Polyhedron Vol. 12, No. 1, pp. 1–5, 1993
Printed in Great Britain

0277–5387/93 $6.00+.00
© 1993 Pergamon Press Ltd

PENDENT ARM MACROCYCLIC COMPLEXES: CRYSTAL STRUCTURES OF Al(TCTA) AND In(TS-TACN)

URSULA BOSSEK, DIETER HANKE and KARL WIEGHARDT*

Lehrstuhl für Anorganische Chemie I, Ruhr-Universität, D-4630 Bochum, Germany

and

BERNHARD NUBER

Anorganisch-Chemisches Institut der Universität, D-6900 Heidelberg, Germany

(*Received* 2 *June* 1992; *accepted* 10 *September* 1992)

Abstract—Complexes of Al^{3+} and In^{3+} containing the pendent arm macrocycles 1,4,7-tris(acetato)-1,4,7-triazacyclononane (TCTA) and 1,4,7-tris(2-mercaptoethyl)-1,4,7-triazacyclononane (TS-TACN), respectively, have been synthesized and their crystal structures determined. Al(TCTA) contains an octahedral *fac*-N_3O_3 donor set, whereas In(TS-TACN) has an octahedral *fac*-N_3S_3 donor set. Average Al—O and In—S distances are 1.846 and 2.397 Å, respectively.

The coordination chemistry of trivalent group 13 metal ions with trianionic pendent-arm macrocyclic ligands (Scheme I) has attracted considerable interest in recent years as potential diagnostic radiopharmaceuticals (Ga, In).[1,2] Their use *in vivo* in nuclear medicine requires kinetic inertness and, in addition, it appears to be desirable that such complexes are electroneutral, have a low molecular weight and are lipophilic in order to cross the blood–brain barrier. Aluminium complexes of this type are also of interest due to the possible involvement of this element in Alzheimer's disease[3] and removal of Al^{3+} from the body. Parker *et al.* and Kaden *et al.* have recently published the synthesis and crystal structures of Ga(TCTA),[4,5] In(R-MeTCTA),[6] In(TCTA-H)Cl[7] and InL[1,8] and tested their utility as radiopharmaceuticals.

Clarke and Martell[9] have established that Ga^{III} and In^{III} bind very strongly to TCTA and noted in accord with Hancock *et al.*'s[10,11] molecular mechanics calculations that this ligand preferentially binds to *small* metal ions. Stability constants ($K_{ML} = [ML]/[L^{3-}][M^{3+}]$) of Ga^{3+} and In^{3+} are $10^{30.98}$ and $10^{26.2}$, respectively. It is to be expected from these studies that Al(TCTA) is even more stable.

Fanwick *et al.*,[5] on the other hand, have introduced a macrocycle with a 1,4,7-triazacyclononane backbone and three 2-mercaptoethyl pendent arms and have reported the structure of Ga(TS-TACN).

In 1982 we reported the synthesis of Al(TCTA),[12]

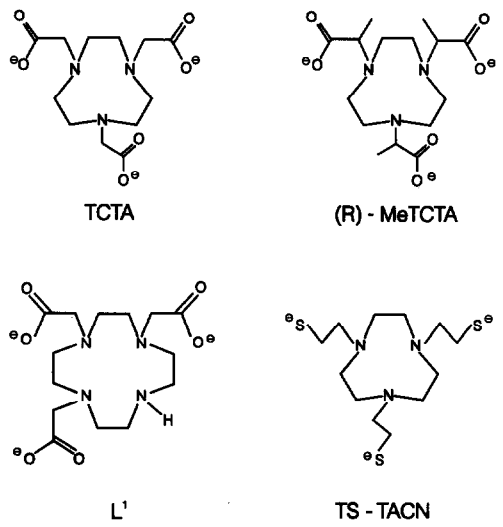

Scheme I.

* Author to whom correspondence should be addressed.

which is extremely stable in aqueous solution over a wide range of pH (0–13) for many days at ambient temperature. We have now determined the crystal structure of this complex. The structure has been briefly reported previously.[13] Since the quality of our structure determination is better we decided to publish our data. Independently of Moore's work,[5] we have prepared the neutral complex In(TS-TACN), the structure of which we also report here.

RESULTS AND DISCUSSION

Colourless crystals suitable for the X-ray crystallography of Al(TCTA) were obtained from the reaction of an aqueous solution of the hexadentate ligand and $AlCl_3 \cdot 6H_2O$, as described in ref. 12. Figure 1 shows the structure; important bond distances and angles are summarized in Table 1. Table 2 gives selected bond lengths and angles of the corresponding complexes of Ga^{III}, In^{III} and Fe^{III}.

As Hancock *et al.*[10] pointed out there are two possible arrangements for the coordinated acetate groups on the pseudo-octahedral complexes of TCTA. The bound base fragment 1,4,7-triazacyclononane is chiral. For a given arrangement of the base fragment, ($\lambda\lambda\lambda$) or ($\delta\delta\delta$) conformation

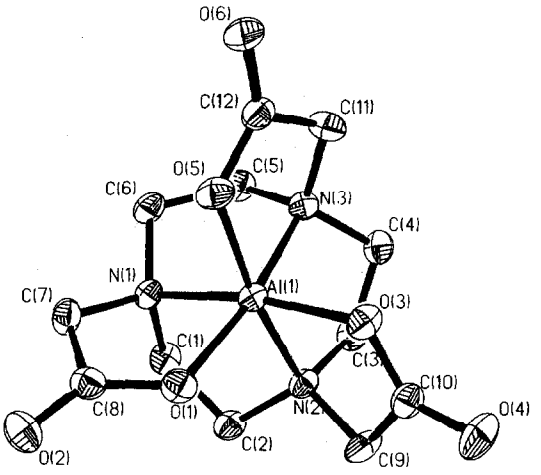

Fig. 1. The structure of Al(TCTA).

of the five-membered M—N—C—C—N chelate rings, the acetate goups may be oriented in a clockwise or anticlockwise fashion (Δ, Λ configuration). The change from type I [Δ($\lambda\lambda\lambda$), Λ($\delta\delta\delta$) enantiomers] to type II [Δ($\delta\delta\delta$), Λ($\lambda\lambda\lambda$) enantiomers][5,9] is a consequence of the increasing M—N bond distance, which forces the metal ion up out of the nine-mem-

Table 1. Selected bond distances (Å) and angles (°) in Al(TCTA) and In(TS-TACN)

Al(TCTA)			
Al—N(1)	2.065(3)	Al—O(1)	1.851(2)
Al—N(2)	2.054(3)	Al—O(3)	1.846(2)
Al—N(3)	2.051(2)	Al—O(5)	1.840(2)
N(1)—Al—N(2)	84.4(1)	N(1)—Al—O(3)	168.1(1)
N(1)—Al—N(3)	84.5(1)	N(2)—Al—O(3)	84.0(1)
N(2)—Al—N(3)	84.4(1)	N(3)—Al—O(3)	96.8(1)
N(1)—Al—O(1)	83.7(1)	O(1)—Al—O(3)	95.1(1)
N(2)—Al—O(2)	96.1(1)	N(1)—Al—O(5)	96.0(1)
N(3)—Al—O(1)	168.0(1)	N(2)—Al—O(5)	168.3(1)
N(3)—Al—O(5)	84.0(1)	O(1)—Al—O(5)	95.6(1)
O(3)—Al—O(5)	95.9(1)		
In(TS-TACN)			
In—S(1)	2.499(1)	In—N(1)	2.379(2)
In—S(2)	2.515(1)	In—N(2)	2.403(2)
In—S(3)	2.518(1)	In—N(3)	2.408(3)
S(1)—In—S(2)	102.6(1)	S(2)—In—S(3)	104.5(1)
S(1)—In—S(3)	106.4(1)	S(2)—In—N(1)	81.3(1)
S(1)—In—N(1)	156.2(1)	S(2)—In—N(2)	155.6(1)
S(1)—In—N(2)	99.0(1)	S(2)—In—N(3)	98.2(1)
S(1)—In—N(3)	81.7(1)	S(3)—In—N(1)	95.0(1)
N(1)—In—N(2)	74.4(1)	S(3)—In—N(2)	79.8(1)
N(1)—In—N(3)	74.5(1)	S(3)—In—N(3)	153.3(1)
N(2)—In—N(3)	73.8(1)		

Table 2. Comparison of structural data of complexes

Complex	av. M—O (Å)	av. M—S (Å)	av. M—N (Å)	C.N.[a]	θ (°)[b]	Ref.
Al(TCTA)	1.846		2.057	6	25.5	This work
Ga(TCTA)	1.933		2.097	6	23.8	4, 11
In(R-MeTCTA)	2.096		2.261	6	10.4	5
InL[1]	2.16–2.20		2.36	7	—	7
Fe(TCTA)	1.962		2.181	6	12.6	12
In(TCTA-H)Cl	2.284, 2.424 2.116		2.332, 2.288 2.331	7	—	6
Ga(TS-TACN)		2.339	2.208	6	24.8	11
In(TS-TACN)		2.511	2.397	6	23	This work

Ligand abbreviations are as in Scheme I.
[a] C.N. = coordination number.
[b] Twist angle as defined in the text.

bered 1,4,7-triazacyclononane ring which causes a strain on the M—O bond. This tension may then be somewhat relieved by switching to the type II structure.[5,9] The twist angle θ is defined as shown below.

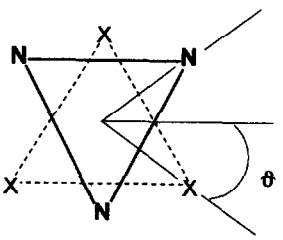

It is 30° for a perfect octahedron and 0° for a trigonal prism. It is clearly seen from the compilation of θ values in Table 2 that Al(TCTA) and Ga(TCTA) have slightly distorted octahedral geometry, whereas for In((R)-MeTCTA) a trigonal prism prevails. This switch from an octahedral to a trigonal prismatic polyhedron relieves the above mentioned strain which is imposed on the ligand by increasing M—N and M—O distances. It is interesting that Ga(TCTA) is octahedral whereas Fe(TCTA) is trigonal prismatic, although the effective ionic radii of six-coordinate Ga^{3+} of 0.76 Å and of high-spin Fe^{3+} of 0.785 Å are actually quite similar.[14] It appears that the configurational switch is triggered within a narrow range of M—N and M—O distances and does not occur gradually.

Not surprisingly, in Al(TCTA) the shortest M—N and M—O distances are observed as compared to those in Ga(TCTA)[4,5] and In((R)-MeTCTA).[6] Consequently, Al(TCTA) and Ga(TCTA) are octahedral (type I), whereas In((R)-MeTCTA) is more trigonal prismatic (type II). The average Al—O distance in Al(TCTA) is very short at 1.846(2) Å and may be compared with the corresponding distance in $[Al(OH_2)_6](NO_3)_3 \cdot 3H_2O$ of 1.877(2) Å.[15]

The reaction of $InBr_3$ dissolved in a sodium methanolate/methanol mixture with the ligand 1,4,7-tris(2-mercaptoethyl)-1,4,7-triazacyclononane at 20°C produced colourless microcrystals of In(TS-TACN). Single crystals were obtained from a hot aqueous solution upon slow cooling. Figure 2 shows the structure, Table 1 summarizes selected bond distances and angles. The ligand is hexadentate providing a *fac*-N_3S_3 donor set around the indium(III) metal ion. As Moore *et al.* have discussed for Ga(TS-TACN) the coordinated ligand TS-TACN has three different sources of chirality. The 1,4,7-triazacyclononane backbone adopts either a $(\delta\delta\delta)_m$ or $(\lambda\lambda\lambda)_m$ conformation, the three pendent arms have either $(\delta\delta\delta)_m$ or $(\lambda\lambda\lambda)_m$ configuration and, in addition, may adopt $(\lambda\lambda\lambda)_p$ or $(\delta\delta\delta)_p$ conformation in either configuration.

In crystals of Ga(TS-TACN)$\cdot 2CH_2Cl_2$ both enantiomeric forms of the neutral complex $\Delta(\lambda\lambda\lambda)_m(\delta\delta\delta)_p$ and $\Lambda(\delta\delta\delta)_m(\lambda\lambda\lambda)_p$ are present in the centric unit cell of the space group $P2_1/n$. In(TS-TACN) crystallizes in the same space group and the same enantiomers are present [$\Delta(\lambda\lambda\lambda)_m(\delta\delta\delta)_p$ and $\Lambda(\delta\delta\delta)_m(\lambda\lambda\lambda)_p$], despite the fact that the M—N and M—S bond distances increase by 0.189 and 0.172 Å, respectively, on going from Ga^{3+} to In^{3+}. These differences reflect quite accurately the enormous difference of effective ionic radii of 0.18 Å between six-coordinate Ga^{3+} and In^{3+}.

We conclude from these observations that the ligand TS-TACN exhibits more flexibility towards

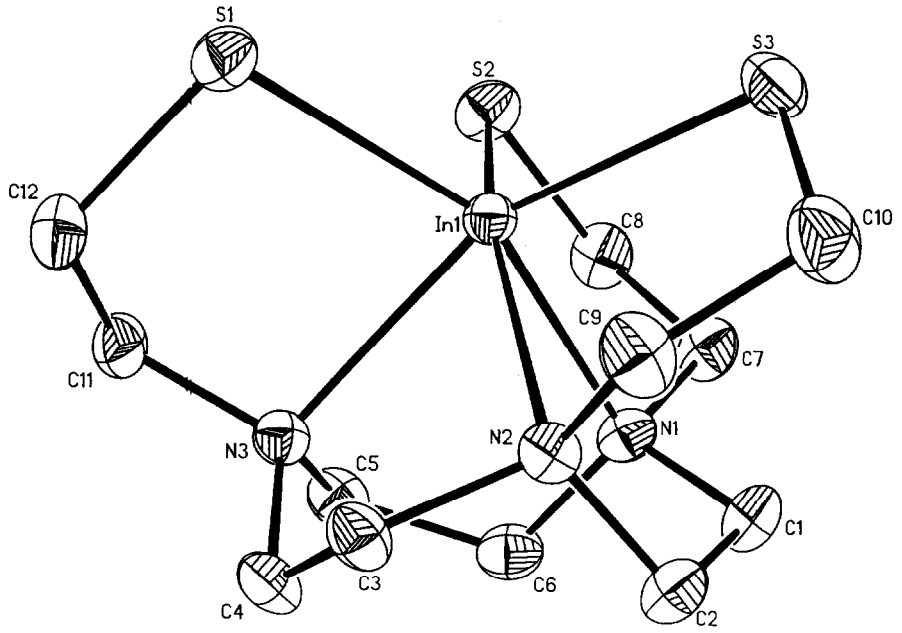

Fig. 2. The structure of In(TS-TACN).

binding of small *and* large metal ions than its counterpart TCTA with three acetate pendent arms.

EXPERIMENTAL

The compound Al(TCTA) and the ligand 1,4,7-tris(2-mercaptoethyl)-1,4,7-triazacyclononane (TS-TACN) were synthesized according to published procedures.[5,12]

Synthesis of In(TS-TACN)

Sodium metal (0.15 g) was carefully dissolved in dry ethanol (25 cm^3) and $InBr_3$ (0.35 g, 1.0 mmol) was added to this solution. To the clear solution the ligand TS-TACN (0.34 g, 1.0 mmol) was added dropwise with stirring at ambient temperature. After 2–3 h a colourless precipitate of In(TS-TACN) formed, which was collected by filtration, washed with ethanol and diethylether and air-dried. Needle shaped, colourless crystals suitable for X-ray crystallography were obtained from recrystallization from a hot water solution (95°C) which was allowed to slowly cool to 20°C (yield: 0.18 g, 43%). Found: C, 34.4; H, 5.8; N, 9.8; S, 22.6. Calc. for $C_{12}H_{24}N_3S_3In$: C, 34.2; H, 5.7; N, 10.0; S, 22.8%.

Crystal structure determinations

Crystal data. $[C_{12}H_{18}N_3O_6Al]$, $M = 327.27$, monoclinic, space group $P2_1/n$, $a = 8.803(6)$, $b = 13.526(9)$, $c = 11.983(6)$ Å, $\beta = 105.43(5)°$, $U = 1375.4$ Å^3 (from 2θ values for 25 reflections measured at $15° < 2\theta < 37°$), $\lambda = 0.71073$ Å, $T = 298$ K, $Z = 4$, $D_c = 1.58$ g cm^{-3}, μ(Mo-K_α) = 0.18 mm^{-1}.

$[C_{12}H_{24}N_3S_3In]$, $M = 421.35$, monoclinic, space group $P2_1/n$, $a = 7.292(1)$, $b = 16.807(4)$, $c = 13.107(2)$ Å, $\beta = 93.69(2)°$, $U = 1603.0$ Å^3 (from 2θ values for 25 reflections measured at $22 < 2\theta < 40°$), $\lambda = 0.71073$ Å, $T = 298$ K, $Z = 4$, $D_c = 1.75$ g cm^{-3}, μ(Mo-K_α) = 1.82 mm^{-1}.

Data processing and structure solution. Intensity data were collected using a Syntex R3 diffractometer, equipped with a graphite monochromator and an Mo-K_α radiation source (ψ-scans). Data were corrected for Lorentz and polarization effects in the usual manner and absorption corrections (ψ-scans of seven reflections) were also carried out in both cases. For Al(TCTA) 4500 reflections were measured ($2\theta_{max} = 60°$, h −11–+8, k 0–16, l 0–16) yielding 2694 with $I \geqslant 2.5\sigma(I)$; for In(TS-TACN) 5144 reflections were measured ($2\theta_{max} = 60°$, h −10–11, k 0–20, l 0–+18) yielding 3809 with $I \geqslant 2.5\sigma(I)$. Both structures were solved by Patterson and difference-Fourier methods, and refined by standard least-squares techniques (SHELXTL PLUS program system). The positions of the hydrogen atoms were calculated and included in the refinement with a common isotropic thermal parameter ($U_{iso} = 0.080$ Å^2); all other atoms were refined with anisotropic thermal parameters. The weighting scheme $w^{-1} = \sigma^2(F)$ was used throughout. For Al(TCTA) refine-

ment converged with $R = 0.049$, $R_w = 0.048$ and for In(TS-TACN) with $R = 0.032$, $R_w = 0.029$. Neutral atom scattering factors and anomalous dispersion data were taken from ref. 16. Final difference maps had no chemically significant maxima.

Thermal parameters, fractional atom coordinates, listings of observed and calculated structure factors have been deposited with the Editor, from whom copies are available on request. Atom coordinates have also been deposited with the Cambridge Crystallographic Data Centre.

REFERENCES

1. M. E. Raichle, *Adv. Chem. Ser.* 1981, **197**, 419.
2. V. L. Alvarez, M. L. Wen, C. Lee, A. D. Lopes, J. D. Rodwell and T. J. McKearn, *Nucl. Med. Biol.* 1986, **13**, 347.
3. J. J. R. F. da Silva and R. J. P. Williams, *The Biological Chemistry of the Elements*. Clarendon Press, Oxford (1991).
4. A. S. Craig, D. Parker, H. Adams and N. A. Bailey, *J. Chem. Soc., Chem. Commun.* 1989, 1793.
5. D. A. Moore, P. E. Fanwick and M. J. Welch, *Inorg. Chem.* 1990, **29**, 672.
6. R. C. Matthews, D. Parker, G. Ferguson, B. Kaitner, A. Harrison and L. Royle, *Polyhedron* 1991, **10**, 1951.
7. A. C. Craig, I. M. Helps, D. Parker, H. Adams, N. A. Bailey, M. G. Williams, J. M. A. Smith and G. Ferguson, *Polyhedron* 1989, **8**, 2481.
8. A. Riesen, T. A. Kaden, W. Ritter and H. R. Mäcke, *J. Chem. Soc., Chem. Commun.* 1989, 460.
9. E. T. Clarke and A. E. Martell, *Inorg. Chim. Acta* 1991, **181**, 273.
10. M. J. van der Merve, J. C. A. Boeyens and R. D. Hancock, *Inorg. Chem.* 1985, **24**, 1208.
11. T. W. Duma, F. Marsicano and R. D. Hancock, *J. Coord. Chem.* 1991, **23**, 221.
12. K. Wieghardt, U. Bossek, P. Chaudhuri, W. Herrmann, B. C. Menke and J. Weiss, *Inorg. Chem.* 1982, **21**, 4308.
13. A. Jyo, Y. Kohno, Y. Terazono and S. Kawano, *Anal. Sci.* 1990, **6**, 629.
14. R. D. Shannon, *Acta Cryst.* 1976, **A32**, 751.
15. D. Lazar, B. Ribár and B. Prelesnik, *Acta Cryst.* 1991, **C47**, 2282.
16. *International Tables for Crystallography*, Vol. IV, pp. 99 and 149. Kynoch Press, Birmingham (1974).

Polyhedron Vol. 12, No. 1, pp. 7–12, 1993
Printed in Great Britain

0277–5387/93 $6.00+.00
© 1993 Pergamon Press Ltd

AXIAL VERSUS EQUATORIAL METAL–LIGAND DISTANCES IN SQUARE-PYRAMIDAL NICKEL(II) COMPLEXES*

EUGEN JÓNA,† MARIÁN KOMAN and ROMAN BOČA

Department of Inorganic Chemistry, Slovak Technical University,
CS-812 37 Bratislava, Czechoslovakia

(*Received* 13 *May* 1992; *accepted* 10 *September* 1992)

Abstract—The integral stereospecific influences in metal complexes have been analysed, namely the equatorial–axial and angular interactions. These concepts have been extended to five-coordinate complexes, in particular to nickel(II) complexes. The experimental findings are supported by the molecular orbital calculations on model complexes.

A few years ago a concept of the equatorial–axial (shortly equ–ax) interactions was proposed on the basis of both the experimental data and theoretical calculations.[1,2] This was motivated by the works of Hathaway[3] and Gažo *et al.*[4] on correlations among structural parameters within square-bipyramidal copper(II) complexes. Later extensions to nickel(II) complexes,[5] as well as to hexafluoro, hexachloro, hexanitro and hexaaqua complexes of the first row transition metals,[6–8] showed a more general validity of structural correlations abbreviated as R_a vs R_e dependences. These dependences manifest themselves in the fact that increasing axial metal–ligand distances (R_a, 2×) decrease the equatorial distances (R_e, 4×) and *vice versa*. Also, other groups[9,10] closely followed our approach and analogous correlations have been reported for cobalt(III), nickel(II) and zinc(II) complexes of the *trans*-$[MX_2(L_N)_4]$ type, $(L_N)_4$ being an N-donor macrocyclic ligand. Recently we found well-defined R_a vs R_e correlations in complexes of the *trans*-$[Ni(NCS)_2(L_N)_4]\cdot nG$ type, G being a guest molecule.[11]

The aim of the present work is to document structural correlations in square-pyramidal nickel(II) complexes. This allows an extension of the equatorial–axial interaction concept to other than square-bipyramidal complexes. The chromophores to be analysed span two classes: $\{NiN_5\}$ and *trans*-$\{NiXL_4\}$, L being an N- or O-donor ligand, X = Cl, Br and I.

In addition, the molecular structure of $[Ni(NCS)_2(3,5\text{-}Me_2pip)_3]$ is reported here. This was motivated by the fact that its coordination polyhedron may be either square-pyramidal or trigonal bipyramidal, and eventually an intermediate between these limiting cases; its position on the R_a vs R_e correlation curve is under question.

ANALYSIS OF STRUCTURAL DATA

Penta-coordinate complexes with square-pyramidal geometry for the chromophore may be characterized by a couple of basal angles, α and β, which for the ideal square-pyramidal system of C_{4v} symmetry adopt values of 180° (Fig. 1). The apical ligand is denoted as X and $\beta \geqslant \alpha$ usually holds. In the majority of square-pyramidal complexes the central atom M shows a displacement out of the basal plane and thus $\alpha = \beta < 180°$. On the contrary,

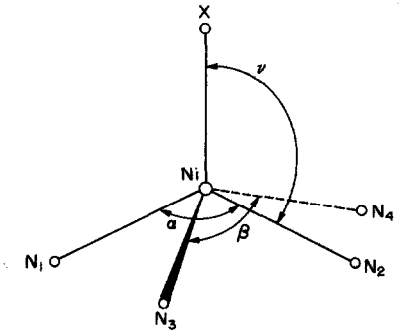

Fig. 1. Definition of structural parameters in square-pyramidal complexes.

*Part 4 of the series Statistical Study of Structural Manifestation of Mutual Influence of Ligands.

†Author to whom correspondence should be addressed.

Table 1. Structural data on penta-coordinate nickel(II) complexes[a]

No.	Complex	R_a	R_e	δ	T	100τ	v_e	Ref.
Group A: {NiN_5} chromophore								
1	$[Ni(C_{11}H_{20}N_5O_2)]\cdot H_2O$	204.9	203.6	1.3	0.994	13.8	96.5	15
2	$[Ni(C_{23}H_{29}N_5)](ClO_4)_2\cdot MeNO_2$	201.1	209.1	−8.0	1.040	3.3	99.0	16
3	$[Ni(C_{14}H_{32}N_4)(VH_3CN)](ClO_4)_2$	198.0	214.3	−16.3	1.082	0.0	99.1	17
4	$[Ni(C_{14}H_{32}N_4)(N_3)](ClO_4)_2$	195.0	210.4	−15.4	1.079	4.3		18
5	$[Ni(C_{16}H_{16}B_{26}N_4O_2)(py)]\cdot 2py$	203.3	202.1	1.2	0.994	9.2	101.1	19
6	$[Ni(dmgBF_2)_2(NH_2CH_2Ph)]_2$	228.0	185.9	42.1	0.815	0.2	97.0	20
7	$[Ni(dmgBF_2)_2(NH_2Ph)]_2$	266.3	187.1	79.2	0.702	4.5		21
8	$\{[Ni(dmgBF_2)_2]_2(4,4'\text{-bipy})\}$	235.0	185.0	50.0	0.787	3.3	96.3	22
9	$[Ni(C_{26}H_{42}N_3)(NCS)_2]$	216.0	195.0	21.0	0.903	5.3	99.3	23
10	$[Ni(3,5\text{-}Me_2pip)_2(NCS)_2]$	204.0	201.9	2.1	0.989	0.5	100.6	24
Group B: {NiL_4X} chromophore								
11	$[Ni(Ph_3AsO)_4Br]Br\cdot 3/2PhCH_3\cdot H_2O$	250.6	200.0	50.6	0.798	3.2	100.4	25
12	$[Ni(C_{10}H_{24}N_4)Cl]Cl$	233.8	207.9	25.9	0.889	2.2	99.4	26
13	$[Ni(C_{11}H_{19}N_4O_2)Br]$	266.2	189.6	76.6	0.712	2.0	97.4	27
14	$[Ni(C_{15}H_{22}N_4)Br]Br\cdot H_2O$	279.1	189.0	90.1	0.677	3.7	95.5	28
15	$[Ni(C_{11}H_{18}BF_2N_4O_2)I]$	283.4	187.4	96.0	0.661	2.8	97.3	29
16	$(Me_2pip)[Ni(dmgBF_2)_2I]$	284.2	187.0	97.2	0.658	4.0	96.0	30

[a] Distances in pm, angles in °.

for the ideal trigonal-bipyramidal geometry (D_{3h} symmetry) the angle α becomes 120°. An intermediate geometry may be characterized by the difference $(\beta-\alpha)$, which for C_{4v} symmetry equals 0° and for D_{3h} symmetry equals 60°. Thus, a distortion parameter $\tau = (\alpha-\beta)/60$ has been introduced[12] for the penta-coordinate systems, which expresses the degree of trigonality as $\tau = 0$ for C_{4v} and $\tau = 1$ for D_{3h} geometries, respectively. Other alternatives for expressing the degree of trigonality have also been reported.[13,14]

A set of X-ray structural data on square-pyramidal nickel(II) complexes has been abstracted from the structural data bases. Only the complexes having {NiN_5} (group A) and {NiL_4X} (group B) chromophores (X = Cl, Br, I, L = N, O) have been subjected to analysis. The relevant data (for $\tau < 0.15$) are collected in Table 1. Of interest are the R_a (1×) and R_e (4×) metal–ligand distances, the degree of tetragonal distortion $\delta = R_a - R_e$, the tetragonality parameter $T = R_e/R_a$, the trigonality parameter $\tau = (\alpha-\beta)/60$ and the mean bonding angle $v_e(L_a—Ni—L_e)$.

MOLECULAR ORBITAL CALCULATIONS

The molecular orbital calculations have been performed by the quasi-relativistic INDO/1 method.[31,32] This method spans the class of all valence, and non-empirical calculations which also account for dominant relativistic effects (*s*- and *p*-orbital contraction side-by-side with *d*-orbital expansion). The geometry optimization has been performed for selected bonding coordinates, keeping the rest of the geometrical degrees of freedom unchanged.

EQU–AX INTERACTIONS IN PENTA-COORDINATE COMPLEXES

The experimental R_a values have been plotted vs R_e and the corresponding dependences are shown in Fig. 2. The linear relationship arises from the least-squares fitting. The nearly linear correlation can be considered significant as the correlation coefficients fulfil the relationship $|r| > r_{crit}$ at the 0.01 and 0.05 levels of significance for groups A and B, respectively. Thus, it may be concluded that an R_a vs R_e correlation with the negative slope exists: with increasing R_a values the mean R_e values decrease and *vice versa*. This finding may be interpreted in terms of equatorial–axial interactions: the weakening of the axial (apical) metal–ligand bond is accompanied by the strengthening of the equatorial (basal) metal–ligand bonds so that the total bonding capacity remains almost constant and it is only redistributed among the existing bonds. However, other, mostly steric, effects exist which apply sim-

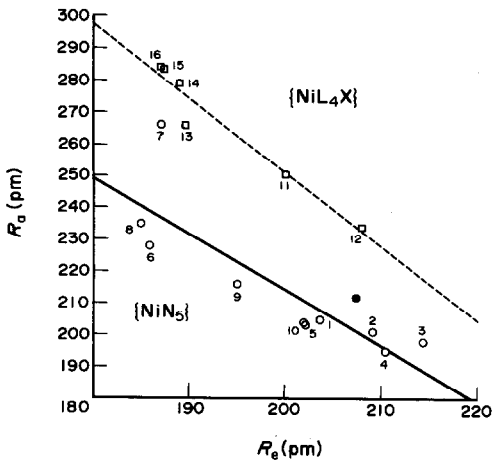

Fig. 2. R_e vs R_e dependences for $\{NiN_5\}$ (group A, hollow circles) and $\{NiL_4X\}$ (group B, hollow squares) chromophores. Filled circle = theoretical result for the $[Ni(NH_3)_3(NCS)_2]$ complex. Numbering according to Table 1.

ultaneously electronic in origin effects and may lead to higher deviations from the ideal (smooth) correlation curve.

The coordination polyhedra of group A prefer an elongated form of the tetragonal pyramid, with tetragonality $T = 0.702$–0.994. Three complexes, however, prefer the slightly compressed tetragonal pyramid. The latter class is less numerous and it covers complexes of the macrocyclic ligands (derivatives of tetramethylcyclam) in the equatorial plane with a monodentate ligand (acetonitrile, azide) occupying the axial position. This finding is contradictory to the behaviour of hexa-coordinate *trans*-$[Ni(L_N)_4(NCS)_2]$ complexes where the macrocycle ligands with a smaller central "hole" prefer an elongated form of the tetragonal bipyramid.[11] Within group A the parameter δ varies from -16.3 to 79.2 pm so that the "length" of the correlation is considerable. The greatest values of δ appear for the bis(difluoroboratodimethylglyoximato) nickel(II) complexes (**6**, **7** and **8**). The molecular geometry of the benzylamine adduct (**6**) closely parallels that of the 4,4′-bipyridine adduct (**7**), but it is markedly in contrast to that of the aniline adduct (**8**). In particular, the plane of the phenyl ring is perpendicular to the macrocycle plane so that a π-interaction between them is impossible. A long axial Ni—N distance in the aniline adduct has been discussed in connection with steric effects.[20]

The $[Ni(3,5\text{-}Me_2pip)_3(NCS)_2]$ complex shows electronic absorption bands and magnetic moment characteristic for penta-coordinate nickel(II) complexes,[33] but these data cannot be used to differentiate between the C_{4v} and D_{3h} symmetry of the $[NiN_5]$ chromophore. According to X-ray data,[24] presented in Fig. 3, the coordination polyhedron is close to a regular tetragonal pyramid, as $\tau = 0.005$. One of the 3,5-Me_2pip ligands occupies the axial position and the remaining ligands (two 3,5-Me_2pip and two NCS ligands) form the equatorial plane. The corresponding R_a and R_e parameters obey the

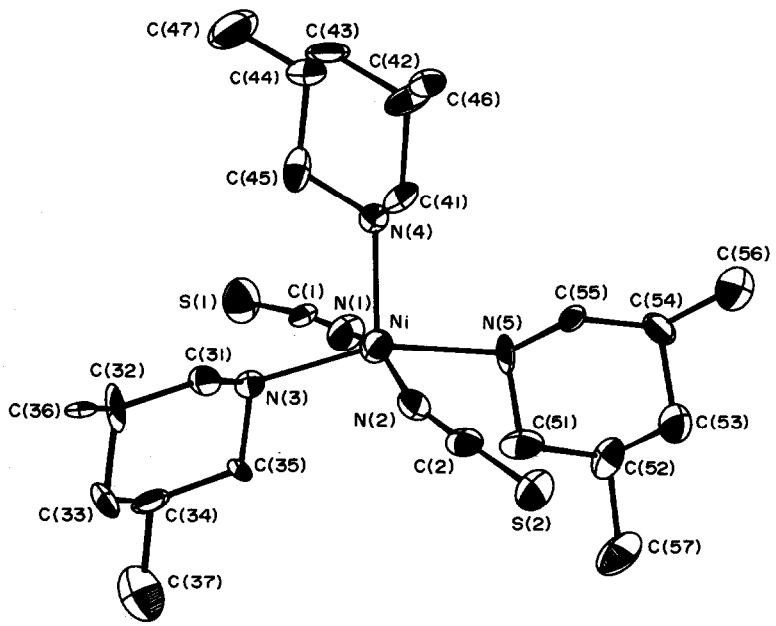

Fig. 3. Molecular structure of the $[Ni(3,5\text{-}Me_2pip)_3(NCS)_2]$ complex.

correlation curve found for the square-pyramidal $\{NiN_5\}$ chromophore (Fig. 2).

The unusual structure of the $[Ni(3,5\text{-}Me_2pip)_3(NCS)_2]$ complex has been subjected to theoretical analysis. Actually, the geometry optimization of the $[Ni(NH_3)_3(NCS)_2]$ complex has been performed with respect to 11 degrees of freedom. The resulting values are: $R_a(Ni—N_a) = 211.9$ (204), $R(N_a—H) = 103.6$, $\nu(Ni—N_a—H) = 107.2$, $R_e(Ni—N_e) = 213.8$ (210, 205), $\nu_e(N_a—Ni—N_e) = 113.1$ (98.9, 102.1), $R(N_e—H) = 103.3$, $\nu(Ni—N_e—H) = 107.7$, $R(Ni—NCS) = 200.9$ (197, 195), $\nu(N_a—Ni—NCS) = 95.5$ (87.4, 104.1), $R(N—C) = 122.2$ (115, 116) and $R(C—S) = 159.4$ (161, 156), where the experimental data are in parentheses (distances in pm, angles in °). The position of this complex within the R_a vs R_e plot is also shown in Fig. 2 (filled circle) and it may be concluded that it spans the range of experimental data.

For group B the tetragonality parameter varies as $T = 0.658$–0.889 and the distortion degree is $\delta = 25.9$–96.0 pm. The greatest degree of distortion is observed for bromine and iodine derivatives. For example, the Ni—Br distance in complex **14** is 279.1 pm, which is significantly longer than that found in hexa-coordinate $[Ni(py)_4Br_2]$ where $R(Ni—Br) = 258$ pm.[34] Thus, the axial nickel–bromine and nickel–iodine interactions in five-coordinate complexes are far weaker than normally observed.

In order to place groups A and B into a common set, a correction for the $R_a(Ni—X)$ value of the differing covalent radii of the halide ions, r_X, has been made: $R_a(cor) = R_a - (r_X - r_N)$. The $R_a(cor)$ vs R_e correlation is shown in Fig. 4, alongside the 99% confidence interval. As the correlation coefficient is $\rho = 0.84$, the correlation is fairly good.

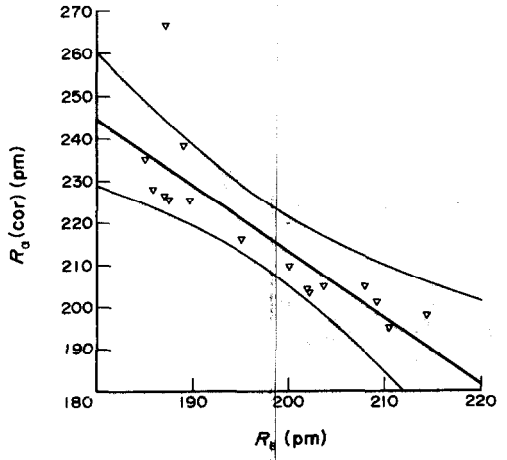

Fig. 4. $R_a(cor)$ vs R_e correlation in penta-coordinate nickel(II) complexes (group A+B). Correlation coefficient $\rho = 0.84$; 99% confidence interval is shown.

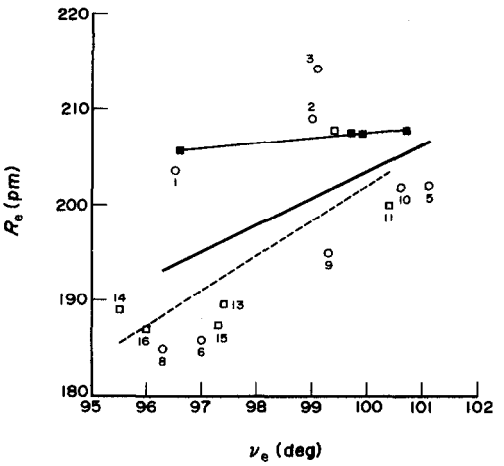

Fig. 5. R_e vs ν_e dependences for $\{NiN_5\}$ (group A, hollow circles) and $\{NiL_4X\}$ (group B, hollow squares) chromophores. Filled squares = theoretical results for $[Ni(NH_3)_4X]^+$ complexes. Numbering according to Table 1.

ANGULAR DEPENDENCE IN PENTA-COORDINATE COMPLEXES

In addition to the R_a vs R_e dependence classified as a manifestation of the equatorial–axial interactions in complexes, another structural correlation has been observed. The bond length R_e is interrelated to the bond angle $\nu_e(X—Ni—N)$ and the corresponding plot is shown in Fig. 5. The R_e vs ν_e dependence is approximated by a straight line and again a significant correlation is proven. Thus, it may be concluded that with increasing R_e values the bond angle ν_e increases. This behaviour may be considered as a new type of integral stereospecific influence in metal complexes, termed hereafter as the "angular dependence".

A common R_e vs ν_e correlation for groups A and B again exists (Fig. 6) with the correlation coefficient $\rho = 0.65$.

The geometry optimization for low-spin $^1[Ni(NH_3)_4X]^+$ complexes has been performed, X being F, Cl, Br and I. Within the square-pyramidal structure of C_{4v} (exactly C_4) symmetry five geometry parameters are independent: distances $R_a(Ni—X)$, $R_e(Ni—N)$ and $R_3(N—H)$ and angles $\nu_e(X—Ni—N)$ and $\nu_1(Ni—N—H)$, or, alternatively, $R_a(N—X)$, $R_1(o\text{-}Ni)$, $R_2(o\text{-}N)$, $R_3(N—H)$ and $\nu_2(o\text{-}N—H)$, where o is the centre of the square defined by four NH_3 groups. As a result of the geometry optimization, the total energy function $E_T = f(R_a, R_e, R_3, \nu_e, \nu_1)$ or $E_T = f(R_a, R_1, R_2, R_3, \nu_2)$ adopts a minimum value.

The relevant equilibrium coordinates are listed in Table 2. The geometry of the NH_3 group is almost

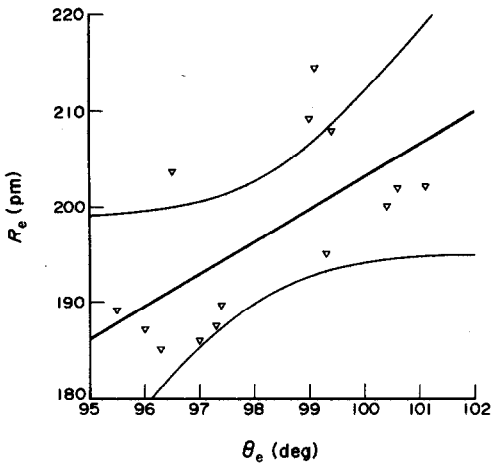

Fig. 6. R_e vs ν_e correlation in penta-coordinate nickel(II) complexes (group A+B). Correlation coefficient $\rho = 0.65$; 99% confidence interval is shown.

constant within the series under study: the angle ν_2(o-N—H) spans the range 108.2–108.7° and the distance keeps the value R_3 = 103.9 pm. The only remarkable change is represented by the out-of-plane displacement of the nickel atom: R_1(o-Ni) = 23.5, 35.7, 35.7 and 38.5 pm. This is the raison d'etre of the bond angle variation ν_e(X—Ni—N) = 96.6, 99.9, 99.9 and 100.7°. It may be concluded that with the decreasing polarity of the apical R_a(Ni—X) bond the out-of-plane displacement R_1(o-Ni) of the nickel atom increases, the ν_e(X—Ni—N) bond angle simultaneously increases and the R_e(Ni—N) bond length also increases. Thus, an R_e vs ν_e correlation is predicted according to an ascending line. The last finding may be rationalized in terms of the extended electron-pair repulsion theory.[35] As far as the iodine atom allows a localization of the bonding electron pair closest to the nickel atom, it repels more effectively the remaining electron pairs at the Ni—N bonds, then the R_e(Ni—N) bond length and the ν_e(X—Ni—N) bond angle increases.

CONCLUSIONS

The bonding capacity of the central atom obeys an integral redistribution among ligands present in the coordination sphere. The integral stereospecific influences may be documented by the equatorial–axial and angular interactions, respectively. They manifest themselves in correlations among structural parameters, namely the R_a vs R_e and R_e vs ν_e dependences.

Table 2. Calculated geometry of $[Ni(NH_3)_4X]^{+1}$ complexes

Geometry parameter	X F	Cl	Br	I
R_a(Ni—X) (pm)	210.4	229.8	239.2	253.3
R_e(Ni—N) (pm)	205.7	207.6	207.5	207.9
ν_e(X—Ni—N) (°)	96.6	99.7	99.9	100.7
R_1(o-Ni) (pm)	23.5	35.7	35.7	38.5
R_2(o-N) (pm)	204.4	204.5	204.4	204.3
ν_2(o-N—H) (°)	108.2	108.5	108.6	108.7
R_3(N—H) (pm)	103.9	103.9	103.9	103.9

REFERENCES

1. J. Gažo, R. Boča, E. Jóna, M. Kabešóva, Ľ. Macá škova, J. Šima, P. Pelikán and F. Valach, *Coord. Chem. Rev.* 1982, **43**, 87.
2. J. Gažo, R. Boča, E. Jóna, M. Kabešová, Ľ. Macá šková and J. Šima, *Pure Appl. Chem.* 1983, **55**, 65.
3. B. J. Hathaway, *Struct. Bonding* 1973, **14**, 49.
4. J. Gažo, I. B. Bersuker, J. Garaj, M. Kabešová, J. Kohout, H. Langfelderová, M. Melnik, M. Serátor and F. Valach, *Coord. Chem. Rev.* 1976, **19**, 253.
5. E. Jóna, F. Valach, J. Gažo, E. Fendrich and T. Šramko, *Koord. Khim.* 1983, **9**, 86.
6. R. Boča, *Chem. Zvesti* 1981, **35**, 769.
7. R. Boča, *Chem. Zvesti* 1981, **35**, 779.
8. R. Boča, *Chem. Zvesti* 1983, **37**, 297.
9. M. Sugimoto, J. Fujita, H. Ito, K. Toriumi and T. Ito, *Inorg. Chem.* 1983, **22**, 995.
10. T. Ito, M. Kato and H. Ito, *Bull. Chem. Soc. Japan* 1984, **57**, 1556.
11. E. Jóna, J. Kožíšek, M. Koman and R. Boča, *Polyhedron* 1992, **11**, 573.
12. A. W. Addison, T. N. Rao, J. Reedijk, J. van Rijn and G. C. Verschoor, *J. Chem. Soc., Dalton Trans.* 1984, 1349.
13. S. Tyagi and B. J. Hathaway, *J. Chem. Soc., Dalton Trans.* 1981, 2029.
14. W. D. Harrison, D. M. Kenedy, M. Power, R. Sheahan and B. J. Hathaway, *J. Chem. Soc., Dalton Trans.* 1981, 1556.
15. R. Machida, E. Kimura and Y. Kushi, *Inorg. Chem.* 1986, **25**, 3461.
16. B. F. Hoskins and F. D. Whillans, *J. Chem. Soc., Dalton Trans.* 1975, 657.
17. J. S. Crick, B. F. Hoskins and P. A. Tregloan, *Inorg. Chim. Acta* 1986, **114**, L33.
18. M. J. D'Aniello Jr, M. T. Mocella, F. Wagner, E. K. Berefield and J. C. Paul, *J. Am. Chem. Soc.* 1975, **97**, 192.
19. R. E. Cobbledick, F. W. B. Einstein, E. C. Lingafelter and P. L. Samuel, *Acta Cryst.* 1986, **C42**, 969.
20. F. S. Stephens and R. S. Vagg, *Inorg. Chim. Acta* 1983, **69**, 103.
21. R. S. Vagg and E. C. Watton, *Acta Cryst.* 1978, **B34**, 2715.

22. F. S. Stephens and R. S. Vagg, *Inorg. Chim. Acta* 1980, **42**, 139.
23. M. DiVaira, *J. Chem. Soc.* (*A*) 1971, 148.
24. M. Koman, E. Jóna and E. Ďurčanská, *Acta Cryst.* 1992, **C48**, 1652.
25. G. Oliva, E. E. Castellano, J. Zukerman-Schpector and A. C. Massabni, *Inorg. Chim. Acta* 1984, **89**, 9.
26. J. G. Gibson and E. D. McKenzie, *J. Chem. Soc., Dalton Trans.* 1974, 989.
27. J. Korvenranta and H. Saarinen, *Fin. Chem. Lett.* 1979, 219.
28. E. B. Fleischer and S. W. Hawkinson, *Inorg. Chem.* 1968, **7**, 2312.
29. F. S. Stephens and R. S. Vagg, *Inorg. Chim. Acta* 1981, **52**, 245.
30. O. P. Anderson, *Acta Cryst.* 1981, **B37**, 1194.
31. R. Boča, *Int. J. Quantum Chem.* 1988, **34**, 385.
32. R. Boča, Program MOSEM7. Slovak Technical University, Bratislava (1989).
33. M. Koman, E. Jóna and E. Ďurčanská, *Inorg. Chim. Acta* 1986, **47**, 121.
34. A. S. Antsyskhina and M. A. Porai-Koshitz, *Krystallographiya* 1958, **3**, 676.
35. D. L. Kepert, in *Inorganic Chemistry Concepts*, Vol. 6. Springer-Verlag, Berlin (1982).

Polyhedron Vol. 12, No. 1, pp. 13–17, 1993
Printed in Great Britain

0277–5387/93 $6.00+.00
© 1993 Pergamon Press Ltd

SYNTHESIS OF A RHODIUM METHYLTHIOLATE AND INSERTION OF CS_2 INTO THE Rh—SCH_3 BOND. STRUCTURE OF THE THIOXANTHATE [$(pp_3)RhSC(S)SCH_3$] [pp_3 = TRIS(2-(DIPHENYLPHOSPHINO)ETHYL)PHOSPHINE]

MASSIMO DI VAIRA, DONELLA ROVAI and PIERO STOPPIONI*

Dipartimento di Chimica, Università di Firenze, Via Maragliano 77, 50144 Firenze, Italy

(*Received* 31 *July* 1992; *accepted* 3 *September* 1992)

Abstract—The reaction between the $(pp_3)Rh^I$ fragment [pp_3 = tris(2-(diphenylphosphino)-ethyl)phosphine, $P(CH_2CH_2PPh_2)_3$] and $NaSCH_3$ readily yields the methylthiolate derivative [$(pp_3)RhSCH_3$]. The sulphur atom of this compound is attacked by the electrophile $CF_3SO_3CH_3$ to yield the stable dimethylsulphide complex [$(pp_3)RhS(CH_3)_2]CF_3SO_3$. Furthermore, the rhodium methylthiolate undergoes CS_2 insertion to form the thioxanthate [$(pp_3)RhSC(S)SCH_3$], which has been characterized by a complete X-ray crystallographic analysis.

Recently, there has been growing interest in mononuclear complexes with the thiolate (M-SR) and hydrosulphide (M-SH) groups, because of the reactivity exhibited by such ligands towards organic substrates.[1] We have recently reported about a family of hydrochalcogenide rhodium derivatives formed by the tripodal polyphosphine tris(2-(diphenylphosphino)ethyl)phosphine, pp_3, and described their reactivity towards electrophiles (H^+, CH_3^+).[2] The chalcogen atom in such compounds appears to be the site for the electrophilic attack, which yields the hydride methyl- or hydro-chalcogenide derivatives of rhodium(III) through a stereospecific internal oxidative addition involving the acidic X—H bond.[3] It has been shown that processes of this type are controlled by the tripodal polyphosphine pp_3, which favours smoother reactions at the metal centre.[4]

With the aim of investigating further the chalcogenide chemistry at the $(pp_3)Rh^I$ fragment, however, avoiding the labile X—H bond, we have undertaken the synthesis of alkylchalcogenolate complexes and the study of their reactivity. Here we report on the isolation and structure determination of a mononuclear rhodium(I) methylthiolate stabilized by the pp_3 ligand and some aspects of its reactivity.

* Author to whom correspondence should be addressed.

EXPERIMENTAL

All reactions and manipulations were performed under an atmosphere of oxygen-free nitrogen. Solvents were freshly distilled under nitrogen from the appropriate drying agents immediately before use. The ^{31}P and ^1H NMR spectra were obtained in CD_2Cl_2 using a Varian VXR 300 spectrometer operating at 121.4 and 300.1 MHz and are referred to external 85% H_3PO_4 and internal TMS, respectively.

Synthetic procedures

Synthesis of the compounds. [$(pp_3)RhSCH_3$]: $NaSCH_3$ (0.21 g, 3 mmol) dissolved in methanol (10 cm^3) was added to a THF (40 cm^3) solution of $[(pp_3)Rh(cod)]^+$ (1 mmol), generated *in situ*.[5] Orange needles of [$(pp_3)RhSCH_3$] were obtained on leaving the resulting solution overnight (yield 85%). Found: C, 62.7; H, 5.6; S, 3.8. Calc. for [$(pp_3)RhSCH_3$], $C_{43}H_{45}P_4RhS$: C, 62.9; H, 5.5; S, 3.9%. NMR data in CD_2Cl_2: ^1H: δ 2.19 (3H, s, SCH_3). ^{31}P: δ 146.3 [1P, dq, $^1J(P_ARh)$ = 126.9 Hz, $^2J(P_AP_M)$ = 17.3 Hz, P_{apical}], 40.3 [3P, dd, $^1J(P_MRh)$ = 147.6 Hz, $P_{meridional}$].

[$(pp_3)RhS(CH_3)_2]CF_3SO_3$: Neat $CF_3SO_3CH_3$ (0.37 mmol) was added to a suspension of [(pp_3) $RhSCH_3$] (0.3 g, 0.37 mmol) in THF (30 cm^3) at 0°C. The complex dissolved in 30 min and red

crystals of $[(pp_3)RhS(CH_3)_2]CF_3SO_3$ were obtained by the addition of benzene (30 cm^3). Yield 80%. Found: C, 54.7; H, 5.0; S, 6.4. Calc. for $[(pp_3)RhS(CH_3)_2]CF_3SO_3$, $C_{45}H_{48}F_3O_3P_4RhS_2$: C, 54.9; H, 4.9; S, 6.5%. NMR data in $(CD_3)_2CO$: ^1H: δ 1.77 [6H, d, $^3J(HRh) = 2.9$ Hz, $S(CH_3)_2$]. ^{31}P: δ 145.2 [1P, dq, $^1J(P_ARh) = 109.1$ Hz, $^2J(P_AP_M) = 17.0$ Hz, P_{apical}], 47.2 [3P, dd, $^1J(P_MRh) = 143.2$ Hz, $P_{meridional}$].

$[(pp_3)RhSC(S)SCH_3]$: Neat CS_2 (0.6 mmol) was added to a suspension of $[(pp_3)RhSCH_3]$ (0.3 g, 0.37 mmol) in THF (30 cm^3) at room temperature. The complex dissolved in 24 h and red crystals of $[(pp_3)RhSC(S)SCH_3]$ were obtained by adding methanol (20 cm^3). Yield 55%. Found: C, 58.9; H, 5.1; S, 10.6. Calc. for $[(pp_3)RhSC(S)SCH_3]$, $C_{44}H_{45}P_4RhS_3$: C, 58.9; H, 5.1; S, 10.7%. NMR data in CD_2Cl_2: ^1H: δ 2.02 (3H, s, SCH_3). ^{31}P: δ 146.7 [1P, dq, $^1J(P_ARh) = 127.0$ Hz, $^2J(P_AP_M) = 17.1$ Hz, P_{apical}], 40.3 [3P, dd, $^1J(P_MRh) = 148.2$ Hz, $P_{meridional}$].

X-ray crystallographic studies

All measurements were carried out at room temperature on an Enraf–Nonius CAD4 diffractometer using graphite-monochromated Mo-K_α radiation ($\lambda = 0.71069$ Å). The crystal used had the dimensions $0.20 \times 0.20 \times 0.25$ mm. Cell constants were obtained from least-squares refinement of the setting angles of 24 reflections ($14 < \theta < 18°$).

Crystal data. $C_{44}H_{45}P_4RhS_3$, $M = 896.84$, trigonal, space group $P3_2$ (No. 145), $a = 17.360(4)$, $c = 11.702(3)$ Å, $V = 3054(1)$ Å^3, $Z = 3$, $D_{calc} = 1.462$ g cm^{-3}, μ(Mo-K_α) = 7.46 cm^{-1}, $F(000) = 1386$.

Data were collected for $2 \leqslant \theta \leqslant 23°$ by ω–2θ scans with $(0.90 + 0.34 \tan\theta)°$ scan width and 1–5° min^{-1} scan speed. No crystal movement or decay was detected over the data collection. Of 3122 independent reflections measured 1788 having $I > 3\sigma(I)$ were used for structure solution and refinement. An empirical absorption correction was applied after the structure had been solved.[6]

The structure was solved by heavy-atom methods and refined by full-matrix least-squares. The principal computer programs used in the crystallographic calculations are listed in refs 6 and 7. The rhodium, phosphorus, sulphur and the carbon atoms of the thioxanthate ligand were refined anisotropically, whereas the other carbon and hydrogen atoms were assigned isotropic temperature factors. The hydrogen atoms were in calculated positions (C—H = 0.96 Å, $U_H = 1.2U_C$) and phenyl groups were refined as rigid bodies with idealized geometry. The z coordinate of rhodium was fixed during refinement due to the polar nature of the space group. The alternative choice of the $P3_1$ space group was rejected on the basis of the R ratio test.[8] Data were weighted according to $w^{-1} = [\sigma^2(F) + 0.0010F^2]$. Refinement converged at $R = \Sigma ||F_o| - |F_c|| / \Sigma |F_o| = 0.054$ and $R_w = [\Sigma (|F_o| - |F_c|)^2 / \Sigma w(F_o)^2]^{1/2} = 0.057$ for 189 parameters. The extreme values of residual electron density in the final ΔF synthesis were 0.65 (on proximity of the rhodium position, without any chemical meaning) and -0.38 e Å^{-3}. Scattering factors were from refs 7 (carbon, hydrogen, phosphorus and sulphur) and 9a (rhodium), those for rhodium being corrected for anomalous dispersion.[9b] Values of selected bond distances and angles are given in Table 1. Tables of final atomic positional and thermal parameters, full lists of bond lengths and angles, tables of hydrogen atoms positions and a list of observed and calculated structure factors have been deposited as supplementary material.

Table 1. Selected bond distances (Å) and angles (°) for $[(pp_3)RhSC(S)SCH_3]$

Rh—P(1)	2.350(5)	S(1)—C(7)	1.675(18)
Rh—P(2)	2.339(5)	S(2)—C(7)	1.647(18)
Rh—P(3)	2.369(5)	S(3)—C(7)	1.666(19)
Rh—P(4)	2.206(4)	S(2)—C(8)	1.748(22)
Rh—S(1)	2.409(5)		
P(1)—Rh—P(2)	119.8(2)	P(3)—Rh—S(1)	104.8(2)
P(1)—Rh—P(3)	119.9(2)	P(4)—Rh—S(1)	168.3(2)
P(1)—Rh—P(4)	83.2(2)	Rh—S(1)—C(7)	122.7(7)
P(2)—Rh—P(3)	116.2(2)	S(1)—C(7)—S(2)	112.6(1.1)
P(2)—Rh—P(4)	82.9(2)	S(1)—C(7)—S(3)	124.0(1.1)
P(3)—Rh—P(4)	83.7(2)	S(2)—C(7)—S(3)	123.3(1.1)
P(1)—Rh—S(1)	99.0(2)	C(7)—S(2)—C(8)	107.9(1.2)
P(2)—Rh—S(1)	86.0(2)		

RESULTS AND DISCUSSION

The methylthiolate $[(pp_3)RhSCH_3]$ derivative was obtained in high yield when a three-fold excess of $NaSCH_3$ was reacted with $[(pp_3)Rh(cod)]^+$, generated *in situ*. The compound was poorly soluble in THF and in chlorinated solvents like $CHCl_3$ and CH_2Cl_2. In the latter solvents it slowly reacted to give chloro complexes. Such sensitivity of metal thiolates to chlorinated hydrocarbon solvents has been observed previously and has been ascribed to the nucleophilicity of the coordinated sulphur atom.[10] Highly diagnostic for the solution stereochemistry of the compound is its $^{31}P\{^1H\}$ NMR spectrum, exhibiting a first-order AM_3X spin system consistent with a trigonal bipyramidal geometry around the metal, with the peripheral phosphorus atoms of the polydentate ligand in the equatorial plane and the central pp_3 phosphorus and the sulphur atom in the axial positions. Both the coupling constants and chemical shifts are in the expected ranges for trigonal bipyramidal compounds of rhodium(I) with tripodal polyphosphines.[11] The proton spectrum of the compound exhibits, in addition to the usual uninformative pattern due to the protons of the pp_3 ligand, a signal whose intensity and chemical shift are consistent with those expected for the group SCH_3.[2]

The methylthiolate derivative suspended in THF readily reacted with a stoichiometric amount of $CF_3SO_3CH_3$ to give the compound $[(pp_3)RhS(CH_3)_2]CF_3SO_3$. The dimethylsulphide derivative was soluble in THF, acetone, CH_2Cl_2 and $CHCl_3$ and its solutions were stable under nitrogen. The $^{31}P\{^1H\}$ NMR spectrum, showing an AM_3X spin system, is consistent with a trigonal bipyramidal arrangement about the metal, similar to that of the parent methylthiolate, and the ^1H NMR spectrum exhibits a resonance whose intensity is in accordance with the proposed formula.

The methylthiolate derivative $[(pp_3)RhSCH_3]$ suspended in THF slowly reacted with carbon disulphide to yield a compound of the formula $[(pp_3)RhSC(S)SCH_3]$. The strong IR band at 995 cm^{-1} is typical for the thioxanthate group.[12] The $^{31}P\{^1H\}$ NMR spectrum of the compound, which consists of a first-order AM_3X spin system, is in agreement with a trigonal bipyramidal geometry around the metal, with the apical phosphorus atom of the ligand in the axial position and the terminal phosphorus atoms in equatorial positions.

Previous studies on thioxanthate complexes, which have been obtained either by reaction of the metal halide with $M(S_2CSR)$, where M is an alkali metal ion,[12,13] or through the less common route of CS_2 insertion into transition metal–thiolate bonds,[14] have shown that the S_2CSR group is bound to the metal centre with two sulphur atoms. Such a feature of the thioxanthate ligand contrasts with the electronic requirements of the $(pp_3)Rh^I$ fragment, which accommodates two-electron donors.[4] In order to ascertain the coordination

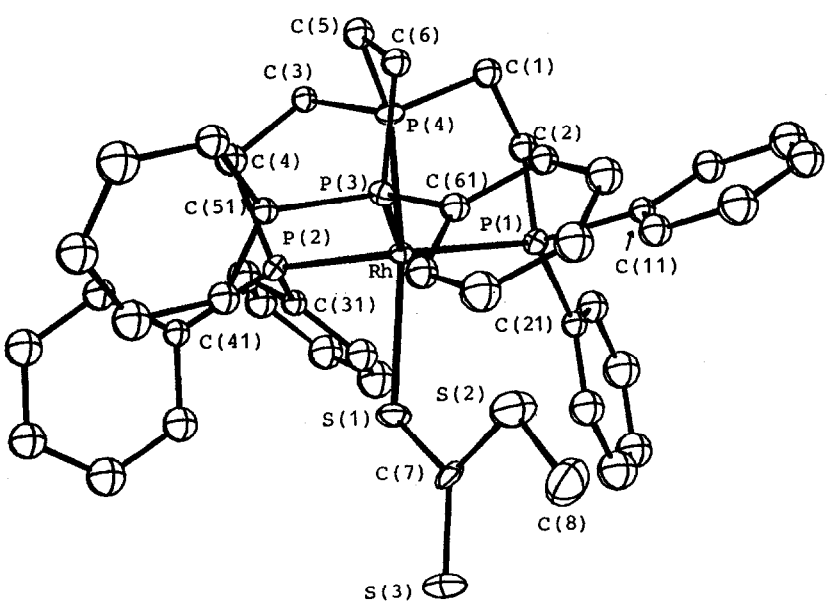

Fig. 1. Perspective view of the $[(pp_3)RhSC(S)SCH_3]$ molecule, with 20% probability ellipsoids. Only the first carbon atom of each phenyl group is labelled for clarity.

mode of the thioxanthate in the present [(pp_3)RhSC(S)SCH_3] compound, its crystal structure was determined by a single crystal X-ray analysis.

The structure of the compound is formed by isolated [(pp_3)RhSC(S)SCH_3] molecules (Fig. 1), in which the metal atom is coordinated by the four phosphorus atoms of the phosphine ligand and one sulphur atom of the thioxanthate group with essentially trigonal bipyramidal geometry. The central phosphorus atom of the pp_3 ligand and the sulphur donor, occupying the axial positions, form with the metal atom an angle [P(4)—Rh—S(1) = 168.3(2)°] which deviates from the idealized 180° value, probably as a consequence of non-bonded interactions between the thioxanthate group and phenyl rings. The metal atom lies 0.27 Å away from the plane through the equatorial phosphorus atoms towards the sulphur donor. The Rh—P distances are comparable to those existing in the [(pp_3)Rh(SH)] complex,[2] and the Rh—S distance is 0.04 Å shorter than in the latter compound. The C—S distances within the thioxanthate ligand are grossly comparable to each other, presumably due to extensive delocalization,[15] and their mean, of 1.66(1) Å, is slightly smaller than the values, in the range 1.67–1.74 Å, reported for the C—S distances in bidentate thioxanthate ligands.[14,15] We are not aware of other structures of metal compounds containing monodentate thioxanthate ligands which might be referred to for better comparisons.

Insertion of CS_2 into transition-metal thiolates has been reported. However, there has been little investigation on the mechanism of CS_2 insertion into metal–thiolate bonds; it has been recently suggested[14] that at least two extremes can be envisioned regarding the initial interaction of the metal complex with the incoming carbon disulphide: (1) pre-coordination of CS_2 at the metal centre; or (2) attack by free CS_2 on the sulphur atom of the thiolate ligand. Qualitative observations on CS_2 insertion into the M—S bonds in the complexes $CpW(CO)_2(PPh_3)SR$[16] and $CpRu(PPh_3)_2SR$[14] suggested pre-coordinated insertion in those cases. On the other hand, the present results seem to favour the second hypothesis. In particular, the straightforward formation of the dimethylsulphide [(pp_3)RhS$(CH_3)_2$]CF_3SO_3 by electrophilic attack clearly shows that the sulphur atom is preferred as a nucleophilic site with respect to the metal atom. Moreover, the structural results showing that the thioxanthate group acts as a monodentate ligand prove that the tripodal pp_3 ligand is tightly bound to the metal. This opposes pre-coordination by CS_2, thus disfavouring the above route (1) in the present case.

We have attempted to rationalize some aspects of the formation of [(pp_3)RhSC(S)SCH_3] by attack of CS_2 on [(pp_3)RhSCH_3] by means of extended Hückel calculations[17,18] using the program CACAO[19] and, in part, by Fenske–Hall calculations[20] on model systems, with atomic parameter data from the literature[18] or as provided with the package.[20] According to the previous considerations and to views presented for similar processes[21] we have considered as the most probable first step the facile attack [Scheme 1, (a)] of the bent CS_2 electrophile on the sulphur nucleophilic site of the parent rhodium complex. This step should be followed by rotation of the S_2CSCH_3 group thus formed, in the course of which the methyl-substituted sulphur atom should be displaced from the metal environment by one of the unsubstituted sulphur atoms. However, a four-centred transition state as shown in (b), with the undeformed (PP_3)Rh moiety, is unlikely as it would imply a high energy barrier. A transition state of this type, not requiring

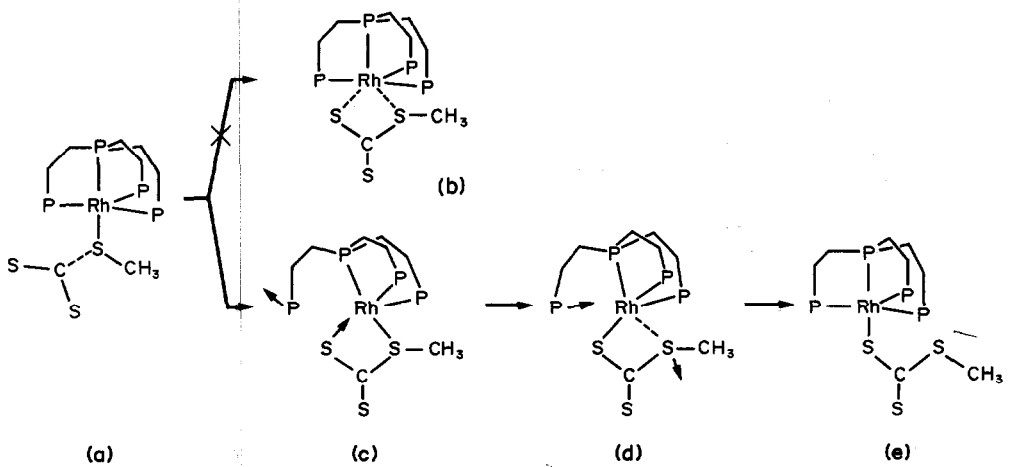

Scheme 1.

an open coordination site, has been proposed for COS or CS_2 attack on the W—O bond of $W(CO)_5OR$ systems on the basis of experimental data.[21] Actually, we find that in the latter systems a set of metal-based low-energy empty orbitals may assist in the course of the process, keeping the energy barrier comparatively low. On the other hand, only one σ-type empty hybrid is available in the $(pp_3)Rh$ moiety, the other virtual orbitals being contracted and at high energies. We suggest that in the present case the rearrangement of the S_2CSCH_3 group should be accompanied by detachment of one arm of the pp_3 ligand. Although, as stated above, the ligand appears to be tightly bound, such a detachment has already been found to occur in solution in the presence of strong incoming ligands.[22] A concerted process, such as that schematized in (c), may sensibly reduce the energy barrier preserving orbital symmetry. Finally, detachment from rhodium of the substituted sulphur atom accompanied by approach to the metal by the phosphorus atom of the uncoordinated arm (d) is an easy process leading to the final product (e).

The overlap populations of both Rh—S bonds in the proposed five-coordinate intermediate, between (c) and (d), may vary considerably with the assumed mutual orientation of the two ligands, although significant energy barriers for rearrangements from the geometry shown in (d) exist. Taking all this into consideration, we find no clear evidence for electronic factors strongly favouring detachment of a specific sulphur atom. The steric hindrance due to the CH_3 group may be the factor disfavouring coordination by the substituted sulphur atom. It could also prevent it from bonding again to the metal through possible iterations in solution of the process described above. On the other hand, exchange occurring in solution between the two unsubstituted sulphur atoms, in the bonding position to the metal atom, cannot be ruled out.

Acknowledgement—We thank the Italian Ministero dell'Università e della Ricerca Scientifica e Technologica for financial support.

REFERENCES

1. (a) D. Sellmann, P. Lechner, F. Knoch and M. Moll, *J. Am. Chem. Soc.* 1992, **114**, 922; (b) P. G. Jessop, S. J. Rettig, C. L. Lee and B. R. James, *Inorg. Chem.* 1991, **30**, 4617; (c) D. P. Klein, G. M. Kloster and R. G. Bergman, *J. Am. Chem. Soc.* 1990, **112**, 2022; (d) J. J. Garcia, H. Torrens, H. Adams, N. A. Bailey and P. M. Maitlis, *J. Chem. Soc., Chem. Commun.* 1991, 74; (e) P. M. Treichel, M. S. Schmidt and R. A. Crane, *Inorg. Chem.* 1991, **30**, 379; (f) W. F. Liaw, C. Kim, M. Y. Darensbourg and A. L. Rheingold, *J. Am. Chem. Soc.* 1989, **111**, 3591.
2. M. Di Vaira, M. Peruzzini and P. Stoppioni, *Inorg. Chem.* 1991, **30**, 1001.
3. M. Di Vaira, D. Rovai, P. Stoppioni and M. Peruzzini, *J. Organomet. Chem.* 1991, **420**, 135.
4. C. Bianchini, D. Masi, A. Meli, M. Peruzzini and F. Zanobini, *J. Am. Chem. Soc.* 1988, **110**, 6411.
5. M. P. Anderson and L. H. Pignolet, *Inorg. Chem.* 1981, **20**, 4101.
6. N. Walker and D. Stuart *Acta Cryst., Sect. A* 1983, **39**, 158.
7. G. M. Sheldrick, SHELX, A Program for Crystal Structure Determination. University of Cambridge, Cambridge, U.K. (1977).
8. W. C. Hamilton, *Acta Cryst.* 1965, **18**, 502.
9. *International Tables for X-ray Crystallography.* Kynoch Press, Birmingham, U.K. (1974): (a) Vol. IV, p. 99; (b) Vol. IV, p. 149.
10. A. Shaver, R. D. Lai, P. H. Bird and W. Wickramasinghe, *Can. J. Chem.* 1985, **63**, 2555 and refs therein.
11. (a) M. Di Vaira, M. Peruzzini, F. Zanobini and P. Stoppioni, *Inorg. Chim. Acta* 1983, **69**, 37; (b) J. J. Gambaro, W. H. Hohman and D. W. Meek, *Inorg. Chem.* 1989, **28**, 4154; (c) C. Bianchini, A. Meli, M. Peruzzini, F. Zanobini and P. Zanello, *Organometallics* 1990, **9**, 241.
12. G. Gattow and W. Behrendt, *Carbon Sulfides and their Inorganic and Complex Chemistry* (Edited by A. Senning); Topics in Sulfur Chemistry 2, p. 183. Georg Thieme, Stuttgart, F.R.G. (1977) and refs therein.
13. (a) T. Wilczewki, M. Bochenska and J. F. Biernat, *J. Organomet. Chem.* 1981, **215**, 87; (b) L. B. Reventos and A. G. Alonso, *J. Organomet. Chem.* 1986, **309**, 179.
14. A. Shaver, P. Plouffe, P. Bird and E. Livingstone, *Inorg. Chem.* 1990, **29**, 1826 and refs therein.
15. D. F. Lewis, S. J. Lippard and J. A. Zubieta, *Inorg. Chem.* 1972, **11**, 823.
16. A. Shaver, B. S. Lum, P. Bird and K. Arnold, *Inorg. Chem.* 1989, **28**, 1900.
17. R. Hoffmann, *J. Chem. Phys.* 1963, **39**, 1397.
18. R. Hoffmann, *Angew. Chem., Int. Edn Engl.* 1982, **21**, 711 and refs therein.
19. C. Mealli and D. M. Proserpio, *J. Chem. Educ.* 1990, **67**, 3399.
20. M. B. Hall and R. F. Fenske, *Inorg. Chem.* 1972, **11**, 768.
21. D. J. Darensbourg, B. L. Mueller, C. J. Bischoff, S. S. Chojnacki and J. H. Reibenspies, *Inorg. Chem.* 1991, **30**, 2418.
22. C. Bianchini, A. Meli, M. Peruzzini, J. A. Ramirez, A. Vacca, F. Vizza and F. Zanobini, *Organometallics* 1989, **8**, 337; C. Bianchini, A. Meli, M. Peruzzini, F. Zanobini and P. Zanello, *Organometallics* 1990, **9**, 241.

Polyhedron Vol. 12, No. 1, pp. 19–26, 1993
Printed in Great Britain

0277–5387/93 $6.00+.00
© 1993 Pergamon Press Ltd

PHOSPHOLYL (PHOSPHACYCLOPENTADIENYL) AND ARSOLYL (ARSACYCLOPENTADIENYL) COMPLEXES OF YTTERBIUM(II) AND SAMARIUM(II). SYNTHETIC, STRUCTURAL AND MULTINUCLEAR (^{31}P AND ^{171}Yb) NMR STUDIES

F. NIEF,† L. RICARD and F. MATHEY

Laboratoire "Heteroatomes et Coordination", CNRS URA 1499, 91128 Palaiseau, France

(*Received* 31 *July* 1992; *accepted* 3 *September* 1992)

Abstract—Bis(η^5-phospholyl) or bis(η^5-arsolyl)M(THF)$_2$ complexes, where M = Sm or Yb, can be obtained either by reaction of potassium phospholides or arsolides with $MI_2(THF)_2$ or by cleavage of the P—P or As—As bond of a biphospholyl or biarsolyl by ytterbium or samarium metal powders. The THF molecules that coordinate to the metal are labile when the ligands are 2,3,4,5-tetramethylphospholyl or arsolyl, but not when they are 2,5-diphenylphospholyl. An X-ray crystal structure of bis(η^5-2,5-diphenylphospholyl)Yb(THF)$_2$ is presented. ^{171}Yb and ^{31}P NMR studies reveal that exchange of ligands is occurring in bis(η^5-2,3,4,5-tetramethylphospholyl)Yb(THF)$_2$; this exchange is slow at room temperature and frozen at −20°C. For bis(η^5-2,5-phenyldiphenylphospholyl)Yb(THF)$_2$ ^{31}P NMR data suggest that no exchange is occurring at room temperature.

In a recent communication[1] we briefly described the synthesis of bis(η^5-2,3,4,5-tetramethylphospholyl) complexes of samarium(II) and ytterbium(II), $L_2M(THF)_2$ (**1**·2THF and **2**·2THF, respectively) by two methods: (a) reaction of an anionic precursor such as L^-K^+ with the lanthanide(II) iodides; or (b) direct reaction of the biphospholyl L—L with ytterbium or samarium as metallic powders (Scheme 1).

At this point, we wanted to check if we could apply these methods to the synthesis of other heterocyclopentadienyl compounds; this led us to develop the use of the η^5-2,3,4,5-tetramethylarsolyl ligand. We also wanted to see whether one could synthesize π-heterocyclopentadienyl compounds, where electron-withdrawing substituents were present on the ring; for this purpose, we used the η^5-2,5-diphenylphospholyl ligand.

† Author to whom correspondence should be addressed.

RESULTS AND DISCUSSION

Arsolyl complexes

The synthesis of the 2,3,4,5-tetramethylarsole ring system has recently been described by Fagan *et al.*,[2] by reaction of $PhAsCl_2$ with zirconacyclopentadienes. Instead of using $PhAsCl_2$, we reacted the zirconacyclopentadiene with $AsCl_3$, thus obtaining a chloroarsole. However, in our hands, this chloroarsole was rather unstable, and, although we were able to successfully transform it into the desired 2,3,4,5,2′,3′,4′,5′-octamethyl-1,1′-biarsolyl (**6**), we chose another route: reaction of zirconacyclopentadiene (**3**) with $PhAsCl_2$ gave 1-phenyl-2,3,4,5-tetramethylarsole **4** in good yield as a reasonably stable yellow oil, as described.[2] Potassium cleavage of **4** yielded potassium 2,3,4,5-tetramethylarsolide (**5**) as an unsolvated stable white salt, which could be coupled with $Bu^n_4N^+Br_3^-$ to give **6** (Scheme 2).

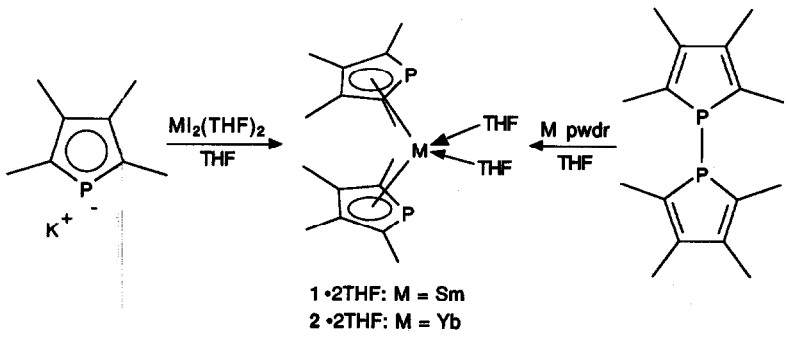

Scheme 1.

Interaction of potassium arsolide (**5**) with YbI_2 and SmI_2 in THF resulted in an immediate colour change, to dark reddish-brown for samarium and to dark red for ytterbium. Evaporation of the solvents led to desolvation of THF and obtention of amorphous powders (**7**: M = Sm, black; **8**: M = Yb, green), of the composition L_2M, as shown by ^1H NMR; the spectra in d_8-THF did not reveal the presence of non-deuterated THF. d_8-THF coordinates to **7** and **8** upon dissolution, as shown by the colour change back to dark reddish-brown for samarium and dark red for ytterbium. With M = Yb, careful evaporation of THF yielded $(C_4Me_4As)_2Yb(THF)_2$(**8**·2THF), as shown by ^1H NMR, but attempted recrystallization of this material led to desolvation and elemental analysis of all arsenic complexes was poor. Complexes **7** and **8** could also be made by the direct interaction of biarsolyl (**6**) with samarium and ytterbium as elements. Thus, overnight stirring of a THF solution of **6** with commercial samarium and ytterbium powders resulted in complete transformation into **7** and **8** respectively. In this way, similar to the previously described synthesis of complexes **1** and **2** from a biphospholyl,[1] the metals samarium and ytterbium are electropositive enough to be able to transfer electrons to the As—As bond of **6**, resulting in cleavage of this bond and stabilization by π-complexation (Scheme 3).

The NMR characteristics of **7**·2THF and **8**·2THF are very similar to those of **1**·2THF and **2**·2THF, respectively, as far as chemical shifts are concerned. One also observes, in **7**·2THF, the paramagnetic shift of the arsolyl ring carbons at high field and that of the methyl groups at low field.

2,5-*Diphenylphospholyl complexes*

A number of published studies in the field of divalent lanthanide π-complexes have used pentamethylcyclopentadienyl (C_5Me_5 or Cp*) as the π-ligand.[3] This ligand increases the solubility and enhances the reactivity of the electron-rich metal in the lower oxidation state. A five-electron π-ligand bearing electron-withdrawing substituent, on the other hand, should stabilize the +II vs the +III oxidation state more than the Cp* ligand. There are few examples of such complexes in the

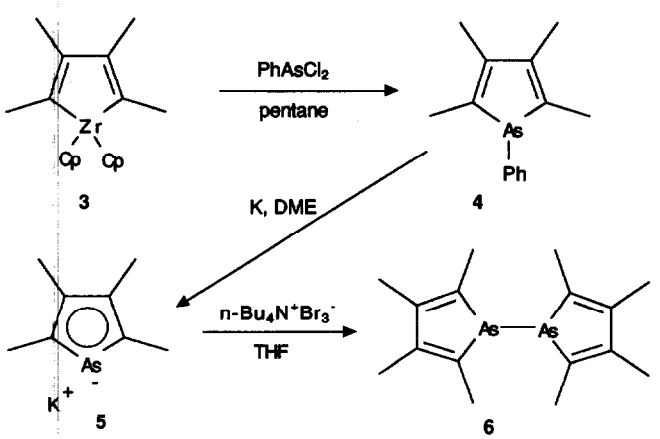

Scheme 2.

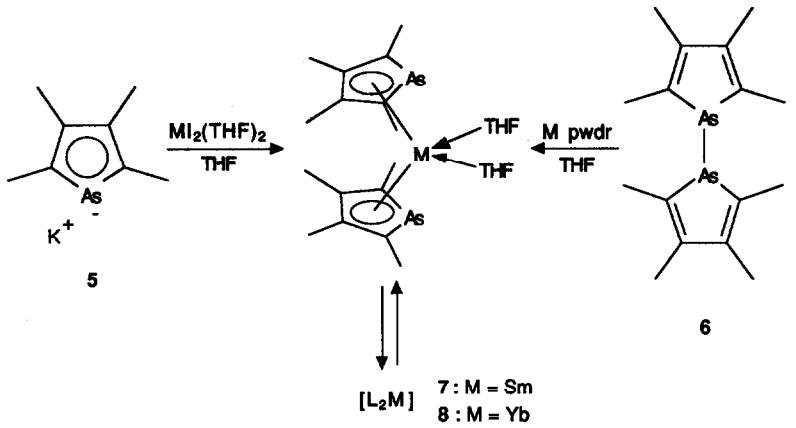

Scheme 3.

literature; one can note the preparation of complexes with silyl-[4] and phosphinyl-substituted[5] cyclopentadienes and also that of indenyl[6] complexes. We, therefore, wanted to devise the synthesis of complexes of samarium and ytterbium with phenyl substituents on the phospholyl rings.

Some time ago, Charrier successfully prepared 2,5,2′,5′-tetraphenyl-1,1′-biphospholyl (**9**).[7] We thought that in order to prepare π-complexes of the 2,5-dimethylphospholyl ligand, the most suitable method would be method (b), which uses the direct interaction of the zero-valent metal with the P—P bond, because in this case no inorganic salt (KI) would interfere with the isolation of the products which are expected to be of low solubility.

When a solution of **9** was stirred in the presence of samarium or ytterbium metal no reaction took place after 24 h at room temperature. If a small (*ca* 20 mg) amount of $HgCl_2$ was added to the reaction mixture, activation of the metals occurred and the reaction proceeded to yield reasonable yields of **10**·2THF and **11**·2THF, respectively, after 16 h (Scheme 4).

These compounds are only slightly soluble in THF and almost totally insoluble in toluene or hexane, and the THF which is coordinated to the metal shows no sign of lability; overnight pumping of the solids did not lead to partial desolvation. **11**·2THF gave a correct microanalysis. The spectral characteristics of **10**·2THF and **11**·2THF fully support their structure. All ^1H and ^{13}C NMR resonances could be resolved and attributed. In **10**·2THF one observes an upfield paramagnetic shift of the heterocyclic ring ^{31}P and ^{13}C atom resonances, and a downfield shift of the H3 proton ($\approx$20 ppm).

Crystal structure of **11**·2*THF*

A suitable crystal of **11**·2THF could be obtained by slow cooling of a warm saturated THF solution. Crystal data and data collection parameters are listed in Table 1. Table 2 lists selected bond lengths and angles for **11**·2THF. There are two nearly identical but independent molecules in the unit cell, and Fig. 1 presents an ORTEP plot of one molecule of **11**·2THF. This structure shows the pseudo-tetrahedral coordination geometry around the ytterbium atom, if one considers the values of the centroid—Yb—centroid and O—Yb—O angles (129° and 82°, respectively). The former angle is slightly smaller than that found in other L_2Yb

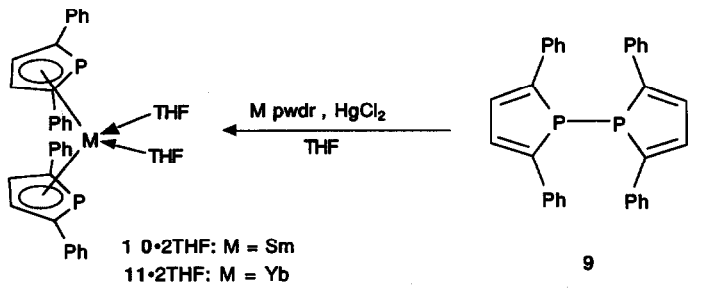

Scheme 4.

Table 1. Crystal data and details of data collection

Empirical formula	$C_{40}H_{40}O_2P_2Yb$
Fw	787.75
Space group	$P2_1/n$ (no. 14)
a (Å)	16.321(2)
b (Å)	17.287(2)
c (Å)	23.934(4)
β (°)	93.40(1)
V (Å^3)	6741(2)
Z	8
Crystal size (mm)	$0.06 \times 0.20 \times 0.30$
ρ_{calc} (g cm^{-1})	1.555
Radiation	Mo-K_α
Monochromator	Graphite
Temperature (°C)	-150 ± 0.5
2θ max (°)	55
Scan type	ω
Unique reflections	12,277
Reflections with $F^2 > 3\sigma(F^2)$	9240
R	0.026
R_w	0.036
Convergence, largest shift/error	0.02

$(THF)_2$ compounds: 133°, 134° and 134°, respectively, in $(Me_3SiC_5H_4)_2Yb(THF)_2$,[4] $(Me_3CC_5H_4)_2Yb(THF)_2$[8] and $[Me_2Pt(Ph_2PC_5H_4)_2Yb(THF)_2]THF$;[5] whereas the O—Yb—O angle is similar to those described. The Yb—O, Yb—C and Yb—P[9] bonds are also quite similar to those already mentioned. The heterocyclic bond angles and distances are not significantly different from those of other π-phospholyl complexes, the most noteworthy feature being the partial double-bond character of the P—C bond (1.77 Å). The phospholyl and the phenyl rings of **11**·2THF are almost planar. The molecule is rather asymmetrical: one of the phenyl rings is almost co-planar to a phospholyl ring (dihedral angle = 5°), and the other phospholyl–phenyl dihedral angles range from 25° to 80°. Furthermore, in the same molecule the phenyl ring *ipso*-carbons of one ligand bend towards the ytterbium atom, whereas for the other ligand the *ipso* carbons bend away from the metal. Packing forces might be responsible for these irregularities.

^{171}Yb and ^{31}P NMR spectra

^{171}Yb NMR has recently been introduced as an additional tool in the study of ytterbium(II) organometallic compounds.[10] A range of chemical shifts and heteronuclear coupling constants is already available.[11] However, no ^{31}P–^{171}Yb coupling constants have ever been reported; fast chemical exchange of the dmpe ligand in $Yb[N(SiMe_3)_2]$(dmpe) precluded the observation of any P—Yb coupling.[10]

In the ^{31}P spectrum of **2**·2THF at room temperature a singlet is observed at 81.2 ppm, with broad humps symmetrically disposed on both sides of the peak. As the temperature is gradually lowered these humps sharpen and at −20°C, their width at half height ($w_{1/2}$) becomes equal to the central peak. For **11**·2THF satellite peaks can be seen at room

Table 2. Selected bond distances (Å) and angles (°)

Yb—P(1)	2.959(1)	Yb—O(40)	2.384(3)
Yb—C(2)	2.784(4)	P(1)—C(2)	1.779(4)
Yb—C(3)	2.784(4)	P(1)—C(5)	1.770(4)
Yb—C(4)	2.818(4)	C(2)—C(3)	1.396(5)
Yb—C(5)	2.831(4)	C(3)—C(4)	1.399(5)
Yb—P(18)	2.986(1)	C(4)—C(5)	1.393(5)
Yb—C(19)	2.867(4)	P(18)—C(19)	1.780(4)
Yb—C(20)	2.812(4)	P(18)—C(22)	1.769(4)
Yb—C(21)	2.784(4)	C(19)—C(20)	1.405(5)
Yb—C(22)	2.812(4)	C(20)—C(21)	1.386(6)
Yb—O(35)	2.405(3)	C(21)—C(22)	1.401(6)

O(35)—Yb—O(40)	82.16(9)	C(2)—P(1)—C(5)	90.2(2)
P(1)—C(2)—C(3)	110.8(3)	C(2)—C(3)—C(4)	113.9(3)
C(3)—C(4)—C(5)	113.3(3)	P(1)—C(5)—C(4)	111.6(3)
P(18)—C(22)—C(21)	111.4(3)	P(18)—C(19)—C(20)	110.6(3)
C(20)—C(21)—C(22)	113.4(4)	C(19)—C(20)—C(21)	114.1(4)
C(19)—P(18)—C(22)	90.4(2)		

Numbers in parentheses are estimated standard deviations in the least significant digits.

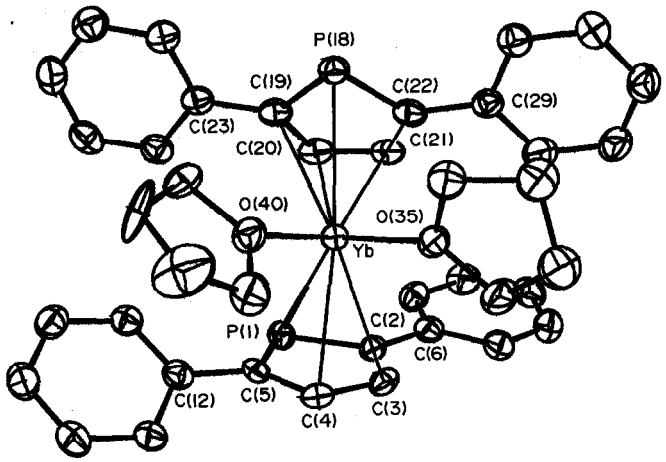

Fig. 1. ORTEP plot of one molecule of **11**·2THF. Thermal ellipsoids are scaled to enclose 50% of the overall electronic density.

temperature (Fig. 2). The separation between the satellite lines is 100 Hz for **2**·2THF and 50 Hz for **11**·2THF. We successfully obtained, at 70 MHz, ^{171}Yb NMR spectra of **2**·2THF and **8**·2THF. Unfortunately, we could not detect the resonance of **11**·2THF, presumably because of the very low solubility of this compound. At −30°C, the resonance of **8**·2THF is a broad ($w_{1/2} \approx 50$ Hz) peak at 316 ppm [downfield from the resonance of $Cp^*_2Yb(THF)_2$ at 0 ppm] and that of **2**·2THF is a reasonably well-resolved 1/2/1 triplet at 242 ppm; the separation between the lines is 100 Hz (Fig. 3). At room temperature, this triplet collapses into a broad ($w_{1/2} \approx 100$ Hz) signal at 185 ppm, where a triplet structure is barely noticeable. These results indicate that: (a) the satellites in the ^{31}P spectra are ^{171}Yb satellites, the measured separation is the ^{31}P–^{171}Yb coupling constant and for **11**·2THF we verified that the separation was the same at different field strengths, thus indicating a coupling constant; (b) that the stoichiometry in solution is indeed $L_2M(THF)_2$, as indicated by the triplet with $J = 100$ Hz in the ^{171}Yb spectrum of **2**·2THF. Temperature dependence of the chemical shift had already been noted;[10] and (c) that an exchange process, slow at room temperature and frozen at −20°C, is occurring for the phospholyl ligands of **2**·2THF in THF solution. The sharp appearance of the ^{171}Yb satellites at 20°C suggests that for this compound, no exchange takes place at this temperature.

Our future goals include the investigation of the

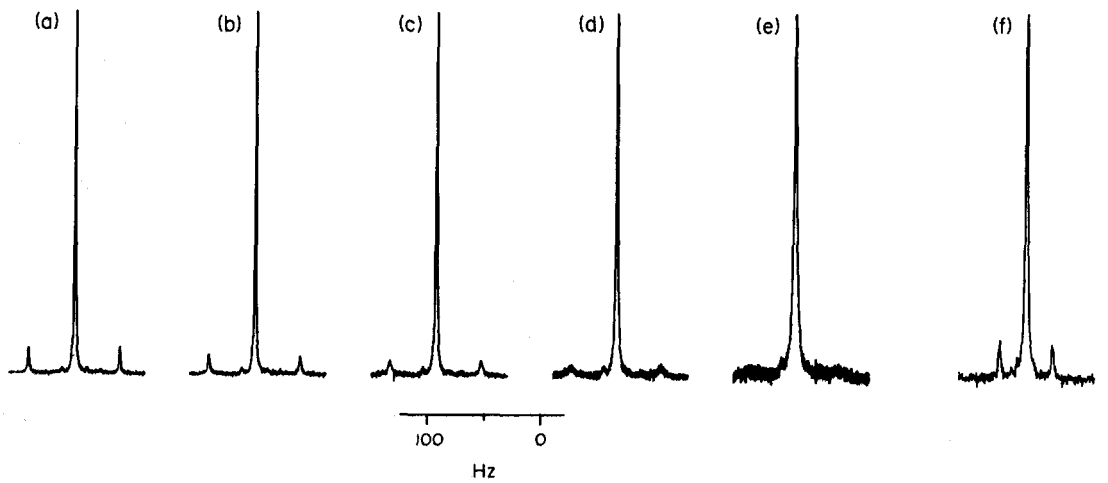

Fig. 2. (a)–(e) ^{31}P NMR spectra of **2**·2THF at different temperatures: (a) −20°C, (b) −10°C, (c) 0°C, (d) +10°C, (e) +20°C; (f) ^{31}P NMR spectrum of **11**·2THF at +20°C.

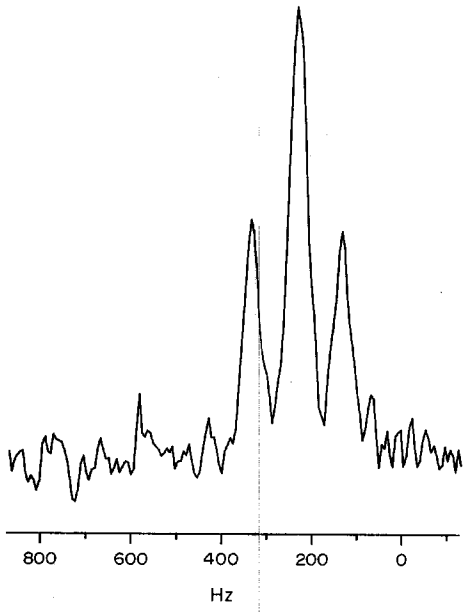

Fig. 3. ^{171}Yb NMR spectrum of **2**·2THF at −30°C.

samarium and ytterbium P—P bond cleavage reaction with simple biphosphines and also the chemistry of the isolated ytterbium and samarium complexes.

EXPERIMENTAL

Due to the extreme air sensitivity of the complexes, all operations were performed under nitrogen with the use of a vacuum-line and dry-box, with dry, carefully degassed solvents. $SmI_2(THF)_2$, $YbI_2(THF)_2$,[12] potassium 2,3,4,5-tetramethylphospholide,[13] 2,3,4,5,2′,3′,4′,5′-octamethyl-1,1′-biphospholyl,[14] $PhAsCl_2$[15] and 2,5,2′,5′-tetraphenyl-1,1′-biphospholyl[7] were prepared as previously described. Tetrabutylammonium tribromide was recrystallized in ethyl acetate. All other reagents were used as received from the commercial suppliers. NMR (^{1}H, ^{13}C, ^{31}P) spectra were measured on Bruker AC 200 or AM 400 instruments. ^{171}Yb spectra were measured at 70 MHz on the AM 400 instrument with a 5 mm multinuclear probe. Elemental microanalyses were obtained at the Centre de Microanalyse du CNRS, Gif-sur-Yvette, France. Mass spectra were obtained on a Shimadzu GC-MS 1000.

1-*Phenyl*-2,3,4,5-*tetramethylarsole* (**4**)[2]

In a 1 dm^3 screw-capped vessel were placed magnesium (8 g, 0.33 g-atom), $HgCl_2$ (9 g, 0.033 mol) and THF (250 cm^3). The magnesium was activated by stirring for 10 min and then a solution of Cp_2ZrCl_2 (17.8 g, 0.061 mol) and 2-butyne (7 g, 0.130 mol) in THF (250 cm^3) was added to the flask. The vessel was stoppered and its contents stirred overnight. The reaction mixture was then filtered and evaporated to dryness. The resulting residue was taken up in n-pentane (500 cm^3) and filtered again. To the dark-red pentane solution cooled to 0°C was added dropwise a pentane (50 cm^3) solution of $PhAsCl_2$ (13 g, 0.058 mol). The reaction mixture was filtered, evaporated to dryness and the residue bulb-to-bulb distilled at 150–160°C/1 mm Hg. 13.05 g (0.050 mol, 86%) of **4** were obtained as a yellow oil. NMR ($CDCl_3$): ^{1}H: 1.87 (Me), 1.98 (Me), 7.24 (Ph). ^{13}C: 14.45 (Me), 14.65 (Me), 128.12 (C *para*), 128.45 (C *ortho*), 132.77 (C *meta*), 137.72 (C *ipso*), 140.99 (C3), 143.42 (C2). Mass spec.: *m/z* 260 (M^+, 100%).

Potassium 2,3,4,5-*tetramethylarsolide* (**5**)

To a solution of **4** (2.68 g, 10.30 mmol) in dimethoxyethane (25 cm^3) was added potassium metal in small lumps (1.0 g, 25 mmol). The reaction mixture was heated at 70°C with vigorous stirring for 2 h. The dark-brown reaction mixture was then filtered on a 5 mm layer of celite and evaporated to dryness. The residue was redissolved in boiling THF (30 cm^3) and slowly cooled to room temperature. The white precipitate which resulted was filtered and rinsed with cold THF (5 cm^3), 1/1 THF/n-pentane (5 cm^3) and n-pentane (10 cm^3) and then dried *in vacuo*. 1.85 g of **5** were obtained as a white powder (8.33 mmol, 81%). NMR (C_4D_8O): ^{1}H: 1.93 (Me), 2.32 (Me). ^{13}C: 14.87 (Me), 18.23 (Me), 126.13 (C3), 145.96 (C2). Found: C, 42.6; H, 5.5. Calc. for $C_8H_{12}AsK$: C, 43.2; H, 5.4%.

2,3,4,5,2′,3′,4′,5′-*Octamethyl*-1,1′-*biarsolyl* (**6**)

$Bu^n{}_4N^+Br_3^-$ (480 mg, 1 mmol) was added to a slurry of **5** (440 mg, 2 mmol) in THF (10 cm^3). After stirring at room temperature for 10 min the reaction mixture was evaporated to dryness. The residue was taken up in n-pentane (20 cm^3), filtered and evaporated to dryness, yielding **6** as a yellow semi-solid (310 mg, 0.84 mmol, 84%) that darkens on standing. NMR (C_6D_6): ^{1}H: 1.72 (Me), 1.86 (Me). ^{13}C: 15.27 (Me), 16.17 (Me), 140.12 (C3 or C2), 143.56 (C2 or C3). Mass spec.: *m/z* 366 (M^+, 75%), 183 (M/2, 100%).

General procedure for the synthesis of bis(heterocyclopentadienyl)lanthanide(II) *complexes*

Method A. To a mixture of one equivalent of solid $MI_2(THF)_2$ (M = Sm, Yb) and two equivalents of

L^-K^+ was added THF (10 to 20 cm^3). The reaction mixtures were stirred for 10 min at room temperature, evaporated to dryness and the residues were repeatedly extracted with toluene until the filtrates were colourless. The combined extracts were then evaporated to dryness and the residues stirred in toluene and filtered.

Method B. To a mixture of the metallic powders (samarium or ytterbium) in a slight excess and the biphospholyl or biarsolyl was added THF (10 cm^3). The reaction mixtures were stirred overnight, evaporated to dryness and usually worked up as described in method A, unless otherwise specified.

Bis(2,3,4,5-*tetramethylphospholyl*)*samarium* (**1**)

Method A. From potassium 2,3,4,5-tetramethylphospholide (400 mg, 2.2 mmol) and $SmI_2(THF)_2$ (620 mg, 1.1 mmol) **1** was obtained as a black powder (265 mg, 0.65 mmol, 58%).

Method B. From 2,3,4,5,2′,3′,4′,5′-octamethyl-1,1′-biphospholyl (500 mg, 1.8 mmol) and samarium (300 mg, 2 mmol) **1** was obtained (400 mg, 0.93 mmol, 50%). NMR data are described in ref. 1. Found: C, 44.7; H, 5.5. Calc. for $C_{16}H_{24}P_2Sm$: C, 44.8; H, 5.6%.

Bis(2,3,4,5-*tetramethylphospholyl*)*ytterbium* (**2**)

Method A. From potassium 2,3,4,5-tetramethylphospholide (400 mg, 2.2 mmol) and $YbI_2(THF)_2$ (640 mg, 1.1 mmol) **2** was obtained as a green powder (310 mg, 0.69 mmol, 61%).

Method B. From 2,3,4,5,2′,3′,4′,5-octamethyl-1,1′-biphospholyl (500 mg, 1.8 mmol) and ytterbium (350 mg, 2 mmol) **1** was obtained (450 mg, 1.1 mmol, 55%). NMR data are described in ref. 1.

Bis(2,3,4,5-*tetramethylarsolyl*)*samarium* (**7**)

Method A. From tetramethylarsolide (**5**) (440 mg, 2 mmol) and $SmI_2(THF)_2$ (550 mg, 1 mmol) **7** was obtained as a black powder (310 mg, 0.60 mmol, 60%).

Method B. From biarsolyl (**6**) (250 mg, 0.68 mmol) and samarium (130 mg, 0.87 mmol) **7** was obtained (200 mg, 0.38 mmol, 57%). NMR (C_4D_8O): ^1H: 3.67 ($w_{1/2} \approx 5$ Hz, Me), 5.64 ($w_{1/2} \approx 5$ Hz, Me). ^{13}C: 0.17 ($w_{1/2} \approx 15$ Hz, C2 or C3), 15.93 ($w_{1/2} \approx 15$ Hz, C3 or C2), 73.12 ($w_{1/2} \approx 6$ Hz, Me), 78.80 ($w_{1/2} \approx 6$ Hz, Me).

Bis(2,3,4,5-*tetramethylarsolyl*)*ytterbium* (**8**)

Method A. From tetramethylarsolide (**5**) (440 mg, 2 mmol) and $YbI_2(THF)_2$ (570 mg, 1 mmol) **8** was obtained as a green powder (300 mg, 0.48 mmol, 48%).

Method B. From biarsolyl (**6**) (300 mg, 0.82 mmol) and ytterbium (170 mg, 1 mmol) **8** was obtained (270 mg, 0.51 mmol, 50%). NMR (C_4D_8O): ^1H: 1.93 (Me), 2.31 (Me). ^{13}C: 15.48 (Me), 18.75 (Me), 131.12 (C3), 150.12 (C2).

Bis(η^5-2,5-*diphenylphospholyl*)*samarium bis*(*tetrahydrofuran*) **10**·2THF

Method B. To biphospholyl (**9**) (470 mg, 1 mmol) and samarium (180 mg, 1.2 mmol) $HgCl_2$ was added ($\approx$20 mg) and the reaction mixture was stirred overnight. The resulting chocolate brown solution was then filtered and the residue was repeatedly extracted with THF until the filtrate was colourless. The filtrate was then reduced to 5 cm^3 and the resulting crystalline precipitate filtered, rinsed with cold THF (2 cm^3) and dried. **10**·2THF was obtained as a chocolate brown microcrystalline powder (500 mg, 0.65 mmol, 65%). NMR (C_4D_8O): ^1H: 1.76 (THF), 3.62 (THF), 7.48 (ps. t., $J_{app.} = 8$, H *para*), 9.44 (ps. t., $J_{app.} = 8$, H *meta*), 9.67 (ps. d., $J_{app.} = 8$, H *ortho*), 19.4 ($w_{1/2} \approx 10$ Hz, H3). ^{13}C: −9 ($w_{1/2} \approx 10$ Hz, C3), 57.5 [d, $w_{1/2} \approx 25$ Hz, J(PC) $\approx$ 40, C2], 128.62 (C *meta*), 134.80 (C *para*), 143.82 [d, J(PC) = 12, C *ortho*], 181.80 [d, J(PC) = 17.5, C *ipso*]. ^{31}P: −417 ($w_{1/2} \approx 25$ Hz).

Bis(η^5-2,5-*diphenylphospholyl*)*ytterbium bis*(*tetrahydrofuran*) **11**·2THF

Method B. From biphospholyl (**9**) (470 mg, 1 mmol) and ytterbium (210 mg, 1.2 mmol) $HgCl_2$ ($\approx$20 mg) was added and the reaction mixture was stirred overnight. The resulting dark purple solution was then worked up as described above to **10**·2THF. Yield: 560 mg (0.71 mmol, 71%) of **11**·2THF as a purple microcrystalline powder. NMR (C_4D_8O): ^1H: 1.77 (THF), 3.61 (THF), 7.07 (ps. d., $J_{app.} = 8$, H *para*), 7.23 (ps. t., $J_{app.} = 8$, H *meta*), 7.26 [d, J(PH) 3.5, H3], 7.67 (ps. t., $J_{app.} = 8$, H *ortho*). ^{13}C: 120.25 (C3), 125.72 (C *para*), 125.84 [d, J(PC) = 12.5, C *ortho*], 129.04 (C meta), 141.13 [d, J(PC) = 19, C *ipso*], 151.93 [d, J(PC) = 46, C2]. ^{31}P: 74.7. Found: C, 61.0; H, 5.0. Calc. for $C_{40}H_{40}O_2P_2Yb$: C, 61.0; H, 5.1%.

X-ray structure determination of **11**·2THF

Data were collected on an Enraf–Nonius CAD4 diffractometer with graphite-monochromated Mo-K_α radiation ($\lambda = 0.71073$ Å, $\mu = 29.0\ cm^{-1}$), using the Enraf–Nonius supplied SDP package. The intensities were corrected for Lorentz–polarization

effects and the structure was solved by the Patterson method. The crystal structure consists of two nearly identical independent molecules. In each molecule one carbon atom of a THF ligand is disordered; refinement of the multiplicity of these atoms showed that the occupancy of each site was equal. The hydrogen atoms were included as fixed contributions in the final stages of least-squares refinement while using anisotropic temperature factors for all the other atoms. A non-Poisson weighting scheme was applied with a p factor equal to 0.05. The final agreement factors were $R = 0.026$, $R_w = 0.036$, G.O.F. = 1.05.

REFERENCES

1. F. Nief and F. Mathey, *Synlett* 1991, 745.
2. P. J. Fagan and W. A. Nugent, *J. Am. Chem. Soc.* 1988, **110**, 2310.
3. K.-G. Wang, E. D. Stevens and S. P. Nolan, *Organometallics* 1992, **11**, 1011; A. Rechnagel, M. Noltemeyer and F. T. Edelmann, *J. Organomet. Chem.* 1991, **410**, 53; W. J. Evans, S. L. Gonzales and J. W. Ziller, *J. Am. Chem. Soc.* 1991, **113**, 2310; C. M. Forsyth, S. P. Nolan and T. J. Marks, *Organometallics* 1991, **10**, 2543; W. J. Evans, T. A. Ulibarri, L. R. Chamberlain, J. W. Ziller and D. Alvarez Jr, *Organometallics* 1990, **9**, 2124; W. J. Evans, R. A. Keyer and J. W. Ziller, *Organometallics* 1990, **9**, 2629; M. R. Gagné, S. P. Nolan and T. J. Marks, *Organometallics* 1990, **9**, 1716; C. J. Burns and R. A. Andersen, *J. Chem. Soc., Chem. Commun.* 1989, 136; R. G. Finke, S. R. Keenan and P. L. Watson, *Organometallics* 1989, **8**, 263; S. J. Swamy, L. Loebel, J. Pickardt and H. Schumann, *J. Organomet. Chem.* 1988, **353**, 27; For a review, see: W. J. Evans, *Polyhedron* 1987, **5**, 803.
4. M. F. Lappert, I. W. Yarrow, J. L. Artwood, R. Shakir and J. Holton, *J. Chem. Soc., Chem. Commun.* 1980, 987.
5. G. B. Deacon, A. Dietrich, C. M. Forsyth and H. Schumann, *Angew. Chem., Int. Edn Engl.* 1989, **28**, 1370.
6. G. B. Deacon and R. H. Newnham, *Aust. J. Chem.* 1985, **38**, 1757.
7. C. Charrier, H. Bonnard, F. Mathey and D. Neibecker, *J. Organomet. Chem.* 1982, **231**, 361.
8. Q. Shen, D. Zheng, L. Lin and Y. Lin, *J. Organomet. Chem.* 1990, **391**, 321.
9. T. Don Tilley, R. A. Andersen and A. Zalkin, *Inorg. Chem.* 1983, **22**, 856; *J. Am. Chem. Soc.* 1982, **104**, 3725.
10. A. G. Avent, M. A. Edelmann, M. F. Lappert and G. A. Lawless, *J. Am. Chem. Soc.* 1989, **111**, 3423.
11. F. G. N. Cloke, G. I. Dalby, P. B. Hitchcock, H. Karamallakis and G. A. Lawless, *J. Chem. Soc., Chem. Commun.* 1991, 779; A. R. Strzelelecki, P. A. Timinski, B. A. Helsel and P. A. Bianconi, *J. Am. Chem. Soc.* 1991, **114**, 3159.
12. P. L. Watson, T. H. Tulip and I. Williams, *Organometallics* 1990, **9**, 1999; J.-L. Namy, P. Girard, H. B. Kagan and P. E. Caro, *Nouv. J. Chim.* 1981, **5**, 479.
13. D. Baudry, M. Ephrithikhine, F. Nief, L. Ricard and F. Mathey, *Angew. Chem., Int. Edn Engl.* 1990, **29**, 1485.
14. T. Douglas and K. Theopold, *Angew. Chem., Int. Edn Engl.* 1989, **28**, 1367.
15. G. Roeder and N. Blasi, *Chem. Ber.* 1914, **47**, 2748.

Polyhedron Vol. 12, No. 1, pp. 27–30, 1993
Printed in Great Britain

0277–5387/93 $6.00+.00
© 1993 Pergamon Press Ltd

SYNTHESIS OF MONO- AND BINUCLEAR [{Mo(CO)$_3$L}$_n$(dpq)] [n = 1,2; L = CO, MeCN, PPh$_3$; dpq = 2,3-BIS(2-PYRIDYL)QUINOXALINE] COMPLEXES AND HETEROBIMETALLIC ADDUCT FORMATION WITH HEXAFLUOROACETYLACETONATECOBALT(II)

J. GRANIFO

Departamento de Ciencias Químicas, Facultad de Ingeniería y Administración, Universidad de La Frontera, Casilla 54-D, Temuco, Chile

(*Received* 17 *July* 1992; *accepted* 3 *September* 1992)

Abstract—The new compounds [{Mo(CO)$_4$}$_n$(dpq)] [n = 1,2; dpq = 2,3-bis(2-pyridyl) quinoxaline] on refluxing in MeCN produce the acetonitrile complexes [{Mo(CO)$_3$(NCMe)}$_n$(dpq)] (n = 1,2). These acetonitrile derivatives behave as precursors for the tricarbonyl-based fragments [{Mo(CO)$_3$}$_n$(dpq)] (n = 1,2); they react in CH_2Cl_2 at room temperature with PPh$_3$ to afford the [{Mo(CO)$_3$(PPh$_3$)}$_n$(dpq)] (n = 1,2) complexes. In addition, the ligating properties of the novel mononuclear products [Mo(CO)$_4$(dpq)] and [Mo(CO)$_3$(PPh$_3$)(dpq)] towards [Co(hfacac)$_2$] are also reported. The new substances were characterized by IR and electronic spectroscopy.

In previous work,[1] the acetonitrile derivatives [Mo(CO)$_3$(NCMe)(NN)] (NN = bipy, phen), obtained by refluxing [Mo(CO)$_4$(NN)] in MeCN,[2] have been used as precursors for the tricarbonyl complexes *fac*-[Mo(CO)$_3$(L)(NN)] (L = P donor ligand) through the replacement of MeCN by the L ligand. Now, as an extension of this synthetic procedure, we are interested in obtaining acetonitrile precursors containing bis(diimine) ligands instead of the diimine ligands NN.

Recently, Ruminski and Johnson[3] have reported that the molybdenum complexes [{Mo(CO)$_4$}$_n$(dpp)] [n = 1,2; dpp = 2,3-bis(2-pyridyl)pyrazine, Fig. 1] suffer thermal decomposition in MeCN. The binuclear complex [{Mo(CO)$_4$}$_2$(dpp)] derives to the mononuclear [Mo(CO)$_4$(dpp)]; the final products of the monometallic [Mo(CO)$_4$(dpp)] compound were not identified. In this work we report different behaviour in the above molybdenum complexes when the 2,3-bis(2-pyridyl)pyrazine ligand is replaced by the closely related ligand 2,3-bis (pyridyl)quinoxaline (dpq, Fig. 1). Therefore, the [{Mo(CO)$_3$(NCMe)}$_n$(dpq)] (n = 1,2) compounds are obtained by refluxing the [{Mo(CO)$_4$}$_n$(dpq)] (n = 1,2) complexes with MeCN. These acetonitrile derivatives show a high reactivity evidenced through the easy displacement of the MeCN ligand by PPh$_3$ to give the [{Mo(CO)$_3$(PPh$_3$)}$_n$(dpq)] (n = 1,2) complexes.

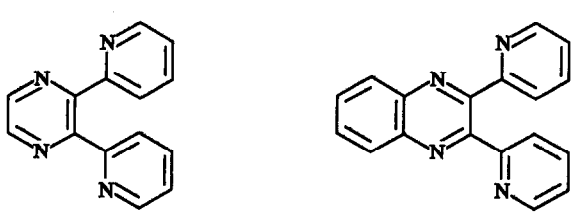

dpp dpq

Fig. 1. Structure of the ligands dpp and dpq.

In addition, we report here the coordinating properties of the above novel and stable mononuclear complexes [Mo(CO)$_4$(dpq)] and [Mo(CO)$_3$(PPh$_3$)(dpq)]. They react with the hexafluoroacetylacetonatecobalt(II) complex [Co(hfacac)$_2$] to yield heterobinuclear complexes with Mo—dpq—Co arrays. The chelating aptitude of the dpq ligand towards [Co(hfacac)$_2$] has been reported recently by Escuer *et al.*[4] by isolating the [Co(dpq)(hfacac)$_2$] complex.

RESULTS AND DISCUSSION

The carbonyl stretching frequencies of the new dpq complexes [{Mo(CO)$_4$}$_n$(dpq)] (n = 1,2) (Table 1) are typical of the *cis*-[Mo(CO)$_4$(NN-donor)]

Table 1. Analytical and IR spectra for the complexes $[\{Mo(CO)_3L\}_n(dpq)]$ (n = 1,2; L = CO, MeCN, PPh_3) and $[(CO)_3(L)Mo(dpq)Co(hfacac)_2]$ (L = CO, PPh_3)

Compound	Analysis (%)[a] C	H	N	IR (cm^{-1})[b] ν(CO)
$[\{Mo(CO)_4\}_2(dpq)]$	44.1(44.6)	1.7(1.7)	8.3(8.0)	2005, 1910, 1870, 1810
$[Mo(CO)_4(dpq)]$	53.2(53.7)	2.4(2.5)	11.6(11.4)	2000, 1890, 1855, 1810
$[\{Mo(CO)_3(NCMe)\}_2(dpq)]$	46.1(46.3)	2.6(2.5)	11.7(11.6)	1905, 1775[c]
$[Mo(CO)_3(NCMe)(dpq)]$	54.2(54.7)	2.8(3.0)	14.0(13.9)	1910, 1780[c]
$[\{Mo(CO)_3(PPh_3)\}_2(dpq)]$	61.6(61.6)	3.5(3.6)	4.7(4.8)	1910, 1815, 1800
$[Mo(CO)_3(PPh_3)(dpq)]$	64.1(64.5)	3.7(3.7)	8.0(7.7)	1905, 1810, 1777
$[(CO)_4Mo(dpq)Co(hfacac)_2]$	40.1(39.8)	1.3(1.5)	6.0(5.8)	2010, 1920, 1880, 1840
$[(CO)_3(PPh_3)Mo(dpq)Co(hfacac)_2]$	49.3(49.1)	2.6(2.4)	4.8(4.7)	1915, 1820[c]

[a] Required values are given in parentheses.
[b] KBr discs, all bands are strong.
[c] Broad.

species.[5] The visible absorption spectra of these mono- and bimetallic compounds are dominated by an intense solvatochromic band (Table 2). On the basis of the similarity to results previously published on related complexes,[3] these solvatochromic bands are assigned to metal-to-ligand charge-transfer (MLCT) transitions dpq(π^*) ← Mo(4d). In the analogous $[\{Mo(CO)_4\}_n(dpp)]$ (n = 1,2) complexes[3] these absorptions are shifted towards the blue region, indicating an increase of the electron-withdrawing ability of the LUMO of dpq in comparison with dpp.

Refluxing the above mono- and binuclear $[\{Mo(CO)_4\}_n(dpq)]$ (n = 1,2) complexes in MeCN results in the formation of the acetonitrile derivatives $[\{Mo(CO)_3(NCMe)\}_n(dpq)]$ (n = 1,2), respectively. The $[\{Mo(CO)_3(NCMe)\}_n(dpq)]$ (n = 1,2) complexes are air-sensitive in the solid state and extremely air-sensitive in solution. Their structures are likely to have a facial tricarbonyl geometry, since the IR spectra in the ν(CO) region (Table 1) have a similar pattern to that from the tricarbonyl complexes *fac*-$[Mo(CO)_3(NCMe)(NN\text{-donor})]$.[2]

Considering the labile character of the MeCN ligand, the novel acetonitrile compounds $[\{Mo(CO)_3(NCMe)\}_n(dpq)]$ (n = 1,2) are expected to act as potential precursors of the $[\{Mo(CO)_3\}_n(dpq)]$ (n = 1,2) fragments. In fact, treatment at room temperature of CH_2Cl_2 solutions of $[\{Mo(CO)_3(NCMe)\}_n(dpq)]$ (n = 1,2) in the presence of PPh_3 gave the crystalline $[\{Mo(CO)_3(PPh_3)\}_n(dpq)]$ (n = 1,2) complexes. These products are air stable and soluble in common organic solvents.

Likewise with the starting $[\{Mo(CO)_3(NCMe)\}_n(dpq)]$ (n = 1,2) complexes, the new mixed derivatives $[\{Mo(CO)_3(PPh_3)\}_n(dpq)]$ (n = 1,2) have the facial structure of the carbonyl groups. In particular, the IR spectra of the $[\{Mo(CO)_3(PPh_3)\}_n(dpq)]$ (n = 1,2) compounds display two strong carbonyl stretching bands (Table 1). The lower frequency band is split into two. The same pattern has been observed in the complexes *fac*-$[Mo(CO)_3(L)(NN\text{-donor})]$, L being a phosphorus donor ligand.[1]

The electronic spectra in the visible region of the triphenylphosphine $[\{Mo(CO)_3(PPh_3)\}_n(dpq)]$ (n =

Table 2. Visible absorption maxima (nm) of the complexes $[\{Mo(CO)_4\}_n(dpq)]$ (n = 1,2) and $[\{Mo(CO)_3(PPh_3)\}_n(dpq)]$ (n = 1,2) in several solvents

Compound	Benzene	$CHCl_3$	THF	CH_2Cl_2	Acetone	MeCN
$[\{Mo(CO)_4\}_2(dpq)]$	706	708	661	685[a]	631	622
$[Mo(CO)_4(dpq)]$	584	582	560	562[b]	540	533
$[\{Mo(CO)_3(PPh_3)\}_2(dpq)]$	854	842	841	830[c]	816	800
$[Mo(CO)_3(PPh_3)(dpq)]$	711	702	696	680[d]	667	646

[a] ε = 13,965 M^{-1} cm^{-1}.
[b] ε = 4886 M^{-1} cm^{-1}.
[c] ε = 18,140 M^{-1} cm^{-1}.
[d] ε = 4221 M^{-1} cm^{-1}.

1,2) complexes consist of one broad and strong solvent sensitive band (Table 2). These bands appear at a lower energy than those of their respective parent complexes [{Mo(CO)$_4$}$_n$(dpq)] (n = 1,2). These results suggest that the observed absorptions in both systems are of the same nature, i.e. MLCT dpq(π^*) ← Mo(4d) transitions. Indeed, when one carbonyl group is substituted by a phosphorus-donor ligand the metal orbitals are destabilized,[1] then a lower dpq(π^*)/Mo(4d) gap for the PPh_3 complexes should occur.

Finally, the capacity of adduct formation of the mononuclear dpq complexes [Mo(CO)$_4$(dpq)] and [Mo(CO)$_3$(PPh$_3$)(dpq)] was demonstrated. Thus, the reaction of an equimolar amount of the mononuclear [Mo(CO)$_4$(dpq)] or [Mo(CO)$_3$(PPh$_3$)(dpq)] complexes with [Co(hfacac)$_2$] in CH_2Cl_2 affords the heterobinuclear adducts [(CO)$_4$Mo(dpq)Co(hfacac)$_2$] or [(CO)$_3$(PPh$_3$)Mo(dpq)Co(hfacac)$_2$]. Both bimetallic compounds are soluble and stable in non-coordinating solvents such as dichloromethane or benzene; nevertheless, in acetone they dissociate into the original [Mo(CO)$_4$(dpq)] or [Mo(CO)$_3$(PPh$_3$)(dpq)] and [Co(hfacac)$_2$] complexes as evidenced by the electronic spectra. The new adducts have ν(CO) modes in their IR spectra that are in close agreement with those which are exhibited by their precedent mononuclear [Mo(CO)$_4$(dpq)] and [Mo(CO)$_3$(PPh$_3$)(dpq)] species (Table 1). Furthermore, in CH_2Cl_2 solutions a pronounced red shift of the MLCT dpq(π^*) ← Mo(4d) transition of the heterometallic [(CO)$_4$Mo(dpq)Co(hfacac)$_2$] (λ_{max} = 643 nm) and [(CO)$_3$(PPh$_3$)Mo(dpq)Co(hfacac)$_2$] (λ_{max} = 777 nm) species vs their respective monometallic components, [Mo(CO)$_4$(dpq)] (λ_{max} = 562 nm) and [Mo(CO)$_3$(PPh$_3$)(dpq)] (λ_{max} = 680 nm), was observed. These shifts in dpq-based complexes[6,7] have been rationalized in terms of a stabilization of the π^*dpq orbital of the monometallic chromophore upon attachment of a second metal centre. On the other hand, the magnetic moments of the complexes [(CO)$_4$Mo(dpq)Co(hfacac)$_2$] (μ_{eff} = 4.8 B.M.) and [(CO)$_3$(PPh$_3$)Mo(dpq)Co(hfacac)$_2$] (μ_{eff} = 4.3 B.M.) are in the range observed by Escuer *et al.*[4] for the six-coordinated cobalt(II) complexes [Co(L)(hfacac)$_2$] [L = bis(diimine) ligand]. However, we failed to determine the ligand field (d–d) transitions of the cobalt(II) centre[4] in the visible region, since they are masked by the more intense MLCT dpq(π^*) ← Mo(4d) transitions.

EXPERIMENTAL

All solvents used in preparing the complexes were reagent grade and used without further purification. [Mo(CO)$_6$] and [Co(hfacac)$_2$]·3H$_2$O were purchased from Aldrich Chemical Company. 2,3-Bis(2-pyridyl)quinoxaline (dpq)[8] and [Mo(CO)$_4$(piperidine)$_2$][9] were prepared by similar methods to those described in the literature. The IR spectra were recorded on a Perkin–Elmer 577 spectrophotometer. The electronic spectra were registered on a Spectronic 3000 diode array spectrophotometer. Magnetic susceptibilities at room temperature were measured by the Faraday method using a Cahn 7600-RTL balance.

Synthesis of [Mo(CO)$_4$(dpq)]

A mixture of dpq (0.300 g, 1.057 mmol) and freshly prepared [Mo(CO)$_4$(piperidine)$_2$] (0.400 g, 1.057 mmol) was stirred in methanol (15 cm^3) for 2 h. The bright black precipitate was filtered and washed three times with 3 cm^3 portions of methanol and dried *in vacuo*. 0.365 g (70% yield) of the crystalline compound were obtained. The results of the elemental analysis are presented in Table 1.

Synthesis of [{Mo(CO)$_4$}$_2$(dpq)]

A mixture of dpq (0.350 g, 1.231 mmol) and [Mo(CO)$_6$] (0.780 g, 2.954 mmol) in benzene (15 cm^3) was heated at reflux for 16 h under nitrogen. The solid was collected by filtration, washed with benzene (10 cm^3), dissolved in CH_2Cl_2 (100 cm^3), filtered and then reprecipitated by the addition of petroleum ether (150 cm^3, 40–60° fraction). The black needle-like crystals were washed with a mixture of CH_2Cl_2 and petroleum ether (30 cm^3, 1 : 2). Yield: 0.700 g (81%). The results of the elemental analysis are presented in Table 1.

Synthesis of [{Mo(CO)$_3$(PPh$_3$)}$_n$(dpq)] (n = 1,2)

These complexes were prepared by an analogous method using fresh samples of [{Mo(CO)$_3$(NCMe)}$_n$(dpq)] (n = 1,2) as the starting material. The following procedure is typical.

[{Mo(CO)$_3$(PPh$_3$)}$_2$(dpq)]. [{Mo(CO)$_4$}$_2$(dpq)] (0.1 g, 0.143 mmol) in MeCN (10 cm^3) was refluxed for 2 h under nitrogen. The green solution was evaporated to dryness to give the black acetonitrile complex [{Mo(CO)$_3$(NCMe)}$_2$(dpq)] and PPh_3 (0.075 g, 0.286 mmol) and CH_2Cl_2 (10 cm^3) were added. The resultant green mixture was stirred at room temperature for 0.5 h, filtered and concentrated to 3–4 cm^3 volume. A very dark green crystalline precipitate was formed on slow addition of MeOH (10 cm^3). The material was separated and washed with MeOH (3 × 4 cm^3).

Yield: 0.130 g (78%). The results of the elemental analyses are presented in Table 1.

Synthesis of $[(CO)_4Mo(dpq)Co(hfacac)_2]$ *and* $[(CO)_3(PPh_3)Mo(dpq)Co(hfacac)_2]$

Both adducts were obtained by direct reaction at room temperature of a mixture of equimolar amounts of $[Mo(CO)_4(dpq)]$ or $[Mo(CO)_3(PPh_3)(dpq)]$ and $[Co(hfacac)_2]\cdot 3H_2O$ in CH_2Cl_2; a typical reaction runs as follows.

$[(CO)_3(PPh_3)Mo(dpq)Co(hfacac)_2]$. To a solution of $[Mo(CO)_3(PPh_3)(dpq)]$ (0.070 g, 0.096 mmol) in CH_2Cl_2 (15 cm^3) was added $[Co(hfacac)_2]\cdot 3H_2O$ (0.051 g, 0.096 mmol). The green solution was stirred for 0.5 h, filtered and then concentrated to 3–4 cm^3 volume. To the concentrate was added petroleum ether (30 cm^3, 40–60° fraction). A black crystalline solid precipitated after 30 min, which was washed with a mixture of CH_2Cl_2/petroleum ether (10 cm^3, 1:10). Yield: 0.052 g (45%). The elemental analyses are presented in Table 1.

Acknowledgements—Financial support given by the Dirección de Investigación y Desarrollo de la Universidad de La Frontera (Project No. 9212) and the Comisión Nacional de Investigación Científica y Tecnológica (Project No. 92-0569) to carry out this work is gratefully acknowledged.

REFERENCES

1. J. Granifo, M. E. Vargas, J. Costamagna and A. M. François, *Polyhedron* 1988, **7**, 489.
2. L. W. Houk and G. R. Dobson, *Inorg. Chem.* 1966, **5**, 2119.
3. R. R. Ruminski and J. O. Johnson, *Inorg. Chem.* 1987, **26**, 210.
4. A. Escuer, R. Vicente, T. Comas, J. Ribas, M. Gomez, X. Solans, D. Gatteschi and C. Zanchini, *Inorg. Chim. Acta* 1991, **181**, 51.
5. M. H. B. Stiddard, *J. Chem. Soc.* 1962, 4712.
6. J. A. Baiano, D. L. Carlson, G. M. Wolosh, D. E. De Jesus, C. F. Knowles, E. G. Szabo and R. Murphy Jr, *Inorg. Chem.* 1990, **29**, 2327.
7. D. B. MacQueen and J. D. Petersen, *Inorg. Chem.* 1990, **29**, 2313.
8. H. A. Goodwin and F. Lions, *J. Am. Chem. Soc.* 1959, **81**, 6415.
9. D. J. Darensbourg and R. L. Kump, *Inorg. Chem.* 1978, **17**, 2680.

Polyhedron Vol. 12, No. 1, pp. 31–36, 1993
Printed in Great Britain

0277–5387/93 $6.00+.00
© 1993 Pergamon Press Ltd

ELECTROCHEMICAL SYNTHESIS OF CADMIUM(II) COMPLEXES OF SCHIFF BASES: THE CRYSTAL STRUCTURE OF 2,2′-BIPYRIDINE BIS{2-[(2-METHOXYPHENYL)-IMINOMETHYL]PYRROLATO}CADMIUM(II)

J. A. CASTRO, J. ROMERO, J. A. GARCIA-VAZQUEZ and A. SOUSA*

Departamento de Química Inorgánica, Universidad de Santiago de Compostela, 15706 Santiago de Compostela, Galicia, Spain

and

E. E. CASTELLANO and J. ZUKERMAN-SCHPECTOR

Universidad de Sao Paulo, Instituto de Física e Química, Sao Carlos, Brazil

(*Received* 13 *July* 1992; *accepted* 3 *September* 1992)

Abstract—The electrochemical oxidation of anodic cadmium in acetonitrile containing both a Schiff base, HL (derived from H-pyrrole-2-carbaldehyde and a substituted aniline), and a nitrogen donor ligand [1,10-phenanthroline(phen) or 2,2′-bipyridine(bipy)] yielded the mixed complexes $CdL_2 \cdot phen$ and $CdL_2 \cdot bipy$. The crystal structure of 2,2′-bipyridine bis{2-[(2-methoxyphenyl)iminomethyl]pyrrolato}cadmium(II) was determined by X ray diffraction.

The synthesis of mixed complexes of nickel and cobalt with pyrrolaldimines and additional ligands by electrolysis of the metal in a solution of the ligands has been the subject of several recent papers from our laboratory.[1,2] In continuation of this series, this paper describes the successful application of the above method to the synthesis of mixed complexes of cadmium(II) with arylpyrrolaldimines (HL) and bidentate nitrogen ligands, such as 2,2′-bipyridine or 1,10-phenanthroline.

The crystal structure of 2,2′-bipyridine bis{2-[(2-methoxyphenyl)iminomethyl]pyrrolato}cadmium(II) is also reported.

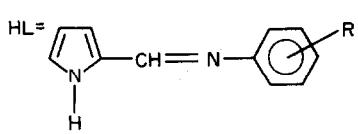

where R = H (HL^1); 4-CH_3 (HL^2); 4-Cl (HL^3); 2-OCH_3 (HL^4) or 4-OCH_3 (HL^5).

* Author to whom correspondence should be addressed.

EXPERIMENTAL

Acetonitrile, pyrrole-2-aldehyde, 1,10-phenanthroline(phen), 2,2′-bipyridine(bipy) and all other reagents were commercial products and were used as supplied. Cadmium (Ega Chemie) was used as *ca* 2 × 2 cm plates.

The ligands were prepared by standard methods by direct reaction of equimolar amounts of the aldehyde and the amine in chloroform, using a Dean–Stark trap. After removal of the water produced in the reaction, the solution was concentrated and the isolated solid was washed with diethyl ether and dried *in vacuo*. Its purity was checked by recording its IR and ^1H NMR spectra.

Electrochemical synthesis

The electrochemical method used was similar to that described by Tuck.[3] The cell was a 100 cm^3 tall-form beaker fitted with a rubber bung, through which the electrochemical leads entered. The anode was suspended from a platinum wire and the cathode was also a platinum wire. The Schiff base and

Table 1. Experimental conditions for the electrochemical syntheses

Ligand HL	Amount of HL (g)	Amount of L′ (g)[a]	Initial voltage (V)[b]	Time (h)	Metal dissolved (mg)	E_f (mol F^{-1})
HL^1	0.26	0.12 (bipy)	12	2	75.9	0.45
HL^1	0.26	0.13 (phen)	15	1	50.4	0.60
HL^2	0.28	0.12 (bipy)	16	2	76.9	0.46
HL^2	0.29	0.13 (phen)	18	2	77.9	0.46
HL^3	0.30	0.12 (bipy)	14	2	75.8	0.45
HL^3	0.32	0.13 (phen)	20	2	86.4	0.52
HL^4	0.15	0.08 (bipy)	15	1	44.8	0.53
HL^4	0.15	0.09 (phen)	10	1	48.4	0.58
HL^5	0.30	0.12 (bipy)	14	2	88.0	0.52
HL^5	0.30	0.13 (phen)	16	2	76.6	0.45

[a] Plus $[NMe_4]ClO_4$ (*ca* 10 mg).
[b] Voltage to produce a current of 20 mA.

the additional ligand (1,10-phenanthroline or 2,2′-bipyridine) were dissolved in acetonitrile and a small amount of tetraethylammonium perchlorate was added to the solution as a current carrier. A direct current was obtained from a purpose-built d.c. power supply. Applied voltages of 15–30 V allowed sufficient current flow for smooth solution of the metal. In all cases, hydrogen was evolved at the cathode. These cells can be summarized as:

$$Pt(-)/CH_3CN + HL + L'/Cd(+),$$

where L′ is phenanthroline or bipyridine.

At the end of electrolysis, the clear solutions were filtered to remove any particles of metal and then left to concentrate, yielding crystalline products. The solids were washed with acetonitrile and diethyl ether and dried at room temperature.

The solution compositions and experimental conditions are set out in Table 1.

Physical measurements

The carbon, nitrogen and hydrogen contents of the complexes (Table 2) were determined on a Carlo–Erba EA1108 microanalyser. IR spectra were recorded in KBr mulls on a Perkin–Elmer 180 spectrophotometer. Proton NMR spectra were recorded on a Bruker WM 250 MHz spectrometer using DMSO as the solvent; chemical shifts were referred to TMS as the internal standard.

Table 2. Analytical data for the compounds

Complex	Found (Calc.) (%) N	C	H
$CdL^1{}_2$bipy	13.8(13.8)	62.6(63.3)	4.5(4.3)
$CdL^1{}_2$phen	13.9(13.3)	64.6(64.7)	4.6(4.1)
$CdL^2{}_2$bipy	13.0(13.2)	64.3(64.3)	4.8(4.7)
$CdL^2{}_2$phen	12.7(12.7)	66.2(65.5)	5.2(4.9)
$CdL^3{}_2$bipy	11.3(12.4)	56.9(56.8)	4.1(3.5)
$CdL^3{}_2$phen	11.3(12.0)	59.8(58.3)	3.8(3.4)
$CdL^4{}_2$bipy·CH_3CN	13.3(13.8)	60.7(61.1)	4.7(4.7)
$CdL^4{}_2$phen	12.6(12.2)	62.3(62.6)	4.4(4.3)
$CdL^5{}_2$bipy	12.5(12.6)	60.9(61.2)	4.9(4.5)
$CdL^5{}_2$phen	12.6(12.2)	62.7(62.6)	4.3(4.3)

Crystal structure determination

Crystal data. $C_{36}CdH_{33}N_7O_2$; $M = 708.11$, orthorhombic, $a = 11.0362(6)$, $b = 17.0351(7)$, $c = 17.6012(7)$ Å, $U = 3309.1(4)$ Å^3 (by least-squares refinement on diffractometer angles for 25 automatically centred reflections, $19 < \theta < 56°$, $\lambda = 1.54184$ Å), space group *Pccn* (No. 56), $Z = 4$, $D_c = 1.421$ g cm^{-3}. Irregular shaped crystals of maximum and minimum linear dimension 0.25 and 0.35 mm were used; μ(Mo-K_α) = 57.53 mm^{-1}.

Data collection and processing

CAD4 diffractometer, $\omega/2\theta$ mode with ω scan width = 0.85+0.15 tan θ, graphite monochromated Cu-K_α radiation, 2845 reflections measured ($0 < \theta < 60°$, $-2 \leqslant h \leqslant 12$, $0 \leqslant l \leqslant 19$), 2313 unique (merging $R = 0.027$), 1842 with $I > 3\sigma(I)$; Lorentz and polarization corrections. Absorption corrections were applied at a later stage in the refinement[4] (max., min. transmission factors = 1.48, 0.46). The intensities of two standard reflections were essentially constant throughout the experiment.

Structure analysis and refinement

Standard direct methods were followed by normal difference Fourier techniques. Blocked-matrix least-squares refinement with all non-hydrogen atoms anisotropic; hydrogens included as fixed contributors were those found in difference syntheses, with an overall isotropic temperature factor of $U_{iso} = 0.08$ Å^2. The function which minimized $\Sigma w(|F_o| - |F_c|)^2$ with the weighting scheme $w = 1/[\sigma^2(F_o) + 0.0002F_o^2]$ gave final $R[= \Sigma w(|F_o| - |F_c|)/\Sigma w(|F_o|]$ and $R'\{= [\Sigma w(|F_o| - |F_c|)^2/\Sigma w|F_o|^2]^{1/2}\}$ values of 0.044 and 0.048, respectively. Programs used: SHELX76[5] and ORTEP;[6] scattering factors for non-hydrogen atoms from Cromer and Mann[7] with corrections for anomalous dispersion from Cromer and Liberman,[8] for hydrogen from Stewart *et al.*[9] These and other crystallographic data have been deposited as supplementary material (No. CSD 56421). Copies can be obtained through the Fachinformationszentrum Energie, Physik, Mathematik D-7514 Eggenstein-Leopoldshafen.

RESULTS AND DISCUSSION

The oxidation of metallic cadmium as the anode of an electrochemical cell containing an acetonitrile solution of the appropriate Schiff base HL and 1,10-phenanthroline or 2,2′-bipyridine as additional ligands was a simple direct route to CdL_2L'. The compounds obtained were yellow crystalline solids that were insoluble in common non-polar solvents, but soluble in polar solvents such as acetonitrile or dimethylsulphoxide.

As in the synthesis of other cadmium complexes, the electrochemical efficiency, E_f, defined as the number of moles of metal dissolved per Faraday of charge (mol F^{-1}), was always close to 0.5. This, and the formation of hydrogen at the cathode, are in keeping with the following mechanism:

$$\text{Cathode: } 2HL + 2e^- \longrightarrow H_{2(g)} + 2L^-$$

$$\text{Anode: } Cd + L' + 2L^- \longrightarrow CdL_2L' + 2e^-$$

$$L' = \text{bipy or phen.}$$

An ORTEP view of the structure of 2,2′-bipyridine bis{2-[(2-methoxyphenyl)iminomethyl]pyrrolato}cadmium(II) is shown in Fig. 1. Bond distances and angles are listed in Table 3. The complex has crystallographic C_2 symmetry, with the cadmium atom located on the two-fold axis and coordinated to the N(1) and N(2) nitrogen atoms of two symmetry-related Schiff bases and to the two nitrogen atoms of the bipyridine moiety, which are also symmetry related by the two-fold axis.

The coordination polyhedron is best described as a distorted trigonal prism in which the bases, formed by atoms N(1), N(2) and N(3), are related by the crystallographic two-fold axis, with a dihedral angle of 171(1)° between them.

The Cd—$N_{(pyrrole)}$ bond length, 2.242(4) Å, is similar to the 2.266(4) Å found in the bis{2-[[2(N,N-dimethyl)aminoethyl]iminomethyl]pyrrolato}cadmium(II), a compound with a CdN_4 core and only a very weak interaction with the tertiary amine nitrogen.[10] The Cd—$N_{(azomethine)}$ distance, 2.524(5) Å, is considerably longer than those found in the above-mentioned complex, 2.277(5) Å,[10] and those found in the hexa-coordinate [(1,2-benzenediamine-N)][N,N″-(2,6-pyridinediyldimethylidene)bis[1,2-benzenediamine]diperchlorate]cadmium(II), 2.377(10) Å.[11] The Cd—$N_{(bipyridine)}$ bond lengths, 2.371(4) Å, are very similar to that found in $Cd(S_2CSC_4H_{9-n})_2 \cdot$ bipy, 2.363(3) Å,[12] and not very different to those found in [(2,2′-bipyridine)bis-(diethyldithiocarbamato)]cadmium(II), 2.430(3) Å.[13] Likewise, the N—Cd—N bite angle, 68.4(2)°, is similar to those reported for the latter complexes, 69.0(1)° and 67.6(3)°, respectively.

The average value of the C—N bond lengths, 1.287(7) Å, is very close to the reported norm for C=N bonds, 1.30 Å.[14] The bond lengths and angles in the pyrrole ring are very similar to those of the free pyrrole molecule. An acetonitrile molecule completes the crystal structure with its two carbon atoms on a crystallographic two-fold axis.

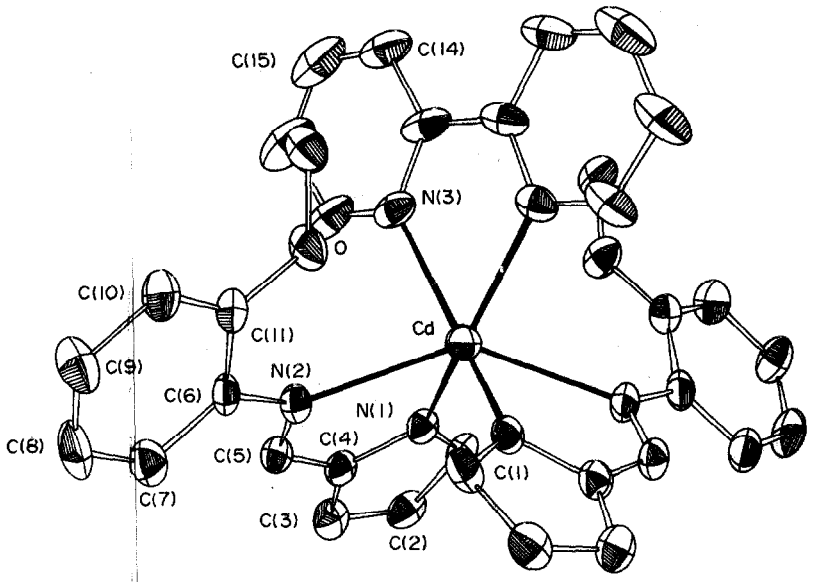

Fig. 1. Crystal structure of 2,2′-bipyridine bis{2-[(2-methoxyphenyl)iminomethyl]pyrrolato}-cadmium(II).

Table 3. Interatomic distances (Å) and bond angles (°)

Cd—N(1)	2.242(4)	Cd—N(2)	2.524(5)
Cd—N(3)	2.371(4)	O—C(11)	1.360(7)
O—C(12)	1.428(7)	N(1)—C(1)	1.342(7)
N(1)—C(4)	1.363(8)	N(2)—C(5)	1.287(7)
N(2)—C(6)	1.421(7)	N(3)—C(13)	1.356(7)
N(3)—C(17)	1.314(9)	N(4)—C(19)	1.29(2)
C(1)—C(2)	1.425(9)	C(2)—C(3)	1.38(1)
C(3)—C(4)	1.400(8)	C(4)—C(5)	1.427(8)
C(6)—C(7)	1.391(8)	C(6)—C(11)	1.401(8)
C(7)—C(8)	1.39(1)	C(8)—C(9)	1.36(1)
C(9)—C(10)	1.38(1)	C(10)—C(11)	1.394(8)
C(13)—C(14)	1.42(1)	C(14)—C(15)	1.34(2)
C(15)—C(16)	1.38(1)	C(16)—C(17)	1.39(1)
C(18)—C(19)	1.29(2)		

N(1)—Cd—N(2)	72.1(1)	N(1)—Cd—N(3)	93.0(2)
N(1)—Cd—N(1^{i})	113.0(2)	N(1)—Cd—N(2^{i})	86.3(1)
N(1)—Cd—N(3^{i})	149.4(2)	N(2)—Cd—N(3)	86.7(2)
N(2)—Cd—N(2^{i})	140.6(1)	N(2)—Cd—N(3^{i})	127.9(2)
N(3)—Cd—N(3^{i})	68.4(2)	C(11)—O—C(12)	116.6(4)
C(1)—N(1)—C(4)	106.9(5)	Cd—N(1)—C(1)	136.6(4)
Cd—N(1)—C(4)	116.1(3)	C(5)—N(2)—C(6)	120.2(5)
Cd—N(2)—C(5)	108.4(3)	Cd—N(2)—C(6)	131.2(3)
C(13)—N(3)—C(17)	120.1(5)	Cd—N(3)—C(13)	118.6(4)
Cd—N(3)—C(17)	121.4(4)	N(1)—C(1)—C(2)	109.7(5)
C(1)—C(2)—C(3)	106.7(6)	C(2)—C(3)—C(4)	105.8(5)
N(1)—C(4)—C(3)	110.9(5)	N(1)—C(4)—C(5)	120.5(5)
C(3)—C(4)—C(5)	128.6(5)	N(2)—C(5)—C(4)	122.6(5)
N(2)—C(6)—C(7)	124.4(5)	N(2)—C(6)—C(11)	118.6(5)
C(7)—C(6)—C(11)	116.9(5)	C(6)—C(7)—C(8)	120.8(6)
C(7)—C(8)—C(9)	121.9(7)	C(8)—C(9)—C(10)	118.6(7)
C(9)—C(10)—C(11)	120.4(6)	O—C(11)—C(6)	115.4(5)
O—C(11)—C(10)	123.1(5)	C(6)—C(11)—C(10)	121.4(5)
N(3)—C(13)—C(14)	118.2(6)	N(3)—C(13)—C(13)	117.2(6)
C(14)—C(13)—C(13)	124.5(6)	C(13)—C(14)—C(15)	120.8(9)
C(14)—C(15)—C(16)	120(1)	C(15)—C(16)—C(17)	117.0(8)
N(3)—C(17)—C(16)	123.5(7)	N(4)—C(19)—C(18)	146(1)

[i]Symmetry operation: $-x, -y, -z$.

Table 4. Selected IR bands of the ligands and complexes

Compound	ν(C=N)	L'(bipy)			L'(phen)			
2,2'-Bipyridine		739	755	1420				
1,10-Phenanthroline					738	854	1427	1510
HL^1	1630							
$CdL^1{}_2$bipy	1600	740	755	1430				
$CdL^1{}_2$phen	1600				730	850	1430	1510
HL^2	1635							
$CdL^2{}_2$bipy	1600	740	755	1430				
$CdL^2{}_2$phen	1610				730	850	1430	1510
HL^3	1615							
$CdL^3{}_2$bipy	1595	745	765	1440				
$CdL^3{}_2$phen	1590				730	860	1430	1510
HL^4	1630							
$CdL^4{}_2$bipy	1595	740	755					
$CdL^4{}_2$phen	1600				730	850	1425	1505
HL^5	1615							
$CdL^5{}_2$bipy	1600	740	755	1430				
$CdL^5{}_2$phen	1600				730	860	1430	1510

The IR spectra of the complexes (Table 4) are consistent with the structural data presented above. The ν(N—H) band of the free bases at 3300 cm^{-1} is absent in the spectra of the complexes, confirming that it is the deprotonated ligand that is present in the latter. The band which appears in the free ligand at 1630–1615 cm^{-1} is shifted to lower frequencies as a consequence of coordination to the imino nitrogen.[15]

In addition, bands at *ca* 1510, 850 and 730 cm^{-1} in the compounds containing 1,10-phenanthroline and at *ca* 760 and 760 cm^{-1} in the 2,2'-bipyridine derivatives confirm the presence of these ligands in the coordination sphere of the metal[16] and hence that cadmium is hexa-coordinate in all these compounds.

The ^1H NMR spectra reinforce the above conclusions. The signal attributed to N—H which appears at 11.8 ppm in the ligand (Table 5) is absent in the complexes, confirming that in the latter the ligand is deprotonated. The azomethine signal (at 8.3–8.6 ppm in the complexes) was slightly shifted downfield from its position in the free ligands. The spectra also show the signals of the additional

Table 5. Selected NMR shifts of the compounds

R	H^a	H^b	H^c	H^d	$H^{3,3'}$	$H^{4,4'}$	$H^{5,5'}$	$H^{6,6'}$	$H^{2,9}$	$H^{4,7}$	$H^{5,6}$	$H^{3,8}$
$CdL^1{}_2$bipy	6.7	6.2	7.0	8.4	8.4	8.0	7.5	8.5				
$CdL^1{}_2$phen	6.8	6.2	7.0	8.4					8.6	8.4	8.0	7.8
$CdL^2{}_2$bipy	6.7	6.2	6.9	8.4	8.3	8.0	7.5	8.4				
$CdL^2{}_2$phen	6.7	6.2	6.8	8.4					8.6	8.3	8.0	7.9
$CdL^3{}_2$bipy	6.7	6.2		8.4	8.4	8.0	7.5	8.6				
$CdL^3{}_2$phen		6.2		8.4					8.6	8.4	8.1	7.8
$CdL^4{}_2$bipy	6.7	6.2	6.8	8.6	8.4	7.9	7.4	8.6				
$CdL^4{}_2$phen	6.7	6.2	6.9	8.6					8.6	8.2	8.1	7.8
$CdL^5{}_2$bipy	6.7	6.2	6.9	8.4	8.3	8.0	7.5	8.4				
$CdL^5{}_2$phen	6.7	6.2		8.3					8.6	8.3	8.0	7.9

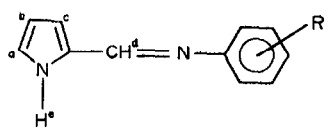

ligands bipy and phen with small shifts with respect to the free molecules, which confirm their coordination to the metal.

REFERENCES

1. J. Castro, J. E. Vilasanchez, J. Romero, J. A. García-Vázquez, M. L. Durán, A. Sousa, E. E. Castellano and J. Zukerman-Schpector, *Z. Anorg. Allg. Chem.*, 1992, **612**, 83.
2. J. Castro, J. Romero, J. A. García-Vázquez, M. L. Durán, A. Sousa, E. E. Castellano and J. Zukerman-Schpector, *Polyhedron* 1992, **11**, 235.
3. C. Oldhan and D. G. Tuck, *J. Chem. Educ.* 1982, **59**, 420.
4. N. Walker and D. Stuart, *Acta Cryst.* 1983, **A39**, 158.
5. G. M. Sheldrick, SHELX-76, Program for Crystal Structure Determination. University of Cambridge (1976).
6. C. K. Johnson, ORTEP, Report ORNL-3794. Oak Ridge Laboratory, Tennessee, U.S.A. (1965).
7. D. T. Cromer and J. B. Mann, *Acta Cryst.* 1968, **A24**, 321.
8. D. T. Cromer and D. Liberman, *J. Chem. Phys.* 1970, **53**, 1891.
9. R. F. Stewart, E. R. Davidson and W. T. Simpson, *J. Chem. Phys.* 1965, **42**, 3175.
10. J. Castro, J. Romero, J. A. García-Vásquez, A. Sousa, E. E. Castellano and J. Zuckerman-Schpector, *J. Coord. Chem.*, in press.
11. S. M. Nelson, F. S. Esho and M. G. B. Drew, *J. Chem. Soc., Dalton Trans.* 1982, 407.
12. S. J. Black, F. W. Z. Einstein, P. C. Hayes, R. Kumar and D. G. Tuck, *Inorg. Chem.* 1986, **25**, 4181.
13. C. Arioldi, S. de Oliveira, S. G. Riggiero and J. R. Lechat, *Inorg. Chim. Acta* 1990, **174**, 103.
14. F. H. Allen, O. Kennard, D. G. Watson, L. Brammer, A. G. Orpen and R. Taylor, *J. Chem. Soc., Perkin Trans. II.* 1987, S1.
15. G. C. Perry and D. G. Thorton, *J. Inorg. Nucl. Chem.* 1972, **34**, 335.
16. A. A. Shift and R. C. Taylor, *J. Inorg. Nucl. Chem.* 1959, **9**, 211; R. G. Inskeep, *J. Inorg. Nucl. Chem.* 1982, **24**, 763.

Polyhedron Vol. 12, No. 1, pp. 37–43, 1993
Printed in Great Britain

0277–5387/93 $6.00+.00
© 1993 Pergamon Press Ltd

REACTIONS OF $[Mo\{HB(3,5\text{-}Me_2pz)_3\}(NO)Cl_2]$ WITH $[Ph_3Sn]_2S$ AND OF $[Et_3NH][Mo\{HB(3,5\text{-}Me_2pz)_3\}(NO)Cl_2]$ WITH ELEMENTAL SULPHUR. THE MOLECULAR STRUCTURE OF μ-DISULPHIDO BIS(CHLORO)NITROSYL-{HYDROTRIS(3-5-DIMETHYLPYRAZOL-1-YL)-BORATO-MOLYBDENUM}, $[Mo\{HB(3,5\text{-}Me_2pz)_3\}(NO)Cl]_2(\mu\text{-}S_2)$

SEAN L. W. McWHINNIE,†‡ CHRISTOPHER J. JONES, JON A. McCLEVERTY,†§ THOMAS A. HAMOR and JEAN-DOMINIQUE F. FOULON

School of Chemistry, The University of Birmingham, PO Box 363, Birmingham B15 2TT, U.K.

(*Received* 4 *June* 1992; *accepted* 3 *September* 1992)

Abstract—$[Mo(NO)L^*Cl_2]$ [L* = hydrotris(3,5-dimethylpyrazol-1-yl)borate] reacted with $S(SnPh_3)_2$ to give $[\{Mo(NO)L^*Cl\}_2(\mu\text{-}S_2)]$ in low yield. The reaction between $[Et_3NH][Mo(NO)L^*Cl_2]$ and elemental sulphur afforded $[\{Mo(NO)L^*\}_2(\mu\text{-}S)_2]$ and $[\{Mo(NO)L^*Cl\}_2(\mu\text{-}S_2)]$. Both compounds undergo reversible one-electron reductions. The molecular structure of one isomer of $[\{Mo(NO)L^*Cl\}_2(\mu\text{-}S_2)]$ was determined crystallographically and the compound contains an Mo—S—S—Mo core with short Mo—S distances of 2.310 Å, but no direct metal–metal bond.

In our studies of bimetallic redox-active molybdenum and tungsten nitrosyl complexes, in which the two metals are bridged by aromatic and aliphatic groups, we have observed[1–3] that the interaction between the two metal centres is, as expected, strongly dependent on the nature of the bridging ligand, i.e. whether it is conjugated or non-conjugated in nature, and on the distance between the two metal centres. The mono-reduced species derived from the general system [M(NO)L*X—Q—M′(NO)L*X] [L* = tris(3,5-dimethylpyrazolyl)borate; X = Cl, I], which are paramagnetic and have one unpaired electron per bimetallic, exhibit the full range of mixed-valence behaviour. That is, the unpaired electron in the species $[M(NO)L^*X—Q—M'(NO)L^*X]^-$ may be localized on one metal ("valence-trapped"), partially localized ("hopping" between metal centres) or fully delocalized, depending on the electronic structure and geometry of Q.[1,3,4–7]

During our synthetic studies of the [M(NO)L*XY] system we have frequently obtained the bimetallic μ-oxo species $[\{M(NO)L^*X\}_2O]$.[5,8] These compounds both contain inequivalent metal sites as shown by ^1H NMR spectroscopy, an observation which was confirmed in $[Mo(NO)L^*I]_2(\mu\text{-}O)$ by an X-ray crystal structure determination.[8] It was expected that the electrochemical interaction between the two metal centres in this type of complex would be very strong and so we would have anticipated two well-separated one-electron reduction processes. However, we have so far detected only one one-electron electrochemical reduction process, although it is possible that the second reduction occurs very close to the potentials for the decomposition processes of the solvent and base electrolyte. Spectroelectrochemical studies of $[\{Mo(NO)L^*Cl\}_2O]^-$ suggest that the unpaired electron is delocalized over the Mo—O—Mo unit.[5]

† Authors to whom correspondence should be addressed.
‡ Present address: Department of Chemistry, Brunel University, Uxbridge, Middlesex UB8 3PH, U.K.
§ Present address: School of Chemistry, University of Bristol, Cantock's Close, Bristol BS8 1TS, U.K.

The closely related μ-sulphido complexes [{Mo(NO)L*X}$_2$S] would clearly be of interest in further exploring the electronic properties of such single-atom bridged systems. The reactions between elemental sulphur and [Mo(CO)$_3$LH] or [Mo(CO)$_3$L*H] [L = hydrotris(pyrazol-1-yl)borate] have afforded [{Mo(CO)$_2$L}$_2$(μ-S)] and [{Mo(CO)$_2$L*}$_2$(μ-S)], respectively,[9] both of which contain a linear [Mo—S—Mo]$^{2+}$ unit. This contrasts with the more general observation that μ-sulphido molybdenum complexes show acute Mo—S—Mo angles (75°).[10] The apparently straightforward synthesis of such μ-sulphido carbonyl species encouraged us initially to investigate the reactions between [Mo(NO)L*I$_2$] and either H_2S or Na_2S, since the reactive di-iodide was readily converted into [{Mo(NO)L*I}$_2$O] on treatment with water. However, although reactions with H_2S and Na_2S undoubtedly occurred, we were unable to isolate characterizeable products.

In contrast, the reactions between [Mo(NO)L*Cl$_2$] and S(SnPh$_3$)$_2$, and between [Et$_3$NH][Mo(NO)L*Cl$_2$] and S_8, have afforded isolable products and in this paper we describe the nature of the products isolated and their characterization.

EXPERIMENTAL

The complexes [Mo(NO)L*Cl$_2$] and [NHEt$_3$][Mo(NO)L*Cl$_2$] were prepared by previously described methods.[11,12] Other reagents were used as supplied and reaction solvents were redistilled from drying agents according to standard methods. All reactions were performed under an atmosphere of dry nitrogen, but most of the reaction products were air-stable. Column chromatography was carried out using silica gel (Merck 70-230 ASTM) columns.

IR spectra were recorded in KBr discs using a PE 297 spectrophotometer and ^{1}H NMR spectra were obtained using Jeol GX270 and Bruker WH400 instruments. Electronic spectra were recorded in dichloromethane solution using a Shimadzu UV-240 spectrometer. Mass spectra were obtained using a Kratos MS80 instrument under EI conditions.

Electrochemical measurements were made using an in-house designed three-electrode cell which incorporated a saturated calomel electrode (SCE), a platinum wire auxiliary electrode and a platinum-bead working electrode. Cyclic voltammetry and differential pulse voltammetry measurements were made at 20 ± 1°C with a PAR 174A potentiostat and a Philips *X–Y* recorder. Cyclic voltammetry measurements for Condecon electrochemical analysis were made over three or four scan rates between 100 and 1000 mV s^{-1} using a PAR 360 potentiostat with an analogue-digital convertor and the data were collected using an Amstrad PC1512 computer. The Condecon software, available from E.G. & G, uses convolutions and deconvolutions in the treatment of digitalized data from cyclic voltammetric experiments. An iterative approach is used to enable modelling of experimental data and, hence, mechanistic details can be deduced. All the electrochemical results were obtained from solutions containing [NBu$_4$]BF$_4$ (*ca* 0.2 mol dm^{-3}) as the supporting electrolyte and the potentials are reported vs SCE, but were calibrated using ferrocene as an internal reference couple.

Synthesis of S(SnPh$_3$)$_2$

SnClPh$_3$ (5.46 g, 14.2 mmol) and Na_2S (0.81 g) in water (100 cm^3) were refluxed for 2 days. The water was then distilled off, acetone was added to dissolve the solid and the solution was filtered. The bulk of the solution was reduced *in vacuo* and the addition of water gave a crystalline white precipitate. The solid was collected by filtration and dried *in vacuo* over P_2O_5 (yield: 2.78 g, 53%). The product was characterized by ^{1}H NMR spectroscopy and by elemental analysis. The presence of sulphur was ascertained by adding acid to an acetone solution of the product and monitoring the evolved gas with lead acetate paper, which turned black.

Reaction of S(SnPh$_3$)$_2$ *with* [Mo(NO)L*Cl$_2$], *isolation of* [{Mo(NO)L*Cl}$_2$(μ-S$_2$)] (1)

[Mo(NO)L*Cl$_2$] (0.203 g, 41 mmol) was refluxed for 5 days in toluene (75 cm^3) containing S(SnPh$_3$)$_2$ (0.133 g, 0.18 mmol). The solution, which had become very dark brown, was cooled and filtered. The filtrate was evaporated to dryness and purified by column chromatography (column dimensions 40 × 4 cm, eluant dichloromethane/hexane, 70/30 v/v). Five fractions were collected, but only the blue second fraction, compound **1**, afforded a solid in a pure form. This compound was identified as [{Mo(NO)L*Cl}$_2$(μ-S$_2$)] from the X-ray study (yield: 7 mg, 3%). Found: C, 38.9; H, 4.6; N, 19.3. Calc. for **1**: C, 38.0; H, 4.7; N, 20.7%. IR (cm^{-1}, KBr disc): ν(BH) 2545, ν(NO) 1685. ^{1}H NMR spectrum [ppm, 270 MHz, $CDCl_3$ (relative area, multiplicity)]: 5.95(2s), 5.87(2s), 5.83(2s), 2.66(6s). 2.47(6s), 2.41(6s), 2.38(6s) and 2.31(6s). Mass spectrum: m/z = 947 ([Mo$_2$(NO)$_2$L*$_2$Cl$_2$S − 1]$^+$), 932 ([Mo$_2$(NO)NL*$_2$Cl$_2$S]$^+$), 493 ([Mo(NO)L*ClS + 1]$^+$), 465 ([Mo(NO)L*Cl]$^+$). Electronic spectrum {λ_{max} [nm, ε (dm^3 mol^{-1} cm^{-1}; $CHCl_3$)]}: 586 (17,250), 410 (67,000), 342 (11,940), 232 (45,240). Electrochemical data (CH_2Cl_2; vs SCE): $E_{1/2}$ =

-0.073 ± 0.005 V, $\Delta E_p = 85\pm10$ mV (ferrocene, $E_{1/2} = +0.555\pm0.005$ V, $\Delta E_p = 100\pm10$ mV). Condecon analysis in dichloromethane showed a one-electron fast transfer process. This process was not fully reversible, with a decomposition rate of *ca* 0.2 s^{-1}.

Reaction of [NHEt$_3$][Mo(NO)L*Cl$_2$] *with elemental sulphur; attempted isolation of* [{Mo(NO)L*S}$_2$] (3)

[NHEt$_3$][Mo(NO)L*Cl$_2$] (250 mg, 0.42 mM) was refluxed with elemental sulphur (125 mg, 3.90 mM) in toluene (50 cm^3). The solution began to darken immediately, but heating was continued for 16 h. The solution was cooled, filtered and evaporated to dryness. Purification was carried out by column chromatography (column dimensions 50×2 cm, eluant 80% dichloromethane/20% hexane) and four fractions (brown, red, blue and purple in order of elution) were isolated. The first fraction was brown (3) and was identified tentatively by ^{1}H NMR and mass spectrometry as [{Mo(NO)L*Cl}$_2$(μ-S)$_2$] contaminated with elemental sulphur, which could not be removed (yield: 13 mg of the impure product). IR spectrum (cm^{-1}, KBr disc): ν(BH) 2555, ν(NO) 1685. ^{1}H NMR spectrum [ppm, 400 MHz, $CDCl_3$ (relative area, multiplicity)]: 5.90(1s), 5.85(2s), 2.50(3s), 2.39(6s), 2.33(6s) and 2.18(3s). Mass spectrum: $m/z = 910$ ([M]$^+$), 489 ([Mo(NO)L*S$_2$]$^+$), 457 ([Mo(NO)L*S]$^+$), 427 ([MoL*S]$^+$). Electronic spectrum {λ_{max} [nm, ε ($dm^3\ mol^{-1}\ cm^{-1}$; $CHCl_3$)]}: 535 (4890), 413 (17,870), 233 (66,400). Electrochemical data (CH_2Cl_2; vs SCE): $E_{1/2} = -0.360\pm0.005$ V, $\Delta E_p = 105\pm10$ mV (ferrocene, $E_{1/2} = +0.555\pm0.005$ V; $\Delta E_p = 95\pm10$ mV). Condecon analysis showed a fast one-electron transfer with a small decomposition process with a rate constant <0.05 s^{-1}.

The remaining fractions were obtained in yields of 3% or less, in insufficient quantities for adequate characterization. However, from mass and IR spectral comparisons the third blue fraction seems to be very similar, if not identical, to **1**.

X-ray crystallographic data obtained from compound **1**

$C_{30}H_{44}B_2Cl_2Mo_2N_{14}O_2S_2$, $M = 981.3$, monoclinic, space group $P2_1$, $a = 10.205(4)$, $b = 16.958(9)$, $c = 12.701(3)$ Å, $\beta = 106.38(3)°$, $V = 2108.8$ Å^3, $Z = 2$, $D_c = 1.545$ g cm^{-3}, $F(000) = 996$, μ(Mo-K_α) = 0.844 mm^{-1}, $\lambda = 0.71069$ Å.

A plate-shaped crystal ($0.3\times0.25\times0.1$ mm) was mounted on an Enraf–Nonius CAD-4 diffractometer, cell dimensions and intensities were measured by $\omega/2\theta$ scans with graphite-monochromated Mo-K_α radiation and scan range (θ) = (1.1+0.35 tan θ)°. 4367 reflections were scanned in the range $2 < \theta < 25°$, of which 3838 were unique ($R_i = 0.04$), and of these 2378 having $I > 2.5\sigma(I)$ were considered observed and used in the analysis. Three standard reflections measured every 2 h showed no significant variation in intensity.

The structure was determined by Patterson and Fourier methods. It was obvious as this stage that the overall molecular conformation approximated closely $\bar{1}$ (C_i) symmetry. It had been noted that the hol reflections having $h+1$ odd were significantly weaker than those having $h+1$ even. The space group thus approximates to the centrosymmetric $P2_1/n$. To overcome the difficulties inherent in refining by least-squares a pseudo-centrosymmetric structure in a non-centrosymmetric space group, a damping factor[13] was included in the calculations and the two halves of the molecules related by the pseudo-centre were refined in separate blocks. Anisotropic thermal parameters were used for the non-hydrogen atoms. Hydrogen atoms were placed in calculated positions. Weights, $w = 1/[\sigma^2(F)+0.001F^2]$, which resulted in a satisfactory weighting analysis, were used in the least-squares refinement. The calculations were terminated when all shift/error ratios were less than 0.35 and R = 0.0477, $R_w = 0.0564$ for 2378 observed reflections. The residual electron density in a final difference map was within the range -0.73 to $+0.91$ e Å^{-3}.

Complex neutral-atom scattering factors were employed. Computations were carried out largely on the University of Birmingham IBM 3090 computer with SHELX 76.[13] The molecular diagram was drawn using PLUTO.[14]

Additional material available from the Cambridge Crystallographic Data Centre comprises atomic coordinates, thermal parameters and the full set of bond lengths and angles.

RESULTS AND DISCUSSION

Synthetic and spectral studies

Because of earlier difficulties in obtaining isolable products from the reactions between H_2S and Na_2S and the labile [Mo(NO)L*I$_2$], we have investigated reactions between [Mo(NO)L*Cl$_2$] and S(SnPh$_3$)$_2$. The tin-containing reagent appeared to be particularly useful for introducing S^{2-} into the molybdenum nitrosyl system because of the very high stability of the Sn—Cl bonds in the $SnClPh_3$ by-product. We have also investigated the reaction between [Mo(NO)L*Cl$_2$]$^-$ and S_8. The reduced molybdenum nitrosyl chloride has proved to be a

most useful intermediate for the introduction of neutral nucleophiles into the molybdenum nitrosyl system, affording species of the type [Mo(NO)L*ClQ].

The reaction between $[Mo(NO)L^*Cl_2]$ and $[Ph_3Sn]_2S$ was carried out in refluxing toluene for several days in order to drive the reaction to near-completion. Five fractions, excluding the starting material, were separated by column chromatography, the first fraction being red, the second dark blue (**1**), the third green, the fourth purple and the fifth dark green (**2**). Of these, we were only able to satisfactorily separate and purify the second and fifth fractions. Among the other compounds which could occasionally be isolated from the reaction mixture during work-up, one white crystalline material was identified as $Ph_3SnSnPh_3$ on the basis of mass spectral measurements.

The fifth fraction yielded compound **2**, identified as $[\{Mo(NO)L^*Cl\}_2(\mu\text{-}O)]$ by ^1H NMR spectroscopy and by comparison with an authentic sample.[5,8] The first fraction could not be identified. However, the IR spectrum of the dark blue second fraction (**1**) contained a single nitrosyl stretch, the ^1H NMR spectrum contained only a single set of signals attributable to L* and the mass spectrum contained a peak assigned to $[Mo_2(NO)_2L^*_2Cl_2S-H]^+$. It was possible to obtain crystals of this compound by slow evaporation of a dichloromethane solution, and an X-ray analysis established that the compound is $[\{Mo(NO)L^*Cl\}_2(\mu\text{-}S_2)]$. Although the yield of the product was very low, the reaction was reproducible. The observation of **1** as a product of the reaction between $[Mo(NO)L^*Cl_2]$ and $S(SnPh_3)_2$ possibly explains the occurrence of $[\{SnPh_3\}_2]$, perhaps formed by reaction of two molecules of the putative intermediate [Mo(NO)L*Cl(SSnPh$_3$)].

The reaction between $[NHEt_3][Mo(NO)L^*Cl_2]$ and an excess of S_8 in refluxing toluene afforded, after cooling, reduction of the solvent and column chromatography gave four fractions, the first being brown (**3**), the second red, the third dark blue (probably **1**) and the fourth purple. All four fractions were separated by column chromatography.

The brown fraction afforded compound **3**, but this was difficult to obtain in pure form as it travelled down the column with elemental sulphur. The sulphur was observed to preferentially precipitate from a dichloromethane/hexane mixture, but it could not be completely removed from the fraction. Attempts were made to sublime the element from the compound mixture, but even this failed to fully purify the compound and thus elemental analysis was precluded. The mass spectrum of this material contained a molecular ion at $m/z = 910$ which corresponds to the formulation $[\{Mo(NO)L^*S\}_2]^+$. The ^1H NMR spectrum of this species was also consistent with this formulation, showing one set of signals assigned to L*, viz. two signals due to the hydrogen atom attached to C(4) of the pyrazolyl ring and four methyl signals, of relative areas 1:2:3:6:6:3. This indicates that the molecule has a plane of symmetry through one pyrazole ring of each L* ligand and this could be consistent with a formulation as $[\{Mo(NO)L^*\}_2(\mu\text{-}S)_2]$, which could exist as two isomers, *cis* and *trans* with respect to the nitrosyl groups (Fig. 1). However, the compound exhibits only one NO stretching frequency and so we conclude that the species may have the *trans* (C_{2h}) form. NOE studies failed to reveal any signal enhancements and so did not distinguish the possibilities.

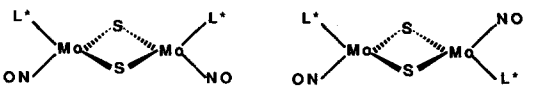

Fig. 1. *Cis* and *Trans* isomers of $[\{Mo(NO)L^*\}(\mu\text{-}S)_2]$ (**3**).

Electronic spectral data obtained from the purified complexes are given in the Experimental. The absorption which appears at *ca* 230 nm can be assigned to a π–π^* transition in L* and the other transitions would appear to be charge-transfer in nature, almost certainly ligand-to-metal, as indicated by their intensities. The transition at 410 nm in **1** is very strong ($\varepsilon = 67{,}000$ dm^3 mol^{-1} cm^{-1}), which causes the complex to be intensely dark blue. It is possible that this band is due to a transition associated with the Mo—S—S—Mo chromophore, implying that there is delocalization within the bridge.[5]

Electrochemical studies

Compound **1** displayed an initial reduction process at -0.073 ± 0.005 V in dichloromethane (platinum electrode, vs SCE). Multiple scans around this wave and scan-rate dependence studies indicated that it was very close to being reversible, so we presume that $[\{Mo(NO)L^*Cl\}_2S_2]^-$ has been formed. Condecon™ electrochemical analysis established that the compound exhibited a fast one-electron addition process with only slight decomposition. Species **1** also revealed additional processes as the voltage was scanned to potentials negative of the initial reduction; viz. two waves close together at around -1.05 ± 0.02v V and a third at *ca* -1.6 ± 0.02 V were detected. These three waves all appeared to be slightly smaller than the initial wave, but were at best only quasi-reversible. In addition, scanning out as far as -1.9 V and then

recycling produced a small product wave with its maximum at +0.2 V. Multiple scans around the first wave at −1.05 V showed that it died away rapidly.

The cyclic voltammogram of **3** showed only one reduction process, perhaps due to the formation of $[\{Mo(NO)L^*S\}_2]^-$, but if the voltage scan was continued well past the wave to negative potentials a small irreversible product was observed on the return sweep, with its maximum at $-0.55+/-0.02$ V. Analysis of the reduction wave using Condecon™ procedures established that the electrode reaction was a fully reversible one-electron process.

X-ray structural studies

Selected geometrical parameters are in Table 1. The structure is illustrated in Fig. 2, which also shows the atomic numbering scheme. The molecule is pseudo-centrosymmetric about the mid-point of the S—S′ bond. The Mo—Mo′ distance is 5.686(2) Å, indicating the absence of any direct interaction between the metal centres.

The coordination about molybdenum is essentially octahedral [maximum angular deviation from ideal octahedral 15.9°, angle S(1)—Mo—N(6) and S(1′)—Mo′—N(6′) both 164.1°, mean deviation 6.4°] and is similar to that found in an analogous bimetallic complex,[3] $[\{Mo(NO)L^*Cl\}_2(\mu\text{-}NC_4H_8N)]$, where the mean angular deviation from octahedral is 5.6°.

The Mo—S and S—S bond lengths, 2.308 (mean) and 2.036(5) Å, respectively, are significantly shorter than the corresponding lengths in the oxo-disulphido molybdate(VI) anion $[\{(S_2)_2MoO\}_2S]_2^{2-}$ of 2.418 and 2.083 Å.[15] This appears to be the only example in the literature of two molybdenum atoms bridged by a single disulphide bridge for which structural parameters have been determined. In $[Fe(\eta^5\text{-}C_5H_4S)_2Mo(NO)L^*]$[16] the Mo—S bond distances are also longer at 2.356(2) and 2.375(2) Å. The bonds to the pyrazolyl rings (2.142–2.215 Å) fall within the range of lengths commonly found in this type of complex. As has been noted previously[3,17] the bond *trans* to the nitrosyl group tends to be long [2.205 Å (mean) in the present structure] due to the *trans* influence of the strongly π-accepting nitrosyl group. The shortest Mo—N(pyrazolyl) bond is *trans* to the chloro substituent. This is also a systematic effect and has been described before.[3,17] The Mo—Cl length, 2.389 Å, is similar to those found in two analogous chloro complexes, 2.408(2)[3] and 2.380(3) Å.[18] The Mo—N(nitrosyl) bond, mean 1.744 Å, is the short-

Table 1. Selected bond lengths (Å) and angles (°) with e.s.d.s in parentheses

Mo(1)—S(1)	2.297(3)	Mo(1′)—S(1′)	2.319(3)
Mo(1)—Cl(1)	2.389(4)	Mo(1′)—Cl(1′)	2.389(4)
Mo(1)—N(1)	1.736(10)	Mo(1′)—N(1′)	1.752(8)
Mo(1)—N(2)	2.196(8)	Mo(1′)—N(2′)	2.215(10)
Mo(1)—N(4)	2.142(9)	Mo(1′)—N(4′)	2.163(10)
Mo(1)—N(6)	2.206(9)	Mo(1′—N(6′)	2.195(10)
O(1)—N(1)	1.246(14)	O(1′)—N(1′)	1.911(11)
S(1)—S(1′)	2.036(5)		

S(1)—Mo—Cl(1)	101.6(1)	S(1′)—Mo(1′)—Cl(1′)	101.1(1)
S(1)—Mo(1)—N(1)	95.1(3)	S(1′)—Mo(1′)—N(1′)	95.4(3)
Cl(1)—Mo(1)—N(1)	90.1(4)	Cl(1′)—Mo(1′)—N(1′)	90.8(3)
S(1)—Mo(1)—N(2)	83.0(2)	S(1′)—Mo(1′)—N(2′)	81.7(3)
Cl(1)—Mo(1)—N(2)	87.1(2)	Cl(1′)—Mo(1′)—N(2′)	86.8(3)
N(1)—Mo(1)—N(2)	176.2(5)	N(1′)—Mo(1′)—N(2′)	175.7(4)
S(1)—Mo(1)—N(4)	90.4(2)	S(1′)—Mo(1′)—N(4′)	91.9(2)
Cl(1)—Mo(1)—N(4)	165.6(3)	Cl(1′)—Mo(1′)—N(4′)	165.1(3)
N(1)—Mo(1)—N(4)	96.7(5)	N(1′)—Mo(1′)—N(4′)	95.3(4)
N(2)—Mo(1)—N(4)	86.5(3)	N(2′)—Mo(1′)—N(4′)	87.9(4)
S(1)—Mo(1)—N(6)	164.1(2)	S(1′)—Mo(1′)—N(6′)	164.1(3)
Cl(1)—Mo(1)—N(6)	87.4(3)	Cl(1′)—Mo(1′)—N(6′)	89.3(3)
N(1)—Mo(1)—N(6)	98.0(4)	N(1′)—Mo(1′)—N(6′)	96.5(4)
N(2)—Mo(1)—N(6)	84.5(3)	N(2′)—Mo(1′)—N(6′)	87.0(4)
N(4)—Mo(1)—N(6)	79.2(3)	N(4′)—Mo(1′)—N(6′)	76.5(4)
Mo(1)—S(1)—S(1′)	111.8(2)	S(1)—S(1′)—Mo(1′)	111.1(2)
Mo(1)—N(1)—O(1)	174.3(11)	Mo(1′)—N(1′)—O(1′)	176.0(9)

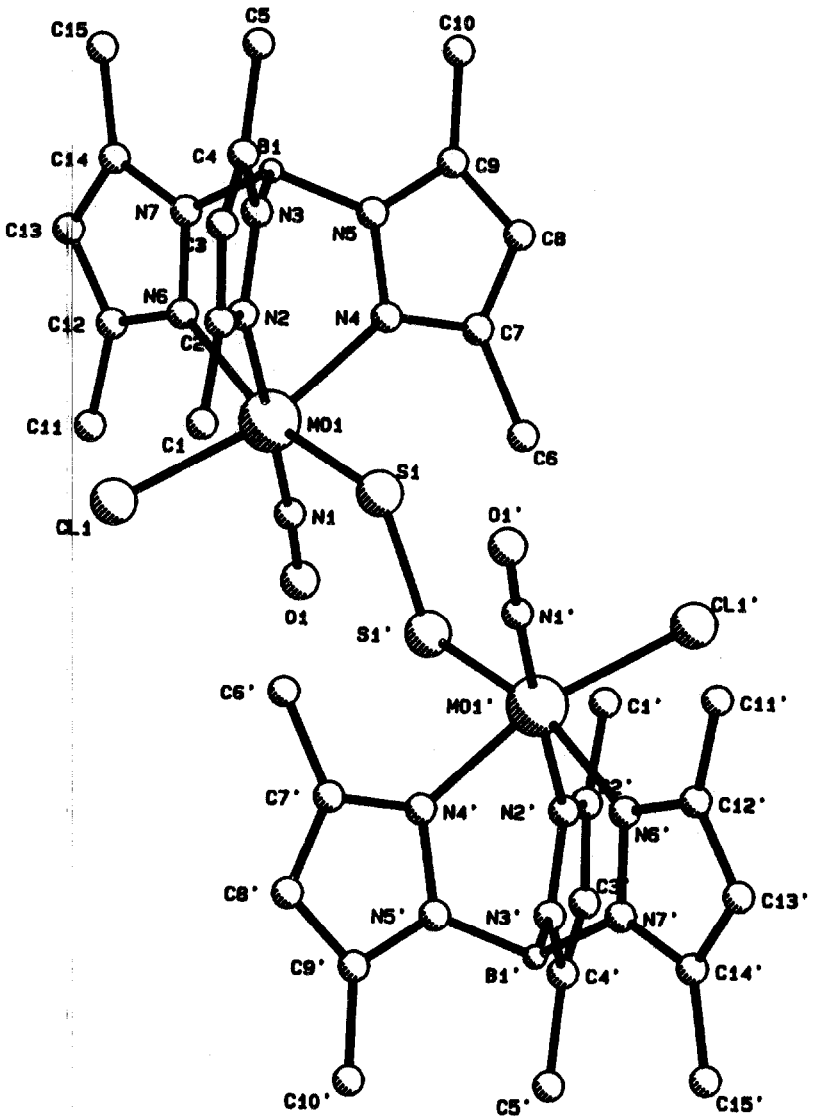

Fig. 2. Structure of [{Mo(NO)L*Cl}(μ-S_2)] (1).

est molybdenum–ligand distance and falls at the lower end of the range (*ca* 1.74–1.80 Å) commonly found[3,17,18] for this bond in complexes containing the $\{Mo(NO)L^*\}^{2+}$ moiety. The slight (mean 4.85°) deviation from linearity of the Mo—N—O grouping is also typical, comparing with deviations ranging from 0.4 to 6.0°, mean 3.0° found in the crystal structures of a number of closely related structures of this type.[16]

Hoffmann has recently described a theoretical investigation into some of the factors effecting bonding in molybdenum sulphur bimetallics.[19] Apparently there are only small energy differences between the various possible bonding alternatives in sulphido bridge molybdenum species and so it is difficult to predict, or even to account for, the structures found in these molecules. Although disulphide links are fairly common in transition metal chemistry,[20] only a few examples of ($\eta^1:\eta^1$-S_2) have been crystallographically characterized, the ($\eta^2:\eta^2$-S_2) bridge being more common. Amongst the examples which have been characterized many contain more than just a single bridge. Examples of other metals bridged by a single S_2 unit include [{Ru$(NH_3)_5$}$_2$(μ-S_2)][21] and [{Co$(CN)_5$}$_2$(μ-S_2)].[22]

REFERENCES

1. S. M. Charsley, C. J. Jones, J. A. McCleverty, B. D. Neaves, S. J. Reynolds and G. Denti, *J. Chem. Soc., Dalton Trans.* 1988, 293.
2. S. M. Charsley, C. J. Jones, J. A. McCleverty, B. D.

Neaves and S. J. Reynolds, *J. Chem. Soc., Dalton Trans.* 1988, 301.
3. N. Al-Obaidi, T. A. Hamor, C. J. Jones, J. A. McCleverty and K. Paxton, *J. Chem. Soc., Dalton Trans.* 1987, 2653.
4. S. L. W. McWhinnie, C. J. Jones and J. A. McCleverty, work to be published; S. L. W. McWhinnie, PhD Thesis, University of Birmingham (1989).
5. S. L. W. McWhinnie, C. J. Jones, J. A. McCleverty and L. J. Yellowlees, *J. Chem. Soc., Dalton Trans*, in press.
6. S. L. W. McWhinnie, W. Hussain, C. J. Jones, J. A. McCleverty, D. Collison, F. E. Mabbs and L. J. Yellowlees, work to be published.
7. S. L. W. McWhinnie, C. J. Jones, J. A. McCleverty, D. Collison and F. E. Mabbs, *J. Chem. Soc., Dalton Trans.* 1990, 940.
8. H. Adams, N. A. Bailey, G. Denti, J. A. McCleverty, J. M. A. Smith and A. Wlodarczyk, *J. Chem. Soc., Dalton Trans.* 1983, 2287.
9. S. Lincoln, S.-L. Soong, S. A. Koch, M. Sato and J. H. Enemark, *Inorg. Chem.* 1985, **24**, 1355.
10. J. H. Enemark and G. Bunzey, *Inorg. Chem.* 1978, **17**, 682.
11. A. S. Drane and J. A. McCleverty, *Polyhedron* 1983, **2**, 53.
12. S. L. W. McWhinnie, C. L. Jones and J. A. McCleverty, D. Collison and F. E. Mabbs, *Polyhedron* 1992, **11**, 2639.
13. G. M. Sheldrick, SHELX 76, Program for Crystal Structure Determination, University of Cambridge (1976).
14. W. D. S. Motherwell and W. Clegg, PLUTO, Program for Drawing Crystal and Molecular Structures, University of Cambridge (1978).
15. D. Coucouvanis and A. Hadjikyriacou, *Inorg. Chem.* 1989, **2**, 1.
16. R. P. Sidebotham, P. D. Beer, T. A. Hamor, C. J. Jones and J. A. McCleverty, *J. Organomet. Chem.* 1989, **371**, C31.
17. J. A. McCleverty, A. E. Rae, I. Wolochowicz, N. A. Bailey and J. M. A. Smith, *J. Chem. Soc., Dalton Trans.* 1982, 429.
18. J. A. McCleverty, D. Seddon, N. A. Bailey and N. W. Walker, *J. Chem. Soc., Dalton Trans.* 1976, 898.
19. W. Tremel, R. Hoffmann and E. D. Jemmis, *Inorg. Chem.* 1989, **28**, 1213.
20. *Comprehensive Coordination Chemistry* (Edited by G. Wilkinson, R. D. Gillard and J. A. McCleverty), Ch. 16.1. Pergamon Press, Oxford (1983).
21. C. R. Boulet, S. S. Isied and H. Taube, *J. Am. Chem. Soc.* 1973, **95**, 4758.
22. M. Di Vaira, S. Midolini and L. Sacconi, *Inorg. Chem.* 1979, **18**, 3466.

Polyhedron Vol. 12, No. 1, pp. 45–53, 1993
Printed in Great Britain

0277–5387/93 $6.00+.00
© 1993 Pergamon Press Ltd

THE SYNTHESIS, ELECTROCHEMISTRY AND THERMAL BEHAVIOUR OF SOME MOLYBDENUM MONONITROSYL COMPLEXES INCORPORATING STILBENAMIDE LIGANDS CARRYING LONG-CHAIN ALKOXY SUBSTITUENTS

BENJAMIN J. COE, CHRISTOPHER J. JONES* and JON A. McCLEVERTY*†

School of Chemistry, The University of Birmingham, Edgbaston, Birmingham B15 2TT, U.K.

and

DUNCAN W. BRUCE

Sheffield Centre for Molecular Materials, Department of Chemistry, The University, Sheffield S3 7HF, U.K.

(*Received* 13 *August* 1992; *accepted* 20 *August* 1992)

Abstract—The new complexes $[Mo(NO)L(X)(NHC_6H_4CH{=}CHC_6H_4OR\text{-}4,4')]$ ($R = C_6H_{13}$, X = Cl, I, OH; $R = C_8H_{17}$ or $C_{12}H_{25}$ and X = Cl or I) and $[Mo(NO)L(NHC_6H_4CH{=}CHC_6H_4OR\text{-}4,4')_2]$ ($R = C_6H_{13}$, C_8H_{17} or $C_{12}H_{25}$) have been synthesized and characterized by spectroscopic methods. All undergo one-electron reduction processes at potentials ranging from −0.74 to −1.20 V (vs S.C.E.). These new compounds have also been examined by differential scanning calorimetry and polarizing hot-stage microscopy, but do not exhibit any liquid crystalline mesophases.

In recent years a variety of transition metal derivatives has been reported to form liquid crystal phases and there is continuing interest in compounds of this type because of their potential for introducing magnetic, redox and optical properties into liquid crystal materials.[1–5] The molybdenum mononitrosyl derivatives [Mo(NO)L(X)(Y)] [L = hydrotris(3,5-dimethylpyrazol-1-yl)borate, X = Cl, I or Y and Y = phenoxide or arylamide][6] are redox active,[7,8] and can, in certain cases, exhibit non-linear optical properties.[9] In order to discover whether suitably derived complexes of this type might form liquid crystal mesophases, we have previously synthesized derivatives of [Mo(NO)L(X)(Y)] containing anilide or phenolate ligands carrying long-chain alkyl substituents in the 4-position of the aryl ring. Although the alkyl substituents served to reduce the melting points of these complexes, no liquid crystal phases were observed.[10] In a continuation of this study we have used ligands containing alkoxylated stilbenyl groups in an attempt to produce molecules which might give rise to mesophases and which might also, in suitably ordered arrays, exhibit non-linear optical properties. The alkoxystilbenamide ligand was selected since molecules of this structural type are known to form liquid crystals and, when attached to the {Mo(NO)L(X)} moiety, the ferrocenylstilbenamide ligand produces NLO materials. Thus, the new complexes $[Mo(NO)L(X)(NHC_6H_4CH{=}CHC_6H_4OR\text{-}4,4')]$ ($R = C_6H_{13}$, X = Cl, I, OH; $R = C_8H_{17}$ or $C_{12}H_{25}$ and X = Cl or I) and $[Mo(NO)L(NHC_6H_4CH{=}CHC_6H_4OR\text{-}4,4')_2]$ ($R = C_6H_{13}$, C_8H_{17} or $C_{12}H_{25}$) (Fig. 1) have been synthesized and studied by differential scanning calorimetry and polarizing hot-stage microscopy.

EXPERIMENTAL

All reagents were used as supplied. $[Mo(NO)\{HB(3,5\text{-}Me_2C_3N_2H)_3\}I_2]$ and $[Mo(NO)\{HB(3,5\text{-}Me_2C_3N_2H)_3\}Cl_2]$ were prepared according to

* Authors to whom correspondence should be addressed.
† Present address: School of Chemistry, University of Bristol, Cantock's Close, Bristol BS8 1TS, U.K.

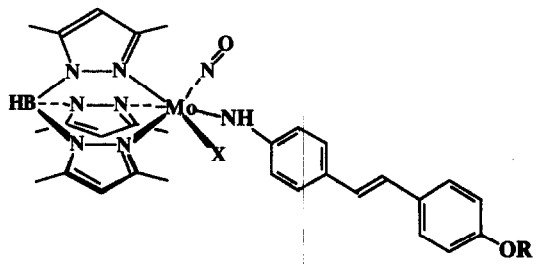

Fig. 1. $[Mo(NO)L(X)(NHC_6H_4CH{=}CHC_6H_4OR)]$ ($R = C_6H_{13}$, C_8H_{17}, $C_{12}H_{25}$; X = Cl, I, $NHC_6H_4CH{=}CHC_6H_4OR$; X = OH, $R = C_6H_{13}$).

previously described methods.[11,12] Solvents used as reaction media were dried according to standard methods and freed of oxygen before use. Silica gel 60 (70–230 mesh) or alumina 90 (70–230 mesh) was used as the stationary phase for column chromatography with column dimensions of 40 × 2 cm unless otherwise specified. Triethylamine was dried over sodium and stored over activated alumina, and hexamine was recrystallized from absolute ethanol and dried under vacuum. Other reagents were used as supplied, and all reaction solvents were redistilled from drying agents according to standard methods prior to use. All reactions were performed under an atmosphere of dry nitrogen but the reaction products were handled in air. Elemental analyses were carried out by the Microanalytical Laboratory, University of Birmingham.

IR spectra were recorded using a PE 297 spectrometer with samples as KBr discs. 270 MHz ^1H NMR spectra were obtained from solutions in $CDCl_3$ using a Jeol GX 270 spectrometer. Cyclic voltammetric measurements were made using a PAR 174A polarograph. Solutions in CH_2Cl_2 were *ca* 10^{-3} mol dm^{-3} in the complex and 0.2 mol dm^{-3} in $[Bu^nN]BF_4$ as the base electrolyte. A platinum bead test electrode was used with a scan rate of 200 mV s^{-1}. An S.C.E. reference electrode was used with ferrocene as an internal standard. Potentials are quoted relative to the S.C.E. and under these conditions E_f for the oxidation of ferrocene was found to be 0.58 V. Differential scanning calorimetry measurements were carried out using a Perkin–Elmer DSC7 instrument with samples (typically 1.4–3 mg) being hermetically sealed in 0.1 cm^3 aluminium pans. In all cases heating and cooling rates of 10 K min^{-1} were used. The microscopy studies were carried out using a CZ Scientific Labpol system equipped with a Link-Am PR600 controller and TH600 hot-stage. Heating rates were 10 K min^{-1} unless otherwise stated.

4-n-*Dodecyloxy-4′-nitrostilbene* (**1**)

A solution of 4-n-dodecyloxybenzaldehyde (4.0 g, 13.8 mmol), 4-nitrophenylacetic acid (2.74 g, 15.1 mmol) and piperidine (10 cm^3) was stirred under reflux in pyridine (50 cm^3) for 22 h. The mixture was cooled and the solvent removed under reduced pressure. The bright yellow product was purified by two recrystallizations from ethanol to yield bright yellow crystals of 4-n-dodecyloxy-4′-nitrostilbene (0.90 g, 16%).

$C_{12}H_{25}OC_6H_4CH{=}CHC_6H_4{-}NO_2$, m.p. 95–113°C. Found: C, 76.5; H, 8.5; N, 3.4. Calc. for $C_{26}H_{35}NO_3$: C, 76.3; H, 8.6; N, 3.4%. $\nu_{max}(NO_2)$: 1500s and 1330s cm^{-1}. $\delta_H(CDCl_3)$: 8.19 and 7.58 [2H, d, J(HH) = 8.8 Hz; 2H, d, J(HH) = 8.8 Hz, $C_6H_4{-}NO_2$], 7.48 and 6.91 [2H, d, J(HH) = 8.8 Hz; 2H, d, J(HH) = 8.8 Hz, $C_6H_4{-}OC_{12}H_{25}$], 7.22 and 6.99 [1H, d, $J(HH)_{trans}$ = 16.3 Hz; 1H, d, $J(HH)_{trans}$ = 16.3 Hz, $CH = CH$], 3.98 [2H, t, J(HH) = 6.6 Hz, $OCH_2{-}C_{11}H_{23}$], 1.80 [2H, qn, $OCH_2{-}CH_2{-}C_{10}H_{21}$], 1.46 [2H, qn, $OCH_2CH_2{-}CH_2{-}C_9H_{19}$], 1.27 [16H, br s, $OC_3H_6{-}C_8H_{16}{-}CH_3$], 0.88 [3H, t, J(HH) = 7.0 Hz, CH_3].

4-n-*Hexyloxy-4′-nitrostilbene* (**2**)

This compound was prepared in an identical manner to **1** using 4-n-hexyloxybenzaldehyde (2.85 g, 13.8 mmol) in place of 4-n-dodecyloxybenzaldehyde. Recrystallization afforded bright yellow crystals of 4-n-hexyloxy-4′-nitrostilbene (0.85 g, 19%).

$C_6H_{13}OC_6H_4CH{=}CHC_6H_4{-}NO_2$, m.p. 99–106°C. Found: C, 73.8; H, 7.0; N, 4.6. Calc. for $C_{20}H_{23}NO_3$: C, 73.8; H, 7.1; N, 4.3%. $\nu_{max}(NO_2)$: 1500s and 1330s cm^{-1}. $\delta_H(CDCl_3)$:* 8.19 and 7.58 [2H, d, J(HH) = 8.8 Hz; 2H, d, J(HH) = 8.8 Hz, $C_6H_4{-}NO_2$], 7.48 and 6.91 [2H, d, J(HH) = 8.8 Hz; 2H, d, J(HH) = 8.8 Hz, $C_6H_4{-}OC_6H_{13}$], 7.22 and 6.99 [1H, d, $J(HH)_{trans}$ = 16.3 Hz; 1H, d, $J(HH)_{trans}$ = 16.3 Hz, $CH = CH$], 3.99 [2H, t, J(HH) = 6.6 Hz, $OCH_2{-}C_5H_{11}$], 1.80 [2H, qn, $OCH_2{-}CH_2{-}C_4H_9$], 1.47 [2H, qn, $OCH_2CH_2{-}CH_2{-}C_3H_7$], 1.37–1.31 [4H, c m, $OC_3H_6{-}C_2H_4{-}CH_3$], 0.91 [3H, t, J(HH) = 7.0 Hz, CH_3].

4-n-*Octyloxy-4′-nitrostilbene* (**3**)

This compound was prepared in an identical manner to **1** using 4-n-octyloxybenzaldehyde (3.23 g, 13.8 mmol) in place of 4-n-dodecyloxybenzaldehyde. Recrystallization afforded bright yellow

* Relative area and multiplicity given in parentheses; s = singlet, d = doublet, t = triplet, m = multiplet with unresolved coupling, b = broad.

needles of 4-n-octyloxy-4′-nitrostilbene (0.98 g, 20%).

$C_8H_{17}OC_6H_4CH{=}CHC_6H_4{-}NO_2$, m.p. 95–109°C. Found: C, 75.1; H, 7.7; N, 4.0. Calc. for $C_{22}H_{27}NO_3$: C, 74.8; H, 7.7; N, 4.0%. $\nu_{max}(NO_2)$: 1500s and 1330s cm^{-1}. $\delta_H(CDCl_3)$: 8.19 and 7.58 [2H, d, J(HH) = 8.8 Hz; 2H, d, J(HH) = 8.8 Hz, $C_6H_4{-}NO_2$], 7.48 and 6.91 [2H, d, J(HH) = 8.8 Hz; 2H, d, J(HH) = 8.8 Hz, $C_6H_4{-}OC_8H_{17}$], 7.22 and 6.99 [1H, d, $J(HH)_{trans}$ = 16.3 Hz; 1H, d, $J(HH)_{trans}$ = 16.3 Hz, $CH = CH$], 3.98 [2H, t, J(HH) = 6.6 Hz, $OCH_2{-}C_7H_{15}$], 1.80 [2H, qn, $OCH_2{-}CH_2{-}C_6H_{13}$], 1.46 [2H, qn, $OCH_2CH_2{-}CH_2{-}C_5H_{11}$], 1.40–1.20 [8H, br m, $OC_3H_6{-}C_4H_8{-}CH_3$], 0.89 [3H, t, J(HH) = 7.0 Hz, CH_3].

4-n-*Hexyloxy-4′-stilbenamine* (**4**)

A solution of **2** (1.1 g, 3.38 mmol) and ammonium chloride (1.1 g, 20.56 mmol) in acetone (100 cm^3) and water (20 cm^3) was heated to reflux. Zinc powder (1.0 g, 15.30 mmol) was added and the mixture stirred under reflux for 1 h. Further ammonium chloride (0.5 g) and zinc powder (0.5 g) were added and the mixture was stirred under reflux for a further 4 h. The colour of the solution changed from yellow to almost colourless during this time. The reaction mixture was cooled and the zinc powder removed by filtration. The acetone was removed *in vacuo* and water (50 cm^3) and dichloromethane (50 cm^3) were added. The pale yellow–orange organic layer was separated and the aqueous layer extracted with further dichloromethane (3 × 20 cm^3). The combined organic extracts were evaporated to yield 4-n-hexyloxy-4′-stilbenamine as a beige powder (0.89 g, 89%).

$C_6H_{13}OC_6H_4CH{=}CHC_6H_4{-}NH_2$. Found: C, 78.7; H, 8.2; N, 4.8. Calc. for $C_{20}H_{25}NO{\cdot}0.13CH_2Cl_2$: C, 78.9; H, 8.3; N, 4.6%. $\nu_{max}(NH_2)$: 3380s and 3315s cm^{-1}. $\delta_H(CDCl_3)$: 7.39 and 6.86 [2H, d, J(HH) = 8.8 Hz; 2H, d, J(HH) = 8.8 Hz, $C_6H_4{-}NH_2$], 7.30 and 6.66 [2H, d, J(HH) = 8.6 Hz; 2H, d, J(HH) = 8.6 Hz, $C_6H_4{-}OC_6H_{13}$], 6.87 [2H, s, $CH{=}CH$], 3.96 [2H, t, J(HH) = 6.6 Hz; $OCH_2{-}C_5H_{11}$], 3.72 [2H, vbr, s, NH_2], 1.78 [2H, qn, $OCH_2{-}CH_2{-}C_4H_9$], 1.45 [2H, qn, $OCH_2CH_2{-}CH_2{-}C_3H_7$], 1.37–1.31 [4H, c m, $OC_3H_6{-}C_2H_4{-}CH_3$], 0.91 [3H, t, J(HH) = 7.0 Hz, CH_3].

4-n-*Octyloxy-4′-stilbenamine* (**5**)

This compound was prepared in an identical manner to **4** using **3** (1.19 g, 3.38 mmol) in place of **2**. Due to lower solubility the reaction was allowed to proceed for a total reflux time of 22 h. This afforded 4-n-octyloxy-4′-stilbenamine as a beige powder (0.69 g, 63%).

$C_8H_{17}OC_6H_4CH{=}CHC_6H_4{-}NH_2$. Found: C, 80.5; H, 8.8; N, 4.5. Calc. for $C_{22}H_{29}NO{\cdot}0.06CH_2Cl_2$: C, 80.6; H, 8.9; N, 4.3%. $\nu_{max}(NH_2)$: 3380s and 3315s cm^{-1}. $\delta_H(CDCl_3)$: 7.39 and 6.86 [2H, d, J(HH) = 8.8 Hz; 2H, d, J(HH) = 8.8 Hz, $C_6H_4{-}NH_2$], 7.30 and 6.66 [2H, d, J(HH) = 8.6 Hz; 2H, d, J(HH) = 8.6 Hz, $C_6H_4{-}OC_8H_{17}$], 6.87 [2H, s, $CH{=}CH$], 3.96 [2H, t, J(HH) = 6.6 Hz; $OCH_2{-}C_7H_{15}$], 3.72 [2H, vbr, s, NH_2], 1.78 [2H, qn, $OCH_2{-}CH_2{-}C_6H_{13}$], 1.45 [2H, qn, $OCH_2CH_2{-}CH_2{-}C_5H_{11}$], 1.40–1.25 [4H, br m, $OC_3H_6{-}C_4H_8{-}CH_3$], 0.89 [3H, t, J(HH) = 7.0 Hz, CH_3].

4-n-*Dodecyloxy-4′-stilbenamine* (**6**)

This compound was prepared in an identical manner to **4** using **1** (1.38 g, 3.38 mmol) in place of **2**. Due to lower solubility the reaction was allowed to proceed for a total reflux time of 22 h. This afforded 4-n-dodecyloxy-4′-stilbenamine as a beige powder (0.62 g, 48%).

$C_{12}H_{25}OC_6H_4CH{=}CHC_6H_4{-}NH_2$. Found: C, 80.6; H, 9.5; N, 3.0. Calc. for $C_{26}H_{37}NO{\cdot}0.11CH_2Cl_2$: C, 80.6; H, 9.6; N, 3.6%. $\nu_{max}(NH_2)$: 3380s and 3315s cm^{-1}. $\delta_H(CDCl_3)$: 7.39 and 6.86 [2H, d, J(HH) = 8.8 Hz; 2H, d, J(HH) = 8.8 Hz, $C_6H_4{-}NH_2$], 7.30 and 6.66 [2H, d, J(HH) = 8.6 Hz; 2H, d, J(HH) = 8.6 Hz, $C_6H_4{-}OC_8H_{17}$], 6.87 [2H, s, $CH{=}CH$], 3.96 [2H, t, J(HH) = 6.6 Hz; $OCH_2{-}C_{11}H_{23}$], 3.72 [2H, vbr, s, NH_2], 1.78 [2H, qn, $OCH_2{-}CH_2{-}C_6H_{13}$], 1.45 [2H, qn, $OCH_2CH_2{-}CH_2{-}C_9H_{19}$], 1.26 [16H, br s, $OC_3H_6{-}C_8H_{16}{-}CH_3$], 0.88 [3H, t, J(HH) = 7.0 Hz, CH_3].

$[Mo(NO)\{HB(3,5\text{-}Me_2C_3N_2H)_3\}Cl(HNC_6H_4CH{=}CHC_6H_4OC_6H_{13})]$ (**7**)

A solution of $Mo(NO)LCl_2$ (0.30 g, 0.61 mmol), 4-hexyloxy-4′-stilbenamine (**4**) (0.22 g, 0.74 mmol) and triethylamine (0.5 cm^3) was stirred under reflux in toluene (20 cm^3) for 2 h. The reaction mixture was cooled and evaporated to dryness under reduced pressure. The resulting solid was purified by column chromatography on silica using 60% dichloromethane/n-hexane as an eluant. The major violet band was collected and the product it contained was recrystallized from dichloromethane/n-hexane to give a deep violet solid (0.32 g, 70%). Found: C, 53.6; H, 6.0; N, 14.5; M^+, 754. Calc. for $C_{35}H_{46}BClMoN_8O_2{\cdot}0.5CH_2Cl_2$: C, 53.6; H, 6.0; N, 14.1%; M, 753. $\nu_{max}(NH)$: 3270w; $\nu_{max}(NO)$: 1655 cm^{-1}. $\delta_H(CDCl_3)$: 12.60 [1H, s, NH], 7.54 and 7.45 [2H, d, J(HH) = 8.7 Hz; 2H, d,

J(HH) = 8.7 Hz, C_6H_4—OC_6H_{13}], 7.45 and 6.90 [2H, d, J(HH) = 8.7 Hz; 2H, d, J(HH) = 8.7 Hz, C_6H_4—NHMo], 7.09 and 6.98 [1H, d, $J(HH)_{trans}$ = 16.3 Hz; 1H, d, $J(HH)_{trans}$ = 16.3 Hz, CH=CH], 5.87 and 5.79 [2H, s; 1H, s, $(Me_2C_3N_2H)_3$], 3.98 [2H, t, J(HH) = 6.4 Hz, C_6H_4—OCH_2—C_5H_{11}], 2.69, 2.42, 2.39, 2.38, 2.37 and 2.03 [3H, s; 3H, s; 3H, s; 3H, s; 3H, s; 3H, s, $(Me_2C_3N_2H)_3$], 1.79 [2H, qn, $C_6H_4OCH_2$—CH_2—C_4H_9], 1.47 [2H, qn, $C_6H_4OC_2H_4$—CH_2—C_3H_7], 1.40–1.30 [4H, c m, OC_3H_6—C_2H_4—CH_3], 0.91 [3H, t, J(HH) = 6.7 Hz, CH_3]. m/z 754 (M^+), 724 (M−NO), 718 (M−Cl), 682 (M−C_5H_{11}), 652 (M−OC_6H_{13}), 628 (M−125), 295 ($H_2NC_6H_4$ CH=$CHC_6H_4OC_6H_{13}$), 252 ($H_2NC_6H_4CH$=$CHC_6H_4OC_3H_6$), 211 ($H_2NC_6H_4CH$=CHC_6H_4 OH), 107 ($H_2CC_6H_4OH$). E_f = −0.78 V, ΔE_p = 140 mV, ΔE_p(Fc) = 105 mV.*

[Mo(NO){HB(3,5-$Me_2C_3N_2H$)$_3$}I(HNC_6H_4CH=$CHC_6H_4OC_6H_{13}$)] (**8**)

This compound was prepared in an identical manner to **7** using [Mo(NO){HB(3,5-$Me_2C_3N_2$ H)$_3$}(I)$_2$]·C_7H_8 (0.40 g, 0.52 mmol) in place of [Mo(NO){HB(3,5-$Me_2C_3N_2H$)$_3$}(Cl)$_2$] and 4-n-hexyloxy-4′-stilbenamine (**4**) (0.20 g, 0.68 mmol). A deep violet solid was obtained (0.33 g, 75%). Found: C, 47.8; H, 5.5; N, 13.5; M^+, 846. Calc. for $C_{35}H_{46}BIMoN_8O_2$·0.5CH_2Cl_2: C, 48.1; H, 5.3; N, 12.6%; M, 844. ν_{max}(NH): 3275w; ν_{max}(NO): 1655 cm^{-1}. δ_H($CDCl_3$): 13.06 [1H, s, NH], 7.61 and 7.46 [2H, d, J(HH) = 8.7 Hz; 2H, d, J(HH) = 8.7 Hz, C_6H_4—OC_6H_{13}], 7.49 and 6.89 [2H, d, J(HH) = 8.7 Hz; 2H, d, J(HH) = 8.7 Hz, C_6H_4—NHMo], 7.18 and 6.94 [1H, d, $J(HH)_{trans}$ = 16.1 Hz; 1H, d, $J(HH)_{trans}$ = 16.1 Hz, CH=CH], 5.93, 5.86 and 5.77 [1H, s; 1H, s; 1H, s, $(Me_2C_3N_2H)_3$], 3.98 [2H, t, J(HH) = 6.7 Hz, C_6H_4—OCH_2—C_5H_{11}], 2.72, 2.48, 2.46, 2.38, 2.37 and 2.00 [3H, s; 3H, s; 3H, s; 3H, s; 3H, s; 3H, s, $(Me_2C_3N_2H)_3$], 1.80 [2H, qn, $C_6H_4OCH_2$—CH_2—C_4H_9], 1.47 [2H, qn, $C_6H_4OC_2H_4$—CH_2—C_3H_7], 1.40–1.30 [4H, c m, OC_3H_6—C_2H_4—CH_3], 0.91 [3H, t, J(HH) = 6.9 Hz, CH_3]. m/z 846 (M^+), 719 (M−125), 295 ($H_2NC_6H_4CH$=$CHC_6H_4OC_6H_{13}$), 211 ($H_2NC_6H_4CH$=CHC_6H_4OH), 128 (I). E_f = −0.78 V, ΔE_p = 125 mV, ΔE_p(Fc) = 100 mV.

[Mo(NO){HB(3,5-$Me_2C_3N_2H$)$_3$}(HNC_6H_4CH=$CHC_6H_4OC_6H_{13}$)$_2$] (**9**)

Sodium (0.1 g, 4.35 mmol) was heated under reflux in dry THF (35 cm^3) for 30 min. Naphthalene (0.1 g, 0.78 mmol) was then added and the mixture stirred for 1 h under reflux, during which time the solution became dark green. The mixture was filtered under dinitrogen to remove excess sodium and 4-n-hexyloxy-4′-stilbenamine (**4**) (0.06 g, 0.20 mmol) was added to the filtrate. After stirring the resulting solution for 30 min at room temperature **8** (0.11 g, 0.13 mmol) was added and the mixture stirred under reflux for a further 2 h. The resulting mixture was cooled and filtered in air and the solvent removed by evaporation under reduced pressure. The crude product was purified by column chromatography on alumina 90 using 40% n-hexane/dichloromethane. This afforded a deep emerald green solid (0.11 g, 84%). Found: C, 63.4; H, 6.9; N, 11.4; M^+, 1013. Calc. for $C_{55}H_{70}BMo$ N_9O_3·0.5CH_2Cl_2: C, 63.2; H, 6.8; N, 12.0%; M, 1012. ν_{max}(NH): 3300m; ν_{max}(NO): 1635 cm^{-1}. δ_H($CDCl_3$): 8.90 [2H, s, 2×NH], 7.40 and 7.27 [4H, d, J(HH) = 8.7 Hz; 4H, d, J(HH) = 8.7 Hz, 2×C_6H_4—OC_6H_{13}], 7.40 and 6.87 [4H, d, J(HH) = 8.7 Hz; 4H, d, J(HH) = 8.7 Hz, 2×C_6H_4—NHMo], 6.93 [4H, s, 2×CH=CH], 5.96 and 5.75 [1H, s; 2H, s, $(Me_2C_3N_2H)_3$], 3.97 [4H, t, J(HH) = 6.6 Hz, 2×C_6H_4—OCH_2—C_5 H_{11}], 2.47, 2.35 and 2.27 [3H, s; 9H, s; 6H, s, $(Me_2C_3N_2H)_3$], 1.78 [4H, qn, 2×$C_6H_4OCH_2$—CH_2—C_4H_9], 1.46 [4H, qn, 2×$C_6H_4OC_2H_4$—CH_2—C_3H_7], 1.40–1.30 [8H, c m, 2×OC_3H_6—C_2H_4—CH_3], 0.91 [6H, t, J(HH) = 6.9 Hz, 2×CH_3]. m/z 1013 (M^+), 989 (M−23), 982 (M−NO), 927 (M−C_6H_{13}), 911 (M−OC_6H_{13}), 295 ($H_2NC_6H_4CH$=$CHC_6H_4OC_6H_{13}$), 211 (H_2NC_6 H_4CH=CHC_6H_4OH). E_f = −1.20 V, ΔE_p = 230 mV, ΔE_p(Fc) = 100 mV.

[Mo(NO){HB(3,5-$Me_2C_3N_2H$)$_3$}OH(HNC_6H_4CH=$CHC_6H_4OC_6H_{13}$)] (**10**)

This compound was prepared by the rapid hydrolysis of **9** (0.10 g, 0.10 mmol) on an activated alumina column in dichloromethane. A dark brown solid was produced (0.046 g, 64%). Found: C, 55.6; H, 6.2; N, 14.3. Calc. for $C_{35}H_{47}BMoN_8O_3$· 0.33CH_2Cl_2: C, 55.6; H, 6.3; N, 14.7%; M, 735. ν_{max}(OH): 3480w br; ν_{max}(NH): 3300w; ν_{max}(NO): 1640 cm^{-1}. δ_H($CDCl_3$): 10.46 [1H, s, NH], 7.46 and 7.26 [2H, d, J(HH) = 8.7 Hz; 2H, d, J(HH) = 8.7 Hz, C_6H_4—OC_6H_{13}], 7.43 and 6.88 [2H, d, J(HH) = 8.7 Hz; 2H, d, J(HH) = 8.7 Hz,

* Electrochemical data: E_f = formal electrode potential for reduction, ΔE_p = separation between cathodic and anodic peak potentials of cyclic voltammogram, ΔE_p(Fc) = value of ΔE_p for ferrocene present as an internal standard. No compensation was made for internal resistance in the cell.

C_6H_4—NHMo], 7.01 and 6.94 [1H, d, $J(HH)_{trans}$ = 16 Hz; 1H, d, $J(HH)_{trans}$ = 16 Hz, C*H*=C*H*], 6.48 [1H, s, O*H*], 5.84, 5.81 and 5.76 [1H, s; 1H, s; 1H, s, $(Me_2C_3N_2H)_3$], 3.97 [2H, t, $J(HH)$ = 6.7 Hz, C_6H_4—OCH_2—C_5H_{11}], 2.61, 2.40, 2.37, 2.36, 2.33 and 2.10 [3H, s; 3H, s; 3H, s; 3H, s; 3H, s; 3H, s; 3H, s, $(MeC_3N_2H)_3$], 1.79 [2H, qn, $C_6H_4OCH_2$—CH_2—C_4H_9], 1.46 [2H, qn, $C_6H_4OC_2H_4$—CH_2—C_3H_7], 1.40–1.30 [4H, c m, OC_3H_6—C_2H_4—CH_3], 0.91 [3H, t, $J(HH)$ = 6.9 Hz, C*H*$_3$]. *m/z* 706 (M − NO), 691 (M − NO − OH), 650 (M − C_6H_{13}), 295 ($H_2NC_6H_4CH$=$CHC_6H_4OC_6H_{13}$), 211 ($H_2NC_6H_4CH$=CHC_6H_4OH). E_f = −1.19 V, ΔE_p = 250 mV, ΔE_p(Fc) = 105 mV.

[Mo(NO){HB(3,5-$Me_2C_3N_2H)_3$}Cl(HNC_6H_4CH=$CHC_6H_4OC_8H_{17}$)] (**11**)

This compound was prepared in a similar manner to **7** using 4-n-octyloxy-4′-stilbenamine (**5**) (0.24 g, 0.74 mmol) in place of **4**. The product was purified by column chromatography on silica using 20% n-hexane/dichloromethane as an eluant. Recrystallization from dichloromethane/n-hexane yielded a deep violet solid (0.31 g, 65%). Found: C, 54.2; H, 6.3; N, 14.0; M^+, 782. Calc. for $C_{37}H_{50}BClMoN_8O_2 \cdot 0.6CH_2Cl_2$: C, 54.3; H, 6.2; N, 13.5%; M, 781. ν_{max}(NH): 3270w; ν_{max}(NO): 1655 cm^{-1}. $\delta_H(CDCl_3)$: 12.60 [1H, s, N*H*], 7.54 and 7.45 [2H, d, $J(HH)$ = 8.7 Hz; 2H, d, $J(HH)$ = 8.7 Hz, C_6H_4—OC_8H_{17}], 7.45 and 6.90 [2H, d, $J(HH)$ = 8.7 Hz; 2H, d, $J(HH)$ = 8.7 Hz, C_6H_4—NHMo], 7.09 and 6.98 [1H, d, $J(HH)_{trans}$ = 16.3 Hz; 1H, d, $J(HH)_{trans}$ = 16.3 Hz, C*H*=C*H*], 5.87 and 5.79 [2H, s; 1H, s, $(Me_2C_3N_2H)_3$], 3.98 [2H, t, $J(HH)$ = 6.4 Hz, C_6H_4—OCH_2—C_7H_{15}], 2.69, 2.42, 2.39, 2.38, 2.37 and 2.03 [3H, s; 3H, s; 3H, s; 3H, s; 3H, s; 3H, s, $(MeC_3N_2H)_3$], 1.79 [2H, qn, $C_6H_4OCH_2$—CH_2—C_6H_{13}], 1.46 [2H, qn, $C_6H_4OC_2H_4$—CH_2—C_5H_{11}], 1.40–1.30 [8H, c m, OC_3H_8—C_4H_8—CH_3], 0.89 [3H, t, $J(HH)$ = 6.7 Hz, C*H*$_3$]. *m/z* 782 (M^+), 752 (M − NO), 746 (M − Cl), 656 (M − 125), 323 ($H_2NC_6H_4CH$=$CHC_6H_4OC_8H_{17}$), 252 ($H_2NC_6H_4CH$=$CHC_6H_4OC_3H_6$), 211 ($H_2NC_6H_4CH$=CHC_6H_4OH), 107 ($H_2CC_6H_4OH$). E_f = −0.78 V, ΔE_p = 160 mV, ΔE_p(Fc) = 100 mV.

[Mo(NO){HB(3,5 - $Me_2C_3N_2H)_3$}I(HNC_6H_4CH=$CHC_6H_4OC_8H_{17}$)] (**12**)

This compound was prepared in an identical manner to **11** using Mo(NO){HB(3,5-$Me_2C_3N_2H)_3$}$(I)_2 \cdot C_7H_8$ (0.40 g, 0.52 mmol) and 4-n-octyloxy-4′-stilbenamine (**5**) (0.22 g, 0.68 mmol). A deep violet solid was obtained (0.38 g, 84%). Found: C, 49.3; H, 5.6; N, 12.2; M^+, 874. Calc. for $C_{37}H_{60}BIMoN_8O_2 \cdot 0.5CH_2Cl_2$: C, 49.2; H, 5.6; N, 12.2%; M, 873. ν_{max}(NH): 3275w; ν_{max}(NO): 1655 cm^{-1}. $\delta_H(CDCl_3)$: 13.06 [1H, s, N*H*], 7.61 and 7.46 [2H, d, $J(HH)$ = 8.7 Hz; 2H, d, $J(HH)$ = 8.7 Hz, C_6H_4—OC_6H_{13}], 7.49 and 6.89 [2H, d, $J(HH)$ = 8.7 Hz; 2H, d, $J(HH)$ = 8.7 Hz, C_6H_4—NHMo], 7.18 and 6.94 [1H, d, $J(HH)_{trans}$ = 16.1 Hz; 1H, d, $J(HH)_{trans}$ = 16.1 Hz, C*H*=C*H*], 5.93, 5.86 and 5.77 [1H, s; 1H, s; 1H, s, $(Me_2C_3N_2H)_3$], 3.98 [2H, t, $J(HH)$ = 6.7 Hz, C_6H_4—OCH_2—C_7H_{15}], 2.72, 2.48, 2.46, 2.38, 2.37 and 2.00 [3H, s; 3H, s; 3H, s; 3H, s; 3H, s; 3H, s, $(MeC_3N_2H)_3$], 1.80 [2H, qn, $C_6H_4OCH_2$—CH_2—C_6H_{13}], 1.47 [2H, qn, $C_6H_4OC_2H_4$—CH_2—C_5H_{11}], 1.40–1.30 [8H, c m, OC_3H_6—C_4H_8—CH_3], 0.89 [3H, t, $J(HH)$ = 6.9 Hz, C*H*$_3$]. *m/z* 874 (M^+), 747 (M − 125), 323 ($H_2NC_6H_4CH$=$CHC_6H_4OC_8H_{17}$), 211 ($H_2NC_6H_4CH$=CHC_6H_4OH), 128 (I). E_f = −0.74 V, ΔE_p = 120 mV, ΔE_p(Fc) = 100 mV.

[Mo(NO){HB(3,5-$Me_2C_3N_2H)_3$}(HNC_6H_4CH=$CHC_6H_4OC_8H_{17})_2$] (**13**)

This compound was prepared in a similar manner to **9** using **12** (0.11 g, 0.13 mmol) and 4-n-octyloxy-4′-stilbenamine (**5**) (0.065 g, 0.20 mmol). Upon the addition of **12** the solution was stirred under reflux for 2 h and cooled before filtration. The product was purified by column chromatography on alumina 90 using 40% n-hexane in dichloromethane. This afforded a deep emerald green solid (0.11 g, 82%). Found: C, 65.3; H, 7.4; N, 10.3; M^+, 1069. Calc. for $C_{59}H_{78}BMoN_9O_3 \cdot 0.25CH_2Cl_2$: C, 65.3; H, 7.3; N, 11.6%; M, 1068. ν_{max}(NH): 3300m; ν_{max}(NO): 1635 cm^{-1}. $\delta_H(CDCl_3)$: 8.90 [2H, s, 2 × N*H*], 7.40 and 7.27 [4H, d, $J(HH)$ = 8.7 Hz; 4H, d, $J(HH)$ = 8.7 Hz, 2 × C_6H_4—OC_8H_{17}], 7.40 and 6.87 [4H, d, $J(HH)$ = 8.7 Hz; 4H, d, $J(HH)$ = 8.7 Hz, 2 × C_6H_4—NHMo], 6.93 [4H, s, 2 × C*H*=C*H*], 5.96 and 5.75 [1H, s; 2H, s, $(Me_2C_3N_2H)_3$], 3.97 [4H, t, $J(HH)$ = 6.6 Hz, 2 × C_6H_4—OCH_2—C_7H_{15}], 2.47, 2.35 and 2.27 [3H, s; 9H, s; 6H, s, $(MeC_3N_2H)_3$], 1.78 [4H, qn, 2 × $C_6H_4OCH_2$—CH_2—C_6H_{13}], 1.46 [4H, qn, 2 × $C_6H_4OC_2H_4$—CH_2—C_5H_{11}], 1.40–1.30 [16H, c m, 2 × OC_3H_6—C_4H_8—CH_3], 0.89 [6H, t, $J(HH)$ = 6.9 Hz, 2 × C*H*$_3$]. *m/z* 1069 (M^+), 1037 (M − NO), 990 (M − 78), 926 (M − C_6H_{13}), 323 ($H_2NC_6H_4CH$=$CHC_6H_4OC_8H_{17}$), 211 ($H_2NC_6H_4CH$=CHC_6H_4OH). E_f = −1.20 V, ΔE_p = 290 mV, ΔE_p(Fc) = 105 mV.

[Mo(NO){HB(3,5-$Me_2C_3N_2H$)$_3$}Cl(HNC$_6$H$_4$CH=CHC$_6$H$_4$OC$_{12}$H$_{25}$)] (**14**)

This compound was prepared in a similar manner to **7** using 4-n-dodecyloxy-4′-stilbenamine (**6**) (0.28 g, 0.74 mmol). The product was purified by column chromatography on silica using 20% n-hexane/dichloromethane as an eluant. Recrystallization from dichloromethane/n-hexane yielded a deep violet solid (0.37 g, 73%). Found: C, 57.6; H, 6.8; N, 12.7; M^+, 838. Calc. for $C_{41}H_{58}BClMoN_8O_2 \cdot 0.3CH_2Cl_2$: C, 57.5; H, 6.8; N, 13.0%; M, 837. ν_{max}(NH): 3270w; ν_{max}(NO) 1655 cm^{-1}. δ_H($CDCl_3$): 12.60 [1H, s, N*H*], 7.54 and 7.45 [2H, d, J(HH) = 8.7 Hz; 2H, d, J(HH) = 8.7 Hz, C_6H_4—$OC_{12}H_{25}$], 7.45 and 6.90 [2H, d, J(HH) = 8.7 Hz; 2H, d, J(HH) = 8.7 Hz, C_6H_4—NHMo], 7.09 and 6.98 [1H, d, $J(HH)_{trans}$ = 16.3 Hz; 1H, d, $J(HH)_{trans}$ = 16.3 Hz, C*H*=C*H*], 5.87 and 5.79 [2H, s; 1H, s, $(Me_2C_3N_2H)_3$], 3.98 [2H, t, J(HH) = 6.4 Hz, C_6H_4—OCH_2—$C_{11}H_{23}$], 2.69, 2.42, 2.39, 2.38, 2.37 and 2.03 [3H, s; 3H, s; 3H, s; 3H, s; 3H, s; 3H, s, $(MeC_3N_2H)_3$], 1.79 [2H, qn, $C_6H_4OCH_2$—CH_2—$C_{10}H_{21}$], 1.46 [2H, qn, $C_6H_4OC_2H_4$—CH_2—C_9H_{19}], 1.40–1.30 [16H, c m, OC_3H_6—C_8H_{16}—CH_3], 0.88 [3H, t, J(HH) = 6.7 Hz, CH_3]. *m/z* 838 (M^+), 807 (M−NO), 802 (M−Cl), 712 (M−125), 379 ($H_2NC_6H_4CH$=$CHC_6H_4OC_{12}H_{25}$), 252 ($H_2NC_6H_4CH$=$CHC_6H_4OC_3H_6$), 211 ($H_2NC_6H_4CH$=CHC_6H_4OH), 107 ($H_2CC_6H_4OH$). E_f = −0.78 V, ΔE_p = 200 mV, ΔE_p(Fc) = 95 mV.

[Mo(NO){HB(3,5-$Me_2C_3N_2H$)$_3$}I(HNC$_6$H$_4$CH=CHC$_6$H$_4$OC$_{12}$H$_{25}$)] (**15**)

This compound was prepared in an identical manner to **14** using [Mo(NO){HB(3,5-$Me_2C_3N_2H$)$_3$}(I)$_2$]·C_7H_8 (0.40 g, 0.52 mmol) and 4-n-dodecyloxy-4′-stilbenamine (**6**) (0.26 g, 0.68 mmol). A deep violet solid was obtained (0.36 g, 75%). Found: C, 50.2; H, 6.0; N, 11.8; M^+, 930. Calc. for $C_{41}H_{58}BIMoN_8O_2 \cdot 0.8CH_2Cl_2$: C, 50.4; H, 6.0; N, 11.2%; M, 929. ν_{max}(NH): 3275w; ν_{max}(NO): 1655 cm^{-1}. δ_H($CDCl_3$): 13.06 [1H, s, N*H*], 7.61 and 7.46 [2H, d, J(HH) = 8.7 Hz; 2H, d, J(HH) = 8.7 Hz, C_6H_4—$OC_{12}H_{25}$], 7.49 and 6.89 [2H, d, J(HH) = 8.7 Hz; 2H, d, J(HH) = 8.7 Hz, C_6H_4—NHMo], 7.18 and 6.94 [1H, d, $J(HH)_{trans}$ = 16.1 Hz; 1H, d, $J(HH)_{trans}$ = 16.1 Hz, C*H*=C*H*], 5.93, 5.86 and 5.77 [1H, s; 1H, s; 1H, s, $(Me_2C_3N_2H)_3$], 3.98 [2H, t, J(HH) = 6.7 Hz, C_6H_4—OCH_2—$C_{11}H_{23}$], 2.72, 2.48, 2.46, 2.38, 2.37 and 2.00 [3H, s; 3H, s; 3H, s; 3H, s; 3H, s; 3H, s, $(Me_2C_3N_2H)_3$], 1.80 [2H, qn, $C_6H_4OCH_2$—CH_2—$C_{10}H_{21}$], 1.47 [2H, qn, $C_6H_4OC_2H_4$—CH_2—C_9H_{19}], 1.40–1.30 [16H, c m, OC_3H_6—C_8H_{16}—CH_3], 0.88 [3H, t, J(HH) = 6.9 Hz, CH_3]. *m/z* 930 (M^+), 803 (M−125), 379 ($H_2NC_6H_4CH$=$CHC_6H_4OC_{12}H_{25}$), 211 ($H_2NC_6H_4CH$=CHC_6H_4OH), 128 (I). E_f = −0.74 V, ΔE_p = 110 mV, ΔE_p(Fc) = 95 mV.

[Mo(NO){HB(3,5-$Me_2C_3N_2H$)$_3$}(HNC$_6$H$_4$CH=CHC$_6$H$_4$OC$_{12}$H$_{25}$)$_2$] (**16**)

This compound was prepared in an identical manner to **9** using **15** (0.12 g, 0.13 mmol) and 4-n-dodecyloxy-4′-stilbenamine (**6**) (0.075 g, 0.20 mmol). Upon the addition of **15** the solution was stirred at reflux for 2 h, and cooled before filtration. The product was purified by column chromatography on alumina 90 using 40% n-hexane in dichloromethane. This afforded a deep emerald green solid (0.070 g, 46%). Found: C, 68.1; H, 8.4; N, 9.4. Calc. for $C_{67}H_{94}BMoN_9O_3$: C, 68.2; H, 8.0; N, 10.7%; M, 1180. ν_{max}(NH): 3300m; ν_{max}(NO): 1635 cm^{-1}. δ_H($CDCl_3$): 8.90 [2H, s, 2×N*H*], 7.40 and 7.27 [4H, d, J(HH) = 8.7 Hz; 4H, d, J(HH) = 8.7 Hz, 2×C_6H_4—$OC_{12}H_{25}$], 7.40 and 6.87 [4H, d, J(HH) = 8.7 Hz; 4H, d, J(HH) = 8.7 Hz, 2×C_6H_4—NHMo], 6.93 [4H, s, 2×C*H*=C*H*], 5.96 and 5.75 [1H, s; 2H, s, $(Me_2C_3N_2H)_3$], 3.97 [4H, t, J(HH) = 6.6 Hz, 2×C_6H_4—OCH_2—$C_{11}H_{23}$], 2.47, 2.35 and 2.27 [3H, s; 9H, s; 6H, s, $(MeC_3N_2H)_3$], 1.78 [4H, qn, 2×$C_6H_4OCH_2$—CH_2—$C_{10}H_{21}$], 1.46 [4H, qn, 2×$C_6H_4OC_2H_4$—CH_2—C_9H_{19}], 1.40–1.30 [32H, c m, 2×OC_3H_6—C_8H_{16}—CH_3], 0.88 [6H, t, J(HH) = 6.9 Hz, 2×CH_3]. *m/z* 1037 (M−NO−C_8H_{17}), 990, 925 (M−$OC_{12}H_{25}$−C_5H_{11}), 895 (M−$OC_{12}H_{25}$−C_5H_{11}−NO), 379 ($H_2NC_6H_4CH$=$CHC_6H_4OC_{12}H_{25}$), 211 ($H_2NC_6H_4CH$=CHC_6H_4OH). E_f = −1.20 V, ΔE_p = 230 mV, ΔE_p(Fc) = 100 mV.

DISCUSSION

Synthetic studies

The new complexes were synthesized according to previously established procedures.[6,13] In the formation of the monoarylamide complexes triethylamine was used to consume the HI or HCl liberated in the halide substitution reactions. In forming the bis-arylamide derivative more forcing conditions involving sodium naphthalenide were used to substitute the remaining iodide in [Mo(NO)LI(NHC$_6$H$_4$CH=CHC$_6$H$_4$OR)].[13]

All the new complexes exhibit ν(BH) at *ca* 2550 cm^{-1} in their IR spectra. In addition, the chloro-monostilbenamide complexes exhibit ν(NH)

at 3270 cm^{-1}, whilst in their iodo containing counterparts this band appears at 3275 cm^{-1} and in [Mo(NO)L(OH)I($NHC_6H_4CH{=}CHC_6H_4OC_6H_{13}$)] it appears at 330 cm^{-1}. The spectra also contain ν(NO) at 1635 cm^{-1} in the cases of the halide complexes and 1640 cm^{-1} in the case of the hydroxy complex. The IR spectra of the bis-stilbenamide complexes contain ν(NH) at 3300 cm^{-1} and ν(NO) at 1635 cm^{-1} in accord with their formulations.[6]

The ^{1}H NMR spectra of the new complexes contain signals from the three pyrazolyl-4-H and six methyl groups in the ligand L, which are indicative of the molecular symmetry. In the absence of overlap nine resonances with the area ratios 1 : 1 : 1 : 3 : 3 : 3 : 3 : 3 : 3 should be present for mono-substituted derivatives, whilst the bis-substituted derivatives should exhibit signals with the area 1 : 2 : 3 : 3 : 6 : 6. The area ratios observed for the new complexes are in all cases in accord with their formulations. The complexes also exhibit signals attributable to the presence of the aryl and alkyl groups in the stilbenamide ligand, which have the appropriate relative areas for mono- or bis-substituted complexes according to their formulations. The ^{1}H NMR spectra of the chloro-mono-stilbenamide complexes contain a broad signal at 12.60 ppm due to the amide proton, whilst in their iodo and hydroxy substituted counterparts this signal appears at 13.06 and 10.46 ppm, respectively. In the bis-stilbenamide complexes this signal appears at 8.90 pm.

Electrochemical studies

The electrochemical properties of the new complexes have been determined by cyclic voltammetry and are in accord with expectations. Previous work has shown that the reduction potentials of the complexes Mo(NO)LXY are highly sensitive to the nature of X and Y. Thus, for X = halide and Y = arylamide a reduction potential of *ca* −0.8 V might be expected, compared to the value *ca* −1.2 V for the bis-arylamide complexes.[7] The ΔE_p values are significantly larger than those of ferrocene, particularly in the case of the bis-stilbenamide complexes, and indicative of kinetically-controlled electron transfer. However, on the cyclic voltammetry time-scale the processes appear to be chemically reversible.

Thermal studies

The nitrostilbene precursors to the stilbenamine ligands used were investigated under the polarizing microscope and the occurrence of extensive fluid birefringence, characteristic of liquid crystalline phases, was observed in all three. Both of the previously reported hexyloxy (**2**) and octyloxy (**3**) derivatives melted at *ca* 100°C and the new dodecyloxy derivative (**4**) at about 80°C. Since their mesogenic properties have already been reported elsewhere,[14] **2** and **3** will not be discussed here. The thermal behaviour of 4-dodecyloxy-4′-nitrostilbene (**1**) has not been described previously and is discussed here; a DSC trace for this compound is shown in Fig. 2.

Under the microscope a crystal-to-fluid transition was observed at about 85°C and the birefringent texture of a smectic A phase was seen until clearing occurred at about 115°C. A DSC study gave more precise evidence for these transitions. On heating at 10 K min^{-1} a minor endo-

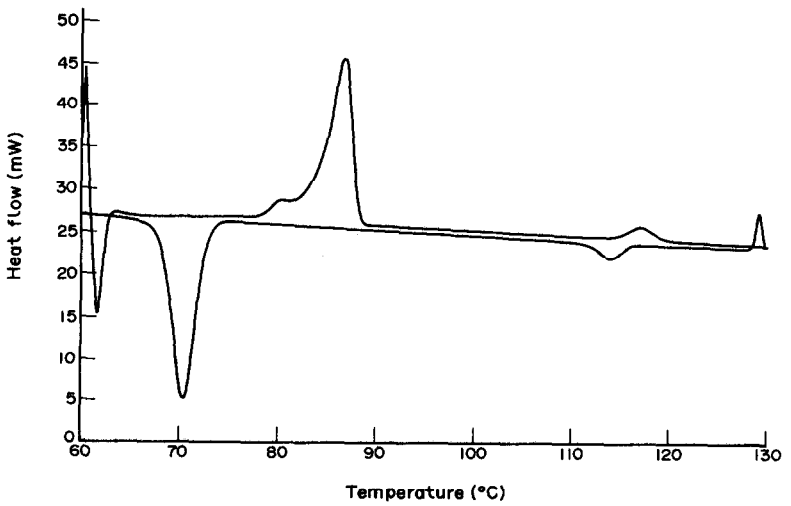

Fig. 2. The DSC trace for 4-dodecyloxy-4′-nitrostilbene. T1 = 77.2°C, T2 = 91.3°C, peak at 86.8°C, area = 406.1 mJ, ΔH = 108.0 J g^{-1}, height = 19.53 mW, onset = 83.5°C.

thermic event peaking at 80.0°C was found before a major event with T_{ON} = 83.5°C (for both events combined ΔH = 108.0 J g^{-1}). The main peak represents the K–S_A (crystal to smectic) transition, but the origin of the small pre-peak is unclear. A second endothermic event corresponding to the S_A–I (smectic to isotropic liquid) transition was detected with T_{ON} = 114.5°C (ΔH = 7.9 J g^{-1}). Upon cooling from 130°C at 10 K min^{-1} both of these events proved to be fully reversible with exothermic events at T_{ON} = 116.1°C (ΔH = −8.0 J g^{-1}) and at T_{ON} = 72.7°C (ΔH = −101.5 J g^{-1}).

The three stilbenamine ligands **4**, **5** and **6** were also investigated. These showed ill-defined behaviour, all melting at *ca* 120°C with no evidence for liquid crystalline phases. This is perhaps unsurprising as terminal amino groups are not generally thought of as desirable for the stabilization of mesophases. The vast majority of known thermotropic organic compounds possess terminal cyano, halo, nitro, alkoxy or alkyl groups,[15] and the absence of mesogenic behaviour in these amines may well reflect the presence of opportunities for hydrogen bonding between the amino hydrogens and the oxygen of the alkoxy function.

DSC and microscopy studies on the new stilbenamide and complexes were carried out, but none revealed signs of any liquid crystalline behaviour. Indeed, under the microscope these compounds were observed to melt over very broad ranges, 10–20°C, and many DSC traces failed to show any detectable events whatsoever. Their extremely strong visible absorptions render even very thin layers highly coloured, and the crystalline samples appeared almost black without the analyser in place. Generally high melting points were observed under the microscope as shown in Table 1. For the octyloxy and dodecyloxy derivatives the iodide complexes melt at considerably lower temperatures than their chloride analogues with the longest chain species having the lowest melting points. However, the hexyloxy/chloride derivative **7** has a far lower melting point than its iodo analogue **8** and than its longer chain homologues **11** and **14**, providing a curious exception to the trends found for other types of complex. The hydroxide derivative **10** is also high melting, with apparent decomposition at 190°C. No evidence for liquid crystalline behaviour was observed in any of these compounds.

The bis-substituted stilbenamide complexes also showed reduced melting points, which were found to decrease with increasing chain length as shown in Table 1. The bis(dodecyloxystilbenamide) complex **16** represents the only compound other than $[Mo(NO)L(OC_6H_4CO_2C_{12}H_{25})_2]$[10] which melts significantly below 100°C. However, these compounds did not show any birefringence under the microscope and DSC study failed to show any features in heating or cooling modes so that again there was no evidence for any liquid crystalline behaviour.

Table 1. Approximate melting points for the stilbenamide complexes $[Mo(NO)L(X)(HNC_6H_4CH{=}CHC_6H_4OC_nH_{2n+1})]$ and $[Mo(NO)L(HNC_6H_4CH{=}CHC_6H_4OC_nH_{2n+1})_2]$

X	*n*	M.p. (°C)	Complex
$[Mo(NO)L(X)(HNC_6H_4CH{=}CHC_6H_4OC_nH_{2n+1})]$			
Cl	6	130	**7**
	8	210	**11**
	12	175	**14**
I	6	210	**8**
	8	130	**12**
	12	110	**15**
OH	6	190	**10**
$[Mo(NO)L(HNC_6H_4CH{=}CHC_6H_4OC_nH_{2n+1})_2]$			
	6	105	**9**
	8	90	**13**
	12	70	**16**

Acknowledgements—We are grateful to Mr T. Green for technical assistance, to the Royal Society (D. W. B.) and the SERC (B. J. C.) for support. The calorimeter and microscope were purchased with the aid of grants from the SERC, the University of Sheffield and the European Community (Twinning Grant No ST2J-0387-C).

REFERENCES

1. D. W. Bruce, in *Inorganic Materials* (Edited by D. W. Bruce and D. O'Hare). Wiley, Chichester (1992); A. M. Giroud-Godquin, *Angew. Chem., Int. Edn Engl.* 1991, **30**, 325.
2. U. T. Mueller-Westerhoff, A. Nazzal, R. J. Cox and A.-M. Giroud, *J. Chem. Soc., Chem. Commun.* 1980, 497.
3. M. Veber, R. Fugnitto and H. Strzeleka, *Molec. Cryst. Liq. Cryst.* 1983, **96**, 221.
4. K. Ohta, A. Takagi, H. Muroki, I. Yamamoto and K. Matsuzaki, *Molec. Cryst. Liq. Cryst.* 1987, **147**, 15.
5. M. Khan, J. Bhatt, B. M. Fung, K. M. Nicholas and E. Wachtel, *Liq. Cryst.* 1989, **5**, 285.
6. J. A. McCleverty, *Chem. Soc. Rev.* 1983, **12**, 331.
7. N. Al-Obaidi, D. Clague, M. Chaudhury, C. J. Jones, J. A. McCleverty, J. C. Pearson and S. S. Salam, *J. Chem. Soc., Dalton Trans.* 1987, 1733.
8. N. Al-Obaidi, S. M. Charsley, W. Hussain, C. J. Jones, J. A. McCleverty, B. D. Neaves and S. J. Reynolds, *Trans. Met. Chem.* 1987, **12**, 143.

9. B. J. Coe, C. J. Jones, J. A. McCleverty, D. Bloor, P. V. Kolinsky and R. J. Jones, *J. Chem. Soc., Chem. Commun.* 1989, 1485.
10. B. J. Coe, C. J. Jones, J. A. McCleverty and D. W. Bruce, *Polyhedron* 1990, **9**, 687.
11. S. J. Reynolds, C. F. Smith, C. J. Jones, J. A. McCleverty, D. C. Bower and J. L. Templeton, *Inorg. Synth.* 1985, **23**, 4.
12. J. A. McCleverty, D. Seddon, N. A. Bailey and N. W. Walker, *J. Chem. Soc., Dalton Trans.* 1976, 898; B. J. Coe, PhD thesis, The University of Birmingham, U.K. (1991).
13. N. Al-Obaidi, T. A. Hamor, C. J. Jones, J. A. McCleverty and K. Paxton, *J. Chem. Soc., Dalton Trans.* 1986, 1525.
14. J.-C. Dubois, A. Zann and N. H. Tinh, *C.R. Seances Acad. Sci. Ser. C* 1977, 284, 137.
15. K. J. Toyne, *Thermotropic Liquid Crystals* (Edited by G. W. Gray), pp. 28–63. John Wiley, Chichester (1987).

Polyhedron Vol. 12, No. 1, pp. 55–58, 1993
Printed in Great Britain

0277–5387/93 $6.00+.00
© 1993 Pergamon Press Ltd

FIRST ELECTROSYNTHESIS OF TRANSITION METAL PEROXO COMPLEXES. SYNTHESIS, CHARACTERIZATION AND REACTIVITY OF MOLYBDENUM AND TUNGSTEN HETEROLIGAND PEROXO COMPLEXES

M. C. CHAKRAVORTI,* SOMENATH GANGULY and MANISH BHATTACHARJEE

Department of Chemistry, Indian Institute of Technology, Kharagpur 721 302, India

(*Received* 26 *May* 1992; *accepted* 3 *September* 1992)

Abstract—Molecular peroxo complexes of molybdenum and tungsten, viz. $[MO(O_2)_2L]$ (M = Mo or W; L = 2,2′-bipyridine, 1,10-phenanthroline or 2,2′-bipyridine-N,N′-dioxide), have been synthesized electrochemically using a sacrificial molybdenum or tungsten anode in the presence of hydrogen peroxide and then precipitating with the corresponding heteroligands. These complexes have also been prepared by the dissolution of metal powders in hydrogen peroxide. They have been characterized by elemental analysis and vibrational spectra. The complexes oxidize triphenylphosphine and triphenylarsine to triphenylphosphine oxide and triphenylarsine oxide, respectively.

Transition metal peroxo compounds play a central role in catalytic and biological oxidation reactions and have generated considerable interest among chemists in recent years.[1–5] The existing methods for the synthesis of peroxo complexes are the reactions between the oxides or oxoanions of the metal with hydrogen peroxide, or the interaction of dioxygen with metal complexes.[6] Until now, there have been no reports on the synthesis of the peroxo complexes by electrochemical or chemical methods starting directly from metals, except for a recent report[7] on the preparation of an ill-characterized peroxopolytungstic acid by the dissolution of tungsten powder in hydrogen peroxide. Electrochemical synthesis provides an easy and direct route to the synthesis of highly pure complexes, starting from sacrificial metal anodes.[8–11] It was thought worthwhile to develop a simple electrosynthetic route for peroxo complexes. A few heteroligand peroxo complexes of molybdenum and tungsten of the type $[MO(O_2)_2L_1L_2]$ and $[MO(O_2)_2L_2]$ have been reported and crystal structures of $[MoO(O_2)_2(HMPA)(H_2O)]$,[12] $[MoO(O_2)_2(bipy)]$,[13] $[MoO(O_2)_2(phen)]$[14] and $[MoO(O_2)_2(glycine)(H_2O)]$[15] have been determined. This paper deals with the first electrosynthesis of molybdenum and tungsten heteroligand peroxo complexes of the type $[MO(O_2)_2L]$ (M = Mo or W; L = 2,2′-bipyridine, 1,10-phenanthroline and 2,2′-bipyridine-N,N′-dioxide). The paper also reports the direct chemical synthesis of these complexes from metal powders. The oxidizing capability of the aforesaid complexes is also determined.

EXPERIMENTAL

Specpure molybdenum and tungsten rods (0.5 cm diameter) were supplied by Johnson Matthey Chemicals Ltd, U.K. Molybdenum powder (4–8 μ), supplied by Koch–Light Laboratories Ltd, U.K., was 99.95% pure. Tungsten powder, supplied by Johnsons of Hendon Ltd, U.K., was 99.0% pure. Other chemicals were of AR/GR quality from reputable manufacturers. The salts $(pyH)_2[Mo_2O_3(O_2)_4(H_2O)_2]$ and $K_2[W_2O_3(O_2)_4(H_2O)_2]\cdot 2H_2O$ were prepared by literature methods.[16,17]

The electric power was supplied by a d.c. power supply (Aplab, India). The electrolytic cell was a tall form beaker (100 cm^3) fitted with a rubber stopper through which two holes were made. The appropriate metal rods which formed the anode

* Author to whom correspondence should be addressed.

were inserted through a hole. In both cases a platinum foil (1 × 1 × 0.15 cm) connected to a platinum wire served as the cathode and was introduced through the second hole.

Peroxide was analysed iodometrically by stirring the aqueous suspensions of the compounds by a magnetic stirrer. Metals were analysed by standard gravimetric methods. Nitrogen was determined by micro Dumas' method. IR spectra were recorded in KBr pellets using a Perkin–Elmer spectrophotometer (No. 883). The laser Raman spectra were recorded on a SPEX Ramalog model 1403 spectrophotometer. The 5145 Å laser line from a Spectra-Physics model 165 argon laser was used as the excitation source. The scattered light at 90° was detected with the help of a cooled RCA 31034 photomultiplier tube, followed by a photon count processing system. The spectra were recorded at ambient temperatures by making pressed pellets of the compounds. Molar conductance was measured using a direct reading conductivity (Systronics, India). Magnetic susceptibility was measured by the Gouy method.

Preparation of the complexes $[MO(O_2)_2L]$ (M = Mo *or* W; L = 2,2′-*bipyridine*; 1,10-*phenanthroline*; 2,2′-*bipyridine-N,N′-dioxide*)

Method A. Hydrogen peroxide (30%, 15 cm^3) was taken in a beaker. The molybdenum or tungsten rod and the platinum foil each connected to platinum wire were dipped in it and connected to the positive and negative terminal of the d.c. power supply, respectively. Electrolysis was carried out at an applied voltage of 15 V for 4 h. Initially the current was very small, but it slowly increased from 0.02 to 0.1 A. The temperature of the reaction medium was maintained at 0–5°C throughout the electrolysis. Gradually, the solution became yellow in the case of molybdenum, while with tungsten the solution remained colourless. After electrolysis, the solution was filtered to remove any disintegrated metal particles. The amount of metal lost was calculated and the ligands 2,2′-bipyridine, 1,10-phenanthroline and 2,2′-bipyridine-N,N′-dioxide (metal : ligand = 1 : 1) dissolved in ethanol (20 cm^3), in the first two cases, and in water (20 cm^3), in the others, were added to the filtrate with stirring. The bipyridine and the phenanthroline complexes precipitated out instantly, while the bipyridine N,N′-dioxide complex was precipitated by adding ethanol (40 cm^3). The complexes were separated by filtration, washed several times with ethanol and dried *in vacuo* over concentrated sulphuric acid. The yields were *ca* 80% and 50% (based on the amount of metal oxidized) for molybdenum and tungsten, respectively.

Method B. Finely powdered molybdenum or tungsten metal (0.25 g) was added to cold hydrogen peroxide (30%, 10 cm^3) and the reaction mixture was allowed to stand for 3 h at 0–5°C, with occasional stirring. Molybdenum dissolved almost completely to form a yellow solution, but a considerable amount of white residue was left with tungsten. The mixture was filtered and the complexes were obtained as described above.

Reactions of $[Mo(O_2)_2L]$ *complexes with triphenylphosphine and triphenylarsine.* $[MO(O_2)_2L]$ (1 mmol) was added to a solution of triphenylphosphine or triphenylarsine (1 mmol) dissolved in acetonitrile (50 cm^3) and the mixture was refluxed for 5 h. The reaction mixture was then filtered and the filtrate was evaporated to dryness. The yellowish white residue was recrystallized from ethanol (yield 70%) and the oxidized products were identified to be triphenylphosphine oxide and triphenylarsine oxide, respectively, by recording their melting points (156–158°C and 188–190°C, respectively) and IR spectra, which were in agreement with those of the authentic samples.

RESULTS AND DISCUSSION

Molybdenum and tungsten powders dissolve readily in cold hydrogen peroxide solution, from which the heteroligand peroxo complexes $[MOO(O_2)_2L]$ can be easily precipitated out by the addition of 2,2′-bipyridine, 1,10-phenanthroline and 2,2′-bipyridine-N,N′-dioxide. While molybdenum dissolves almost completely giving a yellow solution, tungsten gives a colourless solution along with a considerable amount of white residue which does not contain any peroxide. In both cases the solutions are strongly acidic (pH about 1.5). The electronic spectrum of a solution of molybdenum metal in 30% hydrogen peroxide shows a band at 327 nm, which is identical in position to the absorption spectrum of $(pyH)_2[Mo_2O_3(O_2)_4(H_2O)_2]$ in 30% hydrogen peroxide. It is thus believed that molybdenum dissolves in 30% hydrogen peroxide to give the dimeric species $H_2[Mo_2O_3(O_2)_4(H_2O)_2]$ which, however, changes to the monomeric form on addition of the ligands giving the complexes $[MoO(O_2)_2L]$ (L = 2,2′-bipyridine, 1,10-phenanthroline and 2,2′-bipyridine-N,N′-dioxide). This is supported by the fact that the mononuclear complexes $[MO(O_2)_2L]$ (M = Mo or W) are also obtained by the addition of the ligands L to an aqueous solution of the salts $(pyH)_2[Mo_2O_3(O_2)_4(H_2O)_2]$ and $K_2[W_2O_3(O_2)_4(H_2O)_2]\cdot 2H_2O$.

Molybdenum and tungsten rods are unaffected

by 30% hydrogen peroxide in the cold. When platinum foil is dipped in, the evolution of oxygen occurs on the platinum surface at a moderate rate. However, on the application of a voltage molybdenum and tungsten anodes undergo dissolution giving yellow and colourless solutions, respectively. The rate of evolution of oxygen at the platinum cathode is not much affected, but along with dissolution of the metals a slight evolution of oxygen occurs at the tungsten anode, while at the molybdenum anode the evolution of gas is negligible. Initially the current is very small (0.02 A), but with the passage of time it increases steadily with a simultaneous increase in the acidity of the solution, which is ascribed to the formation of $H_2[M_2O_3(O_2)_4]$ (or its hydrated species). The main reaction taking place at the anode may be depicted as follows:

$$2M + 4H_2O_2 + 3H_2O \longrightarrow [M_2O_3(O_2)_4]^{2-} + 14H^+ + 12e,$$

which is evident from the observed electrochemical efficiency (defined as the number of moles of metal oxidized per Faraday) of 0.16 and 0.14 mol F^{-1} for molybdenum and tungsten systems, respectively. The slightly lower value in the latter case may be ascribed to the liberation of oxygen at the anode due to the oxidation of OH^- and/or hydrogen peroxide. Since the rate of liberation of gas at the cathode is not affected by the passage of a current, hydrogen is not liberated at the cathode. The main reaction at the cathode may be as follows:

$$H_2O_2 + 2H^+ + 2e \longrightarrow 2H_2O,$$

which appears highly probable in view of the high value of E^0(1.77 V) in the above redox system.[18]

The complexes $[MO(O_2)_2L]$ can be precipitated out by the addition of the corresponding ligands to the solution remaining after the dissolution of the sacrificial metal anodes. These were identical in all respects to the corresponding complexes formed by the dissolution of metal powders in hydrogen peroxide.

The properties of the complexes are similar to those reported earlier.[16,19] The elemental analyses are satisfactory (Table 1). The molar conductance values measured in dimethylformamide solution

Table 1. Analytical data[a] and vibrational spectral bands (ν, cm^{-1}) of the complexes

Complex	Analysis (%) M	O_2^{2-}	N	Molar conductance (Ω^{-1} cm^2 mol^{-1})	IR	Raman	Assignment
$[MoO(O_2)_2(bipy)]$	28.4	19.0	7.9	11	941s	937, 912	ν(Mo=O)
	(28.9)	(19.2)	(8.4)		850s	869	ν(O—O)
					584m	581	ν_{as}(Mo—O_2)
					534m	527	ν_s(Mo—O_2)
$[MoO(O_2)_2(phen)]$	26.4	17.4	7.8	7	948s	930	ν(Mo=O)
	(27.0)	(18.0)	(7.9)		860s[b]	880	ν(O—O)
					580m	575[b]	ν_{as}(Mo—O_2)
					530	550[b]	ν_s(Mo—O_2)
$[MoO(O_2)_2(bipyO_2)]$	25.8	17.8	7.8	8	950s	950, 930	ν(Mo=O)
	(26.4)	(17.6)	(7.7)		850s[b]	850	ν(O—O)
					585m	566	ν_{as}(Mo—O_2)
					538m	527	ν_s(Mo—O_2)
$[WO(O_2)_2(bipy)]$	43.5	15.1	6.5	1	945s		ν(W=O)
	(43.8)	(15.2)	(6.7)		839s		ν(O—O)
					651m[b]		ν_{as}(W—O_2)
					541m		ν_s(W—O_2)
$[WO(O_2)_2(phen)]$	41.7	14.0	6.5	1	950s		ν(W=O)
	(41.4)	(14.4)	(6.3)		843s[b]		ν(O—O)
					651m		ν_{as}(W—O_2)
					541m		ν_s(W—O_2)
$[WO(O_2)_2(bipyO_2)]$	40.0	14.0	6.4	6	954s		ν(W=O)
	(40.7)	(14.2)	(6.2)		834s[b]		ν(O—O)
					618m		ν_{as}(W—O_2)
					546m		ν_s(W—O_2)

[a] The values in parentheses are calculated.
[b] Overlapped with ligand bands.

(1.0×10^{-3} M) lie in the range 1–11 Ω^{-1} cm^2 mol^{-1} at 25°C, showing their non-electrolytic nature. All the compounds are diamagnetic and the vibrational spectra are in order[19,20] (Table 1).

Having achieved the direct synthesis of these compounds we were interested in studying their reactivity in terms of their ability to transfer oxygen to other substances. All the complexes were found to oxidize triphenylphosphine and triphenylarsine to their oxides in acetonitrile under reflux conditions in good yields. Reactions of the complexes with unsaturated compounds like styrene, cyclohexene and α,β-unsaturated ketone were carried out with a view to examining the epoxidizing capability of the compounds, but no epoxides or other oxidized products could be isolated. This lack of reactivity may be due to their low or moderate solubility in organic solvents.

CONCLUSIONS

This paper reports the first electrosynthesis of some heteroligand peroxo complexes of molybdenum and tungsten, all of which, except [MO$(O_2)_2$(bipyO_2)] (M = Mo or W), are already known.[13,14,16,20] It appears that the method may be extended to other metals to prepare peroxo and heteroligand peroxo complexes.

Acknowledgement—The authors thank the Council of Scientific and Industrial Research for support.

REFERENCES

1. H. Mimoun, *The Chemistry of Peroxides* (Edited by S. Patai), p. 469. John Wiley, New York (1983) and refs therein.
2. H. Mimoun, *Comprehensive Coordination Chemistry* (Edited by G. Wilkinson), Vol. 6, p. 317. Pergamon Press. New York (1987) and refs therein.
3. H. Mimoun, M. Mignard, P. Brechot and L. Sausine, *J. Am. Chem. Soc.* 1986, **108**, 3711.
4. M. N. Hughes, *Comprehensive Coordination Chemistry* (Edited by G. Wilkinson), Vol. 6, p. 665. Pergamon Press, New York (1987) and refs therein.
5. R. Landau, G. A. Sullivan and D. Brown, *Chem. Tech.* 1979, 602.
6. M. H. Gubelmann and A. F. Williams, *Struct. Bonding* 1983, **55**, 1 and refs therein.
7. I. Kudo, H. Okamoto, K. Matsumoto and Y. Sasaki, *Inorg. Chim. Acta* 1986, **111**, L27.
8. V. A. Konev, V. Yu. Kukushkin and Yu. N. Kukushkin, *Russ. J. Inorg. Chem.* 1986, **31**, 838.
9. G. A. Ozin and A. Van der Voet, *Prog. Inorg. Chem.* 1975, **19**, 105.
10. C. Oldham and D. G. Tuck, *J. Chem. Educ.* 1982, **59**, 420.
11. M. C. Chakravorti, G. V. B. Subrahmanyam and D. Bandyopadhyay, *Polyhedron* 1991, **10**, 2605.
12. J. M. Le Carpentier, A. Mitschler and R. Weiss, *Acta Cryst.* 1972, **B28**, 1288.
13. E. O. Schlemper, G. N. Schrauzer and L. A. Hughes, *Polyhedron* 1984, **3**, 377.
14. E. I. Stiefel, *Comprehensive Coordination Chemistry* (Edited by G. Wilkinson), Vol. 6, p. 1400. Pergamon Press, New York (1987).
15. C. Djordjevic, N. Vuletic and E. Sinn, *Inorg. Chim. Acta* 1985, **104**, L7.
16. H. Mimoun, I. Seree De Roch and L. Sajus, *Bull. Soc. Chim. France* 1969, 1481.
17. F. W. B. Einstein and B. R. Penfold, *Acta Cryst.* 1964, **17**, 1127.
18. F. A. Cotton and G. Wilkinson, *Advanced Inorganic Chemistry*, 5th edn, p. 458. John Wiley, New York (1988).
19. W. P. Griffith, *J. Chem. Soc.* 1964, 5428.
20. R. Kergoat and J. E. Guerchais, *C.R. Acad. Sc. Paris, Ser. C* 1969, **268**, 2304.

Polyhedron Vol. 12, No. 1, pp. 59–68, 1993
Printed in Great Britain

0277–5387/93 $6.00+.00
© 1993 Pergamon Press Ltd

PREPARATION AND CHARACTERIZATION OF (ARYLOXY)CHLOROCYCLOTRIPHOSPHAZENES BY PHASE TRANSFER CATALYSIS

Y. W. CHEN-YANG* and B. D. TSAI

Department of Chemistry, Chung Yuan Christian University, Chung Li, Taiwan 32023, R.O.C.

(*Received* 16 *August* 1991; *accepted* 28 *August* 1992)

Abstract—The phase transfer catalysis method (PTC) was used to synthesize seven series of (aryloxy)chlorocyclotriphosphazenes, $N_3P_3Cl_{6-n}(OC_6H_4Y)_n$, n = 1–6, in high yields, where Y = (*o*, *m* and *p*)-Cl, (*o*, *m* and *p*)-Br, *p*-NO_2, and *p*-CH_3. Except for the case with Y = NO_2, all the reactions were successfully carried out in an aqueous/dichloromethane immiscible binary solvent system. Ethylene glycol and benzene were used as solvents for Y = NO_2. It was found that the PTC method is more convenient and efficient for the preparation of the (aryloxy)chlorocyclotriphosphazenes than that reported before. Most of the compounds obtained were isolated by column chromatography and characterized by a combination of IR spectroscopy, elemental analysis, mass spectroscopy and ^{31}P NMR spectroscopy. The distributions of the products are not affected by the side group Y and its position in the lower level of substitution, but are strongly affected by them in the higher level of substitution. The rates of the reactions, with a molar ratio of aryl alcohol and hexachlorocyclotriphosphazene of 2, are all second-order with respect to the concentration of the corresponding aryloxide transferred to the organic phase.

As the application of alkoxy and aryloxy cyclo- and polyphosphazenes is developing rapidly, a large number of these cyclic oligomers and polymers have been synthesized. The synthesis of various (aryloxy)cyclotriphosphazenes has been studied by many groups.[1–13] In these studies the conventional substitution method of the reaction of alkali metal aryloxides with chlorocyclotriphosphazenes in organic media has been used.[1] However, it takes longer, usually about 2 days, to complete the reaction. Therefore, several studies have been reported to improve the preparation.[11,14–17] Most of these studies were concentrated on the preparation of the fully substituted compounds. Nevertheless, as far as the application of the functional phosphazenes is concerned, the preparation of partially substituted derivatives is equally important.[9–18] Hence, a study on preparing partially substituted (phenoxy)cyclotriphosphazenes by the PTC method has been carried out in our laboratory. It was found that the method is not only convenient and economic for preparing hexa(phenoxy)cyclotriphosphazenes, but also efficient for preparing partially substituted derivatives.[19] In this study, the method is further extended to the reaction of hexachlorocyclotriphosphazene (**1**) and some aryl alcohols, YC_6H_4OH, where Y = (*o*, *m* and *p*)-Cl, (*o*, *m* and *p*)-Br, *p*-NO_2 and *p*-CH_3. Five questions are of interest. First, how fast are the reactions by this method? Second, is the reaction mass transfer or kinetically controlled? Third, how is the reaction affected by the side group Y and its position on the benzene ring (*o*-, *m*- *p*-)? Fourth, how does the molar ratio of aryl alcohol and **1**, MR, affect the distribution of the products? Fifth, what is the limitation of the reaction? Therefore, the distributions of the products were measured and the rate constants were determined for the reactions with MR equal to 2 as model reactions. Also discussed is the relation of the chemical shifts and the coupling constants of ^{31}P NMR data to the nucelophilic ability of the aryloxy group and the level of substitution, n.

* Author to whom correspondence should be addressed.

EXPERIMENTAL

Apparatus and materials

^{31}P NMR spectra (in $CDCl_3$) were recorded on a Bruker AC200 spectrometer. $N_3P_3Cl_6$, assigned as 20 ppm relative to 85% H_3PO_4, was used as an internal reference. The IR spectra were obtained as thin films (KBr disks) on a Jasco Report-100 spectrometer. Mass spectra were recorded on a Jeol JMS-HX 110 spectrometer. Elemental analyses were performed on a Heraius CHN-O-RAPID analyser by the Instrument Center of NSC at Tainan, Taiwan. Differential scanning calorimetry (DSC) data were obtained on a Mettler DSC-30 thermal analyser at a heating rate of 10°C min^{-1} in a nitrogen atmosphere. The concentration of aryloxide derivatives in the aqueous phase was determined with a Shimadzu UV160 spectrometer at fixed wavelengths. An Iwaki Glass PC-351 hot plate with magnetic stirrer was used for the synthesis of the individual derivatives.

Hexachlorocyclotriphosphazene (**1**) was kindly provided by the Nippon Fine Chemical Corporation, Japan. Except sodium hydroxide (Osaka Chemical Co., Japan), all the other reagents and solvents were purchased from Merck Chemical Co. The reagents and solvents were all used as received.

Reaction kinetics of the reaction with MR = 2

In this part, the procedure described previously[19] was followed. Hence, a solution of **1** (3.48 g, 0.01 mol) in chloroform (100 cm^3) was mixed with an aqueous solution (200 cm^3) containing aryloxide (0.02 mol), sodium hydroxide (1.60 g, 0.04 mol) and tetrabutylammonium bromide (TBNB) (0.24 g, 0.75 mmol) as the phase transfer catalyst. The reaction mixture was stirred vigorously and taken out with a 20 cm^3 pipette at time intervals of 3 or 6 min. The reaction mixture collected at each time interval was separated into an organic phase and an aqueous phase. The concentration of aryloxide remaining in the aqueous phase was then determined using the UV spectrometer at the corresponding wavelengths listed in Table 1. The dependence of the absorbance on the concentration of a standard solution of each aryloxide at the corresponding wavelength was made for calibration.

Synthesis of aryloxychlorocyclotriphosphazenes, $N_3P_3Cl_{6-n}(OC_6H_4Y)_n$, Y = Cl(-o, -m, -p), Br(-o, -m, -p), NO_2, H *and* CH_3, n = 1–6.

A typical example with $[HOC_6H_4—Y]/[I] = 2$, Y = Cl—*p* was carried out as follows: An aqueous solution (32 cm^3) containing *p*-chlorophenol (3.70 g, 0.029 mol), sodium hydroxide (1.53 g, 0.038 mol) and TBNB (1.25 g, 0.0039 mol) was prepared. On the other hand, dichloromethane solution (50 cm^3) containing **1** (5 g, 0.014 mol) was prepared in a 250 cm^3 three-necked flask. With stirring, the aqueous solution was added dropwise into the dichloromethane solution in an ice bath was was reacted for 40 min at room temperature. When the reaction was over the solution mixture was separated into water and organic layers. The organic layer was dried by magnesium sulphate and filtered, and then the filtrate was concentrated by vacuum evaporation. The residue was separated by column chromatography with n-hexane/chloroform as the eluant. A similar procedure was used for the other reactions. The conditions for the other reactions are listed in Table 2.

Table 1. The absorption characteristics of various aryloxides ($OC_6H_4Y^-$) in UV spectra

Y	Absorption peak (m)
m-Cl	305.0
p-Cl	297.2
o-Cl	307.0
m-Br	280.0
p-Br	289.4
o-Br	308.0
p-CH_3	294.2
p-NO_2	275.0

Synthesis of $N_3P_3(OC_6H_4Y)_6$, Y = o-NO_2 *or* p-NO_2, *in ethylene glycol/benzene solvent system*

Synthesis of $N_3P_3(p\text{-}OC_6H_4NO_2)_6$ (**50**). A solution of *p*-nitrophenol (9.73 g, 0.07 mol), Na_2CO_3 (8.48 g, 0.14 mol) and methyltrioctylammonium chloride (MRNC) (0.9 g, 0.002 mol) in ethylene glycol (20 cm^3) was added dropwise into a solution of $N_3P_3Cl_6$ in benzene (30 cm^3). The mixture was then refluxed for 3.5 h. When the reaction was over, the solvent was removed by vacuum evaporation. The residue was added to hot DMF, decolourized by activated carbon and then filtered. The product was finally crystallized to yield 8.81 g (91.5%) of **50**.

Synthesis of $N_3P_3(o\text{-}OC_6H_4NO_2)_6$ (**51**). The reaction was carried out as above for compound **50** for 2 h. The reaction product was then purified by column chromatography with THF as the eluant. Yield: 91.9%.

Table 2. The conditions of synthesis of $N_3P_3Cl_{6-n}(OC_6H_4Y)_n$, $n = 1$–6[a]

MR	$N_3P_3Cl_6$ (mmol)	HOC_6H_4Y (mmol)	TBNB (mmol)	NaOH (mmol)	H_2O (cm^3)	CH_2Cl_2 (cm^3)
2	14.4	28.7	3.88	38.3	32	50
4	14.4	57.5	7.76	76.5	64	50
5	14.4	71.8	9.70	95.6	80	50
7	14.4	100.6	13.60	133.9	112	50

[a] All the reactions were carried out at room temperature for 40–60 min.

RESULTS AND DISCUSSION

The mechanism of the reaction of aryl alcohol with **1** in the aqueous and organic phases can be described as follows:[20]

$$ArOH + NaOH \Leftrightarrow ArO^-_{[aq.]} + Na^+_{[aq.]} + H_2O \quad [aq.\ phase] \quad (1)$$

$$ArO^-_{[aq.]}Q^+X^-_{[aq.]} \Leftrightarrow Q^+ArO^-_{[aq.]} + X^-_{[aq.]} \quad [aq.\ phase] \quad (2)$$

$$Q^+ArO^-_{[aq.]} \Leftrightarrow Q^+ArO^-_{[org.]} \quad [interface] \quad (3)$$

$$Q^+ArO^-_{[org.]} + N_3P_3Cl_x(OAr)_y \Leftrightarrow N_3P_3Cl_{x-1}(OAr)_{y+1} + Q^+Cl^-_{[org.]} \quad [org.\ phase] \quad (4)$$

$$Q^+Cl^-_{[org.]} \Leftrightarrow Q^+Cl^-_{[aq.]} \quad [interface] \quad (5)$$

$$ArO^-_{[aq.]} + Q^+Cl^-_{[aq.]} \Leftrightarrow Q^+ArO^-_{[aq.]} + Cl^-_{[aq.]} \quad [aq.\ phase] \quad (6)$$

then repeat from eq. (2).

QX, representing tetrabutylammonium bromide, was used as a phase transfer catalyst to transfer aryloxide from the aqueous phase to the organic phase, where the reaction occurred.

Kinetic study of the reactions with [*aryloxide*]/[1] = 2

As described in the previous study,[19] in order to understand the possible kinetics and the relative rate of the reaction in the lower level substitution, a milder condition was used for the model reactions with MR equal to 2. Figure 1 shows the relation between the concentration of aryloxide remaining in the aqueous phase, [B], vs the reaction time. Figure 2 shows that all the reactions followed eq. (7) and are second-order. The corresponding rate constants, k, are determined and listed in Table 3, which indicates that most of the rate constants are in the range 10^{-3}–10^{-1} $dm^3\ mol^{-1}\ s^{-1}$ and the rate, varied with Y, is of the order *m*-Br > *m*-Cl > *p*-Br > *p*-Cl > *o*-Br > *o*-Cl > —H > *p*-CH_3 ≫ *p*-NO_2 for the model reactions.

$$1/[B] - 1/[B]_0 = k't \quad (7)$$

Syntheses of (*aryloxy*)*chlorocyclotriphosphazenes*

The products obtained in each run were separated by column chromatography and identified by a combination of IR spectroscopy, elemental analysis, mass spectroscopy and ^{31}P NMR spectroscopy (Tables 4 and 5).

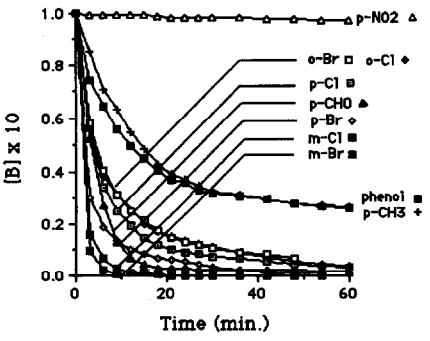

Fig. 1. The effect of various aryl alcohols on the aryloxide concentration transferred from the aqueous phase to the organic phase with the reaction time.

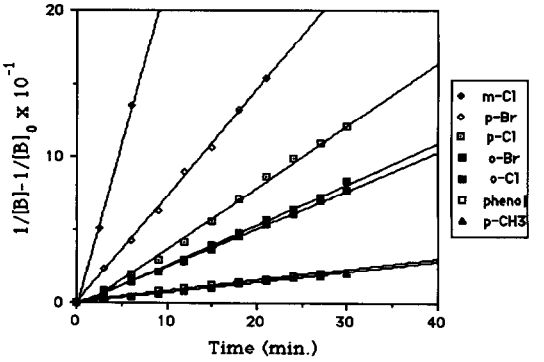

Fig. 2. The effect of various aryl alcohols on the kinetics of the reaction with MR = 2.

Table 3. The effect of Y on the rate constant of the reaction with MR = 2

Y	Reaction order	Rate constant[a] ($dm^3\ mol^{-1}\ S \times 10^3$)
m-Cl	Second	377.2
p-Cl	Second	70.7
o-Cl	Second	43.7
m-Br	Second	Too fast
p-Br	Second	121.7
o-Br	Second	46.6
—H[b]	Second	13.0
p-CH_3	Second	12.0

[a] Unit of the rate constant is S^{-1}.
[b] Recorded from ref. 19 for comparison.

The retention of the cyclic trimeric ring is indicated by the presence of a strong IR absorption at 1100–1300 cm^{-1}. On the other hand, the aromatic nitro groups in **44** and **45** are identified by the absorptions at 1570–1485 and 1370–1320 cm^{-1}.

The assignments of the ^{31}P NMR spectra are based on the simple rule that increasing substitution on a phosphorus atom leads to upfield shifts, viz. $\delta PCl_2 > \delta PCl(OAr) > \delta P(OAr)_2$. Explanations for the spectra are described below.

The mono-substituted derivatives have AX_2 ^{31}P NMR spectra appropriate to their structures. The individual spectrum of the bis derivatives shows a mixture spectrum of two closely spaced AX_2 patterns, representing the *cis* and *trans* isomers, and a low-intensity A_2X pattern, indicating the exis-

Table 4. Characterization data of $N_3P_3Cl_{6-n}(OC_6H_4Y)_n$, $n = 1$–6

Y	Compound number	*n*	Mass spectral data[a] Found	Calc.	Elemental analysis Found	Calc.
m-Cl	**2**	1	440.0	440.0	C, 16.8 N, 9.6 H, 1.0	C, 16.4 N, 9.6 H, 0.9
	3	2	532.0	532.0	C, 26.6 N, 8.0 H, 1.5	C, 27.1 N, 7.9 H, 1.5
	4	3	624.0	624.0	C, 34.7 N, 6.9 H, 2.0	C, 34.6 N, 6.7 H, 1.9
	5	4	716.0	716.0	C, 40.1 N, 6.0 H, 2.2	C, 40.2 N, 5.9 H, 2.2
	6	5	808.0	808.0	C, 45.2 N, 5.3 H, 2.4	C, 44.6 N, 5.2 H, 2.5
	7	6	900.0	900.0	C, 48.1 N, 4.8 H, 2.7	C, 48.0 N, 4.7 H, 2.7
p-Cl	**8**	1	440.0	440.0	C, 16.8 N, 9.5 H, 1.0	C, 16.4 N, 9.6 H, 0.9
	9	2	532.0	532.0	C, 26.6 N, 8.0 H, 1.4	C, 27.1 N, 7.9 H, 1.5
	10	3	624.0	624.0	C, 34.7 N, 6.8 H, 2.0	C, 34.6 N, 6.7 H, 1.9
	11	4	716.0	716.0	C, 40.1 N, 5.8 H, 2.1	C, 40.1 N, 5.9 H, 2.2
	12	5	808.0	808.0	C, 45.2 N, 5.2 H, 2.4	C, 44.6 N, 5.2 H, 2.5
	13	6	900.0	900.0	C, 48.7 N, 4.7 H, 2.8	C, 48.0 N, 4.7 H, 2.7

Table 4.—*continued*

Y	Compound number	n	Mass spectral data[a] Found	Calc.	Elemental analysis Found	Calc.
o-Cl	**14**	1	440.0	440.0	C, 16.0	C, 16.4
					N, 9.2	N, 9.6
					H, 1.0	H, 0.9
	15	2	532.0	532.0	C, 26.2	C, 27.1
					N, 7.8	N, 7.9
					H, 1.5	H, 1.5
	16	3	624.0	624.0	C, 34.6	C, 34.6
					N, 6.6	N, 6.7
					H, 1.9	H, 1.9
	17	4	716.0	716.0	C, 40.2	C, 40.2
					N, 5.9	N, 5.9
					H, 2.2	H, 2.2
	18	5	808.0	808.0	C, 45.4	C, 44.6
					N, 5.2	N, 5.2
					H, 2.4	H, 2.5
	19	6	900.0	900.0	C, 47.9	C, 48.1
					N, 4.5	N, 4.7
					H, 2.6	H, 2.7
m-Br	**20**	1	485.0	484.5	C, 14.6	C, 14.9
					N, 8.4	N, 8.7
					H, 0.8	H, 0.8
	21	2	622.0	621.0	C, 22.5	C, 23.2
					N, 6.7	N, 6.8
					H, 1.4	H, 1.3
	22	3	758.0	757.5	C, 28.4	C, 28.5
					N, 5.6	N, 5.5
					H, 1.6	H, 1.6
	23	4	895.0	894.0	C, 32.2	C, 32.2
					N, 4.7	N, 4.7
					H, 1.8	H, 1.8
	24	5	1031.0	1130.5	C, 34.8	C, 34.9
					N, 4.1	N, 4.1
					H, 2.0	H, 1.9
	25	6	1168.0	1167.0	C, 36.9	C, 37.0
					N, 3.8	N, 3.6
					H, 2.2	H, 2.1
p-Br	**26**	1	485.0	484.5	C, 14.8	C, 14.9
					N, 8.6	N, 8.7
					H, 0.9	H, 0.8
	27	2	622.0	621.0	C, 23.3	C, 23.2
					N, 6.7	N, 6.8
					H, 1.2	H, 1.3
	28	3	758.0	757.5	C, 28.6	C, 28.5
					N, 5.7	N, 5.5
					H, 1.7	H, 1.6
	29	4	895.0	894.0	C, 32.3	C, 32.2
					N, 4.8	N, 4.7
					H, 1.9	H, 1.8
	30	5	1031.0	1130.5	C, 34.8	C, 34.9
					N, 4.2	N, 4.1
					H, 2.0	H, 1.9
	31	6	1168.0	1167.0	C, 36.9	C, 37.0
					N, 3.7	N, 3.6
					H, 2.2	H, 2.1

Table 4.—*continued*

Y	Compound number	n	Mass spectral data[a] Found	Calc.	Elemental analysis Found	Calc.
o-Br	32	1	485.0	484.5	C, 15.1	C, 14.9
					N, 8.6	N, 8.7
					H, 0.9	H, 0.8
	33	2	622.0	621.0	C, 23.8	C, 23.2
					N, 6.7	N, 6.8
					H, 1.2	H, 1.2
	34	3	758.0	757.5	C, 28.7	C, 28.5
					N, 5.4	N, 5.5
					H, 1.6	H, 1.6
	35	4	895.0	894.0	C, 32.5	C, 32.2
					N, 4.8	N, 4.7
					H, 1.9	H, 1.8
	36	5	1031.0	1130.5	C, 35.6	C, 34.9
					N, 4.1	N, 4.1
					H, 2.0	H, 1.9
	37	6	1168.0	1167.0	C, 37.5	C, 37.0
					N, 3.7	N, 3.6
					H, 2.1	H, 2.1
p-CH_3	38	1	420.0	419.5	C, 20.9	C, 20.0
					N, 9.9	N, 10.0
					H, 1.7	H, 1.7
	39	2	492.0	491.0	C, 34.9	C, 34.2
					N, 8.5	N, 8.6
					H, 2.9	H, 2.9
	40	3	562.0	562.5	C, 43.9	C, 44.8
					N, 7.4	N, 7.5
					H, 3.6	H, 3.7
	41	4	634.0	634.0	C, 51.4	C, 53.0
					N, 6.5	N, 6.6
					H, 4.3	H, 4.4
	42	5	706.0	705.5	C, 60.2	C, 59.5
					N, 5.8	N, 6.0
					H, 4.7	H, 5.0
	43	6	563.0[b]	777.0	C, 65.2	C, 64.9
					N, 5.2	N, 5.4
					H, 5.2	H, 5.4
p-NO_2	44	6	[c]	963.0	C, 44.8	C, 44.9
					N, 13.1	N, 13.1
					H, 2.5	H, 2.5
o-NO_2	45	6	964.0	963.0	C, 45.3	C, 44.9
					N, 12.9	N, 13.1
					H, 2.6	H, 2.5

[a] Cl was calculated as 35.5 and the found molecular weight was observed directly from the mass spectra.

[b] The parent peak was not observed.

[c] The highest mass ion observed was the parent minus $NP(OC_6H_4CH_3)_2$.

Table 5. The ^{31}P NMR data of $N_3P_3Cl_{6-n}(OC_6H_4Y)_n$, $n = 1$–6[a]

Y	K_a (10^{-10})	$n = 1$	$n = 2$ Geminal	$n = 2$ Non-geminal	$n = 3$	$n = 4$	$n = 5$	$n = 6$
m-Cl	16.0							
PCl_2		22.5(d)	24.2(d)	24.9(t)	—	—	—	—
PCl(OAr)		12.7(t)	—	15.8(d)	18.5(s)	20.3(d)	21.9(t)	—
$P(OAr)_2$		—	0.0(t)	—	—	4.8(t)	6.5(d)	8.3(s)
J(A—B)		150.5	164.7	158.0	—	198.0	208.0	—
p-Cl	6.3							
PCl_2		22.6(d)	24.1(d)	25.0(t)	—	—	—	—
PCl(OAr)		12.4(t)	—	15.5(d)	18.3(s)	20.4(d)	22.3(t)	—
$P(OAr)_2$		—	−0.7(t)	—	—	5.0(t)	7.0(d)	8.8(s)
J(A—B)		150.4	159.0	160.4	—	196.2	204.2	—
o-Cl	77.0							
PCl_2		22.2(d)	23.9(d)	24.3(t)	—	—	—	—
PCl(OAr)		12.5(t)	—	15.4(d)	18.1(s)	20.0(d)	21.6(t)	—
$P(OAr)_2$		—	−1.1(t)	—	—	4.3(t)	6.0(d)	8.1(s)
J(A—B)		152.7	166.7	159.7	—	202.6	214.2	—
m-Br	14.0							
PCl_2		22.5(d)	24.2(d)	24.8(t)	—	—	—	—
PCl(OAr)		12.8(t)	—	15.8(d)	18.4(s)	20.2(d)	21.7(t)	—
$P(OAr)_2$		—	0.0(t)	—	—	4.8(t)	6.5(d)	8.3(s)
J(A—B)		150.2	164.7	159.0	—	197.9	207.6	—
p-Br	5.6							
PCl_2		22.6(d)	24.1(d)	25.0(t)	—	—	—	—
PCl(OAr)		12.4(t)	—	15.5(d)	18.3(s)	20.4(d)	22.3(t)	—
$P(OAr)_2$		—	−0.7(t)	—	—	5.0(t)	7.0(d)	8.8(s)
J(A—B)		150.4	159.1	160.4	—	196.2	204.2	—
o-Br	41.0							
PCl_2		22.5(d)	23.9(d)	24.2(t)	—	—	—	—
PCl(OAr)		12.8(t)	—	15.1(d)	18.4(s)	20.0(d)	21.4(t)	—
$P(OAr)_2$		—	−1.1(t)	—	—	4.2(t)	5.8(d)	8.0(s)
J(A—B)		150.0	166.7	160.2	—	196.3	215.7	—
p-CH_3	0.67							
PCl_2		22.4(d)	23.6(d)	24.6(t)	—	—	—	—
PCl(OAr)		12.3(t)	—	15.3(d)	18.5(s)	20.5(d)	22.3(t)	—
$P(OAr)_2$		—	−0.3(t)	—	—	5.2(t)	7.2(d)	8.9(s)
J(A—B)		148.6	153.0	164.8	—	187.6	201.5	—

[a] Units of chemical shifts and the coupling constants are ppm and Hz, respectively.

tence of a trace amount of the geminal isomer. Each A_2X spectrum, with A being in the PCl_2 region and X in the general $P(OAr)_2$ region, is consistent only with the corresponding geminal isomer.

The ^{31}P NMR spectra of the tris derivatives mainly show a mixture of non-geminal isomers. A large singlet corresponding to the *cis* isomer and an AB_2 pattern corresponding to the *trans* isomer are indistinguishable in the PCl(OAr) region. A doublet of doublets or triplet (centre lines of doublet of doublets merged) in the PCl_2, PCl(OAr) and $P(OAr)_2$ regions, respectively, is observed in a few cases, indicating the existence of traces of the geminal isomer. A typical spectrum of the tetrakis derivatives again indicates mainly the presence of non-geminal isomers. Two sets of closely spaced A_2X spectra represent the *cis* and *trans* isomers.

Each spectrum of the pentakis derivatives, as expected, exhibits the corresponding AX_2 pattern. A doublet in the $P(OAr)_2$ region and a triplet in PCl(OAr) region are observed. The spectra of the hexakis derivatives have the expected singlet in the $P(OAr)_2$ region.

From the results shown above, it is found that

the non-geminal pathway is favoured in all the reactions. Table 3 lists the chemical shifts and the coupling constants of the compounds isolated. As found for phenoxychlorocyclotriphosphazenes,[21] the chemical shifts and the coupling constants correlate linearly with the level of substitution, n. Furthermore, the chemical shift for $\delta P(OAr)_2$ is generally shifted upfield and that of $\delta PCl(OAr)$ is shifted downfield as the nucleophilic ability of the aryloxide, which is indicated by the K_a value of the corresponding aryl alcohol in Table 4, is increased.

The distributions of the products for the reactions carried out in the aqueous dichloromethane solvent system are listed in Table 6. Except for nitrophenol, the total yields of the other cases were all larger than 85%.

For the reactions with MR < 5 the distributions of the products are similar and the degree of substitution of the major product, yield >60%, is the same as the value of MR, independent of the side

Table 6. The distribution of the products of the syntheses of $N_3P_3Cl_{6-n}(OC_6H_4Y)_n$, $n = 1$–6[a]

Y	K_a[b] (10^{-10})	MR	Reaction time (min)	$n=1$	$n=2$	$n=3$ (%)	$n=4$	$n=5$	$n=6$	Yield (%)
m-Cl	16.0	2	40	18.0	62.0	9.3	—	—	—	89.3
		4	40	—	—	16.0	67.0	7.0	—	90.0
		5	40	—	—	—	22.0	64.0	6.0	92.0
		7	60	—	—	—	—	—	92.0	92.0
p-Cl	6.3	2	40	12.0	70.0	6.0	—	—	—	88.0
		4	40	—	—	14.0	69.0	6.0	—	89.0
		5	40	—	—	—	11.0	74.0	5.0	90.0
		7	40	—	—	—	—	9.2	83.0	92.2
o-Cl	77.0	2	40	15.0	62.0	3.0	—	—	—	90.0
		4	40	—	—	17.0	68.0	7.0	—	92.0
		5	60	—	—	—	25.0	64.0	3.0	92.0
		7	60	—	—	—	10.7	76.4	3.1	90.2
m-Br	14.0	2	40	17.0	68.0	6.3	—	—	—	91.3
		4	40	—	—	13.8	68.4	7.4	—	89.6
		5	40	—	—	—	20.0	62.6	7.6	90.2
		7	60	—	—	—	—	—	93.0	93.0
p-Br	5.6	2	40	14.0	67.0	7.0	—	—	—	88.0
		4	40	—	—	9.0	71.0	6.0	—	86.0
		5	40	—	—	—	13.0	69.0	7.0	89.0
		7	40	—	—	—	—	15.0	78.0	93.0
o-Br	41.0	2	40	19.2	65.5	5.3	—	—	—	90.0
		4	40	—	—	14.5	71.0	4.3	—	89.8
		5	60	—	—	—	22.5	64.0	4.0	90.5
		7	60	—	—	—	9.6	77.4	4.2	91.2
—H	1.0	2	40	8.0	74.0	6.0	—	—	—	88.0
		4	60	—	—	13.0	72.0	3.0	—	88.0
		5	60	—	—	2.0	78.6	9.4	—	90.0
		7	60	—	—	—	62.0	29.0	—	91.0
p-CH_3	6.67	2	40	7.0	75.0	4.0	—	—	—	86.0
		4	60	—	—	13.0	72.0	4.0	—	89.0
		5	60	—	—	—	88.0	4.0	—	92.0
		7	60	—	—	—	76.0	15.0	—	91.0
p-NO_2	690.0	2	60	10.0	7.0	1.0	—	—	—	18.0
		4	60	—	—	9.0	5.0	2.0	—	16.0
		5	60	—	—	—	1.0	17.0	2.0	20.0

[a] All the reactions were carried out at room temperature.
[b] K_a of YC_6H_4OH from ref. 25.

Table 7. The results of the preparation of $N_3P_3(OC_6H_4NO_2)_6$ in the ethylene glycol/benzene (EG/BG) system

Position of Y	MR	Temperature	Solvent	Time (h)	Yield (%)	
p-NO_2	7.0	Reflux	EG/BG	3.5	91.5	This study
o-NO_2	7.0	Reflux	EG/BG	2.0	91.9	This study
p-NO_2	7.5	Reflux	Xylene	28.0	87.0	22
p-NO_2	6.2	Reflux	THF	72.0	81.0	23
p-NO_2	7.0	Reflux	Xylene	14.0	76.0	11

group Y being electron-withdrawing or electron-releasing. This indicates that under the reaction conditions used, the inductive and resonance effects are obviously not present in the formation of the low substituted derivatives, i.e. lower than pentakis derivatives. The reactions were basically mass transfer-controlled in these levels of substitution. Therefore, mono-substituted and tri-substituted derivatives are expected to be obtained predominantly in these cases, if MR equals 1 and 3 are used, respectively, in the reaction. However, it becomes important for the formation of the pentakis and hexakis derivatives due to the increased steric hindrance. The reactions are slowed down and become more kinetically controlled. Hence, for the reactions with Y in the *para* position of aryloxide and MR = 5, the major products are pentakis for those with an electron-withdrawing group, both tetrakis and pentakis for phenol and tetrakis for *p*-creosol, an electron-releasing substituted phenol.

For the reactions with MR = 7 and Y in *para* and *meta* positions, fully substituted derivatives were obtained in high yield for those with electron-withdrawing groups, while a very low yield was obtained for phenol, and none was found for *p*-cresol. On the other hand, for the reaction with Y at the *ortho* position the major product found was pentakis and a low yield of hexakis was obtained due to the steric hindrance effect. These results indicate that the steric hindrance effect enhances the activation energy, and the electron-withdrawing inductive effect and the resonance effect, on the other hand, enhances the reactivity; but, the rate of the reaction depends on the net effect of them.

The extremely low yield for the reaction with nitrophenol, showing a much higher percentage of hydrolysis, is ascribed to the insolubility of nitrophenol in the aqueous alkali solution. In order to overcome this problem, ethylene glycol/benzene, a non-aqueous solvent system, was used. As listed in Table 7 the yield increased remarkably, and the reaction time was much shorter than that reported before.[9,11,22,23] Similar thermal behaviour, reported by Bornstein,[11] is observed for compound **44** by DSC measurement. The compound melted at 248°C and 264°C, indicating two crystalline forms, in the first scan, and mainly at 263°C in the second scan. On the other hand, a single melting point at 158°C is observed in the DSC thermograph, indicating one crystalline form for compound **45**.

CONCLUSION

The results of this study indicate that phase transfer catalysis is a very efficient method for the preparation of the strongly nucleophilic (aryloxy) chlorocyclotriphosphazenes in a suitable binary immiscible solvent system. The partially substituted (aryloxy)chlorocyclotriphosphazenes obtained can be expected to form the basis of the derivation of functional cyclotriphosphazenes. It is also expected that the method can be applied to the successive replacement of chlorine atoms in **1** to prepare mixed substituted aryloxycyclotriphosphazenes. Although the small molecule chemistry of hexachlorocyclotriphosphazene often provides a model for the reactivity of polydichlorophosphazene,[24] the aqueous/organic solvent system will not be suitable for polydichlorophosphazene due to its high sensitivity to water. However, other non-aqueous immiscible binary solvent systems may be applicable. Work concerning this is under investigation in our laboratory.

Acknowledgements—We thank the National Science Council for R.O.C. for the support of this work under project NSC-79-0208-M033-11, and Nippon Fine Chemical Co., Japan, for providing the hexachlorocyclotriphosphazene.

REFERENCES

1. H. R. Allcock, *Phosphorus–Nitrogen Compounds*, pp. 151–155. Academic Press, New York (1972).
2. H. R. Allcock, T. L. Evans and J. L. Fuller, *Inorg. Chem.* 1980, **19**, 1026.

3. H. R. Allcock, M. L. Levin and P. E. Austin, *Inorg. Chem.* 1986, **25**, 2281.
4. H. R. Allcock, M. S. Connelly, J. T. Sisko and S. Al-Shali, *Macromolecules* 1988, **21**, 323.
5. K. Brandt, *Chem. Stow.* 1986, **30**, 255.
6. D. Dell, B. W. Fitzsimmons and R. A. Shaw, *J. Chem. Soc., London* 1965, 4070.
7. B. T. McBee, K. Okuhara and C. J. Morton, *Inorg. Chem.* 1966, 450.
8. M. Gleria, F. Barigelletti, S. Dellonte, S. Lora, F. Minto and P. Bortolus, *Chem. Phys. Lett.* 1981, **83**, 559.
9. M. Gleria, S. Lora, F. Minto, L. Busulini and G. Paolucci, *Chim. Ind.* 1981, **63**, 719.
10. M. Gleria, G. Paolucci, F. Minto and S. Lora, *Chem. Ind.* 1982, **64**, 479.
11. J. Bornstein, D. P. Macajone and P. R. Bergquist, *Inorg. Chem.* 1985, **24**, 625.
12. M. D. Bezoari, U.S. Pat. US 4727176 (1988).
13. M. D. Bezoari, U.S. Pat. US 4727175 (1988).
14. P. E. Austin, G. H. Riding and H. R. Allcock, *Macromolecules* 1983, **16**, 719.
15. L. J. Carr and G. M. Nicklos, US Pat. No 4600791, p. 41 (1986).
16. M. R. Wang and H. S. Wu, *J. Org. Chem.* 1990, **55**, 2344.
17. R. C. Haddon and S. V. Chichester-Hicks, *Macromolecules* 1989, **22**, 1027.
18. K. V. Katti and S. S. Krishnamurthy, *J. Polym. Sci., Polym. Lett. Edn* 1982, **20**, 647.
19. Y. W. Chen-Yang, S. J. Chen and B. D. Tsai, *Ind. Engng Chem. Res.* 1991, **30**, 1314.
20. E. V. Dehmlow and S. S. Dehmlow, in *Phase Transfer Catalysis*, 2nd edn, pp. 52–321. Verlag Chemie GmbH, Weinheim, F.R.G. (1983).
21. J. Reuben, *Magnet. Reson. Chem.* 1987, **25**, 1049.
22. E. Kober, H. Lederle and G. Ottmann, *Inorg. Chem.* 1966, **5**, 2239.
23. H. R. Allcock, P. E. Austin and T. F. Rokowsky, *Macromolecules* 1981, **14**, 1622.
24. H. R. Allcock, *Accts Chem. Res.* 1979, **12**, 351.
25. R. T. Morrison and R. N. Boyd, *Organic Chemistry*, 4th edn. Allyn & Bacon, Inc., Boston (1983).

Polyhedron Vol. 12, No. 1, pp. 69–75, 1993
Printed in Great Britain

0277–5387/93 $6.00+.00
© 1993 Pergamon Press Ltd

A NEW INORGANIC METALLOCYCLE CONTAINING TIN, SULPHUR, PHOSPHORUS AND NITROGEN. CRYSTAL AND MOLECULAR STRUCTURE OF SPIROBICYCLIC $Me_2Sn(SPPh_2NPPh_2S)_2$

IONEL HAIDUC* and CRISTIAN SILVESTRU

Chemistry Department, Babes-Bolyai University, RO-3400 Cluj-Napoca, Romania

and

HERBERT W. ROESKY, HANS-GEORG SCHMIDT and MATHIAS NOLTEMEYER

Institut für Anorganische Chemie der Universität Göttingen, Tammannstr. 4, D-3400 Göttingen, F.R.G.

(*Received* 31 *July* 1992; *accepted* 27 *August* 1992)

Abstract—A new inorganic heterocycle is obtained by reacting potassium tetraphenyldithioimidodiphosphinate with trimethyltin and dimethyltin chlorides, in benzene. X-ray diffraction analysis reveals a spirocyclic structure with the dimethyltin moiety as the coordination centre with non-planar six-membered SnS_2P_2N rings. The coordination at tin is nearly perfectly octahedral, with equal Sn—S [273.3(2) and 273.7(2) pm] and P—S bonds [200.9(3) and 201.9(3) pm]. The S—Sn—S and H_3C—Sn—CH_3 units are co-linear.

The most common inorganic heterocycles[1,2] are non-metal rings. Although metal-containing inorganic heterocycles have been known for some time this area has started flourishing in the last 10 years, mainly by incorporation of metal heteroatoms into cyclothiazene[3] and cyclophosphazene[4] rings. Such rings are attractive as precursors for new types of inorganic polymers.[5] A particular class of carbon-free metallocycles includes inorganic chelate rings[6] and this type of compound may add a new dimension to both coordination chemistry and inorganic ring chemistry.

In addition to phosphazene metallocycles (1),[7] chelate rings (**2**), in which an azadiphosphinate group is attached to a metal through oxygen or sulphur, have been reported.[6] The known compounds of type **2**, with E = sulphur, are chelate rings with M = Mn^{II},[8] Fe^{II},[9] Co^{II},[8c,9a,9c] Ni^{II},[9a,10] Pd^{II},[9a] Pt^{II},[9a] Zn^{II},[9a] Cu^{I},[8c,11] Cu^{II},[9c,12] Ag^{I},[13] Au^{I},[13,14] Bi^{III}[15] or Te^{II}.[16] The only derivatives with an organometallic coordination centre reported so far are a dimeric phenyltellurium(II) compound, $[PhTe(SPPh_2NPh_2PS)]_2$,[17] and monomeric diorganogold(III) derivatives, $R_2Au(SPR_2NR_2PS)$.[14,18]

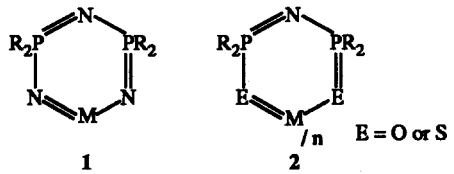

1 **2**

Several years ago one of us reported an organotin derivative, $Me_2Sn(SPPh_2NPh_2PS)_2$, which was not investigated in detail.[19] We now report some spectroscopic properties and a full crystal structure determination of this compound. This was prompted by the renewed interest in this type of chelate ring (e.g. **2**, E = O, M = Al, Ga, In, Sn, Mo, V)[20] and by the possible comparison with organotin dithiophosphates and dithiophosphinates, much investigated in recent years.[21,22] Thus, nearly all diorganotin dithiophosphates and phosphinates whose structures were determined by single-crystal X-ray diffraction show that the ligand is anisobidentate, coordinated to the metal in an unsymmetrical fashion (**3**) and exhibits an intermediate geometry between tetrahedral and octahedral, with

* Author to whom correspondence should be addressed.

short and long Sn—S bonds.[21a,d,e] The only exception known so far in organotin compounds is diphenyltin bis(diisopropyldithiophosphate) (**4**)

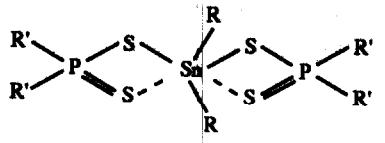

3

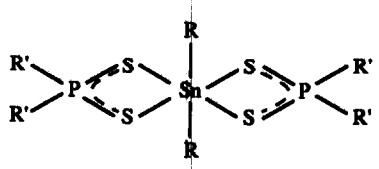

4

(R = Ph, R′ = OPr^i),[23] which exhibits a symmetrical structure with octahedral geometry and identical Sn—S bonds. The fact that the symmetrical structure **4** is the exception rather than the rule makes difficult any prediction. This latter type (isobidentate) of coordination is, however, typical for transition metal dithiophosphates.

In agreement with this data, for an organotin derivative of the dithioimidodiphosphinato ligand either an unsymmetrical structure **5** or a symmetrical structure **6** could be expected (M = Sn).

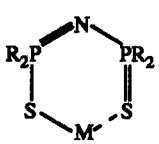

5

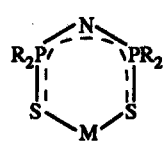

6

The single-crystal X-ray structure determination showed that the symmetrical structure **6** is actually present in the dimethyltin compound.

EXPERIMENTAL

The potassium salt of tetraphenyldithioimidodiphosphinic was prepared from the free acid and Bu^{t}OK.[24] The IR spectra of the starting materials and of the tin compounds were recorded as KBr pellets on a Nicolet 310/320 FT-IR spectrometer. The ^{119m}Sn Mössbauer spectrum of compound **8** was recorded at liquid nitrogen temperature, using $CaCa^{119m}SnO_3$ as a source and standard material for zero velocity.

Preparation of $Me_2Sn[(SPPh_2)_2N]_2$

A solution of Me_2SnCl_2 (0.44 g, 2 mmol) in anhydrous benzene was added to a suspension of $(SPPh_2)_2NK$ (1.95 g, 4 mmol) in the same solvent and the reaction mixture was refluxed for 90 min. The remaining white solid was then filtered off and extracted several times in a Soxhlet apparatus, using acetonitrile as a solvent. Small white–pink crystals of the title compound deposited from the clear acetonitrile solution upon standing for 24 h. Yield: 1.23 g (61%). Found: P, 11.0. Calc for $C_{50}H_{46}N_2P_4S_4Sn$: P, 11.8%.

Preparation of $Me_3Sn(SPPh_2)_2N$

A solution of Me_3SnCl (0.80 g, 4 mmol) in anhydrous benzene was added to a stirred suspension of $(SPPh_2)_2NK$ (1.95 g, 4 mmol) in the same solvent. The mixture was refluxed for 3–4 h and then the resultant KCl was filtered off. The hot, clear solution was allowed to reach room temperature slowly and colourless crystals deposited. Yield: 1.40 g (66%).

Crystallographic data for compound **8**

$C_{50}H_{46}N_2P_4S_4Sn$, $M = 1045.7$, monoclinic, space group $P2_1/n$; $a = 11.099(1)$, $b = 15.551(3)$, $c = 14.442(2)$ Å, $\beta = 103.30(1)°$; $V = 2425.9(6)$ Å^3, $Z = 2$, $d_{calc} = 1.43$ g cm^{-3}, absorption coefficient 0.858 mm^{-1}, $F(000) = 1068$. A colourless crystal of the dimensions $0.3 \times 0.4 \times 0.5$ mm was measured at room temperature on a STOE HED2 (rev. 6.2) four-circle goniometer with graphite monochromatized Mo-K_α radiation in the profile optimizing mode. Within $2\theta < 45°$, 2259 symmetry-independent reflections were collected of which 1678 with $F > 3\sigma(F)$ were used in the least-squares calculations (SHELX-76). The structure was solved by the heavy-atom method implemented in SHELX-86. All non-hydrogen atoms were refined anisotropically and hydrogen atoms positioned geometrically. The final R values are $r = 0.043$ and $Rw = 0.041$ with weights $w^{-1} = \sigma^2(F) + 0.0004\,F^2$. The residual electron density was in the range -0.3 to 0.5 e Å^{-3}. Further details of the crystal structure investigation may be obtained from the Fachinformationszentrum Karlsruhe, Gesellschaft für wissenschaftlich-technische Informations mbH, W-7514 Eggenstein-Leopoldstr. 2 (FRG), on quoting the deposit number CSD 56534, the names of the authors and the journal citation.

RESULTS AND DISCUSSION

The potassium salt of the tetraphenyldithioimidodiphosphinato ligand reacted with trimethyltin chloride, in benzene, to give a crystalline product; m.p. 135°C.

Table 1. IR data for methyltin(IV) derivatives and related compounds (in cm^{-1})

Compound	ν(PN)	ν(P=S)	ν(P···S)	ν(PNP)	ν(SnC_n)	Ref.
$(SPPh_2)_2NH$	928vs 922vs	652s	—	503s	—	25
$(SPPh_2)_2N^-K^+$	1199vs	—	598s 576s	511s	—	25
$Me_2Sn[(SPPh_2)_2N]_2$	1217vs	—	591m 570s	520m 510m	535m	—[a]
$Me_3Sn(SPPh_2)_2N$	1250vs	—	560s	500m	546m 507w	—[a]

[a] This work.

$$Me_3SnCl + K[(SPPh_2)_2N] \longrightarrow Me_3Sn(SPPh_2)_2N + KCl$$
7

Similarly prepared, the dimethyltin derivative was a colourless, crystalline compound; m.p. 265–266°C (from acetonitrile).

$$Me_2SnCl_2 + 2K[(SPPh_2)_2N] \longrightarrow Me_2Sn[(SPPh_2)_2N]_2 + 2KCl$$
8

The IR spectra of the two organotin compounds differ significantly from that of the neutral free ligand. The latter was shown by X-ray diffraction to have the structure of a bis(thiodiphenylphosphinyl)amine (**9**), $Ph_2P(S)NHP(S)Ph_2$.[25] The important bands in the IR spectra of the organotin derivatives are compared with those of the neutral ligand **9** and the potassium salt containing the anion **10** in Table 1.[9c,24] It is quite obvious that in the

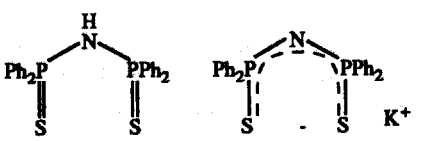

9 **10**

organotin compounds both the ν(PS) and ν(PNP) frequencies are different, due to the delocalization of the negative charge over the whole SPNPS fragment in the anion and changes in the P—S and P—N bond orders, as shown in structures **9** and **10**.

The 1250 and 1217 cm^{-1} bands in $Me_2Sn[(SPPh_2)_2N]_2$ and $Me_3Sn(SPPh_2)_2N$, respectively, were assigned to P···N···P asymmetrical stretching by comparison with a similar band in cyclophosphazenes, $(Ph_2PN)_{3\text{ and }4}$,[26] which exhibit ν_{as}(PNP) in the range 1220–1190 cm^{-1}. The strong bands at 652 and 645 cm^{-1}, characteristic of the P=S double bond in the free ligand **9** and its N-methyl derivative,[24] are replaced by a strong band at 570 and 560 cm^{-1} in the tin compounds, assigned to P···S stretching. This suggests the coordination of all sulphur atoms to tin.

The 535 cm^{-1} band in the diorganotin compound, assigned to SnC_2, indicates a linear arrangement of the two methyl groups in the central $SnMe_2$ moiety. For the trimethyltin(IV) derivative IR data suggest a non-planar orientation of the Sn—C bonds. Since both sulphur atoms seem to be coordinated, its possible solid-state molecular structures could be either monomeric (**11**) [as proposed for $Me_3SnS_2P(OR)_2$, R = Et, Pr^i, on the basis of Mössbauer data[21c]] or dimeric (**12**) with bridging ligands (similar to $Ph_2SbS_2PPh_2$[27]). The coordination geometry of the tin atom would be distorted trigonal bipyramidal in **11**, and octahedral in **12**.

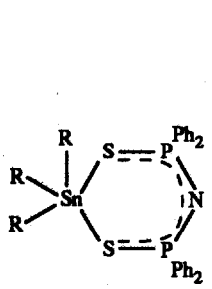

11

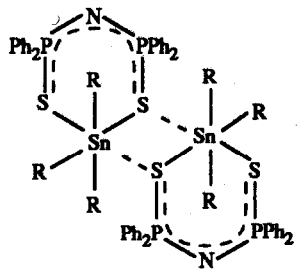

12

The Mössbauer spectrum of the dimethyltin compound (IS = 1.63 mm s^{-1} and QS = 3.98 mm s^{-1}) is in agreement with the presence of tin(IV) with a *trans* configuration of the Me—Sn—Me central unit. On the other hand, both the quadrupole splitting and the QS/IS ratio (ρ = 2.44) are consistent with six-coordinate octahedral geometry around tin.[28]

These data were insufficient to distinguish between the chelate ring structure **5** and metallocycle structure **6** of the tin compounds. The X-ray

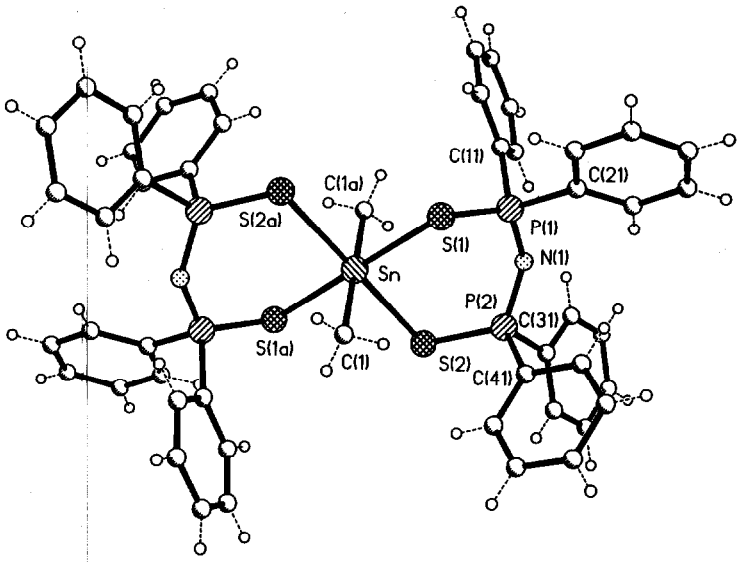

Fig. 1.

molecular structure determination of the trimethyltin compound **7** was not possible because of disorder, but we were successful with the dimethyltin derivative **8**.

Crystal and molecular structure of $Me_2Sn[(SPPh_2)_2N]_2$ (**8**)

The structure of compound **8** is built up of discrete $Me_2Sn[(SPPh_2)_2N]_2$ molecules. Its molecular structure in the crystal, with the atom numbering scheme, is illustrated in Fig. 1. Selected bond lengths and angles are given in Table 2.

The most unexpected feature of this structure is its high symmetry besides its crystallographic centrosymmetry. Both dithioimidodiphosphinato ligands act as isobidentate moieties forming a symmetrical metallocycle, **6**. All four sulphur atoms lie at equal distances [273.3(2) and 273.7(2) pm, respectively] from the tin atom, which are intermediate between the ester-type bonds (P—)S—Sn (average 248.5 pm) and secondary bonds (P=)S···Sn (average 321.5 pm) in $Ph_2Sn[S_2P(OEt)_2]_2$.[21a] As a result, two six-membered metallocycles, SnS_2P_2N, are formed with tin as the *spiro* atom. Moreover, opposite sulphur atoms belonging to different ligand molecules are co-linear [i.e. S(1)—Sn—S(1A) and S(2)—Sn—S(2A) angles are 180.0(1)°]. This leads to a co-planar SnS_4 system in which the angle between the sulphur atoms of the same ligand is greater [S(1)—Sn—S(2) 97.8(1)°] than that arising between *cis*-sulphur atoms belonging to different ligand moieties [S(1)—Sn—S(1A) 82.2(1)°] (**13**). A similar co-planar MS_4 system with co-linear opposite sulphur atoms was present in the tellurium(II) derivative of the same ligand, i.e. $Te[(SPPh_2)_2N]_2$,[16] but here the Te—S bonds are unequivalent [267.5(2) and 269.9(3) pm] and the intraligand S(1)—Sn—S(2) bond angle [86.05(8)°] is lower than the interligand S(2)—Sn—S(2A) angle [93.95(8)°] (**14**).

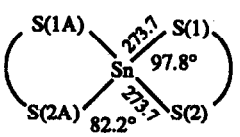

13

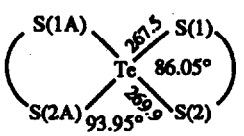

14

In the central dimethyltin unit the tin–carbon bonds are equal [211.1(8) pm] and co-linear [C(1)—Sn—C(1A) 180.0(1)°]. The axis described by the SnC_2 moiety is almost perpendicular to the SnS_4 plane, as suggested by the C—Sn—S angles (range 86.3–93.7°). As a result the tin atom is placed in the centre of a slightly distorted octahedron.

A comparison with other octahedral compounds containing dithiophosphorus ligands will be useful. Thus, the bismuth(III) complex of tetraphenyldithioimidodiphosphinic acid, $Bi[(SPPh_2)_2N]_3$, contains two sets of short and long Bi—S bonds (average values of 276 and 289 pm, respectively), indicating a structure analogous to **5** (M = Bi). The angles between opposite sulphur atoms are lower than 180° (range 166.3–174.4°). The distorted octahedral geometry around the metal atom was discussed as a result of two concurrent factors, i.e. the electrostatic repulsions between bonded pairs

Table 2. Selected bond lengths (pm) and angles (°) for compound **8**

Sn—C(1)	211.1(8)	Sn—S(1)	273.3(2)
Sn—S(2)	273.7(2)	Sn—C(1a)	211.1(8)
Sn—S(1a)	273.3(2)	Sn—S(2a)	273.7(2)
S(1)—P(1)	200.9(3)	P(1)—N(1)	158.2(7)
P(1)—C(11)	181.5(9)	P(1)—C(21)	180.9(8)
N(1)—P(2)	158.2(6)	P(2)—S(2)	201.9(3)
P(2)—C(31)	181.7(8)	P(2)—C(41)	179.7(9)

C(1)—Sn—S(1)	86.3(2)	C(1)—Sn—S(2)	89.9(2)
S(1)—Sn—S(2)	97.8(1)	C(1)—Sn—C(1a)	180.0(1)
S(1)—Sn—C(1a)	93.7(2)	S(2)—Sn—C(1a)	90.1(2)
C(1)—Sn—S(1a)	93.7(2)	S(1)—Sn—S(1a)	180.0(1)
S(2)—Sn—S(1a)	82.2(1)	C(1a)—Sn—S(1a)	86.3(2)
C(1)—Sn—S(2a)	90.1(2)	S(1)—Sn—S(2a)	82.2(1)
S(2)—Sn—S(2a)	180.0(1)	C(1a)—Sn—S(2a)	89.9(2)
S(1a)—Sn—S(2a)	97.8(1)	Sn—S(1)—P(1)	106.1(1)
S(1)—P(1)—N(1)	118.5(2)	S(1)—P(1)—C(11)	111.1(3)
N(1)—P(1)—C(11)	106.4(4)	S(1)—P(1)—C(21)	106.8(3)
N(1)—P(1)—C(21)	109.5(4)	C(11)—P(1)—C(21)	103.5(3)
P(1)—N(1)—P(2)	136.0(4)	N(1)—P(2)—S(2)	118.8(3)
N(1)—P(2)—C(31)	104.5(4)	S(2)—P(2)—C(31)	106.2(2)
N(1)—P(2)—C(41)	112.3(3)	S(2)—P(2)—C(41)	109.6(2)
C(31)—P(2)—C(41)	104.0(4)	Sn—S(2)—P(2)	106.0(1)
P(1)—C(11)—C(12)	120.9(7)	P(1)—C(11)—C(16)	120.9(7)
P(1)—C(21)—C(22)	121.7(6)	P(1)—C(21)—C(26)	120.2(6)
P(2)—C(31)—C(32)	120.4(7)	P(2)—C(31)—C(36)	120.5(6)
P(2)—C(41)—C(42)	119.4(6)	P(2)—C(41)—C(46)	123.0(6)

and the lone pair of the bismuth atom, and the bulky nature of the ligand, respectively.[15b]

The coordination around tin in compound **8** is similar to that found in $Ph_2Sn[S_2P(OPr^i)_2]_2$, with a unique octahedral structure, containing linear Ph—Sn—Ph groups and symmetrically coordinated (isobidentate) dithiophosphato ligands with all four Sn—S bonds identical (average 268.4 pm).[23] In unsymmetrically coordinated (anisobidentate) diethyldithiophosphate, $Ph_2Sn[S_2P(OEt)_2]_2$,[21a] and dimethyltin(IV) bis(dialkyldithiophosphinates), $Me_2Sn(S_2PMe_2)_2$[21d] and $Me_2Sn(S_2PEt_2)_2$,[21e] there are two sets of long and short Sn—S distances (Table 3). The lengths of the P—S bonds also differ in these compounds.

Concerning the tetraphenyldithioimidodiphosphinato ligand, since it is coordinated to tin through both its sulphur atoms, a twist about the P—N bond from the *trans* configuration of the sulphur atoms in the free ligand[25] to the *cis* orientation is required.

Although there are some small differences between the P—S and P—N bond lengths respectively reported in the structure of the free ligand described by different authors,[25] these bonds are of the same magnitude as the P=S double bond in P_4S_{10} (196 pm)[29] and P—N single bonds in $[ClP(S)NMe]_2$ (167 pm)[30] or $(H_2N)_2P(S)$—NMe—$P(S)(NH_2)NHMe$ (173 pm).[31] The isobidentate coordinated ligand in the tin compound **8** has equal phosphorus–sulphur and phosphorus–nitrogen bond lengths, respectively. However, the former are significantly longer and the latter shorter than in the free ligand, thus suggesting a considerable amount of double bond character resulting from the delocalization of the π-electrons on the SnS_2P_2N metallocycle. Moreover, the lengths of the tin–sulphur and phosphorus–sulphur bonds in compound **8** are comparable to those observed in the highly symmetrical molecule of $Ph_2Sn[S_2P(OPr^i)_2]_2$,[23] which also involves an extensive electron delocalization on the SnS_2P ring.

Both S—P—N and P—N—P angles in the dimethyltin(IV) complex are slightly larger than in the free ligand,[25] to permit the symmetrical coordination of the ligand to the metal atom. The electrons of the phosphorus atoms are essentially sp^3 hybridized, resulting in a distorted tetrahedral

Table 3. Comparison of M—S and P—S bond lengths for $Me_2Sn[(SPPh_2)_2N]_2$ and related compounds (in pm)

Compound	Structure type	Bond lengths (average) M—S	P—S	Ref.
$Me_2Sn[(SPPh_2)_2N]_2$	**6**	273.5	201.4	This work
$(SPPh_2)_2NH$	**9**	—	194.3	24a
		—	191.6	24c
$Ph_2Sn[S_2P(OPr^i)_2]_2$	**4**	268.4	200.2	23
$Ph_2Sn[S_2P(OEt)_2]_2$	**3**	248.6	203.5	21a
		321.5	193	
$Me_2Sn(S_2PMe_2)_2$	**3**	248.2	204.7	21d
		333.4	196.9	
$Me_2Sn(S_2PEt_2)_2$	**3**	247.6	205.4	21e
		333.6	196.1	
$Bi[(SPPh_2)_2N]_3$	**5**	275.7	202.1	15b
		289	200.6	
$Te[(SPPPh_2)_2N]_2$	**5**	267.5	202.2	16
		269.9	202.3	

geometry, with X—P—Y (X, Y = C and/or S atoms) angles close to the tetrahedral value (109°28′).

Acknowledgements—We are grateful to E. Merck company for complementary research samples of organotin halides used as starting materials in this work. We also thank Prof. Dr Marcel Gielen, from Vrije Universiteit, Brussels, for providing the ^{119m}Sn Mössbauer spectrum. Support of the Deutsche Forschungsgemeinschaft is highly acknowledged.

REFERENCES

1. (a) I. Haiduc, *The Chemistry of Inorganic Ring Systems*. Wiley-Interscience, London (1970); (b) I. Haiduc and D. B. Sowerby (Editors), *The Chemistry of Inorganic Homo- and Heterocycles*. Academic Press, London (1987).
2. H. G. Heal, *Inorganic Heterocyclic Chemistry of Sulfur, Nitrogen and Phosphorus*. Academic Press, London (1980).
3. (a) H. W. Roesky, J. Anhaus, H.-G. Schmidt, G. M. Sheldrick and M. Noltemeyer, *J. Chem. Soc., Dalton Trans.* 1983, 1207; for reviews, see: (b) T. Chivers and F. Edelmann, *Polyhedron* 1986, **5**, 1661; (c) P. F. Kelly and J. D. Woollins, *Polyhedron* 1986, **5**, 607.
4. H. W. Roesky, *Synlett* 1990, 651.
5. H. W. Roesky, *Polyhedron* 1989, **8**, 1729.
6. For a review, see: I. Haiduc and I. Silaghi-Dumitrescu, *Coord. Chem. Rev.* 1986, **74**, 127.
7. (a) H. W. Roesky, K. V. Katti, U. Seseke, M. Witt, E. Egert, R. Herbst and G. M. Sheldrick, *Angew. Chem.* 1986, **98**, 447; *Angew. Chem., Int. Edn Engl.* 1986, **25**, 477; (b) H. W. Roesky, K. V. Katti, U. Seseke, H.-G. Schmidt, E. Egert, R. Herbst and G. M. Sheldrick, *J. Chem. Soc., Dalton Trans.* 1987, 847; (c) K. V. Katti, H. W. Roesky and M. Rietzel, *Inorg. Chem.* 1987, **26**, 4032; (d) R. Herbst, K. V. Katti, H. W. Roesky and G. M. Sheldrick, *Z. Naturforsch.* 1987, **42b**, 1387; (e) M. Witt and H. W. Roesky, *Polyhedron* 1989, **8**, 1736; (f) H. W. Roesky, P. Olms, M. Witt, K. Keller, D. Stalke, T. Henkel and G. M. Sheldrick, *J. Chem. Soc., Chem. Commun.* 1989, 366; (g) M. Witt, H. W. Roesky, M. Noltemeyer and A. Schmidpeter, *New J. Chem.* 1989, **13**, 403.
8. (a) O. Siiman, M. Wrighton and H. B. Gray, *J. Coord. Chem.* 1972, **2**, 159; (b) O. Siiman and H. B. Gray, *Inorg. Chem.* 1974, **13**, 1185; (c) O. Siiman, *Inorg. Chem.* 1981, **20**, 2285.
9. (a) A. Davison and E. Switkes, *Inorg. Chem.* 1971, **10**, 837; (b) M. R. Churchill and J. Wormald, *Inorg. Chem.* 1971, **10**, 1778; (c) R. Czernuszewicz, E. Maslowsky and K. Nakamoto, *Inorg. Chim. Acta* 1980, **40**, 199.
10. (a) M. R. Churchill, J. Cooke, J. Wormald, A. Davison and E. S. Switkes, *J. Am. Chem. Soc.* 1969, **91**, 6518; (b) M. R. Churchill, J. Cooke, J. P. Fennessey and J. Wormald, *Inorg. Chem.* 1971, **10**, 1031.
11. O. Siiman, C. P. Huber and M. L. Post, *Inorg. Chim. Acta* 1977, **25**, L11.
12. R. D. Bereman, F. T. Wang, J. Nadjdzionek and D. M. Braitsch, *J. Am. Chem. Soc.* 1976, **98**, 7266.
13. R. Uson, A. Laguna and M. Concepcion Gimeno, *J. Chem. Soc., Dalton Trans.* 1989, 1883.
14. A. Laguna, M. Laguna, A. Rojo and M. N. Fraile, *J. Organomet. Chem.* 1986, **315**, 269.
15. (a) D. J. Williams, *Inorg. Nucl. Chem. Lett.* 1980, **16**, 189; (b) D. J. Williams, C. O. Quicksall and K. M.

Barkigia, *Inorg. Chem.* 1982, **21**, 2097; (c) D. J. Williams, J. B. Travis and K. L. Bergbauer, *J. Coord. Chem.* 1987, **16**, 315.
16. S. Bjornevag, S. Husebye and K. Maartmann-Moe, *Acta Chem. Scand.* 1982, **A36**, 195.
17. S. Husebye, K. Maartmann-Moe and O. Mikalsen, *Acta Chem. Scand.* 1990, **44**, 802.
18. H. W. Chen, C. Paparizos and J. P. Fackler Jr, *Inorg. Chim. Acta* 1985, **96**, 137.
19. I. Haiduc, V. P. Botha and A. Ziegler, *1er Symposium Internationale de Chimie Heterocyclique Minerale*, Besancon, 16–19 Juin 1975 (Proceedings), p. 437.
20. (a) M. Rietzel, H. W. Roesky, K. V. Katti, H.-G. Schmidt, R. Herbst-Irmer, M. Noltemeyer, G. M. Sheldrick, M. C. R. Symons and A. Abu-Raqabah, *J. Chem. Soc., Dalton Trans.* 1990, 2387; (b) A. Mazzah, H. J. Gosink, J. Liebermann and H. W. Roesky, *Chem. Ber.* 1991, **124**, 753; (c) M. Rietzel, H. W. Roesky, K. V. Katti, M. Noltemeyer, M. C. R. Symons and A. Abu-Raqabah, *J. Chem. Soc., Dalton Trans.* 1991, 1285; (d) R. O. Day, R. R. Holmes, A. Schmidpeter, K. Stoll and L. Howe, *Chem. Ber.* 1991, **124**, 2443.
21. (a) B. W. Liebich and M. Tomassini, *Acta Cryst.* 1978, **B34**, 944; (b) J. L. Lefferts, K. C. Molloy, J. J. Zuckerman, I. Haiduc, M. Curtui, C. Guta and D. Ruse, *Inorg. Chem.* 1980, **19**, 2861; (c) J. L. Lefferts, K. C. Molloy, J. J. Zuckerman, I. Haiduc, C. Guta and D. Ruse, *Inorg. Chem.* 1980, **19**, 1662; (d) K. C. Molloy, M. B. Hossain, D. Van der Helm, J. J. Zuckerman and F. P. Mullins, *Inorg. Chem.* 1981, **20**, 2172; (e) C. Silvestru, I. Haiduc, S. Klima, U. Thewalt, M. Gielen and J. J. Zuckerman, *J. Organomet. Chem.* 1987, **327**, 181; (f) C. Silvestru, F. Ilies, I. Haiduc, M. Gielen and J. J. Zuckerman, *J. Organomet. Chem.* 1987, **330**, 315; (g) C. Silvestru and I. Haiduc, *J. Organomet. Chem.* 1989, **365**, 83.
22. For reviews, see: (a) R. C. Mehrotra, G. Srivastava and B. P. S. Chauhan, *Coord. Chem. Rev.* 1984, **55**, 207; (b) R. C. Mehrotra, *Silicon, Germanium, Tin Lead Compds*, 1986, **9**, 185.
23. K. C. Molloy, M. B. Hossain, D. Van der Helm, J. J. Zuckerman and I. Haiduc, *Inorg. Chem.* 1980, **19**, 2041.
24. A. Schmidpeter and H. Groeger, *Z. Anorg. Allg. Chem.* 1966, **345**, 106.
25. (a) H. Nöth, *Z. Naturforsch.* 1982, **37b**, 1491; (b) S. Husebye and K. Maartmann-Moe, *Acta Chem. Scand.* 1983, **A37**, 439; (c) P. B. Hitchcock, J. F. Nixon, I. Silaghi-Dumitrescu and I. Haiduc, *Inorg. Chem. Acta* 1985, **96**, 77; (d) R. Cea-Olivares and H. Nöth, *Z. Naturforsch.* 1987, **42b**, 1507.
26. L. C. Thomas, *The Identification of Functional Groups in Organophosphorus Compounds*, p. 62. Academic Press, New York (1974).
27. C. Silvestru, L. Silaghi-Dumitrescu, I. Haiduc, M. J. Begley, M. Nunn and D. B. Sowerby, *J. Chem. Soc., Dalton Trans.* 1986, 1031.
28. R. V. Parish, *NMR, NQR, EPR and Mössbauer Spectroscopy in Inorganic Chemistry*, p. 149. Ellis Harwood Ltd, London (1990).
29. A. Vos and E. M. Wiebenga, *Acta Cryst.* 1955, **8**, 217.
30. J. Weiss and G. Hartman, *Z. Naturforsch.* 1966, **21b**, 891.
31. M. L. Ziegler and J. Weiss, *Z. Anorg. Allg. Chem.* 1968, **361**, 136.

Polyhedron Vol. 12, No. 1, pp. 77–81, 1993
Printed in Great Britain

0277–5387/93 $6.00+.00
© 1993 Pergamon Press Ltd

THE CRYSTAL STRUCTURE OF THE ADDITION COMPOUND OF DECAVANADATE AND GUANIDINE

XIN WANG* and HAI-XIN LIU

Department of Chemistry, Lanzhou University, Lanzhou 730000, P.R.C.

and

XUE-XIANG XU and XIAO-ZENG YOU

Coordination Chemistry Institute, Nanjing University, Nanjing 210008, P.R.C.

(*Received* 17 *June* 1992; *accepted* 27 *August* 1992)

Abstract—$NaVO_3$ reacts with guanidine hydrochloride in aqueous solution to afford the title complex. The X-ray single crystal structure of the complex reveals that the molecular structure consists of a $V_{10}O_{28}^{6-}$ polyanion with 10 VO_6 distorted octahedra, which form two octahedra sharing an edge. Six protons of each decavanadic acid are captured by guanidine. In the crystal, the isopolydecavanadate anion, guanidine and the crystal water are linked together by ionic forces and hydrogen bonding.

Vanadium is an element which can form hetero- and isopolyanions. The degree of aggregation and structures of the vanadates are directly dependent upon the acidity of the medium.[1] The isopolyvanadate and the adducts of isopolyvanadic acid with a variety of Lewis bases are the important intermediate products during the wet process of vanadium metallurgy and some of them may be used to separate vanadium from other elements.[2] In addition, polyvanadic acids are polybasic acids, so they can offer several protons and have the ability to combine with various Lewis bases in different proportions. Therefore, it should be worth while systematically studying this kind of addition compound.

Here, we report the synthesis and the crystal structure of the title compound.

EXPERIMENTAL

Preparation

$NaVO_3$ (4.5 g, 37 mmol) was dissolved in water (25 cm^3) and the pH of the orange solution adjusted to 5–6 by nitric acid (3 mol dm^{-3}). An aqueous solution containing guanidine hydrochloride (5.0 g, 52.3 mmol) was then added with stirring. A yellow precipitate immediately formed and was washed several times with ethanol and cold water. Found: C, 5.1; H, 3.3; N, 17.6. Calc. for $(CN_3H_6)_6[V_{10}O_{28}]\cdot 6H_2O$: C, 5.0; H, 3.4; N, 17.7%. The orange-needle single crystals of the title compound were obtained by recrystallization in hot water.

Determination of the crystal structure

A single crystal with the approximate dimensions $0.20 \times 0.20 \times 0.30$ mm was mounted on a glass fibre. All the intensity data were collected on an Enraf–Nonius CAD4 diffractometer using graphite-monochromated Cu-K_α radiation ($\lambda = 1.5418$ Å) with a scan mode of ω–2θ. 3571 independent reflections were collected in the range $2° < 2\theta < 120°$, and 2910 independent reflections with $I > 3\sigma(I)$ were used for further computation. All data were corrected for Lorentz and polarization effects and empirical absorption corrections, based on ψ scans, were applied (max 0.987, min 0.481).

The title compound is monoclinic, space group $P2_1/n$, $Mr = 1353.91$, with the cell dimensions $a = 9.198(2)$, $b = 21.895(2)$, $c = 11.170(3)$ Å, $\beta = 103.92(2)°$, $V = 2183.4$ Å^3, $Z = 2$, $D_{calc} = 2.06$ g cm^{-3}, $F(000) = 1344$, $\mu = 183.8$ cm^{-1}. The structure analysis was performed on a PDP 11/44 com-

* Author to whom correspondence should be addressed.

puter with the SDP program. The positions of all the vanadium atoms were determined by direct methods. The positions of other non-hydrogen atoms were revealed by difference-Fourier syntheses. The hydrogen atoms, located in a difference map and fixed with isotropic $B = 5.0$ Å^2, were included as a fixed contribution. The structure was refined with unit weights by full-matrix least-squares methods with anisotropic thermal factors for all non-hydrogen atoms. Refinement converged to a final $R = 0.074$ for the 2910 observed reflections; $(\Delta/\sigma)_{max} = 0.76$, $\Delta\rho_{max} = 1.86$ e Å^{-3} and $\Delta\rho_{min} = -0.3$ e Å^{-3}. R is high due to the poor quality of the crystal.

RESULTS AND DISCUSSION

Selected bond angles and distances are summarized in Tables 1 and 2, respectively. The final atomic coordinates and the thermal parameters have been deposited as supplementary material with the Editor, from whom copies are available on request.

The decavanadate polyanion shows the same configuration with $K_2Zn_2V_{10}O_{28}\cdot 16H_2O$,[3] $Ca_3V_{10}O_{28}\cdot 17H_2O$,[4] $Na_6V_{10}O_{28}\cdot 18H_2O$,[5] $Nd_2V_{10}O_{28}\cdot 28H_2O$[6] and $(H_3NCH_2CH_2NH_3)_3V_{10}O_{28}\cdot 6H_2O$.[7]

In the crystal, the existence of the decavanadate polyanions has been confirmed by structure analysis. This kind of isopolynuclear complex anion is a highly condensed system of VO_6 octahedra formed by 10 vanadium atoms and 28 oxygen atoms. It therefore has a high molecular weight, 957.4. The stereoconfiguration of the complex and atomic labels are shown in Fig. 1; the 10 vanadium atoms form two octahedra sharing an edge of which the middle point sits on a crystallographic centre of symmetry.

In the decavanadate group there are three kinds of unique vanadium atoms: V(2) and V(5), V(1) and V(4), and V(3). The first two types of vanadium, V(2), V(5), V(1) and V(4), form oxovanadium(V), i.e. VO^{3+}, with O(3), O(4), O(14) and O(13), respectively. The third type of vanadium atom, V(3), has two short V—O bonds with O(1) and O(2) (the lengths of these bonds are 1.679 and 1.691 Å) and the bond angle O(1)—V(3)—O(2) is 106.94°. This group with a bent configuration might be considered as a separate dioxovanadium(V) ion or the pervanadyl ion VO_2^+.

Both in VO^{3+} and VO_2^+ groups V—O bonds possess high multiple bond character due to the participating π-bonds of the d-orbitals.

On the basis of eight VO^{3+} and two VO_2^+ groups the polydecavanadate anion is formed by linking 10 oxovanadium(V) groups together with 16 oxygen

Table 1. Bond angles for $[V_{10}O_{28}]^{6-}$

O(1)—V(1)—O(6)	74.13(4)	O(1)—V(1)—O(8)	82.15(8)	O(1)—V(1)—O(10)	157.2(2)
O(1)—V(1)—O(11)	84.1(3)	O(1)—V(1)—O(14)	98.8(1)	O(6)—V(1)—O(8)	77.62(8)
O(6)—V(1)—O(10)	83.2(2)	O(6)—V(1)—O(11)	78.2(2)	O(6)—V(1)—O(14)	172.8(1)
O(8)—V(1)—O(10)	90.7(1)	O(8)—V(1)—O(11)	154.6(3)	O(8)—V(1)—O(14)	100.5(1)
O(10)—V(1)—O(11)	93.9(2)	O(10)—V(1)—O(14)	103.7(2)	O(11)—V(1)—O(14)	102.7(2)
O(3)—V(2)—O(5)	99.19(5)	O(3)—V(2)—O(6)	174.36(9)	O(3)—V(2)—O(8)	103.9(2)
O(3)—V(2)—O(9)	101.8(1)	O(3)—V(2)—O(12)	101.4(2)	O(5)—V(2)—O(6)	75.51(5)
O(5)—V(2)—O(8)	155.58(9)	O(5)—V(2)—O(9)	88.8(1)	O(5)—V(2)—O(12)	75.9(1)
O(6)—V(2)—O(8)	81.15(8)	O(6)—V(2)—O(9)	80.2(1)	O(6)—V(2)—O(12)	75.6(2)
O(8)—V(2)—O(9)	94.3(2)	O(8)—V(2)—O(12)	91.6(1)	O(9)—V(2)—O(12)	153.9(3)
O(1)—V(3)—O(2)	106.94(6)	O(1)—V(3)—O(5)	99.10(4)	O(1)—V(3)—O(6)	88.51(8)
O(1)—V(3)—O(6′)	166.35(9)	O(1)—V(3)—O(12)	96.4(2)	O(2)—V(3)—O(5)	97.93(8)
O(2)—V(3)—O(6)	164.37(8)	O(2)—V(3)—O(6′)	86.44(8)	O(2)—V(3)—O(12)	94.9(2)
O(5)—V(3)—O(6)	81.49(4)	O(5)—V(3)—O(6′)	81.37(6)	O(5)—V(3)—O(12)	156.2(1)
O(6)—V(3)—O(6′)	78.03(6)	O(6)—V(3)—O(12)	80.8(1)	O(6′)—V(3)—O(12)	79.4(1)
O(2)—V(4)—O(6)	73.79(4)	O(2)—V(4)—O(7)	83.6(1)	O(2)—V(4)—O(9)	84.5(1)
O(2)—V(4)—O(10)	155.6(3)	O(2)—V(4)—O(13)	101.5(2)	O(6)—V(4)—O(7)	76.8(1)
O(6)—V(4)—O(9)	77.1(1)	O(6)—V(4)—O(10)	81.8(3)	O(6)—V(4)—O(13)	175.3(2)
O(7)—V(4)—O(9)	153.5(2)	O(7)—V(4)—O(10)	90.5(2)	O(7)—V(4)—O(13)	102.4(2)
O(9)—V(4)—O(10)	90.8(1)	O(9)—V(4)—O(13)	103.1(3)	O(10)—V(4)—O(13)	102.9(3)
O(4)—V(5)—O(5)	99.26(7)	O(4)—V(5)—O(6)	174.28(8)	O(4)—V(5)—O(7)	103.96(9)
O(4)—V(5)—O(11)	101.4(1)	O(4)—V(5)—O(12)	101.4(2)	O(5)—V(5)—O(6)	75.17(4)
O(5)—V(5)—O(7)	155.70(3)	O(5)—V(5)—O(11)	88.2(2)	O(5)—V(5)—O(12)	77.3(1)
O(6)—V(5)—O(7)	81.43(8)	O(6)—V(5)—O(11)	80.0(1)	O(6)—V(5)—O(12)	76.3(2)
O(7)—V(5)—O(11)	94.2(4)	O(7)—V(5)—O(12)	91.2(2)	O(11)—V(5)—O(12)	154.6(2)

Table 2. Comparison of bond distances (Å) within the VO_6 octahedra of two decavanadates

	$(CN_3H_6)_6[V_{10}O_{28}]\cdot 6H_2O$	$Na_2[(CH_2)_6N_3NH]_2[H_2V_{10}O_{28}]\cdot 8H_2O$	Δ
V(1)—O(14)	1.599(3)	1.607(3)	−0.008
V(1)—O(10)	1.832(5)	1.849(3)	−0.017
V(1)—O(11)	1.849(6)	1.888(3)	−0.039
V(1)—O(8)	1.909(3)	1.862(3)	+0.047
V(1)—O(1)	2.071(2)	2.019(2)	+0.052
V(1)—O(6)	2.292(1)	2.353(3)	−0.061
V(2)—O(3)	1.604(1)	1.619(3)	−0.015
V(2)—O(8)	1.796(3)	1.817(3)	−0.021
V(2)—O(9)	1.834(5)	1.811(3)	+0.023
V(2)—O(12)	1.992(5)	2.021(2)	−0.029
V(2)—O(5)	2.029(1)	2.024(3)	+0.005
V(2)—O(6)	2.244(1)	2.240(3)	+0.004
V(3)—O(1)	1.679(3)	1.686(2)	−0.007
V(3)—O(2)	1.691(2)	1.679(2)	+0.012
V(3)—O(12)	1.942(5)	1.984(3)	−0.042
V(3)—O(5)	1.886(5)	1.891(3)	−0.005
V(3)—O(6′)	2.075(1)	2.102(3)	−0.027
V(3)—O(6)	2.126(1)	2.140(3)	−0.014
V(4)—O(13)	1.599(2)	1.607(3)	−0.008
V(4)—O(10)	1.827(5)	1.807(3)	+0.020
V(4)—O(9)	1.851(3)	1.913(3)	−0.038
V(4)—O(7)	1.891(4)	1.856(3)	+0.035
V(4)—O(2)	2.018(2)	2.096(3)	−0.078
V(4)—O(6′)	2.346(1)	2.284(2)	+0.062
V(5)—O(4)	1.599(2)	1.606(3)	−0.007
V(5)—O(7)	1.809(5)	1.832(3)	−0.023
V(5)—O(11)	1.837(8)	1.802(3)	+0.035
V(5)—O(12′)	1.962(4)	2.039(2)	−0.077
V(5)—O(5)	2.000(1)	1.989(2)	+0.011
V(5)—O(6)	2.235(2)	2.255(3)	−0.020

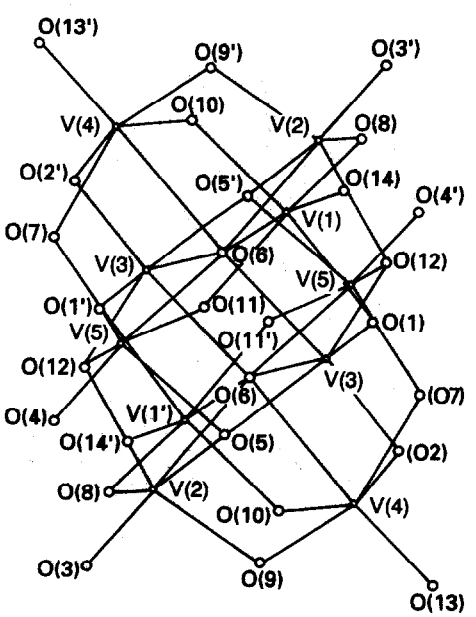

Fig. 1. View of the $V_{10}O_{28}^{6-}$ polyhedron.

atoms. In the polyanion the oxygen atoms may be divided into five classes in which eight oxygen atoms coordinate with only one vanadium atom in each VO^{3+} group; there are four oxygen atoms [O(5), O(5′), O(12) and O(12′)], each coordinates with three vanadium atoms; four bridge atoms involved in VO_2^+ groups coordinate two vanadiums each in an asymmetric way; 10 bridge atoms coordinate two vanadium atoms each and two oxygen atoms lie inside the $V_{10}O_{28}^{6-}$ group and coordinate with six vanadium atoms each.

From Table 2 and Fig. 1 we can recognize that each vanadium atom is coordinated by six oxygen atoms. The characteristic features of the bond type in oxovanadium species are the asymmetry of the V=O multiple bond in the axial direction, with respect to the opposite position, and the coordinate bonds around vanadium may be divided into three distinct classes (strong, medium and weak).

The decavanadic acid is a hexaprotic acid with

Table 3. The contact distances (Å) of nitrogen and oxygen in the crystal

N to O(decavanadate) and O(water)					
O(1)···N(13)	3.067(6)	(1)	O(1)···N(22)	3.094(5)	(2)
O(2)···N(13)	3.153(6)	(3)	O(2)···N(22)	2.906(4)	(4)
O(4)···N(23)	3.221(3)	(5)	O(5)···N(22)	3.244(3)	(6)
O(8)···N(12)	2.970(5)	(1)	O(8)···N(31)	3.172(7)	(4)
O(9)···N(11)	3.091(5)	(7)	O(9)···N(13)	2.945(5)	(7)
O(9)···N(32)	3.000(8)	(4)	O(10)···N(11)	2.990(8)	(4)
O(11)···N(22)	3.150(7)	(2)	O(12)···N(21)	2.938(5)	
O(13)···N(12)	2.984(10)	(4)	O(14)···N(31)	3.220(6)	
O(15)···N(31)	2.896(8)	(8)	O(15)···N(33)	2.844(4)	(8)
O(16)···N(12)	3.075(3)	(9)	O(17)···N(21)	2.993(5)	(10)
O(17)···N(32)	2.878(6)	(11)			
O(water) to O(decavanadate) and O(Water)					
O(15)···O(4)	2.883(8)	(12)	O(15)···O(7)	2.758(8)	(11)
O(16)···O(3)	2.870(9)	(11)	O(16)···O(14)	2.862(8)	(13)
O(17)···O(7)	2.929(7)		O(17)···O(16)	2.762(9)	(10)

(1) $x, y, 1+z$; (2) $1/2-x, 1/2-y, 3/2-z$; (3) $1-x, 1-y, 1-z$; (4) $1/2+x, 1/2-y, 3/2-z$; (5) $1/2-x, -1/2+y, 3/2-z$; (6) $3/2+x, -1/2+y, 1/2+z$; (7) $1+x, y, 1+z$; (8) $1/2+x, 1/2-y, -1/2+z$; (9) $1/2+x, 1/2-y, 1/2+z$; (10) $x, y, -1+z$; (11) $-1/2+x, 1/2-y, -1/2+z$; (12) $3/2-x, 1/2-y, 1/2-z$; (13) x, y, z.

six replaceable hydrogen atoms. Therefore, it may combine with protons or Lewis bases in different ways under varied conditions. In the title complex all the six protons of decavanadic acid are captured by six guanidine molecules so as to yield the bare species of $V_{10}O_{28}^{6-}$.

Table 2 provides a comparison of the V—O bond distances in $(CN_3H_6)_6[V_{10}O_{28}]\cdot 6H_2O$ and $Na_2[(CH_2)_6N_3NH]_2[H_2V_{10}O_{28}]\cdot 8H_2O$.[8] It can be seen from Table 2 that the V—O distances of the title complex (except a few V—O bonds) are shorter than these of $H_2V_{10}O_{28}^{4-}$. As the hydrogen in $H_2V_{10}O_{28}^{4-}$ belonged to O(12) the V(5)—O(12′) and V(4)—O(2) bonds have been shortened significantly from 2.039 and 2.096 Å (the values for $H_2V_{10}O_{28}^{4-}$) to 1.962 and 2.018 Å, respectively. This is a reasonable variation which is associated with a strong O(12)—H bond formation in $H_2V_{10}O_{28}^{4-}$.

As mentioned above, guanidine has a stronger capability of capturing protons than hexamethylenamine.

From Table 3 it can be seen that in directions away from the guanidine groups and the water groups, nitrogen and oxygen atoms of water molecules show close contacts in the ranges 2.906–3.244 and 2.758–2.929 Å, respectively, with oxygen atoms of the anions. The nitrogen atoms make contact with the oxygen atoms of water molecules in the range 2.844–3.075 Å, indicating strong hydrogen bonding to the water molecule. The O(17)···O(16) distance is 2.762 Å, which indicates that there is

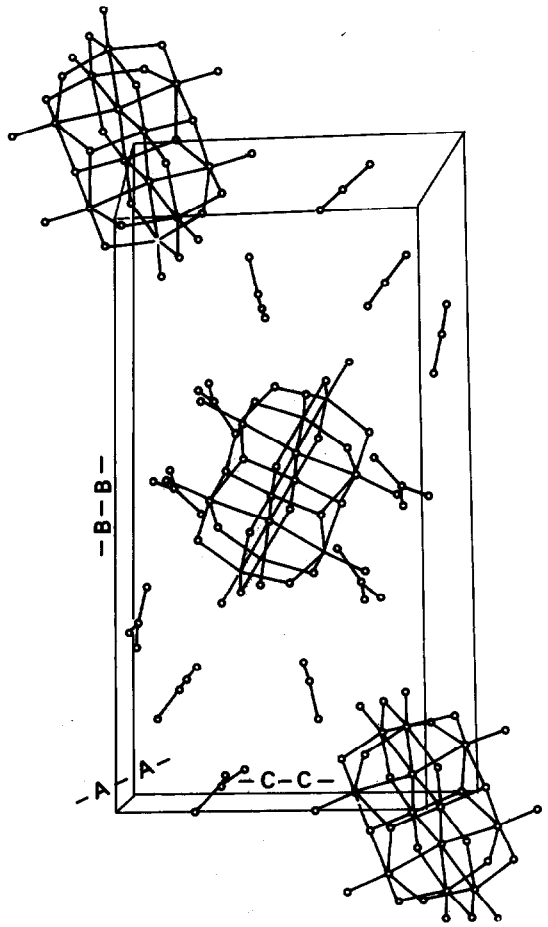

Fig. 2. The unit cell of $(CN_3H_6)_6[V_{10}O_{28}]\cdot 6H_2O$.

strong hydrogen bonding to the water molecules. In the anions all the oxygen atoms show close contacts with the nitrogen atoms of guanidine, except O(6) due to its central position in the polyanion. Therefore, in crystals decavanadate, guanidine and the crystal water are linked together by ionic forces and hydrogen, see Fig. 2.

REFERENCES

1. M. T. Pope, *Heteropoly and Isopoly Oxometalates*, p. 34. Springer Verlag, Berlin, Heidelberg (1983).
2. M. Shao, L. Wang, Z. Zhang and Y. Tang, *Sci. Sin., Ser B (Engl. Edn)* 1984, **5**, 137.
3. H. T. Evans, *Inorg. Chem.* 1966, **5**, 967.
4. A. G. Swallow, F. R. Ahmed and W. H. Barnes, *Acta Cryst.* 1966, **21**, 397.
5. A. Durif, M. T. Averbucb-Pouchot and J. C. Guitel, *Acta Cryst.* 1980, **B36**, 680.
6. Saf'yanov, N. Yu and N. V. Belov, *Soc. Phys. Dokl.* 1976, **21**, 176.
7. M. Shao, L. Wang, Z. Zhang and Y. Tang, *Fenzi Kexue yu Huaxue Yanjiu* (Chinese) 1983, **3**, 1.
8. M. Shao, L. Wang, Z. Zhang and Y. Tang, *Sci. Sin. Ser B (Chin. Edn)* 1985, **9**, 775.

Polyhedron Vol. 12, No. 1, pp. 83–88, 1993
Printed in Great Britain

0277–5387/93 $6.00+.00
© 1993 Pergamon Press Ltd

SYNTHESIS AND CHARACTERIZATION OF COPPER(II) AND NICKEL(II) COMPLEXES WITH LIGANDS HAVING $N_2S_2^*S_2$ (S* = THIOETHER) DONORS: PSEUDO-REVERSIBLE Cu^{III}/Cu^{II} COUPLE

R. SHUKLA, S. MANDAL and P. K. BHARADWAJ†

Department of Chemistry, Indian Institute of Technology, Kanpur 208016, India

(*Received* 2 *June* 1992; *accepted* 27 *August* 1992)

Abstract—Two new hexadentate ligands having thioether and thiolate groups in pairs along with two amide nitrogens have been synthesized. The thiols are protected as their tertiary butyl derivatives. On refluxing the ligands with a copper(II) or a nickel(II) salt in isopropanol, the S-tertiary butyl group was cleaved to form the corresponding hexa-coordinated neutral complex with the chromophore $M^{II}N_2S_2^*S_2$, where the four sulphurs are equatorial and the amide nitrogens are axial. Both the copper(II) complexes show pseudo-reversible responses (ΔE_p = 100 mV) in cyclic voltammograms with $E_{1/2}$ = 0.5 V vs S.C.E. at room temperature in acetonitrile, attributable to a Cu^{III}/Cu^{II} couple. The corresponding nickel(II) complex shows an irreversible response in the region −1.0 to +1.0 V. In their electronic spectra the copper(II) complexes show a strong band near 600 nm, attributable to a σ(thiolate) → Cu^{II} LMCT transition. Each of the copper(II) complexes show ligand field bands typical of a tetragonally distorted octahedral complex. The nickel(II) complexes show three ligand field bands typical of octahedral geometry.

Hexa-coordinated copper(II)-thiolates having the chromophore $CuN_2S_2^*S_2$ (S* = thioether), where the four sulphurs are equatorially bound and the two nitrogens are axially bound, have been reported by us.[1] This arrangement of donor atoms not only lowers the Cu^{II}/Cu^{I} couple, but also makes possible the generation of oxidized copper-thiolate systems electrochemically, which are metastable. Electrochemical studies showed that these oxidized species could be copper(III)-thiolate systems. The importance of these studies lies in the fact that copper(II) has been implicated[2] in the biochemical reactions of some copper proteins. To further probe whether the oxidation is metal centred or ligand based, we have synthesized the two new ligands L_1 and L_2. With copper(II) each forms a hexa-coordinated neutral complex. To identify possible ligand oxidations the corresponding nickel(II) complexes have also been synthesized and probed electrochemically. Besides, nickel has been established as an essential constituent of several hydrogenases.[3,4] Based on physicochemical techniques,[5–8] the nickel site is believed to have the metal ion in a distorted octahedral arrangement with 2/3 sulphur atoms and the rest are nitrogen or oxygen atoms. Nickel bonded to sulphur and nitrogen/oxygen are also present in carbon monoxide dehydrogenases.[9] These findings have stimulated interest in nickel chemistry with mixed sulphur and nitrogen donor ligands.[10–14] Thus, it was considered worthwhile to study nickel(II) complexes having sulphur and nitrogen donor ligands in an octahedral/pseudo-octahedral environment.

EXPERIMENTAL

Materials

Thiosalicylic acid, ethyl chloroformate (Fluka), 1,2-dibromoethane, 1,3-dibromopropane, copper(II) and nickel(II) salts (Aldrich) were reagent grade chemicals and were used as received without further purification. Triethylamine, t-butanol and all solvents were obtained from Glaxo laboratories and purified[15] prior to use. The physical measurements made on the complexes were per-

† Author to whom correspondence should be addressed.

formed as described earlier.[1] Elemental analyses were performed at the Central Drug Research Institute, Lucknow, India.

Syntheses of ligands and complexes

Syntheses of the ligands were achieved as schematically shown in Fig. 1.

S-t-Butylthiosalicylic acid. This was synthesized following a published procedure.[16] A solution of thiosalicylic acid (5 g, 3.2 mmol) in a mixture of 2 (N) hydrochloric acid (15 cm^3) and tertiary butyl alcohol (5 cm^3) was refluxed for 12 h. At the end of reflux excess alcohol and water were removed under reduced pressure. The remaining thick liquid upon cooling to room temperature solidified as a pale yellow solid and was washed several times with water. The solid upon recrystallization from a 1 : 1 ethanol–water mixture gave a pale yellow crystalline solid in 60% yield; m.p. 67–68°C. ^{1}H NMR (80 MHz, d^6-DMSO, δ_{TMS} ppm): 7.4 (m, 4H), aromatic; 1.2 (s, 9H), t-butyl.

1,2-*Bis*(O-*aminophenolthio*)*ethane* (*DAPTE*). The synthesis of this compound was achieved as described earlier.[1]

1,3-*Bis*(O-*aminophenolthio*)*propane*, (*DAPTP*). This compound was synthesized for the first time following the method used for DAPTE, starting with 1,3-dibromopropane and *o*-aminothiophenol.

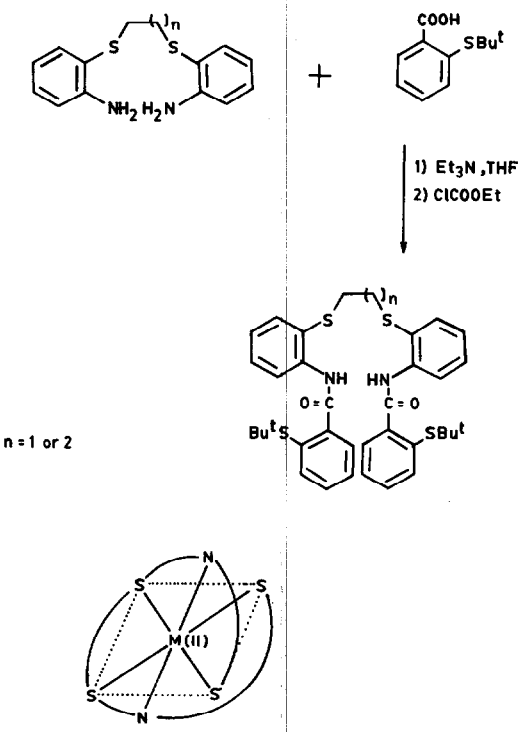

Fig. 1. Synthetic scheme for the ligand syntheses and binding mode of the ligands.

The product was obtained as a semi-solid in a 72% yield. ^{1}H NMR (80 MHz, $CDCl_3$, δ_{TMS} ppm): 7.1 (m, 8H), aromatic; 4.0 (sb, 4H), NH_2; 2.7 (t, 4H), SCH_2; 1.6 (m, 2H), CH_2.

Synthesis of the ligand L_1. This was synthesized by the mixed anhydride method.[1] To an ice cold solution of S-t-butyl thiosalicylic acid (2 g, 9.5 mmol) and triethylamine (0.96 g, 9.5 mmol) was slowly added ethylchloroformate (1.03 g, 9.5 mmol) mixed with THF (30 cm^3). The mixture was allowed to stir at ice cold temperature for 30 min and then allowed to react slowly with a THF solution (40 cm^3) of DAPTE (1.31 g, 4.7 mmol) in an argon atmosphere. The reaction mixture was brought to room temperature after 2 h and allowed to stir for 16 h. The colourless precipitate of triethylamine hydrochloride was filtered off and THF evaporated under reduced pressure to obtain a pale yellow semi-solid. This semi-solid product in $CHCl_3$ was washed several times with H_2O and finally all of the $CHCl_3$ removed in a rotary evaporator to obtain the desired product as a pale yellow semi-solid; yield 78%. ^{1}H NMR (80 MHz, $CDCl_3$, δ_{TMS} ppm): 7.2 (m, 16H), aromatic; 5.5 (sb, 2H), NH; 2.9 (s, 4H), CH_2; 1.3 (s, 18H), t-butyl.

Synthesis of the ligand L_2. The ligand L_2 was synthesized following the same method as used for L_1 using DAPTP and S-tertiary butyl thiosalicyclic acid. The product was obtained as a semi-solid in 75% yield. ^{1}H NMR (80 MHz, $CDCl_3$, δ_{TMS} ppm): 7.3 (m, 16H), aromatic; 6.2 (sb, 2H), NH; 2.8 (t, 4H), SCH_2; 1.6 (m, 2H), CH_2; 1.3 (s, 18H), t-butyl.

Syntheses of thiolato complexes of copper(II) *and nickel*(II). The metal complexes were synthesized by breaking the S-tertiary butyl linkages.[17,18]

Synthesis of **1**. The ligand L_1 (1 g, 1.5 mmol) was dissolved in ethanol (30 cm^3) and a solution of $CuCl_2 \cdot 2H_2O$ (0.26 g, 1.5 mmol) in ethanol (10 cm^3) was added with constant stirring at room temperature. The resulting solution was heated under reflux in a nitrogen atmosphere for 0.5 h until it became deep blue. The deep blue solution was reduced to *ca* 10 cm^3 volume by passing nitrogen through at room temperature. Finally, on keeping at 5°C for 2 h a dark blue powder separated, which was collected by filtration, washed with diethyl ether and dried *in vacuo*; yield 60%.

Synthesis of the copper(II) *complex* **2**. Complex **2** was synthesized by the same method as that adopted for **1**; yield 53%.

Synthesis of the nickel(II) *complex* **3**. $NiCl_2 \cdot 6H_2O$ (0.56 g, 2.3 mmol) and L_1 (1.5 g, 2.3 mmol) were dissolved in iso-butanol and heated under reflux in an argon atmosphere. The colour of the solution changed slowly to dark brown. After refluxing for a total of 2 h the solution was filtered,

Table 1. Analytical, EPR and magnetic susceptibility data for the complexes

Complex	μ_{eff}/μ_B	g_{av}[a]	Analysis (%) C	H	N	S
1	1.93	2.12	54.2(55.3)	3.8(3.6)	4.3(4.6)	21.2(21.0)
2	1.98	2.07	55.6(55.8)	3.7(3.9)	4.6(4.6)	20.0(20.6)
3	3.10		55.3(55.6)	3.4(3.6)	4.3(4.6)	21.2(21.2)
4	3.06		56.0(56.2)	4.0(3.9)	4.1(4.5)	20.8(20.7)

[a] The values given are those obtained on the solid samples at room temperature.

concentrated to *ca* 15 cm^3 and cooled to room temperature, whereupon a dark brown crystalline solid separated. The solid was collected by filtration and air-dried; yield 31%.

Synthesis of the nickel(II) *complex* **4**. Complex **4** was synthesized following the same method used for **3**; yield 34%.

All the complexes could be synthesized using other metal salts, such as acetate, nitrate, perchlorate, etc. Analytical data for the complexes are given in Table 1.

RESULTS AND DISCUSSION

The copper(II)-thiolates are air-stable in the solid state. In solution under argon they are stable for days. However, on exposure to air they are stable only for a few hours, after which they decompose slowly. The nickel(II) complexes are stable in the solid state as well as in solution. All the complexes are non-conducting in dichloromethane or in acetonitrile—the two solvents used in the conductivity measurements.

In the solid state as well as in acetonitrile (*ca* 1×10^{-3} M) **1** and **2** gave isotropic EPR spectra with $g_{av} > g_e$ (Table 1), which were not indicative of their structures. The room temperature magnetic moment values for the complexes were found to be within the normal ranges for hexa-coordinated discrete complexes.[19]

The electronic spectral data for the copper(II) complexes are shown in Table 2 while the spectrum of **1** is shown in Fig. 3. In the case of hexa-coordinated copper(II) complexes with moderate Jahn–Teller distortions, the lowest energy transition ($d_{z^2} \rightarrow d_{x^2-y^2}$) occurs[1,20] around 750–900 nm. In **1** and **2** a broad band appears with λ_{max} near 800 nm (Table 2), which is attributed to the lowest energy transition. Transitions from the components of t_{2g} to $d_{x^2-y^2}$ should then occur as a broad band at higher energy. Both **1** and **2** show a very strong band near 615 nm, which is responsible for their blue colour. In other $CuN_2S_2^*S_2$ (S* = thioether) complexes[1] this band is slightly blue shifted and occurs near 600 nm. This band has been identified[1] as due to a σ(thiolate) → copper(II) LMCT transition. The ligand field transition originating from t_{2g} to $d_{x^2-y^2}$ is not seen due to this intense band. The

Table 2. Cyclic voltammetric and electronic spectral data for the complexes

Complex	M^{III}/M^{II} couple $E_{1/2}$ (V)	ΔE_p (mV)	λ_{max} (nm) (ε/dm^3 mol^{-1} cm^{-1})
1	0.53	100	800(205), 620(2625), 525(sh), 420(2800), 305(7515)
2	0.48	120	805(sh),[a] 625(1520), 525(1315), 465(1575), 280(9615)
3	—	—	1035(40), 895(45), 670(145), 495(230), 295(11,800), 270(16,980)
4	—	—	1030(15), 875(15), 660(60), 490(240), 300(9900), 270(13,260)

[a] sh = shoulder.

high intensity (Table 2) of the band is due to a good overlap of the equatorially bound thiolate (Fig. 1) with the $d_{x^2-y^2}$ orbital of the copper(II) ion. Cu(DAPTP)Cl_2 shows only a small absorption around 600 nm. Molecular model studies also indicated that the complex will be least strained in the binding mode illustrated in Fig. 1. In this mode the four sulphurs are equatorially bound, while the two nitrogens are axially bound. An alternative mode of binding will make the thioethers and amide nitrogens equatorial and the thiolates axial. However, in this mode one carbonyl oxygen will come very close to the other. A similar diphenolate[21] also binds as shown in Fig. 1. A shoulder which appears near 525 nm (Table 2) is attributed to the lower energy π(thiolate) → copper(II) LMCT transition.[1,22]

Electronic absorption bands observed for the nickel(II) complexes **3** and **4** are also listed in Table 2 while the spectrum of **3** is shown in Fig. 4. Octahedral nickel(II) complexes show three spin-allowed ligand field transitions[23] corresponding to excitation from the $^3A_{2g}$ ground state to $^3T_{2g}$, $^3T_{1g}$ and $^3T_{1g}$(P) states. For an ideal octahedral coordination the intensities of these *d–d* bands lie below 30 M^{-1} cm^{-1}. As the geometry distorts from ideal centrosymmetric, the intensities of these bands increase and may result in splitting of some of the bands.[24] The intensities of the ligand field bands in **3** and **4** (Table 2) are consistent with their structures, which are almost regular octahedral. For both the nickel(II) complexes the solvent had no effect in the appearance of the electronic spectral bands. This means that the ligands encapsulate the metal ion, leaving no vacant site for possible solvent interactions.

Cyclic voltammograms for the complexes **1** and **2** in acetonitrile (*ca* 1×10^{-3} M) are shown in Figs 2 and 3. Both the copper(II) complexes show quasi-reversible responses with $E_{1/2}$ near +0.53 V vs S.C.E. and $\Delta E_p \simeq 100$ mV. The following characteristics were observed: the ratio $i_{pa}/i_{pc} = 1.0$ within experimental error for different scan rates, the ratio $i_{pc}/v^{1/2}$ is practically constant and the peak separation, ΔE_p, increases slowly with an increase in the scan rate. To identify possible ligand oxidations, the corresponding nickel(II) complexes **3** and **4** were subjected to cyclic voltammetric investigations. None of these complexes showed any well-defined peaks in the region −1.0 to +1.0 V. Only a broad anodic peak appears at *ca* 1.0 V, but on scan reversal no peak appears. This indicates that the oxidized species undergo rapid chemical decomposition once generated electrochemically. We, therefore, assign this quasi-reversible response to the following redox

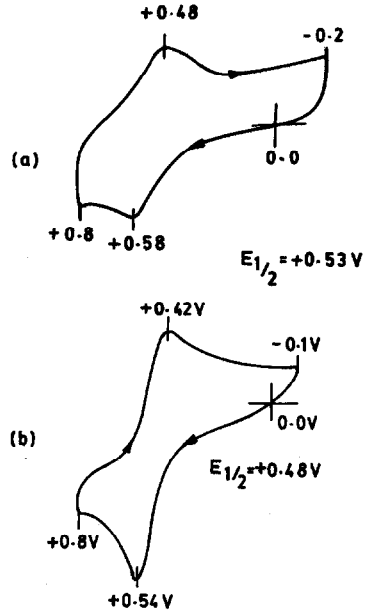

Fig. 2. Cyclic voltammograms for the copper(II) complexes in DMF at the scan rate of 100 mV s^{-1}, using a glassy carbon working electrode and TBAP as the supporting electrolyte: (a) complex **1**, (b) complex **2**.

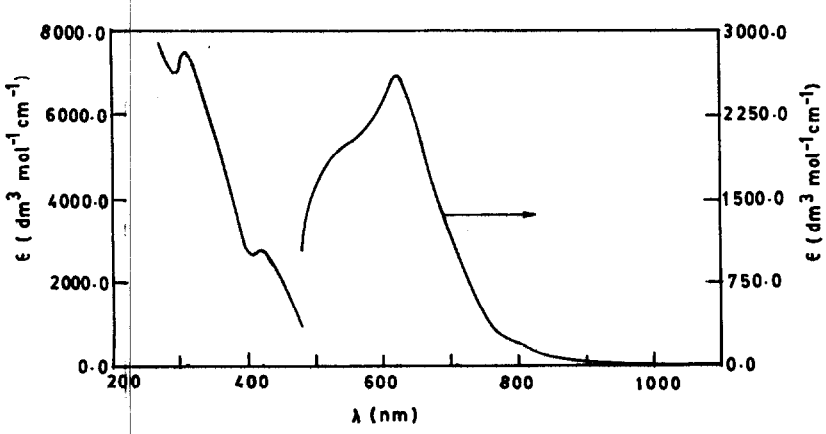

Fig. 3. Electronic spectrum for the copper(II) complex **1** in DMF.

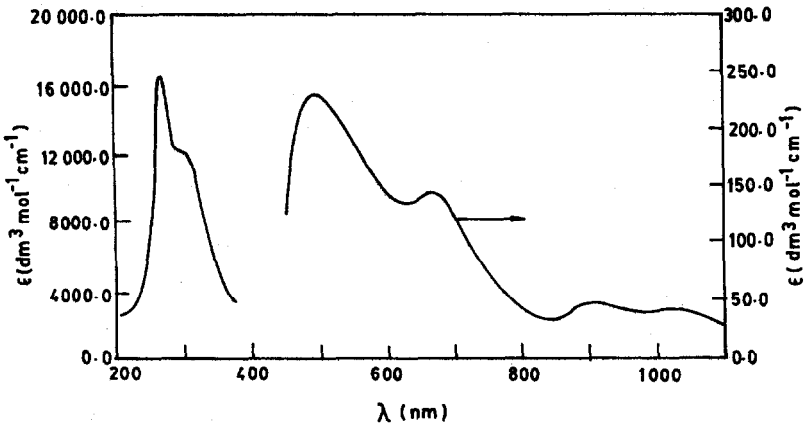

Fig. 4. Electronic spectrum for the nickel(II) complex **3** in DMF.

reactions:

$$1^+ + e^- = 1$$

$$2^+ + e^- = 2.$$

On scanning further on either side, none of the copper(II) complexes showed any well-defined cyclic response. However, when scanned in the negative direction beyond −0.9 V a broad peak appears and on scan reversal an intense peak centring around −0.2 V appears, which is attributable[25] to the oxidation of copper deposited at the electrode. As the data shown in Table 2 indicate, complex **2** is easier to oxidize compared to complex **1**. Both the ligands' donor atoms are somewhat rigid due to the aromatic rings. However, ligand L_2 is less rigid as the thioethers are separated by three carbon atoms, therefore enabling easier self-reorganization upon oxidation, resulting in a lower $E_{1/2}$ value.

CONCLUSION

Hexa-coordinated copper(II) and nickel(II) complexes have been synthesized. The copper complexes are tetragonal and show a quasi-reversible Cu^{III}/Cu^{II} couple while the nickel(II) complexes do not show any well-defined peaks in their cyclic voltammograms. The generation of copper(III) in the cyclic voltammetric time-scale may be associated with the strong equatorial ligation by four sulphur donors, as also observed in the previous cases.[1]

Acknowledgement—We thank the Department of Science and Technology, New Delhi, India, for financial support.

REFERENCES

1. S. Mandal and P. K. Bharadwaj, *Polyhedron* 1992, **11**, 1037; S. Mandal, R. Shukla and P. K. Bharadwaj, *Polyhedron* 1992, **11**, 1855.
2. D. W. Margerum and G. D. Owens, *Metal Ions Biol. Syst.* 1981, **12**, 75.
3. A. J. Thompson, *Nature* 1982, **298**, 602; R. P. Hausinger, *Microbiol. Rev.* 1987, **51**, 22; R. Cammack, in *The Bioinorganic Chemistry of Nickel* (Edited by J. R. Lancaster Jr), Ch. 8. VCH Publishers, New York (1988).
4. J. J. G. Moura, I. Moura, M. Teixeira, A. V. Xavier, G. D. Fauque and J. LeGall, *Metal Ions Biol. Syst.* 1988, **23**, 285.
5. M. K. Eidsnes, R. A. Scott, B. C. Prickril, D. V. DeVartanian, J. LeGall, I. Moura, J. J. Moura and H. D. Peck Jr, *Proc. Natl. Acad. Sci. USA* 1989, **86**, 147.
6. P. A. Lindahl, N. Kojima, R. P. Hausinger, J. A. Fox, B. K. Teo, C. T. Walsh and W. H. Orme-Johnson, *J. Am. Chem. Soc.* 1984, **106**, 3062; R. A. Scott, S. A. Wallin, M. Czechowski, D. V. DeVartannian, J. LeGall, H. D. Peck Jr and I. Moura, *J. Am. Chem. Soc.* 1984, **106**, 6864.
7. A. Chapman, R. Cammack, E. C. Hatchikian, J. McCracken and J. Peisach, *FEBS Lett.* 1988, **242**, 135.
8. M. Teixeira, I. Moura, A. V. Xavier, B. H. Huynh, D. V. DeVartanian, H. D. Peck Jr, J. LeGall and J. J. Moura, *J. Biol. Chem.* 1985, **260**, 8942; R: Camack, D. Patil, E. C. Hatchikian and V. M. Fernandez, *Biochim. Biophys. Acta* 1987, **912**, 98; M. Teixeira, I. Moura, A. V. Xavier, J. J. G. Moura, J. LeGall, D. V. DerVartanian, H. D. Peck Jr and B. H. Huynh, *J. Biol. Chem.* 1989, **264**, 16435.
9. S. W. Ragsdale, L. G. Ljungdahl and D. V. DerVartanian, *Biochem. Biophys. Res. Commun.* 1983, **115**, 658.
10. D. Ray, S. Pal and A. Chakravorty, *Inorg. Chem.* 1986, **25**, 2674; S. Bhanja Chaudhury, D. Ray and A. Chakravorty, *Inorg. Chem.* 1990, **29**, 4603; S. Bhanja Chaudhury, D. Ray and A. Chakravorty, *Inorg. Chem.* 1991, **30**, 4354.
11. H. J. Krugar and R. H. Holm, *J. Am. Chem. Soc.* 1990, **112**, 2955 and refs therein.
12. S. Fox, Y. Wang, A. Silver and M. Millar, *J. Am. Chem. Soc.* 1990, **112**, 3218.

13. M. Zimmer, G. Schulte, X. L. Luo and R. H. Crabtree, *Angew. Chem., Int. Edn Engl.* 1991, **30**, 193.
14. N. Baidya, D. Ndreu, M. M. Olmstead and P. K. Mascharak, *Inorg. Chem.* 1991, **30**, 2448 and refs therein.
15. D. D. Perrin, W. L. F. Armarego and D. R. Perrin, *Purification of Laboratory Chemicals*, 1st edn. Pergamon Press, Oxford (1966).
16. J. J. Pastuszak and A. Chimiak, *J. Org. Chem.* 1981, **46**, 1868.
17. J. Becher, H. Toftlund and P. H. Olesen, *J. Chem. Soc., Chem. Commun.* 1983, 740.
18. T. Yamamura, M. Tadokoro and R. Kuroda, *Chem. Lett.* 1989, 1245.
19. F. A. Cotton and G. Wilkinson, *Advanced Inorganic Chemistry*, 5th edn, Part 3. John Wiley, New York (1988).
20. M. A. Hitchman and T. D. Waite, *Inorg. Chem.* 1976, **15**, 2150.
21. R. D. Cannon, B. Chiswell and L. M. Venanzi, *J. Chem. Soc.* (*A*) 1967, 1277.
22. K. W. Penfield, A. A. Gewirth and E. I. Solomon, *J. Am. Chem. Soc.* 1985, **107**, 4519.
23. A. B. P. Lever, *Inorganic Electronic Spectroscopy*, 2nd edn, pp. 507–511. Elsevier, New York (1984) and refs therein.
24. B. J. Hathaway and A. E. Underhill, *J. Chem. Soc.* (*A*) 1961, 3091.
25. M. I. Pilo, G. Manca, M. A. Zoroddu and R. Seeber, *Inorg. Chim. Acta* 1991, **180**, 225.

Polyhedron Vol. 12, No. 1, pp. 89–94, 1993
Printed in Great Britain

0277–5387/93 $6.00+.00
© 1993 Pergamon Press Ltd

REACTIONS OF $As(NMe_2)_3$ AND $Sb(NMe_2)_3$ WITH ALUMINUM AND MAGNESIUM ALKYLATING AGENTS

C. J. THOMAS, L. K. KRANNICH* and C. L. WATKINS

Department of Chemistry, University of Alabama at Birmingham, AL 35294, U.S.A.

(*Received* 26 *May* 1992; *accepted* 18 *August* 1992)

Abstract—The reactions of aluminum alkyls, R_3Al (R = Me, Et, Pr^n, Bu^n and Bu^i), with $As(NMe_2)_3$ and $Sb(NMe_2)_3$ have been used to synthesize the respective tertiary arsines, R_3As, and tertiary stibines, R_3Sb, in good yields. $As(NMe_2)_3$ also reacts with Grignard reagents, RMgX (R = Et, Pr^n, Pr^i, Bu^n, Bu^i, Bu^t, $CH_2{=}CH{-}$, $CH_3CH{=}CH{-}$, $Me_3SiCH_2{-}$, Ph, *p*-tolyl and mesityl), to give R_3As. Complete ^{13}C and ^1H NMR spectral data on the synthesized R_3Sb and $[R_2AlNMe_2]_2$ are also reported.

Our recent studies on the reactivity of Me_3Al with $Me_{3-n}As(NMe_2)_n$ ($n = 1$–3) established the formation of a mono Al—N—As adduct with Me_2AsNMe_2, mono and bis Al—N—As adducts with $MeAs(NMe_2)_2$ and $As(NMe_2)_3$, and an Al—As adduct of $As(NMe_2)_3$ at −95°C.[1] Subsequent Al—N adduct decomposition with Me moiety transfer from the aluminum to the arsenic atom and As—N bond cleavage gave the next higher Me homologue in the $Me_{3-n}As(NMe_2)_n$ series and $[Me_2AlNMe_2]_2$. From this study, we designed novel and improved high-yield synthetic routes to Me_3As[1] and heteroleptic[2] tertiary arsines.

$$R_3Al + Me_2AsNMe_2 \longrightarrow Me_2AsR + 1/2[R_2AlNMe_2]_2$$

We have been interested for some time in the general reactivity of various alkylating agents with the aminoarsines as potential synthesis routes to organoarsines and have now extended these studies to the aminostibines.

The general synthetic routes to homoleptic tertiary arsines have been previously summarized and the primary literature cited.[3–6] These consist of the reactions of AsX_3 (X = halogen) with Grignard reagents, alkyl lithium, trialkylaluminum, dialkyl zinc and $LiAlR_4$. Yields of R_3As are variable and dependent upon the method used. Trialkylaluminum reagents alkylate As_2O_3 to give moderate yields of the tertiary arsines. They can also be prepared by treating As_2O_3, As_2S_3, arsenic thioacid esters and trialkylarsenites with Grignard reagents. A limited number of tertiary arsines have been synthesized via the reaction of elemental arsenic with SnR_4[7] and alkyl radicals.[8] Our recent studies on the reactions of $\overline{OCH_2CH_2OAs}Cl$ with organoaluminum, -magnesium, -lithium or -zinc reagents established a new general high-yield synthetic route[4] to the tertiary arsines, R_3As.

As in the tertiary arsine syntheses, SbX_3 (X = halogen) serves as a general reagent for the synthesis of R_3Sb. The reactions of SbX_3 with RMgX,[6] R_3Al,[9] $LiAlR_4$,[10] R_4Pb[11] and $(NH_4)_2(RSiF_5)$[12] produce R_3Sb in 45–85% yield. Reactions of Sb_2O_3 with R_3Al give 62–89% yields of R_3Sb, where R = Et, Bu^n, Bu^i and Hex^i.[13] Trimethyl and ethyl stibines have been prepared by the action of Me and Et radicals on elemental antimony.[8] Also, Me_3Sb has been synthesized by heating powdered antimony with Me_2Hg in the presence of $HgCl_2$.[14] The reactions of $(Me_2N)_3Sb$ with RMgX and RLi produce tertiary stibines in 66–78% yield.[15]

In this paper we report a study on the reactivity of $As(NMe_2)_3$ and $Sb(NMe_2)_3$ with R_3Al. From these studies, we obtain good yields of the respective R_3As and R_3Sb compounds (R = Me, Et, Pr^n, Bu^n, Bu^i). The other reaction product, $[R_2AlNMe_2]_2$, has also been isolated and characterized. This paper also gives the ^1H and ^{13}C NMR data on the synthesized tertiary stibines and aminoalanes. In addition, the reactivity of $As(NMe_2)_3$ with RMgX

* Author to whom correspondence should be addressed.

has been studied as an alternate route to R_3As. The merits and limitations of these synthetic routes are discussed. The relative reactivities of $As(NMe_2)_3$ and $Sb(NMe_2)_3$ towards R_3Al are compared.

EXPERIMENTAL

A Vacuum Atmospheres Model HE-43 Dri-lab equipped with a model HE-493 Dri-train was used for the storage and handling of all reagents and products. All reactions and work-ups were carried out under dry nitrogen using common Schlenk techniques. $As(NMe_2)_3$[16] was synthesized by the aminolysis of $AsCl_3$, while $Sb(NMe_2)_3$[17] was prepared by the amination of $SbCl_3$. These were purified by spinning band column distillation and their purities were checked by NMR spectroscopy prior to use. Aluminum alkyls were purchased from Ethyl Corporation and Texas Alkyls. The Grignard reagents, $LiNMe_2$, $AsCl_3$ and $SbCl_3$, were purchased from Aldrich Chemicals, Inc. and used as obtained. Dimethylamine (anhydrous) was purchased from Matheson and used as obtained. Solvents (pentane, Et_2O) were dried over sodium metal, distilled and stored over molecular sieves. Chloroform-d (MSD), benzene-d_6 (MSD) and Me_4Si (Aldrich) were stored over molecular sieves.

The IR spectra of the liquid compounds were recorded neat and of the solid as Kei—F and Nujol mulls on KBr plates using a Nicolet IR/42 FT spectrophotometer. Low-resolution EI-MS data were obtained on a HP 5986A GC/MS spectrometer at 70 eV with a 2400 V electron multiplier. Samples of tertiary arsines and tertiary stibines were introduced into the GC probe as C_6H_6 solutions, while aminoalanes were introduced by the direct insertion probe method.

The NMR spectral data were obtained on a GE(Nicolet) 300 MHz multinuclear FT-NMR spectrometer operating at 300.1 and 75.5 MHz for ^1H and ^{13}C, respectively. Spectra were collected at 24°C using 0.2 M chloroform-d (R_3As) and benzene-d_6 (R_3Sb and $[R_2AlNMe_2]_2$) solutions of the samples with TMS as the internal reference. ^{13}C coupled, $\{^1H\}$ decoupled and APT[18] spectra were obtained for each of the compounds. The ^1H NMR data of the tertiary stibines and aminoalanes are reported in Table 1, while the respective ^{13}C data are given in Table 2. References to earlier reported NMR data are noted in the tables. The NMR data on the tertiary arsines have been previously reported.[4]

All the compounds, except $[Bu^i_2AlNMe_2]_2$, have been mentioned in the literature. Satisfactory carbon, hydrogen and nitrogen analyses were obtained for $[Bu^i_2AlNMe_2]_2$ from E&R Microanalytical Laboratory, Inc., Corona, New York. Found: C, 64.7; H, 12.8; N, 7.7. Calc. for C, 64.9; H, 13.0; N, 7.6%. Melting points were determined in sealed capillaries and were not corrected. All the tertiary arsines that were obtained in this study were previously well-determined.[4] Our NMR, IR and MS data are in excellent agreement with the earlier data.[4] The IR[30,31] and mass spectral data[32,33] of the tertiary stibines are also in very good agreement with the earlier reported values.

IR data

Previously unreported IR data for the aminoalanes synthesized in this study are as follows:

$[Et_2AlNMe_2]_2$. 2984(vs), 2844(vs), 2797(vs), 2725(m), 2687(w), 1478(vs), 1459(vs), 1408(vs), 1375(m), 1234(vs), 1190(vs), 1164(vs), 1120(vs), 1066(s), 1045(vs), 981(vs), 953(vs), 897(vs), 672(vs,br), 588(vs,br), 550(vs), 522(vs), 493(vs) cm^{-1}.

Table 1. ^1H NMR chemical shifts (ppm, TMS) of stibines and aminoalanes

Compound	H(1)	H(2)	H(3)	H(4)	NMe_2
Me_3Sb[19,20]	0.59(s)	—	—	—	—
Et_3Sb[21,22]	1.19(m)	1.19(m)	—	—	—
Pr^n_3Sb	1.32(m)	1.55(m)	0.97(t)	—	—
Bu^n_3Sb	1.36(m)	1.53(m)	1.36(m)	0.90(t)	—
Bu^i_3Sb	1.40(d)	1.86(m)	1.01(d)	1.01(d)	—
$Sb(NMe_2)_3$[17]	—	—	—	—	2.76(s)
$[Me_2AlNMe_2]_2$[23–25]	−0.58(s)	—	—	—	2.05(s)
$[Et_2AlNMe_2]_2$[26]	0.10(q)	1.26(t)	—	—	2.10(s)
$[Pr^n_2AlNMe_2]_2$	0.12(m)	1.58(m)	1.17(t)	—	2.09(s)
$[Bu^n_2AlNMe_2]_2$	0.15(m)	1.53(m)	1.53(m)	1.07(t)	2.14(s)
$[Bu^i_2AlNMe_2]_2$	0.18(d)	2.05(m)	1.12(d)	1.12(d)	2.12(s)

Table 2. ^{13}C NMR chemical shifts (ppm, TMS) of stibines and aminoalanes[a]

Compound	C(1)	C(2)	C(3)	C(4)	NMe_2
Me_3Sb[27]	−3.57(131.6)	—	—	—	—
Et_3Sb[27b]	5.86(132.3)	11.81(127.0)	—	—	—
$Pr^n{}_3Sb$	17.60	21.63	18.24(124.7)	—	—
$Bu^n{}_3Sb$[27]	14.74(128.2)	30.45	26.83(125.0)	13.92(124.4)	—
$Bu^i{}_3Sb$	28.69(129.0)	28.18(125.9)	25.97(124.4)	25.97(124.4)	—
$Sb(NMe_2)_3$	—	—	—	—	40.83(132.6)
$[Me_2AlNMe_2]_2$[1,28,29]	−12.0	—	—	—	41.46(135.5)
$[Et_2AlNMe_2]_2$[29]	−1.5	9.40(124.3)	—	—	41.29(135.4)
$[Pr^n{}_2AlNMe_2]_2$	11.32	19.58(123.8)	21.38(123.6)	—	41.60(135.3)
$[Bu^n{}_2AlNMe_2]_2$	7.90	28.50(124.1)	29.71(124.9)	14.27(124.0)	41.63(135.3)
$[Bu^i{}_2AlNMe_2]_2$	20.94	26.47(124.8)	28.88(123.4)	28.88(123.4)	42.57(135.4)

[a] ^1J(CH) (Hz) in parentheses.
[b] Assignments are reversed in ref. 27.

$[Pr^n{}_2AlNMe_2]_2$. 2984(s), 2953(vs), 2922(vs), 2890(vs), 2859(vs), 2812(vs), 2797(vs), 2781(m), 1477(vs), 1459(vs), 1408(m), 1470(m), 1323(s), 1234(vs), 1206(w), 1166(vs), 1122(vs), 1041(vs), 1019(m), 1004(w), 975(m), 943(w), 900(vs), 882(m,sh), 770(w), 681(vs), 640(vs), 616(vs), 572(s), 523(vs) cm^{-1}.

$[Bu^n{}_2AlNMe_2]_2$. 2984(m,sh), 2953(vs), 2906(vs), 2875(vs), 2843(vs), 2812(m), 2792(m), 1478(m), 1459(vs), 1403(w), 1375(m), 1290(w), 1234(s), 1160(m), 1150(m), 1122(vs), 1075(w,sh), 1057(m), 1047(vs), 990(w), 953(w), 907(vs), 878(w), 869(w), 850(w), 691(s), 616(vs), 578(m), 522(vs) cm^{-1}.

$[Bu^i{}_2AlNMe_2]_2$. 2997(vs), 2950(vs), 2865(bvs), 2800(vs), 2781(vs), 2772(vs), 2716(m), 2641(w), 2603(m), 1477(vs), 1401(vs), 1378(vs), 1361(vs), 1321(vs), 1231(vs), 1286(m), 1182(vs), 1157(vs), 1119(vs), 1062(vs), 1044(vs), 1012(vs), 944(m), 900(vs), 813(s), 675(vs), 637(vs), 594(vs), 525(vs), 431(m) cm^{-1}.

Reactions of $As(NMe_2)_3$ *and* $Sb(NMe_2)_3$ *with* R_3Al

The respective trialkylaluminum, R_3Al (0.15 mol), was slowly added with stirring over a period of 2 h to a sample of $As(NMe_2)_3$ or $Sb(NMe_2)_3$ (0.05 mol) at 0°C. The reaction mixture was slowly warmed to room temperature, stirred for 4 h, and then heated for 12–24 h (see Tables 3 and 4). The optimum reaction conditions were determined by monitoring the reaction mixture with NMR spectroscopy. Fractional distillation gave R_3As or R_3Sb. The aminoalane $[R_2AlNMe_2]_2$ was isolated from the reaction residue by further distillation (R = Et, Pr^n, Bu^n) or sublimation (R = Me, Bu^i).

Table 3. Results obtained from the reactions of $Sb(NMe_2)_3$ with R_3Al

Aluminum alkyl	Reaction conditions	Compounds isolated	Yield (%)	B.p./m.p. (°C/mm Hg)
Me_3Al	12 h/120°C	Me_3Sb	82	48/270
		$[Me_2AlNMe_2]_2$	93	153[a]
Et_3Al	12 h/120°C	Et_3Sb	83	64/26
		$[Et_2AlNMe_2]_2$	89	42/< 1
$Pr^n{}_3Al$	12 h/120°C	$Pr^n{}_3Sb$	80	80/8
		$[Pr^n{}_2AlNMe_2]_2$	91	68/< 1
$Bu^n{}_3Al$	12 h/120°C	$Bu^n{}_3Sb$	87	52/< 1
		$[Bu^n{}_2AlNMe_2]_2$	95	121/< 1
$Bu^i{}_3Al$	12 h/120°C	$Bu^i{}_3Sb$	63	58/< 1
		$[Bu^i{}_2AlNMe_2]_2$	95	46[a]

[a] Melting point.

Table 4. Results obtained from the reactions of $As(NMe_2)_3$ with R_3Al and RMgX

R	Synthetic route[a]	Reaction conditions	Arsine formed	Yield (%)	B.p./m.p. (°C/mm Hg)
Et—	A	12 h/reflux	Et_3As	80	140/76
	B	12 h/120°C		88	
Pr^n—	A	12 h/reflux	$Pr^n{}_3As$	80	73/8
	B	24 h/150°C		60	
Pr^i—	A	12 h/reflux	$Pr^i{}_3As$	10[b]	
Bu^n—	A	12 h/reflux	$Bu^n{}_3As$	78	102/8
	B	24 h/150°C		88	
Bu^i—	A	12 h/reflux	$Bu^i{}_3As$	10[b]	95/8
	B	24 h/150°C		45	
Bu^t—	A	12 h/reflux	—	—	—
CH_2=CH—	A	12 h/reflux	$(CH_2{=}CH)_3As$	60	55/85
CH_3CH=CH—	A	12 h/reflux	$(Allyl)_3As$	80	111/50
Me_3SiCH_2—	A	12 h/reflux	—	—	—
Ph—	A	12 h/reflux	Ph_3As	70	61[c]
p-tolyl—	A	12 h/reflux	$(p\text{-tolyl})_3As$	78	146[c]
mesityl—	A	12 h/reflux	—	—	—

[a] A = Organomagnesium; B = organoaluminum.
[b] Percentage conversion from NMR data.
[c] Melting point.

Yield and m.p./b.p. data are given in Tables 3 and 4.

Reactions of $As(NMe_2)_3$ *with* RMgX

The respective Grignard reagent (0.15 mol) in Et_2O or pentane (100 cm^3) was added to a stirred 0°C solution of $As(NMe_2)_3$ (0.05 mol) in Et_2O or pentane (200 cm^3) over a period of 1 h. The reaction mixture was warmed to room temperature and refluxed for 12 h. Degassed, saturated, aqueous NH_4Cl solution (200 cm^3) was added to hydrolyse any unreacted Grignard reagent. The organic layer was separated and dried over anhydrous Na_2SO_4. After removal of most of the solvent by distillation, the arsine was purified by distillation on a spinning band column. The b.p. and yield data are given in Table 4.

NMR study on the reactions of $As(NMe_2)_3$ *and* $Sb(NMe_2)_3$ *with* R_3Al

R_3Al (1.5 mmol in 2 cm^3 of benzene-d_6) was added to a screw type 10 mm NMR tube (pyrex, Wilmad) containing 0.5 mmol of $As(NMe_2)_3$ or $Sb(NMe_2)_3$ in benzene-d_6 (1 cm^3). The room-temperature ^1H and ^{13}C NMR spectra of the reaction mixture were then recorded at regular time intervals.

RESULTS AND DISCUSSION

Tables 3 and 4 summarize the results obtained from the alkylation reactions of $Sb(NMe_2)_3$ and $As(NMe_2)_3$ with R_3Al, respectively. Both tertiary stibines, R_3Sb (63–87%), and arsines, R_3As (45–88%), are isolated in comparable yields. The NMR spectra of the reaction mixture at 25°C indicate the consumption of starting materials and the presence of R_3As or R_3Sb, $[R_2AlNMe_2]_2$ and Al—N—As or Al—N—Sb bonded species. Thus, heating was essential (see Tables 3 and 4) to achieve complete conversion to R_3As or R_3Sb and $[R_2AlNMe_2]_2$. In the aminostibine reactions the conversion to R_3Sb and $[R_2AlNMe_2]_2$ was more facile than with the aminoarsines. This observation is in agreement with the results of studies on the reactivity of $As(NMe_2)_3$ and $Sb(NMe_2)_3$ towards SO_2,[34] carbonyl compounds[35] and ethylacetate[36] and insertion reactions with amino–imino boranes[37] and ketenes.[38] By analogy to the synthesis of the Me_2AsR arsines,[2] only about a 50% yield of the arsine/stibine results when the distillation is carried out by heating the reaction mixture to *ca* 30°C above the reported boiling point of the product arsine/stibine. Higher yields are obtained by further raising the temperature and reducing the pressure. The yields of $Bu^i{}_3As$ and $Bu^i{}_3Sb$ are much lower than those of the n-butyl analogues. This is also the case in the reported syntheses of $Bu^i{}_3Sb$ (71%) and $Bu^n{}_3Sb$

Table 5. Comparison of yields from R_3Sb syntheses

R	$(Me_2N)_3Sb/R_3Al$	Yield of R_3Sb (%) $(Me_2N)_3Sb/RMgX$ or RLi	$SbCl_3AlR_3$	$SbCl_3/RMgX$
Me	82	—	—	60–70[6]
Et	83	63–66[15]	71[9]	80–85[6]
Pr^n	80	—	66[9]	60–70[6]
Bu^n	87	78[15]	—	70[6]
Bu^i	63	—	77[9]	32[6]

(87%) from the reaction of R_3Al with Sb_2O_3.[13] The yields of R_3Sb from the alkylation of $Sb(NMe_2)_3$ with R_3Al are better than those reported for Grignard (EtMgBr) and alkyl lithium (EtLi and Bu^nLi) alkylating reagents (see Table 5).[15]

The aminoalanes, $[R_2AlNMe]_2$ (R = Me, Et, Pr^n, Bu^n, Bu^i) which are the other products from these reactions, have been isolated in excellent yield. Both $[Me_2AlNMe_2]_2$[28,39–44] and $[Et_2AlNMe_2]_2$[26,29,45] are well-known and well-characterized. The Pr^n[46] and Bu^n[46,47] homologues have been briefly mentioned in the literature and characterized as dimers by cryoscopic molecular weight studies. Our mass spectral data were consistent with the dimeric nature of R_2AlNMe_2 and comparable to the previously reported data for $[Et_2AlNMe_2]_2$.[45] Their spectra show very weak molecular ion peaks. High intensity [M—R] peaks correspond to the loss of the alkyl group bound to the aluminum. The IR spectral data are consistent with those reported for $[Me_2AlNMe_2]_2$.[41] The ν(Al—N) peaks are observed in the region 520–525 cm^{-1}, which is similar to the ν(Al—N) value of 508 cm^{-1} reported for $[Me_2AlNMe_2]_2$.[41]

The results from the reactions of $As(NMe_2)_3$ with the Grignard reagents are summarized in Table 4. Seven of the 12 Grignard reagents gave tertiary arsines, R_3As (R = Et, Pr^n, Bu^n, $CH_2{=}CH{-}$, $CH_3{-}CH{=}CH{-}$, Ph and *p*-tolyl) in 60–80% yield. Although with R = Pr^i, Bu^i, $Me_3SiCH_2^-$ and mesityl there is NMR evidence that the reaction proceeds, we could not isolate the respective tertiary arsines. This is presumably due to incomplete alkylation on the arsenic and probably results from the steric bulk of the R groups. Thus, this method is useful for synthesizing tertiary arsines with less sterically hindered substituents. Possibly these results can be exploited as a potential route to heteroleptic tertiary arsines by first treating $As(NMe_2)_3$ with a sterically bulky Grignard reagent and then with an appropriate amount of a less bulky alkylating agent. For example, we have shown that the reactions of Me_2AsNMe_2 with a wide range of Grignard reagents produce very good yields of heteroleptic tertiary arsines, Me_2AsR.[2] Interestingly, in the reported reaction of $\overline{OCH_2CH_2OAsCl}$ with RMgX tertiary arsines, R_3As, are readily obtained[4] in excellent yield (60–95%) even with bulky R groups.

REFERENCES

1. L. K. Krannich, C. L. Watkins and D. K. Srivastava, *Polyhedron* 1990, **9**, 289.
2. C. J. Thomas, L. K. Krannich and C. L. Watkins, *Synth. React. Inorg. Met–Org. Chem.* 1992, **22**, 461.
3. M. Dub (Editor), *Organometallic Compounds: Methods of Synthesis, Physical Constants and Chemical Reactions. Compounds of As, Sb and Bi*, Vol. 3, 2nd edn. Springer Verlag, New York (1968).
4. D. K. Srivastava, L. K. Krannich and C. L. Watkins, *Inorg. Chem.* 1990, **29**, 3502.
5. W. R. Cullen, in *Advances in Organometallic Chemistry*, Vol. 4, p. 145. Academic Press, New York (1966).
6. G. O. Doak and L. D. Freedman, *Organometallic Compounds of Arsenic, Antimony, and Bismuth*. John Wiley & Sons, Inc., New York (1970).
7. H. Schumann, H. Kopf and H. Schmidt, *Z. Anorg. Allg. Chem.* 1964, **331**, 220.
8. F. A. Paneth and H. Loleit, *J. Chem. Soc.* 1935, 366.
9. L. I. Zakarkin and O. Yu. Okhlobystin, *Bull. Acad. Sci. USSR. Div. Chem. Sci. (Engng)* 1959, 1853.
10. R. S. Dickson and B. O. West, *Aust. J. Chem.* 1962, **15**, 710.
11. M. Wieber, D. Wirth and I. Fetzer, *Z. Anorg. Allg. Chem.* 1983, **505**, 134.
12. R. Muller and C. Dathe, *Chem. Ber.* 1966, **99**, 1609.
13. W. Stamm and A. Breindel, *Angew. Chem., Int. Edn Engl.* 1964, **3**, 1.
14. S. J. W. Price and J. P. Richard, *Can. J. Chem.* 1972, **50**, 966.
15. K. Kiennemann, G. Levy and C. Taniélian, *J. Organomet. Chem.* 1972, **46**, 305.
16. K. Mödritzer, *Chem. Ber.* 1959, **92**, 2637.
17. K. Mödritzer, *Inorg. Chem.* 1964, **3**, 609.

18. S. L. Patt and J. N. Shoolery, *J. Magnet. Reson.* 1982, **46**, 535.
19. R. G. Kostyanovskii, I. I. Chervin, V. V. Yakshin and A. U. Stepanyants, *Izv. Akad. Nauk SSSR, Ser. Khim.* 1967, 1629.
20. J. C. Summers and H. H. Sisler, *Inorg. Chem.* 1970, **9**, 862.
21. N. Tempel, W. Schwarz and J. Weidlein, *J. Organomet. Chem.* 1978, **154**, 21.
22. H. J. Breunig and D. Mueller, *Z. Naturforsch., B: Anorg. Chem., Org. Chem.* 1983, **38B**, 125.
23. O. T. Beachley Jr and J. D. Bernstein, *Inorg. Chem.* 1973, **12**, 183.
24. J. D. Glore and E. P. Schram, *Inorg. Chem.* 1972, **11**, 1532.
25. H. Vahrenkamp and H. Nöth, *J. Organomet. Chem.* 1968, **12**, 281.
26. T. Hirabayashi, H. Imaeda, K. Itoh, S. Sakai and Y. Ishii, *J. Organomet. Chem.* 1969, **19**, 299.
27. G. M. Bodner, C. Gagnon and D. N. Whittern, *J. Organomet. Chem.* 1983, **243**, 305.
28. B. A. Amero and E. P. Schram, *Inorg. Chem.* 1976, **15**, 2842.
29. L. Cocco and D. P. Eyman, *J. Organomet. Chem.* 1979, **179**, 1.
30. F. Oswald, *Z. Anal. Chem.* 1963, **197**, 309.
31. R. L. McKenney and H. H. Sisler, *Inorg. Chem.* 1967, **6**, 1179.
32. R. G. Kostyanovski and V. G. Plekhanov, *Org. Mass Spectrom.* 1972, **6**, 1183.
33. G. M. Bogolyubov, N. N. Girishin and A. A. Petrov, *Zh. Obsh. Khim.* 1969, **39**, 2244.
34. F. Ando, J. Koketsu and Y. Ishii, *Bull. Chem. Soc. Japan* 1978, **51**, 1481.
35. F. Ando, K. Ohashi and J. Koketsu, *Bull. Chem. Soc. Japan* 1976, **49**, 727.
36. P. Krommes and J. Lorberth, *J. Organomet. Chem.* 1975, **97**, 59.
37. A. Brandl, P. Kölle and H. Nöth, *Chem. Ber.* 1989, **122**, 419.
38. F. Ando, Y. Kohmura and J. Koketsu, *Bull. Chem. Soc. Japan* 1987, **60**, 1564.
39. N. Davidson and H. C. Brown, *J. Am. Chem. Soc.* 1942, **64**, 316.
40. H. Hess, A. Hinderer and S. Steinhauser, *Z. Anorg. Allg. Chem.* 1970, **377**, 1.
41. O. T. Beachley, G. E. Coates and G. Kohnstam, *J. Chem. Soc.* 1965, 3248.
42. M. J. S. Dewar, D. B. Patterson and W. I. Simpson, *J. Chem. Soc., Dalton Trans.* 1973, 2381.
43. G. E. Coates and J. Graham, *J. Chem. Soc.* 1963, 233.
44. D. Y. Yee and R. Ehrlich, *J. Inorg. Nucl. Chem.* 1965, **27**, 2681.
45. K. Gosling, J. D. Smith and D. H. W. Wharmby, *J. Chem. Soc. A* 1969, 1738.
46. J. K. Ruff, *J. Org. Chem.* 1962, **27**, 1020.
47. J. K. Ruff, *J. Am. Chem. Soc.* 1961, **83**, 1798.

Polyhedron Vol. 12, No. 1, pp. 95–110, 1993
Printed in Great Britain

0277–5387/93 $6.00+.00
© 1993 Pergamon Press Ltd

PROMOLECULES WITH A SUBSYMMETRY OF O_h. COMBINATORIAL ENUMERATION AND STEREOCHEMICAL PROPERTIES FOR CHARACTERIZING OCTAHEDRAL COMPLEXES

SHINSAKU FUJITA

Ashigara Research Laboratories, Fuji Photo Film Co. Ltd, Minami-Ashigara, Kanagawa 250-01, Japan

(*Received* 31 *July* 1992; *accepted* 12 *August* 1992)

Abstract—The concept of promolecules is presented for enumerating octahedral complexes, where achiral and chiral proligands are considered as substituents for an octahedral O_h skeleton. After the table of marks and its inverse are calculated, octahedral promolecules are enumerated using the USCI (unit-subduced-cycle-index) method. The numbers of isomers are obtained in an itemized manner with respect to their formulae and symmetries. The stereochemical relationships between the isomers are discussed in the light of the SCR (set-of-closet-representation) notation, which is also effective in clarifying stereochemical equivalency and non-equivalency of proligands and specifying the prochirality of octahedral promolecules and molecules.

Since the proposal of the coordination theory by Werner,[1,2] the stereochemistry of octahedral complexes has been widely investigated to verify the theory.[3] In particular, several studies have aimed at synthesizing all the possible geometrical isomers of a specific series.[4] For these purposes, it has been necessary to calculate the number of such isomers; this task has been done for several specific series. However, there have been few studies on systematic and combinatorial enumeration, except pioneering enumerations using Pólya's theorem[5,6] and using a computer.[7] Since these enumerations have been concerned with molecular formulae and have taken no account of symmetries, more systematic enumerations are desirable to comprehend the stereochemistry of octahedral complexes.

The present paper deals with a systematic approach to such enumerations and relevant problems, where we use a method based on unit-subduced-cycle-indices (USCIs).[8,9] Although the USCI method enables us to enumerate any objects in an itemized manner concerning formulae and symmetries, its application to octahedral complexes requires further derivation of several tables for the O_h point group. In this connection the inorganic complexes are examined in terms of the concept of promolecules, which was once proposed for discussing the stereochemical properties of organic compounds.[10] In addition, we discuss the stereochemical properties of the complexes in the light of the concept of chirality fittingness.[11]

RESULTS

Promolecules with a subsymmetry of the O_h *group*

To illustrate the concept of promolecules for octahedral complexes, let us examine the *trans*-tetraamminedichlorocobalt ion (**1**), i.e. *trans*-$[CoCl_2(NH_3)_4]^+$ (Fig. 1). First, we take into consideration the fixed conformer (**1a**) that has the highest attainable symmetry of D_{2d}. By substituting proligands *a* and *b* for the ammine ligands and the chloro ligands (atoms), respectively, the molecule is converted into the corresponding promolecule (**2**). Since proligands have been defined as hypothetical ligands that have chirality/achirality but are structureless,[10] promolecule **2** is concluded to belong to $\mathbf{D}_{4h}$ symmetry. The promolecule is in turn considered to be constructed by substituting a set of proligands (a_4b_2) for the six vertices of the octahedral skeleton of **3** with O_h symmetry.

If we start from another fixed conformer (**1b**) of C_{4v} symmetry, we are able to obtain the same

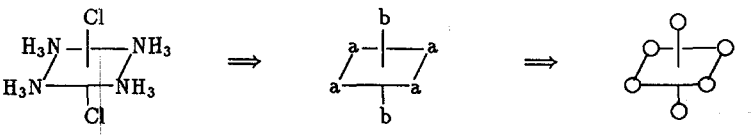

1a D_{2d} (D'_{2d}) 1b C_{4v} 2 D_{4h} 3 O_h

Fig. 1. Molecule, promolecule and skeleton.

promolecule and the same skeleton. This fact indicates that while the tetraamminedichlorocobalt ion has several conformers, the resulting promolecule (**2**) can be regarded as a rigid object.

Although such structures as **2** are frequently used in inorganic chemistry, they have not been well-defined enough to clarify these problems. This means that the conventional treatment has not taken into explicit consideration what happens conceptually when the conversion between **1** and **2** takes place. It follows that one of the main subjects of the present paper is to make clear which symmetrical properties of complexes such as **1** are maintained in the conversion into promolecules such as **2**. This discussion requires (1) combinatorial enumeration of promolecules derived from the octahedral skeleton (**3**), (2) stereochemical properties of the resulting promolecules and (3) a stereochemical relationship between promolecules and molecules.

Tables of marks and USCIs for the O_h *group*

To apply the USCI method to octahedral complexes we should prepare a table of marks, its inverse, and a table of USCIs with respect to the O_h group. The O_h group has an irredundant set of 33 subgroups (SSG):

$$\begin{aligned}\mathrm{SSG}_{O_h} = \{&C_1, C_2, C'_2, C_s, C'_s, C_i, C_3, C_4, S_4, D_2,\\ &D'_2, C_{2v}, C'_{2v}, C''_{2v}, C_{2h}, C'_{2h}, D_3, C_{3v}, C_{3i},\\ &D_4, C_{4v}, C_{4h}, D_{2d}, D'_{2d}, D_{2h}, D'_{2h}, T, D_{3d},\\ &D_{4h}, O, T_h, T_d, O_h\},\end{aligned}$$

where these subgroups are aligned in order of increasing orders. In accord with the SSG we can consider a complete set of coset representations (SCR):

$$\begin{aligned}\mathrm{SCR}_{O_h} = \{&O_h(/C_1), O_h(/C_2), O_h(/C'_2), O_h(/C_s),\\ &O_h(/C'_s), O_h(/C_i), O_h(/C_3), O_h(/C_4),\\ &O_h(/S_4), O_h(/D_2), O_h(/D'_2), O_h(/C_{2v}),\\ &O_h(/C'_{2v}), O_h(/C''_{2v}), O_h(/C_{2h}), O_h(/C'_{2h}),\\ &O_h(/D_3), O_h(/C_{3v}), O_h(/C_{3i}), O_h(/D_4),\\ &O_h(/C_{4v}), O_h(/C_{4h}), O_h(/D_{2d}), O_h(/D'_{2d}),\\ &O_h(/D_{2h}), O_h(/D'_{2h}), O_h(/T), O_h(/D_{3d}),\\ &O_h(/D_{4h}), O_h(/O), O_h(/T_h), O_h(/T_d),\\ &O_h(/O_h)\},\end{aligned}$$

which contains all of the transitive permutation representations concerning the O_h group.

Let G be a group of finite order and G_i and G_j be its subgroups. The mark of the subgroup G_j in a coset representation $G(/G_i)$ is defined as the number of fixed points of $G(/G_i)$ on the action of the subgroup G_j.[12] A table of marks (or a mark table) contains all of the marks concerning the G group. From a multiplication table and a group–subgroup relationship of the O_h group, we calculated a set of coset representations and counted fixed points (marks) for every subgroup. The resulting mark table and its inverse are found in Tables 1 and 2.

In order to construct the table of USCIs for the O_h group, we calculate the subduction of every coset representation (CR) by every subgroup. For example, let us examine the subduction of the $O_h(/C_{4v})$ CR by C_{2v}, which is denoted by the symbol $O_h(/C_{4v})\downarrow C_{2v}$. Since the SSG of the C_{2v} group is represented by

$$\mathrm{SSG}_{C_{2v}} = \{C_1, C_2, C_s, C'_s, C_{2v}\}, \qquad (1)$$

we collect the corresponding marks in the $O_h(/C_{4v})$ row of Table 1 to form a row vector, (62442). Note that C_s and C'_s of $\mathrm{SSG}_{C_{2v}}$ are conjugate within the O_h group. Hence, the value at the intersection between the $O_h(/C_{4v})$ row and the C_s column in Table 1 is doubly placed as the third and fourth elements of the row vector. The row vector is multiplied by the inverse of the mark table of the C_{2v} group[9] as follows:

$$(62442)\begin{bmatrix} 1/4 & 0 & 0 & 0 & 0\\ -1/4 & 1/2 & 0 & 0 & 0\\ -1/4 & 0 & 1/2 & 0 & 0\\ -1/4 & 0 & 0 & 1/2 & 0\\ 1/2 & -1/2 & -1/2 & -1/2 & 1 \end{bmatrix} = (00112). \qquad (2)$$

Table 1. Mark table for O_h group

	C_1	C_2	C_2'	C_s	C_s'	C_i	C_3	C_4	S_4	D_2	D_2'	C_{2v}	C_{2v}'	C_{2v}''	C_{2h}	C_{2h}'	D_3	C_{3v}	C_{3i}	D_4	C_{4v}	C_{4h}	D_{2d}	D_{2d}'	D_{2h}	D_{2h}'	T	D_{3d}	D_{4h}	O	T_h	T_d	O_h
$O_h(/C_1)$	48	0	0	0	0	0	0	0	0	0	0	0	0	0	0	0	0	0	0	0	0	0	0	0	0	0	0	0	0	0	0	0	0
$O_h(/C_2)$	24	8	0	0	0	0	0	0	0	0	0	0	0	0	0	0	0	0	0	0	0	0	0	0	0	0	0	0	0	0	0	0	0
$O_h(/C_2')$	24	0	4	0	0	0	0	0	0	0	0	0	0	0	0	0	0	0	0	0	0	0	0	0	0	0	0	0	0	0	0	0	0
$O_h(/C_s)$	24	0	0	8	0	0	0	0	0	0	0	0	0	0	0	0	0	0	0	0	0	0	0	0	0	0	0	0	0	0	0	0	0
$O_h(/C_s')$	24	0	0	0	4	0	0	0	0	0	0	0	0	0	0	0	0	0	0	0	0	0	0	0	0	0	0	0	0	0	0	0	0
$O_h(/C_i)$	24	0	0	0	0	24	0	0	0	0	0	0	0	0	0	0	0	0	0	0	0	0	0	0	0	0	0	0	0	0	0	0	0
$O_h(/C_3)$	16	0	0	0	0	0	4	0	0	0	0	0	0	0	0	0	0	0	0	0	0	0	0	0	0	0	0	0	0	0	0	0	0
$O_h(/C_4)$	12	4	0	0	0	0	0	4	0	0	0	0	0	0	0	0	0	0	0	0	0	0	0	0	0	0	0	0	0	0	0	0	0
$O_h(/S_4)$	12	4	0	0	0	0	0	0	4	0	0	0	0	0	0	0	0	0	0	0	0	0	0	0	0	0	0	0	0	0	0	0	0
$O_h(/D_2)$	12	12	0	0	0	0	0	0	0	12	0	0	0	0	0	0	0	0	0	0	0	0	0	0	0	0	0	0	0	0	0	0	0
$O_h(/D_2')$	12	4	4	0	0	0	0	0	0	0	4	0	0	0	0	0	0	0	0	0	0	0	0	0	0	0	0	0	0	0	0	0	0
$O_h(/C_{2v})$	12	4	0	8	0	0	0	0	0	0	0	4	0	0	0	0	0	0	0	0	0	0	0	0	0	0	0	0	0	0	0	0	0
$O_h(/C_{2v}')$	12	4	0	0	4	0	0	0	0	0	0	0	4	0	0	0	0	0	0	0	0	0	0	0	0	0	0	0	0	0	0	0	0
$O_h(/C_{2v}'')$	12	0	2	4	2	0	0	0	0	0	0	0	0	2	0	0	0	0	0	0	0	0	0	0	0	0	0	0	0	0	0	0	0
$O_h(/C_{2h})$	12	4	0	4	0	12	0	0	0	0	0	0	0	0	4	0	0	0	0	0	0	0	0	0	0	0	0	0	0	0	0	0	0
$O_h(/C_{2h}')$	12	0	2	0	2	12	0	0	0	0	0	0	0	0	0	2	0	0	0	0	0	0	0	0	0	0	0	0	0	0	0	0	0
$O_h(/D_3)$	8	0	4	0	0	0	2	0	0	0	0	0	0	0	0	0	2	0	0	0	0	0	0	0	0	0	0	0	0	0	0	0	0
$O_h(/C_{3v})$	8	0	0	0	4	0	2	0	0	0	0	0	0	0	0	0	0	2	0	0	0	0	0	0	0	0	0	0	0	0	0	0	0
$O_h(/C_{3i})$	8	0	0	0	0	8	2	0	0	0	0	0	0	0	0	0	0	0	2	0	0	0	0	0	0	0	0	0	0	0	0	0	0
$O_h(/D_4)$	6	6	2	0	0	0	0	2	0	6	2	0	0	0	0	0	0	0	0	2	0	0	0	0	0	0	0	0	0	0	0	0	0
$O_h(/C_{4v})$	6	2	0	4	2	0	0	2	0	0	0	2	2	0	0	0	0	0	0	0	2	0	0	0	0	0	0	0	0	0	0	0	0
$O_h(/C_{4h})$	6	2	0	2	0	6	0	2	2	0	0	0	0	0	2	0	0	0	0	0	0	2	0	0	0	0	0	0	0	0	0	0	0
$O_h(/D_{2d})$	6	6	0	0	2	0	0	0	2	6	0	0	2	0	0	0	0	0	0	0	0	0	2	0	0	0	0	0	0	0	0	0	0
$O_h(/D_{2d}')$	6	2	2	4	0	0	0	0	2	0	2	2	0	0	0	0	0	0	0	0	0	0	0	2	0	0	0	0	0	0	0	0	0
$O_h(/D_{2h})$	6	6	0	6	0	6	0	0	0	6	0	6	0	0	6	0	0	0	0	0	0	0	0	0	6	0	0	0	0	0	0	0	0
$O_h(/D_{2h}')$	6	2	2	2	2	6	0	0	0	0	2	0	2	2	2	2	0	0	0	0	0	0	0	0	0	2	0	0	0	0	0	0	0
$O_h(/T)$	4	4	0	0	0	0	4	0	0	4	0	0	0	0	0	0	0	0	0	0	0	0	0	0	0	0	4	0	0	0	0	0	0
$O_h(/D_{3d})$	4	0	2	0	2	4	1	0	0	0	0	0	0	0	0	2	1	1	1	0	0	0	0	0	0	0	0	1	0	0	0	0	0
$O_h(/D_{4h})$	3	3	1	3	1	3	0	1	1	3	1	3	1	1	3	1	0	0	0	1	1	1	1	1	3	1	0	0	1	0	0	0	0
$O_h(/O)$	2	2	2	0	0	0	2	2	0	2	2	0	0	0	0	0	2	0	0	2	0	0	0	0	0	0	2	0	0	2	0	0	0
$O_h(/T_h)$	2	2	0	2	0	2	2	0	0	2	0	2	0	0	2	0	0	0	2	0	0	0	0	0	2	0	2	0	0	0	2	0	0
$O_h(/T_d)$	2	2	0	0	2	0	2	0	2	2	0	0	2	0	0	0	0	2	0	0	0	0	2	0	0	0	2	0	0	0	0	2	0
$O_h(/O_h)$	1	1	1	1	1	1	1	1	1	1	1	1	1	1	1	1	1	1	1	1	1	1	1	1	1	1	1	1	1	1	1	1	1

Table 2. The inverse of the mark table for the O_h group

	O_h $(/C_1)$	O_h $(/C_2)$	O_h $(/C_s')$	O_h $(/C_s)$	O_h $(/C_s')$	O_h $(/C_i)$	O_h $(/C_3)$	O_h $(/C_4)$	O_h $(/S_4)$	O_h $(/D_2)$	O_h $(/D_2')$	O_h $(/C_{2v})$	O_h $(/C_{2v}')$	O_h $(/C_{2v}'')$	O_h $(/C_{2h})$	O_h $(/C_{2h}')$
C_1	1/48	0	0	0	0	0	0	0	0	0	0	0	0	0	0	0
C_2	−1/16	1/8	0	0	0	0	0	0	0	0	0	0	0	0	0	0
C_2'	−1/8	0	1/4	0	0	0	0	0	0	0	0	0	0	0	0	0
C_s	−1/16	0	0	1/8	0	0	0	0	0	0	0	0	0	0	0	0
C_s'	−1/8	0	0	0	1/4	0	0	0	0	0	0	0	0	0	0	0
C_i	−1/48	0	0	0	0	1/24	0	0	0	0	0	0	0	0	0	0
C_3	−1/12	0	0	0	0	0	1/4	0	0	0	0	0	0	0	0	0
C_4	0	−1/8	0	0	0	0	0	1/4	0	0	0	0	0	0	0	0
S_4	0	−1/8	0	0	0	0	0	0	1/4	0	0	0	0	0	0	0
D_2	1/24	−1/8	0	0	0	0	0	0	0	1/12	0	0	0	0	0	0
D_2'	1/8	−1/8	−1/4	0	0	0	0	0	0	0	1/4	0	0	0	0	0
C_{2v}	1/8	−1/8	0	−1/4	0	0	0	0	0	0	0	1/4	0	0	0	0
C_{2v}'	1/8	−1/8	0	0	−1/4	0	0	0	0	0	0	0	1/4	0	0	0
C_{2v}''	1/4	0	−1/4	−1/4	−1/4	0	0	0	0	0	0	0	0	1/2	0	0
C_{2h}	1/8	−1/8	0	−1/8	0	−1/8	0	0	0	0	0	0	0	0	1/4	0
C_{2h}'	1/4	0	−1/4	0	−1/4	−1/4	0	0	0	0	0	0	0	0	0	1/2
D_3	1/4	0	−1/2	0	0	0	−1/4	0	0	0	0	0	0	0	0	0
C_{3v}	1/4	0	0	0	−1/2	0	−1/4	0	0	0	0	0	0	0	0	0
C_{3i}	1/12	0	0	0	0	−1/6	−1/4	0	0	0	0	0	0	0	0	0
D_4	0	1/4	0	0	0	0	0	−1/4	0	−1/4	1/4	0	0	0	0	0
C_{4v}	0	1/4	0	0	0	0	0	−1/4	0	0	0	−1/4	−1/4	0	0	0
C_{4h}	0	1/4	0	0	0	0	0	−1/4	−1/4	0	0	0	0	0	−1/4	0
D_{2d}	0	1/4	0	0	0	0	0	0	−1/4	−1/4	0	0	−1/4	0	0	0
D_{2d}'	0	1/4	0	0	0	0	0	0	−1/4	0	1/4	−1/4	0	0	0	0
D_{2h}	−1/6	1/4	0	1/4	0	1/12	0	0	0	−1/12	0	−1/4	0	0	−1/4	0
D_{2h}'	−1/2	1/4	1/2	1/4	1/2	1/4	0	0	0	0	1/4	0	−1/4	−1/2	−1/4	−1/2
T	1/12	0	0	0	0	0	−1/4	0	0	−1/12	0	0	0	0	0	0
D_{3d}	−1/2	0	1/2	0	1/2	1/2	1/2	0	0	0	0	0	0	0	0	−1
D_{4h}	0	−1	0	0	0	0	0	1/2	1/2	1/2	1/2	1/2	1/2	0	1/2	0
O	−1/4	0	1/2	0	0	0	1/4	0	0	1/4	0	0	0	0	0	0
T_h	−1/12	0	0	0	0	1/6	1/4	0	0	1/12	0	0	0	0	0	0
T_d	−1/4	0	0	0	1/2	0	1/4	0	0	1/4	0	0	0	0	0	0
O_h	1/2	0	−1/2	0	−1/2	−1/2	−1/2	0	0	−1/2	0	0	0	0	0	1

The resulting vector represents the multiplicities of the coset representations, which correspond to the equation:

$$O_h(/C_{4v})\downarrow C_{2v} = C_{2v}(/C_s) + C_{2v}(/C_s') + 2C_{2v}(/C_{2v}). \tag{3}$$

Each CR on the right-hand side of eq. (3) corresponds to a suborbit that emerges during the restriction of the original O_h symmetry to the subsymmetry C_{2v}. Since we have $|C_{2v}|/|C_s| = 2$, $|C_{2v}|/|C_s'| = 2$ and $|C_{2v}|/|C_{2v}| = 1$, we assign a dummy variable s_2 to the $C_{2v}(/C_s)$ CR and to the $C_{2v}(/C_s')$ CR, and s_1 to the $C_{2v}(/C_{2v})$ CR. Their product is the corresponding USCI, i.e. $s_1^2 s_2^2$, which is assigned to the subduction represented by eq. (3). This procedure is repeated for every subgroup to afford other USCIs, which are collected in Table 3.

On the other hand, we can construct the corresponding unit-subduced-cycle-index with chirality fittingness (USCI-CF) as follows. The three CRs on the right-hand side of eq. (3) are all homospheric, because all the subgroups involved are achiral. Hence, we assign dummy variables: a_2 to the $C_{2v}(/C_s)$ CR, a_2 to the $C_{2v}(/C_s')$ CR and a_1 to the $C_{2v}(/C_{2v})$ CR. We accordingly obtain the USCI-CF, $a_1^2 a_2^2$. The USCI-CFs concerning the $O_h(/C_{4v})$ orbit are obtained as shown in Table 3, where the variable a_d is ascribed to a d-membered homospheric orbit, variable b_d to a d-membered hemispheric orbit and variable c_d to a d-membered enantiospheric orbit. In a similar way, USCIs and USCI-CFs for other CRs have been obtained; however, they are abbreviated for simplicity's sake. The general procedure for constructing tables of USCIs and of USCI-CFs has been described in Chapter 9 of ref. 9.

O_h ($/D_3$)	O_h ($/C_{3v}$)	O_h ($/C_{3i}$)	O_h ($/D_4$)	O_h ($/C_{4v}$)	O_h ($/C_{4h}$)	O_h ($/D_{2d}$)	O_h ($/D'_{2d}$)	O_h ($/D_{2h}$)	O_h ($/D'_{2h}$)	O_h ($/T$)	O_h ($/D_{3d}$)	O_h ($/D_{4h}$)	O_h ($/O$)	O_h ($/T_h$)	O_h ($/T_d$)	O_h ($/O_h$)
0	0	0	0	0	0	0	0	0	0	0	0	0	0	0	0	0
0	0	0	0	0	0	0	0	0	0	0	0	0	0	0	0	0
0	0	0	0	0	0	0	0	0	0	0	0	0	0	0	0	0
0	0	0	0	0	0	0	0	0	0	0	0	0	0	0	0	0
0	0	0	0	0	0	0	0	0	0	0	0	0	0	0	0	0
0	0	0	0	0	0	0	0	0	0	0	0	0	0	0	0	0
0	0	0	0	0	0	0	0	0	0	0	0	0	0	0	0	0
0	0	0	0	0	0	0	0	0	0	0	0	0	0	0	0	0
0	0	0	0	0	0	0	0	0	0	0	0	0	0	0	0	0
0	0	0	0	0	0	0	0	0	0	0	0	0	0	0	0	0
0	0	0	0	0	0	0	0	0	0	0	0	0	0	0	0	0
0	0	0	0	0	0	0	0	0	0	0	0	0	0	0	0	0
0	0	0	0	0	0	0	0	0	0	0	0	0	0	0	0	0
0	0	0	0	0	0	0	0	0	0	0	0	0	0	0	0	0
0	0	0	0	0	0	0	0	0	0	0	0	0	0	0	0	0
0	0	0	0	0	0	0	0	0	0	0	0	0	0	0	0	0
1/2	0	0	0	0	0	0	0	0	0	0	0	0	0	0	0	0
0	1/2	0	0	0	0	0	0	0	0	0	0	0	0	0	0	0
0	0	1/2	0	0	0	0	0	0	0	0	0	0	0	0	0	0
0	0	0	1/2	0	0	0	0	0	0	0	0	0	0	0	0	0
0	0	0	0	1/2	0	0	0	0	0	0	0	0	0	0	0	0
0	0	0	0	0	1/2	0	0	0	0	0	0	0	0	0	0	0
0	0	0	0	0	0	1/2	0	0	0	0	0	0	0	0	0	0
0	0	0	0	0	0	0	1/2	0	0	0	0	0	0	0	0	0
0	0	0	0	0	0	0	0	1/6	0	0	0	0	0	0	0	0
0	0	0	0	0	0	0	0	0	1/2	0	0	0	0	0	0	0
0	0	0	0	0	0	0	0	0	0	1/4	0	0	0	0	0	0
−1/2	−1/2	−1/2	0	0	0	0	0	0	0	0	1	0	0	0	0	0
0	0	0	−1/2	−1/2	−1/2	−1/2	−1/2	−1/2	−1/2	0	0	1	0	0	0	0
−1/2	0	0	−1/2	0	0	0	0	0	0	−1/4	0	0	1/2	0	0	0
0	0	−1/2	0	0	0	0	0	−1/6	0	−1/4	0	0	0	1/2	0	0
0	−1/2	0	0	0	0	−1/2	0	0	0	−1/4	0	0	0	0	1/2	0
1/2	1/2	1/2	1/2	0	0	1/2	0	1/2	0	1/2	−1	−1	−1/2	−1/2	−1/2	1

Enumeration of octahedral promolecules with achiral proligands only

Supposing that the six vertices in the octahedral skeleton (**3**) of O_h symmetry are occupied with a set of achiral proligands selected from *a* to *f*. Then, the problem at issue is to obtain the number of isomers with a given formula and a given symmetry.

The first step is to assign a coset representation (CR) to the orbit of the six vertices. By counting fixed points on the action of every subgroup of SSR_{O_h}, we obtain a fixed-point vector (FPV) represented by (6 2 0 4 2 0 0 2 0 0 0 2 2 0 0 0 0 0 0 0 2 0 0 0 0 0 0 0 0 0 0 0 0 0). Since this vector is identical with the $O_h(/C_{4v})$ row of the mark table (Table 1), the orbit of the six vertices is concluded to be subject to the $O_h(/C_{4v})$ CR. As a result, the derivation of isomeric complexes from the skeleton can be discussed in the light of the subduction listed in Table 3.

The next step is to construct subduced-cycle-indices (SCIs).[8] Since we consider *a*–*f* as proligands, we have a ligand inventory:

$$s_d = a^d + b^d + c^d + d^d + e^d + f^d. \tag{4}$$

This inventory is introduced into the SCIs that are equal to the USCIs listed in Table 3. Thereby, we obtain the following equations:

For C_1:

$$s_1^6 = (a+b+c+d+e+f)^6; \tag{5a}$$

for C_2, C_s, C_{2v}:

$$s_1^2 s_2^2 = (a+b+c+d+e+f)^2 \, (a^2+b^2+c^2+d^2+e^2+f^2)^2; \tag{5b}$$

Table 3. USCIs and USCI-CFs for $O_h(/C_{4v})$

Subgroup $\downarrow G_j$	Subduction $O_h(/C_{4v})\downarrow G_j$	USCI	USCI-CF	Coefficient for CI
C_1	$6C_1(/C_1)$	s_1^6	b_1^6	1/48
C_2	$2C_2(/C_1)+2C_2(/C_2)$	$s_1^2s_2^2$	$b_1^2b_2^2$	1/16
C_2'	$3C_2'(/C_1)$	s_2^3	b_2^3	1/8
C_s	$C_2(/C_1)+4C_s(/C_s)$	$s_1^4s_2$	$a_1^4c_2$	1/16
C_s'	$2C_s'(/C_1)+2C_s'(/C_s)$	$s_1^2s_2^2$	$a_1^2c_2^2$	1/8
C_i	$3C_i(/C_1)$	s_2^3	c_2^3	1/48
C_3	$2C_3(/C_1)$	s_3^2	b_3^2	1/6
C_4	$C_4(/C_1)+2C_4(/C_4)$	$s_1^2s_4$	$b_1^2b_4$	1/8
S_4	$S_s(/C_1)+S_4(/C_2)$	s_2s_4	c_2c_4	1/8
D_2	$D_2(/C_2)+D_2(/C_2')+D_2(/C_2'')$	s_2^3	b_2^3	0
D_2'	$D_2'(/C_1)+D_2'(/C_2)$	s_2s_4	b_2b_4	0
C_{2v}	$C_{2v}(/C_s)+C_{2v}(/C_s')+2C_{2v}(/C_{2v})$	$s_1^2s_2^2$	$a_1^2a_2^2$	0
C_{2v}'	$C_{2v}'(/C_1)+2C_{2v}'(/C_{2v})$	$s_1^2s_4$	$a_1^2c_4$	0
C_{2v}''	$2C_{2v}''(/C_s)+C_{2v}''(/C_s')$	s_2^3	a_2^3	0
C_{2h}	$C_{2h}(/C_2)+C_{2h}(/C_s)$	s_2^3	$a_2^2c_2$	0
C_{2h}'	$C_{2h}'(/C_1)+C_{2h}'(/C_s)$	s_2s_4	a_2c_4	0
D_3	$D_3(/C_1)$	s_6	b_6	0
C_{3v}	$2C_{3v}(/C_s)$	s_3^2	a_3^2	0
C_{3i}	$C_{3i}(/C_1)$	s_6	c_6	1/6
D_4	$D_4(/C_2')+D_4'(/C_4)$	s_2s_4	b_2b_4	0
C_{4v}	$C_{4v}(/C_s)+2C_{4v}(/C_{4v})$	$s_1^2s_4$	$a_1^2a_4$	0
C_{4h}	$C_{4h}(/C_s)+C_{4h}(/C_4)$	s_2s_4	c_2a_4	0
D_{2d}	$D_{2d}(/C_2')+D_{2d}(/C_{2v})$	s_2s_4	a_2c_4	0
D_{2d}'	$D_{2d}'(/C_s)+D_{2d}'(/C_{2v})$	s_2s_4	a_2a_4	0
D_{2h}	$D_{2h}(/C_{2v})+D_{2h}(/C_{2v}')+D_{2h}(/C_{2v}'')$	s_2^3	a_2^3	0
D_{2h}'	$D_{2h}'(/C_s'')+D_{2h}'(/C_{2v})$	s_2s_4	a_2a_4	0
T	$T(/C_2)$	s_6	b_6	0
D_{3d}	$D_{3d}(/C_s)$	s_6	a_6	0
D_{4h}	$D_{4h}(/C_{2v}'')+D_{4h}(/C_{4v})$	s_2s_4	a_2a_4	0
O	$O(/C_4)$	s_6	b_6	0
T_h	$T_h(/C_{2v})$	s_6	a_6	0
T_d	$T_d(/C_{2v})$	s_6	a_6	0
O_h	$O_h(/C_{4v})$	s_6	a_6	0

for C_2', C_i, D_2, C_{2v}'', C_{2h}, D_{2h}:

$$s_2^3=(a^2+b^2+c^2+d^2+e^2+f^2)^3; \quad (5c)$$

for C_s:

$$s_1^4s_2=(a+b+c+d+e+f)^4 (a^2+b^2+c^2+d^2+e^2+f^2); \quad (5d)$$

for C_3, C_{3v}:

$$s_3^2=(a^3+b^3+c^3+d^3+e^3+f^3)^2; \quad (5e)$$

for C_4, C_{2v}', C_{4v}:

$$s_1^2s_4=(a+b+c+d+e+f)^2 (a^4+b^4+c^4+d^4+e^4+f^4); \quad (5f)$$

for S_4, D_2', C_{2h}', D_4, C_{4h}, D_{2d}, D_{2d}', D_{2h}', D_{4h}:

$$s_2s_4=(a^2+b^2+c^2+d^2+e^2+f^2) (a^4+b^4+c^4+d^4+e^4+f^4); \quad (5g)$$

and for D_3, C_{3i}, T, D_{3d}, O, T_h, T_d, O_h:

$$s_6=a^6+b^6+c^6+d^6+e^6+f^6. \quad (5h)$$

After the expansion of each of these equations, we collect the coefficient of the term $a^{\theta_1}b^{\theta_2}c^{\theta_3}d^{\theta_4}e^{\theta_5}f^{\theta_6}$ to construct Table 4. For simplicity's sake, we designate the term by the partition $[\theta_1\theta_2\theta_3\theta_4\theta_5\theta_6]$, where we omit zero elements and presume $\theta_1 \geqq \theta_2 \geqq \theta_3 \geqq \theta_4 \geqq \theta_5 \geqq \theta_6$ without losing generality.

The data of Table 4 are regarded as a matrix, which is multiplied by the inverse (Table 2). The resulting matrix is found in Table 5, which contains

Table 4. Coefficients of generating functions

	C_1	C_2	C_2'	C_s	C_s'	C_i	C_3	C_4	S_4	D_2	D_2'	C_{2v}	C_{2v}'	C_{2v}''	C_{2h}	C_{2h}'	D_3	C_{3v}	C_{3i}	D_4	C_{4v}	C_{4h}	D_{2d}	D_{2d}'	D_{2h}	I
[6]	1	1	1	1	1	1	1	1	1	1	1	1	1	1	1	1	1	1	1	1	1	1	1	1	1	
[51]	6	2	0	4	2	0	0	2	0	0	0	2	2	0	0	0	0	0	0	0	2	0	0	0	0	
[42]	15	3	3	7	3	3	0	1	1	3	1	3	1	3	3	1	0	0	0	1	1	1	1	1	3	
[411]	30	2	0	12	2	0	0	2	0	0	0	2	2	0	0	0	0	0	0	0	2	0	0	0	0	
[33]	20	4	0	8	4	0	2	0	0	0	0	4	0	0	0	0	0	2	0	0	0	0	0	0	0	
[321]	60	4	0	16	4	0	0	0	0	0	0	4	0	0	0	0	0	0	0	0	0	0	0	0	0	
[3111]	120	0	0	24	0	0	0	0	0	0	0	0	0	0	0	0	0	0	0	0	0	0	0	0	0	
[222]	90	6	6	18	6	6	0	0	0	6	0	6	0	6	6	0	0	0	0	0	0	0	0	0	6	
[2211]	180	4	0	24	4	0	0	0	0	0	0	4	0	0	0	0	0	0	0	0	0	0	0	0	0	
[21111]	360	0	0	24	0	0	0	0	0	0	0	0	0	0	0	0	0	0	0	0	0	0	0	0	0	
[111111]	720	0	0	0	0	0	0	0	0	0	0	0	0	0	0	0	0	0	0	0	0	0	0	0	0	

Table 5. The number of promolecules with achiral ligands

	C_1	C_2	C_2'	C_s	C_s'	C_i	C_3	C_4	S_4	D_2	D_2'	C_{2v}	C_{2v}'	C_{2v}''	C_{2h}	C_{2h}'	D_3	C_{3v}	C_{3i}	D_4	C_{4v}	C_{4h}	D_{2d}	D_{2d}'	D_{2h}	D_{2h}'	T
[6]	0	0	0	0	0	0	0	0	0	0	0	0	0	0	0	0	0	0	0	0	0	0	0	0	0	0	0
[51]	0	0	0	0	0	0	0	0	0	0	0	0	0	0	0	0	0	0	0	1	0	0	0	0	0	0	0
[42]	0	0	0	0	0	0	0	0	0	0	0	0	0	1	0	0	0	0	0	0	0	0	0	0	0	0	0
[411]	0	0	0	1	0	0	0	0	0	0	0	0	0	0	0	0	0	0	0	1	0	0	0	0	0	0	0
[33]	0	0	0	0	0	0	0	0	0	0	0	1	0	0	0	0	0	1	0	0	0	0	0	0	0	0	0
[321]	0	0	0	1	1	0	0	0	0	0	0	1	0	0	0	0	0	0	0	0	0	0	0	0	0	0	0
[3111]	1	0	0	3	0	0	0	0	0	0	0	0	0	0	0	0	0	0	0	0	0	0	0	0	0	0	0
[222]	1	0	0	0	0	0	0	0	0	0	0	0	0	3	0	0	0	0	0	0	0	0	0	0	1	0	0
[2211]	2	0	0	2	1	0	0	0	0	0	0	1	0	0	0	0	0	0	0	0	0	0	0	0	0	0	0
[21111]	6	0	0	3	0	0	0	0	0	0	0	0	0	0	0	0	0	0	0	0	0	0	0	0	0	0	0
[111111]	15	0	0	0	0	0	0	0	0	0	0	0	0	0	0	0	0	0	0	0	0	0	0	0	0	0	0

the number of isomers with $[\theta_1\theta_2\theta_3\theta_4\theta_5\theta_6]$ and a given symmetry at the corresponding intersection.

The total number of each row of Table 5 is calculated by means of a cycle index (CI), which is obtained using the USCIs and the coefficients listed in Table 3. The coefficients are calculated by adding the values in every row of Table 2;[13] each of them is non-zero only if the corresponding group is cyclic. By introducing the ligand inventory [eq. (4)], we have a generating function for calculating the number of isomers with a given partition:

$$
\begin{aligned}
&G(a,b,c,d,e,f)\\
&\quad=(1/48)(s_1^6+3s_1^2s_2^2+6s_2^3+3s_1^4s_2+6s_1^2s_2^2\\
&\qquad+s_2^3+8s_3^2+6s_1^2s_4+6s_2s_4+8s_6)\\
&\quad=(1/48)(s_1^6+9s_1^2s_2^2+7s_2^3+3s_1^4s_2+8s_3^2\\
&\qquad+6s_1^2s_4+6s_2s_4+8s_6)\\
&\quad=(a^6+\cdots)+(a^5b+\cdots)+2(a^4b^2+\cdots)\\
&\qquad+2(a^4bc+\cdots)+2(a^3b^3+\cdots)\\
&\qquad+3(a^3b^2c+\cdots)+4(a^3bcd+\cdots)\\
&\qquad+5(a^2b^2c^2+\cdots)+6(a^2bcd+\cdots)\\
&\qquad+9(a^2bcde+\cdots)+15(abcdef+\cdots). \qquad (6)
\end{aligned}
$$

Note that the cycle index is equivalent to that derived by Pólya's theorem;[14] this equivalency has been proved in general.[13] Each of the coefficients appearing in eq. (6) is identical to the corresponding value in the rightmost column of Table 5, which is obtained by summing up every row.

Figure 2 illustrates all the promolecules enumerated in Table 5. It should be noted that an arbitrary enantiomer is depicted as a representative of each pair of enantiomers, since the present method counts a pair of enantiomers once. The drawing of these promolecules is conducted without difficulty, since the values in Table 5 are itemized with respect to the partitions (molecular formulae) as well as to the symmetries.

Enumeration of octahedral promolecules with achiral and chiral proligands.

Let us next consider cases in which proligands are capable of being achiral or chiral. For simplicity's sake, we examine the case in which six proligands for **3** are selected from a set of three achiral proligands (a, b and c) and a pair of enantiomers (p and $\bar{p}$).

In order to obtain the numbers of isomers with a given formula and a given symmetry, we use the following three ligand inventories:

$$a_d = a^d+b^d+c^d, \qquad (7a)$$

$$b_d = a^d+b^d+c^d+p^d+\bar{p}^d, \qquad (7b)$$

$$c_d = a^d+b^d+c^d+2p^{d/2}\bar{p}^{d/2}; \qquad (7c)$$

where a_d is applied to a homospheric orbit, b_d to a hemispheric orbit and c_d to an enantiospheric orbit. These inventories are introduced into the SCI-CFs which are, in this case, identical with the USCI-CFs listed in Table 3. Thereby, we obtain the following

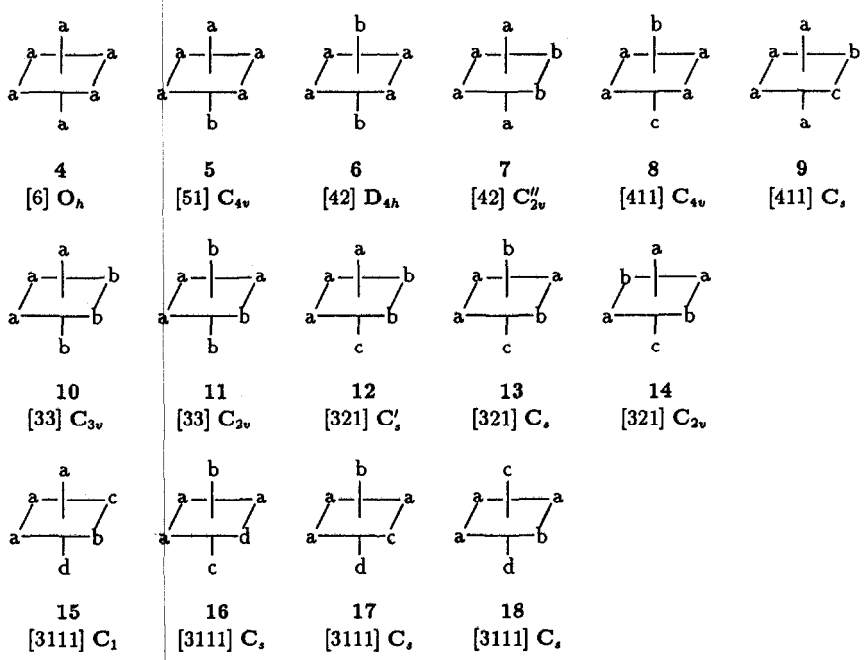

Fig. 2. Octahedral promolecules with achiral proligands.

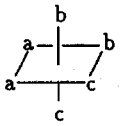

19
[222] C_1

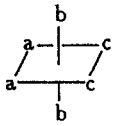

20
[222] C''_{2v}

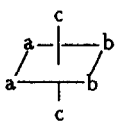

21
[222] C''_{2v}

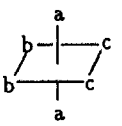

22
[222] C''_{2v}

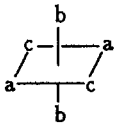

23
[222] D_{2h}

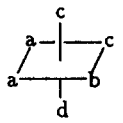

24
[2211] C_1

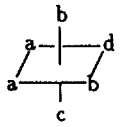

25
[2211] C_1

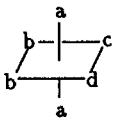

26
[2211] C_s

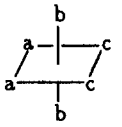

27
[2211] C_s

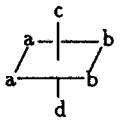

28
[2211] C'_s

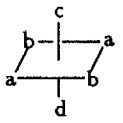

29
[2211] C_{2v}

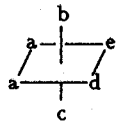

30
[21111] C_1

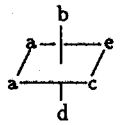

31
[21111] C_1

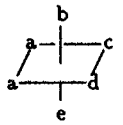

32
[21111] C_1

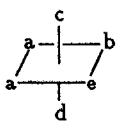

33
[21111] C_1

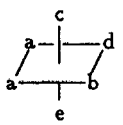

34
[21111] C_1

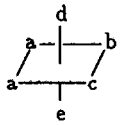

35
[21111] C_1

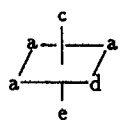

36
[21111] C_s

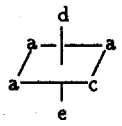

37
[21111] C_s

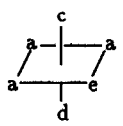

38
[21111] C_s

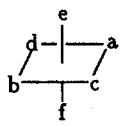

39
[111111] C_1

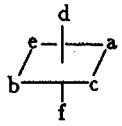

40
[111111] C_1

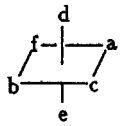

41
[111111] C_1

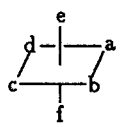

42
[111111] C_1

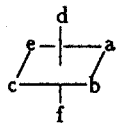

43
[111111] C_1

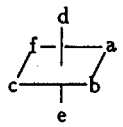

44
[111111] C_1

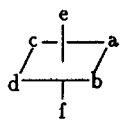

45
[111111] C_1

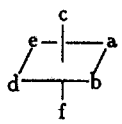

46
[111111] C_1

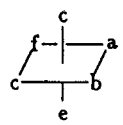

47
[111111] C_1

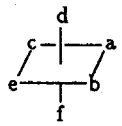

48
[111111] C_1

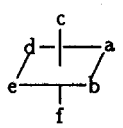

49
[111111] C_1

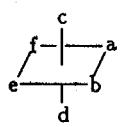

50
[111111] C_1

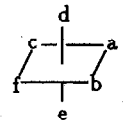

51
[111111] C_1

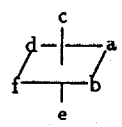

52
[111111] C_1

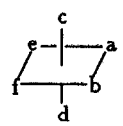

53
[111111] C_1

Fig. 2—*Continued.*

generating functions:

for C_1:

$$b_1^6 = (a+b+c+p+\bar{p})^6; \quad (8a)$$

for C_2:

$$b_1^2 b_2^2 = (a+b+c+p+\bar{p})^2(a^2+b^2+c^2+p^2+\bar{p}^2)^2; \quad (8b)$$

for C_2', D_2:

$$b_2^3 = (a^2+b^2+c^2+p^2+\bar{p}^2)^3; \quad (8c)$$

for C_s:

$$a_1^4 c_2 = (a+b+c)^4(a^2+b^2+c^2+2p\bar{p}); \quad (8d)$$

for C_s':

$$a_1^2 c_2^2 = (a+b+c)^2(a^2+b^2+c^2+2p\bar{p})^2; \quad (8e)$$

for C_i:

$$c_2^3 = (a^2+b^2+c^2+2p\bar{p})^3; \quad (8f)$$

for C_3:

$$b_3^2 = (a^3+b^3+c^3+p^3+\bar{p}^3)^2; \quad (8g)$$

for C_4:

$$b_1^2 b_4 = (a+b+c+p+\bar{p})^2(a^4+b^4+c^4+p^4+\bar{p}^4); \quad (8h)$$

for S_4:

$$c_2 c_4 = (a^2+b^2+c^2+2p\bar{p})(a^4+b^4+c^4+2p^2\bar{p}^2); \quad (8i)$$

for D_2', D_4:

$$b_2 b_4 = (a^2+b^2+c^2+p^2+\bar{p}^2)(a^4+b^4+c^4+p^4+\bar{p}^4); \quad (8j)$$

for C_{2v}:

$$a_1^2 a_2^2 = (a+b+c)^2(a^2+b^2+c^2)^2; \quad (8k)$$

for C_{2v}':

$$a_1^2 c_4 = (a+b+c)^2(a^4+b^4+c^4+2p^2\bar{p}^2); \quad (8l)$$

for C_{2v}'', D_{2h}:

$$a_2^3 = (a^2+b^2+c^2)^3; \quad (8m)$$

for C_{2h}:

$$a_2^2 c_2 = (a^2+b^2+c^2)^2(a^2+b^2+c^2+2p\bar{p}); \quad (8n)$$

for C_{2h}', D_{2d}:

$$a_2 c_4 = (a^2+b^2+c^2)(a^4+b^4+c^4+2p^2\bar{p}^2); \quad (8o)$$

for D_3, T, O:

$$b_6 = a^6+b^6+c^6+p^6+\bar{p}^6; \quad (8p)$$

for C_{3v}:

$$a_3^2 = (a^3+b^3+c^3)^2; \quad (8q)$$

for C_{3i}:

$$c_6 = a^6+b^6+c^6+2p^3\bar{p}^3; \quad (8r)$$

for C_{4v}:

$$s_1^2 s_4 = (a+b+c)^2(a^4+b^4+c^4); \quad (8s)$$

for C_{4h}:

$$c_2 c_4 = (a^2+b^2+c^2+2p\bar{p})(a^4+b^4+c^4+2p^2\bar{p}^2); \quad (8t)$$

for D_{2d}', D_{2h}', D_{4h}:

$$a_2 a_4 = (a^2+b^2+c^2)(a^4+b^4+c^4); \quad (8u)$$

and for D_{3d}, T_h, T_d, O_h:

$$a_6 = a^6+b^6+c^6. \quad (8v)$$

After the expansion of each of the equations, we collect the coefficient of each term, $a^{\theta_1}b^{\theta_2}c^{\theta_3}p^{\theta_4}\bar{p}^{\theta_5}$, to construct Table 6. We designate this term by the symbol $[\theta_1\theta_2\theta_3;\theta_4\theta_5]$, where we omit zero elements; and presume $\theta_1 \geqslant \theta_2 \geqslant \theta_3$ and $\theta_4 \geqslant \theta_5$ without losing generality. Terms containing achiral proligands only (i.e. $\theta_1+\theta_2+\theta_3 = 6$) are abbreviated, since they have already appeared in Table 4. If a promolecule has $[\theta_1\theta_2\theta_3;\theta_4\theta_5]$ in which $\theta_4 \geqslant 1$, $\theta_5 \geqslant 1$ and $\theta_4 \neq \theta_5$, it has an enantiomer that corresponds to $[\theta_1\theta_2\theta_3;\theta_5\theta_4]$. In accord with this fact, the values containing the factor 2* correspond to such cases to obtain the correct results.

The data of Table 6 are regarded as a matrix, which is then multiplied by the inverse (Table 2). The resulting matrix (Table 7) contains the number of isomers with $[\theta_1\theta_2\theta_3;\theta_4\theta_5]$ and a given symmetry at the corresponding intersection.

For verifying the values collected in Table 7, Fig. 3 illustrates all cases in which θ_4 and θ_5 are both equal to 1.

DISCUSSION

Inherent lack and accidental lack

Table 5 involves several columns in which all the values are equal to zero. Such a lack of derivatives of specific subsymmetries can be deduced by means of SCIs derived from USCIs. In general, a derivative of a given point group is inherently absent if the corresponding SCI is identical with the SCI of one of its supergroups. To discuss the octahedral promolecules we can use the USCIs collected in Table 3, since the corresponding skeleton **3** has one orbit. For example, the SCI of the C_2 group $(s_1^2 s_2^2)$ is the same as that of C_{2v}; hence, there inherently emerge no C_2 derivatives. In other words, even if we place ligands a_2b_2cd in agreement of the SCI

Table 6. Coefficients of generating functions

	C_1	C_2	C_2'	C_s	C_s'	C_i	C_3	C_4	S_4	D_2	D_2'	C_{2v}	C_{2v}'	C_{2v}''	C_{2h}	C_{2h}'	D_3	C_{3v}	C_{3i}	D_4	C_{4v}	C_{4h}	D_{2d}	D_{2d}'	D_{2h}	D_{2h}'	T	D_{3d}	D_{4h}	O	T_h	T_d	O_h
[5; 1]	2∗6	2∗2	0	0	0	0	0	2∗2	0	0	0	0	0	0	0	0	0	0	0	0	0	0	0	0	0	0	0	0	0	0	0	0	0
[41; 1]	2∗30	2∗2	0	0	0	0	0	2∗2	0	0	0	0	0	0	0	0	0	0	0	0	0	0	0	0	0	0	0	0	0	0	0	0	0
[4; 2]	2∗15	2∗3	2∗3	0	0	0	0	2∗1	0	2∗3	2∗1	0	0	0	0	0	0	0	0	2∗1	0	0	0	0	0	0	0	0	0	0	0	0	0
[4;11]	30	2	0	2	4	6	0	2	2	0	0	0	0	0	2	0	0	0	0	0	0	2	0	0	0	0	0	0	0	0	0	0	0	0
[32; 1]	2∗60	2∗4	0	0	0	0	0	0	0	0	0	0	0	0	0	0	0	0	0	0	0	0	0	0	0	0	0	0	0	0	0	0	0	0
[311; 1]	2∗120	0	0	0	0	0	0	0	0	0	0	0	0	0	0	0	0	0	0	0	0	0	0	0	0	0	0	0	0	0	0	0	0	0
[31; 2]	2∗60	2∗4	0	0	0	0	0	0	0	0	0	0	0	0	0	0	0	0	0	0	0	0	0	0	0	0	0	0	0	0	0	0	0	0
[31; 11]	120	0	0	8	8	0	0	0	0	0	0	0	0	0	0	0	0	0	0	0	0	0	0	0	0	0	0	0	0	0	0	0	0	0
[3; 3]	2∗20	2∗4	0	0	0	0	2∗2	0	0	0	0	0	0	0	0	0	0	0	0	0	0	0	0	0	0	0	0	0	0	0	0	0	0	0
[3; 21]	2∗60	2∗4	0	0	0	0	0	0	0	0	0	0	0	0	0	0	0	0	0	0	0	0	0	0	0	0	0	0	0	0	0	0	0	0
[221; 1]	2∗180	2∗4	0	0	0	0	0	0	0	0	0	0	0	0	0	0	0	0	0	0	0	0	0	0	0	0	0	0	0	0	0	0	0	0
[22; 2]	2∗90	2∗6	2∗6	0	0	0	0	0	0	2∗6	0	0	0	0	0	2∗2	0	0	0	0	0	0	0	0	0	0	0	0	0	0	0	0	0	0
[22; 11]	180	4	0	12	8	12	0	0	0	0	0	0	0	0	4	0	0	0	0	0	0	0	0	0	0	0	0	0	0	0	0	0	0	0
[211; 2]	2∗180	2∗4	0	0	0	0	0	0	0	0	0	0	0	0	0	0	0	0	0	0	0	0	0	0	0	0	0	0	0	0	0	0	0	0
[211; 11]	360	0	0	24	8	0	0	0	0	0	0	0	0	0	0	0	0	0	0	0	0	0	0	0	0	0	0	0	0	0	0	0	0	0
[21; 3]	2∗60	2∗4	0	0	0	0	0	0	0	0	0	0	0	0	0	0	0	0	0	0	0	0	0	0	0	0	0	0	0	0	0	0	0	0
[21; 21]	2∗180	2∗4	0	0	0	0	0	0	0	0	0	0	0	0	0	0	0	0	0	0	0	0	0	0	0	0	0	0	0	0	0	0	0	0
[2; 4]	2∗15	2∗3	2∗3	0	0	0	0	2∗1	0	2∗3	2∗1	0	0	0	0	0	0	0	0	2∗1	0	0	0	0	0	0	0	0	0	0	0	0	0	0
[2; 31]	2∗60	2∗4	0	0	0	0	0	0	0	0	0	0	0	0	0	0	0	0	0	0	0	0	0	0	0	0	0	0	0	0	0	0	0	0
[2; 22]	90	6	6	0	4	12	0	0	2	6	0	0	2	0	0	2	0	0	0	0	0	0	2	0	0	0	0	0	0	0	0	0	0	0
[111; 3]	2∗120	0	0	0	0	0	0	0	0	0	0	0	0	0	0	0	0	0	0	0	0	0	0	0	0	0	0	0	0	0	0	0	0	0
[111; 21]	2∗360	0	0	0	0	0	0	0	0	0	0	0	0	0	0	0	0	0	0	0	0	0	0	0	0	0	0	0	0	0	0	0	0	0
[11; 4]	2∗30	2∗2	0	0	0	0	0	2∗2	0	0	0	0	0	0	0	0	0	0	0	0	0	0	0	0	0	0	0	0	0	0	0	0	0	0
[11; 31]	2∗120	0	0	0	0	0	0	0	0	0	0	0	0	0	0	0	0	0	0	0	0	0	0	0	0	0	0	0	0	0	0	0	0	0
[11; 22]	180	4	0	0	8	0	0	0	0	0	4	0	0	0	0	0	0	0	0	0	0	0	0	0	0	0	0	0	0	0	0	0	0	0
[1; 5]	2∗6	2∗2	0	0	0	0	0	2∗2	0	0	0	0	0	0	0	0	0	0	0	0	0	0	0	0	0	0	0	0	0	0	0	0	0	0
[1; 41]	2∗30	2∗2	0	0	0	0	0	2∗2	0	0	0	0	0	0	0	0	0	0	0	0	0	0	0	0	0	0	0	0	0	0	0	0	0	0
[1; 32]	2∗60	2∗4	0	0	0	0	0	0	0	0	0	0	0	0	0	0	0	0	0	0	0	0	0	0	0	0	0	0	0	0	0	0	0	0
[; 6]	2∗1	2∗1	2∗1	0	0	0	2∗1	2∗1	0	2∗1	2∗1	0	0	0	0	0	2∗1	0	0	2∗1	0	0	0	0	0	0	2∗1	0	0	2∗1	0	0	0
[; 51]	2∗6	2∗2	0	0	0	0	0	2∗2	0	0	0	0	0	0	0	0	0	0	0	0	0	0	0	0	0	0	0	0	0	0	0	0	0	0
[; 42]	2∗15	2∗3	2∗3	0	0	0	0	2∗1	0	2∗3	2∗1	0	0	0	0	0	0	0	0	2∗1	0	0	0	0	0	0	0	0	0	0	0	0	0	0
[; 33]	20	4	0	0	0	8	2	0	4	0	0	0	0	0	0	0	0	0	2	0	0	0	0	0	0	0	0	0	0	0	0	0	0	0

Table 7. The number of promolecules with achiral and chiral ligands

C_s'	C_i	C_3	C_4	S_4	D_2	D_2'	C_{2v}	C_{2v}'	C_{2v}''	C_{2h}	C_{2h}'	D_3	C_{3v}	C_{3i}	D_4	C_{4v}	C_{4h}	D_{2d}	D_{2d}'	D_{2h}	D_{2h}'	T	D_{3d}	D_{4h}	O	T_h	T_d	O_h
0	0	0	1	0	0	0	0	0	0	0	0	0	0	0	0	0	0	0	0	0	0	0	0	0	0	0	0	0
0	0	0	1	0	0	0	0	0	0	0	0	0	0	0	0	0	0	0	0	0	0	0	0	0	0	0	0	0
0	0	0	0	0	0	0	0	0	0	0	0	0	0	0	1	0	0	0	0	0	0	0	0	0	0	0	0	0
1	0	0	0	0	0	0	0	0	0	0	0	0	0	0	0	0	1	0	0	0	0	0	0	0	0	0	0	0
0	0	0	0	0	0	0	0	0	0	0	0	0	0	0	0	0	0	0	0	0	0	0	0	0	0	0	0	0
0	0	0	0	0	0	0	0	0	0	0	0	0	0	0	0	0	0	0	0	0	0	0	0	0	0	0	0	0
0	0	0	0	0	0	0	0	0	0	0	0	0	0	0	0	0	0	0	0	0	0	0	0	0	0	0	0	0
2	0	0	0	0	0	0	0	0	0	0	0	0	0	0	0	0	0	0	0	0	0	0	0	0	0	0	0	0
0	0	1	0	0	0	0	0	0	0	0	0	0	0	0	0	0	0	0	0	0	0	0	0	0	0	0	0	0
0	0	0	0	0	0	0	0	0	0	0	0	0	0	0	0	0	0	0	0	0	0	0	0	0	0	0	0	0
0	0	0	0	0	0	0	0	0	0	0	0	0	0	0	0	0	0	0	0	0	0	0	0	0	0	0	0	0
0	0	0	0	0	1	0	0	0	0	0	0	0	0	0	0	0	0	0	0	0	0	0	0	0	0	0	0	0
2	0	0	0	0	0	0	0	0	0	1	0	0	0	0	0	0	0	0	0	0	0	0	0	0	0	0	0	0
0	0	0	0	0	0	0	0	0	0	0	0	0	0	0	0	0	0	0	0	0	0	0	0	0	0	0	0	0
2	0	0	0	0	0	0	0	0	0	0	0	0	0	0	0	0	0	0	0	0	0	0	0	0	0	0	0	0
0	0	0	0	0	0	0	0	0	0	0	0	0	0	0	0	0	0	0	0	0	0	0	0	0	0	0	0	0
0	0	0	0	0	0	0	0	0	0	0	0	0	0	0	0	0	0	0	0	0	0	0	0	0	0	0	0	0
0	0	0	0	0	0	0	0	0	0	0	0	0	0	0	1	0	0	0	0	0	0	0	0	0	0	0	0	0
0	0	0	0	0	0	0	0	0	0	0	0	0	0	0	0	0	0	0	0	0	0	0	0	0	0	0	0	0
0	0	0	0	0	0	0	0	0	0	0	1	0	0	0	0	0	0	1	0	0	0	0	0	0	0	0	0	0
0	0	0	0	0	0	0	0	0	0	0	0	0	0	0	0	0	0	0	0	0	0	0	0	0	0	0	0	0
0	0	0	0	0	0	0	0	0	0	0	0	0	0	0	0	0	0	0	0	0	0	0	0	0	0	0	0	0
0	0	0	1	0	0	0	0	0	0	0	0	0	0	0	0	0	0	0	0	0	0	0	0	0	0	0	0	0
0	0	0	0	0	0	0	0	0	0	0	0	0	0	0	0	0	0	0	0	0	0	0	0	0	0	0	0	0
1	0	0	0	0	0	0	0	1	0	0	0	0	0	0	0	0	0	0	0	0	0	0	0	0	0	0	0	0
0	0	0	1	0	0	0	0	0	0	0	0	0	0	0	0	0	0	0	0	0	0	0	0	0	0	0	0	0
0	0	0	1	0	0	0	0	0	0	0	0	0	0	0	0	0	0	0	0	0	0	0	0	0	0	0	0	0
0	0	0	0	0	0	0	0	0	0	0	0	0	0	0	0	0	0	0	0	0	0	0	0	0	0	0	0	0
0	0	0	0	0	0	0	0	0	0	0	0	0	0	0	0	0	0	0	0	0	0	0	0	1	0	0	0	0
0	0	0	1	0	0	0	0	0	0	0	0	0	0	0	0	0	0	0	0	0	0	0	0	0	0	0	0	0
0	0	0	0	0	0	0	0	0	0	0	0	0	0	0	1	0	0	0	0	0	0	0	0	0	0	0	0	0
0	0	0	0	1	0	0	0	0	0	0	0	0	0	1	0	0	0	0	0	0	0	0	0	0	0	0	0	0

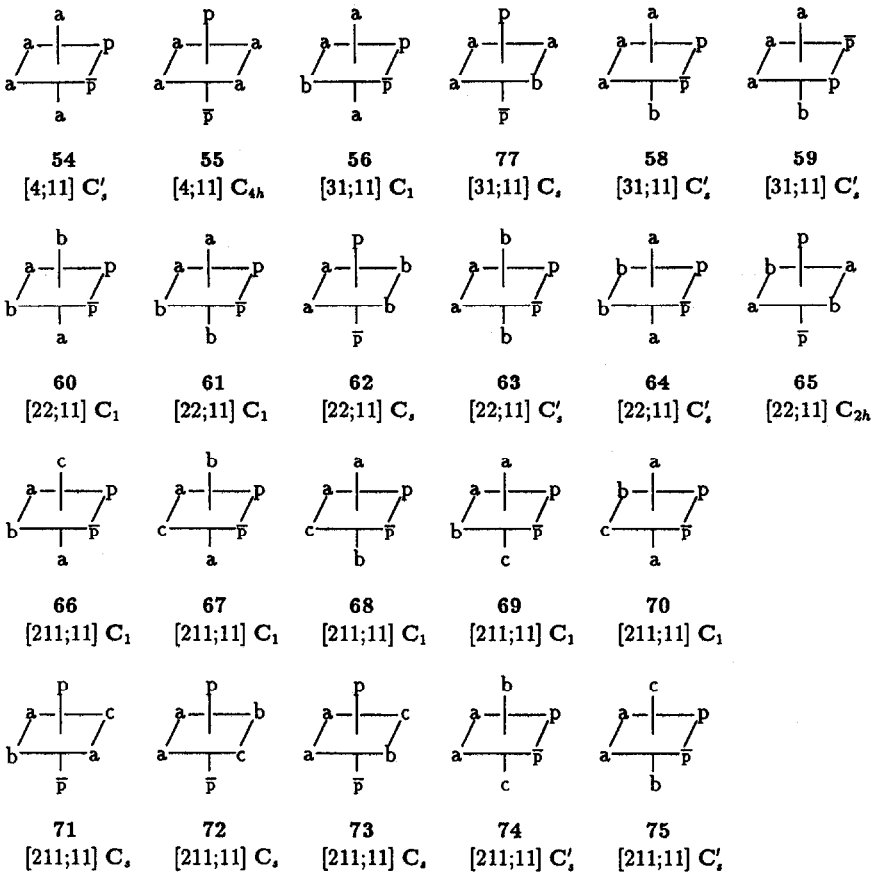

Fig. 3. Octahedral promolecules with achiral and chiral proligands.

$(s_1^2 s_2^2)$ on the vertices of the skeleton, the resulting molecule belongs not to C_2 but to C_{2v}.

By using the data collected in Table 3 and the group–subgroup relationship,[11] the inherent lack of derivatives for the octahedral complexes with achiral proligands is concluded to occur in the following cases:

$$C_2 \Rightarrow C_{2v}(s_1^2 s_2^2)$$

$$C'_2, C_i, D_2, C_{2h} \Rightarrow D_{2h}(s_2^3)$$

$$C_3 \Rightarrow C_{3v}(s_3^2)$$

$$C_4, C'_{2v} \Rightarrow C_{4v}(s_1^2 s_4)$$

$$S_4, D'_2, C'_{2h}, D_4, C_{4h}, D_{2d}, D'_{2d}, D'_{2h} \Rightarrow D_{4h}(s_2 s_4)$$

$$D_3, C_{3i}, T, D_{3d}, O, T_d, T_h \Rightarrow O_h(s_6);$$

where each group on the right-hand side represents a supergroup to be considered.

In the light of the SCI-CFs (derived from USCI-CFs in Table 3) we are able to determine the inherent lack of subsymmetries for cases in which achiral and chiral proligands are permitted:

$$D_3, T \Rightarrow O(b_6),$$

$$D'_{2d}, D'_{2h} \Rightarrow D_{4h}(a_2 a_4)$$

$$D_{3d}, T_d, T_h \Rightarrow O_h(a_6).$$

Table 7 involves the corresponding columns which all have zero values.

Enumeration collected in Table 7 involves another type of lack (C_i and D'_2), which is called *accidental lack*. This means that we can obtain derivatives of such symmetries if we increase the variety of the proligands. Thus, a C_i derivative can be obtained by placing three pairs of antipodal proligands, i.e. $p\bar{p}q\bar{q}r\bar{r}$, in the same line; substitution of $p_4 q_2$ gives a D'_2 derivative.

Algebraically speaking, such accidental lacks can be avoided by using the following ligand inventories in place of eqs (7a)–(7c).

$$a_d = a^d + \cdots + f^d, \tag{9a}$$

$$b_d = (a^d + \cdots + f^d) + (p^d + \bar{p} + \cdots u^d + \bar{u}^d), \tag{9b}$$

$$c_d = (a^d + \cdots + f^d) + 2(p^{d/2}\bar{p}^{d/2} + \cdots + u^{d/2}\bar{u}^{d/2}). \tag{9c}$$

However, the full calculation based on eqs (9a)–(9c) affords too large a list to be tabulated.

SCR notation of octahedral promolecules

We have already proposed the set-of-coset-representation (SCR) notation for characterizing organic compounds.[9,15] The SCR notation determines every coset representation and its members for specifying a compound. The notation is also useful for characterizing octahedral promolecules.

The [51], C_{4v} promolecule (**5**) is designated by the SCR notation, $C_{4v}[/C_s(a_4)\,;\,C_{4v}(a,b)]$. This notation stems from the fact that the four *a*s of **5** construct an orbit corresponding to the $C_{4v}(/C_s)$ CR; the remaining *a* is a member of one $C_{4v}(/C_{4v})$ orbit and *b* is a member of the other $C_{4v}(/C_{4v})$ orbit. The notation for **5** explicitly indicates that the four *a*s are not equivalent to the remaining *a*. Note that $|C_{4v}|/|C_s| = 8/2 = 4$ and $|C_{4v}|/|C_{4v}| = 8/8 = 1$; these values control the number of proligands to be accommodated by each of the orbits. In addition, it should be emphasized that a desymmetrization created by the a_5b (or [51]) substitution is exactly controlled by the subduction

$$O_h(/C_{4v})\downarrow C_{4v} = C_{4v}(/C_s)+2C_{4v}(/C_{4v}), \quad (10)$$

which is collected in the corresponding row of Table 3. Similarly, we obtain the SCR notations for the promolecules depicted in Figs 2 and 3, as found in Tables 8 and 9.

It should be noted that the point group C''_{2v} in $C''_{2v}[/C_s(a_2,b_2),\ /C'_s(a_2)]$ for **7** (also for **20**–**22**) is differentiated from the C_{2v} point group in $C_{2v}[/C_s(a_2),\ /C'_s(b_2),\ /C_{2v}(a,b)]$ *for* **11**, although they are equivalent as point groups after such subductions. Since they indicate different modes of deriving promolecules of the C_{2v} symmetry, such a differentiation between C_{2v} and C''_{2v} is useful when we emphasize the fact that we start from the O_h skeleton (**3**).

The symbols a_2 and $2a$ in the notation $C_s[/C_1(a_2),\ /C_s(2a,\ b,\ c)]$ for **9** (Table 8) indicate two distinct modes of substitution. The two *a*s in a_2 construct a two-membered orbit, while each *a* of $2a$ constructs a distinct one-membered orbit.

The promolecules **6** and **7** correspond to a *trans*--*cis* pair of [42] isomers; they are differentiated by

Table 8. Orbits for octahedral promolecules

	Promolecule	Symmetry	Chirality	SCR notation
[6]	**4**	O_h	Achiral	$O_h[/C_{4v}(a_6)]$
[51]	**5**	C_{4v}	Achiral	$C_{4v}[/C_s(a_4)\,;\,/C_{4v}(a,\ b)]$
[42]	**6**	D_{4h}	Achiral	$D_{4h}[/C''_{2v}(a_4)\,;\,/C_{4v}(b_2)]$
	7	C''_{2v}	Achiral	$C''_{2v}[/C_s(a_2,\ b_2)\,;\,/C'_s(a_2)]$
[411]	**8**	C_{4v}	Achiral	$C_{4v}[/C_s(a_4)\,;\,/C_{4v}(b,\ c)]$
	9	C_s	Prochiral	$C_s[/C_1(a_2)\,;\,/C_s(2a,\ b,\ c)]$
[33]	**10**	C_{3v}	Achiral	$C_{3v}[/C_s(a_3,\ b_3)]$
	11	C_{2v}	Achiral	$C_{2v}[/C_s(a_2)\,;\,/C'_s(b_2),\ /C_{2v}(a,\ b)]$
[321]	**12**	C'_s	Prochiral	$C'_s[/C_1(a_2,\ b_2)\,;\,/C_s(a,\ c)]$
	13	C_s	Prochiral	$C_s[/C_1(a_2)\,;\,/C_s(a,\ 2b,\ c)]$
	14	C_{2v}	Achiral	$C_{2v}[/C_s(a_2)\,;\,/C'_s(b_2),\ /C_{2v}(a,\ c)]$
[3111]	**15**	C_1	Chiral	$C_1[/C_1(3a,\ b,\ c,\ d)]$
	16–18	C_s	Prochiral	$C_s[/C_1(a_2)\,;\,/C_s(a,\ b,\ c,\ d)]$
[222]	**19**	C_1	Chiral	$C_1[/C_1(2a,\ 2b,\ 2c)]$
	20	C''_{2v}	Achiral	$C''_{2v}[/C_s(a_2,\ c_2)\,;\,/C'_s(b_2)]$
	21	C''_{2v}	Achiral	$C''_{2v}[/C_s(a_2,\ b_2)\,;\,/C'_s(c_2)]$
	22	C''_{2v}	Achiral	$C''_{2v}[/C_s(b_2,\ c_2)\,;\,/C'_s(a_2)]$
	23	D_{2h}	Achiral	$D_{2h}[/C_{2v}(a_2)\,;\,/C'_{2v}(b_2),\ /C''_{2v}(c_2)]$
[2211]	**24, 25**	C_1	Chiral	$C_1[/C_1(2a,\ 2b,\ c,\ d)]$
	26	C_s	Prochiral	$C_s[/C_1(a_2)\,;\,/C_s(2b,\ c,\ d)]$
	27	C_s	Prochiral	$C_s[/C_1(b_2)\,;\,/C_s(2a,\ c,\ d)]$
	28	C'_s	Prochiral	$C'_s[/C_1(a_2,\ b_2)\,;\,/C_s(c,\ d)]$
	29	C_{2v}	Achiral	$C_{2v}[/C_s(a_2)\,;\,/C'_s(b_2),\ /C_{2v}(c,\ d)]$
[21111]	**30–35**	C_1	Chiral	$C_1[/C_1(2a,\ b,\ c,\ d,\ e)]$
	31–38	C_s	Prochiral	$C_s[/C_1(a_2)\,;\,/C_s(b,\ c,\ d,\ e)]$
[111111]	**39–53**	C_1	Chiral	$C_1[/C_1(a,\ b,\ c,\ d,\ e,\ f)]$

Table 9. Orbits for octahedral promolecules with a pair of enantiomorphic proligands

	Promolecule	Symmetry	Chirality	SCR notation
[4; 11]	**54**	C_s'	Prochiral	$C_s'[/C_1(a_2, p\bar{p})\,; /C_s(2a)]$
	55	C_{4h}	Prochiral	$C_{4h}[/C_s(a_4)\,; /C_4(p\bar{p})]$
[31; 11]	**56**	C_1	Chiral	$C_1[/C_1(3a, b, p, \bar{p})]$
	57	C_s	Prochiral	$C_s[/C_1(p\bar{p})\,; /C_s(3a, b)]$
	58, 59	C_s'	Prochiral	$C_s'[/C_1(a_2, p\bar{p})\,; /C_s(a, b)]$
[22; 11]	**60, 61**	C_1	Chiral	$C_1[/C_1(2a, 2b, p, \bar{p})]$
	62	C_s	Prochiral	$C_s[/C_1(p\bar{p})\,; /C_s(2a, 2b)]$
	63	C_s'	Prochiral	$C_s'[/C_1(a_2, p\bar{p})\,; /C_s(2b)]$
	64	C_s'	Prochiral	$C_s'[/C_1(b_2, p\bar{p})\,; /C_s(2a)]$
	65	C_{2h}	Prochiral	$C_{2h}[/C_2(p\bar{p})\,; /C_s'(a_2, b_2)]$
[211; 11]	**66–70**	C_1	Chiral	$C_1[/C_1(2a, b, c, p, \bar{p})]$
	71–73	C_s	Prochiral	$C_s[/C_1(p\bar{p})\,; /C_s(2a, b, c)]$
	74, 75	C_s'	Prochiral	$C_s'[/C_1(a_2, p\bar{p})\,; /C_s(b, c)]$

their SCR notations (Table 8). A *fac–mer* relationship for [33] isomers is exemplified by the pair **10** and **11**.

When an octahedral promolecule has a pair of enantiomorphic proligands several cases emerge to be carefully examined. For example, **58** and **59** are both achiral, whereas they contain chiral proligands. These cases correspond to organic compounds of the *meso*-type. Although **58** and **59** can be interchanged by the permutation of chiral proligands p and $\bar{p}$, they are by no means enantiomeric, but are diastereomeric.

Although several diastereomers have the same SCR notation, most promolecules are well characterized by the SCR notations. Thus, the SCR notations have several advantages over simple point-group notations: (1) Stereochemical equivalency and non-equivalency are easily determined; (2) the local symmetry for each ligand is explicitly designated by the symbol after a slash; (3) the coset representations in the square brackets are algebraically determined by the subduction of the original symmetry of the skeleton.

Stereochemical equivalency and non-equivalency

In general, proligands in the same orbit are determined to be stereochemically equivalent; on the other hand, proligands in different orbits are concluded to be stereochemically non-equivalent. The SCR notation described in the preceding subsection involves information for characterizing such equivalency/non-equivalency. Non-equivalent proligands can be differentiated by an appropriate method, such as NMR spectroscopy.

The present method provides us with unambiguous results for such complicated cases that even careful inspection is liable to mistakes. Let us examine the four *a*s in **54**. The two *a*s in the $C_s'(/C_1)$ orbit (on the left edge) are determined, without any confusion, to be equivalent to each other. Since the $C_s'(/C_1)$ orbit is enantiopheric, the relationship between the two *a*s is concluded to be enantiotopic.

On the other hand, the relationship between the remaining two *a*s (top and bottom) may be erroneously determined to be equivalent by a glimpse of the formula **54**. However, as the SCR notation indicates, one a in the $C_s'(/C_s)$ orbit is non-equivalent to the other a belonging to the other $C_s'(/C_s)$ orbit. In other words, they are diastereotopic.

This conclusion is affirmed by the facts that the bottom one of the two *a*s in **54** is replaced by b to produce **58**, that the replacement of the top a creates molecule **59**, and that the replacement of both by two *b*s affords **63**. These derivations are accompanied by no change in the C_s' symmetry, as found in their SCR notations.

In the same line, the two *a*s in **62** are stereochemically non-equivalent to each other; the *b*s in 62 are also non-equivalent. This fact is closely related to the relationship between **62** and **72** of the same C_s symmetry (or between **62** and **73**). The two *a*s in **63** are equivalent, while the two *b*s in **63** are non-equivalent. Compare **63** with **74** (or with **75**).

Prochiralities of octahedral promolecules and molecules

A promolecule that has at least one enantiospheric orbit is defined as being prochiral.[11] When a promolecule contains an enantiospheric orbit in which half the members are chiral proligands of the same kind and the remaining half are the same number of their antipodes, the two halves are equi-

valent and enantiotopic to each other. Even if all the members of an enantiospheric orbit are achiral as fragments, the half is antipodal to the other half when incorporated in the orbit. The equivalency concerning the two halves of the enantiospheric orbit is created only by improper rotations.

The definition of prochirality can be applied to the present cases of octahedral promolecules. The chirality/achirality/prochirality of each promolecule is found in the chirality columns of Tables 8 and 9. For example, **9** is prochiral because of the enantiospheric $C_s(/C_1)$ orbit; thus, the two *a*s in this orbit (at *trans* positions) can be differentiated by an attack of an appropriate chiral reagent. According to the conventional terminology, they are enantiotopic. If one of the *a*s is replaced by *d* during the attack, either **15** or its enantiomer is obtained in agreement with energetical requirements.

The prochirality of the promolecules in Fig. 3 should be carefully examined, since p and $\bar{p}$ can construct a single orbit. For example, **54** is prochiral because of its $C_s'(/C_1)$ orbits that are enantiospheric. Thus, the two-membered enantiospheric orbit is constructed by a pair, p and $\bar{p}$, and the other enantiospheric orbit is composed of a pair of two *a*s. Hence, a chiral synthesis can be realized by differentiating p from $\bar{p}$ (or one *a* from the other **a**) which are enantiotopic.

A molecule is considered to be a derivative of substituting appropriate ligands for the proligands of a promolecule. Let us re-examine **1a** and **1b**, which can be considered to be derived from **2**. The fixed conformer **1a** is represented by the SCR notation:

$$D'_{2d}[/C_1(H_8); /C_s(N_4, H_4); /C_{2v}(Cl_2); /D_{2d}(Co)].$$

The SCR notation of **1b** is

$$C'_{4v}[/C_1(H_8); /C_s(N_4, H_4); /C_{4v}(2Cl, Co)].$$

Since an enantiospheric orbit represents prochirality, these fixed conformers are prochiral.

If we consider rotations of four ammonia ligands we should use the EWP (extended-wreath-product) notation[16] for rotatable **1**,

$$D_{4h}(/C''_{2v})[4C_{3v}[/C_s(H_3); /C_{3v}(N)]] - D_{4h}(/C_{4v})[2C_{\infty v}[/C_{\infty v}(Cl)]],$$

where the symbol for the central cobalt is abbreviated. This EWP notation is obtained from the SCR notation for **6** (= **2**) and those for ammonia and chloro ligands. Since there emerge no enantiospheric orbits in the EWP notation, rotatable **1** is concluded not to be prochiral. The problem of which of these conclusions is predominant for complex **1** is open to further experimental investigation.

CONCLUSION

The USCI (unit-subduced-cycle-index) method has been applied to enumeration problems concerning octahedral complexes after the derivation of a mark table and relevant tables for the O_h point group. The concept of promolecules and the SCR (set-of-coset representation) notation have proved effective in discussing the stereochemical properties of the complexes, such as prochirality and equivalency/non-equivalency.

REFERENCES

1. A. Werner, *Z. Anorg. Chem.* 1893, **3**, 267.
2. A. Werner, *Ann.* 1912, **386**, 1.
3. Y. Shimura, in *Kagaku Sosetu—Chemistry of Octahedral Complexes*, Vol. 13, Ch. 1, pp. 1–12. Chemical Society of Japan, Gakkai Shuppan Center, Tokyo (1976).
4. W. Preetz and H. Homborg, *Z. Anorg. Chem.* 1974, **407**, 1.
5. B. A. Kennedy, D. A. McQuarrie and C. H. Brubaker Jr, *Inorg. Chem.* 1964, **3**, 265.
6. D. H. McDaniel, *Inorg. Chem.* 1972, **11**, 2678.
7. W. E. Bennett, *Inorg. Chem.* 1969, **8**, 1325.
8. S. Fujita, *Theoret. Chim. Acta* 1989, **76**, 247.
9. S. Fujita, *Symmetry and Combinatorial Enumeration in Chemistry*. Springer-Verlag, Berlin (1991).
10. S. Fujita, *Tetrahedron* 1991, **47**, 31.
11. S. Fujita, *J. Am. Chem. Soc.* 1990, **112**, 3390.
12. W. Burnside, *Theory of Groups of Finite Order*, 2nd edn. Cambridge University Press, Cambridge (1911).
13. S. Fujita, *J. Math. Chem.* 1990, **5**, 99.
14. G. Pólya and R. C. Read, *Combinatorial Enumeration of Groups, Graphs and Chemical Compounds*. Springer, New York (1987).
15. S. Fujita, *Bull. Chem. Soc. Japan* 1990, **63**, 203.
16. S. Fujita, *Theoret. Chim. Acta* 1990, **78**, 45.

Polyhedron Vol. 12, No. 1, pp. 111–115, 1993
Printed in Great Britain

0277-5387/93 $6.00+.00
© 1993 Pergamon Press Ltd

THE DESIGN SYNTHESIS AND CRYSTALLOGRAPHIC CHARACTERIZATION OF A NOVEL HETEROTRIMETALLIC LINEAR COMPLEX OF $[Et_4N][(Ph_3P)_2\{CuS_2MoS_2Fe\}Cl_2]$

TIANLU SHENG, SHAOWU DU and XINTAO WU*

State Key Laboratory of Structure Chemistry, Fujian Institute of Research on Structure of Matter, Chinese Academy of Science, Fuzhou, Fujian 350002, P.R.C.

(*Received* 13 *July* 1992; *accepted* 10 *August* 1992)

Abstract—The complex $[Et_4N][(Ph_3P)_2\{CuS_2MoS_2Fe\}Cl_2]$ has been obtained by reaction of $[Et_4N]_2[S_2MoS_2FeCl_2]$ with $Cu(PPh_3)_3Cl$ in $MeCN/CH_2Cl_2$. In this new complex, the bond lengths of the Mo—Fe bond and the Mo—Cu bond are 2.769(2) and 2.786(2) Å, respectively.

The tetrathiometallate anions MoS_4^{2-} and WS_4^{2-} have been shown to be important in various biological processes.[1,2] Thiomolybdates were detected in the hydrolysis product of nitrogenase (Fe–Mo protein of *clostridium pasteurianium*)[1] and most probably are formed in the rumen of grazing animals.[2] Many types of compounds, which are interesting from the stand-point of structural chemistry, are formed with the aid of doubly, triply and quasi-quadruply bridging tetrathiomellate ligands. The complex anion $[S_2MoS_2FeCl_2]^{2-}$ [3] can serve as a precursor for the synthesis of Fe–Mo cofactors (FeMo-co).[4] The MoS_4^{2-} anion has been claimed to be the most effect antagonist[2b] of copper metabolism. Extensive research has been performed on MoS_4^{2-}-Cu[1,5–10] complexes which show a rich structural variety. Meanwhile a number of MoS_4^{2-}-Ag^I complexes[1,5b,10–13] have been obtained. Recently, some heterotrimetallic $[(PPh_3)_2AgS_2MS_2Cu(CN)]^-$ [14] (M = Mo, W) and $[(PPh_3)_2AgS_3MOCu(CN)]^-$ [15] (M = Mo, W) complexes were also synthesized in our laboratory.

The anionic fragment $[MoS_4FeCl_2]^{2-}$ may be expected to combine with another metal complex to form a heterobimetallic complex, for example a $[Cl_2FeS_2MoS_2FeCl_2]^{2-}$ [16] type cluster, but no heterotrimetallic complexes of this series have been reported as yet. In this paper, the designed synthesis of a novel heterotrimetallic complex is reported.

* Author to whom correspondence should be addressed.

EXPERIMENTAL

All operations were carried out under dinitrogen. Solvents and reagents were degassed by repeated evacuation and flushing with pure dinitrogen before use. MeCN was distilled from CaH_2 and CH_2Cl_2 was of A.R. grade and used without further purification. $Cu(PPh_3)_3Cl$ was obtained from a CH_3OH solution of PPh_3 and CuCl (molar ratio 3:1). Elemental analyses were performed by the Elemental Analysis Laboratories in our Institute. The visible and UV electronic spectra were recorded on a Shimadzu UV-3000 spectrophotometer. IR spectra were obtained on a Perkin–Elmer 577 spectrometer.

Preparation of $[Et_4N][(Ph_3P)_2\{CuS_2MoS_2Fe\}Cl_2]$

A solution of $Cu(PPh_3)_3Cl$ (0.886 g, 1.0 mmol) in CH_2Cl_2 (30 cm^3) was slowly added to a solution of $[Et_4N]_2[MoS_4FeCl_2]$ [17] (0.612 g, 1.0 mmol) in MeCN (25 cm^3). After stirring for a while at 35°C, the colour changed from dark to red to black and a red precipitate appeared after 2 min. Pr^iOH (5 cm^3) was added and then filtered. The filtrate was kept in a refrigerator and black crystals of the title compound were obtained the next day. Yield 0.70 g (65.46%). Found: C, 49.5; H, 4.4; N, 1.8; P, 5.3; S, 12.3; Cl, 7.0; Cu, 5.8; Mo, 9.9; Fe, 5.4. Calc. for $C_{44}H_{50}NP_2Cl_2S_4CuMoFe$: C, 49.4; H, 4.7; N, 1.3; P, 5.8; S, 11.9; Cl, 6.6; Cu, 5.9; Mo, 8.9; Fe, 5.2%. IR spectra (KBr pellet, cm^{-1}); δ (C—H) in PPh_3: 750.2 (vs), 696 (vs); Cu—P: 519 (vs), 507.3 (vs);

Mo—μ_2-S: 478.4 (s), 468.5 (vs), 428.9 (w); Fe—Cl: 350.3 (s), 333.2 (vs).

Crystal structure determination

The crystal and refinement data for the structure of the compound are shown in Table 1, together with some experimental details. Data were collected on a Rikagu AFC5R diffractometer using Mo-K_α radiation ($\lambda = 0.71069$ Å) at 296 K. The ω scan speed was varied on the basis of the SEARCH intensity (maximum 16° min^{-1}). Three standard reflections were measured periodically in each case, and the absence of random deviations indicated crystal and electronic stability. The intensity error was defined as $\sigma(F^2) = c + \frac{1}{4}(t_c/t_b)^2(b_1+b_2)+(PI)^2$, where I is the intensity and P a factor which downweights strong reflections, taken to be 0.05. The data were corrected for Lorentz and polarization effects and for absorption using empirical ω scan data and DIFABS.[18] The structure was solved by the Patterson method and direct methods using MITHRIL.[19] The coordinates of the molybdenum atom were obtained from the Patterson function analysis, and the iron and copper atoms were located in the E-map. Most non-hydrogen atoms were successively located using the DIRDIF program;[20] some non-hydrogen atoms were located in the succeeding difference-Fourier syntheses. The structure was refined by a full-matrix least-squares calculation. Molybdenum, iron, copper, chlorine and sulphur in the anion and the two phosphorus atoms were refined with anisotropic temperature factors; all carbon atoms in the PPh_3 ligands and all the carbon atoms in the cations were refined with isotropic temperature factors. Structure details for the title complex anion are shown in Table 1. All calculations were performed on a VAX 785 computer using the TEXSAN program package.[21] Non-hydrogen scattering factors were taken from Cromer and Waber.[22]

Important bond lengths and bond angles for the title complex are given in Tables 2 and 3, respectively.

RESULTS AND DISCUSSION

Synthesis

The substitution reaction between metals or ligands may cause difficulties in obtaining the heterotrimetallic complex. In our procedure, two reac-

Table 1. Crystal data and some experimental details for the title compound

Empirical formula	$C_{44}H_{50}NP_2S_4Cl_2MoCuFe$
Formula weight	1069.31
Crystal system	Triclinic
Lattice parameters	
a (Å)	13.429(3)
b (Å)	15.284(4)
c (Å)	12.285(3)
α (°)	105.50(2)
β (°)	93.21(2)
γ (°)	101.54(2)
V (Å^3)	2365(1)
Space group	$P\bar{1}$ (No. 2)
Z value	2
D_{calc} (g cm^{-3})	1.50
$F(000)$	1092
μ(Mo-K_α) (cm^{-1})	13.86
Diffractometer	Rigaku AFC5R
Radiation	Mo-K_α ($\lambda = 0.71069$ Å)
Temperature (°C)	23
2θ (max) (°)	48.1
No. of observations [$I < 3.00(\sigma(I))$]	3735
No. of variables	280
Residuals: R; Rw	0.059; 0.076
Goodness of fit indicator	1.59
Maximum shift in final cycle	0.01
Largest peak in final difference map (e Å^{-1})	0.75

Table 2. Selected bond lengths

Mo—Fe	2.769(2)	Cu—S(1)	2.310(4)
Mo—Cu	2.786(2)	Cu—S(2)	2.330(4)
Mo—S(1)	2.180(3)	Cu—P(1)	2.321(3)
Mo—S(2)	2.182(3)	Cu—P(2)	2.331(3)
Mo—S(3)	2.223(3)	P(1)—C(131)	1.81(1)
Mo—S(4)	2.229(3)	P(1)—C(111)	1.82(1)
Fe—S(3)	2.272(4)	P(1)—C(121)	1.83(1)
Fe—S(4)	2.281(4)	P(2)—C(211)	1.81(1)
Fe—Cl(1)	2.211(4)	P(2)—C(231)	1.81(1)
Fe—Cl(2)	2.216(4)	P(2)—C(221)	1.82(1)

tions can be presented as follows:

$$[MoS_4FeCl_2]^{2-} + Cu(PPh_3)_3^+ \longrightarrow [(Ph_3P)_2CuS_2MoS_2FeCl_2]^- \quad (1)$$

$$[(Ph_3P)_2CuS_2MoS_2FeCl_2]^- + Cu(PPh_3)_3^+ \rightleftharpoons [(Ph_3P)_2CuS_2MoS_2Cu(PPh_3)] + FeCl_2. \quad (2)$$

Due to eq. (2), the yield of the title compound was lower. If the concentration of $FeCl_2$ is increased, the yield of the title compound will be increased. Obviously, if the concentration of $Cu(Ph_3P)_3^+$ ions is increased, the yield of the title compound will be reduced. However, using $[MoS_4Fe(SPh)_2]^{2-}$ to replace $[MoS_4FeCl_2]^{2-}$, only $[(Ph_3P)_2CuS_2MoS_2Cu(PPh_3)]$ was produced, which may be because the Lewis acid strength of $FeCl_2$ is stronger than that of $Fe(SPh)_2$.

Structure

$[(Ph_3P)_2\{CuS_2MoS_2Fe\}Cl_2]^-$ is shown in Fig. 1. The arrangement of the three atoms Fe—Mo—Cu is approximately linear (Fe—Mo—Cu is 178.41°). C_{2v} is the idealized symmetry of the anion. In the structure of the anion the molybdenum atom retains its tetrahedral coordination by four sulphur atoms as in MoS_4^{2-}. The two metal atoms attached to the MoS_4 moiety all have approximately tetrahedral geometry.

The MoS_2Cu and MoS_2Fe cores are planar to within a maximum of 0.007 and 0.001 Å, respectively. Their dihedral angle is 90.10°, which means they are very closely perpendicular to each other. The Mo—Fe distance [2.769(2) Å] in the title compound is slightly shorter than the Mo—Fe distances [2.786(1) Å] in $[S_2MoS_2FeCl_2]^{2-}$ (**1**)[3] and [2.775(6) Å] $[Cl_2FeS_2MoS_2FeCl_2]^{2-}$ (**2**),[16] respectively. However, the Mo—Cu distance (2.786 Å) in the title compound is slightly longer than the Mo—Cu distance [2.775(2) Å] in $[(Ph_3P)_2CuS_2MoS_2Cu(PPh_3)]\cdot 0.8CH_2Cl_2$.[23] The mean value for the Mo—S (sulphur bonded to the iron atom) bond lengths [2.226(3) Å] in the title compound is slightly longer

Table 3. Selected bond angles

Fe—Mo—Cu	178.41(8)	S(2)—Cu—Mo	49.51(9)
S(1)—Mo—S(2)	108.1(1)	P(2)—Cu—Mo	121.2(1)
S(1)—Mo—S(3)	110.4(1)	Cl(1)—Fe—Cl(2)	111.2(2)
S(1)—Mo—S(4)	111.1(1)	Cl(1)—Fe—S(3)	112.1(2)
S(1)—Mo—Fe	125.8(1)	Cl(1)—Fe—S(4)	109.8(2)
S(2)—Mo—Fe	126.2(1)	Cl(2)—Fe—S(3)	110.0(2)
S(3)—Mo—Fe	52.8(1)	Cl(2)—Fe—S(4)	110.9(2)
S(4)—Mo—Fe	53.0(1)	Cl(1)—Fe—Mo	124.8(1)
S(1)—Mo—Cu	53.8(1)	Cl(2)—Fe—Mo	124.0(1)
S(2)—Mo—Cu	54.3(1)	S(3)—Fe—Mo	51.19(9)
S(3)—Mo—Cu	125.7(1)	S(4)—Fe—Mo	51.3(1)
S(4)—Mo—Cu	128.5(1)	Mo—S(1)—Cu	76.6(1)
S(2)—Mo—S(3)	110.3(1)	Mo—S(2)—Cu	76.2(1)
S(2)—Mo—S(4)	111.3(1)	Mo—S(3)—Fe	76.0(1)
S(3)—Mo—S(4)	105.8(1)	Mo—S(4)—Fe	75.7(1)
S(1)—Cu—P(1)	110.4(1)	S(3)—Fe—S(4)	102.5(1)
S(1)—Cu—S(2)	99.1(1)	C(111)—P(1)—Cu	116.7(4)
S(1)—Cu—P(2)	112.9(1)	C(121)—P(1)—Cu	112.4(4)
P(1)—Cu—S(2)	111.9(1)	C(131)—P(1)—Cu	116.9(4)
P(1)—Cu—P(2)	115.4(1)	C(211)—P(2)—Cu	120.1(4)
S(2)—Cu—P(2)	105.8(1)	C(221)—P(2)—Cu	109.6(4)
S(1)—Cu—Mo	49.58(9)	C(231)—P(2)—Cu	115.7(4)
P(1)—Cu—Mo	123.3(1)		

Table 4. Electronic spectra in DMF

Complex	λ/nm (10^{-3} ε/dm^3 mol^{-1} cm^{-1})	Ref.
$[Et_4N]_2[MoS_4]$	477(14.25), 324(20.60)	10
$[Et_4N]_2[S_2MoS_2FeCl_2]$	468.9(5.0), 433(4.1), 314.8(11.2), 290(9.6)	This work
$[Ph_4P]_2[Cl_2FeS_2MoS_2FeCl_2]$	472(5.8), 432(4.07), 314(12.3)	16
$[Et_4N][(Ph_3P)_2CuS_2MoS_2FeCl_2]$	475.6(4.9), 436.5(4.2), 312.5(15.9), 265.5(25.7)	This work

than the corresponding value of 2.204 Å in **2**; while the mean value for the Mo—S (sulphur is bonded to the copper atom) bond lengths [2.181 (3) Å] is slightly shorter than the corresponding value of 2.208 Å in $[(Ph_3P)_2CuS_2MoS_2Cu(PPh_3)]\cdot 0.8CH_2Cl_2$ (**3**).[24] The Fe—S bond length [2.276(4) Å] in the title compound is longer than the Fe—S bond length [2.263(2) Å] in **1** and shorter than the Fe—S bond length (2.295 Å) in **2**. The Cu—S distance [2.310(4)–2.330(4) Å] in the title compound is slightly longer than the Cu—S distance [2.212(5)–2.315(6) Å] in **3**.

The structure of the anion is quite similar to that of $[Cl_2FeS_2MoS_2FeCl_2]^{2-}$,[16] in which the MoS_4 unit bridges two terminal $FeCl_2$ moieties and the MoS_4^{2-} and $FeCl_2S_2$ fragments show distorted tetrahedral geometry around the metal.

The electronic spectra of the anions of the $[Et_4N]_2[MoS_4]$, $[Et_4N]_2[S_2MoS_2FeCl_2]$, $[Ph_4P]_2[Cl_2FeS_2FeCl_2]$ and $[Et_4N][(Ph_3P)_2CuS_2MoS_2FeCl_2]$ complexes are listed in Table 4. A simple molecular orbital (MO) scheme for MS_4^{2-} (T_d symmetry) may be devised[25] by assuming *nd*, $(n+1)s$ and $(n+1)p$ valence orbitals on M and 3*s* and 3*p* valence orbitals on S. The longest wavelength absorption at 477 nm can be unambiguously assigned[11,25] to the one-electron transition v_1: $t_1(n,\pi) \rightarrow 2e(d)$ on the basis of magnetic circular dichroism measurements. The absorption at 324 nm was plausibly assigned to v_2: $3t_2(\pi,\sigma) \rightarrow 2e(d)$, and the other absorption at 240–280 nm is assigned to v_3: $t_1(n,\pi) \rightarrow 4t_2(d)$. Our results are also consistent with the conclusion[10] that the bi- and trinuclear complexes absorb in the same energy regions as MoS_4^{2-}. It is demonstrated[10,25] that the spectra of the complex are dominated by the internal transitions of $[MoS_4]^{2-}$. The splitting of the v_1 absorption is plausibly due to raising the degeneracy of the $t_1(n,\pi)$ level in the lower symmetry of the complexes $[t_1(T_d) \leftrightarrow a_2+e(D_{2d}) \leftrightarrow a_2+b_1+b_2(C_{2v})]$. The MoS_4^{2-} S→Mo transition in the title compound is split, which is consistent with the Fe—MoS_4^{2-} complexes previously reported,[26] due to lowering in local symmetry about the central atom in the MS_4^{2-} unit from T_d to C_{2v} in the title compound. It is interesting that the longest wavelength band, v_1, in the title compound is somewhat red-shifted after the incorporation of a $Cu(PPh_3)_2^+$ group.

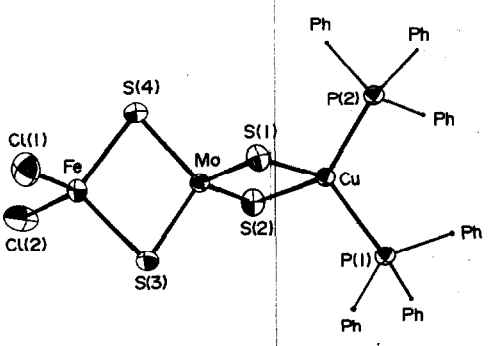

Fig. 1. The ORTEP drawing of the anion $[(PPh_3)_2\{CuS_2MoS_2Fe\}Cl_2]^-$.

Acknowledgements—This research was supported by grants from the State Key Laboratory of the Structural Chemistry, Fujian Institute of Research on the Structure of Matter, Chinese Academy of Sciences and the National Science Foundation of China.

REFERENCES

1. W. G. Zumft, *Eur. J. Biochem.* 1978, **91**, 345.
2. (a) E. J. Underwood, *Trace Elements in Human and Animal Nutrition*, 4th edn. Academic Press, New York (1977); (b) C. F. Mills, *Chem. Ber.* 1979, **15**, 512; *Phil. Trans. R. Soc.* 1979, **B288**, 51 and refs therein; private communication (1980); (c) N. J. Clark and S. H. laurie, *J. Inorg. Biochem.* 1980, **12**, 37.
3. R. H. Tieckelmann, H. C. Silvis, T. A. Kent, B. H. Huynb, J. V. Waszczak, Boon-Keng Teo and B. A. Averill, *J. Am. Chem. Soc.* 1980, **102**, 5550.
4. W. E. Newton, B. K. Burgess and E. I. Stiefel, in *Molybdenum Chemistry of Biological Significance* (Edited by W. E. Newton and S. Otsuka). Plenum Press, New York (1980); V. K. Shan and W. J. Brill, *Proc. Nat. Acad. Sci. USA* 1977, **74**, 3249.
5. (a) A. Müller, R. Jostes and F. A. Cotton, *Angew. Chem., Int. Edn Engl.* 1980, **19**, 875; (b) A. Müller, H. Bögge and U. Schimanski, *Inorg. Chim. Acta* 1983, **69**, 5 and refs therein.

6. F. Sarkar and S. B. S. Mishra, *Coord. Chem. Rev.* 1984, **59**, 239.
7. (a) S. R. Acott, C. D. Garner, J. R. Nicholson and W. Clegg, *J. Chem. Soc., Dalton Trans.* 1983, 713; (b) J. R. Nicholson, A. C. Flood, C. D. Garner and W. Clegg, *J. Chem. Soc., Chem. Commun.* 1983, 1179.
8. F. Secheresse, M. Salis, C. Potvin and J. M. Manoli, *Inorg. Chim. Acta* 1986, **114**, L19; J. M. Manoli, C. Potvin, F. Secheresse and S. Marzak, *Inorg. Chim. Acta* 1988, **150**, 257.
9. (a) X.-T. Wu, S.-F. Lu, L.-Y. Zu, Q.-J. Wu and J.-X. Lu, *Inorg. Chim. Acta* 1987, **133**, 39; (b) S.-F. Lu, N.-Y. Zhu, X.-T. Wu, Q.-J. Wu and J.-X. Lu, *J. Molec. Struct.* 1989, **197**, 15; (c) H.-Q. Zhang, Y.-F. Zheng, X.-T. Wu and J.-X. Lu, *Inorg. Chim. Acta* 1989, **156**, 277; (d) Y.-F. Zheng, H.-Q. Zhang, X.-T. Wu and J.-X. Lu, *Trans. Met. Chem.* 1989, **14**, 161; (e) X.-T. Wu, Y.-F. Zheng, S.-W. Du and N.-Y. Zhu, *Trans. Met. Chem.* 1989, **14**, 157; (f) N.-Y. Zhu, J.-H. Wu and X.-T. Wu, *Acta Cryst., Sect. C* 1991, **C47**, 856; (g) X.-T. Wu, Y.-F. Zheng and S.-W. Du, *Acta Cryst., Sect. C* 1989, **45**, 1070.
10. S. F. Gheller, T. W. Hambley, J. R. Rodgers, R. T. C. Brownlee, M. J. O'Connor, M. R. Snow and A. G. Wedd, *Inorg. Chem.* 1984, **23**, 2519.
11. A. Müller and R. Menge, *Z. Anorg. Allg. Chem.* 1972, **393**, 259; J. C. Huffman, R. S. Roth and A. R. Siedle, *J. Am. Chem. Soc.* 1976, **98**, 4340.
12. A. Müller, H. Bögge, E. Königer-Ahlborn and W. Hellmann, *Inorg. Chem.* 1979, **18**, 2301; A. Müller, H. Böggle and T. K. Kwang, *Inorg. Chem.* 1980, **39**, 73; J. K. Stalick, A. R. Siedle, A. D. Minghell and C. R. Hubbard, *J. Am. Chem. Soc.* 1979, **101**, 2903.
13. C.-C. Lin and Z.-X. Huang, *Jiegou Huaxue* 1990, **9**, 58 (English).
14. S.-W. Du, N.-Y. Zhu, P.-C. Chen, X.-T. Wu and J.-X. Lu, *Polyhedron* 1992, **11**, 109.
15. S.-W. Du, N.-Y. Zhu, P.-C. Chen, X.-T. Wu and J.-X. Lu, *J. Chem. Soc., Dalton Trans.* 1992, 339.
16. D. Coucouvanis, N. C. Baenziger, E. D. Simhon, P. Stremple, D. Swenson, A. Kostikas, A. Simopoulos, V. Petrouleas and V. Papaefthymiou, *J. Am. Chem. Soc.* 1980, **102**, 1732.
17. Preparation of $[Et_4N]_2[MoS_4FeCl_2]$: anhydrous $FeCl_2$ (0.128 g, 1 mmol) and $Et_4Cl \cdot H_2O$ (0.184 g, 1.0 mmol) were dissolved in MeCN (50 cm^3), to which $[Et_4N]_2[MoS_4]$ (0.484 g, 1.0 mmol) was added. The initial brown–yellow solution changed to dark red upon stirring for approximately 5 h at 40°C and then was filtered. The filtrate was kept in a refrigerator and the black crystals were obtained the next day.
18. N. Walker and D. Stuart, DIFABS, *Acta Cryst., Sect. A* 1983, **39**, 159.
19. C. J. Gilmore, MITHRIL, A Computer Program for the Automatic Solution of Crystal Structures from X-ray Data. University of Glasgow (1983).
20. P. T. Beurskens, DIRDIF, Direct Methods for Difference Structures: An Automatic Procedure for Phase Extension and Refinement of Difference Structure Factors, Technical Report 1984/1. Crystallography laboratory, Toernooiveld (1984).
21. TEXSAN, TERAY Structure Analysis Package. Molecular Structure Corporation (MSC), TX (1985).
22. D. T. Cromer and J. T. Waber, *International Tables for X-Ray Crystallography*, Vol. 4, Tables 2.2a and 2.3.1. Kynoch Press, Birmingham (1974).
23. A. Müller, H. Bögge and U. Schimanski, *Inorg. Chim. Acta* 1980, **45**, L249.
24. A. Müller, H. Bögge, H. G. Tölle, R. Jostes, U. Schimanski and M. Dartmann, *Angew. Chem., Ind. Edn Engl.* 1980, **8**, 19.
25. A. Müller, E. Diemann, R. Jostes and H. Bögge, *Angew. Chem., Int. Edn Engl.* 1981, **20**, 934.
26. D. Coucouvanis, *Accts Chem. Res.* 1981, **14**, 201.

Polyhedron Vol. 12, No. 1, pp. 117–124, 1993
Printed in Great Britain

0277–5387/93 $6.00+.00
© 1993 Pergamon Press Ltd

EPR STUDIES ON BIS(DIISOPROPYLDITHIOPHOSPHATO)COPPER(II) MAGNETICALLY DILUTED IN THE CORRESPONDING PALLADIUM(II) AND PLATINUM(II) SINGLE CRYSTALS AND CRYSTAL AND MOLECULAR STRUCTURE OF BIS(DIISOPROPYLDITHIOPHOSPHATO)PALLADIUM(II) HOST LATTICE

N. D. YORDANOV* and M. IVANOVA

Institute of Kinetics and Catalysis, Bulgarian Academy of Sciences, 1113 Sofia, Bulgaria

and

G. GOCHEV

Chemistry Department, University of Sofia, 1126 Sofia, Bulgaria

and

J. MACICEK

Institute of Applied Mineralogy, Bulgarian Academy of Sciences, 1000 Sofia, Bulgaria

(*Received* 23 *June* 1992; *accepted* 10 *August* 1992)

Abstract—The EPR spectra of single-crystal samples of $^{63}Cu[(Pr^i_2O)_2PS_2]_2$ magnetically diluted in the corresponding palladium(II) and platinum(II) host lattices were studied at room temperature and eigen-values of the A and g tensors evaluated. The results obtained show that both the samples have approximately axial symmetry ($\Delta A = A_x - A_y \leqslant 3$ G; $\Delta g = g_x - g_y \leqslant 0.03$) with one molecule per unit cell in both host lattices. It is found that g_z coincides with A_z whereas the angle between g_x and A_x (g_y and A_y) is 27° and 11° for $^{63}Cu/Pt[(Pr^i_2O)_2PS_2]_2$ and $^{63}Cu/Pd[(Pr^i_2O)_2PS_2]_2$, respectively. The data about a quadrupole interaction obtained was considered with special attention, because their values are close to the experimental error. In view of this, the possibility for determiming Q values from simulated powdered EPR spectra was explored. The results show, however, inapplicability of this approach too. The crystal and molecular structure of bis(diisopropyldithiophosphato)palladium(II) was determined.

It is well known that the single-crystal EPR studies of paramagnetic species give comprehensive information about all spin-Hamiltonian parameters. In many cases, however, it is difficult or impossible to grow suitable single crystals. The spin-Hamiltonian parameters can then be determined from EPR spectra of powders and/or frozen solutions, but with less accuracy. However, in a typical case when anisotropy is present, only the principal values of various tensors can be obtained from powder-type EPR spectra and the mutual orientations of the principal directions of these tensors remain unknown. A possible solution of this problem would be the comparison between computer simulated spectra, by varying unknown parameters in reasonable limits, and experimentally obtained ones until satisfactory coincidence occurred. In this manner many authors have made conclusions not only about the strongest coupling constants but also about much weaker interactions such as quadrupole coupling.[1–3] The

* Author to whom correspondence should be addressed.

applicability of this approach can be verified when both single-crystal and powder-type EPR spectra of a given paramagnetic species are available. The constants of the quadrupole interaction evaluated in this way, for copper(II) chelate complexes in different host lattices, differ strongly from each other and do not coincide with the values obtained from the method of ENDOR spectroscopy.

In this paper the results obtained on single-crystal and powder-type experimentally recorded and simulated EPR spectra of bis(diisopropyldithiophosphato)copper(II), $Cu[(C^i_3H_7O)_2PS_2]_2$, magnetically diluted in the corresponding platinum and palladium host lattices, are presented. The molecular and crystal structure of $Pd[(C^i_3H_7O)_2PS_2]_2$ is also presented.

EXPERIMENTAL

Preparation of the samples

The preparation of magnetically diluted samples of $^{63}Cu/Pd[(C^i_3H_7O)_2PS_2]_2$ and $^{63}Cu/Pt[(C^i_3H_7O)_2PS_2]_2$ was performed by the following stages:

Synthesis of the ligand. The preparation of the potassium salt of the ligand $(C^i_3H_7O)_2PSSK$ was made according to the following equations:

$$4C^i_3H_7OH + P_2S_5 \longrightarrow 2(C_3H_7O)_2PS(S)H + H_2S \quad (1)$$

$$(C^i_3H_7O)_2PS(S)H + KOH \longrightarrow (C_3H_7O)_2PS(S)K + H_2O. \quad (2)$$

In a three-necked round-bottomed flask, equipped with a mechanical stirrer, condenser and nitrogen inlet, fine melted P_2S_5 was added in small portions to absolute $C^i_3H_7OH$. Nitrogen was bubbled through dry isopropanol and the mixture was stirred continuously and heated for 3 h at a temperature of 50°C. After that the mixture was cooled to room temperature, filtered and neutralized with KOH. The mixture was then cooled in an ice bath, the precipitate, $[(C^i_3H_7O)_2PS(S)K]$, formed was collected, washed with C_2H_5OH and dried at room temperature.

Preparation of the complexes. The complexes $Cu[(C^i_3H_7O)_2PS_2]_2$, $Pd[(C^i_3H_7O)_2PS_2]_2$ and $Pt[(C^i_3H_7O)_2PS_2]_2$ were obtained by mixing aqueous solutions of the corresponding $^{63}CuCl_2$ (obtained as CuO from AERE, Harwell and transformed in $CuCl_2$), K_2PdCl_4 (Fluka) and K_2PtCl_4 (Fluka) and the potassium salt of the ligand, $(C^i_3H_7O)_2PS(S)K$. The complexes precipitated were collected and recystallized from $CHCl_3$.

Single crystals of $Pd[(C^i_3H_7O)_2PS_2]_2$ suitable for X-ray study were obtained by slow evaporation of a chloroform/n-heptane (1 : 1 v/v) solution of $Pd[(C^i_3H_7O)_2PS_2]_2$ in an open beaker.

Preparation of magnetically diluted $^{63}Cu/Pd[(C^i_3H_7O)_2PS_2]_2$ and $^{63}Cu/Pt[(C^i_3H_7O)_2PS_2]_2$ powder and single-crystal samples. The powdered sample of $^{63}Cu/Pt[(C^i_3H_7O)_2PS_2]_2$ has been obtained by the exchange of approximately 2% platinum(II) with copper(II) from $CHCl_3$–water solutions. After intensive shaking for 30 min, or 12 h staying of the mixture, the organic phase was separated and evaporated.

The sample of $^{63}Cu/Pd[(C^i_3H_7O)_2PS_2]_2$ was prepared by dissolving the corresponding palladium(II) and copper(II) complexes (in a ratio of 98 : 2) in $CHCl_3$, followed by evaporation of the solvent. The magnetically diluted single-crystals of $^{63}Cu/Pt[(C^i_3H_7O)_2PS_2]_2$ and $^{63}Cu/Pd[(C^i_3H_7O)_2PS_2]_2$, suitable for EPR measurements, have been obtained by slow evaporation of their chloroform/n-heptane (1 : 1 v/v) solutions in an open beaker.

EPR measurement

All EPR spectra were recorded on a Bruker ER 200-D SRC X band spectrometer at room temperature using 100 kHz modulation of the magnetic field. The microwave frequency of each EPR spectrum was calculated from the line position of a point standard of powdered DPPH fixed on the bottom side of the cavity. A two-circle goniometer (Bruker G-2) was used for the orientation and rotation of the single-crystal samples in the magnetic field. The EPR spectra were taken every 10° in three mutually perpendicular planes. All spectra were acquired using the specialized module described in reference 4. The post-acquisition processing and manipulation of the spectra were performed on an IBM compatible PC using a special program prepared in this laboratory. A conventional spin-Hamiltonian parameter [eq. (1)] for this kind of paramagnetic species ($S = 1/2$, $I \neq 0$) was used to describe the experimentally obtained EPR spectra.

$$\mathcal{H} = \beta HgS + SAI + IQI - g_n\beta_n HI. \quad (1)$$

All the symbols in eq. (1) have their usual meaning. A perturbation approach with first- and second-order corrections to the energy levels with respect to the hyperfine, quadrupole and nuclear Zeeman coupling was used to get the relationship between the line positions for a given direction of the magnetic field and the components[5,6] of the tensors. Because this relationship is very complex a modified simplex procedure[7] was used to obtain the best estimation of the components of various tensors. A criterion for goodness of fit is the quantity

$$S = \left\{ \frac{1}{N(2I+1)} \sum_{i=1}^{N} \sum_{m_I=-I}^{I} [h\nu_i - f(i, m_I, P_\alpha)]^2 \right\}^{1/2}, \quad (2)$$

where N is the number of single-crystal spectra, ν_i the microwave frequency for the ith spectrum, I the spin of the central nucleus and P_α the components of the tensors. In all cases the minimum value of $S = 0.5 \times 10^{-4}$ cm^{-1}, which is comparable with the experimental error in measuring line positions (0.5 G), was chosen as a goodness-of-fit. After this fitting the g, A and Q tensors were diagonalized and their principal values, as well as their principal direction with respect to the laboratory reference frame, were obtained. Based on these data, powdered spectra of the samples were simulated and the best fit with the experimentally-recorded powdered spectra was found. The powdered EPR spectra were simulated using a computer program written on the basis of Pilbrow's algorithm[8,9] and assuming a Lorentz line shape in all cases.

X-ray study

A brown prismatically-shaped crystal of $Pd[(C^{i}_{3}H_7O)_2PS_2]_2$ with approximate dimensions $0.25 \times 0.28 \times 0.12$ mm was investigated at 290 K on an Enraf–Nonius CAD-4 diffractometer (graphite monochromator, Mo-K_α radiation, $\lambda = 0.70930$ Å). Crystal data: $C_{12}H_{28}PdO_4P_2S_4$, $Mr = 532.96$, triclinic system, space group $P\bar{1}$, $a = 6.379(1)$, $b = 8.449(1)$, $c = 10.977(3)$ Å, $\alpha = 99.89(1)$, $\beta = 97.04(1)$, $\gamma = 99.42(1)°$, $V = 568$ Å^3, $Z = 1$, $D_x = 1.558$ g cm^{-3}, $\mu = 13.1$ cm^{-1}, $F(000) = 272$.

The intensities were collected in an $\omega/2\theta$ scan mode with $\Delta\omega = [0.9 + 0.4 \tan\theta]°$. In total 5464 reflections were measured in the range $\sin\theta/\lambda < 0.660$ (h: -8 to 8, k: -11 to 11, l: -14 to 14). Three standard reflections were monitored every 2 h and exhibited intensity variation less than 0.4%. Lorentz, polarization and empirical absorption corrections (transmission factor 0.9424–0.9996) were applied. From 2732 unique reflections with $R(\text{int}) = 0.012$, 2413 with $I > 3\sigma(I)$ were used in further calculations. The structure was solved by the heavy-atom method by placing a palladium atom in the origin ($Z = 1$). Subsequent full-matrix least-squares refinement on Fs, followed by difference Fourier syntheses, revealed the remaining atoms. The positions of the hydrogen atoms were geometrically regularized and included in the final refinement as riding atoms, with fixed $U = 0.06$ Å^2. Final $R = 0.020$, $wR = 0.033$ and $S = 1.356$; $w = 4F_o^2/[s(F_o)^2]^2$. Max. $(\Delta/\rho) = 0.007$; max. and min. residual densities 0.31 and -0.57 e Å^{-3}. Atomic scattering factors and anomalous-dispersion coefficients were used as coded in the SDP/PDP V3.0 software (Enraf–Nonius, 1985).[10] Positional and thermal parameters have been deposited along with tables of F_o/F_c values.

RESULTS AND DISCUSSION

Single-crystal EPR study

Single crystal EPR spectra of $^{63}Cu/Pt[(C^{i}_{3}H_7O)_2PS_2]_2$ and $^{63}Cu/Pd[(C^{i}_{3}H_7O)_2PS_2]_2$ for two different arbitrarily chosen orientations with respect to the laboratory coordinate system are shown in Figs 1 and 2. Due to the hyperfine (hf) interaction with the ^{63}Cu nucleus ($I = 3/2$), both spectra consist of four hf lines. In addition, each hf line is further split into three lines with relative intensities 1:2:1, as a result of the superhyperfine (shf) interaction between $^{63}Cu^{II}$ unpaired electrons and two equivalent ^{31}P nuclei. Independently of the sample's orientation the shf splitting constant was evaluated to be 9.5 G. This result is in

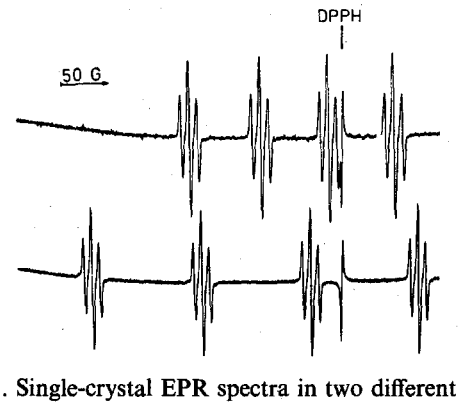

Fig. 1. Single-crystal EPR spectra in two different arbitrarily chosen orientations of the magnetic field of $^{63}Cu/Pd[(C^{i}_{3}H_7O)_2PS_2]_2$.

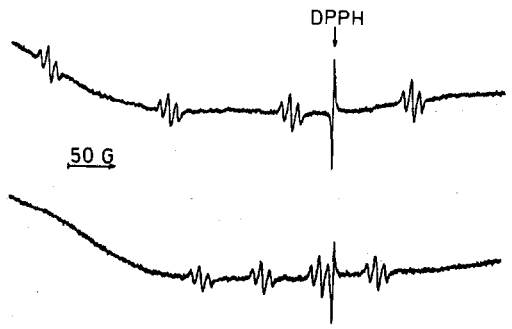

Fig. 2. Single-crystal EPR spectra in two different arbitrarily chosen orientations of the magnetic field of $^{63}Cu/Pt[(C^{i}_{3}H_7O)_2PS_2]_2$.

Table 1. EPR parameters for $^{63}Cu/M[Pr^{i}_{2}dtp]_2$ obtained from single crystal studies

Parameter/direction		x	y	z
Pd	A^a	27.66	33.40	150.30
Pt		30.34	32.31	149.90
Pd	g^b	2.0161	2.0190	2.0833
Pt		2.0161	2.0193	2.0827
Pd	Q	1.6	3.3	−4.9
Pt		4.0	3.4	−7.4
Pd	(A_{ii}, g_{ii})	11.1°	11.1°	0.7°
Pt		27.8°	27.8°	1.0°

[a] The values of hyperfine and quadrupole interactions are in 10^{-4} cm^{-1}. For A values the experimental error was estimated to be 0.5×10^{-4} cm^{-1}.
[b] ± 0.0005.

agreement with the previous studies of other copper/nickel dialkyl-dithiophosphate[11] or -dithiophosphinate single-crystal samples.[12] The appearance of only one set of four hf lines suggests the presence of one molecule per unit cell of the platinum and palladium hosts. This finding is supported by both available crystallographic data for the platinum(II)[13] host and the results of our X-ray structural studies (*vide infra*). The principal values of A, g and Q tensors from single-crystal EPR measurements, as well as the angles between their principal directions, are collected in Table 1. The proximity of g_x and g_y, as well as the relation $g_x \approx g_y < g_z$, suggests nearly axial symmetry of the complexes studied and that the unpaired electron occupies predominantly the $d_{x^2-y^2}$ orbital. It is worthwhile to note, however, that the tensors are nearly axial ($g_x \approx g_y$, $A_x \approx A_y$), and hence the error (see Table 1) in the determination of the angles (g_{xx}, A_{xx}) and (g_{yy}, A_{yy}) is relatively high. Moreover, because the principal values of the quadrupole tensors obtained are much smaller than that of hf and shf interactions and are close to the limit of experimental error, the results were not considered reliable.

Crystallography

The centrosymmetric $Pd[(C^{i}_{3}H_7O)_2PS_2]_2$ molecule and the atom numbering scheme is depicted in Fig. 3. Selected interatomic distances and angles are given in Table 2.

The palladium atom disposed at the centre of symmetry is coordinated by four sulphur atoms at an average distance of 2.340(1) Å, the five-atom assembly being necessarily planar. The intramolecular Pd ··· P distance is 2.975(1) Å. The phosphorus atom deviates from the PdS_4 plane only by 0.077 Å, but the atom-to-plane distances of O(1) and O(2) are significantly different (−1.025 and 1.305 Å, respectively). The PS_2O_2 tetrahedron is highly distorted with angles varying from 95.89(8)° [O(1)—P—O(2)] to 114.64° [S(1)—P—O(2)].

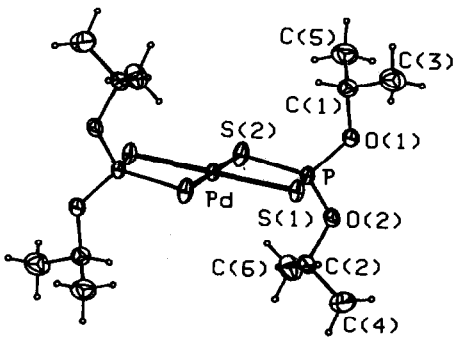

Fig. 3. A molecule of $Pd[(C^{i}_{3}H_7O)_2PS_2]_2$ and its atom numbering scheme.

Packing of the complex molecules is illustrated in Fig. 4. The palladium atom is approached by one

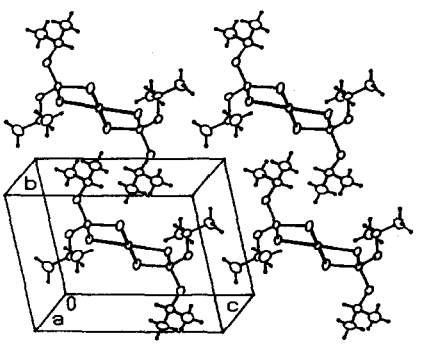

Fig. 4. Packing of the $Pd[(C^{i}_{3}H_7O)_2PS_2]_2$ molecules in the unit cell.

Table 2. Interatomic distances (Å) and angles (°) with e.s.d.s in parentheses

Pd—S(1)	2.3456(6)	O(1)—C(1)	1.466(3)
Pd—S(2)	2.3345(5)	O(2)—C(2)	1.460(3)
S(1)—P	1.9978(7)	C(1)—C(3)	1.517(4)
S(2)—P	1.9937(7)	C(1)—C(5)	1.483(4)
P—O(1)	1.572(1)	C(2)—C(4)	1.488(4)
P—O(2)	1.572(1)	C(2)—C(6)	1.521(4)
S(1)—Pd—S(2)	84.00(2)	C(4)—C(2)—C(6)	112.2(2)
Pd—S(1)—P	86.06(2)	P—O(1)—C(1)	121.2(1)
Pd—S(2)—P	86.46(2)	P—O(2)—C(2)	121.4(1)
S(1)—P—S(2)	103.37(4)	O(1)—C(1)—C(3)	107.3(3)
S(1)—P—O(1)	114.50(7)	O(1)—C(1)—C(5)	107.9(2)
S(1)—P—O(2)	114.64(7)	C(3)—C(1)—C(5)	113.6(2)
S(2)—P—O(1)	114.46(7)	O(2)—C(2)—C(4)	107.4(3)
S(2)—P—O(2)	114.55(7)	O(2)—C(2)—C(6)	107.2(2)
O(1)—P—O(2)	95.89(8)	C(4)—C(2)—C(6)	112.2(2)

sulphur and two carbon atoms, i.e. Pd···S(2) 4.5069(6) $(1+x, y, z)$, Pd···C(3) 4.261(3) $(x, y-1, z)$ and Pd···C(5) 4.304(3) Å $(x, y-1, z)$. The presumed orientation of the methyl hydrogen atoms at C(3) and C(5) is accompanied by the formation of short Pd···H(32) and Pd···H(52) linkages of 3.39 and 3.43 Å $(x, 1-y, z)$, respectively. The shortest Pd···Pd distance of 6.379(1) is realized along the *a*-axis. The palladium complex is isopointal to Pt $[(C^i_3H_7O)_2PS_2]_2$[13] and their molecular geometries are identical within the accuracy limits. It should be mentioned that the observed difference in the two Pd—S bond lengths of 0.01 Å takes place in the platinum complex as well. Hence, the two coordinative bonds are intrinsically different in both structures.

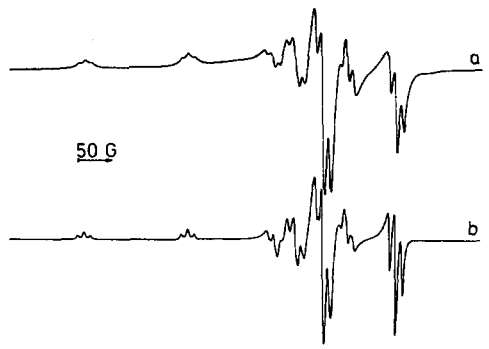

Fig. 5. EPR spectra of $^{63}Cu/Pt[(C^i_3H_7O)_2PS_2]_2$: (a) experimentally-recorded powdered spectrum; and (b) simulated spectrum with the parameters given in Table 5.

Powdered EPR measurements

The experimentally-recorded powdered EPR spectra of the samples $^{63}Cu/Pt[(C^i_3H_7O)_2PS_2]_2$ and $^{63}Cu/Pd[(C^i_3H_7O)_2PS_2]_2$ are shown in Figs 5(a) and 6(a) and their calculated EPR parameters are presented in Table 3. Comparing the principal values of g and A tensors obtained from single-crystal

Table 3. The EPR parameters obtained from powdered spectra of $^{63}Cu/Pd[Pr^i_2dtp]_2$ and $^{63}Cu/Pt[Pr^i_2dtp]_2$

EPR parameters		$^{63}Cu/Pd[Pr^i_2dtp]_2$	$^{63}Cu/Pt[Pr^i_2dtp]_2$
A	xx	34.40	34.30
	yy	34.40	34.30
	zz	150.90	148.86
g	xx	2.0203	2.0227
	yy	2.0203	2.0227
	zz	2.0820	2.0827

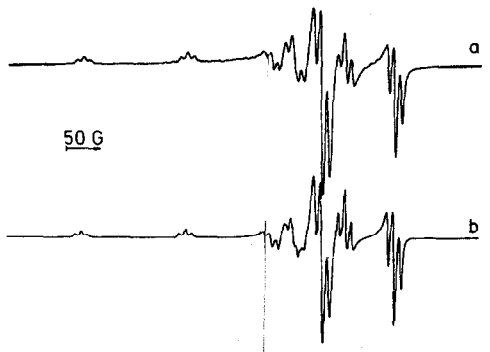

Fig. 6. EPR spectra of $^{63}Cu/Pd[(C_3H_7O)_2PS_2]_2$: (a) experimentally-recorded powdered spectrum; and (b) simulated spectrum with the parameters given in Table 5.

measurements, collected in Table 1, with those received from powdered spectra (Table 3) shows a small difference between them. This difference may be considered as quite normal taking into account the fact that the line-widths in the powdered spectra are greater, and thus the uncertainty in the determination of g and A is relatively high.

An attempt to use computer-aided EPR spectroscopy to verify the quadrupole tensor components and the angles (g_x, A_x) *and* (g_y, A_y). The results of the studies summarized[1-3,12-18] in Table 4 on determining the quadrupole coupling constants from single-crystal EPR and ENDOR measurements of different copper(II) complexes show values which vary over a wide range. The great difference

Table 4. Values of quadrupole interactions obtained in different studies

Sample[a]	Q ($\times 10^{-4}$ cm^{-1})	Method	Ref.
$^{63}Cu/Ni(dto)_2$	0.7	Single-crystal EPR	1
$^{63}Cu/Ni(Et_2dtp)_2$	1.8–1.9	Single-crystal EPR	1
$Cu/Ni(mnt)_2^{2-}$	1.2	Single-crystal EPR	1
$Cu/Ni(mnt')_2$	0.7	Single-crystal EPR	1
$Cu(SdbmO)_2$	1.3	Single-crystal EPR	1
$^{63,65}Cu(acac)_2$	7.3	EPR, frozen ethanol and simulation of spectra	3
$^{63,65}Cu(acac)_2$	6.8	EPR, frozen chloroform and simulation of spectra	3
$^{63,65}Cu(acac)_2$	8.5	EPR, frozen pyridine and simulation of spectra	3
$^{63}Cu/Pd(acac)_2$	8.0	Powder EPR and simulation of spectra	2
	3.4	Single-crystal EPR	14
	7.0	Single-crystal EPR	15
	−2.0 MHz −4.5 MHz 6.5 MHz	Single-crystal ENDOR	16
$^{63}Cu/Ni(dtc)_2$	0.7	Single-crystal EPR	1
$Cu/Zn(dtc)_2$	2.1 0.5 −1.6	Single-crystal EPR	17
$^{63}Cu(dtc)_2$	86 MHz	EPR, frozen pyridine and simulation of spectra	18

[a] Abbreviations used: *Cu(dto)* = *bis(dithiooxalate)cuprate(II)*, *Cu(mnt')* = *bis(1,1-*dicyano-2,2-dithioethylene)cuprate(II), $Cu(mnt)_2$ = bis(1,2-dicyano-1,2-dithioethylene) cuprate(II), $Cu(dtc)_2$ = bis(dithiocarbamate)cuprate(II), $Cu(Et_2dtp)_2$ = bis(diethyldithiophosphate)copper(II), $Cu(SdbmO)_2$ = bis(*cis*-monodithiodibenzoilmethanate) copper(II) and $Cu(acac)_2$ = bis(acetylacetonate)copper(II).

between the results obtained from the EPR studies of the different authors and the deviations from the values resulting from ENDOR spectroscopy, which possess approximately 10^3 times higher resolution than the former one, typically occur. Having this in mind the conclusion was made that single-crystal EPR measurements are not precise enough to obtain values of quadrupole coupling in copper(II) complexes. On the other hand, however, some authors have used a computer-simulation procedure of powdered spectra of copper(II) chelate complexes in order to obtain this kind of data. In view of this we also tried to explore this approach to obtain more precise values on the quadrupole constants as well as about the angles (g_i, A_i).

The simulation of the powdered spectra of $^{63}Cu/Pt[(C^i_3H_7O)_2PS_2]_2$ and $^{63}Cu/Pd[(C^i_3H_7O)_2PS_2]_2$ with the exact values obtained from the single-crystal spectra (Table 1) do not agree well with the experimentally-recorded powdered EPR spectra. Therefore, it was necessary to search such EPR parameters which would lead to the best fit between experimentally obtained and theoretically simulated spectra. In order to find some information about the principal values of Q tensors as well as the angles (g_i, A_i), where $i = x$ or y, we have simulated the powdered EPR spectra using the principal values of g and A tensors shown in Table 1 as a precursor and varying Q_i and angles (g_i, A_i), respectively. The powdered EPR spectra thus simulated and showing best fit with the experimental ones are presented in Figs 5(b) and 6(b); the corresponding parameters are shown in Table 5. It is seen from Table 5 that for the $^{63}Cu/Pt[(C^i_3H_7O)_2PS_2]_2$ sample the principal values of A_x and A_y used for the simulation of the powdered spectra deviate slightly from the single-crystal data (within *ca* 2×10^{-4} cm^{-1}) and are close to higher in-plane values (A_y) obtained by single crystal measurements. For $^{63}Cu/Pd[(C^i_3H_7O)_2PS_2]_2$ the A values used for simulation are averaged between A_x and A_y from the single-crystal data, and the difference is greater (about 6×10^{-4} cm^{-1}). The principal values of the g tensor obtained from single-crystal data used for the simulation are in very good agreement with $^{63}Cu/Pt[(C^i_3H_7O)_2PS_2]_2$, whereas for $^{63}Cu/Pd[(C^i_3H_7O)_2PS_2]_2$ the values of g_x and g_y, in which the best-fit appears, are higher in comparison with single-crystal results. It was found that the angle (g_x, A_x) has no influence on the shape and EPR parameters of the simulated powdered spectra.

In the process of searching for the best fit between simulated and powdered spectra, a series of simulations were performed by varying the quadrupole coupling constants in the range 1×10^{-4}–10×10^{-4} cm^{-1} at fixed g and A values. The best fit was found for Q values shown in Table 5. As can be seen these values vary significantly from those obtained by single-crystal EPR measurements (Table 1). This is not surprising, because the literature data also show considerable differences between the Q values obtained by single-crystal EPR and ENDOR measurements, as well as the computer-simulated powdered spectra. Some of these data are collected in Table 4. All these results show that the determination of the quadrupole coupling constant obtained from single-crystal, powdered and simulated-powdered EPR spectra can give satisfactory information for the order of this interaction only, not for its exact value.

Table 5. The EPR parameters for $^{63}Cu/M[Pr^i_2dtp]_2$, used for the simulation of powder spectra

M	Parameter/direction	x	y	z
Pd		32.00	32.00	150.00
Pt	A	30.50	34.40	150.40
Pd		2.0161	2.0194	2.0827
Pt	g	2.0180	2.0210	2.0835
Pd	Q	3.0		
Pt		1.2		

Acknowledgements—The financial support of the Ministry of Education and Science (project 137) and the Bulgarian Academy of Sciences are gratefully acknowledged.

REFERENCES

1. K. L. White and R. L. Belford, *J. Am. Chem. Soc.* 1976, **98**, 4428.
2. L. D. Rollman and S. I. Chan, *J. Chem. Phys.* 1969, **50**, 3416.
3. R. L. Belford and D. C. Duan, *J. Magnet. Reson.* 1978, **46**, 293.
4. N. M. Nedelchev and N. D. Yordanov, *Rev. Sci. Instr.*, submitted.
5. S. Misra, *Magnet. Reson. Rev.* 1986, **10**, 285.
6. D. G. McGavin, R. A. Palmer, W. A. Singers and W. C. Tennant, *J. Magnet. Reson.* 1980, **40**, 69.
7. S. N. Deming and S. L. Morgan, *Analyt. Chem.* 1973, **45**, 278A.
8. J. R. Pilbrow, *Molec. Phys.* 1973, **25**, 1073.
9. A. D. Toy, H. H. Chaston and J. R. Pilbrow, *Inorg. Chem.* 1971, **10**, 2219.
10. Enraf–Nonius Structural Determination Package, SDP/PDP V3.0, Users Guide. Enraf-Nonius, Delft, The Netherlands (1985).

11. N. D. Yordanov and D. Shopov, *Chem. Phys. Lett.* 1972, **16**, 69; *J. Molec. Struct.* 1973, **19**, 617.
12. N. D. Yordanov, G. Gochev, O. Angelova and J. Macicek, *Polyhedron* 1990, **9**, 2597.
13. V. Tkachev and L. Atovmian, *Koord. Khim.* 1982, **8**, 215.
14. H. So and R. L. Belford, *J. Am. Chem. Soc.* 1969, **91**, 2392.
15. A. H. Maki and B. B. McGarvey, *J. Chem. Phys.* 1978, **29**, 293.
16. M. Iwaizumi and S. Kita, *J. Magnet. Reson.* 1982, **46**, 361.
17. C. P. Keijzers, PhD Thesis. University of Nijmegen (1974).
18. D. L. Liczwek and R. L. Belford, *J. Phys. Chem.* 1983, **87**, 2509.

Polyhedron Vol. 12, No. 1, pp. 125–127, 1993
Printed in Great Britain

0277–5387/93 $6.00+.00
© 1993 Pergamon Press Ltd

COMMUNICATION

INDENYL COMPLEXES OF GERMANIUM(II)

ALAN H. COWLEY* and MIGUEL A. MARDONES

Department of Chemistry and Biochemistry, The University of Texas at Austin, Austin, TX 78712, U.S.A.

and

SALVADOR AVENDAÑO

Facultad de Química, Casilla 306, Correo 22, Universidad Católica de Chile, Santiago, Chile

and

ENRIQUE ROMÁN and JUAN M. MANRIQUEZ

Centro de Investigación Minera y Metalúrgica, Casilla 170, Correo 10, Santiago, Chile

and

CARL J. CARRANO

Department of Chemistry, Southwest Texas State University, San Marcos, TX 78666, U.S.A.

(*Received* 26 *May* 1992; *accepted* 18 *August* 1992)

Abstract—The first indenyl complexes of germanium(II), $Ge(1,3\text{-}(Me_3Si)_2C_9H_5)_2$ (**1**) and $Ge(1,3\text{-}(Me_3Si)_2C_9H_5)(Me_5C_5)$ (**2**), have been prepared by treatment of $Li(1,3\text{-}(Me_3Si)_2C_9H_5)$ with $GeCl_2 \cdot$ dioxane and $[(\eta\text{-}Me_5C_5)Ge]BF_4$, respectively. The structure of **2** has been determined by X-ray crystallography.

The indenyl ligand has proved to be of importance in transition metal chemistry[1] due to the stabilization of the η^3-bonding mode in the cyclopentadienyl ring and the consequent enhanced rate of ligand substitution (the so-called "indenyl effect"[2]). Interestingly, this ligand system has been seldom used in the context of main group chemistry.[3] Here we report $Ge(1,3\text{-}(Me_3Si)_2C_9H_5)_2$ (**1**) and $Ge(1,3\text{-}(Me_3Si)_2C_9H_5)(Me_5C_5)$ (**2**), the first indenyl complexes of germanium. The X-ray crystal structure of **2** has been determined.

1,3-Bis(trimethylsilyl)indenyllithium was prepared from indene using the Bu^nLi/Me_3SiCl procedure described by Merola *et al.*[4] Tetrahydrofuran (80 cm^3) was added via a syringe to a cooled (−78°C) Schlenk flask, which had been loaded previously in a dry-box with $GeCl_2 \cdot$ dioxane (1.0 g, 4.32 mmol) and $Li(1,3\text{-}(Me_3Si)_2C_9H_5)$ (2.29 g, 8.64 mmol). The reaction mixture was allowed to assume ambient temperature and stirring was continued for 1 h thereafter. After removal of the solvent and volatiles by evacuation, the resulting orange residue was recrystallized from pentane to afford yellow crystalline **1** in 59% yield. Analytical

* Author to whom correspondence should be addressed.

data* are in accord with the formula $C_{30}H_{46}GeSi_4$. The ^1H and $^{13}C\{^1H\}$ NMR spectra for **1*** are indicative of a symmetrical sandwich-type structure with either an η^5- or η^3-attachment of germanium to the five-membered rings of the indenyl substituents. Kohler[5] has pointed out that for (unsubstituted) indenyl complexes, the hapticity can be assigned on the basis of the ^{13}C chemical shifts of the ring carbon atoms. For η^3-attachment, for example, the slip-fold distortion of the five-membered ring results in C(1)—C(3) being more shielded than C(8) and C(9).† This is not the case for **1**. Although the C(1)/C(3) resonance is more shielded than that of C(8)/C(9), the C(2) resonance appears at almost the same frequency as the latter. The ^{13}C NMR argument therefore leads to the conclusion that the germanium is attached in an η^5-fashion in **1**. Unfortunately, the crystals of this material proved to be unsatisfactory for X-ray analysis. It was, therefore, necessary to prepare another indenyl derivative of germanium(II).

(Pentamethylcyclopentadienyl)(2,6-bis(trimethylsilyl)indenyl)germanium(II) was prepared in a similar manner to that described for **1** using $[(\eta\text{-}Me_5C_5)Ge]BF_4$[6] (0.6 g, 4.48 mmol) and $Li[1,3\text{-}(Me_3Si)_2C_5H_9]$ (0.54 g, 2.03 mmol). After recrystallization from pentane (−30°C) the yield of orange crystalline **2** was 57% (0.54 g). Analytical data* are consistent with the composition $C_{25}H_{38}GeSi_2$ and the ^1H and $^{13}C\{^1H\}$ NMR data are similar to (a) those of η^5-bonded Me_5C_5-substituted germanium(II) compounds, and (b) those of **1**. An X-ray diffraction study‡ was undertaken to clarify the bonding arrangement in **2**. Individual molecules of **2**, which are well separated in the solid state, comprise a sandwich-type structure in which the germanium is bonded to an Me_5C_5 ring and the five-membered ring of the indenyl group (Fig. 1). Although there is a scatter in the ring-Ge distances due to "ring slippage", the Me_5C_5 group is best regarded as η^5-bonded. The five-membered ring of the indenyl substituent is planar, the maximum deviation from planarity being 0.01 Å. There is a very slight folding of this ring about the C(21)—C(28) vector (3.3°); however, the bonding to germanium is closest to η^5. Interestingly, there is a large difference (~0.4 Å) in the two ring centroid/germanium distances. The observation that this distance is shorter for the Me_5C_5 ring (2.066 Å) than the indenyl ring (2.438 Å) implies that the bonding of the latter to germanium is appreciably weaker. Finally, we note that the ring centroid/germanium/ring centroid angle (163.0°) is very close to that found in the sterically encumbered germanocene $[(C_6H_5CH_2)_5C_5]_2Ge$ (163.1°).[7]

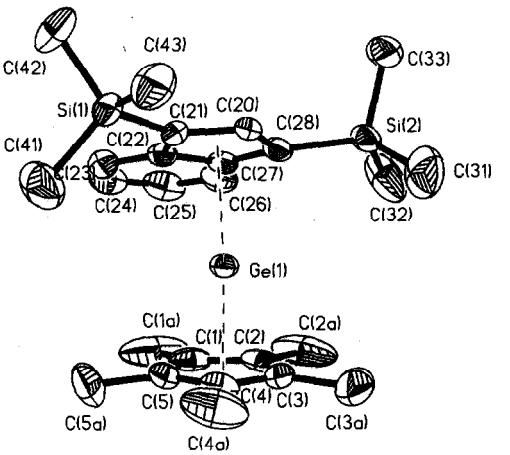

Fig. 1. View (ORTEP) of **2** showing the atom numbering scheme. Important bond distances (Å): Ge—C(1) 2.332(8), Ge—C(2) 2.331(7), Ge—C(3) 2.386(7), Ge—C(4) 2.445(6), Ge—C(5) 2.415(6), Ge—C(20) 2.732(7), Ge—C(21) 2.767(7), Ge—C(22) 2.725(7), Ge—C(27) 2.704(6), Ge—C(28) 2.690(6).

* Analytical data. Found: C, 60.8; H, 7.7. Calc. for **1**: C, 60.9; H, 7.8%. Found: C, 64.0; H, 8.0. Calc. for **2**: C, 64.3; H, 8.1%. ^1H NMR data† (C_6D_6, 25°C, 300.15 MHz): **1**: δ 0.30 (s, 36H, Me_3Si), 6.32 [s, 2H, H(2)], 7.02–7.05 and 7.46–7.49 [AA′BB′ system, 8H, H(4)—H(7)]. **2**: δ 0.45 (s, 18H, Me_3Si), 1.70 (s, br, 15H, Me_5C_5), 6.42 [s, 1H, H(2)], 6.96–7.08 and 7.74–7.86 (AA′BB′ system, 4H, H(4)—H(7)]. $^{13}C\{^1H\}$ NMR data (C_6D_6, 25°C, 75.47 MHz): **1**: δ 0.66 (s, Me_3Si), 113.78 [s, C(1) and C(3)], 123.03–123.11 [s, C(8) and C(9)], 123.52 [s, C(2)], 130.08 [s, C(5) and C(6)], 141.32 [s, C(4) and C(7)]. **2**: δ 0.85 (s, Me_3Si), 9.42 (s, Me_5C_5), 113.70 [s, C(1) and C(3)], 119.51 (s, Me_5C_5), 122.66–123.63 [C(8), C(9) and C(2)], 130.17 [s, C(5) and C(6)], 141.25 [s, C(4) and C(7)].

† Numbering system.

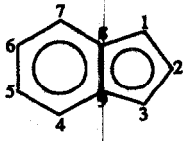

‡ Crystal structure data for **2**: monoclinic, space group $P2_1/n$, $a = 8.583(2)$, $b = 19.961(4)$, $c = 15.779(3)$ Å, $\beta = 92.40(3)°$, $V = 2700.9(10)$ Å^3, $D_c = 1.149$ g cm^{-3}, $Z = 4$, 2788 unique reflections collected from $2\theta = 3.0$–$45.0°$ with $F_o > 2.0\sigma(F)$. Siemens R3m/V diffractometer, Mo-K_α radiation, $\lambda = 0.71073$ Å, $T = 298$ K. The structure was solved by Patterson map interpretations using the SHELXTL PLUS (VMS) software package and refined by full-matrix least-squares methods to $R = 5.56$ and $Rw = 6.49\%$.

Acknowledgements—We are grateful to the National Science Foundation (Grant CHE 9108228), the Robert

A. Welch Foundation (Grant F-135), FONDECYT Chile (Grant 624/89), and UNDP (Grant CHI/87-029).

REFERENCES

1. J. M. O'Connor and C. P. Casey, *Chem. Rev.* 1987, **87**, 307.
2. M. E. Rerek, L.-N. Ji and F. Basolo, *J. Chem. Soc., Chem. Commun.* 1983, 1208.
3. P. Jutzi, *Adv. Organomet. Chem.* 1986, **26**, 217.
4. J. S. Merola and R. T. Kacmarcik, *Organometallics* 1989, **8**, 778.
5. F. H. Kohler, *Chem. Ber.* 1974, **107**, 570.
6. P. Jutzi, B. Hampel, M. B. Hursthouse and A. J. Howes, *Organometallics* 1986, **5**, 1944.
7. H. Schumann, C. Janiak, E. Hahn, C. Kolax, J. Loebel, M. D. Rausch, J. J. Zuckerman and M. J. Heeg, *Chem. Ber.* 1986, **119**, 2656.

Polyhedron Vol. 12, No. 2, pp. 129–131, 1993
Printed in Great Britain

0277–5387/93 $6.00+.00
© 1993 Pergamon Press Ltd

A CONVENIENT PREPARATION OF IODOFERROCENES

IAN R. BUTLER,* STEVEN B. WILKES, SARA J. McDONALD and LOIS J. HOBSON

University of Wales, Bangor, Gwynedd LL57 2UW, U.K.

and

ALPAY TARALP and C. PAUL WILDE

Department of Chemistry, University of Ottawa, Ottawa, Ontario, Canada K1N 9B4

(*Received* 4 *September* 1992; *accepted* 1 *October* 1992)

Abstract—The synthesis of iodoferrocenes using stannylferrocenes as key intermediates is described. The method is suitable for the bulk preparation of iodoferrocenes.

There has been a definite resurgence in the chemistry of metallocenes and in particular ferrocene chemistry in the past year or so. This comes with the recognition that ferrocene may be a useful synthon in the rapidly expanding areas of "new material science", for example in molecular ferromagnets,[1,2] molecular sensors[3,4] and self assembly.[5–7]

A significant proportion of ferrocene-based synthetic work relies on a few key reagents such as lithio-ferrocenes,[8,9] ferrocenylcarboxaldehydes,[10,11] ferrocenylcarboxylic acids[12] and haloferrocenes.[12–14] The conventional synthesis of haloferrocenes has been via either ferrocenylmercury reagents[15–17] or ferrocenyl boronic acids,[18] or the direct reaction of lithioferrocenes with hexachloroethane,[19] tetrabromodichloroethane or iodine[20] (Scheme 1). We have made use of these synthetic procedures for several years and have found them to be satisfactory; however, yields of iodoferrocenes tend to be low and variable. In one of our current research projects we require large quantities of iodoferrocene and, therefore, we decided to look for an alternative synthesis which would give more predictable and higher yields and at the same time be economically acceptable. A reasonable route seemed to be via organo-tin compounds since the halogen/organotin exchange reaction is well established. Wright has published the synthesis and use of 1,1′-bis-(tri-n-butylstannyl)ferrocene and its use as a precursor to monolithioferrocenes:[21] this reagent seemed well suited as a synthetic intermediate since the precursors required are inexpensive.

EXPERIMENTAL

Bis-tri-n-butylstannylferrocene (BSSF) or tri-n-butylstannylferrocene (BSF) were prepared by the literature procedure and purified by repeated chromatography on a neutral alumina support where pure samples were required. In some experiments crude BSSF and BSF were used, which had been purified by one chromatographic separation only. Bis-triphenylstannylferrocenes and triphenylstannylferrocene were prepared by reaction of dilithioferrocene or monolithioferrocene, respectively, with chlorotriphenyltin and were crystallized prior to use.

Reaction of crude BSF or BSSF with I_2

A cooled (approx -70°C) sample of either crude (isolated without column chromatography) BSF or BSSF (0.25 mol) in dichloromethane (1000 cm^3) was treated with I_2 (0.27 mol or 0.54 mol I_2, respectively) under a nitrogen atmosphere. The mixture was allowed to warm to room temperature and was stirred overnight. The mixture was then washed twice with 1 M solutions of sodium thiosulphate (200 cm^3), the organic layer separated and flashed through a small portion of neutral alumina. The

* Author to whom correspondence should be addressed.

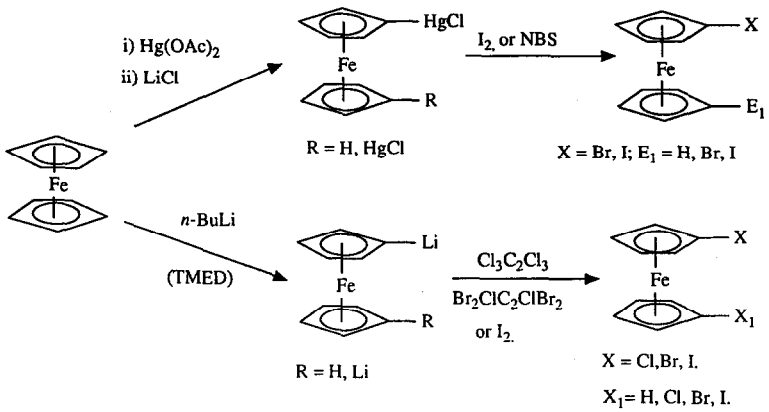

Scheme 1.

solvent was then removed on a rotary evaporator to leave a viscous oil which was dissolved in MeOH (1000 cm^3). Excess KF (50 g) was then added to precipitate the stannyl by-products. The precipitated material ws removed by filtration and the MeOH was removed *in vacuo*. The solid/oil was then extracted with several portions of diethyl ether, again flashed through an alumina plug and the solvent removed to give an amber oil. ^1H NMR indicated the product iodo- or di-iodoferrocene was in each case contaminated with butyl-tin derivatives. Further separation and isolation of the iodo- or di-iodoferrocene were attempted but found to be extremely difficult except on small scale chromatographic purifications on neutral alumina.

Reaction of pure BSF or BSSF with I_2 *or* ICl

Identical reactions to the above method were carried out using pure bis-tri-n-butylstannylferrocene or tri-n-butylstannylferrocene on scales of up to 100 g of the starting compounds. These yielded pure 1,1′-di-iodo- or iodoferrocene, respectively, as amber oils without the need for chromatography. Yields are > 80% on average.

An identical reaction procedure using ICl in place of I_2 gave higher yields (> 90%) of the appropriate iodoferrocene.

Reaction of pure triphenylstannylferrocenes with ICl

The reaction of bis-triphenylstannylferrocene with ICl on a 0.2 mol scale gave bis 1,1′-diiodoferrocene as the sole ferrocene containing product. A similar methodology to the above was used except that it is not necessary to use KF since the by-products are not soluble in weakly polar solvents. For the work-up the solvent was removed from the crude reaction mixture and the product di-iodoferrocene was extracted into the diethyl ether and purified by passing the yellow product solution through an alumina plug. The yields using this procedure were > 85%. Similar treatment of triphenylstannylferrocene with ICl gave iodoferrocene again in high yield.

RESULTS AND DISCUSSION

The syntheses of tri-n-butylstannylferrocene (BSF) and 1,1′-bis-n-(tri-n-butylstannyl)ferrocene (BBSF) are straightforward.[21] The compounds are prepared from lithioferrocenes by reaction with tri-n-butylstannyl chloride and are obtained as golden brown oils. Purification of the product compounds is effected using column chromatography on a neutral alumina support, using hexane as an eluent. In the case of BBSF synthesis when the reactions were scaled up (> 50 g) the chromatographic purification became more difficult unless extremely large quantities of alumina were used. The ferrocene and BSF were easily removed from the BBSF; however, tetrabutyltin was more difficult to remove on a large scale. On treamtent of pure BBSF with I_2 or ICl the 1,1′-di-iodoferrocene cleanly forms in near quantitative yield and thus provides a viable alternative route for the synthesis of di-iodoferrocene. The product iodoferrocenes are isolated by removal of the co-produced stannyl chlorides or iodides. This was achieved by treatment of the crude reaction mixtures with KF in methanol, followed by filtration to remove the precipitated tri-n-butylstannylfluoride. Since it would be advantageous to use crude BSF or BBSF, attempts were made to use unchromatographed samples arising directly from the reaction of lithioferrocenes with tri-n-butylstannyl chloride. However, the actual isolation of the product posed problems, especially when carried out on a large scale (> 50 g). The problem

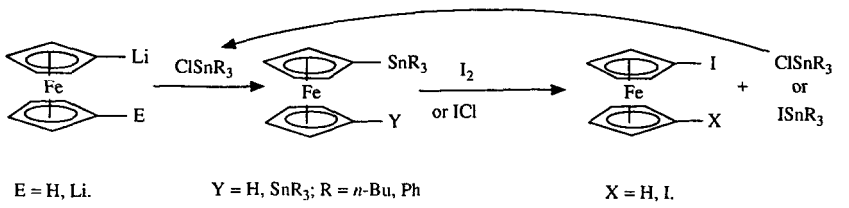

E = H, Li. Y = H, SnR_3; R = *n*-Bu, Ph X = H, I.

Scheme 2.

arises from residual impurities such as tetrabutyltin (formed by reaction of butyllithium with the tributylstannyl chloride) without several chromatographic steps.[22] Therefore, it is important to use pure 1,1′-bis-tri-n-butylstannylferrocene as the starting compound and not to proceed with an impure mixture—the best check of sample purity (BBSF or BSF) is to use the integration of the ^1H NMR cyclopentadienyl signals versus those of the butyl resonances as the basis for evaluation. Using pure 1,1′-bis-tri-n-butyl stannylferrocene we have been able to prepare > 100 g quantities of di-iodoferrocene in one batch. The drawback is that the alumina required for purification of the stannylferrocenes is now rather expensive. We therefore decided to examine the use of tri-phenylstannylferrocenes, which are solids and are easily purified by crystallization. Using the same methodology we have found that di-iodoferrocene is readily obtained in the same manner without the problems caused by impurities. The drawback here, however, is that chlorotriphenyltin is more commercially expensive than the butyl compound so that may limit large scale application.

In principle, the halo-stannyl by-products could be recycled (Scheme 2, step 1). We are currently attempting modifications to the isolation procedure which would allow this. Small scale experiments indicate that the procedure is applicable to the synthesis of bromoferrocenes; however, the yields are considerably diminished presumably caused by the direct side-reaction of bromine with ferrocene.

REFERENCES

1. C. Kollmar, M. Couty and O. Kahn, *J. Am. Chem. Soc.* 1991, **113**, 7994.
2. K. M. Chi, J. C. Calbrese, W. M. Reiff and J. S. Miller, *Organometallics* 1991, **10**, 668.
3. R. W. Wagner, P. A. Brown, T. E. Johnson and J. S. Lindsey, *J. Chem. Soc., Chem. Commun.* 1991, 1463.
4. E. C. Constable, *Angew. Chem., Int. Edn Engl.* 1991, **30**, 407.
5. J. C. Medina, C. Li, S. G. Bott, J. L. Atwood and G. W. Gokel, *J. Am. Chem. Soc.* 1991, **113**, 366.
6. M. C. Grossel, M. R. Goldspink, J. A. Hrijac and S. C. Weston, *Organometallics* 1991, **10**, 851.
7. P. D. Beer, E. L. Tite and A. Ibbotson, *J. Chem. Soc., Dalton Trans.* 1991, 1691.
8. M. D. Rausch and D. J. Clappenelli, *J. Organomet. Chem.* 1967, **10**, 127.
9. M. D. Rausch, G. A. Moser and C. F. Meade, *J. Organomet. Chem.* 1973, **51**, 1.
10. P. L. Pauson and W. E. Watts, *J. Chem. Soc.* 1962, 3880.
11. J. M. Osgerby and P. L. Pauson, *J. Chem. Soc.* 1961, 4604.
12. P. C. Reeves, *Org. Synth.* 1970, **56**, 28.
13. M. D. Rausch, L. P. Klemann, A. Siegel, R. F. Kovar and T. M. Gund, *Synth. Inorg. Met.-Org. Chem.* 1973, **3**, 193.
14. A. N. Nesmeyanov, E. G. Perevalova and A. N. Nesmeyanov, *Dokl. Akad. Nauk., SSSR* 1955, **100**, 1099.
15. R. W. Fish and M. Rosenblum, *J. Org. Chem.* 1965, **30**, 1253.
16. A. N. Nesmeyanov, E. G. Perevalova, R. A. Golovnya and O. A. Nesmeyanov, *Dokl. Akad. Nauk. SSSR* 1954, **97**, 459.
17. *Handbuch der Anorg. Chem.*, 8th edn, Suppl. **14**, A368. Gmelin (1974).
18. H. Shechter and J. F. Helling, *J. Org. Chem.* 1961, **26**, 1034.
19. F. L. Hedberg and H. Rosenberg, *J. Am. Chem. Soc.* 1973, **95**, 870.
20. For a series of general references see *Organometallic Compounds of Iron* (Edited by G. Knox). Chapman and Hall, New York (1985).
21. M. E. Wright, *Organometalics* 1990, **9**, 853.
22. It is very difficult to remove tetrabutyltin from the product iodoferrocenes without repeated rigorous chromatography on small sample quantities. If only slight quantities are present, however, in the case of iodoferrocene synthesis, the iodoferrocene can be successfully crystallized at low temperatures.

Polyhedron Vol. 12, No. 2, pp. 133–140, 1993
Printed in Great Britain

0277–5387/93 $6.00+.00
© 1993 Pergamon Press Ltd

NUCLEAR MAGNETIC RESONANCE STUDIES OF MULTINUCLEAR CHROMIUM ASSEMBLIES

M. M. GLASS, K. BELMORE and J. B. VINCENT*

Department of Chemistry, University of Alabama, Tuscaloosa, AL 35487, U.S.A.

(*Received* 27 *July* 1992; *accepted* 5 *October* 1992)

Abstract—^{1}H NMR and ^{2}H NMR resonances of a series of oxo-centred trinuclear chromium complexes of the form $[Cr_3O(O_2CR)_6(L)_3]^+$ (R = —CH_3, —CH_2CH_3, —Ph, -4-MePh; L = H_2O, py, 2-Mepy, 3-Mepy, 4-Mepy) have been observed and assigned. The role of π- and σ-bonding frameworks in the delocalization of unpaired electron density onto the ligand protons is examined. The π-delocalization mechanism dominates where ligands contain aromatic substituents or carboxylate functionalities, consistent with the presence of a metal centre where unpaired electrons reside solely in t_{2g} orbitals. A comparison of the importance of these mechanisms with that in trinuclear manganese and iron complexes is reported. These results suggest that ^{1}H and ^{2}H NMR studies could be useful probes of proteins containing coupled multinuclear chromium assemblies.

Trinuclear oxo-centred metal carboxylate assemblies of the general composition $[M_3O(O_2CR)_6L_3]^{n+}$ have been of intense interest since the first structure determination by X-ray diffraction in 1965,[1] as emphasized by the appearance of a recent review article.[2] The importance of these compounds rests in their potential to serve as models to test theories of magnetic coupling between metal ions in multinuclear systems.[2–8] Hence, the properties of these systems, most specifically examples where M = Cr, Fe, or Cr and Fe, have been examined by a wide range of magnetic and spectroscopic techniques including variable-temperature magnetic susceptibility, inelastic neutron scattering, Mössbauer spectroscopy, etc.[2,9] However, nuclear magnetic resonance studies have only rarely been reported and are especially lacking on the M = chromium series. The trivalent oxidation level of chromium dominates the chemistry of the chromium-containing trinuclear assemblies. Each octahedrally-coordinated Cr^{III} thus supplies three unpaired electrons; however, antiferromagnetic coupling between the chromium centres reduces the effective magnetic moment of the complexes. As a consequence, observations of paramagnetically-shifted (and broadened) ^{1}H NMR resonances should be possible and provide information on the electronic environment.

In addition, the feasibility of ^{1}H NMR as a probe of chromium-containing proteins can be addressed using these trinuclear assemblies. Low molecular-weight chromium-binding substance is an oligopeptide that reportedly binds four Cr^{III} ions and serves as a chromium detoxifying agent and has a role in the potentiation of insulin action.[10,11] Charge considerations and the high ratio of chromium to amino acid residues (over half of which are aspartate or glutamate)[10,11] suggest that this protein contains an anion-bridged multinuclear chromium carboxylate assembly.

Herein are reported the successful observation and assignment of ^{1}H NMR resonances of $[Cr_3O(O_2CR)_6L_3]^+$ complexes and a discussion of the mode of spin delocalization in these systems.

EXPERIMENTAL

Syntheses

$[Cr_3O(O_2CMe)_6(H_2O)_3]Cl$,[12] $[Cr_3O(O_2CMe)_6(py)_3]ClO_4$,[13] $[Cr_3O(O_2CMe)_6(3\text{-Mepy})_3]ClO_4$,[12] $[Cr_3O(O_2CCH_2CH_3)_6(H_2O)_3]NO_3$,[3] $[Fe_3O(O_2CMe)_6(py)_3]ClO_4$[13] and $[Mn_3O(O_2CMe)_6(py)_3]ClO_4$[6] were prepared as described elsewhere. $[Cr_3O(O_2CMe)_6(X\text{-Mepy})_3]ClO_4$ (X = 2, 3, 4) were pre-

* Author to whom correspondence should be addressed.

pared in an analogous fashion to $[Cr_3O(O_2Me)_6(py)_3]ClO_4$ using the appropriate substituted-pyridine for pyridine. Compounds containing deuterium-labelled ligands were prepared in an analogous fashion to the protio analogues substituting DO_2CD_3, $DO_2CC_5D_5$, D_2O or NC_5D_5 as required. Reagents were obtained commercially and used as received.

$[Cr_3O(O_2CPh)_6(py)_3]ClO_4 \cdot 1.1CH_2Cl_2$. $Cr(ClO_4)_3 \cdot 6H_2O$ (18.70 g, 40.79 mmol) and benzoic acid (12.20 g, 99.90 mmol) were stirred in pyridine (100 cm^3). The mixture was refluxed for 4 h and allowed to cool to room temperature. The solution was filtered to reveal green microcrystals of the product. The microcrystals were washed copiously with diethylether and dried *in vacuo*. Yield: *ca* 65% based on chromium. Recrystallization may be accomplished from CH_2Cl_2/hexanes (or hot MeCN). Found: C, 52.2; H, 3.2; N, 3.2; Cl, 8.4; Cr, 11.4%. Calc. for $C_{58.1}H_{47.2}N_3O_{17}Cl_{3.2}Cr_3$: C, 52.5; H, 3.6; N, 3.2; Cl, 8.5; Cr, 11.7%.

NMR spectroscopy

^1H and ^2H spectra were obtained using a Bruker AM-360 spectrometer and a Bruker AM-500 spectrometer, respectively at *ca* 23°C. Chemical shifts are reported on the δ scale (shifts downfield are positive) using the solvent protio- or deutero-impurity signal(s) as a reference. Assignments were made on the basis of relative intensities and broadening and by substitution of appropriate ligands.

Other methods

Elemental analyses were performed at Galbraith Laboratories, Knoxville, TN, U.S.A. The purity of synthetic compounds was examined by IR (Nujol mull) spectroscopy, using a Perkin–Elmer 283 B spectrophotometer.

RESULTS AND DISCUSSION

Trinuclear oxo-centred metal carboxylate assemblies have the general structure shown in Fig. 1. The three metal centres and the μ_3-oxide are coplanar. Each pair of chromic ions are bridged by two carboxylate ligands; coordination about each octahedral Cr^{3+} ion is completed by a single terminal ligand, usually H_2O or pyridine. Each chromic ion, d^3, has each of its three unpaired electrons occupying a t_{2g} orbital, directed between the ligands. Chromium(III) complexes are thus magnetically isotropic or nearly so, and their dipolar shifts should be quite small or negligible.[14] Hence, isotropic shifts should be essentially solely contact

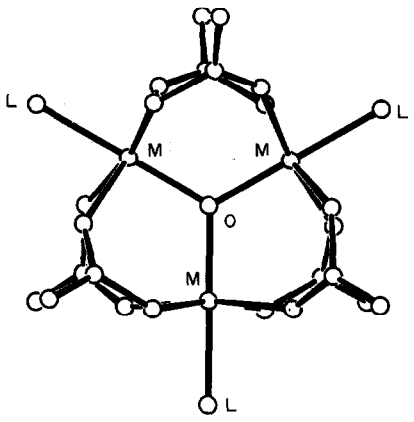

Fig. 1. General structure of oxo-centred trinuclear carboxylate assemblies.

in origin. This is counterbalanced by the long electronic spin-lattice relaxation time of isolated chromic ions, which renders ^1H NMR resonances of their coordination complexes difficult to observe. Reduction of the magnetic moment per Cr^{3+} ion as a result of antiferromagnetic coupling in the carboxylate assemblies (μCr for $[Cr_3O(O_2CMe)_6(py)_3]^+$ is 3.14 μ_B[13] vs *ca* 3.87 μ_B for mononuclear species) might yet allow the observation of such resonances.

The ^1H NMR spectrum of the simplest of these trinuclear compounds, $[Cr_3O(O_2CMe)_6(H_2O)_3]Cl$, displays only a single downfield-shifted, slightly broad ($\sim$ 2.4 ppm wide at half height) resonance in the range -100 to $+200$ ppm (Table 1 and Fig. 2). Comparison of this spectra with those of other acetate complexes where the terminal H_2O is substituted with another ligand (*vide infra*) reveals that this resonance is retained; thus, this signal is readily assigned to the methyl protons of the bridging acetate ligands. This compares favourably with ^2H NMR signals of O_2CCD_3-bridged chromium dimers ($+40$ to $+60$ ppm).[15] The protons of the water ligands because of their proximity to the chromium centres (separated by one oxygen in the σ-bonding framework) are broadened beyond detection. However, by using ^2H NMR signals in a given environment should be narrower than the corresponding ^1H NMR signal by up to $\gamma_H^2/\gamma_D^2 = 42.5$, where γ_H and γ_D are the gyromagnetic ratios of the proton and deuteron, respectively; a narrowing by a factor of 42 has been reported previously for $Cr(acac)_3$.[16] In contrast to the ^1H spectra, the aquo deuteron signal is readily observed by ^2H NMR for the D_2O analogue $[Cr_3O(O_2CMe)_6(D_2O)_3]^+$ (Table 2 and Fig. 3).

The ^1H NMR spectrum of $[Cr_3O(O_2C$

Table 1. ^{1}H chemical shifts (ppm)

Species	H		Chemical shift
$[Cr_3O(O_2CMe)_6(H_2O)_3]^{+a}$	O_2CCH_3		+36.2
$[Cr_3O(O_2CMe)_6(py)_3]^{+b}$	O_2CCH_3		+36.2
		2-H	n.o.[c]
	py	3-H	+11.2
		4-H	−14.4
$[Cr_3O(O_2CMe)_6(NC_5D_5)_3]^{+b}$	O_2CCH_3		+36.4
$[Cr_3O(O_2CCH_2CH_3)_6(H_2O)_3]^{+a}$	$O_2CCH_2CH_3$		+42.2
	$O_2CCH_2CH_3$		−0.1
$[Cr_3O(O_2CMe)_6(4\text{-Mepy})_3]^{+b}$	O_2CCH_3		+36.2
		2-H	n.o.
	4-Mepy	3-H	+11.3
		Me	+26.2
$[Cr_3O(O_2CMe)_6(3\text{-Mepy})_3]^{+b}$	O_2CCH_3		+36.2
		2-H	n.o.
		3-H	+10.1
	3-Mepy	4-H	−14.1
		Me	−6.4
$[Cr_3O(O_2CMe)_6(2\text{-Mepy})_3]^{+b}$	O_2CCH_3		+36.4
		Me	+26.9
	2-Mepy	2-H	n.o.
		3-H	+11.1
		4-H	−14.3
$[Cr_3O(O_2CPh)_6(py)_3]^{+a}$		2-H	n.o.
	py	3-H	+11.2
		4-H	−14.4
		o	v.b.[d]
	O_2CPh	*m*	+7.4
		p	+0.5
$[Cr_3O(O_2CPh)_6(NC_5D_5)_3]^{+a}$		*o*	v.b.
	O_2CPh	*m*	+7.4
		p	+0.5
$[Cr_3O(O_2CC_6D_5)_6(py)_3]^{+a}$		2-H	n.o.
	py	3-H	+11.2
		4-H	−14.4
$[Cr_3O(p\text{-}O_2CC_6H_5Me)_6(py)_3]^{+a}$		2-H	n.o.
	py	3-H	+11.2[e]
		4-H	−14.4
		Me	+11.2
	$O_2CC_5H_5Me$	*o*	v.b.
		m	+7.1

[a] d_3-MeCN.
[b] d_4-MeOH.
[c] Not observed.
[d] Very broad.
[e] Superimposed on methyl resonance from *p*-toluate ligand.

$CH_2CH_3)_6(H_2O)_3]^+$ correspondingly shows two features. The ratio of the areas of the two signals is 1.5 : 1.0, with the least intense signal possessing the greater downfield shift (Table 1); this unambiguously identifies the strongly shifted feature with the methylene protons of the propionate ligand and is consistent with their closer proximity to the metal centres. It is of particular note that the methyl proton signal is shifted *upfield*, opposite the methylene protons. (The methyl proton signal of free propionic acid under similar conditions is at +1.04 ppm.) For bridging carboxylate ligands where the

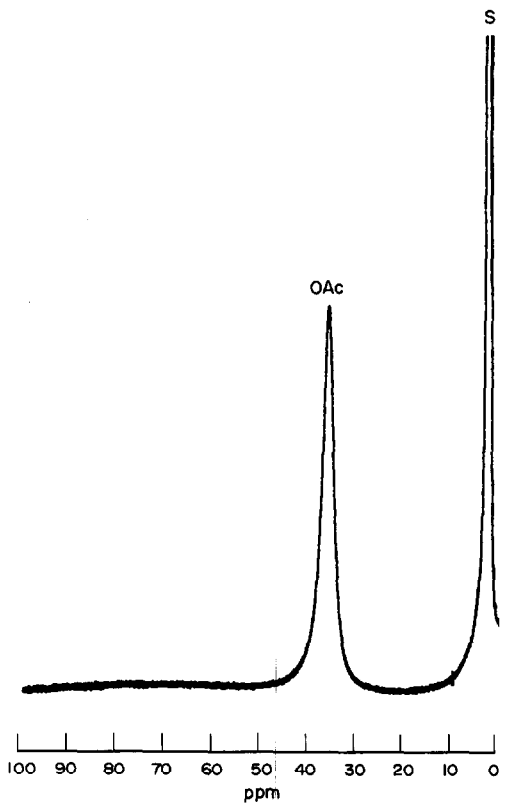

Fig. 2. ^{1}H NMR spectrum of $[Cr_3O(O_2CMe)_6(H_2O)_3]^+$ in d_3-MeCN. The small shoulder at *ca* 0 ppm is a probe artifact. S = protio-solvent impurity.

metals and carboxylate moiety are co-planar, two mechanisms for spin delocalization are expected: σ and π, wth the π-pathway expected to predominate for protons more removed from the metal centre.[17] When substitution of a proton by a methyl group results in the methyl proton signal being shifted in the direction opposite the original proton, a π-spin delocalization is assumed to be in effect. As propionate can be considered to be a methyl-substituted acetate ligand, this provides clear evidence for a dominant π-pathway. In fact, the authors are unaware of any previous example of a bridging proprionate or similar carboxylate ligand where this methyl resonance is shifted upfield from the dimagnetic case, indicating the extreme dominance of this mechanism for chromium(III) complexes. (A shift of -6 ppm has been observed for a crotonate complex; crotonate has an extended π-system compared to propionate.[17])

To test the dominance of this π-delocalization mechanism, complexes with aromatic groups such as benzoate and pyridine (py) were examined. The ^{1}H NMR spectrum of $[Cr_3O(O_2CMe)_6(py)_3]^+$ contains two resonances in addition to that of the acetate methyl protons at +36.2 ppm (*vide supra*) (Table 1). This signal is unambiguously assigned as it is retained in the ^{1}H NMR spectrum of $[Cr_3O(O_2CMe)_6(NC_5D_5)_3]^+$ (Table 1). The upfield resonance from its position and width (0.6 ppm) is assigned to the 4-position proton; the broader (0.7 ppm) downfield resonance then corresponds to the 3-position proton, with the 2-position proton broadened beyond detection. (The signal assigned to the 4-position proton also integrates to appropriately half the area of the other.) Thus, the broadness [H(4) < H(3) < H(2)] and alternating sense of shift between the 3-position and 4-position protons is consistent with a strong π-delocalization pathway. In the ^{2}H NMR spectrum of the NC_5D_5 analogue, the 3-position and 4-position deuteron resonances are readily observable, as well as a third, broader signal, which is shifted strongly upfield and

Table 2. ^{2}H chemical shifts (ppm)

Species	D		Chemical shift
$[Cr_3O(O_2CMe)_6(D_2O)_3]^+$ [a]		D_2O	+180
$[Cr_3O(O_2CMe)_6(D_2O)_3]^+$ [b]		2-H	−45.1
	py	3-H	+11.0
		4-H	−14.2
$[Cr_3O(O_2CPh)_6(NC_5D_5)_3]^+$ [a]		2-H	−44.8
	py	3-H	+11.1
		4-H	−14.4
$[Cr_3O(O_2CC_6D_5)_6(py)_3]^+$ [a]		*o*	+3.2
	O_2CPh	*m*	+7.4
		p	+0.5

[a] MeCN.
[b] MeOH.

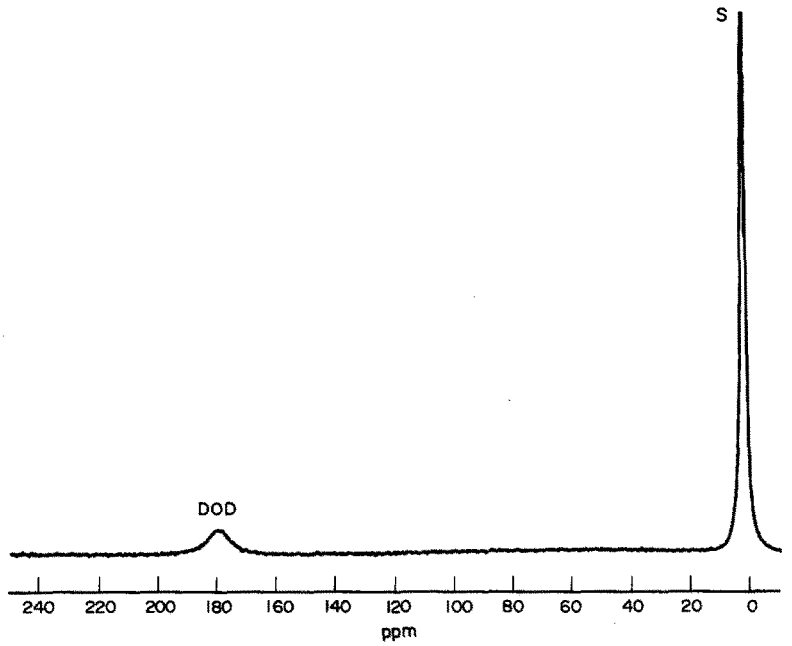

Fig. 3. ^2H NMR spectrum of $[Cr_3O(O_2CMe)_6(D_2O)_3]^+$ in MeCN. S = deutero-solvent impurity.

assigned to the 2-position deuteron (Fig. 4 and Table 2). Substitution of the pyridine with 3-methyl-pyridine or 4-methylpyridine results in a decrease in intensity of or loss of the 3-position proton signal or 4-position proton signal, respectively, with the appearance of a new signal from the methyl group. In both cases, the sense of the isotropic shift of the methyl protons is opposite that of the replaced proton of the pyridine (Table 1), as expected for a π-delocalization pathway. For the 2-methyl-pyridine-

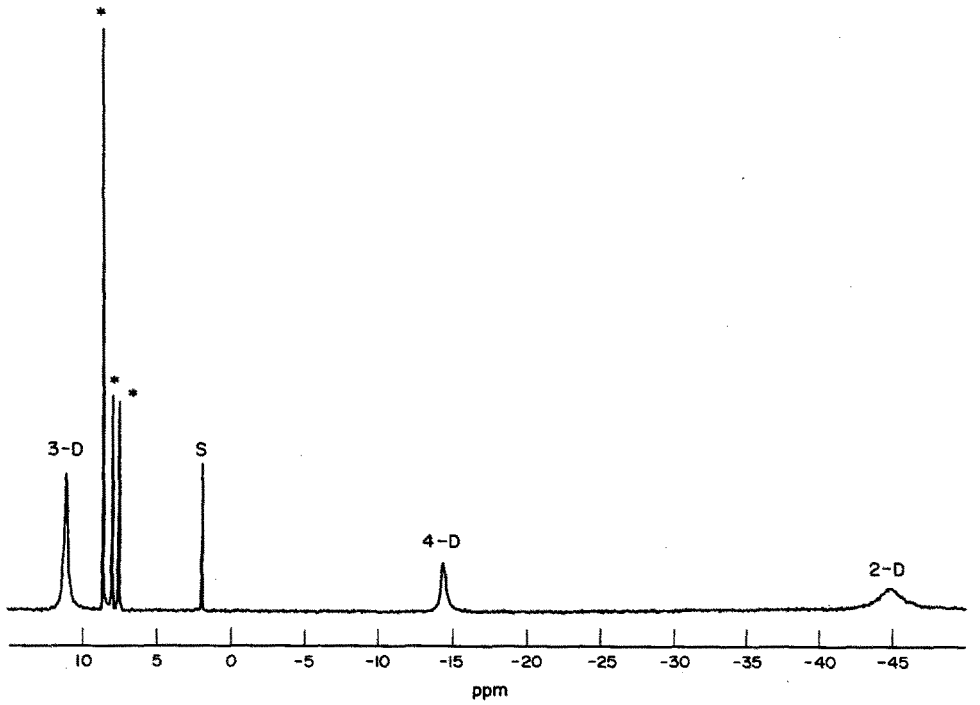

Fig. 4. ^2H NMR spectrum of $[Cr_3O(O_2CMe)_6(NC_5D_5)_3]^+$ in MeOH. * indicates a signal from added NC_5D_5 for comparison; S indicates the deutero-solvent impurity.

substituted complex, the methyl protons are shifted downfield (Table 1), opposed to the upfield shift of the deuterons in the 2-position of the NC_5D_5 complex.

As dipolar contributions to the isotropic shifts should be negligible, the ratio of the magnitude of the contact shifts of the pyridine protons/deuterons of the trinuclear complex and a previously reported mononuclear complex,[18] $[Cr(malonate)_2(d_5\text{-py})_2]^-$ ($\Delta H_{Cr_3}/\Delta H_{Cr}$), should approximate the ratio of the squares of the effective magnetic moments of the two species (μ_{eff}^2/μ_{eff}^2). The magnetic moment of the mononuclear complex has not been reported but can safely be assumed to be approximately the spin-only value for a d^3 system, 3.87 B.M. The ratio of the squares of the moments is then ~ 0.66. The ratio of the shifts (taken as the position of the proton/deuteron in the paramagnetic material compared to free pyridine under similar conditions) is 0.72 for the 3-position, 0.72 for the 4-position, and 0.68 for the 2-position. Thus, the magnitude of the shifts is controlled by the extent of coupling between chromic ions. The ability to detect ^1H NMR signals for the trinuclear compound and the need to use ^2H NMR for the mononuclear complex is a result of the relative broadness of the signals, which is also proportional to the effective magnetic moments and thus also linked to the extent of antiferromagnetic coupling.

This behaviour of alternating shifts about the pyridine ring is strongly in contrast to results previously reported for pyridine complexes of nickel(II) or cobalt(II), which suggest predominate σ-delocalization mechanisms,[19-22] but in agreement with the behaviour of a mononuclear chromium(III) NC_5D_5 complex.[18] This contrasting behaviour can be best understood by comparing the ^1H NMR spectrum of $[Cr_3O(O_2CMe)_6(py)_3]^+$ with those of its isostructural Mn^{III} and Fe^{III} analogues. For the Fe^{III} complex all three py resonances are downfield with the magnitude of the shifts of the order (2H > 3H > 4H) expected for a predominant σ-delocalization mechanism (Table 3 and Fig. 5). This reflects the different electron configuration of the ferric ions, d^5, which have two unpaired electrons in the e_g orbitals, directed along the metal–ligand σ-bonds. Octahedral nickel(II) and cobalt(II) ions also have two unpaired electrons in e_g orbitals. The acetate methyl signal for this complex is readily assigned by its intensity and displays a downfield shift of magnitude similar to the chromium compound.

Octahedral high-spin manganic ions are subject to a Jahn–Teller distortion, which removes the degeneracy of the e_g orbitals. If it is assumed the d_{z^2} orbital of each manganic ion is oriented along a Mn—oxide bond, the d_{z^2} orbital is destabilized and resides at a higher energy than the $d_{x^2-y^2}$ orbital. The $d_{x^2-y^2}$ orbital, which is oriented along the Mn—O (acetate) bonds, is then partially occupied. The d_{z^2} orbital is thus unoccupied. To a first approximation, the pyridine ring disposed *trans* to the oxide ligand would be expected to be influenced by only a π-spin delocalization pathway. Consequently, the pyridine protons experience alternating upfield and downfield shifts, consistent with a dominant π-delocalization mechanism (Table 3). The magnitude of the acetate methyl signal (assigned by its disappearance in the ^1H NMR spectrum of $[Mn_3O(O_2CCD_3)_6(py)_3]^+$) is greater than expected when compared to the magnitude of the pyridine proton signals. The NMR spectrum of the manganese complex is more complex than the chromium or iron compounds; manganese-ligated pyridine appears to be exchanging with free pyridine and perhaps solvent, resulting in a series of broad resonances between 5 and 15 ppm, which seem to obscure the 3-H pyridine resonance.

Table 3. Comparison of $[M_3O(O_2CMe)_6(py)_3]^+$ chemical shifts (ppm)

M	O_2CMe	py 2-H	py 3-H	py 4-H
Cr^{III} [a]	+36.2	n.o.[b]	+11.2	−14.4
Fe^{III} [c]	+30.4	+64.5	+29.0	+8.1
Mn^{III} [c]	+32.0	−63.0	[d]	−21.2

[a] d_4-MeOH.
[b] −45.1 ppm in ^2H NMR of NC_5D_5 analogue.
[c] d_3-MeCN.
[d] Probably obscured by resonances from solvent and free pyridine.

The ^1H NMR spectrum of $[Cr_3O(O_2CPh)_6(py)_3]^+$ displays four distinct resonances, while a very broad band seems barely definable above the baseline over the region *ca* 0–10 ppm. Two of these resonances occur in essentially identical positions as the 3-H and 4-H pyridine resonances of the analogous acetate compound and may be definitively assigned to these signals as they disappear in the spectrum of the NC_5D_5 analogue and are retained in the $O_2CC_5D_5$ analogue (Table 1). The ^2H NMR spectrum of the NC_5D_5 analogue (Table 2) discloses that the 2-D signal is also in a location similar to the acetate compound. These results indicate that the substitution of the bridging acetate ligands with benzoates does not substantially affect the coupling between the chromium ions.

The two remaining features, one with an upfield

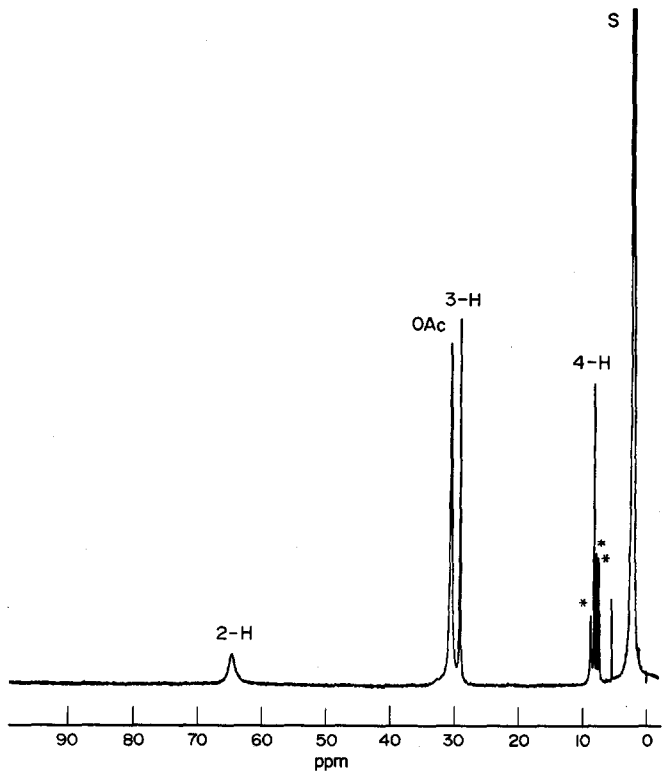

Fig. 5. ^{1}H NMR spectrum of $[Fe_3O(O_2CMe)_6(py)_3]^+$ in d_3-MeCN. S = protio-solvent impurity; * = pyridine solvate.

isotropic shift and the other with a tiny downfield shift, are assigned to the benzoate *para*-proton and *meta*-protons, respectively. This assignment is consistent with their intensities and width. Use of ^{2}D NMR is required to unambiguously observe the signal of the *ortho*-deuteron (proton), which is appreciably broader than the *meta*- or *para*-deuteron signals and upfield shifted, indicating a predominating π-delocalization is in operation (Table 2). This proton is probably responsible for the broad resonance in the ^{1}H NMR. To test which delocalization pathway is dominent, the *para*-toluate derivative was prepared. The *para*-methyl proton resonance is shifted downfield, in contrast to the *para*-proton resonance providing conclusive evidence for the existence of a dominant delocalization pathway (Table 1).

The alternating pattern of upfield and downfield resonances is consistent with the reported ^{1}H NMR of copper(II) benzoate,[23] and the position of the 2-D signal is similar to that reported for $[Cr_3O(2\text{-}d\text{-nicotinateH})_6(H_2O)_3]^{7+}$ in 1 M $HClO_4$.[24] (Listing of this 2-D chemical shift for this compound is the only reported NMR data on these trinuclear chromium complexes.)

CONCLUSIONS

Despite the long electronic spin-lattice relaxation time of Cr^{III} ions, the ^{1}H NMR spectra of oxo-centred trinuclear chromium carboxylate assemblies possess readily discernable signals (although signals due to protons in the closest proximity to the metal centres are broadened beyond detection). Using a combination of ^{1}H NMR and ^{2}H NMR all the proton/deuteron signals could be identified and unambiguously assigned. As the methyl and methylene protons of acetate and propionate are comparable to the α- and β-protons of the carboxylate side-chains of aspartate and glutamate, the results suggest that ^{1}H NMR studies could prove valuable to the study of proteins containing similar assemblies. This utility of ^{1}H NMR derives from the antiferromagnetic coupling between the chromium centres, which reduces the effective magnetic moment per chromium(III).

Acknowledgement—The authors would like to thank N. S. F. for support via the research experiences for minority undergraduate students program (M.M.G.).

REFERENCES

1. B. N. Figgis and G. B. Robertson, *Nature* (*London*) 1965, **205**, 694.
2. R. D. Cannon and R. P. White, *Prog. Inorg. Chem.* 1988, **36**, 195.
3. A. Earnshaw, B. N. Figgis and J. Lewis,, *J. Chem. Soc.* (*A*) 1966, 1656.
4. L. Dubicki and P. Day, *Inorg. Chem.* 1972, **11**, 1868.
5. B. S. Tsukerblat, M. I. Belinski and B. Y. Kuyavskaya, *Inorg. Chem.* 1983, **22**, 995.
6. J. B. Vincent, H.-R. Chang, K. Folting, J. C. Huffman, G. Christou and D. N. Hendrickson, *J. Am. Chem. Soc.* 1987, **109**, 5703.
7. S. M. Oh, D. N. Hendrickson, K. L. Hassett and R. E. Davis, *J. Am. Chem. Soc.* 1984, **106**, 7984.
8. S. M. Oh, D. N. Hendrickson, K. L. Hassett and R. E. Davis, *J. Am. Chem. Soc.* 1985, **107**, 8009.
9. U. A. Jayasooriya, R. D. Cannon, R. P. White and G. D. Kearley, *Angew. Chem., Int. Edn Engl.* 1989, **28**, 930.
10. A. Yamamoto, O. Wada and T. Ono, *Eur. J. Biochem.* 1987, **165**, 627.
11. A. Yamamoto, O. Wada and S. Manabe, *Biochem. Biophys. Res. Commun.* 1989, **163**, 189.
12. M. K. Johnson, D. B. Powell and R. D. Cannon, *Spectrochim. Acta* 1981, **37A**, 995.
13. S. Vemura, A. Spencer and G. Wilkinson, *J. Chem. Soc., Dalton Trans.* 1973, 2565.
14. W. D. Horrocks Jr, in *NMR of Paramagnetic Molecules* (Edited by G. N. LaMar, W. D. Horrocks Jr and R. H. Holm), p. 143. Academic Press, New York (1973).
15. C. A. Green, N. Koine, J. I. Legg and R. D. Willet, *Inorg. Chim. Acta* 1990, **176**, 87.
16. A. Johnson and G. W. Everett, *J. Am. Chem. Soc.* 1972, **94**, 1419.
17. I. M. Arafa, H. M. Goff, S. S. David, B. P. Murch and L. Que Jr, *Inorg. Chem.* 1987, **26**, 2779.
18. W. D. Wheeler, S. Kaizaki and J. I. Legg, *Inorg. Chem.* 1982, **21**, 3248.
19. D. Doddrell and J. D. Roberts, *J. Am. Chem. Soc.* 1970, **92**, 6839.
20. R. H. Holm, G. W. Everett Jr and W. D. Horrock Jr, *J. Am. Chem. Soc.* 1966, **88**, 1071.
21. J. A. Happe and R. L. Ward, *J. Chem. Phys.* 1963, **39**, 1211.
22. R. W. Kluiber and W. D. Horrocks Jr, *Inorg. Chem.* 1967, **6**, 166.
23. R. A. Zelonka and M. C. Baird, *Inorg. Chem.* 1972, **11**, 134.
24. C. A. Green, R. J. Bianchini and J. I. Legg, *Inorg. Chem.* 1984, **23**, 2713.

Polyhedron Vol. 12, No. 2, pp. 141–147, 1993
Printed in Great Britain

0277–5387/93 $6.00+.00
Pergamon Press Ltd

DEHALOSILYLATION REACTIONS INVOLVING $E(SiMe_3)_3$ AND Ph_2InCl. SYNTHESIS AND X-RAY STRUCTURES OF $[Ph_2InE(SiMe_3)_2]_2$ (E = P OR As)

RICHARD L. WELLS,* ANDREW T. McPHAIL, LEONIDAS J. JONES and MARK F. SELF

Department of Chemistry, Paul M. Gross Chemical Laboratory, Duke University, Durham, NC 27708, U.S.A.

(*Received* 24 *July* 1992; *accepted* 1 *October* 1992)

Abstract—Combining $P(SiMe_3)_3$ or $As(SiMe_3)_3$ with Ph_2InCl in a 1 : 1 mole ratio results in the elimination of Me_3SiCl via a dehalosilylation reaction to yield $[Ph_2InP(SiMe_3)_2]_2$ (**I**) and $[Ph_2InAs(SiMe_3)_2]_2$ (**II**), respectively. X-ray structures were determined for **I** and **II**. The $(InP)_2$ core of dimer **I** is planar, whereas in dimer **II** the $(InAs)_2$ ring is slightly puckered.

The quest for suitable single-source precursors to ceramic and/or electronic III–V materials in previous years has resulted in a large number of fundamental reports concerning the structural aspects and reactivities of these compounds.[1,2] Elucidation of this basic chemistry is paramount to the understanding of the nature of the factors that influence the correct design and fabrication of such materials. Research in our laboratory has primarily centred on the use of silylarsines and, of late, silylphosphines in dehalosilylation reactions with a dialkyl group III halide or group III trihalide. These reactions eliminate a silyl halide thus forming a III–V bond.[1,3] This line of investigation has proven to be very fruitful in that a variety of compounds containing $\overline{MEME}$ (M = Ga, E = As;[4–7] M = In, E = P[8] or As[9]) and $\overline{MEMCl}$ (M = Ga, E = As[4,6,7] or P;[10] M = In, E = P[8] or As[9]) cores have been isolated. From the latter compounds, the possibility of replacing the chlorine atom with other functionalities exists.[11] Currently, for the case of compounds with cores consisting of $\overline{MEME}$ (M = In, E = P or As) rings, we have only employed this dehalosilylation methodology to $(Me_3SiCH_2)_2InCl$.[8,9] Herein we report our further explorations into this area with the synthesis and structural characterization of $[Ph_2InP(SiMe_3)_2]_2$ (**I**) and $[Ph_2InAs(SiMe_3)_2]_2$ (**II**).

EXPERIMENTAL

Synthesis

All manipulations were performed using general Schlenk, dry-box and/or high vacuum techniques. Solvents (including those for NMR spectra) were appropriately dried, distilled under argon and degassed prior to use. Literature methods were used to prepare Ph_3In,[12] $P(SiMe_3)_3$[13] and $As(SiMe_3)_3$.[14] Indium(III) chloride was purchased from Alfa Products, Ward Hill, MA, and purified by sublimation. Ph_2InCl was prepared via the equilibration of Ph_3In and indium(III) chloride in refluxing toluene in a 2 : 1 mole ratio and purified by recrystallization. ^1H, $^{13}C\{^1H\}$ and $^{31}P\{^1H\}$ NMR spectra were obtained on a Varian XL-300 at 300.0, 75.4 and 121.4 MHz, respectively. ^1H and ^{13}C spectra were referenced to TMS via the residual protons or carbons of C_6D_6. ^{31}P spectra were referenced to external 80% H_3PO_4 at δ 0.00 ppm. Melting points (uncorrected) were taken in sealed capillaries (Thomas–Hoover Uni-melt). Elemental analyses were performed by E+R Microanalytical Laboratory, Inc., Corona, NY. Single-crystal X-ray data were collected on an Enraf–Nonius CAD-4 diffractometer with graphite-monochromated Cu-K_α radiation.

$[Ph_2InP(SiMe_3)_2]_2$ (I)

Inside the dry-box a one-necked 250 cm^3 round-bottomed flask equipped with a Teflon valve was

* Author to whom correspondence should be addressed.

charged with pentane (15 cm^3) and Ph_2InCl (0.250 g, 0.82 mmol), furnishing a white suspension to which was added dropwise $P(SiMe_3)_3$ (0.206 g, 0.82 mmol) in pentane (20 cm^3). The resulting milky mixture was placed in a sonicating water bath and allowed to react for 48 h after which it became pale yellow. The volatiles were removed *in vacuo* and the crude product was dissolved in warm pentane (15 cm^3). Upon cooling to −15°C for several days, colourless air-sensitive crystals of **I** formed; 0.224 g, 61.2% yield; m.p. 205–240°C (dec). Found: C, 48.4; H, 6.3%. Calc. for $C_{36}H_{56}In_2P_2Si_4$: C, 48.6; H, 6.3%. ^1H NMR: δ 0.34 (t, 36 H, SiMe_3 [J(P—H) = 2.7 Hz]), 7.17 (t, 4H, *para*-C_6H_5), 7.26 (t, 8H, *meta*-C_6H_5), 7.80 (d, 8H, *ortho*-C_6H_5). $^{13}C\{^1H\}$ NMR: δ 4.79 (t, SiMe_3 [J(P—C) = 4.7 Hz]), [127.63–129.17 (m, C_6H_5) partially obscured by solvent], 139.23 (s, C_6H_5). $^{31}P\{^1H\}$ NMR: δ −221.59 (s).

$[Ph_2InAs(SiMe_3)_2]_2$ (II)

In a manner similar to that employed for the preparation of **I**, Ph_2InCl (0.250 g, 0.82 mmol) in pentane (15 cm^3) and $As(SiMe_3)_3$ (0.243 g, 0.82 mmol) in pentane (20 cm^3) were combined. The resulting milky mixture was stirred for 48 h at room temperature giving a yellow solution. The volatiles were removed *in vacuo* and the crude product was dissolved in warm pentane (15 cm^3). Upon cooling to −15°C for several days, colourless air-sensitive crystals of **II** formed; 0.141 g, 35.0% yield; m.p. 185–190°C (dec. to orange liquid). Found: C, 44.5; H, 6.1%. Calc. for $C_{36}H_{56}As_2In_2Si_4$: C, 44.1; H, 5.8%. ^1H NMR: δ 0.35 (s, 36H, SiMe_3), 7.18 (t, 4 H, *para*-C_6H_5), 7.29 (t, 8H, *meta*-C_6H_5), 7.85 (d, 8H, *ortho*-C_6H_5). $^{13}C\{^1H\}$ NMR: δ 5.00 (s, SiMe_3), [127.80 (s, C_6H_5), 128.12 (s, C_6H_5) partially obscured by solvent], 139.00 (s, C_6H_5).

X-ray structural solution and refinement

Colourless crystals of **I** and **II** were mounted inside flame-sealed 0.6 mm thin-walled glass capillaries under an inert argon atmosphere. Oscillation and Weissenberg photographs provided preliminary unit cell parameters and space group information. The monoclinic space groups $P2_1/c$ for **I** and $P2_1/n$ (alternative setting of $P2_1/c$) for **II** were established unequivocally from the Laue symmetry and systematic absences. Crystallographic data are summarized in Table 1. Intensity data ($+h$, $+k$, $\pm l$; 4832 reflections, $\theta_{max} = 75°$ for **I**; 8025 reflections, $\theta_{max} = 65°$ for **II**), recorded on an Enraf–Nonius CAD-4 diffractometer (Cu-K_α radiation, $\lambda = 1.5418$ Å, graphite monochromator), were corrected for the usual Lorentz and polarization effects; empirical absorption corrections (derived from ψ-scans) were also applied. Equivalent reflections were averaged leaving 4598 (**I**) and 7734 (**II**) out of which 2765 and 3625, respectively, with $I > 3.0\sigma(I)$, were retained for the analyses. With two formula units per unit cell, dimer **I** must lie on a crystallographic centre of symmetry. For **II**, on the other hand, the unit cell contains four dimers that may either occupy general positions or two crystallographically independent dimers must lie on centres of symmetry. Initial indium atom coordinates for **I** were derived from a Patterson map. Approximate indium and arsenic coordinates for **II**, obtained from an E-map (MULTAN11/82), indicated that the molecules lay in general positions with no crystallographically-imposed symmetry. The remaining non-hydrogen atoms of **I** and **II** were located in a series of weighted F_o and difference Fourier syntheses phased successively by an increasing number of atoms. Several rounds of full-matrix least-squares adjustment of atomic positional and thermal parameters (at first isotropic, then anisotropic) followed. In the later iterations, hydrogen atoms were incorporated at their calculated positions (C—H = 1.05 Å) and an extinction correction was included as a variable. The parameter refinements converged at $R = 0.038$ ($R_w = 0.050$) for **I** and $R = 0.040$ ($R_w = 0.048$) for **II**. Final difference-Fourier syntheses revealed no unusual features [max. $\Delta\rho$ (e Å^{-3}): 0.54 (**I**) and 0.56 (**II**), both in the vicinity of the indium atom]. The solid-state structures of **I** and **II**, with their atom numbering schemes, are illustrated in Figs 1 and 2, respectively. Selected bond lengths and bond angles are listed in Tables 2 and 3. Crystallographic calculations were performed using the Enraf–Nonius structure determination package[15] on PDP11/44 and MicroVAX computers. For all structure–factor calculations, neutral atom scattering factors and their anomalous dispersion corrections were taken from ref. 16. In the least-squares iterations, $\Sigma w\Delta^2$ [$w = 1/\sigma^2(|F_o|)$, $\Delta = (|F_o| - |F_c|)$] was minimized. Supplementary material: atomic coordinates, thermal parameters, bond lengths and angles and crystal data have been deposited with the Cambridge Crystallographic Data Centre.

RESULTS AND DISCUSSION

We have previously demonstrated the utility of dehalosilylation reactions between an organogroup III halide and a silylarsine[1] or silylphosphine[8,10] to form III–V bonds. Our initial efforts in pursuit of compounds possessing In—E bonds (E = As or P) involved only the reaction of organoindium species

Table 1. Crystallographic data and summary of data collection and refinement for $[Ph_2InP(SiMe_3)_2]_2$ (I) and $[Ph_2InAs(SiMe_3)_2]_2$ (II)

	I	II
Molecular formula	$C_{36}H_{56}In_2P_2Si_4$	$C_{36}H_{56}As_2In_2Si_4$
Formula weight	892.78	980.68
Crystal system	Monoclinic	Monoclinic
Space group	$P2_1/c$ (C_{2h}^5)	$P2_1/n$ (C_{2h}^5)
a (Å)	10.691(1)	16.248(1)
b (Å)	19.821(2)	20.285(1)
c (Å)	11.512(1)	13.887(1)
β (°)	113.34(1)	90.12(1)
No. of orient. reflections; θ, range (°)	25; 36–40	25; 36–40
V (Å^3)	2239.8(8)	4577.0(8)
Z	2	4
D_{calc} (g cm^{-3})	1.324	1.423
Temperature (K)	296	296
Crystal dimensions (mm)	$0.18 \times 0.18 \times 0.40$	$0.21 \times 0.23 \times 0.28$
T_{max} : T_{min}	1.00 : 0.68	1.00 : 0.76
Radiation (wavelength)	Cu-K_α (1.5418 Å)	Cu-K_α (1.5418 Å)
μ (cm^{-1})	103.1	110.4
Scan type	ω–2θ	ω–2θ
Scan width (°)	$0.80+0.14 \tan\theta$	$0.70+0.14 \tan\theta$
θ_{max} (°)	75	65
Intensity control reflections	131, 232, 33$\bar{2}$, 42$\bar{1}$	13$\bar{2}$, 21$\bar{2}$, 33$\bar{1}$, 41$\bar{2}$
Variation; repeat time (h)	< 2%; 2	< 1%; 2
No. of reflections recorded	4832 ($+h$, $+k$, $\pm l$)	8025 ($+h$, $+k$, $\pm l$)
No. of non-equivalent reflections	4598	7734
R(merge)	0.029 on I	0.034 on I
No. of reflections retained, $I > 3.0\sigma(I)$	2765	3625
No. of parameters refined	200	398
Extinction correction	$6.8(4) \times 10^{-7}$	$1.7(1) \times 10^{-7}$
$R(F)$, $R_w(F)$[a]	0.038, 0.050	0.040, 0.048
Goodness-of-fit[b]	1.25	1.17
Max. shift; e.s.d. in final least-squares cycle	0.02	0.01
Final $\Delta\rho$ (e Å^{-3}) max.; min.	0.54; −0.55	0.56; −0.56

[a] $R = \Sigma ||F_o| - |F_c|| / \Sigma |F_o|$; $R_w = [\Sigma w(|F_o| - |F_c|)^2 / \Sigma w|F_o|^2]^{1/2}$; $\Sigma w\Delta^2$[$w = 1/\sigma^2(|F_o|)$, $\Delta = (|F_o| - |F_c|)$] was minimized.
[b] Goodness-of-fit = $[\Sigma w\Delta^2/(N_{obs} - N_{para})]^{1/2}$.

bearing the Me_3SiCH_2 group,[8,9] an organic substituent that was chosen because of its steric bulk and relative stability. In an effort to ascertain the viability of our methodology for other systems, we have begun to explore the use of different organic substituents at the organoindium centre. We now report the synthesis, characterization and X-ray structures of two new compounds containing the In—E bond (E = P or As), $[Ph_2InP(SiMe_3)_2]_2$ (I) and $[Ph_2InAs(SiMe_3)_2]_2$ (II).

The 1 : 1 mole ratio reaction of Ph_2InCl with $E(SiMe_3)_3$ (E = P or As) at room temperature in pentane affords I and II, respectively, via a dehalosilylation reaction [eq. (1)].

$$2Ph_2InCl + 2E(SiMe_3)_3 \longrightarrow [Ph_2InE(SiMe_3)_2]_2 + 2Me_3SiCl \quad (1)$$

Compounds I and II are the second examples of dimeric In—P or In—As species to be prepared in our laboratory through the elimination of Me_3SiCl, with $[(Me_3SiCH_2)_2InP(SiMe_3)_2]_2$ (III)[8] and $[(Me_3SiCH_2)_2InAs(SiMe_3)_2]_2$ (IV)[9] constituting the first. Subsequent to III and IV being reported, Theopold and co-workers demonstrated that $[C_5Me_5(Cl)InP(SiMe_3)_2]_2$ (V)[17] results from a similar reaction. As with III, IV and V the core fragment of I consists of a planar four-membered $(InP)_2$ ring, whereas in II the $(InAs)_2$ ring is slightly puckered (*vide infra*). The ^1H, ^{13}C and for I, ^{31}P room-temperature NMR spectra for each compound are consistent with their solid-state structures. The dimeric nature of I is clearly demonstrated by the virtual coupling of the ring phosphorus atoms with the hydrogen and carbon atoms of the trimethylsilyl

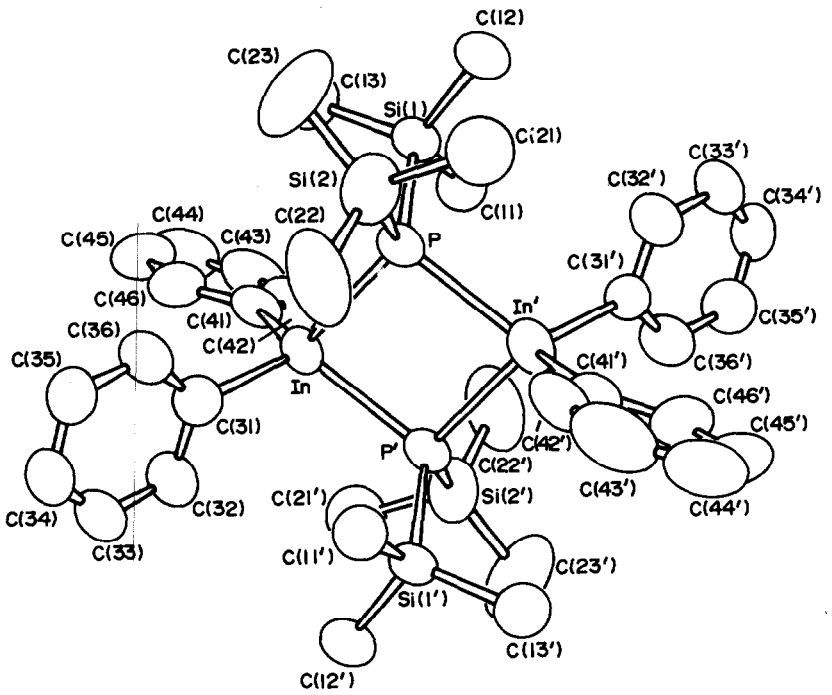

Fig. 1. ORTEP diagram (30% probability ellipsoids) of the solid-state structure of $[Ph_2InP(SiMe_3)_2]_2$ (**I**); primed atoms are related to the unprimed atoms by a crystallographic centre of symmetry. Hydrogen atoms have been omitted for clarity.

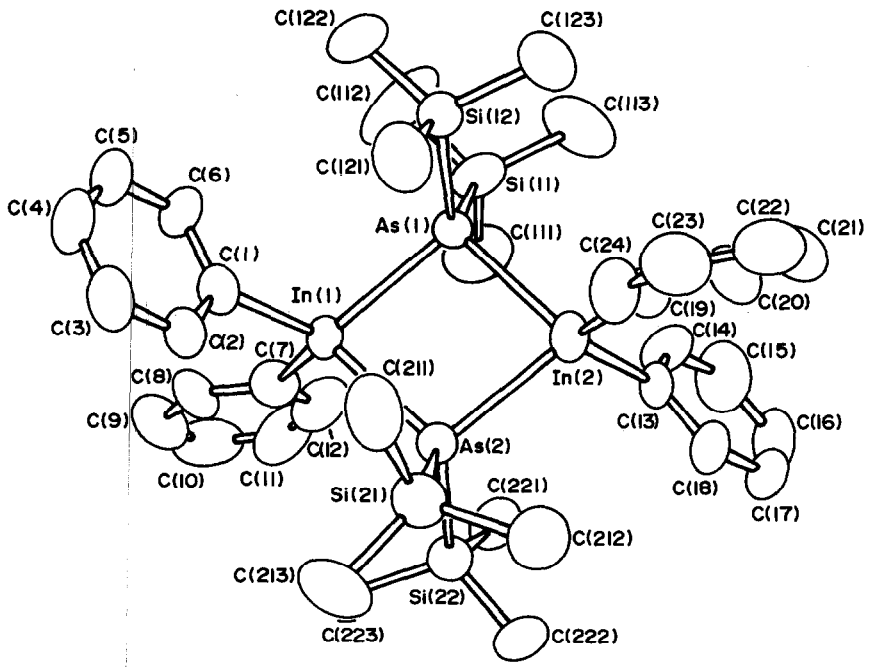

Fig. 2. ORTEP diagram (30% probability ellipsoids) of the solid-state structure of $[Ph_2InAs(SiMe_3)_2]_2$ (**II**). Hydrogen atoms have been omitted for clarity.

Table 2. Selected bond lengths (Å) and angles (°), with e.s.d.s in parentheses, for $[Ph_2InP(SiMe_3)_2]_2$ (I)

(a) Bond lengths			
P—In	2.612(1)	In—C(31)	2.178(6)
P′—In	2.612(1)	In—C(41)	2.185(5)
P—Si(1)	2.262(2)		
P—Si(2)	2.261(3)		
(b) Bond angles			
In—P—In′	92.97(4)	C(31)—In—C(41)	105.7(2)
In—P—Si(1)	107.30(7)	P—Si(1)—C(11)	107.9(2)
In—P—Si(2)	120.62(8)	P—Si(1)—C(12)	111.0(3)
In′—P—Si(1)	112.32(8)	P—Si(1)—C(13)	108.8(3)
In′—P—Si(2)	114.64(7)	P—Si(2)—C(21)	107.1(3)
Si(1)—P—Si(2)	108.26(8)	P—Si(2)—C(22)	108.5(3)
P—In—P′	87.03(4)	P—Si(2)—C(23)	110.2(4)
P—In—C(31)	118.1(2)	In—C(31)—C(32)	118.2(5)
P—In—C(41)	114.3(2)	In—C(31)—C(36)	125.3(5)
P′—In—C(31)	112.7(1)	In—C(41)—C(42)	127.9(5)
P′—In—C(41)	118.8(2)	In—C(41)—C(46)	114.5(5)

Table 3. Selected bond lengths (Å) and angles (°), with e.s.d.s in parentheses, for $[Ph_2InAs(SiMe_3)_2]_2$ (II)

(a) Bond lengths			
As(1)—In(1)	2.689(1)	As(2)—In(1)	2.689(1)
As(1)—In(2)	2.683(1)	As(2)—In(2)	2.682(1)
As(1)—Si(11)	2.344(4)	As(2)—Si(21)	2.370(4)
As(1)—Si(12)	2.352(2)	As(2)—Si(22)	2.353(2)
In(1)—C(1)	2.19(1)	In(2)—C(13)	2.17(1)
In(1)—C(7)	2.17(1)	In(2)—C(19)	2.17(1)
(b) Bond angles			
In(1)—As(1)—In(2)	93.47(4)	In(1)—As(2)—In(2)	93.48(4)
In(1)—As(1)—Si(11)	119.8(1)	In(1)—As(2)—Si(21)	121.6(1)
In(1)—As(1)—Si(12)	110.3(1)	In(1)—As(2)—Si(22)	107.8(1)
In(2)—As(1)—Si(11)	118.2(1)	In(2)—As(2)—Si(21)	116.6(1)
In(2)—As(1)—Si(12)	107.5(1)	In(2)—As(2)—Si(22)	111.3(1)
Si(11)—As(1)—Si(12)	106.7(1)	Si(21)—As(2)—Si(22)	105.6(1)
As(1)—In(1)—As(2)	86.22(4)	As(1)—In(2)—As(2)	86.49(3)
As(1)—In(1)—C(1)	112.5(2)	As(1)—In(2)—C(13)	115.8(3)
As(1)—In(1)—C(7)	117.4(3)	As(1)—In(2)—C(19)	116.4(2)
As(2)—In(1)—C(1)	115.2(3)	As(2)—In(2)—C(13)	114.5(2)
As(2)—In(1)—C(7)	115.4(3)	As(2)—In(2)—C(19)	114.3(3)
C(1)—In(1)—C(7)	108.9(3)	C(13)—In(2)—C(19)	108.2(3)
As(1)—Si(11)—C(111)	109.8(4)	As(2)—Si(21)—C(211)	111.3(5)
As(1)—Si(11)—C(112)	108.8(5)	As(2)—Si(21)—C(212)	106.6(5)
As(1)—Si(11)—C(113)	106.5(5)	As(2)—Si(21)—C(213)	107.7(5)
As(1)—Si(12)—C(121)	106.3(4)	As(2)—Si(22)—C(221)	108.7(4)
As(1)—Si(12)—C(122)	111.0(4)	As(2)—Si(22)—C(222)	110.6(4)
As(1)—Si(12)—C(123)	109.6(4)	As(2)—Si(22)—C(223)	107.7(4)
In(1)—C(1)—C(2)	123(1)	In(2)—C(13)—C(14)	126(1)
In(1)—C(1)—C(6)	119(1)	In(2)—C(13)—C(18)	119(1)
In(1)—C(7)—C(8)	117(1)	In(2)—C(19)—C(20)	119(1)
In(1)—C(7)—C(12)	125(1)	In(2)—C(19)—C(24)	125(1)

substituents at the phosphorus centre. This coupling gives rise to a triplet for these groups in the ^1H and ^{13}C NMR spectra. At room temperature no evidence of solution fluxionality has been observed for either **I** or **II**.

Compound **I** crystallizes in the monoclinic space group $P2_1/c$ with the two dimers in the unit cell lying on crystallographic centres of symmetry and accordingly the $(InP)_2$ ring is required to be strictly planar. The In—P bond lengths are both 2.612(1) Å, a distance which is distinctly shorter than the mean of 2.655 Å in **III**, reflecting the less sterically demanding nature of the phenyl substituents in **I** versus the much bulkier Me_3SiCH_2 moieties in **III**. The mean P—Si bond length of 2.262 Å in **I** is similar to the mean of 2.255 Å in **III**. Bond angles in the $(InP)_2$ core of **I** [In—P—In = 92.97(4)° > P—In—P = 87.03(4)°] are similar to and differ in the same sense as corresponding angles in **III** [93.6(1)°, 86.4° (mean)] and **V** [92.2(1)°, 87.8(1)°]. The C—In—C angle at 105.7(2)° in **I** is very much smaller that the mean of 123.2° in **III** where the considerable enlargement from an approximately tetrahedral value may be ascribed at least in part to the greater steric crowding by the geminal Me_3SiCH_2 substituents. It is relevant to note that the larger the exocyclic bond angle subtended at an opposite pair of ring atoms in four-membered rings, the greater the steric compression exerted on substituents at the other ring centres. It is, therefore, not surprising to find that the Si—P—Si angle of 108.3(1)° in **I** is slightly larger than that of 105.7(2)° in **III**. In contrast to the situations in [In(2,4,6-trimethylphenyl)$_2$I]$_2$,[18] $(Ph_2InOSiMe_3)_2$[19] and $[Ph_2GaAs(CH_2SiMe_3)_2]$,[5] where one of the phenyl ring planes approximately eclipses one of the four-membered ring bonds while the other is in a bisecting orientation, or in $Ph_2GaAs(SiMe_3)_2Ga(Ph)_2Cl$[6] where all are in approximately eclipsing orientations, both of the phenyl rings in **I** are rotated moderately away from either the eclipsing or the bisecting orientation [torsion angles: P—In—C(31)—C(36) = 36.4(6)°, P′—In—C(31)—C(32) = −49.5(5)°; P′—In—C(41)—C(42) = −22.5(6)°, P—In—C(41)—C(42) = 78.1(6)°] to minimize intramolecular non-bonded interactions with the proximal $SiMe_3$ substituents. The indium atom lies close to the C(41)—C(46) least-squares plane (Δ = 0.013 Å), but is displaced significantly (Δ = 0.108 Å) from that through the other phenyl ring atoms [C(31)—C(36)]. Substituent crowding is also indicated in the highly significant differences between the exocyclic bond angles at the *ipso* carbon atoms [In—C(31)—C(36) = 125.3(5)° > In—C(31)—C(32) = 118.2(5)°; In—C(41)—C(42) = 127.9(5)° > In—C(41)—C(46) = 114.5(5)°].

Crystals of dimer **II** also belong to the monoclinic system but they are not isomorphous with those of **I**. Compound **II** crystallizes in the space group $P2_1/n$ with four molecules occupying the general positions. In contrast to the planar $(InAs)_2$ ring in **I**, in **II** the ring is very slightly puckered [As(1)—In(1)—As(2)/As(1)—In(2)—As(2) dihedral angle = 6.0°]. The mean In—As bond length at 2.686 Å in **II** is significantly shorter than the value of 2.728 Å in the planar ring of **IV**; the difference between these distances (Δ = 0.042 Å), which is essentially the same as that between the corresponding bonds (Δ = 0.043 Å) in the phosphorus analogues **I** and **III**, again may be ascribed principally to the different steric demands of the geminal substituents, Ph ≪ Me_3SiCH_2. Endocyclic bond angles [In—As—In = 93.48°(mean) > As—In—As = 86.36°(mean)] in **II** lie close to the corresponding values for **IV** [94.57(5)°, 85.43°(mean)]. The mean As—Si bond length [2.355 Å] and the mean Si—As—Si bond angle [106.2°] in **II** do not differ significantly from those in **IV** [As—Si = 2.348 Å(mean), Si—As—Si = 105.4(2)°]. In addition, the mean In—C bond length at 2.18 Å in **II** is the same as that in **I** (2.182 Å). The mean of the C—In—C angles at 108.5° in **II** is slightly larger than that of 105.7(2)° in **I**, whereas it is much smaller than the mean of 125.4° in **IV** which has the bulky Me_3SiCH_2 substituents at indium. With the reduced symmetry of **II** versus **I**, the dispositions of the phenyl rings with respect to the As—In bonds show more variation [torsion angles: As(2)—In(1)—C(1)—C(2) = −27(1)°, As(1)—In(1)—C(1)—C(6) = 58(1)°; As(1)—In(1)—C(7)—C(12) = 41(1)°, As(2)—In(1)—C(7)—C(2) = −59(1)°; As(1)—In(2)—C(13)—C(14) = 15(1)°; As(2)—In(2)—C(13)—C(18) = −72(1)°; As(2)—In(2)—C(19)—C(24) = −25(1), As(1)—In(2)—C(19)—C(24) = 73(1)°]. The indium atom lies out of each of the phenyl ring planes [Δ = 0.070, 0.108, 0.151 and 0.156 Å, respectively, from the C(1)—C(6), C(7)—C(12), C(13)—C(18) and C(19)—C(24) least-squares planes]. In common with **I**, exocyclic bond angle deformation at the *ipso* carbon centres is also present in **II** [In(1)—C(1)—C(2) = 123(1)° > In(1)—C(1)—C(6) = 119(1)°; In(1)—C(7)—C(12) = 125(1)° > In(1)—C(7)—C(8) = 117(1)°; In(2)—C(13)—C(14) = 126(1)° > In(2)—C(13)—C(18) = 119(1)°; In(2)—C(19)—C(24) = 125(1)° > In(2)—C(19)—C(20) = 119(1)°] to aid in the minimization of intramolecular non-bonded interactions.

Acknowledgement—We are grateful to the Office of Naval Research for their financial support.

REFERENCES

1. R. L. Wells, *Coord. Chem. Rev.* 1992, **112**, 273.
2. A. H. Cowley and R. A. Jones, *Angew. Chem., Int. Edn Engl.* 1989, **28**, 1208.
3. R. L. Wells, R. B. Hallock, A. T. McPhail, C. G. Pitt and J. D. Johansen, *Chem. Mater.* 1991, **3**, 381.
4. R. L. Wells, J. W. Pasterczyk, A. T. McPhail, J. D. Johansen and A. Alvanipour, *J. Organomet. Chem.* 1991, **407**, 17.
5. R. L. Wells, A. P. Purdy, A. T. McPhail and C. G. Pitt, *J. Organomet. Chem.* 1986, **308**, 281.
6. W. K. Holley, R. L. Wells, S. Shaafieezad, A. T. McPhail and C. G. Pitt, *J. Organomet. Chem.* 1990, **381**, 15.
7. R. L. Wells, A. T. McPhail, J. W. Pasterczyk and A. Alvanipour, *Organometallics* 1992, **11**, 226.
8. R. L. Wells, A. T. McPhail and M. F. Self, *Organometallics* 1992, **11**, 221.
9. R. L. Wells, L. J. Jones, A. T. McPhail and A. Alvanipour, *Organometallics* 1991, **10**, 2345.
10. R. L. Wells, S. R. Aubuchon, M. F. Self, J. P. Jasinski, R. C. Woodenberg and R. J. Butcher, *Organometallics*, 1992, **11**, 3370.
11. R. L. Wells, A. T. McPhail, L. J. Jones, M. F. Self and R. Butcher, *Organometallics*, 1992, **11**, 2694.
12. L. Chao and R. D. Rieke, *Syn. React. Inorg. Met.-Org. Chem.* 1974, **4**, 373.
13. G. Becker and W. Hoelderich, *Chem. Ber.* 1975, **108**, 2484.
14. G. Becker, G. Gutekunst and H. J. Wessely, *Z. Anorg. Allg. Chem.* 1980, **462**, 113.
15. Enraf–Nonius Structure Determination Package (SDP 3.0). Enraf–Nonius, Delft, The Netherlands (1985).
16. *International Tables for X-ray Crystallography*, Vol. IV. Kynoch Press, Birmingham (1974).
17. T. Douglas and K. H. Theopold, *Inorg. Chem.* 1991, **30**, 594.
18. J. T. Leman, J. W. Ziller and A. R. Barron, *Organometallics* 1991, **10**, 1766.
19. R. L. Wells, A. T. McPhail and M. F. Self, *J. Coord. Chem.*, in press.

Polyhedron Vol. 12, No. 2, pp. 149–158, 1993
Printed in Great Britain

0277–5387/93 $6.00+.00
© 1993 Pergamon Press Ltd

SYNTHESIS AND CARBONYLATION OF SOME α-ALKOXYALKYL COBALT COMPLEXES, $[RCH(OR')Co(CO)_3PPh_3]$ (R = H, CH_3; R′ = Me, Et)

CHUNG C. TSO and ALAN R. CUTLER*

Department of Chemistry, Rensselaer Polytechnic Institute, Troy, NY 12180, U.S.A.

(*Received* 27 *January* 1992; *accepted* 1 *October* 1992)

Abstract—Cobalt α-alkoxyalkyl compounds $[ROCH_2Co(CO)_3PPh_3]$ (R = Me, Et) and $[CH_3(EtO)CHCo(CO)_3PPh_3]$ have been synthesized and transformed to their acyl derivatives, $[R'CH(OR)C(O)Co(CO)_3PPh_3]$ (R′ = H, CH_3), using 1 atm. of CO. The α-ethoxyethyl complex $[CH_3(EtO)CHCo(CO)_3PPh_3]$ was generated by treating the acetyl compound $[CH_3C(O)Co(CO)_3PPh_3]$ with triethyloxonium hexafluorophosphate in CH_2Cl_2 and then reducing with $LiHBEt_3$. The thermal instability of the resulting $[CH_3(EtO)CHCo(CO)_3PPh_3]$ compound precluded its full characterization, although it transformed into its acyl derivative in 82% isolated yield. The ethoxycarbene intermediate $[CH_3(EtO)C{=}Co(CO)_3PPh_3]^+PF_6^-$, the two alkoxymethyl complexes and the three acyl complexes have been characterized by elemental analysis and IR and NMR (^1H, ^{13}C, ^{31}P) spectroscopy. Attempts to convert the α-alkoxyacyl complexes $[ROCH_2C(O)Co(CO)_3PPh_3]$ and $[CH_3(EtO)CHC(O)Co(CO)_3PPh_3]$ into their alkoxycarbene compounds with a variety of alkylating agents instead afforded $[Co(CO)_3(PPh_3)_2]^+$.

The chain growth of a poly(alkoxymethylene)acyl ligand on an organotransition metal acyl complex (**1**) could incorporate CO [eq. (1)] by coupling acyl ligand reduction (**a** and **b**) and subsequent carbonylation (**c**) steps.[1,2] Although many examples of these ligand reactions are known individually,[3] sequentially iterating them requires careful choice of the organometallic systems ML_x due to their antithetical requirements. Steps **a**/**b** thus require the presence of a coordinatively saturated, non-labile metal centre on ML_x in order to restrict the chemistry to the acyl ligand,[3] whereas the alkyl-CO migratory-insertion step **c** needs a more labile metal centre.[4] Indeed, carbonylating α-alkoxyalkyl complexes is especially demanding.[3] Another consideration concerning the choice of ML_x is the potential use of metal–ligand stereoelectronic inter-

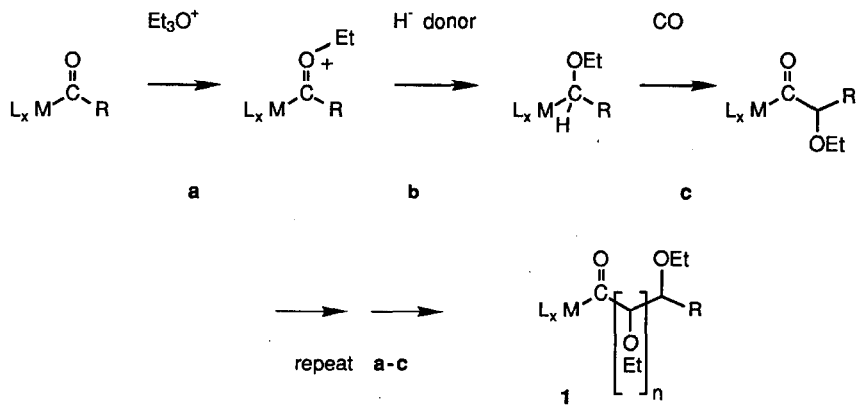

(1)

* Author to whom correspondence should be addressed.

actions[5] to control the stereochemistry at each emerging chiral centre (step **b**).

Two organometallic templates ML_x thus far have proved useful in balancing the antithetical requirements of the acyl ligand reduction and carbonylation sequences. The (η^5-indenyl)iron system $Fe(CO)_2(\eta^5\text{-}C_9H_7)$ supports both steps **a**/**b** as well as the facile carbonylation of α-alkoxyalkyl ligands (step **c**).[2] Facility of this carbonylation step depends on reversible η^5/η^3-indenyl ring slippage on these iron complexes[6] to associate CO under conditions that their CpFe analogues are inert.[7] The other organometallic template is the extremely labile cobalt moiety $[Co(CO)_2(Ph_2PCH_2CH_2PPh_2)]$.[1] With these cobalt complexes, the presence of the η^2-dppe ligand retains the high lability at the cobalt centre that one associates with easy carbonylation of cobalt carbonyl alkyl complexes,[8] in addition to supporting the subsequent acyl ligand reduction sequence **a**,**b**. A gratifying outcome of this cobalt chemistry was our diastereoselective synthesis of the *threo*-diethoxybutanoyl **2**.[1] This diastereofacial selectivity (during iteration of step **b**), which could derive from the disposition of the axial phosphine phenyl rings of the dppe ligand, serves as the impetus for the present study.

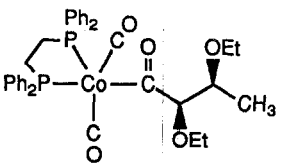

2

The monophosphine-substituted cobalt system $Co(CO)_3(PPh_3)$ was used in the present study as the template for the reaction chemistry engendered in eq. (1), since the now remote phosphine phenyl rings should not contribute to the diastereoselectivity of acyl ligand reduction (steps **a**/**b**). This steric isolation of the phosphine ligand corresponds to the anticipated *trans* array of the phosphine and acyl (or ethoxycarbene) ligands that is depicted for the targeted cobalt acyl complexes **3**. The bis-axial, pseudo-C_{3v} geometry that is predicted for **3** has been established for a number of cobalt alkyl and acyl complexes, $[R'C(O)Co(CO)_3(PR_3)]$.[8,9] Moreover, these cobalt acyl complexes are readily available by carbonylating their alkyl precursors, as demonstrated for the related cobalt methyl $[CH_3Co(CO)_3(PPh_2Me)]$[10] and even methoxymethyl $[MeOCH_2CO(CO)_3(PPh_2Me]$[11] complexes. Our initial objective was to synthesize and to assess the stereochemistry of the cobalt diethoxybutanoyl complex **3** ($n = 1$): according to our previously advanced Felkin–Anh transition-state argument[1] it should form with *threo*-diastereoselectivity that is quite independent of the phosphine ligand.

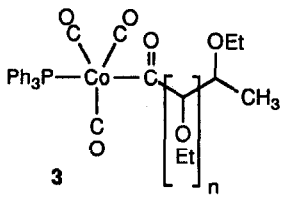

3

EXPERIMENTAL

All synthetic manipulations were performed under a nitrogen atmosphere using standard Schlenk line and syringe/septum bench-top techniques for handling moderately air-sensitive organometallics.[12] Solvents for synthetic work and for recording spectral data were deoxygenated by purging with nitrogen for *ca* 15 min. Camag alumina (neutral, activity 3) was used for column chromatography.

IR spectra were recorded in CH_2Cl_2 solutions (0.10 mmol, 2.5 cm^3) in an NaCl solution cell with an amalgam spacer (0.10 mm) and were recorded on a Perkin–Elmer Model No. 297 spectrophotometer. The ν(CO) frequencies (2100–1600 cm^{-1}) were calibrated against the polystyrene 1601 cm^{-1} band; they are precise to ± 2 below and ± 5 above 2000 cm^{-1}. NMR spectral data were recorded in concentrated $CDCl_3$ solutions after trace amounts of insoluble residues were centrifuged. Varian Model XL-200 and IBM-WP100 instruments were used for recording the NMR spectra, which are reported as δ values downfield from internal $(CH_3)_4Si$ (^1H and $^{13}C\{^1H\}$ NMR spectra) or relative to external H_3PO_4 ($^{31}P\{^1H\}$). The PF_6^- absorption in ^{31}P NMR spectra, centred at -143.2 ppm [$J(PF) = 710$ Hz], also was used as an internal standard.

Organic and inorganic reagents were procured commercially and used as received. THF and diethyl ether were distilled under nitrogen from sodium benzophenone ketyl; methylene chloride likewise was obtained as needed from P_2O_5. Triethyloxonium hexafluorophosphate was recrystallized from nitrobenzene–ether to remove any residual acid.[13]

Preparation of $[Co(CO)_3PPh_3]_2$

Dimeric $[Co(CO)_3PPh_3]_2$ was prepared by a modification of the procedure reported by Manning.[14] A single-neck 300 cm^3 round-bottomed flask fitted with a magnetic stir bar was charged with $[Co(CO)_4]_2$ (10.00 g, 29.24 mmol) and PPh_3

(15.21 g, 58.00 mmol) before sealing with a rubber septum. The atmosphere was replaced by nitrogen and benzene (150 cm^3) was then injected via a syringe into the flask. Vigorous gas evolution ensued and a thick brick-red slurry consisting of $Co(CO)_3(PPh_3)_2{}^+Co(CO)_4{}^-$ formed.

CAUTION: Carbon monoxide (toxic) was vented in the hood through a mineral oil bubbler, which was attached to a syringe needle inserted through the septum of the reaction flask.

This slurry was stirred at 60°C for 10 h. The solvent was then evaporated at room temperature and the remaining red–brown solid was washed with ether (3×100 cm^3) and vacuum dried. $[Co(CO)_3PPh_3]_2$ (21.20 g, 89% yield), IR (Nujol): 1945 cm^{-1} (br). This solid, which is very slightly soluble to insoluble in benzene, ether, THF and CH_2Cl_2, was not further purified.

Synthesis of $CH_3C(O)Co(CO)_3(PPh_3)$ **(4)**

An oven-dried 500 cm^3 three-neck amalgam flask, which was fitted with an overhead ground-glass stirring shaft/teflon stirring paddle and a nitrogen inlet adapter, was cooled to room temperature in a stream of nitrogen. Enough 1.5% sodium amalgam was added to cover the teflon stirrer blade before adding THF (30 cm^3) and $[Co(CO)_3PPh_3]_2$ (5.00 g, 6.17 mmol). The brick red suspension converted slowly to a yellowish–green suspension upon stirring for 12 h; its light yellow–green supernatant liquid corresponded to $Co(CO)_3(PPh_3)^-Na^+$.[15] IR spectrum: ν(CO) 1934 (m), 1857 (s), 1810 (m) cm^{-1}. The anion slurry that remained after draining the amalgam was transferred via a stainless steel transfer needle into a 500 cm^3 one-neck round-bottomed flask, which was then cooled to −78°C. Methyl iodide (0.78 cm^3, 13.0 mmol) was added dropwise by syringe to the stirred suspension. Within 0.5 h, the yellowish green tint had turned dark yellow and its IR spectrum at room temperature (1.5 h) was consistent with conversion to $[CH_3Co(CO)_3(PPh_3)]$:[10,15a,16] ν(CO) 2037 (w), 1958 (s,br) cm^{-1}.

This suspension containing $[CH_3Co(CO)_3(PPh_3)]$ was stirred under 1 atm. of CO for 4 h (with no colour change), the solvent was evaporated on a Buchi rotovaporator and the residue was extracted with methylene chloride (4×10 cm^3). The combined extracts were filtered through celite; the filtrate was concentrated and chromatographed on alumina (2×3 cm column) with methylene chloride. This afforded a yellow band that upon evaporating left $[CH_3C(O)Co(CO)_3(PPh_3)]$ **(4)**[10,17] as a yellow solid (5.13 g, 93% yield). IR (THF): ν(CO) 2048 (w), 1978 (s), 1959 (s), 1677 (m) cm^{-1}.

Synthesis of $CH_3(CH_3CH_2O)C{=}Co(CO)_3(PPh_3)^+PF_6^-$ **(5)**

A solution of $CH_3C(O)Co(CO)_3(PPh_3)$ **(4)** (2.00 g, 4.46 mmol) in methylene chloride (100 cm^3) was treated with purified triethyloxonium hexafluorophosphate (1.66 g, 6.70 mmol) and the ensuing slow reaction was monitored by IR spectroscopy. The starting acetyl complex **(4)** was consumed in 24 h, although the original yellow colour remained. After the yellow solution was evaporated, the residue was extracted with methylene chloride (25 cm^3) and filtered through celite before adding a layer of ether (200 cm^3). White crystals of $Et_3O^+PF_6^-$ formed first (−5°C) at the solvent interface as a vitreous deposit or "ring" on the flask, then yellow crystals deposited on the lower wall of the flask over 12 h. The supernatant liquid was removed with a cannula and the two crystalline deposits were separated. Repeating this crystallization step afforded 2.25 g of a yellow crystalline solid that was characterized as $[CH_3(CH_3CH_2O)C{=}Co(CO)_3(PPh_3)]^+PF_6^-$ **(5)** (81% yield). Found: C, 48.3; H, 3.7. Calc. for $C_{25}H_{23}O_4P_2F_6Co$: C, 48.2; H, 3.7%.

The ethoxycarbene compound **5** is thermodynamically unstable as well as being extremely reactive towards nucleophiles. Either long-term storage of **5** as a solid at −10°C (> 2 days) or in CH_2Cl_2 solution at 22°C (> 12 h) degraded it to $[Co(CO)_3(PPh_3)_2]^+PF_6^-$ **(12)**[18] as the only identifiable cobalt complex. IR (CH_2Cl_2): 2008 cm^{-1} (CO); $^{31}P\{^1H\}$ NMR (CH_2Cl_2): δ 55.4. This degradation product was also found in the CH_2Cl_2–ether filtrates that were collected during the synthesis of **5**. Upon exposure either to traces of moisture (e.g. NaCl plates of an IR cell that had not been flushed with dry solvent) or to 1 equivalent of $Bu^n{}_4N^+I^-$ in methylene chloride, **5** immediately regenerated its acetyl precursor **4**.

Reduction of $[CH_3(CH_3CH_2O)C{=}Co(CO)_3(PPh_3)]^+PF_6^-$ **(5)**

The ethoxycarbene complex **5** (0.50 g, 0.80 mmol) was dissolved in methylene chloride (25 cm^3) at −78°C. To this dark yellow solution a lithium triethylborohydride–THF solution (80 cm^3, 1.0 M) was added dropwise with stirring. The solution immediately turned lighter and IR spectral monitoring was consistent with quantitative conversion to $[CH_3CH(OEt)Co(CO)_3(PPh_3)]$ **(6)**. None of the acetyl complex precursor **4** was detected by IR or ^{31}P NMR spectroscopy (−30°C). Passing the cold (−78°C) solution of **6** quickly through a 2×2 cm column of alumina–CH_2Cl_2 gave the unchanged

yellow–brown eluate, as ascertained by IR spectroscopy. This solution containing **6** slowly (2 h) turned reddish–brown and deposited $[Co(CO)_3(PPh_3)]_2$ as it warmed to room temperature. Rapid evaporation of the solvent from cold (−30°C) methylene chloride solutions of **6** on a vacuum line left a yellow–brown gum, which did not redissolve in CH_2Cl_2. Definitive ^1H NMR spectral data for **6** were not obtained due to paramagnetic broadening.

Synthesis of $[CH_3CH(OCH_2CH_3)C(O)Co(CO)_3(PPh_3)]$ **(7)**

A methylene chloride solution (20 cm^3) of $[CH_3(CH_3CH_2O)C{=}Co(CO)_3(PPh_3)]^+PF_6^-$ **(5)** (0.51 g, 0.82 mmol) was treated with an $LiHBEt_3$–THF solution (0.86 cm^3) (0.95 M, 0.82 mmol) at −78°C. The reaction was judged complete after 15 min (−78°C) by IR spectral monitoring, then the pale yellow solution was passed rapidly through 2 × 2 cm of alumina that had been precooled with CH_2Cl_2 (−78°C). The yellow band that eluted with cold methylene chloride immediately was exposed to 1 atm. of carbon monoxide with agitation for 2 h. The volume of the resulting yellow solution then was reduced and it was chromatographed on alumina (2 × 4 cm column) with CH_2Cl_2 or on silica gel with 1 : 5 THF–hexane. A yellow band eluted from both columns; slowly evaporating this eluate on a Buchi rotovaporator left a small amount of a clear vitreous deposit (borane residues) on the upper wall of the flask and a yellow–brown solid in the bottom of the flask. This yellow–brown material was collected and fractionally reprecipitated again from methylene chloride–hexane, before drying under reduced pressure. It was identified as $[CH_3CH(OCH_2CH_3)C(O)Co(CO)_3(PPh_3)]$ **(7)** (343 mg, 82% yield). Found: C, 61.4; H, 4.8. Calc. for $C_{26}H_{24}O_5PCo$: C, 61.6; H, 4.7%.

Synthesis of alkoxymethyl complexes $[ROCH_2Co(CO)_3(PPh_3)]$ **(8, R = CH_3; 9, R = CH_2CH_3)**

$[CH_3OCH_2Co(CO)_3(PPh_3)]$ **(8)**. A light yellow–green THF suspension (250 cm^3) containing $Co(CO)_3(PPh_3)^-Na^+$ (4.94 mmol) was generated by stirring a reddish-brown slurry of $[Co(CO)_3(PPh_3)]_2$ (2.00 g, 2.47 mmol) over excess 1% Na (Hg) for 8 h. This suspension was transferred via stainless-steel cannula, cooled to −78°C and treated with chloromethyl methyl ether (0.38 cm^3, 5.0 mmol).

CAUTION: Chloromethyl ethers are potentially carcinogenic and must be handled in a hood.

The greenish tint gradually left as the reaction mixture warmed to room temperature over 2 h. It then was evaporated and methylene chloride extracts (30 cm^3) were filtered through celite (all the yellow colour was washed through the celite pad with CH_2Cl_2). The combined filtrates were reduced in volume on a Buchi rotovaporator and chromatographed on alumina (2 × 3 cm) with methylene chloride. The yellow band that eluted cleanly afforded $[CH_3OCH_2Co(CO)_3(PPh_3)]$ **(8)**[19] as a stable yellow solid (1.98 g, 89% yield). Found: C, 61.0; H, 4.3. Calc. for $C_{23}H_{20}O_4PCo$: C, 61.3; H, 4.4%.

$[CH_3CH_2OCH_2Co(CO)_3(PPh_3)]$ **(9)**. The same procedure was repeated using chloromethyl–ethyl ether for alkylating $Co(CO)_3(PPh_3)^-Na^+$, thus affording $[CH_3CH_2OCH_2Co(CO)_3(PPh_3)]$ **(9)** in 83% yield after an identical workup. This stable yellow solid also can be stored for prolonged periods (over a month) in a refrigerator without noticeable decomposition. Found: C, 62.0; H, 4.7. Calc. for $C_{24}H_{22}O_4PCo$: C, 62.0; H, 4.7%.

Carbonylation of alkoxymethyl complexes $[ROCH_2Co(CO)_3(PPh_3)]$ **(8, R = CH_3; 9, R = CH_2CH_3)**

$[CH_3OCH_2C(O)Co(CO)_3(PPh_3)]$ **(10)**. A THF suspension (300 cm^3) containing $[CH_3OCH_2Co(CO)_3(PPh_3)]$ **(8)** (12.34 mmol) was generated from $[Co(CO)_3(PPh_3)]_2$ (5.0 g, 6.17 mmol) and was warmed to room temperature. An IR spectrum of the yellow supernatant solution was consistent with quantitatively forming **8**; ν(CO): 1955 (br) cm^{-1}. Carbon monoxide (1 atm.) was then bubbled into this solution for 3 h; although there was no change in physical appearance, quantitative conversion of **8** to $CH_3OCH_2C(O)Co(CO)_3(PPh_3)$ **(10)** was established by its IR spectrum: $\nu(C{\equiv}O)$ (THF) 2048 (w), 1978 (vs), 1958 (vs) cm^{-1}; $\nu(C{=}O)$ 1675 (br) cm^{-1}. Methylene chloride extracts (30 cm^3) of the evaporated reaction mixture were filtered through celite before they were concentrated and chromatographed on alumina (2 × 3 cm column) with methylene chloride. This cleanly eluted a yellow band that gave $[CH_3OCH_2C(O)Co(CO)_3(PPh_3)]$ **(10)**[17a,19] as a stable yellow solid (5.41 g, 91% yield). Found: C, 60.1; H, 4.2. Calc. for $C_{24}H_{20}O_5PCo$: C, 60.2; H, 4.2.

$[CH_3CH_2OCH_2C(O)Co(CO)_3(PPh_3)]$ **(11)**. Carbon monoxide was bubbled through a methylene chloride solution (75 cm^3) of $[CH_3CH_2OCH_2Co(CO)_3(PPh_3)]$ **(9)** (3.00 g, 6.47 mmol) for 3 h. The light yellow solution, unchanged in appearance, was filtered through 3 cm of alumina and the yellow band that washed through the column was evaporated to give analytically pure $[CH_3CH_2OCH_2C(O)Co(CO)_3(PPh_3)]$ **(11)** as a stable yellowish-tan solid (yield 3.01 g, 95%). Found: C,

60.9; H, 4.4. Calc. for $C_{25}H_{22}O_5PCo$: C, 60.9; H, 4.5%.

RESULTS AND DISCUSSION

In the present study, the ligand reactions corresponding to eq. (1) have been studied using $Co(CO)_3(PPh_3)$ as the ML_x template. The corresponding acyl-alkyl-alkoxy-carbene complexes for this template should offer increased thermodynamic stability with respect to the parent $Co(CO)_4$ compounds,[8,9] but the alkyl complexes should still undergo facile alkyl-CO migratory-insertion.[20] For example, Baird[10] and Cutler,[11] using the related $Co(CO)_3PPh_2Me$ template, carbonylated the methyl and methoxymethyl compounds, respectively, with 1 atm. of CO and isolated the corresponding acyl complexes $[CH_3C(O)Co(CO)_3(PPh_2Me)]$ and $[MeOCH_2C(O)Co(CO)_3(PPh_2Me)]$. Other cobalt acyl complexes, notably the $Co(CO)_3(PPh_3)$ acetyl,[10,17a] methoxyacetyl,[17a,19] hydroxyacetyl and siloxyacetyl[19] compounds, had been synthesized via the classic Heck and Breslow procedure of adding PPh_3 to $RCo(CO)_4/RCOCo(CO)_4$ mixtures.

We switched to using the $Co(CO)_3(PPh_3)$ vs the $Co(CO)_3(PPh_2Me)$[11] system because the alkyl and acyl complexes of the former moiety form as (sometimes crystalline) solids, whereas analogous complexes of the latter cobalt system invariably appear as gums or syrups. Once isolated as gums many of these cobalt alkyl and acyl complexes tend to decompose. The apparent gain in stability in working with $Co(CO)_3(PPh_3)$ alkyl-acyl complexes offsets the minor inconvenience encountered in using the now insoluble dimeric $[Co(CO)_3(PPh_3)]_2$ as our starting material.

Conversion of $[CH_3C(O)Co(CO)_3(PPh_3)]$ (**4**) *to* $[CH_3CH(OCH_2CH_3)C(O)Co(CO)_3(PPh_3)]$ (**7**)

A convenient two-step preparation of the cobalt acetyl complex $[CH_3C(O)Co(CO)_3(PPh_3)]$ (**4**) entails alkylating $Co(CO)_3(PPh_3)^-Na^+$[15] with methyl iodide and then carbonylating the resulting methyl compound, $[CH_3Co(CO)_3(PPh_3)]$, with 1 atm. of CO for 4 h. A 93% yield of **4** as a stable, yellow solid was realized after a work-up procedure involving chromatography on alumina. In addition to being prepared by the Heck and Breslow procedure,[17a] **4** previously had been generated by displacing iodide from $CH_3C(O)Co(CO)_3I^-$ with PPh_3.[17b] Its full ^1H, ^{13}C and ^{31}P NMR spectral properties are detailed in Table 1. (The unstable cobalt methyl precursor $[CH_3Co(CO)_3(PPh_3)]$[10,15a,16] was not characterized.)

We converted **4** to the ethoxypropionyl $[CH_3CH(OEt)C(O)Co(CO)_3(PPh_3)]$ (**7**) by the three-step set of coordinated ligand reactions outlined in eq. (2). In the first step reacting **4** with purified $Et_3O^+PF_6^-$ gave the ethoxycarbene salt **5**, which was isolated analytically pure in 80% yield as a thermally-sensitive yellow solid. The isolation procedure was complicated by the unavoidable presence of unreacted $Et_3O^+PF_6^-$. Because of the sluggishness of this alkylation reaction, excess triethyloxonium salt must be used to drive the reaction to completion before the product decomposes. Even in the presence of 1.5 equivalents of $Et_3O^+PF_6^-$, transforming **4** to **5** requires 18–24 h to consume the starting compound **4**. The thermal sensitivity of the purified ethoxycarbene salt **5** in CH_2Cl_2 solution is evident in its slow degradation at room temperature to the known[18] carbonyl salt $Co(CO)_3(PPh_3)_2^+PF_6^-$ (**12**). Interestingly, the more electron rich $[CH_3C(O)Co(CO)_2(dppe)]$ [acetyl $\nu(C{=}O) = 1630\ cm^{-1}$] transforms within 1 h to its stable ethoxycarbene derivative[1] with 1 equivalent of $Et_3O^+PF_6^-$.

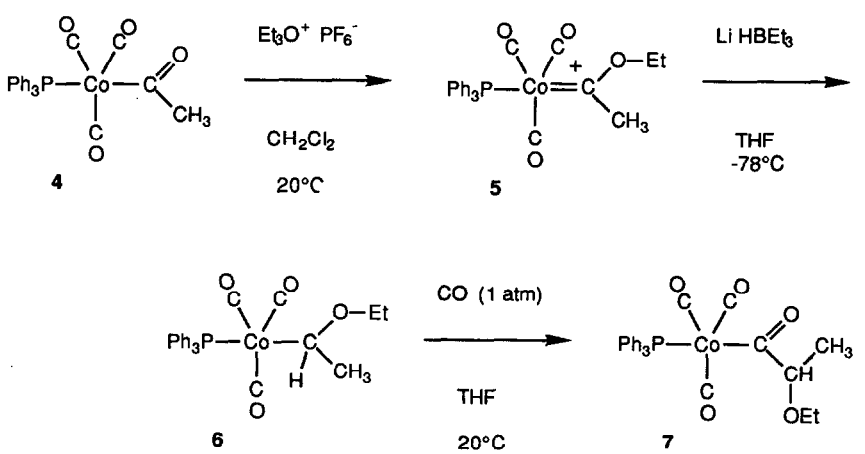

(2)

Table 1. Spectroscopic characterization of $Co(CO)_3PPh_3$ complexes

Complex	IR (CH_2Cl_2) (cm^{-1})	^1H NMR ($CDCl_3$) (ppm)[a]	$^{13}C\{^1H\}$ NMR ($CDCl_3$) (ppm)[a,b]	$^{31}P\{^1H\}$ NMR ($CDCl_3$)
$[CH_3C(O)Co(CO)_3PPh_3]$ **(4)**	2053(w), 1980(vs) 1961(vs) (C≡O) 1666(m) (C=O)	7.45 (s) $CoPPh_3$ 2.78 [d, J(PH) = 1.2] $CoCH_2$	238.6 [d, J(PC) = 33.2] $CoCOCH_3$ 199.7 [br d, J(PC) = 21.2] CO 50.0 [d, J(PC) = 26.0] $CoCOCH_3$	48.2
$[CH_3(CH_3CH_2O)C{=}Co(CO)_3PPh_3]^+PF_6^-$ **(5)**[a,c]	2083(w), 2027(vs) 2013(vs) (C≡O)	4.92 (q, J = 7.0) OCH_2CH_3 3.32 (s) $Co{=}CCH_3$ 1.74 (t, J = 7.0) OCH_2CH_3	317.2 [d, J(PC) = 41.1] $Co{=}C$(OEt)Me 193.8 [br d, J(PC) = 22.6] CO 81.0 (s) OCH_2 45.4 [d, J(PC) = 7.9] $Co{=}CCH_3$ 14.0 (s) OCH_2CH_3	47.1
$[CH_3OCH_2Co(CO)_3PPh_3]$ **(8)**	2037(w), 1959(vs, br) (C≡O)	7.45 (s) $CoPPh_3$ 5.27 [d, J(PH) = 2.1] $CoCH_2$ 3.47 (s) OCH_3	201.4 (br s) CO 69.6 [d. J(PC) = 27.3] $CoCH_2$ 59.9 (s) OCH_3	55.1
$[CH_3CH_2OCH_2Co(CO)_3PPh_3]$ **(9)**	2040(w), 1960(vs, br) (C≡O)	7.43 (br s) $CoPPh_3$ 5.31 (br s) $CoCH_2$ 3.62 (q, J = 6.8) OCH_2CH_3 1.25 (t, J = 6.8) OCH_2CH_3	201.5 (br) CO 67.4 (s) OCH_2 66.5 [d, J(PC) = 27.2] $CoCH_2$ 15.1 (s) OCH_2CH_3	55.9
$[CH_3OCH_2C(O)Co(CO)_3PPh_3]$ **(10)**	2055(w), 1981(vs) 1964(vs) (C≡O) 1671(m) (C=O)	7.46 (br s) $CoPPh_3$ 4.40 (s) $CoCOCH_2$ 3.44 (s) OCH_3	238.5 [d, J(PC) = 31.4] $CoCOCH_2$ 198.7 [d, J(PC) = 20.0] CO 89.4 [d, J(PC) = 27.9] $CoCOCH_2$ 59.4 (s) OCH_3	49.1
$[CH_3CH_2OCH_2C(O)Co(CO)_3PPh_3]$ **(11)**	2058(w), 1983(vs) 1964(vs) (C≡O) 1674(m) (C=O)	7.46 (s) $CoPPh_3$ 4.41 (s) $CoCOCH_2$ 3.60 (q, J = 7.0) OCH_2CH_3 1.24 (t, J = 7.0) OCH_2CH_3	239.1 [d, J(PC) = 31.3] $CoCOCH_2$ 198.8 [d, J(PC) = 21] CO 87.7 [d, J(PC) = 27.9] $CoCOCH_2$ 67.0 (s) OCH_2CH_3 15.0 (s) OCH_2CH_3	50.2
$[CH_3(CH_3CH_2O)CHCo(CO)_3PPh_3]$ **(6)**[d]	2031(w), 1950(vs, br)			54.2
$[CH_3(CH_3CH_2O)CHC(O)Co(CO)_3PPh_3]$ **(7)**	2048(w), 1978(vs) 1962(vs) (C≡O) 1647(m) (C=O)	7.47 (s) $CoPPh_3$ 3.99 (q, J = 5.9) $CoCOCH$ 3.69 (dq, J = 9.1, 7.0) $(OCHHCH_3$ 3.54 (dq, J = 9.1, 7.3) $OCHHCH_3$ 1.34 (d, J = 5.9) $CoCOCHCH_3$ 1.28 (br t, J = 7.1) OCH_2CH_3	247.8 [d, J(PC) = 30.6] CoCOCH 199.0 [d, J(PC) = 20.6] CO 91.4 [d, J(PC) = 23.9] $CoCOCH$ 65.4 (s) OCH_2 17.1 (s) $CoCOCHCH_3$ 15.3 (s) OCH_2CH_3	49.5

[a] Spin–spin splittings (J values) in Hz.

[b] Phenyl assignments for **4**: δ 133.3 [d, J(PC) = 42 Hz, *ipso*-C], 133.0 [d, J(PC) = 12 Hz, *ortho*-C], 130.7 (s, *para*-C), 128.8 [d, J(PC) = 10 Hz, *meta*-C]. These assignments are representative for the alkyl/acyl $Co(CO)_3PPh_3$ complexes.

[c] NMR data correspond to CD_2Cl_2 solutions.

The trigonal bipyramidal structure depicted for the phosphinecobalt ethoxycarbene salt **5** is consistent with its spectral data. The IR spectrum of **5**, for example, exhibits one weak and two closely spaced strong intensity ν(CO) bands for the terminal carbonyls, a band pattern diagnostic for *trans*-axial RCo(CO)$_3$L structures of local C_{3v} symmetry.[8,9,21] The presence of a cationic cobalt centre on **5** is supported by the shifting of its IR terminal carbonyl ν(CO) bands to higher frequencies with respect to those of the starting acetyl complex **4**, and by downfield shifting of its ^{1}H NMR spectral C-methyl resonance at δ 3.32 with respect to that of **4** (2.78 ppm). A 78 ppm downfield shift for the carbenoid carbon in the ^{13}C{^{1}H} NMR spectrum of **5** (to δ 317 ppm) vs **4** further identifies **5** as a Fischer carbene complex.[22]

Complex **5** also has the reactivity of a typical Fischer carbene complex. Treatment of **5** in CH_2Cl_2 solution with 1 equivalent of $Bu^n_4N^+I^-$ immediately and quantitatively released its acetyl precursor **4**, thus satisfying a standard assay for cationic alkoxycarbene compounds.[3,13] In further agreement with its reactivity as a Fischer carbene complex, **5** instantaneously added hydride at the carbenoid centre[3] from $LiHBEt_3$ in THF at -78°C and transformed to its α-ethoxyethyl derivative [$CH_3CH(OEt)Co(CO)_3(PPh_3)$] (**6**). A surprising outcome of this second of the three-step set of coordinated ligand reactions in eq. (2) is that the cobalt α-ethoxyethyl product **6** promptly decomposed upon warming to room temperature. IR and ^{31}P{^{1}H} NMR spectral data for cold solutions of **6** nevertheless closely match that obtained for the stable alkoxymethyl compounds [$ROCH_2Co(CO)_3(PPh_3)$] (**8**, R = Me; **9**, R = Et) (*vide infra*).

Carbonylating **6**, the third step set in eq. (2), between -78°C and room temperature with 1 atm. of CO provided the ethoxypropionyl complex [$CH_3CH(OEt)C(O)Co(CO)_3(PPh_3)$] (**7**). It was isolated as a stable, yellow solid in 82% yield. The IR spectrum of **7** in the terminal carbonyl stretching frequency region resembles those of [$CH_3C(O)Co(CO)_3(PPh_3)$] (**4**) and alkoxyacetyl compounds [$ROCH_2C(O)Co(CO)_3(PPh_3)$] (**10**, **11**), although the 25 cm^{-1} reduction in frequency of the acyl ν(C=O) band for **7** vs **10** and **11** exceeds the previously reported 12 cm^{-1} drop for the ethoxypropionyl vs alkoxyacetyl ligands coordinated to $Fe(CO)_2(\eta^5\text{-}C_9H_7)$.[2]

^{1}H and ^{13}C{^{1}H} NMR spectra of **7** (Table 1) further define the ethoxypropionyl ligand and closely resemble published data for [$CH_3CH(OEt)C(O)Fe(CO)_2(\eta^5\text{-}C_9H_7)]^-$[2] and [$CH_3CH(OEt)C(O)Co(CO)_2$(dppe)].[1] Noteworthy assignments for the ^{13}C{^{1}H} NMR spectrum of **7** (all carbons are assigned) include the doublets at δ 248 for the acyl carbonyl [J(PC) = 31 Hz] and δ 199 for the terminal carbonyls [J(PC) = 21 Hz]. The ^{31}P{^{1}H} spectrum for **7** shows a singlet at δ 50, in agreement with the other acyl complexes reported in this study, and demonstrates the absence of any other phosphorus-containing species.

The increased bench stability of the cobalt acyl complex **7** compared to its alkyl precursor **6** follows the trend that we noted for analogous pairs of acyl and alkyl complexes ligand to $Fe(CO)_2(\eta^5\text{-}C_9H_7)^2$ and $Co(CO)_2$(dppe).[1] Surprisingly, [$CH_3CH(OEt)Co(CO)_3(PPh_3)$] (**6**) readily decomposes at room temperature (cf. the cobalt alkoxymethyl complexes **8** and **9**) to give [$Co(CO)_3(PPh_3)]_2$ as the only organometallic product. Such reactivity is consonant with homolytic Co—C bond dissociation and the formation of a geminate radical pair, an established decomposition pathway of secondary alkyl cobalt(III) complexes.[23] If the unstable cobalt hydride $HCo(CO)_3(PPh_3)$[15a,24] had formed due to the operation of an alternative decomposition pathway, then we would have at least detected it, based on work by Martin and Baird[10] with $HCo(CO)_3(PPh_2Me)$.

Preparation of alkoxyacetyl complexes [$ROCH_2C(O)Co(CO)_3(PPh_3)$] (**10**, R = CH_3; **11**, R = CH_2CH_3)

We prepared the methoxymethyl and ethoxymethyl complexes [$ROCH_2Co(CO)_3(PPh_3)$] (**8** and **9**, respectively) by metallating chloromethyl methyl and ethyl ethers with $Co(CO)_3(PPh_3)^-Na^+$ [eq. (3)]. Both **8** and **9**, stable yellow solids, were isolated analytically pure in 83–89% yields after column chromatography on alumina.

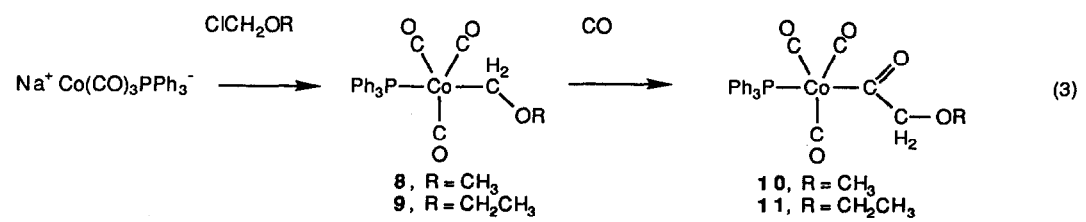

(3)

IR and NMR spectral data adequately characterize **8** and **9** as *trans*-diaxial alkoxymethyl

complexes, $[ROCH_2Co(CO)_3(PPh_3)]$, having local C_{3v} symmetry. Their IR spectra show two terminal carbonyl ν(CO) bands, a weak absorption near 2040 cm^{-1} and a broad, intense band at 2060 cm^{-1} (for the nearly degenerate E mode vibrations) which typify alkyl cobalt complexes, $RCo(CO)_3PR_3$.[8,9,21] NMR spectral absorptions for the $CoCH_2$ group

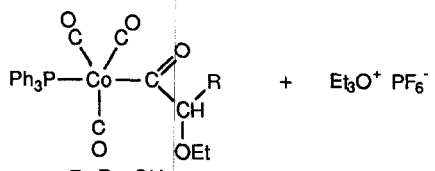

7, R = CH_3
11, R = H

are also diagnostic due to ^{31}P spin coupling: the $CoCH_2$ group absorbs as doublets in both the ^1H and $^{13}C\{^1H\}$ NMR spectra, δ 5.30, J(PH) = 2 Hz and δ 67–70, J(PC) = 27 Hz, respectively.

Carbonylating **8** and **9**, either *in situ* in THF or after purification in CH_2Cl_2, using 1 atm. of CO gives their alkoxyacetyl compounds **10** and **11** in over 90% isolated yields. These alkoxyacetyl compounds were isolated analytically pure as yellow solids that are stable at room temperature. Their IR spectra in relatively polar solvents such as CH_2Cl_2 or THF display one medium intensity acyl ν(C=O) band near 1670 cm^{-1} and three terminal carbonyl ν(C≡O) bands, including two closely spaced and intense E vibrational modes at 1982 and 1964 cm^{-1}. This pattern of carbonyl ν(CO) absorptions is typical for (acyl)$Co(CO)_3(PPh_3)$ compounds. The presence of two intense E vibrational modes for these acyl complexes vs one for the alkyl complexes (alkyl)$Co(CO)_3(PPh_3)$ has been noted previously for analogous pairs of such acyl/alkyl complexes.[21]

Both the methoxymethyl **8** and methoxyacetyl **10** compounds have been previously reported. The Heck–Breslow procedure had been used to generate **10**,[17a] which ejected CO upon warming to give **8**.[19] Although similar decarbonylation reactions have been noted recently under ambient conditions for analogous chloroacetyl[9b] and propargylacyl[25] compounds, we did not discern room-temperature decarbonylation of alkoxyacetyl compounds **10** and **11** to **8** and **9**, respectively, by ^1H or ^{31}P NMR spectroscopy. Our spectral data for **8** and **10** (Table 1) agrees with the previously reported IR and ^1H NMR spectral assignments.[17a,19]

The present high yield access to the alkoxyacetyl compounds **10** and **11** by direct carbonylation is not surprising given our previous report on converting a related ethoxymethyl, $[EtOCH_2Co(CO)_3(PMePh_2)]$ to its acyl derivative, $[EtOCH_2(CO)Co(CO)_3(PMePh_2)]$.[11] The ready availability of the more tractable triphenylphosphine-substituted alkoxyacetyl compounds **10** and **11**, as well as the ethoxypropionyl analogue $[CH_3CH(OEt)C(O)Co(CO)_3(PPh_3)]$ (**7**), make them attractive substrates for attempted chain growth reactions, as outlined in eq. (1) [R = H and Me; ML_x = $Co(CO)_3(PPh_3)$].

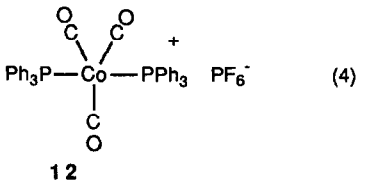

12

Reactions of $Et_3O^+PF_6^-$ *with α-alkoxyacyl complexes* $[CH_3CH(OEt)C(O)Co(CO)_3(PPh_3)]$ (**7**) *and* $[ROCH_2C(O)Co(CO)_3(PPh_3)]$ (**10**, R = Me; **11**, R = Et)

Treatment of either α-alkoxyacyl complex **7** or **11** with purified $Et_3O^+PF_6^-$ (1–1.5 equivalents) in CH_2Cl_2 [eq. (4)] provided identical results. The starting acyl complex was consumed in 8–20 h and the only organocobalt complex detected in significant concentration was the known[18] cobalt carbonyl salt $[Co(CO)_3(PPh_3)_2]^+PF_6^-$ (**12**). Its IR [ν(CO) 2008 cm^{-1}] and $^{31}P\{^1H\}$ NMR [δ 55.4] spectral data match that of independently prepared samples. Only trace amounts of $[Co(CO)_4(PPh_3)]^+PF_6^-$[26] were detected. IR: ν(CO) 2143 (s), 2100 (m), 2071 (vs, sh), 2058 (vs) cm^{-1}; $^{31}P\{^1H\}$ NMR: δ 57.3.

We substituted electrophilic methylating agents for triethyloxonium hexafluorophosphate in its reactions with cobalt acyl complexes. Thus, methyl triflate or $[HC(OMe)_2]^+PF_6^-$ (1.0–1.5 equivalents) upon adding to $[CH_3C(O)Co(CO)_3(PPh_3)]$ (**4**), $[EtOCH_2C(O)Co(CO)_3(PPh_3)]$ (**11**) and $[CH_3CH(OEt)C(O)Co(CO)_3(PPh_3)]$ (**7**) in CH_2Cl_2 at room temperature exclusively formed the same cobalt carbonyl degradation product, **12**. These results (particularly with the cobalt acetyl **4**) are surprising, since both methylating reagents had been used extensively in transforming iron acetyl complexes, $[CH_3C(O)Fe(CO)(L)Cp]$ (L = CO, PPh_3), to their cationic methoxycarbene compounds.[3] Not surprisingly, $HBF_4 \cdot OEt_2$ (1 equivalent) also rapidly converted **4** to **12**.

The ill-defined reactions of the α-ethoxyacyl cobalt compounds **7** and **11** with $Et_3O^+PF_6^-$ [eq. (4)] or other alkylation agents to give $Co(CO)_3(PPh_3)_2^+$ (**12**) do not preclude the desired alkoxycarbene compounds [cf. eqs (1) and (2)] from forming as kinetic products. Analogous $Co(CO)_2$(dppe) alkoxycarbene compounds have been character-

ized.[1] In the present study the anticipated alkoxycarbene intermediates [RCH(OEt)C(OEt)=Co(CO)$_3$(PPh$_3$)]$^+$ then apparently would degrade to **12**. In contrast, the fully characterized cobalt alkoxycarbene compound [CH$_3$C(OEt)=Co(CO)$_3$(PPh$_3$)]$^+$ (**5**) only slowly decomposes to **12**. The slow rates with which cobalt acyl complexes **4**, **7** and **11** reacted with even excess $Et_3O^+PF_6^-$ at room temperature precluded further study at lower temperatures.

CONCLUSIONS

Our inability to synthesize α-alkoxycarbene compounds, [RCH(OEt)C(OEt)=Co(CO)$_3$(PPh$_3$)]$^+$ (R = H, CH$_3$), prevented carrying out the first iteration of the acyl ligand activation–reduction–carbonylation sequence [eq. (1)]. The alkoxycarbene complex [CH$_3$(EtO)C=Co(CO)$_3$(PPh$_3$)]$^+PF_6^-$ (**5**) that was isolated is the first fully characterized, cationic cobalt Fisher carbene compound that we are aware of, although several neutral analogues,[22] e.g. [R(EtO)C=Co(CO)$_3$(MPh$_3$)] (M = Si, Sn, Ge),[27] have been reported. Another unexpected development was the instability of the secondary alkyl complex [CH$_3$CH(OEt)Co(CO)$_3$(PPh$_3$)] (**6**) vs the stable primary analogues [ROCH$_2$Co(CO)$_3$(PPh$_3$)] (**8** and **9**), an observation that merits further study.

Acknowledgements—We gratefully acknowledge receiving a preprint of ref. 19 from G. Pályi (University of Veszprém) and financial support from the Department of Energy, Office of Basic Energy Science.

REFERENCES

1. C. C. Tso and A. R. Cutler, *J. Am. Chem. Soc.* 1987, **109**, 5844.
2. S. A. Levitre, A. R. Cutler and T. C. Forschner, *Organometallics* 1989, **8**, 1133.
3. A. R. Cutler, P. K. Hanna and J. C. Vites, *Chem. Rev.* 1988, **88**, 1363.
4. J. P. Collman, L. S. Hegedus, J. R. Norton and R. G. Finke, *Principles and Applications of Organotransition Metal Chemistry*, Ch. 6. University Science Books, Mill Valley, CA (1987).
5. B. K. Blackburn, S. G. Davies and M. Whittaker, in *Stereochemistry of Organometallic and Inorganic Compounds*, Vol. 3, Ch. 2. Elsevier, Amsterdam (1989).
6. T. C. Forschner, A. R. Cutler and R. K. Kullnig, *J. Organomet. Chem.* 1988, **356**, C12.
7. T. C. Forschner and A. R. Cutler, *Organometallics* 1985, **4**, 1247.
8. (a) R. D. W. Kemmitt and D. R. Russell, in *Comprehensive Organometallic Chemistry* (Edited by G. Wilkinson, F. G. A. Stone and E. W. Abel), Vol. 5, Ch. 34.3. Pergamon Press, Oxford (1982); (b) V. Galamb and G. Pályi, *Coord. Chem. Rev.* 1984, **59**, 203.
9. (a) D. Milstein, *Accts Chem. Res.* 1988, **21**, 428; (b) V. Galamb, G. Pályi, R. Boese and G. Schmid, *Organometallics* 1987, **6**, 861; (c) V. Galamb, G. Pályi, F. Ungváry, L. Markó, R. Boese and G. Schmid, *J. Am. Chem. Soc.* 1986, **108**, 3344.
10. J. T. Martin and M. C. Baird, *Organometallics* 1983, **2**, 1073.
11. C. C. Tso and A. R. Cutler, *Organometallics* 1986, **5**, 1834.
12. D. F. Shriver and M. A. Drezdon, *The Manipulation of Air-Sensitive Compounds*, 2nd edn. Wiley-Interscience, New York (1986).
13. E. J. Crawford, T. W. Bodnar and A. R. Cutler, *J. Am. Chem. Soc.* 1986, **108**, 6702.
14. (a) W. Hieber and W. Freyer, *Chem. Ber.* 1958, **91**, 1230; (b) A. R. Manning, *J. Chem. Soc. A* 1968, 1135; (c) R. L. Sweany and T. L. Brown, *Inorg. Chem.* 1977, **16**, 415.
15. (a) W. Hieber and E. Lindner, *Chem. Ber.* 1961, **94**, 1417; *Z. Naturforsch., B: Anorg. Chem., Org. Chem., Biochem., Biophys., Biol.* 1961, **16B**, 137; (b) M. D. Curtis, *Inorg. Chem.* 1972, **11**, 802; (c) F. Ungváry and A. Wojcicki, *J. Am. Chem. Soc.* 1987, **109**, 6848.
16. R. F. Heck, *J. Am. Chem. Soc.* 1963, **85**, 1220.
17. (a) R. F. Heck and D. S. Breslow, *J. Am. Chem. Soc.* 1962, **84**, 2499; (b) M. Roper, M. Schieren and B. T. Heaton, *J. Organomet. Chem.* 1986, **299**, 131.
18. (a) W. Hieber and H. Duchatsch, *Chem. Ber.* 1965, **98**, 2530; (b) S. Attali and R. Poilblanc, *Inorg. Chim. Acta* 1972, **6**, 475; (c) P. Rigo, M. Bressan and A. Morvillo, *J. Organomet. Chem.* 1976, **105**, 263; (d) M. Abs-Halabi and T. L. Brown, *J. Am. Chem. Soc.* 1977, **99**, 282; (e) H. Schumann, *J. Organomet. Chem.* 1986, **304**, 341; (f) C. Carriedo, P. Gomey-Sal, P. Royo, S. Martinez-Carrera and S. Garcia-Blanco, *J. Organomet. Chem.* 1986, **301**, 79; (g) J. D. Atwood, *Inorg. Chem.* 1987, **26**, 2918; (h) K. Y. Lee and J. K. Kochi, *Inorg. Chem.* 1989, **28**, 567.
19. A. Sisak, E. Sámpár-Szerencsés, V. Galamb, L. Németh, F. Ungváry and G. Pályi, *Organometallics* 1989, **8**, 1096.
20. Z. Nagy-Magos, G. Bor and L. Markó, *J. Organomet. Chem.* 1968, **14**, 205.
21. (a) W. Hieber and E. Lindner, *Chem. Ber.* 1962, **95**, 273; (b) E. Lindner, H. Stich, K. Geibel and H. Kranz, *Chem. Ber.* 1971, **104**, 1524; (c) E. Lindner and M. Zipper, *Chem. Ber.* 1974, **107**, 1444.
22. (a) J. P. Collman, L. S. Hegedus, J. R. Norton and R. G. Finke, *Principles and Applications of Organotransition Metal Chemistry*, p. 119. University Science Books, Mill Valley, CA (1987); (b) K. H. Dotz, H. Fischer, P. Hofmann, F. R. Kreissl, U. Schubert and K. Weiss, *Transition Metal Carbene Complexes*. Verlag Chemie, Deerfield Beach, FL (1983).
23. F. T. T. Ng, G. L. Rempel, C. Mancuso and J. Halpern, *Organometallics* 1990, **9**, 2762.
24. E. J. Moore, J. M. Sullivan and J. R. Norton, *J. Am. Chem. Soc.* 1986, **108**, 2257.

25. F. Ungváry and A. Wojcicki, *J. Organomet. Chem.* 1990, **396**, 95.
26. W. Hieber and H. Duchatsch, *Chem. Ber.* 1965, **98**, 1745.
27. (a) A. C. Filippou, E. Herdtweck and H. G. Alt, *J. Organomet. Chem.* 1988, **355**, 437; (b) G. Cerveau, E. Colomer, R. J. P. Corriu and J. C. Young, *J. Organomet. Chem.* 1981, **205**, 31; (c) F. Carre, G. Cerveau, E. Colomer, R. J. P. Corriu, J. C. Young, L. Ricard and R. Weiss, *J. Organomet. Chem.* 1979, **179**, 215; (d) D. J. Darensbourg and M. Y. Darensbourg, *Inorg. Chem.* 1970, **9**, 1691.

Polyhedron Vol. 12, No. 2, pp. 159–163, 1993
Printed in Great Britain

0277–5387/93 $6.00+.00
© 1993 Pergamon Press Ltd

REACTIVITY OF BIS(ACETYLACETONATO)DINITROSYLMOLYBDENUM(0) TOWARDS SCHIFF BASES DERIVED FROM SALICYLALDEHYDE OR *o*-VANILLIN AND BENZOYLHYDRAZIDE, OR ISONICOTINOYLHYDRAZIDE*

MANNAR R. MAURYA,† S. GOPINATHAN and C. GOPINATHAN

Inorganic Chemistry Division, National Chemical Laboratory, Pune 411 008, India

and

RAM C. MAURYA

Department of Chemistry, R.D. University, Jabalpur, M.P. 482 001, India

(*Received* 18 *August* 1992; *accepted* 1 *October* 1992)

Abstract—The synthesis of dinitrosylmolybdenum(0) complexes of Schiff bases by a single-step ligand-exchange process has been reported for the first time by the reaction of $[Mo(NO)_2(acac)_2]$ with the Schiff bases (LH_2) obtained by the condensation of salicylaldehyde or *o*-vanillin and benzoylhydrazide, or isonicotinoylhydrazide, and are of the type $[Mo(NO)_2(LH)_2]$. The Schiff bases behave as monobasic bidentate ligands coordinating through the azomethine nitrogen and enolic oxygen after deprotonation. Two geometric isomers having nitrosyl groups *trans* to each other have been observed in solution. Another complex, $[MoO_2(sal\text{-}INH)\cdot MeOH]$, has also been synthesized for comparison.

In recent years there has been a great deal of interest in dinitrosylmolybdenum(0) complexes because of their use as homogeneous catalysts.[1,2] The widely applied routes to prepare these complexes are: (1) the reaction of $[\{Mo(NO)_2X_2\}_n]$ (X = halogens) with ligands[3] and (2) reaction of nitrosyl halides with molybdenum hexacarbonyl or its derivatives.[4] Bencze *et al.*[5] have generated dinitrosylmolybdenum(0) species by the reductive reaction of nitric oxide with molybdenum pentachloride. The generation of dinitrosylmolybdenum(0) species in aqueous-aerobic conditions and its stabilization using mono- and bidentate ligands have been reported recently.[6]

In spite of the considerable growth of literature on Schiff base complexes of dioxomolybdenum(VI),[7] no attempts have so far been reported of the synthesis of analogous dinitrosylmolybdenum(0) complexes.[8] In order to find a suitable starting material and to develop a more versatile synthetic route to dinitrosyl molybdenum(0) complexes, we have studied the reactivity of $[Mo(NO)_2(acac)_2]$ (acacH = acetylacetone) towards Schiff bases. Some dinitrosylmolybdenum(0) complexes of the following Schiff bases (**1** and **2**) have thus been isolated in a

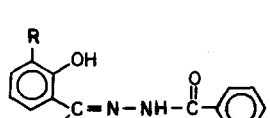

1

(**1a**) R = H(H_2sal-BZH),
(**1b**) R = OMe(H_2van-BZH).

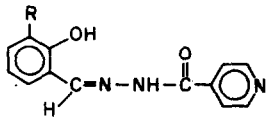

2

(**2a**) R = H(H_2sal-INH),
(**2b**) R = OMe(H_2van-INH).

* NCL communication No. 5579.

† Author to whom correspondence should be addressed.

single-step process and their spectral studies are reported here.

EXPERIMENTAL

Preparations

All reagents were of analytical grade and were used without further purification. The Schiff bases **1** and **2** were synthesized following the literature procedures.[9–11] $[Mo(NO)_2(acac)_2]$[6a] and $[MoO_2(acac)_2]$[12] were prepared by the methods described previously.

Preparation of $[Mo(NO)_2(Hsal\text{-}BZH)_2]$

A solution of $[Mo(NO)_2(acac)_2]$ (0.354 g, 0.001 mol) in methanol (10 cm^3) was added to a hot solution of **1a** (0.48 g, 0.002 mol) in methanol (25 cm^3) and the reaction mixture was refluxed on a water bath for 30 h. The separated yellow solid was filtered, washed with methanol and dried at 100°C. Yield: 0.39 g (60%). Found: C, 53.3; H, 3.3; N, 13.0; Mo, 15.5. Calc. for $C_{28}H_{22}N_6O_6Mo$: C, 53.0; H, 3.5; N, 13.2; Mo, 15.1%.

The following complexes were similarly prepared.

$[Mo(NO)_2(Hvan\text{-}BZH)_2]$. Yield: 0.35 g (50%). Found: C, 51.3; H, 3.7; N, 12.4; Mo, 13.6. Calc. for $C_{30}H_{26}N_6O_8Mo$: C, 51.9; H, 3.8; N, 12.1; Mo, 13.8%.

$[Mo(NO)_2(Hsal\text{-}INH)_2]$. Yield: 0.31 g (49%). Found: C, 49.2; H, 3.3; N, 17.3; Mo, 14.7. Calc. for $C_{26}H_{22}N_8O_6Mo$: C, 48.9; H, 3.5; N, 17.5; Mo, 15.0%.

$[Mo(NO)_2(Hvan\text{-}INH)_2]$. Yield: 0.39 g (56%). Found: C, 48.5; H, 3.8; N, 15.7; Mo, 13.4. Calc. for $C_{28}H_{26}N_8O_8Mo$: C, 48.1; H, 3.7; N, 16.0; Mo, 13.7%.

Preparation of $[MoO_2(sal\text{-}INH)\cdot MeOH]$

The Schiff base **2a** (0.482 g, 0.002 mol) was dissolved in methanol (25 cm^3) and to this $[MoO_2(acac)_2]$ (0.66 g, 0.002 mol) was added with vigorous stirring. The reaction mixture was boiled under reflux on a water bath for 3 h and the orange–yellow precipitate which separated was filtered, washed with methanol and dried *in vacuo* at room temperature. Yield: 0.27 g (68%). Found: C, 42.4; H, 3.2; N, 10.3; Mo, 23.9. Calc. for $C_{14}H_{13}N_3O_5Mo$: C, 42.1; H, 3.3; N, 10.5; Mo, 24.1%.

Measurements

Elemental analyses were performed by the microanalytical section of this laboratory. Molybdenum content was determined gravimetrically as bis(8-hydroxyquinolinato)dioxomolybdenum (VI) after decomposing the complexes with concentrated HNO_3. IR spectra were recorded as Nujol mulls and in KBr on a Perkin–Elmer Model 1620 FT-IR spectrophotometer. ^1H NMR spectra were obtained using a Bruker WH-90 spectrometer in DMSO-d_6 using tetramethylsilane as an internal standard. The electrical conductance measurements were performed in 1×10^{-3} M dimethylformamide solutions using a Toshniwal conductivity bridge (Type CL01-02A) and a dip-type cell calibrated with potassium chloride solutions. The molecular weight measurement was carried out by Rast's method[13] using diphenyl as the solvent.

RESULTS

$[MoO_2(acac)_2]$ has been used as a precursor to prepare dioxomolybdenum(VI) complexes by ligand exchange reactions involving protonated Schiff bases as well as other ligands.[7] $[MoO_2(sal\text{-}INH)\cdot MeOH]$ reported here has also been synthesized similarly using $[MoO_2(acac)_2]$ and **2a**. This complex has also been synthesized recently by Zhai *et al.*[14] using $[MoO_2(butanediolato)_2\cdot 2(butanediol)]$. The Schiff base behaves as a dibasic tridentate ligand and methanol occupies the sixth position.

The use of $[Mo(NO)_2(acac)_2]$ as a starting material for dinitrosylmolybdenum(0) complexes has not yet been reported in the literature. We have found this precursor very useful in preparing such complexes of the Schiff bases. Thus, $[Mo(NO)_2(acac)_2]$ undergoes ligand exchange reaction with the Schiff bases **1** and **2** in refluxing methanol to yield the corresponding dinitrosyl complexes of the type $[Mo(NO)_2(LH)_2]$ (LH_2 = Schiff bases **1** and **2**).

$$[Mo(NO)_2(acac)_2] + 2LH_2 \xrightarrow{MeOH} [Mo(NO)_2(LH)_2] + 2acacH$$

Under these reaction conditions complete removal of coordinated acetylacetone occurred and two molecules of the Schiff bases, which behave as monobasic bidentate ligands (*vide infra*), occupied four positions of the octahedron. Analytical data support the above formulation of the complexes. The decomposition temperature (> 250°C) indicates increased stability of the complexes. These diamagnetic complexes are insoluble in most of the

organic solvents but soluble in coordinating solvents like pyridine, DMF and DMSO. The nitrosyl complexes do not lose weight on heating at 150°C for 1 h but the dioxo complex does, corresponding to the loss of one molecule of methanol; information which confirms the coordination of methanol in $[MoO_2(sal\text{-}INH)\cdot MeOH]$. The coordinated monodentate ligands in dioxomolybdenum(VI) complexes of the type $MoO_2L\cdot X$ (X = monodentate ligand) are known to undergo cleavage on heating due to weak coordination and their labile nature.[15]

The low molar conductance values (3.0–8.0 Ω mol^{-1} cm^2) of the complexes in DMF indicate their non-electrolytic behaviour. Although molecular weight measurement on $[MoO_2(sal\text{-}INH)\cdot MeOH]$ indicated its monomeric nature (found: 382, calc.: 399), such measurements on nitrosyl complexes were not possible due to their poor solubility in suitable organic solvents. The monomeric nature of the dinitrosyl complex $[Mo(NO)_2(pic)_2]$ (pic = 2-picolinic acid) has, however, been confirmed by an X-ray study.[6c] Thus, we also suggest a monomeric nature with octahedral geometry for the nitrosyl complexes reported here.

IR spectra

A partial listing of the IR spectra of the ligands and their complexes is given in Table 1. The IR spectra of the complexes show distinct changes in their band positions relative to those of the starting material. For example, the IR spectrum of $[Mo(NO)_2(acac)_2]$ is reported to show two strong bands at 1763 and 1645 cm^{-1} due to ν(NO) stretches of the *cis*-$\{Mo(NO)_2\}^6$ moiety.[6a] In the dinitrosyl complexes reported here, the IR spectra show only one band centred at 1665–1678 cm^{-1} due to ν(NO), suggesting a *trans* disposition of the NO group.

The Schiff bases exhibit a broad band at 2800–3000 cm^{-1}, which is assigned to the intramolecularly hydrogen-bonded ν(OH) stretch. The absence of this band and appearance of a broad band at 3400 cm^{-1} suggests the existence of a free phenolic group in the nitrosyl complexes. In $[MoO_2(sal\text{-}INH)\cdot MeOH]$ this band may be due to the ν(OH) stretch of the coordinated methanol. This is further supported by the appearance of a new band at 1005 cm^{-1} due to the ν(C—O); the ν(C—O) stretch in methanol occurs at 1034 cm^{-1}.[16] Bands due to ν(C=O) and ν(NH) in the free Schiff bases appear in the regions 1650–1692 and 3200–3270 cm^{-1}, respectively. These bands disappear in the complexes indicating the destruction of the carbonyl moiety due to enolization and consequent proton replacement with the metal. A new band appearing in the region 1225–1256 cm^{-1} is assigned to the ν(C—O)(enolic) mode.[17] The ν(C=N) stretch of the ligands (1607–1626 cm^{-1}) shifts to a lower frequency by 6–24 cm^{-1}, indicating the coordination of the azomethine nitrogen.[18] A band at 900–1000 cm^{-1} due to the ν(N—N) stretch of the ligands shifts to a higher frequency by 11–48 cm^{-1} upon complexation. The magnitude of this shift indicates the monodentate coordination[19] of the >N—N< residue, as a shift of > 50 cm^{-1} is usually observed in bidentate coordination. A shift to a higher frequency in ν(N—N) is expected due to the reduction of the lone pair–lone pair repulsive forces of the adjacent nitrogen atoms.[20] Thus, the IR data suggest the monobasic bidentate nature of the Schiff bases in the nitrosyl complexes in which they coordinate through the azomethine nitrogen and deprotonated oxygen of the hydrazide moiety. Similar bidentate behaviour of the Schiff base H_2sal-BZH has been suggested in the complex $[UO_2(Hsal\text{-}BZH)_2]$.[9] In $[MoO_2(sal\text{-}INH)\cdot MeOH]$

Table 1. IR spectral data (in cm^{-1}) of $[Mo(NO)_2(LH)_2]$ and $[MoO_2(sal\text{-}INH)\cdot MeOH]$ complexes

Compounds	ν(C=O)	ν(NO)	ν(C=N)	ν(C—O) (enolic)	ν(N—N)
$[H_2sal\text{-}BZH]$	1668		1621		980
$[Mo(NO)_2(Hsal\text{-}BZH)_2]$		1678	1604	1225	1028
$[H_2van\text{-}BZH]$	1650		1607		966
$[Mo(NO)_2(Hvan\text{-}BZH)_2]$		1671	1592	1252	977
$[H_2sal\text{-}INH]$	1680		1625		1000
$[Mo(NO)_2(Hsal\text{-}INH)_2]$		1665	1602	1225	1026
$[H_2van\text{-}INH]$	1692		1626		1000
$[Mo(NO)_2(Hvan\text{-}INH)_2]$		1678	1602	1256	1027
$[MoO_2(sal\text{-}INH)\cdot MeOH]$			1619	1251	1016

the Schiff base behaves as a dibasic tridentate ONO donor ligand.

NMR spectra

Further evidence for the coordinating mode of the ligands is derived from the ^{1}H NMR spectra. The NMR spectra of the representative ligands and their complexes are given in Table 2. The sharp singlet due to the azomethine proton shifts downfield and splits into two signals. This downfield shift suggests the coordination of the azomethine nitrogen to molybdenum[21] while splitting of the signal may be due to the presence of two isomeric forms in solution as discussed later. The Schiff bases also exhibit signals at 11.15–11.23 and 12.0–12.28 ppm (singlet, 1H each) due to NH and phenolic protons, respectively. These signals are identified by the D_2O exchange experiments. The absence of NH proton resonance on complexation suggests the enolization of the keto group and subsequent coordination of the enolic oxygen. Further, two resonances are observed due to the phenolic OH which suggest the existence of the free phenolic group in the nitrosyl complexes. A slightly upfield shift of the resonances is expected due to the breaking of the hydrogen bond between the phenolic hydrogen and azomethine nitrogen atoms. The absence of both NH and phenolic proton resonances and the downfield shift of the azomethine proton resonance in $[MoO_2(sal\text{-}INH)\cdot MeOH]$ are in agreement with the dibasic tridentate behaviour of the ligand in the complex. The methyl protons of the methanol appear at 3.64 ppm.

DISCUSSION

The most common method used for the synthesis of dinitrosyl complexes is the reaction of $[\{Mo(NO)_2X_2\}_n]$ (X = halogen) with the free ligands. However, poor stability and high reactivity of this precursor towards air and moisture limit its use to an inert atmosphere. The synthetic route described here is a one-step ligand-exchange reaction between $[Mo(NO)_2(acac)_2]$ and the Schiff bases, which can be prepared in aerobic conditions using a simple set-up. It is interesting to note that during the exchange reaction the nitrosyl groups remain intact and do not oxidize to dioxo species as in the complex $[MoO_2(sal\text{-}INH)\cdot MeOH]$, which shows two bands at 938 and 911 cm^{-1} characteristic of ν_{sym}(O=Mo=O) and ν_{asym}(O=Mo=O) stretches, respectively. The nitrosyl complexes do not furnish any band in the O=Mo=O stretching region. Further, the presence of only one band at 1665–1680 cm^{-1} due to the ν(NO) stretch strongly suggests isomerization of the nitrosyl groups from *cis* in the precursor, $[Mo(NO)_2(acac)_2]$, to *trans* in the Schiff base complexes. The presence of the nitrosyl group was further confirmed qualitatively by using the Griess reagent.[22]

On the basis of *trans*-dinitrosyl geometry, the complexes are expected to show two geometrical isomers (**3** and **4**) and both the isomers are expected

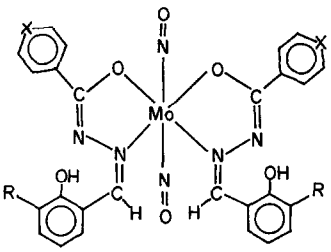

3

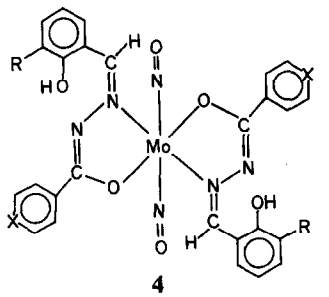

4

X = H or N
R = H or OMe

Table 2. ^{1}H NMR spectral data (δ in ppm) of $[Mo(NO)_2(LH)_2]$ and $[MoO_2(sal\text{-}INH)\cdot MeOH]$ complexes[a]

Compounds	—CH=N	Aromatic	NH	OH
$[H_2sal\text{-}BZH]$	8.53(s)	6.67–8.0(m)	11.23(s)	12.0(s)
$[Mo(NO)_2(Hsal\text{-}BZH)_2]$	9.19(s), 9.22(s)	6.78–9.0(m)	—	11.71(s), 11.82(s)
$[H_2sal\text{-}INH]$	8.70(s)	6.90–7.85(m) 8.80(d)	11.15(s)	12.28(s)
$[Mo(NO)_2(Hsal\text{-}INH)_2]$	9.27(s), 9.36(s)	6.85–9.10	—	11.06(s), 11.25(s)
$[MoO_2(sal\text{-}INH)\cdot MeOH]$	9.11(s)	6.93–8.11(m)	—	—

[a] Letters given in parentheses indicate the type of signal. s = singlet, d = doublet, m = multiplet.

to show only one signal each for the azomethine and phenolic protons. However, chemical shifts may be different due to the different arrangement of the ligands around the molybdenum ion. The NMR spectra in fact show two sets of signals for each proton, indicating the presence of both isomers in solution. Based on the height of the signals and integration ratios, the percentage of these isomers in solution are approximated to be 60 : 40. However, it is not possible at present to distinguish between the set of the signals for each particular isomer. Unfortunately, the complexes reported here have not been suitable for X-ray diffraction.

CONCLUSIONS

The complexes prepared herein are the first examples of neutral dinitrosyl molybdenum(0) complexes of Schiff bases. Using $[Mo(NO)_2(acac)_2]$ as a precursor, it is now possible to prepare a variety of this kind of complex. Further investigation of the physical and chemical properties of these novel complexes and extension of this work is underway.

Acknowledgement—One of the authors (MRM) is thankful to the Council of Scientific and Industrial Research, New Delhi, for the award of Pool Officership.

REFERENCES

1. E. A. Zuech, *J. Chem. Soc., Chem. Commun.* 1968, 1182.
2. E. A. Zuech, W. B. Hughes, D. H. Kubicek and E. T. Kittleman, *J. Am. Chem. Soc.* 1970, **92**, 528.
3. D. Ballivet-Tkatchenko, C. Bremard, F. Abraham and G. Nowogrocki, *J. Chem. Soc., Dalton Trans.* 1983, 1137 and refs therein.
4. M. Green and S. H. Taylor, *J. Chem. Soc., Dalton Trans.* 1973, 2629.
5. K. Bencze, J. Kohan, B. Mohai and L. Marko, *J. Organomet. Chem.* 1974, **70**, 421.
6. (a) S. Sarkar and P. Subramanian, *Inorg. Chim. Acta* 1979, **35**, L357; (b) R. G. Bhattacharya, G. P. Bhattarcharjee and A. M. Saha, *Trans. Met. Chem.* 1983, **8**, 255; (c) M. F. Perpinan, L. Ballester, A. Santos, A. Monge, C. Ruiz-Valero and E. G. Puebla, *Polyhedron* 1987, **6**, 1523; (d) R. G. Bhattarcharya and S. Ghosh, *Ind. J. Chem.* 1991, **30A**, 35; (e) T. K. Banerjee, S. K. Brahma and S. P. Bag, *Ind. J. Chem.* 1991, **30A**, 281.
7. A. Syamal and M. R. Maurya, *Coord. Chem. Rev.* 1989, **95**, 183.
8. J. H. Ememark and R. D. Feltham, *Coord. Chem. Rev.* 1974, **13**, 339.
9. A. Syamal and B. K. Gupta, *Rev. Roum. Chim.* 1981, **26**, 857.
10. K. N. Srivastava, S. Das and R. A. Lal, *Ind. J. Chem.* 1986, **25A**, 85.
11. B. V. Agrawal, S. Hingorani and G. A. N. Gowda, *Inorg. Chim. Acta* 1990, **176**, 149.
12. G. G. J. Chen, J. W. McDonald and W. E. Newton, *Inorg. Chem.* 1976, **15**, 2612.
13. F. G. Mann and B. C. Saunders, *Practical Organic Chemistry*, p. 435. Longmans, London (1961).
14. Y. L. Zhai, X. X. Xu and X. Wang, *Polyhedron* 1992, **11**, 415.
15. (a) O. A. Rajan and A. Chakravorty, *Inorg. Chem.* 1981, **20**, 660; (b) A. Syamal and M. R. Maurya, *Trans. Met. Chem.* 1986, **11**, 255.
16. G. Hertzberg, *Molecular Spectra and Molecular Structure*, Vol. 2, p. 435. Van Nostrand Co., New York (1959).
17. (a) A. Syamal and K. S. Kale, *Ind. J. Chem.* 1980, **19A**, 225; (b) A. Syamal and M. R. Maurya, *Trans. Met. Chem.* 1986, **11**, 205.
18. P. Teyssi and J. J. Charrettee, *Spectrochim. Acta* 1963, **19**, 1407.
19. A. Baribanti, F. Dallvalle, M. A. Pellinghel and E. Laporati, *Inorg. Chem.* 1968, **7**, 1430.
20. S. P. Perlepes, D. Nicholls and M. R. Harrison, *Inorg. Chim. Acta* 1985, **102**, 137.
21. E. C. Alyea, A. Malek and A. I. Kazi, *Trans. Met. Chem.* 1981, **6**, 223.
22. Griess reagent: A solution of sulphanilic acid and α-naphthylamine in acetic acid which gives a pink colour on reaction with the solution obtained after decomposition of nitrosyl complexes; P. Griess, *Chem. Ber.* 1879, **12**, 427.

Polyhedron Vol. 12, No. 2, pp. 165–170, 1993
Printed in Great Britain

0277–5387/93 $6.00+.00
© 1993 Pergamon Press Ltd

STUDIES ON ACETYLFERROCENYLNAPHTHOYLHYDRAZONE (AND DIACYL HYDRAZONE) AND ITS COORDINATION COMPOUNDS WITH LEAD(II)

ZHANG HONGYUN,* LI FENG, CHEN PEIKUN, CHE DEJI, CHEN DONGLI and ZHANG HONGQUAN

Chemistry Department, Zhengzhou University, Zhengzhou 450052, China

(*Received* 10 *August* 1992; *accepted* 1 *October* 1992)

Abstract—Acetylferrocenylnaphthoylhydrazone, acetylferrocenyl-3-hydroxyl-2-naphthoylhydrazone, 1,1′-diacetylferrocenylnaphthoylhydrazone and 1,1′-diacetylferrocenyl-3-hydroxyl-2-naphthoylhydrazone have been synthesized by the condensation of acetylferrocene or 1,1′-diacetylferrocene with naphthoylhydrazine or 3-hydroxyl-2-naphthoylhydrazine, respectively. Their lead(II) coordination compounds have been prepared and characterized by elemental analyses, IR, ^{1}H NMR, UV, TG–DTA and molar conductivities. Results show that the ligands coordinate in the enolic form with lead(II) and the thermostabilities of the coordination compounds are higher than that of the corresponding ligand due to the formation of the chelate ring.

The special structure of ferrocene has attracted wide interest and a series of derivatives have been synthesized.[1–3] Due to the formation of stable coordination compounds with heavy metals ions the aroylhydrazone ligands are promising as specific reagents in analytical and extractive chemistry.[4] This type of compound possesses strong biological activity and can inhibit many vital enzymatic reactions catalysed by heavy metals.[5] It is reported that the replacement of aromatic groups by the ferrocenyl moiety in penicillin and cephalosporin molecules improves their antibiotic activity.[6] In recent years the research on ferrocenylaroylhydrazone and their coordination compounds has become more extensive.[7–9] In this paper, we report the syntheses of acetylferrocenylnaphthoylhydrazone, acetylferrocenyl-3-hydroxyl-2-naphthoylhydrazone, 1,1′-diacetylferrocenylnaphthoylhydrazone and 1,1′-diacetylferrocenyl-3-hydroxyl-2-naphthoylhydrazone and their coordination compounds with lead(II). The form in which the ligands coordinate lead(II), the composition and properties of the coordination compounds were elucidated by elemental analyses, IR, ^{1}H NMR, UV, TG–DTA and molar conductance measurements.

* Author to whom correspondence should be addressed.

EXPERIMENTAL

Measurements

UV–vis spectra were recorded on a HITACHI 220A UV spectrophotometer in the 200–500 nm region using a solution in DMF. IR spectra were obtained using KBr discs with a SHIMADZU IR-435 spectrophotometer in the 4000–400 cm^{-1} region. ^{1}H NMR were measured with an AC-80 NMR spectrophotometer using DMSO as a solvent and TMS as an internal standard. TG–DTA data were measured with a RIGAKU thermal analyser in a nitrogen atmosphere from room temperature to 800°C. Molar conductance values were obtained with a DDS-11 conductometer from Shanghai Second Analytical Equipment Factory, using DMF as a solvent at 20°C. Carbon, hydrogen and nitrogen were measured with a CARLO-ERBA 1106 elemental analyser.

Materials

The ferrocene used was the industrial product from state operated 504 factory after purifying. Acetylferrocene and 1,1′-diacetylferrocene were prepared[10,11] and purified[12] by the method described in the literature. Naphthoylhydrazine and

3-hydroxyl-2-naphthoylhydrazine have been prepared, respectively, by the condensation of methyl naphthoate and methyl 3-hydroxyl-2-naphthoate with hydrazine hydrate. Acetates and other related reagents were of analytically pure grade.

Synthesis of ligand HL^1 (**1**)

Naphthoylhydrazine (3.72 g, 0.02 mol) and acetylferrocene (4.56 g, 0.02 mol) in anhydrous alcohol were heated under reflux with stirring at 85°C for 8 h, cooled and filtered. The crude product was recrystallized twice in anhydrous alcohol to obtain brown–red crystals and dried *in vacuo*. Yield 80%, m.p. 211–212°C.

Synthesis of ligand H_2L^2 (**2**)

H_2L^2 was synthesized with a molar ratio of 1 : 2 of 1,1′-diacetylferrocene and naphthoylhydrazine in anhydrous alcohol with the same operation as HL^1. The crude product was dissolved in DMF and filtered. Anhydrous alcohol was added to the filtrate with stirring and then the golden yellow powder was separated. Yield 65%, m.p. 209–210°C.

Synthesis of ligand HL^3 (**3**)

A mixture of acetylferrocene and 3-hydroxyl-2-naphthoylhydrazine in a molar ratio of 1 : 1 was reacted in anhydrous alcohol under reflux using the same operation as HL^1. The product was recrystallized with a mixed solvent of anhydrous alcohol and cyclohexane (1 : 1) and dried *in vacuo*, and reddish-orange crystals were obtained. Yield 85%, m.p. 187.5–188.5°C.

Synthesis of ligand H_2L^4 (**4**)

The reaction mixture of 1,1′-diacetylferrocene and 3-hydroxyl-2-naphthoylhydrazine in a molar ratio of 1 : 2 was heated under reflux with stirring until the precipitate appeared, and continuously refluxed for 5 h, following the operation used for H_2L^2. The orange–yellow precipitate was obtained. Yield 80%.

Syntheses of coordination compounds PbL_2^1 (**5**) *and* PbL_2^3 (**7**)

A solution of $Pb(O_2CMe)_2 \cdot 3H_2O$ (0.379 g, 1 mmol) in anhydrous alcohol (10 cm^3) was added dropwise to a solution of HL^1 (0.792 g, 2.02 mmol) or HL^3 (0.824 g, 2.02 mmol) in anhydrous alcohol (30 cm^3). The reaction mixture was heated under reflux with stirring at 85°C for 6 h. The crystals which separated out on cooling were filtered and washed successively three times with 0.5% HNO_3, water and anhydrous alcohol, and dried *in vacuo*. PbL_2^1 is a yellow coordination compound, yield 68%, and PbL_2^3 is a yellow coordination compound, yield 80%.

Synthesis of coordination compound PbL^2 (**6**)

A solution of $Pb(O_2CMe)_2 \cdot 3H_2O$ (0.379 g, 1 mmol) in anhydrous alcohol (10 cm^3) was added dropwise with stirring to a solution of H_2L^2 (0.606 g, 1 mmol) in anhydrous alcohol and DMF (1 : 3) (30 cm^3). Following the operation for PbL_2^1, a yellow coordination compound was obtained. Yield 65%.

Synthesis of coordination compound PbL^4 (**8**)

A solution of $Pb(O_2CMe)_2 \cdot 3H_2O$ (0.190 g, 0.5 mmol) in anhydrous alcohol (15 cm^3) and triethyl orthoformate (4 cm^3) was added dropwise to a solution of HL^4 (0.32 g, 0.5 mmol) in anhydrous alcohol (15 cm^3), and triethylamine (0.4 cm^3) was added. The reaction mixture was heated under reflux at 85°C for 8 h, then evaporated to remove unreacted triethylamine and a little ethanol, and cooled and filtered. The precipitate was washed three times with hot alcohol and dried *in vacuo*. An orange–red coordination compound was obtained. Yield 65%.

RESULTS AND DISCUSSION

Elemental analyses and some physical properties

The ligands **1** and **3** are soluble in hot ethyl alcohol, but **2** and **4** are insoluble. They dissolve in strong polar solvents such as DMF and DMSO. Four coordination compounds of lead do not dissolve in common organic solvents such as ethyl alcohol, but are soluble in DMF. The results of the elemental analyses of the ligands and coordination compounds are given in Table 1. The ligands **1** and **3** coordinate to lead(II) with a molar ratio of 2 : 1, but **2** and **4** coordinate as 1 : 1. As the solubility of these lead(II) coordination compounds is less, we attempted to prepare the single crystal, but did not succeed. The polymerization number *n* of the structural formula of **6** and **8** in Fig. 1 considers chiefly that the coordination between ferrocenyl diaroylhydrazone and metals decreases the steric effect.

IR spectra and ^1H *NMR spectra*

The important IR absorption frequencies of the ligands and lead(II) coordination compounds are

Table 1. Elemental analyses of the ligands and lead(II) coordination compounds

Formula	Molecular weight	M.p.[a] (°C)	Colour	Elemental analyses (%)[b] C	H	N
HL^1	396.26	211.5	Brown–red	69.5 (69.7)	5.1 (5.1)	6.9 (7.1)
H_2L^2	606.49	209	Orange–red	70.5 (71.3)	5.0 (5.0)	9.1 (9.2)
HL^3	412.26	188	Orange–red	66.9 (67.0)	5.4 (4.9)	6.7 (6.8)
H_2L^4	638.50	256	Orange–yellow	67.4 (67.7)	4.9 (4.7)	8.9 (8.7)
PbL_2^1	997.72	285	Yellow	54.9 (55.4)	3.7 (3.8)	5.5 (5.6)
$PbL^2 \cdot 2H_2O$	847.72	269	Yellow	50.7 (51.0)	4.3 (3.8)	7.2 (6.6)
$PbL_2^3 \cdot H_2O$	1047.74	316	Yellow	52.2 (52.7)	4.0 (3.8)	5.9 (5.3)
PbL^4	843.69	266	Orange	51.0 (51.2)	3.6 (3.3)	6.9 (6.6)

[a] M.p.s of all coordination compounds are their decomposition temperatures.
[b] Calculated values are given in parentheses.

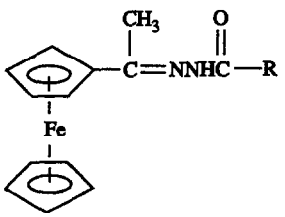

1(a), 3(b)

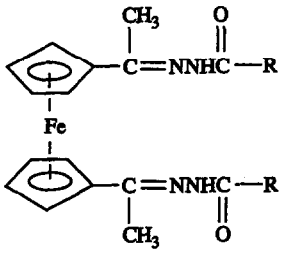

2(a), 4(b)

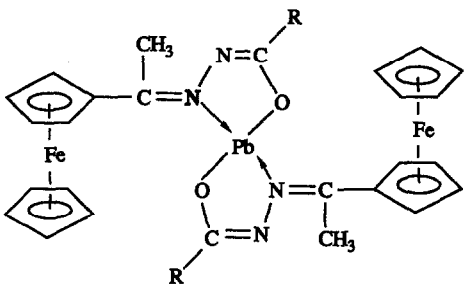

5(a), 7(b)

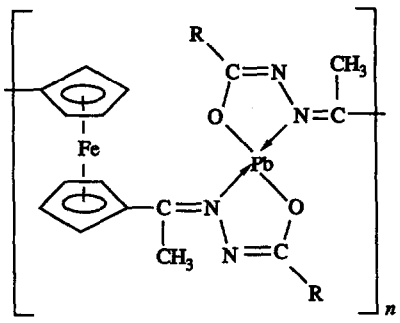

6(a), 8(b)

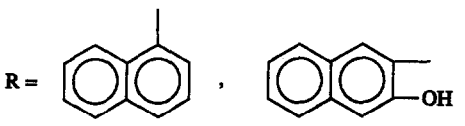

(a) (b)

Fig. 1. Proposed structure for the ligands **1a**, **2a**, **3b** and **4b**, and the complexes **5a**, **6a**, **7b** and **8b**.

Table 2. Important IR absorption frequencies (cm^{-1}) of the ligands and their lead(II) coordination compounds

Formula	ν(N—H)	ν(C=O)	ν(C=N—N=C)	ν(C=N)	ν(C—O)	ν(N—N)
HL^1	3140(s)	1635(vs)	—	1540(vs)	—	905(w)
PbL_2^1	—	—	1578(s)	1500(vs)	1075(m)	910(m)
H_2L^2	3180(s)	1642(vs)	—	1535(vs)	—	910(m)
$PbL^2 \cdot 2H_2O$	—	—	1650(vs)	1510(vs)	1040(m)	912(m)
HL^3	3290(s)	1613(vs)	—	1542(vs)	—	906(m)
$PbL_2^3 \cdot H_2O$	—	—	1631(vs)	1514(vs)	999(m)	905(m)
H_2L^4	3260(s)	1640(vs)	—	1622(vs)	—	936(m)
PbL^4	—	—	1628(vs)	1560(vs)	1242(m)	941(m)

Abbreviations: vs = very strong, s = strong, m = medium, w = weak.

listed in Table 2, and ^{1}H NMR data in Table 3. It is shown in Table 2 that the characteristic absorption frequencies of ν(N—H), ν(C=O), ν(C=N) and ν(N—N) appeared in the 3140–3260, 1613–1642, 1500–1622 and 905–936 cm^{-1} regions, respectively. The results indicate that there is an acylhydrazonyl group in the molecule of all the ligands, which exists in the keto form in the solid state.[5]

The results in Table 3 show that the single peak (5H) of unsubstituted cyclopentadiene and multiple peak (4H) of substituted cyclopentadiene appear in the range 4.00–4.74 ppm in the ^{1}H NMR spectra of HL^1 and HL^3. A multiple peak (4H) of substituted cyclopentadiene was observed in the range 4.09–4.97 ppm in the ^{1}H NMR spectra of H_2L^2 and H_2L^4. A multiple peak (7H or 6H) of the naphthene ring appears at 7.52–8.01 ppm, and the single peaks (1H) of N—H were observed in the 10.70–13.88 ppm region in the ^{1}H NMR spectra of the four ligands. A single peak (1H) of O—H was observed in the region 8.22–8.61 ppm in the ^{1}H NMR spectra of HL^3 and H_2L^4.[13] The results of ^{1}H NMR further prove that the free ligands exist in the keto form.

The IR spectra of the coordination compounds show significant changes as compared with those of the corresponding ligands. The characteristic absorption bands due to ν(N—H) and ν(C=O) disappeared, but two new absorption bands were observed in the 1578–1650 and 999–1242 cm^{-1} regions, respectively, which can be attributed to the stretching vibration of conjugate 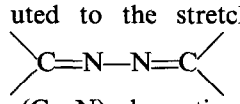 and C—O groups.[8] The ν(C=N) absorption band was shifted to a lower frequency by 25–62 cm^{-1}, while the band attributed to ν(N—N) was shifted to a higher frequency by 2–5 cm^{-1}. The changes in these frequencies show that the ligands coordinate to lead(II) to form neutral coordination compounds through the methylenimine group nitrogen atom and amide oxygen negative ion,[8] and the ligands are present in the enolic form in the corresponding coordination compounds. The coordination compounds $PbL^2 \cdot 2H_2O$ and PbL^4 are insoluble in deuterated DMSO. The proton peak due to the N—H group disappeared in the ^{1}H NMR spectra of PbL_2^1 and $PbL_2^3 \cdot H_2O$,

Table 3. ^{1}H NMR of ligands (ppm)

Formula	Methyl group	Ferrocenyl group	Naphthenyl group	N—H	O—H
HL^1	2.18 3H(s)	4.00–4.74 5H(s), 4H(m)	7.52–8.00 7H(m)	10.70 1H(s)	
H_2L^2	2.26 3H(s)	4.09–4.77 4H(m)	7.55–7.99 7H(m)	10.76 1H(s)	
HL^3	2.22 3H(s)	4.24–4.71 5H(s), 4H(m)	7.35–8.01 6H(m)	11.34 1H(s)	8.61 1H(s)
H_2^4	2.09 3H(s)	4.49–4.97 4H(m)	6.69–7.26 6H(m)	13.88 1H(s)	8.22 1H(s)

which supported the conclusion of the IR spectra above. The characteristic absorption bands of the naphthene ring were observed in the IR spectra of the ligands and coordination compounds at 1570–1595 and 733–742 cm^{-1}. The characteristic absorption bands observed at 3085, 1442, 1105, 830, 503 and 482 cm^{-1} were attributed to the ferrocenyl group as ν(C—H), ν(C—C), δ(C—H), π(C—H) and δ(Fe-ring), respectively.[5]

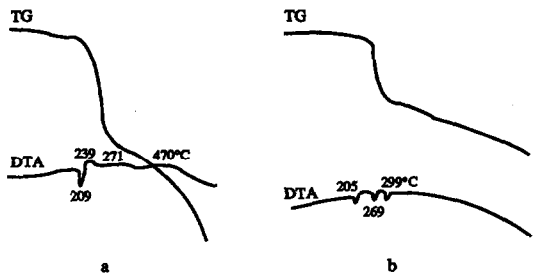

Fig. 2. The TG–DTA diagram of (a) the ligand H_2L^2 and (b) complex $PbL^2 \cdot 2H_2O$.

UV–vis spectra

UV–vis absorption bands of the ligands and lead(II) coordination compounds are shown in Table 4. It can be seen that there is a shoulder peak in the UV–vis spectra of the ligands and coordination compounds near 270 nm, which was attributed to the B band of cyclopentadiene. There is a weak and broad absorption band at *ca* 420–422 nm, arising from the transition of the 3*d* electrons on iron to either the non-bonding or antibonding orbitals of the cyclopentadienyl ring.[8] A strong K absorption band ($\pi \rightarrow \pi^*$ transition) appeared in the UV spectra of the ligands at 286–314 nm, while that of the coordination compounds is shifted to a longer wavelength by 2–20 nm. The results indicate that the ligands coordinate to lead(II) in the enol form, respectively, to form a greater conjugated system which decreased the energy of the whole system.

Thermal analysis

The results of TG–DTA for the ligand H_2L^2 and coordination compound $PbL^2 \cdot 2H_2O$ are shown in Fig. 2(a,b). It can be seen that the ligand H_2L^2 melted at 209°C, accompanied by the endothermal effect, then decomposed exothermally at 239°C. A weak endothermal peak appeared at 271°C. The whole weight loss is about 38.3% until 358°C, which suggests that two naphthalene rings break away from the molecule (calc. *ca* 42%). The weak and broad exothermal peak was observed at 470°C, and weight loss was 39% until 800°C, which was attributed to the decomposition of the ferrocenyl and acylhydrazonyl groups (the residue was iron). A weak endothermal peak and two endothermic decomposed peaks appear at 205, 269 and 299°C, respectively, in Fig. 2(b), $PbL^2 \cdot 2H_2O$. The three weight losses cannot be distinguished. It may be that it loses two molecules of water and two naphthalene groups, accompanied by the whole weight loss of *ca* 35.2% (calc. 34.2%). The two molecules of water lost at 205°C perhaps exist as coordination water. The chelate continues to decompose until 800°C to lose 26.4% of its weight. This suggests that whole coordination compounds decomposed completely and the remaining mixture perhaps is lead, iron and parts of the ferrocenyl group. The decomposition temperature of lead(II) coordination compounds is higher than that of the corresponding ligand, which suggests that the formation of the stable chelate ring in coordination compounds increased their thermal stable properties.

Molar conductance

The molar conductances of the ligands and coordination compounds in DMF are listed in Table

Table 4. UV–vis absorption bands of the ligands and coordination compounds (nm, λ_{max} DMF)

Formula	λ_{max} DMF I	II	III
HL^1	270sh	293	434
H_2L^2	270sh	286	438
HL^3	266	306	440
H_2L^4	270	314	440
PbL_2^1	270sh	295	431
$PbL^2 \cdot 2H_2O$	266sh	294	420
$PbL_2^3 \cdot H_2O$	266	326	440
PbL^4	270	326	442

Table 5. Molar conductance of the ligands and coordination compounds in DMF (Λ, $\Omega^{-1}\,cm^2\,mol^{-1}$), 20°C

Formula	Concentration (M)	Λ ($\Omega^{-1}\,cm^2\,mol^{-1}$)
HL^1	9.34×10^{-4}	6.76
H_2L^2	1.80×10^{-5}	38.40
HL^3	7.76×10^{-5}	45.10
H_2L^4	9.40×10^{-5}	46.00
PbL_2^1	1.91×10^{-4}	21.20
$PbL^2 \cdot 2H_2O$	1.30×10^{-5}	17.90
$PbL^3 \cdot H_2O$	1.00×10^{-5}	27.73
PbL^4	2.00×10^{-5}	47.00

5. The results from Table 5 show that the molar conductances are in the region 6.76–47.0 Ω^{-1} cm^2 mol^{-1} due to the ligands and coordination compounds being weak electrolytes (the reference values for 1 : 1 electrolytes have been taken as 65–90 Ω^{-1} cm^2 mol^{-1} in DMF).[14] Thus, it can be deduced that the ligand coordinates to lead(II) to form a stable neutral coordination compound, accompanied by the release of acetate.

REFERENCES

1. G. Marr and B. W. Rockett, *J. Organomet. Chem.* 1976, **106**, 259.
2. B. W. Rockett and G. Marr, *J. Organomet. Chem.* 1976, **123**, 205.
3. B. W. Rockett and G. Marr, *J. Organomet. Chem.* 1974, **79**, 223.
4. M. Gallego, M. Garcia-Vargas and M. Valcarcel, *Analyst* 1979, **104**, 613.
5. S. R. Patil, U. N. Kantank and D. N. Sen, *Inorg. Chim. Acta* 1982, **63**, 261.
6. E. I. Edwards, R. Epton and G. Marr, *J. Organomet. Chem.* 1975, **C23**, 85.
7. S. R. Patil, U. N. Kantank and D. N. Sen, *Inorg. Chim. Acta* 1983, **68**, 1.
8. Zhao Gang, Li Feng, Xie Jishan and Ma Yongxiang, *Polyhedron* 1988, **7**, 393.
9. Ma Yongxiang, Zeng Zhengzhi, Ma Yun and Zhao Gang, *Inorg. Chim. Acta* 1989, **165**, 185.
10. P. J. Graham, R. V. Lindsey, G. W. Parshall, M. L. Petersen and G. M. Whitman, *J. Am. Chem. Soc.* 1957, **79**, 3416.
11. M. Rosenblum and R. B. Woodward, *J. Am. Chem. Soc.* 1958, **80**, 5443.
12. Zhang Hongyun, Chen Dongli, Jia Handong and Che Deji, *Chem. World* 1991, **2**, 63.
13. Ma Yongxiang, Li Feng, Sun Hongsui and Xie Jishan, *Inorg. Chim. Acta* 1988, **149**, 209.
14. W. J. Geary, *Coord. Chem. Rev.* 1971, **7**, 81.

Polyhedron Vol. 12, No. 2, pp. 171–180, 1993
Printed in Great Britain

0277–5387/93 $6.00+.00
© 1993 Pergamon Press Ltd

SYNTHESIS AND CHARACTERIZATION OF CYCLOMETALLATED PALLADIUM(II) COMPLEXES WITH $Ph_2PCH_2PPh_2$ (dppm), *TRANS*-$Ph_2PCH{=}CHPPh_2$ (*TRANS*-dppe), *CIS*-$Ph_2PCH{=}CHPPh_2$ (*CIS*-dppe) AND $Ph_2P(CH_2)_4PPh_2$ (dppb). THE X-RAY CRYSTAL STRUCTURE OF DI-μ-BROMO-BIS[N-(4-METHYLBENZYLIDENE)CYCLOHEXYLAMINATO-C6,N]DIPALLADIUM(II)

J. M. VILA,* M. GAYOSO, M. T. PEREIRA, J. M. ORTIGUEIRA and A. FERNANDEZ

Department of Inorganic Chemistry, University of Santiago, Santiago de Compostela E-15706, Spain

and

NEIL A. BAILEY and HARRY ADAMS

Department of Chemistry, The University of Sheffield, Sheffield S3 7HF, U.K.

(*Received* 17 *July* 1992; *accepted* 1 *October* 1992)

Abstract—Treatment of the Schiff bases 4-$MeC_6H_4C(H){=}NCy$ (**a**), 3-Me-4-$MeOC_6H_3$—$C(H){=}N$-2′,4′,6′-$Me_3C_6H_2$ (**b**) or 2,4-$Me_2C_6H_3C(H){=}N$-2′,4′,6′-$Me_3C_6H_2$ (**c**) with palladium(II) acetate gave the cyclometallated complexes **1a**, **1b** and **1c**. These reacted with NaX to give the halide-bridged complexes **2a**, **2b** and **2c** (X = Cl), **3a**, **3b** and **3c** (X = Br) and **4c** (X = I). Reaction of the halide-bridged dimers with $Ph_2PCH_2PPh_2$(dppm), *trans*-$Ph_2PCH{=}CHPPh_2$ (*trans*-dppe), *cis*-$Ph_2PCH{=}CHPPh_2$ (*cis*-dppe) or $Ph_2P(CH_2)_4PPh_2$ (dppb), as appropriate, in a dimer/diphosphine 1 : 1 or 1 : 2 molar ratio gave the dinuclear phosphine-bridged **4a**, **5a**, **4b**, **5b**, **5c–7c** and **8c–10c** and mononuclear **6a**, **6b**, **11c** and **12c** complexes, respectively. The structure of the bromo-bridged palladium(II) complex $[Pd\{4\text{-}Me\text{—}C_6H_3C(H){=}NCy\}(Br)]_2$ (**3a**) has been determined by X-ray crystallography. The structure has two asymmetrically bridging bromine atoms and a non-bonding Pd···Pd distance of 341.8(2) pm.

Cyclometallated complexes are an important part of organometallic chemistry and reviews covering them have appeared.[1–4] Many types of ligands may undergo cyclometallation reactions and we have studied those complexes derived from Schiff bases,[5] phenylimidazoles,[6] benzylidene hydrazones[7] and bis(N-benzylidene)-1,4-phenylenediamines.[8] The halide-bridged cyclometallated dimers are good starting materials for reactions with nucleophiles such as tertiary phosphines or diphosphines, pyridine, thallium acetylacetonate or thallium cyclopentadienyl. In particular, they react with tertiary diphosphines to give dinuclear or mononuclear species, depending on the dimer/diphosphine molar ratio.[9,10] The dinuclear compounds have bridging diphosphine and halide ligands. When the larger "bite" diphosphines are used the metal–metal distance is increased and complexes with a bridging disphosphine and terminal metal–halogen bonds are to be expected; such is the case of compounds with $Ph_2PCH_2CH_2PPh_2$.[11] In the present paper we report the synthesis and characterization of cyclometallated palladium(II) dinuclear and mononuclear complexes with the diphosphines $Ph_2PCH_2PPh_2$ (dppm), *trans*-$Ph_2PCH{=}CHPPh_2$ (*trans*-

* Author to whom correspondence should be addressed.

dppe), *cis*-$Ph_2PCH{=}CHPPh_2$ (*cis*-dppe) and $Ph_2P(CH_2)_4PPh_2$ (dppb). The "bite" of the diphosphine is also related to the symmetry of the compounds, as is described.

Another feature of the halide-bridged compounds is the question of whether they are dimeric or polymeric in nature. Spectroscopic results alone are not sufficient to resolve this problem; the most suitable method being X-ray diffraction. However, crystals of these complexes are often difficult to obtain, due to their low solubility, although some examples of chloro-bridged complexes are found in the literature.[12–16] For the bromo-bridged complexes only one cyclometallated bromine dimer has been reported[17] with monodentate Schiff base ligands (a novel tetranuclear bromine-bridged complex has also been described recently[8]). In the present paper we also report the X-ray crystal structure of one of the bromo-bridged complexes.

RESULTS AND DISCUSSION

Treatment of 4-$MeC_6H_4C(H){=}NCy$ (**a**), 3-Me-4-$MeOC_6H_3C(H){=}N$-2′,4′,6′-$Me_3C_6H_2$ (**b**) or 2,4-$Me_2C_6H_3C(H){=}N$-2′,4′,6′-$Me_3C_6H_2$ (**c**) with palladium(II) acetate in boiling glacial acetic acid under dinitrogen gave the cyclometallated acetato-bridged complexes **1a**, **1b** and **1c**, respectively, as air-stable solids. These were converted into the corresponding halide-bridged analogues by treatment in acetone with aqueous sodium chloride or sodium bromide to give the chloro-bridged **2a–2c**, bromo-bridged **3a–3c** and iodo-bridged **4c** complexes, respectively, as air-stable solids (see Experimental and Tables 1 and 2). Compounds **1b**, **2b** and **3b** have been prepared by us[18] earlier (corrected and more complete NMR data is given in this paper) and they have been used here as starting materials for the synthesis of the diphosphine complexes. The

Table 1. Microanalytical, colour, yield and IR data

	Colour	Yield (%)	Analytical data, Found (Calc.) (%) C	H	N	IR data (cm^{-1}) ν(C=N)[a]	ν(Pd—Cl)$_b$	ν(Pd—Cl)$_t$
1a[b]	Yellow	73	52.2(52.5)	6.1(5.8)	4.3(3.8)	1610m		
2a	Pale yellow	95	49.1(46.8)	5.3(5.2)	4.1(3.7)	1611s	318m 248m	
3a	Yellow	94	44.1(43.5)	5.1(4.7)	3.6(3.6)	1608m		
4a	Pale yellow	91	60.1(59.6)	5.9(5.5)	2.6(2.6)	1617vs		272m
5a	Yellow	66	54.5(55.0)	5.3(5.1)	2.7(2.4)	1616vs		
6a	White	95	56.5(56.0)	5.3(4.8)	1.9(1.7)	1614m		
1b[b]	Orange	76	55.4(55.6)	5.7(5.4)	3.1(3.2)	1605m		
2b	Yellow	86	52.3(52.9)	5.3(4.9)	3.4(3.4)	1612m	307m 280m	
3b	Yellow	82	46.2(47.7)	4.6(4.5)	2.9(3.1)	1613m		
4b	Pale yellow	83	59.6(61.0)	5.5(5.2)	2.3(2.3)	1613m		290m
5b	Yellow	65	56.4(56.8)	5.1(4.9)	2.2(2.2)	1617m		
6b	Yellow	95	57.6(57.4)	4.9(4.5)	1.9(1.6)	1608m		
1c[b]	Yellow	55	57.6(57.7)	5.4(5.5)	3.7(3.4)	1608sh,s		
2c	Yellow	70	55.6(55.1)	5.3(5.1)	3.3(3.6)	1610m	321m 270m	
3c	Yellow	80	49.2(49.5)	4.7(4.6)	3.2(3.2)	1610m		
4c	White	92	44.4(44.7)	4.1(4.1)	2.9(2.9)	1605s		
5c	White	93	62.6(63.0)	5.0(5.3)	2.3(2.4)	1612m		280m
6c	Pale yellow	69	58.0(58.6)	4.7(4.9)	2.2(2.2)	1610m		
7c	Pale yellow	70	54.6(54.6)	4.6(4.6)	2.3(2.1)	1610s		
8c	White	84	63.6(63.5)	5.2(5.6)	2.1(2.3)	1606s		281m
9c	Pale yellow	51	59.4(59.1)	5.1(5.3)	1.8(2.1)	1610m		
10c	Orange	40	55.3(55.1)	5.2(4.9)	2.0(2.0)	1614m		
11c	White	80	58.7(58.7)	4.9(4.7)	1.9(1.6)	1610m		
12c	Yellow	87	59.4(59.5)	5.2(5.2)	1.4(1.5)	1604m		

[a] ν(C=N) values for **a** = 1642vs, **b** = 1635m and **c** = 1625s (cm^{-1}).

[b] ν(COO) values for **1a**: ν_{as}(COO) = 1578m, ν_s(COO) = 1415s; **2a**: ν_{as}(COO) = 1582s; ν_s(COO) = 1412m; ν_{as}(COO) = 1586, ν_s(COO) = 1408s (cm^{-1}).

acetato- and halide-bridged dimers show the typical features of similar complexes prepared by us.[5] Thus, the IR spectrum of complexes **1a–1c** shows the ν_{as}(COO) and ν_s(COO) stretching modes of the acetato ligands at 1578m, 1415s (**1a**), 1582s, 1412m (**1b**) and 1586s, 1408s cm^{-1} (**1c**); the separation between them is in agreement with bridging acetato groups.[19] The shift of the ν(C=N) vibration towards lower wavenumbers[20] and the shift of the *H*C=N resonance towards lower frequency[20] and the shift of the *H*C=N resonances towards lower frequency[21] in the ^{1}H NMR spectrum (*ca* 0.5–1.0 ppm) show that the palladium atom is bonded through the nitrogen atom of the C=N group (see Tables 1 and 2). Only one singlet (integrating for 6H) is observed in the ^{1}H NMR spectrum for the *Me*CO_2 resonances, indicating that the Schiff base ligands are in a *trans* disposition.[5a,10]

Treatment of the halide-bridged dimer complexes with $Ph_2PCH_2PPh_2$ (dppm), *trans*-Ph_2PCH=$CHPPh_2$ (*trans*-dppe) or $Ph_2P(CH_2)_4PPh_2$ (dppb) in a dimer/diphosphine 1 : 1 molar ratio gave the dinuclear complexes **4a**, **5a**, **4b** and **5b** as 1 : 1 electrolytes, and **5c–7c** and **8c–10c** as molecular compounds (see Scheme 1). They have been fully characterized by elemental analysis (carbon, hydrogen, nitrogen) and IR, $^{31}P\{^1H\}$ and ^{1}H NMR spectroscopy. The larger "bite" disphosphines *trans*-

Table 2. $^{31}P\{^1H\}^a$ and $^1H^b$ NMR data[c,d]

	δ(HC=N)	δ[H(2)]	δ[H(3)]	δ[H(5)]	δ($C_6H'_2$)[e]	δ(MeO)	δ(Me)[f]	δ(Me)[g]	δ(Me)[h]	δ(P)
a[i]	8.26s		7.40dd						2.36s	
1a[j]	7.21s	6.92d	6.77d	6.88s					2.28s	
		^3J[H(2)H(3)] = 7.8								
2a	7.79s	7.07d	6.84d	7.20s					2.32s	
		^3J[H(2)H(3)] = 8.0								
3a	7.82s	7.09d	6.84d	7.39s					2.32s	
		^3J[H(2)H(3)] = 7.8								
4a	7.93d	7.06d	6.65d	5.74d					1.65s	27.9s
	^4J(PH) = 8.6	^3J[H(2)H(3)] = 7.8		^4J(PH) = 6.0						
5a	7.96d	7.08d	6.68d	5.71d					1.64s	27.7s
	^4J(PH) = 8.2	^3J[H(2)H(3)] = 7.7		^4J(PH) = 6.6						
6a[k,l]	8.19d	7.07d	6.91d	6.44t					1.93s	27.6d
	^3J(PH) = 7.7	^3J[H(2)H(3)] = 8.0		^4J(PH) = 8.5						4.2d
b[i]	8.06s	7.76d		6.86d	6.85s	3.85s	2.10s	2.26s	2.27s	
1b[j]	7.48s	7.04s		6.89s	6.49s	3.66s	2.19s	2.26s	2.52s	
2b	7.56s	7.05s		6.69s	6.85s	3.78s	2.11s	2.26s	2.32s	
3b	7.59d	7.05s		6.86s	6.85s	3.79s	2.10s	2.27s	2.31s	
4b	7.76d	6.99s		5.72d	6.94s	2.86s	1.93s	2.32s	2.37s	30.52s
	^4J(PH) = 8.0			^4J(PH) = 6.0						
5b	7.77d	6.99s		5.68d	6.93s	2.87s	1.93s	2.33s	2.36s	31.09s
	^4J(PH) = 8.0			^4J(PH) = 6.5						
6b[k,l]	7.89d			6.20dd	6.69s	3.12s	2.10s	2.13s	2.24s	30.42d
	^4J(PH) = 6.7			^4J(PH) = 10.4						5.33d
				^4J(PH) = 7.9						
c[i]	8.64s		6.79s	7.15d	6.91s		2.14s	2.30	2.52s	
									2.39s	
1c[j]	7.88s		6.66s	6.35s	6.86s		2.17s	2.29s	2.34s	
									2.31s	
2c	7.91s		6.62s	6.84s	6.90s		2.17s	2.30s	2.34s	
									2.31s	
3c	7.95s		6.61s	7.03s	6.89s		2.16s	2.30s	2.42s	
									2.35s	
4c	8.03s		6.62s	6.85s	6.93s		2.17s	2.32s	2.60s	
									2.36s	
5c[m]	8.25d		6.48s	6.04d	6.91s		2.17s	2.42s	2.42s	34.93d
	^4J(PH) = 7.8			^4J(PH) = 5.3					1.67s	
6c[m]	8.28d		6.48s	6.05d	6.93s		2.26s	2.42s	2.42s	33.14s
	^4J(PH) = 7.7			^4J(PH) = 5.5					1.66s	

Table 2.—*continued*

	δ(HC=N)	δ[H(2)]	δ[H(3)]	δ[H(5)]	δ($C_6H'_2$)[e]	δ(MeO)	δ(Me)[f]	δ(Me)[g]	δ(Me)[h]	δ(P)
7c[m]	8.32d		6.48s	6.01d	6.93s		2.17s	2.42s	2.43s	36.75s
	^4J(PH) = 7.6			^4J(PH) = 6.0					1.63s	
8c	8.25d		6.49s	6.02d	6.90s		2.18s	2.31s	2.35s	32.11s
	^4J(PH) = 7.8			^4J(PH) = 5.9					1.69s	
9c	8.27d		6.49s	5.98d	6.90s		2.18s	2.31s	2.36s	33.83s
	^4J(PH) = 7.7			^4J(PH) = 5.8					1.69s	
10c	8.31d		6.50s	5.92d	6.91s		2.17s	2.42s	2.42ss	29.04s
	^4J(PH) = 7.6			^4J(PH) = 6.8					1.68s	
11c[k,l]	8.25d		6.72s	6.68t	6.45s		2.16s	2.42s	2.42s	58.75d
	^4J(PH) = 7.8			^4J(PH) = 7.4					1.90s	45.88d
12c[k,l]	8.21d		6.60s	6.38t	6.42s		2.15s	2.43s	2.43s	30.80d
	^4J(PH) = 7.0			^4J(PH) = 7.4					1.70s	11.08d

[a] Spectra measured at 100.6 MHz (*ca* ±20°C); chemical shifts (δ) in ppm (±0.1) to a high frequency of 85% H_3PO_4.

[b] Spectra measured at 250 MHz (*ca* ±20°C); chemical shifts (δ) in ppm (±0.01) to a high frequency of $SiMe_4$.

[c] Coupling constants in Hz.

[d] s, singlet; d, doublet; dd, doublet of doublets; t, triplet.

[e] Proton resonances of the aniline ring.

[f] δ(Me) corresponds to the 2′-Me and 6′-Me groups; integration is for 6H.

[g] δ(Me) corresponds to the 4′-Me group; integration is for 3H.

[h] Corresponds to the C(4)-*Me* group in **a**, **1a–6a**; to the C(3)-*Me* group in **b**, **1b–6b**; and to the C(2)-*Me* and C(4)-*Me* groups in **c**, **1c–12c**. In **5c–12c** the lower value is for C(4)-*Me*.

[i] δ(H6) values: **1**, the H2, H3, H5 and H6 resonances appear as an apparent doublet of doublets (AA′XX′ spin system) centred at 7.40 ppm; **b**, 7.62dd, ^3J[H(5)H(6)] = 8.3, ^4J[H(5)H(6)] = 2.0; **c**, 8.0d, ^3J[H(5)H(6)] = 8.0.

[j] δ(O_2CMe) values: **1a**, 2.14s, 6H; **1b**, 1.70s, 6H; **1c**, 1.65s, 6H.

[k] Coupling constants: **6a**, ^2J(PP) = 63; **6b**, ^2J(PP) = 63; **11c**, ^3J(PP) = 11.6; **12b**, ^5J(pp) = 12.0 Hz.

[l] The higher value corresponds to P_A and the lower one to P_B.

[m] δ[PC(*H*)=C(*H*)P] values for: **5c**, δ6.97; **6c**, δ6.80; **7c**, δ6.68. N values *ca* 42Hz.

dppe and dppb, as opposed to the smaller "bite" diphosphines *trans*-dppe and dppb, as opposed to the smaller "bite" diphosphine dppm, preclude the possibility of a bridging halogen atom between the metal centres in **5c–7c** and **8c–10c**. Also noticeable is that for both cyclometallated moieties in each complex, only one set of signals is observed in the ^{1}H NMR spectrum and only one singlet in the $^{31}P\{^1H\}$ spectrum for both phosphorus atoms, showing the compounds to be symmetric, i.e. in complexes **4a**, **5a**, **4b** and **5b** the Schiff base ligands are in a parallel arrangement, whereas in complexes **5c–7c** and **8c–10c** they are in an antiparallel arrangement. As an example, the C(4)—*Me* and C(4)—*MeO* resonances (see Table 2) appear shifted to a lower frequency due to the shielding effect of the phosphine phenyl ring.[18] In antiparallel (**4a**, **5a**, **4b** and **5b**) and parallel (**5c–7c** and **8c–10c**) arrangements, one would observe two signals in each case, one shielded and one non-shielded by the phosphine ligand. This also evidences the geometry around the palladium atom with the phosphorus atom always *trans* to the nitrogen atom. Therefore, we may conclude that complexes **4a**, **5a**, **4b** and **5b** are symmetric across a two-fold axis and that complexes **5c–7c** and **8c–10c** are centrosymmetric. In complexes **5c–7c** the apparent triplet at *ca* 6.9–6.7 ppm was assigned to the PC*H*=C*H*P proton resonances (AA′XX′ spin system) with N *ca* 42 Hz.

Treatment of the halide-bridged dimer compounds with $Ph_2PCH_2PPh_2$ (dppm), *cis*-Ph_2PCH=$CHPPh_2$ (*cis*-dppe) or $Ph_2P(CH_2)_4PPh_2$ (dppb), and NH_4PF_6, in a dimer/diphosphine 1:2 molar ratio afforded the mononuclear species **6a**, **6b**, **11c** and **12c** as air-stable solids (see Experimental and Tables 1 and 2). The final products in each case are identical whether one uses the choro, bromo- or iodo-bridged dimer as the starting material, because the halogen is exchanged by the hexafluorophosphate ion (see Scheme 1). The $^{31}P\{^1H\}$ NMR spectrum showed two doublets for the two inequivalent phosphorus nuclei. The lower frequency doublet is assigned to the phosphorus nucleus *trans* to the phenyl carbon and the higher frequency one to the phosphorus nucleus *trans* to the nitrogen atom, assuming that a ligand of greater *trans* influ-

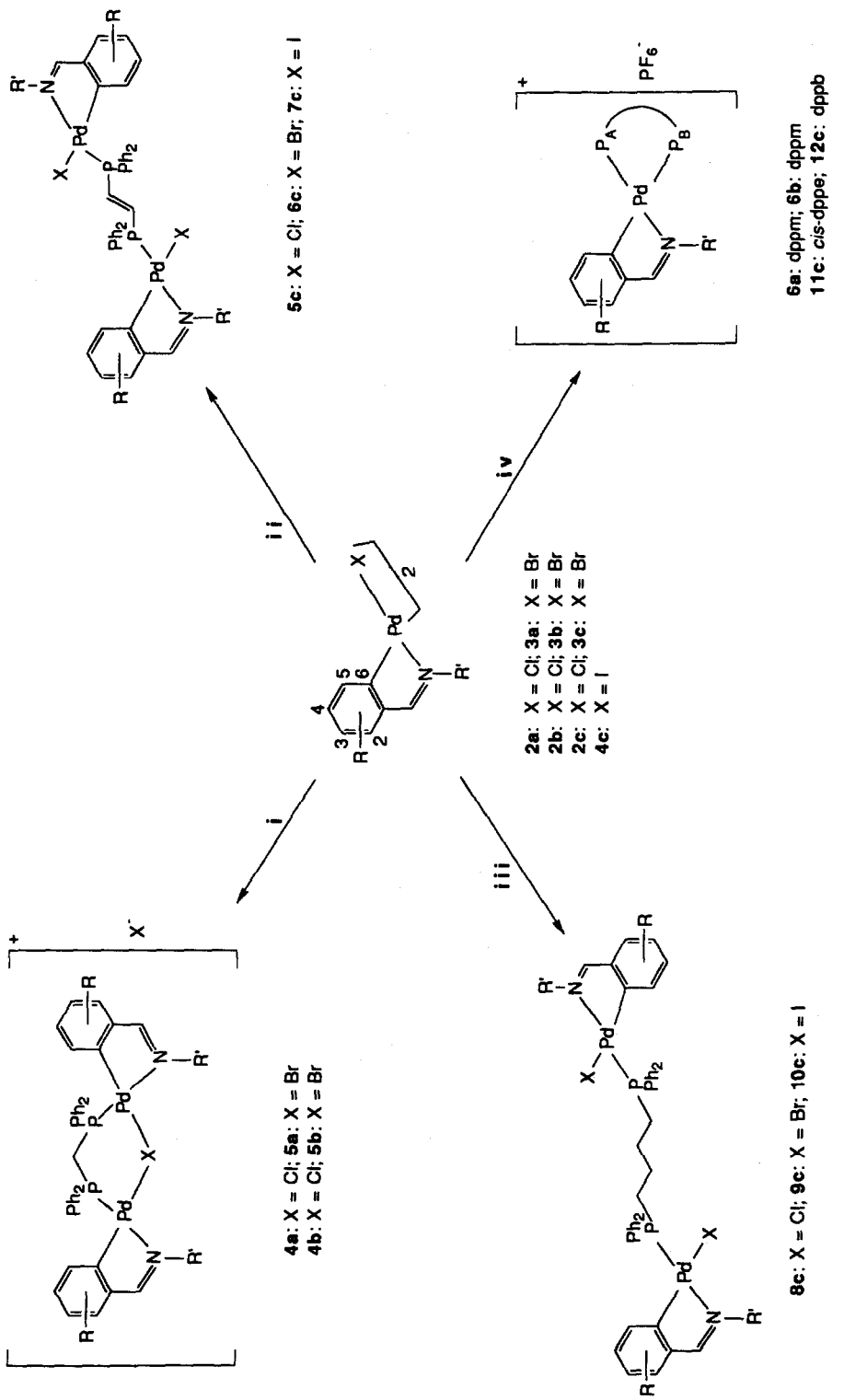

i: 1 equiv. of dppm; ii: 1 equiv. of *trans*-dppe ; iii: 1 equiv. of dppb; iv: 2 equiv. of dppm, *cis*-dppe or dppb, + NH_4PF_6
a: R = 4-Me, R' = Cy; **b**: R = 3-Me, 4-MeO; R' = 2',4',6'-$Me_3C_6H_2$; **c**: R = 2,4-Me_2; R' = 2',4',6'-$Me_3C_6H_2$

Scheme 1.

ence shifts the ^{31}P resonance of the phosphorus *trans* to it to a lower frequency.[22] The *H*C=N resonance is coupled to only one phosphorus nucleus, i.e. that *trans* to it [^4J(PH) = *ca* 7.0–8.0 Hz]. Selective decoupling experiments confirmed this. Selective irradiation of the P_A or P_B resonances reduces the *H*(5) resonance to a doublet [^4J(PH) = *ca* 6.0–10 Hz] and the *H*C=N resonance to a singlet (irradiating at P_A) or to a doublet (irradiating at P_B). In complexes **11c** and **12c** the PC*H*=C*H*P resonances are probably shielded by the phosphine phenyl rings and are shifted to a higher frequency, where they are occluded by the phenyl proton resonances and hence were not assigned.

Crystal structure of **3b**

Suitable crystals of compound **3b** were obtained by slowly evaporating a chloroform solution. The molecular structure and its numbering scheme are shown in Fig. 1 and the unit cell is shown in Fig. 2. Selected interatomic distances and angles are given in Table 3.

The molecule is dimeric, with two square-planar coordinated palladium atoms asymmetrically bridged by two bromine ligands [Pd(1)—Br(1) 259.7(2), Pd(1)—Br(2) 244.9(2), Pd(2)—Br(1) 245.0(2) and Pd(2)—Br(2) 257.8(2) pm]. The asymmetry results from the differing *trans* influence of the phenyl carbon and nitrogen atoms of the Schiff base ligand. The remaining coordination sites on each palladium are occupied by an aromatic carbon and an imino nitrogen atom of the bidentate ligand N-(4-methylbenzylidene)cyclohexylamine-C6,N [Pd(1)—C(1) 199.3(10), Pd(1)—N(1) 203.4(9), Pd(2)—C(16) 199.5(12) and Pd(2)—N(2) 204.9(7) pm]. The two cyclometallated ligands are in an overall antiparallel arrangement about the Pd_2Br_2 core, similar to that observed in other dimers.[17,23–26] The Pd—C bond lengths are shorter than the expected value of 208.1 pm based on the sum of the covalent radii for carbon and palladium, 77.1 and 131 pm, respectively;[27] this shortening observed in related complexes[8,17,25] is probably due to partial double bond character in the Pd—C linkage. The Pd—N bond distances are slightly longer than the value of

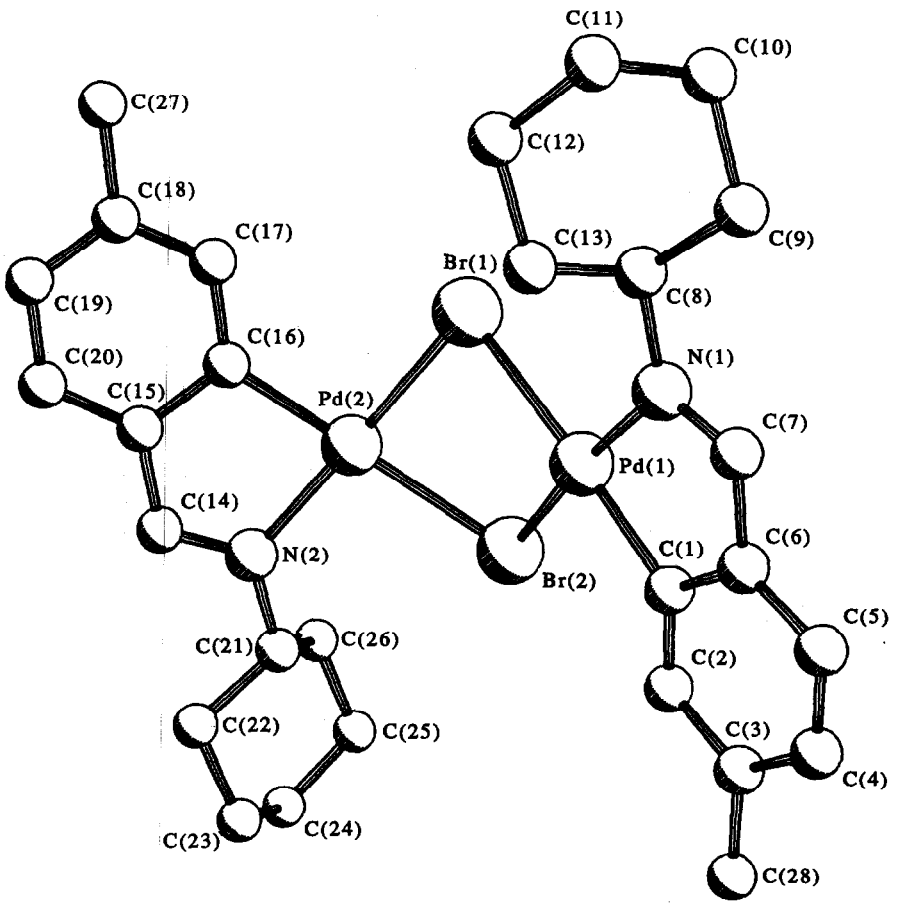

Fig. 1. Molecular and numbering scheme of compound **3a**.

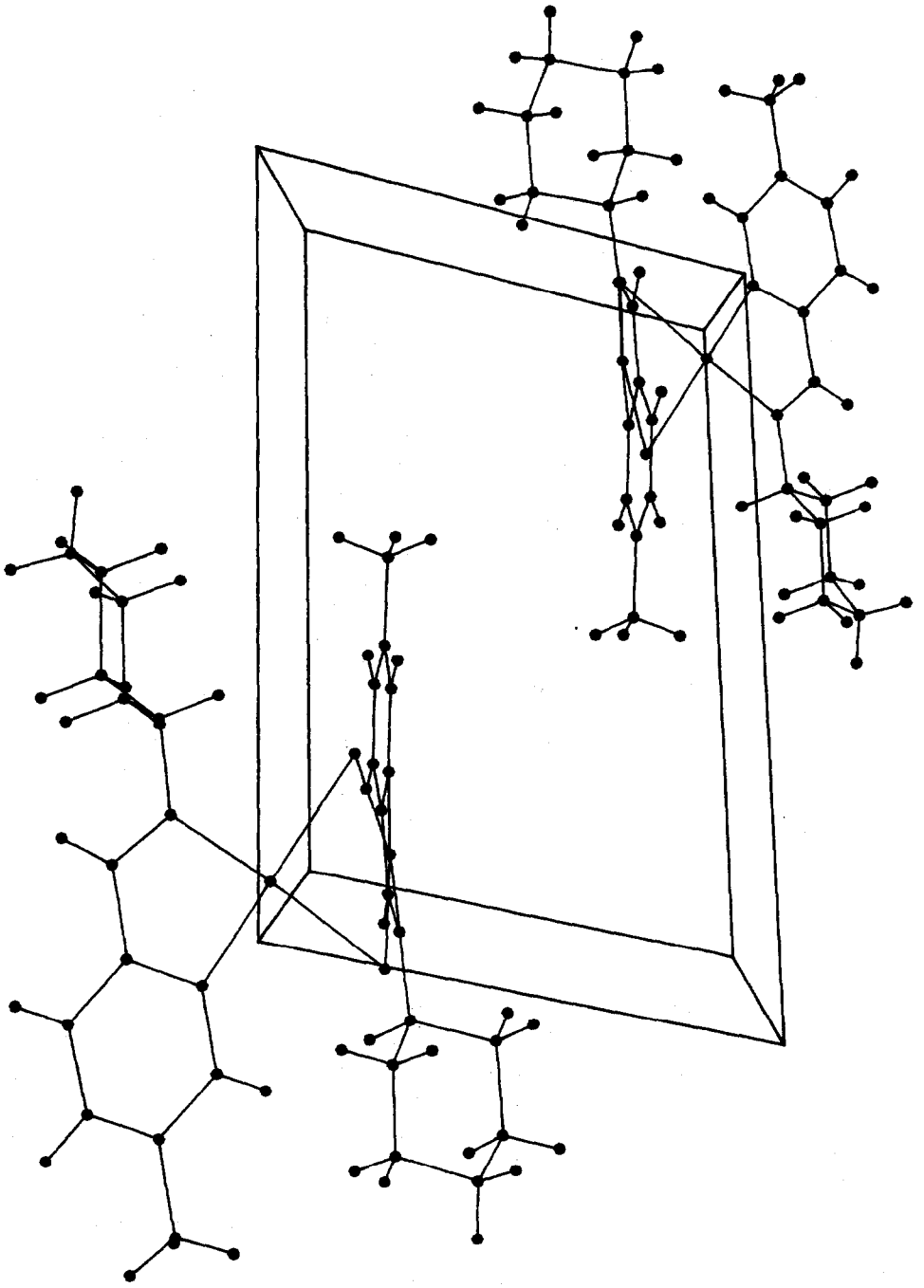

Fig. 2. Unit cell of compound **3a**.

201 pm obtained from the sum of the covalent radius for N(sp^2), 70 pm, and for palladium, 131 pm. The C=N distances [N(1)—C(7) 128.0(4) and N(2)—C(14) 129.0(6)] are somewhat longer than the value of 123.7(3) which is observed for a related free ligand;[28] this lengthening is typical of a coordinated Schiff base ligand[29] where the nitrogen atom is involved in a σ-bond to a metal atom and has been observed by us before.[8,17]

The bond angles at palladium do not deviate greatly from 90°, the most deviant being in the chelate rings [N(1)—Pd(1)—C(1) 81.2(4)° and N(2)—Pd(2)—C(16) 82.0(4)°]. The coordination of the palladium atoms is approximately planar, as expected for Pd^{2+} (r.m.s. deviations of coordinating atoms 4.4 and 6.0 pm), with the metals only 0.2 and 10.7 pm from the mean planes; the loss of five-atom co-planarity is represented by a symmetric

Table 3. Selected bond lengths (pm) and angles (°) in compound **3a**

Pd(1)—Br(1)	259.7(2)	Pd(1)—Br(2)	244.9(2)
Pd(1)—N(1)	203.4(9)	Pd(1)—C(1)	199.3(10)
Pd(2)—Br(1)	245.0(2)	Pd(2)—Br(2)	257.8(2)
Pd(2)—N(2)	204.9(7)	Pd(2)—C(16)	199.5(12)
N(1)—C(7)	128.0(14)	N(1)—C(8)	148.6(13)
N(2)—C(14)	129.0(16)	C(1)—C(6)	139.6(16)
C(1)—C(2)	136.2(13)	C(3)—C(4)	134.3(18)
C(2)—C(3)	139.9(15)	C(4)—C(5)	137.8(15)
C(3)—C(28)	153.6(15)	C(6)—C(7)	143.7(14)
C(5)—C(6)	138.9(16)	C(8)—C(13)	151.1(15)
C(8)—C(9)	150.4(17)	C(10)—C(11)	148.9(19)
C(9)—C(10)	155.9(15)	C(12)—C(13)	151.5(15)
C(11)—C(12)	149.2(19)	C(14)—C(15)	141.4(17)
Br(1)—Pd(1)—Br(2)	84.7(1)	Br(1)—Pd(1)—N(1)	99.8(2)
Br(2)—Pd(1)—N(1)	175.0(3)	Br(1)—Pd(1)—C(1)	177.7(2)
Br(2)—Pd(1)—C(1)	94.5(3)	N(1)—Pd(1)—C(1)	81.2(4)
Br(1)—Pd(2)—Br(2)	85.1(1)	Pd(1)—Br(2)—Pd(2)	85.6(1)
Br(2)—Pd(2)—N(2)	97.9(3)	Br(1)—Pd(2)—N(2)	170.8(2)
Br(2)—Pd(2)—C(16)	177.6(3)	Br(1)—Pd(2)—C(16)	94.8(3)
Pd(1)—Br(1)—Pds(2)	85.2(1)	N(2)—Pd(2)—C(16)	82.0(4)
Pd(1)—N(1)—C(7)	114.9(7)	Pd(1)—N(1)—C(8)	124.2(7)
C(7)—N(1)—C(8)	120.9(9)	Pd(1)—C(1)—C(6)	111.5(7)
Pd(1)—C(1)—C(2)	129.5(9)	C(1)—C(2)—C(3)	118.6(11)
C(2)—C(1)—C(6)	119.0(10)	C(3)—C(4)—C(5)	121.4(11)
C(4)—C(3)—C(28)	121.5(11)	C(1)—C(6)—C(5)	120.5(9)
C(4)—C(5)—C(6)	118.7(12)	C(5)—C(6)—C(7)	123.2(11)
C(1)—C(6)—C(7)	116.3(9)	N(1)—C(8)—C(9)	115.6(9)
N(1)—C(7)—C(6)	116.0(10)	N(1)—C(8)—C(13)	108.7(6)
Pd(1)···Pd(2)	341.8(2)		

tetrahedral twist of 3.4° around Pd(1), and an asymmetric pyramidalization of 8.7° about Pd(2) (both bromines lie on the same side of the PdNC plane by 36.5 and 10.6 pm). The Pd_2Br_2 bridge is not planar, but is hinged about Br···Br by 46.4°; this contrasts with the situation observed in a similar complex[17] where the Pd_2Br_2 unit is planar and centrosymmetric. The chelate rings are planar (r.m.s. deviations 0.1 and 0.1 pm) with palladium deviations of 7.7 and 26.9 pm. The two aromatic rings are planar (r.m.s. deviations 0.9 and 1.4 pm, metal deviations 1.9 and 14.9 pm), and are twisted by 2.5° and 5.2° with respect to the adjacent chelate planes. The cyclohexyl fragments adopt chair conformations [plane of C(9) C(10), C(12), C(13) r.m.s. deviation 0.6 pm, displacements of C(8) and C(11) 69.5 and −61.3 pm; plane of C(22), C(23), C(25), C(26) r.m.s. deviation 1.8 pm, displacements of C(21) and C(24) 72.8 and −64.3 pm]. It is evident that the environment of Pd(2) is less regular than that of Pd(1).

The inter-palladium distance of 341.8(2) pm is shorter than the one observed for a related dibromo-bridged complex[17] of 354.9(9) pm reflecting the non-planarity of the Pd_2Br_2 unit in this case; nevertheless, this value excludes any metal–metal bonding.

There are no noteworthy intermolecular contacts.

EXPERIMENTAL

Solvents were purified by the standard methods.[30] Chemicals were reagent grade. Palladium(II) acetate, dppm and dppb were purchased from Aldrich Chemie and Strem Chemicals; *trans*- and *cis*-dppe were prepared as reported in ref. 31 but using *trans*- and *cis*-ClCH=CHCl, as appropriate. Elemental analyses were performed by Mr J. Ulloa in the Servicio de Analysis Elemental of the University of Santiago using a Carlo–Erba elemental analyser model 1108. IR spectra were recorded as Nujol mulls or polythene discs on a Perkin–Elmer 1330 spectrophotometer. $^{31}P\{^1H\}$ and ^1H NMR spectra were obtained as $CDCl_3$ solutions, referred to a high frequency of 85% H_3PO_4 or $SiMe_4$,

respectively, and recorded on a Bruker WM-250 spectrometer.

The Schiff base ligands and the acetato- and halide-bridged compounds were prepared as reported for similar compounds.[5,17]

Preparation of $[\{Pd[4\text{-}MeC_6H_3C(H)=NCy]\}_2(\mu\text{-}Ph_2PCH_2PPh_2)(\mu\text{-}Cl)]Cl$ (**4a**)

To a suspension of the chloro-bridged dimer **2a** (30.28 mg, 0.044 mmol) in acetone (*ca* 5 cm^3) was added dppm (16.98 mg, 0.044 mmol). The mixture was stirred at room temperature for 2 h, after which time it had become clear. After a further 2 h a yellow precipitate formed, which was filtered off and dried *in vacuo*. Recrystallization from dichloromethane–n-hexane gave the final product was a yellow solid. Complexes **5a**, **4b**, **5b**, **5c–7c** and **8c–10c** were made similarly.

Preparation of $[\{Pd[4\text{-}MeC_6H_3C(H)=NCy]\}(Ph_2PCH_2PPh_2\text{-}P,P)]PF_6$ (**6a**)

To a suspension of the chloro-bridged dimer (30.00 mg, 0.044 mmol) in acetone (*ca* 5 cm^3) was added dppm (33.65 mg, 0.088 mmol). The mixture was stirred at room temperature for 2 h, NH_4PF_6 (0.014 mg, 0.088 mmol) was added and the solution stirred for a further 2 h. Water was then added and the resulting solid filtered off and dried *in vacuo*. Recrystallization from dichloromethane–*n*-hexane gave the final compound as a white solid. Compounds **6b**, **11c** and **12c** were made similarly.

Single crystal X-ray diffraction analysis

Three-dimensional, room-temperature X-ray data were collected in the range $3.5 < 2\theta < 50°$ on a Nicolet R3 diffractometer by the ω-scan method. The 3580 independent reflections (of 5007 measured) for which $|F|/o(|F|) > 3.0$ were corrected for Lorentz and polarization effects, and for absorption by analysis of eight azimuthal scans (minimum and maximum transmission coefficients 0.262 and 0.522). The structure was solved by Patterson and Fourier techniques and refined by blocked-cascade least-squares methods. Hydrogen atoms were included in calculated positions with isotropic thermal parameters related to those of the supporting atom. Refinement converged at a final $R = 0.0596$ ($R_w = 0.0549$, 307 parameters, final mean and maximum Δ/σ 0.001 and 0.003, respectively), with allowance for the thermal anisotropy of all non-hydrogen atoms. A final difference electron density synthesis showed minimum and maximum values of -0.80 and $+1.35$ e $Å^{-3}$. Complex scattering factors were taken from ref. 32 and from the program package SHELXTL,[33] as implemented on the Data General Nova 3 computer. A weighting scheme $w^{-1} = [\sigma^2(F) + 0.00076(F)^2]$ was used in the latter stages of refinement.

Crystal data. $[Pd\{4\text{-}MeC_6H_3C(H)=NC_y\}Br]_2$, $C_{28}H_{36}Br_2N_2Pd_2$; $M = 773.22$. Crystallizes from solvent as yellow blocks; crystal dimensions $0.40 \times 0.20 \times 0.15$ mm. Triclinic, $a = 854.3(3)$, $b = 1309.7(3)$, $c = 1426.1(5)$ pm, $\alpha = 110.874(23)$, $\beta = 107.044(30)$, $\gamma = 97.003(27)°$, $U = 1.3793(9)$ nm^3; $D_c = 1.862$ g cm^{-3}, $Z = 2$. Space group $P\bar{1}$, $\lambda(Mo\text{-}K_\alpha) = 71.069$ pm, $\mu(Mo\text{-}K_\alpha) = 41.77$ cm^{-1}, $F(000) = 759.91$.

Acknowledgement—We wish to thank the Xunta de Galicia (Spain) for grants to J.M.O. and to A.F.

REFERENCES

1. I. Omae, *Chem. Rev.* 1979, **79**, 289.
2. E. C. Constable, *Polyhedron* 1984, **3**, 1037.
3. V. V. Dunina, O. A. Zalevskaya and V. M. Potapov, *Russ. Chem. Rev.* 1988, **571**, 250.
4. A. D. Ryabov, *Chem. Rev.* 1990, **90**, 403.
5. (a) M. T. Pereira, J. M. Vila, E. Gayoso, W. Hiller, J. Strahle and M. Gayoso, *J. Coord. Chem.* 1988, **18**, 245; (b) M. T. Pereira, J. M. Vila, A. Suarez, E. Gayoso and M. Gayoso, *Gazz. Chim. Ital.* 1988, **118**, 783; (c) J. M. Vila, A. Suarez, M. T. Pereira, E. Gayoso and M. Gayoso, *Synth. React. Inorg. Met.-Org. Chem.* 1988, **18**, 47.
6. A. Suarez, J. M. Vila, M. T. Pereira, E. Gayoso and M. Gayoso, *J. Organomet. Chem.* 1987, **335**, 359.
7. J. L. Casas, E. Gayoso, J. M. Vila, M. T. Pereira and M. Gayoso, *Synth. React. Inorg. Met.-Org. Chem.* 1991, **21**, 263.
8. J. M. Vila, M. Gayoso, M. T. Pereira, M. C. Rodriguez, J. M. Ortigueira and M. Thornton-Pett, *J. Organomet. Chem.* 1992, **426**, 267.
9. J. M. Vila, M. Gayoso, J. J. Fernandez, J. M. Ortiguiera and A. Suarez, *Polyhedron* 1990, **9**, 2741.
10. J. M. Vila, J. M. Ortigueira, E. Gayoso, M. Gayoso, A. Castineiras, W. Hiller and J. Strahle, *Inorg. Chim. Acta* 1991, **179**, 171.
11. J. Dehand, M. Pfeffer and M. Zinsius, *Inorg. Chim. Acta* 1975, **13**, 229.
12. A. G. Constable, W. S. McDonald, L. C. Sawkins and B. L. Shaw, *J. Chem. Soc., Dalton Trans.* 1980, 1992.
13. B. Galli, F. Gasparini, B. E. Mann, L. Maresca, G. Natile, A. M. Manotti-Lanfredi and A. Tiripicchio, *J. Chem. Soc., Dalton Trans.* 1985, 1155.
14. A. A. Watson, D. A. House and P. J. Steel, *J. Organomet. Chem.* 1986, **311**, 387.
15. R. C. Elder, R. D. P. Cruea and R. F. Morrison, *Inorg. Chem.* 1976, **15**, 1623.

16. N. Barr, S. F. Dyke, G. Smith, C. H. L. Kennard and V. McKee, *J. Organomet. Chem.* 1985, **288**, 109.
17. J. M.Vila, M. Gayoso, M. T. Pereira, A. Romar, J. J. Fernandez and M. Thornton-Pett, *J. Organomet. Chem.* 1991, **401**, 385.
18. J. M. Vila, A. Suarez, M. P. Pereira, E. Gayoso and M. Gayoso, *Polyhedron* 1987, **6**, 1003 and refs therein.
19. K. Nakamaoto, *IR and Raman Spectra of Inorganic and Coordination Compounds*, 4th edn. Wiley-Interscience, New York (1986).
20. H. Onoue and I. Moritani, *J. Organomet. Chem.* 1972, **43**, 431.
21. Y. A. Ustinyuk, V. A. Chertov and J. V. Barinov, *J. Organomet. Chem.* 1971, **29**, C53.
22. P. S. Pregosin and R. W. Kuntz, *^{31}P and ^{13}C NMR of Transition Metal Phosphine Complexes*, in *NMR 16* (Edited by P. Diehl, E. Fluck and R. Kosfeld). Springer, Berlin (1979).
23. W. Hiller, A. Castineiras, J. M. Vila, A. Suarez and M. Gayoso, *Acta Cryst.* 1986, **C42**, 1136.
24. M. Alonso, J. M. Vila, E. Blas Rivero, W. Hiller, J. Strahle and M. Gayoso, *Acta Cryst.* 1988, **C44**, 929.
25. J. Selbin, K. Abboud, S. F. Watkins, M. A. Gutierrez and F. R. Fronczek, *J. Organomet. Chem.* 1983, **241**, 259.
26. Wehman, G. van Koten, J. T. B. H. Jastrzebsji, H. Ossor and M. Pfeffer, *J. Chem. Soc., Dalton Trans.* 1988, 2975.
27. L. Pauling, *The Nature of the Chemical Bond*, 3rd edn. Cornell University Press, New York (1960).
28. H. B. Burgi and J. D. Dunitz, *Helv. Chim. Acta* 1970, **53**, 1747.
29. J. Granell, D. Sainz, J. Sales and X. Solans, *J. Chem. Soc., Dalton Trans.* 1986, 1785.
30. D. D. Perrin, W. L. F. Armarego and D. P. Perrin, *Purification of Laboratory Chemicals*, 2nd edn. Pergamon Press, Oxford (1983).
31. W. Hewertson and H. R. Watson, *J. Chem. Soc.* 1962, 1490.
32. *International Tables for X-ray Crystallography*, Vol. 4. Kynoch Press, Birmingham (1974).
33. G. M.Sheldrick, SHELXTL, An Integrated System for Solving, Refining and Displaying Crystal Structures from Diffraction Data (Revision 5.1). University of Göttingen, Germany (1985).

Polyhedron Vol. 12, No. 2, pp. 181–185, 1993
Printed in Great Britain.

0277-5387/93 $6.00+.00
© 1993 Pergamon Press Ltd

REDOX INTERCALATION REACTION OF CRYSTALLINE $VOPO_4 \cdot 2H_2O$ WITH NaI SOLUTION IN ACETONE

RENÁTA ŠIŠKOVÁ, LUDVÍK BENEŠ, VÍTĚZSLAV ZIMA and MILAN VLČEK

Joint Laboratory of Solid State Chemistry of Czechoslovak Academy of Sciences, 53210 Pardubice, Czechoslovakia

and

JIŘÍ VOTINSKÝ* and JAROSLAVA KALOUSOVÁ

Institute of Chemical Technology, 53210 Pardubice, Czechoslovakia

(*Received* 13 *July* 1992; *accepted* 1 *October* 1992)

Abstract—Polycrystalline layered $VOPO_4 \cdot 2H_2O$ reacts very readily with NaI solution in acetone producing green solids and releasing molecular iodine. This redox intercalation is joined with Na^+ ion insertion between layers of the host and with reduction of vanadium (V^V to V^{IV}). Three solid phases are created gradually with the compositions $Na_{0.3}V^{IV}_{0.3}V^V_{0.7}OPO_4 \cdot 2H_2O$, $Na_{0.5}V^{IV}_{0.5}V^V_{0.5}OPO_4 \cdot 2H_2O$ and $NaV^{IV}OPO_4 \cdot H_2O$. These phases are stages 3, 2 and 1 and agree with situations in which the host is intercalated from 33, 50 and 100%. Basal spacings of all three stages were measured. Changes in phase ratio in the solid reaction products were determined by X-ray phase analysis for the reaction time 0–500 h and temperature range 20–40°C. Magnetic susceptibility (−170–30°C), a.c. conductivity and thermal properties (20–600°C) of these phases were investigated.

The structure of $VOPO_4 \cdot 2H_2O$ was described by Ladwig,[1] Tietze[2] and Tachéz[3] as a layered tetragonal lattice, built up of neutral $(VOPO_4)_\infty$ networks and interlayer water molecules. Water can be easily replaced in this lattice by other molecules, for example aliphatic alcohols,[4,5] amines,[6] carboxylic acids,[7] pyridine,[8] *etc.* Some of these intercalation reactions have a redox character.

Also, the reaction of crystalline $VOPO_4 \cdot 2H_2O$ with an ethanolic solution of NaI, which is rapid and spontaneous at room temperature, is a redox process.[9–11]

$$V^VOPO_4 \cdot 2H_2O + x\text{NaI} \xrightarrow{C_2H_5OH} Na_xV^{IV}_xV^V_{1-x}OPO_4 \cdot 2H_2O + x/2I_2$$

The structure of the host layers is preserved during the reaction, but the distance between adjacent $(VOPO_4)_\omega$ layers decreases. The sodium ions which penetrate into the interlayer space among the water molecules modify the arrangement of the water layer and cause its contraction. It was shown that a good reducing agent (I^-, $S_2O_3^{2-}$, SO_2, N_2H_5Cl, etc.) present in the system enables other cations (Li^+, K^+, Rb^+, Cs^+, Mg^{2+}, Mn^{2+}, Co^{2+}, Ni^{2+} and Zn^{2+}) to intercalate into $VOPO_4 \cdot 2H_2O$.[12,13] An isostructural compound, $VOAsO_4 \cdot 2H_2O$, similarly undergoes this type of reaction.[11]

In this paper we present results of a study of intercalation in the modified system $VOPO_4 \cdot 2H_2O$–NaI–acetone. We replaced the ethanol in the system mentioned above by acetone because acetone is not able to form intercalates with $VOPO_4 \cdot 2H_2O$, in contrast to alcohols, and NaI is very soluble in it.

We attempted to identify the intermediate phases formed and to determine their ratio in the solid reaction product and their dependence on reaction time. Some properties of the products were studied.

EXPERIMENTAL

$VOPO_4 \cdot 2H_2O$ was prepared by prolonged boiling of a mixture of V_2O_5 and H_3PO_4 in water.[1]

* Author to whom correspondence should be addressed.

The removal of all the reducing materials from the chemicals used was necessary to eliminate the presence of V^{IV} in the resulting products.

Products of the intercalation reaction described by the formula $Na_xVOPO_4 \cdot yH_3O$ ($0 < x < 1$; $1 < y < 2$) were prepared in sealed glass tubes (*ca* 50 cm^3) by contact of a polycrystalline (size of particles: 0.1–0.2 mm) host (*ca* 0.4 g) with NaI (0.5 M) acetone solution (20 cm^3). Systems were shaken at constant temperature (20, 30 or 40 ± 0.1°C). Acetone was distilled before use and its water content was fixed at 2% (weight).

Dependence of the sodium content in the solid products on reaction time was studied on a series of simultaneous experiments which were interrupted after a definite period of time (from 5 min to 500 h). The solid phase was washed thoroughly with pure acetone immediately after interruption. The sodium content of the solids was determined by amperometric titration of released iodine with thiosulphate and by EDX microanalysis of sodium vanadium and phosphorus content.

The powder data of the solid reaction products were obtained with an X-ray diffractometer HZG-4 (Freiburg Prazision Mechanik, Germany); the methods of measurement and checking have been described in our previous work.[4]

All reaction products and their relative ratios were determined by X-ray phase analysis. Relative contents w_i of solid phases were calculated from the equation:

$$w_i = I_i(002) \Big/ \sum_n I_i(002), \qquad (1)$$

where $I_i(002)$ is the intensity of the diffraction line (002) of the ith phase and n is the number of present phases. The sodium content in phases x_i was calculated by multidimensional linear regression of the equation:

$$x = \sum_n x_i w_i, \qquad (2)$$

where x is the total sodium content in the samples (as a stoichiometric coefficient) determined by the titration and w_i is the relative content of the single phases in the sample.

Magnetic susceptibilities were measured in the range 90–300 K using a variable-temperature Gouy balance (Newport Instruments, England); the molar magnetic susceptibilities were corrected for diamagnetism. Magnetic moments were calculated from the Curie–Weiss equation.

DT and TG analyses were performed using a Derivatograph MOM (Hungary). The measurements were carried out under air between 20 and 900°C at a heating rate of 5°C min^{-1}. The weight of the samples was 100 mg.

An a.c. conductivity of solid products was investigated by means of an impedance meter, Tesla BM 507 (Czechoslovakia), working in the frequency region 100–500 kHz. The real and imaginary parts of impedance were determined for all the samples measured. Complex impedance plots of the samples in all cases showed arc-shaped curves, typical of solid ionic conductors.[14] The simplest equivalent electronic circuit describing curves of this type is a resistance connected in parallel with a constant phase element (CPE). An equation describing the dependence of impedance on frequency was derived for this circuit. Parameters of this equation were estimated from experimental values by the complex non-linear least-squares fittings,[15] and the conductivities of the samples were calculated. Rectangular pellets were prepared from microcrystalline intercalates before impedance measurements. A dry powder sample (0.150 ± 0.006 g) was pressed under pressure (95 kN cm^{-2}) in a rectangular matrix; platelets of intercalate under pressure are preferably orientated with layers of $(VOPO_4)_\infty$ perpendicular to the direction of the pressure. Samples of cuboid shape with the dimensions 7 × 3 × 2 mm were obtained in this way. This cuboid was placed between electrodes so that a.c. conductance was measured along the layers of $(VOPO_4)_\infty$. Better sample–electrode contacts are obtained using electrodes painted with graphite paste.

For the thermopower measurements a cuboid was mounted on the top of two stainless steel blocks with platinum contacts. One of the blocks was heated by a kanthal wire to create a temperature gradient across the sample. The temperature difference was monitored by a nickel/chromium–nickel thermocouple.

RESULTS AND DISCUSSION

X-ray diffraction analyses of all the solid products obtained in the $VOPO_4 \cdot 2H_2O$–NaI–acetone system showed that the samples are composed of three phases; their signature (column 1), lattice parameters (column 2) and line indicates (column 3) are given in Table 1.

It is obvious from phase diffractograms that the phases S3, S2 and S1 have typical layered structures. The periodicity of their structure along a layer is very similar to the periodicity of $VOPO_4 \cdot 2H_2O$, and their parameters, a, therefore, differ very slightly. Parameter c or its fraction decreases in the set $VOPO_4 \cdot 2H_2O$—S3—S2—S1 ($c = 0.7403$, $c/2 = 0.6685$, $c/2 = 0.6531$ and $c/2 = 0.5665$ nm).

Table 1. Composition and X-ray diffraction data of the reaction product

Phase signature	Calculated lattice constants[a] (nm)	Found diffraction lines	Stoichiometric coefficients x and y found for $Na_xVOPO_4 \cdot yH_2O$
S3	$a = 0.6240$ $c = 1.3370$	002, 102, 104 004, 200, 006 201, 202, 106 008	$x = 0.30 \pm 0.06$ $y = 2.0 \pm 0.1$
S2	$a = 0.6284$ $c = 1.3063$	002, 101, 102 004, 200, 201 202, 006, 106 310	$x = 0.50 \pm 0.01$ $y = 2.0 \pm 0.1$
S1	$a =$ — $c = 1.1330$	002, 004, 006	$x = 1.07 \pm 0.17$ $y = 1.00 \pm 0.05$

[a] Lattice constants of the host $VOPO_4 \cdot 2H_2O$: $a = 0.6202$, $2c = 1.4806$.

The need to use double values for parameters c to describe S3, S2 and S1 phase unit cells is probably caused by the tangential shift of $(VOPO_4)_\infty$ during intercalation. The time course of the S3 to the S1 phase formation is given in Fig. 1, where the relative phase ratio (% mol.) in the solid product is plotted against reaction time. The S3 phase is formed first at all temperatures (20, 30 and 40°C) and only this phase is present in the system in such a short period and so it is not possible to observe the kinetics of the S1 phase formation for the NaI concentration used. Therefore, only a decrease in the S3 phase is apparent, which is caused by S2 phase formation. The largest amount of the S2 phase is achieved after *ca* 20 h at 40°C. While at 20°C the first signs of the S1 phase appear after *ca* 270 h, at 40°C the S1 phase begins to form much sooner, even when the S3 phase has not totally disappeared. The reaction solid contains only 10% S1 phase at 20°C after 500 h, while at 40°C it contains 80% after the same amount of time.

Figure 2 shows the dependence of the total

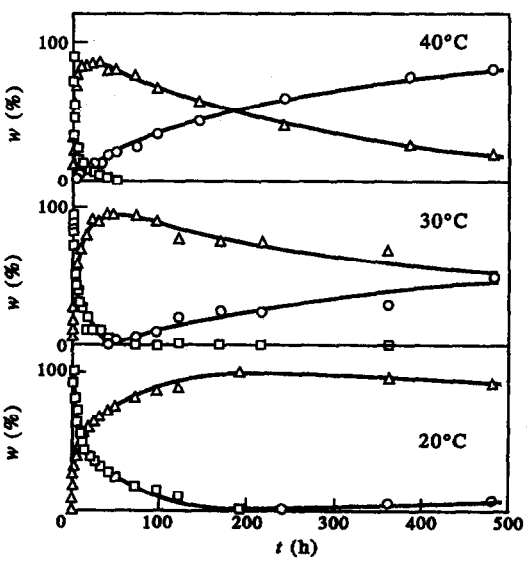

Fig. 1. Dependence of relative content w of the S3 (□), S2 (△) and S1 (○) phases in $Na_xVOPO_4 \cdot yH_2O$ on time t at 20, 30 and 40°C.

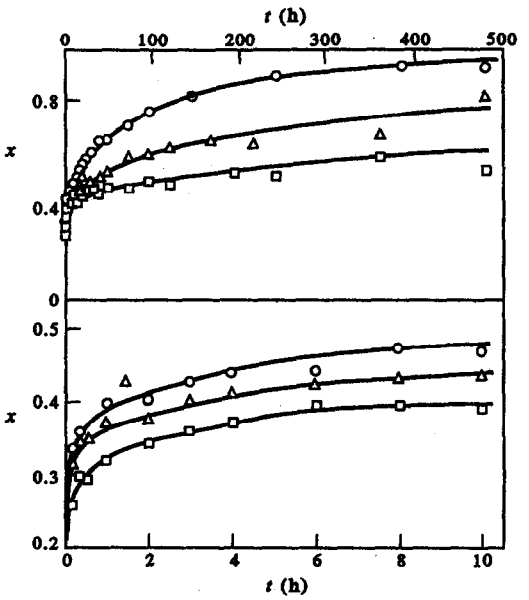

Fig. 2. Dependence of sodium content x in $Na_x VOPO_4 \cdot yH_2O$ on time t (□ 20°C, △ 30°C, ○ 40°C).

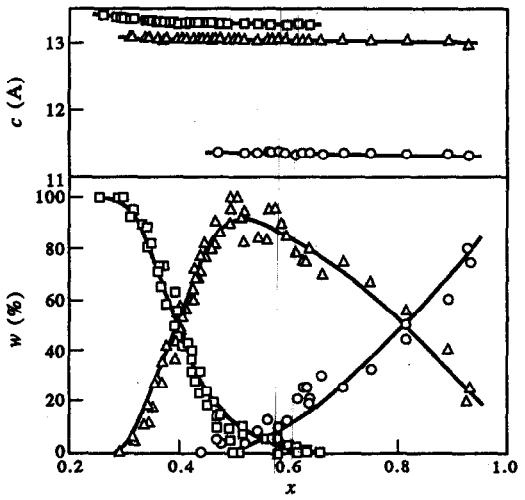

Fig. 3. Dependence of basal spacing c and relative content w of the stages 3 (□), 2 (△) and 1 (○) on sodium content x in $Na_xVOPO_4 \cdot yH_2O$.

sodium content, x, in $Na_xVOPO_4 \cdot yH_2O$ on the reaction time. This dependence is given in the lower part of this figure for three temperatures from 0 to 10 h; the upper part of the figure shows the same dependence from 0 to 500 h. We found no significant effect of light on the reaction rate.

Figure 3 shows the dependence of basal spacing c and relative content w for all three phases on the sodium content, x, in the solid reaction product. Values of x for all phases (Table 1, column 4) were determined by the multidimensional linear regression of the data. Coincident values of a phase composition found from experiments carried out at 20, 30 and 40°C show that temperature has no influence on the phase composition, but only on the rate of phase forming and transforming.

The upper part of Fig. 3 shows the parameters c obtained by X-ray diffraction analysis. A minimal scatter of basal spacings c calculated from 001 and *hkl* lines was found after treatment of X-ray diffractograms. There are no oscillations of diffraction lines connected with the formation of the statistic distribution of the intercalated and unintercalated layers (Hendricks–Teller effect[16]).

All the facts described suggest that the heterogeneous redox reaction of $VOPO_4 \cdot 2H_2O$ with NaI in acetone is an intercalation process. At first sodium ions enter into each third interlayer space among the water molecules. This process is associated with a contraction of the interlayer distance. This S3 phase (stage 3) has been described on the whole set of layered complexes, its basal spacing is in this case lower than in the parent host. The introduction of Na^+ is accompanied by reduction of vanadium in the host layers. Regarding the electroneutrality of the host crystal, the number of reduced vanadium atoms (V^V–V^{IV}) is equal to the number of intercalated sodium ions. When the reaction continues intercalated and non-intercalated water molecule layers are present in a 1 : 1 ratio in phase S2 (stage 2). The process is complete when only the S1 phase (stage 1) is present.

The solid reaction products with different sodium contents were studied by TG and DT analyses. The only process which occurs in the temperature region up to 600°C is the endothermic releasing of water. While $VOPO_4 \cdot 2H_2O$ releases water at 115°C ($VOPO_4 \cdot 2H_2O$ and $VOPO_4 \cdot 1H_2O$) and 150°C (formation of dehydrated $VOPO_4$), samples with the S3 phase predominance release water in two endothermic steps again but at 148 and 205°C. The S2 phase is dehydrated at 185 and 205°C, whilst the S1 phase loses water in one step at 265°C. Figure 4 shows the dependence of the sodium content x in solid products on y values calculated from a decrease of weight by dehydration. Two molecules of water pertain to one atom of phosphorus in the S3 and S2 phases, but in the S1 phase only one water molecule pertains to one atom of phosphorus. Probably the reduction of more than half of the vanadium atoms in the host layers leads to the breakdown of the water interlayer structure and the removal of half of the water molecules.

Results of magnetic susceptibility measurements confirm the presence of V^{IV} atoms in the reaction products. In contrast to diamagnetic $VOPO_4 \cdot 2H_2O$, the reaction products are markedly paramagnetic. Dependencies of reciprocal values of the corrected molar magnetic susceptibility on temperature are linear in the whole region of

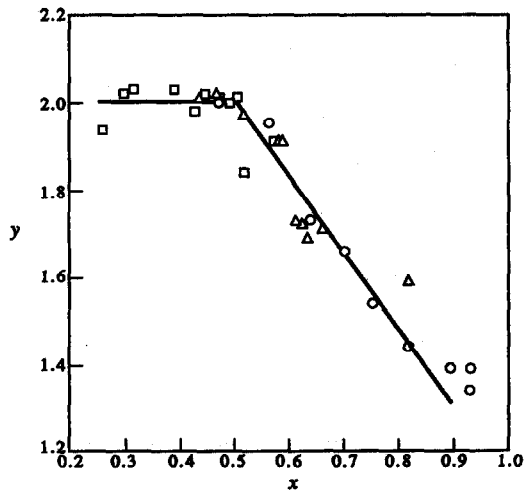

Fig. 4. Dependence of crystal water content y in $Na_xVOPO_4 \cdot yH_2O$ on sodium conent x (□ 20°C, △ 30°C, ○ 40°C).

measurements and there is no evidence of a Néel temperature. The samples with lower sodium content, formed by the S3 and S2 phases, have magnetic moments μ from 1.80 to 1.76 B.M. and Weiss constant θ values which range from -2 to -4 K. This magnetic moment value is in agreement with the pure spin contribution of the d^1 electron of the V^{IV} atom and therefore it is possible to assume the phases are magnetically dilute. The magnetic moments of the samples with high sodium content (high S1 phase content) range from $\mu = 1.7$ to 1.72 B.M. Weiss constant values of $\theta = -6$ to -8 K provide evidence about more significant coupling of paramagnetic V^{IV} centres. Apparently, there is an interaction in the V^{IV}—O—P—O—V^{IV} chain in the $(VOPO_4)_\infty$ layer or across the adjacent layers (V^{IV}—O—H···O—V^{IV}).

Pellets made by pressing the powdered $VOPO_4 \cdot 2H_2O$, with preferential orientation of platelet crystals, present relatively high conductivities ($\sigma_m = 3.10^{-5}$–$4.10^{-5}\ \Omega^{-1}\ cm^{-1}$) in a direction nearly parallel with the $(VOPO_4)_\infty$ layers, whilst pellets of dehydrated $VOPO_4$ show very low conductivity ($\sigma_m < 10^{-7}\ \Omega^{-1}\ cm^{-1}$). Conductivity across the layers in $VOPO_4 \cdot 2H_2O$ is about four-fold lower. Polarity measurements (Seebeck effect) on the same pellets demonstrate the positive charge of the charge carriers in $VOPO_4 \cdot 2H_2O$. Therefore, it is presumed that protons are charge carriers in the $VOPO_4 \cdot 2H_2O$ structure.

It was shown above that intercalation of $VOPO_4 \cdot 2H_2O$ by NaI acetone solution causes the reduction of vanadium, penetration of sodium ions into the water layer and elimination of water with S1 phase formation (as soon as the reaction passes 50%). Each of these changes by itself must cause a decrease in conductivity of the solid reaction product. The basicity of the water molecules coordinating vanadium atoms is increased by the reduction of vanadium, thus proton activity and mobility decrease. Penetration of the Na^+ ions into the host structure must also diminish the proton mobility in the water layers. The elimination of water from an interlayer space must have a similar effect.

These conclusions are in an agreement with the results of the conductivity measurements of the solid reaction products. The conductivity of the solid phase decreases linearly (Fig. 5) with the content of Na^+ ions ($x = 0.25$–0.5). When the S1 phase is formed ($x = 0.5$), conductivity σ_m becomes less dependent on the content of sodium x.

Our results could not explain the mechanism of this intercalation reaction. It is clear only that the electron transfer is not realized in the non-conducting $(VOPO_4)_\infty$ layer. Transport of voluminous iodide ions through the water layer into the solid phase to the vanadium atoms which are reduced also seems to be improbable.

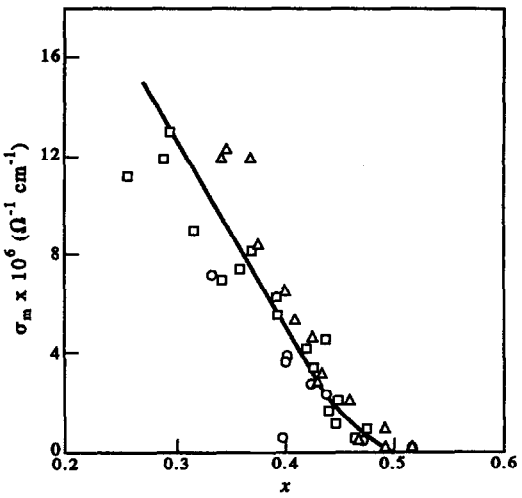

Fig. 5. Dependence of conductivity σ_m of Na_x-$VOPO_4 \cdot yH_2O$ pellets on sodium content x (□ 20°C, △ 30°C, ○ 40°C).

REFERENCES

1. G. Ladwig, *Z. Anorg. Allg. Chem.* 1965, **338**, 266.
2. H. R. Tietze, *Aust. J. Chem.* 1981, **34**, 2035.
3. M. Tachez, F. Theobald, J. Bernard and A. W. Hewat, *Rev. Chim. Miner.* 1982, **19**, 291.
4. L. Beneš, J. Votinský, J. Kalousová and J. Klikorka, *Inorg. Chim. Acta* 1986, **114**, 47.
5. J. Votinský, L. Beneš, J. Kalousová and J. Klikorka, *Inorg. Chim. Acta* 1987, **126**, 19.
6. L. Beneš, R. Hyklová, J. Kalousová and J. Votinský, *Inorg. Chim. Acta* 1990, **177**, 71.
7. L. Beneš, J. Votinský, J. Kalousová and K. Handlíř, *Inorg. Chim. Acta* 1990, **176**, 255.
8. J. W. Johnson, A. J. Jacobson, J. F. Brody and S. M. Rich, *Inorg. Chem.* 1982, **21**, 3820.
9. J. W. Johnson and A. J. Jacobson, *Angew. Chem., Int. Edn Engl.* 1983, **22**, 412.
10. J. W. Johnson and A. J. Jacobson, *Angew. Chem.* 1983, **95**, 422.
11. A. J. Jacobson, J. W. Johnson, J. F. Brody, J. C. Scanlon and J. T. Lewandowski, *Inorg. Chem.* 1985, **24**, 1782.
12. V. A. Zazhigalow, A. I. Pyatnitskaya, I. V. Bachevikova, G. A. Komashko, G. Ladwig and V. M. Belousov, *React. Kinet. Catal. Lett.* 1983, **23**, 119.
13. N. Casan-Pastor, D. Beltran-Porter and E. Martinez-Tamayo, *Neuv. J. Etude Equil. Phases* 1983, 77.
14. J. R. MacDonald and W. B. Johnson, in *Impedance Spectroscopy* (Edited by J. R. MacDonald), p. 17. John Wiley & Sons, New York (1987).
15. See ref. 14, p. 180.
16. S. Hendricks and E. Teller, *J. Chem. Phys.* 1942, **10**, 147.

Polyhedron Vol. 12, No. 2, pp. 187–193, 1993
Printed in Great Britain.

0277–5387/93 $6.00+.00
© 1993 Pergamon Press Ltd

TECHNETIUM COMPLEXES WITH THIOETHER LIGANDS—II. SYNTHESIS AND STRUCTURAL CHARACTERIZATION OF NEUTRAL OXOTECHNETIUM(V) COMPLEXES WITH DITHIOETHERS. X-RAY STRUCTURE ANALYSIS OF μ-OXO-BIS(5,8-DITHIADODECANE)DICHLOROOXOTECHNETIUM(V) AND (8-HYDROXY-3,6-DITHIAOCTAN-1-OLATO)DICHLOROOXOTECHNETIUM(V)

HANS-JUERGEN PIETZSCH and HARTMUT SPIES*

Forschungszentrum Rossendorf e.V., Institut für Bioanorganische und Radiopharmazeutische Chemie, D-8051 Dresden, PF 19, Germany

and

PETER LEIBNITZ and GUENTER RECK

Bundesanstalt für Materialforschung, D-1199 Berlin, Germany

and

JOERG BEGER and RENATE JACOBI

Bergakademie Freiberg, D-9200 Freiberg, Germany

(*Received* 31 *July* 1992; *accepted* 29 *September* 1992)

Abstract—Neutral, bidentate thioethers such as 5,8-dithiadodecane, 3,6-dithiaoctane ("S_2") as well as the dithia-diole 1,8-dihydroxy-3,6-dithiaoctane ["$S_2(OH)_2$"] react with tetrachlorooxotechnetate ($TcOCl_4^-$) in acetone to give binuclear oxo species of the type [TcO("S_2")Cl_2]$_2$O with dithiaalkanes and [TcO("$S_2O(OH)$")Cl_2] with the dithia-diole, respectively. The complexes have been characterized by elemental analysis and spectroscopic methods. The crystal structures of [TcO(5,8-dithiadodecane)Cl_2]$_2$O (**1**) and [TcO(8-hydroxy-3,6-dithiaoctan-1-olato)Cl_2] (**3**) were determined from X-ray data: **1** consists of two independent [TcO("S_2")Cl_2] units bridged by an oxygen atom. Each technetium atom is centred in a distorted octahedron with the equatorial plane formed by the S_2Cl_2 donor set. The sulphur and chlorine atoms of the units are in the *anti* position with respect to the bridging oxygen. The structural analysis of **3** shows that the metal has distorted octahedral coordination, with the equatorial plane formed by the sulphur and chlorine atoms. Furthermore, one terminal oxygen is coordinated in the *trans* position to the $Tc{=}O^{3+}$ core, while the second hydroxy group is non-coordinated.

The well-known coordination chemistry of thioethers with transition metals such as ruthenium, platinum and palladium[1–3] implies that a variety of thioether complexes of technetium with the metal in various oxidation states may also be anticipated. The first fully characterized technetium complex in which thioether groups are involved in the coordination sphere, the cationic *trans*-dioxotechnetium(V) complex $[TcO_2(S_2N_2)]^+$ (S_2N_2: 1,4-dithia-8,11-diazacyclotetradecane), has been described by Ianoz *et al.* in 1989.[4,5] More recently we found that cationic technetium(III) complexes containing neutral tetradentate thioethers and monothioles as co-ligands are formed when an appro-

* Author to whom correspondence should be addressed.

priate technetium precursor is reduced by stannous chloride in the presence of both a tetrathiaalkane and a mono-thiole.[6]

As earlier observed,[7] the reaction of pertechnetate with two equivalents of stannous chloride in the presence of e.g. R—S—CH_2CH_2—S—R ("S_2", R = alkyl) in acetone or acetic acid delivers yellow–green coloured products. These species are reactive in ligand exchange reactions with e.g. 2,3-dimercaptosuccinic acid dimethylester, resulting in the formation of the known bis(dithiolato)oxotechnetate(V) complexes.[8] Therefore, we assume our new species to be in the oxidation state +V. This prompted us to attempt the isolation and characterization of definite technetium(V) complexes with dithiaalkanes and related compounds. Experiments for the preparation of technetium(V) complexes with the neutral dithiaalkanes 5,8-dithiadodecane and 3,6-dithiaoctane ("S_2") as well as with 1,8-dihydroxy-3,6-dithiaoctane ["$S_2(OH)_2$"], which will be described in this paper, were successful with tetrachlorooxotechnetate(V) as a precursor, but failed when the less reactive technetium(V) was used. The resulting compounds, μ-oxo-bis-[(5,8-dithia-dodecane)dichlorooxotechnetium(V)], [TcO("S_2")Cl_2]$_2$O, and [8-hydroxy-3,6-dithiaoctan-1-olato-(O,S,S)]dichlorooxotechnetium(V), [TcO("$S_2O(OH)$")Cl_2], were characterized by single-crystal X-ray structural analysis.

EXPERIMENTAL

UV–vis spectra were recorded on a Specord M 40 spectrometer from Carl–Zeiss Jena (solvent acetone). IR spectra were measured on KBr discs on a Specord M 80 spectrometer from Carl–Zeiss Jena. The content of technetium was determined by liquid-scintillation counting.

Abbreviations

"S_2" = 3,6-dithiaoctane and 5,8-dithiadodecane, "$S_2(OH)_2$" = 1,8-dihydroxy-3,6-dithiaoctane.

Synthesis of μ-oxo-bis[(5,8-dithiadodecane)dichlorooxotechnetium(V)] (1)

5,8-Dithiadodecane (42 mg, 200 μmol) dissolved in acetone (1 cm^3) was added to NBu_4TcOCl_4 (50 mg, 100 μmol) dissolved in acetone (1 cm^3). After addition of methanol (2 cm^3) the mixture was stirred for 1 h. Slow evaporation of the reaction mixture overnight to a volume of 1 cm^3 yielded yellow–green crystals suitable for X-ray analysis. Yield: 18 mg (45% relative to NBu_4TcOCl_4); m.p. 174–175°C. Found: C, 30.2; H, 5.4; S, 15.9; Cl, 17.5; Tc, 25.1. Calc. for $C_{20}H_{44}Cl_4O_3S_4Tc_2$: C, 30.0; H, 5.5; S, 16.0; Cl, 17.7; Tc, 24.8%. IR (KBr): 2880–3080 cm^{-1}, aliphatic CH; 920 cm^{-1}, Tc=O. UV–vis (acetone) [λ_{max} (log ε)]: 400 nm (3.9).

μ-Oxo-bis[(3,6-dithiaoctane)dichlorooxotechnetium(V)] (2)

This compound was prepared with 3,6-dithiaoctane (30 mg) following the procedure described above. Yield: 14 mg (40% relative to NBu_4TcOCl_4); m.p. 193–194°C. Found: C, 21.1; H, 4.3; S, 18.4; Cl, 20.2; Tc, 29.1. Calc. for $C_{12}H_{28}Cl_4O_3S_4Tc_2$: C, 20.9; H, 4.1; S, 18.6; Cl, 20.6; Tc, 28.8%. IR (KBr): 2880–3080 cm^{-1}, aliphatic CH; 920 cm^{-1}, Tc=O. UV–vis (acetone) [λ_{max} (log ε)]: 400 nm (3.8).

Synthesis of (8-hydroxy-3,6-dithiaoctan-1-olato-(O,S,S))dichlorooxotechnetium(V) (3)

1,8-Dihydroxy-3,6-dithiaoctane (36 mg, 200 μmol) dissolved in acetone (1 cm^3) was added to NBu_4TcOCl_4 (50 mg, 100 μmol) dissolved in acetone (1 cm^3). After the addition of methanol (2 cm^3) the colour changed to green and the mixture was stirred for 30 min. Standing of the reaction mixture in the refrigerator overnight yielded green crystals suitable for X-ray analysis. Yield: 22 mg (60% relative to NBu_4TcOCl_4); m.p. 148–149°C. Found: C, 19.5; H, 3.3; S, 17.6; Cl, 18.7; Tc, 27.2. Calc. for $C_6H_{13}Cl_2O_3S_2Tc$: C, 19.6; H, 3.5; S, 17.4; Cl, 19.3; Tc, 27.0%. IR (KBr): 2880–3080 cm^{-1}, aliphatic CH; 920 cm^{-1}, Tc=O. UV–vis (acetone) [λ_{max} (log ε)]: 405 nm (3.8).

Structure determination and crystal data

The X-ray data of both complexes were collected at room temperature (296 K) on an Enraf–Nonius CAD 4 diffractometer, using graphite monochromatized Mo-K_α radiation (λ = 0.71073 Å). A summary of the crystallographic data is given in Table 1. The positions of the non-hydrogen atoms were determined by the heavy-atom technique. After anisotropic refinement of the positions of these, the hydrogen positions were calculated according to ideal geometries. Empirical absorption corrections with the program DIFABS[9] were made at two stages during the structure refinement. Most of the calculations were carried out in the Enraf–Nonius SDP system with some local modifications. Relevant bond lengths and angles are contained in Tables 2 and 3. Difficulties in the structure refinement of both complexes arose from a partial

Table 1. Experimental crystallographic data for [TcO(5,8-dithiadodecane)$_2$Cl$_2$]$_2$O and [TcO{7-hydroxy-3,6-dithiaoctan-1-olato-(O,S,S)}Cl$_2$]

Crystal data		
Molecular formula	$C_6H_{13}S_2O_3Cl_2Tc$	$C_{20}H_{44}S_4Cl_4O_3Tc_2$
Molecular weight	367.313	800.46
a (Å)	8.086(3)	16.474(7)
b (Å)	11.189(9)	17.044(6)
c (Å)	27.426(4)	23.756(9)
α (°)	90.01(3)	89.96(3)
β (°)	90.05(2)	89.75(5)
γ (°)	90.11(7)	90.00(4)
V (Å^3)	2481.6	6670.3
Space group; No.	*Pbca*; 61	*Pbca*; 61
Z; $F(000)$; d_{calc}	8; 1456; 1.9661	8; 3248; 1.594
T (K)	296	296
Data collection		
Crystal size (mm^3)	0.05 × 0.58 × 0.98	0.05 × 0.25 × 0.6
Mo-K_α (Å)	0.71073	0.71073
μ (cm^{-1})	18.705	13.80
Data sphere (°)	$3 < 2\theta < 50$	$3 < 2\theta < 40$
Scan mode	ω–2θ	ω–2θ
Scan rate (° min^{-1})	Variable 1.2–4.8	Variable 1.1–4.8
Miller index range	h 0–9 k 0–13 l 0–32	h 0–15 k 0–16 l 0–22
Unique reflections measured	2534	3472
Unique reflections used [$I0 > 3\sigma(I)$]	1472	1760
Check reflections	5 1 8 4 2 8 7 4 6	5 1 8 4 2 8 7 4 6
Intensity variations	< 1.42 relative	< 3.82 relative
Absorption corrections	Yes	Yes
$R = \Sigma[F_o - F_c]/\Sigma F_o$	0.069	0.078

structural disorder caused by strong thermal motion of some substituents and by a flip-flop mechanism in the ring Tc(2), S(4), C(3), C(4), S(3) in [TcO("S_2")Cl$_2$]$_2$ and Tc, S(1), C(3), C(4), S(2) in [TcO("S_2O(OH)")Cl$_2$], respectively. This explains the very high temperature factors of some atoms and the relatively high R values. Atomic positional and thermal parameters, full lists of bond lengths and angles and F_o/F_c values have been deposited as supplementary material.

Health precautions

In view of the radioactivity of ^{99}Tc some health precautions were taken. All operations were carried out in a fume cupboard with gloves. ^{99}Tc is only a weak β^--emitter so that apart from some elementary precautions no further safety measures are required. Normal glassware gives adequate protection against the weak β^--emission. Bremsstrahlung becomes important if ^{99}Tc is handled on a larger scale.

RESULTS AND DISCUSSION

Preparation of new definite technetium(V) complexes were successful with tetrachlorooxotechnetate(V) as a precursor, but not with the less reactive technetium(V) gluconate. Dithialkanes as well as the potentially tetradentate 1,8-dihydroxydithiaoctane react with $TcOCl_4^-$ under the partial exchange of chloride ligands by sulphur atoms of dithia ligands. 3,6-Dithiaoctane (R = C_2H_5) and 5,8-dithiadodecane (R = C_4H_9) deliver in acetone/methanol analytically pure yellow–green oxo complexes of the type [TcO("S_2")Cl$_2$]$_2$O, which

Table 2. Bond lengths (Å) and angles (°) for $[TcO(5,8\text{-dithiadodecane})_2Cl_2]_2O$

Tc(1)—Cl(1)	2.396(2)	Tc(2)—O(3)	1.899(3)
Tc(1)—Cl(2)	2.418(2)	S(1)—C(2)	1.785(8)
Tc(1)—S(1)	2.464(2)	S(1)—C(5)	1.843(6)
Tc(1)—S(2)	2.425(2)	S(2)—C(1)	1.880(8)
Tc(1)—O(1)	1.665(4)	S(2)—C(9)	1.805(9)
Tc(1)—O(3)	1.898(3)	S(3)—C(4)	1.928(10)
Tc(2)—Cl(3)	2.400(2)	S(3)—C(13)	1.842(7)
Tc(2)—Cl(4)	2.395(2)	S(4)—C(3)	1.732(13)
Tc(2)—S(3)	2.433(2)	S(4)—C(17)	1.823(9)
Tc(2)—S(4)	2.445(2)	C(1)—C(2)	1.486(11)
Tc(2)—O(2)	1.674(4)	C(3)—C(4)	1.416(15)
Cl(1)—Tc(1)—Cl(2)	91.03(7)	Cl(3)—Tc(2)—Cl(4)	90.69(8)
Cl(1)—Tc(1)—S(1)	90.28(7)	Cl(3)—Tc(2)—S(3)	92.10(8)
Cl(1)—Tc(1)—S(2)	173.40(7)	Cl(3)—Tc(2)—S(4)	173.65(6)
Cl(1)—Tc(1)—O(1)	98.0(2)	Cl(3)—Tc(2)—O(2)	98.4(2)
Cl(1)—Tc(1)—O(3)	92.4(1)	Cl(3)—Tc(2)—O(3)	91.2(1)
Cl(2)—Tc(1)—S(1)	173.70(6)	Cl(4)—Tc(2)—S(3)	174.03(7)
Cl(2)—Tc(1)—S(2)	93.43(7)	Cl(4)—Tc(2)—S(4)	89.99(8)
Cl(2)—Tc(1)—O(1)	97.1(2)	Cl(4)—Tc(2)—O(2)	98.7(2)
Cl(2)—Tc(1)—O(3)	91.6(1)	Cl(4)—Tc(2)—O(3)	92.9(1)
S(1)—Tc(1)—S(2)	84.78(7)	S(3)—Tc(2)—S(4)	86.66(8)
S(1)—Tc(1)—O(1)	88.8(2)	S(3)—Tc(2)—O(2)	86.1(2)
S(1)—Tc(1)—O(3)	91.6(1)	S(3)—Tc(2)—O(3)	81.8(1)
S(2)—Tc(1)—O(1)	86.3(2)	S(4)—Tc(2)—O(2)	87.8(2)
S(2)—Tc(1)—O(3)	82.6(1)	S(4)—Tc(2)—O(3)	82.5(1)
O(1)—Tc(1)—O(3)	166.3(2)	O(2)—Tc(2)—O(3)	164.9(2)

Table 3. Bond lengths (Å) and angles (°) for [TcO{8-hydroxy-3,6-dithiaoctan-1-olato-(O,S,S)}Cl_2]

Tc—Cl(1)	2.461(1)	S(2)—C(4)	1.845(8)
Tc—Cl(2)	2.408(1)	S(2)—C(5)	1.814(7)
Tc—S(1)	2.446(2)	O(2)—C(2)	1.399(8)
Tc—S(2)	2.439(2)	O(3)—C(6)	1.389(0)
Tc—O(1)	1.680(4)	O(3)′—C(6)	1.286(0)
Tc—O(2)	1.895(4)	C(1)—C(2)	1.543(11)
S(1)—C(1)	1.799(8)	C(3)—C(4)	1.405(11)
S(1)—C(3)	1.854(8)	C(5)—C(6)	1.517(8)
Cl(1)—Tc—Cl(2)	92.03(6)	Tc—S(1)—C(1)	97.8(3)
Cl(1)—Tc—S(1)	89.40(6)	Tc—S(1)—C(3)	102.1(2)
Cl(1)—Tc—S(2)	173.72(6)	C(1)—S(1)—C(3)	102.9(4)
Cl(1)—Tc—O(1)	93.7(2)	Tc—S(2)—C(4)	98.4(3)
Cl(1)—Tc—O(2)	92.2(2)	Tc—S(2)—C(5)	106.0(2)
Cl(2)—Tc—S(1)	169.40(6)	C(4)—S(2)—C(5)	101.6(4)
Cl(2)—Tc—S(2)	93.60(5)	Tc—O(2)—C(2)	130.7(4)
Cl(2)—Tc—O(1)	104.4(2)	S(1)—C(1)—C(2)	107.2(5)
Cl(2)—Tc—O(2)	90.8(1)	O(2)—C(2)—C(1)	107.8(6)
S(1)—Tc—S(2)	84.56(6)	S(1)—C(3)—C(4)	113.0(5)
S(1)—Tc—O(1)	86.0(2)	S(2)—C(4)—C(3)	110.2(6)
S(1)—Tc—O(2)	78.7(1)	S(2)—C(5)—C(6)	114.8(4)
S(2)—Tc—O(1)	87.6(2)	C(5)—C(6)—O(3)	100.1(4)
S(2)—Tc—O(2)	84.9(2)	C(5)—C(6)—O(3)′	127.0(4)
O(1)—Tc—O(2)	163.5(2)	O(3)—C(6)—O(3)′	122.58(0)

precipitate from the reaction mixtures. In a similar manner 1,8-dihydroxy-3,6-dithiaoctane (R = CH_2CH_2—OH) reacts to give dark green crystals of [TcO("$S_2O(OH)$")Cl_2].

$$TcOCl_4^- \xrightarrow[\text{acetone/methanol}]{\text{"}S_2\text{"}} [TcO(\text{"}S_2\text{"})Cl_2]_2O$$

1: "S_2" = $C_4H_9SCH_2CH_2SC_4H_9$
2: "S_2" = $C_2H_5SCH_2CH_2SC_2H_5$

$$TcOCl_4^- \xrightarrow[\text{acetone/methanol}]{\text{"}S_2(OH)_2\text{"}} [TcO(\text{"}S_2O(OH)\text{"})Cl_2]$$

3: "$S_2(OH)_2$" =
HO—$CH_2CH_2SCH_2CH_2SCH_2CH_2$—OH

The neutral complexes are stable in air and, except for acetone and acetonitrile, insoluble in the common organic solvents. Elemental analyses are consistent with the proposed formulations.

In the IR spectra strong absorptions at 920 cm^{-1}, as well for **1**, **2** and **3**, indicate the Tc=O^{3+} core; ν(Tc—Cl) is not assigned owing to the absorption of other vibrations in the region 300–250 cm^{-1}.

In order to obtain an unambiguous structural assignment the structures of the complexes **1** and **3** were determined by X-ray structure analyses. Suitable crystals were obtained from acetone/methanol.

Drawings of **1** are shown in Figs 1 and 2 and of **3** in Fig. 3. Selected bond angles and distances are listed in Tables 2 and 3 and as supplementary material. In both complexes flip-flop mechanisms in the rings Tc(2), S(4), C(3), C(4), S(3) (complex **1**) and Tc, S(1), C(3), C(4), S(2) (complex **3**), respectively, are observed. This leads to a smearing of electron density of the C(4) atoms of both molecules.

The crystal structure of **1** consists of two independent TcO("S_2")Cl_2 units bridged by an oxygen atom. The characteristic feature is the presence of the O=Tc—O—Tc=O group. In this respect the structure of **1** is comparable to those of [TcO(salpd)]$_2$O [salpd = N,N′-propane-1,3-diylbis (salicylideneiminate)][10] and [TcO(N_2S_2)]$_2$O [N_2S_2 = N,N′-ethylene-bis(thioacetylacetoneiminate)].[11] The technetium atoms are centred in a flattened octahedron with the equatorial plane formed by the S_2Cl_2 donor set, in which the technetium atoms Tc(1) and Tc(2) are 0.12 Å out-of-plane towards O(1) and O(2), respectively. The S_2Cl_2 planes are almost parallel with a small deviation of 0.013 Å; the dihedral angle is 2.6°. The sulphur and chlorine donor atoms of the units are in the *anti* position with respect to the bridging oxygen.

The bond lengths of the Tc=O cores with 1.665 and 1.674 Å, respectively, are in the range generally found for those units (1.61–1.75 Å), but they are in between those in the octahedral O=Tc=O compounds and in square-pyramidal Tc=O complexes. This corresponds to the relatively low value of Tc=O absorption in the IR spectrum. The bridging Tc—O distances (Tc(1)—O(3) 1.898 and Tc(2)—O(3) 1.899 Å) are intermediate between the average Tc=O length and the average Tc—O bond

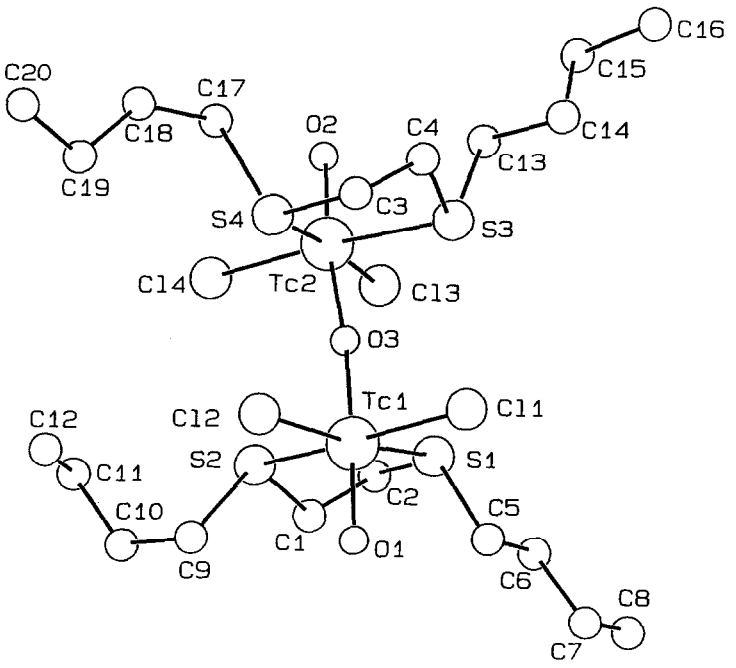

Fig. 1. CELLGRAF drawing of [TcO(5,8-dithiadodecane)$_2Cl_2$]$_2$O.

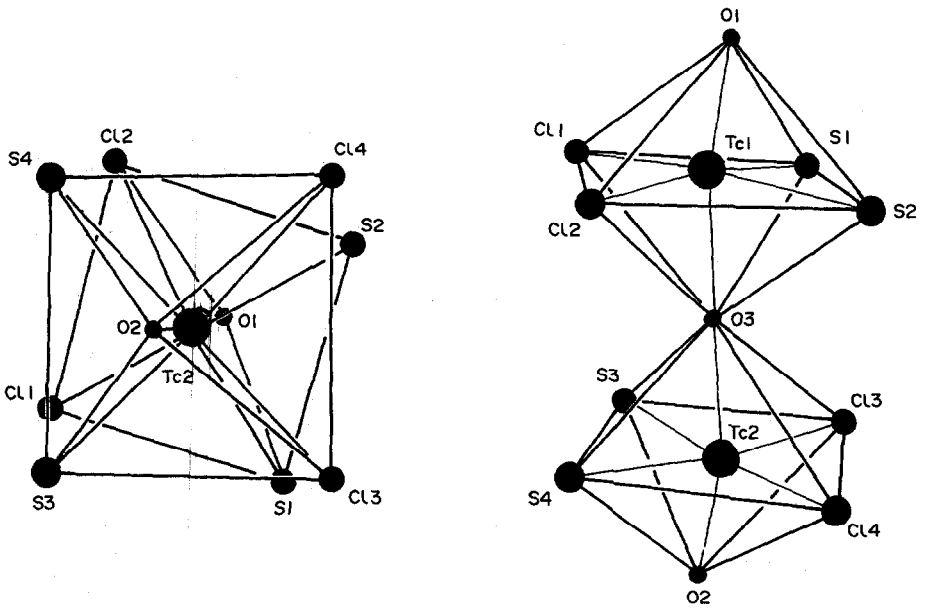

Fig. 2. Molecular geometry of $[TcO(5,8\text{-dithiadodecane})_2Cl_2]_2O$ viewed (a) perpendicular and (b) parallel to the O_1, Tc_1, O_3, Tc_2, O_2 axis.

distance, which are observed in the range 1.98–2.09 Å.[12–14]

As illustrated in Fig. 3, complex **3** consists of discrete monomolecular units containing the O= Tc—O— core. In general, the structure strongly resembles that of the complex derived from dithiaoctane. However, while in the dinuclear species the *trans* position is occupied by a bridging oxygen which may come from traces of water present in the reaction mixture, the *trans* position in complex **3** is occupied by an oxygen of one of the terminal hydroxy groups. The second hydroxy group remains "free". The CELLGRAF[15] drawing in Fig. 3 shows the two possible positions for the non-coordinated hydroxy group caused by a rotation disorder about the bond C(5), C(6). The sulphur atoms of the dithioether and the two chlorine atoms which remain at the metal due to the incomplete exchange at the tetrachlorooxotechnetium ion form a *cis* arrangement in the equatorial plane.

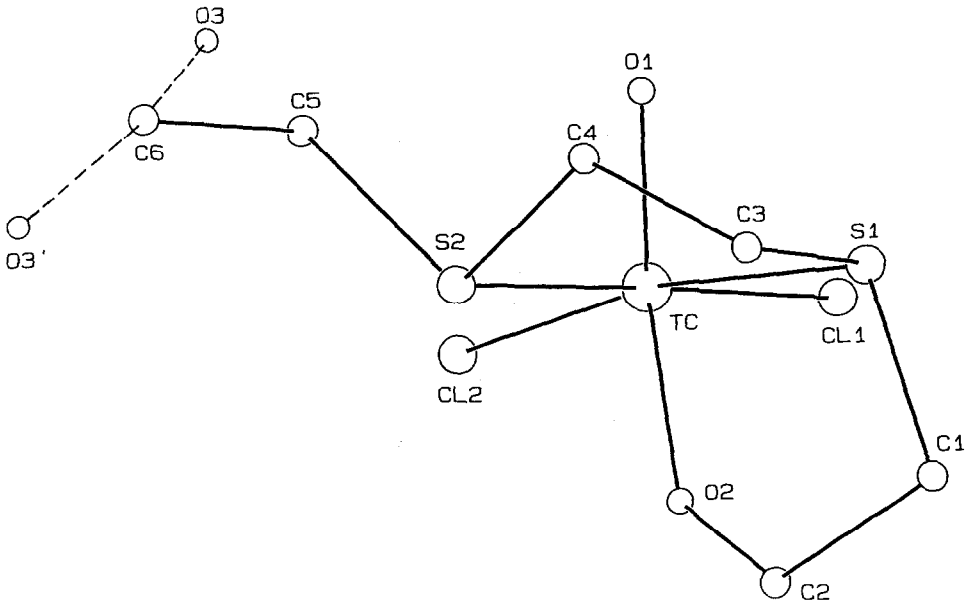

Fig. 3. CELLGRAF drawing of $[TcO\{8\text{-hydroxy-}3,6\text{-dithiaoctan-}1\text{-olato-}(O,S,S)\}Cl_2]$.

Compounds with single-bonded oxygen *trans* to the Tc=O core are scarcely described. The length of the Tc—O bond (1.912 Å) is comparable to that found in other *trans*-O=Tc—O^- groups.[15-18]

Special interest should be devoted to this new class of technetium complexes as many subsequent reactions may be anticipated to occur. In ligand exchange reactions diversity is given by various leaving groups in the coordination sphere. For complex **3** additional reactivity may be caused by the non-coordinated hydroxy group at the side chain. Therefore, new radiopharmacologically relevant compounds may be rendered accessible. Studies on the reactivity of the described complexes will follow.

Additional material concerning this paper can be ordered from Fachinformationszentrum Energie, Physik, Mathematik GmbH, D-W-7514 Eggenstein-Leopoldshafen 2, Germany, quoting CSD No. 55698 ([TcO("S_2")Cl_2]$_2$O, [TcO("S_2O_2")Cl_2]), authors' names as well as the title of the paper.

Acknowledgements—This work was supported by a grant from the Fond der Chemischen Industrie. The authors thank Prof. E. Hoyer (Universität Leipzig) for the ligand 1,8-dihydroxy-3,6-dithiaoctane.

REFERENCES

1. S. G. Murray and F. R. Hartley, *Chem. Rev.* 1981, **81**, 365.
2. S. R. Cooper and S. C. Rawle, *Struct. Bonding* 1990, **72**, 1.
3. C. G. Kuehn and S. S. Isied, *Prog. Inorg. Chem.* 1980, **27**, 153.
4. S. Truffer, E. Ianoz, P. Lerch and M. Kosinski, *Inorg. Chim. Acta* 1988, **149**, 217.
5. E. Ianoz, D. Mantegazzi, P. Lerch, F. Nicolo and G. Chapius, *Inorg. Chim. Acta* 1989, **156**, 235.
6. H. J. Pietzsch, H. Spies, P. Leibnitz, G. Reck, J. Beger and R. Jacobi, *Polyhedron* 1992, **11**, 1623.
7. H. J. Pietzsch and H. Spies, internal report, Rossendorf (1990).
8. H. Spies and H. Scheller, *Inorg. Chim. Acta* 1986, **116**, 1.
9. N. Walker and D. Stuart, *Acta Cryst.* 1983, **A39**, 158.
10. G. Bandoli, M. Nicolini, U. Mazzi and F. Refosco, *J. Chem. Soc., Dalton Trans.* 1984, 2505.
11. F. Tisato, F. Refosco and U. Mazzi, *J. Chem. Soc., Dalton Trans.* 1991, 1301.
12. G. Bandoli, U. Mazzi, E. Roncari and E. Deutsch, *Coord. Chem. Rev.* 1982, **44**, 191.
13. M. Melnik and J. E. Van Lier, *Coord. Chem. Rev.* 1987, **77**, 27.
14. U. Mazzi, *Polyhedron* 1989, **8**, 1683.
15. G. Reck and R. G. Kretschmer, CELLGRAF, a Program for Representation of Organic and Inorganic Crystal Structures. Analytical Centre, Berlin (1989/1991).
16. K. J. Franklin, H. E. Howard-Lock and C. J. L. Lock, *Inorg. Chem.* 1982, **21**, 1941.
17. S. Jurisson, L. F. Lindoy, K. P. Dancey, M. McPartlin, P. A. Tasker, D. K. Uppal and E. Deutsch, *Inorg. Chem.* 1984, **23**, 227.
18. P. H. Fackler, M. E. Kastner and M. J. Clarke, *Inorg. Chem.* 1984, **23**, 3968.

Polyhedron Vol. 12, No. 2, pp. 195–201, 1993
Printed in Great Britain

0277–5387/93 $6.00+.00
© 1993 Pergamon Press Ltd

MONONUCLEAR CHIRAL RUTHENIUM(II) SCHIFF BASE COMPLEXES; SYNTHESIS, PHYSICOCHEMICAL STUDIES AND REACTIVITY WITH π-ACCEPTOR LIGANDS

R. I. KURESHY† and N. H. KHAN

Discipline of Coordination Chemistry and Homogeneous Catalysis,
Central Salt and Marine Chemicals Research Institute, Bhavnagar 364 002, India

(*Received* 20 *August* 1992; *accepted* 11 *September* 1992)

Abstract—Some ruthenium(II) chiral Schiff base complexes of the composition $[RuL(PPh_3)(H_2O)_2]$ (**1–3**), where L = chiral Schiff bases derived from salicylaldehyde and L-amino acids, namely L-phenylalanine, L-tyrosine and L-methionine, have been synthesized. The interaction of the complexes with π-acceptor ligands such as 2,2′-bipyridyl and 1,10-phenanthroline gives substituted mixed-ligand complexes. The characterization of the complexes was accomplished by microanalysis, IR, UV–vis, ^1H, $^{13}C[^1H]$ and $^{31}P[^1H]$ NMR spectroscopy, conductance measurements, electrochemical studies, optical rotation and circular dichroism spectra. The conformational aspects regarding the asymmetric arrangement of substituents at the amino acid moiety of the Schiff bases, as well as the effect of the π-acceptor ligand around the ruthenium(II) metal ion, have been discussed. The complexes show irreversible behaviour and the redox potentials of the Ru^{II}/Ru^{I} couples are less negative in **4–9** than those of the parent chiral Schiff base complexes.

The use of classical transition metal complexes containing nitrogen and oxygen donor ligands as effective and sometimes stereospecific catalysts for oxidation,[1,2] reduction,[3] hydrolysis[4,5] and other transformations of organic compounds[6] is a challenging area of both organic and inorganic chemistry. One of many possible avenues of exploration in this field is the design and synthesis of transition metal complexes bearing additional functional side groups incapable of interaction with the central metal ion but capable of non-covalent interaction with an organic substrate.[6]

The structural studies of metal chelates of amino acids and aminopolycarboxylic acids show examples where the carboxyl function plays a variety of roles. In addition to free and metal bonded carboxylic groups (and metal chelates) free mono-, bi- and tridentate carboxylato groups are known in metal chelate compounds.[7–9] Amino acids themselves play an important role in the function performed by haeme proteins, either by controlling the size of the cavity available to the substrate molecule when it binds to the haeme or by modifying the local dielectric constant or polar character of this cavity.[10]

In continuation of our previous work[11,12] we describe here the synthesis of novel, neutral, chiral ruthenium(II) Schiff base complexes derived from salicylaldehyde, L-phenylalanine, L-tyrosine and L-methionine and substitution of these complexes with π-acceptor ligands such as 2,2′-bipyridyl and 1,10-phenanthroline. A variety of physicochemical methods including IR, ^1H, $^{13}C[^1H]$, $^{31}P[^1H]$, electronic and circular dichroism spectroscopy, optical rotation and electrochemistry have been used to study the extent of the π-back bonding from the ruthenium(II) metal ion to the unsaturated ligands. Here we are concerned that such an interaction may be partly responsible for the currently inexplicable differences in intensity between LMCT absorptions, CD patterns and electrochemical behaviour.

RESULTS AND DISCUSSION

The stoichiometric composition of all the mononuclear ruthenium(II) complexes **1–9** is consistent with the microanalysis of the complexes (Table 1). Millimolar solutions of the complexes in methanol

† Author to whom correspondence should be addressed.

Table 1. Elemental analyses, molar conductance, absolute configuration and optical rotation of chiral ruthenium(II) Schiff base complexes

S. No.	Complexes	Analysis (%)[a] C	H	N	Molar conductance (M) (Ω^{-1} cm^2 mol^{-1})	Absolute configuration	$[\alpha]_D$ ° cm^{-2} g^{-1} (MeOH)
1.	Sal(L-methtriphenylphosphino-diaquoruthenate(II))	56.5 (56.8)	4.9 (5.1)	2.0 (2.2)	06	*S*	+71.71
2.	Sal(L-tyrtriphenylphosphino-diaquoruthenate(II))	62.1 (62.8)	4.2 (4.9)	2.0 (2.1)	08	*R*	−72.40
3.	Sal(L-phealatriphenylphosphino-diaquoruthenate(II))	64.2 (64.7)	4.2 (4.5)	2.1 (2.2)	05	*R*	−63.23
4.	Sal(L-methtriphenylphosphino-2,2-dipyruthenate(II))	62.0 (62.3)	4.0 (4.7)	5.1 (5.4)	04	*S*	+66.23
5.	Sal(L-methtriphenylphosphino-1,10-phenruthenate(II))	63.1 (63.5)	4.2 (4.6)	5.0 (5.3)	06	*S*	+87.33
6.	Sal(L-tyrtriphenylphosphino-2,2-dipyruthenate(II))	66.3 (66.8)	4.0 (4.4)	4.9 (5.1)	09	*R*	−56.33
7.	Sal(L-tyrtriphenylphosphino-1,10-phenruthenate(II))	65.2 (65.8)	4.1 (4.6)	5.0 (5.2)	08	*R*	−75.60
8.	Sal(L-phealatriphenylphosphino-2,2-dipyruthenate(II))	66.9 (67.2)	4.0 (4.6)	5.1 (5.3)	07	*R*	−43.58
9.	Sal(L-phealatriphenylphosphino-1,10-phenruthenate(II))	68.0 (68.1)	4.0 (4.5)	5.0 (5.2)	05	*R*	−60.48

[a] Calculated numbers are in parentheses.

are non-electrolytic in nature. Some of the water is retained by the complexes in the solid state, as indicated by ν(OH) bands at 3300–3400 cm^{-1}, along with the deformation and rocking modes of water at 1620 and 620 cm^{-1} in the IR and far IR regions,[13] and also by elemental analysis. The imine structure of the chiral Schiff bases is also clearly indicated by intense bands near 1635–1610 cm^{-1}, which overlap with $\nu_{asym}(COO^-)$ stretching modes. This band undergoes a modest decrease on complexation to the metal ion, inferring coordination through the carboxylato oxygen and nitrogen of the azomethine group to the metal ion.[14] The symmetric (COO^-) stretching vibration absorbs at 1440 cm^{-1}. Other significant bands are listed in Table 2.

In the far-IR region the bands at 550 and 345 cm^{-1} are due to ν(Ru—P) and ν(Ru—N), respectively.

The electronic spectra of complexes **1–3** were recorded in dichloromethane and show high intensity bands in the UV region near 238 (ε = 1627) to 379 nm (ε = 2049), which are assigned to the $\pi \rightarrow \pi^*$ transition from the benzene ring and the double bond of the azomethene group. The absorption bands in the 449 nm region (ε = 458) are due to the $n \rightarrow \pi^*$ transition of the non-bonded electron present on the azomethine nitrogen of the Schiff bases. In the complexes this band undergoes a blue-shift due to coordination to the metal through the azomethine nitrogen atom. An allowed band in the range 612 (ε = 627) to 655 nm (ε = 468) is assigned to a $t_2(Ru) \rightarrow \pi^*(L)$ transition, i.e. an LMCT band. The position of the LMCT band depends on the R group attached to the azomethine group of the amino acid moiety.[15] The energy of the band decreases in the order Sal Meth > Sal Tyr > Salpheala, which is in agreement with those reported earlier.[11,12]

The circular dichroism data for all the complexes in CH_2Cl_2/MeOH are given in Table 3. Three representative circular dichroism spectra (Fig. 1) of

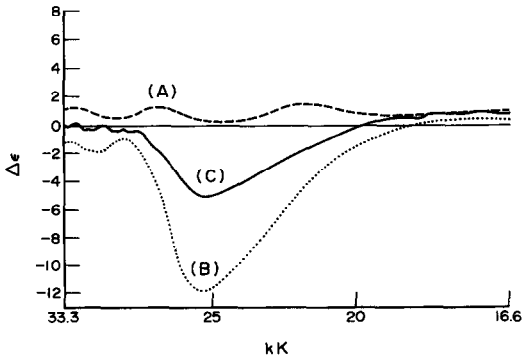

Fig. 1. Circular dichroism spectra of (A) Sal(L-methtriphenylphosphinodiaquoruthenate(II)), (B) Sal(L-tyrtriphenylphosphinodiaquoruthenate(II)), and (C) Sal(L-phealatriphenylphosphinodiaquoruthenate(II)).

Table 2. Selected IR absorption bands in chiral ruthenium(II) Schiff base complexes

S. No.	Complexes	H—C=N $\nu_{asym}(COO^-)$	ν(C=O)	ν(Ru—P)	ν(Ru—N)	Bands due to heterocyclic bases
1.	Sal(L-methtriphenylphosphino-diaquoruthenate(II))	1605(s)	1710(s)	545	340	—
2.	Sal(L-tyrtriphenylphosphino-diaquoruthenate(II))	1610(s)	1715(s)	540	345	—
3.	Sal(L-phealatriphenylphosphino-diaquoruthenate(II))	1590(s)	1710(s)	550	345	—
4.	Sal(L-methtriphenylphosphino-2,2-dipyruthenate(II))	1600(s)	1720(s)	545	340	1460(s), 1440(s), 1160(s), 768(s), 700(s), 405
5.	Sal(L-methtriphenylphosphino-1,10-phenruthenate(II))	1610(s)	1735(s)	550	345	1425(s), 1145(m), 845(m), 725(m), 638(m)
6.	Sal(L-tyrtriphenylphosphino-2,2-dipyruthenate(II))	1605(s)	1710(s)	550	340	1465(s), 1440(s), 1150, 760, 700, 408
7.	Sal(L-tyrtriphenylphosphino-1,10-phenruthenate(II))	1595(s)	1720(s)	540	345	1430(s), 1150(s), 840(s), 720(s), 640
8.	Sal(L-phealatriphenylphosphino-2,2-dipyruthenate(II))	1590(s)	1725(s)	545	340	1460(s), 1445(s), 1165(s), 770(s), 705(s), 410
9.	Sal(L-phealatriphenylphosphino-1,10-phenruthenate(II))	1600(s)	1730(s)	550	340	1430(s), 1150(s), 840(s), 725(s), 630(s)

Table 3. Electronic absorption and CD spectral data of chiral ruthenium(II) Schiff base complexes

S. No.	Complexes	λ_{max} (M^{-1} cm^{-1})	ν kK ($\Delta\varepsilon$)
1.	Sal(L-methtriphenylphosphino-diaquoruthenate(II))	238(1627), 378(564), 449(458), 655(468)	32.3(+1.4), 27.4(+1.2), 24.7(+0.4), 17.4 (+0.8)
2.	Sal(L-tyrtriphenylphosphino-diaquoruthenate(II))	385(2192), 615(868)	31.3(−1.8), 25.3(−11.5), 17.5(+0.4)
3.	Sal(L-phealatriphenylphosphino-diaquoruthenate(II))	379(2049), 612(627)	31.3(−0.2), 25.3(−4.8), 17.9(+0.8)
4.	Sal(L-methtriphenylphosphino-2,2-dipyruthenate(II))	227(2333), 419(790), 451(807), 525sh(677), 585sh(545), 713sh(394)	34.5(+4.1), 30.8(+3.7), 27.8(+9.6), 24.7(+9.2), 21.0(+1.2), 17.2(+5.5)
5.	Sal(L-methtriphenylphosphino-1,10-phenruthenate(II))	227(2317), 419(823), 453(823), 521sh(670), 718sh(131)	35.0(+8.3), 31.0(+8.7), 27.4(−0.4), 23.8(+5.4), 19.2(+5.0)
6	Sal(L-tyrtriphenylphosphino-2,2-dipyruthenate(II))	225(3910), 390sh(1158), 451(1250), 521(627)	29.9(+5.2), 26.6(−10.1), 21.7(−1.5), 17.5(−0.5)
7	Sal(L-tyrtriphenylphosphino-1,10-phenruthenate(II))	225(2442), 420(781), 452(809), 526sh(767), 565sh(670), 781sh(301)	33.3(+1.8), 27.0(−11.8), 22.7(−8), 17.5(−1.4)
8.	Sal(L-phealatriphenylphosphino-2,2-dipyruthenate(II))	229(2089), 420(758), 452(790), 525sh(729), 575sh(600)	28.16(+3.5), 24.8(−11.9), 19.19(−3.2), 18.28(−1.8)
9.	Sal(L-phealatriphenylphosphino-1,10-phenruthenate(II))	229(2073), 419(759), 451(791), 525sh(734), 575sh(583)	30.3(+4), 26.2(−11.5), 22.9(−7.5), 18.5(+1.6)

chiral ruthenium(II) Schiff base complexes derived from L-Meth (**A**), L-Tyr (**B**) and L-Pheala (**C**) show that although all amino acids have the same absolute configuration, complexes **B** and **C** are stereospecifically coordinated to the ruthenium moiety so that the *gauche* chelate ring is located in the δ form with a very small preference for the λ isomer while complex **A** prefers only the λ conformation. For the amine, diamine and dipeptide[16] complexes with sulphur donor atoms the complex undergoes a non-bonded interaction between the (COO^-) group and the —S.CH_3 group of the methionine moiety, while the complexes derived from L-pheala and L-Tyro do not show such an interaction. This suggests that the strain for the conformation of the ligand affects the circular dichroism intensity without a pattern. Due to the steric interaction between the SCH_3 group and the —(COO^-) group, complex **A** acquires the *S*(*S*) configuration in dichloromethane solution, which is also evidenced by its optical rotation $[\alpha]_D^t = +[71.71]$. The two complexes **B** and **C** acquire the *R* configuration. Similar behaviour was also observed elsewhere.[12,15,17]

In the ligand field region, at 17.39–17.85 kK, circular dichroism bands of the positive Cotton effect are displayed which are assigned to both the *d–d* bands and spin-forbidden ligand bands. These bands undergo a blue shift with an increase in donor strength of the R group in the Schiff base complexes.[15] In the charge-transfer region the bands $d \rightarrow \pi^*$ lie in the range 24.69–25.31 kK and the ligand $\pi \rightarrow \pi^*$ (azomethine) transition bands are seen in the higher energy region at 27.39–32.25 kK. The shift in both the charge transfer and ligand transition with azomethine substituents is consistent with the inductive effect of the substituent R on the ligand π-levels.[18]

^{1}H NMR spectra of complexes **1–3** were recorded in $CDCl_3$ and show signals in the range 7.25–7.51 ppm, which are assigned to the phenyl protons of the triphenyl phosphino group, the salicylaldehyde moiety as well as the R group attached to the amino acid moiety (Table 4). The azomethine proton at 8.1 ppm in all chiral Schiff base ligands shows a downfield shift after complexation to the metal ion and lies at 8.30–8.47 ppm, inferring coordination

Table 4. [^{1}H] and ^{13}C[^{1}H] NMR data of chiral ruthenium(II) Schiff base complexes

S. No.	Complexes	[^{1}H] NMR assignment (ppm) —CH	—CH=N	Aromatic/N-heterocyclic	^{13}C[^{1}H] NMR assignment (ppm) —CH	COO^-	Aromatic/N-heterocyclic
1.	Sal(L-methtriphenylphosphino-diaquoruthenate(II))	4.22(t)	8.30(s)	7.51, 7.26	62.08	199.97	132.05, 129.30, 127.14
2.	Sal(L-tyrtriphenylphosphino-diaquoruthenate(II))	2.93(t)	8.47(s)	7.58, 7.34	56.20	204.42	130.06, 128.6, 128.14
3.	Sal)L-phealatriphenylphosphino-diaquoruthenate(II))	3.51(t)	8.41(s)	7.52, 7.27	58.36	206.54	126.96, 129.07
4.	Sal(L-methtriphenylphosphino-2,2-dipyruthenate(II))	4.30	8.41(s)	7.56, 7.25, 9.5, 9.24, 9.17	61.90	201.05	132.6, 128.5, 126.35, 156.77, 124.3, 137.36, 126.2, 151.09
5.	Sal(L-methtriphenylphosphino-1,10-phenruthenate(II))	4.29	8.70(s)	7.57, 7.29, 9.60, 9.14, 9.24	62.01	199.80	131.50, 129.5, 127.6, 152.57, 130.65, 127.55
6.	Sal(L-tyrtriphenylphosphino-2,2-dipyruthenate(II))	3.30	8.39(s)	7.57, 7.04, 9.74, 9.24, 9.17	56.26	203.62	130.05, 128.77, 156.70, 137.30, 151.0
7.	Sal(L-tyrtriphenylphosphino-1,10-phenruthenate(II))	3.31	8.32(s)	7.57, 7.22, 9.59, 9.62, 9.16	57.21	204.55	133.5, 129.6, 127.4, 150.5, 136.6, 127.8
8.	Sal(L-phealatriphenylphosphino-2,2-dipyruthenate(II))	3.30	8.42(s)	7.56, 7.26, 9.5, 9.26, 9.18	58.40	206.06	132.5, 130.06, 129.5, 156.3, 124.4, 127.3
9.	Sal(L-phealatriphenylphosphino-1,10-phenruthenate(II))	3.29	8.7(s)	7.50, 7.29, 9.62, 9.24, 9.17	58.60	205.91	131.6, 134.4, 127.6, 151.9, 130.6, 127.8

through the azomethine nitrogen atom. In the case of complex **2** the signal at 5.95 ppm is due to the hydrogen-bonded phenolic group of the tyrosine moiety. After shaking the complex with D_2O this signal disappears due to proton exchange. Complexes **1–3** have a triplet in the region 2.93–4.22 ppm due to protons of the asymmetric —CH group, which are also reported by others.[19–21]

The $^{13}C[^1H]$ chemical shift data of all the complexes are given in Table 4. In the $^{13}C[^1H]$ NMR spectra of complexes **1–3** the signals due to the carbon of the carboxylato group and the azomethine carbon atom undergo a downfield shift from those of the free Schiff bases, which reflects that the complexes of ruthenium(II) functioned as terdentate O—N—O. However, the signals due to the ring carbon, asymmetric carbon and carbon of the $—CH_2$ group lie in the ranges 127–135, 56–62 and 27.9–30 ppm. In the case of complex **1** a signal at 16.21 ppm is due to a CH_3 group directly attached to the non-bonded sulphur atom, which is in agreement with data reported earlier.[16,22–24]

The $^{31}P[^1H]$ NMR spectra of all the complexes recorded in dichloromethane show only one signal in the range 29.5–32 ppm, which shows that only one phosphorus is in an axial position and is *trans* to the nitrogen of the azomethine group.[25,26]

The cyclic and differential pulse voltammograms of complexes **1–3**, in CH_2Cl_2 using tetrabutyl ammonium perchlorate as the supporting electrolyte with Ag/AgCl as the reference electrode, show irreversible behaviour. In the differential pulse voltammogram the $E_{1/2}$ value of the Ru^{II}/Ru^{I} reduction potential lies in the range -0.50 to -0.84 V. The more negative value of the redox potential in complex **1** is due to the presence of the methionine moiety, which increases the electron density at the metal centre and the $E_{1/2}$ value lies at the more cathodic side.[15,27]

The substitution reactions of complexes **1–3**, with π-acceptor ligands such as 2,2-bipyridyl and 1,10-phenanthroline, is summarized in Scheme 1.

Complexes **1–3** interact with 2,2-bipyridyl and 1,10-phenanthroline in refluxing CH_2Cl_2/MeOH with the replacement of two water molecules and show a colour change from green to brownish red, yielding the complexes **4–9**. All the complexes are non-electrolytes in methanol. The electronic spectra of the complexes in methanol show a high intensity charge-transfer band in the range 225 ($\varepsilon = 2442$) to 229 nm ($\varepsilon = 2089$), while the $n \rightarrow \pi^*$ bands lie at 419 ($\varepsilon = 759$) to 452 nm ($\varepsilon = 790$).[28] The appearance of shoulders in the region 521–585 nm and also 713 nm are due to ruthenium(II) $d \rightarrow \pi^*$ (2,2-bipy and 1,10-phenon), and a d–d transition which has also been reported by others.[29]

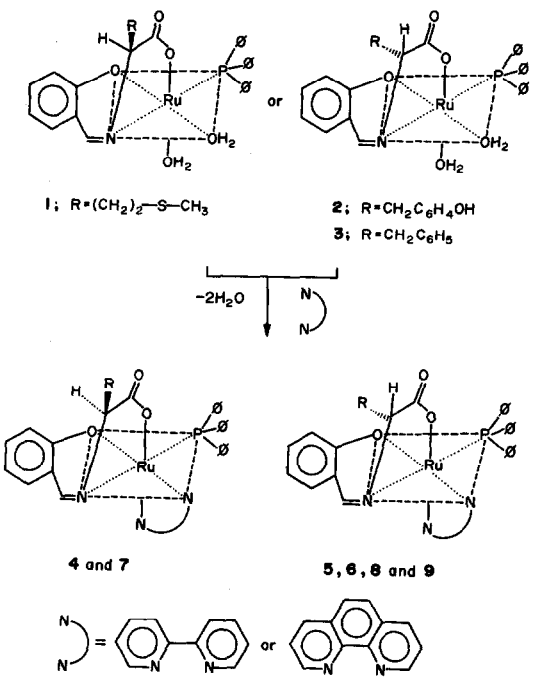

Scheme 1.

The IR spectra of the complexes **4–9** show bands at 1605, 1575, 1460, 1440, 1315, 1242, 1160 and 770 cm^{-1} and 1600, 1575, 1425, 1145, 845 and 725 cm^{-1} due to coordination of 2,2-bipyridyl and 1,10-phenanthroline, which are merged with the IR bands of the symmetric or asymmetric (COO^-) group and some of the ring bands.[30]

The circular dichroism spectra of the complexes **4–9** were recorded in methanol and show great differences in intensity compared to the parent complexes, which is comparable to the circular dichroism effect due to the presence of π-acceptor ligands. The strain for conformation affects the circular dichroism intensity without the pattern, see Fig. 2.

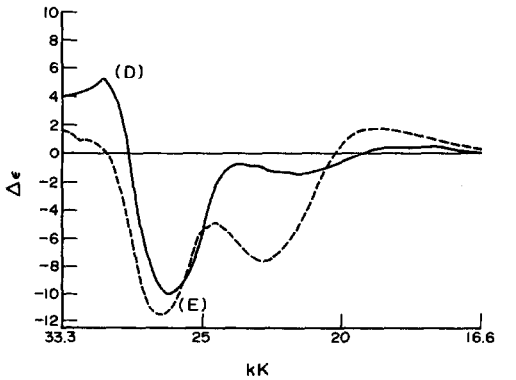

Fig. 2. Circular dichroism spectra of (D) Sal(L-tyrtriphenylphosphino(2,2-dipy)ruthenate(II)) and (E) Sal(L-tyrtriphenylphosphino(1,10-Phen)ruthenate(II)).

In the higher energy region the ligand $\pi \rightarrow \pi^*$ transition bands lie at 29.85–34.48 kK, while the charge-transfer band lies near 27.77 kK. The bands in the range 21.05–22.72 kK are due to the ruthenium(II) transition $d\pi \rightarrow \pi^*$ (2,2-bipy and 1,10-phenanthroline). In the ligand field region the circular dichroism bands with a positive Cotton effect lie in the region 17.24–19.23 kK and have been assigned to both *d–d* bands and spin-forbidden ligand bands which undergo a blue shift with an increase in donor strength of the R group attached to the amino acid moiety.[15]

The [^{1}H] NMR spectra of complexes **4–9** were recorded in a deuterated methanol and show signals in the range 7.89–9.60 ppm due to the ring protons of coordinated π-acceptor ligands such as 2,2-bipy and 1,10-phenanthroline. These assignments have also been reported elsewhere.[31]

The ^{13}C[^{1}H] NMR spectra of the complexes **4**, **6** and **8** in methanol show a signal at 151.01–156.77 ppm due to the carbon atom directly attached to the coordinated nitrogen atom of the 2,2′-bipyridyl ligand, while the rest of the carbon signals lie in the range 124.30–127.67 ppm and in complexes **5**, **7** and **9** the signal due to carbons attached to nitrogens lie in the range 152.50–152.67 ppm. The other carbon signals lie in the region 126.16–136.12 ppm which has also been reported earlier.[32]

The substituted complexes **4–9** are irreversible in nature in methanol using tetrabutylammonium perchlorate as the supporting electrolyte, Ag/AgCl as the reference electrodes. Their Ru^{II}/Ru^{I} reduction couple is less negative in the range -0.69 to -0.52 V compared to the parent complexes **1–3**. This is due to the π-accepting tendency of the substituents, such as 2,2-bipy and 1,10-phen, directly attached to the metal[33] and also to the inductive effect of the R group of the amino acid moiety. All these electronic effects are transmitted through the ligands to the ruthenium metal ion.[12,15]

EXPERIMENTAL

$RuCl_3 \cdot 3H_2O$ was obtained from Johnson Matthey. Triphenylphosphine (Sisco), salicylaldehyde, L-methionine, L-phenylalanine and L-tyrosine (Aldrich) were used as received. All the Schiff bases derived from salicylaldehyde and the L-amino acids were prepared by reported procedures.[11,12] The metal complex $RuCl_2(PPh_3)_3$ was synthesized by a known method.[34]

Preparation of the complexes **1**, **2** *and* **3**

$RuCl_2(PPh_3)_2$ (1.0 mmol) in acetone was refluxed with a methanolic solution of the chiral Schiff bases (1.0 mmol) under an inert atmosphere for 6–8 h. The completion of the reaction was ensured using TLC intermittently. After completion of the reaction the solution was filtered under argon. The filtrate was concentrated to *ca* 10 cm^3 and the complexes were precipitated by diethyl ether. The complexes were filtered and again washed with diethyl ether to remove excess PPh_3, recrystallized in methanol/dichloromethane and dried *in vacuo*. Yield: 70–75%.

Synthesis of the complexes [RuL(PPh$_3$)(2,2-bipy)] (**4**, **6** *and* **8**)

A hot solution of complexes **1**, **2** and **3** (0.01 mmol) in dichloromethane and methanol was refluxed with 2,2-bipyridyl (0.01 mmol) for 8–10 h with constant stirring. The resulting solution was filtered and concentrated to 10 cm^3 in a rotatory evaporator and the complexes were precipitated with diethyl ether, filtered, recrystallized and dried *in vacuo*. Yield: 60–65%.

Synthesis of the complexes [RuL(PPh)$_3$(1,10-phen)] (**5**, **7** *and* **9**)

Complexes **1**, **2** and **3** (0.01 mmol) were dissolved in dichloromethane/methanol and refluxed with 1,10-phenanthroline (0.01 mmol) dissolved in methanol for 10 h. The solution was filtered, concentrated and precipitated with diethyl ether. The complexes were then filtered, washed with the same solvent, recrystallized and dried *in vacuo*. Yield: 65–68%.

Physical measurements

Microanalyses of the complexes were performed on a Carlo–Erba analyser Model 1106. Molar conductance values were measured at room temperature on a Digisun Electronic Conductivity bridge DI-909. The IR spectra were recorded on Carl–Zeiss–Specord M-80 spectrophotometer in Nujol mulls/KBr. Electronic spectra were recorded on a Shimadzu UV–vis recording spectrophotometer model 160. [^{1}H], ^{13}C[^{1}H] and ^{31}P[^{1}H] NMR spectra were obtained on a Jeol FX-100 NMR spectrometer in $CDCl_3$ and chloroform using [$Si(CH_3)_4$] as an internal standard and operating at 99.55, 24.99 and 40.27 MHz. Cyclic voltammograms and differential pulse voltammogram polarograms were recorded with a Princeton Applied Research (PAR) instrument using tetrabutylammonium perchlorate as the supporting electrolyte in dichloromethane/MeOH. The optical rotation of the complexes in dichloromethane/

methanol was measured using a polarimeter Atago, Japan. The circular dichroism spectra were recorded in dichloromethane/methanol by JASCO Machine Model J-20, Japan.

Acknowledgement—We sincerely thank Prof. P. Natarajan, Director, Central Salt and Marine Chemicals Research Institute for his valuable guidance and cooperation in allowing us to send the paper for publication.

REFERENCES

1. E. Kimura, R. Machida and M. Kodama, *J. Am. Chem. Soc.* 1984, **106**, 5497.
2. J. Collins, *J. Chem. Soc., Chem. Commun.* 1987, 803.
3. Y. Aoyama, T. Fujisawa, T. Walanawe, H. Toi and H. Ogashi, *J. Am. Chem. Soc.* 1986, **108**, 943.
4. Y. Murakami, Y. Aoyama and M. Kida, *J. Chem. Soc., Perkin Trans.* 1980, **2**, 1665.
5. R. S. Brawn, M. Zamakani and J. L. Coho, *J. Am. Chem. Soc.* 1984, **106**, 5222.
6. T. R. Kelly, A. Whitting and N. S. Chandrakumar, *J. Am. Chem. Soc.* 1986, **108**, 3510.
7. J. M. Gonzalez Perez, J. N. Gutierrez, N.-H. Dung, B. Viossat, A. Busnot and M. Wintenberger, *Inorg. Chim. Acta* 1991, **189**, 243.
8. L. L. Martin and R. A. Jacobson, *Inorg. Chem.* 1972, **11**, 2785.
9. N. H. Dung, B. Viossat, A. Busnot, E. Abarca, Garcia, M. F. Gardette and J. N. Gutiennez, *Inorg. Chim. Acta* 1990, **169**, 9.
10. E. Mikros, F. Gaudemer and A. Gaudemer, *Inorg. Chim. Acta* 1991, **30**, 1806.
11. M. M. Taqui Khan, R. I. Kureshy and N. H. Khan, *Tetrahedron Asym.* 1991, **2**, 1015.
12. M. M. Taqui Khan, N. H. Khan and R. I. Kureshy, *Tetrahedron Asym.* 1992, **3**, 307.
13. L. Casella, M. Gullotti, A. Pintar, L. Messori, A. Rockenbauer and M. Gyor, *Inorg. Chem.* 1987, **26**, 1032.
14. D. A. Edwards and R. Richards, *J. Chem. Soc., Dalton Trans.* 1975, 637.
15. K. Nakajima, K. Kojima, M. Kojima and J. Fujita, *Bull. Chem. Soc. Japan* 1990, **63**, 2620.
16. K. Okamoto, M. T. T. Yonemura, T. Konno and J. Hidaka, *Inorg. Chim. Acta* 1990, **175**, 31.
17. L. J. Boucher and C. G. Coe, *Inorg. Chem.* 1976, **15**, 1334.
18. L. J. Boucher, *Inorg. Nucl. Chem.* 1974, **36**, 531.
19. W. S. Sheldrick and S. Heeb, *Inorg. Chim. Acta* 1990, **168**, 93.
20. M. Nazimuddin, M. A. Ali and F. E. Smith, *Polyhedron* 1991, **10**, 1327.
21. R. Bastida, T. Lage, C. Parrado, T. Rodrigues, A. Sousa and D. E. Fentan, *J. Chem. Soc., Dalton Trans.* 1990, 2101.
22. K. Okamoto, M. Takari, T. Yonemura, T. Konno and J. Hidaka, *Inorg. Chim. Acta* 1990, **175**, 31.
23. M. T. Nunes and V. M. S. Gil, *Inorg. Chim. Acta* 1990, **170**, 59.
24. P. A. Hunt, B. P. Straughan, A. A. M. Ali, R. K. Harris and B. J. Say, *J. Chem. Soc., Dalton Trans.* 1990, 2131.
25. F. M. Conroy-Lewis, A. D. Redhouse and S. J. Simpeen, *J. Organomet. Chem.* 1990, **399**, 307.
26. C. Bianchini, P. J. Perez, M. Peruzzini, F. Zanobini and A. Vacca, *Inorg. Chem.* 1991, **30**, 279.
27. M. M. Taqui Khan, R. I. Kureshy and N. H. Khan, *Polyhedron* 1992, **11**, 1053.
28. R. R. Ruminski, K. D. V. Tassel and J. D. Peterson, *Inorg. Chem.* 1984, **23**, 4380.
29. H. E. Toma and J. M. Malin, *Inorg. Chem.* 1973, **12**, 1039.
30. U. C. Sharma, S. C. Sarkar, B. C. Paul and R. K. Poddar, *Inorg. Chim. Acta* 1990, **173**, 195.
31. E. C. Constable, R. P. G. Henney, T. A. Leese and D. A. Tocher, *J. Chem. Soc., Dalton Trans.* 1990, 443.
32. M. J. Cook, A. P. Lewis, G. S. G. McAuliffe and A. J. Thomson, *Inorg. Chim. Acta* 1982, **64**, L25.
33. M. J. Root, B. P. Sullivan, T. J. Meyer and E. Dentsch, *Inorg. Chem.* 1985, **24**, 2731.
34. T. F. Calson and S. D. Robinson, *Inorg. Chim. Acta* 1988, **149**, 13.

Polyhedron Vol. 12, No. 2, pp. 203–208, 1993
Printed in Great Britain

0277–5387/93 $6.00+.00
© 1993 Pergamon Press Ltd

METAL PHENOXYALKANOIC ACID INTERACTIONS—36. THE PREPARATION AND CRYSTAL STRUCTURES OF TETRAAQUABIS(2-PHENOXYBENZOATO)NICKEL(II) DIHYDRATE, DIAQUABIS(4-FLUOROPHENOXYACETATO)ZINC(II), *CATENA*-DIAQUABIS(PHENOXYACETATO)COBALT(II) AND TETRAKIS-μ-[(PENTAFLUOROPHENOXY)ACETATO(O,O′)]BIS[AQUACOPPER(II)]

GRAHAM SMITH* and DANIEL E. LYNCH

School of Chemistry, Queensland University of Technology, PO Box 2434, Brisbane 4001, Australia

and

THOMAS C. W. MAK and WAI-HING YIP

Department of Chemistry, The Chinese University of Hong Kong, Shatin, New Territories, Hong Kong

and

COLIN H. L. KENNARD

Department of Chemistry, The University of Queensland, Brisbane 4072, Australia

(*Received* 10 *August* 1992; *accepted* 10 *September* 1992)

Abstract—The structures of four complexes involving divalent first-row transition metals and phenoxy substituted carboxylic acids have been determind by X-ray diffraction. These are tetraaquabis(2-phenoxybenzoato)nickel(II) dihydrate (**1**), diaquabis(4-fluorophenoxyacetato)zinc(II) (**2**), diaquabis(phenoxyacetato)cobalt(II) (**3**) and tetrakis-μ-(pentafluorophenoxyacetato)bis[aquacopper(II)] (**4**). Complex **1** is regular octahedral with *trans*-related unidentate carboxylates [Ni—O (carboxylate) 2.031(1) Å] and four waters [Ni—O 2.049, 2.104(2) Å]. Complex **2** has a skew trapezoidal bipyramidal stereochemistry, involving four oxygens from two asymmetric bidentate carboxylates [Zn—O 2.107, 2.332(3) Å] and two waters [Zn—O 1.989(4) Å]. The polymeric complex **3** is isomorphous and isostructural with the manganese(II) analogue, with centrosymmetric octahedral CoO_6 stereochemistry comprising four bonds to carboxylate oxygens (both bridging) [Co—O 2.076, 2.087(3) Å] and two to waters [Co—O 2.134(3) Å]. Complex **4** is a pseudo-centrosymmetric tetracarboxylate bridged dimer of the copper(II) acetate hydrate type with a Cu—Cu separation of 2.644(4) Å. Bond distances to copper are 1.96(1) (average, equatorial) and 2.15(1) Å (average, axial, to water).

The structural systematics of both phenoxyalkanoic acids and their complexes with metal ions have been an area of considerable research interest in our laboratories for a number of years. More than 60 metal complexes have been prepared and characterized, largely by single-crystal X-ray diffraction methods.[1,2] Complex **1**, tetraaquabis(2-phenoxybenzoato)nickel(II)dihydrate, represents the second known complex with 2-phenoxybenzoic acid (2-PBAH), the previous example being a tetracarboxylate-bridged dimer, $[Cu_2(2\text{-PBA})_4(2\text{-PBAH})_2]$.[3] Complex **2**, diaquabis(4-fluorophenoxyacetato)-

* Author to whom correspondence should be addressed.

zinc(II), has the same stoichiometric formula as the previously reported anhydrous zinc complexes of phenoxyacetic acid (PAH) and 4-chlorophenoxyacetic acid (4-CPAH), $[Zn(PA)_2(H_2O)_2]$ and $[Zn(4\text{-}CPA)_2(H_2O)_2]$, respectively.[4] Other complexes of 4-FPAH are $[Cu(4\text{-}FPA)_2(H_2O)_2]\cdot 2(4\text{-}FPAH)\cdot 2H_2O$,[5] $[Cu_2(4\text{-}FPA)_4(ampym)_2]$ (ampym = 2-aminopyrimidine),[5] $[Cu_{1.5}(4\text{-}FPA)_3(H_2O)_{5.5}]$[6] and $[Ag_2(4\text{-}FPA)_2(H_2O)_2]$.[7]

Complexes of phenoxyacetic acid (PAH) and 4-chlorophenoxyacetic acid (4-CPAH) give two different complex series with the metals zinc(II),[4] manganese(II), magnesium(II) and cobalt(II),[1] which are all isomorphous and isostructural. The structure of diaquabis(phenoxyacetato)cobalt(II) (**3**) confirms this isomorphism. No other structurally characterized complexes of cobalt(II) with phenoxyalkanoic acids are known. The structures of (pentafluorophenoxy)acetic acid (PFPAH) and its complexes with silver(I), $[Ag_2(PFPA)_2]$, and mercury(I), $[Hg(PFPA)]_n$, are also known.[8] The structure reported here, tetrakis[(pentafluorophenoxy)acetato(O,O′)]bis[aquacopper(II)], $[Cu_2(PFPA)_4(H_2O)_2]$ (**4**), represents the only example of a complex of PFPAH with a first-row transition series metal.

EXPERIMENTAL

Preparation of complexes

Complex **1** was prepared by digesting 2 : 1 molar quantities of $NiCO_3\cdot 2Ni(OH)_2\cdot 4H_2O$ and 2-phenoxybenzoic acid (2-PBAH) in 80% ethanol/water for 5 h at 90°C. Pale blue needle crystals were obtained from the filtrate after *ca* 2 months. The complexes **2**–**4** were prepared using a previously described procedure[1] by reacting 50% aqueous ethanolic solutions of the acids with the appropriate metal carbonate. Crystals were obtained after partial room temperature evaporation of the respective filtrates. The acids were synthesized using the general procedure of Synerholm and Zimmerman.[9] Elemental analyses, density measurement and preliminary single-crystal X-ray preliminary data suggested the formulae $Ni(2\text{-}PBA)_2(H_2O)_6$ (**1**), $Zn(4\text{-}FPA)_2(H_2O)_2$ (**2**), $Co(PA)_2(H_2O)_2$ (**3**) and $Cu(PFPA)_2(H_2O)$ (**4**). The dark green colour of **4** indicated that a tetracarboxylate-bridged dimer of the copper(II) acetate hydrate type was probable.

Crystal data, structure determination and refinement

Table 1 lists information about crystal data, data acquisition, structure solution and refinement for compounds **1**, **2**, **3** and **4**. Data were collected at room temperature (293 K) on Nicolet R3m (**1**–**3**) or Enraf–Nonius (**4**) four-circle diffractometers, using graphite crystal monochromatized Mo-K_α radiation ($\lambda = 0.71073$ Å). Structures were solved by heavy-atom methods using SHELX 76[10] and refined by full-matrix least-squares with anisotropic thermal parameters for all non-hydrogen atoms. Hydrogens were located by difference-Fourier methods and included in the respective refinements with both positional and isotropic thermal parameters refined (**1**, **2** and **4**) or with coordinates refined and isotropic U values set invariant at 0.05 Å^2 (**3**). No corrections were made for absorption or extinction. The high residual for **4** is the result of poor crystal quality because of twinning. Final atomic coordinates, anisotropic thermal parameters, intraligand bond distances and angles and observed and calculated structure factors have been deposited and are available from the Editor or the authors. Bond distances and angles about the respective coordination polyhedra are given in Table 2.

DISCUSSION

$[Ni(2\text{-}PBA)_2(H_2O)_4]\cdot 2H_2O$ (**1**)

The structure of complex **1** is typical of most nickel(II) carboxylates. The first complex of this type involving a phenoxyalkanoic acid was, $[Ni(PA)(H_2O)_4]$,[11] for which the structure was determined but only partially refined. The present complex also has regular octahedral NiO_6 coordination (Fig. 1), involving two centrosymmetrically related unidentate carboxylate ligands [Ni—O 2.031(1) Å] and four water molecules [Ni—O 2.049, 2.104(2) Å]. These values compare with other complexes of nickel(II) from the series with the general formula $[Ni(L)_2(H_2O)_4]$:

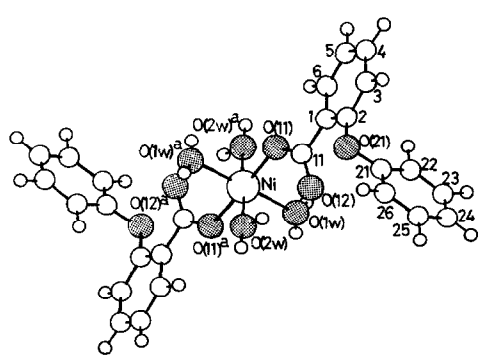

Fig. 1. Molecular configuration and atom naming scheme for $[Ni(2\text{-}PBA)_2(H_2O)_4]\cdot 2H_2O$ (**1**). Unless otherwise indicated, atoms are carbon.

Table 1. Crystal data for $[Ni(2\text{-PBA})_2(H_2O)_4]\cdot 2H_2O$ (**1**), $[Zn(4\text{-FPA})_2(H_2O)_2]\cdot 2H_2O$ (**2**), $[Co(PA)_2(H_2O)_2]$ (**3**) and $[Cu_2(PFPA)_4(H_2O)_2]$ (**4**)

Formula	$C_{26}H_{30}NiO_{12}$	$C_{16}H_{16}F_2O_8Zn$	$C_{16}H_{18}CoO_8$	$C_{32}H_{12}Cu_2F_{20}O_{14}$
Mr	593.3	439.7	397.2	1127.5
a (Å)	5.7604(5)	11.648(7)	6.850(1)	7.635(5)
b (Å)	7.6779(2)	5.2052(8)	7.606(1)	12.958(4)
c (Å)	29.057(7)	28.193(9)	33.302(8)	37.45(3)
α (°)	90	90	90	90
β (°)	92.79(2)	99.15(2)	90	94.45(4)
γ (°)	90	90	90	90
V (Å^3)	1283.5(4)	1687.6(7)	1735.1(5)	3794(4)
D_c (g cm^{-3})	1.534	1.730	1.521	2.026
D_m (g cm^{-3})	1.54	1.74	1.55	2.00
Z	2	4	4	4
μ (cm^{-1})	8.2	15.5	10.2	13.2
F(000)	620	896	820	2216
Space group	$P2_1/c$	$C2/c$	*Pbca*	$P2_1/c$
Data collection				
Crystal size (mm)	$0.20\times0.32\times0.40$	$0.44\times0.36\times0.12$	$0.36\times0.34\times0.08$	$0.29\times0.19\times0.08$
$2\theta_{max}$ (°)	55	55	54	50
Unique data	2944	1790	1977	6461
Data used	2357	1376	1321	2436
Discrimination	$I > 2.5\sigma(I)$	$I > 2.5\sigma(I)$	$I > 2.5\sigma(I)$	$I > 2.5\sigma(I)$
R	0.034	0.060	0.043	0.064
*R*w	0.041	0.058	0.050	0.064
w^a *A*	1.0	4.2	3.2	1.0
B	3.6×10^{-3}	4.5×10^{-4}	4.1×10^{-4}	8.8×10^{-4}

[a] $w = A/[\sigma^2(F_o)+B(F_o)^2]$.

L = (2-carbamoylphenoxy)acetate:[12] 2.072, 2.063, 2.076(2) Å; L = (4-carboxyphenoxy)acetate:[13] 2.058, 2.026, 2.084(4) Å; L = hydrogen benzene-1,2-dioxydiacetate:[14] 2.064(10), 2.092(7), 2.047(7) Å, respectively. This general stereochemistry is in contrast to the skew trapezoidal bipyramidal six-coordination of the isostructural yellow phenoxybutyrate complexes, $NiL_2(H_2O)_2$ [L = 4-phenoxybutyrate (a) and 4(4-chlorophenoxy)butyrate (b)].[15] With these, the carboxylate groups are only slightly asymmetrically bidentate chelate in their coordination mode [Ni—O(carboxyl), 2.181, 2.062(2) Å (a); 2.175, 2.068(2) Å (b). Ni—O (water), 2.020(2) Å (a); 2.016(2) Å (b)].

$[Zn(4\text{-FPA})_2(H_2O)_2]$ (2)

The zinc(II) complex of 4-fluorophenoxyacetic acid, $[Zn(4\text{-FPA})_2(H_2O)_2]$ (**2**), has distorted trapezoidal bipyramidal stereochemistry about zinc (Fig. 2), similar to that found for the isomorphous complexes $[Zn(PA)_2(H_2O)_2]$,[4] $[Zn(4\text{-CPA})_2(H_2O)_2]$[4] and $[Cd(PA)(H_2O)_2]$[16] (PA = phenoxyacetate; 4-CPA = 4-chlorophenoxyacetate). This is also found in the complex $[ZnL_2(H_2O)_2]$ [L = (2-formyl-6-methoxyphenoxy)acetate[17]]. Although it is surprising that isomorphism does not extend right through the series, $[Zn(PA)_2(H_2O)_2]$, $[Zn(4\text{-CPA})_2(H_2O)_2]$ to $[Zn(4\text{-FPA})_2(H_2O)_2]$ (**2**), all complexes possess the same crystallographically imposed two-fold rotational symmetry. Similar structural characteristics and stereochemistry are possessed by a number of other zinc(II) and cadmium(II) carboxylates. The six-

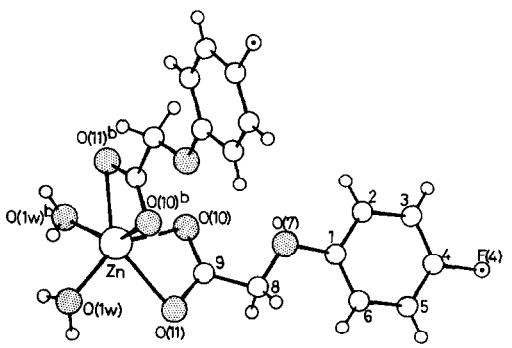

Fig. 2. Molecular configuration and atom naming scheme for $[Zn(4\text{-FPA})_2(H_2O)_2]$ (**2**).

Table 2. Bond distances (Å) and angles (°) about the coordination polyhedra for compounds **1–4**

Distances			
	1		
Ni—O(11)	2.031(1)	Ni—O(2w)	2.049(2)
Ni—O(1w)	2.104(2)		
	2		
Zn—O(10)	2.332(3)	Zn—O(1w)	1.989(4)
Zn—O(11)	2.107(3)		
	3		
Co—O(10)	2.087(3)	Co—O(1w)	2.134(3)
Co—O(11)[a]	2.076(3)		
	4		
Cu(1)—O(11A)	1.95(1)	Cu(2)—O(11C)	1.95(1)
Cu(1)—O(11B)	1.98(1)	Cu(2)—O(11D)	1.97(1)
Cu(1)—O(10C)	1.98(1)	Cu(1)—O(1w)	2.17(1)
Cu(1)—O(10D)	1.93(1)	Cu(2)—O(2w)	2.13(1)
Cu(2)—O(10A)	1.94(1)	Cu(1)—Cu(2)	2.644(4)
Cu(2)—O(10B)	1.95(1)		
Angles			
	1		
O(11)—Ni—O(1w)	91.2(2)	O(1w)—Ni—O(2w)	89.5(1)
O(11)—Ni—O(2w)	91.7(1)	Ni—O(11)—C(9)	128.3(1)
	2		
O(10)—Zn—O(11)	58.6(1)	O(10)—Zn—O(11)[b]	94.5(1)
O(10)—Zn—O(1w)	99.2(1)	O(10)—Zn—O(1w)[b]	141.9(2)
O(11)—Zn—O(1w)	122.3(2)	O(11)—Zn—O(1w)[b]	84.1(2)
O(10)—Zn—O(10)[b]	91.5(1)	Zn—O(10)—C(9)	95.1(3)
O(11)—Zn—O(11)[b]	143.0(1)	Zn—O(11)—C(9)	84.9(3)
O(1w)—Zn—O(1w)[b]	94.5(2)		
	3		
O(10)—Co—O(11)[a]	82.2(1)	Co—O(10)—C(9)	130.2(3)
O(10)—Co—O(1w)	86.6(1)	Co—O(11)[a]—C(9)[a]	134.6(3)
O(11)[a]—Co—O(1w)	88.8(1)		
	4		
O(1w)—Cu(1)—O(11A)	93.0(5)	O(10A)—Cu(2)—O(10B)	89.3(5)
O(1w)—Cu(1)—O(11B)	97.0(4)	O(10A)—Cu(2)—O(11C)	167.4(5)
O(1w)—Cu(1)—O(10C)	98.4(5)	O(10A)—Cu(2)—O(11D)	86.5(5)
O(1w)—Cu(1)—O(10D)	94.9(5)	O(10B)—Cu(2)—O(11C)	91.8(5)
O(11A)—Cu(1)—O(11B)	89.3(5)	O(10B)—Cu(2)—O(11D)	167.8(5)
O(11A)—Cu(1)—O(10C)	168.3(5)	O(11C)—Cu(2)—O(11D)	89.9(5)
O(11A)—Cu(1)—O(10D)	91.5(5)	Cu(1)—O(11A)—C(9A)	122(1)
O(11B)—Cu(1)—O(10C)	86.9(5)	Cu(1)—O(11B)—C(9B)	120(1)
O(11B)—Cu(1)—O(10D)	168.0(5)	Cu(1)—O(10C)—C(9C)	122(1)
O(10C)—Cu(1)—O(10D)	90.0(5)	Cu(1)—O(10D)—C(9D)	126(1)
O(2w)—Cu(2)—O(10A)	97.9(5)	Cu(2)—O(10A)—C(9A)	123(1)
O(2w)—Cu(2)—O(10B)	95.4(4)	Cu(2)—O(10B)—C(9B)	126(1)
O(2w)—Cu(2)—O(11C)	94.5(5)	Cu(2)—O(11C)—C(9C)	124(1)
O(2w)—Cu(2)—O(11D)	96.6(5)	Cu(2)—O(11D)—C(9D)	120(1)

[a] $\frac{1}{2}-x, \frac{1}{2}+y, z$.
[b] $-x, y, \frac{1}{2}-z$.

coordination comprises four oxygens from two bidentate chelate carboxylates [Zn—O, 2.107, 2.332(3) Å] and two water molecules [Zn—O, 1.989(4) Å]. The corresponding distances in [Zn $(PA)_2(H_2O)_2$] are 2.118, 2.337(1) and 1.994(1) Å, while with the formyl complex these are 2.073, 2.381(2) and 1.997(2) Å, respectively. Among the zinc structures, compound **2** is intermediate between the terahedral and octahedral structural types. Both types are found in the phenoxyalkanoate complex $[Zn(L)_2(H_2O)_2][Zn(L)_2(H_2O)_4]$ (L = 2,4-dichlorophenoxyacetate).[18] No other tetrahedral examples are known but the octahedral types with the general formula $[Zn(L)_2(H_2O)_4]$ are relatively common (L = 2-formylphenoxyacetate,[19] 2-fluorophenoxyacetate[20] or 2-chlorophenoxyacetate[17]). As for other similar examples of this series, no significant stabilizing intermolecular associations are involved in the packing of the complex monomers in the unit cell. The 4-fluorophenoxyacetate residues retain the planar conformation of the parent acid,[21] while the bond distances and angles are closely comparable.

$[Co(PA)_2(H_2O)_2]_n$ (**3**)

The structure determination of complex **3**, *catena*-[diaquabis(phenoxyacetato)cobalt(II)], confirms that it is isomorphous and isostructural with the manganese(II) complex $[Mn(PA)_2(H_2O)_2]_n$.[1] Single-crystal and powder X-ray diffraction studies previously indicated the isomorphism, which extends through to magnesium(II) and includes the 4-chlorophenoxyacetate analogues. The comparative cell for $[Mn(PA)(H_2O)_2]_n$ is $a = 7.007(4)$, $b = 7.699(4)$, $c = 33.22(2)$ Å, giving a volume which is 57 Å^3 larger than the present example. This is consistent with the increase in effective ionic radius going from cobalt (0.74 Å) to manganese (0.82 Å).[22] The coordination sphere about cobalt is centrosymmetric octahedral, comprising two bonds to *trans*-related waters and four to carboxylate oxygens of bidentate bridging phenoxyacetate ligands (Fig. 3). As for the manganese(II) analogue the Co—Ow (water) bonds are slightly elongated compared to the Co—O (carboxyl) oxygens. These bonds are also shorter and more regular than for the manganese analogue [Co 2.134, 2.076, 2.987(3) Å; Mn 2.216, 2.148, 2.155(2) Å]. As for the zinc(II) complexes (including compound 2) it is surprising that the series isomorphism does not extend to the 4-fluorophenoxyacetate complexes, although it

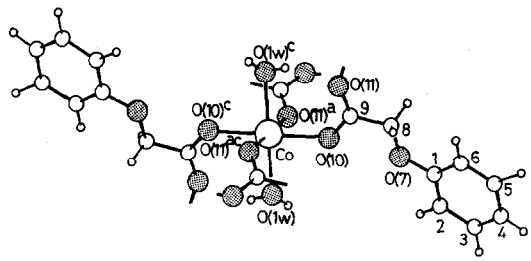

Fig. 3. Molecular configuration and atom naming scheme for $[Co(PA)_2(H_2O)_2]_n$ (**3**). An inversion symmetry operation is indicated by *c*.

does include those with phenoxyacetic acid and 4-chlorophenoxyacetic acid. For cobalt(II), preliminary single crystal data for the compound $[Co(4\text{-}FPA)_2(H_2O)_4]$[23] indicate that it is a regular centrosymmetric octahedral complex with one formula unit in the cell.*

$[Cu_2(PFPA)_4(H_2O)_2]$ (**4**)

The copper(II) complex of (pentafluorophenoxy)acetic acid, $[Cu(PFPA)_4(H_2O)_2]$, is a pseudo-centrosymmetric tetracarboxylato-(O,O′)-bridged dimer of the copper(II) acetate hydrate type[24] (Fig. 4). The dimer has a Cu—Cu separation of 2.644(4) Å with a mean Cu—O (equatorial) bond distance of 1.96(1) Å and a Cu—Ow (axial) bond distance of 2.15(1) Å. These distances are typical of the values found for five other known examples of dimeric copper(II) phenoxyalkanoates, all characteristically dark green in colour. However, the only completely analogous monomeric example in the series, having a general formula $[Cu_2(L)_4(H_2O)_2]\cdot nH_2O$, is copper(2,4-dichlorophenoxy)-acetate hydrate[25] (L = 2,4-D; $n = 2$), while ad-

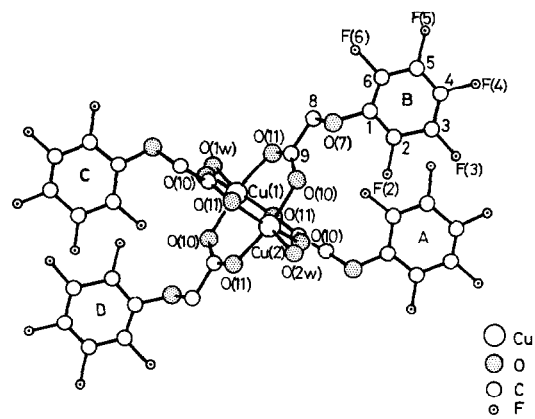

Fig. 4. Molecular configuration and atom naming scheme for $[Cu_2(PFPA)_4(H_2O)_2]$ (**4**).

*Cell data for $[Co(4\text{-}FPA)_2(H_2O)_4]$: $a = 5.051(2)$, $b = 6.814(5)$, $c = 14.75(2)$ Å, $\alpha = 84.87(9)$, $\beta = 85.03(8)$, $\gamma = 71.32(5)$ °; $Z = 1$, space group $P\bar{1}$.

ducts with nitrogen bases replacing the axial water in the dimer system are also known. These have the general formula $[Cu_2(L)_4(X)_2]$ [L = (2,4,5-trichlorophenoxy)acetate, X = pyridine;[25] L = (4-chlorophenoxy)isobutyrate, X = 2-aminopyrimidine[26]]. Polymeric modifications also exist, having the formula $[Cu_2(L)_4]_n$ [L = (2-chlorophenoxy)acetate[27]] or $[Cu_2(L)_4X]_n$ [L = 2-chlorophenoxy)acetate; X = 2-aminopyrimidine (providing a bifunctional bridging group)[27]].

Consistent with other analogous members of this dimeric series, the packing of the molecules in the unit cell shows no significant interdimer hydrogen bonding interactions. However, packing effects influence the conformation of the (pentafluorophenoxy)acetate residues, which results in the substituted ring systems all lying approximately parallel and forming stacks down the *b* cell direction, consistent with the perfect basal cleavage possessed by crystals of this compound. The result is that the side-chain conformation for the pair of residues which are *trans*-related (A and C) are similar but differ from the other pair (B and D). This is reflected in the side-chain torsion angles [C(2)—C(1)—O(7)—C(8), C(1)—O(7)—C(8)—C(9) and O(7)—C(8)—C(9)—O(10)], which are (−99.3, +133.9, −9.0)°, (−150.1, −99.1, −5.3)°, (+99.7, −133.7, +9.2)° and (+146.5, +103.9, +6.4)° for residues A, C, B and D, respectively. The corresponding angles in the parent (pentafluorophenoxy)acetic acid are +50.8°, −110.0° and −2.7°.[8]

Acknowledgements—The authors thank The Chinese University of Hong Kong, The University of Queensland and the Queensland University of Technology for financial support.

REFERENCES

1. Part 1: G. Smith, E. J. O'Reilly and C. H. L. Kennard, *J. Chem. Soc., Dalton Trans.* 1980, 2462.
2. R. C. Bott, D. S. Sagatys, D. E. Lynch, G. Smith and C. H. L. Kennard, *Aust. J. Chem.* 1992, **45**, 947.
3. T. C. W. Mak, W.-H. Yip, C. H. L. Kennard and G. Smith, *Polyhedron* 1990, **9**, 1667.
4. G. Smith, E. J. O'Reilly, C. H. L. Kennard, K. Stadnicka and B. Oleksyn, *Inorg. Chim. Acta* 1981, **47**, 111.
5. E. J. O'Reilly, G. Smith and C. H. L. Kennard, *Inorg. Chim. Acta* 1984, **90**, 63.
6. G. Smith and C. H. L. Kennard, *Inorg. Chim. Acta* 1989, **161**, 3.
7. G. Smith, D. S. Sagatys, C. Campbell, D. E. Lynch and C. H. L. Kennard, *Aust. J. Chem.* 1990, **43**, 1707.
8. T. C. W. Mak, W.-H. Yip, C. H. L. Kennard, G. Smith and E. J. O'Reilly, *Aust. J. Chem.* 1988, **41**, 683.
9. M. E. Synerholm and P. W. Zimmerman, *Contrib. Boyce Thompson Inst.* 1945, **14**, 91.
10. G. M. Sheldrick, SHELX 76, Program for Crystal Structure Determination. University of Cambridge, U.K. (1976).
11. C. K. Prout, C. Walker and F. J. C. Rossotti, *J. Chem. Soc. A* 1972, 1852.
12. T. C. W. Mak, W.-H. Yip, G. Smith, E. J. O'Reilly and C. H. L. Kennard, *Inorg. Chim. Acta* 1986, **112**, 53.
13. C. H. L. Kennard, G. Smith and P. T. Manoharan, *Inorg. Chim. Acta* 1984, **82**, 35.
14. G. Smith, E. J. O'Reilly and C. H. L. Kennard, *Polyhedron* 1987, **6**, 871.
15. G. Smith, S. M. Shariff, E. J. O'Reilly and C. H. L. Kennard, *Polyhedron* 1989, **8**, 39.
16. T. C. W. Mak, W.-H. Yip, E. J. O'Reilly, G. Smith and C. H. L. Kennard, *Inorg. Chim. Acta* 1985, **100**, 267.
17. E. J. O'Reilly, G. Smith, C. H. L. Kennard and T. C. W. Mak, *Aust. J. Chem.* 1987, **40**, 1147.
18. C. H. L. Kennard, G. Smith, E. J. O'Reilly, K. Stadnicka and B. Oleksin, *Inorg. Chim. Acta* 1982, **59**, 241.
19. C. H. L. Kennard, E. J. O'Reilly, G. Smith and T. C. W. Mak, *Aust. J. Chem.* 1985, **38**, 1381.
20. C. H. L. Kennard, E. J. O'Reilly, S. Schiller, G. Smith and A. H. White, *Aust. J. Chem.* 1986, **39**, 1823.
21. G. Smith, D. E. Lynch, D. S. Sagatys, C. H. L. Kennard and G. F. Katekar, *Aust. J. Chem.* 1992, **45**, 1101.
22. J. E. Huheey, *Inorganic Chemistry*, 1st edn, p. 74. Harper and Row, London (1972).
23. G. Smith and C. H. L. Kennard, unpublished work.
24. J. N. van Neikerk and F. R. L. Schoening, *Acta Cryst.* 1953, **6**, 227.
25. G. Smith, E. J. O'Reilly and C. H. L. Kennard, *Inorg. Chim. Acta* 1981, **49**, 53.
26. T. C. W. Mak, C. H. L. Kennard, G. Smith, E. J. O'Reilly, D. S. Sagatys and J. Fulwood, *Polyhedron* 1987, **6**, 855.
27. G. Smith, E. J. O'Reilly, C. H. L. Kennard and A. H. White, *J. Chem. Soc., Dalton Trans.* 1985, 243.

Polyhedron Vol. 12, No. 2, pp. 209–219, 1993
Printed in Great Britain

0277–5387/93 $6.00+.00
© 1993 Pergamon Press Ltd

SOLUBLE AND VOLATILE BARIUM ARYLOXIDE DERIVATIVES: SYNTHESIS AND MOLECULAR STRUCTURE OF $Ba_5(\mu_5\text{-}OH)(\mu_3\text{-}OAr)_4(\mu_2\text{-}OAr)_4(OAr)(THF)_5$, $[Ba(\mu_1,\mu_2\text{-}dpm)(dpm)(HOAr)_2(THF)]_2$ AND $[Ba(H_2NCH_2CH_2OH)(\mu_1,\mu_2\text{-}H_2NCH_2CH_2OH)(\mu_2\text{-}OH)(\mu_2\text{-}OAr)(HOAr)]_\infty$ (Ar = $C_6H_3Bu^t_2$-3,5; dpm = $Bu^tC(O)CHC(O)Bu^t$)

PHILIPPE MIELE, JEAN-DOMINIQUE FOULON and NADINE HOVNANIAN*

Laboratoire de Physicochimie des Matériaux, URA 1312, ENSCM 8 rue Ecole Normale, 34053 Montpellier Cédex 1, France

(*Received* 31 *July* 1992; *accepted* 10 *September* 1992)

Abstract—Various barium aryloxide derivatives have been investigated. $Ba_5(\mu_5\text{-}OH)(\mu_3\text{-}OAr)_4(\mu_2\text{-}OAr)_4(OAr)(THF)_5$ (**I**), obtained by the reaction of barium metal granules in THF with 3,5-di-tert-butylphenol using gaseous ammonia as a catalyst, has been characterized by X-ray diffraction. The high nuclearity of this square-pyramidal pentahydroxyaryloxide complex accounts for its poor volatility. Complex **I** reacts with dpmH or $H_2NCH_2CH_2OH$ (2 mol) to yield $[Ba(\mu_1,\mu_2\text{-}dpm)(dpm)(HOAr)_2(THF)]_2$ (**II**) and $[Ba(H_2NCH_2CH_2OH)(\mu_1,\mu_2\text{-}H_2NCH_2CH_2OH)(\mu_2\text{-}OH)(\mu_2\text{-}OAr)(HOAr)]_\infty$ (**III**), respectively. The molecular structure of **II** shows a dimeric nature with two bridging-chelating β-diketonate ligands. Each metal atom is eight-coordinated with dodecahedral geometry. This complex is volatile and dissociates upon heating into a barium containing compound for which the spectroscopic data are in accord with the formula $[Ba(dpm)_2(HOAr)]_n$, $n \geqslant 2$. Complex **III** consists of a chain structure based on the infinite repetition of $[Ba(H_2NCH_2CH_2OH)(\mu_1,\mu_2\text{-}H_2NCH_2CH_2OH)(\mu_2\text{-}OH)(\mu_2\text{-}OAr)(HOAr)]$ units. This polymeric compound which presents some intramolecular hydrogen bonding is soluble but not volatile.

Molecular compounds of barium such as barium amides,[1] alkoxides[2] and aryloxides[3] have drawn increasing attention as sources of oxide precursors for MOCVD applications. In fact, barium oxides are involved in various advanced materials such as high-Tc superconducting ceramics[4] and materials with valuable electronic properties.[5]

The main behaviour of the alkaline-earth metals is dominated by their ionic character and their high metal coordination number (5–9 for barium) in their molecular compounds. We have been interested in producing compounds containing sterically hindered ligands in order to have low degrees of molecular aggregation which can allow better volatility. The substituted phenols have proved to be a source of interesting metal aryloxides which in general are hydrocarbon-soluble and volatile;[6] they are often available with an unusual metal coordination number.[7]

Herein the synthesis, the characterization and the reactivity towards polydentate compounds of a barium hydroxyaryloxide complex derived from the substituted phenol 3,5-di-tert-butylphenol will be described. The molecular structures of $Ba_5(\mu_5\text{-}OH)(\mu_3\text{-}OAr)_4(\mu_2\text{-}OAr)_4(OAr)(THF)_5$, $[Ba(\mu_1,\mu_2\text{-}dpm)(dpm)(HOAr)_2(THF)]_2$ and $[Ba(H_2NCH_2CH_2OH)(\mu_1,\mu_2\text{-}H_2NCH_2CH_2OH)(\mu_2\text{-}OH)(\mu_2\text{-}OAr)(HOAr)]_\infty$ will be reported. Their thermal behaviour will also be discussed.

EXPERIMENTAL

All manipulations were routinely performed under argon using Schlenk tubes and vacuum-line techniques with solvents purified by standard methods. Dipyvaloylmethane [dpmH = Bu^tC

* Author to whom correspondence should be addressed.

$(O)CH_2C(O)Bu^t$] was purified and 3,5-di-tert-butylphenol was sublimed before use; barium granules were used as received. ^1H NMR and IR spectra were run on Bruker AC-250 and IR FT Nicolet ZDX spectrometers, respectively. IR spectra were obtained as Nujol mulls between KBr plates. Mass spectra were recorded on a 300 DX JEOL by Electronic Impact or Fast-Atom Bombardment positive-ion[8] with an NBA matrix (NBA = *meta*-nitrobenzylalcohol). Thermogravimetric analysis was made under an argon atmosphere and the heating rate was 5°C min^{-1}. Analytical data were obtained from the Centre de Microanalyses du CNRS et de l'ENSCM.

Synthesis of $Ba_5(\mu_5\text{-}OH)(\mu_3\text{-}OAr)_4(\mu_2\text{-}OAr)_4(OAr)(THF)_5$ **(I)**

Barium metal granules (1.37 g, 10 mmol), 3,5-di-tert-butylphenol (4.12 g, 20 mmol) and THF (40 cm^3) were stirred together. Ammonia gas was bubbled at intermittent intervals of 5 min until all the barium metal was consumed (4 h). The solvent and an excess of ammonia were removed *in vacuo*. The precipitate was redissolved in toluene/THF (40/20) and the mixture was filtered. The yellow–green filtrate was left to crystallize at 5°C for 12 h. A large crop of colourless crystals was formed. Yield: 98%, based on barium. Found: C, 61.2; H, 7.9; Ba, 21.0. Calc. for $C_{146}H_{230}O_{15}Ba_5$: C, 60.2; H, 7.9; Ba, 23.6%. IR (cm^{-1}): 3590 [ν(O—H)], 1581, 1362, 1320, 1243, 1230, 1204, 1114, 1043, 1027, 995, 964, 901, 851, 816, 727, 711; 584, 542, 442 [ν(Ba—O)]. ^1H NMR ($CDCl_3$, ppm): 6.62 s (CH, 1H); 6.49 s (CH, 2H); 3.45 t (CH_2, 2H); 1.72 t (CH_2, 2H); 1.10 s (CH_3, 18H). SM (*m/z*, FAB^+): Ar = $C_6H_3Bu^t$-3,5; Bz = $(C_6H_4CH_2)NO_2$-3: $Ba_2(OAr)_3$ (10%), $Ba(OAr)_2Ba(OBz)$ (8%), $Ba(C_{12}H_{15}O)_2$ (5%), Ba(OAr) (100%), Ba(OBz) (35%), Ba(OPh) (35%). Soluble in THF, $CHCl_3$ and CH_2Cl_2, partially soluble in pentane and toluene.

Alternative synthesis of **I**

Barium metal granules (0.28 g, 2 mmol) and 3,5-di-tert-butylphenol (0.84 g, 4 mmol) were stirred in THF (40 cm^3) at reflux temperature until all the metal was consumed (60 h). The solvent was evaporated to dryness to yield a white solid. It was crystallized in hexane at 5°C. The same spectroscopic data were obtained for this compound.

Synthesis of $[Ba(dpm)_2(HOAr)_2(THF)]_2$ **(II)**

DpmH (0.41 cm^3, 2 mmol) was added to a solution of $Ba_5(\mu_5\text{-}OH)(\mu_3\text{-}OAr)_4(\mu_2\text{-}OAr)_4(OAr)(THF)_5$ (0.58 g, 0.2 mmol) in toluene/THF (7 cm^3/1 cm^3). The mixture was stirred at room temperature for 2 h. After concentration, the crystallization at 5°C yielded a large crop of parallelopiped colourless crystals. Yield: 80%, based on barium. Found: C, 65.9; H, 9.3. Calc. for $C_{108}H_{180}O_{14}Ba_2$: C, 65.6; H, 9.1%. IR (cm^{-1}): 3070 [ν(O—H)], 1593, 1575, 1562, 1530, 1461, 1419, 1395, 1382, 1361, 1303, 1271, 1250, 1237, 1224, 1200, 1181, 1123, 1049, 1025, 999, 959, 951, 933, 898, 880, 864, 853, 795, 787, 774, 753, 737, 727, 713, 671, 647, 616, 592, 565, 537, 476, 386, 357. ^1H NMR ($CDCl_3$, ppm): 6.98 t (CH, 1H, ^3J = 1.2 Hz); 6.68 d (CH, 2H, ^3J = 1.2 Hz); 5.53 s (CH, 1H); 3.75 t (CH_2, 2H); 4.87 broad (OH); 1.86 t (CH_2, 2H); 1.29 s (CH_3, 18H); 0.99 s (CH_3, 18H). SM (m/z^+, IE): $Ba_2(dpm)(THF)(OAr)(Bu^tCO)$ (82%), $Ba_2(OAr)(THF)_2$ (5%), $Ba(OAr)(THF)(C(O)CH_2C(O)Bu^t)$ (7%), $Ba(OAr)(C(O)CH_2C(O)Bu^t)$ (15%), Ba(dpm) (100%), ArOH-Me (40%), $C(O)CH_2C(O)Bu^t$ (14%), Bu^t(95%). Soluble in THF, $CHCl_3$, CH_2Cl_2, heptane and toluene, partially soluble in pentane.

Synthesis of $[Ba(H_2NCH_2CH_2OH)(\mu_1,\mu_2\text{-}H_2NCH_2CH_2OH)(\mu_2\text{-}OH)(\mu_2\text{-}OAr)(HOAr)]_\infty$ **(III)**

$H_2NCH_2CH_2OH$ (0.12 cm^3, 2 mmol) was added to a solution of $Ba_5(\mu_5\text{-}OH)(\mu_3\text{-}OAr)_4(\mu_2\text{-}OAr)(THF)_5$ (0.58 g, 0.2 mmol) in toluene/THF (7 cm^3/1 cm^3). A reaction occurred and the colour of the medium changed from green to yellow. The mixture was stirred for 2 h. Colourless needles were obtained after concentration and crystallization at room temperature. Yield: 88%, based on barium. Found: C, 56.9; H, 8.3; N, 4.2. Calc. for $C_{32}H_{58}N_2O_5Ba$: C, 55.8; H, 8.4; N, 4.1%. IR (cm^{-1}): 3490, 3360 [ν(NH or/and OH)], 1581, 1323, 1244, 1261, 1242, 1204, 1170, 1157, 1107, 1027, 996, 964, 934, 898, 864, 843, 815, 774, 722, 585, 538. ^1H NMR (CD_2Cl_2, ppm): 6.58 s (CH, 1H); 6.48 s (CH, 2H); 3.29 broad (OCH_2, 2H); 2.34 broad (NCH_2, 2H); 1.23 s (CH_3, 18H). SM (m/z^+, IE): Ba(Ph)(OAr)$(HNC_2H_4O)(H_2NC_2H_4OH)$ (1%), Ba(HOAr)$(H_2NC_2H_4OH)_2$ (2%), Ba(OAr-Bu^t)$(H_2NC_2H_4OH)_2$ (3%), Ba(OAr-Bu^t)$(H_2NC_2H_4OH)(C_2H_4OH)$ (1%), Ba(OPh)$(H_2NC_2H_4OH)_2$ (4%), Ba(OAr-Bu^t)(CH_3OH) (2%), Ba(OH)(OPh)(CH_3OH) (20%), Ba(OPh)(CH_3OH) (5%), ArOH (23%), ArOH-CH_3 (90%), Bu^t (100%), NC_2H_4 (30%). Soluble in toluene, heptane, THF, $CHCl_3$ and CH_2Cl_2, partially soluble in pentane.

Crystallographic studies

The selected crystals of **I**, **II** and **III** were mounted onto a Siemens P3 automatic diffractometer. Accur-

ate unit cell dimensions and crystal orientation matrices, together with their estimated standard deviations, were obtained from least-squares refinement of the setting angles of 25 (compound **I**), 21 (compound **II**) and 22 (compound **III**) reflections. Crystallographic data and other pertinent information are summarized in Table 1. The data of **I** were corrected for linear decay by batch scaling from one set of checks to the next. Corrections were made for Lorentz and polarization effects. No correction for absorption was made. All calculations for these three investigations were performed on a VAX 3100. Complex neutral-atom scattering factors were employed. Anomalous dispersion terms were used. For the three investigated compounds the positions of the barium atom were found by analysis of a three-dimensional Patterson map using SHELXS 86[9] and was confirmed by direct methods using SIR.[10] All remaining non-hydrogen atoms were found by successive electron density map calculations using SHELX 76.[11] Anisotropic temperature factors were introduced for all non-hydrogen atoms in **II**. Due to a medium quality of the crystal of **I**, the data contained a large

Table 1. Summary of crystallographic data of **I**, **II** and **III**

	I	**II**	**III**
Compound	$C_{146}H_{230}O_{15}Ba_5$	$C_{108}H_{180}O_{14}Ba_2$	$C_{32}H_{58}N_2O_5Ba$
Molecular weight	2912	1977.3	698.2
Crystal system	Triclinic	Triclinic	Orthorhombic
Space group	$P\bar{1}$	$P\bar{1}$	$Pna2_1$
a (Å)	16.629(3)	13.190(3)	26.872(7)
b (Å)	18.456(3)	16.081(4)	18.006(3)
c (Å)	26.843(6)	16.152(4)	7.660(1)
α (°)	94.43(2)	112.43(2)	90
β (°)	97.28(2)	97.27(2)	90
γ (°)	97.01(1)	109.06(2)	90
V (Å^3)	8074(3)	2866(1)	3706(1)
Z	2	1	4
D_{calc} (g cm^{-3})	1.98	1.145	1.233
$F(000)$ (e$^-$)	3012	1052	1440
Diffractometer	Siemens P3	Siemens P3	Siemens P3
Temperature (K)	293	293	293
Radiation	Mo-K_α	Mo-K_α	Mo-K_α
Scan type	ω–2θ	ω–2θ	ω
Scan width	$0.90+0.35\tan\theta$	$1.00+0.35\tan\theta$	$1.00+0.35\tan\theta$
Scan range	$2 \leqslant \theta \leqslant 20$	$2 \leqslant \theta \leqslant 22.5$	$2 \leqslant \theta \leqslant 22.5$
hkl limits	$\pm h, \pm k, +l$	$\pm h, \pm k, +l$	$+h, +k, +l$
Reference reflections	4 every 50 reflections	3 every 50 reflections	3 every 100 reflections
Intensity stability	30% of decay (during data collection)	Variation less than 5%	Variation $\leqslant$ 5%
Data collected	16,489	7869	3746
Unique data used ($F_o^2 > 3\sigma(F_o)^2$)	7520	6238	2265
μ (cm^{-1})	12.5	7.3	11.0
Absorption correction	None	None	None
R^a	0.0953	0.0384	0.0558
$R_w{}^a$	0.1072	0.0434	0.0677
Number of parameters refined	698	560	275
Ratio of observation to parameter	10.8	11.1	8.2
$(\Delta/\sigma)_{max}{}^b$	0.01	0.01	0.01
Residual electron density (e Å^{-3})	1.2 to −1.6	0.6 to −0.4	±1.1

[a] The quantity minimized in the least-squares procedure is: $w(|F_o|-|F_c|)^2$. $R = \Sigma\,||F_o|-|F_c||/\Sigma\,|F_o|$; $R_w = [\Sigma\, w(|F_o|-|F_c|)^2/\Sigma\, w(F_o)^2]^{1/2}$.

[b] Maximum ratio of the rms shift to standard deviation observed for the last cycle of refinement.

proportion of weak reflections. Therefore, only barium atoms were allowed to move anisotropically in **I** in order to keep the ratio of observation-to-parameter higher than 10. For the same reason, in complex **III** the carbon atoms of the Bu^t groups as well as the solvent molecule were kept isotropic whereas the other atoms were refined anisotropically. For **II** and **III** hydrogen atoms were placed in calculated positions (C—H = 1.08 Å) and were not further refined but recalculated after each cycle. They were ignored in compound **I**. In complex **I**, in two THF groups, the distances between the carbon atoms refined to unreasonable values. The three carbon atoms involved were thus fixed in their found positions, leading to satisfactory bond lengths in these two THF groups. The solvent toluene molecule in the lattice was not refined (atoms were just included in found positions with a fixed isotropic temperature factor). The criteria for a satisfactory complete analysis were the ratios of the rms shift-to-standard deviation being less than 0.1 and no significant features in the final different map. Positional parameters and equivalent isotropic or isotropic parameters are given as supplementary material.

RESULTS AND DISCUSSION

We have investigated the synthesis of 3,5-di-tert-butylphenoxide of barium and its reactivity towards dpmH and ethanolamine (Scheme 1). Each compound was characterized by elemental analysis and the usual spectroscopic methods: IR, NMR and mass spectroscopy. The complete structural characterization of $Ba_5(\mu_5\text{-}OH)(\mu_3\text{-}OAr)_4(\mu_2\text{-}OAr)_4(OAr)(THF)_5$, $[Ba(\mu_1,\mu_2\text{-}dpm)(dpm)(HOAr)_2(THF)]_2$ and $[Ba(H_2NCH_2CH_2OH)(\mu_1,\mu_2\text{-}H_2NCH_2CH_2OH)(\mu_2\text{-}OH)(\mu_2\text{-}OAr)(HOAr)]_\infty$ was achieved by X-ray diffraction. The thermal stability and volatility of each aryloxide derivative have been studied by heating the complexes *in vacuo* (10^{-2} mmHg) and by thermogravimetric analyses.

Synthesis and characterization of I

The pentahydroxyaryloxide aggregate of barium, $Ba_5(\mu_5\text{-}OH)(\mu_3\text{-}OAr)_4(\mu_2\text{-}OAr)_4(OAr)(THF)_5$ (**I**), was obtained by reaction between barium metal and 3,5-di-tert-butylphenol using ammonia gas as the catalyst in a 98% yield. This route has already been mentioned by Caulton;[12] it allows an easy and fast reaction of alkaline-earth metals by very sterically encumbered ligands in an oxygenated medium.[13] The direct reaction of the barium metal with 3,5-di-tert-butylphenol in THF has also been achieved by heating, but an alternate synthesis of **I** is very long (the reaction will be longer as the ArO ligand increases in size).

Despite the sterically hindered ligands, this compound presents a high nuclearity which accounts for its poor volatility. It decomposes by loss of ArOH at 100°C/10^{-1} mmHg. The thermogravimetric analysis of **I** shows a two-step process: a rapid weight loss in the range 100–120°C and a second one in the range 250–300°C. The percentage of weight loss corresponds to the THF and ArOH removal, respectively. The aggregate also displays good solubility.

The IR spectra display essentially the absorption bands of the ligands. The presence of the hydroxy group is obvious with a characteristic O—H stretching vibration at 3590 cm^{-1}. The ^{1}H NMR spectra show a single set of ArO and THF resonances. The solvent also acts as a Lewis base; it stabilizes the complex in which the coordination number of the barium is reached.

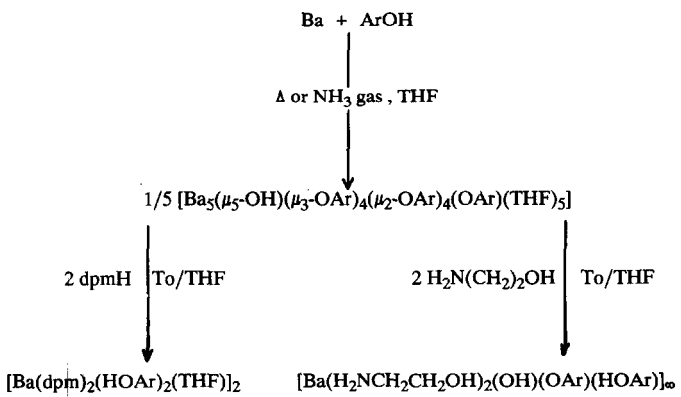

Scheme 1

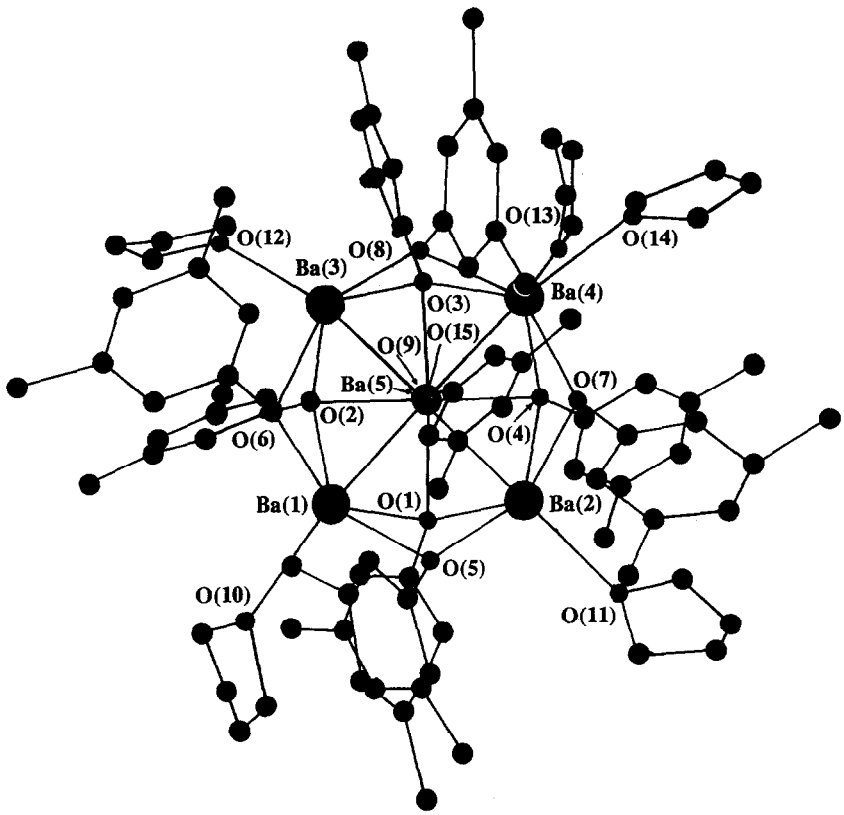

Fig. 1. Atomic numbering scheme for $Ba_5(\mu_5\text{-}OH)(\mu_3\text{-}OAr)_4(\mu_2\text{-}OAr)_4(OAr)(THF)_5$ (the terminal methyl groups of the Bu^t ligands are omitted for clarity).

Solid-state structure of $Ba_5(\mu_5\text{-}OH)(\mu_3\text{-}OAr)_4(\mu_2\text{-}OAr)_4(OAr)(THF)_5$

Since the spectroscopic data offer limited structural information, X-ray diffraction studies were carried out on $Ba_5(\mu_5\text{-}OH)(\mu_3\text{-}OAr)_4(\mu_2\text{-}OAr)_4(OAr)(THF)_5$. The molecular structure of **I** is a square-based pyramid of barium atoms with a single OH^- ligand lying 2.01(2) Å above the plane defined by the four basal barium centres (Fig. 1). The aryloxides are of three types: four triply bridging, four doubly bridging and one terminal. The μ_2- and μ_3-OAr groups are thus responsible for the stability of the structural arrangement. The μ_3-OAr groups occupy the four triangular faces of the square pyramid; the μ_2-OAr ligands bridge the four basal metal atoms and the single OAr terminal ligand bonds to the apical barium. Selected bond distances and angles are given in Table 2.

The same square pyramidal Ba_5 geometry found in $Ba_5(OH)(OAr)_9(THF)_5$ is also adopted in $HBa_5(O)(OPh)_9(THF)_8$.[3b] The distribution of the OAr ligands, four μ_3, four μ_2 and one terminal, duplicates that reported here. The lengths of analogous bonds in these two molecules are very similar. The structural differences are essentially due to the number and the coordination of the THF molecules. (1) In the aryloxide complex **I** three of the basal barium atoms are bonded to one THF molecule—they, and the apical barium, are hexa-coordinated—whereas the fourth basal barium bonded to two THF molecules is hepta-coordinated. (2) In the phenoxide complex each basal atom is bonded to two THF molecules—so they are ligated to seven oxygen atoms—whereas the apical barium is only six-coordinated.

Presumably the number of THF molecules is lower in **I** than in the phenoxide analogue because of the steric hindrance provided by the bulky Bu^t groups of the OAr ligand. The range of Ba—O(THF) distances is large (2.69–2.85 Å), indicating the different degree of steric hindrance imposed on each THF ligand.

The Ba—O(OAr) distances illustrate the different types of OAr groups: the more these groups are coordinated, the higher the bond length. This could be expected on the basis of electronic effects. These bond lengths are in good agreement with previous values reported in the literature.[3] In particular, the Ba—O(OAr terminal) bond length is typical of a

Table 2. Selected bond lengths (Å) and angles (°) for $Ba_5(\mu_5\text{-}OH)(\mu_3\text{-}OAr)_4(\mu_2\text{-}OAr)_4(OAr)(THF)_5$ (I) (standard deviations in parentheses)

Bond lengths					
Ba(1)—O(1)	2.708(18)	Ba(1)—O(2)	2.740(18)	Ba(1)—O(5)	2.662(22)
Ba(1)—O(6)	2.551(23)	Ba(1)—O(10)	2.786(25)	Ba(1)—O(15)	2.775(17)
Ba(2)—O(1)	2.695(13)	Ba(2)—O(4)	2.711(17)	Ba(2)—O(5)	2.552(21)
Ba(2)—O(7)	2.603(21)	Ba(2)—O(11)	2.700(33)	Ba(2)—O(15)	2.801(18)
Ba(3)—O(2)	2.670(17)	Ba(3)—O(3)	2.702(17)	Ba(3)—O(6)	2.711(22)
Ba(3)—O(8)	2.558(20)	Ba(3)—O(12)	2.783(28)	Ba(3)—O(15)	2.804(19)
Ba(4)—O(3)	2.772(17)	Ba(4)—O(4)	2.678(17)	Ba(4)—O(7)	2.648(23)
Ba(4)—O(8)	2.605(20)	Ba(4)—O(13)	2.855(22)	Ba(4)—O(14)	2.826(24)
Ba(4)—O(15)	2.862(17)	Ba(5)—O(1)	2.676(18)	Ba(5)—O(2)	2.702(18)
Ba(5)—O(3)	2.685(15)	Ba(5)—O(4)	2.688(18)	Ba(5)—O(9)	2.397(26)
Ba(5)—O(15)	3.084(18)				
Selected bond averaged for the four basal barium atoms					
$(\mu_3\text{-}O)$—Ba—$(\mu_3\text{-}O)$	78.1(5)			$(\mu_3\text{-}O)$—Ba—$(\mu_2\text{-}O)$	74.3(6)
$(\mu_2\text{-}O)$—Ba—$(\mu_3\text{-}O)$	134.5(6)			$(\mu_3\text{-}O)$—Ba—$(\mu_5\text{-}O)$	67.7(5)
$(\mu_2\text{-}O)$—Ba—$(\mu_5\text{-}O)$	73.1(6)				
Bond angles involving THF oxygen atoms[a]					
$(\mu_2\text{-}O)$—Ba—O(THF)		85.9(7)–129.3(7)			
$(\mu_3\text{-}O)$—Ba—O(THF)		73.9(6)–136.6(6)			
Bond angles involving the apical barium atom					
O(3)—Ba(5)—O(1)	128.0(5)			O(3)—Ba(5)—O(2)	77.7(5)
O(4)—Ba(5)—O(1)	79.6(5)			O(4)—Ba(5)—O(2)	127.7(5)
O(4)—Ba(5)—O(3)	78.7(5)			O(9)—Ba(5)—O(1)	122.9(7)
O(9)—Ba(2)—O(1)	113.1(7)			O(9)—Ba(5)—O(3)	109.0(7)
O(9)—Ba(5)—O(4)	118.6(7)			O(15)—Ba(5)—O(1)	63.6(5)
O(15)—Ba(5)—O(2)	63.9(5)			O(15)—Ba(5)—O(3)	64.4(5)
O(15)—Ba(5)—O(4)	63.9(5)			O(15)—Ba(5)—O(9)	172.8(7)

[a] Bond angles involving THF oxygen atoms cover a wide range of values, which does not permit any average. Minimum and maximum values for the different angles are reported below.

formal OAr^- group. Therefore, although the presence of the hydrogen atom in the neighbouring μ^5-O was not evident from the X-ray work, the μ^5-oxygen atom was definitively considered as a hydroxy group since it was the only possibility for the remaining hydrogen atom. Such an unambiguous assignment was not possible in the case of $HBa_5(O)(OPh)_9(THF)_8$. Furthermore, the hydroxy-ligand is observed in the IR spectra [ν(O—H) = 3590 cm^{-1}]; also, it allows the electroneutrality of the compound. Although the origin of the hydroxy ligand is not elucidated, its formation by "accidental" hydrolysis seems improbable since the isolation of the hydroxyaryloxide in high yield is reproducible.

The square-pyramidal configuration $M_5(\mu_5\text{-}O)(\mu_3\text{-}OR)_4(\mu_2\text{-}OR)_4$ has also been found for several alkoxide compounds, such as $M_5O(OPr^i)_{13}$ (Y,[14] In,[15] Yb[16]) and $(\eta^5Cp)_5Y_5O(OMe)_8$.[17] The molecular structures of alkaline-earth metal aryloxides remain relatively scarce; only mononuclear metal compounds with very sterically hindered ligands, such as $Ca(OCH_2Bu^t_2\text{-}2,6\text{-}Me\text{-}4)_2(THF)_3$[18] and $Ba(OC_6H_3Bu^t_2\text{-}3,5)_2(HOCH_2CH_2NMe_2)_4$,[3a] or metal clusters with phenoxide ligands, such as $HBa_5(O)(OPh)_9(THF)_8$[3b] and $Sr_4(OPh)_8(PhOH)_2(THF)_6$,[19] have been recently reported. By the metathetical reaction of an alkali metal aryloxide with a barium halide an oxoaryloxide cluster is obtained, $[Ba_4(\mu_4\text{-}O)\mu_2\text{-}OC_6H_2(CH_2NMe_2)_3\text{-}2,4,6)_6]\cdot 3(toluene)$,[3d] even with very encumbered ligands. None of them are volatile.

Reactivity of **I**

The reactions of **I** towards oxygenated compounds such as β-diketone (dpmH) and amino-alcohol ($H_2NCH_2CH_2OH$) have been studied. Such

polydentate compounds may be potentially useful in stabilizing the aryloxide complex **I** while reducing its polymerization. Complex **II**, $[Ba(dpm)_2(HOAr)_2(THF)]_2$, and complex **III**, $[Ba(H_2NCH_2CH_2OH)(\mu_1,\mu_2\text{-}H_2NCH_2CH_2OH)(\mu_2\text{-}OH)(\mu_2\text{-}OAr)(HOAr)]_\infty$, were obtained by reacting complex **I** with dpmH (2 mol) and $H_2NCH_2CH_2OH$ (2 mol), at room temperature in a mixture of toluene and THF.

Complex **II** displays a broad O—H stretching vibration in the IR spectrum at 3070 cm^{-1}. The ^1H NMR spectrum of this compound reveals a single average environment for the β-diketonate and the aryloxide groups. A broad resonance at 4.87 ppm is attributed to the alcohol proton. The ion with the highest molecular mass, $[Ba_2(dpm)(THF)(OAr)(Bu^tCO)]$ (82%), is present in the electron ionization mass spectrum, suggesting a dimeric nature for this complex. This is confirmed by X-ray crystal structure determination. It displays a good solubility and it dissociates upon heating between 200 and 220°C/10^{-2} mmHg into a barium-containing compound (EDX analyses), which shows the dpm and OAr ligands in ^1H NMR spectra. The elemental analysis of this sublimate compound agrees with the formula $[Ba(dpm)_2(HOAr)]_n$, $n \geqslant 2$. This sublimation with decomposition is obtained in a high yield (90% based on Ba). Thermogravimetric analyses have shown three weight losses of 7.3, 41.7 and 37.1% in the ranges 80–110°C, 160–310°C and 310–580°C, corresponding to THF, ArOH and dpmH removal, respectively. Thus, the volatility and the high solubility of complex **II** make it an attractive precursor for MOCVD and sol–gel processes. The ease with which complex **II** is obtained from **I** in very mild conditions proves the fragility of the polyhedron hydroxyaryloxide structure. The β-diketone dpmH causes the degree of molecular aggregation to decrease and enhances the volatility. Only very few volatile molecular barium compounds have been reported in the literature;[20,21] they often display a low degree of molecular aggregation (monomer or dimer) depending on whether or not the β-diketonate ligands are fluorinated.

The IR spectrum of complex **III** displays essentially the absorption bands of the ligands as well as broad stretching vibrations at 3490 and 3360 cm^{-1}, characteristic of ν(O—H) and/or μ(N—H) vibrations. The room-temperature ^1H NMR spectrum in CD_2Cl_2 reveals a single environment for the aryloxide groups and for the ethanolamine ligands. Integration establishes the presence of one ArO group for one ethanolamine. The alcohol and amine proton resonances are not observed. The polymeric nature of this compound has been determined by an X-ray crystal structure study. This and the presence of intramolecular hydrogen bondings in the building account for its non-volatility. A TG analysis presents a total weight loss of 78% in the range 100–700°C in various and badly defined steps. However, complex **III** is highly soluble.

Solid-state structure of $[Ba(\mu_1,\mu_2\text{-dpm})(dpm)(HOAr)_2(THF)]_2$ **(II)**

The structure of the $[Ba(dpm)_2(HOAr)_2(THF)]_2$ complex is shown in Fig. 2 and selected bond distances and angles are given in Table 3. The molecule is centrosymmetric and consists of a dimeric unit where barium atoms are bonded to eight oxygen atoms in a roughly dodecahedral environment. Both independant β-diketonate ligands are bidentate, but one occupies a terminal position whereas the other acts as a bridge between the two barium atoms of the dimeric complex. Such a pattern of dpm ligands is also encountered in related dimeric barium β-diketonate species, $[Ba(dpm)_2\cdot 2NH_3]_2$ and $[Ba(dpm)_2\cdot Et_2O]_2$.[21] However, in the latter compound each carbonyl oxygen of the two bridging dpm ligands is μ_2-coordinated, whereas in the studied complex **II** the dpm bridges are achieved by μ_1-O and μ_2-O carbonyl ligands. In addition, in the dpm ligands each metal centre is ligated to one THF and two ArOH molecules in terminal positions, yielding a coordination number of eight. Although the hydrogen atoms of the ArOH groups were not crystallographically located, an unambiguous assignment as coordinated alcohol was made on the basis of the long terminal Ba(1)—O(31) and Ba(1)—O(41) bond lengths of 3.003(3) and 2.815(5) Å, respectively. The alcohol group is confirmed by the spectroscopic data. This is also necessary in order to ensure the electroneutrality of the complex. The Ba—O distances are in good agreement with the expected ones. Ba—μ_1-O(dpm) bond lengths are shorter than Ba—μ_2-O(dpm) due to electronic effects. The Ba—O(THF) bond length is rather small compared to the Ba—O(THF) range observed in compound **I**. The present bond length indicates little steric hindrance from the other ligands to the THF ligand. The Ba—O(ArOH) distances are very long and thus ArOH groups should be considered as only interacting with the metal atom and not directly bonding to it.

Solid-state structure of $[Ba(H_2NCH_2CH_2OH)(\mu_1,\mu_2\text{-}H_2NCH_2CH_2OH)(\mu_2\text{-}OH)(\mu_2\text{-}OAr)(HOAr)]_\infty$

The structure of complex **III** is shown in Fig. 3. Relevant bond lengths and angles are collected in Table 4. The complex is shown to be polymeric and its chain structure is based on monomeric $[Ba(H_2N$

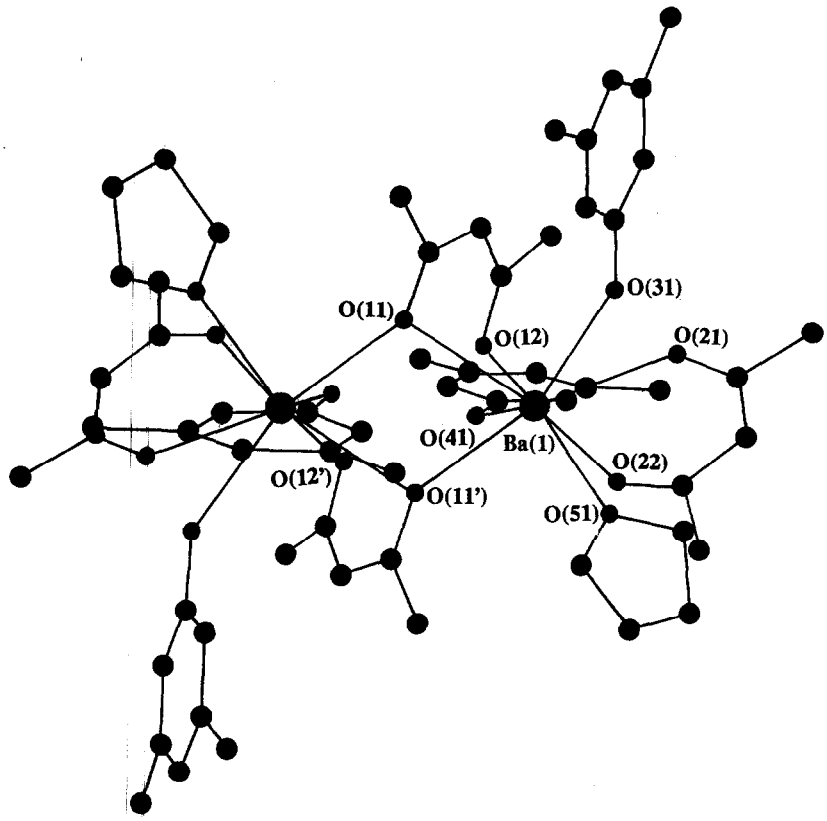

Fig. 2. Atomic numbering scheme for $[Ba(\mu_1,\mu_2\text{-dpm})(dpm)(HOAr)_2(THF)]_2$ (the terminal methyl groups of the Bu^t ligands are omitted for clarity).

Table 3. Selected bond lengths (Å) and angles (°) for $[Ba(\mu_1,\mu_2\text{-dpm})(dpm)(HOAr)_2(THF)]_2$ (II)[a] (standard deviations between parentheses)

Bond lengths			
Ba(1)—O(11)	2.833(3)	Ba(1)—O(11′)	2.670
Ba(1)—O(12)	2.777(4)	Ba(1)—O(51)	2.888(5)
Ba(1)—O(21)	2.713(3)	Ba(1)—O(22)	2.625(4)
Ba(1)—O(31)	3.003(3)	Ba(1)—O(41)	2.815(5)
O(21)···O(31)	2.558(6)	O(12′)···O(41)	2.675(6)
Bond angles			
O(12)—Ba(1)—O(11)	59.7(1)	O(21)—Ba(1)—O(11)	127.2(1)
O(21)—Ba(1)—O(12)	93.9(1)	O(22)—Ba(1)—O(11)	134.6(1)
O(22)—Ba(1)—O(12)	76.7(1)	O(22)—Ba(1)—O(21)	63.9(1)
O(31)—Ba(1)—O(11)	92.6(1)	O(31)—Ba(1)—O(12)	111.4(1)
O(31)—Ba(1)—O(21)	52.9(1)	O(31)—Ba(1)—O(22)	116.4(1)
O(41)—Ba(1)—O(11)	75.3(1)	O(41)—Ba(1)—O(12)	134.2(1)
O(41)—Ba(1)—O(21)	121.6(1)	O(41)—Ba(1)—O(22)	142.3(1)
O(41)—Ba(1)—O(31)	76.4(1)	Ba(1)—O(11)—Ba(1)	111.9(1)
O(11′)—Ba(1)—O(11)	68.1(1)	O(11′)—Ba(1)—O(12)	84.3(1)
O(11′)—Ba(1)—O(21)	160.6(1)	O(11′)—Ba(1)—O(22)	96.9(1)
O(11′)—Ba(1)—O(31)	145.2(1)	O(11′)—Ba(1)—O(41)	70.9(1)
O(51)—Ba(1)—O(11)	142.3(1)	O(51)—Ba(1)—O(11′)	90.7(1)
O(51)—Ba(1)—O(12)	152.0(1)	O(51)—Ba(1)—O(21)	81.8(1)
O(51)—Ba(1)—O(22)	76.5(1)	O(51)—Ba(1)—O(31)	88.1(1)
O(51)—Ba(1)—O(41)	68.3(1)		

[a] Atoms marked with primes are related by the inversion centre.

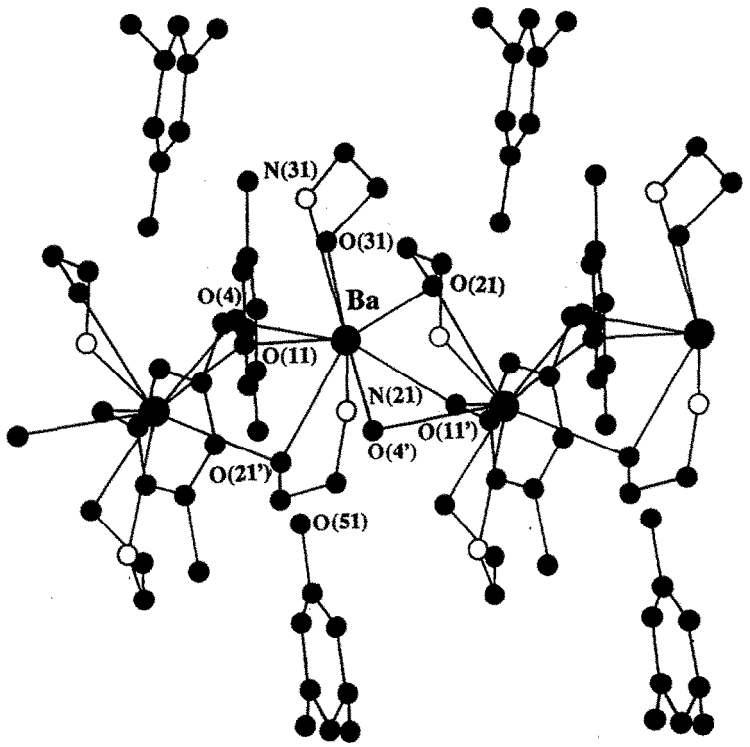

Fig. 3. Atomic numbering scheme for [Ba($H_2NCH_2CH_2OH$)(μ_1,μ_2-$H_2NCH_2CH_2OH$)(μ_2-OH)(μ_2-OAr)(HOAr)]$_\infty$ (the terminal methyl groups of the Bu^t ligands are omitted for clarity.

CH_2CH_2OH)(μ_1,μ_2-$H_2NCH_2CH_2OH$)(μ_2-OH)(μ_2-OAr)(HOAr)] units. The chains are growing along the *c*-axis through a 2_1 screw axis. The monomeric unit can be formulated in four different ways: (1) [Ba($H_2NCH_2CH_2OH$)(μ_1,μ_2-$H_2NCH_2CH_2OH$)(μ_2-OAr)(OAr)], (2) [Ba($H_2NCH_2CH_2OH$)(μ_1,μ_2-$H_2NCH_2CH_2O$)(μ_2-OH_2)(μ_2-OAr)(HOAr)], (3) [Ba($H_2NCH_2CH_2OH$)(μ_1,μ_2-$H_2NCH_2CH_2OH$)(μ_2-OH)(μ_2-OAr)(HOAr)] and (4) [Ba($H_2NCH_2CH_2O$)(μ_1,μ_2-$H_2NCH_2CH_2OH$)(μ_2-OH_2)(μ_2-OAr)(HOAr)].

Each of these four different possibilities allows for the electroneutrality of the molecule and arises from the non-location of the hydrogen atoms in the X-ray diffraction analysis. Nevertheless, the ethanolamine ligands are likely to be neutral according to the Ba—N (3 Å) and Ba—O (2.87 Å) bond distances, which fall in the range of the values previously reported in the literature.[22] Therefore, the formulation of the monomeric unit can only be 1 or 3. These two forms are tautomeric through the hydrogen bonding, according to the short oxygen–oxygen distances [O(4)—O(51) = 2.57, O(4)—O(31) = 2.59 and O(51)—O(21) = 2.58 Å], and it is impossible to differentiate one from the other in the present work. Nevertheless, we prefer to consider the isolated ArO(H) molecule as a solvent molecule rather than as a counter-ion, since generally isolated solvent molecules are more often encountered than isolated ions. Thus, in a further discussion complex **III** will be referred to as [Ba($H_2NCH_2CH_2OH$)(μ_1, μ_2-$H_2NCH_2CH_2OH$)(μ_2-OH)(μ_2-OAr)(HOAr)]$_\infty$, knowing that it could be otherwise.

The barium atoms are linked together by a chelating-bridging ethanolamine ligand, a doubly-bridging aryloxide ligand and a doubly-bridging hydroxy group. Their coordination is completed by a terminal ethanolamine ligand, resulting in a high degree of coordination of nine. The presence of relatively small ligands as ethanolamine or hydroxy groups reinforced by hydrogen bonding between them takes an important part in this high coordination of the metal centre. The Ba—O and the Ba—N bond lengths are usually observed for the different ligands.[22,23] It is noted that ethanolamine ligands play, in compound **III**, a similar role to the dpm ligands in compound **II**, as illustrated by the identical mode of coordination for these two ligands. In fact, since both complexes **II** and **III** originate from the reaction of dpmH and ethanolamine on the same complex (**I**), respectively, it appears to be a logical consequence to observe similar structural arrangements around the barium

Table 4. Selected bond lengths (Å) and angles (°) for $[Ba(H_2NCH_2CH_2OH)(\mu_1,\mu_2\text{-}H_2NCH_2CH_2OH)(\mu_2\text{-}OH)(\mu_2\text{-}OAr)(HOAr)]_\infty$ **(III)**[a] (standard deviations in parentheses)

Bond lengths			
Ba(1)—O(11)	2.733(11)	Ba(1)—O(11′)	2.676(11)
Ba(1)—O(21)	2.855(14)	Ba(1)—O(21′)	2.885(14)
Ba(1)—N(21)	3.027(18)	Ba(1)—O(31)	2.856(16)
Ba(1)—N(31)	3.045(17)	Ba(1)—O(4)	2.867(13)
Ba(1)—O(4′)	2.960(13)		
O(4)···O(31)	2.639(25)	O(51)···O(21)	2.566(24)
O(51)···O(4)	2.614(25)		
Bond angles			
O(21)—Ba(1)—O(11)	97.3(4)	N(21)—Ba(1)—O(11)	123.4(6)
N(21)—Ba(1)—O(21)	138.4(5)	O(31)—Ba(1)—O(11)	108.3(5)
O(31)—Ba(1)—O(21)	106.4(4)	O(31)—Ba(1)—N(21)	71.1(6)
N(31)—Ba(1)—O(11)	74.6(5)	N(31)—Ba(1)—O(21)	77.4(5)
N(31)—Ba(1)—N(21)	118.5(6)	N(31)—Ba(1)—O(31)	48.4(5)
O(4)—Ba(1)—O(11)	68.7(3)	O(4)—Ba(1)—O(21)	146.8(3)
O(4)—Ba(1)—N(21)	66.8(3)	O(4)—Ba(1)—O(31)	54.8(3)
O(4)—Ba(1)—N(31)	69.9(5)	O(11′)—Ba(1)—O(11)	138.2(4)
O(11′)—Ba(1)—O(21)	72.5(4)	O(11′)—Ba(1)—N(21)	71.3(6)
O(11′)—Ba(1)—O(31)	113.5(5)	O(11′)—Ba(1)—N(31)	137.3(5)
O(11′)—Ba(1)—O(4)	137.9(3)	O(11′)—Ba(1)—O(21′)	89.9(4)
O(11′)—Ba(1)—O(4′)	68.2(3)	O(21′)—Ba(1)—O(11)	71.2(4)
O(21′)—Ba(1)—O(21)	138.9(4)	O(21′)—Ba(1)—N(21)	60.3(5)
O(21′)—Ba(1)—O(31)	114.7(4)	O(21′)—Ba(1)—N(31)	132.1(5)
O(21′)—Ba(1)—O(4)	66.9(3)	O(21′)—Ba(1)—O(4′)	72.8(3)
O(4′)—Ba(1)—O(11)	70.6(3)	O(4′)—Ba(1)—O(21)	66.2(3)
O(4′)—Ba(1)—N(21)	116.4(5)	O(4′)—Ba(1)—O(31)	172.0(3)
O(4′)—Ba(1)—N(31)	124.7(5)	O(4′)—Ba(1)—O(4)	129.7(4)
Ba(1)—O(11)—Ba(1)	104.1(3)		

[a] Atoms marked with primes are related by the 2_1 screw axis.

atom in complexes **II** and **III**. The infinite chains obtained in complex **III** are presumably a consequence of the relatively small size of the ethanolamine ligand compared to the dpm ligand, which precludes the polymerization due to the steric hindrance of the bulky Bu^t groups.

Acknowledgement—We thank the CNRS-PIRMAT for financial support.

REFERENCES

1. (a) J. M. Boncella, C. J. Coston and J. K. Cammack, *Polyhedron* 1991, **10**, 769; (b) B. A. Vaartstra, J. C. Huffman, W. E. Streib and K. G. Caulton, *Inorg. Chem.* 1991, **30**, 121; (c) M. Westerhausen, *Inorg. Chem.* 1991, **30**, 96; (d) D. C. Bradley, M. B. Hursthouse, A. A. Ibrahim, K. M. Abdul Malik, M. Motevalli, R. Möseler, H. Powell, J. D. Runnacles and A. C. Sullivan, *Polyhedron* 1990, **24**, 2959.
2. (a) O. Poncelet, L. G. Hubert-Pfalzgraf, L. Toupet and J.-C. Daran, *Polyhedron* 1991, **10**, 2045; (b) K. G. Caulton, M. H. Chisholm, S. R. Drake and J. C. Huffman, *J. Chem. Soc., Chem. Commun.* 1990, 1498; (c) W. S. Rees Jr and D. A. Moreno, *J. Chem. Soc., Chem. Commun.* 1991, 1759.
3. (a) K. G. Caulton, M. H. Chisholm, S. R. Drake and K. Folting, *Inorg. Chem.* 1991, **30**, 1500; (b) K. G. Caulton, M. H. Chisholm, S. R. Drake and K. Folting, *J. Chem. Soc., Chem. Commun.* 1990, 1349; (c) P. B. Hitchcock, M. F. Lappert, G. A. Lawless and B. Royo, *J. Chem. Soc., Chem. Commun.* 1990, 1141, (d) K. F. Tesh and T. P. Hanusa, *J. Chem. Soc., Chem. Commun.* 1991, 879; (e) H. W. Roesky, M. Scholz and M. Noltemeyer, *Chem. Ber.* 1990, **123**, 2303.
4. (a) C. N. R. Rao and B. Raveau, *Accts Chem. Res.* 1989, **22**, 106; (b) S. Nomura, L. Toyama and K. Kaneta, *Jap. J. Appl. Phys.* 1982, **21**, L624; (c) C. W. Chu, P. H. Hor, R. L. Meng, L. Gao, Z. J. Huang, Y. Q. Wang, J. Bechtold, D. Campbell, M. K. Wu, J. Ashburn and C. Y. Huong, *Phys. Rev. Lett.* 1987, **58**, 405.

5. S. S. Flachen, *J. Am. Chem. Soc.* 1955, **77**, 6194.
6. (a) R. A. Andersen and G. E. Coates, *J. Chem. Soc., Dalton Trans.* 1972, 2153; (b) P. B. Hitchcock, M. F. Lappert and R. G. Smith, *Inorg. Chim. Acta* 1987, **139**, 183; (c) P. B. Hitchcock, M. F. Lappert and A. Singh, *J. Chem. Soc., Chem. Commun.* 1983, 1499; (d) R. L. Geerts, J. C. Huffman and K. G. Caulton, *Inorg. Chem.* 1986, **25**, 1803.
7. P. G. Eller, D. C. Bradley, M. B. Hursthouse and D. W. Meek, *Coord. Chem. Rev.* 1977, **24**, 1.
8. J.-L. Aubagnac, L. Cot, N. Hovnanian and P. Miele, *Bull. Soc. Chim. Belg.* 1992, **101**, 689.
9. G. M. Sheldrick, SHELXS-86, Program for the Solution of Crystal Structures. University of Göttingen, F.R.G. (1987).
10. M. C. Burla, M. Camalli, S. Cascaravo, C. Giacovazzo, G. Polidoni, R. Spagna and D. Viterbo, *J. Appl. Cryst.* 1989, **22**, 389.
11. G. M. Sheldrick, SHELX 76, Program for Crystal Structure Determination. University of Cambridge (1976).
12. K. G. Caulton, M. H. Chisholm, S. R. Drake and K. Folting, *Inorg. Chem.* 1991, **30**, 1500.
13. (a) S. R. Drake and D. J. Otway, *J. Chem. Soc., Chem. Commun.* 1991, 517; (b) S. R. Drake and D. J. Otway, *Polyhedron* 1992, **11**, 517.
14. O. Poncelet, W. J. Sartain, L. G. Hubert-Pfalzgraf, K. Folting and K. G. Caulton, *Inorg. Chem.* 1989, **28**, 263.
15. D. C. Bradley, H. Chudzynska, D. M. Frigo, M. B. Hursthouse and M. A. Mazid, *J. Chem. Soc., Chem. Commun.* 1988, 1258.
16. D. C. Bradley, H. Chudzynska, D. M. Frigo, M. E. Hammond, M. B. Hursthouse and M. A. Mazid, *Polyhedron* 1990, **9**, 719.
17. W. J. Evans and M. S. Sollberger, *J. Am. Chem. Soc.* 1986, **108**, 6095.
18. P. B. Hitchcock, M. F. Lappert, G. A. Lawless and B. Royo, *J. Chem. Soc., Chem. Commun.* 1990, 1141.
19. S. R. Drake, W. E. Streib, M. H. Chisholm and K. G. Caulton, *Inorg. Chem.* 1990, **29**, 2708.
20. (a) A. Gleizes, S. Sans-Lenain, D. Medus and R. Morancho, *C. R. Acad. Sci. Paris* 1991, **312**, series II, 983; (b) A. Gleizes, S. Sans-Lenain and D. Medus, *C. R. Acad. Sci. Ser. II*, 1991, **131**, 761; (c) J. A. T. Norman and G. P. Pez, *J. Chem. Soc., Chem. Commun.* 1991, 971; (d) A. P. Purdy, A. D. Berry, R. T. Holm, M. Fatemi and D. K. Gaskill, *Inorg. Chem.* 1989, **28**, 2799; (e) K. Timmer and H. A. Meinema, *Inorg. Chim. Acta*, submitted; (f) S. B. Turnipseed, R. D. Barkley and R. E. Sievers, *Inorg. Chem.* 1991, **30**, 1164.
21. W. S. Rees Jr, M. W. Carris and W. Hesse, *Inorg. Chem.* 1991, **30**, 4479; G. Rossetto, A. Polo, F. Benetollo, M. Porchia and P. Zanella, *Polyhedron* 1992, **11**, 979.
22. K. G. Caulton, M. H. Chisholm, S. R. Drake and K. Folting, *Inorg. Chem.* 1991, **30**, 1500.
23. O. Poncelet, L. G. Hubert-Pfalzgraf, L. Toupet and J.-C. Daran, *Polyhedron* 1991, **17**, 2045.

Polyhedron Vol. 12, No. 2, pp. 221–225, 1993
Printed in Great Britain

0277–5387/93 $6.00+.00
© 1993 Pergamon Press Ltd

THE PREPARATION OF RHENIUM(V) OXO AND IMIDO COMPLEXES WITH $Et_2NCSNHCOPh$ AND $Et_2NCSNC(NH)Ph$. THE X-RAY CRYSTAL STRUCTURE OF $[ReOCl(PhCONCSNEt_2)_2]$*

JONATHAN R. DILWORTH,† JASON S. LEWIS, JOHN R. MILLER and YIFAN ZHENG

Department of Chemistry and Biological Chemistry, University of Essex, Wivenhoe Park, Colchester, Essex CO4 3SQ, U.K.

(*Received* 31 *July* 1992; *accepted* 10 *September* 1992)

Abstract—Reaction of $[Bu^n_4N][ReOCl_4]$ with two equivalents of the bidentate (1−) oxygen/sulphur donor ligand N,N-diethyl-N′-benzoylthiourea (DEBTH) or the sulphur/nitrogen donor ligand N,N-diethyl-N′-benzoyliminothiourea (DEBITH) in dry methanol leads to the formation of the neutral complexes $[ReOCl(DEBT)_2]$ (**1**) and $[ReOCl(DEBIT)_2]$ (**2**). The X-ray crystal structure of **1** shows the complex has a pseudo-octahedral geometry with the oxo and chloride ligands in *cis* positions. Complex **1** reacts with substituted anilines, $ArNH_2$, to give the imido complexes $[ReCl(NAr)(DEBT)_2]$ in good yield and with PPh_3 to form the rhenium(III) complex $[Re(DEBT)_2(PPh_3)_2]^+$. The spectroscopic and electrochemical properties of these complexes are discussed.

The coordination chemistry of bidentate sulphur–oxygen ligands has been widely investigated,[1] and the sulphur donor can be thiolate,[2–8] thioether[9–16] or other forms of neutral sulphur.[17–29] However, the coordination chemistry of N,N-diethylbenzoylthiourea (DEBTH, see Fig. 1) and N,N-diethyl-N′-benzoyliminothiourea (DEBITH, Fig. 1) have been comparatively little investigated apart from some complexes of first row transition metals,[30] although some technetium nitrido-complexes of DEBIT have recently been reported by Abram *et al.*[31] We have for some time been interested in the possibilities of using the thioamide group as a potential masked source of anionic sulphur by virtue of the thiol–thione tautomerism, and have reported the chemistry of thiohydrazide ($RCSNHNHR'$) ligands with a variety of metals. We are currently investigating the coordination chemistry of technetium with a wide range of such ligands and here we describe the chemistry of rhenium with DEBTH and DEBITH. Due to the strong analogies between technetium and rhenium, this can provide useful indications of how technetium may behave. Here we describe the preparation and structure of a rhenium(V) oxo complex with DEBT and its reaction with anilines to give arylimido complexes, together with some related chemistry of the DEBIT ligand system. The analogous technetium chemistry will be reported elsewhere.

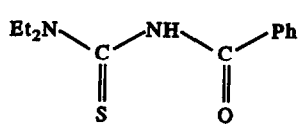

DEBTH

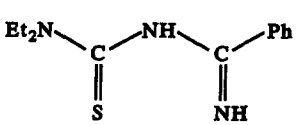

DEBITH

Fig. 1. The structures of DEBTH and DEBITH.

* Chloro-bis(N,N-diethyl-N′-benzoylthiourea)oxorhenium(V).

† Author to whom correspondence should be addressed.

EXPERIMENTAL

General

All manipulations were carried out under an inert atmosphere of dry dinitrogen gas. Standard Schlenk tube–vacuum line and syringe techniques were utilized where appropriate. Elemental analyses were performed by MEDAC Ltd, University of Brunel, using either a CEC 240XA or Carlo Erba 1106 instrument. Fast atom bombardment mass spectra were performed using 3-nitrobenzyl alcohol as a matrix material. IR spectra were recorded in the range 200–4000 cm^{-1} as Nujol mulls on KBr plates on a Perkin–Elmer 1330 spectrophotometer. ^1H and ^{13}C NMR were measured using a EX270 Jeol (270 MHz) NMR spectrophotometer in $CDCl_3$ solutions. UV–vis data were recorded on a Phillips PU8730 UV–vis spectrophotometer in the range 190–630 nm using dichloromethane solution in quartz cells. Cyclic voltammetry measurements were made at 200 K using an EG and G PAR model 362 scanning potentiostat linked to a PC with a Condecon 310 interface and software. A three-electrode cell configuration was used, with a platinum wire working electrode, platinum wire secondary electrode and a silver wire pseudo-reference electrode. The solvent was dichloromethane with 0.2 M tetrabutylammonium tetrafluoroborate as the support electrode. Potentials are quoted relative to the ferrocene/ferrocenium couple in the same system. $[Bu^n_4N][ReOCl_4]$ and DEBTH were made by the standard literature methods.[32,33]

Preparation of the complexes

Synthesis of $[ReOCl(DEBT)_2]$ (**1**). $[ReOCl_4][Bu^n_4N]$ (0.5 g, 0.85 mmol) was dissolved in degassed methanol (25 cm^3) and DEBTH (0.6 g, 2.56 mmol) was added. The solution was stirred at room temperature for 2 h producing a microcrystalline blue/green solid. The solid was washed with methanol and diethylether. The complex was recrystallized from dichloromethane/diethylether as dark green prisms. Found: C, 40.5; H, 4.2; N, 7.8. Calc. for $ReC_{24}H_{30}N_4O_3S_2Cl$: C, 40.7; H, 4.3; N, 8.0%.

Reaction of $[ReOCl(DEBT)_2]$ *with 4′-aminoacetophenone.* $[ReOCl(DEBT)_2]$ (0.2 g, 0.28 mmol) and $CH_3COC_6H_4NH_2$ (0.2 g, 1.41 mmol) were taken up in toluene (25 cm^3) and a few drops of triethylamine were added. The mixture was heated under reflux for 30 min until a dark green solution was formed. The toluene was removed under reduced pressure and methanol (20 cm^3) was then added. A dark green solid was formed. The complex recrystallized from CH_2Cl_2/Et_2O as a dark green complex (yield: 62%). Found: C, 46.8; H, 4.2; N, 8.3. Calc. for $ReC_{20}H_{22}N_5O_3S_2Cl$: C, 46.5; H, 4.5; N, 8.5%.

Reaction of $[ReOCl(DEBT)_2]$ *with 4-methoxyaniline.* The reaction was performed as above with $[ReOCl(DEBT)_2]$ (0.2 g, 0.28 mmol). The complex recrystallized from CH_2Cl_2/Et_2O as a dark green complex (yield: 64%). Found: C, 46.0; H, 4.2; N, 8.4. Calc. for $ReC_{19}H_{21}N_5O_3S_2Cl$: C, 45.8; H, 4.6; N, 8.6%.

Reaction of $[ReOCl(DEBT)_2]$ *with 2,6-diisopropylaniline.* The reaction was performed as above with $[ReOCl(DEBT)_2]$ (0.2 g, 0.28 mmol). The complex recrystallized from CH_2Cl_2/Et_2O as a dark green complex (yield: 59%). Found: C, 50.0; H, 5.2; N, 8.4. Calc. for $ReC_{21}H_{25}N_5O_2S_2Cl$: C, 45.8; H, 4.6; N, 8.6%.

Reaction of $[ReOCl(DEBT)_2]$ *with* PPh_3. $[ReOCl(DEBT)_2]$ (0.2 g, 0.28 mmol) and PPh_3 (0.22 g, 0.85 mmol) were heated under reflux in methanol (20 cm^3) to give a deep purple solution. Addition of $Na[BPh_4]$ gave the product as a red–brown solid, which was recrystallized from CH_2Cl_2–isopropanol (yield: 52%). Found: C, 61.9; H, 5.1; N, 4.4. Calc. for $ReBC_{79}H_{71}N_5O_2P_2S_5$: C, 61.8; H, 3.9; N, 4.8%. ^{31}P NMR: singlet, 14.0 ppm. ^{13}C NMR: 188.1 (*C*=O) and 173.7 ppm (*C*=S).

Preparation of $[ReOCl(DEBIT)_2]$ (**2**). $[Bu^n_4N][ReOCl_4]$ (0.25 g, 0.42 mmol) and DEBITH (0.3 g, 1.27 mmol) were stirred in methanol (20 cm^3) at room temperature to give the product as an emerald green solid. Found: C, 40.8; H, 4.2; N, 11.8. Calc. for $ReC_{19}H_{23}N_7OS_2$: C, 40.9; H, 4.3; N, 11.9%. ^{13}C NMR: 190.8 and 183.6 (*C*=O), 174.2 and 171.4 ppm (*C*=S). FAB mass spectrum: M^+ 707 with correct isotope splitting pattern.

X-ray crystal structure determination for $[ReOCl(DEBT)_2]$

A suitable single crystal was grown from dichloromethane–methanol and was mounted in air on a glass fibre.

Crystal data. $C_{24}H_{30}ClReN_4O_3S_2$, $M = 708.31$, orthorhombic space group *Pbca*, $a = 15.395(1)$, $b = 17.541(1)$, $c = 20.684(1)$ Å. $U = 5585.3$ Å, $Z = 8$, $D_c = 1.68\ g\ cm^{-3}$, $F(000) = 2800$, blue green prisms, crystal dimensions $= 0.30 \times 0.4 \times 0.30$ mm, $\mu(Mo\text{-}K_\alpha) = 46.8\ cm^{-1}$, $T = 18°C$.

Crystal collection and processing. Enraf–Nonius CAD4 diffractometer, graphite crystal monochromated Mo-K_α radiation ($\lambda = 0.71073$ Å), ω–2θ scan, ω scan speed 1–7.0° min^{-1}, scan width (°) $= 0.5 + 0.340 \tan\theta$, 5090 reflections measured ($1.5 < \theta < 25°$), 4906 unique.

Table 1. Some selected bond angles (°) and lengths (Å) for complex (1)

Re—O(1)	2.138(5)	Re—S(1)	2.353(2)
Re—O(2)	2.022(6)	Re—S(2)	2.320(2)
Re—O(3)	1.684(7)	Re—Cl	2.427(2)
O(1)—Re—O(2)	79.3(2)	O(3)—Re—S(1)	99.9(3)
O(1)—Re—Cl	79.5(1)	O(3)—Re—S(2)	102.1(3)
O(1)—Re—S(1)	80.8(1)	O(1)—Re—O(3)	169.8(3)
O(1)—Re—S(2)	88.1(1)	Cl—Re—S(2)	167.63(7)
O(3)—Re—O(2)	100.1(3)	S(1)—Re—O(2)	159.9(2)
O(3)—Re—Cl	90.3(3)	S(2)—Re—O(2)	91.3(2)

Structure analysis and refinement. The structure analysis is based upon 3039 observed reflections with $F_o > 3.0\sigma$; the intensities were corrected for absorption using empirical scan data and for Lorentz and polarization factors. The structure was solved by Patterson and difference-Fourier methods and was refined by full-matrix least-squares techniques with anisotropic thermal parameters for all non-hydrogen atoms (316 variables). Final $R = 0.031$, $R_w = 0.038$, $S = 3.68$, $(\Delta/\sigma)_{max} = 0.10$. The final difference electron density synthesis showed maximum positive and negative features of 0.84 and -0.16 e $Å^{-3}$. All calculations were performed on a micro VAX using MolEN (Enraf–Nonius). The neutral atom scattering factors were taken from international tables. Selected bond lengths and angles are given in Table 1.

RESULTS AND DISCUSSION

Reaction of the rhenium(V) precursor $[ReOCl_4]^-$ with DEBTH or DEBITH in methanol at room temperature gives the neutral rhenium(V) oxo complexes $[ReOClL_2]$ rapidly in high yields. Attempts to prepare the same complexes from $[ReOCl_3(PPh_3)_2]$ were not successful, and intractable mixtures resulted. The emerald green complexes are air-stable in the solid state and in solution, and non-electrolytes in dichloromethane solution. The ^{13}C NMR spectra of both complexes show two distinct pairs of resonances for the carbonyl and thiocarbonyl carbons, indicating that the two ligands are not in equivalent environments. This is consistent with a *cis* arrangement of the bidentate ligands. The FAB mass spectra show the expected mass ions and isotope distribution patterns, and the UV spectra display a charge transfer band at *ca* 400 nm. The presence of the Re=O group is confirmed by the appearance of an intense IR band close to 1000 cm^{-1}.

The formation of the neutral pseudo-octahedral rhenium complexes is in contrast to the behaviour of technetium where cationic, square pyramidal complexes of the type $[TcO(DEBT)_2]^+$ are formed. This presumably reflects the greater lability of the chloride ligand *trans* to the oxo-group on technetium.

Cyclic voltammetry of $[ReOCl(DEBT)_2]$ (1) *and* $[ReOCl(DEBIT)_2]$ (2)

The cyclic voltammogram of complex 1 in dichloromethane at room temperature (Fig. 2) was mea-

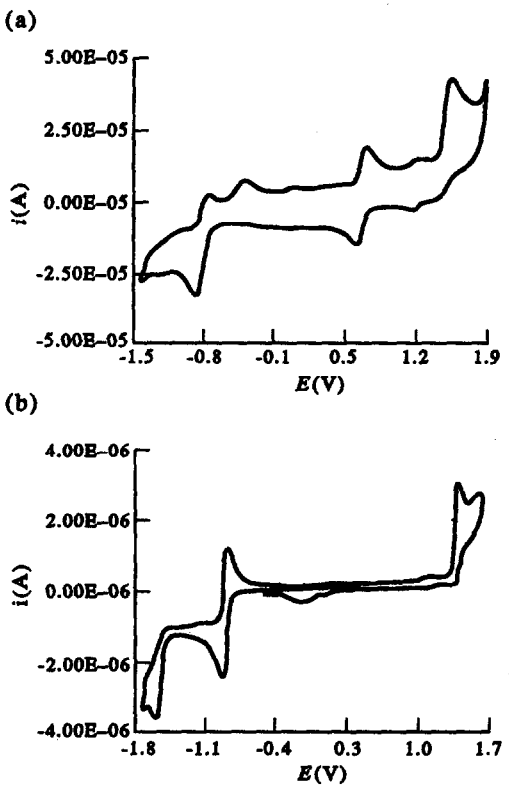

Fig. 2. The cyclic voltammogram of complex 1, in CH_2Cl_2 at room temperature and -80°C at a platinum electrode with 0.2 M $[Bu^n_4][BF_4]$ as the supporting electrolyte and a silver wire pseudo-reference electrode at a scan rate of 200 mV s^{-1}. The reversible couple at *ca*+0.7 V on the scale shown is due to ferrocene and is used as the internal standard of 0.0 V to quote potentials.

sured at a platinum electrode with 0.2 M $[Bu^n_4][BF_4]$ as the supporting electrolyte and a silver wire pseudo-reference electrode at a scan rate of 200 mV s^{-1}. There is a partially reversible reduction process at $E_{1/2} = -1.52$ V with an irreversible wave due to a product at -1.12 V (all potentials are quoted relative to an internal reference, the ferrocene–ferrocenium couple, taken as 0.0 V). In addition, an irreversible oxidation process occurs at $+0.88$ V. Convolution and deconvolution analyses of the primary processes indicate that both involve one electron. Addition of a large excess of chloride ion to the cell has no effect on the reduction at -1.52 V, strongly suggesting that the chemical process responsible for the irreversibility is not the expulsion of chloride. This reduction remained non-Nernstian, even at the fastest scan rates available, but became completely reversible at -80°C (Fig. 2). However, the oxidation process remained irreversible even at the low temperature. Convolution and deconvolution analyses confirmed that the -1.52 V process is entirely Nernstian at low temperature and involves one electron. A further completely irreversible reduction occurs at -2.27 V. The cyclic voltammogram of [ReOCl(DEBIT)$_2$] at room temperature is remarkably similar to that of **1**, with an irreversible reduction at -1.55 V and an irreversible oxidation at $+0.91$ V. The reduction process is noticeably less reversible at room temperature than the corresponding process for complex **1**. These results indicate a marginal stability for the rhenium(IV) anionic species at room temperature.

Reactions of [ReOCl(DEBT)$_2$]

The reaction of complex **1** with anilines in methanol under reflux gives the deep green imido complexes [Re(NAr)Cl(DEBT)$_2$] in good yield in the presence of triethylamine. The reaction does not proceed at all in the absence of additional base, which is in interesting contrast to the reaction of aromatic amines with $[ReOCl_3(PPh_3)_2]$ which does not require base catalysis. The imido complexes are formally 18-electron systems with the imide ligand functioning as a four-electron donor. The ^{13}C NMR spectra show an analogous four-peak pattern for the thiocarbonyl and carbonyl carbons, indicating a similar *cis* geometry to the oxo complexes. The FAB mass spectra all exhibit the expected mass ions and isotope distribution patterns.

Attempts to access rhenium(III) complexes by reaction of precursors such as $[ReCl_3(MeCN)(PPh_3)_2]$ with DEBTH or DEBITH were unsuccessful, complex mixtures of products being formed. However, reaction of **1** with excess triphenylphosphine in methanol under reflux gave the brown cationic rhenium(III) species $[Re(DEBT)_2(PPh_3)_2]^+$ in good yield. This showed a singlet in its ^{31}P NMR spectrum and only one carbonyl and one thiocarbonyl ^{13}C NMR peaks. These data are consistent with a *trans* disposition of the PPh_3 ligands, presumably as this geometry minimises steric repulsions with the bulky phosphine ligands.

The crystal structure of [ReOCl(DEBT)$_2$]

A perspective view of the molecule appears in Fig. 3, and selected bond lengths and angles are presented in Table 1. The geometry about the rhenium atom is essentially octahedral, with the chloride and oxo ligands *cis*. The Re—Cl and Re=O distances lie in the normal ranges found for rhenium(V) oxo complexes. The disposition of the two DEBT ligands is such that the sulphur and oxygen donor atoms are *cis*, and the phenyl groups are therefore located on the same side of the molecule. There is some steric interaction between them, and this causes a significant distortion in the Re—S(1)—C(10)—N(10)—C(11)—O(1) chelate ring. The rhenium atom lies 0.37 Å below and S(1) 0.49 Å above the least-squares plane through the six atoms of the chelate ring system. The other chelated ligand is comparatively close to being planar. The distortions within one chelate ring are reflected in the differing bite angles of 80.8(1)° and 91.3(2)°.

There is extensive delocalization throughout both chelate ring systems as evidenced by the remarkably uniform C—N distances of close to 1.33 Å, even for the exocyclic nitrogens N(11) and N(21). The geometry about N(11) and N(21) is essentially trigonal planar, and the N—CH_2 bonds are virtually coplanar with the chelate rings, which indicates that delocalization extends well into the chelate sub-

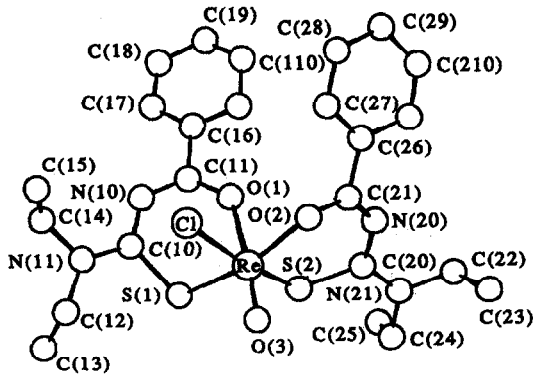

Fig. 3. A perspective view of the structure of [ReOCl(DEBT)$_2$] showing the atom labelling scheme.

stituents. The steric interaction between the two phenyl groups causes some deviations from coplanarity with the chelate rings, and the interplanar angles are 27.8° [S(1)—O(1) chelate] and 17.7°.

CONCLUSIONS

The ligands DEBT and DEBIT have been shown to behave similarly in forming neutral, six-coordinate rhenium(V) oxo complexes of the type $[ReOClL_2]$. The oxo group is relatively labile, and can be abstracted by PPh_3 to generate a rhenium(III) cation and can also be replaced by an arylimido ligand by reaction with aniline in a base catalysed reaction.

Acknowledgements—We thank Joanne Warmsley, University of Essex, for the NMR spectra, Edgar Potter, University of Essex, for the mass spectra and Neil Barnard, University of Essex, for the electrochemical results. We would also like to thank Hermann Stark GMBH, Berlin, for the generous gift of rhenium metal and Antony J. Hutson for the $[Bu^n_4N][ReOCl_4]$ preparation. One of us (JSL) thanks Hampshire LEA for the funding and ICI plc, U.K., for an additional grant payment.

REFERENCES

1. H. F. De Brabander and L. C. Van Poucke, *J. Coord. Chem.* 1974, **3**, 301.
2. H. F. De Brabander, J. J. Tombeux and L. C. Van Poucke, *J. Coord. Chem.* 1974, **4**, 87; C. M. Harris and S. E. Livingstone, in *Chelating Agents and Metal Chelates* (Edited by F. P. Dwyer and D. P. Mellor), p. 124. Academic Press, New York (1964).
3. A. G. Jones, B. V. De Phamphilis and A. Davidson, *Inorg. Chem.* 1981, **20**, 1617.
4. U. Casellato, P. A. Vigato, R. Graziani, M. Vidali and B. Acone, *Inorg. Chim. Acta* 1980, **45**, L79.
5. R. Graziani, M. Vidali, U. Casellato and P. A. Vigato, *Trans. Met. Chem.* 1981, **6**, 166.
6. R. G. Garvey, J. H. Nelson and R. O. Ragsdale, *Coord. Chem. Rev.* 1973, **11**, 93.
7. N. M. Karayannis, L. L. Pytlewski and C. M. Mikulski, *Coord. Chem. Rev.* 1973, **11**, 93.
8. N. M. Karayannis, A. N. Speca, D. E. Chasen and L. L. Pytlewski, *Coord. Chem. Rev.* 1976, **20**, 37.
9. J. D. Lydon, K. J. Mulligan, R. C. Elder and E. Deutsch, *Inorg Chem.* 1980, **19**, 2083; S. G. Murray and F. R. Hartley, *Chem. Rev.* 1981, **81**, 365.
10. G. J. Gainsford, W. G. Jackson and A. M. Sargeson, *Aust. J. Chem.* 1980, **33**, 707.
11. K. Mennemann and R. Mattes, *Angew. Chem., Int. Edn Engl.* 1977, **16**, 260.
12. G. J. Ford, P. Gans, L. D. Pettit and C. Sherrington, *J. Chem. Soc., Dalton Trans.* 1972, 1763.
13. L. D. Pettit, *Q. Rev., Chem. Soc.* 1971, **25**, 1.
14. A. Ouchi, M. Shimoi, T. Takeuchi and H. Saito, *Bull. Chem. Soc. Japan* 1981, **54**, 2290.
15. T. Ogawa, M. Shimoi and A. Ouchi, *Acta Cryst., Sect. B* 1980, **36**, 3114.
16. T. Ogawa, M. Shimoi and A. Ouchi, *Bull. Chem. Soc. Japan* 1982, **55**, 126.
17. K. Yamanari, J. Hidaka and Y. Shimura, *Bull. Chem. Soc. Japan* 1977, **50**, 2299; R. C. Elder, G. J. Kennard, M. D. Payne and E. Deutsch, *Inorg. Chem.* 1978, **17**, 1296.
18. M. Kojima and J. Fujita, *Bull. Chem. Soc. Japan* 1983, **56**, 2958.
19. M. R. Udupa, B. Krebs and U. Seyer, *Inorg. Chim. Acta* 1980, **41**, 31.
20. G. J. Kubas, R. R. Ryan and V. McCarty, *Inorg. Chem.* 1980, **19**, 3003.
21. G. D. Jarvinen, G. J. Kubas and R. R. Ryan, *J. Chem. Soc., Chem. Commun.* 1981, 305.
22. D. C. Moody and R. R. Ryan, *J. Chem. Soc., Chem. Commun.* 1980, 1230.
23. T. R. Gaffney and J. A. Ibers, *Inorg. Chem.* 1982, **21**, 2860.
24. R. D. Bereman, D. M. Baird, J. R. Dorfman and J. Bordner, *Inorg. Chem.* 1982, **21**, 2365.
25. J. B. McCormick, R. D. Pereman and D. M. Baird, *Coord. Chem. Rev.* 1984, **54**, 9.
26. S. Mizukami and K. Nagata, *Coord. Chem. Rev.* 1968, **3**, 267.
27. Y. Egawa, K. Umino, Y. Ito and T. J. Okuda, *J. Antibiot.* 1971, **24**, 124, 140.
28. D. P. Freyberg, K. Abu-Dari and K. N. Raymond, *Inorg. Chem.* 1979, **18**, 3037.
29. K. Abu-Dari and K. N. Raymond, *Inorg. Chem.* 1982, **21**, 1676.
30. L. Beyer, E. Hoyer, J. Liebscher and H. Hartmann, *Zeit. Chem.* 1981, **21**, 81 and refs therein.
31. U. Abram, R. Meunze, J. Hartung, L. Beyer, R. Kirmse, K. Koeher, J. Stach, H. Behm and P. T. Beurskens, *Inorg. Chem.* 1989, **28**, 834.
32. J. R. Dilworth, W. Hussain, A. J. Hutson, C. J. Jones and F. S. McQuillan, *Inorg. Synth.*, in press
33. J. Hartung, G. Weber, L. Beyer and R. Szargan, *Z. Anorg. Allg. Chem.* 1985, **523**, 153.

Polyhedron Vol. 12, No. 2, pp. 227–234, 1993
Printed in Great Britain.

0277–5387/93 $6.00+.00
© 1993 Pergamon Press Ltd

SYNTHESIS AND SPECTROSCOPIC CHARACTERIZATION OF MIXED-FLUORO COMPLEXES OF UO_2^{2+} CONTAINING AMINO ACIDS, ACETYLACETONATE OR ACETATE AS THE CO-LIGANDS AND THE FIRST REPORT ON THE HEPTAFLUORODIOXOURANATE(VI) COMPLEX $[UO_2F_7]^{5-}$

MIHIR K. CHAUDHURI* and PENDYALA SRINIVAS

Department of Chemistry, North-Eastern Hill University, Shillong 793 003, India

and

DARLANDO T. KHATHING

Department of Physics, North-Eastern Hill University, Shillong 793 003, India

(*Received* 17 *July* 1992; *accepted* 10 *September* 1992)

Abstract—The synthesis of mixed-ligand fluoro complexes of UO_2^{2+} of the types $A_3[UO_2(GlyH)_2F_5]\cdot 3H_2O$ [A = K (**1**) or NH_4^+ (**2**)], $K_3[UO_2(AlanH)_2F_5]\cdot 2H_2O$ (**3**), $(NH_4)_5[UO_2(CysH)_2F_5]\cdot 2H_2O$ (**4**), $[UO_2(acac)F(H_2O)_2]\cdot 3H_2O$ (**6**), $K_2[UO_2(acac)F_3]$ (**8**) and $[UO_2(CH_3COO)F(H_2O)_2]$ (**9**) (GlyH = glycine, AlanH = alanine, $CysH^-$ = cysteinate and $acac^-$ = acetylacetonate) is described. The complexes have been characterized by a combination of chemical analyses, solution conductance measurements and spectroscopic studies. Vibrational spectroscopy has been used for their structural assessment. Laser Raman spectrum could be recorded only for $K_2[UO_2(acac)F_3]$ (**8**), while an extensive fluorescence foiled such attempts on the other complexes. Each of the three amino acid co-ligands acts in a unidentate manner, being coordinated to UO_2^{2+} through the caroxylate oxygen atom. While glycine and alanine occur in the zwitter-ionic form, cysteine seems to be present as a uninegative ligand. The reaction of $[UO_2(acac)F(H_2O)_2]\cdot 3H_2O$ (**6**) with aqueous HF produced $[UO_2F_2]\cdot 3H_2O$ (**7**). Treatment of $K_3[UO_2(GlyH)_2F_5]\cdot 3H_2O$ (**1**) with water afforded the hitherto unreported potassium heptafluorodioxouranate(VI) dihydrate, $K_5[UO_2F_7]\cdot 2H_2O$ (**5**), in a high yield with satisfactory analysis and electrical conductance measurement (590 Ω^{-1} cm^2 mol^{-1}). IR and laser Raman spectra provide clear evidence for the presence of *trans*-linked O=U=O and coordinated flouride. The solution Raman spectrum of **5** is similar to that of its solid indicating that the structure in aqueous solution is the same as the solid. Scanning electron microscopy has been used to ascertain its homogeneity and crystalline nature.

Uranium(VI) generally occurring as uranyl (UO_2^{2+}) has been known to form stable fluoro and mixed-ligand fluoro complexes.[1] Notable among the binary fluoro complexes[1,2] are $[UO_2F_3]^-$, $[UO_2F_4]^{2-}$, $[UO_2F_5]^{3-}$ and $[(UO_2)_3F_7]^-$. For the mixed-ligand fluoro complexes of UO_2^{2+} the co-ligands were drawn largely from sulphate,[3] carbonate,[3b] oxalate,[4] acetate,[1c] acetylacetonate,[5] propionate[6] and malonate.[6]

Interestingly, the fluoro complexes of the types $[UO_2F_6]^{4-}$ and $[UO_2F_7]^{5-}$ were not included in the earlier reports. We addressed ourselves to these complexes and the first synthesis of $(NH_4)_4[UO_2F_6]$ has been achieved very recently.[7] A fortuitous synthesis of heptafluorodioxouranate(VI), obtained as $K_5[UO_2F_7]\cdot 2H_2O$ (**5**), enables us now to make the first report on the complex. In addition, we have been interested in the complex chemistry of UO_2^{2+}[8–11] and some of our previous publications have dealt with mixed-ligand peroxo complexes, including fluoroperoxouranates(VI).[11]

* Author to whom correspondence should be addressed.

In this investigation we included the synthesis of a few selective mixed fluoro complexes with amino acids, such as glycine, L-alanine and L-cysteine, acetylacetonate and acetate as the co-ligands.

Incidentally, amino acids,[12–15] acetylacetonate[16] and acetate[1c,1d] have been known for a long time to form complexes with UO_2^{2+}, although their isolation in the solid state varied from case to case. In addition, the reaction solution pH conducive to the formation of such complexes, particularly with regard to amino acids and acetylacetonate ligands, seems to be an important parameter. One of our main concerns in this context was to ascertain appropriate experimental conditions leading to the synthesis of the desired complexes.

Herein are reported the synthesis of the mixed-fluoro complexes $A_3[UO_2(GlyH)_2F_5]\cdot 3H_2O$ [A = K (**1**) or NH_4^+ (**2**); GlyH = glycine], $K_3[UO_2(AlanH)_2F_5]\cdot 2H_2O$ (**3**) (AlanH = L-alanine), $(NH_4)_5[UO_2(CysH)_2F_5]\cdot 2H_2O$ (**4**) ($CysH^-$ = cysteinate), $[UO_2(acac)F(H_2O)_2]\cdot 3H_2O$ (**6**), $K_2[UO_2(acac)F_3]$ (**8**) ($acac^-$ = acetylacetonate) and $[UO_2(CH_3COO)F(H_2O)_2]$ (**9**), their spectroscopic characterization and the interaction of **1** with water, thus enabling us to make the first report on the heptafluorodioxouranate(VI) complex $K_5[UO_2F_7]\cdot 2H_2O$ (**5**).

EXPERIMENTAL

The chemicals used were of reagent grade quality and acetylacetone was distilled before use. IR spectra were recorded on a Perkin–Elmer Model 983 spectrophotometer and laser Raman (LR) on a SPEX Ramalog 1403 spectrophotometer using the 4880 Å laser line from a Spectra-Physics Model 165 argon laser. The pH values of the reaction solutions were measured using a Systronics type 335 digital pH meter and BDH indicator paper. Solution electrical conductances were measured using a Systronics type 304 digital direct reading conductivity meter. Bis(acetylacetonato)dioxouranium(VI) dihydrate, $UO_2(C_5H_7O_2)_2\cdot 2H_2O$, was prepared by a method developed in this laboratory.[16,17]

Preparation of $UO_3\cdot 4H_2O$

Uranyl nitrate hexahydrate, $UO_2(NO_3)_2\cdot 6H_2O$ (5.0 g, 9.96 mmol), was dissolved in water (100 cm^3), to which was added pyridine (10 cm^3) whereupon a yellow precipitate appeared. This was separated by decantation, washed three or four times with water, twice with acetone and finally dried on a steam bath to obtain yellow uranium trioxide, $UO_3\cdot 4H_2O$ (yield: 2.8 g; 78.4%).

Syntheses

$A_3[UO_2(GlyH)_2F_5]\cdot 3H_2O$ [A = K (**1**) *or* NH_4^+ (**2**)]. $UO_3\cdot 4H_2O$ (1.0 g, 2.79 mmol) was dissolved in an aqueous solution of a combination of aqueous HF (12 mmol) and AF (8.38 mmol) (A = K or NH_4^+). To the clear lemon yellow solution thus obtained was added an aqueous solution (5 cm^3) of glycine (0.42 g, 5.57 mmol) and the solution was stirred for *ca* 10 min. The solution after concentration by heating on a steam bath to nearly half of its volume afforded a lemon–yellow solid. The pH of the reaction solution was recorded to be *ca* 2.5. The compound was isolated by filtration and dried *in vacuo* over concentrated H_2SO_4. The yields of $K_3[UO_2(GlyH)_2F_5]\cdot 3H_2O$ (**1**) and $(NH_4)_3[UO_2(GlyH)_2F_5]\cdot 3H_2O$ (**2**) were 1.2 g (63%) and 1.1 g (65%), respectively.

$K_3[UO_2(AlanH)_2F_5]\cdot 2H_2O$ (**3**) *and* $(NH_4)_5[UO_2(CysH)_2F_5]\cdot 2H_2O$ (**4**). These complexes were prepared by a method similar to that employed for **1** and **2**, except that AHF_2 was used as the fluorinating agent instead of AF and HF. $UO_3\cdot 4H_2O$ (1.0 g, 2.79 mmol) was dissolved in an aqueous solution (5 cm^3) of AHF_2 (8.37 mmol). This was followed by the addition of L-alanine or L-cysteine (5.57 mmol). The pH of the resulting clear solution was *ca* 2.5. The solution upon concentration over a steam-bath produced **3** and **4**, respectively. The compounds were isolated in a manner similar to that of **1** and **2**. The yields of **3** and **4** were 1.3 g (66%) and 1.4 g (68%), respectively.

Treatment of **1** *with water and isolation of* $K_5[UO_2F_7]\cdot 2H_2O$ (**5**). A suspension of $K_3[UO_2(GlyH)_2F_5]\cdot 3H_2O$ (**1**) (1.0 g, 1.46 mmol) in water (10 cm^3) was stirred constantly for *ca* 5 min, whereupon the solid slowly dissolved. On further agitation, the solution deposited a bright lemon–yellow crystalline solid. The pH of the mother liquor was recorded to be *ca* 1.7. The solid thus obtained was collected by filtration and finally dried *in vacuo* over concentrated H_2SO_4 (yield: 0.7 g; 76%).

Synthesis of $[UO_2(acac)F(H_2O)_2]\cdot 3H_2O$ (**6**). (1) $UO_3\cdot 4H_2O$ (1.0 g, 2.79 mmol) in water (5 cm^3) was reacted with 48% HF (0.2 cm^3, 4.8 mmol) in the presence of acacH (1.0 cm^3, 10 mmol) and the resultant reaction mixture was stirred constantly on a steam bath for *ca* 15 min, whereupon a yellow solid precipitated out. The pH of the reaction solution was found to be *ca* 3.5. The yellow solid was collected by filtration and washed with ethanol (yield: 1.0 g; 77%).

(2) Alternatively, to an aqueous suspension (5 cm^3) of $UO_2(acac)_2\cdot 2H_2O$ (1.0 g, 1.98 mmol) was added 48% HF (0.2 cm^3, 4.8 mmol). The reaction solution upon stirring on a steam bath for *ca* 15

min afforded a yellow solid. The pH of the reaction solution measured at this stage was *ca* 3.5 (yield: 0.7 g; 74%).

Synthesis of $K_2[UO_2(acac)F_3]$ (**8**). Uranyl nitrate hexahydrate, $UO_2(NO_3)_2 \cdot 6H_2O$ (1.0 g, 1.99 mmol), was dissolved in water (15 cm^3) and 20% KOH solution was added until the yellow precipitate formation was complete. The precipitate was filtered off and washed free from alkali and nitrate. To a suspension of the yellow precipitate in an excess of acetylacetone (10 cm^3, 100 mmol) was added KF (0.7 g, 12 mmol), maintaining the atom ratio of U:F at 1:6. The reaction solution was stirred constantly over a steam bath for *ca* 2 h until the formation of a bright yellow compound was complete. The pH of the reaction solution at this stage was measured to be *ca* 3.5. The compound was separated by filtration and dried *in vacuo* over concentrated H_2SO_4 (yield, 0.7 g; 70%).

Synthesis of $[UO_2(CH_3COO)F(H_2O)_2]$ (**9**). $UO_3 \cdot 4H_2O$ (1.0 g, 2.79 mmol) was dissolved in a minimum amount of glacial acetic acid (2 cm^3, 35 mmol). To the resulting clear solution was added 48% HF (0.2 cm^3, 4.8 mmol) and the reaction solution was concentrated over a steam bath to afford a lemon–yellow solid. The pH of the reaction solution was *ca* 2.5. The solid was isolated by filtration, washed with ethanol and finally dried *in vacuo* over concentrated H_2SO_4 (yield: 0.8 g; 74%).

Elemental analyses

Uranium was estimated gravimetrically as uranyl oxinate.[18a] Fluoride was precipitated as PbClF and chloride estimated by Volhard's method, from which the fluoride content was also calculated.[18b] Carbon, nitrogen and hydrogen were determined by the Micro Analytical Laboratory of our university. Potassium was estimated using a Perkin–Elmer Model 2380 atomic absorption spectrophotometer. The uranium content was also checked using the Perkin–Elmer Model 2380 atomic absorption spectrophotometer.

RESULTS AND DISCUSSION

The synthesis of mixed-ligand fluorodioxouranates(VI) with the co-ligands drawn from amino acids, such as glycine, L-alanine and L-cysteine, and acetylacetonate and acetate required first the development of the appropriate experimental conditions. It is known[19] that amino acids do not coordinate with UO_2^{2+} below pH *ca* 1.8, while above pH 4–4.5 there is a strong tendency for hydrolysis of the complexes. Evidence for the formation of binary amino acid-uranyl complexes at pH *ca* 2 has been provided by pH titration and solvent extraction experiments.[14] Thus, it was anticipated that a pH range 2–4.5 might be conducive to the coordination of an amino acid to UO_2^{2+} in the presence of F^-. Incidentally, the reaction of $UO_3 \cdot 4H_2O$ with AHF_2 in the case of L-alanine and L-cysteine or a combination of AF and HF in the case of glycine gave rise to a natural pH of *ca* 2.5. The complexes were thus isolated as $A_3[UO_2(GlyH)_2F_5] \cdot 3H_2O$ [A = K (**1**) or NH_4^+ (**2**)], $K_3[UO_2(AlanH)_2F_5] \cdot 2H_2O$ (**3**) and $(NH_4)_5[UO_2(CysH)_2F_5] \cdot H_2O$ (**4**), respectively, in high yields.

The mixed-ligand amino acid fluoro complexes of UO_2^{2+} were unstable in aqueous solutions, undergoing decomposition to form intractable products, except for $K_3[UO_2(GlyH)_2F_5] \cdot 3H_2O$ (**1**). Significantly, **1** underwent hydrolysis affording a well-defined but hitherto unknown binary fluoro complex, $K_5[UO_2F_7] \cdot 2H_2O$ (**5**), enabling us to make the first report on the heptafluorodioxouranate(VI) species. Although it is difficult to say how exactly the formation of **5** from **1** occurred, presumably at least the hydrolysis of the complex $[UO_2(GlyH)_2F_5]^{3-}$ and a reorganization of the coordination sphere of the UO_2^{2+} ion must have occurred to afford the complex $[UO_2F_7]^{5-}$. The solution pH on the formation of the compound $K_5[UO_2F_7] \cdot 2H_2O$ (**5**) was recorded to be 1.7, which might have facilitated dissociation of the co-ligand GlyH.

In some recent reports, direct syntheses of $UO_2(acac)_2 \cdot 2H_2O$ have been dealt with.[16,17] A pH of 5–5.5 was ascertained to be necessary for coordination of $acac^-$ to UO_2^{2+}. In order to design suitable experimental conditions for the synthesis of fluoro(acetylacetonato)dioxouranium(VI) complexes it was felt that the pH of the reaction medium might be important.

Our experience in dealing with uranyl systems[7–11] led us to believe that the reactions of $UO_2(acac)_2 \cdot 2H_2O$ with a controlled amount of F^- in acidic medium should be appropriate for accessing fluoro(acetylacetonato)dioxouranates(VI). It was important in this context to avoid a higher F^- ion concentration which would inhibit the formation of binary fluoro complexes. As shown here (see Experimental), the reaction of $UO_3 \cdot 4H_2O$ with aqueous HF and acacH at pH 3.5 (attained spontaneously) afforded the molecular complex $[UO_2(acac)F(H_2O)_2] \cdot 3H_2O$ (**6**). However, on lowering the pH to *ca* 2 by the addition of aqueous HF, a known fluoro compound, $[UO_2F_2] \cdot 3H_2O$[1a] (**7**), resulted. It should be mentioned that in two separate reactions $[UO_2(acac)_2] \cdot 2H_2O$ and $[UO_2(acac)F(H_2O)_2] \cdot 3H_2O$ (**6**) were reacted with excess aqueous HF to yield **6** and **7**, respectively.

An important implication of the observed sequential loss of coordinated acetylacetonate ligands from $[UO_2(acac)_2]\cdot 2H_2O$ at the pH values *ca* 3.5 and *ca* 2 is that an enhanced acidity appears to be detrimental to the formation of fluoro-(acetylacetonato) complexes of the metal. In other words, $[UO_2(acac)F(H_2O)_2]\cdot 3H_2O$ (**6**) may be regarded as an isolable intermediate in the process $[UO_2(acac)_2]\cdot 2H_2O$ to $[UO_2F_2]\cdot 3H_2O$.

5–9 are stable in water under the present experimental conditions. It may be important to mention that the reported solution electrical conductances for the salts of the complex ions $[UO_2F_3]^-$, $[UO_2F_4]^{2-}$ and $[UO_2F_6]^{4-}$ were *ca* 130,[22a] 216[22b] and 495[7] Ω^{-1} cm^2 mol^{-1}, respectively.

The common features of the IR spectra of complexes **1–9** are the bands at *ca* 900 and 375 cm^{-1},

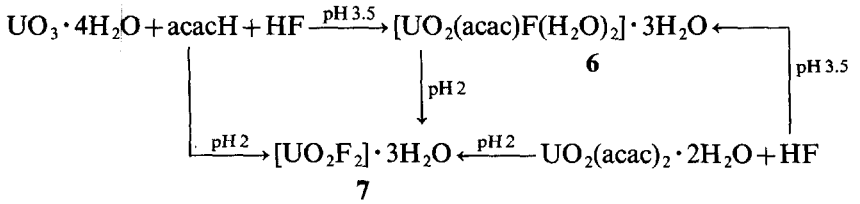

The knowledge obtained from the preceeding results suggested that if a reaction of UO_2^{2+} with acacH and an excess of fluoride were conducted at pH *ca* 3.5, it would be possible to gain access to the anionic fluoro(acetylacetonato) complex of UO_2^{2+}. Indeed this is what has happened in one of the reactions where $K_2U_2O_7$ was reacted with KF and acetylacetone at pH 3.5 leading to $K_2[UO_2(acac)F_3]$ (**8**).

Our success in the synthesis of $[UO_2(acac)F(H_2O)_2]\cdot 3H_2O$ (**6**) caused us to anticipate that the adoption of a similar synthetic methodology might enable the preparation of analogous molecular mixed fluoro complexes with the co-ligand derived from a weak acid. To test this, the strategy was applied to a fluoro-acetato system and the compound $[UO_2(CH_3COO)F(H_2O)_2]$ (**9**) has been successfully synthesized.

The compounds are either yellow or lemon–yellow in colour and stable in the solid state. Their analytical data, molar conductance values and important IR and LR spectral bands along with their assignments are summarized in Tables 1 and 2, respectively. The results of the conductance experiments are of particular value in determining the mode of ionization of coordination compounds.[20,21] The conductances of dilute (10^{-3} M) solutions of 1 : 1, 1 : 2, 1 : 3, 1 : 4 and 1 : 5 types of electrolytic complexes are expected[20] to be *ca* 120, 240, 360, 480 and 600 Ω^{-1} cm^2 mol^{-1}, respectively, with the average value of ion conductance being *ca* 60 Ω^{-1} cm^2 mol^{-1}. For complexes **1–4** conductance measurements were not attempted due to their instability in aqueous solution; however, the solution (10^{-3} M) electrical conductances for compounds **5**, **6**, **7**, **8** and **9** were 590, 5, 7, 175 and 6 Ω^{-1} cm^2 mol^{-1}, respectively, which conforms to the formulations. This also implies that complexes assigned to ν(U=O)[23] (*trans* linked O=U=O) and ν(U—F)[23c] modes, respectively. The amino acids glycine and L-alanine form complexes with metals in either their zwitter-ionic or ionic forms,[24–26] and coordinate either through the N,O atoms in a bidentate manner or through the carboxylate oxygen atoms in a monodentate fashion. In addition to glycine and L-alanine, L-cysteine[27] was the other amino acid co-ligand included in the study which contained a sulphhydryl group as an additional coordination site.

Incidentally, the chosen amino acids are interesting probes useful in the IR spectroscopic determination of their modes of coordination.[26] There was a general pattern in the spectra of complexes **1–3**; for instance, the bands at *ca* 1600s [$\nu_{as}(COO^-)$], 1400s [$\nu_s(COO^-)$], 1120 m [$\rho_r(NH_3^+)$], 680m [$\rho_w(COO^-)$] and 580m [$\delta(COO^-)$] cm^{-1}. The observed pattern and band positions are clear reflections of the occurrence of glycine and alanine in their zwitter-ionic forms,[26,28a] thus being coordinated through their carboxylate oxygen atoms in the respective complexes. However, unlike complexes **1–3**, cysteine in **4** occurs in its cysteinate form ($CysH^-$). Important in this context have been the absorptions at 2565 cm^{-1} due to the S—H stretch[27] and at 1650s and 1385s owing to $\nu_{as}(COO^-)$ and $\nu_s(COO^-)$ modes, respectively. Notably, the observed shifts of $\nu_{as}(COO^-)$ to higher and $\nu_s(COO^-)$ to lower wave numbers than the corresponding values of free cysteine[27] provide evidence for the coordination of $CysH^-$ through its carboxylate oxygen atom. The complementary ν(U—O) mode was observed at 451m cm^{-1}. The fact that the nitrogen atom has not involved itself in coordination is clear from the unaltered NH_3^+ deformation band[27] observed at 1483 cm^{-1} for **4**. Thus, based upon the IR results described above, it

Table 1. Analytical data and solution electrical conductances of the compounds

Compound (colour)	Conductance (Ω^{-1} cm^2 mol^{-1})	Analysis: Found (Calc.) U	F	C	N	H	K
$K_3[UO_2(GlyH)_2F_5]\cdot 3H_2O$ (**1**)	d	34.1	13.6	7.1	4.0	2.4	17.3
(lemon–yellow)		(34.7)	(13.8)	(7.0)	(4.1)	(2.4)	(17.1)
$(NH_4)_3[UO_2(GlyH)_2F_5]\cdot 3H_2O$ (**2**)	d	37.7	15.4	7.6	11.1	4.7	—
(lemon–yellow)		(38.2)	(15.2)	(7.7)	(11.2)	(4.5)	
$K_3[UO_2(AlanH)_2F_5]\cdot 2H_2O$ (**3**)	d	34.2	13.5	10.2	4.0	2.8	16.8
(lemon–yellow)		(34.2)	(13.6)	(10.3)	(4.0)	(2.6)	(16.8)
$(NH_4)_5[UO_2(CysH)_2F_5]\cdot 2H_2O$ (**4**)	d	32.3	13.6	9.6	13.3	4.7	—
(green)		(32.5)	(13.0)	(9.9)	(13.4)	(5.0)	
$K_5[UO_2F_7]\cdot 2H_2O$ (**5**)	590	37.4	21.1	—	—	—	30.6
(lemon–yellow)		(37.5)	(21.0)				(30.8)
$[UO_2(acac)F(H_2O)_2]\cdot 3H_2O$ (**6**)	5	49.5	4.1	12.6	—	3.6	—
(yellow)		(49.8)	(4.0)	(12.6)		(3.6)	
$[UO_2F_2]\cdot 3H_2O$ (**7**)	7	65.9	10.3	—	—	1.8	—
(yellow)		(65.7)	(10.5)			(1.7)	
$K_2[UO_2(acac)F_3]$ (**8**)	175	46.8	11.5	11.4	—	1.7	15.6
(yellow)		(47.2)	(11.3)	(11.9)		(1.4)	(15.5)
$[UO_2(CH_3COO)F(H_2O)_2]$ (**9**)	6	60.8	4.4	5.8	—	1.7	—
(yellow)		(62.0)	(5.0)	(6.3)		(1.8)	

d = decomposed in water, GlyH = glycine ($C_2H_5NO_2$), AlanH = L-alanine ($C_3H_7NO_2$), $CysH^-$ = cysteinate ($C_3H_6NS^-$), $acac^-$ = acetylacetonate ($C_5H_7O_2^-$).

may be assumed that the amino acid in complexes **1–4** has acted as a monodentate ligand, coordinated with the metal centre through the carboxylate oxygen atom. In addition, the spectra exhibited the lattice water modes in their usual positions[28b] (Table 2). Unfortunately, no information could be extracted from laser Raman spectroscopic experiments on complexes **1–4** owing to extensive fluorescence.

The IR spectrum of potassium heptafluorodioxouranate(VI) dihydrate, $K_5[UO_2F_7]\cdot 2H_2O$ (**5**), is very straightforward. As expected, the spectrum exhibited only a few prominent bands; for instance, one at 866s [ν(U=O), *trans*-linked O=U=O] and another at 373 cm^{-1} [ν(U—F)], in addition to the ν(OH) and δ(HOH) modes of lattice water at 1640 and 3455 cm^{-1}, respectively. It may be mentioned that the ν(O—H) band at *ca* 3450 has been generally observed for complexes containing lattice water.[28a] Indeed, the ν(O—H) value of 3455 cm^{-1} has been argued to be rather typical of uncoordinated H_2O.[29] Incidentally, this is one of the few compounds, from among those reported herein, which exhibited a laser Raman spectrum with signals located at 920 cm^{-1} due to ν(U=O) (*trans*-linked O=U=O) and 314 cm^{-1} attributed to ν(U—F). These results not only complement the corresponding IR spectral observation but also augment our assumptions on the characteristic spectral features of the complex $[UO_2F_7]^{5-}$ species. The stability of the complex in water enabled recording its solution Raman spectrum. Significantly, the principal features of the spectrum include the appearance of the ν(U=O) and ν(U—F) signals at 915 and 325 cm^{-1}, respectively. The pattern resembles that of the corresponding solid, thus indicating that the structure of the complex $[UO_2F_7]^{5-}$ ion in aqueous solution is the same as the solid. It may be worth noting that the recently characterized[7] complex $[UO_2F_6]^{4-}$ displayed related bands at 951 and 340 cm^{-1}. The corresponding ν(U=O) and ν(U—F) modes for $[UO_2F_5]^{3-}$ were observed at *ca* 865s and 387m cm^{-1}, respectively, in the IR spectra[30,31] of the complex.

In order to gain an idea about the crystallinity and homogeneity of the product (**5**), it was subjected to Scanning Electron Microscopy (SEM). The SE micrograph (Fig. 1) attests to the homogeneity of the product as well as its crystalline character.

For compounds **6**, **8** and **9** the IR spectra provide, in addition to ν(U=O) and ν(U—F) bands, a pattern typical of chelated acetylacetonate[28c] for **6** and **8**, and bidentate acetate[28d] for **9**. Some of the charac-

Table 2. IR and LR spectral data of the complexes with their assignments

Compound	IR (cm^{-1})	LR (cm^{-1})	Assignment
$K_3[UO_2(GlyH)_2F_5]\cdot 3H_2O$ (1)	377m	—	ν(U—F)
	900s		ν(U=O)
	1585s		$\nu_{as}(COO^-)$
	1400s		$\nu_s(COO^-)$
	1120m		$\rho_r(NH_3^+)$
	680m		$\rho_w(COO^-)$
	580m		$\delta(COO^-)$
	1645		δ(H—O—H)
	3450		ν(O—H)
$(NH_4)_3[UO_2(GlyH)_2F_5]\cdot 3H_2O$ (2)	372m	—	ν(U—F)
	910s		ν(U=O)
	1590s		$\nu_{as}(COO^-)$
	1402s		$\nu_s(COO^-)$
	1115m		$\rho_r(NH_3^+)$
	680m		$\rho_w(COO^-)$
	585m		$\delta(COO^-)$
	1640		δ(H—O—H)
	3445		ν(O—H)
	1420s		ν(N—H)ν_4
$K_3[UO_2(AlanH)_2F_5]\cdot 2H_2O$ (3)	374m	—	ν(U—F)
	905s		ν(U=O)
	1600s		$\nu_{as}(COO^-)$
	1395s		$\nu_s(COO^-)$
	1110m		$\rho_r(NH_3^+)$
	685m		$\rho_w(COO^-)$
	575n		$\delta(COO^-)$
	1630		δ(H—O—H)
	3440		ν(O—H)
$(NH_4)_5[UO_2(CysH)_2F_5]\cdot 2H_2O$ (4)	372m	—	ν(U—F)
	902s		ν(U=O)
	1650s		$\nu_{as}(COO^-)$
	1385s		$\nu_s(COO^-)$
	451m		ν(U—O)
	2568m		ν(S—H)
	1418s		ν(N—H)ν_4
	1483m		NH_3^+ (symm. def.)
	1640		δ(H—O—H)
	3440		ν(O—H)
$K_5[UO_2F_7]\cdot 2H_2O$ (5)	373	314	ν(U—F)
	866	920	ν(U=O)
	1640		δ(H—O—H)
	3460		ν(O—H)
$[UO_2(acac)F(H_2O)_2]\cdot 3H_2O$ (6)	369	—	ν(U—F)
	890		ν(U=O)
	612		ring def. + ν(U—O)
	295		ν(U—O)
	725		$\rho_r(H_2O)$
	1635		δ(H—O—H)
	3450		ν(O—H)
$[UO_2F_2]\cdot 3H_2O$ (7)	374	425	ν(U—F)
	857	866	ν(U=O)
	1625		δ(H—O—H)
	3358		ν(O—H)

Table 2—*continued*

Compound	IR (cm^{-1})	LR (cm^{-1})	Assignment
$K_2[UO_2(acac)F_3]$ (**8**)	366	438	ν(U—F)
	900	890	ν(U═O)
	615		ring def. + ν(U—O)
	290		ν(U—O)
$[UO_2(CH_3COO)F(H_2O)_2]$ (**9**)	387	—	ν(U—F)
	905		ν(U═O)
	1468s		ν_s(OCO)
	1545s		ν_{as}(OCO)
	725m		$\rho_r(H_2O)$
	670m		δ(OCO)

Fig. 1.

teristic bands have been cited in Table 2. In agreement with their formulae the IR spectra of **6** and **9** showed a band at *ca* 725 cm^{-1}. We believe this originates from the rocking mode of coordinated water.[28b] The absence of a similar mode in the spectrum of **8** lends support to the aforementioned assignment. The only other compound which gave a good LR spectrum was **7**. In the region 1200–200 cm^{-1} there have been only two signals, one at 867 cm^{-1} assigned to ν(U═O) (*trans*-linked O═U═O) and another centred at 425 cm^{-1} due to ν(U—F), with the latter being broad.

Acknowledgement—Financial assistance from the Department of Atomic Energy is gratefully acknowledged.

REFERENCES

1. S. Ahrland, K. W. Bagnall, D. Brown, R. M. Dell, S. H. Eberle, C. Keller, J. A. Lee, J. O. Liljenzin, P. G. Mardon, J. A. C. Marples, G. W. C. Milner, G. Phillips, P. E. Potter and J. Rydberg, in *Pergamon Texts in Inorganic Chemistry*, Vol. 10. Pergamon Press, Oxford (1975); (a) p. 178; (b) p. 179; (c) p. 451; (d) p. 462; (e) *Gmelin Handbook of Inorganic Chemistry*, Uran, Suppl. Vol. C.8. Springer-Verlag, Berlin (1980).
2. K. W. Bagnall, in *Comprehensive Coordination Chemistry* (Edited by G. Wilkinson), Vol. 3, p. 1211. Pergamon Press, Oxford (1987).
3. (a) N. W. Alcock, M. M. Roberts and M. C. Chakravorti, *Acta Cryst.* 1980, **B36**, 687; (b) I. I. Chernyaev, G. V. Ellert, L. K. Shubochkin and R. N. Shehelokov, *Zh. Neorgan. Khim.* 1963, **8**, 1584 (*Chem. Abstr.* 1964, **59**, 8344e); 1963, **8**, 2332 (*Chem. Abstr.* 1964, **60**, 1325c).
4. M. C. Chakravorti, P. K. Bhardwaj, S. C. Pandit and B. K. Mathur, *J. Inorg. Nucl. Chem.* 1978, **40**, 1365.
5. K. C. Satpathy, R. Mishra and G. C. Pradhan, *Acta Cienc. Indica.* [*Ser.*] *Chem.* 1982, **8**, 139 (*Chem. Abstr.* 1983, **98**, 136563s).
6. M. C. Chakravorti and M. Chowdhury, *J. Ind. Chem. Soc.* 1985, **62**, 399; 1986, **63**, 472.
7. M. K. Chaudhuri, D. T. Khathing and P. Srinivas, *J. Fluorine Chem.* 1992, **56**, 305.
8. M. Bhattachajee, M. K. Chaudhuri and R. N. Dutta

Purkayastha, *J. Chem. Soc., Dalton Trans.* 1990, 2883.
9. M. Bhattachajee, M. K. Chaudhuri and R. N. Dutta Purkayastha, *Inorg. Chem.* 1986, **25**, 2354.
10. J. K. Basumatary, M. K. Chaudhuri, R. N. Dutta Purkayastha and Z. Hiese, *J. Chem. Soc., Dalton Trans.* 1986, 709.
11. M. N. Bhattachajee, M. K. Chaudhuri and R. N. Dutta Purkayastha, *J. Chem. Soc., Dalton Trans.* 1985, 409.
12. M. Cefola, R. C. Taylor, P. S. Gentile and A. V. Celiano, *J. Phys. Chem.* 1962, **66**, 790.
13. N. C. Li, E. Doody and J. M. White, *J. Am. Chem. Soc.* 1958, **80**, 5901.
14. I. Feldman and L. Koval, *Inorg. Chem.* 1963, **2**, 145.
15. N. W. Alcock, D. J. Flanders, T. J. Kemp and M. A. Shand, *J. Chem. Soc., Dalton Trans.* 1985, 517.
16. M. N. Bhattacharjee, M. K. Chaudhuri, M. Devi, R. N. Dutta Purkayastha, Z. Hiese and D. T. Khathing, *Int. J. Mass. Spectr. Ion Processes* 1986, **71**, 109 and refs therein.
17. M. K. Chaudhuri, P. C. Paul and P. Srinivas, *Proc. Ind. Acad. Sci.* 1992, **104**, 479.
18. A. I. Vogel, *A Text Book of Quantitative Inorganic Analysis*, 4th edn. Longmans Green, New York (1978); (a) p. 343; (b) p. 488.
19. V. V. Ramanujam, K. Rengaraj and B. Sivasankar, *Bull. Chem. Soc. Japan* 1979, **52**, 2713.
20. S. Glasston, *Text Book of Physical Chemistry*, p. 901. Macmillan, London (1956); M. C. Day and J. Selbin, *Theoretical Inorganic Chemistry* p. 394. Affiliated East–West Press, New Delhi (1977).
21. W. J. Geary, *Coord. Chem. Rev.* 1971, **7**, 81.
22. (a) M. C. Chakravorti and N. Bandyopadhyay, *J. Inorg. Nucl. Chem.* 1972, **34**, 2867; (b) 1971, **33**, 2565.
23. (a) L. H. Jones, *J. Chem. Phys.* 1955, **23**, 2105; (b) K. Nakamoto, *Infrared and Raman Spectra of Inorganic and Coordination Compounds*, 4th edn, p. 109. Wiley Interscience, London (1986); (c) B. Frlec and H. H. Hyman, *Inorg. Chem.* 1967, **6**, 2233.
24. I. M. Kolthoff and C. Auerbach, *J. Am. Chem. Soc.* 1952, **74**, 1452.
25. R. L. Pecsok, *Anal. Chem.* 1953, **25**, 561.
26. M. Bhattacharjee, M. K. Chaudhuri, N. S. Islam and P. C. Paul, *Inorg. Chim. Acta* 1990, **169**, 97.
27. H. Shindo and L. Brown, *J. Am. Chem. Soc.* 1965, **87**, 1905; M. Chandrasekharam, M. R. Udupa and G. Aravamudhan, *Inorg. Chim. Acta* 1973, **7**, 88.
28. K. Nakamoto, *Infrared and Raman Spectra of Inorganic and Coordination Compounds*. 4th edn. Wiley Interscience, London (1986); (a) p. 234; (b) p. 228; (c) p. 260; (d) p. 233.
29. N. F. Curtis, *J. Chem. Soc.* (*A*) 1968, 1584.
30. S. P. McGlynn, J. K. Smith and W. C. Neely, *J. Chem. Phys.* 1961, **35**, 105.
31. W. Wendling and S. Mahamoudi, *Bull. Soc. Chim. France* 1972, 40.

Polyhedron Vol. 12, No. 2, pp. 235–239, 1993
Printed in Great Britain

0277–5387/93 $6.00+.00
© 1993 Pergamon Press Ltd

8-QUINOLINOLATE COMPLEXES OF RUTHENIUM(II). SYNTHESIS, CHARACTERIZATION AND ELECTRON TRANSFER PROPERTIES

SAMARESH BHATTACHARYA

Department of Chemistry, Inorganic Chemistry Section, Jadavpur University, Calcutta 700032, India

(*Received* 23 *June* 1992; *accepted* 10 *September* 1992)

Abstract—Two stable 8-quinolinolate complexes of ruthenium(II), $[Ru(bpy)(Q)]ClO_4$ and $[Ru(tap)_2(Q)]ClO_4$ [bpy = 2,2′-bipyridine, Q = 8-quinolinolate anion, tap = 2-(*m*-tolylazo)pyridine] have been synthesized. The complexes are diamagnetic and show strong absorption near 1100 cm^{-1} in the IR spectra due to the presence of ClO_4^-. In acetonitrile solution they behave as 1 : 1 electrolytes. The complexes display intense absorption bands in the visible region (400–700 nm) which are assigned to MLCT transitions. The formal potential (E^0_{298}), determined cyclic voltammetrically for the ruthenium(II)–ruthenium(III) oxidation, is 0.48 V vs SCE for $[Ru(bpy)_2(Q)]^+$. The same oxidation takes place irreversibly at 1.00 V vs SCE (E_{pa} value) in the case of $[Ru(tap)_2(Q)]^+$. Reductions of the bound bpy and tap ligands are also observed.

The anion obtained from 8-quinolinol (HQ, 1; H is the dissociable phenolic proton) binds metal ions as a bidentate N,O coordinator forming five-membered chelate rings (**2**). The coordination chemistry of this ligand is rich and well studied.[1–12] However,

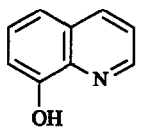

8-Quinolinol (HQ)

1

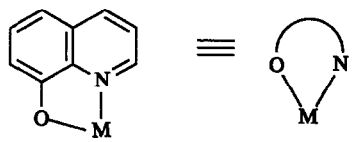

2

very few well-characterized 8-quinolinolate complexes of ruthenium exist in the literature.[6–12] The present work originated from the search for stable Ru^{II}-Q complexes. It is well documented in the literature that the 8-quinolinolate anion alone cannot afford stable complexes of ruthenium(II).[6] Therefore, 2,2′-bipyridine (bpy, **3**) and 2-(*m*-tolylazo)pyridine (tap, **4**) were used as co-ligands to stabilize the bivalent state of ruthenium. Synthesis, characterization and redox properties of two mixed ligand Ru^{II}-Q complexes are reported in this paper.

EXPERIMENTAL

Materials

Commercial ruthenium trichloride (Arora Matthey, Calcutta, India) was converted to $RuCl_3 \cdot 3H_2O$ by repeated evaporation to dryness with concentrated hydrochloric acid. 2,2′-Bipyridine and 8-quinolinol were purchased from S.D. Fine-Chemicals, Bombay, India. 2-(*m*-Tolylazo)pyridine, *cis*-$Ru(bpy)_2Cl_2 \cdot 2H_2O$ and ctc-$Ru(tap)_2Cl_2$ were prepared following reported procedures.[13,14] BDH silica gel (60–120 mesh) was used for chromatography. Purification of acetonitrile and the preparation of tetraethylammonium perchlorate (TEAP) for electrochemical work were per-

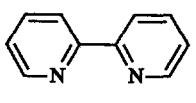

2,2'- Bipyridine (bpy)

3

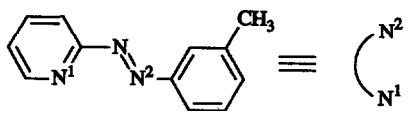

2- (*m* - Tolylazo) pyridine (tap)

4

formed as reported in the literature.[15,16] Dinitrogen gas was purified by successively bubbling it through alkaline dithionite and concentrated sulphuric acid. All other chemicals and solvents were reagent-grade commercial materials.

Preparation of complexes

(8-*Quinolinolato*)*bis*(2,2′-*bipyridine*)*ruthenium*(II) *perchlorate*, $[Ru(bpy)_2(Q)]ClO_4$. $Ru(bpy)_2Cl_2 \cdot 2H_2O$ (100 mg, 0.19 mmol) was taken in warm ethanol (30 cm^3). To this was added $AgClO_4$ (80 mg, 0.38 mmol) and the mixture was stirred for 15 min. The deposited AgCl was separated by filtration and to the filtrate was added 8-quinolinol (60 mg, 0.41 mmol) and sodium acetate (60 mg, 0.44 mmol). The resulting mixture was stirred for 18 h. Ethanol was then evaporated under reduced pressure to give a gummy solid, which was washed with water and dried *in vacuo* over P_4O_{10}. Recrystallization of the crude product from acetonitrile–benzene afforded $[Ru(bpy)_2(Q)]ClO_4$ as a crystalline solid; yield 88 mg, 70%.

(8-*Quinolinolato*)*bis*(2-(*m*-*tolylazo*)*pyridine*)*ruthenium*(II) *perchlorate*, $[Ru(tap)_2(Q)]ClO_4$. ctc-$Ru(tap)_2Cl_2$ (100 mg, 0.18 mmol) was taken in warm ethanol (30 cm^3) and $AgClO_4$ (75 mg, 0.36 mmol) was added to it. The mixture was stirred for 15 min. The deposited AgCl was then separated by filtration and to the filtrate was added 8-quinolinol (60 mg, 0.41 mmol) and sodium acetate (60 mg, 0.44 mmol). The resulting mixture was stirred for 20 h. Ethanol was then removed under reduced pressure and the resulting solid was dissolved in a minimum volume of acetonitrile. This solution was filtered to separate any insoluble material and the filtrate was chromatographed through a silica gel column. With chloroform as the eluant, a yellow band appeared first which was rejected. Using a 1 : 1 chloroform–acetonitrile solution as the eluant, a second deep blue-violet band separated. This fraction was collected and evaporation of the solvents gave crystalline $[Ru(tap)_2(Q)]ClO_4$; yield 85 mg, 65%.

Physical measurements

Electronic spectra were recorded on a Hitachi 330 spectrophotometer. IR spectra were obtained on a Perkin–Elmer 783 spectrometer with samples prepared as KBr pellets. ^1H NMR spectra were recorded on a Varian T-60A spectrometer. Solution electrical conductivity was measured using a Philips PR 9500 bridge with a solute concentration of 10^{-3} M. Magnetic susceptibilities were measured with the help of a PAR 155 vibrating sample magnetometer fitted with a Walker Scientific L75FBAL magnet. Electrochemical measurements were made using the PAR model 370-4 electrochemistry system incorporating the following components: 174A polarographic analyser, 175 universal programmer, RE0074 *X–Y* recorder, 173 potentiostat, 179 digital coulometer, 377 cell system. All electrochemical experiments were performed under a dinitrogen atmosphere. A planar Beckman 39273 platinum-inlay working electrode, a platinum-wire auxiliary electrode and an aqueous saturated calomel reference electrode (SCE) were used in a three electrode configuration. A platinum-wire gauge working electrode was used in the coulometric experiments. All electrochemical data were collected at 298 K and are uncorrected for junction potentials. Microanalyses (C, H, N) were performed using a Perkin–Elmer 240C elemental analyser.

RESULTS AND DISCUSSION

$[Ru(bpy)_2(Q)]^+$ has been synthesized from $Ru(bpy)_2Cl_2$ following the synthetic route shown in eq. (1).

$$Ru(bpy)_2Cl_2 \xrightarrow[EtOH]{Ag^+} [Ru(bpy)_2(EtOH)_2]^{2+} \xrightarrow[NaOAc]{HQ} [Ru(bpy)_2(Q)]^+ \quad (1)$$

The complex cation has been isolated in a good yield as the perchlorate salt in the solid state. $[Ru(tap)_2(Q)]ClO_4$ has similarly been prepared starting from ctc-$Ru(tap)_2Cl_2$ (**5**), as shown in eq. (2). The synthetic route used to obtain

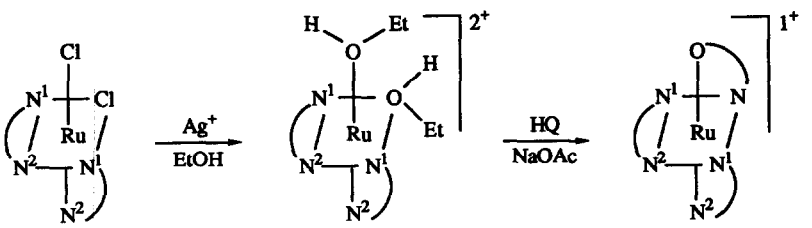

ctc - Ru (tap)$_2$ Cl$_2$ — **5**

[Ru (tap)$_2$ (Q)]$^+$ — **6**

(2)

Table 1. Microanalytical, molar conductivity, electronic spectral and cyclic voltammetric data

Compound	Analytical data[a] %C	%H	%N	Molar conductivity[b] Λ_M (Ω^{-1} cm^2 M^{-1})	Electronic spectral data[b] λ_{max} (nm) (ε,[c] M^{-1} cm^{-1})	Cyclic voltammetric data[d] E^0_{298}, V(ΔE_p, mV) Ru^{III}–Ru^{II}	Ligand reductions
$[Ru(bpy)_2(Q)]ClO_4$	53.2 (53.0)	3.3 (3.3)	10.5 (10.7)	140	580[e](3890), 505(11,900), 460[e](9000)	0.48(80)	−1.55(60), −1.77(60)
$[Ru(tap)_2(Q)]ClO_4$	53.8 (53.6)	3.7 (3.8)	13.2 (13.3)	155	670(2500), 560(11,000), 450(6440)	1.00[f](—)	−0.37(60), −0.93(60), −1.70(80)

[a] Calculated values are in parentheses.
[b] In acetonitrile solution.
[c] Extinction coefficient.
[d] Conditions: solvent, acetonitrile; supporting electrolyte, TEAP (0.1 M); working electrode, platinum; reference electrode, SCE; solute concentration, 10^{-3} M; $E^0_{298} = 0.5(E_{pa}+E_{pc})$, where E_{pa} and E_{pc} are anodic and cathodic peak potentials respectively; $\Delta E_p = E_{pa} - E_{pc}$; scan rate, 50 mV s^{-1}.
[e] Shoulder.
[f] E_{pa} value.

$[Ru(tap)_2(Q)]^+$ is known to be stereoretentive.[17] Therefore, structure **6** is assigned to the tap complex. As the 8-quinolinolate anion is an unsymmetrical bidentate ligand, the two tap ligands are non-equivalent in $[Ru(tap)_2(Q)]^+$. Two equally intense ^1H NMR methyl signals from the two tap ligands are observed at 2.16 and 2.23 ppm in $CDCl_3$ solution, as expected.

Microanalytical data (Table 1) confirm the formulations of the two complexes. The IR spectra of the complexes contain several sharp bands of different intensities. Individual band assignment has not been attempted. However, a very strong vibration near 1100 cm^{-1} is observed for both complexes due to the presence of ClO_4^-. The ν(OH) band observed in free HQ at ~ 3150 cm^{-1} is, of course, absent in these complexes. The complexes are diamagnetic as expected for low-spin d^6, $S = 0$ systems and in acetonitrile solution they behave as 1:1 electrolytes (Table 1). Both complexes display three intense absorption bands in the visible region (400–700 nm) in acetonitrile solution, which are assigned to MLCT transitions. Spectra are shown in Fig. 1 and data are given in Table 1.

The electron-transfer properties of the two complexes have been studied in acetonitrile solution by cyclic voltammetry. Voltammograms are shown in Fig. 2 and voltammetric data are given in Table 1. Both complexes show metal oxidation and ligand reductions. The ruthenium(II)–ruthenium(III) oxidation in $[Ru(bpy)_2(Q)]^+$ [eq. (3)] takes place reversibly at a formal potential (E^0_{298}) of 0.48 V vs SCE. The value of i_{pa}/i_{pc} (i_{pa} = anodic peak current; i_{pc} = cathodic peak current) for this couple is 1, as expected for a reversible couple. The one-electron stoichiometry of this ruthenium(II)–ruthenium(III) couple has been confirmed by constant potential coulometry. In RuQ_3 the same couple appears at −0.70 V vs SCE.[6] Therefore, the use of bpy as a co-ligand indeed stabilized the bivalent state of the metal to an appreciable extent.

$$[Ru^{II}(bpy)_2(Q)]^+ \rightleftharpoons [Ru^{III}(bpy)_2(Q)]^{2+} + e^- \quad (3)$$

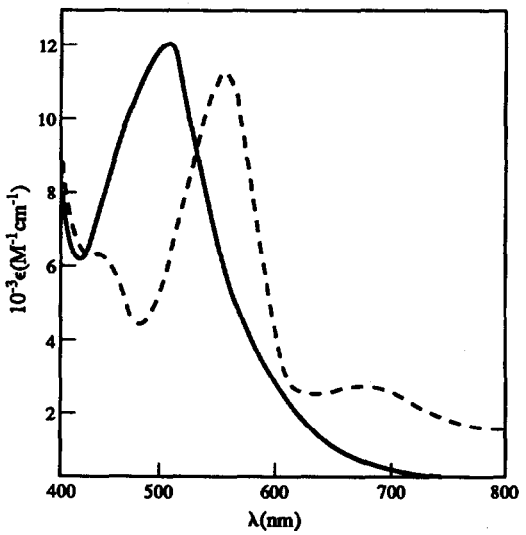

Fig. 1. Electronic spectra of $[Ru(bpy)_2(Q)]ClO_4$ (——) and $[Ru(tap)_2(Q)]ClO_4$ (– – –) in acetonitrile.

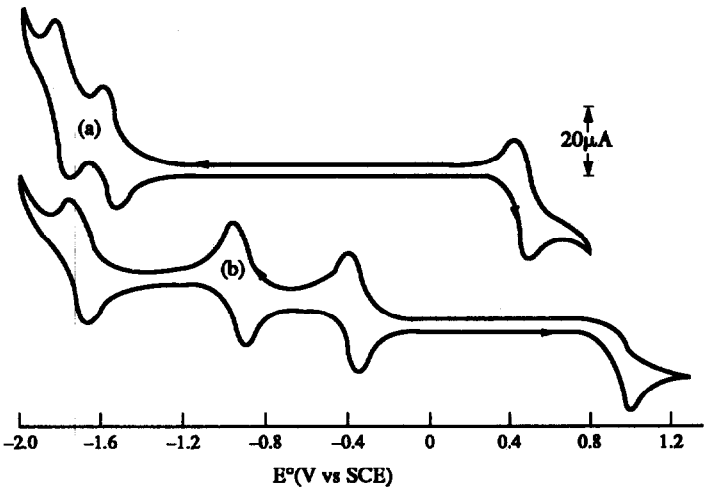

Fig. 2. Cyclic voltammograms of (a) $[Ru(bpy)_2(Q)]ClO_4$ and (b) $[Ru(tap)_2(Q)]ClO_4$ in acetonitrile (0.1 M TEAP) at a scan rate of 50 mV s^{-1}. The solute concentration in each case was *ca* 10^{-3} M.

In $[Ru(tap)_2(Q)]^+$ the ruthenium(II)–ruthenium(III) oxidation is irreversible [eq. (4)]. The anodic peak potential (E_{pa}) is 1.00 V vs SCE. The cathodic response corresponding to the reduction of $[Ru^{III}(tap)_2(Q)]^{2+}$, formed during the anodic scan, has not been observed, presumably due to the fast decomposition of $[Ru^{III}(tap)_2(Q)]^{2+}$. The one-electron nature of this oxidation is established from current height considerations. The tap ligand is found to be a better stabilizer of ruthenium(II), which is due to its better π-accepting ability as observed before.[17,18]

$$[Ru^{II}(tap)_2(Q)]^+ \longrightarrow [Ru^{III}(tap)_2(Q)]^{2+} + e^- \quad (4)$$

On the negative side of SCE $[Ru(bpy)_2(Q)]^+$ displays two successive reversible one-electron reductions at -1.55 and -1.77 V vs SCE, which are assgined to the reductions of the two bpy ligands as shown in eqs (5) and (6). The i_{pa}/i_{pc} values for these two couples are very close to 1, indicating their reversible nature. It is well documented[19,20] that bpy is a potential carrier of electron-transfer, each bpy successively accepting two electrons in one electrochemically accessible lowest unoccupied molecular orbital.

$$[Ru^{II}(bpy)_2(Q)]^+ + e^- \rightleftharpoons [Ru^{II}(bpy)(bp\dot{y})(Q)] \quad (5)$$

$$[Ru^{II}(bpy)(bp\dot{y})(Q)] + e^- \rightleftharpoons [Ru^{II}(bp\dot{y})_2(Q)]^- \quad (6)$$

Hence, in $[Ru(bpy)_2(Q)]^+$ four successive reductions are expected. Out of the expected four only two reductions have been experimentally observed. The remaining two reductions are not observed due to solvent cut-off. The formal potential of the first reduction of bpy in $[Ru(bpy)_2(Q)]^+$ [eq. (5)] is more positive than that of free bpy (-2.17 V)[20] due to the coordination of bpy to bivalent ruthenium. The two reduction potentials in the present complex compare well with those observed for $[Ru(bpy)_2(T)]^+$ (T = triazene-1-oxidato anion).[18]

The tap complex, $[Ru(tap)_2(Q)]^+$, displays three successive reversible one-electron reductions at -0.37, -0.93 and -1.70 V vs SCE, which are assigned to reductions of the bound tap ligands as shown in eqs (7)–(9).

$$[Ru^{II}(tap)_2(Q)]^+ + e^- \rightleftharpoons [Ru^{II}(tap)(t\dot{a}p)(Q)] \quad (7)$$

$$[Ru^{II}(tap)(t\dot{a}p)(Q)] + e^- \rightleftharpoons [Ru^{II}(t\dot{a}p)_2(Q)]^- \quad (8)$$

$$[Ru^{II}(t\dot{a}p)_2(Q)]^- + e^- \rightleftharpoons [Ru^{II}(t\dot{a}p)(t\dot{a}\dot{p})(Q)]^{2-} \quad (9)$$

As expected for reversible couples, the observed i_{pa}/i_{pc} values for these couples are all close to 1. Each tap ligand is known[17] to accept two electrons in its lowest unoccupied molecular orbital, which is largely azo in nature. Thus, four reductions are expected in $[Ru(tap)_2(Q)]^+$, three of which are observed but the fourth is not due to solvent cut-off. The free tap ligand shows[17] two reductions at -1.30 and -1.60 V. Due to coordination to ruthenium(II), the potentials of the first reduction

are shifted towards more positive values in $[Ru(tap)_2(Q)]^+$. The observed reduction potentials are comparable to those in $[Ru(tap)_2(T)]^+$.[17]

Concluding remarks

In combination with bpy and tap, the 8-quinolinolate anion can be bound to ruthenium(II) to form the stable species $[Ru^{II}(bpy)_2(Q)]^+$ and $[Ru^{II}(tap)_2(Q)]^+$. The ruthenium(II)–ruthenium(III) oxidation is observed on the positive side of SCE in these two complexes. The redox stability of the ruthenium(II) state is greater in the tap complex paralleling the π-acceptor order bpy < tap. Reductions of the bound tap and bpy ligands are also observed in these two complexes.

Acknowledgements—Financial support received from the Department of Chemistry, Jadavpur University, Calcutta, India, is gratefully acknowledged. The author thanks Professor Animesh Chakravorty of the Indian Association for the Cultivation of Science, Calcutta, India, for providing instrumental facilities and helpful discussions.

REFERENCES

1. N. Ohakaku and K. Nakamoto, *Inorg. Chem.* 1971, **10**, 798 and refs therein.
2. A. F. Isbell Jr and D. T. Sawyer, *Inorg. Chem.* 1971, **10**, 2449; T. L. Riechel and D. T. Sawyer, *Inorg. Chem.* 1975, **14**, 1869; E. T. Seo, T. L. Riechel and D. T. Sawyer, *Inorg. Chem.* 1977, **16**, 734.
3. C. J. Weber and R. D. Archer, *Inorg. Chem.* 1983, **22**, 4149; R. D. Archer and C. J. Weber, *Inorg. Chem.* 1984, **23**, 4158.
4. W. J. Cheng, *J. Coord. Chem.* 1983, **11**, 57.
5. J. Chatt, B. A. L. Crichton, J. R. Dilworth, P. Dahlstrom and J. A. Zubieta, *J. Chem. Soc., Dalton Trans.* 1982, 1041; S. Yamada, C. Katayama, J. Tanaka and M. Taneka, *Inorg. Chem.* 1984, **23**, 253; B. E. Wilcox, M. J. Heeg and E. Deutsch, *Inorg. Chem.* 1984, **23**, 2962.
6. G. K. Lahiri, S. Bhattacharya, B. K. Ghosh and A. Chakravorty, *Inorg. Chem.* 1987, **26**, 4324.
7. S. A. Luchkina and T. P. Sergeeva, *Russ. J. Inorg. Chem.* (English) 1983, **28**, 1466.
8. N. E. Domracheva, V. N. Konstantinov, S. A. Luchkina and I. V. Orchinnikov, *Koord. Khim.* 1985, **11**, 503; *Chem. Abstr.* 1985, **103**, 63742j.
9. G. S. Rodman and J. K. Nagle, *Inorg. Chim. Acta* 1985, **105**, 205.
10. P. Powell, *J. Organomet. Chem.* 1974, **65**, 89.
11. J. A. Van Doorn and P. W. N. M. Van Leeuween, *J. Organomet. Chem.* 1981, **222**, 299.
12. S. Gopinathan, S. S. Deshpande and C. Gopinathan, *Z. Anorg. Allg. Chem.* 1985, **527**, 203; *Chem. Abstr.* 1986, **104**, 27831z.
13. P. J. Giordino, C. R. Bock and M. S. Wrighton, *J. Am. Chem. Soc.* 1978, **100**, 6960.
14. S. Goswami, A. R. Chakravarty and A. Chakravorty, *Inorg. Chem.* 1981, **20**, 2246; 1982, **21**, 2737.
15. D. T. Sawyer and J. L. Roberts Jr, *Experimental Electrochemistry for Chemists*, pp. 167–215. Wiley, New York (1974).
16. M. Walter and L. Ramaley, *Anal. Chem.* 1973, **45**, 165.
17. S. Goswami, R. N. Mukherjee and A. Chakravorty, *Inorg. Chem.* 1983, **22**, 2825.
18. R. N. Mukherjee and A. Chakravorty, *J. Chem. Soc., Dalton Trans.* 1983, 2179.
19. A. A. Vlcek, *Coord. Chem. Rev.* 1982, **43**, 39.
20. J. L. Kahl, K. W. Hanck and K. DeArmond, *J. Phys. Chem.* 1978, **82**, 540.

Polyhedron Vol. 12, No. 2, pp. 241–246, 1993
Printed in Great Britain

0277–5387/93 $6.00+.00
© 1993 Pergamon Press Ltd

SYNTHESIS AND CHARACTERIZATION OF URANIUM(IV) COMPOUNDS WITH PIPERAZINES

B. S. MANHAS*, S. PAL and A. K. TRIKHA

Department of Chemistry, Punjabi University, Patiala 147002, India

(*Received* 18 *March* 1992; *accepted* 10 *September* 1992)

Abstract—Compounds of the empirical formula $[UX_4 \cdot n(L) \cdot m\text{THF}]$ (where X = thiocyanate, perchlorate, bromide and iodide; n = 1–3; L = piperazine, 1-methyl-, 2-methyl-, 1-phenyl-, 1,4-dimethyl-, 2,5-dimethyl- and 2,6-dimethylpiperazine; m = 0 and 1) have been prepared and characterized by physical studies. IR spectra indicate the mode of coordination. Electronic spectral and variable-temperature magnetic data have been employed to ascertain the stereochemical environment of uranium. Except for the perchlorate compounds, which are 1 : 1 electrolytes, all other compounds are non-electrolytes.

Piperazines which exist in the chair conformation in their free state can form complexes in which they are either in (a) the boat form or (b) in the chair form, giving chelated and non-chelated polymeric complexes, respectively. Due to our interest in such

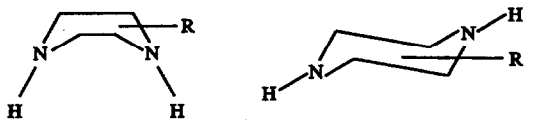

R=CH_3, C_6H_5

systems we report the complexes of uranium(IV) thiocyanate, perchlorate, bromide and iodide with piperazine (L_1), 1-methylpiperazine (L_2), 2-methylpiperazine (L_3), 1-phenylpiperazine (L_4), 1,4-dimethylpiperazine (L_5), 2,5-dimethylpiperazine (L_6) and 2,6-dimethylpiperazine (L_7) in this paper.

RESULTS AND DISCUSSION

Synthesis

The complexes were prepared by direct interaction of uranium(IV) salts with piperazines.[1] Complexes of various shades of green colour and of the formula $[UX_4 \cdot n(L) \cdot m\text{THF}]$ (where X = NCS, ClO_4, Br and I; n = 1–3; L = various piperazines; m = 0 and 1) were obtained by mixing solutions of piperazines in THF with the THF solutions of uranium(IV) salts, prepared *in situ* from UCl_4 according to reaction (1):

$$UCl_4 + 4MX \longrightarrow UX_4 + 4MCl \qquad (1)$$

X = Br, I and NCS for M = K and X = ClO_4 for M = Ag.

The products were filtered and dried under anhydrous conditions. The complexes of 1-phenylpiperazine, however, separated as dark green oils from which green solids were obtained after successive treatments with diethyl ether and THF.

All the complexes are stable at room temperature only in vacuum-sealed ampoules. They do not melt even when heated at 300°C, but decompose in the temperature range 51–182°. Some of the complexes are soluble in common organic solvents like ethanol, methanol, nitrobenzene, nitromethane, methyl cyanide, etc., but the solubility is too low to determine the molecular weights. Some relevant data are given in Table 1.

IR spectral studies (4000–250 cm^{-1}).

The NH stretch which appears at *ca* 3400 cm^{-1} for free piperazines is observed as a broad band in the region 3400–3150 cm^{-1} for the present complexes. This downward shift[2,3] is indicative of coordination of the NH nitrogen atom and is supported by the shift in the δ(NH) frequency, which

* Author to whom correspondence should be addressed.

Table 1. Analytical, magnetic and electronic spectral data of the complexes

Sr. No.	Complex	Analysis[a] (%) M	Br/I/S	C	H	N	Magnetism S' (cgs units)	θ^c (K)	$\chi_M \times 10^{-6}$ (cgs units) (μ_{eff}) 77 K	296 K	Principal electronic spectral bands (nm)
1	$U(NCS)_4 \cdot (L_1)$	42.5 (42.8)	23.0 (23.0)	17.3 (17.2)	1.1 (1.7)	15.2 (15.1)	1.96	−245	1582 (0.98)	942 (1.49)	600, 1450, 1950
2	$U(NCS)_4 \cdot (L_2)$	41.2 (41.7)	22.3 (22.4)	19.0 (18.9)	2.1 (2.1)	14.5 (14.7)	0.84	−207	4193 (1.60)	2367 (2.36)	560, 640, 670, 925, 1135, 1475
3	$U(NCS)_4 \cdot (L_3)$	40.9 (41.7)	22.2 (22.4)	18.1 (18.9)	2.1 (2.1)	14.0 (14.7)	1.87	−142	2430 (1.22)	1215 (1.68)	670,1100
4	$U(NCS)_4 \cdot 2(L_4)$	30.0 (29.9)	15.9 (16.1)	36.0 (36.2)	3.1 (3.5)	14.0 (14.1)	1.09	−107	5246 (1.79)	2332 (2.34)	500, 580, 690, 945, 1135, 1445
5	$U(NCS)_4 \cdot (L_5)$	40.4 (40.7)	21.9 (21.9)	20.3 (20.5)	2.3 (2.3)	14.8 (14.3)	0.99	−209	3515 (1.47)	1992 (2.17)	500, 575, 690, 1080, 1170
6	$U(NCS)_4 \cdot (L_6)$	40.1 (40.7)	22.0 (21.9)	20.6 (20.5)	2.7 (2.3)	14.0 (14.3)	0.77	−161	4519 (1.66)	2553 (2.45)	500, 580, 695, 1120, 1145, 1450
7	$U(NCS)_4 \cdot (L_7)$	39.4 (40.7)	21.4 (21.9)	20.8 (20.5)	2.9 (2.3)	14.5 (14.3)	1.08	−144	4181 (1.60)	2102 (2.23)	500, 570, 670, 930, 1135, 1445
8	$U(ClO_4)_4 \cdot (L_1)THF$	29.1 (29.9)	—	11.8 (12.0)	2.2 (2.2)	3.4 (3.5)	3.87	−66	1080 (1.05)	747 (1.29)	430, 1140, 1440, 1950
9	$U(ClO_4)_4 \cdot 3(L_2)$	24.8 (25.4)	—	19.2 (19.2)	3.8 (3.8)	8.8 (8.9)	54.70	−32	166 (0.32)	56 (0.36)	505, 550, 620, 645, 1020, 1100, 1265, 1460, 1610, 1750
10	$U(ClO_4)_4 \cdot 3(L_3)$	25.3 (25.4)	—	19.0 (19.2)	3.4 (3.8)	8.7 (8.9)	2.53	−52	3050 (1.37)	1160 (1.64)	450, 1135, 1500, 1680, 1950
11	$U(ClO_4)_4 \cdot 2(L_4)$	25.0 (24.7)	—	24.2 (24.9)	2.5 (2.9)	5.7 (5.8)	0.74	−58	9850 (2.46)	3900 (2.98)	465, 550, 620, 655, 940, 1100, 1420, 1700
12	$U(ClO_4)_4 \cdot 2(L_5)THF$	25.9 (25.3)	—	20.4 (20.4)	3.8 (3.8)	5.8 (5.9)	1.59	−22	6666 (2.03)	2125 (2.22)	440, 620, 1040, 11, 1450, 1720
13	$U(ClO_4)_4 \cdot 2(L_6)THF$	25.7 (25.4)	—	20.5 (20.4)	3.9 (3.8)	5.7 (5.9)	2.67	−31	3460 (1.46)	1170 (1.64)	625, 655, 1100, 1430, 1720

14	$U(ClO_4)_4 \cdot 2(L_7)THF$	26.0 (25.4)	—	20.4 (20.4)	3.6 (3.8)	6.1 (5.9)	—	—	—	—	470, 650, 1100, 1450, 1700
15	$UBr_4 \cdot (L_1)THF$	33.0 (33.2)	44.5 (44.6)	13.2 (13.4)	2.5 (2.5)	3.8 (3.9)	1.32	−167	3095 (1.38)	1631 (1.96)	480, 1120, 1410, 1500, 1700, 1950
16	$UBr_4 \cdot (L_2)THF$	32.7 (32.6)	42.9 (43.8)	14.7 (14.8)	2.7 (2.7)	3.7 (3.8)	0.84	−258	3515 (1.47)	2126 (2.43)	480, 560, 1090, 1430, 1700, 1950
17	$UBr_4 \cdot (L_3)$	36.0 (36.1)	48.5 (48.6)	9.2 (9.1)	1.9 (1.8)	4.2 (4.2)	357	−85	1720 (1.03)	746 (1.31)	1030, 1100, 1460, 1730, 1980
18	$UBr_4 \cdot (L_4)$	27.0 (26.9)	36.0 (36.2)	27.2 (27.2)	3.1 (3.1)	6.3 (6.3)	0.58	−137	7939 (2.21)	3932 (3.05)	480, 550, 660, 1120, 1410, 1700
19	$UBr_4 \cdot (L_5)THF$	27.7 (27.7)	37.2 (37.2)	22.3 (22.3)	4.1 (4.1)	6.6 (6.5)	0.87	−216	3905 (1.55)	2235 (2.30)	835, 1100
20	$UBr_4 \cdot (L_6)THF$	27.4 (27.7)	37.3 (37.2)	22.3 (22.3)	4.1 (4.1)	6.5 (6.5)	0.71	−200	5044 (1.76)	2818 (2.58)	475, 545, 645, 800, 1100, 1400, 1710
21	$UBr_4 \cdot 2(L_7)THF$	27.7 (27.7)	37.2 (37.2)	22.3 (22.3)	4.2 (4.1)	6.5 (6.5)	0.59	−280	4740 (1.70)	2936 (2.63)	480, 540, 600, 650, 940, 1100, 1440, 1730, 1960
22	$UI_4 \cdot (L_1)$	28.4 (28.6)	60.5 (61.0)	5.8 (5.7)	1.2 (1.2)	3.2 (3.3)	1.08	−144	4182 (1.60)	2102 (2.23)	465, 610, 665, 1150, 1430, 1700, 1900
23	$UI_4 \cdot (L_2)$	28.7 (28.1)	58.5 (60.0)	7.0 (7.0)	1.3 (1.4)	3.1 (3.3)	1.57	−44	5262 (1.80)	1872 (2.10)	630, 660, 920, 1100, 1450, 1720
24	$UI_4 \cdot (L_3)THF$	26.0 (25.9)	55.2 (55.3)	11.5 (11.7)	2.0 (2.1)	3.1 (3.0)	1.85	−114	2818 (1.31)	1313 (1.76)	450, 650, 1100, 1450, 1720, 1930, 1980
25	$UI_4 \cdot 2(L_4)THF$	20.1 (20.8)	45.0 (44.4)	25.1 (25.2)	3.4 (3.1)	4.9 (4.9)	0.49	−154	8751 (2.32)	4495 (3.26)	480, 555, 670, 950, 1130, 1430, 1700
26	$UI_4 \cdot 2(L_5)$	24.4 (24.4)	52.1 (52.1)	14.7 (14.7)	2.9 (2.8)	5.8 (5.7)	0.63	−181	6087 (1.94)	3294 (2.79)	540, 660, 920, 1100, 1400, 1710, 1960
27	$UI_4 \cdot 2(L_6)$	24.7 (24.4)	52.1 (52.1)	14.7 (14.7)	2.8 (2.8)	5.7 (5.7)	0.57	−117	9037 (2.37)	4236 (3.17)	470, 555, 620, 655, 940, 1040, 1100, 1420, 1760
28	$UI_4 \cdot 2(L_7)$	24.5 (24.4)	51.8 (52.1)	14.7 (14.7)	3.0 (2.8)	5.5 (5.7)	0.40	−115	—	5959 (3.75)	550, 630, 665, 920, 1040, 1120

[a] Required values are given in parentheses.
[b] Slopes of plots $1/\chi_M$ vs T.
[c] Obtained by extrapolating the plots mentioned in b to $1/\chi_M = 0$.

appears at *ca* 1650 cm^{-1} for free piperazines and in the range 1625–1620 cm^{-1} for the complexes.[2] The broadness of the band due to ν(NH) may be caused by hydrogen bonding.[4] The CH stretches of NCH_3 which appear at 2750 and 2810 cm^{-1} in the IR spectra of 1-methyl- and 1,4-dimethylpiperazine are not observed in the IR spectra of the complexes. They presumably shift to higher frequencies and become mixed with the other CH bands occurring around 2900 cm^{-1}, on coordination of the NCH_3 nitrogen atom.[5]

The IR spectrum[6] of the 1,4-dimethylpiperazine complex of $PdCl_2$, in which piperazine has been shown to exist in the boat form by X-ray diffraction studies,[7] exhibits a large number of new bands of low and medium intensity in addition to changes in the bands characteristic of the free ligand. Except for the additional bands due to the metal–ligand and anions, the IR spectra of the present complexes are quite simple and no new bands of low and medium intensity assignable to the boat conformation[6] appear, thus showing that the piperazines retain their chair conformation in the complexes. The complexes are thus non-chelated polymers.

The COC frequency which appears at 1076 cm^{-1} in free THF[4] could not be identified in the complexes studied due to a strong ligand absorption at *ca* 1080 cm^{-1}. Therefore, IR studies do not say anything about the coordination of THF. However, TGA studies on the complex $[U(ClO_4)_4 \cdot (L_1) \cdot THF]$ indicate a weight loss at 132°C corresponding to one THF molecule, thus showing the presence of coordinated THF.

In the IR spectra of the thiocyanate complexes studied two prominent bands, one at *ca* 2050 cm^{-1} and the other at *ca* 2300 cm^{-1}, assignable to the CN stretch, are observed. This indicates that two types of thiocyanate groups, N-bonded and bridging, are present in the complexes.[8,9] In the perchlorate compounds with ligands L_1, L_2, L_3 and L_6, all the three known types of perchlorate are shown to be present since the broad band (ν_3) at *ca* 1110 cm^{-1}, due to ionic (T_d) perchlorate, a doublet at *ca* 1020 and 1135 cm^{-1} and a triplet at *ca* 1035, 1160 and 1270 cm^{-1} assignable to uni-(C_{3v}) and bidentate (C_{2v}) perchlorates, respectively, are observed.[8,10,11] The complexes with L_5 and L_7 contain unidentate and ionic perchlorates, while that with L_4 contains bidentate and ionic perchlorates only.

In the far-IR spectra of these complexes bands at *ca* 460 and 380 cm^{-1} (refs 3 and 4) have tentatively been assigned to the UO and UN stretches. The ligands exhibit two bands at 520 and 480 cm^{-1} assignable to rocking modes.

All of these compounds are genuine uranium(IV) complexes since all were green in colour and no bands assignable to the uranyl stretch were observed.

The molar conductance values in $\Omega^{-1}\,cm^2\,mol^{-1}$ of the millimolar solutions of the complexes of uranium(IV) bromide, thiocyanate and iodide determined in methanol, ethanol, dimethylsulphoxide and dimethylformamide range from 7.51 to 8.31, 2.14 to 3.87, 2.32 to 4.33 and 2.17 to 4.65. These complexes are thus considered to be non-ionic in nature.[12] The perchlorate complexes behave as 1 : 1 electrolytes since the values in methanol, dimethylsulphoxide and dimethylformamide lie in the ranges 59.77–76.65, 24.51–27.31 and 21.26–27.40.

Electronic reflectance spectra (200–2000 nm) *and magnetic susceptibility measurements*

The electronic reflectance spectra of the present complexes can be placed into three classes on the basis of intensity:[13] weak, strong and medium. The uranium atom may be present in a six-coordinate centrosymmetrical environment (compounds with Sr. No. 1, 3, 8, 10, 15, 17, 22 and 24),[13,14] eight-coordinate cubic environment without a centre of symmetry (compounds with Sr. No. 2, 4–7, 16, 18, 20, 21, 23, 25–28)[15] or an environment where eight-coordinate cubic or six-coordinate octahedral symmetry is destroyed by the presence of non-equivalent ligands (compounds with Sr. No. 9, 11–13).[13] This inference is based both on the nature of the spectrum and the positions of various bands. The band positions (Table 1) of the medium intensity spectra can be correlated more closely with those of the strong rather than the weak intensity type.

In the case of compounds indicated to be eight-coordinate by electronic reflectance spectra, the plot of $1/\chi_M$ (Fig. 1), corrected by least-squares, against temperature was linear and susceptibility varied according to the Curie–Weiss law, $1/\chi_M = S(T-\theta)$, over the temperature range 77–296 K. The susceptibility is, therefore, defined by the parameters S and θ (Table 1). The temperature dependence of the observed paramagnetic susceptibility and the room-temperature effective magnetic moment are both suggestive of the ligand field of a cube for these uranium(IV) compounds.[15–17] However, the small variation in magnetic susceptibility in the complexes where coordination geometry other than the cube (Fig. 1) is indicated by electronic spectra, may be due to a small distortion in the octahedral symmetry. A smaller magnitude of magnetic susceptibility at room temperature for these complexes is in close analogy with an earlier report.[18]

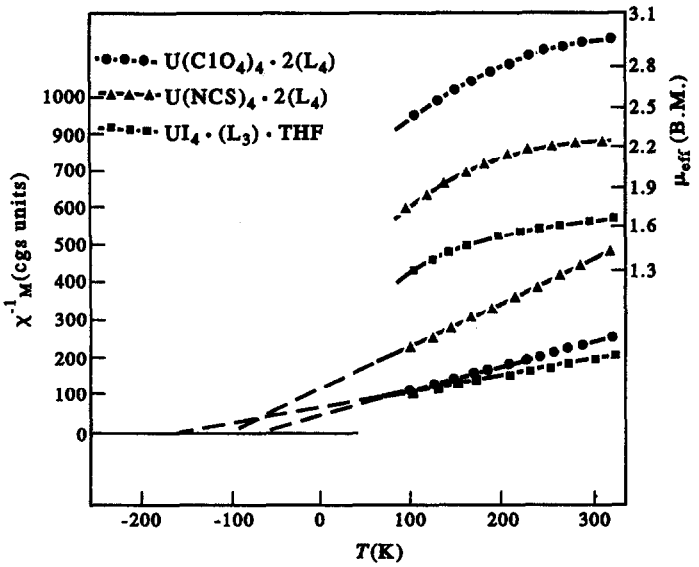

Fig. 1. Variation of molar magnetic susceptibility and effective Bohr magneton numbers with temperature of some representative compounds.

EXPERIMENTAL

The experimental manipulations were performed using Schlenk techniques. The solvents, piperazines and other starting materials were obtained and dried as described earlier.[1,19,20]

Preparation of the complexes

A three-fold excess of the ice-cooled ligand dissolved in THF (10 cm^3) was added to uranium(IV) bromide, iodide, thiocyanate and perchlorate (1.24–1.96 g, 2.63 mmol), prepared *in situ* in the same solvent as described below. The green complex which precipitated immediately was separated by addition of excess dry diethyl ether (*ca* 50 cm^3). The complex was then filtered in a G_4 filtration unit under anhydrous conditions, washed five to six times with ether and finally dried *in vacuo*. A continuous flow of purified nitrogen was maintained throughout the solution during this preparation.

The solutions of uranium(IV) salts employed in this study were obtained as follows:[1] To a solution of UCl_4 (1.00 g, 2.63 mmol) in THF (50 cm^3) were added solid KBr (1.25 g), KI (1.75 g), KNCS (1.02 g) and $AgClO_4$ (2.18 g) in a mole ratio of 1:4. In the preparation of the perchlorate, AgCl separated immediately on mixing. The mixtures for the preparation of the bromide, iodide and thiocyanate had to be stirred for 12 h to allow complete separation of the potassium salts. The green filtrate obtained after filtering out the precipitated salts was used for the preparation of the complexes.

Physical and analytical studies

IR[1,18] and electronic[1] spectra, magnetic[1] and molar conductance[19] measurements, and TGA[1,18] and elemental analysis[1] were performed as described earlier.

Acknowledgements—One of the authors (S. Pal) is thankful to Punjabi University, Patiala, India, for the award of a research scholarship. Professor K. Chandra, University of Roorkee, India, is thanked for the magnetic measurements.

REFERENCES

1. B. S. Manhas and A. K. Trikha, *J. Chem. Soc., Dalton Trans.* 1985, 1985.
2. J. Selbin, J. D. Ortego and M. Schober, *J. Inorg. Nucl. Chem.* 1966, **28**, 1385.
3. N. N. Greenwood and K. Wade, *J. Chem. Soc.* (*A*) 1960, 1130.
4. M. Avram and G. Mateescu, *Infrared Spectroscopy*, p. 257. Wiley-Interscience, New York (1966).
5. J. T. Braunholtz, E. A. V. Ebsworth, F. G. Mann and N. Sheppard, *J. Chem. Soc.* (*A*) 1958, 2780.
6. P. J. Hendra and D. B. Powell, *J. Chem. Soc.* (*A*) 1960, 5105.
7. O. Hassel and B. F. Pederson, *Proc. Chem. Soc.* 1959, 394.

8. K. Nakamoto, *Infrared and Raman Spectra of Inorganic and Coordination Compounds*, 3rd edn. Wiley-Interscience, New York (1980).
9. P. C. H. Mitchell and R. J. P. Williams, *J. Chem. Soc.* (*A*) 1960, 1912.
10. F. A. Cotton and G. Wilkinson, *Advanced Inorganic Chemistry*, 4th edn. Wiley-Interscience, New York (1980).
11. B. J. Hathaway and A. E. Underhill, *J. Chem. Soc.* (*A*) 1961, 3091.
12. W. J. Geary, *Coord. Chem. Rev.* 1971, **7**, 81.
13. P. Gans, B. J. Hathaway and B. C. Smith, *Spectrochim. Acta* 1965, **21**, 1589.
14. J. G. H. du Preez, H. E. Rohwer, B. J. A. M. van Brecht, B. Zeelie, U. Casellato and R. Graziani, *Inorg. Chim. Acta* 1991, **189**, 67.
15. P. Gans and J. Marriage, *J. Chem. Soc., Dalton Trans.* 1972, 46.
16. P. Gans and J. Marriage, *J. Chem. Soc., Dalton Trans.* 1972, 1738.
17. B. N. Figgis, *Introduction to Ligand Fields*. Wiley-Interscience, New York (1966).
18. J. P. Day and L. M. Venanzi, *J. Chem. Soc.* (*A*) 1967, 197.
19. B. S. Manhas, S. Pal and A. K. Trikha, *Ind. J. Chem., Sect. A* 1987, **26**, 759.
20. B. S. Manhas, S. Pal and A. K. Trikha, *Synth. React. Inorg. Met.-Org. Chem.* 1987, **17**, 201.

Polyhedron Vol. 12, No. 2, pp. 247–253, 1993
Printed in Great Britain

0277–5387/93 $6.00+.00
© 1993 Pergamon Press Ltd

OXIDANTS CONTAINING RHODIUM.[1] X-RAY PHOTOELECTRON SPECTRA OF DICAESIUM HEXACHLORORHODATE(IV), CLAUS' BLUE AND MODEL COMPOUNDS

A. N. BUCKLEY

CSIRO Division of Coal and Energy Technology, P.O. Box 136, North Ryde, NSW 2113, Australia

and

J. A. BUSBY

Johnson Matthey Research Centre, Blounts Court, Sonning Common, Kidmore End, Reading RG4 9NH, U.K.

and

I. J. ELLISON and R. D. GILLARD*

School of Chemistry and Applied Chemistry, University of Wales College of Cardiff, P.O. Box 912, Cardiff CF1 3TB, U.K.

(*Received* 13 *July* 1992; *accepted* 3 *August* 1992)

Abstract—The X-ray photoelectron spectra of dicaesium hexachlororhodate(IV), tricaesium hexachlororhodate(III), a hydrated rhodium(III) oxide, and the barium salt of Claus' blue—previously formulated as a rhodate(VI)—suggest that the latter has rhodium(III) ions in an oxygen environment. ESR and Raman spectra of this blue solid confirm that the superoxide moiety is present. Prior work on higher oxidation states of rhodium in various environments is critically re-assessed. The compounds $Cs_2[MCl_6]$ (M = Rh, Pt and Ir) are isomorphous by X-ray powder diffraction.

Blue or violet aqueous solutions of rhodium species[2] can be made in two principal ways. First is the oxidation of rhodium(III) using various oxidants; many have been used, including peroxodisulphate, bismuthate, dichlorine or dibromine (or the equivalent hypochlorite or hypobromite) and inert anodes. The products have been variously formulated as containing rhodium(IV), (V) or (VI) and are often the bases of analyses for rhodium. One such blue solution[3] results from the action of dichlorine on an alkaline solution of rhodium(III) chloride. This solution is called "Claus' blue" and has been formulated as containing $[RhO_4]^{2-}$ ions; an anion precipitates with barium hydroxide. The second way is to oxidize complex compounds of rhodium—containing such nitrogenous ligands as pyridine, bipyridyl or 1,2-diamino-ethane—using a preformed source of the dioxygen link, such as peroxide, ozone or dioxygen. The products here are superoxides of rhodium(III).

All these blue and violet products, however made, in fact have very similar visible and ESR spectra, strongly suggesting[3] that they all contain the superoxide moiety.

There are a few oxidized inorganic complex compounds of rhodium where the electron deficiency is undoubtedly at the rhodium, rather than on ligands. $Cs_2[RhCl_6]$ is the simplest and best known[4] generated in an aqueous medium. We report here our results on the X-ray photoelectron spectra (XPS)

* Author to whom correspondence should be addressed.

of this green compound, its pink rhodium(III) analogue, $Cs_3[RhCl_6]$, an oxide of rhodium(III) and Claus' blue, as its barium salt. The results, coupled with ESR and Raman measurements, support the formulation of Claus' blue as a bridged μ-superoxo-dirhodium(III,III) species.

It is clear from the quite extensive prior work[5] concerning the influence of the oxidation state of rhodium (in pure well-defined compounds) on its photoelectron binding energies that the higher the oxidation state, the higher the binding energy.

It must be strongly emphasized that comparisons of binding energies from distinct studies may *not* yield satisfactory agreement. The binding energy range for the commonly utilized $Rh(3d)_{5/2}$ level is[5,6] from 307 eV for rhodium(0) in rhodium metal to 310.6 eV for the very stable $K_3[Rh(CN)_6]$. The range would be rather larger if the value for "$K_3[Rh(NO_3)_6]$" (sic) was included, but that substance is of very doubtful provenance and character. Similarly, one study[5b] of the $Rh(3d)_{5/2}$ binding energy in various compounds containing di-, tri- and tetravalent rhodium reported absolute values that were appreciably higher than our own, although this may be in part due to the unusually high value (291.3 eV) used there for the reference C(1*s*) peak. Furthermore, reported binding energies for Rh_2O_3 vary widely; as discussed later, this may be because of different degrees of hydration of the oxide studied. Ultimately, caution must be exercised when comparing absolute XPS electron binding energies that derive from different laboratories.

EXPERIMENTAL

Tricaesium hexachlororhodate(III)

This pink compound was precipitated from an ice-cold solution of sodium hexachlororhodate(III) using caesium chloride. Sodium hexachlororhodate(III) was producted by vigorously boiling stoichiometric amounts of rhodium trichloride and sodium chloride in *ca* 6 M HCl, using the absorption spectrum (λ_{max} = 518, 412 nm) to follow the course of the reaction.

Dicaesium hexachlororhodate(IV)

The preparation, based on that of Dwyer *et al.*,[4a] oxidized dry, solid samples of $Cs_3[RhCl_6]$ with a 10-fold excess of 1 M $(NH_4)_2[Ce(NO_3)_6]$ solution. The green product was washed thoroughly with acetone. Samples were stored over P_2O_5 at atmospheric pressure.

Photoelectron spectra for this compound were measured on a sample which had been kept dry for about 1 month after its synthesis. Specimens of this compound were prepared for examination under nitrogen in a chamber attached to the spectrometer. Samples were inserted into the nitrogen-flushed spectrometer immediately after preparation, so that dry, inert conditions were maintained throughout. One specimen was examined at ambient temperature, another was cooled to -25°C before being subjected to X-ray irradiation. In the latter case, several Rh(3*d*) spectra were determined, each one contemporaneous with a C(1*s*) spectrum, i.e. scan 1 of the Rh(3*d*) spectrum, then scan 1 of the C(1*s*) spectrum, then scan 2 of the Rh(3*d*) spectrum, and so on. The initial Rh(3*d*) and C(1*s*) spectra were determined in the minimum time for an acceptable S/N ratio (about 35 min total, with the X-ray source separated at 10 kV, 10 mA).

Rhodium(III) *oxide hydrate*

NaOH (0.5 M) was added to a solution of rhodium trichloride forming a flocculent yellow precipitate. The solid was collected by filtration, washed with water (to remove chloride ions) and then dissolved in dilute perchloric acid. This scheme was then repeated twice.

Barium salt of Claus' blue

This was prepared[3] by passing dichlorine into the yellow solution from rhodium(III) trichloride and potassium hydroxide until a deep purple solution was produced (λ_{max} = 520 nm). The solid was formed on the addition of an excess of barium hydroxide. The dark blue precipitate was collected under nitrogen to prevent contamination by barium carbonate.

Dicaesium hexachloroplatinate(IV)

To a solution of chlorinated dihydrogen hexachloroplatinate(IV) (λ_{max} = 262, 202 nm) was added caesium chloride solution. The pale yellow solid was washed with a little water and dried over P_2O_5.

Dicaesium hexachloroiridate(IV)

$Na_3[IrCl_6]$ solution was chlorinated until the absorption spectrum showed that all iridium had been oxidized to the tetravalent state (λ_{max} = 488, 434, 410 nm). The deep red caesium salt was isolated by the addition of caesium chloride solution, washing with water and drying over P_2O_5.

Raman spectra were recorded in 1 M HCl solution on a Jeol JRS-S1 laser Raman spectrometer

equipped with rotating sample cells and 488 nm excitation. X-ray powder diffraction patterns were produced using a Debye–Scherrer camera (radius 57.3 mm) and Cu-K_α radiation.

Two distinct sets of XPS measurements were made upon different samples. All were mounted on double-sided adhesive tape and the oxides were also examined when pressed into indium foil. (a) refers to a Kratos XSAM 800 spectrometer using Mg-K_α radiation at 150 W with 80/40 eV pass energies and 7.5 mm slits. As in earlier work,[7] (b) relates to a Vacuum Generator ESCA3 spectrometer, unmonochromatized Mg radiation, 20 eV pass energy and 2 mm slits.

RESULTS

X-ray powder diffraction patterns (Table 1) confirmed close isomorphism between $Cs_2[MCl_6]$ (M = Rh, Pt and Ir), strongly supporting the presence of quadrivalent rhodium in the green compound. Our measured electron binding energies are given in Table 2.

A narrow and symmetrical Rh($3d$)$_{5/2}$ peak centred between 309.2 and 309.6 eV for $Cs_3[RhCl_6]$ is consistent with the trivalent oxidation state. Similarly, the Cl($2p$) and Cs($3d$) spectra are indicative of one major electronic environment for each element.

For $Cs_2[RhCl_6]$, all Rh($3d$) spectra remained essentially the same throughout the period of examination: the doublet peaks, however, were broader than for $Cs_3[RhCl_6]$, probably because of the presence of two components. The Rh($3d$)$_{5/2}$ peak maximum binding energy was situated at 309.9 eV; the shift of all peaks due to charging diminished by only 0.2 eV during 6 h of irradiation. This Rh($3d$)$_{5/2}$ binding energy is up to 0.6 eV greater than the corresponding value for $Cs_3[RhCl_6]$. The Cl($2p$) spectrum appeared to consist of two doublets, one at 197.9 eV (accounting for 75–80% of the intensity) and another shifted *ca* 1.2 eV to a higher binding energy. The Cs($3d$)$_{5/2}$ peak, at 723.6 eV, was significantly broader than for $Cs_3[RhCl_6]$ (*ca* 2.1 eV cf. *ca* 1.7 eV), suggesting the possibility of two caesium environments. The Cl($2p$) and Cs($3d$) spectra for the specimen cooled to −25°C were essentially identical to the corresponding spectra from the specimen examined at ambient temperature. Thus, the existence of more than one environment for the chlorine and caesium atoms was not an artefact of the cooling. Assuming that there should be only one distinguishable electronic environment for caesium, rhodium and chlorine atoms in $Cs_2[RhCl_6]$—and the elemental analyses of the compound confirm this stoichiometry—it appears that we have a mix-

Table 1. Measured X-ray powder diffraction d-values and intensities for $Cs_2[MCl_6]$ compounds (M = Ir, Pt and Rh)

$Cs_2[IrCl_6]$	$Cs_2[PtCl_6]$	$Cs_2[RhCl_6]$
—	8.230(10)	—
—	—	7.109(20)
7.053(20)	7.053(20)	7.081(30)
6.511(40)	6.511(50)	—
6.130(20)	6.130(30)	—
5.887(90)	5.867(90)	5.867(60)
—	5.068(10)	5.096(20)
4.484(10)	4.450(20)	—
4.322(20)	4.311(40)	4.332(20)
3.986(50)	3.978(60)	3.986(50)
3.786(30)	3.746(30)	3.746(30)
3.590(100)	3.590(100)	3.534(100)[a]
3.473(10)	—	—
3.345(20)	3.395(20)	—
3.255(20)	3.261(10)	3.255(40)
3.198(10)	3.198(5)	—
3.143(30)	3.126(5)	—
3.069(60)	3.069(60)	3.063(50)
2.945(50)	2.936(50)	2.936(80)
2.823(40)	2.818(50)	2.818(40)
2.659(30)	2.656(40)	2.660(10)
—	2.574(20)	—
2.546(80)	2.543(80)	2.543(80)
2.522(5)	2.501(5)	—
2.452(5)	—	2.458(5)
2.344(30)	2.335(20)	2.445(10)[a]
2.301(40)	2.304(30)	—
2.225(30)	—	—
2.168(40)	2.163(40)	2.168(20)
2.080(70)	2.076(70)	2.080(50)
2.051(10)	2.042(10)	—
1.994(30)	1.989(30)	1.993(30)
1.957(40)	1.957(40)	1.961(20)
1.893(40)	1.907(20)	1.912(30)
1.852(20)	1.872(30)	1.850(30)
1.783(70)	1.797(70)	1.801(60)
1.789(10)	1.783(10)	—
1.722(50)	1.720(50)	1.720(20)
1.681(10)	1.678(10)	1.698(10)
—	1.626(5)	—
1.609(60)	1.608(50)	1.608(40)
1.552(5)	1.576(5)	—
1.536(10)	1.551(10)	1.536(40)
1.509(20)	1.533(10)	1.510(40)
—	1.487(10)	—
1.470(50)	1.469(40)	1.468(20)
1.428(30)	1.372(30)[a]	1.430(40)
1.361(20)	1.351(50)	1.361(5)
1.327(50)	1.326(30)	1.326(10)
1.274(20)	1.273(10)	—
—	1.260(5)	—
1.201(20)	1.199(30)	—
—	1.176(10)	—
—	1.005(30)	—

[a] Not within ±0.050 agreement.

Table 2. Measured electron binding energies (eV) of rhodium complexes

Compound	C(1*s*)[a]	Cs(3*d*)$_{5/2}$	Rh(3*d*)$_{5/2}$	Cl(2*p*)	O(1*s*)	Notes
$Cs_3[RhCl_6]$[b]	284.8	723.9	309.2	197.9		Cs : Rh = 3 Cl : Rh = 6
[c]	284.7	723.9	309.6	198.1		[d]
$Cs_2[RhCl_6]$[b]	284.8	723.4	309.8	198.1		Cs : Rh = 1.6 Cl : Rh = 7
[c]	284.7	723.6	309.9	197.9 199.1		[e]
$Rh_2O_3 \cdot xH_2O$[b]	284.8		309.3		531.2	Na(1*s*) = 1070.7[f]
[c]	284.7		309.5			[g]
"$Ba[RhO_4]$"[b]	284.8		309.2		530.9 531.3 530.7 531.6	Ba(3*d*)$_{5/2}$ = 779.4 Ba : Rh = 1
[c]	284.7		309.3			

[a] Reference used to correct for sample charging effects.
[b] Kratos XSAM 800 spectrometer.
[c] Vacuum Generators ESCA3 spectrometer.
[d] After several hours irradiation, the Rh(3*d*)$_{5/2}$ spectrum displayed a component shifted to 308.1 eV. This was not due to differential charging effects, since no similar asymmetry of the Cs(3*d*) peak was seen. This component may be rhodium(I) produced by photoreduction.
[e] Cl(2*p*) indicated two environments, as discussed in the text.
[f] This contamination is from NaOH in the preparative method.
[g] Carbonate C(1*s*) peak at 289.2 eV.

ture of trivalent and quadrivalent ions. The two environments observed for chlorine might imply ready decomposition of $Cs_2[RhCl_6]$ and we have certainly seen strong EPR signals from (Cl_2^-) in aged samples. This signifies the *instability* of rhodium(IV) compared to that of rhodium(III).

The barium salt of Claus' blue had a binding energy for rhodium virtually identical to that in rhodium(III) oxide; no change in the Rh(3d) spectrum was observed during the extended period of study. Line widths for our rhodium oxide pressed into indium foil were identical with those measured for the double-sided tape.

DISCUSSION

Werner's original bridged superoxo-dimetal complex ions contained not rhodium but its eutrope cobalt. The question of the formulation of the ion in salts like those of $[(en)_2Co(\mu\text{-}NH_2, \mu\text{-}O_2)Co(en)_2]^{4+}$ (with one unpaired electron) as containing either Co^{III}—$(O_2)^{2-}$—Co^{IV} or Co^{III}—$(O_2)^-$—Co^{III} was initially resolved[8] by Weil and his associates, who showed that the *g*-factor in the ESR spectrum was close to 2.02 (typical of superoxide) and that the signal was split into 15 lines from the equal input of the two ^{59}Co ions ($I = 7/2$). Further, an elegant experiment[8b] using ^{17}O in the bridge showed that the unpaired electron was shared by the cobalt ions via the dioxobridge. Unfortunately, in the case of rhodium, the gyromagnetic ratio of the ^{103}Rh nucleus (albeit 100% abundant) is so small as to render nugatory similar measurements of hyperfine structure. Nevertheless, the *g*-value offers a good means of establishing the presence of superoxide ligands, and such values have been tabulated.[1]

The X-ray photoelectron spectrum offers a better means of commenting on the complementary question of the *oxidation states* of rhodium. Our measured energies are collected in Table 2. These are corrected for the effects of charging using the C(1*s*) signal of adventitious carbon. Table 3 assembles some values for the rhodium levels ($3d_{5/2}$) from compounds with varying oxidation states. This includes values for rhodium with chloride ligands in several environments. One should note that $(NH_4)_3[Rh(S_5)_3] \cdot 2H_2O$ is without doubt a compound of rhodium(III) and the Rh(3*d*)$_{5/2}$ binding energy is discussed in ref. 7 as being at the low end of the range for rhodium(III). Table 4 collects values for rhodium in oxygen environments, including the few available for blue compounds.

The higher oxidation state, rhodium(IV), in $Cs_2[RhCl_6]$ gives a mean binding energy for Rh(3*d*)$_{5/2}$ of 309.9 eV against 309.4 eV for rhodium(III) in $Cs_3[RhCl_6]$. We would expect

Table 3. Electron binding energies (eV) for rhodium in differing oxidation states and for chlorine combined with rhodium

Compound/system	$Rh(3d)_{5/2}$	$Cl(2p)_{3/2}$	Ref.
Rh metal	307.1		5
RhCl(COD)[a,b]	308.1[f]	197.9	16
$[RhCl(COD)]_2$[a]	308.6[f]	198.7	17
$RhCl_3$	310.2[f]	198.8	18
$RhCl_3$ on zeolite	310.2[f]	199.3	18
$[Rh(NH_3)_5Cl]Cl_2$	310.2[f]	198.5	18
$(NH_4)_3[Rh(S_5)_3] \cdot 2H_2O$	308.2		7
$Cs_3[RhCl_6]$[c]	309.2	197.9	This work
$Cs_3[RhCl_6]$[d]	309.6	198.1	This work
$Cs_2[RhCl_6]$[c]	309.8	198.1	This work
$Cs_2[RhCl_6]$[d]	309.9	197.9[e]	This work

[a] COD = 1,5-cyclo-octadiene.
[b] Attached to phosphinated polystyrene.
[c] Kratos XSAM 800 spectrometer.
[d] Vacuum Generators ESCA3 spectrometer.
[e] Major component only.
[f] This value is higher than ours; see text.

at least as large a shift (if not far greater) in an oxygen ligand environment from rhodium(III) in the six-coordinated oxide lattice of Rh_2O_3 hydrate to rhodium(VI) in $Ba[RhO_4]$ if Claus' blue really did involve the $[RhO_4]^{2-}$ ion. In fact, the binding energies are 309.3 and 309.2 eV, respectively, which strongly supports a formulation of Claus' blue as containing rhodium(III) ions. "$Ba[RhO_4]$" might possibly react rapidly on exposure to air to produce a surface layer of a rhodium(III) oxide species. We think such a reaction unlikely because there was no evidence of carbonate in the C(1*s*) spectrum. The formation of carbonate usually accompanies such surface changes in air under ambient conditions. By contrast, a peak near 289.2 eV due to carbonate was evident in the C(1*s*) spectra of the rhodium oxide samples studied. The presence of a superoxide bridging two rhodium ions is indicated by the *g*-value ($g_{iso} = 2.044$)[1,3] and Raman spectrum (strong, broad absorption centred at 1088 cm^{-1}).

The barium salt of Claus' blue has been analysed several times by gravimetry and other classical bulk microanalytical methods leading to a Ba : Rh ratio of 1 : 1. The present observation on relative intensities of the signals for $Ba(3d)_{5/2}$ at 779.4 eV and $Rh(3d)_{5/2}$ of Rh at 309.2 eV confirms this stoi-

Table 4. Binding energies (eV) for rhodium [$Rh(3d)_{5/2}$] in differing oxygen environments

Compound/system	$Rh(3d)_{5/2}$	Ref.
$Rh_2O_3 \cdot xH_2O$[a]	309.3	This work
[b]	309.5	This work
	309.7	19
Rh_2O_3	309.2	17
	308.7	20
	308.5	19
"$Ba[RhO_4]$"[a]	309.2	This work
[b]	309.3	This work
$\{[(H_2O)(py)_3Rh]_2(\mu\text{-}O_2)(\mu\text{-}OH)\}(ClO_4)_3$[c]	310.0	21

[a] Kratos XSAM 800 spectrometer.
[b] Vacuum Generators ESCA3 spectrometer.
[c] This value may be high, since it is quoted without the binding energy of the standard and with no experimental detail.

chiometry; this ratio has been taken as consistent with the original formulation $Ba[RhO_4]$—it is, of course, equally consistent with $Ba_2\{[(H_2O)_4Rh]_2(\mu\text{-}O_2)(\mu\text{-}OH)\}$. Similar blue or violet paramagnetic species containing the $[Rh^{III}—(\mu\text{-}O_2)—Rh^{III}]^{5+}$ moiety, or more commonly the $[Rh^{III}—(\mu\text{-}O_2),(\mu\text{-}OH)—Rh^{III}]^{4+}$ fragment, with various ligands are known; crystallographic studies of compounds containing these moieties and their peroxo derivatives support the conclusion that the ESR signal derives from the superoxide bridge.[9]

This simple, elemental, microanalytical ratio is well founded. Otherwise, the analytical determination of properties helping to formulate such oxidized compounds of rhodium is complicated by three major factors. First, in titrations using reductants, there are catalytic effects (due to the very nature of rhodium) which may lead to irrelevant apparent stoichiometries. Secondly, elemental analyses rarely distinguish between compositions involving, say $(Rh^{IV}—OH)^{3+}$ or $(Rh^{III}—OH_2)^{3+}$, or between $Rh^{IV}—(O_2)^{2-}$ and $Rh^{III}—(O_2)^{-}$. Finally, the non-superoxo ligands on rhodium(III) are a combination of halide- and aquo-derived; for example, the solution of Claus' blue is a mixture of many different aquo, hydroxo, chloro, dimeric superoxo species (and possibly monomeric and peroxo species depending on the extent of chlorination). These problems with chemical analyses render spectroscopic studies particularly valuable.

The synthesis of Claus' blue *in the absence of oxygen* by passing dichlorine gas through an alkaline solution of rhodium(III) represents the unusual formation of an O—O link in the aqueous medium. We suspect that the O—O link comes from the dichlorine oxidation of hydroxide ions (which may be coordinated to rhodium in dimeric precursors) to form quantities of hydrogen peroxide (which, as its conjugate anion, may be coordinated). The peroxo-rhodium precursor may subsequently be involved in further dimerization and oxidation processes; problems arise in assigning[3] intermediates due to complicated spectroscopic signals observed in the course of the preparation.

We have used rhodium(III) oxide (precipitated from basic aqueous medium) here only as a reference. However, we should comment on some of the quite extensive prior work on the nature of rhodium centres in oxide matrices, since most of these substances were made in similar ways to our own. Most work was done in the context of heterogeneous catalysis and surface science, and has used, in general, either X-ray photoelectron spectra or ESR spectra as a means of commenting on the nature of the rhodium centres present, before and after modification.

There is a fair range of values for the $(3d)_{5/2}$ binding energies in samples described as $Rh_2O_3\cdot nH_2O$, of which ours (mean = 309.4 eV) could be regarded as typical. (Rhodium oxide is not a simple entity, and it is not always clear what form has been studied.) The parent oxide is, of course, diamagnetic, but there are several studies which have generated paramagnetic centres, variously described as rhodium(II) or rhodium(IV). The nature of such centres in isolated compounds is, of course, very much the nub of the present paper.

RhO_2 exists.[10a] It is $Rh^{IV}—(O^{2-})_2$ with the rutile structure and metallic conductance. It is not easy to make; very high pressures and temperatures are needed, even in the presence of such powerful oxidants as 7 M nitric or 2.7 M chloric acids. Similarly, Van Arkel[10b] and his colleagues made $Li_2[RhO_3]$ only by oxidizing rhodium sponge in lithium carbonate using O_2 at 600–1000°C for 20 h. It was isomorphous with $Li_2[TiO_3]$ and presumably contained rhodium(IV) ions.

Alternatively, various rather ill-defined dark solids have been made during the past century by relatively mild aqueous methods and classified as oxides of rhodium in higher oxidation states. This seems inconsistent, and our view is that they are probably all rhodium(III) superoxides and (perhaps) peroxides. They include $RhO_2\cdot xH_2O$, produced[11a] by electrochemical oxidation or by chlorination (cf. Claus' blue) of rhodium(III) in water. Likewise, Kalinina and Lyakushina[11b] precipitated "$RhO_2\cdot 2H_2O$" from dilute rhodium chloride by heating with hypobromite. This dissolved in dilute perchloric acid to give a dark red solution said to be of rhodium(IV) perchlorate. In bulk, it loses dioxygen at 800–900°C, forming Rh_2O_3.

In a sample of $RhO\cdot OH$ (with the orthorhombic InOOH structure) heated in air at 300°C, new EPR signals at $g_1 = 2.25$, $g_2 = 2.08$ and $g_3 = 1.94$ were attributed to rhodium(IV) centres. In rhodium on alumina exposed to dioxygen at 500°C, Yao and Shelef located an EPR signal at $g = 2.14$, which they likewise assigned[12] to rhodium(IV) centres. Consequently, the origin of other signals near this region in similar oxide systems comes into question. These included[13] the spectrum for rhodium on silica exposed to dioxygen at 200°C, with $g_1 = 2.092$, $g_2 = 2.031$ and $g_3 = 1.963$.

In much the same way, Goldfarb and Kevan exchanged[14] $[Rh(NH_3)_5Cl]Cl_2$ from its aqueous solution into the zeolite Linde-13X (NaX) at room temperature, exposed this to dioxygen at temperatures from 240°C upward and observed an ESR signal at $g = 2.06$. They assigned this to a paramagnetic rhodium ion whereas we consider it to arise from a superoxo-rhodium(III) species. This

may well be an amine-superoxide (rather than an oxide-superoxide) since the chloro-pentammine-rhodium(III) ion is quite thermally stable: not all the ammonia ligands would dissociate at 240°C unless there is a specific local destabilizing effect in the zeolite. Further, monomeric $[Rh—O_2]^{2+}$ and dimeric $[Rh—O_2—Rh]^{5+}$ units are well known[2] in solid amine and substituted amine compounds, such as the salts of $\{[Rh(en)_2Cl]_2(\mu\text{-}O_2)\}^{3+}$ (en = 1,2-diamino-ethane).

The factors which control the detailed nature of the products from the oxidation of platinum group element compounds are still unclear. However, Griffith[15a] and Holm[15b] have summarized the range of oxocomplexes of the transition elements and pointed out that all formations of terminal M—O bonds (formally double or triple) depend largely on the interaction of a filled $2p_\pi$ donor pair on oxygen with empty Lewis acceptor orbitals on M^{n+}. These orbitals are empty only for d^n configurations where $n \leqslant 4$ (cf. $n = 0$ for RuO_4 and $n = 2$ for $[RuO_4]^{2-}$); rhodates do not fulfil this criterion. Since many compounds of the iso-electronic ruthenium(IV) ($4d^4$) and (V) ($4d^3$) have been made, oxocompounds of rhodium in oxidation states higher than (III) may occur. There are as yet very few well-defined examples.

Acknowledgements—We wish to thank Monika Moszner (Institute of Chemistry, University of Wrocław) and Wrocław Polytechnic for measuring Raman spectra and Malcolm Anderson (Department of Physics, U.W.C.C.) for recording X.R.P.D. patterns on our behalf.

REFERENCES

1. This is Part 11. Part 9, R. D. Gillard, *Polyhedron* 1992, **11**, 1737.
2. P. S. Sheridan and F. Jardine, in *Comprehensive Coordination Chemistry* (Edited by G. Wilkinson, R. D. Gillard and J. A. McCleverty), Vol. 4, p. 901. Pergamon Press, Oxford (1987) and refs therein.
3. I. J. Ellison and R. D. Gillard, *J. Chem. Soc., Chem. Commun.* 1992, 851.
4. (a) F. P. Dwyer, R. S. Nyholm and L. E. Rogers, *J. Proc. Roy. Soc. (NSW)* 1947, **81**, 267; (b) C. K. Jorgensen, *Molec. Phys.* 1961, **4**, 231; (c) A. D. Westland, *Can. J. Chem.* 1968, **48**, 3591; (d) I. Feldman, R. S. Nyholm and E. C. Watton, *J. Chem. Soc.* 1965, 4724.
5. (a) C. D. Wagner, W. M. Riggs, L. E. Davis, J. F. Moulden and G. E. Muilenberg, *Handbook of X-ray Photo-electron Spectroscopy*, p. 108. Perkin–Elmer Corporation, Eden Prairie, Minnesota (1979); (b) R. S. Hay-Motherwell, G. Wilkinson, B. Hussain-Bates and M. B. Hursthouse, *Polyhedron* 1990, **9**, 2071; (c) V. I. Nefedov, E. F. Shubochkina, I. S. Kolomnikov, I. B. Baranovskii, V. P. Kukolev, M. A. Golubnichaya, L. K. Shubochkin, M. A. Porai-Koshits and M. E. Vol'pin, *Russ. J. Inorg. Chem.* 1973, **18**, 444: this study used a defined standard value of 310.8 eV for $[Rh(NH_3)_6]Cl_3$ and consequently gives a range from 311.0 eV for $K_3[Rh(CN)_6]$ to 309.6 eV for a rhodium(I) compound.
6. J. S. Brinen and A. Melera, *J. Phys. Chem.* 1972, **76**, 2525.
7. A. N. Buckley, H. J. Wouterlood, P. S. Cartwright and R. D. Gillard, *Inorg. Chim. Acta* 1988, **143**, 77.
8. (a) D. L. Duffy, D. A. House and J. A. Weil, *J. Inorg. Nucl. Chem.* 1969, **31**, 2053; (b) J. A. Weil and J. K. Kinnaird, *J. Phys. Chem.* 1967, **71**, 3341.
9. N. S. A. Edwards, I. J. Ellison, R. D. Gillard, B. Mile and J. Maher, *Polyhedron* 1992, in press.
10. (a) E. M. Miguelez, M. A. A. Franco and J. Soria, *J. Solid State Chem.* 1983, **46**, 156 and refs therein; (b) J. J. Scher, A. E. Van Arkel and R. D. Heyding, *Can. J. Chem.* 1955, **33**, 683.
11. (a) L. Wohler and K. F. A. Ewald, *Z. Anorg. Allg. Chem.* 1931, **201**, 145; (b) V. E. Kalinina and V. M. Lyakushina, *Izv. Vyssh. Uchebn. Zaved. Khim. Khim. Tekhnol.* 1976, **19**, 1287.
12. H. C. Yao and M. Shelef, Proceedings of the International Conference on Catalysis, p. 329. Tokyo (1980).
13. (a) A. Raizman, J. Suss and S. Szapiro, *Phys. Lett. (A)* 1970, **32**, 30; (b) V. B. Kazanskii, V. E. Shubin and V. A. Shvets, *Kinet. Catal.* 1978, **19**, 1026.
14. D. Goldfarb and L. Kevan, *J. Phys. Chem.* 1986, **90**, 264.
15. (a) W. P. Griffith, *Trans. Met. Chem.* 1990, **15**, 251; (b) R. H. Holm, *Chem. Rev.* 1987, **87**, 1401.
16. P. Terreros, E. Pastor, J. M. Palacios and J. L. G. Fierro, *Surf. Interface Anal.* 1990, **15**, 279.
17. J. L. G. Fierro, J. M. Palacios and F. Tomas, *Surf. Interface Anal.* 1988, **13**, 25.
18. S. L. T. Andersson and M. S. Scurrell, *J. Catal.* 1981, **71**, 233.
19. H. Y. Hall and P. M. A. Sherwood, *J. Chem. Soc., Faraday Trans.* 1984, **80**, 2867.
20. O. Johnson, *Chem. Scr.* 1975, **8**, 162.
21. I. B. Baranovskii, A. N. Zhilyaev, L. M. Dikareva and A. V. Rotov, *Russ. J. Inorg. Chem.* 1986, **31**, 1661 (English translation).

Polyhedron Vol. 12, No. 2, pp. 255–257, 1993
Printed in Great Britain

0277–5387/93 $6.00+.00
© 1993 Pergamon Press Ltd

AN UNUSUAL LABILITY OF 2,2′-BIPYRIDYL CHELATED TO PLATINUM(II)[1]

JUSTINE COLLINS, R. D. GILLARD* and MICHAEL B. HURSTHOUSE

School of Chemistry and Applied Chemistry, University of Wales College of Cardiff, P.O. Box 912, Cardiff CF1 3TB, U.K.

(*Received* 31 *July* 1992; *accepted* 18 *August* 1992)

Abstract—The pentakaidekasulphidoplatinate(IV) ion, $[Pt(S_5)_3]^{2-}$, is a product when dichloro-2,2′-bipyridyl-platinum(II) reacts with yellow ammonium sulphide. Pentasulphido-2,2′-bipyridylplatinum(II) has also been made.

The well-known chelated 1 : 1 derivatives (**I**) of the N-heterocyclic ligands 2,2′-bipyridyl and 1,10-phenanthroline with platinum(II) and (in some cases) palladium(II) have again attracted a great deal of interest recently. Wimmer *et al.* have recently extended our knowledge[2] of the systems based on **I** (M = Pt; X = OH; Y = OH_2; overall charges are omitted for simplicity; the chelating ligand is shown as bipyridyl, although several examples discussed here actually relate to 1,10-phenanthroline). The bis-aquo-bipyridylplatinum(II) cation (**I**, X = Y = H_2O) has been used as a bifunctional carrier for spin labels[3] and platinum has been bonded to polymers through the functionalized bipyridyl, to give[4] a hydrogenation catalyst.

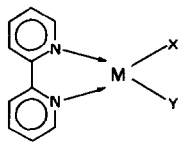

(I)

Many compounds (**I**) have been made, and their stabilities (both thermodynamic and against nucleophilic substitution) repeatedly described. Typically, for **I**, X = Y = ½en, the 2,2′-bipyridyl is inert[5a] (for weeks) to substitution by 1,2-diaminoethane. Similarly, the same compound was found[5b] by Watt and Upchurch to react with potassium in liquid ammonia, but only to deprotonate the NH_2 units of the 1,2-diaminoethane.

In 0.1 M potassium methylsulphonate, log K_{110} for **I** (M = Pt and Pd) are[6] 19.8 and 20.7, respectively. Some descriptions imply[7] that the stability of the 1 : 1 moiety is unusual, $[Pd(phen)]^{2+}_{aq}$ being described as "a new aromatic system".

We describe here a surprising displacement of 2,2′-bipyridyl from a 1 : 1 system with platinum.

The compound $[Pt(PR_3)_2(S_4)]$ (**II**) is made[8] from **III** by reaction (1).

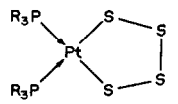

(II)

$$(NH_4)_2[Pt(S_5)_3] + 12PR_3 \longrightarrow [Pt(PR_3)_2(S_4)] + (NH_4)_2S + 10SPR_3 \quad (1)$$

(III) **(II)**

It is well characterized.[9] A similar palladium(II) compound (**IV**) exists, made[10] by the distinct route shown in eq. (2).

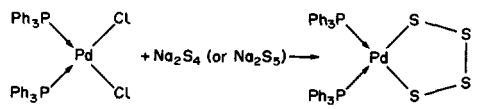

(2)

(IV)

We attempted to make the N-heterocyclic chelated (bipyridyl) analogue of the eutrope of **IV** by a related route, combining **I** (M = Pt; X = Y = Cl) with oligosulphide (S_n^{2-}; $4 \leqslant n \leqslant 6$) from aqueous yellow ammonium sulphide. We obtained both the desired product, with $n = 5$, and, in low yield, the unexpected product (**III**) as its ammonium salt

* Author to whom correspondence should be addressed.

$(NH_4)_2[Pt(S_5)_3]\cdot 2H_2O$. The form produced in the present work is a known[11] dimorph. Its formation represents a surprising contrast with the behaviour expected from eq. (1), where **III** is a factor rather than a product.

EXPERIMENTAL

K_2PtCl_4 (0.50 g) in hot water (300 cm^3) heated for 1 h with 2,2′-bipyridyl (1.95 g) in hydrochloric acid (2 M) gave 0.43 g (91%) of $[Pt(bipy)Cl_2]$. This compound (0.15 g) was treated with ammonium polysulphide (BDH yellow ammonium sulphide, 10 cm^3) and left for several hours until it had become olive green. The mixture was kept at 85°C, passing through yellow–orange to orange–red to dark brown. The brown product, pentasulphido-2,2′-bipyridylplatinum(II), $[Pt(bipy)(S_5)]$ (0.15 g), was removed by filtration and the filtrate kept at room temperature in a closed container.

$(NH_4)_2[Pt(S_5)_3]\cdot 2H_2O$

During 3–4 weeks, the filtrate gave crystals, initially of 2,2′-bipyridyl and finally of the bright red product. These were collected and dried over silica gel *in vacuo*. The bipyridyl dissolved in toluene and was extracted from it into ferrous sulphate in dilute HCl (2 M), giving the characteristic $[Fe(bipy)_3]^{2+}$.

Analyses are in Table 1 and properties in Table 2. IR spectra for $[Pt(bipy)X_2]$ (A, X = Cl; B, X = $\frac{1}{2}S_5$) were essentially similar from 3050 to 700 cm^{-1}, those absorptions arising from 2,2′-bipyridyl. A strong absorption at 355 cm^{-1} in A (arising from its $PtCl_2$ moiety) is very much weaker in B. Similarly, other new weak bands at 650 and 460 cm^{-1} in B may be assigned to S—S modes.

Table 2. Identity of $(NH_4)_2[Pt(S_5)_3]\cdot 2H_2O$ (unit cell sizes; Å)

	Present product	Dimorph A (*Cc*)[11]	Dimorph B (*C2/c*)[11]
a	15.71	15.73	16.93
b	9.95	9.83	8.92
c	13.00	12.83	27.31
β (°)	93.71	92.61	101.44

DISCUSSION

There are a number of possible mechanisms for this extraordinary reaction. It may not merely involve substitution at the d^8-centre. The driving force probably does relate to solution stability rather than displacement of an equilibrium toward an insoluble product. That is, the formation of solvated $[Pt(S_5)_3]^{2-}$ is indeed favoured because its ammonium salt, the product, is actually far more water soluble than the other platinum-containing compounds which could be formed as solids, such as $[Pt(bipy)(S_5)]$ or $[Pt(bipy)Cl_2]$. Nucleophilic attack on [Pt(bipy)XY] is slow,[12] although nucleophilic sulphur does react with $[Pt(bipy)_2]^{2+}$ via[13] a rather stable 1 : 1 adduct (possibly, however, involving a C—S bond rather than a Pt—S bond) as an intermediate. Indeed, some more polarizable nucleophiles, like cyanide, do slowly displace chelated bipyridyl, both from platinum(II) and the isoelectronic gold(III) in $[Au(phen)(Cl_2)]^+$, where the products include[14] $[Au(CN)_2Cl_2]^-$ and 1,10-phenanthroline.

In view of the ease of formation of the thioplatinate(IV) anion $[Pt(S_5)_3]^{2-}$ from platinum(II) chlorides [eq. (3)], or from bis-pentasulphidoplatinate(II) ions [eq. (4)], it may be that oligo-

Table 1. Analysis of products

Compound	Sample	Analysis C Calc.	C Found	H Calc.	H Found	N Calc.	N Found
$[Pt(bipy)Cl_2]$	1	28.4	28.8	1.9	1.9	6.6	6.7
	2	28.4	29.2	1.9	2.0	6.6	6.7
	2	28.4	28.8	1.9	1.9	6.6	6.6
$[Pt(bipy)(S_5)]$	1	23.5	23.2	1.6	1.7	5.5	5.8
	2	23.5	23.6	1.6	1.7	5.5	5.8
	2	23.5	23.8	1.6	1.8	5.5	5.7
$(NH_4)_2[Pt(S_5)_3]\cdot 2H_2O$	1	0	0	1.61	1.6	3.74	3.8
	2	0	0	1.61	1.5	3.74	3.8

sulphide oxidizes the factor or an intermediate.

$$[PtCl_4]^{2-} + 4S_5^{2-} \longrightarrow [Pt(S_5)_3]^{2-} + 4Cl^- + S_2^{2-} + S_3^{2-} \quad (3)$$

$$[Pt(S_5)_2]^{2-} + 2S_5^{2-} \longrightarrow [Pt(S_5)_3]^{2-} + S_2^{2-} + S_3^{2-} \quad (4)$$

The mere oxidation of N-heterocyclic chelates [Pt(bipy)XY] to platinum(IV) species does not of itself labilize the heterocyclic ligand. $[Pt(bipy)(en)]^{2+}$ may be oxidized[15] to $[Pt(bipy)(en)Cl_2]^{2+}$, and this will undergo reactions[16] within the ligands without metal–ligand bond breakage.

In studies[1] aimed at producing $[PtS_x]^{2-}$, with $12 \leqslant x \leqslant 21$ from platinum(IV) precursors, far and away the most common products were salts of the $[Pt(S_5)_3]^{2-}$ ion, and this has again formed here by an utterly distinct route.

The mixed compound is analogous to a number of other species (**I**), [M(NN)(X)(Y)], where M = Pd or Pt, NN = a chelating N-heterocycle bipy or phen, and X+Y = a doubly charged anion chelated through group 16 atoms. Examples include[17] [Pt(phen)(OCH_2CH_2O)] and [Pd(phen)(SCH_2CH_2S)], although there seems to be no other example of [Pt(bipy)(X)(Y)] where XY is bonded through two sulphur atoms.

Finally, we list the few displacements known to us of N-heterocyclic chelates from species **I**: these involve palladium(II) as the central metal ion, and non-aqueous conditions:

(a)[18] $[Pd(bipy)(C_6Cl_5)_2] + dppe \longrightarrow [Pd(dppe)(C_6Cl_5)_2]$

(dppe = 1,2-diphenylphosphinoethane)

(b)[19] $[Pd(NN)Cl_2]$ (in DMF) + en $\longrightarrow$ $[Pd(NN)(en)]^{2+} \longrightarrow [Pd(en)_2]^{2+}$,

the second step, in an excess of 1,2-diaminoethane, being very fast.

REFERENCES

1. (a) This is Part 13 of Sulfides of the platinum group metals. Part 11 is R. D. Gillard and E. R. J. Sillanpää, in *Stability of Minerals*, abstracts volume, p. 30, Min. Soc. GB Winter Meeting, U.C. London, December (1989); (b) Part 12: P. S. Cartwright, R. D. Gillard, E. R. J. Sillanpää and J. Valkonen, *Polyhedron* 1991, **10**, 2501.
2. S. Wimmer, P. Castan, F. L. Wimmer and N. P. Johnson, *Inorg. Chim. Acta* 1988, **142**, 13 and refs therein: cf. S. G. Fox, MSc thesis, University of Wales (1985).
3. Y. Y. H. Chao, A. Holtzer and S. H. Mastin, *J. Am. Chem. Soc.* 1977, **99**, 8024.
4. R. S. Drago, E. D. Nyberg and A. G. El A'mma, *Inorg. Chem.* 1981, **20**, 2461.
5. (a) M. Cusumano, G. Guglielmo and V. Ricevuto, *J. Chem. Soc., Dalton Trans.* 1981, 1722; (b) G. W. Watt and D. G. Upchurch, *J. Am. Chem. Soc.* 1967, **89**, 177.
6. G. Anderegg and H. Wanner, *Inorg. Chim. Acta* 1986, **113**, 101.
7. (a) V. Parthasarathy and C. K. Jorgensen, *Chimica* 1975, **29**, 210; (b) L. Rasmussen and C. K. Jorgensen, *Inorg. Chim. Acta* 1969, **4**, 65.
8. D. Dudis and J. P. Fackler, *Inorg. Chem.* 1982, **21**, 3577.
9. C. E. Briant, M. J. Calhorda, T. S. A. Hor, N. D. Howells and D. M. P. Mingos, *J. Chem. Soc., Dalton Trans.* 1983, 1325.
10. M. Schmidt and G. G. Hoffman, *Z. Naturforsch (B)* 1972, **27**, 461.
11. E. H. M. Evans, R. D. Gillard, J. P. G. Richards and F. L. Wimmer, *Nouv. J. Chim.* 1986, **10**, 783.
12. A. Peloso, *J. Chem. Soc., Dalton Trans.* 1976, 984.
13. O. Wernberg, *J. Chem. Soc., Dalton Trans.* 1986, 725.
14. L. Cattalini, G. Marangoni, G. Paolucci, B. Pittari and M. L. Tobe, *Inorg. Chem.* 1987, **26**, 2450.
15. G. T. Morgan and F. H. Burstall, *J. Chem. Soc.* 1934, 965.
16. W. A. Freeman, *J. Am. Chem. Soc.* 1983, **105**, 2725.
17. S. G. Fox and R. D. Gillard, *Polyhedron* 1988, **7**, 349.
18. R. Uson and J. Fornes, *Adv. Organomet. Chem.* 1988, **28**, 219 and refs therein.
19. M. Cusumano, G. Guglielmo and V. Ricevuto, *J. Chem. Soc., Dalton Trans.* 1980, 1722.

Polyhedron Vol. 12, No. 2, pp. 259–261, 1993
Printed in Great Britain

0277–5387/93 $6.00+.00
© 1993 Pergamon Press Ltd

COMMUNICATION

THE FIRST EXAMPLE OF VIB METAL–METAL TRIPLY BONDED COMPLEXES CONTAINING FUNCTIONALLY SUBSTITUTED CYCLOPENTADIENYL LIGAND. SYNTHESIS AND X-RAY STRUCTURE OF $[\eta^5\text{-EtO}_2\text{CC}_5\text{H}_4\text{W(CO)}_2]_2$

LI-CHENG SONG,† JI-QUAN WANG and QING-MEI HU

Department of Chemistry, Nankai University, Tianjin 300071, P.R.C.

and

RU-JI WANG and HONG-GEN WANG

Central Laboratory, Nankai University, Tianjin 300071, P.R.C.

(*Received* 30 *September* 1992; *accepted* 22 *October* 1992)

Abstract—Through thermolysis of $[\eta^5\text{-EtO}_2\text{CC}_5\text{H}_4\text{W(CO)}_3]_2$ the title complex **1** has been prepared and characterized by elemental, spectroscopic and X-ray analyses. The X-ray analysis revealed that the $\text{Cp}^*_{\text{centre}}$—W—W′ axis of **1**, on the contrary to the linear configuration of the $\text{Cp}_{\text{centre}}$—Mo—Mo axis in its molybdenum analogue, is bent with a 20.1° departure from linearity.

Although the VIB metal–metal triply bonded complexes containing mixed cyclopentadienyl carbonyl ligands, such as $(\eta^5\text{-C}_5\text{R}_5)\text{M}_2(\text{CO})_4$ (M = Cr, Mo, W; R = H, Me), have been extensively studied,[1–6] the crystal molecular structure of any tungsten complex of this type has never been determined and the functionally substituted cyclopentadienyl-carbonyl W—W triply bonded derivatives have not been prepared even now. We now report the synthesis, characterization and X-ray structure analysis of the ethoxycarbonyl substituted cyclopentadienyl-carbonyl W—W triply bonded compound, **1**.

A solution of the corresponding W—W singly bonded complex[7] $[\eta^5\text{-EtO}_2\text{CC}_5\text{H}_4\text{W(CO)}_3]_2$ (0.648 g, 0.8 mmol) in diglyme (25 cm^3) was heated at 140°C for 9 h to give 0.137 g of $[\eta^5\text{-EtO}_2\text{CC}_5\text{H}_4\text{W(CO)}_2]_2$ (**1**) in 23% yield after column chromatography. It is an air-stable red–brown solid but quite air-sensitive in solution. The characterizing data‡ are in good agreement with the formulation of **1**. The IR data of 1909 and 1852 cm^{-1} are too low for normal terminal carbonyls and actually are characteristic of linear semi-bridging carbonyls (*vide infra*).

The structure of **1** is presented in Fig. 1,§ which includes some important bond lengths and angles.

As seen from Fig. 1, the molecule consists of

† Author to whom correspondence should be addressed.

‡ Characterization data: Found: C, 31.8; H, 2.4. Calc. for $C_{20}H_{18}O_8W_2$: C, 31.9; H, 2.4%. IR (KBr disc): ν(C≡O), 1909 s, 1852 s, ν(C=O), 1713 s. ^{1}H NMR ($CDCl_3$): δ 1.33 (t, 6H, J = 7.0 Hz, $2CH_3$), 4.30 (q, 4H, J = 7.0 Hz, $2CH_2$), 5.50 (br. s, 4H, ring's H^3, H^4), 5.89 (br. s, 4H, ring's H^2, H^5). MS (EI): m/z 754 (M^+, 17%).

§ Crystal data for **1**: monoclinic, space group $P2_1/c$, a = 6.847(1), b = 11.644(2), c = 13.541(4) Å, β = 101.02(2)°, V = 1059.7 Å^3, Z = 2, Mr = 754.14, D_x = 2.40 g cm^{-3}, μ = 113 cm^{-1}, $F(000)$ = 700. A total of 1614 independent reflections were collected in the range $2° \leqslant \theta \leqslant 25°$ with Mo-K_α radiation by the ω–2θ scan mode, of which 1213 reflections were considered to be observed with $I \geqslant 3\sigma(I)$ and used in structure solution and refinement. The structure was solved by the Patterson method and refined to R = 0.025 and Rw = 0.029. Final atomic coordinates, thermal parameters and structure factor tables have been deposited with the Editor as supplementary material.

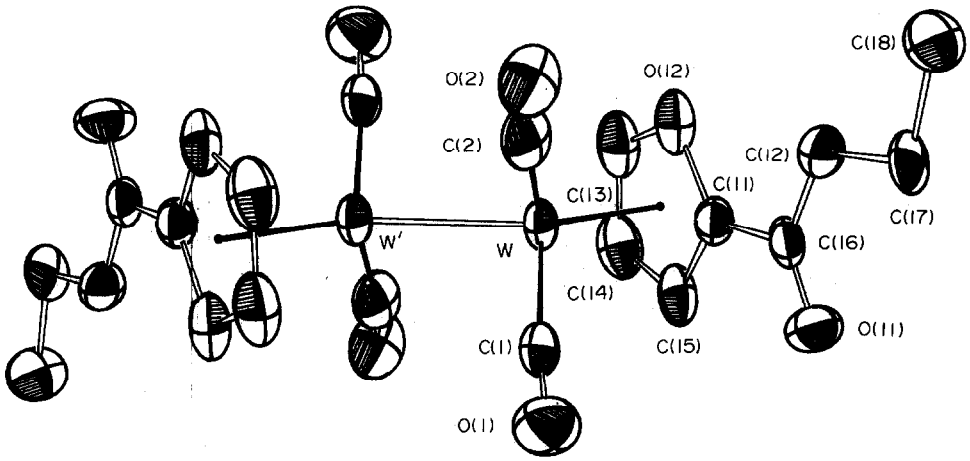

Fig. 1. The molecular structure of $[\eta^5\text{-}EtO_2CC_5H_4W_2(CO)_2]_2$ showing the numbering scheme. Selected bond lengths (Å) and angles (°): W—W′ 2.5064(6), W—C(1) 1.948(8), W—C(2) 1.946(9), W′—W—C(1) 81.9(2), W′—W—C(2) 71.3 (2), W—C(1)—O(1) 174.9(6), W—C(2)—O(2) 172.2(6). Symmetrical transformation: $' = (-x, 1-y, 1-z)$.

two $[\eta^5\text{-}EtO_2CC_5H_4W(CO)_2]$ moieties linked by a W—W bond. The W—W bond length of 2.5064 Å is about 0.72 Å shorter than that of $[\eta^5\text{-}C_5H_5W(CO)_3]_2$,[8] but almost the same as that (2.503 Å) of $L_2W_2(CO)_4$ ($L^- = [(C_5H_5)Co\{P(O)(OC_2H_5)_2\}_3]^-$).[9] On the basis of these facts and the 18-electron rule, a triple bond, W≡W, can be assigned for the bonding between the two tungsten atoms in **1**. As required from its space group, **1** is centrosymmetric and the two cyclopentadienyl rings are parallel to each other. The five non-hydrogen atoms of the functional substituent EtO_2C lie in a plane, which forms a dihedral angle of 6.8° with the cyclopentadienyl ring. So, the substituent ethoxycarbonyl is conjugated quite well with the cyclopentadienyl system. The average W—C—O angle for carbonyl is 173.5° which is close to 180°, and the average W′—W—C angle is 76.6°. Thus, the four carbonyls are bent back over the W—W bond, forming a semi-bridging structure. In this structural unit, the average "short" W—C distance is 1.947 Å and the average "long" W···C distance is 2.802 Å. The linear semi-bridging carbonyls are also observed in its chromium[3,4] and molybdenum[5,6,10] analogues, which donate their lone electron pairs of carbon atoms, as a two electron ligand, to the near metal and concurrently utilize their π^*-orbitals to accept π-electrons from M≡M.[6] The degree of bridge asymmetry, i.e. asymmetry parameter $a = (D_2 - D_1)/D_1$, equals 0.31, which is greater than those of $Cp_2Cr_2(CO)_4$ (0.29) and $Cp_2Mo_2(CO)_4$ (0.20).[4,5]

It is interesting to note that the angle of Cp^*_{centre}—W—W′ is 159.1° ($Cp^* = \eta^5\text{-}EtO_2CC_5H_4$); namely, the configuration of Cp^*_{centre}—W—W′ is bent, as those of Cp_{centre}—Cr—Cr in $Cp_2Cr_2(CO)_4$[4] and Cp''_{centre}—Cr—Cr in $Cp''_2Cr_2(CO)_4$[3] ($Cp'' = \eta^5\text{-}Me_5C_5$), but it is contrary to the linear Cp_{centre}—Mo—Mo in $Cp_2Mo_2(CO)_4$.[5] For the Cp'''_{centre}—M—M configurations in the $Cp'''_2M_2(CO)_4$ (M = Cr, Cp‴ = Cp, η^5-Me_5C_5; M = Mo, Cp‴ = Cp) complex Curtis[5] and Hall[6] proposed two explanations on the basis of electronic and steric factors, respectively. Obviously the bending configuration of Cp^*_{centre}—W—W′ in **1** cannot be explained according to the magnitude of the metal atom since tungsten is larger than molybdenum. In such a case the electronic and steric effects of the functionally substituted EtO_2C must play an important role in deciding the bent configuration of Cp^*_{centre}—W—W′ in **1**. However, further structural studies and the detailed preparative procedures of **1** and other functional substituted complexes of this type will be given in a full paper.

Acknowledgement—We are grateful to the National Science Foundation of China for financial support of this work.

REFERENCES

1. G. Wilkinson, F. G. A. Stone and E. W. Abel (Editors), *Comprehensive Organometallic Chemistry*, Vol. 6. Pergamon Press, Oxford (1982).
2. F. A. Cotton and R. A. Walton, *Multiple Bonds Between Metal Atoms*, Ch. 5. Wiley-Interscience, New York (1982).
3. J. Potenza, P. Giordano, D. Mastropaols and A. Efraty, *Inorg. Chem.* 1974, **13**, 2540.
4. M. D. Curtis and W. M. Butler, *J. Organomet. Chem.* 1978, **155**, 131.

5. R. J. Klinger, W. M. Butler and M. D. Curtis, *J. Am. Chem. Soc.* 1978, **100**, 5034.
6. B. J. Morris-Sherwood, C. B. Pewell and M. B. Hall, *J. Am. Chem. Soc.* 1984, **106**, 5079.
7. L.-C. Song and J.-Y. Shen, *Chem. J. Chim. Univ.* 1992, **13**, 1227.
8. R. D. Adams, D. M. Collins and F. A. Cotton, *Inorg. Chem.* 1974, **13**, 1086.
9. W. Kläul, A. Müller, R. Herbst and E. Egert, *Organometallics* 1987, **6**, 1824.
10. J.-S. Huang and L. F. Dahl, *J. Organomet. Chem.* 1983, **243**, 57.

Polyhedron Vol. 12, No. 2, pp. 263–266, 1993
Printed in Great Britain

0277–5387/93 $6.00+.00
© 1993 Pergamon Press Ltd

COMMUNICATION

TETRAHEDRAL AND SQUARE-PYRAMIDAL SULPHUR-RICH COMPLEXES OF MANGANESE(II)

SHI-BAO YU and R. H. HOLM*

Department of Chemistry, Harvard University, Cambridge, MA 02138, U.S.A.

(*Received* 24 *July* 1992; *accepted* 22 *October* 1992)

Abstract—The reaction system $MnCl_2/2Na_2S_2/2.2CS_2/Et_4NSH/2Et_4NCl$ in acetonitrile affords $(Et_4N)_3[Mn(CS_4)_2Cl]$ in high yield. Upon prolonged standing, $(Et_4N)_2[Mn(S_6)_2]$ was isolated from the reaction mixture filtrate. The structures of these compounds were determined by X-ray crystallography. $[Mn(CS_4)_2Cl]^{3-}$ exhibits a distorted square pyramidal stereochemistry with chloride in the apical position and two five-membered chelate rings formed by the infrequently encountered perthiocarbonate ligand. Indistinguishable C—S bond distances to coordinated and free sulphur atoms at a common carbon atom indicate ligand delocalization. In $[Mn(S_6)_2]^{2-}$ the manganese atom occurs in an irregular tetrahedral coordination formed by two chelating hexasulphido ligands. This work adds to the small group of sulphur-rich manganese complexes of established structures.

The chemistry of metal complexes of sulphur-rich ligands has implications in both bioinorganic chemistry and catalysis. Although the majority of such complexes, with ligands such as polysulphide (S_x^{2-}) and the rare perthiocarbonate (CS_4^{2-}), have been prepared with molybdenum, tungsten and other second and third row transition elements,[1–3] several manganese species have also been characterized. Three structurally defined per- and polysulphide complexes of manganese are known. The first reported is $[Cp_2Mn_2(CO)_6S_2]$, in which two $CpMn(CO)_3$ units are bridged by persulphide.[4] Subsequently, tetrahedral $[MnS_{11}]^{2-}$, in which manganese(II) is coordinated by the polysulphide ligands S_5^{2-} and S_6^{2-},[5] and the related tetrahedral complex $[Mn(Se)_4]^{2-}$[6–8] have been described, as has octahedral $[L'Mn(S_4)(OH_2)]$[9] (L′ = N, N′,N″-trimethyl-1,4,7-triazacyclononane). Among perthiocarbonate complexes, $[Mn(CS_4)_2]^{2-}$ and $[Mn(CS_4)S_6)]^{2-}$ have been prepared[5] but not structurally characterized. Binuclear centrosymmetric $[Mn_2(CO)_6(CS_4)_2]^{2-}$ has been obtained by an unprecedented phase-transfer-catalysed reaction between $[Mn_2(CO)_9Br]^{1-}$ and sulphur; two $Mn(CO)_3$ units are linked by the perthiocarbonate ions, each acting as a bridging and terminal ligand to complete octahedral coordination.[10] We report here two additions to this small group of sulphur-rich manganese compounds, $(Et_4N)_3[Mn(CS_4)_2Cl]$ and a by-product of its preparation, $(Et_4N)_2[MnS_{12}]$.

EXPERIMENTAL

All operations were performed under a pure dinitrogen atmosphere using standard Schlenk techniques.

$(Et_4N)_3[Mn(CS_4)_2Cl]$ (1)

To a slurry of anhydrous $MnCl_2$ (0.50 g, 4.0 mmol), Na_2S_2 (0.88 g, 8.0 mmol), Et_4NCl (1.40 g, 8.4 mmol) and Et_4NSH (0.65 g, 4.0 mmol) in acetonitrile (100 cm^3), CS_2 (0.52 cm^3, 8.8 mmol) was added dropwise. The initial greenish colour quickly turned to red and a clear solution formed. The solution was stirred overnight, during which time an orange solid separated. This material was collected by filtration and recrystallized by adding ether to a concentrated acetonitrile solution. The product was obtained as 2.65 g (87%) of an orange

* Author to whom correspondence should be addressed.

microcrystalline solid. Absorption spectrum (acetonitrile): λ_{max} nm (ε_M M^{-1} cm^{-1}), 337 (23,300), 416 (11,400). IR spectrum (Nujol): 993 (s) cm^{-1}. Found: C, 40.5; H, 7.5; Cl, 4.7; Mn, 7.2; N, 5.4; S, 33.2. Calc. for $C_{26}H_{60}ClMnN_3S_8$: C, 41.0; H, 7.9; Cl, 4.6; Mn, 7.2; N, 5.5; S, 33.7%.

$(Et_4N)_2[Mn(S_6)_2]$ (**2**)

When the filtrate from the preceding preparation was stored at −20°C for 1 month, orange needle-like crystals developed. These were collected and identified by single-crystal X-ray diffraction.

Block-shaped orange crystals of **1** were grown in a 1:1 (v/v) acetonitrile/ether solution over several days at room temperature. Crystals of **2** were grown in the reaction filtrate. X-ray data collection and processing and structure solution and refinement were performed using the instrumentation and programs described elsewhere.[11] Three standard reflections monitored every 97 reflections exhibited no significant decay over the course of data collection. The asymmetric unit of **1** consists of one-half trianion with manganese and chlorine atoms residing on a two-fold axis, one full cation and one-half cation with its nitrogen atom on a two-fold axis. The asymmetric unit of **2** contains the dianion and two cations. In one of the cations each of the four methylene carbon atoms is disordered over two positions; these were modelled with equal site occupancies. Excluding disordered atoms, all non-hydrogen atoms for **1** and **2** were refined with anisotropic thermal parameters. In the final stages of the refinements hydrogen atoms were introduced on the non-disordered carbon atoms.

Crystallographic data using Mo-K_α ($\lambda = 0.71069$ Å) at $T = 297$ K: **1**, $C_{26}H_{60}ClMnN_3S_8$, $M = 761.7$, monoclinic, $C/2c$, $a = 21.991(7)$, $b = 13.302(3)$, $c = 13.275(2)$ Å, $\beta = 92.15(2)°$, $V = 3881(2)$ Å^3, $Z = 4$, $D_c = 1.30$ g cm^{-3}, $\mu = 8.31$ cm^{-1}, 2θ limits 3–45°, 3024 reflections collected, $R = 4.03$ ($R_w = 6.63$) for 2256 ($I > 3\sigma$) unique observed reflections. **2**, $C_{16}H_{40}MnN_2S_{12}$, $M = 700.2$, monoclinic, $P2_1/c$, $a = 12.747(3)$, $b = 17.725(3)$, $c = 14.501(2)$ Å, $\beta = 96.53(2)°$, $V = 3255(1)$ Å^3, $Z = 4$, $D_c = 1.43$ g cm^{-3}, $\mu = 11.4$ cm^{-1}, 2θ limits 3–48°, 6424 reflections collected, $R = 9.06$ ($R_w = 8.31$) for 2533 ($I > 4\sigma$) unique reflections.

RESULTS AND DISCUSSION

The apparent stoichiometry for the formation of $[Mn(CS_4)_2Cl]^{3-}$, which was isolated in 87% yield as its Et_4N^+ salt, is represented by reaction (1).

$$MnCl_2 + 2S_2^{2-} + 2CS_2 \longrightarrow [Mn(CS_4)_2Cl]^{3-} + Cl^- \quad (1)$$

While Et_4NSH does not appear in this reaction, its presence is required to obtain high yields. We conjecture that nucleophilic attack of HS^- on CS_2 generates CS_3^{2-}, which is stabilized by chelation. Insertion of sulphur from persulphide in the Mn—S bond affords coordinated perthiocarbonate and releases sulphide. In this picture hydrosulphide or sulphide is a catalyst in the formation of the product complex. Perthiocarbonate complexes are generally efficiently prepared by the reaction of CS_2 with species containing MS_4 chelate rings,[5,12] no doubt because nucleophilic and electrophilic sulphur atoms are present in the same structural fragment. Further, it has been demonstrated that the conversion $[Ni(CS_3)_2]^{2-} \rightarrow [Ni(CS_4)_2]^{2-}$ upon reaction of the trithiocarbonate complex with sulphur is nearly quantitative.[13] The means of formation of $[Mn(S_6)_2]^{2-}$ is obscure, but may result from adventitious oxidation of persulphide (despite anaerobic conditions) during prolonged storage of the reaction filtrate. We have not attempted to devise a synthesis of this species.

The structure of $[Mn(CS_4)_2Cl]^{3-}$ is presented in Fig. 1 and bond distances and angles are listed in Table 1. The complex is best described as distorted square pyramidal, with the nearly planar chelate rings in the *trans* orientation, required by the imposed C_2 axis along the Mn—Cl bond. The S_4 base of the pyramid is not planar; atoms S(1′,2′) deviate by 0.90 Å from the plane of the other three sulphur atoms. The overall structure is similar to that of $[MoS(CS_4)_2]^{2-}$.[12] The manganese atom is displaced toward the apical chloride ligand and the Mn—Cl distance of 2.400(2) Å is quite close to the corresponding distances (2.35–2.41 Å) in other square pyramidal manganese(II) complexes.[14–16] The Mn—S bond lengths (2.51–2.56 Å) are longer than those in tetrahedral Mn^{II}—S_4 complexes[5,17,18] (*vide infra*) and approach the value (2.57 Å) found in the octahedral tetrasulphide complex.[9] The C—S and S—S bond distances and angles approach those

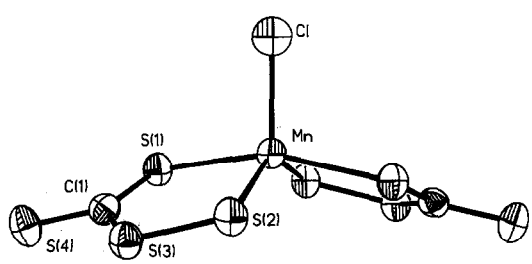

Fig. 1. The structure of $[Mn(CS_4)Cl]^{3-}$, showing the atom labelling scheme and 50% probability ellipsoids. An imposed C_2 axis passes through the manganese and chlorine atoms.

Table 1. Selected bond distances (Å) and angles (°)[a] for $(Et_4N)_3[Mn(CS_4)_2Cl]$ (1)

Mn—Cl	2.400(2)		
Mn—S(1)	2.564(1)	Mn—S(2)	2.505(1)
S(2)—S(3)	2.048(2)	S(3)—C(1)	1.755(5)
S(1)—C(1)	1.685(5)	S(4)—C(1)	1.677(5)
Cl—Mn—S(1)	100.4(1)	Cl—Mn—S(2)	111.6(1)
S(1)—Mn—S(2)	85.8(1)	S(1)—Mn—S(1′)	159.1(1)
S(2)—Mn—S(1′)	86.6(1)	S(2)—Mn—S(2′)	136.8(1)
Mn—S(1)—C(1)	111.8(2)	Mn—S(2)—S(3)	108.2(1)
S(2)—S(3)—C(1)	111.5(2)	S(1)—C(1)—S(3)	122.7(3)
S(1)—C(1)—S(4)	125.4(3)	S(3)—C(1)—S(4)	111.9(3)

[a] Primed and unprimed atoms are related by a C_2 axis.

Table 2. Selected bond distances (Å) and angles (°) for $(Et_4N)_2[Mn(S_6)_2]$ (2)

Mn—S(1)	2.429(4)		Mn—S(7)	2.437(4)
Mn—S(6)	2.472(5)		Mn—S(12)	2.409(4)
S—S	range	1.996(7)–2.054(7) Å		
	average	2.01(1)		
S(1)—Mn—S(6)	112.7(2)		S(7)—Mn—S(12)	120.2(1)
S(1)—Mn—S(12)	110.7(1)		S(6)—Mn—S(12)	107.2(2)
S(1)—Mn—S(7)	101.6(1)		S(6)—Mn—S(7)	104.5(2)
Mn—S(1)—S(2)	100.9(2)		Mn—S(6)—S(5)	113.6(2)
Mn—S(7)—S(8)	104.6(2)		Mn—S(12)—S(11)	109.5(2)
S—S—S	range	107.0(3)–111.1(3)		
	average	109(1)		

exhibited by $[Ni(CS_4)_2]^{2-}$,[5] $[MoS(CS_4)_2]^{2-}$[12] and $[Mo_2S_4(CS_4)_2]^{2-}$,[12] the only other structurally characterized perthiocarbonate complexes, but there are certain significant differences.

The indistinguishability of the S(4)—C(1) and S(1)—C(1) bond lengths indicates delocalization of this portion of the ligand. This situation is very similar to that found with one of the two inequivalent anions in the structure of $K_2CS_4 \cdot MeOH$,[19] in which the corresponding bonds have the identical distance of 1.705 Å. In the other anion these distances differ by 0.086 Å, with one of these (1.745 Å) being appreciably longer than the S(4,1)—C(1) bonds in $[Mn(CS_4)_2Cl]^{3-}$. Ligand delocalization is also found in $[Ni(CS_4)_2]^{2-}$, where the two C—S distances differ by only 0.03 Å.[5] However, this feature is not an invariant property inasmuch as bond length differences in $[MoS(CS_4)_2]^{2-}$ (0.09 Å) and $[Mo_2S_2(CS_4)_2]^{2-}$ (0.17 Å)[12] are indicative of a far more localized ligand structure.

The structure of $[Mn(S_6)_2]^{2-}$ is set out in Fig. 2 and metric data are collected in Table 2. The complex contains manganese(II) in distorted tetrahedral coordination and is structurally very similar to $[Mn(S_5)(S_6)]^{2-}$.[5] The MnS_6 rings adopt a chair-type conformation very similar to those observed for some other complexes containing the S_6^{2-} ligand[2,20] and for cyclo-S_7.[21]

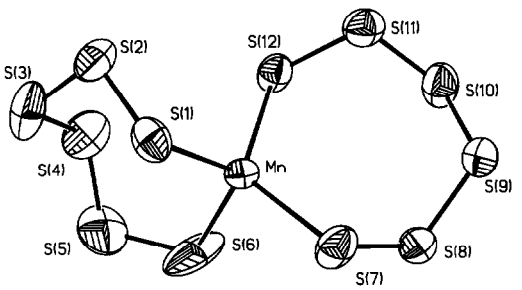

Fig. 2. The structure of $[Mn(S_6)_2]^{2-}$, showing the atom labelling scheme and 50% probability ellipsoids.

Acknowledgements—This research was supported by NIH Grant GM 28856. X-ray diffraction equipment was obtained by NIH Grant 1 S10 RR 02247. We thank M. J. Scott for useful discussions.

REFERENCES

1. M. Draganjac and T. B. Rauchfuss, *Angew. Chem., Int. Edn Engl.* 1985, **24**, 742.

2. A. Müller and E. Diemann, *Adv. Inorg. Chem.* 1987, **31**, 89.
3. D. Coucouvanis, A. Toupadakis, S.-M. Koo and A. Hadjikyriacou, *Polyhedron* 1989, **8**, 1705.
4. M. Herberhold, D. Reiner, B. Zimmer-Gasser and U. Schubert, *Z. Naturforsch.* 1980, **35b**, 1281.
5. D. Coucouvanis, P. R. Patil, M. G. Kanatzidis, B. Detering and N. C. Baenziger, *Inorg. Chem.* 1985, **24**, 24.
6. G. Kraüter, M.-L. Ha-Eierdanz, U. Müller and K. Dehnicke, *Z. Naturforsch.* 1990, **45**, 695.
7. S. C. O'Neal, W. T. Pennington and J. W. Kolis, *Inorg. Chem.* 1990, **29**, 3134.
8. M. A. Ansari, C. H. Mahler, G. S. Chorghade, Y.-J. Lu and J. A. Ibers, *Inorg. Chem.* 1990, **29**, 3832.
9. K. Wieghardt, U. Bossek, B. Nuber and J. Weiss, *Inorg. Chim. Acta* 1987, **126**, 39.
10. H. Alper, F. Sibtain, F. W. B. Einstein and A. C. Willis, *Organometallics* 1985, **4**, 604.
11. S.-B. Yu, G. C. Papaefthymiou and R. H. Holm, *Inorg. Chem.* 1991, **30**, 3476.
12. D. Coucouvanis and M. Draganjac, *J. Am. Chem. Soc.* 1982, **104**, 6820.
13. D. Coucouvanis and J. P. Fackler Jr, *J. Am. Chem. Soc.* 1967, **87**, 1346.
14. M. B. Ferrari, G. G. Fava, C. Pelizzi, P. Tarasconi and G. Tosi, *J. Chem. Soc., Dalton Trans.* 1987, 227.
15. H.-R. Chang, S. K. Larsen, P. D. W. Boyd, C. G. Pierpont and D. N. Hendrickson, *J. Am. Chem. Soc.* 1988, **110**, 4565.
16. M. Di Viara and F. Mani, *J. Chem. Soc., Dalton Trans.* 1990, 191.
17. T. Costa, J. R. Dorfman, K. S. Hagen and R. H. Holm, *Inorg. Chem.* 1983, **22**, 4091.
18. K. Greiwe, B. Krebs and G. Henkel, *Inorg. Chem.* 1989, **28**, 3713.
19. W. A. Bueno, A. Lautie, C. Sourisseau, D. Zins and M. Robineau, *J. Chem. Soc. Perkin II* 1978, 1011.
20. (a) A. Müller, M. Römer, H. Bögge, E. Krickemeyer, F.-W. Baumann and K. Schmitz, *Inorg. Chim. Acta* 1984, **89**, L7; (b) A. Müller, F.-W. Baumann, H. Bögge, M. Römer, E. Krickemeyer and K. Schmitz, *Angew. Chem., Int. Edn Engl.* 1984, **23**, 632; (c) A. Müller, J. Schimanski, U. Schimanski and H. Bögge, *Z. Naturforsch.* 1985, **40b**, 1277; (d) R. Sillanpaa, P. S. Cartwright, R. D. Gillard and J. Valkonen, *Polyhedron* 1988, **7**, 1801; (e) Y. Watasuki, H. Yamazaki and C.-B. Cheng, *J. Organomet. Chem.* 1989, **372**, 437; (f) R. M. H. Banda, I. G. Dance, T. D. Bailey, D. C. Craig and M. L. Scudder, *Inorg. Chem.* 1989, **28**, 1862.
21. R. Steudel, R. Reinhardt and F. Schuster, *Angew. Chem., Int. Edn Engl.* 1977, **16**, 715.

Polyhedron Vol. 12, No. 3, pp. 267–271, 1993
Printed in Great Britain

0277–5387/93 $6.00+.00
© 1993 Pergamon Press Ltd

SYNTHESIS AND X-RAY CRYSTAL STRUCTURE OF A MONONUCLEAR ARYLOXIDE-CROWN ETHER OF BARIUM: [Ba(OAr)$_2$(18-crown-6)] · (2ArOH)(18-crown-6) (Ar = $C_6H_3Bu^t_2$-3,5)

PHILIPPE MIELE, JEAN-DOMINIQUE FOULON, NADINE HOVNANIAN* and LOUIS COT

Laboratoire de Physicochimie des Matériaux, URA 1312, ENSCM 8 rue Ecole Normale, 34075 Montpellier Cedex, France

(*Received* 17 *June* 1992; *accepted* 6 *October* 1992)

Abstract—The reaction of elemental barium with 3,5-di-tert-butylphenol and 18-crown-6 in THF at reflux temperature and/or using gaseous ammonia as catalyst yields a monomeric barium compound. The complex has been characterized by IR, ^{1}H NMR, mass spectroscopy, elemental analysis and single-crystal X-ray studies and shown to be an alcohol and crown-ether solvate: [Ba(OAr)$_2$(18-crown-6)] · (2ArOH)(18-crown-6). The structure consists of two ArO ligands, one above and one below the planar barium-coordinating polyether resulting in an eight-coordination for the barium atom. The bulky aryloxide anions are hydrogen-bonded to the OH group of the 3,5-di-tert-butylphenol molecule and one free 18-crown-6 molecule fits between two [Ba(OAr)$_2$(18-crown-6)] · 2ArOH units. The poor thermal stability of this monomeric complex accounts for its non-volatility, whereas its high solubility is attractive for sol–gel processes.

The chemistry of alkaline-earth alkoxides has shown a growing interest over the last 5 years.[1,2] This is due to its new applications, including Chemical Vapour Deposition (CVD), for the preparation of high-temperature superconducting ceramics thin films.[3] Although there are satisfactory OMCVD sources for depositing copper and yttrium oxides,[4] only a very few compounds of barium having an adequate volatility are known.[1b,5] They often display fluorinated β-diketonate, macrocyclic polyether and alkoxide ligands.

Since the volatility of these species is consistent with a low degree of molecular aggregation, we approach the problem by attempting to prepare a mononuclear barium aryloxide-crown ether using two sterically hindered ligands: 3,5-di-tert-butyphenol and 18-crown-6 (1,4,7,10,13,16-hexaoxacyclooctadecane).

We describe here the synthesis and the characterization including X-ray diffraction crystal structure of [Ba(OAr)$_2$(18-crown-6)] · (2ArOH)(18-crown-6).

EXPERIMENTAL

All manipulations were routinely performed under argon using Schlenk tubes and vacuum-line techniques with solvents purified by standard methods. The 3,5-di-tert-butylphenol was sublimed before use; barium metal granules and 18-crown-6 were commercially available from Strem Chemicals and Aldrich-chemie, respectively. ^{1}H NMR and IR spectra were run on a Bruker AC-250 and an IR FT Nicolet ZDX spectrometer. IR spectra were obtained as Nujol mulls between KBr plates. Mass spectra were recorded on a 300 DX JEOL by Fast-Atom Bombardment, positive-ions[6] with an NBA matrix (NBA = *ortho*-nitrobenzylalcohol). Thermogravimetric analysis was made under argon atmosphere with an heating rate of 5°C min^{-1}. Analytical data were obtained from the Centre de Microanalyses du CNRS.

Synthesis of [Ba(OAr)$_2$(18-crown-6)] · (2ArOH)(18-crown-6) (**I**)

Barium metal granules (0.78 g, 5.7 mmol), 3,5-di-tert-butylphenol (2.35 g, 11.4 mmol) and 18-

* Author to whom correspondence should be addressed.

crown-6 (1.51 g, 5.7 mmol) were stirred together with THF (50 cm^3) at reflux temperature. Then ammonia gas was bubbled into the reaction medium in order to accelerate and complete the reaction. A beige precipitate appeared when all the barium metal was consumed. The mixture was concentrated to dryness. Extraction with 20 cm^3 of toluene and filtration yielded an orange–brown filtrate. Large crystals were easily obtained at −20°C, but then dissolved quickly at room temperature. The mixture was heated under reflux and after slow concentration, crystals suitable for X-ray were formed as air-sensitive colourless rods. Yield: 49% based on barium. Found: C, 64.2; H, 9.0. Calc. for $C_{80}H_{134}O_{16}Ba$: C, 64.5; H, 9.0%. IR (cm^{-1}): 3205 [ν(OH)], 1581, 1328, 1244, 1202, 1096, 1026, 998, 963, 899, 864, 836, 716, 583, 562. ^{1}H NMR ($CDCl_3$, 293 K, ppm): 6.57 t (CH, 1H); 6.54 d (CH, 2H); 3.69 s (CH_2, 12H); 1.21 s (CH_3, 18H). SM (*m/z*, FAB$^+$): Ar = $C_6H_3Bu^t_2$-3,5; Ar′ = $C_6H_4NO_2$-2, $Ba(OAr)_2$(18-crown-6) (3%), Ba(OAr)(18-crown-6) (100%), Ba(HOAr′)(18-crown-6) (25%), Ba(OPh)(18-crown-6) (8%), $Ba(OCH_2Ph)$(OAr) (25%), Ba(18-crown-6) (22%), Ba(OAr) (40%), Ba(OH) (45%). Several kinds of crystals may be obtained from the same synthesis, depending on the crystallization conditions. Despite their poor quality, which precluded an X-ray diffraction study, we have noted that their difference comes from the solvatation of the 18-crown-6 ether according to their spectroscopic data and elemental analysis.

Alternate synthesis of **I**

Barium metal granules (0.4 g, 2.9 mmol), 3,5-di-tert-butylphenol (2.4 g, 11.6 mmol) and 18-crown-6 (1.53 g, 5.8 mmol) were stirred together with THF (40 cm^3) under reflux for 1 week. When all the metal was consumed the mixture was filtered and concentrated. The filtrate was left to crystallize at 5°C, leading to crystals of **I**. Yield: 90% based on barium.

Crystallographic studies

A single-crystal of **I** was sealed in a Lindemann glass capillary and was mounted onto a Siemens P3 automatic diffractometer at room temperature. Accurate unit cell dimensions and crystal orientation matrix, together with their estimated standard deviations, were obtained from least-squares refinement of the setting angles of 22 reflections. Crystallographic data and other pertinent information are summarized in Table 1. Corrections were made for Lorentz and polarization effects. No correction for absorption was done. All calculations were performed on a VAX 3100. Complex neutral-atom scattering factors were employed. Anomalous dispersion terms were used. The position of the barium atoms was found by analysis of a three-dimensional Patterson map using SHELXS 86[7] and was confirmed by direct methods using SIR.[8] All remaining non-hydrogen atoms were found by successive electron density map calculations using SHELX 76.[9] In view of keeping the data/variables ratio higher than 10:1, only atoms from the chelated polyether and the phenyl ring were allowed to move anisotropically. This choice results in relatively high values for R of 0.0791 and for R_w of 0.0907. Refinement with anisotropic thermal parameters for all the non-hydrogen atoms leads to more reasonable values of 0.0484 and 0.0522 for both R and R_w, respectively, which does not reveal any problem of crystal quality. However, this latter refinement appears to be less accurate because of the small data/variables ratio of 6.7:1. For this reason, we decided to report here the results obtained from the first refinement type. Hydrogen atoms were placed in calculated positions (C—H = 1.08 Å) and were not further refined but recalculated after each cycle. Positional parameters and thermal parameters are given as supplementary material.

RESULTS AND DISCUSSION

[$Ba(OAr)_2$(18-crown-6)]·(2ArOH)(18-crown-6) was obtained by mixing metallic barium, 3,5-di-tert-butylphenol and 18-crown-6 (ratio 1:2:1, respectively) with THF in the presence of ammonia gas as a catalyst. Such a route has already been mentioned.[2e,10] It consists of a fast reaction of alkaline-earth metals with sterically hindered ligands in oxygenated medium using ammonia gas as a catalyst. However, the same compound can be selectively obtained in 90% yield with a molecular ratio of 1:4:2 for Ba:ArOH:18-crown-6, in THF under reflux.

The X-ray crystal structure of **I** is shown in Fig. 1. It comprises monomeric $Ba(OAr)_2$(18-crown-6) units solvated by alcohol and 18-crown-6 ether molecules. Selected bond lengths and angles are listed in Table 2. The barium atom is surrounded by the polyether ring forming an almost BaO_6 planar configuration (maximum deviation of 0.15 Å) and by two aryloxide ligands lying perpendicularly on both sides of this plane. Each oxygen atom of the aryloxide ligand has short contacts (2.48 Å), implying hydrogen bonding with the oxygen atom of the neighbouring 3,5-di-tert-butylphenol molecule. Finally, one free 18-crown-6 molecule fits between

Table 1. Summary of crystallographic data

Compound	$C_{80}H_{134}O_{16}Ba$
Molecular weight	1489.3
Crystal system	Triclinic
Space group	$P\bar{1}$
a (Å)	9.548(2)
b (Å)	14.525(3)
c (Å)	16.984(5)
α (°)	111.74(2)
β (°)	91.61(2)
γ (°)	95.15(2)
V (Å^3)	2174.3(9)
Z	1
D_{calc} (g cm^{-3})	1.137
$F(000)$ (e$^-$)	798
Diffractometer	Siemens P3
Temperature (K)	293
Radiation	Mo-K_α
Scan type	ω–2θ
Scan width	$1.00+0.35 \tan\theta$
Scan range	$2 \leqslant \theta \leqslant 20$
hkl limits	$\pm h, \pm k, +l$
Reference reflections	3 every 100 reflections
Intensity stability	Variation $\leqslant 3\%$
Data collected	4262
Unique data used ($F_o^2 > 3\sigma(F_o)^2$)	2938
μ (cm^{-1})	5.1
Absorption correction	None
R^a	0.0791
$R_w{}^a$	0.0907
Weight	$w = 1$
Number of parameters refined	289
Ratio of observation to parameter	10.2
$(\Delta/\sigma)_{max}{}^b$	$\leqslant 0.001$
Residual electron density (e Å^{-3})	−0.5–1.0

[a] The quantity minimized in the least-squares procedure is: $w(|F_o| - |F_c|)^2$. $R = \Sigma||F_o| - |F_c||/\Sigma|F_o|$; $R_w = [\Sigma w(|F_o| - |F_c|)^2/\Sigma w(F_o)^2]^{1/2}$.

[b] Maximum ratio of the rms shift to standard deviation observed for the last cycle of refinement.

two [Ba(OAr)$_2$(18-crown-6)]·2ArOH units. The barium atom is coordinated by eight oxygen atoms defining a hexagonal bipyramid. The Ba—O (polyether) distances are in good agreement with the ones previously reported for other barium derivatives with crown ether ligands,[5b,c] whereas the Ba—O(OAr) bond length is significantly longer than the usual Ba—O(aryloxide) distances.[2] This could be partly attributed to the already mentioned hydrogen bonding reinforced by the steric hin-

Table 2. Selected bond lengths (Å) and angles (°)

Ba—O(1)	2.570(8)	Ba—O(21)	2.785(9)
Ba—O(23)	2.806(10)	Ba—O(22)	2.808(11)
Ba···O(3)	3.76(2)	O(1)···O(3)	2.48(2)
O(1)—Ba—O(21)	82.3(3)	O(1)—Ba—O(23)	82.8(3)
O(1)—Ba—O(22)	84.7(3)	O(21)—Ba—O(23)	119.0(4)
O(21)—Ba—O(22)	60.0(4)	O(22)—Ba—O(23)	60.0(4)

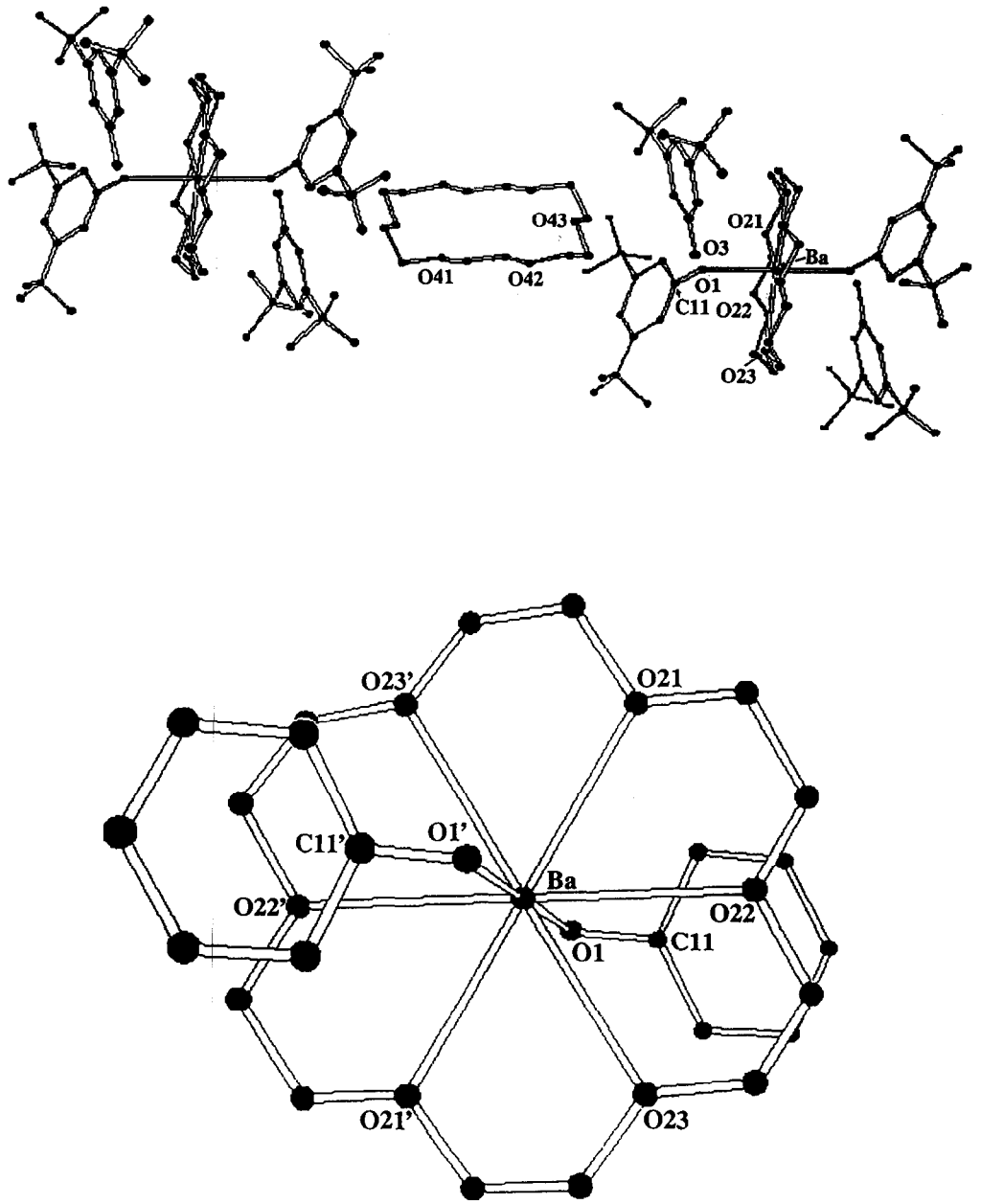

Fig. 1. Atomic numbering schemes of $[Ba(OAr)_2(18\text{-crown-}6)]\cdot(2ArOH)(18\text{-crown-}6)$ and of the monomeric moiety $[Ba(OAr)_2(18\text{-crown-}6)]$ (the Bu^t ligands are omitted for clarity).

drance from the bulky polyether ligand. Moreover, although the Ba—O(1)—C(11) bond angle of 136.1° is in favour of π-donation, the dihedral angle of 89.3° between the Ba—O(1)—C(11) plane and its adjacent phenyl ring allows no conjugation limiting the π-donation effect.

The coordination number of the barium–oxygen derivatives is generally high (5–10); multidentate Lewis base ligands as the cyclic polyether 18-crown-6 yield coordinatively saturated barium monomeric species. Some other molecular barium crown ether derivatives have been reported in the literature.[5b,c,d] They are generally associated with fluorinated β-diketonate ligands (such as 1,1,1,5,5,5-hexafluoro-2,4-pentanedionate) and their structure is similar to the $Ba(OAr)_2(18\text{-crown-}6)$ moiety. In fact, they consist of two β-diketonate ligands, one above and one below the planar barium-coordinating polyether. $[Ba(OAr)_2(18\text{-crown-}6)]\cdot(2ArOH)(18\text{-crown-}6)$ is the first example of an aryloxide crown ether complex of barium.

The monomeric nature of the compound is confirmed by Fast-Atom Bombardment positive-ion mass spectral data, which exhibit the parent molec-

ular ion without any ion of higher molecular mass. The IR spectrum displays essentially the absorption bands of the ligands as well as a broad ν(O—H) stretching vibration at 3205 cm^{-1}, characteristic of hydrogen-bonding. The room-temperature ^1H NMR spectrum in $CDCl_3$ reveals a single average environment for the aryloxide groups and for the cyclic polyether molecules. Integration establishes four ArO groups for two polyether molecules. A variable-temperature study shows that the aryloxo ligands remain unchanged; they are non-fluxional on the NMR time-scale. On cooling to 276 K two singlets of equal intensity appear at 3.69 and 3.66 ppm, assignable to the free and coordinated 18-crown-6, respectively. On decreasing the temperature in the range 276–255 K, only the signal of the coordinated crown ether moves to the high field. The alcohol proton resonance is not observed.

Since monomeric compounds are better candidates than oligomers for volatility properties, the monomeric studied complex could reasonably be expected to be volatile. Unfortunately, its poor thermal stability does not allow it to be volatile. In fact, compound **I** decomposes on heating *in vacuo* (10^{-1} mm of Hg) with sublimation of the 18-crown-6 and alcohol. Preliminary TGA results have shown two weight losses of 59 and 19% in the range 200–300°C and 380–450°C, respectively. It could be thought that the decomposition leads to coordinatively unsaturated barium species, which have a strong tendency to form non-volatile intermolecular aggregates. The compound is, thus, of no use for CVD applications; nevertheless, its hydrocarbon-solubility makes it interesting for sol–gel and pyro–sol methods.

Acknowledgement—We thank the CNRS-PIRMAT for financial support.

REFERENCES

1. (a) O. Poncelet, L. Hubert-Pfalzgraf, L. Toupet and J. C. Daran, *Polyhedron* 1991, **10**, 2045; (b) K. G. Caulton, M. H. Chisholm, S. R. Drake and J. C. Huffman, *J. Chem. Soc., Chem. Commun.* 1990, 1498; (c) S. C. Goel, M. A. Matchett, Y. Chiang and W. E. Buhro, *J. Am. Chem. Soc.* 1991, **113**, 1844.
2. (a) P. B. Hitchcock, M. F. Lappert, G. A. Lawless and B. Royo, *J. Chem. Soc., Chem. Commun.* 1990, 1141; (b) S. R. Drake, W. E. Streib, M. H. Chisholm and K. G. Caulton, *Inorg. Chem.* 1990, **29**, 2707; (c) F. G. N. Cloke, P. B. Hitchcock, M. F. Lappert, G. A. Lawless and B. Royo, *J. Chem. Soc., Chem. Commun.* 1991, 724; (d) K. F. Tesh and T. P. Hanusa, *J. Chem. Soc., Chem. Commun.* 1991, 879; (e) K. G. Caulton, M. H. Chisholm, S. R. Drake and K. Folting, *Inorg. Chem.* 1991, **30**, 1500.
3. (a) F. Schmaderer, R. Huber, H. Oetzmann and G. Wahl, Proceedings of the Eight European Conference on Chemical Vapour Deposition, 1991, Glasgow, Scotland, 9–13 September, **C2**, 539 (edited M. L. Hitchman and N. J. Archer. idem E. Fitzer, H. Oetzmann, F. Schmaderer and G. Wahl), **C2**, 713.
4. $Cu(dpm)_2$ and $Y(dpm)_3$ are commonly used as OMCVD sources of copper and yttrium oxide.
5. (a) W. S. Rees Jr, M. W. Carris and W. Hesse, *Inorg. Chem.* 1991, **30**, 4479; (b) J. A. Norman and G. P. Pez, *J. Chem. Soc., Chem. Commun.* 1991, 971; (c) P. Van Der Sluis, A. L. Spek, K. Timmer and H. A. Meinema, *Acta Cryst.* 1990, **C46**, 1741; (d) K. Timmer and H. A. Meinema, *Inorg. Chim. Acta* 1991, **187**, 99; A. P. Purdy and C. F. George, *Inorg. Chem.* 1991, **30**, 1969; A. P. Purdy and C. F. George, *Inorg. Chem.* 1991, **30**, 2812.
6. J.-L. Aubagnac, L. Cot, N. Hovnanian and P. Miele, *Bull. Soc. Chim. Belg.* 1992, **101**, 689.
7. G. M. Sheldrick, SHELXS-86, Program for the Solution of Crystal Structures. University of Göttingen, Germany (1987).
8. M. C. Burla, M. Camalli, S. Cascaravo, C. Giacovazzo, G. Polidoni, R. Spagna and D. Viterbo, *J. Appl. Cryst.* 1989, **22**, 389.
9. G. M. Sheldrick, SHELX 76, Program for Crystal Structure Determination. University of Cambridge (1976).
10. S. R. Drake and D. J. Otway, *J. Chem. Soc., Chem. Commun.* 1991, 517.

Polyhedron Vol. 12, No. 3, pp. 273–278, 1993
Printed in Great Britain

0277-5387/93 $6.00+.00
© 1993 Pergamon Press Ltd

SYNTHESIS, STRUCTURE AND REDOX PROPERTIES OF (μ-OXO)BIS(μ-CARBOXYLATO)DIRUTHENIUM(III) COMPLEXES CONTAINING THREE DIFFERENT TERMINAL LIGANDS

ARIYANCHIRA SYAMALA and AKHIL R. CHAKRAVARTY*

Department of Inorganic and Physical Chemistry, Indian Institute of Science, Bangalore 560 012, India

(*Received* 10 *September* 1992; *accepted* 1 *October* 1992)

Abstract—Blue coloured, unstable, essentially diamagnetic and non-electrolytic diruthenium(III) complexes of the formulation $[Ru_2O(O_2CR)_4(en)_2(PPh_3)_2]$ were prepared by reacting $[Ru_2O(O_2CR)_4(PPh_3)_2]$ with 1,2-diaminoethane (en) in CH_2Cl_2 (R = C_6H_4-*p*-X; X = H, Me and OMe). The molecular structure of the complexes is proposed as $[\{(\eta^1\text{-}O_2CR)(\eta^1\text{-en})(PPh_3)Ru\}_2(\mu\text{-}O)(\mu\text{-}O_2CR)_2]$ based on the ^1H NMR spectral data. The electronic spectra of the complexes display a band near 569 nm with a shoulder at 630 nm. In CH_2Cl_2–0.1 M $[Bu^n{}_4N]ClO_4$, the complexes exhibit redox couples $Ru_2^{III,III}/Ru_2^{III,IV}$ and $Ru_2^{III,IV}/Ru_2^{IV,IV}$ near 0.1 and 1.2 V (vs SCE), respectively. The potentials are the lowest among diruthenium(III) complexes with a similar core structure.

The present work stems from our interest in studying the role played by the terminal ligands in stabilizing and altering the electronic structure of (μ-oxo)bis(μ-carboxylato)diruthenium(III) complexes. It is recognized[1] that the chemistry at terminal positions is important in the biological activity of oxo-bridged diiron proteins. Although diiron complexes have been extensively studied[2] in recent years, the reaction chemistry at the terminal sites of analogous diruthenium complexes is virtually unknown. For such an investigation diruthenium(III) complexes having substitutionally inert heterocyclic bases[3] or capping tridentate ligands[4–6] are not suitable as precursors.

The higher stability of the $[Ru_2(\mu\text{-}O)(\mu\text{-}O_2CR)_2{}^{2+}]$ core and the ready availability of a synthon like $[Ru_2O(O_2CR)_4(PPh_3)_2]$ (**1a–1c**)[7–9] (R = C_6H_4-*p*-X; X = H, **a**; OMe, **b**; Me, **c**) have prompted us to explore the reaction chemistry of this precursor at the labile carboxylato terminal sites of the core. We have chosen the σ-only and potentially bidentate N,N-donor 1,2-diaminoethane (en) to initiate our programme. We have been able to isolate an unstable complex of the formulation $[Ru_2O(O_2CR)_4(en)_2(PPh_3)_2]$ (R = C_6H_4-*p*-X; X = H, **2a**; OMe, **2b**; Me, **2c**) from a reaction of the precursor with en in CH_2Cl_2. The molecular structures of **2a–2c**, deduced from spectral studies, show the presence of three different unidentate terminal ligands. Such an observation is of interest in the chemistry of (μ-oxo)bis(μ-carboxylato) dimetal(III) complexes.[2–9] The electrochemical behaviour of **2a–2c** is also found to be unusual. Herein, we report the synthesis, structure, spectral and redox properties of **2a–2c**.

RESULTS AND DISCUSSION

Synthesis and stability of 2a–2c

The complexes were prepared in high yield by reacting $[Ru_2O(O_2CR)_4(PPh_3)_2]$ with 1,2-diaminoethane (en) in CH_2Cl_2 at 0°C under a dinitrogen atmosphere [eq. (1)]. Conductivity measurements in nitromethane show the non-conducting nature of **2a–2c**.

$$[Ru_2O(O_2CR)_4(PPh_3)_2] + en \longrightarrow [Ru_2O(O_2CR)_4(en)_2(PPh_3)_2] \quad (1)$$

The complexes are highly soluble in acetone, CH_2Cl_2, $CHCl_3$ and aromatic hydrocarbons, less soluble in MeOH and MeCN, and essentially insoluble in aliphatic hydrocarbons and H_2O. The com-

* Author to whom correspondence should be addressed.

plexes, which are moderately stable in the solid state at low temperature, are unstable in solution.

Spectral nature and the molecular structure

The electronic spectra of the complexes **2a–2c** in CH_2Cl_2 show a strong visible absorption at 569 nm and a weak shoulder at 630 nm. The peak is diagnostic of the presence of a (μ-oxo)bis(μ-carboxylato)diruthenium(III) core in these complexes. The origin of the band is believed to be charge-transfer in nature, involving the Ru^{III}–$d\pi$ and μ-oxo-$p\pi$ orbitals.[3,5]

In **1a–1c** the band is observed[7,8] at 562 nm. It is interesting that the ligation of the σ-only donor ligand en has caused a shift of the band to a lower energy. In a structurally similar complex, $[Ru_2O(O_2CR)_2(PPh_3)_2\{NH_2CH_2CH_2NHC(Me)NH\}_2]^{2+}$, the visible band is seen[10] at 565 nm. The electronic spectral results suggest a *cis*-ligation of the η^1-O_2CR ligand, which is isoelectronic with the amidine moiety. The *trans* effect of the μ-oxo ligand is expected to facilitate removal of the *trans* ligand in the precursor.

The molecular structure of the complexes was deduced from the ^1H NMR spectral data (Table 1). A representative spectrum is shown in Fig. 1. The presence of two types of carboxylato ligands in a 1:1 ratio is observed from the peak integrations of the methyl resonances. Further, a 1:2:1 ratio of en : RCO_2^- : PPh_3 is evident in the spectrum. Considering the non-electrolytic behaviour of **2a–2c** and the electronic spectral feature showing the presence of an $[Ru_2(\mu\text{-}O)(\mu\text{-}O_2CR)_2^{2+}]$ core, the molecular structure of **2a–2c** is proposed as $[\{(\eta^1\text{-}O_2CR)(\eta^1\text{-en})(PPh_3)Ru\}_2(\mu\text{-}O)(\mu\text{-}O_2CR)_2]$. The structure is believed to be stabilized by hydrogen-bond formation involving the η^1-en and η^1-O_2CR ligands as shown below.

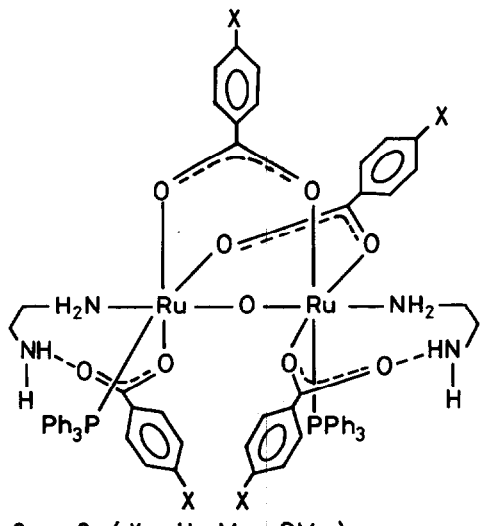

2a – 2c (X = H, Me, OMe)

Table 1. ^1H NMR spectral[a] and electrochemical[b] data for $[Ru_2O(O_2CR)_4(en)_2(PPh_3)_2]$ (**2a–2c**)

	2a (R = C_6H_5)	**2b** (R = C_6H_4-*p*-OMe)	**2c** (R = C_6H_4-*p*-Me)
^1H NMR : δ (ppm) [nH ; *J* (Hz)]			
Me(O_2CR)		3.78 s[6H], 3.84 s[6H]	2.38 s[6H], 2.42 s[6H]
CH_2[c]	2.40 br[2H], 5.46 br[2H]	2.24 br[2H], 4.75 br[2H]	2.41 br[2H], 4.36 br[2H]
NH_2[d]	12.67 br[2H], 13.52 br [2H]	11.64 br[2H], 13.01 br[2H]	12.57 br[2H], 13.52 br[2H]
CH_2,[c] NH_2,[d] R,[e] PPh_3[f]	6.00–8.78[58H][e-f]	6.68, 6.79, 7.73, 7.88 d[16H,9][e]	6.97, 7.10, 7.63, 7.84[16H,8][e]
		6.35–8.78[38H][e,d,f]	6.35–8.50[38H][e,d,f]
Redox data : [$E_{1/2}$ (V) (ΔE_p/mV)]			
$Ru_2^{III,III}/Ru_2^{III,IV}$	0.18(90)	0.12(80)	0.12(90)
$Ru_2^{III,IV}/Ru_2^{IV,IV}$	1.22(120)	1.19(130)	1.15(100)

[a] $CDCl_3$, Me_4Si as a standard ; s, singlet ; d, doublet ; br, broad.

[b] $E_{1/2} = 0.5$ V ($E_{pa} + E_{pc}$) ; $\Delta E_p = E_{pa} - E_{pc}$; E_{pa} and E_{pc} are the anodic and cathodic peak potentials, respectively. All potentials are referred to SCE, a platinum button was used as the working electrode. CH_2Cl_2–0.1 M $[NBu^n_4]ClO_4$, scan rate = 20 mV s^{-1}.

[c] CH_2 protons of en. [d] Amino protons of en. [e] Aryl group protons of the carboxylate. [f] PPh_3 protons.

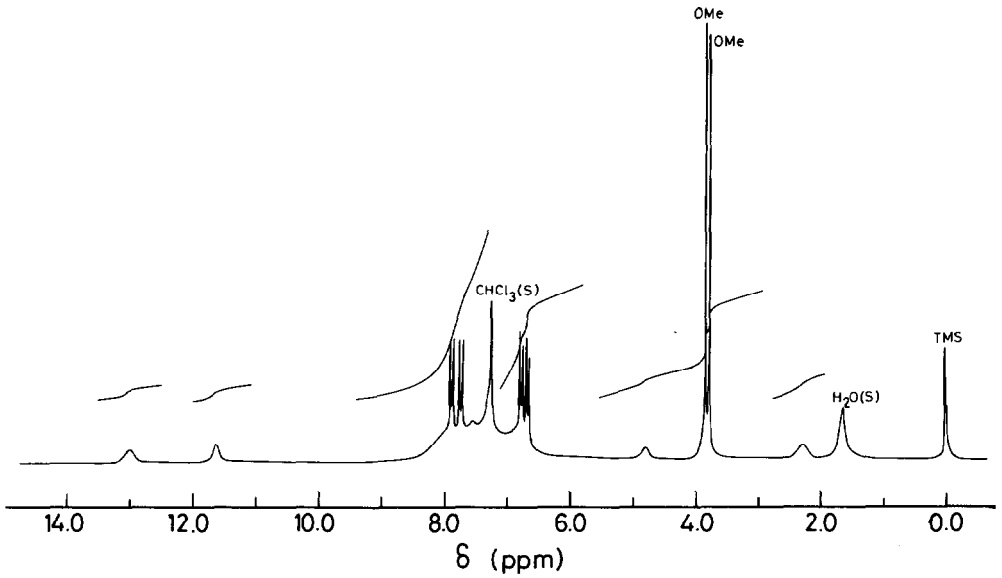

Fig. 1. ^1H NMR spectrum of $[Ru_2O(O_2CC_6H_4\text{-}p\text{-}OMe)_4(en)_2(PPh_3)_2]$ (**2b**) in $CDCl_3$ (S: solvent peak).

The complexes display two broad peaks in the ranges δ 11.6–12.6 and δ 13.0–13.5. Each signal corresponds to a single proton. On D_2O exchange, these two peaks disappear and a new peak is observed within δ 12.1–12.9. This peak, however, disappears completely after 10 h. The singlets are assignable to an amino group involved in the hydrogen bond formation. The amino protons *trans* to the μ-oxo ligand, appearing in the aromatic region at δ 7.6, also undergo exchange with D_2O.

The *trans* ligation of the η^1-en ligand in **2a–2c** could be rationalized from the X-ray structure of **1b**, which shows a longer Ru—O(*trans*) bond length than Ru—O(*cis*).[8] Sasaki *et al.*[3] have shown that in $[Ru_2O(O_2CMe)_2(py)_6]^{2+}$ a regioselective *trans*-pyridine exchange with py-d_5 in CD_3CN takes place exclusively without any exchange at the *cis* ligand. This suggests a selective chelate ring opening in **1a–1c** by η^1-en at the *trans* terminal position in preference to the *cis* site following a dissociative pathway.[3] However, the presence of two potentially bidentate O_2CR and en ligands in a unidentate fashion makes the complex unstable. In polar solvents the complex is unstable and converts to a purple diamagnetic complex, which is isolated as a perchlorate salt and characterized as $[Ru_2O(O_2CR)_2(en)_2(PPh_3)_2](ClO_4)_2$.[11] In non-polar solvents the formation of a mixture of products containing paramagnetic species is observed.

Redox properties

The electrochemical behaviour of **2a–2c** was studied to investigate the effect of terminal ligands on the stability and the electronic structure of the core. The cyclic voltammograms of **2c** are shown in Fig. 2. and the relevant data are presented in Table 1.

Diruthenium(III,III)–*diruthenium*(III,IV) *couple*

The complexes display a one-electron redox process occurring near 0.1 V (vs SCE) in CH_2Cl_2–0.1 M $[NBu^n_4]ClO_4$. A controlled potential electrolysis performed at a potential 200 mV higher than the anodic peak potential (E_{pa}) and 200 mV lower than the cathodic peak potential (E_{pc}) showed that the redox process occurring at 0.1 V is a one-electron oxidation [eq. (2)]. The peak-to-peak separation (ΔE_p) of > 58 mV and an i_{pa}/i_{pc} ratio of 1.0 at various scan rates (20–200 mV s^{-1}) indicate the quasi-reversible nature of the electron transfer (i_{pa} and i_{pc} are anodic and cathodic peak currents, respectively).

$$\{Ru_2^{III,IV}(\mu\text{-}O)(\mu\text{-}O_2CR)_2{}^{3+}\} \underset{-e^-}{\overset{+e^-}{\rightleftharpoons}} \{Ru_2^{III,III}(\mu\text{-}O)(\mu\text{-}O_2CR)_2{}^{2+}\} \quad (2)$$

The potentials of the $Ru_2^{III,III}/Ru_2^{III,IV}$ couple in **2a–2c** are the lowest among the known[3–10] diruthenium(III) complexes with an analogous core structure. Such a low potential accounts for the instability of the complexes in solution as well as in the solid phase. The unusual feature is that the facile oxidation takes place even in the presence of a π-acceptor ligand like PPh_3. The observed potential is significantly lower than that reported[4] in an anal-

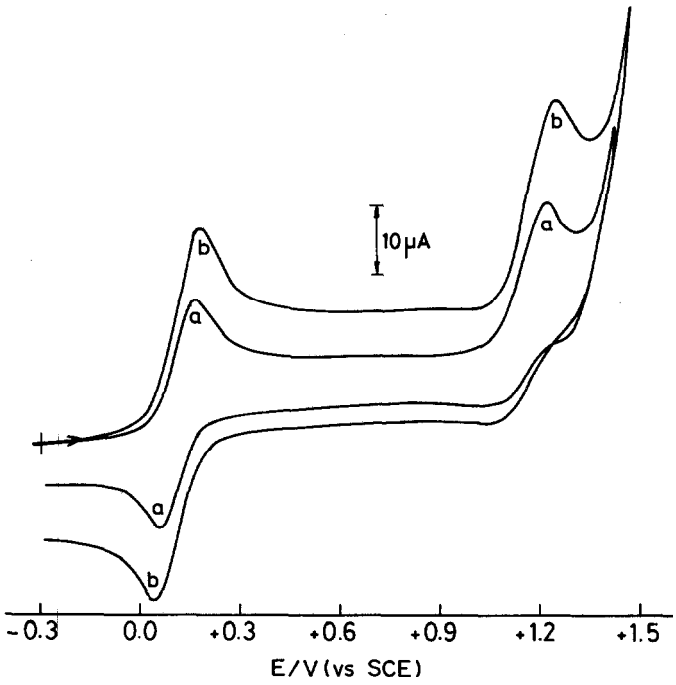

Fig. 2. Cyclic voltammograms of $[Ru_2O(O_2CC_6H_4\text{-}p\text{-}Me)_4(en)_2(PPh_3)_2]$ (**2c**) in CH_2Cl_2 containing 0.1 M $[NBu^n_4](ClO_4)$. Scan rates: (a) 20 and (b) 50 mV s^{-1}.

ogous complex containing a σ-only donor tridentate triazacyclononane capping ligand. A general trend, observed so far in the diruthenium(III) complexes, shows that a π-acceptor terminal ligand stabilizes the +2 and +3 oxidation states of ruthenium and the complex displays a low-energy visible band in the electronic spectrum. From the visible spectral and electrochemical data on several $[Ru_2(\mu\text{-}O)(\mu\text{-}O_2CR)_2]^{2+}$ complexes, given in Table 2, it is evident that complexes **2a**–**2c** stand as an exception to the general trend. The paucity of the experimental data, however, precludes us from drawing any definite conclusion on the unusual behaviour of **2a**–**2c**.

Diruthenium(III,IV)–*diruthenium*(IV,IV) *couple*

This couple is observed as an oxidation wave near 1.2 V with a broad and relatively ill-defined cathodic response showing diminished peak current. The one-electron stoichiometry of the redox process is

Table 2. A comparison of the redox data on the $Ru_2^{III,III}/Ru_2^{III,IV}$ couple and the low-energy visible band in (μ-oxo)bis(μ-carboxylato)diruthenium(III) complexes

Complex	$E_{1/2}$ (V)	λ_{max} (nm)	Ref.
$[Ru_2O(O_2CPh)_2(L)_2(PF_6)_2]^a$	0.69[b]	549	4
$[Ru_2O(O_2CMe)_2(py)_6(PF_6)_2]$	0.60[c]	581	3
$[Ru_2O(O_2CMe)_2(bpy)_2(py)_2(PF_6)_2]$	0.56[c]	599	3
$[Ru_2O(O_2CMe)_2(L')_2(ClO_4)_2]^d$	0.85[e]	564	6
$[Ru_2O(O_2CMe)_2(tpm)_2(PF_6)_2]^f$	1.07[e]	576	5
$[Ru_2O(O_2CC_6H_5)_4(en)_2(PPh_3)_2]$	0.18[e]	569	This work
$[Ru_2O(O_2CC_6H_4\text{-}p\text{-}OMe)_2(PPh_3)_2(L'')_2(ClO_4)_2]^g$	0.91[e]	565	10

[a] L = 1,4,7-trimethyl-1,4,7-triazacyclononane.
[b] Ref. to n.h.e.
[c] Ref. to Ag–AgCl.
[d] L′ = (2-pyridylethyl)(2-pyridylmethyl)methylamine.
[e] Ref. to SCE.
[f] tpm = trispyrazolylmethane.
[g] L″ = $NH_2CH_2CH_2NHC(Me)NH$.

determined from the i_{pa} values of this response with that of the $Ru_2^{III,III}/Ru_2^{III,IV}$ couple [eq. (3)].

$$[Ru_2^{IV,IV}(\mu\text{-O})(\mu\text{-}O_2CR)_2{}^{4+}] \underset{-e^-}{\overset{+e^-}{\rightleftharpoons}} [Ru_2^{IV,III}(\mu\text{-O})(\mu\text{-}O_2CR)_2{}^{3+}] \quad (3)$$

The i_{pc}/i_{pa} ratio of < 1.0 indicates a slow $Ru_2^{IV,IV} \rightarrow Ru_2^{IV,III}$ electron-transfer process. Prior to this work, there are only two reports[3,6] of observing this couple at a much higher potential in related diruthenium(III) complexes.

CONCLUSIONS

This work presents new diruthenium(III) complexes having three different terminal ligands of varied σ-donor and π-acceptor abilities. This gives us an opportunity to study the influence of the *trans*- and *cis*-oxo ligands on the spectral and redox properties of the $[Ru_2(\mu\text{-O})(\mu\text{-}O_2CR)_2{}^{2+}]$ core. The observation of a $Ru_2^{III,III}/Ru_2^{III,IV}$ couple at a near zero potential in **2a–2c** is of significance. Finally, the present study has shown that using suitable precursors having labile terminal sites, the chemistry of the $[Ru_2(\mu\text{-O})(\mu\text{-}O_2CR)_2{}^{2+}]$ complexes can be developed by selective incorporation of σ-donor as well as π-acceptor ligands at the terminal positions to tune the electronic structure of the core.

EXPERIMENTAL

Materials

Precursor complexes $[Ru_2Cl(O_2CMe)_4]$,[7] $[Ru_2Cl(O_2CR)_4]$[12] and $[Ru_2O(O_2CR)_4(PPh_3)_2]$[8] (**1**) (R = C_6H_4-*p*-X; H, **a**; OMe, **b**; Me, **c**) were prepared by published methods.

Preparation of $[Ru_2O(O_2CR)_4(en)_2(PPh_3)_2]$ (R = C_6H_4-*p*-X: X = H, **2a**; OMe, **2b**; Me, **2c**)

The complexes were prepared by following a general procedure. A representative one is given below.

A sample of **1b** (68 mg, 0.05 mmol) in CH_2Cl_2 (5 cm^3) was reacted with 0.3 M en solution (0.42 cm^3, 0.11 mmol) in CH_2Cl_2. The mixture was stirred for 1 h at 0°C under dinitrogen. Immediately after the addition of en, the colour of the purple reaction mixture changed to blue. A blue solid of **2b** was precipitated by adding petroleum ether (b.p. 60–80°C) to the reaction mixture. The product was filtered off, washed with a CH_2Cl_2–petroleum ether (1:20 v/v) mixture and dried over P_4O_{10} *in vacuo*. Yield: 45 mg (*ca* 65%). Found: C, 58.4; H, 5.2; N, 3.7. Calc. for $C_{72}H_{74}N_4O_{13}P_2Ru_2$: C, 58.9; H, 5.1; N, 3.8%. Λ_M (nitromethane, 25°C) = 15 Ω^{-1} cm^2 mol^{-1}. Electronic spectral data in CH_2Cl_2 at 25°C [λ_{max} (nm) (ε/M^{-1} cm^{-1})]: 630(sh), 569(12,200), 359(sh), 339(12,900), 289(sh). Complex **2a**: yield: *ca* 60%. Found: C, 60.2; H, 5.0; N, 4.3. Calc. for $C_{68}H_{66}N_4O_9P_2Ru_2$: C, 60.6; H, 4.9; N, 4.2%. Λ_M (nitromethane, 25°C) = 18 Ω^{-1} cm^2 mol^{-1}. Electronic spectral data [λ_{max} (nm) (ε/M^{-1} cm^{-1})] in CH_2Cl_2 at 25°C: 630(sh), 569(9700), 359(11,200), 333(sh), 296(sh). Complex **2c**: yield, *ca* 60%. Found: C, 61.2; H, 5.4; N, 3.9. Calc. for $C_{72}H_{74}N_4O_9P_2Ru_2$: C, 61.6; H, 5.3; N, 4.0%. Λ_M (nitromethane, 25°C) = 15 Ω^{-1} cm^2 mol^{-1}. Electronic spectral data [λ_{max} (nm) (ε/M^{-1} cm^{-1})] in CH_2Cl_2 at 25°C: 569(9400), 359(9600), 325(sh), 296(10,000). The complexes **2a–2c** are unstable in the solution phase and attempts to isolate single crystals suitable for X-ray diffraction studies were unsuccessful.

Physical measurements

The elemental analyses were made with a Heraeus CHN-O Rapid instrument. Electronic spectra were obtained from a Hitachi U-3400 spectrophotometer. The ^1H NMR spectra were recorded on Bruker WH-270 and AC(AF)200 MHz spectrometers. Conductivity measurements were performed on a Century CC603 digital conductivity meter. Cyclic voltammetric measurements were done using a three-electrode set-up on PAR model 174A polarographic analyser connected with a Houston Instruments Omnigraphic *X–Y* recorder. A platinum button, a platinum wire and a saturated calomel electrode (SCE) were used as working, auxiliary and reference electrodes, respectively. The measurements were performed at 25°C in CH_2Cl_2 containing 0.1 M $[NBu^n_4]ClO_4$ as a supporting electrolyte. The data reported are uncorrected for junction potentials. Ferrocene, $(\eta^5\text{-Cp})_2Fe$, was used as a standard to verify the potentials observed against the SCE and to obtain the electron-transfer stoichiometries of the redox couples by peak current measurements. The Fe^{II}/Fe^{III} couple of ferrocene was observed at 0.50 V (vs SCE) under similar experimental conditions in CH_2Cl_2–0.1 M $[Bu^n_4N]ClO_4$.

Acknowledgement—We thank the Department of Science and Technology, Government of India, for financial support.

REFERENCES

1. J. Sanders-Loehr, *Iron Carriers and Iron Proteins*, T. M. Loehr (Editor), p. 373. VCH Publishers, New York (1989).

2. (a) S. J. Lippard, *Angew. Chem., Int. Edn Engl.* 1988, **27**, 344; (b) D. M. Kurtz Jr, *Chem. Rev.* 1990, **90**, 585; (c) L. Que Jr and A. E. True, *Prog. Inorg. Chem.* 1990, **38**, 97.
3. Y. Sasaki, M. Suzuki, A. Nagasawa, A. Tokiwa, M. Ebihara, T. Yamaguchi, C. Kabuto, T. Ochi and T. Ito, *Inorg. Chem.* 1991, **30**, 4903.
4. P. Neubold, K. Wieghardt, B. Nuber and J. Weiss, *Inorg. Chem.* 1989, **28**, 459.
5. A. Llobet, M. E. Curry, H. T. Evans and T. J. Meyer, *Inorg. Chem.* 1989, **28**, 3131.
6. N. Gupta, S. Mukerjee, S. Mahapatra, M. Roy and R. N. Mukherjee, *Inorg. Chem.* 1992, **31**, 139.
7. R. W. Mitchell, A. Spencer and G. Wilkinson, *J. Chem. Soc., Dalton Trans.* 1973, 846.
8. B. K. Das and A. R. Chakravarty, *Inorg. Chem.* 1990, **29**, 2078.
9. M. C. Barral, R. Jamenez-Aparicio, E. C. Royer, F. A. Urbanos, A. Monge and C. Ruiz-Valero, *Polyhedron* 1991, **10**, 113.
10. A. Syamala and A. R. Chakravarty, *Inorg. Chem.* 1991, **30**, 4699.
11. A. Syamala and A. R. Chakravarty, unpublished work.
12. B. K. Das and A. R. Chakravarty, *Polyhedron* 1988, **7**, 685.

Polyhedron Vol. 12, No. 3, pp. 279–284, 1993
Printed in Great Britain

0277–5387/93 $6.00+.00
© 1993 Pergamon Press Ltd

POSSIBLE STRUCTURE OF PARATHIOCYANOGEN—II. ELECTROCHEMICAL SYNTHESIS, ^{13}C NMR AND CONDUCTIVITY MEASUREMENTS ON UNDOPED AND IODINE DOPED SAMPLES

FRANCO CATALDO*

PROGEGA s.n.c., Via Mario Mencatelli 14, Rome 00128, Italy

and

PAOLO FIORDIPONTI

Area della Ricerca del CNR, Monterotondo Stazione, Rome 00100, Italy

(*Received* 10 *September* 1992; *accepted* 1 *October* 1992)

Abstract—Parathiocyanogen or polythiocyanogen $(SCN)_x$ has been synthesized by the anodic oxidation of NaSCN solutions in methanol. The structure of parathiocyanogen $(SCN)_x$ has been studied by means of elemental analysis, IR, UV, ^{13}C NMR and ESR spectroscopy and also by comparison with a triazine-based model compound. All data collected clearly show that parathiocyanogen is structurally different from the triazine-based structure. On the basis of the data collected, the most probable structure should be a linear one, very similar to the one accepted for polysulphur nitride. Upon doping with iodine vapour the specific conductivity of parathiocyanogen increases by several orders of magnitude, as expected from a semi-conductive polymer.

A chemical route for the synthesis of parathiocyanogen $(SCN)_x$ was recently reported,[1] and its possible structure based on its IR and UV spectra was discussed. It was pointed out that $(SCN)_x$ should not have a 1,3,5-triazine structure as had been believed in the past, but it should have a linear structure very similar to that accepted for polysulphur nitride $(SN)_x$.[1]

In this work an electrochemical route in organic solvent is reported for the synthesis of parathiocyanogen, and it is shown that "electrochemical" $(SCN)_x$ has the same structure as "chemical" $(SCN)_x$. Moreover, we report a ^{13}C NMR and ESR study on parathiocyanogen versus a triazine-based model compound, as well as conductivity measurements on compressed pellets of undoped and iodine doped $(SCN)_x$.

* Author to whom correspondence should be addressed.

EXPERIMENTAL

Physical and analytical measurements

^{13}C NMR spectra were measured in N,N-dimethylformamide solutions of each sample using a Bruker AC 200 spectrometer operating at 50.33 MHz, with $\langle^1H\rangle$ Waltz decoupling or without any decoupling. No differences have been noted between decoupled and undecoupled spectra. Spectral conditions are: size = 64 K, time domain 64 K; pulse width 60°, corresponding to 5 μs acquisition time, 2.75 s; sweep width 12,000 Hz and at least 12,000 scans. Chemical shifts are given in ppm from TMS, but were actually measured from the carbonyl of DMF.

The IR and UV spectra and elemental analyses were carried out as previously described.[1] ESR spectra were kindly obtained on solid samples at room temperature by Dr Luciano Montanari; the EPR spectrometer was a Varian E-3.

Electrochemical synthesis of parathiocyanogen

NaSCN (60.5 g) was dissolved in anhydrous methanol (270 cm^3) and the solution was electrolysed between two platinum electrodes under nitrogen, in a H-shaped cell at 45°C. The anodic compartment of the H-shaped cell was divided from the cathodic compartment by a G3 fritted glass septum. The syntheses were performed at 24 V with a current density at the platinum anode of *ca* 0.040 A cm^{-2}. During the electrolysis the cell was put into an ultrasonic cleaning bath and sonicated. The cavitation due to ultrasound stirred the solution and prevented the growth of a thick film on the anode surface, which could cause a drop in the passage of the current. After the first 10 min of electrolysis a brick-red–orange precipitate appeared. After 22,900 C (0.24 F) had passed through the cell the electrolysis was stopped. Parathiocyanogen was collected by filtration of the anodic solution. The polymer appeared as a very fine powder due to the mechanical effects of ultrasound; it was extracted in a Soxhlet apparatus with acetone for 20 h and then dried *in vacuo* for several days. The yield was 6.8 g (100% current yield). Found: C, 18.6; H, 0.73; N, 21.2; S, 53.3. Calc. for $(SCN)_x$: C, 20.7; N, 24.1; S, 55.2%. Similar results can be obtained by working in glacial acetic acid instead of methanol as the solvent. As a reference, chemically prepared parathiocyanogen was obtained, as described in part I of this work.[1]

Preparation of triazine-based model compound

This synthesis was accomplished by the nucleophilic substitution of chlorine with 2,4,6-trichloro-1,3,5-triazine and sodium disulphide as described previously.[1] Found: C, 12.0; H, 1.0; N, 15.3; S, 64.3. Calc. for $C_3N_3S_6H_2Na$ (model compound): C, 12.2; H, 0.68; N, 14.2; S, 65.1; Na, 7.8%. The IR spectrum has been reported previously.[1]

Doping of parathiocyanogen with iodine

A weighed sample of parathiocyanogen, prepared by electrochemical methods, was placed into a flask and left to absorb under reduced pressure, at 25°C, the iodine vapours escaping from the solid iodine present in the same flask from a separate vessel. After 4 days of treatment the polymer sample became black with the iodine absorbed, calculated from the total weight of the doped sample, being *ca* 30%; the conductivity of a compressed pellet of the sample was 2.0×10^{-6} S cm^{-1}. After 7 days in the same conditions the iodine content of the total weight of the doped sample was about 63%, and the conductivity of a compressed pellet was measured to be 1.2×10^{-4} S cm^{-1}. Undoped compressed pellets of parathiocyanogen showed a conductivity of 6.8×10^{-10} S cm^{-1}. A sample of parathiocyanogen doped with bromine vapours for 7 days in the same way as was used for iodine doping gave a conductivity of 1.3×10^{-7} S cm^{-1}. All the above-mentioned samples showed an ohmic response in the range 3.0–30 V. All conductivity measurements were performed using DC and the two-probe method, in air.

RESULTS AND DISCUSSION

The anodic oxidation of potassium thiocyanate in methanol at low temperatures has been described by early investigators[2] to yield a solution of thiocyanogen $(SCN)_2$. By heating the methanolic thiocyanogen solution at room temperature parathiocyanogen polymerizes into a brick-red amorphous material. We have optimized a procedure for the anodic oxidation of thiocyanates in methanol or glacial acetic acid at higher temperatures (45°C), to obtain parathiocyanogen directly without having to pass through thiocyanogen, assuming that the direct formation of parathiocyanogen by anodic oxidation occurs as shown in eqs (1) and (2).

$$x\mathrm{SCN}^- \rightarrow x\mathrm{SCN}^{\cdot} + xe \quad (1)$$

$$x\mathrm{SCN}^{\cdot} \rightarrow (\mathrm{SCN})_x \quad (2)$$

During electrolysis, in order to avoid direct film formation of the polymer on the electrode surface which could cause a drop in current and low yields, the cell was sonicated with ultrasound. Cavitation due to ultrasound detaches the polymer from the anode and allows current flow, even when large amounts of polymer had been obtained. There is also the possibility of obtaining thin films of the polymer on a platinum leaf used as the electrode (w/o ultrasound).

Elemental analyses performed on electrochemically prepared $(SCN)_x$ show the stoichiometric ratios C/N and C/S always close to 1.0. In order to obtain an acceptable elemental analysis it is necessary to use a H-shaped cell with a cathode compartment separated from the anode compartment by a fritted glass septum and also to stop electrolysis at relatively low conversions, as shown in the Experimental.

The IR spectra of parathiocyanogen obtained through the two different routes are presented in Fig. 1. They can be completely overlapped and clearly show the same structure. Moreover, these spectra are in agreement with the IR spectrum of

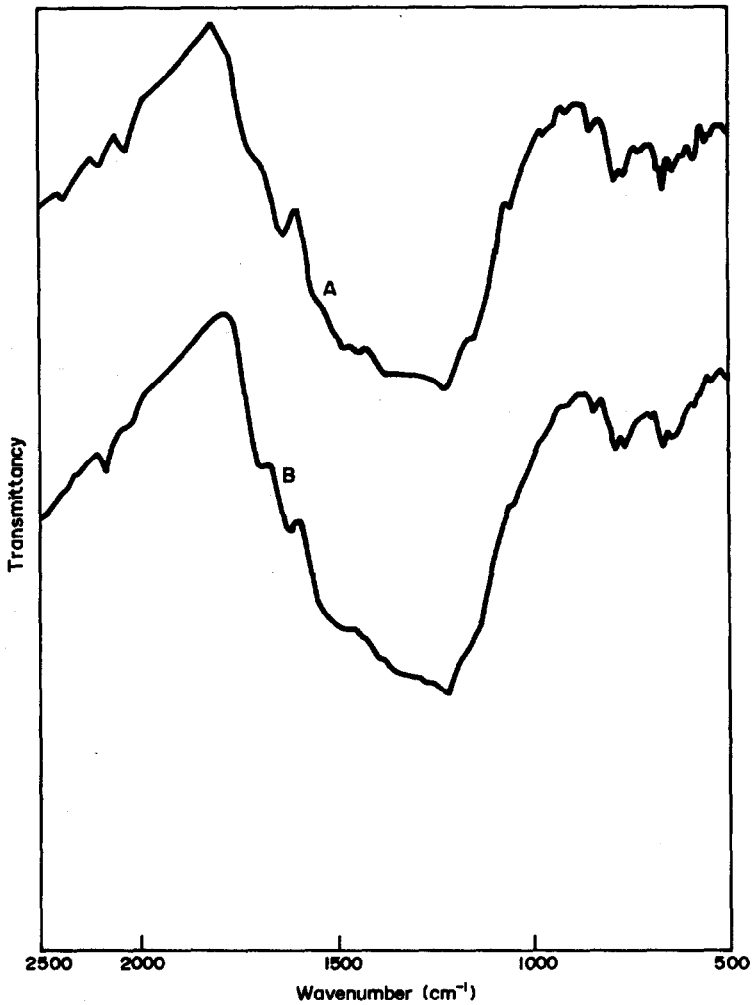

Fig. 1. IR spectra in KBr pellets of: (A) $(SCN)_x$ prepared electrochemically and (B) $(SCN)_x$ prepared chemically.

parathiocyanogen obtained from the anodic oxidation of molten thiocyanate salts, recorded by Pucciarelli *et al.*[3] A detailed discussion of the IR spectrum of $(SCN)_x$ in relation to its possible linear structure and in comparison to a triazine-based model compound can be found in the previous report.[1]

The ^{13}C NMR spectrum of a triazine-based model compound shows a neat narrow signal at 145.0 ppm, clearly due to sp^2 hybridized carbons of the triazine rings (Fig. 2). The ^{13}C NMR spectra of parathiocyanogen samples (Fig. 3) prepared through different routes (electrochemical or chemical) show only a very weak signal at 143.9 ppm. It is different both in chemical shift and mainly in intensity from the spectrum of the triazine-based model compound. No other signals were recorded from parathiocyanogen; these differences in its ^{13}C NMR spectrum compared with that of the triazine-based model compound are adduced as further proof to support the idea that parathiocyanogen has its own peculiar structure different from the triazine structure.

It should be noted that the ^{13}C NMR signal of carbon of an isothiocyanate —N=C=S group is expected in the range 120–140 ppm,[4] while potassium thiocyanate has a signal at 134.3 ppm. This means that in the parathiocyanogen ^{13}C NMR spectrum there is no trace of free thiocyanate ions. Also, the isothiocyanate groups, if present as the end groups of the linear structure proposed for parathiocyanogen, are practically not detectable.

Further evidence indicating that parathiocyanogen has a peculiar structure is shown in the UV spectra measured in N,N-dimethylformamide, shown in Fig. 4, in comparison with that of the triazine-based model compound and with a solution of NaSCN in the same solvent. Parathiocyanogen shows a maximum at 268 nm followed by a weak shoulder at *ca* 300 nm and

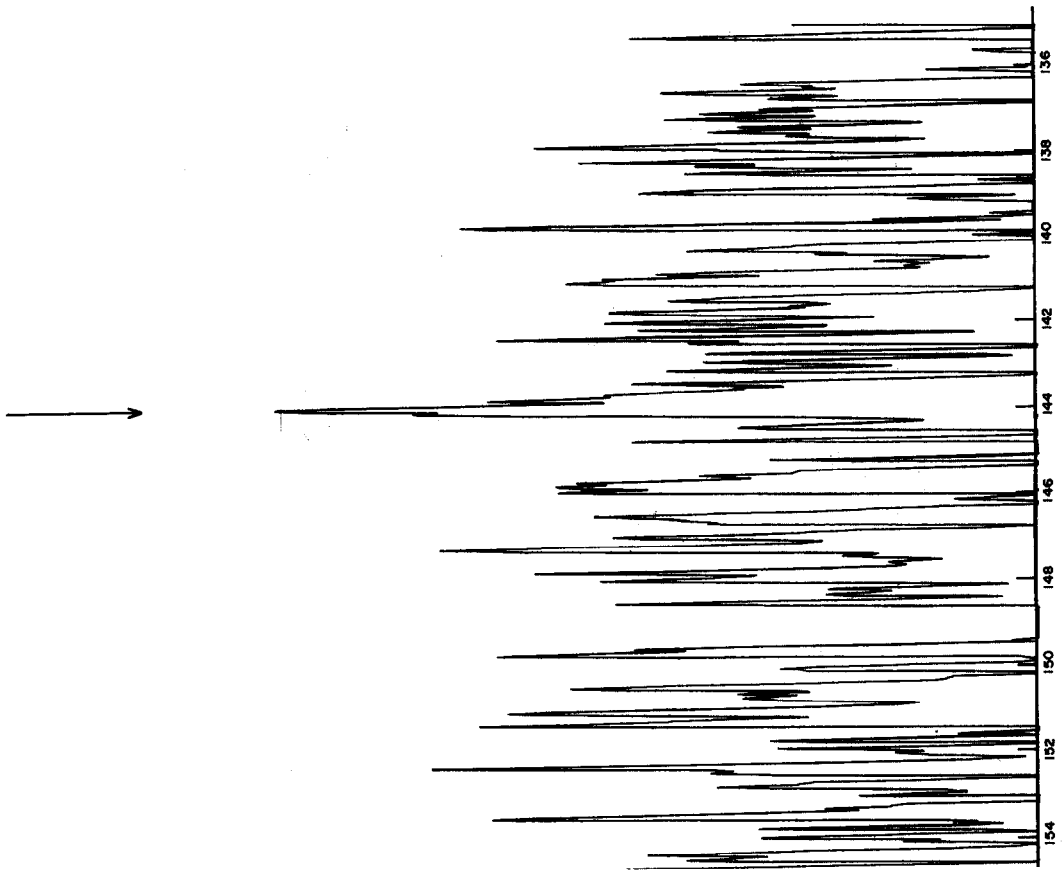

Fig. 3. C NMR spectra on $(SCN)_x$ prepared electrochemically.

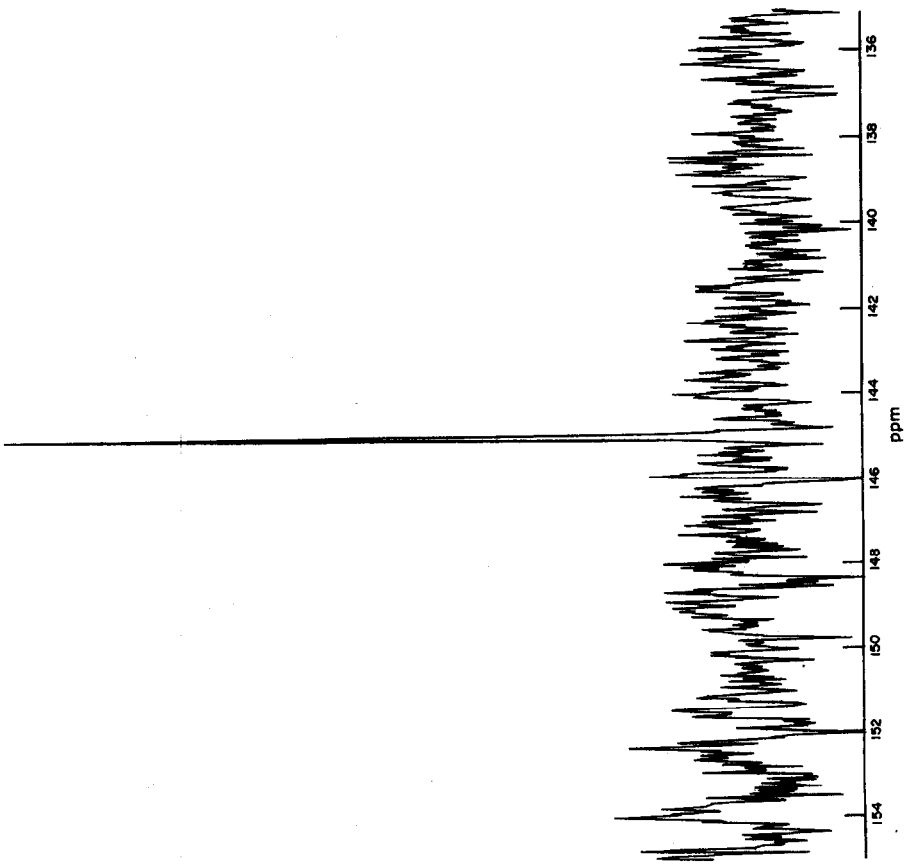

Fig. 2. C NMR spectra of the triazine-based model compound.

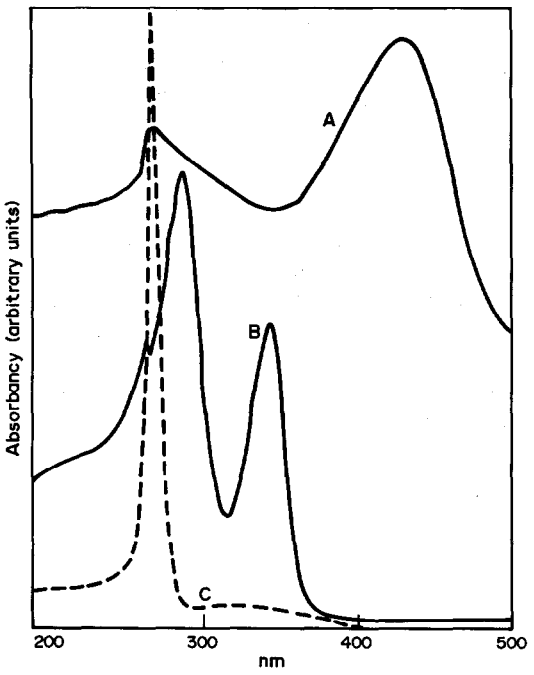

Fig. 4. Electronic spectra in N,N-dimethylformamide: (A) $(SCN)_x$ prepared electrochemically, (B) model compound containing a 1,3,5-triazine ring and (C) (dotted) NaSCN solution.

another maximum at 441 nm. However, the thiocyanate ion in the same solvent shows only a narrow absorption at 266 nm. Therefore, the new strong maximum shown by parathiocyanogen at 441 nm could account for conjugation along the polymeric chain, in agreement with the proposed linear structure.

The ESR spectrum was measured at room temperature, only for qualitative purposes, on the solid undoped sample of electrochemically-prepared parathiocyanogen for comparison with a solid sample of the triazine compound (Fig. 5). Parathiocyanogen showed a signal indicating the presence of a large number of unpaired spins. On the other hand, the ESR spectrum of the triazine model compound did not show any signal.

It is well known that conjugated polymers like polyacetylene or paracyanogen $(CN)_x$ have a very large number of unpaired spins due to the presence of defective structures along the polymeric chain.[5] Therefore, we should postulate the presence of unpaired electrons also in the case of parathiocyanogen, with the proposed linear structure. Unpaired electrons have not been detected in the compound having a triazine ring in its structure. We have measured a specific conductivity of 6.8×10^{-10} S cm^{-1} on compressed undoped pellets of electrochemically prepared parathiocyanogen.

Doping with iodine or bromine increases the specific conductivity of parathiocyanogen (see Experimental), as happens with other known conductive polymers. There should be an interaction between dopant and polymeric chain analogous to that between iodine or bromine and polysulphurnitride or polyacetylene chains, possibly with the formation of I^-, I_3^- and I_5^- or Br_3^-.[6] The maximum conductivity achieved with iodine doped samples of parathiocyanogen is somewhat lower

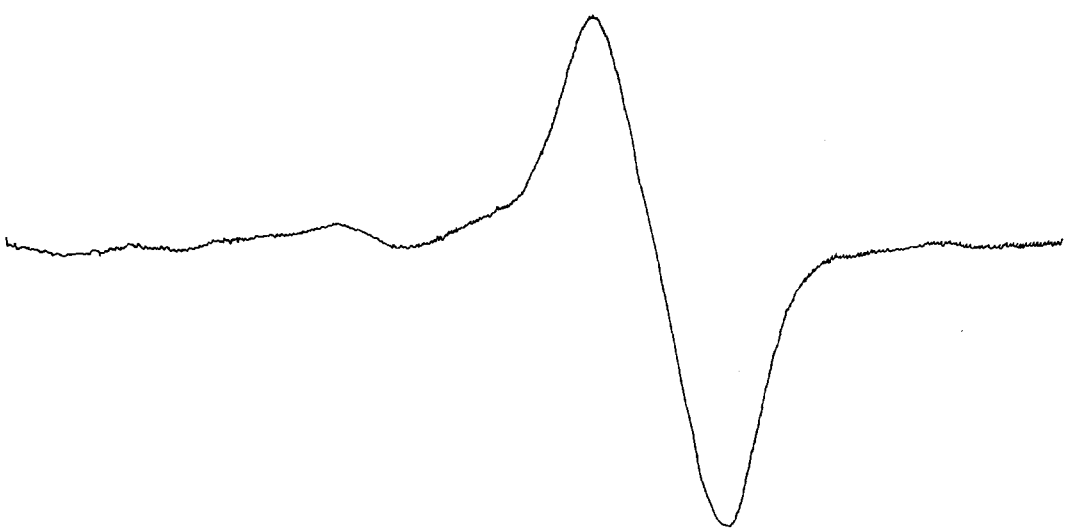

Fig. 5. Solid-state ESR spectrum of $(SCN)_x$ prepared electrochemically. The triazine model compound does not show a signal (practically).

than that reported for doped polysulphurnitride or polyacetylene samples.[6] It may be that the insertion of a carbon atom between sulphur and nitrogen lowers the delocalization of electrons along the polymeric chain. Hence, parathiocyanogen is only a high resistive semi-conductor while polysulphurnitride has quasi-metallic behaviour.

Acknowledgements—We thank Dr A. Segre of the "Istituto di Strutturistica Chimica L. Giacomello", Monterotondo (Rome), for ^{13}C NMR spectra and helpful discussion, Dr L. Montanari for ESR spectra and Prof. Nuti for the elemental analyses.

REFERENCES

1. F. Cataldo, *Polyhedron* 1992, **11**, 79.
2. H. Kerstein and R. Hoffmann, *Chem. Ber.* 1924, **57**, 491.
3. F. Pucciarelli, P. Cescon and H. Heyrowsky, *J. Electrochem. Soc.* 1979, **126**, 972.
4. G. C. Levy, R. L. Lichter and G. L. Nelson, *Carbon-13 Nuclear Magnetic Resonance for Organic Chemists*, p. 133. John Wiley, New York (1980).
5. Ya. M. Paushkin, T. P. Vishnyakova, A. F. Lunin and S. A. Nizova, *Organic Polymeric Semiconductors*. John Wiley, New York (1974).
6. M. M. Labes, P. Love and L. F. Nichols, *Chem. Rev.* 1979, **79**, 1.

Polyhedron Vol. 12, No. 3, pp. 285–289, 1993
Printed in Great Britain

0277–5387/93 $6.00+.00
© 1993 Pergamon Press Ltd

SYNTHESIS OF SOME NOVEL PENTA-COORDINATED COMPLEXES OF RUTHENIUM(II) CONTAINING AROMATIC ALDEHYDE AND OTHER MONODENTATE LIGANDS AND CATALYTIC OXIDATION OF TRIPHENYLPHOSPHINE USING SOME OF THEM

BIPUL C. PAUL, K. P. SARMA* and RAJ K. PODDAR†

Department of Chemistry, North-Eastern Hill University, Bijni Complex, Shillong 793003, India

(*Received* 31 *July* 1992; *accepted* 1 *October* 1992)

Abstract—The synthesis and characterization of some penta-coordinated ruthenium(II) complexes, viz. $[RuX_2(MPh_3)(C_4H_3OCHO)_2]$ (X = Cl or Br; M = P or As), $[RuBr_2(MPh_3)(C_6H_5CHO)_2]$ (M = P or As) and $[RuBr_2(CO)(PPh_3)_2]$, are described. The compounds were characterized using analytical data and various physical methods. $[RuBr_2(PPh_3)L_2]$ (L = C_4H_3OCHO or C_6H_5CHO) complexes catalysed the oxidation of PPh_3 by molecular oxygen.

Reports on the studies of ruthenium(II) and ruthenium(III) with weak donor ligands, such as dimethylsulphoxide, acetonitrile, benzaldehyde and other aldehydes, are more scarce compared to other donor ligands.[1–8] Complexes of ruthenium(II) containing weak donor ligands, or having both strong and weak donor ligands, have a strong potential to act as catalysts in various homogeneous reactions.[1]

Most of the complexes reported with weak donor ligands[1–8] have six coordination around the metal ion. Penta-coordinated complexes of ruthenium(II) and ruthenium(III) have a strong potential to act as catalysts in various homogeneous reactions.[9] Some of the complexes containing bromide and monodentate ligands, such as triphenylphosphine or dimethylsulphoxide, were found to be better catalysts than their corresponding chloro analogues.[10–12] Considering the above, we report here the synthesis and characterization of some of the penta-coordinated complexes of ruthenium(II) containing chloride or bromide, triphenylphosphine or triphenylarsine and benzaldehyde or furfural, and explore the catalytic activity of some of these complexes towards oxidation of triphenylphosphine to triphenylphosphine oxide by molecular oxygen.

* Present address: Assam Engineering College, Guwahati.

† Author to whom correspondence should be addressed.

EXPERIMENTAL

All the solvents were freshly distilled before use. $RuCl_3 \cdot 3H_2O$ was obtained from Arora–Matthey Ltd, Calcutta. The analyses for the chlorides and bromides were carried out by standard methods[13] after decomposition with a KOH and KNO_3 mixture. Carbon and hydrogen analyses were obtained from the Microanalytical section of the Department of Chemistry, NEHU, Shillong. The analytical data are presented in Table 1. IR spectra were recorded on a Perkin–Elmer 983 spectrometer in the 4000–200 cm^{-1} range. ^1H NMR spectra were recorded on a Varian EM-390, 90 MHz spectrometer, in $CDCl_3$. Electronic absorption spectra were recorded in solution on a Hitachi-330 spectrophotometer in the 1000–250 nm range. The results are given in Table 2. Magnetic susceptibilities were measured on an EG & G PARC Vibrating Sample Magnetometer at room temperature. Conductivity measurements were made on a Wayne Kerr, Automatic Precision Bridge B905 conductivity meter with millimolar solutions in acetonitrile.

Preparations

$[RuCl_2(MPh_3)(C_4H_3OCHO)_2]$ (M = P *or* As). To a solution of ruthenium trichloride trihydrate (0.1 g) in ethanol (10 cm^3) was added furfural (1

Table 1. Physical and analytical data of new ruthenium(II) complexes

Compound	Colour	Melting point (°C)	Found (Calc.) (%) C	H	X
$[RuCl_2(PPh_3)(C_4H_3OCHO)_2]$	Yellow–brown	180	54.1 (53.7)	3.7 (3.7)	11.1 (11.3)
$[RuCl_2(AsPh_3)(C_4H_3OCHO)_2]$	Light green	205	50.7 (50.1)	3.5 (3.4)	10.4 (10.6)
$[RuBr_2(PPh_3)(C_4H_3OCHO)_2]$	Dark violet	225	46.6 (47.0)	3.5 (3.2)	21.9 (22.4)
$[RuBr_2(AsPh_3)(C_4H_3OCHO)_2]$	Dark violet	210	44.3 (44.3)	3.5 (3.0)	21.4 (21.1)
$[RuBr_2(AsPh_3)(C_6H_5CHO)_2]$	Reddish-brown	205	49.5 (49.3)	3.5 (3.5)	20.0 (20.5)
$[RuBr_2(PPh_3)(C_6H_5CHO)_2]$	Brown	185	52.1 (52.2)	3.6 (3.7)	21.8 (21.8)
$[RuBr_2(CO)(PPh_3)_2]$	Brown	190	54.6 (54.6)	3.4 (3.7)	19.1 (19.7)

X = Cl or Br.

cm^3) and the mixture was refluxed for 1 h. A solution of triphenylphosphine (0.5 g) or triphenylarsine (0.6 g) in ethanol (5 cm^3) was then added to the hot solution. The resulting solution was refluxed for a further period of 30 min, when a yellow–brown compound in the case of triphenylphosphine and light green in the case of triphenylarsine separated out. This compound was centrifuged and washed

Table 2. ^1H NMR and electronic absorption spectral data of the ruthenium(II) complexes

Compound	δ (ppm)[a]	λ_{max} (nm)	(ε)
$[RuCl_2(PPh_3)(C_4H_3OCHO)_2]$	9.83, 7.81, 7.57, 7.39, 6.70	820	(280)
		400	(1620)
		345	(2350)
		295	(10,430)
$[RuCl_2(AsPh_3)(C_4H_3OCHO)_2]$	9.90, 7.65, 7.51, 7.44	900	(160)
		530sh	(290)
		400	(1310)
		305	(6845)
$[RuBr_2(PPh_3)(C_4H_3OCHO)_2]$	9.83, 7.75, 7.56, 7.33, 6.70	680sh	(240)
		480	(1700)
		270	(18,660)
$[RuBr_2(AsPh_3)(C_4H_3OCHO)_2]$	9.94, 7.80, 7.50, 7.24	680sh	(175)
		580sh	(550)
		490	(990)
		270	(14,010)
$[RuBr_2(AsPh_3)(C_6H_5CHO)_2]$	10.15, 7.66, 7.39	680sh	(310)
		580sh	(656)
		490	(1270)
		315	(8200)
$[RuBr_2(PPh_3)(C_6H_5CHO)_2]$	10.10, 7.96, 7.53	680sh	(185)
		480	(1280)
		300	(11,630)

[a] NMR in $CDCl_3$; sh: shoulder.

with methanol and dried *in vacuo*. The compounds were analysed for $[RuCl_2(MPh_3)(C_4H_3OCHO)_2]$ (M = P or As); yield: 70–75%.

$[RuBr_2(MPh_3)(C_4H_3OCHO)_2]$ (M = P *or* As). Hydrated ruthenium trichloride (0.1 g) was dissolved in ethanol (10 cm^3) and LiBr (0.4 g) was added to the solution and the mixture was refluxed for 1 h. To the clear solution furfural (1 cm^3) was added and the mixture was refluxed for a further 30 min. A solution of triphenylphosphine (0.5 g) or triphenylarsine (0.6 g) in ethanol (5 cm^3) was added to the hot reaction mixture and the mixture was refluxed for 45 min, when a compound separated out. It was isolated as in the preparation for $[RuCl_2(MPh_3)(C_4H_3OCHO)_2]$. The compounds were analysed for $[RuBr_2(MPh_3)(C_4H_3OCHO)_2]$ (M = P or As); yield: 65–70%.

$[RuBr_2(PPh_3)(C_6H_5CHO)_2]$. (a) To a solution of hydrated ruthenium trichloride (0.1 g) in n-butanol (10 cm^3) were added LiBr (0.4 g) and HBr (0.5 cm^3) and the mixture was refluxed for 30 min. Benzaldehyde (1 cm^3) was added to the mixture, refluxed for a further 15 min and a solution of triphenylphosphine (0.5 g) in n-butanol (5 cm^3) was added. The resulting solution was refluxed for a further period of 30 min, when a reddish-brown crystalline compound separated out. This compound was centrifuged, washed first with methanol and then with diethylether and dried *in vacuo*. It was analysed for $[RuBr_2(PPh_3)(C_6H_5CHO)_2]$; yield: 0.18 g, 64%.

(b) A reaction similar to that of $[RuBr_2(MPh_3)(C_4H_3OCHO)_2]$ was performed using benzaldehyde (1 cm^3) instead of furfural and the refluxing time for the final mixture was 3 h. A reddish-brown compound was isolated as in the preparation of $[RuCl_2(MPh_3)(C_4H_3OCHO)_2]$. It was analysed for $[RuBr_2(PPh_3)(C_6H_5CHO)_2]$; yield: 0.16 g, 57%.

$[RuBr_2(CO)(PPh_3)_2]$. A reaction similar to (a) was performed without using HBr and the product was isolated similarly. It was analysed for $[RuBr_2(CO)(PPh_3)_2]$; yield: 0.25 g, 80%.

$[RuBr_2(AsPh_3)(C_6H_5CHO)_2]$. A reaction similar to (a) was performed without using HBr and triphenylarsine (0.6 g) was added instead of triphenylphosphine and the mixture was refluxed for 1 h. The compound was isolated in a similar manner to (a). It was analysed for $[RuBr_2(AsPh_3)(C_6H_5CHO)_2]$; yield: 0.18 g, 60%.

Catalytic oxidation of triphenylphosphine

The catalytic oxidation of triphenylphosphine was performed using different molar ratios of catalyst: PPh_3 (1:5 to 1:20). The catalysts used were $[RuBr_2(PPh_3)L_2]$ (L = C_4H_3OCHO or C_6H_5CHO). The results are given in Table 3. A typical reaction using $[RuBr_2(PPh_3)(C_4H_3OCHO)_2]$ as the catalyst and PPh_3 (molar ratio 1:15) is described below.

A solution of $[RuBr_2(PPh_3)(C_4H_3OCHO)_2]$ (0.3 g) in n-butanol (10 cm^3) was added to a solution of triphenylphosphine (1.65 g) in n-butanol (15 cm^3) and the mixture was refluxed to boiling on an oil bath for 5 h, while oxygen was slowly bubbled through the solution. The solution was cooled to room temperature and a compound was separated by centrifugation. The solvent was removed from the mother liquor under reduced pressure and a white mass was obtained. It was washed several times with diethylether to free it from PPh_3 and dried *in vacuo*. It was analysed for $OPPh_3$; m.p. 155–157°C; yield: 1.48 g, 85%.

A reaction similar to that above was performed using $[RuCl_2(PPh_3)(C_4H_3OCHO)_2]$. The product isolated from the mother liquor after reaction for 5 h was found to be unoxidized PPh_3 only.

RESULTS AND DISCUSSION

$[RuX_2(MPh_3)(C_4H_3OCHO)_2]$ (X = Cl *or* Br; M = P *or* As]

New compounds containing halides, furfural and triphenylphosphine or triphenylarsine have the

Table 3. Oxidation of triphenylphosphine with ruthenium(II) compounds

Catalyst	Molar ratio catalyst: PPh_3	Quantity (g) Catalyst	PPh_3	$OPPh_3$	Yield (%)
$[RuBr_2(PPh_3)(C_4H_3OCHO)_2]$	1:5	0.3	0.55	0.52	89
$[RuBr_2(PPh_3)(C_4H_3OCHO)_2]$	1:10	0.3	1.10	1.00	86
$[RuBr_2(PPh_3)(C_4H_3OCHO)_2]$	1:15	0.3	1.65	1.48	85
$[RuBr_2(PPh_3)(C_4H_3OCHO)_2]$	1:20	0.3	2.20	1.85	80
$[RuBr_2(PPh_3)(C_6H_5CHO)_2]$	1:5	0.3	0.53	0.50	88
$[RuBr_2(PPh_3)(C_6H_5CHO)_2]$	1:20	0.3	2.12	1.90	84
$[RuCl_2(PPh_3)(C_4H_3OCHO)_2]$	1:5	0.3	0.63	0.00	
No catalyst		0.0	1.00	0.00	

composition $[RuX_2(MPh_3)(C_4H_3OCHO)_2]$ (X = Cl or Br; M = P or As). The ^1H NMR spectra of $[RuCl_2(PPh_3)(C_4H_3OCHO)_2]$ and $[RuBr_2(PPh_3)(C_4H_3OCHO)_2]$ are superimposable (Table 2). The spectra showed one weak signal at δ 9.83 and four signals in the region δ 7.81–6.70. The ratio of the area under the signal at δ 9.83 and those in the region 7.81–6.7 δ is 2:21. The aldehydic proton is normally observed in the 10.1–9.5 δ range,[14] and thus, the signal at δ 9.83 could be assigned to the aldehydic proton of furfural. The proton signals in the aromatic region (δ 7.81–6.70) could be assigned to the phenyl and furan groups of triphenylphosphine and furfural, respectively. The ratio of the area for the aldehydic protons to the area under the signals in the aromatic region is as expected, 2:21. Similarly, the ^1H NMR spectra of the triphenylarsine analogues, viz. $[RuX_2(AsPh_3)(C_4H_3OCHO)_2]$ (X = Cl or Br), showed one signal at δ 9.9 and three signals in the region δ 7.80–7.24. The ratio of the area under the signals at δ 9.9 to those in the aromatic proton region is again 2:21, as expected for two aldehydic protons and 21 protons of phenyl and furan groups for the aforementioned compositions.

The IR spectra of the complexes $[RuX_2(MPh_3)(C_4H_3OCHO)_2]$ (X = Cl or Br; M = P or As) showed all the characteristic bands due to triphenylphosphine or triphenylarsine and furfural. A strong sharp band around 1605 cm^{-1} in the complexes may be due to ν(CO) of the furfural coordinated to the ruthenium [ν(CO) for free furfural is observed at 1700 cm^{-1}, which upon coordination is shifted to a lower frequency[15]]. A medium band at 326 cm^{-1} was observed for $[RuCl_2(PPh_3)(C_4H_3OCHO)_2]$, which was absent (no absorption in the region 400–250 cm^{-1}) in the case of $[RuBr_2(PPh_3)(C_4H_3OCHO)_2]$. This could be assigned to ν(Ru—Cl) of the complex. A strong band at 321 cm^{-1} was observed for $[RuCl_2(AsPh_3)(C_4H_3OCHO)_2]$, whereas a medium band at 318 cm^{-1} was observed for $[RuBr_2(AsPh_3)(C_4H_3OCHO)_2]$. The band in the case of the chloro compound could be assigned to a coupled vibration of ν(Ru—Cl) and characteristic vibrations due to triphenylarsine, whereas in the case of the bromo compound this band must be due to the vibration of the triphenylarsine molecule.[16]

$[RuBr_2(MPh_3)(C_6H_5CHO)_2]$ (M = P *or* As) *and* $[RuBr_2(CO)(PPh_3)_2]$

$[RuCl_2(MPh_3)(C_6H_5CHO)_2]$ (M = P or As) were reported earlier from our research group. Presently $[RuBr_2(MPh_3)(C_6H_5CHO)_2]$ (M = P or As) have been synthesized by the metathesis of chloride in $RuCl_3$ with LiBr, following a similar method as described earlier.[8] For the synthesis of $[RuBr_2(PPh_3)(C_6H_5CHO)_2]$ HBr was used in addition to $RuCl_3$, LiBr, PPh_3 and C_6H_5CHO, and n-butanol was used as a solvent. HBr was not required when ethanol was used as a solvent, similar to the preparation of its furfural analogue. In n-butanol the reaction took place at a higher temperature than in ethanol, which favoured the decarbonylation of benzaldehyde in the presence of PPh_3 leading to the formation of $[RuBr_2(CO)(PPh_3)_2]$. The addition of HBr (n-butanol as solvent) prevented decarbonylation, which may be due to the protonation of benzaldehyde. The ^1H NMR spectrum of $[RuBr_2(AsPh_3)(C_6H_5CHO)_2]$ in $CDCl_3$ showed one signal around δ 10.1 and two signals in the region δ 7.96–7.39. The proton signal around δ 10.1 is assigned to the aldehyde proton and the rest is due to the presence of the phenyl groups of benzaldehyde and triphenylphosphine or triphenylarsine. The ratio of the area under the signal around δ 10.1 and in the aromatic proton region is 2:25, thereby confirming the presence of two benzaldehyde and one PPh_3 or $AsPh_3$ molecules in the complex. The IR spectra of $[RuBr_2(MPh_3)(C_6H_5CHO)_2]$ (M = P or As) showed all the bands due to benzaldehyde and triphenylphosphine or triphenylarsine. Three bands of medium intensity at 1613, 1595 and 1575 cm^{-1} were observed, one of which could be due to ν(CO) of coordinated benzaldehyde.[8] The absence of any coordinated benzaldehyde group in $[RuBr_2(CO)(PPh_3)_2]$ is confirmed by IR and ^1H NMR spectra. The IR spectra show a strong and sharp band at 1935 cm^{-1} assignable to ν(CO) (terminal). A compound of the same molecular formula was reported by James *et al.*[17]

All the complexes discussed above show diamagnetic behaviour at room temperature, confirming a low-spin d^6 configuration of ruthenium(II). These complexes are non-electrolytic ($\Lambda_M \simeq 2$–$5\ \Omega^{-1}\ cm^2\ mol^{-1}$ in MeCN), thereby confirming covalent coordination of the halides with the metal ions.

Electronic spectra

The electronic absorption spectra of the complexes $[RuX_2(MPh_3)L_2]$ (L = C_4H_3OCHO, X = Cl or Br, M = P or As; L = C_6H_5CHO, X = Br, M = P or As) in chloroform show a general pattern of the three absorption bands; the first between 900 and 500 nm, the second between 500 and 400 nm and the third between 315 and 270 nm. Since the complexes are five-coordinate assuming an axial distortion from the octahedral geometry, the first and second absorption bands could be assigned to

$^1A_1 \rightarrow {}^1E$ and $^1A_1 \rightarrow {}^1A_2$ transitions, respectively.[18] The molar extinction coefficient for the second absorption band is of the order 10^3, which is higher than the *d–d* transition in second row transition metals. Hence, the band between 500 and 400 nm may have a contribution from the charge-transfer transition [ruthenium(II) → ligand], besides being due to $^1A_1 \rightarrow {}^1A_2$. In the case of $[RuCl_2(MPh_3)(C_4H_3OCHO)_2]$ (M = P or As), the band between 900 and 800 nm is characteristic of a penta-coordinated square pyramidal ruthenium(II) complex.[8,16] The third absorption band in the region 315–270 nm has a molar extinction coefficient of the order 10^4, which suggests it to be either a charge-transfer band or an allowed transition as observed in the ligand. The absorption at 270 nm in the case of $[RuBr_2(MPh_3)(C_4H_3OCHO)_2]$ (M = P or As) may be assigned to the $\pi \rightarrow \pi^*$ transition of the carbonyl group of the furfural molecules[19] and the absorption between 295 and 305 nm in the cases of $[RuCl_2(MPh_3)(C_4H_3OCHO)_2]$ (M = P or As) could be assigned to a combination of $\pi \rightarrow \pi^*$ of the furfural and ruthenium(II) → Cl charge-transfer transitions.

Catalytic activity of $[RuBr_2(PPh_3)L_2]$ (L = C_4H_3OCHO *or* C_6H_5CHO)

A reaction of PPh_3 with molecular oxygen took place in refluxing n-butanol in the presence of $[RuBr_2(PPh_3)L_2]$ (L = C_4H_3OCHO or C_6H_5CHO) to yield $OPPh_3$. Reactions were carried out by taking different molar ratios of catalyst : PPh_3 (1 : 5 to 1 : 20) (Table 3) and in all cases *ca* 80–90% of $OPPh_3$ was obtained. When a blank reaction without a catalyst was performed, no $OPPh_3$ could be isolated. $OPPh_3$ was characterized by carbon and hydrogen analyses, melting point determination and IR spectroscopy [a strong sharp band at 1190 cm^{-1} characteristic of $\nu(P{=}O)$ was observed[5]]. The complex isolated after the reaction using $[RuBr_2(PPh_3)(C_4H_3OCHO)_2]$ as a catalyst was analysed for $[RuBr_2(CO)(PPh_3)_2]$. The compound is the same as reported in the preceding part of the work. The mechanism of oxidation of PPh_3 by molecular oxygen using $[RuBr_2(PPh_3)L_2]$ (L = C_4H_3OCHO or C_6H_5CHO) may involve the loss of one aldehyde molecule in the first step, followed by the addition of one PPh_3 molecule. In the next step the addition of O_2 *cis to* the two PPh_3 molecules occurs, which is similar to that described by Graham *et al.*[20] An attempt to oxidize PPh_3 by molecular oxygen using $[RuCl_2(PPh_3)(C_4H_3OCHO)_2]$ as a catalyst was unsuccessful.

Acknowledgements—One of the authors (B.C.P.) is thankful to CSIR, New Delhi, for the award of a Senior Research Fellowship. The authors thank RSIC-NEHU, Shillong, for recording IR and ^1H NMR spectra.

REFERENCES

1. J. A. Davies and F. R. Hartley, *Chem. Rev.* 1981, **81**, 79.
2. J. Chatt, G. J. Leigh and A. P. Storace, *J. Chem. Soc.* (*A*) 1971, 1380.
3. J. D. Gilbert, D. Rose and G. Wilkinson, *J. Chem. Soc.* (*A*) 1970, 2765.
4. I. P. Evans, A. Spencer and G. Wilkinson, *J. Chem. Soc., Dalton Trans.* 1973, 204.
5. B. C. Paul, U. C. Sarma and R. K. Poddar, *Inorg. Chim. Acta* 1991, **17**, 179.
6. U. C. Sarma, K. P. Sarma and R. K. Poddar, *Polyhedron* 1988, **17**, 1727.
7. U. C. Sarma and R. K. Poddar, *Polyhedron* 1988, **7**, 1737.
8. R. K. Poddar, K. P. Sarma and U. C. Sarma, *Polyhedron* 1985, **4**, 1419.
9. M. M. Taqui Khan and A. E. Martell, *Homogeneous Catalysis by Metal Complexes*. Academic Press, New York (1974).
10. D. P. Riley and R. Shumate, *J. Am. Chem. Soc.* 1984, **106**, 3179.
11. D. P. Riley, *Inorg. Chim. Acta* 1985, **5**, 99.
12. M. A. Ledlie, K. G. Allum, I. V. Howell and R. C. Pitkethly, *J. Chem. Soc., Perkin Trans. I* 1976, 1734.
13. A. I. Vogel, *Inorganic Quantitative Analysis*, 3rd edn. ELBS and Longman, London (1961).
14. J. R. Dyer, *Applications of Absorption Spectroscopy of Organic Compounds*, p. 88. Prentice-Hall, New York (1978).
15. L. H. Rogers and D. Williams, *J. Am. Chem. Soc.* 1938, **60**, 2619.
16. R. K. Poddar and U. Agarwala, *J. Inorg. Nucl. Chem.* 1973, **35**, 567.
17. B. R. James, L. D. Markhan, B. C. Hui and G. L. Rempel, *J. Chem. Soc., Dalton Trans.* 1973, 2247.
18. R. K. Poddar, U. Agarwala and P. T. Manoharan, *J. Inorg. Nucl. Chem.* 1974, **36**, 2275.
19. R. H. Abu-Eittah and M. M. Hammed, *Bull. Chem. Soc. Japan* 1984, **57**, 844.
20. B. W. Graham, K. R. Laing, C. J. O'Connor and W. R. Ropper, *J. Chem. Soc., Dalton Trans.* 1972, 1237.

Polyhedron Vol. 12, No. 3, pp. 291–296, 1993
Printed in Great Britain

0277–5387/93 $6.00+.00
© 1993 Pergamon Press Ltd

THIOETHER-LIGATED NICKEL. SYNTHESIS, X-RAY CRYSTAL STRUCTURE AND REDOX BEHAVIOUR OF COMPLEXES OF HEXADENTATE LIGANDS INCORPORATING THIOETHER AND TRIAZENE-1-OXIDE FUNCTIONS

SOMA KARMAKAR, SURANJAN BHANJA CHOUDHURY, DEBASHIS RAY and ANIMESH CHAKRAVORTY*

Department of Inorganic Chemistry, Indian Association for the Cultivation of Science, Calcutta 700 032, India

(*Received* 20 *August* 1992; *accepted* 29 *September* 1992)

Abstract—The hexadentate ligands $RN(O)NNHC_6H_4S(CH_2)_3SC_6H_4NHN(O)NR$ (H_2L^1: R = Me; H_2L^2: R = Pr^n; general abbreviation H_2L) and their nickel(II) complexes, [NiL^1] and [NiL^2], have been synthesized. The X-ray structure of [NiL^1] has revealed the presence of a severely distorted $NiN_2O_2S_2$ coordination sphere with longer than normal Ni—S distances: 2.494(4) and 2.526(3) Å. The low symmetry of the ligand field is reflected in large splittings of octahedral ν_1 and ν_2 bands. In dichloromethane solution the nickel(III)–nickel(II) redox couple is observable cyclic voltammetrically and the $E_{1/2}$ values are: [NiL^1] = 0.74 and [NiL^2] = 0.75 V (vs SCE). Frozen (77 K) solutions of the electrogenerated nickel(III) species display rhombic EPR spectra: $g_1 = 2.195$, $g_2 = 2.145$, $g_3 = 2.038$ for [NiL^1]$^+$; $g_1 = 2.199$, $g_2 = 2.138$, $g_3 = 2.035$ for [NiL^2]$^+$. The g_1 and g_2 parameters for each complex can be considered as split components of $g_\perp$ of the idealized geometry affording the inequality $g_\perp > g_\parallel$, which corresponds to an effective axial elongation and $(d_{z^2})^1$ ground state.

An isolated thioether function is a poor coordinating agent[1] for bivalent nickel. However, macrocyclic ligation can stabilize the nickel(II)-thioether binding and a number of complexes of this type have been characterized.[2,3] Such stabilization should in principle be achievable also in the case of polydentate acyclic ligands which can achieve multiple chelation. This work forms part of our programme[4–6] on the use of this strategy for synthesizing stable complexes of nickel(II) derived from acyclic chelators incorporating the thioether function. A pair of new hexadentate ligands having thioether and triazene-1-oxide functions have been synthesized and these have afforded stable nickel(II) complexes of the coordination type $NiN_2O_2S_2$. The X-ray structure of one of these is reported. There is a large distortion of the coordination sphere from idealized octahedron and this is also reflected in large splittings of ligand field bands. The complexes are electroactive due to metal redox and the EPR spectra of nickel(III) congeners generated in solution are reported. The binding of redox-active nickel-to-sulphur ligands is of bioinorganic interest.[7,8]

* Author to whom correspondence should be addressed.

EXPERIMENTAL

Materials

Commercially available reagents were used for the synthesis of ligands and complexes. 1,3-Bis(2-aminophenylthio)propane was prepared following a reported method.[9] The N-methyl- and N-*n*-propylhydroxylamines were prepared by the reduction of the corresponding nitro compounds with zinc dust and ammonium chloride in neutral aqueous medium.[10] The preparation of tetraethylammonium perchlorate (TEAP) and purification of dichloromethane for electrochemical/spectroscopic work were performed as before.[11]

Physical measurements

Microanalytical data (carbon, hydrogen, nitrogen) were obtained with a Perkin–Elmer model 240C elemental analyser. Electronic and IR spectra were recorded with Hitachi model 330 and Perkin–Elmer model 783 IR spectrophotometers, respectively. Electrochemical measurements were performed using the PAR model 370-4 electrochemistry system as before[12] and all potentials are referenced to SCE. Magnetic susceptibilities were measured on a PAR-155 vibrating-sample magnetometer fitted with a Walker Scientific magnet. The EPR spectra were recorded in the *X*-band with a Varian E-109C spectrometer fitted with a quartz Dewar flask for measurements at 77 K (liquid nitrogen) and diphenylpicrylhydrazyl (dpph) ($g = 2.0037$) was used for their calibration.

Synthesis of the ligands

The ligands H_2L^1 and H_2L^2 are synthesized as pale yellow solids by the reaction of diazotized amines with the hydroxylamines. Details are given for the representative case of H_2L^1, 1,3-bis[*o*-(1-methyltriazene-1-oxido)phenylthio]propane. 1,3-Bis(2-aminophenylthio)propane (3.50 g) taken in concentrated HCl (8 cm^3) and water (8 cm^3) was diazotized at 0°C with $NaNO_2$ (1.7 g) dissolved in water (10 cm^3). The diazotized solution was added with stirring to N-methylhydroxylaminehydrochloride (2.05 g) in water (40 cm^3) cooled to 0°C. The pH of the reaction mixture was kept in the range 3–5 by gradual addition of an aqueous solution (50 cm^3) of sodium acetate (12 g). The solution was stirred for 20 min. After the addition of diazonium salt solution was completed, the solid ligand separated out. This was filtered and recrystallized from alcohol to yield pale yellow needles. Yield: 70%. Found: C, 50.2; H, 5.4; N, 20.6. Calc. for $C_{17}H_{22}N_6O_2S_2$: C, 50.3; H, 5.4; N, 20.7%. The ligand H_2L^2 was synthesized similarly in 65% yield. Found: C, 54.5; H, 6.4; N, 18.2. Calc. for $C_{21}H_{30}N_6O_2S_2$: C, 54.6; H, 6.5; N, 18.2%.

Synthesis of the complexes

The same general procedure was followed for both the complexes. Details are given for $[NiL^1]$. An aqueous solution of nickel(II) acetate tetrahydrate (250 mg, 1.0 mmol) was added to a hot ethanol solution of H_2L^1 (400 mg, 1.0 mmol). The mass was then refluxed for 30 min and on concentration, a pale brown crystalline compound separated out. The complex was washed with cold alcohol and water and dried *in vacuo* over P_4O_{10}. Yield: 70%. Found: C, 44.1; H, 4.3; N, 18.1. Calc. for $C_{17}H_{20}N_6O_2S_2Ni$: C, 44.1; H, 4.3; N, 18.1%.

The complex $[NiL^2]$ was synthesized similarly in a 73% yield. Found: C, 48.5; H, 5.4; N, 16.1. Calc. for $C_{21}H_{28}N_6O_2S_2Ni$: C, 48.6; H, 5.4; N, 16.2%.

X-ray structure determination

Single crystals of $[NiL^1]$ were grown by slow diffusion of hexane into a dichloromethane solution. Cell dimensions were obtained by the least-squares refinement of diffractometer angles of 30 automatically centred reflections. Data were collected at 296 K on a Nicolet R3m/V diffractometer with graphite monochromated Mo-K_α ($\lambda = 0.71073$ Å) radiation in the ω–2θ scan mode. Two check reflections measured after every 98 reflections showed no significant variations. Lorentz and polarization corrections were followed by semi-empirical absorption correction on the basis of azimuthal scans.[13] The structure was solved by direct methods

Table 1. Crystal data, intensity data collection and structural refinement for $[NiL^1]$

Formula	$C_{17}H_{20}N_6O_2S_2Ni$
Crystal size (mm)	$0.28 \times 0.30 \times 0.22$
Crystal system	Orthorhombic
Space group	$P2_12_12_1$
a (Å)	7.795(2)
b (Å)	9.729(5)
c (Å)	26.220(9)
U (Å^3)	1988.4(13)
Z	4
M	463.2
D_c (g cm^{-3})	1.547
μ(Mo-K_α) (cm^{-1})	12.12
F(000)	960
2θ range (°)	2–55
Total no. of reflections	2651
No. of unique reflections	2620
No. of observed reflections $[I > 3\sigma(I)]$	1519
Transmission factors	0.8736
Weighing scheme g in $w = 1/[\sigma^2(F)+gF^2]$	0.0005
No. of parameters refined	254
Final R	0.0576
Final R_w	0.0658
Goodness-of-fit	1.77
Largest and mean Δ/σ	0.001, 0.000
Data-to-parameter ratio	6.0 : 1
Largest difference peak (e Å^{-3})	0.44
Largest difference hole (e Å^{-3})	−0.32

and was refined by full-matrix least-squares procedures. All the non-hydrogen atoms were refined anisotropically. Hydrogen atoms were included at the calculated positions in the final refinement cycle with isotropic thermal parameters (0.08 Å^2). Crystal data and other details are collected in Table 1. Computations were carried out on a MicroVAX II computer using the SHELXTL-PLUS program system.[14]

Tables of atomic coordinates, anisotropic thermal parameters, full listing of bond lengths and angles, and observed and calculated structure factors are available as supplementary material from the Editor.

RESULTS AND DISCUSSION

Synthesis and characterization

Triazene-1-oxides can be generated[15] by coupling a diazotized aromatic amine with a substituted hydroxylamine, eq. (1).

$$ArN_2^+ + RNHOH \longrightarrow RN(O){=}NNHAr + H^+ \quad (1)$$

The hexadentate ligands (**1**) utilized in the present work are H_2L^1 and H_2L^2 (general abbreviation

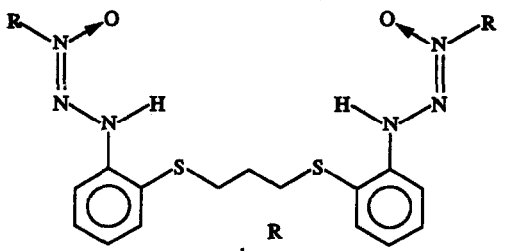

(1)

H_2L). These were prepared as pale yellow solids in good yields by reacting N-methyl- or N-*n*-propylhydroxylamine (2 mol) with a fully diazotized solution of the diamine 1,3-bis(2-aminophenylthio)propane. The H_2L ligands react with nickel(II) acetate in aqueous ethanol affording brown crystalline complexes of the type [NiL]. Selected characterization data are given in Table 2.

The complexes behave as two-electron paramagnets. In dichloromethane solution four relatively weak bands/shoulders are observed in the region 500–1500 nm. The two bands at ~ 1400 nm and ~ 1000 nm are assigned to the octahedral ν_1 transition split by low symmetry ligand field components. Similarly, the absorptions at *ca* 650 and 500 nm are attributed to split components of the ν_2 transition. The relatively large magnitudes of these splittings (3000–5000 cm^{-1}) are indicative of a severe distortion of the coordination sphere and this is in agreement with the X-ray structure of [NiL^1] reported below. The expected ν_3 transition is not observable due to the presence of other intense bands in the UV region. Two characteristic vibrations[16] of the triazene-1-oxide chelate ring corresponding to the N_3 and NO moieties are observed in the present complexes (Table 2).

X-ray structure of [NiL^1]

The lattice consists of discrete hexa-coordinated molecules. A perspective view is shown in Fig. 1 and a selected list of bond parameters is collected in Table 3. The thioether sulphur atoms are ligated to the metal, affording the coordination sphere $NiN_2O_2S_2$. Angular distortions from formal octahedral symmetry are large. For example, the angles S(1)—Ni—O(1), 156.9(2)°, and S(2)—Ni—O(2), 156.7(2)°, fall far short of 180°. The angles at the metal between atoms coordinated in *cis* positions span a wide range, 76.7(3)–106.6(3)°.

In conformity with the triazene-1-oxide formulation (—N(O)=N—N—) of the coordinated ligand N(1)—N(2) and N(5)—N(6) distances—

Table 2. Magnetic moment,[a] electronic spectra[b] and IR spectra[c] of [NiL]

Compound	μ_{eff} (B.M.)	λ (nm) (ε, (dm^3 mol^{-1} cm^{-1}))	ν(NO) (cm^{-1})	$\nu(N_3)$ (cm^{-1})
[NiL^1]	3.18	1425(26), 1025(68), 650(42), 500[d](100), 350(34,745)	1280	1455
[NiL^2]	3.31	1425(26), 1000(77), 650(44), 525[d](77), 350(34,025)	1220	1455

[a] In the solid state at 298 K.
[b] In dichloromethane.
[c] In KBr discs.
[d] Shoulder.

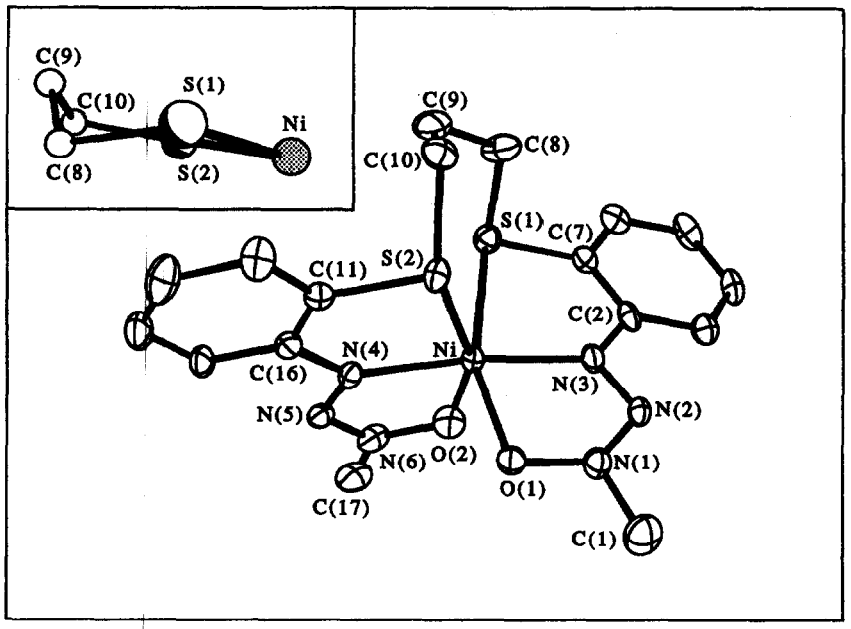

Fig. 1. Perspective view and atom labelling scheme of [NiL^1]. Atoms are shown as 50% thermal probability ellipsoids. The inset shows the half-chair conformation of the Ni—S(1)—C(8)—C(9)—C(10)—S(2) ring.

1.264(13) and 1.268(13) Å—are shorter than the N(2)—N(3) and N(4)—N(5) distances—1.307(12) and 1.332(12) Å. The ligand anionic charge primarily resides on N(3) and N(4). This is reflected in the Ni—N distances [1.984(8) and 1.993(8) Å] being significantly shorter than the Ni—O distances [2.075(8) and 2.060(7) Å].

In known nickel(II)-thioether complexes the Ni—S distances span the range 2.39–2.44 Å.[4,5,17] The sum of ionic radii has been estimated to be 2.44 Å.[1] An unusual feature of the present complex is that the Ni—S distances lie outside the above range, 2.494(4) and 2.526(4) Å. The nickel(II)–thioether bonds in [NiL^1] appear to be weaker than normal.

All the five-membered chelate rings are nearly perfectly planar (mean deviations 0.002–0.02 Å), except the ring incorporating S(1) which is moderately planar (mean deviation 0.09 Å). The six-membered NiS_2C_3 ring can be considered as a half-chair (inset in Fig. 1).

Table 3. Selected bond distances (Å) and angles (°)[a] for NiL^1

Ni—S(1)	2.494(4)	Ni—S(2)	2.526(3)
Ni—N(3)	1.984(8)	Ni—N(4)	1.993(8)
Ni—O(1)	2.075(8)	Ni—O(2)	2.060(7)
N(1)—N(2)	1.264(13)	N(1)—O(1)	1.331(12)
N(2)—N(3)	1.307(12)	N(4)—N(5)	1.332(12)
N(5)—N(6)	1.268(13)	N(6)—O(2)	1.345(12)
S(1)—Ni—S(2)	94.9(1)	S(1)—Ni—N(3)	80.7(3)
S(2)—Ni—N(3)	106.6(3)	S(1)—Ni—N(4)	103.3(3)
S(2)—Ni—N(4)	79.7(2)	N(3)—Ni—N(4)	172.4(3)
S(1)—Ni—O(1)	156.9(2)	S(2)—Ni—O(1)	86.8(3)
N(3)—Ni—O(1)	76.7(3)	N(4)—Ni—O(1)	99.7(3)
S(1)—Ni—O(2)	89.6(3)	S(2)—Ni—O(2)	156.7(2)
N(3)—Ni—O(2)	96.7(3)	N(4)—Ni—O(2)	77.0(3)
O(1)—Ni—O(2)	97.9(3)		

[a] Estimated standard deviations are given in parentheses.

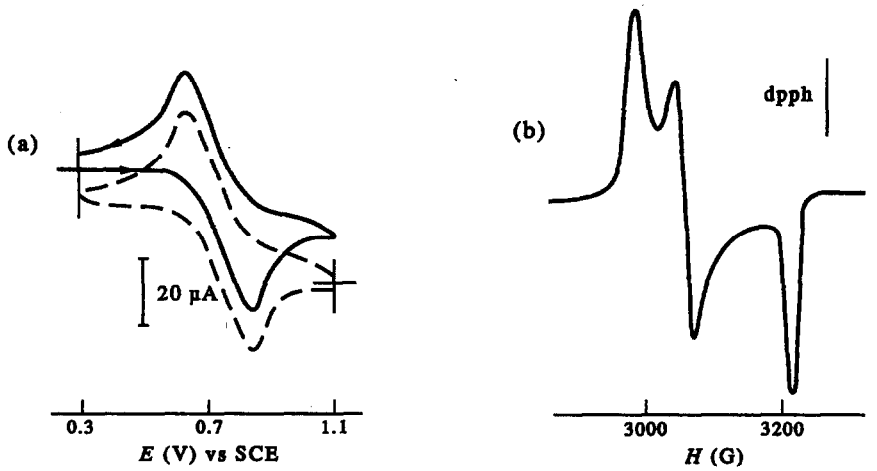

Fig. 2. (a) Cyclic voltammogram (scan rate 50 mV s^{-1}) of 10^{-3} mol dm^{-3} solutions of [NiL^1] (——) and electro-generated (298 K) [NiL^1]$^+$ (– – –) in dichloromethane (0.1 mol dm^{-3} NEt_4ClO_4) at a platinum electrode at 298 K. (b) *X*-band (9.11 GHz) EPR spectrum of [NiL^1]$^+$ in frozen (77 K) dichloromethane.

Electrochemistry

In dichloromethane solution [NiL] displays a quasi-reversible cyclic voltammetric response near 0.7 V (vs SCE), see Fig. 2. The voltammogram is assigned to the metal redox couple of eq. (2).

$$[Ni^{III}L]^+ + e \rightleftharpoons [Ni^{II}L] \qquad (2)$$

The one-electron nature of the couple is revealed by constant potential (1.04 V) coulometry. The $E_{1/2}$ values and coulometric data are collected in Table 4. Among currently known nickel complexes incorporating thioether sulphur bonding, the nickel (III)–nickel(II) reduction potentials span the range 0.3–0.8 V[4–6,18] and the $E_{1/2}$ values of the present complexes lie at the higher end of this range.

We have not succeeded in isolating [NiL]$^+$ as pure salts, but coulometrically generated (258–298 K) brown solutions of [NiL]$^+$ have the same voltammogram (initial scan cathodic) as the cor-

Table 4. Electrochemical and EPR data

(a) Electrochemical data[a]

Couple	$E_{1/2}$ (V)[b]	ΔE_p (mV)[c]	n[d]	E (V)[e]
[NiL^1]$^+$ + e ⇌ [NiL^1]	0.74	200	0.95	1.04
[NiL^2]$^+$ + e ⇌ [NiL^2]	0.75	220	1.08	1.06

(b) EPR data[f]

Compound	g_1	g_2	g_3
[NiL^1]$^+$	2.195	2.145	2.038
[NiL^2]$^+$	2.199	2.138	2.035

[a] In CH_2Cl_2 (0.1 M TEAP) at a platinum electrode with an SCE reference.
[b] From cyclic voltammetry at a scan rate of 50 mV s^{-1}.
[c] Peak-to-peak separation.
[d] n is the ratio of observed : calculated coulomb counts.
[e] Potential used for coulometry of [NiL].
[f] In frozen (77 K) dichloromethane solution.

responding nickel(II) parent (initial scan anodic), see Fig. 2. Upon coulometric reduction (0.4 V) of the oxidized solutions, the original [NiL] complex is regenerated. It is, therefore, logical to assume that there is no gross structural change upon metal redox and the $NiN_2O_2S_2$ coordination is retained in the oxidized complex $[NiL]^+$.

EPR spectra of $[NiL]^+$

That the oxidized complexes indeed contain trivalent nickel has been confirmed by EPR spectra of frozen (77 K) electro-oxidized solutions. The spectrum of $[NiL^1]^+$ is shown in Fig. 2 and g values are listed in Table 4. The spectra (all gs > 2) are compatible with low-spin trivalent nickel (d^7, $S = 1/2$).[4,19–21]

Due to the low symmetry of the $NiN_2O_2S_2$ coordination sphere the spectra are as expected rhombic. If g_1 and g_2 are considered to be split components of $g_\perp$, the axial limit of the spctrum is defined by $g_\perp = 1/2(g_1+g_2)$ and $g_\parallel = g_3$. In this formalism the $[NiL]^+$ complexes belong to the type $g_\perp > g_\parallel$, which corresponds to an effective axial elongation, $(d_{z^2})^1$ ground state.[19,20]

CONCLUSIONS

The hexadentate ligand system H_2L, incorporating triazene-1-oxide and thioether functions, binds nickel(II) affording [NiL], in which the $NiN_2O_2S_2$ coordination sphere is severely distorted. The Ni—S(thioether) bond is longer than normal and the ligand field bands display large splittings. Oxidation to the nickel(III) congener $[NiL]^+$ is electrochemically achievable. The frozen solution EPR spectrum of $[NiL]^+$ is rhombic with the ground state (d_{z^2}).[1]

Acknowledgements—Crystallographic work was done at the National Single Crystal Diffractometer Facility established by the Department of Science and Technology, New Delhi, at the Department of Inorganic Chemistry, Indian Association for the Cultivation of Science, Calcutta. Financial support received from the Council of Scientific and Industrial Research, New Delhi, India, is also acknowledged.

REFERENCES

1. S. G. Murrey and F. R. Hartley, *Chem. Rev.* 1981, **81**, 365.
2. S. R. Cooper and S. C. Rawle, *Struct. Bonding* 1990, **72**, 1.
3. A. J. Blake and M. Schröder, *Adv. Inorg. Chem.* 1990, **35**, 1.
4. S. Bhanja Choudhury, D. Ray and A. Chakravorty, *J. Chem. Soc., Dalton Trans.*, 1992, 107.
5. S. Bhanja Choudhury, D. Ray and A. Chakravorty, *Inorg. Chem.* 1991, **30**, 4354.
6. D. Ray, S. Pal and A. Chakravorty, *Inorg. Chem.* 1986, **25**, 2674.
7. J. R. Lancaster Jr, *The Bioinorganic Chemistry of Nickel.* VCH Publishers, New York (1988).
8. R. Cammack, *Adv. Inorg. Chem.* 1988, **32**, 297.
9. O. Unger, *Chem. Ber.* 1897, **30**, 607.
10. A. Chakravorty, B. Behera and P. S. Zacharias, *Inorg. Chim. Acta* 1968, **2**, 85.
11. G. K. Lahiri, S. Bhattacharya, B. K. Ghosh and A. Chakravorty, *Inorg. Chem.* 1987, **26**, 4324.
12. P. Basu, S. Bhanja Choudhury, S. Pal and A. Chakravorty, *Inorg. Chem.* 1989, **28**, 2680.
13. A. C. T. North, D. C. Philips an F. S. Mathews, *Acta Cryst.* 1968, **424**, 351.
14. G. M. Sheldrick, SHELXTL-Plus 88, Structure Determination Software Programs. Nicolet Instrument Corporation, Madison (1988).
15. (a) R. N. Mukherjee and A. Chakravorty, *Inorg. Chem.* 1984, **23**, 4753 and refs therein; (b) P. S. Zacharias and A. Chakravorty, *Inorg. Chem.* 1971, **10**, 1961.
16. R. L. Dutta and R. Sharma, *J. Inorg. Nucl. Chem.* 1980, **42**, 1204.
17. S. R. Cooper, S. C. Rawle, J. A. R. Hartman, E. J. Hintsa and G. A. Admans, *Inorg. Chem.* 1988, **27**, 1209.
18. (a) K. Weighardt, H.-J. Küppers and J. Weiss, *Inorg. Chem.* 1985, **24**, 3067; (b) D. Fortier and A. McAuley, *Inorg. Chem.* 1989, **28**, 655; (c) L. Fabbrizzi and D. M. Proserpio, *J. Chem. Soc., Dalton Trans.* 1982, 229.
19. K. Nag and A. Chakravorty, *Coord. Chem. Rev.* 1980, **33**, 87.
20. S. Bhattacharya, R. N. Mukherjee and A. Chakravorty, *Inorg. Chem.* 1986, **25**, 3448.
21. S. A. Jacobs and D. W. Mergerum, *Inorg. Chem.* 1984, **23**, 1195.

Polyhedron Vol. 12, No. 3, pp. 297–301, 1993
Printed in Great Britain

0277–5387/93 $6.00+.00
© 1993 Pergamon Press Ltd

REACTION OF PENTACARBONYLIRON WITH A NITROGEN HETEROCYCLE. X-RAY CRYSTAL STRUCTURE OF BIS[(CARBONYL)(QUINOLINE-2-THIOLATE-N,S)]IRON(II)

A. E. MAURO,* O. L. CASAGRANDE JR and V. M. NOGUEIRA

Instituto de Química de Araraquara, UNESP, C.P. 355, 14800-900 Araraquara, SP, Brazil

and

R. H. A. SANTOS, M. T. P. GAMBARDELLA and J. R. LECHAT

Instituto de Física e Química de São Carlos, USP, C.P. 369, 13560 São Carlos, SP, Brazil

and

M. F. J. FILHO

Departamento de Química, UFMG, 31270, Belo Horizonte, MG, Brazil

(*Received* 18 *August* 1992; *accepted* 29 *September* 1992)

Abstract—The monomeric compound bis[(carbonyl)(quinoline-2-thiolate-N,S)]iron(II) was synthesized and studied by IR and Mössbauer spectroscopy, cyclic voltammetry and X-ray diffraction. The molecule has two terminal carbonyl groups and two quinoline-2-thiolate anions coordinated as N,S-donor chelates, and the iron atom shows an octahedral coordination geometry.

The first reaction of a metal carbonyl with an amine N-oxide was described[1] in 1959. Since then, notably in the last few years, there has been an increase in the use of trimethylamine N-oxide (TMNO) as a reagent to induce decarbonylation.[2–5] Such promoted decarbonylation reactions constitute an interesting alternative synthetic route to novel or known molecules, and in this paper we report the one-pot synthesis of the mononuclear compound $[Fe(qnS)_2(CO)_2]$ (qnS = quinoline-2-thiolate), which was subjected to a full IR, Mössbauer, cyclic voltammetry and X-ray crystallographic characterization. There are two main reasons for carrying out this work. First, considerable interest has been demonstrated during the past few years in compounds containing heterocyclic thiols as ligands, stemming from the similarity of these ligands with thiolated nucleosides. Secondly, several coordination possibilities[6] have been observed for the heterocyclic ligand employed in this study. Indeed, depending upon reactions conditions, such as pH, it can coordinate to the metallic centre as the free ligand (qnSH) or as the conjugated base (qnS^-) and in this last case it can act as a monodentate N- or S-bonded ion, or as an N,S-donor chelate or bridging anion.

EXPERIMENTAL

Synthesis of $[Fe(qnS)_2(CO)_2]$

All operations involved in the synthesis, except the weighings, were performed in an atmosphere of purified nitrogen in a Schlenk apparatus. A solution containing 2-quinolinethiol (0.8 g, 5 mmol) and trimethylamine N-oxide (0.6 g, 5.5 mmol) dissolved in ethanol (15.0 cm^3) was added dropwise to a solution of $[Fe(CO)_5]$ (0.6 cm^3, 4.56 mmol) in ethanol (3 cm^3). The mixture was stirred for 2 h and the brown solid obtained was filtered off, washed with ethanol and ether and dried *in vacuo*. Recry-

* Author to whom correspondence should be addressed.

stallization from ethanol gave brown crystals suitable for X-ray analysis. The elemental analysis results were in agreement with the proposed formula.

IR spectrum

The IR spectrum of the title compound was measured as a Nujol mull between CsI plates on a Nicolet 730-FT spectrophotometer.

Mössbauer spectrum

The Mössbauer spectrum was obtained at room temperature and 85 K in the standard transmission geometry with a Wiss-El transducer. The source employed was ^{57}Co in rhodium. The sample was kept *in vacuo* in order to avoid oxidation during the measurements. The lines were fitted with Lorentzians without constraining any parameter and the isomer shift was made relative to metallic iron.

Electrochemical measurements

The electrochemical measurements were carried out under nitrogen at 25°C. The cyclic voltammograms and the coulometric investigation were performed with a PAR model 273 Potentiostat–Galvanostat in conjunction with a Hewlett–Packard 7090A *X–Y* recorder. All experiments were performed using a conventional three-electrode cell. A platinum disc was used as the working electrode in cyclic voltammetry and a platinum gauze was used as the working electrode in the controlled potential electrolysis. The reference electrode was Ag/Ag^+ (10^{-2} M), 0.5 M $NaClO_4$ (supporting electrolyte) in acetonitrile, which was purified by standard methods used in electrochemical studies. The auxiliary electrode was a platinum wire.

Crystal structure determination of $[Fe(qnS)_2(CO)_2]$

A crystal of the title compound was mounted on an Enraf–Nonius CAD4 diffractometer. Using graphite monochromated Mo-K_α radiation, unit cell parameters (by automatic centring of 25 reflections) and intensity data were obtained. Table 1 gives the data collection and refinement conditions. The data were corrected for Lorentz and polarization effects and for absorption [μ(Mo-K_α) = 9.94 cm^{-1}]. The structure was solved by the Patterson method.[7] The refinement was by full-matrix least-squares.[8] The hydrogen atoms were placed at their calculated positions (C—H 1.08 Å) and allowed to ride on their respective carbon atoms. Scattering factors for the non-hydrogen atoms were taken from Cromer and Mann[9] with an anomalous dispersion correction from Cromer and Liberman[10] and for hydrogen atoms from Stewart *et al.*[11] Lists of atomic parameters, tables of bond lengths and angles, observed and calculated structure factors and anisotropic thermal parameters have been deposited with the Editor as supplementary material.

RESULTS AND DISCUSSION

Among the cyclic molecules showing the tautomeric forms —NH—C(X)— $\rightleftharpoons$ —N=C(XH)— (X = O or S) are relevant biological compounds and sulphur ligands as thiols.[12] Taking into account both the important aspects of the coordination chemistry of the thiols as well as the synthetic potentialities of decarbonylation reactions induced by trimethylamine N-oxide, we performed the reaction of $[Fe(CO)_5]$ with quinoline-2-thiol (qnSH), which afforded the microcrystalline compound $[Fe(qnS)_2(CO)_2]$. The new compound was found to be quite stable in the atmosphere. Some important points emerged from the analysis of the IR spectrum[13] of this complex. First, only two ν(CO) stretching bands were observed at 2030s and 1969vs cm^{-1}. Secondly, when a comparison was made with the IR spectrum of the free ligand, no bands assignable to ν(NH) (3500–3200 cm^{-1}) or ν(SH) (2500–2400 cm^{-1}) modes were detected. These facts allowed us to conclude that only CO terminal groups are present and furthermore that the heterocyclic ligand is coordinated to the iron atom in a deprotonated form.

In order to better elucidate these aspects related to the geometry around the iron atom and the metal oxidation state, we made use of Mössbauer spectroscopy. The Mössbauer spectrum of the title compound consisted of a single quadrupole splitting. The small quadrupole splitting observed, $QS = 0.51$ mm s^{-1}, is typical of iron complexes with an octahedral structure. In addition the isomer shift value, $IS = 0.07$ mm s^{-1}, is similar[14] to those of other low-spin iron(II) compounds

It is instructive at this point to relate the preceding results with those of the electrochemical investigation. The electrochemical oxidation of $[Fe(qnS)_2(CO)_2]$ was studied by cyclic voltammetry and controlled potential electrolysis in 0.5 M $NaClO_4$ (acetonitrile). Figure 1 shows the cyclic voltammogram for the compound, obtained on a platinum electrode at a potential scan rate $v = 50$ mV s^{-1} and 25°C. In the range from −0.20 to +1.0 V (vs Ag/Ag^+) only one anodic current peak is observed at +0.83 V, independent of the scan rate. This result suggests that at this potential the iron(II) → iron(III) oxidation probably occurs, pro-

Table 1. Summary of data collection and refinement for $[Fe(qnS)_2(CO)_2]$

Molecular formula	$FeS_2O_2N_2C_{20}H_{12}$
Molecular weight	432.30
Crystal system	Monoclinic
Space group	$C2/c$
Z	8
D_c (g cm^{-3})	1.56
a (Å)	18.105(4)
b (Å)	7.087(2)
c (Å)	29.556(6)
β (°)	104.03(1)
V (Å^3)	3679(4)
$F(000)$	1760
Crystal size (mm)	$0.75 \times 0.35 \times 0.08$
λ (Å)	0.7107
Scan mode	ω–2θ
θ range (°)	2–23
Range in hkl	−19, 19; 0, 7; 0, 32
Unique reflections	2552
Reflections used ($I \geqslant 3\sigma(I)$)	2183
No. of variables (two blocks)	147, 147
Goodness of fit	2.93
R, R_w	0.050, 0.052
R_{all}	0.066
Max. shift (e.s.d.)	0.3
Max. density in difference map (e Å^{-3})	0.53
Minimized function	$\Sigma w(\|F_o\|-\|F_o\|)^2$
Weight system, w for observed	$[\sigma^2(F_o)+0.00017\|F_o\|^2]^{-1}$
Weight system, w for unobserved	0

ducing a non-electrochemically active species.[15] The number of electrons obtained from the controlled potential electrolysis was one, supporting the proposal of an iron(II) → iron(III) oxidation. The cyclic voltammogram after exhaustive electrolysis at the anodic potential peak showed the disappearance of this peak. The electrochemical behaviour of $[Fe(qnS)_2(CO)_2]$ was described as one-electron oxidation, with an irreversible electrochemical reaction on the platinum electrode.

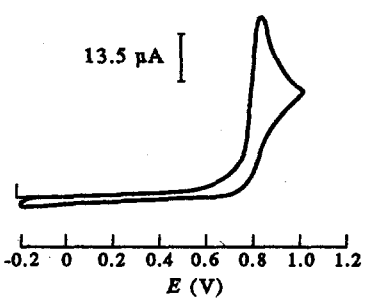

Fig. 1. Cyclic voltammogram for $NaClO_4$ (0.5 M) in acetonitrile solution with $[Fe(qnS)_2(CO)_2]$ (1.0×10^{-3} M) at a platinum electrode, 25°C and $v = 50$ mV s^{-1}.

The monomeric nature of the compound and the important structural features suggested by IR and Mössbauer spectroscopies and supported by its electrochemical behaviour were definitely proved by the crystal and molecular structural X-ray analysis. The structure of the compound with the labelling scheme is presented in Fig. 2. Selected bond lengths and angles are given in Table 2. Two carbonyl groups and two quinoline-2-thiolate anions coordinated as N,S-donor chelates achieve a slightly distorted octahedral environment about the iron atom. The average Fe—C and C—O distances, 1.778(6) and 1.122(8) Å, respectively, and the average Fe—C—O angle, 177.5(6)°, are in agreement with the average values[16,17] observed in other iron carbonyl compounds.

In addition, inspection of the polyhedra around the iron atom showed that the carbonyl groups are disposed in a *cis* arrangement with the angle C(A)—Fe—C(B) being 92.3(3)°. Moreover, the influence of the atom in a *trans* position to the carbon atoms on Fe—C distances can be clearly verified since the bond length *trans* to nitrogen [Fe—C(A) = 1.768(6) Å] is shorter than the one *trans* to sulphur [Fe—C(B) = 1.788(6) Å]. Fur-

Table 2. Selected distances (Å) and angles (°) for $[Fe(qnS)_2(CO)_2]$

Fe—C(A)	1.768(6)	Fe—C(B)	1.788(6)
Fe—S(1)	2.348(2)	Fe—S(11)	2.318(2)
Fe—N(1)	1.996(4)	Fe—N(11)	2.010(5)
S(1)—C(1)	1.715(6)	S(11)—C(11)	1.738(6)
N(1)—C(1)	1.342(6)	N(11)—C(11)	1.322(8)
N(1)—C(9)	1.365(7)	N(11)—C(91)	1.400(7)
C(A)—O(A)	1.140(7)	C(B)—O(B)	1.104(8)
C(A)—Fe—C(B)	92.3(3)	S(1)—Fe—S(11)	93.5(7)
C(A)—Fe—S(1)	88.9(2)	C(A)—Fe—S(11)	98.4(3)
C(A)—Fe—N(11)	168.2(2)	C(B)—Fe—N(11)	91.5(2)
C(B)—Fe—S(1)	176.2(2)	C(B)—Fe—S(11)	89.9(2)
C(A)—Fe—N(1)	91.5(2)	C(B)—Fe—N(1)	105.7(2)
S(1)—Fe—N(1)	70.6(1)	S(1)—Fe—N(11)	88.0(1)
N(1)—Fe—S(11)	161.2(1)	N(11)—Fe—S(11)	70.5(1)
N(1)—Fe—N(11)	98.1(2)		
Fe—C(A)—O(A)	178.6(5)	Fe—C(B)—O(B)	176.3(6)
Fe—S(1)—C(1)	77.9(2)	Fe—S(11)—C(11)	78.4(2)
Fe—N(1)—C(1)	100.5(3)	Fe—N(11)—C(11)	100.7(4)
Fe—N(1)—C(9)	139.7(3)	Fe—N(11)—C(91)	139.1(4)

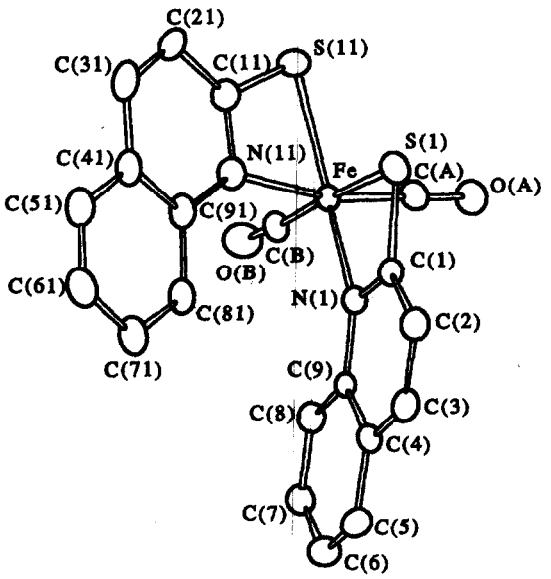

Fig. 2. Molecular structure of $[Fe(qnS)_2(CO)_2]$.

thermore, the angles C(1)—N(1)—C(9) and C(11)—N(11)—C(91) of 119.8(4)° and 119.7(4)°, respectively, are within the range expected for deprotonated N-heterocycles[18] and demonstrate that the chelates (qnS) are effectively deprotonated.

Finally, it is important to note the advantages of the synthetic strategy adopted in this work, due to the fact that the reactions of iron pentacarbonyl with nitrogen-based ligands usually lead to iron disproportionation to ferrous complexes and groups of ferrate ions, depending on the base and the reactions conditions.[19] Accordingly, the present procedure relies on the formation of NMe_3 from the decarbonilating TMNO. This strong base is effective for *in situ* deprotonation reactions such as those involved in the formation of $[Fe(qnS)_2(CO)_2]$. Other syntheses are being carried out in order to extend this preparative route to a wide class of nitrogen and phosphorus based ligands.

Acknowledgements—We thank CNPq, FAPESP and FINEP for financial support.

REFERENCES

1. W. Hieber and L. Lipp, *Chem. Ber.* 1959, **92**, 2085.
2. H. Alper and J. T. Edward, *Can. J. Chem.* 1970, **48**, 1543.
3. J. Elzinga and H. Hogeveen, *J. Org. Chem.* 1980, **45**, 3957.
4. T. S. A. Hor and H. S. O. Chan, *Inorg. Chim. Acta* 1989, **160**, 53.
5. T. S. A. Hor and L. P. Thang, *Polyhedron* 1990, **9**, 2305.
6. E. S. Raper, *Coord. Chem. Rev.* 1985, **61**, 115.
7. G. M. Sheldrick, SHELX 86, Program for the Solution of Crystal Structures. University of Göttingen, Germany (1986).
8. G. M. Sheldrick, SHELX 76, Program for Crystal Structure Determination. University of Cambridge, England (1976).
9. D. T. Cromer and J. B. Mann, *Acta Cryst.* 1986, **A24**, 321.
10. D. T. Cromer and L. Liberman, *J. Chem. Phys.* 1970, **53**, 1891.

11. R. F. Stewart, E. R. Davidson and W. T. Simpson, *J. Chem. Phys.* 1965, **42**, 3175.
12. P. Mura, B. G. Olby and S. D. Robinson, *J. Chem. Soc., Dalton Trans.* 1985, 2101.
13. K. Nakamoto, *Infrared Spectra of Inorganic and Coordination Compounds*. Wiley Interscience, New York (1970).
14. G. M. Bancroft, M. J. Mays and B. E. Prater, *J. Chem. Soc. (A)* 1970, 956.
15. R. S. Nicholson and I. Shain, *Analyt. Chem.* 1964, **36**, 706.
16. A. E. Mauro, R. H. A. Santos, M. T. P. Gambardella and R. H. P. Francisco, *Polyhedron* 1987, **6**, 1273.
17. A. E. Mauro, S. H. Pulcinelli, R. H. A. Santos and M. T. P. Gambardella, *Polyhedron* 1992, **11**, 799.
18. E. M. Padilla, J. H. Yamamoto and C. M. Jensen, *Inorg. Chim. Acta* 1990, **174**, 209.
19. A. P. Ginsberg, *Trans. Met. Chem.* 1965, **1**, 112.

Polyhedron Vol. 12, No. 3, pp. 303–311, 1993
Printed in Great Britain

0277–5387/93 $6.00+.00
© 1993 Pergamon Press Ltd

COMPLEXES OF MoO_2Cl_2 AND WO_2Cl_2 WITH THE LIGANDS N,N,N′,N′-TETRAMETHYLETHYLENEDIAMINE, N,N′-DI-t-BUTYL-1,4-DIAZA-1,3-BUTADIENE AND N,N′-DIMETHYLPIPERAZINE. *CIS,TRANS,CIS* VS ALL *CIS* COORDINATION IN BIDENTATE N-DONOR COMPLEXES OF WO_2Cl_2 AND MoO_2Cl_2. CRYSTAL STRUCTURES OF MoO_2Cl_2(N,N,N′,N′-TETRAMETHYLETHYLENEDIAMINE) AND MoO_2Cl_2(N,N′-DI-t-BUTYL-1,4-DIAZA-1,3-BUTADIENE)

KLAUS DREISCH,* CARLAXEL ANDERSSON and CLAES STÅLHANDSKE

Department of Inorganic Chemistry, Chemical Centre, University of Lund, P.O. Box 124, S 22100 Lund, Sweden

(*Received* 31 *July* 1992; *accepted* 10 *September* 1992)

Abstract—The complexes [MoO_2Cl_2(Bu^t-dab)], [WO_2Cl_2(Bu^t-dab)] (Bu^t-dab = N,N′-di-t-butyl-1,4-diaza-1,3-butadiene), [MoO_2Cl_2(dmp)] and [WO_2Cl(dmp)] (dmp = N,N′-dimethylpiperazine) have been prepared and characterized by IR, Raman, ^{1}H and ^{13}C NMR spectroscopy. [MO_2Cl_2(dmp)] (M = Mo, W) has *cis*-dichloroligands and [MoO_2Cl_2(dmp)] shows fluxional behaviour of the coordinated ligand in CH_2Cl_2 solution, as monitored by ^{1}H NMR spectroscopy. The structures of [MoO_2Cl_2(tmen)] (tmen= N,N,N′,N′-tetramethylethylenediamine) and [MoO_2Cl_2(Bu^t-dab)] are reported. Both compounds are built up of discrete molecules with distorted octahedral geometry and *cis*-dioxoligands, the former having the unusual *cis*-dichloro and the latter the common *trans*-dichloro arrangement. MoO_2Cl_2(tmen) has Mo=O distances of 1.681(4) and 1.697(4) Å with an O—Mo—O angle of 103.1(2)°. The *trans* influence of the oxo-ligands is shown by two different Mo—Cl distances [2.449(2) Å *trans* to O and 2.338(2) Å *trans* to N] and two different Mo—N distances [2.464(4) Å *trans* to O and 2.278(4) Å *trans* to Cl]. MoO_2Cl_2(Bu^t-dab) has an Mo=O distance of 1.688(3) and an O—Mo—O angle of 104.5(2)°. The *trans*-dichloro ligands have equal distances to molybdenum, *d*(Mo—Cl) = 2.356(1) Å. The Mo—N distances of the nitrogen atoms *trans* to the oxo groups are 2.399(2) and 2.388(2) Å.

The syntheses of catalytically active alkylidene and alkylidyne complexes,[1,2] of importance in industrial processes such as the olefin metathesis reaction and ring opening polymerization, have recently initiated large interest in the chemistry of high valent molybdenum and tungsten complexes. Moreover, molybdenum complexes containing the *cis*-dioxomolybdenum(VI) cation, $[MoO_2]^{2+}$, coordinated to ligands containing nitrogen, oxygen and/or sulphur donors, are intensely investigated because such complexes are proposed as model compounds for the active site in a number of oxo-transfer molybdato enzymes.[3,4] We are currently studying high valent molybdenum and tungsten complexes in relation to the olefin metathesis reaction and we have recently described the synthesis and structure of [WO_2Cl_2(tmen)] (tmen = N,N,N′,N′-tetramethylethylenediamine).[5] This complex was found to be structurally unique among known octahedral [$WO_2X_2L_2$] complexes (X = anionic ligand and L = neutral ligand) in that the configuration of the ligating atoms O, X = Cl, L = N around the tungsten atom is all-*cis* and not the commonly en-

* Author to whom correspondence should be addressed.

countered *cis,trans,cis* of O, X, L. $[MoO_2Cl_2(tmen)]$ was also prepared in that study and found to be isostructural to its tungsten analogue, but a lack of suitable crystals precluded an X-ray structure determination. Despite the very large number of structurally known octahedral molybdenum complexes derived from $[MoO_2]^{2+}$ with different kinds of mono- to tetradentate ligands there seems to be only one additional example[6] with an all *cis* configuration, the ligand in that case being a dianionic tetradentate ligand of the Schiff base type, X = O, L = N.

A less repulsive interligand interaction, i.e. chlorine–N-methyl interaction, in an all *cis* configuration as compared to a hypothetical *cis,trans,cis* configuration was the suggested reason for the unusual all *cis* arrangement of the ligands in both $[MoO_2Cl_2(tmen)]$ and $[WO_2Cl_2(tmen)]$. To test this hypothesis of interligand repulsion as a factor governing the coordination geometry of MO_2Cl_2 complexes (M = Mo and W) we have performed further studies using bidentate N-donor ligands by varying the steric demands of the ligands along two lines. Firstly, using N,N′-dimethylethylenediamine (dmed) with two methyl groups less than tmen or N,N′-dimethylpiperazine (dmp), where the two methyls are replaced by two methylene groups, might lead to a reduced steric bulk, which could cause a structural change to a *trans*-dichloro arrangement. However, our attempts to prepare complexes with dmed as the ligand have been unsuccessful, giving analytically impure products most probably because of aminolysis as a side-reaction. Secondly, 2,2′-bipyridyl (bipy) and *o*-phenanthroline (*o*-phen) are the bidentate N-donor ligands often used. These are known to form *cis,trans,cis* configurated complexes $[MO_2X_2(L_2)]$ (M = Mo, W; L_2 = bipy or *o*-phen) in which these ligands are close to planar.[7–14]

The question raised in relation to ligands such as e.g. bipy was if the introduction of sterically bulky groups in the 3,3′ position of bipy would lead to all *cis* configurated complexes. N,N′-disubstituted 1,4-diaza-1,3-butadienes, R—N=CH—CH=N—R (R-dab), are easily accessible ligands related to 3,3′-disubstituted bipy. Such ligands have been widely applied to the stabilization of low-valent metal complexes,[15] but rarely used for high-valent ones.[16,17] In fact, no molybdenum(VI) or tungsten(VI) complex containing R-dab is reported in the literature. Due to their bulkiness R-dab ligands are known to alter stabilities and the structures of R-dab metal complexes relative to their bipy- and *o*-phen analogues.[18] Bu^t-dab was considered as an obvious choice for a sterically demanding R-dab ligand since the tert-butyl groups introduce bulkiness perpendicular to the plane of the N=C—C=N skeleton. In this report we present the X-ray structures of $[MoO_2Cl_2(tmen)]$ (**1**) and $[MoO_2Cl_2(Bu^t\text{-dab})]$ (**2**) and the spectroscopic characterization of **2**, $[WO_2Cl_2(Bu^t\text{-dab})]$ (**3**), $[MoO_2Cl_2(dmp)]$ (**4**) and $[WO_2Cl_2(dmp)]$ (**5**).

RESULTS AND DISCUSSION

Synthesis and general characteristics of the complexes

The synthesis and characterization of complex **1** have been described earlier[5] and the same general preparative principles have been used here. Thus, the new compounds **2–5** were synthesized in a straightforward way from the corresponding dme complexes and a slight excess (5%) of the ligand, by dme/ligand exchange. For complexes **2** and **3** the reactions were performed in CH_2Cl_2 at room temperature, but for complexes **4** and **5** the temperature must not exceed 0°C otherwise extensive decomposition to insoluble and untractable products occurs. The molybdenum complexes **2** and **4** were also prepared by direct reaction between molybdenum dioxodichloride and the corresponding ligand. The tungsten complex **3** was additionally synthesized from $WOCl_4$, $O(SiMe_3)_2$ and Bu^t-dab, as described for the preparation of $[WO_2Cl_2(dme)]$[20] and $[WO_2Cl_2(bipy)]$.[8]

All the complexes (**1–5**) are susceptible to hydrolysis. For a given metal the hydrolytic stability decreases in the following order: Bu^t-dab > tmen ≫ dmp. The bipy complexes, $[MO_2Cl_2(bipy)]$ (M = Mo, W), are indefinitely air-stable;[8] **2** is at least 3 days stable as the present X-ray structure determination performed in air proves, but the dmp complexes **4** and especially **5** are rather sensitive and should be kept under inert gas in the freezer (−30°C). Furthermore, complexes **4** and **5** are light-sensitive showing a grey–blue colour after some days exposure to daylight, therefore, no acceptable Raman spectrum of **5** could be obtained.

Description and discussion of the structures of $[MoO_2Cl_2(tmen)]$ (**1**) *and* $[MoO_2Cl_2(Bu^t\text{-dab})]$ (**2**)

Views of the molecules **1** and **2** with atomic numbering are shown in Figs 1 and 2, respectively. Selected bond distances and angles are given in Table 1.

The bond distances and angles of **1** are close to those of the isostructural tungsten complex $[WO_2Cl_2(tmen)]$, as is also the case in the isostructural complexes $[MO_2Cl_2(dme)]$ (M = Mo,[19]

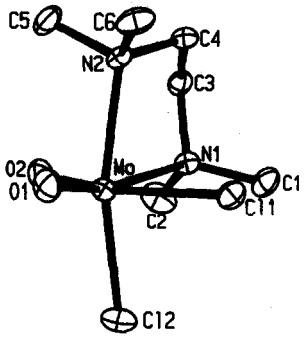

Fig. 1. A perspective view of the MoO_2Cl_2(tmen) (**1**) molecule.

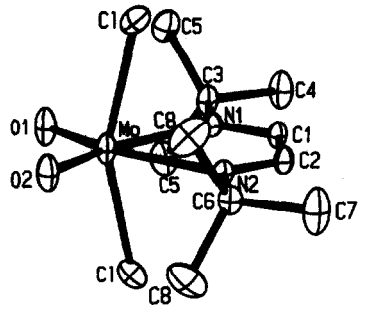

Fig. 2. A perspective view of the MoO_2Cl_2(Bu^t-dab) (**2**) molecule.

Table 1. Selected bond distances (Å) and angles (°) for MoO_2Cl_2(tmen) (**1**) and MoO_2Cl_2(Bu^t-dab) (**2**)

MoO_2Cl_2(tmen) (**1**)

Bond distances (Å)

Mo—O(2)	1.681(4)	N(1)—C(1)	1.48(1)
Mo—O(1)	1.697(4)	N(1)—C(2)	1.48(1)
Mo—N(2)	2.278(4)	N(1)—C(3)	1.48(1)
Mo—Cl(2)	2.338(2)	C(3)—C(4)	1.49(1)
Mo—Cl(1)	2.449(2)	C(4)—N(2)	1.49(1)
Mo—N(1)	2.464(4)	N(2)—C(5)	1.50(1)
		N(2)—C(6)	1.49(1)

Bond angles (°)

O(1)—Mo—O(2)	103.1(2)	Mo—N(1)—C(3)	103.3(3)
O(2)—Mo—N(1)	80.5(2)	N(1)—C(3)—C(4)	111.8(5)
N(1)—Mo—Cl(1)	82.1(1)	C(3)—C(4)—N(2)	111.3(5)
Cl(1)—Mo—O(1)	92.7(2)	C(4)—N(2)—Mo	109.3(3)
N(2)—Mo—Cl(2)	165.2(1)		
Cl(1)—Mo—Cl(2)	87.49(6)		
N(1)—Mo—N(2)	76.7(1)		

MoO_2Cl_2(Bu^t-dab) (**2**)

Bond distances (Å)

Mo—O(1)	1.688(3)	N(1)—C(3)	1.513(3)
Mo—O(2)	1.688(3)	N(1)—C(1)	1.271(4)
Mo—2Cl	2.356(1)	C(1)—C(2)	1.476(4)
Mo—N(2)	2.388(2)	C(2)—N(2)	1.267(4)
Mo—N(1)	2.399(2)	N(2)—C(6)	1.508(4)
		C(3)—C(4)	1.525(5)
		C(3)—2C(5)	1.527(4)
		C(6)—C(7)	1.514(5)
		C(6)—2C(8)	1.514(6)

Bond angles (°)

O(1)—Mo—O(2)	104.5(1)	Mo—N(1)—C(3)	125.5(2)
O(2)—Mo—N(2)	93.4(1)	Mo—N(1)—C(1)	114.4(2)
N(2)—Mo—N(1)	70.3(1)	N(1)—C(1)—C(2)	120.0(3)
N(1)—Mo—O(1)	91.8(1)	C(1)—C(2)—N(2)	120.4(3)
Cl—Mo—Cl	156.61(5)	C(2)—N(2)—C(6)	120.2(2)
		C(2)—N(2)—Mo	114.8(2)
		C(6)—N(2)—Mo	125.0(2)

W[20]). This is not surprising in view of the very small difference between molybdenum and tungsten in their atomic and covalent radii.[21]

Both **1** and **2** have a distorted octahedral arrangement of the six ligand atoms around the molybdenum centre with *cis*-dioxo ligands, as is commonly found in other d^0 six-coordinated dioxo-complexes.[22] There is no significant difference in molybdenum–oxygen distances between complexes **1** and **2** and their O=Mo=O angles differ by only 1.4°, which emphasizes the structural rigidity of the MO_2^{2+} moiety when no competing π-donors are present *trans* to the oxo ligands. The mean Mo=O distances of **1** (1.689 Å) and **2** (1.688 Å) are close to the average value of 1.704 Å reported for a wide range of molybdenum dioxo-complexes.[22]

With respect to the overall geometry the two compounds differ in that MoO_2Cl_2(tmen) (**1**) has *cis*-dichloro ligands as its tungsten analogue,[5] but MoO_2Cl_2(Bu^t-dab) (**2**) has *trans*-dichloro ligands. Consequently, each of the two nitrogen atoms and each of the two chlorine atoms in complex **1** have different *trans* ligands, while in complex **2** both nitrogen and both chlorine atoms have one kind of *trans* ligand, oxo and chloro respectively. The *trans* influence of the multiply bonded oxo ligands in **1** is demonstrated by longer molybdenum–nitrogen and molybdenum–chlorine distances *trans* to oxo; Mo—N(1), 2.464(4) Å, as compared to Mo—N(2), 2.278(4) Å, and Mo—Cl(1), 2.449(2) Å, as compared to Mo—Cl(2), 2.338(2) Å. Thus, the *trans*-lengthening effect of O(1) relative to Cl(2) on the molybdenum nitrogen distances is 0.186 Å and of O(2) relative to N(2) on the molybdenum chlorine distances is 0.111 Å, which compares well with the *trans*-lengthening observed in the tungsten analogue.[5] The molybdenum–chlorine distance in **2**, 2.356(1) Å, is similar to that in other dioxo-dichloromolybdenum complexes with *trans*-chloro ligands,[7,19,23–27] while the Mo—Cl(2) distance in **1** *trans* to N(2), 2.278(4) Å, is shorter. Thus, the relative *trans* influence of the donors on the molybdenum–chlorine bond follows the order: $O^{2-} > Cl^- > N$.

A comparison of the molybdenum–nitrogen distances *trans* to oxo in complex **2** [2.399(2) and 2.388(2) Å] and in complex **1** [2.464(4) Å] reveals that they are significantly shorter in the former than in the latter. The higher degree of alkyl substitution and the sp^3 hybridization of the nitrogen atoms in tmen imply a higher basicity and donor ability of tmen relative to Bu^t-dab; taking only donor strength arguments into consideration shorter molybdenum–nitrogen distances could, therefore, be expected in the tmen complex **1**. The alkyl substituents of tmen increase its steric bulk leading to repulsive interligand interactions in the complex, which may hamper the aforementioned bond strengthening inductive effect. The full donor capacity of the tmen ligand might therefore not be reflected in the Mo—N(1) bond distance.

Our motive for preparing **2** was to see if the use of the Bu^t-dab ligand with the two bulky t-butyl groups would result in the formation of an all *cis* configurated $MO_2Cl_2L_2$ complex. Despite the bulkiness of the ligand the configuration around the molybdenum atom in **2** is, however, the commonly encountered *cis,trans,cis*. The nitrogen atoms N(1) and N(2), the carbon atoms C(1) and C(2) of the five-membered metallacycle, the tertiary carbon atoms C(3) and C(6) and one of the methyl carbon atoms in each tertiary butyl group, C(4) and C(7), all lie in the plane of the molybdenum atom and the oxo ligands (Fig. 2). C(4) and C(7) are directed away from the MoO_2 moiety. This particular conformation of Bu^t-dab is adopted because here the distances between the methyl and the oxo groups are maximal: 3.250(4) and 3.272(5) Å for O(1)···C(5) and O(2)···C(8), respectively. Considering the sum of the van der Waals' radii of oxygen and carbon which is approximately 3.25 Å,[21] any rotation of the methyl groups around C(6)—N(2) or C(3)—N(1) would lead to methyl–oxygen repulsion. Molecule **2** has C_s symmetry very close to C_{2v}. The chlorine atoms in **2** are bent towards the Bu^t-dab ligand resulting in a Cl—Mo—Cl angle of 156.6°, a deviation from linearity commonly encountered in MoO_2^{2+} complexes and caused by the high π-electron density in the two Mo=O bonds.[13]

Since the *o*-phen ligand can formally be regarded as a bis-imine ligand, [MoO_2Cl_2(*o*-phen)] is a complex of MoO_2Cl_2 closely related to complex **2**. Comparing the $MoO_2Cl_2N_2$ cores of these two molecules shows that in complex **2** the mean Mo—N distance, 2.393 Å, is much larger than that in [MoO_2Cl_2(*o*-phen)], 2.308 Å.[7] The mean M=O distance is slightly longer in the *o*-phen complex, 1.695(3) Å, than in complex **2**, 1.688 Å. These differences may arise from the π-donor/π-acceptor properties of the two ligands *o*-phen and Bu^t-dab: 1,4 diaza-1,3-butadienes like Bu^t-dab are known to be exceptionally good π-acceptors and consequently weaker π-donors compared to *o*-phen,[18,28] and π-donation from *o*-phen into empty *d*-orbitals of molybdenum(VI) reduces the electrophilicity of the metal centre. This in turn reduces to some extent the π-donation from the oxo ligands to molybdenum. Thus, the Mo=O bond is weakened and the Mo—N bond strengthened relative to the case of the Bu^t-dab ligand, as reflected in the metal–ligand bond lengths in the two complexes. The Mo=O

stretching vibrations of $[MoO_2Cl_2(o\text{-phen})]$[29] at 935 and 902 cm^{-1} (IR) and those of complex **2** at 948 and 915 cm^{-1} (IR) support this interpretation.

Another difference between complex **2** and $[MoO_2Cl_2(o\text{-phen})]$ concerns the inner ligand distances and is a consequence of the aromaticity of the *o*-phen ligand. The central C(1)—C(2) bond between the two imino-carbon atoms in **2** is a pure sigma bond [1.476(4) Å] and relatively unaffected by complexation [free Bu^t-dab :[30] 1.496(20) Å], while in the *o*-phen ligand it has double bond character [1.423(6) Å].

Spectroscopic characterization of the complexes

Crystals of the dmp complexes **4** and **5** could not be obtained; conclusions concerning their configuration must therefore rely on vibrational and NMR spectroscopy.

As shown in the Experimental complexes **2**–**5** show two intense IR and Raman peaks between 890 and 960 cm^{-1}. These peaks belong to the symmetric and antisymmetric M=O stretching vibrations of MO_2^{2+} complexes with a *cis*-dioxo arrangement.[4,31] For the Bu^t-dab complexes **2** and **3** two peaks appear between 200 and 260 cm^{-1}. Based on assignments made on some diazabutadienemetaltetracarbonyl complexes, $M(CO)_4$(R-dab)],[32] these bands can be tentatively assigned to antisymmetric and symmetric metal–nitrogen stretching vibrations. Preliminary force-field calculations[33] on the molybdenum complex **2**, the structure of which has been presented above, are also in agreement with these assignments. On the other hand, in the vibrational spectra of complexes $MoO_2Cl_2X_2$ with X = an oxygen donor[34] IR absorptions of medium intensity between 250 and 260 cm^{-1} are always present and are considered to be molybdenum–oxygen rocking vibrations of the *cis*-O=Mo=O moiety; ^{15}N labelling experiments might therefore help to reach a definite conclusion concerning the metal–nitrogen vibrations.

Neither the metal–oxo nor the metal–nitrogen vibrations are of value in distinguishing between an all *cis* or a *cis,trans,cis* configuration of $MO_2Cl_2N_2$ complexes, but the vibrational spectra in the metal–chlorine stretching region may hold some information on this matter. The metal–chlorine stretching vibrations in complexes **2** and **3** follow the intensity patterns usually found in other *trans*-dichloro complexes,[34] the band at a higher wave number [ν_{as}(M—Cl)] has medium to high intensity in IR and low intensity in Raman, whilst the band at a lower wave number [ν_s(M—Cl)] shows appreciable intensity in Raman while the IR absorption is weak. In the two hitherto characterized octahedral complexes with *cis*-dichloro configuration, $[WO_2Cl_2$(t-men)][5] and $[MoO_2Cl_2$(tmen)] (**1**), the IR spectra show two metal–chlorine stretching vibrations at 345(m), 307(vw) and 350(m), 303(vw) cm^{-1}, respectively, thus exhibiting the same intensity patterns as *trans*-dichloro complexes. The assignments of the symmetric stretching vibrations made here are reassignments to those suggested earlier.[5] Contrary to the IR intensities there is a difference in the Raman spectra between *cis,trans,cis* configurated complexes, such as $[MoO_2Cl_2$(Bu^t-dab)] and $[MoO_2Cl_2$(bipy)], and the all *cis* configurated complex $[MoO_2Cl_2$(tmen)] (**1**). In the latter case the Raman intensities of the symmetric and asymmetric stretching vibrations at 303 and 343 cm^{-1} are of about equal intensity, while in the former complexes the Raman intensity of the asymmetric stretching vibrations is weak (see Fig. 3). Thus, two Raman peaks of about equal intensity in the Mo—Cl stretching region might be a useful criterion for distinguishing between *cis*- and *trans*-dichloro configurated complexes, $MoO_2Cl_2L_2$. When applied to the molybdenum complex **4** this criterion implies that it has a *cis*-dichloro configuration like its monocyclic counterpart **1**. Due to the lack of a Raman spectrum no conclusion can be drawn for $[WO_2Cl_2$(dmp)] (**5**). However, the NMR spectra of **5** and **4** discussed below indicate a *cis*-dichloro arrangement for both complexes. The NMR spectra of complexes **2** and **3** consist of two singlets in the ^1H NMR spectra and three resonances in the $^{13}C\{^1H\}$ spectra (see Experimental), i.e. there is only a single set of signals for the two ligand halves of Bu^t-dab. In accord with the solid-state structure of **2** this shows that Bu^t-dab is symmetrically bound to MoO_2Cl_2 with the nitrogen atoms *trans* to the oxo ligands. The NMR spectra of **3** exhibit the same patterns as those of **2**, implying that **3** in solution

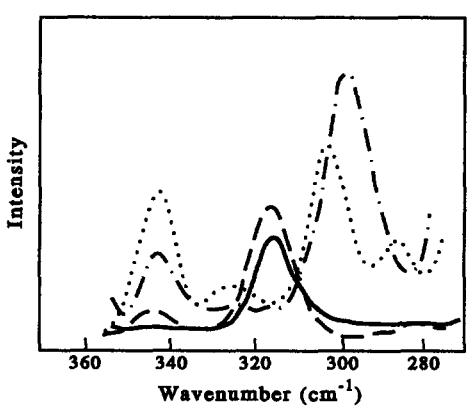

Fig. 3. Raman spectra of: —— MoO_2Cl_2(bipy); ---- MoO_2Cl_2(Bu^t-dab) (**2**); ····· MoO_2Cl_2(tmen) (**1**); and –·–·– MoO_2Cl_2(dmp) (**4**).

also has the chelating ligand symmetrically bound. X-ray powder photograms reveal that the two complexes are not isostructural in the solid state, but this does not imply that the molecular structure of the two complexes are different. The ^1H and ^{13}C NMR resonances of the azomethine groups in complexes **3** and **4** are typical for Bu^t-dab in the σ,σ'-bidentate coordination mode.[35] To avoid decomposition during acquisition the NMR spectra of $[MoO_2Cl_2(dmp)]$ (**4**) and $[WO_2Cl_2(dmp)]$ (**5**) were obtained at $-34°C$ in CD_2Cl_2. At this temperature five resonances at 3.84, 3.54, 2.88, 2.77 and 2.56 ppm (**4**) and 3.87, 3.70, 3.06, 2.97 and 2.83 ppm (**5**) appeared in ^1H NMR with the relative intensities 2:2:6:2:2. The four resonances each representing two protons are broad, having approximately 17 Hz half-width, while the single peak of the two methyl groups has only 2.5 Hz half-width. The $^{13}C\{^1H\}$ NMR spectra show two methylene resonances at 59.5 and 56.4 ppm (**4**), 60.8 and 57.3 ppm (**5**) and a methyl resonance at 47.3 and 47.5 ppm for **4** and **5**, respectively. Compared to the free ligand all proton and carbon resonances in complexes **4** and **5** are shifted to lower field, as is also observed for complexes **2** and **3**. Two possible configurations of **4** are shown in Figs 4(a) and (b). The NMR data presented above make the symmetrical configuration of **4** [Fig. 4(b)] unlikely. It has C_{2v} symmetry, thus only two sets of proton resonances (for protons *e* and *f*), a singlet for the methyl groups and two carbon resonances, one for the four methylenes and one for the methyls, should appear. On the other hand, if the configuration seen in Fig. 4(a) is adopted the observed NMR spectra can be rationalized. The spatial proximity of the protons *a* to Cl(2) and *b* to O(1) makes *a* chemically inequivalent to *b* and consequently *d* inequivalent to *c*. The carbon nuclei to which the hydrogen atoms *a*, *d* and *b*, *c*, respectively, are attached are magnetically equivalent. There are two isolated AA′BB′ spin systems present in the ^1H NMR spectrum, one consisting of protons *a* and *d* and the other consisting of protons *b* and *c*. The AA′BB′ splitting patterns as a result of geminal and vicinal couplings are not resolved and this may explain part of the broadening of the resonances assigned to these protons. Furthermore, it is reasonable that in the diazamolybdena[2.2.1]bicycloheptane frame the *exo* protons *a* and *b*, which are directed towards Cl(2) and O(1), respectively, are more deshielded than the *endo* protons *d* and *c* which are directed away from these ligands. Somewhat unexpectedly both N-methyl groups have the same chemical shift implying that they are affected by O(2) and Cl(1) to the same extent. This observation is, however, in contrast to the NMR spectra observed for MoO_2Cl_2(tmen) (**1**) and its tungsten analogue[5] where the four N-methyl groups appear as four singlets in ^1H and $^{13}C\{^1H\}$ NMR.

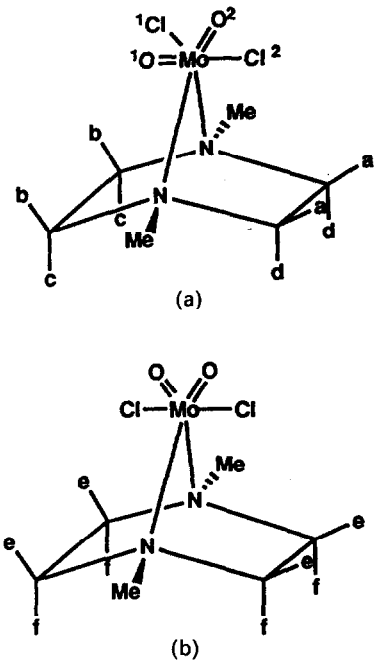

Fig. 4. Two possible configurations of $MoO_2Cl_2(dmp)$ (**4**). Hydrogen atoms a–f are omitted for clarity. (a) All *cis* and (b) *cis,trans,cis*.

Interestingly, in the ^1H NMR spectrum of complex **4** at 0°C the resonances of the protons *a*, *b* and *d*, *c* coalesce, while the methyl resonance at 2.88 ppm is not affected in position or in half-width. This effect has not been possible to confirm in the tungsten complex **5** because it is more unstable than the molybdenum complex **4** at this higher temperature.

An explanation for the observed fluxional behaviour cannot be given to date, but it can be proposed that fast scrambling on the NMR time-scale of the oxygen and chlorine atoms *cis* to the bridge-head nitrogen atoms by some not yet identified process make the protons *a* and *b* and consequently *d* and *c* equivalent.

CONCLUSIONS

In the complex $[MoO_2Cl_2(tmen)]$ (**1**), which adopts the unusual all *cis* configuration, there are two methyl groups directed above and two below a plane defined as that containing the metal atom and the nitrogen atoms. Thus, there are similarities between $[MoO_2Cl_2(Bu^t\text{-dab})]$ (**2**) and the tmen complex (**1**) with regard to the orientation of the four methyl substituents on sp^3 hybridized atoms to the MoO_2Cl_2 core. One important difference between **1** and **2** is at hand, however. In the tmen complex

(1) the sp^3-hybridized atoms are nitrogen atoms directly linked to the metal atom, thereby placing the methyl groups close to the apical ligands; in the case of the Bu^t-dab complex (2) the methyl groups are attached to the carbon atoms of the tertiary butyl groups which are not directly linked to the metal centre, thereby placing these methyl groups further away from the MoO_2Cl_2 core. Since the tmen complex (1) and the Bu^t-dab complex (2) adopt different configurations of the MoO_2Cl_2 core we find it reasonable to conclude that indeed interligand repulsions between the methyl groups of the bidentate dinitrogen ligands and the chloro and oxo ligands are of importance in determining the overall structures of the complexes **1** and **2**.

EXPERIMENTAL

All manipulations were performed on a vacuum line using standard Schlenk techniques and argon as an inert gas. Diethylether and dimethoxyethane (dme) were distilled over $LiAlH_4$ and hexamethyldisiloxane (Janssen) and solvents were dried over activated molecular sieves. N,N′-Dimethylpiperazine (dmp) (Janssen) was distilled over CaH_2; N,N′-di-t-butyl-1,4-diaza-1,3-butadiene (Bu^t-dab),[36] $WOCl_4$,[37] MoO_2Cl_2,[37] $[MoO_2Cl_2(dme)]$,[19] $[MoO_2Cl_2(tmen)]$ (**1**)[5] and $[WO_2Cl_2(dme)]$[20] were prepared according to published methods. Elemental analyses were performed by Analytische laboratorien Malissa und Reuter, Gummersbach, F.R.G. The tungsten analysis was done gravimetrically as WO_3. IR spectra (Nujol mulls between CsI plates) were recorded using a Nicolet 20SXC spectrometer. Raman spectra were recorded with a Bruker FRA 106 instrument [excitation radiation 1064 nm, resolution 4 cm^{-1}, 1000 scans, laser power 10 (**4**) to 50 mW (**2**, **3**)]. ^1H and ^{13}C spectra in $CDCl_3/CH_2Cl_2$ (**2**, **3**) or CD_2Cl_2 (**4**, **5**) solution were recorded with a Varian XL 300 spectrometer (300 MHz, $T = 298$ K (**2**, **3**), $T = 239$ K (**4**, **5**); $SiMe_4$ was the internal standard with $\delta = 0$ ppm).

X-ray crystallography

Crystals of $[MoO_2Cl_2(tmen)]$ (**1**) and $[MoO_2Cl_2(Bu^t\text{-dab})]$ (**2**) were obtained from CH_2Cl_2/heptane and CH_2Cl_2/ether, respectively. For the data collections, only the single crystals of $[MoO_2Cl_2(tmen)]$ (**1**) had to be enclosed in a capillary to keep it from air. The two data sets were corrected by Lorentz, polarization and absorption effects, the latter by an empirical method.[38] Some crystal data for complexes **1** and **2** are collected in Table 2.

Table 2. Crystal and data collection parameters for $MoO_2Cl_2(tmen)$ (**1**) and $MoO_2Cl_2(Bu^t\text{-dab})$ (**2**)

	Crystal data	
Formula	$MoC_6H_{16}Cl_2N_2O_2$ (**1**)	$MoC_{10}H_{20}Cl_2N_2O_2$ (**2**)
Molecular weight	315.05	367.13
Size	$0.30 \times 0.10 \times 0.10$	$0.20 \times 0.20 \times 0.19$
Space group	*Pbca*	*Pnma*
a (Å)	12.960(3)	19.927(7)
b (Å)	11.666(3)	9.224(2)
c (Å)	15.765(3)	8.201(2)
V (Å^3)	2383.5(5)	1507.4(4)
z	8	4
D_c (g cm^{-3})	1.76	1.62
μ(Mo-K_α) (cm^{-1})	15.0	12.0
Temperature (°C)	23	23
	Data collection and structure refinement	
Diffractometer	CAD4	
Radiation	Mo-K_α (= 0.71073 Å)	
Monochromator	Graphite	
Data collection ($2\theta_{max}$)	50	64
Scan mode	ω–2θ	ω
Independent reflections	2086	2745
Observed reflections [$I > 3\sigma(I)$]	1180	1698
Weighting scheme (w^{-1})	$\sigma^2(F_o)+(0.015F_o)^2+5.0$	$\sigma^2(F_o)+(0.04F_o)^2$
R	0.025	0.027
R_w	0.029	0.037
$\Sigma(\rho_{max})$ (e Å^{-3})	0.31	0.58

The structure of $[MoO_2Cl_2(tmen)]$ (**1**) was refined with starting parameters from the isostructural tungsten compound and the structure of $[MoO_2Cl_2(Bu^t\text{-dab})]$ (**2**) was solved by direct methods (MULTAN 87), which gave the positions of the atoms in the MoO_2Cl_2 core. The remaining atoms were located from subsequent difference Fourier syntheses. In the final refinements all non-hydrogen atoms were refined with anisotropic parameters and the hydrogen atoms with isotropic temperature factors.

Preparations

$[MoO_2Cl_2(Bu^t\text{-dab})]$ (**2**). Bu^t-dab (0.97 g, 5.7 mmol) was added to a solution of $[MoO_2Cl_2(dme)]$ (1.61 g, 5.6 mmol) in CH_2Cl_2 (90 cm^3). Alternatively, MoO_2Cl_2 (1.11 g, 5.6 mmol) suspended in CH_2Cl_2 (90 cm^3) was applied. After stirring overnight and filtering the filtrate was concentrated to approximately 30 cm^3. The white crystals which precipitated after the addition of diethylether (40 cm^3) and cooling at −30°C were collected, repeatedly washed with ether and dried *in vacuo*. Yield: 1.57 g, 77.2%. Found: C, 32.9; H, 5.3; N, 7.7; Cl, 19.2. Calc. for $C_6H_{20}Cl_2MoN_2O_2$: C, 32.7; H, 5.4; N, 7.6; Cl, 19.3%. IR and *Raman* data (in cm^{-1}): 1587w, *1588s* [ν(C=N)]; 948vs, 912vs; *948vs*, *915m* [ν(Mo=O)]; 349s, 314vw, *344w*, *316m* [ν(Mo—Cl)]; 248s, *250m*, *215s* [ν(Mo—N)]. NMR data: ^1H: 8.24 (s, 2H, —C*H*=N—) and 1.70 [s, 18H, =N—C(CH_3)$_3$]; $^{13}C\{^1H\}$: 153.8 (—*C*H=N—), 66.1 [=N—*C*(CH_3)$_3$], 28.9 [=N—C(*C*H_3)$_3$].

$[WO_2Cl_2(Bu^t\text{-dab})]$ (**3**). (a) Bu^t-dab (1.29 g, 7.7 mmol) was added to $[WO_2Cl_2(dme)]$ (2.76 g, 7.3 mmol) in CH_2Cl_2 (130 cm^3). Bu^t-dab dissolved immediately to give a clear colourless solution. After stirring for 4 h the reaction mixture was filtered and the filtrate concentrated to approximately 90 cm^3. The addition of ether (50 cm^3) and cooling at −30°C gave **3** as a white powder, which was isolated by filtration, washed thoroughly with ether (4 × 10 cm^3) and dried *in vacuo*. Yield 2.19 g, 65.7%. If the product is grey it can be recrystallized from hot acetonitrile.

(b) Hexamethyldisiloxane (1.67 g, 10.3 mmol) was added to a suspension of $WOCl_4$ (3.35 g, 9.8 mmol) in CH_2Cl_2 (150 cm^3). After vigorously stirring for 75 min solid Bu^t-dab (1.65 g, 9.8 mmol) was added to the yellow suspension. Stirring was continued for 2 h, meanwhile most of the yellow solid dissolved. The reaction mixture was filtered and the pink filtrate stored at −30°C overnight to give 1.8 g of the white product, which was isolated by filtration. Further concentration of the filtrate and cooling at −78°C gave another fraction of 1.34 g of $WO_2Cl_2(Bu^t\text{-dab})$. The solids were combined and repeatedly washed with ether and dried *in vacuo*. Yield: 3.14 g, 70.4%. Found: C, 26.7; H, 4.5; N, 6.2; Cl, 15.8; W, 40.5. Calc. for $C_6H_{20}Cl_2O_2W$: C, 26.3; H, 4.4; N, 6.1; Cl, 15.5; W, 40.4%. IR and *Raman* data (in cm^{-1}): 1606w, *1608m* [ν(C=N)]; 960vs, 925vs, *960vs*, *928m* [ν(W=O)]; 339s, 303vw, *337m*, *303vw* [ν(W—Cl)]; 247vs, *245vs*, *224m* [ν(W—N)]. NMR data: ^1H: 8.43 (s, 2H, —C*H*=N—) and 1.66 [s, 18H, =N—C(CH_3)$_3$]; $^{13}C\{^1H\}$: 155.7 (—*C*H=N—), 67.1 [=N—*C*(CH_3)$_3$], 28.8 [=N—C(*C*H_3)$_3$].

$[MoO_2Cl_2(dmp)]$ (**4**). Dmp (0.19 g, 1.7 mmol) dissolved in CH_2Cl_2 (20 cm^3) was added dropwise either to a solution of $[MoO_2Cl_2(dme)]$ (0.47 g, 1.6 mmol) in CH_2Cl_2 (15 cm^3) at −78°C or a suspension of MoO_2Cl_2 (0.32 g, 1.6 mmol) in CH_2Cl_2 (15 cm^3) at −78°C. After the addition of dmp (10 min) the cooling was removed and the clear orange–brown solution was stirred at approximately −10°C for 90 min. The brown–green precipitate which formed was filtered and the filtrate quickly evaporated to dryness. The remaining light brown powder was dried *in vacuo*. Yield: 0.33 g, 66%. Found: C, 23.2; H, 4.6; N, 8.8; Cl, 22.6. Calc. for $C_8H_{14}Cl_2MoN_2O_2$: C, 23.0; H, 4.5; N, 8.9; Cl, 22.6%. IR and *Raman* data (in cm^{-1}): 933vs, *933vs* [ν_s(Mo=O)]; 896vs, *902vs* [ν_{as}(Mo=O)]; 340s,b, 296w, *342w*, *297m* [ν(Mo—Cl)]. NMR data: ^1H: 3.84 (m, 2H, CH_2), 3.54 (m, 2H, CH_2), 2.88 (s, 6H, CH_3), 2.77 (m, 2H, CH_2), 2.56 (m, 2H, CH_2); $^{13}C\{^1H\}$: 59.5 (*C*H_2), 56.4 (*C*H_2), 47.3 (*C*H_3).

$WO_2Cl_2(dmp)]$ (**5**). This compound was obtained under the same reaction conditions as $[MoO_2Cl_2(dmp)]$: $[WO_2Cl_2(dme)]$ (1.43 g, 3.79 mmol) and dmp (0.45 g, 3.98 mmol) in CH_2Cl_2 (70 cm^3) gave **5** as a grey, light-sensitive powder. Yield: 0.67 g, 42.0%. Found: C, 17.8; H, 3.7; N, 6.8; Cl, 17.8; W, 45.4. Calc. for $C_8H_{14}Cl_2N_2O_2W$: C, 17.9; H, 3.5; N, 6.9; Cl, 17.6; W, 45.8%. IR data (in cm^{-1}): 953vs [ν_s(W=O)], 907vs [ν_{as}(W=O)], 340s,b, 298w [ν(W—Cl)]. NMR data: ^1H: 3.87 (m, 2H, CH_2), 3.7 (m, 2H, CH_2), 3.06 (s, 6H, CH_3), 2.97 (m, 2H, CH_2), 2.83 (m, 2H, CH_2); $^{13}C\{^1H\}$: 60.8 (*C*H_2), 57.3 (*C*H_2), 47.5 (*C*H_3).

Acknowledgements—Financial support from NUTEK (Swedish National Board for Industrial and Technical Development) and TFR (Swedish Research Council for Engineering Sciences) is gratefully acknowledged.

REFERENCES

1. G. Schoettel, J. Kress and J. A. Osborn, *J. Chem. Soc., Chem. Commun.* 1989, 1062.

2. R. R. Schrock, R. T. DePue, J. Feldman, Y. B. Yap, D. C. Yang, D. M. Gavis, L. Park, M. DiMare, M. Schofield, J. Anhaus, E. Walborsky, E. Evitt, C. Krüger and P. Betz, *Organometallics* 1990, **9**, 2262.
3. R. H. Holm, *Chem. Rev.* 1987, **87**, 1401.
4. E. I. Stiefel, *Prog. Inorg. Chem.* 1977, **22**, 1.
5. K. Dreisch, C. Andersson and C. Stålhandske, *Polyhedron* 1992, **11**, 2143.
6. M. Gullotti, A. Pasini, G. M. Zanderighi, G. Ciani and A. Sironi, *J. Chem. Soc., Dalton Trans.* 1980, 902.
7. P. B. Viossat and N. Rodier, *Acta Cryst.* 1979, **B35**, 2715.
8. W. A. Herrmann, W. R. Thiel and E. Herdtweck, *Chem. Ber.* 1990, **123**, 271.
9. G. N. Schrauzer, L. A. Hughes, N. Strampach, P. R. Robinson and E. O. Schlemper, *Organometallics* 1982, **1**, 44.
10. G. N. Schrauzer, L. A. Hughes, N. Strampach, F. Ross, D. Ross and E. O. Schlemper, *Organometallics* 1983, **2**, 481.
11. C. Zhang, E. O. Schlemper and G. N. Schrauzer, *Organometallics* 1990, **9**, 1016.
12. C. Zhang, X. Zhang, N. H. Liu, G. N. Schrauzer and E. O. Schlemper, *Organometallics* 1990, **9**, 1307.
13. I. Sense, H. Stenger, U. Müller and K. Dehnicke, *Z. Anorg. Allg. Chem.* 1992, **610**, 117.
14. G. N. Schrauzer, E. O. Schlemper, N. H. Liu, Qu. Wang, K. Rubin, X. Zhang, X. Long and C. S. Chin, *Organometallics* 1986, **5**, 2452.
15. G. V. Koten and K. Vrieze, *Advances in Organometallic Chemistry* (Edited by F. G. A. Stone and R. West), Vol. 21, p. 151 (1982).
16. A. J. L. Pombeiro and M. F. N. N. Carvalho, *Rev. Port. Quim.* 1981, **23**, 23.
17. A. J. L. Pombeiro and R. L. Richards, *Trans. Met. Chem.* 1981, **6**, 255.
18. L. H. Staal, G. V. Koten and K. Vrieze, *J. Organomet. Chem.* 1979, **175**, 73.
19. B. Kamenar, M. Penavic, B. Korpar-Colig and B. Markovic, *Inorg. Chim. Acta* 1982, **65**, L245.
20. K. Dreisch, C. Andersson and C. Stålhandske, *Polyhedron* 1991, **10**, 2417.
21. J. Elmsley, *The Elements*. Clarendon Press, Oxford (1991).
22. J. A. Mayer, *Inorg. Chem.* 1988, **27**, 3899.
23. L. R. Florian and E. R. Corey, *Inorg. Chem.* 1968, **7**, 722.
24. B. Kamenar and M. Penavic, *Acta Cryst.* 1976, **B32**, 3323.
25. C. G. Pierpont and H. H. Downs, *Inorg. Chem.* 1977, **16**, 2970.
26. P. B. Viossat, P. Khodadad and N. Rodier, *Acta Cryst.* 1977, **B33**, 2523.
27. R. J. Butcher, B. R. Penfold and E. Sinn, *J. Chem. Soc., Dalton Trans.* 1979, 668.
28. J. Reinhold, R. Benedix, P. Birner and H. Hennig, *Inorg. Chim. Acta* 1979, **33**, 209.
29. W. M. Carmichael, D. A. Edwards, G. W. A. Fowles and P. R. Marshall, *Inorg. Chim. Acta* 1967, **1**, 93.
30. I. Hargittai and R. Seip, *Acta Chem. Scand.* 1976, **A30**, 540.
31. W. P. Griffith and T. D. Wickins, *J. Chem. Soc. A* 1968, 400.
32. L. H. Staal, D. J. Stufkens and A. Oskam, *Inorg. Chim. Acta* 1978, **26**, 255.
33. W. Zablinskas, personal communication.
34. R. J. Butcher, H. P. Gunz, R. G. A. R. Maclagan, H. K. J. Powell, C. J. Wilkins and Y. A. Hiam, *J. Chem. Soc., Dalton Trans.* 1975, 1223.
35. L. H. Staal, A. Oskam and K. Vrieze, *J. Organomet. Chem.* 1979, **170**, 235.
36. J. M. Klirgman and R. G. Barnes, *Tetrahedron* 1970, **26**, 2555.
37. V. C. Gibson, T. P. Kee and A. Shaw, *Polyhedron* 1990, **9**, 2293.
38. N. Walker and D. Stuart, *Acta Cryst.* 1983, **A39**, 158.

Polyhedron Vol. 12, No. 3, pp. 313–317, 1993
Printed in Great Britain

0277–5387/93 $6.00+.00
© 1993 Pergamon Press Ltd

SYNTHESIS AND SPECTROSCOPIC STUDIES OF OXOVANADIUM(IV) COMPLEXES WITH 16- AND 18-MEMBERED MACROCYCLIC LIGANDS

H. S. YADAV

Chemistry Division, North Eastern Regional Institute of Science and Technology, Nirjuli 791 109, Itanagar, Arunachal Pradesh, India

(*Received* 23 *June* 1992; *accepted* 10 *September* 1992)

Abstract—Oxovanadium(IV) complexes of the type $[VO(L)](SO_4)$ (where L = ligands derived by reaction between 2,6-pyridinedicarboxylic acid and ethylenediamine or propanediamine in a 1 : 2 molar ratio) have been prepared by *in situ* synthesis. These complexes react with different β-diketones to yield macrocyclic products of the type $[VO(mac)](SO_4)$ (where mac = macrocyclic ligands). Tentative structures of the complexes have been proposed on the basis of elemental analyses, magnetic moments and spectral (IR, electronic and ESR) data. The *X*-band ESR spectra of all the complexes were recorded at room temperature and at liquid nitrogen temperature (177 K). The values of $|g|$, $g_\parallel$, $g_\perp$, $|A|$, $A_\parallel$ and $A_\perp$ were obtained. The room temperature ESR spectra do not show anisotropy because of rapid tumbling of the molecules in solution, but it is clearly visible at 177 K. The spectral studies support square pyramidal geometry for the five-coordinate oxovanadium(IV) complexes.

Vanadium is widely distributed in the biosphere[1] and its essential role has been recognized in both plants and animals.[2–8] The oxovanadium(IV) cation has been found to inhibit the plasma membrane ATPase of *Neurospora crassa*[9] and *Saccharomyces cerevisiae*,[10] the proton translocating ATPase of *Mycobacterium phlei*[11] and Ca^{2+}-ATPase of red cell membranes.[12] It has been observed that the free vanadyl ion is oxidized to vanadate within a few minutes in aqueous solution exposed to air at neutral pH. However, the tetravalent state appears to be stable when complexed with intracellular proteins or smaller molecules.[13] Thus, the complex formation of the oxovanadium(IV) cation with macrocyclic ligands appears to be interesting, particularly in order to explore the biochemical importance of the oxovanadium(IV) cation *in vitro* at neutral pH. In this communication, the synthesis and characterization of oxovanadium(IV) complexes with ligands derived from 2,6-pyridinedicarboxylic acid and ethylenediamine or propanediamine (type I) are reported. The reactions of these complexes with β-diketones such as acetylacetone, benzoylacetone and dibenzoylmethane, leading to the formation of macrocyclic products (type II), are also reported.

EXPERIMENTAL

The oxovanadium(IV) complexes of type I were prepared by mild heating and stirring the solutions of vanadyl sulphate, 2,6-pyridinedicarboxylic acid and ethylenediamine or propanediamine in 1 : 1 : 2 molar ratios in ethanol for 1 h. The resulting green precipitate was filtered, thoroughly washed with ethanol and dried at 110°C. A suspension of complex **I** in ethanol was mixed with an appropriate β-diketone solution in ethanol in a 1 : 1 molar ratio and the reaction mixture was stirred with mild heating for 1 h. The resulting deep-green coloured complexes were filtered, thoroughly washed with ethanol and dried at 110°C.

Microanalyses for carbon, hydrogen and nitrogen were performed by the CDRI, Lucknow. Sulphur was estimated as barium sulphate.[14] The vanadium was estimated gravimetrically as its vanadate after decomposing the complex with concentrated nitric acid.[15] The magnetic susceptibility measurements and electronic spectra of complexes were performed at the Faculty of Science, University of Gorakhpur. IR spectra were recorded in KBr medium on a Perkin–Elmer Model 983 spec-

trometer at RSIC, NEHU, Shillong. The ESR spectra were recorded on a Varian-E-4 spectrometer (*X*-band) in DMSO at RSIC, IIT, Madras.

RESULTS AND DISCUSSION

The oxovanadium(IV) complexes of type I were synthesized *in situ* by stirring with mild heating of the reaction mixture containing vanadyl sulphate, 2,6-pyridinedicarboxylic acid, ethylenediamine or propanediamine in 1 : 1 : 2 molar ratios in aqueous ethanol medium. The reactions appear to proceed as follows:

$$VOSO_4 \cdot H_2O + \text{2,6-pyridinedicarboxylic acid} \xrightarrow[\text{ethanol}]{+\text{ethylenediamine or propanediamine}} \underset{\textbf{(I)}}{[VO(L)]SO_4} + 3H_2O;$$

where L = ligand derived by reaction of 2,6-pyridinedicarboxylic acid with ethylenediamine or propanediamine.

The reaction of complex **I** with different β-diketones in 1 : 1 molar ratios results in the condensation of the terminal amino group of complex **I** with ketonic groups of the β-diketones yielding macrocyclic complexes of type **II**, [VO(mac)](SO$_4$). The elemental analyses (Table 1) of complexes show 1 : 1 metal-to-ligand stoichiometry.

IR spectra

The important IR bands for the complexes are listed in Table 2. The oxovanadium(IV) complexes of type I show bands at 1690, 1510, 1230 and 470 cm^{-1}, assignable[16] to amide-I [ν(C=O)], amide-II [ν(CN) + δNH], amide-III (δNH) and amide-IV (ϕCO) vibrations, respectively. It is evident that in the complexes the amide-II and amide-III bands are lowered ($\sim$ 30 cm^{-1}), whereas the amide-I and amide-IV bands are unperturbed in comparison to the free ligands. This indicates the coordination of amide nitrogen atoms and the non-coordination of amide oxygen atoms.[17] The bands appearing at 3350 and 3180 cm^{-1} may be assigned to asymmetrical and symmetrical N—H stretching modes of the coordinated terminal amino group.[18] The coordination of nitrogen atoms to vanadium is further supported by the appearance of a band at *ca* 310 cm^{-1}, which may be assigned to the ν(V—N) vibrations.[19] The unchanged pyridine ring

Table 1. Physical and analytical data of the complexes

Complex	Empirical formula	Colour	Decomposition temperature (°C)	Calc. (Found) % C	H	N	V	S	μ_{eff} (B.M.) (300 K)
[VO(L^1)](SO$_4$)	$C_{11}H_{17}N_5O_7SV$	Green	190	31.9 (31.8)	4.1 (4.0)	16.9 (16.8)	12.3 (12.3)	7.7 (7.6)	1.71
[VO(L^2)](SO$_4$)	$C_{13}H_{21}N_5O_7SV$	Green	189	35.3 (35.1)	4.8 (4.8)	15.8 (15.7)	11.5 (11.5)	7.2 (7.1)	1.73
[VO(mac^1)](SO$_4$)	$C_{16}H_{21}N_5O_7SV$	Green	196	40.2 (40.1)	4.4 (4.3)	14.6 (14.6)	10.6 (10.5)	6.7 (6.5)	1.76
[VO(mac^2)](SO$_4$)	$C_{21}H_{23}N_5O_7SV$	Green	198	46.7 (46.6)	4.3 (4.3)	12.9 (12.7)	9.4 (9.4)	5.9 (5.8)	1.74
[VO(mac^3)](SO$_4$)	$C_{26}H_{25}N_5O_7SV$	Green	191	51.8 (51.7)	4.1 (4.0)	11.6 (11.5)	8.4 (8.4)	5.3 (5.2)	1.74
[VO(mac^4)](SO$_4$)	$C_{18}H_{25}N_5O_7SV$	Green	190	42.7 (42.6)	4.9 (4.8)	13.8 (13.8)	10.0 (9.9)	6.3 (6.1)	1.75
[VO(mac^5)](SO$_4$)	$C_{23}H_{27}N_5O_7SV$	Green	192	48.6 (48.4)	4.8 (4.8)	12.3 (12.1)	8.9 (8.9)	5.6 (5.5)	1.76
[VO(mac^6)](SO$_4$)	$C_{28}H_{29}N_5O_7SV$	Green	195	53.3 (53.1)	4.6 (4.5)	11.1 (11.1)	8.0 (8.0)	5.0 (5.0)	1.74

L^1 and L^2 = Ligands derived by reaction between 2,6-pyridinedicarboxylic acid and ethylenediamine or propanediamine, respectively.

mac^1, mac^2 and mac^3 = Macrocyclic ligands derived by reaction between L^1 and acetylacetone or benzoylacetone or dibenzoylmethane, respectively.

mac^4, mac^5 and mac^6 = Macrocyclic ligands derived by reaction between L^2 and acetylacetone or benzoylacetone or dibenzoylmethane, respectively.

Table 2. Some characteristic IR spectral bands of the complexes

Complex	IR spectra (cm^{-1})							
	Amide-II [ν(CN)+ δNH]	Amide-III (δNH)	ν_{asym}(NH)	ν_{sym}(NH)	ν(>NH)	ν(V—N)	ν(V=O)	$\nu(SO_4^{2-})$
$[VO(L^1)](SO_4)$	1510s	1230m	3350s	3180s	—	310s	980s	1130m, 955w, 605m
$[VO(L^2)](SO_4)$	1515m	1230s	3345m	3175m	—	305m	980m	1135m, 955m, 610w
$[VO(mac^1)](SO_4)$	1510s	1225m	3350s	3180m	3210s	310m	980s	1135s, 960m, 610m
$[VO(mac^2)](SO_4)$	1510s	1230m	3350m	3170s	3210m	300s	980s	1135m, 960w, 610w
$[VO(mac^3)](SO_4)$	1515m	1225m	3345s	3180m	3210s	305m	980m	1130s, 960m, 600m
$[VO(mac^4)](SO_4)$	1510s	1230s	3350s	3180m	3205m	305s	980s	1135m, 955w, 605m
$[VO(mac^5)](SO_4)$	1515m	1225m	3345m	3175s	3210s	310m	980s	1130m, 955m, 610s
$[VO(mac^6)](SO_4)$	1510s	1230m	3350s	3180m	3205m	310s	980m	1135s, 960m, 610w

s = strong; m = medium; w = weak.

vibrations[20,21] occuring at 1580 (8a, pyridine ring deformation), 610 (6a, in-plane ring deformation) and 400 cm^{-1} (16b, out-of-plane ring deformation) in the complexes indicate non-coordination of the pyridine nitrogen to vanadium. The oxovanadium(IV) complexes show a band at 980 cm^{-1}, which is assigned to the ν(V=O) vibration.[22] The presence of an ionic sulphate group in the complexes is confirmed by the appearance of three bands at *ca* 1130–1135 (ν_3), 955–960 (ν_1) and 600–610 cm^{-1} (ν_4). The absence of a ν_2 band and non-splitting of the ν_3 band indicate that *Td* symmetry is retained.[16] The IR spectra of macrocyclic complexes show the same pattern of bands, except a new band at 1610–1615 cm^{-1} which is assigned to the coordinated ν(>C=N) group.[23] The two bands due to asymmetric and symmetric N—H stretching modes also disappear in the macrocyclic complexes and only one band is observed in the ν(NH) region at 3210 cm^{-1} which may be due to a secondary amino group, establishing the condensation of a primary amino group of type I complexes with the carbonyl group of diketones.

Magnetic moments and electronic spectra

Oxovanadium(IV) complexes show magnetic moment values in the range 1.70–1.76 B.M. at room temperature. These values are in the range reported for oxovanadium(IV) complexes with one unpaired electron.[24] The electronic spectra show bands in the regions 11,040–11,980, 15,040–15,920 and 21,090–22,380 cm^{-1}. These spectra are similar to other five coordinate oxovanadium(IV) complexes involving nitrogen donor atoms. Such a spectrum has been predicted for five-coordinate complexes possessing the effective C_v symmetry of a square pyramid. Wasson *et al.*[25] have reported an energy level scheme ($d_{xy} < d_{yz} < d_{xz} < d_{x^2-y^2} < d_{z^2}$) to interpret the electronic spectra of distorted, five-coordinate square-pyramidal oxovanadium(IV) complexes. Accordingly, the observed bands can be assigned to $^2B_2 \rightarrow {}^2E$, $^2B_2 \rightarrow {}^2B_1$ and $^2B_2 \rightarrow {}^2A_1$ transitions, respectively. One more band is observed in the region 35,280–35,780 cm^{-1}, which may be due to transitions of the azomethine linkages.[26]

ESR spectra

The *X*-band ESR spectra of an oxovanadium(IV) complex recorded in DMSO at room temperature and at liquid nitrogen temperature (177 K) is shown in Figs 1(a) and 1(b), respectively. The ESR spectra of the complexes were analysed by the method of Kneubuhl,[27] Sands[28] and Garman *et al.*[29] The room-temperature ESR spectra show eight lines, which are due to hyperfine splitting arising from the interaction of the unpaired electron with a ^{51}V nucleus having the nuclear spin number $I = 7/2$. This confirms the presence of a single oxovanadium(IV) cation as the metallic centre in the complex. The anisotropy is not observed due to rapid tumbling of molecules in solution at room temperature and only *g*-average values are obtained. The anisotropy is clearly visible in the spectra at liquid nitrogen temperature and eight bands each due to $g_\parallel$ and $g_\perp$ are observed separately. The $g_\parallel$, $g_\perp$, $A_\parallel$ and $A_\perp$ values (Table 3) are measured from the spectra, which are in good agreement for a square-pyramidal structure.[30–32] The g_{iso} value from mobile solution at room temperature and g_{av} from frozen solution at liquid nitrogen temperature do not agree very closely since the *g* and *A* tensors are corrected for second-order. Furthermore, the *g*

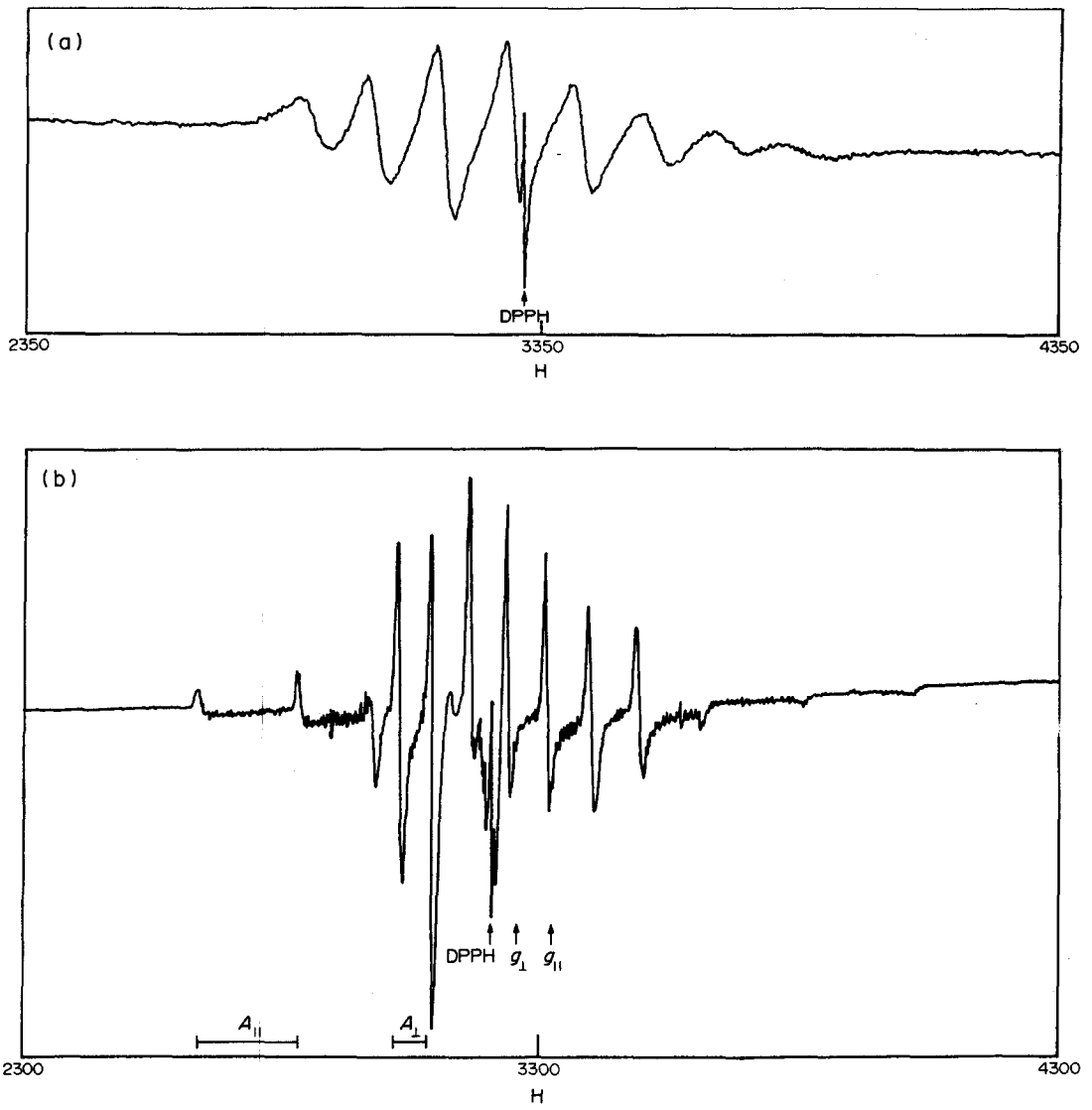

Fig. 1. EPR spectra of $[VO(L^1)](SO_4)$ in DMSO at (a) room temperature and (b) liquid nitrogen temperature.

Table 3. Room temperature g values and liquid nitrogen temperature g and A values of oxovanadium(IV) complexes

Complex	Room temperature	Liquid nitrogen temperature					
	$\|g\|$	$g_\parallel$	$g_\perp$	$\|g\|$	$A_\parallel$	$A_\perp$	$\|A\|$
$[VO(L^1)](SO_4)$	1.973	1.931	1.971	1.957	190.70	66.40	107.83
$[VO(L^2)](SO_4)$	1.982	1.934	1.978	1.963	191.65	65.81	107.75
$[VO(mac^1)](SO_4)$	1.988	1.935	1.979	1.977	188.54	64.82	106.06
$[VO(mac^2)](SO_4)$	1.978	1.932	1.976	1.961	185.46	65.50	105.55
$[VO(mac^3)](SO_4)$	1.980	1.938	1.984	1.968	186.45	66.74	106.64
$[VO(mac^4)](SO_4)$	1.979	1.933	1.976	1.961	184.38	64.50	104.46
$[VO(mac^5)](SO_4)$	1.976	1.938	1.983	1.968	188.25	66.79	107.27
$[VO(mac^6)](SO_4)$	1.978	1.935	1.978	1.963	187.46	66.59	106.88

values are all very close to the spin-only value (free electron value) of 2.0023, suggesting little spin-orbit coupling.

On the basis of the above studies, the following tentative structures may be proposed for these oxovanadium(IV) complexes.

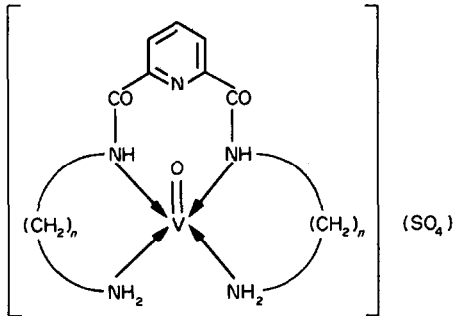

I

where $n = 2$ for ethylenediamine,
$n = 3$ for propanediamine.

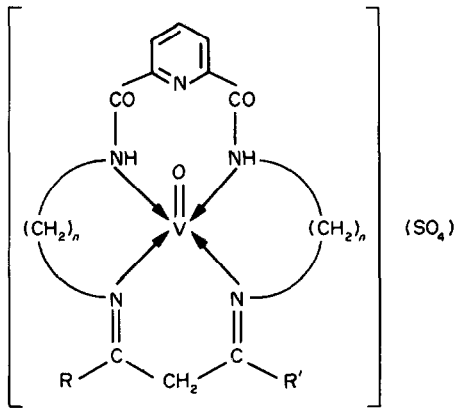

II

where $n = 2$ for ethylenediamine,
$n = 3$ for propanediamine

and

R	R′	β-Diketone
CH_3	CH_3	Acetylacetone
C_6H_5	CH_3	Benzoylacetone
C_6H_5	C_6H_5	Dibenzoylmethane

Acknowledgements—The author thanks the C.S.I.R., New Delhi, for financial help and Dr Harish Chand, Department of Chemistry, NEHU, Shillong, for his valuable discussions on the ESR spectra.

REFERENCES

1. G. Wilkinson (Editor), *Comprehensive Coordination Chemistry*, Vol. 6, p. 665. Pergamon Press, Oxford (1987).
2. E. J. Underwood, *Trace Elements in Human and Animal Nutrition*, p. 416. Academic Press, London (1971).
3. K. Kustin and I. G. Macara, *Comments Inorg. Chem.* 1982, **2**, 1.
4. N. D. Chasteen, *Struct. Bonding* 1983, **53**, 105.
5. E. J. Baren, *Quimica Bio-inorganica*. Ediciones Faba. La Plata, Argentina (1984).
6. R. L. Robson, R. R. Eady, T. H. Richardson, R. W. Miller, M. Hawkins and J. R. Postagate, *Nature* 1986, **322**, 288.
7. R. Cammack, *Nature* 1986, **322**, 312.
8. B. J. Hates, E. E. Case, J. E. Morningstar, M. F. Dzeda and L. A. Mauterer, *Biochemistry* 1986, **25**, 7251.
9. B. J. Bowman and C. W. Slayman, *J. Biol. Chem.* 1979, **254**, 2928.
10. G. R. Willsky, *J. Biol. Chem.* 1979, **254**, 3326.
11. F. Yoshimura and A. F. Brodie, *J. Biol. Chem.* 1981, **256**, 12239.
12. J. P. F. C. Rossi, P. J. Garrahan and A. F. Rega, *Biochim. Biophys. Acta* 1981, **648**, 145.
13. P. North and R. L. Post, *J. Biol. Chem.* 1984, **259**, 4971.
14. A. J. Vogel, *A Text Book of Practical Organic Chemistry*, 4th edn. Longmans Green Co. Ltd, London (1978).
15. A. I. Vogel, *A Text Book of Quantitative Inorganic Analysis*, 4th edn. Longmans Green Co. Ltd, London (1968).
16. M. Nonoyama, S. Tomita and K. Yamasaki, *Inorg. Chim. Acta* 1975, **12**, 33.
17. S. K. Sahni, *Trans. Met. Chem.* 1979, **4**, 73.
18. J. R. Dyer, *Applications of Absorption Spectroscopy of Organic Compounds*. Prentice-Hall, Inc., Englewood Cliffs, NJ (1965).
19. J. R. Ferraro, *Low Frequency Vibrations of Inorganic and Coordination Compounds*. Plenum Press, New York (1971).
20. D. P. Madden, M. M. daMota and S. M. Nelson, *J. Chem. Soc. A* 1970, 890.
21. D. P. Madden and S. M. Nelson, *J. Chem. Soc. A* 1968, 2342.
22. K. Sakata, M. Kuroda, S. Yanagida and M. Hashimoto, *Inorg. Chim. Acta* 1989, **156**, 107.
23. H. S. Yadav, *Bull. Soc. Chim. France* 1990, **127**, 641.
24. A. Syamal, *Coord. Chem. Rev.* 1975, **21**, 309.
25. H. J. Stocklosa, J. R. Wasson and M. J. McCormick, *Inorg. Chem.* 1964, **13**, 592.
26. P. C. H. Mitchell and J. A. Valero, *Inorg. Chim. Acta* 1983, **71**, 179.
27. F. K. Kneubuhl, *J. Chem. Phys.* 1960, **33**, 1074.
28. R. H. Sands, *Phys. Rev.* 1955, **99**, 1222.
29. H. R. Garman and J. D. Swalen, *J. Chem. Phys.* 1962, **56**, 3221.
30. A. Syamal and K. S. Kale, *Ind. J. Chem.* 1979, **17A**, 518.
31. L. J. Boucher, E. C. Tynan and T. F. Yen, *Inorg. Chem.* 1968, **A**, 731.
32. L. J. Boucher and T. F. Yen, *Inorg. Chem.* 1969, **8**, 689.

Polyhedron Vol. 12, No. 3, pp. 319–325, 1993
Printed in Great Britain

0277–5387/93 $6.00+.00
Pergamon Press Ltd

SYNTHESES AND CRYSTAL STRUCTURES OF $[Rh(1\text{-}3:5,6\text{-}\eta^5\text{-}C_8H_{11})(\eta^5\text{-}7,8\text{-}C_2B_9H_9Me_2)]$ AND $[RhCl(PMe_3)_2(\eta^5\text{-}7,8\text{-}C_2B_9H_9Me_2)]$ AND RELATED STUDIES

JOHN C. JEFFERY, F. GORDON A. STONE* AND ISIL TOPALOĞLU

School of Chemistry, The University of Bristol, Bristol BS8 1TS, U.K.

(*Received* 25 *August* 1992; *accepted* 28 *August* 1992)

Abstract—Treatment of $[NEt_4][Rh(cod)(\eta^5\text{-}7,8\text{-}C_2B_9H_9Me_2)]$ (cod = cyclo-octa-1,5-diene) in THF with $[CPh_3][BF_4]$ affords the complex $[Rh(1\text{-}3:5,6\text{-}\eta^5\text{-}C_8H_{11})(\eta^5\text{-}7,8\text{-}C_2B_9H_9Me_2)]$, the structure of which has been established by X-ray diffraction. The *nido*-$7,8\text{-}C_2B_9H_9Me_2$ ligand is attached to the rhodium in the usual pentahapto manner, while the cyclo-octadienyl C_8H_{11} group ligates the metal centre in a $1\text{-}3:5,6\text{-}\eta^5$ bonding mode. The complex $[Rh(\eta^3\text{-}C_8H_{13})(\eta^5\text{-}7,8\text{-}C_2B_9H_9Me_2)]$ in CH_2Cl_2 adds a molecule of CO to afford $[Rh(CO)(\eta^3\text{-}C_8H_{13})(\eta^5\text{-}7,8\text{-}C_2B_9H_9Me_2)]$, and reacts with excess PMe_3 and PEt_3 to give $[RhCl(PMe_3)_2(\eta^5\text{-}7,8\text{-}C_2B_9H_9Me_2)]$ (whose structure was determined by X-ray crystallography) and $[RhH(PEt_3)_2(\eta^5\text{-}7,8\text{-}C_2B_9H_9Me_2)]$, respectively.

We have reported elsewhere the syntheses of complexes in which rhodium is bonded to rhenium, cobalt, iridium, platinum or gold using as reagents the salts $[NEt_4][Rh(CO)(L)(\eta^5\text{-}7,8\text{-}C_2B_9H_9R_2)]$ (L = PPh_3 or CO, R = H or Me).[1] In a recent extension of this study we have employed the salt $[NEt_4][Rh(cod)(\eta^5\text{-}7,8\text{-}C_2B_9H_9Me_2)]$ (**1**) to obtain dimetal species with bonds between rhodium and copper and manganese.[2] The anionic complex $[Rh(cod)(\eta^5\text{-}7,8\text{-}C_2B_9H_9Me_2)]^-$ was first prepared by Hawthorne and co-workers,[3] who isolated it as the $[N(PPh_3)_2]$ salt. It was found that protonation with CF_3CO_2H afforded initially an unstable intermediate with a C—H→Rh interaction, which rearranged to give an unusually stable 16-electron allylic complex, $[Rh(\eta^3\text{-}C_8H_{13})(\eta^5\text{-}7,8\text{-}C_2B_9H_9Me_2)]$ (**2**). In this paper we report the results of treating **1** with the hydride abstracting reagent $[CPh_3][BF_4]$, and reactions of compound **2** with CO, PMe_3 and PEt_3.

RESULTS AND DISCUSSION

The reaction between **1** and $[CPh_3][BF_4]$ in THF gave the complex $[Rh(1\text{-}3:5,6\text{-}\eta^5\text{-}C_8H_{11})(\eta^5\text{-}7,8\text{-}C_2B_9H_9Me_2)]$ (**3**) (Scheme 1), characterized by microanalysis and NMR spectroscopy (Tables 1 and 2). The molecular structure of **3** was fully established by a single-crystal X-ray diffraction study, data from which are listed in Table 3. The molecular structure is shown in Fig. 1.

The rhodium atom is penta-coordinated by the open face of the *nido*-icosahedral $7,8\text{-}C_2B_9H_9Me_2$ fragment in the usual manner,† with Rh—C_2B_3 ring distances in the range 2.181(3)–2.272(3) Å. In compound **2** the corresponding connectivities are 2.12–2.20 Å.[3] The cyclo-octadienyl ligand in **3** ligates the metal via carbon atoms C(21), C(22), C(24), C(25) and C(26) [Rh—C(21) 2.251(3), Rh—C(22) 2.258(3), Rh—C(24) 2.331(4), Rh—C(25) 2.166(4), Rh—C(26) 2.202(3) Å]. The allyl function is not symmetrically bound to the rhodium, with Rh—C(24) being the longest separation and Rh—C(25) the shortest, and Rh—C(26) being intermediate between the two. This may be partly due to the conformation adopted by the C_8H_{11} moiety and partly to give sufficient clearance for the

* Author to whom correspondence should be addressed (at the Department of Chemistry, Baylor University, Waco, TX 76798-7348, U.S.A.).

† In this paper, and in related articles,[1] we designate the four-electron donor carbaborane cage as $\eta^5\text{-}7,8\text{-}C_2B_9H_9Me_2$ in order to emphasize its relationship with the five-electron donor $\eta^5\text{-}C_5H_5$ group. However, in **3** the rhodium atom and the carbaborane framework form a *closo*-$1,2\text{-}Me_2\text{-}3,1,2\text{-}RhC_2B_9H_9$ structure.

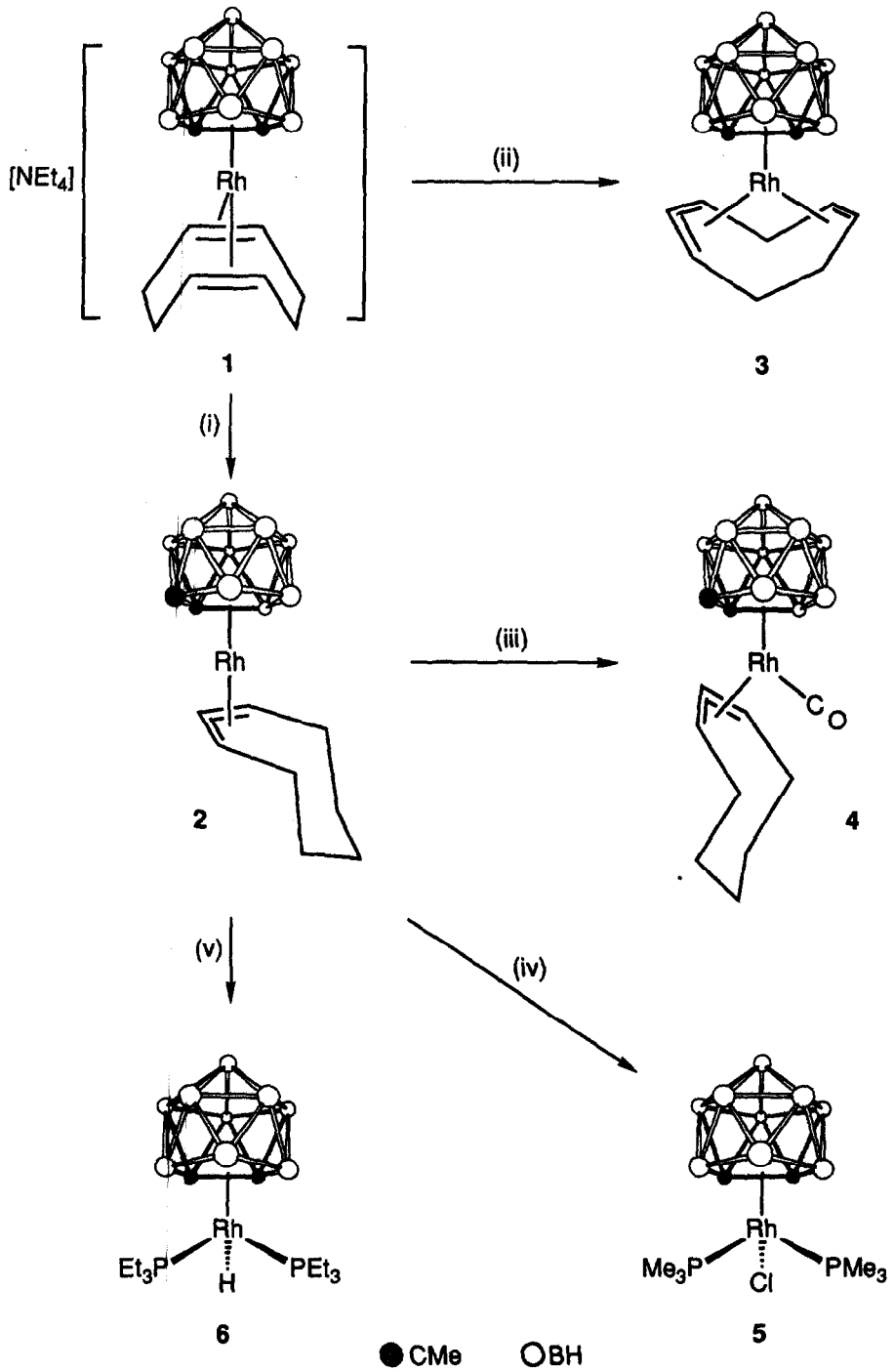

Scheme 1. (i) CF_3CO_2H/CH_2Cl_2, (ii) $[CPh_3][BF_4]/CH_2Cl_2$, (iii) CO, (iv) PMe_3/CH_2Cl_2 and (v) PEt_3/CH_2Cl_2.

$C(23)H_2$ group, the single methylene fragment separating the η^3-allyl and η^2-alkene functions. In contrast with the asymmetric allylic-rhodium bonding in **3**, that in complex **2** is essentially symmetric (Rh—η^3-C_3 2.136, 2.167 and 2.130 Å).[3]

The 1-3 : 5,6-η^5-C_8H_{11} bonding in **3** is similar to that established by X-ray crystallography in the compound $[Ru(1\text{-}3 : 5,6\text{-}\eta^5\text{-}C_8H_{11})(\eta^6\text{-}C_8H_{10})][PF_6]$ (η^6-C_8H_{10} = 1,3,5-cyclo-octatriene).[4] In this complex also the allyl function is not symmetrically bound to the metal [Ru—η^3-C_3 2.20(2), 2.21(2) and 2.46(3) Å]. As in **3** the longer connectivity is associated with the CH group separated by only one CH_2 fragment from the η^2-CH=CH moiety.

Table 1. Analytical[a] and other data for the rhodium complexes

	Compound[b]	Colour	Yield (%)	Analysis (%) C	H
3	[Rh(1-3 : 5,6-η^5-C_8H_{11})(η^5-7,8-$C_2B_9H_9Me_2$)]	Yellow	61	38.7 (38.5)	7.2 (7.2)
4	[Rh(CO)(η^3-C_8H_{13})(η^5-7,8-$C_2B_9H_9Me_2$)]	Orange	85	38.2 (38.9)	6.1 (6.9)
5	[RhCl(PMe_3)$_2$(η^5-7,8-$C_2B_9H_9Me_2$)][c]	Yellow	71	24.5 (24.7)	6.8 (6.6)
6	[RhH(PEt_3)$_2$(η^5-7,8-$C_2B_9H_9Me_2$)]	Brick red	51	37.5 (38.3)	9.1 (8.1)

[a] Calculated values are given in parentheses.

[b] In their IR spectra all the compounds showed a broad band at *ca* 2550 cm^{-1} due to B—H. In addition, complex **4** displayed a very strong ν_{max}(CO) absorption at 2047 cm^{-1}.

[c] Complex crystallizes with a molecule of CH_2Cl_2.

The ^1H and $^{13}C\{^1H\}$ NMR data for **3** (Table 2) are in agreement with the molecular structure established by X-ray crystallography. The ^1H assignments were determined from a 2D-COSY spectrum and are further supported by similar data obtained for the 1-3 : 5,6-η^5-C_8H_{11} ligand in [Ru(1-3 : 5,6-η^5-C_8H_{11})(η^6-C_8H_{10})][PF_6] and related molecules.[4] The $^{13}C\{^1H\}$ NMR spectrum of **3** shows eight resonances for the non-equivalent carbons of the C_8H_{11} ring. The assignments in Table 2 are made on the basis of the very detailed measurements made in the ruthenium species containing the 1-3 : 5,6-η^5-C_8H_{11} moiety.[4]

The rhodium atom in **3** can be regarded as being

Table 2. ^1H and ^{13}C NMR data for the rhodium complexes[a]

Compound	^1H[b] (δ)	^{13}C[c] (δ)
3[d]	1.84 (s, 3H, CMe), 1.93 (m, 1H, H^8), 2.31 (s, 3H, CMe), 2.34 (m, 1H, H^8), 2.82 (m, 2H, H^7), 3.07, 3.26 (m × 2, 2H, H^4), 3.60 [d of d of d, 1H, H^5, *J*(HH) 8, 8 and 8], 3.97 [d of d of d, 1H, H^3, *J*(HH) 8, 8 and 8], 4.35 [d of d, 1H, H^2, *J*(HH) 8 and 8], 5.70 (m, 1H, H^6), 5.84 [d of d of d, 1H, H^1, *J*(HH) 8, 8 and 8]	100.1 [d, C^2 or C^6, *J*(RhC) 4], 98.4 [d, C^2 or C^6, *J*(RhC) 9], 76.6 [d, C^1, *J*(RhC) 12], 71.5, 66.4 (*C*Me), 63.9 [d, C^5, *J*(RhC) 3], 33.5 (C^3, C^4, C^7 or C^8), 29.8 (C*Me*), 27.0, 25.5, 20.4 (C^3, C^4, C^7 or C^8)
4[d,e]	1.05 (m, 2H, CH_2), 1.37 (m, 2H, CH_2), 1.76 (m, 4H, CH_2), 2.16 (s, 6H, CMe), 2.53 (m, 2H, CH_2), 4.65 (t, 1H, CH), 5.81 (q, 2H, CH)	105.7 (C^2), 83.5 (2C, C^1 and C^3), 68.2 (br, *C*Me), 32.4 (2C, C^4 and C^8 or C^5 and C^7), 30.0 (C*Me*), 28.2 (C^4 and C^8 or C^5 and C^7), 22.5 (C^6)
5[f,g]	1.76 (m, 18H, Me_3P), 2.01 (s, 6H, CMe)	26.1 (C*Me*), 19.4 (m, MeP)
6[h]	−9.87 [t, 1H, HRh, *J*(PH) 31], 1.10 [d of t, 9H, CH_2*Me*, *J*(HH) 7, *J*(PH) 16], 1.87 [d of q, 6H, C*H*$_2$Me, *J*(HH) 7, *J*(PH) 20], 2.16 (s, 6H, CMe)	62.1 (*C*Me), 31.9 (C*Me*), 19.6 (m, *C*H_2Me), 7.80 (CH_2*Me*)

[a] Chemical shifts (δ) in ppm, coupling constants in Hz. Measurements in CD_2Cl_2 at ambient temperatures.

[b] Resonances for BH protons occur as unresolved broad and weak signals in the range δ 0–3.

[c] Hydrogen-1 decoupled chemical shifts are positive to high frequency of $SiMe_4$.

[d] For the 1-3 : 5,6-η^5-C_8H_{11} ligand the hydrogen and carbon atoms are labelled as shown.

[e] CO resonance not observed due to weak spectrum.

[f] $^{31}P\{^1H\}$ NMR : δ 3.17 [d, *J*(RhP) 125].

[g] The *C*Me resonance was not observed due to a poor signal-to-noise ratio.

[h] $^{31}P\{^1H\}$ NMR : δ 32.6 [d, *J*(RhP) 135].

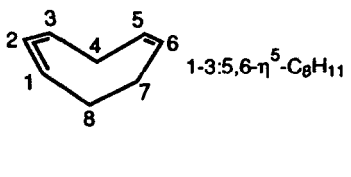

Table 3. Selected internuclear distances (Å) and angles (°) for [Rh(1-3 : 5,6-η^5-C_8H_{11})(η^5-7,8-$C_2B_9H_9Me_2$)] (**3**)

Rh—C(1)	2.272(3)	Rh—C(2)	2.239(3)	Rh—B(3)	2.185(3)	Rh—B(4)	2.216(3)
Rh—B(5)	2.181(3)	Rh—C(21)	2.251(3)	Rh—C(22)	2.258(3)	Rh—C(24)	2.331(4)
Rh—C(25)	2.166(4)	Rh—C(26)	2.202(3)	C(1)—C(2)	1.611(4)	C(1)—C(3)	1.527(4)
C(1)—B(5)	1.738(4)	C(1)—B(6)	1.723(4)	C(1)—B(10)	1.702(5)	C(2)—C(4)	1.526(5)
C(2)—B(3)	1.767(5)	C(2)—B(6)	1.736(5)	C(2)—B(7)	1.703(5)	B(3)—B(4)	1.796(4)
B(3)—B(7)	1.776(5)	B(3)—B(8)	1.777(5)	B(4)—B(5)	1.830(4)	B(4)—B(8)	1.781(5)
B(4)—B(9)	1.786(5)	B(5)—B(9)	1.775(5)	B(5)—B(10)	1.789(5)	B(6)—B(7)	1.752(5)
B(6)—B(10)	1.731(5)	B(6)—B(11)	1.737(6)	B(7)—B(8)	1.757(6)	B(7)—B(11)	1.762(6)
B(8)—B(9)	1.777(5)	B(8)—B(11)	1.767(6)	B(9)—B(10)	1.774(5)	B(9)—B(11)	1.781(6)
B(10)—B(11)	1.756(5)	C(21)—C(22)	1.370(5)	C(21)—C(28)	1.516(6)	C(22)—C(23)	1.497(6)
C(23)—C(24)	1.493(5)	C(24)—C(25)	1.377(5)	C(25)—C(26)	1.396(5)	C(26)—C(27)	1.528(5)
C(27)—C(28)	1.484(6)						

C(1)—Rh—C(2)	41.8(1)	C(1)—Rh—B(3)	77.7(1)	C(2)—Rh—B(3)	47.1(1)
C(1)—Rh—B(4)	80.1(1)	C(2)—Rh—B(4)	79.9(1)	B(3)—Rh—B(4)	48.2(1)
C(1)—Rh—B(5)	45.9(1)	C(2)—Rh—B(5)	76.6(1)	B(3)—Rh—B(5)	81.5(1)
B(4)—Rh—B(5)	49.2(1)	C(1)—Rh—C(21)	120.4(1)	C(2)—Rh—C(21)	161.2(1)
B(3)—Rh—C(21)	134.8(1)	B(4)—Rh—C(21)	91.6(1)	B(5)—Rh—C(21)	85.1(1)
C(1)—Rh—C(22)	105.5(1)	C(2)—Rh—C(22)	140.5(1)	B(3)—Rh—C(22)	170.0(1)
B(4)—Rh—C(22)	122.4(1)	B(5)—Rh—C(22)	93.9(1)	C(21)—Rh—C(22)	35.4(1)
C(1)—Rh—C(24)	111.1(1)	C(2)—Rh—C(24)	104.7(1)	B(3)—Rh—C(24)	127.2(1)
B(4)—Rh—C(24)	167.5(1)	B(5)—Rh—C(24)	142.8(1)	C(21)—Rh—C(24)	87.2(1)
C(22)—Rh—C(24)	61.1(1)	C(1)—Rh—C(25)	129.8(1)	C(2)—Rh—C(25)	99.7(1)
B(3)—Rh—C(25)	97.8(1)	B(4)—Rh—C(25)	133.0(1)	B(5)—Rh—C(25)	175.7(1)
C(21)—Rh—C(25)	98.3(1)	C(22)—Rh—C(25)	87.5(1)	C(24)—Rh—C(25)	35.4(1)
C(1)—Rh—C(26)	160.6(1)	C(2)—Rh—C(26)	119.1(1)	B(3)—Rh—C(26)	89.4(1)
B(4)—Rh—C(26)	102.0(1)	B(5)—Rh—C(26)	146.7(1)	C(21)—Rh—C(26)	78.9(1)
C(22)—Rh—C(26)	89.8(1)	C(24)—Rh—C(26)	65.6(1)	C(25)—Rh—C(26)	37.3(1)
C(22)—C(21)—C(28)	128.2(3)	C(21)—C(22)—C(23)	127.4(3)	C(22)—C(23)—C(24)	102.6(3)
C(23)—C(24)—C(25)	126.3(4)	C(24)—C(25)—C(26)	124.9(3)	C(25)—C(26)—C(27)	123.9(3)
C(21)—C(28)—C(27)	113.6(3)				

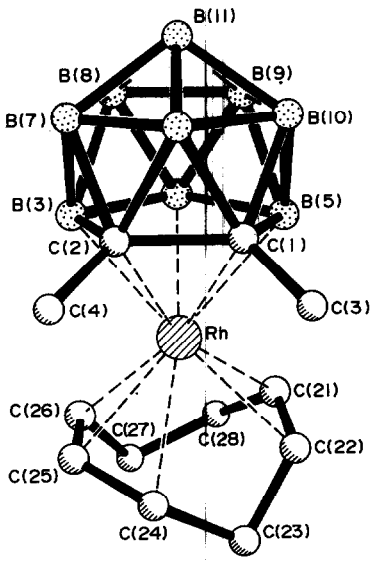

Fig. 1. Molecular structure of [Rh(1-3 : 5,6-η^5-C_8H_{11})(η^5-7,8-$C_2B_9H_9Me_2$)] (**3**) showing the crystallographic numbering scheme.

essentially octahedrally coordinated, assuming that the carbaborane group is a tridentate ligand, the allyl function occupies two sites and the alkene function occupies one. The molecule is also electronically saturated with the rhodium atom having an 18-electron closed shell. This is in contrast with the coordinatively- and electronically-unsaturated 16-electron rhodium species **2**, features which encouraged us to investigate reactions between **2** and some donor molecules.

If CH_2Cl_2 solutions of **2** are treated at ambient temperatures and pressures with CO the electronically and coordinatively saturated complex [Rh(CO)(η^3-C_8H_{13})(η^5-7,8-$C_2B_9H_9Me_2$)] (**4**) is formed (Scheme 1). Data characterizing this species are given in Tables 1 and 2. The ^{1}H NMR spectrum revealed characteristic allylic resonances; a quartet at δ 5.81 corresponding to two hydrogens [J(HH) 8] and a triplet at δ 4.65 with an intensity for one hydrogen [J(HH) 8]. The methyl groups of the carbaborane cage display a single signal at δ

2.16. The equivalence of these CMe fragments indicates a degree of symmetry, discussed further below.

The $^{13}C\{^1H\}$ NMR spectrum did not show a CO peak and we attribute this to the signal-to-noise ratio in the spectrum being inadequate. Nevertheless, the IR spectrum of the molecule displayed a strong CO stretch at 2047 cm^{-1}. The number of resonances seen in the $^{13}C\{^1H\}$ spectrum indicate that there is a plane of symmetry through the C—C connectivity of the C_2B_9 cage, the metal atom and two of the carbons of the C_8H_{13} ring, namely, the central carbon of the η^3-allyl moiety and the carbon of the CH_2 group separated from the allyl fragment by two other methylene groups. The presence of such a plane renders the carbaborane cage CMe groups equivalent, leading to the observation of two resonances (δ 68.2, *C*Me and 30.0, C*Me*). It also results in the occurrence of five rather than eight resonances for the carbons of the C_8H_{13} ligand since two CH and four CH_2 groups are symmetrically related in pairs on either side of the plane of symmetry.

The reaction between PMe_3 and **2** was anticipated to yield a complex structurally analogous to **4**, with a phosphine ligand present instead of a CO molecule. However, in CH_2Cl_2 solution the product was [RhCl(PMe_3)$_2$(η^5-7,8-$C_2B_9H_9Me_2$)] (**5**), characterized by an X-ray diffraction study (Table 4 and Fig. 2).

The rhodium atom carries the carbaborane cage in the usual manner and is also ligated by the two PMe_3 molecules [Rh—P_{av} 2.332 Å] and the chloride

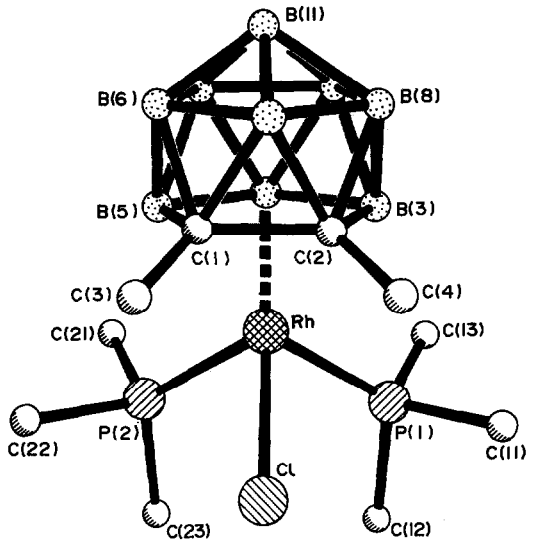

Fig. 2. Molecular structure of [RhCl(PMe_3)$_2$(η^5-7,8-$C_2B_9H_9Me_2$)] (**5**) showing the crystallographic numbering scheme.

[Rh—Cl 2.435(2) Å]. The molecule **5** is closely related to [RhCl(PPh_3)$_2$(η^5-7,8-$C_2B_9H_{11}$)].[5,6] Although the structure of the latter has not been determined by X-ray crystallography, that of the monophosphine complex [RhCl(PPh_3)(η^5-7,9-$C_2B_9H_{11}$)] has. The Rh—Cl [2.215(4) Å] and Rh—P [2.329(1) Å] separations in this species are significantly shorter than those in **5**, in accord with the former having an electron deficient metal centre.[5] Evidently

Table 4. Selected internuclear distances (Å) and angles (°) for [RhCl(PMe_3)$_2$(η^5-$C_2B_9H_9Me_2$)]·CH_2Cl_2 (**5**)

Rh—P(1)	2.335(2)	Rh—P(2)	2.328(2)	Rh—Cl	2.435(2)	Rh—C(1)	2.261(7)
Rh—C(2)	2.273(7)	Rh—B(3)	2.212(8)	Rh—B(4)	2.203(9)	Rh—B(5)	2.225(9)
C(1)—C(2)	1.667(11)	C(1)—C(3)	1.542(12)	C(1)—B(5)	1.700(12)	C(1)—B(6)	1.710(12)
C(1)—B(7)	1.763(13)	C(2)—C(4)	1.515(12)	C(2)—B(3)	1.733(12)	C(2)—B(7)	1.739(13)
C(2)—B(8)	1.730(12)	B(3)—B(4)	1.813(12)	B(3)—B(8)	1.791(13)	B(3)—B(9)	1.778(13)
B(4)—B(5)	1.823(13)	B(4)—B(9)	1.797(13)	B(4)—B(10)	1.789(13)	B(5)—B(6)	1.758(13)
B(5)—B(10)	1.751(14)	B(6)—B(7)	1.764(14)	B(6)—B(10)	1.742(14)	B(6)—B(11)	1.747(14)
B(7)—B(8)	1.760(15)	B(7)—B(11)	1.765(15)	B(8)—B(9)	1.774(14)	B(8)—B(11)	1.778(14)
B(9)—B(10)	1.771(14)	B(9)—B(11)	1.766(14)	B(10)—B(11)	1.756(15)		

P(1)—Rh—P(2)	96.7(1)	P(1)—Rh—Cl	83.7(1)	P(2)—Rh—Cl	83.1(1)
P(1)—Rh—C(1)	153.3(2)	P(2)—Rh—C(1)	110.0(2)	Cl—Rh—C(1)	98.4(2)
P(1)—Rh—C(2)	110.1(2)	P(2)—Rh—C(2)	153.2(2)	Cl—Rh—C(2)	98.5(2)
C(1)—Rh—C(2)	43.1(3)	P(1)—Rh—B(3)	81.7(2)	P(2)—Rh—B(3)	145.2(2)
Cl—Rh—B(3)	130.7(2)	C(1)—Rh—B(3)	76.8(3)	C(2)—Rh—B(3)	45.4(3)
P(1)—Rh—B(4)	98.6(2)	P(2)—Rh—B(4)	98.1(2)	Cl—Rh—B(4)	177.3(2)
C(1)—Rh—B(4)	78.9(3)	C(2)—Rh—B(4)	79.3(3)	B(3)—Rh—B(4)	48.5(3)
P(1)—Rh—B(5)	145.9(2)	P(2)—Rh—B(5)	81.9(2)	Cl—Rh—B(5)	129.4(2)
C(1)—Rh—B(5)	44.5(3)	C(2)—Rh—B(5)	76.4(3)	B(3)—Rh—B(5)	80.7(3)
B(4)—Rh—B(5)	48.6(3)				

the chlorine ligand is derived from the CH_2Cl_2 solvent used in the reaction, and this feature is discussed further below. The ^1H and $^{13}C\{^1H\}$ NMR spectra of **5** showed no peaks due to the η^3-C_8H_{13} group, as expected, and the $^{31}P\{^1H\}$ NMR spectrum displayed a doublet signal at δ 3.17 [J(RhP) 125].

The reaction between **2** and PEt_3 also results in displacement of the 1-3-η^3-C_8H_{13} ligand, the product being the hydrido-rhodium complex [RhH$(PEt_3)_2(\eta^5$-7,8-$C_2B_9H_9Me_2)$] (**6**). The ^1H NMR spectrum revealed a high-field resonance at δ −9.87 as a triplet [J(PH) 31], and the $^{31}P\{^1H\}$ NMR spectrum displayed a doublet at δ 32.6 [J(RhP) 135]. These data may be compared with those for [RhH$(PEt_3)_2(\eta^5$-7,8-$C_2B_9H_{11})$] [^1H δ −14.1, J(PH) 29, J(RhH) 16; $^{31}P\{^1H\}$, δ 30.6, J(RhP) 120], reported by Hawthorne and coworkers.[5]

We suggest that compound **6** forms via the following steps. Addition of a PEt_3 molecule to **2** affords an intermediate [Rh$(PEt_3)(\eta^3$-$C_8H_{13})(\eta^5$-7,8-$C_2B_9H_9Me_2)$], which is structurally akin to **4**. Although such an intermediate is ostensibly electronically saturated at the rhodium, slippage of the metal atom to an exopolyhedral site on the carbaborane cage, a process well documented,[5] could lead to an unsaturated rhodium centre, thereby facilitating transfer of hydride to the metal from the hydrocarbon group. The latter, having lost a hydrogen atom, would be released as cyclo-octa-1,3- or -1,5-diene. The resulting metal-containing species, [RhH$(PEt_3)(\eta^5$-7,8-$C_2B_9H_9Me_2)$], would readily add a further molecule of PEt_3 to yield **6**. We assume that the synthesis of **5** proceeds via a complex [RhH$(PMe_3)_n(\eta^5$-7,8-$C_2B_9H_9Me_2)$] (n = 1 or 2), the hydrido ligand of which is replaced by Cl from CH_2Cl_2. Evidence supporting this proposal comes from the observation that [RhCl$(PMe_2Ph)_2$ $(\eta^5$-7,8-$C_2B_9H_{11})$] was obtained in quantitative yield by crystallizing [RhH$(PMe_2Ph)_2(\eta^5$-7,8-$C_2B_9H_{11})$] from CH_2Cl_2.[5]

EXPERIMENTAL

Light petroleum refers to the fraction of b.p. 40–60°C, and all solvents were freshly distilled over appropriate drying agents prior to use. Alumina used in chromatography columns (*ca* 20 cm in length and 3.0 cm in diameter) was BDH aluminium oxide (Brockmann Activity II). Experiments were carried out using Schlenk-tube techniques under nitrogen. IR spectra were measured with a Perkin–Elmer FT1600 spectrometer and NMR spectra recorded with JEOL JNM FX 90Q and GX 270 spectrometers. The $^{31}P\{^1H\}$ NMR chemical shifts are in ppm to high frequency of 85% H_3PO_4 (external). The reagent, [NEt_4][Rh(cod)$(\eta^5$-7,8-$C_2B_9H_9Me_2)$], was prepared by treating [$Rh_2(\mu$-Cl$)_2$(cod$)_2$] with two molar equivalents of Tl[$TlC_2B_9H_9Me_2$][7] in THF, followed by the addition of [NEt_4]Cl.

Synthesis of the complex [Rh(1-3 : 5,6-η^5-$C_8H_{11})(\eta^5$-7,8-$C_2B_9H_9Me_2)$]

The salt **1** (0.20 g, 0.39 mmol) was dissolved in THF (10 cm^3) and treated with [CPh_3][BF_4] (0.13 g, 0.39 mmol), and the mixture stirred for 2 h. Solvent was removed *in vacuo*, the residue dissolved in CH_2Cl_2 (*ca* 3 cm^3) and the solution chromatographed. Elution of the column with CH_2Cl_2–light petroleum (1 : 1) removed a yellow band, which afforded yellow microcrystals of [Rh(1-3 : 5,6-η^5-$C_8H_{11})(\eta^5$-7,8-$C_2B_9H_9Me_2)$] (**3**) (0.09 g), on removal of the solvent *in vacuo*.

Reactions of the complex [Rh(1-3-η^3-$C_8H_{13})(\eta^5$-7,8-$C_2B_9H_9Me_2)$]

(1) Compound **2** (0.20 g, 0.52 mmol) was dissolved in CH_2Cl_2 (10 cm^3) and CO was bubbled through the solution for 10 min, producing a colour change from orange to yellow. The solvent was removed *in vacuo* and the residue was recrystallized twice from CH_2Cl_2–light petroleum (10 cm^3, 1 : 4) to give yellow microcrystals of [Rh(CO)(1-3-η^3-$C_8H_{13})(\eta^5$-7,8-$C_2B_9H_9Me_2)$] (**4**) (0.18 g).

(2) Similarly, **2** (0.20 g, 0.52 mmol) was treated with excess PMe_3 (*ca* 2 mmol) in CH_2Cl_2 (15 cm^3) and the mixture stirred for *ca* 3 h. Solvent was removed *in vacuo*, the residue dissolved in CH_2Cl_2 (*ca* 5 cm^3) and chromatographed. Elution of the column with CH_2Cl_2–light petroleum (1 : 2) removed a yellow fraction, which afforded, after the removal of the solvent *in vacuo*, yellow microcrystals of [RhCl$(PMe_3)_2(\eta^5$-7,8-$C_2B_9H_9Me_2)$] (**5**) (0.17 g). Use of less than an excess of PMe_3 in the reaction afforded only complex mixtures.

(3) In a similar experiment, employing an excess of PEt_3 in CH_2Cl_2, compound **2** (0.20 g, 0.52 mmol) gave orange microcrystals of [RhH$(PEt_3)_2(\eta^5$-7,8-$C_2B_9H_9Me_2)$] (**6**) (0.13 g).

Crystal structure determinations and refinement

Data were collected using a Siemens R3m/V four-circle diffractometer (293 K, Mo-K_α X-radiation, graphite monochromator, $\bar{\lambda}$ = 0.71073 Å). The data were corrected for Lorentz, polarization and X-ray absorption effects, the latter by an empirical method based upon azimuthal scan data.[8] The

structures were solved by conventional heavy-atom or direct methods and successive difference-Fourier syntheses were used to locate all non-hydrogen atoms. All calculations were performed on a DEC micro-Vax II computer with the SHELXTL PLUS system of programs.[8] Scattering factors with corrections for anomalous dispersion were taken from ref. 9. Additional material available from the Cambridge Crystallographic Data Centre comprises the atom coordinates, thermal parameters and remaining bond lengths and angles.

Crystals of **3** were grown from CH_2Cl_2–light petroleum as yellow prisms and that used had the dimensions *ca* $0.65 \times 0.50 \times 0.20$ mm. Of the 4358 data collected (Wyckoff ω-scan, $2\theta \leqslant 55°$), 3253 unique data had $F \geqslant 5\sigma(F)$, and only these were used for structure solution and refinement.

Crystal data for $C_{12}H_{26}B_9Rh$. $M = 370.5$, monoclinic, space group $C2/c$, $a = 17.972(3)$, $b = 8.131(2)$, $c = 23.757(4)$ Å, $\beta = 99.63(2)°$, $U = 3423(1)$ Å^3, $Z = 8$, $D_c = 1.44$ g cm^{-3}, $F(000) = 1504$, μ(Mo-K_α) = 9.7 cm^{-1}.

All non-hydrogen atoms were refined with anisotropic thermal parameters. Methyl hydrogen atoms were included in calculated positions (C—H 0.96 Å) with fixed isotropic thermal parameters ($U_{iso} = 0.08$ Å^2). The positions of the remaining hydrogen atoms were refined with fixed isotropic thermal parameters ($U_{iso} = 0.05$ Å^2). Final $R = 0.027$ ($R' = 0.028$) with a weighting scheme of the form $w^{-1} = [\sigma^2(F) + 0.0002F^2]$. The final electron-density difference synthesis showed no peaks > 0.46 or < -0.32 e Å^{-3}.

Crystals of **5** were grown as for **3**, and that used had the dimensions *ca* $0.60 \times 0.51 \times 0.40$ mm. Of the 3289 data collected (Wyckoff ω-scan, $2\theta \leqslant 55°$), 2566 unique data had $F \geqslant 5\sigma(F)$ and only these were used for structure solution and refinement.

Crystal data for $C_{10}H_{33}B_9ClP_2Rh \cdot CH_2Cl_2$. $M = 535.9$, orthorhombic, space group $P2_12_12_1$, $a = 10.443(3)$, $b = 12.606(4)$, $c = 19.033(4)$ Å, $U = 2506(1)$ Å^3, $Z = 4$, $D_c = 1.42$ g cm^{-3}, $F(000) = 1088$, μ(Mo-K_α) = 11.2 cm^{-1}.

All non-hydrogen atoms were refined with anisotropic thermal parameters. Methyl hydrogen atoms and the methylene hydrogen atoms of the CH_2Cl_2 solvent of crystallization were included in calculated positions (C—H 0.96 Å) with fixed isotropic thermal parameters [$U_{iso} = 0.08$ (Me) and 0.10 (CH_2) Å^2]. The positions of the remaining hydrogen atoms were refined with fixed isotropic thermal parameters ($U_{iso} = 0.08$ Å^2). Final $R = 0.040$ ($R' = 0.041$), with a weighting scheme of the form $w^{-1} = [\sigma^2(F) + 0.001F^2]$. The final electron-density difference synthesis showed no peaks > 0.57 or < -0.48 e Å^{-3}.

Acknowledgement—We thank the Turkish Government and the University of Ege for a scholarship (to I.T.).

REFERENCES

1. J. E. Goldberg and F. G. A. Stone, *Polyhedron* 1992, **11**, 2841 and refs therein.
2. J. C. Jeffery, F. G. A. Stone and I. Topaloğlu, *J. Organomet. Chem.* 1992, in press.
3. D. M. Speckman, C. B. Knobler and M. F. Hawthorne, *Organometallics* 1985, **4**, 426.
4. T. V. Ashworth, A. A. Chalmers, D. C. Liles, E. Meintzies and E. Singleton, *Organometallics* 1987, **6**, 1543.
5. R. T. Baker, M. S. Delaney, R. E. King, C. B. Knobler, J. A. Long, T. B. Marder, T. E. Paxson, R. G. Teller and M. F. Hawthorne, *J. Am. Chem. Soc.* 1984, **106**, 2965.
6. A. R. Siedle, *J. Organomet. Chem.* 1975, **90**, 249.
7. J. L. Spencer, M. Green and F. G. A. Stone, *J. Chem. Soc., Chem. Commun.* 1972, 1178.
8. SHELXTL PLUS program system (S320), Nicolet Instrument Corporation (1987); SHELXTL PLUS™ program system, Siemens Analytical X-Ray instruments (1989).
9. *International Tables for X-Ray Crystallography*, Vol. 4. Kynoch Press, Birmingham (1974).

Polyhedron Vol. 12, No. 3, pp. 327–336, 1993
Printed in Great Britain

0277–5387/93 $6.00+.00
Pergamon Press Ltd

REDOX ACTIVITY OF BIMETALLIC MOLYBDENUM AND TUNGSTEN NITROSYLS CONTAINING LIGANDS BASED ON 4-HYDROXYPHENYLALKANOLS

AMITAVA DAS,† CHRISTOPHER J. JONES and JON A. McCLEVERTY†‡

School of Chemistry, University of Birmingham, Edgbaston, Birmingham B15 2TT, U.K.

(*Received* 10 *August* 1992; *accepted* 18 *August* 1992)

Abstract—The redox-active bimetallic complexes, $[\{M(NO)L^*X\}_2Q]$ [L* = tris(3,5-dimethylpyrazolyl)borate, $HB(3,5\text{-}Me_2pyz)_3$; M = Mo, X = Cl or I; M = W, X = Cl; Q = $OC_6H_4(CH_2)_nO$ (n = 1–3) or $NHC_6H_4(CH_2)_nO$ (n = 2, 3)], have been prepared and characterized spectroscopically and electrochemically (cyclic voltammetry, coulometry). The electrochemical data indicate that there can be weak interactions between the two metal-based redox centres.

Cyclic voltammetric (CV) studies of the bimetallic tris(3,5-dimethylpyrazolyl)borato molybdenum and tungsten complexes, $[\{M(NO)L^*X\}_2Q]$ (where M = Mo or W, X = halide and Q = O, OC_6H_4O, $NHC_6H_4OC_6H_4NH$, etc.)[1,2] reveal that they undergo two one-electron addition processes. In many cases there was evidence for significant interactions between the two metal redox centres, and in that situation, the E_f values of the first and second reductions are more anodic and more cathodic, respectively, than the E_f value for the reduction of the corresponding *monometallic* species. These CV results further revealed that the extent of the interaction between the two metal centres, as measured by ΔE_f, the separation in mV between the two reduction potentials, was strongly dependent on the nature of Q, being greatest when Q = O or EC_6H_4E (E = O or NH).[1–3]

However, in our studies of the electrochemistry of these bimetallic species we noticed that the inclusion of saturated groups within the bridging system caused a significant reduction in the interaction between the metal centres. This effect was especially noticeable in $[\{Mo(NO)L^*I\}_2(OCH_2C_6H_4CH_2O)]$, where ΔE_f is $\geqslant$100 mV, whereas in $[\{Mo(NO)L^*Cl\}_2OC_6H_4O\text{-}p]$ ΔE_f is 460 mV, and it is reasonable to suppose that the attenuation of ΔE_f is due in part to the "insulating" effect of the aliphatic linkages.[1,2] In this paper, we report further studies of the effect inserted methylene groups have on the electrochemistry of the complexes $[\{M(NO)L^*X\}_2\{OC_6H_4(CH_2)_nO\}]$ (n = 1–3) and in related anilido species $[\{M(NO)L^*X\}_2\{NHC_6H_4(CH_2)_nO\}]$.

EXPERIMENTAL

All reactions were carried out under oxygen-free dry nitrogen. Dry freshly distilled dichloromethane and toluene were used for all reactions. All other commercial reagents were used as received. The starting materials $[ML(NO)X_2]$ (M = Mo/W, X = Cl, I) were prepared following known procedures.[4] New compounds were purified by column chromatography using silica gel 60 (70–230 mesh) and CH_2Cl_2 and CH_2Cl_2/n-hexane mixtures as the eluant; the bimetallic species were stable in solution and in the presence of air for short periods. IR spectra were recorded using either PE357 or PE1600 FTIR spectrophotometers and ^1H NMR spectra were recorded using a JEOL JN Max 270 spectrometer. Cyclic voltammetric and differential pulse polarographic data were obtained using a PAR174 instrument using dry CH_2Cl_2 as a solvent and $[NBu^n_4][PF_6]$ (0.2 mol dm^{-3}) as a supporting electrolyte. The data obtained were reproducible, the experimental error being $\pm$10 mV. Some of the experiments were repeated in THF, but a variation of only up to +20 mV, with respect to CH_2Cl_2, was detected. Thus, it seems reasonable to compare the

† Present address: School of Chemistry, University of Bristol, Cantocks Close, Bristol BS8 1TS, U.K.

‡ Author to whom correspondence should be addressed.

results obtained in CH_2Cl_2 with those obtained in CH_3CN.

[Mo(NO)L*Cl($OC_6H_4CH_2OH$)]

A solution of [Mo(NO)L*Cl_2] (0.207 g, 0.4 mM) and 4-hydroxybenzyl alcohol (0.099 g, 0.8 mM) was refluxed in CH_2Cl_2 (30 cm^3) for 4 h. The solution was then evaporated to a small volume and thin-layer chromatography (tlc) showed the residue to be a mixture of two compounds. Using column chromatography the second major brown fraction was collected and identified as [Mo(NO)L*Cl ($OC_6H_4CH_2OH$)], which was recrystallized from dichloromethane/n-hexane mixtures giving the complex as a dark brown powder (yield: 0.13 g, 53%).

[{Mo(NO)L*Cl}$_2$($OC_6H_4CH_2O$)]

Method 1. A mixture of [MoL*(NO)Cl(OC_6H_4 CH_2OH)] (0.10 g, 0.17 mM), [Mo(NO)L*Cl_2] (0.84 g, 0.17 mM) and triethylamine (0.17 g, 0.17 mM) was refluxed in toluene (50 cm^3) for 90 min. The reaction mixture was then evaporated *in vacuo*, the residue redissolved in CH_2Cl_2 and filtered. The filtrate was evaporated to low volume and chromatographed using CH_2Cl_2/n-hexane (20% v/v) as an eluant. The first major fraction was collected, the solvent evaporated *in vacuo* and the residue recrystallized from dichloromethane/n-hexane affording the complex as a brown powder (yield: 0.04 g, 25%).

Method 2. [Mo(NO)L*Cl_2] (0.207 g, 0.4 mM) was stirred in CH_2Cl_2 (30 cm^3) containing $AgBF_4$ (0.078 g, 0.4 mM) at room temperature for 1 h under nitrogen. The resulting mixture was then filtered under nitrogen and to the filtrate was added 4-hydroxybenzyl alcohol (0.0245 g, 0.2 mM), the mixture then being refluxed for 18 h. The solution was then evaporated to low volume and purified by column chromatography, the complex being isolated as brown microcrystals (yield: 0.04 g, 20%).

[Mo(NO)L*I($OC_6H_4CH_2OH$)]

This compound was prepared in the same way as [Mo(NO)L*Cl($OC_6H_4CH_2OH$)] using [Mo (NO)L*I_2] instead of [Mo(NO)L*Cl_2] as the starting material, the reaction mixture then being refluxed for 2 h. The complex was obtained as a red–brown powder after recrystallization from dichloromethane/n-hexane (yield: 0.14 g, 52%).

[{Mo(NO)L*I}$_2$($OC_6H_4CH_2O$)]

This compound was prepared following the same method described in Method 1 above for [{Mo(NO)L*Cl}$_2$($OC_6H_4CH_2O$)], but using [Mo(NO)L*I_2] and hexamine. After work-up and recrystallization from CH_2Cl_2/n-hexane, the compound was isolated as a dark red–brown powder (yield: 0.04 g, 30%).

[{MoL*(NO)Cl}$_2$($OC_6H_4CH_2CH_2O$)]

A mixture of [Mo(NO)L*Cl_2] (0.207 g, 0.4 mM) and 2-(4-hydroxyphenyl)ethanol (0.027 g, 0.2 mM) was refluxed in toluene (50 cm^3) in the presence of triethylamine for 8 h. The reaction mixture was then evaporated *in vacuo*, the residue redissolved in CH_2Cl_2 and chromatographed using n-hexane/ dichloromethane (30% v/v) as an eluant. The first major fraction was collected, evaporated to low volume and the red–brown product was precipitated by adding n-hexane (yield: 0.072 g, 35%).

[{MoL*(NO)I}$_2$($OC_6H_4CH_2CH_2O$)]

A mixture of [Mo(NO)L*I_2] (0.27 g, 0.4 mM), 2-(4-hydroxyphenyl)ethanol (0.027 g, 0.2 mM) and hexamine (0.34 g, 0.4 mM) was refluxed in toluene (50 cm^3) for 8 h. The mixture was evaporated *in vacuo*, the residue redissolved in CH_2Cl_2 and the resulting solution filtered. The filtrate was then evaporated to low volume and chromatographed using n-hexane/dichloromethane (25% v/v) as an eluant. The complex was isolated as a brown powder after work-up and recrystallization from CH_2Cl_2/n-hexane (yield: 0.10 g, 37%).

[{Mo(NO)L*Cl}$_2$($OC_6H_4CH_2CH_2CH_2O$)]

This compound was synthesized in the same way as [{MoL*(NO)Cl}$_2$($OC_6H_4CH_2CH_2O$)] using 3-(4-hydroxyphenyl)propanol in place of 2-(4-hydroxyphenyl)ethanol and was obtained as a brown microcrystalline solid (yield: 0.07 g, 34%).

[{Mo(NO)L*I}$_2$($OC_6H_4CH_2CH_2CH_2O$)]

This compound was prepared in the same way as [{Mo(NO)L*I}$_2$($OC_6H_4CH_2CH_2O$)]. 3-(4-Hydroxyphenyl)propanol was used instead of 2-(4-hydroxyphenyl)ethanol, and the compound was isolated as a dark brown microcrystalline solid (yield: 0.81 g, 30%).

[{Mo(NO)L*Cl}$_2$($NHC_6H_4CH_2CH_2O$)]

This compound was prepared in a way similar to [{Mo(NO)L*Cl}$_2$($OC_6H_4CH_2CH_2O$)] described above, using 2-(4-aminophenyl)ethanol (0.03 g, 0.02 mM) in refluxing toluene (50 cm^3) over 6 h.

Table 1. Elemental analyses for [ML*(NO)XY]

M	X	Y	n^a	C (Found/Calc.)	H (Found/Calc.)	N (Found/Calc.)
Mo	Cl	$OC_6H_4CH_2OH$	0	45.6(45.44)	3.9(3.8)	16.8(16.86)
Mo	I	$OC_6H_4CH_2OH$	$\frac{1}{6}C_6H_{14}$	40.4(41.25)	4.6(4.69)	14.3(14.56)
Mo	Cl	$OC_6H_4CH_2OMoL^*(NO)Cl$	0	42.6(42.76)	4.8(4.55)	19.0(18.86)
Mo	I	$OC_6H_4CH_2OMoL^*(NO)I$	0	36.5(36.36)	4.1(4.13)	16.2(16.04)
W	Cl	$OC_6H_4CH_2OWL^*(NO)Cl$	$\frac{1}{3}CH_2Cl_2$	36.0(36.57)	4.1(4.15)	15.8(16.14)
Mo	Cl	$OC_6H_4CH_4CH_2OMoL^*(NO)Cl$	0	43.5(43.37)	5.1(5.07)	18.7(18.69)
Mo	I	$OC_6H_4CH_2CH_2OMoL^*(NO)I$	$\frac{1}{3}CH_2Cl_2$	36.4(36.92)	4.1(4.24)	15.5(15.86)
W	Cl	$OC_6H_4CH_2CH_2OWL^*(NO)Cl$	0	37.3(37.19)	4.3(4.27)	15.9(15.98)
Mo	Cl	$OC_6H_4CH_2CH_2CH_2OMoL^*(NO)Cl$	$\frac{1}{6}C_6H_{14}$	43.5(43.88)	5.0(5.1)	18.1(18.37)
Mo	I	$OC_6H_4CH_2CH_2CH_2OMoL^*(NO)I$	$\frac{1}{6}C_6H_{14}$	37.2(37.47)	4.3(4.35)	15.5(15.68)
W	Cl	$OC_6H_4CH_2CH_2CH_2OWL^*(NO)Cl$	0	37.6(37.65)	4.4(4.38)	15.7(15.77)
Mo	Cl	$NHC_6H_4CH_2CH_2OMoL^*(NO)Cl$	0	43.3(43.37)	5.1(5.07)	20.1(19.96)
Mo	I	$NHC_6H_4CH_2CH_2OMoL^*(NO)I$	$\frac{1}{3}C_6H_{14}$	38.0(36.95)	4.6(4.33)	16.6(17.01)
W	Cl	$NHC_6H_4CH_2CH_2OWL^*(NO)Cl$	0	36.6(36.57)	4.2(4.15)	16.1(16.14)

^{a} Number of moles of C_6H_{14} or CH_2Cl_2; this factor also confirmed by independent ^{1}H NMR spectral analysis.

The complex was obtained as a red–brown powder (yield: 0.06 g, 28%).

[{Mo(NO)L*I}$_2$(NHC$_6$H$_4$CH$_2$CH$_2$O)]

This compound was prepared in the same way as [{Mo(NO)L*I}$_2$(OC$_6$H$_4$CH$_2$CH$_2$O)} using 2-(4-aminophenyl)ethanol (0.03 g, 0.2 mM) and was refluxed for 5 h. The complex was isolated as black microcrystals (yield: 0.09 g, 33%).

[{W(NO)L*Cl}$_2$Q] (Q = OC$_6$H$_4$CH$_2$O, OC$_6$H$_4$CH$_2$CH$_2$O, OC$_6$H$_4$CH$_2$CH$_2$CH$_2$O *and* HNC$_6$H$_4$CH$_2$CH$_2$O)

These complexes were prepared following the same method as for [{Mo(NO)L*Cl}$_2$(OC$_6$H$_4$CH$_2$CH$_2$O)], but were refluxed for 12 h. Yields of the respective tungsten complexes were generally 35%.

RESULTS AND DISCUSSION

Synthetic studies

The monometallic species [Mo(NO)L*X(OC$_6$H$_4$CH$_2$OH)] (X = Cl or I) were obtained by direct reaction between [Mo(NO)L*X$_2$] and HOC$_6$H$_4$CH$_2$OH in dichloromethane. The bimetallic complexes [{M(NO)L*X}$_2$EC$_6$H$_4$(CH$_2$)$_n$O] (M = Mo, X = Cl or I; M = W, X = Cl; E = O or NH), however, could be prepared by two methods: either by refluxing 2 mole equivalents of [M(NO)L*X$_2$] with 1 mole equivalent of the desired bridging ligand in toluene, or by preforming [M(NO)L*X{EC$_6$H$_4$(CH$_2$)$_n$OH}] and treating that with 1 mole equivalent of [M(NO)L*X$_2$] in the presence of amine (triethylamine or hexamine). It was also possible to produce the bimetallic species by reaction of [Mo(NO)L*X$_2$] with Ag$^+$ in dichloromethane, followed by addition of the desired bridging ligand but, in general, reactions in toluene were more rapid, presumably because of the higher reaction temperature.

In these reactions with bifunctional ligands, [M(NO)L*X$_2$] preferentially selected the alkoxy group and earlier work has shown that arylamines react in preference to phenoxy ligands.[5] The yields of bimetallic complexes were relatively low, those of the molybdenum complexes being significantly lower than those of their tungsten analogues.

The new compounds were obtained as microcrystalline powders, whose formulations are based on elemental analyses (Table 1), spectroscopic (Table 2) and electrochemical studies (Table 3).

Spectroscopic studies

The IR spectra of the new complexes exhibited bands characteristic of the tris(3,5-dimethylpyrazolyl)borato ligand and the bridging ligand, with ν(BH) at *ca* 2550 cm^{-1} and ν(NH) at *ca* 3228 cm^{-1}. The monometallic species [Mo(NO)L*X(OC$_6$H$_4$CH$_2$OH)] exhibited ν(NO) at *ca* 1680 cm^{-1} [X = Cl and 1670 cm^{-1} (X = I)], typical of this class of phenolato compounds, as

Table 2. NO stretching frequencies and ^{1}H NMR spectra of [M(NO)L*XY] (M = Mo, W; X = Cl or I)

M	X	Y	ν(NO) (cm^{-1})[a]	δ (ppm)[b]	Assignment
Mo	Cl	$OC_6H_4CH_2OH$	1681	9.976(1)s	—CH_2OH
				7.69(4)m	—C_6H_4—, AA′BB′; δ_A 7.69, δ_B 7.42
				5.94(2)s 5.77(1)s	$Me_2C_3HN_2$
				4.7(2)m	—CH_2OH
				2.52(3)s 2.44(3)s 2.42(3)s 2.39(3)s 2.17(3)s 2.05(3)s	$(CH_3)_2C_3HN_2$
Mo	I	$OC_6H_4CH_2OH$	1677	10.15(1)s	N*H*
				7.86(4)m	—C_6H_4—, AA′BB′; δ_A 8.13, δ_B 7.52
				5.95(2)s 5.80(1)s	$Me_2C_3HN_2$
				4.8(2)m	—CH_2OH
				2.52(3)s 2.48(3)s 2.41(3)s 2.39(3)s 2.16(3)s 2.06(3)s	$(CH_3)_2C_3HN_2$
W	Cl	$OC_6H_4CH_2OH$	1637	9.97(1)s	—CH_2OH
				7.69(4)m	—C_6H_4—, AA′BB′; δ_A 7.95, δ_B 7.42
				5.94(2)s 5.77(1)s	$Me_2C_3HN_2$
				4.65(2)m	—CH_2OH
				2.55(3)s 2.46(3)s 2.40(3)s 2.36(3)s 2.17(3)s 2.06(3)s	$(CH_3)_2C_3HN_2$
Mo	Cl	$OC_6H_4CH_2OMoL^*(NO)Cl$	1682; 1662	7.38(4)m	—C_6H_4—, AA′BB′; δ_A 7.48, δ_B 7.27
				6.42(2)m	—OCH_2—
				5.91(2)s 5.80(2)s 5.76(2)s	$Me_2C_3HN_2$
				2.50(3)s 2.45(3)s 2.41(6)s 2.39(6)s 2.36(3)s 2.20(6)s 2.17(6)s 2.06(3)s	$(CH_3)_2C_3HN_2$

Table 2.—*continued*

M	X	Y	ν(NO) (cm^{-1})[a]	δ (ppm)[b]	Assignment
Mo	I	$OC_6H_4CH_2OMoL^*(NO)I$	1677; 1661	6.97(4)m	—C_6H_4—, AA′BB′; δ_A 7.50, δ_B 6.44
				6.44(2)m	—OCH_2—
				5.97(4)s 5.74(2)s	$Me_2C_3HN_2$
				2.54(3)s 2.47(6)s 2.43(6)s 2.36(3)s 2.32(3)s 2.18(6)s 2.09(3)s	$(CH_3)_2C_3HN_2$
W	Cl	$OC_6H_4CH_2OWL^*(NO)Cl$	1633(br)	7.34(4)m	—C_6H_4—, AA′BB′; δ_A 7.42, δ_B 7.26
				6.5(2)m	—OCH_2—
				5.94(2)s 5.82(2)s 5.74(2)s	$Me_2C_3HN_2$
				2.52(3)s 2.49(3)s 2.47(6)s 2.43(6)s 2.36(3)s 2.30(6)s 2.18(3)s 2.06(3)s	$(CH_3)_2C_3HN_2$
Mo	Cl	$OC_6H_4CH_2CH_2OMoL^*(NO)Cl$	1682; 1665	7.30(4)m	—C_6H_4—, AA′BB′; δ_A 7.34, δ_B 7.26
				6.10(2)m	—OCH_2—
				5.93(2)s 5.90(2)s 5.78(2)s	$Me_2C_3HN_2$
				3.50(2)m	β-CH_2—
				2.58(3)s 2.53(6)s 2.50(12)s 2.42(6)s 2.31(3)s 2.19(3)s 2.07(3)s	$(CH_3)_2C_3HN_2$
Mo	I	$OC_6H_4CH_2CH_2OMoL^*(NO)I$	1677; 1662	7.34(4)m	—C_6H_4—, AA′BB′; δ_A 7.42, δ_B 7.25
				6.21(2)m	—OCH_2—
				5.89(2)s 5.81(2)s 5.74(2)s	$Me_2C_3HN_2$
				3.23(2)m	β-CH_2—
				2.57(3)s 2.50(6)s 2.46(9)s 2.39(6)s 2.30(6)s 2.18(3)s 2.09(3)s	$(CH_3)_2C_3HN_2$

Table 2.—*continued*

M	X	Y	ν(NO) (cm^{-1})[a]	δ (ppm)[b]	Assignment
W	Cl	$OC_6H_4CH_2CH_2OWL^*(NO)Cl$	1633(br)	7.25(4)m	$—C_6H_4—$, AA′BB′; δ_A 7.32, δ_B 7.17
				6.02(2)m	$—OCH_2—$
				5.92(2)s 5.87(2)s 5.80(2)s	$Me_2C_3HN_2$
				3.18(2)m	β-CH_2—
				2.66(3)s 2.62(3)s 2.58(9)s 2.53(6)s 2.46(6)s 2.36(3)s 2.24(3)s 2.18(3)s	$(CH_3)_2C_3HN_2$
Mo	Cl	$HNC_6H_4CH_2CH_2OMoL^*(NO)Cl$	1650; 1662	12.62(1)br	—N*H*—
				7.33(4)m	$—C_6H_4—$, AA′BB′; δ_A 7.40, δ_B 7.25
				6.14(2)m	$—OCH_2—$
				5.95(2)m 5.88(2)m 5.81(2)m	$(C_3H)Me_2N_2$
				3.2(2)m	β-CH_2—
				2.68(3)s 2.52(9)s 2.50(6)s 2.44(6)s 2.38(6)s 2.31(3)s 2.04(3)s	$(CH_3)_2C_3HN_2$
Mo	I	$HNC_6H_4CH_2CH_2OMoL^*(NO)I$	1660(br)	13.17(1)br	—N*H*—
				7.44(4)m	$—C_6H_4—$, AA′BB′; δ_A 7.52, δ_B 7.35
				6.08(2)m	$—OCH_2—$
				5.91(2)s 5.87(2)s 5.80(2)s	$Me_2C_3HN_2$
				3.26(2)m	β-CH_2—
				2.71(3)s 2.51(3)s 2.47(6)s 2.42(6)s 2.36(9)s 2.27(6)s 2.10(3)s	$(CH_3)_2C_3HN_2$
W	Cl	$HNC_6H_4CH_2CH_2OWL^*(NO)Cl$	1626(br)	10.81(1)br	—N*H*—
				7.29(4)m	$—C_6H_4—$, AA′BB′; δ_A 7.31, δ_B 7.26
				6.04(2)m	$—OCH_2—$
				5.94(2)s 5.87(2)s 5.82(2)s	$Me_2C_3NN_2$

Table 2.—*continued*

M	X	Y	ν(NO) (cm^{-1})[a]	δ (ppm)[b]	Assignment
				3.18(2)m	β-CH_2—
				2.72(3)s 2.69(6)s 2.63(6)s 2.50(6)s 2.45(6)s 2.42(3)s 2.35(3)s 2.16(3)s	$(CH_3)_2C_3HN_2$
Mo	Cl	$OC_6H_4CH_2CH_2CH_2OMoL^*(NO)Cl$	1681; 1663	7.31(4)m	—C_6H_4—, AA′BB′; δ_A 7.39, δ_B 7.22
				6.15(2)m	—OCH_2—
				5.89(4)s 5.83(2)s	$Me_2C_3HN_2$
				2.76(2)m	β-CH_2—
				2.57(3)s 2.51(6)s 2.48(6)s 2.44(3)s 2.38(6)s	$(CH_3)_2C_3HN_2$ + γ-CH_2—
				2.30(6)s 2.28(4)s 2.16(4)s	
Mo	I	$OC_6H_4CH_2CH_2CH_2OMoL^*(NO)I$	1677; 1661	7.30(4)m	—C_6H_4—, AA′BB′; δ_A 7.38, δ_B 7.21
				6.20(2)m	—OCH_2—
				5.88(4)s 5.83(2)s	$Me_2C_3HN_2$
				2.77(2)m	β-CH_2—
				2.57(3)s 2.51(3)s 2.48(3)s 2.44(3)s 2.39(9)s	$(CH_3)_2C_3HN_2$ + γ-CH_2—
				2.30(6)s 2.24(6)s 2.15(2)s 2.05(3)s	
W	Cl	$OC_6H_4CH_2CH_2CH_2OWL^*(NO)Cl$	1681(br)	7.21(4)m	—C_6H_4—, AA′BB′; δ_A 7.23, δ_B 7.18
				6.10(2)m	—OCH_2—
				5.94(4)s 5.82(2)s	$Me_2C_3HN_2$
				2.70(2)m	β-CH_2—
				2.66(3)s 2.60(6)s 2.58(6)s 2.51(6)s 2.43(3)s	$(CH_3)_2C_3HN_2$ + γ-CH_2—
				2.35(4)s 2.30(4)s 2.14(4)s	

[a] In KBr discs.

[b] In CD_2Cl_2 (relative area), multiplicity; all complexes exhibited the very broad B*H* resonance at *ca* δ 4.6 ppm.

Table 3. Electrochemical data obtained from [ML*(NO)XY]

M	X	Y	E_f[a]	ΔE[b] (mV)	Comment[c]
Mo	Cl	Cl	+0.09[d]	70	R
Mo	I	I	+0.22[d]	120	EC
W	Cl	Cl	−0.42[d]	80	R
Mo	I	$OCH_2C_6H_4CH_2OMoL^*(NO)I$	−0.52[d]	160	—
W	Cl	$OCH_2C_6H_4CH_2OWL^*(NO)Cl$	−1.16[d]	190	R
Mo	Cl	$OC_6H_4CH_2OH$	−0.30	80	R
	I	$OC_6H_4CH_2OH$	−0.28	110	
Mo	Cl	$OC_6H_4CH_2OMoL^*(NO)Cl$	−0.23	85	R
			−0.74	120	
Mo	I	$OC_6H_4CH_2OMoL^*(NO)I$	−0.22	80	EC
			−0.72	115	
W	Cl	$OC_6H_4CH_2OWL^*(NO)Cl$	−0.81	80	R
			−1.29	130	
Mo	Cl	$OC_6H_4CH_2OMoL^*(NO)Cl$	−0.34	70	R
			−0.67	100	
Mo	I	$OC_6H_4CH_2CH_2OMoL^*(NO)I$	−0.32	75	EC
			−0.58	100	
W	Cl	$OC_6H_4CH_2CH_2OWL^*(NO)Cl$	−0.88	80	R
			−1.21	130	
Mo	Cl	$OC_6H_4CH_2CH_2CH_2OMoL^*(NO)Cl$	−0.37	70	R
			−0.68	85	
Mo	I	$OC_6H_4CH_2CH_2CH_2OMoL^*(NO)I$	−0.33	80	EC
			−0.58	95	
W	Cl	$OC_6H_4CH_2CH_2CH_2OWL^*(NO)Cl$	−0.88	85	R
			−1.22	125	
Mo	Cl	$NHC_6H_4CH_2CH_2OMoL^*(NO)Cl$	−0.60	75	R
			−0.90	90	
Mo	I	$NHC_6H_4CH_2CH_2OMoL^*(NO)I$	−0.51	70	EC
			−0.82	85	
W	Cl	$NHC_6H_4CH_2CH_2OWL^*(NO)Cl$	−1.14	110	
			−1.3	—	

[a] Studied in CH_2Cl_2 vs SCE using a platinum bead electrode, unless otherwise stated: bimetallic species exhibited two reduction processes.

[b] Separation between cathodic and anodic CV peak for one-electron process values is 90 ± 10 mV for $[FeCp_2/[FeCp_2]^+$ couple.

[c] R = reversible process; EC = reversible process accompanied by a chemical reaction.

[d] Measured in CH_3CN.

observed earlier.[5] The bimetallic complexes exhibited two NO stretching frequencies, one for each metal–donor atom arrangement. Thus, for complexes of the type [Mo(NO)L*Cl{$OC_6H_4(CH_2)_nO$}Mo(NO)*X] these NO stretching frequencies are in the range 1680–1685 cm^{-1} and at 1670 cm^{-1}, and from comparisons with spectral data taken from related mono- and bimetallic species, the former absorptions are associated with the *phenoxide* {Mo(NO)L*Cl(OAr)} fragment and the latter with the *alkoxide* {Mo(NO)L*Cl[$O(CH_2)_nAr$]} fragment. In the related iodo complexes, these two sets of absorptions occur at 1655–1660 and 1665–1670 cm^{-1}, respectively. In the spectra of the related tungsten complexes, ν(NO) occurred at 1640, 1630 and 1625 cm^{-1}, associated with phenolato, arylamide and alkoxy fragments, respectively.

The ^1H NMR spectra of the new complexes (Table 2) were generally unexceptional and are consistent with the formulation of the complexes. Thus, in all complexes, the 4-H protons of the pyrazole rings occurred in the range δ 5.7–6.1 ppm, appearing either as two signals of relative intensity 2:1 or three of relative intensity 1:1:1. The latter is expected because of the asymmetric ML*(NO)X centre and it can be presumed that a 2:1 pattern arises because the non-equivalence of two of the protons is not resovled. The absence of a plane of

symmetry is confirmed by the methyl signals of the pyrazolyl rings which appeared as a set of six lines in the region δ 2.04–2.68 ppm. In a few cases, the pyrazolyl ring signals were more complex probably because of the presence of diastereoisomers of $[\{ML^*(NO)X\}_2Q]$, which we were unable to separate (each metal centre is chiral). In the spectra of the bimetallic species, the ratio of integrated intensities for the protons of the methyl groups in the pyrazole ring relative to the 4-H protons was close to 36:6, while that relative to the aromatic ring protons was 36:4. These observations are consistent with the bimetallic nature of the complexes. Solvent of crystallization could be detected in the spectra of those complexes, whose elemental analytical data indicated that it was present.

In the ^1H NMR spectra of $[\{Mo(NO)L^*X\}_2\{OC_6H_4(CH_2)_nCH_2O\}]$ ($n = 1, 2$) signals due to L* appeared at very similar δ values, irrespective of n. The aromatic protons resonated at δ 7.3–7.4 ppm, a slightly lower field than in the monometallic $[Mo(NO)L^*X(OC_6H_4CH_2OH)]$. The methylene protons on the carbon atoms α to the oxygen atom of the alkoxy group occurred at *ca* δ 6.2 ppm, whereas those associated with the other methylenic groups appeared in more normal positions. In the spectrum of $[\{WL^*(NO)Cl\}_2\{OC_6H_4(CH_2)_nCH_2O\}]$ ($n = 1, 2$), the aromatic signals also occurred at δ 7.2, the α-C protons also appeared near 6.2 ppm due to the strong electronegativity of $\{M(NO)L^*X\}$.[5] The resonances of the α-methylene protons in $[\{M(NO)L^*X\}_2OC_6H_4CH_2O]$ [δ 6.4–6.5 (M = Mo); δ 6.5 (M = W)] were slightly more deshielded than those found in $[\{Mo(NO)L^*I\}_2OCH_2C_6H_4CH_2O]$ (δ = 6.5–6.9 ppm),[2] suggesting that the electron-withdrawing ability of the $\{Mo(NO)L^*(X)OC_6H_4\}$ group is somewhat stronger than that of the $\{Mo(NO)L^*XOCH_2C_6H_4\}$ group.

As the metal in $[Mo(NO)L^*Cl(OR)]$ is chiral, the methylene protons within the alkoxide group are inequivalent, and differential couplings to the aromatic protons should occur. This appears to be generally the case in the spectra examined, but we were unable to obtain reliable assignments due to the difficulty of separating the diastereomeric mixtures. In most complexes the aromatic proton signals appeared as AA'BB' multiplets which revealed additional fine structure, almost certainly due to coupling with the inequivalent α-C methylene protons in the alkoxide group.

In the spectra of the molybdenum arylamido iodo complexes $[\{M(NO)L^*X\}_2NHC_6H_4CH_2CH_2O]$ δ(NH) occurred at low field, the value depending on M and X, as expected. In general the spectra were similar to those of $[\{M(NO)L^*X\}_2OC_6H_4CH_2CH_2O]$, the methylene protons on the carbon atom α to the alkoxide oxygen atom also being significantly deshielded, as expected, because of the electronegativity of the $[M(NO)L^*X]$ centre.[5]

Electrochemical studies

The electrochemical behaviour of the new complexes was investigated by cyclic voltammetry (Table 3) and by differential pulse polarographic techniques, using a platinum bead electrode in dichloromethane, unless otherwise stated. The electrochemical behaviour of a few complexes was also determined in CH_3CN, but the data were almost identical to those obtained in dichloromethane. In accord with earlier findings, the complexes exhibited a poorly defined irreversible oxidation process at potentials more anodic than +0.5 V for the molybdenum complexes and +0.8 V for the tungsten complexes. A number of the reductive electrode processes were reversible or nearly so, this being established by comparison of wave shape with that of the electrode behaviour of ferrocene under the same conditions. The separation of peaks in the reversible system (i.e. ΔE_p) varied from 80 to 120 mV depending on the solvent and the cells used for the measurements.

The nature of the reduction processes was established by plotting the cyclic voltammogram scan rate (v) vs $i_p v^{1/2}$, for reversible processes a straight line was obtained; further tests relied on the constancy of the dependency of E_f values on $v^{1/2}$. The reduction processes of iodo complexes $[\{MoL^*(NO)I\}_2Q]$ were presumed to be electrochemically reversible, but were coupled to a subsequent chemical reaction, as observed earlier.[6] In a few selected cases the number of electrons in each transfer was checked by coulometry. The data obtained are presented in Table 3 along with some previously reported data from $[\{M(NO)L^*X\}_nY]$ (Y = OPh, $n = 1$, and $OCH_2C_6H_4CH_2O$, $n = 2$).[2,7] It is assumed that the new complexes undergo discrete one-electron transfer processes, the wave shapes being analysed by comparison with known one-electron transfer species (e.g. $[Mo(NO)L^*Cl_2]$ and $[Mo(NO)L^*Cl(OPh)]$).

$[Mo(NO)L^*Cl_2]$ and $[W(NO)L^*Cl_2]$ undergo a one-electron reversible reduction, whereas $[Mo(NO)L^*I_2]$ exhibits a one-electron quasi-reversible reduction process, the E_f values being −0.09, −0.46 and +0.22 V vs SCE, respectively, in CH_3CN.[8] $[Mo(NO)L^*Cl(OPh)]$ was reduced in CH_2Cl_2 at *ca* −0.4 V, while its iodo analogue was reduced at −0.25 to −0.28 V.[7] The reduction potentials for $[Mo(NO)L^*I(OEt)]$ have been reported at *ca* −0.61 V[6] and those for $[Mo(NO)L^*I(OCH_2C_6H_4CH_2OH)]$ at −0.53 V,[2] while the

E_f values for the arylamido [Mo(NO)LX(NHPh)] derivatives occurred at *ca* −0.85 (X = Cl) and −0.83 (X = I) V, respectively.[9] The reduction potentials for phenoxy, benzyloxy and arylamido derivative of [W(NO)L*Cl_2] were −0.86, −1.10 and −1.30 V, respectively, the values being slightly solvent dependent.[2,9]

On the basis of the above data, it may be concluded that for [{Mo(NO)L*X}$_2$ $OC_6H_4(CH_2)_nCH_2O$] (X = Cl or I, n = 1 or 2), the molybdenum centre linked to the phenoxy end of the bridging ligand is reduced in the potential range −0.32 to −0.37 V, while that attached to the alkoxy function is reduced in the range −0.67 to −0.58 V. In [{W(NO)L*Cl}$_2$$OC_6H_4(CH_2)_nCH_2O$] ($n$ = 1 or 2), these values are −0.88 and −1.22 V, respectively.

For [{Mo(NO)L*X}$_2$$NHC_6H_4CH_2CH_2O$] the alkoxy- and arylamido-linked metal centres are reduced in the regions −0.5 to −0.6 V and −0.82 to −0.9 V, respectively. The alkoxy- and arylamido-linked metal centres are presumed to be reduced reversibly as E_f is independent of the CV scan rate, but in both cases electrochemical reduction is followed by a chemical reaction as proposed earlier.[6] Metal phenoxide centres are either reduced reversibly or the rate of chemical decomposition of the reduced species is low, and comparing the cathodic reduction peak shape for alkoxy and arylamido derivatives with that for phenoxy derivatives and ferrocene we suggest that electron transfer rates for the aryl amido and alkoxy derivative are relatively slow. If we compare the E_f values for the reduction processes for these bimetallic and the corresponding monometallic complexes, it is evident that there is not much variation (±30 mV), i.e. ΔE_f is almost 0, which clearly indicates that there is little interaction between the two metal centres in the bimetallic complexes.

However, the situation is slightly different in [{Mo(NO)L*X}$_2$($OC_6H_4CH_2O$). Metal centres linked to the phenoxy end of the ligand are reduced at values 70 mV more *anodic* than the corresponding monometallic complexes, while alkoxy linked metal centres are reduced at values approximately 20 mV more *cathodic* than the expected potentials. This suggests that there *is* an interaction between the two metal centres, although its extent is much lower than that occurring in [{Mo(NO)L*Cl}$_2$$OC_6H_4O$-*p*] ($\Delta E_f$ = 460 mV). Thus, it can be concluded that insertion of CH_2 groups into the bridging ligand significantly reduces the extent of interaction between two metal centres, partly because of the attenuation of conjugation. These findings may be contrasted with the situation in the ruthenium complexes [{$(NH_3)_5Ru$}$_2$ {NC_5H_4—X—C_5H_4N-4,4′}]$^{4+}$ (X = nothing, S-S), where the incorporation of the S_2 bridge leads to the four-fold increase in the intermetallic interaction, measured electrochemically by ΔE_f.[10]

Acknowledgements—We are grateful to the Indian Government and the UK Foreign and Commonwealth Office for the award of a Nehru Centenary British Fellowship (AD), to the University of Birmingham for facilities and to Mr T. Green for technical assistance.

REFERENCES

1. S. M. Charsley, C. J. Jones, J. A. McCleverty, B. D. Neaves, S. J. Reynolds and G. Denti, *J. Chem. Soc., Dalton Trans.* 1988, 293.
2. S. M. Charsley, C. J. Jones, J. A. McCleverty, B. D. Neaves and S. J. Reynolds, *J. Chem. Soc., Dalton Trans.* 1988, 301.
3. S. L. M. McWhinnie, S. M. Charsley, C. J. Jones, J. A. McCleverty and L. J. Yellowlees, *J. Chem. Soc., Dalton Trans.* 1992, submitted.
4. S. J. Reynolds, C. F. Smith, C. J. Jones and J. A. McCleverty, *Inorg. Synth.* 1985, **23**, 4.
5. J. A. McCleverty, *Chem. Soc. Rev.* 1983, **12**, 331.
6. C. J. Jones, J. A. McCleverty, B. D. Neaves, S. J. Reynolds, H. Adams, N. A. Bailey and G. Denti, *J. Chem. Soc., Dalton Trans.* 1986, 733.
7. N. Al Obaidi, M. Chaudhury, D. Clague, C. J. Jones, J. C. Pearson, J. A. McCleverty and S. S. Salam, *J. Chem. Soc., Dalton Trans.* 1987, 1733.
8. T. N. Briggs, C. J. Jones, J. A. McCleverty, B. D. Neaves, N. El Murr and H. M. Colquhoun, *J. Chem. Soc., Dalton Trans.* 1985, 1249.
9. N. Al Obaidi, S. M. Charsley, W. Hussain, C. J. Jones, J. A. McCleverty, B. D. Neaves and S. J. Reynolds, *Trans. Met. Chem.* 1987, **12**, 143.
10. I. de S. Moreira and D. W. Franco, *J. Chem. Soc., Chem. Commun.* 1992, 450.

Polyhedron Vol. 12, No. 3, pp. 337–341, 1993
Printed in Great Britain

0277–5387/93 $6.00+.00
Pergamon Press Ltd

COMMUNICATION

SYNTHESIS AND X-RAY STUDIES OF THE SEVEN-COORDINATE Ti^{IV}(THPED) DIMER

DENNIS F. EVANS,✝ JONATHAN PARR, SAMIMA RAHMAN, ALEXANDRA M. Z. SLAWIN, DAVID J. WILLIAMS,* CHIH Y. WONG and J. DEREK WOOLLINS*

The Evans and Chemical Crystallographic Laboratories, Department of Chemistry, Imperial College, London SW7 2AY, U.K.

(*Received* 1 *October* 1992; *accepted* 13 *November* 1992)

Abstract—The synthesis and X-ray structure of the seven-coordinate Ti^{IV}(THPED) dimer, where H_4THPED = N,N,N′,N′-tetrakis-(2-hydroxypropyl)ethylenediamine, is described. The structure is dimeric with each titanium atom chelating to an N_2O_5 donor set. One oxygen atom in each ligand is binucleating, thus forming a central Ti_2O_2 ring.

Recently we have reported the synthesis of zirconium(IV) and hafnium(IV) complexes with the encapsulating octadentate ligand ethylene glycol-O,O′-bis-(2-aminoethyl)-N,N,N′,N′-tetraacetic acid, which possesses an N_2O_6 donor set.[1] Titanium(IV) has a much reduced ionic radius compared to zirconium(IV) and hafnium(IV) and its complexes also have a tendency to hydrolyse to compounds containing Ti—O linkages and/or oxo-bridges. X-ray studies have been carried out on $Ti^{IV}(EDTA)\cdot H_2O$,[2] $[NEt_3H][Ti^{IV}(Htripace)]\cdot 1.5\,CH_3CN$[3] and Ti^{IV}-crown-ether[4] derivatives and to our knowledge these represent the only titanium complexes reported which utilize ligands with denticity greater than or equal to six.

The titanium tartrate complexes developed by Sharpless and co-workers[5,6] which are responsible for a number of highly successful asymmetric epoxidation reactions remain the principal route to many enantiospecific products. The data available support a dimeric species, $[Ti_2(tartrate)_2(OR)_4]$, as the catalyst, but the structure has been assigned on the basis of the related dibenzyltartramide analogue.[7] This complex utilizes hydroxylate oxygen donors, which bridge to form a Ti_2O_2 ring.

Here, we describe the synthesis and X-ray characterization of the air stable complex $[Ti^{IV}(THPED)]_2\cdot C_7H_8$, where H_4THPED = N,N,N′,N′-tetrakis-(2-hydroxypropyl)ethylenediamine (Quadrol, Fig. 1), formed by the reaction shown in eq. (1).†

$$2Ti(OPr^i)_4 + 2H_4THPED \longrightarrow [Ti(THPED)]_2 + 8HOPr^i \quad (1)$$

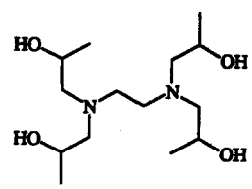

Fig. 1. The structure of H_4THPED.

* Authors to whom correspondence should be addressed.

† Preparation of $[Ti^{IV}(THPED)]_2\cdot C_7H_8$. Titanium(IV) isopropoxide (4.07 cm^3, 13.7 mmol) was added to a solution of H_4THPED (4.0 g, 13.7 mmol) in dichloromethane. The mixture was refluxed for 24 h, evaporated to dryness and recrystallized from hot toluene. Yield: 4.36 g, 42%. Found: C, 53.5; H, 8.5; N, 7.5. Calc. for $[Ti^{IV}(THPED)]_2\cdot C_7H_8$: C, 55.0; H, 8.4; N, 7.3%. Mass spectrum (FAB$^+$, glycerol + thioglycerol + trifluoroacetic acid matrix): $m/z = 337$ and 673, which corresponds to $[Ti^{IV}(THPED)H]^+$ and $\{[Ti^{IV}(THPED)]_2H\}^+$, respectively.

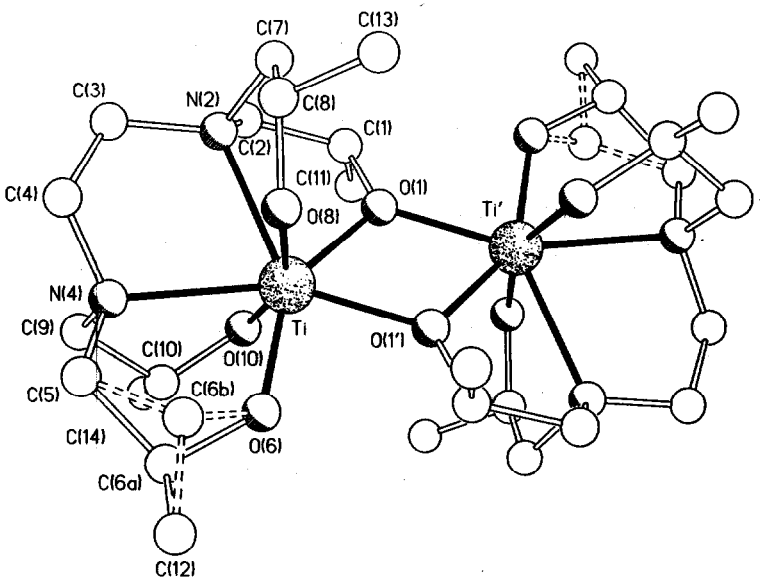

Fig. 2. The X-ray structure of $[Ti(THPED)]_2$ in $[Ti(THPED)]_2 \cdot C_7H_8$. The dotted bonds to C(6b) show the two disordered configurations that exist for this portion of the ligand in the crystal.

* Crystals of $[Ti^{IV}(THPED)]_2 \cdot C_7H_8$ suitable for X-ray diffraction measurements were recrystallized from toluene.

Crystal data. $[Ti^{IV}(THPED)]_2 \cdot C_7H_8$: $C_{35}H_{64}N_4O_8Ti_2$, $M = 764.7$, monoclinic, $a = 22.476(9)$, $b = 10.176(9)$, $c = 18.403(9)$ Å, $\beta = 112.43(4)°$, $U = 3891$ Å^3, space group $C2/c$, $Z = 4$. The complex has crystallographic C_i symmetry. $D_c = 1.305$ Mg m^{-3}. Clear block, dimensions $0.33 \times 0.40 \times 0.43$ mm, μ(Mo-K_α) = 0.463 mm^{-1}, $\lambda = 0.71073$ Å, $F(000) = 1640$.

Data collection and processing. Siemens P4/PC diffractometer, room temperature, ω scan method (2θ range 3.0–50.0°), graphite monochromated Mo-K_α radiation; 3427 independent measured reflections, 2325 observed [$|F_o| > 4.0\sigma(|F_o|)$], corrected for Lorentz and polarization factors.

Structure analysis and refinement. The structure was solved by direct methods and all the non-hydrogen atoms refined anisotropically. A ΔF map revealed the presence of disorder for one of the CH groups [C(6)]. This disorder corresponds to an inversion of this centre and two positions [C(6a) and C(6b) each of occupancy 50%] were refined anisotropically. The positions of hydrogen atoms were idealized (C—H = 0.96 Å), assigned isotropic thermal parameters $U(H) = 1.2U_{eq}(C)$ and allowed to ride on their parent carbons. The methyl groups were refined as rigid bodies. Refinement was by full-matrix least-squares to $R = 0.054$ ($R = \Sigma[|F_o| - |F_c|]/\Sigma|F_o|$), $R_w = 0.054$ [$w^{-1} = \sigma^2(F) + 0.0007F^2$]. The mean and maximum shifts/errors in the final refinement cycle were 0.014 and 0.743, respectively. The maximum and minimum residual electron densities were 0.50 and -0.36 e Å^{-3}, respectively. Computations were carried out on an IBM 386/70 using SHELXTL PC.[8]

The X-ray crystal structure* shows the molecule to be dimeric (Fig. 2) with each titanium atom being seven-coordinate, binding to all six of the potential donor atoms of the ligand. One oxygen atom [O(1)] of the ligand is binucleating, serving to bridge between adjacent titanium centres. The binuclear molecule is centrosymmetric with a crystallographic centre of symmetry at the centre of the planar Ti_2O_2 ring. The transannular Ti···Ti′ and O(1)···O(1′) distances are 3.41 and 2.29 Å and the O(1)—Ti—O(1′) and Ti—O(1)—Ti′ angles are 67.8(1)° and 112.2(1)°, respectively. Although the ligand is capable of binding the metal with a high degree of symmetry the potential molecular C_2 symmetry is broken both by C(10) and by one of the two disordered C(6) configurations (see below). The coordination polyhedron can be considered as either a distorted monocapped trigonal prism [Fig. 3(a)] with O(1)···N(2)···O(10) and O(1′)···O(6)···O(8) forming the prism and with N(4) as the capping atom or as a distorted pentagonal biprism [Fig. 3(b)] with O(8)···O(10) forming the principal axis. The lengths of the edges for the monocapped prism are in the range 2.29 [O(1)···O(1′)] to 2.99 Å [N(2)···O(10)] and those for the pentagonal biprism are in the range 2.29 [O(1)···O(1′)] to 3.20 Å [O(1′)···O(10)]. The Ti—O coordination distances (Table 1) are in the range 1.880(3) [Ti—O(6)] to 2.078(3) Å [Ti—O(1)]. These distances, with the exception of those involving the bridging oxygen atoms [O(1) and O(1′)], are noticeably shorter than those in $Ti(EDTA) \cdot H_2O$

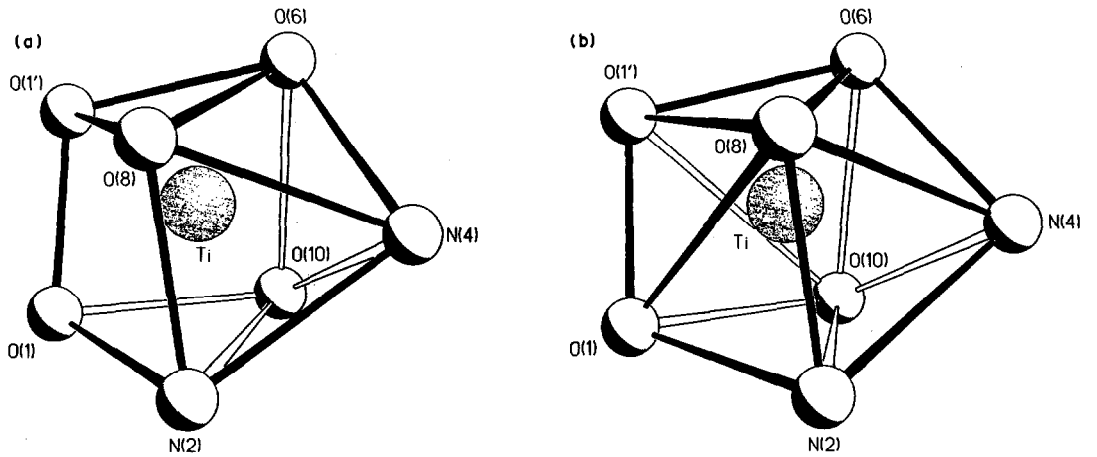

Fig. 3. (a) Distorted monocapped trigonal prismatic and (b) distorted pentagonal biprismatic representations of the coordination sphere about each titanium atom. In the binuclear structure the polyhedra are linked edge to edge about O(1)···O(1').

[range 1.922(2)–1.985(2) Å]. In contrast, both Ti—N distances [2.349(4), N(2); 2.386(5) Å, N(4)] are significantly longer than those in Ti(EDTA)·H_2O [mean 2.302(3) Å].[2] The similar structure of the seven-coordinate binuclear oxygen-bridged titanium cation $[\{TiCl(\mu\text{-}O)(12\text{-crown-}4)\}_2]^{2+}$ contains μ-oxo groups where, as expected, the bridging Ti—O distances are significantly shorter at 1.811(3) and 1.823(4) Å than those observed here [2.078(3), Ti—O(1); 2.025(4), Ti—O(1')].[4] In contrast, the Ti—O distances of the six-coordinate binuclear hydroxylate bridged $Ti_2(DBTA)_2(OPr^i)_4$ complex, where H_2DBTA = (*R*,*R*)-N,N'-dibenzyltartramide, are comparable [2.160(9) and 1.973(9) Å].[7]

As each ligand contains four chiral centres, there is the potential to form, in a binuclear structure, i.e. 2562,[8] configurational isomers. However, many of these must be sterically unfavourable when the ligand is complexed to a metal centre, although the disorder that is observed at C(6) (which corresponds to an inversion at this centre) clearly indicates that more than one configuration for the complexed ligand can exist in the solid state. As the binuclear complex is centrosymmetric the relative configurations about the two titanium centres are enantiomeric.

Attempts to characterize the complex in solution by NMR spectroscopy confirmed the presence of numerous isomers. The ^1H NMR spectrum of the complex showed that racemization was slow on the

Table 1. Selected bond lengths (Å) and angles (°) with e.s.d.s in parentheses

Ti—O(1)	2.078(3)	Ti—N(2)	2.349(4)
Ti—N(4)	2.386(5)	Ti—O(6)	1.880(3)
Ti—O(8)	1.905(3)	Ti—O(10)	1.891(3)
Ti—O(1')	2.025(4)		
O(1)—Ti—N(2)	70.5(1)	O(1)—Ti—N(4)	136.8(1)
N(2)—Ti—N(4)	72.2(1)	O(1)—Ti—O(6)	145.9(1)
N(2)—Ti—O(6)	143.4(2)	N(4)—Ti—O(6)	73.0(1)
O(1)—Ti—O(8)	104.8(1)	N(2)—Ti—O(8)	73.3(1)
N(4)—Ti—O(8)	84.4(1)	O(6)—Ti—O(8)	92.4(1)
O(1)—Ti—O(10)	82.8(1)	N(2)—Ti—O(10)	88.8(1)
N(4)—Ti—O(10)	75.3(1)	O(6)—Ti—O(10)	93.1(1)
O(8)—Ti—O(10)	156.4(2)	O(1)—Ti—O(1')	67.8(1)
N(2)—Ti—O(1')	131.3(1)	N(4)—Ti—O(1')	154.9(1)
O(6)—Ti—O(1')	82.1(1)	O(8)—Ti—O(1')	94.0(1)
O(10)—Ti—O(1')	109.5(1)	Ti—O(1)—Ti'	112.2(1)

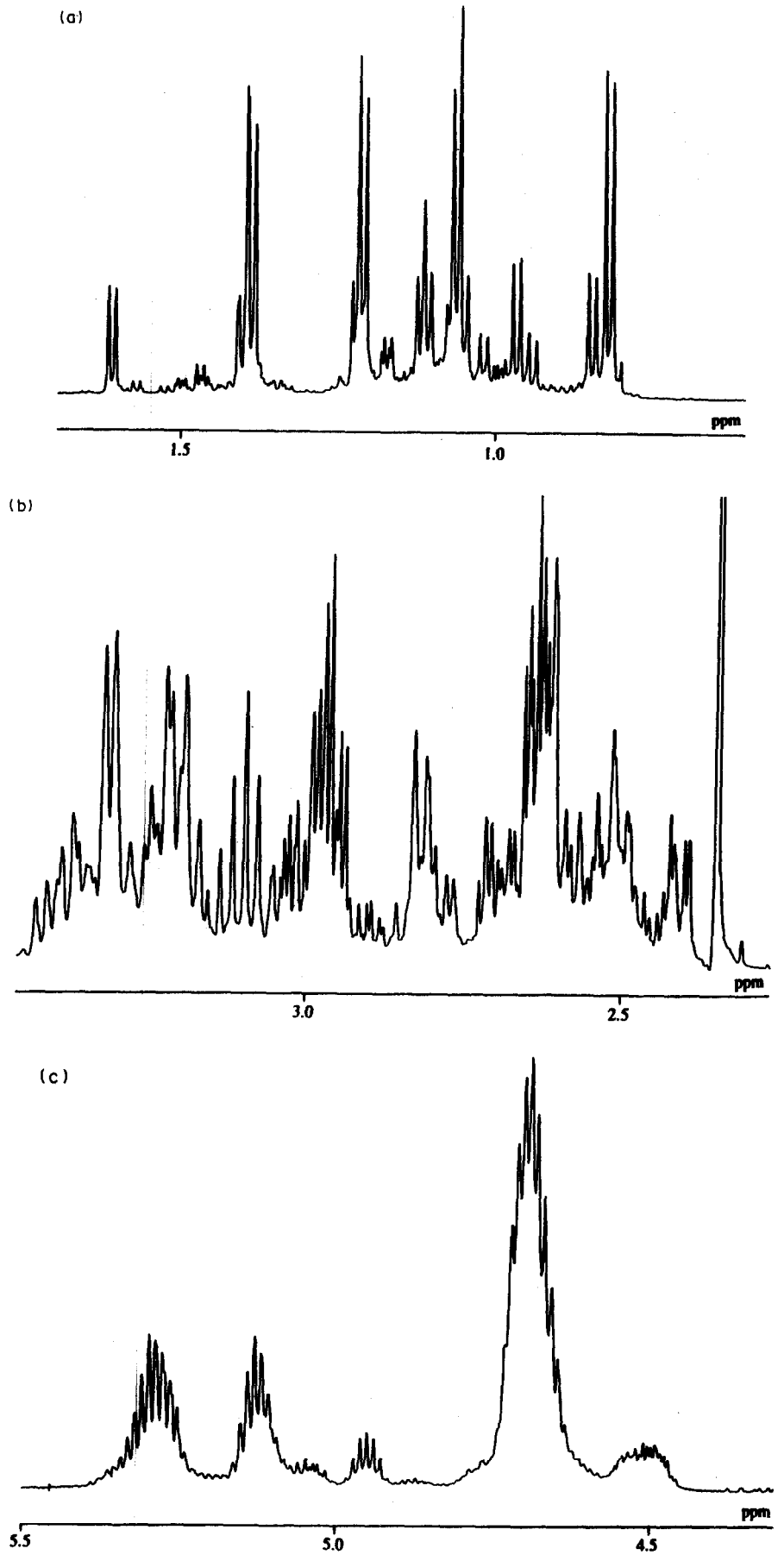

Fig. 4. ^1H NMR (500 MHz, $CDCl_3$) spectrum of $[Ti(THPED)]_2 \cdot C_7H_8$; (a) CH_3 resonances, δ 0.60–1.70 ppm; (b) CH_2 resonances, δ 2.25–3.45 ppm; (c) CH resonances, δ 4.30–5.50 ppm.

NMR time-scale with different isomers separated in the spectrum (Fig. 4). There is a certain degree of overlap due to the inability of NMR to distinguish between diastereomers, however, this leads to only a small reduction in the complexity of the system, thus individual assignments cannot be made.

The complex described is an example of a titanium dimer which utilizes a bridging hydroxylate moiety from the ligand to form a Ti_2O_2 ring analogous to titanium catalysts used in asymmetric organic syntheses. However, the success of the titanium catalysts depends on the orientation of the ligands and the mechanism of the reaction is believed to involve six-coordinate titanium intermediates.[5] In contrast, the $[Ti(THPED)]_2$ complex described here is a stable dimer with seven-coordinate titanium atoms. The observations reported here may stimulate investigations to evaluate the possibility of seven-coordinated titanium intermediates in catalysis.

Acknowledgements—We are grateful to the SERC for an equipment grant. We also thank Mr R. N. Sheppard for the 500 MHz NMR spectra and Mr M. Domin for the mass spectrum. One of us (C.Y.W.) thanks the SERC for a grant.

REFERENCES

1. D. F. Evans, G. W. Griffiths, C. A. O'Mahoney, D. J. Williams, C. Y. Wong and J. D. Woollins, *J. Chem. Soc., Dalton Trans.* 1992, 2475.
2. J. P. Fackler Jr, F. J. Kristine, A. M. Mazany, T. J. Moyer and R. E. Shepperd, *Inorg. Chem.* 1985, **24**, 1857.
3. F. E. Hahn, S. Rupprecht and K. H. Moock, *J. Chem. Soc., Chem. Commun.* 1991, 224.
4. G. R. Willey, J. Palin and N. W. Alcock, *J. Chem. Soc., Dalton Trans.* 1992, 1117 and refs therein.
5. R. A. Johnson and K. B. Sharpless, *Comprehensive Organic Synthesis—Selectivity, Strategy and Efficiency in Modern Organic Chemistry*, Vol. 7, *Oxidation* (Edited by B. M. Trost and I. Fleming). Pergamon Press, Oxford (1991) and refs therein.
6. M. G. Finn and K. B. Sharpless, *Asymmetric Synthesis* (Edited by J. D. Morrison), Vol. 5, p. 247. Academic Press, New York (1985) and refs therein.
7. I. D. Williams, S. F. Pedersen, K. B. Sharpless and S. J. Lippard, *J. Am. Chem. Soc.* 1984, **106**, 6430.
8. SHELXTL PC Version 4.2, Siemens X-Ray Analytical Instruments (1991).

Polyhedron Vol. 12, No. 3, pp. 343–345, 1993
Printed in Great Britain

0277–5387/93 $6.00+.00
© 1993 Pergamon Press Ltd

COMMUNICATION

TWO NEW STRUCTURAL TYPES FOR d^3–d^3 DIMERS OF MOLYBDENUM AND TUNGSTEN: $[K(18\text{-crown-6})]^+[Mo_2(OCH_2Bu^t)_7]^-$ AND $[W_2\{P(c\text{-hexyl})_2\}_3(OCH_2Bu^t)_3\{HP(c\text{-hexyl})_2\}]$

THEODORE A. BUDZICHOWSKI, MALCOLM H. CHISHOLM,* JAMES D. MARTIN, JOHN C. HUFFMAN, K. G. MOODLEY and WILLIAM E. STREIB

Department of Chemistry and Molecular Structure Center, Indiana University, Bloomington, IN 47405, U.S.A.

(*Received* 1 *October* 1992; *accepted* 13 *November* 1992)

Abstract—The syntheses and structures (determined by single-crystal X-ray diffraction techniques) are reported for $[K(18\text{-crown-6})]^+[Mo_2(OCH_2Bu^t)_7]^-$ and $[W_2\{P(c\text{-hexyl})_3\}_3(OCH_2Bu^t)_3\{HP(c\text{-hexyl})_2\}]$. The former contains a single bridging (μ-OCH_2Bu^t) ligand, six terminal alkoxide ligands and an M≡M triple bond. The latter contains three bridging (μ-PR_2) ligands and an M—M bond distance that is most consistent with the presence of a single bond. These two compounds are the first examples of M_2L_7 complexes with bridging ligands. They highlight the delicate balance of metal–metal vs metal–ligand bonding in the coordination chemistry of d^3–d^3 dimers of molybdenum and tungsten.

The coordination chemistry of M_2^{6+} containing compounds, where M = molybdenum and tungsten, is extremely rich because of the subtle interplay between metal–ligand and metal–metal bonding.[1] Compounds of the form M_2L_6 generally adopt an ethane-like geometry, $L_3M{\equiv}ML_3$, for L = alkyl, alkoxide, thiolate and amide. This type of geometry is also found for numerous mixed-ligand sets, as in $M_2(NMe_2)_4X_2$ compounds, where X = halide or alkyl. The compounds $M_2(OR)_6$ react reversibly with donor ligands L such as pyridine and PMe_3 to give adducts $M_2(OR)_6L_2$, which contain two roughly square-planar four-coordinate metal atoms united by an unbridged M≡M bond.[2] The monoligated adducts $M_2(CH_2Ph)_2(OPr^i)_4(PMe_3)$[3] and $W_2(p\text{-tolyl})_2(OPr^i)_4(HNMe_2)$[4] provide the only known examples of d^3–d^3 dimers having seven ligands and in each case there is an unbridged M≡M bond between three- and four-coordinated metal atoms, as might have been anticipated by the removal of one of the neutral ligands from an $M_2(OR)_6L_2$ compound. Nevertheless, it seemed reasonable to suppose that for compounds with seven ligands bridged structures should be accessible. Indeed bridged structures were implicated by two earlier observations. (1) The reversible addition of PMe_3 to $(Pr^iO)_2(PhCH_2)Mo{\equiv}Mo(CH_2Ph)(OPr^i)_2$ yielded $(PMe_3)(Pr^iO)(PhCH_2)_2Mo{\equiv}Mo(OPr^i)_3$ by way of facile benzyl/alkoxide ligand migrations.[3] (2) In the amide for halide substitution involving $(Me_3SiCH_2)_2BrMo{\equiv}MoBr(CH_2SiMe_3)_2$ and $LiNMe_2$ (2 equivalents) the compound $(Me_3SiCH_2)(Me_2N)_2Mo{\equiv}Mo(CH_2SiMe_3)_3$ was formed, whereas by an alternate synthesis the 1,2-isomer $(Me_3SiCH_2)_2(Me_2N)Mo{\equiv}Mo(NMe_2)(CH_2SiMe_3)_2$ was formed.[5] Furthermore, although 1,1- and 1,2-isomers of the formula $M_2X_4Y_2$ do not interconvert readily in solution, when $X = NMe_2$ and $Y = PR_2$, we have observed an equilibrium involving the 1,2-ethane-like dimers and bridged isomers $W_2(\mu\text{-}PR_2)_2(NMe_2)_4$. In the latter metal–phosphorus bonding is maximized at the expense of metal–metal bonding.[6]

The addition of 1 equivalent of an alkoxide anion Q^+OR^- (1 equivalent) to hydrocarbon solutions of $M_2(OR)_6$ compounds [M = Mo, R = Pr^i and CH_2Bu^t, and M = W, R = Bu^t; $Q^+ = K^+$ (18-

* Author to whom correspondence should be addressed.

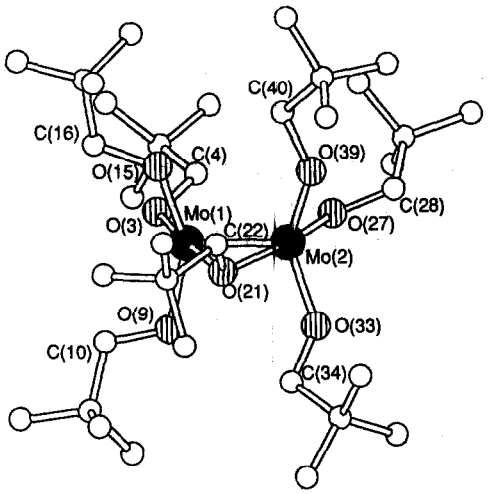

Fig. 1. A ball-and-stick drawing of one of the $Mo_2(OCH_2Bu^t)_7^-$ anions found in the structure of $[K(18\text{-crown-6})]^+[Mo_2(OCH_2Bu^t)_7]^- \cdot 2.5C_6H_6$. Selected averaged distances (Å) and angles (°) are Mo—Mo = 2.218(3), Mo—μ-O = 2.15(2), Mo—O terminal 1.92–1.97, *trans*-O(bridge)—Mo—O = 175 and 170, equatorial O terminal—Mo—O terminal = 146, 132, 147 and 131, and Mo—O(bridge)—Mo = 62.

crown-6)] yields a colour change from yellow–orange to purple. By ^1H NMR spectroscopy only one type of OR ligand is observed at room temperature in benzene-d_6 and at −40°C in pyridine-d_5. Adduct formation was confirmed in the solid state by a single-crystal X-ray structural determination of the $[K(18\text{-crown-6})]^+[Mo_2(OCH_2Bu^t)_7]^-$ salt.* A drawing of the anion is shown in Fig. 1.

The $Mo_2(OCH_2Bu^t)_7^-$ anion contains two four-coordinate molybdenum atoms that share a single bridging OR ligand. The Mo—Mo distance, 2.22 Å, is essentially the same as that in the ethane-like unbridged parent compound $Mo_2(OCH_2Bu^t)_6$, Mo—Mo = 2.222(2) Å.[7] The formation of an Mo—Mo triple bond in the $Mo_2(OR)_7^-$ anion can be anticipated based on a consideration of the Mo_2O_7 skeleton, which contains an acute Mo—O—Mo angle (62°). The coordination geometry about each molybdenum atom can be considered to be derived from a trigonal bipyramid, wherein one equatorial site is vacant. The bridging OR ligand occupies a common apical site and the frontier orbitals of the two d^3-ML_4 fragments interact to form an M—M triplebond having one σ- and two π-components, as shown below.

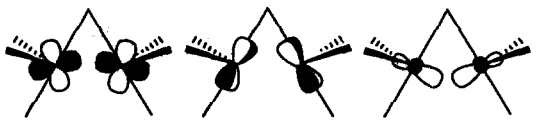

In the unit cell there are two independent $Mo_2(OCH_2Bu^t)_7^-$ anions and in both the oxygen atom of the bridging OR ligand is distinctly pyramidal: Σ angles at μ-O = 318.6 and 322.2. This is unusual for μ-OR ligands, but can be understood in terms of the formation of an Mo—Mo triple bond having one σ- and two π-components. A trigonal-planar bridging oxygen would introduce a filled oxygen p_π-orbital of the correct symmetry to interact with a filled M—M π-orbital. This filled–filled orbital interaction is avoided by the pyramidal rather than trigonal hybridization at the bridging oxygen.

In the reaction between $W_2(p\text{-tolyl})_2(OCH_2Bu^t)_4$ and HP(c-hexyl)$_2$ (4 equivalents) in benzene at room temperature a red crystalline compound is formed in *ca* 60% yield, based on tungsten and was shown to be $[W_2(OCH_2Bu^t)_3\{P(c\text{-hexyl})_2\}_3\{HP(hexyl)_2\}]$ by single-crystal X-ray crystallography.[7] A ball-and-stick drawing of the molecule is given in Fig. 2. The two tungsten atoms are united by three μ-PR_2 ligands. One tungsten atom,

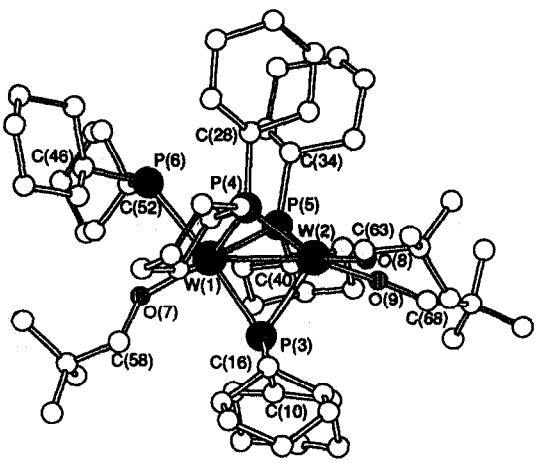

Fig. 2. A ball-and-stick drawing of the $[W_2\{\mu\text{-P(c-hexyl)}_2\}_3(OCH_2Bu^t)_3\{HP(c\text{-hexyl})_2\}]$ molecule. Selected distances (Å): W—W = 2.618(1), W—μ-P = 2.36–2.44 and W(1)—P(6) = 2.548(2), W(1)—O = 1.99(1), W(2)—O(8) = 2.00(1) and W(2)—O(9) = 1.97(1).

*Crystal data (i) for $[K(18\text{-crown-6-})]^+[Mo_2(OCH_2Bu^t)_7]^- \cdot 2.5C_6H_6$ at −165°C: a = 19.653(4), b = 22.244(4), c = 19.228(3) Å, α = 110.99(1)°, β = 107.51(1)°, γ = 98.19(1)°, Z = 4, d_{calc} = 1.22 g cm^{-3}, and space group $P\bar{1}$; (ii) for $[W_2\{P(c\text{-hexyl})_2\}_3(OCH_2Bu^t)_3\{HP(c\text{-hexyl})_2\}] \cdot 1.5C_6H_6$ at −156°C: a = 14.824(5), b = 19.262(7), c = 13.845(5) Å, α = 93.84(2)°, β = 108.10(2)°, γ = 95.62(2)°, Z = 2, d_{calc} = 1.37 g cm^{-3} and space group $P\bar{1}$.

W(2), has two terminal OR ligands and its WP_3O_2 geometry may be described as square pyramidal with the bridging phosphido ligand P(3) occupying the apical site. The other tungsten atom W(1) is in a pseudo-trigonal bipyramidal geometry, wherein the bridging phosphido ligand P(3) and the terminal phosphine ligand occupy axial sites.[8] There is only one terminal RO ligand bound to W(1). In solution the molecule is stereochemically labile so that on the ^{31}P NMR time-scale at room temperature all three bridges are equivalent, $\delta = 235$, but show coupling to two inequivalent tungsten nuclei, $^1J(^{183}W—^{31}P) = 247$ and 303 Hz. The phosphine ligand appears as a singlet at $\delta = 27.5$. Evidently, proton transfer between the phosphine and the phosphido ligands is slow. At $-80°C$ in toluene-d_8 there is evidence for the freezing-out of two types of μ-PR_2 ligands, δ 241 and 202, as expected based on the observed solid-state structure.

Although we are not sure how the phosphido bridged compound is formed in the reaction between $W_2(p\text{-tolyl})_2(OCH_2Bu^t)_4$ and dicyclohexylphosphine, we report it here because its structure represents a situation where metal–ligand bonding in the form of three bridging phosphido ligands is favoured at the expense of metal–metal bonding. Note the W—W distance of 2.62 Å. This contrasts with the structure of the $Mo_2(OCH_2Bu^t)_7^-$ anion, where the essential elements of the triple bond are preserved.

In conclusion, we note that the present structural characterizations provide the first examples of bridged M_2^{6+}-containing compounds supported by seven ligands and add to the wealth of structural diversity in the chemistry of d^3–d^3 dimers of molybdenum and tungsten. In one case we see the preference for M—M bonding, while in the other M—M bonding is sacrificed in favour of metal–ligand bonding. The structure and fluxional behaviour of the $Mo_2(OR)_7^-$ anion provide insight into the likely mechanism of facile ligand transfer between the metal atoms that occurs when seven ligands are present at the dinuclear centre. Ligand transfer does not occur rapidly when only six ligands are present.*

Further studies are in progress.

Supplementary material available. Listing of atomic coordinates and isotropic thermal parameters have been deposited with the Cambridge Crystallographic Data Center.

Acknowledgements—We thank the National Science Foundation for financial support. KGM thanks the South African CSIR for financial assistance and the University of Durban–Westville for a sabbatical leave.

REFERENCES

1. (a) M. H. Chisholm, *Accts Chem. Res.* 1990, **23**, 419; (b) F. A. Cotton and R. A. Walton, in *Multiple Bonds Between Metal Atoms*. John Wiley, New York (1982).
2. M. H. Chisholm, *Polyhedron* 1983, **2**, 681.
3. (a) M. H. Chisholm, J. C. Huffman and R. J. Tatz, *J. Am. Chem. Soc.* 1984, **106**, 5385; (b) M. H. Chisholm, K. Folting, J. C. Huffman, K. S. Kramer and R. J. Tatz, *Organometallics* 1992, **11**, 4029.
4. M. H. Chisholm, B. W. Eichhorn, K. Folting, J. C. Huffman and R. J. Tatz, *Organometallics* 1986, **5**, 1599.
5. M. H. Chisholm, K. Folting, J. C. Huffman and I. P. Rothwell, *Organometallics* 1982, **1**, 251.
6. W. E. Buhro, M. H. Chisholm, J. D. Martin, K. Folting, J. C. Huffman and W. E. Streib, *J. Am. Chem. Soc.* 1992, **114**, 557.
7. M. H. Chisholm, F. A. Cotton, C. A. Murillo and W. W. Reichert, *Inorg. Chem.* 1977, **16**, 1801.
8. In this regard the structure is different from those seen for $W_2(OBu^t)_6(\mu\text{-}CX)$ molecules where (a) X = O: M. H. Chisholm, D. M. Hofman and J. C. Huffman, *Organometallics* 1985, **4**, 987; P. J. Blower, M. H. Chisholm, D. L. Clark and B. W. Eichhorn, *Organometallics* 1986, **5**, 2125; (b) X = Nxylyl: M. H. Chisholm, D. L. Clark, D. Ho and J. C. Huffman, *Organometallics* 1987, **6**, 1532.

* The 1,1- and 1,2-$Mo_2(NMe_2)_2(CH_2SiMe_3)_4$ isomers do not interconvert at 80°C in benzene-d_6 over a period of hours.[5] Even when a bridged isomer is accessible as in some $W_2(\mu\text{-}PR_2)_2(NMe_2)_4$ complexes, the free energy of activation for bridge closure/rupture is *ca* 25 kcal mol^{-1} at 22°C.[6]

Polyhedron Vol. 12, No. 3, pp. 347–349, 1993
Printed in Great Britain

0277–5387/93 $6.00+.00
© 1993 Pergamon Press Ltd

COMMUNICATION

INCORPORATION OF CHELATING 2,2′-BIPYRIDINE (bipy) LIGANDS AT THE EQUATORIAL SITES OF $Cu_2(\mu\text{-}O_2CMe)_4(H_2O)_2$: AN X-RAY STRUCTURE OF $[Cu_2(\mu\text{-}O_2CMe)_2(H_2O)(bipy)_2](PF_6)_2$

SHANMUGAM MEENAKUMARI and AKHIL R. CHAKRAVARTY*

Department of Inorganic and Physical Chemistry, Indian Institute of Science, Bangalore 560 012, India

(*Received* 13 *August* 1992; *accepted* 1 *October* 1992)

Abstract—The asymmetric dicopper(II) title complex with a $[Cu_2(\mu\text{-}O_2CMe)_2]^{2+}$ core was isolated from the reaction between $Cu_2(\mu\text{-}O_2CMe)_4(H_2O)_2$ and bipy in EtOH in the presence of NH_4PF_6 and has been characterized by X-ray diffraction analysis.

Perlepes *et al.* have recently reported[1] the isolation of a dicopper(II) complex, $[Cu_2(\mu\text{-}O_2CMe)_2(H_2O)_2(bipy)_2](ClO_4)_2 \cdot H_2O$, from the reaction between $[Cu_2(OH)_2(bipy)_2](ClO_4)_2$ and $MeCO_2H$. In this communication we report an unusual and hitherto unknown $Cu_2(\mu\text{-}O_2CMe)_4 \rightarrow Cu_2(\mu\text{-}O_2CMe)_2^{2+}$ core conversion, resulting in the formation of $[Cu_2(\mu\text{-}O_2CMe)_2(H_2O)(bipy)_2](PF_6)_2$ (**1**). The reactivity of the tetra-μ-acetatodicopper(II) precursor towards bipy has been extensively studied.[1–4] However, previous attempts to isolate a complex with a $[Cu_2(\mu\text{-}O_2CMe)_2]^{2+}$ core using this precursor remained unsuccessful. Complex **1**, having bipy ligands at the equatorial sites, is unique in showing different coordination geometries at two copper(II) centres.

The reaction between $Cu_2(\mu\text{-}O_2CMe)_4(H_2O)_2$ and bipy in EtOH, followed by the addition of NH_4PF_6, led to the formation of a mixture of dicopper(II)[1–3] and tricopper(II)[4] complexes. Complex **1** was isolated as a minor product from this mixture by fractional crystallization. The molecular structure of **1** has been determined by X-ray diffraction.[5]†

An ORTEP view[6] of the cationic complex is shown in Fig. 1. Selected bond distances and angles are given in Table 1. The structure consists of a dicopper(II) unit held by two acetato bridges. The chelating bipy ligands occupy the equatorial sites and are in *syn* positions stabilized by stacking interactions. The coordination geometries of two copper(II) centres are square-planar and square-pyramidal. The removal of two bridging acetato ligands from the precursor has resulted in an increased Cu—Cu separation from 2.616(1) to 2.965(3) Å in **1**. The Cu—Cu distance in **1** is, however, the shortest among the reported[1,7] di-

* Author to whom correspondence should be addressed.

† Analytical and crystal data for $[Cu_2(\mu\text{-}O_2CMe)_2(H_2O)(bipy)_2](PF_6)_2$ (**1**): Found: C, 33.1; H, 3.3; N, 6.4. Calc. for $C_{24}H_{24}N_4O_5F_{12}P_2Cu_2$: C, 33.3; H, 2.8; N, 6.5%. Mol. wt = 865.5, monoclinic, $a = 16.120(2)$, $b = 12.482(4)$, $c = 17.467(2)$ Å, $\beta = 113.98(1)°$, $U = 3211(1)$ Å^3, $Z = 4$, space group $P2_1/n$, $D_c = 1.79$ g cm^{-3}, $T = 290$ K, $\mu = 15.34$ cm^{-1}, $F(000) = 1728$, $R(R_w) = 0.0808$ (0.0904) for 3176 reflections with $I > 3\sigma(I)$, weighting scheme $w = 1.0000/(\sigma^2 |F_o| + 0.000115 |F_o|^2)$. The higher values of the R indices could be due to the presence of highly disordered PF_6 anions in the crystal lattice. Intensity data, collected on an Enraf–Nonius CAD4 diffractometer (Mo-K_α radiation, $\lambda = 0.7107$ Å), were corrected for Lorentz, polarization and absorption effects (transmission coefficients 0.92–1.00). The structure was solved and refined using the SHELX 76 program[5a] with Fourier syntheses and full-matrix least-squares. Atomic coordinates, full lists of bond lengths and angles, and thermal parameters have been deposited at the Cambridge Crystallographic Data Centre.

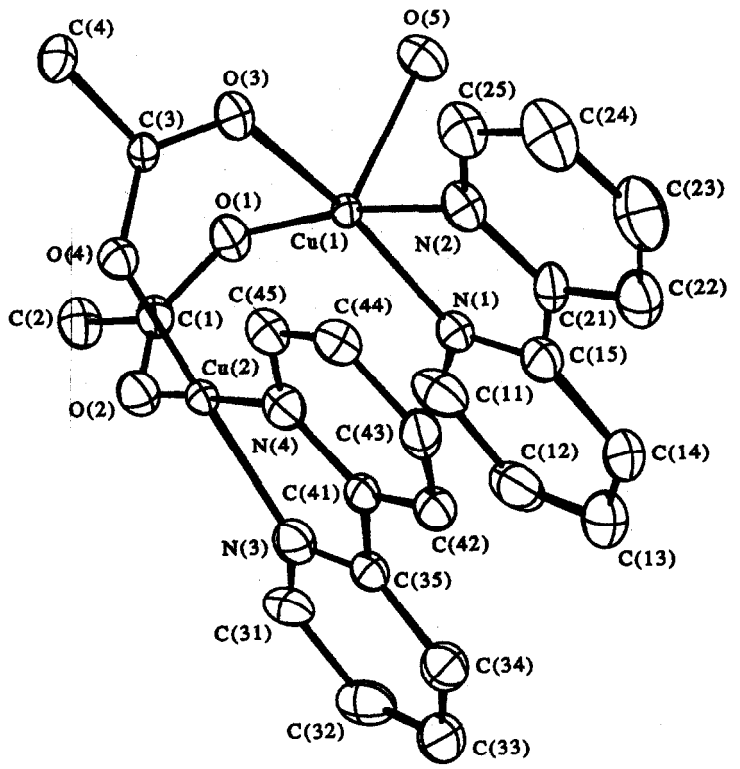

Fig. 1. An ORTEP view of the complex cation $[Cu_2(\mu\text{-}O_2CMe)_2(H_2O)(bipy)_2]^{2+}$ along with the atom numbering scheme.

copper(II) complexes containing a $[Cu_2(\mu\text{-}O_2CR)_2]^{2+}$ core (R = alkyl group) and two axial ligands. Complex **1** exemplifies the first dicopper(II) complex containing one axial ligand bonded to the di-μ-acetatodicopper(II) core.

The ESR spectrum of **1**, recorded at *X*-band in frozen methanol and shown in Fig. 2, exhibits well-resolved resonances which correspond to $\Delta M_s = \pm 1$, giving $g_\parallel$ and $g_\perp$ values of 2.28 and 2.06 ($A_\parallel = 165$ G, $A_\perp = 14$ G; $1\text{G} = 10^{-4}$ T), respectively. The fact that $g_\parallel > g_\perp$ is consistent with the X-ray structure. The ESR results indicate a weak antiferromagnetic interaction between the copper (II) centres as is observed[1] in analogous complexes. Further synthetic and magneto-chemical work on **1** is in progress.

Table 1. Selected bond distances (Å) and angles (°) for $[Cu_2(\mu\text{-}O_2CMe)_2(H_2O)(bipy)_2](PF_6)_2$ (**1**)

Cu(1)—Cu(2)	2.965(3)	Cu(1)—O(1)	1.939(8)
Cu(1)—N(1)	1.993(9)	Cu(1)—O(3)	1.957(8)
Cu(1)—N(2)	1.943(10)	Cu(1)—O(5)	2.253(9)
Cu(2)—N(3)	1.991(9)	Cu(2)—O(2)	1.934(7)
Cu(2)—N(4)	1.981(9)	Cu(2)—O(4)	1.914(7)

O(3)—Cu(1)—O(5)	95.0(3)	N(4)—Cu(2)—O(4)	95.1(4)
O(1)—Cu(1)—O(5)	90.6(3)	N(4)—Cu(2)—O(2)	173.3(4)
O(1)—Cu(1)—O(3)	89.6(4)	O(2)—Cu(2)—O(4)	90.3(4)
N(2)—Cu(1)—O(3)	93.4(4)	N(3)—Cu(2)—O(4)	176.3(4)
N(2)—Cu(1)—O(1)	172.6(4)	N(3)—Cu(2)—O(2)	93.4(4)
N(1)—Cu(1)—O(3)	167.7(3)	N(3)—Cu(2)—N(4)	81.2(4)
N(1)—Cu(1)—O(1)	94.1(4)	Cu(2)—Cu(1)—O(5)	167.6(3)
N(1)—Cu(1)—O(5)	96.7(3)	N(1)—Cu(1)—N(2)	81.6(4)

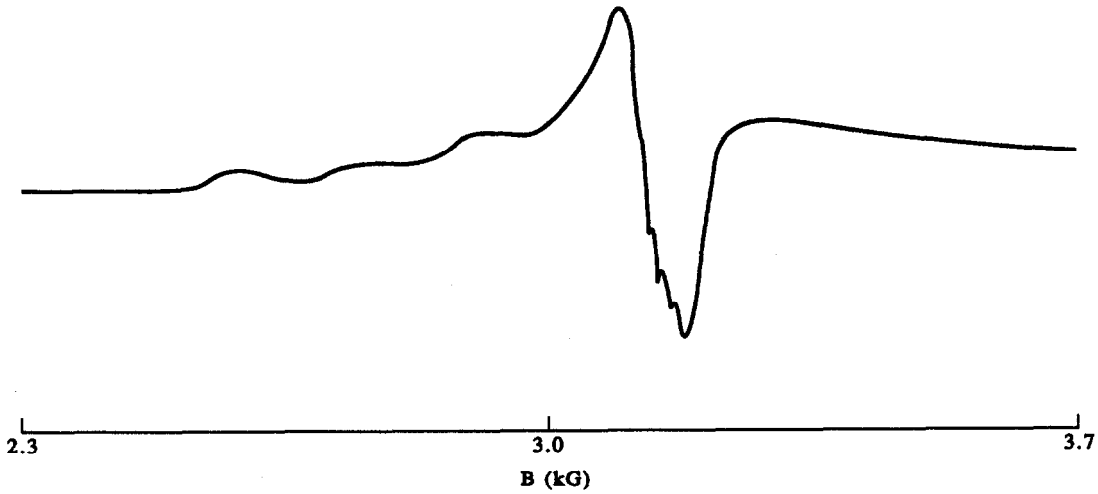

Fig. 2. The ESR spectrum of complex **1** in methanol glass at 77 K (microwave frequency 9.05 GHz, microwave power 2 mW, modulation frequency 100 kHz and modulation amplitude 4 × 1 G on a Varian E-line Century series *X*-band spectrometer).

Acknowledgement—This work was supported by UGC, India.

REFERENCES

1. S. P. Perlepes, J. C. Huffman and G. Christou, *Polyhedron* 1992, **11**, 1471.
2. G. Christou, S. P. Perlepes, E. Libby, K. Folting, J. C. Huffman, R. J. Webb and D. N. Hendrickson, *Inorg. Chem.* 1990, **29**, 3657.
3. S. P. Perlepes, J. C. Huffman and G. Christou, *Polyhedron* 1991, **10**, 2301.
4. S. Meenakumari and A. R. Chakravarty, *J. Chem. Soc., Dalton Trans.* 1992, 2749.
5. (a) G. M. Sheldrick, SHELX 76, Program for Crystal Structure Determination. University of Cambridge (1976); (b) *International Tables for X-Ray Crystallography*, Vol. 4. Kynoch Press, Birmingham (1974).
6. C. K. Johnson, ORTEP-II, A Program for Thermal Ellipsoid Plotting. Oak Ridge National Laboratory, Oak Ridge, Tennessee (1976).
7. (a) T. Tokii, N. Watanabe, M. Nakashima, Y. Muto, M. Morooka, S. Ohba and Y. Saito, *Bull. Chem. Soc. Japan* 1990, **63**, 364; (b) E. Dubler, U. K. Haring, K. H. Scheller, P. Baltzer and H. Sigel, *Inorg. Chem.* 1984, **23**, 3785; (c) M. Mikuriya, S. Kida, I. Veda, T. Tokii and Y. Muto, *Bull. Chem. Soc. Japan* 1977, **50**, 2464; (d) D. B. W. Yawney, J. A. Moreland and R. J. Doedens, *J. Am. Chem. Soc.* 1973, **95**, 1164; (e) T. Tokii, S. Emori and Y. Muto, *Bull. Chem. Soc. Japan* 1974, **47**, 2887; (f) T. Tokii and Y. Muto, *Bull. Chem. Soc. Japan* 1976, **49**, 1849.

Polyhedron Vol. 12, No. 3, p. 351, 1993
Pergamon Press Ltd. Printed in Great Britain

CAUTIONARY NOTE

The compound $[Co(NH_3)_5(H_2O)](ClO_4)_3$ (solid) decomposed in an explosive way when the researcher who had prepared the sample placed it on a porcelain capsule, producing serious injuries to his eyes and hands.

The substance has been used in our laboratory for 25 years as a precursor of other compounds, e.g. **Synthesis and characterization of *trans*-$[Co(NH_3)_4(NH_2CH_3)L]^{3+}$ [L = $(CH_3)_2SO$ or $(CH_3)_2NCHO$] complexes,** B. Sienra and A. Massaferro, *Polyhedron* 1991, **10**, 2075. On this occasion the usual steps for its preparation and recrystallization had been followed. The only plausible hypothesis to explain the accident is that deprotonation could have been caused by localized heating produced by friction in the solid.

Beatriz Sienra
Facultad de Química
C.C. 1157
Montevideo
Uruguay
Fax: 598-2-941906.

Polyhedron Vol. 12, No. 4, pp. 353–356, 1993
Printed in Great Britain

0277–5387/93 $6.00+.00
© 1993 Pergamon Press Ltd

TEMPLATE SYNTHESIS OF A NEW DINUCLEAR NICKEL(II) COMPLEX OF A BIS(MACROBICYCLIC) LIGAND

SHIN-GEOL KANG,* SOO-KYUNG JUNG, JAE KEUN KWEON and MI-SEON KIM

Department of Chemistry, Taegu University, Kyungsan 713-714, Korea

(*Received* 10 *September* 1992; *accepted* 28 *October* 1992)

Abstract—A one-pot condensation reaction of 1,4,8-triazaoctane, ethylenediamine and formaldehyde in the presence of nickel(II) produced a new dinuclear nickel(II) complex of a bis(macrobicyclic) ligand, $[Ni_2(\mathbf{D})](ClO_4)_4$, in which two fully saturated hexaazamacrobicycles are linked together by an ethylene chain. Each macrobicyclic subunit of the complex contains one 1,3-diazacyclohexane ring and has a square-planar geometry with a 5–6–5–6 chelate ring sequence. The electronic spectra and electrochemical properties show that metal–metal interactions of the dinuclear complex are negligible.

Dinuclear complexes of polyazamacrocycles are important in the study of intramolecular metal–metal interactions and multielectron catalysts.[1–3] Although various types of such compounds have been prepared and investigated, those of fully saturated bis(macrocyclic) ligands are relatively rare[4–6] and in most cases the synthetic routes require several steps.

A one-pot metal template condensation reaction of amines and formaldehyde has been employed in the preparation of mononuclear complexes of fully saturated macrocyclic ligands.[7–13] The nickel(II) complexes of **A** and **B** have been synthesized by the reactions of eqs (1)[7] and (2),[9] respectively. Recently, this type of reaction was extended to the synthesis of dinuclear complexes of bis(macrocyclic) ligands.[14,15] For example, the dinuclear nickel(II) complex of **C** was prepared in our group by the reaction [eq. (3)] of the nickel(II) ion with ethylenediamine, methylamine and formaldehyde.[14] Utilizing the characteristics of the reactions, we have designed and prepared a new dinuclear nickel(II) complex of the bis(macrobicyclic) ligand **D** that contains two fully saturated hexaazamacrocyclic subunits with one 1,3-diazacyclohexane ring, by the one-pot reaction [eq. (4)] of 1,4,8-triazaoctane, ethylenediamine and formaldehyde in the presence of the metal ion. The synthesis and characterization of the dinuclear complex $[Ni_2(\mathbf{D})]^{4+}$ are reported. Comparisons of the properties of the dinuclear complex with those of $[Ni(\mathbf{B})]^{2+}$ and $[Ni_2(\mathbf{C})]^{4+}$ are also presented.

* Author to whom correspondence should be addressed.

EXPERIMENTAL

Materials and measurements

All chemicals used in the syntheses were of reagent grade. Solvents for spectral and electrochemical measurements were of spectroscopic and electroanalytical reagent grade, respectively.

IR spectra were obtained using a Shimadzu IR-440 spectrophotometer. Visible spectra were recorded with a Kontron Uvikon 860 UV–vis spectrophotometer. Conductance measurements were made using a Metrohm Herisau Conductometer E518. NMR spectra were recorded on a Bruker WP 300 FT NMR spectrometer. Elemental analyses were performed at the Koloin R&D center, Kumi, Korea. The cyclic voltammograms were recorded using a Yanaco Voltammetric Analyser p-1000 equipped with an FG-121B function generator and a Watanabe *X–Y* recorder. The cyclic voltammetric data were obtained by published methods.[7]

Synthesis

$[Ni_2(\mathbf{D})](ClO_4)_4$. To a methanol solution (25 cm^3) of $NiCl_2 \cdot 6H_2O$ (3.0 g) were added 97% 1,4,8-triazaoctane (1.3 cm^3), 99% ethylenediamine (1.7 cm^3) and *para*-formaldehyde (2.1 g). The mixture

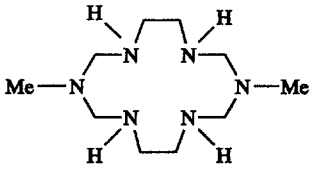

A

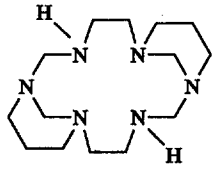

B

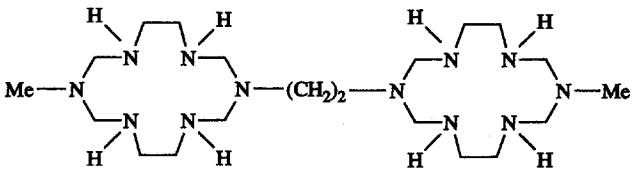

C

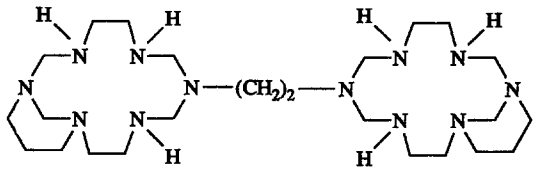

D

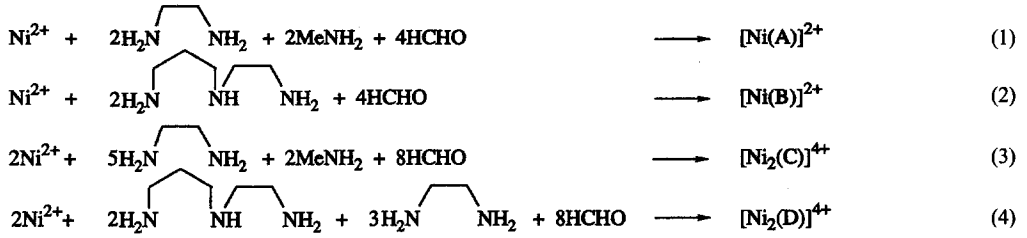

(1)

(2)

(3)

(4)

was heated at reflux for 24 h until a dark orange–red solution resulted and then cooled to room temperature. Excess perchloric acid was added dropwise to the solution with stirring and then yellow solids were precipitated. The solids collected by filtration contain the dinuclear complex and a small amount (<5%) of orange [Ni(**B**)]$(ClO_4)_2$ as a by-product. The crude product was dissolved in the minimum volume of hot water and then cooled to room temperature. The first crop of the precipitates contained mainly [Ni_2(**D**)]$(ClO_4)_4$. The pure product was obtained by fractional recrystallizations of the crude product from hot water. Yield: *ca* 20%. Found: C, 28.4; H, 5.4; N, 16.1 Calc. for $Ni_2C_{24}H_{54}N_{12}Cl_4O_{16}$: C, 28.1; H, 5.3; N, 16.4%. IR: 3200 [ν(N—H)], 1100 cm^{-1} [$\nu(ClO_4^-)$].

[Ni_2(**D**)]$(PF_6)_4$. To a hot saturated solution of the above complex was added excess NH_4PF_6 dissolved in water. The yellow solids formed were filtered, washed with a cold water–methanol (1:1) mixture and dried in air. Found: C, 24.0; H, 4.7; N, 13.7. Calc. for $Ni_2C_{24}H_{54}N_{12}P_4F_{24}$: C, 23.8; H, 4.5; N, 13.9%. ^{13}C NMR (CD_3NO_2): δ 23.5, 44.1, 47.0, 47.5, 48.5, 49.1, 55.8, 58.2, 68.2, 68.3, 70.5, 74.1 ppm.

RESULTS AND DISCUSSION

The reaction of excess formaldehyde with a 2:2:3 molar mixture of nickel(II) ions, 1,4,8-triazaoctane and ethylenediamine, followed by the addition of excess perchloric acid, yields a mixture of the bis(macrobicyclic) complex [Ni_2(**D**)]$(ClO_4)_4$ and a small amount of the mononuclear complex [Ni(**B**)]$(ClO_4)_2$ as a by-product. However, the major product is the dinuclear complex, which can be easily isolated by fractional recrystallizations of the mixture from hot water. The proportion of the by-product in the crude product can be reduced to less than 5% by employing a 2:1:6:4 molar mixture of the reactants (see Experimental). The routes to give the dinuclear complex of **D** may be similar to

those reported for the complexes of **A**–**C**.[7,9,14] The bis(macrobicyclic) complex is extremely stable in the solid state and is decomposed very slowly even at low pH. The visible spectra of the complex (2.0×10^{-3} M) in HNO_3 solution (0.3 M) show that only about 10% of the complex is decomposed in 10 h at 20°C. The slow decomposition in acidic solutions was also observed for the complexes of **A**–**C**.[7,9,14]

The ^{13}C NMR spectrum of $[Ni_2(D)](PF_6)_4$ measured in CD_3NO_2 shows 12 resonances, indicating that the complex contains 12 pairs of non-equivalent carbon atoms and this is consistent with the ligand structure. Four carbon peaks of N—C—N linkages are observed at 74.1, 70.5, 68.3 and 68.2 ppm. A peak of the N—C—C—N chain, that links two macrobicyclic subunits, is observed at 44.1 ppm and peaks of the chains on the macrobicyclic rings at 47.0, 47.5, 48.5 and 49.1 ppm. Other peaks at 23.5, 55.8 and 58.2 ppm are assigned to the carbons of the N—C—C—C—N linkages. The IR spectrum of $[Ni_2(D)](ClO_4)_4$ shows a single strong absorption at 3200 cm^{-1}, which is attributed to N—H stretching vibrations of the coordinated secondary amino groups. No peak near 1600 cm^{-1} assignable to primary amines was observed, indicating that the cyclization reaction took place. The values of molar conductance measured in aqueous and acetonitrile solutions of the dinuclear complex (2.0×10^{-4} M) are 498 and 506 Ω^{-1} mol^{-1} cm^2, respectively, showing that the complex is a 1 : 4 electrolyte.

The visible spectra of $[Ni_2(D)](ClO_4)_4$ in nitromethane and aqueous solutions show the *d–d* transition band at 455 ($\varepsilon = 150$ M^{-1} cm^{-1}) and 452 nm ($\varepsilon = 107$ M^{-1} cm^{-1}), respectively, indicating that each metal ion of the complex is in a square planar Ni—N_4 environment.[7–15] In each solvent the wavelength of the band is intermediate between those of the dinuclear complex of **C** (~444 nm)[14] and the mononuclear complex of **B** (~465 nm).[9] The molar extinction coefficient for the complex of **D** in nitromethane solution also falls between that for **C** (135 M^{-1} cm^{-1})[14] and twice that for **B** (95 M^{-1} cm^{-1}).[9] It is likely that the two chromophores of the dinuclear complex of **D** behave independently, likewise the complexes of **C** and other bis(macrocyclic) ligands in which two macrocyclic subunits are linked together by a $-(CH_2)_n-$ chain.[14,15] Therefore, the weaker ligand field strength of **D**, compared to that of **C**, can be attributed to the increased Ni—N bond length caused by the formation of the 1,3-diazacyclohexane ring.[9,12] The visible spectra also show that the molar extinction coefficient of the bis(macrobicyclic) complex is much lower in water than in nitromethane. This indicates that the complex dissolves in water to give an equilibrium mixture of the square planar $[Ni_2(D)]^{4+}$ and octahedral $[Ni_2(D)(H_2O)_4]^{4+}$ species, as shown in eq. (5).[7,10–14]

$$[Ni_2(D)]^{4+} + 4H_2O \overset{K}{\rightleftharpoons} [Ni_2(D)(H_2O)_4]^{4+} \quad (5)$$

The equilibrium constant (K) for the reaction determined by published methods[7,12,14] at 25°C is 0.40, which is larger than that for **C** (0.26).[14] This trend is quite similar to the reported result that the K value (0.77) of the mononuclear nickel(II) complex of **B**[12] containing two 1,3-diazacyclohexane rings is much larger than that for **A** (0.44).[7]

The cyclic voltammograms of $[Ni_2(D)](ClO_4)_4$ obtained in 0.1 M $(Bu^n)_4NClO_4$ acetonitrile solution showed only one anodic and cathodic peak corresponding to a Ni^{II}/Ni^{III} process. This implies that the interactions between the two metal ions are negligible and each metal ion is able to release one electron nearly at the same potentials.[6,14,15] The oxidation potential (+1.08 V vs S.C.E. at 20°C) of the complex also falls between those for the nickel (II) complexes of **C** (+0.97 V)[14] and **B** (+1.34 V).[12] It has been widely observed that the stepwise alkylation on the coordinated secondary nitrogens of the macrocyclic ligands makes the oxidation of the nickel(II) complexes a more unfavourable process.[16]

Summary

The results show that the new compound prepared in this work is the dinuclear nickel(II) complex of **D**, in which four nitrogen atoms of each macrobicyclic subunit are coordinated to the metal ion with a square-planar geometry. The present synthetic method is interesting because formation and linking of the two macrobicycles with small ring moieties are performed by the simple one-pot reaction. Furthermore, relatively simple reagents are required for the reaction. This work also supports the idea that the intramolecular metal–metal interactions of dinuclear complexes, in which two uncoordinated nitrogen atoms of fully saturated macrocyclic subunits are linked together by an ethylene chain, are negligible. Comparisons of the spectral and chemical properties of the dinuclear complex with those of **B** and **C** show that these properties are largely affected by the number of 1,3-diazacyclohexane ring moieties fused to the ligands.

REFERENCES

1. J.-P. Collin, A. Jouaity and J. P. Sauvage, *Inorg. Chem.* 1988, **27**, 1986.
2. J. P. Collman, C. S. Bensosme, R. R. Durand, R. P.

Kreh and F. A. Anson, *J. Am. Chem. Soc.* 1983, **105**, 2699 and refs therein.
3. L. P. Battaglia, A. Bianchi, A. C. Corradi, E. Gercia-Espana, N. Micheloni and M. Julve, *Inorg. Chem.* 1988, **27**, 4174 and refs therein.
4. M. Ciampolini, M. Micheloni, N. Nardi, F. Vizza, A. Buttafava, L. Fabbrizzi and A. Perotti, *J. Chem. Soc., Chem. Commun.* 1984, 998.
5. K. Wieghardt, I. Tolksdorf and W. Herrmann, *Inorg. Chem.* 1985, **24**, 1230.
6. L. Fabbrizzi, L. Montagna, A. Poggi, T. A. Kaden and L. C. Siegfried, *J. Chem. Soc., Dalton Trans.* 1987, 2631.
7. M. P. Suh and S.-G. Kang, *Inorg. Chem.* 1988, **27**, 2544.
8. S.-K. Jung, S.-G. Kang and M. P. Suh, *Bull. Korean Chem. Soc.* 1989, **10**, 362.
9. M. P. Suh, W. Shin, S.-G. Kang, M. S. Lah and T. M. Chung, *Inorg. Chem.* 1989, **28**, 1602.
10. M. P. Suh, J. Choi, S.-G. Kang and W. Shin, *Inorg. Chem.* 1989, **28**, 1763.
11. S.-G. Kang, S.-K. Jung and J. K. Kweon, *Bull. Korean Chem. Soc.* 1990, **11**, 431.
12. M. P. Suh, S.-G. Kang, V. L. Goedken and S.-H. Park, *Inorg. Chem.* 1991, **30**, 365.
13. L. Fabbrizzi, A. M. M. Lanfred, P. Pallavicini, A. Perotti, A. Taglietti and F. Ugozzoli, *J. Chem. Soc., Dalton Trans.* 1991, 3262.
14. S.-G. Kang, S.-K. Jung and J. K. Kweon, *Bull. Korean Chem. Soc.* 1991, **12**, 219.
15. S. V. Rosokha and Y. D. Lampeka, *J. Chem. Soc., Chem. Commun.* 1991, 1077.
16. E. K. Barefield, G. M. Freeman and D. G. V. Derveer, *Inorg. Chem.* 1986, **25**, 552.

Polyhedron Vol. 12, No. 4, pp. 357–362, 1993
Printed in Great Britain

0277–5387/93 $6.00+.00
© 1993 Pergamon Press Ltd

THE PREPARATION AND REACTIONS WITH DONOR LIGANDS OF $[MoBrI(CO)_3(NCMe)_2]$

PAUL K. BAKER,* KEVIN R. FLOWER, H. MARGARET NAYLOR and KATHERINA VOIGT

Department of Chemistry, University of Wales, Bangor, Gwynedd LL57 2UW, U.K.

(*Received* 8 *October* 1992; *accepted* 15 *October* 1992)

Abstract—Equimolar quantities of *fac*-$[Mo(CO)_3(NCMe)_3]$ {prepared *in situ* by reacting $[Mo(CO)_6]$ in refluxing acetonitrile for 24 h} and BrI react at 0°C to give the seven-coordinate complex $[MoBrI(CO)_3(NCMe)_2]$ (**1**). Complex **1** reacts with 1 equivalent of L (L = PPh_3, $AsPh_3$ or $SbPh_3$) to initially give the mono(acetonitrile) complexes $[MoBrI(CO)_3(NCMe)L]$, which subsequently dimerize to afford $[Mo(\mu\text{-}I)Br(CO)_3L]_2$. Reaction of **1** with 2 equivalents of L (L = PPh_3, $AsPh_3$ or $SbPh_3$) gives the bis(ligand) compounds $[MoBrI(CO)_3L_2]$. The preparation and characterization of a series of new mixed-ligand complexes $[MoBrI(CO)_3LL']$ [L = PPh_3, L′ = $AsPh_3$; L = PPh_3, L′ = $SbPh_3$; L = $AsPh_3$, L′ = $SbPh_3$; L = PPh_3, $AsPh_3$ and $SbPh_3$; L′ = $SPPh_3$, $SC(NH_2)_2$ and $SC(NMe_2)_2$] are also described. Equimolar quantities of $\widehat{LL}$ [$\widehat{LL}$ = $Ph_2P(CH_2)_nPPh_2$ (n = 1–3); 1,10-phen] and $[MoBrI(CO)_3(NCMe)_2]$ react to afford the acetonitrile displaced products $[MoBrI(CO)_3(\widehat{LL})]$ in high yield. The synthesis of the novel, dicarbonyl five different ligand compound $[MoBrI(CO)_2(NCMe)(SbPh_3)_2]$ is also reported.

In 1986[1] we reported the preparation of the highly versatile seven-coordinate diiodo complexes $[MI_2(CO)_3(NCMe)_2]$ (M = Mo or W). These compounds react with both donor ligands[2–5] and alkynes[6,7] to give a range of new organometallic complexes. In order to increase the number of different ligands attached to a transition-metal centre we herein describe the preparation of the new mixed-halide seven-coordinate complex $[MoBrI(CO)_3(NCMe)_2]$ and discuss some of its reaction chemistry.

EXPERIMENTAL

All the reactions described in this paper were performed under an atmosphere of dry nitrogen using standard Schlenk-line techniques. The solvents CH_2Cl_2 and NCMe were dried over P_4O_{10}, acetone was dried over molecular sieves (4 Å) and diethyl ether was dried over sodium. All solvents were distilled before use and were free from dioxygen. The complex *fac*-$[Mo(CO)_3(NCMe)_3]$ was prepared *in situ* by the published method.[8] All chemicals were purchased from commercial sources except BrI, which was also synthesized by a literature method.[9]

Elemental analyses (carbon, hydrogen and nitrogen) were determined using a Carlo–Erba Elemental Analyser MOD 1106 (using helium as a carrier gas). IR spectra were recorded as $CHCl_3$ films between NaCl plates on a Perkin–Elmer 197 IR spectrophotometer. ^1H NMR spectra were recorded on a Bruker AC 250 CP/MAS NMR spectrometer. All spectra were referenced to tetramethylsilane.

$[MoBrI(CO)_3(NCMe)_2]$ (1)

A suspension of $[Mo(CO)_6]$ (3.96 g, 0.015 mmol) in degassed acetonitrile (150 cm^3) was heated under reflux in a nitrogen atmosphere for 24 h. The solution was cooled to 0°C and BrI (3.18 g, 0.015 mmol) was added to the solution. The mixture immediately

* Author to whom correspondence should be addressed.

became brown. The solvent was removed *in vacuo* to give a light-brown crystalline complex, $[MoBrI(CO)_3(NCMe)_2]$ (**1**), which was recrystallized from $MeCN/Et_2O$. Yield = 6.54 g, 92%.

Reactions of $[MoBrI(CO)_3(NCMe)_2]$ (**1**) *with* 1 *equivalent of L to give* $[MoBrI(CO)_3(NCMe)L]$

In a typical reaction: To $[MoBrI(CO)_3(NCMe)_2]$ (0.496 g, 1.05 mmol) dissolved in CH_2Cl_2 (15 cm^3) with continuous stirring under a stream of dry nitrogen was added PPh_3 (0.278 g, 1.1 mmol). After stirring the solution for 30 min the mixture was filtered. Removal of the solvent *in vacuo* gave mid-brown crystals of $[MoBrI(CO)_3(NCMe)(PPh_3)]\cdot\frac{1}{2}CH_2Cl_2$ (**2**), which were recrystallized from CH_2Cl_2/Et_2O. Yield = 0.492 g, 64%.

Similar reactions of $[MoBrI(CO)_3(NCMe)_2]$ with an equimolar amount of L (L = $AsPh_3$ or $SbPh_3$) in CH_2Cl_2 at room temperature gave after 30 min the new complexes $[MoBrI(CO)_3(NCMe)L]$ (**3** and **4**). For physical and analytical data see Table 1.

Reactions of $[MoBrI(CO)_3(NCMe)_2]$ *with* 1 *equivalent of L to give* $[Mo(\mu\text{-}I)Br(CO)_3L]_2$

In a typical reaction: To $[MoBrI(CO)_3(NCMe)_2]$ (0.5 g, 1.066 mmol) dissolved in CH_2Cl_2 (15 cm^3) with continuous stirring under a stream of dry nitrogen was added PPh_3 (0.28 g, 1.066 mmol). After stirring the solution for 4 h, the mixture was filtered. Removal of the solvent *in vacuo* gave mid-brown crystals of $[Mo(\mu\text{-}I)Br(CO)_3(PPh_3)]_2$ (**5**), which were recrystallized from CH_2Cl_2/Et_2O. Yield = 0.35 g, 50%.

Similar reactions of $[MoBrI(CO)_3(NCMe)_2]$ with an equimolar amount of L (L = $AsPh_3$ or $SbPh_3$) in CH_2Cl_2 at room temperature gave after 4 h the new compounds $[Mo(\mu\text{-}I)Br(CO)_3L]_2$ (**6** and **7**). For physical and analytical data see Table 1.

Reactions of $[MoBrI(CO)_3(NCMe)_2]$ *with* 2 *equivalents of L to give* $[MoBrI(CO)_3L_2]$

In a typical reaction: To $[MoBrI(CO)_3(NCMe)_2]$ (0.460 g, 0.98 mmol) dissolved in CH_2Cl_2 (15 cm^3) with continuous stirring under a stream of dry nitrogen at room temperature was added $AsPh_3$ (0.600 g, 1.96 mmol). After stirring the solution for 150 min the mixture was filtered. Removal of the solvent *in vacuo* gave brown crystals of $[MoBrI(CO)_3(AsPh_3)_2]$ (**9**), which were recrystallized from CH_2Cl_2/Et_2O. Yield = 0.578 g, 59%.

Similar reactions of $[MoBrI(CO)_3(NCMe)_2]$ with 2 equivalents of L (L = PPh_3 or $SbPh_3$) gave the new complexes $[MoBrI(CO)_3L_2]$ (**8** and **10**). For physical and analytical data see Table 1.

Reactions of $[MoBrI(CO)_3(NCMe)_2]$ *with L, followed by L′ to give* $[MoBrI(CO)_3LL']$

In a typical reaction: To $[MoBrI(CO)_3(NCMe)_2]$ (0.271 g, 0.58 mmol) dissolved in CH_2Cl_2 (15 cm^3) with continuous stirring under a stream of dry nitrogen at room temperature was added $SbPh_3$ (0.204 g, 0.58 mmol). After stirring the solution for 5 min $SPPh_3$ (0.170 g, 0.58 mmol) was added and the mixture was stirred for a further 30 min. Filtration, followed by removal of the solvent *in vacuo*, gave the dark orange solid $[MoBrI(CO)_3(SbPh_3)(SPPh_3)]$ (**16**), which was recrystallized from CH_2Cl_2. Yield = 0.354 g, 59%.

Similar reactions of $[MoBrI(CO)_3(NCMe)_2]$ with 1 equivalent of L [L = PPh_3 (1 min), $AsPh_3$ (3 min) or $SbPh_3$ (5 min)], followed by an equimolar amount of L′ {L′ = PPh_3, $AsPh_3$, $SbPh_3$, $SPPh_3$, $SC(NH_2)_2$ [reactions carried out in acetone with $SC(NH_2)_2$], $SC(NMe_2)_2$} (all 30 min), gave the new mixed-ligand complexes $[MoBrI(CO)_3LL']$ (**11–15**, **17–22**). For physical and analytical data see Table 1.

Reactions of $[MoBrI(CO)_3(NCMe)_2]$ *with an equimolar quantity of* $\widehat{LL}$ *to give* $[MoBrI(CO)_3(\widehat{LL})]$

In a typical reaction: To $[MoBrI(CO)_3(NCMe)_2]$ (0.5 g, 1.066 mmol) dissolved in CH_2Cl_2 (15 cm^3) with continuous stirring under a stream of dry nitrogen at room temperature was added $Ph_2P(CH_2)PPh_2$ (0.41 g, 1.066 mmol). After stirring the solution for 2 h the mixture was filtered. Removal of the solvent *in vacuo* gave mid-brown crystals of $[MoBrI(CO)_3\{Ph_2P(CH_2)PPh_2\}]\cdot\frac{1}{2}CH_2Cl_2$ (**23**), which were recrystallized from CH_2Cl_2/Et_2O. Yield = 0.53 g, 61%.

Similar reactions of $[MoBrI(CO)_3(NCMe)_2]$ with an equimolar quantity of $\widehat{LL}$ [$\widehat{LL}$ = $Ph_2P(CH_2)_n PPh_2$ (n = 2 and 3), 1,10-phen] in CH_2Cl_2 at room temperature gave $[MoBrI(CO)_3(\widehat{LL})]$ (**24–26**). For physical and analytical data see Table 1.

Bubbling a stream of nitrogen through a solution of $[MoBrI(CO)_3(SbPh_3)_2]$ *in acetonitrile to give* $[MoBrI(CO)_2(NCMe)(SbPh_3)_2]$ (**27**)

A stream of nitrogen gas was bubbled into a stirred suspension of $[MoBrI(CO)_3(SbPh_3)_2]$ (0.543 g, 0.5 mmol) in acetonitrile (15 cm^3) at room temperature. After 3 h the three bands of the tricarbonyl complex had been replaced by two new carbonyl bands of equal intensity. At this stage, the

Table 1. Physical and analytical data for the seven-coordinate complex $[MoBrI(CO)_3(NCMe)_2]$ and its derivatives

Complex	Colour	Yield (%)	Analysis[a] C(%)	H(%)	N(%)
$[MoBrI(CO)_3(NCMe)_2]$ (**1**)	Light brown	92	15.6 (17.9)	1.5 (1.5)	5.9 (6.0)
$[MoBrI(CO)_3(NCMe)(PPh_3)] \cdot \frac{1}{2}CH_2Cl_2$ (**2**)	Mid-brown	64	38.6 (38.5)	2.7 (2.6)	1.6 (1.9)
$[MoBrI(CO)_3(NCMe)(AsPh_3)]$ (**3**)	Orange	59	37.3 (37.6)	2.8 (2.5)	1.6 (1.9)
$[MoBrI(CO)_3(NCMe)(SbPh_3)] \cdot \frac{1}{2}CH_2Cl_2$ (**4**)	Red–rust	75	34.3 (34.3)	2.4 (2.3)	1.2 (1.7)
$[Mo(\mu\text{-}I)Br(CO)_3(PPh_3)]_2$ (**5**)	Mid-brown	50	38.7 (38.9)	2.7 (2.3)	— —
$[Mo(\mu\text{-}I)Br(CO)_3(AsPh_3)]_2$ (**6**)	Dark green	52	36.5 (36.8)	2.6 (2.2)	— —
$[Mo(\mu\text{-}I)Br(CO)_3(SbPh_3)]_2$ (**7**)	Red	49	33.6 (34.1)	2.4 (2.1)	— —
$[MoBrI(CO)_3(PPh_3)_2]$ (**8**)	Mid-brown	63	51.3 (51.4)	3.7 (3.3)	— —
$[MoBrI(CO)_3(AsPh_3)_2]$ (**9**)	Brown	59	46.7 (46.9)	3.1 (3.0)	— —
$[MoBrI(CO)_3(SbPh_3)_2]$ (**10**)	Orange	68	43.1 (42.9)	2.9 (2.8)	— —
$[MoBrI(CO)_3(PPh_3)(AsPh_3)]$ (**11**)	Green	73	48.2 (49.3)	3.4 (3.2)	— —
$[MoBrI(CO)_3(PPh_3)(SbPh_3)]$ (**12**)	Orange–brown	65	46.4 (46.7)	3.2 (3.0)	— —
$[MoBrI(CO)_3(AsPh_3)(SbPh_3)]$ (**13**)	Orange	69	44.6 (44.8)	3.0 (2.9)	— —
$[MoBrI(CO)_3(PPh_3)(SPPh_3)]$ (**14**)	Green–brown	62	49.3 (49.7)	3.2 (3.2)	— —
$[MoBrI(CO)_3(AsPh_3)(SPPh_3)]$ (**15**)	Brown	65	47.7 (47.4)	3.0 (3.1)	— —
$[MoBrI(CO)_3(SbPh_3)(SPPh_3)]$ (**16**)	Dark orange	59	45.0 (45.3)	3.3 (3.1)	— —
$[MoBrI(CO)_3(PPh_3)\{SC(NH_2)_2\}]$ (**17**)	Mid-brown	58	35.8 (36.4)	3.1 (2.6)	4.1 (3.9)
$[MoBrI(CO)_3(AsPh_3)\{SC(NH_2)_2\}]$ (**18**)	Red–brown	46	34.5 (34.4)	3.0 (2.5)	3.8 (3.6)
$[MoBrI(CO)_3(SbPh_3)\{SC(NH_2)_2\}]$ (**19**)	Rust	54	31.5 (32.4)	2.7 (2.4)	3.4 (3.4)
$[MoBrI(CO)_3(PPh_3)\{SC(NMe_2)_2\}]$ (**20**)	Green	62	40.6 (40.0)	3.7 (3.5)	3.2 (3.6)
$[MoBrI(CO)_3(AsPh_3)\{SC(NMe_2)_2\}]$ (**21**)	Light brown	59	38.4 (37.8)	3.3 (3.3)	2.9 (3.4)
$[MoBrI(CO)_3(SbPh_3)\{SC(NMe_2)_2\}]$ (**22**)	Orange–brown	67	35.5 (35.8)	3.3 (3.1)	2.9 (3.2)
$[MoBrI(CO)_3(dppm)] \cdot \frac{1}{2}CH_2Cl_2$ (**23**)	Mid-brown	61	42.8 (42.1)	3.1 (2.9)	— —
$[MoBrI(CO)_3(dppe)] \cdot \frac{1}{2}CH_2Cl_2$ (**24**)	Light brown	73	43.3 (42.8)	3.4 (3.1)	— —
$[MoBrI(CO)_3(dppp)] \cdot \frac{1}{2}CH_2Cl_2$ (**25**)	Green–brown	67	43.2 (43.5)	3.5 (3.2)	— —
$[MoBrI(CO)_3(1,10\text{-phen})]$ (**26**)	Dark brown	59	30.1 (30.8)	1.6 (1.4)	4.8 (4.8)
$[MoBrI(CO)_2(NCMe)(SbPh_3)_2]$ (**27**)	Pale yellow	99	43.6 (44.5)	3.1 (3.0)	1.1 (1.3)

[a] Calculated values are given in parentheses.

solvent was removed *in vacuo* to give pale yellow crystals of $[MoBrI(CO)_2(NCMe)(SbPh_3)_2]$ (**27**), which were recrystallized from CH_2Cl_2/Et_2O (yield = 0.548 g, 99%).

RESULTS AND DISCUSSION

It is interesting to note that in their original paper in 1962 describing the preparation of the tris (acetonitrile) complexes *fac*-$[M(CO)_3(NCMe)_3]$ (M = Cr, Mo, W),[8] Tate, Knipple and Augl reported that "reaction of $[W(CO)_3(NCMe)_3]$ with an equimolar quantity of iodine in methanol gave a non-carbonyl containing product". From our previous work we have found that reaction of *fac*-$[M(CO)_3(NCMe)_3]$ *in situ*, i.e. in acetonitrile with equimolar quantities of I_2 (M = Mo or W),[1] $SnCl_4$ (M = Mo)[10] and $GeCl_4$ (M = Mo),[11] gave the seven-coordinate bis(acetonitrile) compounds $[MI_2(CO)_3(NCMe)_2]$, $[MoCl(SnCl_3)(CO)_3(NCMe)_2]$ and $[MoCl(GeCl_3)(CO)_3(NCMe)_2]$, respectively.

Equimolar quantities of *fac*-$[Mo(CO)_3(NCMe)_3]$ {prepared *in situ* by reacting $[Mo(CO)_6]$ in refluxing acetonitrile[8]} and BrI react to give high yields of the light brown crystalline complex $[MoBrI(CO)_3(NCMe)_2]$ (**1**). Complex **1** is very air-sensitive in solution and also air-sensitive in the solid state. It is considerably more sensitive and less stable compared to the diiodo-analogue $[MoI_2(CO)_3(NCMe)_2]$.[1] Compound **1** has been characterized by elemental analysis (carbon, hydrogen and nitrogen) (it was very difficult to obtain good analytical results for this complex due to its air-sensitivity), IR and ^1H NMR spectroscopy (Tables 1–3). Since the IR and ^1H NMR spectral properties of **1** closely resemble those of the diiodo-complex (which has been structurally characterized by X-ray crystallography),[12] the most likely struc-

Table 2. IR[a] data for the seven-coordinate complex $[MoBrI(CO)_3(NCMe)_2]$ and its derivatives

Complex	$\nu(C{\equiv}O)$ (cm^{-1})			$\nu(C{\equiv}N)$ (cm^{-1})	
1	1893(w)	1957(s)	2034(s)	2288(m)	2316(m)
2	1884(m)	1981(s)	2040(m)	2287(w)	
3	1925(m)	1981(m)	2041(m)	2285(w)	
4	1870(m)	1962(s)	2040(s)	2282(w)	
5	1910(s)	1965(s)	2038(s)		
6	1912(m)	1956(m)	2020(m)		
7	1919(m)	1960(s)	2023(m)		
8	1888(s)	1975(m)	2020(s)		
9	1926(m)	1961(s)	2028(m)		
10	1857(m)	1959(s)	2024(m)		
11	1883(s)	1960(s)	2025(m)		
12	1888(s)	1960(s)	2023(s)		
13	1862(m)	1959(s)	2024(m)		
14	1924(w)	1981(m)	2040(w)		
15	1925(m)	1980(s)	2039(m)		
16	1868(m)	1962(s)	2026(m)		
17	1919(s)	1965(s)	2023(m)		
18	1925(m)	1958(m)	2024(w)		
19	1918(m)	1962(m)	2025(m)		
20	1902(m)	1960(s)	2023(m)		
21	1900(s)	1960(s)	2024(s)		
22	1928(m)	1959(m)	2023(m)		
23	1926(m)	1972(s)	2045(m)		
24	1940(s)	1975(s)	2041(m)		
25	1930(m)	1965(s)	2041(m)		
26	1923(m)	1974(m)	2072(m)		
27	1851(s)	1941(s)		2271(m)	

[a] Spectra recorded as thin films in $CHCl_3$ between NaCl plates. s, strong; m, medium; w, weak.

ture for **1** is capped octahedral with a carbonyl ligand in the capping position with the more bulky iodide ligand *trans* to the more crowded capped face (Fig. 1.).

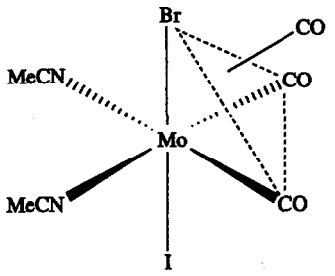

Fig. 1. Most likely structure for $[MoBrI(CO)_3(NCMe)_2]$ (**1**).

The reaction of **1** with an equimolar amount of L (L = PPh_3, $AsPh_3$ or $SbPh_3$) in CH_2Cl_2 at room temperature initially gave the monomers $[MoBrI(CO)_3(NCMe)L]$ (**2–4**), which were isolated and characterized (Tables 1–3). However, the complexes $[MoBrI(CO)_3(NCMe)L]\cdot\frac{1}{2}CH_2Cl_2$ (**2**) (L = PPh_3) and **4** (L = $SbPh_3$) were confirmed as $\frac{1}{2}CH_2Cl_2$ solvates by repeated elemental analyses and ^1H NMR spectroscopy. Stirring CH_2Cl_2 solutions of the monomers (**2–4**) at room temperature for 4 h gave the fully characterized (Tables 1–3) dimers $[Mo(\mu\text{-}I)Br(CO)_3L]_2$ (**5–7**) in good yield. These results are very similar to the reactions of $[MI_2(CO)_3(NCMe)_2]$ (M = Mo or W) with L (L = PPh_3, $AsPh_3$ and $SbPh_3$) in CH_2Cl_2 at room temperature, which gave $[MI_2(CO)_3(NCMe)L]$ and subsequently upon further stirring in CH_2Cl_2 gave the dimers $[M(\mu\text{-}I)I(CO)_3L]_2$.[4]

Table 3. ^1H NMR data[a] for the seven-coordinate complex $[MoBrI(CO)_3(NCMe)_2]$ and its derivatives

Complex	^1H (δ, ppm)
1	2.0(s,br,CH_3)
2	2.0(s,br,3H,CH_3); 5.3(s,1H,CH_2Cl_2); 7.2–8.0(m,15H,C_6H_5)
3	2.0(s,br,3H,CH_3); 7.3–7.7(m,15H,C_6H_5)
4	2.0(s,br,3H,CH_3); 5.3(s,1H,CH_2Cl_2); 7.3–7.7(m,15H,C_6H_5)
5	7.2–7.7(m,C_6H_5)
6	7.3–7.7(m,C_6H_5)
7	7.2–7.7(m,C_6H_5)
8	7.2–7.9(m,C_6H_5)
9	7.2–7.6(m,C_6H_5)
10	7.2–7.7(m,C_6H_5)
11	7.2–7.8(m,C_6H_5)
12	7.1–7.8(m,C_6H_5)
13	7.2–7.8(m,C_6H_5)
14	7.3–7.9(m,C_6H_5)
15	7.3–7.8(m,C_6H_5)
16	7.3–7.8(m,C_6H_5)
17[b]	4.5(s,4H,NH_2); 7.3–8.0(m,15H,C_6H_5)
18[b]	4.7(s,4H,NH_2); 7.3–7.8(m,15H,C_6H_5)
19[b]	4.5(s,4H,NH_2); 7.3–7.9(m,15H,C_6H_5)
20[b]	3.0(s,12H,CH_3); 7.2–8.0(m,15H,C_6H_5)
21[b]	3.3(s,br,12H,CH_3); 7.3–7.8(m,15H,C_6H_5)
22[b]	3.2(s,br,12H,CH_3); 7.2–7.9(m,15H,C_6H_5)
23	4.9(s,br,2H,CH_2); 5.3(s,1H,CH_2Cl_2); 7.2–7.8(m,20H,C_6H_5)
24	2.9(s,br,4H,CH_2); 5.3(s,1H,CH_2Cl_2); 7.0–8.1(m,20H,C_6H_5)
25	1.7(s,br,2H,CH_2); 4.0(s,4H,CH_2); 5.3(s,1H,CH_2Cl_2); 7.1–7.7(m,20H,C_6H_5)
26	7.9(m,2H,5-$C_{12}N_2H_8$); 8.1(m,2H,5-$C_{12}N_2H_8$); 8.6(m,2H,3-$C_{12}N_2H_8$); 9.7(m,2H,2-$C_{12}N_2H_8$)
27[b]	2.1(s,br,3H,CH_3); 7.3–8.2(m,30H,C_6H_5)

[a] Spectra recorded in $CDCl_3$ at +25°C.
[b] Spectra recorded in $(CD_3)_2CO$ at +25°C.

Two equivalents of the ligands L (L = PPh_3, $AsPh_3$ and $SbPh_3$) reacted with **1** in CH_2Cl_2 at room temperature to afford the bis(ligand) compounds $[MoBrI(CO)_3L_2]$ (**8–10**) in high yields. Compounds **8–10** have been characterized by elemental analysis (carbon, hydrogen and nitrogen), IR and ^1H NMR spectroscopy (Tables 1–3). Since a number of seven-coordinate complexes of the type $[MX_2(CO)_3L_2]$ have been structurally characterized, and have been shown to have capped octahedral geometry,[13–18] the geometry of **8–10** and other mononuclear complexes described in this paper are likely to be capped octahedral. Unfortunately, many attempts to grow suitable single crystals for X-ray crystallography of several complexes were unsuccessful.

Reactions of $[MoBrI(CO)_3(NCMe)_2]$ with an equimolar quantity of L (L = PPh_3, $AsPh_3$ or $SbPh_3$) initially gave $[MoBrI(CO)_3(NCMe)L]$, which when reacted *in situ* with an equimolar amount of L′ [L′ = PPh_3, $AsPh_3$, $SbPh_3$, $SPPh_3$, $SC(NH_2)_2$ or $SC(NMe_2)_2$] in CH_2Cl_2 at room temperature or acetone [for L′ = $SC(NH_2)_2$] afforded the mixed-ligand compounds $[MoBrI(CO)_3LL']$ (**11–22**) in good yield. These new complexes were characterized by elemental analysis (carbon, hydrogen and nitrogen) (Table 1), IR (Table 2) and ^1H NMR spectroscopy (Table 3). The complexes are soluble in chlorinated solvents such as CH_2Cl_2, $CHCl_3$ and acetone [for $SC(NH_2)_2$ and $SC(NMe_2)_2$] complexes, however, they are insoluble in hydrocarbon solvents and diethyl ether.

Equimolar quantities of **1** and $\widehat{LL}$ [$\widehat{LL}$ = $Ph_2P(CH_2)_nPPh_2$ (n = 1–3) and 1,10-phen] react in CH_2Cl_2 at room temperature to give the acetonitrile displaced products $[MoBrI(CO)_3(\widehat{LL})]$ (**23–26**) in high yield. Characterization of (**23–26**) was obtained by elemental analysis (carbon, hydrogen and nitrogen), IR and ^1H NMR spectroscopy (Tables 1–3). Complexes **23–25** were shown to be $\frac{1}{2}CH_2Cl_2$ solvates by repeated elemental analyses and ^1H NMR spectroscopy.

It is interesting to note that bubbling a stream of dry nitrogen through an acetonitrile solution of $[MoBrI(CO)_3(SbPh_3)_2]$ gave the seven-coordinate dicarbonyl compound $[MoBrI(CO)_2(NCMe)(SbPh_3)_2]$ with five different ligands attached to the molybdenum. It should be noted that Brisdon and Hodson[19] have reported the preparation and characterization of the related dihalo-complexes $[MX_2(CO)_2(NCMe)L_2]$ (for M = Mo, X = Br, L = $PEtPh_2$, PMe_2Ph or PEt_2Ph, X = Cl, Br or I, L = $PMePh_2$; for M = W, X = Br, L = PMe_2Ph, $PMePh_2$).

In summary, the mixed-halide complex $[MoBrI(CO)_3(NCMe)_2]$ is much less stable compared to its diiodide analogue; however, the reaction chemistry of **1** is very similar to $[MoI_2(CO)_3(NCMe)_2]$. The reaction products derived from **1** are very similar to $[MoI_2(CO)_3(NCMe)_2]$ and the reaction products derived from **1** were considerably more stable than **1**. Hence, full characterization of **2–27** was achieved.

Acknowledgements—We thank the SERC for support (K.R.F.) and the ERASMUS scheme for supporting K.V.

REFERENCES

1. P. K. Baker, S. G. Fraser and E. M. Keys, *J. Organomet. Chem.* 1986, **309**, 319.
2. P. K. Baker and S. G. Fraser, *Inorg. Chim. Acta* 1986, **116**, L1.
3. P. K. Baker and S. G. Fraser, *Inorg. Chim. Acta* 1986, **116**, L3.
4. P. K. Baker and S. G. Fraser, *Trans. Met. Chem.* 1987, **12**, 560.
5. P. K. Baker, S. G. Fraser and M. G. B. Drew, *J. Chem. Soc., Dalton Trans.* 1988, 2729.
6. E. M. Armstrong, P. K. Baker and S. G. Fraser, *J. Chem. Res. (S)* 1988, 52; *J. Chem. Res. (M)* 1988, 410.
7. E. M. Armstrong, P. K. Baker and M. G. B. Drew, *Organometallics* 1988, **7**, 319.
8. D. P. Tate, W. R. Knipple and J. M. Augl, *Inorg. Chem.* 1962, **1**, 433.
9. *Handbook of Preparative Inorganic Chemistry*, Vol. 1, 2nd edn. Academic Press, New York (1963).
10. P. K. Baker and A. Bury, *J. Organomet. Chem.* 1989, **359**, 189.
11. P. K. Baker and D. ap Kendrick, *Inorg. Chim. Acta* 1991, **188**, 5.
12. M. G. B. Drew, P. K. Baker, E. M. Armstrong and S. G. Fraser, *Polyhedron* 1988, **7**, 245.
13. M. G. B. Drew, A. W. Johans and A. P. Wolters, *J. Chem. Soc., Chem. Commun.* 1971, 819.
14. A. Mawby and G. E. Pringle, *J. Inorg. Nucl. Chem.* 1972, **34**, 514.
15. M. G. B. Drew, *J. Chem. Soc., Dalton Trans* 1972, 626.
16. M. G. B. Drew, *J. Chem. Soc., Dalton Trans.* 1972, 1329.
17. M. G. B. Drew and A. P. Wolters, *Acta Cryst.* 1977, **B33**, 205.
18. M. G. B. Drew and J. D. Wilkins, *J. Chem. Soc., Dalton Trans.* 1977, 194.
19. B. J. Brisdon and A. G. W. Hodson, *Inorg. Chim. Acta* 1987, **128**, 51.

Polyhedron Vol. 12, No. 4, pp. 363–370, 1993
Printed in Great Britain

0277–5387/93 $6.00+.00
© 1993 Pergamon Press Ltd

SYNTHESIS AND CHARACTERIZATION OF 1,2-BIS(PHOSPHINO)BENZENE (DIPHOS) AND RELATED COMPLEXES OF VANADIUM, CHROMIUM, IRON AND COBALT. X-RAY CRYSTAL STRUCTURES OF $MCl_2(DIPHOS)_2$ (M = V, Cr and Fe) AND $[Fe(DIPHOS)_2(MeCN)_2](BPh_4)_2$

CARL REDSHAW and GEOFFREY WILKINSON*

Johnson Matthey Laboratory, Chemistry Department, Imperial College, London SW7 2AY, U.K.

and

BILQUIS HUSSAIN-BATES and MICHAEL B. HURSTHOUSE*

School of Chemistry and Applied Chemistry, University of Wales Cardiff, P.O. Box 912, Cardiff CF1 3TB, U.K.

(*Received* 1 *October* 1992; *accepted* 15 *October* 1992)

Abstract—The interaction of transition metal dichlorides with the chelating diphosphine (diphos) ligands 1,2-bis(phosphino) benzene, 1,2-bis(2-propylphosphino) benzene and 1,2-bis(dimethylphosphino) benzene leads to the octahedral complexes *trans*-$MCl_2(diphos)_2$, (M = V, Cr, Fe or Co). Interaction of $FeCl_2[1,2\text{-}(Me_2P)C_6H_4]_2$ with $NaBPh_4$ in refluxing MeCN gives the nitrile complex *trans*-$[Fe(NCMe)_2(diphos)_2](BPh_4)_2$, whereas $VCl_2[1,2\text{-}(C_3H_7PH)_2C_4H_4]_2$ gives only the complex $[V(CNMe)_6](BPh_4)_2$. This difference is attributed to the weaker basicity (exemplified by the longer M—P bond lengths) of the secondary phosphine ligand. X-ray crystal structures of the following compounds have been determined: $MCl_2[1,2\text{-}(C_3H_7PH)_2C_6H_4]_2$ (M = V, Cr or Fe) and $[Fe(NCMe)_2\{1,2\text{-}(Me_2P)C_6H_4\}_2](BPh_4)_2$. In all cases the octahedral complexes have *trans*-Cl or MeCN groups.

We have previously described the synthesis and X-ray crystal structures of 1,2-bis(dimethylphosphino)ethane (dmpe) complexes of divalent first row transition metals, *trans*-$MX_2(dmpe)_2$ (M = Ti, V, Cr, Mn or Fe; X = Me or halide).[1] While dmpe,[1,2a–c] dppe,[2d] dippe, [1,2-bis(diisopropylphosphino)ethane],[2e] 1,2-bis(diphenylphosphino)-ethane[3a] complexes and the salts of the cations *trans*-$[M(NCR)_2(dmpe)_2]^{2+}$ (M = V,[2a] Cr[2b] and Fe;[2c] R = Me or Et) and dmpp, 1,3-bis(dimethylphosphino)propane,[3b] have been thoroughly investigated, similar ditertiary aryl phosphines of the type $1,2\text{-}C_6H_4(PR_2)_2$ have been less studied. The bis-dimethyl[3c] group has been shown to stabilize high oxidation state complexes of first row elements as readily as the more commonly studied diarsine $1,2\text{-}(Me_2As)_2C_6H_4$.[3d]

By contrast, few studies on bis(primary/secondary) phosphinobenzene have been reported.[4] Analogues of dmpe types[1,2] have not been described; these are now reported for $1,2\text{-}(H_2P)_2C_6H_4$ and $1,2\text{-}(R^1R^2P)_2C_6H_4$ (R^1 = H, R^2 = $C^i{}_3H_7$; R^1 = R^2 = Me.

Analytical data for new compounds are given in Table 1.

RESULTS AND DISCUSSION

Halide complexes

Interaction of the THF solvates of the metal dichlorides with bis (primary/secondary/tertiary)

* Authors to whom correspondence should be addressed.

Table 1. Analytical and physical data for new compounds[a]

Compound	Colour	M.p. (°C)	Analysis (%) C	H	Other
1 $VCl_2[C_6H_4(PH_2)_2]_2$	Green	*ca* 140 (decomp.)	29.2 (35.5)	3.7[b] (4.0)	
2 $VCl_2[C_6H_4(C_3H_7PH)_2]_2$	Yellow	*ca* 160	50.7 (50.2)	7.0 (7.0)	
3 $VCl_2\{C_6H_4[P(Me)_2]_2\}_2$	Tan	*ca* 130–140	47.3 (46.4)	6.5 (6.2)	
4 $CrCl_2[C_6H_4(PH_2)_2]_2$	Orange–tan	> 150 (decomp.)	34.7 (35.4)	4.9 (3.9)	
5 $CrCl_2[C_6H_4(C_3H_7PH)_2]_2$	Red	230	50.8 (50.0)	7.3 (7.0)	
6 $CrCl_2\{C_6H_4[P(Me)_2]_2\}_2$	Red–orange		47.3 (46.3)	7.0 (6.2)	
7 $FeCl_2[C_6H_4(C_3H_7PH)_2]_2$	Green	*ca* 190	50.0 (49.8)	7.0 (7.0)	21.6P (21.4)P
8 $[FeCl_2(NCMe)_2\{C_6H_4[P(Me)_2]_2\}_2](BPh_4)_2$	Yellow	256	71.5 (72.7)	6.6 (6.7)	4.5N (4.5)N
9 $CoCl_2[C_6H_4(C_3H_7PH)_2]_2 \cdot CH_2Cl_2$	Green	*ca* 220–225	45.2 (45.0)	6.2 (6.3)	

[a] For mass spectra see Experimental.
[b] See text.

phosphino benzenes (diphos) in toluene at ambient temperature readily gives the adducts *trans*-MCl_2(diphos)$_2$. However, all attempts to prepare *trans*-$MnCl_2$(diphos)$_2$, where diphos = primary or secondary phosphino benzene, were unsuccessful. The tertiary phosphino benzene complex $MnCl_2(1,2\text{-}(Me_2P)_2C_6H_4]_2$ has previously been reported.[3c].

All the present MCl_2(diphos)$_2$ complexes have IR spectra showing strong bands typical of P—H groups (*ca* 2340 cm^{-1}) as well as a single M—Cl band except for $CrCl[1,2\text{-}(Me_2P)_2C_6H_4]_2$ (**6**) and $CoCl_2[1,2\text{-}(C_3H_7PH)_2C_6H_4]_2$ (**9**) that have split bands and hence may have *cis* and *trans* isomers—see below), consistent with the monomeric *trans* geometry confirmed by X-ray diffraction studies as quoted for the manganese compound.[3c]

The low solubility of the primary phosphine complexes in non-coordinating organic solvents, even at elevated temperatures, precludes crystallization and further characterization. In the case of $VCl_2[C_6H_4(PH_2)_2]_2$ (**1**), analytical data (see Table 1) suggests small contamination of the product with zinc salts, as is well known.[5] However, use of the secondary phosphine $[1,2\text{-}(C_3H_7PH)_2C_6H_4]$ results in more soluble species, and crystals suitable for X-ray diffraction were obtained for M = V, Cr and Fe. The vanadium and chromium compounds are air sensitive, especially in solution, but the iron and cobalt complexes may be handled as solids in air.

The *X*-band EPR spectrum for $VCl_2[1,2\text{-}(C_3H_7PH)_2C_6H_4]_2$ (**2**) as a frozen toluene solution at −196°C comprises broad low-field features at *ca* $g = 4.2$ and 2.8, and several weaker transitions to higher field, similar to those previously reported for $VCl_2(dmpe)_2$.[1] By contrast, $VCl_2[1,2\text{-}(Me_2P)_2C_6H_4]_2$ (**3**) possesses an isotropic spectrum ($g = 1.995$) at room temperature with poorly defined splitting; as a frozen MeCN solution (−196°C) the splitting is only slightly more resolved. The ^1H NMR spectra are broad and uninformative, except for the iron(II) low-spin d^6 complex (see Experimental), which gives a red–brown solution at room temperature. The ^{31}P NMR spectrum of $FeCl_2[1,2\text{-}(C_3H_7PH)_2C_6H_4]_2$ is consistent with extensive isomerization in solution. A singlet at $\delta = 82$ ppm can be assigned to the *trans* isomer **7**, whilst two triplets ($\delta = 70.4$ and 96.2 ppm, A_2B_2 coupling) are consistent with the two sets of equivalent P present in the *cis*-isomer. Similar isomerism is anticipated for $CoCl_2[1,2\text{-}(C_3H_7PH)_2C_6H_4]_2$ (**9**); the split band at *ca* 290 cm^{-1} in the IR spectrum is consistent with *cis* and *trans* isomers. Interestingly, a recent report[6] concerning two diphosphines of comparable steric bulk to $1,2\text{-}(C_3H_7PH)_2C_6H_4$, namely DEPE [1,2-bis(diethylphosphino)ethane] and DPrPE [1,2-bis(di-n-propylphosphino)ethane], describes solution paramagnetism for iron(II) complexes and associates this with partial reversible dissociation of phosphine.

In addition, we have also synthesized by the same method other complexes, $MCl_2[(Me_2P)_2C_6H_4]_2$.

Three complexes have been studied by X-ray

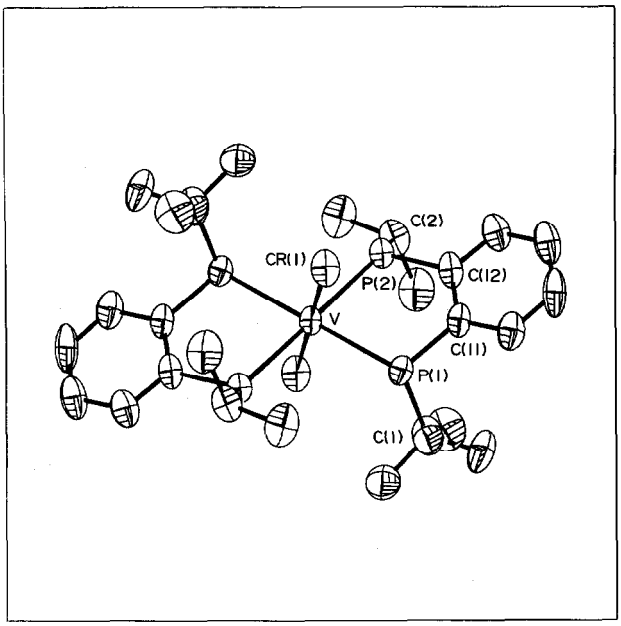

Fig. 1. The structure of *trans*-$VCl_2[(Pr^iHP)_2C_6H_4]_2$.

crystallography (M = V, Cr, Fe); surprisingly, the crystal structures are all different (the vanadium complex is solvated) but the molecular structures are analogous. In each case the metal atoms lie on centres of symmetry and in each diphos ligand the isopropyl groups are *syn*. The crystal structures of the chromium and iron complexes each contain two independent centrosymmetric molecules. A diagram of the vanadium complex is shown in Fig. 1; bond lengths and angles for all three complexes are given in Table 2.

The structures are analogous to those previously determined[1] for the related dmpe complexes[1] of titanium, vanadium and chromium, and it is interesting to compare geometry parameters for the two groups. Relevant data are plotted in Fig. 2, from which it can be seen that the M—Cl bond lengths here are slightly shorter than in the comparable bonds in the dmpe complexes, while only the V—P bond lengths are slightly longer (*ca* 0.02 Å). Clearly, similar variations exist within each series. Whereas in the dmpe complexes the M—P bond is longer

Table 2. Selected bond lengths (Å) and angles (°) for the complexes $MCl_2(diphos)_2$, M = V, Cr and Fe. The atomic numbering relates to that in Fig. 1

	V	Cr		Fe	
M—Cl	2.427(1)	2.336(4)	2.334(4)	2.333(4)	2.329(4)
M—P(1)	2.520(1)	2.373(4)	2.387(4)	2.237(4)	2.234(4)
M—P(2)	2.511(1)	2.379(4)	2.376(4)	2.233(3)	2.227(3)
P(1)—C(1)	1.829(3)	1.88(1)	1.85(1)	1.85(1)	1.87(1)
P(1)—C(11)	1.835(3)	1.84(1)	1.83(1)	1.83(1)	1.82(1)
P(2)—C(2)	1.849(3)	1.86(1)	1.84(1)	1.86(1)	1.86(1)
P(2)—C(12)	1.830(3)	1.85(1)	1.82(1)	1.83(1)	1.82(1)
Cl—M—P(1)	84.7(1)	85.8(2)	84.0(2)	84.5(3)	85.6(3)
Cl—M—P(2)	83.5(1)	85.6(2)	84.7(2)	84.8(3)	86.5(3)
P(1)—M—P(2)	79.0(1)	80.6(2)	81.7(2)	84.2(2)	84.2(3)
M—P(1)—C(1)	126.4(2)	118.1(4)	127.5(4)	126.8(4)	120.4(4)
M—P(1)—C(11)	109.0(2)	108.4(3)	108.9(4)	108.5(3)	108.1(3)
C(1)—P(1)—C(11)	104.3(2)	104.8(5)	101.5(5)	103.5(4)	104.8(4)
M—P(2)—C(2)	126.5(2)	118.8(4)	122.3(5)	120.6(3)	122.2(4)
M—P(2)—C(21)	109.4(2)	108.2(3)	109.7(3)	108.6(3)	108.7(3)
C(2)—P(1)—C(21)	105.0(2)	107.4(4)	104.3(5)	105.6(4)	107.1(4)

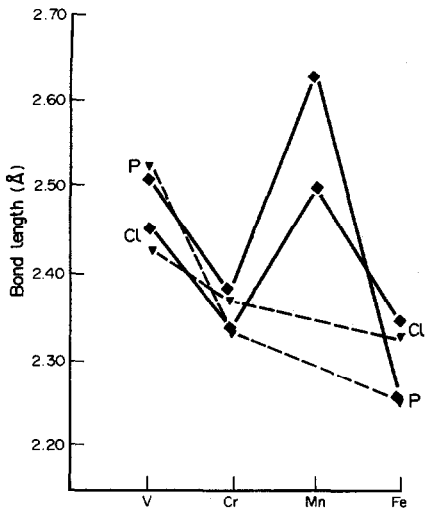

Fig. 2. Variations in M—Cl and M—P distances: ◆ $MCl_2(dmpe)_2$ from ref. 1; ▼ $MCl_2[(Pr^iHP)_2C_6H_4]_2$.

than the M—Cl bond for vanadium, chromium and manganese but shorter for iron, in the bis-isopropyl phosphine complexes the M—P bond is longer than the M—Cl bond only for vanadium; for chromium and iron it is shorter.

The cross-over for the $FeCl_2(dmpe)_2$ case was explained[1] in terms of greater $p\pi$–$d\pi$ back-bonding for d^6-Fe^{II}; in the present complexes it seems to have occurred already for d^4-Cr.

The diphos ligand bonds symmetrically with essentially equal M—P—C angles, which differ from complex to complex in correlation with M—P bond lengths and P—M—P angles (see Table 2); the angles at C in P—C—C—P are fairly constant at 115–117°. This contrasts strongly with the geometry of the diphosphido bonding in the complexes $[L_nM\{P(Ph)C_6H_4PPh\}]$, where M = Zr and Sn[4b] and where the M—P—C(benz), M—P—C (phenyl) and P—M—P angles, and, in the case of the zirconium complex, Zr—P distances, vary considerably. This may well arise from steric factors, since the other ligands in these two complexes are very bulky. Comparison between these structures and our phosphines cannot be taken too far, however, in view of the formal chemical differences between the phosphorus atoms and their associated stereochemistries.

One final point of note in the present complexes is the small tilts of the M—Cl bonds relative to the MP_4 planes, as a result of steric interactions, and between the chlorine atoms and the *syn*-isopropyl substituents.

Attempts to alkylate $MCl_2[(C_3H_7PH)_2C_6H_4]_2$ with MeLi were generally unsuccessful. This could be in part due to the increased strength of the M—Cl bonds (cf. dmpe complexes[1]) or simply due to the greater steric constraints of the isopropyl groups.

Nitrile complexes

Interaction of $FeCl_2[1,2\text{-}(Me_2P)_2C_6H_4]_2$ with excess $NaBPh_4$ in refluxing acetonitrile yields bright yellow, diamagnetic crystals of *trans*-$[Fe(diphos)_2(MeCN)_2](BPh_4)_2 \cdot MeCN$. The complex has two weak C≡N stretches in the IR spectrum (2285 and 2246 cm^{-1}), consistent with a lowering of $\nu(C{\equiv}N)$ upon coordination, and is a 1:2 electrolyte in MeCN. Unlike the analogous chromium dmpe complex, this iron complex, like its iron dmpe analogue, does not react with oxygen or with methanol.[2b,c]

The structure, as the MeCN solvate, has been confirmed by X-ray crystallography. A diagram of the cation is shown in Fig. 3; selected bond lengths and angles are given in Table 3. The structure is analogous to the closely related cationic M^{II}

Table 3. Selected bond lengths (Å) and angles (°) for $[Fe(diphos)_2(MeCN)_2](BPh_4)_2 \cdot MeCN$

N(1)—Fe	1.903(7)	P(1)—Fe	2.263(4)
P(2)—Fe	2.270(4)	C(1)—P(1)	1.811(12)
C(2)—P(1)	1.787(11)	C(3)—P(2)	1.831(9)
C(4)—P(2)	1.834(9)	C(11)—P(1)	1.834(11)
C(12)—P(2)	1.832(10)	C(12)—C(11)	1.371(10)
P(2)—Fe—P(1)	85.5(2)	P(1)—Fe—N(1)	91.8(3)
P(2)—Fe—N(1)	91.6(3)	P(1)—Fe—P(1B)	180.0(1)
P(2)—Fe—P(2B)	180.0(1)	N(1)—Fe—N(1B)	180.0(1)
P(1)—Fe—P(2B)	94.5(2)	P(1)—Fe—N(1B)	88.2(2)
P(2)—Fe—N(1B)	88.6(2)	C(01)—N(1)—Fe	178.7(5)
C(11)—P(1)—Fe	109.3(3)	C(1)—P(1)—Fe	117.7(5)
C(2)—P(1)—Fe	119.2(4)	C(12)—P(2)—Fe	108.8(3)
C(3)—P(2)—Fe	119.1(4)	C(4)—P(2)—Fe	118.6(5)
C(1)—P(1)—C(11)	102.3(5)	C(2)—P(1)—C(11)	102.6(5)
C(3)—P(2)—C(12)	104.5(5)	C(4)—P(2)—C(12)	101.6(5)

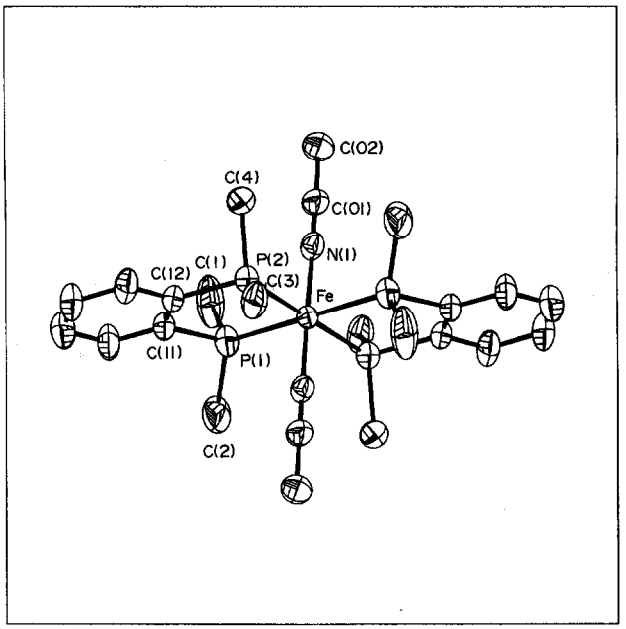

Fig. 3. The structure of *trans*-$\{Fe[(Me_2P)_2C_6H_4]_2(NCMe)_2\}^{2+}$ in the tetraphenylborate, MeCN solvate.

species $[M(NCMe)_2(dmpe)_2]^{2+}$ (M = V, Cr or Fe)[2]. Indeed, the Fe—P distances are essentially comparable (2.268–2.278 Å) to those of the dmpe complex (2.264–2.270 Å), whilst the Fe—N(nitrile) distances (1.92 Å) are slightly larger compared to 1.905 Å in the dmpe complexes. This is to be expected for complexes containing chelating bis-phosphines with similar basicity and series constraints at P.

A similar reaction using $VCl_2[(C_3H_7PH)_2C_6H_4]_2$ gives only the hexakis(acetonitrile)vanadium(II) salt $[V(NCMe)_6](BPh_4)_2$, characterized by analysis and spectra.[2a]

Failure to give $\{V(MeCN)_2[(C_3H_7PH)_2C_6H_4]_2\}(BPh_4)_2$ is presumably due to the weaker M—P bonding associated with the secondary phosphine with lesser involvement of $Md\pi \rightarrow Pd\pi$ back-bonding in the M—P bond. The influence of $d\pi$–$d\pi$ back-bonding will of course be greater for iron (increasing *d*-electron count).

Further work is in progress in an effort to obtain crystal structures of metal organoimido/diphos complexes for comparison with the previously reported *trans*-$[Cr^{IV}Cl(NEt)(dmpe)_2]CF_3SO_3$ and *trans*-$[Cr^{IV}(N{=}CHMe_2)(dmpe)_2](BPh_4)_2$.[2b]

EXPERIMENTAL

General procedures and instrumentation have been described.[7] Microanalyses were by Pascher, Remagen and MEDAC Ltd, Brunel University. The precursors $[V_2(\mu\text{-}Cl)_3(THF)_6]_2[Zn_2Cl_6]$[8] and $CrCl_2 \cdot THF$[9] were prepared as previouly described. 1,2-Bis(phosphino)benzene and related alkylated ligands were prepared by the method of Kyba *et al.*[10] All operations were carried out under oxygen-free nitrogen or argon. NMR spectra: Bruker WM 250 MHz (^1H, ^{31}P) δ in ppm referred to Me_4Si and 85% H_3PO_4 (external), respectively. IR spectra: (cm^{-1}) in Nujol mulls. Mass spectra: *m/z*% in fast atom bombardment (matrix, *m*-nitrobenzyl alcohol) unless otherwise stated. Commercial chemicals are from Aldrich.

Trans-*bis*[1,2-*bis*(*phosphino*)*benzene*]*dichlorovanadium*(II) (1)

To a suspension of $[V_2(\mu\text{-}Cl)_3(THF)_6]_2(Zn_2Cl_6)$ (0.6 g, 2.26 mmol) in toluene (*ca* 40 cm^3) was added 1,2-bis(phosphino)benzene (0.64 cm^3, 4.51 mmol). After 24 h the apple-green precipitate was collected, washed with toluene (2×20 cm^3) and hexane (*ca* 30 cm^3) and dried *in vacuo*. Yield 80–90%. IR: 3332w, 2727w, 2672w, 2329w, [*v*(P—H)], 1716w, 1296w, 1261m, 1170m, 1149m, 1067m, 1026s, 915m, 880s, 820s, 749m, 722m, 683w, 454w, 329m, 302s.

Trans-*bis*[1,2-*bis*(2-*propylphosphino*)*benzene*]-*dichlorovanadium*(II) (2)

To a suspension of $[V_2(\mu\text{-}Cl)_3(THF)_6][Zn_2Cl_6]$ (0.33 g, 1.24 mmol) in toluene (*ca* 40 cm^3) was added 1,2-bis(2-propylphosphino)benzene (0.57 cm^3, 2.52 mmol). The suspension slowly developed a yellow–

brown colour and was stirred for 24 h. The suspension was concentrated to *ca* 25 cm^3, warmed to dissolve all solid and cooled to −20°C. The large golden brown prisms were collected: further crops could be obtained by concentration and cooling of the supernatant. Yield *ca* 70%. IR: 2729w, 2307s [*ν*(PH)], 1722w, 1603w, 1575w, 1558w, 1495m, 1300w, 1275w, 1256w, 1239s, 1163m, 1134s, 1081w, 1061s, 1048m, 1029w, 966w, 931m, 887s, 877s, 865s, 808s, 766s, 728s, 695m, 641s, 628m, 498s, 467s, 467w, 436m, 405w, 324s [*ν*(VCl)]. EPR: see text.

Trans-*bis*[1,2-*bis*(*dimethylphosphino*)*benzene*]-*dichlorovanadium*(II) (**3**)

To a suspension of $[V_2(\mu\text{-}Cl)_3(THF)_6](Zn_2Cl_6)$ (0.3 g, 1.13 mmol) in toluene (*ca* 30 cm^3) was added 1,2-bis(dimethylphosphino)benzene (0.45 cm^3, 2.27 mmol). After 24 h the yellow–brown precipitate was collected, washed with toluene (2 × 25 cm^3) and hexane (30 cm^3) and dried *in vacuo*. Yield: *ca* 80%. IR: 1717w, 1494w, 1422s, 1299s, 1262m, 1149s, 1115s, 1057m, 1040m, 955s, 910s, 874m, 802w, 764s, 737s, 696m, 465s, 379w, 357w, 326w, 280s. EPR: see text.

Trans-*bis*[1,2-*bis*(*phosphino*)*benzene*]*dichlorochromium*(II) (**4**)

To a suspension of $CrCl_2 \cdot THF$ (0.27 g, 1.39 mmol) in toluene (*ca* 40 cm^3) was added [1,2-bis(phosphino)benzene (0.4 g, 2.81 mmol). The suspension rapidly developed a deep orange colour and was stirred for 24 h. The pale orange–tan precipitate was collected, washed with toluene (2 × 25 cm^3) and hexane (30 cm^3) and dried *in vacuo*. Yield *ca* 80%. IR: 2324 [*ν*(P—H)], 1720w, 1552w, 1303w, 1258m, 1156w, 1107m, 1053m, 1043m, 1027m, 894w, 834s, 757s, 723s, 448s, 337s [*ν*(CrCl)]. MS (E.I.): M^+ 407.

Trans-*bis*[1,2-*bis*(2-*propylphosphino*)*benzene*]-*dichlorochromium*(II) (**5**)

To a suspension of $CrCl_2 \cdot THF$ (0.24 g, 1.23 mmol) in toluene (*ca* 30 cm^3) was added 1,2-bis(2-propylphosphino)benzene (0.55 g, 2.43 mmol). The solution rapidly developed a deep red colour. After 4 h the solution was filtered, concentrated to *ca* 20 cm^3 and cooled to −20°C. The large red prisms were collected: further crops may be obtained by concentration and cooling of the supernatant. Yield: *ca* 80%. IR: 2290m, 2271m, [*ν*(PH)], 1717w, 1558w, 1280w, 1261m, 1241m, 1164m, 1132w, 1112s, 1058s, 1033s, 929w, 895s, 878s, 821s, 809s, 764s, 755s, 723m, 67w, 629s, 501s, 461m, 443w, 348s, [*ν*(CrCl)]. MS: 574 (M^+), 539 $(M-Cl)^+$, 348 $(M-L)^+$, 313 $(M-L-Cl)^+$.

Trans-*bis*[1,2-*bis*(*dimethylphosphino*)*benzene*]-*dichlorochromium*(II) (**6**)

To a suspension of $CrCl_2 \cdot THF$ (0.2 g, 1.03 mmol) in toluene (*ca* 30 cm^3) was added 1,2-bis(dimethylphosphino)benzene (0.4 g, 2.02 mmol). The solution rapidly developed a blood-red colour. After 24 h the solution was concentrated and the product precipitated hexane (*ca* 30 cm^3) and dried *in vacuo*. Yield *ca* 80%. IR: 1723w, 1420s, 1292s, 1278s, 1246m, 1156w, 1134w, 1104m, 1047w, 1037m, 1019m, 942s, 902s, 866s, 837m, 802w, 769s, 728s, 688s, 655w, 458sm, 431s, 341s, 306s.

Trans-*bis*[1,2-*bis*(2-*propylphosphino*)*benzene*]-*dichloroiron*(II) (**7**)

To a suspension of $FeCl_2$ (0.62 g, 4.88 mmol) in toluene (*ca* 325 cm^3) was added 1,2-bis(2-propylphosphino)benzene (2.19 g, 9.68 mmol). The solution slowly developed a red–brown colour and was stirred for 12 h. The solution was filtered, a hexane layer (*ca* 30 cm^3) added and cooled to 0°C. Emerald green crystals of the complex were obtained. Yield: *ca* 30%. IR: 2720w, 2322s [*ν*(PH)], 1713w, 1560w, 1361m, 1283m, 1246m, 1167w, 1135w, 1118s, 1091w, 1059s, 929m, 893s, 880s, 853s, 834s, 759s, 731s, 673m, 638s, 512m, 504s, 484s, 461m, 449w, 376w, 349m [*ν*(FeCl)], 317w, 263w. MS: 578 (M^+), 543 ($M^+ - Cl$), 448 ($2L - 2H_2$), 317 ($M - L - Cl$). $^{31}P\{^1H\}$ ($CDCl_3$, 250 mHz): δ = 81.8 (s, *trans* isomer), 77.4 [t, J(P—P) = 47.6 Hz, *cis* isomer], 96.2 [t, J(P—P) = 47.7 Hz, *cis* isomer].

Trans-*bis*(*acetonitrile*)*bis*[1,2-*bis*(*dimethylphosphino*)*benzene*]*iron*(II)*bis*(*tetraphenylborate*) (**8**)

To *trans*-$[FeCl_2\text{-}1,2\text{-}(Me_2P)_2C_6H_4]$[3c] (1.0 g, 1.19 mmol) in MeCN (*ca* 40 cm^3) was added $NaBPh_4$ (1.31 g, 3.83 mmol). The solution was refluxed vigorously for 12 h, cooled and then filtered. Concentrating and cooling (−20°C) the orange solution gave golden yellow prisms. Yield: *ca* 90%. IR: 2285w ("free" MeCN), 2246m [coordinated nitrile *ν*(C≡N)], 1714w, 1579m, 1562w, 1426s, 1367s, 1308m, 1301m, 1287m, 1267w, 1253w, 1182w, 1143m, 1118m, 1066w, 1032m, 941s, 905s, 862w, 841m, 759m, 731s, 704s, 691m, 614m, 481s, 461m, 417w, 374w. MS: 534.3 (M^{2+}), 492 (M^{2+} − MeCN). Conductivity (MeCN): Λ_M = 183 Ω cm^2 mol^{-1}.

Table 4. Crystal data, details of intensity measurements and structure refinements

Formula	$[C_{24}H_{336}Cl_2P_4V][C_7H_8]$	$[C_{24}H_{36}Cl_2P_4Cr]$	$[C_{24}H_{36}Cl_2P_4Fe]$	$[C_{24}H_{38}N_2P_4Fe][C_{24}H_{20}B][C_2H_3N]$
M	662.43	715.49	611.48	627.45
Crystal system	Triclinic	Monoclinic	Triclinic	Monoclinic
Space group	$P\bar{1}$	$P2_1/c$	$P\bar{1}$	$P2_1/n$
a (Å)	9.365(2)	10.298(2)	9.049(2)	16.245(14)
b (Å)	9.781(2)	16.477(6)	10.104(2)	10.219(16)
c (Å)	10.745(5)	17.565(14)	16.258(2)	22.157(13)
α (°)	84.29(1)	90	83.12(2)	90
β (°)	75.41(1)	98.09(2)	83.28(2)	107.47(15)
γ (°)	68.67(1)	90	82.48(2)	90
U (Å^3)	887.22	2950.77	1455.31	3508.57
Z	1	4	2	2
D_c (g cm^{-1})	1.240	1.611	1.395	1.370
$F(000)$	347	1480	672	1520
μ (cm^{-1})	6.18	8.03	9.32	3.5
Total no. of reflections	3283	14122	8102	25057
No. of unique reflections	2940	7385	6053	8340
No. of observed reflections $[F_0 > 3\sigma(F_0)]$	2459	2738	3688	2914
No. of refined parameters	245	346	313	434
Weighting scheme parameter g in $w = 1/[\sigma^2(F)+gF^2]$	0	0	0	0
Final R	0.0501	0.0528	0.0582	0.0615
Final Rw	0.0533	0.0571	0.0647	0.0651

Trans-*bis*[1,2-*bis*(2-*propylphosphino*)*benzene*]-*dichlorocobalt*(II) (**9**)

To a suspension of $CoCl_2 \cdot THF$ (0.25 g, 1.26 mmol) in toluene (*ca* 35 cm^3) was added 1,2-bis(2-propylphosphino)benzene (0.56 g, 2.48 mmol). After 12 h the solvent was removed and the residue extracted with CH_2Cl_2 (*ca* 30 cm^3). Concentration and cooling (−20°C) gave a bright green microcrystalline solid. Yield: *ca* 30%. IR: 2328w (νPH), 1567w, 1424w, 1365w, 1288w, 1257m, 1245m, 1158w, 1136w, 1121m, 1089w, 1064m, 1038s, 967w, 928m, 885s, 859s, 842s, 769s, 746s, 735s, 708s, 675m, 637s, 518s, 504s, 470s, 460s, 441m, 390w, 372w, 297s, 285s.

X-ray crystal structures

Crystals of all four complexes were sealed under argon in thin walled glass capillaries. Cell dimensions and intensity data were recorded using a FAST TV area detector diffractometer, as previously described.[11] The structures were solved and developed via the heavy atom method and refined via full-matrix least-squares. An absorption correction was applied using the DIFABS method.[12] Non-hydrogen atoms were refined anisotropically and organic hydrogens were included in idealized positions and assigned group U_{iso} values. The phosphine hydrogens were not located or included. In the vanadium complex one of the isopropyl groups shows 70/30 disorder over two orientations. Crystal data and experimental details are given in Table 4. Tables of coordinates and other data have been deposited as supplementary material with the Editor, from whom copies are available on request. Atomic coordinates have also been deposited at the Cambridge Crystallographic Data Centre.

Acknowledgements—We thank the SERC for support and for provision of X-ray facilities.

REFERENCES

1. G. S. Girolami, G. Wilkinson, A. M. R. Galas, M. Thornton-Pett and M. B. Hursthouse, *J. Chem. Soc., Dalton Trans.* 1985, 1339.
2. (a) S. J. Anderson, F. J. Wells, G. Wilkinson, B. Hussain and M. B. Hursthouse, *Polyhedron* 1988, **7**, 2615; (b) A. R. Barron, J. E. Salt, G. Wilkinson, M. Motevalli and M. B. Hursthouse, *J. Chem. Soc., Dalton Trans.* 1987, 2947; J. E. Salt, G. Wilkinson, M. Motevalli and M. B. Hursthouse, *J. Chem. Soc., Dalton Trans.* 1986, 1141; (c) A. R. Barron, G. Wilkinson, M. Motevalli and M. B. Hursthouse, *Polyhedron* 1987, 1089; (d) see, for example, A. R. Barron, S. J. Anderson, K. McGregor and G. Wilkinson, *Polyhedron* 1989, **8**, 2599; (e) A. R. Hermes and G. S. Girolami, *Inorg. Chem.* 1990, **29**, 313 and refs therein.
3. (a) R. J. Puddephat, *Chem. Soc. Rev.* 1983, 99;

(b) N. Bampos, L. D. Field and T. W. Hamby, *Polyhedron* 1992, **11**, 1213; (c) L. F. Warren and M. A. Bennett, *Inorg. Chem.* 1976, **15**, 3216; (d) for $Ph_2PCHCHPPh_2$ and various 1,2-C_6H_4 complexes with $AsMe_2$, PMe_2 and NMe_2 groups, see L. R. Gray, A. L. Hale, W. Levason, F. P. McCullough and M. Webster, *J. Chem. Soc., Dalton Trans.* 1983, 2573.

4. (a) E. Hey, *J. Organomet. Chem.* 1989, **378**, 375; (b) R. Bohra, P. B. Hitchcock, M. F. Lappert and W. A. Leung, *J. Chem. Soc., Chem. Commun.* 1989, 728; (c) C. Redshaw, G. Wilkinson, B. Hussain-Bates and M. B. Hursthouse, *J. Chem. Soc., Dalton Trans.* 1992, 1803; (d) E. P. Kyba, M. C. Kerby, R. P. Kashyap, J. A. Mountzouris and R. E. Davis, *Organometallics* 1989, **8**, 852 and refs therein.
5. M. Pomerantz, G. L. Combs Jr and N. L. Dassanayake, *Inorg. Synth.* 1982, **21**, 185.
6. M. V. Baker, L. D. Field and T. W. Hambley, *Inorg. Chem.* 1988, **27**, 2872.
7. A. A. Danopoulos, A. C. C. Wong, G. Wilkinson, B. Hussain-Bates and M. B. Hursthouse, *J. Chem. Soc., Dalton Trans.* 1990, 315.
8. R. J. Boruma, J.-H. Teuben, W. R. Beukema, R. L. Bansemer, J. C. Huffman and K. G. Caulton, *Inorg. Chem.* 1984, **23**, 2715.
9. L. F. Larkworthy and M. H. O. Nelson-Richardson, *Chem. Ind. (London)* 1974, 164.
10. E. P. Kyba, S. T. Liu and R. L. Harris, *Organometallics* 1983, **2**, 1877.
11. A. A. Danopoulos, G. Wilkinson, B. Hussain-Bates and M. B. Hursthouse, *J. Chem. Soc., Dalton Trans.* 1991, 1855.
12. N. P. C. Walker and D. Stuart, *Acta Cryst., Sect. A* 1983, **39**, 1980.

Polyhedron Vol. 12, No. 4, pp. 371–374, 1993
Printed in Great Britain

0277–5387/93 $6.00+.00
© 1993 Pergamon Press Ltd

THE ELECTRON SPIN RESONANCE SPECTRA OF THE PROTOTYPE SUPEROXO-DIRHODIUM(III,III) SALT[1]

NICOLA S. A. EDWARDS, IAN J. ELLISON, R. D. GILLARD† and B. MILE

School of Chemistry and Applied Chemistry, University of Wales Cardiff, P.O. Box 912, Cardiff CF1 3TB, U.K.

and

J. MAHER

School of Chemistry, University of Bristol, Cantock's Close, Bristol BS8 1TS, U.K.

(*Received* 1 *September* 1992; *accepted* 12 *October* 1992)

Abstract—The ESR spectra of the ion *trans*-$[Cl(py)_4Rh(\mu\text{-}O_2)Rh(py)_4Cl]^{3+}$, pure and magnetically dilute in diamagnetic *trans*-$[Rh(py)_4Cl_2]Cl \cdot 5H_2O$, are given to confirm the presence of the superoxide bridge; structural studies support this assignment.

The blue superoxo-dirhodium(III,III) moiety $[Rh_2(\mu\text{-}O_2)]^{5+}$ was discovered[2] in a search for the cause of the green colourations common during the preparation of *trans*-dichlorotetrakispyridine-rhodium(III) chloride, itself yellow, from aqueous rhodium trichloride and pyridine, catalysed by ethanol. The greening is observed particularly for aqueous ethanolic solutions left in air. The blue species responsible is[2] the μ-superoxo-bis(*trans*-chlorotetrakispyridine)dirhodium(III,III) cation (**A**). Such blue compounds with a range of ligands are now quite common.[3,4]

The most convenient demonstration of the presence of the μ-superoxo-dirhodium(III,III) unit is its ESR spectrum, since many of these complexes contain ClO_4^- anions; perchlorate can obscure the vibrational spectra of dioxygen compounds. A few compounds containing the superoxide moiety are listed in Table 1; all show the average g-value (g_{av}) at *ca* 2.03 ± 0.01. One crystallographic study[4] of $[\{(CH_3CN)(py)_3Rh\}_2(\mu\text{-}O_2)(\mu\text{-}OH)](ClO_4)_4 \cdot H_2O$ established that the species giving the characteristic ESR signals ($g_{av} = 2.035$) was indeed the superoxide; the oxygen–oxygen bond length is 133.6 pm, typical of O_2^-.[3c] The measured[4] Rh—O distances for the $Rh^{(III)}$—$(\mu\text{-}O_2)$—$Rh^{(III)}$ moiety were 198.6 and 194.9 pm.

† Author to whom correspondence should be addressed.

For the prototype cation **A**, as its perchlorate, a rhodium–rhodium vector of 487 pm was measured.[5] Oddly, Zehnder attributed this to the structural unit **B**, but acknowledged[5] that this led to the extraordinary Rh—O bond length of 243.7 pm.

$$[Rh^{(IV)}\text{—}O\text{—}Rh^{(III)}]^{5+}$$
B

In the tetrafluoroborate of **A** (isostructural with the perchlorate) this laboratory found that the Rh—Rh vector was similarly 486.2 pm, but[6] there was disorder in exactly the region of the rhodium–oxygen components.

Metal–oxygen interatomic distances decrease as the oxidation state of the metal increases. This is reflected in the Rh—O bond lengths of coordinated *terminal* water ligands; the longest M—O distances for aqueous generated rhodium(II) and rhodium(III) species are 233.2[7] and 216.2 pm.[8] Indeed, the only genuine linear, oxo-bridged dirhodium species[9] contains rhodium(IV) ions, $[Rh^{(IV)}\text{—}O\text{—}Rh^{(IV)}]^{6+}$, with an Rh—O distance of *ca* 190 pm. Contrary to this trend, reduction of unit **B** was said to result in a *shortening* of the Rh—O bond by 32.5 pm.[5]

We now show that for the original system,[2] the ESR spectrum is indeed that of a superoxide: the g-value, shape and intensity of the ESR spectrum

Table 1. ESR spectra for superoxide and its complexes

Complex ion or species	g_{zz}	g_{yy}	g_{xx}	g_{av}	Ref.
$[O_2]^-$ (in Na_2O_2)	2.190	2.016	2.016	2.076	This work
$[O_2]^-$ (in H_2O)	2.101	2.001	2.001	2.035	14
$(CH_3)_3CO_2$ (in d^6-benzene)[a]	2.040	2.009	2.003	2.017	11
$(CH_3)_3SiO_2$ (in cyclopropane)[a]	2.059	2.008	2.002	2.023	11
$(CH_3)_3GeO_2$ (in d^6-benzene)[a]	2.054	2.008	2.002	2.021	11
$(CH_3)_3SnO_2$ (in d^6-benzene)[a]	2.060	2.008	2.003	2.024	11
$(CH_3)_3PbO_2$ (in d^6-benzene)[a]	2.080	2.008	2.001	2.029	11
$\{[Co(NH_3)_5]_2(\mu\text{-}O_2)\}^{5+}$	2.076	2.003	2.003	2.028	12
$\{[Rh(en)_2Cl]_2(\mu\text{-}O_2)\}^{3+}$	2.097	2.030	1.989	2.040	15
$\{[Rh(bipy)_2Cl]_2(\mu\text{-}O_2)\}^{3+}$	2.088	2.020	2.004	2.038	16
$\{[Rh(bipy)_2(H_2O)]_2(\mu\text{-}O_2)\}^{5+}$	2.089	2.021	1.992	2.034	16
$\{[Rh(py)_4Cl]_2(\mu\text{-}O_2)\}^{3+}$ (in $[Rh(py)_4Cl_2]Cl \cdot 5H_2O$)	2.100	2.032	1.990	2.041	This work
$\{[Rh(py)_4Cl]_2(\mu\text{-}O_2)\}(ClO_4)_3 \cdot 8H_2O$[b]	1.976	1.938	1.938	1.951	This work

bipy = 2,2′-bipyridyl; py = pyridine; en = ethylenediamine.
[a] As a solid matrix.
[b] Crystalline sample.

would be very different[10] if the complex did contain rhodium(IV), i.e. the fragment **B**.

The powder ESR spectrum of $\{[Rh(py)_4Cl]_2(\mu\text{-}O_2)\}^{3+}$ in $[Rh(py)_4Cl_2]Cl$, shown in Fig. 1, is typical of a species having an orthorhombic g-tensor with no hyperfine interactions with either the rhodium or nitrogen nuclei; the spectrum of pure solid $\{[Rh(py)_4Cl]_2(\mu\text{-}O_2)\}(ClO_4)_3 \cdot 8H_2O$ is given in Fig. 2 for comparison.

The magnetically dilute sample of paramagnetic $\{[Rh(py)_4Cl]_2(\mu\text{-}O_2)\}^{3+}$ illustrated in Fig. 1 appears to contain a second minor superoxide species, as shown by the shoulders positioned at $g_{xx} = 2.001$ and $g_{zz} = 2.092$. However, the absorptions due to the minor species can be regarded as non-reproducible, since the shoulders are variable, sometimes negligible, in intensity. The principal g-values (determined from the turning points of the derivative spectrum), the value of g_{av} and the ESR parameters for other paramagnetic superoxo species are listed in Table 1. The g_{av} value of 2.041 is larger than that of organic superoxides (*ca* $g_{iso} = 2.015$),[11] smaller than that of O_2^- in alkali metal matrices, but similar to the values for O_2^- in dipolar matrices. These features strongly indicate that the unpaired electron resides mainly in one of the $1\pi_g^*$ antibonding orbitals of the bridging dioxygen with minimal spin density at the rhodium centres, i.e. the description $[Rh^{(III)}—(\mu\text{-}O_2)—Rh^{(III)}]^{5+}$ is accurate.

The principal values of the g-tensor in the x, y and z directions for the magnetically dilute sample correspond very closely to that of superoxide-bridged dirhodium(III,III) complexes with other nitrogenous ligands. g_{zz} shows the largest deviation from free spin ($g_e = 2.0023$) and must correspond to the case where the field is along the O—O bond axis. The value of g_{xx} is close to g_e, thus identifying the x-axis as that of the orbital containing the unpaired electron, i.e. π_x^*. The deviation of g_{yy} from g_e is larger in these rhodium complexes than in other superoxides and the small but significant difference between g_{yy} and g_{xx} requires non-axial symmetry around the O—O bond, suggesting that the Rh—O—O—Rh bond is not co-linear or co-planar in the dinuclear complexes. The larger shift in g_{yy} is associated with a lowering of the energy gap between the $2p\sigma_g$ and the $2p\pi_g^*$ orbitals, presumably through a repulsive interaction between d_{zy} and σ_g electrons. Comparison of the g-tensors for the rhodium species with those of the similar $\{[Co(NH_3)_5]_2(\mu\text{-}O_2)\}^{5+}$ suggests[12] that the greater shift away from the free electron value in the rhodium complexes is also due, in part, to the larger spin orbit coupling constant for rhodium.

EXPERIMENTAL

The ESR spectra of magnetically dilute $\{[Rh(py)_4Cl]_2(\mu\text{-}O_2)\}^{3+}$ in *trans*-$[Rh(py)_4Cl_2]Cl \cdot 5H_2O$ and NaO_2 in Na_2O_2 were recorded on a Bruker 300E ESR spectrometer at 77K; calibration of the magnetic field was achieved using α,α′-diphenyl-β-picrylhydrazyl. The ESR spectrum of μ-superoxo-bis(*trans*-chlorotetrakispyridine)dirhodium(III,III) triperchlorate octahydrate crystals was obtained using a JES RE2X spectrometer with

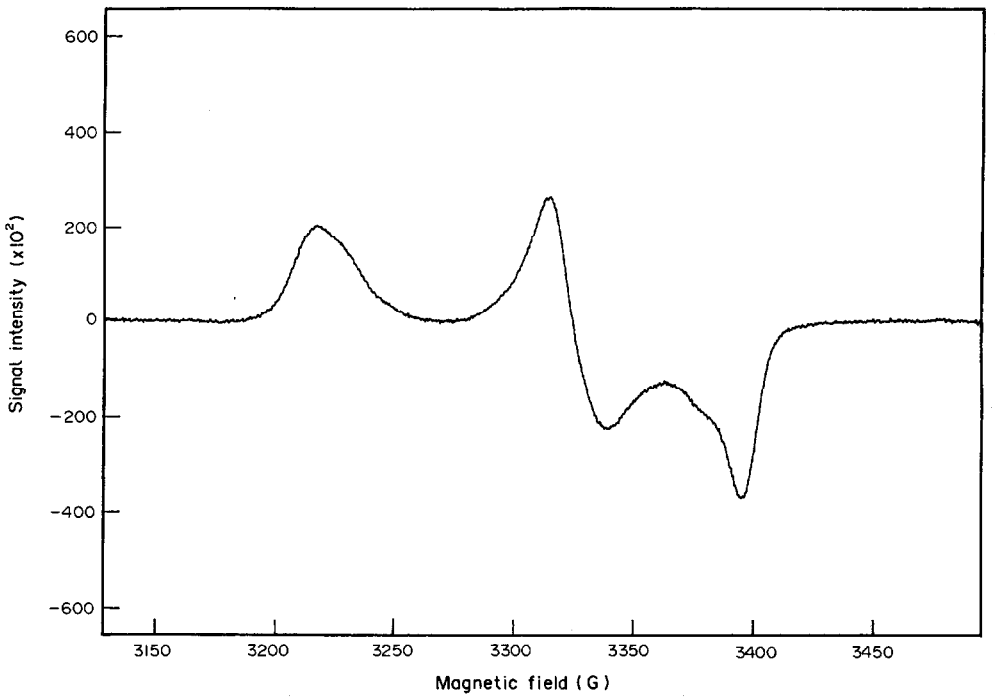

Fig. 1. The ESR spectrum of $[\{Rh(py)_4Cl\}_2(\mu\text{-}O_2)]^{3+}$ in diamagnetic *trans*-$[Rh(py)_4Cl_2]Cl \cdot 5H_2O$ at 77 K.

manganese markers. Crystallographic studies were carried out using a single-crystal diffractometer.

Sodium peroxide beads, containing sodium superoxide as an impurity, were used without further treatment.

Trans-dichlorotetrakispyridinerhodium(III) chloride was prepared by the method of Gillard and Wilkinson[13] using a catalyst of ethanol rather than sodium hypophosphite. This preparation[13] states that the yield may be increased by allowing the filtrate to stand for a few days; during this time the ethanolic solution slowly becomes green, indicating the formation of the paramagnetic species. Evaporation gives the green crystals of the diluted superoxide complex.

Preparations of $\{[Rh(py)_4Cl]_2(\mu\text{-}O_2)\}(X)_3 \cdot nH_2O$,

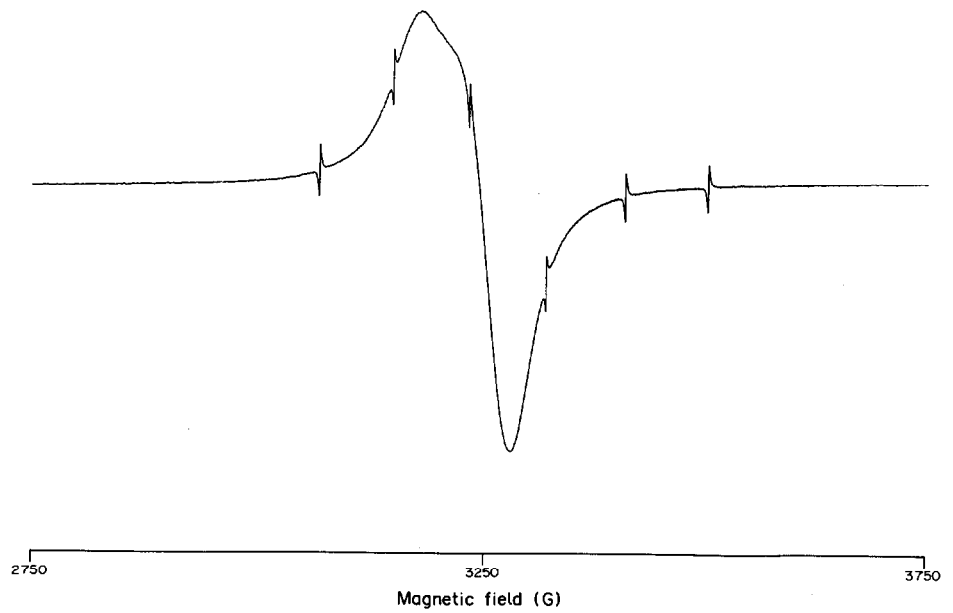

Fig. 2. The ESR spectrum of crystalline $\{[Rh(py)_4Cl]_2(\mu\text{-}O_2)\}(ClO_4)_3 \cdot 8H_2O$ with manganese markers.

where X is the perchlorate anion ($n = 8$) or the tetrafluoroborate anion ($n = 0$), were based on the method reported elsewhere.[2] However, crystals from the blue solution ($\lambda = 646$ nm), resulting[2] from ozonolysis of an alkaline ethanolic solution of $[Rh(py)_4Cl_2]Cl$, were isolated in a different fashion.

The addition of excess solid $NaClO_4$ to a freshly prepared sample of the blue solution gave a silver/blue precipitate. After filtering and washing with a small volume of water, the solid was redissolved in the minimum quantity of boiling $HClO_4$ (0.5 M); alternatively, to generate the tetrafluoroborate salt, excess boiling $NaBF_4$ solution was added to this perchlorate acid solution. The hot solution was immediately placed in a sealed dewar and allowed to crystallize (refrigerator) for 48 h. Once collected, the crystals were washed with a little acetone.

It should be noted that although some degree of twinning of crystals took place using the conditions described above, recrystallization of the salts in any medium other than an aqueous acidic solution of anion (e.g. pyridine, acetone, etc.) resulted in the decay of the compound or the twinning of all crystals.

Acknowledgements—I.J.E., R.D.G. and J.M. wish to thank SERC and the Universities of Bristol and Bath for the purchase of the Bruker 300E ESR spectrometer. Further, I.J.E. and R.D.G. wish to express their gratitude to M. B. Hursthouse, C. W. Lehmann and A. B. Lehmann (SERC crystallographic group, Cardiff) for structural studies.

REFERENCES

1. This is part 12 of *Oxidants containing Rhodium*: further studies can be found in: I. J. Ellison and R. D. Gillard, *J. Chem. Soc. Chem. Commun.* 1992, 851; A. N. Buckley, J. A. Busby, I. J. Ellison and R. D. Gillard, *Polyhedron* 1993, **12**, 247; I. J. Ellison, R. D. Gillard and J. P. Maher, *Polyhedron* 1992, **11**, 2757.
2. A. W. Addison and R. D. Gillard, *J. Chem. Soc.* (*A*) 1970, 2523.
3. (a) I. B. Baranovskii, A. N. Zhilyaev, L. M. Dikareva and A. V. Rotov, *Russ. J. Inorg. Chem.* (English translation) 1986, **31**, 1661; (b) M. Moszner and J. J. Ziolkowski, *Inorg. Chim. Acta* 1988, **145**, 299; (c) J. Springborg and M. Zehnder, *Helv. Chim. Acta* 1984, **67**, 2218.
4. L. M. Dikareva, V. I. Andrianov, A. N. Zhilyaev, I. B. Baranovskii and M. A. Porai-Koshits, *Russ. J. Inorg. Chem.* (English translation) 1988, **33**, 539.
5. M. Zehnder, *Chimia* 1984, **38**, 243.
6. I. J. Ellison, R. D. Gillard, M. B. Hursthouse, A. B. Lehmann and C. W. Lehmann, unpublished results.
7. J. D. Korp, I. Bernal and J. L. Bear, *Inorg. Chim. Acta* 1981, **51**, 1.
8. T. Glowiak, M. Kubiak and T. Szymanska-Buzar, *Acta Cryst.* (*B*) 1977, **33**, 1732.
9. R. S. Hay-Motherwell, G. Wilkinson, B. Hussain-Bates and M. B. Hursthouse, *Polyhedron* 1990, **9**, 2071.
10. I. J. Ellison and R. D. Gillard, in preparation; A. D. Westland, *Can. J. Chem.* 1968, **46**, 3591.
11. J. E. Bennett and J. A. Howard, *J. Am. Chem. Soc.* 1972, **94**, 8244.
12. M. Mori, J. A. Weil and J. K. Kinnaird, *J. Phys. Chem.* 1967, **71**, 103 and refs therein.
13. R. D. Gillard and G. Wilkinson, *Inorg. Synth.* 1967, **10**, 64.
14. J. E. Bennett, B. Mile and A. Thomas, *Trans. Faraday Soc.* 1968, **64**, 3200.
15. J. B. Raynor, R. D. Gillard and J. D. Pedrosa de Jesus, *J. Chem. Soc., Dalton Trans.* 1982, 1165.
16. H. Caldemaru, K. DeArmond and K. Henck, *Inorg. Chem.* 1978, **17**, 2030.

Polyhedron Vol. 12, No. 4, pp. 375–381, 1993
Printed in Great Britain

0277-5387/93 $6.00+.00
© 1993 Pergamon Press Ltd

THE NATURE OF THE OXIDATION PRODUCTS OF DICYANORUTHENIUM PHTHALOCYANINE IN AQUEOUS AND NON-AQUEOUS SOLVENTS

TEBELLO NYOKONG

Chemistry Department, Rhodes University, Grahamstown 6140, Republic of South Africa

(*Received* 13 *July* 1992; *accepted* 12 *October* 1992)

Abstract—The cyclic voltammetry of $[(CN)_2Ru^{II}Pc]^{2-}$ in acetonitrile or dichloromethane shows two oxidation couples at $E_{1/2} = 0.31$ and 0.85 V (vs S.C.E.) in CH_2Cl_2 and $E_{1/2} = 0.45$ and 1.15 V (vs S.C.E.) in acetonitrile. The spectroelectrochemistry of $[(CN)_2Ru^{II}Pc]^{2-}$ in these solvents showed that oxidations occur at the phthalocyanine ligand. $K_2[(CN)_2Ru^{II}Pc]$ dissolves in water at pHs greater than 5. The cyclic voltammetry of this complex showed oxidation couples at 0.32 and 0.29 V (vs S.C.E.) for aqueous solutions containing sodium sulphate (0.1 M) and for buffered solutions (pH = 9), respectively. Both cyclic voltammetry and controlled potential coulometry gave evidence of electrocrystallization of the oxidation product. Chemical oxidations of $[(CN)_2Ru^{II}Pc]^{2-}$ in water also showed phthalocyanine ligand oxidation.

Phthalocyanine complexes have established themselves industrially as green or blue dyes. Potential applications of metal phthalocyanine (MPc; Pc = phthalocyanine dianion) complexes include uses in catalysis, pollution control, electronic devices, photovoltaic devices and many others. Most of these applications involve the exchange of one or two electrons per reaction and hence, an understanding of the redox properties of the phthalocyanine complexes is very important. There is also an interest in metal-based drugs that can act against the rapid toxic effects of cyanide, and for this metalloporphyrin complexes have been suggested.[1–5] Phthalocyanines are structurally similar to the porphyrins and hence, studies of the cyano complexes of MPc complexes are of interest; a number of $(CN)_2MPc$ complexes have been reported.[6–8]

Cyclic voltammetry (CV) studies of a series of dicyanometallo phthalocyanines have been reported.[6] In these studies the first oxidation potential in $[(CN)_2Ru^{II}Pc]$ was assigned to the oxidation of the ruthenium metal to ruthenium(III), based on the comparison with the CV results of ruthenium porphyrin complexes. In this work, we take a closer look at the electrochemical properties of the $[(CN)_2Ru^{II}Pc]$ complex. The CV studies will be coupled with controlled potential coulometry and the site of the first and second oxidations will be determined.

Phthalocyanine complexes are normally insoluble in water. Attaching sulphonic acid groups to the outer periphery of the phthalocyanine ring renders these complexes soluble in water.[9–12] Sulphonated phthalocyanine complexes, however, aggregate in aqueous solution and are photoinactive. $[(CN)_2Ru^{II}Pc]$ shows solubility in water; the redox properties of this complex in water are reported in this work.

EXPERIMENTAL

Materials

Crude RuPc was synthesized from $RuCl_3 \cdot 3H_2O$ and *o*-cyanobenzamide and extracted with glacial acetic acid following the method of Dolphin *et al.*[13]

$K_2[(CN)_2RuPc]$ was prepared according to synthetic procedures for other $[(CN)_2MPc]^{2-}$ complexes.[7,8] Crude RuPc (0.05 g, 0.08 mmol) and KCN (0.05 g, 0.77 mmol) were suspended in absolute ethanol or DMF (10 cm^3) and refluxed for 3 h, giving a blue solution. The solution of $K_2[(CN)_2$ RuPc] was filtered to remove the insoluble RuPc and the filtrate evaporated to dryness, giving a purple solid which was washed in hexanes and recrystallized from acetone, giving 40 mg (66%) of $K_2[(CN)_2RuPc] \cdot 3H_2O$.

$K_2[(CN)_2RuPc]$ could also be prepared by reacting $[(DMSO)_2RuPc \cdot 2DMSO]$ (0.02 g, 0.02 mmol) with KCN (0.03 g, 0.46 mmol) in DMF (10 cm^3), following the procedure outlined above, giving 0.013 g (80%) of $K_2[(CN)_2RuPc] \cdot 3H_2O$. $(DMSO)_2RuPc \cdot 2DMSO$ was prepared following procedures outlined previously.[14] Found: C, 50.9; H, 3.3; N, 17.1. Calc. for $K_2C_{34}H_{22}N_{10}O_3Ru$: C, 51.2; H, 2.8; N, 17.6%. IR spectra (KBr discs): ν(Ru—CN), 2075; ν(O—H), 3440 cm^{-1}. UV–vis (CH_3CN) λ_{max} (nm): 620 (ε = 46,000), 565, 345.

CH_2Cl_2 and CH_3CN were dried over calcium hydride and phosphorus pentoxide, respectively, and then distilled. DMF and DMSO were stirred with alumina, distilled under reduced pressure and stored over molecular sieves. Distilled deionized water was used for studies in aqueous solutions. Tetrabutylammonium perchlorate (TBAP), tetraethylammonium perchlorate (TEAP) and Na_2SO_4 were recrystallized and used as electrolytes for electrochemical studies. Ferrocene was recrystallized from ethanol before use as an internal standard. All other materials were reagent grade and used without further purification.

Methods

Electrochemical data were collected with the BAS CV 27 voltammograph connected to an HP 7047A *X–Y* recorder. All electrochemical measurements were carried out under an atmosphere of nitrogen. For cyclic voltammetry a platinum disc (1.6 mm diameter) was used as the working electrode and a platinum wire as the auxiliary electrode. A silver wire coated with silver chloride was used as a quasi-reference electrode. Potentials were referenced internally to the ferrocenium/ferrocene (Fc^+/Fc) couple.[15,16] The Fc^+/Fc couple was measured as 0.47 V vs S.C.E. in CH_2Cl_2 containing TBAP and 0.44 vs S.C.E. in CH_3CN containing TBAP or TEAP. Platinum sheet working and auxiliary electrodes and an Ag/AgCl reference were employed for bulk electrolysis, the auxiliary electrode being separated from the compartment housing the reference and working electrodes by a fine glass frit. TBAP or TEAP (0.03–0.1 M) in CH_3CN or CH_2Cl_2 were used as supporting electrolytes for electrochemical studies in non-aqueous solutions. Sodium sulphate (0.1 M) and phthalate and phosphate buffers were employed as electrolytes for electrochemical experiments in aqueous solutions. HCl and NaOH were used to adjust pH in unbuffered aqueous solutions.

A Quanta Ray Neodynium Yag pumped dye laser with a DCM dye for irradiation at 640 nm was used as a source of the ns pulses. EPR measurements were carried out at room temperature or in liquid nitrogen with the Bruker ESR spectrometer. IR spectra (KBr discs) were collected with a Perkin–Elmer Model 180 IR spectrometer. Electronic absorption spectra were recorded with a Varian Techtron UV–vis spectrophotometer, model 635.

RESULTS AND DISCUSSION

Studies in non-aqueous solvents

Both ruthenium(II) and ruthenium(III) porphyrin complexes are known to form cyano complexes.[2] As has been observed before[6] the oxidation state of ruthenium in $(CN)_2RuPc$ is +2. The $(CN)_2RuPc$ complex prepared in this work is EPR inactive, consistent with an oxidation state of +2 for ruthenium and the formulation of the complex as $[(CN)_2Ru^{II}Pc]^{2-}$. The Ru—CN vibration is observed at 2075 cm^{-1}.

Cyclic voltammetry. Two successive ring oxidations from the non-degenerate $a_{1u}(\pi)$ orbital of the phthalocyanine ligand and four successive ring reductions into the doubly degenerate $e_g(\pi^*)$ orbital are theoretically possible in metal phthalocyanine complexes. Some MPc complexes show redox activity at the central metal.[17–19] CV and controlled potential coulometry studies of $[(L)_2Ru^{II}Pc]$ complexes show that oxidations occur at the phthalocyanine ligand in these complexes.[13,19]

Figure 1 shows the CV of $[(CN)_2Ru^{II}Pc]^{2-}$ in CH_2Cl_2 containing TBAP. Two oxidation couples

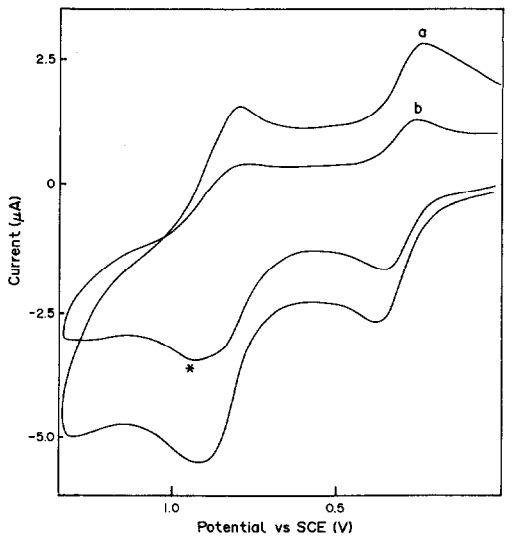

Fig. 1. Cyclic voltammogram of $[(CN)_2Ru^{II}Pc]^{2-}$ in dichloromethane containing TBAP (0.05 M). Scan rate (a) 50 and (b) 200 mV s^{-1}. * refers to the irreversible peak following the second oxidation couple.

Table 1. Half-wave[a] potentials of the $[(CN)_2RuPc]$ complex in various solvents and electrolytes

Solvent/electrolyte	Pc^-/Pc^{2-} (V)	Pc^0/Pc^- (V)
CH_3CN/TEAP	0.45 (0.01)	1.15 (0.71)
CH_2Cl_2/TBAP	0.31 (−0.16)	0.85 (0.38)
H_2O/Na_2SO_4	0.34	
H_2O/pH 9 buffer	0.29	

[a] Note: Numbers in brackets are half-wave potentials ($E_{1/2}$) vs the ferrocenium/ferrocene (Fc^+/Fc) couple. $E_{1/2}$ values vs S.C.E. were obtained by adding $E_{1/2}$ (Fc^+/Fc) = 0.47 V vs S.C.E. (for dichloromethane solutions) or 0.44 V vs S.C.E. (for acetonitrile solutions) to $E_{1/2}$ vs Fc^+/Fc values in brackets.

were observed: the first at a half-wave potential ($E_{1/2}$) of 0.31 V and the second at 0.85 V, Table 1. The first oxidation couple is quasi-reversible with an anodic-to-cathodic peak separation of approximately 100 mV. The second oxidation couple is reversible with a peak separation of 59 mV. The second couple is immediately followed by an irreversible peak at a potential of 0.97 V. This peak is more prominent at low scan rates, Fig. 1(a).

The oxidation potential of 0.31 V observed for $[(CN)_2Ru^{II}Pc]^{2-}$ is lower than potentials generally observed for the first ligand oxidation of MPc complexes.[19] However, all $[(L)_2Ru^{II}Pc]$ complex studies so far[13,19,20] show oxidation at the phthalocyanine ligand and not at the ruthenium metal. Thus, it is suggested here that the first oxidation in $[(CN)_2Ru^{II}Pc]^{2-}$ occurs at the phthalocyanine ligand giving an $[Ru^{II}Pc]^-$ π-cation radical species. The quasi-reversible nature of the first oxidation couple could be due to axial ligand exchange or the formation of five-coordinate intermediates. Five-coordinate ruthenium(II) porphyrins are known.[2] The second oxidation couple at 0.85 V vs S.C.E. is assigned to the removal of the second electron from the phthalocyanine ligand. Spectroelectrochemistry is used to confirm these CV assignments.

CV results similar to those reported in CH_2Cl_2 were also obtained when acetonitrile was employed as a solvent. The oxidation potentials were observed at 0.45 and 1.15 V for the first and second oxidation potentials, respectively (Table 1).

Spectroelectrochemistry. Oxidation at the phthalocyanine ligand in MPc complexes occurs by the removal of electrons from the $1a_{1u}$ highest occupied molecular orbital, resulting in a drastic change in transitions that arise from this orbital. Data presently available for the MPc^- π-cation radical species show that the formation of this species is accompanied by the loss of intensity of the Q band, which arises from the $1a_{1u}$ orbital, and the formation of a broad band centred at approximately 500 nm.[13,16,19-21] Metal centred oxidation would result in a shift in the Q band without much change in intensity.[19,22]

Figure 2, shows the absorption spectral changes observed when solutions of $[(CN)_2Ru^{II}Pc]^{2-}$ in acetonitrile containing TBAP (0.05 M) were exhaustively electrolysed at potentials 50 mV positive of the first oxidation potential, viz. 0.5 V. As electrolysis proceeds the Q band decreases in intensity,

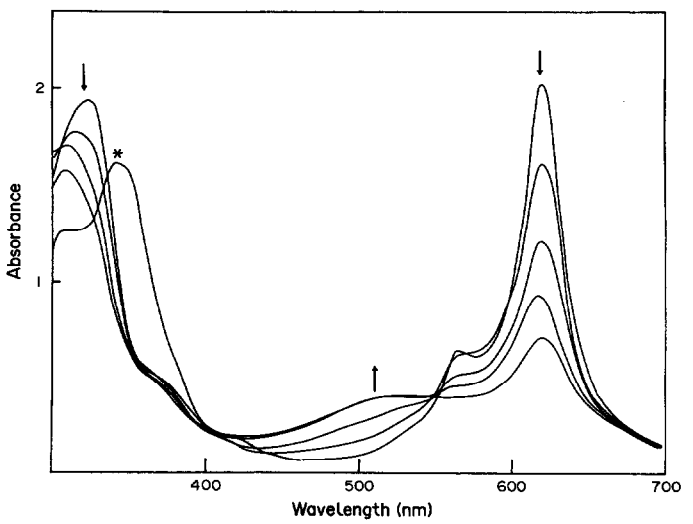

Fig. 2. Absorption spectral changes observed when solutions of $[(CN)_2Ru^{II}Pc]^{2-}$ in acetonitrile containing TBAP (0.05 M) were exhaustively electrolysed at 0.5 V vs S.C.E. * refers to the Soret band of the original complex.

Table 2. Electronic absorption spectral data for $[(CN)_2RuPc]$ in various solvents, showing only the main band centres

Complex[a]	Solvent	Data	
$RuPc^{2-}$	CH_3CN	345	620
	CH_2Cl_2/TBAP	345	623
	H_2O	313	
$RuPc^-$	CH_3CN	358	520[b]
	CH_3CN	308	520[c]
	CH_2Cl_2	300	520[c]
	H_2O	308	550[d]
$RuPc^0$	CH_2Cl_2	~400[c]	

[a] Axial ligands have been excluded.
[b] Ferric chloride oxidized.
[c] Electrochemically oxidized.
[d] Bromine oxidized.

the Soret band shifts from 345 to 325 nm and finally to 308 nm at the end of the electrolysis (Table 2). The spectra of the final oxidation product with a broad band at 520 nm is typical of the spectra of the MPc^- π-cation radical species. Thus, the first oxidation in $[(CN)_2Ru^{II}Pc]$ occurs at the phthalocyanine macrocycle and not at the metal, contrary to that suggested before.[6] Values of $n = 1 \pm 10\%$ (where n is the number of electrons involved in the electron transfer step) were obtained for oxidation at the first oxidation potentials of the $[(CN)_2Ru^{II}Pc]$ complex. The EPR spectra, at 77 K, of the oxidized complex show a signal centred at $g = 2.00$. Reduction of the oxidized species at 0 V vs S.C.E. does not regenerate the original species with the Soret band at 345 nm, but regenerates the intermediate species, the Soret band centred at 325 nm. The original species is only observed on addition of CN^- to the reduced species, implying that the oxidation of $[(CN)_2Ru^{II}Pc]$ to the π-cation radical species is accompanied by loss of cyanide. Loss of both cyanide ligands is unlikely as unligated RuPc is highly insoluble. It is likely that the lost CN^- is replaced by the electrolyte ClO_4, to give $[(CN)(ClO_4)RuPc]^-$.

Similar results were observed when solutions of $[(CN)_2Ru^{II}Pc]$ in dichloromethane containing TBAP (0.05 M) were exhaustively electrolysed at 0.4 V. The spectral changes are again typical of the formation of a π-cation radical species, accompanied by the exchange of axial ligands.

Exhaustive electrolysis at the potentials of the second oxidation gave the spectral changes shown in Fig. 3. The first step is the formation of the $RuPc^-$ complex with a typical broad peak at 520 nm. As the electrolysis proceeds the 520 nm peak is reduced in intensity and a new broad peak is observed at *ca* 400 nm; we tentatively assign the final oxidation product of this electrolysis to the formation of the $RuPc^0$ dication radical. There is considerable decomposition accompanying the formation of these species. The oxidation of the cyanide ligand is known to occur at approximately

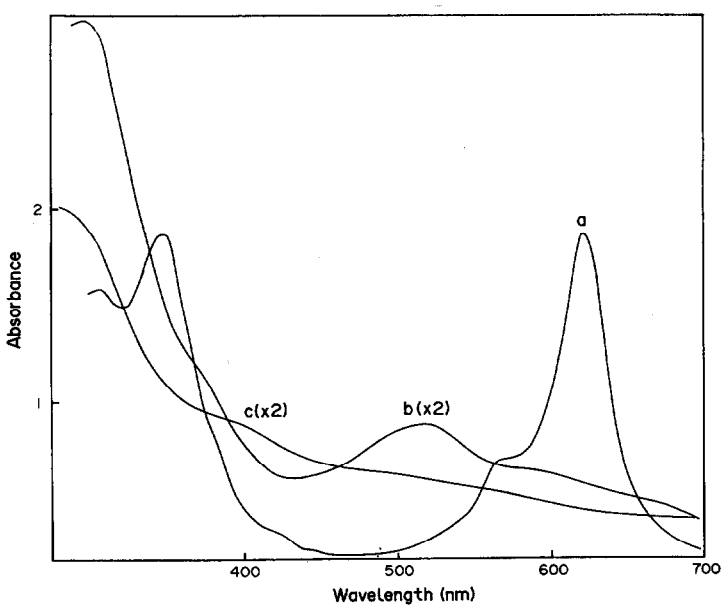

Fig. 3. Absorption spectral changes observed when solutions of $[(CN)_2Ru^{II}Pc]^{2-}$ in dichloromethane containing TBAP (0.05 M) were exhaustively electrolysed at 0.9 V vs S.C.E. (a) Unoxidized complex: (b) π-cation radical species; and (c) final species obtained on oxidation.

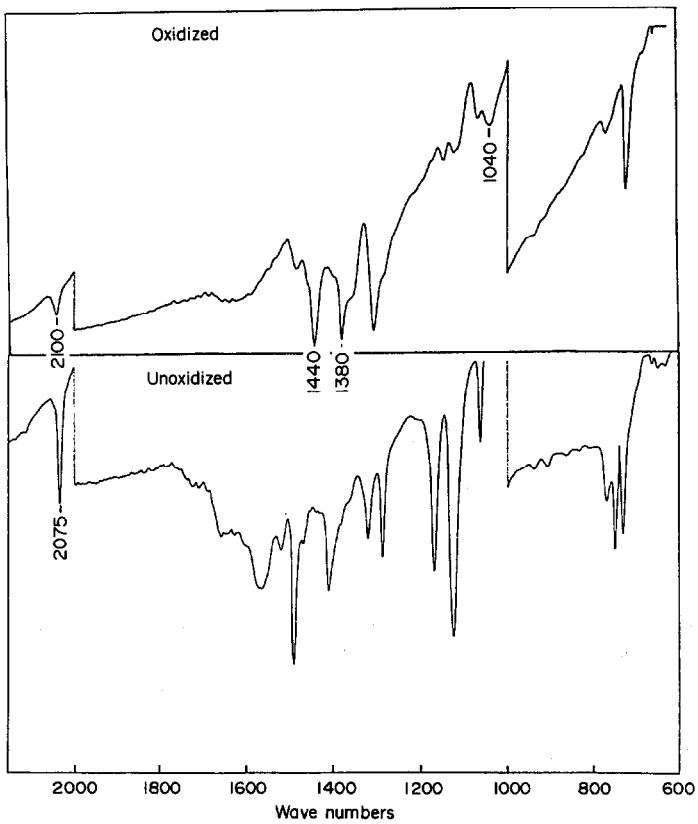

Fig. 4. The IR spectra (KBr discs) of the bromine-oxidized and unoxidized $K_2[(CN)_2Ru^{II}Pc]$.

1.0 V,[23] hence, the shoulder observed at 0.97 V is associated with the oxidation of the CN^- ligand.

Chemical oxidation. Bromine oxidation of $[(CN)_2Ru^{II}Pc]$ in acetonitrile forms the π-cation radical species with clear isosbestic points, with no evidence for axial ligand exchange. Reduction of the oxidized species with $Na_2S_2O_4$ completely regenerates the spectra due to the neutral species.

The IR spectra of the bromine-oxidized $[(CN)_2Ru^{II}Pc]^-$ complex is not complicated by vibrations of the electrolyte and in Fig. 4 we compare the IR spectra of $[(CN)_2Ru^{II}Pc]^{2-}$ and of the oxidized species. The oxidized species for IR were obtained by evaporating off the solvent from acetonitrile solutions of the bromine-oxidized $[(CN)_2Ru^{II}Pc]^-$ complex. The oxidized complex shows the Ru—CN vibration at 2100 cm^{-1}, an increase of 25 cm^{-1} from the frequency of the original species at 2075 cm^{-1} (Fig. 4). The increase in energy of the M—CN^- frequency when MPc^- are formed has been observed before.[6] The IR spectra of the MPc^- species are of lower intensity than those of the neutral species.[6,24] Bands typical of the MPc^- complexes[6,24] are observed at 1040, 1380 and 1440 cm^{-1}.

The reaction between ferric chloride and $[(CN)_2Ru^{II}Pc]$ proceeds through several stages. Initially, the Q band broadens and shifts to slightly lower energies [Fig. 5(b)]. The spectra are still typical of $[(L)_2Ru^{II}Pc]$ complexes, hence maybe assigned to the exchange of axial ligands, probably the formation of the $[(Cl)(CN)Ru^{II}Pc]$ complex. Similar spectral changes were observed during the oxidation of cobalt tetraneopentoxyphthalocyanine by $SOCl_2$[25] and were assigned to axial ligation effects. Further addition of ferric chloride results in the formation of the π-cation radical species [Fig. 5(b)] with an Ru—CN vibration at 2090 cm^{-1}, thus, confirming that at least one cyanide ligand remains coordinated to the $RuPc^-$ complex.

Studies in water

Phthalocyanine complexes that are not substituted peripherally by sulphonic acid groups are insoluble in water. $K_2[(CN)_2RuPc]\cdot 3H_2O$, however, dissolves in water with an extinction coefficient (at $\lambda = 630$ nm) of 3×10^4 $dm^3\,mol^{-1}\,cm^{-1}$. This value is of the same order of magnitude as the value reported for other $(L)_2RuPc$ complexes.[13]

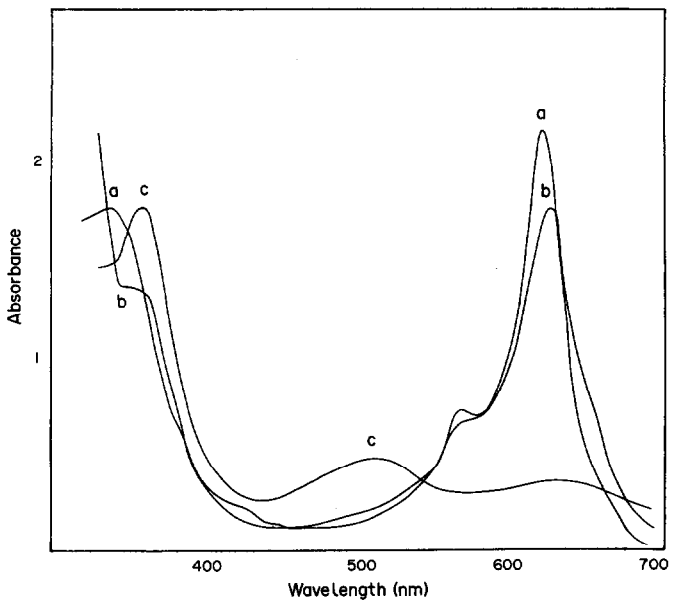

Fig. 5. Absorption spectral changes observed on addition of ferric chloride to acetonitrile solutions of $[(CN)_2Ru^{II}Pc]$. (a) No $FeCl_3$ added; (b) complex formed on addition of small amounts of $FeCl_3$; and (c) oxidized complex, excess $FeCl_3$ added.

$K_2[(CN)_2RuPc]\cdot 3H_2O$ dissolves in aqueous solutions above pH = 5, forming blue–green solutions. Beer's law is obeyed in the concentration range 10^{-6}–10^{-3} M. Below pH = 5, the solubility of $[(CN)_2Ru^{II}Pc]$ is considerably decreased. In this pH range a green solution is obtained with an uncharacteristically broad Q band centred at *ca* 670 nm, Fig. 6. Addition of hydroxide or cyanide to the green solution results in the regeneration of the blue–green solution and the narrowing of the Q band as it shifts back to 630 nm. Addition of SO_2 or $Na_2S_2O_4$ to basic solutions of $[(CN)_2Ru^{II}Pc]$ also resulted in the broadening of the Q band shown in Fig. 6(c). The dependence of the spectra on pH has been observed before in ruthenium(II) porphyrin complexes and has been attributed to the loss of the cyanide ligands at low pH.[2] We similarly assign the species at low pH to an $Ru^{II}Pc$ complex which has lost the cyanide ligands.

Cyclic voltammetry of the $[(CN)_2Ru^{II}Pc]$ com-

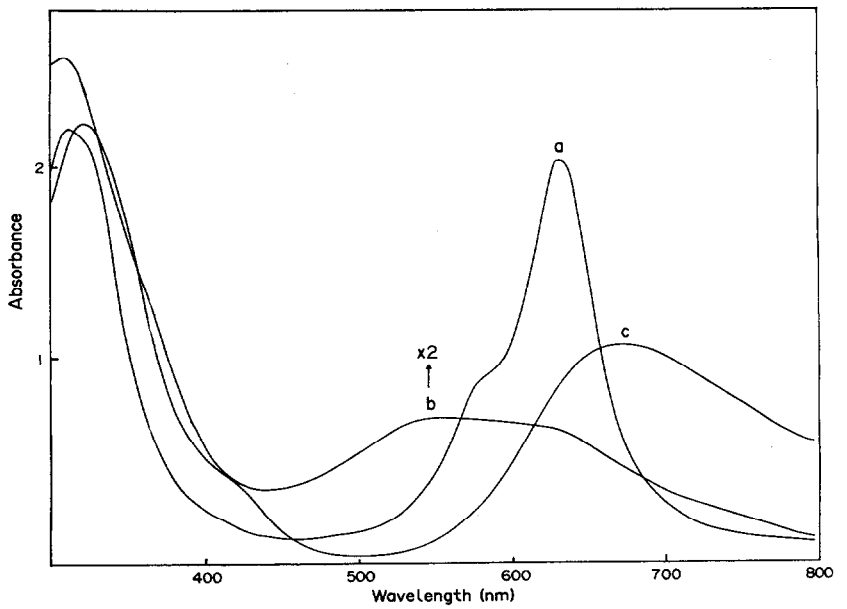

Fig. 6. Absorption spectra of (a) unoxidized $[(CN)_2Ru^{II}Pc]^{2-}$ dissolved in pH = 9 buffer; (b) bromine oxidized $[(CN)_2Ru^{II}Pc]^-$, pH = 9; and (c) $[(CN)_2Ru^{II}Pc]$ in water at pH < 5.

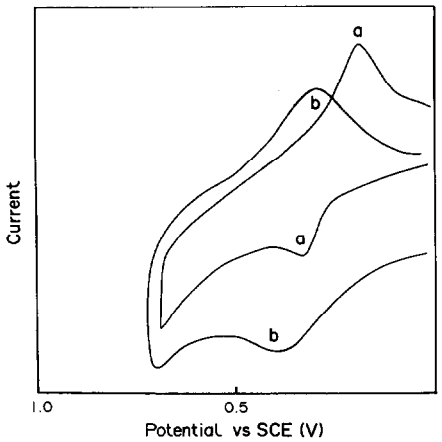

Fig. 7. Cyclic voltammogram of solutions of $[(CN)_2Ru^{II}Pc]$ in (a) pH 9 buffer; scan rate 200 mV s^{-1}; and (b) water containing sodium sulphate (0.1 M); scan rate = 1 V s^{-1}.

plex in buffered solutions (pH = 9) or in water containing sodium sulphate (0.1 M) shows a quasi-reversible oxidation couple at 0.29 and 0.34 V, respectively (Fig. 7). These potentials are in the range reported above for the first oxidation of the phthalocyanine macrocycle, showing that oxidation of the $[(CN)_2Ru^{II}Pc]$ complex in water also occurs at the phthalocyanine ligand. The cathodic currents for these oxidation couples (Fig. 7) are greatly enhanced when compared to the anodic currents. This behaviour is typical of a weakly adsorbed product.[26] Indeed exhaustive electrolysis at 0.4 V resulted in considerable electrocrystallization and adsorption of the product to the electrodes. However, bromine oxidation of $[(CN)_2Ru^{II}Pc]$ in basic aqueous solutions gave spectral changes which are characteristic of the formation of the MPc^- π-cation radical species with a broad band at 550 nm [Table 2 and Fig. 6(b)]. Reduction of the oxidized species with sodium borohydride regenerates more than 95% of the original species.

Laser irradiations of basic solutions of $[(CN)_2Ru^{II}Pc]$ at wavelengths of the Q band produced a short-lived ligand-centred $^3\pi\pi^*$ state at a wavelength of 520 nm and with a half-life of 75 ns. Such short-lived species have been observed in other RuPc complexes.[27]

Acknowledgements—This work was supported by Rhodes University through the Joint Research Committee. I wish to thank the Radiation Laboratory of the University of Notre Dame, Indiana, U.S.A. for the use of the ESR and laser equipment.

REFERENCES

1. S. Mosseri, P. Neta, A. Harriman and P. Hambright, *J. Inorg. Biochem.* 1990, **39**, 93.
2. P. Hambright, *Inorg. Chim. Acta* 1989, **157**, 95.
3. S. Modi, V. P. Shedbalkar and D. V. Behere, *Inorg. Chim. Acta* 1990, **173**, 9.
4. P. Hambright and R. Langley, *Inorg. Chim. Acta* 1987, **137**, 209.
5. P. Hambright and R. Langley, *J. Inorg. Biochem.* 1988, **32**, 197.
6. R. Behnisch and M. Hanack, *Synth. Met.* 1990, **36**, 387.
7. Y. Orihashi, H. Ohno, E. Tsuchida, H. Matsuda, H. Nakanishi and M. Kato, *Chem. Lett.* 1987, 601.
8. J. Metz and M. Hanack, *J. Am. Chem. Soc.* 1983, **105**, 828.
9. R. H. Campbell, G. A. Heath, G. T. Hefter and R. C. S. McQueen, *J. Chem. Soc., Chem. Commun.* 1983, 1123.
10. J. R. Darwent, I. McCubbin and D. Phillips, *J. Chem. Soc., Faraday Trans. 2* 1982, **78**, 347.
11. J. R. Darwent, I. McCubbin and G. Porter, *J. Chem. Soc., Faraday Trans. 2* 1982, **78**, 903.
12. K. Schmatz, S. Muralidharan, K. Madden, R. Fessenden and G. Ferraudi, *Inorg. Chim. Acta* 1981, **64**, L23.
13. D. Dolphin, B. R. James, A. J. Murray and J. R. Thornback, *Can. J. Chem.* 1980, **58**, 1125.
14. W. Kobel and M. Hanack, *Inorg. Chem.* 1989, **25**, 103.
15. R. R. Gagne, C. A. Koval and G. C. Lisensky, *Inorg. Chem.* 1980, **19**, 2855.
16. T. Nyokong, Z. Gasyna and M. J. Stillman, *Inorg. Chem.* 1987, **26**, 548.
17. A. B. P. Lever, P. C. Minor and J. P. Wilshire, *Inorg. Chem.* 1981, **20**, 2550.
18. A. B. P. Lever, M. R. Hempstead, C. C. Leznoff, W. Liu, M. Melnik, W. A. Nevin and P. Seymour, *Pure Appl. Chem.* 1986, **58**, 1467.
19. T. Nyokong, Z. Gasyna and M. J. Stillman, *ACS Symp. Ser.* 1986, **321**, 309.
20. T. Nyokong, Z. Gazyna and M. J. Stillman, *Inorg. Chim. Acta* 1986, **112**, 11.
21. P. C. Minor, M. Gouterman and A. B. P. Lever, *Inorg. Chem.* 1985, **24**, 1894.
22. N. Kobayashi, M. Koshiyama, K. Fumayana, T. Osa, H. Shirai and K. Hanabusa, *J. Chem. Soc., Chem. Commun.* 1983, 913.
23. S. Andreades and E. W. Zahnow, *J. Am. Chem. Soc.* 1969, **91**, 4181.
24. J. F. Myers, G. W. Rayner Canham and A. B. P. Lever, *Inorg. Chem.* 1975, **14**, 461.
25. P. A. Bernstein and A. B. P. Lever, *Inorg. Chem.* 1990, **29**, 608.
26. A. J. Bard and L. R. Faulkner, *Electrochemical Methods, Fundamentals and Applications*, p. 530. John Wiley & Sons, Inc., New York (1980).
27. G. Ferraudi and D. R. Prasad, *J. Chem. Soc., Dalton Trans.* 1984, 2137.

Polyhedron Vol. 12, No. 4, pp. 383–387, 1993
Printed in Great Britain

0277–5387/93 $6.00+.00
© 1993 Pergamon Press Ltd

SYNTHESIS AND CHARACTERIZATION OF COMPLEXES OF COBALT(II), NICKEL(II), ZINC(II), CADMIUM(II) AND MERCURY(II) WITH *p*-ACETAMIDOBENZALDEHYDE THIOSEMICARBAZONE

G. KANAGARAJ and G. N. RAO*

Chemistry Department, Indian Institute of Technology, New Delhi 110016, India

(*Received* 1 *September* 1992; *accepted* 9 *October* 1992)

Abstract—Some complexes of *p*-acetamidobenzaldehyde thiosemicarbazone (thiacetazone) with cobalt(II), nickel(II), zinc(II), cadmium(II) and mercury(II) have been prepared and their magnetic, spectral and thermal data suggest that the thiacetazone acts as a neutral bidentate ligand binding the metal ion through the hydrazine nirogen and the carbothioamide sulphur. A brown-coloured nickel(II) complex, $Ni(TA)_2$, was isolated and found to be diamagnetic and it contains a monoanionic bidentate ligand (thiol form). All the metal complexes of the type $M(TAH)_2X_2$ (where X is Cl, Br, NO_3 and SCN) are octahedral, while $Ni(TA)_2$ is square planar in structure.

p-Acetamidobenzaldehyde thiosemicarbazone (thiacetazone) is used to treat mycobacterial infections that are resistant to isoniazid, a well-known antituberculosis drug. Leibermeister showed that copper ions enhanced the anti-tubercular activity of thiacetazone.[1] The copper complex of thiacetazone was reported by Kuhn and Zilliken in 1954 and its use in chemotherapy of tuberculosis has been discussed briefly.[2] Copper(II) and nickel(II) complexes of the type $[ML_2]SO_4$ and ML_2 were reported with magnetic susceptibility, electronic and IR spectral data.[3]

This paper presents detailed information on the preparation and properties of the complexes formed by thiacetazone with cobalt(II), nickel(II), zinc(II) and mercury(II).

EXPERIMENTAL

Thiacetazone was procured from Sigma Chemical Co. (USA) and was used without further purification. All the metal salts used were of Analar reagent grade.

The metal halide (2.5 mmol) dissolved in acetone or methanol (10 cm^3) was added slowly to a refluxing acetone solution (100 cm^3) of the ligand thiacetazone (2.5 mmol). The solid which separates out on concentration of the solution was filtered, washed with a small amount of acetone and then dried in a vacuum desiccator.

Cobalt(II) nitrate hexahydrate was used to prepare the cobalt(II) complex containing nitrate as the anion. An alcoholic ammonia solution (1 : 1) was added to the reaction mixture of nickel(II) chloride and thiacetazone until a brownish product appeared and the reaction mixture was refluxed for 1 h to isolate the brown colour complex of nickel (II), $Ni(TA)_2$. For the preparation of the nickel (II) complex with isothiocyanate anion a stoichiometric amount of ammonium thiocyanate (in a small amount of water) was added to the reaction mixture of nickel(II) chloride and thiacetazone. The yield of all the metal complexes was found to be in the range 60–80%.

Physical measurements

Elemental analyses for carbon, hydrogen and nitrogen were carried out on a Perkin–Elmer 240°C microanalyser. The amount of metal present in the complexes was determined using a Pye–Unicam SP191 atomic absorption spectrophotometer. Conductivities of the metal complexes were measured in dimethylformamide at room temperature using a Metrohm 660 conductometer. Magnetic susceptibilities of the metal complexes were measured

* Author to whom correspondence should be addressed.

using a Cahn 2000 Faraday magnetic balance calibrated with $Hg[Co(NCS)_4]$ at room temperature.

Diffuse reflectance spectra were recorded on a Hitachi 300 UV–vis spectrophotometer, fitted with a standard reflectance attachment. IR spectra were recorded on a Nicolet DX FTIR instrument and a Perkin–Elmer 1700X FT far-IR spectrophotometer. Proton magnetic resonance spectra were recorded on a JEOL JNM FX-100 FT NMR spectrometer, using tetramethylsilane as a reference in d^6-DMSO at room temperature. Thermograms were recorded on a Stanton Redcroft STA 780 thermal analyser.

RESULTS AND DISCUSSION

The analytical data for the metal-thiacetazone complexes (see Table 1) were found to be in agreement with the proposed molecular formulae.

Conductivity

Thiacetazone and its metal complexes were found to be non-conducting in acetone. In dimethylformamide, however, thiacetazone complexes of cobalt(II) chloride(110), zinc(II) chloride (104) and cadmium(II) chloride (119) were found to have molar conductivities (Ω^{-1} cm^2 mol^{-1}) in the range expected for 1 : 1 electrolytes. The mercury(II) complex (17) and $Ni(TA)_2$ (10) behaved as non-electrolytes at room temperature. Other metal complexes including that of cobalt(II) bromide (356), cobalt(II) nitrate (707) and nickel(II) isothiocyanate (443) were found to have high molar conductivities, possibly due to solvolysis in dimethylformamide.[4]

Magnetic susceptibility

The effective magnetic moment values (in B.M.) for thiacetazone complexes of cobalt(II) bromide (4.58), cobalt(II) nitrate (4.98) and nickel(II) isothiocyanate (2.99) were obtained from susceptibility measurements at room temperature and suggest that the ligand field environment around cobalt(II) and nickel(II) ions is octahedral with three and two unpaired electrons, respectively.[5] The brown coloured $Ni(TA)_2$ was found to be diamagnetic, thereby suggesting a spin paired square-planar stereochemistry for the d^8 Ni^{2+} complex.

IR spectral study[6]

Thiacetazone exhibits four prominent IR bands in the regions 3310, 3250, 3220 and 3145 cm^{-1}. Although it is very difficult to assign each band to any symmetric or asymmetric stretchings of the three different NH groups present, namely acetamide NH, hydrazine NH and carbothioamide NH_2, the overall positive shifts of these bands in the IR spectra of metal complexes indicate the non-involvement of the NH group in metal binding (Table 2).[7] Other IR bands due to NH_2 bending (1610 and 1590 cm^{-1}), amide **III** (1325 and 1285 cm^{-1}), ρ (NH_2) (1270 and 1180 cm^{-1}), ω (NH_2) (1015 cm^{-1}) and δ (NCS) (460 and 440 cm^{-1}) showed no shift on coordination of the ligand to the metal ion.

A strong band at 1680 cm^{-1} (due to carbonyl stretching) in the case of both thiacetazone and its metal complexes indicates the presence of the acetamide carbonyl group free from metal binding. Two vibrational bands at 1115 and 815 cm^{-1} in the spectrum of thiacetazone might be due to C=S

Table 1. Physical and analytical data of thiacetazone and its metal complexes

Compound[a]	Colour	M.p. (°C)[b]	Calc. (%) M	C	H	N	Elemental analysis Found (%) M	C	H	N
Thiacetazone	Light Yellow	225d	—	50.8	5.2	23.7	—	51.2	5.6	23.9
$Co(TAH)_2Cl_2$	Green	226d	9.8	39.9	4.0	18.6	9.9	39.7	4.4	18.5
$Co(TAH)_2Br_2$	Green	220d	8.5	34.7	3.5	16.2	8.0	34.5	3.7	16.9
$Co(TAH)_2(NO_3)_2$	Brown	120d	9.0	36.6	3.7	21.4	8.9	36.2	3.8	21.6
$[Ni(TAH)_2(NCS)_2]2H_2O$	Yellow	210d	8.6	38.7	4.1	20.5	8.4	38.5	4.1	20.3
$Ni(TA)_2$	Dark brown	305d	11.1	45.4	4.2	21.2	11.8	45.6	4.2	21.4
$Zn(TAH)_2Cl_2$	Yellow	235d	10.7	39.4	4.0	18.4	10.0	39.1	3.5	18.7
$Cd_2(TAH)Cl_4$	Light Yellow	320	37.3	19.9	2.0	9.3	37.6	19.1	2.9	9.1
$Hg(TAH)_2Cl_2$	Light Yellow	278d	27.0	32.3	3.2	15.1	26.4	32.5	3.5	15.3

[a] TAH = thiacetazone; TA = deprotonated thiacetazone.
[b] d = decomposing.

Table 2. IR spectral data of thiacetazone and its metal complexes[a]

Proton[b]	Thiacetazone	$Zn(TAH)_2Cl_2$	$Cd_2(TAH)Cl_4$	$Hg(TAH)_2Cl_2$
H^a	11.37	11.37	11.40	12.15
H^b	10.09	10.09	10.08	10.13
H^c	8.12	8.14	8.12	8.09
H^d	7.97	7.80	7.99	8.82
	7.90	—	—	8.74
H^e	7.77	7.78	7.77	7.82
	7.68	7.69	7.68	7.74
	7.64	7.66	7.64	7.66
	7.54	7.57	7.55	7.58
H^f	2.07	2.07	2.05	2.07

[a] Chemical shifts in δ ppm; the solvent used, d^6-DMSO.
[b] H^a = hydrazine NH, H^b = acetamide NH, H^c = methylene CH, H^d = carbothioamide NH_2, H^e = aromatic CH and H^f = acetamide CH_3.

stretching, perhaps coupled with N—C—N stretching. These bands showed a negative shift of 35–50 cm^{-1} (1060–1080 cm^{-1}) and of relatively less magnitude, 5–10 cm^{-1} (800–810 cm^{-1}), in the case of all metal complexes.[8] These observations indicate the involvement of the C=S group in bonding to the metal ion. In the spectrum of $Ni(TA)_2$ only the band at 820 cm^{-1} was observed. The disappearance of the other band in the range 1115–1060 cm^{-1} indicates the loss of C=S double bond character on coodination.[7] Thiacetazone, in this case, probably acts as an anion (deprotonated thiol form), binding the nickel(II) ion through sulphur.

Additional IR bands at 2060 [ν(C=N)], 820 [ν(C=S)], 445 and 500 cm^{-1} [δ(NCS)] in the spectrum of the nickel(II) isothiocyanate complex of thiacetazone suggest that the coordination of the isothiocyanate anion to the nickel(II) ion is through nitrogen.[9] In the far -IR spectra of the metal complexes absorptions due to metal–ligand stretching vibrations are identified, which can be assigned to various M—L (M—N and M—S) and M—X (M—Cl, M—Br and M—NO_3) bondings (Table 2).

Electronic spectral study

Diffuse reflectance spectra recorded for the cobalt(II) complexes of thiacetazone showed two principal regions of absorptions, one in the range 8000–10,000 cm^{-1} due to the $^4T_{2g} \leftarrow {}^4T_{1g}$ electronic transition (ν_1) and the other in the range 18,000–21,000 cm^{-1} due to the $^4T_{1g}$(P) electronic transition (ν_3) (Table 3). In the case of $[Co(TAH)_2(NO_3)_2]$ a weak absorption observed at 15,870 cm^{-1} could be due to the $^4A_{2g} \leftarrow {}^4T_{1g}$ transition (ν_3). These observations suggest an octahedral ligand field environment around the d^7 cobalt(II) ion in the complexes prepared.[10]

The three electronic bands observed at 11,430 16,390 and 26,320 cm^{-1} (shoulder) in the spectrum of $[Ni(TAH)_2(NCS)_2]\cdot 2H_2O$ indicate octahedral stereochemistry for the d^8 nickel(II) ion with $^3A_{2g}$ as a ground electronic state in the complex (Table 3). In the case of the diamagnetic $Ni(TA)_2$ complex only one absorption band at 19,610 cm^{-1} was observed. This could be attributed to the $^1B_{2g}$ (XY) $\leftarrow {}^1A_{1g}$ transition in a square-planar ligand field environment around the nickel(II) ion.

^{1}H NMR spectral study

The number of protons related to all the chemical shifts observed in the spectrum of thiacetazone remained unchanged in the spectra of the diamagnetic metal complexes (Table 4). This shows the non-deprotonated nature of the ligand in the complexes of zinc(II), cadmium(II) and mercury (II). The chemical shifts,[11] in δ ppm, due to acetamide NH (10.09) and hydrazine NH (11.37) protons remained unchanged in the spectra of zinc(II) and cadmium(II) complexes. This indicates neither acetamide NH nitrogen nor hydrazine NH nitrogen are involved in metal coordination of the ligand.

The split in the proton signal due to carbothioamide-NH_2 groups (7.97 and 7.90 δ ppm) observed in the spectrum of the ligand disappeared and only one stronger signal corresponding to two protons was found in the case of zinc(II) and cadmium(II) complexes (Table 4). This split in the proton signal due to the NH_2 group can be explained on the basis that because of the partial double-bond character of the C—N bond (due to resonance in the

Table 3. Electronic spectral data of thiacetazone and some of its metal complexes

Compound	Diffuse reflectance wavelength (cm^{-1})[a]	Electronic transition assignment
Thiacetazone	39,220	
$Co(TAH)_2Cl_2$	26,320 (sh.)	Charge transfer
	19,610	$^4T_{1g}(P) \leftarrow {}^4T_{1g}(\nu_3)$
	10,870	$^4T_{2g} \leftarrow {}^4T_{1g}(\nu_1)$
$Co(TAH)_2Cl_2$	26,320 (sh.)	Charge transfer
	18,870	$^4T_{1g}(P) \leftarrow {}^4T_{1g}(\nu_3)$
	10,750	$^4T_{2g} \leftarrow {}^4T_{1g}(\nu_1)$
$Co(TAH)_2(NO_3)_2$	26,320 (sh.)	Charge transfer
	21,740	$^4T_{1g}(P) \leftarrow {}^4T_{1g}(\nu_3)$
	15,870	$^4A_{2g} \leftarrow {}^4T_{1g}(\nu_2)$
	8,330	$^4T_{2g} \leftarrow {}^4T_{1g}(\nu_1)$
$[Ni(TAH)_2NCS)_2]\cdot 2H_2O$	26,320 (sh.)	$^3T_{1g}(P) \leftarrow {}^3A_{2g}(\nu_3)$
	16,390	$^3T_{1g} \leftarrow {}^3A_{2g}(\nu_2)$
	11,430	$^3T_{2g} \leftarrow {}^3A_{2g}(\nu_1)$
$Ni(TA)_2$	19,610 (sh.)	$^1B_{1g}(xy) \leftarrow {}^1A_{1g}$

[a] sh. = shoulder.

carbothioamide moiety

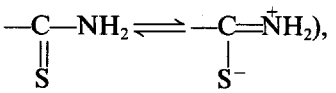

the two NH_2 protons have a different environment (*cis* and *trans*).[12] The presence of only one signal due to the NH_2 protons in these complexes indicates a substantial reduction in the double-bond character of the C—N bond, which allows free single-bond rotation at room temperature, thereby making the two NH_2 protons equivalent.

In the spectrum of $Hg(TAH)_2Cl_2$, however, the doublet nature of the proton signal due to the carbothioamide NH_2 group (8.82 and 8.74 δ ppm) was observed. The downfield shift of this proton signal when compared to that of thiacetazone, $Zn(TAH)_2Cl_2$ and $Cd_2(TAH)Cl_4$ could be attributed to the change in the structure of the ligand from thione to thiol forms. The presence of the thiol form of the ligand in the mercury(II) complex is further supported by the broad signal observed at 12.15 δ ppm, which could be due to the SH proton. The absence of the proton signal (11.37 δ ppm) cor-

Table 4. Proton magnetic resonance spectral data of thiacetazone and its diamagnetic metal complexes[a]

Assignment	1	2	3	4	5	6	7	8	9
ν(NH)	3310s	3380s	3390s	3340s	—	—	3380s	3410s	3400s
	3250s	3310s	3280s	3320s	—	3320s	—	3300s	—
	3220s	3250s	—	3180s	3250s	—	3250s	3240s	3235s
	3140s	3170s	3160s	3050s	3170s	3130s	3170s	3150s	3140s
ν(C=N)(SCN^-)	—	—	—	—	2060s	—	—	—	—
ν(C=O)	1680s	1680s	1670s	1690s	1680s	1690s	1670s	1670s	1670s
ν(C=S^+)	1115s	1060s	1070s	1070s	1060s	—	1060s	1080s	1080s
ν(N—C—N)	815s	810s	810s	810s	800s	820s	815s	820s	815s
ν(C=S)(SCN^-)	—	—	—	—	820s	—	—	—	—
ν(M=L)	—	290	295	290	290	385	250	260	260
	—	270	275	270	—	—	—	—	—
ν(M=X)	—	320	250	280	—	—	270	295	280

[a] Spectra recorded in KBr; vibrational frequencies in cm^{-1}; s = strong.

1 = thiacetazone, **2** = $Co(TAH)_2Cl_2$, **3** = $Co(TAH)_2Br_2$, **4** = $Co(TAH)_2(NO_3)_2$, **5** = $[Ni(TAH)_2(NCS)_2]\cdot 2H_2O$, **6** = $Ni(TA)_2$, **7** = $Zn(TAH)_2Cl_2$, **8** = $Cd_2(TAH)Cl_4$ and **9** = $Hg(TAH)_2Cl_2$.

responding to the hydrazine NH proton in the spectrum of $Hg(TAH)_2Cl_2$ indicates the involvement of this proton in thione–thiol tautomerism.[13]

Thermal decomposition study[14]

Thiacetazone was found to be stable up to 280°C, above which the ligand decomposed, continuously exhibiting a broad exotherm centred at 585°C. On heating thiacetazone complexes of cobalt(II) with chloride, bromide and nitrate as anions decomposed exothermically, resulting in the formation of cobalt(II) oxides, probably a mixture of CoO and Co_3O_4.

The thermogram of the nickel(II) isothiocyanate complex of thiacetazone showed an initial weight loss of 5.0% around 120°C. This indicates the presence of at least two water molecules of hydration in the complex. The anhydrous compound [Ni $(TAH)_2(NCS)_2$] was found to be decomposing further exothermically, resulting in the formation of nickel(II) oxide, NiO (above 750°C). The brown coloured $Ni(TA)_2$ complex was found to be stable up to 300°C. On further heating of the sample a constant weight residue, probably a mixture of NiS and NiO, was obtained around 660°C.

$Zn(TAH)_2Cl_2$ and $Cd_2(TAH)Cl_4$ complexes gave exothermic decompositions, yielding their respective metal oxides. $Hg(TAH)_2Cl_2$, which was found to be stable up to 320°C, gave a complete loss of the sample due to continuous exothermic decomposition at higher temperature.

REFERENCES

1. K. Liebermeister, *Z. Naturforsch.* 1950, **B5**, 79.
2. R. Kuhn and F. Zilliken, U.S. Patent No. 2,695,911, November (1954).
3. C. B. Mahto, *J. Ind. Chem. Soc.* 1980, **57**, 481.
4. W. J. Geary, *Coord. Chem. Rev.* 1971, **7**, 81.
5. R. S. Drago, *Physical Methods in Chemistry*, 1st edn, p. 411. W. B. Saunders, Philadelphia (1977).
6. M. J. M. Campbell, *Coord. Chem. Rev.* 1975, **15**, 279.
7. B. A. Gingras, R. L. Samorjai and C. H. Bayley, *Can. J. Chem.* 1961, **39**, 973.
8. D. M. Wiles, B. A. Gingras and T. Suprunchuk, *Can. J. Chem.* 1967, **45**, 469.
9. K. Nakamoto, *Infrared and Raman Spectra of Inorganic and Coordination Compounds*, 3rd edn, p. 270. Wiley-Interscience, New York (1978).
10. A. B. P. Lever (Editor), *Inorganic Electronic Spectroscopy*, 2nd edn. Elsevier, Amsterdam (1984).
11. *Handbook of Proton-NMR Spectra and Data*, Asahi Research Center (Editors). Academic Press, Tokyo (1987).
12. I. L. Finar, *Organic Chemistry*, Vol. 1, 6th edn, p. 263. Longman, Essex (1985).
13. S. Padhye and G. B. Kauffman, *Coord. Chem. Rev.* 1985, **63**, 127.
14. C. Duval, *Inorganic Thermogravimetric Analysis*, 2nd edn. Elsevier, Amsterdam (1963).

Polyhedron Vol. 12, No. 4, pp. 389–399, 1993
Printed in Great Britain

0277–5387/93 $6.00+.00
© 1993 Pergamon Press Ltd

REACTIVITY OF $(Me_3Al)_2$ WITH SELECTED AMINOARSINES AND SECONDARY AMINES

C. J. THOMAS, L. K. KRANNICH and C. L. WATKINS*

Department of Chemistry, University of Alabama at Birmingham, AL 35294, U.S.A.

(*Received* 14 *August* 1992; *accepted* 5 *October* 1992)

Abstract—The reactions of $(Me_3Al)_2$ with 11 aminoarsines, Me_2AsR (R = Et_2N, $Pr^n{}_2N$, $Pr^i{}_2N$, $Bu^n{}_2N$, $Bu^i{}_2N$, C_4H_8N, $C_5H_{10}N$, $C_6H_{12}N$, $CH_3NC_4H_8N$, Ph_2N and Bzl_2N, where Bzl = $PhCH_2$—), have been studied by multinuclear NMR spectroscopy. The results are compared with those of our previous studies on the Me_3Al/Me_2AsNMe_2 system. In each case, except Me_2AsNPh_2, the final reaction products are $[Me_2AlR]_2$ and Me_3As. The reaction intermediates have been identified and, in most cases, the As—N—Al adducts and $Me_2AlR \cdot AlMe_3$ are observed. With Me_2AsNPh_2 the product is $Me_3As \cdot Me_2AlNPh_2$. The influence of steric and electronic effects on arsenic vs nitrogen bonding site preference, adduct stability, complexity of overall reaction and ease of forming Me_3As and $[Me_2AlR]_2$ are discussed. $[Me_2AlR]_2$, $Me_2AlR \cdot AlMe_3$ and $Me_3Al \cdot HR$ have been independently synthesized and characterized. A comparison of the ^{13}C NMR chemical shift values for Me_2AsR and $Me_2AsR \cdot AlMe_3$ provides information on steric interactions that influence adduct stability.

Numerous reactions of trialkylaluminum species with compounds containing group 15 elements have been reported.[1–7] $(Me_3Al)_2$ reacts readily with secondary amines to form adducts of the type $Me_3Al \cdot HNR_2$, which upon heating undergo alkane elimination to yield Al—N cyclic dimers.[8–11] For example, thermolysis of $Me_3Al \cdot HNMe_2$ at 120°C yields CH_4 and $[Me_2AlNMe_2]_2$.[8] The reactions of $(Me_3Al)_2$ with multidentate nitrogen compounds such as diamines,[3,4] triamines[12] and open-chain[13–16] and cyclic[17–20] amines have also been investigated. In certain cases, the resulting Al—N bonded species may contain penta-[13,15] and hexa-coordinate[16,20] aluminum.

Aluminum alkyls have also been reacted with compounds that contain adjacent, competing, group 15 Lewis base sites, i.e. N—N,[21,22] P—N,[23] As—N,[6,24–26] Sb—N,[26] P—N—N[27] and P—N—P[23,28,29] bonds. Typically when the Lewis base molecule contains an N—H bond, alkane elimination occurs with the formation of a condensed Al—N bonded species. For example, in the reaction of $(Ph_2P)_2NH$ with $(R_3Al)_2$ (R = Me, Et), the aluminum-containing product is $[R_2AlNPPh_2]_2$, which in the Me case contains a six-membered AlNPAlNP ring.[29] With P—N bond containing species having no NH bonds the reaction is not as straightforward, but appears to depend upon the bulkiness of the substituents on phosphorus and nitrogen. For example, in the reaction of $(Et_3Al)_2$ with Me_2PNMe_2 an Al—P adduct, $Et_3Al \cdot Me_2PNMe_2$,[23] is formed; with Ph_2PNEt_2 no adduct formation has been observed,[23] and with $(Ph_2P)_2NR$ (R = Me, Et, Pr^n, Bu^n) only Al—P bonded 1:1 adducts[23,28] are obtained.

Reports on the reactivity of trialkylaluminum with As—N bonded compounds are limited.[6,24–26] Unlike in the P—N systems, the As—N bond is cleaved by $(Me_3Al)_2$. For example, with Me_2AsNMe_2 there is initial formation of the Al—N bonded adduct, $Me_2AsNMe_2 \cdot AlMe_3$,[6] which decomposes in solution at room temperature to Me_3As and $[Me_2AlNMe_2]_2$.[6] Although analogous products are obtained with $MeAs(NMe_2)_2$ and $As(NMe_2)_3$,[6] the As—N bond is more labile than with Me_2AsNMe_2. These reactions have been exploited as synthetic pathways to Me_3As,[6] R_3As[26] and Me_2AsR[25] (R = Et, Pr^n, Bu^n, and Bu^i) by reacting $As(NMe_3)_3$ and Me_2AsNMe_2 with the appropriate R_3Al. As the bulkiness of the R group increases, higher temperatues are needed to achieve

* Author to whom correspondence should be addressed.

adduct decomposition to the respective Me_2AsR and $[R_2AlNMe_2]_2$ species.

We were also interested in investigating the generality of the $(Me_3Al)_2/Me_2AsNMe_2$ reaction when the amino substituent is varied in order to study the influence of substituent steric and electronic effects on arsenic vs nitrogen binding site preference, adduct stability, complexity of decomposition pathways and ease of forming Me_3As and the respective aminoalane. In this paper, we report an NMR (^1H and ^{13}C) investigation of the reactions of trimethylaluminum with 11 aminoarsines, Me_2AsR (R = Et_2N, $Pr^n{}_2N$, $Pr^i{}_2N$, $Bu^n{}_2N$, $Bu^i{}_2N$, C_4H_8N, $C_5H_{10}N$, $C_6H_{12}N$, $CH_3NC_4H_8N$, Ph_2N and Bzl_2N, where Bzl = $PhCH_2$—). The results obtained from these reactions are then compared with those from the Me_2AsNMe_2 system. Because the $(Me_3Al)_2/Me_2AsR$ systems yield $[Me_2AlR]_2$, we independently synthesized 12 aminoalanes by the reaction of $(Me_3Al)_2$ with the respective secondary amine.[8] These reactions initially gave the $Me_3Al\cdot$amine adducts, which were then isolated and subsequently pyrolysed to the aminoalanes. The $Me_3Al\cdot$amine adducts and the aminoalanes were characterized by IR, MS, ^1H, ^{13}C and ^{27}Al NMR and elemental analysis. These data are reported for 11 adducts (eight previously unreported) and 12 aminoalane dimers (five previously unreported).

EXPERIMENTAL

Standard high vacuum-line techniques in conjunction with a Vacuum Atmospheres HE-43 Dri-Lab equipped with Model HE-493 Dri-Train was used for the synthesis and subsequent manipulations of all compounds. All the amines employed in this study, except Me_2NH (Matheson Gas Products) and $Bu^i{}_2NH$ (Fluka), were purchased from Aldrich Chemicals, Inc. Ph_2NH was recrystallized from a mixture of C_6H_6 and hexane, while the other amines were dried over sodium and distilled before use. Me_2AsNMe_2 (b.p. 108°C) was synthesized by the aminolysis[30] of Me_2AsCl, which was obtained by the reduction of $Me_2As(O)OH$.[31] Me_2AsNPh_2 was synthesized by the amination[32] of Me_2AsCl with Ph_2NK. The other aminoarsines were obtained by a modified transamination[32] reaction involving Me_2AsNMe_2 and the respective amine. The aminoarsines were distilled on a spinning band column and their purities were checked by ^1H and ^{13}C NMR spectroscopy. Diethylether, benzene and hexane were dried over sodium metal and distilled before use. Benzene-d_6 and Me_4Si were purchased from Aldrich Chemicals, Inc. and stored over molecular sieves.

A Nicolet 300 MHz multinuclear FT NMR spectrometer operating at 300.1, 75.4 and 78.2 MHz was used to record the ^1H, ^{13}C and ^{27}Al NMR spectra, respectively. The ^1H and ^{13}C chemical shift values of $Me_3Al\cdot HR$ and $[Me_2AlR]_2$ were measured as 0.2 M solutions of the compounds in C_6D_6 with TMS as the internal standard. For ^{27}Al data were obtained on C_6D_6 (0.1 M) solutions with $[Al(H_2O)_6{}^{3+}](NO_3)_3$ as the external reference. Both ^{13}C coupled and $\{^1H\}$ decoupled, and APT[33] spectra, were obtained for each compound. The NMR data of the Al—N adducts and dimers are reported in Tables 1–4. Previously reported NMR data are referenced. The following numbering system is used for the NMR data. Position 1 is assigned to the carbon bound to the nitrogen in the alkyl derivatives and to the nitrogen bound to aluminum in the cyclic amine derivatives. Position 7 is assigned to the exocyclic carbon. Normal aromatic ring numbering is used.

IR spectra were obtained as KeI-F/Nujol mulls or as neat liquids on KBr plates using a Nicolet IR/42 FT spectrophotometer. Low resolution EI-MS data were recorded on a HP5986A GC/MS spectrometer operated at 70 eV with a 2400 V electron multiplier. Samples were introduced directly into the probe in the vapour phase. Carbon, hydrogen and nitrogen analyses of the previously uncharacterized solid adducts and aminoalanes were obtained from E&R Microanalytical laboratory, Inc., Corona, NY (see Table 5). Melting points were determined in sealed capillaries and are uncorrected.

IR data

Previously unreported IR data for the $Me_3Al\cdot HR$ adducts and $[Me_2AlR]_2$ synthesized in this study are as follows:

$Me_3Al\cdot HNEt_2$. 3250(vs), 2984(vs), 2922(vs), 2891(vs), 2814(s), 1478(m), 1470(m), 1459(m), 1440(w), 1422(w), 1388(m), 1366(w), 1122(m), 1075(sh; m), 1057(s), 1012(sh; s), 1001(s), 904(m), 900(m), 846(s), 794(s), 783(s), 695(br; vs), 625(vs), 577(s), 521(s).

$Me_3Al\cdot HNPr^n{}_2$. 3250(vs), 2969(vs), 2921(vs), 2875(vs), 2810(vs), 1472(vs), 1459(vs), 1432(m), 1421(s), 1387(s), 1314(w), 1266(w), 1181(vs), 1125(m), 1069(s), 1060(s), 1035(vs), 1017(s), 1008(m), 953(vs), 943(vs), 887(m), 859(m), 850(m), 784(m), 746(sh; s), 700(br; vs), 625(vs), 578(s), 522(vs).

$Me_3Al\cdot HNPr^i{}_2$. 3235(s), 3000(br; s), 2983(vs), 2921(vs), 2890(vs), 2828(m), 1469(m), 1459(m), 1437(w), 1422(w), 1390(vs), 1378(vs), 1363(w), 1338(w), 1305(w), 1203(sh; s), 1188(vs), 1164(s), 1142(vs), 1115(m), 1090(m), 1047(vs), 970(w),

Table 1. Synthesized aminoalanes and adducts

Compound	Compound number	$\delta(^{27}Al$, ppm)	M.p.	ν(NH)
$[Me_2AlNMe_2]_2$	I[8,11,26]	169	153	—
$Me_3Al \cdot HNMe_2$	XIII[8,34]	174	51	3250
$[Me_2AlNEt_2]_2$	II[11,35]	167	42	—
$Me_3Al \cdot HNEt_2$	XIV[34]	173	[a]	3250
$[Me_2AlNPr^n_2]_2$	III	170	45	—
$Me_3Al \cdot HNPr^n_2$	XV	178	[a]	3250
$[Me_2AlNPr^i_2]_2$	IV[36]	164	127	—
$Me_3Al \cdot HNPr^i_2$	XVI	173	[a]	3235
$[Me_2AlNBu^n_2]_2$	V	172	67	—
$Me_3Al \cdot HNBu^n_2$	XVII	176	[a]	3250
$[Me_2AlNBu^i_2]_2$	VI	170	66	—
$Me_3Al \cdot HNBu^i_2$	XVIII	179	[a]	3288
$[Me_2AlNC_4H_8]_2$	VII[37]	168	58	—
$Me_3Al \cdot HNC_4H_8$	XIX	171	65	3227
$[Me_2AlNC_5H_{10}]_2$	VIII[10,37]	166	73	—
$Me_3Al \cdot HNC_5H_{10}$	XX[10]	171	63	3219
$[Me_2AlNC_6H_{12}]_2$	IX	171	68	—
$Me_3Al \cdot HNC_6H_{12}$	XXI	174	74	3249
$[Me_2AlNC_5H_{11}N]_2$	X	166	125	—
$Me_3Al \cdot HNC_5H_{11}N$	XXII	173	95	3083
$[Me_2AlNPh_2]_2$	XI[9,11,38]	181	130 dec.	—
$Me_3Al \cdot HNPh_2$	XXIII	[b]	[b]	[b]
$[Me_2AlNBzl_2]_2$	XII[11]	176	136	—
$Me_3Al \cdot HNBzl_2$	XXIV	169	65	3256

[a] Liquid.
[b] Decomposition at room temperature.

915(w), 836(m), 803(w), 755(m), 700(br; vs), 638(s), 623(s), 587(m), 569(m), 528(m).

$Me_3Al \cdot HNBu^n_2$. 3250(s), 2969(vs), 2922(vs), 2875(vs), 2818(s), 1468(s), 1462(m), 1435(w), 1418(m), 1381(m), 1186(vs), 1127(m), 1100(m), 1073(s), 1046(s), 981(w), 953(m), 934(m), 915(m), 887(m), 878(m), 831(m), 774(s), 700(br; vs), 625(vs), 578(s), 522(vs).

$Me_3Al \cdot HNBu^i_2$. 3288(s), 2969(vs), 2922(vs), 2880(vs), 2843(vs), 2820(s), 1472(vs), 1412(s), 1395(s), 1375(s), 1241(w), 1189(vs), 1138(m), 1103(m), 1060(vs), 1037(vs), 981(s), 972(s), 939(vs), 898(m), 869(m), 859(s), 822(s), 812(s), 775(sh; s), 700(br; vs), 625(vs), 578(vs), 522(vs).

$Me_3Al \cdot HNC_4H_8$. 3227(m), 2972(vs), 2930(vs), 2881(vs), 2822(s), 1464(s), 1405(w), 1347(w), 1180(s), 1112(w), 1040(w), 906(w), 710(s), 620(m), 588(w).

$Me_3Al \cdot HNC_5H_{10}$. 3219(s), 2966(m), 2948(vs), 2922(vs), 2883(s), 2865(s), 1468(m), 1454(vs), 1438(w), 1420(m), 1375(w), 1184(m), 1166(m), 1113(m), 1094(s), 1084(sh; s), 1041(m), 1028(m), 943(m), 868(s), 845(s), 812(s), 737(s), 700(br; s), 600(s).

$Me_3Al \cdot HNC_6H_{12}$. 3249(vs), 2960(s), 2927(vs), 2885(s), 2862(s), 2816(m), 1469(vs), 1435(vs), 1423(m), 1382(m), 1312(w), 1291(w), 1220(w), 1206(s), 1187(vs), 1169(s), 1113(vs), 1086(s), 1070(vs), 1032(s), 1000(s), 962(m), 906(w), 884(sh; m), 877(s), 845(s), 822(s), 805(s), 700(br; vs), 620(vs), 522(s).

$Me_3Al \cdot HNC_5H_{11}N$. 3083(s), 2980(s), 2950(s), 2930(vs), 2918(vs), 2885(vs), 2754(w), 1470(w), 1456(vs), 1372(m), 1333(m), 1304(w), 1284(vs), 1222(vs), 1181(br; vs), 1143(vs), 1117(w), 1098(vs), 1067(s), 1042(s), 1023(m), 1000(vs), 907(s), 777(s), 699(br; vs), 614(vs), 527(w), 434(w).

$Me_3Al \cdot HN(CH_2C_6H_5)_2$. 3256(vs), 3088(w), 3067(m), 3030(s), 3005(w), 2977(w), 2988(s), 2928(vs), 2885(vs), 2815(s), 1605(w), 1585(w), 1498(vs), 1465(vs), 1456(vs), 1410(s), 1368(sh; s), 1349(m), 1339(w), 1329(w), 1275(w), 1213(w), 1206(m), 1190(vs), 1184(vs), 1174(vs), 1155(s), 1116(s), 1100(m), 1065(s), 1029(m), 1020(s), 990(s), 936(s), 921(s), 906(m), 887(m), 840(w), 821(m), 747(vs), 691(br; vs), 634(sh; vs), 625(sh; vs), 592(s), 571(s), 528(s), 500(s), 443(w).

$[Me_2AlNPr^n_2]_2$. 2961(vs), 2935(vs), 2878(s),

Table 2. Aminoalane dimer and Me_3Al·amine adduct ^{13}C NMR data (ppm, TMS)

Compound	Me—Al	C(1)	C(2)	C(3)	C(4)	C(5)	C(6)	C(7)
Aminoalane dimers								
I[26]	−12.0	41.48	—	—	—	—	—	—
II[39]	−9.9	39.90	11.99	—	—	—	—	—
III	−10.2	49.21	20.62	11.68	—	—	—	—
IV	−4.0	51.25	26.96	26.96	—	—	—	—
V	−10.0	47.17	29.56	21.04	14.17	—	—	—
VI	−6.6	55.91	27.01	22.50	22.50	—	—	—
VII	−11.6	—	49.73	25.11	25.11	49.73	—	—
VIII	−10.5	—	49.86	26.85	24.39	26.85	49.86	—
IX	−9.6	—	51.79	28.60	28.07	28.07	28.60	51.79
X	−10.4	—	48.90	56.09	—	56.09	48.90	46.53
XI	−3.4	151.11	128.30	129.00	125.27	129.00	128.30	—
XII	−7.6	136.63	129.31	128.08	127.25	128.08	129.31	52.65
Me_3Al·amine adducts								
XIII	−9.7	36.65	—	—	—	—	—	—
XIV	−8.2	41.12	12.24	—	—	—	—	—
XV	−8.2	49.61	20.81	11.13	—	—	—	—
XVI	−5.4	46.97	21.70	21.70	—	—	—	—
			21.29	21.29				
XVII	−8.2	47.61	29.53	20.20	13.69	—	—	—
XVIII	−8.3	57.14	25.77	19.88	19.88	—	—	—
XIX	−9.4	—	46.40	24.70	24.70	46.40	—	—
XX	−9.4	—	45.34	25.44	23.06	25.44	45.34	—
XXI	−9.1	—	46.92	26.35	28.53	28.53	26.35	46.92
XXII	−9.4	—	44.45	54.23	—	54.23	44.45	45.90
XXIV	−8.1	135.71	129.30	128.90	128.36	128.90	129.30	51.60

1469(vs), 1459(s), 1380(s), 1305(m), 1255(m), 1225(w), 1197(vs), 1178(s), 1140(s), 1113(s), 1067(vs), 1038(m), 1019(s), 953(vs), 877(s), 849(vs), 760(m), 747(s), 691(vs), 672(vs), 606(vs), 555(w).

$[Me_2AlNPr^i_2]_2$. 3024(m), 2996(s), 2968(vs), 2936(vs), 2926(vs), 2895(s), 1473(s), 1403(s), 1391(m), 1372(vs), 1305(w), 1198(s), 1174(m), 1162(s), 1134(s), 1127(s), 954(m), 915(m), 835(m), 765(s), 700(sh; s), 681(vs), 672(vs), 644(m), 578(w), 569(w), 442(w).

$[Me_2AlNBu^n_2]_2$. 2952(vs), 2931(vs), 2866(vs), 1378(s), 1372(vs), 1196(s), 1172(w), 1118(m), 1069(m), 1027(w), 904(w), 878(m), 730(sh; m), 693(vs), 670(sh; s), 610(m).

$[Me_2AlNBu^i_2]_2$. 2961(vs), 2871(vs), 1472(s), 1393(m), 1370(w), 1199(s), 978(m), 862(w), 830(w), 808(w), 690(vs), 666(m), 595(w).

$[Me_2AlNC_4H_8]_2$. 2969(vs), 2930(vs), 2875(s), 2825(w), 1464(vs), 1346(m), 1292(w), 1246(m), 1212(m), 1196(vs), 1103(w), 1053(s), 954(w), 916(vs), 849(w), 825(w), 724(br; s), 691(vs), 577(m), 504(w).

$[Me_2AlNC_5H_{10}]_2$. 2969(vs), 2937(vs), 2894(m), 2856(s), 2850(s), 1464(s), 1455(vs), 1448(s), 1377(s), 1356(w), 1347(w), 1356(m), 1308(s), 1280(m), 1199(vs), 1147(m), 1090(vs), 1047(vs), 1031(vs), 954(w), 881(vs), 856(s), 814(vs), 803(s), 688(br; vs), 648(s), 573(vs), 500(m), 487(m).

$[Me_2AlNC_6H_{12}]_2$. 3020(sh; w), 2964(vs), 2936(vs), 2847(vs), 2728(m), 2698(m), 2669(m), 1472(s), 1465(s), 1456(s), 1447(s), 1441(s), 1384(s), 1378(m), 1355(sh; w), 1269(w), 1197(vs), 1167(w), 1113(s), 1089(w), 1028(m), 1007(m), 989(w), 963(w), 843(s), 816(w), 745(s), 689(br; vs), 640(m), 598(m), 583(m).

$[Me_2AlNC_5H_{11}N]_2$. 2970(m), 2956(s), 2937(s), 2925(vs), 2894(s), 2856(m), 2794(s), 2744(m), 1461(s), 1454(s), 1445(s), 1366(s), 1317(s), 1292(vs), 1285(vs), 1194(vs), 1152(s), 1137(s), 1105(vs), 1089(s), 1060(m), 1055(m), 1047(m), 1000(s), 912(s), 887(sh; s), 875(sh; s), 775(m), 695(br; vs), 575(s), 500(m).

General reaction of $(Me_3Al)_2$ *with the aminoarsines*, Me_2AsR

In a typical reaction $(Me_3Al)_2$ (0.5 mmol) in C_6D_6 (2 cm^3) was added to a screw-top Wilmad NMR

Table 3. Aminoalane dimer and Me_3Al·adduct ^1H NMR data (ppm, TMS)

Compound	Me_2Al	NH	H(1)	H(2)	H(3)	H(4)	H(5)	H(6)	H(7)
Aminoalane dimers									
I[26]	−0.59	—	2.06	—	—	—	—	—	—
II[11,35]	−0.50	—	2.66	0.76	—	—	—	—	—
III	−0.42	—	2.69	1.30	0.71	—	—	—	—
IV	−0.27	—	3.63	1.19	1.19	—	—	—	—
V	−0.38	—	2.81	1.39	1.16	0.84	—	—	—
VI	−0.28	—	2.80	2.01	0.86	0.86	—	—	—
VII[37]	−0.57	—	—	2.61	1.32	1.32	2.61	—	—
VIII[10,37]	−0.48	—	—	2.59	1.26	1.26	1.26	2.59	—
IX	−0.44	—	—	2.83	1.43	1.33	1.33	1.43	2.83
X	−0.50	—	—	2.75	2.10	—	2.10	2.75	1.99
XI[11,38,40,41]	−0.26	—	—	7.24	6.91	6.80	6.91	7.24	—
XII[11]	−0.08	—	—	7.0	7.0	7.0	7.0	7.0	4.16
Me_3Al·amine adducts									
XIII	−0.59	0.67	1.51	—	—	—	—	—	—
XIV	−0.49	1.00	2.30	0.52	—	—	—	—	—
			2.02						
XV	−0.45	1.37	2.20	1.04	0.49	—	—	—	—
XVI	−0.36	1.42	2.87	0.788	0.788	—	—	—	—
				0.731	0.731				
XVII	−0.43	1.41	2.3	1.07	0.90	0.70	—	—	—
XVIII	−0.42	1.87	2.2	1.59	0.52	0.52	—	—	—
XIX	−0.52	1.42	—	2.17	0.92	0.92	2.17	—	—
XX[10]	−0.48	1.00	—	2.29	0.71	0.88	0.71	2.29	—
XXI	−0.46	1.31	—	2.40	0.93	0.93	0.93	0.93	2.40
XXII	−0.48	0.97	—	2.40	1.51	—	1.51	2.40	1.77
XXIV	−0.38	2.34	—	6.62	6.94	6.94	6.94	6.62	3.52

tube (10 mm, pyrex, with a PTFE insert) containing Me_2AsR (1 mmol) in C_6D_6 (1 cm^3) at room temperature. The reaction mixture composition was monitored by ^1H and ^{13}C NMR spectroscopy as a function of time. During storage, the tubes were wrapped in aluminum foil to minimize exposure of the reaction mixtures to light. The products formed and the time required for the completion of each reaction are listed in Table 6. Products were identified by comparing their chemical shifts with those of the authentic samples. Variable-temperature NMR studies were also carried out on $(Me_3Al)_2$ reactions with Me_2AsR (R = Me_2N, Ph_2N and Bzl_2N) using the previously described procedure.[6]

General synthesis of Me_3Al·HR

The secondary amine (10 mmol) was added to a 50 cm^3 reaction flask containing trimethylaluminum (10 mmol) at −76°C. The reaction mixture was slowly warmed to room temperature with stirring. At room temperature white solid adducts formed when R = Me_2N, C_4H_8N, $C_5H_{10}N$, $C_6H_{12}N$, $CH_3NC_4H_8N$ and Bzl_2N. The solid adducts were purified by sublimation at *ca* 50°C/10^{-5} torr Hg to give nearly quantitative yields of Me_3Al·HR, except in the case of R = $NC_4H_8NCH_3$ (70%). In the case of the liquid adducts (R = Et_2N, $Pr^n{}_2N$, $Pr^i{}_2N$, $Bu^n{}_2N$ and $Bu^i{}_2N$), further purification was not necessary. The physical, NMR spectral and analytical data for the adducts are given in Tables 1–5.

General procedure for the synthesis of $[Me_2AlR]_2$

The adduct Me_3Al·HR (5 mmol) was heated slowly (100–140°C) in a 50 cm^3 flask equipped with a reflux condensor and a nitrogen by-pass until gas evolution was observed. Heating was continued at that temperature until gas evolution ceased. After cooling to room temperature the resulting product was sublimed at 100–130°C/10^{-5} torr Hg to give white crystalline materials, $[Me_2AlR]_2$, in greater than 90% yield. However, $[Me_2AlN(Bzl)_2]_2$ could not be sublimed, because it decomposed when heated above 150°C. The unsublimed sample of $[Me_2AlN(Bzl)_2]_2$ was found to be analytically pure.

Table 4. ^1H and ^{13}C NMR data for $Me_2AlR \cdot AlMe_3$

R	H(1)	H(2)	H(3)	H(4)	H(5)	H(6)	H(7)
Et_2N	2.58	0.69	—	—	—	—	—
$Pr^n{}_2N$	2.55	1.18	0.65	—	—	—	—
$Pr^i{}_2N$	3.36	1.03	1.03	—	—	—	—
$Bu^n{}_2N$	2.66	1.27	1.10	0.80	—	—	—
$Bu^i{}_2N$	2.61	1.80	0.76	0.76	—	—	—
C_4H_8N	—	2.52	1.24	1.24	2.52	—	—
$C_5H_{10}N$	—	2.51	1.17	1.17	1.17	2.51	—
$C_6H_{12}N$	—	2.70	1.33	1.29	1.29	1.33	2.70
Bzl_2N	—	6.9	7.0	7.0	7.0	6.9	4.0
	C(1)	C(2)	C(3)	C(4)	C(5)	C(6)	C(7)
Et_2N	38.61	11.84	—	—	—	—	—
$Pr^n{}_2N$	47.57	20.53	11.48	—	—	—	—
$Pr^i{}_2N$	49.22	25.05	25.05	—	—	—	—
$Bu^n{}_2N$	45.56	29.43	20.79	14.07	—	—	—
$Bu^i{}_2N$	53.56	26.74	21.97	21.97	—	—	—
C_4H_8N	—	49.26	24.94	24.94	49.26	—	—
$C_5H_{10}N$	—	48.62	26.66	24.13	26.66	48.62	
$C_6H_{12}N$	—	50.90	28.85	27.31	27.31	28.85	50.90
Bzl_2N	136.22	128.94	128.30	127.40	128.30	128.94	50.84

The physical, NMR spectral and analytical data of the aminoalane dimers are listed in Tables 1–5. Since pure $[Me_2AlNPh_2]_2$ could not be obtained by this procedure, it was synthesized by the following alternate route.

Synthesis of $[Me_2AlNPh_2]_2$

To a solution of Ph_2NH (169 mg, 1 mmol) in C_6D_6 (2 cm^3) was added slowly Me_6Al_2 (72 mg, 0.5 mmol) in C_6D_6 (1 cm^3) at room temperature. Upon mixing, gas evolution occurred. The reaction mixture composition was monitored by ^1H and ^{13}C NMR spectroscopy as a function of time. Within 3 days, the NMR spectrum indicated the complete disappearance of the parent peaks. The solvent was removed under reduced pressure and the white, light-sensitive solid $[Me_2AlNPh_2]_2$ was obtained in quantitative yield. Physical, spectroscopic and analytical data are given in Tables 1–5.

Table 5. Elemental analysis of synthesized adducts and aminoalanes

Compound	C(%) Calc.	C(%) Found	H(%) Calc.	H(%) Found	N(%) Calc.	N(%) Found
Aminoalanes						
$[Me_2AlNPr^n{}_2]_2$	61.21	61.29	12.74	12.91	8.92	8.93
$[Me_2AlNPr^i{}_2]_2$	61.21	61.12	12.74	12.91	8.92	8.71
$[Me_2AlNBu^n{}_2]_2$	64.92	64.89	12.97	13.00	7.56	7.44
$[Me_2AlNBu^i{}_2]_2$	64.92	64.79	12.97	13.09	7.56	7.36
$[Me_2AlNC_6H_{12}]_2$	61.99	62.13	11.61	11.84	9.03	8.88
$[Me_2AlNC_5H_{11}N]_2$	53.81	53.65	10.91	10.91	17.92	17.94
Adducts						
$Me_3Al \cdot HNC_4H_8$	58.71	58.75	12.67	12.57	9.78	9.98
$Me_3Al \cdot HNC_6H_{12}$	63.12	63.10	12.86	12.99	8.19	8.00
$Me_3Al \cdot HNC_5H_{11}N$	55.78	55.56	12.29	12.39	16.25	16.35
$Me_2Al \cdot HNBzl_2$	75.79	75.57	8.98	8.82	5.19	5.38

Table 6. Summary of the reactions of Me_6Al_2 with aminoarsines

Aminoarsines	Species formed	Final products	Time for completion
Me_2AsNMe_2	$Me_2AsNMe_2 \cdot AlMe_3$ Me_3As, $[Me_2AlNMe_2]_2$	Me_3As $[Me_2AlNMe_2]_2$	1 week
Me_2AsNEt_2	$Me_2AsNEt_2 \cdot AlMe_3$ $Me_2AlNEt_2 \cdot AlMe_3$ Me_3As, $[Me_2AlNEt_2]_2$	Me_3As $[Me_2AlNEt_2]_2$	1 week
$Me_2AsNPr^n_2$	$Me_2AsNPr^n_2 \cdot AlMe_3$ $Me_2AlNPr^n_2 \cdot AlMe_3$ Me_3As, $[Me_2AlNPr^n_2]_2$	Me_3As $[Me_2AlNPr^n_2]_2$	2 weeks
$Me_2AsNPr^i_2$	$Me_2AsNPr^i_2 \cdot AlMe_3$ $Me_2AlNPr^i_2 \cdot AlMe_3$ $Me_3As \cdot AlMe_3$ Me_3As, $[Me_2AlNPr^i_2]_2$	Me_3As $[Me_2AlNPr^i_2]_2$	3 months
$Me_2AsNBu^n_2$	$Me_2AsNBu^n_2 \cdot AlMe_3$ $Me_2AlNBu^n_2 \cdot AlMe_3$ Me_3As, $[Me_2AlNBu^n_2]_2$	Me_3As $[Me_2AlNBu^n_2]_2$	2 weeks
$Me_2AsNBu^i_2$	$Me_2AsNBu^i_2 \cdot AlMe_3$ $Me_2AlNBu^i_2 \cdot AlMe_3$ $Me_3As \cdot AlMe_3$ Me_3As, $[Me_2AlNBu^i_2]_2$	Me_3As $[Me_2AlNBu^i_2]_2$	1 month
$Me_2AsNC_4H_8$	$Me_2AsNC_4H_8 \cdot AlMe_3$ $Me_2AlNC_4H_8 \cdot AlMe_3$ Me_3As, $[Me_2AlNC_4H_8]_2$	Me_3As $[Me_2AlNC_4H_8]_2$	6 months
$Me_2AsNC_5H_{10}$	$Me_2AsNC_5H_{10} \cdot AlMe_3$ $Me_2AlNC_5H_{10} \cdot AlMe_3$ Me_3As, $[Me_2AlNC_5H_{10}]_2$	Me_3As $[Me_2AlNC_5H_{10}]_2$	2 months
$Me_2AsNC_6H_{12}$	$Me_2AsNC_6H_{12} \cdot AlMe_3$ $Me_2AlNC_6H_{12} \cdot AlMe_3$ Me_3As $[Me_2AlNC_6H_{12}]_2$	Me_3As $[Me_2AlNC_6H_{12}]_2$	4 months
$Me_2AsNC_4H_8NMe$	Complex mixture		
Me_2AsNPh_2	$Me_3As \cdot Me_2AlNPh_2$ $Me_3As \cdot [Me_2AlNPh_2]_2$ Me_3As, $[Me_2AlNPh_2]_2$	$Me_3As \cdot Me_2AlNPh_2$	2 days
$Me_2AsNBzl_2$	$Me_2AsNBzl_2 \cdot AlMe_3$ $Me_2AlNBzl_2 \cdot AlMe_3$ $Me_3As \cdot AlMe_3$ Me_3As, $[Me_2AlNBzl_2]_2$	Me_3As $[Me_2AlNBzl_2]_2$	2 days

RESULTS AND DISCUSSION

Reactions of $(Me_3Al)_2$ *with aminoarsines*

The results obtained from the NMR study of the reactivity of trimethylaluminum with the various aminoarsines are summarized in Table 6. In the room temperature studies the Al—N bonded adducts, $Me_2AsR \cdot AlMe_3$, are initially observed, except for Me_2AsNPh_2 and $Me_2AsNBzl_2$. $Me_2AsNC_4H_8NMe$, the spectra imply the prese of additional, uncharacterized Al—N bon species. With time, the Al—N adducts decom to yield ultimately Me_3As and the respective am alane dimer $[Me_2AlR]_2$.

The reaction of $(Me_3Al)_2$ with Me_2AsN yields initially $Me_2AsNMe_2 \cdot AlMe_3$, which converts to Me_3As and $[Me_2AlNMe_2]_2$, wit

week. Initially $(Me_3Al)_2$ reacts with Me_2AsNEt_2 to form $Me_2AsNEt_2 \cdot AlMe_3$. However, within 1 day we note the formation of a small amount of $Me_2AlNEt_2 \cdot AlMe_3$, with an accompanying shift in the NMR spectrum of the As—N—Al adduct peaks toward those of the parent aminoarsine. The analogous $Me_2AlNR'_2 \cdot AlMe_3$ species have been reported, where R′ = Me,[42], Ph[43] or Me_3Si.[44] In the Me case the adduct is not isolable at room temperature.[42] As discussed below, we have independently synthesized and determined the NMR chemical shift values of the $Me_2AlR \cdot AlMe_3$ adducts, where R = Et_2N, $Pr^n{}_2N$, $Pr^i{}_2N$, $Bu^n{}_2N$, $Bu^i{}_2N$, C_4H_8N, $C_5H_{10}N$, $C_6H_{12}N$ and Bzl_2N. $Me_2AlNEt_2 \cdot AlMe_2$ possibly results from the competition of Me_2AlNEt_2 for the $AlMe_3$ bound in $Me_2AsNEt_2 \cdot AlMe_3$. The resulting parent Me_2AsNEt_2 is then exchanged with $Me_2AsNEt_2 \cdot AlMe_3$. With $Me_2AsNPr^n{}_2$ and $Me_2AsNBu^n{}_2$ there is incomplete initial As—N—Al adduct formation. Line-width broadening of adduct peaks in the ^1H spectrum suggests adduct/parent aminoarsine exchange. As $Me_2AlR \cdot AlMe_3$ forms the line width narrows and the resonances shift towards those of the parent aminoarsine. Aminoalane dimer forms as peaks associated with $Me_2AlR \cdot AlMe_3$ and $Me_2AsR \cdot AlMe_3$ decrease in intensity. Complete conversion to products and consumption of reactants takes *ca* 2 weeks. When $Me_2AsNPr^i{}_2$ and $Me_2AsNBu^i{}_2$ are mixed with $(Me_3Al)_2$, not only are the $AlMe_3$ adducts of the parent aminoarsines and the aminoalanes formed and observed to be in exchange, but an exchange averaged adduct, $Me_3As \cdot AlMe_3$, is also observed. Thus, with the more sterically demanding Bu^i and Pr^i moieties, Me_3As is effective in competing for $AlMe_3$. Now the conversion to final products takes approximately 1 and 3 months, respectively.

In the case of the cyclic amine substituents As—N—Al adducts are formed, except with $Me_2AsNC_4H_8NMe$. The nature of the cyclic amine substituent influences adduct stability. With $Me_2AsNC_4H_8$ the As—N—Al adduct slowly converts, over 6 months, to Me_3As and the aminoalane dimer. This is accompanied by the formation of a small amount of $Me_2AlNC_4H_8 \cdot AlMe_3$. For $Me_2AsNC_6H_{12}$, a slow conversion (4 months) to Me_3As and the respective aminoalane dimer also occurs. In this case the NMR spectra indicate that a slightly greater amount of $Me_2AlNC_6H_{12} \cdot AlMe_3$ forms, which is in exchange with $Me_2AsNC_6H_{12} \cdot AlMe_3$. In the case of $Me_2AsNC_5H_{10}$, the As—N—Al adduct converts to Me_3As and the aminoalane dimer over a 2 month period. A significant amount of $Me_2AlNC_5H_{10} \cdot AlMe_3$ is observed prior to dimer formation.

The reaction of $(Me_3Al)_2$ with $Me_2AsNBzl_2$ at room temperature gives a mixture of $Me_3Al \cdot Me_2AlNBzl_2$, $Me_3Al \cdot AsMe_3$, Me_3As and unreacted $Me_2AsNBzl_2$. Chemical shift data and line-width broadening indicate exchange involving $Me_3Al \cdot AsMe_3$ and Me_3As and an $Me_3Al \cdot Me_2AsNBzl_2$ adduct and $Me_2AsNBzl_2$. Upon standing for 1 day, the reaction is almost complete with the final products being $[Me_2AlNBzl_2]_2$ and Me_3As.

In order to further investigate the reaction of $(Me_3Al)_2$ with the aminoarsines, a variable-temperature, multinuclear NMR study was carried out on the 1 : 1 $Me_3Al/Me_2AsNBzl_2$ system. At −80°C, NMR resonances are observed that can be assigned to both $Me_2AsNBzl_2$ and $Me_3Al \cdot Me_2AsNBzl_2$ in slow exchange. With increasing temperature rapid exchange averaging occurs up to 0°C without any observed decomposition reaction. The sample was recooled to −80°C and the reversibility of the exchange process was established. Upon standing at 0°C, decomposition occurred to yield peaks assignable to $Me_3Al \cdot AsMe_3$ and $Me_3Al \cdot Me_2AlNBzl_2$. With increasing temperature further reaction occurs; chemical shift data and line-width broadening indicate subsequent exchange involving $Me_3Al \cdot AsMe_3$ and Me_3As, and there is additional formation of $Me_3Al \cdot Me_2AlNBzl_2$. With time at room temperature decomposition proceeds, $[Me_2AlNBzl_2]_2$ forms and the amount of free Me_3As increases.

These results suggest that the nature of the amino substituent impacts the relative importance of various exchange reactions that involve the As—N—Al bonded adduct, aminoalane monomer, aminoalane · $AlMe_3$ adduct, $Me_3As \cdot AlMe_3$ and Me_3As. These influence the time required for complete conversion to Me_3As and $[Me_2AlNR]_2$.

Thus, the following reactions can occur in these Me_3Al/Me_2AsR reaction systems:

$$Me_2AsR + 1/2(Me_3Al)_2 \rightleftharpoons Me_2AsR \cdot AlMe_3 \quad (1)$$

$$Me_2AsR + 1/2(Me_3Al)_2 \rightleftharpoons Me_2AsR \cdot AlMe_3 \longrightarrow Me_3As + Me_2AlR \quad (2)$$

$$Me_2AlR + 1/2(Me_3Al)_2 \rightleftharpoons Me_2AlR \cdot AlMe_3 \quad (3)$$

$$Me_2AlR + Me_2AsR \cdot AlMe_3 \rightleftharpoons Me_2AlR \cdot AlMe_3 + Me_2AsR \quad (4)$$

$$Me_3As + 1/2(Me_3Al)_2 \rightleftharpoons Me_3As \cdot AlMe_3 \quad (5)$$

$$Me_3As \cdot AlMe_3 + Me_2AsR \longrightarrow Me_3As + Me_2AsR \cdot AlMe_3 \quad (6)$$

$$Me_3As \cdot AlMe_3 + Me_2AlR \longrightarrow Me_3As + Me_2AlR \cdot AlMe_3 \quad (7)$$

$$Me_2AlR \longrightarrow 1/2[Me_2AlR]_2. \quad (8)$$

The nature of the substituent on the N of the amino moiety influences the relative importance of certain reactions in solution. Increasing bulkiness favours incomplete formation of $Me_2AsR \cdot AlMe_3$ and its involvement in exchange in solution [eqs (1) and (4)], decreased stability of $Me_2AsR \cdot AlMe_3$ [eq. (2)], stabilization of Me_2AlR through adduct formation and exchange [eqs (3), (4) and (7)], formation of $Me_3As \cdot AlMe_3$ and its involvement in exchange in solution [eqs (5), (6) and (7)] and slower formation of final reaction products, Me_3As and $[Me_2AlR]_2$ [eqs (2) and (8)]. On the basis of our study, we cannot distinguish whether conversion of $Me_2AsR \cdot AlMe_3$ to Me_3As and $[Me_2AlR]_2$ arises by decomposition of $Me_2AsR \cdot AlMe_3$ or through dissociation to the original reactants and then subsequent effective recombination that proceeds to a concerted formation of products.[45,46]

In contrast, $(Me_3Al)_2$ reacts with Me_2AsNPh_2 at room temperature to give a mixture of Me_3As, $Me_3As \cdot Me_2AlNPh_2$, $Me_3As \cdot [Me_2AlNPh_2]_2$ and $[Me_2AlNPh_2]_2$. There is no evidence for the formation of an Al—N bonded adduct of Me_2AsNPh_2. Upon standing, the reaction proceeds to give predominantly $Me_3As \cdot Me_2AlNPh_2$. Because these results suggested that Me_3As reacts with $[Me_2AlNPh_2]_2$ to yield $Me_3As \cdot Me_2AlNPh_2$, the independent reactions of Me_3As with $[Me_2AlNPh_2]_2$ in 1:1 and 2:1 stoichiometries were performed. In the 1:1 case reaction occurred upon mixing to give a mixture of $Me_3As \cdot Me_2AlNPh_2$, $Me_3As \cdot [Me_2AlNPh_2]_2$ and $[Me_2AlNPh_2]_2$. With a 2:1 stoichiometry, all the $[Me_2AlNPh_2]_2$ was consumed.

Because the $(Me_3Al)_2/Me_2AsNPh_2$ reaction system gave unique results in comparison with the other aminoarsine systems, a variable-temperature (−90–25°C) NMR study was conducted on the reaction of $(Me_3Al)_2$ with Me_2AsNPh_2 in a 1:1 Al:N mole ratio. At low temperature the NMR data indicate the formation of an Al—As adduct, $Me_3Al \cdot Me_2AsNPh_2$, which is in exchange with $(Me_3Al)_2$ and Me_2AsNPh_2. At −80°C a decomposition reaction leads to the formation of $Me_3As \cdot AlMe_3$ and $Me_2AlNPh_2 \cdot AlMe_3$. With increasing temperature the Al—As adduct dissociates and further reaction occurs (−50°C) to yield $Me_3As \cdot AlMe_3$ and $[Me_2AlNPh_2]_2$. By −40°C all the original adduct has disappeared. With increasing temperature more $Me_3As \cdot AlMe_3$ and $[Me_2AlNPh_2]_2$ are formed and the presence of $Me_3As \cdot Me_2AlNPh_2$ and $Me_3As \cdot [Me_2AlNPh_2]_2$ are noted as the original reactants are consumed. At 25°C the results are analogous to those obtained from the room temperature study.

A comparison of the ^{13}C NMR chemical shift values for the parent aminoarsine, Me_2AsR, and its Me_3Al adduct (Table 7) gives insight into the steric interactions that influence adduct stability. The underscored entries in Table 7 highlight the greatest changes in chemical shifts that occur upon adduct formation. ^{13}C NMR chemical shifts are known to be very sensitive to steric effects and have been used to study conformational equilibria in the coordination of borane with nitrogen heterocycles.[47] When Me_3Al adducts to the C_4H_8N derivative there is a large change in the C(2)/C(5) ^{13}C chemical shift, which indicates that the five-membered ring is

Table 7. Differences in ^{13}C NMR chemical shifts—$\delta(Me_2AsR \cdot AlMe_3) - \delta(Me_2AsR)$[30]

R	Me_2As	C(1)	C(2)	C(3)	C(4)	C(5)	C(6)	C(7)
Me_2N	0.50	−1.02	—	—	—	—	—	—
Et_2N	−0.51	0.72	−4.06	—	—	—	—	—
$Pr^n{}_2N$	−0.58	0.58	−3.66	0.03	—	—	—	—
$Pr^i{}_2N$	−1.63	−0.71	−0.40	−0.40	—	—	—	—
$Bu^n{}_2N$	−0.48	0.95	−4.38	0.41	−0.38	—	—	—
$Bu^i{}_2N$	−1.57	−0.34	−0.19	0.17	0.17	—	—	—
C_4H_8N	2.07	—	2.12	0.44	0.44	2.12	—	—
$C_5H_{10}N$	1.82	—	−0.99	−4.87	−1.90	−4.87	−0.99	—
$C_6H_{12}N$	1.04	—	−0.21	−3.19	−1.33	−1.33	−3.19	−0.21
$NC_5H_{11}N$	0.07	—	−6.02	−3.18	—	−3.18	−6.02	−6.37

sufficiently flexible to minimize steric repulsions and this enhances adduct stability. In contrast with the $C_5H_{10}N$ and $C_6H_{12}N$ derivatives large ^{13}C chemical shift changes occur at the C(3) position. This is indicative of strong 1,3-diaxial interactions[47] between the Me_3Al group upon binding to the nitrogen and the proton at C(3), which adversely affect adduct stability. This is consistent with the classic studies of Brown *et al.* on the binding of Me_3B with C_4H_8NH and $C_5H_{10}NH$[48] and our results on the times required for the conversion of the Me_3Al adducts of Me_2AsR (R = C_4H_8N, $C_5H_{10}N$ and $C_6H_{12}N$) to Me_3As and the respective aminoalane.

Steric effects, as evidenced by the ^{13}C chemical shift data, are also observed in the alkyl amino derivatives. Significant changes in the C(2) ^{13}C chemical shifts are noted for the Et, Pr^n and Bu^n derivatives upon adduct formation, but are not observed for the Pr^i and Bu^i derivatives. With the latter, the adduct formation is incomplete and the Me_3As that is produced effectively competes for the unbound Me_3Al in the reaction mixture.

Reaction of $(Me_3Al)_2$ *with secondary amines*

The reactions of $(Me_3Al)_2$ with the secondary amines in a 1 : 1 Al : N mole ratio give quantitative yields of the respective Al—N adducts, $Me_3Al \cdot HR$, which were isolated and characterized except in the $HNPh_2$ case. The Et_2N—, $Pr^n{}_2N$—, $Pr^i{}_2N$—, $Bu^n{}_2N$— and $Bu^i{}_2N$— derivatives were isolated as liquids and the others as white crystalline solids. Since $Me_3Al \cdot HNPh_2$ readily decomposes at room temperature, only the dimer $[Me_2AlNPh_2]_2$ was isolated from the reaction. Although **XIII**,[8,34] **XIV**[34] and **XX**[10] have been previously synthesized, their characterization is reported in this paper.

Thermolysis of the $Me_3Al \cdot$ amine adducts gives excellent yields of the white crystalline aminoalane dimers, $[Me_2AlR]_2$, which were purified by sublimation. Although the previously reported[9,38] preparation of $[Me_2AlNPh_2]_2$ involved heating a mixture of $(Me_3Al)_2$ and $HNPh_2$, we observed that this also gives side products. On the other hand, the simple room-temperature decomposition of $Me_3Al \cdot HNPh_2$ affords the pure dimer. All the $Me_3Al \cdot$ amine adducts and the aminoalane dimers were characterized by IR, MS and NMR (^1H, ^{13}C and ^{27}Al) spectroscopy.

The IR spectra of the adducts, $Me_3Al \cdot HR$, show an intense band in the NH region, 3080–3290 cm^{-1} (see Table 1), which is *ca* 30–180 cm^{-1} less than the values observed in the free amines. This band is absent from the spectra of the product aminoalanes. The mass spectra of the adducts usually exhibit a high intensity peak at $[M-15]^+$, with molecular ion peaks also being observed for **XIV** and **XVI**. The mass spectra of the aminoalanes typically give low intensity $[M]^+$ and fairly intense $[M-15]^+$ peaks. This is consistent with the known dimeric nature of **I**,[8,11] **II**,[11,35] **IV**,[36] **VII**,[37] **VIII**,[10] **XI**[8,11,38] and **XII**[11] and previously reported mass spectral data.[10,26,37,49] The ^{27}Al NMR data are consistent for a tetra-coordinate aluminum bound to a nitrogen[50] in both the adducts and the aminoalanes. The $\delta(^{27}Al)$ values for the aminoalanes are generally 3–9 ppm upfield of those for the parent adducts. The benzyl derivatives are an exception to this trend, where the parent adduct $\delta(^{27}Al)$ value is 7 ppm upfield of that for the aminoalane. Although **XV**, **XVI**, **XVII** and **XVIII** could not be distilled, the IR, MS and NMR data support the conclusion that these are molecular adducts and not 1 : 1 stoichiometric mixtures of Me_3Al and the amine. Compounds **XIII** and **XIV** are known to be molecular adducts from thermodynamic studies.[34]

The reactions of $(Me_3Al)_2$ with the secondary amines in a 3 : 1 Al : N mole ratio were carried out for the purpose of synthesizing the $Me_2AlR \cdot AlMe_3$ adducts, which were observed as reaction intermediates in the Me_3Al/Me_2AsR systems. The NMR data (Table 4) of these adducts were identical with those observed in the various reaction systems. Attempts to isolate and purify the adducts were unsuccessful because removal of excess Me_3Al causes concomitant Al—N dimer formation. These results are consistent with those previously reported for $Me_2AlNPh_2 \cdot AlMe_3$.[40]

REFERENCES

1. M. Cesari and S. Cucinella, in *The Chemistry of Inorganic Homo- and Heterocycles* (Edited by I. Haiduc and D. B. Sowerby), Vol. 1, p. 167. Academic Press, London (1987).
2. M. F. Lappert, P. P. Power, A. R. Sanger and R. C. Srivastava, *Metal and Metalloid Amides*. Ellis Horwood/Wiley, New York (1980).
3. J. J. Eisch, in *Comprehensive Organometallic Chemistry* (Edited by G. Wilkinson, F. G. A. Stone and E. W. Abel), Vol. 1, p. 555. Pergamon Press, Oxford (1982).
4. T. Mole and E. A. Jeffery, *Organoaluminum Compounds*. Elsevier, Amsterdam (1972).
5. G. E. Coates, M. L. H. Green and K. Wade, *Organometallic Compounds*, 3rd edn, Vol. 1. Methuen, London (1967).
6. L. K. Krannich, C. L. Watkins and D. K. Srivastava, *Polyhedron* 1990, **9**, 289.
7. A. McKillop, J. D. Smith and I. J. Worrall, *Organometallic Compounds of Aluminum, Gallium, Indium, and Thallium*. Chapman and Hall, London (1985).

8. N. Davison and H. C. Brown, *J. Am. Chem. Soc.* 1942, **64**, 316.
9. G. E. Coates and J. Graham, *J. Chem. Soc.* 1963, 233.
10. B. Sen and G. L. White, *J. Inorg. Nucl. Chem.* 1973, **35**, 2207.
11. J. D. Bernstein, The Chemistry of Amine Lewis Base Complexes of Dimethylalane, PhD Dissertation, State University of New York at Buffalo, NY (1975).
12. G. H. Robinson and S. A. Sangokoya, *J. Am. Chem. Soc.* 1987, **109**, 6852.
13. G. H. Robinson, S. A. Sangokoya, F. Moise and W. T. Pennington, *Organometallics* 1988, **7**, 1887.
14. G. H. Robinson, F. Moise, W. T. Pennington and S. A. Sangokoya, *J. Cryst. Spectrosc. Res.* 1988, **18**, 387.
15. G. H. Robinson, F. Moise, W. T. Pennington and S. A. Sangokoya, *Polyhedron* 1989, **8**, 1279.
16. F. Moise, W. T. Pennington and G. H. Robinson, *J. Coord. Chem.* 1991, **24**, 93.
17. G. H. Robinson, A. D. Rae, C. F. Campana and S. K. Byram, *Organometallics* 1987, **6**, 1227.
18. G. H. Robinson, H. Zhang and J. L. Atwood, *J. Organomet. Chem.* 1987, **331**, 153.
19. G. H. Robinson, E. S. Appel, S. A. Sangokoya, H. Zhang and J. L. Atwood, *J. Coord. Chem.* 1988, **17**, 373.
20. G. H. Robinson, M. F. Self, S. A. Sangokoya and W. T. Pennington, *J. Am. Chem. Soc.* 1989, **111**, 1520.
21. D. F. Clemens, W. S. Brey and H. H. Sisler, *Inorg. Chem.* 1963, **2**, 1251.
22. R. P. Nielsen and H. H. Sisler, *J. Chem. Soc.* 1962, 3818.
23. D. F. Clemens, H. H. Sisler and W. S. Brey Jr, *Inorg. Chem.* 1966, **5**, 527.
24. P. B. Hitchcock, H. A. Jasim, M. F. Lappert and H. D. Williams, *J. Chem. Soc., Chem. Commun.* 1986, 1634.
25. C. J. Thomas, L. K. Krannich and C. L. Watkins, *Synth. React. Inorg. Met.-Org. Chem.* 1992, **22**, 461.
26. C. J. Thomas, L. K. Krannich and C. L. Watkins, *Polyhedron* 1993, **12**, 89.
27. S. F. Spangenberg and H. H. Sisler, *Inorg. Chem.* 1969, **8**, 1004.
28. D. F. Clemens, R. B. Smith and J. G. Dickinson, *Can. J. Chem.* 1973, **51**, 3187.
29. H. Schmidbaur, S. Lauteschläger and B. Milewski-Mahrla, *Chem. Ber.* 1983, **116**, 1403.
30. K. Modritzer, *Chem. Ber.* 1959, **92**, 2637.
31. W. Steinkopf and W. Meig, *Chem. Ber.* 1920, **53B**, 1013.
32. C. J. Thomas, L. K. Krannich and C. L. Watkins, *Synth. React. Inorg. Met.-Org. Chem.* 1991, **21**, 427.
33. S. L. Patt and J. Shoolery, *J. Magnet. Reson.* 1982, **46**, 535.
34. C. H. Henrickson, D. Duffy and D. P. Eyman, *Inorg. Chem.* 1968, **7**, 1047.
35. N. Koide, K. Iimura and M. Takeda, *J. Polym. Sci., Polym. Chem. Edn* 1973, **11**, 3161.
36. D. C. Bradley, M. M. Faktor, D. M. Frigo and K. V. Young, *Chemtronics* 1988, **3**, 50.
37. A. Storr and B. S. Thomas, *J. Chem. Soc. A* 1971, 3850.
38. M. Kawai, T. Ogawa and K. Hirota, *Bull. Chem. Soc. Japan* 1964, **37**, 1302.
39. L. Cocco and D. P. Eyman, *J. Organomet. Chem.* 1979, **179**, 1.
40. J. E. Rie and J. P. Oliver, *J. Organomet. Chem.* 1974, **80**, 219.
41. J. E. Rie and J. P. Oliver, *J. Organomet. Chem.* 1977, **133**, 147.
42. E. P. Schram, R. E. Hall and J. D. Glore, *J. Am. Chem. Soc.* 1969, **91**, 6643.
43. V. R. Magnuson and G. D. Stucky, *J. Am. Chem. Soc.* 1968, **90**, 3269.
44. M. Veith, *Adv. Organomet. Chem.* 1990, **31**, 269.
45. O. T. Beachley Jr, *Inorg. Chem.* 1981, **20**, 2825.
46. O. T. Beachley Jr and C. Tessier-Youngs, *Inorg. Chem.* 1979, **18**, 3188.
47. A. Flores-Parra, N. Farfán, A. I. Hernandez-Bautista, L. Ferńandez-Sánchez and R. Contreras, *Tetrahedron* 1991, **47**, 6903.
48. H. C. Brown and M. Gerstein, *J. Am. Chem. Soc.* 1950, **72**, 2926.
49. K. Gosling, J. D. Smith and D. H. W. Wharmby, *J. Chem. Soc. A* 1969, 1738.
50. R. Benn and A. Rufińska, *Angew. Chem., Int. Edn Engl.* 1986, **25**, 861.

Polyhedron Vol. 12, No. 4, pp. 401–405, 1993
Printed in Great Britain

0277–5387/93 $6.00+.00
© 1993 Pergamon Press Ltd

THEORETICAL STUDY OF THE INFLUENCE OF THE HALIDE LIGANDS ON THE METAL–METAL QUADRUPLE BOND IN THE $M_2X_4(PH_3)_4$ (M = Mo, W; X = Br, Cl, I) SERIES OF COMPLEXES

MARIA C. MILLETTI

Department of Chemistry, Eastern Michigan University, Ypsilanti, MI 48197, U.S.A.

(*Received* 23 *March* 1992; *accepted* 5 *October* 1992)

Abstract—The relationship between the metal–metal bond length and the nature of the halide ligands in complexes of the type $M_2X_4(PH_3)_4$ (M = Mo, W; X = Br, Cl, I) is investigated using the Fenske–Hall semi-empirical molecular orbital method. The relative positions of the molecular orbitals follow the pattern predicted by electronic spectral data, with the ^{1}(delta → delta*), HOMO–LUMO transition and the higher-energy LMCT transition both red-shifting as the halide ligand changes from chlorine to bromine to iodine. This pattern is present for both the molybdenum and the tungsten complexes. Although halide ligand contributions to the metal–metal valence molecular orbitals are significant and are a strong function of ligand identity, this does not seem to influence the metal–metal bond length. This would suggest that changes in the bond order brought about by changes in the identity of the halide ligands are not large enough to cause a significant variation in the metal–metal bond length.

The largest known group of compounds containing quadruple bonds are those formed by molybdenum. Among these are a category of molybdenum neutral complexes of the type $M_2X_4L_4$, containing both halide and uncharged sigma-donor ligands.[1] As for other transition-metal complexes containing M—M quadruple bonds, the delta overlap between metal centres is the focus of widespread experimental efforts to elucidate the electronic characteristics of the interaction between the two metals. Although bond order cannot always be used to faithfully predict M—M bond lengths, partially because bond orders are not objectively measurable, in general an increase in the amount of delta overlap between metal centres is expected to result in a shortening of the M—M bond length. Even though the actual extent of orbital overlap is also not directly measurable, often the energy of the ^{1}(delta → delta*) transition is taken as an indicator of the strength of the delta bond. In fact, several works have shown a nearly linear relationship between the metal–metal bond distance and the energy of the ^{1}(delta → delta*) band in several limited series of complexes.[2]

At this time, compounds of the type $M_2X_4(PMe_3)_4$ (M = Mo, W; X = Cl, Br, I) have been investigated through electronic, vibrational and photoelectron spectroscopy, in conjunction with X-ray crystallography, in order to enhance the understanding of the molecular and electronic structure of quadruply bonded complexes.[3] The results for the $Mo_2X_4(PMe_3)_4$ series indicate that although the metal–metal distances of these species appear to be independent of the nature of the X ligand, the electronic absorption spectra show that the ^{1}(delta → delta*) transition does have a marked sensitivity to the nature of the X ligand.[3a] In fact, previous SCF-Xalpha-SW calculations confirm that the metal-localized delta- and pi-bonding levels possess non-negligible halogen orbital character.[4] The question arises, therefore, of why the close similarity of the metal–metal bonding suggested by the crystal structures of the complexes is not reflected in the energies and intensities of their ^{1}(delta → delta*) transitions. This work analyses the bonding in the series of compounds $Mo_2X_4(PH_3)_4$ and $W_2X_4(PH_3)_4$ via molecular orbital calculations and suggests an answer to the above question.

COMPUTATIONAL PROCEDURE

Calculations have been carried out using the Fenske–Hall semi-empirical method[5] on a VAX

mainframe computer. Atomic basis functions were employed; for phosphorus, chlorine, bromine and iodine Clementi's double-zeta functions were used,[6] except for 1*s* and 2*s* functions, which were curve-fit to single-zeta using the maximum overlap criterion.[7] For bromine and iodine, *d*-basis set functions were employed. The hydrogen exponent was set to 1.16. The molybdenum functions were developed by the method of Bursten *et al.*,[8] in which Slater functions are fitted to the numeric functions generated by Xalpha methods for atomic orbitals. The tungsten functions were taken from the results of Richardson *et al.*[9] The 5*s* and 5*p* exponents for molybdenum were set to 1.85 and the 6*s* and 6*p* exponents for tungsten were set to 1.852 to avoid working with metal outer functions that are too diffuse, which often leads to meaningless results.

The geometry used for $Mo_2Cl_4(PH_3)_4$ and $W_2Cl_4(PH_3)_4$ was taken from the X-ray structures determined by Cotton *et al.*;[2b] the X-ray structures for $Mo_2Br_4(PMe_3)_4$ and $Mo_2I_4(PMe_3)_4$ were determined by Gray *et al.*[3a] The geometry of the remaining tungsten compounds was extrapolated from that of the corresponding molybdenum complexes. For simplicity of interpretation and greater ease in the calculations, the trimethylphosphine groups present in each of the complexes have been substituted with phosphine groups. The P—H distance was set to 1.350 Å.[4]

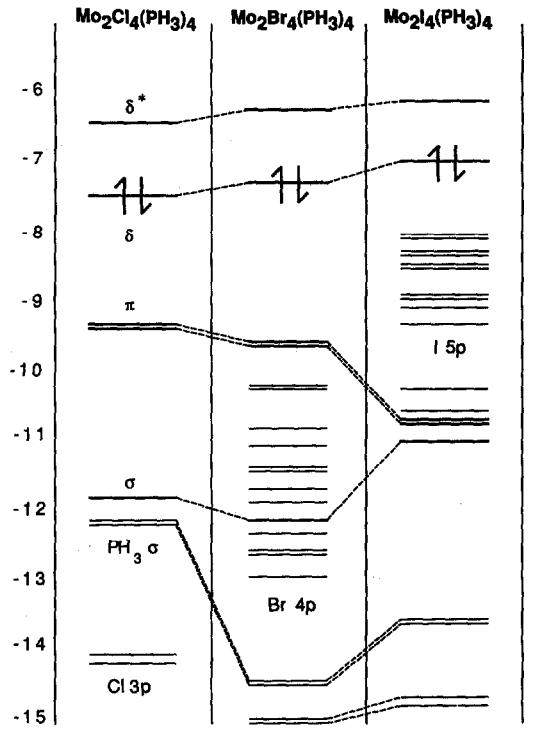

Fig. 1. Comparison molecular orbital diagram for $Mo_2Cl_4(PH_3)_4$, $Mo_2Br_4(PH_3)_4$ and $Mo_2I_4(PH_3)_4$.

RESULTS AND DISCUSSION

The analysis of the bonding in the series of $M_2X_4(PH_3)_4$ compounds will start from an examination of each species' molecular orbital diagram and its relationship with the electronic spectrum. Subsequently, trends in energy and composition of each complex's molecular orbitals will be used to explain the influence of the identity of the halide ligand on metal–metal distance.

Figure 1 shows a comparison molecular orbital diagram of the molecules $Mo_2Cl_4(PH_3)_4$, $Mo_2Br_4(PH_3)_4$ and $Mo_2I_4(PH_3)_4$. In all cases, the HOMO–LUMO transition, which corresponds to the lowest energy band of the electronic spectrum, is clearly a delta → delta* transition. Also, the energetic pattern of orbitals representing M—M bonds remains the same for all three molecules, namely sigma, pi and delta in order of increasing energy. On the other hand, as the halide ligands change from chlorine (more electronegative) to iodine (less electronegative), the halogen *p*-orbitals rise in energy and contribute heavily first to the band of orbitals between the sigma and pi M—M orbitals (for bromine) and eventually to the band above the pi M—M orbitals (in the case of iodine). Consequently, while in the case of $Mo_2Cl_4(PMe_3)_4$ and $Mo_2Br_4(PMe_3)_4$ the second electronic transition is primarily a ^{1}(pi → delta*) transition, for $Mo_2I_4(PH_3)_4$ it acquires a large LMCT character.

In the past there has been some disagreement as to whether the phosphine sigma orbitals fall between the pi and delta M—M orbitals[4] or whether they are lower in energy than any of the metal orbitals.[10] The present Fenske–Hall calculations show that the sigma orbitals of the phosphine ligands lie at a lower energy than either the M—M bonding orbitals or the halide *p*-orbitals in all of the systems under consideration, and therefore do not participate in the first several electronic transitions. This is confirmed by photoelectron data on $W_2Cl_4(PMe_3)_4$.[11]

Figure 2 shows a comparison molecular orbital diagram, similar to that of Fig. 1, for molecules $W_2Cl_4(PH_3)_4$, $W_2Br_4(PH_3)_4$ and $W_2I_4(PH_3)_4$. The observed pattern is the same as that shown in Fig. 1, with the delta and delta* M—M orbitals being the HOMO and the LUMO, respectively, followed by the two degenerate pi orbitals and the sigma orbital at lower energies. Again, as the halide ligand changes from chlorine to bromine to iodine the halogen *p*-orbitals rise in energy as the electro-

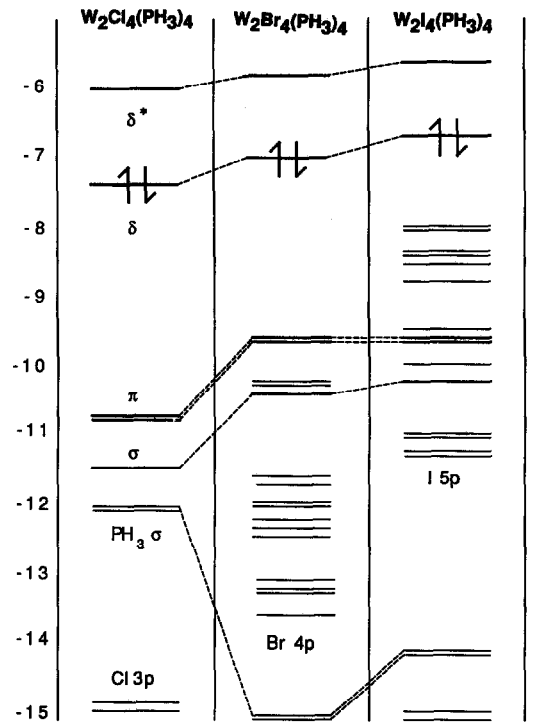

Fig. 2. Comparison molecular orbital diagram for $W_2Cl_4(PH_3)_4$, $W_2Br_4(PH_3)_4$ and $W_2I_4(PH_3)_4$.

negativity of the atom decreases. This causes some bromine 4*p*-symmetry-combination orbitals to appear between the sigma and pi M—M orbitals and most of the iodine 5*p*-orbitals to become the levels below the HOMO in $Mo_2I_4(PH_3)_4$. It should also be noted that for $Mo_2Br_4(PH_3)_4$ and $Mo_2I_4(PH_3)_4$, the rise of the outer *p*-halide orbitals causes a certain degree of scattering of the metal sigma and pi character among sets of two or three molecular orbitals. The orbitals indicated in Fig. 2 as sigma and pi for $Mo_2Br_4(PH_3)_4$ and $Mo_2I_4(PH_3)_4$ are in fact those carrying the larger metal contribution. Minor metal–metal sigma and pi contributions also appear in a few other molecular orbitals.

By comparing the energy patterns observed in Figs 1 and 2 it can be concluded that as the halide ligand changes from chlorine to bromine to iodine, there is a gradual decrease both in the HOMO–LUMO gap and in the separation between the set of molecular orbitals below the HOMO (either the M—M pi set or the halide *p*-band, depending on the complex) and the LUMO. This pattern is consistent with experimental observations that show the low-energy band of the electronic spectra for these compounds red-shifting as the halide ligands change from chlorine to iodine.[3a] On the other hand, in going from molybdenum to tungsten, the energy separation between these levels in the MO diagram is observed to increase. This trend can most clearly be seen in Fig. 3, where complexes with identical ligands but different metal centres are compared. However, electronic spectra show that while a blue shift in band I (the HOMO to LUMO transition)

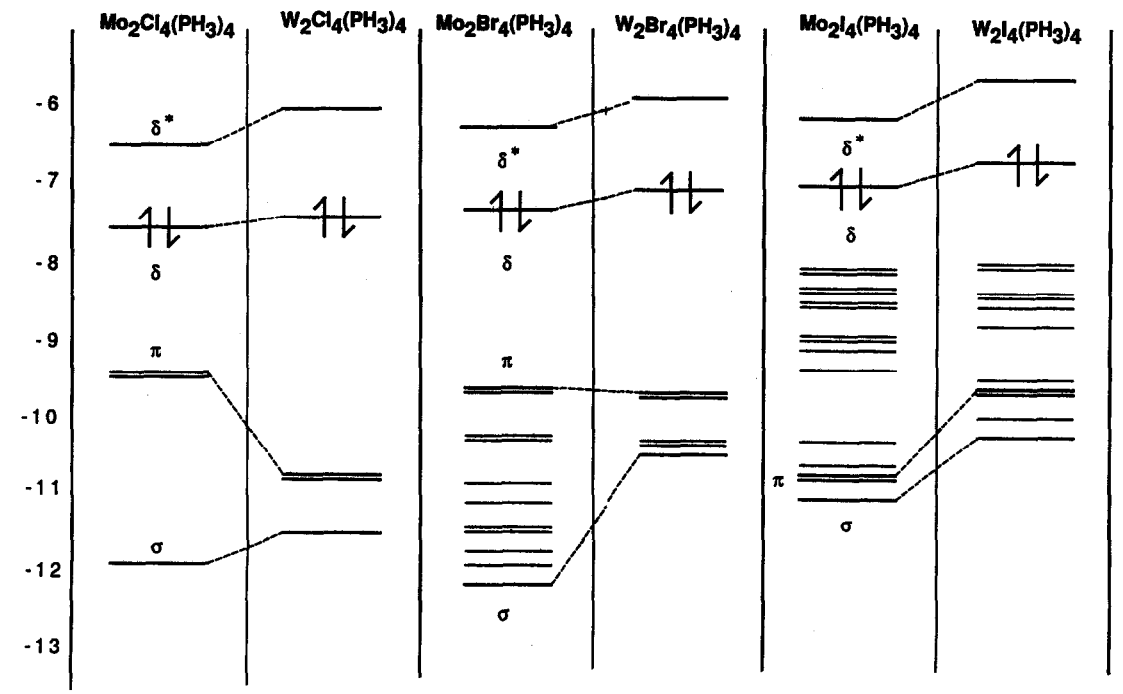

Fig. 3. Comparison of valence molecular orbitals for molecules with the same set of ligands but different metal centres.

Table 1. Metal and halide contributions to M—M bonds

	$Mo_2Cl_4(PH_3)_4$		$Mo_2Br_4(PH_3)_4$		$Mo_2I_4(PH_3)_4$	
	%M	%X	%M	%X	%M	%X
Delta*	75	11	69	17	60	26
Delta	78	14	70	22	53	40
Pi	83	11	59	31	54	40
Sigma	90	6	56	35	79	7
	$W_2Cl_4(PH_3)_4$		$W_2Br_4(PH_3)_4$		$W_2I_4(PH_3)_4$	
	%M	%X	%M	%X	%M	%X
Delta*	62	18	56	26	46	37
Delta	65	23	56	34	40	53
Pi	67	21	41	50	24	50
Sigma	71	5	48	23	58	27

is observed on replacing tungsten by molybdenum complexes, the same comparison reveals a red shift for band II.[3a]

Now that the general energy and composition patterns for the molecular orbitals of interest have been examined, we turn to the question of the influence of the halide ligands on the metal–metal bond. Previous theoretical calculations on $M_2L_4X_4$ compounds suggest that the halide *p*-orbitals contribute significantly to the M—M bonding orbitals in the molecule.[4] This would imply that changing the identity of the halide ligand should have an impact on the strength and length of the quadruple bond between the metal centres for the molecules under consideration. Indeed, the calculations performed in this work also confirm that the valence M—M orbitals contain a significant percentage of X ligand character (see Table 1). More specifically, the amount of contribution to the metal–metal bonds from the halogen *p*-orbitals seems to increase as X = Cl → Br → I. The current calculations show that the nature of the halide ligands also influences the amount of overlap between metal centres. More specifically, the metal–metal overlap decreases as the halide ligand changes and the contribution from the ligand to the M—M orbitals increases. This is true for both molybdenum and tungsten complexes. Table 2 shows that the total amount of overlap between metal centres decreases in going from chlorine to bromine to iodine, by an amount between 2% and 5% each time. This would suggest that the metal–metal quadruple bond is weakened by halide ligands with low electronegativity (such as I), the *p*-orbitals of which heavily mix in with the metal orbitals.

However, these observations are not consistent with the fact that the metal–metal bond distance does not change significantly throughout the halide series, at least for the molybdenum metal.[3a] On closer scrutiny of Table 2 one notices that the amount of change in the sigma overlap is very small, except for the $W_2I_4(PH_3)_4$ molecule, in which it increases significantly. This would suggest that the length of the metal–metal bond is mainly a function of the sigma overlap in the molecule. In fact, both molecular orbital calculations[10] and experimental results[3,4] indicate that the sigma portion of the overlap between the two metal centres is of little importance to the strength of the bond. Alternatively, the lack of change in the metal–metal bond lengths might suggest that the changes in the bond order brought about by changes in the halide ligands are not large enough to cause a significant variation in the bond length. This is supported by the fact that bond lengths for several cation complexes show that quadruple bonds are not substantially shorter than triple bonds.[10a]

Table 2. Mulliken overlap populations between metal centres

	Sigma	Pi	Delta	Total
$Mo_2Cl_4(PH_3)_4$	0.162	0.480	0.088	0.730
$Mo_2Br_4(PH_3)_4$	0.161	0.474	0.082	0.717
$Mo_2I_4(PH_3)_4$	0.163	0.454	0.071	0.688
$W_2Cl_4(PH_3)_4$	0.143	0.472	0.097	0.712
$W_2Br_4(PH_3)_4$	0.142	0.468	0.088	0.698
$W_2I_4(PH_3)_4$	0.204	0.408	0.076	0.688

CONCLUSIONS

The results of the calculations confirm the accepted description of metal–metal bonding in

quadruply bonded tungsten and molybdenum complexes[1] and follow the electronic spectral band assignments.[3a] The metal–metal bonding molecular orbitals appear to have significant halide contributions, which also affect the amount of pi and delta metal–metal overlap. Crystal structure data, however, indicate that these changes in electron distribution have essentially no influence on the M—M bond length.

REFERENCES

1. F. A. Cotton and R. A. Walton, *Multiple Bonds Between Metal Atoms*. John Wiley, New York (1982).
2. (a) A. P. Sattelberger and J. P. Fackler, *J. Am. Chem. Soc.* 1977, **99**, 1258; (b) F. A. Cotton, M. W. Extine, T. R. Felthouse, B. W. S. Kolthammer and D. G. Lay, *J. Am. Chem. Soc.* 1981, **103**, 4040; (c) R. J. H. Clark and N. R. D'Urso, *J. Am. Chem. Soc.* 1975, **97**, 2691; (d) D. M. Collins, F. A. Cotton, S. Koch, M. Millar and C. A. Murillo, *J. Am. Chem. Soc.* 1977, **99**, 1259; (e) F. A. Cotton, S. Koch, K. Mertis, M. Millar and G. Wilkinson, *J. Am. Chem. Soc.* 1977, **99**, 4989; (f) W. H. Bohmer, K. Madeja, E. Kurras and U. Rosenthal, *Z. Chem.* 1978, **18**, 453; (g) F. A. Cotton, G. N. Mott, R. R. Schrock and L. G. Sturgeoff, *J. Am. Chem. Soc.* 1982, **104**, 6781; (h) P. E. Fanwick, B. E. Bursten and G. B. Kaufmann, *Inorg. Chem.* 1985, **24**, 1165.
3. (a) M. D. Hopkins, W. P. Schaefer, M. J. Bronikowski, W. H. Woodruff, V. M. Miskowski, R. F. Dallinger and H. B. Gray, *J. Am. Chem. Soc.* 1987, **109**, 408; (b) M. D. Hopkins, V. M. Miskowski and H. B. Gray, *J. Am. Chem. Soc.* 1988, **110**, 1787.
4. F. A. Cotton, J. L. Hubbard, D. L. Lichtenberger and I. Shim, *J. Am. Chem. Soc.* 1982, **104**, 679.
5. M. B. Hall and R. F. Fenske, *Inorg. Chem.* 1972, **11**, 768.
6. E. Clementi, *J. Chem. Phys.* 1964, **40**, 1944.
7. D. D. Radtke, PhD Thesis, University of Wisconsin, Madison, WI (1966).
8. B. E. Bursten, J. R. Jensen and R. F. Fenske, *J. Chem. Phys.* 1987, **68**, 2320.
9. J. W. Richardson, W. C. Niewpoort, R. R. Powell and W. F. Edgell, *J. Chem. Phys.* 1962, **36**, 1057.
10. (a) T. Ziegler, *J. Am. Chem. Soc.* 1984, **106**, 5901; (b) T. Zeigler, *J. Am. Chem. Soc.* 1985, **107**, 4453.
11. D. R. Root, C. H. Blevins, D. L. Lichtenberger, A. P. Sattelberger and R. A. Walton, *J. Am. Chem. Soc.* 1986, **108**, 953.

Polyhedron Vol. 12, No. 4, pp. 407–414, 1993
Printed in Great Britain

0277–5387/93 $6.00+.00
Pergamon Press Ltd

DEOXYGENATION OF OXOVANADIUM(IV) COMPLEXES UNDER MILD CONDITIONS: CONVERSION OF VANADYL SPECIES TO THE CORRESPONDING DIHALIDES WITH CARBOXYLIC ACID HALIDES

JOHN G. REYNOLDS* and EDWARD L. JONES

Lawrence Livermore National Laboratory, University of California, Livermore, CA 94550, U.S.A.

and

JOHN C. HUFFMAN and GEORGE CHRISTOU*

Department of Chemistry and Molecular Structure Center, Indiana University, Bloomington, IN 47405, U.S.A.

(*Received* 5 *June* 1992; *accepted* 5 *October* 1992)

Abstract—A new procedure for the deoxygenation of VO^{2+} complexes utilizing carboxylic acid halides in toluene or methylene chloride has been successfully applied to several vanadyl complexes with different ligand types. Facile conversion of vanadyl β-diketonates, dialkyldithiocarbamates, β-ketiiminates, 8-quinolinolate and porphyrin complexes to the corresponding dihalide complexes has been achieved, demonstrating the general application of the synthetic method. The β-diketonate complexes were studied in the greatest detail. $VX_2(Y)_2$ (X = Cl, Br; Y = $CH_3COCHCOCH_3$, $CH_3COCHCOC_6H_5$) were synthesized in high yield, and the single-crystal X-ray structure of $VCl_2(CH_3COCHCOCH_3)_2$ was obtained. The structure contains a mononuclear unit with *trans*-chloride ligands and distorted octahedral symmetry. The complexes were examined by IR; the spectra exhibited the characteristic loss of the V=O band at approximately 1000 cm^{-1}. For $VX_2(CH_3COCHCOCH_3)_2$ the ligand bands indicate more delocalization of charge onto the ligands compared with the vanadyl starting material, which is consistent with the *trans* octahedral geometry of $VCl_2(CH_3COCHCOCH_3)_2$ and its co-planar chelate ligands. The UV–vis spectra show a weak maximum around 600–700 nm with ε_m of approximately 2000 dm^3 mol cm^{-1}, typical of dihalogenated complexes.

Recently we reported a new, more convenient method of synthesizing V^{IV} dihalide complexes involving the reactions of vanadyl starting materials with acetyl halides.[1] Vanadyl dialkyldithiocarbamates were shown to readily convert to the corresponding dihalide compounds in high yield. For example, vanadyl diethyldithiocarbamate reacts with 3.0 equivalents of acetyl chloride or acetyl bromide to produce dichloro-bis(diethyldithiocarbamate)vanadium(IV) (**1**) or dibromo-bis(diethyldithiocarbamate)vanadium(IV) (**2**), respectively. Single X-ray examination of these complexes shows the halides to be *cis*, consistent with spectroscopic properties that indicate less ligand–metal interactions due to distortions out of the ligand bonding plane. Although the synthetic method works well with dithiocarbamates, we have felt it important to explore application of the procedure to $VO(acac)_2$ ($acac^- = CH_3COCHCOCH_3^-$) and related species for two reasons: (1) $VO(acac)_2$ is an excellent starting material (cheap and air stable); and (2) even though $VCl_2(acac)_2$ has been known for many years, controversy surrounds the precise arrangement of the chlorine atoms because no single-crystal X-ray

* Authors to whom correspondence should be addressed.

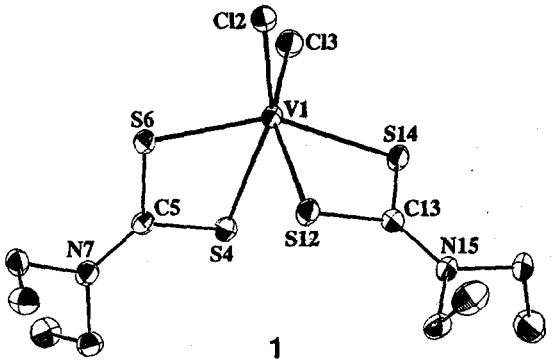

1

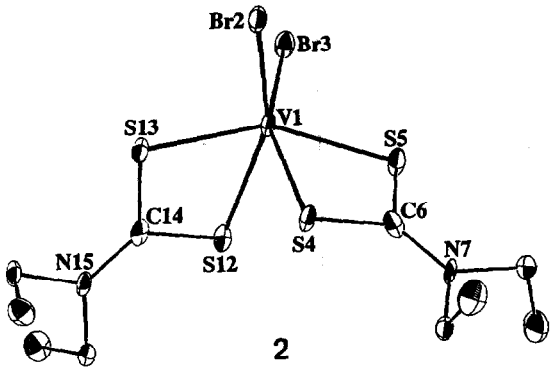

2

examination has been reported; spectroscopic studies on dihalide β-diketonates have suggested both *trans* and *cis* arrangements.[2-5]

In this report, we describe the extension of the deoyxgenation reaction of acetyl halides to a broader group of vanadyl complexes, generalizing the utility of the method. In addition we report the single-crystal X-ray analysis of $VCl_2(acac)_2$, the only structurally characterized dichloro V^{IV} β-diketonate complex. The structure is very similar to that of VCl_2(salen-N-Bu^t)$_2$ in possessing *trans*-chlorine atoms.[6,7]

EXPERIMENTAL

All syntheses were carried out in a dry/inert atmosphere of purified dinitrogen employing standard Schlenk glassware. Air-sensitive samples for spectroscopic study were prepared in a dinitrogen glove-bag or Vacuum Atmospheres glove-box. IR spectra were recorded as KBr pellets with the Mattson Polaris Model 10410 spectrophotometer. Far-IR spectra were recorded on a Perkin–Elmer Model 283 spectrophotometer. Electronic spectra were recorded in CH_2Cl_2 solutions using a Varian Model 503 spectrophotometer and Spectrochem quartz anaerobic cells. Because the dihalide complexes readily convert back to the corresponding vanadyl complexes upon exposure to even trace quantities of water, excess acetyl chloride (AcCl) or acetyl bromide (AcBr) was added to the solutions. Elemental analyses were performed by Galbraith Laboratories, Inc., Knoxville, TN.

Reagents

Spectroanalytical grade methylene chloride (0.006% water), toluene and hexanes were obtained from Burdick and Jackson Laboratories. Methylene chloride and toluene were dried using CaH_2 (Aldrich Chemical Co.) and the hexanes were dried using $LiAlH_4$ (Aldrich Chemical Co.). All solvents were dried under dinitrogen and degassed before use. AcCl, AcBr and benzoyl chloride (BzCl) were purchased from Aldrich Chemical Co. The AcBr was distilled before use and the AcCl and BzCl were used as purchased.

Synthesis of the complexes

The vanadyl complexes $VO(acac)_2$ [acac = acetylacetonate] and VO(TPP) (TPP = 5,10,15,20-tetraphenyl-porphine) were obtained from Aldrich Chemical Co.; VO(PTC) (PTC = phthalocyanine) and $VOOH(8HQ)_2$ (8HQ = 8-hydroxyquinolinate) were obtained from Pfaltz & Bauer Chemicals, Inc.; $VO(bzac)_2$ (bzac = 1-phenyl-1,3-butanedionate) was obtained from Eastman Kodak Co.; $VO(S_2CNMe_2)_2$ (S_2CNMe_2 = dimethyldithiocarbamate), $VO(S_2CNEt_2)_2$ (S_2CNEt_2 = diethyldithiocarbamate) and $VO(S_2CNPy)_2$ (S_2CNPy = pyrrolidinedithiocarbamate) were prepared by the method of McCormick[8] and recrystallized from methylene chloride; $VO(edt)_2(PPh_4)_2$ (edt = ethanedithiolate) was prepared by the method of Wiggins *et al.*;[9] VO(bzen) (bzen = bisbenzoylacetoneethylenediiminate) and VO(acen) (acen = bisacetylacetoneethylenediiminate) were prepared by the method of Boucher *et al.*;[10] $VO(quin)_2$ (quin = 2-methyl-8-quinolinolate) was prepared by the method of Stoklosa *et al.*[11]

Dichlorobis(acetylacetonato)vanadium(IV), $VCl_2(acac)_2$. $VO(acac)_2$ (6.00 g, 0.0226 mol) was dissolved in toluene (200 cm^3) to give a dark green solution. The solution was degassed and AcCl (4.8 cm^3, 0.068 mol) was added while stirring. The green solution slowly turned dark blue. The reaction mixture was stirred at room temperature overnight, then layered with hexanes (125 cm^3) and placed in a freezer. Storage at -10°C for 3 days led to the formation of purple–black crystals. The crystals were filtered and dried *in vacuo*. The yield of crude product was 85% based on vanadium. Recrystallization from a CH_2Cl_2/hexanes mixture (layered) led to a

pure material as determined by IR, UV–vis and elemental analysis. The preparation was also performed by heating the reaction mixture for 3 h at approximately 100°C, followed by the above crystallizing procedure. Found: C, 37.4; H, 4.6; V, 15.9%. Calc. for $C_{10}H_{14}O_4Cl_2V$: C, 37.5; H, 4.4; V, 15.9%. Mol. wt = 320.07. Electronic absorption maxima, λ(nm) (ε_m, dm^{-3} mol^{-1} cm^{-1}): 628.9 (1849), 396.0sh (2179), 348.0sh (3942).

$VCl_2(acac)_2$ was also prepared by reacting $VO(acac)_2$ (6.00 g, 0.0226 mol) with BzCl (7.9 cm^3, 0.068 mol) in a manner similar to the above procedure. The crude product yield was 60% with respect to vanadium.

The other V^{IV} dihalogen complexes were prepared by the method above described for $VCl_2(acac)_2$, utilizing either AcCl or AcBr with the corresponding vanadyl starting material. The products were identified by comparisons with spectroscopic data found in the literature. For $VBr_2(acac)_2$ [λ (nm), (ε_m, dm^{-3} mol^{-1} cm^{-1})]: 715.8 (1799), 468.0sh (1689); $VCl_2(bzac)_2$: 638.3 (2183), 384.4sh (6541); $VBr_2(bzac)_2$: 706.4 (2243), 627.0sh (1990), 395.0sh (5626). The products were isolated and recrystallized using the same solvents and procedures as above. Crude yields, with respect to vanadium, were 75, 81 and 65%, respectively.

X-ray crystallography and structure solution

Data were collected on a Picker four-circle diffractometer using standard low-temperature facilities. Details of the diffractometry, low-temperature facilities and computational procedures employed by the Molecular Structure Center are available elsewhere.[12] Data collection parameters are summarized in Table 1 for $VCl_2(acac)_2$. The structures were solved by a combination of MULTAN and Fourier techniques, and refined by full-matrix least-squares.

For $VCl_2(acac)_2$ a systematic search of a limited hemisphere of reciprocal space located a set of diffraction maxima with symmetry and systematic absences indicating the unique space group $P2_1/c$. Subsequent solution and refinement of the structure confirmed this choice. A total of 1870 reflections were collected. Following the usual data processing, 1739 unique reflections remained. Of the 1739 reflections, 884 were considered observed [$F > 2.33\sigma(F)$]. All non-hydrogen atoms were readily located and refined with anisotropic thermal parameters. A difference Fourier synthesis revealed the location of some, but not all, hydrogen atoms. All hydrogen atom positions were therefore calculated using ideal geometries and d(C—H) = 0.95 Å, and the hydrogen atoms were included as fixed contributors in the final refinement cycles. The final difference map was essentially featureless, with the largest peak being 1.24 e $Å^{-3}$ at the vanadium site.

Table 1. Crystallographic data for *trans*-$VCl_2(acac)_2$

Space group	$P2_1/c$
a (Å)	7.964(5)
b (Å)	12.454(8)
c (Å)	13.341(9)
β (°)	93.80(4)
Z	4
V ($Å^3$)	1320.35
Formula	$V_{10}H_{14}O_4Cl_2$
M_r (g mol^{-1})	320.07
ρ_{calc} (g cm^{-3})	1.610
μ (cm^{-1})	11.339
T (°C)	−155
λ (Å)	0.71069
Range	$6° \leqslant 2\theta \leqslant 45°$
Observed data	884
$R(R_w)$ (%)	8.45(8.69)
Crystal dimensions (mm)	$0.35 \times 0.15 \times 0.20$
Colour of crystal	Brown

RESULTS AND DISCUSSION

Synthesis

Vanadyl complexes can be deoxygenated by a variety of reagents ($SOCl_2$, $SOBr_2$, PCl_5, $SeOCl_2$ and $COCl_2$)[3,7,13,14] to yield the corresponding dihalide derivatives. These reagents, however, are caustic and often react with the ligands. In addition, some dihalide complexes can be made by the direct reaction of VCl_4 (which is difficult to handle) with the ligand,[5] and by less direct methods including via thiuram disulphide intermediates.[15] We have now discovered carboxylic acid halides can also be used to synthesize V^{IV} dihalide complexes. The cheap and relatively easy-to-handle RX reagents (X = Cl, Br; R = CH_3CO, $C_6H_5CH_2CO$) directly afford the dihalide complexes, overcoming potential side-reactions of the other reagents. As a result we have recently reported the synthesis of, directly from the corresponding vanadyl complexes, $VCl_2(S_2CNMe_2)_2$, $VCl_2(S_2CNEt_2)_2$, $VBr_2(S_2CNEt_2)_2$ and $VCl_2(S_2CNPy)_2$ by eq. (1). Previous attempts in the literature to synthesize such compounds using the other halogenating agents mentioned above often led to poorly characterized, impure products, probably due to the halogenating agent reacting with the ligand.

Although we have reported the characterization of the dihalodithiocarbamates, our original development of carboxylic acid halides as vanadyl deoxy-

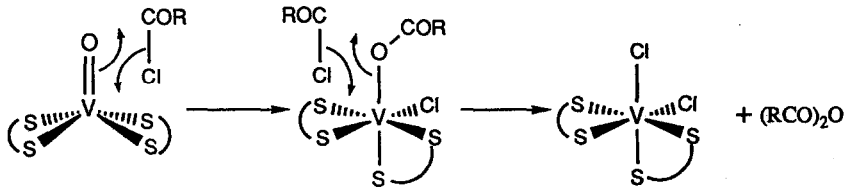

Scheme 1.

genation reagents was with the vanadyl β-diketonates. $VCl_2(acac)_2$, $VBr_2(acac)_2$, $VCl_2(bzac)_2$ and $VBr_2(bzac)_2$ can all be successfully prepared by eq. (1). The procedure yields very clean products, which has made single-crystal growth facile. All the complexes are relatively easily isolated and may be purified by recrystallization from CH_2Cl_2/hexanes (layered). As a result, a single-crystal X-ray analysis of $VCl_2(acac)_2$ has been performed to unequivocally establish the geometry around the metal.

$$VO(L)_2 + 2RX \longrightarrow VX_2(L)_2 + R_2O \qquad (1)$$

(X = Cl, Br; R = CH_3CO, $C_6H_5CH_2CO$)

An excess (50%) of RX has been routinely employed after observation of incomplete conversion with stoichiometric amounts of reagents (probably due to hydrolysis by adventitious water) in preliminary experiments.

Although we have not experimentally verified the mechanism of the reaction, it probably involves electrophilic attack by the carboxylic acid halide at the VO^{2+} oxygen atom to lead to a bound acetate group that can then undergo attack by a second acid halide molecule (Scheme 1). This sequence would suggest a *cis* isomer might result, as found in the dithio carbamate complexes, but it is likely that *cis*/*trans* isomerization will be rapid, allowing for the formation of the observed *trans* isomer for the β-diketonate complexes. The extreme rapidity of the reaction and the paramagnetic nature of the V^{IV} species have precluded attempts to probe this point further by normal spectroscopic methods.

To explore the scope of the deoxygenation reaction further, several other representative vanadium(IV) complexes and one vanadium(V) species were mixed with AcCl, AcBr or BzCl in CH_2Cl_2. (We assume the reactivity displayed when only AcCl was used will extend to other carboxylic acid halides.) Table 2 summarizes the results. The identification of products was either by full analysis, including X-ray crystallography, or in some cases,

Table 2. Summary of products from the reaction of vanadyl complexes with carboxylic acid halides in CH_2Cl_2

Vanadium starting complex	Acid halide	Vanadium product	Evidence	Purified yield (%)[a]
$VO(S_2CNEt_2)_2$	AcCl	$VCl_2(S_2CNEt_2)_2$	X-ray, IR, UV–vis	41
$VO(S_2CNEt_2)_2$	AcBr	$VBr_2(S_2CNEt_2)_2$	X-ray, IR, UV–vis	42
$VO(S_2CNEt_2)_2$	BzCl	$VCl_2(S_2CNEt_2)_2$	IR, UV–vis	39
$VO(S_2CNMe_2)_2$	AcCl	$VCl_2(S_2CNMe_2)_2$	IR, UV–vis	33
$VO(S_2CNPy)_2$	AcCl	$VCl_2(S_2CNPy)_2$	IR, UV–vis	34
$VO(acac)_2$	AcCl	$VCl_2(acac)_2$	X-ray, IR, UV–vis	56
$VO(acac)_2$	AcBr	$VBr_2(acac)_2$	IR, UV–vis	50
$VO(bzac)_2$	AcCl	$VCl_2(bzac)_2$	IR, UV–vis	54
$VO(bzac)_2$	AcBr	$VBr_2(bzac)_2$	IR, UV–vis	42
$VO(edt)_2^{2-}$	AcCl	$VOCl_4^-$	X-ray, IR	[b]
VO(PTC)	AcCl	No reaction	Insoluble	[c]
VOOH(8HQ)	AcCl	Partial reaction	IR	[d]
VO(acen)	AcCl	VCl_2(acen)	IR	[d]
VO(bzen)	AcCl	VCl_2(bzen)	IR	[d]
$VO(quin)_2$	AcCl	$VCl_2(quin)_2$	IR	[d]
VO(TPP)	AcCl	VCl_2(TPP)	UV–vis	[d]

[a] Per cent yield based on moles of vanadium in starting material.
[b] Not measured.
[c] Does not apply.
[d] Reactions performed on spectroscopic scale for identification only.

by diagnostic spectroscopic changes. As can be seen in Table 2, the reaction by eq. (1) is able to efficiently convert several different types of vanadyl compounds to the corresponding dihalide complexes. The vanadyl β-diketonate, dialkyldithiocarbamate, β-ketiiminate, 8-quinolinate and tetrapyrrole complexes demonstrate the utility of the reaction. However, VO(PTC) did not exhibit any reactivity, probably due to its low solubility (higher temperatures were not used); $VOOH(8HQ)_2$ appeared to only partially react as evidenced by IR; $VO(edt)_2^{2-}$ was extremely reactive, producing $VOCl_4^-$. In the sequence of the latter reaction a dark blue intermediate was formed, which could possibly be the dihalide product.[16] This intermediate was so short-lived that it could not be isolated by standard techniques. Further attempts to isolate this material are in progress.

Description of structure

Figure 1 shows the structure of *trans*-$VCl_2(acac)_2$ with the atom numbering scheme. Selected structural parameters are collected in Table 3. The crystal is composed of discrete molecules of $VCl_2(acac)_2$ with the expected octahedral coordination around the vanadium. The molecule has virtual C_{2v} symmetry with the chlorine atoms *trans* to the equatorial plane formed by the oxygen atoms of the acetylacetonate groups. A very similar coordination and geometry is observed in VCl_2(salen-N-Bu^t)$_2$, the only other reported[6] example of a structurally characterized V^{IV} dihalide with *trans* chlorine atoms. In that case the equatorial plane is formed by

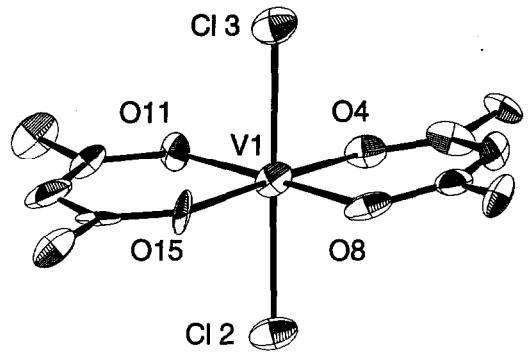

Fig. 1. ORTEP drawing of *trans*-$VCl_2(acac)_2$ showing the appropriate atom numbering scheme.

two nitrogen and two oxygen atoms. Several studies (EPR and IR) have suggested the existence of both *trans* and *cis* isomers is possible and the geometrical preference seems to be based on the polarity of the solvent medium.[2-5] Whereas the *cis* configuration is predicted in polar solvents, we have isolated the *trans* isomer from CH_2Cl_2.

Table 3 shows the V—Cl bond lengths to be essentially the same. Comparing to other reported dichloride structures, the average V—Cl bond length is longer than those reported for *cis*-$VCl_2(S_2CNEt_2)_2$ (2.25 and 2.26 Å) and is consistent with the argument of a more efficient delocalization of charge onto the chelate ligands in *trans*-type structures.[3] The V—Cl bond lengths of $VCl_2(acac)_2$, however, are slightly shorter than those reported for VCl_2(salen-N-Bu^t)$_2$ (2.35 Å),[6] probably an effect of the different ligand types. The ligand type[17-19] and substituents on the ligand[20] have been shown

Table 3. Selected bond distances (Å) and bond angles (°) for *trans*-$VCl_2(acac)_2$

V(1)—Cl(2)	2.326(7)	O(15)—C(14)	1.299(25)
V(1)—Cl(3)	2.307(7)	C(6)—C(7)	1.35(3)
V(1)—O(4)	1.904(15)	C(5)—C(6)	1.41(3)
V(1)—O(8)	1.906(15)	C(5)—C(9)	1.45(3)
V(1)—O(11)	1.916(14)	C(7)—C(10)	1.50(3)
V(1)—O(15)	1.904(14)	C(12)—C(13)	1.44(3)
O(4)—C(5)	1.303(24)	C(12)—C(16)	1.497(26)
O(8)—C(7)	1.281(27)	C(13)—C(14)	1.36(3)
O(11)—C(12)	1.242(25)	C(14)—C(17)	1.453(27)

Cl(2)—V(1)—Cl(3)	179.1(3)	O(4)—V(1)—O(8)	87.1(7)
Cl(2)—V(1)—O(4)	91.8(5)	O(4)—V(1)—O(11)	92.0(6)
Cl(2)—V(1)—O(8)	88.3(4)	O(4)—V(1)—O(15)	177.2(7)
Cl(2)—V(1)—O(11)	89.9(5)	O(8)—V(1)—O(11)	178.0(6)
Cl(2)—V(1)—O(15)	89.3(5)	O(8)—V(1)—O(15)	95.5(6)
Cl(3)—V(1)—O(4)	88.5(5)	O(11)—V(1)—O(15)	85.5(6)
Cl(3)—V(1)—O(8)	90.9(5)	V(1)—O(4)—C(5)	132.5(14)
Cl(3)—V(1)—O(11)	90.9(5)	V(1)—O(8)—C(7)	129.7(14)
Cl(3)—V(1)—O(15)	90.4(5)	V(1)—O(11)—C(12)	134.2(13)
		V(1)—O(15)—C(14)	134.5(12)

Table 4. Comparison of selected structural information for $VO(acac)_2$, *trans*-$VCl_2(acac)_2$ and $V(acac)_3^+$

Property	$VO(acac)_2$[17]	$VCl_2(acac)_2$	$V(acac)_3^+$[24]
V—O	1.97 Å	1.91 Å	1.91 Å
C—O	1.28 Å	1.28 Å	1.28 Å[a]
O—V—O[b]	87.2°	85.5°	85.8°

[a] Only average value reported.
[b] Internal ligand angle.

Table 5. IR data for selected vanadyl and vanadium(IV) β-diketonate complexes (cm^{-1})

Complex	ν(C—O)	ν(C—C)	ν(V=O)
$VO(acac)_2$	1558	1532	998
$VCl_2(acac)_2$	1529		
$VBr_2(acac)_2$	1529		
$VO(bzac)_2$	1588	1521	998
$VCl_2(bzac)_2$	1595	1522	
$VBr_2(bzac)_2$	1596	1539	

to affect the V=O bond distance in vanadyl complexes. Little structural comparison among V^{IV} dihalide complexes to establish this point can be made due to the paucity of comparable structures. However, $VCl_2(acac)_2$ has an O_4Cl_2 first coordination sphere, while VCl_2(salen-N-Bu^t)$_2$ has an $O_2N_2Cl_2$ coordination sphere. The average V—Cl bond length of *trans*-$VCl_2(acac)_2$ is also similar to the average V—Cl bond length in $VOCl_2(C_5H_{12}N_2O)_2$ (2.34 Å)[21] and $VOCl_2(C_4H_8O)_2H_2O$ (2.39 Å),[22] but is longer than that of $VOCl_2(NMe_3)_2$ (2.25 Å).[23] These former two vanadyl dichlorides have square-pyramidal geometry with chlorine atoms on opposite sides of the basal plane (roughly *trans* configuration). The latter vanadyl dichloride has a trigonal bipyramidal structure with the chlorine atoms adjacent to each other similar to the chlorine atoms in *cis*-$VCl_2(S_2CNEt_2)_2$.

The four V—O bonds of $VCl_2(acac)_2$ are essentially equivalent as well as the four C—O bonds, as expected. Since the single-crystal X-ray structure has also been performed on the vanadyl starting material,[17] an interesting comparison can be made to see what effects the chlorine atom substitution for the oxygen atom have on the $[V(acac)_2]^{2+}$ subunit structure. Table 4 lists the comparison for selected bond distances and angles. Also included are some structural features of $[V(acac)_3][SbCl_6]$, another non-vanadyl V^{IV} β-diketonate.[24] The dihalo complex is shown to be more planar as a result of substitution of the chlorine atoms. This is evident in the average V—O bond lengths of the dichloro complex as compared to the average V—O of the vanadyl starting material. The dichloro derivative also exhibits V—O bond lengths similar to $V(acac)_3^+$. However, this difference does not appear to extend past the first coordination sphere, because the average C—O bond lengths are the same for the three complexes.

IR spectra

Table 5 lists the most important and characteristic bands of the IR spectra of $VCl_2(acac)_2$, $VBr_2(acac)_2$, $VCl_2(bzac)_2$ and $VBr_2(bzac)_2$. Included are the same characteristic bands for the corresponding vanadyl starting material. For all the dihalide derivatives, as expected, the strong V=O band is absent, indicating the conversion to the dihalide. We used this method as our best indicator of completeness of reaction.

For $VCl_2(acac)_2$ and $VBr_2(acac)_2$ the principal ligand bands in the 1500–1550 cm^{-1} range combine to form one unresolved peak. This does not agree with the assignments of Behzadi and Thompson[14] for the same compounds. [X-ray powder pattern diffraction data of our preparation of $VCl_2(acac)_2$ were consistent with their reported values.] However, $[V(acac)_3][SbCl_6]$ exhibits only one unresolved peak for these ligand bands.[24] The position of this combined band for both $VCl_2(acac)_2$ and $VBr_2(acac)_2$ is lower in energy than either of those assigned in the vanadyl precursor. This is consistent with the ligand band position of other vanadium(IV) dihalide complexes that have or are considered to have *trans* geometry when compared to the corresponding vanadyl starting materials. In these cases on going from the vanadyl structure (where the metal is somewhat out of the basal plane) to the *trans* structure (where the metal is in the equatorial plane), the σ-bonding d_{xy} orbital is slightly destabilized and the π-bonding $d_{x^2-y^2}$ orbital is greatly destabilized due to increased orbital overlap. This overlap increases delocalization, effectively reducing the charge on the ligand and therefore shifts the position of the diagnostic ligand bands to lower energy.

For $VCl_2(bzac)_2$ and $VBr_2(bzac)_2$ the principal bands are resolved and are shifted to higher energy than the corresponding bands for the vanadyl starting materials. This is not consistent with the observation of Behzadi and Thompson[14] for $VCl_2(bzac)_2$, who reported much lower energies for the C—O and C—C bands. However, our assignments are consistent with their assignment of these bands for $VBr_2(bzac)_2$ and are very similar to assignments of these bands for other vanadium(IV)

complexes with bzac as a ligand [for example, V(cat)(bzac)$_2$,[25] [V(bzac)$_3$][SbCl$_6$][24] and V(dtbc)(bzac)$_2$[25]].

The shift of the ligand bands for the bzac cases when going from VO(bzac)$_2$ to the dihalide complexes is opposite to the shift of the corresponding bands in the acac cases discussed above and for the salen-N-Bu^t case. One expectation is that VCl$_2$(bzac)$_2$ and VBr$_2$(bzac)$_2$ might have *cis* geometry, based on the behaviour of the analogous dithiocarbamate complexes.[1] [The principal ligand bands of VCl$_2$(S$_2$CNEt$_2$)$_2$ and VBr$_2$(S$_2$CNEt$_2$)$_2$ are shifted to a higher frequency than the corresponding bands for VO(S$_2$CNEt$_2$)$_2$ and this has been accounted for by the *cis* geometry reducing delocalization from the ligand plane.] However, Von Dreele and Fay[5] determined the geometry of VCl$_2$(*t*-C$_4$H$_9$COCHCO-*t*-C$_4$H$_9$)$_2$ by examining the V—Cl bands in the far-IR. Their assignment of 362 cm^{-1} for the *trans* geometry matches ours of 359 cm^{-1} for VCl$_2$(bzac)$_2$ and 365 cm^{-1} for VCl$_2$(acac)$_2$. The expected position for the *cis* geometry would be around 385 cm^{-1}. This evidence indicates VCl$_2$(bzac)$_2$ and VBr$_2$(bzac)$_2$ also have *trans* geometry and that the shift to higher wave-numbers is probably due to electronic effects of the aromatic ring of the ligand.

CONCLUSIONS

The new and convenient synthetic method of converting vanadyl dialkyldithiocarbamate complexes to the corresponding vanadium(IV) dihalide complexes using carboxylic acid halides has been successfully applied to a wide variety of vanadyl systems. In general, as verified by spectroscopic methods, the reaction was found to work well with β-diketonates, β-ketiiminates, 8-quinolinolate and some tetrapyrroles, as well as dithiocarbamates. In specific, the reaction using VO(acac)$_2$ and AcCl produced a highly crystalline product which, when characterized by single-crystal X-ray analysis, showed the chlorides to be *trans* with respect to the bonding plane formed by the acac ligands. This geometry is similar to that of VCl$_2$(salen-N-Bu^t)$_2$, but contrary to the *cis* structures of VX$_2$(S$_2$CNEt$_2$)$_2$ (X = Cl, Br). Regardless of the structural differences of these products, the reaction using carboxylic acid halides appears to be a general method to produce dihalide derivatives from vanadyl complexes without the deleterious side-reactions seen for syntheses using some other, more well-known halogenating reagents.

Supplementary material. Complete listings of atomic coordinates, isotropic and anisotropic thermal parameters, bond distances and angles (20 pages); listings of observed and calculated structure factors for VCl$_2$(acac)$_2$ are available on request. Ordering information is given on any current masthead page. The complete MSC structure report (No. 89164) is available on request from the Indiana Chemistry Library.

Acknowledgements—Work at the Lawrence Livermore National Laboratory was performed under the auspices of the U.S. Department of Energy under contract number W-7405-ENG-48. Work at Indiana University was supported by the Office of Basic Energy Sciences, Division of Chemical Sciences, U.S. Department of Energy under Grant DE-FG02-87ER13702. We especially thank the Affirmative Action Equal Employment Opportunity Program at Lawrence Livermore National Laboratory for additional support. We also thank Ann M. Murray, Katherine E. Nelson and Melissa Chi-Lin Chu of Lawrence Livermore National Laboratory, Norman R. Dean of Indiana University and Thomas F. Finger of Chevron Research Company for experimental assistance.

REFERENCES

1. E. L. Jones, J. G. Reynolds, J. C. Huffman and G. Christou, *Polyhedron* 1991, **10**, 1817.
2. A. Jezierski and J. B. Raynor, *Inorg. Chim. Acta* 1980, **44**, L153.
3. A. Jezierski and J. B. Raynor, *J. Chem. Soc., Dalton Trans.* 1981, 1.
4. A. Jezierski, *Inorg. Chim. Acta* 1985, **98**, L1.
5. R. B. Von Dreele and R. C. Fay, *J. Am. Chem. Soc.* 1972, **94**, 7935.
6. M. Pasquali, F. Marchetti and C. Floriani, *Inorg. Chem.* 1979, **18**, 2401.
7. M. Pasquali, A. Torres-Filho and C. Floriani, *J. Chem. Soc., Chem. Commun.* 1975, 534.
8. B. J. McCormick, *Inorg. Chem.* 1968, **7**, 1965.
9. R. W. Wiggins, J. C. Huffman and G. Christou, *J. Chem. Soc., Chem. Commun.* 1983, 1313.
10. L. J. Boucher, E. C. Tynan and T. F. Yen, *Inorg. Chem.* 1968, **7**, 731.
11. H. J. Stoklosa, J. R. Wasson and B. J. McCormick, *Inorg. Chem.* 1974, **13**, 592.
12. M. H. Chisholm, K. Folting, J. C. Huffman and C. C. Kirkpatrick, *Inorg. Chem.* 1984, **23**, 1021.
13. P. Richard, J. L. Poncet, J. M. Barbe, R. Guilard, J. Goulon, D. Rinaldi, A. Cartier and P. J. Tola, *J. Chem. Soc., Dalton Trans.* 1982, 1451.
14. K. Behzadi and A. J. Thompson, *J. Less-Comm. Met.* 1987, **128**, 281.
15. I. Cuadrado and M. Moran, *Trans. Met. Chem.* 1986, **11**, 375.
16. J. G. Reynolds, J. C. Huffman and G. Christou, unpublished data.
17. R. P. Dodge, D. H. Templeton and A. Zalkin, *J. Chem. Phys.* 1961, **35**, 55.
18. K. Henrick, C. Raston and A. White, *J. Chem. Soc., Dalton Trans.* 1976, 26.

19. D. Bruins and D. L. Weaver, *Inorg. Chem.* 1970, **9**, 130.
20. M. Pasquali, F. Marchetti, C. Floriani and S. Merlino, *J. Chem. Soc., Dalton Trans.* 1977, 139.
21. J. Coetzer, *Acta Cryst.* 1970, **B26**, 872.
22. J. G. Reynolds, J. C. Huffman and G. Christou, unpublished data.
23. J. E. Drake, J. Vekris and J. S. Woods, *J. Chem. Soc. (A)* 1968, 1000.
24. T. W. Hambley, C. J. Hawkins and T. A. Kabanos, *Inorg. Chem.* 1987, **26**, 3740.
25. C. J. Hawkins and T. A. Kabanos, *Inorg. Chem.* 1989, **28**, 1084.

Polyhedron Vol. 12, No. 4, pp. 415–422, 1993
Printed in Great Britain

0277–5387/93 $6.00+.00
© 1993 Pergamon Press Ltd

THE DIMOLYBDENUM PENTAPIVALATE ANION: X-RAY CRYSTAL STRUCTURE AND DYNAMIC SOLUTION BEHAVIOUR AND COMMENTS ON THE SUBSTITUTIONAL LABILITY OF M–M CONTAINING COMPOUNDS

R. H. CAYTON, S. T. CHACON, M. H. CHISHOLM† and K. FOLTING

Department of Chemistry and Molecular Structure Center, Indiana University, Bloomington, IN 47405, U.S.A.

(*Received* 1 *September* 1992; *accepted* 1 *October* 1992)

Abstract—The reaction between $Mo_2(O_2CBu^t)_4$ and $[Bu^n_4N]^+[Bu^tCO_2]^-$ in toluene yields the yellow toluene-soluble salt $[Bu^n_4N]^+[Mo_2(O_2CBu^t)_5]^-$ as large yellow plates upon crystallization. The molecular structure of the anion contains the now common paddle-wheel or lantern $M_2(O_2C)_4$ core, Mo–Mo = 2.1035(7) and Mo—O = 2.12(2) Å (av), with a monodentate pivalate ligand coordinated to one metal atom, Mo—O = 2.298(5) Å in the axial position and Mo—Mo—O (η^1-pivalate) = 176.6(1)°. In CD_2Cl_2 and toluene-d_8 solutions the anion shows fluxional behaviour such that exchange between all pivalates is rapid on the NMR time-scale at room temperature. At −80°C this fluxional process becomes sufficiently slow to lead to the expected 4:1 ratio for the Bu^t protons. In pyridine-d_5 the exchange of pivalates is slower but still sufficiently fast to lead to coalescence at elevated temperatures. In pyridine solution the predominant species are $Mo_2(O_2CBu^t)_4(py)_2$ and $[Bu^n_4N]^+[Bu^tCO_2]^-$. These findings complement earlier work wherein $[Et_4N]^+[Mo_2(O_2CCF_3)_5]^-$ was prepared (Garner and Senior, *J. Chem. Soc., Dalton Trans.* 1975, 1171) and the exchange of $CF_3CO_2^-$ groups in the reaction between $Mo_2(O_2CCF_3)_4$ and NaO_2CCF_3 in CH_3CN was studied (Sasaki *et al.*, *Bull. Chem. Soc. Japan* 1979, **52**, 446). The facile intramolecular exchange of pivalate ligands in the $Mo_2(O_2CBu^t)_5^-$ anion emphasizes that Mo_2^{4+} containing compounds are kinetically labile to associative nucleophilic substitution reactions. Possible reaction pathways leading to exchange of $Bu^tCO_2^-$ are discussed.

The mechanisms and rates of ligand exchange reactions involving mononuclear transition metal ions are strongly influenced by the electronic configuration of the metal ion.[1] For example, octahedral complexes with the t_{2g}^6 configurations are generally substitutionally inert and react via dissociative or interchange dissociative mechanisms, while the pseudo-octahedral complexes with the electronic configuration $t_{2g}^3e_g^1$ or $t_{2g}^6e_g^3$ are generally super-labile. Compare the rates of $k_{exch}(H_2O)$ for the $M(H_2O)_6^{n+}$ ions which span the range 10^{-8}–10^9 s^{-1} in water at 25°C.[2] In organometallic chemistry the electronic configuration of the complex is also important. Typically, 18-electron complexes undergo nucleophilic substitution by dissociative mechanisms and are relatively inert. When associative behaviour is observed there is most often a special explanation such as a rearrangement of the binding of a coordinated ligand (e.g. a ring slippage η^5 to η^3 or a bending of linear nitrosyl) or there is a reversible attack on a coordinated ligand, which in turn facilitates ligand loss.[3] By contrast, 17- and 19-electron organometallic species are generally kinetically labile to associative and dissociative processes, respectively.[4]

For some time we have been interested in the reactivity of dinuclear compounds containing M—M multiple bonds and we recently noted[5] that the structurally related compounds of the formula $M_2(O_2CMe)_2(NCCH_3)_4^{2+}(BF_4^-)_2$, where M = molybdenum[6,7] and rhodium,[6] showed very different

† Author to whom correspondence should be addressed.

substitution chemistry. Specifically, the acetonitrile ligands were extremely labile to exchange in CD_3CN solvent at $-40°C$ for M = molybdenum, whereas the CH_3CN ligands bound to the Rh_2 complex were inert at room temperature. Indeed the $t_{1/2}$ for MeCN bound to $Rh_2(O_2CMe)_2(NCCH_3)_4^{2+}$ dissolved in CD_3CN as a solvent was of the order 4 h at $+100°C$. Studies of the kinetics of CH_3CN for CD_3CN exchange as a function of temperature led to the activation parameters $\Delta H^{\ddagger} = 33(1)$ kcal mol^{-1} and $\Delta S^{\ddagger} = +11(3)$ eu for M = rhodium, suggestive of bond breaking being most important in the transition state. Since there is no reason to believe that molybdenum–nitrogen or –oxygen bonds are weaker than their rhodium analogues, we speculated that the difference in lability was due to a difference in mechanism and that this in turn was influenced by the M—M bonding electronic configuration Mo—Mo $\sigma^2\pi^4\delta^2$ vs Rh—Rh $\sigma^2\pi^4\delta^2\delta^{*2}\pi^{*}$.[4]

In this paper we describe our preparation and characterization of the $Mo_2(O_2CBu^t)_5^-$ anion, which allows us to probe the exchange mechanism between free and Mo_2^{4+}-coordinated carboxylate ligands.

RESULTS AND DISCUSSION

Synthesis

The reaction between $Mo_2(O_2CBu^t)_4$ and $[Bu^n_4N]^+[Bu^tCO_2]^-$ in toluene yields the yellow crystalline compound $[Bu^n_4N]^+[Mo_2(O_2CBu^t_5]^-$.

This synthetic procedure has precedence in the work of Garner and Senior,[8] who studied the reactions of the trifluoroacetate complex $Mo_2(O_2CCF_3)_4$ with $[Et_4N]^+X^-$ which yielded 1 : 1 salts, $[Et_4N]^+[Mo_2(O_2CCF_3)_4X]^-$, where X = Cl, Br, I, CF_3CO_2 and $SnCl_3$, as well as 2 : 1 salts, $[Et_4N]_2[Mo_2(O_2CCF_3)_4X_2]$, where X = Br and I.

Table 1. Summary of crystal data for $[Bu^n_4N][Mo_2(O_2CBu^t)_5]$

Empirical formula	$C_{41}H_{81}Mo_2NO_{10}$
Colour of crystal	Clear yellow
Crystal dimensions (mm)	$0.08 \times 0.30 \times 0.32$
Space group	$P2_1/n$
Cell dimensions	
Temperature (°C)	−181
a (Å)	13.459(3)
b (Å)	24.045(5)
c (Å)	15.590(3)
β (°)	103.32(1)
Z (molecules/cell)	4
Volume (Å^3)	4909.81
Calculated density (g cm^{-3})	1.272
Wavelength (Å)	0.71069
Molecular weight	939.97
Linear absorption coefficient (cm^{-1})	5.447
Detector to sample distance (cm)	22.5
Sample to source distance (cm)	23.5
Average Ω scan width at half height	0.25
Scan speed (° min^{-1})	6.0
Scan width (° + dispersion)	1.7
Individual background (s)	6
Aperture size (mm)	3.0×4.0
2θ range (°)	6–45
Total number of reflections collected	8015
Number of unique intensities	6442
Number with $F > 0.0$	5799
Number with $F > 3.00\sigma(F)$	4042
R(F)	0.0477
Rw(F)	0.0475
Goodness of fit for the last cycle	1.045
Maximum delta/sigma for last cycle	0.03

Table 2. Selected bond lengths (Å) for $Mo_2(O_2CBu^t)_5^-$

Mo(1)—Mo(2)	2.1035(7)	O(3)—C(4)	1.276(8)
Mo(1)—O(3)	2.137(5)	O(5)—C(4)	1.286(8)
Mo(1)—O(10)	2.123(4)	O(10)—C(11)	1.260(8)
Mo(1)—O(17)	2.142(5)	O(12)—C(11)	1.296(8)
Mo(1)—O(24)	2.124(4)	O(17)—C(18)	1.266(7)
Mo(1)—O(31)	2.298(5)	O(19)—C(18)	1.290(8)
Mo(2)—O(5)	2.094(5)	O(24)—C(25)	1.269(8)
Mo(2)—O(12)	2.122(4)	O(26)—C(25)	1.266(8)
Mo(2)—O(19)	2.120(5)	O(31)—C(32)	1.266(8)
Mo(2)—O(26)	2.100(4)	O(33)—C(32)	1.251(8)

Molecular structure of $[Bu^n_4N]^+[Mo_2(O_2CBu^t)_5]^-$

A summary of crystal data is given in Table 1 and selected bond distances and bond angles are given in Tables 2 and 3, respectively. A molecular drawing of the anion showing the atom number scheme is given in Fig. 1.

The molecular structure of the $Mo_2(O_2CBu^t)_5^-$ anion contains the typical $Mo_2(O_2C)_4$ lantern or paddle-wheel structure seen now in so many structures of $Mo_2(O_2CR)_4$ compounds.[9] The Mo—Mo distance of 2.1035(7) Å is typical of those for Mo$\overset{4}{-}$Mo bonds.[9] The Mo—O(μ-O_2CBu^t) distances, 2.12(2) Å (av.), are slightly longer than those in the parent compound $Mo_2(O_2CBu^t)_4$, 2.105(10) Å (av.).[10] Also on average the Mo(1)—O distances are slightly longer, 2.132 Å, than those for Mo(2)—O, 2.109 Å. Although only a small difference, this is not surprising in view of the fact that Mo(1) is ligated by five oxygen atoms while Mo(2) has only four. The axially aligned η^1-O_2CBu^t ligand, Mo(2)—Mo(1)—O(31) = 176.6(1)°, has an Mo(1)—O(31) distance, 2.298(5) Å, somewhat longer than the other Mo—O distances. This is consistent with the general observation of rather long axial Mo—L bonds in $Mo_2(O_2CR)_4L_2$ complexes[9] and most certainly reflects the strong *trans* influence[11] of the Mo$\overset{4}{-}$Mo bond.

It should be noted that the structure of $Mo_2(O_2CBu^t)_5^-$ reported here is analogous to that predicted on the basis of spectroscopic studies by Garner and Senior[8] for the $Mo_2(O_2CCF_3)_5^-$ anion.

^{1}H *NMR studies*

The solution behaviour of $[Bu^n_4N]^+[Mo_2(O_2CBu^t)_5]^-$ with and without added $[Bu^n_4N]^+[Bu^tCO_2]^-$ has been investigated in the solvents toluene-d_8, CD_2Cl_2 and pyridine-d_5.

In pyridine-d_5 the ^{1}H spectrum of $[Bu^n_4N]^+[Mo_2(O_2CBu^t)_5]^-$ at 22°C shows two signals in the ratio 4:1 assignable to $Mo_2(O_2CBu^t)_4(py)_2$ and the free carboxylate anion $Bu^tCO_2^-$. The chemical shift position of the signal assignable to $Mo_2(O_2CBu^t)_4$ is the same as that arising when pure $Mo_2(O_2CBu^t)_4$ is dissolved in pyridine-d_5. Addition of an excess of $[Bu^n_4N]^+[Bu^tCO_2]^-$ to $[Bu^n_4N]^+[Mo_2(O_2CBu^t_5)]^-$ in pyridine-d_5 causes an increase in the signal assigned to $[Bu^n_4N]^+[Bu^tCO_2]^-$, but does not influence that assigned to $Mo_2(O_2CBu^t)_4$. Upon raising the temperature the signals assigned to free and coordinated Bu^tCO_2 ligands initially broaden and coalesce at +70°C.

These findings parallel the behaviour of the ex-

Table 3. Selected bond angles (°) for $Mo_2(O_2CBu^t)_5^-$

Mo(2)—Mo(1)—O(3)	90.39(13)	Mo(1)—Mo(2)—O(19)	93.15(13)
Mo(2)—Mo(1)—O(10)	91.17(12)	Mo(1)—Mo(2)—O(26)	92.91(12)
Mo(2)—Mo(1)—O(17)	90.07(12)	O(5)—Mo(2)—O(12)	88.85(18)
Mo(2)—Mo(1)—O(24)	90.33(12)	O(5)—Mo(2)—O(19)	173.96(18)
Mo(2)—Mo(1)—O(31)	176.55(11)	O(5)—Mo(2)—O(26)	91.33(18)
O(3)—Mo(1)—O(10)	89.01(17)	O(12)—Mo(2)—O(19)	90.38(17)
O(3)—Mo(1)—O(17)	179.25(16)	O(12)—Mo(2)—O(26)	174.49(17)
O(3)—Mo(1)—O(24)	90.68(17)	O(19)—Mo(2)—O(26)	88.87(17)
O(3)—Mo(1)—O(31)	90.89(18)	Mo(1)—O(3)—C(4)	118.3(4)
O(10)—Mo(1)—O(17)	90.39(17)	Mo(2)—O(5)—C(4)	118.0(5)
O(10)—Mo(1)—O(24)	178.47(16)	Mo(1)—O(10)—C(11)	117.8(4)
O(10)—Mo(1)—O(31)	92.06(16)	Mo(2)—O(12)—C(11)	115.7(4)
O(17)—Mo(1)—O(24)	89.91(17)	Mo(1)—O(17)—C(18)	119.1(5)
O(17)—Mo(1)—O(31)	88.68(18)	Mo(2)—O(19)—C(18)	116.7(4)
O(24)—Mo(1)—O(31)	86.45(16)	Mo(1)—O(24)—C(25)	117.6(4)
Mo(1)—Mo(2)—O(5)	92.87(12)	Mo(2)—O(26)—C(25)	116.5(4)
Mo(1)—Mo(2)—O(12)	92.59(12)	Mo(1)—O(31)—C(32)	166.0(5)

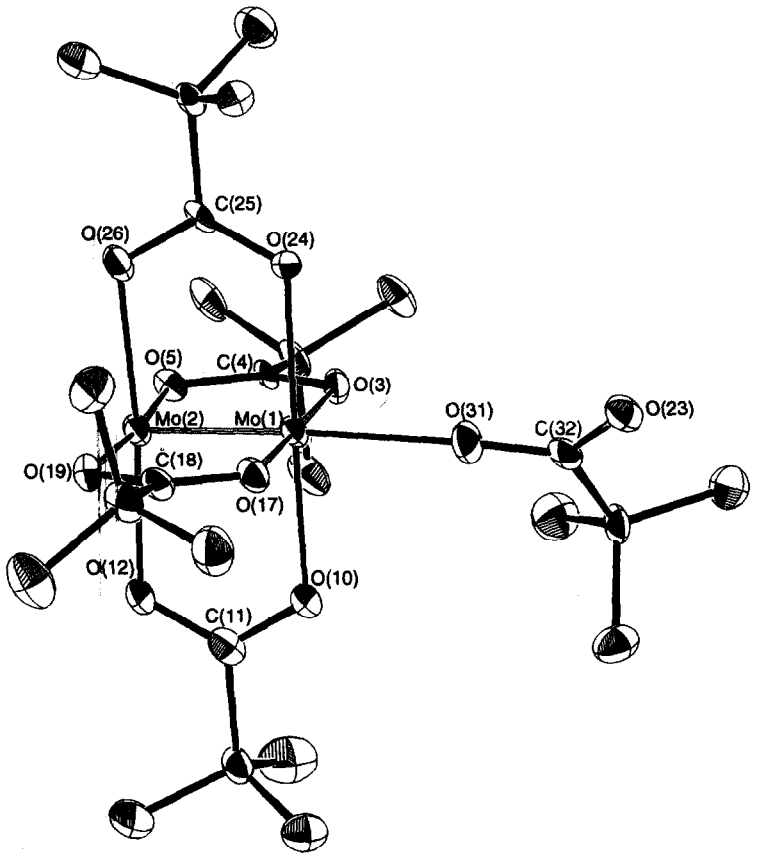

Fig. 1. A ball-and-stick drawing of the $Mo_2(O_2CBu^t)_5^-$ anion found in the crystal structure of $[Bu^n_4N][Mo_2(O_2CBu^t)_5]$. The hydrogen atoms have been omitted for clarity.

change of free $CF_3CO_2^-$ with the coordinated ligands in $Mo_2(O_2CCF_3)_4$ previously studied by chemists in Japan.[12]

In the solvents CD_2Cl_2 and toluene-d_8 at 22°C there is only one broad ^1H signal for the $Mo_2(O_2CBu^t)_5^-$ anion, implying rapid exchange of all $Bu^tCO_2^-$ ligands on the ^1H NMR time-scale. Upon lowering the temperature the signal broadens further and then splits into two signals in the ratio 1 : 4 at −80°C. Neither ^1H signal has the chemical shift assignable to free $Bu^tCO_2^-$ (as its $Bu^n_4N^+$ salt) or $Mo_2(O_2CBu^t)_4$. Thus, at low temperature the ^1H spectrum is consistent with expectations based on the solid-state structure.

If more than 1 equivalent of $[Bu^n_4N]^+[Bu^tCO_2]^-$ is added to a solution of $Mo_2(O_2CBu^t)_4$ in CD_2Cl_2, the NMR spectra at −80°C reveal the presence of the free pivalate anion and the signals associated with $Mo_2(O_2CBu^t)_5^-$ noted above. Thus, if $Mo_2(O_2CBu^t)_6^{2-}$ is formed in solution, it is formed reversibly and by an equilibrium that, at relatively low concentrations of $Bu^tCO_2^-$, favours $Mo_2(O_2CBu^t)_5^-$ and free $Bu^tCO_2^-$.

Discussion of the mechanism of carboxylate exchange

Sasaki, Saito and their co-workers[12] proposed the reaction scheme shown in eq. (1) for the exchange of $CF_3CO_2^-$ groups in the reaction between $Mo_2(O_2CCF_3)_4$ and NaO_2CCF_3 in CH_3CN. (They showed that NaO_2CCF_3 was effectively ionized in CH_3CN solutions.)

(i) $Mo_2(O_2CCF_3)_4(\underline{NCCH_3})_2 + {}^*CF_3CO_2^- \rightleftharpoons$

$Mo_2(O_2CCF_3)_4(\underline{NCCH_3})(\underline{O^2C}{}^*\underline{CF_3})^-$

$+ CH_3CN$ (1)

(ii) $Mo_2(O_2CCF_3)_4(\underline{NCCH_3})(\underline{O_2C}{}^*\underline{CF_3})^- \rightleftharpoons$

$Mo_2(O_2CCF_3)_3(O_2C{}^*CF_3)(\underline{NCCH_3})(\underline{O_2CCF_3})^-$

The ligands underlined in eq. (1) represent axial ligands, i.e. those aligned along the axis. From their studies they were able to rule out the importance of the dianionic species $Mo_2(O_2CCF_3)_4(\underline{O_2CCF_3})_2^{2-}$. Furthermore, they determined that the equilibrium eq. 1(i) in CH_3CN lies well to the left. By ^{19}F NMR spectroscopy at −40°C only the signals associated

with $Mo_2(O_2CCF_3)_4(\underline{NCCH_3})_2$ and free $CF_3CO_2^-$ were seen. This directly parallels the carboxylate exchange of $[Bu^n_4N]^+[Mo_2(O_2CBu^t)_5]^-$ dissolved in pyridine. Pyridine is a relatively good ligand to the Mo_2^{4+} centre and when present as the solvent readily displaces the axially coordinated $Bu^tCO_2^-$ ligand of the $Mo_2(O_2CBu^t)_5^-$ anion. The rate of carboxylate exchange in pyridine-d_5 is slower than that in CD_2Cl_2 or toluene-d_8 (as evidenced by the higher temperature of coalescence in the ^1H NMR spectrum) because the free carboxylate ligand must compete with pyridine for axial ligation prior to ligand scrambling.

In the solvents CD_2Cl_2 and toluene-d_8, the ^1H NMR spectra are indicative of the exchange process shown in eq. (2) which parallels that proposed for $CF_3CO_2^-$ exchange in eq. 1(ii).

$$[Mo_2(O_2CBu^t)_4(O_2\underline{C}^*\underline{Bu^t})(\underline{solvent})]^- \rightleftharpoons$$
$$[Mo_2(O_2CBu^t)_3(O_2C^*Bu^t)(\underline{solvent})(\underline{O_2CBu^t}]^- \quad (2)$$

From the coalescence temperature we can estimate the energy of activation for axial $\eta^1 \rightleftarrows \mu\text{-}O_2CR$ exchange to be *ca* 11 kcal mol^{-1}.[13] The exchange between free carboxylate and $\mu\text{-}O_2CR$ ligands is not much higher in energy because the axial sites of ligation, those along the M—M axis, are easily and reversibly accessed.

How is axial $\eta^1\text{-}O_2CR$ and $\mu\text{-}O_2CR$ site exchange so easily achieved? What is the reaction coordinate? Bond breaking cannot be very important when $\Delta G^\dagger = 11$ kcal mol^{-1}. Only weak bonds can be broken or as bonds break new bonds must be formed.

There are known structurally characterized d^3–d^3 compounds of the formulae $W_2(O_2CNMe_2)_6$,[14] $W_2(O_2CBu^t)_6$[15] and $W_2(O_2CNEt_2)_4(Me)_2$.[14] These contain tungsten atoms that form five W—L bonds in a pentagonal plane roughly perpendicular to the W—W bond axis. Based on this structural motif one might speculate about a symmetrical transition state or reactive intermediate of the type shown in **A**. Defining the *Z*-axis to be coincident with the M—M axis, then the d_{xy} and $d_{x^2-y^2}$ orbitals must be involved in metal–ligand bonding. It is easy to formulate an M—M triple bond of configuration $\sigma^2\pi^4$ for a d^3–d^3 dimer by the use of metal atomic orbitals d_{z^2} and d_{xy}, d_{yz}. However, for a d^4–d^4 dimer we would have to populate a relatively high energy metal-based orbital, formally derived from metal p_z–p_z interactions. Because of the mixing of *s*, d_{z^2} and p_z in M—M σ-interactions, this orbital could be either weakly bonding or weakly antibonding. Perhaps it is best to describe it as σ non-bonding. In order to proceed from the ground state structure of $Mo_2(O_2CBu^t)_4(\eta^1\text{-}O_2CBu^t)^-$ to **A**, two Mo—O bonds are formed in the *xy* plane and one relatively weak axial Mo—O bond is lost, along with some loss of M—M bonding being equivalent to at least the δ-component.

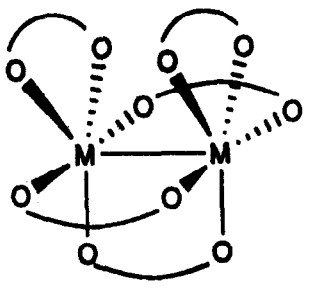

A

The other alternative that we present is shown in Scheme 1. This reaction involves a sort of merry-go-round of ligands or a slippage of carboxylates.[16] The intermediate shown in **B** is a distorted bi-octahedron sharing an edge. The formation of **B** represents a formal increase in metal–oxygen bonding, 10 Mo—O bonds vs nine Mo—O bonds in the ground-state structure $Mo_2(O_2CBu^t)_4(\eta^1\text{-}O_2CBu^t)^-$ and a loss of M—M bonding. The ordering of the δ and δ^* orbitals in edge-shared bioctahedra is often inverted as a result of oxygen p_π–metal *d* interactions[17] and so we might represent the M—M bonding in **B** as $\sigma^2\pi^2(\delta/\delta^*)$,[4] which emphasizes that both δ and δ^* would be occupied. The formation of **B** thus sacrifices M—M bonding in going from Mo–$\overset{4}{}$M to Mo–$\overset{2}{}$Mo.

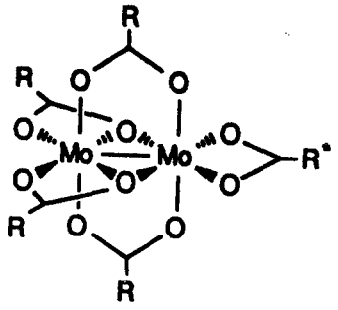

B

Further speculation is pointless, suffice to say that the presence of the low energy empty metal-based δ^* orbitals makes the $Mo_2(O_2CR)_4$ compounds labile to associative nucleophilic substitution reactions. In a simple picture we can envisage nucleophilic attack as shown below in **C**.

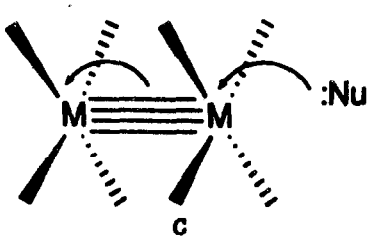

C

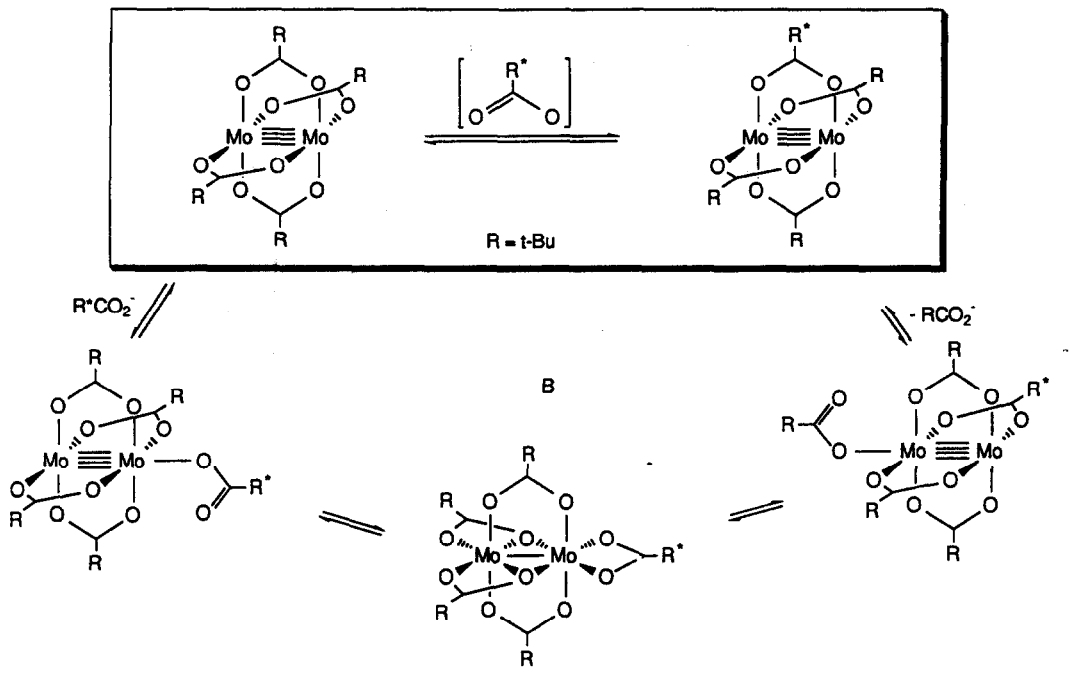

Scheme 1. A possible mechanism for carboxylate group scrambling in the reaction between $Mo_2(O_2CR)_4$ and RCO_2^-. The activated complex or reactive intermediate shown in **B** is an edge-shared bioctahedron, which is an alternative to **A** discussed in the text.

The formation of a fifth bond in a pentagonal plane at one molybdenum atom destroys the Mo—Mo δ-bond and places a pair of electrons at the other metal centre in the metal based d_{xy} orbital. The new metal–ligand bond may then assist in the displacement of either the axial ligand (or solvent molecule) or one of the other ligands in the equatorial pentagonal plane. Once the fifth ligand is lost from the pentagonal plane by either dissociation or migration to the axial site as the original axial ligand or solvent leaves, the δ-bond is restored.

An estimate of the δ-bond strength based on a rotational barrier in a Mo_2(porphyrin)$_2$ complex is *ca* 11 kcal mol^{-1}.[18] Since our proposed mechanism for substitution involves the loss of the Mo—Mo δ-bond but with the accompanying formation of a new metal–ligand bond, it is not unreasonable to suppose that the enthalpy of activation for substitution at dinuclear centres containing the M^4–M bonds of electronic configuration $\sigma^2\pi^4\delta^2$ will be limited by (1) the loss of M—M bonding upon the formation of a new metal–ligand bond and (2) steric factors. Consequently, we predict that compounds with M^4–M bonds will in general be substitutionally labile and will react via associative or interchange associative mechanisms with Lewis bases.

Finally, it is worth noting that Espenson and Webb[19] studied the bromide-for-chloride exchange reaction shown in eq. (3). The halide ligands adopt the axial sites. They noted that the reaction in CH_3CN was catalysed by the presence of various nucleophiles [H_2O, py, THF, $(Me_2N)_2C{=}O$]. We suggest that the dissociation of Cl^- is facilitated in this reaction by the associative interchange mechanism involving the nucleophiles as described in this paper.

$$Cl{-}Re(\mu\text{-}O_2CEt)_4Re{-}Cl + Br^- \longrightarrow Cl{-}Re(\mu\text{-}O_2CEt)_4Re{-}Br + Cl^- \quad (3)$$

In aqueous trifluorosulphonic acid, the Mo_2^{4+} aquo ion shows substitutional lability comparable to the MO^{2+} aquo ions (M = Ti, V) toward NCS^- and the analogy between metal–metal and metal–ligand multiply-bonded systems was noted by Sykes and co-workers some 10 years ago.[20]

EXPERIMENTAL

^{1}H NMR spectra were recorded on a Varian XL300 spectrometer at 300 MHz in dry and oxygen-free pyridine-d_5, toluene-d_8 and methylene chloride-d_2. All ^{1}H NMR chemical shifts are reported in ppm relative to the protio impurity resonance at 7.19 ppm for pyridine-d_5, 2.09 ppm for toluene-d_8 and 5.32 ppm for methylene chloride-d_2.

All reactions were carried out under an atmosphere of dry and oxygen-free nitrogen using standard Schlenk and glove-box techniques. All solvents were dried and degassed by standard methods and distilled prior to use. Pivalic acid and tetra-n-butyl ammonium hydroxide were purchased from Aldrich and used as received. Dimolybdenum tetrapivalate was prepared by a published procedure.[21]

$[Bu^n_4N]^+[Bu^tCO_2]^-$

To a flask containing pivalic acid (0.5107 g, 5.0 mmol) dissolved in benzene (15 cm^3) was added a solution of tetra-n-butyl ammonium hydroxide (5 cm^3, 1.0 M) in methanol. The volatile components were removed *in vacuo* and dried for 1 h to yield a white solid. The material was slurried in pentane, the volatile components were again removed under vacuum and the resulting white powder was dried *in vacuo* at 70°C for 12 h. The powder was washed with 5 × 10 cm^3 of pentane, filtered and dried under vacuum for 3 h to yield 1.380 g (80%).

$[Bu^n_4N]^+[Mo_2(O_2CBu^t)_5]^-$

To a flask containing $Mo_2(O_2CBu^t)_4$ (0.090 g, 0.15 mmol) and $[Bu^n_4N]^+[Bu^tCO_2]^-$ (0.075 g, 0.22 mmol) was added toluene (10 cm^3). The mixture was heated until all the material dissolved giving a clear yellow solution. Slow cooling of this solution to room temperature afforded 0.120 g (85%) of large yellow plates. ^1H NMR (−80°C), methylene chloride-d_2: δ 0.85 (s, 9H), 0.91 (t, 12H), 1.27 (m, 8H), 1.35 (s, 36H), 1.48 (m, 8H), 3.05 (m, 8H). Coalescence temperatures: T_c = +30°C in toluene-d_8 and +70°C in pyridine-d_5.

Crystallographic study

General operating procedures and listings of programs have been described.[22]

A suitable crystal was selected by using inert atmosphere handling techniques and transferred to the goniostat, where it was cooled to −181°C for characterization and data collection. A systematic search of a limited hemisphere of reciprocal space yielded a set of reflections which exhibited monoclinic ($2_1/m$) symmetry. The systematic extinction of $0k0$ for $k = 2n+1$ and of $h01$ for $h+1 = 2n+1$ uniquely identified the space group as $P2_1/n$. The structure was solved by a combination of direct methods and Fourier techniques. Following the initial refinement almost all of the hydrogen atoms were located; this included at least two on each of the methyl groups. The hydrogen atom positions were idealized and introduced in the least-squares refinement. The full-matrix least-squares refinement was completed using anisotropic thermal parameters on all non-hydrogen atoms. The hydrogen atoms were refined using isotropic thermal parameters.

The closest approach between Mo(2) and the cation is 3.8 Å. The distance between Mo(2) and the n-butylammonium cation nitrogen atom is 4.645(6) Å. The closest distance from O(33) to atoms in the cation is 3.133(8) Å.

The final difference map was essentially featureless, the largest peak being 0.66 e $Å^{-3}$ in the vicinity of Mo(1).

Acknowledgements—We thank the National Science Foundation for financial support and R.H.C. acknowledges an NSF postdoctoral fellowship, 1989–1991.

REFERENCES

1. F. Basolo and R. G. Pearson, in *Mechanisms of Inorganic Reactions: A Study of Metal Complexes in Solution*, 2nd edn. John Wiley, New York (1968).
2. See ref. 1, Table 3.11, p. 152 and references therein.
3. F. Basolo, *Polyhedron* 1990, **9**, 1503.
4. D. R. Tyler, *Accts Chem. Res.* 1991, **24**, 324.
5. J. M. Casas, R. H. Cayton and M. H. Chisholm, *Inorg. Chem.* 1991, **30**, 358.
6. C. D. Garner, W. Clegg and G. Pimblett, *J. Chem. Soc., Dalton Trans.* 1986, 1257.
7. F. A. Cotton, A. H. Reid Jr and W. Schwotzer, *Inorg. Chem.* 1985, **24**, 3965.
8. C. D. Garner and R. G. Senior, *J. Chem. Soc., Dalton Trans.* 1975, 1171. The structure of the acetic acid solvate $Mo_2(O_2CMe)_4 \cdot Na^+[MeCO_2H \cdots O_2CMe]^-$ has been reported. D. L. Kepert, B. W. Skelton and A. H. White, *Aust. J. Chem.* 1980, **33**, 1847. The Mo···O axial distance is 2.575(4) Å.
9. F. A. Cotton and R. A. Walton, in *Multiple Bonds Between Metal Atoms*. John Wiley, New York (1982).
10. F. A. Cotton, M. W. Extine and L. D. Gage, *Inorg. Chem.* 1978, **17**, 172.
11. T. G. Appleton, H. C. Clark and L. E. Manzer, *Coord. Chem. Rev.* 1973, **10**, 335.
12. K. Teramoto, Y. Sasaki, K. Migita, M. Iwaizumi and K. Saito, *Bull. Chem. Soc. Japan* 1979, **52**, 446.
13. R. S. Drago, in *Physical Methods in Chemistry*, Ch. 8. W. B. Saunders Publishers, New York (1977).
14. M. H. Chisholm, F. A. Cotton, M. W. Extine and B. R. Stults, *Inorg. Chem.* 1977, **16**, 603.
15. M. H. Chisholm, J. A. Heppert, D. M. Hoffman and J. C. Huffman, *Inorg. Chem.* 1985, **24**, 3214.
16. For examples of μ-η^1,η^2-O_2CR ligands, see G. Christou, *Polyhedron*, submitted.
17. (a) F. A. Cotton, *Polyhedron* 1987, **6**, 667; (b) S. Shaik, R. Hoffmann, C. R. Fisel and R. H. Summerville, *J. Am. Chem. Soc.* 1980, **102**, 4555.

18. J. P. Collman and L. K. Woo, *Proc. Natn. Acad. Sci. U.S.A.* 1984, **81**, 2592; J. P. Collman, J. M. Garner, R. T. Hembre and Y. Ha, *J. Am. Chem. Soc.* 1992, **114**, 1292.
19. J. H. Espenson and T. R. Webb, *J. Am. Chem. Soc.* 1974, **96**, 6289.
20. J. E. Finholt, P. Leupin and A. G. Sykes, *Inorg. Chem.* 1983, **22**, 3315.
21. F. A. Cotton and A. G. Brignote, *Inorg. Synth.* 1972, **13**, 81.
22. M. H. Chisholm, K. Folting, J. C. Huffman and C. C. Kirkpatrick, *Inorg. Chem.* 1984, **23**, 1021.

Polyhedron Vol. 12, No. 4, pp. 423–426, 1993
Printed in Great Britain

0277–5387/93 $6.00+.00
© 1993 Pergamon Press Ltd

PREPARATION AND CHARACTERIZATION OF SOME COMPLEXES OF CHROMIUM(III), COBALT(III) AND RHODIUM(III) IONS CONTAINING 1,4,8,12-TETRA-AZACYCLOPENTADECANE

M. SAIDUL ISLAM* and M. MASIR UDDIN

Department of Chemistry, Rajshahi University, Rajshahi 6205, Bangladesh

(*Received* 20 *August* 1992; *accepted* 1 *October* 1992)

Abstract—Some new complexes of chromium(III), cobalt(III) and rhodium(III) containing 1,4,8,12-tetra-azacyclopentadecane and imido ligands have been prepared and characterized by elemental analyses, conductometric, magnetic, IR and electronic spectral studies. The complexes have the general formula *trans*-$[ML(im)_2]ClO_4$ [where M = chromium(III), cobalt(III) or rhodium(III); L = 1,4,8,12-tetra-azacyclopentadecane; im = anion of succinimide (sim^-) or phthalimide (pim^-)]. A proposed *trans* configuration for the complexes is supported by spectral data.

Imides and their metal complexes have wide applications in pharmacological,[1,2] industrial[3,4] and analytical[5,6] fields. The role of synthetic macrocyclic complexes as models for their natural counterparts is now well recognized.[7,8] The coordination chemistry of chromium(III),[9–11] cobalt(III)[12–14] and rhodium(III)[15,16] with 14-membered, saturated cyclic tetraamines has been studied in some detail, but only limited information is available on the complexes of these metal ions with 1,4,8,12-tetra-azacyclopentadecane (L).[17–20] The ligand L normally gives complexes of the type *trans*-$[MLA_2]$ (M = chromium(III), cobalt(III) or rhodium(III); A = monodentate ligand],[18–20] and only in the presence of chelating ligands have complexes with a *cis* geometry been reported.[18,19] Keeping these facts in view, we herein report the preparation and characterization of some complexes of chromium(III), cobalt(III) and rhodium(III) ions containing 1,4,8,12-tetra-azacyclopentadecane (L) and imido anions.

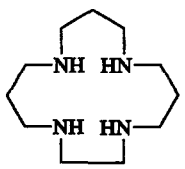

L
(1,4,8,12-tetra-azacyclopentadecane)

* Author to whom correspondence should be addressed.

EXPERIMENTAL

Physical measurements

IR spectra (as KBr discs) were recorded on a Pye–Unicam SP3-300 IR spectrophotometer. Electronic spectra in acetonitrile were recorded on a Ultrospec K-4053 spectrophotometer. Magnetic measurements were made on a Johnson–Matthey magnetic susceptibility balance. Conductivities of 1.0×10^{-3} mol dm^{-3} solutions of the complexes in acetonitrile were measured at 28°C using a WPA CM35 conductivity meter and a dip-type cell with platinized electrodes.

Reagents

All the chemicals used were of reagent grade and were used as such. The potassium salts of the imides (succinimide and phthalimide) were prepared by mixing saturated ethanolic solutions of an imide and potassium hydroxide. The macrocyclic ligand 1,4,8,12-tetra-azacyclopentadecane was synthesized according to a literature method.[21]

Analyses

Carbon, hydrogen and nitrogen analyses were carried out by the Regional Sophisticated Instrumentation Centre, Central Drug Research Institute, Lucknow, India.

Preparation of the complexes

Trans - *dichloro*(1,4,8,12 - *tetra* - *azacyclopentadecane*)*chromium*(III) *perchlorate*, trans-$[CrLCl_2]ClO_4$. A solution of chromium(III) chloride hexahydrate (1.6 g, 0.006 mol) in dimethylformamide (30 cm^3) was boiled for 0.5 h and then cooled to *ca* 90°C. A solution of L (1.29 g, 0.006 mol) in dimethylformamide (20 cm^3) was added to the chromium(III) solution. Water (100 cm^3) was then added to the above mixture followed by the addition of concentrated hydrochloric acid (10 cm^3) and $NaClO_4 \cdot H_2O$ (1.5 g). The volume of the solution was reduced to *ca* 50 cm^3 by heating the mixture on a steam-bath and then leaving to cool. The green crystalline product which deposited was filtered off, recrystallized from hot hydrochloric acid (6 mol dm^{-3}), washed with 2-propanol and then dried in a vacuum desiccator over anhydrous silica gel. Found: C, 30.0; H, 6.1; N, 12.7. Calc. for $C_{11}H_{26}Cl_3CrN_4O_4$: C, 30.2; H, 6.0; N, 12.8%.

Trans - *dichloro*(1,4,8,12 - *tetra* - *azacyclopentadecane*)*cobalt*(III) *perchlorate*, trans-$[CoLCl_2]ClO_4$. Cobalt(II) chloride hexahydrate (1.42 g, 0.006 mol) and the ligand L (1.30 g, 0.006 mol) were dissolved in methanol (100 cm^3) to give a deep brown solution. Air was bubbled through this solution for 2 h. Concentrated hydrochloric acid was then added dropwise until the brown solution turned green (3 cm^3). Aeration was continued until the volume of the solution was reduced to *ca* 50 cm^3. Water (25 cm^3) was then added followed by $NaClO_4 \cdot H_2O$ (1.5 g). The volume of the solution was reduced to *ca* 25 cm^3 by heating on a steam-bath and then cooled. The bright green crystals formed were filtered off, recrystallized from hot hydrochloric acid (6 mol dm^{-3}), washed with 2-propanol and then dried *in vacuo* over silica gel. Found: C, 29.4; H, 5.8; N, 12.4. Calc. for $C_{11}H_{26}Cl_3CoN_4O_4$: C, 29.8; H, 5.9; N, 12.6%.

Trans - *dichloro*(1,4,8,12 - *tetra* - *azacyclopentadecane*)*rhodium*(III) *perchlorate*, trans-$[RhLCl_2]ClO_4$. Rhodium(III) chloride trihydrate (1.58 g, 0.006 mol) and the ligand L (1.30 g, 0.006 mol) were dissolved in methanol (100 cm^3) and heated under reflux for 48 h. The resulting solution was evaporated to dryness and the residue dissolved in water (25 cm^3). NaCl (1.0 g) was then added to this solution followed by the addition of $NaClO_4 \cdot H_2O$ (1.5 g). The solution was then warmed and stirred. The orange–yellow precipitate which formed was filtered off, recrystallized from hot water and dried *in vacuo* over silica gel. Found: C, 26.9; H, 5.4; N, 11.4. Calc. for $C_{11}H_{26}Cl_3RhN_4O_4$: C, 27.1; H, 5.4; N, 11.5%.

General method for the preparation of complexes **1–6**: trans-$[ML(im)_2]ClO_4$ (M = Cr^{III}, Co^{III} *or* Rh^{III}; L = 1,4,8,12-*tetra-azacyclopentadecane*; *im* = *anion of succinimide or phthalimide*). A methanolic solution of the sodium salt of an imide [prepared by adding a saturated methanolic solution of the potassium salt of an imide (0.002 mol) to a saturated methanolic solution of $NaClO_4 \cdot H_2O$ (0.5 g) and filtering off the insoluble $KClO_4$] was added to a solution of *trans*-$[MLCl_2]ClO_4$ (0.001 mol) in methanol (30 cm^3). The mixture was refluxed on a steam-bath for *ca* 4 h and filtered while hot. The filtrate was cooled in an ice–salt bath. The crystals formed were filtered off and recrystallized from hot methanol. The crystals collected were washed with ice-cooled methanol and diethyl ether and then dried *in vacuo* over silica gel.

RESULTS AND DISCUSSION

The complexes of the type *trans*-$[MLCl_2]ClO_4$ were prepared by some variations of the published methods.[18–20] Using the dichloro complexes as precursors, the desired diimido complexes were prepared. Treatment of *trans*-$[MLCl_2]ClO_4$ with a stoichiometric amount of the sodium salt of an imide resulted in the replacement of two chlorine atoms from the coordination sphere, leading to the formation of *trans*-$[ML(im)_2]ClO_4$.

The analytical and physical data of the complexes (**1–6**) are collected in Table 1. The complexes are soluble in water, acetonitrile and dimethylsulphoxide. The molar conductance values (Table 1) indicate that all the complexes are 1 : 1 electrolytes in acetonitrile.[22] The analytical and physical data are consistent with six-fold coordination of the metal atoms.

IR spectral data of the complexes are summarized in Table 2. An imide anion may be coordinated through its carbonyl oxygen or imido nitrogen (N^-). On the basis of the Lewis acid–base concept, it may be established that the negatively charged imido nitrogen is more likely to be coordinated to the metal ion and coordination through the carbonyl oxygen is expected to be inhibited by steric hindrance.[23] Again, any change (due to coordination) in the imido nitrogen which is directly linked to the carbonyl group will alter the molecular environment and, hence, the absorption frequency of the latter even if it is not coordinated.[24] In the present complexes the ν(C=O) mode is found at $\sim$ 1685 cm^{-1} compared to $\sim$ 1720 cm^{-1} in free succinimide or phthalimide.[25] This decrease in frequency may be due to the mass effect.[26] The observed ν(C—N) mode of free succinimide or phthalimide at $\sim$ 1310 cm^{-1} is shifted to 1340–

Table 1. Analytical and physical data of the complexes

Compound	No.	Colour	% Carbon Calc.	% Carbon Found	% Hydrogen Calc.	% Hydrogen Found	% Nitrogen Calc.	% Nitrogen Found	Effective magnetic moment (B.M.)	Molar conductance ($\Omega^{-1}cm^2$ mol^{-1})
$[CrL(sim)_2]ClO_4$	**1**	Purple	40.6	40.2	6.1	6.1	14.9	14.8	3.97	124
$[CrL(pim)_2]ClO_4$	**2**	Purple	49.3	48.9	5.2	5.3	12.8	12.5	4.12	145
$[CoL(sim)_2]ClO_4$	**3**	Brown	40.1	39.8	6.0	6.0	14.8	14.6	0.31	109
$[CoL(pim)_2]ClO_4$	**4**	Brown	48.8	48.3	5.1	5.0	12.6	12.4	0.48	136
$[RhL(sim)_2]ClO_4$	**5**	Yellow	37.2	36.9	5.6	5.6	13.7	13.6	0.25	132
$[RhL(pim)_2]ClO_4$	**6**	Yellow	45.7	45.4	4.8	4.9	11.8	11.6	0.14	118

L = $C_{11}H_{26}N_4$, sim^- = $C_4H_4O_2N$, pim^- = $C_8H_4O_2N$.

Table 2. IR spectral data (cm^{-1})[a]

Compound	ν(NH)	ν(C—N)	ν(ClO_4^-)	ν(M—N)
1	3160s	1355m	1100vs 625s	450w
2	3140s	1360m	1095vs 625s	430w
3	3175m	1365m	1095vs 620s	460m
4	3160s	1350m	1095vs 625s	470m
5	3185m	1345m	1100vs 625s	445m
6	3150m	1340m	1095vs 625s	430m

[a] Relative band intensities are denoted by vs, s, m and w meaning very strong, strong, medium and weak, respectively.

Table 3. Electronic spectral data of the complexes (extinction cofficients in dm^3 mol^{-1} cm^{-1} are given in parentheses)

Compound	Spectral band maxima (cm^{-1})
1	17,730 (34), 23,923 (40)
2	17,182 (25), 23,041 (47)
3	16,420 (62)
4	16,835 (38)
5	23,640 (59)
6	22,988 (83)

1365 cm^{-1} in the spectra of the complexes, thereby suggesting N^- formation and coordination.[25,27]

All the complexes show characteristic absorption for the secondary NH stretching mode in the region 3140–3185 cm^{-1}, indicating coordination of the macrocycle through the nitrogen atoms. The presence of M—N bonds is evident from the appearance of ν(M—N) vibrations at 430–470 cm^{-1} in the spectra of the complexes.[18] The complexes show strong bands at ~ 1095 and ~ 625 cm^{-1}, characteristic of ionic perchlorate.

The observed values of effective magnetic moments at room temperature are given in Table 1. The chromium(III) complexes yield effective magnetic moments (3.92 and 4.12 B.M.) corresponding to three unpaired electrons, consistent with essentially octahedral stereochemistry. The effective magnetic moments of cobalt(III) and rhodium(III) complexes (0.14–0.48 B.M.) indicate that the complexes are low-spin diamagnetic species and this revealed that there was no change in the oxidation state of the metal ions upon complex formation.

The electronic spectral data of the complexes are given in Table 3. The chromium(III) complexes gave two bands in the regions 17,182–17,730 and 23,041–23,923 cm^{-1} corresponding to the transitions $^4A_{2g} \rightarrow {}^4T_{2g}$ and $^4A_{2g} \rightarrow {}^4T_{1g}$(F), respectively.[11,18] The cobalt(III) and rhodium(III) complexes produced a single band at 16,420–16,835 and 22,988–23,640 cm^{-1}, respectively, corresponding to the transition $^1A_{1g} \rightarrow {}^1T_{1g}$.[19,20] A *trans* structure is suggested for these complexes from the low energy of the *d–d* bands present and their low extinction coefficients (Table 3).

Acknowledgement—We are grateful to the Bangladesh University Grants Commission for the award of a Research Fellowship to one of us (M.M.U.).

REFERENCES

1. Z. M. Elden, A. M. Shubber, M. A. Naji, A. Khayat and H. Ghantous, *J. Med. Chem.-Chem. Ther.* 1980, **15**, 85.

2. P. Rocchi, P. Perocco, W. Alberghini, A. Fini and G. Prodi, *Arch. Toxicol.* 1980, **45**, 101.
3. E. S. Yamaguchi and T. V. Liston, U.S. Patent, US 4443360 (Cl. 252-46.7; C10M1/48), 17 April 1984.
4. R. C. Schlicht and A. P. Skrobul, U.S. Patent, US 4446038 (Cl. 252-51.5A; C10M1/32), 1 May 1984.
5. F. Grases, R. Forteza, J. G. March and V. Cerda, *Analyt. Chim. Acta* 1983, **155**, 299.
6. G. L. Hatch, *Analyt. Chem.* 1984, **56**, 2238.
7. N. F. Curtis, *Coord. Chem. Rev.* 1968, **3**, 3.
8. L. F. Lindoy and D. H. Busch, *Preparative Inorganic Reactions* (Edited by W. L. Jolly), Vol. 6, p. 1. John Wiley, New York (1971).
9. J. Ferguson and M. L. Tobe, *Inorg. Chim. Acta* 1970, **4**, 109.
10. C. K. Poon and K. C. Pun, *Inorg. Chem.* 1980, **19**, 568.
11. D. A. House, R. W. Hay and M. A. Ali, *Inorg. Chim. Acta* 1983, **72**, 239.
12. B. Bosnich, C. K. Poon and M. L. Tobe, *Inorg. Chem.* 1965, **4**, 1102.
13. C. K. Poon and M. L. Tobe, *J. Chem. Soc. A* 1967, 2069.
14. C. K. Poon and M. L. Tobe, *J. Chem. Soc. A* 1968, 1549.
15. E. J. Bounsall and S. R. Koprich, *Can. J. Chem.* 1970, **48**, 1481.
16. N. F. Curtis and D. F. Cook, *J. Chem. Soc., Dalton Trans.* 1972, 691.
17. D. T. Tichens, I. K. Adzamli, P. Leupin and A. G. Sykes, *Inorg. Chem.* 1984, **23**, 3065.
18. R. W. Hay and M. T. H. Tarafder, *J. Chem. Soc., Dalton Trans.* 1991, 823.
19. Y. Hung, L. Y. Martin, S. C. Jackels, A. M. Tait and D. H. Busch, *J. Am. Chem. Soc.* 1977, **99**, 4029.
20. P. K. Bhattacharya, *J. Chem. Soc., Dalton Trans.* 1980, 810.
21. L. Y. Martin, C. R. Sperati and D. H. Busch, *J. Am. Chem. Soc.* 1977, **99**, 2968.
22. W. J. Geary, *Coord. Chem. Rev.* 1971, **7**, 81.
23. J. C. Bailar, *The Chemistry of Coordination Compounds*, pp. 179–180. Reinhold, New York (1956).
24. S. Strimn, *J. Chem. Phys.* 1955, **23**, 1371.
25. M. S. Alam, Q. Islam and M. S. Islam, *Pakistan J. Sci. Ind. Res.* 1991, **34**, 177.
26. G. F. Svatos, C. Curran and J. V. Quagliano, *J. Am. Chem. Soc.* 1955, **77**, 6159.
27. P. C. H. Mitchell, *J. Inorg. Nucl. Chem.* 1963, **25**, 963.

Polyhedron Vol. 12, No. 4, pp. 427–434, 1993
Printed in Great Britain

0277–5387/93 $6.00+.00
© 1993 Pergamon Press Ltd

OLIGOPHOSPHINE LIGANDS—XXXVII.* STEREOCHEMICAL FEATURES OF COMPLEXES CONTAINING THE *cis*-L_4Ru FRAGMENT: MOLECULAR STRUCTURES OF $(Me_3P)_4RuH_2$ AND $\{P[(CH_2)_3PMe_2]_3\}RuH_2$

LUTZ DAHLENBURG† and KAY-MICHAEL FROSIN

Institut für Anorganische Chemie der Universität Hamburg, Martin-Luther-King-Platz 6, D-2000 Hamburg 13, Germany

(*Received* 20 *August* 1992; *accepted* 29 *September* 1992)

Abstract—The title compounds have been studied by single-crystal X-ray diffraction. Both structures can be described as distorted octahedra. P—Ru—P angles between phosphorus atoms at mutually *cis* positions are considerably larger than 90°, with the sum of the *cis* angles amounting to 495.6° for $(Me_3P)_4RuH_2$ (**1**) and to 486.2° for $\{P[(CH_2)_3PMe_2]_3\}RuH_2$ (**2**). These structural parameters and the observed bending over of the two axial donor sets toward the hydrido ligands, which results in *trans* P—Ru—P angles of 151.5° for complex **1** and of 153° for structure **2** averaged over four crystallographically independent molecules, suggest a considerably higher degree of steric encumbrance in *cis*-$(Me_3P)_4Ru$ than in $\{P[(CH_2)_3PMe_2]_3\}Ru$ systems. They thus correspond to both the well-known ability of the $\{P[(CH_2)_3PMe_2]_3\}Ru(0)$ fragment to insert across C—H bonds of non-coordinated hydrocarbons and the propensity of *cis*-$(Me_3P)_4Ru(0)$ to undergo spontaneous cyclometallation. Selected bond lengths of compound **1** are: Ru—P (*trans* ligand H), 2.306(1) and 2.306(2) Å; Ru—P (*trans* to each other), 2.276(1) and 2.289(2) Å. For the averaged structure **2**, the mean distances between the central metal and the donor atoms are 2.270(5) Å for the bridging phosphorus atom, 2.292(6) Å for the PMe_2 group *trans* to hydrogen, and 2.281(7) and 2.284(10) Å for the PMe_2 substituents situated at mutually *trans* positions.

Within the scope of our studies with the $(pp_3)Ru$ metal/ligand system ($pp_3 = P[(CH_2)_3PMe_2]_3$)[4–11] we also came across several complexes derived from the closely related *cis*-$(Me_3P)_4Ru$ fragment, which have been synthesized in great variety, first by Wilkinson,[12–17] then by Schmidbaur,[18] Werner[19] and Green,[20] and recently by Andersen and Bergman[21–27] as well as Osakada and Yamamoto.[28] The structurally characterized ruthenium complexes *cis*-$L_4Ru(X)(Y)$, with trimethylphosphine as the common ligand L, include the alkyl $L_4Ru(H)(Et)$,[17] the aryl $L_4Ru(OH)(Ph)$,[23b] the arylamide and -oxide $L_4Ru(H)(NHPh)$[26] and $L_4Ru(H)(OC_6H_4$ Me-4),[26,28] the mercury-bridged heterotrimetallic $[L_4Ru(Me)]_2Hg$,[16] as well as a series of further derivatives where the *cis*-L_4Ru moiety is part of a three- to five-membered metallaheterocycle, including $L_4Ru(CH_2CH_2)$,[17] $L_4Ru(C_6H_4)$,[23] $L_4Ru[CH_2C(O)CH_2]$,[27b,d] $L_4Ru[CH_2C(=CHCMe_3)O]$[27d] and several *ortho*-metallated systems, such as $L_4Ru(o\text{-}C_6H_4CH_2)$,[29] $L_4Ru(o\text{-}C_6H_4OCH_2)$,[30] $L_4Ru[o\text{-}C_6H_4C(=CH_2)O]$[27c] and $L_4Ru(o\text{-}C_6H_4C(Ph)=N)$.[23b]

Here we report the results of two X-ray structure determinations performed on the parent dihydride of the above derivatives, *cis*-$(Me_3P)_4RuH_2$ (**1**), and its closely related analogue, $(pp_3)RuH_2$ (**2**). Dihydride **1** represents a key-compound in ruthenium trimethylphosphine chemistry. The complex has

* For parts XXXIV to XXXVI, see refs 1–3.

† Author to whom all correspondence should be addressed at his new address at the Institut für Anorganische Chemie der Friedrich-Alexander-Universität Erlangen-Nürnberg, Egerlandstraße 1, D. 8520 Erlangen, Germany.

thus been shown to undergo H/D exchange with C_6D_6 solvent,[24] to assist proton-transfer processes with OH acids[26,28] and even with the weaker NH acids,[26] presumably on a pathway that involves the reversible formation of a non-classical cation $[(Me_3P)_4RuH_3]^+$ containing both a hydride and a dihydrogen ligand.[26,28] $(Me_3P)_4RuH_2$ furthermore serves as an efficient catalyst for the homo-dimerization of terminal alkynes, RC≡CH, to yield 1,4-disubstituted but-1-en-3-ynes, RCH=CHC≡CR,[31] as well as for the co-dimerization of 1-alkynes with buta-1,3-diene to afford substituted hex-3-en-5-ynes, $CH_3CH_2CH{=}CHC{\equiv}CR$.[32] Upon photolytic conversion with Me_3SiH to $(Me_3P)_3RuH_3(SiMe_3)$, dihydride **1** finally mediates the dehydrogenative coupling of trialkylsilanes to generate carbosilanes as a net result of silane Si—H and C—H activation and organosilicon Si—C bond formation.[33]

The two structural analyses were performed on the principal expectation that their results would help to improve our understanding of factors that govern the competition between *intra-* and *inter*molecular C—H oxidative addition reactions occurring on coordinatively unsaturated phosphine complexes of ruthenium: A common problem with reactive poly(trimethylphosphine) systems such as $(Me_3P)_4Ru$ is their propensity for undergoing ligand cyclometallation rather than hydrocarbon C—H bond activation.[19,24] Metal/ligand fragments with chelating phosphines, e.g. $(Me_2PCH_2CH_2PMe_2)_2Ru$[34,35] or $\{P[(CH_2)_3PMe_2]_3\}Ru$,[3,6,9–11] on the other hand, are in general capable of intermolecular reactivity. The control of balance between *intra-* and *inter*molecular C—H cleavage on transition metal complexes has been attributed to arise from two opposing effects; (1) conformational strain within the ligand sphere, retarding the metallation of ligand C—H bonds due to an extra amount of activation energy required to bend the ligand over in the proper orientation; and (2) steric congestion about the metal centre, which prevents additional molecules from entering into the coordination sphere but may bring coordinated ligands a bit closer to the central metal atom and may therefore be thought to drive the sterically more encumbered systems toward *intra*molecular reactivity.[36] Both **1** and **2** appear to be particularly suited for evaluating the degree of steric encumbrance and/or conformational strain in chelated and non-chelated L_4Ru systems, as it can be anticipated that the additional two hydrido ligands required to stabilize the otherwise highly reactive 16e fragments will distort the phosphine coordination less than sterically more demanding substituents such as halides or alkyl groups.

EXPERIMENTAL

$(Me_3P)_4RuH_2$[15,16,19,24] (**1**) was prepared from $(Me_3P)_3Ru(H)(CH_2PMe_2)$ by reaction with methanol as described by Werner and Werner[19a,c] and was isolated in 71% yield by repeated high-vacuum sublimation at 50–80°C. Dihydride **2** was obtained from $(pp_3)RuCl_2$ and $LiAlH_4$, as reported previously,[5] and was also purified by sublimation at *ca* 70°C in the dynamic vacuum of a mercury diffusion pump. Single crystals of **1** grew when hexane solutions were allowed to evaporate slowly at ambient conditions; crystals of **2** suitable for X-ray analysis were collected from re-sublimed samples of the compound.

X-ray measurements were carried out at 20 ± 2°C on a Syntex $P2_1$ diffractometer using Mo-K_α radiation, as described elsewhere.[37] Data were corrected for Lorentz and polarization effects, but not for absorption or extinction.

In each structure the ruthenium, as well as several of the phosphorus atoms, were readily located by comparison of the Patterson map with the results of the TREF direct-methods attempts of SHELXS-86.[38] Subsequent alternate cycles of difference-Fourier synthesis and least-squares refinement (full-matrix for **1**, block-diagonal for **2**), employing the SHELX-76 program package[39] with scattering factors from the sources given therein, revealed the positions of the remaining non-hydrogen atoms. The structure models resulting for the two complexes were refined with allowance for anisotropic thermal motion of all non-hydrogen atoms. In both structures, many of the hydrogen atoms present were also located experimentally, although most of those belonging to the phosphine methyl and methylene groups did not refine well. Hence, only the ruthenium-bound hydrogens (as far as detected) were freely refined with isotropic thermal parameters, whilst those on the phosphine ligands were included into the molecular models in geometrically idealized positions with C—H distances constrained to 0.96 Å. No attempts were made to resolve the disorder of the methyl groups attached to the phosphorus atom P(4) in structure **1**, which became obvious from high values of the displacement factor coefficients characterizing the anisotropic thermal motion of the respective carbon atoms.

A summary of relevant crystallographic information and results is collected in Table 1. Atomic positional coordinates, thermal parameters, full lists of bond lengths and angles and lists of observed and calculated structure factors have been deposited as supplementary material with the Editor, from whom copies are available upon request.

Table 1. Summary of crystal data, intensity collection and structure refinement

	1	2
Crystal data		
Empirical formula	$C_{12}H_{38}P_4Ru$	$C_{15}H_{38}P_4Ru$
Molecular mass	407.40	443.43
Crystal system	Orthorhombic	
Space group	$P2_12_12_1$	$Pn2_1a$
a (Å)	9.359(2)	18.150(9)
b (Å)	15.141(4)	30.165(20)
c (Å)	15.260(4)	15.857(8)
V (Å^3)	2162.3(9)	8682(8)
Z	4	16
d_{calc} (g cm^{-3})	1.252	1.357
μ(Mo-K_α) (cm^{-1})	9.90	9.92
Intensity collection		
$2\theta_{min}$; $2\theta_{max}$ (deg.)	4.5; 65.0	4.5; 55.0
Recip. latt. segment	h: 0 → 15	h: 0 → 24
	k: 0 → 23	k: 0 → 40
	l: 0 → 24	l: 0 → 21
Number of data		
collected	4417	10,902
unique	4390	9553
used ($\|F_o\| > 4\sigma$)	3440	5194
Structure refinement		
Data/parameter ratio	21.10	7.00
R	0.047	0.064
R_w	0.57	0.068
Weighting scheme	$[\sigma^2(F_o)+0.001(F_o)^2]^{-1}$	
Largest diff. peak (e Å^{-3})	1.09	1.08
Largest diff. hole (e Å^{-3})	1.05	0.84

Atomic coordinates have also been deposited with the Cambridge Crystallographic Data Centre.

RESULTS

Complex **1** crystallized in the space group $P2_12_12_1$ (No. 19). Selected bond lengths and angles are collected in Table 2. A SCHAKAL drawing[40] of the molecule is shown in Fig. 1. Dihydride **2** was found to crystallize in space group $Pn2_1a$ (unconventional setting of $Pna2_1$, No. 33) with four crystallographically independent molecules that had structures similar to each other. A perspective view of one of these molecules is given in Fig. 2. Table 3

Table 2. Selected bond lengths and angles for dihydride **1**

Lengths (Å)	Angles (°) Ru	P(2)	P(3)	P(4)	H(1)	H(2)
2.306(1)	P(1)	98.8(1)	98.4(1)	99.2(1)	175.8(4)	87.3(3)
2.306(2)	P(2)		97.4(1)	101.8(1)	80.9(4)	173.9(3)
2.276(1)	P(3)			151.5(1)	77.6(4)	82.1(3)
2.289(2)	P(4)				84.9(3)	76.6(3)
1.507(9)	H(1)					93.0(5)
1.659(10)	H(2)					

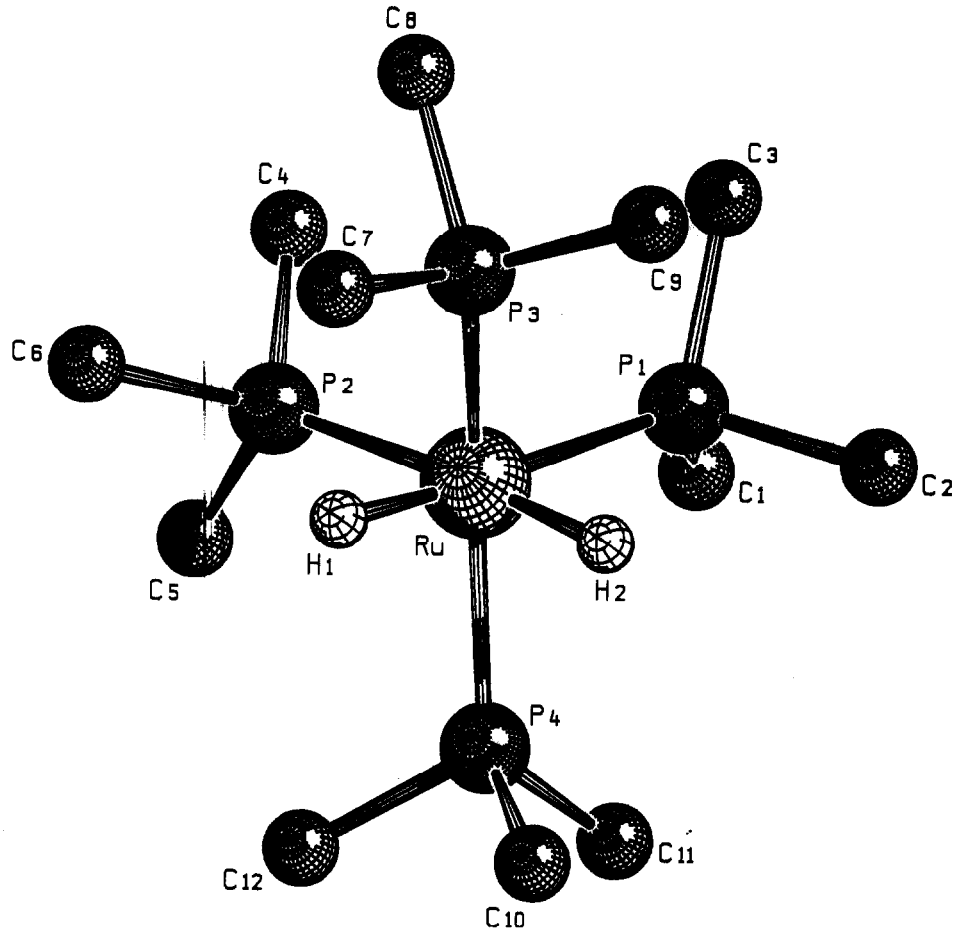

Fig. 1. Structure of $(Me_3P)_4RuH_2$ (**1**) with atom labelling (methyl hydrogen atoms omitted).

summarizes relevant interatomic distances and bond angles. For simplicity, only averaged values of the latter, such as also presented in Table 3, will be used throughout further discussion.

DISCUSSION

In both structures, the four phoshorus atoms and the two hydrogens bonded to the ruthenium atom are situated at the coordination sites of distorted octahedra.

For molecule **1** the distances between the central metal and the phosphorus atoms P(1) and P(2) *trans* to the hydride ligands are equally long, 2.306(2) Å, and are significantly elongated relative to those between the ruthenium centre and the phosphorus atoms P(3) and P(4), situated at mutually *trans* positions [2.276(1) and 2.289(2) Å]. Although this is expected from the usual *trans* influencing properties of metal-bound hydride and phosphine, respectively, all these distances remain remarkably short as compared to the Ru—P bond lengths for PMe_3 ligands located *trans* to Ru—H or *trans* to a second phosphine in other hydrido(trimethylphosphine)-ruthenium complexes of the composition *cis*-$(Me_3P)_4Ru(H)(X)$; X = Et,[17] NHPh,[26] OC_6H_4Me-4.[26,28] In these latter systems, the Ru—P separations for the phospine *trans* to the hydride substituent range from 2.326(3) Å in the ethyl compound[17] to 2.359(5) Å (averaged for two independent molecules) in the anilido complex[26] to 2.371(5) Å (mean value from two independent structure determinations) in the *p*-cresolato derivative,[26,28] with the metal–phosphorus bond lengths for the phosphines *trans* to each other varying between 2.313(3) Å in $(Me_3P)_4Ru(H)(Et)$[17] and 2.329(6) Å (average of 10 values) in $(Me_3P)_4Ru(H)(NHPh)$[26] and $(Me_3P)_4Ru(H)(OC_6H_4Me$-4),[26,28] respectively. The *trans* P—Ru—P distances measured for **1** are approximately as short as those reported for the Ru—P bonds opposite to the poor *trans* influence ligand $PhNH^{(-)}$ in the crystallographically independent molecules of *cis*-$(Me_3P)_4Ru(H)(NHPh)$, 2.268(2) and 2.271(2) Å,

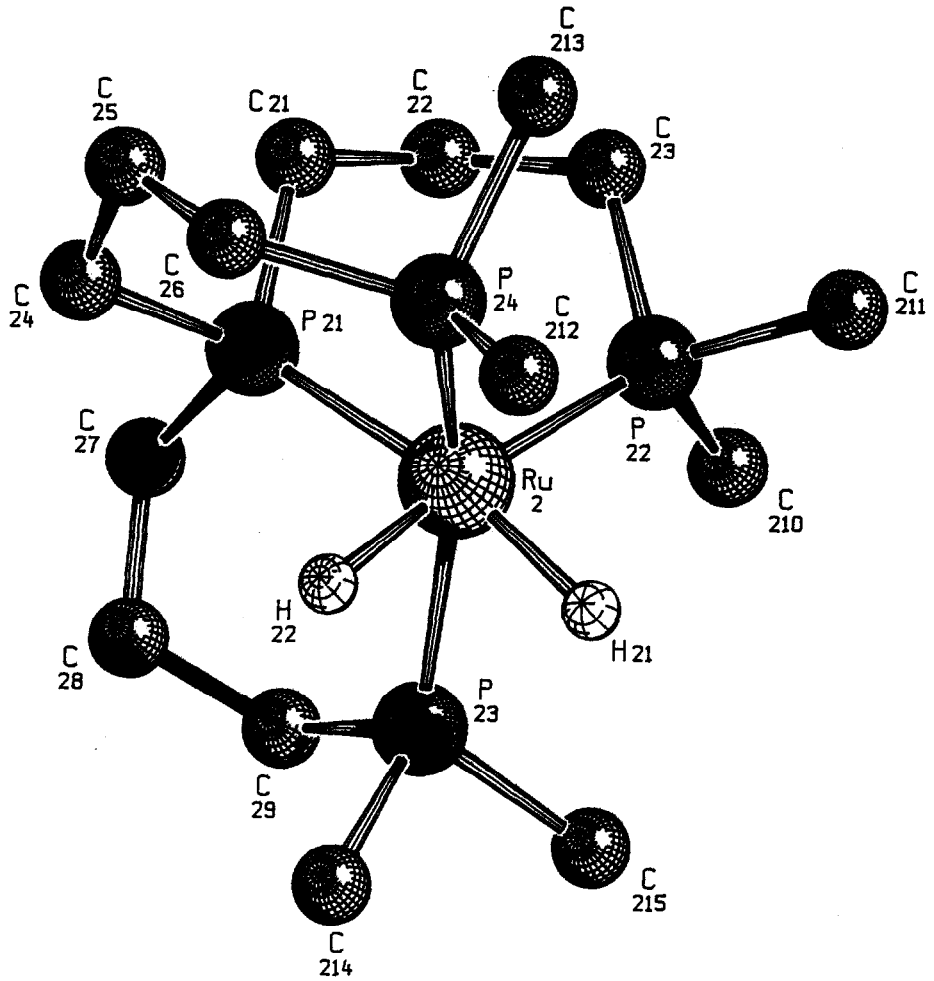

Fig. 2. Perspective view of one of the four independent molecules of $\{P[(CH_2)_3PMe_2]_3\}RuH_2$ (2) defining the atomic numbering scheme (phosphine hydrogen atoms removed for clarity).

respectively.[26] The contraction of the metal–phosphine separations in **1** is attributed to the stereochemically undemanding nature of hydride substituents relative to that of other anionic groups linked to ruthenium, since the wealth of structural data available for trimethylphosphine derivatives, *cis*-$(Me_3P)_4Ru(X)(Y)$, suggest that the separations *d*(Ru—P) for the mutually *trans*-arranged phosphines are particularly sensitive to the steric demand of the two additional ligands X and Y, increasing in the order X, Y = H, H [2.283(7) Å] < H, Et [2.313(3) Å][17] < $—CH_2CH_2—$ [2.326(3) Å][17] ≈ H, NHPh [2.329(9) Å][26] ≈ H, OC_6H_4Me-4 [2.330(3) Å][26,28] < $—CH_2C(=CHR)O—$* [2.343(2) Å][27d] < $—CH_2C(O)CH_2—$† [2.355(3) Å][27d] ≈ —*o*-$C_6H_4C(=CH_2)O—$‡ [2.357(1) Å],[27c] as shown by the distances given parenthetically as mean values for the two *trans* bonds.

For the four independent molecules of structure **2**, the average separation between the central atom and the terminal Me_2P group *trans* to one of the hydride ligands, 2.292(6) Å, is longer than that of 2.270(5) Å between the metal and the bridging phosphorus atom of the tripodal-tetradentate pp_3 system, but is barely elongated when set against the average length of the Ru—P bonds in the *trans* P—Ru—P moieties of the four molecules, 2.282(9) Å. These parameters can be compared directly with those of several aryl(hydrido)ruthenium(II) derivatives of the pp_3 ligand, as there exist only marginal differences in *trans* influencing properties between the hydride and aryl groups. For a series of $(pp_3)Ru(H)(Ar)$ compounds with Ar = C_6H_5, C_6H_4Me-3, $C_6H_3Me_2$-3,4, $C_6H_3Me_2$-3,5 and $C_6H_4CF_3$-3, the length of the bond between the

* Ligand portion of a flat four-membered metallacycle (dihedral angle, 1.9°).[27d]

† Ligand portion of a tilted four-membered metallacycle (dihedral angle, 45.6°).[27d]

‡ Ligand portion of a twisted five-membered metallacycle (twist angle, 3.0°).[27c]

Table 3. Selected bond lengths and angles for dihydride **2**

Molecule 1						
Lengths	Angles (°)					
(Å)	Ru(1)	P(12)	P(13)	P(14)		H(12)
2.275(4)	P(11)	94.3(2)	96.0(2)	90.9(2)		90(1)
2.283(5)	P(12)		102.9(2)	102.0(2)		176(1)
2.291(4)	P(13)			153.5(2)		76(2)
2.276(4)	P(14)					79(2)
H(11) not localized						
1.65(1)	H(12)					
Molecule 2						
Lengths	Angles (°)					
(Å)	Ru(2)	P(22)	P(23)	P(24)	H(21)	H(22)
2.262(5)	P(21)	93.0(2)	96.1(2)	91.2(2)	170(1)	91(1)
2.299(5)	P(22)		102.4(2)	102.2(2)	94(2)	171(1)
2.292(4)	P(23)			153.9(2)	76(2)	78(2)
2.291(5)	P(24)				93(2)	77(2)
1.75(4)	H(21)					77(2)
1.78(6)	H(22)					
Molecule 3						
Lengths	Angles (°)					
(Å)	Ru(3)	P(32)	P(33)	P(34)		
2.273(4)	P(31)	93.4(2)	96.2(2)	91.7(2)		
2.296(5)	P(32)		103.6(2)	103.3(2)		
2.267(5)	P(33)			151.4(2)		
2.272(4)	P(34)					
H(31) not well refined						
H(32) not localized						
Molecule 4						
Lengths	Angles (°)					
(Å)	Ru(4)	P(42)	P(43)	P(44)		
2.269(4)	P(41)	93.2(1)	96.4(2)	90.8(2)		
2.288(5)	P(42)		102.4(2)	102.1(2)		
2.284(4)	P(43)			154.0(2)		
2.285(5)	P(44)					
H(41) not well refined						
H(42) not localized						
Averaged values:						
Lengths	Angles (°)					
(Å)	Ru	P(2)	P(3)	P(4)		
2.270(5)	P(1)	93.5(5)	96.3(2)	91.2(4)		
2.292(6)	P(2)		102.8(5)	102.4(5)		
2.284(10)	P(3)			153.2(1.0)		
2.281(7)	P(4)					

ruthenium atom and the Me_2P substituent opposite to Ru—H has previously been determined as 2.342(5) Å, on average.[9–11] Thus, the distance of the Me_2P group *trans* to hydrogen from the central metal is considerably shorter in $(pp_3)RuH_2$ than in $(pp_3)Ru(H)(Ar)$, and the same applies to the average values obtained for $d(Ru—PMe_2)$ in the *trans* P—Ru—P portions of the different molecules, 2.282(9) Å for **2** but 2.310(6) Å for the aryl hydrides,[9–11] as well as to the separations between the ruthenium centre and the bridging phosphorus atom *trans* to hydride or aryl, 2.270(5) Å for dihydride **2** vs 2.289(3) Å for the various aryl hydrido complexes.[9–11] $Ru—PMe_2$ bonds *trans* to hydrogen or phosphorus that are significantly longer than in structure **2** have also been observed for $(pp_3)Ru(H)(Cl)$, where the mutually *trans*-coordinated Me_2P substituents and the Me_2P group *trans* to the Ru—H linkage are at distances from the ruthenium atom of 2.310(2) and 2.343(2) Å, respectively.[7] Thus, the two families of complexes *cis*-$(Me_3P)_4Ru(H)(X)$ and $(pp_3)Ru(H)(X)$ (X = alkyl, aryl, arylamide, aryloxide, halide) are structurally similar in that in both series of compounds it is the dihydride that is characterized by the shortest Ru—P distances, as long as bonds opposite to the very weak *trans* influence ligands containing highly electronegative donor atoms are not considered.

In structures **1** and **2** all P—Ru—P angles between phosphorus atoms at mutually *cis* positions are considerably larger than 90°, while the axial Ru—P bonds *trans* to each other are bent towards the hydride ligands with P—Ru—P angles much smaller than 180°. Both deformations result from steric repulsions that are larger between the methyl substituents on the phosphorus atoms *cis* to each other than those between the metal-bound hydrogens and the *cis*-located PMe_3 ligands and Me_2P substituents, respectively. In agreement with the stereochemically undemanding nature of the hydride, as compared to other anionic ligands, these distortions are much more pronounced in dihydrides **1** and **2** than in *cis*-$(Me_3P)_4Ru(H)(X)$ or $(pp_3)Ru(H)(X)$, where X = alkyl, aryl, amide, alkoxide or halide. Thus, the sum of *cis* angles, $\Sigma(PRuP)_{cis}$, which would be 450° for an ideal octahedron, adds up to 495.6° for compound **1** and 486.2° for the averaged structure **2**. Values of $\Sigma(PRuP)_{cis}$ found for other *cis*-L_4Ru complexes with trimethylphosphine ligands are $\approx$ 479° for $L_4Ru(CH_2CH_2)$,[17] 482–483° for $L_4Ru(H)(Et)$[17] and $L_4Ru(H)(NHPh)$,[26] and *ca* 484° for $L_4Ru(H)(OC_6H_4Me\text{-}4)$.[26,28] In the structures of $(pp_3)Ru(H)(Cl)$[7] and $(pp_3)Ru(H)(Ar)$[9–11] (for aryl ligands Ar, see above), *cis* P—Ru—P angles, resulting in approximately constant sums of 476–477°, have been observed in previous work.

The finding that the angle sum $\Sigma(PRuP)_{cis}$ obtained for dihydride **1** exceeds that of its chelated analogue **2** by nearly 10°, and the observation that the angle *trans* P—Ru—P determined as 151.5° for *cis*-$(Me_3P)_4RuH_2$ tends to be some two to three degrees smaller than that of 153.5–154.0° measured for three of the four independent molecules of structure **2***, are in agreement with the view that there is a higher degree of steric crowding about the central metal in *cis*-$(Me_3P)_4Ru$ than in $(pp_3)Ru$ systems.[6] Hence, a 16e fragment, *cis*-$L_4Ru(0)$, coordinated by the tripodal-tetradentate $P[(CH_2)_3PMe_2]_3$ ligand can indeed be thought of as being more open and more accessible at the central metal than a formally related fragment with four monodentate PMe_3 ligands bonded to the ruthenium atom. This in turn corresponds to the observed propensity of *cis*-$(Me_3P)_4Ru(0)$ to stabilize by metal atom insertion across C—H bonds of its own ligands,[19,24] as contrasted with the ability of $(pp_3)Ru(0)$ to form stable products by oxidative addition of solvent C—H bonds.[3,6,9–11]

In view of the limited accuracy obtained for the positions of the hydrido ligands of both **1** and **2**, it is difficult to discuss and compare Ru—H bond lengths and angles.

Acknowledgements—We gratefully acknowledge generous support by the Volkswagen-Stiftung (Hannover) and the Fonds der Chemischen Industrie (Frankfurt/Main). We are furthermore indebted to Degussa AG (Hanau) for generous gifts of previous metal salts.

REFERENCES

1. A. Saare and L. Dahlenburg, *Z. Naturforsch., B: Anorg. Chem., Org. Chem.* 1992, **47b**, 247.
2. A. Saare and L. Dahlenburg, *GIT Fachz. Lab.* 1992, **36**, 738.
3. L. Dahlenburg, in *Organic Synthesis via Organometallics, Proc. 4th Symp., Aachen, July* 15–18, 1992 (Edited by D. Enders and H.-J. Gais). Friedr. Vieweg & Sohn Verlagsgesellschaft, Braunschweig, in press.
4. M. Antberg, C. Prengel and L. Dahlenburg, *Inorg. Chem.* 1984, **23**, 4170.
5. M. Antberg and L. Dahlenburg, *Inorg. Chim. Acta* 1986, **111**, 73.
6. M. Antberg and L. Dahlenburg, *Angew. Chem.* 1986, **98**, 274; *Angew. Chem., Int. Edn Engl.* 1986, **25**, 260.

* The corresponding angle in molecule 3 of structure **2** is smaller, 151.4°, presumably due to solid-state effects rather than different steric crowding within the coordination spheres of the individual molecules.

7. M. Antberg and L. Dahlenburg, *Acta Cryst.* 1986, **C42**, 997.
8. M. Antberg and L. Dahlenburg, *J. Organomet. Chem.* 1986, **312**, C67.
9. M. Antberg, L. Dahlenburg, K.-M. Frosin and N. Höck, *Chem. Ber.* 1988, **121**, 859.
10. L. Dahlenburg and K.-M. Frosin, *Chem. Ber.* 1988, **121**, 865.
11. L. Dahlenburg, K.-M. Frosin, S. Kerstan and D. Werner, *J. Organomet. Chem.* 1991, **407**, 115.
12. (a) R. A. Andersen, R. A. Jones, G. Wilkinson, M. B. Hursthouse and K. M. A. Malik, *J. Chem. Soc., Chem. Commun.* 1977, 283; (b) R. A. Andersen, R. A. Jones and G. Wilkinson, *J. Chem. Soc., Dalton Trans.* 1978, 446.
13. R. A. Jones and G. Wilkinson, *J. Chem. Soc., Dalton Trans.* 1979, 472.
14. R. A. Jones, F. Mayor Real, G. Wilkinson, A. M. R. Galas, M. B. Hursthouse and K. M. A. Malik, *J. Chem. Soc., Dalton Trans.* 1980, 511.
15. R. A. Jones, G. Wilkinson, I. J. Colquohoun, W. McFarlane, A. M. R. Galas and M. B. Hursthouse, *J. Chem. Soc., Dalton Trans.* 1980, 2480.
16. J. A. Statler, G. Wilkinson, M. Thornton-Pett and M. B. Hursthouse, *J. Chem. Soc., Dalton Trans.* 1984, 1731.
17. W.-K. Wong, K. W. Chiu, J. A. Statler, G. Wilkinson, M. Motevalli and M. B. Hursthouse, *Polyhedron* 1984, **3**, 1255.
18. H. Schmidbaur and G. Blaschke, *Z. Naturforsch., B: Anorg. Chem., Org. Chem.* 1980, **35b**, 584.
19. (a) R. Werner, Dissertation, Universität Würzburg (1981); (b) H. Werner and R. Werner, *J. Organomet. Chem.* 1981, **209**, C60; (c) J. Gotzig, R. Werner and H. Werner, *J. Organomet. Chem.* 1985, **285**, 99.
20. (a) C. E. Graimann and M. L. H. Green, *J. Organomet. Chem.* 1984, **275**, C12; (b) V. C. Gibson, C. E. Graimann, P. M. Hare, M. L. H. Green, J. A. Bandy, P. D. Grebenik and K. Prout, *J. Chem. Soc., Dalton Trans.* 1985, 2025.
21. V. V. Mainz and R. A. Andersen, *Organometallics* 1984, **3**, 675.
22. J. F. Hartwig, R. G. Bergman and R. A. Andersen, *J. Organomet. Chem.* 1990, **394**, 417.
23. (a) J. F. Hartwig, R. A. Andersen and R. G. Bergman, *J. Am. Chem. Soc.* 1989, **111**, 2717; (b) J. F. Hartwig, R. G. Bergman and R. A. Andersen, *J. Am. Chem. Soc.* 1991, **113**, 3404.
24. J. F. Hartwig, R. A. Andersen and R. G. Bergman, *J. Am. Chem. Soc.* 1991, **113**, 6492.
25. J. F. Hartwig, R. G. Bergman and R. A. Andersen, *J. Am. Chem. Soc.* 1991, **113**, 6499.
26. J. F. Hartwig, R. A. Andersen and R. G. Bergman, *Organometallics* 1991, **10**, 1875.
27. (a) J. F. Hartwig, R. G. Bergman and R. A. Andersen, *J. Am. Chem. Soc.* 1990, **112**, 3234; (b) J. F. Hartwig, R. A. Andersen and R. G. Bergman, *J. Am. Chem. Soc.* 1990, **112**, 5670; (c) J. F. Hartwig, R. G. Bergman and R. A. Andersen, *Organometallics* 1991, **10**, 3326; (d) J. F. Hartwig, R. G. Bergman and R. A. Andersen, *Organometallics* 1991, **10**, 3344.
28. K. Osakada, K. Oshiro and A. Yamamoto, *Organometallics* 1991, **10**, 404.
29. J. C. Calabrese, M. C. Colton, T. Herskovitz, U. Klabunde, G. W. Parshall, D. L. Thorn and T. H. Tulip, *Ann. N.Y. Acad. Sci.* 1983, **415**, 302.
30. M. B. Hursthouse and K. M. A. Malik, personal communication to R. A. Jones and G. Wilkinson.[13]
31. K.-M. Frosin, Dissertation, Universität Hamburg (1989); see also ref. 11.
32. (a) T. Mitsudo, Y. Nakagawa, H. Watanabe, K. Watanabe, H. Misawa and Y. Watanabe, *J. Chem. Soc., Chem. Commun.* 1981, 496; (b) T. Mitsudo, Y. Nakagawa, K. Watanabe, Y. Hori, H. Misawa, H. Watanabe and Y. Watanabe, *J. Org. Chem.* 1985, **50**, 565.
33. L. J. Procopio and D. H. Berry, *J. Am. Chem. Soc.* 1991, **113**, 4039.
34. J. Chatt and J. M. Davidson, *J. Chem. Soc.* 1965, 843.
35. (a) S. D. Ittel, C. A. Tolman, A. D. English and J. P. Jesson, *J. Am. Chem. Soc.* 1976, **98**, 6073; (b) C. A. Tolman, S. D. Ittel, A. D. English and J. P. Jesson, *J. Am. Chem. Soc.* 1978, **100**, 4080; (c) S. D. Ittel, C. A. Tolman, A. D. English and J. P. Jesson, *J. Am. Chem. Soc.* 1978, **100**, 7577; (d) C. A. Tolman, S. D. Ittel, A. D. English and J. P. Jesson, *J. Am. Chem. Soc.* 1979, **101**, 1742.
36. R. H. Crabtree, *Chem. Rev.* 1985, **85**, 245.
37. K.-M. Frosin and L. Dahlenburg, *Inorg. Chim. Acta* 1990, **167**, 83.
38. G. M. Sheldrick, SHELXS-86, a FORTRAN-77 Program for the Solution of Crystal Structures from Diffraction Data. Universität Göttingen (1986).
39. G. M. Sheldrick, SHELX-76, a Program for Crystal Structure Determination. University of Cambridge (1976).
40. E. Keller, SCHAKAL, a FORTRAN Program for the Graphical Representation of Molecular Models. Universität Freiburg (1988).

Polyhedron Vol. 12, No. 4, pp. 435–444, 1993
Printed in Great Britain

0277–5387/93 $6.00+.00
© 1993 Pergamon Press Ltd

C-SPIROPHOSPHORANE-SUBSTITUTED PHOSPHORUS YLIDES*

IGOR V. SHEVCHENKO, AXEL FISCHER, PETER G. JONES and REINHARD SCHMUTZLER†

Institut für Anorganische und Analytische Chemie der Technischen Universität, Hagenring 30, 3300 Braunschweig, Germany

(*Received* 10 *August* 1992; *accepted* 29 *September* 1992)

Abstract—The methylenephosphinophosphorane **2** was methylated by MeI forming the phosphonium salt **4**, which is stable in crystalline form but rearranges into isomer **10** when heated in chloroform solution at 80°C in a sealed tube for 16 h. The isomerization occurs by elimination of N,N′-dimethylcarbodiimide and formation of the methylenephosphonium phosphonate **5**. Compound **5** reacts with the carbodiimide via its ylide form **5a** to give the ylide **9**, which is transformed reversibly into **10**. Compound **2** shows unusual properties, such as its reaction with hexafluoroacetone via its ylide form **2a** forming the addition product **12**. The ylide structure of **12** was confirmed by X-ray analysis. The coordination geometry at P(2) is distorted trigonal bipyramidal, with axial substituents O (of the chelate ring) and N (of the four-membered ring). The bond lengths and angles at the ylidic carbon confirm the partial multiple bond character of the P—C bonds. There is evidence for a C—H···O hydrogen bond from the carbon atom bearing the CF_3 groups. The ylide **13** was obtained by the elimination of HI from **4** with triethylamine. Compound **2** reacted with CCl_4 to give the P-chloroylide **15**, as well as a small amount of **16**, which contains two phosphorus atoms of opposite formal charge and different coordination number (λ^4P^+, λ^6P^-). Compound **16** is isomeric to **3**, which we obtained earlier and investigated by X-ray analysis.

In previous work[1,2] we described a new rearrangement in phosphorus chemistry; the spirophosphorane **1** was transformed gradually into the isomeric compound **2**. The methylenephosphinophosphorane **2**, containing one phosphine and one spirophosphorane phosphorus atom bridged via a methylene group, is a new type of compound and shows unusual chemical properties. For example, its oxidation with tetrachloroorthobenzoquinone (TOB) leads to the formation of the unusual zwitterionic compound **3**, containing two phosphorus atoms of opposite formal charge and different coordination number (λ^4P^+, λ^6P^-) [eq. (1)]. The formation of **3** is probably the result of the addition of TOB to the two phosphorus atoms of compound **2**.[2]

* Dedicated to Professor Robert W. Parry on the occasion of his 75th birthday.

† Author to whom correspondence should be addressed.

RESULTS AND DISCUSSION

The chemical properties exhibited by the methylenephosphinophosphorane **2** are closely connected to the presence of the methylene group between two electronegative phosphorus groups. The hydrogen atoms possess high acidity, which, together with the presence of bulky substituents at the phosphorus atoms, should promote the formation of stable ylides. This article is devoted to the investigation of this feature.

The methylenephosphinophosphorane **2** reacts with methyl iodide to give the phosphonium salt **4**. The nucleophilic properties of the trivalent phosphorus atom of **2** are substantially reduced and its methylation occurs slowly; it is completed in 10–16 h when a large excess of alkylation agent is used [eq. (2)]. The phosphonium salt **4** is a colourless crystalline product, insoluble in non-polar organic solvents. The structure of **4** is confirmed by its analytical and NMR spectroscopic data. The ^1H NMR spectrum shows a characteristic double doublet for

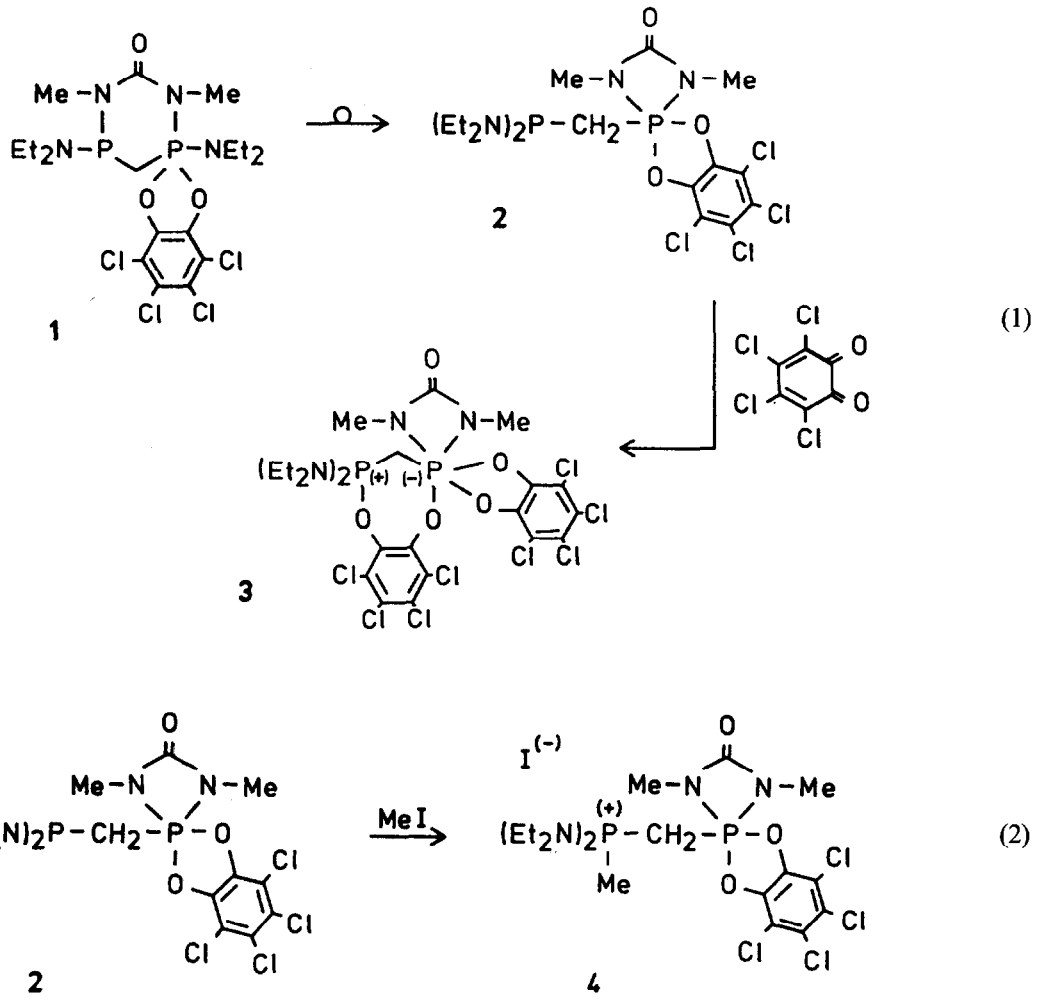

the methylene group P—CH_2—P at 3.99 ppm, which testifies to the high acidity of the methylene protons. In the ^{31}P NMR spectrum there are two doublets at 53.39 and −34.14 ppm. The coupling constant $^2J(PP)$ is small, amounting to only 5.1 Hz, although its value in the starting product **2** is 96 Hz.

The phosphonium salt **4** is very sensitive to moisture. Its hydrolysis proceeds according to eq. (3). The addition of the first molecule of water leads to the elimination of N,N′-dimethylurea (**7**) and to the formation of the methylenephosphonium phosphonate (**5**).

Compound **5** was isolated as a colourless crystalline product. The phosphonium and the tetrachlorophenoxyphosphonate groups—two powerful electron-withdrawing groups, attached to the bridging methylene group—make this compound a strong C—H acid. The CH_2 group manifests itself in the ^1H NMR spectrum as a characteristic double doublet with a large $\delta(H)$ value, 5.12 ppm.

Like the starting phosphonium salt **4**, compound **5** is very sensitive to moisture. Careful hydrolysis of **5** leads to the cleavage of the dioxaphosphole ring with the formation of compound **6**. This process gives no by-products and **6** is, therefore, obtained in the reaction solution in NMR spectrally pure form. The cleavage of one of the P—O bonds of the phosphole heterocycle is confirmed by the ^1H NMR spectrum, where the CH_2 group gives rise to a double doublet at only 3.93 ppm. For the two OH groups of **6** one broad signal at 10.35 ppm can be seen, probably because of exchange processes. The ^{13}C NMR spectrum of **6** shows six signals for the carbon atoms of the benzene ring, one of them being a doublet with $^1J(PC) = 9.85$ Hz.

Further hydrolysis of **6** takes place considerably more slowly and leads to the elimination of the *o*-dioxytetrachlorophenyl group.

The phosphonium salt **4** is stable in its crystalline form. Upon heating the crystals to 100°C no changes are seen in the ^{31}P and ^1H NMR spectra. However, heating **4** in chloroform solution in a sealed tube at 80°C for 16 h brings about the elimination of N,N′-dimethylcarbodiimide (**8**) with the formation of **5** [eq. (4)].

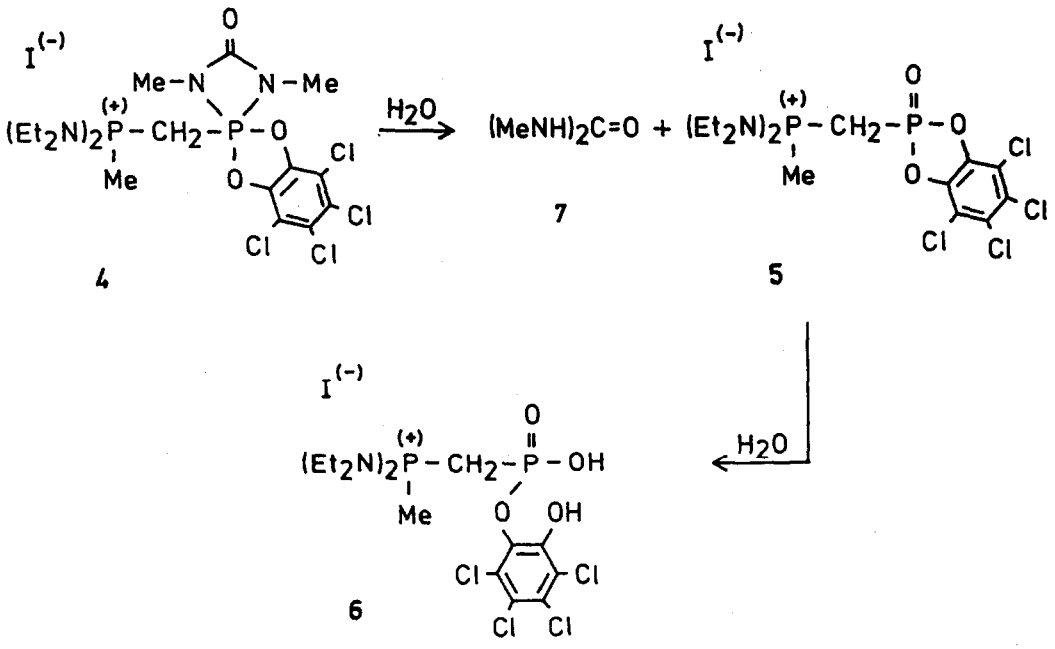

(3)

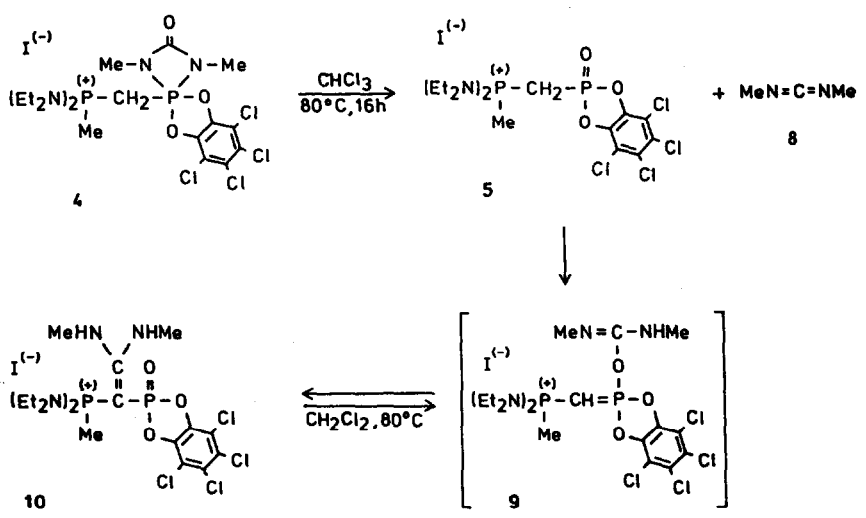

(4)

Under the reaction conditions some of compound **5** reacts with the carbodiimide to give the addition product **9**, which has an ylide structure. The ^{31}P NMR spectrum of the reaction mixture shows the presence of **5** and **9**. Compound **5** can be quantitatively isolated from the mixture as a crystalline product. Samples of **5** obtained by two independent methods (see above) gave the same NMR spectroscopic parameters. After the separation of **5** the reaction solution contains, judging by the ^{31}P NMR spectrum, only compound **9**, exhibiting two doublets at 53.82 and 58.43 ppm with $^2J(PP) = 65.3$ Hz. Compound **9** is stable only in solution and cannot be isolated in a pure state. Careful removal of the solvent *in vacuo* (0.05 mm) gives rise to its isomerization into compound **10**.

The crystalline compound **10** remaining after removing the solvent yields the addition product of the protons of the active methylene group to the carbodiimide. We were unable to recrystallize **10** to investigate its structure by X-ray analysis. However, the structure of **10** was confirmed by ^1H and ^{31}P NMR spectra and is in agreement with the results of the elemental analysis.

The formation of **10** is also suggested by literature data. For example, it is known that strong CH acids add to carbodiimides with the formation of a C=C double bond.[3–5] For phosphorus-containing CH acids the analogous addition reaction has been carried out by Fild *et al.*[6]

Compounds **4** and **10** are isomers, but the reverse transformation **10** → **4** cannot be realized. How-

ever, **10** can again be partly transformed into the ylide form **9**. After dissolving **10** in methylene chloride and heating the solution for 10 h at 80°C in a sealed tube, the formation of the intermediate ylide form **9** is observed by ^{31}P NMR spectroscopy.

The suggested structure of **9** is confirmed by its readiness to undergo the Wittig reaction with benzaldehyde. It is interesting that this process is accompanied by the patial isomerization of **9** into **10**. Isomer **10** does not possess an ylide structure and does not react with benzaldehyde.

The structure of **9** is also confirmed by independent synthesis. Compound **5** reacted under the same conditions (heating in chloroform or methylene chloride at 80°C in a sealed tube) with dicyclohexylcarbodiimide with the formation of a product with the same signals in the ^{31}P NMR spectrum. Compound **5** added to carbodiimide not as a CH acid, but as the ylide form **5a** [eq. (5)]. The ability of the phosphoryl group to undergo enolization has been known since 1976.[7] This process requires the presence of sufficiently strong acidifying substituents (for example, the phosphonium group) at the central carbon atom of the $P—CH_2—P$ group.[8,9]

The suggested mode of formation of **9** was indirectly confirmed by the reaction of the methylenephosphinophosphorane **2** with hexafluoroacetone. In spite of an excess of hexafluoroacetone, the reaction did not lead to the oxidation product **11**, but to the ylide **12** which is an addition product of **2** to the carbonyl group of hexafluoroacetone. The reaction presumably proceeds through the ylide form **2a**, which, as in the case of compound **5**, cannot be detected by NMR spectral methods [eq. (6)].

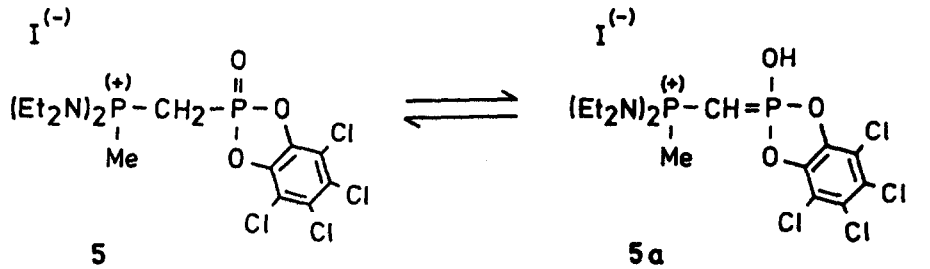

(5)

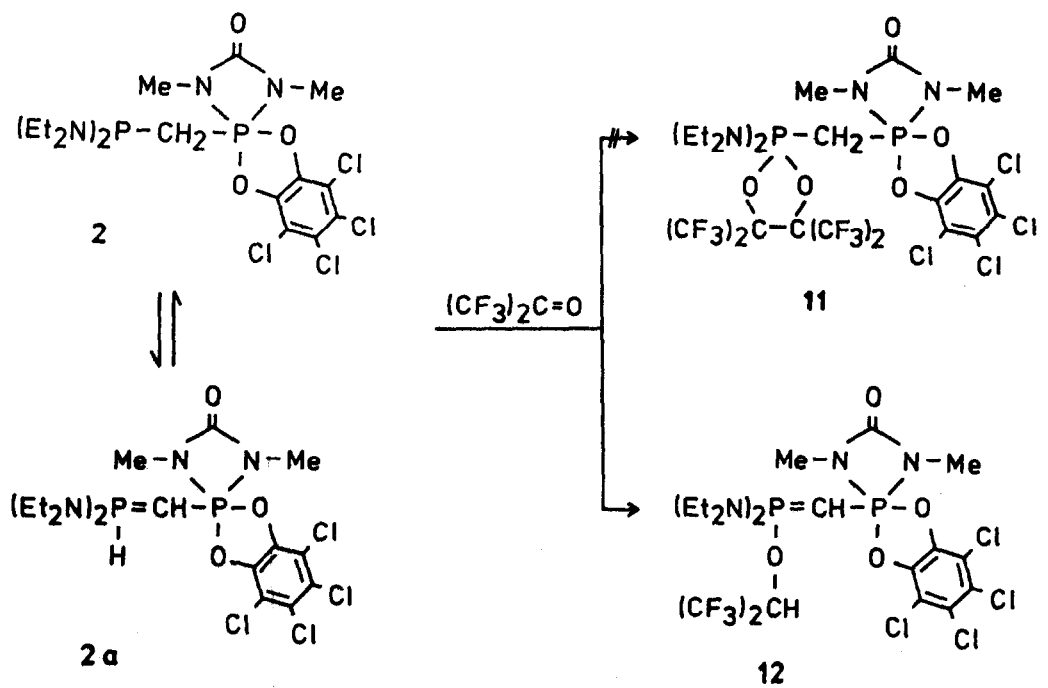

(6)

Ylide **12** is a colourless stable crystalline product, the structure of which is in accordance with the NMR spectral and analytical data. The ^{31}P NMR spectrum contains two characteristic doublets

(64.35 and −29.65 ppm) with a similar value of the ^2J(PP) coupling constant (49.7 Hz) as in **9**. The ^{1}H NMR spectrum has a low-field signal for the $(CF_3)_2CH$ proton (5.43 ppm) as a well-resolved double quartet. The detailed structure of **12** was established by X-ray analysis (Fig. 1 and Table 1).

The coordination geometry at P(1) is tetrahedral, although O(3)—P(1)—N(4) (98.7°) is narrower and O(3)—P(1)—C(7) and N(4)—P(1)—C(7) (114.4, 120.2°) wider than the ideal angles. There is no obvious reason for these irregularities.

The atom P(2) displays trigonal bipyramidal coordination geometry; the axial substituents are O(1) and N(1) [O(1)—P(2)—N(1) 165.0°], with N(2), O(2) and C(7) equatorial. The four-membered ring (which is planar, r.m.s. deviation 0.5 pm) is necessarily a major cause of distortion from ideal angles [e.g. N(1)—P(2)—N(2) 74.0°]. The axial bonds are *ca* 10 pm longer than equatorial bonds to the same element.

The bonding at the ylidic carbon C(7) is described by the parameters P(1)—C(7), 169.4, P(2)—C(7), 168.8 pm (indicating appreciable multiple bond character), P(1)—C(7)—P(2), 130.9°.

The hydrogen atom at C(10), the central carbon atom derived from the hexafluoracetone molecule, should possess some acidic character; consistent with this, a short contact C(10)···O(4) $(1-x, 1-y, -z)$, 315 pm, is observed, which may be a C—H···O hydrogen bond.

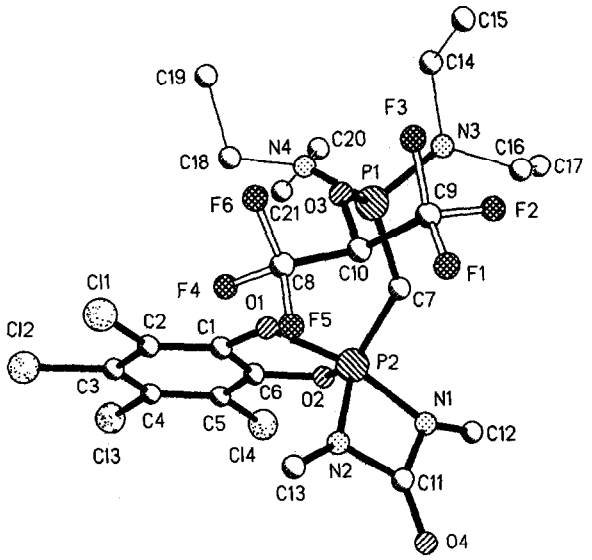

Fig. 1. A molecule of compound **12** in the crystal. Radii are arbitrary; hydrogen atoms are omitted.

The synthesis of ylides on the basis of the methylenephosphinophosphorane **2** can be carried

Table 1. Selected bond lengths (pm) and angles (°) for compound **12**

P(1)—O(3)	162.7(2)	P(1)—N(3)	163.1(3)
P(1)—N(4)	162.6(3)	P(1)—C(7)	169.4(3)
P(2)—O(1)	175.9(2)	P(2)—O(2)	167.4(2)
P(2)—N(1)	176.3(3)	P(2)—N(2)	169.2(3)
P(2)—C(7)	168.8(4)	P(2)···C(11)	228.5(4)
O(4)—C(11)	121.1(4)	N(1)—C(11)	135.8(4)
N(1)—C(12)	145.1(4)	N(2)—C(11)	140.1(4)
N(2)—C(13)	145.1(4)		

O(3)—P(1)—N(3)	107.2(1)	O(3)—P(1)—N(4)	98.7(1)
N(3)—P(1)—N(4)	107.1(2)	O(3)—P(1)—C(7)	114.4(1)
N(3)—P(1)—C(7)	108.3(2)	N(4)—P(1)—C(7)	120.2(2)
O(1)—P(2)—O(2)	89.3(1)	O(1)—P(2)—N(1)	165.0(1)
O(2)—P(2)—N(1)	90.8(1)	O(1)—P(2)—N(2)	91.9(2)
O(2)—P(2)—N(2)	110.7(1)	N(1)—P(2)—N(2)	74.0(1)
O(1)—P(2)—C(7)	95.2(1)	O(2)—P(2)—C(7)	119.8(1)
N(1)—P(2)—C(7)	97.8(2)	N(2)—P(2)—C(7)	129.0(2)
P(2)—N(1)—C(11)	93.2(2)	P(2)—N(1)—C(12)	135.3(2)
C(11)—N(1)—C(12)	125.5(3)	P(2)—N(2)—C(11)	94.8(2)
P(2)—N(2)—C(13)	136.9(2)	C(11)—N(2)—C(13)	125.5(3)
P(1)—N(3)—C(14)	119.4(3)	P(1)—N(3)—C(16)	126.6(3)
C(14)—N(3)—C(16)	113.0(3)	P(1)—N(4)—C(18)	126.6(2)
P(1)—N(4)—C(20)	117.3(2)	C(18)—N(4)—C(20)	115.8(3)
P(1)—C(7)—P(2)	130.9(2)	O(4)—C(11)—N(1)	132.6(3)
O(4)—C(11)—N(2)	129.5(3)	N(1)—C(11)—N(2)	97.9(3)
N(3)—C(14)—C(15)	118.5(4)	N(3)—C(16)—C(17)	111.8(6)
N(4)—C(18)—C(19)	113.6(3)	N(4)—C(20)—C(21)	115.1(3)

out in another way. The methylation of **2** by MeI led to the phosphonium salt **4** containing an iodide anion and a mobile α-CH hydrogen atom as a potential leaving group. The elimination of HI occurs very rapidly under the action of triethylamine with the formation of the P—Me substituted ylide **13** [eq. (7)].

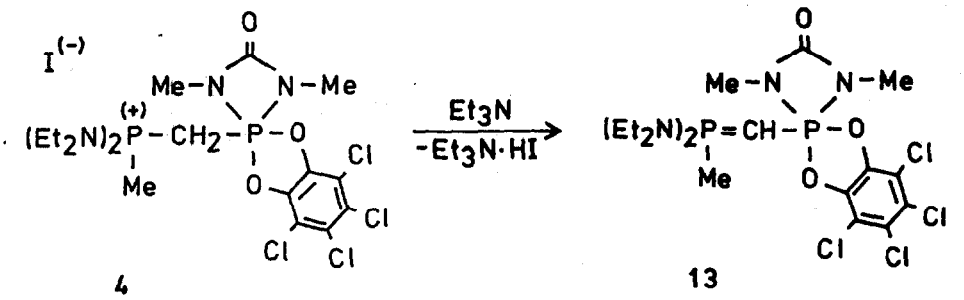

4 13 (7)

The ylide **13** was isolated as a colourless crystalline product, the structure of which was confirmed by analytical and NMR spectral methods.

It is known that phosphines containing a mobile C—H bond in the α-position to a trivalent phosphorus atom react very readily (even at −78°C) with carbon tetrahalides with the formation of P-halogenoylides.[10] In this respect the methylenephosphinophosphorane **2** represents an interesting starting material. It was found that the nucleophilic properties of **2** are substantially reduced; reaction with CCl_4 takes place only when it is used as a solvent, and upon heating [eq. (8)].

After 10 min at 80°C the ^{31}P NMR spectrum of the reaction mixture shows only the signals of the ylide **14** as two doublets at 74.10 and −32.75 ppm. The coupling constant $^2J(PP)$ is 46.2 Hz. Compound **14** can be obtained in good yield, but it is stable only in solution. All our attempts to isolate this compound in pure crystalline form failed and only a slow decomposition with the formation of a complicated mixture of products was observed.

Further heating of the mixture of **2** with CCl_4 at 80°C led to the appearance of small amounts of **15** and **16**, containing six-coordinate phosphorus atoms, as well as small quantities of other unidentified products. The phosphorate **16** was observed ^{31}P NMR spectroscopically in a yield of *ca* 1–2% ($\delta_P = -103$ ppm). Earlier we obtained this compound in another way and confirmed its structure

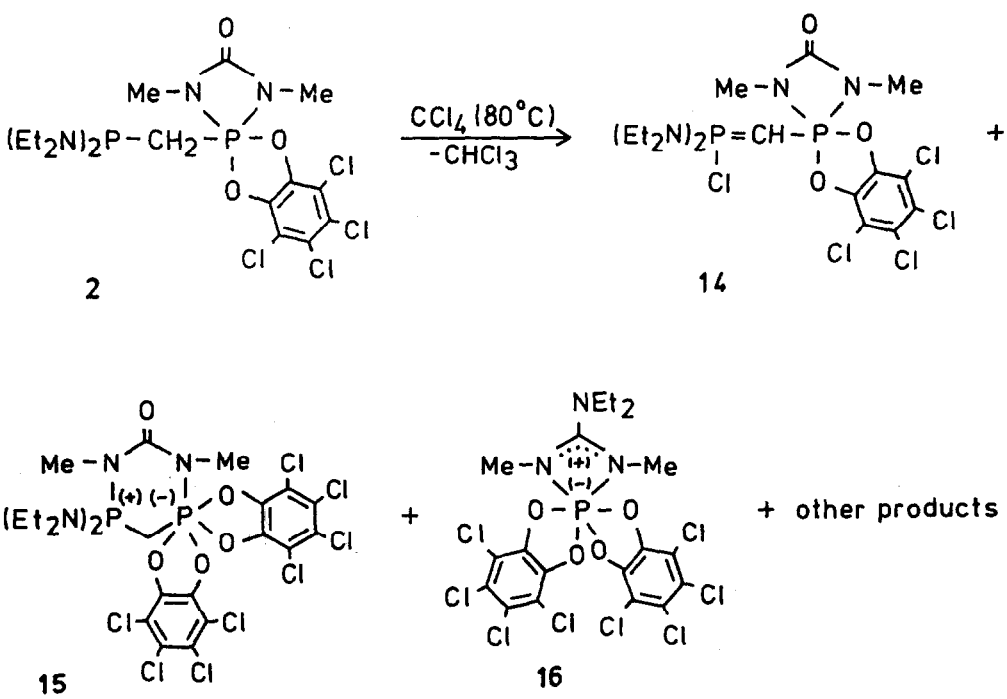

by single-crystal X-ray structure analysis.[1] The content of **15** in the reaction mixture is not more than 6–8% and does not increase on heating for a longer time.

The formation of **15** and **16** in reaction (8) is not yet understood. It is possible that this process is connected with the presence of small amounts of by-products, together with the starting material **2**,

Compound **15** is an isomer of compound **3**, the structure of which we have also confirmed by X-ray analysis.[1] The isomers **3** and **15** exist independently of each other and do not undergo mutual isomerization [eq. (10)]. Unlike **15**, isomer **3** is thermally unstable and decomposes in boiling toluene with the formation of a complicated mixture of products that does not contain **15**.

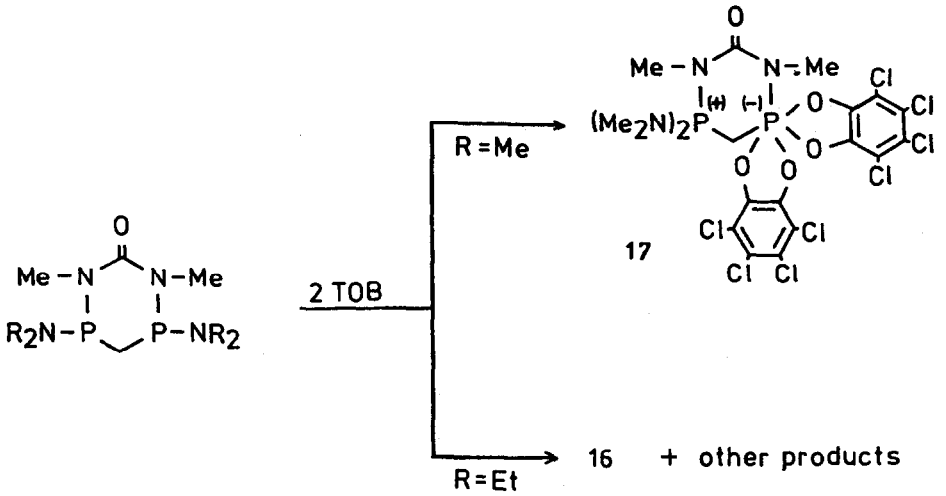

(9)

which was obtained according to our procedure[2] and was used without further purification.

Compound **15**, containing two phosphorus atoms of opposite charge and different coordination number, was isolated as a colourless, high-melting crystalline product, which, owing to its zwitter-ionic structure, is insoluble in non-polar and poorly soluble in polar organic solvents. The ^{31}P NMR spectrum shows two characteristic doublets at 55 and -115 ppm with a coupling constant $^{2}J(PP)$ of only 3.5 Hz.

Compound **15** is a homologue of **17**, which we had obtained earlier [eq. (9)][11] and subjected to X-ray analysis. Compound **15** shows spectral characteristics similar to **17** and thus presumably has an analogous structure. Compound **15** cannot be obtained in the same way; cleavage of the original heterocycle is observed with the formation of **16** and other products.[1]

The hydrolysis of isomer **15** confirmed its structure. The process proceeds in two stages [eq. (11)]. At first, cleavage of the two P—O bonds at the six-coordinate phosphorus atom takes place to give the zwitter-ionic product **18**. The second stage of the hydrolysis is substantially slower, thus allowing **18** to be obtained in solution in spectroscopically pure form. The ^{31}P NMR spectrum shows two doublets at 10.39 and 52.52 ppm [$^{2}J(PP) = 6.6$ Hz] and the ^{1}H NMR spectrum two doublets due to the non-equivalent N—Me groups of the urea unit. After removal of the solvent there remains a crystalline product, for which elemental analysis confirms the presence of only one *o*-dioxytetrachlorophenyl group in the molecule.

Further hydrolysis proceeds slowly with the cleavage of the 1,5-diaza-2,4-diphosphorinane-6-one heterocycle and formation of **19**. This process

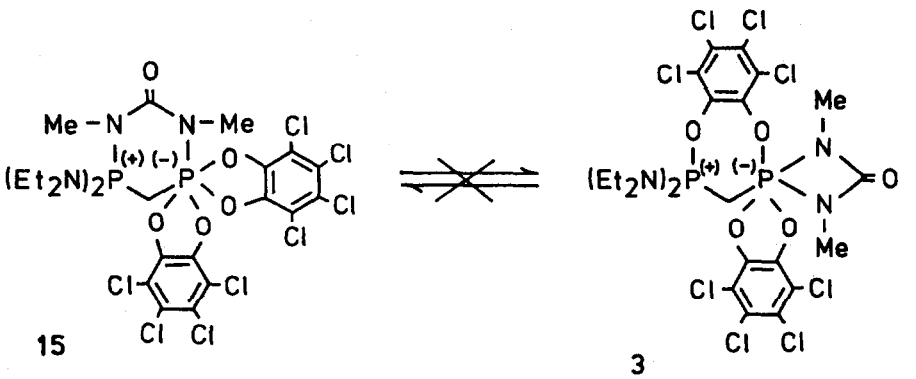

(10)

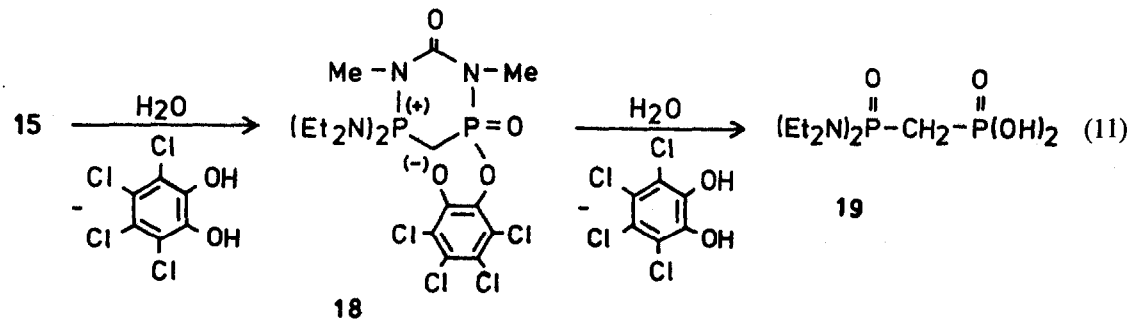

(11)

is illustrated by the disappearance of the signals of **18** and the appearance of two new doublets at 16.5 and 30.5 [^2J(PP) = 10.1 Hz] in the ^{31}P NMR spectrum. Unfortunately, the isolation of **19** and a more detailed investigation of **18** are complicated by the very low yield of the starting material **15**.

EXPERIMENTAL

Materials and spectroscopy

All experiments were conducted with the exclusion of moisture in sealed systems in an atmosphere of dried nitrogen (BASF BTS catalyst). Solvents were purified and dried according to the usual methods.[12,13] NMR spectra: Bruker AC 200 (^{1}H at 200.1 MHz; ^{13}C at 50.3 MHz; ^{31}P at 81.3 MHz). Reference substances were $SiMe_4$ (TMS) ext. (^{1}H, ^{13}C) and 85% H_3PO_4 ext. (^{31}P). High-field shifts were given negative, low-field shifts positive signs. Materials: the methylenephosphinophosphorane **2** was synthesized according to ref. 2 and was used without further purification.

Synthesis of **4**

To **2** (1.0 g, 1.81 mmol) was added MeI (1.28 g, 9.05 mmol) and the mixture was stirred for 5 h at 20°C. Excess MeI was removed *in vacuo* (0.5 mm); the residue was washed with ether (3 × 10 cm^3) and dried *in vacuo* (0.05 mm). The colourless crystalline product (1.12 g, 89%; m.p. 138–142°C) was dissolved in CH_2Cl_2 (3 cm^3) and ether was added dropwise while stirring until the solution just remained clear. The solution was allowed to stand at 20°C for 2 days and for 1 day at −20°C. The crystals formed were separated and dried *in vacuo* (0.05 mm). Yield after crystallization: 0.64 g (51%); m.p. 149–151°C. ^{1}H NMR ($CDCl_3$): 1.12 [t, ^3J(HH) = 6.9 Hz, CH_3—CH_2—N]; 1.15 [t, ^3J(HH) = 6.9 Hz, CH_3—CH_2—N]; 2.33 [d, ^2J(PH) = 13.3 Hz, CH_3P]; 2.93 [d, ^3J(PH) = 13.2 Hz, CH_3N]; 3.15 (m, CH_3—CH_2—N); 3.99 [dd, ^2J(PH) = 18.03 Hz, ^2J(PH) = 20.51 Hz, P—CH_2—P]. ^{31}P NMR ($CDCl_3$): 53.39 [d, ^2J(PP) = 5.1 Hz]; −34.14 [d, ^2J(PP) = 5.1 Hz]. Found: C, 32.7; H, 4.7; N, 7.9. Calc. for $C_{19}H_{31}Cl_4IN_4O_3P_2$ (694.15): C, 32.9; H, 4.5; N, 8.1%.

Formation of **5**

A solution of **4** (1 g, 1.44 mmol) in $CHCl_3$ (10 cm^3) was heated at 80°C for 16 h in a sealed tube. The solvent was removed *in vacuo* (0.5 mm). The residue was immediately dissolved in CH_2Cl_2 (2.5 cm^3) and ether was slowly added dropwise while stirring at room temperature until the solution just remained clear. The crystals of **5** formed after 48 h at 20°C were separated from the mother liquor and dried *in vacuo* (0.05 mm). Colourless product m.p. 206–208°C; yield 0.38 g (39.6%). ^{1}H NMR ($CDCl_3$) δ: 1.28 [t, ^3J(HH) = 7.1 Hz, N—CH_2—CH_3]; 2.52 [d, ^2J(PH) = 14.3 Hz, P—CH_3]; 3.2–3.5 (m, N—CH_2—CH_3); 5.12 [dd, ^2J(PH) = 16.2 Hz; ^2J(PH) = 23.3 Hz; P—CH_2—P]; 5.24 (s, CH_2Cl_2). ^{31}P NMR ($CDCl_3$): 52.61; 39.38 ppm. ^2J(PP) could not be determined. Found: C, 30.0; H, 4.3; Cl, 27.1; I, 19.9; N, 4.9; P, 8.4. Calc. for $C_{16}H_{25}Cl_4IN_2O_3P_2 \cdot 1/2CH_2Cl_2$ (666.52): C, 29.7; H, 3.9; Cl, 26.6; I, 19.0; N, 4.2; P, 9.3%.

Hydrolysis of compound **5**

A stream of moist nitrogen was slowly bubbled through a stirred solution of **5** (0.15 g, 0.23 mmol) in $CDCl_3$ (2 cm^3) until the signals of **5** completely disappeared (^{31}P NMR control). The solution of **6** thus formed shows the following NMR spectroscopic parameters: ^{1}H NMR ($CDCl_3$) δ: 1.19 [t, ^3J(HH) = 7.1 Hz, CH_3—CH_2—N]; 2.35 [d, ^2J(PH) = 13.5 Hz, CH_3—P]; 3.01–3.35 (m, CH_3—CH_2—N); 3.93 [dd, ^2J(PH) = 16.5 Hz; ^2J(PH) = 22.2 Hz, P—CH_2—P]; 10.35 (P—OH, Ar—OH). ^{13}C NMR ($CDCl_3$): 12.85 [d, ^1J(PC) = 84.5 Hz, CH_3—P]; 14.20, 14.23 (CH_3—CH_2—N); 25.76 [dd, ^1J(PC) = 75.9 Hz, ^1J(PC) = 133.8 Hz, P—CH_2—P]; 40.59, 40.68 (CH_3—CH_2—N); 122.22 (Ar); 123.80 (Ar); 125.85

(Ar); 129.45 (Ar); 136.14 [d, ^2J(PC) = 9.9 Hz, Ar]; 145.50 (Ar). ^{31}P NMR ($CDCl_3$): 14.38; 54.79 [^2J(PP) coupling was not resolved].

Formation of compounds **9** *and* **10**

The mother liquor left after the separation of compound **5** (see above) contained mainly compound **9**, which was stable only in solution. ^{31}P NMR of **9** (C_6D_6 solvent): 53.82 [d, ^2J(PP) = 65.32 Hz]; 58.43 [d, ^2J(PP) = 65.32 Hz].

After removing the solvent and drying the residue *in vacuo* (0.05 mm) for 2 h, **10** remained as a crystalline product which was washed with ether (2 × 10 cm^3) and dried *in vacuo* (0.05 mm). Colourless crystals; yield 0.49 g. ^{1}H NMR ($CDCl_3$): 1.18 [t, ^3J(HH) = 7.1 Hz, N—CH_2—CH_3]; 2.23 [d, ^2J(PH) = 13.5 Hz, P—CH_3]; 2.97 (NH—CH_3); 2.99 (NH—CH_3); 3.0–3.3 (m, N—CH_2—CH_3); 3.49 (s, NH). ^{31}P NMR ($CDCl_3$): 9.58; 58.46 [^2J(PP) coupling was not resolved]. Found: C, 33.6; H, 4.7; N, 8.7. Calc. for $C_{19}H_{31}Cl_4IN_4O_3P_2$ (694.15): C, 32.9; H, 4.5; N, 8.1%.

Synthesis of compound **12**

To a flask containing a solution of **2** (0.85 g, 1.54 mmol) in ether (15 cm^3) cooled to −20°C was added hexafluoroacetone (150 cm^3, 1.11 g, 6.70 mmol) with a syringe while stirring. After 10 min the reaction mixture was allowed to warm to 20°C; after 1 h the mixture was cooled to −20°C and the crystals formed after 24 h were separated from the mother liquor and dried *in vacuo* (0.05 mm). Colourless product; m.p. 166–168°C; yield 0.43 g (40%). ^{1}H NMR ($CDCl_3$) δ: 1.03 [t, ^3J(HH) = 7.1 Hz, CH_3—CH_2—N]; 2.72 [dd, ^2J(PH) = 12.1 Hz, the second ^2J(PH) was not resolved, P—CH_2—P]; 2.72 [d, ^3J(PH) = 12.1 Hz, CH_3—N]; 2.7–3.3 (m, CH_3—CH_2—N); 5.43 [dq, ^3J(PH) = 19.3 Hz, ^3J(FH) = 6.3 Hz, CF_3—CH—CF_3]. ^{13}C NMR ($CDCl_3$) δ: 13.84, 13.87 (CH_3—CH_2—N); 17.89 [dd, J(PC) = 59.5 Hz, J(PC) = 185.7 Hz, P—CH—P]; 26.21, 26.25 (CH_3—CH_2—N); 40.69, 40.79 (CH_3—N); 114.48 [d, ^2J(PC) = 12.6 Hz, Ar]; 124.07 (Ar); 142.42 (Ar), 157.23 [d, ^2J(PC) = 14.5 Hz, C=O]. ^{19}F NMR ($CDCl_3$) δ: −72.78. ^{31}P NMR: 64.35 d, ^2J(PP) = 49.7 Hz; −29.65 d, ^2J(PP) = 49.7 Hz. Found: C, 35.4; H, 4.1; N, 7.7. Calc. for $C_{21}H_{28}Cl_4F_6N_4O_4P_2$ (718.23): C, 35.1; H, 3.9; N, 7.8%.

Synthesis of compound **13**

A solution of **4** (0.5 g, 0.72 mmol, recrystallized) in CH_2Cl_2 (6 cm^3) was cooled to −20°C and triethylamine (0.73 g, 7.2 mmol) was added. After 20 min the solvent was removed *in vacuo* and the residue was dried *in vacuo* (0.05 mm) for 1 h. The remaining colourless crystalline product was extracted with boiling petroleum ether (60–70°C; 2 × 20 cm^3). The colourless crystals formed after the extract were allowed to stand at −20°C for 24 h, were separated and dried *in vacuo* (0.05 mm); m.p. 128–129°C; yield 0.26 g (63%). ^{1}H NMR ($CDCl_3$) δ: 1.05 [t, ^3J(HH) = 7.06 Hz, CH_3—CH_2N]; 1.62 [d, ^2J(PH) = 13.49 Hz, CH_3—P]; 2.15 [dd, ^2J(PH) = 13.92 Hz, ^2J(PH) = 22.31 Hz, P—CH_2—P]; 2.73 [d, ^3J(PH) = 11.83 Hz, CH_3—N]; 2.9–3.2 (m, CH_3—CH_2—N). ^{13}C NMR ($CDCl_3$) δ: 13.76, 13.81 (CH_3—CH_2—N); 16.23 [d, J(PC) = 98.1 Hz, CH_3—P]; 19.49 [dd, J(PC) = 147.0 Hz, J(PC) = 233.5 Hz, P—CH—P]; 26.31, 26.36 (CH_3—CH_2—N); 38.95, 39.05 (CH_3—N); 113.93 [d, ^2J(PC) = 12.29 Hz, Ar]; 123.04 (2C, Ar); 142.71 (2C, Ar); 157.96 [d, ^2J(PC) = 11.5 Hz, C=O]. ^{31}P NMR ($CDCl_3$): 62.8 [d, ^2J(PP) = 44.3 Hz]; −29.7 [d, ^2J(PP) = 44.3 Hz]. Mass spectrum: M_{calc} = 566.24. M_{exp}(EI) = 566. Found: C, 39.9; H, 5.3; N, 9.5. Calc. for $C_{19}H_{30}Cl_4N_4O_3P_2$ (566.24): C, 40.3; H, 5.3; N, 9.9%.

Interaction of **2** *with* CCl_4

A solution of **2** (1.0 g, 1.81 mmol) in CCl_4 (4 cm^3) was heated at 80°C for 10 min in a sealed tube. The reaction mixture after this time contained only the P-chloroylide **14** with the following ^{31}P NMR data: 74.10 [d, ^2J(PP) = 46.2 Hz]; −32.75 [d, ^2J(PP) = 46.2 Hz].

The reaction mixture was heated further at 80°C for 24 h. The colourless crystalline product **15** was separated and washed with ether (4 cm^3) and CH_2Cl_2 (1.5 cm^3), and was recrystallized from acetonitrile (yield 80 mg); mp. 250–252°C. ^{1}H NMR ($CDCl_3$) δ: 1.20 [t, ^3J(HH) = 7.1 Hz, CH_3—CH_2—N]; 2.65 [dd, ^2J(PH) = 15.1 Hz; ^2J(PH) = 16.8 Hz, P—CH_2—P]; 3.00 [d, ^3J(PH) = 6.46 Hz; CH_3—N]; 3.02 [d, ^3J(PH) = 8.8 Hz, CH_3—N]; 3.12–3.40 (m, CH_3—CH_2—N). ^{31}P NMR ($CDCl_3$) δ: 55.12 [d, ^2J(PP) = 3.5 Hz]; −114.39 [d, ^2J(PP) = 3.5 Hz]. Mass spectrum: M_{calc} = 798.09; M_{exp}(FAB) = 799 [M+H$^+$]. Found: C, 35.8; H, 3.7; N, 6.8. Calc. for $C_{24}H_{28}Cl_8N_4O_5P_2$ (798.09): C, 36.1; H, 3.5; N, 7.0%.

Hydrolysis of compound **15**

A mixture of **15** (50 mg), $CDCl_3$ (2 cm^3) and water (0.1 cm^3) was stirred at 20°C until **15** had

dissolved and its ^{31}P NMR signals disappeared. The resulting solution of **18** showed the following NMR parameters: ^1H NMR ($CDCl_3$) δ: 1.17 [t, $^3J(HH) = 7.0$ Hz, CH_3—CH_2—N]; 2.74 [d, $^3J(PH) = 4.8$ Hz, CH_3—N]; 3.00 [d, $^3J(PH) = 10.2$ Hz, CH_3—N]; 3.05–3.3 (m, CH_3—CH_2—N, P—CH_2—P). ^{31}P NMR ($CDCl_3$): 10.39 [d, $^2J(PP) = 6.6$ Hz]; 52.52 [d, $^2J(PP) = 6.6$ Hz].

After removing the solvent **18** remained as a white crystalline product with the following analytical data: Found: C, 36.9; H, 4.9; Cl, 26.5. Calc. for $C_{18}H_{28}Cl_4N_4O_4P_2$ (568.21): C, 38.0; H, 5.0; Cl, 25.0%.

Crystal structure analysis of compound **12**

Crystal data. $C_{21}H_{28}Cl_4F_6N_4O_4P_2$, $M = 718.2$, triclinic, space group $P\bar{1}$, $a = 1090.1(3)$, $b = 1134.9(3)$, $c = 1250.9(3)$ pm, $\alpha = 82.05(2)$, $\beta = 85.41(2)$, $\gamma = 79.85(2)°$, $U = 1.5063$ nm^3, $Z = 2$, $D_x = 1.584$ Mg m^{-3}, λ(Mo-K_α) = 71.069 pm, $\mu = 0.57$ nm^{-1}, $F(000) = 732$, $T = -95°C$.

Data collection and reduction. Data were collected from two colourless prisms, *ca* $0.3 \times 0.3 \times 0.3$/$0.5 \times 0.45 \times 0.2$ mm, which were mounted on glass fibres with inert oil and transferred to the cold gas stream of the diffractometer (Siemens R3 with LT-2 low temperature attachment). 3162/5028 intensities were registered to $2\theta_{max}$ 50°, of which (after appropriate scaling, $R_{int} = 0.022$) 5314 were independent and 3969 considered significant ($> 4\sigma(F)$). Cell constants were refined from diffractometer angles of 50 reflections in the 2θ range 20–23°.

Structure solution and refinement. The program system "Siemens SHELXTL PLUS" was used. The structure was solved by direct methods and refined anisotropically. Hydrogen atoms were included using a riding model. The weighting scheme was $w^{-1} = \sigma^2(F) + 0.0003F^2$. The final R value was 0.043, with $wR = 0.040$. 376 parameters; $S = 1.8$; max. Δ/σ 0.001; max. $\Delta\rho$ 1.1×10^{-6} e pm^{-3} near C(17), which probably indicates some disorder of the associated ethyl group.

Full details of the structure determination (including structure factors) have been deposited at the Fachinformationszentrum Karlsruhe, Gesellschaft für Wissenschaftlich-technische Information mbH, W-7514 Eggenstein-Leopoldshafen 2, Germany. Any request for this material should quote a full literature citation and the reference number CSD 56910.

Acknowledgements—I. V. Shevchenko acknowledges a post-doctoral Fellowship of the Alexander von Humboldt-Stiftung. We are grateful to Dr H. M. Schiebel and Frau D. Döring for recording mass spectra. BASF AG, BAYER AG and HOECHST AG are thanked for generous gifts of chemicals used in this research. The support of the Fonds der Chemischen Industrie is gratefully acknowledged.

REFERENCES

1. I. V. Shevchenko, A. Fischer, P. G. Jones and R. Schmutzler, *Chem. Ber.* 1992, **125**, 1325.
2. I. V. Shevchenko and R. Schmutzler, *Heteroat. Chem.* 1993, **4**, in press.
3. R. Gompper and R. Kunz, *Chem. Ber.* 1965, **98**, 1391.
4. F. Kurzer and K. Douraghi-Zadeh, *Chem. Rev.* 1967, **67**, 107.
5. W. E. Tischtshenko and N. W. Koshkin, *Zh. Obshch. Khim.* 1934, **4**, 1021.
6. M. Fild, W. Handke and H.-P. Rieck, *Chem.-Ztg.* 1988, **112**, 107.
7. O. I. Kolodiazhnyi, *Zh. Obshch. Khim.* 1976, **46**, 2386.
8. T. A. Mastryukova, I. M. Aladzheva, O. V. Bykhovskaya, P. V. Petrovskii, M. Yu. Antipin, Yu. T. Struchkov and M. I. Kabachnik, *Dokl. Akad. Nauk SSSR* 1982, **264**, 1396.
9. I. M. Aladzheva, I. V. Leontyeva, P. V. Petrovskii, T. A. Mastryukova and M. I. Kabachnik, *Zh. Obshch. Khim.* 1988, **58**, 1396.
10. O. I. Kolodiazhnyi, *Phosphorus Sulfur* 1990, **49/50**, 239.
11. I. V. Shevchenko, A. Fischer, P. G. Jones and R. Schmutzler, *Heteroatom. Chem.* 1992, **3**, 177.
12. Autorenkollektiv, *Organikum*, Reprint of the 15th edn, p. 783 ff. VEB Deutscher Verlag der Wissenschaften, Berlin (1977).
13. D. D. Perrin, W. L. F. Armarego and D. R. Perrin, *Purification of Laboratory Chemicals.* Pergamon Press, Oxford (1966).

Polyhedron Vol. 12, No. 5, pp. 445–454, 1993
Printed in Great Britain

0277–5387/93 $6.00+.00
© 1993 Pergamon Press Ltd

SOLVATION AND REACTIVITY OF THE LOW-SPIN TRIS-DIIMINE IRON(II) COMPLEX OF THE SCHIFF BASE LIGAND DERIVED FROM 2-BENZOYLPYRIDINE AND 3,4-DIMETHYLANILINE, $[Fe(Me_2bsb)_3]^{2+}$

S. ALSHEHRI, M. J. BLANDAMER and J. BURGESS†

Chemistry Department, University of Leicester, Leicester LE1 7RH, U.K.

and

P. GUARDADO

Departamento de Quimica Fisica, Universidad de Sevilla, 41012 Sevilla, Spain

and

C. D. HUBBARD

Department of Chemistry, University of New Hampshire, Durham, NH 03824, U.S.A.

(*Received* 28 *September* 1992; *accepted* 20 *November* 1992)

Abstract—The reactivity and solvation of the iron(II) tris complex made from the bidentate ligand obtained by condensing phenyl 2-pyridyl ketone and 3,4-dimethylaniline have been examined in aqueous solution and in aqueous solvent mixtures. Base hydrolysis kinetics measurements upon the complex ion, $[Fe(Me_2bsb)_3]^{2+}$, show an increasing rate of dissociation with increasing co-solvent concentration, due largely to the destabilization of the hydroxide ion. The predicted preference the lipophilic complex would exhibit toward solvents less polar than water is an expectation that is realized when transfer (from water to aqueous solvent mixtures) chemical potential trends are analysed. The latter parameters were obtained from solubility measurements. When corresponding transfer chemical potentials for the transition state are also considered, the factors controlling reactivity patterns are shown; this is described by an initial state—transition state analysis. Base hydrolysis kinetics carried out at high pressures (up to 1 kbar) yield the volumes of activation, ΔV^*, which provide a complementary view of solvation. Some measurements with a similar complex, $[Fe(Me_2tsb)_2]^{2+}$, are reported for comparison.

Kinetics of the reaction of iron(II) complexes of ligands of the 2,2′-bipyridyl (bipy, **1**) and 1,10-phenanthroline (phen, **2**) type have been extensively studied for many years.[1] A reasonable range of substituents can be introduced into these ligands by appropriate synthetic approaches, but at times the organic chemistry is difficult, involving multistage syntheses including two Skraup reactions.[2] An alternative approach to the introduction of substituents into diimine ligands is to prepare them from pyridine 2-carboxaldehyde, 2-acetyl pyridine, 2-benzoyl pyridine[3,4] or from 2,3-butanedione[3,5] and substituted anilines, which are available in great profusion, to give ligands of the type **3** or **4**. We have studied the kinetics of a selection of substitution and redox reactions of such complexes, particularly those of type **3**.[4,6] In recent years we have been particularly interested in solvation and reactivity of iron(II)-diimine complexes in binary aqueous solvent mixtures.[7,8] Several years ago we showed that ligand variation has a dramatic effect on the

† Author to whom correspondence should be addressed.

hydrophilic/hydrophobic properties of such complexes,[9,10] with complexes of such ligands as gmi (**5**) or the hexadentate Schiff base **6** (hxsbH) showing only a very slight preference for alcohols over water; however, much more hydrophobic ligands, such as **7** (= **3** with R = Ph, X = 3,4-Me_2), are strongly preferentially solvated by organic co-solvents. Thus, the cation derived from **7** is stabilized by *ca* 50 kJ mol^{-1} on transfer from water into methanol. We have studied solvation and base hydrolysis kinetics of the almost hydrophilic complexes $[Fe(gmi)_3]^{2+}$ and $[Fe(hxsbH)]^{2+}$ extensively establishing reactivity trends and activation volumes in several series of binary aqueous solvent mixtures.[10–12] A parallel study of the extremely hydrophobic complex containing ligand **7**, $[Fe(Me_2bsb)_3]^{2+}$, has been fraught with difficulties, both of preparation of pure materials and of reproducibility of kinetic and solubility measurements. It has become clear that most of the problems arise from the production of varying amounts of *mer* and *fac* isomers when preparing salts of this complex under various conditions. This matter has been fully investigated and documented recently for the analogous tris complex of the ligand **8**, derived from 2-acetyl pyridine and methylamine (**8** = **3** with R = Me and N—C_6H_5 replaced by N—CH_3),[13] whose kinetic and spectroscopic properties (^{1}H NMR and visible absorption spectra) are particularly favourable for the resolution of this isomer problem. We are now in a position to resolve most of the problems with the $[Fe(Me_2bsb)_3]^{2+}$ cation, so now present the results of our kinetic studies on base hydrolysis of this most hydrophobic complex, particularly in relation to co-solvent effects on reactivity trends and on activation volumes. In the latter connection we report activation volumes for some related complexes which also have very bulky and

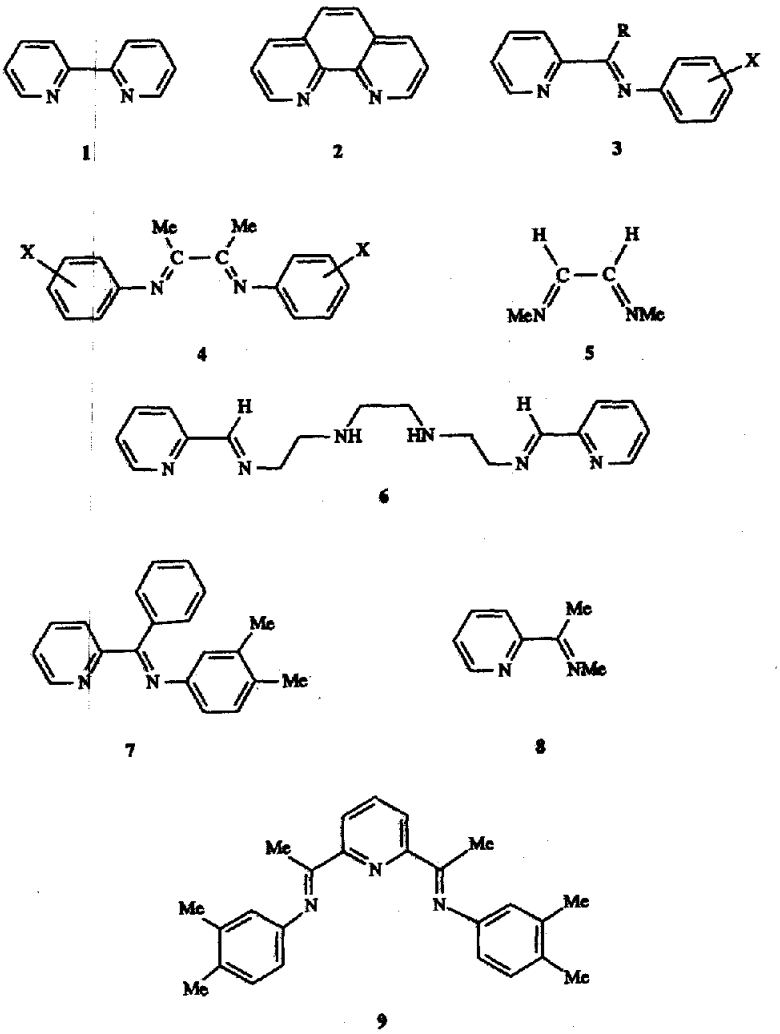

hydrophobic leaving ligands. These ligands include the 3-methyl and 4-methoxy analogues of **7** and the terdentate analogue **9** (Me_2tsb).

EXPERIMENTAL

Materials

Samples of $[Fe(Me_2bsb)_3](ClO_4)_2$ were either those obtained earlier[11] or were prepared during this study according to established methods.[14,15] The perchlorate salt of $[Fe(Me_2tsb)_2]^{2+}$ was prepared as reported in earlier work.[7] Reagents used in dissociation studies, sodium hydroxide and sodium chloride were Analar grade. Co-solvents used in solubility and kinetics measurements were high-grade commercial products and employed without further purification.

Methods

Solubility measurements were made according to the method described earlier,[7] but a longer period of absorbance sampling was carried out for the bidentate containing complex (references to and discussion of complex ion isomerism, the reason for modification of the method, are found in earlier and in later parts of this paper). The wavelengths of maximum absorbance of $[Fe(Me_2bsb)_3]^{2+}$ and $[Fe(Me_2tsb)_2]^{2+}$ are 585 and 592 nm, respectively. Absorbance measurements were made on a Pye–Unicam SP 8-100 spectrophotometer or on a Cary 219 spectrophotometer. Dissociation kinetics at atmospheric pressure were carried out on a Pye–Unicam SP 8-100, Unicam SP 1800 or a Cary 219 spectrophotometer, with temperature controlled to 298.2 ± 0.1 K, at the appropriate wavelength to monitor the loss of the complex ion. Data were either processed manually or with data treatment software indicated elsewhere.[7,16]

The reactions were carried out under first-order conditions with the hydroxide ion in a large excess over the metal complex concentration. In many solvent mixtures the first-order rate constant, k_{obs}, was obtained at several different hydroxide concentrations. A linear dependence of k_{obs} on hydroxide ion concentration was observed when $[OH^-] < 0.15$ mol dm^{-3}. The slopes of these plots, when available, were used to calculate k_2, the second-order rate constant. Otherwise, for comparison of dissociation in different solvent mixtures k_{obs} at a given hydroxide ion concentration was used. For both methods the hydroxide concentrations were sufficiently low to avoid any higher order terms than first in the rate equation. With increasing co-solvent concentration the non-linear dependence portion of the k_{obs} versus hydroxide plot occurs at lower hydroxide ion concentrations. All solvent mixtures have compositions given, which refer to the composition before mixing.

Kinetics at high pressure were carried out in the range 1 bar to 1.3 kbar, as described earlier.[11,17] The rate constants obtained (k_p) were used in plots of $\ln(k_p/k_0)$ vs pressure, where k_0 is the rate constant at 1 atmos. for an aliquot of the same solution employed in the high pressure experiment. The slopes of such plots (there was no detectable curvature indicating a negligible compressibility of activation) yield ΔV^*, the volume of activation. Values quoted in this paper refer to the volume of activation at 1 bar. In the high pressure measurements hydroxide ion concentrations were always below those where complications of higher order terms can arise.[18]

RESULTS AND DISCUSSION

Solvation

We deal first with the hydrophobicity of the complex $[Fe(Me_2bsb)_3]^{2+}$, as reflected in solvation in binary aqueous solvent mixtures. Here the isomer problem presents considerable difficulties in regard to obtaining precise solubilities and transfer chemical potentials, but does not prevent us from presenting an informative semi-quantitative picture. It is clear that the transfer chemical potentials for the *mer* and *fac* isomers do not differ by more than 10% and that solubility measurements carried out under constant conditions (equilibration for 24 h) can give results which are reliable, reproducible and consistent to this order of uncertainty. In view of the large changes in transfer chemical potential with solvent composition, the solvation pattern shown in Fig. 1 can be deemed reliable, even if individual

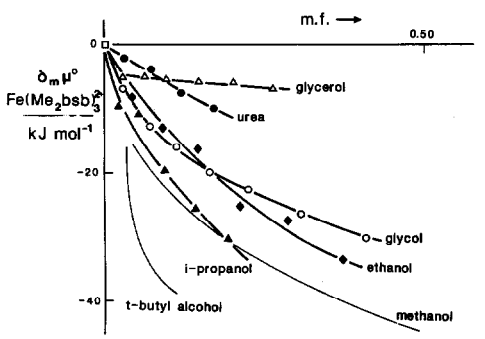

Fig. 1. Transfer chemical potentials (kJ mol^{-1}) from water into aqueous solvent mixtures for the $[Fe(Me_2bsb)_3]^{2+}$ species vs solvent composition (mole fraction) at 298.2 K.

values have larger uncertainties than usual. The results in this figure are derived from published data[9,19,20] and from previously unpublished solubilities. Details are given in Table 1. The pattern is similar to that of other iron(II)-diimine complexes, but transfer chemical potentials are generally larger than for most other such complexes. This is illustrated for the typical case of methanol–water in Fig. 2[7,21] (exceptionally, in urea–water mixtures differences between trends for various complexes are very

Table 1. Derivation of transfer chemical potentials for the $[Fe(Me_2bsb)]^{2+}$ cation from measured solubilities of its perchlorate salt. Solubilities are in mol dm^{-3}; transfer chemical potentials (Δ) are in kJ mol^{-1} on the molar scale and the TATB assumption. All values are at 298.2 K

Ethanol: vol%[a]	0	10	20	30	40	50	60
m.f.	0	0.042	0.089	0.143	0.207	0.281	0.370
Abs. sat. soln[b]	0.39	1.10	2.18	3.0	8.8	9.2	16.1
10^4 soly[c]	0.30	0.85	1.7	2.3	6.8	7.1	12.4
Δ(salt)		−7.7	−12.8	−15.2	−23.2	−23.5	−27.7
$\Delta(ClO_4^-)$[d]		+0.2	+0.2	+0.4	+1.0	+2.0	+2.9
Δ(complex)		−8.1	−13.2	−16.0	−25.2	−27.5	−33.5

i-Propanol: vol%	0	10	30	40	50
m.f.	0	0.026	0.092	0.136	0.190
Abs. sat. soln	0.39	1.29	3.9	7.2	8.2
10^4 soly	0.30	0.99	3.0	5.5	6.3
Δ(salt)		−8.9	−17.1	−21.7	−22.6
$\Delta(ClO_4^-)$[d]		+0.2	+1.2	+2.2	+3.8
Δ(complex)		−9.3	−19.5	−26.1	−30.2

1,2-Ethanediol: vol%	0	10	20	30	40	50	60	70
m.f.	0	0.031	0.068	0.111	0.162	0.225	0.303	0.404
Abs. sat. soln	0.39	0.82	1.57	2.1	4.3	5.8	8.9	14.3
10^4 soly	0.30	0.64	1.2	1.6	3.3	4.5	6.9	11.0
Δ(salt)		−5.5	−10.3	−12.5	−17.8	−20	−23	−27
$\Delta(ClO_4^-)$[e]		+0.5	+1.3	+1.6	+1.2	+1.0	+1.6	+1.8
Δ(complex)		−6.5	−12.9	−15.7	−20.2	−22	−27	−30

1,2,3-Propanetriol: wt%	0	12.3	24.0	35.1	47.1	55.8	64.5
m.f.	0	0.027	0.058	0.096	0.148	0.198	0.262
Abs. sat. soln	0.39	0.81	0.83	0.91	0.92	0.94	1.12
10^4 soly	0.30	0.62	0.64	0.70	0.71	0.72	0.92
Δ(salt)		−5.4	−5.6	−6.3	−6.4	−6.6	−7.8
$\Delta(ClO_4^-)$[e]		−0.3	−0.5	−0.5	−0.4	−0.4	−0.6
Δ(complex)		−4.8	−4.6	−5.3	−5.6	−5.8	−6.6

Urea: wt%	0	10	20	30	40
m.f.	0	0.032	0.070	0.114	0.167
Abs. sat. soln	0.39	1.14	2.25	3.8	5.9
10^4 soly	0.30	0.88	1.73	2.9	4.5
Δ(salt)		−8.0	−13.0	−16.9	−20.2
Soly · $KClO_4$[f]	0.146	0.167	0.183	0.184	0.190
$\Delta(KClO_4)$		−0.6	−1.0	−1.0	−1.2
$\Delta(K^+)$[g]		+2.4	+3.6	+3.5	+3.9
$\Delta(ClO_4^-)$		−3.0	−4.6	−4.5	−5.1
Δ(complex)		−2.0	−3.8	−7.9	−10.0

[a] Volume percentages are by volume before mixing (cf. text).
[b] Absorbance of saturated solution, i.e. measured absorbance times dilution (where needed).
[c] ε = 13,000 at 585 nm.
[d] From ref. 30.
[e] From ref. 20.
[f] Flame photometric determinations.
[g] From ref. 31—also on the TATB single ion assumption.

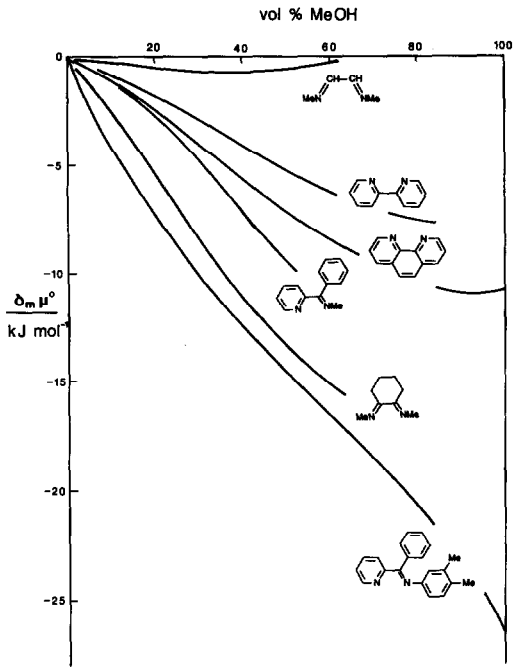

Fig. 2. Transfer chemical potentials (kJ mol^{-1}) from water into aqueous methanol vs per cent methanol (v/v) for various iron(II)-tris-diimine complexes (ligand formulae indicated on each plot), at 298.2 K.

much less marked[19]). As discussed below such marked stabilization by most organic co-solvents has a dominant effect when reactivity trends are analysed into their initial state and transition state contributions.

Kinetics

Base hydrolysis kinetic runs were carried out on solutions of the complex which had been aged (allowed to stand for at least 24 h) and, therefore, contained predominantly the more stable (presumably *mer*) isomer. These runs showed no significant deviation from first-order behaviour (hydroxide always present in a large excess) over at least three half-lives. First-order rate constants calculated, as is our normal custom,[7] from absorbance changes monitored over the first 2.5 half-lives are reported in Table 2. The general rate law for hydroxide attack at iron(II)-diimine complexes is:

$$-\mathrm{d[complex]}/\mathrm{d}t = \{k_1 + k_2[\mathrm{OH^-}] + k_3[\mathrm{OH^-}]^2 \ldots\}[\mathrm{complex}].$$

For hydroxide concentrations up to *ca* 0.15 mol dm^{-3} contributions from $[OH^-]^2$ and higher terms

Table 2. First-order rate constants for base hydrolysis of $[Fe(Me_2bsb)_3]^{2+}$ at 298.2 K (ionic strength 0.15 mol dm^{-3})

Co-solvent: vol. (%)		$10^5 k_{obs}$ (s^{-1})						$10^4 k_2$
$[OH^-]$ (mol dm^{-3}):		0.025	0.050	0.073	0.100	0.120	0.150	(mol dm^{-3} s^{-1})
1,2-Ethanediol	20	1.7	3.0	4.2	6.2	7.3	10.2	6.3
	30	1.6	2.5	4.4	5.3		7.8	5.5
	40		3.0	4.3	6.0		8.9	6.0
	50			6.0				8
	60			6.3				9
	70			6.5				9
Glycerol	10		2.7	4.0	5.6		8.0	5.2
	20			4.6				6
	30	1.2	1.8	2.4	2.6		3.8	2.5
	40			1.6				2
	50			2.1				3
Ethanol	10			8.3				11
	20			10.5				14
	30			18.3				25
	40			29				40
	50		54	88	122		190	110
	60	25		113				155
i-Propanol	10			8.8				12
	20	4.7		14				19
	30			42				58
	40			76				104
	50		118	147	227		329	220
t-Butyl alcohol	17			13				18

are negligible for this complex, although the square term begins to be significant at higher hydroxide concentrations.[11] The k_1 term is also vanishingly small here. Values of k_2 are included in Table 2. They, together with published data on this reaction,[11] are plotted in Fig. 3 to give an overall picture of reactivity. This again shows a similarity to such patterns for the other iron(II)-diimine complexes. One common and important feature is the steadily increasing effect of mono-hydroxylic alcohols as their carbon content increases, to which the transfer chemical potential trends and consequent nucleophilicity of the hydroxide contribute. The effect of added dimethyl sulphoxide is somewhat less than perhaps intuitively expected, but is in fact exactly similar to that in base hydrolysis of the $[Fe(phen)_3]^{2+}$ cation.[22]

Initial state–transition state analysis

Solvation effects on reactivity can be probed informatively through dissection into initial state and transition state components.[23,24] This is illustrated for methanol–water solvent media in Figs 4 and 5 (see also Table 3), and for ethane-1,2-diol in Fig. 6. We have chosen these two mixed solvent series firstly because kinetic measurements cover a wide range of compositions and secondly because hydroxide is destabilized on transfer to aqueous methanol[7] but stabilized on transfer to aqueous ethane-1,2-diol.[20] The complex is of course greatly stabilized in both cases. Two representations have been provided for the methanol–water system, since one emphasizes the relation between the magnitude of the solvation changes and that of the activation barrier (ΔG^*), the other emphasizes how solvation of the periphery of the complex dominates initial and transition state trends. This is, of course, also the case for other co-solvents. The picture is

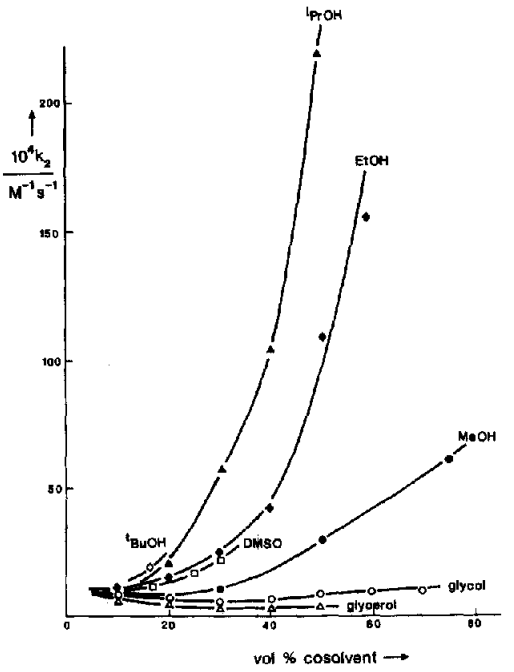

Fig. 3. Second-order rate constant, k_2, for base hydrolysis of $[Fe(Me_2bsb)_3]^{2+}$ vs solvent composition at 298.2 K and an ionic strength of 0.33 mol dm^{-3}.

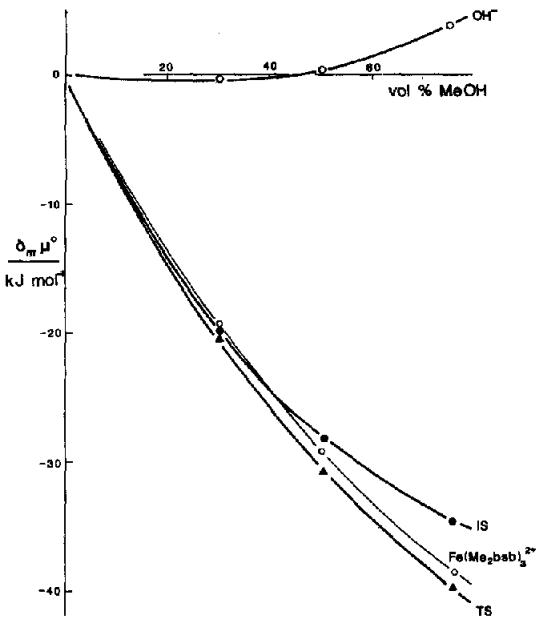

Fig. 4. Initial state–transition state analysis of base hydrolysis of $[Fe(Me_2bsb)_3]^{2+}$ in aqueous methanol at 298.2 K: transfer trends normalized to water.

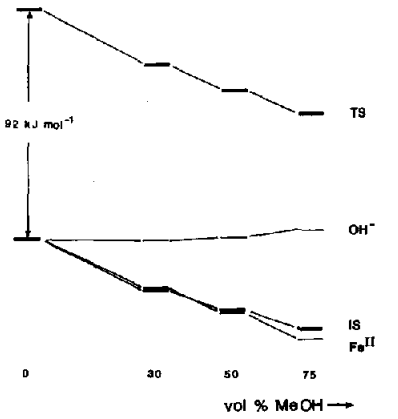

Fig. 5. Initial state–transition state analysis of base hydrolysis of $[Fe(Me_2bsb)_3]^{2+}$ in aqueous methanol at 298.2 K: relation of transfer quantities to the activation barrier in water.

Table 3. Initial state–transition state analyses of reactivity trends for base hydrolysis of the $[Fe(Me_2bsb)_3]^{2+}$ cation in methanol–water and 1,2-ethanediol–water media. All transfer parameters, Δ, are in kJ mol^{-1}, on the molar scale, on the TPTB (for MeOH) or TATB (for glycol) assumption; all data refer to 298.2 K

Vol. MeOH (%)	0	30	50	75
k_{obs} (0.1 M NaOH) (s^{-1})[a]	5.1	6.4	15.5	31.7
$\Delta(\Delta G^*)$ (kJ mol^{-1})		−0.5	−2.7	−4.5
Δ(complex)[b]		−19.5	−29	−39
$\Delta(OH^-)$[c]		−0.2	+0.5	+4
Δ(initial state)		−20	−28	−35
Δ(transition state)		−21	−31	−40

Vol. glycol (%)	20	30	40	50	60
$\Delta(\Delta G^{\ddagger})$[d]	−0.5	−0.2	−0.4	−1.1	−1.4
Δ(complex)[e]	−12.9	−15.7	−20	−22	−27
$\Delta(OH^-)$[f]	−1.3	−1.7	−2.5	−3.4	−4
Δ(initial state)	−14.2	−17.4	−23	−26	−31
Δ(transition state)	−14.7	−17.6	−23	−27	−32

[a] From ref. 11.
[b] Interpolated from results in refs 9 and 11.
[c] From ref. 7.
[d] From Table 2 rate constants (k_2 values).
[e] From Table 1.
[f] From ref. 20.

markedly different from those for the much less hydrophobic complexes $[Fe(gmi)_3]^{2+}$ [7,8] and $[Fe(hxsbH)]^{2+}$.[12] Even for $[Fe(bipy)_3]^{2+}$, which is moderately hydrophibic, it is hydroxide solvation variation rather than complex solvation which dominates the base hydrolysis reactivity trend in dimethyl sulphoxide–water media.[22]

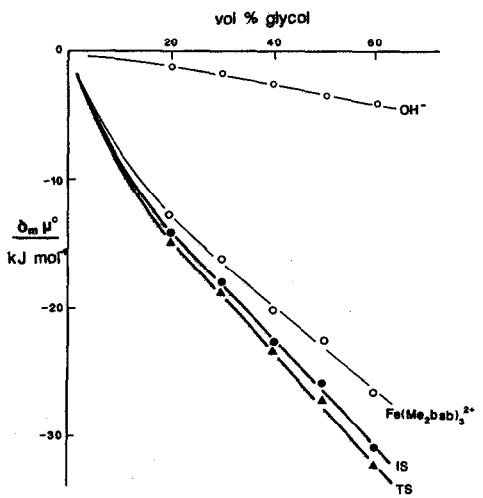

Fig. 6. Initial state–transition state analysis for base hydrolysis of $[Fe(Me_2bsb)_3]^{2+}$ in aqueous 1,2-ethanediol mixtures at 298.2 K.

Activation volumes

Values of ΔV^* for the reaction of hydroxide with $[Fe(Me_2bsb)_3]^{2+}$ in water have been interpreted as arising from a dominant contribution from the solvation component.[11] Specifically, desolvation of the incoming hydroxide ion gives rise to a contribution of just over 20 cm^3 mol^{-1}, as the expected ΔV^* value from an intrinsic contribution alone would be −10 cm^3 mol^{-1} for an associative mechanism.[25] The relative insensitivity of the observed ΔV^* to the nature of the iron(II) diimine cation has been recorded previously,[26] and is here reinforced for bsb type ligands by recalling that the ΔV^* values for the iron(II) tris complexes of the 3Me- and 4MeO-bsb ligands (3) are 13 and 12 cm^3 mol^{-1}, respectively.

At first examination the changes in ΔV^* with co-solvent addition (see Table 4) are paradoxical in that a large increase in the values indicates a loss of restricted solvent, the alcohol co-solvent, from the very lipophilic cation upon forming the transition state, with the hydroxide ion being similarly desolvated as it is in purely aqueous solution. Yet since the charge upon the reactant cation is reduced by one as the transition state is formed, it could be argued that this would permit increased solvation by the co-solvent to occur. There is no doubt that

Table 4. Ratios of rate constants for base hydrolysis of $[Fe(Me_2bsb)_3]^{2+}$ at high pressures (k_p) to those at atmospheric pressure (k_0), in methanol–water media at 298.2 K [I = 0.33 mol dm^{-3} (NaCl)] and derived activation volumes, ΔV^*

Co-solvent	Vol. (%)	[NaOH] (M)	ln(k_p/k_0) (p kbar^{-1}) 0.34	0.68	0.85	1.01	ΔV^* (cm^3 mol^{-1})
$[Fe(Me_2bsb)_3]^{2+}$							
Ethanol	20	0.073	−0.242	−0.463		−0.590	+15[a]
	40	0.073	−0.247	−0.461		−0.748	+17
	60	0.025	−0.212	−0.470		−0.795	+18
i-Propanol	20	0.025	−0.213	−0.468[b]		−0.693[b]	+17
t-Butyl alcohol	17	0.073	−0.350	−0.820		−1.020[c]	+27
	40	0.100	−0.446	−0.714	−0.769	−0.882	+21
1,2-Ethanediol	20	0.073	−0.129	−0.203		−0.451	+11
	40	0.073	−0.210	−0.419			+15
$[Fe(3Mebsb)_3]^{2+}$							
Methanol	67	0.073[d]	−0.398	−0.795		−1.085[e]	+26[f]
$[Fe(4OMebsb)_3]^{2+}$							
Methanol	67	0.073[d]	−0.228	−0.468	−0.467	−0.813	+19[g]
$[Fe(Me_2tsb)_2]^{2+}$							
t-Butyl alcohol	0	0.33		−0.196		−0.256	+6
	17	0.33	−0.279	−0.527			+19

[a] $\Delta V^* = +11$ cm^3 mol^{-1} in water.[11]
[b] [NaOH] = 0.073 mol dm^{-3}.
[c] Also −1.310 at 1.34 kbar.
[d] KOH/KCl.
[e] Also −1.204 at 1.17 kbar.
[f] $\Delta V^* = +14$ cm^3 mol^{-1} in water.[26]
[g] $\Delta V^* = +12$ cm^3 mol^{-1} in water.[26]

the initial state iron complex cation is strongly solvated by the co-solvent as the transfer chemical potentials, for example from water into aqueous methanol at 41 kJ mol^{-1} to mole fraction of methanol 0.64,[9] indicate. Therefore, it must be surmised that the consequence of charge reduction is very small for such a huge cation, and that the hydroxide ion upon penetrating the periphery of the heavily solvated cation, en route to the central iron and effectively breaking the first iron–nitrogen bond, perturbs a considerable array (in the case of methanol) of solvent molecules. To reinforce the point of a small charge–change/size ratio it is recalled that $\delta_m\mu^\circ$ ($[Fe(Me_2bsb)_3]^{2+}$) > $\delta_m\mu^\circ$ (Ph_4As^+) or $\delta_m\mu^\circ$ (Ph_4B^-).[7] In Fig. 7 it can be seen that, as reported earlier,[9] ΔV^* increases in an approximately proportional manner with increasing per cent of methanol after an initial jump from 11 to almost 20 cm^3 mol^{-1} at 33% co-solvent, with a value of 27 cm^3 mol^{-1} being reached at 93% methanol. There is nothing unique about methanol as the results for ethanol and isopropanol-aqueous mixtures mostly mirror this trend, although less markedly so. This could reflect fewer of the larger mono-ols initially solvating the complex cation and thus fewer are released upon reaction, but this is quite speculative. There is a dramatic effect obtained using t-butyl alcohol as the co-solvent. The increase to 24 cm^3

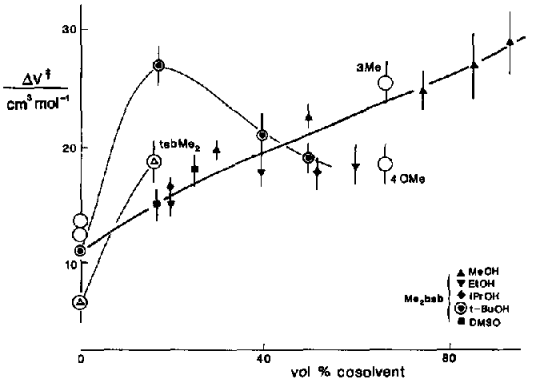

Fig. 7. Volumes of activation vs aqueous solvent mixture compositions for base hydrolysis of $[Fe(Me_2bsb)_3]^{2+}$ and $[Fe(Me_2tsb)_2]^{2+}$ at 298.2 K, ionic strength 0.33 mol dm^{-3}.

mol^{-1} at 17% co-solvent has been noted earlier. Due to the magnitude of this effect and the error range obtained earlier[9] this point has been redetermined and is now established as 26 ± 2 cm^3 mol^{-1}, with a subsequent decrease to *ca* 20 cm^3 mol^{-1} at 40 and 50% t-butyl alcohol. Given the extreme bulkiness of this alcohol relative to the lower homologues these changes are probably a consequence of a big volume change per released co-solvent molecule. Actually the maximum value of ΔV^* is the same in both methanol and t-butyl alcohol, but with the maximum occurring at a much lower mole fraction for the bigger mono-ol. This is not unexpected given the structural changes to water proposed by the two mono-ols in question and the co-solvent concentrations where these effects are manifested.[27] Modelling studies in progress[28] should help to address these hypotheses and enable a semi-quantitative explanation to emerge. The occupancy by solvent molecules of the spaces between ligand entities, within the complex cation, clearly a feature of the system addressed here, has been discussed earlier for the $[Fe(phen)_3]^{2+}$ complex cation.[21] While exactly the same values of ΔV^* are not obtained in water or in 67% methanol, for base hydrolysis of the tris complexes of the 4-methoxy and 3-methyl analogues of Me_2bsb (see Table 4), the closeness of the values and the general trends are the same, indicating parallel solvation changes. Collectively for the three complex cations this is in contrast to the pattern of ΔV^* values and associated solvation changes for the complex ions $[Fe(hxsbH)]^{2+}$ [9] and $[Fe(gmi)_3]^{2+}$.[10] We note here that a trend of activation volumes increasing with increasing mole fraction of organic co-solvent has recently been reported for homolysis of cobaloxime derivatives in n-propanol–water mixtures and interpreted in terms of a cage effect controlled by solvent structural effects.[29]

The large effect of t-butyl alcohol is not restricted to the bsb-type complexes. The terdentate ligand Me_2tsb forms a bidentate complex with iron(II); the kinetics of base hydrolysis of this complex over a range of pressures yield ΔV^* values of $+6$ and $+18$ cm^3 mol^{-1}, respectively, in water and in 17% t-butyl alcohol. The difference in ΔV^* values, considering the quantities for 17% t-butyl alcohol and water solution, are very similar for the complexes of Me_2bsb and Me_2tsb. In each case $\Delta(\Delta V^*)$ is *ca* 13 cm^3 mol^{-1}, which is a reflection of the similar lipophilic exteriors of the complex ions.

What is now really needed for a fuller understanding of the trends discussed in the preceding paragraphs is a full set of partial molar volumes for the complexes in question in the mixed solvents studied. Unfortunately, this is a major research exercise in itself, for it would be necessary to establish partial molar volumes for a number of salts in each solvent mixture before it would be possible to deduce single ion values for such reference ions as $AsPh_4^+$ and BPh_4^- and thence values for our charged iron(II) complexes.

Acknowledgements—We thank the Royal Society and the SERC for grants towards the purchase of the Unicam SP8-100 and the construction of the high pressure apparatus, respectively. The National Science Foundation grant (CHE-7908399) used for the purchase of the Cary 219 spectrophotometer is gratefully acknowledged. S.A. thanks the Saudi Arabian National Guard for financial support and the King Khalid Military Academy for leave of absence; P.G. thanks the British Council (Vicente Canada Blanch Foundation) for financial assistance.

REFERENCES

1. F. Basolo and R. G. Pearson, *Mechanisms of Inorganic Reactions*, 2nd edn. Wiley, New York (1967).
2. For example: F. H. Case, Z. B. Jacobs, R. S. Cook and J. Dickstein, *J. Org. Chem.* 1957, **22**, 390.
3. P. Krumholz, *Struct. Bonding* 1971, **9**, 139.
4. J. Burgess and R. H. Prince, *J. Chem. Soc. A* 1967, 434, 955; J. Burgess, *J. Chem. Soc. A* 1968, 497.
5. H. A. Sinn, PhD thesis. Technische Hochschule Darmstadt (1966).
6. J. Burgess, G. E. Ellis, D. J. Evans, A. Porter, R. Wane and R. D. Wyvill, *J. Chem. Soc. A* 1971, 44; M. J. Blandamer, J. Burgess, R. I. Haines, F. M. Mekhail and P. Askalani, *J. Chem. Soc., Dalton Trans.* 1978, 1001; J. Burgess and G. M. Burton, *Revista Latinoamer. Quim.* 1980, **11**, 107.
7. M. J. Blandamer, J. Burgess, B. Clark, P. P. Duce, A. W. Hakin, N. Gosal, S. Radulović, P. Guardado, F. Sanchez, C. D. Hubbard and E. A. Abu-Gharib, *J. Chem. Soc., Faraday Trans. I* 1986, **82**, 1471.
8. M. J. Blandamer, B. Briggs, J. Burgess, D. Elvidge, P. Guardado, A. W. Hakin, S. Radulović and C. D. Hubbard, *J. Chem. Soc., Faraday Trans. I* 1988, **84**, 2703.
9. J. Burgess and C. D. Hubbard, *J. Chem. Soc., Chem. Commun.* 1983, 1482.
10. M. J. Blandamer, J. Burgess, P. Guardado, C. D. Hubbard, S. Nuttall, L. J. S. Prouse, S. Radulović and D. R. Russell, *Inorg. Chem.* 1991, **30**, 1383.
11. J. Burgess and C. D. Hubbard, *J. Am. Chem. Soc.* 1984, **106**, 1717.
12. J. Burgess and C. D. Hubbard, *Inorg. Chem.* 1988, **27**, 2548.
13. M. J. Blandamer, J. Burgess, D. L. Elvidge, P. Guardado, A. W. Hakin, L. J. S. Prouse, S. Radulović and D. R. Russell, *Trans. Met. Chem.* 1991, **16**, 82.
14. A. J. Duffield, PhD thesis. University of Leicester (1980).
15. R. Sherry, PhD thesis. University of Leicester (1982).
16. P. P. Duce, PhD thesis. University of Leicester (1982).

17. N. Hallinan, P. McArdle, J. Burgess and P. Guardado, *J. Organomet. Chem.* 1987, **333**, 77.
18. D. W. Margerum and L. P. Morgenthaler, *J. Am. Chem. Soc.* 1962, **84**, 706.
19. M. J. Blandamer, J. Burgess, A. W. Hakin, P. Guardado, S. Nuttall and S. Radulović, *J. Chem. Soc., Faraday Trans. I* 1987, **83**, 559.
20. M. J. Blandamer, J. Burgess, P. P. Duce, D. L. Elvidge, P. Guardado, C. D. Hubbard and J. Ibechem, *J. Chem. Soc., Faraday Trans.* 1992, **88**, 215.
21. F. M. van Meter and H. M. Neumann, *J. Am. Chem. Soc.* 1976, **98**, 1382.
22. A. Al-Alousy, S. Alshehri, M. J. Blandamer, J. Burgess, H. J. Cowles and S. Radulović, *J. Chem. Soc., Faraday Trans.*, accepted for publication.
23. A. J. Parker, *Chem. Rev.* 1969, **69**, 1.
24. M. J. Blandamer and J. Burgess, *Pure Appl. Chem.* 1979, **51**, 2087; 1982, **54**, 2285; 1983, **55**, 55; *Coord. Chem. Rev.* 1980, **31**, 93.
25. T. Asano and W. J. LeNoble, *Chem. Rev.* 1978, **73**, 407.
26. J. Burgess, S. A. Galema and C. D. Hubbard, *Polyhedron* 1991, **10**, 703.
27. F. Franks and D. J. G. Ives, *Q. Rev. Chem. Soc.* 1966, **20**, 1.
28. D. M. P. Mingos, J. Burgess, P. Guardado and C. D. Hubbard, calculations in progress.
29. M. W. G. de Bolster and R. A. C. Kranenburg, *Inorg. Chim. Acta* 1991, **183**, 119.
30. M. J. Blandamer, B. Briggs, J. Burgess, D. Elvidge, P. Guardado, A. W. Hakin, S. Radulović and C. D. Hubbard, *J. Chem. Soc., Faraday Trans. I* 1988, **84**, 2703.
31. K. K. Kundu and A. K. Das, *J. Solution Chem.* 1976, **5**, 431; 1979, **8**, 259.

Polyhedron Vol. 12, No. 5, pp. 455–459, 1993
Printed in Great Britain

0277–5387/93 $6.00+.00
© 1993 Pergamon Press Ltd

X-RAY CRYSTAL STRUCTURE OF $InCl_3 \cdot 2THF$, A NEUTRAL FIVE-COORDINATE BIS-ADDUCT OF AN INDIUM(III) TRIHALIDE

MARK F. SELF, ANDREW T. McPHAIL and RICHARD L. WELLS*

Department of Chemistry, Paul M. Gross Chemical Laboratory, Duke University, Durham, NC 27708, U.S.A.

(*Received* 14 *September* 1992; *accepted* 20 *November* 1992)

Abstract—The 2 : 1 mole ratio reaction of $InCl_3$ and $P(SiMe_3)_3$ in a toluene/THF mixture was investigated. The reaction appears to occur in a 1 : 1 mole fashion, since the products obtained are unreacted $InCl_3$ (48.5% recovered) as $InCl_3 \cdot 2THF$ and a fine powder which appears to be $[Cl_2In_3P_3(SiMe_3)_2]_n$. The latter was characterized by melting point and partial elemental analysis. The X-ray crystal structure of $InCl_3 \cdot 2THF$ shows it to be a neutral penta-coordinated bis-adduct of an indium(III) trihalide. The crystal structure consists of discrete monomeric units with no abnormally short intermolecular separations. The geometry about the indium atom approximates to trigonal bipyramidal with oxygen atoms of each of the THF molecules occupying axial positions [In—O = 2.257(9) Å, O—In—O = 178.5(3)°], while the three chlorine atoms (mean In—Cl = 2.321 Å) lie in the equatorial plane.

For some time our laboratory has been investigating convenient and facile routes to the formation of novel compounds containing Ga—As bonds.[1] In fact, one such compound with the empirical formula $(AsCl_3Ga_2)_n$ (**I**) can be easily converted into nanocrystalline GaAs itself.[2] Compound **I** results from the 2 : 1 mole ratio reaction of $GaCl_3$ and $As(SiMe_3)_3$. In related work, Barron and co-workers recently reported that the 1 : 1 mole ratio reaction of $InCl_3$ and $P(SiMe_3)_3$ at low temperature yields $[Cl_2InP(SiMe_3)_2]_x$ (**II**).[3] In that we have now begun to direct considerable attention to the production of compounds containing In—P bonds,[4–7] it was decided that the In/P analogue of the reaction leading to the formation of **I** should be investigated [i.e. the 2 : 1 reaction of $InCl_3$ and $P(SiMe_3)_3$], the goal being the possible isolation of the new precursor $(PCl_3In_2)_n$. We report that although the 2 : 1 reaction of $GaCl_3$ and $As(SiMe_3)_3$ to produce **I** occurs cleanly and readily, the corresponding reaction of $InCl_3$ and $P(SiMe_3)_3$ affords $[Cl_2In_3P_3(SiMe_3)_2]_n$ (**III**) and unreacted $InCl_3$ (48.5% of the starting $InCl_3$) in a solvated form [$InCl_3 \cdot 2THF$ (**IV**)]. Compound **III** (characterized by melting point and partial elemental analysis) was isolated as a relatively unreactive fine orange powder. It is insoluble in hydrocarbon solvents, THF and Et_2O and air-stable for several hours at room temperature. Complex **IV** has been previously synthesized and quite extensively characterized by Fairbrother *et al.*,[8] but no solid-state structure was ever obtained. Herein, we report the crystal structure of **IV** as it represents a novel example of a neutral penta-coordinated bis-adduct of an indium (III) trihalide.

EXPERIMENTAL

Synthesis

All manipulations were performed using general Schlenk techniques. Colourless crystals of **IV** were obtained by the 2 : 1 mole reaction of $P(SiMe_3)_3$[9] and $InCl_3$ (purchased from Strem chemicals). In the dry-box (Vacuum/Atmospheres HE-493 Dri-Lab containing an argon atmosphere) $P(SiMe_3)_3$ (0.250 g, 0.998 mmol) was dissolved in anhydrous, degassed toluene (25 cm^3; distilled from sodium/benzophenone ketyl) in a 100 cm^3 one-necked round-bottomed flask equipped with a Teflon valve and a microstir-bar. A suspension of $InCl_3$ (0.441

* Author to whom correspondence should be addressed.

g, 1.99 mmol) in toluene (15 cm^3) and anhydrous, degassed THF (15 cm^3) (distilled from sodium/benzophenone ketyl) was slowly added dropwise. Immediately upon addition the reaction mixture became yellow–orange and quite turbid. The reaction mixture was stirred at room temperature for 2 days and then allowed to settle undisturbed for 1 day. Decantation of the colourless mother liquor from the bright orange powder gave $[Cl_2In_3P_3(SiMe_3)_2]_n$ (**III**), 0.204 g, 47% yield based on In; m.p. = 200–260°C (dec. to black). Found: C, 11.4, 11.6; H, 2.6, 2.5; Cl, 10.7, 10.9. Calc. for $C_6H_{18}Cl_2In_3P_3Si_2$: C, 11.0; H, 2.7; Cl, 10.8%. Subsequent cooling at −15°C for 3 days afforded crystals of **IV** (0.352 g, 48.5% yield based on In), suitable for X-ray analysis.

X-ray structural solution and refinement

Crystallographic data are summarized in Table 1. The crystal used was a colourless block mounted inside a flame-sealed 0.6 mm thin-walled glass capillary under an inert argon atmosphere. Oscillation and Weissenberg photographs yielded preliminary unit cell parameters and space group information. X-ray intensity data were recorded on an Enraf–Nonius CAD-4 diffractometer at 25°C using graphite-monochromated Cu-K_α radiation (λ = 1.5418 Å). Lorentz and polarization corrections were applied, as was an empirical absorption correction. The crystal structure was solved by direct methods. Initial coordinates for the indium and chlorine atoms were derived from an *E*-map. Carbon and oxygen atoms were located in a difference-Fourier synthesis phased by these atoms. Several rounds of full-matrix least-squares adjustment of non-hydrogen atom positional and thermal parameters (at first isotropic, then anisotropic) followed. Hydrogen atoms were incorporated at their calculated positions (C—H = 1.05 Å) in the later iterations which converged (max. shift: e.s.d. = 0.02) at R = 0.042 (R_w = 0.058). A final difference-Fourier synthesis revealed no unusual features (max. 0.56, min. −0.41 e $Å^{-3}$, both in the vicinity of the indium atom). Crystallographic calculations were performed using the Enraf–Nonius Structure Deter-

Table 1. Crystallographic data for $InCl_3 \cdot 2THF$ (**IV**)

Molecular formula	$C_8H_{16}Cl_3InO_2$
Formula weight	365.39
Crystal system	Orthorhombic
Space group	*Pbcn* (D_{2h}^{14}) No. 60
a (Å)	10.802(1)
b (Å)	10.101(1)
c (Å)	13.083(1)
No. of orientation reflections; θ range (°)	25; 36–40
V ($Å^3$)	1427.5(4)
Z	4
D_{calc} (g cm^{-3})	1.700
μ(Cu-K_α radiation, λ = 1.5418 Å)	186.9
Temperature (°C)	25
Crystal dimensions (mm)	0.16 × 0.18 × 0.20
T_{max} : T_{min}	1.00 : 0.71
Scan type	ω–2θ
Scan width (°)	0.80 + 0.14 tan θ
$\theta_{max.}$ (°)	75
Intensity control reflections	111, 122, 133, 114
Variation; repeat time (h)	<1%; 2
Total no. of reflections (+h, +k, +l) recorded	1471
No. of reflections retained [$I > 3.0\sigma(I)$]	537
No. of parameters refined	65
R (R_w)[a]	0.042 (0.058)
Goodness-of-fit[b]	1.16
Max. shift : e.s.d. in final least-squares cycle	0.02
Final $\Delta\rho$ (e $Å^{-3}$) max.; min.	0.56; −0.41

[a] $R = \Sigma||F_o|-|F_c||/\Sigma|F_o|$; $R_w = [\Sigma w(|F_o|-|F_c|)^2/\Sigma w|F_o|^2]^{1/2}$; $\Sigma w\Delta^2$ [$w = 1/\sigma^2(|F_o|)$, $\Delta = (|F_o|-|F_c|)$] was minimized.

[b] Goodness-of-fit = $[\Sigma w\Delta^2/(N_{obs}-N_{par})]^{1/2}$.

Table 2. Interatomic distances (Å) and angles[a] (°) for $InCl_3 \cdot 2THF$ (**IV**), with e.s.d.s in parentheses

In—Cl(1)	2.330(4)	O(1)—C(5)	1.49(2)
In—Cl(2)	2.312(5)	C(2)—C(3)	1.53(3)
In—O(1)	2.257(9)	C(3)—C(4)	1.45(3)
O(1)—C(2)	1.46(2)	C(4)—C(5)	1.50(2)
Cl(1)—In—Cl(1′)	117.8(2)	In—O(1)—C(2)	122(1)
Cl(1)—In—Cl(2)	121.1(1)	In—O(1)—C(5)	122(1)
Cl(1)—In—O(1)	90.5(3)	C(2)—O(1)—C(5)	109(1)
Cl(1)—In—O(1′)	90.3(3)	O(1)—C(2)—C(3)	104(1)
Cl(2)—In—O(1)	89.2(2)	C(2)—C(3)—C(4)	105(1)
O(1)—In—O(1′)	178.5(3)	C(3)—C(4)—C(5)	104(1)
		O(1)—C(5)—C(4)	104(1)

[a] Primed atoms are related to unprimed atoms by the following transformation: $-x, y, 1/2-z$.

mination Package (SDP).[10] For all structure-factor calculations, neutral atom scattering factors and their anomalous dispersion corrections were taken from ref. 11. Selected distances and angles are provided in Table 2. An ORTEP diagram showing the atom labelling scheme and solid-state conformation of **IV** is presented in Fig. 1; the packing arrangement of molecules of **IV** in the crystal is illustrated in Fig. 2. Full information concerning conditions for crystallographic data collection and structure refinement, atomic coordinates, positional parameters, anisotropic thermal parameters and observed and calculated structure factors have been deposited with the Cambridge Crystallographic Data Centre.

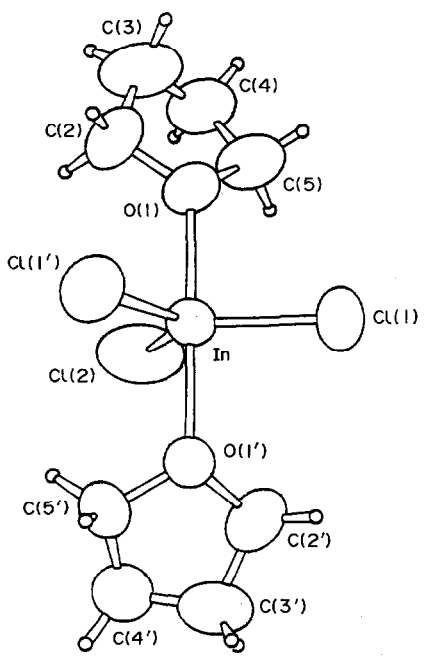

Fig. 1. ORTEP diagram (50% probability ellipsoids) showing the atom numbering scheme and solid-state conformation of $InCl_3 \cdot 2THF$ (**IV**); primed atoms are related to the unprimed atoms by a crystallographic C_2 symmetry axis passing through In and Cl(2). Small circles represent hydrogen atoms.

RESULTS AND DISCUSSION

Although the structural chemistry of five-coordinate aluminum and gallium compounds has been well examined, corresponding investigations of such indium compounds have remained more sparse.[12] Currently, there are seven penta-coordinate indium(III) trihalide bis-adducts which have been crystallographically characterized [viz. $InX_3 \cdot L_2$: X = Cl; L = PPh_3 (**V**),[13] HMPA ($OP\{N(Me)_2\}_3$) (**VI**),[14] NMe_3 (**VII**),[15] $SPMe_3$ (**VIII**),[16] $SAsMe_3$ (**IX**)[16]; X = Br; L = $SPMe_3$ (**X**),[16] $SAsMe_3$ (**XI**)[16]]. Of these, it is interesting to note that five (**VII–XI**) were only reported within the last 6 years and **IV** is only the second such compound containing In—O bonds to be structurally characterized, the first being **VI**.

The crystal structure of **IV** consists of discrete monomeric units which have one of their In—Cl bonds lying on a crystallographic C_2 symmetry axis (see Fig. 1). In common with the other $InX_3 \cdot L_2$ adducts, the coordination geometry about the indium atoms is trigonal-bipyramidal with three chlorine atoms defining the equatorial plane and the oxygen atoms of the THF molecules occupying the axial sites. The O—In—O angle at 178.5(3)° in **IV** deviates only slightly from an exactly linear value

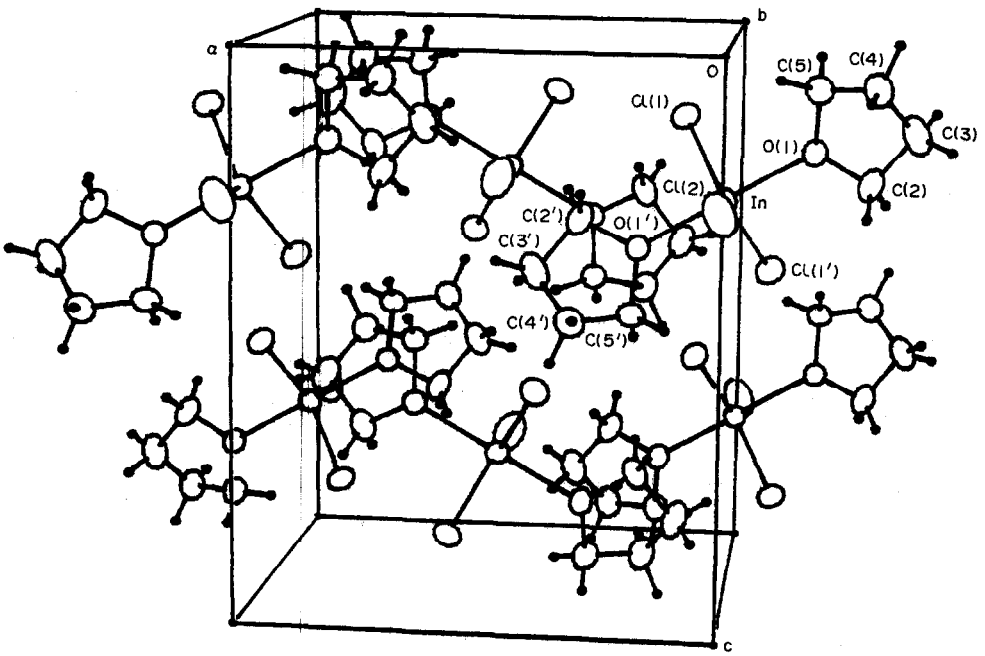

Fig. 2. Packing arrangement of molecules of $InCl_3 \cdot 2THF$ (**IV**) in the crystal.

and lies close to that of 178.0(2)° in **VI**. The In—O bond length of 2.257(9) Å in **IV** is significantly longer and thus weaker than the corresponding bonds in **VI**, where they average 2.180 Å; this difference may be ascribed to the increased electron-donating ability of the oxygen atom in the HMPA ligand. The mean In—Cl bond length at 2.321 Å in **IV** is shorter than that of 2.359 Å in **VI**, as well as the corresponding lengths of 2.360–2.412 Å in **V** and **VII–IX**. The observed decrease in the equatorial bond lengths in **IV** vs **VI** is correlated with the aforementioned lengthened axial bond distance in the former. Endocyclic torsion angles characterizing the conformation of the THF molecule are related by an approximate C_2 symmetry axis which passes through the oxygen atom and the mid-point of the C(3)—C(4) bond, and, accordingly, this ring is in a half-chair conformation. The mean bond angle subtended at the oxygen atom is 118° and thus the geometry about this atom lies closer to trigonal planar than to tetrahedral. X-ray crystallographic studies[16] on the series $InX_3 \cdot L_2$ (X = Cl, Br; L = $SPMe_3$, $SAsMe_3$) have shown that in the solid state the angle subtended at the axial sulphur atom is dependent on intermolecular as well as intramolecular non-bonded interactions. The orientation of the In—O bond with respect to the THF ring in crystals of **IV** produces no unusually short intramolecular Cl···H non-bonded distances (min. Cl···H = 3.29 Å). Crystal packing requirements involving two equidistant intermolecular interactions between Cl(2) in the reference molecule and one of the hydrogen atoms at C(2) in neighbouring molecules [Cl(2)···H(2) = 2.87 Å] apparently dictate the geometry at the oxygen atom in the solid state.

Acknowledgement—This work was financially supported by the Office of Naval Research.

REFERENCES

1. For a general review, see: R. L. Wells, *Coord. Chem. Rev.* 1992, **112**, 273.
2. R. L. Wells, R. B. Hallock, A. T. McPhail, C. G. Pitt and J. D. Johansen, *Chem. Mat.* 1991, **3**, 381.
3. M. D. Healy, P. E. Laibinis, P. D. Stupik and A. R. Barron, *J. Chem. Soc., Chem. Commun.* 1989, 359.
4. R. L. Wells, A. T. McPhail and M. F. Self, *Organometallics* 1992, **11**, 221.
5. R. L. Wells, A. T. McPhail, L. J. Jones, M. F. Self and R. J. Butcher, *Organometallics* 992, **11**, 2694.
6. R. L. Wells, A. T. McPhail and M. F. Self, *J. Coord. Chem.* 1993, in press.
7. R. L. Wells, A. T. McPhail, L. J. Jones and M. F. Self, *J. Organomet. Chem.* 1993, in press.
8. F. Fairbrother, N. Flitcroft and H. Prophet, *J. Less-Common Met.* 1960, **2**, 49.
9. G. Becker and W. Holderich, *Chem. Ber.* 1975, **108**, 2484.
10. Enraf–Nonius Structure Determination Package (SDP 3.0). Enraf–Nonius, Delft, The Netherlands (1985).

11. *International Tables for X-ray Crystallography*, Vol. IV. Kynoch Press, Birmingham (1974).
12. (a) D. G. Tuck, in *Comprehensive Organometallic Chemistry* (Edited by G. Wilkinson), Vol. 1, Ch. 7, pp. 683–723. Pergamon Press, Oxford (1982); (b) D. G. Tuck, in *Comprehensive Coordination Chemistry* (Edited by G. Wilkinson, R. D. Gillard and J. A. McCleverty), Vol. 3, Ch. 25.2, pp. 153–182. Pergamon Press, Oxford (1987).
13. M. V. Veidis and G. J. Palenik, *J. Chem. Soc. D* 1969, 586.
14. S. P. Sinha, T. T. Pakkanen, T. A. Pakkanen and L. Niinisto, *Polyhedron* 1982, **1**, 355.
15. R. Karia, G. R. Willey and M. G. B Drew, *Acta Cryst., Sect. C., Cryst. Struct. Comm.* 1986, **C42**, 558.
16. W. T. Robinson, C. J. Wilkins and Z. Zeying, *J. Chem. Soc., Dalton Trans.* 1988, 2187.

Polyhedron Vol. 12, No. 5, pp. 461–465, 1993
Printed in Great Britain

0277–5387/93 $6.00+.00
© 1993 Pergamon Press Ltd

SINDO STUDIES OF $[M(CN)_5CO]^{n-}$ COMPLEX IONS FOR M = IRON, MANGANESE AND CHROMIUM

EWA WASIELEWSKA† and ELWIRA ILKOWSKA

Faculty of Chemistry, Jagiellonian University, ul. Ingardena 3, 30 060 Kraków, Poland

(*Received* 10 *November* 1992; *accepted* 16 *November* 1992)

Abstract—SINDO type calculations were performed for $[M(CN)_5CO]^{n-}$ complexes (where M = Fe, Mn or Cr) in different oxidation states. The results seem to predict that $[Mn^{II}(CN)_5CO]^{3-}$ and $[Cr^{II}(CN)_5CO]^{3-}$ could be synthesized as thermally stable complex ions, besides $[Fe^{II}(CN)_5CO]^{3-}$ which is already known. On the basis of the results of the calculations the changes in properties of the CO molecule upon coordination are discussed.

The hexacyano complexes of iron, manganese and chromium form an interesting group of compounds which have been studied extensively, both experimentally and theoretically.[1–3] Also several complexes of the $[M(CN)_5NO]^{n-}$ type, in which the CN^- ligand is replaced by the isoelectronic NO^+ molecule, are known and well characterized.[4] On the contrary only one example of carbonylpentacyanometallates has been reported as a stable complex, namely $[Fe^{II}(CN)_5CO]^{3-}$ [5,6] (also $[Fe(CN)_5CO]^{2-}$ could be observed but only within minutes[7]). The existence of more compounds of the type $[M(CN)_5CO]^{n-}$ should be expected on the basis of the properties of the CO group, which has intermediate acceptor properties between isoelectronic molecules CN^- and NO^+.[8] The intermediate character of the CO ligand should result in the $[M(CN)_5CO]^{1-n}$ properties being intermediate between those of $[M(CN)_6]^{n-}$ and $[M(CN)_5NO]^{2-n}$.

In order to confirm these expectations we decided to undertake a theoretical study of the properties of carbonylpentacyano complexes of iron, manganese and chromium in different oxidation states. There have been no such calculations reported in the literature until now. The calculations were performed by means of the SINDO method which has proven to give reasonable results for different cyano and mixed cyano complexes. On the basis of the SINDO method the influence of the central atom and its oxidation state on physical properties as well as the thermal reactivity of $[M(CN)_5NO]^{n-}$ complexes has been explained.[4–9] The characteristics of the excited states obtained by the SINDO method has enabled the photochemical behaviour of $[Fe(CN)_5NO]^{2-}$, $[Fe(CN)_6]^{4-}$ and $[Cr(CN)_6]^{3-}$ complexes to be interpreted.[10–12]

METHOD AND DETAILS OF CALCULATIONS

SINDO[13] is a scaled version of the INDO method with integrals depending on the actual charge and configuration of the constituent atoms. Two centre electron repulsion integrals are approximated using Ohno's formula. As far as the electronic structure is concerned there are no parameters of molecular origin in this treatment. Core–core repulsion terms on the other hand, which are estimated by a method taken from the MINDO/2 procedure, require such parameters. For pairs of ligand atoms they have been estimated from experimental bond energies and bond lengths of simple diatomic molecules.[9] Due to the lack of appropriate experimental data the estimation of parameters for metal–ligand core–core repulsion terms was not unequivocal.

The bond lengths for which actual calculations have been performed have been chosen on the basis of the trends in the changes of the strength of metal–ligand bonds accompanying the substitution of the CN^- ligand by a CO molecule with fixed geometry. Two centre contributions to the total energy with one centre referring to the metal atom and the other to the atoms of the ligand, together with the bond order, have been selected here as the indices characterizing the bond strength. The results

† Author to whom correspondence should be addressed.

Table 1. Comparison of M—CO and M—CN bonds in $[M(CN)_5CO]^{n-}$ complexes; p^{π} denotes π-electronic bond order and E^{cov}_{A-B} is the covalent diatomic contribution to the total energy (in eV)

	$[Fe(CN)_5CO]^{3-}$	$[Mn(CN)_5CO]^{4-}$	$[Cr(CN)_5CO]^{5-}$
p^{π}_{M-CO}	1.492	1.626	1.636
E^{cov}_{M-CO}	−45.34	−43.71	−41.16
$p^{\pi}_{M-CN_{eq}}$	0.905	1.009	1.060
$E^{cov}_{M-CN_{eq}}$	−41.99	−39.49	−37.04
$p^{\pi}_{M-CN_{ax}}$	0.864	0.924	0.926
$E^{cov}_{M-CN_{ax}}$	−41.84	−38.94	−36.10

of the calculations for the isoelectronic series $[Fe(CN)_5CO]^{3-}$, $[Mn(CN)_5CO]^{4-}$ and $[Cr(CN)_5CO]^{5-}$ are presented in Table 1. In this table p^{π} contribution to the bond order and the sum of the covalent diatomic contribution to the total energy for the metal —CO ligand, equatorial CN^- and axial CN^- ligand are listed. It is clear from Table 1 that both these indicies for M—CO are always significantly different from those characteristic for M—CN bonds, whereas the differences between axial and equatorial M—CN fragments are small. On the other hand it can be shown that the influence of iron oxidation states as well as ligand substitution on the Fe—CN bond strength is insignificant (compare, for example, the values of p^{π}_{Fe-CN} equal to 0.998 and 0.924 eV and E^{cov}_{Fe-CN} equal to −42.44 and −42.12 eV, respectively, for $[Fe^{II}(CN)_6]^{4-}$ and $[Fe^{III}(CN)_6]^{3-}$). This behaviour of the CN^- ligand is consistent with the experimental data. According to the X-ray measurements the Fe—CN bond length is equal to 1.93 for $[Fe^{II}(CN)_6]^{4-}$ and 1.95 Å for $[Fe^{III}(CN)_6]^{3-}$. The experimental data for $[Fe^{II}(CN)_5CO]^{3-}$ are not known, but the length of Fe—CN bonds in $[Fe^{II}(CN)_5NO]^{2-}$ is only 0.03 Å shorter than in $[Fe(CN)_6]^{4-}$. As NO^+ is an even stronger acceptor than the CO molecule one can expect that also in the $[Fe(CN)_5CO]^{3-}$ complex the Fe—CN bond length should not change very much. Consequently, we fixed the M—CN bond lengths equal to the experimentally known value for appropriate hexacyanometallates in all calculations.

The same procedure could not be applied to the M—CO bond length. In each case we performed a series of calculations in which the M—CO distance was varied from the smallest value, equal to the M—NO distance in $[M(CN)_5NO]^{2-n}$, to the largest value, equal to the experimentally observed M—CN bond length in $[M(CN)_6]^{n-}$. In Table 2 the properties of the CO ligand in the case of $[Fe(CN)_5CO]^{3-}$ are listed and compared with those obtained for the free CO molecule. Here the results are given for two selected values of Fe—CO bond lengths, where 1.93 Å is the Fe—CN distance in $[Fe(CN)_6]^{4-}$ and 1.63 Å is the Fe—NO distance in $[Fe(CN)_5NO]^{2-}$. These results were obtained for R(C—O) kept constant at 1.13 Å, characteristic for the free molecule. We have also made calculations for the intermediate values of the distance and we

Table 2. Characteristics of free CO against coordinated to the $[Fe^{II}(CN)_5]^{3-}$ moiety; q_x denotes here net charge on X, p = appropriate bond orders, E^{cov}_{C-O} = covalent diatomic contribution and E^{tot}_{C-O} = full diatomic contribution to the total energy (in eV)

	CO	$[Fe(CN)_5CO]^{3-}$	$[Fe(CN)_5CO]^{3-}$
R (Fe—C) (Å)		1.93	1.63
q_C	0.448	0.795	0.712
q_O	−0.448	−0.803	−0.903
q_{CO}	0.0	−0.008	−0.191
p^{σ}_{C-O}	1.791	1.890	1.900
p^{π}_{C-O}	1.565	1.040	0.830
E^{cov}_{C-O}	−70.62	−64.28	−61.70
E^{tot}_{C-O}	−71.14	−68.23	−66.29

have found that the properties changed only gradually in this range. From the analysis of the results given in Table 2 the following conclusions may be drawn. The bond strength within CO decreases upon coordination, which is illustrated by bond order and energetical parameters. This decrease comes mainly from the π-contribution, which can be seen from the large changes in p^{π}_{CO} values in contrast to the values of p^{σ}_{CO}. This result is consistent with the experiment which gives the frequencies ν_{CO} in the $[Fe(CN)_5CO]^{3-}$ ion *ca* 160 cm^{-1} smaller than in the free molecule.[6] The polarization in the CO bond increases upon coordination and on decreasing the distance between the CO ligand and the metal atom. The charge transfer from the central atom to the CO ligand is larger for the smaller distances. These properties suggest that for the complexes studied here the Fe—CO distance should be smaller than for Fe—CN, whereas the carbon–oxygen distance should be greater than that in the free molecule.

Finally, we assume the Fe—CO bond to be shorter by 0.1 Å than the Fe—CN bond and the CO distance equal to 1.16 Å for all $[Fe(CN)_5CO]^{n-}$ complexes. The same geometrical parameters for the M—CO fragment in other complexes under consideration were selected by analogy. Nevertheless, the additional calculations for slightly different geometries were performed in order to check the validity of this assumption. The results have shown that the small variation of the M—C—O geometry does not influence the general conclusions.

DISCUSSION

Carbonylpentacyano complexes of iron

$[Fe^{II}(CN)_5CO]^{3-}$. Electronic features of the carbonylpentacyanoferrates studied are listed in Table 3. The ground state configuration for $[Fe(CN)_5CO]^{3-}$ is $2b_2^2 8e^4$, the same as for the isoelectronic $[Fe(CN)_5NO]^{2-}$ complex. The two highest occupied molecular orbitals lie very close in energy, −5.74 and −5.32 eV, respectively. The LUMO orbital is that of 9*e* symmetry, again in full accordance with the electronic structure of the $[Fe(CN)_5NO]^{3-}$ ion. Ligand π^* orbitals contribute significantly to all discussed frontier orbitals. Orbital $2b_2$ is a mixture of metal *d* (58%) and π^*CN (42%) orbitals. In both orbitals of *e* symmetry π^*CO also plays an important role. Its contribution (bonding) to the 8*e* orbital is equal to 13%, whereas in the 9*e* orbital the contribution is as high as 72% and it is antibonding. The energies of the HOMO and LUMO orbitals decrease in the isoelectronic series: $[Fe^{II}(CN)_6]^{4-} > [Fe^{II}(CN)_5CO]^{3-} > [Fe^{II}(CN)_5NO]^{2-}$. This tendency explains the experimentally observed redox properties in this series. $[Fe(CN)_6]^{4-}$, with the highest HOMO energies (close to 0.0 eV), is indeed known as a reducer. On the other hand the oxidative properties of the $[Fe(CN)_5NO]^{2-}$ complex may be explained on the basis of the value of the LUMO energy (−10.86 eV), which is the lowest in the series. The intermediate complex $[Fe(CN)_5CO]^{3-}$ should not easily undergo redox reactions since its HOMO energy is

Table 3. Characteristics of the $[Fe(CN)_5CO]^{n-}$ complexes; ε denotes orbital energy (in eV), ΔE = charge in total energy of the complex caused by one-electron oxidation (in eV); for other quantities see Tables 1 and 2

	$[Fe^{II}(CN)_5CO]^{3-}$	$[Fe^{III}(CN)_5CO]^{2-}$	$[Fe^{I}(CN)_5CO]^{4-}$
No. of electrons	66	65	67
Ground state configuration	$2b_2^2 8e^4$	$8e^4 2b_2^1$	$2b_2^2 8e^4 9e^1$
q_{Fe}	−0.562	−0.275	−0.473
q_C	0.765	0.934	0.326
q_O	−0.860	−0.740	−0.887
q_{CO}	−0.095	0.194	−0.561
E^{cov}_{C-O}	−60.40	−63.58	−60.08
E^{cov}_{Fe-CO}	−51.08	−44.21	−45.08
$E^{cov}_{Fe-CN_{ax}}$	−41.80	−41.29	−42.68
$E^{cov}_{Fe-CN_{eq}}$	−41.86	−41.84	−41.12
$\varepsilon(2b_2)$	−5.74	−4.66	−0.85
$\varepsilon(8e)$	−5.32	−10.90	−0.80
$\varepsilon(9e)$	+5.94	+0.42	+9.47
ΔE	−4.13	−2.02	−13.28

too low and LUMO energy too high to facilitate appropriate electron loss or gain.

$[Fe^{III}(CN)_5CO]^{2-}$. The highest occupied orbitals in the case of $[Fe(CN)_5CO]^{3-}$ are closely distributed and it was not clear from which of them one electron should be removed in the oxidation process, thus a series of calculations was performed. The configuration $8e^4 2b_2^1$ appears to be the most favourable (see Table 3), independently of the assumed bond distances. The oxidation of $[Fe(CN)_5CO]^{3-}$ results in a decrease of electron density, mainly of the iron atom ($\Delta q = +0.287$) and CO ligand ($\Delta q = +0.289$), leading even to a positive charge in the latter. This is accompanied by the strengthening of CO and weakening of Fe—CO bonds. Iron–cyano bonds both in axial and equatorial positions are influenced only slightly. The low orbital energy (−4.66 eV) of the semi-occupied $2b_2$ orbital should facilitate reduction of the complex. Moreover, the positive charge on the CO group, together with a small positive value of LUMO energy and a large contribution of π^*CO (85%), should lead to great susceptibility towards nucleophilic attack. The expected high reactivity of the $[Fe(CN)_5NO]^{2-}$ ion is confirmed by experiment and this species is observed only as a short lived moiety.[7]

$[Fe^{I}(CN)_5CO)]^{4-}$. The ground state configuration of this complex has been established as $2b_2^2 8e^4 9e^1$ (Table 3). The ground state energy term is the double degenerate ^{2}E one. We can expect that the geometrical structure of $[Fe(CN)_5CO]^{4-}$ would be unstable. The reduction of $[Fe(CN)_5CO]^{3-}$ results in a great increase in electron density on the CO ligand, and simultaneously the Fe—CO bond undergoes considerable weakening. The complex should behave as a stronger reducer than $[Fe(CN)_6]^{4-}$ due to the considerable negative charge on the CO group ($q = -0.561$), high positive energy of the $9e$ orbital with one unpaired electron (+9.47 eV) and significant decrease in the total energy of the complex caused by one-electron oxidation ($\Delta E = -13.28$ eV). All these factors lead to the conclusion that the probability of the existence of $[Fe^{I}(CN)_5CO]^{4-}$ is very low.

Carbonylpentacyano complexes of manganese and chromium

The results of calculations for $[Mn(CN)_5CO]^{n-}$ and $[Cr(CN)_5CO]^{n-}$ complexes are gathered in Tables 4 and 5. The complexes which are isoelectronic with $[Fe^{II}(CN)_5CO]^{3-}$ are $[Mn^{I}(CN)_5CO]^{4-}$ and $[Cr^{0}(CN)_5CO]^{5-}$, respectively. The ground state of both these complexes is again $2b_2^2 8e^4$. The negative net charge on the CO group increases in the series Fe < Mn < Cr. The same trend is observed for the HOMO orbital energies. This ability to change electronic properties leads to the conclusion that the $[Mn(CN)_5CO]^{4-}$ complex should be more active in oxidation reactions than the $[Fe(CN)_5CO]^{3-}$ ion. The $[Cr(CN)_5CO]^{5-}$ complex is expected to be an extremely strong reducer (note the values of $q_{CO} = -0.619$ and $\varepsilon_{HOMO} = +14.73$ eV). Significant lowering of the total energy which follows one-electron oxidation fully supports this conclusion ($\Delta E = -15$ eV).

In the case of the manganese complex we have studied its oxidized and reduced form. Similarly, as in the case of iron complexes, their ground state configurations are $8e^4 2b_2^1$ and $2b_2^2 8e^4 9e^1$, respec-

Table 4. Characteristics of the $[Mn(CN)_5CO]^{n-}$ complexes (see Table 3)

	$[Mn^{I}(CN)_5CO]^{4-}$	$[Mn^{II}(CN)_5CO]^{3-}$	$[Mn^{0}(CN)_5CO]^{5-}$
No. of electrons	66	65	67
Ground state configuration	$2b_2^2 8e^4$	$8e^4 2b_2^1$	$2b_2^2 8e^4 9e^1$
q_{Mn}	−0.536	−0.288	−0.380
q_C	0.512	0.682	0.153
q_O	−0.908	−0.837	−0.948
q_{CO}	−0.396	−0.155	−0.795
E^{cov}_{C-O}	−59.95	−61.51	−58.74
E^{cov}_{Mn-CO}	−46.40	−45.48	−44.78
$E^{cov}_{Mn-CN_{ax}}$	−38.81	−38.53	−39.82
$E^{cov}_{Mn-CN_{eq}}$	−39.38	−38.85	−39.52
$\varepsilon(2b_2)$	+0.599	+0.810	+5.187
$\varepsilon(8e)$	+0.876	−4.712	+5.232
$\varepsilon(9e)$	+10.43	+5.72	+13.88
ΔE	−10.09	−6.11	−18.77

Table 5. Characteristics of the $[Cr(CN)_5CO]^{n-}$ complexes (see Table 3)

	$[Cr^0(CN)_5CO]^{5-}$	$[Cr^I(CN)_5CO]^{4-}$	$[Cr^{II}(CN)_5CO]^{3-}$
No. of electrons	66	65	64
Ground state configuration	$2b_2^2 8e^4$	$8e^4 2b_2^1$	$8e^4$
q_{Cr}	−0.753	−0.494	−0.394
q_C	0.346	0.481	0.589
q_O	−0.965	−0.910	−0.855
q_{CO}	−0.619	−0.429	−0.266
E^{cov}_{C-O}	−58.72	−59.88	−58.15
E^{cov}_{Cr-CO}	−45.03	−44.92	−45.43
$E^{cov}_{Cr-CN_{ax}}$	−35.95	−35.83	−35.60
$E^{cov}_{Cr-CN_{eq}}$	−36.93	−36.06	−35.67
$\varepsilon(2b_2)$	+6.25	+5.78	+4.62
$\varepsilon(8e)$	+6.13	+0.95	−3.88
$\varepsilon(9e)$	+14.73	+10.39	+6.12
ΔE	−15.00	−10.00	−5.18

tively. The trends in the changes of electronic structure factors caused by oxidation/reduction are the same as for iron complexes. Nevertheless, for $[Mn^{II}(CN)_5CO]^{3-}$ no oxidative properties can be expected. It remains a weak reducer ($q_{CO} = -0.155$). However, the reduced form $[Mn(CN)_5CO]^{5-}$ should be very active in redox reactions with even stronger reducing properties than $[Fe(CN)_5CO]^{4-}$ ($q_{CO} = -0.795$, $\varepsilon_{HOMO} = +13.88$ eV, $\Delta E = -18.77$ eV).

The isoelectronic species to the iron(II) complex is the $[Cr^0(CN)_5CO]^{5-}$ ion so only its oxidized forms have been taken into account. $[Cr^I(CN)_5CO]^{4-}$ can be expected to exhibit fairly strong reducing properties, which together with an unstable ground state configuration seem to indicate that this complex should not be observed experimentally. The ground state configuration of the $[Cr^{II}(CN)_5CO]^{3-}$ complex is $8e^4$. The net charge on the CO ligand ($q = -0.266$) and the HOMO orbital energy ($\varepsilon = -3.88$ eV) enable this complex to show at least mild reducing behaviour.

On the basis of the results discussed some general conclusions regarding the relative thermal stabilities of carbonylpentacyano complexes of iron, manganese and chromium can be drawn. Obviously the most stable complex should be $[Fe^{II}(CN)_5CO]^{3-}$, which is indeed observed experimentally. Its oxidized form, $[Fe^{III}(CN)_5CO]^{2-}$, may be expected to be the only oxidant within the studied compounds. The weak reducing properties and stable electronic configurations of $[Mn^{II}(CN)_5CO]^{3-}$ and $[Cr^{II}(CN)_5CO]^{3-}$ suggest that these complexes could be the next candidates for a successful synthesis.

REFERENCES

1. A. G. Sharpe, *The Chemistry of Cyano Complexes of the Transition Metals*. Academic Press, New York (1976).
2. A. G. Sharpe, in *Comprehensive Coordination Chemistry* (Edited by G. Wilkinson), Vol. 2, 1st edn, p. 7. Pergamon Press, New York (1987).
3. B. Sieklucka, *Prog. React. Kinet.* 1989, **15**, 175 and refs therein.
4. E. Wasielewska and Z. Stasicka, in *Coordination Chemistry and Catalysis* (Edited by J. J. Ziółkowski), p. 440. World Scientific, Singapore (1987) and refs therein.
5. A. Vogler and H. Kunkely, *Z. Naturforsch.* 1975, **B30**, 335.
6. H. E. Toma, E. Fluck, H. Binder and S. Yanagisawa, *Z. Anorg. Allg. Chem.* 1981, **483**, 75.
7. H. E. Toma and F. T. P. Lellis, *An. Acad. Bras. Cienc.* 1987, **59**, 165.
8. Z. Stasicka, Proc. 12th CCC, p. 359. Bratislava-Smolenice, Czechoslovakia (1989).
9. E. Wasielewska and A. Gołębiewski, *Pol. J. Chem.* 1981, **55**, 1099.
10. A. Gołębiewski and E. Wasielewska, *J. Molec. Struct.* 1980, **67**, 183.
11. E. Wasielewska and Z. Stasicka, *J. Inform. Rec. Mater.* 1989, **17**, 441.
12. E. Wasielewska, *Inorg. Chim. Acta* 1986, **122**, L1.
13. A. Gołębiewski and M. Witko, *Acta Phys. Polon.* 1980, **A57**, 585.

Polyhedron Vol. 12, No. 5, pp. 467–472, 1993
Printed in Great Britain

0277–5387/93 $6.00+.00
© 1993 Pergamon Press Ltd

REACTIONS OF LANTHANIDE NITRATES WITH DIMETHYLBENZOYLPHOSPHONATE

ANDREW W. G. PLATT

Chemistry Division, Staffordshire University, College Road, Stoke-on-Trent ST4 2DE, U.K.

(*Received* 30 *September* 1992; *accepted* 6 *November* 1992)

Abstract—The reactions between lanthanide nitrates and $(MeO)_2P(:O)C(:O)Ph$ in methanol have been studied. The products of the reaction are $(MeO)_2P(:O)H$, $[(MeO)_2P(:O)]_2C(OH)Ph$ and $PhC(:O)OMe$. At high concentrations of reactants the complexes $Ln(NO_3)_3\{[(MeO)_2P(:O)]_2C(OH)Ph\}_2$ are formed (Ln = La, Ce) whilst loss of nitrate occurs for the heavier metals giving $Ln(PO_4)\{(MeO)_2P(:O)H\}_2 \cdot H_2O$ (Ln = Yb). The kinetics of the reaction in dilute solution have been studied and a mechanism proposed. Derivation of a rate equation from the full mechanism is not possible but the kinetics data have been fitted to an approximate expression and the results compared with first order analysis. Supporting evidence for the proposed mechanism (mainly ^{31}P NMR spectroscopy) is also presented.

Alpha ketophosphonates readily undergo acid or base catalysed cleavage of the P—C bond[1–3] and calculations suggest that protonation of the phosphoryl oxygen is followed by P—C bond breaking with zero activation energy.[4] Complex formation with metals might be considered to be analogous to protonation, and indeed catalytic decomposition of α-ketophosphonates by Lewis acids has been mentioned but no details were reported.[4] Despite this there are several reports of stable complexes being formed between α-ketophosphonates and metals in both aprotic[5] and protic systems.[6,7] We report here studies on the reactions between lanthanide nitrates and dimethylbenzoylphosphonate, $(MeO)_2P(:O)C(:O)Ph$, in methanol.

RESULTS AND DISCUSSION

Attempts to prepare lanthanide nitrate complexes with dimethylbenzoyl phosphonate (**1**) were not successful. On reaction with lanthanide nitrates, $Ln(NO_3)_3$ (Ln = La, Ce, Pr, Dy, Er and Yb), in warm methanol the yellow colour of **1** was rapidly discharged. On cooling the new complexes **2** crystallized, where Ln = La or Ce.

$$Ln(NO_3)_3[\{(MeO)_2P(:O)\}_2C(OH)Ph]_2$$

2

2a Ln = La

2b Ln = Ce

The complexes were characterized by elemental analysis and IR spectroscopy, which showed strong bands consistent with the presence of bidentate nitrate groups at 1450 and1385 cm^{-1},[8–10] and a strong absorption at 1210 cm^{-1} due to the coordinated PO group. There were no bands attributable to the CO group of the original phosphonate. The complexes were insoluble in all common organic solvents, but did dissolve in water with decomposition to give the free ligand in solution.

Cerium(III) nitrate reacted in an identical manner. Both dysprosium and ytterbium nitrates caused rapid decolourization of the solutions giving the same phosphorus containing products (^{31}P NMR evidence). However, no dysprosium or ytterbium complexes analogous to **2** could be crystallized from solution. In the case of dysprosium no solid material could be obtained, whilst reduction of the solvent by slow evaporation of the ytterbium nitrate solution produced an amorphous solid whose IR spectrum indicated the presence of coordinated phosphite [ν(PH) 2415 cm^{-1} compared with 2440 cm^{-1} for dimethylphosphite] and phosphate groups, with no bands attributable to nitrate. This was supported by elemental analysis, which gave an approximate composition of $Yb(PO_4) \cdot [(MeO)_2P(:O)H]_2 \cdot H_2O$.

The reaction can be conveniently monitored in dilute solution by ^{31}P NMR spectroscopy, as shown in the case of lanthanum nitrate in Fig. 1. In lanthanum nitrate solution (10 mmol dm^{-3}) spectra

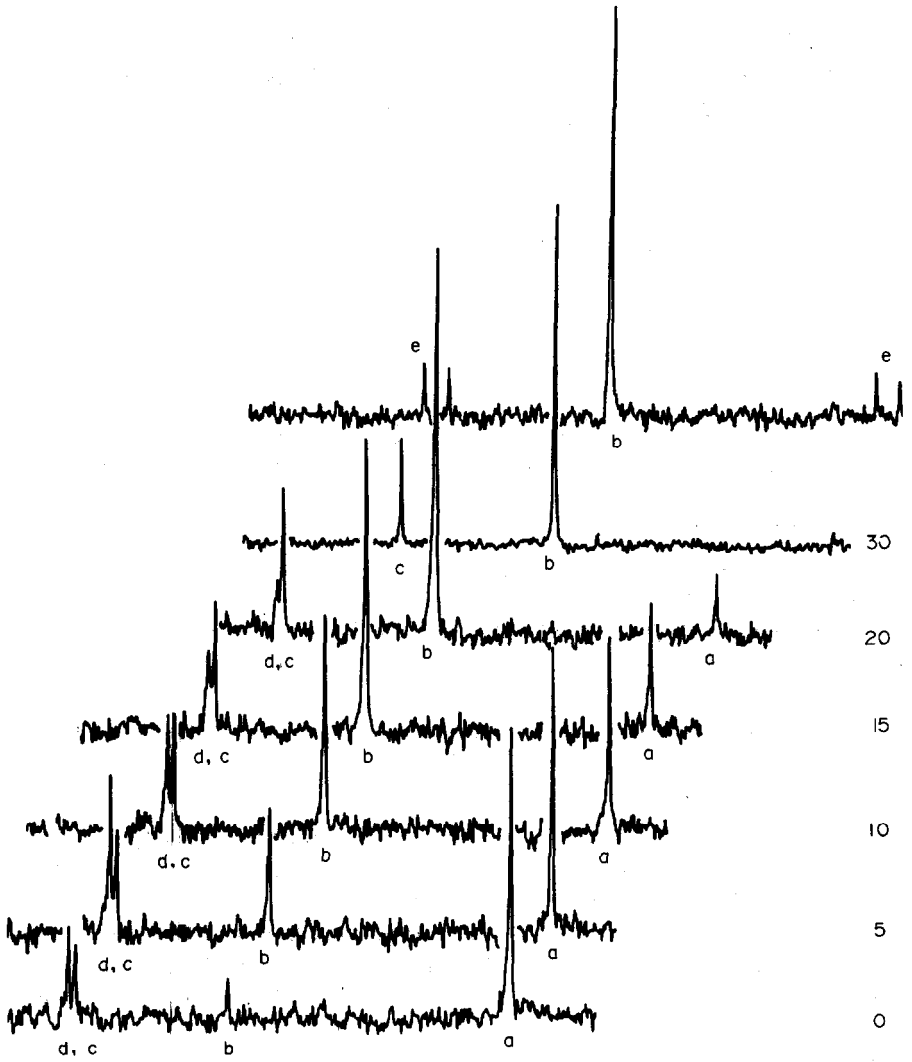

Fig. 1. ^{31}P NMR spectra taken from the reaction between $La(NO_3)_3$ (10 mmol dm^{-3}) and $(MeO)_2P(:O)C(:O)Ph$ in methanol as a function of time (min). The top trace is for the reaction mixture after the addition of a trace of triethylamine. Key: a = $(MeO)_2P(:O)C(:O)Ph$, b = $(MeO)_2P(:O)H$, c = $[(MeO)_2P(:O)]_2C(OH)Ph$, d = $(MeO)_2P(:O)C(OH)(OMe)Ph$, e = $(MeO)_2P(:O)OCH(Ph)P(:O)(OMe)_2$.

show that in the initial stages of the reaction the products are dimethylphosphite, the methanol adduct of the original phosphonate, $(MeO)_2P(:O)C(OH)(OMe)Ph$, and $[(MeO)_2P(:O)]_2C(OH)Ph$, formed by reaction between dimethylphosphite and the dimethylbenzoyl phosphonate. At the end of the reaction dimethylphosphite and the diphosphonate are the only phosphorus containing species. The identity of $[(MeO)_2P(:O)]_2C(OH)Ph$ was confirmed by its isomerization by either heating or by adding traces of triethylamine to the mixed phosphate–phosphonate $(MeO)_2P(O)OCH(Ph)P(O)(OMe)_2$,[11] which exhibits two characteristic doublets at δ 19.8 and 0.7 ppm, $^3J(PP)$ 33 Hz (see Fig. 1, signals "e"). A possible mechanism for the solvolysis of the phosphonate **1** in dilute solution is shown in Scheme 1.

The following observations support this mechanism.

(1) Reaction (1) can be observed independently by electronic spectroscopy and ^{31}P NMR spectroscopy, which shows the gradual appearance of a resonance at 18.0 ppm assigned to **3**, in addition to that of **1** at 0.3 ppm. The assignment to **3** is in good agreement with the value of 17.9 quoted for the corresponding hydrate.[1] First order kinetics were observed for this reaction with the rate coefficient corresponding to k_1+k_{-1}.

(2) Complex **4** could not be observed in solutions containing lanthanum nitrate and **1** by either NMR

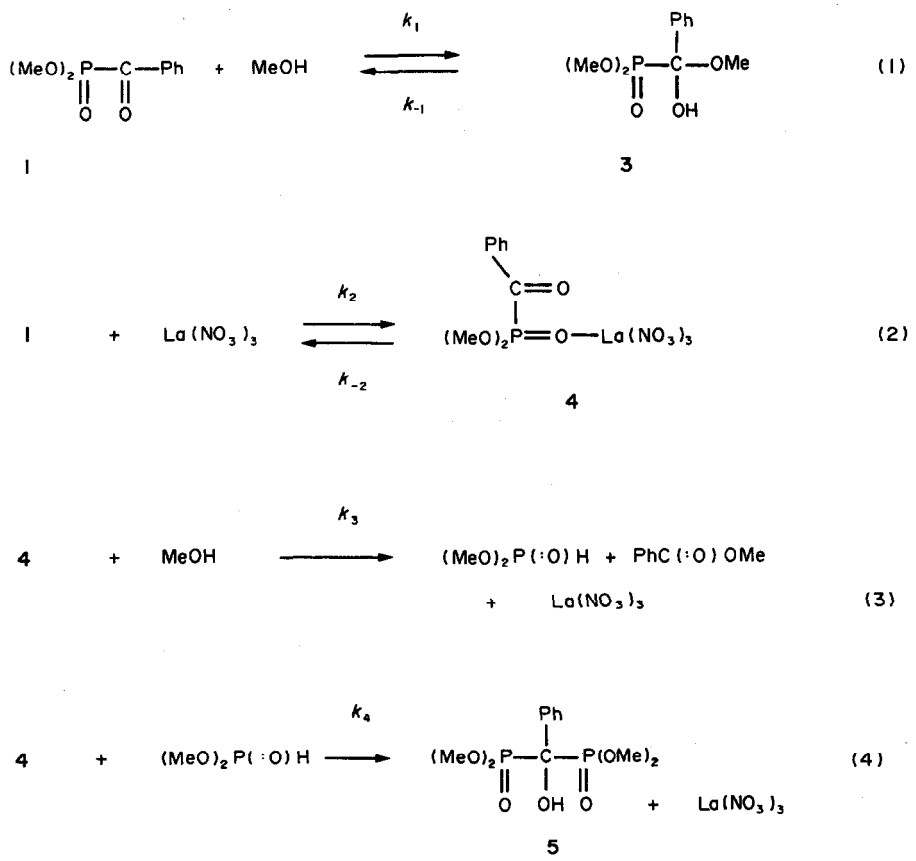

Scheme 1.

or UV–vis spectroscopy, which implies that it is only present in low concentration. The fact that coordination of $(MeO)_2P(:O)C(:O)Ph$ to the metal [eq. (2)] is important in the decomposition was demonstrated by the reduced rate of solvolysis in the presence of O-dimethyl-methylphosphonate, $(MeO)_2MeP(:O)$, and when the complex $Lu(NO_3)_3\{(EtO)_2P(:O)CH_2C(:O)OEt)_2$[12] was used instead of lanthanum nitrate. In both these instances there would be increased competition for the coordination sphere of the metal.

(3) In step (3) the cleavage of the P—C bond could be brought about by reaction with methanol or possibly water coordinated to the lanthanide (hydrated salts were used throughout). The reaction carried out in CH_3OD shows unambiguously that $(MeO)_2P(:O)D$ [δ 11.2 ppm, $^1J(PD) = 108$ Hz; lit. δ 11.2 ppm, $^1J(PD) = 107$ Hz[13]] is the major product. Methylbenzoate was detected by gas chromatography of the reaction mixture.

(4) The phosphonate **1** does not react with dimethylphosphite in methanol in the absence of lanthanum nitrate. Thus, it seems reasonable to suppose that reaction (4) in the scheme is the likely route to the formation of the diphosphonate **5**.

Kinetic studies were carried out by monitoring the n–π^* transition at 365 nm. This band was chosen rather than the more sensitive π–π^* band due to the fact that nitrate and the aromatic containing products absorb in this region in addition to **1**.

Analysis of the data as a pseudo-first-order process gave reasonable fits with experimental data, as indicated in Table 1. However, the experimental data points appear to oscillate about the best-fit line rather than give a random scatter. An example is shown in Fig. 2, which shows the residuals (calculated minus observed absorbances) as a function of time. This is compared with the residuals from fitting the same data to eq. (1) (see below).

Full analysis of the scheme, assuming a steady-state approximation for complex **4**, leads to a set of differential equations which cannot be solved analytically to give an expression for C_1. However, if it is assumed that, as a first approximation, reaction (4) is of minor importance [the ratio of diphosphonate (**5**) to dimethylphosphite in the reaction mixture at completion was approximately 1 : 5, as measured by ^{31}P NMR spectroscopy in the presence of chromium trisacetylacetonate as a relaxation reagent] then the analysis gives the simultaneous differential equations:

$$DC_1 = -aC_1 + bC_3$$

$$DC_3 = dC_1 - bC_3,$$

Table 1. Results of the analysis of kinetic data for the hydrolysis of **1** catalysed by lanthanum nitrate in methanol

$[La(NO_3)_3]$ (mmol dm^{-3})	k_{obs} (min^{-1})[a]	Sum of squares[b]	$x(1)$[c]	Sum of squares[b]
10.8	0.165	6.0	0.250	18.0
6.3	0.132	5.2	0.128	4.7
4.3	0.105	5.8	0.100	4.6
2.5	0.080	13.0	0.076	6.4
1.3	0.061	5.4	0.058	3.8
0.0	0.015[d]	0.1		

[a] Values obtained from first-order analysis.
[b] $\Sigma(A_{calc}-A_{obs})^2 \times 10^3$ for 30 data points.
[c] Values obtained by fitting to eq. (5).
[d] k_1+k_{-1} derived from first-order analysis.

The equilibrium constant was estimated as 0.94, giving values of $k_1 = 0.0073$ and $k_{-1} = 0.0078$ min^{-1}.

where $D = d/dt$, $a = k_1+k_2k_3C_{La}/(k_{-2}+k_3)$, $b = k_{-1}$, $d = k_1$ and C_1 and C_3 are the concentrations of **1** and **3**, and C_{La} is the concentration of lanthanum nitrate. Eliminating C_3 gives

$$[D^2+(a+b)D+(ab-bd)]C_1 = 0,$$

which can be solved to give

$$C_1 = \exp\left(-\frac{t}{2}[x(1)+2b]\right) \times \left\{x(2)\exp\left(\frac{t}{2}\sqrt{x(1)^2+4bd}\right) + x(3)\exp\left(-\frac{t}{2}\sqrt{x(1)^2+4bd}\right)\right\}+x(4), \quad (5)$$

where $x(1)$ to $x(4)$ are constants whose values are found by fitting the experimental data to eq. (5).

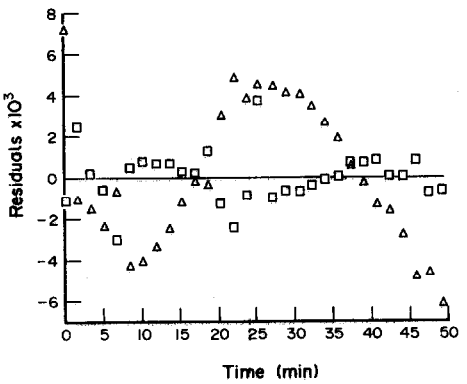

Fig. 2. Plot of the residuals, $(A_{calc}-A_{obs}) \times 10^3$, for kinetic data from the solvolysis of **1** in lanthanum nitrate (2.5 mmol dm^{-3}) fitted to a first-order equation (△) and to eq. (5) (□).

The parameter $x(1)$ corresponds to $(a-b)$. From the initial conditions the sum $x(2)+x(3)$ equals the initial concentration of phosphonate whilst $x(4)$ represents a baseline correction. In practice it was found that the sum $x(2)+x(3)+x(4)$ invariably equalled the initial absorbance value, giving some confidence that the fit to eq. (5) is chemically sensible. The results analysed by fitting to eq. (5) generally give better results than a simple first-order analysis, as indicated by a lower sum of squares, although the values of coefficients obtained are virtually the same. The fit to eq. (5) becomes progressively better as the concentration of lanthanum nitrate is decreased. Figure 2 shows that whilst the residuals are smaller than obtained from the first-order plot, there is still a periodic pattern evident.

If eqs (5) accurately represent the reaction then a plot of $x(1)$ vs C_{La} should give a straight line. A reasonable straight line ($R^2 = 0.97$) is obtained for C_{La} in the region 1–10 mmol dm^{-3}, as shown in Fig. 3. The intercept of 0.021(15) agrees fairly well with the expected value of around zero (corresponding to k_1-k_{-1}). The probable reason for the small discrepancy is the exclusion of reaction (4) in the scheme from the rate equation. The fact that the fit to eq. (5) becomes progressively worse with increasing concentration of lanthanum nitrate may be due to other reactions becoming significant at higher concentrations. One possibility is complex formation between **3** and the metal leading to P—C bond breaking. Although it is not possible to take this into account in the rate equation, some experimental evidence for the reaction can be obtained from ^{31}P NMR measurements on an equilibrated mixture of **1** and **3** in methanol. Thus, addition of small amounts of gadolinium nitrate caused pref-

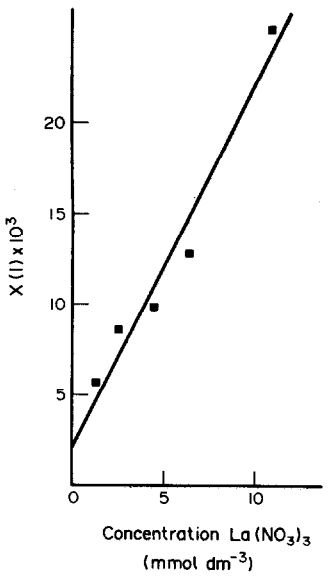

Fig. 3. Plot of $x(1)$ vs concentration of $La(NO_3)_3$.

erential broadening of the signal due to **3**, whilst that due to **1** remained relatively sharp. Also, addition of praseodynium nitrate caused a rapid decrease in the concentration of **3**, whereas the signal due to **1** decreased at a slower rate. Both these observations support the fact that **3** forms complexes with the lanthanide nitrates more readily than **1**, and that this process also leads to P—C bond breaking.

Thus, although the kinetic data cannot be used to support the proposed mechanism directly, the first three reactions in the scheme do give a reasonable approximation. The overall rate of solvolysis would indicate that steps (3) and (4) in the scheme are rate determining. The rate of complex formation is known to be of the order $10^9\ s^{-1}$ for lanthanide ions with simple monodentate ligands.[14] If this process was followed by bond breaking with zero activation energy, as proposed for the analogous protonated systems,[4] then the overall catalysis would be much more rapid. The observation that **1** does not undergo rapid solvolysis in 0.01 M $HClO_4$ in methanol and the fact that previous work has shown that the rate of hydrolysis in aqueous solution decreases with decreasing pH[1,3] indicate that the results of such calculations are not directly applicable to the chemistry in the protic solvents studied.

EXPERIMENTAL

Dimethylbenzoyl phosphonate was prepared by the reaction of trimethylphosphite with freshly distilled benzoyl chloride[11] in 89% yield.

Preparation of $Ln(NO_3)_3\{[(MeO)_2P(:O)]_2C(OH)Ph\}_2$ (**2a** *and* **2b**)

Ln = La. $La(NO_3)_3 \cdot 6H_2O$ (1 g, 2.3 mmol) was dissolved in methanol (10 cm^3) and the phosphonate (2 g, 9.3 mmol) was added. The solution was warmed to 50°C for 2 min, during which time the yellow colour of the phosphonate was discharged. The mixture was allowed to cool to room temperature and on standing crystals of the colourless complex were formed. Filtration followed by washing with ethanol and diethyl ether gave 0.51 g (22%) of **2a**. Found: C, 27.2; H, 3.8; N, 4.1. Calc.: C, 27.1; H, 3.7; N, 4.3%.

Ln = Ce. $Ce(NO_3)_3 \cdot 6H_2O$ (1 g, 2.3 mmol) was reacted as above to give the corresponding cerium complex as colourless crystals. Yield 0.5 g (22%) of **2b**. Found: C, 27.4; H, 4.0; N, 4.2. Calc.: C, 27.1; H, 3.7; N, 4.3%.

Reaction of ytterbium nitrate with **1**

$Yb(NO_3)_3 \cdot 6H_2O$ (1 g, 2.14 mmol) was allowed to react with **1** (2 g) in methanol as above. On standing for 1 week a white amorphous solid was deposited from the decolourized solution (0.5 g). Found: C, 8.8; H, 3.0. Calc.: for $Yb(PO_4)[(MeO)_2P(:O)H]_2 \cdot H_2O$: C, 9.5; H, 3.2%.

Kinetic measurements were performed using a Varian DMS 100 in cells thermostated to 25°C. Optical density data were collected over *ca* three half-lives using 30 points. For first-order kinetics the data were fitted by a non-linear least-squares program with the rate coefficient, initial and infinity absorbancies as the adjustable parameters. Data were fitted to eq. (5) using an iterative procedure by a NAG subroutine.[15] The values are averages of at least three independent runs and were reproducible to within 5%. ^{31}P NMR spectra were run on a JEOL FX90Q.

Acknowledgements—Thanks are due to Dr C. D. Adam for his invaluable assistance with the program for fitting the data to eq. (5) and to Dr J. T. Thompson for the use of the non-linear least-squares program and for valuable discussions.

REFERENCES

1. K. D. Berlin and K. S. Narayanan, *J. Am. Chem. Soc.* 1979, **101**, 109.
2. E. Breuer, R. Karaman, A. Goldblum and H. Leader, *J. Chem. Soc. Perkin (II)* 1988, 2029.
3. R. Kluger and J. Chin, *J. Am. Chem. Soc.* 1978, **100**, 7383.
4. E. Breuer, R. Karaman, H. Leader, A. Goldblum and R. Moshe, *Phosphorus Sulfur* 1988, **30**, 113.

5. A. N. Pudovik, A. A. Muratova, O. B. Sobanova and E. G. Yarkov, *J. Gen. Chem. (USSR)* 1977, **47**, 1330.
6. C. M. Mikulski, W. Henry, L. L. Pytlewski and N. M. Karayannis, *J. Inorg. Nucl. Chem.* 1978, **40**, 769.
7. C. M. Mikulski, W. Henry, L. L. Pytlewski and N. M. Karayannis, *Trans. Met. Chem.* 1977, **2**, 135.
8. R. Babecki, A. W. G. Platt and J. Fawcett, *J. Chem. Soc., Dalton. Trans.* 1992, 675.
9. Y. Kawano and V. K. Lakatos Osorio, *J. Inorg. Nucl. Chem.* 1977, **39**, 701.
10. D. G. Hendricker and R. J. Foster, *J. Inorg. Nucl. Chem.* 1972, **34**, 1949.
11. D. A. Nicholson and H. Vaughn, *J. Org. Chem.* 1971, **36**, 3843.
12. A. Lothian and A. W. G. Platt, *Polyhedron* 1992, **11**, 2983.
13. W. J. Stec, *Z. Naturforsch.* 1974, **298**, 109.
14. S. F. Lincoln, *Adv. Inorg. Bioinorg. Mech.* 1986, **4**, 217.
15. NAG subroutine library EO4 FDF (1987).

Polyhedron Vol. 12, No. 5, pp. 473–477, 1993
Printed in Great Britain

0277–5387/93 $6.00+.00
© 1993 Pergamon Press Ltd

FORMATION OF ISOPOLYOXOMETALLATE(VI) ANIONS IN THE REACTION BETWEEN $M(CO)_6$ (M = W, Mo) AND ACETIC ACID: X-RAY CRYSTAL STRUCTURE OF $[W_3(\mu_3\text{-}O)_2(\mu_2\eta^2\text{-}O_2CCH_3)_6(H_2O)_3]_2[W_{10}O_{32}]\cdot$SOLVENT

ANNE MADDEN, MALACHY McCANN* and HELEN RYAN

Chemistry Department, St Patrick's College, Maynooth, Co. Kildare, Ireland

and

CHRISTINE CARDIN* and MAIRE CONVERY

Chemistry Department, Trinity College, Dublin, Ireland

(*Received* 30 *September* 1992; *accepted* 4 *November* 1992)

Abstract—$W(CO)_6$ reacts with a mixture of acetic acid/acetic anhydride to give $[W_3(\mu_3\text{-}O)_2(\mu_2\eta^2\text{-}O_2CCH_3)_6(H_2O)_3](CH_3CO_2)_2$ (**1**), which was converted by $HClO_4$ to $[W_3(\mu_3\text{-}O)_2(\mu_2\eta^2\text{-}O_2CCH_3)_6(H_2O)_3](ClO_4)_2$ (**2**). Addition of CH_3CO_2Na to the above reaction mixture, and prolonged exposure of the solution to air, results in the formation of the W^{IV}/W^{VI} complex salt $[W_3(\mu_3\text{-}O)_2(\mu_2\eta^2\text{-}O_2CCH_3)_6(H_2O)_3]_2[W_{10}O_{32}]\cdot$solvent (**3**). Complex **3** was also prepared by reacting **1** with $Na_2WO_4\cdot 2H_2O$ in acetic acid, and it has been characterized by X-ray crystallography. Addition of $[CH_3(CH_2)_3]_4N(ClO_4)$ to the reaction filtrate remaining after the preparation of $[Mo_2(\mu\text{-}O_2CCH_3)_4]$ [from $Mo(CO)_6$, CH_3CO_2H and $(CH_3CO)_2O$], followed by exposure to air, gives $([CH_3(CH_2)_3]_4N)_2[Mo_6O_{19}]$ (**4**).

One of the most commonly encountered structural units in tungsten(IV) carboxylate chemistry is the bioxo-capped trinuclear cluster $[W_3(\mu_3\text{-}O)_2(\mu_2\eta^2\text{-}O_2CR)_6(H_2O)_3]^{2+}$.[1–4] The acetate dication $[W_3(\mu_3\text{-}O)_2(\mu_2\eta^2\text{-}O_2CCH_3)_6(H_2O)_3]^{2+}$ can be prepared either by the oxidation of W^0 [as $W(CO)_6$] in acetic acid/acetic anhydride[4] or by the reduction of W^{VI} (as WO_4^{2-}) with zinc in acetic anhydride.[1] These routes have led to the structurally characterized salts $[W_3(\mu_3\text{-}O)_2(\mu_2\eta^2\text{-}O_2CCH_3)_6(H_2O)_3](CF_3SO_3)_2$ and $[W_3(\mu_3\text{-}O)_2(\mu_2\eta^2\text{-}O_2CCH_3)_6(H_2O)_3][ZnBr_4]\cdot 8H_2O$, respectively.

In this paper we outline the preparation of the trinuclear tungsten(IV) acetate and perchlorate salts $[W_3(\mu_3\text{-}O)_2(\mu_2\eta^2\text{-}O_2CCH_3)_6(H_2O)_3](CH_3CO_2)_2$ (**1**) and $[W_3(\mu_3\text{-}O)_2(\mu_2\eta^2\text{-}O_2CCH_3)_6(H_2O)_3](ClO_4)_2$ (**2**), together with the synthesis and structure of the W^{IV}/W^{VI} complex salt $[W_3(\mu_3\text{-}O)_2(\mu_2\eta^2\text{-}O_2CCH_3)_6(H_2O)_3]_2[W_{10}O_{32}]\cdot$solvent (**3**). In addition, the isolation of the isopolyoxomolybdate(VI) ion $[Mo_6O_{19}]^{2-}$ from a reaction involving $Mo(CO)_6$ and acetic acid/acetic anhydride is also discussed.

* Authors to whom correspondence should be addressed.

RESULTS AND DISCUSSION

Tungsten

Routes to the tungsten complexes are summarized in Scheme 1. During the reaction of $W(CO)_6$ with acetic acid/acetic anhydride the reaction mixture undergoes a number of subtle colour changes, finally giving a yellow–black solution. Furthermore, the pattern of these colour changes appears to be essentially the same when the reaction is conducted in air or under nitrogen. When the yellow–black solution is exposed to air for a short time during concentration the diacetate salt **1** is recovered. The perchlorate salt **2** is recovered in a similar manner following addition of perchloric acid to the yellow–black solution prior to concentration. However, if the initial yellow–black

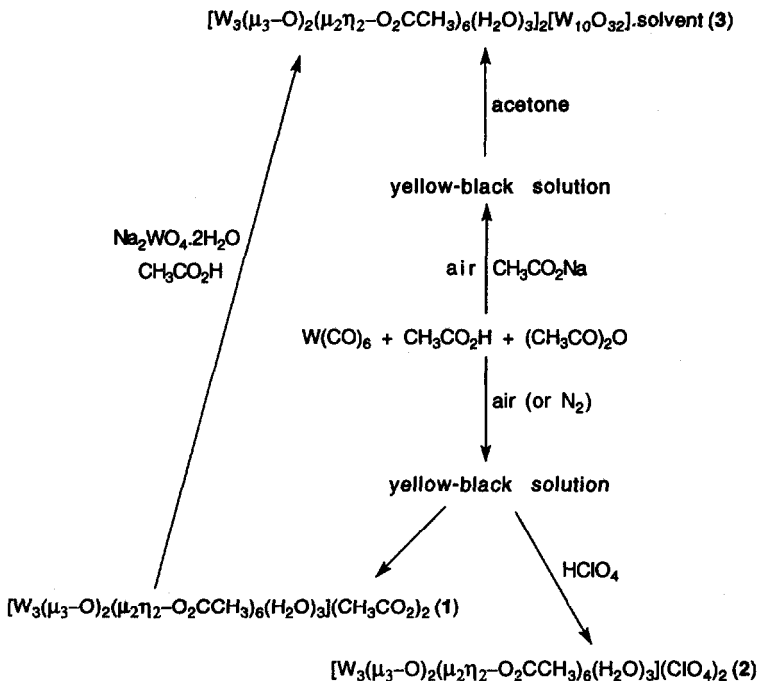

Scheme 1.

solution (containing some added sodium acetate) is allowed to stand in air for a long time (*ca* 3 months), then crystals of **3** are formed. Having discovered from X-ray crystallography (see later) that **3** contained trinuclear tungsten(IV) cations and a decanuclear tungsten(VI) anion, it was decided to try and make **3** by reacting **1** with a source of tungsten(VI), namely $Na_2WO_4 \cdot 2H_2O$. This method did indeed yield **3**.

The IR spectra of **1**, **2** and **3** all showed bands for the bridging bidentate acetate ligands in the region 1450–1550 cm^{-1}. Complex **1** exhibited $\nu_{asym}(CO_2)$ and $\nu_{sym}(CO_2)$ bands for the two non-coordinated acetate groups at 1635 and 1270 cm^{-1}, respectively,[5] whilst strong bands were present at 1085–1145 and 625 cm^{-1} for the perchlorate ions in **2**.[6] The spectrum of **3** contained prominent bands at 805, 895 and 960 cm^{-1}, arising from W—O—W and W=O vibrations of the $[W_{10}O_{32}]^{4-}$ ion.[7,8] None of these latter bands were present in the spectra of **1** and **2**.

In the first paper to be published on the reaction of $W(CO)_6$ with acetic acid/acetic anhydride (under nitrogen) Stephenson and Whittaker[9] tentatively formulated their yellow–brown microcrystalline product as $W_3O(CH_3CO_2)_8(OH)L$ ($L = H_2O$ or CH_3OH, depending on the reaction work-up procedure). On the basis of the present and previous work,[4] it seems likely that their compound was $[W_3(\mu_3\text{-}O)_2(\mu_2\eta^2\text{-}O_2CCH_3)_6(H_2O)_3](CH_3CO_2)_2$ (**1**). Furthermore, they reported that when an acetic acid solution of $W_3O(CH_3CO_2)_8(OH)CH_3OH$ was exposed to oxygen a deep yellow solid precipitated. Although the authors did not report any microanalytical data for this solid they did, however, mention that its IR spectrum was identical to that of $W_3O(CH_3CO_2)_8(OH)CH_3OH$, except for the growth of bands at 820 and 890 cm^{-1}, which they attributed to W—O—W and W=O vibrations, respectively. We believe that this deep yellow solid is a close relative of our present complex, $[W_3(\mu_3\text{-}O)_2(\mu_2\eta^2\text{-}O_2CCH_3)_6(H_2O)_3]_2[W_{10}O_{32}] \cdot$ solvent (**3**).

The crystal structure of **3** consists of two separate trinuclear tungsten(IV) dications, $[W_3(\mu_3\text{-}O)_2(\mu_2\eta^2\text{-}O_2CCH_3)_6(H_2O)_3]^{2+}$ (Fig. 1), and one decanuclear isopolyoxotungstate(VI) tetraanion, $[W_{10}O_{32}]^{4-}$ (Fig. 2). Although separate X-ray crystal structures of the cation[1,4] $[W_3(\mu_3\text{-}O)_2(\mu_2\eta^2\text{-}O_2CCH_3)_6(H_2O)_3]^{2+}$ and the anion[8] $[W_{10}O_{32}]^{4-}$ have previously been reported, complex **3** represents the first example of a structurally characterized tungsten salt in which the cation contains the metal in one oxidation state [tungsten(IV)] and the anion having the metal in a different oxidation state [tungsten(VI)]. The average values of the W—W and W—O bond lengths in **3** were found to be very similar to those listed in the literature for the independent ions (Table 1).

Molybdenum

When $Mo(CO)_6$ is refluxed under nitrogen with an acetic acid/acetic anhydride mixture yellow crys-

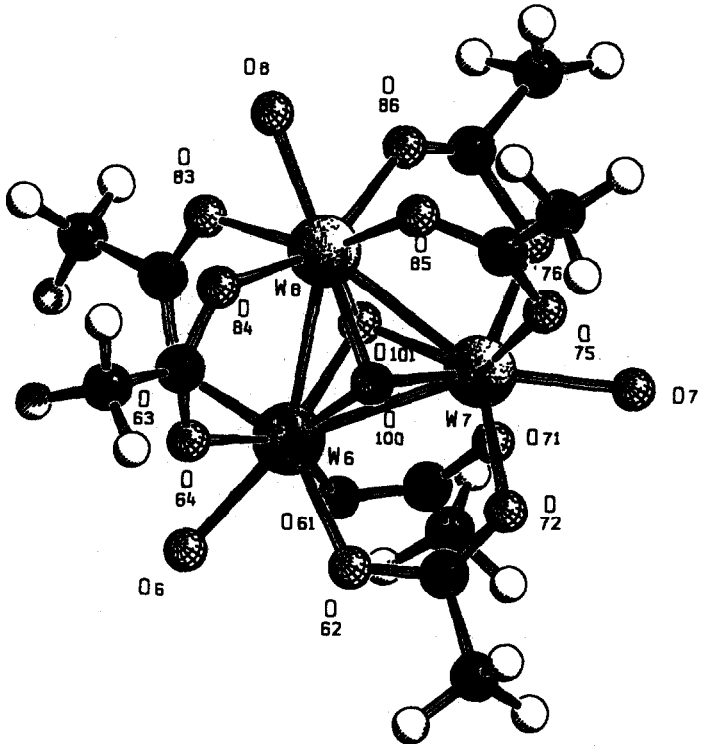

Fig. 1. One of the two trinuclear tungsten(IV) dications, $[W_3(\mu_3\text{-}O)_2(\mu_2\eta^2\text{-}O_2CCH_3)_6(H_2O)_3]^{2+}$, present in **3**·decanuclear isopolyoxotungstate(VI) tetraanion $[W_{10}O_{32}]^{4-}$.

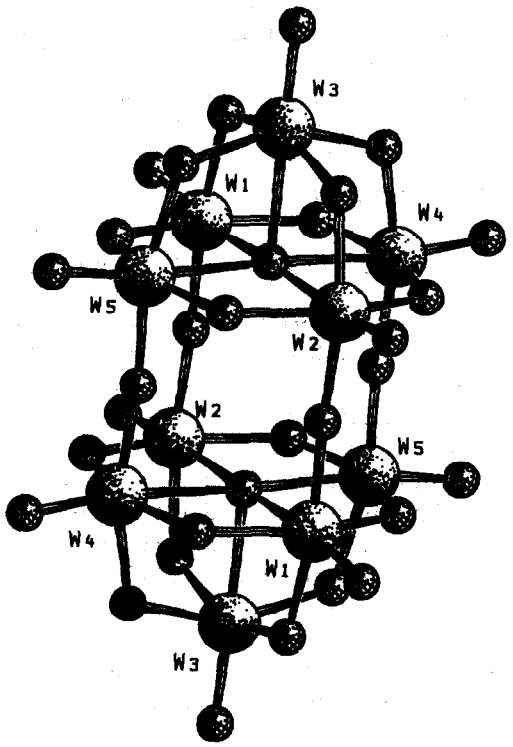

Fig. 2. The decanuclear isopolyoxotungstate(VI) tetraanion $[W_{10}O_{32}]^{4-}$ present in **3**.

tals of $[Mo_2(\mu\text{-}O_2CCH_3)_4]$ are deposited in a low[10] to moderate[11] yield at the bottom of a dark brown supernatant. If the above reaction is conducted in air,[12,13] or if the dark brown filtrate is subsequently exposed to air,[14] then a series of trinuclear cluster

Table 1. Comparison between tungsten ions and their previously determined structures. All bond lengths quoted are averages for similar bonds in the structures, therefore, no errors are listed

$[W_3(\mu_3\text{-}O)_2(\mu_2\eta^2\text{-}O_2CCH_3)_6(H_2O)_3]^{2+}$	This work (Å)	Ref. 1 (Å)
W—W	2.741	2.735
W—capping O	1.99	1.98
W—O	2.09	2.09
$[W_{10}O_{32}]^{4-}$	This work (Å)	Ref. 8 (Å)
W—central O	2.30	2.31
W—terminal O	1.68	1.67
W—bridging O	1.90	1.93
W—W	3.269	3.289

complexes of the type $[Mo_3(\mu_3\text{-}X)_2(\mu_3\text{-}Y)_2(\mu_2\eta^2\text{-}O_2CCH_3)_6(H_2O)_3](anion)_x \cdot yH_2O$ are formed. We have found that if the above-mentioned dark brown filtrate is treated with $[CH_3(CH_2)_3]_4N(ClO_4)$, and then exposure to air for a few days, yellow crystals of the known[15-17] isopolyoxomolybdate(VI) salt $([CH_3(CH_2)_3]_4N)_2[Mo_6O_{19}]$ (**4**) slowly form.

In conclusion, this work has established that in reactions between $M(CO)_6$ (M = W, Mo) and acetic acid/acetic anhydride (under aerobic conditions) the fate of some of the metal lies in the formation of isopolyoxometallate(VI) anions of the type $[M_xO_y]^{n-}$. Work is currently in progress on tyring to improve the yield of complex **3** in order that its reaction chemistry can be investigated further.

EXPERIMENTAL

Chemicals were purchased from commercial sources and, unless specified, were used without further purification. Diglyme was dried by distilling from sodium. IR spectra (KBr discs) were recorded in the region 4000–200 cm^{-1} on a Perkin–Elmer 783 grating spectrometer. Elemental analyses were carried out by the Microanalytical Laboratory, University College Cork, Ireland.

Crystallography

Crystal data for $[W_3(\mu_3\text{-}O)_2(\mu_2\eta^2\text{-}O_2CCH_3)_6(H_2O)_3]_2[W_{10}O_{32}]\cdot$solvent (**3**). Formula: $C_{12}H_{24}O_{33}W_8$ (in asymmetric unit), solvent: $C_{14.5}$. Mr = 2341.25, monoclinic, $P2_1/n$, a = 14.104(2), b = 14.097(1), c = 26.217(4) Å, β = 89.996(8)°, U = 5212(1) $Å^3$, D_c = 2.983 g cm^{-3}, Z = 4, $F(000)$ = 4156, μ(Mo-K_α) = 180.85 cm^{-1}.

A yellow–brown needle shaped crystal was mounted on an Enraf–Nonius CAD4 diffractometer and intensities of 6799 reflections were measured in the range $1° < \theta < 22°$ using graphite monochromated Mo-K_α radiation. The final cell coordinates were obtained by least-squares refinement of the setting angles for 25 automatically centred reflections, in the range $15° < \theta < 18°$. The crystal class was checked by examining a series of equivalent reflections. The data were not corrected for decay, but an empirical absorption correction was carried out using psi-scan data from three reflections. The data was reduced to give 5632 unique reflections (merging R of 0.0175), of these 4837 had $|I| > 4\sigma|I|$ and were used in the structure solution and refinement.

The structure was solved by the Patterson method of SHELXS. A $[W_3O_2(O_2CCH_3)_6(H_2O)_3]^{2+}$ cation and half of the $[W_{10}O_{32}]^{4-}$ anion, along with a number of solvent molecules, were found to be in the asymmetric unit. The structure was refined by blocked full-matrix least-squares of 507 parameters to give a final R value of 0.0323; the tungsten and oxygen atoms were all refined with anisotropic temperature factors. There were no significant correlations in the refinement. Difficulty was experienced in resolving the solvent molecules in the structure. A disordered acetic acid dimer was identified. The other positions of high electron density were assumed to be partially occupied acetones, and all atoms were refined with carbon structure factors. The weighting scheme was refined to give a flat analysis of variance, R_w = 0.0324. The final difference-Fourier had a goodness of fit of 1.77 and a highest peak in the difference map of 1.26 e $Å^{-1}$, adjacent to a tungsten atom.

SHELXS-86 and SHELX-76 were used by kind permission of G. M. Sheldrick, University of Göttingen.

$[W_3(\mu_3\text{-}O)_2(\mu_2\eta^2\text{-}O_2CCH_3)_6(H_2O)_3](CH_3CO_2)_2$ (1)

$W(CO)_6$ (0.5 g, 1.42 mmol), glacial acetic acid (10 cm^3) and acetic anhydride (4 cm^3) were refluxed together for 48 h under nitrogen. The initial pale yellow colour of the mixture gradually changed to orange–brown and finally to yellow–black. The solution was concentrated to low volume and the green product precipitated. The solid was filtered off, washed with acetone and then dried *in vacuo*. Yield 0.26 g (49%). The complex was very soluble in water and was slightly soluble in ethanol and methanol. Found: C, 17.7; H, 2.3. Calc.: C, 17.3; H, 2.7%. IR: 3400, 1635, 1510, 1460, 1270, 1020, 690, 642, 600, 350 cm^{-1}.

$[W_3(\mu_3\text{-}O)_2(\mu_2\eta^2\text{-}O_2CCH_3)_6(H_2O)_3](ClO_4)_2$ (2)

$W(CO)_6$ (0.4 g, 1.14 mmol), glacial acetic acid (10 cm^3) and acetic anhydride (10 cm^3) were refluxed together in air for 36 h. The initial pale yellow colour of the mixture gradually changed to orange–brown and finally to yellow–black. To the hot solution was slowly added $HClO_4$ (60%, 5 cm^3). The solution immediately changed to a light-brown colour and the green product precipitated. After cooling to room temperature the solid was filtered off, washed with acetone and then dried *in vacuo*. The complex was very soluble in water, ethanol and methanol and was slightly soluble in acetone, ether and chloroform. Found: C, 12.2; H, 2.2; Cl, 6.1. Calc.: C, 12.1; H, 2.0; Cl, 6.0%. IR: 3300, 1535, 1460, 1145, 1115, 1085, 690, 650, 625, 360, 340 cm^{-1}.

$[W_3(\mu_3\text{-}O)_2(\mu_2\eta^2\text{-}O_2CCH_3)_6(H_2O)_3]_2[W_{10}O_{32}]$ · solvent (**3**)

Method (*a*). $W(CO)_6$ (0.6 g, 1.70 mmol), glacial acetic acid (20 cm^3), acetic anhydride (10 cm^3) and sodium acetate (0.1 g, 1.2 mmol) were refluxed together in air for 36 h. The resulting yellow–black solution was allowed to cool to room temperature and then filtered to remove any undissolved solid. Acetone was then added to the filtrate, and on standing in air for *ca* 3 months a small amount of the product formed as yellow–brown crystals. One of these crystals was selected for the structure determination.

Method (*b*). Complex **1** (0.08 g, 0.07 mmol) and $Na_2WO_4 \cdot 2H_2O$ (0.12 g, 0.36 mmol) were refluxed in glacial acetic acid for 6 days in air. The mustard suspension was filtered whilst hot to give a yellow solid (0.1 g) and a yellow filtrate. The solid was washed with a little acetone and these acetone washings were added to the initial filtrate. Upon standing in air for *ca* 10 days crystals of **3** formed in the filtrate. Found: C, 7.3; H, 1.5%. IR: 3440, 2930, 1540, 1460, 1382, 960, 895, 805, 690, 645, 430, 400, 350 cm^{-1}.

$([CH_3(CH_2)_3]_4N)_2[Mo_6O_{19}]$ (**4**)

$Mo(CO)_6$ (3.0 g, 11.36 mmol), glacial acetic acid (40 cm^3), acetic anhydride (8 cm^3) and dry diglyme (45 cm^3) were refluxed together under nitrogen for 5 h, during which time yellow crystals of $[Mo_2(\mu\text{-}O_2CCH_3)_4]$ slowly precipitated from the dark brown solution. When $[Mo_2(\mu\text{-}O_2CCH_3)_4]$ (1.55 g) was filtered off $[CH_3(CH_2)_3]_4N(ClO_4)$ (0.5 g, 1.46 mmol) was added to the remaining dark brown filtrate. Upon standing in air for *ca* 4 days the solution deposited large yellow crystals of **4** (0.2 g). The solid was filtered off, washed with a little dry methanol and then dried *in vacuo*. Found: C, 28.5; H, 5.5; N, 2.2. Calc.: C, 28.2; H, 5.3; N, 2.1%. IR: 2970, 2880, 1470, 1382, 955, 800, 595, 430 cm^{-1}.

REFERENCES

1. Y. Xiu-Fen and X. Li, *Jiegou Huaxue* (*J. Struct. Chem.*) 1990, **9**, 145.
2. X. Li and Y. Xiu-Fen, *Jiegou Huaxue* (*J. Struct. Chem.*) 1990, **9**, 199.
3. A. Bino, F. A. Cotton, Z. Dori, M. Shaia-Gottlieb and M. Kapon, *Inorg. Chem.* 1988, **27**, 3592.
4. A. Bino, F. A. Cotton, Z. Dori, S. Koch, H. Küppers, M. Millar and J. C. Sekutowski, *Inorg. Chem.* 1978, **17**, 3245.
5. R. C. Mehrotra and R. Bohra, *Metal Carboxylates*, p. 49. Academic Press, London (1983) and refs therein.
6. K. Nakamoto, *Infrared and Raman Spectra of Inorganic and Coordination Compounds*, 3rd edn, p. 242. Wiley, New York (1978).
7. A. Chemseddine, C. Sanchez, J. Livage, J. P. Launay and M. Fournier, *Inorg. Chem.* 1984, **23**, 2609.
8. J. Fuchs, H. Hartl, W. Schiller and U. Gerlach, *Acta Cryst., Sect. B* 1976, **B32**, 740.
9. T. A. Stephenson and D. Whittaker, *Inorg. Nucl. Chem. Lett.* 1969, **5**, 569.
10. T. A. Stephenson, E. Bannister and G. Wilkinson, *J. Chem. Soc.* 1964, 2538.
11. J. C. Menezes and C. C. Romão, *Polyhedron* 1990, **9**, 1237.
12. A. Bino, F. A. Cotton and Z. Dori, *J. Am. Chem. Soc.* 1981, **103**, 243.
13. M. Ardon, A. Bino, F. A. Cotton, Z. Dori, M. Kaftory and G. Reisner, *Inorg. Chem.* 1982, **21**, 1912.
14. A. Bino, M. Ardon, I. Maor, M. Kaftory and Z. Dori, *J. Am. Chem. Soc.* 1976, **98**, 7093.
15. J. Fuchs and K. F. Jahr, *Z. Naturforsch. B* 1968, **23**, 1380.
16. V. R. Mattes, H. Bierbüsse and J. Fuchs, *Z. Anorg. Allg. Chem.* 1971, **385**, 230.
17. H. R. Allcock, E. C. Bissell and E. T. Shawl, *Inorg. Chem.* 1973, **12**, 2963.

Polyhedron Vol. 12, No. 5, pp. 479–488, 1993
Printed in Great Britain

0277–5387/93 $6.00+.00
© 1993 Pergamon Press Ltd

N-(2-PYRIDYL)-3-PHENYL-2-PROPENE AMIDE (O-N) COMPLEXES OF COPPER(II), NICKEL(II), COBALT(II) AND PALLADIUM(II). CRYSTAL AND MOLECULAR STRUCTURE OF $Cu(O\text{-}N)_2(CF_3SO_3)_2$

ABDESSALAM BOUAYAD and NAJIB BITIT

Laboratoire de Chimie Organique, Faculté des Sciences,
Université Sidi Mohamed Ben Abdelha, BP 1776 Fès, Maroc

and

ERIC DEYDIER, MARIE-JOELLE MENU, MICHELE DARTIGUENAVE* and YVES DARTIGUENAVE

Laboratoire de Chimie Inorganique, Université Paul Sabatier,
118 route de Narbonne, 31062 Toulouse, France

and

HUBERT DURAN and LILIANE GORRICHON

Laboratoire de Synthèse et Physicochimie Organique, URA CNRS 471,
Université Paul Sabatier, 118 route de Narbonne, 31062 Toulouse, France

and

MICHEL SIMARD and ANDRE L. BEAUCHAMP*

Département de Chimie, Université de Montréal, CP 6128, Succ. A., Montréal,
Québec, Canada H3C 3J7

(*Received* 30 *September* 1992; *accepted* 4 *November* 1992)

Abstract—The reaction of the title ligand N-(2-pyridyl)-3-phenyl-2-propene amide (O-N) with MX_2 salts yields compounds of the type $M(O\text{-}N)_2X_2$ and $[M(O\text{-}N)_2(H_2O)_2]X_2$, which were characterized by elemental analysis, magnetic moments and IR and EPR spectroscopies. From the IR spectra the ligand is found to be bidentate via the pyridyl nitrogen and the amide oxygen, except in $[Pd(O\text{-}N)_2Cl_2]$ where only the pyridyl ring is coordinated. The magnetic moments, IR spectra and thermograms of the $M(O\text{-}N)_2(NO_3)_2 \cdot 3H_2O$ compounds [M = nickel(II), cobalt(II)] are consistent with the presence of *trans*-$[M(O\text{-}N)_2(H_2O)_2]^{2+}$ ions, similar to the *trans*-$[Zn(O\text{-}N)_2(CH_3OH)_2]^{2+}$ species observed earlier. The EPR spectra of the *trans*-$Cu(O\text{-}N)_2X_2$ compounds ($X = NO_3^-$, $CF_3SO_3^-$) indicate an elongated octahedral coordination with equatorial bidentate (O-N) ligands and solvent molecules or anions in axial sites. The solid-state spectra reveal the presence of more than one type of copper(II) centre. The crystal structure of *trans*-$Cu(O\text{-}N)_2(CF_3SO_3)_2$ was determined by X-ray diffraction. The unit cell contains two types of discrete *trans*-$Cu(O\text{-}N)_2(CF_3SO_3)_2$ molecules, in which bidentate (O-N) ligands are strongly bonded to the equatorial sites of a tetragonally distorted octahedron. The axial positions are filled by

* Authors to whom correspondence should be addressed.

more weakly bonded unidentate triflate anions completing an all-*trans* stereochemistry. In the molecules sitting on crystallographic inversion centres, departure from D_{4h} symmetry in the copper coordination sphere is small and the roughly planar (O-N) ligands lie close to the equatorial plane. Molecules of the second type have no crystallographic symmetry and they are severely distorted: one of the axial copper–triflate bonds is very long, the equatorial CuN_2O_2 plane exhibits a significant tetrahedral distortion and the (O-N) ligands make angles of *ca* 17° with this plane.

The biosynthesis of lignin in plants is catalysed by the enzyme CAD, in which the active site contains a Zn^{2+} centre.[1-3] Efforts have recently been devoted to the synthesis of tailor-made molecules, which would be better ligands for zinc than the enzyme and thus might prevent or reduce lignin biosynthesis. Encouraging results have been obtained *in vitro* using the following type of molecule:[4,5]

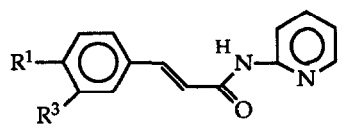

$R^1 = H$; $R^3 = H$ (O-N)
$R^1 = OH$; $R^3 = OMe$

These compounds contain both an amido oxygen and a pyridyl nitrogen as donor atoms, properly oriented to close a chelate ring around the metal ion. Their chelating ability, however, is still poorly documented, except for a few publications dealing with the related ligand 2-pyridylacetamide (aapH).[6-9]

We describe here the complexes of Cu^{2+}, Ni^{2+} and Co^{2+} obtained by reacting the (O-N) molecule with the corresponding metal salts. A Pd^{2+} complex has also been prepared to evaluate the influence of this second row metal on the mode of coordination. To our knowledge, the effect of these metal ions on the enzymatic reaction *in vitro* is still unknown. The X-ray structure of the molecular copper complex $Cu(O\text{-}N)_2(CF_3SO_3)_2$ has been determined. It illustrates how a complicated interplay of electronic and steric effects triggered by inter- and intramolecular steric hindrance contributes to stabilize drastically different structures without disrupting the tetragonally distorted octahedron geometry about copper. Comparisons with the cationic zinc analogue[10] show that the differences are essentially steric in nature and may be due to the smaller Cu^{2+} radius (0.62 Å) compared to Zn^{2+} (0.72 Å).

EXPERIMENTAL

The ligand N-(2-pyridyl)-3-phenyl-2-propene amide (O-N)[4] was synthesized according to published procedures. $Cu(CF_3SO_3)_2$ was obtained from Aldrich.

$Cu(O\text{-}N)_2(CF_3SO_3)_2$ (1)

To an acetonitrile solution (10 cm^3) of $Cu(CF_3SO_3)_2$ (0.34 g, 0.9 mmol) was added a THF solution (10 cm^3) of (O-N) (0.4 g, 1.8 mmol) at room temperature with constant stirring. The green precipitate immediately formed was filtered, washed with THF and dried *in vacuo*. Recrystallization from an acetonitrile: THF 1:1 mixture gave green crystals of **1**. Yield: 75%. Found: C, 44.4; H, 3.0; N, 7.0; F, 14.5; S, 7.7; Cu, 7.7. Calc. for $C_{30}H_{24}F_6N_4O_8S_2Cu$: C, 44.5; H, 3.0; N, 6.9; F, 14.1; S, 7.9; Cu, 7.8%.

$Cu(O\text{-}N)_2(NO_3)_2 \cdot H_2O$ (2), $Ni(O\text{-}N)_2(NO_3)_2 \cdot 3H_2O$ (3), $Co(O\text{-}N)_2(NO_3)_2 \cdot 3H_2O$ (4)

To $Cu(NO_3)_2 \cdot 3H_2O$ (0.3 g, 1.24 mmol) dissolved in methanol (10 cm^3) was added (O-N) (0.55 g, 2.45 mmol) in the same solvent. The green precipitate was filtered, washed several times with methanol and ether, and dried *in vacuo*. Recrystallization from hot methanol gave a green microcrystalline powder. Yield: 65%. Found: C, 51.6; H, 3.7; N, 12.8. Calc. for $C_{28}H_{26}N_6O_9Cu$: C, 51.4; H, 3.8; N, 12.8%.

Similar synthetic procedures were used for the nickel and cobalt compounds.

$Ni(O\text{-}N)_2(NO_3)_2 \cdot 3H_2O$ was precipitated from THF. Light blue crystals were obtained by recrystallization in hot methanol. Yield: 72%. Found: C, 49.3; H, 4.3; N, 11.9. Calc. for $C_{28}H_{30}N_6O_{11}Ni$: C, 49.1; H, 4.4; N, 12.3%. $Co(O\text{-}N)_2(NO_3)_2 \cdot 3H_2O$ was precipitated as a powder from methanol. Orange crystals were grown by recrystallization from hot methanol. Yield: 69%. Found: C, 49.6; H, 4.4; N, 11.7. Calc. for $C_{28}H_{30}N_6O_{11}Co$: C, 49.1; H, 4.4; N, 12.3%.

$Pd(O\text{-}N)_2Cl_2$ (5)

Water was added to K_2PdCl_4 (0.33 g, 1.02 mmol) suspended in THF (10 cm^3) until the salt completely

dissolved (70 cm^3). Upon addition of (O-N) (0.46 g, 2.04 mmol) dissolved in ethanol, the colour of the solution changed from red to yellow. A light yellow powder precipitated, which was filtered, washed several times with ethanol and ether. Yield: 45%. Found: C, 53.0; H, 3.7; N, 8.8. Calc. for $C_{28}H_{24}Cl_2N_4O_2Pd$: C, 53.7; H, 3.8; N, 8.9%.

Measurements

The analytical data were obtained from the Laboratoire de Microanalyse du CNRS (Lyon, France) and the Centre de Microanalyse de l'INP (Toulouse, France).

The magnetic moments were determined in the solid state by the Faraday method, using a Cahn microbalance coupled with a Drusch electromagnet. Measurements were performed at room temperature and $HgCo(NCS)_4$ was used as standard ($Xg = 16.44 \times 10^{-6}$ cgs emu). The experimental values were corrected for the diamagnetism of the ligands.[11] The ESR spectra were measured on a Bruker ER 200 TT spectrometer operating at an *X*-band frequency between 90 and 300 K. The IR spectra were recorded on a Perkin–Elmer 1600 FTIR spectrophotometer in Nujol or KBr. TGA curves were recorded with a Mettler B85 system.

Crystal data

$[Cu(C_{14}H_{12}N_2O)_2](CF_3SO_3)_2$ (**1**). Formula: $CuC_{30}H_{24}F_6N_4O_8S_2$, $fw = 810.20$, triclinic, *P*-1; $a = 10.648(9)$, $b = 14.080(7)$, $c = 18.294(10)$ Å, $\alpha = 81.86(4)°$, $\beta = 77.06(6)°$, $\gamma = 71.21(5)°$, $V = 2523.4$ Å^3, $D_c = 1.599$ g cm^{-3}, $Z = 3$, μ(Mo-K_α) = 8.54 cm^{-1}, λ(Mo-K_α) = 0.71069 Å, $T = 190$ K.

Crystallographic measurement and structure determination

Crystals suitable for X-ray work were obtained by recrystallization of the crude product from an MeCN–THF mixture. The specimen used was a parallelepiped with the following dimensions (mm) between the indicated pairs of faces: 0.48 (100–100) × 0.11 (012–012) × 0.17 (011–011). The crystallographic work was performed on an Enraf–Nonius CAD-4 diffractometer. The unit cell was determined from 25 reflections ($10 \leqslant \theta \leqslant 11°$) found by the automatic search routine and centred in the counter aperture. This cell was checked with axial photographs taken along each of the three axes. The Niggli parameters ruled out all lattices of higher symmetry. The intensity data were collected over one half of the Laue sphere *hkl*, *hk̄l*, *hkl̄*, *hk̄l̄* ($2\theta_{max} = 50°$) by the ω-scan technique. The $\Delta\omega$ range was $(1.00 + 0.35 \tan\theta)°$ and a constant scan rate of 4° min^{-1} was used. Intensity was checked every hour on seven standard reflections, which showed fluctuations within ±1.9% during data collection. The same standard reflections were used to check orientations every 200 measurements. A total of 8891 independent reflections were measured, of which 3468 reflections [$I > 3\sigma(I)$] were retained for structure resolution and refinement.

The structure was solved by the heavy-atom method. The copper atoms were located from a Patterson map and the remaining non-hydrogen atoms were found from difference Fourier (ΔF) maps calculated with the SHELX program.[12] Refinement was based on $|F|$ (initially by full-matrix least-squares, last cycles with the block-diagonal approximation). All non-hydrogen atoms were refined anisotropically. The hydrogens were visible in the ΔF map. They were introduced at idealized positions [C(N)—H = 0.95 Å, $B_{iso} = 4.0$ Å^2]. Their coordinates were recalculated after each least-squares cycle. The final agreement factors were $R = \Sigma||F_o|-|F_c||/\Sigma|F_o| = 0.049$ and $R_w = (\Sigma w||F_o|-|F_c||^2/\Sigma|F_o|^2)^{1/2} = 0.038$ (weights based on counting statistics). The goodness-of-fit ratio was 1.39 for 692 parameters refined. Electron density fluctuations in the final ΔF map were within ±0.42 e Å^{-3}.

The scattering curves were from standard sources. The anomalous dispersion contributions of copper and sulphur were taken into account.[13,14]

RESULTS AND DISCUSSION

The complexes are all obtained in good yields. They are air stable, but poorly soluble in usual solvents. Decomposition temperatures determined from thermograms indicate that **3** and **4** lose three water molecules between 20 and 200°C. Then, decomposition starts at 250°C for nickel and 220°C for cobalt.

The palladium complex is diamagnetic (Table 1), whereas the nickel and cobalt complexes have magnetic susceptibilities typical of high-spin octahedral species.[15,16]

The most significant IR frequencies are reported in Table 1. The strong band corresponding to the amide ν(C=O) vibration at 1694 cm^{-1} in the free ligand is shifted by ~ 30 cm^{-1} to lower wave numbers for complexes **1**–**4**, showing that the carbonyl oxygen is coordinated to the metal.[6] The characteristic deformation band of the pyridine ring, at 621 cm^{-1} in the free ligand, undergoes shifts to higher wave numbers for the copper, nickel and cobalt compounds, as expected for coordination

Table 1. Spectroscopic and magnetic data for the ligand and its complexes

Compound	IR ν(CO) (cm^{-1})	IR δ(pyridine) (cm^{-1})	Magnetic moment (B.M.)	ESR (G)
O-N	1694	621		
$Co(O\text{-}N)_2(CF_3SO_3)_2$ (**1**)	1657	651	1.88	$g_\parallel = 2.296$, $g_\perp = 2.060$, $A_\parallel = 141$; solid, room temperature $\langle g \rangle = 2.082$; solid, 90 K $g_\parallel = 2.280$, $g_\perp = 2.061$, $A_\parallel = 146$; MeOH, 90 K
$Cu(O\text{-}N)_2(NO_3)_2 \cdot H_2O$ (**2**)	1668	650	1.89	$\langle g \rangle = 2.050$; solid, room temperature $\langle g \rangle = 2.067$; solid, 90 K $g_\parallel = 2.288$, $g_\perp = 2.070$, $A_\parallel = 145$; MeOH, 90 K
$Ni(O\text{-}N)_2(NO_3)_2 \cdot 3H_2O$ (**3**)	1667	646	3.18	
$Co(O\text{-}N)_2(NO_3)_2 \cdot 3H_2O$ (**4**)	1666	645	4.96	
$Pd(O\text{-}N)_2Cl_2$ (**5**)	1694	658	diamagnetic	

through the ring nitrogen atom.[17a] Interestingly, the palladium complex **5** shows appreciable shift only for the pyridine band, indicating that ligand coordination to this second-row metal occurs only through the ring nitrogen and leaves the amide group unbonded.[6]

No evidence for the coordination of $CF_3SO_3^-$ to Cu^{2+} can be deduced from the IR spectrum. This complex presents a single strong $\nu(SO_3)$ stretch at 1031 cm^{-1}, the other vibrations being masked by ligand bands. The presence of uncoordinated NO_3^- anions in **3** and **4** is very likely, since both compounds exhibit only one strong and broad ν_3 vibration at 1375 cm^{-1}, in the range for free NO_3^-. On the other hand, two stretching bands at 1378 and 1340 cm^{-1} in **2** suggest that the two NO_3^- groups are not equivalent and that one of them might be coordinated to Cu^{2+}.[17b,18a,19,20]

These data are all consistent with the O-N ligand acting as a chelating agent. The coordination geometries suggested by the analytical and magnetic data are square planar for palladium and octahedral for nickel and cobalt. Therefore, assuming *trans*-stereochemistry the two axial sites in **3** and **4** should be occupied by water molecules, as observed in $[Ni(aapH)_2(H_2O)_2](NO_3)_2$.[8]

Complexes **1** and **2** have room-temperature magnetic moments (1.88 and 1.89 B.M., respectively) characteristic of copper(II) compounds.[21] The ESR spectrum of **1**, recorded at room temperature in the solid state, consists of an intense absorption at high field and a set of three broad and weaker signals at lower field ($g_\parallel = 2.296$, $g_\perp = 2.06$, $A_\parallel = 141$ G). Spectrum broadening by exchange narrowing is observed when the temperature is decreased ($\langle g \rangle = 2.082$), in agreement with the presence of copper atoms with different environments (*vide infra*). When dissolved in methanol **1** gives an anisotropic axial spectrum with $g_\parallel = 2.280$, $g_\perp = 2.061$ and $A_\parallel = 146$ G at 90 K. These spectra with $g_\parallel > g_\perp > 2$ are typical of copper(II) compounds with a $d_{x^2-y^2}$ ground state and an elongated octahedral geometry resulting from Jahn–Teller effects. The ESR spectra of **2**, recorded at room temperature and 90 K on the polycrystalline powder, reveal in both cases a quasi-isotropic signal at $\langle g \rangle = 2.050$ (room temperature) and 2.067 (90 K). Moreover, a weak absorption corresponding to the $\Delta M = 2$ transition is apparent in the half-field region (at $\sim$ 1650 G). This line is held to be indicative of the presence of Cu—Cu exchange interaction in the solid.[22] Such an absorption is commonly seen for powdered samples of copper(II) dimers, but it has also been reported for the polymeric chains in a pyrazine copper(II) nitrate complex[23] and in potassium dioxalatocuprate.[24] The five-line pattern expected for an elongated octahedral geometry is again observed for **2** when dissolved in methanol at 90 K, with $g_\parallel = 2.288$, $g_\perp = 2.070$ and $A_\parallel = 145$ G.

Due to the plasticity of the coordination sphere, such differences between the solid and solution structures are common in copper chemistry. To see if these ESR data can be used to establish a reliable spectra–structure relationship, attempts were made to grow single crystals of **1** and **2**. To our knowledge no complete structural work has been carried out yet on copper(II) complexes with N-phenolamide model ligands. Only **1** gave a suitable crystalline material. Its X-ray crystal structure was determined.

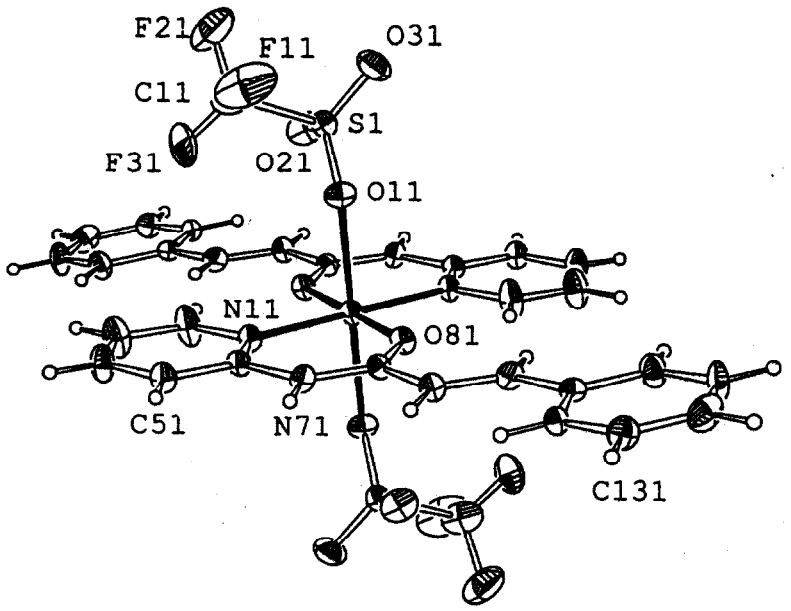

Fig. 1. ORTEP drawing of the *trans*-$[Cu(O\text{-}N)_2(CF_3SO_3)_2]$ complex, molecule **A**. The central Cu(1) atom occupies a crystallographic inversion centre. Atom numbering is explained in Fig. 3. Ellipsoids correspond to 35%, except for hydrogens, which are shown as spheres of arbitrary size.

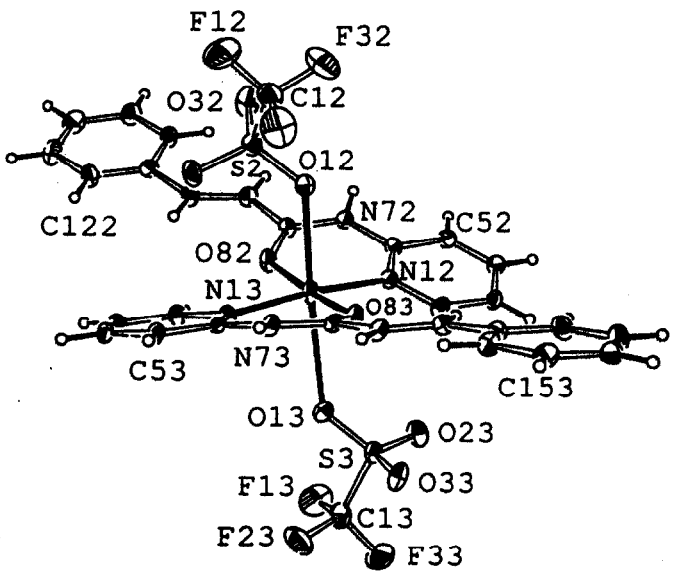

Fig. 2. ORTEP drawing of the *trans*-$[Cu(O\text{-}N)_2(CF_3SO_3)_2]$ complex, molecule **B**. The central atom is Cu(2). Other conditions as in Fig. 1.

The structure consists of well-separated $Cu(O\text{-}N)_2(CF_3SO_3)_2$ entities. The unit cell contains two symmetry independent kinds of molecules shown in Fig. 1 (molecule **A**) and Fig. 2 (molecule **B**). The atoms are labelled following the numbering scheme of Fig. 3, with an extra (right-most) digit added to identify the ligands individually.† Interatomic distances and bond angles are listed in Table 2.

The environment of both types of copper atoms can be described as an octahedral arrangement of four strongly bonded, roughly co-planar, equatorial donors and two semi-coordinated axial ligands. The equatorial positions are occupied by pyridine nitrogens N(1) and amide oxygens O(8) of two chelating

† When the ligands are discussed collectively, the atoms are represented by the unparenthesized symbols of Fig. 3. To designate one particular ligand, individual parenthesized symbols are used.

Table 2. Interatomic distances and bond angles

	Cu(1) ($n = 1$)	Cu(2) ($n = 2$)	Cu(2) ($n = 3$)
	Distances (Å)		
Cu—O(1*n*)	2.356(5)	2.466(5)	2.800(5)
Cu—O(8*n*)	1.926(4)	1.915(4)	1.918(4)
Cu—N(1*n*)	2.069(6)	2.018(6)	2.016(6)
O(8*n*)—C(8*n*)	1.237(9)	1.241(8)	1.241(9)
N(1*n*)—C(2*n*)	1.348(9)	1.355(8)	1.361(8)
N(1*n*)—C(6*n*)	1.316(9)	1.334(8)	1.329(8)
N(7*n*)—C(6*n*)	1.392(9)	1.391(8)	1.404(8)
N(7*n*)—C(8*n*)	1.354(10)	1.352(9)	1.347(9)
C(2*n*)—C(3*n*)	1.355(14)	1.361(11)	1.353(11)
C(3*n*)—C(4*n*)	1.366(12)	1.362(10)	1.382(10)
C(4*n*)—C(5*n*)	1.346(10)	1.363(10)	1.362(10)
C(5*n*)—C(6*n*)	1.388(11)	1.401(11)	1.392(10)
C(8*n*)—C(9*n*)	1.481(9)	1.452(9)	1.460(9)
C(9*n*)—C(10*n*)	1.327(11)	1.319(11)	1.341(10)
C(10*n*)—C(11*n*)	1.461(9)	1.467(9)	1.452(9)
C(11*n*)—C(12*n*)	1.387(11)	1.388(11)	1.389(11)
C(11*n*)—C(16*n*)	1.397(12)	1.394(10)	1.383(10)
C(12*n*)—C(13*n*)	1.384(10)	1.376(10)	1.373(10)
C(13*n*)—C(14*n*)	1.345(13)	1.353(12)	1.357(12)
C(14*n*)—C(15*n*)	1.379(13)	1.388(12)	1.388(12)
C(15*n*)—C(16*n*)	1.366(11)	1.367(10)	1.368(10)
S(*n*)—O(1*n*)	1.435(5)	1.442(6)	1.440(5)
S(*n*)—O(2*n*)	1.418(5)	1.432(6)	1.431(6)
S(*n*)—O(3*n*)	1.408(6)	1.444(6)	1.434(5)
S(*n*)—C(1*n*)	1.808(11)	1.774(9)	1.806(9)
F(1*n*)—C(1*n*)	1.376(12)	1.342(11)	1.312(10)
F(2*n*)—C(1*n*)	1.328(11)	1.305(10)	1.322(11)
F(3*n*)—C(1*n*)	1.229(12)	1.328(11)	1.313(10)
	Angles (°)		
O(11)—Cu—O(81)	85.6(2)		
O(11)—Cu—O(81)[a]	94.4(2)		
O(11)—Cu—N(11)	87.2(2)		
O(11)—Cu—O(11)[a]	180.0		
O(11)—Cu—N(11)[a]	92.8(2)		
O(81)—Cu—N(11)	89.2(2)		
O(81)—Cu—O(81)[a]	180.0		
O(81)—Cu—N(11)[a]	90.8(2)		
N(11)—Cu—N(11)[a]	180.0		
O(12)—Cu—O(13)		174.4(2)	
O(12)—Cu—O(8*n*)		84.7(2)	89.5(2)
O(12)—Cu—N(1*n*)		93.9(2)	92.4(2)
O(13)—Cu—O(8*n*)		100.9(2)	85.0(2)
O(13)—Cu—N(1*n*)		85.8(2)	87.9(2)
O(82)—Cu—O(83)		174.2(2)	
N(12)—Cu—O(8*n*)		89.9(2)	90.3(2)
N(12)—Cu—N(13)		173.6(2)	
N(13)—Cu—O(8*n*)		90.2(2)	90.1(2)
Cu—O(8*n*)—C(8*n*)	131.0(5)	128.4(5)	128.1(4)
Cu—N(1*n*)—C(2*n*)	117.4(5)	118.8(4)	118.1(4)
Cu—N(1*n*)—C(6*n*)	125.1(5)	124.2(5)	124.8(4)
C(2*n*)—N(1*n*)—C(6*n*)	117.5(6)	116.9(6)	116.9(6)
C(6*n*)—N(7*n*)—C(8*n*)	128.9(6)	129.2(6)	128.9(6)
N(1*n*)—C(2*n*)—C(3*n*)	122.8(8)	123.4(6)	123.3(6)
C(2*n*)—C(3*n*)—C(4*n*)	119.0(8)	118.9(7)	118.4(7)
C(3*n*)—C(4*n*)—C(5*n*)	119.2(8)	119.9(7)	120.1(7)

Table 2—*continued*

	Cu(1) (n = 1)	Cu(2) (n = 2)	Cu(2) (n = 3)
C(4*n*)—C(5*n*)—C(6*n*)	119.2(7)	118.4(7)	117.9(7)
N(1*n*)—C(6*n*)—N(7*n*)	121.6(6)	120.6(6)	120.3(6)
N(1*n*)—C(6*n*)—C(5*n*)	122.3(7)	122.4(6)	123.3(6)
N(7*n*)—C(6*n*)—C(5*n*)	116.0(6)	117.0(6)	116.4(6)
O(8*n*)—C(8*n*)—N(7*n*)	124.1(6)	122.8(6)	124.1(6)
O(8*n*)—C(8*n*)—C(9*n*)	122.8(6)	122.0(6)	121.0(6)
N(7*n*)—C(8*n*)—C(9*n*)	113.0(6)	115.2(6)	114.9(6)
C(8*n*)—C(9*n*)—C(10*n*)	120.3(7)	122.8(7)	120.3(6)
C(9*n*)—C(10*n*)—C(11*n*)	126.3(7)	126.6(7)	128.0(7)
C(10*n*)—C(11*n*)—C(12*n*)	122.1(7)	118.7(7)	119.0(6)
C(10*n*)—C(11*n*)—C(16*n*)	119.8(7)	121.4(7)	123.2(6)
C(12*n*)—C(11*n*)—C(16*n*)	118.0(7)	119.9(7)	117.8(7)
C(11*n*)—C(12*n*)—C(13*n*)	119.9(7)	119.1(7)	121.5(7)
C(12*n*)—C(13*n*)—C(14*n*)	121.8(8)	120.2(8)	119.8(8)
C(13*n*)—C(14*n*)—C(15*n*)	119.0(8)	122.0(8)	120.0(7)
C(14*n*)—C(15*n*)—C(16*n*)	120.9(8)	118.2(7)	120.0(7)
C(11*n*)—C(16*n*)—C(15*n*)	120.4(8)	120.6(7)	120.9(7)
Cu—O(1*n*)—S(*n*)	134.7(3)	130.0(3)	134.6(3)
O(1*n*)—S(*n*)—O(1*n*)	113.7(3)	115.9(3)	116.4(3)
O(1*n*)—S(*n*)—O(3*n*)	115.9(4)	113.4(3)	112.6(3)
O(1*n*)—S(*n*)—C(1*n*)	103.0(4)	103.3(4)	104.2(4)
O(2*n*)—S(*n*)—O(3*n*)	114.6(4)	115.1(3)	114.5(3)
O(2*n*)—S(*n*)—C(1*n*)	101.3(4)	103.4(4)	104.1(4)
O(3*n*)—S(*n*)—C(1*n*)	106.2(4)	103.5(4)	103.1(4)
S(*n*)—C(1*n*)—F(1*n*)	105.5(7)	111.8(6)	111.4(6)
S(*n*)—C(1*n*)—F(2*n*)	109.7(7)	113.4(6)	111.3(6)
S(*n*)—C(1*n*)—F(3*n*)	113.2(7)	111.5(6)	112.4(6)
F(1*n*)—C(1*n*)—F(2*n*)	105.1(8)	105.9(7)	107.6(7)
F(1*n*)—C(1*n*)—F(3*n*)	110.8(9)	106.6(7)	106.3(7)
F(2*n*)—C(1*n*)—F(3*n*)	112.1(9)	107.1(7)	107.7(7)

[a] $-x, -y, -z$.

(O-N) molecules. The two axial sites are filled by unidentate $CF_3SO_3^-$ ligands, completing an all-*trans* coordination about the metal. This type of tetragonally distorted (4+2) coordination is widespread in the chemistry of copper(II), a d^9 metal centre with a non-spherical *d*-shell particularly sensitive to the Jahn–Teller effects.[25] A similar all-*trans* arrangement has been observed for a related cationic zinc complex,[10] in which methanol molecules occupy the axial positions filled here by triflate oxygens.

In molecule **A** the metal sits on a crystallographic inversion centre. Therefore, all *trans* bond angles are exactly equal to 180° and the four copper–donor bonds in each of the three principal planes are rigorously co-planar. Departure from ideal D_{4h} sym-

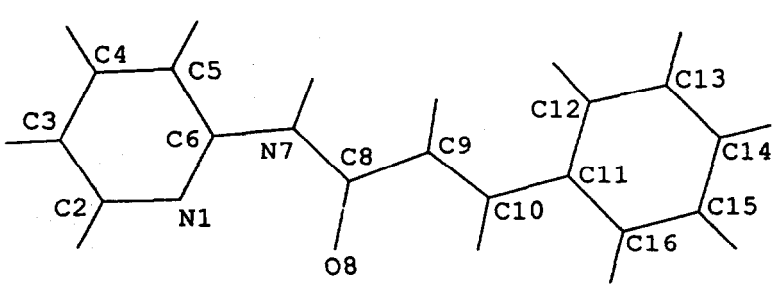

Fig. 3. Numbering scheme used for the ligand atoms. An extra digit representing the ligand number is added at the right-most position.

metry in the $CuN_2O_2(trif)_2$ framework is small, as can be appreciated from the dihedral angles between the principal planes being all close to 90°: $CuN_2O_2/CuN_2(trif)_2 = 85.6°$, $CuN_2O_2/CuO_2(trif)_2 = 87.3°$ and $CuN_2(trif)_2/CuO_2(trif)_2 = 89.3°$. The "bite" of the (O-N) ligand allows the *cis* bond angles in the equatorial plane [89.2(2)° and 90.8(2)°] to be close to ideal values. As usual, the angles involving the axial groups [85.6(2)°, 87.2(2)°] show greater deviation from 90°. Binding of oxo-anions off the axial direction is commonly encountered in such systems and large distortions sometimes lead to coordination numbers > 6 by allowing more than one oxygen to lie within bonding distance from the metal.[18b] However, in the present case the anions remain monodentate and the copper–triflate bonds deviate by only 5.2° from the axial direction.

In the chelate ring, the N(11), N(71), C(81) and O(81) atoms are co-planar, whereas C(61) is displaced from this plane by 0.044(7) Å, defining a significant, but small "envelope" conformation. Also, the angle between the plane of these four atoms and the CuN_2O_2 plane is only 1.2° (Table 3). Thus, molecule **A** shows only minor distortions.

Molecule **B** (Fig. 2) has no crystallographically-imposed symmetry and it is severely distorted, although the immediate environment of copper is affected only to a limited extent. The *cis* angles in the equatorial plane remain in the 89.9(2)–90.3(2)° range. The deviation from 180° for the *trans* angles [174.2(2)°, 173.6(2)°] is due to a tetrahedral distortion in the CuO_2N_2 "plane". The distances to the least-squares plane are: O(82), 0.090(5); O(83), 0.087(5); N(12), −0.122(5); N(13), −0.119(5); Cu(2), −0.008(1). The tetrahedral deformation can be envisioned as resulting from the N(12)—Cu(2)—O(82) and N(13)—Cu(2)—O(83) planes being twisted by 6.5° in opposite directions about their common bisector. Displacement of the triflate oxygens from the axial direction is more important, the angles with the equatorial donors ranging from 84.7(2) to 100.9(2)°. Although somewhat greater than in molecule **A**, the distortions *in the coordination sphere* of **B** remain relatively small.

The peripheral part of molecule **B**, however, is found to be severely distorted. A larger "envelope" effect is noted in the chelate rings: C(62) and C(63) are displaced by 0.142(7) and 0.078(6) Å, respectively, from the plane of the other four atoms. Furthermore, folding about the N(1)—O(8) line displaces considerably both ligands on the O(12) side. The angle between the ring and the Cu—N(1)—O(8) plane, which is 1.2° for molecule **A**, is now 17.6° for ligand 2 and 16.1° for ligand 3 (Table 3).

The Cu—N bond distances are significantly different in **A** and **B** but remain in the range of the values reported for [(pyridine-2-acetamide)$_2$ Cu]$(ClO_4)_2$,[26] pyridine-2-carboxamide compound,[27] pyrazine-2,3-dicarboxamide complex[28] and a series of N-donor compounds.[29–33]

$CuL_4(triflate)_2$ compounds are known with L = isoquinoline[32] and pyridine.[33] They have roughly D_{4h} symmetry and contain similar axially coordinated triflate anions with Cu—O(triflate) distances from 2.425(4) to 2.472(9) Å. Thus, the value of 2.356(5) Å can be regarded as relatively short in molecule **A**, where Cu(1)—N(11) is longer [2.069(6) Å]. In molecule **B**, where shorter Cu—N bonds [mean 2.017(6) Å] are found, one of the Cu—O(triflate) bonds is normal at 2.466(5) Å, whereas the other is much longer [2.800(5) Å], but still within the limit (~ 3 Å) normally accepted for semi-coordination of an oxo-anion.[34] Although the long Cu—O(13) bond could suggest that the octahedron is *on its way* to a square pyramid, the expected displacement of the metal from the CuO_2N_2 plane towards the *short* O(12) bond is not observed here, the Cu(2) atom lying only 0.008(1) Å from the plane and on the *opposite* side. It is noteworthy that bending along the N(1)—O(8) lines brings both chelate rings to the O(12) side, thereby ruling out the possibility that the long Cu—O(13) bond could result from *intramolecular* steric hindrance.

The dihedral angles between the four individually planar units (pyridine, chelate, olefin region and phenyl) are listed in Table 3 (details in supplementary material). As found in the zinc analogue they are all significantly different from 0, but they remain relatively small and the ligand can still be regarded as an uninterrupted system of π-electrons.

The triflate ligands show the usual ethane-like staggered conformation with mean values for bond lengths and angles similar to those found in other complexes.[32,33,35–37] Even though the S—O(1) distances involving the coordinated oxygens O(1) tend to be slightly greater than the two others, the dis-

Table 3. Dihedral angles (°) between subunits in the coordinated ligands

	Ligand number		
	1	2	3
CuN_2O_2–chelate[a]	1.2	17.6	16.1
Chelate–pyridine	3.3	11.3	4.8
Chelate–olefin[b]	2.8	6.8	4.9
Olefin–phenyl	3.4	4.7	4.8

[a] N(1)—N(7)—C(8)—O(8).
[b] C(8)—C(9)—C(10)—C(11).

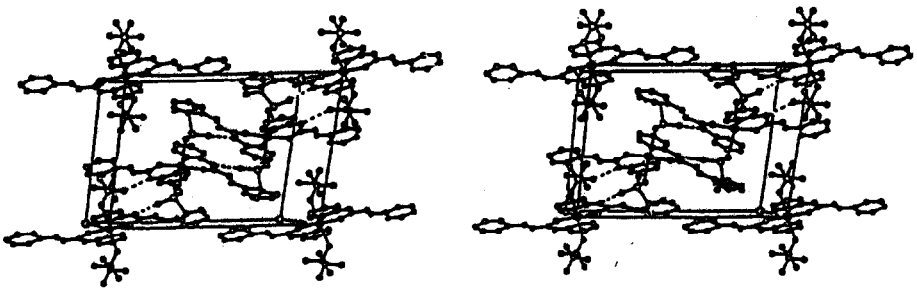

Fig. 4. View of the unit cell of *trans*-$[Cu(O\text{-}N)_2(CF_3SO_3)_2]$ down the a^*-axis. The b- and c-axes are roughly vertical and horizontal, respectively, in the plane of the figure. The copper atoms are shown as black spheres and the remaining non-hydrogen atoms can be identified by comparison with Figs 1 and 2. Hydrogens are omitted for simplicity. The unit cell origin is occupied by molecules of type **A**, whereas molecules of type **B** are inside the unit cell. Dashed lines represent hydrogen bonds.

tinction between coordinated and non-coordinated S—O bond lengths is not very clear because of the presence of hydrogen bonds involving one oxygen on each triflate ligand.

A view of the unit cell is given in Fig. 4, which illustrates the presence of intermolecular interactions. The amide N—H groups, which are the only hydrogen-bond donors present in the structure, each form a moderately strong N—H···O bond with one of the triflate oxygens [N···O = 2.778(8)–2.819(8) Å, N—H—O = 170–173°]. Besides these localized bonds, intermolecular interactions consist mainly of van der Waals forces, namely in the copper environment. The long axial Cu—O(triflate) bond and the puckered arrangement in molecule **B** undoubtedly contribute to optimizing molecular packing without being themselves too energy costly.

The large distortions found in **B** were not predictable and they should not be retained in the free molecule, so that molecule **A** probably better represents the normal geometry of the complex. Nevertheless, the equatorial plane remains a constricted region. It has been noted previously[10] that co-planar arrangement in the *trans*-$Zn(O\text{-}N)_2$ unit introduces short contacts between H(2) of one ligand and the H(10)—O(8) region of the other. Steric strain is likely to be still more important here than in the Zn^{2+} analogue,[10] since the metal–ligand bonds are *ca* 0.1 Å shorter, as expected from the difference between the radii of Cu^{2+} (0.62 Å) and Zn^{2+} (0.72 Å).[38] In molecule **A** the inter-ligand distances are 2.34 [H(2)···H(10)] and 2.19 Å [H(2)···O(8)], definitely shorter than the normal van der Waals separations of 2.4 and 2.7 Å, respectively. Although these values are derived from calculated hydrogen coordinates and displacement from these idealized positions could increase the separations, very close inter-ligand contacts are certainly present, especially between H(2) and O(8). In molecule **B**, folding along the N(1)—O(8) line allows the ligands to become non-co-planar, resulting in greater non-bonded distances of 2.62 (H···H) and 2.26 Å (H···O).

The differences observed between the Cu—N bond lengths are probably correlated with these steric features. In molecule **B** normal Cu—N distances of *ca* 2.017 Å are observed, whereas in molecule **A** the Cu(1)—N(11) bonds are stretched by *ca* 0.05 Å in order to counteract the greater inter-ligand repulsions. In turn, the extent of Cu—N binding in the equatorial plane seems to affect the binding to the axial sites. Thus, the long Cu—N bonds in **A** apparently reduce electron donation to copper in the equatorial plane, thereby improving the acceptor character of the axial sites, where the copper-triflate bond is found to be relatively short (2.35 Å). In molecule **B**, where the Cu—N bonds are of normal lengths and donation in the equatorial plane is better, no such short Cu(2)–triflate bonds are observed.

Thus, a complicated interplay of electronic and geometric effects triggered by inter- and intramolecular steric hindrance contributes to make the overall structures of the two $Cu(O\text{-}N)_2(CF_3SO_3)_2$ units drastically different, without disrupting the tetragonally distorted octahedron about copper.

Supplementary material available. Anisotropic temperature factors, idealized hydrogen coordinates, geometry of the hydrogen bonds, weighted least-squares planes and structure factor amplitudes (41 pages). Copies may be obtained upon request from A.L.B.

Acknowledgements—We are grateful to the Université Paul Sabatier, to the France–Quebec Exchange Programme (Projet Intégré) (travel and research support to E.D.) and to the Natural Sciences and Engineering Research Council (Canada) for financial support.

REFERENCES

1. A. Boudet, L. Cazaux, L. Gorrichon and C. Grand, Patent Fr. Demande FR2, 559,763 (1985) (*Chem. Abstr.* **104**, 168156 w).
2. H. Grisebach, *Naturwissenschaften* 1977, **64**, 619.
3. G. G. Gross, J. Stoeckigt, R. L. Mansell and M. H. Zenk, *Febs Lett.* 1973, **31**, 283.
4. H. Duran, E. Duran, M. Ben Bakkar, L. Gorrichon and C. Grand, *Bull. Soc. Chem. France* 1987, 672.
5. A. M. Boudet and C. Grand, *Monogr. Br. Crq. Prot. Counc.* 1987, **36**, 67.
6. M. Nonoyama, S. Tomita and K. Yamasaki, *Inorg. Chim. Acta* 1975, **12**, 33.
7. M. F. El-Shazly, A. El-Dissowky, T. Salem and M. Osman, *Inorg. Chim. Acta* 1980, **40**, 1.
8. V. Scheller-Krattiger, K. H. Scheller, E. Sinn and R. B. Martin, *Inorg. Chim. Acta* 1982, **60**, 45.
9. H. Sigel and R. B. Martin, *Chem. Rev.* 1982, **82**, 385.
10. A. Bouayad, N. Bitit, E. Deydier, M. J. Menu, M. Dartiguenave, Y. Dartiguenave, H. Duran, L. Gorrichon, M. Simard and A. L. Beauchamp, *Inorg. Chim. Acta* 1992, **190**, 79.
11. G. Foëx, *Table de constantes et données numériques—Diamagnétisme et Paramagnétisme*. Masson, Paris (1957).
12. G. Sheldrick, SHELX76, A Crystallographic Computation System for Crystal Structure Determination. University of Cambridge, U.K. (1976).
13. D. T. Cromer and J. T. Waber, *Acta Cryst.* 1965, **18**, 104; D. T. Cromer, *Acta Cryst.* 1965, **18**, 17.
14. R. F. Stewart, E. R. Davidson and W. T. Simpson, *J. Chem. Phys.* 1965, **42**, 3175.
15. R. C. Aggarwal, R. Bala and R. L. Prasad, *Ind. J. Chem.* 1983, **22A**, 568.
16. B. N. Figgis and J. Lewis, *Prog. Inorg. Chem.* 1964, **6**, 37.
17. K. Nakamoto, *Infrared and Raman Spectra of Inorganic and Coordination Compounds*, 4th edn. Wiley, New York (1986); (a) p. 212; (b) p. 254.
18. B. J. Hathaway, *Comprehensive Coordination Chemistry* (Edited by G. Wilkinson, R. D. Gillard and J. McCleverty), Vol. 5, Ch. 53, (a) p. 596; (b) p. 614. Pergamon Press, New York (1987).
19. B. J. Hathaway, *Comprehensive Coordination Chemistry* (Edited by G. Wilkinson, R. D. Gillard and J. McCleverty), Vol. 2, Ch. 15.5, p. 419. Pergamon Press, New York (1987).
20. H. Nakai, S. Ooi and H. Kuroya, *Bull. Soc. Chem. Japan* 1977, **50**, 531.
21. M. Kato, H. B. Jonassen and J. C. Fanning, *Chem. Rev.* 1964, **64**, 99.
22. C. Benelli, D. Gatteschi and R. L. Carlin, *Inorg. Chem.* 1985, **24**, 3081.
23. J. F. Villa and W. E. Hatfield, *J. Am. Chem. Soc.* 1971, **93**, 4081.
24. D. Y. Jeter and W. E. Hatfield, *Inorg. Chim. Acta* 1972, **6**, 523.
25. B. J. Hathaway and D. E. Billing, *Coord. Chem. Rev.* 1970, **5**, 143; B. J. Hathaway, *Struct. Bonding (Berlin)* 1984, **57**, 55.
26. M. Sekizaki, F. Marumo, K. Yamasaki and Y. Saito, *Bull. Chem. Soc. Japan* 1971, **44**, 1731.
27. D. H. Brown, D. R. MacSween, M. Mercer and D. W. A. Sharp, *J. Chem. Soc. A* 1971, 1574; S. Tsuboyama, T. Sakurai, K. Kobayashi, N. Azuma, Y. Kajikawa and K. Ishizu, *Acta Cryst.* 1984, **B40**, 466; M. Sekizaki, *Acta Cryst.* 1973, **B29**, 327.
28. M. Sekizaki, *Bull. Chem. Soc. Japan* 1981, **54**, 146.
29. H. Nakai, *Bull. Chem. Soc. Japan* 1971, **44**, 2412; 1983, **56**, 1637; S. P. S. Rao, H. Manohar, K. Aoki, H. Yamazaki and R. Bau, *J. Chem. Soc., Chem. Commun.* 1986, 4; L. Antolini, L. P. Battaglia, A. B. Corradi, L. Menabue, G. Micera and M. Saladini, *Inorg. Chem.* 1986, **25**, 3301.
30. B. Morosin, *Acta Cryst.* 1975, **B31**, 632.
31. C. Mealli and L. Sacconi, *Acta Cryst.* 1977, **B33**, 710.
32. K. Al Sarraj, J. Gouteron, S. Jeannin and Y. Jeannin, *Acta Cryst.* 1987, **C43**, 1261.
33. J. S. Haynes, S. J. Rettig, J. R. Sams, J. Trotter and R. C. Thompson, *Inorg. Chem.* 1988, **27**, 1237.
34. G. J. M. Ivarsson, *Acta Chem. Scand.* 1979, **A33**, 323; N. Ray, S. Tyagi and B. Hathaway, *Acta Cryst.* 1982, **B38**, 1574; J. Foley, D. Kennefick, D. Phelan, S. Tyagi and B. Hathaway, *J. Chem. Soc., Dalton Trans.* 1983, 2333.
35. S. Komiya, J. C. Huffman and J. K. Kochi, *Inorg. Chem.* 1977, **16**, 2138.
36. J. S. Haynes, S. J. Rettig, J. R. Sams, R. C. Thompson and J. Trotter, *Can. J. Chem.* 1986, **64**, 429.
37. M. B. Humphrey, W. M. Lamanna, M. Brookhart and G. R. Husk, *Inorg. Chem.* 1983, **22**, 3355.
38. J. E. Huheey, *Inorganic Chemistry, Principles of Structure and Reactivity*, p. 73. Harper & Row, London (1983).

Polyhedron Vol. 12, No. 5, pp. 489–492, 1993
Printed in Great Britain

0277–5387/93 $6.00+.00
© 1993 Pergamon Press Ltd

A ^{31}P AND ^{95}Mo NMR STUDY OF SOME MOLYBDENUM AND TUNGSTEN CARBONYL COMPLEXES OF A SMALL AIR-STABLE ALIPHATIC PHOSPHINE, 1,3,5-TRIAZA-7-PHOSPHAADAMANTANE (PTA)

ELMER C. ALYEA,* KEITH J. FISHER,† SENG FOO and BRUNO PHILIP

Guelph–Waterloo Centre for Graduate Work in Chemistry, Guelph Campus, Department of Chemistry and Biochemistry, University of Guelph, Guelph, Ontario, Canada N1G 2W1

(*Received* 15 *September* 1992; *accepted* 4 *November* 1992)

Abstract—Complexes of molybdenum and tungsten of the type $M(CO)_5L$, $M(CO)_4L_2$ and $M(CO)_3L_3$ have been prepared, where L = 1,3,5-triaza-7-phosphaadamantane (PTA), a small air-stable aliphatic phosphine. The ^{31}P coordination chemical shifts indicate a strong σ-interaction between the metals and PTA. The ^{95}Mo chemical shifts also indicate a large nephelauxetic effect and/or a significant π-interaction of the ligand with molybdenum. Some PTA methyl iodide derivatives of these metal carbonyls have also been prepared and these also have a strong interaction with molybdenum and tungsten through the phosphorus atom of the novel ligand.

1,3,5-Triaza-7-phosphaadamantane (PTA) is a small air-stable aliphatic phosphine first prepared by Daigle and co-workers in 1974.[1] Fluck *et al.*[2] determined the crystal structure of PTA and prepared halogen and benzyl chloride derivatives. The study of a few metal carbonyl complexes of PTA and the determination of the crystal structure of $Mo(CO)_5PTA$ by Darensbourg and co-workers[3,4] seem to be the only complexation studies of this potentially important ligand. That work showed the similarity of the force constants of the carbonyl stretching frequencies and also of the ^{31}P coordination chemical shifts in the complexes $Mo(CO)_5L$ (L = Me_3P, PTA). The crystal structure of $Mo(CO)_5PTA$ indicated that PTA has a smaller cone angle (102°) than Me_3P (118°) and that the Mo—P bond length is 2.48 Å.[4] This bond length is short compared with 2.56 Å in $Mo(CO)_5PPh_3$ and 2.51 Å in $Mo(CO)_5P(CH_2CH_2CN)_3$.[5] The possibility that PTA may be a suitable alternative to PMe_3 as a ligand for transition metals due to its attractive properties (such as water solubility) attracted our attention; in addition, the specific nature of its interaction with molybdenum and other transition metals needs exploration.

Our current investigations of the coordinating ability of PTA include the syntheses and NMR characterization of some water soluble derivatives,[6] a solid-state ^{31}P CP-MAS NMR study of mercury(II) complexes[7] and an exploration of PTA complexation with various other metal salts (e.g. Co, Ni, Cu, Ph, Rd, Pt, Au).[8] In the present study we sought to extend the range of molybdenum and tungsten complexes of PTA and to utilize ^{31}P and ^{95}Mo NMR parameters to characterize the Mo—P bonding interaction. Various ^{95}Mo NMR studies in our laboratory,[9] as well as others,[10] have demonstrated the sensitivity of $\delta(^{95}Mo)$ values to the nature of phosphorus ligands.

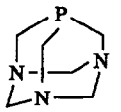

PTA

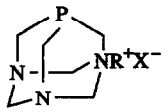

PTAR$^+$X$^-$

EXPERIMENTAL

General procedures

All operations were carried out under oxygen-free dry dinitrogen and all solvents were degassed.

* Author to whom correspondence should be addressed.
† Present address: School of Chemistry, The University of New South Wales, P.O. Box 1, Kensington, N.S.W. 2033, Australia.

^{31}P NMR spectra were recorded at ambient temperature on Bruker WH-400 or Bruker AM-250 spectrometers in the FT mode using 85% H_3PO_4 as an external standard. ^{95}Mo spectra were recorded at ambient temperature on a Bruker WH-400 spectrometer tuned to 26.08 MHz at a field strength of 9.3956 T. 2 M K_2MoO_4 in an aqueous solution of pH 11 was used as a standard.

Synthesis of $Mo(CO)_5PTA$

$Me_3NO \cdot 2H_2O$ (0.21 g 1.89 mmol) was added to a solution of $Mo(CO)_6$ (0.50 g 1.89 mmol) in acetonitrile (20 cm^3). After 30 min stirring at room temperature a solution of PTA (0.30 g 1.90 mmol) in methanol (20 cm^3) was added to the yellow acetonitrile solution. The resulting solution was refluxed for 30 min. The solvent was removed *in vacuo* and the solid washed in cold hexane (10 cm^3) and water (10 cm^3) and recrystallized from hexane. Yield 0.46 g (62% theory). Found: C, 33.1; H, 3.0; N, 10.6. Calc. for $Mo(CO)_5[PN_3(CH_2)_6]$: C, 33.6; H, 3.1; N, 10.7%.

Synthesis of $W(CO)_5PTA$

$W(CO)_5PTA$ was prepared in a similar manner to that described above for the molybdenum analogue, except that the reaction of $Me_3NO \cdot 2H_2O$ with $W(CO)_6$ took about 2 h at room temperature. Found: C, 27.5; H, 2.5; N, 9.0. Calc. for $W(CO)_5[PN_3(CH_2)_6]$: C, 27.4; H, 2.5; N, 8.7%.

Synthesis of cis-$Mo(CO)_4(PTA)_2$

A solution of PTA (0.83 g 5.3 mmol) in methanol (15 cm^3) was added to a solution of $Mo(CO)_4(NHC_5H_{10})_2$ (1.00 g 2.6 mmol) in dichloromethane (15 cm^3). The solution was stirred for 30 min and the yellow colour faded. The solvent was removed *in vacuo* and the resulting solid recrystallized from acetonitrile. Yield 1.10 g (80% theory). Found: C, 36.5; H, 4.7; N, 16.0. Calc. for $Mo(CO)_4[P_2N_6(CH_2)_{12}]$: C, 36.8; H, 4.6; N, 16.1%. IR CO: 2012, 1932, 1910 cm^{-1} (trichloroethylene). FTICR *m/z*: 524 (^{98}Mo).

Synthesis of cis-$W(CO)_4(PTA)_2$

$W(CO)_4(PTA)_2$ was prepared in a similar manner to the analogous molybdenum compound. Found: C, 31.2; H, 4.0; N, 13.7. Calc. for $W(CO)_4[P_2N_6(CH_2)_{12}]$: C, 31.5; H, 3.9; N, 13.8%. IR CO: 2016, 1928, 1904, 1848 cm^{-1}. FTICR *m/z*: 610 (^{184}W).

Attempts to prepare the *trans*-$M(CO)_4(PTA)_2$ derivatives by isomerization in boiling toluene were unsuccessful.

Syntheses of $M(CO)_3(PTA)_3$ *compounds*

Reactions of PTA with $Mo(CO)_6$ or $W(CO)_6$ in boiling acetonitrile for several days produced solutions containing mainly the $M(CO)_4(PTA)_2$ derivatives with some insoluble polymeric material. Reaction of PTA with $M(CO)_3(CH_3CN)_3$ solutions gave mixed products of mainly $M(CO)_4(PTA)_2$ and some $M(CO)_3(PTA)_3$. Pure compounds could not be isolated so they were studied in acetonitrile reaction solutions.

Syntheses of methyl iodide derivatives

The methyl iodide derivatives were prepared by the reaction of methyl iodide with the PTA metal carbonyl complexes in acetonitrile or by the reaction of PTAMeI with $M(CO)_5NMe_3$[11] or $M(CO)_4(NHC_5H_{10})_2$.[12] Similar spectra were obtained using either method.

RESULTS AND DISCUSSION

$Mo(CO)_5PTA$ and $W(CO)_5PTA$ were prepared by the reaction of PTA with the trimethylamine derivatives $M(CO)_5NMe_3$.[11] These compounds were previously synthesized by Darensbourg[3,4] using refluxing diglyme or a photochemical synthesis of $Mo(CO)_5THF$.

Cis-$Mo(CO)_4(PTA)_2$ and *cis*-$W(CO)_4(PTA)_2$ were prepared using the piperidine derivatives.[12] The IR spectrum of *cis*-$Mo(CO)_4(PTA)_2$ was similar to a *cis*-$Mo(CO)_4L_2$ spectrum reported by Darensbourg.[12] Isomerization to the *trans* isomer is expected to be very slow, as indicated by Darensbourg;[12] we found no evidence of isomerism in these complexes, possibly due to the small cone angle of PTA causing ligand dissociation to be negligible.

Although pure compounds were not obtained for the tri-substituted complexes by the acetonitrile method,[13] the ^{95}Mo NMR spectrum (a quartet) indicated the presence of a species with three equivalent phosphorus atoms, indicating the formation of the *fac*-isomer of $Mo(CO)_3(PTA)_3$.

The ^{31}P and ^{95}Mo data are given in Table 1 for the molybdenum carbonyl complexes and included in Table 1 are ^{31}P data for the tungsten carbonyl complexes.

The molybdenum complexes all give substantial ^{31}P coordination chemical shifts, relative to the complexes of PMe_3 and PEt_3 (Table 2), confirming a strong σ-interaction. The $J(^{31}P—^{95}Mo)$ obtained

Table 1. ^{31}P and ^{95}Mo NMR data of some PTA complexes in acetonitrile

Complex	$\delta^{31}P$	Δ^a	J (Hz)	$\delta^{95}Mo$
$Mo(CO)_5PTA$	−55.9	44.9	126	−1877
$Mo(CO)_4(PTA)_2$	−54.9	45.9	126	−1837
$Mo(CO)_3(PTA)_3$	−54.7	46.1	126	−1759
$Mo(CO)_5PTAMeI^b$	−30.2	54.1	127	−1860
$Mo(CO)_4(PTAMeI)_2^b$	−32.2	52.2	127	−1819
$W(CO)_5(PTA)$	−78.4	25.4	224	—
$W(CO)_4(PTA)_2$	−75.0	25.8	210	—
$W(CO)_3(PTA)_3$	−74.5	26.3	204	—
$W(CO)_5PTAMeI^b$	−53.7	30.6	236	—

[a] PTAMeI in CH_3CN, δ = −84.3 ppm.
[b] PTAMeI = 1-methyl-1-azonia-3,5-diaza-7-phosphaadamantane.

from the ^{95}Mo spectrum are all similar and are in the range generally observed for triaryl- and trialkylphosphines.[9,10]

The $\delta(^{95}Mo)$ value for the complex $Mo(CO)_5$PTA (−1877 ppm) indicates that the molybdenum shielding is even greater than that found for $Mo(CO)_6$ (−1855 ppm in acetonitrile) or the related complex $Mo(CO)_5PEt_3$ (−1854 ppm). This surprising result implies that either a large nephelauxetic effect and/or a significant π-interaction is operative, as well as the strong σ-interaction.[9,10] The short Mo—P bond of 2.48 Å found in $Mo(CO)_5$PTA[4] strongly suggests the presence of considerable π-bonding as the major factor, especially since PTA is less basic than PEt_3 (pK_a = 6.0 vs 8.69 for PEt_3; protonation actually occurs at one nitrogen atom, not at the phosphorus atom).[6] The three $\delta(^{95}Mo)$ values for the $Mo(CO)_{6-n}PTA_n$ (n = 1–3) complexes are very similar to those known for $Mo(CO)_{6-n}[P(OMe)_3]_n$ (n = 1–3; −1864, −1827 and −1756 ppm, respectively),[9,10] where $P(OMe)_3$ is acknowledged to be a strong π-acceptor ligand. By comparison, the $\delta(^{95}Mo)$ values for the three $Mo(CO)_{6-n}(PMe_3)_n$ (n = 1–3) complexes, which are −1819, −1723 and −1583 ppm,[9,10] respectively, signify that π-bonding is not a significant factor in the complexes of this basic aliphatic phosphine ligand. The ^{95}Mo chemical shift data thus shows that PTA has bonding properties which are much closer to those of $P(OMe)_3$ than PMe_3. This behaviour is obviously a consequence of the restricted C—P—C angles in the adamantane structure of PTA.

Previous workers[14–16] have shown that there is a good correlation between $\Delta\delta^{31}P$ of metal complexes and the free ligand chemical shift δ using the equation:

$$\Delta = A\delta + B.$$

We have used recent values of the parameters A and B, determined by Nelson,[16] but find our values give a poor fit to this equation (Table 2). We also note that data for Me_3P and Et_3P[17] also give a poor fit to this equation, as shown in Table 2. It may be that data used by Nelson was only applicable for arylphosphines of similar cone angle and the correlations may break down when small cone angle phosphines with quite different electronic properties such as Me_3P or PTA are used. It is interesting that our data for the *fac* isomers gives a better fit, although Nelson's data gave the poorest correlation with the least number of compounds.

Earlier work[3,6] showed that coordinated PTA might be alkylated by adding MeI and that the alkylated derivatives might also be prepared by the reaction of the hexacarbonyl with the alkylated derivative of PTA. We were able to prepare two such molybdenum derivatives and their ^{31}P data

Table 2. Observed and calculated values of the ^{31}P coordination chemical shift

Compound	Δ_{obs}	Δ_{calc}[a]	Diff.
$Mo(CO)_5$PTA	44.9	54.3	9.4
$Mo(CO)_5PMe_3$	43.7	48.9	5.2
$Mo(CO)_5PEt_3$	39.0	42.9	3.9
cis-$Mo(CO)_4$(PTA)	45.9	57.6	11.7
cis-$Mo(CO)_4(PMe_3)_2$	46.5	52.2	5.7
cis-$Mo(CO)_4(PEt_3)_2$	32.0	46.5	14.5
fac-$Mo(CO)_3(PTA)_3$	46.1	47.1	1.0
fac-$Mo(CO)_3(PMe_3)_3$	42.3	42.9	0.6
fac-$Mo(CO)_3(PEt_3)_3$	27.0	38.5	11.5

[a] Calculated using values given by Nelson.[16]
$LMo(CO)_5$; A = −0.142, B = 40.19.
cis-$L_2Mo(CO)_4$; A = −0.136, B = 43.90.
fac-$L_3Mo(CO)_3$; A = −0.105, B = 36.49.

indicate an even stronger σ-interaction with molybdenum. The ^{95}Mo data indicates a smaller σ- or nephelauxetic effect and/or a lower π-acceptor ability of PTAMeI. Previous $\delta(^{95}Mo)$ data[9,10] for phosphine and phosphite-substituted molybdenum carbonyl complexes showed that the better π-acceptor ligands caused molybdenum to be most shielded, presumably due mainly to their effect on the HUMO–LUMO separation, and hence the paramagnetic shift term for this quadrupolar nuclei ($I = 5/2$, 15.7% natural abudance).

The tungsten carbonyl complexes give much lower ^{31}P coordination chemical shifts than for the analogous molybdenum complexes, as observed for other phosphines.[10] These data also give a poor fit to the coordination chemical shift correlation equation.[16] The value for *fac*-$(PTA)_3W(CO)_3$ is close (observed $\Delta = 26.3$ ppm, calculated 27.2 ppm), but as the original data is only based on three determinations the agreement may be fortuitous.

The $J(^{31}P—^{183}W)$ coupling constants observed for the complexes are low. The value of 224 Hz for $W(CO)_5PTA$ would make PTA a poorer donor than PBu_3^n (227 Hz) and a much poorer donor than PPh_3 (245 Hz). The $J(^{31}P—^{183}W)$ values show significant and intriguing differences in the complexes studied. Other metal complexes are being investigated to provide a better assessment of $J(^{31}P—^{n}M)$ values and the nature of M—PTA bonds.

Acknowledgements—We are grateful to N.S.E.R.C. (Canada) for continued financial support and to the Southwestern Ontario NMR Centre for access to the Bruker WH-400 spectrometer.

REFERENCES

1. D. J. Daigle, A. B. Pepperman Jr and S. L. Vail, *J. Heterocyclic Chem.* 1974, **17**, 407.
2. E. Fluck, J. E. Forster, J. Weidlein and E. Hadicke, *Z. Naturforsch.* 1977, **32b**, 499.
3. M. Y. Darensbourg and D. J. Daigle, *Inorg. Chem.* 1975, **14**, 1217.
4. J. R. Delerno, L. M. Trefonas, M. Y. Darensbourg and R. J. Majeste, *Inorg. Chem.* 1976, **15**, 816.
5. F. A. Cotton, D. J. Darensbourg and W. H. Isley, *Inorg. Chem.* 1981, **20**, 578.
6. K. J. Fisher, E. C. Alyea and N. Shahnazarian, *Phosphorus, Sulphur, Silicon* 1990, **48**, 37.
7. E. C. Alyea, K. J. Fisher and S. Johnson, *Can. J. Chem.* **67**, 1319.
8. (a) E. C. Alyea and K. J. Fisher, Third Chemical Congress of North America, Toronto, June 5–10 1988, INOR 172 and 420; (b) E. C. Alyea and K. J. Fisher, XXVI ICCC, Porto Portugal, 28 August–2 September 1988, Abstract A41.
9. (a) E. C. Alyea and A. Somogyvari, *Trans. Met. Chem.* 1987, **12**, 310; (b) E. C. Alyea and A. Somogyvari, *Can. J. Chem.* 1988, **66**, 397; (c) E. C. Alyea and S. Song, *Inorg. Chem.* 1992, **31**, 4909.
10. M. Minelli, J. H. Enemark, R. T. C. Brownlee, M. J. O'Connor and A. G. Wedd, *Coord. Chem. Rev.* 1985, **68**, 169.
11. T. S. Andy Hor, *J. Organomet. Chem.* 1987, **319**, 213.
12. D. J. Darensbourg and R. L. Kump, *Inorg. Chem.* 1978, **17**, 2680.
13. D. P. Tate, W. R. Knipple and J. M. Augl, *Inorg. Chem.* 1962, **1**, 433.
14. B. E. Mann, C. Masters, B. L. Shaw, R. M. Slade and R. E. Stainbank, *Inorg. Nucl. Chem. Lett.* 1971, **7**, 881.
15. L. W. Cary, J. H. Nelson and A. W. Verstuyft, *Inorg. Nucl. Chem. Lett.* 1976, **12**, 53.
16. S. Affandi, J. H. Nelson, N. W. Alcock, O. W. Howarth, E. C. Alyea and G. M. Sheldrick, *Organometallics* 1988, **7**, 1724.
17. R. Mathieu, M. Lenzi and R. Poilblanc, *Inorg. Chem.* 1970, **9**, 2030.

Polyhedron Vol. 12, No. 5, pp. 493–496, 1993
Printed in Great Britain

0277-5387/93 $6.00+.00
© 1993 Pergamon Press Ltd

AN *IN SITU* STOPPED-EXCHANGE SOLUTION ^{31}P NMR COMPARISON STUDY OF 1-PHENYLDIBENZOPHOSPHOLE AND TRIPHENYLPHOSPHINE LIGANDS IN $[Hg(DMF)_{4-n}L_n][ClO_4]_2$ ($n = 1$–4)

ELMER C. ALYEA* and JOHN MALITO

Guelph–Waterloo Centre for Graduate Work in Chemistry, Guelph Campus, Department of Chemistry and Biochemistry, University of Guelph, Guelph, Ontario, Canada N1G 2W1

(*Received* 9 *September* 1992; *accepted* 22 *October* 1992)

Abstract—Upon dissolution in DMF $Hg(ClO_4)_2$ is solvated to give $[Hg(DMF)_4][ClO_4]_2$, which reacts with 1-phenyldibenzophosphole (DBP) or triphenylphosphine (PPh_3) to give $[Hg(DMF)_{4-n}L_n][ClO_4]_2$ (n = 1–3 for DBP and 1–2 for PPh_3). One-bond Hg—P coupling constants, which reach 11,014 Hz in the $[Hg(DMF)_3(DBP)]^{2+}$ cation, and coordination chemical shifts are higher and lower, respectively, for the DBP species. The former and latter observations are ascribed to electronic and steric effects, respectively. The ultimate $n = 4$ species are not observed in DMF solution but form readily in the non-coordinating solvent CH_2Cl_2. Overall, the PPh_3 species show higher kinetic lability, which contrasts with the opposite behaviour observed earlier for group 11 complexes.

Mercuric complexes of the type HgX_2L_2 (X = halide, pseudohalide; L = tertiary phosphine) have been well studied;[1] our earlier contributions focussed on ligand steric and electronic effects active within these and related complexes.[2] These reports established that for a given X and variable L relative Hg—P bond strengths are indicated by the magnitudes for $^1J(^{199}Hg—^{31}P)$[3], which in turn are sensitive to the steric and electronic properties of L. For weakly or non-coordinating X cationic species of variable stoichiometry are possible, dependent upon the natures of both X and L[4].

In this paper we apply the above knowledge in undertaking an *in situ* solution ^{31}P NMR study to compare the relative ligating properties of 1-phenyldibenzophosphole (DBP) and triphenyl phosphine (PPh_3) in reactions with $Hg(ClO_4)_2$. We have already reported complexation studies of DBP, which is both less sterically demanding[5a] and less basic than its nearest tertiary phosphine analogue PPh_3, with group 6 and 11 metals.[5]

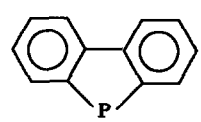

DBP

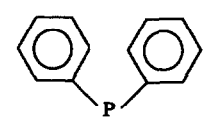

Ph_3P

EXPERIMENTAL

1-Phenyldibenzophosphole was supplied by Professor John H. Nelson (University of Nevada, Reno) while triphenylphosphine was purchased from a commercial source; each of these ligands was used as received. All syntheses were carried out under dinitrogen in 10 mm OD NMR tubes for stoichiometric additions of ligand solutions to $Hg(ClO_4)_2$ solutions (1 equivalent = 0.1 mmol). DMF and CH_2Cl_2 solvents were deoxygenated and of spectroscopic grades.

^{31}P NMR spectra were recorded at 223 K on a Bruker WH-400 spectrometer operating at 161.98 MHz and chemical shifts are reported relative to an external standard of aqueous 85% H_3PO_4. Chemical shifts for ^{199}Hg are reported relative to a 0.50 M solution of $HgCl_2$ in EtOH, set to −1497.0 ppm

* Author to whom correspondence should be addressed.

relative to neat $HgMe_2$ at 0.00 ppm.[6] The magnet was shimmed for sample ^1H FID spectra (^{31}P NMR) or deuterium in pure D_2O (^{199}Hg NMR). In all cases chemical shifts to higher frequency (i.e. downfield) are considered positive.

RESULTS AND DISCUSSION

The magnitude of the one-bond coupling constant $^1J(^{199}Hg—^{31}P)$, for species of the type HgX_2L_2, is sensitive to both experimental conditions of measurement[7] and the ligand properties of X and L. For strongly coordinating X the coupling constant magnitudes increase linearly with increasing tertiary phosphine basicities.[2,3,7] A similar trend has been reported for the analogous system CdX_2L_2.[8] If, however, X is weakly bonded or non-coordinating, then the trend is reversed and coupling constant magnitudes increase with decreasing basicities.[9] These trends, consistent with a Hg—P bond dominated by σ-character, are summarized, for a collection of literature data for three different anions,[2,3,7,9] in Fig. 1.

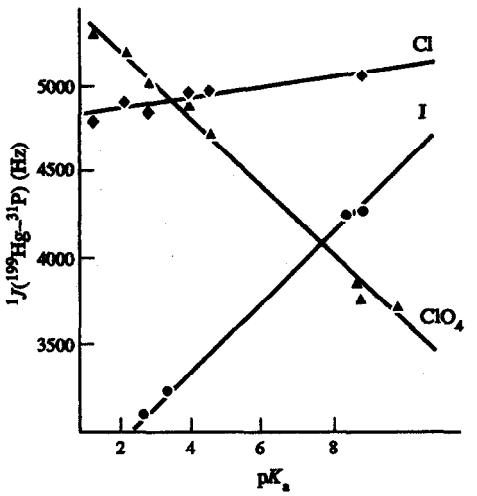

Fig. 1. Plots for $^1J(^{199}Hg—^{31}P)$ (Hz) vs ligand pK_a for HgX_2L_2 (X = Cl, I, ClO_4; L = tertiary phosphine).

For a given L, the coupling constant magnitude increases as (X=) CN < I < SCN < Br < Cl < OAc < NO_3 < ClO_4,[3,7-10] or as the Hg—X bond becomes more ionic. This is consistent with Bent's rule[11] and implies that as X becomes more electronegative, the bonding orbitals on mercury directed toward X and P gain in *p*- and *s*-character, respectively. Thus, $^1J(^{199}Hg—^{31}P)$ values, which reflect the amount of *s*-character in the Hg—P bond, should and do reflect Hg—P bond strengths.[3,10,12]

Our comparison studies for DBP and PPh_3 confirm the trends discussed above. In an earlier short paper[5b] we reported that for HgX_2L_2 (X = I, SCN; L = DBP, PPh_3) $J(^{199}Hg—^{31}P)$ values increase in magnitude as I < SCN and DBP < PPh_3. For $[Hg(DMF)_{4-n}L_n][ClO_4]_2$ (n = 1–3) (see Table 1), however, coupling constants are larger for L = DBP. For the n = 4 species, the coupling constants should be,[5b] but are not, equal in magnitude. Thus, which of DBP or PPh_3 forms the stronger bond with mercury(II) will depend on what other ligands are also bound to the same mercury(II) centre.

The maximum coordination species, $[HgL_4][ClO_4]_2$, are not observed in DMF solution even for a 10 times molar excess of added L. These species are observed, however, in the much less interactive solvent CH_2Cl_2. Thus, the assignments made in Table 1 assume complete solvation of $Hg(ClO_4)_2$ in DMF to give $[Hg(DMF)_4][ClO_4]_2$. Similar solvent interactions with mercury(II) have been previously suggested for DMF,[10a] as well as MeOH[4a], py[4a] and DMSO.[13] As part of this study we have observed that for saturated solutions of $Hg(ClO_4)_2$, the ^{199}Hg chemical shift moves upfield as acetone (−1504

Table 1. ^{31}P NMR data for $[Hg(DMF)_{4-n}L_n][ClO_4]_2$

Species	L = DBP $\Delta\delta^{31}P^{a,b}$ (ppm)	L = DBP $^1J(^{199}Hg—^{31}P)$ (Hz)	L = PPh_3 $\Delta\delta^{31}P^{a,c}$ (ppm)	L = PPh_3 $^1J(^{199}Hg—^{31}P)$ (Hz)	Solvent
$[Hg(DMF)_3L]^{2+}$	34.1	11,014	39.6	10,547	DMF
$[Hg(DMF)_2L_2]^{2+}$	44.0	6868	48.6	6413	DMF
$[Hg(DMF)L_3]^{2+}$	40.7	3888	[d]	[d]	DMF
$[HgL_4]^{2+}$	25.2	2051	32.4	2076	CH_2CH_2

[a] $\Delta\delta = \delta^{31}P$ (P coordinated) − $\delta^{31}P$ (P free).
[b] $\delta^{31}P$ (DBP free) = −11.0 ppm in DMF; −11.9 ppm in CH_2CH_2.
[c] $\delta^{31}P$ (PPh_3 free) = −6.8 ppm in DMF; −5.6 ppm in CH_2Cl_2.
[d] Not observed.

ppm) < H_2O (−2264 ppm) < DMSO (−2320 ppm) < DMF (−2346 ppm), i.e. as the solvent nucleophilicity increases.[14] In support of this, Sens *et al.*[15] have reported that shielding of mercury(II) in $HgMe_2$ increases with solvent Lewis basicity for 20 different solvents. Therefore, reaction of DBP or PPh_3 with $[Hg(DMF)_4][ClO_4]_2$ must involve displacement of a coordinated DMF molecule.

The ligands were added sequentially in stoichiometric quantities to DMF solutions of $Hg(ClO_4)_2$. Ensuing reactions were monitored *in situ* by ^{31}P NMR spectrometry at 223 K. This low temperature is required to resolve the ^{199}Hg satellites to measure $^1J(^{199}Hg—^{31}P)$. At this temperature, except for those cases where exchange occurs (*vide infra*), the line widths are typically 10 Hz or less and assignments are unambiguous.

Cationic species of the type $[HgL]^{2+}$ have been previously reported for phosphite ligands,[16] but comparable species for L = tertiary phosphine also contain either coordinated anions[17] or solvent molecules.[4a,10a,13] In DMF there is a very smooth stepwise formation observed for $[Hg(DMF)_{4-n}(DBP)_n]^{2+}$ (to $n = 3$) as DBP is added. Once three equivalents of DBP are added, a resonance assignable to free (or uncoordinated) DBP is observed and all resonances begin to broaden, indicating exchange of free ligand with $[Hg(DMF)(DBP)_3]^{2+}$. The case for PPh_3 is very different. The maximum coordination species observed is $[Hg(DMF)_2(PPh_3)_2]^{2+}$ and a resonance assignable to free PPh_3 does not appear until at least six equivalents of PPh_3 are added. The $n = 1$ and $n = 2$ species appear to be in equilibrium with each other and with free PPh_3.

It is clear that DBP competes more effectively than PPh_3 with DMF for coordination sites on mercury(II). This is most likely due to the smaller size of DBP, relative to PPh_3, in spite of the lower basicity for DBP. It is also clear that the PPh_3 species are much more kinetically labile than their DBP counterparts, contrary to our earlier observations for the group 11 metals,[5b] but consistent with results from our more recent study for L_nAuCl.[18]

Assignments for the PPh_3 species in Table 1 are consistent with data for similar species reported in the current literature.[4,9,19] The higher $^1J(^{199}Hg—^{31}P)$ values measured for the DBP species are also consistent with expectations based on relevant literature data.[9] These larger coupling constants, however, correspond with smaller complex coordination chemical shifts [$\Delta\delta = \delta$(coordinated P) − δ(free P)], opposite to what is usually observed for tertiary phosphine ligands.[2d,7b,10a] This suggests that the $\Delta\delta$ parameter, in this case, merely reflects larger C—P—C bond angle changes upon coordination for PPh_3 than for the more rigid DBP molecule.[5a] Also, $\Delta\delta$ appears to be maximized for the $n = 2$ species, indicating that steric crowding is a factor that is active for $[Hg(DMF)_{4-n}L_n]^{2+}$, as has been observed for other related species.[5b,9b]

Our comparison studies, including multinuclear NMR techniques, of the ligating properties of phosphole and dibenzophosphole ligands with their tertiary phosphine analogues continue. Nevertheless, it can be said at this point that whether DBP or PPh_3 is the "better" ligand depends upon several factors, including the nature of the metal centre and whatever ancillary ligands are also present.

Acknowledgements—E.C.A. thanks N.S.E.R.C. Canada for an operating grant.

REFERENCES

1. (a) R. C. Evans, F. G. Mann, H. S. Peiser and D. Purdie, *J. Chem. Soc.* 1940, 1209; (b) G. B. Deacon and B. O. West, *J. Inorg. Nucl. Chem.* 1962, **24**, 169; (c) G. E. Coates and D. Ridley, *J. Chem. Soc.* 1964, 166; (d) G. E. Coates and A. Lunder, *J. Chem. Soc.* 1965, 1875; (e) G. B. Deacon, J. H. S. Green and D. J. Harrison, *Spectrochim. Acta* 1968, **24**, 1921; (f) R. C. Makhija, A. L. Beauchamp and R. Rivest, *J. Chem. Soc., Dalton Trans.* 1973, 2447; (g) S. C. Jain and R. Rivest, *Inorg. Chim. Acta* 1970, **4**, 291; (h) T. S. Lobana, *Coord. Chem. Rev.* 1985, **63**, 161.
2. (a) E. C. Alyea, S. A. Dias, R. G. Goel and W. O. Ogini, *Can. J. Chem.* 1977, **55**, 4227; (b) E. C. Alyea, S. A. Dias, G. Ferguson, M. A. Khan and P. J. Roberts, *Inorg. Chem.* 1979, **18**, 2433; (c) E. C. Alyea, S. A. Dias, G. Ferguson and M. A. Khan, *J. Chem. Res. (S)* 1979, 360; (d) E. C. Alyea and S. A. Dias, *Can. J. Chem.* 1979, **57**, 83; (e) E. C. Alyea, S. A. Dias, G. Ferguson and M. A. Khan, *Can. J. Chem.* 1984, **57**, 2217,
3. (a) H. G. Buergi, R. W. Kunz and P. S. Pregosin, *Inorg. Chem.* 1980, **19**, 3707; (b) T. Allman and R. E. Lenkinski, *Inorg. Chem.* 1986, **25**, 3202.
4. (a) P. Peringer and M. Lusser, *Inorg. Chim. Acta* 1986, **118**, L7; (b) T. Allman, R. G. Goel and A. L. Beauchamp, *Acta Cryst.* 1988, **C44**, 1557.
5. (a) E. C. Alyea, G. Ferguson, J. Malito and B. L. Ruhl, *Acta Cryst.* 1986, **C42**, 882; (b) E. C. Alyea, J. Malito and J. H. Nelson, *Inorg. Chem.* 1987, **26**, 4294; (c) S. Affandi, J. H. Nelson, N. W. Alcock, O. W. Howarth, E. C. Alyea and G. M. Sheldrick, *Organometallics* 1988, **7**, 1724; (d) S. Attar, W. H. Bearden, N. W. Alcock, E. C. Alyea and J. H. Nelson, *Inorg. Chem.* 1990, **29**, 425.
6. R. K. Harris and B. E. Mann, *NMR and the Periodic Table*. Academic Press, London (1978).
7. (a) S. O. Grim and D. P. Shah, *Inorg. Nucl. Chem. Lett.* 1978, **14**, 105; (b) S. O. Grim, D. P. Shah,

C. K. Haas, J. M. Ressmer and P. M. Smith, *Inorg. Chim. Acta* 1979, **36**, 139; (c) T. Allman and R. G. Goel, *Can. J. Chem.* 1984, **62**, 615; 1984, **62**, 621.
8. R. G. Goel, W. P. Henry and R. C. Srivastava, *Inorg. Chem.* 1981, **20**, 1727.
9. (a) T. Allman and R. G. Goel, *Inorg. Nucl. Chem. Lett* 1979, **15**, 199; (b) R. Colton and D. Dakternieks, *Aust. J. Chem.* 1981, **34**, 323.
10. (a) E. C. Alyea, S. A. Dias, R. G. Goel, W. O. Ogini, P. Pilon and D. W. Meek, *Inorg. Chem.* 1978, **17**, 1697; (b) H. B. Buergi, E. Fischer, R. W. Kunz, M. Parvez and P. S. Pregosin, *Inorg. Chem.* 1982, **21**, 1246; (c) R. W. Kunz, P. S. Pregosin, H. Camalli, F. Caruso and L. Zambonelli, *Helv. Chim. Acta* 1983, **66**, 1661; (d) H. Motschi, P. S. Pregosin and L. M. Venanzi, *Helv. Chim. Acta* 1979, **62**, 667; (e) D. P. Arnold and M. A. Bennett, *Inorg. Chem.* 1984, **23**, 2117.
11. H. A. Bent, *Chem. Rev.* 1961, **61**, 275.
12. Ronald W. Kunz, Strukturuntersuchung an Quecksilberkomplexen mittels NMR-Röntgenstrukturund MO-Methoden, PhD Thesis, Eidgenössichen Technischen Hochschule, Zurich (1979).
13. P. Peringer and H. Lusser, *Polyhedron* 1987, **6**, 665.
14. V. Gutmann and R. Schmid, *Coord. Chem. Rev.* 1976, **18**, 225.
15. M. A. Sens, N. K. Wilson, P. D. Ellis and J. D. Odom, *J. Magnet. Reson.* 1975, **19**, 323.
16. P. Peringer and D. Obendorf, *Inorg. Chim. Acta* 1983, **77**, L147.
17. (a) P. L. Goggin, R. J. Goodfellow, S. R. Haddock and J. G. Eary, *J. Chem. Soc., Dalton Trans.* 1972, 647; (b) P. L. Goggin, R. J. Goodfellow, D. M. McEwan, A. J. Griffith and K. Kessler, *J. Chem. Res. (M)* 1979, 2315.
18. E. C. Alyea, J. Malito, S. Attar and J. H. Nelson, *Polyhedron* 1992, **11**, 2409.
19. D. Dakternicks, *Inorg. Chim. Acta* 1984, **89**, 209.

Polyhedron Vol. 12, No. 5, pp. 497–500, 1993
Printed in Great Britain

0277–5387/93 $6.00+.00
© 1993 Pergamon Press Ltd

PREPARATION OF $Mn(C_6F_5)_2$ COMPOUNDS BY TREATMENT OF $Hg(C_6F_5)_2$ WITH MANGANESE METAL—A NOVEL SYNTHESIS OF *d*-BLOCK ORGANOMETALLICS

GLEN B. DEACON,* RON S. DICKSON, JOZEF L. LATTEN and BRUCE O. WEST

Chemistry Department, Monash University, Clayton, Victoria 3168, Australia

(*Received* 27 *October* 1992; *accepted* 2 *November* 1992)

Abstract—Prolonged reaction of manganese metal with bis(pentafluorophenyl)mercury in thf or 1,2-dimethoxyethane (dme) yields $Mn(C_6F_5)_2(thf)_2$ or $Mn(C_6F_5)_2(dme)$. The latter reacts with N,N,N′,N′-tetramethylethane-1,2-diamine (tmen) in toluene to give $Mn(C_6F_5)_2$(tmen). Mass spectra indicate the complexes have associated structures. Impure $Mn(p\text{-}HC_6F_4)_2(dme)$ was obtained from manganese metal and $Hg(p\text{-}HC_6F_4)_2$.

Redox transmetallation between organomercurials and main group elements (e.g. Li, Mg, Al and Sn) is a well-established route to their organic derivatives [eq. (1)].[1,2]

$$E + n/2HgR_2 \longrightarrow ER_n + n/2Hg \downarrow \qquad (1)$$

The method is applicable to a number of main group polyfluorophenyl derivatives,[2,3] but has only limited use for perfluoroalkyls.[2] These syntheses are generally carried out in the absence of a solvent or in hydrocarbon media, at elevated temperatures, hence thermally stable target molecules are required. A free radical mechanism is likely for most reactions, although alternatives have been proposed for some of the few cases where mild conditions are used.[1] The main advantage of reaction (1) is that it provides a "halide-free" synthesis. In addition, where no solvent or a hydrocarbon solvent is used solvent coordination is avoided. There is no clear example of the use of reaction (1) in the synthesis of a *d*-block organometallic. In a related preparation ferrocene has been obtained in modest yield (24–30%) from treatment of iron powder with the crude product [stated to be a mixture of $Hg(C_5H_5)_2$ and $Hg(C_5H_5)Cl$] of the reaction of sodium acetate, cyclopentadiene and mercuric chloride.[4] However, the synthesis is not "halide-free" and the initial stoichiometry (C_5H_6:$HgCl_2$ = 1:1) favours $Hg(C_5H_5)Cl$ rather than $Hg(C_5H_5)_2$ as the main reactant. Widespread application of reaction (1) to the synthesis of *d*-block organometallics appears unlikely, because there are a number of low energy decomposition paths for these compounds. However, it has been shown that some *f*-block organometallics, including the thermally-unstable $Ln(C_6F_5)_2$ (Ln = Eu or Yb) derivatives,[5,6] can be prepared by redox transmetallation in ether solvents.[7,8] These may be envisaged as involving carbanion transfer to the highly electropositive lanthanide metal rather than a free radical mechanism.[5] The possibility of extension to *d*-block organometallics can be viewed as speculative, since the metals, apart from the neolanthanides Sc and Y, are much less electropositive than the lanthanide elements. Nevertheless, we now report the synthesis of bis(pentafluorophenyl)manganese by redox transmetallation.

RESULTS AND DISCUSSION

Prolonged reaction of bis(pentafluorophenyl)-mercury with manganese metal flake in thf at room temperature gave $Mn(C_6F_5)_2(thf)_2$ in reasonable yield after a difficult purification [eq. (1), E = Mn, R = C_6F_5, n = 2]. Reaction between the mercurial and manganese metal powder in refluxing 1,2-dimethoxyethane (dme) for a much shorter time gave $Mn(C_6F_5)_2(dme)$. Although microanalytical data deviated somewhat from calculated values, the variations were not excessive for highly air- and moisture-sensitive compounds. Moreover, acidolysis of $Mn(C_6F_5)_2(dme)$ [eq. (2)], which had the less satisfactory analyses, and determination of the C_6F_5H : dme ratio confirmed the composition.

* Author to whom correspondence should be addressed.

$$Mn(C_6F_5)_2(dme) + 2H^+ \longrightarrow Mn^{2+} + 2C_6F_5H + dme \quad (2)$$

In addition, the complex was converted by ligand exchange with N,N,N′,N′-tetramethylethane-1,2-diamine (tmen) into $Mn(C_6F_5)_2(tmen)$ [eq. (3)], which gave good microanalysis data.

$$Mn(C_6F_5)_2(dme) + tmen \longrightarrow Mn(C_6F_5)_2(tmen) + dme \quad (3)$$

Impure $Mn(p\text{-}HC_6F_4)_2(dme)$ was also obtained by redox transmetallation [eq. (1), R = p-HC_6F_4, n = 2, E = Mn).

The pentafluorophenylmanganese complexes showed IR absorptions characteristic[3,9] of pentafluorophenylorganometallics at *ca* 1630 and 1500 cm^{-1} [ν(CC)] and 1045 and 945 cm^{-1} [ν(CF)]. In addition, the thf complex showed intense features at 1019 and 862 cm^{-1} attributable to ring C—O stretching of coordinated thf, shifted characteristically from free ligand values.[10] Main group element[9] and some *d*-block pentafluorophenyls[11] show an "X-sensitive" mode involving metal–carbon stretching at 850–760 cm^{-1}. No corresponding absorption could be observed for $Mn(C_6F_5)_2L$ [L = $(thf)_2$, dme or tmen]. Bands for the thf and dme complexes at *ca* 860 cm^{-1} cannot be assigned to this mode, as there is no analogous absorption for $Mn(C_6F_5)_2(tmen)$. The absence of such a feature is consistent with the predominantly ionic character for the Mn—C bonds. Likewise, no clear assignment of this mode could be made for highly ionic $Yb(C_6F_5)_2(thf)_4$.[5] The IR spectrum of $Mn(p\text{-}HC_6F_4)_2(dme)$ showed the distinctively different ν(CF) bands (1200–1100; 879 cm^{-1}) exhibited by 2,3,5,6-tetrafluorophenylorganometallics.[5]

Magnetic moments consistent with high-spin manganese(II) were observed for the complexes. No parent ions or $Mn(C_6F_5)_2^+$ ions were observed in the mass spectra. However, several Mn_2^+-containing ions appeared with $Mn_2F(C_6F_5)_3^+$, $Mn_2H(C_6F_5)_3^+$, $Mn_2F_2(C_6F_5)_2^+$ and $Mn_2HF(C_6F_5)_2^+$ common to the spectra of the three $Mn(C_6F_5)_2L$ complexes and $Mn_2(C_6F_5)_2C_6F_4^+$, $Mn_2(C_6F_5)_2^+$ and $Mn_2F(C_6F_5)^+$ present in two (see Experimental). Only one ion containing a single manganese was evident, viz. $Mn(C_6F_5)dme^+$. These features indicate an associated, possibly dimeric, structure for the complexes. Although all ligands, even thf,[12] potentially can be bridging, the observation of dimers as dominant species under gas phase, mass spectrometric conditions at 200°C implies bridging pentafluorophenyl groups. Possible structures include a six-coordinate polymer with four bridging C_6F_5 groups per manganese or a five-coordinate dimer with two bridging and one terminal C_6F_5 group per manganese. Dimeric structures with bridging organic groups are known for organomanganese(II) Lewis base complexes.[13,14] Crystals suitable for X-ray crystallography could not be obtained.

Formation of $Mn_2F(C_6F_5)_3^+$ as the highest observed ion can be envisaged as resulting from loss of tetrafluorobenzyne from the desolvated dimer $Mn_2(C_6F_5)_4$. An ion with the composition $Mn_2(C_6F_5)_2C_6F_4^+$ has been observed for two compounds. This may plausibly be a 2-nonafluorobiphenylyl species, $Mn_2(C_6F_5)(2\text{-}C_{12}F_9)^+$, formed by insertion of tetrafluorobenzyne into an Mn—C_6F_5 bond. Analogous insertions are a well-established decomposition path for highly ionic C_6F_5Li[3] and C_6F_5-lanthanide[6] compounds. The ion $(C_6F_5)_2^+$ may be indicative of thermal decomposition into decafluorobiphenyl via pentafluorophenyl radicals.

The use of redox transmetallation between mercurials and manganese metal has provided a route to the first pentafluorophenylmanganese(II) complexes. It is the first authentic use of this synthetic method in *d*-block organometallic chemistry, and it indicates that use of polar solvents and mild reaction conditions for prolonged times can enable redox transmetallation to be used for the preparation of compounds with facile thermal decomposition paths. The discovery that a commercial form of manganese metal is sufficiently reactive to undergo redox transmetallation with mercurials offers the possibility that others of the more electropositive *d*-block metals may undergo convenient analogous reactions.

EXPERIMENTAL

All work was carried out under argon using standard Schlenk and dry-box techniques, as the products are very air-sensitive. Thf and 1,2-dimethoxyethane were distilled from sodium and benzophenone, whilst toluene and N,N,N′,N′-tetramethylethane-1,2-diamine were distilled from sodium and hexane from sodium–potassium alloy. Manganese flake was obtained from Aldrich; manganese powder was obtained by grinding the flake with a mortar and pestle in a recirculating atmosphere dry-box. Bis(pentafluorophenyl) mercury(II)[15] and bis(2,3,5,6-tetrafluorophenyl) mercury(II)[16] were prepared according to literature methods. Elemental analyses were carried out by National Analytical Laboratories, on preweighted encapsulated samples. IR spectra were recorded as Nujol mulls with a Perkin–Elmer 1600 Series FTIR spectrometer. Mass spectra were recorded on a VG

Micromass 7070F mass spectrometer, using a sample holder which could be loaded in the dry-box. Magnetic moments were determined using a Johnson–Matthey magnetic susceptibility balance calibrated with $Ni(en)_3S_2O_3$.

$Mn(C_6F_5)_2(thf)_2$ (1)

Manganese flake (0.28 g, 5.1 mmol) and bis(pentafluorophenyl)mercury (2.51 g, 4.7 mmol) were stirred in thf (20 cm^3) at room temperature for 2.5 months, giving a brown solution which was evaporated to dryness under a vacuum. The residue was extracted with boiling toluene and filtered. On cooling the extract to room temperature, fine needles were deposited, which were isolated by decanting the mother liquor, washed with hexane and dried *in vacuo*. A second crop was isolated by concentration of the mother liquor to saturation at its boiling point. Fine pale brown needles (1.17 g, 2.2 mmol, 47%) were obtained after a second recrystallization from boiling toluene. Found: C, 46.0; H, 3.2. Calc. for $C_{20}H_{16}F_{10}MnO_2$: C, 45.0; H, 3.0%. IR: 1670w, 1631m, 1606w, 1583w, 1498s, 1321m, 1279w, 1070w, sh, 1046vs, 1019s, 945vs, 862s, 750m, 722m, 713w, 676w, 593w, 480w cm^{-1}. $\mu_{eff} = 5.8$ B.M. MS (*m/z*): 630 ($[Mn_2F(C_6F_5)_3]^+$), 612 ($[Mn_2H(C_6F_5)_3]^+$), 482 ($[Mn_2F_2(C_6F_5)_2]^+$), 464 ($[Mn_2HF(C_6F_5)_2]^+$), 334 ($[C_6F_5C_6F_5]^+$), 316 ($[C_6F_5C_6F_4H]^+$), 168 (100%, $[C_6F_5H]^+$), 99 ($[C_5F_2H]^+$), 72 (thf^+).

$Mn(C_6F_5)_2(dme)$ (2)

Manganese powder (0.27 g, 4.9 mmol) and bis(pentafluorophenyl)mercury (2.31 g, 4.3 mmol) were stirred in refluxing 1,2-dimethoxyethane (10 cm^3) for 1 week. The resulting brown suspension was cooled and evaporated to dryness under reduced pressure. Extraction of the residue with boiling toluene, filtration and cooling to room temperature gave pale brown crystals, which were isolated by decanting the mother liquor, washed with hexane and dried *in vacuo*. A second crop was isolated by concentration of the mother liquor to saturation at its boiling point. Fine pale brown needles (0.83 g, 1.7 mmol, 40%) were obtained after a second recrystallization from boiling toluene. Found: C, 41.6; H, 2.6. Calc. for $C_{16}H_{10}F_{10}MnO_2$: C, 40.1; H, 2.1%. IR: 1633m, 1500m, 1324m, 1278w, 1254m, 1194w, 1093w, 1071m, 1049vs, 1003m, 944vs, 865s, 823w, 759w, 722m, br, 592m, 483m cm^{-1}. $\mu_{eff} = 5.8$ B.M. MS (*m/z*): 630 ($[Mn_2F(C_6F_5)_3]^+$), 612 ($[Mn_2H(C_6F_5)_3]^+$), 592 ($[Mn_2(C_6F_5)_2(C_6F_4)]^+$), 482 ($[Mn_2F_2(C_6F_5)_2]^+$), 464 ($[Mn_2HF(C_6F_5)_2]^+$), 444 ($[Mn_2(C_6F_5)_2]^+$), 334 ($[C_6F_5C_6F_5]^+$), 316 ($[C_6F_5C_6F_4H]^+$), 312 ($[Mn(C_6F_5)(dme)]^+$), 296 ($[Mn_2F(C_6F_5)]^+$), 168 ($[C_6F_5H]^+$), 99 ($[C_5F_2H]^+$), 98 ($[C_5F_2]^+$), 90 ($dme^+$), 60 (100%, $[OCH_2CH_2O]^+$).

$Mn(C_6F_5)_2(tmen)$ (3)

$Mn(C_6F_5)_2(dme)$ (0.74 g, 1.6 mmol), N,N,N'N'-tetramethylethane-1,2-diamine (0.5 cm^3, 3.3 mmol) and toluene (10 cm^3) were heated under reflux for 10 min. The brown solution was cooled and evaporated to dryness under reduced pressure. The residue was extracted with boiling toluene and filtered. Cooling the extract to room temperature gave brown needles, which were isolated by decanting the mother liquor, washed with hexane and dried *in vacuo*. Fine pale brown needles (0.43 g, 0.85 mmol, 55%) were obtained after a second recrystallization from boiling toluene. Found: C, 42.9; H, 3.1; N, 5.8. Calc. for $C_{18}H_{16}F_{10}MnN_2$: C, 42.8; H, 3.2; N, 5.5%. IR: 1628m, 1533w, 1496m, 1319w, 1282w, 1246m, 1168w, 1120w, 1073m, 1060m, 1041s, 1019w, 1006m, 951s, 944s, 798m, 769w, 750w, 722s, 592w, 587w, 479w cm^{-1}. $\mu_{eff} = 5.8$ B.M. MS (*m/z*): 630 ($[Mn_2F(C_6F_5)_3]^+$), 612 ($[Mn_2H(C_6F_5)_3]^+$), 592 ($[Mn_2(C_6F_5)_2(C_6F_4)]^+$), 482 ($[Mn_2F_2(C_6F_5)_2]^+$), 464 ($[Mn_2HF(C_6F_5)_2]^+$), 444 ($[Mn_2(C_6F_5)_2]^+$), 334 ($[C_6F_5C_6F_5]^+$), 316 ($[C_6F_5C_6F_4H]^+$), 298 ($[Mn_2(tmen)(C_4H_{10}N)]^+$), 296 ($[Mn_2F(C_6F_5)]^+$), 168 ($[C_6F_5H]^+$), 116 ($tmen^+$), 99 ($[C_5F_2H]^+$), 58 (100%, $[Me_2NCH_2]^+$).

$Mn(p\text{-}HC_6F_4)_2(dme)$ (4)

Manganese powder (0.39 g, 7.1 mmol) and Hg $(p\text{-}HC_6F_4)_2$ (1.52 g, 3.1 mmol) were heated under reflux in 1,2-dimethoxyethane (10 cm^3) for 11 days. The clear solution slowly turned cloudy and a fine grey precipitate formed. The suspension was evaporated to dryness under reduced pressure. The residue was recrystallized from boiling toluene, filtered and slowly cooled to room temperature giving colourless crystals. These were isolated by decanting the mother liquor, washed with hexane and dried *in vacuo*. A second crop was obtained by concentration of the mother liquor. Yield: 0.44 g, 0.99 mmol, 32%. Found: C, 40.3; H, 3.1. Calc. for $C_{16}H_{12}F_8MnO_2$: C, 43.4; H, 2.7%. IR: 3090w, 1771w, 1663w, 1599s, 1571w, 1533w, 1318w, 1308s, 1278m, 1239m, 1200s, 1172vs, 1089s, 1044vs, 1018m, 998m, 974w, 935w, 879vs, 858vs, 832s, 820m, 798w, 793w, 722s, 697s, 658m, 502w, 491m cm^{-1}. $\mu_{eff} = 6.0$ B.M.

Acidolysis of **2**

Compound **2** (20 mg, 42 μmol) was dissolved in pyridine-d_5 (0.7 cm^3) and frozen in a liquid nitrogen bath. Trifluoroacetic acid (0.1 cm^3, 1.3 mmol) was added to the frozen mixture, which was then allowed to thaw. On reaching room temperature a pale orange solution formed. The volatile components of the orange solution were vacuum distilled in a closed system and collected in a flask cooled in a liquid nitrogen bath. The solid residue was gently warmed to ensure that all volatiles had evaporated. An ^1H NMR spectrum of the condensed volatiles showed peaks at δ 7.39 (C_6F_5H), 3.49 ($MeOCH_2)_2$ and 3.27 ppm ($MeOCH_2)_2$ in a peak area ratio of 1 : 2 : 3, as required for hydrolysis of **2** [eq. (2)].

Acknowledgement—We are grateful to the Australian Research Council for support.

REFERENCES

1. L. G. Makarova, *Organomet. React.* 1970, **1**, 190; 248.
2. Houben-Weyl, *Methoden der Organischen Chemie*, Vol. XIII/2b, 40th edn, pp. 277–281. Georg Thieme Verlag, Stuttgart (1974).
3. S. C. Cohen and A. G. Massey, *Adv. Fluorine Chem.* 1970, **6**, 83.
4. K. Issleib and A. Brack, *Z. Naturforsch.* 1956, **11b**, 420.
5. G. B. Deacon, W. D. Raverty and D. G. Vince, *J. Organomet. Chem.* 1977, **135**, 103.
6. G. B. Deacon, A. J. Koplick, W. D. Raverty and D. G. Vince, *J. Organomet. Chem.* 1979, **182**, 121.
7. H. Schumann and W. Genthe, *Organometallic Compounds of the Rare Earths* (Edited by K. A. Gschneidner and L. Eyring), Vol. 7, Ch. 53. Elsevier, Amsterdam (1984).
8. W. J. Evans, *Polyhedron* 1987, **6**, 803.
9. G. B. Deacon and J. H. S. Green, *Spectrochim. Acta (A)* 1968, **24**, 1125.
10. J. Lewis, J. R. Miller, R. L. Richards and A. Thompson, *J. Chem. Soc.* 1965, 5850.
11. G. B. Deacon and I. L. Grayson, *Trans. Met. Chem.* 1982, **7**, 97.
12. G. B. Deacon, B. M. Gatehouse, S. Nickel and S. N. Platts, *Aust. J. Chem.* 1991, **44**, 613 and refs therein.
13. J. I. Davies, C. G. Howard, A. C. Skapski and G. Wilkinson, *J. Chem. Soc., Chem. Commun.* 1982, 1077.
14. C. G. Howard, G. Wilkinson, M. Thornton-Pett and M. B. Hursthouse, *J. Chem. Soc., Dalton Trans.* 1983, 2025.
15. G. B. Deacon and R. N. M. Smith, *J. Org. Chem. USSR* 1982, **18**, 1584.
16. G. B. Deacon and D. Tunaley, *J. Organomet. Chem.* 1978, **156**, 403.

Polyhedron Vol. 12, No. 5, pp. 501–505, 1993
Printed in Great Britain

0277–5387/93 $6.00+.00
© 1993 Pergamon Press Ltd

COMPLEXES OF MOLYBDENUM(V) WITH DITHIOCARBAMATE DERIVED FROM α-AMINO ACIDS

B. MACIAS,* J. J. CRIADO, M. V. VILLA, M. R. IGLESIAS and M. CASTILLO

Departamento de Química Inorgánica, Facultad de Farmacia, Universidad de Salamanca, Avda. Campo Charro s.n., 37007 Salamanca, Spain

(*Received* 15 *October* 1992; *accepted* 26 *October* 1992)

Abstract—Complexes formed through reaction of dithiocarbamate derived from α-amino acids with molybdenum(V) chloride in an inert atmosphere have been synthesized. These same complexes have also been prepared by the reduction of sodium molybdate with dithionite in an acidic medium. Chemical analyses for the complexes indicate the general formula $[Mo_2O_4(dtc\ a.a.)_2]\cdot 2H_2O$, where a.a. is the corresponding amino acid. No absorption band for the $Mo_2O_4^{2+}$ moiety was recorded in the visible range. IR spectra indicate that the carboxyl group is in the acid form, without binding to the metal cation. X-ray photoelectron spectra confirm the oxidation state of the molybdenum ions (Mo^{5+}), and that both sulphur atoms of the dithiocarbamate unit are equivalent.

The coordination chemistry of molybdenum has received much attention in the last decades, especially studies on the high oxidation states of this metal, as found in molybdoenzymes.[1–3] The complexes synthesized so far have provided information about the chemical behaviour of this element, and as it has been reported that molybdenum–sulphur bonds exist in these molybdoenzymes much effort has focussed on preparing and characterizing complexes with donor sulphur atoms.[4–6] Within this group of compounds, dialkyldithiocarbamate complexes have been studied, as they can undergo redox reactions as in molybdoenzymes.[4,7,8] These dialkyldithiocarbamate are easily synthesized through the reaction of the amine with carbon sulphide in a basic medium. However, if an α-amino acid is used instead of an amine, dithiocarbamate derivatives of α-amino acids are obtained[9,10] with the general formula:

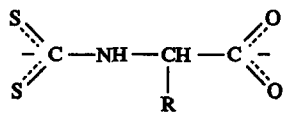

The simultaneous presence of the dithiocarbamate and the carboxylic groups makes these ligands very interesting, as both can coordinate the metallic cation and will modify the solubility of the complexes because of their polar properties. On the other hand, the nature of the side chain (R) is characteristic of the starting α-amino acid and may also affect the donor properties of the dithiocarbamate moiety.

In order to analyse the effect of this side-chain on the properties of the complexes thus formed, we have selected a series of α-amino acids with branched or linear side-chains of different lengths: R = H, glycine (gly); $-CH_3$, alanine (ala); $-CH_2-CH_3$, α-aminobutyric acid (α-ambut); $-CH_2-CH_2-CH_3$, norvaline (norval); $-CH-(CH_3)_2$, valine (val); $-CH_2-CH_2-CH_2-CH_3$, norleucine (norleu); $-CH_2-CH-(CH_3)_2$, leucine (leu); $-CH-(CH_2-CH_3)(CH_3)$, isoleucine (isoleu). The complexes formed upon reaction of these dithiocarbamate derivatives with molybdenum(V) chloride have been characterized.

EXPERIMENTAL

Materials and methods

All amino acids (in the DL form), $Na_2MoO_4\cdot 2H_2O$, $Na_2S_2O_4$ and CS_2 were from Fluka (p.a.). $MoCl_5$ was from Aldrich and the organic solvents, acetone and dimethylformamide (DMF),

* Author to whom correspondence should be addressed.

were from Carlo–Erba (RPE). All reactions were performed under a nitrogen atmosphere using standard Schlenk techniques.

Chemical analyses for carbon, hydrogen and nitrogen were performed using a Perkin–Elmer model 2400 analyser; sulphur contents were determined in the Instituto Bio-Organica de Barcelona (CSIC); the molybdenum content was determined using a Perkin–Elmer model 2380 Plasma-2 ICP spectrometer. Magnetic susceptibilities were determined by the Gouy method using a Stanton MC-5 microbalance, with $Hg[Co(SCN)_4]$ as the reference. FT-IR spectra were recorded using a Perkin–Elmer FT-IR 1730 spectrometer, with KBr pellets. Electronic spectra were recorded in a Shidmazu model UV-240 double beam spectrophotometer, using a diffuse reflectance accessory for solid samples and MgO as a reference. X-ray photoelectron spectra were recorded in the Departamento de Química Inorgánica (University of Sevilla), using a Leybold Heraeus LHS-10 apparatus, with Al-K_α radiation, an intensity of 20 mA, the samples being outgassed *in situ* at a residual pressure of 10^{-9} Torr, and using the C(1s) signal at 284.6 eV as a reference.

Preparation of the complexes

$MoCl_5$ (0.004 mol) was dissolved in doubly distilled water (15 cm^3), previously degassed, and the freshly prepared dithiocarbamate derivative (0.006 mol) of the α-amino acid (dissolved in 10 cm^3 of doubly distilled water) was slowly added with continuous stirring. After the addition of the first drops a brown–purple precipitate was observed, which increased in amount as the process continued. The precipitate was filtered using Schlenk flasks and washed three times with doubly distilled, degassed water (20 cm^3). The brown–ochre solid was dried *in vacuo* in the same flask. The yield ranges from 60% (for long-chain derivatives) to 40% (for short-chain derivatives).

These same complexes can also be prepared through reaction of the dithiocarbamate derivatives with sodium molybdate, using $Na_2S_2O_4$ as the reducing agent. The reaction takes place also under nitrogen. A solution was prepared by dissolving $Na_2MoO_4 \cdot 2H_2O$ (0.015 mol) in doubly distilled water (10 cm^3) and the sodium salt (0.025 mol) of the dithiocarbamate derivative in doubly distilled water (25 cm^3); to this solution, another containing sodium dithionite (0.045 mol) in NaOH (15 cm^3, 0.2 M) was added. Then, HCl (15 cm^3, 6 M) was slowly added dropwise to the former solution and a brown precipitate was formed, while the colour of the solution changed to orange. The precipitate was filtered and washed several times with doubly distilled water in order to remove excess dithionate, and was finally dried *in vacuo*. The yield was only 15–20% as more washing cycles were needed, due to the larger number of chemicals and reaction products.

RESULTS AND DISCUSSION

Data for chemical analyses for the complexes obtained following the two methods outlined above are included in Table 1. The general formula calculated from these data corresponds to $[Mo_2O_4(dtc\ a.a.)_2] \cdot 2H_2O$. Complexes containing the $Mo_2O_4^{2+}$ moiety have been previously described in the literature,[4,8,11] and they usually contain a two-oxygen atom bridge and two terminal oxygen atoms in *cis* positions; the oxidation state of molybdenum is Mo^{5+}. Solubility in water is low for all complexes prepared and so the low yields attained for the short-chain compounds can be associated with their higher solubility due to their lower organic character. Solubility is also low in methanol and acetone,

Table 1. Analytical data for dithiocarbamate complexes

	Found					Calc.				
	% C	% H	% N	% S	% Mo	% C	% H	% N	% S	% Mo
$[Mo_2O_4(dtc\ gly)_2]$	11.8	2.0	4.6	22.2	32.0	12.2	2.0	4.7	21.6	32.4
$[Mo_2O_4(dtc\ ala)_2]$	14.9	2.4	4.4	n.m.	30.9	15.5	2.6	4.5	20.7	30.9
$[Mo_2O_4(dtc\ \alpha\text{-ambut})_2]$	17.9	2.9	4.1	20.1	30.0	18.5	3.1	4.3	19.8	29.6
$[Mo_2O_4(dtc\ norval)_2]$	21.0	3.5	4.0	n.m.	28.7	21.3	3.6	4.1	19.0	28.4
$[Mo_2O_4(dtc\ val)_2]$	21.0	3.5	4.0	19.1	29.0	21.3	3.6	4.1	19.0	28.4
$[Mo_2O_4(dtc\ norleu)_2]$	23.9	4.0	3.9	n.m.	27.3	23.9	4.0	4.0	18.2	27.2
$[Mo_2O_4(dtc\ leu)_2]$	23.6	4.1	3.9	18.5	27.5	23.9	4.0	4.0	18.2	27.2
$[Mo_2O_4(dtc\ isoleu)_2]$	24.0	4.1	3.9	18.4	27.3	23.9	4.0	4.0	18.2	27.2

n.m. = not measured.

where they decompose slowly at room temperature; on the contrary, solubility is higher in DMF, forming brown coloured solutions. In any case, due to the low stability in solution crystals could not be obtained and the molecular structure could not be determined.

All compounds are diamagnetic, with pairing between the odd electrons in both molybdenum atoms of the $Mo_2O_4^{2+}$ moiety occurring through the bridging oxygen atoms. No absorption band was recorded in the visible range. Only a band at 330 nm was recorded when acetone was used as a solvent, with a molar extinction coefficient of 6500 $dm^3\ mol^{-1}\ cm^{-1}$. This band can be associated with a S → Mo charge-transfer process. A band recorded at 280 nm in DMF with a very large extinction coefficient (21,000 $dm^3\ mol^{-1}\ cm^{-1}$) can be due to intraligand electron transfer. A broad band recorded in the solid state may contain both of the absorptions detected separately in solution. This sort of finding has already been reported in the literature for dinuclear molybdenum complexes with a two-oxygen bridge and containing the $Mo_2O_4^{2+}$ moiety; for complexes with a one-oxygen bridge ($Mo_2O_3^{4+}$), the band is recorded at 500 nm.[4,8,12–14]

The positions of the most significant FT-IR bands are included in Table 2. The band due to the C—N stretching mode is recorded at *ca* 1530 cm^{-1} in all cases, thus indicating a fairly large bond order. According to the valence bond theory, the structure of these dithiocarbamate units can be depicted as:

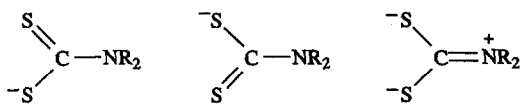

(a) (b) (c)

and so structure **c** would contribute to a larger extent than the others to the real structure, as confirmed by X-ray diffraction studies for some dithiocarbamate complexes, showing that the C—N distance is between those corresponding to a single and a double bond.[15–18] It has been reported[16,19–21] that this band shifts towards lower wave numbers as the length of the side-chain increases, because of the increasing molecular mass, but this effect is hardly observed in our case, probably due to the presence of the relatively heavy carboxylic group which make the relative differences between the point masses less important. The C—N stretching mode between the carbon atom and the nitrogen atom from the amino acid fragment is also recorded (see Table 2) and corresponds to a single C—N bond.[22,23]

Table 2. Proposed assignments for selected vibrational frequencies (cm^{-1}) in molybdenum complexes

	ν(C—N)	ν(N—C′)	ν(N—H)	ν(C=O)	ν(C—O)+δ(O—H)	ν(O—H)	ν(Mo=O)	ν(Mo—O—Mo)	ν(S—Mo)
$[Mo_2O_4(dtc\ gly)_2]$	1543(vs)	1100(m)	3220(s)	1729(s)	1403(s), 1238(w)	3440(m)	969(vs)	726(m)	371(m)
$[Mo_2O_4(dtc\ ala)_2]$	1533(vs)	1138(m)	3208(s)	1724(s)	1416(s), 1228(w)	3436(m)	972(vs)	711(m)	359(m)
$[Mo_2O_4(dtc\ \alpha\text{-ambut})_2]$	1531(vs)	1140(m)	3215(s)	1724(s)	1417(s), 1257(w)	3436(m)	973(vs)	712(m)	342(m)
$[Mo_2O_4(dtc\ norval)_2]$	1531(vs)	1143(m)	3208(s)	1723(s)	1417(s), 1239(w)	3436(m)	971(vs)	714(m)	386(m)
$[Mo_2O_4(dtc\ val)_2]$	1531(vs)	1141(m)	3205(s)	1723(s)	1412(s), 1261(w)	3436(m)	972(vs)	715(m)	397(m)
$[Mo_2O_4(dtc\ norleu)_2]$	1526(vs)	1141(m)	3192(s)	1724(s)	1416(s), 1231(w)	3436(m)	973(vs)	728(m)	375(m)
$[Mo_2O_4(dtc\ leu)_2]$	1531(vs)	1154(m)	3192(s)	1724(s)	1412(s), 1242(w)	3436(m)	973(vs)	714(m)	391(m)
$[Mo_2O_4(dtc\ isoleu)_2]$	1526(vs)	1139(m)	3196(s)	1723(s)	1414(s), 1258(w)	3436(m)	972(vs)	716(m)	411(m)

vs = very strong, s = strong, m = medium, w = weak.

As in both synthetic routes outlined above the complexes are prepared in an acidic medium. The carboxylic group of the amino acid remains as such (i.e. it is not ionized to the carboxylate form) and thus does not participate in bonding to the molybdenum cation. This fact was confirmed by the presence of a single strong band for all complexes at 1724 cm^{-1}, due to the C=O stretching mode, together with the band due to the C—O stretching and OH in-plane deformation modes at 1410 and 1240 cm^{-1}, and the O—H stretching band at 3435 cm^{-1}.

With regard to bands due to vibrations involving the molybdenum atom, a strong band at 970 cm^{-1} can be assigned to the ν(Mo=O) mode; a well-defined medium intensity band at 725 cm^{-1} is also recorded, and it has been previously reported[24,25] for two-oxygen bridged molybdenum(V) units. Finally, the band due to the ν(S—Mo) mode is recorded in the expected[26–28] range.

Ionization energies for the most representative energy levels of the atoms forming these complexes, as measured by XPS, do not show significant differences from one complex to another. The peak due to O(1*s*) levels is recorded as a complex feature, due to the existence of oxygen atoms in different chemical environments, but the maximum is centred at 531.4 eV. For N(1*s*) the peak is recorded at 400.0 eV in all cases, a value slightly higher than that reported[29] for dithiocarbamate complexes of copper(II), nickel(II) and cobalt(II), thus confirming that resonance form **c** mainly contributes to the structure of the complexes, in agreement with the FT-IR results. A peak at 396.7 eV, i.e. close to that for N(1*s*), should be ascribed to the Mo(2*p*) level.

However, the most interesting signals to analyse the donor ability of dithiocarbamate are those due to the sulphur atoms. The value recorded for S(2*p*) is at 162.7–162.8 eV, slightly larger than that reported by Walton[30] for dithiocarbamate complexes, thus suggesting a larger donor capacity of these atoms in our case. Only the expected $2p_{1/2}$–$2p_{3/2}$ splitting is observed, indicating that both sulphur atoms are chemically equivalent; the ligand thus acting as bidentate, as in most of the dithiocarbamate complexes reported in the literature.[31,32] The Mo($3d_{3/2}$) and Mo($3d_{5/2}$) signals are recorded at 230.8 and 234.0 eV (the difference reported in the literature is 3.1 eV). The value for the Mo($3d_{5/2}$) level, usually taken to compare the ionization energy of molybdenum species, coincides with that reported for complexes of molybdenum(V) with polysulphides,[33] where it is coordinated solely by sulphur atoms, and is very close to that for complexes of molybdenum(V) with cystein (231.1 eV) and penicylamine (231.0 eV).[34,35] For $Mo_2S_4(dtc)_2$ (dtc = diethyldithiocarbamate) the value is 229.6 eV,[36] as in this case only sulphur atoms are bonded to Mo^{5+} and the more electronegative oxygen atoms (present as bridging and terminal atoms in our case) are absent.

Acknowledgements—Financial support from CAICYT (Grant No. 800-84) and from Universidad de Salamanca (Acciones Concertadas) is gratefully acknowledged. The authors thank Professor V. Rives (Universidad de Salamanca) for his fruitful discussions.

REFERENCES

1. M. T. Pope, E. R. Still and R. J. P. Williams, *Molybdenum and Molybdenum-Containing Enzymes* (Edited by M. P. Coughlan). Pergamon Press, Oxford (1980).
2. R. C. Bray and G. N. George, *Biochem. Soc. Trans.* 1985, **13**, 560.
3. S. J. N. Burgmayer and E. I. Stiefel, *J. Chem. Educ.* 1985, **62**, 943.
4. E. I. Stiefel, *Prog. Inorg. Chem.* 1977, **22**, 1.
5. K. V. Rajagopalan, S. Kramer and S. Gardlik, *Polyhedron* 1986, **5**, 573.
6. R. H. Holm, *Coord. Chem. Rev.* 1990, **100**, 183.
7. P. W. Schneider, D. C. Bravard, J. W. McDonald and W. E. Newton, *J. Am. Chem. Soc.* 1972, **94**, 8640.
8. W. E. Newton, J. L. Corbin, D. C. Bravard, J. E. Searles and J. W. McDonald, *Inorg. Chem.* 1974, **13**, 1100.
9. M. Castillo, J. J. Criado, B. Macias and M. V. Vaquero, *Inorg. Chim. Acta* 1986, **124**, 127.
10. M. Castillo, J. J. Criado, B. Macias and M. V. Vaquero, *Trans. Met. Chem.* 1986, **11**, 476.
11. F. A. Schultz, V. R. Ott, D. S. Rolison, D. C. Bravard, J. W. McDonald and W. E. Newton, *Inorg. Chem.* 1978, **17**, 1758.
12. R. N. Jowitt and P. C. H. Mitchell, *J. Chem. Soc. (A)* 1970, 1702.
13. A. T. Casey, D. J. Mackey, R. L. Martin and A. H. White, *Austral. J. Chem.* 1972, **25**, 477.
14. W. E. Newton, J. L. Corbin and J. W. McDonald, *J. Chem. Soc., Dalton Trans.* 1974, 1044.
15. W. Beck, M. Girnth, M. Castillo and H. Zippel, *Chem. Ber.* 1978, **111**, 1246.
16. B. J. McCormick, *Inorg. Chem.* 1968, **7**, 1965.
17. D. Coucouvanis and J. P. Fackler Jr, *Inorg. Chem.* 1967, **6**, 2047.
18. L. J. Bellamy, *The Infrared Spectra of Complex Molecules*, Vol. 1, 2nd edn, p. 401. Chapman and Hall, London (1980).
19. F. W. Moore and M. L. Larson, *Inorg. Chem.* 1967, **6**, 998.
20. S. Wajda and K. Drabent, *Bull. Acad. Polon. Sci., Ser. Sci. Chim.* 1977, **25**, 963.
21. T. N. Srivastava, V. Kumar and R. B. Rastogi, *J. Inorg. Nucl. Chem.* 1978, **40**, 399.

22. K. Nakamoto, *Infrared and Raman Spectra of Inorganic and Coordination Compounds*, 4th edn, p. 234. John Wiley and Sons, New York (1986).
23. R. A. Condrate and K. Nakamoto, *J. Chem. Phys.* 1965, **42**, 2590.
24. W. E. Newton and J. W. MacDonald, *J. Less-Common Met.* 1977, **54**, 51.
25. G. J. J. Chen, J. W. McDonald, D. C. Bravard and W. E. Newton, *Inorg. Chem.* 1985, **24**, 2327.
26. A. Nieuwpoort, J. H. E. Moonem and J. A. Cras, *Rec. Trav. Chim. Pays-Bas.* 1973, **92**, 1086.
27. M. Chaudhury, *Polyhedron* 1986, **5**, 387.
28. S. Baran Kumar and M. Chaudhury, *J. Chem. Soc., Dalton Trans.* 1991, 1149.
29. G. Polzonetti, C. Preti and G. Tosi, *Polyhedron* 1986, **5**, 1969.
30. R. A. Walton, *Coord. Chem. Rev.* 1980, **31**, 183.
31. C. Furlani, G. Polzonetti, C. Preti and G. Tosi, *Gazz. Chim. Ital.* 1983, **113**, 609.
32. A. A. Achilleos, L. R. Gahan, T. W. Hambley, P. C. Healy and D. M. Weedon, *Inorg. Chim. Acta* 1989, **157**, 209.
33. R. Bhattacharyya, P. K. Chakrabarty, P. N. Ghosh, A. K. Mukherjee, D. Podder and M. Mukherjee, *Inorg. Chem.* 1991, **30**, 3948.
34. V. Srinivasan, E. I. Stiefel, A. Elsberry and R. A. Walton, *J. Am. Chem. Soc.* 1979, **101**, 2611.
35. W. S. Mialki, E. I. Stiefel, A. E. Bruce and R. A. Walton, *Inorg. Chem.* 1981, **20**, 1614.
36. A. Müller, R. Jostes, W. Eltzner, C.-S. Nie, E. Diemann, H. Bogge, M. Zimmermann, M. Dartmann, U. Reinsch-Vogell, S. Che, S. J. Cyvin and B. N. Cyvin, *Inorg. Chem.* 1985, **24**, 2872.

Polyhedron Vol. 12, No. 5, pp. 507–512, 1993
Printed in Great Britain

0277–5387/93 $6.00+.00
© 1993 Pergamon Press Ltd

SYNTHESIS AND STRUCTURAL STUDIES ON Z-2-BENZYLTHIO-4-HYDROXIMINOMETHYL-1-*p*-METHOXYPHENYL IMIDAZOLE METAL COMPLEXES

R. LOPEZ-GARZON, M. N. MORENO-CARRETERO,* M. A. SALAS-PEREGRIN and J. M. SALAS-PEREGRIN

Departamento de Química Inorgánica, Facultad de Ciencias Experimentales, Universidad de Granada, 23071 Jaén, Spain

(*Received* 30 *September* 1992; *accepted* 22 *October* 1992)

Abstract—Complexes of Z-2-benzylthio-4-hydroximinomethyl-1-*p*-methoxyphenyl imidazole (Z-OXLME) with Co^{II}, Ni^{II}, Cu^{II}, Zn^{II}, Cd^{II} and Hg^{II} were prepared and characterized by IR, UV–vis–NIR diffuse reflectance, ^{1}H and ^{13}C NMR spectroscopies and magnetic and thermal measurements. In all the complexes the organic compound acts as a chelator through $N(3)_{imid}$ and N_{oxime} atoms.

Organic compounds containing the oxime group are of great biological interest. In 1950, Wilson found that the hydroxylamine acts as a regenerator of the phosphorylated acetylcholinesterase.[1] Since then, many other oximic derivatives have been obtained with the aim of improving their toxicity; among these derivatives several N-methyl derivatives of pyridinaldoximes,[2] the compound 1-dodecyl-2-hydroximinomethyl pyridinium[3–5] and the quaternary salts derived from the 2-hydroximinomethyl imidazole may be highlighted. Other oximic derivatives, e.g. the α-cetoglutamic oxime acid and the dimethylglyoxime exhibit *in vitro* antitumor activity.[6–8] In some cases this activity is enhanced in the presence of certain metal ions; so, Takamiya proved that the *in vitro* antitumor activity of the α-cetoglutamic oxime acid is minor compared with that of their Fe^{II} and Cu^{II} metal chelates. Likewise, in the case of the dimethylglyoxime the *in vitro* antitumor activity is enhanced when the compound is supplied together with Cu^{II} ions, but not with other metal ions like Ni^{II}, Co^{II}, Zn^{II}, Fe^{II}, Mn^{II}, Hg^{I} or Hg^{II}.[6] This suggests that the antitumoral activity of a metal chelate depends not only on its permeability through the cellular membrane, but of the structural characteristics of both metal ion and chelating agent. Thus, dimethylglyoxime-copper and bis-(acetylmonoxime)-copper(II) are both of them permeable to Erhlich carcinoma and 180 Crocker sarcoma cellules; nevertheless, only the former inhibited tumor development.

Other oxime complexes, *trans*-bis[salicylaldoximate]copper(II) and *trans*-bis[resorcylaldoximato]copper(II), also show strong *in vitro* and *in vivo* anticancer activities against Leukaemia L1210 and Erhlich *ascites carcinome*.[9]

As a continuation of a previous work,[10] in which the coordination ability of the compound E-1-*p*-ethoxyphenyl-4-hydroximinomethyl imidazole (EALDH) against several metal ions was studied, the present paper is focussed on the synthesis and characterization of metal complexes from the monoximic derivative Z-2-benzylthio-4-hydroximinomethyl-1-*p*-methoxyphenyl imidazole (Z-OXLME) with Co^{II}, Ni^{II}, Cu^{II}, Zn^{II}, Cd^{II} and Hg^{II}. The compound Z-OXLME differs structurally from the former in the presence of a benzylthio group substituted on C(2) of the imidazolic ring. These compounds are analogous to some others which are regenerators of the phosphorylated acetylcholinesterase.[11]

EXPERIMENTAL

Preparation of the ligands and complexes

The compound used as the ligand, Z-OXLME, was prepared according to a reported procedure.[11]

The complexes were obtained by adding with stirring the corresponding metallic chloride (1 mmol) to an ethanolic solution (75 cm^3) of Z-

* Author to whom correspondence should be addressed.

OXLME (0.339 g, 1 mmol). The resulting solutions were evaporated in air until precipitation of the complexes occurred (about 3 days later), except in the case of the copper(II) complex, which precipitated almost immediately.

Apparatus and methods

Microanalyses of carbon, hydrogen and nitrogen were performed in the Technical Services of University of Granada (STUGRA). IR spectra were obtained on a Perkin–Elmer 983G spectrophotometer, from KBr pellets in the 4000–250 cm^{-1} range and polyethylene pellets in the 600–180 cm^{-1} range. ^1H and ^{13}C NMR spectra were recorded on a Bruker AM-300 machine, using DMSO-d_6 as a solvent and TMS as the internal standard. UV–vis–NIR reflectance spectra of the complexes in the 240–1400 nm range were obtained from pellets of the corresponding samples, using a Shimadzu MPC-3100 spectrophotometer and $BaSO_4$ as a reference. Magnetic susceptibilities of the ligand and complexes at room temperature were measured using Faraday–Bruker Magnet Mod. B-E15 equipment. Dependence of susceptibility values on the temperature was measured on a Mannics DSM-8 susceptometer. The temperature range investigated was 80–280 K. The ESR spectrum of $CuCl_2$(Z-OXLME)·$2H_2O$ was obtained in the *X*-band using a Bruker E.S.P.-300 spectrometer. Finally, the thermal study of the ligand and complexes was performed using a Mettler TA-3000 system, provided with a Mettler TG-50 thermobalance and a DSC-20 differential scanning calorimeter. TG curves were obtained on heating samples of the corresponding solids in a dynamic pure air atmosphere (100 cm^3 min^{-1}) in the 35–850°C temperature range, whereas DSC plots were recorded under a static air atmosphere in the temperature range between 35 and 450°C. In both cases a heating rate of 10°C min^{-1} and samples varying in weight from 1 to 10 mg were utilized.

RESULTS AND DISCUSSION

The assignments of the bands of the IR spectra of Z-OXLME were performed in accordance with the literature.[12–17] These assignments (Table 1) point out that the tautomeric form of Z-OXLME in the solid state is the hydroxioximic one instead of the nitronic one. The assignments of the broad band at 2844 cm^{-1} at ν(OH) of the oxime group and that of 1681 cm^{-1} at δ(OH) in plane deformation due to hydrogen bridged OH groups were proved by the shifting from 2720 to 2200 cm^{-1} of the former and the disappearance of the second upon deuteration of Z-OXLME.

The low wave number value and widening of the ν(OH) band (2844 cm^{-1}), together with the appearance of the δ(OH) band in the IR spectrum of Z-OXLME, prove the existence of an intramolecular hydrogen bridge[12] between the OH group and probably the N(3) atom of the imidazole ring (as shown in Fig. 1), which is favoured by the *Z* conformation of the compound.

NMR data are summarized in Table 2. It is noticeable that the value of the chemical shift of the hydroxylic hydrogen atoms in the ^1H NMR spectrum of Z-OXLME is high (11.60 ppm) compared to the one corresponding for EALDH (10.80 ppm),[10] in which an intramolecular hydrogen bridge of the above type is prevented; this fact is also in accordance with the structure depicted in Fig. 1. Moreover, the higher melting enthalpy of the compound EALDH (51 kJ mol^{-1}) than Z-OXLME (22 kJ mol^{-1}), measured from their corresponding DSC plots, is also in accordance with the existence of stronger intramolecular interactions in the former compound than in the latter.

The assignments of the signals corresponding to

Table 1. IR spectral data (cm^{-1})

Compound	ν(OH)	δ(OH)	ν(C=N)$_{oxime}$	ν(NO)	ν(M—Cl)	[ν(C=C), ν(C=N)]$_{ar.}$
Z-OXLME	2844 s,b	1681 m	1609–1648 m	917 s	—	1457 s, 1512 s
$CoCl_2$(Z-OXLME)$_2$	2844 m	1721 m	1607–1639 m	1018 s	232 b,s	1444, 1510 s
$NiCl_2$(Z-OXLME)$_2$	3194 m	1722 m	1607–1648 m	1021 s	327 s	1449, 1510 s
$CuCl_2$(Z-OXLME)·$2H_2O$	3442 m,b	—	1605–1639 m	997 s	357 a,s	1441 m, 1508 s
$ZnCl_2$(Z-OXLME)	3238 s	—	1605–1647 m	1032 s	303, 346 s	1449, 1510 s
$CdCl_2$(Z-OXLME)$_2$	3294 m	1721 m	1606–1640 m	1013 s	230 s	1443, 1510 s
$CdCl_2$(Z-OXLME)·H_2O	3295 m	—	1606–1652 vs	1012 m	253 a,s	1462 s, 1512, vs, 1579 vs
$HgCl_2$(Z-OXLME)·H_2O	3311 m	—	1609–1631 m	1015 s	283 s	1443 s, 1510

a = double band; b = broad; s = strong; m = medium; w = weak; vs = very strong.

Table 2. NMR data (δ, ppm)

Compound	^{1}H NMR			^{13}C NMR			
	OH_{oxime}	C(5)—$H_{imid.}$	C_α—H_{oxime}	$C\alpha_{oxime}$	$C(2)_{imid.}$	$C(4)_{imid.}$	$C(5)_{imid.}$
Z-OXLME	11.60	7.47	7.95	140.30	141.50	137.16	126.69–132.64
$ZnCl_2$(Z-OXLME)	10.95	7.63	8.05	142.21–142.35[a]	142.21–142.35[a]	137.26	131.42
$CdCl_2$(Z-OXLME)·H_2O	10.90	7.61	8.00	142.22[a]	142.22[a]	137.28	—[b]

[a] Doublet.
[b] Not detected due to its low solubility.

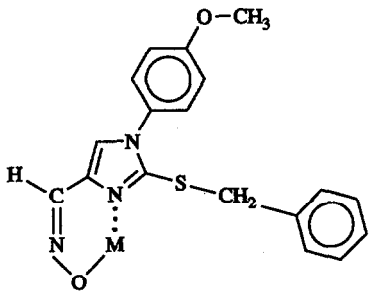

Fig. 1. Structure of the compound Z-OXLME.

the carbon atoms of the imidazolic moiety together with that of C_α oxime, which are of special interest in order to supply information about the coordination pattern of Z-OXLME to the metal ions, are given in Table 2. The assignments were carried out on the basis of those ones for analogous compounds,[11,12] together with the information provided by the DEPT technique.

The colour, analytical data and proposed formulae for the metal complexes are given in Table 3. All of them contain the organic ligand in the neutral form and the metal/organic ligand stoichiometries are either 1/1 (Cu^{II}, Zn^{II}, Cd^{II} and Hg^{II} complexes) or 1/2 (Co^{II}, Ni^{II} and Cd^{II} complexes). The complexes are fairly soluble in water, except copper(II), and ethanol. The hydrated character of $M^{II}Cl_2$(Z-OXLME)·H_2O complexes (M^{II} = Cu, Hg and Cd) was determined from their TG and DSC curves; nevertheless, the accurate determination of dehydration energies has not been possible because the corresponding endothermic effects overlap with the exothermic effects, due to the pyrolysis of the organic ligand in the three hydrated complexes.

The pyrolytic decomposition of Z-OXLME starts at 220°C via an intramolecular dehydration according to the following process:

$$R—HC{=}N—OH \longrightarrow H_2O + R—C{\equiv}N.$$

The complexes show similar thermal behaviour. They start pyrolytic decomposition at the above temperature (except Hg^{II} which starts the pyrolysis at 190°C by the sublimation of $HgCl_2$, as proved by the disappearance of the ν(Cl—Hg) band in the IR spectrum of a sample heated up to the temperature 195°C). The above dehydration process gave rise to the disappearance of the ν(OH) and δ(OH) characteristic bands of the oxime group in the IR spectra of the ligand and their metal complexes. The decompositions of the compounds proceed steadily up to the formation of Co_3O_4, CuO, ZnO and CdO residues. In the case of the mercury(II) complex no residue was found at the end of the pyrolysis, due to the whole sublimation of $HgCl_2$.

Z-OXLME ligand binding mode

IR spectral data of the seven complexes in Table 1 show the shifting at higher wave number values

Table 3. Colour, analytical data (found, calc) and proposed formulae for the complexes

Compound	Colour	C (%)	H (%)	N (%)
$CoCl_2$(Z-OXLME)$_2$	Carmine	53.4 (53.5)	4.2 (4.2)	10.1 (10.4)
$NiCl_2$(Z-OXLME)$_2$	Green	54.8 (53.5)	4.2 (4.2)	10.3 (10.4)
$CuCl_2$(Z-OXLME)·$2H_2O$	Green	42.8 (42.4)	3.2 (4.1)	7.9 (8.2)
$ZnCl_2$(Z-OXLME)	White	46.2 (45.4)	3.7 (3.6)	8.7 (8.8)
$CdCl_2$(Z-OXLME)$_2$	White	50.2 (50.1)	3.9 (3.9)	9.4 (9.7)
$CdCl_2$(Z-OXLME)·H_2O	White	40.4 (40.0)	3.5 (3.5)	7.3 (7.8)
$HgCl_2$(Z-OXLME)·H_2O	White	34.5 (34.4)	3.0 (3.0)	6.5 (6.7)

of the ν(NO) oxime characteristic band, which suggests, in accordance with the literature data,[12,18] that the coordination takes place through the N_{oxime} atom instead of the O_{oxime} atom. This hypothesis is also supported by the increase in wave number of $\nu(C{=}N)_{oxime}$ bands;[12] when the ligand acts as a chelator upon coordination, the possibility of retrodonating metal → ligand bonds gave rise to an increase in the π-electronic delocalization, which is opposed to the above cited expected increase in $\nu(C{=}N)_{oxime}$. This fact would explain the variable increments in the frequency of the above cited band observed in the spectra of the complexes.

From low-frequency IR data no evidence of ν(M—N) bands were obtained, due to the high absorbance of the ligand. Nevertheless, in all cases a new and strong band was observed, which is assignable to the ν(M—Cl) mode which suggests that the chloride ions are directly linked to the metal ions in all the complexes. The presence of only one band for this vibration mode indicates that chloride ligands are probably in *trans* positions.[19]

The IR spectra of those complexes having ligand: metal stoichiometries of 2:1 show in-plane deformation δ(OH) bands characteristic of O···H···O grouping, which suggests probable planar structures in which the interactions between the oxime groups of the two Z-OXLME molecules give rise to the above arrangement.

The NMR spectra of the $CdCl_2$(Z-OXLME) complex could not be obtained with enough resolution because of its poor solubility; that of $HgCl_2$(Z-OXLME)·H_2O, despite its good resolution, is equal to that of free Z-OXLME, due probably to its total dissociation in solution. Thus, only the NMR spectra of $ZnCl_2$(Z-OXLME) and $CdCl_2$(Z-OXLME)·H_2O were available. The assignment of the corresponding signals are summarized in Table 2, together with those of Z-OXLME. The downfield shift of the $C_\alpha H$ signal is due to the deshielding of a hydrogen atom on coordinating N_{oxime} atoms to metal ions, whereas the strong shift to higher field in NOH signals of both complexes can be explained on the basis of a change from the *Z* to the *E* isomer upon coordination to metal ions. This change becomes the breaking of the intramolecular hydrogen bridge interaction characteristic of the *Z* isomers, which produces a strong shielding in the OH hydrogen atom.[20] Finally, the shifting to lower field values in the $C(5)H_{imid}$ signal could be caused by a change in the electronic density of the imidazole moiety, this fact being consistent with the coordination of the $N(3)_{imid}$ atom to the metal ions.

^{13}C NMR data also corroborate this hypothesis; namely, the deshielding of C_α and $C(5)_{imid}$ signals is in accordance with a chelation of the ligand in the *E* isomeric form, through the N(3) atom of the imidazolic ring and the N atom of the oxime group.[10] It is interesting to point out that the deshielding in $C(5)_{imid}$ in Z-OXLME has also been observed upon the protonation of $N(3)_{imid}$.[11]

Thus, the similarity in the IR spectra of all complexes, together with their formulae, suggests that the organic ligand Z-OXLME acts as a chelator, which is linked to the metal ions through the nitrogen atom of the oxime group and the N(3) atom of the imidazolic ring.

Coordination environment of metal ions

The magnetic moment value at room temperature for $CoCl_2$(Z-OXLME)$_2$ complex, 4.80 B.M., is considerably higher than that corresponding to the expected spin-only value for a d^7-system with three unpaired electrons.[12] The existence of an orbital contribution suggests an octahedral arrangement of the two halogen atoms and the two bidentate Z-OXLME molecules, in which the two chlorine atoms, according to far-IR data, are in *trans* positions.

In accordance with this fact, the NIR–vis reflectance spectrum of this complex shows three bands assignable to the three expected transitions in octahedral complexes of cobalt(II) ions;[21] thus, the band at 7.9 kK is assigned to the $^4T_{2g}(F) \leftarrow {}^4T_{1g}$ transition and the two remaining at 13.8 and 18.6 kK (the first one being the weakest) are assigned to $^4A_{2g}(F) \leftarrow {}^4T_{1g}$ and $^4T_{1g}(P) \leftarrow {}^4T_{1g}$ transitions, respectively.

The above IR spectral data of the $NiCl_2$(Z-OXLME)$_2$ complex suggest that the two Cl^- ions are coordinated to nickel(II) in *trans* positions. On the other hand, the magnetic moment at room temperature for this complex is 2.90 B.M., which is in agreement with the expected one for the spin-only moment in a d^8-system with two unpaired electrons.[12] In accordance with this the two bidentate Z-OXLME molecules and the two Cl^- ions could be in a distorted $NiCl_2N_4$ octahedral arrangement. The three expected bands for octahedral complexes of nickel(II), corresponding to $^3T_{1g}(P) \leftarrow {}^3A_{2g}$, $^3T_{1g}(F) \leftarrow {}^3A_{2g}$ and $^3T_{2g}(F) \leftarrow 3A_{2g}$ transitions,[21] appear in the NIR–vis reflectance spectrum of the complex at 27.0, 15.6 and 10.0 kK, respectively. The most probable structure for these cobalt(II) and nickel(II) complexes is shown in Fig. 2.

Spectral data for the $CuCl_2$(Z-OXLME)·$2H_2O$ complex suggest that the two water molecules are not coordinated to the metal ion, whereas the two Cl^- ions are directly bound to copper ions.

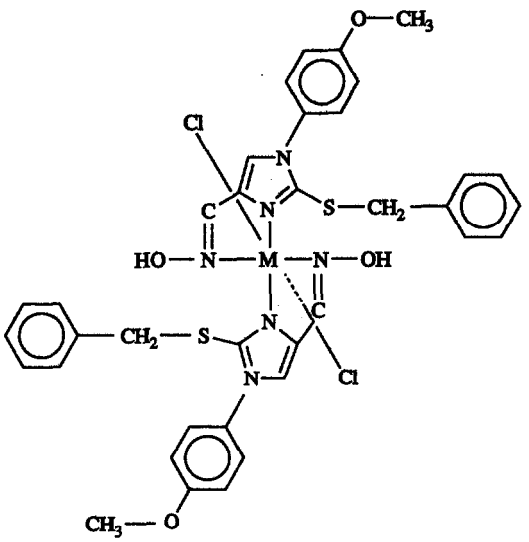

Fig. 2. Structure of $CoCl_2$(Z-OXLME)$_2$, $NiCl_2$(Z-OXLME)$_2$ and $CdCl_2$(Z-OXLME)$_2$ complexes.

All these data suggest a four-coordinated $CuCl_2N_2$ sphere for the metal ion in this complex. The magnetic moment at room temperature, 1.42 B.M., is considerably lower than that expected for the spin-only contribution in a d^9-system;[12,22] this fact suggests a probable antiferromagnetic interaction between copper(II) ions and consequently a planar or distorted tetrahedral arrangement of the four donor atoms around each copper(II) ion. In order to explain this fact magnetic susceptibility values of the complex were measured in the 80–280 K temperature range; the results are presented in Fig. 3, which shows the variation of χ_M and $1/\chi_M$ versus T values.

These data indicate that the complex follows

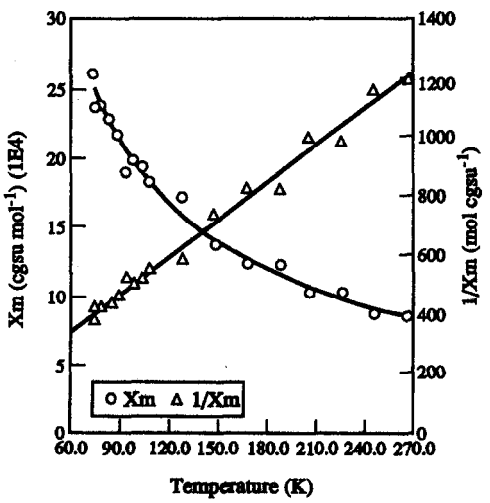

Fig. 3. Variation of χ_M and $1/\chi_M$ vs T for the $CuCl_2$(Z-OXLME)$\cdot 2H_2O$ complex.

Curie–Weiss behaviour in the studied temperature range:

$$1/\chi_M = (T+\theta)/C;$$

$C = 0.242$ cm^3 K mol^{-1}; $\theta = 23.29$ K; $\mu = 1.40 \pm 0.03$ B.M. (r value of $1/\chi_M$ vs T plot = 0.9932).

In order to elucidate if this deviation from Curie's law is due to the existence of temperature-independent paramagnetism (TIP), χ_M observed values have been plotted versus T. The resulting curve has been adjusted, using the ENZFITTER non-linear regression data analysis program (R. J. Leatherbarrow, Elsevier-Biosoft, 1987), to the general equation:

$$\chi_M = \chi_T + \chi_{TIP} = \frac{C}{T+\theta} + \chi_{TIP},$$

in which both temperature-dependent and -independent contributions to the total value of paramagnetism have been taken into account. From this plot (Fig. 3) the following values have been obtained: $\chi_{TIP} = 1.237 \times 10^{-4}$ cm^3 mol^{-1}, $\theta = 9.9$ K and $C = 0.202$ cm^3 K mol^{-1}. The agreement factor of this plot, defined as $\Sigma(\chi_{obs} - \chi_{calc})^2/\Sigma\chi_{obs}^2$, was 1.5×10^{-3}. The θ value indicates this compound displays a Curie behaviour in its temperature-dependent component. Knowing the χ_{TIP} value, the magnetic moment of the Cu^{2+} ion in this complex has been calculated using the molar susceptibility of the compound corrected by both diamagnetic and TIP contributions. The value obtained for the magnetic moment is 1.26 ± 0.03 B.M. This gives a μ_{TIP} value of 0.14 B.M., which is in accordance with the values found in the literature for this magnitude.[22]

The ESR spectrum of $CuCl_2$(Z-OXLME)$\cdot 2H_2O$ shows an isotropic signal at a g value of 2.11. This would suggest the presence of a copper(II) ion in a complex containing grossly misaligned tetragonal axes; this situation being, according to Hathaway and Billing,[23] the most common reason for the observation of an isotropic ESR spectrum. The reflectance spectrum of the complex presents an asymmetric band centred at 12.5 kK which may involve several $d \rightarrow d$ transitions in square-planar or slightly distorted tetrahedral copper(II) complexes.[21]

From exposed experimental data for the complexes $ZnCl_2$(Z-OXLME), $CdCl_2$(Z-OXLME) and $HgCl_2$(Z-OXLME)$\cdot H_2O$, tetrahedral structures, as shown in Fig. 4, can be proposed.

In the $CdCl_2$(Z-OXLME)$_2$ complex, a CdN_4Cl_2 octahedral arrangement of the six donor atoms with the two Cl^- ions in *trans* positions would be expected (see Fig. 2).

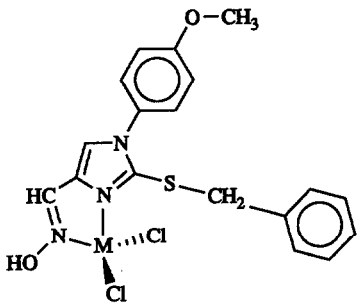

Fig. 4. Structure of $ZnCl_2$(Z-OXLME), $CdCl_2$(Z-OXLME)·H_2O and $HgCl_2$(Z-OXLME)·H_2O complexes.

REFERENCES

1. I. B. Wilson and F. Bergman, *J. Biol. Chem.* 1950, **185**, 479.
2. I. B. Wilson and G. Ginsburg, *Arch. Biochem. Biophys.* 1955, **54**, 570.
3. I. B. Wilson, *Biochem. Biophys. Acta* 1958, **27**, 196.
4. E. J. Poziomek, B. E. Mackley and G. M. Steinberg, *J. Org. Chem.* 1958, **23**, 714.
5. Y. Ashani, H. E. Dery, J. Zahavy, W. Kunberg and S. Cohen, *Isr. J. Chem.* 1985, **3**, 133.
6. K. Takamiya, *Nature* 1960, **185**, 190.
7. K. Klkuchl and M. Matsuzawa, *J. Antibiotics* (*Japan*) 1955, Ser. B, **8**, 170.
8. H. Kamata, *J. Antibiotics* (*Japan*) 1958, Ser. B, **11**, 1.
9. P. O. Lumme and H. O. Elo, *Inorg. Chim. Acta* 1958, **107**, L15 and refs therein.
10. R. López-Garzón, M. A. Romero-Molina, A. Navarrete-Guijosa, J. M. López-González, G. Alvarez-Cienfuegos and M. Herrador-Pino, *J. Inorg. Biochem.* 1990, **38**, 139.
11. M. Herrador-Pino and J. Sáenz de Buruaga, *Anal. Quim.* 1983, **69C**, 99.
12. K. Burger, *Coordination Chemistry. Experimental Methods.* Butterworth, London (1973).
13. R. E. Rundle and M. Parasol, *J. Chem. Phys.* 1952, **20**, 1847.
14. B. Orel, M. Penko and D. Hadzi, *Spectrochim. Acta* 1980, **36**, 859.
15. L. J. Bellamy, *The Infrared Spectra of Complex Molecules*, Vol. 11. Chapman and Hall, London (1980).
16. R. Blinc and D. Hadzi, *Spectrochim. Acta* 1960, **16**, 853.
17. R. Blinc and D. Hadzi, *J. Chem. Soc.* 1958, 4537.
18. M. E. Keeney and K. Osseo-Asare, *Coord. Chem. Rev.* 1984, **59**, 141.
19. R. López-Garzón, D. Gutierrez-Valero, C. Valenzuela-Calahorro, N. Cruz-Pérez and A. García-Rodríguez, *Monat. Chem.* 1987, **118**, 553.
20. R. López-Garzón, D. Gutiérrez-Valero, M. Melguizo-Guijarro, M. Nogueras-Montiel and A. Sánchez-Rodrigo, *Thermochim. Acta*, in press.
21. A. B. P. Lever, *Inorganic Electronic Spectroscopy*, 2nd edn. Elsevier, New York (1986).
22. R. L. Carlin, *Magnetochemistry*. Springer Verlag, New York (1986).
23. B. J. Hathaway and E. Billing, *Coord. Chem. Rev.* 1970, **5**, 143.

Polyhedron Vol. 12, No. 5, pp. 513–522, 1993
Printed in Great Britain

0277–5387/93 $6.00+.00
© 1993 Pergamon Press Ltd

THE CLEAVAGE OF THE N—N BOND OF N,N-DISUBSTITUTED HYDRAZINES ON RHENIUM. THE PREPARATION, REACTIONS AND X-RAY CRYSTAL STRUCTURES OF $[ReCl_2(NH_3)(NNCOC_6H_4\text{-}4\text{-}R)(PPh_3)_2]$ (R = H, —OMe, —NO_2), $[ReCl_3(NNPh_2)(PPh_3)_2]$, $[ReCl_2(N)(NNPh_2)(PPh_3)]$ and $[ReCl(N)(Me_2CNNCOPh)(PPh_3)_2]$†

JONATHAN R. DILWORTH,* PANNA JOBANPUTRA, JOHN R. MILLER and SUZANNE J. PARROTT

Department of Chemistry and Biological Chemistry, University of Essex, Wivenhoe Park, Colchester, Essex CO4 3SQ, U.K.

and

QIN CHEN and JON ZUBIETA

Department of Chemistry, University of Syracuse, Syracuse, NY 13244, U.S.A.

(*Received* 18 *August* 1992; *accepted* 22 *October* 1992)

Abstract—Reaction of the N,O-chelated complexes $[ReCl_2(N_2COC_6H_4\text{-}4\text{-}R)(PPh_3)_2]$ (R = H, Me, NO_2) with N,N- and certain N-substituted hydrazines gave the ammine complexes $[ReCl_2(NH_3)(NNCOC_6H_4\text{-}4\text{-}R)(PPh_3)_2]$ [R = H (**1**), R = Me (**2**), R = NO_2 (**3**)]. The mechanism is believed to involve intermolecular homolytic cleavage of the N—N bond. The X-ray structure of **1** revealed a pseudo-octahedral geometry with *trans*-phosphines. The ammine ligand is *cis* to the benzoyldiazenido group and the ammine hydrogens are hydrogen-bonded to the carbonyl oxygen.

Reaction of $[ReOCl_3(PPh_3)_2]$ with excess $Ph_2NNH_2 \cdot HCl$ in ethanol gave both $[ReCl_3(NNPh_2)(PPh_3)_2]$ (**6**) and $[ReCl_2(N)(NNPh_2)(PPh_3)]$ (**7**). In the presence of base the rhenium(VII) cation $[ReCl_2(NNPh_2)_2(PPh_3)]^+$ was formed. The geometry of **7** was shown by X-ray structural determination to be a distorted square-based pyramid, with the nitride in the apical position. Attempted derivatization of **7** led to N—N bond cleavage and the generation of nitrido complexes.

The nitrido complex $[ReCl(N)(Me_2CNNCOPh)(PPh_3)_2]$ (**8**) was unexpectedly formed in the reaction of $[ReOCl_3(PPh_3)_2]$ with $Me_2C{=}NNHCOPh$ in ethanol in the presence of HCl. The X-ray crystal structure of **8** showed a pseudo-octahedral geometry with the nitride ligand *trans* to the oxygen of the N,O-chelated hydrazonato(1-) ligand. The possible mechanisms of N—N bond cleavage are discussed.

Despite intensive investigations, the exact details of the N—N bond cleavage step in the protonation of coordinated dinitrogen remain obscure.[1] The cleavage of the N—N bond of hydrazines on reaction with metals can be viewed as a possible model for this step and many examples have been reported. One of the most intensively investigated systems has involved the reactions of hydrazine or phenylhydrazine hydrochlorides with $[ReOCl_3(PPh_3)_2]$ to give $[ReCl_2N(PPh_3)_2]$ and $[NH_4]Cl$ or $PhNH_2 \cdot HCl$, respectively. Ethanol was shown to be essential and $[ReO(OEt)Cl_2(PPh_3)_2]$ is a key intermediate.[2] Superficially, the reaction is a condensation-type process and might be expected to involve intermediates such as $Re{=}NNH_2$.

* Author to whom correspondence should be addressed.

† Benzoyldiazenidodichloro(ammine)dichlorobis(triphenylphosphine)rhenium(III); dichlorodiphenylhydrazido(2-)nitridotriphenylphosphinerhenium(VII); chloronitridoacetonebenzoylhydrazonato(1-)bistriphenylphosphinerhenium(V).

However, additional PPh_3 is required and triphenylphosphine oxide can be identified in the reaction mixture.[3] It therefore appears possible that the reaction proceeds via oxygen abstraction with PPh_3 and halide metathesis to give species such as $[ReCl_2(NHNH_2)(PPh_3)_2]$. Here we report three further examples of N—N bond cleavage on rhenium under a variety of circumstances and discuss the mechanisms involved.

RESULTS AND DISCUSSION

The formation of $[ReCl_2(NH_3)(NNCOC_6H_4\text{-}4R)(PPh_3)_2]$ [R = H (**1**), Me (**2**), NO_2 (**3**)]

It has previously been reported that the reaction of the chelated derivative $[ReCl_2(N_2COPh)(PPh_3)_2]$[3] with benzoylhydrazine under relatively dilute conditions gives $[ReCl_2(NNHCOPh)(NHNHCOPh)(PPh_3)_2]$. The identity of the product as a hydrazido(2-) hydrazido(1-) complex was confirmed by an X-ray structure determination.[12] We have had some difficulty in repeating this reaction, and now report the surprizing observation that when this reaction is carried out at higher concentrations, the ammonia complex $[ReCl_2(NH_3)(NNCOPh)(PPh_3)_2]$ is formed rapidly in quantitative yield. This occurs both on reaction with benzoylhydrazine and certain other N- and N,N-substituted hydrazines of the types $RNHNH_2$ (R = Me, Ph) and R_2NNH_2 (R_2 = MePh, Me_2, Ph_2). The NH_3 complex is directly analogous to $[ReCl_2(NH_3)(NNPh)(PMe_2Ph)_2]$, formed by reaction of $[ReCl_3(PMe_2Ph)_3]$ with $PhNHNH_2$.[4]

The reaction of $[ReCl_2(NNCOPh)(PPh_3)_2]$ with hydrazines proceeds rapidly in dichloromethane or toluene in air or under dinitrogen, and yields of the ammonia complex are consistently $\geq 90\%$.[5] Monitoring of the reaction in benzene by ^{31}P NMR revealed a relatively short-lived intermediate and the reaction is essentially complete in less than 2 min at room temperature. It appears very likely that this intermediate is of the type $[ReCl_2(H_2NNR_2)(NNCOPh)(PPh_3)_2]$, since the chelated complex $[ReCl_2(NNCOPh)(PPh_3)_2]$[3] is known to undergo facile ring opening reactions with Lewis bases such as MeCN to give benzoyldiazenido complexes of the type $[ReCl_2(NCMe)(NNCOPh)(PPh_3)_2]$.[3]

The formation of ammonia from the proposed hydrazide intermediate requires two electrons and two protons. There is, however, no obvious source of electrons as the reaction proceeds in a high overall yield. If the metal or the hydrazine were providing the electrons the yields would have to be much lower at the 1:1 stoichiometry. We accordingly suggest that the N—N bond cleavage reaction occurs *homolytically* with the formation of rhenium(IV), $[ReCl_2(NH_2)(NNCOPh)(PPh_3)_2]$, and an N-based radical such as HNCOPh. Analysis of the organic by-products, from the reaction with $MePhNNH_2$, revealed the presence of $MeC_6H_4NH_2$. The formation of the aniline we propose is from the radical scavenging of a hydrogen radical by the aniline radical. We also note the formation of other organonitrogen species by GLC, which is consistent with the radical mechanism. Further support for the concept of homolytic N—N bond cleavage comes from the greater ease of N—N bond cleavage found for Ph_2NNH_2, where the Ph_2N radical has higher stability.

We have also observed that the cleavage of the N—N bond of the 1-arylhydrazines $4\text{-}RC_6H_4NHNH_2$ on reaction with $[ReCl_2(NNCOPh)(PPh_3)_2]$ is markedly dependent on the nature of R. With R = H, or an electron-withdrawing substituent such as $4\text{-}NO_2$, then N—N bond cleavage occurs rapidly to give the ammonia complex **7**. However, when the substituent is electron donating (Me, MeO), then the N—N bond is retained and the hydrazidodiazenido complexes $[ReCl_2(NNH_nCOPh)(NNH_mAr)(PPh_3)_2]$ ($n, m = 0$ or 1) appear. NMR and IR spectroscopy do not distinguish between the proton being located on the PhCONN or PhNN fragments. In view of the relatively greater basicity of the ArN nitrogen, this seems to be the most probable location for the hydrogen. These reactions serve to emphasize further the relatively subtle factors that determine whether N—N bond cleavage occurs, and an understanding of these is particularly important in the context of the design of radiopharmaceuticals incorporating hydrazide and diazenide fragments. Further details of the benzoyldiazenidoarylhydrazide complexes will be published elsewhere.

Spectroscopy alone was unable to distinguish whether complexes **1**, **2** and **3** were $[ReCl_2(NH)(NNCOC_6H_4\text{-}4\text{-}R)(PPh_3)_2]$ or the ammonia complexes. The IR spectra all showed a band at 1575 cm^{-1} characteristic of the benzoyldiazenide ligand, and a sharp band at *ca* 3200 cm^{-1}, due to ν(N—H). The N—H protons appeared as a very broad singlet at 3.20 ppm in the ^1H NMR spectrum, and the peak width made accurate integration difficult. Accordingly, a single-crystal X-ray structure determination of complex **1** was undertaken.

Structure of $[ReCl_2(NH_3)(NNCOPh)(PPh_3)_2]\cdot Et_2O$ (**1**)

A perspective view of the structure of complex **1** appears in Fig. 1, and some selected bond lengths

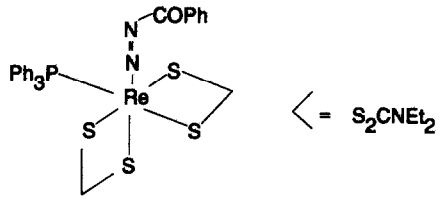

Fig. 1. Proposed structures of the complexes of the type $[Re(NNCOAr)(S_2CNEt_2)_2(PPh_3)]$ (Ar = phenyl or 4-substituted phenyl group).

and angles are given in Table 1. The overall geometry about the rhenium is best described as pseudo-octahedral, with the bulky PPh_3 ligands occupying *trans* sites. The chloride ligands are *trans* to the nitrogen ligands and the Re—Cl distances are unexceptional. The Re—N—N angle is 178(1)°, which, when coupled with the Re—N(1) distance of 1.77(1) Å, indicates that the diazenide ligand is functioning as a three-electron donor. The Re—N(3) bond length of 2.16(1) Å is typical for a metal ammonia complex, and the N(3)—O(1) distance of 2.89(2) Å is indicative of a strong hydrogen-bonding interaction between the ammonia hydrogens and the carbonyl oxygen.

Table 1. Table of selected bond distances (Å) and angles (°) of **1**

Re—Cl(1)	2.439(5)
Re—Cl(2)	2.419(5)
Re—P(1)	2.457(5)
Re—P(2)	2.473(5)
Re—N(1)	1.77(2)
Re—N(3)	2.16(2)
N(1)—N(2)	1.24(2)
Cl(1)—Re—Cl(2)	92.0(2)
Cl(1)—Re—P(1)	92.0(2)
Cl(1)—Re—P(2)	89.5(2)
Cl(1)—Re—N(1)	98.2(4)
Cl(1)—Re—N(3)	172.9(4)
Cl(2)—Re—P(2)	88.2(2)
Cl(2)—Re—N(1)	169.8(5)
Cl(2)—Re—N(3)	80.9(4)
P(1)—Re—P(2)	176.4(2)
P(1)—Re—N(1)	91.1(5)
P(1)—Re—N(3)	88.8(4)
P(2)—Re—N(1)	92.0(5)
P(2)—Re—N(3)	89.4(4)
N(1)—Re—N(3)	88.9(6)
Re—N(1)—N(2)	177.0(1)

Substitution reactions of **1**, **2** *and* **3**

Sodium diethyldithiocarbamate reacts readily with **1**, **2** or **3** to give the brown crystalline complexes $[Re(NNCOC_6H_4\text{-}4\text{-}R)(S_2CNEt_2)_2(PPh_3)]$ in high yield. The ^1H NMR spectrum of each complex shows four triplets for the dithiocarbamate CH_3 protons, suggesting that the complexes have a structure with *cis*-dithiocarbamato-ligands (Fig. 2). The observation of two different environments for the

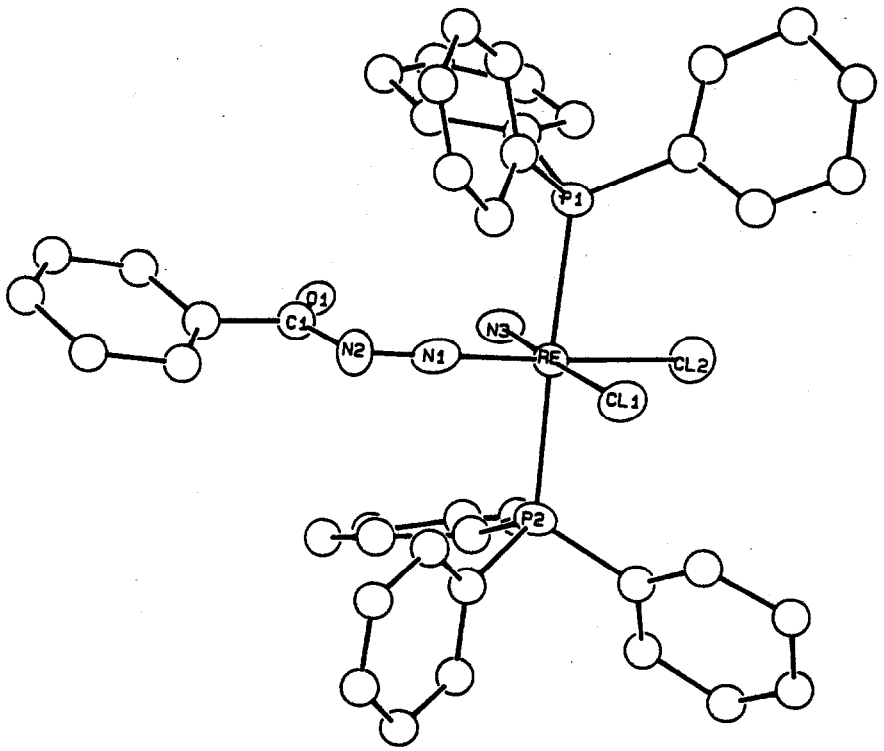

Fig. 2. A perspective view of the structure of $[ReCl_2(NH_3)(NNCOPh)(PPh_3)_2]$, showing the atom labelling scheme.

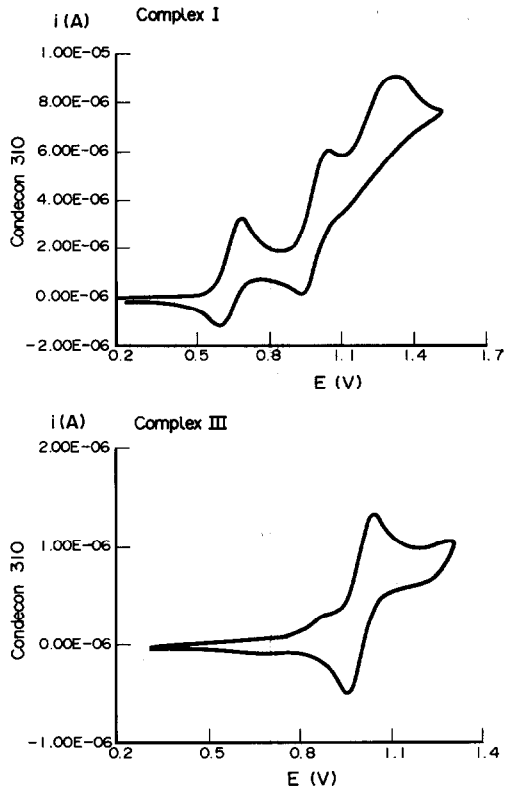

Fig. 3. Cyclic voltammograms for $[ReCl_2(NH_3)(NNCOPh)(PPh_3)_2]$ and $[ReCl_2(NNCOC_6H_4\text{-}4\text{-}NO_2)(PPh_3)_2]$. Recorded at room temperature in CH_2Cl_2 at a platinum wire auxiliary electrode and silver wire pseudo-reference electrode.

dithiocarbamate ligands confirms that the complexes are not fluxional at room temperature.

Electrochemistry of complexes **1** *and* **3**

The cyclic voltammogram of complex **1** (Fig. 3) was recorded at room temperature in dichloromethane solution at a platinum wire working electrode with 0.2 M $[Bu^n_4N][BF_4]$ as the supporting electrolyte. Potentials are quoted relative to the ferrocene–ferrocenium couple, taken as 0.0 V, and details are quoted in Table 2. The complex shows three one electron oxidation processes, the first two appearing reversible and the last irreversible. The oxidations correspond to the formation of a rhenium(IV) monocation, a rhenium(V) dication and a rhenium(VI) trication.

The introduction of the 4-NO_2 group in complex **3** causes a profound shift in potentials and a single reversible one-electron oxidation at $E_{1/2} = +0.56$ V occurs. This corresponds to the formation of a monocationic rhenium(IV) species. The electron-withdrawing 4-NO_2 group raises the potential for the second and third oxidation beyond the observable range. There are a number of reduction processes associated with the NO_2 group which were not analysed further. Attempts to monitor the reaction by cyclic voltammetry were not successful as the reaction was too fast in the accessible temperature range.

Reaction of $[ReOCl_3(PPh_3)_2]$ *with* 1,1-*diphenylhydrazine*

Two products were obtained on reaction of $[ReOCl_3(PPh_3)_2]$ with an excess of diphenylhydrazine hydrochloride in methanol under reflux. The first is a rather insoluble orange precipitate of the rhenium(V) complex $[ReCl_3(NNPh_2)(PPh_3)_2]$ (**6**) in 42% yield. The yellow filtrate gave yellow crystalline rhenium(VII), $[ReCl_2(N)(NNPh_2)(PPh_3)]$ (**7**), in 30% yield on reduction in volume and addition of diethyl ether. By contrast, we showed earlier[6] that reaction of $[ReOCl_3(PPh_3)_2]$ with $PhMeNNH_2$ gave $[ReCl_2(NNMePh)_2(PPh_3)]^+$, and here the analogous complex $[ReCl_2(NNPh_2)_2(PPh_3)]^+$ (**8**) is formed only when $Ph_2NNH_2 \cdot HCl$ is used in the presence of Et_3N. This confirms that the N—N bond cleavage reaction is highly pH sensitive. The fact that it

Table 2. Cyclic voltammetry of the complexes $[ReCl_2(NH_3)(NNCOC_6H_4\text{-}4\text{-}R)(PPh_3)_2]$ (R = H, NO_2)

Process	i_{pa}/i_{pc}	E_{pa} (V)[a]	E_{pc} (V)[a]	ΔE_p (mV)	$E_{1/2}$ (V)
$[ReCl_2(NH_3)(NNCOPh)(PPh_3)_2]$					
Oxidation 1	1.05	+0.04	−0.03	70	+0.00
Oxidation 2	0.98	+0.33	+0.27	60	+0.30
Oxidation 3	—	+0.53	—	—	—
$[ReCl_2(NH_3)(NNCOC_6H_4NO_2)(PPh_3)_2]$					
Oxidation 1	1.01	+0.60	+0.52	80	+0.56

[a] All potentials are quoted relative to the ferrocenium/ferrocene couple taken as 0.0 V. Ferrocene was added to the cell for each measurement. Scan rate: 0.2 V s^{-1}.

does not occur in the presence of base strongly suggests that in this instance the cleavage occurs by electron transfer from the metal and protonation. A rhenium(V) intermediate such as $[ReCl_2(NNPh_2)(NHNPh_2)(PPh_3)_2]$ seems likely. All these complexes showed the expected mass ion in their FAB mass spectra.

We have also observed that the N—N bond of complex **6** is cleaved readily on attempted metathesis reactions. Thus, reaction of **6** with sodium diethyl dithiocarbamate results in a near quantitative yield of the known $[ReN(S_2CNEt_2)_2]$. The source of electrons for the cleavage of the N—N bond are not clear, but it could be the dithiocarbamate anion. However, we cannot entirely rule out that this system involves a similar homolytic bond cleavage reaction to that discussed in the last section.

Structure of $[ReCl_2(N)(NNPh_2)(PPh_3)]$ **(7)**

There are very few examples of the nitride ligand occurring in combination with other multiply-bonded ligands and those that are known generally involve oxo-ligands (e.g. $[OsO_3N]^{3-}$).[6] Accordingly, a single-crystal X-ray structural determination of complex **7** was undertaken and a perspective view of the structure appears in Fig. 4, together with a partial atom labelling scheme. Selected bond lengths and angles appear in Table 3. The structure can be compared to the recently reported $[Tc_2N_2(N_2Ph_2)(2,4,6\text{-}Pr^i_3C_6H_2S)_4]\cdot 0.5(C_2H_5)_2O$.[7]

The structure, as for the technetium complex, is best described as distorted square-based pyramid with the nitride ligand at the apex. The metal–nitride distance of 1.653(5) Å [technetium complex 1.64(1) Å] lies within the range normally found for terminal metal nitrido complexes.[8] The diphenylhydrazido(2-) ligand occupies a basal site and is

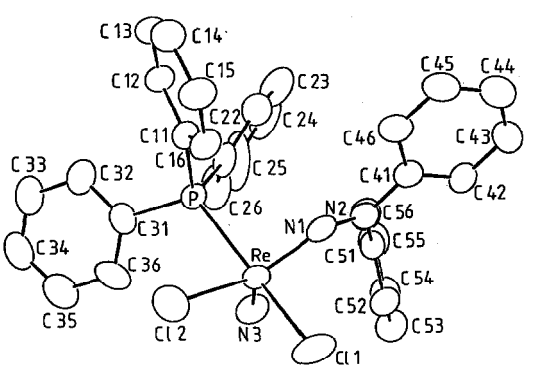

Fig. 4. A perspective view of the structure of $[ReCl_2N(NNPh_2)(PPh_3)_2]$, together with an atom labelling scheme.

Table 3. Table of selected bond distances (Å) and angles (°) of **7**

Re—Cl(1)	2.396(2)
Re—Cl(2)	2.388(2)
Re—P	2.445(1)
Re—N(1)	1.837(5)
Re—N(3)	1.653(5)
N(1)—N(2)	1.280(6)
N(2)—C(41)	1.437(7)
N(2)—C(51)	1.455(7)
Cl(1)—Re—Cl(2)	84.46(6)
Cl(1)—Re—P	161.78(5)
Cl(1)—Re—N(1)	89.2(1)
Cl(1)—Re—N(3)	104.2(2)
Cl(2)—Re—P	84.21(5)
Cl(2)—Re—N(1)	140.0(2)
Cl(2)—Re—N(3)	112.4(2)
P—Re—N(1)	90.4(1)
P—Re—N(3)	93.3(2)
N(1)—Re—N(3)	107.5(2)
Re—N(1)—N(2)	142.9(4)

significantly bent at N(1) [Re—N(1)—N(4) angle = 142.9(4)°, average Tc—N—N angle 140.4(4)°]. This suggests the hydrazide ligand is functioning as a two-electron donor and this is supported by the Re—N(1) distance of 1.837(5) and N(1)—N(2) distance of 1.280(6) Å. This compares with Tc—N 1.87(1) and 1.89(1) Å and N—N 1.25(1) and 1.24(2) Å for $[Tc_2N_2(N_2Ph_2)(2,4,6\text{-}Pr^i_3C_6H_2S)_4]$. For $[Re(NNMePh)_2(S_2CNMe_2)_2]^+$[5] the Re—N and N—N distances are 1.78 and 1.30 Å, where each hydrazido(2-) ligand is virtually linear and formally donating four electrons. The 18-electron rule is not invariably useful for predicting the bonding of hydrazide ligands, and in this case an 18-electron configuration would require the hydrazide to be a four-electron donor. The strongly π-donating nitride ligand competes for the empty metal orbitals and prevents donation of the lone pair on N(1).

The preparation of $[ReCl(N)(Me_2CNNCOPh)(PPh_3)_2]$ **(8)**

We have previously shown that reaction of $[ReOCl_3(PPh_3)_2]$ with $PhCONHNH_2$ in acetone gives the complex $[ReOCl_2(Me_2CNNCOPh)(PPh_3)]$ with a chelated benzoyl hydrazonato(1-) ligand.[3] If, however, $[ReOCl_3(PPh_3)_2]$ is reacted with $Me_2C{=}NNHCOPh$ in ethanol in the presence of dilute HCl, the orange nitrido complex $[ReCl(N)(Me_2NNCOPh)(PPh_3)_2]$ is formed in high yield. The reaction presumably involves partial hydrolysis of the hydrazone to the free hydrazine and subsequent N—N bond cleavage to give the nitride. This reaction of the hydrazone is in interesting con-

trast to the reaction of PhNHNHCOPh, which under related conditions undergoes N—N bond cleavage to form the imide $[ReCl_3(NPh)(PPh_3)_2]$ in high yield.[9]

Structure of $[ReClN(Me_2CNNCOPh)(PPh_3)_2]$ (**8**)

A perspective view of the structure of complex **8** appears in Fig. 5, together with a partial atom labelling scheme and some selected bond lengths and angles are given in Table 4. The geometry about the rhenium is pseudo-octahedral with *trans*-phosphine ligands. The metal–nitride distance of 1.662(6) Å is typical for rhenium(V) nitrido-complexes, and the metal–chlorine and metal–phosphorus distances are unremarkable. The bond distances within the hydrazonato ligand confirm the loss of the proton on N(3). The C(1)—N(3) distance of 1.30(1) Å is typical for a C=N bond.

Table 4. Table of selected bond distances (Å) and angles (°) in **8**

Re—Cl	2.413(2)
Re—P(1)	2.478(2)
Re—P(2)	2.476(2)
Re—O	2.166(5)
Re—N(1)	1.662(6)
Re—N(2)	2.153(6)
N(2)—N(3)	1.433(8)
N(2)—C(2)	1.297(9)
C(1)—O(1)	1.298(8)
Cl—Re—P(1)	87.77(2)
Cl—Re—P(2)	88.00(7)
Cl—Re—O	87.7(1)
Cl—Re—N(1)	101.1(2)
Cl—Re—N(2)	161.4(2)
P(1)—Re—P(2)	168.35(7)
P(1)—Re—O	85.0(1)
P(1)—Re—N(1)	95.5(2)
P(1)—Re—N(2)	91.1(2)
P(2)—Re—O	84.0(1)
P(2)—Re—N(1)	171.2(2)
O—Re—N(1)	73.7(2)
N(1)—Re—N(2)	97.5(3)
Re—O—Cl	113.8(4)
Re—N(2)—N(3)	115.1(4)

EXPERIMENTAL

All manipulations were carried out under an inert atmosphere of dry dinitrogen gas unless stated

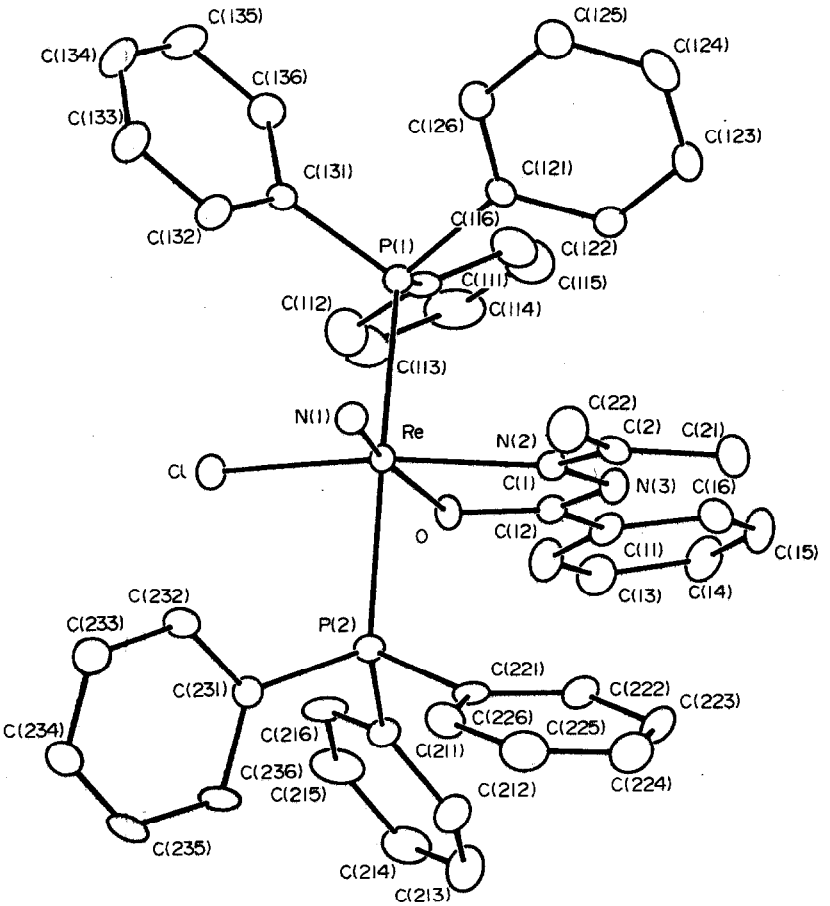

Fig. 5. A perspective view of the structure of $[ReCl(N)(Me_2C{=}NNCOPh)(PPh_3)_2]$, together with an atom labelling scheme.

otherwise. Standard Schlenk-tube, vacuum-line and syringe techniques were employed throughout where appropriate. Elemental analyses were performed by Medac Ltd, University of Brunel. IR spectra were measured in the range 200–4000 cm^{-1} as Nujol mulls (KBr plates) on a Perkin–Elmer 1330 IR spectrometer. ^1H NMR and $^{31}P\{^1H\}$ NMR spectra were measured using a JEOL EX270 spectrometer. Fast-atom bombardment mass spectra were obtained from the SERC service at University College of Swansea, using either thioglycerol or 3-nitrobenzyl alcohol (3-NOBA) as matrix materials. All isotope distributions were compared to a computer generated distribution pattern written by one of us (J.R.M.). HPLC measurements were taken using a Gilson model 702 isocratic HPLC system fitted with a poly(styrene-divinylbenzene) copolymer column and UV detection module HM Holochrome (set at 250 nm). UV studies were performed on a Phillips PU8730 spectrophotometer in dried dichloromethane using quartz cells. Methanol and dichloromethane were dried by standard methods.[10] All other materials and reagents were obtained commercially (Aldrich, Fisons) and used without further purification. $[ReOCl_3(PPh_3)_2]$[11] and $[ReCl_2(N_2COPh)(PPh_3)_2]$[12] were prepared from rhenium metal using the published procedures.

Cyclic voltammetry measurements were made at 200 K using an EG and G PAR model 362 scanning potentiostat linked to a PC with a Condecon 310 interface and software. A three-electrode cell configuration was used, with a platinum wire working electrode, platinum wire secondary electrode and a silver wire pseudo-reference electrode. The solvent was dichloromethane with 0.2 M tetrabutylammonium tetrafluoroborate as the supporting electrolyte. Potentials are quoted relative to the ferrocene/ferrocenium couple in the same system.

Preparation of $[ReCl_2(NH_3)(N_2COPh)(PPh_3)_2]$ **(1)**

$[ReCl_2(N_2COPh)(PPh_3)_2]$ (0.3 g, 0.4 mmol) and $MePhNNH_2$ (0.2 cm^3, 1.7 mmol) were heated under reflux in ethanol (20 cm^3) for 30 min. The emerald green suspension changed to a dark brown solution with the presence of an olive green solid, which was filtered off and washed with diethylether and dried *in vacuo*. The olive green product was recrystallized from CH_2Cl_2/Et_2O; yield 0.24 g, 80%. The reaction proceeds equally well at room temperature. IR (KBr): 1510, 1610 cm^{-1} (NNCOPh ligand). ^1H NMR ($CDCl_3$): 3.7 ppm [3H, s, br, NH_3], 7.2–7.9 ppm [35H, multiplet, phenyl H]. $^{31}P\{^1H\}$ NMR ($CDCl_3$): 0.46 ppm (singlet). Found: C, 55.6; H, 4.1; N, 4.4. Calc. for $ReC_{43}H_{35}N_3Cl_2P_2O_2$: C, 55.4; H, 4.1; N, 4.5%. FAB mass spectrum *m/z* (%): (932, 8), $[ReCl_2(NH_3)(N_2COPh)(PPh_3)_2]^+$ (915, 10), $[ReCl_2(N_2COPh)(PPh_3)_2]^+$.

Preparation of $[ReBr_2(NH_3)(N_2COPh)(PPh_3)_2]$

$[ReBr_2(N_2COPh)(PPh_3)_2]$ (0.3 g, 0.3 mmol) and $MePhNNH_2$ (0.2 cm^3, 1.6 mmol) were heated under reflux in ethanol (20 cm^3) for 30 min. The emerald green suspension changed to a dark brown solution with the presence of an olive green solid, which was filtered off, washed with diethylether and dried *in vacuo*. The olive green product was recrystallized from CH_2Cl_2/Et_2O; yield 0.18 g, 55%. IR, ^1H and ^{31}P NMR as for complex **1**. Found: C, 50.6; H, 3.9; N, 4.2. Calc. for $ReC_{43}H_{35}N_3Br_2P_2O_2$: C, 50.6; H, 3.8; N, 4.1%.

Preparation of $[ReCl_2(NH_3)(N_2COC_6H_4\text{-}OMe)(PPh_3)_2]$ **(2)**

Reaction of $[ReCl_2(NH_3)(N_2COC_6H_4\text{-}OMe)(PPh_3)_2]$ (0.2 g, 0.2 mmol) with $MePhNNH_2$ (0.1 cm^3, 1.2 mmol) as above yielded the ammine/4-OMe-benzoyldiazenido complex; yield 0.16 g, 70%. IR: 1510, 1610 cm^{-1} (NNCOPh ligand). ^1H NMR ($CDCl_3$): 3.7 [3H, s, br, NH_3], 7.2–7.9 [35H, multiplet, phenyl H], 3.8 ppm [3H, s, OCH_3]. $^{31}P\{^1H\}$ NMR ($CDCl_3$): 0.46 ppm (singlet). ^{13}C NMR ($CDCl_3$): 170.4 [*C*—O] and 55.2 ppm [O*C*H_3]. Found: C, 54.8; H, 4.7; N, 4.1. Calc. for $ReC_{44}H_{36}N_3Cl_2P_2O_2$: C, 54.9; H, 4.2; N, 4.4%. FAB mass spectrum, *m/z* (%): (963, 10), $[ReCl_2(NH_3)(N_2COC_6H_4\text{-}OMe)(PPh_3)_2]^+$; (781, 27), $[ReCl_2(PPh_3)_2]^+$; (519, 24), $[ReCl_2(PPh_3)^+$; (263, 100), $[PPh_3]^+$.

Preparation of $[ReCl_2(NH_3)(N_2COC_6H_4\text{-}4\text{-}NO_2)(PPh_3)_2]\cdot H_2O$ **(3)**

Reaction of $[ReCl_2(N_2COC_6H_4\text{-}4\text{-}NO_2)(PPh_3)_2]$ (0.2 g, 0.3 mmol) with $MePhNNH_2$ (0.2 g, 2.6 mmol) as above yielded the ammine/4-NO_2 benzoyldiazenide complex, yield 0.14 g, 58%. IR: 1510, 1610 (NNCOPh ligand), 1160 and 850 cm^{-1} (NO_2). ^1H NMR ($CDCl_3$): 4.0 [3H, br, s, NH_3], 7.2–8.4 ppm [35H, multiplet, phenyl H]. $^{31}P\{^1H\}$ NMR ($CDCl_3$): −0.55 ppm (singlet). Found: C, 51.4; H, 3.8; N, 5.7. Calc. for $ReC_{43}H_{36}N_4Cl_2P_2O_4$: C, 51.9; H, 3.9; N, 5.6%. FAB mass spectrum, *m/z* (%): (976, 40), $[ReCl_2(NH_3)(N_2COC_6H_4\text{-}NO_2)(PPh_3)_2]$; (924, 15), $[ReCl_2(N_2COC_6H_4\text{-}NO_2)(PPh_3)_2]^+$; (781, 100), $[ReCl_2(PPh_3)_2]^+$.

Preparation of $[Re(S_2CNEt_2)_2(N_2COPh)(PPh_3)]$ **(4)**

$[ReCl_2(NH_3)(N_2COPh)(PPh_3)_2]$ (0.3 g, 0.3 mmol) and NaS_2CNEt_2 (0.3 g, 1.6 mmol) were heated under reflux in ethanol (20 cm^3) for 1 h. The green suspension gave way to a dark brown solution and a brown solid, which was filtered off and washed with diethylether. IR: 1620 (dithiocarbamate C—N) and 1580, 1490 cm^{-1} (NNCOPh). ^1H NMR ($CDCl_3$): 0.8–1.4 [CH_3, 3t, 12H], 3.0–4.0 ppm [CH_2, m, 8H]. $^{31}P\{^1H\}$ NMR ($CDCl_3$): 16.6 ppm (singlet). $^{13}C\{^1H\}$ NMR ($CDCl_3$): 12 [CH_3, 4], 43–44 [CH_2, 4 singlets], 127–135 [phenyl], 171.7 [CS_2] and 203.8 ppm [CO]. Found: C, 47.6; H, 4.6; N,

Table 5. Summary of experimental details for the X-ray crystal structures of $[ReCl_2(NH_3)(NNCOPh)(PPh_3)_2]\cdot Et_2O$ **(1)**, $[ReCl_2(N)(NNPh_2)(PPh_3)]$ **(7)** and $[ReNCl(Me_2CNNCOPh)(PPh_3)_2]$ **(8)**

(a) Crystal parameters at 298 K			
Compound	**1**	**7**	**8**
a (Å)	18.528(3)	13.937(3)	15.291(3)
b (Å)	22.932(3)	9.774(1)	11.550(2)
c (Å)	10.455(2)	20.400(5)	23.137(6)
α (°)	90	90	90
β (°)	90	91.16(1)	94.53(2)
γ (°)	90	90	90
V (Å)	4438(1)	2778(1)	4073(2)
Space group	$P2_12_12_1$	$P2_1/c$	$P2_1/c$
P_{calc} (g cm^{-3})	1.505	1.711	1.486
$F(000)$	2024	1400	na
Z	4	4	4
Mr	$C_{43}H_{38}N_3OP_2Cl_2Re$	$C_{30}H_{25}N_3PCl_2Re$	$C_{46}H_{41}N_3OP_2ClRe$
(b) Measurement of intensity data			
Compound	**1**	**7**	**8**
Crystal dimensions (mm)	0.1 × 0.2 × 0.3	0.2 × 0.4 × 0.5	0.2 × 0.3 × 0.3
Instrument	Rigaku AFC5S	Enraf-Nonius CAD4	Rigaku AFC5S
Radiation	Mo-K_α	Mo-K_α	Mo-K_α (λ = 0.71073 Å)
Scan rate (° min^{-1})	8	1.3–5.5	6
Scan mode	ω–2θ	ω–2θ	ω–2θ
Scan length	1.5 + 0.35 tan θ	1.2 + 0.34 tan θ	1.5 + 0.35 tan θ
Scan range	$2\theta < 55°$	$2\theta < 50°$	$2\theta < 55°$
No. of reflections collected	5677	5152	5755
No. of reflections used in solution $F > 3\sigma(F_0)$:	3446	4213	4063

(c) Reduction of intensity data and summary of structure solution and refinement.
Data corrected for background attenuators, Lorentz and polarization factors in the usual fashion.
Structure solution: Patterson method yielded the heavy atom positions. All remaining non-hydrogen atoms were located via standard Fourier techniques. Neutral atom scattering factors were used throughout the analysis.

Final discrepancy factors:			
Compound	**1**	**7**	**8**
R	0.055	0.034	0.031
Rw	0.058	0.043	0.037
Goodness-of-fit	1.63	1.67	1.49

(d) References
ORTEP[13]
Structure solution methods: PHASE,[14] DIRDIF.[15]
Least squares:
Function minimized: $\Sigma w(|F_o| - |F_c|)^2$
Where $w = 4F_o^2/s^2(F_o^2)$
$s^2(F_o^2) = [S^2(C + R^2B) + (pF_o^2)^2Lp^2$
S = Scan rate, C = Total integrated peak count, R = ratio of scan time to total background counting time, B = total background count, Lp = Lorentz polarization factor, p = p-factor.
Standard deviation of an observation of unit weight:
$[\Sigma w(|F_o| - |F_c|)^2/(N_o - N_v)]^{1/2}$
Where: N_o = number of observations, N_v = number of variables.
For other crystallographic data see refs 16, 17, 18 and 19.

6.3. Calc. for $ReC_{35}H_{50}N_4S_4P_1O_1$: C, 47.6; H, 4.7; N, 6.2%.

Preparation of $[Re(S_2CNEt_2)_2(N_2COC_6H_4$-4-OMe)$(PPh_3)]$ **(5)**

$[ReCl_2(NH_3)(N_2COC_6H_4$-4-OMe$)(PPh_3)_2]$ (0.3 g, 0.3 mmol) and NaS_2CNEt_2 (0.3 g, 1.6 mmol) were reacted as above, yield 0.25 g, 89%. IR: 1500, 1610 (NNCOPh) and 1595 cm^{-1} (dithiocarbamate C—N). ^1H NMR ($CDCl_3$): 3.8 [OCH_3, s, 3H], 0.8–1.4 [CH_3, t, 12H], 3.0–4.0 [CH_2, m, 8H] and 6.7–7.7 ppm [phenyl, m, 15H]. $^{31}P\{^1H\}$ ($CDCl_3$): 16.9 ppm (singlet). $^{13}C\{^1H\}$ ($CDCl_3$): 12 [CH_3, 3], 43–44 [CH_2, 4 singlets], 55.2 [OCH_3], 203.9 [CO, 152.7, 162.1 [NCS], 110–140 ppm [phenyl]. Found: C, 47.3; H, 4.6; N, 6.0. Calc. for $ReC_{36}H_{53}N_4S_4P_1O_2$: C, 47.6; H, 4.7; N, 6.2%.

Preparation of $[ReCl_3(NNPh_2)(PPh_3)_2]$ **(6)** and $[ReCl_2(N)(NNPh_2)(PPh_3)]$ **(7)**

$[ReOCl_3(PPh_3)_2]$ (0.4 g, 0.5 mmol) and $Ph_2NNH_2 \cdot HCl$ (0.5 g, 2.4 mmol) were heated under reflux in methanol (40 cm^3) for 1 h. The resulting orange solid was filtered off and washed with Et_2O. The filtrate was reduced to *ca* 20 cm^3 and left overnight, and the resulting dark yellow crystals were filtered and washed with Et_2O; yield of orange solid, $[ReCl_3(NNPh_2)(PPh_3)_2]$, 0.2 g, 42%. IR: 1580 cm^{-1} (N=N). ^1H NMR ($CDCl_3$): 6.4–8.2 ppm [m, phenyl H]. $^{31}P\{^1H\}$ NMR ($CDCl_3$): −22.2 ppm (singlet). Found: C, 57.7; H, 4.0; N, 2.8. Calc. for $ReC_{48}H_{40}N_2Cl_3P_2$: C, 57.3; H, 4.1; N, 2.8%. FAB mass spectrum, *m/z* (%): (998, 45), $[ReCl_3(NNPh_2)(PPh_3)_2]^+$; (963, 70), $[ReCl_2(NNPh_2)(PPh_3)_2]^+$; (736, 100), $[ReCl_3(NNPh_2)(PPh_3)]^+$; (701, 65), $[ReCl_2(NNPh_2)(PPh_3)]^+$; (533, 70), $[ReCl_2(N)(PPh_3)]$.

Yield of yellow crystals, $[ReCl_2(N)(NNPh_2)(PPh_3)]$, 0.2 g, 40%. IR: 1580 cm^{-1} (N=N). ^1H NMR ($CDCl_3$): 7.0–8.1 ppm [m, phenyl H]. $^{31}P\{^1H\}$ NMR ($CDCl_3$): 42.5 ppm (singlet). Found: C, 50.8; H, 3.5; N, 5.8; Cl, 10.0. Calc. for $ReC_{48}H_{40}N_2Cl_3P_3$: C, 50.4; H, 3.5; N, 5.9; Cl, 9.9%. FAB mass spectrum, *m/z* (%): (716, 10), $[ReCl_2(N)(NNPh_2)(PPh_3)]^+$; (680, 100), $[ReCl(N)(NNPh_2)(PPh_3)]^+$; (461, 15) $[ReN(PPh_3)]^+$; (446, 80), $[Re(PPh_3)]^+$.

Preparation of $[ReNCl_2(NNCOPhC(Me_2))(PPh_3)_2]$ **(8)**

$[ReOCl_3(PPh_3)_2]$ (1.0 g, 1.2 mmol), PPh_3 (1.0 g, 3.8 mmol), concentrated HCl (0.5 cm^3) and $PhC(O)N(H)NC(CH_3)_2$ (1.0 g, 5.7 mmol) were heated under reflux in methanol (25 cm^3) for 1.5 h. The orange solid obtained was filtered, washed with Et_2O and dried; yield 0.46 g, 40%. Recrystallized from CH_2Cl_2/MeOH. IR: 1570 (NN), 1550 (CN) and 1000 cm^{-1} (ReN). ^1H NMR ($CDCl_3$): 1.4 and 2.6 [CH_3, s, 3H] and 7.1–7.8 [phenyl H, m, 35H] ppm. $^{31}P\{^1H\}$ ($CDCl_3$): 14.3 ppm (singlet). Found: C, 58.5; H, 4.4; N, 4.3. Calc. for $ReC_{35}H_{50}N_4S_4P_1O_1$: C, 59.1; H, 4.4; N, 4.5%.

Determination of X-ray crystal structures

Full details of the three structure determinations are summarized in Table 5.

Acknowledgements—Two of us (J.P. and S.P.) thank the SERC for studentships, and we are indebted to Herman Starck GMBH for the generous gift of rhenium powder. We are also grateful to Joanne Warmsley for recording the NMR spectra and Neil Barnard for the electrochemical measurements, and the SERC mass spectroscopy service for the FAB mass spectra.

REFERENCES

1. J. Chatt, R. R. Eady, D. J. Lowe, M. J. O'Donnell, J. R. Postgate, R. L. Richards, B. E. Smith and R. N. F. Thorneley, in *Nitrogen Fixation*, Vol. 1, p. 190. University Park Press, Baltimore, MA (1980).
2. J. Chatt, C. D. Falk, G. J. Leigh and R. J. Paske, *J. Chem. Soc A.* 1969, 2288.
3. J. Chatt, J. R. Dilworth and G. J. Leigh, *J. Chem. Soc., Dalton Trans.* 1973, 612.
4. R. Mason, K. M. Thomas, J. A. Zubieta and B. L. Shaw, *J. Am. Chem. Soc.* 1974, **96**, 260.
5. J. R. Dilworth, P. Jobanputra, S. J. Parrott, R. M. Thompson, O. C. Povey and J. A. Zubieta, *Polyhedron* 1992, **11**, 147.
6. S. R. Fletcher, *Inorg. Nucl. Chem. Lett.* 1973, **9**, 1117.
7. M. J. Abrams, Q. Chen, N. Shaikh and J. A. Zubieta, *Inorg. Chim. Acta* 1990, **176**, 11.
8. W. P. Griffiths, *Coord. Chem. Rev.* 1972, **8**, 369.
9. J. Chatt and G. J. Leigh, *J. Chem. Soc.* (*A*) 1970, 2239.
10. D. D. Perrin and W. L. F. Armarego, *Purification of Laboratory Chemicals*, 3rd edn, Ch. 1, p. 16. Pergamon Press, Oxford (1989).
11. J. Chatt and G. J. Rowe, *J. Chem. Soc.* (*A*) 1962, 4019.
12. T. Nicholson and J. A. Zubieta, *J. Chem. Soc., Chem. Commun.* 1985, 367.
13. C. K. Johnson, ORTEPII, Report ORNL-5138. Oak Ridge National Laboratory, Oak Ridge, TN (1976).
14. J. C. Calbrese, Ph.D. thesis, PHASE-Patterson

Heavy Atom Solution Extractor. University of Wisconsin-Madison (1972).
15. P. T. Beurskens, DIRDIF: Direct Methods for Difference Structures—an automatic procedure for phase extension and refinement of difference structure factors, Technical report 1984/1. Crystallography Laboratory, Toernooiveld, 6526 Ed Nijmegen, The Netherlands.
16. D. T. Cromer and J. T. Waber, *International Tables for X-ray Crystallography*, Vol. IV, Table 2.2a. Kynoch Press, Birmingham (1974).
17. J. A. Ibers and W. C. Hamilton, *Acta Cryst.* 1964, **17**, 781.
18. D. T. Cromer, *International Tables for X-ray Crystallography*, Vol. IV, Table 2.3.1. Kynoch Press, Birmingham (1974).
19. TEXAN-TEXRAY, Structure Analysis Package. Molecular Structure Corporation (1985).

Polyhedron Vol. 12, No. 5, pp. 523–525, 1993
Printed in Great Britain

0277–5387/93 $6.00+.00
© 1993 Pergamon Press Ltd

SYNTHESIS, CRYSTAL STRUCTURE AND PROPERTIES OF A FIVE-COORDINATE COPPER(II) COMPLEX

ZONG-HUI JIANG,* LIN-GUN BAI, DAI-ZHENG LIAO, JIN-HUI HUANG and GEN-LIN WANG

Department of Chemistry, Nankai University, Tianjin, China

and

HONG-GEN WANG and XIN-KAN YAO

Central Laboratory, Nankai University, Tianjin, China

(*Received* 23 *June* 1992; *accepted* 22 *October* 1992)

Abstract—The five-coordinate copper(II) complex [(3,3′-trimethylenedinitrilo)bis(2-butanone oximato)]copper(II) bromide (CuHLBr) has been prepared and its crystal structure has been determined. The complex has a square-pyramidal structure with the copper displaced 0.43 Å out of the basal nitrogen plane. The Cu—Br distance is 2.955 Å. The differences in the structures of the copper(II) and copper(I) complexes is discussed. Covalency of the coordinate bond for the title complex is also discussed based on ESR spectra.

There has been recent interest in the study of macrocyclic complexes containing copper atoms as possible models for biochemically important proteins and enzymes.[1–3] In this paper the structural features of the complex of copper(II) with 3,3′-(trimethylenedinitrilo)bis(2-butanone dioxime) (H_2L) are reported.

EXPERIMENTAL

The ligand H_2L was prepared by the literature method.[3]

Synthesis of the complex

Copper(II) bromide and H_2L (mole ratio 1:1) were dissolved in warm acetone. The solutions were mixed and set aside for 2 days to give dark green crystals of the complex. Found: C, 34.6; H, 5.0; N, 14.7. Calc. for $C_{11}H_{19}N_4O_2CuBr$: C, 34.5; H, 5.0; N, 14.6%.

Instruments

PE-240 elemental analysis meter; Shimadzu IR-408 spectrometer; Perkin–Elmer Hitachi-240 spectrophotometer; Enraf–Nonius CAD4 automated diffractometer, JES-FEIXG ESR spectrometer.

X-ray structure determination

A single crystal of the complex having the approximate dimensions $0.2 \times 0.3 \times 0.3$ mm^3 was mounted on a glass fibre. Determination of the unit cell and data collection were performed with Mo-K_α radiation ($\lambda = 0.71073$ Å) on a CAD4 diffractometer equipped with a graphite monochromator. A total of 2845 independent reflections were collected by the ω–2θ scan technique in the range $2 \leqslant \theta \leqslant 25°$, from which 1154 reflections [$I \geqslant 3\sigma(I)$] were considered to be observed. Intensity data were corrected for Lorentz and polarization factors.

The structure was solved by direct methods (MULTAN82). The copper atom was located from an E-map. The other non-hydrogen atoms were

* Author to whom correspondence should be addressed.

Table 1. Related bond lengths (Å) and angles (°)

Cu—N(1)	1.967(7)	N(1)—Cu—N(3)	154.1(4)
Cu—N(2)	1.961(7)	N(2)—Cu—N(4)	155.6(3)
Cu—N(3)	1.949(7)	N(1)—Cu—N(4)	80.2(3)
Cu—N(4)	1.993(7)	N(2)—Cu—N(3)	81.6(3)
Cu—Br	2.534(1)	N(3)—Cu—N(4)	93.4(3)
		N(1)—Cu—N(2)	94.4(3)
		Br—Cu—N(1)	103.2(3)
		Br—Cu—N(2)	105.9(3)
		Br—Cu—N(3)	102.5(2)
		Br—Cu—N(4)	98.5(2)

determined with successive difference-Fourier syntheses. The final refinement by the full-matrix least-squares method with anisotropic thermal parameters for the non-hydrogen atoms converged with the unweighted and weighted agreement factors 0.065 and 0.083, respectively (unit weights for all observed reflections). The highest peak in the final difference Fourier map had a height of 0.79 e $Å^{-3}$. All calculations were performed on a PDP 11/44 computer using the SDP-PLUS program system. The related bond lengths and angles for the complex are given in Table 1.

RESULTS AND DISCUSSION

Elemental analyses, IR and electronic spectra have indicated that the reaction of the ligand H_2L with $CuBr_2$ yielded the title complex. In the electronic absorption spectra of an aqueous solution of the complex a broad absorption at 510 nm ($\varepsilon = 5 \times 10^2\ M^{-1}\ cm^{-1}$) and a strong absorption at 228 nm ($\varepsilon = 2 \times 10^5\ M^{-1}\ cm^{-1}$) were observed. The former may be attributed to the *d–d* transition and the latter to the charge-transfer absorption bands. Features of the optical spectra are consistent with the expected five-coordinate copper(II) complex.[4]

The crystal structure of the complex

The complex crystallizes in the monoclinic space group $P2_1/c$ with $a = 13.329(4)$, $b = 7.535(2)$, $c = 14.773(6)$ Å and $\beta = 103.68(3)°$, $V = 1441.55$ $Å^3$, $Mr = 382.7$, $Z = 4$, $D_x = 1.759$ g cm^{-3}, $F(000) = 772$.

Figure 1 shows the structure and labelling scheme of the five-coordinated copper(II) complex. The copper atom sits in an asymmetrical square-pyramidal environment and is displaced 0.43 Å from the basal plane of the four nitrogen atoms. The bromine atom coordinates at the apex of the square-pyramid with a Cu—Br distance of 2.534(1) Å. Both copper and bromine atoms sit at the same side of the basal plane. Cu—N bond lengths ranging from 1.961(7) to 1.993(7) Å (mean 1.967 Å) characterize the equatorial asymmetry. The *trans*-N—Cu—N angles are 154.1(4) and 155.6(3)° and the *cis*-N—Cu—N angles range from 80.2(3) to 94.4(3)°.

There is an intramolecular hydrogen bond between the oxime oxygens.[3] A structural determination of copper(I) coordinated to H_2L has been reported.[1] Due to the smaller size of the copper(II) ion, it is not surprising that the geometry of the coordination is different. The Cu—N bond lengths in the copper(II) complex reported here average 0.165 Å shorter than those in the copper(I) complex of H_2L. The copper(I) ion is displaced 0.96 Å out of the plane of the equatorial nitrogen atoms,[3] but there is a smaller displacement of the metal atom from the plane of the four nitrogen atoms in Cu(HL)Br. The planarity of the basal plane of the four nitrogens in the copper(II) complex Cu(HL)Br is better than the one in the copper(I) complex. The basal plane deviates from planarity as evidenced by a dihedral angle of 31.9° between the N(1)—C(12)—N(4) and N(2)—C(23)—C(22)—N(3)

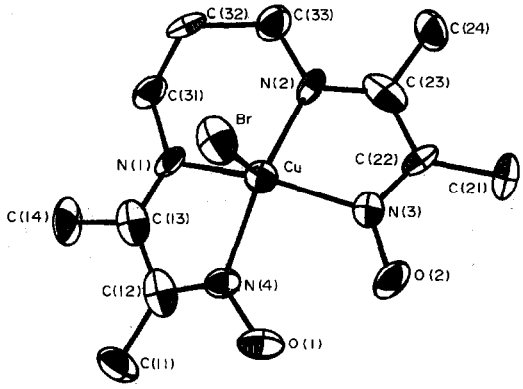

Fig. 1. The structure of the copper(II) complex.

planes. This angle is 60.0° for the copper(I) complex.

ESR spectra

The *X*-band powder ESR spectrum of the complex at room temperature is shown in Fig. 2. $g_{\parallel} = 2.155$ and $g_{\perp} = 2.053$ are obtained; $g_{\parallel} > g_{\perp} > g_e$ and this fact implies that the $3d$ unpaired electron of the copper(II) ion should occupy the $d_{x^2-y^2}$ orbital and the coordination compound would have elongated tetragonal octahedral, square planar or square pyramidal stereochemistry. The latter is in agreement with the result of the X-ray structure determination.

The ESR spectra of the complex in both glass and solution states are shown in Fig. 3. An approximate estimation of $g_{\parallel}$, $g_{\perp}$, $A_{\parallel}$ and $A_{\perp}$ was first performed following the suggestions of Kivelsen and Neiman.[5] These were then used in a computer simulation program[6] and varied on a trial and error basis until a reasonable fit was obtained. The final computer simulation spectrum of Fig. 3(b) is shown in Fig. 3(c). The ESR and bonding parameters of the complex are as follows: $g_{av} = 2.090$, $a_{av} = 84.6$ G for room temperature solution; $g_{\parallel} = 2.155$, $g_{\perp} = 2.056$, $A_{\parallel} = 0.0199$, $A_{\perp} = 0.0026$ cm^{-1}, $g_{av} = 2.089$ $((g_{\parallel}+2g_{\perp})/3)$, $a_{av} = 84.3$ G, $\alpha^2 = 0.72$, $K = 0.0115$ cm^{-1} for the glass.

The g values in powder and frozen solution states are the same, which indicates that the complex is very stable in solution and the molecular configuration in both states is not changed. The ESR parameters have been used to obtain the bonding parameter α^2 and Fermi contact interaction term K.[7] If $\alpha^2 = 1$, the bond would be completely ionic. If $\alpha^2 = 0.5$, the bond would be completely covalent. The smaller value of α^2 ($\alpha^2 = 0.72$) of this complex indicates that the σ-bonding is quite covalent in nature. This is in agreement with the result of the crystal structure determination in which the Cu^{II}—N bond lengths are short. The K value of the complex shows that the polarization is responsible for the isotropic hyperfine interaction between the copper nucleus and the unpaired electron.

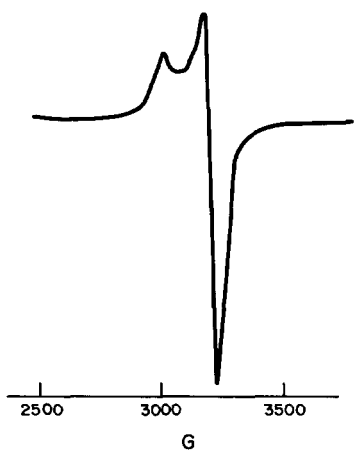

Fig. 2. Powder *X*-band ESR spectra of the complex.

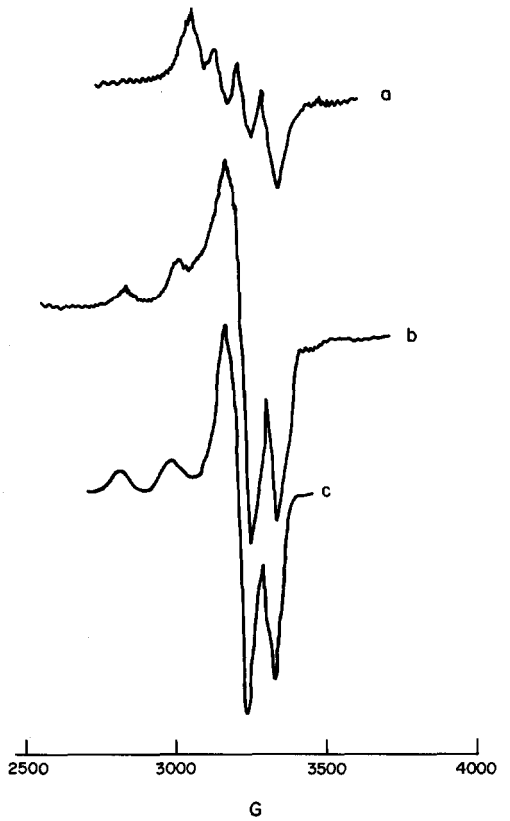

Fig. 3. The ESR spectra of the complex in solution: (a) at room temperature; (b) at −150°C; and (c) computer simulation spectrum of (b).

Acknowledgement—This project was supported by the National Natural Science Foundation of China.

REFERENCES

1. N. Sorrell, *Tetrahedron* 1989, **45**, 3.
2. Z.-H. Jiang, D.-Z. Liao and S.-Q. Hao, *Polyhedron* 1991, **10**, 941.
3. R. R. Gagne, J. L. Allison, R. S. Gall and C. A. Koval, *J. Am. Chem. Soc.* 1977, **99**, 7170.
4. W. K. Musker and M. S. Husain, *Inorg. Chem.* 1969, **8**, 528.
5. R. Neiman and D. Kivelson, *J. Chem. Phys.* 1961, **35**, 156.
6. L.-J. Bai, *Chin. J. Microwave Radio-Freq. Spectrosc.* 1986, **3**, 131.
7. P. W. Lau and W. C. Lin, *J. Inorg. Nucl. Chem.* 1975, **37**, 2389.

Polyhedron Vol. 12, No. 5, pp. 527–532, 1993
Printed in Great Britain

0277–5387/93 $6.00+.00
Pergamon Press Ltd

CONVERSION OF A METALLAENOLATE COMPLEX TO A BIMETALLIC μ-KETENE COMPLEX: MOLECULAR STRUCTURE OF $(\eta^5\text{-}C_5Me_5)(NO)(PPh_3)Re[\mu\text{-}(COCH_2)\text{-}C^1\text{:}C^2]Re(CO)_4(PPh_3)$

JOSEPH M. O'CONNOR,* ROGER UHRHAMMER and RAJ K. CHADHA†

Department of Chemistry (0506), University of California at San Diego, La Jolla, CA 92093-0506, U.S.A.

(*Received* 11 *August* 1992; *accepted* 22 *October* 1992)

Abstract—Reaction of rhenaenolates $[(\eta^5\text{-}C_5Me_5)(NO)(PPh_3)Re(COCH_2Li)]$ (**2**) and $[Re(CO)_4(PPh_3)(OSO_2CF_3)]$ in THF at −78°C gave the μ-ketene complex $[(\eta^5\text{-}C_5Me_5)(NO)(PPh_3)Re[\mu\text{-}(COCH_2)\text{-}C^1\text{:}C^2]Re(CO)_4(PPh_3)]$ (**5**). The structure of (**5**) was determined by single-crystal X-ray analysis.

The reaction of metallaenolates and metal carbonyl electrophiles represents a potentially useful and straightforward route towards μ-(C,C)-ketene complexes.[1] However, the only well-characterized example of this synthetic approach involves reaction of $[(\eta^5\text{-}C_5H_5)Fe(CO)(PPh_3)(COCH_2)]^-Li^+$ and the non-carbonyl containing metal halide $(PPh_3)AuCl$ to give a μ-(C,C)-ketene complex, $(\eta^5\text{-}C_5H_5)Fe(CO)(PPh_3)(COCH_2)Au(PPh_3)$ (**1**, Scheme 1).[2] Akita and Kondoh found that the related enolate $[(\eta^5\text{-}C_5H_5)Fe(CO)_2(COCH_2)]^-Li^+$ gave bimetallic complexes with no ketene ligand upon reaction with either $(\eta^5\text{-}C_5H_5)Fe(CO)_2Cl$ or $(\eta^5\text{-}C_5H_5)Mo(CO)_3I$[3]. In this case it is not clear if the μ-ketene complexes were initially formed. Geoffroy reported spectroscopic observation of an unisolable μ-ketene complex from $[(\eta^5\text{-}C_5H_5)Fe(CO)(PPh_3)(COCH_2)]^-Li^+$ and $M(CO)_5Br$ (M = Re, Mn).[1a] We recently reported that the rhenium enolate $(\eta^5\text{-}C_5Me_5)(NO)(PPh_3)Re(COCH_2Li)$ (**2**)[4] reacts with a carbon monoxide ligand of $(CO)_5ReBr$ to generate the lithium chelating malonyl complex $\{(\eta^5\text{-}C_5Me_5)(NO)(PPh_3)Re[\mu\text{-}(COCH_2CO)\text{-}C^1\text{:}C^3]Re(CO)_4(Br)\}^-Li^+$ (**3**, Scheme 2).[3e] Abstraction of the lithium cation in **3** with 12-crown-4 led to the loss of LiBr and formation of a chelating malonyl complex, $(\eta^5\text{-}C_5Me_5)(NO)(PPh_3)Re[\mu\text{-}(COCH_2CO)\text{-}C^1\text{:}C^3, O^1]Re(CO)_4$ (**4**). We have now discovered that modification of the metal electrophile utilized in reaction with **2** results in the formation of an isolable bimetallic ketene complex, $(\eta^5\text{-}C_5Me_5)(NO)(PP_3)Re[(COCH_2)\text{-}C^1\text{:}C^2]Re(CO)_4(PPh_3)$ (**5**, Scheme 3).

EXPERIMENTAL

General

All manipulations, unless otherwise stated, were performed under purified nitrogen using Schlenk techniques or a Vacuum Atmospheres nitrogen box equipped with Dri-Train MO 40-1 purifier. IR spectra were recorded on a Perkin–Elmer 1330 IR spectrometer. Melting points were determined in sealed capillaries using an electrothermal melting point apparatus equipped with a calibrated thermometer. Mass spectra were performed at the University of California, Riverside Mass Spectroscopy (UCRMS) facility. Elemental analyses were performed by Galbraith Laboratories. ^1H, ^{13}C and ^{31}P NMR spectra were recorded at ambient probe temperature unless otherwise stated on either a GE QE NMR or a Varian UNITY 500 NMR spectrometer. ^1H NMR chemical shifts are reported relative to the residual protio-solvent resonance: $CHCl_3$, δ 7.24; THF-d_7, 3.58. ^{13}C NMR chemical shifts are reported relative to the solvent resonance: $CDCl_3$, δ 77.0; THF-d_8, 67.4. ^{31}P NMR chemical shifts are reported

*Author to whom correspondence should be addressed at: Department of Chemistry, 216, University of Nevada, Reno, NV 89557-0020, U.S.A.

† For correspondence concerning the crystallographic details, contact R.K.C. at: Department of Chemistry, The Scripps Research Institute, 10666 North Torrey Pines Road, La Jolla, CA 92037, U.S.A.

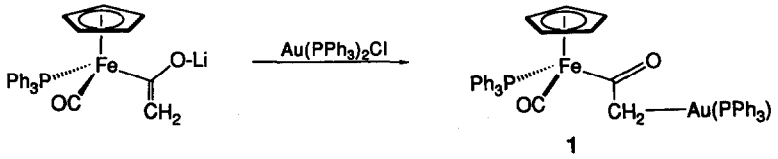

1

Scheme 1.

relative to external H_3PO_4 (85%). Thoroughly dried and degassed solvents were used throughout. (η^5-C_5Me_5)(NO)(PPh_3)Re($COCH_3$) was prepared according to published procedures.[4]

Preparation of cis-$(CO)_4(PPh_3)Re(OSO_2CF_3)$.

A procedure similar to that for $(CO)_5Re(OSO_2CF_3)$ was employed.[6] A round-bottomed flask equipped with a magnetic stir bar was charged with $(CO)_4(PPh_3)ReBr$ (1.00 g, 1.56 mmol, 31 mM), $Ag(OSO_2CF_3)$ (0.44 g, 1.71 mmol) and CH_2Cl_2 (50 cm^3) and stirred in the dark for 2 h. The solution was concentrated under vacuum to *ca* 5 cm^3 and filtered. Hexanes (20 cm^3) were slowly added and large clear plates of *cis*-$(CO)_4(PPh_3)Re(OSO_2CF_3)$ were isolated by filtration, along with small patches of a black solid. The crude *cis*-$(CO)_4(PPh_3)Re(OSO_2CF_3)$ was dissolved in CH_2Cl_2 (10 cm^3) and filtered. Hexanes were added to the filtrate and *cis*-$(CO)_4(PPh_3)Re(OSO_2CF_3)$ was isolated as a white solid by filtration (0.75 g, 1.06 mmol, 68%); m.p. 113–117°C. IR (CH_2Cl_2): 2120 (s), 2015 (vs), 1964 (s), 1335 (m), 1233 (m), 1200 (s), 1095 (m), 1008 (m) cm^{-1}. $^{13}C\{^1H\}$ NMR ($CDCl_3$): δ 186.3 (d, $J = 9.4$ Hz, *cis*-Re*C*O), 184.9 (d, $J = 5.8$ Hz, *cis*-Re*C*O), 182.6 (d, $J = 54.9$ Hz, *trans*-Re*C*O), 133.2 (d, $J = 10.8$ Hz, C_6H_5), 131.6 (d, $J = 2.6$ Hz, C_6H_5), 130.4 (d, $J = 49.9$ Hz, C_6H_5), 129.2 (d, $J = 10.3$ Hz, C_6H_5). FAB MS: 561 (M^+-OTf), 1271 *m/z* ($2M^+$-OTf). Found: C, 38.7; H, 2.1. Calc for $C_{23}H_{15}F_3O_7PReS$: C, 38.9; H, 2.1.

Preparation of (η^5-C_5Me_5)(NO)(PPr_3)Re[(CO CH_2)C^1:C^2]Re($CO)_4$(PPh_3) (**5**)

A round-bottomed flask equipped with a magnetic stir bar was charged with the acyl complex (η^5-C_5Me_5)Re(NO)(PPh_3)($COCH_3$) (525 mg, 0.800 mol, 27 mM), THF (30 cm^3) and cooled to −78°C. A 1.6 M solution of n-BuLi in hexanes (0.5 cm^3, 0.802 mmol) was added and the deep red solution stirred for 0.5 h at −78°C. This solution was then added to a stirred −78°C THF (45 cm^3) solution of $(CO)_4(PPh_3)Re(OSO_2CF_3)$ (569 mg, 0.802 mmol, 18 mM) and warmed to room temperature. The solvent was removed *in vacuo* and the residue was chromatographed under an atmosphere of nitrogen on activated silica. An orange band was eluted with 4:3 hexanes/THF (v/v). After removal of the solvent under vacuum the residue was recrystallized twice with $CHCl_3$/hexanes to give **5** as an orange crystalline solid (212 mg, 0.174 mmol, 22%); m.p. 147–151°C (dec). FAB HRMS: 1214. 2051 *m/z* (MH^+), calc. 1214.2016. IR (CH_2Cl_2): 2075 (m), 1975 (vs), 1920 (s), 1625 (m), 1481 (w), 1431 (w) cm^{-1}. ^1H NMR ($CDCl_3$): δ 7.25–7.39 (m, 30H), 2.32 (dd, $J = 11.7$, 5.8 Hz, 1H), 1.86 (dd, $J = 11.7$, 8.2 Hz, 1H), 1.68 (s, 15 H). $^{13}C\{^1H\}$ NMR ($CDCl_3$): δ 263.9 (dd, $J = 8.2$, 3.1

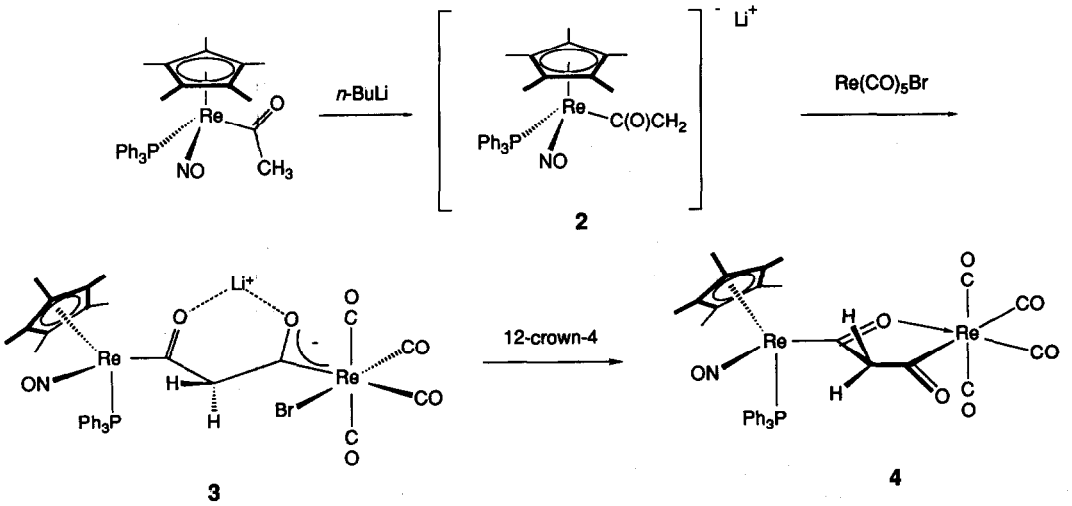

Scheme 2.

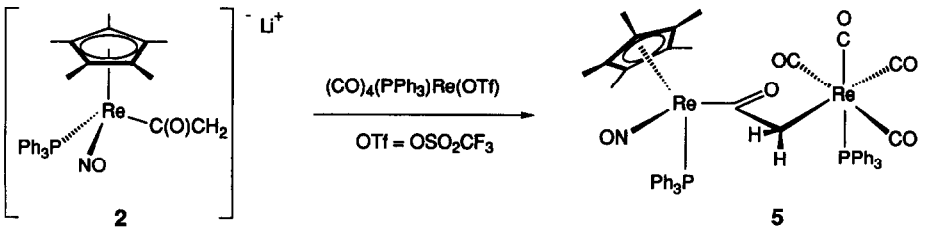

Scheme 3.

Hz, $ReCOCH_2$), 193.1 (d, $J = 10.1$ Hz, *cis*-ReCO), 192.8 (d, $J = 9.8$ Hz, *cis*-ReCO), 190.1 (d, $J = 53.4$ Hz, *trans*-ReCO), 188.5 (d, $J = 7.0$ Hz, *cis*-ReCO), 135.6 (d, $J = 53$ Hz, C_6H_5), 134.1 (d, $J = 11.1$ Hz, C_6H_5), 133.6 (d, $J = 45.3$ Hz, C_6H_5), 133.6 (d, $J = 10.1$ Hz, C_6H_5), 130.1 (d, $J = 2.0$ Hz, C_6H_5), 129.5 (C_6H_5), 128.4 (d, $J = 10.1$ Hz, C_6H_5), 127.7 (d, $J = 10.1$ Hz, C_6H_5), 101.8 (d, $J = 2.0$ Hz, C_5Me_5), 39.8 (ps, t, $J = 3.0$, 2.6 Hz, CH_2), 9.8 (C_5Me_5). $^{31}P\{^1H\}$ NMR ($CDCl_3$): δ 23.2, 8.5. Found: C, 47.4; H, 3.6; N, 1.04. Calc. for $C_{52}H_{47}NO_6P_2Re_2 \cdot CHCl_3$: C, 47.7; H, 3.6; N, 1.0. A sample was also recrystallized from CH_2Cl_2/pentane. Found: C, 48.53; H, 3.74; N, 1.29. Calc. for $C_{52}H_{47}NO_6P_2Re_2 \cdot 0.7CH_2Cl_2$ [CH_2Cl_2 observed by ^1H NMR ($CDCl_3$) spectroscopy]: C, 48.80; H, 3.76; N, 1.08.

X-ray structure determination for $(\eta^5\text{-}C_5Me_5)(NO)(PPh_3)Re[\mu\text{-}(COCH_2)\text{-}C^1{:}C^2]Re(CO)_4(PPh_3)$ (**5**)

An orange crystal of **5** containing a CH_2Cl_2 molecule of crystallization was obtained from layering of a CH_2Cl_2 solution with pentane and mounted on a glass fibre along the longest dimension. Data collection parameters are summarized in Table 1. The unit cell dimensions were obtained from 20 reflections in the range $15 < 2\theta < 30°$. Intensities of monitor reflections (three measured every 200 reflections) decreased by ~8% during 48 h of X-ray exposure. All non-hydrogen atoms were refined anisotropically using Patterson methods and a full-matrix least-squares refinement method. Hydrogen atoms were included in ideal positions with U fixed at 0.08 Å^2. A residual peak (1.46 e Å^{-3}) near the chlorine atoms of the solvent molecule suggested disorder in CH_2Cl_2. No evidence of secondary extinction was observed, therefore, no correction was applied. No systematic absences suggested the space group $P\bar{1}$, which was confirmed by successful solution of the structure.

RESULTS AND DISCUSSION

Treatment of a THF solution of the known acyl complex $[(\eta^5\text{-}C_5Me_5)Re(NO)(PPh_3)(COCH_3)]$ with n-BuLi generated the rhenolate anion **2**, to which was added a cold THF solution of $[(CO)_4(PPh_3)Re(OSO_2CF_3)]$. Evaporation of the volatiles, chromatography of the residue and recrystallization of the resultant orange solid led to isolation of an orange crystalline product, identified as the μ-ketene complex **5** (34% yield; Scheme 3).

In the IR spectrum of **5** a band at 1625 cm^{-1} is attributed to coincidental overlap of ν(C≡O) and ν(N≡O) bands. In the ^1H NMR spectrum ($CDCl_3$) the diastereotopic methylene hydrogens of the ketene ligand are observed at δ 2.32 [dd, J(HH) = 11.7 Hz, J(PH) = 5.8 Hz, 1H] and 1.85 [dd, J(HH) = 11.7 Hz, J(PH) = 8.2 Hz, 1H]. In the $^{13}C\{^1H\}$ NMR spectrum ($CDCl_3$) of **5** the COs *cis* to the PPh_3 ligand appear at 192.8 (d, $J = 9.8$ Hz), 193.1 (d, $J = 10.1$ Hz) and 188.5 (d, $J = 7.0$ Hz). This observation that CO ligands *trans* to one another are diastereotopic is an unusual one. The carbonyl carbon of the ketene ligand is observed at 264 ppm [dd, ^2J(PC) = 8.2 Hz, ^3J(PC) = 3.1 Hz]. For comparison, $(\eta^5\text{-}C_5Me_5)Re(NO)(PPh_3)(CO CH_2Ph)$ (**6**) exhibits ν(CO) and ν(NO) bands in the IR spectrum ($CHCl_3$) at 1574 and 1636 cm^{-1}, respectively, whereas the methylene hydrogens appear in the ^1H NMR spectrum ($CDCl_3$) at δ 3.66 (d, $J = 11.3$ Hz) and 2.83 (d, $J = 11.3$ Hz), and the carbonyl carbon appears at 261.2 ppm (d, $J = 10.3$ Hz) in the $^{13}C\{^1H\}$ NMR spectrum ($CDCl_3$).[4] The analogous spectroscopic data for the malonyl **3** are as follows: IR (CH_2Cl_2): 1648 ν(N≡O) and 1482 ν(C≡O), 1560 ν(C≡O). ^1H NMR (CD_2Cl_2): δ 1.93 (d, $J = 15.2$ Hz) and 5.82 (d, $J = 15.1$ Hz). $^{13}C\{^1H\}$ NMR spectrum (CD_2Cl_2): 270.8 (d, $J = 9.5$ Hz) and 270.7 (s) ppm.[5e] The 67 cm^{-1} shift to a higher frequency for ν(C≡O) on going from acyl **6** to ketene **5** is in the reverse direction to that observed (−35 cm^{-1}) on going from $(\eta^5\text{-}C_5H_5)Fe(CO)_2(COCH_3)$ to the μ-(C,C)-ketene complex $(\eta^5\text{-}C_5H_5)Fe(CO)_2(COCH_2)Fe(CO)_2(\eta^5\text{-}C_5H_5)$ (**7**). In the case of **7** the shift to lower frequency has been attributed to a contribution of the π-complex **II**, in addition to the expected oxycarbene structure **III** (Scheme 4).[1d]

The solid state structure of **5** was determined by

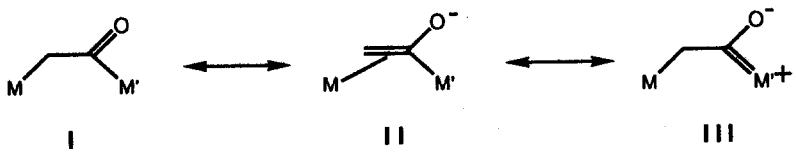

Scheme 4.

X-ray crystallography and is illustrated in Fig. 1. Crystal data, data collection and refinement parameters are summarized in Table 1. Selected bond distances and angles are given in Table 2. As was observed for the structures of related malonyl complexes, the ON—Re(1)—C(12)—O(11) torsion angle θ, as defined by Gladysz,[4] is 179.9°. Table 3 lists the structural parameters for the ketene ligand in **5** along with those for other (C,C)-ketene and acyl complexes.[1d] It is clear from a comparison of these parameters that **5** exhibits the least degree of π-complex character (**II**) in the bimetallic ketenes structurally characterized to date. Complex **5** adopts a conformation with an Re(2)—C(11)—C(12)—O(11) torsion angle φ of 54.7°, which places Re(2) opposite the ketene ligand plane from P(1) and bent away from the C_5Me_5 ligand. As previously discussed by Akita, the angle φ is one of the structural parameters pertinant to the question of a π-complex contribution (**II**) in **5** and other μ-(C,C)-ketene complexes.[1d] A dihedral angle of 90° would maximize overlap between the Re(2)—C(11) bond and the carbonyl *p*-orbital on C(12). Comparison of the *b*, *c* and *d* structural parameters in **5** to those for the rhenium acyl (η^5-C_5Me_5)

Table 1. Crystal and data collection and refinement parameters for **5**

Formula	$C_{53}H_{49}NO_6P_2Cl_2Re_2$
Lattice type	Triclinic
Space group	$P\bar{1}$
a (Å)	10.708(3)
b (Å)	10.846(3)
c (Å)	22.163(12)
α (°)	98.82(3)
β (°)	93.35(4)
γ (°)	90.71(2)
V (Å^3)	2539(2)
Z	2
Crystal dimensions (mm)	0.08 × 0.16 × 0.22
Crystal colour	Orange
D_{calc} (g cm^{-3})	1.702
μ (mm^{-1})	5.045 (Mo-K_α)
Temperature (°C)	23
T_{min}/T_{max}	0.4428/0.6708
Radiation type	Mo-K_α (λ = 0.71073 Å)
2θ range (°)	4.0–45.0
Read	6655
Unique	6655
Unique observed	4314
R (F) (%)	3.91
R (wF) (%)	4.73
GOF	1.11
$\Delta(\rho)$ (e Å^{-3})	1.46

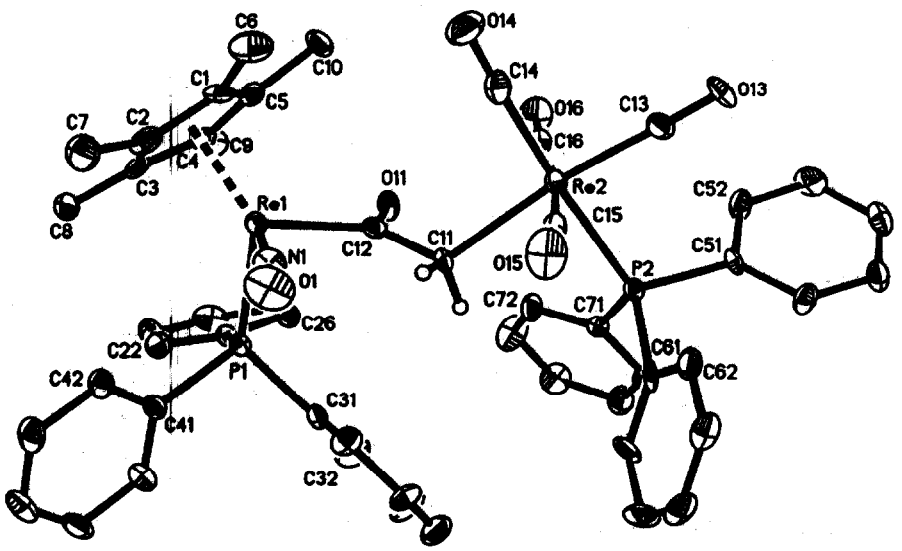

Fig. 1. Structure of the μ-ketene complex (η^5-C_5Me_5)(NO)(PPh_3)Re[μ-($COCH_2$)-C^1:C^2]Re(CO)$_4$(PPh_3) (**5**).

Table 2. Selected bond distances and angles for **5**

Re(2)—C(15)	2.009(14)	C(12)—Re(1)	2.105(13)
Re(2)—C(13)	1.946(15)	Re(1)—N(1)	1.743(17)
Re(2)—C(16)	1.996(15)	Re(1)—P(1)	2.367(3)
Re(2)—C(14)	1.954(17)	N(1)—O(1)	1.188(16)
Re(2)—C(11)	2.296(12)	C(12)—O(11)	1.239(15)
Re(2)—P(2)	2.488(4)	C(14)—O(14)	1.134(21)
C(11)—C(12)	1.527(19)	C(13)—O(13)	1.142(18)
C(16)—O(16)	1.128(17)	C(15)—O(15)	1.117(18)

C(14)—Re(2)—P(2)	176.0(5)	C(14)—Re(2)—C(15)	88.0(6)
C(14)—Re(2)—C(16)	88.7(6)	C(14)—Re(2)—C(13)	89.4(6)
C(14)—Re(2)—C(11)	95.5(6)	C(13)—Re(2)—C(11)	172.0(5)
C(13)—Re(2)—C(15)	95.1(6)	C(13)—Re(2)—C(16)	93.3(6)
C(13)—Re(2)—P(2)	87.2(4)	C(15)—Re(2)—C(11)	78.9(5)
C(15)—Re(2)—C(16)	171.0(6)	C(15)—Re(2)—P(2)	94.4(4)
C(16)—Re(2)—C(11)	93.1(5)	C(16)—Re(2)—P(2)	89.4(4)
Re(2)—C(11)—C(12)	116.7(8)	Re(1)—C(12)—C(11)	119.2(8)
C(12)—Re(1)—N(1)	100.1(5)	C(12)—Re(1)—P(1)	86.2(3)
P(1)—Re(1)—N(1)	93.0(4)	Re(1)—C(12)—O(11)	121.4(10)
O(11)—C(12)—C(11)	119.4(11)		

$Re(NO)(PPh_3)(COCHMeCH_2Ph)$ (**8**)[7] also indicates negligible structural differences; once again mitigating against a significant π-contribution (**II**) to the structure of **5**. The C(11)—C(12) bond length in **5** is the longest reported to date for a μ-(C,C)-ketene complex.

When $(CO)_4(PPh_3)ReBr$ was utilized in reaction with metallaenolate **2** and the product recrystallized from CH_2Cl_2/ether, a mixture of two new products (**9**) was isolated in a ~90:10 ratio (45% yield), with no evidence for the formation of ketene **5**. The ^1H and ^{13}C NMR spectra of these two compounds were very similar. In the ^1H NMR spectrum ($CDCl_3$), methylene hydrogen resonances are observed at δ 4.87 (d, J = 20.4 Hz) and 3.61 (dd, J = 20.6, 1.1. Hz) for the major isomer and 3.68 (d, J = 19.5 Hz) and 4.48 (d, J = 19.4 Hz) for the minor isomer. The observed geminal coupling constant of ~20 Hz is consistent with a five-membered chelate ring as observed for the malonyl complex **4** (δ 2.84, d, J = 20.7 Hz; 3.13, d, J = 20.7 Hz).[5e] In the $^{13}C\{^1H\}$ NMR spectrum ($CDCl_3$) acyl carbon resonances were observed as doublets at 300.0 (J = 10.3 Hz) and 270.2 ppm (J = 8.8 Hz) for the major isomer, and at 300.4 (J = 9.4 Hz) and 270.1 ppm (J = 9.4 Hz) for the minor isomer. These low-field shifts are again consistent with a malonyl structure similar to that of **4**. When the malonyl complexes (**9**) were dissolved in THF-d_8 and allowed to stand for 2 days, complete decomposition occured to give the μ-ketene complex **5** in 21% yield, along with uncharacterized other products. It thus appears that the formation of **5** occurs by initial attack of the enolate on the carbonyl ligand of

Table 3. Structural parameters of selected bridging ketene and simple acyl ligands

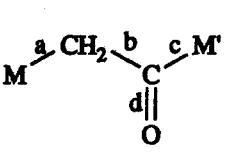

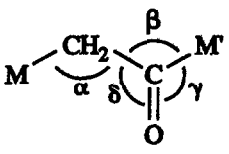

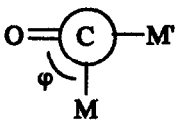

Complex	*a*	*b*	*c*	*d*	α	β	γ	δ	φ	ν(C=O)
5	2.296	1.527	2.105	1.239	116.7	119.2	121.4	119.4	55	1625
$(C_5Me_5)(NO)(PPh_3)ReC(=O)R$ (**8**)	—	1.531	2.081	1.252	—	121.4	122.7	115.6	—	1548
$[(OC)_2(Cp)Fe(CH_2CO)Ni(Cp(CO)]$	2.088	1.482	1.940	1.205	111.9	117.3	118.0	124.6	88	1649
$[(OC)_2(Cp)Fe(CH_2CO)Mo(CO)_5]$	2.082	1.486	2.173	1.212	114.0	119.6	118.4	122.0	64	1581
$[(OC)_2(Cp)Fe]_2CH_2CO]$	2.073	1.481	2.008	1.219	114.0	117.1	120.9	121.6	76	1612
$([(OC)_2(Cp)Fe]_2CH_2CH_2CO)$	2.071	1.534	1.991	1.203	114.6	117.4	122.3	120.2	79	1645

the electrophile and not direct attack at the metal centre.

Acknowledgement—Partial support from the National Science Foundation is gratefully acknowledged.

REFERENCES

1. For leading references to ketene complexes: (a) G. L. Geoffroy and S. L. Bassner, *Adv. Organomet. Chem.* 1988, **28**, 1; (b) M. Akita, A. Kondoh and Y. Moro-oka, *J. Chem. Soc., Chem. Commun.* 1986, 1296; (c) M. Akita, A. Kondoh, T. Kawahara and Y. Moro-oka, *J. Organomet. Chem.* 1987, 1296; (d) M. Akita, A. Kondoh and Y. Moro-oka, *J. Chem. Soc., Dalton Trans.* 1989, 1627; (e) Y. C. Lin, J. C. Calabrese and S. S. Wreford, *J. Am. Chem. Soc.* 1983, **105**, 1679; (f) N. M. Doherty, M. J. Fildes, N. J. Forrow, S. A. R. Knox, K. A. Macpherson and A. G. Orpen, *J. Chem. Soc., Chem. Commun.* 1986, 1355; (g) P. Hofmann, L. A. Perez-Moya, O. Steigelmann and J. Riede, *Organometallics* 1992, **11**, 1167 and refs therein; (h) C. Ruechardt and G. N. Schrauzer, *Chem. Ber.* 1960, **93**, 1840; (i) W. A. Herrmann and J. Plank, *Angew. Chem., Int. Edn Engl.* 1979, **17**, 525; (j) E. D. Morrison and G. L. Geoffroy, *J. Am. Chem. Soc.* 1985, **107**, 3545; (k) B. Denise, D. Navarre, H. Rudler and J. C. Daran, *J. Organomet. Chem.* 1989, **375**, 273; (l) T. W. Bodnar and A. R. Cutler, *J. Am. Chem. Soc.* 1983, **105**, 5926; (m) W. Schulze, H. Hartl and K. Seppelt, *Angew. Chem., Int. Edn Engl.* 1986, **25**, 185.
2. I. Weinstock, C. Floriani, A. Chiesi-Villa and C. Guastini, *J. Am. Chem. Soc.* 1986, **108**, 8298.
3. M. Akita and A. Kondoh, *J. Organomet. Chem.* 1986, **299**, 369.
4. P. C. Heath, A. T. Patton and J. A. Gladysz, *J. Am. Chem. Soc.* 1986, **108**, 1185.
5. (a) J. M. O'Connor, R. Uhrhammer and A. L. Rheingold, *Organometallics* 1987, **6**, 1987; (b) J. M. O'Connor, R. Uhrhammer and A. L. Rheingold, *Organometallics* 1988, **7**, 2422; (c) J. M. O'Connor and R. Uhrhammer, *J. Am. Chem. Soc.* 1988, **110**, 4448; (d) J. M. O'Connor, R. Uhrhammer, A. L. Rheingold and D. L. Staley, *J. Am. Chem. Soc.* 1989, **111**, 7633; (e) J. M. O'Connor, R. Uhrhammer, A. L. Rheingold, S. L. Staley and R. K. Chadha, *J. Am. Chem. Soc.* 1990, **112**, 7585; (f) J. M. O'Connor, R. Uhrhammer, A. L. Rheingold and R. K. Chadha, *J. Organomet. Chem.* 1993, accepted.
6. S. P. Schmidt, J. Nitschke and W. C. Trogler, *Inorg. Syn.* 1989, **26**, 113.
7. G. S. Bodner, A. T. Patton, D. E. Smith, S. Georgiou, W. Tam, W.-K. Wong, C. E. Strouse and J. A. Gladysz, *Organometallics* 1987, **6**, 1954.

Polyhedron Vol. 12, No. 5, pp. 533–542, 1993
Printed in Great Britain

0277–5387/93 $6.00+.00
© 1993 Pergamon Press Ltd

SYNTHESIS AND PROTONATION OF MIXED DIPHOSPHORUS LIGAND-BRIDGED DERIVATIVES OF DI-IRON NONACARBONYL

KANDASAMY G. MOODLEY*

Department of Chemistry, University of Durban–Westville, Private Bag X54001, Durban 4000, Republic of South Africa

and

DENNIS W. ENGEL

Department of Physics, University of Durban–Westville, Private Bag X54001, Durban 4000, Republic of South Africa

and

JOHN S. FIELD and RAYMOND J. HAINES

Unit of Metal Cluster Chemistry, Department of Chemistry, University of Natal, PO Box 375, Pietermaritzburg, Republic of South Africa

(*Received* 17 *July* 1992; *accepted* 6 *October* 1992)

Abstract—Reaction of the di-iron heptacarbonyl compounds $[Fe_2(\mu\text{-CO})(CO)_6(\mu\text{-}R_2PCH_2PR_2)_2]$ (R = Me or Ph) with a range of diphosphorus or diarsenic ligands under photochemical conditions affords the ligand-bridged pentacarbonyl derivatives $[Fe_2(\mu\text{-CO})(CO)_4(\mu\text{-}Me_2PCH_2PMe_2)(\mu\text{-L-L})]$ [L-L = $(MeO)_2PN(Et)P(OMe)_2$ or $(EtO)_2PN(Me)P(OEt)_2$] and $[Fe_2(\mu\text{-CO})(CO)_4(\mu\text{-}Ph_2PCH_2PPh_2)(\mu\text{-L-L})]$ [L-L = $Me_2PCH_2PMe_2$, $Ph_2PN(Et)PPh_2$, $Ph_2AsCH_2AsPh_2$, $(MeO)_2PN(Et)P(OMe)_2$ and $(EtO)_2PN(Me)P(OEt)_2$] in good yield. Treatment of these mixed ligand-bridged complexes with the protic acids $HBF_4 \cdot Et_2O$ or CF_3COOH leads exclusively to the formation of the hydride-bridged species $[Fe_2(\mu\text{-H})(\mu\text{-CO})(CO)_4(\mu\text{-}R_2PCH_2PR_2)(\mu\text{-L-L})]^+$ isolated as the tetrafluoroborate salts. Hydride-bridged products are also obtained by protonation of $[Fe_2(\mu\text{-CO})(CO)_4\{\mu\text{-}(R'O)_2PN(R'')P(OR')_2\}_2]$ (R'' = Me, R' = Et; R'' = Et, R' = Me, Pr^i or Ph) and $[Fe_2(\mu\text{-CO})(CO)_4(\mu\text{-}R_2PCH_2PR_2)_2]$ (R = Me or Ph), but whereas the diphosphazane-bridged species $[Fe_2(\mu\text{-H})(\mu\text{-CO})(CO)_4\{\mu\text{-}(R'O)_2PN(R'')P(OR')_2\}_2]^+$ are only stable to deprotonation in the presence of excess acid, the ditertiary phosphine-bridged species $[Fe_2(\mu\text{-H})(\mu\text{-CO})(CO)_4(\mu\text{-}R_2PCH_2PR_2)_2]^+$ can only be deprotonated by strong bases such as $NaBH_4$. The structure of $[Fe_2(\mu\text{-CO})(CO)_4(\mu\text{-}Ph_2PCH_2PPh_2)_2]$ has been established X-ray crystallographically. The two iron atoms, which are bridged by a carbonyl group as well as by the two ditertiary phosphine ligands, are separated by a distance of 2.742(4) Å, corresponding to a formal iron–iron bond.

Although it is widely accepted that the reactivity and structures of homo-dinuclear compounds bridged by two bidentate diphosphorus ligands are governed by the electronic and stereochemical properties of the bridging ligands, the number of systematic studies aimed at probing these factors has been somewhat limited.[1] Nevertheless, Puddephatt *et al.* have shown, in their studies of di-

* Author to whom correspondence should be addressed.

platinum compounds bridged by ditertiary phosphines, that the nature of the product formed in the reaction of $[Pt_2(\mu\text{-}H)H_2(\mu\text{-}R_2PCH_2PR_2)_2]^+$ with $R_2PCH_2PR_2$ (R = Et or Ph) is dependent on the identity of the ditertiary phosphine,[2,3] while we have established that the structures of the diphosphazane-bridged dirhodium compounds of stoichiometry $[Rh_2Cl_2(CO)_2\{\mu\text{-}(RO)_2PN(Et)P(OR)_2\}_2]$ and $[Rh_2Cl_2(CO)\{\mu\text{-}(RO)_2PN(Et)P(OR)_2\}_2]$ (R = Me, Et, Pr^i or Ph) vary with the alkoxy or aryloxy groups attached to the phosphorus atoms.[4,5] Furthermore, studies by Eisenberg *et al.*, Kubiak *et al.* and Cowie *et al.* on the reactivity of the dirhodium and diiridium derivatives $[Rh_2(CO)_3(\mu\text{-dppm})_2]$,[6,7] $[Rh_2(CO)_3(\mu\text{-dmpm})_2]$,[8] $[Ir_2(CO)_3(\mu\text{-dppm})_2]$[9,10] and $[Ir_2(CO)_3(\mu\text{-dmpm})_2]$[11,12] (dppm = $Ph_2PCH_2PPh_2$, dmpm = $Me_2PCH_2PMe_2$), as well as of related isocyanide derivatives,[12-14] towards various substrates have revealed that the reactivity patterns for the dmpm-bridged species are often quite different to those for the corresponding dppm-bridged derivatives.

We have also established that while the reactions of the tetra-alkoxydiphosphazane-bridged diruthenium compounds $[Ru_2(\mu\text{-}CO)(CO)_4\{\mu\text{-}(RO)_2PN(Et)P(OR)_2\}_2]$ (R = Me or Pr^i) with acids of non-coordinating conjugate bases, e.g. HBF_4 and HPF_6, give protonated products of the type $[Ru_2H(CO)_5\{\mu\text{-}(RO)_2PN(Et)P(OR)_2\}_2]^+$, which from spectroscopic evidence occur as mixtures of the two isomers **1** and **2** in solution, in which the hydride ligand is coordinated terminally at either an axial or an equatorial site,[15] the protonation of the corresponding dppm- and dmpm-bridged derivatives, $[Ru_2(\mu\text{-}CO)(CO)_4(\mu\text{-dppm})_2]$ and $[Ru_2(\mu\text{-}CO)(CO)_4(\mu\text{-dmpm})_2]$, by these acids affords products resulting from the formal addition of a proton across the two ruthenium atoms, viz. $[Ru_2(\mu\text{-}H)(\mu\text{-}CO)_4(\mu\text{-dppm})_2]^+$ (**3**, R = Ph) and $[Ru_2(\mu\text{-}H)(\mu\text{-}CO(CO)_4(\mu\text{-dmpm})_2]^+$ (**3**, R = Me), respectively.[15a,16] With the object of establishing whether a similar reactivity pattern is observed for the corresponding di-iron complexes, the protonation behaviour of a range of these compounds using tetrafluoroboric acid diethyletherate as the source of protons was investigated. Also, in order to probe further the effect of the nature of the bridging ligand on the reactivity of the iron centres in these compounds, a range of mixed ligand complexes of the type $[Fe_2(\mu\text{-}CO)(CO)_4(\mu\text{-dppm})(\mu\text{-L-L})]$ and $[Fe_2(\mu\text{-}CO)(CO)_4(\mu\text{-dmpm})(\mu\text{-L-L})]$, where L-L represents various diphosphine (R_2PYPR_2) or diphosphite $\{(RO)_2PYP(OR)_2\}$ type ligands, were synthesized and their protonation behaviour also studied. The results of these investigations are reported here.

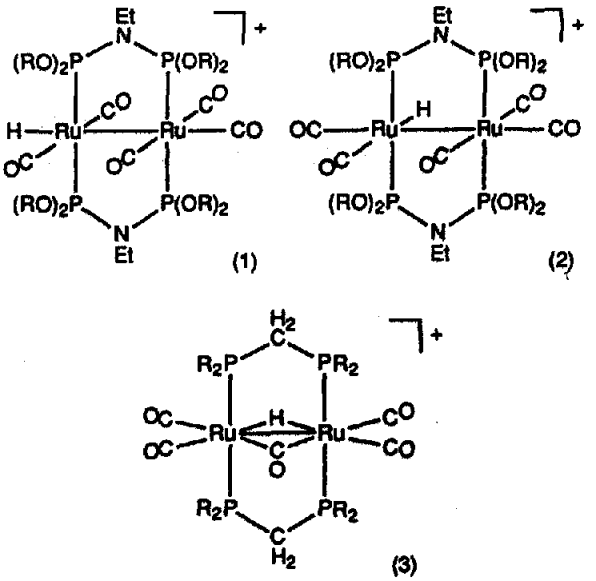

RESULTS AND DISCUSSION

Synthesis of the mixed-ligand derivatives, $[Fe_2(\mu\text{-}CO)(CO)_4(\mu\text{-L-L})(\mu\text{-L'-L'})]$

Cotton and Troup were the first to report the synthesis of a simple substituted derivative of $[Fe_2(CO)_9]$ and, in particular, they showed that the reaction of this binary carbonyl with a half molar amount of bis(diphenylphosphino)methane (dppm) under thermal conditions affords a product mixture containing primarily the heptacarbonyl derivative $[Fe_2(\mu\text{-}CO)(CO)_6(\mu\text{-dppm})]$ (**4**).[17] We subsequently established that this compound as well as a range of related diphosphazane- and pyrophosphite-bridged complexes can be synthesized in high yield[18] photochemically. Furthermore, we also established that treatment of these substituted heptacarbonyl derivatives with an excess of the corresponding ligand under photochemical conditions leads to the formation of pentacarbonyl products of the type $[Fe_2(\mu\text{-}CO)(CO)_4(\mu\text{-L-L})_2]$ [L-L = $Ph_2PCH_2PPh_2$, $(EtO)_2POP(OEt)_2$, $(MeO)_2PN(Et)P(OMe)_2$, etc.] in good yield.[18]

We have now found that this procedure is excellent for the synthesis of the mixed-ligand derivatives $[Fe_2(\mu\text{-}CO)(CO)_4(\mu\text{-L-L})(\mu\text{-L'-L'})]$ [L-L = $Ph_2PCH_2PPh_2$ or $Me_2PCH_2PMe_2$, L'-L' = $(MeO)_2PN(Et)P(OMe)_2$, etc.]. In particular, photolysis of a solution of $[Fe_2(\mu\text{-}CO)(CO)_6(\mu\text{-dppm})]$ and an excess of bis(dimethylphosphino)methane (dmpm) or the diphosphazane ligands $R_2PN(R')PR_2$ (R' = Et, R = Ph or OMe; R' = Me, R = OEt) or bis(diphenylarsino)methane (dpam) was found to yield crystalline or microcrystalline products characterized by means of IR and ^1H and ^{31}P NMR spectroscopy, as well as from elemental analysis as

the mixed-ligand derivatives $[Fe_2(\mu\text{-CO})(CO)_4(\mu\text{-dppm})(\mu\text{-dmpm})]$, $[Fe_2(\mu\text{-CO})(CO)_4(\mu\text{-dppm})\{\mu\text{-R}_2PN(R')PR_2\}]$ or $[Fe_2(\mu\text{-CO})(CO)_4(\mu\text{-dppm})(\mu\text{-dpam})]$, respectively.

Both the solid-state and the solution IR spectra of these compounds exhibited band patterns in the C—O stretching region similar to those for $[Fe_2(\mu\text{-CO})(CO)_4(\mu\text{-dppm})_2]$ and $[Fe_2(\mu\text{-CO})(CO)_4(\mu\text{-dmpm})_2]$,[18] the structures of which have been established X-ray crystallographically (*vide infra* and ref. 19), while the $^{31}P\{^1H\}$ NMR spectra of $[Fe_2(\mu\text{-CO})(CO)_4(\mu\text{-dppm})(\mu\text{-dmpm})]$ and $[Fe_2(\mu\text{-CO})(CO)_4(\mu\text{-dppm})\{\mu\text{-R}_2PN(R')PR_2\}]$ contained sets of resonances of AA'BB' patterns. These results are interpreted in terms of the structures illustrated in **5** and **6** respectively; the singlet observed in the $^{31}P\{^1H\}$ NMR spectrum of $[Fe_2(\mu\text{-CO})(CO)_4(\mu\text{-dppm})(\mu\text{-dpam})]$ is consistent with **7**. Significantly, in contrast to $[Fe_2(\mu\text{-CO})(CO)_4(\mu\text{-dppm})_2]$, which degrades on alumina or silica gel columns or even on standing in solution in aromatic solvents, the above mixed-ligand complexes could be purified by column chromatography; any degradation is readily monitored by means of $^{31}P\{^1H\}$ NMR spectroscopy. A compound of the type $[Fe_2(\mu\text{-CO})(CO)_4(\mu\text{-dppm})\{\mu\text{-R}_2PN(R')PR_2\}]$, for instance, would afford two singlets instead of an AA'BB' pattern of peaks if it underwent ligand scrambling to give $[Fe_2(\mu\text{-CO})(CO)_4(\mu\text{-dppm})_2]$ and $[Fe_2(\mu\text{-CO})(CO)_4\{\mu\text{-R}_2PN(R')PR_2\}_2]$. Furthermore, the solubility of $[Fe_2(\mu\text{-CO})(CO)_4(\mu\text{-dppm})_2]$ is limited even in solvents such as dichloromethane, whereas the mixed dppm/tetraalkoxydiphosphazane-bridged derivatives are relatively soluble and as a consequence are far more amenable for further study.

Mixed-ligand pentacarbonyl derivatives derived from $[Fe_2(\mu\text{-CO})(CO)_6(\mu\text{-dmpm})]$ have also been synthesized. Thus, treatment of a solution of the latter, readily synthesized from $[Fe_2(CO)_9]$ and dmpm, with an excess of $(MeO)_2PN(Et)P(OMe)_2$ or $(EtO)_2PN(Me)P(OEt)_2$ and irradiation of the resultant solution with UV light was shown to produce the mixed-ligand complexes $[Fe_2(\mu\text{-CO})(CO)_4(\mu\text{-dmpm})\{\mu\text{-(RO)}_2PN(R')P(OR)_2\}]$ (R' = Et, R = Me; R' = Me, R = Et) (**8**), characterized by elemental analysis as well as by spectroscopic (IR and $^{31}P\{^1H\}$ NMR) methods.

Attempts were made to synthesize $[Fe_2(\mu\text{-CO})(CO)_4(\mu\text{-dpam})_2]$ and $[Fe_2(\mu\text{-CO})(CO)_4(\mu\text{-dppea})_2]$ [dppea = $Ph_2PN(Et)PPh_2$], but in contrast to the relative ease of synthesis of $[Fe_2(\mu\text{-CO})(CO)_4(\mu\text{-dppm})_2]$ and $[Fe_2(\mu\text{-CO})(CO)_4(\mu\text{-dmpm})_2]$ all efforts proved unsuccessful. Furthermore, the dppea-bridged heptacarbonyl species $[Fe_2(\mu\text{-CO})(CO)_6(\mu\text{-dppea})]$ (**9**), which could be isolated as a brown microcrystalline solid from light petroleum, was found to readily degrade in toluene solution to the mononuclear derivative $[Fe(CO)_3(dppea)]$, characterized X-ray crystallographically.[20]

Crystal structure of $[Fe_2(\mu\text{-CO})CO)_4(\mu\text{-dppm})_2]\cdot 2Me_2CO$

In attempts to obtain single crystals of the mixed-ligand complex $[Fe_2(\mu\text{-CO})(CO)_4(\mu\text{-dppm})(\mu\text{-dppea})]$ it was found that the first batch of crystals which separated on crystallizing this species from acetone at −10°C were in fact of $[Fe_2(\mu\text{-CO})(CO)_4(\mu\text{-ddpm})_2]$. Second and subsequent crops afforded single crystals of $[Fe_2(\mu\text{-CO})(CO)_4(\mu\text{-dppm})(\mu\text{-dppea})]$, but these were found to be disordered. The structure of $[Fe_2(\mu\text{-CO(CO)}_4(\mu\text{-}$

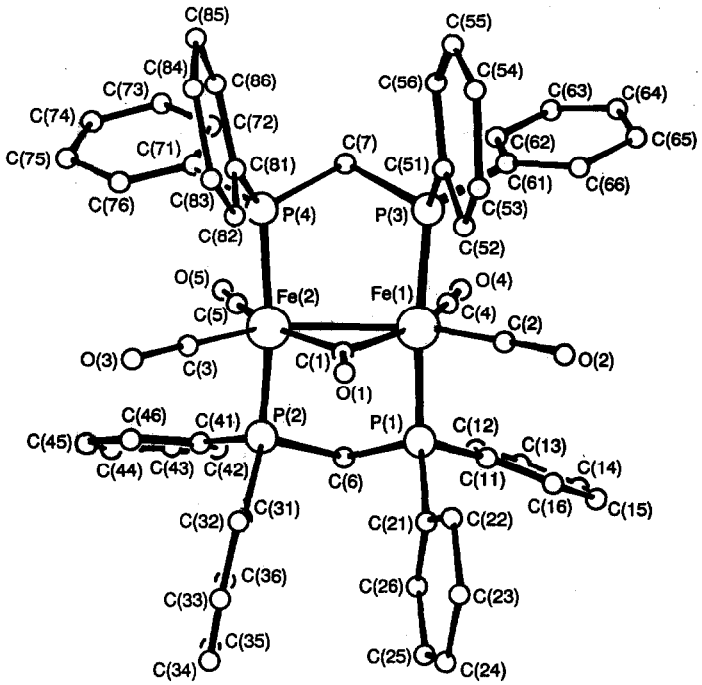

Fig. 1. Molecular stereochemistry of $[Fe_2(\mu\text{-CO})(CO)_4(\mu\text{-dppm})_2]$, showing the atom labelling scheme.

dppm)$_2$] was established X-ray crystallographically and the stereochemistry of the compound is illustrated in Fig. 1. The two iron atoms, which are separated by a distance of 2.742(4) Å corresponding to a formal iron–iron bond, are bridged by the two dppm ligands, *trans* disposed with respect to each other, as well as by a carbonyl group, symmetrically positioned with respect to the iron–iron vector. The remaining four carbonyls are terminal and essentially co-planar with the bridging carbonyl and the two iron atoms, with the plane defined by these groups being essentially orthogonal to the one defined by the four phosphorus and the two iron atoms. The two equatorial carbonyls subtend angles of 111.1(7)° and 113.6(7)° with the iron–iron vector, while the two axial carbonyls subtend angles of 140.8(7)° and 146.7(8)° with it. The structure is thus analogous to those established previously for $[Fe_2(\mu\text{-CO})(CO)_4\{\mu\text{-(EtO)}_2\text{POP(OEt)}_2\}_2]$,[21] $[Fe_2(\mu\text{-CO})(CO)_4\{\mu\text{-F}_2\text{PN(Me)PF}_2\}_2]$,[22] $[Fe_2(\mu\text{-CO})(CO)_4\{\mu\text{-Me}_2\text{PCH}_2\text{PMe}_2\}_2]$[19] and $[Ru_2(\mu\text{-CO})(CO)_4\{\mu\text{-(MeO)}_2\text{PN(Et)P(OMe)}_2\}_2]$.[18]

Protonation studies

As communicated previously[15a] reaction of the diphosphazane-bridged derivatives $[Fe_2(\mu\text{-CO})(CO)_4\{\mu\text{-(RO)}_2\text{PN(R')P(OR)}_2\}_2]$ (R' = Et, R = Me, Pr^i or Ph; R' = Me, R = Et) (**10**) with tetrafluoroboric acid diethyletherate in either ether or benzene was found to afford products identified as $[Fe_2(\mu\text{-H})(CO)_4\{\mu\text{-(RO)}_2\text{PN(Et)P(OR)}_2\}_2]BF_4$ (**11**, BF_4), which, according to IR and NMR spectroscopic evidence, contain a bridging hydride as well as bridging diphosphazane ligands. These protonations are reversible, however, with the cationic hydrides being readily deprotonated in the absence of excess acid by the solvent utilized and with the ease of deprotonation increasing along the series R = Et < Pr^i < Me < Ph.

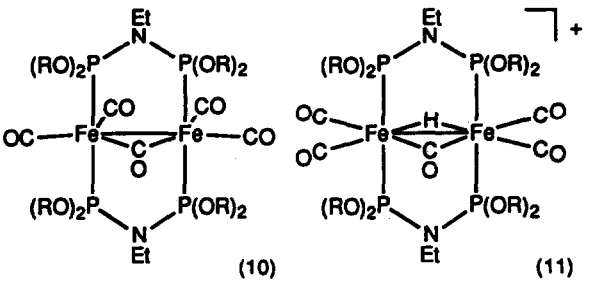

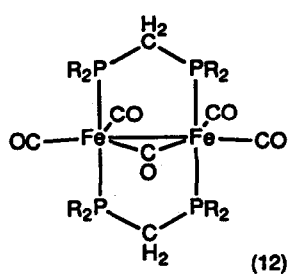

Protonation of the dppm- and dmpm-bridged derivatives $[Fe_2(\mu\text{-}CO)(CO)_4(\mu\text{-}dppm)_2]$ (**12**, R = Ph) and $[Fe_2(\mu\text{-}CO)(CO)_4(\mu\text{-}dmpm)_2]$ (**12**, R = Me) by both tetrafluoroboric acid diethyletherate and trifluoroacetic acid was also shown to lead to the formation of hydride-bridged products, viz. $[Fe_2(\mu\text{-}H)(\mu\text{-}CO)(CO)_4(\mu\text{-}dppm)_2]$Anion (Anion = BF_4 or CF_3COO) (**13**, Anion; R = Ph) and $[Fe_2(\mu\text{-}H)(\mu\text{-}CO)(CO)_4(\mu\text{-}dmpm)_2]$Anion (**13**, Anion; R = Me). However, in contrast to the corresponding diphosphazane-bridged derivatives, these compounds are relatively stable to deprotonation, with strong bases such as $NaBH_4$ being required to remove the proton.

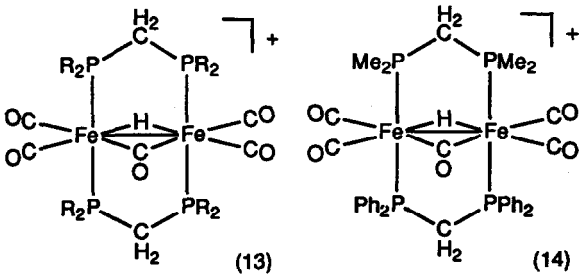

(13)

(14)

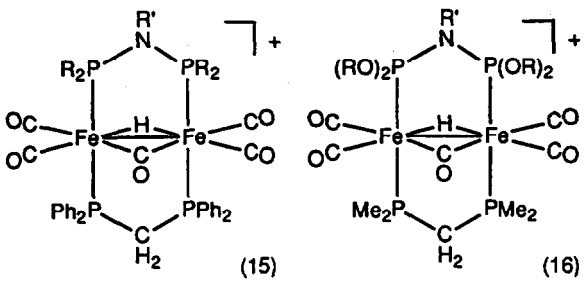

(15)

(16)

Not surprisingly hydride-bridged products, viz. $[Fe_2(\mu\text{-}H)(\mu\text{-}CO)(CO)_4(\mu\text{-}dppm)(\mu\text{-}dmpm)]BF_4$ (**14**, BF_4), $[Fe_2(\mu\text{-}H)(\mu\text{-}CO)(CO)_4(\mu\text{-}dppm)\{\mu\text{-}(RO)_2PN(R')P(OR)_2\}]BF_4$ (**15**, BF_4) and $[Fe_2(\mu\text{-}H)(\mu\text{-}CO)(CO)_4(\mu\text{-}dmpm)\{\mu\text{-}(RO)_2PN(R')P(OR)_2\}]BF_4$ (**16**, BF_4), were isolated from the reactions of the mixed-ligand complexes $[Fe_2(\mu\text{-}CO)(CO)_4(\mu\text{-}dppm(\mu\text{-}dmpm)]$ (**5**), $[Fe_2(\mu\text{-}CO)(CO)_4(\mu\text{-}dppm)\{\mu\text{-}R_2PN(R')PR_2\}]$ (R' = Et, R = Ph or OMe; R' = Me, R = OEt) (**6**) and $[Fe_2(\mu\text{-}CO)(CO)_4(\mu\text{-}dmpm)\{\mu\text{-}(RO)_2PN(R')P(OR)_2\}]$ (R' = Et, R = OMe; R' = Me, R = OEt) (**8**), respectively, with HBF_4 etherate. Selected examples of these compounds were characterized fully, while the others were identified spectroscopically; the relevant spectral features of these compounds were the presence of a set of four peaks of a particular pattern in the terminal carbonyl stretching region and a single peak in the bridging carbonyl region of their IR spectra, a quintet readily assigned to a bridging hydride in their ^1H NMR spectra and either an AA'BB' or an AA'XX' pattern of peaks in their $^{31}P\{^1H\}$ NMR spectra (*vide* Figs 2 and 3, respectively). Significantly, these complexes are considerably more stable to deprotonation than the diphosphazane-bridged species $[Fe_2(\mu\text{-}H)(\mu\text{-}CO)(CO)_4\{\mu\text{-}(RO)_2PN(Et)P(OR)_2\}_2]BF_4$ (**11**, BF_4), and at the same time considerably more soluble in the more common polar organic solvents than $[Fe_2(\mu\text{-}H)(\mu\text{-}CO)(CO)_4(\mu\text{-}dppm)_2]BF_4$ (**13**, BF_4, R = Ph) and as such, similar to their parent compounds, are ideal precursors for further study.

EXPERIMENTAL

All reactions were carried out using Schlenk line techniques under nitrogen. Chromatographic separations (on silica gel columns) and photochemical experiments were performed under nitrogen and argon atmospheres, respectively. All solvents (best grade available) were pre-dried using recommended agents and were freshly distilled prior to use. The IR spectra were recorded with Philips Pye–Unicam SP3-200 spectrophotometer using cells with KBr windows, while NMR spectra were measured on a Varian FT80A instrument using TMS (internal) and H_3PO_4 (external) as references for the ^1H NMR and $^{31}P\{^1H\}$ NMR spectral measurements, respectively. The ligands $Ph_2PCH_2PPh_2$, $Ph_2AsCH_2AsPh_2$ and $Me_2PCH_2PMe_2$ were purchased from Strem Chemicals and used without further purification. The diphosphazane ligands $Ph_2PN(Et)PPh_2$ and $(RO)_2PN(R')P(OR)_2$ (R' = Et, R = Me, Pr^i or Ph; R' = Me, R = Et) were synthesized according to known methods,[23,24] which were modified to improve yields. $[Fe_2(\mu\text{-}CO)(CO)_4(\mu\text{-}dppm)_2]$, $[Fe_2(\mu\text{-}CO)(CO)_4(\mu\text{-}dmpm)_2]$, $[Fe_2(\mu\text{-}CO)(CO)_4\{\mu\text{-}(RO)_2PN(Et)P(OR)_2\}_2]$ (R = Me, Pr^i or Ph), $[Fe_2(\mu\text{-}CO)(CO)_6(\mu\text{-}dppm)]$ and $[Fe_2(\mu\text{-}CO)(CO)_6(\mu\text{-}dpmpm)]$ were also synthesized according to literature procedures.[17,18] Elemental analyses (carbon, hydrogen and nitrogen) were performed by the Microanalytical Section of the Department of Chemistry, University of Natal, Pietermaritzburg.

Synthesis of mixed-ligand complexes

All mixed-ligand complexes were synthesized by very similar methods. Typically, the red–brown oil of $[Fe_2(\mu\text{-}CO)(CO)_6(\mu\text{-}dppm)]$ or $[Fe_2(\mu\text{-}CO)(CO)_6(\mu\text{-}dmpm)]$, obtained from the reaction of $[Fe_2(CO)_9]$ with $Ph_2PCH_2PPh_2$ and $Me_2PCH_2PMe_2$, respectively, was transferred to the photochemical reactor, together with light petroleum (*ca* 120 cm^3; 60–80°C), and a stoichiometric amount of the second ligand dissolved in a suitable solvent (3–5 cm^3) was added. The stirred reaction mixture

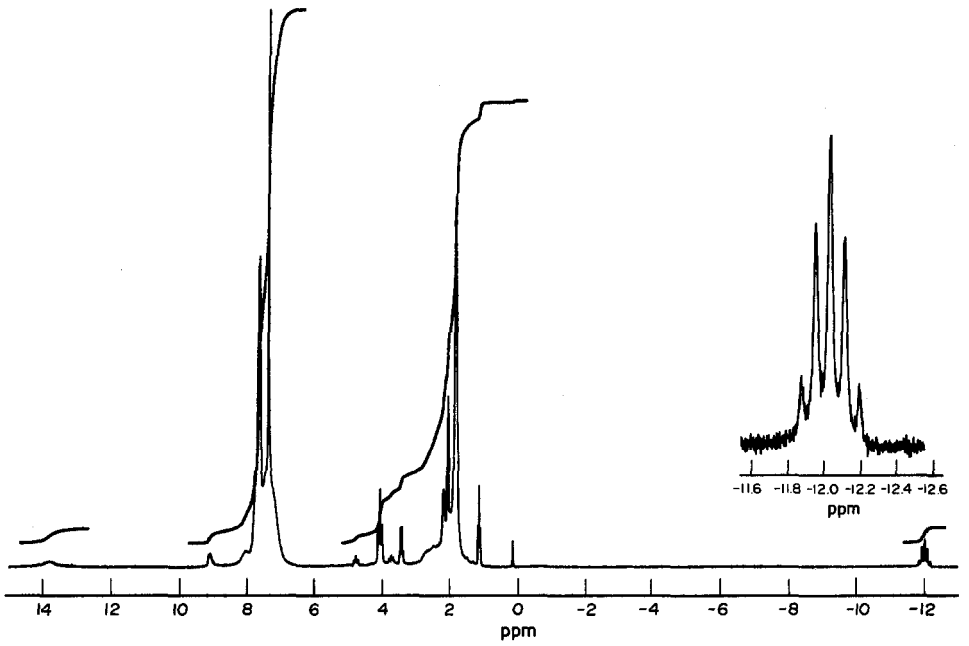

Fig. 2. ^1H NMR spectrum of $[Fe_2(\mu\text{-}H)(\mu\text{-}CO(CO)_4(\mu\text{-}dppm)(\mu\text{-}dmpm)]BF_4$ measured in acetone-d_6.

(under an atmosphere of argon) was irradiated by means of a 125 W or a 250 W medium-pressure mercury vapour lamp for a period of 6–30 h. The yield of the product, isolated as a light to dark brown microcrystalline material from this reaction mixture, ranged from 50 to 85%. The analyses and the spectral data for the compounds synthesized are summarized in Tables 1 and 2, respectively.

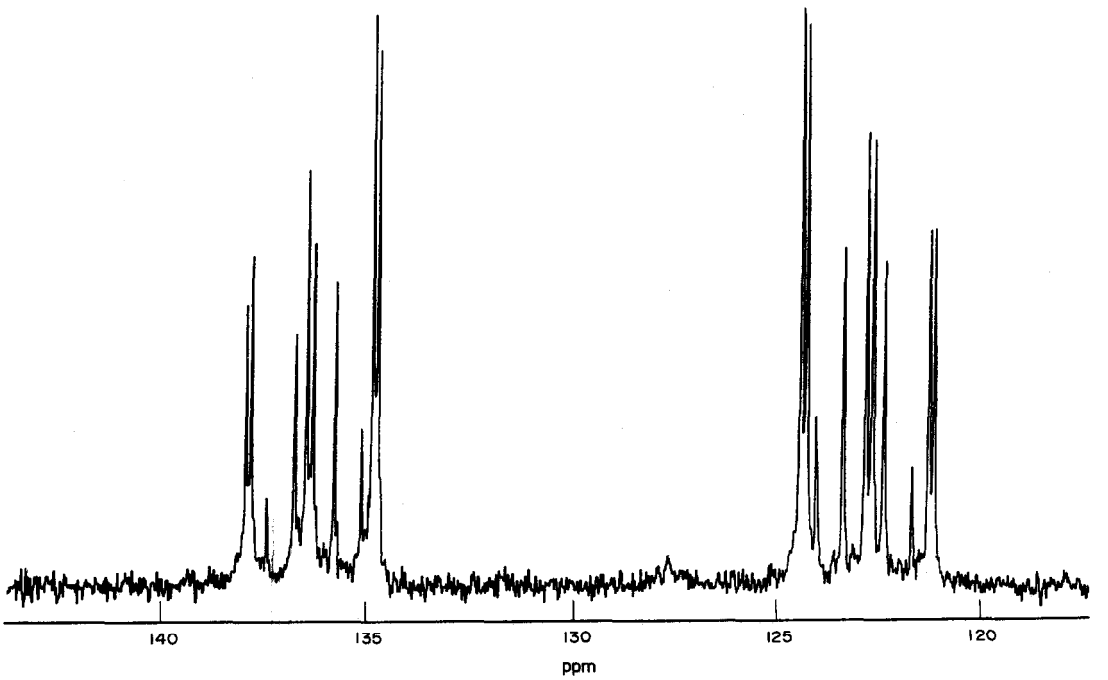

Fig. 3. $^{31}P\{^1H\}$ NMR spectrum of $[Fe_2(\mu\text{-}H)(\mu\text{-}CO)(CO)_4(\mu\text{-}dppm)(\mu\text{-}dmpm)]BF_4$ measured in acetone-d_6.

Table 1. Microanalytical data

Compound	Analysis: Found (Calc) (%) C	H	N
$[Fe_2(\mu\text{-CO})(CO)_4(\mu\text{-(dppm)}_2)(\mu\text{-L-L})]$			
L-L			
$(Me)_2PCH_2P(Me)_2$	46.1	2.8	—
	(46.7)	(2.9)	—
$(Ph)_2PN(Et)P(Ph)_2$	64.0	4.4	1.3
	(64.1)	(4.5)	(1.3)
$(Ph)_2AsCH_2As(Ph)_2$	59.4	3.9	—
	(59.6)	(4.0)	—
$(MeO)_2PN(Et)P(OMe)_2$	49.9	4.5	1.6
	(50.0)	(4.5)	(1.6)
$(EtO)_2PN(Me)P(OEt)_2$	51.5	4.8	1.5
	(51.6)	(5.0)	(1.5)
$[Fe_2(\mu\text{-CO})(CO)_4(\mu\text{-(dmpm)}_2)(\mu\text{-L-L})]$			
L-L			
$(MeO)_2PN(Et)P(OMe)_2$	30.9	5.0	2.0
	(31.1)	(5.0)	(2.3)
$(EtO)_2PN(Me)P(OEt)_2$	34.2	5.3	2.1
	(34.6)	(5.6)	(2.1)
$[Fe_2(\mu\text{-H})(\mu\text{-CO})(CO)_4(\mu\text{-dppm})(\mu\text{-L-L})]BF_4$			
L-L			
$Ph_2PCH_2PPh_2$	59.6	4.1	—
	(59.0)	(4.2)	—
$Me_2PCH_2PMe_2$	48.2	4.2	—
	(48.9)	(4.3)	—
$[Fe_2(\mu\text{-H})(\mu\text{-CO})(CO)_4(\mu\text{-dmpm})(\mu\text{-L-L})]BF_4$			
L-L			
$(MeO)_2PN(Et)P(OMe)_2$	27.0	4.4	1.9
	(27.3)	(4.4)	(2.0)
$(EtO)_2PN(Me)P(OEt)_2$	30.1	5.0	1.8
	(30.5)	(5.1)	(1.9)

Protonation reactions

All protonation reactions were carried out using the same general procedure. A slight excess of tetrafluoroboric acid diethyletherate in ether or trifluoroacetic acid in benzene (*ca* 30 cm^3) was added dropwise to a stirred solution of $[Fe_2(\mu\text{-CO})(CO)_4(\mu\text{-dppm})_2]$, $[Fe_2(\mu\text{-CO})(CO)_4(\mu\text{-dmpm})_2]$ or the mixed-ligand complex (0.1–0.2 mmol) in benzene (*ca* 30 cm^3) at room temperature and stirring continued until the reaction was complete, as determined by monitoring by means of IR spectroscopy. The red–orange solid that separated from solution was isolated, washed with dry pentane and crystallized from acetone/pentane at −20°C. Yields of the crystalline protonated products varied from 40 to 60%.

The protonated products of the diphosphazane derivatives $[Fe_2(\mu\text{-CO})(CO)_4\{\mu\text{-(RO)}_2PN(Et)P(OR)_2\}_2]$ could not be isolated as a solid material and were identified by spectroscopic means only.

Crystal structure determination

Crystal data. $C_{61}H_{56}Fe_2O_7P_4$, $M = 1136.7$, triclinic, space group $P\bar{1}$, $a = 13.549(8)$, $b = 14.455(9)$, $c = 16.065(9)$ Å, $\alpha = 89.99(4)$, $\beta = 68.75(6)$, $\gamma = 68.63(5)°$, $V = 2698.98$ $Å^3$, $D_c = 1.399$ g cm^{-3}, $Z = 2$, Mo-K_α radiation, $\lambda = 0.71069$ Å, $\mu = 7.053$ cm^{-1}, $F(000) = 1108$.

Intensity data were collected on a Nonius CAD-4 diffractometer using graphite monochromated Mo-K_α radiation. A least-squares fit of 25 high angle reflections ($\theta > 12°$) was used to obtain accurate cell constants. Diffraction intensities were measured in the range $3 < 2\theta < 46°$ using the ω–2θ scan technique, with background counts made for half the total scan time on each side of the peak. Three

Table 2.

Compound	ν(CO)[a] (cm^{-1})	$^{31}P\{^1H\}$ NMR[b]	^1H NMR[c]
$[Fe_2(\mu\text{-CO})(CO)_4(\mu\text{-dppm})(\mu\text{-L-L})]$			
$Me_2PCH_2PMe_2$	1955(s), 1905(vs), 1878(ms), 1856(sh), 1689(m)[d]		
	1949(s), 1902(ms), 1883(ms) 1855(m), 1680(s)[f]	129.7[e]	—
$Ph_2PN(Et)PPh_2$	1972(ms), 1917(vs), 1894(vs), 1873(ms), 1702(m), 1689(m)[d]		
	1969(ms), 1919(ms), 1889(ms), 1871(ms), 1688(ms)[f]	123.6[e]	—
$Ph_2AsCH_2AsPh_2$	1960(s), 1910(vs), 1884(ms), 1862(sh), 1700(m)[d]		
	1960(s), 1910(ms), 1879(ms), 1864(sh), 1695(s)[f]	180.7[g]	—
$(MeO)_2PN(Et)P(OMe)_2$	1979(ms), 1938(vs), 1903(vs), 1881(ms), 1700(ms)[d]		
	1980(ms), 1928(ms), 1900(ms), 1869(ms), 1696(ms)[f]	197.6,[h] 81.7[i]	—
$(EtO)_2PN(Me)P(OEt)_2$	1980(m), 1929(ms), 1901(ms), 1882(sh), 1703(m)[d]		
	1990(w), 1974(s), 1942(m), 1920(ms), 1891(ms), 1876(m), 1717(m), 1696(m)[f]	195.9[h], 86.9[i]	—
$[Fe_2(\mu\text{-CO})(CO)_4(\mu\text{-dmpm})(\mu\text{-L-L})]$			
$(MeO)_2PN(Et)P(OMe)_2$	1972(ms), 1921(vs), 1896(vs), 1872(ms), 1700(m), 1688(w, sh)[d]		
	1980(s), 1928(ms), 1903(ms), 1881(ms), 1682(s)[f]	280.6,[h] 129.6[i]	—
$(EtO)_2PN(Me)P(OEt)_2$	1972(s), 1922(ms), 1895(ms) 1774(ms), 1700(m), 1690(m)[d]		
	1974(ms), 1918(ms), 1686(ms) 1673(ms), 1701(ms)[f]	260.0,[h] 133.7[i]	—
$[Fe_2(\mu\text{-CO})(CO)_4(\mu\text{-L-L})_2]BF_4$			
$Ph_2PCH_2PPh_2$	2010(s), 1957(ms), 1730(ms)[d]	190.2[g]	−11.6[j]
$Me_2PCH_2PMe_2$	1998(s), 1952(vs), 1720(ms)[d]	149.8[g]	−10.7[j]
$(EtO)_2PN(Me)P(OEt)_2$	2025(s), 1985(vs), 1747(s)[f]	—	−9.5[j]
$(PhO)_2PN(Et)P(OPh)_2$	2070(w), 2008(s), 1990(s), 1760(vw)[d]	—	Unstable
$(MeO)_2PN(Et)P(OMe)_2$	2020(s), 1975(s), 1958(s)[f]	—	−10.5[j]
$(Pr^iO)_2PN(Et)P(OPr^i)_2$	2060(w), 2005(s), 1975(s), 1760(vw)[d]	—	Unstable
$[Fe_2(\mu\text{-H})(\mu\text{-CO})(CO)_4(\mu\text{-dppm})(\mu\text{-L-L})]BF_4$			
$Me_2PCH_2PMe_2$	2010(s), 1965(vs), 1730(ms)[d]	130.0[e]	−12.0[j]
$(MeO)_2PN(Et)P(OMe)_2$	2010(vs), 1980(vs), 1740(ms)[d]	187.9,[h] 71.4[i]	−11.6[j]
$Ph_2PN(Et)PPh_2$	2010(s), 1975(s), 1725(m)[d]	166.9[e]	−11.0[j]
$(EtO)_2PN(Me)P(OEt)_2$	2060(w), 2017(s), 1997(vs) 1920(w)[d]	180.2,[h] 71.2[i]	−11.5[j]
$[Fe_2(\mu\text{-H})(\mu\text{-CO})(CO)_4(\mu\text{-dmpm})(\mu\text{-L-L})]BF_4$			
$(MeO)_2PN(Et)P(OMe)_2$	2015(s), 1980(vs), 1742(ms)[d]	134.6[e]	−11.0[j]
$(EtO)_2PN(Me)P(OEt)_2$	2000(s), 1975(s), 1725(ms)[d]	140.3[e]	−10.3[j]

[a] Abbreviations: vs, very strong; s, strong; ms, medium strong; m, medium; w, weak; sh, shoulder; vw, very weak.

[b] Measured in acetone-d_6; δ scale in ppm relative to H_3PO_4.

[c] Measured in acetone-d_6; δ scale in ppm relative to TMS.

[d] Measured in CH_2Cl_2.

[e] Centre of an AA′BB′ pattern of peaks.

[f] Measured as a Nujol mull.

[g] Singlet.

[h] Centre of AA′ part of AA′XX′ spectrum.

[i] Centre of XX′ part of AA′XX′ spectrum.

[j] Quintet assigned to a bridging hydride.

Table 3. Selected interatomic distances (Å) for $[Fe_2(\mu\text{-CO})(CO)_4(\mu\text{-dppm})_2]\cdot 2Me_2CO$

Fe(1)—Fe(2)	2.742(4)	Fe(1)—P(1)	2.265(7)
Fe(1)—P(3)	2.275(7)	Fe(1)—C(1)	2.00(2)
Fe(1)—C(2)	1.77(2)	Fe(1)—C(4)	1.82(2)
Fe(2)—P(2)	2.261(7)	Fe(2)—P(4)	2.258(7)
Fe(2)—C(1)	1.99(2)	Fe(2)—C(3)	1.76(2)
Fe(2)—C(5)	1.85(2)	P(1)—C(6)	1.83(2)
P(2)—C(6)	1.89(2)	P(3)—C(7)	1.83(2)
P(4)—C(7)	1.83(2)		

Table 4. Selected interatomic angles (°) for $[Fe_2(\mu\text{-CO})(CO)_4(\mu\text{-dppm})_2]\cdot 2Me_2CO$

Fe(2)—Fe(1)—P(1)	92.8(2)	Fe(2)—Fe(1)—P(3)	92.7(2)
P(1)—Fe(1)—P(3)	174.4(3)	Fe(2)—Fe(1)—C(1)	46.4(6)
P(1)—Fe(1)—C(1)	91.3(6)	P(3)—Fe(1)—C(1)	91.8(6)
Fe(2)—Fe(1)—C(2)	146.7(8)	P(1)—Fe(1)—C(2)	88.1(7)
P(3)—Fe(1)—C(2)	86.7(7)	P(1)—Fe(1)—C(4)	91.2(7)
Fe(2)—Fe(1)—C(4)	111.1(7)	Fe(1)—Fe(2)—P(2)	93.9(2)
P(3)—Fe(1)—C(4)	87.8(7)	C(2)—Fe(1)—C(4)	102.1(10)
Fe(1)—Fe(2)—P(4)	93.2(2)	P(2)—Fe(2)—P(4)	171.5(3)
Fe(1)—Fe(2)—C(1)	46.8(6)	P(2)—Fe(2)—C(1)	94.2(6)
P(4)—Fe(2)—C(1)	94.1(6)	Fe(1)—Fe(2)—C(3)	140.8(7)
P(2)—Fe(2)—C(3)	88.2(7)	P(4)—Fe(2)—C(3)	89.2(7)
C(1)—Fe(2)—C(3)	94.1(9)	Fe(1)—Fe(2)—C(5)	113.6(7)
P(2)—Fe(2)—C(5)	86.5(7)	Fe(1)—P(1)—C(6)	111.7(8)
C(1)—Fe(2)—C(5)	160.3(9)	Fe(1)—P(3)—C(7)	108.3(7)
Fe(2)—P(2)—C(6)	111.3(7)	Fe(1)—C(1)—Fe(2)	86.9(8)
Fe(2)—P(4)—C(7)	109.7(7)	P(1)—C(6)—P(2)	107.7(12)
P(3)—C(7)—P(4)	108.8(10)		

standard reflections measured every hour showed no decrease in intensity during data collection. Lorentz and polarization as well as empirical absorption corrections were made. Of the 6716 unique reflections measured 2892 were classed as observed $[I > 3\sigma(I)]$ and these were used for the solution and refinement of the structure.

The structure was solved by conventional Patterson and Fourier techniques. Hydrogen atoms were not located and, because of disorder problems, both of the acetone solvent molecules were refined as rigid groups. All of the non-hydrogen atoms were assigned anisotropic temperature factors, except the phenyl carbon atoms which were assigned isotropic thermal parameters. The phenyl rings were also refined as rigid groups. A weighted full-matrix least-squares refinement (319 variables) converged at $R = 0.099$, $R_w = 0.106$. A final difference Fourier was featureless. Complex neutral scattering factors were taken from tables[25] and the program SHELX-76 was used for the calculations.[26] Selected interatomic distances and angles are given in Tables 3 and 4, respectively.*

Acknowledgements—The authors express their sincere thanks to the Foundation for Research Development, and the Universities of Durban–Westville and Natal for financial support, Dr D. H. Pienaar and Mr M. Watson for the measurement of NMR spectra, Miss N. Ramesar for intensity data collection and Miss I. Govender for experimental assistance.

REFERENCES

1. R. J. Puddephatt, *Chem. Soc. Rev.* 1983, **12**, 99.
2. R. H. Hill and R. J. Puddephatt, *J. Am. Chem. Soc.* 1983, **105**, 5797; M. P. Brown, J. R. Fischer, R. H. Hill, R. J. Puddephatt and K. R. Seddon, *Inorg. Chem.* 1981, **20**, 3516; Lj. Manojlovic-Muir and K. W. Muir, *J. Organomet. Chem.* 1981, **219**, 129.
3. A. J. McLennan and R. J. Puddephatt, *J. Chem. Soc., Chem. Commun.* 1986, 422.

*Atomic coordinates have been deposited at the Cambridge Crystallographic Data Centre.

4. E. Meintjies, unpublished results; R. J. Haines, M. Laing and E. Meintjies, *Inorg. Chim. Acta Lett.* 1979, **36**, L403.
5. R. J. Haines, M. Laing, E. Meintjies and P. Sommerville, *J. Organomet. Chem.* 1981, **215**, C17.
6. C. P. Kubiak and R. Eisenberg, *J. Am. Chem. Soc.* 1980, **102**, 3637; C. P. Kubiak, C. Woodcock and R. Eisenberg, *Inorg. Chem.* 1982, **21**, 2119; C. Woodcock and R. Eisenberg, *Inorg. Chem.* 1984, **23**, 4207; C. Woodcock and R. Eisenberg, *Inorg. Chem.* 1985, **24**, 1285.
7. D. H. Berry and R. Eisenberg, *J. Am. Chem. Soc.* 1985, **107**, 7181; D. H. Berry and R. Eisenberg, *Organometallics* 1987, **6**, 1796.
8. J. A. Jenkins and M. Cowie, *Organometallics* 1992, **11**, 2767.
9. B. R. Sutherland and M. Cowie, *Organometallics* 1985, **4**, 1637.
10. R. McDonald and M. Cowie, *Organometallics* 1990, **9**, 2468.
11. M. K. Reinking, J. Ni, P. E. Fanwick and C. P. Kubiak, *J. Am. Chem. Soc.* 1989, **111**, 6459.
12. C. P. Kubiak, personal communication.
13. J. Wu, M. K. Reinking, P. E. Fanwick and C. P. Kubiak, *Inorg. Chem.* 1987, **26**, 247.
14. J. Wu, P. E. Fanwick and C. P. Kubiak, *J. Am. Chem. Soc.* 1989, **111**, 7812.
15. (a) J. S. Field, R. J. Haines, C. N. Sampson, J. Sundermeyer and K. G. Moodley, *J. Organomet. Chem.* 1987, **322**, C7; (b) J. S. Field, R. J. Haines, E. Minshall, C. N. Sampson, J. Sundermeyer and S. F. Woollam, *J. Chem. Soc., Dalton Trans.* 1992, 2629.
16. K. A. Johnson and W. L. Gladfelter, *Organometallics* 1989, **8**, 2866.
17. F. A. Cotton and J. M. Troup, *J. Am. Chem. Soc.* 1974, **96**, 4422.
18. G. de Leeuw, J. S. Field, R. J. Haines, B. McCulloch, E. Meintjies, C. Monberg, G. M. Olivier, P. Ramdial, C. N. Sampson, B. Sigwarth, N. D. Steen and K. G. Moodley, *J. Organomet. Chem.* 1984, **275**, 99.
19. W. K. Wong, K. W. Chiu, G. Wilkinson, M. Motevalli and M. B. Hursthouse, *Polyhedron* 1985, **4**, 1231.
20. E. C. Horsfield, D. W. Engel and K. G. Moodley, *Acta Cryst.* 1988, **C44**, 80.
21. F. A. Cotton, R. J. Haines, B. E. Hanson and J. C. Sekutowski, *Inorg. Chem.* 1978, **17**, 2010.
22. M. G. Newton, R. B. King, M. Chang and J. Gimeno, *Inorg. Chem.* 1978, **17**, 2390.
23. G. Ewart, A. P. Lane, J. McKechinie and D. S. Payne, *J. Chem. Soc.* 1964, 1543.
24. E. Meintjies, PhD thesis, University of Natal (1981).
25. *International Tables for X-ray Crystallography*, Vol. IV. Kynoch Press, Birmingham (1974).
26. G. M. Sheldrick, SHELX-76, Program for Crystal Structure Determination. University of Cambridge (1976).

Polyhedron Vol. 12, No. 5, pp. 543–548, 1993
Printed in Great Britain

0277–5387/93 $6.00+.00
© 1993 Pergamon Press Ltd

RIGIDITY OF DONOR ATOMS' TOPOLOGY: SYNTHESIS AND SPECTROSCOPIC CHARACTERIZATION OF COPPER(II) AND COPPER(II)-DOPED ZINC(II) COMPLEXES HAVING THE CHROMOPHORE MN_4

S. MANDAL and P. K. BHARADWAJ*

Department of Chemistry, Indian Institute of Technology, Kanpur 208016, India

(*Received* 13 *May* 1992; *accepted* 6 *October* 1992)

Abstract—A new acyclic ligand has been synthesized by Schiff base condensation of 2-dimethylaminoethyl amine with diisobutyraldehyde disulphide, which can coordinate to a metal ion through four nitrogens. Introduction of a large bite angle for two nitrogens forces the coordination geometry around a metal ion to distort from planarity towards tetrahedral. The presence of a disulphide linkage along with two imine linkages make the ligand somewhat neoplastic so that the four nitrogens can impose a pseudo-tetrahedral geometry upon a metal ion overcoming its own preference for a particular geometry. The electronic spectral results when compared with the square planar complex $Cu(L)_2(ClO_4)_2$ (L = 2-dimethylaminoethyl amine) are consistent with a pseudo-tetrahedral coordination geometry for copper(II). We have tested the rigidity of the donor atoms' topology through synthesis and characterization of neat copper(II) and copper(II)-doped zinc(II) complexes. ESR spectral results show that the neat copper(II) as well as the copper(II)-doped zinc(II) complexes give axial spectra and almost identical $g_\parallel$ and $A_\parallel$ values, which are attributable to similar pseudo-tetrahedral coordination. Thus, the ligand-field driven tendencies of zinc(II) to form tetrahedral complexes of copper(II) to form square planar complexes with four nitrogen donors are overcome through ligand design. The neat copper(II) complex shows a quasi-reversible copper(II)/copper(I) couple at $E_{1/2} = +0.18$ V (vs SCE), which is shifted by more than +450 mV compared to the square-planar analogue $Cu(L)_2(ClO_4)_2$.

Simple monodentate or bidentate N-donor ligands favourably form square-planar complexes with copper(II) and tetrahedral complexes with zinc(II) ions. Thus, it is possible, in principle, to test the rigidity of the donor atoms' topology of any ligand by complexing it with copper(II), as well as zinc(II), and observing whether imposition of a particular coordination geometry can be effected onto the aforesaid metal ions. Studies of this kind have bioinorganic relevance. Metalloproteins having intrinsic active sites[1] are often characterized by low symmetry of coordination geometry. In these proteins the amino acid side-chains of the protein backbone provide the donor atoms imposing a low symmetry of coordination onto the metal ions. The low symmetry arises due to conformationally imposed constraints upon amino acid side-chains that comprise the donors. This imposition of an irregular geometry is designed by nature[2] to achieve a condition energetically favourable to carry out its assigned biological role(s). Recently, the synthesis of a geometrically constrained bidentate imidazole derivative has been reported,[3] which forms pseudo-tetrahedral (D_{2d}) complexes with copper(II), nickel (II), cobalt(II) and zinc(II). Our interest in the imposition of a desired coordination geometry onto metal ions[4] has led us to synthesize the ligand L_1. Examination of molecular models revealed that the ligand with a constrained donor set and a large bite angle should be able to impose a coordination which would be substantially distorted from planarity. To test the rigidity of the donor set a zinc(II) complex with copper(II) as the dopant has been synthesized, in addition to a neat copper(II) complex, and subjected to EPR studies as both g and A values

* Author to whom correspondence should be addressed.

are quite sensitive to the symmetry of coordination.[5] The ligand L is known[6] to form a square-planar complex with copper(II) perchlorate hexahydrate. This complex is included in the present study to compare the spectroscopic and electrochemical characteristics of the copper(II) complexes formed with L and L_1.

EXPERIMENTAL

Materials

Sulphur monochloride and 2-dimethylaminoethyl amine (Merck) were used as received without further purification. Perchlorate salts of copper(II) and zinc(II) were synthesized by treating the corresponding carbonate with aqueous perchloric acid. Isobutyraldehyde (Merck) was distilled prior to use. All the solvents were purified following standard procedures.[7]

Physical measurements were made as reported earlier.[8] Elemental analyses were performed at the Central Drug Research Institute, Lucknow, India.

Synthesis of the ligand and complexes

Synthesis of the ligand was achieved in several steps, as shown schematically in Fig. 1.

Diisobutyraldehyde disulphide. The dialdehyde was prepared by homolytic cleavage of the S—Cl bond by isobutyraldehyde, following a published procedure.[9] Sulphur monochloride (20 g, 0.15 mol) in dry CCl_4 (25 cm^3) was added dropwise to a solution of freshly distilled isobutyraldehyde (21.4 g, 0.30 mol) mixed with dry CCl_4 (40 cm^3), maintaining the temperature at 40–45°C throughout. At the beginning the temperature of the reaction mixture increased rapidly and cooling was necessary. As soon as sulphur monochloride came into contact with isobutyraldehyde copius evolution of HCl gas occurred, which was driven out of the reaction vessel by occasional passage of nitrogen gas. The total addition time was 3 h, after which time the reaction mixture was maintained at 40°C for 48 h for completion of the reaction. To collect the product CCl_4 was evaporated off and the resulting pale yellow, thick liquid was washed several times with distilled water to remove dissolved HCl and finally allowed to distil under reduced pressure. The dialdehyde was obtained as a pale yellow oily liquid (15 mm; 90–100°C; lit.[9] 1 mm; 110–115°C) in 81% yield. ^1H NMR (80 MHz; $CDCl_3$; TMS, ppm): 1.1 (s, 12H), $4CH_3$; 9.0 (s, 2H), 2CHO. The NMR spectral data were in agreement with the reported data.[9] The dialdehyde can easily form Schiff bases with different amines. The X-ray structure of one such compound is available.[10]

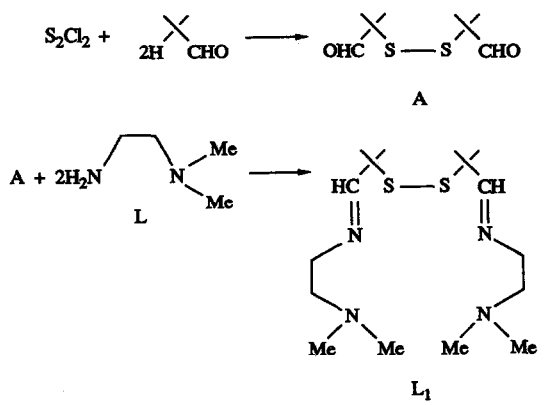

Fig. 1. Schematic diagram for the synthesis of the ligands.

Synthesis of L_1. Diisobutyraldehyde disulphide (2 g, 0.01 mol) was allowed to reflux in the dark and in an atmosphere of purified nitrogen with 2-dimethylaminoethyl amine (1.7 g, 0.02 mol) in dry ethanol (20 cm^3) for 2 h to give an orange solution of the Schiff base. Ethanol was removed completely under reduced pressure and the thick orange liquid was used for complexation without further purification.

Synthesis of $Cu(L_1)\cdot 2ClO_4$ (**1**). When $Cu(H_2O)_6(ClO_4)_2$ (1 g, 0.003 mol) was allowed to react with the ligand L_1 (0.93 g, 0.003 mol) in ethyl acetate a green crystalline solid separated immediately. The solid was collected by filtration and dried *in vacuo*. Yield 42%.

Synthesis of copper(II)*-doped* $Zn(L_1)\cdot 2ClO_4$ (**2**). This was synthesized as above using acetone instead of ethyl acetate as the medium, with nominal 2% doping of copper(II). In a typical experiment a mixture of $Zn(H_2O)_6(ClO)_2$ (1.2 g, 0.003 mol) and $Cu(H_2O)_6(ClO_4)_2$ (0.001 g, 0.003 mmol) was heated with the ligand L_1 (0.95 g, 0.003 mol) in acetone for 30 min. The colour of the solution turned pale green, which on evaporation afforded the product as a pale yellow solid in 53% yield.

Synthesis of $Cu(L)(ClO_4)_2$ (**3**). $Cu(H_2O)_6(ClO_4)_2$ was allowed to stir at room temperature with 2-dimethylaminoethyl amine (L) in a 1 : 2 molar ratio in ethanol to obtain a dark blue solution, which on slow evaporation yielded dark blue plates of **3** in 80% yield.

Analytical data for the complexes are given in Table 1.

RESULTS AND DISCUSSION

Conductivity data (Table 1) ethanol and acetonitrile are consistent[11] with the 1 : 2 electrolytic

Table 1. Conductivity and analytical data[a] for the complexes

Complex	Conductance in CH_3CN (Ω^{-1} cm^2 mol^{-1})	Conductance in Ethanol (Ω^{-1} cm^2 mol^{-1})	Analysis (%) C	H	N
1	263	82	31.9(31.5)	6.1(5.6)	9.0(9.2)
3	266	83	21.5(21.9)	5.3(5.5)	12.6(12.8)

[a] Calculated values are given in parentheses.

nature of the complexes. IR spectra of the complexes **1–3** show a strong peak around 1610 cm^{-1}. The downward shift in imine stretching frequency is consistent with the fact that the imine nitrogens are coordinated to the metal ion.

Magnetic moment values (Table 2) for the neat copper(II) complexes after diamagnetic corrections are indicative of discrete mononuclear species.[12] EPR data for **1–3** and related complexes are collected in Table 2. In the solid state **1** shows a broad EPR spectrum with $g_{av} = 2.10$, while in acetonitrile solution at room temperature a four-line EPR spectrum ($A_{av} = 79 \times 10^{-4}$ cm^{-1}) is obtained. In acetonitrile glass (liquid nitrogen temperature) **1** shows an axial spectrum which is very similar to that of **2**. The axial nature of the EPR spectra exhibited by each complex is characteristic of copper(II) with the $d_{x^2-y^2}$ ground state. However, the $g_\parallel$ and $A_\parallel$ values (Table 2) are consistent with a geometry that is substantially distorted from planarity[13] for a CuN_4 chromophore. For tetragonal geometry the expressions for $g_\parallel$ and $g_\perp$ are:[1]

$$g_\parallel = g_e + \frac{-8\xi}{\Delta E_{xy}}$$

and

$$g_\perp = g_e + \frac{-2\xi}{\Delta E_{xz,yz}}. \quad (1)$$

E_{xy} is the energy difference between d_{xy} and $d_{x^2-y^2}$ (ground state); similar for $E_{xz,yz}$; ξ is the one electron spin-orbit coupling parameter. The hyperfine couplings are expressed as:

$$A_\parallel = P_d[-\chi - 4/7\alpha^2 + (g_\parallel - 2) + 3/7(g_\perp - 2)]$$

and

$$A_\perp = P_d[-\chi + 2/7\alpha^2 + 11/14(g_\perp - 2)]; \quad (2)$$

where χ is the contribution from the indirect Fermi contact, and the second term is the anisotropic dipolar contribution; P_d is a constant which is *ca* 350×10^{-4} cm^{-1} for the free copper ion. As these equations indicate, $g_\parallel$ and $A_\parallel$ values are dependent on the ligand field strength, specifically in the equatorial plane. Increasing the strength of the ligand field, keeping the geometry unaltered, will lead to a lower value for $g_\parallel$ and a higher value for $A_\parallel$. As the geometry distorts from planar (D_{4h}) towards flattened tetrahedral (D_{2d}), the ligand field strength

Table 2. Room-temperature magnetic and ESR spectral data for the complexes used in this study and related ones

Complex	μ_{eff}/μ_3	$g_\parallel$	$A_\parallel^{Cu}$[a]	Ref.
1	2.01	2.32	150	This work
3		2.33	148	This work
3	2.07	2.218	185	This work
$Cu(en)_2(ClO_4)_2$		2.209	207	14
$Cu(L')_2(ClO_4)_2$		2.25	147	3
Copper(II)-doped $Zn(L')_2(ClO_4)_2$		2.32	118	3
Haemocyanin, half-met nitrite		2.302	125	17
Tyrosinase, half-met nitrite		2.296	131	17
Cu/Zn SOD[b]		2.316	116	18

[a] Unit is 1×10^{-4} cm^{-1}.

[b] Spectrum taken after doping copper(II) into the zinc(II) site.

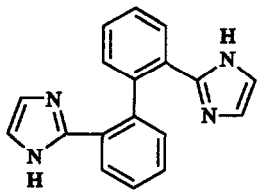

L'

Fig. 2. Ligand L' from ref. 3.

decreases and consequently the $g_{\parallel}$ value increases while $A_{\parallel}$ decreases.[1] Hence, for **1** compared with **3** the increase in $g_{\parallel}(\Delta g_{\parallel} = 0.10)$ and decrease in $A_{\parallel}(\Delta A_{\parallel} = 35 \times 10^{-4}\ cm^{-1})$ are attributable to the distortion of the coordination geometry towards pseudo-tetrahedral. For **2** the $g_{\parallel}$ as well as the $A_{\parallel}$ values do not differ to any significant extent with respect to those found in **1**. This result is consistent with grossly the same coordination geometry in both cases. Schugar *et al.*[3] found that comparing the EPR spectral data for neat copper(II) and copper(II)-doped zinc(II) complexes of the ligand 2,2'-bis(imidazolyl)biphenyl (Fig. 2), the $g_{\parallel}$ as well as the $A_{\parallel}$ values (Table 3) change significantly for a slight change in the dihedral angle describing the tetrahedral geometry.

Electronic spectral data for the complexes are collected in Table 3. Complex **1** in the solid state has features similar to those in acetonitrile solution. This suggests that the chromophore is preserved in acetonitrile solution. Ligand field bands are quite sensitive to the coordination geometry. As the coordination geometry distorts from planarity towards tetrahedral, the overall splitting of the *d*-orbital energy levels will decrease resulting in a red shift for the *d–d* bands.[14] Attempts have been made to relate the band maxima with the value of the dihedral angle.[15] Any conclusion based on such correlations, however, should be made only for closely related ligands. The X-ray crystallographically-characterized pseudo-tetrahedral CuN_4 chromophore shows[3] more than one ligand field band. However, for both **1** and **3** only one broad asymmetric band appears in the ligand field region; a situation not so uncommon for copper(II) complexes.[16] This band is considerably red-shifted (135 nm) in **1** compared to that in **3**, signifying appreciable distortion of the geometry from planarity as envisaged. Electronic spectra of the bis-copper(II) complexes with the ligand $H_2NCH_2CH_2NH_2$ (en) and its alkyl derivatives have been studied in detail.[6,17] The parent square planar complex $[Cu(en)_2]2ClO_4$ absorbs at 240 nm, which is attributable to the (N) → Cu^{II} LMCT transition. Alkylation of the nitrogen atoms lowers the ionization potential of the amine[18] and results in a systematic red-shift of this band. The observed correlation between the position of this band and the estimated first ionization potential of the free diamines[6] suggests this transition to occur at 285 nm for $[Cu(L_1)_2]2ClO_4$. Thus, for **1** the peak that appears at 280 nm is attributable to the (N) → Cu^{II} LMCT transition. The ligand moiety absorbs significantly at higher energies, but we did not probe further.

A DMF solution of **3** (*ca* 1×10^{-3} M) gives a quasi-reversible response (Fig. 3) at $E_{1/2} = -0.28$ V vs SCE with $\Delta E_p = 130$ mV (room temperature, 100 mV s^{-1}). The i_{pa}/i_{pc} ratio is found to be 1.05, which is independent of sweep rate. The quasi-reversible response is attributable to the Cu^{II}/Cu^{I} couple, as shown below:

$$3 + e \longrightarrow 3^{-}. \qquad (3)$$

When scanned further on the negative side a small peak appears at −0.9 V, which disappears in the reverse scan. However, a very sharp rise in anodic current occurs which peaks at 0.15 V. This is attributable to the oxidation of metallic copper

Table 3. Cyclic voltammetric[a] and electronic spectral data for the complexes

Complex	$E_{1/2}$ (V)	ΔE_p (mV)	λ_{max} (nm) (ε/dm^3 mol^{-1} cm^{-1})	Assignment	Ref.
1	+0.28	80	730(25)	LF	This work
			280(1750)	σN → Cu^{II} LMCT	
3	−0.18	110	595(30)	LF	This work
			280(1600)	σN → Cu^{II} LMCT	
$Cu(L')_2(ClO_4)_2$	+0.11	90	650(260)	LF	3
			800(120)	LF	

[a] Results for **1** and **3** were obtained at 298 K at a scan rate of 100 mV s^{-1} and referenced to SCE; $E_{1/2} = 0.5\ (E_{pc} + E_{pa})$; E_{pc} and E_{pa} are cathodic and anodic peak potentials, respectively.

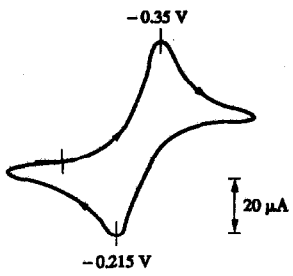

Fig. 3. Cyclic voltammogram (100 mV s^{-1}) of **3** in DMF at a glassy carbon electrode.

deposited at the electrode surface. Examples of this behaviour of copper complexes are known.[19] The peak at −0.9 V is then due to the reduction of copper(I) to copper(O), which partly gets deposited at the electrode surface. Under these circumstances, the anodic peak, which appears at the same position, dramatically increases in current height. Complex **1** in DMF (*ca* 1×10^{-3} M) gives a cyclic response (Fig. 4) at $E_{1/2} = +0.18$ V vs SCE with $\Delta E_p = 80$ mV (room temperature, 100 mV s^{-1}). ΔE_p increases with increasing scan rate. The response is due to the following electrochemical reaction:

$$\mathbf{1} + e \longrightarrow \mathbf{1}^-. \quad (4)$$

The i_{pa}/i_{pc} ratio here is 1.3, which does not alter with the scan rate. The slightly higher magnitude of the anodic current is due to the oxidation of the ligand moiety in addition to the metal ion. No other well-defined peak appears on scanning further on either side, except one attributable to the desorption of metallic copper from the electrode surface when scanned further on the negative side (as found for **3**). These results indicate that as coordination geometry around copper(II) distorts from planar in **3** to distorted tetrahedral in **1**, $E_{1/2}$ shifts positively by 0.46 V. Copper(I) favours tetrahedral geometry; as the geometry distorts towards tetrahedral it becomes easier to reduce copper(II) to copper(I).

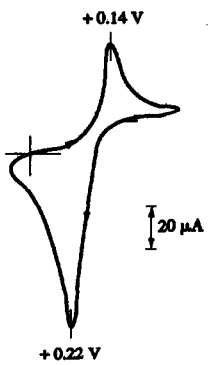

Fig. 4. Cyclic voltammogram (100 mV s^{-1}) of **1** in DMF at a glassy carbon electrode.

CONCLUSION

We have studied the ligating behaviour of a tetradentate nitrogen donor ligand towards copper(II) and zinc(II). Electronic spectral, ESR and electrochemical data are consistent with a pseudo-tetrahedral geometry in both **1** and **2**. The ligand design has made the four nitrogen donors somewhat neoplastic, so that they are capable of imposing a desired coordination geometry onto the above metal ions. In an intrinsic active site of a metalloprotein the geometry around the metal is often much distorted as a result of conformationally imposed constraints upon amino acid side-chains that comprise the donors. In mimicking such sites multidonor ligands with rigid topology are likely to provide the best results.

Acknowledgement—We thank the Department of Science and Technology, New Delhi, India, for financial support.

REFERENCES

1. E. I. Solomon, K. W. Penfield and D. E. Wilcox, *Struct. Bonding* 1983, **1**, 53.
2. B. L. Vallee and R. J. P. Williams, *Proc. Natl. Acad. Sci. USA* 1968, **59**, 398.
3. S. Knapp, T. P. Keenan, X. Zhang, R. Fikar. J. A. Potenza and H. J. Schugar, *J. Am. Chem. Soc.* 1990, **112**, 3452.
4. P. K. Bharadwaj, *J. Sci. Ind. Res. (India)*, in press.
5. H. Yokoi and A. W. Addison, *Inorg. Chem.* 1977, **16**, 1341.
6. H. Yokoi and T. Isobe, *Bull. Soc. Chem. Japan* 1969, **42**, 2187.
7. D. D. Perin, W. L. F. Armarego and D. R. Perrin, *Purification of Laboratory Chemicals*, 1st edn. Pergamon Press, Oxford (1966).
8. S. Mandal and P. K. Bharadwaj, *Polyhedron* 1992, **11**, 1037.
9. J. J. D'Amico and W. E. Dahl, *J. Org. Chem.* 1975, **40**, 1224.
10. P. K. Bharadwaj, J. A. Potenza and H. J. Schugar, *Acta Cryst.* 1988, **C43**, 2365.
11. W. J. Grey, *Coord. Chem. Rev.* 1971, **7**, 81.
12. F. A. Cotton and G. Wilkinson, *Advanced Inorganic Chemistry*, 5th edn, p. 768. John Wiley, New York (1988).
13. W. E. Blumberg and J. Peisach, *Arch. Biochem. Biophys.* 1974, **165**, 691.
14. R. D. Willet, J. A. Haugen, J. Lebsack and J. Morrey, *Inorg. Chem.* 1974, **13**, 2510.
15. (a) R. L. Harlow, W. J. Wells III, G. W. Watt and S. H. Simonsen, *Inorg. Chem.* 1975, **14**, 1768; (b) D. W. Smith, *J. Chem. Soc. (A)* 1969, 2529; 1970, 2900;

(c) L. P. Battaglia, A. B. Corradi, G. Marcotrigiano, L. Menabue and G. C. Pellacani, *Inorg. Chem.* 1979, **18**, 148; (d) M. I. Ban, J. Czaszar and M. Hegyhati, *J. Molec. Struct.* 1973, **19**, 455.

16. B. J. Hathaway, *J. Chem. Soc., Dalton Trans.* 1972, 1196.
17. (a) B. P. Kennedy and A. B. P. Lever, *J. Am. Chem. Soc.* 1973, **95**, 6907; (b) S. Mandal and P. K. Bharadwaj, *Ind. J. Chem.* 1991, 948.
18. M. B. Robin, *Higher Excited States of Polyatomic Molecules*, Vol. 1, pp. 210–214. Academic Press, New York (1974).
19. M. I. Pilo, G. Manca, M. A. Zoroddu and R. Seeber, *Inorg. Chim. Acta* 1991, **180**, 225.

Polyhedron Vol. 12, No. 5, pp. 549–562, 1993
Printed in Great Britain

0277–5387/93 $6.00+.00
© 1993 Pergamon Press Ltd

INTERACTION OF NEUTRAL AND ANIONIC O-DONOR ORGANIC LIGANDS WITH EUROPIUM(III) IN THE MACROCYCLIC COMPLEX $[Eu(CH_3COO)_2(C_{22}H_{26}N_6)]Cl \cdot 4H_2O$ AND CRYSTAL STRUCTURE OF $[Eu(CH_3COO)_2(C_{22}H_{26}N_6)](CH_3COO) \cdot 9H_2O$

K. K. FONDA, D. L. SMAILES and L. M. VALLARINO*

Department of Chemistry, Virginia Commonwealth University, Richmond, VA 23284, U.S.A.

and

G. BOMBIERI

Istituto di Chimica Farmaceutica, Universitá di Milano, Milano, Italy

and

F. BENETOLLO and A. POLO

Istituto di Chimica e Tecnologia dei Radioelementi, C.N.R., Corso Stati Uniti 4, Padova, Italy

and

L. DE COLA

Istituto Chimico "G. Ciamician" dell'Universitá, Bologna, Italy

(*Received* 20 *April* 1992; *accepted* 18 *August* 1992)

Abstract—The interaction of the paramagnetic complex $[Eu(CH_3COO)_2L]Cl \cdot 4H_2O$, where L is the six N-donor macrocyclic ligand $C_{22}H_{26}N_6$, with a series of organic substrates having potential O-donor atoms has been investigated. The ^1H NMR resonances of anionic or acidic substrates were greatly shifted in the presence of the europium complex, whereas those of uncharged substrates remained essentially unchanged. The $^5D_0 \rightarrow {}^7F_2$ emission of the europium complex was considerably enhanced in the presence of certain heteroaromatic carboxylates; new complexes of the formula $[Eu(RCOO)_2L]Cl \cdot nH_2O$, where R is $-C_6H_5$, $-C_4H_3O$, $-C_4H_3S$, $-C_4H_3NH$ or $-C_5H_4N$ and $n = 2$–4, were isolated in the solid state. The crystal and molecular structure of the triacetate, $[Eu(CH_3COO)_2L](CH_3COO) \cdot 9H_2O$, was established by single-crystal X-ray crystallography. The structure is ionic, with a 10-coordinate europium(III) linked to the six N-donor atoms of the macrocyclic ligand and to two bidentate chelating acetates situated on opposite sides of the macrocycle. An ionic acetate and a network of hydrogen-bonded H_2O molecules (nine per complex unit) completed the crystal lattice.

The compounds of europium(III) have recently attracted considerable interest in two unrelated areas: certain europium(III) salts and substituted tris-β-diketonates have found useful applications as NMR shift reagents in organic analysis,[1] while a number of luminescent complexes of chelating

* Author to whom correspondence should be addressed.

ligands have been suggested as markers in cytology and immunology.[2] As NMR shift reagents, the complexes of europium(III)—an f^6 system—offer the advantage of producing relatively large paramagnetic shifts in the spectra of organic substrates, without excessive broadening of the resonances. As luminescent markers, they offer the advantage of long-lived, narrow emissions in the visible region of the spectrum, thus avoiding interference with any intrinsic fluorescence of the bio-substrate. The usefulness of europium(III) compounds in these two areas, however, is often severely limited either by lack of solubility in the desired solvent, especially water, or by the ease with which most lanthanide (III) complexes are decomposed by acids and competing ligands, including strong donor solvents.

In view of these limitations, the $[Eu(CH_3COO)_2L]Cl \cdot 4H_2O$ complex, where L is the six N-donor macrocyclic ligand $C_{22}H_{26}N_6$ illustrated in Fig. 1,[3,4] offers interesting new possibilities. This complex is very soluble in water as well as in organic solvents, and the {EuL} entity is substitution-inert and retains its identity in solution even at acidic pH and in the presence of strongly competing ligands; in contrast, the exocyclic acetate ligands are labile and easily exchanged. This complex, therefore, may provide a useful alternative to existing NMR shift reagents[5] and may serve as a prototype for a new class of luminescent bio-markers.[6]

The present paper reports a study of the interaction between the $[Eu(CH_3COO)_2L]Cl \cdot 4H_2O$ complex and a representative series of oxygen-containing organic substrates—alcohols, phenols, ketones, carboxylic acids and their anions—with the dual purpose of evaluating its performance as an NMR shift reagent and to identify exocyclic ligands that might enhance its luminescence intensity to practically useful levels. Preliminary results of these studies have been reported.[7,8] In order to establish the maximum number of exocyclic carboxylates which can actually coordinate to the metal centre of the {EuL} macrocyclic moiety, a triacetate complex, $EuL(CH_3COO)_3 \cdot 9H_2O$, was synthesized and its structure determined by X-ray crystallography.

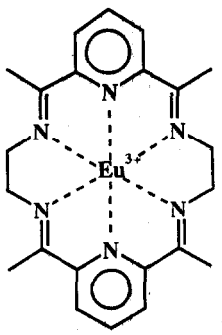

Fig. 1. Schematic formula of the {EuL} moiety, $L = C_{22}H_{26}N_6$.

EXPERIMENTAL

Starting materials

Hydrated europium(III) acetate, 2,6-diacetylpyridine, 1,2-diaminoethane, the organic compounds investigated as substrates (acetone, methanol, 1-butanol, 2-butanol, 2-methyl-2-butanol, phenol, catechol; sodium carboxylates: formate, acetate, propanoate, butanoate, succinate, benzoate) and the carboxylic acids used in luminescence studies (benzoic, 2-furancarboxylic, 2-thiophenecarboxylic, 2-pyrrolecarboxylic, 2-pyridinecarboxylic) were commercially available products; they were checked for purity by NMR and/or IR spectroscopy and recrystallized or distilled whenever necessary. The complex $[Eu(CH_3COO)_2L]Cl \cdot 4H_2O$ was prepared and characterized as previously described.[4] Deuterated solvents for NMR studies (deuterochloroform, deuterium oxide and methanol-d_4, all from Aldrich) and spectrograde solvents for luminescence measurements were used as received.

$[Eu(CH_3COO)_2L](CH_3COO) \cdot 9H_2O$

This complex was prepared similarly to $[Eu(CH_3COO)_2L]Cl \cdot 4H_2O$, except that freshly distilled 1,2-diaminoethane was used as the starting material instead of a mixture of the diamine dihydrochloride and KOH. The product was recrystallized several times from methanol–diethyl ether and obtained as off-white shiny crystals; yields *ca* 80%. The complex is very soluble in water, alcohols, chloroform and other polar organic solvents; it is insoluble in ethers, alkanes and carbon tetrachloride. The IR spectrum is nearly identical to that of $EuL(CH_3COO)_2Cl \cdot 4H_2O$[4] and $YL(CH_3COO)_2Cl \cdot 4H_2O$,[9] except for an additional strong absorption at 1571 cm^{-1} (antisymmetric stretching mode of ionic acetate). Crystallographic analysis data are given in a following section.

$[Eu(RCOO)_2L]Cl \cdot nH_2O$ (R = —C_6H_5, —C_4H_3O, —C_4H_3S, —C_4H_3NH *and* —C_5H_4N; n = 2–4)

These complexes were prepared by the following general procedure, employing a 2:1 mole ratio of carboxylic acid to europium complex. The solid carboxylic acid was added to a solution of

$[Eu(CH_3COO)_2L]Cl \cdot 4H_2O$ (0.10 mmol in 5 cm^3 $CHCl_3$) and the mixture was stirred at 40–50°C for 10 min, or until the acid had dissolved. The resulting slightly cloudy solution was filtered; the clear filtrate was diluted with 10–15 cm^3 of diethyl ether and chilled for several hours in a freezer. The colourless crystalline solid that formed was filtered with suction, washed on the filter with a 1:3 mixture of chloroform–diethyl ether and dried at 60°C. Yields were nearly quantitative. The products thus obtained were analytically pure; however, samples used for luminescence measurements were recrystallized from methanol–diethyl ether. Microanalyses (Atlantic Microlab, Atlanta, GA): $[Eu(C_6H_5COO)_2L]Cl \cdot 3H_2O$: Found: C, 50.4; H, 4.9; N, 9.2. Calc.: C, 50.2; H, 4.9; N, 9.3%. $[Eu(C_4H_3OCOO)_2L]Cl \cdot 4H_2O$: Found: C, 44.9; H, 4.9; N, 9.9. Calc.: C, 44.8; H, 4.7; N, 9.8%. $[Eu(C_4H_3SCOO)_2L]Cl \cdot 2H_2O$: Found: C, 45.3; H, 4.2; N, 9.5. Calc.: C, 45.0; H, 4.2; N, 9.8%. $[Eu(C_5H_4NCOO)_2L]Cl \cdot 4H_2O$: Found: C, 46.4; H, 4.8; N, 12.6. Calc.: C, 46.4; H, 4.8; N, 12.7%. $[Eu(C_4H_4NCOO)_2L]Cl \cdot 3H_2O \cdot 0.5CH_3OH$: Found: C, 45.8; H, 4.8; N, 13.0. Calc.: C, 45.8; H, 5.0; N, 13.1%. The IR spectra of the solid complexes showed in each case the absorptions of the macrocyclic ligand,[9] together with those of the respective anionic ligand: benzoate,[9] 2-furancarboxylate,[10] 2-pyrrolecarboxylate[11] and 2-pyridinecarboxylate.[12] For 2-thiophenecarboxylate the absorptions (not available in the literature) were: 3474 w, br, 3089 w, 3075 w, 1619 sh, 1593 sh, 1555 vs, br, 1522 m (only partly resolved), 1428 vs, 1396 vs, 1381 sh, 1343 s, 1225 w, 1111 m, 1073 vw, 1040 m, 999 sh, 921 vvw, 858 s, 803 s, 776 vs, 691 vs, 653 m, 563 vvw and 479 w cm^{-1}.

Identical products (yields *ca* 35% based on the starting europium diacetate chloride complex) were obtained when the reaction was carried out with a 1:1 mole ratio of RCOOH to europium. Reactions with ratios higher than 2:1 resulted again in the same products, but these were contaminated by variable amounts of unreacted acids.

NMR spectra

Experiments were carried out with a GE QE-300 spectrometer at ambient temperature, using high-precision Pyrex 5 mm o.d. NMR tubes (Wilmad). Spectra in $CDCl_3$ and CD_3OD were referenced either to TMS or to the residual protonated solvent resonance. Spectra in D_2O were referenced to the HOD resonance, which was not shifted in the presence of the europium(III) complex. (The DSS resonance usually employed in aqueous solution was unsuitable because it is shifted in the presence of $[Eu(CH_3COO)_2L]Cl \cdot 4H_2O$.)

The following general procedure was used in the study of the {EuL}–substrate interaction. The proton spectrum of a 3.0×10^{-2} M solution of substrate in the chosen solvent was recorded. An equivalent molar amount of solid europium reagent was added to the substrate solution, and the spectrum was recorded again. When multiple substrate:europium ratios were studied, further equivalent molar aliquots of (solid or liquid) substrate were added stepwise, and the spectrum was recorded after each addition.

Absorption, emission and excitation spectra; excited state lifetimes

Absorption spectra of the $[Eu(RCOO)_2L]Cl \cdot nH_2O$ complexes (R = $—C_6H_5$, $—C_4H_3O$, $—C_4H_3S$, $—C_4H_3NH$, $—C_5H_4N$) in methanol or ethanol (1.0×10^{-4} M) were obtained with Shimadzu 265 UV–vis and Perkin–Elmer 6 spectrophotometers. The spectra were nearly identical to one another and consisted of two broad absorptions centred at *ca* 250 ($\varepsilon = 3.9–4.0 \times 10^4$) and 300 nm ($\varepsilon = 1.6–1.8 \times 10^4$), the latter with a shoulder at 310–320 nm. An SLM 8000 and a Perkin–Elmer L 50 spectrofluorimeter were used for excitation and emission spectra of the complexes in ethanol or methanol at various concentrations (10^{-4}–10^{-5} M). The excitation spectra, for $\lambda_{em} = 614$ nm, were very similar for all complexes and matched the absorption spectra, except for a lower relative intensity of the high energy band. The emission spectra were all identical in regard to pattern and energies, but differed greatly in intensity; under identical experimental conditions, the relative intensities varied with R approximately as follows: $—CH_3$, 1; $—C_4H_3NH$, 1; $—C_6H_5$, 1; $—C_4H_3O$, 7; $—C_5H_4N$, 8; $—C_4H_3S$, 12.

Luminescence "titrations" of $[Eu(CH_3COO)_2L]Cl \cdot 4H_2O$ with the RCOOH acids (R = $—C_6H_5$, $—C_4H_3O$, $—C_4H_3S$, $—C_4H_3NH$, $—C_5H_4N$) consisted of measuring the emission intensities of methanol or ethanol solutions containing the same concentration (2.0×10^{-4} M) of $[Eu(CH_3COO)_2L]Cl \cdot 4H_2O$ and increasing RCOOH:Eu mole ratios (0.5, 1.0, 1.5, 2.0, 2.5 and 10). For R = $—C_4H_3S$, $—C_4H_3O$ and $—C_5H_4N$, the emission intensity gradually increased with the RCOOH:{EuL} ratio and reached a maximum for ratios slightly exceeding 2:1. No enhancement was observed for R = $—C_4H_3NH$ or $—C_6H_5$. Excited-state lifetimes, obtained with a Perkin–Elmer L 50 spectrofluorimeter for freshly prepared ethanol solutions (1.0×10^{-4} M) of the $[Eu(RCOO)_2L]Cl \cdot nH_2O$

complexes, were single exponentials in the 1–2 ms range ($\tau = 1.7$ and 1.4 ms for R = —C_4H_3S and —CH_3, respectively).

IR spectra

Spectra of the solid complexes were obtained on a Perkin–Elmer Model 1600 Fourier-transform instrument. Samples were examined both as KBr pellets and as mulls in hexachlorobutadiene (4000–1800 and 1500–1300 cm^{-1}, supported on NaCl disks) and Nujol (1800–1500 and 1300–400 cm^{-1}, supported on KBr disks). No difference was observed between the spectra obtained in KBr pellets and those in mulls.

X-ray measurements and structure determination

The crystal and refinement data of $[Eu(CH_3COO)_2L](CH_3COO)\cdot 9H_2O$ (pale yellow, almost spherical irregular prisms) are summarized in Table 1. A crystal of dimensions $0.50 \times 0.54 \times 0.42$ mm was lodged in a Lindemann glass capillary and centred on a four-circle Phillips PW 1100 diffractometer with graphite-monochromated Mo-K_α radiation. The orientation matrix and preliminary unit cell dimensions were determined from 25 reflections obtained by mounting the crystal at random and varying each of the orientation angles χ and ϕ over the range 120°, with $5° \leqslant \theta \leqslant 7°$. For the determination of the precise lattice parameters, 25 strong reflections with $10° \leqslant \theta \leqslant 13°$ were considered. Integrated intensities for *hkl* reflections with $h = \pm 14$, $k = \pm 20$ and $l = 16$ were measured, and three standard reflections, 2,1,2, −4,3,1 and −7,−1,3 were monitored every 180 min. There were no significant fluctuations of intensities other than those expected from Poisson statistics.

The intensity data were corrected for Lorentz–polarization effects and for absorption, following the method of North *et al.*;[13] no correction was made for extinction. The structure was solved by three-dimensional Patterson and Fourier techniques and was refined with anisotropic thermal parameters assigned to all non-hydrogen atoms. The hydrogen atoms of the methyl groups (macrocycle and acetates) were introduced at calculated

Table 1. Crystal and refinement data for $[Eu(CH_3COO)_2L]$ $CH_3COO\cdot 9H_2O$

Formula	$EuO_{15}N_6C_{28}H_{53}$
M	865.72
Crystal system	Triclinic
a (Å)	11.006(2)
b (Å)	15.318(3)
c (Å)	12.663(2)
α (°)	84.56(2)
β (°)	115.14(3)
γ (°)	94.20(2)
V (A^3)	1922.68
Space group	$P\bar{1}$
$\rho_{calc.}$ (g cm^{-3})	1.49
Z	2
$F(000)$	892
Radiation	Mo-K_α
μ (cm^{-1})	15.88
Reflections measured	7915
Scan method	$\theta/2\theta$
Scan speed (° min^{-1})	1.8
Scan width (°)	1.20
Background counts (s)	20
$2\theta_{max}$ (°)	50
σ limit [$I \geqslant n\sigma(I)$]	3
Unique observed data with [$I \geqslant 3\sigma(I)$]	7107
No. of parameters	529
$R = \Sigma[\|F_o - F_c\|]/\Sigma\|F_o\|$	0.026
Max Δ/σ	0.034
G.O.F.	1.215

positions and allowed to ride on associated carbon atoms during the least-squares refinement [d(C—H) = 0.98 Å and U = 0.08 Å^2]. Other carbon-attached hydrogen atoms were introduced at the positions observed in the final difference-Fourier map. The hydrogen atoms of the water molecules were disordered and were not introduced. The function minimized was $\Sigma w\Delta^2$ with $\Delta = (|F_o| - |F_c|)$. The anomalous dispersion terms[14] for europium were taken into account in the refinement which reached convergency at $R = 0.026$. Atomic scattering factors were taken from ref. 15. Data processing and computation were carried out with the SHELX 76 program package;[15] PLUTO[16] and ORTEP[17] were used for drawing. Atomic fractional coordinates and thermal parameters, fractional hydrogen coordinates and observed as well as calculated structure factors (× 10) are available as supplementary material (Tables A–C).

RESULTS AND DISCUSSION

Effect of $[Eu(CH_3COO)_2L]Cl \cdot 4H_2O$ *on the proton NMR spectra of potential* O-*donor compounds*

The interaction between the $[Eu(CH_3COO)_2L]Cl \cdot 4H_2O$ complex and a representative series of potential O-donor substrates, including both uncharged and negatively charged species, was investigated in solution by proton NMR spectroscopy. In each case spectra were recorded for the organic substrate alone as well as for mixtures of the substrate and the {EuL} diacetate chloride complex.

(a) *Alcohols, phenols and ketones.* A first group of substrates included acetone, methanol, 1-butanol, 2-butanol and 2-methyl-2-butanol; the three butanols provided examples of increasing steric hindrance near the potential europium-binding site of the substrate. The ^1H NMR spectra, recorded both in D_2O and $CDCl_3$, did not reveal significant shifts or loss of resolution for any of the substrate resonances at a 1 : 1 mole ratio of substrate to {EuL} complex, indicating no interaction of these uncharged substrates with the paramagnetic europium centre. Results are available as supplementary material (Table D). A similar conclusion had been previously reached for uncharged N-donor substrates.[18] Since even in chloroform solution the acetate ligands of $[Eu(CH_3COO)_2L]Cl \cdot 4H_2O$ are partly ionized,[19] leaving the europium centre accessible to other ligands, the failure of uncharged organic substrates to bind to europium must result chiefly from the preferred coordination of the H_2O molecules present in the original complex.

Slightly different results were obtained with phenol and catechol. Although the changes in the chemical shifts observed for 1 : 1 mixtures of the substrate and the {EuL} complex were minor, significant broadening of the resonances did occur even in D_2O solution. Figure 2 illustrates the situation for catechol: the resonance of the protons at the 2 and 5 positions, which are closer to the O-donor atoms, is considerably more broadened than that of the protons at positions 3 and 4. These results show that phenols, which are somewhat more acidic than alcohols, interact to a small extent with the paramagnetic europium(III) centre even in a strongly coordinating solvent.

(b) *Carboxylates.* The interaction of $[Eu(CH_3COO)_2L]Cl \cdot 4H_2O$ with a series of sodium carboxylates (formate, acetate, propanoate, butanoate, benzoate and succinate) was investigated in D_2O. In each case significant downfield shifts of the substrate resonances were observed, and the proton(s) closest to the carboxylate group underwent the greatest shift. The magnitude of the shifts increased with increasing europium content of the mixture; additionally, loss of multiplicity invariably occurred. Spectral data are reported in Table 2. These results show that a substitution equilibrium is established between the carboxylate substrate and the acetate ligands of the original complex; this equilibrium must be rapid on the NMR time-scale since separate sets of resonances for bound and unbound species were never observed for either the substrates or the acetates.

The resonance of the formate proton, unlike those of all other carboxylates examined in this work, was shifted upfield in the presence of $[Eu(CH_3COO)_2L]Cl \cdot 4H_2O$. This anomalous behaviour suggests that the formate proton, being only three bonds away from the metal centre, may experience a predominantly contact shift; an upfield shift of the formate proton resonance would indeed be expected if the contact shift for formate were to approximate the value calculated for the acetate protons of $[Eu(CH_3COO)_2L]Cl \cdot 4H_2O$.[20]

Comparison of $Eu(NO_3)_3$ *and* $[Eu(CH_3COO)_2L]Cl \cdot 4H_2O$ *as aqueous shift reagents*

Simple salts of europium(III), such as $Eu(NO_3)_3$, $EuBr_3$ and $EuCl_3$, are known to act as upfield NMR shift reagents in aqueous solution.[1] The results reported in the preceding sections are therefore somewhat unexpected in that all anionic substrates studied, except formate, shifted downfield in the presence of $[Eu(CH_3COO)_2L]Cl \cdot 4H_2O$. To provide a direct comparison, the proton NMR spectra of sodium butanoate and sodium succinate were recorded in D_2O in the presence of equimolar

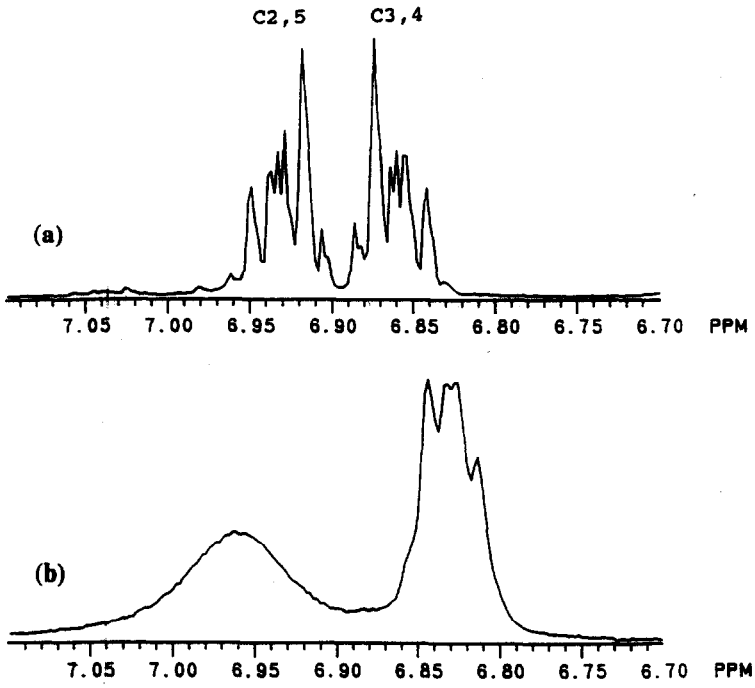

Fig. 2. Proton NMR spectra of: (a) catechol alone and (b) a 1:1 mixture of catechol and $[Eu(CH_3COO)_2L]Cl \cdot 4H_2O$.

amounts of $Eu(NO_3)_3$. As expected, all shifts were in an upfield direction; also, their magnitude was much smaller than for $[Eu(CH_3COO)_2L]Cl \cdot 4H_2O$: for succinate, the shift was −0.93 ppm (upfield) for $Eu(NO_3)_3$, and +7.42 ppm (downfield) for $[Eu(CH_3COO)_2L]Cl \cdot 4H_2O$. The data are presented in Table 3.

The downfield direction of the shifts induced by $[Eu(CH_3COO)_2L]Cl \cdot 4H_2O$ may in itself be a distinct advantage, since the upfield shifts caused by simple europium(III) salts tend to move normally low-field resonances closer to the aliphatic resonances, which are more likely to remain unshifted by a paramagnetic reagent.

An intrinsic limitation in the use of $[Eu(CH_3COO)_2L]Cl \cdot 4H_2O$ as an NMR shift reagent is that at least three of its four resonances occur between 0 and 10 ppm, where they may overlap with resonances of the substrate. This limitation, however, is not serious; the resonances of the europium complex are easily identified because their positions remain very nearly constant in any

Table 2. Proton NMR data for carboxylate substrates and catechol in D_2O with $[Eu(CH_3COO)_2L]Cl \cdot 4H_2O$

Substrate	Position	Chemical shift			
		0.03 M Substrate	Substrate : Eu = 3 : 1	Substrate : Eu = 2 : 1	Substrate : Eu = 1 : 1
Formate		8.46 s	8.17 s	8.15 s	8.12 s
Acetate		1.93 s	5.84 s	6.66 s	7.31 s
Propanoate	2	2.20 q (J = 7.8 Hz)	Severely broadened resonances are unassignable		
	3	1.07 t (J = 7.8 Hz)			
Butanoate	2	2.17 t (J = 7.5 Hz)	6.35 br s	7.68 br s	9.30 br s
	3	1.58 sx (J = 7.5 Hz)	Not seen	5.34 br s	6.13 br s
	4	0.91 t (J = 7.5 Hz)	2.57 br s	3.10 br s	3.72 br s
Benzoate	2	7.89 m	9.94 s	10.18m	11.25 m
	3,4	7.53 m	8.11 s	8.18 m	8.38 m
Succinate		2.47 s	6.57 br s	7.64 br s	9.89 br s
Catechol[a]	3,6	6.93 m			6.86 m
	4,5	6.96 br			6.83 br s

[a] Hydroxy protons unobservable due to deuterium exchange.

Table 3. Proton NMR data for carboxylate substrates in D_2O with $Eu(NO_3)_3$

Substrate	Position	0.03 M Substrate	Substrate: europium = 1:1
Butanoate	2	2.17 t (J = 7.5 Hz)	−0.74 br m
	3	1.58 sx (J = 7.5 Hz)	−0.12 br s
	4	0.91 t (J = 7.5 Hz)	
Succinate		2.47 s	1.54 br s

given solvent and because the characteristic multiplicities of the pyridine resonances generally are retained. Synthesis of a predeuterated version of the macrocyclic species would of course eliminate this problem.

Effect of aromatic and heteroaromatic carboxylic acids on the luminescence of $[Eu(CH_3COO)_2L]Cl \cdot 4H_2O$

The absorption and luminescence spectra of $[Eu(CH_3COO)_2L]Cl \cdot 4H_2O$ have been previously investigated in detail.[20] Low-lying metal–ligand charge-transfer states were shown to be absent and the broad, intense absorptions in the near-UV region were ascribed to electronic transitions of the macrocyclic ligand. Excitation into the $^5D_6$ level of europium(III) at 394 nm resulted in efficient emission for the $^5D_0 \rightarrow {}^7F_2$ europium(III) line ($\Phi_{em} = ca\ 10^{-1}$), but excitation into the intra-ligand absorptions caused only faint luminescence ($\Phi_{em} = ca\ 10^{-3}$ for λ_{ex} = 300 nm).[21] It could be expected that the luminescence of the {EuL} moiety might be enhanced by axial coordination of organic ligands that are better chromophores than acetates in a region suitable for energy transfer to europium(III), and a variety of uncharged as well as anionic O-donor ligands were screened as potential enhancers.[8] Several heteroaromatic monocarboxylic acids showed promise.[21–24] Their effect on the luminescence of the {EuL} moiety was further investigated in the present work, both by performing luminescence "titrations" of the diacetate chloride with the free heteroaromatic acid, RCOOH, and by obtaining the emission/excitation spectra of the $[Eu(RCOO)_2L]Cl \cdot nH_2O$ complexes synthesized for this purpose (see the following section). Coincident results were obtained in the two sets of experiments.

No enhancement relative to the corresponding diacetate chloride occurs for the $[Eu(RCOO)_2L]Cl \cdot nH_2O$ complexes containing benzoate or 2-pyrrolecarboxylate, whereas complexes containing 2-thiophenecarboxylate, 2-pyridinecarboxylate or 2-furancarboxylate show an appreciable (7–12 fold) increase in emission intensity. This luminescence enhancement is not accompanied by any change in either the shape or the position of the emission bands (Fig. 3), indicating that the coordination sphere of the europium(III) emitter still has essentially the same symmetry as in the diacetate chloride complex. Furthermore, the absorption spectra are virtually identical for all the $[Eu(RCOO)_2L]Cl \cdot nH_2O$ complexes, regardless of their emission intensity, and closely resemble the corresponding spectra of the diacetate chloride analogue. The luminescence enhancement observed for R = —C_4H_3S, —C_4H_3O and —C_5H_4N may, therefore, be attributed chiefly to more effective protection of the excited europium(III) centre from vibrational deactivation by solvent molecules or other high-frequency oscillators. This conclusion is in agreement with the somewhat longer luminescence decay time of $[Eu(C_4H_3S—COO)_2L]Cl \cdot 2H_2O$ compared to the diacetate chloride analogue.

Synthesis and IR spectra of $[Eu(RCOO)_2L]Cl \cdot nH_2O$ *complexes*

To provide a better understanding of the luminescence enhancement of the {EuL} moiety in the presence of certain heteroaromatic carboxylates, new complexes were prepared by metathesis between $[Eu(CH_3COO)_2L]Cl \cdot 4H_2O$ and a series of aromatic and heteroaromatic monocarboxylic acids. Independent of the complex-to-carboxylic acids ratio employed, the products had the general formula $EuL(RCOO)_2Cl \cdot nH_2O$, where R is —$C_6H_5$, —$C_4H_3O$, —$C_4H_3S$, —$C_4H_3NH$ or —C_5H_4N. These complexes are colourless crystalline solids, soluble in water and polar organic solvents; their IR spectra show absorptions characteristics of the macrocyclic ligand[9] as well as those arising from the respective carboxylates. Single crystals suitable for X-ray analysis were not obtained for any of these compounds; however, the values of the symmetric and antisymmetric stretching frequencies of the —COO^- groups and their frequency separation, Δ (Table 4), provide a reliable

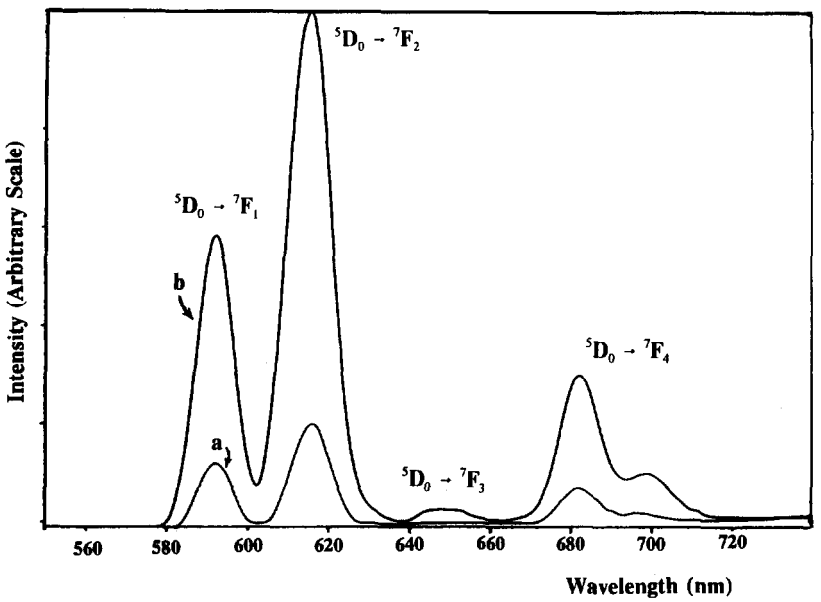

Fig. 3. Emission spectra of 1.0×10^{-4} M methanol solutions of: (a) $[Eu(CH_3COO)_2L]Cl \cdot 4H_2O$ and (b) $[Eu(C_4H_3SCOO)_2L]Cl \cdot 2H_2O$ (both for $\lambda_{ex} = 320$ nm).

basis for structural assignments. A Δ value smaller than that of the sodium salt is indicative of bidentate chelating coordination, whereas a greater Δ value is considered diagnostic of monodentate coordination; bidentate bridging carboxylates exhibit a Δ value close to that of the free ion.[25]

The —COO^- absorptions summarized in Table 4 show that in the solid complexes both $RCOO^-$ groups are coordinated to the europium(III) centre; the coordination formula is almost certainly $[Eu(RCOO)_2L]Cl \cdot nH_2O$, as in the corresponding diacetate chloride[4] and in the triacetate, the X-ray analysis of which is discussed in a following section. The Δ values (cm^{-1}) further suggest that in the complexes containing benzoate, 2-furancarboxylate, 2-pyrrolecarboxylate or 2-thiophenecarboxylate the —COO^- groups act as bidentate chelating ligands. However, the decrease in Δ relative to the sodium salt (−15 for benzoate, −10 for 2-thiophenecarboxylate, −10 for 2-pyrrolecarboxylate and −49 for 2-furancarboxylate) is in each case much smaller than for the diacetate and triacetate complexes (−79 and −73, respectively) and suggests a higher ionic character of the metal–carboxylate bond. The presence of bridging carboxylates, sometimes observed in complexes of these anions,[26,27] may be ruled out for the $EuL(RCOO)_2Cl \cdot nH_2O$ species in view of their solubility in organic solvents and by analogy with the corresponding diacetate chloride and triacetate complexes. The bidentate chelation of the carboxylate group further leads to the conclusion that in these complexes the ring heteroatom cannot be coordinated to the europium (III) centre, since the "bite" of the ligands is not

Table 4. Symmetric and antisymmetric IR stretching frequencies of the carboxylates of isolated $[Eu(RCOO)_2L]Cl \cdot nH_2O$ species

R	Sodium salt ν_a(COO)	ν_s(COO)	$[Eu(RCOO)_2L]Cl \cdot nH_2O$ ν_a(COO)	ν_s(COO)
Methyl	1578	1414	1542	1452
	$\Delta = 164$		$\Delta = 90$	
Phenyl	1551	1413	1534	1411
	$\Delta = 138$		$\Delta = 123$	
2-Furanoyl	1594	1425	1542	1418
	$\Delta = 169$		$\Delta = 124$	
2-Thiophenyl	1555	1396	1543	1394
	$\Delta = 159$		$\Delta = 149$	
2-Pyrrolyl	1529	1444	1526	1447
	$\Delta = 85$		$\Delta = 79$	

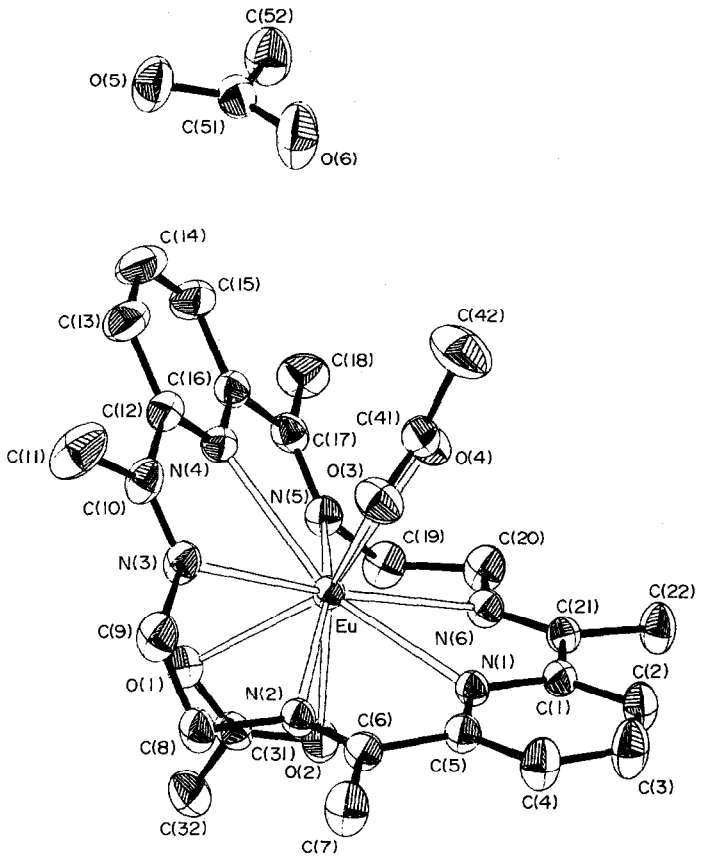

Fig. 4. ORTEP view of the cation and anion units in the $[Eu(CH_3COO)_2L]CH_3COO \cdot 9H_2O$ complex. The water molecules are omitted for clarity.

sufficient to permit tridentate chelation. Non-coordination of the ring heteroatom has also been observed in other complexes of these five-membered heteroaromatic carboxylates for which crystal structures are known.[24,28–30]

The spectrum of the 2-pyridinecarboxylate complex indicates instead monodentate coordination of the —COO group, since its Δ value is somewhat greater than in the sodium salt. Again, the difference is quite small (+10), showing that the metal–carboxylate bond has a highly ionic character. It is reasonable to conclude that the ligand nitrogen heteroatom must also be coordinated, forming a relatively unstrained five-membered chelate ring with europium(III). This mode of binding is common for mononuclear 2-pyridinecarboxylate complexes.[13,31–34]

Proton NMR spectra of $[Eu(RCOO)_2L]Cl \cdot nH_2O$ *complexes*

The spectra of the $[Eu(RCOO)_2L]Cl \cdot nH_2O$ complexes in CD_3OD are reported in Table 5. All resonances are broadened and considerably shifted downfield relative to those of the free acids, showing that in this solvent coordination of the carboxylates to europium(III) is largely maintained. To further investigate these systems, spectra were also determined for mixtures of $[Eu(CH_3COO)_2L]Cl \cdot 4H_2O$ and the free acids, at 1 : 1, 1 : 2 and 1 : 3 mole ratios. The solvent used was again CD_3OD, both for solubility reasons and to allow direct comparison with the luminescence studies. All resonances of the carboxylic acids were broadened and shifted downfield by addition of the {EuL} diacetate chloride complex. The magnitude of shifts for 1 : 2 and 1 : 3 mixtures (Table 5) were generally comparable to those of the $[Eu(RCOO)_2L]Cl \cdot nH_2O$ complexes themselves, indicating that under these conditions the $RCOO^-$ anions largely replace the acetates within the coordination sphere of the complex. The shifts observed for these carboxylic acid–$[Eu(CH_3COO)_2L]Cl \cdot 4H_2O$ mixtures are, however, smaller than those observed for the sodium carboxylate mixtures discussed in a preceding section. For example, the resonance of the C(2) proton of benzoic acid (in CD_3OD) moved only by 1.86 ppm, whereas that of sodium benzoate (in D_2O) moved by 3.36 ppm. This difference must reflect the combination of ligand substitution and acid–base equilibria present in solution; although benzoic acid ($pK_a = 4.2$)[35] is slightly stronger than acetic acid

Table 5. Proton NMR data for carboxylic acid substrates in CD_3OD with $[Eu(CH_3COO)_2L]Cl \cdot 4(H_2O)$ and isolated $[Eu(RCOO)_2L]Cl$ adducts[a]

Substrate	Position	0.03 M Substrate	Eu complex	Chemical shift Substrate : Eu = 3 : 1	Substrate : Eu = 2 : 1	Substrate : Eu = 1 : 1
Benzoic	2	8.02 dm	10.53 br s	9.07 br s	9.79 v br s	9.88 v br s
	3,4	7.46, 7.59 tm	8.25 m	7.81 m	8.01 br d	8.03 br s
2-Pyridinecarboxylic	3	8.19 d	10.06 br s	9.24 br s	9.97 br s	10.88 br s
	4	7.66 ddd	8.95 s	8.41 s	8.85 s	9.06 s
	5	8.06 ddd	9.23 s	9.00 s	9.11 s	9.33 s
	6	8.68 dd	11.70 br s	10.23 br s	11.36 br s	12.46 br s
2-Furancarboxylic	3	7.20 d	8.70 br s	8.64 s	8.88 d	8.90 s
	4	6.59 dd	7.65 br s	7.57 s	7.83 d	7.86 s
	5	7.72 d	9.67 br s	9.45 br s	10.07 d	10.17 br s
2-Pyrrolecarboxylic	3	6.85 dd	7.96 s	7.42 s	7.52 s	8.29 s
	4	6.18 dd	6.35 s	6.29 s	6.31 s	6.50 s
	5	6.94 dd	6.95 br s	6.99 s	7.00 s	7.14 br s
2-Thiophenecarboxylic	3	7.71 dd	8.40 d	8.01 d	8.07 d	8.31 d
	4	7.14 dd	7.96 s	7.51 dd	7.60 dd	7.85 dd
	5	7.77 dd	10.67 br s	9.15 br s	9.48 br s	10.5 br s

[a] Assignments of shifted resonances are unconfirmed.

($pK_a = 4.7$), the benzoic acid–acetate equilibrium does not result in a concentration of benzoate ion equivalent to that present in sodium benzoate at the same molarity.

Crystal structure of $[Eu(CH_3COO)_2L](CH_3COO) \cdot 9H_2O$

The complex was prepared to provide information concerning the maximum number of carboxylates that can coordinate to the {EuL} moiety. The compound is ionic; the complex cation consists of 10-coordinate europium(III) linked to the six N-donor atoms of the macrocyclic ligand and to two bidentate chelating acetates situated on opposite sides of the macrocycle. A non-coordinated acetate balances the ionic charge of the complex cation. Clathrated water molecules (nine per complex unit) form an extensive network of hydrogen bonds that runs in channels through the crystal and includes the oxygen atoms of the coordinated and ionic acetates. An ORTEP view of the cation and anion is shown in Fig. 4. The crystal packing, including water molecules, is illustrated in Fig. 5. Selected bond lengths and angles are listed in Table 6; torsion angles are listed in Table 7.

A comparison between the complex cation present in this triacetate complex and the formally identical cation present in the diacetate chloride species $[Eu(CH_3COO)_2L]Cl \cdot 4H_2O$[4] reveals qualitative similarities as well as quantitative differences. In both compounds the macrocycle has the "folded butterfly" conformation common to other complexes of this ligand and consists of two approximately planar sections that include the pyridine rings and are hinged at the $—CH_2—CH_2—$ side-chains. The folding of the macrocycle, however, is considerably more pronounced in the triacetate complex; the angle between the two planar sections being 122.50(7)° vs 132.37(6)° in the diacetate chloride. Also, the torsion angles of the two $—CH_2—CH_2—$ side-chains of the triacetate, although fairly close to one another [N(5)—C(19)—C(20)—N(6) = 51.7(5)° and N(2)—C(8)—C(9)—N(3) = 50.9(5)°], differ significantly from the corresponding angles [55.4(4)° and 56.6(5)°] of the diacetate chloride. In both compounds the two acetates are staggered; the angle between the two O—C—O planes is 79.2(2)° in the triacetate and 94.8(2)° in the diacetate chloride.

In both compounds the acetate on the concave side of the macrocycle is oriented approximately along the fold line of the macrocycle and leans toward one of the two planar sections; in the triacetate the angle formed by the O—C—O plane with the plane of the N(2)N(1)N(6) macrocyclic section is 69.5(1)° and that formed with the plane of the N(5)N(3)N(4) section is 125.5(2)°; in the diacetate chloride the corresponding angles are 55.1(2)° and 102.6(2)°, respectively. The two $Eu—O_{acetate}$ bond lengths on the concave side of the macrocycle [Eu—O(3) = 2.491(3) and Eu—O(4) = 2.519(3) Å] are more symmetrical, as well as

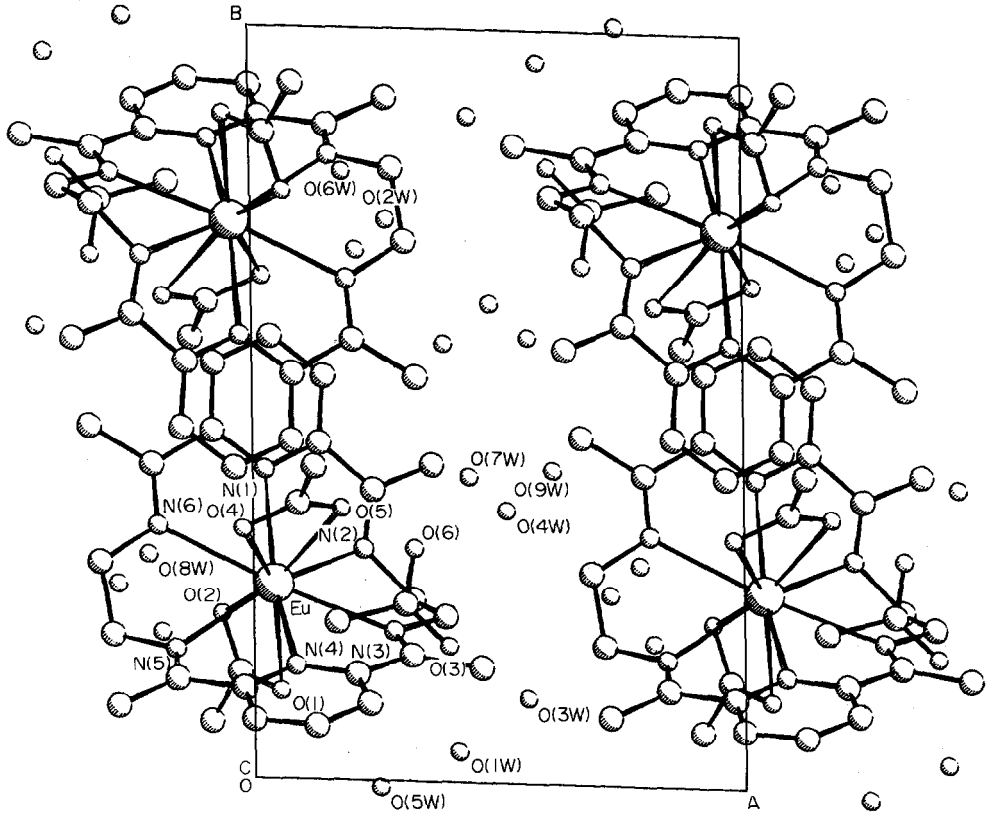

Fig. 5. Crystal packing of $[Eu(CH_3COO)_2L]CH_3COO \cdot 9H_2O$, including water molecules.

slightly longer than those on the convex side [Eu—O(1) = 2.495(3) Å and Eu—O(2) = 2.459(3) Å]. Conversely, the two shortest acetate–nitrogen separations on the concave side [O(3)—N(1) = 3.111(4) and O(4)—N(4) = 2.990(4) Å] are both appreciably shorter than the two shortest acetate–nitrogen separations on the convex side [O(2)—N(1) = 3.209(4) and O(6)—N(4) = 3.222(4) Å].

In the triacetate complex, the Eu—N bond lengths fall into three equal pairs, with values increasing in the order Eu—$N_{imine\text{-}2,5}$ = 2.570(2), Eu—$N_{pyridine}$ = 2.604(3) and Eu—$N_{imine\text{-}3,6}$ = 2.642(3) Å. The same order is found in the diacetate chloride, where, however, all distances are slightly longer: Eu—$N_{imine\text{-}2,5}$ = 2.607(3), Eu—$N_{pyridine}$ = 2.638(3) and Eu—$N_{imine\text{-}3,6}$ = 2.658(3) Å.

A ring-puckering analysis[36] for the six nitrogen system of the triacetate complex shows a slightly twisted conformation with puckering constants Q = 1.035(3), Θ = 90.6(1)° and Φ = 38.7(2)°, whereas the diacetate chloride has a twist-boat conformation with Q = 0.957(3), Θ = 91.6(2)° and Φ = 71.1(2)°. The conformational differences observed among various complexes of the L macrocycle have previously been attributed to changes in the metal size and in the number as well as steric requirements of the exocyclic ligands (anions and solvent molecules). The present work offers the opportunity to compare formally identical metal-macrocycle species in compounds that differ only in the (uncoordinated) counter-ion and in the extent of hydration. Any variations in bond lengths, angles and geometries observed for $[Eu(CH_3COO)_2L](CH_3COO) \cdot 9H_2O$ and $[Eu(CH_3COO)_2L]Cl \cdot 4H_2O$ must necessarily arise from factors outside the coordination sphere. In particular, the numerous water molecules of the triacetate appear to play an important role, for they are involved in hydrogen bonding not only among themselves but also with the oxygens of the coordinated and ionic acetates. These considerations show that the L macrocycle is extremely susceptible to conformational changes that may be induced—for the same metal centre—not only by the exocyclic ligands but also by interaction with species external to the coordination sphere.

CONCLUSIONS

The results of this work lead to several general conclusions. First, the interaction between the $[Eu(CH_3COO)_2L]Cl \cdot 4H_2O$ complex and the O-donor organic substrates—ketones, alcohols, phenols and carboxylic acids—is clearly charge-dependent. Among the substrates investigated, only those which are either anionic or sufficiently acidic to

Table 6. Bond lengths (Å) and angles (°) for $[Eu(CH_3COO)_2L]CH_3COO \cdot 9H_2O$ with e.s.d.s in parentheses

(a) Europium environment			
Eu—N(1)	2.610(3)	Eu—N(2)	2.572(3)
Eu—N(3)	2.649(3)	Eu—N(4)	2.599(3)
Eu—N(5)	2.568(3)	Eu—N(6)	2.634(3)
Eu—O(1)	2.495(3)	Eu—O(2)	2.454(3)
Eu—O(3)	2.491(3)	Eu—O(4)	2.519(3)
N(1)—Eu—N(2)	61.2(1)	N(1)—Eu—N(6)	60.6(1)
N(2)—Eu—N(3)	62.6(1)	N(3)—Eu—N(4)	60.5(1)
N(4)—Eu—N(5)	61.6(1)	N(5)—Eu—N(6)	64.1(1)
O(1)—Eu—O(2)	52.2(1)	O(3)—Eu—O(4)	51.4(1)
(b) Ligands			
N—C(py)	1.342(5)	C—C(py)	1.379(6)
C—C(aliphatic)	1.497(6)		
Eu—N(py)—C	119.7(2)	Eu—N(aliphatic)—C	118.8(3)
O(1)—C(31)	1.259(4)	O(3)—C(41)	1.262(6)
O(2)—C(31)	1.257(4)	O(4)—C(41)	1.242(5)
C(31)—C(32)	1.490(6)	C(41)—C(42)	1.504(8)
O(5)—C(51)	1.238(5)		
O(6)—C(51)	1.226(6)		
C(51)—C(52)	1.513(7)		
Eu—N(1)—C(1)	120.8(2)	C(10)—C(12)—C(13)	122.7(4)
Eu—N(1)—C(5)	118.9(2)	N(4)—C(12)—C(13)	121.1(4)
N(1)—C(1)—C(2)	122.0(4)	C(12)—C(13)—C(14)	118.9(4)
C(2)—C(1)—C(21)	122.5(4)	C(13)—C(14)—C(15)	119.8(5)
C(1)—C(2)—C(3)	118.6(4)	C(14)—C(15)—C(16)	119.2(5)
C(2)—C(3)—C(4)	119.6(4)	C(15)—C(16)—C(17)	122.7(4)
C(3)—C(4)—C(5)	118.7(5)	C(15)—C(16)—N(4)	121.4(4)
N(1)—C(5)—C(4)	122.0(4)	Eu—N(4)—C(12)	119.8(3)
C(4)—C(5)—C(6)	122.1(4)	Eu—N(4)—C(16)	119.2(2)
C(5)—C(6)—C(7)	118.7(3)	C(16)—C(17)—C(18)	117.9(4)
C(7)—C(6)—N(2)	125.0(4)	N(5)—C(17)—C(18)	125.9(4)
Eu—N(2)—C(6)	123.2(3)	Eu—N(5)—C(17)	123.3(3)
Eu—N(2)—C(8)	113.8(2)	Eu—N(5)—C(19)	113.5(2)
Eu—N(3)—C(9)	118.9(3)	Eu—N(6)—C(20)	117.6(2)
Eu—N(3)—C(10)	121.0(3)	Eu—N(6)—C(21)	122.5(3)
N(3)—C(10)—C(11)	124.5(4)	N(6)—C(21)—C(22)	124.4(4)
C(11)—C(10)—C(12)	118.8(4)	C(1)—C(21)—C(22)	119.0(3)
O(1)—C(31)—O(2)	119.7(3)	O(3)—C(41)—O(4)	120.3(4)
Eu—O(1)—C(31)	92.6(2)	Eu—O(3)—C(41)	94.4(3)
Eu—O(2)—C(31)	94.6(2)	Eu—O(4)—C(41)	93.6(3)
O(1)—C(31)—C(32)	120.5(4)	O(3)—C(41)—C(42)	119.5(5)
O(2)—C(31)—C(32)	119.8(4)	O(4)—C(41)—C(42)	120.2(5)
O(5)—C(51)—O(6)	124.8(5)		
O(5)—C(51)—C(52)	117.3(4)		
O(6)—C(51)—C(52)	117.9(4)		

produce an appreciable concentration of anions experience NMR shifts in the presence of the paramagnetic europium(III) complex; similarly, ligands that enhance the intrinsic luminescence of the {EuL} moiety are invariably anionic or acidic in character. This conclusion agrees with the results of a parallel study involving N-donor substrates;[19] of the uncharged substrates studied in that work, including some that are good chelating ligands for the free europium(III) ion (e.g. 1,10-phenanthroline and 2,2′-bipyridyl), none showed any sign of interaction with the europium(III) centre of $Eu(CH_3COO)_2L]Cl \cdot 4H_2O$. With anionic or potentially anionic substrates, the interaction undoubtedly involves an equilibrium substitution of the acetate ligands; aromatic and heteroaromatic

Table 7. Macrocycle torsion angles (°) for $[Eu(CH_3COO)_2L]CH_3COO \cdot 9H_2O$

Atoms	Distances 2–3 (Å)	Angles 1–2–3 (°)	Torsion angles 1–2–3–4 (°)
C(1)—N(1)—C(5)—C(6)	1.342(5)	118.9(3)	−174.0(3)
N(1)—C(5)—C(6)—N(2)	1.489(5)	115.8(3)	−3.5(5)
C(5)—C(6)—N(2)—C(8)	1.269(5)	116.2(4)	179.9(4)
C(6)—N(2)—C(8)—C(9)	1.464(5)	121.4(4)	107.4(4)
N(2)—C(8)—C(9)—N(3)	1.492(6)	108.5(4)	50.9(5)
C(8)—C(9)—N(3)—C(10)	1.473(6)	109.0(4)	−170.4(4)
C(9)—N(3)—C(10)—C(12)	1.263(5)	118.8(4)	−175.4(4)
N(3)—C(10)—C(12)—N(4)	1.487(6)	116.6(4)	2.9(6)
C(10)—C(12)—N(4)—C(16)	1.341(4)	116.0(3)	−172.4(4)
C(12)—N(4)—C(16)—C(17)	1.342(6)	119.5(3)	−177.2(4)
N(4)—C(16)—C(17)—N(5)	1.495(4)	116.0(3)	−2.8(5)
C(16)—C(17)—N(5)—C(19)	1.271(5)	116.3(3)	177.4(4)
C(17)—N(5)—C(19)—C(20)	1.463(4)	121.5(4)	109.5(4)
N(5)—C(19)—C(20)—N(6)	1.503(6)	109.0(4)	51.7(5)
C(19)—C(20)—N(6)—C(21)	1.470(5)	110.1(4)	−165.7(4)
C(20)—N(6)—C(21)—C(1)	1.272(4)	119.0(4)	−177.9(3)
N(6)—C(21)—C(1)—N(1)	1.494(5)	116.6(3)	3.8(5)
C(21)—C(1)—N(1)—C(5)	1.342(5)	115.5(3)	174.9(3)

monocarboxylates actually yield fully substituted products of the formula $[Eu(RCOO)_2L]Cl \cdot nH_2O$. Crystallographic evidence for the triacetate complex $[Eu(CH_3COO)_2L](CH_3COO) \cdot 9H_2O$ suggests that in macrocyclic species of this type the europium(III) will bind at most four exocyclic donor atoms, even when additional suitable ligands are available.

A second general conclusion is that $[Eu(CH_3COO)_2L]Cl \cdot 4H_2O$ can function as an effective NMR shift reagent, both in water and in organic solvents, toward those O-donor substrates that are or can become anionic. The complex is especially promising as an aqueous shift reagent because it retains its identity and solubility over a wide pH range; in addition, it produces downfield shifts that are considerably larger than the upfield shifts induced by simple europium(III) salts.

Finally, this work has shown that replacement of the acetates of $[Eu(CH_3COO)_2L]Cl \cdot 4H_2O$ with certain other carboxylates can substantially enhance the luminescence of the {EuL} moiety. These counter-ions allow more efficient absorption of light via an "antenna effect" and also serve to reduce quenching by protic solvents. A search for even more effective enhancers is in progress.

Acknowledgements—This work has been supported in part by Coulter Electronics, Hialeah, Florida, by a Virginia Commonwealth University Grant-in-Aid, and by N.A.T.O. Bilateral Project No. 184-185.

REFERENCES

1. T. J. Wenzel, *NMR Shift Reagents*. CRC Press, Boca Raton, FL (1987).
2. (a) R. C. Leif, S. P. Clay, H. G. Gratzner, H. G. Haines, K. V. Rao and L. M. Vallarino, in *The Automation of Uterine Cancer Cytology* (Edited by G. L. Wied, G. F. Bahr and P. H. Bartels), Tutorials of Cytology, p. 313. Chicago, IL (1976); (b) E. Soini and T. Lovgren, *CRC Critical Rev. Analyt. Chem.* 1987, **18**, 105; (c) E. Soini and I. Hemmila, U.S. Patent 4,374,120, 1983; (d) H. Mikola, V. M. Mukkala and I. Hemmila, WO Patent 03698, 1984; (e) I. Hemmila, S. Dakubu, V. M. Mukkala, H. Sitari and T. Lovgren, *Analyt. Biochem.* 1984, **137**, 335; (f) R. A. Evangelista, A. Pollak and B. Allore, *Clin. Biochem.* 1988, **21**, 173; (g) M. J. Khosravi and E. P. Diamandis, *Clin. Chem.* 1989, **35**, 181; (h) E. Soini, L. J. Pelliniemi, I. J. Hemmila, V. M. Mukkala, J. J. Kankare and K. Frojdman, *J. Histochem. Cytochem.* 1988, **36**, 1449; (i) R. C. Leif, R. A. Thomas, T. A. Yopp, B. D. Watson, V. R. Guarino, D. H. K. Hindman, N. Lefkove and L. M. Vallarino, *Clin. Chem.* 1977, **23**, 1492.
3. L. De Cola, D. L. Smailes and L. M. Vallarino, *Inorg. Chem.* 1986, **25**, 1729.
4. F. Benetollo, A. Polo, G. Bombieri, K. K. Fonda and L. M. Vallarino, *Polyhedron* 1990, **9**, 1411.
5. T. C. Morrill, M. DiSano and E. George, Presented at the 199th National Meeting of the American Chemical Society, Boston, MA (1990), paper ORGN 208.
6. R. C. Leif and L. M. Vallarino, in *Cell Separation Science and Technology* (Edited by D. H. Kompala

and P. Todd), ACS Symposium Series 464, pp. 41–58. American Chemical Society, Washington, DC (1991).
7. G. Bombieri, F. Benetollo, L. De Cola, K. K. Fonda, A. Polo and L. M. Vallarino, Presented at the 200th National Meeting of the American Chemical Society, Washington, DC (1990), paper INOR 458.
8. L. De Cola, D. L. Smailes and L. M. Vallarino, Presented at the X Convegno Nazionale di Fotochimica, Ravenna, Italy (1985).
9. G. Bombieri, F. Benetollo, W. T. Hawkins, A. Polo and L. M. Vallarino, *Polyhedron* 1989, **8**, 1923.
10. K. Machida, A. Kuvae, Y. Saito and T. Uno, *Spectrochim. Acta, Part A* 1978, **34**, 793.
11. J. H. S. Green and D. J. Harrison, *Spectrochim. Acta, Part A* 1977, **33**, 843.
12. A. Lautié, M. H. Limage and A. Novak, *Spectrochim. Acta, Part A* 1977, **33**, 121.
13. J. G. Leipoldt, G. J. Lamprecht and D. E. Graham, *Inorg. Chim. Acta* 1985, **101**, 123.
14. A. C. T. North, D. C. Phillips and F. S. Mathews, *Acta Cryst.* 1968, **24A**, 351.
15. *International Tables for X-Ray Crystallography*, Vol. 4. Kynoch Press, Birmingham (1974).
16. G. M. Sheldrick, SHELX 76, University of Cambridge, Cambridge, U.K. (1976).
17. W. D. S. Motherwell and W. Clegg, PLUTO, University of Cambridge, Cambridge, U.K. (1978).
18. C. K. Johnson, ORTEP II, Report ORNL-5138. Oak Ridge National Laboratory, TN (1976).
19. G. Bombieri, F. Benetollo, A. Polo, K. K. Fonda and L. M. Vallarino, *Polyhedron* 1991, **10**, 1385.
20. K. K. Fonda and L. M. Vallarino, unpublished results.
21. N. Sabbatini, L. De Cola, L. M. Vallarino and G. Blasse, *J. Phys. Chem.* 1987, **91**, 4681.
22. G. R. Choppin, M. P. Goedken and T. F. Gritmon, *J. Inorg. Nucl. Chem.* 1977, **39**, 2025.
23. T. F. Gritmon, M. P. Goedken and G. R. Choppin, *J. Inorg. Nucl. Chem.* 1977, **39**, 2021.
24. K. S. Gharia, M. Singh, S. Mathur and B. S. Sankhla, *J. Ind. Chem. Soc.* 1983, **60**, 315.
25. A. K. Solanki, S. Wadhwa and A. M. Bhandari, *Ind. J. Chem.* 1980, **19A**, 1020.
26. K. Nakamoto, *Infrared and Raman Spectra of Inorganic and Coordination Compounds*, pp. 231–233. John Wiley and Sons, New York (1986).
27. D. D. Heinrich, K. Folting, W. E. Streib, J. C. Huffman and G. Christou, *J. Chem. Soc., Chem. Commun.* 1989, 1441.
28. F. Charbonnier, M. Petit-Ramel, R. Faure and H. Loiseleur, *Rev. Chim. Miner.* 1984, **21**, 601.
29. A. E. Koziol, W. Brzyska, B. Klimek, A. Król and K. Stepniak, *J. Coord. Chem.* 1987, **15**, 367.
30. H. Preut, M. Domagala and F. Huber, *Acta Cryst.* 1987, **C43**, 416.
31. M. Domagala, H. Preut and F. Huber, *Acta Cryst.* 1988, **C44**, 830.
32. H. Mimoun, L. Saussine, E. Daire, M. Postel, J. Fischer and R. Weiss, *J. Am. Chem. Soc.* 1983, **105**, 3101.
33. P. Chaumette, H. Mimoun, L. Saussine, J. Fischer and A. Mitschler, *J. Organomet. Chem.* 1983, **250**, 291.
34. H. Mimoun, M. Postel, F. Casabianca, J. Fischer and A. Mitschler, *Inorg. Chem.* 1982, **21**, 1303.
35. F. Bottomley, E. Hahn, J. Pickardt, H. Schumann, M. Mukaida and H. Kakihana, *J. Chem. Soc., Dalton Trans.* 1985, 2427.
36. D. Cramer and J. A. Pople, *J. Am. Chem. Soc.* 1975, **97**, 1354.

Polyhedron Vol. 12, No. 5, pp. 563–565, 1993
Printed in Great Britain

0277–5387/93 $6.00+.00
© 1993 Pergamon Press Ltd

COMMUNICATION

SYNTHESIS AND X-RAY CRYSTAL STRUCTURES OF THE HOMOLEPTIC TRIS(1,3-DIPHENYLACETAMIDINATO) COMPLEXES $[M\{PhN{\cdots}C(Me){\cdots}NPh\}_3]$ (M = Ru, Rh), THE RHODIUM(III) TRIAZENIDO ANALOGUE $[Rh(PhN{\cdots}N{\cdots}NPh)_3]$ AND THE CORRESPONDING RHODIUM(II) DERIVATIVE $[Rh_2(PhN{\cdots}N{\cdots}NPh)_4]$

MICHAEL B. HURSTHOUSE* and MUHAMMED A. MAZID

School of Chemistry and Applied Chemistry, University of Wales College of Cardiff, PO Box 912, Cardiff CF1 3TB, U.K.

and

TERRY CLARK and STEPHEN D. ROBINSON*

Department of Chemistry, King's College London, Strand, London WC2R 2LS, U.K.

(*Received* 13 *October* 1992; *accepted* 2 *December* 1992)

Abstract—The synthesis and X-ray crystal structures of the acetamidinato complexes $[M\{PhN{\cdots}C(Me){\cdots}NPh\}_3]$ (M = Ru, Rh) and the triazenido complexes $[Rh(PhN{\cdots}N{\cdots}NPh)_3]$ and $[Rh_2(PhN{\cdots}N{\cdots}NPh)_4]$ are reported.

The "small bite" 1,3-diaryltriazenide anions $ArN{\cdots}N{\cdots}NAr^-$ and their 1,3-diarylamidinate analogues $ArN{\cdots}C(R){\cdots}NAr^-$ have recently attracted much attention as bridging ligands in binuclear "lantern" structures of the general form $[M_2(ArN{\cdots}X{\cdots}NAr)_4]$ (X = N or CR; R = H, alkyl or aryl).[1,2] Their ability to act as chelate ligands and thereby generate highly strained, four-membered chelate rings is also of considerable interest.[1] However, whereas homoleptic tris(1,3-diaryltriazenido) chelates $[M(ArN{\cdots}N{\cdots}NAr)_3]$ have been reported for a wide range of trivalent transition metal ions, notably chromium,[3] iron,[4] ruthenium,[5] osmium,[5] cobalt,[6,7] rhodium[5] and iridium,[5] the only examples of *d*-block tris (amidinato) complexes are provided by the rather air- and moisture-sensitive iron(III) species $[Fe\{PhN{\cdots}C(R){\cdots}NPh\}_3]$ (R = H, Me, Ph) of indeterminate structure.[8] We have now prepared the ruthenium(III) and rhodium(III) tris(acetamidinato) chelates $[M\{PhN{\cdots}C(Me){\cdots}NPh\}_3]$ and have determined the crystal structures of both compounds. For the purpose of comparison we have also determined the X-ray crystal structure of the analogous rhodium(III) tris(1,3-diphenyltriazenido) complex $[Rh(PhN{\cdots}N{\cdots}NPh)_3]$. Finally, we have established the crystal structure of the hitherto unknown rhodium(II) triazenido complex $[Rh_2(PhN{\cdots}N{\cdots}NPh)_4]$ using a single crystal isolated as a by-product during the synthesis of the corresponding rhodium(III) derivative.

1,3-Diphenylacetamidine, PhN=C(Me)—NHPh, reacts with $RuCl_3 \cdot 3H_2O$ and $RhCl_3 \cdot 3H_2O$ in boiling ethanol in the presence of base (NEt_3) to generate green (M = Ru) or red–brown (M = Rh) air-stable isostructural crystalline com-

* Authors to whom correspondence should be addressed.

plexes, $[M\{PhN\cdots C(Me)\cdots NPh\}_3]$, in *ca* 30% yield. The molecular and crystal structure of $[Ru\{PhN\cdots C(Me)\cdots NPh\}_3]$ (**1**) and $[Rh\{PhN\cdots C(Me)\cdots NPh\}_3]$ (**2**) are essentially identical* and are shown in Fig. 1 together with selected bond lengths and angles. In both structures small but apparently significant differences in Rh—N and, to a lesser degree, N—C bond lengths within each chelate ring suggest the presence of some asymmetry in the metal amidinate bonding.

The corresponding rhodium(III) triazenido complex $[Rh(PhN\cdots N\cdots NPh)_3]$ was prepared by adding 1,3-diphenyltriazene to a boiling ethanolic solution of $RhCl_3 \cdot 3H_2O$ in the presence of base (NEt_3) and was isolated as maroon crystals. The molecular structure of $[Rh(PhN\cdots N\cdots NPh)_3]$ (**3**) is shown in Fig. 2, together with selected bond length and angle data. The molecule has a crystallographic diad axis. The molecular dimensions [Rh—N_{av} 2.030(6) Å, <N—Rh—N_{av} 60.9(3)°] are very similar to those observed for the rhodium tris(acetamidinato) complex [Rh—N_{av} 2.046(7) Å <N—Rh—N_{av} 62.8(3)°]. The slightly smaller angles subtended at the rhodium by the triazenide ligands relative to the acetamidinate ligands may be an indirect consequence of the greater steric requirements of the lone pair on the central nitrogen atoms of the former.

An atypical dark red crystal selected from a sample of $[Rh(PhN\cdots N\cdots NPh)_3]$ was also subjected to X-ray structure determination and found to be $[Rh_2(PhN\cdots N\cdots NPh)_4]$, the first example of the long anticipated[9] but hitherto unknown class of rhodium(II) triazenido derivatives of the general form $[Rh_2(ArN\cdots N\cdots NAr)_4]$. The molecular structure of $[Rh_2(PhN\cdots N\cdots NPh)_4]$ (**4**) is shown in Fig. 3, together with selected bond lengths and angles. The Rh—Rh bond length [2.377(3) Å] is very similar to those found for the closely related rhodium(II) formamidinato, $[Rh_2\{ArN\cdots C(H)\cdots NAr\}_4]$ (Ar = *p*-tolyl),[10] and benzamidinato, $[Rh_2\{PhN\cdots C(Ph)\cdots NPh\}_4]$,[11] derivatives, where the Rh—Rh distances are 2.4336

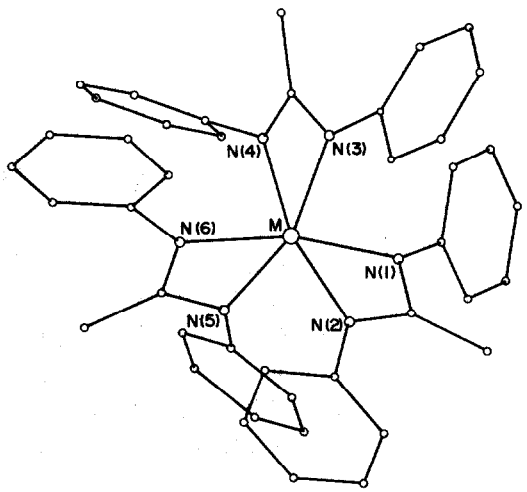

Fig. 1. Molecular structure of **1** (M = Ru) and **2** (M = Rh). Hydrogen atoms are omitted for clarity. Selected distances (Å) and angles (°): **1** (M = Ru): N(1)—Ru(1) 2.049(9), N(2)—Ru(1) 2.080(7), N(3)—Ru(1) 2.071(7), N(4)—Ru(1) 2.048(7), N(5)—Ru(1) 2.040(7), N(6)—Ru(1) 2.069(9), C(7)—N(1) 1.320(10), N(2)—C(7) 1.326(9), C(21)—N(3) 1.332(9), N(4)—C(21) 1.298(9), C(35)—N(5) 1.328(10), N(6)—C(35) 1.321(10); N(2)—Ru(1)—N(1) 62.5(3), N(4)—Ru(1)—N(3) 62.4(3), N(6)—Ru(1)—N(5) 63.1(3), C(7)—N(1)—Ru(1) 95.5(6), C(7)—N(2)—Ru(1) 93.9(5), C(21)—N(3)—Ru(1) 93.3(5), C(21)—N(4)—Ru(1) 95.4(5), C(35)—N(5)—Ru(1) 94.6(5), C(35)—N(6)—Ru(1) 93.5(6). **2** (M = Rh): N(1)—Rh(1) 2.030(9), N(2)—Rh(1) 2.072(7), N(3)—Rh(1) 2.068(7), N(4)—Rh(1) 2.026(7), N(5)—Rh(1) 2.028(7), N(6)—Rh(1) 2.051(9), C(7)—N(1) 1.319(10), N(2)—C(7) 1.328(9), C(21)—N(3) 1.317(8), N(4)—C(21) 1.304(8), C(35)—N(5) 1.321(9), N(6)—C(35) 1.314(9); N(2)—Rh(1)—N(1) 62.8(3), N(4)—Rh(1)—N(3) 62.5(3), N(6)—Rh(1)—N(5) 63.0(3), C(7)—N(1)—Rh(1) 95.8(6), C(7)—N(2)—Rh(1) 93.6(5), C(21)—N(3)—Rh(1) 93.1(4), C(21)—N(4)—Rh(1) 95.5(4), C(35)—N(5)—Rh(1) 94.9(5), C(35)—N(6)—Rh(1) 94.0(6).

* *Crystal data for* **1**. $C_{42}H_{39}N_6Ru$, $M = 728.88$, orthorhombic, $a = 30.840(9)$, $b = 10.843(1)$, $c = 10.766(2)$ Å, $U = 3600.13$ Å^3, $D_c = 1.345$ g cm^{-3}, $Z = 4$, space group $Pca2_1$, Mo-K_α radiation ($\lambda = 0.71069$ Å), μ(Mo-K_α) = 4.63 cm^{-1}, $F(000) = 1508$. Final $R = 0.039$ and $R_w = 0.044$ for 5165 unique reflections with $|F_o| > 3\sigma(|F_o|)$. **2**. $C_{42}H_{39}N_6Rh$, $M = 730.72$, orthorhombic, $a = 30.7659(11)$, $b = 10.833(1)$, $c = 10.780(1)$ Å, $U = 3593.06$ Å^3, $D_c = 1.351$ g cm^{-3}, $Z = 4$, space group $Pca2_1$, Mo-K_α radiation, μ(Mo-K_α) = 5.033 cm^{-1}, $F(000) = 1512$. Final $R = 0.032$ and $R_w = 0.036$ for 4834 unique reflections with $|F_o| > 3\sigma(|F_o|)$. **3**. $C_{36}H_{30}N_9Rh$, $M = 691.60$, orthorhombic, $a = 23.784(6)$, $b = 14.423(3)$, $c = 9.443(4)$ Å, $U = 3239.30$ Å^3, $D_c = 1.418$ g cm^{-3}, $Z = 4$, space group *Pnna*, Mo-K_α radiation, μ(Mo-K_α) = 5.565 cm^{-1}, $F(000) = 1416$. Final $R = 0.041$ and $R_w = 0.044$ for 3856 unique reflections with $|F_o| > 3\sigma(|F_o|)$. **4**. $C_{48}H_{40}N_{12}Rh_2$, $M = 990.74$, triclinic, $a = 10.405(2)$, $b = 13.687(3)$, $c = 15.939(2)$ Å, $\alpha = 100.071(1)$, $\beta = 103.23(1)$, $\gamma = 94.61(1)°$, $U = 2158.41$ Å^3, $D_c = 1.524$ g cm^{-3}, $Z = 2$, space group $P\bar{1}$, Mo-K_α radiation, μ(Mo-K_α) = 8.00 cm^{-1}, $F(000) = 1004$. Final $R = 0.038$ and $R_w = 0.043$ for 5494 unique reflections with $|F_o| > 3\sigma(|F_o|)$.

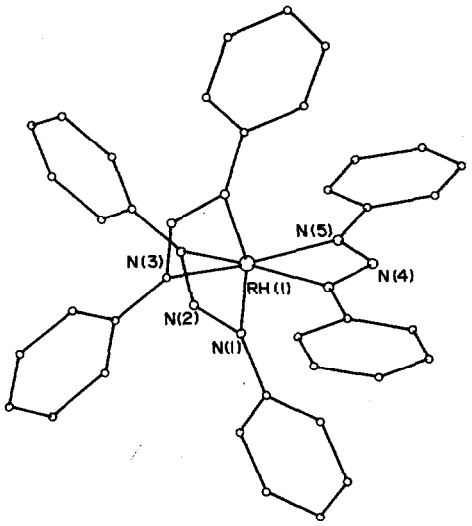

Fig. 2. Molecular structure of **3**. Hydrogen atoms are omitted for clarity. Selected distances (Å) and angles (°): N(1)—Rh(1) 2.030(6), N(3)—Rh(1) 2.035(6), N(5)—Rh(1) 2.025(6), N(2)—N(1) 1.323(6), N(3)—N(2) 1.316(7), N(5)—N(4) 1.300(6); N(3)—Rh(1)—N(1) 61.0(3), N(5)—Rh(1)—N(5a) 60.7(3), N(2)—N(1)—Rh(1) 98.1(4), N(2)—N(3)—Rh(1) 98.1(4), N(4)—N(5)—Rh(1) 97.8(4). (a) $x, \frac{1}{2}-y, \frac{1}{2}-z$.

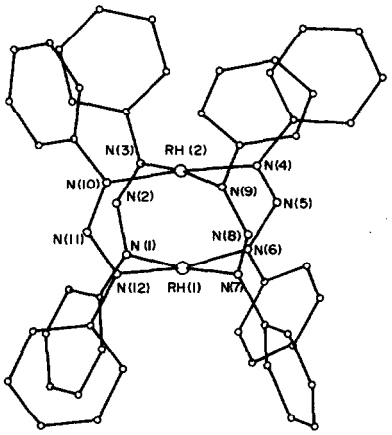

Fig. 3. Molecular structure of **4**. Hydrogen atoms are omitted for clarity. Selected distances (Å) and angles (°): Rh(2)—Rh(1) 2.377(3), N(1)—Rh(1) 2.040(6), N(6)—Rh(1) 2.078(7), N(7)—Rh(1) 2.054(6), N(12)—Rh(1) 2.055(7), N(3)—Rh(2) 2.064(6), N(4)—Rh(2) 2.021(7), N(9)—Rh(2) 2.045(6), N(10)—Rh(2) 2.027(7), N(2)—N(1) 1.315(7), N(3)—N(2) 1.298(6), N(5)—N(4) 1.293(7), N(6)—N(5) 1.308(7), N(8)—N(7) 1.300(6), N(9)—N(8) 1.302(8), N(11)—N(10) 1.314(7), N(12)—N(11) 1.297(7); N(1)—Rh(1)—Rh(2) 88.4(2), N(6)—Rh(1)—Rh(2) 85.7(2), N(6)—Rh(1)—N(1) 89.8(3), N(7)—Rh(1)—Rh(2) 86.7(2), N(7)—Rh(1)—N(6) 90.8(3), N(12)—Rh(1)—Rh(2) 86.4(2), N(12)—Rh(1)—N(1) 87.9(3), N(12)—Rh(1)—N(7) 90.8(3), N(3)—Rh(2)—Rh(1) 85.4(2), N(4)—Rh(2)—Rh(1) 87.4(2), N(4)—Rh(2)—N(3) 92.4(3), N(9)—Rh(2)—Rh(1) 87.5(2), N(9)—Rh(2)—N(4) 86.4(3), N(10)—Rh(2)—Rh(1) 87.9(2), N(10)—Rh(2)—N(3) 89.8(3), N(10)—Rh(2)—N(9) 90.8(3).

and 2.389 Å, respectively. Rhodium–nitrogen bond lengths at 2.050 Å (average) are essentially the same in all three complexes.

Data collection

Unit cell dimensions and intensity data for compounds **1**, **2**, **3** and **4** were obtained at 295 K using an Enraf–Nonius area detector diffractometer and graphite monochromated Mo-K_α radiation, following previously described procedures ($D = 40$ mm, $2\theta = 18$).[12] The structures were solved by Patterson and Fourier techniques and refined by blocked full-matrix least-squares methods.[13] Hydrogen atoms were included in calculated positions with isotropic thermal parameters related to those of the parent atoms and refined in riding mode. All four sets of data were corrected for absorption using the DIFABS procedure,[14] adapted for FAST geometry by A. Karaulov, University of Cardiff (1991). Atomic coordinates, bond lengths and angles, and thermal parameters have been deposited at the Cambridge Data Centre.

All calculations were made on a T800 transputer hosted by an IBM/AT personal computer.

REFERENCES

1. D. S. Moore and S. D. Robinson, *Adv. Inorg. Chem. Radiochem.* 1986, **30**, 1 and refs therein.
2. F. A. Cotton and M. Matusz, *J. Am. Chem. Soc.* 1988, **110**, 5761.
3. F. A. Cotton, G. W. Rice and J. C. Sekutowski, *Inorg. Chem.* 1979, **18**, 1143.
4. F. E. Brinckman and H. S. Haiss, *Chem. Ind. (London)* 1963, 1124.
5. S. F. Colson and S. D. Robinson, *Polyhedron* 1990, **9**, 1737.
6. M. Corbett and B. F. Hoskins, *J. Am. Chem. Soc.* 1967, **89**, 1530.
7. W. R. Krigbaum and B. Rubin, *Acta Cryst., Sect. B* 1973, **29**, 749.
8. J. A. Clark, M. Kilner and A. Pietrzykowski, *Inorg. Chim. Acta* 1984, **82**, 85.
9. F. A. Cotton and X. Feng, *Inorg. Chem.* 1989, **28**, 1180.
10. P. Piraino, G. Bruno, S. Lo Schiavo, F. Laschi and P. Zanello, *Inorg. Chem.* 1987, **26**, 2205.
11. J. C. Le, M. Y. Chavan, L. K. Chau, J. L. Bear and K. M. Kadish, *J. Am. Chem. Soc.* 1985, **107**, 7195.
12. A. A. Danopoulos, G. Wilkinson, B. Hussain-Bates and M. B. Hursthouse, *J. Chem. Soc., Dalton Trans.* 1991, 1855.
13. G. M. Sheldrick, SHELX. University of Göttingen, F.R.G. (1986).
14. N. Walker and D. Stuart, *Acta Cryst.* 1983, **A39**, 158.

Polyhedron Vol. 12, No. 5, pp. 567–570, 1993
Printed in Great Britain

0277–5387/93 $6.00+.00
© 1993 Pergamon Press Ltd

COMMUNICATION

PRESSURE DEPENDENCE OF THE HYDROLYSIS RATES OF INORGANIC CONDENSED PHOSPHATE OLIGOMERS WITH POLYMERIZATION DEGREES OF 6 AND 8

GENICHIRO KURA* and HIDEAKI ARIGATA

Department of Chemistry, Fukuoka University of Education, Akama Munakata, Fukuoka 811-41, Japan

and

SHIGENORI UTOH

Department of Physics, Fukuoka University of Education, Akama, Munakata, Fukuoka 811-41, Japan

(*Received* 13 *October* 1992; *accepted* 10 *November* 1992)

Abstract—The rate constants for the hydrolysis reactions of cyclic and linear condensed phosphate oligomers were determined as a function of pressure at 40°C in a 0.1 M HCl solution. The hydrolysis rates increased with the increase in pressure. The volumes of activation were determined from the linear relations between $\ln k$ vs P. The volumes of activation, which were negative and ranged from -3.8 to -5.7 cm^3 mol^{-1}, were obtained. The mechanism of these hydrolysis reactions is discussed.

Condensed phosphates have been known as important polyvalent inorganic electrolytes and have been used for various purposes.[1] They have been prepared by dehydrating monophosphates, and two of them, one with an open chain and the other with cyclic structure, are well known. When treating these condensed phosphates in the aqueous state, much attention should be given to the hydrolysis reaction. The hydrolysis reactions of condensed phosphate oligomers have been investigated from different points of view and reaction mechanisms have been extensively discussed.[2–8]

In this study the pressure dependence of the hydrolysis rate constants of the cyclic hexamer and octamer and the corresponding linear hexamer and octamer were determined, and the volumes of activation for the hydrolysis reactions were estimated. The hydrolysis rates for the above four phosphates increased with the increase in pressure of the reaction cell. All the volumes of activation determined were negative and thus the molecular volumes of the activated complexes decreased.

Sodium cyclo-hexa- and cyclo-octaphosphate were prepared following the methods described in the literature.[9,10] Other chemicals used were reagent grade and commercially available.

The initial concentration of the phosphate to be degraded was 2.5×10^{-3} M in 0.1 M HCl. The temperature of the reacting solution was maintained at 40°C in a high pressure cell. The sample cell used was part of an injector and the dimensions were 10 mm in diameter and 70 mm in length, as shown in Fig. 1. The high-pressure vessel shown in

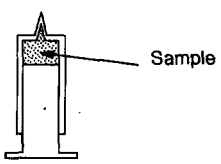

Fig. 1. Sample cell.

* Author to whom correspondence should be addressed.

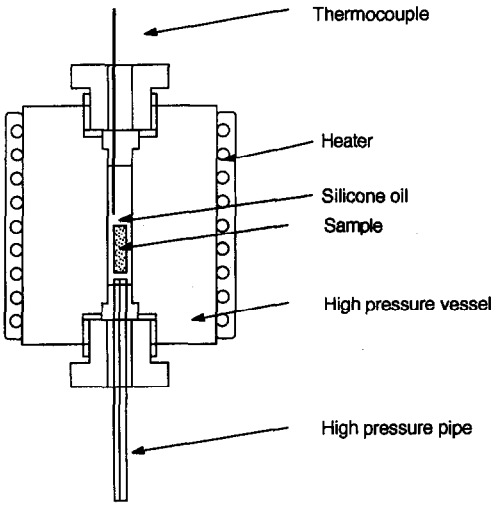

Fig. 2. High pressure vessel.

Fig. 2 was connected to a high-pressure generating pump. Silicone oil was used as a pressure-transmitting medium and the pressure was measured with a Heise gauge attached to a calibrated manganin wire: the accuracy of the pressure measured was ± 0.5 MPa. The temperature of the reaction cell was measured with an alumel–chromel thermocouple inserted in the silicone oil near the cell.

The hydrolysis samples were analysed using the chromatographic system described in our previous paper.[6]

The hydrolytic degradations of cyclic and linear condensed phosphates (abbreviated as P_{nm} and P_n, respectively; in both cases, n indicates the polymerization degree) are characterized by the following equation:

$$P_{nm} \xrightarrow{k_m} P_n \xrightarrow{k_n} P_{n-1}, P_{n-2}, \ldots, P_1, P_{3m},$$

where k_m and k_n are the first-order rate constant of cyclic and linear phosphates, respectively. At first, the cyclic oligomers are hydrolysed to linear oligomers with the same polymerization degree, and then to lower linear phosphates. The hydrolysis rate has been known to be first-order and, therefore, the rate equations can be written as:

$$-\frac{dx}{dt} = k_m x \quad (1)$$

$$-\frac{dy}{dt} = k_n y - k_m x \quad (2)$$

where x and y are the concentrations of cyclic and linear phosphates at time t. These differential equations are solved by assuming that the initial values of x and y are x_0 and y_0, respectively.

$$x = x_0 \exp(-k_m t) \quad (3)$$

$$y = \frac{k_m x_0}{(k_n - k_m)} \exp(-k_m t) + \left\{ y_0 - \frac{k_m x_0}{(k_n - k_m)} \right\} \exp(-k_n t) \quad (4)$$

Equation (3) can be rewritten as:

$$\log \frac{x}{x_0} = -\frac{k_m t}{2.303}. \quad (5)$$

Hydrolysis samples were analysed by the liquid chromatographic system devised by us, and thus, from the chromatograms obtained, x and y were determined as a function of time t. For the hydrolysis of cyclo-hexa- and cyclo-octaphosphate in a 0.1 M HCl solution at 40°C and at various pressures, $\log(x/x_0)$ vs t plots are shown in Figs 3 and 4. Good linear relations were obtained and the first-order rate constants were calculated from the slopes of the straight lines for each pressure. The hydrolysis rates of both cyclic phosphates increased with an increase in pressure. From the chromatograms of the hydrolysis samples of cyclic phosphates, the concentration of linear phosphates with the same polymerization degree as the cyclic phosphates, y, was also determined. Finally, using equation (4), the first-order rate constant k_n was estimated by the least-squares procedure. As an example, for the hydrolysis of hexaphosphate in a 0.1 M HCl solution at 40°C and at 400 MPa, the value of y was

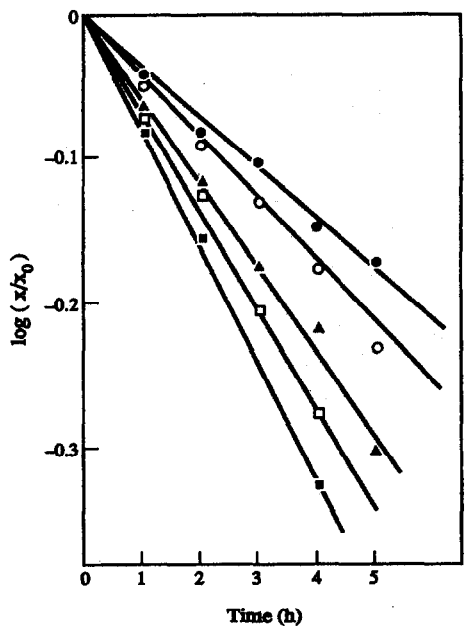

Fig. 3. First-order rate data for cyclo-hexaphosphate hydrolysis in 0.1 M HCl at 40°C and at various pressures: ●, 100 MPa; ○, 200 MPa; ▲, 300 MPa; □, 400 MPa; ■, 500 MPa.

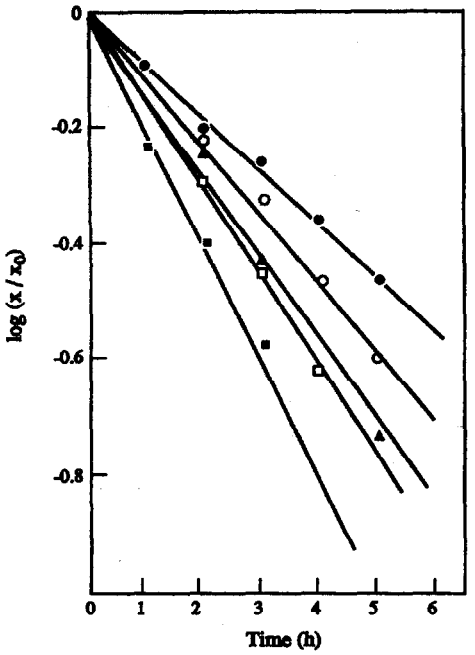

Fig. 4. First-order rate data for cyclo-octaphosphate hydrolysis in 0.1 M HCl at 40°C and at various pressures: ●, 100 MPa; ○, 200 MPa; ▲, 300 MPa; □, 400 MPa; ■, 500 MPa.

plotted as a function of time. The solid line in this figure indicates the value of y calculated by substituting k_m and k_n in equation (4), and the black circles are experimental points. Table 1 presents the rate constants of each phosphate thus obtained.

Table 1. Rate constants (h^{-1}) at various pressures and volumes of activation in 0.1 M HCl at 40°C

Pressure (MPa)	P_{6m}	P_6	P_{8m}	P_8
0.1	0.061	0.348	0.150	0.624
100	0.081	0.574	0.210	1.30
200	0.098	0.639	0.266	1.74
300	0.134	0.750	0.316	1.60
400	0.156	0.878	0.351	1.50
500	0.184	0.970	0.457	1.68
$\Delta V^{\ddagger}$ ($cm^3\ mol^{-1}$)	−5.67	−3.81	−5.35	−3.87

As mentioned above, the rate constants of each phosphate increased with an increase in pressure. According to the transition-state theory, if the volume of activation is defined as $\Delta V^{\ddagger}$, the rate constant can be related to pressure by the following equation:

$$\frac{d(\ln k)}{dP} = -\frac{\Delta V^{\ddagger}}{RT}. \quad (6)$$

If $\Delta V^{\ddagger}$ does not depend on pressure, equation (6) can be integrated to give:

$$\ln k = \ln k_0 - \frac{\Delta V^{\ddagger}}{RT} P, \quad (7)$$

where k_0 is the rate constant at pressure 0 and can be regarded as the value at atmospheric pressure (0.1 MPa). In Fig. 6, for cyclo-hexaphosphate hydrolysis, the pressure dependence of $\log k$ is shown and a linear model is adequate to describe the data. From the slopes of the straight lines the

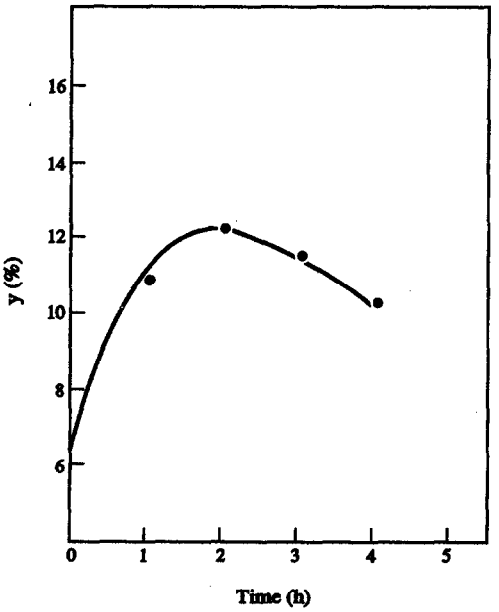

Fig. 5. First-order rate data for linear hexaphosphate hydrolysis in 0.1 M HCl at 40°C and 400 MPa.

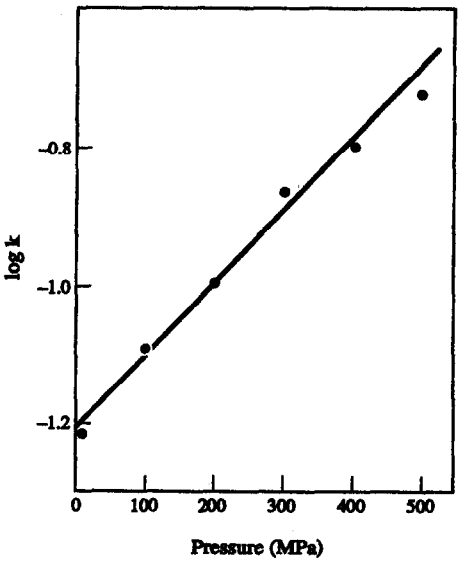

Fig. 6. Pressure dependence of the rate constant of cyclo-hexaphosphate in 0.1 M HCl at 40°C.

volumes of activation, the various $\Delta V^{\ddagger}$, were determined and are shown in Table 1. For all phosphates $\Delta V^{\ddagger}$, represented by the difference in molar volume between the transition state and the reactants of the condensed phosphates in acidic solutions, are regarded to proceed via nucleophilic attack on phosphorus atoms by H_2O molecules. Although the H_2O molecule bonds to the phosphate in the transition state, the molar volume of the activated complex is decreased. One of the hydrating water molecules which are loosely bound to the phosphate becomes more tightly bonded to the phosphorus atom in the activated complex and this association processes the rate determining step, thus causing the decrease in the molar volume. In our previous papers,[2,3] we pointed out that hydrogen ions strongly accelerate the hydrolysis rates of condensed phosphates. Although a pressure dependence for the degree of bonding of H^+ with the phosphate anions cannot be estimated, it has generally been known that many acids dissociate with an increase in pressure.[11] If this were so, the pressure increase should cause a decrease in the protonation of phosphate anions and thus a decrease in the hydrolysis rate. However, the changes in activation volumes are more effective and the rates actually increased. Negative volumes of activation have been observed for the hydrolysis reactions of various esters, which may be bimolecular reactions similar to the scission of P—O—P bonds in the phosphates, caused by the reaction between water molecules and phosphates.

REFERENCES

1. J. R. Van Wazer, *Phosphorus and its Compounds*, Vol. I. Interscience, New York (1958).
2. G. Kura, *Bull. Chem. Soc. Japan* 1983, **56**, 3769.
3. G. Kura, *Polyhedron* 1987, **6**, 531.
4. G. Kura, *Bull. Chem. Soc. Japan* 1987, **60**, 2857.
5. G. Kura, *Polyhedron* 1987, **6**, 1863.
6. G. Kura, *J. Chromatogr.* 1988, **447**, 91.
7. G. Kura, *Polyhedron* 1990, **9**, 2177.
8. G. Kura, *Polyhedron* 1991, **10**, 697.
9. E. J. Griffith and R. L. Buxton, *Inorg. Chem.* 1965, **4**, 549.
10. U. Schülke, *Z. Anorg. Allg. Chem.* 1968, **360**, 231.
11. R. van Eldik (Editor), *Inorganic High Pressure Chemistry: Kinetics and Mechanism.* Elsevier, Amsterdam (1986).

Polyhedron Vol. 12, No. 6, pp. 571–589, 1993
Printed in Great Britain

0277-5387/93 $6.00+.00
Pergamon Press Ltd

POLYHEDRON REPORT NUMBER 46

A THERMODYNAMIC SCALE FOR OXYGEN ATOM TRANSFER REACTIONS

R. H. HOLM† and JAMES P. DONAHUE

Department of Chemistry, Harvard University, Cambridge, MA 02138, U.S.A.

CONTENTS

1. INTRODUCTION 571

2. THERMODYNAMIC REACTION COUPLES 572
   2.1. Gas phase 576
   2.2. Solid and liquid phases and aqueous solution 578

3. APPLICATIONS 578
   3.1. Strong oxo donors 578
   3.2. Other oxo donors 580
   3.3. Oxo acceptors 580

4. THE OXO TRANSFER CHEMISTRY OF RHENIUM 581
   4.1. Oxorhenium functional groups 582
   4.2. Oxo transfer reactions 582

5. OXO TRANSFER REACTION DIAGRAMS 584

1. INTRODUCTION

In our previous analysis of metal-centred oxygen atom (oxo) transfer reactions[1] the three most common reaction types, eqs (1)–(3), were identified, in which X/XO is a generalized oxygen atom acceptor/donor. In the *primary* oxo transfer reaction, eq. (1), the metal oxidation state is altered by two units. In the *incomplete* intermetal oxo transfer reaction, eq. (2), a binuclear μ-oxo species is formed and the oxidation state of the metal is increased by one unit. In the *complete* intermetal oxo transfer reaction, eq. (3a), metal centres act as the oxo donor and acceptor, an intermediate μ-oxo species is formed and the oxidation state changes are the same as in reaction (1). Much less frequently encountered is the complete intermetal oxo transfer reaction, eq. (3b), in which metal oxidation states are altered by one unit and products have the same number of oxo atoms. Reactions (2)–(3b) are obviously specific cases of reaction (1), in which metal complexes function as X/XO. For this set of reactions, ligand numbers n are not necessarily the same in reactant and product, $a = 0$–3, and products X and XO may be coordinated in the forward and reverse, respectively, of reaction (1). These processes are readily extended to two different metals in reactions (2)–(3b) and to higher

† Author to whom correspondence should be addressed.

Abbreviations used: cat = catecholate(2-); Cp = η^5-cyclopentadienyl; Cp* = η^5-pentamethylcyclopentadienyl; cyclam = 1,4,8,11-tetraazacyclotetradecane; diox = dioxane; hq = 8-hydroxyquinolinate(1-); L = ligand; *m*-CPBA = *m*-chloroperoxybenzoic acid; mes = mesityl; Me_3tacn = N,N′,N″-trimethyl-1,4,7-triazacyclononane; P = porphyrinate(2-); py = pyridine; pyO = pyridine N-oxide; pz = pyrazole; quin = quinuclidine; and tacn = 1,4,7-triazacyclononane.

nuclearities in all reactions. This report deals with *thermodynamic* aspects of oxo transfer; reaction kinetics, some data for which have been summarized,[1] are not considered.

$$M^zO_aL_n + XO \rightleftharpoons M^{z+2}O_{a+1}L_n + X \quad (1)$$

$$M^zO_aL_n + M^{z+2}O_{a+1}L_n \rightleftharpoons [L_nM^{z+1}O_a]_2O \quad (2)$$

$$M^zO_aL_n + M^{z+2}O_{a+1}L'_n \rightleftharpoons M^{z+2}O_{a+1}L_n + M^zO_aL'_n \quad (3a)$$

$$M^zO_aL_n + M^{z+2}O_{a+2}L'_n \rightleftharpoons M^{z+1}O_{a+1}L_n + M^{z+1}O_{a+1}L'_n \quad (3b)$$

In order to provide a predictive basis for the outcome of primary oxo transfer reactions, we have introduced a simple reactivity scale that reduces substrate reactions to a common thermodynamic basis.[1-3] Consider generalized reactions (4) and (5), whose enthalpy changes are the differences in the standard molar heats of formation ($\Delta_fH^0_m$) of product and reactant. If $|T\Delta S| \ll |\Delta H|$ and $\Delta H_{X/XO} > \Delta H_{Y/YO}$, reaction (6) is spontaneous. With the use of reaction (7) the bond dissociation energies, D, in reaction (8) can be calculated for an oxidized molecule such as $XO_{(g)}$.

$$X + \tfrac{1}{2}O_{2(g)} \longrightarrow XO \qquad \Delta H_{X/XO} \quad (4)$$

$$Y + \tfrac{1}{2}O_{2(g)} \longrightarrow YO \qquad \Delta H_{Y/YO} \quad (5)$$

$$XO + Y \rightleftharpoons X + YO \qquad \Delta H = \Delta H_{Y/YO} - \Delta H_{X/XO} \quad (6)$$

$$\tfrac{1}{2}O_{2(g)} \longrightarrow O_{(g)} \qquad \Delta_fH^0_m = 59.55 \text{ kcal mol}^{-1}\ ^{15} \quad (7)$$

$$XO_{(g)} \longrightarrow X_{(g)} + O_{(g)} \qquad D = -\Delta H_{X/XO} + \Delta_fH^0_m(O_{(g)}) \quad (8)$$

A series of reactions, or *couples*, such as eqs (4) and (5), when compiled in a descending order of decreasing ΔH, has a utility analogous to that of a table of standard reduction potentials: the reduced member Y of a couple Y/YO with a smaller (more negative) ΔH is thermodynamically competent to reduce the oxidized member XO of a couple X/XO with a larger ΔH. With a sufficient body of data such a compilation would allow prediction of the directions of a large number of oxo transfer reactions and, in a number of gas phase cases, the differences in X—O and Y—O bond energies. Provided the structural differences between X and fragment X in XO and Y and fragment Y in YO are small, ΔH of reaction (6) is a measure of $D_{X-O} - D_{Y-O}$.

Our initial compilation, which was relatively short, was limited to enthalpies of oxidation couples that consisted mainly of the more common oxo donors and acceptors in the solution and gas phases.[1] Since that time new $\Delta_fH^0_m$ and $\Delta_fG^0_m$ data have become available, uncertainties in several previously quoted data have been clarified and examples of the utilization of the reactivity scale in our own work[2-7] and that of others[8-10] have appeared. Indeed, Tolman and co-workers[8,9] have independently obtained a scale of heats of oxidation which they have employed in considerations of alkane oxidation. In view of the importance of and current interest in atom transfer reactions we have sought to formulate a more extensive reactivity scale. Towards that end we have examined the extensive $\Delta_fH^0_m$ and $\Delta_fG^0_m$ data bases.[11-19] Additionally, recent measurements of standard molar heats of combustion and sublimation have permitted calculation of new or more accurate gas phase $\Delta_fH^0_m$ values and X—O bond dissociation energies. Useful examples include a series of N-oxides[20-25] and Ph_3AsO.[26]

2. THERMODYNAMIC REACTION COUPLES

Enthalpies and free energies (where available) for an extensive series of reaction couples are presented in Tables 1–4. Several aspects of these compilations are briefly noted. In order that they contain a considerable quantity of useful information but be limited in size compounds X and XO are restricted to the same pure phase in each of Tables 1–3; aqueous solution data are given in Table 4. The large majority of data refer to standard states of the various compounds. However, because this is not entirely the case the enthalpy and free energy symbols do not indicate standard state. In the few instances in which data from two or more sources were not in agreement results were taken from the 1982 NBS tables[15] when available. Estimated errors are not included, but can be obtained from the original sources in most cases. A general guideline is $\pm$(2-3) kcal mol^{-1} in ΔG and ΔH values. For those oxo donor and acceptors in reasonably common use, the tabulations

Table 1. Oxo transfer thermodynamic reactivity scale: gas phase

$$X_{(g)} + \tfrac{1}{2}O_{2(g)} = XO_{(g)}$$

X	XO	$\Delta G^{298}_{X/XO}$ (kcal mol^{-1})	$\Delta H_{X/XO}$ (kcal mol^{-1})	Ref.
O_2	O_3	+39.0	+34.1	15
H_2O	H_2O_2	+29.4	+25.2	15
N_2	N_2O	+24.9	+19.6	15
Cl_2	Cl_2O	+23.4	+19.2	15
Bu^{t}OH	Bu^{t}OOH	—	+15.9	16
Me_2O	MeOOMe	—	+14.0	16
ClO_2	ClO_3	—	+13.0	15
2,4,6-$Me_3C_6H_2CN$	2,4,6-$Me_3C_6H_2CNO$ (1)	—	+6.4	20
2,4,6-$(MeO)_3C_6H_2CN$	2,4,6-$(MeO)_3C_6H_2CNO$	—	+3.9	20
Bu$^t{}_2O$	Bu^{t}OOBu^t	—	+3.1	16
$SeCl_2$	$SeOCl_2$	—	+1.6	15
ClO	ClO_2	+5.35	+0.2	15
PhCH=NPh	PhCH=N(O)Ph (2)	—	−3.8	21
PhCH=NBu^t	PhCN=N(O)Bu^t (2)	—	−8.2	22
EtONO	$EtONO_2$	—	−11.9	15
C_5H_5N	C_5H_4NO (4)	—	−12.6	23
OsO_3	OsO_4	—	−12.8	15
MeONO	$MeONO_2$	—	−13.3	15
NO	NO_2	−8.42	−13.6	15
PhN=NPh	PhN=N(O)Ph (3)	—	−17.3	21
N_2O_3	N_2O_4	−9.94	−17.8	15
PrN=NPr	PrN=N(O)Pr (3)	—	−19.7	21
SO_2	SO_3	−16.9	−23.6	15
$H_2C=CH_2$	C_2H_4O	−19.4	−25.1	15
RuO_3	RuO_4	—	−25.3	15
$MeCH=CH_2$	$MeCHCH_2O$	—	−27.0	16
Me_2S	Me_2SO	−21.2	−27.1	15
Ph_2S	Ph_2SO	—	−29.7	16
CH_4	MeOH	−26.6	−30.1	15
$SOCl_2$	SO_2Cl_2	—	−33.3	11, 18
$MoCl_4$	$MoOCl_4$	−48	−41	14
Ph_3As	Ph_3AsO	—	−43.1	26
SCl_2	$SOCl_2$	—	−44.7	11, 19
$(MeO)_2SO$	$(MeO)_2SO_2$	—	−48.4	16
SOF_2	SO_2F_2	—	−50.3	18
Sn_2Et_6	$(Et_3Sn)_2O$	—	−52.6	13
Me_2SO	Me_2SO_2	−45.7	−52.7	15
Ge_2Et_6	$(Et_3Ge)_2O$	—	−58.0	13
O	O_2	−55.4	−59.6	15
MeCHO	$MeCO_2H$	−58.6	−63.6	15
HCHO	HCO_2H	—	−64.5	15
PCl_3	$POCl_3$	−58.6	−64.9	15
WCl_4	$WOCl_4$	—	−67.2	15
CO	CO_2	−61.5	−67.6	15
SO	SO_2	−67.0	−72.4	15
Ph_3P	Ph_3PO	—	−73.8[a]	12, 27
WF_4	WOF_4	−74	—	14
Me_3P	Me_3PO	—	−79.7	12
MoO_2	MoO_3	—	−81.0	15
WO_2	WO_3	—	−82.0	15
$(EtO)_3P$	$(EtO)_3PO$	—	−88.6	12
$NbCl_3$	$NbOCl_3$	—	−93.8	15
Si_2Me_6	$(Me_3Si)_2O$	—	−99.0	13

[a] Obtained using an estimated ΔH_{sub} value.[27]

Table 2. Oxo transfer thermodynamic reactivity scale: solid phase[a]

$$X_{(s)} + \tfrac{1}{2}O_{2(g)} = XO$$

X	XO	$\Delta G^{298}_{X/XO}$ (kcal mol^{-1})	$\Delta H_{X/XO}$ (kcal mol^{-1})
$NOClO_4$	NO_2ClO_4	—	+45.6
$KBrO_3$	$KBrO_4$	+23.1	+17.3
$K_2S_2O_7$	$K_2S_2O_8$	+22.5	+16.8
SeO_2	SeO_3	—	+14.0
$NaIO_3$	$NaIO_4$	—	+12.5
KIO_3	KIO_4	+13.6	+8.16
$PhCO_2H$	$PhCO_3H$	—	+4.3[16]
CrO_2	CrO_3	—	−0.1
$NaClO_3$	$NaClO_4$	+1.8	−4.9
PbO (red)	PbO_2	−6.8	−14.0
$NaClO_2$	$NaClO_3$	—	−14.0
$[Co(NH_3)_5NO_2]I_2$	$[Co(NH_3)_5NO_3]I_2$	—	−17.8
$AgNO_2$	$AgNO_3$	−12.6	−19.0
Na_2O	Na_2O_2	−17.3	−23.1
NH_4NO_2	NH_4NO_3	—	−26.1
$Na_2S_2O_3$	$Na_2S_2O_4$	—	−26.1
$NaNO_2$	$NaNO_3$	−19.7	−26.1
V_2O_4	V_2O_5	−24.2	−29.5
K_2O	K_2O_2	—	−31.7
MnO	MnO_2	−24.4	−32.2
ReO_2	ReO_3	−27[14]	−34[14]
MoO_2	MoO_3	−32.3	−37.3
$MoCl_4$	$MoOCl_4$	—	−38.2
WCl_4	$WOCl_4$	—	−49.6
$MoBr_3$	$MoOBr_3$	−39[14]	−49[14]
V_2O_3	V_2O_4	−42.8	−49.8
$Na_2S_2O_5$	$Na_2S_2O_6$	—	−52.8
$Na_2S_2O_6$	$Na_2S_2O_7$	—	−54.0
Ph_3As	Ph_3AsO	—	−55.3[12,26]
$Na_2S_2O_4$	$Na_2S_2O_5$	—	−58.8
UBr_2	$UOBr_3$	−54.1	−60.9
WO_2	WO_3	−55.0	−60.5
$MoCl_3$	$MoOCl_3$	−59.0[14]	−54.9[14]
Na_2SO_3	Na_2SO_4	−61.6	−68.4
GeO	GeO_2	−62.1	−69.1
Ph_3P	Ph_3PO	—	−69.9[12]
SnO	SnO_2	−62.8	−70.5
$GaCl_3 \cdot PCl_3$	$GaCl_3 \cdot POCl_3$	−65[14]	−71[14]
UCl_3	$UOCl_3$	−65.0	−70.9
NaH	NaOH	−82.7	−88.3
TiO	TiO_2	—	−101
Mg	MgO	−136	−144
Ca	CaO	−144	−152

[a] Data from ref. 15 unless otherwise noted.

contain all available data. Also presented are values for infrequently employed or potential oxo transfer reaction couples, some of which, because of their familiar constituents (e.g. $NO_{(g)}/NO_{2(g)}$), may serve as "calibration" points for the scale. In this regard ΔH values for the gas-phase couples CH_4/CH_3OH (−30.2 kcal mol^{-1}) and H_2/H_2O (−57.8 kcal mol^{-1}) attend the same purpose. Lastly, with practically no exceptions, ΔG and ΔH data parallel each other in Tables 1–3 and thus lead to the same predictions of relative reactivity. The much more extensive body of enthalpy data is utilized in the considerations that follow.

Table 3. Oxo transfer thermodynamic reactivity scale: liquid phase[a]

$$X_{(l)} + \tfrac{1}{2}O_{2(g)} = XO_{(l)}$$

X	XO	$\Delta G^{298}_{X/XO}$ (kcal mol^{-1})	$\Delta H_{X/XO}$ (kcal mol^{-1})
H_2O	H_2O_2	+27.9	+23.4
$C_6H_{11}OH$	$C_6H_{11}OOH$	—	+17.9[16]
Bu^tOH	Bu^tOOH	—	+15.7[12]
EtOH	EtOOH	—	+8.3
EtONO	$EtONO_2$	—	−14.7
N_2O_3	N_2O_4	—	−16.7
SO_2	SO_3	—	−28.8
Me_2S	Me_2SO	−25.1	−33.0
$SOCl_2$	SO_2Cl_2	—	−35.5
SCl_2	$SOCl_2$	—	−46.7
MeNC	MeNCO	—	−50.0
Sn_2Et_6	$(Et_3Sn)_2O$	—	−50.1[13]
Ge_2Et_6	$(Et_3Ge)_2O$	—	−57.0[13]
PCl_3	$POCl_3$	—	−66.3
MeCHO	$MeCO_2H$	−62.4	−69.8
$(EtO)_3P$	$(EtO)_3PO$	—	−92.3[12]
Si_2Me_6	$(Me_3Si)_2O$	—	−98.9[13]

[a] Data from ref. 15 unless otherwise noted.

Table 4. Oxo transfer thermodynamic reactivity scale: aqueous solution[a]

$$X_{(aq)} + \tfrac{1}{2}O_{2(g)} = XO_{(aq)}$$

X	XO	$\Delta G^{298}_{X/XO}$ (kcal mol^{-1})	$\Delta H_{X/XO}$ (kcal mol^{-1})
O_2	O_3	—	+32.9[14]
H_2O	H_2O_2	—	+22.6[14]
BrO_3^-	BrO_4^-	+23.8	+19.1
Cl^-	ClO^-	+22.6	+14.4
OH^-	HO_2^-	+21.5	+16.7[14]
Br^-	BrO^-	+16.9	+6.56
IO_3^-	IO_4^-	+16.6	+16.7
$S_2O_7^{2-}$	$S_2O_8^{2-}$	—	+13.5
ClO^-	ClO_2^-	+12.9	+9.70
I^-	IO^-	+3.12	−12.5
ClO_3^-	ClO_4^-	−0.14	−6.06
ClO_2^-	ClO_3^-	−6.00	−8.95
$HSeO_3^-$	$HSeO_4^-$	−9.76	−16.0
TeO_3^{2-}	TeO_4^{2-}	−15.3[14]	—
SeO_3^{2-}	SeO_4^{2-}	−17.1	−21.5
$S_2O_3^{2-}$	$S_2O_4^{2-}$	−18.7	−24.3
$HTeO_3^-$	$HTeO_4^-$	−18.3[14]	—
NO_2^-	NO_3^-	−18.9	−24.0
$H_2AsO_3^-$	$H_2AsO_4^-$	−39.7	−46.6
$S_2O_6^{2-}$	$S_2O_7^{2-}$	—	−48.5
$S_2O_5^{2-}$	$S_2O_6^{2-}$	—	−53.8[14]
V^{2+}	VO^{2+}	−52.9[1]	—
HSO_3^-	HSO_4^-	−54.5	−62.4
HCO_2^-	HCO_3^-	−56.3	−63.7
SO_3^{2-}	SO_4^{2-}	−61.7	−65.4
HCHO	HCO_2H	—	−67.8
CN^-	OCN^-	−64.5	−70.9

[a] Data from ref. 15 unless otherwise noted.

Table 5. Selected bond dissociation energies

$$XO_{(g)} = X_{(g)} + O_{(g)}$$

XO	D (kcal mol^{-1})
O_3	21
N_2O	34
2,4,6-$Me_3C_6H_2CNO$	53
$SeOCl_2$	58
PhCH=N(O)Ph	63
C_5H_5NO	72
$Pr^nN{=}N(O)Pr^n$	79
SO_3	83
Me_2SO	87
$MoOCl_4$	101
Ph_3AsO	103
$SOCl_2$	104
Me_2SO_2	118
$POCl_3$	124
$WOCl_4$	127
Ph_3PO	133
$(EtO)_3PO$	148

2.1. *Gas phase*

The thermodynamics of gas-phase couples provide the best measure of *intrinsic* oxo donor and acceptor reactivity. Data for some 53 couples, which are of two types, are included in Table 1. The large majority involve species in which a bond to a single atom is made or broken in the course of oxo transfer, as in reaction (6). Bond energies of oxo donors are readily calculated from reaction (8); selected examples are given in Table 5. In several couples, exemplified by Si_2Cl_6/Si_2OCl_6, the oxygen atom is inserted between two acceptor atoms, permitting the estimation of a mean X—O bond energy. Examples of the applications of various oxo donors and acceptors noted below in atom transfer reactions through 1986 are given elsewhere.[1] Certain more recent applications are summarized below.

It is immediately evident that the strongest oxo donor is ozone, followed by hydrogen peroxide and nitrous oxide. Being a highly reactive gas, ozone is an inconvenient and often indiscriminant reagent. The use of hydrogen peroxide is largely confined to aqueous or mixed-aqueous solvent systems. Nitrous oxide is a relatively unreactive gas with a high activation energy for dissociation (*ca* 60 kcal mol^{-1}).[28] Its utility as an oxo donor has been largely limited to low valent compounds of titanium, zirconium, vanadium and chromium. Dichlorine monoxide,[29] a gas under ordinary conditions, has found restricted use as an oxo source. Solutions of Cl_2O can be prepared in certain anhydrous organic solvents such as CCl_4.[30] In the presence of water the compound hydrolyses to HOCl; hypochlorite is an effective oxo transfer agent in both aqueous and non-aqueous solvents. The most practical strong donor is t-butylhydroperoxide, which is conventionally employed as a solution in an organic solvent; other compounds of the types ROOH and ROOR[31] are presumably of comparable strength.

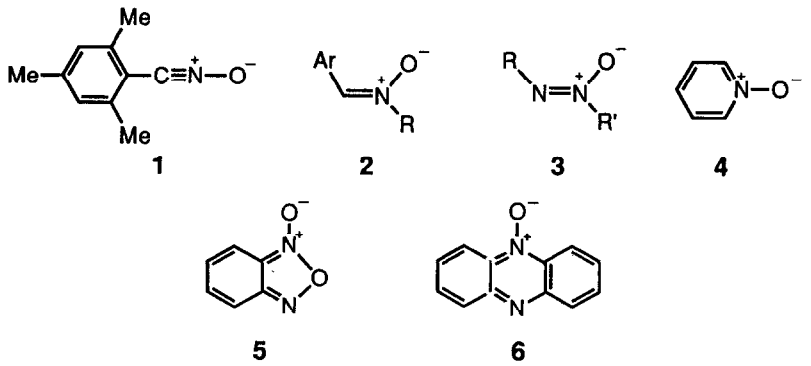

1 2 3 4

5 6

The next portion of the scale is primarily composed of various N-oxides, beginning with the nitrile oxide **1** and including azomethine (**2**), diazine (**3**) and pyridine (**4**) oxides. The available data, due to Acree, Pilcher and co-workers,[20–25] define a graded class of compounds with $6 \geqslant \Delta H \geqslant -20$ kcal mol^{-1}, corresponding to the bond energies $83 \geqslant D \geqslant 53$ kcal mol^{-1} (Table 5). Also part of this set are benzofuroxan (**5**, $\Delta H = -0.4$ kcal mol^{-1}) and phenazine N-oxide (**6**, $\Delta H = -12.7$ kcal mol^{-1}).[24] Azomethine and diazine N-oxides are usually found in the solid state as the *trans* forms **2** and **3**, respectively, but there are exceptions.[32,33] The *cis* and *trans* isomers can be interconverted thermally or photochemically in solution.[32–34] While the *cis* isomer is the less sterically hindered, the formation of an O-bonded complex of **2**, $Cp(CO)_2Fe—O—N(Ph)=CH(p\text{-}C_6H_4OMe)$,[35] indicates that a *trans* isomer with substituents as large as phenyl can approach a simulated metal oxo acceptor site that is relatively unhindered. Organic N-oxides and S-oxides are the only sets of compounds for which there are extensive, comparative thermodynamic data for the common fragment, element O. Aside from pyridine N-oxides, the oxo transfer propensities of N—O compounds are essentially uninvestigated. Given the range of ΔH values, they may find use as selective oxidants.

The remainder of the reactivity series in Table 1, from -20 to -99 kcal mol^{-1}, contain a variety of organic and inorganic donors and acceptors. Of acceptors and donors of moderate strength, sulphides and sulphoxides, respectively, are frequently useful. There is a considerable body of $\Delta_f H^0_m$

data, summarized by Herron,[36] for sulphides, sulphoxides and sulphones, and also for sulphite and sulphate esters. The limited data presented in Table 1 suffice to place sulphide/sulphoxide and sulphoxide/sulphone couples at meaningful positions in the reactivity scale. Dissociation energies of S—O bonds vary very little within the two classes of compounds. For common aliphatic sulphoxides and Ph_2SO the range is only 87–90 kcal mol^{-1}, and for aliphatic sulphones and Ph_2SO_2 it is 111–114 kcal mol^{-1}. Note that the positions of $SeCl_2/SeOCl_2$ and $SCl_2/SOCl_2$ follow the expected periodic trend, with the S—O bond energy exceeding that of the Se—O bond by 46 kcal mol^{-1} (Table 5). Related behaviour is found for the couples $MoCl_4/MoOCl_4$ and $WCl_4/WOCl_4$, for which $D_{W=O} - D_{Mo=O} = 26$ kcal mol^{-1}. The most familiar generally useful oxo acceptors are the tertiary phosphines and phosphites. Of all the compounds for which data are available hexamethyldisilane is the strongest acceptor. While we are incognizant of significant uses of this compound as an atom transfer reductant, Si_2Cl_6 is a most effective reductant of tertiary phosphine oxides.[37] Consequently, ΔH for the Si_2Cl_6/Si_2OCl_6 couple must be less than *ca* -80 kcal mol^{-1}, provided, as the evidence suggests, that Si_2OCl_6 is a primary product of oxo transfer itself and does not arise from another reaction event. The reductions of chiral phosphine oxides by this method proceed with a high degree of stereospecificity and with inversion of configuration.[37]

Table 1 is extensive and, *inter alia*, includes ΔH values for strong oxo donors and acceptors. However, the thermodynamic data required to calculate values for couples involving certain other strong oxo donors have not been reported. Among such donors are the iodosylarenes (**7**),[38–40] percarboxylic acids (**8**),[41] dioxiranes (**9**),[42,43] carbonyl oxides (**10**)[44] and tertiary amine N-oxides such as Me_3NO. While **7**–**10** would appear to be comparable in strength with at least t-butylhydro-

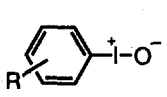

7

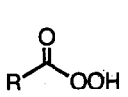

8

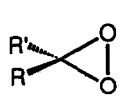

9

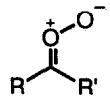

10

peroxide, at this point they cannot be precisely fixed in the reactivity scale. Iodosylarenes, in particular, have been widely employed as strong oxidants, including the formation of highly reactive oxometallates capable of hydrocarbon activation.[1,45,46]

The reactivity scale of Table 1 can be applied only when the system in question has the overall stoichiometry of reaction (6). In such cases a given couple X/XO, lacking the thermodynamic data required for the evaluation of ΔH, can be approximately placed in the scale on the basis of the occurrence of one or two reactions with components of other couples. For example, if compound X reduces PrN=N(O)Pr to PrN=NPr and compound XO oxidizes Ph_3As to Ph_3AsO, then for X/XO $-20 \geqslant \Delta H \geqslant -43$ kcal mol^{-1}. If only one reaction is examined, it is possible to assign an upper or lower limit to ΔH. This procedure has been used to estimate upper limits for several $Mo^{IV}O/Mo^{VI}O_2$ couples.[2] It is most effective if reactions are complete or equilibria are decisively shifted, but even limiting or widely bracketed ΔH values are preferable to none at all. Throughout, it must be borne in mind that the reactivity scale is based on gas phase data. However, we are aware of only several reactions with appreciable enthalpic driving forces ($\Delta H < -20$ kcal mol^{-1}) from gas phase data that do not follow the predictions of the scale when conducted in solution. One case is reaction (9), which is reported not to proceed in refluxing benzene over a 3 day period,[37] despite the apparent driving force of -25 kcal mol^{-1}. Reactions (10)–(13), arranged in probable order of increasing driving force, proceed in good yields under mild conditions.[37] Despite a highly favourable enthalpy change, reaction (14) does not occur when the reactants are maintained at 189° for at least 1 h.[47] Reduction of Me_2SO can be accomplished with a variety of tertiary phosphines, but elevated temperatures and longer reaction times are required for appreciable yields.[48] In contrast, reactions (14)–(16) in DMF solution proceed readily at room temperature in the presence of an $Mo^{VI}O_2$ catalyst.[4,49] In the absence of the catalyst, neither system (15) or (16) showed any detectable reaction (from ^{19}F NMR spectra) for at least 120 h at 25°C. These examples of very slow kinetics of uncatalysed reactions emphasize that any placement in the scale of a couple with an unknown ΔH value should be made on the basis of an observed reaction rather than the lack of reaction.

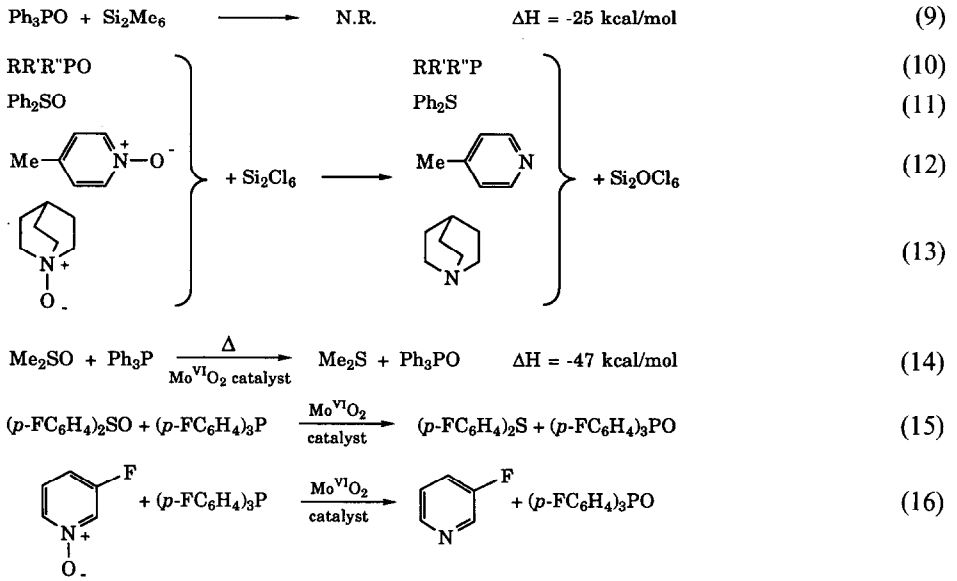

2.2. *Solid and liquid phases and aqueous solution*

Values of ΔH based on thermodynamic data for solids and liquids are set out in Tables 2 and 3, respectively. These values differ from those in Table 1 by the differences in the heats of sublimation or vaporization of X and XO. In the case of solids this relationship tends to alter the order of certain couples in the listings compared to that of Table 1. For liquids the order is the same as in the gas phase, owing to an effective cancellation of the heats of vaporization of members of a given couple. Table 2 serves to suggest oxo donors and acceptors that may find use in heterogeneous reaction systems.

A reactivity scale for aqueous solutions is presented in Table 4. The ΔH values were derived from thermodynamic data. Earlier, we had provided a scale in terms of $\Delta G^0{}_{298}$ values[1] that were calculated from standard potentials.[14] There are some minor numerical discrepancies between those data (not tabulated here) and the $\Delta G_{X/XO}$ values, presumably in part because potentials and thermodynamic data were not measured under identical solution conditions. However, the order of reaction couples is the same and each reactivity series can be utilized in an internally consistent manner. In Table 4 the strongest common oxo donors are hydrogen peroxide and the hypochlorite ion, and the strongest acceptor is the cyanide ion. However, because dioxiranes oxidize chloride to hypochlorite[42] their ΔH values in aqueous solution are considerably above +14 kcal mol^{-1}. As indicated by this and other reactivity aspects, dioxiranes are decidedly strong oxo transfer agents and thus should be placed near the tops of Tables 1 and 4.

We next consider selected recent applications of oxo donors and acceptors which have been reported since our previous treatment of the subject.[1]

3. APPLICATIONS

Applications of donors and acceptors in metal-centred oxo transfer reactions are summarized in order to illustrate recent uses of these reagents, where possible in relation to their positions on the thermodynamic reactivity scale. The principal applications of oxo transfer have been in metal-centred oxidation, involving reagents at the top of Table 1 and also **7** and **8** and, to a very limited extent, **9** and **10**. In addition we note the use of other, less powerful oxidants and of certain reductants.

3.1. *Strong oxo donors*

The very strong donors PhIO, H_2O_2, ROOH, RCO_3H and OCl^- continue to find extensive use in the generation of high-valent oxochromium,[50,51] oxomanganese[52-57] and oxoiron[51,58-66] porphyrin species in reactions (17)–(19). Reactions (17) and (18) are examples of primary oxo transfer, reaction (1). Reaction (19) results in oxidation of the metal and porphyrinate ligand,

the latter to a π-radical. Reaction (17), with M = Fe and Mn, has also been accomplished with dimethyldioxirane in acetone at low temperatures.[67] The oxidation of Mn(TMP)Cl with dioxygen under phase transfer conditions (aqueous NaOH, chloroform) is thought to occur via the carbonyl oxide Cl_2COO formed from dichlorocarbene and dioxygen.[52] While Fe(TPP) can be oxidized in reaction (17) with N-methylmorpholine N-oxide or Me_3NO,[68] the available evidence indicates that stronger donors are required in reactions (18) and (19). The minimal donor strength on the reactivity scale of Table 1 has not been established. There does not appear to be a common mechanism for all oxidants, XO. With peroxidic reagents, YOOH, the simplest pathway involves heterolytic O—O bond cleavage, oxidative addition of the nascent oxygen atom to the metal centre and departure of YOH. A summary of the leading mechanistic aspects of these reactions has been provided by Bruice.[69]

$$M^{II}(P)+XO \longrightarrow M^{IV}O(P)+X \qquad (M = Cr, Mn, Fe) \tag{17}$$

$$Mn^{III}(P)L+XO \longrightarrow Mn^{V}O(P)L+X \tag{18}$$

$$Fe^{III}(P)L+XO \longrightarrow Fe^{IV}O(P^{\cdot})L+X \tag{19}$$

Catalytic systems for the epoxidation of olefins and the hydroxylation of saturated hydrocarbons are based on reactions (18) and (19) for the generation of the oxometal catalyst. The epoxidation of olefins is frequently regarded as indicative of the formation of (highly reactive) oxometal species, at least with iron and earlier transition metals. The chemistry of these metals otherwise includes such species whose existence has been demonstrated spectroscopically, as with iron, or by X-ray structure determinations for compounds of groups 4–7. Meunier[70] has presented a comprehensive account of the formation and catalytic reactions of oxometalloporphyrins. The formation of active Fe=O species by atom transfer from strong oxo donors is not restricted to porphyrins, as inferred from hydrocarbon oxidation in non-haeme systems (PhIO, H_2O_2, Bu^{t}OOH)[71,72] and by the antitumor antibiotic bleomycin (PhIO, H_2O_2) and its synthetic analogues.[73]

The active oxidants in the foregoing hydrocarbon activation systems have proven difficult to isolate and characterize because of their reactive nature. However, with suitably stable ligand systems and strong oxo donors Collins and co-workers[74–77] have shown that it is possible to prepare, isolate and structurally characterize high-valent oxochromium and oxomanganese complexes. Thus, the primary oxo transfer reaction (20) of the Mn^{III} complex **11** affords the $Mn^{V}O$ product **12**.[76] Complexes **13**–**15** were obtained in good yields by the reaction of metal(II) precursors with excess Bu^{t}OOH,[74,75] in reactions that must involve both electron and atom transfer. Oxo transfer with strong donors has also been effective in building up polynuclear clusters from smaller precursors. As one example, treatment of mixed-valence $Mn_3O(O_2CPh)_6(py)_2(OH_2)$ with 1.33 equivalents of PhIO in acetonitrile results in full incorporation of oxygen in the manganese(III) product cluster $Mn_9O_7(O_2CPh)_{13}(py)_2$.[78]

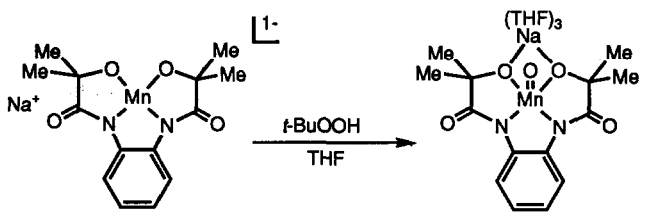

11 **12** (20)

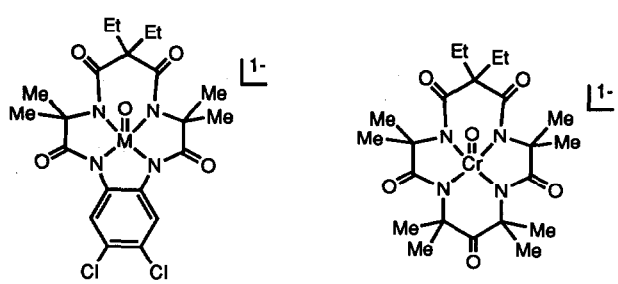

13: M = Cr
14: M = Mn

15

Two of the more powerful oxidants in Table 1, Cl_2O and N_2O, both with $\Delta H \approx +19$ kcal mol^{-1}, have found limited applications. Dichlorine monoxide as a solution in CCl_4 oxidizes manganese(III) porphyrins to higher-valent compounds, probably including $Mn^{IV}O(P)$, but none of these oxidized species have been definitely identified.[30] Solutions of this reagent are described as containing chlorine, which complicates the oxidation chemistry. Reactions of N_2O with Cp^*_2Ti and Cp_2V in toluene produce polynuclear products with no terminal oxo ligands.[1,79,80] In a recent significant development, it has been found that the presence of pyridine shunts related reaction system (21) to the mononuclear oxo product **17**,[81] formed by a primary oxo transfer to the dicarbonyl **16**. Compound **17** is a stabilized derivative of Cp^*_2ZrO, which has been generated by the thermolysis of $Cp^*_2Zr(Ph)(OH)$ and trapped as oxametallocycles by reactions with unsaturated organic compounds.[82] These developments open the chemistry of the heretofore elusive Zr=O group. The Hf=O group is presently unknown, although the potential precursor $Cp^*_2Hf(Ph)(OH)$ has been prepared by treatment of $Cp^*_2HfH(Ph)$ with N_2O in a reaction that demonstrates oxo insertion in a metal–ligand bond when metal-centred oxidation is not possible.[83]

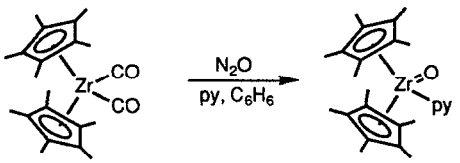

(21)

16 **17**

3.2. *Other oxo donors*

Epoxides have been found to effect a number of primary oxo transfer reactions, among them reactions (22)–(24).[84–87] For these M^n/M^{n+2} couples ΔH is evidently less than *ca* -25 kcal mol^{-1}, indicating that these vanadium(III) and tungsten(II,IV) compounds are oxo acceptors of at least moderate strength. Pyridine N-oxide, Me_3NO and Me_2SO have been found to effect the $Tc^{III} \rightarrow Tc^{V}O$ transformation of tris(2,4,6-trimethylbenzenethiolate) complexes.[88] Lastly, the $W^{IV}O_5(OH_2)$ unit in a heteropolytungstate "brown" anion has been shown to undergo primary oxo transfer, leading to a $W^{VI}O(O)_5$ product.[89] Oxidation is effected by Me_2SO, Ph_2SO or Ph_3AsO at elevated temperatures in toluene or acetonitrile solutions and by PhNO at 25°C in these solvents. However, $(MeO)_2SO_2$, Me_2SO_2, PhNCO and Ph_3PO were not reduced, even after prolonged reaction times. Consequently, for the $W^{IV}/W^{VI}O$ couple $\Delta H < -43$ kcal mol^{-1} as an upper limit, but the lower limit cannot be securely set on the basis of lack of reaction.

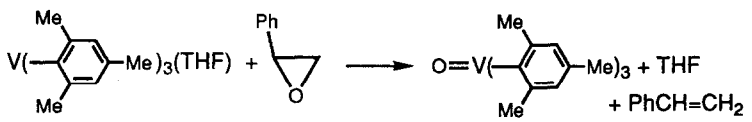

(22)[84]

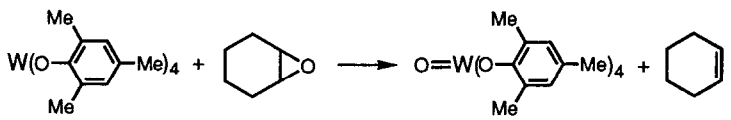

(23)[85]

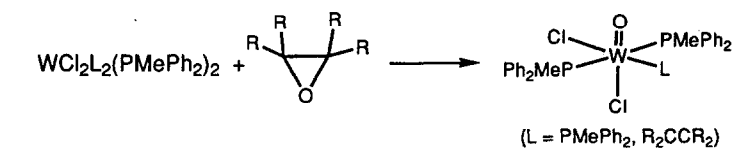

(24)[86,87]

3.3. *Oxo acceptors*

Tertiary phosphines and phosphites are the most commonly employed oxo acceptors. With the exception of Si_2Cl_6 and possibly Si_2Me_6, no soluble non-metal compounds of known ΔH values are

more powerful acceptors. There are numerous recent applications of these compounds as oxo acceptors. Here we note two instances of the infrequent reductive transformation $W^{VI}O_2 \rightarrow W^{IV}O$ by atom transfer. Reaction (25) proceeds readily at room temperature to afford the μ-oxo $W^{V}{}_2O_3$ product in 86% yield.[6] By analogy to well-studied molybdenum systems,[1] the product is consistent with the initial formation of the $W^{IV}O$ compound followed by an inner sphere electron transfer reaction with the $W^{VI}O_2$ reactant. In reaction (26), conducted at 67°C for 7 h, the $W^{IV}O$ product was isolated in 55% yield as the triethylphosphine adduct.[90] Excess phosphine suppressed the formation of the μ-oxo compound. The $W^{IV}O$ group is of general interest because, at parity of the ligand, it should be a more powerful oxo acceptor than the $Mo^{IV}O$ group, a matter that, however, has not been adequately tested.

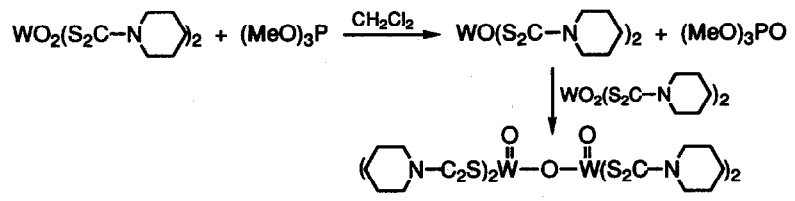

(25)

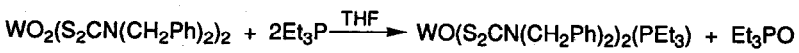

(26)

Mayer and co-workers[91–96] have demonstrated that W^{II} compounds of the type $WCl_2(PR_3)_4$ are among the most powerful oxo acceptors known. Thus, the prototypical complex $WCl_2(PMePh_2)_4$ oxidatively adds carbon dioxide and deoxygenates ketones,[92,93] alcohols,[94] epoxides[91,95] and $Ph_2PCH_2CH_2P(O)Ph_2$.[96] Leading transformations are summarized in eq. (27). Reactions are not necessarily general for a given substrate type and minority products are sometimes observed. Reactions with ketones afford tungsten(VI) oxo alkylidenes. Other products contain tungsten(IV) and occur in primary oxo transfer reactions, resulting in the reduction of XO and coordination of reduced product X. Reduction of the phosphine oxide is the only known metal-mediated reaction of this type. When taken together with the finding that PPh_3 does not react under the same conditions, it has been proposed[96] that the reduction of tertiary phosphine oxides $OPRPh_2$ is thermodynamically favourable but kinetically unfavourable owing to weak binding of the phosphine oxide to the metal centre. If correct, the couple $WCl_2(PMePh_2)_4/WOCl_2(PMePh_2)_3 + PMePh_2$ is placed at $\Delta H < -74$ kcal mol^{-1} on the reactivity scale. $WCl_2(PMePh_2)_4$ should find further applications as a powerful oxo acceptor.

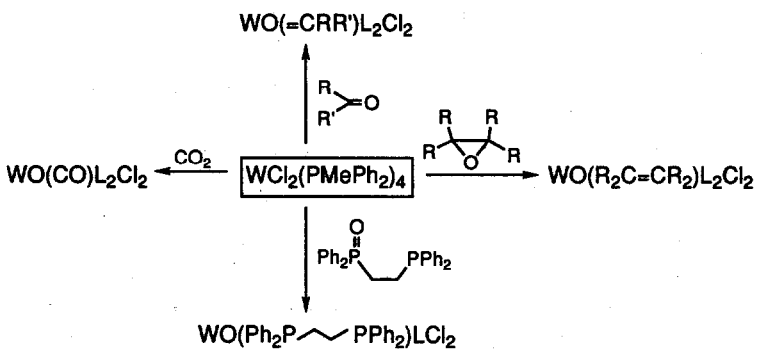

(27)

4. THE OXO TRANSFER CHEMISTRY OF RHENIUM

Of all metals, the oxo chemistry of rhenium has been expanded to the largest extent relative to the situation in 1987.[1] At that time, the great majority of reactions resulted in oxo transfer from rhenium to the substrate. Significant new information has been gained in the last half a dozen years on the synthesis and structures of oxorhenium groups and on oxo transfer reactions resulting in oxidative and reductive transformations of these groups. Consequently, the current use of oxo

transfer reagents and, where possible, of the thermodynamic reactivity scale are well illustrated by leading developments in the oxo transfer chemistry of rhenium, taken together with the foregoing applications. Contemporary advancement of oxorhenium chemistry is due nearly exclusively to the investigations of Herrmann, Hoffman, Mayer and their co-workers, and has been largely motivated by interest in high-valent organometallic oxides, alkyls and unsaturated organic derivatives. Certain parts of the early work of the Herrmann group have been summarized.[1,97-99] In the sections that follow, examples of structures and reactions are confined to those reported in the last 6 years. The coverage is comprehensive in that all significant structural and reaction types are included, but it is not exhaustive.

4.1. *Oxorhenium functional groups*

We begin our considerations by noting the three types of oxorhenium functional groups, ReO, ReO_2 and ReO_3. Due to the possibilities of different oxidation states and structures, there are seven known groups in this set. These are depicted as **18**–**24** in Table 6, which lists structurally proven examples of each.[100-122] *Cis* (**19**) and *trans* (**20**) versions of the $Re^{V}O_2$ group are known. Efficient syntheses of compounds containing these groups have been reported,[123-125] including *cis* and *trans* forms of pyridyl/bipyridyl complexes.[125] The $Re^{VI/VII}O_2$ groups are known only in the *cis* forms **21**/**22**, while the $Re^{VII}O_3$ group is pyramidal (**23**) in nominally six-coordinate complexes and $MeReO_3$ but is planar (**24**) in five-coordinate, 16-electron species. These groups may then be implicated in the binuclear bridged units **25**–**31**, some of which may be formalized in terms of combinations of mononuclear groups with and without electron transfer. For example, **26** is a combination of **18** and **22** and **30** is a combination of **18** and **23**, both with electron transfer, while **31** is an adduct of **22** and **23**/**24** and **29** is a dimer of **19**/**20**. The extent of metal–metal bonding in certain complexes containing units **28** and **29** has been discussed elsewhere.[126] While other elements exhibit MO_{1-3} functional groups,[1,127] no other element forms groups with as many oxidation states and stereochemistries and displays the diversity of binuclear units as does rhenium. As will be seen the majority of groups and binuclear units in Table 6 are formed by or are reactive in oxo transfer processes. Not included in this table are certain low-valent oxorhenium groups in complexes derived from alkynes,[128-130] where the metal oxidation state may be regarded as less clearly defined than in **18**–**24**.

4.2. *Oxo transfer reactions*

Examples of the leading types of metal-centred oxo transfer reactions, eqs (28)–(42), of rhenium are provided in Table 7. Reaction products X/XO are obvious and are not specified. Several other reactions involving alkyne complexes with less well-defined oxidation states have been reported,[131] but are not tabulated. Reactions (28)–(31) are of the primary oxo transfer type (1); as indicated, reaction (31) involves the oxidation of only one rhenium atom in the binuclear precursor complex. In examining the $Re^{III} \rightleftarrows Re^{V}O$ transformations of reactions (28) and (29) Conry and Mayer[10] observed that oxo transfer to the substrate occurs when the X—O bond strength exceeds 133 kcal mol^{-1} (Ph_3P), and the reverse reaction transpires when the bond strength falls below 110 kcal mol^{-1} (Bu^tNCO), using $\Delta H_{MeNC/MeNCO}$ = 50 kcal mol^{-1} (liquid phase†) for the substrate. A more reliable upper limit may be 103 kcal mol^{-1}, based on Ph_3AsO (Table 5). With the use of these and other bond energies in a thermodynamic cycle it has been estimated that D(Re=O) = 149(9) kcal mol^{-1} for $[ReOCl_2(Me_3tacn)]^+$.[10] By similar means D(W=O) in $WOCl_2(PMePh_2)_3$ has been estimated to be > 138 kcal mol^{-1}.[92] Since $[ReOCl_2(Me_3tacn)]^+$ is reduced by tertiary phosphines but the tungsten compound is not, the Re=O bond may be weaker than the W=O bond in these two compounds.

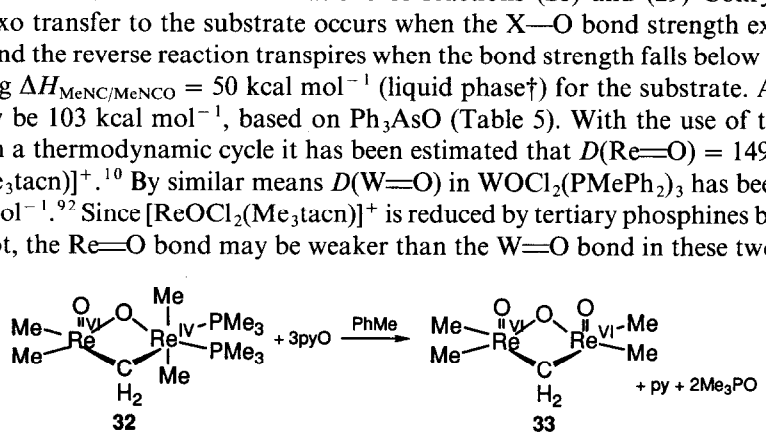

32 **33** (31)

† This value was incorrectly ascribed to the gas phase.[1]

Table 6. Oxorhenium functional groups and binuclear units

Group/Unit	Examples[a]	∠O—Re—O[b] (°)	Ref.
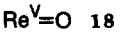 **18**	$ReO(CH_2SiMe_3)_3(PMe_3)$	—	100
	$ReOMe_2Cl(PMe_3)_2$	—	101
19 (bent)	$[ReO_2(CH_2CMe_3)_2]^{1-}$	127–138[c]	103, 104
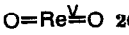 **20** (linear)	$[ReO_2(cyclam)]^{1+}$	180	105
21 (bent)	$ReO_2(mes)_2$	122	106
	$ReO_2(2,6\text{-}Me_2C_6H_3)_2$	117	107
22 (bent)	$[ReO_2(cat)_2]^{1-}$	99	102
	$ReO_2(CH_2CMe_3)_3$	117	108
	$ReO_2(CH_2CMe_3)_2Br(py)$	107	119
	$ReO_2Me(cat)(py)$	108	109
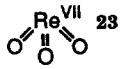 **23** (pyramidal)	$[ReO_3(9S3)]^{1+}$	107	110
	$MeCpReO_3$	105	111
	Cp^*ReO_3	107	113
	$MeReO_3$	113	113
	$EtReO_3(quin)$	118	112
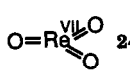 **24** (planar)	$Me_3SiCH_2ReO_3(quin)$	118	112
25 (linear)	$Re_2O_3Cl_4(3,5\text{-}Me_2pz)_4$	173	114
	$[Re_2O_3(CN)_8]^{4-}$	180	115
26	$Re_2O_3Me_6$	[d]	121
	$Re_2O_3Me_2Cl_4(OPPh_3)_2$	[d]	116
27	$Re_2O_3(\mu\text{-}CH_2)Me_4$	[d]	122
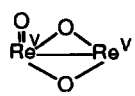 **28**	$Cp^*_2Re_2O_3Cl_2$	114,[e] 83[f]	117
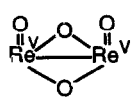 **29**	$Cp^*_2Re_2O_4$	109,[e] 73[f]	117
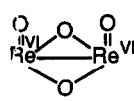 **30**	$Re_2O_4(CH_2CMe_3)_4$	121, 87[f]	103
	$Re_2O_4Me_4$	[d]	120
31	$Re_2O_5(CH_2CMe_3)_4$[g]	109,[h] 100,[e] 151[e]	118
	$Re_2O_5Me_2(hq)_2$[i]	106,[h] 106[e]	109

[a] For additional examples, cf. ref. 1.
[b] Mean value where appropriate.
[c] Cation-dependent.
[d] Not reported.
[e] Terminal-bridge angle.
[f] Bridge angle.
[g] Re—O—Re = 166°.
[h] Terminal oxygen angle.
[i] Re—O—Re = 180°.

Reactions (32)–(35) are examples of the incomplete intermetal oxo transfer process (2). The conversion reaction (32) does not proceed by oxo removal from the initial binuclear complex. Instead, this species is subject to a ligand-assisted dissociation to form $Re^{V}O$ and $Re^{VII}O_2$ complexes; the latter is reduced to the former by $X = Me_3P$ in a primary oxo transfer process. The same pathway is likely for reaction (33). In reaction (34) $XO = pyO$ oxidizes the dissociated $Re^{V}O$ complex to the $Re^{VII}O_2$ product, while in reaction (35) Ph_3P affects the reverse conversion. Underlying these four reactions is the inner sphere electron transfer, eq. (43), analogous to the numerous examples of the formation and dissociation of the μ-oxo $Mo^{V}_2O_3$ unit.[1]

$$Re^{V}_2O_3(CH_2SiMe_3)_6 + Me_3P \rightleftharpoons Re^{V}O(PMe_3)(CH_2SiMe_3)_3 + Re^{VII}O_2(CH_2SiMe_3)_3 \quad (32)$$

$$Re^{V}O(PMe_3)(CH_2SiMe_3)_3 + XO \rightleftharpoons Re^{VII}O_2(CH_2SiMe_3)_3 + X \quad (34,35)$$

Reactions (36)–(38) appear to involve a primary oxo step followed by non-redox ligand substitution. In reaction (36) the second oxygen ligand is derived from the water solvent. In reaction (37) Ph_3P acts as the oxo acceptor and Me_3SiCl functions to remove oxide while concomitantly supplying chloride ligands. This reaction type can be extended to the formation of the non-oxo rhenium(V) product Cp^*ReCl_4 from Cp^*ReO_3.[117] Similar comments apply to reaction (38), in which $GeCl_2$ has the effective dual function of oxo and oxide acceptor and chloride donor. Reactions (39) and (40) are easily interpreted in terms of the non-redox group dimerization reaction, eq. (44). The course of reaction (41) is less clear but may involve process (43) with the mononuclear components subject to ligation by chloride and Ph_3PO. Reaction (42) results in the formation of that bridge unit with the most terminal oxo ligands, as might be expected for rhenium(VII), rather than retaining a bis(μ-oxo) structure.

$$[ReO_3(tacn)]^{1+} + Ph_3P + 2Me_3SiCl \longrightarrow [ReOCl_2(tacn)]^{1+} + Ph_3PO + (Me_3Si)_2O \quad (37)$$

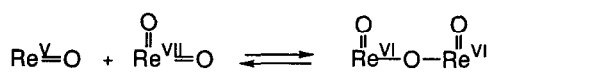

(43)

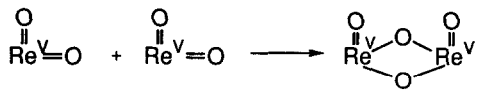

(44)

5. OXO TRANSFER REACTION DIAGRAMS

The elements vanadium, chromium, molybdenum, tungsten, manganese, rhenium and ruthenium each sustain a metal-centred oxo transfer reaction chemistry that is substantial in terms of numbers of reported reactions, varieties of oxometal functional groups and oxo-bridged units, and the range of oxidation states. As on previous occasions[7,132] we suggest that reaction patterns can be effectively summarized in the form of oxo transfer reaction diagrams. Those for vanadium[7] and molybdenum[132] are set out in Schemes 1 and 2, respectively. The diagram for rhenium is presented in Scheme 3 and is based on the reaction types in Table 7 and other examples presented previously.[1] These diagrams, which are restricted to mono- and binuclear oxometal species, recapitulate all known primary oxo transfer reactions of these elements in terms of transformations between functional groups and bridged units.

Oxometal groups joined by straight line segments are accessible in uni- or bidirectional reactions, signified by single- and double-headed curved arrows. The schemes are generalized; not all transformations are spontaneous with a given functional group in different molecules nor with a given oxo donor/acceptor. Scheme 2 does not include peroxide species which may be formed in part by oxo transfer. Several important transformations between groups and bridging units that do not

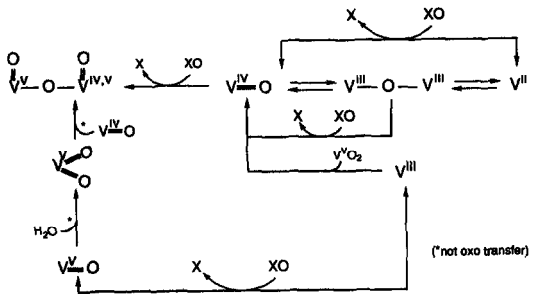

Scheme 1. Oxo transfer reactions of vanadium.

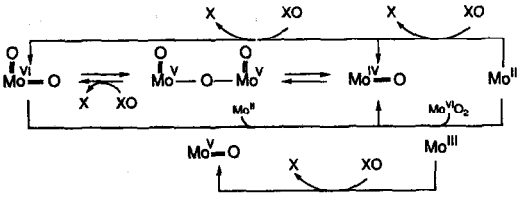

Scheme 2. Oxo transfer reactions of molybdenum.

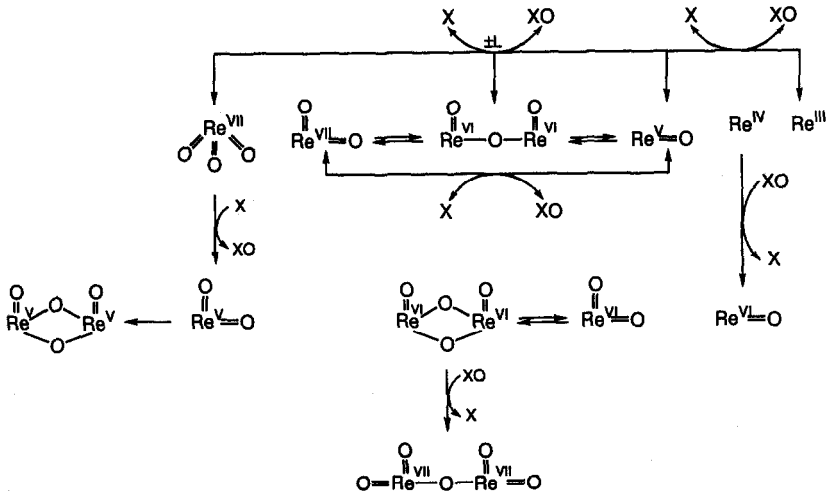

Scheme 3. Oxo transfer reactions of rhenium.

proceed solely by atom transfer are included in this scheme because these species and reactions are encountered with some frequency. This is also the case in Scheme 3 where ancillary ligands are involved in the $Re^{V}O \rightleftarrows Re^{VII}O_3$ transformations. These diagrams suggest what reactions might be possible with new complexes of these elements and what transformations might be accomplished that have not been reported. The thermodynamic reactivity scale can be of significant assistance in planning reactions within the chemistry of a given element once a small body of empirical reactivity information has been gathered. Reactions of X/XO in the middle of the scale (Table 1) are particularly useful in providing rough limits on ΔH values for oxometal species. In this respect, we find the Ph_3As/Ph_3AsO couple, at -41 kcal mol^{-1}, a useful indicator of the thermodynamic oxo transfer

Table 7. Oxo transfer reactions of rhenium

Reactant	X/XO	Product		Ref.
	$Re^{III} \rightleftharpoons Re^{V}O$ (**18**)			
$[ReLCl_2(Me_3tacn)]^{1+}$ (L = MeCN, Me_2CO, py, Ph_3PO)	Me_2SO, Ph_3AsO, pyO, Me_3NO, Bu^tNCO	$[ReOCl_2(Me_3tacn)]^{1+}$	(28)	10
$[ReOCl_2(Me_3tacn)]^{1-}$	Ph_3P	$[ReCl_2(Me_3tacn)(MeCN)]^{1+}$	(29)	10
Cp^*ReOCl_2	Me_3P	$Cp^*ReCl_2(PMe_3)_2$	(30)	117
	$Re^{IV} \longrightarrow Re^{VI}O$			
$ReOMe_2(\mu\text{-}O)(\mu\text{-}CH_2)ReMe_2(PMe_3)_2$ (**32**)	pyO	$Re_2O_2(\mu\text{-}O)(\mu\text{-}CH_2)Me_4$ (**33**)	(31)	122
	(**18**) $Re^{V}O \longleftarrow Re^{VI}{}_2O_3$ (**26**)[a]			
$Re_2O_3(CH_2SiMe_3)_6$	Me_3P	$ReO(CH_2SiMe_3)_3(PMe_3)$	(32)	100
$Re_2O_3Me_6$	$PhMe_2P$	$ReOMe_3(PMe_2Ph)$	(33)	101
	(**22**) $Re^{VII}O_2 \rightleftharpoons Re^{VI}{}_2O_3$ (**26**)			
$Re_2O_3(CH_2SiMe_3)_6$	pyO	$ReO_2(CH_2SiMe_3)_3$	(34)	100
$ReO_2(CH_2SiMe_3)_3$	Ph_3P	$Re_2O_3(CH_2SiMe_3)_6$	(35)	100
	(**18**) $Re^{V}O \rightleftharpoons Re^{VII}O_3$ (**23**)			
$[ReOCl_2(tacn)]^{1+}$	Me_2SO, *m*-CPBA, H_2O_2/H_2O	$[ReO_3(tacn)]^{1+}$	(36)	10
$[ReO_3(tacn)]^{1+}$	Ph_3P/Me_2SiCl	$[ReOCl_2(tacn)]^{1+}$	(37)	10
Cp^*ReO_3	$GeCl_2 \cdot diox$	Cp^*ReOCl_2	(38)	117
	(**23**) $Re^{VII}O_3 \longrightarrow Re^{V}{}_2O_4$ (**28**)			
$[ReO_3(tacn)]^{1+}$	Ph_3P	$[Re_2O_4(tacn)_2]^{2+}$	(39)	10
Cp^*ReO_3	Ph_3P	$Cp^*{}_2Re_2O_4$	(40)	117
	(**23**) $Re^{VII}O_3 \longrightarrow Re^{VI}{}_2O_3$ (**26**)			
$MeReO_3$	Ph_3P/Me_3SiCl	$Re_2O_3Me_2Cl_4(OPPh_3)_2$	(41)	116
	(**30**) $Re^{VI}{}_2O_4 \longrightarrow Re^{VII}{}_2O_5$ (**31**)			
$Re_2O_4(CH_2CMe_3)_4$	pyO	$Re_2O_5(CH_2CMe_3)_4$	(42)	118

[a] cf. ref. 131 for an apparent $Re^{IV}{}_2O_3 \rightarrow Re^{V}O_2$ transformation.

propensity of metal species. Regrettably, there is virtually no thermodynamic information on oxometal complexes that permits their placement in the scale.

Watt *et al.*, in a pioneering study,[133] performed direct calorimetric measurements of reactions of $Mo^{IV,V,VI}$ dithiocarbamate complexes in 1,2-dichloroethane solutions. Among these reactions was the oxidation of $MoO(S_2CNEt_2)_2$ by dioxygen to $MoO_2(S_2CNEt_2)_2$, for which $\Delta H = -35(3)$ kcal mol^{-1}. This value predicts that the $Mo^{IV}O$ complex will reduce Me_2SO (-8 kcal mol^{-1}), azoxybenzene (-18 kcal mol^{-1}) and pyO (-22 kcal mol^{-1}) because of the favourable apparent enthalpic driving forces indicated. These reactions have been observed.[134] However, this complex is not expected to reduce Ph_3AsO because of an apparently unfavourable enthalpy change ($+8$ kcal mol^{-1}). Yet from the reaction system $MoO(S_2CNEt_2)_2/Ph_3AsO$ in benzene (20 h, 40°C), Ph_3As has been isolated in 84–98% yield.[134] This result suggests that users of the gas phase reactivity scale of Table 1 for solution reactions should exercise discretion when enthalpy differences are relatively small, with perhaps 10 kcal mol^{-1} being a cautionary value.

Acknowledgements—Research on oxo atom transfer chemistry in this laboratory is supported by NSF Grant CHE 92-08387. J.P.D. is the recipient of a National Defense Science and Education Grant Predoctoral Fellowship sponsored by the U.S. Air Force.

REFERENCES

1. R. H. Holm, *Chem. Rev.* 1987, **87**, 1401.
2. E. W. Harlan, J. M. Berg and R. H. Holm, *J. Am. Chem. Soc.* 1986, **108**, 6992.
3. J. M. Berg and R. H. Holm, *Accts Chem. Res.* 1986, **19**, 363.
4. J. P. Caradonna, P. R. Reddy and R. H. Holm, *J. Am. Chem. Soc.* 1988, **110**, 2139.
5. J. A. Craig and R. H. Holm, *J. Am. Chem. Soc.* 1989, **111**, 2111.
6. S.-B. Yu and R. H. Holm, *Inorg. Chem.* 1989, **28**, 4385.
7. Y. Zhang and R. H. Holm, *Inorg. Chem.* 1990, **29**, 911.
8. C. A. Tolman and N. Herron, in *Oxygen Complexes and Oxygen Activation by Transition Metals* (Edited by D. T. Sawyer and A. E. Martell), pp. 283–303. Plenum Press, New York (1988).
9. C. A. Tolman, J. D. Druliner, M. J. Nappa and N. Herron, in *Activation and Functionalization of Alkanes* (Edited by C. L. Hill), Ch. X. Wiley-Interscience, New York (1989).
10. R. R. Conry and J. M. Mayer, *Inorg. Chem.* 1990, **29**, 4862.
11. D. D. Wagman, W. H. Evans, V. B. Parker, I. Halow, S. M. Bailey and R. H. Schumm, *Selected Values of Chemical Thermodynamic Properties*; Natl. Bur. Stand. Tech. Note 270-3. U.S. Government Printing Office, Washington, DC (1968).
12. J. D. Cox and G. Pilcher, *Thermochemistry of Organic and Organometallic Compounds*, pp. 478–482. Academic Press, New York (1970).
13. J. B. Pedley and J. Rylance, Sussex-NPL Computer-Analyzed Thermochemical Data: Organic and Organometallic Compounds. University of Sussex, Brighton (1977).
14. *Standard Electrode Potentials in Aqueous Solution* (Edited by A. J. Bard, R. Parsons and J. Jordan). Marcel Dekker, Inc., New York (1985).
15. *The NBS Tables of Chemical Thermodynamic Properties* (Edited by D. R. Lide). American Chemical Society and the American Institute for Physics, Washington, DC; *J. Phys. Chem. Ref. Data* 1982, **11**, Supplement No. 2.
16. J. B. Pedley, R. D. Naylor and S. P. Kirkby, *Thermochemical Data of Organic Compounds*, pp. 87–232, 619–620. Chapman and Hall, New York (1966).
17. *TRC Thermodynamic Tables, Non-Hydrocarbons*. Thermodynamics Research Center, The Texas A&M University System, College Station, Texas.
18. M. W. Chase, J. L. Curnutt, A. T. Hu, H. Prophet, A. N. Syverud and L. C. Walker, *JANAF Thermodynamic Tables*, 1974 Supplement; *J. Phys. Chem. Ref. Data* 1974, **3**, 311.
19. G. A. Takacs, *J. Chem. Engng Data* 1978, **23**, 174.
20. W. E. Acree Jr, S. A. Tucker, A. I. Zvaigzne, M.-Y. Yang, G. Pilcher and M. D. M. C. Ribeiro da Silva, *J. Chem. Thermodyn.* 1991, **23**, 31.
21. J. J. Kirchner, W. E. Acree Jr, G. Pilcher, G. Li and S. Li, *J. Chem. Thermodyn.* 1986, **18**, 793.
22. W. E. Acree Jr, J. J. Kirchner, S. A. Tucker, G. Pilcher and M. D. M. C. Ribeiro da Silva, *J. Chem. Thermodyn.* 1989, **21**, 443.
23. S. Li and G. Pilcher, *J. Chem. Thermodyn.* 1988, **20**, 463.
24. M. L. P. Leitao, G. Pilcher, W. E. Acree Jr, A. I. Zvaigzne, S. A. Tucker and M. D. M. C. Ribeiro da Silva, *J. Chem. Thermodyn.* 1990, **22**, 923.
25. W. E. Acree Jr, S. A. Tucker and G. Pilcher, *J. Chem. Thermodyn.* 1992, **24**, 213.
26. D. S. Barnes, P. M. Burkinshaw and C. T. Mortimer, *Thermochim. Acta* 1988, **131**, 107.
27. A. F. Bedford and C. T. Mortimer, *J. Chem. Soc.* 1960, 1622.
28. N. N. Greenwood and A. Earnshaw, *Chemistry of the Elements*, p. 510. Pergamon Press, New York (1984).
29. J. J. Renard and H. I. Bolker, *Chem. Rev.* 1976, **76**, 487.
30. K. R. Rodgers and H. M. Goff, *J. Am. Chem. Soc.* 1987, **109**, 611; 1988, **110**, 7049.
31. R. A. Sheldon, in *The Chemistry of Peroxides* (Edited by S. Patai), Ch. 6. John Wiley, New York (1983).
32. M. G. McCarty, in *The Chemistry of the Carbon–Nitrogen Double Bond* (Edited by S. Patai), Ch. 9. Interscience, New York (1970).
33. L. Hoesch and H. P. Weber, *Helv. Chim. Acta* 1977, **60**, 3015.
34. D. L. Webb and H. H. Jaffé, *J. Am. Chem. Soc.* 1964, **86**, 2419.
35. W.-J. Peng, A. S. Gamble, J. L. Templeton and M. Brookhart, *Inorg. Chem.* 1990, **29**, 463.
36. J. T. Herron, in *The Chemistry of Sulphones and Sulphoxides* (Edited by S. Patai, Z. Rappoport and C. J. M. Stirling), Ch. 4. John Wiley, New York (1988).
37. K. Naumann, G. Zon and K. Mislow, *J. Am. Chem. Soc.* 1969, **91**, 2788, 7012.
38. H. Saltzman and J. G. Sharefkin, *Org. Synth.* 1963, **43**, 60.
39. M. Schmeisser, K. Dahmen and P. Sartori, *Chem. Ber.* 1967, **100**, 1633.
40. B. C. Schardt and C. L. Hill, *Inorg. Chem.* 1983, **22**, 1563.
41. G. Bouillon, C. Lick and K. Schank, in *The Chemistry of Peroxides* (Edited by S. Patai), Ch. 10. John Wiley, New York (1983).

42. W. Adam, R. Curci and J. O. Edwards, *Accts Chem. Res.* 1989, **22**, 205.
43. R. W. Murray, *Chem. Rev.* 1989, **89**, 1187.
44. W. H. Bunnelle, *Chem. Rev.* 1991, **91**, 335.
45. C. L. Hill, in *Activation and Functionalization of Alkanes* (Edited by C. L. Hill), Ch. VII. John Wiley, New York (1989).
46. D. Ostović and T. C. Bruice, *Accts Chem. Res.* 1992, **25**, 314.
47. H. E. Szmant and O. Cox, *J. Org. Chem.* 1966, **31**, 159.
48. E. H. Amonoo-Neizer, S. K. Ray, R. A. Shaw and B. C. Smith, *J. Chem. Soc.* 1965, 4296.
49. J. M. Berg and R. H. Holm, *J. Am. Chem. Soc.* 1985, **107**, 925.
50. J. M. Garrison, D. Ostović and T. C. Bruice, *J. Am. Chem. Soc.* 1989, **111**, 4960.
51. W. A. Lee, L.-C. Yuan and T. C. Bruice, *J. Am. Chem. Soc.* 1988, **110**, 4277.
52. J. T. Groves and M. K. Stern, *J. Am. Chem. Soc.* 1988, **110**, 8628.
53. P. Battioni, J. P. Renaud, J. F. Bartoli, M. Reina-Artiles, M. Fort and D. Mansuy, *J. Am. Chem. Soc.* 1988, **110**, 8462.
54. R. W. Lee, P. C. Nakagaki and T. C. Bruice, *J. Am. Chem. Soc.* 1989, **111**, 1368,
55. J. P. Collman, H. Tanaka, R. T. Hembre and J. I. Brauman, *J. Am. Chem. Soc.* 1990, **112**, 3689.
56. J. P. Collman, J. I. Brauman, P. D. Hampton, H. Tanaka, D. S. Bohle and R. T. Hembre, *J. Am. Chem. Soc.* 1990, **112**, 7980.
57. E. N. Jacobsen, W. Zhang, A. R. Muci, J. R. Ecker and L. Deng, *J. Am. Chem. Soc.* 1991, **113**, 7063.
58. J. T. Groves and Y. Watanabe, *J. Am. Chem. Soc.* 1988, **110**, 8443.
59. P. N. Balasubramanian, J. R. L. Smith, M. J. Davies, T. W. Kaaret and T. C. Bruice, *J. Am. Chem. Soc.* 1989, **111**, 1477.
60. T. G. Traylor and J. P. Ciccone, *J. Am. Chem. Soc.* 1989, **111**, 8413.
61. R. D. Arasasingham, C. R. Cornman and A. L. Balch, *J. Am. Chem. Soc.* 1989, **111**, 7800.
62. T. G. Traylor, W.-P. Fann and D. Bandyopadhyay, *J. Am. Chem. Soc.* 1989, **111**, 8009.
63. P. N. Balasubramanian, R. W. Lee and T. C. Bruice, *J. Am. Chem. Soc.* 1989, **111**, 8714.
64. T. G. Traylor and F. Xu, *J. Am. Chem. Soc.* 1990, **112**, 178.
65. R. Panicucci and T. C. Bruice, *J. Am. Chem. Soc.* 1990, **112**, 6063.
66. K. Murata, R. Panicucci, E. Gopinath and T. C. Bruice, *J. Am. Chem. Soc.* 1990, **112**, 6072.
67. S. Wolowiec and J. K. Kochi, *J. Chem. Soc., Chem. Commun.* 1990, 1782.
68. K. Shin and H. M. Goff, *J. Am. Chem. Soc.* 1987, **109**, 3140.
69. T. C. Bruice, *Aldrichim. Acta* 1988, **21**, 87.
70. B. Meunier, *Chem. Rev.* 1992, **92**, 1411.
71. A. Stassinopoulos and J. P. Caradonna, *J. Am. Chem. Soc.* 1990, **112**, 7071.
72. R. A. Leising, B. A. Brennan, L. Que Jr, B. G. Fox and E. Münck, *J. Am. Chem. Soc.* 1991, **113**, 3988.
73. D. Y. Dawson, S. E. Hudson and P. K. Mascharak, *J. Inorg. Biochem.* 1992, **47**, 109 and refs therein.
74. T. J. Collins, C. Slebodnick and E. S. Uffelman, *Inorg. Chem.* 1990, **29**, 3433.
75. T. J. Collins and S. W. Gordon-Wylie, *J. Am. Chem. Soc.* 1989, **111**, 4511.
76. T. J. Collins, R. D. Powell, C. Slebodnick and E. S. Uffelman, *J. Am. Chem. Soc.* 1990, **112**, 899.
77. J. M. Workman, R. D. Powell, A. D. Procyk, T. J. Collins and D. F. Bocian, *Inorg. Chem.* 1992, **31**, 1550.
78. D. W. Low, D. M. Eichhorn, A. Draganescu and W. H. Armstrong, *Inorg. Chem.* 1991, **30**, 878.
79. F. Bottomley and L. Sutin, *Adv. Organomet. Chem.* 1988, **29**, 339.
80. F. Bottomley, *Polyhedron* 1992, **11**, 1707.
81. G. J. Parkin, personal communication.
82. M. J. Carney, P. J. Walsh, F. J. Hollander and R. G. Bergman, *Organometallics* 1992, **11**, 761.
83. G. A. Vaughan, P. A. Rupert and G. L. Hillhouse, *J. Am. Chem. Soc.* 1987, **109**, 5538.
84. J. Ruiz, M. Vivanco, C. Floriani, A. Chiesi-Villa and C. Guastini, *J. Chem. Soc., Chem. Commun.* 1991, 762.
85. M. L. Listemann, R. R. Schrock, J. C. Dewan and R. M. Kolodziej, *Inorg. Chem.* 1988, **27**, 264.
86. F.-M. Su, J. C. Bryan, S. Jang and J. M. Mayer, *Polyhedron* 1989, **8**, 1261.
87. L. M. Atagi, D. E. Over, D. R. McAlister and J. M. Mayer, *J. Am. Chem. Soc.* 1991, **113**, 870.
88. N. de Vries, A. G. Jones and A. Davison, *Inorg. Chem.* 1989, **28**, 3728.
89. K. Peipgrass and M. T. Pope, *J. Am. Chem. Soc.* 1989, **111**, 753.
90. S. Lee, D. L. Staley, A. L. Rheingold and N. J. Cooper, *Inorg. Chem.* 1990, **29**, 4391.
91. J. C. Bryan, S. J. Geib, A. L. Rheingold and J. M. Mayer, *J. Am. Chem. Soc.* 1987, **109**, 2826.
92. J. C. Bryan and J. M. Mayer, *J. Am. Chem. Soc.* 1990, **112**, 2298.
93. J. C. Bryan and J. M. Mayer, *J. Am. Chem. Soc.* 1987, **109**, 7213.
94. S. Jang, L. M. Atagi and J. M. Mayer, *J. Am. Chem. Soc.* 1990, **112**, 6413.
95. L. M. Atagi, D. E. Over, D. R. McAlister and J. M. Mayer, *J. Am. Chem. Soc.* 1991, **113**, 870.
96. S. L. Brock and J. M. Mayer, *Inorg. Chem.* 1991, **30**, 2138.

97. W. A. Herrmann, *J. Organomet. Chem.* 1986, **300**, 111; 1990, **382**, 1; *Angew. Chem., Int. Edn Engl.* 1988, **27**, 1297.
98. W. A. Herrmann, D. Marz, E. Herdtweck, A. Schäfer, W. Wagner and H.-J. Kneuper, *Angew. Chem., Int. Edn Engl.* 1987, **26**, 462.
99. W. A. Herrmann, E. Herdtweck, M. Flöel, J. Kulpe, U. Küsthardt and J. Okuda, *Polyhedron* 1987, **6**, 1165.
100. S. Cai, D. M. Hoffman, D. Lappas, H.-G. Woo and J. C. Huffman, *Organometallics* 1987, **6**, 2273.
101. D. M. Hoffman and D. A. Wierda, *Polyhedron* 1989, **8**, 959.
102. J. R. Dilworth, S. K. Ibrahim, S. R. Khan, M. B. Hursthouse and A. A. Karaulov, *Polyhedron* 1990, **9**, 1323.
103. S. Cai, D. M. Hoffman, J. C. Huffman, D. A. Wierda and H.-G. Woo, *Inorg. Chem.* 1987, **26**, 3693.
104. S. Cai, D. M. Hoffman and D. A. Wierda, *Polyhedron* 1990, **9**, 957.
105. A. J. Blake, J. A. Greig and M. Schröder, *J. Chem. Soc., Dalton Trans.* 1988, 2645.
106. P. Stavropoulos, P. G. Edwards, T. Behling, G. Wilkinson, M. Motevalli and M. B. Hursthouse, *J. Chem. Soc., Dalton Trans.* 1987, 169.
107. C. J. Longley, P. D. Savage, G. Wilkinson, B. Hussain and M. B. Hursthouse, *Polyhedron* 1988, **7**, 1079.
108. S. Cai, D. M. Hoffmann and D. A. Wierda, *J. Chem. Soc., Chem. Commun.* 1988, 313.
109. J. Takacs, P. Kiprof, J. Riede and W. A. Herrmann, *Organometallics* 1990, **9**, 782.
110. H.-J. Küppers, B. Nuber, J. Weiss and S. R. Cooper, *J. Chem. Soc., Chem. Commun.* 1990, 979.
111. W. A. Herrmann, M. Taillefer, C. de M. de Bellefon and J. Behm, *Inorg. Chem.* 1991, **30**, 3247.
112. W. A. Herrmann, C. C. Romao, R. W. Fischer, P. Kiprof, C. de M. de Bellefon, *Angew. Chem., Int. Edn Engl.* 1991, **30**, 185.
113. W. A. Herrmann, P. Kiprof, K. Rypdal, J. Tremmel, R. Blom, R. Alberto, J. Behm, R. W. Albach, H. Bock, B. Solouki, J. Mink, D. Lichtenberger and N. E. Gruhn, *J. Am. Chem. Soc.* 1991, **113**, 6527.
114. G. Backes-Dahmann and J. H. Enemark, *Inorg. Chem.* 1987, **26**, 3960.
115. P. O. Lumme, U. Turpeinen and Z. Stasicka, *Acta Cryst.* 1991, **C47**, 501.
116. J. K. Felixberger, J. G. Kuchler, E. Herdtweck, R. A. Paciello and W. A. Herrmann, *Angew. Chem., Int. Edn Engl.* 1988, **27**, 946.
117. W. A. Herrmann, M. Flöel, J. Kulpe, J. K. Felixberger and E. Herdtweck, *J. Organomet. Chem.* 1988, **355**, 297.
118. S. Cai, D. M. Hoffman and D. A. Wierda, *Inorg. Chem.* 1989, **28**, 3784.
119. S. Cai, D. M. Hoffman and D. A. Wierda, *Organometallics* 1988, **7**, 2069.
120. W. A. Herrmann, J. G. Kuchler, J. K. Felixberger, E. Herdtweck and W. Wagner, *Angew. Chem., Int. Edn Engl.* 1988, **27**, 394.
121. P. Stavropoulos, P. G. Edwards, G. Wilkinson, M. Motevalli, K. M. Abdul Malik and M. B. Hursthouse, *J. Chem. Soc., Dalton Trans.* 1985, 2167.
122. D. M. Hoffman and D. A. Wierda, *J. Am. Chem. Soc.* 1990, **112**, 7056.
123. D. Parker and P. S. Roy, *Inorg. Chem.* 1988, **27**, 4127.
124. J. C. Brewer and H. B. Gray, *Inorg. Chem.* 1989, **28**, 3334.
125. M. S. Ram and J. T. Hupp, *Inorg. Chem.* 1991, **30**, 130.
126. G. Böhm, K. Wieghardt, B. Nuber and J. Weiss, *Inorg. Chem.* 1991, **30**, 3464.
127. W. A. Nugent and J. M. Mayer, *Metal–Ligand Multiple Bonds*. Wiley-Interscience, New York (1988).
128. J. M. Mayer, T. H. Tulip, J. C. Calabrese and E. Valencia, *J. Am. Chem. Soc.* 1987, **109**, 157.
129. T. K. G. Erikson, J. C. Bryan and J. M. Mayer, *Organometallics* 1988, **7**, 1930.
130. E. Spaltenstein, T. K. G. Erikson, S. C. Critchlow and J. M. Mayer, *J. Am. Chem. Soc.* 1989, **111**, 617.
131. W. A. Herrmann, J. K. Felixberger, J. G. Kuchler and E. Z. Herdtweck, *Z. Naturforsch.* 1990, **45b**, 876.
132. E. W. Harlan and R. H. Holm, *J. Am. Chem. Soc.* 1990, **112**, 186.
133. G. D. Watt, J. W. McDonald and W. E. Newton, *J. Less-Common Met.* 1977, **54**, 415.
134. X. Lu, J. Sun and X. Tao, *Synthesis* 1982, 185.

Polyhedron Vol. 12, No. 6, pp. 591–599, 1993
Printed in Great Britain

0277–5387/93 $6.00+.00
© 1993 Pergamon Press Ltd

OXIDE-BASE ADDUCTS OF ALUMINUM: X-RAY CRYSTAL STRUCTURES OF $Me_3Al(OPPh_3)$, $Me_3Al(ONMe_3)$ AND $[(CH_3)_3SiO]_3Al(OPPh_3)$

FRANK J. FEHER,† THEODORE A. BUDZICHOWSKI and KEITH J. WELLER

Department of Chemistry, University of California, Irvine, CA 92717, U.S.A.

(*Received* 15 *September* 1992; *accepted* 23 *November* 1992)

Abstract—The crystalline molecular structures of three Lewis adducts of aluminum are reported. The structures of the 1:1 adducts between trimethylaluminum and triphenylphosphine oxide, **1**: $Me_3Al(OPPh_3)$, trimethylaluminum and trimethylamine-N-oxide; **2**: $Me_3Al(ONMe_3)$; and **3**: $[(CH_3)_3SiO]_3Al(OPPh_3)$ are discussed, and a comparison is made to the previously characterized aluminosilsesquioxane complex $(c\text{-}C_6H_{11})_7Si_7O_{12}Al(OPPh_3)$ (**5**).

As part of our efforts to develop useful chemical models for silica and aluminosilicate surfaces,[1] we recently synthesized the first well-characterized examples of polyhedral aluminosilsesquioxanes.[2] Complexes **5**, **6** and **7**, which are readily available from the reactions of **4** with Ph_3PO, Me_3NO and $Me_4SbOSbMe_4$, respectively, exhibit a number of structural similarities to aluminosilicate frameworks, suggesting that aluminosilsesquioxanes will be excellent models for the aluminoferrous sites in zeolites.

In an earlier paper we compared the structural data for **5** with metrical data available from the numerous structural studies on aluminosilicates and zeolites.[2a] At that time **5** was the only crystallographically characterized phosphine oxide complex of aluminum and it was not possible to compare metrical data for the Al—O—P moiety with other chemically similar complexes.[3] Since the appearance of our original paper, Burford *et al.* have reported the structural and spectroscopic characterization of several aluminum/phosphine oxide

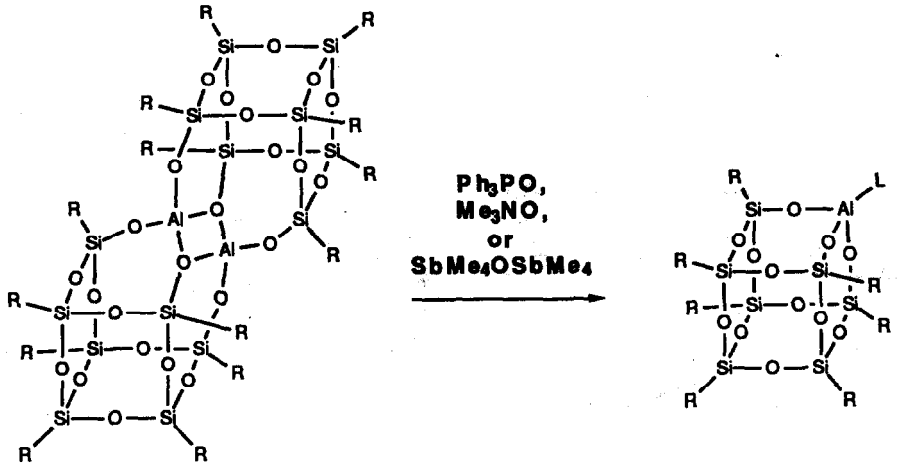

4 R = $c\text{-}C_6H_{11}$

5 L = $OPPh_3$
6 $ONMe_3$
7 $OSbMe_4^-$

† Author to whom correspondence should be addressed.

adducts, including the single-crystal X-ray diffraction studies of $Cl_3AlOPPh_3$ (**8**) and $Br_3AlOPPh_3$ (**9**).[4] In this paper we report the results from X-ray crystallographic studies of **1**, $Me_3Al(OPPh_3)$, **2**, $Me_3Al(ONMe_3)$ and **3**, $[(CH_3)_3SiO]_3Al(OPPh_3)$, and compare these results to the other structurally characterized phosphine oxide adducts of aluminum.

RESULTS AND DISCUSSION

1, $Me_3Al(OPPh_3)$

The molecular structure of **1** is shown in Figs 1(a) and 1(b), a summary of crystallographic data appears in Table 1, and selected bond distances and angles are collected in Table 2. The complex crystallizes from benzene/hexane as colourless rhombohedra in the space group $R\bar{3}$, with the Al—O—P linkage aligned along the crystallographic three-fold rotational axis. Thus, the Al—O—P bond angle is crystallographically imposed at 180°. This interesting structural feature has also been observed in the solid state and in solution for the triphenylphosphine oxide adducts of $AlCl_3$ (**8**) and $AlBr_3$ (**9**) and is indicative of π-delocalization over the Al—O—P linkage (*vide infra*).[4] As expected, the aromatic rings on phosphorus adopt a propeller-like orientation and are staggered from the methyl groups on aluminum. The C(1)—Al—P—C(2b) dihedral angle is 45. [Fig. 1(b)]. There are no significant non-bondi interactions between adjacent molecules in the u cell.

Comparisons of metrical data for **1** with fr Me_3Al[5] and Ph_3PO[6] indicate that the largest stru tural changes occur at the aluminum centre (Tab 3). The trigonal Me_3Al molecule undergoes pyr midalization upon the coordination of Ph_3P [C—Al—C = 113.3(1)°] and the Al—C bond di tances increase slightly from 1.957 to 1.965(3) as pyramidalization increases the percentage of character in the Al—C bonds. Changes in tl molecular structure of Ph_3PO upon coordinatic of Me_3Al are more difficult to quantify becau the molecular structures of Ph_3PO occur in low symmetry space groups with a relatively wide ran of metrical data.[6] The P—O bond distance increas slightly from 1.484(1) to 1.500(2) Å, while the P— bond distances become somewhat (0.01 Å) shorte The C—P—C bond angles also appear to becom more obtuse, but all of these changes are not fa outside their limits of statistical significance.

2, $Me_3Al(ONMe_3)$

The molecular structure of **2** is shown in Fig 2(a) and 2(b), a summary of crystallographic dat appears in Table 1, and selected bond distance and angles are collected in Table 4. The comple

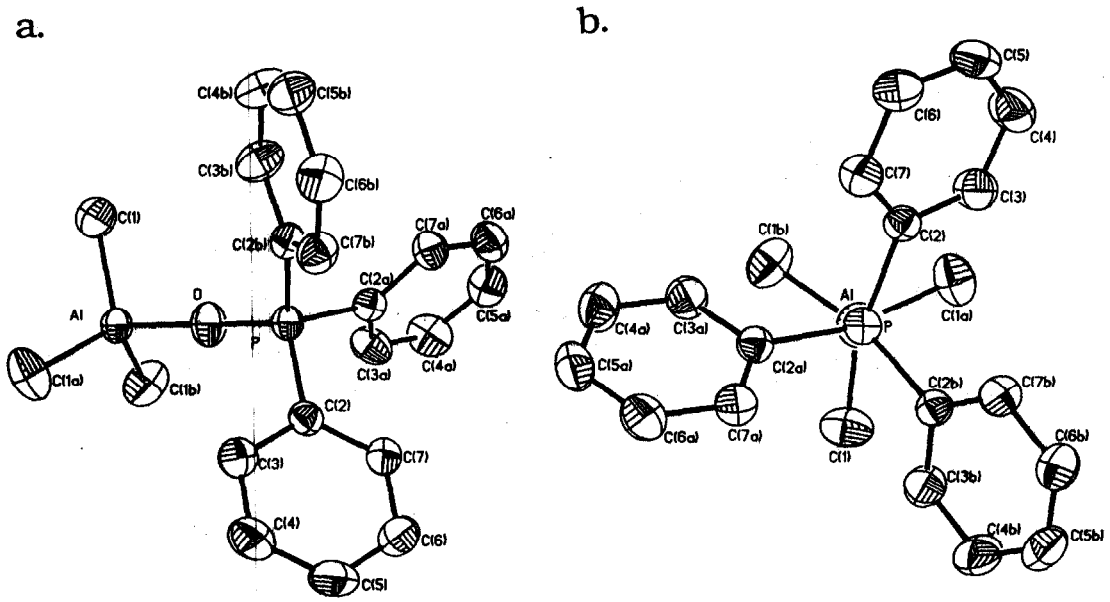

Fig. 1. (a) Perspective ORTEP plot of $Me_3Al(OPPh_3)$ showing 50% thermal ellipsoids for all non-hydrogen atoms in a least-squares plane. (b) ORTEP plot of $Me_3Al(OPPh_3)$ viewed down the crystallographic C_3 axis.

Table 1. Summary of crystallographic data for complexes **1–3**

Compound	**1**	**2**	**3**
Empirical formula	$C_{21}H_{24}OAlP$	$C_6H_{18}NOAl$	$C_{27}H_{42}O_4AlSi_3P$
Formula weight	350.4	147.2	572.8
Colour; habit	Clear rhombohedra	Clear plates	Clear cubes
Crystal size (mm)	$0.32 \times 0.40 \times 0.42$	$0.50 \times 0.30 \times 0.20$	$0.17 \times 0.17 \times 0.23$
Space group	*R3bar*	$P2_1/n$	*P1bar*
Unit cell dimensions			
a (Å)	13.842(2)	7.831(2)	10.265(2)
b (Å)		14.318(3)	10.532(2)
c (Å)	18.159(4)	8.872(2)	16.031(3)
α (°)			101.07(1)
β (°)		92.48(3)	90.60(2)
γ (°)			103.26(2)
Temperature (K)	183	183	183
V (Å^3)	3013.1(9)	993.8(4)	1652.9(5)
Z	6	4	2
D_{calc} (g cm^{-3})	1.158	0.984	1.151
Abs. coef. (mm^{-1})	0.179	0.141	0.240
2θ range (°)	4–57.5	4–55	4–45
Reflections collected	2813	2560	4678
Independent reflections	1757	2090	3826
Observed reflections	1364 ($F > 4.0\sigma F$)	1647 ($F > 4.0\sigma F$)	3137 ($F > 3.0\sigma F$)
$R(F)$	0.0454	0.0476	0.0603
$R_w(F)$	0.0519	0.0485	0.0626
Goodness-of-fit	1.55	1.77	1.32
Number of variables	106	155	325
Data-to-parameter ratio	12.9:1	10.6:1	9.7:1
Largest and mean Δ/σ	0.001, 0.000	0.001, 0.000	0.001, 0.000

Table 2. Interatomic distances (Å) and angles (°) for $Me_3Al(OPPh_3)$ (**1**)

Al—O	1.837(2)	Al—C(1)	1.965(3)
P—O	1.500(2)	P—C(2)	1.789(2)
Al—O—P	180.0	O—P—C(2)	111.1(1)
C(1)—Al—O	105.3(1)	C(2)—P—C(2A)	107.8(1)
C(1)—Al—C(1A)	113.3(1)		

Table 3. Selected bond distances (Å) and angles (°) for Me_3Al,[5] Ph_3PO[6] and Me_3NO[7]

	C—Al	C—Al—C		
Me_3Al	1.957	120.0		
	O—(P)	C—P(N)	O—P(N)—C	C—P(N)—C
Me_3NO	1.388(5)	1.479(8) av.	109.9(5)	109.1(2) av.
Ph_3PO	1.484(1)	1.802(3) av.	112.3(8) av.	106.6(3) av.

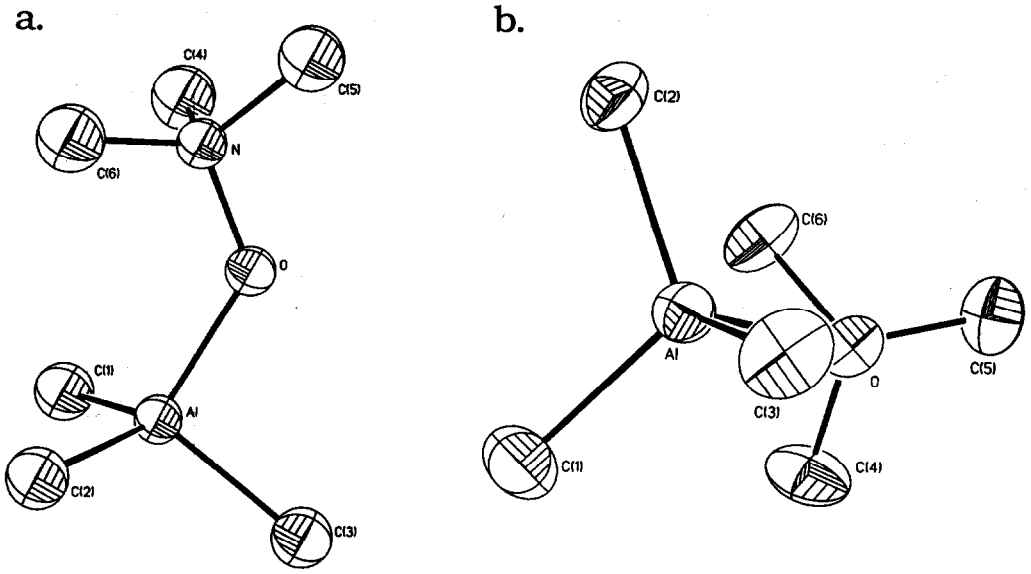

Fig. 2. (a) Perspective ORTEP plot of $Me_3Al(ONMe_3)$ showing 50% thermal ellipsoids for all non-hydrogen atoms in a least-squares plane. (b) ORTEP plot of $Me_3Al(ONMe_3)$ viewed down the O—N bond.

crystallizes from benzene/hexane as colourless plates in the space group $P2_1/n$. The molecule is situated at a general position with no exceptional intermolecular contacts between the four molecules which comprise the unit cell.

In stark contrast to the crystallographically C_{3v} symmetric phosphine oxide adduct **1**, the trimethylamine oxide adduct **2** is bent, with an Al—O—N bond angle of 128.2(1)° (Table 4). Although this angle differs by more than 50° from that in **1**, the Al—O bond distance [1.857(2) Å] is lengthened by only 0.02 Å. The Me_3Al moiety is pyramidalized with average Al—C distances of 1.981 Å and average C—Al—C bond angles of 112.6°. As observed in **1** coordination of $AlMe_3$ to Me_3NO leads to a slight lengthening of the N— bond and appears to flatten the C_3N moiety. Mo of these changes are, however, only minor and the significance is questionable. One of the more inte esting features of the structure is the O—Al—C(bond angle of 99.3(1)°, which is approximately 1(more acute than the other two O—Al—C angl [109.2 and 109.8(1)°] in the adduct. Normal tetr hedral angles are observed for the free amine oxide

3, $[(CH_3)_3SiO]_3Al(OPPh_3)$

The molecular structure of **3** is shown in Fig. a summary of crystallographic data appears i Table 1, and selected bond distances and angles a

Table 4. Interatomic distances (Å) and angles (°) for $Me_3Al(ONMc_3)$ (**2**)

Al—O	1.857(2)	N—O	1.410(2)
Al—C(1)	1.983(3)	N—C(4)	1.485(3)
Al—C(2)	1.986(3)	N—C(5)	1.487(3)
Al—C(3)	1.975(3)	N—C(6)	1.486(3)
Al—O—N	128.2(1)	C(4)—N—O	108.8(2)
C(1)—Al—O	109.2(1)	C(5)—N—O	106.2(2)
C(2)—Al—O	109.8(1)	C(6)—N—O	110.9(2)
C(3)—Al—O	99.3(1)	C(4)—N—C(5)	109.6(2)
C(1)—Al—C(2)	112.5(1)	C(4)—N—C(6)	111.1(2)
C(1)—Al—C(3)	113.2(1)	C(5)—N—C(6)	110.0(2)
C(2)—Al—C(3)	112.0(1)		

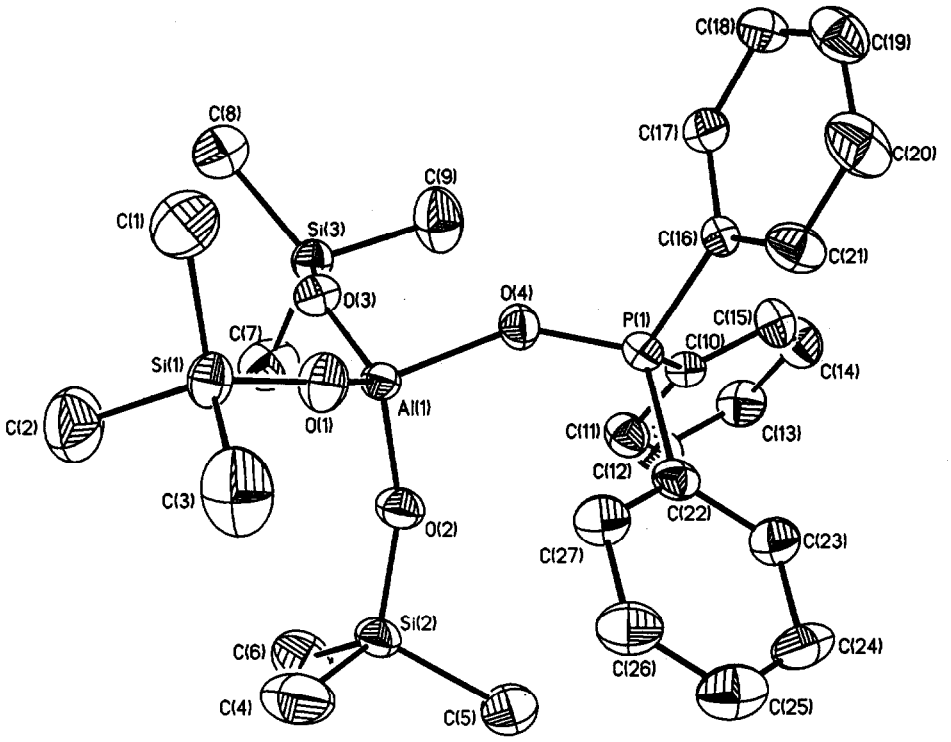

Fig. 3. Perspective ORTEP plot of $[(CH_3)_3SiO]_3Al(OPPh_3)$ showing 50% thermal ellipsoids for all non-hydrogen atoms.

collected in Table 5. The complex crystallizes from benzene/hexane in the triclinic space group $P\bar{1}$. The molecule resides at a general position within the unit cell and displays no significant non-bonded interactions.

The Al—O—P linkage is bent [146.7(2)°] with Al—O(P) and P—O bond lengths of 1.807(4) and 1.517(4) Å, respectively. In this complex the Si—O—Al linkages are also quite obtuse [149.8(2)° av.] and may reflect the cumulative effects of steric interactions and weak Al(Si)—O π-bonding. Again, the phenyl rings adopt a propellar-like arrangement and are staggered from the ligands bound to the aluminum centre. Both the aluminum and phosphorus centres are very nearly tetrahedral: the only statistically significant structural change which

Table 5. Interatomic distances (Å) and angles (°) for $(Me_3SiO)_3Al(OPPh_3)$ (3)

Al(1)—O(1)	1.708(4)	P(1)—C(16)	1.780(5)
Al(1)—O(2)	1.718(4)	P(1)—C(22)	1.793(5)
Al(1)—O(3)	1.709(3)	Si(1)—O(1)	1.603(4)
Al(1)—O(4)	1.807(4)	Si(2)—O(2)	1.607(4)
P(1)—O(4)	1.517(4)	Si(3)—O(3)	1.606(3)
P(1)—C(10)	1.796(5)		

Al(1)—O[4]—P(1)	146.7(2)	O(2)—Al(1)—O(4)	104.7(2)
Al(1)—O(1)—Si(1)	152.7(2)	O(3)—Al(1)—O(4)	105.2(2)
Al(1)—O(2)—Si(2)	151.9(3)	O(4)—P(1)—C(10)	110.9(2)
Al(3)—O(3)—Si(3)	144.7(2)	O(4)—P(1)—C(16)	109.2(2)
O(1)—Al(1)—O(2)	114.3(2)	O(4)—P(1)—C(22)	110.8(2)
O(1)—Al(1)—O(3)	113.9(2)	C(10)—P(1)—C(16)	109.3(2)
O(1)—Al(1)—O(4)	104.0(2)	C(10)—P(1)—C(22)	108.1(2)
O(2)—Al(1)—O(3)	113.2(2)	C(16)—P(1)—C(22)	108.5(2)

occurs in the phosphine oxide is the increase in P—O bond length. As in complexes **1** and **2** (Tables 2 and 4), the substituents about the aluminum centre in **3** are skewed slightly towards the Lewis base [O—Al—O = 113.8° av., O—Al—O(P) = 104.6° av.].

Nature of π-bonding in Lewis oxide-adducts

The presence of linear Al—O—P linkages in phosphine-oxide adducts of aluminum suggests that extensive π-delocalization occurs in these systems.[4] A number of such complexes have been structurally characterized, and it is now possible to postulate about the origins of such interactions. In particular we have determined the structures of three closely related complexes (**1**, **3** and **5**) by single-crystal X-ray diffraction on the same diffractometer system and at the same temperature (−90°C). For convenience, the pertinent bond distances and angles for the complexes described here, as well as several other related species, are collected in Table 6.

The following observations have been made. For adducts of the type E—O—D, where E is an electrophilic group 13 element and its ligands and D is a nucleophilic oxide of a group 15 element and its ligands, a 180° bond angle is observed only for those cases where E and D are from the third row (or greater) of the periodic table. Thus, **2** and F_3B—O—PPh_3[8] are bent, with bond angles of 146.7(2)° and 134.5(2)°, respectively. Also linear Al—O—P linkages are observed only in those cases where the ligands about the aluminum and phosphorus centres are not significant π-donors. Interestingly, Burford and Rogers have recently shown that chemically analogous phosphine-selenide and phosphine-sulphide complexes do not show the same tendency towards linearity, presumably because of weaker π-bonding.[9]

Although it would be tempting to suggest that *d*-orbitals are responsible for the observed behaviour, the role of $d\pi$–$p\pi$ bonding in main group syster in general has been refuted based on numero theoretical[10] and experimental studies.[11] Fu thermore, the significance of π-bonding for alun num complexes has recently come into question. An alternative possibility recently advanced by Ba ron,[13] which is also consistent with the above obse vations, is the interaction of π-symmetry-fill orbitals on oxygen with empty π-symmetry σ orbitals on both the group 13 and group 15 elemen involved in the linkage (Fig. 4). This type of inte action is very weak, but can have significant stru tural impact on bonds with soft flexing potentia such as the Al—O—P linkages described here.

As a result of π–$\sigma^*\pi$ interaction concomita lengthening of the σ-bonds may be observed.[1] Although statistically significant changes are n observed in the systems discussed thus far [perha due to only weak interaction spread over three di tinct M—L bonds, Figs 4(a) and 4(b)], this result not inconsistent with recent theoretical calculatio for this type of interaction.[10c] For **2** and **3** whe cylindrical symmetry at oxygen is not observed the solid state, interesting variations in the Al— and P—C bond distances occur. The lower syn metry causes differing effects and bonds with c orbitals directed at the presumed location of t lone pair orbitals on oxygen are somewhat long [Al—A and P—A in Fig. 4(c)]. In **2** Al—C(1) ar Al—C(2) are approximately 0.01 Å longer tha Al—C(3) [Fig. 2(b)]. Nitrogen, a first row elemen forms strong covalent bonds to carbon and do not display significant N—C bond alterations. I **3** Al—O(2) is 0.01 Å longer than Al—O(1) ar Al—O(3), while P—C(10) and P—C(22) are 0.0 Å longer than P—C(16) (Fig. 3). It should b pointed out that, while consistent with a π–σ^* interaction, these changes are not outside of the statistical limits of significance and may be the resu of other factors such as crystal packing and ster forces.

Table 6. Data for phosphine(amine) oxide adducts of aluminum

	R	X	Al—O	P(N)—O	P—O—Al	δ ^{31}P	Ref.
R_3POAlX_3	Ph	$O_3Si_7O_9$	1.770(5)	1.508(4)	160.4(3)	42.2	2
	Ph	Cl	1.733(4)	1.519(4)	180	44.9	4
	Ph	Br	1.736(4)	1.513(7)	180	45.7	4[a]
	Ph	OTMS	1.807(4)	1.517(4)	146.7(2)	40.6	This work
	Ph	Me	1.837(2)	1.500(2)	180	36.5	This work
R_3NOAlX_3	Me	Me	1.857(2)	1.410(2)	128.2(1)	na	This work

[a] Br positions disordered (see ref. 4 for details).

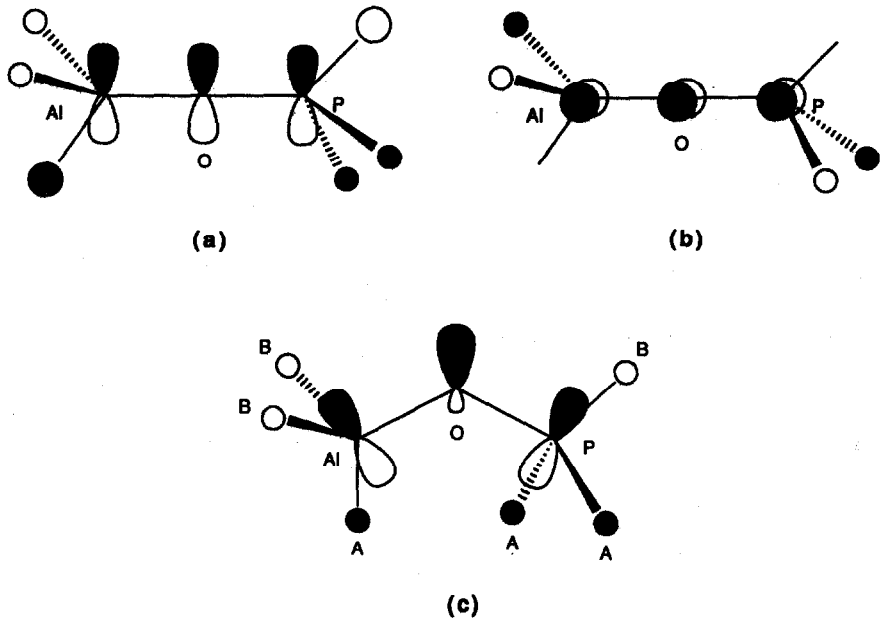

Fig. 4. Interaction of oxygen lone pair orbitals with aluminum and phosphorus σ^*.

Effects of the ligands on Lewis acidity

After a brief inspection of Table 6 it is immediately obvious that there is little correlation between Al—O bond distance and Al—O—P bond angle. This result is not surprising and has been previously noted for alkoxide complexes of the early transition metals[14] and main group elements.[15] Equally obvious, however, is the large range for Al—O(P) bond distances. While this range may or may not be due to the influence of π-bonding, it is no doubt a reflection of the electrophilicity of the aluminum centres in these complexes. Aluminosilsesquioxane **5** has one of the shortest Al—O bond distances and the aluminum centre is presumably much more electrophilic than the corresponding simple alkoxide and siloxide complexes such as **3**.

Burford *et al.* recently noted that the ^{31}P chemical shifts for phosphine oxide complexes are dramatically shifted downfield upon ligation by Lewis acids and suggested that this was the result of significant P—O bond disruption.[9] While there does not appear to be a good correlation between the ^{31}P chemical shift and the P—O bond distance (Table 6), there is an excellent correlation between the latter and the observed Al—O(P) distances (Fig. 5). The lack of correlation between δ ^{31}P and *d* P—O is readily explained by the small range of values observed for P—O separations (0.019 Å compared to 0.067 Å for *d* Al—O), considering the accuracy with which bond distances are determined by X-ray diffraction. The spectroscopic data also suggest that the aluminum centre in **5** is significantly more electrophilic than in the corresponding simple siloxide **3**.

EXPERIMENTAL

All manipulations were performed in a Vacuum Atmospheres Corporation Dri-lab. Benzene and hexanes were distilled from dark purple solutions of potassium benzophenone ketyl containing tetraglyme under nitrogen. Trimethylaluminum (Aldrich) was vacuum distilled and stored under nitrogen prior to use. Triphenylphosphine oxide (Aldrich) was filtered through silica gel

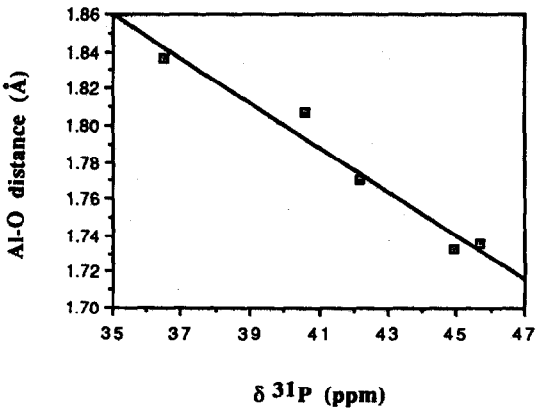

Fig. 5. Plot of Al—O distance (Å) versus δ ^{31}P (ppm) for complexes **1**, **3**, **5**, **8** and **9**. Data from Table 6.

($EtOH/CHCl_3$) and recrystallized from ether. Anhydrous trimethylamine-N-oxide (Aldrich) was obtained by azeotropic dehydration of $Me_3NO \cdot 2H_2O$ (toluene, 110°C) and vacuum sublimation. Paratone-N (viscous lubricant) was degassed under a dynamic vacuum (0.01 torr) overnight. NMR spectra were recorded on a General Electric GN-500 spectrometer ($^{31}P\{^1H\}C_6D_6$, 25°C) and were referenced to H_3PO_4 (0.00 ppm). The spectrum for **5** was originally misreferenced[2a] and was re-recorded under identical conditions to **1** and **2**.

Preparation of **1** *and* **2**

The Lewis adducts were prepared by the addition of an equimolar amount of neat trimethylaluminum to a benzene solution of either triphenylphosphine oxide or trimethylamine-N-oxide.[3e,f] After stirring for 15 min the volatiles were removed *in vacuo* (10^{-3} Torr, 25°C) to afford quantitative yields (NMR) of the respective compounds. Suitable single crystals for X-ray diffraction studies were obtained by the slow diffusion of hexane into benzene solutions of the adducts. The crystals used for X-ray diffraction studies were manipulated under a protective layer of Paratone-N.

Preparation of **3**

This adduct was prepared according to the literature procedure.[16] Suitable crystals for X-ray diffraction were obtained by slow diffusion of hexanes into a saturated benzene solution of **3**.

Collection of X-ray diffraction data

Crystals suitable for X-ray diffraction were cut from larger crystalline masses and mounted using standard procedures under a stream of nitrogen at −90°C on a Syntex P3 automated four-circle diffractometer equipped with a locally modified Syntex LT-1 low-temperature device.[12] Unit cell parameters and intensity data were obtained using standard procedures which have been described previously.[2,17] Low-temperature intensity data were collected using the θ–2θ scan technique with graphite-monochromated Mo-K_α radiation (λ = 0.71069 Å) under the conditions listed in Table 5. All crystallographic calculations were performed using the SHELXTL PLUS program set. The structures were solved by direct methods, which yielded one set of phase relationships with high internal consistency for each adduct. In each case a series of difference-Fourier syntheses revealed the positions of all atoms, including hydrogen atoms for **1** and **2**. For **3** hydrogen atoms were placed in calculated positions with δ C—H = 0.96 Å. Complete details of the refinements are listed in Table 5. In all cases, final difference-Fourier syntheses showed no significant features.

Acknowledgements—We express our thanks to Dr Joseph W. Ziller for assistance with the X-ray structural studies. These studies were supported by the National Science Foundation (CHE-8703016). Funds for the purchase of the X-ray diffraction equipment were made available from NSF Grant CHE-85-14495. Financial support from the UCI Academic Senate Committee on Research is also gratefully acknowledged. One of us (TAB) gratefully acknowledges financial support from the Fannie and John Hertz Foundation as a pre-doctoral fellowship.

REFERENCES

1. (a) F. J. Feher, D. A. Newman and J. F. Walzer, *J. Am. Chem. Soc.* 1989, **111**, 1741; (b) F. J. Feher and D. A. Newman, *J. Am. Chem. Soc.* 1990, **112**, 1931; (c) F. J. Feher, T. A. Budzichowski, K. Rahimian and J. W. Ziller, *J. Am. Chem. Soc.* 1992, **114**, 3859.
2. (a) F. J. Feher, T. A. Budzichowski and K. J. Weller, *J. Am. Chem. Soc.* 1989, **111**, 7288; (b) F. J. Feher and K. J. Weller, *Organometallics* 1990, **9**, 2638.
3. (a) Other R'_3AlOPR_3 complexes are known,[3b–f] but have not been structurally characterized; (b) I. P. Romm, E. N. Gur'yanova, V. M. Ryaboi and E. P. Buchikhin, *Zh. Obsch. Khim.* 1979, **49**, 2098; (c) E. A. Kanevskii, E. P. Buchikhin, T. V. Zagorskaya and V. I. Ulanov, *Zh. Neorg. Khim.* 1979, **24**, 2032; (d) K. M. Nykerk and D. P. Eyman, *Inorg. Nucl. Chem. Lett.* 1968, **4**, 253; (e) F. Schindler and H. Schmidbaur, *Chem. Ber.* 1967, **100**, 3655; (f) F. Schindler and H. Schmidbaur, *Chem. Ber.* 1967, **98**, 3345.
4. N. Burford, B. W. Royan, R. E. v. H. Spence, T. S. Cameron, A. Linden and R. D. Rogers, *J. Chem. Soc., Dalton Trans.* 1990, 1521.
5. G. A. Anderson, F. R. Forgaard and A. Haaland, *Acta Chem. Scand.* 1972, **26**, 1947.
6. (a) A. L. Spek, *Acta Cryst.* 1987, **C43**, 1233; (b) G. Ruban and V. Zabel, *Cryst. Struct. Commun.* 1976, **6**, 671; (c) G. Bandoli, G. Bortolozzo, D. A. Clemente, U. Croatto and C. Pannattoni, *J. Chem. Soc. (A)* 1970, 2778.
7. A. Caron, G. J. Palenik, E. Goldish and J. Donohue, *Acta Cryst.* 1964, **17**, 102.
8. An X-ray diffraction study of $F_3B(OPPh_3)$ was performed in our laboratory at −90°C: monoclinic, $P2_1/n$, a = 9.411(2), b = 17.941(5), c = 10.007(2) Å, β = 104.08(1)°, V = 1639.0(6) Å^3, Z = 4, R_F = 3.93%, R_{wF} = 4.60%. However, since the determination of this structure a room-temperature structure has recently appeared: N. Burford, R. E. v. H. Spence, A Linden and T. S. Cameron, *Acta Cryst., Sect. C* 1990, **C46**, 92. Our results are essentially the same as those described in the literature.
9. N. Burford, B. W. Royan, R. E. v. H. Spence and

R. D. Rogers, *J. Chem. Soc., Dalton Trans.* 1990, 2111.

10. (a) W. J. Cruickshank, *J. Molec. Struct.* 1985, **130**, 1771; (b) S. Shambayati, J. F. Blake, S. G. Wierschke, W. L. Jorgenson and S. L. Schrieber, *J. Am. Chem. Soc.* 1990, **112**, 697 and refs therein; (c) G. Sini, G. Ohanessian, P. Hiberty and S. S. Shaik, *J. Am. Chem. Soc.* 1990, **112**, 1407 and refs therein; (d) A. L. Reed and P. v. R. Schleyer, *J. Am. Chem. Soc.* 1990, **112**, 1434 and refs therein; (e) Y. Apeloig, in *The Chemistry of Organic Silicon Compounds* (Edited by S. Patai and Z. Rappoport). Wiley, Chichester (1989); (f) S.-X. Xiao, W. C. Trogler, D. E. Ellis and Z. Berkovich-Yellin, *J. Am. Chem. Soc.* 1983, **105**, 7033; (g) D. S. Marynick, *J. Am. Chem. Soc.* 1984, **106**, 4064; (h) C. G. Pitt, *J. Organomet. Chem.* 1973, **61**, 49.
11. (a) D. B. Beach and W. L. Jolly, *Inorg. Chem.* 1984, **23**, 4774; (b) A. G. Orpen and N. G. Connelly, *J. Chem. Soc., Chem. Commun.* 1985, 1310; (c) B. J. Dunne, R. B. Morris and A. G. Orpen, *J. Chem. Soc., Dalton Trans.* 1991, 653.
12. (a) R. H. Cayton, M. H. Chisholm, E. R. Davidson, V. F. Distasi, P. Du and J. C. Huffman, *Inorg. Chem.* 1991, **30**, 1020; (b) M. A. Petrie, M. M. Olmstead and P. P. Power, *J. Am. Chem. Soc.* 1991, **113**, 8704.
13. M. D. Healy, D. A. Wierda and A. R. Barron, *Organometallics* 1988, **7**, 2543.
14. (a) T. W. Coffindaffer, B. D. Steffy, I. P. Rothwell, K. Folting, J. C. Huffman and W. E. Strieb, *J. Am. Chem. Soc.* 1989, **111**, 4742; (b) B. D. Steffey, P. E. Fanwick and I. P. Rothwell, *Polyhedron* 1990, **9**, 963.
15. (a) M. D. Healy, J. W. Ziller and A. R. Barron, *Organometallics* 1991, **10**, 597; (b) G. D. Smith, P. E. Fanwick and I. P. Rothwell, *Inorg. Chem.* 1990, **29**, 3221.
16. F. Schindler and H. Schmidbaur, *Chem. Ber.* 1968, **101**, 1656.
17. M. R. Churchill, R. A. Lashewycz and F. J. Rotella, *Inorg. Chem.* 1977, **16**, 265.

Polyhedron Vol. 12, No. 6, pp. 601–606, 1993
Printed in Great Britain

0277–5387/93 $6.00+.00
© 1993 Pergamon Press Ltd.

SYNTHESIS AND CHARACTERIZATION OF THE MOLYBDENUM(IV) OXO-SELENOLATE COMPLEX [MoO($Ph_2P(O)CH_2CH_2P(Ph)CH_2CH_2PPh_2$)(Se-2,4,6-$(CH_3)_3C_6H_2)_2$]

P. MICHAEL BOORMAN,* HEINZ-BERNHARD KRAATZ and MASOOD PARVEZ

Department of Chemistry, University of Calgary, Calgary, Alberta, Canada T2N 1N4

(*Received* 5 *October* 1992; *accepted* 20 *November* 1992)

Abstract—The presence of adventitious oxygen in the reaction of [(Triphos)$MoCl_3$] (Triphos = $Ph_2PCH_2CH_2P(Ph)CH_2CH_2PPh_2$) with $NaSeC_6H_2Me_3$-2,4,6 in THF leads to the formation of [*fac*-MoO($Ph_2P(O)CH_2CH_2P(Ph)CH_2CH_2PPh_2$)($SeC_6H_2Me_3$-2,4,6)$_2$]. This is the first example of a structurally characterized molybdenum(IV)oxo-selenolato complex. It contains a chelating triphosphine mono-oxide ligand. The formation can be understood in terms of an oxidative addition of dioxygen to the metal centre followed by oxygen atom transfer to the triphos ligand and reduction of molybdenum to molybdenum(IV).

In recent years oxo transfer processes have been receiving an increasing amount of attention, stimulated by the involvement of metal-oxo species in biological systems,[1] as well as in industrially relevant processes.[2] In particular molybdenum-oxo systems have been the focus of intense research into the mechanism of the oxygen transfer from the metal to a substrate due to their biorelevance.[3] Since EXAFS results suggest the presence of MoO or MoO_2 units and of thiolate ligands in these enzymes,[4] it is not surprising that modelling studies have mainly focussed on systems combining these features. Furthermore, it has been noted that systems with chelating and monodentate sulphur-based ligands are particularly suitable to study oxygen transfer reactions. Phosphines have been widely used in such studies to abstract an oxygen from the metal centre to form a very stable phosphine oxide[5] (see e.g. ref. 3), according to eq. (1).

$$L_mMo^{(n)}{=}O + R_3P \longrightarrow L_mMo^{(n-2)} + R_3P{=}O \quad (1)$$

To our knowledge, there are no reports of oxygen atom transfer processes involving complexes with selenolate spectator ligands. This is understandable considering the small number of well-characterized selenolate complexes.[6] As part of our ongoing study of the reactivity of early transition metal selenolates we have inadvertently prepared a molybdenum(IV) oxo-selenolate-triphosphine mono-oxide complex and we now report its synthesis and crystal structure and a possible pathway for its formation involving molecular oxygen.

EXPERIMENTAL

All operations were carried out under argon using standard double-manifold techniques. Analytical grade THF was dried with sodium and distilled from Na/benzophenone. $MoCl_3(MeCN)_3$[7] and NaSeMes[8] were prepared according to the literature procedures. Bis(2-diphenylphosphinoethyl)phenylphosphine (Triphos) was purchased from Aldrich and was used as received. Elemental analyses were performed by the University of Calgary, Department of Chemistry, Analytical Service Laboratory. IR spectra (2000–200 cm^{-1}) were recorded as Nujol mulls between CsI plates using a Mattson 4030 Galaxy Series FT-IR spectrometer. Routine ^1H NMR spectra were recorded on a Bruker ACE-200 spectrometer (referenced to external $SiMe_4$). ^{31}P NMR spectra were recorded on a Varian XL-200 spectrometer (referenced to external H_3PO_4).

* Author to whom correspondence should be addressed.

Synthesis of $MoCl_3$(Triphos) (**1**)

$MoCl_3(MeCN)_3$ (0.2 g, 0.615 mmol) and bis-(2-diphenylphosphinoethyl)phenylphosphine (Triphos) (0.33 g, 0.615 mmol) were charged into a Schlenk flask and acetonitrile (20 cm^3) was added. The reaction mixture was stirred for 30 min at room temperature, giving a yellow–brown solution. The volatiles were then removed and the resulting yellow–brown solid redissolved in a minimum amount of CH_2Cl_2 (15 cm^3) and cooled to −25°C to give **1** as a microcrystalline yellow powder. Yield: 0.44 g; 87%. Found: C, 51.8; H, 3.9. Calc. for $C_{34}H_{33}P_3Cl_3Mo \cdot CH_2Cl_2$: C, 51.1; H, 4.2%. ^{1}H NMR ($CDCl_3$, 200 MHz), δ (in ppm): 8.1–6.8 (br, aromatics), 1.6 br s, aliphatics). IR (cm^{-1}): 322 (br) ν(Mo—Cl).

Preparation of [MoO($Ph_2P(O)CH_2CH_2P(Ph)CH_2CH_2PPh_2$)(Se-2,4,6-$(CH_3)C_6H_2)_2$] (**2**)

A mixture of **1** (0.39 g, 0.48 mmol) and NaSeMes (0.41 g, 1.95 mmol) was cooled to −196°C and degassed THF (20 cm^3) was added. The reaction mixture was then degassed three times (freeze–thaw cycles) and allowed to warm up to room temperature. The solution turned dark green over a period of 40 min. The solvent was removed *in vacuo* and all organics were removed by Et_2O extraction leaving a green solid. This solid was redissolved in THF (10 cm^3) and the same amount of hexanes was added. Dark green X-ray quality crystals deposited over a period of 2 weeks. Compound **2** crystallizes as a THF solvate. Yield: 0.177 g; 25%. Found: C, 58.1; H, 4.6. Calc. for $C_{52}H_{55}MoO_2P_3Se_2$: C, 59.0; H, 5.2%. (The poor analysis is probably due to some solvent loss.) ^{31}P NMR, δ: 107.9, 84.8, 69.7 ppm. IR (cm^{-1}): 1152 (vs), 1132 (vs) (P=O), 1082 (s), 1024 (m), 970 (m), 936 (vs) (Mo=O), 844 (w), 694(s), 570 (w), 542 (w), 518 (mw), 341 (mw), 250 (w).

X-ray crystallography study

Crystal data for [MoO($Ph_2P(O)CH_2CH_2P(Ph)CH_2CH_2PPh_2$)(Se-2,4,6-$(CH_3)_3C_6H_2)_2$] · THF. $C_{56}H_{63}P_3Se_2MoO_3$, M = 1130.89, triclinic, space group $P\bar{1}$ (No. 2), a = 12.244(6), b = 19.303(1), c = 11.872(4) Å, α = 91.17(5)°, β = 104.34(3)°, γ = 103.12(5)°, V = 2638(2) Å^3 (−121.0°C), Z = 2, λ(Mo-K_α) = 0.710 Å (graphite monochromated), D_c = 1.423 g cm^{-3}, F(000) = 1156.0, μ(Mo-K_α) = 17.38 cm^{-1}, R = 0.059, R_w = 0.058.

Data collection and refinement. A dark diamond-shaped crystal of dimensions 0.20 × 0.15 × 0.25 mm was mounted onto a glass fibre and coated with epoxy resin. Accurate cell dimensions and the crystal orientation matrix were determined on a Rigaku AFC6S diffractometer by a least-squares refinement of 25 reflections (ω scan average peak width 0.38°) (28.7 < θ < 36.5°). The choice of space group was $P\bar{1}$ (No. 2). Intensity data were collected using the ω–2θ scan method, using a scan speed of 4.0° per minute in ω and monochromatized Mo-K_α radiation (λ = 0.71069 Å) in the range 2° < θ < 25°. The intensities of 9357 reflections were measured, of which 5526 had $I > 3.00\sigma(I)$. The data were corrected for Lorentz and polarization effects. An empirical absorption correction was applied (transmission factors: 0.9101–0.9994). The data were also corrected to account for crystal decay (average drop in intensity of 3.24% for three standard reflections).

The structure was solved using direct methods using the TEXSAN[9] program package. Refinement of the structure was by full-matrix least-squares calculations, minimizing the function $\Sigma(F_o - F_c)^2$, initially with isotropic temperature factors for the non-hydrogen atoms. At an intermediate stage in the refinement a difference map revealed most of the hydrogen atoms. These were included in the subsequent cycles at geometrically idealized positions (C—H 0.95 Å) and fixed isotropic temperature factors. The refinement converged with R = 0.059 and R_w = 0.058. In the refinement cycles, weights were derived from the counting statistics. Scattering factors were those of Cromer and Mann[10] and Stewart *et al.*[11] Allowance was made for anomalous dispersion.[12] A difference map at the end of the refinement had no chemically significant features ($\Delta\rho$ of −0.92–1.33 e Å^{-3}). Figure 1 was plotted using ORTEP II.[13]

RESULTS AND DISCUSSION

Structure of **2**

Selected interatomic distances and interbond angles are given in Table 1. The crystal structure of **2** contains well-separated molecules with the molybdenum being in a distorted octahedral environment (Fig. 1). The molybdenum is bound to two selenolates *cis* to a terminal oxo group and a chelating Triphos-mono-oxide. The two bulky selenolates are bent away from the terminal oxo group [O(2)—Mo(1)—Se(1) 105.8(3); O(2)—Mo(1)—Se(2) 98.5(3)] in order to minimize their steric interaction. The Mo=O distance compares well to that of other molybdenum(IV)-oxo complexes[14] [Mo(1)—O(2) = 1.682(8) Å]. The complex adopts a facial geometry with respect to the chelating tripodal ligand. The phosphine groups are acting as a tether bringing the phosphine oxide group close to the metal centre and allowing its coordination

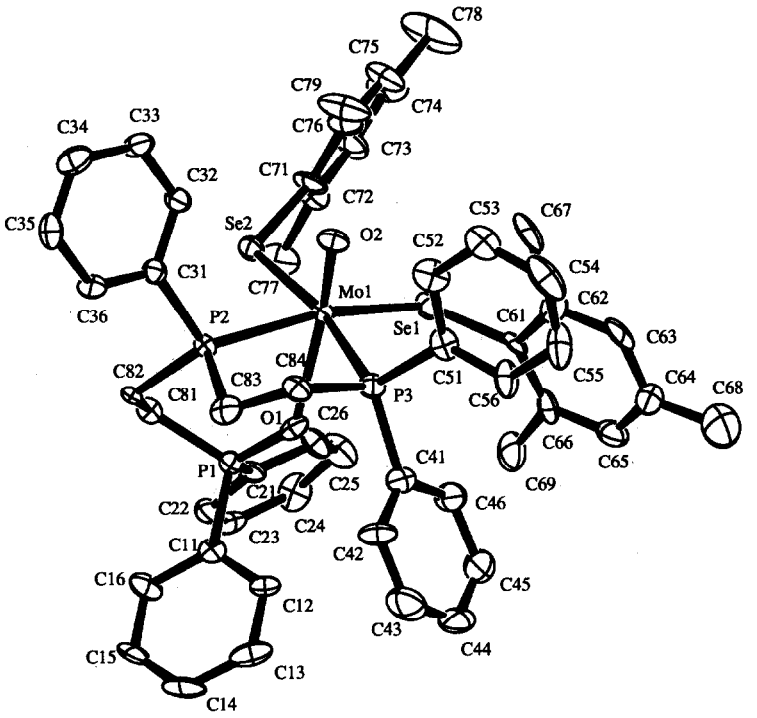

Fig. 1. An ORTEP plot (50% probability ellipsoids) of complex **2**.

Table 1. Selected bond distances (Å) and angles (°) for MoO(Ph$_2$P(O)CH$_2$CH$_2$P(Ph)CH$_2$CH$_2$PPh$_2$)(SeC$_6$H$_2$Me$_2$-2,4,6)$_2$

(a) About the molybdenum atom

Mo(1)—Se(1)	2.553(2)	Mo(1)—Se(2)	2.592(2)
Mo(1)—P(3)	2.559(4)	Mo(1)—P(2)	2.522(4)
Mo(1)—O(1)	2.288(8)	Mo(1)—O(2)	1.682(8)

Se(1)—Mo(1)—Se(2)	83.81(6)	Se(1)—Mo(1)—P(3)	104.8(1)
Se(1)—Mo(1)—P(2)	163.30(9)	Se(1)—Mo(1)—O(1)	90.5(2)
Se(1)—Mo(1)—O(2)	105.8(3)	Se(2)—Mo(1)—P(3)	170.0(1)
Se(2)—Mo(1)—P(2)	90.4(1)	Se(2)—Mo(1)—O(1)	94.0(2)
Se(2)—Mo(1)—O(2)	98.5(3)	P(3)—Mo(1)—P(2)	79.9(1)
P(3)—Mo(1)—O(1)	81.2(2)	P(3)—Mo(1)—O(2)	84.1(3)
P(2)—Mo(1)—O(1)	74.3(2)	P(2)—Mo(1)—O(2)	90.5(3)
O(1)—Mo(1)—O(2)	160.4(3)		

(b) In the phosphine oxide group

P(1)—O(1)	1.51(1)	P(1)—C(11)	1.79(1)
P(1)—C(21)	1.80(1)	P(1)—C(81)	1.78(1)

Mo(1)—O(1)—P(1)	135.6(5)	C(11)—P(1)—C(21)	108.4(5)
C(11)—P(1)—C(81)	106.3(5)	C(21)—P(1)—C(81)	109.9(6)
O(1)—P(1)—C(11)	110.6(5)	O(1)—P(1)—C(21)	110.0(5)
O(1)—P(1)—C(81)	111.5(5)		

(c) About the selenium atoms

Se(1)—C(61)	1.90(1)	Se(2)—C(71)	1.94(1)
Mo(1)—Se(1)—C(61)	113.4(3)	Mo(1)—Se(2)—C(71)	113.7(4)

trans to the oxo group [O(1)—Mo(1)—O(2) = 160.4(3)°] and *cis* to the phosphine groups [O(1)—Mo(1)—P(2) = 74.3(2)°; O(1)—Mo(1)—P(3) = 81.2(2)°]. This geometry is understandable in terms of the arguments brought forward by Mayer and co-workers.[15] According to this the position *trans* to an oxo group is favourable for hard donors in d^2 complexes. The positions *cis* to an oxo group will be preferred by soft π-donors and acids.

The phosphine oxide group does not show any unusual features and has the dimensions P(1)—O(1) = 1.51(1), P—C = 1.79 Å (mean) and the angles O(1)—P(1)—C in the range 110.0–111.5°. It has been noted that the M—O—P linkage is very flexible and can accommodate a wide range of angles.[16a] However, the Mo(1)—O(1)—P(1) angle observed for **2** is notably smaller [135.6(5)°] compared to those found in complexes containing monodentate phosphine oxide ligands.[16] This rather small angle is probably a consequence of the steric interactions of the ligands and the requirements of the six-membered chelate ring and compares well with those observed in chelating diphosphine mono-oxide complexes. The steric requirements of the chelate ring in the molybdenum(V) complex $[MoCl_3O\{Et_2PCH_2CH_2P(O)Et_2\}]$[17] are seen as the cause for the small Mo—O—P angle of 142.3(1)°. The even more rigid aromatic backbone of the chelating ligand in $[RuCl_2\{o\text{-}C_6H_4(PMePh)_2\}\{o\text{-}C_6H_4(PMePh)(P(O)MePh)\}]$[18] leads to an even smaller M—O—P angle of 134.9(3)°.

Origin of **2**

In an attempt to prepare the triselenolato complex [(Triphos)Mo(SeMes)$_3$] (**3**) [$MoCl_3$(Triphos)] (**1**) and a stoichiometric amount of NaSeMes was stirred in THF to give a dark green solution. No resonances were observable in the ^{31}P NMR, indicating the presence of a paramagnetic intermediate (*vide infra*). After the removal of the solvent *in vacuo* and repeated washing of the remaining solid with ether it was crystallized from THF, giving X-ray quality crystals of **2**.

The presence of the MoO and OPR_3 moieties can be seen as indicators for the presence of small amounts of oxygen in the reaction mixture, as has been seen previously.[17] Only minute amounts of

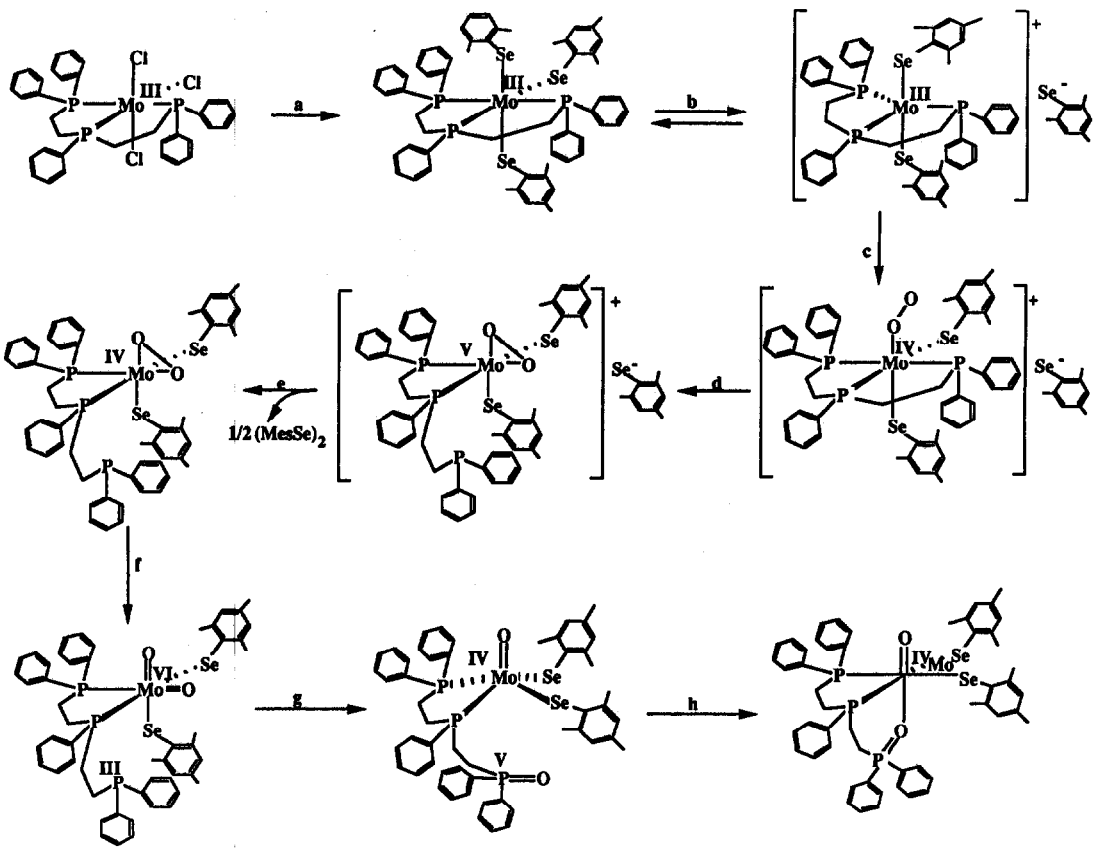

Scheme 1.

adventitious oxygen are needed to yield oxo-molybdenum species, which usually crystallize well from solution.

The likely pathway for the reaction is outlined in Scheme 1. The triphosphine-molybdenum trichloride (**1**) is most likely the *mer* isomer, analogous to similar polydentate phosphine molybdenum(III) complexes.[19] After the initial metathetical reaction of **1** with NaSeMes (a) the target complex (Triphos)Mo(SeMes)$_3$ is formed. Due to steric pressure this complex is in equilibrium (b) with the ionic complex [(Triphos)Mo(SeMes)$_2$][SeMes]. Similar cationic complexes with polydentate ligands have been observed before.[20] Molybdenum(III), which is a molybdenum-based radical species, can react with dioxygen, initially forming a superoxo complex (c). Such interactions are thought of being of importance in the reversible coordination of O_2 in oxyhaemoglobin and related model complexes.[21] Conversion of the η^1-superoxo group to an η^2-peroxo group will oxidize the molybdenum(IV) to molybdenum(V), which can be reduced with selenolate (e) to give back a molybdenum(IV) complex. The selenyl radical will dimerize to give the corresponding diselenide. In the ^{77}Se NMR spectrum a signal at δ 368 indicates the presence of mesityl diselenide. The high stability of the Mo=O linkage[22] will drive the reaction towards the conversion into an $Mo^{VI}O_2$ complex with a dangling phosphine (f). These complexes are known to be easily reduced by phosphines, leading to molybdenum(IV) complexes and phosphine oxides.[3] Hence, the dangling phosphine will reduce the $Mo^{VI}O_2$ complex to a molybdenum(IV) mono-oxo complex (g). Since the phosphine oxide is attached to the coordinated phosphines, it will stay in close proximity to the molybdenum(IV) centre, allowing it to coordinate to the metal centre (h) to yield the observed complex **2**.

Supplementary material available. Tables of distances and angles, atomic coordinates of all atoms, anisotropic and isotropic thermal parameters of all non-hydrogen atoms, listings of calculated and observed ($10F_o/10F_c$) structure factors and a stereoscopic view of the packing diagram for **2** have been deposited with the Editor.

Acknowledgements—Financial support from NSERC (Canada) and the Department of Chemistry for a Graduate Scholarship (to H.-B.K.) is gratefully acknowledged.

REFERENCES

1. (a) J. T. Groves and G. A. McClusky, *J. Am. Chem. Soc.* 1984, **106**, 2177 and refs therein; (b) T. G. Spiro (Editor), *Molybdenum Enzymes*. Wiley, New York (1985).
2. W. A. Nugent and J. M. Mayer, *Metal–Ligand Multiple Bonds*, Ch. 7, pp. 288–319. Wiley, New York (1988).
3. (a) R. H. Holm and J. M. Berg, *Accts Chem. Res.* 1986, **19**, 363; (b) R. H. Holm, *Chem. Rev.* 1987, **87**, 1401; (c) J. M. Berg and R. H. Holm, *J. Am. Chem. Soc.* 1985, **107**, 917; (d) J. M. Berg and R. H. Holm, *J. Am. Chem. Soc.* 1985, **107**, 925.
4. (a) S. P. Cramer, R. Wahl and K. V. Rajagopalan, *J. Am. Chem. Soc.* 1981, **103**, 7721; (b) S. P. Cramer, L. P. Solomonson, M. W. W. Adams and L. E. Mortenson, *J. Am. Chem. Soc.* 1984, **106**, 1467; (c) S. P. Cramer and R. Hille, *J. Am. Chem. Soc.* 1985, **107**, 8164.
5. According to Hudson, the P—O bond strength in $Ph_3P{=}O$ is 127 kcal mol^{-1} R. F. Hudson, in *Structure and Mechanism in Organo-Phosphorus Chemistry*. Academic Press, New York (1965). Holm states that the reaction $MoO_2L_2 + PPh_3 \rightarrow MoOL_2 + OPPh_3$ has a ΔH of -29.0 ± 2.5 kcal mol^{-1} [see ref. 3(b)].
6. H. J. Gysling, *The Chemistry of Organic Selenium and Tellurium Compounds* (Edited by S. Patai and Z. Rappoport), Vol. 1, Ch. 18, pp. 741–754. Wiley, New York (1986).
7. P. T. Bishop and J. R. Dilworth, *Inorg. Synth.* 1990, **28**, 37.
8. J. M. Ball, P. M. Boorman, J. F. Fait, A. S. Hinman and P. J. Lundmark, *Can. J. Chem.* 1988, **67**, 751.
9. TEXSAN (1992), Single Crystal Structure Analysis Software, Version 1.2. Molecular Structures Corporation, Woodland, TX (1992).
10. D. T. Cromer and J. B. Mann, *Acta Cryst.* 1968, **A24**, 321.
11. R. F. Stewart, E. R. Davidson and W. T. Simpson, *J. Chem. Phys.* 1965, **42**, 3175.
12. D. T. Cromer and D. Liberman, *J. Chem. Phys.* 1970, **53**, 1891.
13. C. K. Johnson, ORTEP II, Report ORNL-5138. Oak Ridge National Laboratory, TN (1976).
14. W. A. Nugent and J. M. Mayer, *Metal–Ligand Multiple Bonds*, Ch. 5, pp. 145–219 (especially pp. 168–169). Wiley, New York (1988).
15. (a) J. A. Mayer, *Comm. Inorg. Chem.* 1988, **8**, 125; (b) J. C. Bryan, R. E. Stenkamp, T. H. Tulip and J. M. Mayer, *Inorg. Chem.* 1987, **26**, 2283; (c) J. M. Mayer, D. L. Thorn and T. H. Tulip, *J. Am. Chem. Soc.* 1985, **107**, 7454.
16. (a) C. D. Garner, N. C. Howlader, F. E. Mabbs, A. T. McPhail and K. D. Onan, *J. Chem. Soc., Dalton Trans.* 1978, 1848; (b) R. J. Butcher, B. R. Penfold and E. Sinn, *J. Chem. Soc., Dalton Trans.* 1979, 668.
17. See e.g. M. A. Bakar, A. Hills, D. L. Hughes and G. J. Leigh, *J. Chem. Soc., Dalton Trans.* 1989, 1417.
18. S. R. Hall, B. W. Skelton and A. H. White, *Aust. J. Chem.* 1983, **36**, 267.
19. M. J. Fernández-Trujillo, M. G. Basallote, P. Valerga, M. C. Puerta and D. L. Hughes, *J. Chem. Soc., Dalton Trans.* 1991, 3149.
20. (a) R. R. Conry and J. M. Mayer, *Inorg. Chem.* 1990, **29**, 4862; (b) W. Levason, C. A. McAuliffe and F. P. McCullough, *Inorg. Chim. Acta* 1977, **24**, L13.

21. J. P. Collman, L. S. Hegedus, J. R. Norton and R. G. Finke, *Principles and Applications of Organotransition Metal Chemistry*, pp. 199–203. University Science Books, Mill Valley, CA (1987).
22. W. A. Nugent and J. M. Mayer, *Metal–Ligand Multiple Bonds*, pp. 32–33. Wiley, New York (1988): $Mo(O)_2(S_2CNR_2)_2 \rightarrow Mo(O)(S_2CNR_2)_2 + [O]$, $\Delta H =$ 98 kcal mol^{-1}. According to ref. 2, *ab initio* calculations were performed by Rappé and Goddard: A. K. Rappé and W. A. Goddard III, *J. Am. Chem. Soc.* 1982, **104**, 448. The Mo=O bond energies of $MoOCl_4$ and MoO_2Cl_2 are 102 and 79 kcal mol^{-1}, respectively.

Polyhedron Vol. 12, No. 6, pp. 607–611, 1993
Printed in Great Britain

0277–5387/93 $6.00+.00
© 1993 Pergamon Press Ltd

MOLECULAR STRUCTURE AND MAGNETIC PROPERTIES OF A LINEAR CHAIN COMPOUND, $Ru_2(O_2CCMePh_2)_4Cl$

F. ALBERT COTTON,* YOUNGMEE KIM and TONG REN

Department of Chemistry and Laboratory for Molecular Structure and Bonding, Texas A & M University, College Station, TX 77843, U.S.A.

(*Received* 16 *September* 1992; *accepted* 20 *November* 1992)

Abstract—The linear-chain compound $Ru_2(O_2CCMePh_2)_4Cl$ was prepared by reaction of $Ru_2(O_2CCH_3)_4Cl$ with 2,2-diphenylpropionic acid. The compound has been characterized by X-ray crystallography and magnetic susceptibility measurements from *ca* 2 to 300 K. The chloride ligands bridge the dinuclear units into linear chains. The Ru—Ru′, Ru—O (carboxylate) and Ru—Cl distances are 2.2893(9), 2.030(5) and 2.5016(6) Å, respectively. There is an antiferromagnetic electronic interaction between dinuclear units with J (coupling constant) $= -10.9\ cm^{-1}$. The magnetic moment of $Ru_2(O_2CCMePh_2)_4Cl$ at 300 K is 4.4 μ_B, which indicates three unpaired electrons in each dinuclear unit.

The first carboxylato-bridged diruthenium compound to be structurally characterized,[1] $Ru_2(O_2CC_3H_7)_4Cl$, was found to have the $Ru_2(O_2CC_3H_7)_4^+$ units linked into infinite chains by bridging chloride ions, with equal Ru—Cl distances and an Ru—Cl—Ru angle of 125.4°. Subsequently, another compound with zigzag chains has been reported.[2] In two similar compounds, however, there are chains in which the Ru—Cl—Ru bridges are perfectly linear and symmetrical.[3,4] All available data for such chain structures are summarized in Table 1. Since the $Ru_2(O_2CR)_4^+$ unit has a ground state with $S = 3/2$, the question arises as to whether there is measurable coupling between the $Ru_2(O_2CR)_4^+$ units across the Cl^- bridges. This question has already been addressed in the case of the butyrate,[5] where it was concluded that no detectable coupling exists. Since the manner in which bridging Cl^- ions might effectuate magnetic coupling between $Ru_2(O_2CR)_4^+$ units is not understood in detail, we wondered whether linear bridges might be effective even though the bent ones in the butyrate system are not.

We have chosen to carry out a magnetic study on a new linear system instead of employing one of the two previously known compounds. The reason for this was that the R group, $CMePh_2$, in the new compound is very large and thus keeps the chains well separated. It is, therefore, more likely that any magnetic coupling that might be observed would be correctly attributed to interactions along the chains through the bridging Cl^- ions. Naturally, it was necessary to determine the crystal structure of the new compound in order to be sure it fulfils the requirements of linearity and substantial separation of the chains.

EXPERIMENTAL

$Ru_2(O_2CCH_3)_4Cl$ was prepared using a literature procedure.[6] 2,2-Diphenylpropionic acid was purchased from Aldrich Chemical Company and used as received.

Synthesis

A sample (235 mg, 0.5 mmol) of $Ru_2(O_2CCH_3)_4Cl$ was dissolved in a 1:1 methanol–water (v/v) mixture (50 cm^3). 2,2-Diphenylpropionic acid (570 mg, 2.5 mmol) was added to this solution. The reaction mixture was refluxed for 5 h and the brown precipitate was collected after cooling down. It was washed with methanol and diethylether and dried *in vacuo*: yield 390 mg (68%). The product was recrystallized from CH_2Cl_2 several times. The single crystal for X-ray data collection was prepared by slow diffusion of hexane into a dichloromethane

* Author to whom correspondence should be addressed.

Table 1. Some structural data for compounds having infinite chains of $Ru_2(O_2CR)_4^+$ connected by axial Cl^- ions

	Ru—Ru (Å)	Ru—Cl (Å)	Ru—Cl—Ru (°)	Ref.
$Ru_2(O_2CC_3H_7)_4Cl$	2.281(4)	2.587(5)	125.4[a]	1
$Ru_2(O_2CC_6H_4$-*p*-$OCH_3)_4Cl$[b]	2.284(1)	2.554(2)	117.8(1)	2
	2.290(1)	2.583(2)	124.2(1)	
	2.283(1)	2.563(2)		
		2.568(3)		
$Ru_2(O_2CCH_3)_4Cl \cdot 2H_2O$	2.267(1)	2.566(1)	180	3
$Ru_2(O_2CC_2H_5)_4Cl$	2.292(7)	2.566(4)	180	3
$Ru_2(O_2CCH_3)_4Cl$	2.287(2)	2.577(1)	180	4
$Ru_2(O_2CCMePh_2)_4Cl$	2.2893(9)	2.5016(6)	180	This work

[a] This result was not stated in ref. 1. It was calculated from the reported atomic positional parameters.

[b] Three crystallographically independent $Ru_2(O_2CR)_4^+$ and two independent μ-Cl^- ions.

solution of $Ru_2(O_2CCMePh_2)_4Cl$. IR (Nujol mull, cm^{-1}): 1595 w, 1075 w, 1027 w, 845 w, 790 w, 762 w, 752 w, 733 m, 721 w, 700 m, 669 m, 580 w, 560 w, 540 w, 485 w. UV–vis (CH_2Cl_2 solution; λ, nm (ε, $M^{-1}\,cm^{-1}$): 485 (1637), 324 (5216).

Structure determination

A dark-brown needle crystal of $Ru_2(O_2CCMePh_2)_4Cl$ was wedged in a Lindemann capillary with a mixture of its mother liquor and mineral oil. The diffraction data were collected on a Nicolet P3/F diffractometer equipped with graphite-monochromated Mo-K_α ($\lambda = 0.71073$ Å). The determination of the crystal system, data collection procedures, structure solution and refinements were all carried out by procedures that have been described before.[7,8]

The unit cell parameters and orientation matrix were refined by a least-squares fit to the positions of 25 reflections in the range $21 < 2\theta < 30°$. The data were collected using the 2θ–ω scan technique in the range $4 < 2\theta < 50°$. The overall decay of intensity during the period of data collection was 0.3%. A correction was applied.[9] The space group was determined as $P\bar{4}2_1c$ (No. 114) based on the systematic absences. The crystallographic data are summarized in Table 2 and the final positional parameters are available as supplementary material.*

The Patterson map revealed the position of a ruthenium atom; the positions of the other non-hydrogen atoms were obtained by an alternating sequence of difference Fourier maps and least-squares refinements. All atoms were refined with anisotropic thermal parameters.

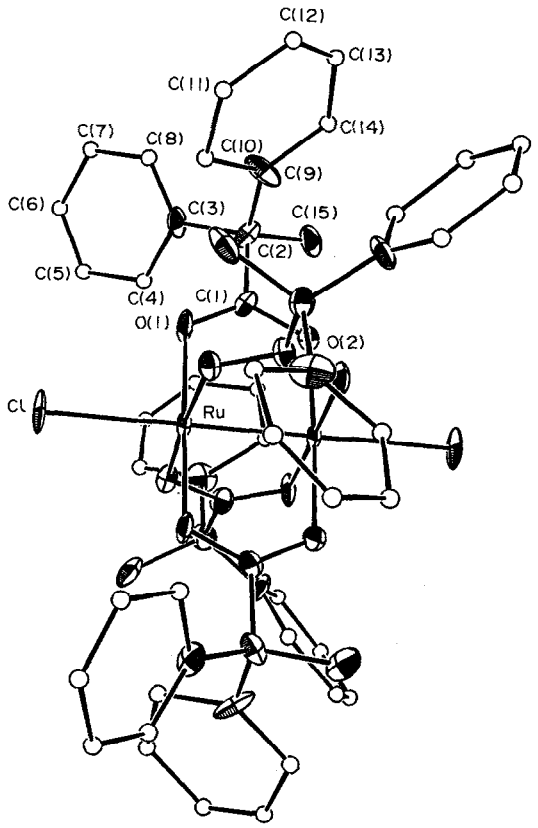

Fig. 1. ORTEP drawing of $Ru_2(O_2CCMePh_2)_4Cl$ with 30% probability ellipsoids shown for all of the atoms, except the phenyl carbon atoms.

* Supplementary material available: Full tables of positional parameters, anisotropic thermal parameters, bond length and angle data, variable-temperature magnetic susceptibility data and a listing of observed and calculated structure factors (total of 15 pages).

Table 2. Crystal data for $Ru_2(O_2CCMePh_2)_4Cl$

Formula	$Ru_2ClO_8C_{60}H_{52}$
Formula weight	1138.67
Space group	$P\bar{4}2_1c$ (No. 114)
a (Å)	20.658(3)
b (Å)	20.658(3)
c (Å)	7.293(2)
α (°)	90.00(0)
β (°)	90.00(0)
γ (°)	90.00(0)
V (Å^3)	3112(1)
Z	2
d_{calc} (g cm^{-3})	1.215
Crystal size (mm)	0.35 × 0.35 × 0.85
μ(Mo-K_α) (cm^{-1})	5.632
Data collection instrument	Nicolet P3/F
Radiation monochromated in incident beam (Mo-K_α, Å)	0.71073
Orientation reflections Number, range (2θ)	25; $21.0 < 2\theta < 29.4$
Temperature (°C)	20
Scan method	2θ–ω
Data collection range, 2θ (°)	$4 < 2\theta < 50$
No. of unique data; total with $F^2_o > 3\sigma(F^2_o)$	1584, 1051
No. of parameters refined	161
Transmission factors: max., min.	1.00, 0.98
R^a	0.041
R^b_w	0.072
Quality-of-fit indicator^c	1.732
Largest shift/e.s.d. final cycle	0.003
Largest peak (e Å^{-3})	0.447

$^a R = \Sigma\|F_o|-|F_c\|/\Sigma|F_o|$.
$^b Rw = [\Sigma w(|F_o|-|F_c|)^2/\Sigma w|F_o|^2]$; $w = 1/\sigma^2(|F_o|)$.
^{c} Quality-of-fit $= [\Sigma w(|F_o|-|F_c|)^2/(N_{obs}-N_{para})]^{1/2}$.

Measurements

The IR spectrum was recorded from 4000 to 400 cm^{-1} on a Perkin–Elmer 783 spectrophotometer. The electronic spectrum was recorded as a solution on a Cary 17D UV–vis spectrophotometer. Magnetic susceptibility measurements were carried out on polycrystalline samples in the 2.0–300 K temperature range with a SQUID (superconducting quantum interference device) at Northwestern University. The sample was quenched in a field of 5 kG.

RESULTS AND DISCUSSION

Structure

The tetragonal unit cell contains two formula units. The ruthenium atom and the chlorine atom reside on a $\bar{4}$ axis at 0,0,z and 0,0, 1/2, respectively. The chlorine atoms connect the Ru_2 units into linear chains. Figure 1 shows one $Ru_2(O_2CCMePh_2)_4Cl$ unit and Fig. 2 shows the stereoview of the linear chains through one unit cell and its neighbours. The chains are exactly linear (Ru—Cl—Ru′ = 180°). The Ru—Ru′ distance is 2.2893(9) Å and the Ru—Cl distance is 2.5016(6) Å (Table 3).

Magnetic properties

The magnetic susceptibilities of $Ru_2(O_2CCMePh_2)_4Cl$ were measured from *ca* 2 to 300 K. The molar magnetic susceptibilities χ_M were calculated from the measured magnetic susceptibilities (χ_g) and molar diamagnetic corrections (χ_D) were calculated from a table of Pascal constants.[10] The measured susceptibilities and the simulated curve of $Ru_2(O_2CCMePh_2)_4Cl$ are plotted in Fig. 3. The measured susceptibility plot shows a typical

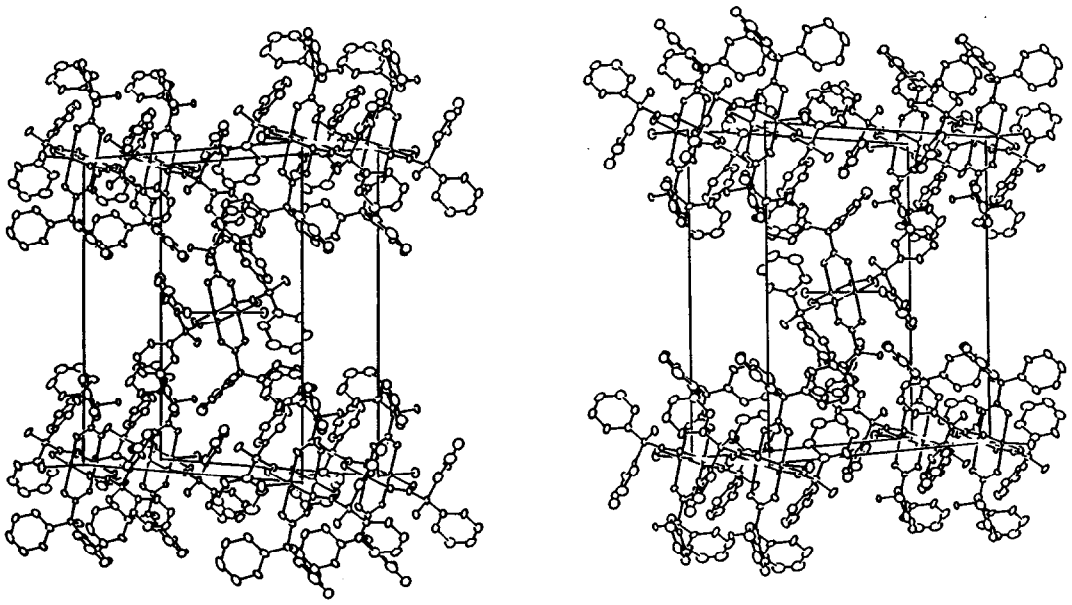

Fig. 2. Stereo ORTEP drawing of the unit cell of $Ru_2(O_2CCMePh_2)_4Cl$, showing the alignment of the linear chains.

paramagnetic impurity tail at low temperature and a turning point at *ca* 70 K. This turning point indicates that there is an antiferromagnetic exchange coupling between the $Ru_2(O_2CCMePh_2)_4^+$ units, which we believe must be through the bridging chloride ligands. These data were fitted to the one-dimensional Ising model developed by Suzuki and co-workers[11] for an infinite linear chain of antiferromagnetic exchange-coupled $S = 3/2$ units. The equation is quite long and will not be written here. The measured susceptibility of $Ru_2(O_2CCMePh_2)_4Cl$ shows the presence of a paramagnetic impurity in the low temperature region. The measured susceptibility for $Ru_2(O_2CC_3H_7)_4Cl$[5] was used to make a correction for the impurity. The measured molar susceptibility of $Ru_2(O_2CCMePh_2)_4Cl$ can be expressed as

$$\chi_M = (1-\alpha)\chi_o + \alpha\chi_{imp} + \text{tip},$$

where χ_o comes from the equation for the one-dimensional Ising model. As mentioned above χ_{imp} is the measured susceptibility for $Ru_2(O_2CC_3H_7)_4Cl$

Table 3. Selected bond distances (Å) and angles (°) for $Ru_2(O_2CCMePh_2)_4Cl$

Ru—Ru′	2.2893(9)	O(1)—C(1)	1.26(1)
Ru—Cl	2.5016(6)	O(2)—C(1)	1.27(1)
Ru—O(1)	2.029(6)	C(1)—C(2)	1.54(1)
Ru—O(2)	2.031(5)	C(2)—C(3)	1.54(1)
C(2)—C(9)	1.50(1)	C(2)—C(15)	1.55(1)

Ru′—Ru—Cl	180.0(0)	O(2)—Ru—O(2)	177.0(2)
Ru′—Ru—O(1)	89.6(1)	Ru—Cl—Ru′	180.0(0)
Ru′—Ru—O(2)	88.5(2)	Ru—O(1)—C(1)	119.2(5)
Cl—Ru—O(1)	90.4(1)	Ru—O(2)—C(1)	119.9(5)
Cl—Ru—O(2)	91.5(2)	O(1)—C(1)—O(2)	122.8(7)
O(1)—Ru—O(1)	179.2(2)	O(1)—C(1)—C(2)	120.4(9)
O(1)—Ru—O(2)	89.8(2)	O(2)—C(1)—C(2)	116.8(8)
O(1)—Ru′—O(2)	90.1(2)		

Numbers in parentheses are estimated standard deviations in the least significant digits.

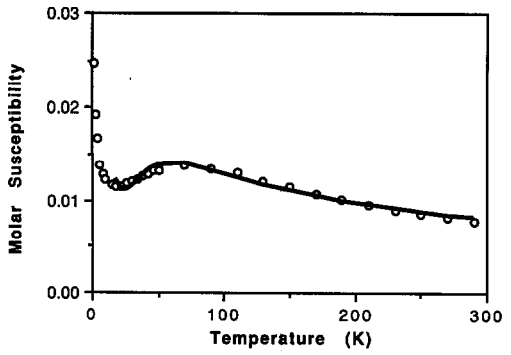

Fig. 3. Molar susceptibility per $Ru_2(O_2CCMePh_2)_4Cl$ molecule as a function of temperature. The solid line results from a least-squares fit to the theoretical equation for an infinite linear chain of antiferromagnetic exchange-coupled $S = 3/2$ units.

and α is the molar fraction of the impurity. The tip is the temperature independent paramagnetism. A g value fixed at 2.0 was used during fitting. The coupling constant J that gave the best fit is -10.9 cm^{-1}. This J is defined by expressing the coupling energy as $-2JS_1 \cdot S_2$.

Concluding remarks

The results of this study suggest that antiferromagnetic coupling between $Ru_2(O_2CR)_4^+$ units linked by Cl^- ions into infinite chains is possible, but only when the chains are linear or at least not bent at Cl^- to angles as small as 125°. It must be noted that there is one respect, other than the linearity at Cl^-, in which the present compound differs from the compounds having zigzag chains, namely, in the shorter Ru—Cl distances, 2.502 Å vs an average of 2.57 Å in the zigzag structures. It is uncertain whether this is a critical difference or not. Interestingly, the three previously known linear compounds also have Ru—Cl distances of *ca* 2.57 Å. In any event, the one-dimensional Ising model[11] for an infinite chain of coupled $S = 3/2$ units can account satisfactorily for the magnetic susceptibility of $Ru_2(O_2CCMePh_2)_4Cl$ as a function of temperature, with a significant coupling constant of -10.9 cm^{-1}. In only one other case[12] has evidence been presented for a similar situation, but the coupling was evidently much weaker and no attempt was made to fit the data to a theoretical expression.

Acknowledgements—We thank the National Science Foundation for support. We are also grateful to Professor T. J. Marks and Mr Douglas Schulz for the SQUID measurements.

REFERENCES

1. M. J. Bennett, K. G. Caulton and F. A. Cotton, *Inorg. Chem.* 1969, **8**, 1.
2. B. K. Das and A. R. Chakravarty, *Polyhedron* 1991, **10**, 491.
3. A. Bino, F. A. Cotton and T. R. Felthouse, *Inorg. Chem.* 1979, **18**, 2599.
4. D. S. Martin, R. A. Newman and L. M. Vlasnik, *Inorg. Chem.* 1980, **19**, 3404.
5. J. Telser and R. S. Drago, *Inorg. Chem.* 1984, **23**, 3114.
6. T. A. Stephenson and G. Wilkinson, *J. Inorg. Nucl. Chem.* 1966, **28**, 2285.
7. A. Bino, F. A. Cotton and P. E. Fanwick, *Inorg. Chem.* 1979, **18**, 3558.
8. F. A. Cotton, B. A. Frenz, G. Deganello and A. Shaver, *J. Organomet. Chem.* 1973, **50**, 227.
9. A. C. T. North, D. C. Phillips and F. S. Mathews, *Acta Cryst., Sect. A.: Cryst. Phys., Diffr., Theor. Gen. Cryst.* 1968, **24A**, 351.
10. L. N. Mulay, *Magnetic Susceptibility*. Interscience/John Wiley, New York (1963).
11. M. Suzuki, B. Tsujiyama and S. Katsura, *J. Math. Phys.* 1967, **8**, 124.
12. F. A. Cotton, Y. Kim and T. Ren, *Inorg. Chem.* 1992, **31**, 2723.

Polyhedron Vol. 12, No. 6, pp. 613–616, 1993
Printed in Great Britain

0277–5387/93 $6.00+.00
© 1993 Pergamon Press Ltd

SYNTHESIS, MAGNETIC PROPERTIES AND STRUCTURE OF THE $[Co_4(\mu_3\text{-}Cl)_2(\mu_2\text{-}Cl)_4Cl_2(THF)_6]$ COMPLEX*

PIOTR SOBOTA,† ZOFIA OLEJNIK, JÓZEF UTKO and TADEUSZ LIS

Institute of Chemistry, University of Wrocław, 14 F. Joliot-Curie, 50-383 Wrocław, Poland

(*Received* 1 *October* 1992; *accepted* 13 *November* 1992)

Abstract—The X-ray analysis showed that the title compound is isomorphous with the iron analogue reported previously. It exists as the centrosymmetric tetramer with two different types of cobalt(II) centres corresponding to octahedral $CoCl_4O_2$ and trigonal bipyramidal $CoCl_4O$ chromophores. The four cobalt atoms, bridged by two μ_3- and four μ_2-chlorine atoms, constitute a rhombus of dimensions: 3.686(3), 3.646(3) (edges) and 3.630(3), 6.37(1) Å (diagonals). The magnetic susceptibility measured over the range 4.2–293 K suggests overall ferromagnetic interactions in the tetrameric molecule. Attempts have been made to simulate the magnetism of the tetramer with the isotropic Heisenberg model. The magnetic properties of the title compound are compared to those of its iron analogue.

The formation of the first-row transition metal chloride complexes with THF such as *cis*- and *trans*-$[TiCl_4(THF)_2]$,[1] [*mer*-$MCl_3(THF)_3$], M = Sc, Ti, V, Cr,[2–4] and $[FeCl_3(THF)]$,[5] $[FeCl_3(THF)_2]$[6] is well documented. However, at the lower oxidation state only the remarkable tetrameric compound $[Fe_4(\mu_3\text{-}Cl)_2(\mu\text{-}Cl)_4Cl_2(THF)_6]$ is known.[7,8] The composition of the cobalt $CoCl_2 \cdot 1.5(THF)$ adduct[9] is similar to that of the iron tetramer $[FeCl_2 \cdot 1.5(THF)]_4$, thus the iron and the cobalt complexes could be isostructural.

In this paper the crystal structure and magnetic properties of the title compound are described.

EXPERIMENTAL

All manipulations were carried out under an inert atmosphere using a standard Schlenk system and a vacuum line. Cobalt dichloride was the commercial material. Solvents were dried and purified by standard techniques. Magnetic susceptibilities were measured by the Faraday method within the temperature range 4.2–293 K. Corrections for diamagnetism were made with Pascal's constants.[10] The following spectrophotometers were used: Specord Perkin–Elmer 180 for IR and Beckman UV 5240 for UV–vis spectroscopy.

Syntheses

A suspension of $CoCl_2$ (1.6 g, 1.25 mmol) in THF (50 cm^3) was refluxed for 10 h and the dark blue solution was filtered off and left in a refrigerator for crystallization. After 1 week the blue needles were filtered off, washed with n-hexane (3×5 cm^3) and dried *in vacuo*. Yield: 0.8 g (the yield is low because only part of $CoCl_2$ undergoes dissolution in THF). Found: Cl, 29.6; Co, 24.6. Calc. for $C_{24}H_{48}Cl_8Co_4O_6$: Cl, 29.8; Co, 24.8%. IR (Nujol): ν(Co—Cl) 310vs, 258s, 204vs cm^{-1}; other 676m, 720m, 876vs, br, 908s, 1032vs, 1172m, 1246m, 1296m cm^{-1}. UV–vis in THF: 7692, 15,530, 16,260 and 17,240 cm^{-1}. Reflectance spectrum: 14,300, 15,400, 17,200sh, 19,300sh and 23,400 cm^{-1}.

X-ray crystallography

A sample of dimensions $0.8 \times 0.8 \times 0.6$ mm was cut from a large crystal and sealed in a capillary. A Syntex $P2_1$ diffractometer (Mo-K_α radiation, graphite monochromator, $\theta/2\theta$ scanning, $2\theta_{max} < 42°$) was used. 2023 reflections were measured, from which 1852 with $I > 3\sigma(I)$ were used for calculations. Crystals were triclinic: $a = 9.931(7)$, $b = 10.573(9)$, $c = 10.919(9)$ Å, $\alpha = 62.63(7)$, $\beta = 67.88(7)$, $\gamma = 81.64(7)°$, $Z = 1$, space group $P\bar{1}$, $V = 942.7(16)$ Å^3, $d_{calc} = 1.677(4)$ g cm^{-3}, $d_{meas} = 1.69$ g cm^{-3}, $\mu = 23.3$ cm^{-1}. The structure was solved by direct methods and refined by

* Bis-μ_3-Cl-tetrakis-μ_2-Cl-dichlorohexakis(tetrahydrofuran-O)tetracobalt(II).

† Author to whom correspondence should be addressed.

full-matrix least-squares using the SHELX76 program.[11] The hydrogen atoms were placed in geometrically calculated positions. Absorption corrections following the DIFABS procedure[12] were applied; minimum and maximum absorption corrections were 0.953 and 1.091. Neutral-atom scattering factors were taken from ref. 13 and the real and imaginary components of anomalous dispersion were included for all non-hydrogen atoms. The final R was 0.0348 and $R_w = 0.0464$. For the last cycle of the refinement the maximal Δ/σ ratio was 0.04. The maximal peaks on the final difference map were 0.32 e $Å^{-3}$.

RESULTS AND DISCUSSION

Properties and structure of $[Co_4(\mu_3\text{-}Cl)_2(\mu_2\text{-}Cl)_4Cl_2(THF)_6]$

The direct reaction of anhydrous $CoCl_2$ with THF yields the blue $CoCl_2 \cdot 1.5(THF)$ compound, which can be stored under dinitrogen.

The IR spectrum shows bands at 204vs, 258s and 310vs cm^{-1}, assigned to Co—Cl vibrations. The electronic spectrum of the compound in THF solution shows bands at 7763 cm^{-1} [$^4A_2 \rightarrow {}^4T_1$(F)] and three transitions at 14,700, 15,800 and 17,200 cm^{-1} being the result of splitting of $^4T_{1g} \rightarrow {}^4T_1$(P), as in those observed for tetrahedral high-spin d^7 compounds, cf. $[Bu_4N][CoCl_4]$.[14] The complex as a solid shows bands at 14,300, 15,400, 17,200sh, 19,300sh and 23,400 cm^{-1} in its diffuse reflectance spectrum. The electronic spectra suggest that the structure of the $CoCl_2$ THF adduct possesses different solution and solid-state structures.

Crystals of the title compound are isomorphous with those of $[Fe_4(\mu_3\text{-}Cl)_2(\mu_2\text{-}Cl)_4Cl_2(THF)_6]$. The reduced cell parameters of the iron compound for the data reported in other papers[7,8] are similar to those of the cobalt compound. The structure presented here consists of centrosymmetric tetranuclear molecules. Its overall view and the numbering scheme are shown in Fig. 1. Selected bond lengths and angles are listed in Table 1. In the tetramer a nearly regular Co_4 rhombus is bridged by two μ_3-chlorine atoms Cl(1) and Cl(1′), one above and one below the Co_4 plane and in addition μ_2-chlorine atoms bridge Co—Co edges. The $[Co_4(\mu_3\text{-}Cl)_2(\mu_2\text{-}Cl)_4Cl_2(THF)_6]$ molecule contains two types of cobalt centres: the six-coordinate Co(1) atoms and the five-coordinate Co(2) atoms. The coordination sphere around Co(1) is a slightly distorted octahedron formed by two μ_3-Cl atoms, two μ_2-Cl atoms and two oxygen atoms from THF ligands (in *cis* positions). The Co(1)—Cl bond distances [2.435(2)–2.465(2) Å] are of the order of

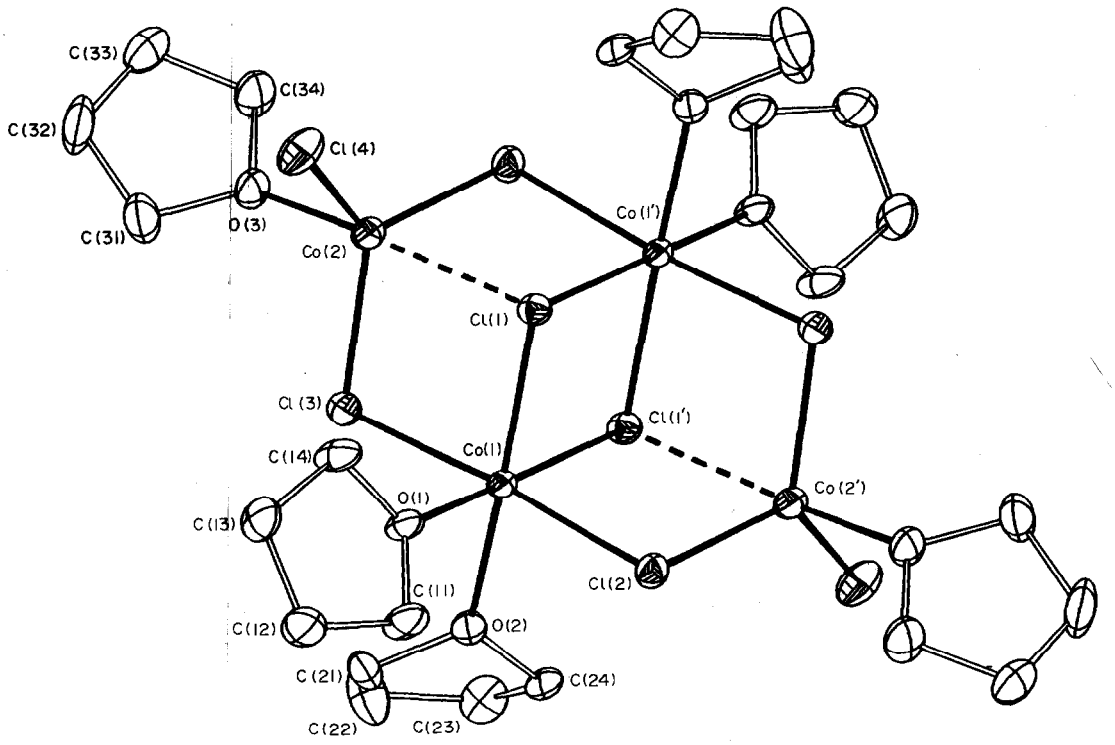

Fig. 1. Molecular structure of $[Co_4(\mu_3\text{-}Cl)_2(\mu_2\text{-}Cl)_4Cl_2(THF)_6]$. Primed and unprimed atoms are related by the inversion centre.

Table 1. Selected interatomic distances (Å) and bond angles (°) for $[Co_4(\mu_3\text{-}Cl)_2(\mu_2\text{-}Cl)_4Cl_2(THF)_6]$[a]

Co(1)—Cl(1)	2.450(2)	Co(2)—Cl(1)	2.844(3)
Co(1)—Cl(1′)	2.435(2)	Co(1)—O(1)	2.072(5)
Co(1)—Cl(2)	2.454(2)	Co(1)—O(2)	2.102(4)
Co(1)—Cl(3)	2.465(2)	Co(2)—O(3)	2.076(5)
Co(2)—Cl(3)	2.285(2)	Co(1)···Co(1′)	3.630(2)
Co(2)—Cl(2′)	2.285(2)	Co(1)···Co(2)	3.686(2)
Co(2)—Cl(4)	2.216(2)	Co(1)···Co(2′)	3.646(2)

Cl(1)—Co(1)—Cl(1′)	84.0(1)	Cl(1)—Co(2)—Cl(2′)	82.4(1)
Cl(1)—Co(1)—Cl(2)	96.6(1)	Cl(1)—Co(2)—Cl(4)	88.6(1)
Cl(1)—Co(1)—O(2)	176.1(2)	Cl(1)—Co(2)—O(3)	174.0(2)
Cl(1)—Co(1)—O(1)	92.4(2)	Cl(2′)—Co(2)—O(3)	95.6(2)
Cl(1)—Co(1)—Cl(3)	87.2(1)	Cl(2′)—Co(2)—Cl(4)	122.1(1)
Cl(1′)—Co(1)—O(1)	175.4(2)	Cl(3)—Co(2)—Cl(2′)	113.0(1)
Cl(2)—Co(1)—Cl(3)	175.7(1)	Cl(3)—Co(2)—Cl(4)	122.1(1)
Cl(2)—Co(1)—O(1)	89.3(2)	Cl(3)—Co(2)—O(3)	93.7(2)
Cl(2)—Co(1)—O(2)	86.8(2)	Cl(4)—Co(2)—O(3)	97.3(2)
Cl(3)—Co(1)—Cl(1′)	94.2(1)	Co(1)—Cl(1)—Co(1′)	96.0(1)
Cl(3)—Co(1)—O(1)	88.5(2)	Co(1)—Cl(2)—Co(2′)	100.5(1)
Cl(3)—Co(1)—O(2)	89.5(2)	Co(1)—Cl(3)—Co(2)	101.7(1)
O(1)—Co(1)—O(2)	89.6(2)	Co(1)—Cl(1)—Co(2)	87.9(1)

[a] Primed atoms are related to unprimed atoms by $1-x$, $1-y$, $1-z$.

other Co—Cl distances that have been observed in the octahedral structures of the cobalt(II) compounds.[15,16] However, the average Co(1)—(μ_2-Cl) distance of 2.46(1) Å is slightly longer than the average Co(1)—(μ_3-Cl) distance of 2.44(2) Å; in contrast to the order of corresponding Fe—Cl distances, Fe—(μ_3-Cl) is larger than Fe—(μ_2-Cl), found in the iron analogue. The Co(2) atoms have trigonal bipyramidal geometry with Cl(1)—Co(2)—O(3) [174.0(2)°] representing the nearly linear group. The equatorial plane of each bipyramid is formed by three chlorine atoms (one terminal and two μ_2-Cl type). The bridging Co(2)—(μ_2-Cl) bonds of 2.285(2) Å are slightly elongated compared to the terminal Co(2)—Cl bond of 2.216(2) Å, but all equatorial Co(2)—Cl distances are within the range observed for the tetrahedrally coordinated cobalt(II) compounds.[15] Since the Co(2) distance to the μ_3-Cl(1) atom at one apex of the bipyramid is long [2.844(3) Å] and the Co(2) atom is displaced from the equatorial plane by 0.2 Å towards the O(3) atom, the coordination of this cobalt atom can also be described as a distorted tetrahedron. It is noteworthy that in the iron tetramer the corresponding Fe—(μ_3-Cl) bond of 2.736(3) Å is shorter and the iron atom almost lies in its equatorial plane.

The THF molecules containing O(1) and O(2) atoms have the envelope conformations with oxygen atoms at the apex and the THF molecule with the O(3) atom has the twist conformation.

Magnetic properties

The temperature dependence of the magnetic moment per cobalt(II) ion, observed for the title compound, is shown in Fig. 2. The high temperature limit of μ_{eff} (4.91 B.M.) is the typical value of the magnetically isolated high-spin cobalt(II) complexes.[17] The increase of the magnetic moment on lowering the temperature (up to 7.1 B.M. at 4.2 K) suggests the overall ferromagnetic interactions in the tetrameric molecule.

The simplest isotropic Heisenberg approximation was used to interpret these magnetic properties, although in the case of orbitally degenerated cobalt(II) ions it could give only the rough estimate

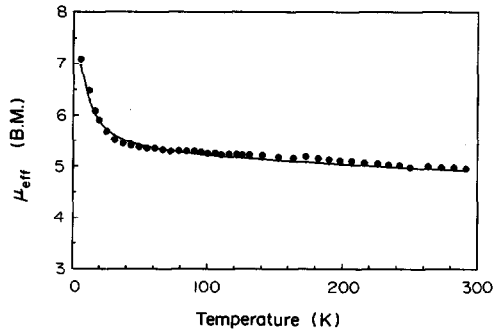

Fig. 2. Effective magnetic moment per cobalt(II) ion vs temperature curve for $[Co_4(\mu_3\text{-}Cl)_2(\mu_2\text{-}Cl)_4Cl_2(THF)_6]$. The solid line represents a fit to the theoretical expression (see text).

of the exchange interactions. The magnetic analysis was carried out with the susceptibility equation based on the Hamiltonian (1), where $S_i = 3/2$ and the numbering scheme for S_iS_j terms is that used in Fig. 1. The J_a parameter refers to the coupling of each of the six-coordinated cobalt ions with each of its five-coordinated neighbours, while the J_b parameter describes the interaction of the two six-coordinate cobalt ions.

$$H = -J_a(S_1S_2 + S_2S'_1 + S'_1S'_2 + S'_2S_1) - J_b(S_1S'_1) \quad (1)$$

A relative error minimization procedure was carried out for various fixed values of the g factor. The best-fit obtained for $g = 2.3$, $J_a = 1.8 \pm 0.5$ cm^{-1} and $J_b = 91 \pm 22$ cm^{-1} is shown by the solid line in Fig. 2. As expected the fit is not quantitative, but the agreement is remarkably good ($r = 2\%$). The low accuracy of the J_b parameter indicates that the interaction represented by this parameter has little effect on the magnetic properties, which are principally determined by four interactions represented by the J_a parameter. The insensitivity of fitting the data to the value of J_b has already been observed for other tetramers,[18] the magnetism of which has been interpreted on the basis of the same Hamiltonian as used here.

The magnetic parameters for the $[Fe_4(\mu_3\text{-}Cl)_2(\mu_2\text{-}Cl)_4Cl_2(THF)_6]$ compound have been reported.[7] The J_b value for our compound corresponds well to the ferromagnetic constant (*ca* 50 cm^{-1}) stated for the interaction between the two six-coordinated iron(II) ions in the iron tetramer. It is noteworthy that the geometries of the central dimers in both tetramers are very similar, e.g. the chlorine bridging angles are 96.0(1)° and 96.6(1)° for the cobalt and iron compound, respectively. Instead, there is the difference in the interactions (J_a) between the six- and five-coordinated metal ions, which are negative for the iron tetramer (*ca* -3 cm^{-1}) and positive for cobalt. This difference cannot be rationalized in terms of angular dependence of superexchange,[19] because the Co(1)—(μ_2-Cl)—Co(2) angles of 101.1° on averaging are larger than corresponding Fe—Cl—Fe angles of 98.7°. The theory predicts a change from ferro- to antiferromagnetic interactions upon increasing the bridging metal–ligand–metal angle.

Acknowledgement—This work was supported financially by KBN.

REFERENCES

1. T. Lis, J. Ejfler, J. Utko and P. Sobota, *Pol. J. Chem.* 1992, **66**, 93.
2. J. L. Atwood and K. D. Smith, *J. Chem. Soc., Chem. Commun.* 1983, 1377.
3. M. Handloviv, D. Miklov and M. Zikmund, *Acta Cryst., Sect. B* 1981, **37**, 811.
4. F. A. Cotton, S. A. Duraj, G. L. Powell and W. J. Roth, *Inorg. Chim. Acta* 1986, **113**, 81.
5. F. A. Cotton, R. L. Luck and K.-A. Son, *Acta Cryst., Sect. C* 1990, **46**, 1424.
6. L. V. Nakina, N. R. Strel'sova, V. K. Bel'ski, P. A. Storochenko, B. M. Bulychev and A. B. Tarasov, *Zh. Obshch. Khim.* 1987, **57**, 1600.
7. V. K. Bel'ski, V. M. Ishchenko, B. M. Bulychev, A. N. Protskii, G. L. Soloveichik, O. G. Ellert, Z. M. Seifulina, Yu. V. Rakitin and V. M. Novotortsev, *Inorg. Chim. Acta* 1985, **96**, 123.
8. F. A. Cotton, R. L. Luck and K.-A. Son, *Inorg. Chim. Acta* 1991, **179**, 11.
9. R. J. Kern, *J. Inorg. Nucl. Chem.* 1962, **24**, 1105; G. W. Flowles, D. A. Rice and R. A. Walton, *J. Inorg. Nucl. Chem.* 1969, **31**, 3119.
10. A. Earnshaw, *Introduction to Magnetochemistry*, p. 5. Academic Press, London (1968).
11. G. M. Sheldrick, SHELX76. University of Cambridge, U.K. (1976).
12. N. Walker and D. Stuart, *Acta Cryst., Sect. A* 1983, **39**, 158.
13. *International Tables for X-ray Crystallography*, Vol. IV. Kynoch Press, Birmingham (1974).
14. F. A. Cotton and D. M. L. Goodgame, *J. Am. Chem. Soc.* 1961, **83**, 4690.
15. I. Bkouche-Waksman and P. L'Haridon, *Acta Cryst., Sect. B* 1977, **33**, 11 and refs therein.
16. A. J. Kinneging, W. J. Vermin and S. Gorter, *Acta Cryst., Sect. B* 1982, **38**, 1824.
17. L. Banci, A. Bencini, C. Benelli, D. Gatteschi and C. Zanchini, *Struct. Bonding (Berlin)* 1982, **52**, 37.
18. J. K. McCusker, J. B. Vincent, E. A. Schmitt, M. L. Mino, K. Shin, D. K. Coggin, P. M. Hagen, J. C. Huffman, G. Christou and D. N. Hendrickson, *J. Am. Chem. Soc.* 1991, **113**, 3012.
19. K. Motida, *J. Phys. Soc. Japan* 1978, **44**, 1498.

Polyhedron Vol. 12, No. 6, pp. 617–619, 1993
Printed in Great Britain

0277-5387/93 $6.00+.00
© 1993 Pergamon Press Ltd

SPECTROSCOPIC STUDIES ON SOME BIVALENT METALLIC COMPLEXES FORMED WITH THREE DIFFERENT BIDENTATE POLYAMINES

S. ZAMEERUDDIN and B. A. SASTRY*

Molecular and Solid State Physics Laboratory, Physics Department, Osmania University, Hyderabad 500007, India

and

G. PONTICELLI and M. MASSACESI

Dipartimento di Chimica E Technologie Inorganiche E Metallorganiche, Universita Degli Studi Di Cagliari, via Ospedale 72, 09124 Cagliari, Italy

(*Received* 30 *September* 1992; *accepted* 11 *November* 1992)

Abstract—Tris(bis-chelate)metallic complexes formed with non-equivalent ligands having the general formula $[ML_1L_2L_3](B\emptyset_4)_2$ [where M = Cu, Zn, Cd; L_1 = 1,2-diaminoethane (en), tetramethyl en ($enMe_4$); L_2 = 1,2-diaminopropane (1,2-Pn); L_3 = 1,3-diaminopropane (1,3-Pn); $B\emptyset_4$ = tetraphenylborate] have been synthesized and characterized using IR, electronic and EPR techniques in the solid state in order to understand the nature of the coordination geometries of these complexes using copper(II) as a paramagnetic probe. The small variations observed in magnetic and metal–ligand bond parameters of these complexes are interpreted in terms of the changes in their structure and coordination geometries, depending on the type of metal ion and the value of the sample temperature.

Even though tris(bis-chelate)copper(II) complexes with equivalent ligands were studied in diluted and undiluted forms to study genuine Jahn–Teller distortion,[1–3] none of the workers so far have studied the nature of the coordination geometries of complexes with non-equivalent bidentate ligands. In the case of non-equivalent ligands one inevitably expects small differences in bond lengths and angles, hence the existence of three equivalent potential wells of the adiabatic potential energy surface does not arise, leading to the elimination of dynamic Jahn–Teller distortion. Still, one can expect either only one or two lowest potential wells to give rise to pseudo-Jahn–Teller distortions. Due to this we have taken up the synthesis and spectroscopic studies of a series of nine metallic complexes formed with non-equivalent ligands having the general formula $[ML_1L_2L_3](B\emptyset_4)_2$, where M, L_1, L_2, L_3 and $B\emptyset_4$ are copper(II), zinc(II) and cadmium(II), 1,2-diaminoethane (en), tetramethyl en ($enMe_4$) and diethyl en ($enEt_2$), 1,2-diaminopropane (1,2-Pn) and 1,3-diaminopropane (1,3-Pn) and tetraphenylborate, respectively, to study the difference between the coordination geometries of equivalent and non-equivalent nitrogens in the coordination sphere of CuN_6 complexes and the fluxional nature using IR, electronic and EPR spectral techniques.

EXPERIMENTAL

En, $enMe_4$, $enEt_2$, 1,2-Pn, 1,3-Pn, $NaB\emptyset_4$ and metal chlorides of copper, zinc and cadmium were commercially available. The present complexes were obtained by adding L_1 (11 mmol), L_2 (11 mmol) and L_3 (11 mmol) (dissolved in water) to a hot aqueous solution of the corresponding metal chloride (10 mmol). A hot aqueous solution of $NaB\emptyset_4$ (20 mmol) was then added dropwise to the above mixture. The complexes were filtered and washed in water and dried for several days over P_4O_{10}. Copper(II) doped zinc and cadmium complexes were obtained by the usual procedure of

* Author to whom correspondence should be addressed.

evaporation of the aqueous solution containing copper(II) and zinc(II) or cadmium(II) complexes (Cu : Zn/Cd = 1 : 100). The IR, electronic and EPR measurements were collected as previously described.[4]

RESULTS AND DISCUSSION

Table 1 gives the analytical data of these complexes, along with their vibrational modes in the far-IR region and the reflectance electronic spectral values. In undiluted copper(II) complexes copper(II) hyperfine lines are obtained, perhaps due to the presence of the bulky anion. The values of g, A, $\Delta A_{\parallel}$% and the metal–ligand σ-bond parameter, α_{σ}^{2}, obtained from the expression[5] given below, are given in Table 2, along with the corresponding values in complexes having equivalent ligands.

$$\alpha_{\sigma}^{2} = \frac{|A_{\parallel}|}{P} + (g_{\parallel} - 2.0023) + \frac{3}{7}(g_{\perp} - 2.0023) + 0.04 \quad (1)$$

A negative shift of *ca* 35 cm^{-1} from free ligand values in the IR bands of $\nu_s(NH_2)$ (3260–3330 cm^{-1}), $\nu_{as}(NH_2)$ (3230–3270 cm^{-1}), ν(NH) (3120–3160 cm^{-1}) and $\delta(NH_2)$ (1570–1612 cm^{-1}),[8] the absence of any band in the frequency range 2820–2760 cm^{-1} of alkylated complexes[9] and the bands in the range 460–480 cm^{-1}, which correspond to ν(M—N), ensure that all the six nitrogens in these complexes are bonded to the metal ions. The ligand reflectance spectra of copper(II) complexes are asymmetric with a prominent peak in the range 17,800–18,500 cm^{-1}, which indicates tetragonally distorted octahedral coordination geometry.[10] The asymmetric nature of these spectra is also indicative of a second peak at lower energies (7–9000 cm^{-1}), similar to that of other $[Cu(chelate)_3]^{2-}$ cations.[3,6,11] The correct value of this low energy peak can only be obtained when a Gaussian analysis of the reflectance spectra is made.[12]

From Table 2, it is evident that the values of g, A and α_{σ}^{2} for equivalent and non-equivalent ligands are different, indicating differences both in the structure and the metal–ligand σ-bond strengths of these complexes. No sudden change in the EPR spectra was found at low temperatures in the present complexes, unlike the case of equivalent ligand complexes. The small differences noticed in $g_{\parallel}$ and $A_{\parallel}$ values of all the present complexes, except in $[Cu/Zn(enEt_2)(1,2\text{-Pn})(1,3\text{-Pn})](B\text{Ø}_4)_2$ where no change is observed in $g_{\parallel}$ and $A_{\parallel}$ values, with temperature can be attributed both to the temperature dependent structural changes and to the fluxional nature of the coordination geometries. The metal–ligand σ-bonds of the present complexes are found to have almost the same strength with moderate covalency.

Table 1. Analytical data, far-IR bands (cm^{-1}) and electronic reflectance spectral values (ΔE) of the mixed ligand complexes

Complex	Found (Calc.) (%) C	H	N	ν(M—N)	ΔE (cm^{-1})
$[Cu(en)(1,2\text{-Pn})(1,3\text{-Pn})](B\text{Ø}_4)_2$	75.2 (74.7)	7.5 (7.0)	9.2 (9.0)	460m, 468s	18,520
$[Zn(en)(1,2\text{-Pn})(1,3\text{-Pn})](B\text{Ø}_4)_2$	75.0 (74.3)	7.5 (7.5)	9.2 (9.3)	468s	—
$[Cd(en)(1,2\text{-Pn})(1,3\text{-Pn})](B\text{Ø}_4)_2$	72.0 (71.3)	7.9 (7.5)	8.3 (8.5)	468s	—
$[Cu(enMe_4)(1,2\text{-Pn})(1,3\text{-Pn})](B\text{Ø}_4)_2$	74.6 (74.1)	7.9 (7.7)	8.8 (8.2)	470mbr	17,860
$[Zn(enMe_4)(1,2\text{-Pn})(1,3\text{-Pn})](B\text{Ø}_4)_2$	74.4 (74.1)	7.7 (8.1)	8.7 (8.7)	477m	—
$[Cd(enMe_4)(1,2\text{-Pn})(1,3\text{-Pn})](B\text{Ø}_4)_2$	71.0 (70.2)	7.5 (7.6)	8.3 (8.0)	470s	—
$[Cu(enEt_2)(1,2\text{-Pn})(1,3\text{-Pn})](B\text{Ø}_4)_2$	74.6 (74.1)	7.2 (7.6)	8.8 (8.4)	470sbr	17,860
$[Zn(enEt_2)(1,2\text{-Pn})(1,3\text{-Pn})](B\text{Ø}_4)_2$	74.4 (74.1)	7.9 (8.1)	8.7 (8.7)	475mbr	—
$[Cd(enEt_2)(1,2\text{-Pn})(1,3\text{-Pn})](B\text{Ø}_4)_2$	71.0 (70.7)	7.5 (7.4)	8.3 (8.0)	464s 480sh	—

Table 2. g, A, $\Delta A_{\parallel}\%$ and α_{σ}^{2} values of copper(II) in different metallic complexes of mixed ligands

Complex	Temperature (K)	$g_{\parallel}$	$g_{\perp}$	$A_{\parallel}$ ($\times 10^{4}$ cm^{-1})	$\Delta A_{\parallel}\%$	α_{σ}^{2}
[Cu(en)(1,2-Pn)(1,3-Pn)](BØ$_4$)$_2$	300	2.192	2.063	193.6	0.80	0.80
	77	2.209	2.068	195.2	0.80	0.82
[Cu/Zn(en)(1,2-Pn)(1,3-Pn)](BØ$_4$)$_2$	300	2.221	2.058	183.3	2.90	0.80
	77	2.223	2.059	188.6	2.90	0.81
[Cu/Cd(en)(1,2-Pn)(1,3-Pn)](BØ$_4$)$_2$	300	2.216	2.059	182.7	4.50	0.79
	77	2.218	2.055	190.8	4.50	0.81
[Cu(enMe$_4$)(1,2-Pn)(1,3-Pn)](BØ$_4$)$_2$	300	2.196	2.066	194.0	2.70	0.80
	77	2.199	2.075	199.4	2.70	0.83
[Cu/Zn(enMe$_4$)(1,2-Pn)(1,3-Pn)](BØ$_4$)$_2$	300	2.215	2.055	185.4	3.00	0.80
	77	2.221	2.057	191.1	3.00	0.82
[Cu/Cd(enMe$_4$)(1,2-Pn)(1,3-Pn)](BØ$_4$)$_2$	300	2.216	2.056	182.9	4.50	0.79
	77	2.219	2.059	190.9	4.50	0.81
[Cu(enEt$_2$)(1,2-Pn)(1,3-Pn)](BØ$_4$)$_2$	300	2.193	2.069	193.8	0.30	0.80
	77	2.202	2.081	194.5	0.30	0.82
[Cu/Zn(enEt$_2$)(1,2-Pn)(1,3-Pn)](BØ$_4$)$_2$	300	2.214	2.058	190.5	0.00	0.81
	77	2.217	2.057	190.6	0.00	0.81
[Cu/Cd(enEt$_2$)(1,2-Pn)(1,3-Pn)](BØ$_4$)$_2$	300	2.218	2.056	180.5	5.60	0.78
	77	2.217	2.068	190.7	5.60	0.82
[3][Cu/Zn(en)$_3$]NO$_3$	(below 77)	2.248	2.082	168.0	—	0.78
[6]Cu(bipy)$_3$ClO$_4$	300	2.249	2.080(g_x) 2.052(g_y)	—	—	—
[6]Cu(phen)$_3$ClO$_4$	300	2.241	2.090(g_x) 2.075(g_y)	150.0	—	0.74
[7][Cu/Zn(Phen)$_3$](NO$_3$)$_2$·2H$_2$O	77	2.273	2.064	160.0	—	0.78

REFERENCES

1. B. J. Hathaway, *Coord. Chem. Rev.* 1981, **35**, 211.
2. B. J. Hathaway, *Comprehensive Coordination Chemistry: The Synthesis, Reactions, Properties and Applications of Coordination Compounds*, Vol. 5, Sec. 53. Pergamon Press, Oxford (1988).
3. I. Bertini, D. Gatteschi and A. Scozzafava, *Inorg. Chem.* 1977, **16**, 1973 and refs therein.
4. B. A. Sastry, K. S. Chary, R. Subramanian, G. Ponticelli and G. Puggioni, *Spectrochim. Acta* 1992, **48A**, 557.
5. D. Kivelson and R. Neiman, *J. Chem. Phys.* 1961, **35**, 149.
6. B. J. Hathaway, P. G. Hondgson and P. C. Power, *Inorg. Chem.* 1974, **13**, 2009.
7. G. F. Kokaszka, C. W. Reimann, H. C. Allen Jr and G. Gordon, *Inorg. Chem.* 1967, **6**, 1657.
8. G. Devoto and G. Ponticelli, *J. Inorg. Nucl. Chem.* 1975, **37**, 1153.
9. D. A. Baldwin and G. J. Leigh, *J. Chem. Soc. (A)* 1968, 1431.
10. B. J. Hathaway, *J. Chem. Soc., Dalton. Trans.* 1972, 1196.
11. M. Duggan, B. J. Hathaway and J. Mullane, *J. Chem. Soc., Dalton Trans.* 1980, 690.
12. I. M. Procter, B. J. Hathaway and P. Nicholls, *J. Chem. Soc. (A)* 1968, 1678.

Polyhedron Vol. 12, No. 6, pp. 621–625, 1993
Printed in Great Britain

0277–5387/93 $6.00+.00
© 1993 Pergamon Press Ltd

STUDIES ON CROWN ETHER COMPLEXES—XXVII. SYNTHESIS, CHARACTERIZATION AND CRYSTAL STRUCTURE OF $[Y(NO_3)_3(OH_2)_3]\cdot$(DIBENZO-24-CROWN-8)

TONGBU LU, XINMIN GAN* and MINYU TAN

Department of Chemistry, Lanzhou University, Lanzhou 730000, P.R.C.

and

KAIBEI YU

Chengdu Centre of Analysis and Measurement, Academia Sinica, Chengdu 610041, P.R.C.

(*Received* 18 *August* 1992; *accepted* 11 *November* 1992)

Abstract—The complex $[Y(NO_3)_3(OH_2)_3]\cdot$(dibenzo-24-crown-8) (DB24C8) has been prepared and characterized by elemental analyses, IR spectra and molar conductance. The structure of the complex has been determined by single-crystal X-ray diffraction. The yttrium(III) ion is nine-coordinate, bonded to three bidentate nitrate groups and three water molecules. The crown ether molecule is hydrogen bonded to these three water molecules. The average Y—O(nitrate) and Y—O(water) distances are 2.426(4) Å and 2.344(4) Å, respectively. The average O(water)···O(crown) hydrogen bonded separation is 2.787 Å. The coordination geometry of the yttrium(III) ion is a distorted, tricapped trigonal prism.

Recently, Rogers *et al.*[1–7] reported a series of hydrogen bonded complexes of rare earth ions with crown ethers. In their studies, it was found that hydrated yttrium nitrate reacted with 12-crown-4 in CH_3CN or in a 3/1 CH_3CN:HOMe mixture to form the anhydrous product $Y(NO_3)_3$(12-crown-4).[8] However, under the same conditions hydrated yttrium nitrate reacted with 15-crown-5 to yield $[Y(NO_3)_2(OH_2)_5](NO_3)\cdot 2$(15-crown-5).[2]

In order to investigate the possibility that one crown ether is bonded directly to two yttrium ions in one molecule, we recently prepared the complexes of hydrated yttrium nitrate with DB24C8 and dibenzo-30-crown-10 (DB30C10) in acetonitrile. Under the same conditions of preparation, we obtained two different kinds of complex: $[Y(NO_3)_2(DB30C10)(OH_2)_2]_2\cdot[Y(NO_3)_5]$ and $[Y(NO_3)_3(OH_2)_3]\cdot$(DB24C8). In the former complex, the Y^{3+} ions are directly bonded to three of the crown ether oxygen atoms[9] and in the latter complex the Y^{3+} ion is not directly bonded to the crown ether oxygen atoms. In this paper, we report the synthesis, characterization and crystal structure of a hydrogen-bonded DB24C8 complex with yttrium nitrate.

EXPERIMENTAL

Reagents

Hydrated yttrium nitrate was prepared by dissolving the Y_2O_3 (Anala R) in 1:1 nitrate acid. The ligand was obtained from Shanghai Reagent Company and purified by recrystallization from ethanol before using, m.p. = 101.5–102.0°C.

Chemical and physical measurements

The yttrium ion content was determined by EDTA titration using Xylenol-orange as an indicator. Carbon, nitrogen and hydrogen were determined using a Carlo–Erba 1106 elemental analyser. The IR spectra were recorded in the 4000–200 cm^{-1} region using KBr pellets and a 170 SX FTIR spectrometer. Conductivity measurements were obtained with a DDS-11A type conductivity bridge for a freshly prepared solution in acetone at 25°C.

* Author to whom correspondence should be addressed.

X-ray diffraction intensities were collected at room temperature on an R3M/E diffractometer with graphite-monochromated Mo-K_α radiation.

Preparation

A solution of $Y(NO_3)_3 \cdot 6H_2O$ (0.42 mmol) in acetonitrile (3 cm^3) was added dropwise to a solution of DB24C8 (0.2 mmol) in acetonitrile (3 cm^3). The mixture was stirred at room temperature over 24 h. The precipitated solid complex was filtered, washed with acetonitrile and then dissolved in nitromethane. The solution was placed in a desiccator over $CaCl_2$ at room temperature. After *ca* 2 weeks the colourless crystal of the title complex formed from the solution. Found: C, 37.2; H, 4.9; N, 5.7; Y, 11.4. Calc. for $C_{24}H_{38}N_3O_{20}Y$: C, 37.1; H, 4.9; N, 5.4; Y, 11.4%.

X-ray structure determination

The structure was solved by the Patterson method and subsequent difference Fourier techniques and refined by full-matrix least-squares methods with anisotropic thermal factors for all non-hydrogen atoms. The crown ether hydrogen atoms were placed in calculated positions. All calculations were performed using the SHELXTL system of computer programs. The final values $R = 0.0531$ and $Rw = 0.0435$ were obtained. The crystal data are listed in Table 1.

Table 1. Crystal data

Formula	$C_{24}H_{38}N_3O_{20}Y$
Crystal dimensions (mm)	$0.20 \times 0.24 \times 0.48$
System	Monoclinic
Space group	$P2_1/n$
Lattice parameters:	
a (Å)	10.530(2)
b (Å)	20.319(3)
c (Å)	15.639(3)
β (°)	98.76(1)
V (Å^3)	3307(9)
Z	4
D_c (g cm^{-3})	1.56
D_o (g cm^{-3})	1.57
μ(calc.) (cm^{-1})	18.56
$F(000)$	1608
Scan type and rate (° min^{-1})	$\theta/2\theta$, 8
Standard reflections	−2,4,0; −4,0,6
2θ range (°)	2–45
Unique data measured	4797
Unique data with $I \geqslant 3.0\sigma(I)$	2869
No. of variables	554
S	0.0968
R	0.0531
Rw	0.0435

RESULTS AND DISCUSSION

Solubility and molar conductance

The complex is sparingly soluble in benzene and tetrachloromethane, slightly soluble in ethyl acetate, diethyl ether and chloroform, and partly soluble in acetonitrile, nitromethane and acetone. The molar conductance measured in acetone at 25°C is 4.2 Ω^{-1} cm^2 mol^{-1}, indicating that the complex is a non-electrolyte.[10] This indicates that all the nitrate groups in the complex are coordinated to the yttrium ion, consistent with the results of the IR spectra and the crystal structure determination.

IR spectra

After the formation of the complex the characteristic frequencies of the free ligand, ν(Ar—O—R) at 1256 and 1224 cm^{-1} and ν(R—O—R) at 1126 and 1102 cm^{-1}, showed small shifts of 5 and 33 cm^{-1} and 13 and 22 cm^{-1}, respectively, towards lower wave numbers. Moreover, no bands assignable to the ν(Y—O_{crown}) stretching frequency in the 380–400 cm^{-1} region[11] were found in the IR spectrum of the complex, suggesting that the ligand does not directly coordinate to the yttrium ion.

In the IR spectrum of the complex the absorptions appearing at 3258, 1664 and 571 cm^{-1} due to ν(OH), δ(HOH) and ρ_γ(HOH) indicate that coordinated water molecules exist in the complex.[12] Compared with the normal ν(OH) band (*ca* 3400 cm^{-1}) of the water molecule, the absorptions of ν(OH) of this complex show a red shift, which suggests that hydrogen bonds exist in this complex.[13,14] This inference was verified by the result of the structure determination.

The characteristic frequencies of the coordinating nitrate groups appear at 1777($\nu_2+\nu_5$), 1734($\nu_2+\nu_6$), 1503(ν_1), 1295(ν_4), 1031(ν_2) and 815(ν_3) cm^{-1}, and the difference between two strongest absorptions (ν_1 and ν_4) of the nitrate groups is over 200 cm^{-1}, indicating that the nitrate groups in the complex coordinate to the yttrium ion as bidentate ligands.[12]

Structural studies

The selected bond lengths and bond angles are given in Tables 2 and 3. Figure 1 shows the molecular structure of the complex and Fig. 2 illustrates the molecular packing arrangement in the unit cell.

Table 2. Selected bond lengths (Å)

Y—O(9)	2.417(4)	Y—O(10)	2.413(5)
Y—O(12)	2.434(4)	Y—O(13)	2.431(4)
Y—O(15)	2.434(4)	Y—O(16)	2.427(5)
Y—O(18)	2.361(4)	Y—O(19)	2.345(4)
Y—O(20)	2.326(5)	N(1)—O(9)	1.280(7)
N(1)—O(10)	1.277(7)	N(1)—O(11)	1.218(8)
N(2)—O(12)	1.269(7)	N(2)—O(13)	1.271(8)
N(2)—O(14)	1.222(7)	N(3)—O(15)	1.258(7)
N(3)—O(16)	1.269(7)	N(3)—O(17)	1.220(7)

Yttrium(III) *coordination*

The Y^{3+} ion is nine-coordinated with three bidentate nitrate groups and three water molecules, forming a distorted tricapped trigonal prism (Fig. 3) with nitrate oxygen atoms capping each quadrilateral face: O(9), O(12) and O(15). This same geometry was observed for $[Y(NO_3)_2(DB30C10)(OH_2)_2]^+$,[9] $[Y(NO_3)_3(OH_2)_2(NCMe)][Y(NO_3)_3(OH_2)_2(HOMe)]\cdot 2(B15C5)\cdot HOMe$[6] and $[MCl(OH_2)_2(18C6)]^{2+}$ (M = Y, Dy).[3]

The average Y—O(nitrate) and Y—O(water) bond lengths are 2.426(4) and 2.344(4) Å, respectively. These are in good agreement with other Y^{3+} complexes of similar geometry; $[Y(NO_3)_2(OH_2)_2(DB30C10)]^+$:[9] Y—O(nitrate) = 2.427, Y—O(water) = 2.353 Å; $[Y(NO_3)_3(OH_2)_2(NCMe)][Y(NO_3)_3(OH_2)_2(HOMe)]\cdot(B15C5)\cdot OHMe$:[6] Y—O(nitrate) = 2.42(3), Y—O(water) = 2.33(3) Å; $Y(NO_3)_3(OH_2)_3\cdot 2(C_{10}H_8N_2)$:[15] Y—O(nitrate) = 2.45(3), Y—O(water) = 2.32(1) Å.

Table 3. Selected bond angles (°)

O(9)—Y—O(10)	53.1(2)	O(9)—Y—O(12)	115.7(1)
O(10)—Y—O(12)	124.1(2)	O(9)—Y—O(13)	73.5(2)
O(10)—Y—O(13)	74.5(2)	O(12)—Y—O(13)	52.3(2)
O(9)—Y—O(15)	117.7(2)	O(10)—Y—O(15)	72.6(2)
O(12)—Y—O(15)	119.2(1)	O(13)—Y—O(15)	122.1(2)
O(9)—Y—O(16)	127.7(2)	O(10)—Y—O(16)	78.7(2)
O(12)—Y—O(16)	72.9(2)	O(13)—Y—O(16)	75.4(2)
O(15)—Y—O(16)	52.3(2)	O(9)—Y—O(18)	79.5(1)
O(10)—Y—O(18)	88.7(2)	O(12)—Y—O(18)	147.1(2)
O(13)—Y—O(18)	153.0(2)	O(15)—Y—O(18)	70.3(1)
O(16)—Y—O(18)	122.5(1)	O(9)—Y—O(19)	70.8(2)
O(10)—Y—O(19)	123.9(2)	O(12)—Y—O(19)	78.6(1)
O(13)—Y—O(19)	92.1(2)	O(15)—Y—O(19)	145.8(1)
O(16)—Y—O(19)	150.8(1)	O(18)—Y—O(19)	79.7(1)
O(9)—Y—O(20)	146.6(2)	O(10)—Y—O(20)	151.0(2)
O(12)—Y—O(20)	72.7(2)	O(13)—Y—O(20)	124.8(2)
O(15)—Y—O(20)	78.5(2)	O(16)—Y—O(20)	85.6(2)
O(18)—Y—O(20)	79.4(2)	O(19)—Y—O(20)	80.1(2)
O(9)—N(1)—O(10)	115.0(5)	O(9)—N(1)—O(11)	121.6(5)
O(10)—N(1)—O(11)	123.4(6)	O(12)—N(2)—O(13)	115.3(5)
O(12)—N(2)—O(14)	122.8(6)	O(13)—N(2)—O(14)	121.9(6)
O(15)—N(3)—O(16)	116.1(5)	O(15)—N(3)—O(17)	123.3(5)
O(16)—N(3)—O(17)	120.7(6)	C(6)—O(1)—C(7)	113.0(5)
C(8)—O(2)—C(9)	114.0(5)	C(10)—O(3)—C(11)	111.8(6)
C(12)—O(4)—C(13)	112.2(5)	C(18)—O(5)—C(19)	118.4(5)
C(20)—O(6)—C(21)	112.1(5)	C(22)—O(7)—C(23)	114.6(5)
C(1)—O(8)—C(24)	117.6(5)	O(8)—C(1)—C(2)	126.2(6)
O(8)—C(1)—C(6)	115.1(5)	O(1)—C(6)—C(1)	119.5(5)
O(1)—C(6)—C(5)	121.0(6)	O(1)—C(7)—C(8)	110.2(6)
O(2)—C(8)—C(7)	113.2(6)	O(2)—C(9)—C(10)	109.2(7)
O(3)—C(10)—C(9)	111.7(7)	O(3)—C(11)—C(12)	107.2(7)
O(4)—C(12)—C(11)	110.9(5)	O(4)—C(13)—C(14)	120.0(6)
O(4)—C(13)—C(I8)	118.8(6)	O(5)—C(18)—C(13)	114.7(6)
O(5)—C(18)—C(17)	127.0(6)	O(5)—C(19)—C(20)	108.0(6)
O(6)—C(20)—C(19)	109.8(6)	O(6)—C(21)—C(22)	111.0(6)
O(7)—C(22)—C(21)	111.6(6)	O(7)—C(23)—C(24)	110.9(6)
O(8)—C(24)—C(23)	106.5(5)		

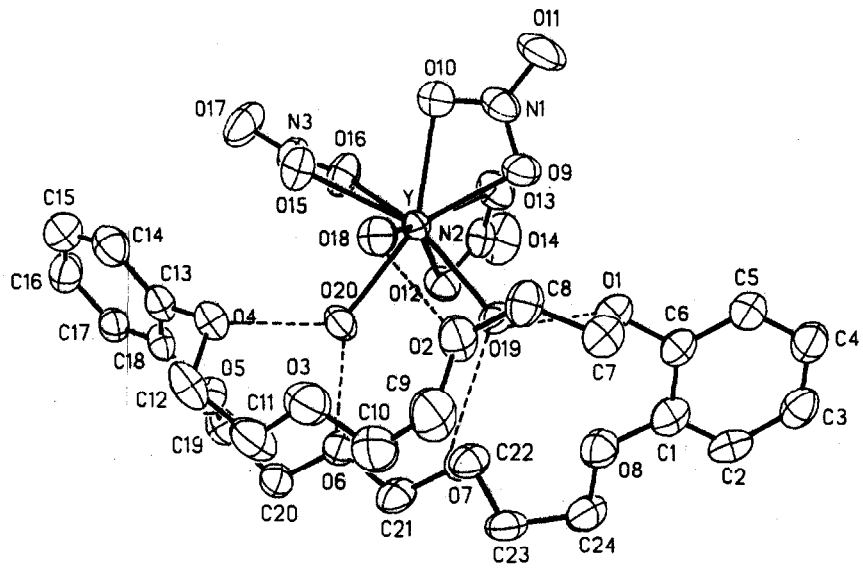

Fig. 1. The molecular structure of the complex.

Hydrogen bonding

Since it was not possible to locate the coordinated water hydrogen atoms, the presence of hydrogen bonding must be inferred from close O···O non-bonded contacts.[1] It can be seen that the five hydrogen atoms in three coordinated water molecules are bonded to five oxygen atoms in the crown ether. The HO—H···O contacts range from 2.705 to 2.839 Å and average 2.787 Å (see Table 4); this value is close to those observed in $[Y(OH_2)_8]Cl_3 \cdot$(15-crown-5) [average 2.76(7) Å],[1] $[UO_2(NO_3)_2(OH_2)_2] \cdot$(dibenzo-18-crown-6)$_2$ [range from 2.800 to 2.840 Å][16] and $[Y(NO_3)_3(OH_2)_2(NCMe)][Y(NO_3)_3(OH_2)_2(OHMe)] \cdot 2(B15C5) \cdot HOMe$ [average 2.77(7) Å].[6]

Crown ether conformation

Even the relatively weak forces involved in hydrogen bonding to crown ether oxygen atoms are known to influence the crown ether conformation.[17,18] The hydrogen bonding in the title complex makes the symmetry of the crown ether lower, from C_i in the free crown ether[19] to C_1 in the title complex. From the torsion angles given in Table 5 it can be seen that in order to form the

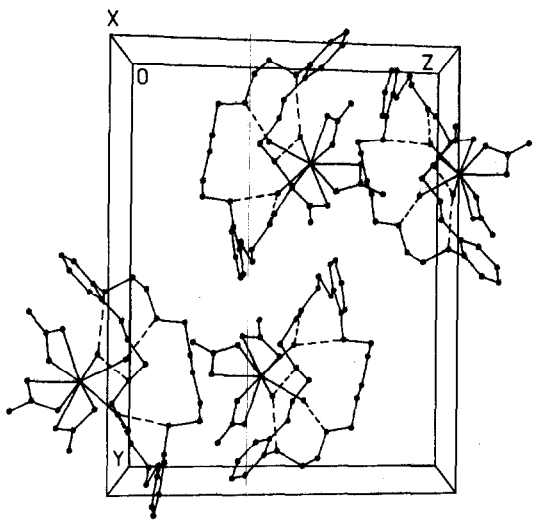

Fig. 2. The molecular packing arrangement in the unit cell.

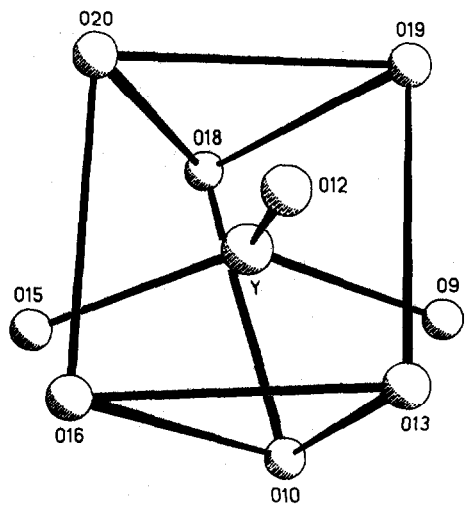

Fig. 3. The coordination geometry of the Y^{3+} ion.

Table 4. Hydrogen bonding contacts (Å)

O(18)···O(2)	2.705	O(19)···O(1)	2.839
O(19)···O(7)	2.770	O(20)···O(4)	2.793
O(20)···O(6)	2.829		
O(1)···O(19)···O(7)	108.8°	O(4)···O(20)···O(6)	107.1°

Table 5. Torsion angles (°)

O(8)—C(1)—C(6)—O(1)	−2.1(9)
O(1)—C(7)—C(8)—O(2)	67.2(8)
O(2)—C(9)—C(10)—O(3)	−64.7(8)
O(3)—C(11)—C(12)—O(4)	72.8(7)
O(4)—C(13)—C(18)—O(5)	1.3(8)
O(5)—C(19)—C(20)—O(6)	−62.8(7)
O(6)—C(21)—C(22)—O(7)	73.8(7)
O(7)—C(23)—C(24)—O(8)	61.0(7)

hydrogen bonding more efficiently the alkyl O—C—C—O angles (range: 61.0–72.8°) become smaller compared with those of the free crown ether (range: 78.0–84.1°). This change can also be found in $[(KNCS)_2(DB24C8)]$,[20] in which the mean C—O(alkyl) distance is 1.44(1) Å and the alkyl O—C—C—O angles range from 61° to 68°. The average distances and angles are: C—O(alkyl) = 1.428(9), C—O(aryl) = 1.380(8), C—C(alkyl) = 1.480(10), C—C(aryl, crown only) = 1.397(9) Å; O—C—C(alkyl) = 110.0(6)°, O—C—C(aryl) = 120.3(6)°, C(alkyl)—O—C(alkyl) = 113.1(5)°, C(alkyl)—O—C(aryl) = 115.3(5)°.

CONCLUSIONS

The ionic diameter of yttrium(III) is small and the cavity diameter of DB24C8 is too large; furthermore, compared with DB30C10, the flexibility of DB24C8 is less and so DB24C8 cannot adopt the folded conformation necessary to achieve the correct Y—O distance. In the presence of nitrate groups, Y^{3+} ion cannot directly coordinate to DB24C8 and it exists in the lattice by hydrogen bonding through the coordinated water molecules.

Acknowledgement—The authors are grateful to the China National Natural Science Foundation for financial support.

REFERENCES

1. R. D. Rogers and L. K. Kurihara, *Inorg. Chim. Acta* 1986, **116**, 171.
2. R. D. Rogers and L. K. Kurihara, *J. Less-Common Met.* 1987, **127**, 199.
3. R. D. Rogers, L. K. Kurihara and E. J. Voss, *Inorg. Chem.* 1987, **26**, 2360.
4. R. D. Rogers and L. K. Kurihara, *Inorg. Chim. Acta* 1987, **130**, 131.
5. R. D. Rogers and L. K. Kurihara, *Inorg. Chim. Acta* 1987, **129**, 277.
6. R. D. Rogers and E. J. Voss, *J. Coord. Chem.* 1988, **16**, 405.
7. R. D. Rogers, *J. Coord. Chem.* 1988, **16**, 415.
8. R. D. Rogers and L. K. Kurihara, *J. Inclusion Phenom.* 1986, **4**, 351.
9. T. Lu, X. Gan, M. Tan and K. Yu, *J. Coord. Chem.*, in press.
10. W. J. Geary, *Coord. Chem. Rev.* 1971, **7**, 81.
11. T. Lu, X. Gan, N. Tang and M. Tan, *Polyhedron* 1990, **9**, 2371.
12. K. Nakamoto, *Infrared and Raman Spectra of Inorganic and Coordination Compounds*, 3rd edn. John Wiley, New York (1978).
13. X. Gan, N. Tang, Y. Zhu, Y. Zhai and M. Tan, *J. Chin. Rare Earth Soc.* 1990, **8**, 10.
14. L. J. Bellamy, *The Infra-red Spectra of Complex Molecules*. Science Press, Beijing (1975).
15. T. J. R. Weakley, *Inorg. Chim. Acta* 1982, **63**, 161.
16. X. Gan, N. Tang, X. Wang, Y. Zhu and M. Tan, *J. Coord. Chem.* 1989, **20**, 21.
17. E. Mason and H. A. Eick, *Acta Cryst.* 1982, **B38**, 1821.
18. F. P. Van Remoortere and F. P. Boer, *Inorg. Chem.* 1974, **13**, 2071.
19. I. R. Hanson, D. L. Hughes and M. R. Truter, *J. Chem. Soc., Perkin II* 1976, **8**, 972.
20. M. Mercer and M. R. Truter, *J. Chem. Soc., Dalton Trans.* 1973, **22**, 2469.

Polyhedron Vol. 12, No. 6, pp. 627–633, 1993
Printed in Great Britain

0277–5387/93 $6.00+.00
© 1993 Pergamon Press Ltd

OPTICAL AND ESR STUDIES ON DIMERIZATION OF METALLOTETRA-CROWNED PHTHALOCYANINES

DAMODAR REDDY and T. K. CHANDRASHEKAR*

Department of Chemistry, Indian Institute of Technology, Kanpur 208016, India

(*Received* 31 *July* 1992; *accepted* 10 *November* 1992)

Abstract—The cation and solvent induced dimerization of free base tetra-crowned phthalocyanine (H_2tCRPc) and its metal derivatives (Ag^{2+} and VO^{2+}) have been studied by optical and ESR methods. Dimerization induces a blue shift of Q and Soret bands in the optical spectrum with a reduction in intensity. The exciton formalism accounts for the spectral blue shift upon dimerization. ESR studies reveal the formation of a cofacial dimer with axial symmetry upon the addition of cations. The measured zero-field splitting values in parallel and perpendicular regions suggest that the two paramagnetic centres are separated by 4.9 Å in VOtCRPc and 4.8 Å in AgtCRPc. In the micellar medium, the dimerization effects are observed only in 0.1 M SDS, while the tetra-crowned phthalocyanines remain aggregated in 0.1 M CTAB and in 5% TX-100.

Alkali cations are known to induce dimerization in porphyrins and phthalocyanines appended with crown ether cavities.[1,2] Many recent studies on these systems have been directed towards an understanding of the dynamics of the dimerization process.[3–5] Kobayashi and Lever have recently studied the dimerization of various metallocrowned phthalocyanines and have presented evidence for the formation of both non-cofacial and cofacial dimers in solution upon the addition of cations.[6] We have been interested in the dimerization of porphyrin systems and our previous studies have shown that the dimerization in porphyrins can be promoted by addition of crown ethers and cations.[7–9] In continuation of our efforts towards an understanding of the dimerization process we have investigated cation- and solvent-induced dimerization of Ag^{2+} and VO^{2+} derivatives of tetra-crowned phthalocyanines (Fig. 1). Being good paramagnetic probes, Ag^{2+} and VO^{2+} ions offer an opportunity to study dimerization by the ESR technique. Furthermore, the dimerization is also followed in micellar medium. It is shown that the dimerization effects are observed only in anionic sodium dodecyl sulphate (SDS), while in cationic cetyl trimethyl ammonium bromide (CTAB) and neutral triton-X-100 (TX-100) the crowned phthalocyanines remain aggregated even in dilute solution.

RESULTS AND DISCUSSION

Optical absorption studies

(1) *Non-aqueous medium.* The VO^{2+} and Ag^{2+} derivatives of tetra-crowned phthalocyanines in

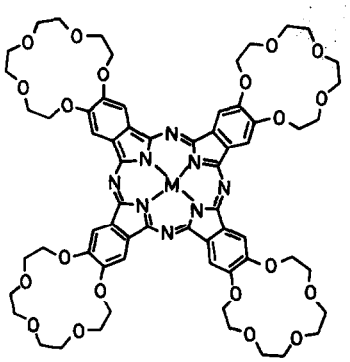

M = 2H ; H_2tCRPc
VO^{2+} ; VOtCRPc
Ag^{2+} ; AgtCRPc
Cu^{2+} ; CutCRPc

Fig. 1. Structure of the free base and metallotetra-crowned phthalocyanines.

* Author to whom correspondence should be addressed.

$CHCl_3$ exhibit well-defined Q and Soret bands in the visible region. The addition of increasing amounts of K^+ ions to a $CHCl_3$ solution results in the following changes: (a) the Q bands are shifted to blue (46 nm for VO^{2+} and 37 nm Ag^{2+}) with broadening and reduced absorbance; and (b) Soret bands also experience a small blue shift (8–10 nm) with reduced absorbance (Table 1). Figure 2 shows the absorption spectra of VOtCRPc before and after the addition of K^+ ions. These results suggest the existence of an equilibrium involving two species.[6] Based on our earlier findings[7–9] and literature reports,[1–3] it is concluded that the two species involved are monomers and dimers of MtCRPc. In the absence of K^+, under our experimental conditions, both VO^{2+} and Ag^{2+} derivatives exist as monomers and the addition of K^+ ions strongly drives the equilibrium to the dimer side. The driving force for the formation of the dimer is the affinity of appended crown ethers for alkali cations[10] to form a cation crown ether complex, thereby bringing the two phthalocyanine rings in close proximity and promoting interaction between the two π-systems.

The inset in Fig. 2 gives a plot of the intensity changes of the Q bands of AgtCRPc due to monomeric and dimeric species upon the addition of increasing amounts of K^+ ions. The shape of the curve reveals that the process of dimer formation involves more than one step. A non-sandwich type dimer of the type MtCRPC-K^+-MtCRPc, involving only one K^+ ion per dimer, and a sandwich type dimer involving two or more cations can be visualized from the fact that crown ethers are known to form both sandwich and non-sandwich type complexes with alkali cations.[10] The intensity decrease (monomer peak) and increase (dimer peak) is sharp at lower concentrations of K^+ ions, probably suggesting the formation of a non-sandwich type dimer. At higher concentrations of K^+ the non-sandwich type dimer encapsulates more K^+ ions to change over to a sandwich type dimer, bringing two phthalocyanine rings in a cofacial geometry.[6] ESR studies (*vide infra*) further confirm the presence of two phthalocyanine rings in a face-to-face geometry.

In order to see whether different cations have different effects on dimer formation optical spectra of solutions containing the same concentration of MtCRPc (7.96×10^{-6} M) and KCl (1.6×10^{-5} M), $NH_4(CH_3COO)_2$, NaCl, LiCl and CsCl were recorded. It was found that complete dimerization was observed in the presence of K^+ and NH^+_4 ions, about 70% dimerization with Cs^+ ions, while no detectable cofacial dimer was observed with Li^+ and Na^+ ions. However, the addition of high concentrations of Na^+ ions did decrease the absorb-

Table 1. Optical data of monomers and dimers of tetra-crowned phthalocyanines

Compound	In $CHCl_3$:CH_3OH (98:2) Q bands λ_{max} (nm) ($\varepsilon \times 10^{-3}$)			In $CHCl_3$:CH_3OH (98:2) Soret bands λ_{max} (nm) ($\varepsilon \times 10^{-3}$)			In 0.1 M SDS solution Q bands λ_{max} (nm) ($\varepsilon \times 10^{-3}$)			In 0.1 M SDS solution Soret bands λ_{max} (nm) ($\varepsilon \times 10^{-3}$)			log K
H_2tCRPc	701	662	644	602	416	348	698	661	640(sh)	410	344	294	—
	(33.4)	(27.4)	(11.6)	(6.2)	(8.1)	(30.8)	(53.1)	(50.5)	(31.9)	(17.9)	(45.9)	(34.6)	
[H_2tCRPc]$_2$[NH_4]$_4$	640.5	—	—	—	393.5	335	632		—	404	334	294	13.0 ± 1.5
AgtCRPc	674	642			342	287	674		637	418	344	279	—
	(12.82)	(9.45)			(12.32)	(12.39)							
[AgtCRPc]$_2$[NH_4]$_4$	636	—			343	282	630		—	418	340	280	—
[AgtCRPc]$_2$$K_4$	637	—			339	284	—		—	—	—	—	—
[AgtCRPc]$_2$[Cs]$_4$	637	—			343	287	—		—	—	—	—	—
CutCRPc	677	646.5	613		408.5	341	674		642	402	341	292	—
	(129.4)		(31.2)		(23.3)	(57.4)	(71.8)		(28.8)	(13.6)	(38.98)	(33.0)	
[CutCRPc]$_2$[NH_4]$_4$	635.5	—	—		338	333	623		—	402	334	291	12.0 ± 1.5
VOtCRPc	700	632	421		346	—							
[VOtCRPc]$_2$$K_4$	654	—	—		338	—							

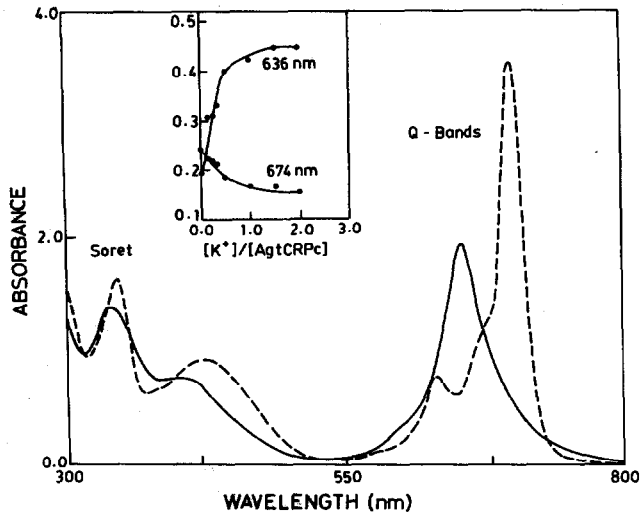

Fig. 2. Absorption spectra of VOtCRPc (2.0×10^{-5} M) in the presence and absence of K^+ ions. Inset: absorption changes of AgtCRPc as a function of increasing concentration of K^+ ions in $CHCl_3$: CH_3OH (98 : 2 V/V).

ance of the monomer peak, probably suggesting a non-sandwich type complex formation. Similar effects were observed for several crown-ether linked porphyrins and phthalocyanines upon complexation with alkali metal cations.[2,3,6] The nature of the complex (sandwich type or non-sandwich type) depends on the size of the crown ether cavity and the ionic radii of the cation. Benzo-15-crown-5 (the crown ether linked to the phthalocyanine ring in the present study) is known to form stable sandwich-type complexes with K^+ and NH^+_4 ions, while the stability of the sandwich type complex formed by Cs^+ ions is much less relative to K^+. On the other hand, Na^+ ions form a non-sandwich type complex where the Na^+ ions are encapsulated in the cavity of the crown ether, whilst no detectable complex formation is observed with Li^+ ions.[10,11] Thus, the observed effects in the electronic spectra are in line with these results.

Effect of solvents

The intensity and position of the Q bands of VO^{2+} and Ag^{2+} derivatives are highly dependent upon the solvent used. Figure 3(a) shows the effect of various solvents on the absorption spectrum of AgtCRPc. The Q bands at 674 and 642 nm (shoulder) in $CHCl_3$ correspond to the monomeric AgtCRPc. In polar solvents like ethanol and butan-1-ol the monomeric band at 674 nm loses considerable intensity and a new band at *ca* 630 nm gains intensity, indicating the presence of dimeric and higher aggregates in solution. However, in methanol the band structure is completely lost and a featureless, broad absorption in the Q band region clearly suggests the formation of oligomeric AgtCRPc in solution. The addition of a small amount of methanol to a $CHCl_3$ solution of AgtCRPc generates the dimeric species and the amount of dimeric species formed was found to be dependent on the concentration of methanol. Figure 3(b) shows the effect of increasing methanol concentration on the absorbance of the peak at 633 nm, due to the dimeric species. It is apparent from the plot that at *ca* 10% methanol concentration (v/v) in $CHCl_3$ solution maximum dimeric species are formed and any further increase leads to the formation of the high aggregates. Thus, at lower concentrations of methanol ($\leqslant$ 10%) the change in the absorption spectrum exactly parallels that observed upon the addition of K^+ or NH^+_4 ions, implying that the dimerization can also be induced by the solvents. VOtCRPc also shows a similar behaviour. These data are consistent with earlier reports on the metallo-crowned phthalocyanines.[6]

(2) *Micellar medium.* The optical absorption spectrum of a *ca* 10^{-6} M solution of H_2tCRPc in SDS (0.1 M) shows well-defined Q and Soret bands, while in CTAB (0.1 M) and 5% TX-100 the absorption bands are broad and featureless, suggesting that H_2tCRPc remains monomeric in SDS while the same is aggregated in CTAB and TX-100. The metal derivatives also show a similar behaviour.

The effect of the addition of increasing concentrations of NH^+_4 ions to a 2.5×10^{-5} M solution of H_2tCRPc in SDS (0.1 M) is displayed in Fig. 4.

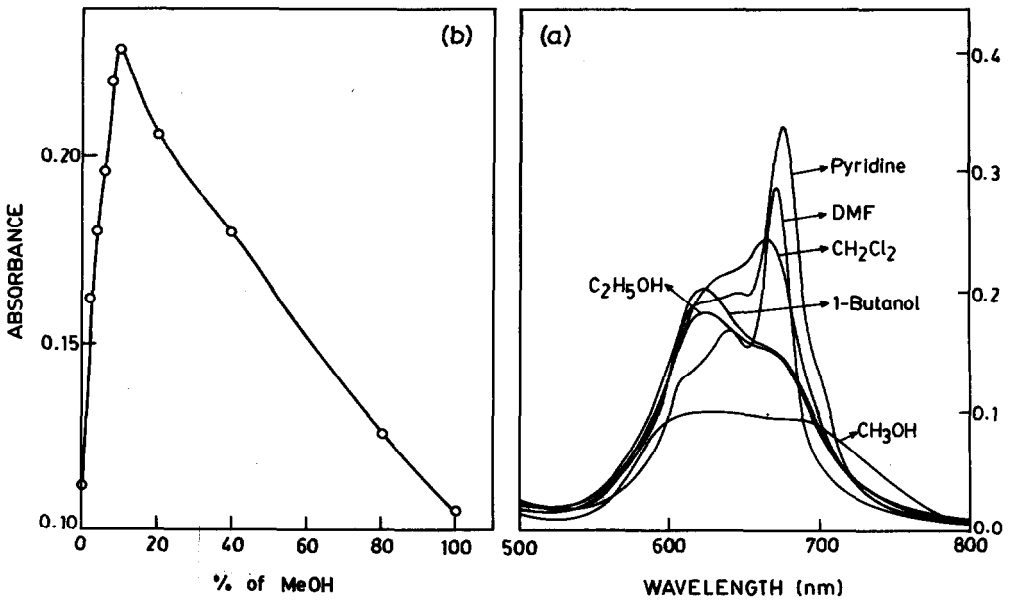

Fig. 3. (a) Absorption spectra of AgtCRPc (1.52×10^{-5} M) in different solvents. (b) Absorption changes of AgtCRPc at 633 nm (dimer peak) with increasing concentrations of CH_3OH in $CHCl_3$ solution.

The inset shows the plot of intensity changes of prominent Q-band(s) for H_2tCRPc and CutCRPc vs the concentration of NH^+_4 ions. The observed changes are similar to those seen in non-aqueous medium for the dimerization process. The progressive decrease in absorbance on the addition of cations are analysed by a method described previously[9] to evaluate the formation constants for the

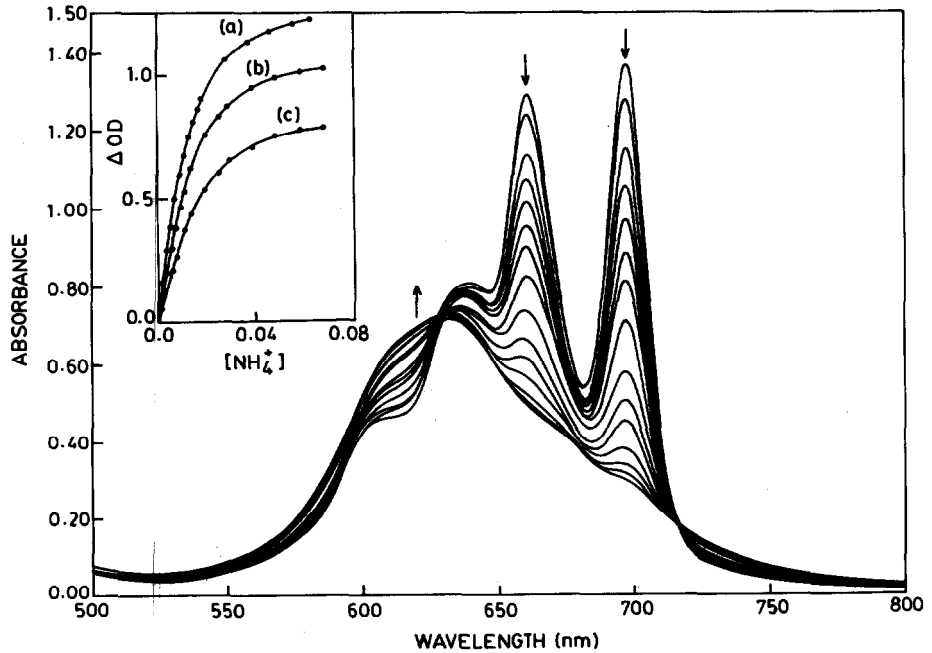

Fig. 4. Effect of the addition of increasing amounts of NH_4^+ ions (1.94×10^{-3}–6.80×10^{-2} M) on the absorption spectrum of H_2tCRPc (2.5×10^{-5} M) in SDS (0.1 M). Inset: intensity changes of prominent Q band(s) of (a) CutCRPc (674 nm), (b) H_2tCRPc (700 nm), and (c) H_2tCRPc (660 nm) on the addition of increasing amounts of NH_4^+ ions in SDS (0.1 M).

dimerization process, which can be represented as

$$2P + nC^+ \rightleftharpoons^{K} (P_2C_n)^{n+},$$

where P stands for phthalocyanine containing crown ether rings, C^+ represents the alkali cation added to induce the dimerization process and n is the number of cations. The value of n was varied from 1 to 4. A computer program was devised to carry out the calculations using the Newton–Raphson iterative method. Calculations were performed varying the value of n from 1 to 4 and in all the cases the best fit was observed when $n = 4$, suggesting that four cations are involved per dimer unit. The magnitudes of the formation constants are comparable to those observed for the cation–crown ether induced dimerization of water soluble porphyrins.[3,9]

Origin of dimerization induced shifts

Assuming a cofacial geometry of two phthalocyanine rings, the spectral blue shift upon dimerization can be explained using exciton theory.[12] The transition $^1A_{1g} \rightarrow {}^1E_u$ gives rise to a Q band absorption in metallophthalocyanines. The coupling of the doubly-degenerate excited states of the two monomers gives rise to two excited states, ^1E_g and ^1E_u. The nature of the coupling depends on the dimer geometry.[13] In the case of the cofacial dimer the higher energy transition ($^1A_{1g} \rightarrow {}^1E_u$) is allowed, whereas the lower energy transition ($^1A_{1g} \rightarrow {}^1E_g$) is forbidden. Thus, the blue shift obtained upon dimerization is in accordance with this prediction. The exciton splitting parameter (V), estimated as twice the energy difference between the monomeric Q band and the dimeric Q band energy, is 1556 cm^{-1} for AgtCRPc and 2009 cm^{-1} for VOtCRPc. This compares well with those observed for Nit CRPc (1760 cm^{-1}), CotCRPc (1960 cm^{-1}), Cut CRPc (1910 cm^{-1}) and ZntCRPc (1960 cm^{-1}).[6]

ESR spectral studies

The frozen solution ESR spectra of VOtCRPc before and after the addition of K^+ ions is displayed in Fig. 5. The spectrum observed in the presence of K^+ ions is typical of a triplet state with axial symmetry, the hyperfine splitting indicating the presence of two equivalent interacting VO^{2+} nuclei. The eight-line pattern arising from both the parallel and perpendicular regions is now decomposed due to zero-field splitting into two sets, each containing 15 lines corresponding to a total spin of 7 ($I = 7/2$ for the VO^{2+} ion). Due to the similarity of $g_\parallel$ and $g_\perp$ values, the lines from both parts are superimposed.[14] Furthermore, the appearance of a weak transition ($\Delta M_s = \pm 2$) arising from the triplet state ($S = 1$) in the half field ($g = 4$) region provides strong support for the existence of a dimer in solution.[15] The spin-Hamiltonian parameters evaluated from the spectra by the standard literature method[16] are listed in Table 2.

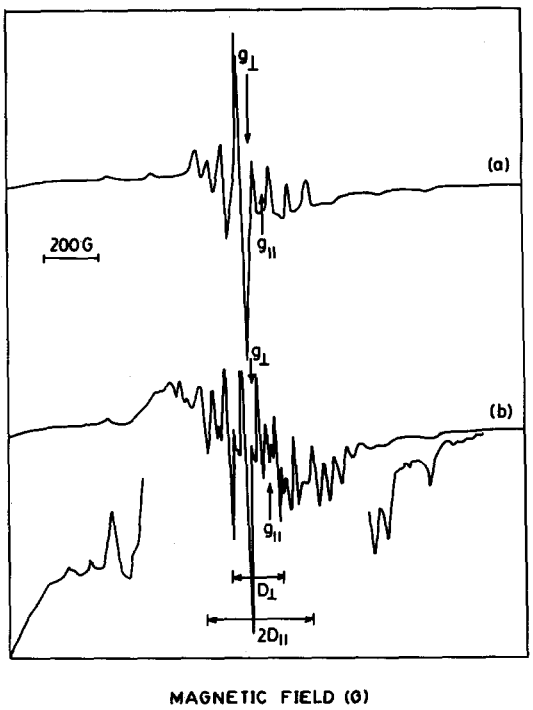

Fig. 5. ESR spectra of (a) VOtCRPc and (b) VOt CRPc + K^+ ions in $CHCl_3$: CH_3OH (98 : 2 V/V) at 100 K. Approximately 1×10^{-4} M of phthalocyanine solution was used for recording the spectra.

AgtCRPc also shows a well-resolved spectrum for the monomeric species. The g and hyperfine values evaluated (Table 2) compare well with those reported for Ag^{2+} ($I = 3/2$) porphyrins. The addition of K^+ ions results in the appearance of additional lines due to dimer formation. However, the dimer spectrum was contaminated with monomer lines in the $g = 2$ region. Nevertheless, the spectrum was resolved enough to evaluate the zero-field splitting parameter.

The zero-field splitting parameter, D, evaluated both in parallel and perpendicular regions, was used to compute the (V—V) and (Ag—Ag) distance in the dimer, making use of the expression developed by Chasteen and Belford[17] (Table 2). The V—V distances calculated in the present study compare well with those observed for the vanadyl tetracrownporphyrin dimer (4.7 Å) and the dimer of vanadyl tetrasulphonato-phthalocyanine[18] (4.5 Å), probably indicating similar solution structures (Fig.

Table 2. ESR parameters of VO^{2+} and Ag^{2+} tetra-crowned phthalocyanines

Compound	$g_\parallel$	$g_\perp$	$10^4 A_\parallel^M$ (cm^{-1})	$10^4 A_\perp^M$ (cm^{-1})	$D_\parallel$ (G)	$D_\perp$ (G)	R(M—M) (Å)
AgtCRPc	2.147	2.042	—	—	—	—	—
AgtCRPc+KCl	2.144	2.052	—	—	240	250	4.8
VOtCRPc	1.967	1.988	159.5	56.9	—	—	—
VOtCRPc+KCl	1.964	1.984	73.7	40.0	230	230	4.9
VOTCP[a]	1.964	1.985	154.7	52.96	—	—	—
VOTCP+KCl[a]	1.967	1.987	77.15	25.98	268.5	261	4.7

[a] VO^{2+} = tetra-crowned porphyrin.[4]

6). The Ag—Ag distance estimated in the present study also compares well with the only reported Ag—Ag distance of 5 Å for the silver meso-porphyrin dimethylester dimer.[19]

EXPERIMENTAL

The electronic spectra were recorded on a Shimadzu UV-160 spectrophotometer. ESR measurements were made using a Varian E-109 *X*-band spectrometer at liquid nitrogen temperature. Benzo-15-crown-5, SDS, CTAB and TX-100 were procured from Aldrich Chemical Company, U.S.A. 4,5-Dibromobenzo-15-crown-5, 4,5-dicyanobenzo-15-crown-5, H_2tCRPc and CutCRPc were prepared using literature procedure.[3,5]

Preparation of vanadyl tetra-crowned phthalocyanine (VOtCRPc)

H_2tCRPc (40 mg) and vanadyl sulphate (100 mg) were dissolved in dry DMF (100 cm^3) and the mixture was refluxed for 7 days. The solvent was then removed under reduced pressure. The dark green powder obtained was washed with excess water to remove unreacted $VOSO_4$. The crude product was purified by column chromatography over basic alumina. The unreacted H_2tCRPc moved as a light green band in $CHCl_3$:CH_3OH (98:2 V/V). VOt CRPc was eluted as a bluish-green band in $CHCl_3$:CH_3OH (95:5 V/V). Yield: 13 mg (30%).

Preparation of silver tetra-crowned phthalocyanine (AgtCRPc)

H_2tCRPc (20 mg), $AgNO_3$ (20 mg) and sodium acetate (20 mg) were taken in a mixture of 1,2-dichloroethane (15 cm^3) and acetic acid (20 cm^3) and the mixture was refluxed for 2.5 h. The reaction mixture was filtered and the resulting solid was washed with excess water. The crude product was dissolved in chloroform and subjected to column chromatography over basic alumina. An initial light green band eluted in $CHCl_3$:CH_3OH (98:2 V/V)

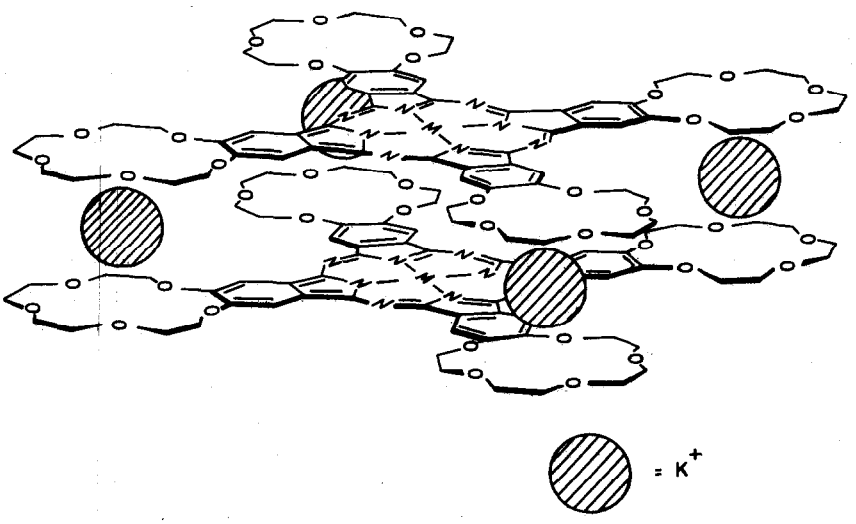

Fig. 6. Proposed cofacial dimer structure.

to give unreacted H_2tCRPc. The bluish-green band eluted in $CHCl_3$: CH_3OH (95 : 5 V/V) gave the pure AgtCRPc. Yield : 8 mg (40%).

Acknowledgements—T.K.C. thanks DST for financial support and D.R. thanks CSIR for a fellowship.

REFERENCES

1. (a) N. Kobayashi and Y. Nishiyama, *J. Chem. Soc., Chem. Commun.* 1986, 1462; (b) R. Hendriks, Ot E. Sielcken, W. Drenth and R. J. M. Nolte, *J. Chem. Soc., Chem. Commun.* 1986, 1464.
2. V. Thanabal and V. Krishnan, *J. Am. Chem. Soc.* 1982, **104**, 3643.
3. Ot E. Sielcken, M. M. Van Tilborg, M. F. M. Roks, R. Hendriks, W. Drenth and R. J. M. Nolte, *J. Am. Chem. Soc.* 1987, **109**, 4261.
4. V. Thanabal and V. Krishnan, *Inorg. Chem.* 1982, **21**, 3606.
5. V. Ahsen, E. Yilmazer, M. Ertas and O. Bekaroglu, *J. Chem. Soc., Dalton Trans.* 1988, 401.
6. N. Kobayashi and A. B. P. Lever, *J. Am. Chem. Soc.* 1987, **109**, 7433.
7. (a) T. K. Chandrashekar and H. Van Willigen, *J. Am. Chem. Soc.* 1983, **105**, 6323; (b) T. K. Chandrashekar, H. Van Willigen and M. H. Ebersole, *J. Phys. Chem.* 1984, **88**, 4326; (c) T. K. Chandrashekar and H. Van Willigen, *Chem. Phys. Lett.* 1984, **106**, 237.
8. (a) T. K. Chandrashekar, H. Van Wiligen and M. H. Ebersole, *J. Phys. Chem.* 1985, **89**, 3453; (b) H. Van Willigen and T. K. Chandrashekar, *J. Am. Chem. Soc.* 1986, **108**, 709.
9. M. Ravikant, D. Reddy and T. K. Chandrashekar, *J. Chem. Soc., Dalton Trans.* 1991, 2103.
10. C. J. Pedersen, *J. Am. Chem. Soc.* 1967, **89**, 7017.
11. H. K. Frensdorff, *J. Am. Chem. Soc.* 1971, **93**, 600.
12. (a) M. Kasha, H. R. Rawls and M. El-Bayoumi, *Pure Appl. Chem.* 1965, **11**, 371; (b) M. Gouterman, D. Holton and E. Lieberman, *Chem. Phys.* 1977, **25**, 139; (c) C. A. Hunter, J. K. M. Sanders and A. J. Stone, *Chem. Phys.* 1989, **133**, 395.
13. E. S. Dodsworth, A. B. P. Lever, P. Seymour and C. C. Leznoff, *J. Phys. Chem.* 1985, **89**, 5698.
14. W. C. Lin, *The Porphyrins* (Edited by D. Dolphin), Vol. IV, p. 355. Academic Press, New York (1979).
15. (a) F. Kim and C. K. Jen, *J. Magnet. Reson.* 1974, **15**, 420; (b) M. Sato and T. Kwan, *J. Chem. Phys.* 1969, **50**, 558; (c) R. H. Sands, *Phys. Rev.* 1955, **99**, 1222; (d) G. Bleaney, *Phil. Magnet.* 1951, **42**, 441.
16. A. MacGraph, C. B. Storm and W. S. Koshi, *J. Am. Chem. Soc.* 1965, **87**, 1470.
17. N. D. Chasteen and R. L. Belford, *Inorg. Chem.* 1970, **9**, 169.
18. P. W. D. Boyd and T. D. Smith, *J. Chem. Soc., Dalton Trans.* 1972, 839.
19. L. Banci, *Inorg. Chem.* 1985, **24**, 782.

Polyhedron Vol. 12, No. 6, pp. 635–639, 1993
Printed in Great Britain

0277–5387/93 $6.00+.00
© 1993 Pergamon Press Ltd

ENDOR STUDY OF $VO(acac)_2$ AND ITS INTERACTION WITH CHLOROFORM IN FROZEN SOLUTION

N. D. YORDANOV* and M. ZDRAVKOVA

Institute of Kinetics and Catalysis, Bulgarian Academy of Sciences, 1113 Sofia, Bulgaria

(*Received* 15 *October* 1992; *accepted* 6 *November* 1992)

Abstract—Proton ENDOR studies in the region between the turning points of the EPR spectrum of $VO(acac)_2$ dissolved in toluene-d_8/$CDCl_3$, as well as in toluene-d_8/$CHCl_3$, are reported. Structural information about the position of the methyl and 3-C protons of the acetylacetonate ligand are extracted from the spectra and compared with data available from X-ray structural analysis and previous ENDOR studies. The formation of outer-sphere complexes between molecules of chloroform and $VO(acac)_2$ has been recorded. This complex is suggested to be formed via hydrogen bonding between the hydrogen atom of $CHCl_3$ and an oxygen atom of the chelate ligand. Another molecule of chloroform is coordinated along the *z*-axis of $VO(acac)_2$ via a hydrogen bond with the oxygen atom from the V=O moiety.

It is well known that the ligand superhyperfine structure in the EPR spectra of oxovanadium complexes is unresolved because of the non-bonding character of the orbital d_{xy}, in which the unpaired electron is situated,[1,2] and of the limited resolution of the EPR method itself.[3] Thus, the information which can be obtained about the electronic and geometric structure of these complexes from their EPR spectra is limited to only the chromophore (VOX_4), where X are donor atoms of the ligand.[2] The spectra obtained by ENDOR spectroscopy are much more informative due to its nearly 10^3 times higher resolution.[3] In view of this advantage the structure of some adducts of VO^{2+} complexes in solution were determined within the last decade by means of ENDOR spectroscopy.[4,5] In these communications the ENDOR spectra were taken at the "turning points" of the EPR spectra of the related compound.[6] Recently, it has been suggested[7–10] that the studies of the region between the turning points give more detailed and exact information about the true values of the hyperfine coupling, as well as about the position of the atoms with respect to the *g*-tensor axes (or *z*-axis of the molecule). Such a study has been reported[11] on the 3-C protons from a molecule of $VO(acac)_2$ in frozen solution.

In the present paper we report more precise results obtained for the structure of $VO(acac)_2$ in frozen solution, as well as for its interaction with chloroform molecules. The results are interpreted using the method previously described.[10] The results obtained were checked with a computer-aided ENDOR spectroscopy, the programme of which was developed in this laboratory.

EXPERIMENTAL

$VO(acac)_2$ (Merk) was used after recrystallization from toluene.

Toluene (p.a.) was used; ethanol, typically available in commercial chloroform as a stabilizer, has been removed by washing several times with water, drying for a few days over $CaCl_2$ and distilling as described.[12] Deuterated solvents, toluene-d_8 and chloroform-d_1 were used as obtained from Merck.

Samples suitable for ENDOR measurements were prepared by filling quartz EPR sample tubes (o.d. 4.5 mm, i.d. 3.5 mm) with a solution of $VO(acac)_2$ (approx. 2×10^{-2} M) dissolved in a solvent mixture of toluene/chloroform in the ratio 1 : 1 v/v. The oxygen was removed from the solutions on a vacuum line by several freeze–pump–thaw cycles until the pressure reached the value of *ca* 1×10^{-3} mm Hg. After that the sample tubes were sealed.

ENDOR spectra were recorded on a Bruker ER

* Author to whom correspondence should be addressed.

200 D-SRC spectrometer equipped with a computer controlled ENDOR accessory. The EPR and ENDOR spectra acquisition as well as post-acquisition processings were performed on a Bruker Aspect 2000 computer. All the EPR and ENDOR measurements were performed at 100 K. Typical experimental conditions for the ENDOR measurements were: microwave power 50 mW, radio-frequency power 200–300 W, modulation frequency 12.5 kHz, modulation depth 60–80 kHz. Magnetic field modulation was not used while recording the ENDOR spectra. The spectra for the computer-aided ENDOR studies were generated using a special program written in this laboratory for IBM PC.[13]

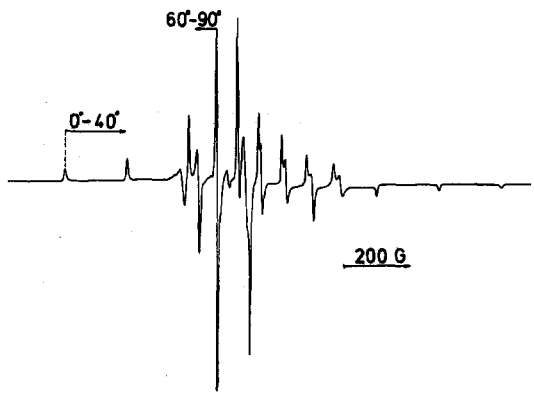

Fig. 1. EPR spectrum of a frozen solution of $VO(acac)_2$ (2×10^2 M) in toluene-d_8/$CDCl_3$; $T = 77$ K.

RESULTS AND DISCUSSION

EPR spectra of VO^{2+} *complexes*

The electronic configuration of the moiety VO^{2+} is $3d^1$ and a hyperfine structure with eight lines ($I = 7/2$) is observed in the EPR spectra of VO^{2+} complexes at room temperature. Since to a first approximation VO^{2+} complexes possess an axial symmetry, their frozen solution EPR spectra typically show an EPR spectrum consisting of eight parallel and eight perpendicular lines.

The EPR spectrum of $VO(acac)_2$ in a frozen solution of toluene-d_8/chloroform-d_1 recorded by us (Fig. 1) shows a slight rhombic distortion. EPR parameters derived from that spectrum as well as those reported by other authors are collected in Table 1. Since the rhombic distortion $g_{xx} - g_{yy} \leqslant 0.006$ is relatively low it may be assumed that the $VO(acac)_2$ complex is axially symmetric with a g-value in the perpendicular region of 1.979.

^1H *ENDOR spectroscopy of* $VO(acac)_2$

The ENDOR study of a paramagnetic system, where the nuclear spin of the central metal atom is larger than 1/2, usually avoids positions in the EPR spectrum where contributions from more than one m_I value would be observed, as they make the resulting ENDOR spectrum more complex.[14] For that reason, in the case of VO^{2+} complexes, typically the regions with $M_I = -7/2$ in the parallel orientation and $M_I = -3/2$ in the perpendicular are chosen in order to take ENDOR spectra from only one EPR transition.[14] These regions, in which the magnetic field was consecutively set in order to cover the whole range, $0° \leqslant \theta \leqslant 90°$, of polar angles θ, are shown in Fig. 1.

Some experimentally obtained ENDOR spectra taken at different settings of the magnetic field in the region $0° \leqslant \theta \leqslant 90°$ are shown in Fig. 2(a). Inspecting Fig. 2(a) it is clear that one intensive pair of lines with a splitting of *ca* 0.72 MHz exists in all the spectra. After selective deuteration of the 3-C protons[4] these lines have been assigned to the methyl protons of $VO(acac)_2$. They were the only lines observed before at $\theta = 0°$; the lack of lines from 3-C protons being explained by the fact that they are very weak and probably obscured by the strong methyl proton peaks.[2] As can be seen in Fig. 2 we have first recorded a pair of lines due to 3-C protons at 0°. These resonance peaks with a splitting of 1.2 MHz are really very weak.

The spectrum taken at 90° is exactly the same as in the literature. Lines with splitting of 3.40 MHz (see Fig. 3) are from 3-C protons, and lines with

Table 1. EPR parameters for the $VO(acac)_2$ complex

Solvent	$g_\parallel$	$g_\perp$	$A_\parallel$	$A_\perp$	Ref.
Toluene	1.942	1.979, 1.983	172.8	64.2, 61.6	4
Toluene/$CHCl_3$	1.945	1.979	170.7	62.0	4
Toluene/CH_2Cl_2	1.951	1.984, 1.988	182	65, 63	11
Toluene/$CHCl_3$	1.947	1.976, 1.985	184.6	65, 63	This work

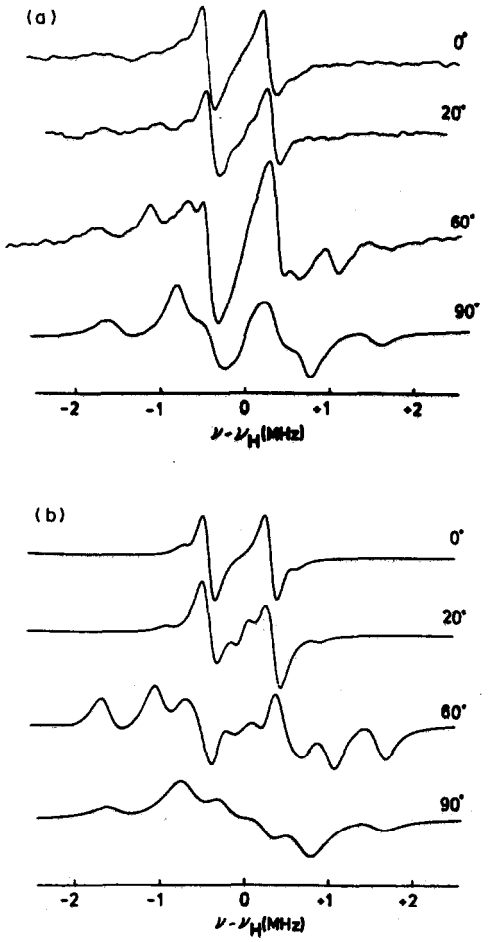

Fig. 2. Proton ENDOR spectra of $VO(acac)_2$ in toluene-d_8/$CDCl_3$ (1 : 1) at differents angles θ: (a) experimental spectra, $T = 100$ K; and (b) simulated spectra.

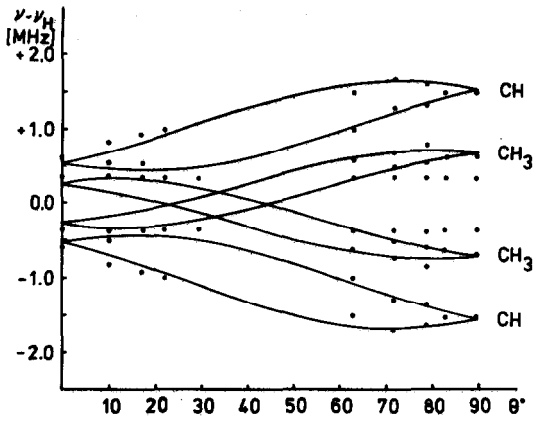

Fig. 3. Angular dependence of proton ENDOR transitions of $VO(acac)_2$ in toluene-d_8/$CDCl_3$. The experimental values are shown with points.

splitting of 1.40 MHz are assigned to the methyl protons.

The experimental proton hyperfine splittings found at settings of the magnetic field at different values of θ in the region $0° < \theta < 90°$ are presented in Fig. 3 (points). The magnitudes of A_{aniso}, A_{iso} and α for 3-C and methyl protons were calculated on the basis of the experimental data and they are all collected in Table 2. In Table 2 are also shown the distances between the vanadium ion and the corresponding proton, which are calculated from the values of A_{aniso} using the point-dipole approximation.

The X-ray structural analysis of the $VO(acac)_2$ complex[15] and a recent publication on a gas-phase electron diffraction study[16] show that methyl and 3-C protons are situated below the equatorial plane. The angle between the two pseudo-aromatic rings and V=O axis is found to be 106°. Approximately the same angle, 109°, was reported on the basis of the ENDOR study.[11] These data are also in good agreement with our results, showing that 3-C protons are situated at an angle of 17° from the xy-plane.

The principal values of the hyperfine splitting for CH_3 and 3-C protons were also calculated and the results are shown in Table 3. The parameters thus obtained were used for simulation of the ENDOR spectra at different angles of the EPR observer (Fig. 2b). Hyperfine splittings determined from the simulated spectra are plotted with solid lines on Fig. 3. It should be noted that in Fig. 3 are presented only their angle-depending parts, which are the most important. As can be seen the coincidence between experiment and theoretical calculations is quite good.

ENDOR study of the interaction between $VO(acac)_2$ *and* $CHCl_3$

The addition of chloroform (alcohol free) to a toluene solution of $VO(acac)_2$ does not change the shape and parameters of its EPR spectrum. However, the ENDOR spectra shown in Fig. 4(a) reveal new large splitting due to the interaction of the unpaired electron with a proton from the chloroform, indicating a well-defined $VO(acac)_2$–

Table 2. Parameters of proton hyperfine splitting (MHz), angles H—V=O (°) and distances V—H (Å)

Proton	A_{iso}	A_{aniso}	α	r
3-C	1.70	0.83	73	4.57
Methyl	0.12	0.67	81	4.90

Table 3. Proton hyperfine splitting parameters (MHz) for the $VO(acac)_2$ complex

Proton	A_{xx}	A_{yy}	A_{zz}	Ref.
Methyl	1.34	−0.71	−0.63	4
	1.45	−0.72	−0.60	This work
3-C	3.37	0.2(?)	0.90(?)	4
	3.69	−1.09	1.41	11
	3.35	−1.10	0.87	This work

$CHCl_3$ interaction. The splittings at 0° and 90° are 2.17 and 2.12 MHz, respectively. In a previous study of this adduct by the method of the "turning points"[4] it was suggested that the most likely binding site is the vanadyl oxygen via a hydrogen bond.

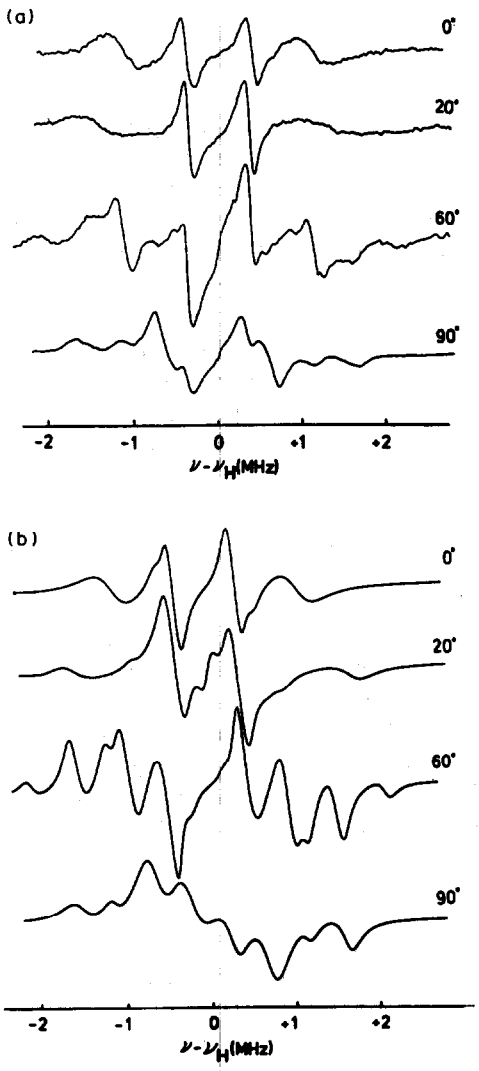

Fig. 4. Proton ENDOR spectra of $VO(acac)_2$ in toluene-$d_8/CHCl_3$ (1:1) at different angles θ: (a) experimental spectra, $T = 100$ K; and (b) simulated spectra.

The authors have calculated the tensor of *hf* coupling, assuming an O···H distance of 1.75 Å and a V=O···H angle of 120°. Nevertheless, they emphasize that the exact geometry of the adduct is not known. Our study of the region between turning points of the $VO(acac)_2$ complex shows that in fact two ENDOR transitions from two differently situated molecules of chloroform are observed. In Fig. 5 they are marked as A and B. The following values were found: for transition B: $A_{aniso} = 1.15$ MHz, $A_{iso} = 0$ MHz, $\alpha = 8.5°$; for transition A: $A_{aniso} = 2.33$ MHz, $A_{iso} = 0$ MHz and $\alpha = 46°$. Some ENDOR spectra simulated with the values thus obtained are shown in Fig. 4(b).

Transition B is due to a proton coordinated by a hydrogen atom, bound to the oxygen atom from the V=O moiety and situated practically along the z-axis of the complex. The distance of 4.10 Å between the proton and the vanadium was calculated. Bearing in mind that the bond length V=O is 1.56 Å,[15] it was found that the O···H distance was 2.57 Å, which is very close to that typical of hydrogen bonds.[17]

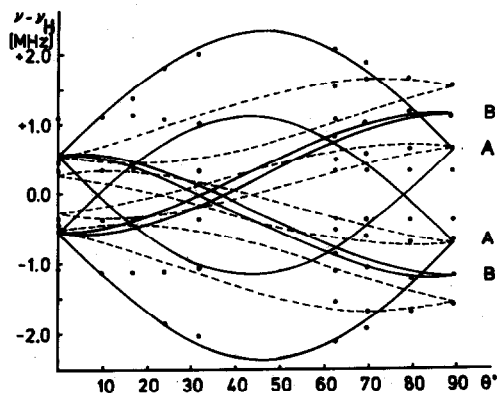

Fig. 5. Angular dependence of proton ENDOR transitions of $VO(acac)_2$ in toluene-$d_8/CHCl_3$: transitions due to the interaction with chloroform are marked with full lines; transitions due to protons of $VO(acac)_2$ are indicated with dashed lines.

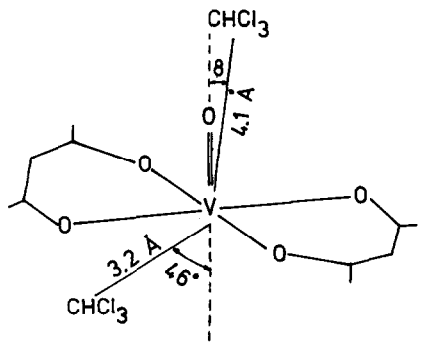

Fig. 6. The proposed model of the outersphere complex between $VO(acac)_2$ and $CHCl_3$.

Transition A is due to the interaction of the unpaired electron with a proton situated at a distance of 3.24 Å from vanadium and at an angle of 46° from the z-axis of the complex. This proton seems to be coordinated to the donor oxygen atoms from the acetylacetonate ligand. Such outersphere complexes, in which chloroform and oxygen atoms from chelate ligands of the metal complexes, including β-diketonate complexes of transition metal ions, from hydrogen bonds, have been studied before by NMR.[18] For example, the distance between the proton of the solvent ($CHCl_3$ or CH_2Cl_2) molecule and cobalt(II) from $CO(acac)_2py_2$ was estimated to be 4.0 ± 0.2 Å, and the angle between the direction Co···H and the z-axis of the complex to be 32°.[19]

The results obtained above on the basis of ENDOR studies suggest that the coordination structure of the outersphere complex between $VO(acac)_2$ and chloroform is as shown in Fig. 6.

Acknowledgements—The financial support from the Ministry of Science and Higher Education (project 137) and the Bulgarian Academy of Sciences is gratefully acknowledged.

REFERENCES

1. N. D. Chasteen, in *Biological Magnetic Resonance*, Vol. 3, p. 53. Plenum Press, New York (1982).
2. H. A. Kuska and M. T. Rogers, in *Radial Ions* (Edited by E. T. Kaiser and L. Kevan). Wiley-Interscience, New York (1968).
3. L. Kevan and l. D. Kispert, *Electron Spin Double Resonance*. Wiley Interscience, New York (1976); *Multiple Electron Resonance Spectroscopy* (Edited by M. Dorio and J. H. Freed). Plenum Press, New York (1979): A. Schweiger, *Struct. Bonding* 1982, **50**, 1.
4. B. Kirste and H. van Willigen, *J. Phys. Chem.* 1982, **86**, 2743.
5. D. Mustafi and M. W. Makinen, *Inorg. Chem.* 1988, **27**, 3360.
6. G. H. Rist and S. Hyde, *J. Chem. Phys.* 1970, **52**, 4633.
7. B. M. Hoffman, J. Martinsen and R. A. Venters, *J. Magnet. Reson.* 1984, **59**, 110.
8. N. D. Yordanov and M. Zdravkova, *Proc. Congress AMPERE*, p. 612. Zurich (1984).
9. G. C. Hurst, T. A. Henderson and R. W. Kreilick, *J. Am. Chem. Soc.* 1985, **107**, 7294.
10. N. D. Yordanov, M. Zdravkova, D. Shopov, *Chem. Phys. Lett.* 1986, **124**, 191.
11. G. J. Baker and J. B. Raynor, *J. Chem. Soc., Faraday Trans. I* 1988, **84**, 4267.
12. *Organic Solvents* (Edited by Arnold Weissberger), p. 410. Interscience Publishers, Inc., New York (1955).
13. G. Gochev and N. D. Yordanov, *J. Magnet. Reson.* 1993, **101**.
14. N. D. Yordanov and M. Zdravkova, *Acta Phys. Hung.* 1987, **61**, 127.
15. R. P. Dodge, D. U. Templeton and A. Zalkin, *J. Chem. Phys.* 1961, **35**, 55.
16. G. A. Forsyth, D. A. Rice and K. Hagen, *Polyhedron* 1990, **9**, 1603.
17. *Hydrogen bond* (Edited by N. D. Sokolov and V. M. Chulanovskii). Mir, Moscow (1964).
18. A. N. Kitaigorodskii, V. M. Nekipelov and K. I. Zamaraev, *Zh. Struct. Khim.* 1978, **19**, 796.
19. V. M. Nekipelov, A. N. Shupik and K. I. Zamaraev, *Zh. Fiz. Khim.* 1975, **49**, 1028.

Polyhedron Vol. 12, No. 6, pp. 641–649, 1993
Printed in Great Britain

0277–5387/93 $6.00+.00
© 1993 Pergamon Press Ltd

ELECTROCHEMICAL STUDIES OF IRON(III) SCHIFF BASE COMPLEXES—I. THE MONOMERIC $Fe^{III}(N_2O_2)Cl$ COMPLEXES

B. CARRÉ

Laboratoire de Synthèse et d'Etudes Physicochimiques Organiques, Faculté des Sciences, Parc de Gramont, 37200 Tours, France

and

J.-P. COSTES, J.-B. TOMMASINO and D. DE MONTAUZON

Laboratoire de Chimie de Coordination du CNRS, UP 8241, lié par conventions à l'Université Paul Sabatier et à l'Institut National Polytechnique de Toulouse, 205 route de Narbonne, 31077 Toulouse Cedex, France

and

F. SOULET and P.-L. FABRE*

Laboratoire de Chimie Inorganique, Université Paul Sabatier, 118 route de Narbonne, 31062 Toulouse Cedex, France

(*Received* 30 *September* 1992; *accepted* 4 *November* 1992)

Abstract—The electrochemical reduction of $Fe^{III}(L)Cl$, where L is a Schiff base, has been investigated in aprotic solvents by cyclic voltammetry and coulometry with UV–vis spectroscopy. Six complexes derived from Schiff base ligands with N_2O_2 environments are described. The reduction of $Fe^{III}(L)Cl$ into $Fe^{II}(L)Cl$ occurs at a potential around -0.5 V vs S.C.E. through an EC mechanism where the following reaction concerns the decomposition of iron(II), a highly reactive complex. A high electronic delocalization of the Schiff base, such as in SALOPH, stabilizes the oxidation state II of iron and shifts the redox potential anodically. The study reveals the extreme reactivity of iron(II) towards dioxygen. Traces of dioxygen with $Fe^{II}(L)Cl$ yield the μ-oxo bridged Fe^{III} dimers (L)Fe—O—Fe(L), whose reduction potentials lie around -1 V vs S.C.E. The redox couple $Fe^{II}(L)/Fe^{III}(L)$ is potentially a good electrochemical mediator for redox catalysis.

In the chemistry of dioxygen activation, iron is one of the most involved metals.[1,2] In this context, the μ-oxo-bridged dinuclear complexes Fe—O—Fe have received extensive studies on the structural, magnetic and spectroscopic properties and are potentially models of biological systems.[2,3]

In this way the chemistry of iron Schiff base complexes has been investigated.[4] The monomeric complexes which are obtained under aerobic conditions exhibit the Fe^{III} oxidation state and present a distorted square-pyramidal structure with $Fe^{III}(L)X$ (L = Schiff base and X = anionic axial ligand, such as halide, pseudohalide, carboxylate, phenolate, thiolate, etc.) or six-coordinate species with a bidentate extra ligand.[4,5]

The iron(II) oxidation state may be reached under drastic anaerobic conditions and isolated as $Fe^{II}(L)$ species.[4] These complexes are extremely sensitive to dioxygen and lead to the formation upon oxygenation of the μ-oxo-bridged dinuclear complexes $(L)Fe^{III}—O—Fe^{III}(L)$, whose synthetic route is, by contrast, an acid–base reaction.[6–8]

$$2Fe(SALEN)^+ + H_2O \Leftrightarrow \mu\text{-O-}[Fe(SALEN)]_2 + 2H^+$$

$$K_D = 5 \times 10^{-13} \text{ mol dm}^{-3}\ ^{8,9} \quad (1)$$

* Author to whom correspondence should be addressed.

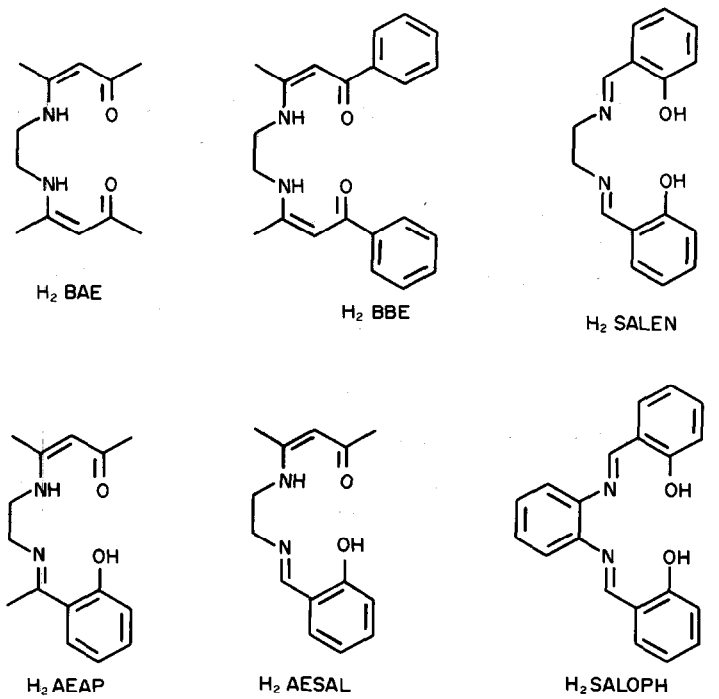

Fig. 1. Chemical schemes and abbreviations of the acid couple of the studied Schiff bases.

Unfortunately, little work has been undertaken on the electrochemistry of such complexes. The interaction with dioxygen involves redox processes and the determination of the electrochemical behaviour of these complexes must provide a clearer understanding of the oxygenation reaction.

In the course of investigating redox catalysis by coordination compounds, we engaged in the study of metal (Schiff base) redox properties.[10] The iron complexes have been found to be electrochemical mediators for the reduction of dioxygen. In this paper (Part I) we describe the electrochemical behaviour of several complexes, $Fe^{III}(L)Cl$, where L is an N_2O_2 Schiff base (SALEN type, Fig. 1): H_2BAE = N,N′-ethylene-bis(acetylacetoneimine);[11] H_2AESAL = N,N′-ethylene(acetylacetoneimine)(salicylideneimine);[12] H_2AEAP = N,N′-ethylene(acetylacetoneimine)(hydroxyacetophenoneimine);[12] H_2BBE = N,N′-ethylene-bis(benzoylacetoneimine);[11] H_2SALEN = N,N′-ethylene-bis(salicylideneimine);[13] and $H_2SALOPH$ = N,N′-orthophenylene-bis(salicylideneimine).[13] The complexes are referred to as Fe(BAE)Cl,[14] Fe(AESAL)Cl,[15] Fe(AEAP)Cl,[16] Fe(BBE)Cl,[14] Fe(SALEN)Cl[13] and Fe(SALOPH)Cl.[13]

RESULTS AND DISCUSSION

Within the electroactivity domain of the solvent, the voltammograms show distinct electrode processes (Fig. 2):

(1) An oxidation process around 1 V, which has been described to be the Schiff base oxidation. It leads to deposition of the complex at the electrode.[17]

(2) A reduction process around −0.5 V, which corresponds to the electrochemical system.[4,8,20]

$$Fe(L)Cl + e \Leftrightarrow Fe(L)Cl^- \qquad (2)$$

This system appears reversible if the potential sweep is restricted to the observation of this electrochemical process [Fig. 2(a), curve (+ + +)].

(3) A second reduction process around −1 V, which is observed when dioxygen is still present. It corresponds to the reduction of the μ-oxo bridged dinuclear complex (L)Fe—O—Fe(L).[10,18,21] With no dioxygen [Fig. 2(b), curve (—)], the voltamperogram presents only the Fe^{II}/Fe^{III} redox couple. With an incomplete deoxygenation [Fig. 2(b), curve(···)], the voltamperogram shows two successive reduction processes. The first one is slightly displaced anodically and corresponds to the original signal. The following system at −1.2 V comes from the oxygenation of Fe^{II}. If we compare with the voltamperogram of μ-oxo (L)Fe—O—Fe(L) [Fig. 2(b), curve (+ + +)], we observe that the reduction potentials are of the same order of magnitude. Then, the final product of the oxygenation of $Fe^{II}(L)$ is the dimer $(L)Fe^{III}—O—Fe^{III}(L)$. This reaction is very fast and no intermediates could be detected using cyclic voltammetry at a scan speed up to 2000 V s^{-1}.[22]

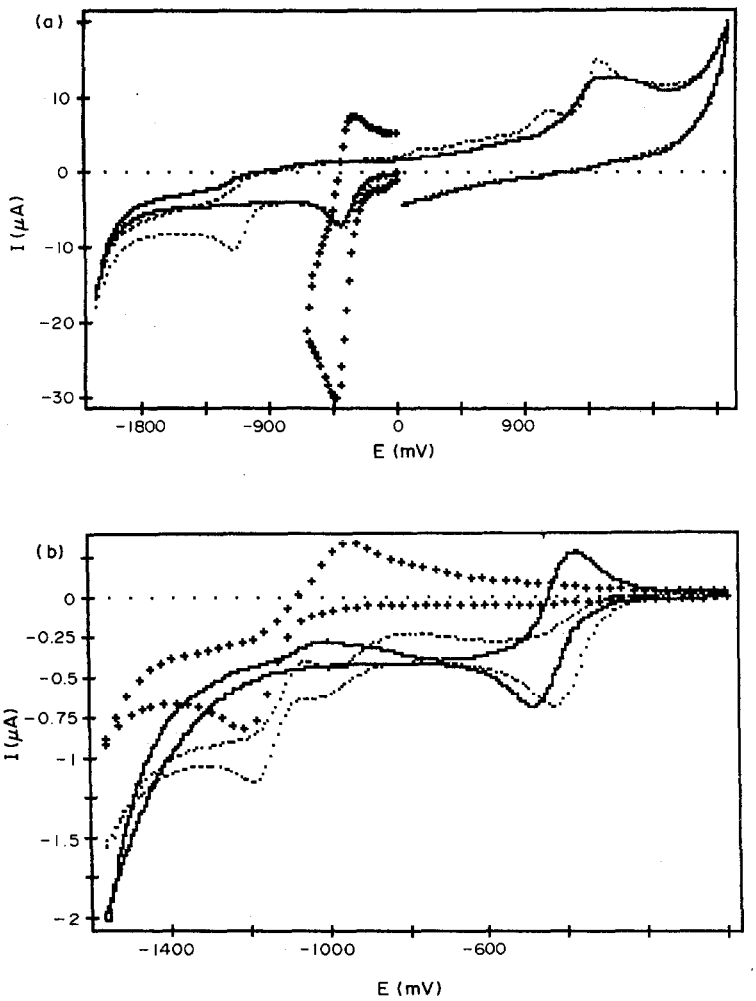

Fig. 2. General voltamperogram of $Fe^{III}(L)Cl$ complexes at a platinum electrode: (a) in CH_3CN–TBAHFP (0.1 mol dm^{-3}) and Fe(SALEN) (1 mmol dm^{-3}), Pt diameter 2 mm, potential sweep rate 0.1 (——) and (...) 2 V s^{-1} (+ + +); (b) in CH_2Cl_2–TBAHFP (0.1 mol dm^{-3}), potential sweep rate 0.1 V s^{-1}, Pt diameter 0.5 mm. (SALEN)Fe—O—Fe(SALEN) (1 mmol dm^{-3}) (+ + +); Fe(SALEN) (1 mmol dm^{-3}), under Ar (——) and with O_2 traces (· · ·).

(4) In CH_3CN or DMF on a gold electrode, voltammograms may show a reduction process around −1.8 V, which has been attributed to a second reduction of iron:[19,23]

$$Fe^{II}(L)+e \Leftrightarrow Fe^{I}(L) \qquad (3)$$

In the sequel the study is restricted to the electrochemical reduction of Fe^{III} into Fe^{II}. Exhaustive electrolysis of $Fe^{III}(L)Cl$ at the potential −0.6 to −0.8 V confirms that there is a monoelectronic exchange. With L = SALEN, the orange–brown solution (λ = 480 nm) turns light yellow (λ = 280 nm); reoxidation of the solution gives back the initial solution. It must be pointed out that electrolysis must be conducted under rigorously anaerobic conditions. $Fe^{II}(L)Cl$ solutions are extremely sensitive to dioxygen and yield the μ-oxo-bridged dinuclear complex. Even with bubbling Argon U as a blanket, we noticed the oxygenation of $Fe^{II}(L)Cl$.

As expected, the potential of this couple depends on the nature of the Schiff base (Fig. 3). Quantitative evaluations of the effect on the redox potential of changing the ligand structure have been made for Schiff base complexes of cobalt(II), nickel(II) and copper(II).[24] The increase in the electronic delocalization of the Schiff base ring (from BAE to SALOPH) shifts the redox potential towards the anodic side. It makes the electrochemical reduction of Fe^{III} into Fe^{II} easier. According to the general equation of the potential shifts with the complexation constants:[25]

$$E'^{0} = E^{0} + 0.058 \log \frac{\alpha Fe^{II}}{\alpha Fe^{III}},$$

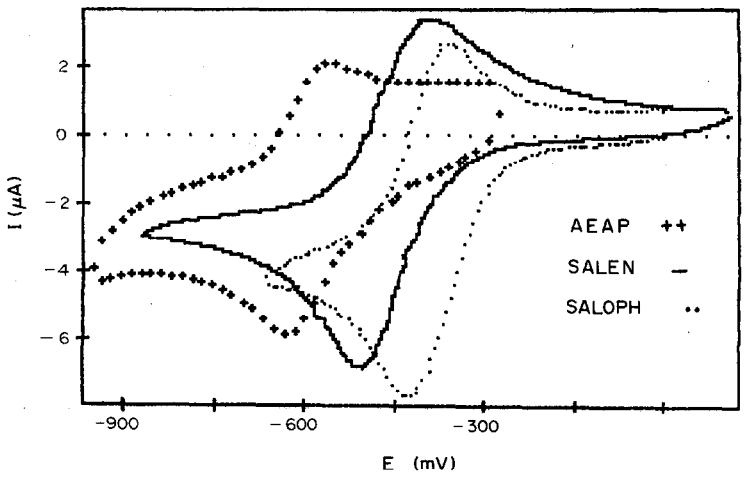

Fig. 3. Cyclic voltamperograms in CH_2Cl_2–TBAHFP (0.1 mol dm^{-3}) of $Fe^{III}(L)Cl$ (1 mmol dm^{-3}), potential sweep rate 0.1 V s^{-1}. L = AEAP (+ + +), SALEN (——), SALOPH (···).

where E'^0 is the observed redox potential, E^0 is the redox potential of Fe^{2+}/Fe^{3+} [26] and α represents the complexation coefficient and is a linear function of the complexation constants $(1+\beta_X[L])$, it appears that vs the free Fe^{2+}/Fe^{3+} redox couple the potential of these complexes is more cathodic: Fe^{3+} is more complexed than Fe^{2+}, $\beta_{III} > \beta_{II}$. $Fe^{II}(L)Cl$ complexes are powerful reducers. When delocalization is introduced on the ligand, the anodic shift of the potential traduces an increase in the complexation of Fe^{2+} vs Fe^{3+}. The potential shift is almost proportional to the ratio of the complexation constants of $Fe^{III}(L)Cl$ and $Fe^{II}(L)Cl$. The ratio β_{III}/β_{II} decreases when the delocalization increases which means that delocalized bases are better stabilizers for Fe^{2+}.

Besides the thermodynamic influence of the Schiff base, the delocalization on the base increases the kinetics of the electron transfer. By cyclic voltammetry (Table 2) the peak separation ΔE_p is decreased and the peak ratio RI_p tends to 1 from BAE to SALOPH (see below).

Stationary conditions, Table 1

At a rotating platinum disc electrode, the voltammograms show the diffusion controlled wave of the reduction of Fe^{III} into Fe^{II}. The waves can be badly defined and show the presence of a slow electron-transfer, according to the nature of the Schiff base and also to the electrode surface. We observed some passivation phenomena, especially

Table 1. Electrochemical characteristics under stationary conditions of $Fe^{III}(L)Cl$ complexes (1 mmol dm^{-3}); Pt rotating electrode 1000 t min^{-1}

	$E_{1/2}$ (mV)	I_D (μA)	p (mV)[a]
Solvent CH_2Cl_2, TBAHFP (0.1 mol dm^{-3})			
Fe(BAE)Cl	−662	−15.1	134
Fe(AEAP)Cl	−552	−18.3	100
Fe(AESAL)Cl	−491	−12.5	122
Fe(BBE)Cl	−513	−23.4	74
Fe(SALEN)Cl	−447	−16.4	72
Fe(SALOPH)Cl	−379	−15.3	70
Solvent CH_3CN, TBAHFP (0.1 mol dm^{-3})			
Fe(AEAP)Cl	−563	−16.6	108
Fe(BBE)Cl	−515	−18.3	94
Fe(SALEN)Cl	−400	−20.1	79
Fe(SALOPH)Cl	−314	−21.8	92

[a] p = slope of the linear regression of $E = f(\log|I_D - I/I|)$.

when the potential sweeps the whole electroactivity domain. The reduction passivation may be attributed to the imine bond reduction of the base (L),[27] yielding C—C bonds and then polymeric deposits. This implies direct reduction of the base or electron-transfer from the metal to the base.[28] In each case when the voltamperogram was badly defined the electrode was cleaned until the spectra were reproducible.

In CH_3CN or CH_2Cl_2 the limiting currents obey the Levich law; they are proportional to the square root of the electrode rotation speed (from 500 t min^{-1} to 4000 t min^{-1}) as for a diffusion controlled process. However, from Table 1 we can see a large discrepancy for the diffusion currents in dichloromethane, especially for Fe^{III}(BBE)Cl. We cannot explain this behaviour: it could be a surface phenomenon because in acetonitrile the diffusion current of Fe^{III}(BBE) is of the same order of magnitude. If we assume that Fe^{III}(SALEN)Cl and Fe^{III}(SALOPH)Cl present the behaviour of a simple reversible system, we obtain in dichloromethane a diffusion coefficient of 6×10^{-6} cm^2 s^{-1}. Versus this reference, when the currents are lower than the reference, passivation phenomena can be invoked and the wave is broadened. When the currents are higher than the reference a redox reaction (catalytic dioxygen reduction, for example) may explain this observation as for Fe^{III}(BBE)Cl.

The study of the variation of the limiting currents as a function of the complex concentration shows two types of behaviour. In CH_3CN, a dissociative solvent,[27,29] limiting currents are proportional to the concentration in the usual domain (up to 5 mmol dm^{-3}). In CH_2Cl_2, a non-dissociative and non-donor solvent[25,29] (Fig. 4), the linearity between the diffusion current and concentration is only observed at low concentrations, the upper limit depends on the nature of the base: 0.6 for AESAL, 1 for BBE, 2 for SALOPH, 3 mmol dm^{-3} for AEAP, etc. We tried to explain the different behaviours according to the solvent by solvation of the species. In the solid phase RX diffraction reveals dimeric structures,[13] which is hexa-coordination of iron with a distorted Schiff base. The sixth coordination comes from an oxygen of a proximal Schiff base.[13,30] Then, in low dissociative solvents such as dichloromethane, the deviation from linearity of $I_D = f(C)$ may come from the formation of dimers at high concentrations, traducing a limited solvation:

$$[Fe(L)Cl]_2 \longrightarrow 2Fe(L)Cl \quad (4)$$

$$Fe(L)Cl + e \Leftrightarrow Fe(L)Cl^- \quad (5)$$

Least-squares fittings of the curves $I_D = f(C)$ do not give satisfactory results and UV–vis spectroscopy does not prove this formation. However, it would explain the different behaviour between acetonitrile and dichloromethane. In dissociative and donor solvent such as CH_3CN the hexa-coordination of iron may be reached with the help of the solvent:

$$Fe(L)Cl + CH_3CN \longrightarrow Fe(L)Cl(CH_3CN) \quad (6)$$

Such solvation can go further, as in DMSO where the axial Cl^- ligand is replaced by the solvent.[18,31] However, we did not observe free Cl^- in CH_3CN, which is detected by an oxidation potential around 0.9 V. CH_3CN is too weak a donor solvent to replace the axial Cl^- ligand.

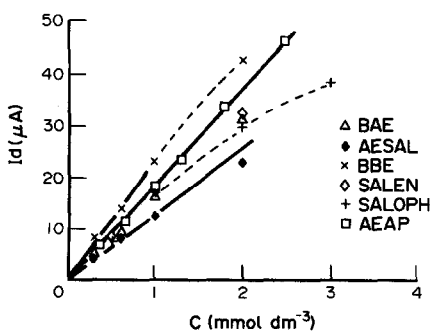

Fig. 4. Limiting current $|I_D|$ vs concentration for Fe(L)Cl complexes in CH_2Cl_2–TBAHFP (0.1 mol dm^{-3}); electrode rotation speed $\omega = 1000$ t min^{-1}.

Cyclic voltammetry, Table 2 (Figs 3 and 5)

At a platinum electrode, the voltammograms of the redox couple Fe^{II}/Fe^{III} present the shape of reversible systems (Fig. 5). As under stationary conditions passivation phenomena disturb the recordings: the peaks are broadened and the peak separation ΔE_p is increased. However, as mentioned above, the reported values are taken with the best drawn voltamperograms.

In fact, the electrochemical process is not restricted to a mono-electronic transfer; the reduction of Fe^{III} yields a more or less stable Fe^{II}, whose accepted electron may be transferred to the Schiff base[27] or to a substrate in solution. Thus, the apparent reversibility depends on the stability of Fe^{II}; if the potential sweep rate is increased the decomposition of Fe^{II} is limited and the peak ratio RI_p increases according to an EC scheme. The electronic delocalization of the Schiff base increases the stability of Fe^{II}: the peak ratio RI_p (Fig. 6) increases with the number of aromatic rings in the base and approaches 1 for Fe^{III}(SALOPH)Cl. Furthermore, the delocalization of the base im-

Table 2. Electrochemical characteristics by cyclic voltammetry of $Fe^{III}(L)Cl$ complexes (1 mmol dm^{-3}); Pt electrode, potential scan speed 0.1 V s^{-1}

	E_p red (mV)	ΔE_p (mV)[a]	I_p red (μA)	RI_p[b]
Solvent CH_2Cl_2, TBAHFP (0.1 mol dm^{-3})				
Fe(BAE)Cl	−682	115	−3.5	0.55
Fe(AEAP)Cl	−624	60	−3.7	0.77
Fe(AESAL)Cl	−521	139	−6.7	0.61
Fe(BBE)Cl	−567	71	−5.5	0.60
Fe(SALEN)Cl	−502	92	−6.2	0.83
Fe(SALOPH)Cl	−425	65	−7.1	0.92
Solvent CH_3CN, TBAHFP (0.1 mol dm^{-3})				
Fe(AEAP)Cl	−592	194	−6.2	0.44
Fe(BBE)Cl	−560	78	−5.8	0.72
Fe(SALEN)Cl	−485	86	−6.4	0.80
Fe(SALOPH)Cl	−362	80	−7.5	0.72

[a] $\Delta E_p = E_{p\,backward} - E_{p\,forward} = E_{p\,ox} - E_{p\,red}$.
[b] $RI_p = |I_{p\,backward}/I_{p\,forward}| = |I_{p\,ox}/I_{p\,red}|$.

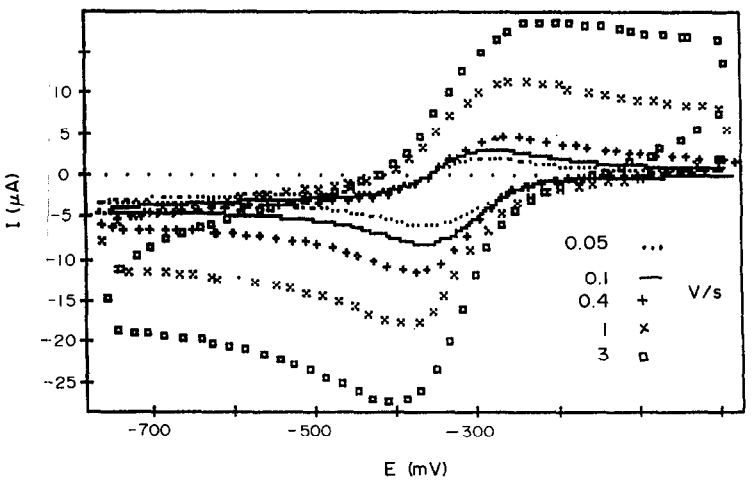

Fig. 5. Cyclic voltamperograms in CH_3CN–TBAHFP (0.1 mol dm^{-3}) of Fe^{III}(SALOPH)Cl (1 mmol dm^{-3}) for various potential sweep rates.

proves the electron transfer: the peak separation ΔE_p (Table 2) decreases with the number of aromatic rings in the base. Taking into account the above results and the chemical reactivity of these complexes, the electrochemical process is expressed by the following scheme:

$$Fe^{III}(L)Cl + e \Leftrightarrow Fe^{II}(L)Cl^- \qquad E$$

$$Fe^{II}(L)Cl^- \xrightarrow{k_1} Fe^{III}(L^\circ)Cl^- \longrightarrow$$

$$\text{dimers} \longrightarrow \text{polymers} \qquad C1$$

$$Fe^{II}(L)Cl^- + S \xrightarrow{k'_1} Fe^{III}(L)Cl + S^\circ \longrightarrow \text{pdts} \qquad C'1$$

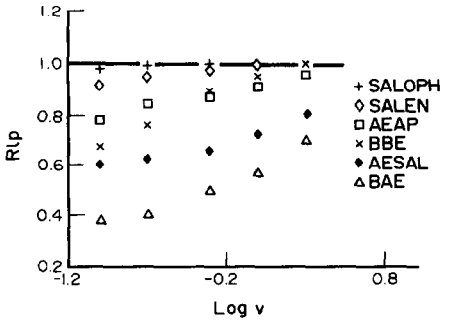

Fig. 6. Plots of RI_p ($= |Ip_{ox}/Ip_{red}|$) vs log V (potential scan rate) for Fe(L)Cl (1 mmol dm^{-3}) in CH_2Cl_2 and TBAHFP (0.1 mol dm^{-3}).

Reactions C1 and C'1 represent the following reaction of an EC scheme: C1 is the intramolecular electron transfer which should yield dimeric species bridged by a C—C bond of the imine of the base and C'1 is a bimolecular redox reaction in solution.

Exhaustive electrolysis of Fe^{III}(SALEN)Cl does not yield dimeric species as in the chemical reduction with sodium[27,28] or in the electrochemical reduction of Ni^{II}(SALOPH).[32] When electrolysis was performed with high concentrations of the complex (10^{-2} mol dm^{-3}), passivation phenomena occurred and the electrolysis was blocked at ~0.8–0.9 Faraday per mole with a red-brownish deposit on the working electrode. If the electrolysis was conducted in CH_3CN–Et_4NBF_4 and the reddish solution after electrolysis evaporated, then, by the addition of CH_2Cl_2 the complex was dissolved and separated from the supporting electrolyte. After evaporation of the solvent a reddish powder was recovered. The mass spectrum of this powder gave by impact electronic ionization (70 eV) the pattern of the initial compound Fe^{III}(SALEN)Cl: m/z at 357 then m/z at 322 (loss of Cl); no higher mass was detected. Moreover, the mass spectrum of the deposit on the electrode gave, by NH_3 chemical ionization, quite a simple spectrum: MH^+/z at 661 corresponding to the μ-oxo-bridged dinuclear complex (L)Fe—O—Fe(L) then MH^+/z at 340 for (L)Fe—O and MH^+/z at 323 for Fe(L). The appearance of this compound derives from dioxygen traces of Argon U, which is used as a blanket in the electrochemical cell. According to these results, we do not give the evidence of the reaction C1 but of the reaction C'1. Due to the high reactivity of iron(II), dioxygen traces (or residual water) are reduced. The process is not catalytic because the final product is the μ-oxo (L)Fe—O—Fe(L) complex:

$$2Fe^{II}(SALEN)CL + \tfrac{1}{2}O_2 \longrightarrow \mu\text{-O-[Fe(SALEN)]}_2. \quad (7)$$

It appears that the electrochemical behaviour of iron complexes is different from that of the nickel analogues.[32] The reduction of Ni^{II}(SALOPH) yields a dimer according to:

$$Ni^{II}(L) + e \Leftrightarrow [Ni^{II}(L^{\circ})]^- \quad (8)$$

$$2[Ni^{II}(L^{\circ})]^- \longrightarrow [Ni^{II}(L)]_2^{2-}; \quad (9)$$

this dimer, being electroactive, is easily electrochemically detected. This electrochemical difference may be attributed to the energy level of the reduction, that is the potential. The Ni^{II}(L) reduction is around 1 V more negative than the Fe^{III}(L)Cl reduction: the intramolecular electron-transfer towards the ligand may proceed in the reduced form of Ni^{II}(L).

Coming back to the kinetics view of the electrochemical system, the analysis of the I_p peak current vs the square root of the potential sweep rate shows different behaviour between CH_3CN and CH_2Cl_2. In CH_3CN peak currents are proportional to the square root of the potential sweep rate, whatever the nature of the base. The plots I_p vs $\sqrt{v}$ present almost the same slope. The electrochemical system follows the EC1' pathway. The peak ratio RI_p is generally lower than in CH_2Cl_2, indicating a higher constant, k'_1 (or higher amounts of O_2 traces), in CH_3CN than in CH_2Cl_2. In CH_2Cl_2 (Fig. 7) different types of behaviour are observed, according to the Schiff base vs the theoretical law[33] of a reversible system [with $D = 6 \times 10^{-6}$ cm^2 s^{-1}, average value gathered from the Levich law under stationary conditions for Fe^{III}(SALEN)Cl and Fe^{III}(SALOPH)Cl]. Among the complexes only those derived from SALEN and SALOPH present $I_p/\sqrt{v}$ plots which follow this law. The complexes of BAE, AESAL and AEAP show $I_p/\sqrt{v}$ plots with values of peak currents lower than expected, indicating that the process is controlled by a preceding step. This limiting step may be the dimerization reaction[4] already invoked under stationary conditions. This reaction is complete in dissociative and donor solvents, where the Fe(L)Cl complex can reach hexa-coordination by ligating a solvent molecule.

CONCLUSION

Up until now, not much data have been given on the electrochemical properties of Fe^{III} Schiff base complexes. This is surprising because iron is one of the most engaged metals in the bio-activation of dioxygen. Only iron porphyrin-type complexes have been fully described. We have presented the electrochemical behaviour of six iron N_2O_2 donor-Schiff base complexes (SALEN type) in an aprotic solvent. It appears that Fe^{II} is much more stabilized

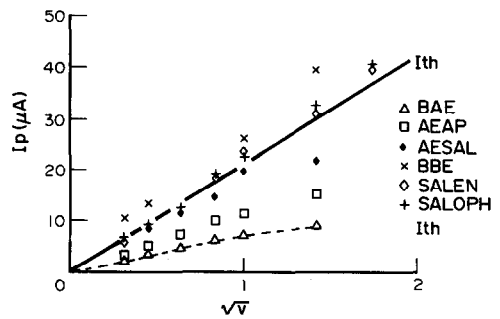

Fig. 7. Plots of $|I_{p\,red}|$ vs $\sqrt{v}$ (potential scan rate) for Fe(L)Cl (1 mmol dm^{-3}) in CH_2Cl_2–TBAHFP.

by a high electronic delocalization of the ligand than Fe^{III}. Moreover, these complexes tend to reach hexa-coordination either by dimerization in non-dissociative solvents, as in the solid phase, or by solvent coordination. This free position, as well as the replaceable Cl axial ligand, is promising for activation of molecules by redox catalysis. Furthermore, $Fe^{II}(L)Cl$ is extremely reactive and presents good opportunities for mediated electrochemical reduction. We must keep in mind that the working potential can be adjusted by the nature of the Schiff base. The reactivity of Fe^{II} with the dioxygen traces of Argon U has been noted. Reaction with O_2 yields the μ-oxo-bridged dinuclear complex (L)Fe—O—Fe(L), which appears as a thermodynamic well.[23] However, the $Fe^{III}(L)Cl$ complexes can manage the dioxygen activation through $Fe^{II}(L)Cl$. This will be the subject of a forthcoming paper.

EXPERIMENTAL

Products

The Schiff bases are prepared according to literature methods through the well-known amine–aldehyde (or –ketone) condensation: H_2BAE,[11] H_2AESAL,[12] H_2AEAP,[12] H_2BBE,[11] H_2SALEN[13] and $H_2SALOPH$.[13]

The monomeric complexes Fe(L)Cl are synthesized by the complexation of $FeCl_3$ with the protonated ligand H_2L in basic methanol.

Fe(AESAL)Cl. To a methanolic solution (20 cm^3) of H_2AESAL (0.5 g, 2.03 mmol) were added triethylamine, NEt_3 (0.6 cm^3), and $FeCl_3$ (0.33 g, 2.03 mmol) dissolved in methanol (20 cm^3). The solution was refluxed for 40 min and then concentrated *in vacuo* to *ca* 20 cm^3. On cooling, the black microcrystalline solid which precipitated was filtered and dried (0.41 g, 60%). Found: C, 50.8; H, 4.6; N, 8.6. Calc. for $C_{14}H_{16}FeN_2O_2$: C, 50.1; H, 4.8; N, 8.3%. The synthesis of this compound was first described[15] according to a complex process through a copper complex which was demetallated before the iron complexation.

The other complexes were prepared according to literature methods: Fe(BAE)Cl,[14] Fe(AEAP)Cl,[16] Fe(BBE)Cl,[15] Fe(SALEN)Cl[13] and Fe(SALOPH)Cl.[13]

Physical measurements

Electrochemical measurements were carried out with a home-made potentiostat controlled by an Apple IIe micro-computer.[34] The electrochemical cell was a conventional one with three electrodes [working electrode: Pt (diameter 2 mm, EDI, Tacusse, or diameter 0.5 mm) for analytical purposes and Pt foil for electrolysis; counter electrode: Pt wire; reference electrode: Ag/AgCl, KCl (0.1 mol dm^{-3}) or S.C.E.]; the potentials are measured vs S.C.E. The supporting electrolyte Bu_4NPF_6 (TBAHPF, Aldrich analytical grade) was used as received. Acetonitrile, CH_3CN (Aldrich, Gold Label), was used without any further purification, whilst dichloromethane, CH_2Cl_2 (SDS, purex), was passed over alumina prior to use. UV–vis spectroscopic measurements were conducted with an UVIKON 930 spectrophotometer (Kontron Instruments).

Acknowledgements—We thank Suzy Richelme [Service de Spectrométrie de Masse (Nermag R10-10), Université Paul Sabatier, Toulouse] for her technical assistance with the mass spectra.

REFERENCES

1. J. P. Collman, T. R. Halbert and K. S. Suslik, in *Metal Ion Activation of Oxygen* (Edited by T. Spiro). Wiley Interscience, New York (1980); *Molecular Mechanisms of Oxygen Activation* (Edited by O. Hayaishi). Academic Press, New York (1974).
2. L. Que Jr, *Coord. Chem. Rev.* 1983, **50**, 73; L. Que Jr and A. E. True, *Prog. Inorg. Chem.* 1990, **38**, 97.
3. K. S. Murray, *Coord. Chem. Rev.* 1974, **12**, 1.
4. R. N. Mukherjee, A. J. Abrahamson, G. S. Patterson, T. D. P. Stack and R. H. Holm, *Inorg. Chem.* 1988, **27**, 2137 and refs therein.
5. R. B. Lauffer, R. H. Heistand and L. Que Jr, *Inorg. Chem.* 1983, **22**, 50.
6. F. Corazza, C. Floriani and M. Zehnder, *J. Chem. Soc., Dalton Trans.* 1987, 709.
7. J. Lewis, F. E. Mabbs and A. Richards, *J. Chem. Soc. (A)* 1967, 1014.
8. F. Lloret, J. Moratal and J. Faus, *J. Chem. Soc., Dalton Trans.* 1983, 1749.
9. F. Lloret, M. Mollar, J. Faus, M. Julve, I. Castro and W. Diaz, *Inorg. Chim. Acta* 1991, **189**, 195.
10. J.-P. Costes, D. de Montauzon, P.-L. Fabre, J.-B. Tommasino and B. Carre, *J. Electrochim. 91,* May 1991, CA 4.5.
11. P. J. McCarthy, R. J. Hovey, K. Deno and A. E. Martell, *J. Am. Chem. Soc.* 1955, **77**, 5820.
12. J.-P. Costes, G. Cros, M.-H. Darbieu and J.-P. Laurent, *Inorg. Chim. Acta* 1982, **60**, 111.
13. P. Pfeiffer, E. Breith, E. Lübbe and T. Tsumaki, *Justus Liebigs Ann. Chem.* 1933, **503**, 84.
14. B. W. Fitzsimmons, A. W. Smith, L. F. Larkworthy and K. A. Rogers, *J. Chem. Soc., Dalton Trans.* 1973, 676.
15. N. Matsumoto, K. Kimoto, A. Ohyoshi and Y. Maeda, *Bull. Chem. Soc. Japan* 1984, **57**, 3307.
16. N. Masumoto, K. Kimoto, K. Nishida, A. Ohyoshi and Y. Maeda, *Chem. Lett.* 1984, 479.

17. P. Audebert, P. Capdevielle and M. Maumy, *New J. Chem.* 1991, **15**, 235.
18. S. E. Wenk and F. A. Schultz, *J. Electroanalyt. Chem.* 1979, **101**, 89.
19. L. S. Jovanovic and L. J. Bjelica, *J. Electroanalyt. Chem.* 1988, **252**, 345.
20. L. J. Bjelica and L. S. Jovanovic, *J. Electroanalyt. Chem.* 1986, **213**, 85.
21. J.-P. Costes and P.-L. Fabre, Part II, to be published.
22. J.-B. Tommasino, Thèse d'Université, Toulouse (1992).
23. C. Floriani and F. Calderazzo, *J. Chem. Soc. (A)* 1971, 3665.
24. G. S. Patterson and R. H. Holm, *Bioinorg. Chem.* 1975, **4**, 257; J. A. Streeky, D. G. Pillsbury and D. H. Busch, *Inorg. Chem.* 1980, **19**, 3148; L. M. Araya, J. A. Vargas and J. A. Costamagna, *Trans. Met. Chem.* 1986, **11**, 312; P. Zanello and A. Cinquantini, *Trans. Met. Chem.* 1985, **10**, 370.
25. G. Charlot and B. Tremillon, *Les réactions chimiques dans les solvants et les sels fondus.* Gauthier-Villars, Paris (1963).
26. P. Kanatharana and M. S. Spritzer, *Analyt. Chem.* 1974, **46**, 958.
27. S. Gambarotto, F. Urso, C. Floriani, A. Chiesi-Villa and C. Guastini, *Inorg. Chem.* 1983, **22**, 3966.
28. S. Gambarotta, C. Floriani, A. Chiesi-Villa and C. Guastini, *J. Chem. Soc., Chem. Commun.* 1982, 756; S. Gambarotta, M. Mazzati, C. Floriani and M. Zehnder, *J. Chem. Soc., Chem. Commun.* 1984, 116.
29. V. Gutmann, *Struct. Bonding* 1973, **15**, 141.
30. J. L. Resce, J. C. Fanning, C. S. Day, S. J. Uhm, A. F. Croisy and L. K. Keefer, *Acta Cryst.* 1987, **C43**, 2100.
31. L. A. Constant and D. G. Davis, *Analyt. Chem.* 1975, **47**, 2253.
32. A. A. Isse, A. Gennaro and E. Vianello, *Electrochim. Acta* 1992, **37**, 113.
33. R. S. Nicholson and I. Shain, *Analyt. Chem.* 1964, **36**, 706.
34. P. Cassoux, R. Dartiguepeyron, P.-L. Fabre and D. de Montauzon, *Actual Chim.* 1985, **1–2**, 79; *Electrochim. Acta* 1985, **30**, 1485.

Polyhedron Vol. 12, No. 6, pp. 651–660, 1993
Printed in Great Britain

0277–5387/93 $6.00+.00
© 1993 Pergamon Press Ltd

ESR STUDIES OF LOW-SPIN [N^1,N^4-BIS(SALICYLIDENE)-S-ALKYL-ISOTHIOSEMICARBAZONATO]COBALT(II) COMPLEXES—II. ADDUCTS OF NITROGEN-, PHOSPHORUS-, ARSENIC-, OXYGEN- AND SULPHUR-DONOR BASES

KRZYSZTOF DRABENT,† JULIUSZ A. WOLNY, PIOTR J. CHMIELEWSKI, KAZIMIERZ GATNER and MIKOŁAJ F. RUDOLF

Institute of Chemistry, University of Wrocław, F. Joliot-Curie 14, 50-383 Wrocław, Poland

(*Received* 13 *October* 1992; *accepted* 2 *November* 1992)

Abstract—ESR spectra of [Co(Me,H,H)·H_2O] [Me,H,H = N^1,N^4-bis(salicylidene)-S-methyl-isothiosemicarbazone^{2-}] and its adducts with ligands containing nitrogen (pyridine, 4-CN pyridine, α- and γ-picoline, N-methyl- and N-ethylimidazole), phosphorus (tributyl-, triphenyl-, diphenylmethyl-, diphenylethylphosphine, triphenyl- and triethylphosphite), arsenic (triphenyl arsine), oxygen (DMF, THF) and sulphur (dimethyl-, diethyl-, diphenyl- and methylphenylsulphide) donor bases were studied in frozen solutions. All spectra were indicative of low-spin cobalt(II) centres with predominantly d_{z^2} character of the ground state. The determined values of A^{Co} and g tensor components and superhyperfine coupling constants observed for base donor atoms indicated the formation of five-coordinate mono-adducts. For some nitrogen bases (pyridine, 4-CN pyridine and γ-picoline) the formation of 1 : 2 six-coordinate bis-adducts was also observed. The bonding parameters were calculated. The activity of the N-donor adducts towards dioxygen is also reported.

Cobalt(II) Schiff-base complexes have attracted much attention because of their extensive coordination chemistry. In particular, the formation of adducts with Lewis bases and reversible dioxygen binding are well recognized features of these chelates.[1] The parent four-coordinate chelates and their adducts may be low-spin,[2] high-spin or exhibit spin cross-over properties.[3] Hitchman[4] has shown that for square pyramidal [Co(N_2O_2)·B] complexes a decrease in the in-plane ligand field strength and a shift of the cobalt(II) atom above the macrocycle plane are decisive for achieving the high-spin configuration. The addition of a second axial ligand may result in six-coordinate cross-over systems with an abrupt spin-state transition, as demonstrated by Charpin *et al.*[5] for bis(pyridine)[N,N′-ethylene-bis(3-carboxy-salicylaldimino)] cobalt(II). Although extensive efforts have been focused on tetradentate cobalt(II) Schiff-base complexes, some essential problems remain open: i.e. (1) the factors determining the formation and spin state of the six-coordinate species of the Co(Schiff base)(Lewis base)$_2$ type; and (2) the relation between structural features of the molecule and the affinity/reversibility of dioxygen binding.

Recently, a new type of four-coordinate Schiff base ligand has been reported. In the course of template condensation of salicylaldehyde S-alkyl-isothiosemicarbazone with a salicylaldehyde molecule in the presence of VO^{II}, Cu^{II}, Ni^{II}, Fe^{III} and Zn^{II} ions the corresponding chelates $M(R^1R^2R^3)$ of N^1,N^4-bis(salicylidene)-S-alkylisothiosemicarbazone as the ligand are formed (see Scheme 1).[6,7]

Demetallation of the nickel(II) complex with gaseous HCl yields the free ligand hydrochloride.[8] Gerbeleu *et al.*[9,10] synthesized the cobalt(II) complexes [Co($R^1R^2R^3$)·H_2O] (R^1 = Me, Et, Pr^n; $R^2 = R^3$ = H) from cobalt(II) diacetate tetrahydrate and the appropriate ligand hydrochloride. The complexes were characterized by their IR and electronic spectra. Magnetic susceptibility measurements proved the complexes to be low-spin.

In our recent paper a more convenient synthetic route to the above complexes involving the direct template synthesis has been reported, together with ESR studies of CoL·H_2O complexes doped into

† Author to whom correspondence should be addressed.

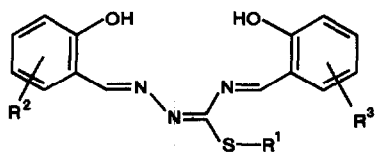

$[R^1R^2R^3]$

R^1 = Me, Et, Pr^n, Bu^n

$R^2 = R^3 = H$

Scheme 1.

the corresponding $ZnL \cdot H_2O$ host lattices.[11] In the present paper ESR studies of five- and six-coordinate adducts of the title complexes are presented. The redox properties and reactivity of base adducts towards dioxygen are also reported.

EXPERIMENTAL

Preparation of the ligands and complexes

The S-alkyl isothiosemicarbazone ligands were prepared according to the method described by Gerbeleu *et al.*[6] The complexes were synthesized as previously reported[11] by the direct template reaction of salicylaldehyde S-alkyl isothiosemicarbazones and salicylaldehyde in the presence of cobalt(II) diacetate tetrahydrate under a purified dinitrogen atmosphere in standard Schlenk-type glassware. The dehydration of the $[Co(R^1R^2R^3) \cdot H_2O]$ complexes was performed *in vacuo* at 100°C for a period of 1 h, yielding the unsolvated chelates.

ESR sample preparation

Samples for ESR studies were prepared under anaerobic conditions. The appropriate complex (1 mg) was placed in a quartz tube sealed with a serum-type stopper and toluene/CH_2Cl_2 (1:3, *ca* 0.25 cm^3), deoxygenated using the double syringe technique, was added. Toluene solutions of Lewis bases were added to the sample solutions with the use of a gas tight microsyringe.

Nematic phase solutions of $[Co(Me,H,H) \cdot H_2O]$ and $[Co(Me,H,H) \cdot py]$ in MBBA were oriented according to ref. 12 at 300 K with a magnetic field of 800 mT for 15 min and then rapidly frozen at 77 K.

Physicochemical methods

Magnetic susceptibilities were measured for the solid samples by the Gouy method at 80–295 K. Diamagnetic corrections were calculated from Pascal constants. Electronic spectra were measured at room temperature on a Beckman UV 5240 spectrometer. ESR spectra were recorded using an *X*-band SE/X spectrometer (Radiopan, Poland) equipped with a NMR magnetometer and MnO/MgO as the *g* calibrant. If not otherwise indicated the spectra were measured at 77 K. The details of the electrochemical experiments and processing data are given in ref. 13.

Calculations

ESR spectra were simulated using the computer program previously described.[11] The principal axes of the *g*, hyperfine and line-width tensors were assumed to be coincident in all but one case (*vide infra*). Quadrupole effects were neglected. An orientation dependent line-width was allowed for by means of a line-width tensor. Spectra were fitted by means of the Marquardt method.[14]

RESULTS AND DISCUSSION

Formation of five- and six-coordinate adducts of Lewis bases

The ESR spectra of five- and six-coordinate complexes were measured upon the addition of the appropriate nitrogen, phosphorus, arsenic, oxygen and sulphur donor bases to the toluene/dichloromethane solutions of $[Co(Me,H,H) \cdot H_2O]$. The amounts of bases needed to observe the spectra of adducts as well as the corresponding spectral patterns do not depend on whether samples of hydrated or dehydrated $Co(R^1R^2R^3)$ chelates have been used. However, it is noteworthy that the initial spectrum, i.e. that before the addition of the base, is strongly solvent dependent. If the solid complex (monohydrate or dehydrated) was dissolved in dry, freshly distilled CH_2Cl_2 and/or toluene only a broad, unresolved signal with $g \cong 2.3$ was observed at 77 K. On the other hand, if wet CH_2Cl_2 (saturated in H_2O) was used a neatly resolved spectrum was observed (Fig. 1). Similar effects were observed for complexes with R^1 = Et, Pr^n and Bu^n. The reason for the above behaviour is not obvious, but most likely results from association of the four-coordinate species, particularly at lower temperatures. Addition of the Lewis base resulted in the development of the spectrum of the adduct.

Nitrogen donor Lewis bases. For pyridine, γ-picoline, 4-cyanopyridine, N-methyl- and N-ethylimidazole (py, γ-pic, 4-CNpy, MeIm and EtIm,

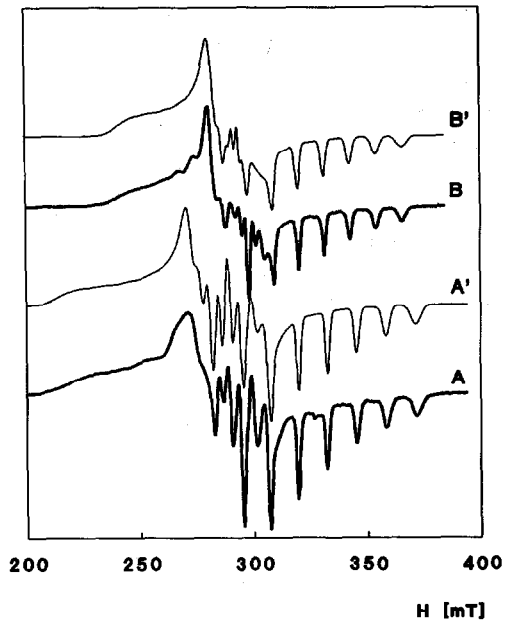

Fig. 1. ESR spectra of (A) [Co(Me,H,H)·H_2O], (B) [Co(Me,H,H)·Et_2S] in CH_2Cl_2/toluene at 77 K. (A′) and (B′) are best fits of (A) and (B), respectively.

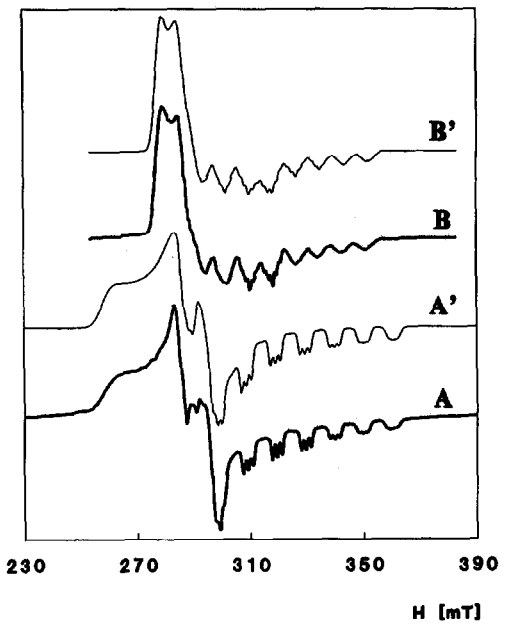

Fig. 2. ESR spectra of (A) [Co(Me,H,H,)·4-CNpy], (B) [Co(Me,H,H)·(4-CNpy)$_2$] in CH_2Cl_2/toluene at 77 K. (A′) and (B′) are best fits of (A) and (B), respectively.

respectively) the spectra of CoL·B complexes were observed at chelate-to-base ratios as low as 1 : 1.5 (at this ratio the last traces of the initial spectrum vanish). The spectra are orthorhombic, showing superhyperfine structure in the high-field region due to one ^{14}N nucleus. For py, γ-pic and 4-CNpy a further spectral evolution was observed, eventually yielding the spectra of the low-spin six-coordinate bis-adducts at a chelate-to-base ratio as low as 1 : 2.5. In these spectra superhyperfine splitting due to two equivalent ^{14}N nuclei is observed. The anisotropy of the spectrum is reduced in comparison with that of the monoadduct, as might be expected.[2] Similar behaviour was observed for all R^1-substituted complexes. This implies that introducing a substituent having a longer chain on the equatorial ligand does not produce any considerable steric hindrance and the formation of bis-adducts is still possible. On the other hand, the steric overcrowding plays an important role if present on the axial ligand. For α-picoline (α-pic) the formation of bis-adducts was not observed, even at a chelate-to-base ratio as large as 1 : 200. This might be interpreted in terms of steric effects of the α-methyl group, resulting in an appreciable shift of the central ion out of the N_2O_2 plane of the Schiff base upon coordination, which is more pronounced than in the case of less sterically demanding bases, and therefore preventing the coordination of a second base molecule.

For N-methyl- and N-ethylimidazole an increase of the base concentration resulted in a gradual disappearance of the initially observed mono-adduct spectrum. Hence, the formation of a high-spin, ESR silent six-coordinate species is inferred.

Typical spectra of five- and six-coordinate nitrogen donor adducts are presented in Fig. 2.

As mentioned above, the formation of mono- and bis-pyridine adducts of [Co(R^1HH)·H_2O], where R^1 = Et, Pr^n and Bu^n, has been studied. In all cases both types of adducts were formed. However, the ESR parameters were virtually identical to those observed for R^1 = Me adducts and, therefore, no detailed studies were performed for these systems.

The adduct formation at room temperature was also investigated by means of electronic spectroscopy. The titration of a CH_2Cl_2 solution of [Co(Me,H,H)·H_2O] with pyridine and 4-cyanopyridine revealed an alteration of the spectral pattern. In both cases the intensities of bands at *ca* 8000, 17,500, 23,200 and 25,000 cm^{-1} decrease. A new band at *ca* 20,000 cm^{-1} and an ill-defined shoulder at *ca* 11,000 cm^{-1} were observed with increasing amine concentration. The lack of isosbestic points implies the simultaneous presence of mono- and dipyridine adducts, beside the starting chelate.

Phosphorus donor Lewis bases. The five-coordinated adducts of the general formula [Co(Me,H,H)·B] [B = PPh_3, PPh_2Me, PPh_2Et, $P(OPh)_3$ and

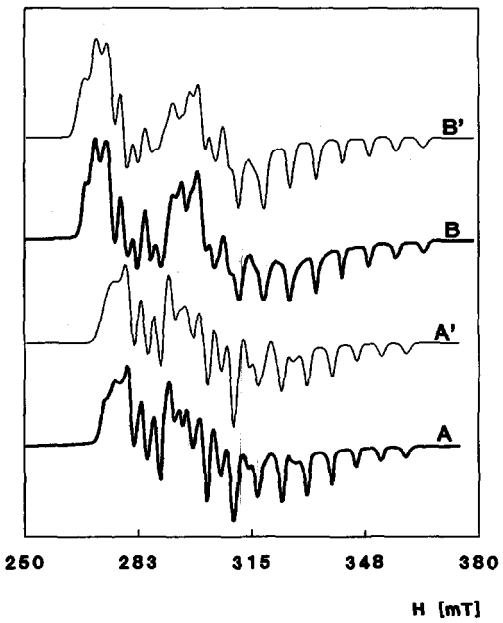

Fig. 3. ESR spectra of (A) [Co(Me,H,H)·PBu_3] and (B) [Co(Me,H,H)·$P(OEt)_3$] in CH_2Cl_2/toluene at 77 K. (A′) and (B′) are best fits of (A) and (B), respectively.

$P(OEt)_3$] are formed upon the addition of phosphorus Lewis bases (see Fig. 3). No traces of the starting complex (aquo-adduct) were detected at a chelate-to-base ratio of *ca* 1 : 5. A further increase of the base concentration does not produce any change in the spectrum up to a complex-to-base ratio of 1 : 100. The spectra are typical for phosphorus donor adducts observed previously for low-spin cobalt(II) complexes of Schiff bases,[15–17] porphyrins,[18] dimethylglyoximates[19] and tetraazamacrocycles.[20,21]

Oxygen, sulphur and arsenic donor ligands. The spectra of [Co(Me,H,H)·H_2O] in dimethylformamide and tetrahydrofurane resemble those of Co[saloph] in the corresponding solvents, reported by Haas and von Zelewsky.[15] One cannot definitely say whether these spectra are due to five- and six-coordinate complexes. However, the titration of a toluene/CH_2Cl_2 solution of [Co(R,H,H)·H_2O] with DMF results in the spectrum observed for a frozen solution of [Co(Me,H,H)·H_2O] in neat DMF, suggesting that the spectrum corresponds to the complex with one coordinated solvent molecule. Unfortunately, the spectrum of [Co(Me,H,H)·H_2O] in a DMSO/toluene frozen solution indicates the presence of *ca* 50% of the starting monoaquo adduct, the spectrum thereof being superimposed on a signal which is most likely due to the DMSO adduct. Therefore, the ESR parameters of the latter were not determined.

The addition of dialkyl and arylalkyl sulphides to solutions of [Co(Me,H,H)·H_2O] resulted in spectral changes and at a *ca* 50-fold excess of sulphide the initial spectrum disappeared [see Fig. 1(B)]. During the addition of sulphide we observed only two types of spectra: the initial one due to [Co(Me,H,H)·H_2O] and that formed after the addition of sulphide. On this basis we believe that the latter might be attributed to coordination of one sulphide molecule.

It seems that the thioether sulphur donor atom has a much higher affinity to the cobalt(II) centre than the oxygen atom in ethers. In contrast to diethyl sulphide comparable or even higher concentrations of added diethyl ether do not affect the ESR spectrum of [Co(Me,H,H)·H_2O].

The triphenylarsine monoadduct formation was established on the basis of the superhyperfine splitting, due to the ^{75}As ($I = 3/2$) nucleus, observed in the central and low-field part of the spectrum (Fig. 4).

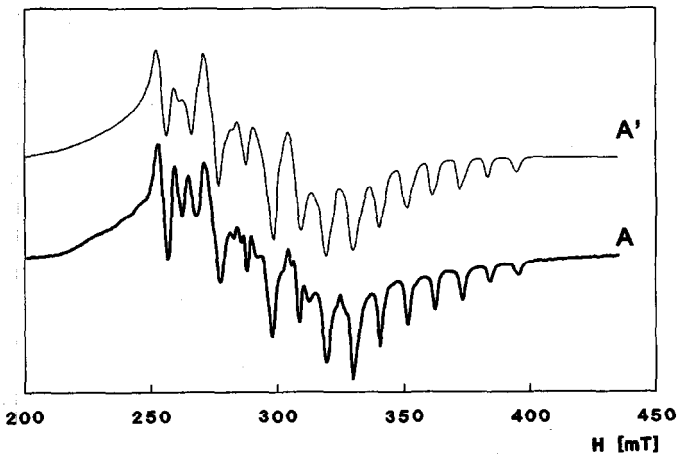

Fig. 4. ESR spectrum of (A) [Co(Me,H,H)·$AsPh_3$] in CH_2Cl_2/toluene at 77 K. (A′) is the best fit of (A).

It has to be pointed out that in no case, either for solid doped samples[11] or solutions, have traces of signals which might correspond to a four-coordinate species been observed.

Interpretation of the ESR spectra

In order to assign the principal magnetic axes of the systems under study the ESR spectra in an oriented nematic liquid crystal were studied. A rapidly frozen MBBA solution of [Co(Me,H,H)·H_2O] exhibits an ESR spectrum with a different pattern than that observed for frozen CH_2Cl_2/toluene solutions. The superhyperfine splitting observed on the high-field lines of the spectra in MBBA ($g = 2.010$, $A^{Co} = 107 \times 10^{-4}$ and $A^{N} = 13 \times 10^{-4}$ cm^{-1}) indicate coordination of one nitrogen atom to the cobalt(II) ion. This could be attributed to the coordination of the azomethine nitrogen atom of the MBBA molecule. On the other hand, a frozen MBBA solution of the [Co(Me,H,H)·py] adduct shows a spectrum with parameters identical to those observed for [Co(Me,H,H)·py] in non-coordinating solvents (see Table 1), but differing from those observed for the postulated [Co(Me,H,H)·MBBA] adduct. Consequently, we believe that neither the pyridine molecule can be replaced by MBBA in [Co(Me,H,H)·py] nor the sixth coordination site of the cobalt(II) centre occupied by an MBBA liquid crystal molecule.

The spectra showed an orientation dependence typical for planar complexes aligned in the direction of the long axis of the liquid crystal.[12] At an orientation of 0° (no rotation) the high-field component of the spectrum was quenched, giving rise to sharp features after sample rotation of 90° (Fig. 5). Accordingly, this component could be assigned as parallel to the z-axis of the complex, being normal to the plane established by the equatorial ligand.[12] The smallest value of the out-of-plane component of the g tensor is indicative of a d_{z^2} ground state.[22] Therefore, the largest component of g was assigned to the x component.

The spin-Hamiltonian parameters for cobalt(II) complexes under study are collected in Table 1. All these parameters were obtained from computer simulations of the experimental spectra. For the analysis of the g and cobalt hyperfine tensors

Table 1. Spin-Hamiltonian parameters for [Co(Me,H,H)·B] and [Co(Me,H,H)·2B] adducts

L[a]	A_x[b]	A_y[b]	A_z[b]	g_x[b]	g_y[b]	g_z[b]	$\langle A \rangle$	$\langle g \rangle$	A_x^B	A_y^B	A_z^B
CoL·H_2O	114.7	47.6	116.4	2.606	2.258	1.997	92.9	2.287			
CoL·THF	52.7	29.3	113.3	2.500	2.258	2.014	65.1	2.257			
CoL·DMF	39.1	16.4	104.7	2.443	2.223	2.020	53.4	2.229			
CoL·Me_2S	37.1	13.7	99.6	2.341	2.194	2.014	50.1	2.183			
CoL·Et_2S	73.8	24.6	106.4	2.462	2.221	2.004	69.3	2.229			
CoL·Ph_2S	106.9	42.1	120.0	2.570	2.257	2.000	89.7	2.276			
CoL·MePhS	64.3	37.0	112.9	2.450	2.197	2.007	71.4	2.218			
CoL·py	34.2	7.7	92.0	2.349	2.199	2.010	44.6	2.201	11.4	16.3	16.3
CoL·py_2	−22.5	−39.8	76.4	2.284	2.177	2.028	4.7	2.163	10.3	0.0	13.7
CoL·(γ-pic)	30.7	6.0	92.0	2.399	2.205	2.017	42.9	2.207	18.4	23.2	17.6
CoL·$(\gamma\text{-pic})_2$	−24.6	−42.8	74.9	2.282	2.175	2.028	2.5	2.162	2.1	0.0	14.2
CoL·(4-CNpy)	37.4	4.4	97.9	2.411	2.199	2.014	46.6	2.208	14.6	0.0	16.6
CoL·$(4\text{-CNpy})_2$	−20.9	−38.4	79.4	2.288	2.178	2.027	6.7	2.164	4.0	4.0	14.8
CoL·(α-pic)	61.0	19.2	99.4	2.518	2.225	2.009	59.9	2.251	10.0	15.4	16.0
CoL·(N-MeIm)	27.3	7.4	91.5	2.380	2.204	2.013	42.1	2.199	11.7	18.3	17.6
CoL·(N-EtIm)	25.9	7.1	91.0	2.380	2.207	2.016	41.3	2.201	11.7	19.6	17.6
CoL·PBu_3	−18.6	−40.4	66.6	2.265	2.155	2.014	2.5	2.145	167.7	174.0	203.2
CoL·$P\Phi_2Me$	−5.3	−30.7	72.5	2.271	2.157	2.010	12.2	2.146	171.9	171.0	195.6
CoL·$P\Phi_2Et$	−28.3	−36.9	68.4	2.231	2.152	2.014	1.1	2.132	162.1	167.4	197.4
CoL·$P\Phi_3$	−13.9	−15.2	81.1	2.314	2.176	2.012	17.6	2.167	180.7	159.2	183.3
CoL·$P(O\Phi)_3$	−38.9	−11.8	83.3	2.260	2.229	2.013	10.9	2.167	267.8	260.5	299.7
CoL·$P(OEt)_3$	−39.0	−12.0	72.0	2.240	2.360	2.020	7.0	2.204	230.6	252.0	283.0
CoL·$As\Phi_3$	98.0	−29.6	104.2	2.459	2.230	2.011	57.5	2.233	127.0	170.4	194.6

[a] L = (Me,H,H).

[b] Parameters estimated on the basis of the computer simulations. The ^{59}Co hyperfine A_i and appropriate base superhyperfine A_i^B constants are in 10^{-4} cm^{-1}. Error limits are: for $A_i \pm 1 \times 10^{-4}$ cm^{-1}; for $g_i \pm 0.001$.

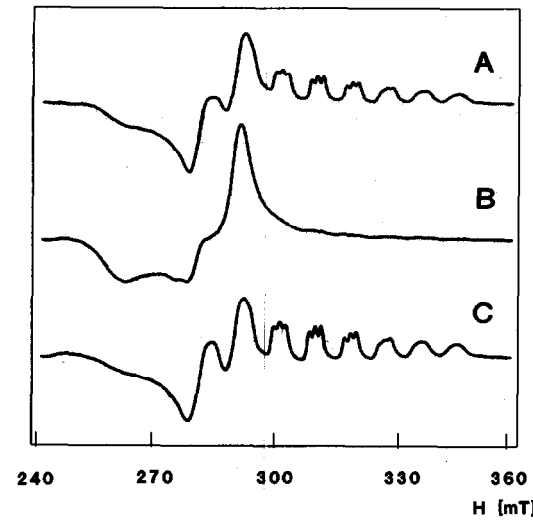

Fig. 5. ESR spectra of a frozen nematic (MBBA) solution of [Co(Me,H,H)·py]. (A) Non-oriented sample, (B) orientation 0°, and (C) orientation 90°.

McGarvey's theory of low-spin d^7 ions has been applied.[23]

As there are more unknowns than equations we have assumed, following Raynor *et al.*,[16,17] $c_3 = c_4 = c_5$, $c_6 = 0$ and $a^2 + b^2 = 1$ (where a and b are the contributions of the d_{z^2} and $d_{x^2-y^2}$ orbitals in the ground state function, respectively).

The values of the energy separations $\Delta B_1(d_{z^2}-d_{xz})$, $\Delta B_2(d_{z^2}-d_{yz})$ and ΔQ (average energy of quartet states) have been calculated from McGarvey's coefficients c_i $(i = 1/3)$, considering $c_i = (\rho_{3d}\lambda)/\Delta E_i$. The spin density in the d_{z^2} orbital ρ_{3d} was calculated as P/P^{2+}, with $P^{2+} = 0.0254$ cm^{-1},[23] and the free ion spin-orbit coupling parameter λ for the Co^{2+} ion has been chosen to be 533 cm^{-1}.[24] The cobalt 4s spin densities ρ_{4s} have been estimated according to eq. (1):[25]

$$-kP = \rho_{4s}a^*_{4s}(^{59}Co) + \rho_{3d}a^*_{3d}(^{59}Co) \qquad (1)$$

with $a^*_{4s}(^{59}Co) = 0.1232$, $a^*_{3d}(^{59}Co) = -0.0084$ cm^{-1}.[15]

The calculated values of c_i $(i = 1/3)$, a^2, b^2, P, k, ρ_{3d}, ρ_{4s}, ΔB_1, ΔB_2 and ΔQ are given in Table 2.

The signs for the cobalt coupling constants were established from the best fit of the experimental data, taking into account that P must be positive.

Table 2. The calculated values of c_i $(i = 1/3)$, a^2, b^2, P, k, ρ_{3d}, ρ_{4s}, ΔB_1, ΔB_2 and ΔQ and [Co(Me,H,H)·B] and [Co(Me,H,H)·2B] adducts

L[a]	c_1	c_2	c_3	a^2	b^2	P[b]	k	ρ_{3d}	ρ_{4s}	ΔB_1[c]	ΔB_2[c]	ΔQ[c]
CoL·H_2O	0.043	0.113	0.102	0.992	0.008	145	−0.364	0.570	0.082	7100	2680	2980
CoL·THF	0.047	0.076	0.113	0.997	0.003	219	−0.064	0.862	0.070	9830	6030	4050
CoL·DMF	0.038	0.067	0.119	0.998	0.002	199	−0.071	0.783	0.065	11,000	6230	3510
CoL·Me_2S	0.031	0.055	0.096	1.000	0.000	156	−0.160	0.614	0.062	10,620	5920	3410
CoL·Et_2S	0.036	0.082	0.089	0.997	0.003	152	−0.231	0.599	0.069	8900	3900	3630
CoL·Ph_2S	0.043	0.103	0.101	0.996	0.004	164	−0.283	0.645	0.082	8060	3340	3420
CoL·MePhS	0.035	0.072	0.091	0.999	0.001	153	−0.263	0.603	0.074	9270	4490	3530
CoL·py	0.033	0.064	0.091	1.000	0.000	161	−0.093	0.635	0.055	10,150	5320	3680
CoL·py_2	0.026	0.042	0.122	1.000	0.000	209	0.101	0.824	0.039	16,970	10,350	3600
CoL·(γ-pic)	0.034	0.062	0.109	1.000	0.000	172	−0.069	0.676	0.056	10,730	5760	3310
CoL·$(\gamma\text{-pic})_2$	0.025	0.042	0.122	1.000	0.000	210	0.111	0.828	0.038	17,340	10,460	3620
CoL·(4-CNpy)	0.033	0.066	0.104	1.000	0.000	181	−0.073	0.712	0.059	11,630	5760	3660
CoL·$(4\text{-CNpy})_2$	0.026	0.043	0.120	1.000	0.000	213	0.095	0.840	0.041	17,020	10,370	3720
CoL·(α-pic)	0.039	0.084	0.106	1.000	0.000	173	−0.114	0.682	0.063	9330	4350	3420
CoL·(N-MeIm)	0.034	0.060	0.097	1.000	0.000	166	−0.074	0.656	0.055	10,220	5840	3590
CoL·(N-EtIm)	0.034	0.059	0.104	1.000	0.000	169	−0.068	0.666	0.055	10,330	5990	3400
CoL·PBu_3	0.024	0.043	0.089	1.000	0.000	175	0.110	0.690	0.031	15,430	8630	4150
CoL·$P\Phi_2Me$	0.024	0.045	0.078	0.999	0.001	166	0.058	0.652	0.037	14,200	7700	4460
CoL·$P\Phi_2Et$	0.024	0.036	0.086	1.000	0.000	176	0.107	0.694	0.032	15,460	10,300	4300
CoL·$P\Phi_3$	0.031	0.047	0.087	0.997	0.003	189	0.056	0.746	0.042	12,960	8410	4570
CoL·$P(O\Phi)_3$	0.041	0.038	0.088	0.994	0.006	218	0.097	0.859	0.041	11,170	11,950	5220
CoL·$P(OEt)_3$	0.058	0.038	0.113	1.000	0.000	225	0.147	0.887	0.034	8200	12,500	4200
CoL·$As\Phi_3$	0.032	0.099	0.113	0.966	0.034	233	−0.037	0.918	0.070	15,390	4970	4330

[a] L = (Me,H,H).
[b] In 10^{-4} cm^{-1}.
[c] In cm^{-1}.

The values of g_i and A_i^{Co} for five- and six-coordinate adducts with oxygen, nitrogen and phosphorus donors lie in the ranges typical for cobalt(II) complexes of tetradentate Schiff bases.[2,15–17] Among the five-coordinate systems the higher anisotropy of g tensors is found for oxygen and sulphur donors, whereas the lowest was established for phosphorus bases reflecting the alteration of axial perturbation.[22] The link between the axial perturbation and anisotropy of g is also illustrated in the case of the α-picoline adduct. Due to the steric effect of the methyl group α-picoline should reveal weaker donor properties than other pyridine derivatives. In fact, adduct formation is observed at higher base concentrations and the spectrum displays appreciably higher g anisotropy than that of pyridine, γ-picoline and 4-cyanopyridine adducts (Table 1).

It is also to be noted that g anisotropy is considerably smaller for six-coordinate than for five-coordinate complexes in all cases where both adducts are formed. One can observe changes in the values of $\Delta_{xy}(g_x - g_y)$, usually taken as a measure of the rhombic distortion,[19,26] on going from five- to six-coordinate adducts. The value of Δ_{xy} observed for the six-coordinate bis-adducts is about half that calculated for the five-coordinate species. Such behaviour was found for the nitrogen base adducts of Co(saloph)[15] and phosphorus donor adducts of $Co(Hdmg)_2$ ($Hdmg^-$ = dimethylglyoximate),[19] and interpreted in terms of changes of the metal ion position with respect to equatorial ligands.[4,19,22]

The values of calculated energy gaps (ΔB_1 and ΔB_2, Table 2) between the ground state ($^2A_1$) and two doublet excited states ($^2B_1$ and $^2B_2$, respectively) fit well the range of those reported previously for the low-spin cobalt(II) chelates. Also, the values of average energy difference between the ground state and lowest lying quartets are close to those calculated for other systems.[15–17,19] A comparison of the calculated energy separations with those deduced from the electronic spectra agrees only roughly. The intense CT bands in the visible region reaching 14,000 cm^{-1} obviously obscure the much weaker *d–d* bands in this region. Nevertheless, at least part of the bands observed in the electronic spectra can be assigned to certain *d–d* transitions, mainly on the basis of spectral changes observed upon ligation of the nitrogen base (*vide supra*). Thus, the band at *ca* 8000 cm^{-1} can be assigned as the $^2A_1 \rightarrow {}^2B_1$ transition for [Co(Me,H,H)·H_2O] (calculated $\Delta B_1 = 7100\ cm^{-1}$). The intensity of this band decreases with increasing base concentration, which is consistent with the predicted absence of any transition in this range for mono- and bis-adducts (Table 2). The shoulder observed near 11,000 cm^{-1} in the presence of the base can be attributed to the $^2A_1 \rightarrow {}^2B_1$ transition in the monoadduct or to the $^2A_1 \rightarrow {}^2B_2$ transition in the bis-adduct.

It has to be noted that for all but two adducts $\Delta B_1 > \Delta B_2$ holds and the difference between these values ranges from 4000 to 7000 cm^{-1}. The exceptions are the diethyl- and diphenylphosphite adducts, where the relation between these energies is reversed. Such an exception has not been observed for other cobalt(II) Schiff base and dimethylglyoxamate complexes.[15,19]

For mono-adducts of oxygen, sulphur and nitrogen bases the signs of all A tensor components are positive, whereas for bis-adducts of nitrogen and phosphorus donor ligands the A_x^{Co} and A_y^{Co} components are negative.

For the adducts with nitrogen bases, for which the steric factors in the vicinity of the nitrogen donor seem to be similar (i.e. for all but α-pic), a dependence of the cobalt hyperfine tensor components on the basicity of the ligand is observed. For the 1 : 1 adducts A_x values decrease in the order 4-CNpy > py > γ-pic > MeIm = EtIm. A similar ordering is observed for $\langle A \rangle$. In the case of six-coordinated complexes values of both A_x and A_z follow the same trend. These tendencies are obviously due to the variations of the donor ability of the nitrogen base ligand being in line with predictions drawn for the dependence of hyperfine constants on axial perturbation.[22]

The fact that both 1 : 1 and 1 : 2 adducts for various pyridines are observed gives us the opportunity to discuss the influence of the coordination number on the spin density parameters. The ρ_{3d} values are considerably higher in the case of six-coordinate complexes, while the opposite trend is observed for ρ_{4s}. A similar observation for the ρ_{4s} parameter was reported by Symons and Wilkinson for the C-bonded ligands.[25] On the other hand, we did not observe any pronounced dependence of both spin densities on the basicity of the N-bonded donors. For adducts with phosphorus donors the ρ_{3d} and ρ_{4s} spin densities on the cobalt atom lie in the range observed previously for adducts of other four-coordinate cobalt(II) Schiff base complexes.[15–17]

The values of all phosphorus superhyperfine tensor components are assumed to be positive. The values of A_i^P obtained from fitting the spectra are similar to those reported for other cobalt(II) Schiff base phosphorus adducts,[15–17] but for the compounds under investigation the values of A_x^P are appreciably higher in the case of the triphenylphosphine adduct.

The isotropic hyperfine coupling constants ($\langle A^P \rangle$) for ^{31}P yield the 3*s* spin density, $\rho_{3s} = \langle A^P \rangle /$

Table 3. The ρ_{3s} and ρ_{3p} spin densities on the phosphorus atoms

L[a]	ρ_{3s}	ρ_{3p}
CoL·PBu_3	0.054	0.112
CoL·$P\Phi_2Me$	0.053	0.084
CoL·$P\Phi_2Et$	0.052	0.113
CoL·$P\Phi_3$	0.051	0.046
CoL·$P(O\Phi)_3$	0.081	0.123
CoL·$P(OEt)_3$	0.075	0.145

[a] Ligand (Me,H,H).

0.3396. The anisotropic coupling gives $3p$ spin density, $\rho_{3p} = (A_z^P - \langle A^P \rangle)/0.01922$.[21] The calculated values of ρ_{3s} and ρ_{3p} are collected in Table 3. Comparison of data presented in this table with those concerning the spin densities on the cobalt $3d$ orbital (see Table 2) led us to the conclusion that, as reported previously,[16,17-19] the more spin density that is localized on the cobalt atom the larger the spin densities on the phosphorus atom.

Redox properties and dioxygen binding

Cyclic voltammetry studies were carried out for [Co(Me,H,H)·H_2O] in dichloromethane and dichloromethane/pyridine solutions with the use of tetrabutylammonium perchlorate as a supporting electrolyte. The voltammogram of [Co(Me,H,H)·H_2O] in CH_2Cl_2 is shown in Fig. 6(a). The complex exhibits one quasi-reversible ($\Delta E_p = 120$ mV) peak at 0.594 V (vs S.C.E.), assigned to the Co^{III}/Co^{II} couple. No additional peaks reported for the corresponding VO^{II} and Ni^{II} complexes in DMF[26] were observed. An ill-defined irreversible cathodic response was additionally found at *ca* −0.95 V. The picture becomes more complicated if the parent chelate is dissolved in dichloromethane containing 1% v/v of pyridine [Fig. 6(b)]. Here, a quasi-reversible peak ($\Delta E_p = 100$ mV) is observed at −0.15 V. This peak was assigned to the Co^{III}/Co^{II} couple of the pyridine adduct. Such a decrease of the oxidation potential upon coordination of an axial N-base is typical for Co-Schiff base systems and is crucial for reversible dioxygen binding.[1a] The anodic peak of the above couple, particularly at low scan rates, is not clearly resolved, being followed by a plateau. This indicates a subsequent homogeneous reaction. By applying the method described by Savéant *et al.*[27] the homogeneous rate constant, $k = 5\ s^{-1}$, was determined. Passing dioxygen through the above solution for *ca* 5 min causes a change in colour from dark green to reddish-brown.

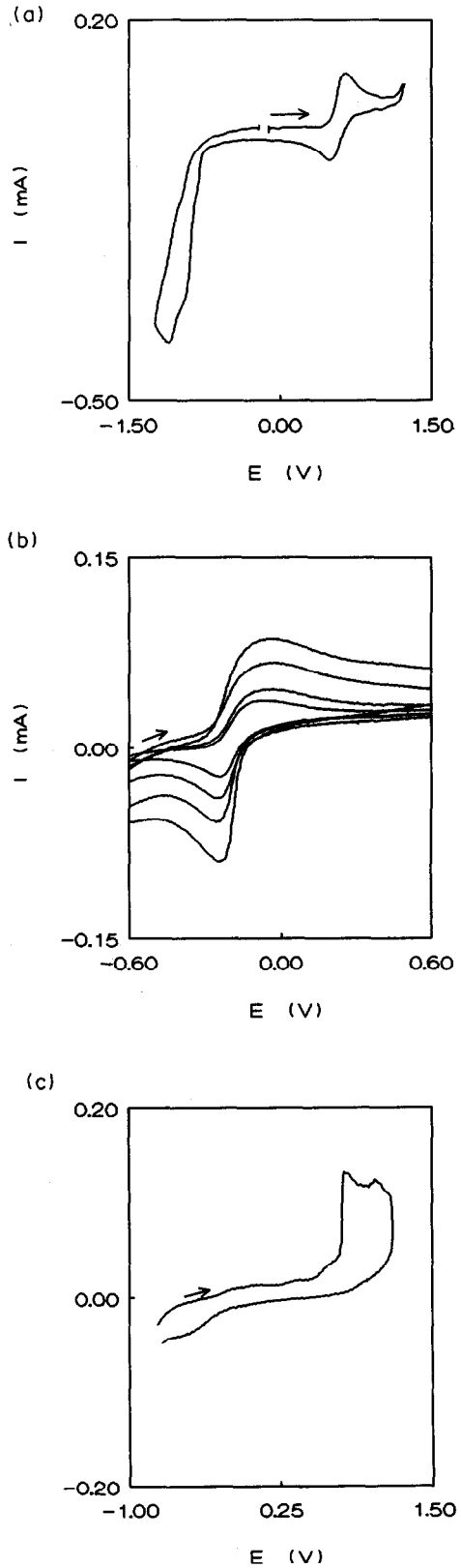

Fig. 6. Cyclic voltammograms of (a) $Co(Me,H,H)^-$ in CH_2Cl_2, (b) Co(Me,H,H) in CH_2Cl_2 containing 1% v/v of pyridine, and (c) as for (b) after passing dioxygen through. Scan rates 100 mV s^{-1}; supporting electrolyte = tetrabutylammonium perchlorate (0.1 M).

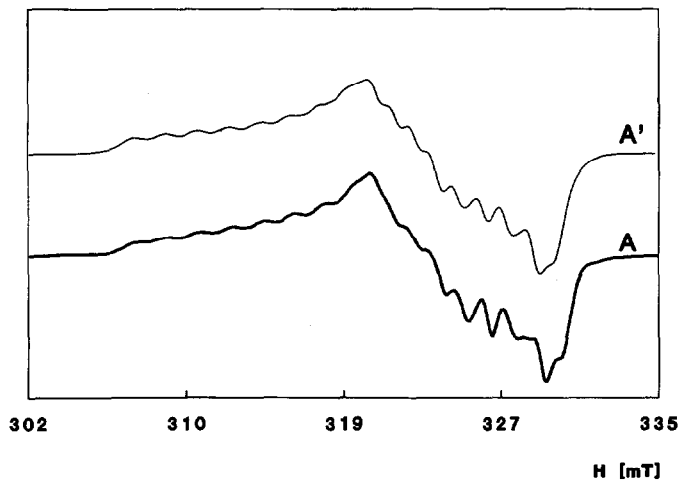

Fig. 7. ESR spectrum of (A) [Co(Me,H,H)·py·O_2] in CH_2Cl_2/toluene at 77 K. (A') is the best fit of (A).

The cyclic voltammetric curve [Fig. 6(c)] reveals only two irreversible peaks at 0.79 and 1.03 V. Bubbling with dinitrogen did not result in any change of the voltammetric pattern. The ESR spectrum of this solution does not display any distinct signals. It is therefore clear that, at least at room temperature, the oxygenation of [Co(Me,H,H)·py] is highly irreversible. This conclusion was further supported by ESR studies. The formation of the oxygenated species was observed only at low temperatures, and the ESR spectrum due to the dioxygen adduct was detected solely in frozen solutions. A complete conversion of the [Co(Me,H,H)·py] and [Co(Me,H,H)·2py] adducts to the [Co(Me,H,H)·O_2·py] dioxygen adduct was possible only by passing pure oxygen through the solution kept over the liquid nitrogen (see Fig. 7). Simulation of the ESR spectrum of [Co(Me,H,H)·py·O_2], using the monoclinic spin-Hamiltonian,[28] yielded the following parameters: $g_x = 2.011$, $g_y = 2.080$, $g_z = 1.994$, $A_x = 7.0 \times 10^{-4}$ cm^{-1}, $A_y = 18.0 \times 10^{-4}$ cm^{-1}, $A_z = 8.1 \times 10^{-4}$ cm^{-1} and $\alpha = 31°$. These values are in the typical range for cobalt superoxo complexes with O_2N_3 donor sets.[29]

Passing argon through the oxygenated sample resulted in recovery of the initial spectrum of five- or six-coordinate adducts of appreciably reduced intensity. In the next repeated oxygenation–deoxygenation cycles the spectral intensities of both oxygenated and deoxygenated forms decreased, resulting in a lack of any ESR signals (after five cycles). The observed disappearance of the ESR active species may be due to either formation of the diamagnetic μ-peroxo dimers or other irreversible processes involving, e.g. oxidation of the ligand or direct oxidation of the cobalt atom.

Acknowledgement—The financial support of the National Research Committee under Grants 1012/S/ICh/92/8 and 2015/W/ICh/92/17 is gratefully acknowledged.

REFERENCES

1. (a) R. D. Jones, D. A. Summerville and F. Basolo, *Chem. Rev.* 1979, **79**, 139; (b) D. Chen, A. E. Martell and Y. Sun, *Inorg. Chem.* 1989, **28**, 2647; (c) D. H. Busch, *Oxygen Complexes and Oxygen Activation by Transition Metals* (Edited by A. E. Martell and D. T. Sawyer). Plenum Press, New York (1988).
2. C. Daul, C. W. Schläpfer and A. von Zelewsky, *Struct. Bonding (Berlin)* 1979, **36**, 129.
3. (a) K. Migita, M. Chikira and M. Iwaizumi, *J. Chem. Soc., Dalton Trans.* 1983, 2281; (b) B. J. Kennedy and K. S. Murray, *Inorg. Chim. Acta* 1987, **134**, 249.
4. M. A. Hitchmann, *Inorg. Chim. Acta* 1977, **26**, 237.
5. P. Charpin, M. Nierlich, D. Vigner, M. Lance, P. Thuery, J. Zarembowitch and F. D'Yvoire, *J. Cryst. Spectrosc. Res.* 1988, **18**, 429.
6. N. V. Gerbeleu, *Reaktsii na Matritsakh.* Shtiintsa, Kishinev (1980).
7. V. M. Leovac, V. Divjakovic and V. I. Cesljevic, *Polyhedron* 1987, **6**, 1901.
8. M. D. Revenko, N. V. Gerbeleu and K. M. Indritchan, *Teoret. Eksperim. Khim.* 1985, **21**, 604.
9. N. V. Gerbeleu, M. D. Revenko and V. G. Rusu, *Zh. Neorg. Khim.* 1987, **32**, 946.
10. V. V. Zelentsov, G. I. Lapushkin, N. V. Gerbeleu, M. D. Revenko and V. G. Rusu, *Zh. Neorg. Khim.* 1987, **32**, 1651.
11. K. Drabent, J. A. Wolny, M. F. Rudolf and P. J. Chmielewski, *Polyhedron* 1992, **11**, 271.
12. J. P. Fackler Jr, J. D. Levy and J. A. Smith, *J. Am. Chem. Soc.* 1972, **94**, 2436.
13. M. F. Rudolf, Z. Ciunik, K. Gatner and J. A. Wolny, *Polyhedron* 1992, **11**, 2591.

14. P. R. Bevington, *Data Reduction and Error Analysis for the Physical Sciences*. McGraw-Hill, New York (1969).
15. O. Haas and A. von Zelewsky, *J. Chem. Res.* 1980, 1201.
16. G. Labauze and J. B. Raynor, *J. Chem. Soc., Dalton Trans.* 1980, 2389.
17. G. Labauze and J. B. Raynor, *J. Chem. Soc., Dalton Trans.* 1981, 590.
18. (a) F. A. Walker, *J. Am. Chem. Soc.* 1970, **92**, 1970; (b) B. B. Wayland and M. E. Abd-Elmageed, *J. Am. Chem. Soc.* 1974, **96**, 4809; (c) B. B. Wayland, M. E. Abd-Elmageed and F. L. Mehne, *Inorg. Chem.* 1975, **14**, 1456.
19. B. de Castro, M. Rangel and J. B. Raynor, *J. Chem. Soc., Dalton Trans.* 1990, 3311.
20. A. Pezeshk, F. T. Greenaway, J. C. Dabrowiak and G. Vincow, *Inorg. Chem.* 1978, **17**, 1717.
21. A. Pezeshk, F. T. Greenaway and G. Vincow, *Inorg. Chem.* 1978, **17**, 3421.
22. M. A. Hitchman, *Inorg. Chem.* 1977, **16**, 1985.
23. B. R. McGarvey, *Can. J. Chem.* 1975, **53**, 2498.
24. B. A. Goodman and J. B. Raynor, *Adv. Inorg. Chem. Radiochem.* 1970, **13**, 135.
25. M. C. R. Symons and G. Wilkinson, *J. Chem. Soc. (A)* 1971, 2069.
26. G. K. Budnikov, N. V. Gerbeleu, V. S. Pakhopol, O. Yu. Kargina, V. I. Morozov and M. D. Revenko, *Koord. Khim.* 1987, **13**, 487.
27. J. M. Savéant and E. Vianello, *Electrochim. Acta* 1965, **10**, 905.
28. T. D. Smith and J. R. Pilbrow, *Coord. Chem. Rev.* 1981, **39**, 295.
29. M. Tirant, T. D. Smith and J. R. Pilbrow, *J. Chem. Soc., Dalton Trans.* 1987, 2341.

Polyhedron Vol. 12, No. 6, pp. 661–670, 1993
Printed in Great Britain

0277–5387/93 $6.00+.00
© 1993 Pergamon Press Ltd

PREPARATION AND SPECTROSCOPIC STUDY OF *TRANS*-[$PtCl_2(C_2H_4)L$] (L = QNO, IQNO, 4-ClQNO, 2-MeQNO, 4-MeQNO). LIGAND EXCHANGE OF *TRANS*-[$PtCl_2(C_2H_4)$(4-MeQNO)]

MARIA-AGLAIA D. STIAKAKI and ARISTIDES CHRISTOFIDES†

Department of General and Inorganic Chemistry, Aristotelian University of Thessaloniki, P.O.B. 135, Thessaloniki 540 06, Greece

(*Received* 9 *August* 1990; *accepted* 2 *November* 1992)

Abstract—A series of *trans*-[$PtCl_2(C_2H_4)L$] [L = QNO (quinoline N-oxide), IQNO (isoquinoline N-oxide), 4-ClQNO, 2-MeQNO and 4-MeQNO] complexes have been prepared by the addition of L to aqueous solutions of Zeise's salt. ^1H NMR and IR studies have been employed to compare the coordination ability of L and ethylene towards platinum metal. The reactions of [$PtCl_2(C_2H_4)$(4-MeQNO)] with L′ [L′ = CO, PPh_3, py(pyridine) and 4-NMe_2py] afforded the *trans* complexes [$PtCl_2$L′(4-MeQNO)], [$PtCl_2$L′$_2$] and [$PtCl_2(C_2H_4)$(4-NMe_2py)]. Furthermore, the ability of [$PtCl_2(C_2H_4)$L] to react towards styrene resulted in the formation of five novel complexes of the type *trans*-[$PtCl_2$(styrene)L], which have been characterized by spectroscopic means (^1H, ^{13}C NMR and IR).

The formation of the first platinum(II) complex, containing N-oxide, was achieved several years ago by stirring [$PtCl_3(C_2H_4)$]K, Zeise's salt, with pyridine N-oxide.[1] Similarly, a small number of other platinum(II) complexes have been prepared using pyridine N-oxides bearing different substituents in the 4-position.[2,3] All these compounds have been characterized by spectroscopic means and in some cases, specifically dichloro(pyridine-1-oxide)-ethyleneplatinum(II) complexes, ^1H NMR studies have been performed.[4] However, reports of platinum(II) complexes incorporating either quinoline N-oxide or its substituted derivatives are scarce, and only the preparation of [$PtCl_2(C_2H_4)$(QNO)] has been reported so far.[5]

We have recently described the synthesis and study of some rhodium(I) quinoline N-oxide complexes[6] and now we report the preparation and spectroscopic study of five platinum(II) complexes.

EXPERIMENTAL

IR spectra were recorded on a Perkin–Elmer Model 1430 ratio recording spectrophotometer (over the range 4000–200 cm^{-1}) with calibration against the absorption band of polystyrene at 1601 cm^{-1}, and samples prepared as KBr discs. The ^1H NMR spectra were measured on Jeol FX-90 QFT and Jeol G×400 spectrometers by the staff of the NMR Service of the School of Chemistry, University of Bristol, U.K., and those of the styrene compounds were recorded on a Bruker AW-80 instrument in our department. The ^{13}C spectra were measured on a Bruker AC-200 spectrometer. The mass spectra were obtained on an RMU-6L Hitachi–Perkin–Elmer mass spectrometer. The thermoanalytical curves of **4** were obtained with a Dupont 951 thermogravimetric analyser. Quinoline N-oxide and its derivatives were prepared by published procedures,[6] whereas [$PtCl_3(C_2H_4)$]K was purchased from Aldrich Chem. Co. All reactions, unless otherwise stated, were conducted in air at room temperature.

Electrochemical studies were carried out using an AMEL Electrochemolab instrument in conjunction with a three-electrode cell. Nitrogen presaturated with solvent (CH_2Cl_2) was used to deoxygenate the solution. The working electrode was a platinum bead, the auxiliary electrode a platinum wire and the reference an aqueous saturated calomel electrode (S.C.E.), separated from the test solution by a fine-porosity frit and an agar bridge saturated

† Author to whom correspondence should be addressed.

with KCl. Solutions were 0.5×10^{-3} mol dm^{-3} in complexes and 0.1 mol dm^{-3} in $[NBu^n_4][PF_6]$ as the supporting electrolyte. Under these conditions, E° for the couple $Fe(\eta^5\text{-}C_5H_5)_2^+/Fe(\eta^5\text{-}C_5H_5)_2$ is -0.47 V.

Preparation of complexes of the type $[PtCl_2(C_2H_4)L]$ **(1–4)**

To a solution of Zeise's salt (0.184 g, 0.5 mmol) in water (25 cm^3), the quinoline N-oxide L was added under constant stirring, the molar ratio being 1 : 2 or 1 : 1, respectively. The yellow solution was stirred for a few minutes affording a precipitate of $[PtCl_2(C_2H_4)L]$, which was selected by suctional filtration, washed with water (2×5 cm^3) and dried *in vacuo*.

Reactions of $[PtCl_2(C_2H_4)(4\text{-MeQNO})]$

(1) Addition of PPh_3 (0.2 mmol) and excess py (0.6 cm^3) to chloroform solutions of **4** (0.1 mmol) caused the complete displacement of organic ligands; concentration under vacuum and addition of diethylether afforded microcrystals of *trans*-$[PtCl_2(PPh_3)_2]$[7] and *trans*-$[PtCl_2py_2]$.[8]

(2) A solution of **4** (0.3 mmol) in chloroform was treated with an equimolar amount of 4-NMe_2py affording *trans*-$[PtCl_2(C_2H_4)(4\text{-}NMe_2py)]$[9] [work-up was as in (1)].

Preparation of complexes of the type $[PtCl_2(styrene)L]$ **(5–9)**

(1) $[PtCl_2(C_2H_4)L]$ (0.2 mmol) was dissolved in hot benzene (20 cm^3). To this solution degassed $C_6H_5CH{=}CH_2$ (0.1 cm^3) was added via a syringe with constant stirring. Minute bubbles of gas were evolved immediately, meanwhile the colour changed from pale yellow to orange. The solution was filtered and the clear orange filtrate was concentrated to one third of its original volume. The mixture was diluted with an equal volume of petroleum ether and after stirring and subsequent cooling on an ice bath afforded yellow microcrystals, which were washed with petroleum ether (b.p. 70–80°C) (4×5 cm^3) and dried in air.

(2) $[PtCl_3(styrene)]K$, which was used as a starting material in this preparation, was prepared by a published method.[2,10]

$[PtCl_3(styrene)]K$ (0.044 g, 0.1 mmol) was dissolved in acetone (15 cm^3). To this yellow solution the ligand L (0.2 mmol) was added and the mixture was stirred for 15 min. The solution was concentrated to a small volume (1 cm^3) and addition of diethylether (10 cm^3) caused the precipitation of yellow microcrystals. The supernatant liquid was discarded, the crystals were washed with diethylether (4×3 cm^3) and dried in air.

Preparation of $[PtCl_2(CO)(4\text{-MeQNO})]$

The complex $[PtCl_2(C_2H_4)(4\text{-MeQNO})]$ (0.045 g, 0.1 mmol) was dissolved in dry and freshly distilled chloroform (5 cm^3), contained in a Schlenk tube. Carbon monoxide was bubbled through the solution until the first sign of a colour change. The treatment was then interrupted and the solution concentrated to a small volume (*ca* 1 cm^3). The addition of petroleum ether (10 cm^3) (b.p. 70–80°C) precipitated a residue which was further washed with petroleum ether (4×3 cm^3) to give khaki microcrystals of $[PtCl_2(CO)(4\text{-MeQNO})]$ (**10**), and dried in air. Yield: 0.03 g, 66%. Found: C, 29.0; H, 2.7; N, 3.2. Calc. for $C_{11}H_9N_1Cl_2Pt_1O_2$: C, 29.2; H, 2.0; N, 3.1%.

RESULTS AND DISCUSSION

Treatment of aqueous solutions of $[PtCl_3(C_2H_4)]K$ with either an excess or a stoichiometric amount of L (L = IQNO, 4-ClQNO, 2-MeQNO, 4-MeQNO) results in the displacement of the chloride opposite to ethylene and the formation of complexes **1–4**.

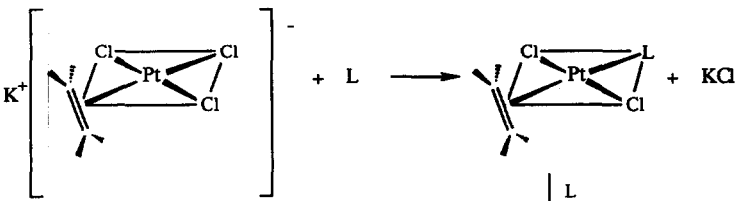

	L
1	IQNO
2	4-ClQNO
3	2-MeQNO
4	4-MeQNO

Table 1. Analytical and other physical data for complexes **1–4**

Complex		Colour	M.p. (°C)[a]	Yield (%)	Elemental analysis[b] %C	%H	%N
$[PtCl_2(C_2H_4)(IQNO)]$	(**1**)	Pale yellow	151–152	88	30.1 (29.3)	2.5 (2.5)	3.2 (3.1)
$[PtCl_2(C_2H_4)(4\text{-}ClQNO)]$	(**2**)	Pale yellow	168–169	90	27.9 (27.2)	2.1 (2.2)	3.0 (3.1)
$[PtCl_2(C_2H_4)(2\text{-}MeQNO)]$	(**3**)	Pale yellow	143[c]	80	31.8 (32.1)	2.9 (2.9)	3.1 (3.0)
$[PtCl_2(C_2H_4)(4\text{-}MeQNO)]$	(**4**)	Yellow–green	152[c]	94	31.8 (30.5)	2.9 (2.9)	3.1 (2.9)

[a] Melting points were determined in open tubes.
[b] Found values are given in parentheses.
[c] Decomposition temperatures.

In a preliminary report we announced some data concerning the title complexes.[11] Due to the strong *trans*-directing effect of the ethylene, the entering quinoline N-oxide displaces the chloride *trans* to ethylene.[12] However, neither $4\text{-}NO_2QNO$ nor 2-PhQNO react with Zeise's salt.

The elemental analyses (carbon, hydrogen and nitrogen) of all the compounds compare well to those expected, indicating that the new complexes precipitate in pure form and they do not need recrystallization. Their yields are quite high and they melt with decomposition. Table 1 displays the analytical and other data for the new complexes **1–4**.

In the mass spectrum of **3** there is a small peak at *m/z* 453, indicating the presence of molecular ions, and more intense peaks at *m/z* 143, 159 and 223, which can be assigned to $[2\text{-MeQN}]^{+\cdot}$, $[2\text{-MeQNO}]^{+\cdot}$ and $[Pt(C_2H_4)]^+$, respectively.

The ^1H NMR spectra of all the complexes show peaks at *ca* 4.36 ppm with $^{195}Pt\text{–}C\text{–}^1H$ coupling constants at *ca* 69 Hz (Table 2), indicating η^2-ethylene–platinum bonding arrangements.[13] In this series of compounds the $J(Pt\text{—}H)$ values of coordinated C_2H_4 are slightly higher than those of their pyridine N-oxide counterparts, which reflect better bonding of this ligand and a correspondingly lower *trans*-influence of quinoline N-oxides than the analogous pyridine ones. No safe conclusion can be drawn from the chemical shifts of ethylene protons (Table 2), since they do not show appreciable differences, mainly due to the fact that the nature of the *cis*-ligand in all complexes remains unchanged. Interestingly, all the spectra exhibit sharp peaks and well-defined platinum satellites and only in the spectrum of **2** has a slight broadening of all peaks been observed, in contrast with previous data.[4] The ^1H NMR spectra of $[PtCl_2(C_2H_4)(QNO)]$ and **4**, taken in deuterated methylene chloride at $-60°C$, displayed a single resonance for the ethylene protons, indicating that the ethylene moiety still rotates about the ligand–metal bond (Fig. 1). The low-temperature spectra measured with a high-resolution instrument (400 MHz) do not exhibit platinum satellites although the ethylene continues to be bonded to the metal. The disappearance of satellites is an implication of a dominant ^{195}Pt chemical shift anisotropy relaxation mechanism, since the spectra were taken at high field and low temperature.[14]

Table 2. ^1H NMR data[a] of $[PtCl_2(C_2H_4)L]$ compounds

Complex	δ ^1H (Ethylene)	$J(^{195}Pt\text{—}^1H)$ (Hz)	Substituted quinoline N-oxide —CH_3
$[PtCl_2(C_2H_4)(QNO)]$	4.37	69.1	
$[PtCl_2(C_2H_4)(IQNO)]$	4.39	69.1	
$[PtCl_2(C_2H_4)(4\text{-}ClQNO)]$	4.38	70.0	
$[PtCl_2(C_2H_4)(2\text{-}MeQNO)]$	4.34	69.0	3.16
$[PtCl_2(C_2H_4)(4\text{-}MeQNO)]$	4.34	68.3	2.89

[a] Measured in $\{^2H_1\}$ chloroform, δ values (ppm).

Fig. 1. ^{1}H NMR spectrum of $[PtCl_2(C_2H_4)(4\text{-MeQNO})]$ at room temperature and at $-60°C$, recorded at 90 MHz in $CDCl_3$ and 400 MHz in CD_2Cl_2, respectively.

Attempts to measure the ^{13}C NMR spectra of **1–4** were unsuccessful due to their low solubility.

IR spectra

The IR spectra of all these complexes show bands characteristic of the coordinated quinoline N-oxides, along with absorptions due to the Pt—Cl bonds. Table 3 lists the main stretching frequencies of the investigated complexes. Generally, their spectra show strong bands in the 1146–1300 cm^{-1} region, assignable to ν(N—O) of the coordinated quinoline N-oxides. As far as the complexes of QNO, IQNO and 2-MeQNO are concerned their ν(N—O) bands are shifted to lower frequencies, compared to those of the free ligands. However, in the spectra of 4-ClQNO and 4-MeQNO compounds the corresponding bands are shifted to higher frequencies for the former, whereas the latter does not show any appreciable shift. It is known that the (C=C) stretching frequency is a low intensity band for olefins such as ethylene; on the other hand, the band in question may be confused with the aromatic (C=C) stretching modes, since the studied complexes incorporate aromatic systems. Therefore, it is apparent that unambiguous assignments concerning this band cannot be made.[2,3] Complexes of QNO and 4-MeQNO show weak peaks at 323 and 318 cm^{-1}, respectively, which could be attributed to Pt—O bonds; such peaks probably are obscured in the spectra of the other complexes.[10,12] Bands due to platinum–olefin stretching frequencies were observed at 412 and 410 cm^{-1} for 4-ClQNO and 4-MeQNO compounds, respectively. The rest of the complexes either do not show such a band (IQNO complex) or the corresponding bands occur around

Table 3. IR data (cm^{-1}) of [$PtCl_2(C_2H_4)L$] and [$PtCl_2$(styrene)L] complexes

Complex–ligand	Ligand ν(N—O)	Complex ν(N—O)	$\Delta\nu$(N—O)	ν(Pt—Cl)
QNO	1229			
[$PtCl_2(C_2H_4)$(QNO)]		1212	−17	347
[$PtCl_2$(styrene)(QNO)]		1228	—	334
IQNO	1180			
[$PtCl_2(C_2H_4)$(IQNO)]		1146	−34	348
[$PtCl_2$(styrene)(IQNO)]		1182	+2	350
4-ClQNO	1302, 1251			
[$PtCl_2(C_2H_4)$(4-ClQNO)]		1300, 1261	−2, +10	340
[$PtCl_2$(styrene)(4-ClQNO)]		1300, 1260	−2, +9	343
2-MeQNO	1204			
[$PtCl_2(C_2H_4)$(2-MeQNO)]		1181	−23	345
[$PtCl_2$(styrene)(2-MeQNO)]		1178	−26	339
4-MeQNO	1236, 1206			
[$PtCl_2(C_2H_4)$(4-MeQNO)]		1207, 1150	−29, −56	344
[$PtCl_2$(styrene)(4-MeQNO)]		1210, 1152	−26, −54	336

400 cm^{-1} (QNO and 2-MeQNO complexes).[12] In all the complexes there is only one Pt—Cl stretching band around 345 cm^{-1}, indicating the *trans* arrangement of the two chlorines. This observation, combined with the NMR data showing the usual η^2-ethylene–platinum bonding, justified by the ^{195}Pt—C–^1H coupling constant of 69 Hz, shows that there is a square planar arrangement around the platinum atom.[13]

Ligand exchange reactions

Siedle *et al.*[13] pointed out that the non-bonded interaction between the *peri* hydrogens of the nitrogen containing ligand and the chlorine atoms in [$PtCl_2(C_2H_4)$(phz)] (phz = phenazine) leads to a twisting of the heterocyclic ligand, being almost perpendicular to the plane defined by the $PtCl_2$ moiety. This configuration leads to the limited reactivity of the complex towards attacking reagents, since its free coordination sites are blocked by the *peri* hydrogens of the ligand. Furthermore, the ethylene of [$PtCl_2(C_2H_4)$(phz)] cannot be displaced easily because the π^*-orbitals of the two unsaturated ligands, being orthogonal, do not compete for the same 5*d* electrons to achieve back-bonding, thereby strengthening their linkages to the metal. In our complexes, however, the incorporated quinoline N-oxides provide only one *peri* hydrogen, which is more distant from the metal atom than those of the phenazine in [$PtCl_2(C_2H_4)$(phz)]. Therefore, their reactivity is as expected and found to be more pronounced.

Displacement of ethylene by styrene in **1**–**4** proceeds rapidly in hot benzene, affording the new complexes *trans*-[$PtCl_2$(styrene)L] [L = QNO, IQNO, 4-ClQNO, 2-MeQNO, 4-MeQNO) (**5**–**9**) in satisfactory yields] (Table 4). Bubbling carbon monoxide through a chloroform solution of **4** also results in the displacement of ethylene and the formation of *trans*-[$PtCl_2$(CO)(4-MeQNO)] (**10**).

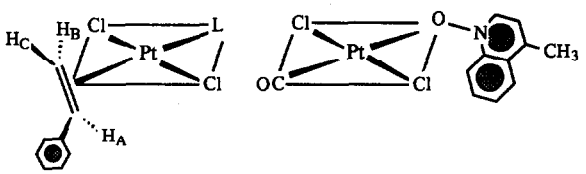

(10)

	L
5	QNO
6	IQNO
7	4-ClQNO
8	2-MeQNO
9	4-MeQNO

The spectroscopic data (IR, ^1H NMR) of **5**–**9** support the above structure. The ^1H NMR spectra of all styrene complexes show the expected peaks; their chemical shifts as well as their coupling constants (Table 5) are rather close to those reported for similar complexes.[15] The pattern is complicated, because the olefinic protons are coupled to each other and with the platinum-195 nucleus (Fig. 2). In particular, the H_A protons give rise to a doublet of doublets centred at *ca* 6.28 ppm with $^3J(H_A, H_B)$ at *ca* 8.2, $^3J(H_A, H_C)$ at *ca* 13.5 and $J(^{195}Pt—H_A)$ at *ca* 79.3 Hz. The H_B protons exhibit a doublet centred at *ca* 4.30 ppm with $^3J(H_B, H_A)$ at *ca* 8.1 and

Table 4. Analytical and other data for complexes **5–9**

Complex		Colour	M.p. (°C)[a]	Yield (%)	Elemental analysis[b] %C	%H	%N
$[PtCl_2(styrene)(QNO)]$	(**5**)	Bright yellow	118–120	80	39.6	2.9	2.7
					(40.1)	(2.9)	(2.6)
$[PtCl_2(styrene)(IQNO)]$	(**6**)	Light yellow	128[c]	91	39.6	2.9	2.7
					(39.6)	(2.9)	(2.8)
$[PtCl_2(styrene)(4\text{-}ClQNO)]$	(**7**)	Light yellow	145[c]	65	37.1	2.6	2.6
					(36.7)	(2.6)	(2.4)
$[PtCl_2(styrene)(2\text{-}MeQNO)]$	(**8**)	Bright yellow	143[c]	77	40.8	3.2	2.7
					(40.1)	(3.2)	(2.5)
$[PtCl_2(styrene)(4\text{-}MeQNO)]$	(**9**)	Yellow	119[c]	87	40.8	3.2	2.7
					(40.1)	(3.4)	(2.7)

[a] Melting points were determined in open tubes.
[b] Found values are given in parentheses.
[c] Decomposition temperatures.

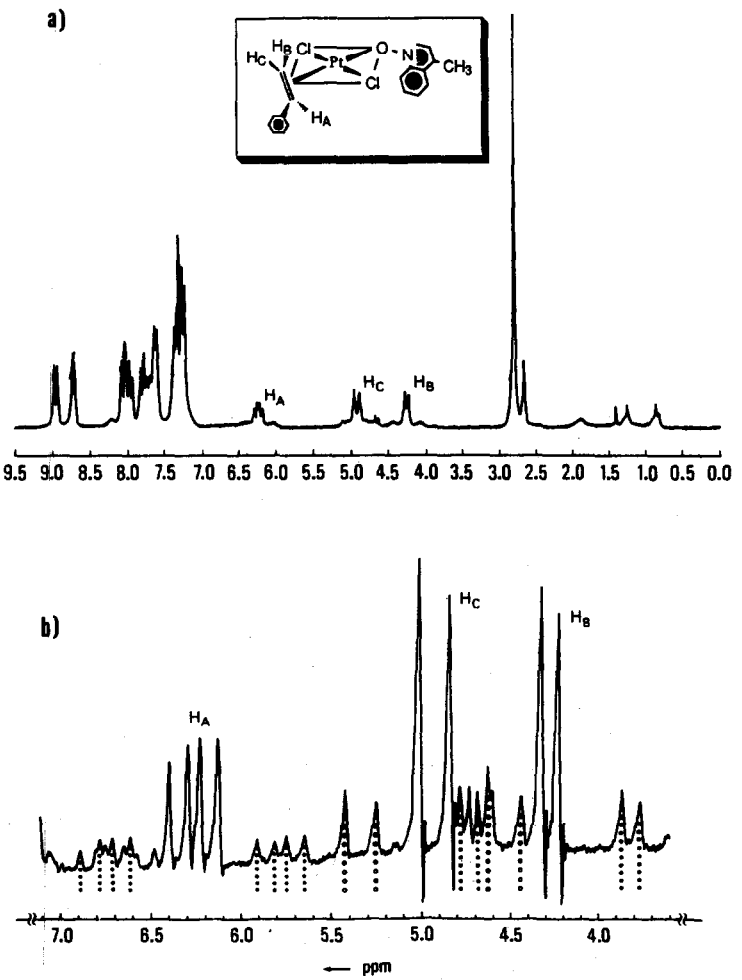

Fig. 2. (a) ^1H NMR spectrum of $[PtCl_2(styrene)(4\text{-}MeQNO)]$ recorded at 80 MHz in $CDCl_3$, and (b) expansion of the olefinic hydrogen area.

Table 5. ^1H NMR data[a] of [$PtCl_2$(styrene)L] compounds (δ in ppm, J in Hz)

Complex	$\delta(H_A)$	$J(H_A, H_B)$	$J(H_A, H_C)$	$J(Pt, H_A)$	$\delta(H_B)$	$J(H_B, H_A)$	$J(Pt, H_B)$	$\delta(H_C)$	$J(H_C, H_A)$	$J(Pt, H_C)$	$\delta(-CH_3)$[b]
[$PtCl_2$(styrene)(QNO)]	6.29dd[c]	8.2	13.5	80.0	4.31d[d]	7.7	73.5	4.97d	13.5	65.3	
[$PtCl_2$(styrene)(IQNO)]	6.30dd	8.3	13.8	79.0	4.34d	8.4	74.2	4.98d	13.2	66.2	
[$PtCl_2$(styrene)(4-ClQNO)]	6.30dd	8.3	13.7	81.2	4.32d	8.2	78.0	4.98d	13.7	65.7	
[$PtCl_2$(styrene)(2-MeQNO)]	6.26dd	8.1	13.5	78.1	4.25d	8.2	73.5	4.92d	13.6	65.2	3.06
[$PtCl_2$(styrene)(4-MeQNO)]	6.24dd	8.2	13.2	78.1	4.26d	8.1	74.0	4.92d	13.6	64.9	2.79

[a] In $CDCl_3$, on a Bruker AW-80 spectrometer.
[b] Methyl protons of substituted quinoline N-oxides.
[c] Doublet of doublets.
[d] Doublet.

$J(^{195}Pt—H_B)$ at *ca* 74.6 Hz. The H_C protons also exhibit a doublet at *ca* 4.95 ppm with $^3J(H_C, H_A)$ at *ca* 13.5 and $J(^{195}Pt—H_C)$ at 65.5 Hz; coupling between H_B and H_C was not observed. The mean value of $J(^{195}Pt—H) = 73.1$ Hz is indicative of π-coordinated styrene; moreover, the resonances of the H_A, H_B and H_C hydrogens are shifted upfield compared to those of the free ligand (H_A 6.71, H_B 5.27, H_C 5.82 ppm).[15] The value of $J(^{195}Pt—H_A) = 79.3$ Hz may suggest that H_A is closer to the platinum atom than the other hydrogens, although other factors can contribute as well to the magnitude of this constant.[16] The same arguments could also be applied for the interpretation of the differences of the corresponding coupling constants of H_B and H_C. The ^{13}C NMR spectra of **5**, **7** and **9** (Table 6) are not very informative due to their low solubility in deuterated chloroform; however, resonances assignable to olefinic carbons of styrene can be seen at *ca* 49.97 and *ca* 82.34 ppm, the former corresponding to the carbon atom attached to the phenyl group. Both resonances are significantly shifted upfield compared to those of the free ligand (112.3 and 135.8 ppm) upon coordination. No ^{195}Pt–carbon coupling, which would be a valuable source of information, could be seen under the conditions of the experiment. Unfortunately, the very low solubility of **6** and **8** excludes the possibility of measuring their ^{13}C NMR spectra on the available instrument.

The IR spectra of **5**–**9** show strong absorption bands in the range 1152–1300 cm^{-1}, assignable to ν(N—O) of quinoline N-oxide ligands (Table 3). They appear to be negatively shifted in complexes of IQNO, 2-MeQNO and 4-MeQNO, compared to those of the free ligands, but there is a slight positive shift in the 4-ClQNO complex; as for [$PtCl_2$(styrene)(QNO)] (**5**), no appreciable shifting was observed. The negative shift could well be an indication that the involved ligands coordinate to the metal via the oxygen atom, but there are two complexes which do not follow the trend. This behaviour is akin to other pyridine and quinoline N-complexes and no safe conclusion can be drawn, from the IR data only, on the effect of coordination on the N—O bond, since ν(N—O) bands are coupled with the vibrations of the aromatic ring.[17] The IR spectrum of **10** exhibits two very strong ν(CO) bands at 2102 and 2115 cm^{-1}, the latter being a little less intense than the former, as well as a medium absorption ν(NO) at 1217 cm^{-1}, indicating coordination of 4-MeQNO. All styrene compounds and the carbonyl complex exhibit single ν(Pt—Cl) bands around 341 cm^{-1}, justifying their *trans*-configuration.

Reactions of **4** in chloroform with two equi-

Table 6. Ethylenic carbon chemical shifts of some $[PtCl_2(PhCH^{2}{=}CH_2^{1})L]$ compounds

Complex[a]	$\delta(CH_2^{1}{=})$	$\delta(CH^{2}{=})$	Substituted quinoline N-oxide —CH_3
$[PtCl_2(Ph{-}CH{=}CH_2)(QNO)]$	49.98	82.22	
$[PtCl_2(Ph{-}CH{=}CH_2)(4\text{-}ClQNO)]$	50.03	82.82	
$[PtCl_2(Ph{-}CH{=}CH_2)(4\text{-}MeQNO)]$	49.96	81.97	19.15

[a] In $CDCl_3$, on a Bruker AC-200 MHz.

valents of PPh_3 and excess pyridine result in the formation of the known complexes *trans*-$[PtCl_2(PPh_3)_2]$[18] and *trans*-$[PtCl_2py_2]$,[8] presumably by first displacing the 4-MeQNO. The products were identified by their colours, IR spectra and elemental analyses. The reaction between **4** and PPh_3 in a 1:2 molar ratio proceeds rapidly, giving the product in high yield (83%) with satisfactory elemental analysis (carbon and hydrogen). This ready preparation of *trans*-$[PtCl_2(PPh_3)_2]$ may imply replacement of its synthesis reported by Mastin *et al.*,[7] which involves irradiation of the *cis* isomer with UV light at 366 nm, lower yield (42%) and is more laborious than the proposed one. Reaction of **4** with 4-(NMe_2)py in a 1:1 molar ratio affords the known complex *trans*-$[PtCl_2(C_2H_4)(4\text{-}NMe_2py)]$.[9] The characterization of this product was achieved as above, as well as by its ^1H NMR spectrum, which has not been reported so far (Fig. 3). The above-mentioned spectrum shows two double resonances centred at δ 8.42 and 6.50 ppm, assignable to H_α and H_β hydrogens, respectively, coupled to each other by $^3J(H_\alpha, H_\beta) = ca\ 7.4$ Hz. The ethylenic protons give rise to a single sharp peak at δ 4.75 ppm, accompanied by platinum-195 satellites, $J(^{195}Pt{-}H) = 58.6$ Hz, indicative of a π-complexed spinning ethylene. The sharp single peak at 3.10 ppm is attributed to the six protons of the methyls. Obviously, the ^1H NMR data favour the proposed *trans* structure. Moreover, they give decisive evidence that coordination of 4-NMe_2py occurs via the heterocyclic nitrogen, since only the H_α hydrogens are shifted downfield compared to those of the free ligand [δ 8.25d (H_α), 6.50d (H_β), 3.00 ppm (—NMe_2)]. Perhaps the most important fact supporting the above mode of coordination is the existence of two sets of platinum satellites attached to the doublet at 8.42 ppm. An expansion of this part of the spectrum enabled us to measure with certainty the $J(^{195}Pt{-}H_\alpha)$ coupling constant, the value

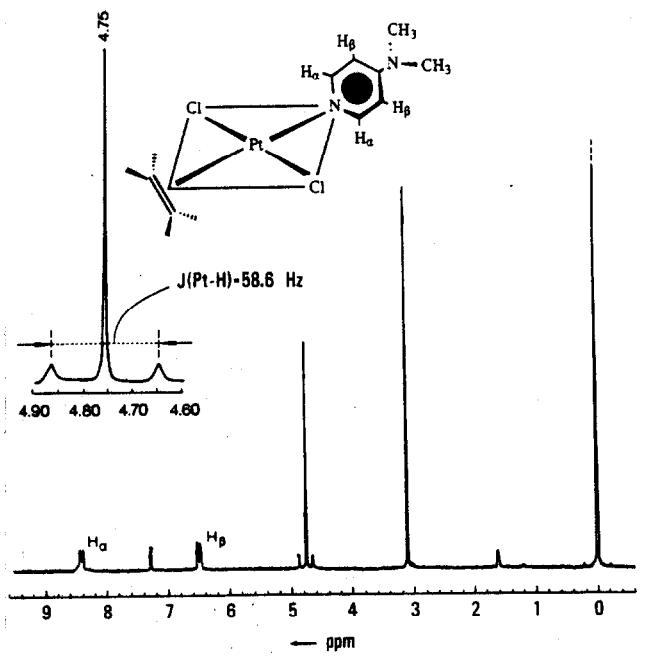

Fig. 3. ^1H NMR spectrum of $[PtCl_2(C_2H_4)(4\text{-}NMe_2py)]$ recorded at 270 MHz in $CDCl_3$.

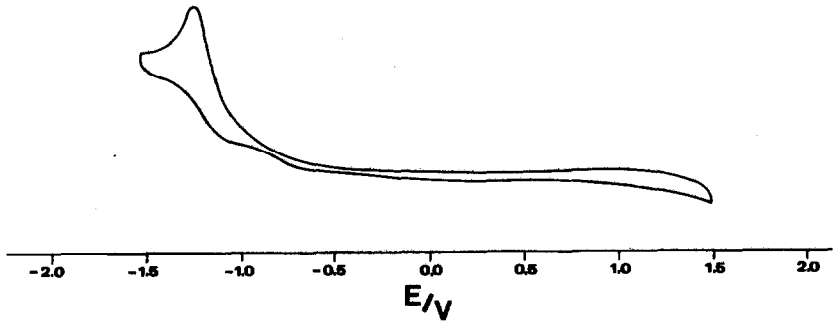

Fig. 4. The single scan cyclic voltammogram of $[PtCl_2(C_2H_4)(4\text{-MeQNO})]$ (**4**) in CH_2Cl_2, at a platinum bead electrode. Scan rate = 200 mV s^{-1}.

of which was 32.5 Hz. The phosphine, pyridine and 4-NMe_2py complexes exhibit a single ν(Pt—Cl) band around 341 cm^{-1} in their IR spectra, indicative of their *trans* configuration.

As can be seen from a survey of the ligand exchange reactions, either the new or known products adopt the *trans* configuration, the main reason for this preference being the strong *trans*-directing effect of ethylene. In addition, it is well known that the *trans* isomers are the most stable thermodynamically due to entropy reasons.[19] On the other hand, π-acceptor ligands displace preferably π-coordinated ethylene. These facts can be explained assuming that quinoline N-oxides lessen the extent of back-donation from platinum to ethylene, thereby facilitating its displacement by ligands with a similar nature.[20] There are also equilibrium reasons favouring the displacement of ethylene. In the case of the reaction with styrene the entering ligand is less volatile,[21] whereas the reaction with CO takes place in a solution saturated with the reacting ligand.

Other studies

The thermogravimetric curve (TG) of **4** shows that it loses 39.0% of its weight in two consecutive steps up to 410°C. The corresponding mass losses indicate clearly that ethylene (6.8%, Calc. 6.2%) is evolved during the first step, whereas removal of 4-MeQNO (32.2%, Calc. 31.6%) is accomplished during the second step. The percentage of the residue left (61.2%) is very close to the calculated one (62.2%), if it is considered to be $\{PtOCl_2\}$.

Platinum complexes may undergo one-electron reversible reduction if they contain ligands capable of supporting a delocalized negative charge.[22] In most cases, however, the reduction is an irreversible two-electron process producing metallic platinum.[23] In order to find out whether the quinoline N-oxide ligands are capable of supporting a delocalized negative charge, we studied **4** by cyclic voltammetry. However, our expectations proved wrong since reduction of **4** dichloromethane/$(C_4H_9)_4NPF_6$ at a scan rate of 200 mV s^{-1} discloses one irreversible reduction wave at $E^\circ = -1.20$ V, leading to decomposition products (Fig. 4).

REFERENCES

1. L. Garcia and M. Orchin, *J. Chem. Soc.* 1961, 2254.
2. M. Orchin and P. J. Schmidt, *Coord. Chem. Rev.* 1968, **3**, 345.
3. S. I. Shupack and M. Orchin, *J. Am. Chem. Soc.* 1963, **85**, 902.
4. P. D. Kaplan and M. Orchin, *Inorg. Chem.* 1965, **4**, 1393.
5. J. L. Davidson, P. N. Preston and M. V. Russo, *J. Chem. Soc., Dalton Trans.* 1983, 783.
6. A. Christofides, *Inorg. Chim. Acta* 1987, **133**, 29.
7. S. H. Mastin and P. Haake, *J. Chem. Soc., Chem. Commun.* 1970, 202.
8. D. Mansuy, J. F. Bartoli and J. C. Chottard, *J. Organomet. Chem.* 1974, **73**, C39.
9. H. Motschi, S. N. Sze and P. S. Pregosin, *Helv. Chim. Acta* 1979, **62**, 2086.
10. F. E. Dickson, E. W. Gowling and F. E. Bentley, *Inorg. Chem.* 1967, **6**, 1099.
11. A. Christofides and M.-A. Stiakaki, 7th Fechem Conference on Organometallic Chemistry, Toledo, 1987. Real Sociedad Española de Química, Toledo (1987); Abstracts EVII, p. 49.
12. S. I. Shupack and M. Orchin, *Inorg. Chem.* 1964, **3**, 374.
13. A. R. Siedle, K. R. Mann, D. A. Bohling, G. Filipovich, P. E. Toren, F. J. Palensky, R. A. Newmark, R. W. Duerst, W. L. Stebbings, H. E. Mishmash and K. Melancon, *Inorg. Chem.* 1985, **24**, 2216.
14. I. M. Ismail, S. J. S. Kerrison and P. J. Sadler, *Polyhedron* 1982, **1**, 57.
15. A. Albinati, W. R. Caseri and P. S. Pregosin, *Organometallics* 1987, **6**, 788.
16. H. P. Fritz, K. E. Schwarzhans and D. Sellmann, *J. Organomet. Chem.* 1966, **6**, 551.

17. L. C. Nathan and R. O. Ragsdale, *Inorg. Chim. Acta* 1969, **3**, 473.
18. F. R. Hartley, *Organomet. Chem. Rev. A* 1970, **6**, 119.
19. U. Belluco, *Organometallic and Coordination Chemistry of Platinum* (Edited by P. M. Maitlis, F. G. A. Stone and R. West), Ch. I, p. 81. Academic Press, New York (1974).
20. C. Cocevar, G. Mestroni and A. Camus, *J. Organomet. Chem.* 1972, **35**, 389.
21. J. R. Joy and M. Orchin, *J. Am. Chem. Soc.* 1959, **81**, 305.
22. J. A. McCleverty, *Progress in Inorganic Chemistry* (Edited by F. A. Cotton), Vol. 10, p. 49. Interscience, New York (1968).
23. J. F. Llopis and F. Colom, in *Encyclopedia of Electrochemistry of the Elements* (Edited by A. J. Bard), Vol. 6, p. 169. Marcel-Dekker, New York (1976).

Polyhedron Vol. 12, No. 6, pp. 671–676, 1993
Printed in Great Britain

0277–5387/93 $6.00+.00
© 1993 Pergamon Press Ltd

SYNTHESIS AND STRUCTURE OF A SERIES OF LANTHANIDE(III) THIOCYANATE DERIVATIVES WITH THF, $[Ln(NCS)_3(THF)_4]$

GIOVANNI DEPAOLI,* PAOLO GANIS† and PIER LUIGI ZANONATO

Dipartimento di Chimica Inorganica Metallorganica ed Analitica, Università di Padova, Via L. Loredan 4, 35100 Padova, Italy

and

GIOVANNI VALLE

Centro Studi sui biopolimeri del CNR, Via Marzolo 1, 35141 Padova, Italy

(*Received* 30 *September* 1992; *accepted* 22 *October* 1992)

Abstract—The thiocyanate complexes $Ln(NCS)_3 \cdot (THF)_4$ (Ln = Nd, Eu and Er) have been prepared and their structure was studied in the solid state by X-ray diffractometric methods. They crystallize in the monoclinic space group $P2_1/a$ with a ranging from 19.279(9) for Nd to 18.980(9) Å for Er; b, c and β have almost constant values: $b = 8.11 \pm 0.01$ Å, $c = 17.68 \pm 0.05$ Å and $\beta = 111.0 \pm 0.03°$. A peculiar feature of these complexes is the octa-coordination, the dimeric nature and the fact that in the molecule the NCS groups are coordinated as mono (Ln—NCS) and bidentate (Ln—NCS—LN) ligands. The structural units assume an almost undistorted square antiprismatic coordination geometry; they are linked through bridges of NCS groups. The Ln···S distances range from 3.10 (Nd) to 3.26 Å (Er); these values correspond to rather weak bond interactions, but are unambiguously recognized as coordinating values in geometrical terms.

The ability of the thiocyanate ion to form complexes with transition elements in a mono (M—NCS, M—SCN) or bidentate (M—NCS—M) ligation mode has been extensively investigated.[1] In the majority of reported complexes the NCS group is coordinated to the metal as a monodentate ligand. Examples of bridging thiocyanate are rather rare[2] and the case in which both ligation modes co-exist in the same molecule is confined to the cobalt compound $Co(NCS)_2 \cdot PPQ$.‡[3] To our knowledge no examples of this type are hitherto known for the f elements.

This paper reports the crystal and molecular structure of the homologous complexes $Ln(NCS)_3(THF)_4$ with Ln = Nd, Eu and Er, in which the unusual dual behaviour of the NCS ligand is found. This study was carried out with the aim of checking the effect of the lanthanide contraction on the ligation mode of the NCS group and understanding the influence of the ionic dimension on the coordination arrangement in the solid state.

EXPERIMENTAL

The reactions, manipulation and preparation of the samples for the X-ray data collection were carried out under nitrogen in a glove-box (oxygen

* Author to whom correspondence should be addressed.
† On sabbatical leave from Dipartimento di Chimica, Università di Napoli, Italy.
‡ PPQ = 2-(2′-pyridyl)-3-(N-2-picolylimido)-4-oxo-1,2,3,4-tetrahydroquinoline.

content 5 ppm, water content 1 ppm). Anhydrous $LnCl_3$ were prepared according to reported methods.[4] Commercially available potassium thiocyanate was purified according to ref. 5. The solvents (THF and pentane) were purified by distillation from lithium aluminium hydride and potassium-benzophenone under nitrogen. The analyses of the metals were performed according to ref. 6.

Synthesis of the complexes $Ln(NCS)_3 \cdot (THF)_4$

In a typical reaction to $LnCl_3$ (2.8 mmol) suspended in THF (50 cm^3) KNCS (8.4 mmol) was added. The mixture was stirred for 1 day at room temperature and successively refluxed for 3 h in an inert atmosphere. The resulting solution was centrifuged, the solid (KCl) removed and the crude product isolated by evaporation of the solvent under reduced pressure. The $Ln(NCS)_3 \cdot (THF)_4$ complexes were recrystallized by adding pentane to their THF solutions. Found: Nd, 23.1; Eu, 24.5; Gd, 25.1; Er, 26.2. Calc. for $C_{19}H_{32}LnN_3O_4S_3$: Nd, 23.8; Eu, 24.7; Gd, 25.4; Er, 26.5%.

Crystallography: crystal data

Single crystals of the complexes $Er(NCS)_3(THF)_4$, $Eu(NCS)_3(THF)_4$ and $Nd(NCS)_3(THF)_4$ were sealed under nitrogen in Lindeman capillaries. Suitable crystals for X-ray analysis were mounted on a Philips PW-100 computer-controlled four-circle diffractometer with a graphite monochromator. Standard centring and auto-indexing procedures indicated the primitive monoclinic lattices $P2_1/a$ for **A**, **B** and **C**. The orientation matrix and accurate unit cell dimensions were determined from a least-squares fit of 25 symmetry-related reflections. Intensity data were collected at 25° using the θ–2θ scan method; two standard reflections, monitored every 150 reflection measurements, fluctuated within 2–3% of their mean value. The intensities were corrected for Lorentz and polarization effects but not for absorption owing to the relatively low values of μ. Crystal data and details of intensity collection are reported in Table 1.

Solution and refinement of the structures

The positions of the lanthanide atoms were determined from three-dimensional Patterson syntheses. The light atoms were located from subsequent Fourier maps. The positions of the hydrogen atoms were geometrically calculated, assigned isotropic thermal parameters [with $U(H) = 1.2\ U_{eq}(C)$] and allowed to ride on their parent carbon atom. They were included in the final calculations but not refined. Anisotropic thermal parameters were used for all the non-hydrogen atoms. Blocked-cascade least-squares refinements were used: they converged to the conventional R indexes reported in Table 1. A unitary weighting scheme was used. Scattering

Table 1. Summary of the crystal data and intensity collection for the complexes $Ln(NCS)_3 \cdot 4THF$ (Ln = Nd, Eu and Er)

	$Nd(NCS)_3(THF)_4$	$Eu(NCS)_3 \cdot (THF)_4$	$Er(NCS)_3 \cdot (THF)_4$
Formula	$NdS_3O_4N_3C_{19}H_{32}$	$EuS_3O_4N_3C_{19}H_{32}$	$ErS_3O_4N_3C_{19}H_{32}$
M	606.90	614.62	629.94
a (Å)	19.279(9)	19.150(9)	18.980(9)
b (Å)	8.112(5)	8.103(5)	8.120(5)
c (Å)	17.703(8)	17.631(8)	17.687(8)
β (°)	111.8(3)	111.6(3)	110.8(3)
V (Å^3)	2570.6	2543.7	2548.2
Z		4	
D_c (g cm^{-3})	1.57	1.60	1.64
Space group		$P2_1/a$	
Crystal dimensions (mm)	0.25 × 0.35 × 0.20	0.15 × 0.30 × 0.20	0.20 × 0.30 × 0.20
T (K)		298	
μ (cm^{-1})	23.02	27.33	36.04
Take-off angle (°)		3	
Scan speed (° min^{-1})		2.0 in the 2θ mode	
2θ range (°)		$3.0 \leqslant 2\theta \leqslant 45$	
Unique data $[F_o^2 \geqslant 2\sigma(F_o^2)]$	6035	5556	6153
R (on F_o)	0.051	0.045	0.047

Table 2. Unit cell parameters for the complexes $Ln(NCS)_3 \cdot (THF)_4$

Element	a	b	c	β
Ce		Not crystallizable		
Pr		Not crystallizable		
Nd	19.279(9)	8.112(5)	17.703(8)	111.8(3)
Sm	19.199(9)	8.104(5)	17.680(8)	111.8(3)
Eu	19.150(9)	8.103(5)	17.631(8)	111.6(3)
Gd	19.132(9)	8.100(5)	17.562(8)	111.5(3)
Tb	19.087(9)	8.110(5)	17.592(8)	111.9(3)
Dy	19.045(9)	8.114(5)	17.561(8)	111.2(3)
Ho	19.013(9)	8.111(5)	17.710(8)	111.5(3)
Er	18.980(9)	8.112(5)	17.687(8)	110.8(3)

factors for the atoms were taken from Cromer and Weber;[7] the scattering factors for the lanthanide atoms were corrected for the real and imaginary parts of anomalous dispersion using Cromer's values.[8] All computations were carried out on a Cyber-76 computer using the SHELX-76 program.[9] Full details of the analysis are available in the additional material deposited with the Cambridge Crystallographic Data Centre.

DISCUSSION

By reacting anhydrous lanthanide(III) chlorides with potassium thiocyanate at room temperature according to the equation:

$$LnCl_3 + 3KNCS \xrightarrow[\text{room temperature}]{THF} Ln(NCS)_3 \cdot (THF)_4 + 3KCl,$$

two homologous series of compounds have been obtained. We reported here the results concerning the first series, which includes the lanthanide elements to erbium; crystals suitable for X-ray analysis could be obtained only for Ln ranging from Nd to Er. Preliminary crystallographic data showed that all these crystals belong to the monoclinic space group $P2_1/a$ and have almost constant values of the unit cell parameters b (8.11 ± 0.01 Å), c (17.68 ± 0.05 Å) and β (111.0 ± 0.03°), while a decreases linearly with atomic number from 19.279 for Ln = Nd to 18.980 Å for Ln = Er (Table 2). On account of this we restricted the full crystallographic analysis to only the three complexes having Ln = Nd, Eu and Er. The structural features of these compounds are basically determined by two distinctive perculiarities; the expected lanthanide contraction and the quite rare behaviour of NCS groups as bidentate and monodentate ligands in the same molecule.

The molecular structures can be described in terms of slightly distorted square antiprismatic octa-coordination.[10]

Except for the eighth coordination site, almost in the theoretical direction and occupied by the sulphur atom of one of the NCS groups of the adjacent centrosymmetrical unit, all the stereochemical parameters correspond to predictable values for such geometry; we report for instance the α angles[11] between each metal–ligand bond with the pseudo-eight-fold inversion axis of the molecular unit (Table 3).*

These values can be considered to be in good agreement with the theoretical value of 59.26° for octa (unidentate ligand) complexes,[10] if one realistically takes into account the approximate location of the eight-fold inversion axis and possible distortions due to steric constraints between the non-identical eight ligands. Figure 1 shows a projection of the resulting square antiprism as viewed parallel and normal to the eight-fold inversion axis.

The metal–ligand distances decrease regularly in the order Nd to Er (Table 4), according to the

Table 3. α angle (°) made by the metal–ligand bond with the pseudo-eight-fold inversion axis passing through the metal atom Ln

Bond	Er	Eu	Nd
Ln—N(1)	65.9	64.5	63.8
Ln—N(2)	48.0	49.7	50.7
Ln—N(3)	55.7	54.9	53.6
Ln—O(1)	53.1	52.5	53.1
Ln—O(2)	48.9	51.1	51.1
Ln—O(3)	61.3	61.2	61.6
Ln—O(4)	69.7	67.1	66.0
Ln—S(1)′	52.7	54.1	54.8

* This axis refers to the eight atoms directly bonded to the metal atom.

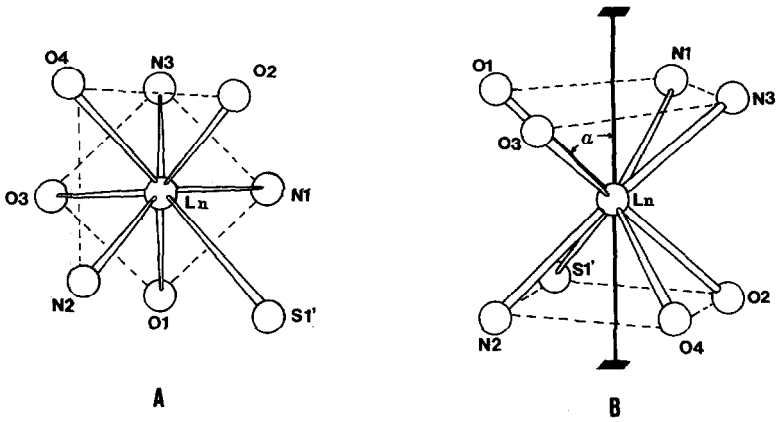

Fig. 1. Schematic perspective of the square antiprism as viewed: (A) parallel and (B) normal to the pseudo-eight-fold inversion axis; only the atoms directly bonded to Ln are drawn.

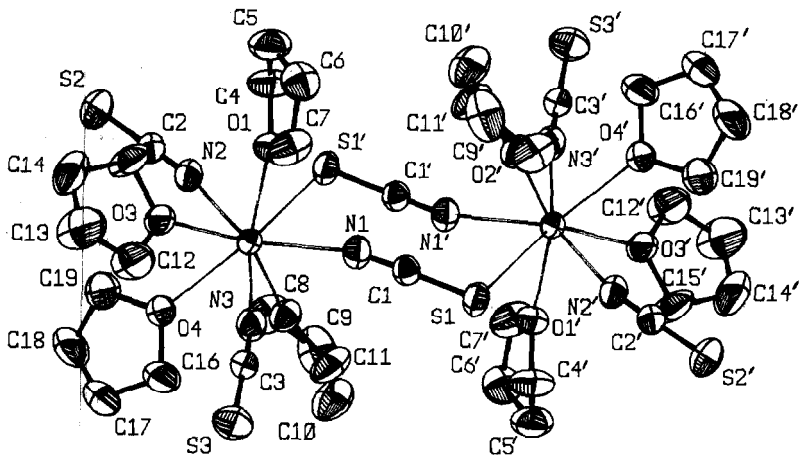

Fig. 2. Projection of the dimer of $Ln(NCS)_3(THF)_4$ down the *b*-axis. The atoms are labelled according to Table 2.

lanthanide contraction. Moreover, the mean variation of these distances (0.054 from Nd to Eu and 0.062 Å from Eu to Er) is almost the same as the corresponding variation of the 3+ ionic radium of the element (0.045 and 0.062 Å, respectively).[12] The large values of Ln—O(3) and Ln—O(4) are likely due to repulsive interactions between bulky groups in the more over-crowded regions of the coordination sphere of the metal; however, they could also be an indication of some amount of *trans* influence of the S-bonded NCS group.[13]

The eighth coordination site is the result of an association through NCS bridges of two $Ln(NCS)_3(THF)_4$ units located about inversion centres (Fig. 2). The metal–metal vector of the dimers is nearly parallel to the *c*-axis. The metal–sulphur distances range from 3.28 for Er to 3.10 Å for Nd; albeit remarkably larger than theoretically evaluable bond lengths, i.e. *ca* 2.84 for Er and up to 2.96 Å for Nd, respectively.* We believe that they can be interpreted with confidence as bond distances. As a matter of fact, these data are in evident contrast with the increasing ionic radius of the metal for Er to Nd and can only be explained in terms of stronger and stronger metal–sulphur bond interactions in the same order. Therefore, the shortening of this bond from 3.28 for Er to 3.10 Å for Nd arises from a gradually expanding coordination sphere of the metal and thus from less and

*These values are calculated from the relation $r_{AB} = r_A + r_B - 0.09D_{AB}$, where r_A and r_B are the ionic radii of the bonded elements and D_{AB} the differences in their electronegativity. The *r* values are taken from Shannon[12] and the D_{AB} values from Allred-Rochow.[14]

less hindered insertion of the sulphur atom therein. Moreover, this analysis shows that the value of *ca* 3.10 Å seems to be a lower limit for the metal–sulphur bond in these complexes; it almost does not change from Eu to Nd (Table 3), in spite of the relatively large increase of the metal–ligand distances which would likely produce unbearable molecular constraints within the dimers. This fact probably explains the instability of the derivatives of Ce and Pr. On the other hand, the value of *ca* 3.28 Å for Er seems to be the upper limit; beyond this value the metal–sulphur bond would be too weak to allow an eight-coordination, so that the next $Ln(NCS)_3 \cdot (THF)_4$ complexes change their molecular configuration.[15] It is to be noted that data on Ln···S bond distances are quite rare; so far we know that they are mostly confined to lanthanum(III) complexes.[16,17] The other conformational parameters of the structural unit are quite normal and do not need any particular comment (see Table 4).

Figure 3 shows the mode of packing which is almost identical for all these complexes as viewed down the *b*-axis. In the *a*-direction the packing is mainly controlled by intermolecular contact distances about two-fold screw axes at (1/4, *y*, 0). These distances are supposed to decrease with increasing metal–ligand bond lengths from Er to Nd, but are instead preserved at constant values by increasing the *a*-axis in an almost equal amount (Table 5). In the *c*-direction the packing is characterized by a stacking of the outermost THF centrosymmetrical units [O(3), C(12), C(14), C(15)], located at *ca* 1/4 and 3/4 of *b* between inversion centres at distances of *ca* 4.0 Å. To a small increase in the metal–ligand distances follows a small slippage of the THF units amidst one another, without appreciable effects on the dimensions of *b* and *c*.

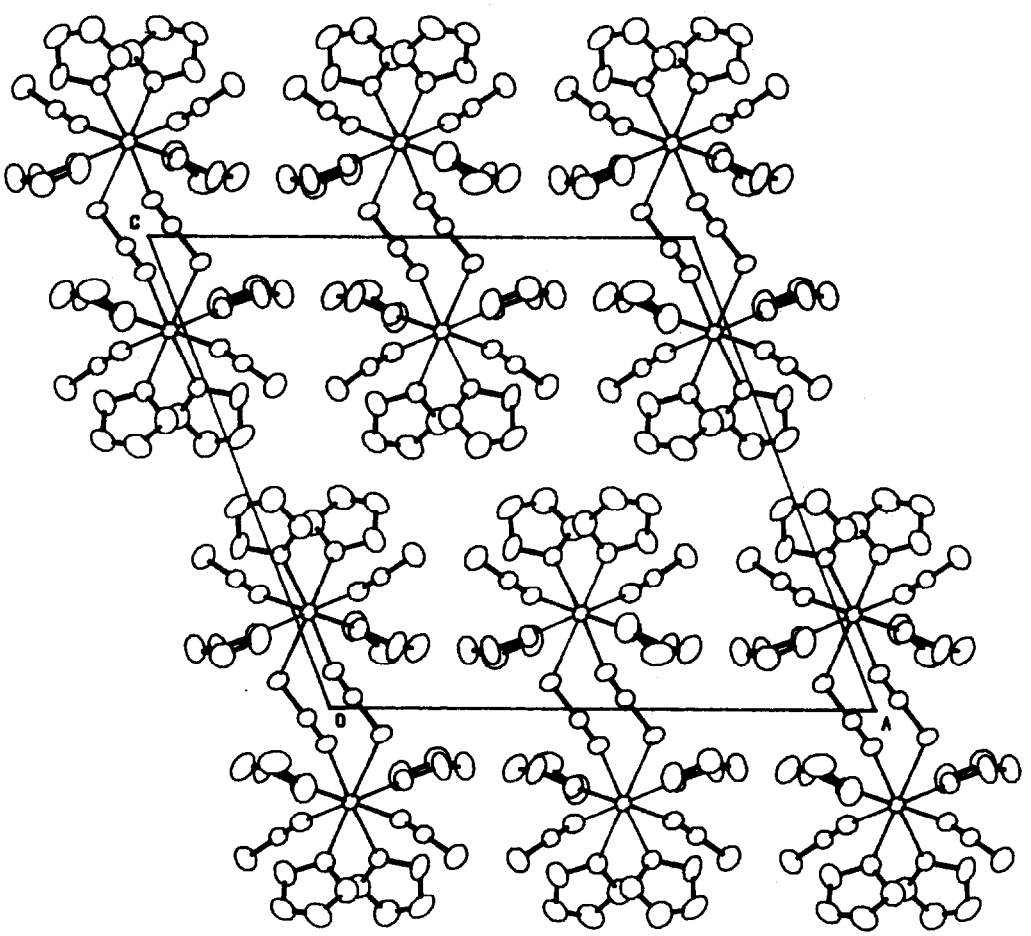

Fig. 3. Mode of the packing of $Ln(NCS)_3(THF)_4$ down the *b*-axis.

Table 4. Selected bond distances (Å) and angles (°) for $Ln(NCS)_3(THF)_4$ (Ln = Er, Eu and Nd)

Ln–atom	Er	Eu	Nd
	Bond distances (Å)		
Ln—N(1)	2.383(6)	2.450(5)	2.507(8)
Ln—N(2)	2.327(6)	2.401(5)	2.462(9)
Ln—N(3)	2.327(6)	2.389(5)	2.471(8)
Ln—O(1)	2.373(4)	2.439(3)	2.496(6)
Ln—O(2)	2.346(5)	2.430(4)	2.470(7)
Ln—O(3)	2.482(5)	2.535(4)	2.578(8)
Ln—O(4)	2.519(4)	2.550(3)	2.592(6)
Ln—S(1)′	3.283(4)	3.112(3)	3.100(9)
	Bond angles (°)		
N(1)—Ln—N(3)	76.0(2)	74.2(1)	73.4(2)
N(1)—Ln—O(1)	76.3(2)	76.1(1)	76.0(2)
N(1)—Ln—S(1)	71.3(2)	73.7(1)	74.5(2)
N(1)—Ln—O(2)	79.1(2)	79.0(1)	78.9(2)
N(3)—Ln—O(3)	76.4(2)	75.8(2)	75.5(2)
N(3)—Ln—O(2)	88.4(2)	86.4(2)	86.5(2)
N(3)—Ln—O(4)	76.2(2)	76.5(1)	76.9(2)
O(3)—Ln—O(1)	72.1(1)	71.5(1)	71.6(2)
O(3)—Ln—N(2)	80.6(2)	79.4(1)	79.1(2)
O(3)—Ln—O(4)	72.0(2)	72.1(1)	72.7(2)
O(1)—Ln—S(1)	76.4(2)	78.4(1)	78.3(2)
O(1)—Ln—N(2)	83.3(2)	83.8(2)	83.5(2)

Table 5. Some relevant intermolecular contact distances between molecules about 2_1 axes in the direction *a*

Atom–Atom	Er	Eu	Nd
S(2)—C(16)	3.63	3.69	3.63
S(3)—C(14)	3.85	3.87	3.87
S(3)—C(15)	3.49	3.54	3.50
C(4)—C(10)	3.71	3.74	3.74
C(5)—C(11)	3.85	3.83	3.87

Acknowledgement—We thank Mr M. Griggio for technical assistance.

REFERENCES

1. R. A. Bailey, S. L. Kozak, T. W. Michelsen and W. N. Mills, *Coord. Chem. Rev.* 1971, **6**, 407; M. F. Lappert and H. Pyszora, *Adv. Inorg. Chem. Radiochem.* 1966, **9**, 133; J. S. Thayer and R. West, *Adv. Organomet. Chem.* 1967, **5**, 169; J. L. Burmeister, *Coord. Chem. Rev.* 1966, **7**, 205; J. L. Burmeister, *Coord. Chem. Rev.* 1968, **3**, 255; A. H. Norbury and A. I. Sinha, *Q. Rev., Chem. Rev.* 1970, **24**, 69; R. T. M. Fraser, *Adv. Chem. Ser.* 1965, **62**, 295; Z. Iqbal, *Struct. Bonding (Berlin)* 1972, **10**, 25; A. H. Norbury, *Adv. Inorg. Chem. Radiochem.* 1975, **17**, 231; S. Ahrland, K. W. Bagnall and D. Brow, *The Chemistry of the Actinides*, p. 212. Pergamon Press, Oxford (1975).
2. M. Nardelli, G. Fava Gasparri, A, Musatti and A. Manfredotti, *Acta Cryst.* 1966, **21**, 910; U. A. Gregory, J. A. J. Jarvis and P. G. Owston, *J. Chem. Soc. (A)* 1970, 2770; A. V. Butcher, D. J. Phillips and J. P. Redfern, *J. Chem. Soc. (A)* 1971, 1640.
3. A. Mangia, M. Nardelli and G. Pelizzi, *Acta Cryst.* 1974, **B30**, 487.
4. M. D. Taylor and C. P. Carter, *J. Inorg. Nucl. Chem.* 1962, **24**, 378.
5. D. D. Perrin, W. L. Armargeo and D. R. Perrin, *Purification of Laboratory Chemicals*, p. 517. Pergamon Press, Oxford (1985).
6. S. L. Lyle and Md. M. Rahmer, *Talanta* 1963, 1177.
7. D. T. Cromer and J. T. Waber, *Acta Cryst.* 1965, **18**, 184.
8. D. T. Cromer, *Acta Cryst.* 1965, **18**, 17.
9. G. M. Sheldrick, SHELX-76, Program for Crystal Structure Determination. Cambridge University, U.K. (1976).
10. D. L. Kepert, *Progress in Inorganic Chemistry*, Vol. 24, pp. 179–249. John Wiley & Sons, Inc., New York (1978) and refs therein.
11. D. L. Kepert, *J. Chem. Soc.* 1965, 4736; E. L. Muetterties and C. M. Wright, *Q. Rev., Chem. Soc. (London)* 1967, **21**, 109; L. D. C. Bok, J. G. Leipoldt and S. S. Basson, *Acta Cryst.* 1970, **B26**, 684.
12. R. D. Shannon, *Acta Cryst.* 1976, **A32**, 751.
13. L. Zhenyang and M. B. Hall, *Inorg. Chem.* 1991, **30**, 646.
14. J. G. Palenik, in *Systematics and Properties of the Lanthanides*, p. 153. D. Reidel Publishing Co., Dordrecht (1982) and refs therein.
15. G. Depaoli, P. L. Zanonato and G. Valle, Proceedings of the Conference Rare Earth '92, Kyoto (Japan), June (1992).
16. T. Malmborg and A. Oskarsson, *Acta Chem. Scand.* 1973, **27**, 2923 and refs therein.
17. *GMELIN Handbuch der Anorganische Chemie, Rare Earth Elements, Coordination Compounds*, Part D1, Vol. 39, pp. 1–256. Springer Verlag, Berlin (1980).

Polyhedron Vol. 12, No. 6, pp. 677–681, 1993
Printed in Great Britain

0277–5387/93 $6.00+.00
© 1993 Pergamon Press Ltd

CRYSTAL STRUCTURE AND MAGNETIC PROPERTIES OF DICYCLOPENTADIENYLHOLMIUM CHLORIDE $[(C_5H_5)_2HoCl]_2$

ZHONGZHI WU,* ZHENG XU, XIAOZENG YOU and HUAQING WANG

The National Key Laboratory of Coordination Chemistry, Nanjing University, Nanjing 210008, Jiangsu, P.R.C.

and

XIGEN ZHOU

Institute of Organic Chemistry, Anhui Normal University, Wuhu 241000, Anhui, P.R.C.

(*Received* 10 *September* 1992; *accepted* 22 *October* 1992)

Abstract—Single crystals of $(Cp_2HoCl)_2$ ($Cp = C_5H_5$) were grown from CH_2Cl_2 solution and studied by X-ray crystallography. The molecule of the title compound is a centrosymmetric dimer with two chloride atoms bridging. The holmium atom is coordinated by two Cp ring centroids and two chloride atoms to form a distorted tetrahedral geometry. The average Ho—Cl and Ho—C(Cp) bond distances are 2.674(5) and 2.60(2) Å, respectively. A comparison of some significant structural parameters along the structural series Cp_2MCl_2 (M = Sc, Ho, Er and Yb) with metal ionic radii was made. The magnetic susceptibility of the title compound has been measured in the range 74–300 K and shows linear Curie–Weiss behaviour with $C = 14.3$, $\theta = 1.2$ K and $\mu_{eff} = 10.77$ B.M. There is no evidence of any magnetic interaction between metal centres.

Recently, studies on the magnetic properties of coordination and organometallic compounds of the *d*-block elements have been widely reported.[1] The magnetic properties of organolanthanide polynuclear compounds, however, are rarely studied.[2–4] Compounds of the type Cp_2LnCl would appear to be relevant to these investigations because of their polymeric nature.[3–11] Recent studies have shown that the crystal structures of the Cp_2LnCl-type compounds are dependent on both the conditions of crystal growth and metallic ionic radii.[5,10–12] We are interested in the influence of the conditions of crystal growth and metallic ionic radii on the crystal structures of the Cp_2LnCl-type compounds and their magnetic properties. In order to investigate the crystal structure and magnetic properties of the Cp_2HoCl compound, we herein report the X-ray crystal structure and magnetic properties of $(Cp_2HoCl)_2$ by growing single crystals of the compound from CH_2Cl_2 solution. At the same time we discuss the comparison of some significant structural parameters along the structural series Cp_2LnCl (Ln = Sc, Ho, Er and Yb).

* Author to whom correspondence should be addressed.

RESULTS AND DISCUSSION

Description and discussion of the crystal structure

The crystal structure of the title compound consists of discrete dimers. The molecular structure of the compound $(Cp_2HoCl)_2$ is shown in Fig. 1. Selected bond lengths and angles are listed in Table 1. The molecular structure contains two holmium atoms, each with two η^5-bonded Cp groups, which are centrosymmetrically bridged by two chlorine atoms. The Ho—Cl bond lengths are 2.676(4) and 2.671(5) Å, respectively, averaging 2.674(5) Å. The Cp rings are almost symmetrically bonded to the holmium atoms with Ho—C bond distances ranging from 2.53(3) to 2.67(3) Å and averaging 2.60(5) Å. The bridging unit Ho_2Cl_2 is almost square, with Ho—Cl—Ho and Cl—Ho—Cl angles of 97.9(2)° and 82.1(1)°, respectively.

The coordination of the holmium atom in this

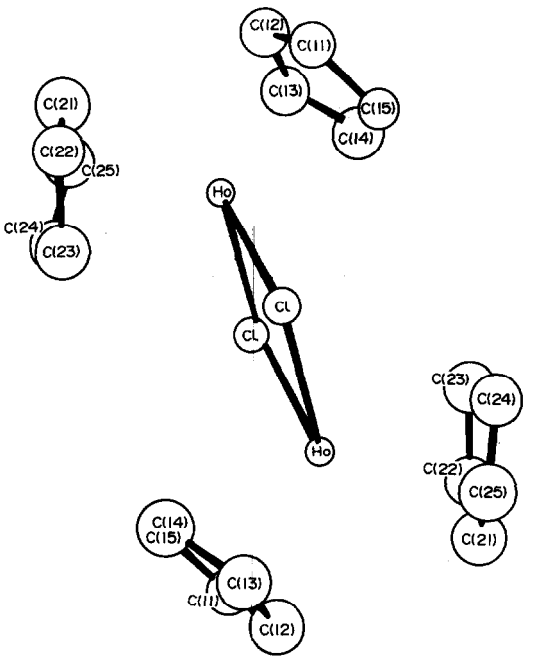

Fig. 1. The molecular structure of the compound $(Cp_2HoCl)_2$ with hydrogen atoms omitted for clarity.

structure can be described as slightly distorted tetrahedral, with the centroids of the two Cp rings and two chlorine atoms forming the apices of the tetrahedron. The vectors from the centroid of each Cp ring to the holmium atoms and from either chlorine to the holmium atoms form two angles (108.5° and 112.3°; 106.4° and 107.9°), which are similar to those reported for the corresponding dimeric compound $[(MeCp)_2YbCl]_2$.[7] The vectors from the centre of either Cp ring to the holmium form an angle of 129.3°, which is similar to that found in the compound $(Cp_2YbCl)_2$ (130.1°),[12] but 2.6° larger than that in compound $(MeCp_2YbCl)_2$. This deviation can be attributed to the difference in the organic ligands. Due to the large steric volume of the MeCp group relative to the Cp group, the steric repulsion existing between two bent metallocene Cp_2Yb subunits should be greater than that in the corresponding compounds $(Cp_2HoCl)_2$ and $(Cp_2YbCl)_2$, thus leading to shortening of the Cent—Yb—Cent angle.

The very fact that there are 15 lanthanide elements which have such a close mutual resemblance means that we can study fairly closely the influence of metal ionic radius on crystal structure. Table 2 compares some significant structural parameters along the structural series $(Cp_2LnCl)_2$ (Ln = Ho, Er, Yb and Sc). It is interesting to note that the bond lengths of Ln—C and Ln—Cl and non-bonded lengths of Cl—Cl and Ln—Ln present a decreasing trend as metal ionic radii decrease. This result is in agreement with the effect of the "lanthanide contraction". In view of the data in

Table 1. Main bond distances (Å) and angles (°)

Ho—Ho	4.031(2)	Cl—Cl	3.511(5)
Ho—Cl	2.671(5)	Ho—Cl	2.676(4)
Ho—C(11)	2.57(2)	Ho—C(12)	2.58(2)
Ho—C(13)	2.56(2)	Ho—C(14)	2.63(2)
Ho—C(15)	2.59(2)	Ho—C(21)	2.63(3)
Ho—C(22)	2.64(2)	Ho—C(23)	2.55(2)
Ho—C(24)	2.67(3)	Ho—C(25)	2.53(3)
C(11)—C(12)	1.46(3)	C(12)—C(13)	1.41(3)
C(13)—C(14)	1.38(4)	C(14)—C(15)	1.46(3)
C(15)—C(11)	1.38(3)	C(21)—C(22)	1.31(3)
C(22)—C(23)	1.48(3)	C(23)—C(24)	1.44(4)
C(24)—C(25)	1.32(3)	C(25)—C(21)	1.30(3)
[a]Cent(1)—Ho	2.308(3)	Ho—Cav.(Cp)	2.60(2)
Cent(2)—Ho	2.347(2)		

Ho—Cl—Ho	97.9(2)	Cl—Ho—Cl	82.1(1)
C(11)—C(12)—C(13)	112.(2)	C(12)—C(13)—C(14)	104.(2)
C(13)—C(14)—C(15)	110.(2)	C(14)—C(15)—C(11)	108.(2)
C(15)—C(11)—C(12)	104.(2)	C(21)—C(22)—C(23)	107.(2)
C(22)—C(23)—C(24)	101.(2)	C(23)—C(24)—C(25)	107.(2)
C(24)—C(25)—C(21)	111.(2)	C(25)—C(21)—C(22)	111.(2)
Cent(1)—Ho—Cl	108.5	Cent(1)—Ho—Cl	112.3
Cent(2)—Ho—Cl	106.4	Cent(2)—Ho—Cl	107.9
Cent(1)—Ho—Cent(2)	129.3		

[a] Cent = cyclopentadinyl ring centroid.

Table 2. Significant structural parameters, conditions of crystal growth and some crystallographic data in the structural series $(Cp_2LnCl)_2$

Compound	Ln^{3+} radii (Å)[13]	Ln—C(Cp)$_{av.}$ (Å)	Ln—Cl$_{av.}$ (Å)	Ln—Ln (Å)	Cl—Cl (Å)	Ln—Cl—Ln (°)	Cl—Ln—Cl (°)	Space group	Z	Condition of crystal growth	Ref.
$(Cp_2HoCl)_2$	0.894	2.60	2.673	4.031	3.511	97.9	82.1	$P2_1/c$	2	CH_2Cl_2	This work
$(Cp_2ErCl)_2$	0.881	2.59	2.66	4.014	3.493	97.94	82.06	$P2_1/c$	2	Sublimation	5
$(Cp_2YbCl)_2$	0.858	2.58	2.642	3.987	3.464	98.0	82.0	$P2_1/c$	2	Sublimation	4
$(Cp_2YbCl)_2$	0.858	2.577	2.649	3.996	3.456	98.3	81.8	$P2_1/c$	6	*n*-hexane	12
$(Cp'_2YbCl)_2$[a]	0.858	2.585	2.637	3.979	3.462	97.95	82.05	C_2/c	4	Benzene	7
$(Cp_2ScCl)_2$	0.732	2.46	2.575	3.904		98.5	81.6	$P2_1/c$	6	Sublimation	6

[a] $Cp' = CH_3C_5H_4$.

Table 2, however, we found that the angles of Ln—Cl—Ln and Cl—Ln—Cl are similar, despite the different metal ionic radius.

A recent study has shown that the compound $(Cp_2YbCl)_2$ can crystallize as in both its Sc ($Z = 6$)[6] and Er ($Z = 2$)[5] analogues (the former obtained by sublimation, the latter from solution). In order to investigate the influence of conditions of crystal growth on crystal structure of the compound Cp_2HoCl, we have grown single crystals of this compound from CH_2Cl_2 solution. However, the single-crystal diffraction study indicates that Cp_2HoCl is isostructural to the compound Cp_2ErCl.[5] A comparison of the conditions of crystal growth and some important crystallographic parameters (Table 2) revealed also that although the conditions of crystal growth are different, the structures of Ho, Er, Yb and Sc compounds are all dimeric, whereas the structures of Gd and Dy compounds are tetrameric and one-dimensional infinite polymeric, respectively.[10,11] The main variable factor between these compounds is the metal ionic radii. Therefore, we postulated that this result is due to "lanthanide contraction", Gd^{3+} and Dy^{3+} ions having larger ionic radii than Ho^{3+}, Er^{3+} and Yb^{3+} ions; Gd and Dy compounds should have much greater steric and coordination unsaturation than Ho, Er and Yb compounds, thus leading to the polymeric structures. In view of the above result, we deduce that the structures of Cp_2LnCl-type compounds with larger metal ionic radii than the Gd^{3+} ion may be polymeric.

Investigation of the magnetic properties of the compound $(Cp_2HoCl)_2$

The magnetic susceptibility of the title compound as a function of temperature is shown in Fig. 2. The

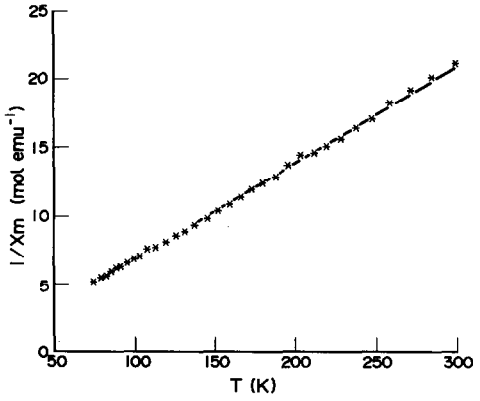

Fig. 2. Inverse molar susceptibility vs temperature for $(Cp_2HoCl)_2$ in the range 74–300 K. The straight line is a least-squares fit to the data

straight line is a least-squares fit to the data. The compound exhibits simple Curie–Weiss behaviour, with $\chi = C/T-\theta$ ($C = 14.3$ and $\theta = 1.2$ K, derived from the straight line). The corresponding value of μ_{eff}, calculated from the slope, is 10.77 B.M. This value is close to those reported for the free ion (10.58 B.M.) and room-temperature magnetic moment (10.3 B.M.) of $(Cp_2HoCl)_2$.[13,14] This result is consistent with those found in the compounds $(Cp_2LnBr)_2$ (Ln = Dy, Er), $(Cp_3Yb)_2C_4H_4N_2$ and $(Cp_2YbX)_2$ (X = Cl, Br).[2-4] Thus, the variable-temperature magnetic susceptibility (74–300 K) of the compound $(Cp_2HoCl)_2$ shows no magnetic interaction between metal centres.

EXPERIMENTAL

Preparation

Due to the extreme sensitivity of the compound to air and moisture, all reactions and handling were facilitated using Schlenk techniques or in a glove-box under dried oxygen-free argon. Tetrahydrofuran was dried over anhydrous $MgSO_4$ and refluxed over sodium-benzophenone ketyl. CH_2Cl_2 was dried and distilled over $LiAlH_4$. All solvents were distilled immediately prior to use.

Anhydrous $HoCl_3$ was prepared according to the literature method.[15] The title compound was pro-

Table 3. Summary of crystal and intensity collection data

Formula	$C_{20}H_{20}Cl_2Ho_2$
Fw	661.14
Crystal size (mm^3)	$0.18\times0.31\times0.25$
Crystal system	Monoclinic
Space group	$P2_1/c$
Cell constants	
a (Å)	11.0944(4)
b (Å)	8.0563(3)
c (Å)	12.1184(4)
β (°)	110.12
V ($Å^3$)	1016.9
D_{calc} (g cm^{-3})	2.159
Z	2
Radiation (Å)	Mo-K_α ($\lambda = 0.71073$)
μ_c (cm^{-1})	80.82
Scan method	ω–2θ
Scan speed (° min^{-1})	7.0 fixed
Scan width (°)	$0.99+0.35\tan\theta$
2θ range (°)	1–50
Data collected	1965
Data unique	1579
Data used in refinement with $I \geqslant 3\sigma(I)$	1123
F(000)	616
Number of refined parameters	149
ρ_{max} (e $Å^{-3}$)	0.58
Max. shift/error	0.09
ρ factor in weighting scheme[a]	0.04
R[b]	0.055
Rw[c]	0.057
GOF[d]	3.088

[a] The weighting scheme for the final refinement was $w = 1/(\sigma_F)^2$, where $\sigma_F = \sigma_{F^2}/2F$ and $\sigma_{F^2} = [(\sigma_I)^2+(\rho F^2)^2]^{1/2}$.

[b] $R = \Sigma\|F_o|-|F_c\|/\Sigma F_o$.

[c] $Rw = [w(F_o-|F_o|)^2/\Sigma w(F_o)^2]^{1/2}$.

[d] $GOF = [\Sigma w(F_o-|F_c|)^2/(N_o-N_v)]^{1/2}$ (N_o and N_v are the number of observations and variables, respectively).

duced by the room temperature reaction of a 1:2:5 molar ratio of $HoCl_3$, Na and C_5H_6 in tetrahydrofuran for 24 h and purified by vacuum sublimation at 200°C/10^{-3} Torr. The yellow sublimate was dissolved in CH_2Cl_2 at room temperature. Crystals suitable for the X-ray diffraction experiment were grown by slow cooling of the saturated CH_2Cl_2 solution.

Structure investigation

Intensities for structure determination were collected on an Enraf–Nonius CAD4 automatic diffractometer using graphite monochromated Mo-K_α radiation at room temperature. Lattice parameters were determined by the least-squares refinement of the setting angles of 25 computer-centred reflections in the range $10° \leqslant \theta \leqslant 15°$. Three standard reflections were monitored every 200 reflections to check crystal stability. No decrease in intensity during data collection was observed. A summary of crystallographic data is listed in Table 3. The calculations were performed on a PDP 11/44 computer (Digital Equipment Corporation) using the SDP programme system. Scattering factors for neutral atoms were taken from the international Tables for crystallography.[16]

The intensity data were corrected for Lorentz–polarization and absorption. The structure was solved by direct methods and refined by full-matrix least-squares techniques, converged to a conventional R factor of 0.055 using 1123 reflections with $I \geqslant 3\sigma(I)$. The positions of the hydrogen atoms were calculated with a C—H bond length of 0.95 Å. In the final calculations the hydrogen atoms ride on the external bisectors of the C—C—C angles. Non-hydrogen atoms were refined using anisotropic temperature factors and hydrogen atoms using isotropic temperature factors. Tables of atomic coordinates, thermal parameters, bond lengths and angles have been deposited at the Cambridge Crystallographic Data Center.

Magnetic susceptibility measurements

Variable-temperature (74–300 K) magnetic susceptibility measurements of crystal samples of the title compound (weighted 0.81 mg) were carried out on a CAHN-2000 Faraday balance with $Ni(en)_3S_2O_3$ as a standard[17] at 6000 G magnetic field. The resulting susceptibility was corrected for underlying diamagnetism.[18]

Acknowledgements—We would like to thank Dr Yunjiang Liu for experimental assistance with the magnetic susceptibility. This research was supported by the National Natural Science Foundation.

REFERENCES

1. J. S. Miller and D. A. Dougherty, *Molec. Cryst. Liq. Cryst.* 1989, **176**, 000 and refs therein.
2. H. Lueken, W. Lamberts and P. Hannibal, *Inorg. Chim. Acta* 1987, **132**, 111.
3. E. C. Baker and K. N. Raymond, *Inorg. Chem.* 1977, **16**, 2710.
4. H. Lueken, J. Schmitz, W. Lamberts, P. Hannibal and K. Handrick, *Inorg. Chim. Acta* 1989, **156**, 119.
5. W. Lamberts, H. Lueken and B. Hessner, *Inorg. Chim. Acta* 1987, **134**, 155.
6. J. L. Atwood and K. D. Smith, *J. Chem. Soc., Dalton Trans.* 1973, 2487.
7. E. C. Baker, L. D. Brown and K. N. Raymond, *Inorg. Chem.* 1975, **14**, 1376.
8. M. F. Lappert, A. Singh, J. L. Atwood and W. E. Hunter, *J. Chem. Soc., Chem. Commun.* 1981, 1190.
9. K. O. Hodgson and K. N. Raymond, *Inorg. Chem.* 1972, **4**, 171.
10. W. Lamberts, B. Hessner and H. Lueken, *Inorg. Chim. Acta* 1987, **139**, 215.
11. W. Lamberts and H. Lueken, *Inorg. Chim. Acta* 1987, **132**, 119.
12. T. Akhnoukh, J. Muller, K. Qiao, X. F. Li and R. D. Fischer, *J. Organomet. Chem.* 1991, **408**, 47.
13. R. C. Weast, *CRC Handbook of Chemistry and Physics*, 66th edn. CRC Press, Inc., Boca Raton, Florida (1985–1986).
14. R. E. Maginn, S. Manastyrskyj and M. Dubeck, *J. Am. Chem. Soc.* 1963, **85**, 672.
15. M. D. Taylor and C. P. Carter, *J. Inorg. Nucl. Chem.* 1962, **24**, 387.
16. D. T. Cromer and J. T. Waber, *International Tables for X-ray Crystallography*. Kynoch Press, Birmingham (1974).
17. L. F. Lindoy, V. Kalovic and D. H. Busch, *J. Chem. Educ.* 1972, **49**, 117.
18. P. W. Selwood, *Magnetochemistry*, 2nd edn. Interscience, New York (1956).

Polyhedron Vol. 12, No. 6, pp. 683–687, 1993
Printed in Great Britain

0277–5387/93 $6.00+.00
© 1993 Pergamon Press Ltd

FIRST ELECTROSYNTHESIS OF TRANSITION METAL PEROXOFLUORO COMPLEXES. SYNTHESIS, CHARACTERIZATION AND REACTIVITY OF SOME PEROXOFLUORO COMPLEXES

M. C. CHAKRAVORTI,* SOMENATH GANGULY, G. V. B. SUBRAHMANYAM and MANISH BHATTACHARJEE

Department of Chemistry, Indian Institute of Technology, Kharagpur 721 302, India

(*Received* 8 *October* 1992; *accepted* 15 *October* 1992)

Abstract—Peroxofluoro complexes of the transition metals, viz. V, Nb, Ta, Mo and W, have been synthesized electrochemically using the sacrificial metal anodes in the presence of hydrogen peroxide (15%) and hydrofluoric acid (10%). These complexes have also been prepared by the dissolution of the metal powders in a mixture of hydrogen peroxide and hydrofluoric acid. While the monoperoxo complexes are formed at lower pH, higher pH is conducive to the formation of diperoxo complexes. The compounds have been characterized by elemental analysis and vibrational spectral studies. $K_2[MoO(O_2)F_4]\cdot H_2O$ and $K_2[WO(O_2)F_4]\cdot H_2O$ can oxidize triphenylphosphine to triphenylphosphine oxide in high yield.

Previous communications from this laboratory reported that many transition metals when used as anodes readily go into solution in the presence of aqueous hydrofluoric acid or hydrogen peroxide, giving rise to fluoro and peroxo complexes.[1–3] It is expected that mixed-ligand peroxofluoro complexes may result from an electrolyte containing a mixture of the two and different species may be isolated by the appropriate adjustment of pH. The importance of the latter in the synthesis of peroxo complexes has already been emphasized in the literature.[4,5] Fluoride is known to stabilize transition metal peroxo complexes[6,7] and a number of peroxofluoro complexes of various metals, viz. $[Ti(O_2)F_5]^{3-}$,[6] $[Ti(O_2)_2F_2]^{2-}$,[8] $[VO(O_2)_2F]^{2-}$,[9] $[M(O_2)F_5]^{2-}$,[6] $[M(O_2)_2F_4]^{3-}$ (M = Nb or Ta),[10] $[MO(O_2)F_4]^{2-}$ (M = Mo or W),[6] $[MoO(O_2)_2F_2]^{2-}$,[11] etc., have been prepared. Some of their structures have been studied by X-ray spectroscopy. Peroxo complexes are of considerable interest because of their involvement in catalytic and biological oxidation reactions.[12] The present work deals with the first electrosynthesis of peroxofluoro complexes of vanadium, niobium, tantalum, molybdenum and tungsten. A few complexes have also been synthesized chemically by dissolving the metal powders in hydrofluoric acid and hydrogen peroxide mixture. The paper also deals with the studies on the reactivity of some of the synthesized peroxofluoro complexes.

* Author to whom correspondence should be addressed.

EXPERIMENTAL

Spec-pure molybdenum and tungsten rods (0.5 cm diameter) were supplied by Johnson Matthey Chemicals Ltd, U.K. Molybdenum powder (4–8 μ), supplied by Koch-Light Laboratories Ltd, U.K., was 99.95% pure. Tungsten powder supplied by Johnsons of Hendon Ltd, U.K., was 99% pure. Vanadium powder (99.5% pure) was supplied by Aldrich Chemical Co., U.S.A. Niobium and tantalum rods (0.6 cm diameter), supplied by Aldrich Chemical Co., were 99.8% pure. Titanium powder (purity >99%) was supplied by BDH Chemicals Ltd, U.K. Platinum foil having 99.95% purity was supplied by Arora-Matthey Ltd. Other chemicals were of AR/GR quality of reputable manufacturers.

The electric power was supplied by a d.c. power supply (Aplab, India). The electrolytic cell was a tall polythene beaker (100 cm^3) fitted with a rubber stopper, through which two holes were made. The

Table 1. Experimental conditions and electrochemical efficiency for the synthesis of the complexes

Compound	Voltage[a] (V)	Current (A)	Time (min)	Metal dissolved (g)	Yield (g)	Yield (%)	E_F (mol F^{-1})
$K_2[Nb(O_2)F_5]\cdot H_2O$	5–15	0.05	180	0.117	0.33	82	0.22
$K_2[Ta(O_2)F_5]\cdot H_2O$	5–18	0.05	180	0.205	0.40	87	0.20
$K_2[MoO(O_2)F_4]\cdot H_2O$	5–8	0.05	150	0.080	0.21	80	0.18
$K_2[WO(O_2)F_4]\cdot H_2O$	5–10	0.05	120	0.130	0.24	84	0.19
$K_2[VO(O_2)_2F]$	2–3	0.1	180	0.107	0.30	70	0.19
$K_3[Nb(O_2)_2F_4]$	5–15	0.05	180	0.117	0.40	90	0.22
$K_3[Ta(O_2)_2F_4]$	5–18	0.05	180	0.205	0.40	80	0.20
$K_2[MoO(O_2)_2F_2]$	5–8	0.05	120	0.065	0.12	60	0.18

[a] Voltage was adjusted occasionally to keep the current constant.

appropriate metal rods which formed the anode were inserted through a hole. In all cases a platinum foil (1 × 1 × 0.05 cm) served as the cathode and was inserted through the second hole.

Peroxide was determined iodometrically. Fluoride was determined by titration with $Th(NO_3)_4$ after steam distillation of $H_2[SiF_6]$. Metals were analysed by standard methods. IR spectra were recorded in KBr pellets and Nujol mulls using a Perkin–Elmer (model 883) spectrophotometer. Raman spectra were recorded using a DILOR Z24 Raman spectrometer (exciting line 488.0 nm). Molar conductance measurements were performed in conductivity grade water using a direct-reading conductivity meter from Systronics, India. Magnetic susceptibility was measured by the Gouy method.

Preparation of the complexes

Method A. Electrochemical synthesis. $K_2[M(O_2)F_5]\cdot H_2O$ (M = Nb or Ta) and $K_2[MO(O_2)F_4]\cdot H_2O$ (M = Mo or W): Hydrogen peroxide (30%, 5 cm^3) and hydrofluoric acid (20%, 5 cm^3) were taken in the beaker. The metal rod and the platinum foil each joined to the platinum wire were connected to positive and negative terminals of the d.c. power supply, respectively, and were dipped in the electrolyte. The voltage was adjusted to give a current of 0.05 or 0.1 A and the electrolysis was carried out for 2–3 h. The details of the experimental conditions and E_F values are given in Table 1. The temperature of the electrolyte was maintained at 0–5°C throughout the electrolysis. Gradually the solution became yellow in the case of molybdenum, while it remained colourless in the other cases. After electrolysis the solution was filtered to remove any disintegrated metal particle. To the filtrate a solution of KF (2 g) in a minimum volume of HF (20%) was added, whereupon niobium and tantalum complexes of the type $K_2[M(O_2)F_5]\cdot H_2O$ and molybdenum and tungsten complexes of the type $K_2[MO(O_2)F_4]\cdot H_2O$ were precipitated. These were then filtered, washed with ethanol and dried over KOH. The yield is given in Table 1.

$K_2[VO(O_2)_2F]$ and $K_3[M(O_2)_2F_4]$ (M = Nb or Ta): These were prepared in a manner analogous to that described above, except that instead of adding a solution of KF the pH of the electrolysed solution was adjusted by the addition of 30% KOH solution. At pH 5 $K_2[VO(O_2)_2F]$ was precipitated out by the addition of ethanol. $K_3[M(O_2)_2F_4]$ (M = Nb or Ta) precipitated out when the pH of the electrolysed solution was raised to 7.

$K_2[MoO(O_2)_2F_2]$: The electrolyte used was a solution of KF (2 g) in H_2O_2 (30%, 10 cm^3). The details of the experimental conditions are given in Table 1. After the electrolysis the solution was filtered and the filtrate was allowed to stand for *ca* 2 h over concentrated H_2SO_4 in a desiccator, whereupon the complex precipitated out in a microcrystalline state.

Method B. Chemical method. $K_3[Ti(O_2)F_5]\cdot H_2O$, $K_2[Ti(O_2)_2F_2]$, $K_2[VO(O_2)_2F]$ and $K_2[MO(O_2)F_4]\cdot H_2O$ (M = Mo or W): Metal powder (0.25 g*) was dissolved in a mixture of hydrofluoric acid (20%, 5 cm^3) and hydrogen peroxide (30%, 5 cm^3) with stirring. The temperature of the reaction medium was maintained below 10°C. After dissolution of the metal the solution was filtered to remove any fine particles. $K_3[Ti(O_2)F_5]\cdot H_2O$, $K_2[Ti(O_2)_2F_2]$ and $K_2[VO(O_2)_2F]$ were obtained by raising the pH of the solution to 4–5, 8–9 and 4–5, respectively, by adding 30% KOH solution followed by the addition of ethanol. The other two complexes, viz. $K_2[MO(O_2)F_4]\cdot H_2O$ (M = Mo or W), were precipitated out by the addition of KF (1 g) dissolved in hydrofluoric acid (20%, 3 cm^3). All the

* In the case of titanium 1 g of metal was used.

complexes were separated and dried as described before. The yields were 60–70%.

Studies on the reactivity of $K_2[MO(O_2)F_4]\cdot H_2O$ (M = Mo *or* W)

Since the method is a general one, only a representative procedure is given. To a solution of triphenylphosphine (1 mmol) in dimethylsulphoxide (10 cm^3) was added $K_2[MO(O_2)F_4]\cdot H_2O$ (M = Mo or W) (1 mmol) and the mixture was heated under reflux for *ca* 5 h. The reaction mixture was then cooled and filtered to remove any residual inorganic compound and the filtrate was treated with water (15 cm^3), whereupon a dirty white product was precipitated. This was filtered, washed with water and recrystallized from ethanol to yield a light yellowish-white compound, identified as triphenylphosphine oxide by melting point determination (154–156°C). The IR spectrum was identical with that of an authentic sample. The yield of triphenylphosphine oxide was *ca* 80%.

RESULTS AND DISCUSSION

When electrolysis is carried out in a cell depicted as:

$$Pt(-)/H_2O_2(15\%)+HF(10\%)/M(+),$$

the metals (Mo, W, V, Nb and Ta) smoothly go into solution. The reaction at the anode may be represented by the equation:

$$M - ne \longrightarrow M^{n+},$$

where $n = 6$ for Mo and W and 5 for V, Nb and Ta (instead of M^{n+}, an oxo metal ion is more probable). This is evident from the observed electrochemical efficiency (defined as the number of moles of metal oxidized per Faraday), which is close to $1/n$ mol F^{-1} (see Table 1). The most probable reaction at the cathode is:

$$H_2O_2+2H^+ + 2e \longrightarrow 2H_2O,$$

which is proposed in view of the very high (1.77 V) standard reduction potential of the above redox system.[13] Thus, it is expected that hydrogen peroxide will be reduced at the cathode in preference to protons. This is also supported by the fact that in the above electrochemical cell the slight liberation of gas (presumably oxygen) occurs on the platinum surface in the absence of applied voltage, and the rate of gas evolution does not increase during the course of electrolysis. The metal ion liberated in solution then reacts with excess H_2O_2 and HF to produce peroxofluorometallates. At the prevailing low pH (1–2) monoperoxo species, viz. $[MO(O_2)F_4]^{2-}$ (M = Mo or W) and $[M(O_2)F_5]^{2-}$ (M = Nb or Ta), are formed which are precipitated as their potassium salts (monohydrate) on the addition of potassium fluoride dissolved in aqueous hydrofluoric acid. If the pH of the solution left after electrolysis using niobium and tantalum anode is raised to about 7 by the addition of potassium hydroxide, diperoxo species, viz. $[M(O_2)_2F_4]^{3-}$, are formed. This is in conformity with the previous observation[4,5] that a higher pH is conducive to the formation of diperoxo species. Electrolysis of a solution containing potassium fluoride and hydrogen peroxide using a molybdenum anode and a platinum cathode gives a red solution having a pH of *ca* 7, from which the diperoxo complex $K_2[MoO(O_2)_2F_2]$ can be crystallized. No diperoxo compound of tungsten could be prepared by either of the methods described above.

Finely divided titanium or vanadium readily dissolves in a mixture containing equal volumes of 20% HF and 30% H_2O_2 and the solution when treated with KOH solution gives $K_3[Ti(O_2)F_5]\cdot H_2O$ at pH 5 and $K_2[Ti(O_2)_2F_2]$ at pH 9 in the case of titanium. In the case of vanadium $K_2[VO(O_2)_2F]$ is formed at pH 4–5. Molybdenum and tungsten powder also dissolve in the HF and H_2O_2 mixture, from which the monoperoxo complexes, viz. $K_2[MO(O_2)F_4]\cdot H_2O$ (M = Mo or W), are precipitated out by the addition of KF dissolved in aqueous HF. No diperoxo complex could be prepared starting from molybdenum or tungsten powder.

Molybdenum, titanium and vanadium complexes are yellow, whereas niobium, tantalum and tungsten complexes are colourless. All the complexes are soluble in water but insoluble in common organic solvents. Molar conductivity measurements carried out in conductivity grade water agree with their electrolytic nature and also show that the compounds are fairly stable in aqueous solution. However, in acidic solution they decompose rendering it easy to determine the peroxide contents by standard iodometric methods. The results of the analysis of peroxide, fluoride and metal contents agree well with the formulae of the compounds (see Table 2). They are all diamagnetic. The hydrated compounds lose the water molecule on heating at 120°C (Table 2) and the chemical analysis of the residue is compatible with the formulation of the anhydrous compounds.

The common features of the IR and Raman spectra of all the complexes (see Table 2) are the vibrational modes due to bonded peroxide, viz. ν(O—O), ν_s(M—O_2) and ν_{as}(M—O_2), which appear in the regions 900–800 and 630–530 cm^{-1}, respectively, as observed earlier.[14] Another common fea-

Table 2. Analytical data[a] of the complexes and bands in IR and Raman[b] spectra (cm^{-1})

Compound	% Metal	% Peroxide	% Fluorine	% Weight loss at 120°C	ν(M=O)	ν(O—O)	ν_{as}(M—O_2)	ν_s(M—O_2)	ν(M—F)
$K_3[Ti(O_2)F_5]\cdot H_2O$	16.1(15.4)	9.8(10.3)	31.0(30.6)	5.8(5.9)		905	605	535	435
						884[b]	623[b]	560[b]	497[b]
$K_2[Ti(O_2)_2F_2]$	21.7(21.0)	28.1(28.0)	17.2(16.7)			841	629		471
						878, 853[b]	595[b]		
$K_2[VO(O_2)_2F]$	23.0(22.3)	27.6(28.0)	7.7(8.3)		962	882, 879	638		469
$K_2[Nb(O_2)F_5]\cdot H_2O$	28.8(29.4)	10.1(10.1)	30.6(30.0)	5.7(5.7)		902	580	500	
						887[b]	620, 599[b]		
$K_3[Nb(O_2)_2F_4]$	27.1(26.5)	18.6(18.3)	21.4(21.7)			884, 858		532	431
						898[b]	592[b]		
$K_2[Ta(O_2)F_5]\cdot H_2O$	44.1(44.8)	7.8(7.9)	24.2(23.5)	4.3(4.5)		862	620	530	
						853[b]	624, 589[b]	556[b]	
$K_3[Ta(O_2)_2F_4]$	40.9(41.3)	15.2(14.6)	17.7(17.3)			866		518	440(br)
						865[b]	592[b]		502[b]
$K_2[MoO(O_2)F_4]\cdot H_2O$	30.7(30.3)	10.3(10.1)	24.4(24.0)	5.7(5.7)	972, 935	862	600	567	
					945[b]	885[b]		545[b]	
$K_2[MoO(O_2)_2F_2]$	33.0(32.8)	21.6(21.9)	13.9(13.0)		964	874, 858	579	545	487
					928[b]	890[b]	640, 613[b]		
$K_2[WO(O_2)F_4]\cdot H_2O$	44.9(45.5)	8.3(7.9)	19.4(18.8)	4.7(4.7)	978	901		540	500(br)
					947[b]	929[b]		555[b]	

[a] Values in parentheses indicate the calculated ones.
[b] Raman spectral data.

ture of the vibrational spectra is the metal–fluorine stretching mode which appears around 500 cm^{-1} and shows the presence of terminal fluoride.[15] Of course, the M—F band may also be overlapped with the symmetric (M—O_2) vibration. Apart from these bands vanadium, molybdenum and tungsten fluoroperoxo complexes show strong absorptions in the region 960–980 cm^{-1}, which can be assigned to terminal ν(M=O) vibrations. The hydrated compounds also give additional bands due to water. The vibrational spectral bands of all the complexes (except the Raman spectra of $K_2[VO(O_2)_2F]$, $K_3[Nb(O_2)_2F_4]$ and $K_3[Ta(O_2)_2F_4]$) are available in the literature.[5,6–11,14] Our data are in agreement with the reported values for the corresponding compounds.

Having achieved the synthesis of the compounds, we were interested in studying their reactivity, especially in terms of oxygen transfer reactions. It should be mentioned here that although all the complexes are reported, no information is available regarding their reactivity. A solution of triphenylphosphine in dimethylsulphoxide when heated under reflux with $K_2[MO(O_2)F_4]\cdot H_2O$ (M = Mo or W) afforded triphenylphosphine oxide in high yield (*ca* 80%).

CONCLUSION

The existing methods[16] for the synthesis of the peroxo complexes are the reactions between the oxides or oxo anions of the metal with hydrogen peroxide or the interaction of dioxygen with metal complexes. The present paper provides a general method for electrochemical as well as chemical synthesis of transition metal peroxofluoro complexes starting directly from metals. Coupled with our previous communication[3] on the synthesis of other heteroligand peroxo complexes of molybdenum and tungsten by a similar method, this opens up a completely new route to the synthesis of peroxo complexes.

Acknowledgement—The authors thank the Council of Scientific and Industrial Research, New Delhi, for support.

REFERENCES

1. M. C. Chakravorti, G. V. B. Subrahmanyam and D. Bandyopadhyay, *Polyhedron* 1991, **10**, 2605.
2. M. C. Chakravorti and G. V. B. Subrahmanyam, *J. Chem. Educ.* 1991, **68**, 961.
3. M. C. Chakravorti, S. Ganguly and M. Bhattacharjee, *Polyhedron* 1993, **12**, 55.
4. M. K. Chaudhuri and S. K. Ghosh, *Inorg. Chem.* 1984, **23**, 534; 1982, **21**, 4020; *J. Chem. Soc., Dalton Trans.* 1984, 507.
5. J. A. Connor and F. A. V. Ebsworth, *Adv. Inorg. Chem. Radiochem.* 1964, **6**, 280.
6. W. P. Griffith and T. D. Wickins, *J. Chem. Soc.* (*A*) 1968, 397.
7. D. F. Evans, W. P. Griffith and L. Pratt, *J. Chem. Soc.* 1965, 2182.
8. M. K. Chaudhuri and B. Das, *Inorg. Chem.* 1986, **25**, 168.
9. M. K. Chaudhuri and S. K. Ghosh, *Polyhderon* 1982, **1**, 553.
10. N. Vuletic and C. Djordjevic, *J. Less-Common Met.* 1976, **45**, 85.
11. M. C. Chakravorti and D. Bandyopadhyay, *Inorg. Chim. Acta* 1988, **143**, 247.
12. H. Mimoun, *Comprehensive Coordination Chemistry* (Edited by G. Wilkinson), Vol. 6, p. 317. Pergamon Press, New York (1987) and refs therein.
13. F. A. Cotton and G. Wilkinson, *Advanced Inorganic Chemistry*, 5th edn, p. 458. John Wiley, New York (1988).
14. W. P. Griffith, *J. Chem. Soc.* 1964, 5428.
15. R. J. H. Clark and C. S. Williams, *Inorg. Chem.* 1965, **4**, 350.
16. M. H. Gubelmann and A. F. Williams, *Struct. Bonding* 1983, **55**, 1 and refs therein.

Polyhedron Vol. 12, No. 6, pp. 689–708, 1993
Printed in Great Britain

0277–5387/93 $6.00+.00
© 1993 Pergamon Press Ltd

ARYL IMIDO COMPLEXES OF THE GROUP 4 METALS: STRUCTURAL ASPECTS AND MECHANISTIC STUDY OF FORMATION

CESAR H. ZAMBRANO, ROBERT D. PROFILET, JOHN E. HILL, PHILLIP E. FANWICK and IAN P. ROTHWELL*

Department of Chemistry, 1393 Brown Building, Purdue University, West Lafayette, IN 47907, U.S.A.

(*Received* 24 *July* 1992; *accepted* 9 *October* 1992)

Abstract—The addition of aniline ($PhNH_2 \geqslant 2$ equivalents) to the organometallic compounds $[Ti(OC_6H_3Pr^i_2\text{-}2,6)_2(\eta^2\text{-}Bu^tNCCH_2Ph)(CH_2Ph)]$, $[Ti(OC_6H_3Ph_2\text{-}2,6)_2(C_4Et_4)]$ and $[Zr(OC_6H_3Bu^t_2\text{-}2,6)_2(CH_3)_2]$ in hydrocarbon solvents leads to the formation of the mononuclear bis(phenylamido) derivatives $[M(OAr)_2(NHPh)_2]$ [M = Ti, OAr = $OC_6H_3Pr^i_2$-2,6 (**1**); M = Ti, OAr = $OC_6H_3Ph_2$-2,6 (**2**); M = Zr, OAr = $OC_6H_3Bu^t_2$-2,6 (**3**)]. Treatment of $[Hf(CH_2Ph)_4]$ first with $PhNH_2$ (4 equivalents), followed by $HOC_6H_3Bu^t_2$-2,6 (2 equivalents), leads to the related bis(phenylamido) compound **4** (M = Hf; OAr = $OC_6H_3Bu^t_2$-2,6). The two homoleptic aryl amido compounds $[M(NHC_6H_3Pr^i_2\text{-}2,6)_4]$ [M = Zr (**5**); Hf (**6**)] have also been obtained by addition of 2,6-diisopropylaniline to the tetra-benzyl compounds $[M(CH_2Ph)_4]$ (M = Zr, Hf). The addition of 4-pyrrolidinopyridine (py′) to all of the aryl amido compounds except **4** leads to elimination of 1 equivalent of aryl amine and the formation of a series of five-coordinate aryl imido derivatives of the general formula $[M(OAr)_2(=NPh)(py')_2]$ [M = Ti, OAr = $OC_6H_3Pr^i_2$-2,6 (**7**); M = Ti, OAr = $OC_6H_3Ph_2$-2,6 (**8**); M = Zr, OAr = $OC_6H_3Bu^t_2$-2,6 (**9**); and $[M(NHAr)_2(=NAr)(py')_2]$; M = Zr, Ar = $C_6H_3Pr^i_2$-2,6 (**10**); M = Hf, Ar = $C_6H_3Pr^i_2$-2,6 (**11**)]. In the case of the hafnium bis(phenylamido) complex **4**, addition of 4-pyrrolidinopyridine resulted in the formation of a simple adduct, $[Hf(OC_6H_3Bu^t_2\text{-}2,6)_2(NHPh)_2(py')]$, [**4**·py′]. (A similar adduct, [**3**·py′], was detected in the conversion of **3**–**9**.) No elimination of aniline from [**4**·py′] and formation of a phenylimido derivative were observed. Both 2,2′-bipyridine and 1,10-phenanthroline were found to eliminate aniline from compounds **1**–**3** to produce insoluble products. Addition of 3,4,7,8-tetramethyl-1,10-phenanthroline to **2**, however, yielded a soluble phenylimido derivative (**12**). The four-coordinate aryl amido compounds **2**, **3** and **5** were found to be pseudo-tetrahedral in the solid state, while the five-coordinate aryl imido compounds **7**, **9**, **10** and **11** are best described as distorted trigonal-bipyramidal with *trans*-axial pyridine ligands. In the phenanthroline derivative **12** a distorted trigonal-bipyramidal geometry exists about the titanium atom with an aryloxide oxygen atom *trans* to a phenanthroline nitrogen. The bonding of the aryl imido, aryl amido and pyridine groups is discussed. A detailed study of the reaction of a series of bis(aryl amido) complexes, $[Zr(OAr)_2(NHC_6H_4\text{-}4X)_2]$ $(\mathbf{3})^X$ (X = H, F, CH_3, OMe, Br), with a variety of pyridine ligands was undertaken. The mono-pyridine adduct $[\mathbf{3}^X \cdot py]$ is rapidly formed, followed by the slow formation of the corresponding aryl imido complex $[Zr(OAr)_2(=NHC_6H_4\text{-}4X)(py)_2]$ $[\mathbf{9}^X]$ and an equivalent of substituted aniline. Equilibrium constants for the reaction $[\mathbf{3}^X py] + py = [\mathbf{9}^X] + ArNH_2$ were measured. Formation of the aryl imido ligand was found to be favoured by a more basic pyridine ligand and by electron-withdrawing substituents on the aryl ring of the initial aryl amido group. The rate of attainment of the equilibrium situation from [**3**] and py was investigated and various pathways for the reaction are considered. X-ray crystal structures were determined for **2**, **3**, **5**, **7**, **9**, **10**, **11** and **12**.

* Author to whom correspondence should be addressed.

The last two decades have seen a growth both in the scope and importance of the chemistry of transition metal compounds containing multiple metal–ligand bonds.[1] In particular, M=CR$_2$,[2] M≡CR,[3] M=NR[4] and M=O[5] functional groups have been shown to be important in various stoichiometric and catalytic reactions. Until very recently a major gap in this area of chemistry had been the dearth of group 4 metal derivatives containing these functional groups. Recent work by a number of research groups has now shown that such ligands can demonstrate a high degree of reactivity when attached to these early *d*-block metals.[6–9] In particular, both titanium and zirconium imido linkages (typically generated *in situ*) have the ability to activate carbon–hydrogen bonds.[6,7] This reactivity combined with the scarcity of group 4 metal imido compounds highlights the importance of studying the structure and bonding of such compounds as well as investigating the mechanistic pathways whereby they are produced. In this paper we report on the synthesis of a series of aryl imido derivatives of titanium, zirconium and hafnium. The structure and bonding in these compounds is discussed as well as the results of a mechanistic study of their formation by ligand-induced elimination of aryl amines from bis(aryl amido) precursors.

RESULTS AND DISCUSSION

Synthesis of aryl amido compounds

Early transition metal dialkylamido compounds represent an important class of starting materials in inorganic chemistry.[10] Over the years many methods for the synthesis of such compounds have been devised with by far the most common involving the reaction of the metal halide with either an amine/base mixture or with an alkaline metal amide salt. In the area of metal aryloxide chemistry our group has demonstrated the utility of organometallic compounds as starting points for the introduction of aryloxide ligands by reaction with the parent phenol.[11] We have investigated the same synthetic method for the synthesis of aryl amido derivatives of the group 4 metals (Scheme 1). The organometallic bis(aryloxide) compounds [Ti(OC$_6$H$_3$Pr$^i_2$-2,6)$_2$(η^2-Bu^{t}NCCH$_2$Ph)(CH$_2$Ph)],[12] [Ti(OC$_6$H$_3$Ph$_2$-2,6)$_2$(C$_4$Et$_4$)][13] and [Zr(OC$_6$H$_3$Bu$^t_2$-2,6)$_2$(CH$_3$)$_2$][14,15] react slowly with aniline (≥ 2 equivalents) in hydrocarbon solvents to produce the corresponding bis(phenyl amido) compounds along with two equivalents of alkane (Scheme 1). In contrast, the hafnium bis(benzyl) compound [Hf(OC$_6$H$_3$Bu$^t_2$-2,6)$_2$(CH$_2$Ph)$_2$] failed to react

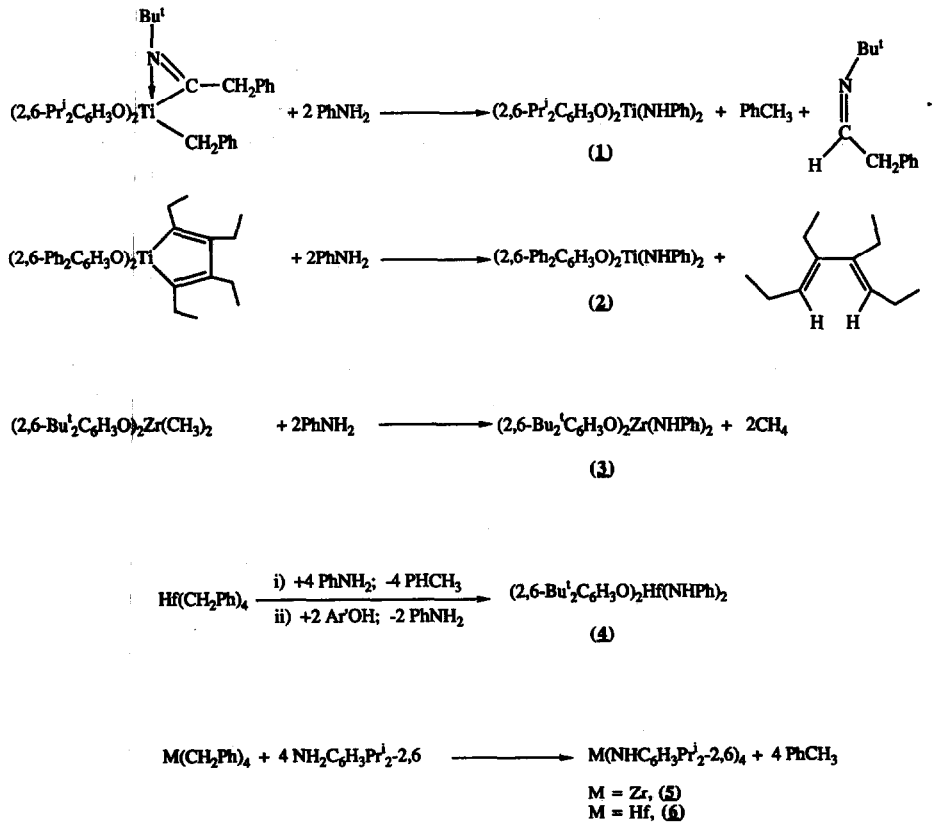

Scheme 1.

(NMR) with aniline over 2 weeks in benzene solution. However, the hafnium bis(phenyl amido) compound $[Hf(OC_6H_3Bu^t_2\text{-}2,6)_2(NHPh)_2]$ (**4**) was obtained by treating $[Hf(CH_2Ph)_4]$ first with aniline (4 equivalents) followed by 2,6-di-tert-butylphenol (2 equivalents, Scheme 1). The homoleptic aryl amido compounds $[M(NHC_6H_3Pr^i_2\text{-}2,6)_4]$ [M = Zr (**5**); Hf (**6**)] can also be obtained by stirring a mixture of 2,6-diisopropylaniline and the corresponding $[M(CH_2Ph)_4]$[16] substrate. The spectroscopic properties of compounds **1–6** are consistent with their formulation as aryl amido compounds and not aryl imido, aniline complexes. In the ^1H NMR spectra of **1–6** the positions and intensities of the aliphatic and aromatic protons appear as expected. An interesting feature of these spectra is the position of the M—N*H*Ar proton. These protons are found to resonate downfield close to the aromatic region of the spectrum and to be sensitive to the metal centre. Progressing down the group 4 triad, from titanium through zirconium to hafnium, this proton resonates to higher field, cf. δ(N*H*) values of 8.22, 7.38 and 6.63 ppm for compounds **1**, **3** and **4**, respectively. A similar upfield shift of the M—N*H* proton is observed between the zirconium compound (**5**), 6.98 δ ppm, and its hafnium analogue (**6**), 6.16 δ ppm.[11,12] An upfield shifting of α-protons is observed for the compounds $[M(OC_6H_3Bu^t_2\text{-}2,6)_2(CH_2Ph)_2]$ on moving from M = titanium, δ 3.19 ppm, to zirconium, δ 2.84 ppm, to hafnium, δ 2.65 ppm. A rationale for this behaviour involves an increase in diamagnetic shielding of adjacent nuclei by the metal centre as the number of core electrons increases.[17]

In order to gain more insight into the bonding in these aryl amido and related aryl imido (*vide infra*) derivatives, compounds **2**, **3** and **5** were subjected to single-crystal X-ray diffraction analyses. Selected bond distances and angles are contained in Tables 1–3 while ORTEP views of the molecules are shown in Figs 1–3. The relevance of the metal–ligand bond distances in these molecules is discussed below. The pair of bis(phenyl amido) compounds **2** and **3** have certain features in common. Within the pseudo-tetrahedral environment about the metal centre the O—M—O angles are larger, 120.1(1)° and 119.8(3)° for **2** and **3**, than the corresponding N—M—N angles, 105.2(1)° and 104.4(4)°. This effect is also seen in other bis(aryloxide), bis(amido) compounds of titanium, cf. O—Ti—O and N—Ti—N angles of 115.2(2)° and 98.6(2)° in $[Ti(OC_6H_2Bu^t_3\text{-}2,4,6)_2(NMe_2)_2]$,[18] 118.5(2)° and 103.8(3)° in $[Ti(OC_6H_2Bu^t_2\text{-}2,6\text{-}Ph\text{-}4)_2(NMe_2)_2]$[19] and 113.1(1)° and 98.5(1)° in $[Ti(OC_6H_3Bu^t_2\text{-}2,6)_2(NMe_2)_2]$.[19] In contrast to this behaviour the O—M—O angles are *smaller* than the N—M—N angles in related group 14 metal derivatives, cf. corresponding angles of 99.8(2)° and 111.9(3)° for $[Ge(OC_6H_3Ph_2\text{-}2,6)_2(NMe_2)_2]$ and 104.5(1)° and 109.6(2)° in $[Sn(OC_6H_3Bu^t_2\text{-}2,6)_2(NMe_2)_2]$.[20] There is also a dis-

Table 1. Selected bond distances (Å) and angles (°) for $[Ti(OC_6H_3Ph_2\text{-}2,6)_2(NHPh)_2]$ (**2**)

Ti—O(10)	1.789(2)	Ti—N(30)	1.881(3)
Ti—O(20)	1.786(2)	Ti—N(4)	1.898(3)
O(10)—Ti—O(20)	120.1(1)	Ti—O(10)—C(11)	147.9(2)
O(10)—Ti—N(30)	110.1(1)	Ti—O(20)—C(21)	159.8(2)
O(10)—Ti—N(40)	104.6(1)	Ti—N(30)—C(31)	134.2(3)
O(20)—Ti—N(30)	103.1(1)	Ti—N(40)—C(41)	132.8(3)
O(20)—Ti—N(40)	113.0(1)	Ti—N(40)—H(40)	113.0(2)
N(30)—Ti—N(40)	105.2(1)	Ti—N(30)—H(30)	113.0(2)

Table 2. Selected bond distances (Å) and angles (°) for $[Zr(OC_6H_3Bu^t_2\text{-}2,6)_2(NHPh)_2]$ (**3**)

Zr—O(1)	1.893(7)	Zr—N(3)	2.041(9)
Zr—O(2)	1.941(7)	Zr—N(4)	2.06(1)
O(1)—Zr—O(2)	119.8(3)	N(3)—Zr—N(4)	104.4(4)
O(1)—Zr—N(3)	107.6(3)	Zr—O(1)—C(11)	174.6(7)
O(1)—Zr—N(4)	107.0(4)	Zr—O(2)—C(21)	170.9(8)
O(2)—Zr—N(3)	109.1(3)	Zr—N(3)—C(31)	130.2(8)
O(2)—Zr—N(4)	107.9(4)	Zr—N(4)—C(41)	132.0(8)

Table 3. Selected bond distances (Å) and angles (°) for [Zr(NHC$_6$H$_3$Pr$^i_2$-2,6)$_4$] (5)

Zr—N(10)	2.035(7)	Zr—N(30)	2.053(7)
Zr—N(20)	2.057(7)	Zr—N(40)	2.027(7)
N(10)—Zr—N(20)	105.2(3)	N(30)—Zr—N(40)	99.7(3)
N(10)—Zr—N(30)	108.1(3)	Zr—N(10)—C(11)	140.2(6)
N(10)—Zr—N(40)	116.8(3)	Zr—N(20)—C(21)	142.4(6)
N(20)—Zr—N(30)	115.3(3)	Zr—N(30)—C(31)	131.9(6)
N(20)—Zr—N(40)	112.0(3)	Zr—N(40)—C(41)	149.3(7)

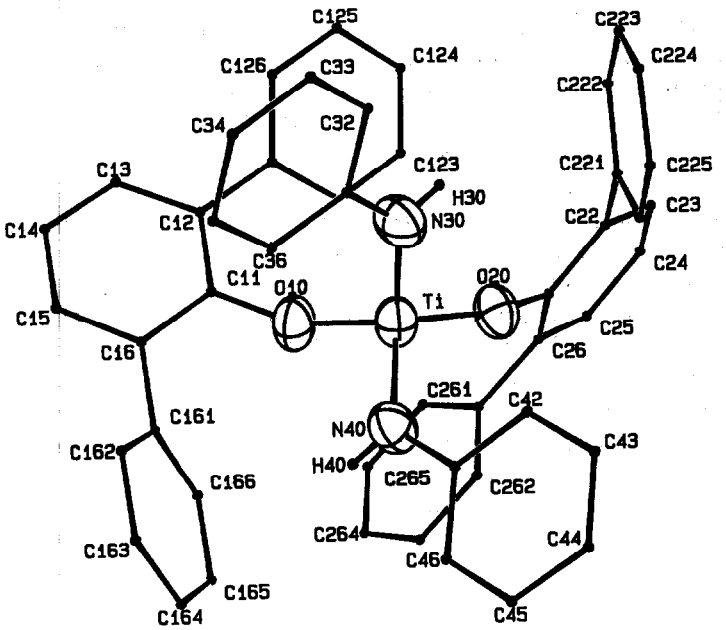

Fig. 1. ORTEP view of [Ti(OC$_6$H$_3$Ph$_2$-2,6)$_2$(NHPh)$_2$] (2).

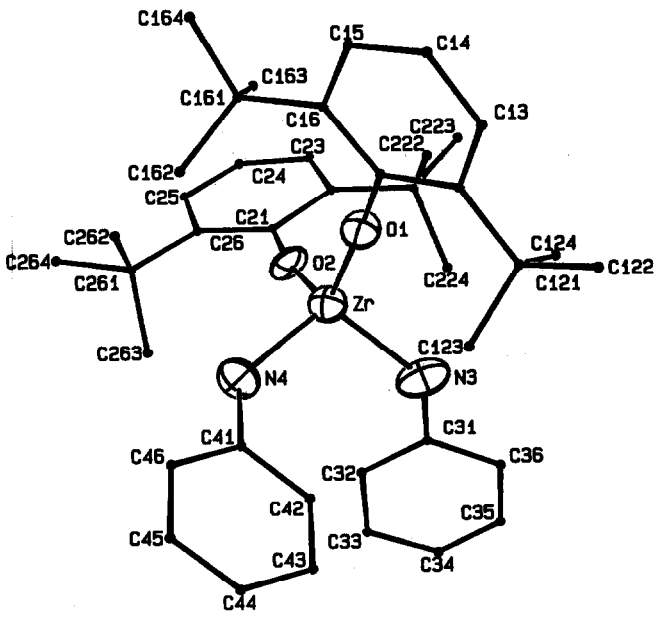

Fig. 2. ORTEP view of [Zr(OC$_6$H$_3$Bu$^t_2$-2,6)$_2$(NHPh)$_2$] (3).

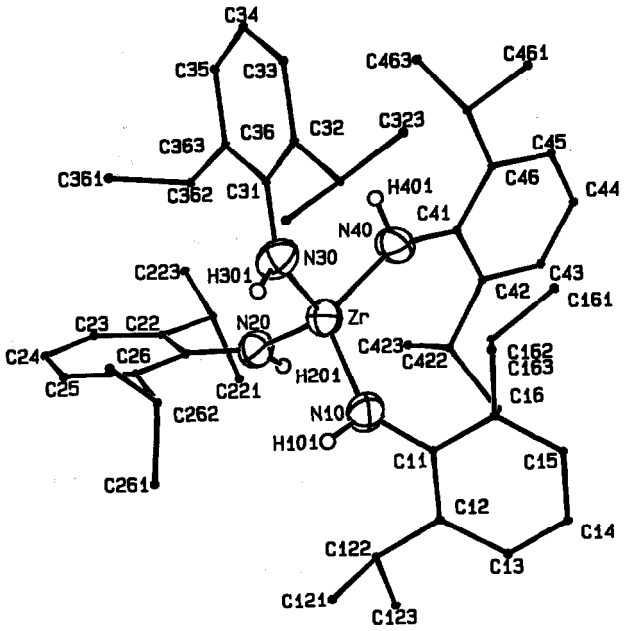

Fig. 3. ORTEP view of $[Zr(NHC_6H_3Pr^i_2\text{-}2,6)_4]$ (**5**).

tortion away from tetrahedral geometry in the tetra(aryl amido) compound **5** with N—Zr—N angles varying from 99.7(3)° to 116.8(3)°. Another interesting feature of these molecules are the M—NH—Ar angles. In the more extensively studied, symmetrical dialkylamido derivatives of the early *d*-block metals the two M—N—C angles are typically close to 120°, rarely exceeding 130°.[10] The nitrogen atom is normally described as being sp^2-hybridized with N-*p*-to-M-*d* π-bonding occurring from a filled p_z orbital on nitrogen into any empty metal *d*-orbitals of the correct symmetry. The structural database for mono-alkyl or aryl amido compounds of the early *d*-block metals is much smaller.[10] However, there is much more variation beyond 120° for the M—NH—C angles. Large M—NH—Si angles have been reported for group 4 metal silyl amido complexes.[7] In the bis(phenyl amido) compounds **2** and **3** the M—NH—Ph angles lie in the narrow range 130–135°, while for the bulkier 2,6-diisopropylphenylamido compound **5** the angles vary from 131.9(6)° to 149.3(7)°.

Synthesis of aryl imido complexes

There is no evidence that the aryl amido compounds **1–6** undergo spontaneous proton transfer to produce aryl imido ligands and aryl amines (either free or bound). Addition of aniline ($PhNH_2$) to C_6D_6 solutions of the zirconium bis(phenyl amido) complex (**3**) did not lead to the formation of any new complexes or adducts, as judged by ^1H NMR spectroscopy. Two sharp, distinct sets of N—*H* and N—*Ph* resonances are observed for free $PhNH_2$ and the aryl amido resonances of **3** for this mixture. The addition of aniline-d_7 (excess) to a C_6D_6 solution of **3** was found to produce only small quantities of protio-aniline after 15 min at 25°C. However, monitoring the solution by ^1H NMR showed the liberation of free $C_6H_5NH_2$(NHD) over hours. Hence, exchange of free aniline and the coordinated phenyl amido groups in **3** can occur over hours at ambient temperatures. Furthermore, exchange of ND_2 (aniline) and NH (amido) protons is not rapid. Based upon the results obtained with pyridine ligands we believe this exchange occurs via an undetected five-coordinate adduct of the formula $[(ArO)_2Zr(NHPh)_2(NH_2Ph)]$; intramolecular transfer of protons within the complex then leading to exchange of initially bound phenyl amido groups and free aniline.

We have also investigated the reaction of these aryl amido compounds with pyridine ligands. In previous work we have found the base 4-pyrrolidinopyridine (py′) to be a good ligand of choice due to its high basicity and tendency to help derivatives crystallize from solution. The addition of py′ (2 equivalents) to solutions of compounds **1–3** and **5–6** was found to generate a series of aryl imido compounds with the elimination of 1 equivalent of aryl amine (Scheme 2). The displacement of aniline from the titanium compounds **1** and **2** and 2,6-diisopropylaniline from **5** and **6** was found to occur with no detectable (^1H NMR) intermediates. In the case of the zirconium bis(phenyl amido) compound (**3**) an intermediate pyridine adduct, [**3**·py′], was

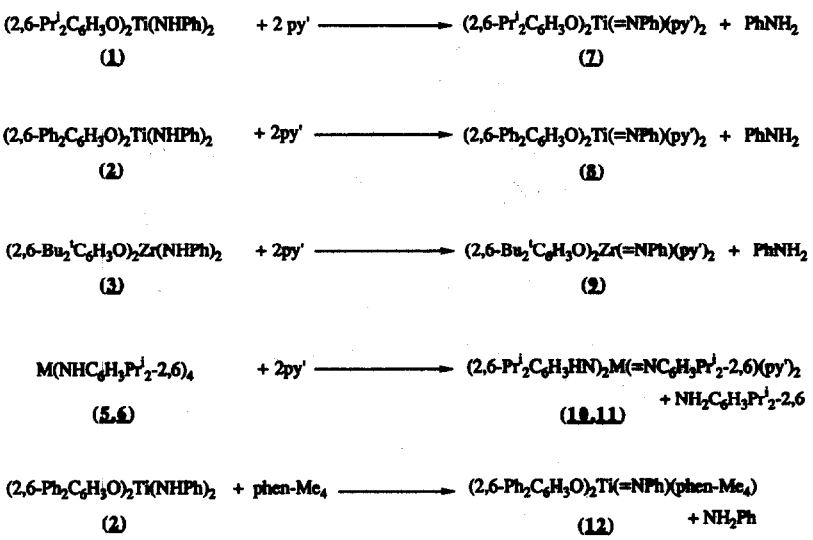

Scheme 2.

detected by ^{1}H NMR. In the case of the hafnium analogue (**4**) the corresponding adduct [**4**·py'] was formed and found to be stable, no aniline being displaced even in the presence of a large excess (> 30 equivalents) of py'. The structure and reactivity of the adducts [**3**·py'] and [**4**·py'] are discussed in the mechanistic section below.

The spectroscopic properties of the aryl imido compounds **7**–**11** are consistent with their formulation. In the ^{1}H NMR spectrum of the phenyl imido compounds **7**, **8** and **9** there are the expected resonances for the aryloxide and 4-pyrrolidinopyridine ligands. The *ortho* and *meta* protons on the pyridine rings are well resolved, appearing as multiplets respectively downfield and upfield of the normal aromatic region. In the case of the mixed aryl imido, aryl amido compounds **10** and **11** the ^{1}H and ^{13}C NMR spectra show two well resolved sets of 2,6-diisopropylphenyl resonances in the ratio 2:1. Hence, exchange of aryl amido and aryl imido ligands by proton transfer between nitrogen atoms is slow on the NMR time-scale. The protons attached to the amido nitrogen atoms are observed at δ 6.90 and 6.28 ppm for **10** and **11**, respectively.

At the present time the number of structurally characterized terminal imido derivatives of the group 4 metals is small but growing steadily. Because of this scarcity of structural data we have subjected the titanium, zirconium and hafnium aryl imido compounds **7**, **9**, **10** and **11** to single-crystal X-ray diffraction analysis. Selected bond distances and angles are collected in Tables 4–7 while ORTEP drawings are shown in Figs 4–7, emphasizing the central coordination sphere. All four compounds can be seen to be structurally related, lying somewhere between trigonal-bipyramidal and square-pyramidal geometries (*vide infra*). The pyridine donor ligands are arranged mutually *trans*, consistent with the lack of diastereotopic isopropylmethyl groups in solution ^{1}H NMR spectra, either for the aryl oxide ligands in **7** or the aryl amido

Table 4. Selected bond distances (Å) and angles (°) for [Ti(OC$_6$H$_3$Pr$^i_2$-2,6)$_2$(=NPh)(py')$_2$] (**7**)

Ti—N(30)	1.719(3)	Ti—O(10)	1.880(3)
Ti—N(41)	2.206(3)	Ti—O(20)	1.867(3)
Ti—N(51)	2.223(3)	Ti—N(30)	1.719(3)
O(10)—Ti—O(20)	133.2(1)	N(30)—Ti—N(41)	96.4(1)
O(10)—Ti—N(30)	114.0(1)	N(30)—Ti—N(51)	97.7(1)
O(10)—Ti—N(41)	86.4(1)	N(40)—Ti—N(51)	165.8(1)
O(10)—Ti—N(51)	87.9(1)	Ti—O(10)—C(11)	172.0(2)
O(20)—Ti—N(30)	112.8(1)	Ti—O(20)—C(21)	173.8(3)
O(20)—Ti—N(41)	88.4(1)	Ti—N(30)—C(31)	173.1(3)
O(20)—Ti—N(51)	86.2(1)		

Table 5. Selected bond distances (Å) and angles (°) for [Zr($OC_6H_3Bu^t_2$-2,6)$_2$(=NPh)(py′)$_2$] (**9**)

Zr—N(1)	1.844(9)	Zr—O(20)	2.030(6)
Zr—N(41)	2.359(9)	Zr—O(30)	2.047(7)
Zr—N(51)	2.366(9)		
O(20)—Zr—O(30)	145.4(3)	N(1)—Zr—N(41)	97.1(4)
O(20)—Zr—N(1)	106.1(3)	N(1)—Zr—N(51)	102.8(4)
O(20)—Zr—N(41)	88.3(3)	N(41)—Zr—N(51)	160.1(3)
O(20)—Zr—N(51)	87.5(3)	Zr—O(20)—C(21)	173.7(7)
O(30)—Zr—N(1)	108.4(3)	Zr—O(30)—C(31)	174.4(7)
O(30)—Zr—N(41)	85.9(3)	Zr—N(1)—C(11)	175.5(8)
O(30)—Zr—N(51)	86.6(3)		

Table 6. Selected bond distances (Å) and angles (°) for [Zr($NHC_6H_3Pr^i_2$-2,6)$_2$(=$NC_6H_3Pr^i_2$-2,6)(py′)$_2$] (**10**)

Zr—N(50)	2.159(3)	Zr—N(21)	2.358(3)
Zr—N(40)	2.134(4)	Zr—N(31)	2.381(3)
Zr—N(10)	1.868(3)		
N(10)—Zr—N(21)	99.6(1)	N(31)—Zr—N(40)	86.1(1)
N(10)—Zr—N(31)	100.4(1)	N(31)—Zr—N(50)	84.2(1)
N(10)—Zr—N(40)	100.9(1)	N(40)—Zr—N(50)	141.3(1)
N(10)—Zr—N(50)	117.7(1)	Zr—N(10)—C(11)	174.9(3)
N(21)—Zr—N(31)	160.0(1)	Zr—N(40)—C(41)	148.0(3)
N(21)—Zr—N(40)	88.6(1)	Zr—N(50)—C(51)	152.5(3)
N(21)—Zr—N(50)	88.0(1)		

Table 7. Selected bond distances (Å) and angles (°) for [Hf($NHC_6H_3Pr^i_2$-2,6)$_2$(=$NC_6H_3Pr^i_2$-2,6)(py′)$_2$] (**11**)

Hf—N(1)	1.850(3)	Hf—N(41)	2.332(3)
Hf—N(2)	2.126(3)	Hf—N(51)	2.331(3)
Hf—N(3)	2.114(3)		
N(1)—Hf—N(2)	113.9(1)	N(3)—Hf—N(41)	87.3(1)
N(1)—Hf—N(3)	103.1(1)	N(3)—Hf—N(51)	86.6(1)
N(1)—Hf—N(41)	101.4(1)	N(41)—Hf—N(51)	155.7(1)
N(1)—Hf—N(51)	102.9(1)	Hf—N(1)—C(11)	174.4(3)
N(2)—Hf—N(3)	143.0(1)	Hf—N(2)—C(21)	149.2(3)
N(2)—Hf—N(41)	87.0(1)	Hf—N(3)—C(31)	144.8(3)
N(2)—Hf—N(51)	83.9(1)		

ligands in **10** and **11**. In order to generate an aryl imido compound with a different geometry we investigated the reaction of bidentate ligands such as 2,2′-bipyridine and 1,10-phenanthroline with aryl amido compounds **1**–**6**. Although addition of these ligands was found to lead to the elimination of aniline, the resulting transition metal compounds were found to be only sparingly soluble. The addition of 3,4,7,8-tetramethyl-1,10-phenanthroline (phen-Me_4) to the bis(phenyl amido) complex (**2**) did yield a soluble phenyl imido complex (**12**) and it was structurally characterized (Scheme 2, Table 8, Fig. 8).

Discussion of the structure and bonding in the aryl imido compounds

In discussing the structure of five-coordinate compounds two idealized geometries, the trigonal-bipyramid (D_{3h}) and square-pyramid (C_{4v}) are typ-

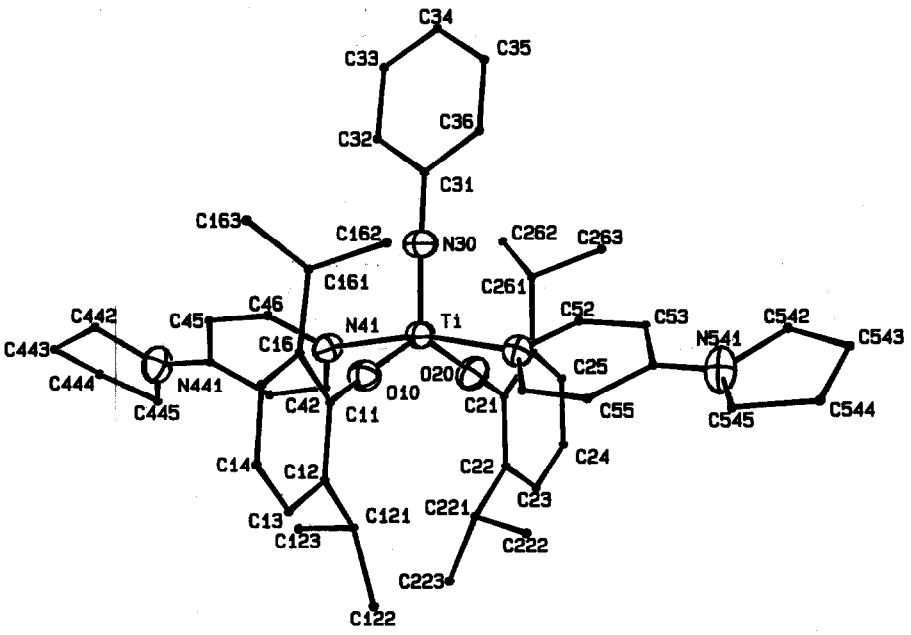

Fig. 4. ORTEP view of $[Ti(OC_6H_3Pr^i_2\text{-}2,6)_2(=NPh)(py')_2]$ (**7**).

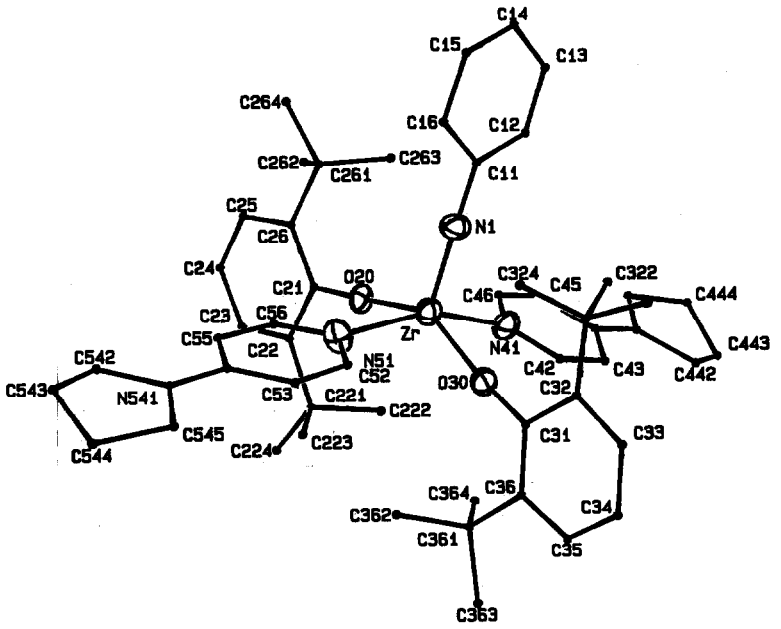

Fig. 5. ORTEP view of $[Zr(OC_6H_3Bu^t_2\text{-}2,6)_2(=NPh)(py')_2]$ (**9**).

ically invoked. A thorough theoretical analysis of transition metal penta-coordination has been published by Rossi and Hoffmann.[21] They have considered these two geometries and the site preference of strong/weak σ-donor ligands as well as the impact of π-donor/acceptor orbitals on the ligands. The five-coordinate aryl imido compounds **7**, **9**, **10** and **11** have a general formula, $[M(=NAr)(X)_2(py')_2]$, where X = aryl oxide or aryl amide. In Table 9 are listed the important angles about the metal centre that help describe the coordination geometry. In the titanium complex **7** the py′—Ti—py′ angle of 165.8(1)° and ArO—Ti—OAr angle of 133.2(1)° are close to the angles (180°, 120°) expected for a trigonal-bipyramidal structure with *trans*-axial py′ groups, but

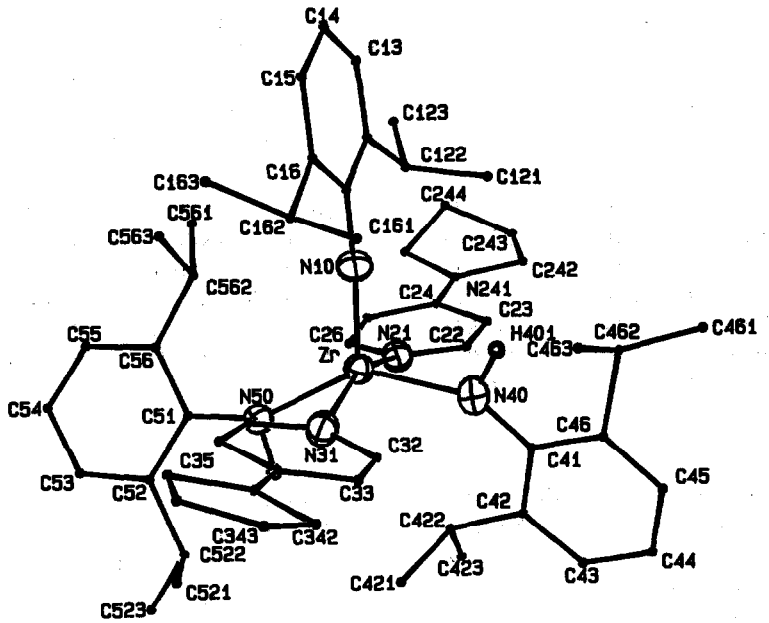

Fig. 6. ORTEP view of $[Zr(NHC_6H_3Pr^i_2\text{-}2,6)_2(=NC_6H_3Pr^i_2\text{-}2,6)(py')_2]$ (**10**).

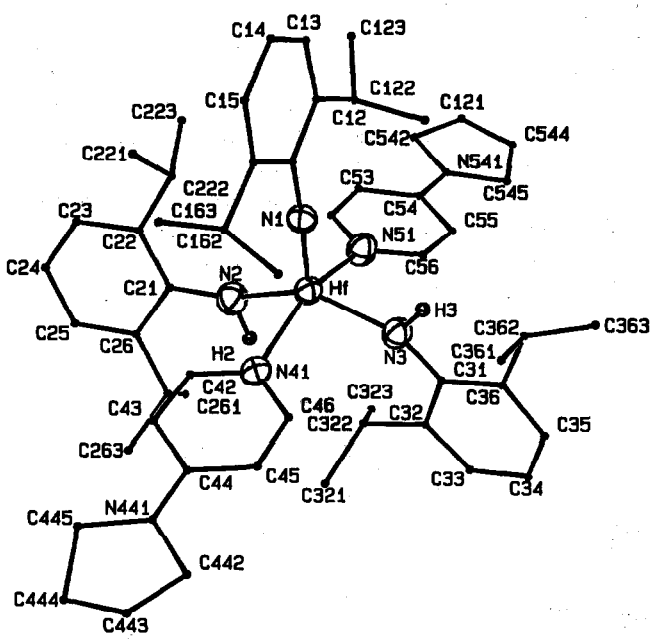

Fig. 7. ORTEP view of $[Hf(NHC_6H_3Pr^i_2\text{-}2,6)_2(=NC_6H_3Pr^i_2\text{-}2,6)(py')_2]$ (**11**).

with a definite distortion towards a square-pyramidal geometry. This distortion is much more evident in the zirconium aryl imido compound (**9**), where the PhN—Zr—py′ and PhN—Zr—OAr angles are approaching one another; 97.1(4)–108.4(3)°. In the mixed aryl amido, aryl imido compounds **10** and **11** the mutually *trans*, aryl amido ligands adopt a conformation in which the planar *ipso*-carbon–N—H propellers lie almost parallel with the M=N—Ar group. One of these groups has the N—H bond pointing towards the imido nitrogen, while the other points away. The difference in the ArN—M—NHAr angles; 100.9(1), 117.7(1)° for **10** and 103.1(1), 113.9(1)° for **11** is almost certainly a reflection of steric repulsion between these groups. We, therefore, conclude that molecules **7** and **9**–**11** adopt structures that lie between a trigonal-bipyramid (with axial py′

Table 8. Selected bond distances (Å) and angles (°) for [Ti($OC_6H_3Ph_2$-2,6)$_2$(=NPh)(phen-Me_4)] (**12**)

Ti—N(40)	1.723(4)	Ti—O(20)	1.882(3)
Ti—N(1)	2.220(3)	Ti—O(30)	1.931(3)
Ti—N(10)	2.216(3)		
O(20)—Ti—O(30)	100.1(1)	N(1)—Ti—N(10)	71.8(1)
O(20)—Ti—N(10)	129.0(1)	N(1)—Ti—N(40)	113.6(1)
O(20)—Ti—N(10)	87.1(1)	N(10)—Ti—N(40)	89.0(1)
O(20)—Ti—N(40)	111.9(2)	Ti—O(20)—C(21)	149.4(3)
O(30)—Ti—N(1)	86.0(1)	Ti—O(30)—C(31)	125.2(3)
O(30)—Ti—N(10)	155.8(1)	Ti—N(40)—C(41)	158.8(3)
O(30)—Ti—N(40)	109.2(1)		

ligands) and a square-pyramid (with apical aryl imido group). In their analysis of the bonding in five-coordinate transition metal compounds, Rossi and Hoffman reached a number of conclusions for a d^0-metal configuration. In the case of only σ-bonding they found that the axial bonds should be weaker in a trigonal-pyramidal structure with stronger σ-donor ligands preferring equatorial positions. In the case of a square-pyramid the preferred position for a stronger σ-donor is apical. In the case of ligands containing cylindrical π-donor orbitals (cf. aryloxide groups), the preference is for an equatorial position in a trigonal-bipyramid and in the basal site of a nearly flat square-pyramid. An increase in the pyramidality of a square-pyramid beyond 90° makes the apical position the most favourable. The authors also point out "a general problem for many of the complexes under consideration is that it is difficult to determine what part of an observed conformational preference is due to the electronic effects, and what part is set by the often large steric requirements of the coordinated ligands". The geometries adopted by the molecules in Table 9 clearly are a compromise between these two forces.

Of particular importance to this work is the bonding of the aryl imido ligand to these group 4 metals and the values of the associated metal–nitrogen bond lengths. To begin this discussion a fully formed triple bond between an aryl or alkyl imido nitrogen and a metal centre would occur in a square-pyramidal compound, [(ArN)MX_4], where the aryl imido group occupied the apical site, the ligands X undergo purely σ-bonding with M and the electron configuration of the metal was d^n, $n \leqslant 2$. In this case, the *sp* hybridized imido nitrogen would be

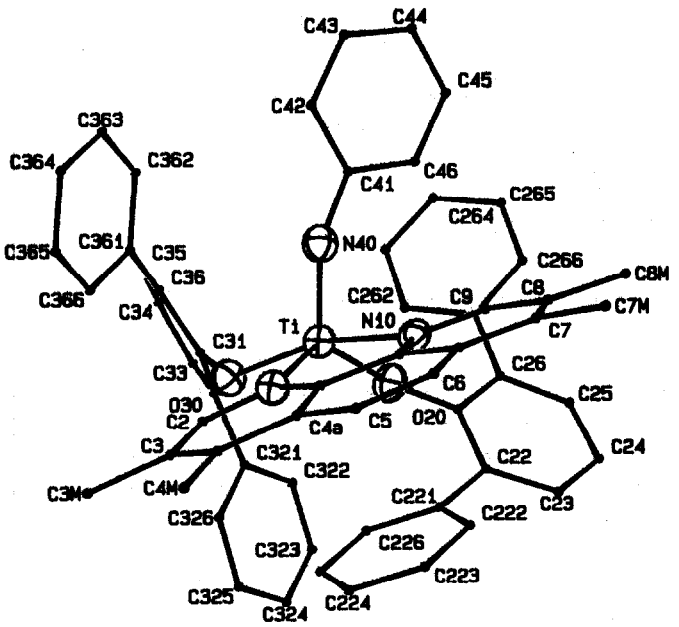

Fig. 8. ORTEP view of [Ti($OC_6H_3Ph_2$-2,6)$_2$(=NPh)(phen-Me_4)] (**12**).

Table 9. Selected bond angles (°) to five-coordinate aryl imido compounds

	X—M—X[a]	(py)N—M—N(py)	ArN=M—N(py)	ArN=M—X[a]
7	133.2(1)	165.8(1)	96.4(1)	112.8(1)
			97.7(1)	114.0(1)
9	145.4(3)	160.1(3)	97.1(4)	106.1(3)
			102.8(4)	108.4(3)
10	141.3(1)	160.0(1)	99.6(1)	100.9(1)
			100.4(1)	117.7(1)
11	143.0(1)	155.7(1)	101.4(1)	103.1(1)
			102.9(1)	113.9(2)
12[b]	100.1(1)	71.8(1)	113.6(1)	111.9(2)

[a] X = OAr or NHAr.
[b] Contains a chelating phenanthroline.

able to form two π-bonds to M, utilizing its p_x and p_y orbitals and the d_{xz} and d_{yz} (e symmetry) metal atomic orbitals. Any electron density on the metal, d^1 and d^2, would reside in the essentially non-bonding d_{xy} metal orbital. The molecules **7** and **9–11** contain two types of ligands besides the aryl imido function. The 4-pyrrolidinopyridine groups can be considered as simple donor ligands that will interact with the metal in a σ-fashion. The aryl oxide and aryl amido ligands, however, bear cylindrical and single-faced π-donor orbitals, respectively. The aryl oxide ligands in compounds **7** and **9** possess almost linear M—O—Ar angles of 172.0(2) and 173.8(3)° for the titanium complex and 173.7(7) and 174.4(7)° for the zirconium complex. Hence, the mutually *trans*-aryl oxide oxygen atoms will compete with each other in π-donating into the empty d_{xy} orbital, as well as competing with the aryl imido nitrogen atom for the d_{xz} orbital. In the case of the compounds **10** and **11** that contain *trans*-aryl amido ligands in the basal plane, their conformation is such that their π-orbitals are both oriented perpendicular to the M—N(imido) axis. They are, therefore, both competing with each other for the empty d_{xy} orbital and are oriented such that they cannot interfere with the metal–imido triple bond. A theoretical (EHMO) analysis of the model compounds $[Zr(NH)(NH_2)_2(NH_3)_2]$ using both the structural parameters for **10** as well as idealized geometries confirmed these ideas. The HOMO was found to be a non-bonding molecular orbital localized on the amido nitrogen atoms, followed first in energy by the amido–metal–amido π-bond and then the two, almost degenerate imido–metal π-bonds (Fig. 9).

We, therefore, conclude that the geometry adopted by the five-coordinate aryl imido compounds **7** and **9–11** does not inhibit, in itself, π-bonding between the aryl imido nitrogen and the metal centre. The geometry is expected, however, to result in decreased π-bonding between the metal centre and aryloxide oxygen atoms in **7** and **9** or the aryl amido nitrogen atoms in **10** and **11**. This is born out by a comparison of the M—O and M—N bond lengths found in the aryl amido compounds **2**, **3** and **5** and the aryl imido compounds **7**, **9** and **10** (Tables 2, 3, 5, 7, 9 and 10). The Ti—OAr bond lengths are 1.789(2) and 1.786(2) Å in tetrahedral **2**, while in the aryl imido complex **7** they are 1.880(3) and 1.867(3) Å. A comparable elongation in Zr—OAr lengths is seen moving from **5** [1.893(7), 1.941(7) Å], to **9** [2.030(6), 2.047(7) Å]. The six Ar—N(amido) distances in compounds **3** and **5** lie in the narrow range 2.027(7)–2.06(1) Å, but are longer in five-coordinate **10**, 2.159(3) and 2.134(4) Å.

In Table 10 are listed the Ti—N distances for

Table 10. Metal–nitrogen distances for group 4 metal imido compounds

Compound	Ti—N (Å)	Ref.
7	1.719(3)	This work
12	1.723(4)	This work
$Ti(OAr)_2(NAr)(C_6H_{14}N_2)$	1.708(5)	4d
$TiCl_2(py)_3[NP(S)Ph_2]$	1.720(4)	4i
$TiCl_2(OPPh_3)_2(NBu^t)$	1.672(7)	4j
$TiCl_2$(TMEDA)(NPh)	1.699(4)	4k
	Zr—N (Å)	
9	1.844(9)	This work
10	1.868(3)	This work
$Cp_2Zr(thf)(NBu^t)$	1.826(4)	6
$[(Bu^t_3SiNH)_2Zr(thf)(NSiBu^t_3)]$	1.974(6)	8a
11	1.850(3)	This work

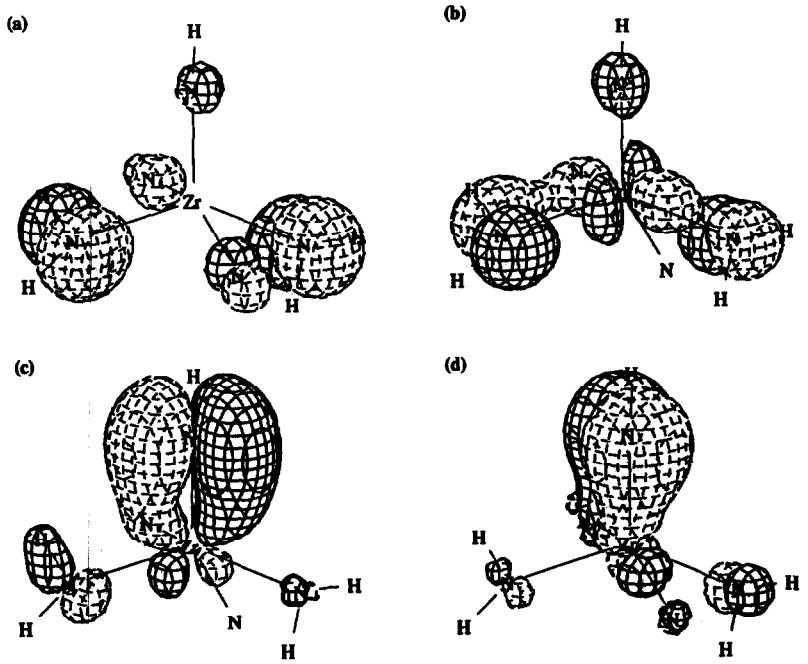

Fig. 9. Plots of the four highest occupied molecular orbitals within the molecule $[Zr(=NH)(NH_2)_2(NH_3)]$. Calculated (EHMO) orbital energies (eV) are: (a) −13.333; (b) −13.836; (c) −13.959; and (d) −14.035.

terminal imido derivatives of titanium(IV) reported in the literature. The aryl imido compounds synthesized in this laboratory have Ti—N (imido) distances in the range 1.708(5)–1.723(4) Å. This is comparable to the distance of 1.720(4) Å reported by Roesky *et al.* for six-coordinate $[TiCl_2(py)_3\{NP(S)Ph_2\}]$. However, these distances are *ca* 0.04 Å longer than found for the tert-butyl imido complex $[TiCl_2(O{=}PPh_3)_2(NBu^t)]$, 1.672(7) Å. The shorter distance for the latter compound may reflect the electronic nature of the nitrogen substituent. It has been shown that M—OR (alkoxide) distances are slightly smaller than M—OAr (aryl oxide) bond distances for these ligands bound to the same metal centre.[22] The presence of the aryl substituent in aryl oxide ligands has been shown to decrease the amount of oxygen-*p* to metal-*d* π-donation compared to their saturated alkoxide counterparts.[23]

There are four terminal imido derivatives of zirconium, including **9** and **10**. In this case the Zr—N distances vary considerably from 1.826(4) in $[Cp_2Zr(thf)(NBu^t)]$ to 1.974(6) Å in the silyl imido complex $[(Bu^t_3SiNH)_2Zr(NSiBu^t_3)(thf)]$. In the zirconocene compound the π-donation of all of the cylindrical π-density on nitrogen would be expected to be destabilizing, leading to a formal 20-electron compound. A long Zr—NBu^t distance is, therefore, to be expected. However, this is the shortest distance so far reported. If we use the contraction observed for titanium of 0.04 Å on moving from an aryl imido ligand to a tert-butyl imido ligand then a distance of *ca* 1.8 Å would seem reasonable. In the case of the silyl imido derivative prepared by Wolczanski *et al.* the long Zr—N bond distance may be a consequence of the silicon substituent on the nitrogen. This remarkably long distance may also explain the high reactivity of this and related silyl imido bonds.[7,8]

Mechanistic study of metal–imido bond formation from bis(aryl amido) precursors

Equilibrium studies. The new group 4 metal aryl imido compounds obtained in this study are formed by the ligand-induced elimination of an aryl amine from a bis(aryl amido) precursor. This process has certain similarities to the α-hydrogen abstraction process that generates metal alkylidene functionalities.[2] In order to gain more insight into this process the elimination of aniline from the zirconium bis(phenylamido) compound (**3**) upon addition of 4-pyrrolidinopyridine (py′) was examined in detail. As noted previously, the careful addition of ⩽ 1 equivalent of py′ to a solution of **3** in C_6D_6 was found to lead to the rapid formation of an adduct, [**3**·py′], as detected by ^1H NMR spectroscopy. Both the aryloxide Bu^t groups and phenyl amido N*H* protons undergo significant chemical shift changes upon adduct formation.

Addition of further equivalents of py′ to solutions of the adduct was found (^{1}H NMR) to *slowly* (hours, at 30°C) lead to the formation of an *equilibrium mixture* of the adduct [**3** · py′] and the phenyl imido derivative **9**. As more ligand py′ was added the equilibrium was found to slowly shift in favour of the phenyl imido compound. Removal of solvent from these mixtures ($\leqslant$ 2 equivalents of py′) led to isolation of only **9** presumably due to the removal of volatile aniline from the mixture. The addition of aniline to solutions of the phenyl imido **9** again led (^{1}H NMR) to a mixture of [**3** · py′], free py′ and **9**. Analysis of various (equilibrated) mixtures of **3** plus py′ (2–30 equivalents), sometimes in the presence of added $PhNH_2$ (1–5 equivalents), yielded consistent values for an equilibrium constant derived from the expression $k = [\mathbf{9}][PhNH_2]/[\mathbf{3} \cdot py'][py']$.

This study was then extended in the following manner. (a) The use of unsubstituted pyridine (py) and 4-methyl-pyridine (py-4Me), instead of 4-pyrrolidinopyridine (py′), was found to also lead to equilibrium mixtures of adduct and phenyl imido derivatives. The equilibrium constants were again measured by NMR methods (Table 11). (b) By using various 4-substituted anilines the corresponding bis(aryl amido) compounds $\mathbf{3}^X$ (X = H, F, CH_3, OMe, Br) of zirconium were isolated. The position of equilibrium upon addition of py, py-4Me and py′ was again measured (^{1}H NMR) (Table 11).

Some conclusions can be drawn from the list of equilibrium constants obtained in this study (Table 11). The degree of formation of any given aryl imido compound increases as the basicity of the pyridine ligand is increased. This is seen on moving from pyridine to 4-methyl-pyridine and is dramatically illustrated for the highly basic 4-pyrrolidinopyridine, where the equilibrium constant (for aryl imido formation) is approximately two orders of magnitude larger. This trend is reasonable given the nature of the final aryl imido products. However, an interpretation of the effect of substituents within the aromatic ring of the bis(aryl amido) precursor is not as straightforward. It can be seen that for any given pyridine, formation of the aryl imido complex (elimination of substituted aniline) is favoured by electron-withdrawing groups (4-Br) and disfavoured by electron-donating groups (4-CH_3, 4-OCH_3). Substituents at this position will simultaneously affect a number of parts of the equilibrium. An important impact will be on the electron donating ability of the aryl amido ligands in $\mathbf{3}^X$ and the aryl imido ligand in $\mathbf{9}^X$. Electron-withdrawing substituents should have the effect of slightly increasing the Lewis acidity of the metal centre and hence increase the binding of the pyridine ligands, therefore, making formation of the aryl imido complex more favourable.

Table 11. Equilibrium constants (C_6D_6, 30°C) for the reaction

$$[\mathbf{3}^X \cdot py] + py \rightleftharpoons [\mathbf{9}^X] + Ar^XNH_2$$

$$\mathbf{3}^X = (2,6\text{-}Bu^t_2C_6H_3O)_2Zr(NHC_6H_4\text{-}4X)_2$$

X	py	py—Me	py′
H	0.017(2)	0.077(8)	3.85(30)
F	0.017(2)	0.078(8)	3.69(30)
CH_3	0.0049(5)	0.012(1)	0.96(9)
OCH_3	0.0060(6)	0.028(3)	1.93(20)
Br	0.053(5)	0.093(9)	5.17(50)

Kinetic studies. A mechanistic investigation by Wolczanski *et al.* of the elimination of $Bu^t_3SiNH_2$ from $[(Bu^t_3SiNH)_3TiCl]$ to form $[(Bu^t_3SiNH)(thf)ClTi{=}NSiBu^t_3]$ in the presence of added thf showed a zero-order dependence on the [thf]. This and other observations, along with a significant primary kinetic isotope effect of 5.9(6) at 90.4°C, were taken as indicative of hydrogen transfer and amine elimination occurring prior to association of the thf. We have considered a number of pathways for the conversion of the mono-pyridine adduct [**3** · py] into the corresponding phenyl imido compound **9** (Scheme 3). The various pathways can be broken down into two groups by focusing upon the important hydrogen transfer step whereby the zirconium imido function is generated. In the first pathway [A] the proton transfer occurs in a six-coordinate complex (**I**) formed by the addition of a second equivalent of pyridine to [**3** · py]. Proton transfer then leads to a six-coordinate phenyl imido complex (**II**), which dissociates aniline to form the product. The other two viable pathways [B] and [C] involve hydrogen transfer occurring within [**3** · py] to generate the five-coordinate phenyl imido complex (**III**). Exchange of pyridine for aniline to produce the product may then occur via a dissociative step through **IV** or an associate exchange process via **II**. The highly circuitous pathway [**3** · py] → **I** → **II** → **III** → **IV** → **9** has also been considered and ruled highly unlikely. Some comments upon the lability of the adduct [**3** · py] and the phenyl imido product **9** are necessary. As pointed out previously the addition of pyridine (py) to the bis(phenyl amido) complex **3** leads to rapid formation of [**3** · py] in solution. It is not possible at room temperature to distinguish (^{1}H NMR) between free and coordinated pyridine in these solutions. Only one set of pyridine resonances is observed at a weighted

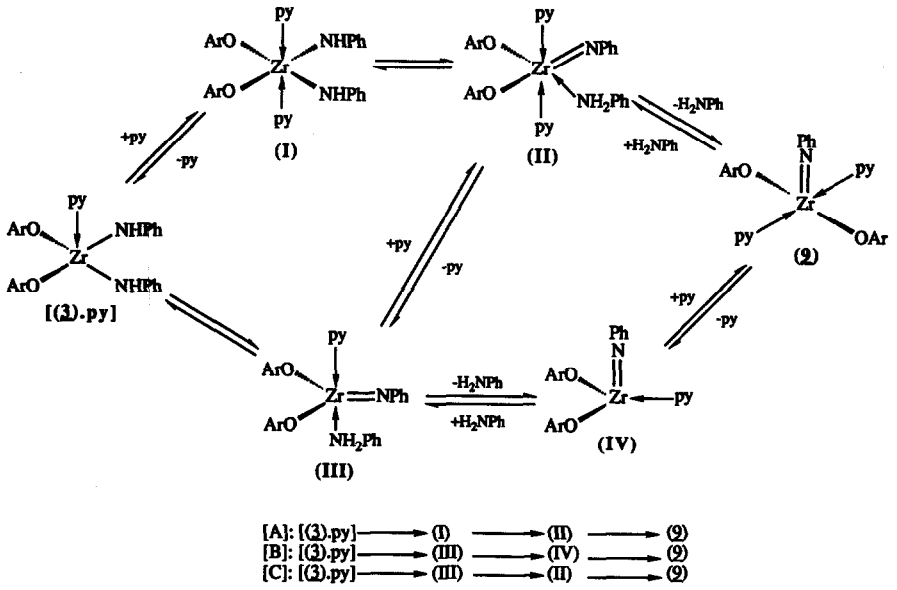

Scheme 3.

average position. Hence, exchange of the pyridine ligand in [**3**·py] occurs rapidly on the NMR time-scale with free py in solution. A dissociative pathway for the rapid exchange seems likely given the fact that upon addition of py (< 1 equivalent) to **3** only one set of ligand resonances are observed, indicating that exchange between **3** and [**3**·py] is also rapid on the NMR time-scale. For all of the five-coordinate aryl imido ligands obtained in this study, exchange of coordinated and free pyridine ligands is slow on the ^{1}H NMR time scale. A sharp, well resolved set of coordinated pyridine ligands is observed even in the presence of a large excess of free pyridine in solution.

The fact that the bis(phenyl amido) complexes react with pyridine ligands to produce an equilibrium mixture of the corresponding phenyl imido complex and aniline and the reversibility of the reaction complicates a kinetic analysis. Initial kinetic experiments involved observing the approach to equilibrium of the pyridine adduct [**3**·py] in the presence of both excess pyridine (30 equivalents) and aniline (5 equivalents) in C_6D_6 solution by ^{1}H NMR methods. A kinetic analysis of this data using a model of two reversible first-order (or pseudo-first-order) reactions gave reasonable linear plots.[24] However, when the kinetic runs were carried out only in the presence of excess pyridine (no added aniline) the resulting data was found to lead to curvature when plotted according to a kinetic model involving a (pseudo-) first-order forward reaction and second-order reverse reaction. The addition of 30 equivalents of pyridine to a known concentration of **3** was found to lead to the more favourable equilibrium faster than when only 15 equivalents of pyridine were used. This implies that the rate of formation of the phenyl imido complex from the adduct is pyridine concentration dependent. However, the inability to fit this data to kinetic models involving reversible first- or second-order reactions is unsettling. Furthermore, the possibility that added pyridine acts as a catalyst for hydrogen (proton) transfer between aryl amido groups complicates the picture even more. In the absence of a system more amenable to kinetic study the detailed mechanism of formation of these aryl imido complexes is still uncertain.

It is interesting to speculate on the lack of observed elimination of aniline from the hafnium compound **4**. The addition of 4-pyrrolidinopyridine (1 equivalent) to solutions of **4** results in rapid and complete formation of an adduct [**4**·py′]. However, addition of even a large excess of py′ does not lead to detectable (^{1}H NMR) amounts of the corresponding hafnium phenyl imido complex. The lack of ligand induced elimination of aniline from [**4**·py′] may be kinetic or thermodynamic in origin. The fact that the hafnium 2,6-diisopropylphenylimido complex (**11**) can be obtained by elimination of 2,6-diisopropyl aniline upon addition of py′ lends support for a kinetic effect. One possible explanation would involve a strong reluctance on the part of hafnium to form a bis-pyridine intermediate, [**4**·(py)$_2$], from which aniline can be eliminated. The reason for the lack of expansion of the coordination sphere may be due to steric effects. X-ray diffraction studies of isomorphous zirconium and hafnium compounds typically show

the hafnium–ligand distances to be slightly smaller than the corresponding zirconium–ligand distances. This can be clearly seen for the isostructural aryl imido complexes **10** and **11**. The Hf—N distances in **11** are consistently shorter than the corresponding Zr—N distance by *ca* 0.02 Å. On this basis the mono-pyridine adduct [**4** · py′] is less likely to associate a second py′ on steric grounds compared to [**3** · py′].

EXPERIMENTAL

All operations were carried out under dry nitrogen, either in a Vacuum Atmospheres Drilab or by standard Schlenck techniques. Hydrocarbon solvents were dried by distillation from sodium benzophenone under nitrogen. The compounds $[M(CH_2Ph)_4]$ (M = Zr, Hf),[16] $[Ti(OC_6H_3Pr^i_2\text{-}2,6)_2(\eta^2\text{-}Bu^tNCCH_2Ph)(CH_2Ph)]$,[12] $[Ti(OC_6H_3Ph_2\text{-}2,6)_2(C_4Et_4)]$,[13] $[Zr(OC_6H_3Bu^t_2\text{-}2,6)_2(CH_2Ph)_2]$, $[Zr(OC_6H_3Bu^t_2\text{-}2,6)_2(CH_3)_2]$ and $[Hf(OC_6H_3Bu^t_2\text{-}2,6)_2(CH_2Ph)_2]$[14,15] were synthesized by previously reported methods. Pyridine (py), 4-methylpyridine (py-4Me) and 4-pyrrolidinopyridine (py′) and substituted anilines were obtained commercially (Aldrich). Pyridine and 4-methylpyridine were dried over NaOH pellets and molecular sieves prior to use. ^1H and ^{13}C NMR were recorded on a Varian Associates Gemini-200 spectrometer and selected spectroscopic data are reported. A Perkin–Elmer 1800 spectrophotometer was used to record IR spectra of compounds as mineral oil (Nujol) mulls, supported on CsI plates in the 4000–150 cm^{-1} region.

Synthesis of $[Ti(OC_6H_3Pr^i_2\text{-}2,6)_2(NHPh)_2]$ (**1**)

To a benzene (25 cm^3) solution of $[Ti(OC_6H_3Pr^i_2\text{-}2,6)_2(\eta^2\text{-}Bu^tNCCH_2Ph)(CH_2Ph)]$ (0.5 g, 0.75 mmol) was added aniline (0.14 g, 2 equivalents). The reaction was heated in a sealed flask for 24 h at 100°C. The solvent and other volatiles were removed *in vacuo* leaving the products as a dark red oil. ^1H NMR (C_6D_6, 30°C): δ 9.29 (s, N*H*Ph); 6.6–7.2 (m, phenyl protons); 3.63 [septet, C*H*$(CH_3)_2$]; 1.12 [d, CH(C*H*$_3)_2$].

Synthesis of $[Ti(OC_6H_3Ph_2\text{-}2,6)_2(NHPh)_2]$ (**2**)

To a 50 : 50 hexane/benzene (25 cm^3) solution of $[Ti(OC_6H_3Ph_2\text{-}2,6)_2(C_4Et_4)]$ (0.5 g, 0.72 mmol) was added aniline (9.13 g, 2 equivalents). After 14 h, large red crystals of the product precipitated out of solution. The product was washed with hexane and dried *in vacuo*. Found: C, 80.3; H, 5.4; N, 5.3. Calc. for $TiC_{48}H_{38}N_2O_2$: C, 79.8; H, 5.3; N, 3.9%. ^1H NMR (C_6D_6, 30°C): δ 8.22 (s, N*H*Ph); 6.44 (dd, *ortho*-NH*Ph*); 6.60 (tt, *para*-NH*Ph*); 6.77–7.42 (m, aromatics). ^{13}C NMR (C_6D_6, 30°C): δ 159.9 (*ipso*-$OC_6H_3Ph_2$-2,6); 152.3 (*ipso*-NHC_6H_5); 129.5 (*meta*-NHC_6H_5); 122.7 (*para*-NHC_6H_5); 116.9 (*ortho*-NHC_6H_5); 140.0 (*ortho*-OC_6H_5); 133.0 (*ipso*-$OC_6H_3Ph_2$-2,6). IR spectrum (Nujol mull): 3300 cm^{-1} (w) $\bar{\nu}$ (NH).

Synthesis of $[Zr(OC_6H_3Bu^t_2\text{-}2,6)_2(NHPh)_2]$ (**3**)

To a benzene (30 cm^3) solution of $[(ArO)_2Zr(CH_3)_2]$ (ArO = 2,6-di-*tert*-butylphenoxide) (1.24 g, 2.33 mmol) was added aniline (0.43 g, 2 equivalents). Stirring was carried out overnight before removal of the solvent *in vacuo*. The solid residue was recrystallized from hot toluene to yield 0.47 g of pale yellow crystals (30% yield based on zirconium). Found: C, 69.0; H, 8.4; N, 3.9. Calc. for $ZrN_2O_2C_{40}H_{54}$: C, 70.0; H, 7.9; N, 4.1%. ^1H NMR (C_6D_6, 30°C): δ 7.37 (s, Zr-*N*H); 1.47 (s, $OC_6H_3Bu^t_2$-2,6); 7.22 (d, *meta*-$OC_6H_3Bu^t_2$-2,6); 6.8–7.2 (m, aromatics). ^{13}C NMR (C_6D_6, 30°C): δ 31.7 (CMe_3); 35.2 (CMe_3); 151.0 (*ipso*-NHC_6H_5); 161.3 (*ipso*-$OC_6H_3Bu^t_2$-2,6). IR spectrum (Nujol mull): 3344 (w) and 3262 cm^{-1} (w), $\bar{\nu}$(NH).

Synthesis of $[Hf(OC_6H_3Bu^t_2\text{-}2,6)_2(NHPh)_2]$ (**4**)

To a benzene (50 cm^3) solution of $Hf(CH_2Ph)_4$ (3.07 g, 5.66 mmol) was added aniline (2.11 g, 4 equivalents). Stirring for 2 days, followed by removal of the solvent *in vacuo* left an insoluble precipitate. To a benzene (25 cm^3) suspension of this precipitate was added 2,6-di-tertbutylphenol (2.33 g, 2 equivalents) and the solution allowed to stir for 4 days. Removal of the solvent left a pale white solid which was washed with hexane to yield 2.35 g of product (54% based upon hafnium). ^1H NMR (C_6D_6, 30°C): δ 6.63 (s, N—*H*); 1.46 (s, $OC_6H_3Bu^t_2$-2,6); 7.21 (d, *meta*-$OC_6H_3Bu^t_2$-2,6); 6.8–7.1 (m, aromatics). ^{13}C NMR (C_6D_6, 30°C): δ 31.7 (CMe_3); 35.1 (CMe_3); 150.7 (*ipso*-NC_6H_5); 161.2 (*ipso*-$OC_6H_3Bu^t_2$-2,6). IR spectrum (Nujol mull): 3324 (w) and 3258 cm^{-1} (w), ν(NH).

Synthesis of $[Zr(NHC_6H_3Pr^i_2\text{-}2,6)_4]$ (**5**)

To a benzene solution (10 cm^3) of $[Zr(CH_2Ph)_4]$ (1.95 g, 4.3 mmol) was added 2,6-diisopropylaniline (3.03 g, $\geqslant$ 4 equivalents). After the reaction mixture had been stirred at room temperature for 24 h, the solvent was removed *in vacuo* to leave the crude product as a yellow solid. The product was recrystallized from cold hexane. Yields were typically 60–70%. Found: C, 72.1; H, 9.4; N, 7.4. Calc. for

$ZrN_4C_{48}H_{72}$: C, 72.4; H, 9.1; N, 7.0%. ^{1}H NMR (C_6D_6, 30°C): δ 6.98 (s, Zr—N*H*); 3.26 (septet, C*H*Me$_2$); 1.18 (d, CH*Me*$_2$). ^{13}C NMR (C_6D_6, 30°C): δ 23.8 [CH(*C*H$_3$)$_2$; 31.1 (*C*HMe$_2$)]; 148.0 (*ipso*-NH*C*$_6$H$_5$). IR spectrum (Nujol mull): 3326, 3294, 3248 and 3278 cm^{-1} (w). $\bar{\nu}$ NH bands.

Synthesis of [Hf(NHC$_6$H$_3$Pr$^i_2$-2,6)$_4$] (**6**)

To a benzene solution (10 cm^3) of Hf(CH$_2$Ph)$_4$ (0.349 g, 0.064 mmol) was added 2,6-diisopropylaniline (4.60 g, $\geqslant$ 4 equivalents). After the reaction mixture had stirred for 72 h at room temperature the solvent was removed *in vacuo* to leave the product as a pale yellow solid. The product was recrystallized from cold hexane. Yields were typically 40–50%. Found: C, 65.6; H, 8.4; N, 5.6. Calc. for $HfN_4C_{48}H_{72}$: C, 65.2; H, 8.2; N, 6.3%. ^{1}H NMR (C_6D_6, 30°C): δ 6.16 (s, Hf—N*H*); 3.32 (septet, C*H*Me$_2$); 1.18 (d, CH*Me*$_2$). ^{13}C NMR (C_6D_6, 30°C): δ 23.9 [CH(*C*H$_3$)$_2$]; 31.0 (*C*HMe$_2$); 148.0 (*ipso*-NH*C*$_6$H$_5$).

Synthesis of [Ti(OC$_6$H$_3$Pr$^i_2$-2,6)$_2$(=NPh)(py′)$_2$] (**7**)

To a benzene (25 cm^3) solution of [Ti(OC$_6$H$_3$Pr$^i_2$-2,6)$_2$(η-Bu^{t}NCCH$_2$Ph)(CH$_2$Ph)] (0.5 g, 0.75 mol) was added 4-pyrrolidinopyridine (0.22 g, 2 equivalents). This was followed by the addition of aniline (0.069 g, 1 equivalent) and the solution was allowed to stir for 14 h. The solvent was removed *in vacuo* and the resulting residue redissolved in a minimum of toluene. Slow diffusion of hexane into the toluene solution produced orange–red crystals of the desired product. Found: C, 72.4; H, 8.5; N, 8.5. Calc. for $TiC_{48}H_{63}N_5O_2$: C, 73.0; H, 8.0; N, 8.9%. ^{1}H NMR (C_6D_6, 30°C): δ 8.79 (d, *ortho*-py′); 6.69–7.35 (m, aromatics); 5.67 (d, *meta*-py′); 4.57 [septet, C*H*(CH$_3$)$_2$]; 2.31 (m, α-CH$_2$—py′); 1.13 (m, β-CH$_2$—py′); 1.49 [d, CH(C*H*$_3$)$_2$]. ^{13}C NMR (C_6D_6, 30°C): δ 161.7 (*ipso*-N*C*$_6$H$_5$); 159.8 (*ipso*-O*C*$_6$H$_3$Pr$^i_2$-2,6); 137.7 (*ortho*-O*C*$_6$H$_3$Pr$^i_2$-2,6); 152.0 (*para*-py′); 149.8 (*ortho*-py′); 106.7 (*meta*-py′); 46.2 (α-*C*H$_2$-py′); 24.5 (β-*C*H$_2$-py′); 26.4 [*C*H(CH$_3$)$_2$]; 24.1 [CH(*C*H$_3$)$_2$].

Synthesis of [Ti(OC$_6$H$_3$Ph$_2$-2,6)$_2$(=NPh)(py′)$_2$] (**8**)

(a) To a benzene (25 cm^3) solution of **2** (0.5 g, 0.69 mmol) was added 4-pyrrolidinopyridine (0.21 g, 1.38 mmol). Slow diffusion of hexane induced the formation of yellow–orange crystals of the desired product. The product was washed with hexane and dried *in vacuo*. (b) To a benzene (20 cm^3) solution of Ti(OC$_6$H$_3$Ph$_2$-2,6)$_2$(Ph$_2$) (0.34 g, 0.5 mmols) was added 2 equivalents of aniline. The red solution was allowed to stir for 36 h. The solvent was removed *in vacuo* to give [Ti(OC$_6$H$_3$Ph$_2$-2,6)(NHPh)$_2$]. The subsequent addition of 2 equivalents of 4-pyrrolidinopyridine (py′) to a benzene solution of [Ti(OC$_6$H$_3$Ph$_2$-2,6)$_2$(NHPh)$_2$] yielded, after stirring and removal of solvent, [Ti(OC$_6$H$_3$Ph$_2$-2,6)(=NPh)(py′)$_2$]. Found: C, 72.5; H, 6.1; N, 7.0. Calc. for $TiC_{60}H_{55}N_5O_2$: C, 72.8; H, 6.0; N, 7.6%. ^{1}H NMR (C_6D_6, 30°C): δ 8.06 (broad s, *ortho*-py′); 6.53–7.76 (m, aromatics); 5.48 (broad, *meta*-py′); 2.59 (m, α-CH$_2$—py′); 1.56 (β-CH$_2$—py′). ^{13}C NMR (C_6D_6, 30°C): δ 161.4 (*ipso*-N*C*$_6$H$_5$); 161.3 (*ipso*-O*C*$_6$H$_3$Ph$_2$-2,6)$_2$; 151.9 (*para*-py′); 149.8 (*ortho*-py′); 142.5 (*ortho*-O*C*$_6$H$_3$Ph$_2$-2,6); 133.6 (*ipso*-OC$_6$H$_3$*Ph*$_2$-2,6); 129.0 (*para*-N*C*$_6$H$_5$); 122.7 (*ortho*-N*C*$_6$H$_5$); 118.7 (*meta*-N*C*$_6$H$_5$); 106.8 (*meta*-py′); 46.8 (α-*C*H$_2$—py′); 25.3 (β-*C*H$_2$—py′).

Synthesis of [Zr(OC$_6$H$_3$Bu$^t_2$-2,6)$_2$(=NPh)(py′)$_2$] (**9**)

A benzene (25 cm^3) solution of Zr(OC$_6$H$_3$Bu$^t_2$-2,6)$_2$ (2.36 g, 3.46 mmol) was reacted with 4-pyrrolidinopyridine (1.02 g, 2 equivalents). After overnight stirring the solvent and generated aniline were removed *in vacuo*. Recrystallization of the crude product from hot toluene yielded 1.22 g of product (40% yield based upon zirconium). Found: C, 70.3; H, 8.5; N, 7.5. Calc. for $ZrC_{52}H_{71}O_2N_5$: C, 70.2; H, 8.0; N, 7.9%. ^{1}H NMR (C_6D_6, 30°C): δ 1.86 (s, OC$_6$H$_3$*Bu*$^t_2$-2,6); 7.65 (d, *meta*-OC$_6$*H*$_3$Bu$^t_2$-2,6). ^{13}C NMR (C_6D_6, 30°C): 32.1 (*CMe*); 36.5 (*C*Me$_3$); 160.0 (*ipso*-O*C*$_6$H$_3$Bu$^t_2$-2,6); 163.8 (*ipso*-N*C*$_6$H$_5$).

Synthesis of [Zr(HNC$_6$H$_3$Pr$^i_2$-2,6)$_2$(=NC$_6$H$_3$Pr$^i_2$-2,6)(py′)$_2$] (**10**)

To a solution of **5** (0.67 g, 0.8 mmol) in benzene (10 cm^3) was added 4-pyrrolidinopyridine (0.26 g, 1.7 mmol). The solution was allowed to stir for 9 h at room temperature. The solvent was removed *in vacuo* to give a yellow–brown solid. The solid was washed with hexane to remove the 2,6-diisopropylaniline produced in the reaction. The resulting crude product was crystallized from hot toluene. Yields were typically 50–70%. Found: C, 70.4; H, 8.6; N, 10.3. Calc. for $ZrC_{54}H_{77}N_7$: C, 70.8; H, 8.5; N, 10.7%. ^{1}H NMR (C_6D_6, 30°C): δ 6.90 (s, Zr—N*H*); 3.92 (septet, imido-C*H*Me$_2$); 3.77 (septet, amido-C*H*Me$_2$); 1.29 (d, imido–CH*Me*$_2$); 1.43 (d, amido-CH*Me*$_2$); 8.87 (d, *ortho*-py′); 5.62 (d, *meta*-py′); 2.32 (m, α-CH$_2$—py′); 1.07 (m, β-CH$_2$—py′). ^{13}C NMR (C_6D_6, 30°C): δ 24.2 [imido-CH(*C*H$_3$)$_2$]; 30.4 [amido *C*H(CH$_3$)$_2$]; 156.1 (*ipso*-N*C*$_6$H$_5$); 151.3 (*ipso*-NH*C*$_6$H$_5$). IR spectrum

(Nujol mull): four bands at 3489, 3403, 3330 and 3269 cm^{-1}.

Synthesis of [Hf(NHC$_6$H$_3$Pr$^i_2$-2,6)$_2$(=NC$_6$H$_3$Pr$^i_2$-2,6)(py′)$_2$] (**11**)

To a solution of **6** (1.12 g, 1.3 mmol) in benzene (10 cm^3) was added 4-pyrrolidinopyridine (0.39 g, 2.7 mmol). The solution was allowed to stir for 72 h at room temperature. The solvent was removed *in vacuo* to give a yellow solid. The solid was washed with hexane to remove the 2,6-diisopropylaniline produced in the reaction and the resulting crude product was recrystrallized from hot toluene. Yields were typically 40–50%. ^{1}H NMR (C_6D_6, 30°C): δ 6.28 (s, Hf—N*H*); 3.84 (septet, imido-C*H*Me$_2$); 3.78 (septet, amido-C*H*Me$_2$); 1.29 (d, imido-CH*Me*$_2$); 1.40 (d, amido-CH*Me*$_2$); 8.91 (d, *ortho*-py′); 5.62 (d, *meta*-py′); 2.30 (m, α-CH$_2$—py′); 1.03 (m, β-CH$_2$—py′). ^{13}C NMR (C_6D_6, 30°C): δ 24.2 [imido CH(*C*H$_3$)$_2$]; 24.6 [amido CH(*C*H$_3$)$_2$]; 28.8 [imido *C*H(CH$_3$)$_2$]; 30.3 [amido-*C*H(CH$_3$)$_2$]; 157.7 (*ipso*-N*C*$_6$H$_5$); 152.0 (*ipso*-NH*C*$_6$H$_5$).

Synthesis of [Ti(OC$_6$H$_3$Ph$_2$-2,6)$_2$(=NPh)(phen-Me$_4$)] (**12**)

To a benzene solution (25 cm^3) of **2** (0.25 g, 0.35 mmol) was added 3,4,7,8-tetramethyl-1,10-phenanthroline (phen-Me$_4$) (0.08 g, 1 equivalent). The reaction was heated for 14 h at 110°C in a sealed flask, then allowed to cool slowly to room temperature. The bright red crystals which formed from the solution were washed with hexane and dried *in vacuo*. Found: C, 81.5; H, 5.7; N, 4.8. Calc. for TiC$_{58}$H$_{47}$N$_3$O$_2$·C$_6$H$_6$: C, 81.4; H, 5.7; N, 4.4%. ^{1}H NMR (C_6D_6, 30°C): δ 8.78 (s, *ortho*-phen); 7.75 (d, *ortho*-OC$_6$H$_3$*Ph*$_2$-2,6); 6.53–7.44 (m, aromatics); 6.09 (d, *ortho*-NC$_6$*H*$_5$); 1.82, 1.68 (2s, C*H*$_3$).

Equilibrium studies

The equilibrium constants (Table 11) for reaction of py, py-4Me and py′ with the various bis(phenylamido) complexes **3**^{X} (X = H, F, CH$_3$, OMe, Br) to produce the corresponding imido derivatives were measured by ^{1}H NMR methods. A C_6D_6 solution of the bis(phenylamido) complex of known concentrated was reacted with various amounts of pyridine ligand. The resulting mixture was allowed to reach equilibrium and the concentration of the adduct [**3** · py] and the resulting imido complex were determined by integrations. In all cases the equilibrium constant was determined using at least two different concentrations of pyridine ligand. The results are collected in Table 11. Selected spectroscopic data for the various substituted phenyl amido derivatives are given below. Selected spectroscopic data for the zirconium imido compounds is contained in Table 12.

^{1}H *NMR* (C_6D_6, 30°C) *for* **3**^{X}, X = F, CH$_3$, OCH$_3$, Br

[Zr(OC$_6$H$_3$Bu$^t_2$-2,6)$_2$(NHC$_6$H$_4$-4F)$_2$]. δ 7.16 (s, Zr—N*H*); 1.44 (s, OC$_6$H$_3$*Bu*$^t_2$-2,6); 6.67–6.74 (m,

Table 12. Selected spectroscopic data for zirconium imido compounds (^{1}H NMR, C_6D_6, 30°C; ArO = 2,6-ditert-butylphenoxide)

Compound	Bu^t, s (ppm)	ArO *meta*-protons, d (ppm)	py *ortho*-protons, dd (ppm)	py *meta*-protons dd (ppm)
(ArO)$_2$Zr(=NPh)(py)$_2$	1.62	7.49	[a]	[a]
(ArO)$_2$Zr(=NC$_6$H$_4$-4F)(py)$_2$	1.62	7.54	[a]	[a]
(ArO)$_2$Zr(=NC$_6$H$_4$-4CH$_3$)(py)$_2$	1.68	7.54	[a]	[a]
(ArO)$_2$Zr(=NC$_6$H$_4$-4OCH$_3$)(py)$_2$	1.67	7.54	[a]	[a]
(ArO)$_2$Zr(=NC$_6$H$_4$-4Br)(py)$_2$	1.62	7.53	[a]	[a]
(ArO)$_2$Zr(=NC$_6$H$_4$-4F)(py′)$_2$	1.88	7.63	8.78	5.52
(ArO)$_2$Zr(=NC$_6$H$_4$-4CH$_3$)(py′)$_2$	1.86	7.65	8.82	5.48
(ArO)$_2$Zr(=NC$_6$H$_4$-4OCH$_3$)(py′)$_2$	1.88	7.66	8.82	5.52
(ArO)$_2$Zr(=NC$_6$H$_4$-4Br)(py′)$_2$	1.84	7.64	8.75	5.48
(ArO)$_2$Zr(=NPh)(py-4Me)$_2$	1.68	7.57	8.95	6.14
(ArO)$_2$Zr(=NC$_6$H$_4$-4F)(py-4Me)$_2$	1.68	7.57	8.92	6.15
(ArO)$_2$Zr(=NC$_6$H$_4$-4CH$_3$)(py-4Me)$_2$	1.71	7.56	8.96	6.08
(ArO)$_2$Zr(=NC$_6$H$_4$-4OCH$_3$)(py-4Me)$_2$	1.74	7.58	8.96	6.10
(ArO)$_2$Zr(=NC$_6$H$_4$-4Br)(py-4Me)$_2$	1.65	7.55	8.88	6.02

[a] Reactions were carried out using pyridine-d$_5$.

Table 13. Crystal data and data collection parameters

	2	3	5	7
Formula	$TiO_2N_2C_{48}H_{38}$	$ZrO_2N_2C_{40}H_{54}$	$ZrN_4C_{48}H_{72}$	$TiO_2N_5C_{48}H_{63}$
Formula weight	722.75	686.11	796.36	789.97
Space group	$P2_1/n$ (No. 14)	$P2_1/c$ (No. 14)	*Pbca* (No. 61)	$P2_1/n$ (No. 14)
a (Å)	11.427(3)	9.934(5)	11.941(1)	14.234(4)
b (Å)	18.722(3)	20.025(5)	19.110(3)	13.818(3)
c (Å)	18.811(5)	18.688(8)	41.155(4)	23.087(6)
α (°)	90	90	90	90
β (°)	105.25(1)	97.42(5)	90	95.99(1)
γ (°)	90	90	90	90
V (Å^3)	3882(3)	3686(5)	9391(3)	4515(4)
Z	4	4	8	4
d_{calc} (g cm^{-3})	1.236	1.236	1.126	1.162
Crystal dimensions (mm)	0.40 × 0.40 × 0.34	0.38 × 0.22 × 0.13	0.63 × 0.40 × 0.20	0.52 × 0.32 × 0.21
Temperature (°C)	20	20	20	−100
Linear absorption coefficient (cm^{-1})	2.56	3.25	2.61	2.26
Absorption correction applied	None	Empirical	Empirical	Empirical
Scan method	ω–2θ	ω–2θ	ω–2θ	ω–2θ
h, k, l limits	−12–11, 0–20, 0–20	−10–10, 0–21, 0–2	0–12, 0–20, 0–4	−15–15, 0–14, 0–24
2θ range (°)	4.00–45.00	4.00–45.00	4.00–45.00	4.00–45.00
Scan width (°)	0.41 + 0.35 tan (θ)	0.38 + 0.35 tan (θ)	0.51 − 0.35 tan (θ)	0.75 + 0.35 tan (θ)
Take-off angle (°)	3.15	3.15	2.95	3.15
F(000)	1512.0	1456.0	3424.0	1696.0
p-factor used in weighting	0.040	0.040	0.040	0.040
Data collected	5262	4999	6811	6196
Unique data	5262	4999	6811	6196
Data with $I > 3.0\sigma(I)$	2919	1918	2401	3687
Number of variables	486	286	478	505
Largest shift/e.s.d. in final cycle	0.0	0.51	0.05	0.01
R	0.041	0.077	0.052	0.054
R_w	0.048	0.096	0.056	0.065
Goodness-of-fit	1.246	1.962	1.252	1.493

overlapped *meta*- and *ortho*-NHC_6H_4F); 7.24 (d, *meta*-$OC_6H_3Bu^t_2$-2,6).

[$Zr(OC_6H_3Bu^t_2$-2,6)$_2(NHC_6H_4$-4$CH_3)_2$]. δ 7.38 (s, Zr—N*H*); 1.50 (s, $OC_6H_3Bu^t_2$-2,6); 6.96 (d, *ortho*-$NHC_6H_4CH_3$); 7.24 (d, *meta*-$OC_6H_3Bu^t_2$-2,6); 2.08 (s, $NHC_6H_4CH_3$).

[$Zr(OC_6H_3Bu^t_2$-2,6)$_2(NHC_6H_4$-4$OCH_3)_2$]. δ 7.34 (s, Zr—N*H*); 1.51 (s, $OC_6H_3Bu^t_2$-2,6); 6.70 (dd, *meta*-$NHC_6H_4OCH_3$); 6.97 (dd, *ortho*-$NHC_6H_4OCH_3$); 7.24 (d, *meta*-$OC_6H_3Bu^t_2$-2,6); 6.86 (t, *para*-$OC_6H_3Bu^t_2$-2,6); 3.27 (s, $NHC_6H_4OCH_3$).

[$Zr(OC_6H_3Bu^t_2$-2,6)$_2(NHC_6H_4$-4Br)$_2$]. δ 7.15 (s, Zr—N*H*); 1.40 (s, $OC_6H_3Bu^t_2$-2,6); 6.62 (dd, *meta*-NHC_6H_4Br); 7.08 (dd, *ortho*-NHC_6H_4Br); 7.20 (d, *meta*-$OC_6H_3Bu^t_2$-2,6); 6.84 (t, *para*-$OC_6H_3Bu^t_2$-2,6.

Crystallographic data

Details of the crystal data and data collected parameters are listed in Table 13. Further experimental details of the crystal structure determinations are contained in the supplementary material.

Acknowledgements—We thank the National Science Foundation (Grant CHE-8915573) for support of this research.

REFERENCES

1. W. A. Nugent and J. A. Mayer, *Metal–Ligand Multiple Bonds*, Wiley-Interscience, New York (1988).
2. (a) R. R. Schrock, *J. Organomet. Chem.* 1986, **300**, 249; (b) R. R. Schrock, *Accts Chem. Res.* 1979, **12**, 98; (c) J. Feldman and R. R. Schrock, *Prog. Inorg. Chem.* 1991, **39**, 1; (d) M. Brookhart and W. B. Studabaker, *Chem. Rev.* 1987, **87**, 411; (e) M. P. Doyle, *Chem. Rev.* 1986, **86**, 919; (f) K. A. Brown Wensley, S. L. Buchwald, L. Cannizzo, L. Clawson, S. Ho, D. Meinhart, J. R. Stille, D. Straus and R. H. Grubbs, *Pure Appl. Chem.* 1983, **55**, 1733; (g) F. A.

Table 13—*continued*

	9	**10**	**11**	**12**
Formula	$ZrO_2N_5C_{73}H_{95}$	$ZrN_7C_{75}H_{101}$	$HfN_7C_{68}H_{93}$	$TiO_2N_3C_{61}H_{50}$
Formula weight	1165.82	1191.91	1176.04	905.00
Space group	$Pna2_1$ (No. 33)	$P\bar{1}$ (No. 2)	$P2_1/c$ (No. 14)	$P2_1/n$ (No. 14)
a (Å)	25.101(1)	13.473(4)	14.629(2)	11.894(3)
b (Å)	10.145(2)	14.445(3)	18.641(5)	19.286(3)
c (Å)	25.721(2)	17.981(3)	23.256(4)	20.779(3)
α (°)	90	82.78(1)	90	90
β (°)	90	76.59(2)	105.258(8)	100.02(2)
γ (°)	90	87.51(2)	90	90
V (Å^3)	6549(2)	3376(2)	6381(4)	4694(3)
Z	4	2	4	4
d_{calc} (g cm^{-3})	1.182	1.172	1.235	1.281
Crystal dimensions (mm)	0.40 × 0.25 × 0.20	0.40 × 0.38 × 0.25	0.61 × 0.50 × 0.38	0.63 × 0.17 × 0.14
Temperature (°C)	−64	−102	−66	−50
Linear absorption coefficient (cm^{-1})	2.09	2.03	16.61	2.26
Absorption correction applied	Empirical	Empirical	Empirical	None
Scan method	ω–2θ	ω–2θ	ω–2θ	ω–2θ
h, k, l limits	−27–0, 0–10, 0–27	−14–14, −15–15, 0–19	0–15, 0–20, −26–25	−12–12, 0–20, 0–20
2θ range (°)	4.00–45.00	4.00–45.00	4.00–45.00	4.00–45.00
Scan width (°)	0.57 + 0.35 tan θ	0.93 + 0.35 tan θ	0.51 + 0.35 tan θ	0.88 + 0.35 tan θ
Take-off angle (°)	2.95	2.95	2.95	2.95
F(000)	2496.0	1280.0	2488.0	1900.0
p-factor used in weighting	0.040	0.040	0.040	0.040
Data collected	4799	8835	8639	6336
Unique data	4799	8835	8639	6336
Data with $I > 3.0\sigma(I)$	2691	6536	6963	3491
Number of variables	508	757	650	589
Largest shift/e.s.d. in final cycle	0.64	0.43	0.36	0.00
R	0.053	0.066	0.033	0.046
R_w	0.061	0.082	0.047	0.053
Goodness-of-fit	1.274	1.980	1.674	1.190

Cotton and C. M. Lukehart, *Prog. Inorg. Chem.* 1972, **16**, 487; (h) D. Seyferth (Editor), *Transition Metal Carbene Complexes*. Verlog Chemie, Weinheim (1983) and refs therein; (i) P. S. Braterman (Editor), *Reactions of Coordinated Ligands*, Vol. 1, Ch. 3, 4 and 5. Plenum Press, New York (1986) and refs therein.

3. (a) H. Fisher, F. R. Kreissl, R. R. Schrock, V. Schubert, P. Hofmann and K. Weiss, *Carbyne Complexes*. VCH Publishers, Weinheim (1988) and refs therein; (b) R. R. Schrock, *Accts Chem. Res.* 1986, **19**, 342; (b) W. R. Roper, *J. Organomet. Chem.* 1986, **300**, 167; (d) R. R. Schrock, *Accts Chem. Res.* 1979, **12**, 98; (e) P. E. Fanwick, A. E. Ogilvy and I. P. Rothwell, *Organometallics* 1987, **6**, 73; (f) A. Mayr and G. A. McDermott, *J. Am. Chem. Soc.* 1986, **108**, 548; (g) M. H. Chisholm, K. Folting, J. C. Huffman and E. A. Lucas, *Organometallics* 1991, **10**, 535; (h) A. F. Hill, *J. Molec. Catal.* 1991, **65**, 85.

4. (a) M. H. Chisholm and I. P. Rothwell, in *Comprehensive Coordination Chemistry*, Vol. 2, Ch. 13.4. Pergamon Press, New York (1987); (b) W. A. Nugent and B. L. Haymore, *Coord. Chem. Rev.* 1980, **31**, 123; (c) I. A. Weinstock, R. R. Schrock and W. M. Davis, *J. Am. Chem. Soc.* 1991, **113**, 135; (d) J. E Hill, P. E. Fanwick and I. P. Rothwell, *Inorg. Chem.* 1991, **30**, 1143; (e) T. E. Glassman, M. G. Vale and R. R. Schrock, *Organometallics* 1991, **10**, 4046; (f) A. A. Donopoulos, G. Wilkinson and D. J. Williams, *J. Chem. Soc., Chem. Commun.* 1991, 181; (g) J. E. Hill, R. D. Profilet, P. E. Fanwick and I. P. Rothwell, *Angew. Chem., Int. Edn Engl.* 1990, **29**, 664; (h) R. D. Profilet, C. H. Zambrano, P. E. Fanwick, J. J. Nash and I. P. Rothwell, *Inorg. Chem.* 1990, **29**, 4362; (i) H. W. Roesky, H. Voelker, M. Witt and M. Noltemeyer, *Angew. Chem., Int. Edn Engl.* 1990, **29**, 669; (j) C. H. Winter, P. H. Sheridan, T. S. Lewkebandova, M. J. Heeg and J. W. Proscia, *J.*

Am. Chem. Soc. 1992, **114**, 1095; (k) R. Duchateau, A. J. Williams, S. Gambarotta and M. Y. Chiang, *Inorg. Chem.* 1991, **30**, 4863; (l) Y. W. Chao, P. A. Wexler and D. E. Wigley, *Inorg. Chem.* 1990, **29**, 4592.

5. (a) M. J. Carney, P. J. Walsh, F. J. Hollander and R. G. Bergman, *Organometallics* 1992, **11**, 761; (b) W. A. Herrmann, *Angew. Chem., Int. Edn Engl.* 1988, **27**, 1297; (c) W. A. Herrmann and J. Okuda, *J. Molec. Catal.* 1987, **41**, 109; (d) W. P. Griffith, *Coord. Chem. Rev.* 1970, **5**, 459; (e) M. J. Carney, P. J. Walsh and R. G. Bergman, *J. Am. Chem. Soc.* 1990, **112**, 6426; (f) G. Perkin and J. E. Bercaw, *Polyhedron* 1988, 7, 2053; (g) R. H. Holm, *Chem. Rev.* 1987, **87**, 1401; (h) J. W. Faller and M. Ma, *Organometallics* 1988, **7**, 559; (i) P. Legzdins, E. C. Phillips, S. J. Rettig, L. Sanchez, J. Trotter and V. C. Lee, *Organometallics* 1988, **7**, 1877; (j) F. Bottomley and L. Sutin, *Adv. Organomet. Chem.* 1988, **28**, 339; (k) S. Cai, D. M. Hoffman and D. A. Wierda, *J. Chem. Soc., Chem. Commun.* 1988, 1489 and refs therein.
6. P. J. Walsh, F. J. Hollander and R. G. Bergman, *J. Am. Chem. Soc.* 1988, **110**, 8729.
7. C. C. Cummins, S. M. Baxter and P. T. Wolczanski, *J. Am. Chem. Soc.* 1988, **110**, 8731.
8. (a) C. C. Cummins, C. P. Schaller, G. D. Van Duyne, P. T. Wolczanski, A. W. Edith Chan and R. Hoffman, *J. Am. Chem. Soc.* 1991, **113**, 2985; (b) E. W. Harlan and R. H. Holm, *J. Am. Chem. Soc.* 1990, **112**, 186.
9. (a) D. S. Williams, M. H. Schofield, J. T. Anhaus and R. R. Schrock, *J. Am. Chem. Soc.* 1990, **112**, 6728; (b) G. C. Bazan, E. Khosravi, R. R. Schrock, W. J. Feast, V. C. Gibson, M. B. O'Regan, J. K. Thomas and W. M. Davis, *J. Am. Chem. Soc.* 1990, **112**, 8378; (c) M. H. Schofield, R. R. Schrock and L. Y. Park, *Organometallics* 1991, **10**, 1844.
10. (a) M. F. Lappert, P. P. Power, A. R. Sanger and R. C. Srivastara, *Metal and Metalloid Amides*. John Wiley, New York (1980); (b) P. J. Davidson, M. F. Lappert and R. Pearce, *Accts Chem. Res.* 1974, **7**, 209; (c) D. C. Bradley and M. H. Chisholm, *Accts Chem. Res.* 1976, **9**, 273; (d) W. A. Nugent and B. L. Haymore, *Coord. Chem. Rev.* 1980, **31**, 123; (e) K. Dehnicke, *Adv. Inorg. Chem.* 1983, **26**, 169; (f) D. J. Cardin, M. F. Lappert and C. L. Raston, *Chemistry of Organo-zirconium and -hafnium Compounds*. John Wiley, New York (1986).
11. (a) S. L. Latesky, A. K. McMullen, G. P. Niccola, I. P. Rothwell and J. C. Huffman, *Organometallics* 1985, **4**, 902; (b) P. E. Fanwick, A. E. Ogilvy and I. P. Rothwell, *Organometallics* 1987, **6**, 73.
12. L. D. Durfee, J. E. Hill, P. E. Fanwick and I. P. Rothwell, *Organometallics* 1990, **9**, 75.
13. J. E. Hill, P. E. Fanwick and I. P. Rothwell, *Organometallics* 1990, **9**, 2211.
14. S. L. Latesky, A. K. McMullen, G. P. Niccola, I. P. Rothwell and J. E. Huffman, *Organometallics* 1985, **4**, 1896.
15. C. H. Zambrano, A. K. McMullen, L. M. Kobriger, P. E. Fanwick and I. P. Rothwell, *J. Am. Chem. Soc.* 1990, **112**, 6565.
16. G. R. Davies, J. A. J. Jarvis and B. T. Kilbourn, *J. Chem. Soc., Chem. Commun.* 1971, 1511.
17. G. M. Bodner, *Inorg. Chem.* 1975, **14**, 2694.
18. R. A. Jones, J. G. Hefner and T. C. Wright, *Polyhedron* 1984, **3**, 1121.
19. V. Visciglio, P. E. Fanwick and I. P. Rothwell, manuscript in preparation.
20. G. D. Smith, P. E. Fanwick and I. P. Rothwell, *Inorg. Chem.* 1990, **29**, 3221.
21. A. R. Rossi and R. Hoffman, *Inorg. Chem.* 1975, **14**, 365.
22. T. W. Coffindaffer, I. P. Rothwell and J. C. Huffman, *Inorg. Chem.* 1983, **22**, 2906.
23. L. R. Chamberlain and I. P. Rothwell, *J. Chem. Soc., Dalton Trans.* 1987, 163.
24. A. A. Frost and R. C. Pearson, in *Kinetics and Mechanisms*, 2nd edn, pp. 185–196. John Wiley, New York (1961).

Polyhedron Vol. 12, No. 6, pp. 709–713, 1993
Printed in Great Britain

0277–5387/93 $6.00+.00
© 1993 Pergamon Press Ltd

PREPARATION AND CRYSTAL STRUCTURE OF POLYMERIC AMMONIUM SILVER(I) CITRATE HYDRATE, $\{NH_4[Ag_2(C_6H_5O_7)(H_2O)]\}_n$

DALIUS S. SAGATYS, GRAHAM SMITH,* RAYMOND C. BOTT and DANIEL E. LYNCH

School of Chemistry, Queensland University of Technology, GPO Box 2434, Brisbane 4001, Australia

and

COLIN H. L. KENNARD

Chemistry Department, The University of Queensland, Brisbane 4072, Australia

(*Received* 13 *August* 1992; *accepted* 20 *August* 1992)

Abstract—The polymeric silver(I) citrate complex $\{NH_4[Ag_2(C_6H_5O_7)(H_2O)]\}_n$ has been synthesized and its structure determined by X-ray diffraction methods and refined to $R = 0.046$ for 2520 observed reflections. This compound represents the first reported complexes of a silver(I) citrate. In the structural repeating unit there are two independent but different carboxylato(O,O′) bridged silver dimers [Ag—Ag, 2.845, 2.846(1) Å] linked into infinite linear chains by the terminal carboxyl groups of the citrato(3−) ligands. With one dimer, the Ag—O (axial) bonds are to oxygens from the sub-terminal carboxylate groups of two independent silver citrate chains. The second silver dimer also forms links with adjacent chains via axial Ag—O(carboxylate) bonds, while in the remaining axial sites are water molecules. The mean Ag—O distance is 2.377(4) Å. The result is a novel convoluted anionic chain sheet structure.

As a program of investigation in our laboratories into the mode of interaction of silver(I) with carboxylic acids, particularly the phenoxyalkanoic acids [which include a number of herbicidally active commercial members, e.g. 2,4-D (2,4-dichlorophenoxyacetic acid), 2,4,5-T (2,4,5-trichlorophenoxyacetic acid) and MCPA (4-chloro-2-methylphenoxyacetic acid)[1]], a number of structures have been determined and general structural systematics described.[2] The basic structural unit found for the majority of silver(I) carboxylates is a bis(carboxylato-O,O′) dimer, which involves each carboxyl group in a *syn–syn* mode.

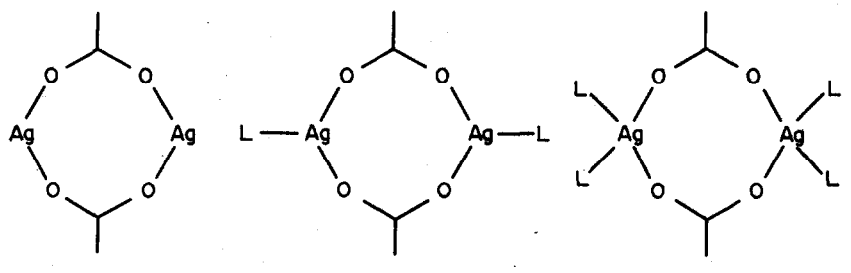

Type 1 Type 2 Type 3

These are classified as Type 1 dimers,[2] such as is found in silver(I) benzoate,[3] silver(I) 4-hydroxy-

* Author to whom correspondence should be addressed.

benzoate hemihydrate,[3] silver(I) 2-hydroxybenzoate,[4] silver(I) 2,6-dihydroxybenzoate,[4] silver(I) pentafluorophenoxyacetate[5] and silver(I) glycylglycine nitrate.[6] Alternatively, the dimer may be extended into a tetramer [bis{bis-μ-(4-fluorophenoxyacetato-O,O′)-bis{aquasilver(I)}}][7] or a polymer (types 2 and 3) via one or two additional terminal oxygens, completing either three- or four-coordinate centres about silver. Examples of the polymeric types among the phenoxyacid complexes are silver(I) phenoxyacetate[7] and silver(I) 2-carbamoylphenoxyacetate.[2] Often terminal positions may be occupied by non-bridging oxygen donor groups, such as H_2O[7] or ClO_4^- [in silver(I) 2-chlorophenoxyacetate-silver(I) perchlorate[8]]. Among all of these types, the Ag—Ag separation ranges from 2.78 [silver(I) 3-hydroxy-2,2,3-trimethylcyclohexanecarboxylate[9]] to 3.00 Å [silver(I) 2-carbamoylphenoxyacetate[2]].

Only two examples are known which are not based on the dimer motif; both are one-dimensional polymers. The first, the isomorphous silver(I) 2,4-dichlorophenoxyacetate and silver(I) 4-chloro-2-methylphenoxyacetate polytypes,[8] form zig-zag polymer chains through *anti–syn* carboxylate linkages. The second, silver(I) pyridinebetaine nitrate, is the only known example of a *syn–syn* bridged one-dimensional polymer.[10]

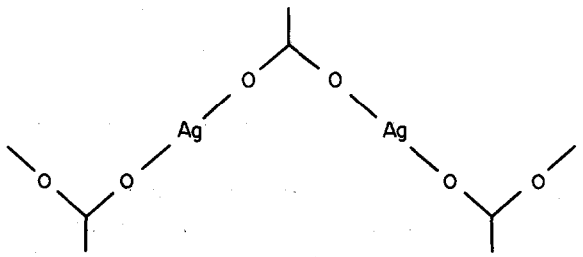

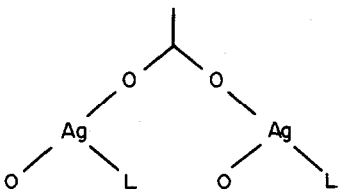

However, when considering the interaction of silver(I) with hydroxy acids, little information is available,[11] with only a few stability constants reported. Generally, only weak complexes are formed, with a tendency to undergo reduction to silver in aqueous solution. This is the case with ascorbate and tartrate and provides a qualitative basis for distinguishing between tartaric and citric acid.[12] Despite the resistance of citrate to oxidation by silver(I), and the availability of silver citrate as a commercial chemical, no structure of a silver citrate compound has previously been reported. Crystals of the title compound, ammonium silver(I) citrate, $\{NH_4[Ag_2(C_6H_5O_7)(H_2O)]\}_n$, were successfully grown from an aqueous ammoniacal solution containing silver nitrate and citric acid. Preliminary qualitative tests and IR spectra indicated the presence of an ammonium ion. Subsequently, the crystal structure was determined by X-ray diffraction.

EXPERIMENTAL

Preparation

The compound was prepared by adding ammonia solution to an aqueous solution containing 2 : 1 stoichiometric amounts of silver nitrate and citric acid. Allowing the resultant solution to partially evaporate at room temperature yielded large colourlesss crystals after several weeks.

Crystal data

$C_6H_{11}Ag_2NO_8$: $Mr = 440.9$; space group $P\bar{1}$, $a = 6.435(1)$, $b = 7.610(1)$, $c = 11.744(2)$ Å, $\alpha = 71.75(1)$, $\beta = 79.74(1)$, $\gamma = 74.87(1)°$, $V = 524.3(1)$ Å^3, $Z = 2$, $D_{calc} = 2.791$ g cm^{-3}, $D_{obs} = 2.83$ g cm^{-3}, $F(000) = 424$, μ(Mo-K_α) = 37.2 cm^{-1}, $T = 298$ K.

Data collection, structure solution and refinement

X-ray diffraction data were collected from a crystal of dimensions $0.26 \times 0.20 \times 0.05$ mm mounted on an Enraf–Nonius CAD-4 diffractometer using graphite-crystal monochromatized Mo-K_α X-radiation ($\lambda = 0.71073$ Å). Of 2915 reflections collected up to $2\theta_{max} = 50°$, 2680 were unique ($R_{int} = 0.008$) while 2520 with $I > 2.5\sigma(I)$ were considered observed and used in structure refinement. Collection range was h, -8 to 8; k -10 to 10; l, 0 to 16. The data were corrected for Lorentz and polarization effects and for absorption (empirical corrections: maximum and minimum transmission factors: 1.00, 0.72). An average loss of 2.1% in the intensities of three standards monitored over the 34 h data collection period indicates negligible crystal decay. The structure was solved using direct methods (SHELXS-86[13]) and refined to residuals $R = 0.046$ and $R_w = 0.052$ ($s = 3.95$) (SHELX 76[14]) using blocked-matrix least-squares, with anisotropic thermal parameters for all non-

Table 1. Bond distances (Å) and angles (°)

O(11)—Ag(1)	2.258(4)	O(311)[b]—Ag(1)	2.455(4)
O(12)[a]—Ag(1)	2.246(4)	O(312)[c]—Ag(1)	2.398(4)
Ag(1)—Ag(1)[a]	2.845(1)	O(51)[e]—Ag(2)	2.203(4)
O(12)[d]—Ag(2)	2.486(4)	O(52)—Ag(2)	2.242(4)
Ag(2)—Ag(2)[e]	2.846(1)	Ow—Ag(2)	2.731(4)
O(11)—C(1)	1.254(5)	O(12)—C(1)	1.263(6)
C(2)—C(1)	1.519(7)	C(3)—C(2)	1.524(7)
O(3)—C(3)	1.423(6)	C(31)—C(3)	1.541(7)
C(4)—C(3)	1.552(7)	O(311)—C(31)	1.239(7)
O(312)—C(31)	1.256(7)	C(5)—C(4)	1.505(7)
O(51)—C(5)	1.271(6)	O(52)—C(5)	1.257(6)
O(11)—Ag(1)—O(12)[a]	154.4(2)	Ag(1)[a]—O(12)—Ag(2)[f]	109.0(2)
O(11)—Ag(1)—O(311)[b]	97.6(2)	C(1)—O(12)—Ag(2)[f]	123.2(4)
O(11)—Ag(1)—O(312)[c]	90.4(1)	O(51)[e]—Ag(2)—O(52)	148.2(1)
O(12)[a]—Ag(1)—O(311)[b]	102.4(2)	O(51)[e]—Ag(2)—O(12)[d]	98.3(1)
O(12)[a]—Ag(1)—O(312)[c]	104.5(2)	O(51)[e]—Ag(2)—Ow	119.7(1)
O(311)[b]—Ag(1)—O(312)[c]	92.8(2)	O(52)—Ag(2)—O(12)[d]	96.1(1)
Ag(1)—O(311)[b]—C(31)[b]	163.5(4)	O(52)—Ag(2)—Ow	83.3(1)
Ag(1)—O(312)[c]—C(31)[c]	132.0(4)	O(12)[d]—Ag(2)—Ow	104.9(1)
Ag(1)—O(11)—C(1)	119.5(4)	Ag(2)—O(52)—C(5)	122.8(3)
Ag(1)[a]—O(12)—C(1)	126.4(4)	Ag(2)—O(51)[e]—C(5)[e]	119.1(3)
O(12)—C(1)—O(11)	124.8(5)	C(2)—C(1)—O(11)	119.2(4)
C(2)—C(1)—O(12)	115.9(5)	C(3)—C(2)—C(1)	114.7(4)
O(3)—C(3)—C(2)	111.5(4)	C(31)—C(3)—C(2)	110.6(4)
C(31)—C(3)—O(3)	108.2(4)	C(4)—C(3)—C(2)	107.4(4)
C(4)—C(3)—O(3)	110.7(4)	C(4)—C(3)—C(31)	108.5(4)
O(311)—C(31)—C(3)	116.4(5)	O(312)—C(31)—C(3)	118.0(5)
O(311)—C(31)—O(312)	125.6(4)	C(5)—C(4)—C(3)	112.3(4)
O(51)—C(5)—C(4)	118.3(5)	O(52)—C(5)—C(4)	118.0(5)
O(52)—C(5)—O(51)	123.7(5)		

Symmetry operations: [a] $= 1-x, 1-y, 1-z$; [b] $= 1+x, y, z$; [c] $= -x, 2-y, 1-z$; [d] $= -1+x, 1+y, z$; [e] $= -1-x, 3-y, -z$; [f] $= 1+x, -1+y, z$.

hydrogen atoms. A weighting scheme with $w = [\sigma^2(F_o)+8.0\times10^{-5}(F_o)^2]^{-1}$ was used. Hydrogens were located by difference methods and were included in the refinement with coordinates refined but with isotropic U values invariant at 0.5 Å^2.

Atomic coordinates, anisotropic thermal parameters, observed and calculated structure factors and intraligand bond distances and angles have been deposited with the Editor as supplementary material; copies are available on request. Atomic coordinates have also been deposited with the Cambridge Crystallographic Data Centre. Bond distances and angles are given in Table 1. The atom numbering scheme follows the convention used for previous structures of this series determined in our laboratories.[15]

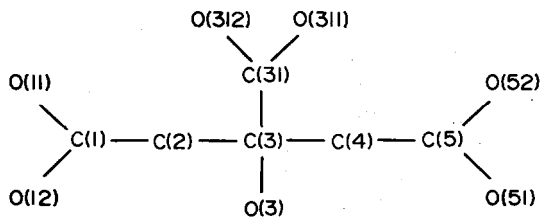

DISCUSSION

The structure determination has revealed a unique sheet polymer structure (Fig. 1), based upon two independent and different bis(carboxylato-O,O′) dimers (**1** and **2**). Both are Type 3 centrosymmetric dimers[2] with Ag—Ag′ separations of 2.845 and 2.846(1) Å for **1** and **2**, respectively. All silver centres are four-coordinate with the terminal O—Ag—O angles close to 90°. In the first dimer, silver is bonded to one terminal carboxylate group of the citrate residue [Ag(1)—O(11), 2.258(4), Ag(1)[a]—O(12). 2.246(4) Å ([a] $= 1-x, 1-y, 1-z$)], while the second silver is bonded to the other terminal carboxylate [Ag(2)—O(52), 2.242(4), Ag(2)[e]—O(51), 2.203(4) Å ([e] $= -1-x, 3-y, -z$)]. The coordination about Ag(1) is completed by bonds to two oxygens from different central citrate

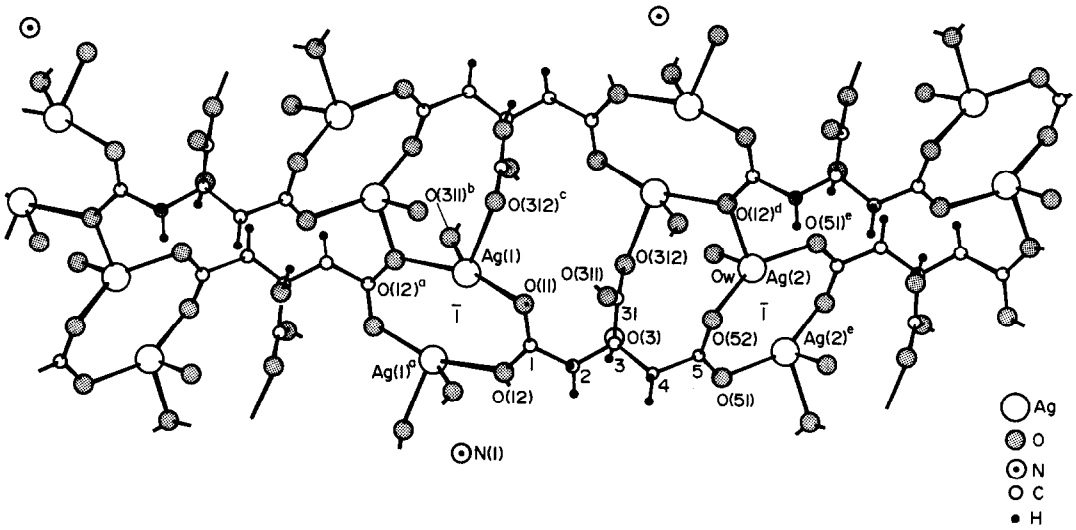

Fig. 1. The structure of $\{NH_4[Ag_2(C_6H_5O_7)(H_2O)]\}_n$. Unless otherwise indicated, atoms are carbons.

carboxylate groups [Ag—O(311)^b, 2.455(4) ($^b = 1+x, y, z$); Ag—O(312)^c, 2.398(4) Å ($^c = -x, 2-y, 1-z$)]. These form links both within and between the polymer sheets. About Ag(2), the terminal coordination comprises a bridging link to a carboxyl oxygen of an adjacent citrate residue [Ag(2)—O(12)^d, 2.486(4) ($^d = -1+x, 1+y, z$)] and a water molecule [Ag(2)—Ow, 2.731(4) Å]. The hydroxyl oxygens are not involved in any direct bonding to the metals but are hydrogen bonded to a carboxyl oxygen [O(51), 2.72(1); $-x, 2-y, -z$] and the coordinated water [2.89(1) Å; $-1-x, 3-y, -z$]. This water is in turn associated with a symmetry generated water [2.92(a) Å; $-2-x, 3-y, -z$]. The ammonium ions are also associated with the coordinated carboxyl oxygens, O(311) [2.80(1) Å; $1+x, y, z$], O(312) [2.77(1) Å; x, y, z] and O(52) [2.91(1) Å; $1+x, y, z$].

Considerable data appears in the literature on the structural systematics of citrates.[16] In the present example, the citrate residue has the extended conformation with the terminal carboxylate groups asymmetrically rotated [torsion angles: C(3)—C(2)—C(1)—O(12), $-131.1(6)°$ and C(3)—C(4)—C(5)—O(51), $+110.8(6)°$]. The central carboxylate group lies essentially perpendicular to the main citrate chain.

Acknowledgements—The authors acknowledge financial support from the Australian Research Council, The University of Queensland and the Queensland University of Technology.

REFERENCES

1. E. Y. Spencer, *Guide to the Chemicals used in Crop Protection*, 4th edn. Agriculture, Canada, Ottawa (1974).
2. T. C. W. Mak, W. H. Yip, C. H. L. Kennard, G. Smith and E. J. O'Reilly, *Aust. J. Chem.* 1986, **39**, 541.
3. B. T. Usubaliev, E. M. Movsumov, I. R. Amiraslanov, A. I. Akhmedov, A. A. Musaev and Mamedov, *J. Struct. Chem.* 1981, **22**, 73.
4. G. Smith, C. H. L. Kennard and T. C. W. Mak, *Z. Kristallogr.* 1988, **184**, 275.
5. T. C. W. Mak, W.-H. Yip, C. H. L. Kennard, G. Smith and E. J. O'Reilly, *Aust. J. Chem.* 1988, **41**, 683.
6. C. B. Acland and H. C. Freeman, *J. Chem. Soc., Chem. Commun.* 1971, 1016.
7. G. Smith, D. S. Sagatys, C. A. Campbell, D. E. Lynch and C. H. L. Kennard, *Aust. J. Chem.* 1990, **43**, 1707.
8. T. C. W. Mak, W. H. Yip, C. H. L. Kennard, G. Smith and E. J. O'Reilly, *J. Chem. Soc., Dalton Trans.* 1988, 2353.
9. P. Coggon and A. T. McPhail, *J. Chem. Soc., Chem. Commun.* 1972, 91.
10. X.-M. Chen and T. C. W. Mak, *Polyhedron* 1991, **10**, 1723.
11. R. J. Lancashire, in *Comprehensive Coordination Chemistry* (Edited by G. A. Wilkinson), Vol. 5, p. 810. Pergamon Press, Oxford (1987).
12. F. G. Mann and B. C. Saunders, *Practical Organic Chemistry*, 4th edn, p. 350. Longman, London (1960).
13. G. M. Sheldrick, SHELX-86, Structure Solution Package. University of Göttingen, Germany (1986).

14. G. M. Sheldrick, SHELX-76, Program for Crystal Structure Determination. University of Cambridge (1976).
15. R. C. Bott, D. S. Sagatys, D. E. Lynch, G. Smith, C. H. L. Kennard and T. C. W. Mak, *Aust. J. Chem.* 1991, **44**, 1495: $\{(NH_4)_4[Cu(C_6H_5O_7)_2]\}$; D. W. Hartley, G. Smith, D. S. Sagatys and C. H. L. Kennard, *J. Chem. Soc., Dalton Trans.* 1991, 2735: $[Ag_2Sb_2(C_6H_6O_7)_4]$, $\{[MNaSb(C_6H_6O_7)_2(H_2O)_2]\cdot H_2O\}$; G. Smith, D. S. Sagatys, R. C. Bott, D. E. Lynch and C. H. L. Kennard, *Polyhedron* 1992, **11**, 631: $\{[CuSb(C_6H_6O_7)(C_6H_5O_7)(H_2O)_2]\cdot 2.5H_2O\}$.
16. J. P. Glusker, *J. Molec. Biol.* 1968, **38**, 149; J. P. Glusker, *Accts Chem. Res.* 1980, **13**, 345; R. E. Tapscott, *Trans. Met. Chem.* 1982, **8**, 253.

Polyhedron Vol. 12, No. 7, pp. 715–719, 1993
Printed in Great Britain

0277–5387/93 $6.00+.00
Pergamon Press Ltd

NEW PARAMAGNETIC PYRAZOLE COMPLEXES OF TRIS(3,5-DIMETHYLPYRAZOLYL)BORATO MOLYBDENUM NITROSYL CHLORIDE AND IODIDE AND THE STRUCTURE OF [Mo(NO){HB(3,5-$Me_2C_3HN_2)_3$}Cl(3,5-$Me_2C_3HN_2H$)]

ANDRZEJ WLODARCZYK and STEFAN S. KUREK

Institute of Chemical Engineering and Physical Chemistry, Technical University of Krakow, 31-155 Krakow, Poland

and

JOHN P. MAHER, ANDREI S. BATSANOV,† JUDITH A. K. HOWARD† and JON A. McCLEVERTY‡

School of Chemistry, University of Bristol, Cantocks Close, Bristol BS8 1TS, U.K.

(*Received* 13 *October* 1992; *accepted* 2 *December* 1992)

Abstract—Reduction of [Mo(NO)L*Cl_2] [L* = HB(3,5-$Me_2C_3HN_2)_3$] with n-butyl lithium in the presence of $SnBu^n_3Cl$ afforded the paramagnetic (17-electron) [Mo(NO)L*Cl(3,5-$Me_2C_3HN_2H$)] (**1**). Related compounds, [Mo(NO)L*XQ] (Q = pyrazole, 3,5-dimethylpyrazole, 4-bromopyrazole and 4-bromo-3,5-dimethylpyrazole; X = Cl or I), were prepared by the reduction of [Mo(NO)L*X_2] by Q (X = I) or by n-butyl lithium in the presence of Q (X = Cl). IR and EPR spectroscopic characterization of these species is reported and the X-ray structure of [Mo(NO)L*Cl(3,5-$Me_2C_3HN_2H$)]·1/2CH_2Cl_2, in which the molybdenum atom has octahedral coordination with disordered Cl and NO ligands, is described.

In an attempt to functionalize the pyrazolyl rings of the tris(3,5-dimethylpyrazolyl)borato ligand HB(3,5-$Me_2C_3HN_2)_3$ (L*) at the 4-positions we have investigated the reactions of [Mo(NO)L*Cl_2] with $LiBu^n$ and $SnBu^n_3Cl$, our intention being to introduce the $SnBu^n_3$ group onto at least one pyrazole ring in the coordinated tripodal ligand. In previous studies of the reactions of [Mo(NO)L*I_2] with organo-lithium reagents we had observed that the reduction of the metal complex rather than displacement of I^- by a carbanion was the dominant reaction.[1] This we could rationalize in terms of the reducing nature of the lithium organyl and the particularly accessible reduction potential of the molybdenum di-iodide (+0.33 V vs S.C.E. in CH_3CN) and also in terms of the apparent steric difficulty in generating a potential four-centred intermediate or transition state necessary to effect interchange of I by an organic group at the metal in the hindered {Mo(NO)L*I} entity. Indeed, treatment of [Mo(NO)L*I_2] with tolyl lithium in ether afforded [Mo(NO)L*$I_2Li(OEt_2)_2$], which contains the paramagnetic [Mo(NO)L*I_2]$^-$ centre stabilized by the $\{Li(OEt_2)_2\}^+$ fragment. However, the reduction potential of [Mo(NO)L*Cl_2] is significantly more anodic (−0.01 V vs S.C.E. in CH_3CN) than that of its iodo-analogue, and we reasoned that, because of this and the well-understood steric protection afforded by L* at the Mo centre,[2] reactivity might be diverted preferentially to the pyrazolyl rings of L*.

In this paper we describe the reactions of [Mo(NO)L*X_2] (X = Cl or I) with n-butyl lithium and $SnBu^n_3Cl$, in which partial decomposition of the nitrosyl complex with disruption of the tris(pyrazolyl)borato ligand and reduction of the basic halide

† Present address: Department of Chemistry, University of Durham, South Road, Durham DH1 3LE, U.K.

‡ Author to whom correspondence should be addressed.

system occurred, and we report on the consequent formation of the paramagnetic 3,5-dimethylpyrazole complex [Mo(NO)L*X(3,5-$Me_2C_3HN_2H$)] (**1**). Using reductive procedures we have also prepared related complexes containing pyrazole ($C_3H_3N_2H$), 4-bromo-(4-$BrC_3H_2N_2H$) and 4-bromo-3,5-dimethylpyrazole (3,5-Me_2-4-BrC_3N_2H). These paramagnetic pyrazole complexes are closely related to the pyridine and 4,4′-bipyridyl complexes [Mo(NO)L*Cl(py)] and [Mo(NO)L*Cl(NC_5H_4—C_5H_4N)], which have been briefly described elsewhere.[3]

EXPERIMENTAL

Synthetic studies

All reactions were carried out in an atmosphere of dry nitrogen. Toluene was redistilled from sodium benzophenone before use. [Mo(NO)L*Cl_2] was prepared as described elsewhere,[4] butyl lithium was used as a 1.6 M solution in hexane and other reagents were used as received. Column chromatography was carried out using 70–230 mesh silica gel. IR spectra were recorded in KBr discs using a PE 1600 FTIR spectrometer and EPR spectra were recorded in dichloromethane using a Bruker ESP 300E instrument.

General procedure for the synthesis of [Mo(NO)L*IQ] (Q = $C_3H_3N_2H$, 4-BrC_3HN_2H, 3,5-$Me_2C_3H_2H$ *and* 3,5-Me_2-4-BrC_3N_2H)

A solution of [Mo(NO)L*I_2] (0.3 g) and pyrazole (0.09 g) or substituted pyrazole (1 : 2 mole ratio) in toluene (30 cm^3) was stirred at 80–90°C for 15–60 min, depending on the kind of pyrazole. The solution became deep green and the solvent was removed *in vacuo*, the residue being redissolved in dichloromethane. The solution was chromatographed on silica gel, using dichloromethane as an eluant, and the main green fraction was collected. The solvent was evaporated and the residue recrystallized from dichloromethane/petroleum ether (b.p. 40–60°C), affording green crystals. The yields were variable (30–50%).

General procedure for the synthesis of [Mo(NO)L*ClQ] (Q = $C_3H_3N_2H$ *and* 3,5-$Me_2C_3HN_2H$]

A solution of [Mo(NO)L*Cl_2] (0.3 g) and the appropriate pyrazole (2 moles per mole of molybdenum complex) was warmed to facilitate dissolution of the molybdenum complex and then cooled to *ca* 60°C. Butyl lithium in hexane (0.8 cm^3) was added and the reaction mixture stirred for 1 h, during which time the solution became grey–green in colour. Petroleum ether (b.p. 40–60°C) was added to precipitate salts and the solution was filtered, evaporated to dryness *in vacuo* and redissolved in the minimum volume of dichloromethane. The product was then obtained in the same way as the corresponding iodo complex and was isolated as green crystals (yields variable, 25–35%).

Crystal structure determination of [Mo(NO)L*Cl(3,5-$Me_2C_3HN_2H$)] (**1**)

A suitable crystal of the compound (a green plate sized $0.25 \times 0.35 \times 0.40$ mm) was grown from dichloromethane/petroleum ether (b.p. 60–80°C).

Crystal data. $C_{20}H_{30}N_9OBClMo \cdot 1/2CH_2Cl_2$, $M = 597.2$, monoclinic, space group $C2/c$, $a = 20.625(5)$, $b = 10.858(2)$, $c = 24.413(6)$ Å, $\beta = 96.23(2)°$, $U = 5.435(2)$ $Å^3$, $Z = 8$, $D_c = 1.46$ g cm^{-3}, $F(000) = 2.448$, graphite-monochromated Mo-K_α radiation, $\lambda = 0.71069$ Å, $\mu = 7.1$ cm^{-1}.

A total of 4000 independent reflections with $2\theta < 47°$ were collected in the Wyckoff (limited ω) scan mode. The reflection intensities were corrected for absorption, using the semi-empirical method,[5] based on 396 azimuthal scans of 11 reflections (min. and max. transmission coefficients 0.5524 and 0.5744, respectively). The structure was solved by Patterson and Fourier methods and refined by full-matrix least-squares using SHELXTLPLUS[6] programs. Difference-Fourier maps revealed a disorder in the coordination sphere of the molybdenum atom, the Cl and NO ligands mixing at each site. Their occupancy factors were refined, yielding 0.65(2) for positions A and 0.35(2) for B (of both ligands). In the final refinement these atoms were treated in isotropic approximation, while all other non-hydrogen atoms were refined with anisotropic displacement parameters. Most of the hydrogen atoms were revealed by difference-Fourier syntheses, but all of them were included in the refinement in riding model in idealized positions, with the distances C—H 0.96, N—H 0.90 and B—H (from Fourier map) 1.07 Å. The refinement of 310 variables converged at $R = 0.041$ and $R' = 0.052$ for 3298 reflections with $I > 2\sigma(I)$. The weighting scheme $w^{-1} = \sigma^2(F) + 0.002F^2$ was used; goodness of fit was 2.22. The maximum and minimum residuals in the final ΔF map were 0.56 and -0.42 e $Å^{-3}$ (around the disordered atoms).

Selected bond lengths and angles are given in Table 1. Additional data (atom coordinates, thermal parameters and remaining bond lengths and angles) are available from the Cambridge Crystallographic Data Centre.

Table 1. Selected bond lengths (Å) and angles (°)

Mo—Cl(1A)	2.420(4)	Mo—Cl(1B)	2.423(9)
Mo—N(0A)	1.782(12)	Mo—N(0B)	1.797(22)
Mo—N(1)	2.199(4)	Mo—N(11)	2.162(4)
Mo—N(21)	2.217(4)	Mo—N(31)	2.204(4)
N(0A)—O(1A)	1.127(18)	N(0B)—O(1B)	1.199(34)
N(1)—N(2)	1.359(6)	N(1)—C(5)	1.335(6)
N(2)—C(3)	1.343(6)	C(3)—C(4)	1.349(7)
C(3)—C(6)	1.498(8)	C(4)—C(5)	1.390(7)
C(5)—C(7)	1.494(8)	N(11)—N(12)	1.374(6)
N(11)—C(15)	1.333(6)	N(12)—C(13)	1.357(6)
N(12)—B	1.529(7)	C(13)—C(14)	1.361(9)
C(13)—C(16)	1.495(8)	C(14)—C(15)	1.376(8)
C(15)—C(17)	1.477(8)	N(21)—N(22)	1.375(5)
N(21)—C(25)	1.342(6)	N(22)—C(23)	1.346(6)
N(22)—B	1.541(7)	C(23)—C(24)	1.382(8)
C(23)—C(26)	1.497(8)	C(24)—C(25)	1.381(7)
C(25)—C(27)	1.486(7)	N(31)—N(32)	1.385(5)
N(31)—C(35)	1.342(6)	N(32)—C(33)	1.356(6)
N(32)—B	1.531(7)	C(33)—C(34)	1.360(7)
C(33)—C(36)	1.493(8)	C(34)—C(35)	1.391(7)
C(35)—C(37)	1.474(8)	Cl(10)—C(10)	1.680(9)

Cl(1B)—Mo—N(0B)	91.4(5)	Cl(1A)—Mo—N(0A)	93.3(3)
Cl(1B)—Mo—N(1)	91.9(2)	Cl(1A)—Mo—N(1)	89.2(1)
N(0B)—Mo—N(1)	91.6(6)	N(0A)—Mo—N(1)	91.5(3)
Cl(1B)—Mo—N(11)	95.3(2)	Cl(1A)—Mo—N(11)	93.6(1)
N(0B)—Mo—N(11)	91.4(6)	N(0A)—Mo—N(11)	95.7(3)
Cl(1A)—Mo—N(21)	91.1(1)	N(1)—Mo—N(11)	172.1(1)
N(0A)—Mo—N(21)	175.5(3)	Cl(1B)—Mo—N(21)	175.0(2)
N(1)—Mo—N(21)	87.6(1)	N(0B)—Mo—N(21)	93.5(5)
Cl(1A)—Mo—N(31)	174.8(1)	N(11)—Mo—N(21)	84.9(1)
N(0A)—Mo—N(31)	91.5(3)	Cl(1B)—Mo—N(31)	90.9(2)
N(1)—Mo—N(31)	92.7(1)	N(0B)—Mo—N(31)	175.0(6)
N(21)—Mo—N(31)	84.1(1)	N(11)—Mo—N(31)	84.0(1)
		Mo—N(0A)—O(1A)	178.2(8)

RESULTS AND DISCUSSION

Synthetic and spectral studies

On addition of n-butyl lithium to [Mo(NO)L*Cl_2] partially dissolved in toluene, in a mole ratio of 2 : 1, a red colour developed, but further addition of $LiBu^n$ was necessary to complete dissolution of the molybdenum chloride and generate a homogeneous deep red solution. On addition of $SnBu^n_3Cl$ the solution darkened and on work-up, which involved chromatography over silica, paramagnetic **1** was formed as green crystals. This species was characterized by elemental analysis (Table 2) and by IR and EPR spectroscopy. The yield of the species was of the order 20% and it is clear that the generation of this 17-electron 3,5-dimethylpyrazole species must occur via decomposition of the starting material, possibly via the reduced, 17-electron species [Mo(NO)L*Cl_2]$^-$. Furthermore, we had also previously observed that in reaction of [Mo(NO)L*I_2] with oxacyclohexane[7] reduction of the molybdenum species and formation of the 3,5-dimethylpyrazole adduct, [Mo(NO)L*I(3,5-$Me_2C_3HN_2H$)], occurred.

In a similar reaction with [Mo(NO)L*I_2] **1** was again formed, probably because of the inclusion of $SnBu^n_3Cl$ in the reaction mixture. We have observed on numerous occasions that iodine may be replaced by chlorine in reaction systems derived from [Mo(NO)L*I_2] in the presence of chlorinated hydrocarbons.[8] The yield of the pyrazole complexes was *ca* 20%.

In a modification of the route to these 17-electron heterocycle complexes [Mo(NO)L*Cl_2] was reduced by $LiBu^n$ in the presence of a suitable

Table 2. Elemental analytical data and NO stretching frequencies for [Mo(NO)L*XQ]

Compound	Calculated C	H	N	Found C	H	N	IR ν(NO) (cm^{-1})
[Mo(NO)L*Cl($Me_2C_3HN_2H$)]	43.3	5.4	22.7	42.9	5.9	21.7	1610
[Mo(NO)L*Cl($C_3H_3N_2H$)]	41.0	5.0	23.9	41.2	5.1	23.8	1610
[Mo(NO)L*I($Me_2C_3HN_2H$)]	37.2	4.7	19.5	36.2	4.9	19.5	1617
[Mo(NO)L*I($C_3H_3N_2H$)]	35.0	4.2	20.4	36.3	4.7	20.3	1616
[Mo(NO)L*I($BrC_3H_2N_2H$)]	31.0	3.6	18.1	31.3	3.8	18.7	1618
[Mo(NO)L*I($Me_2BrC_3N_2H$)]	33.1	4.0	17.4	33.5	4.2	17.8	1617

pyrazole Q ($C_3H_3N_2H$, 3,5-$Me_2C_3HN_2H$, 4-$BrC_3H_2N_2H$), the desired complex [Mo(NO)L*ClQ] being isolated in yields varying from 25 to 35%. However, [Mo(NO)L*I_2] reacted directly with the pyrazoles Q ($C_3H_3N_2H$, 3,5-$Me_2C_3HN_2H$, 4-$BrC_3H_2N_2H$ and 4-Br-3,5-$Me_2C_3N_2H$), without the necessity of the lithium organyl, affording modest yields of the 17-electron [Mo(NO)L*IQ]. This last reaction may be compared with our earlier observations[9] that the di-iodide reacted with an excess of pyrazole Q ($C_3H_3N_2H$, 3,5-$Me_2C_3HN_2H$), affording the *cationic* 17-electron species $[Mo(NO)L^*Q_2]^+$.

The IR spectra of the new compounds are entirely consistent with our formulations. In addition to exhibiting the normal stretching modes associated with L* [e.g. ν(BH) at *ca* 2550 cm^{-1}] they show an NO stretching frequency in the range 1610–1618 cm^{-1}, which is broadly comparable to the position in the related pyridine species [Mo(NO)L*Cl(py)],[3] but significantly lower than the corresponding bis(pyrazole) species $[Mo(NO)L^*Q_2]^+$,[9] as would be expected on the grounds of the nature of the ligands and positive charge.

The complexes [Mo(NO)L*XQ] (X = Cl, Q = $C_3H_3N_2H$ and 3,5-$Me_2C_3HN_2H$; X = I, Q = $C_3H_3N_2H$) exhibit EPR spectra (Table 3) containing a signal at g_{iso} close to 1.976, with additional hyperfine coupling, $A_{av.}$, of *ca* 46×10^{-4} cm^{-1}, due to the $I = 5/2$ isotopes [^{95}Mo (15.9%) and ^{97}Mo (9.6%)]. These spectral parameters are similar to those obtained from [Mo(NO)L*Cl(py)] (g_{iso} 1.970, $A_{av.}$ 45.7×10^{-4} cm^{-1})[3] and [Mo(NO)L*(pyrazole)$_2$]$^+$ (g_{iso} 1.973–1.977, A_{Mo} 43.8–46.0 $\times 10^{-4}$ cm^{-1}).[9] The data are broadly consistent with localization of the unpaired electron on the metal centre. However, the EPR spectrum of [Mo(NO)L*I(3,5-$Me_2C_3HN_2H$)] shows $g_{iso} = 2.0036$ and $A_{av.} = 43.2 \times 10^{-4}$ cm^{-1}, which differs significantly from the other three species. We have no simple explanation for this observation, but it may arise from some form of distortion in the molecule.

Crystal structure of [Mo(NO)L*Cl(3,5-$Me_2C_3HN_2H$)] (**1**)

The asymmetric unit of the structure contains one molecule of **1** in a general position and half of a CH_2Cl_2 molecule, whose carbon atom is situated on a two-fold axis, thus corresponding to the stoichiometry [Mo(NO)L*Cl(3,5-$Me_2C_3HN_2H$)]·$1/2CH_2Cl_2$.

The molybdenum atom has distorted octahedral coordination, with one chlorine and five nitrogen atoms. The disorder (mixing) of Cl and NO ligands can be explained in terms of both *R* and *S* enantiomers of **1** occupying statistically the same crystallographic position (the crystal itself being centrosymmetric and racemic).

The Mo—N bond lengths associated with the tris(pyrazolyl)borate and the 3,5-dimethylpyrazole ligands are similar (average 2.20 Å) and reveal little difference in *trans* influence due to the Cl and NO groups (this also being a result of the nature of the disorder). As expected the Mo—N—O bond angle is essentially linear and the Mo—N(O) distance (mean 1.79 Å) is close to the usual (1.76–1.80 Å).[10]

In nitrosyl complexes of molybdenum with filled d_{xz} and d_{yz} orbitals, other ligands having filled p_π-orbitals or lone electron pairs tend to adopt the orientation with these orbitals approximately

Table 3. EPR spectral data obtained from [Mo(NO)L*XQ]

X	Q	g_{iso}	$A_{av.} \times 10^4$ (cm^{-1})
Cl	$C_3H_3N_2H$	1.9768	46.2
Cl	3,5-$Me_2C_3HN_2H$	1.9768	46.1
I	$C_3H_3N_2H$	1.9760	45.34
I	3,5-$Me_2C_3HN_2H$	2.0036	43.22

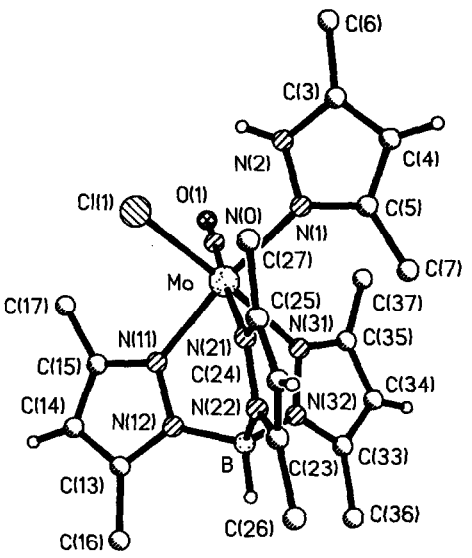

Fig. 1. Molecular structure of [Mo(NO)L*Cl(3,5-$Me_2C_3HN_2H$] (**1**). For clarity, only the major (A) positions of Cl and NO ligands are shown (in B positions these ligands are interconverted), and all methyl hydrogens are omitted.

orthogonal to the NO group, thereby maximizing the d_{xy}–p overlap.[11] In **1** such an orientation is impossible due to the steric hindrance imposed by the methyl substituents of the pyrazolyl rings; torsion angles N(OA)—Mo—N(1)—N(2) and N(OB)—Mo—N(1)—N(2) are 53.6° and −37.3°, respectively. The pyrazole ring C (Fig. 1) is aligned approximately along the bisectral plane between rings E and F, whose interplanar angle of 117.3° is perhaps surprisingly the smallest of the three interplanar angles with L*, viz. D to E 120.3° and D to F 120.5°.

The only active hydrogen atom, at N(2), does not participate in hydrogen bonding.

Acknowledgements—We are grateful to the British Council, through a Tripartite Acciones Integradas Programme, for partial support of this work (S.K. and A.W.), to the Politechnika Krakowska, Poland, for leave of absence (S.K. and A. W.), to the Royal Society for a Visiting Fellowship (A.S.B.) and to the SERC for financial assistance (EPR spectrometer).

REFERENCES

1. T. N. Briggs, C. J. Jones, J. Colquhoun, N. El Murr, J. A. McCleverty, B. D. Neaves, H. Adams and N. A. Bailey, *J. Chem. Soc., Dalton Trans.* 1985, 1249.
2. J. A. McCleverty, *Chem. Soc. Rev.* 1983, **12**, 331.
3. S. L. W. McWhinnie, C. J. Jones, J. A. McCleverty, D. Collison and F. E. Mabbs, *J. Chem. Soc., Chem. Commun.* 1990, 940.
4. S. J. Reynolds, C. F. Smith, S. J. Jones and J. A. McCleverty, *Inorg. Synth.* 1985, **23**, 4; S. Trofimenko, *J. Am. Chem. Soc.* 1967, **89**, 3904; 1969, **91**, 588.
5. A. C. T. North, D. C. Phillips and F. S. Mathews, *Acta Cryst., Sect. A* 1968, **24**, 351.
6. G. Sheldrick, Göttingen and Siemens plc (1990).
7. N. J. Al Obaidi, C. J. Jones and J. A. McCleverty, *J. Chem. Soc., Dalton Trans.* 1990, 3329.
8. B. Coe, C. J. Jones, J. A. McCleverty, S. L. W. McWhinnie and F. McQuillan, work to be published.
9. N. Al Obaidi, A. J. Edwards, C. J. Jones, J. A. McCleverty, B. D. Neaves, F. E. Mabbs and D. Collinson, *J. Chem. Soc., Dalton Trans.* 1989, 127.
10. A. G. Orpen, L. Brammer, F. H. Allen, O. Kennard, D. G. Watson and R. Taylor, *J. Chem. Soc., Dalton Trans.* 1989, S1.
11. M. T. Ashby and J. H. Enemark, *J. Am. Chem. Soc.* 1986, **108**, 730; S. A. Roberts and J. H. Enemark, *Acta Cryst., Sect. C* 1989, **45**, 1292.

Polyhedron Vol. 12, No. 7, pp. 721–729, 1993
Printed in Great Britain

0277–5387/93 $6.00+.00
© 1993 Pergamon Press Ltd

MIXED BIPHOSPHINE COMPLEXES OF PALLADIUM(0); THE STRUCTURE OF {BIS(DIPHENYLPHOSPHINO)ETHANE}-{BIS(DICYCLOHEXYLPHOSPHINO)ETHANE} PALLADIUM(0)

GILLIAN T. L. BROADWOOD-STRONG, PENNY A. CHALONER* and PETER B. HITCHCOCK

School of Chemistry and Molecular Sciences, University of Sussex, Falmer, Brighton BN1 9QJ, U.K.

(*Received* 1 *October* 1992; *accepted* 2 *December* 1992)

Abstract—A range of mixed biphosphine complexes of palladium(0) has been prepared and characterized by ^{31}P NMR spectroscopy. The complexes disproportionate in solution at rates which depend on the nature of the ligands. The structure of [Pd(dcpe)(dppe)] has been established in an X-ray diffraction study.

Studies of the palladium(0) oxidation state have been dominated by investigations of phosphine complexes. Their most significant reactivity involves dissociation and oxidative addition. The complexes are generally prepared by reduction of palladium(II) complexes and a wide variety of reducing agents have been employed. However, most of the simple complexes studied, whether two-, three- or four-coordinate, have contained a single type of phosphine ligand. In this work we report the preparation of mixed biphosphine complexes, their characterization by ^{31}P NMR spectroscopy, their stability with respect to exchange or disproportionation and the determination of the crystal structure of one example in the series. Related mixed chelating biphosphine complexes of platinum have been prepared,[1] by reduction of $[PtCl_2L]$ with $Na[BH_4]$ in the presence of L′. In this case the first product is $[PtLL']^{2+}$, which is then reduced by the borohydride.

RESULTS AND DISCUSSION

Reactions of $[Pd(C_2H_4)(dppe)]$ *with biphosphines*

The complex $[Pd(C_2H_4)(dppe)]$ [dppe = 1,2-bis(diphenylphosphino)ethane], in common with other palladium ethene complexes, is relatively unstable. The synthesis of $[Pd(C_2H_4)(PR_3)_2]$ by reduction of $[Pd(acac)_2]$ (acacH = pentane-2,4-dione) by $AlEt_2OEt$ in the presence of PR_3 and ethene has previously been reported.[2] However, we found it more convenient to prepare $[Pd(C_2H_4)(dppe)]$ *in situ* by the reduction of $[PdCl_2(dppe)]$ with $Li[Et_3BH]$ in the presence of excess ethene. The complex could be characterized spectroscopically at low temperature and ^{31}P NMR spectroscopic data for the phosphine ligand, $[PdCl_2(LL)]$, $[Pd(C_2H_4)(LL)]$ and $[Pd(LL)_2]$ (these complexes were prepared independently from $[Pd(C_2H_4)(LL)]$ and LL for comparison), are collected in Table 1.

Reaction of $[Pd(C_2H_4)(dppe)]$ with dppp [dppp = 1,3-bis(diphenylphosphino)propane] at room temperature gave a solution containing four complexes, identified by ^{31}P NMR spectroscopy as $[Pd(dppe)_2]$, $[Pd(dppp)_2]$, $[Pd(C_2H_4)(dppe)]$ and $[Pd(C_2H_4)(dppp)]$. This suggests that extensive disproportionation had occurred. The presence of $[Pd(C_2H_4)(dppp)]$ and $[Pd(dppp)_2]$ is surprising, since it suggests that dppp is able to displace dppe, which is normally considered to be a much more tightly binding chelating ligand. Even more surprising is the observation that ethene seems to be preferred as a ligand over a chelating biphosphine. The mechanism of formation of $[Pd(C_2H_4)(dppp)]$ is not clear, but two pathways may be envisaged. Either dppp displaces dppe from $[Pd(C_2H_4)(dppe)]$ or ethene displaces one of the biphosphines in $[Pd(dppe)(dppp)]$ or $[Pd(dppp)_2]$. Neither option would have been predicted from conventional wisdom concerning the relative binding abilities of the

* Author to whom correspondence should be addressed.

Table 1. $^{31}P\{^1H\}$ NMR spectroscopic data (solvent THF) for LL, $[PdCl_2(LL)]$ and $[Pd(C_2H_4)(LL)]$

(LL)	δ(LL)[a]	$\delta[PdCl_2(LL)]$[a]	$\delta[Pd(C_2H_4)(LL)]$[b]	$\delta[Pd(LL)_2]$[a]
dppe	−12.6	68.3	34.0	30.4
dppp	−17.3	13.0	10.0	4.0
dppb	−17.1	32.8	18.4	5.0
dppf	−16.9	34.8	16.0	7.4
dcpe	1.47	96.3	54.0	36.0
dmpe	−48.4		−5.0	1.0
dmpp	−16.9[c]	13.6[c,d]	10.9[c,e]	23.0[c,f]
	−52.9[g]	−2.7[g]	−22.4[g]	10.0[g]
triphos	−27.0	19.0[h]	6.0[i]	7.0[h,j]
		−31.0[k]		−3.0[h,j]
				−27.0[k]

[a] 298 K.
[b] 203 K.
[c] —PPh_2
[d] $^2J(PP) = 13$ Hz.
[e] $^2J(PP) = 39$ Hz.
[f] $^2J(PP) = 25$ Hz.
[g] —PMe_2.
[h] Coordinated to palladium.
[i] All three PPh_2 groups are coordinated to palladium.
[j] $^2J(PP) = 24.4$ Hz.
[k] Uncoordinated.

ligands involved. When the reaction was repeated at 203 K the mixed complex [Pd(dppe)(dppp)] was formed, as essentially the sole product. The ^{31}P NMR spectrum (Table 2) could be readily assigned by comparison with the chemical shifts for $[Pd(dppe)_2]$ and $[Pd(dppp)_2]$. When the temperature was raised to 283 K intense signals for the two ethene complexes were observed, this change being

Table 2. $^{31}P\{^1H\}$ NMR spectroscopic data (THF as solvent) for complexes [Pd(LL)(LL′)]

Complex	Temperature (K)	P^a	δP^a	P^b	δP^b	$^2J(P^aP^b)$ (Hz)
[Pd(dppe)(dppp)]	203	dppe	35.3	dppp	10.0	22
[Pd(dppe)(dppb)]	253	dppe	25.5	dppb	14.5	28
[Pd(dppe)(dppf)]	203	dppe	22.6	dppf	13.0	31
[Pd(dppe)(dcpe)]	203	dppe	28.0	dcpe	46.3	26
[Pd(dppe)(dmpe)]	203	dppe	35.7	dmpe	−3.8	28
[Pd(dppe)(dmpp)]	203	dppe	32.0	dmpp	7.0[a]	[b]
					−33.0[c]	
[Pd(dppp)(dppf)]	223	dppp	−0.3	dppf	11.4	24
[Pd(dppp)(dcpe)]	203	dppp	1.5	dcpe	37.5	21
[Pd(dppp)(dmpe)]	253	dppp	11.0	dmpe	−5.8	20
[Pd(dppb)(dmpe)]	203	dppb	19.0	dmpe	−6.0	29
[Pd(dppf)(dcpe)]	203	dppf	12.4	dcpe	27.4	32
[Pd(dppf)(dmpe)]	243	dppf	18.2	dmpe	−7.4	31
[Pd(dcpe)(dmpe)]	243	dcpe	53.3	dmpe	−5.6	25
[Pd(dcpe)(dppm)]	203	dcpe	48.6	dppm	−20.1	16

[a] —PPh_2, P^a.
[b] $^2J(P^aP^b) = 36$ Hz, $^2J(P^aP^c) = 30$ Hz, $^2J(P^bP^c) = 28$ Hz; P^c is assigned as the phosphines of dppe.
[c] —PMe_2, P^b.

partially reversible when the solution was recooled.

Reaction of $[Pd(C_2H_4)(dppe)]$ with dppb [dppb = 1,4-bis(diphenylphosphin)butane] at 203 K gave $[Pd(dppe)(dppb)]$ and $[Pd(dppe)_2]$. No signals due to $[Pd(dppb)_2]$ or free dppb could be observed, possibly because they are rather insoluble at this temperature. Above 263 K the spectrum was appreciably broadened by a dynamic process.

The reaction of $[Pd(C_2H_4)(dppe)]$ with dcpe [dcpe = 1,2-bis(dicyclohexylphosphino)ethane] at 203 K was clean and practically instantaneous. No disproportionation or fluxional processes were noted, even at room temperature, and large bright yellow crystals of [Pd(dcpe)(dppe)] were deposited slowly from solution in the absence of light.

With dppf [dppf = 1,1′-bis(diphenylphosphino)-ferrocene] as the added phosphine the products formed were [Pd(dppe)(dppf)], $[Pd(dppf)_2]$ and $[Pd(dppe)_2]$. On warming the mixed complex became the dominant species and this was stable towards disproportionation at 243 K for several weeks. By contrast, although the reaction with dmpe [dmpe = 1,2-bis(dimethylphosphino)ethane] gave the mixed complex [Pd(dppe)(dmpe)] as the initial product at 203 K, this disproportionated in solution at 243 K over a few days.

Reaction of $[Pd(C_2H_4)(dppe)]$ with the unsymmetrical biphosphine 1-dimethylphosphino-3-diphenylphosphinopropane (dmpp)[3,4] gave a mixture of $[Pd(dppe)_2]$, $[Pd(dmpp)_2]$ and the mixed complex [Pd(dmpp)(dppe)]. Computer simulation allowed the calculation of chemical shifts and coupling constants for the three distinct phosphorus atoms.

Reactions of $[Pd(C_2H_4)(dppp)]$ *with biphosphines*

The addition of 1 molar equivalent of dcpe to $[Pd(C_2H_4)(dppp)]$ at 203 K gave mainly $[Pd(dcpe)_2]$ and $[Pd(dppp)_2]$. On warming to 263 K signals due to a small amount of the mixed species could be seen in the ^{31}P NMR spectrum. Recooling the sample to 203 K resulted in the crystallization of $[Pd(dcpe)_2]$ as a bright yellow microcrystalline solid. Even at low temperature the ^{31}P NMR signal assigned to $[Pd(dppp)_2]$ remained a singlet. This is in contrast to $[Pt(dppp)_2]$ which gives rise to an A_2B_2 pattern in its ^{31}P NMR spectrum at low temperature.[5] At 183 K the signal had broadened slightly, but practical considerations precluded further cooling.

Reaction of $[Pd(C_2H_4)(dppp)]$ with dmpe at 203 K gave a solution containing, as well as the starting material, $[Pd(dppp)_2]$, $[Pd(C_2H_4)(dmpe)]$ and $[Pd(dmpe)_2]$ (Fig. 1). On warming to 253 K the mixed complex [Pd(dmpe)(dppp)] was observed as the predominant component of the mixture, although $[Pd(dmpe)_2]$ and $[Pd(dppp)_2]$ were also present. The mixed complex was stable in THF solution at 243 K for several days.

At 203 K dppf reacted with $[Pd(C_2H_4)(dppp)]$ to give [Pd(dppf)(dppp)] as the main product, together with $[Pd(dppp)_2]$ and $[Pd(C_2H_4)(dppf)]$. At 273 K there was more $[Pd(dppp)_2]$, but the change was reversed on cooling.

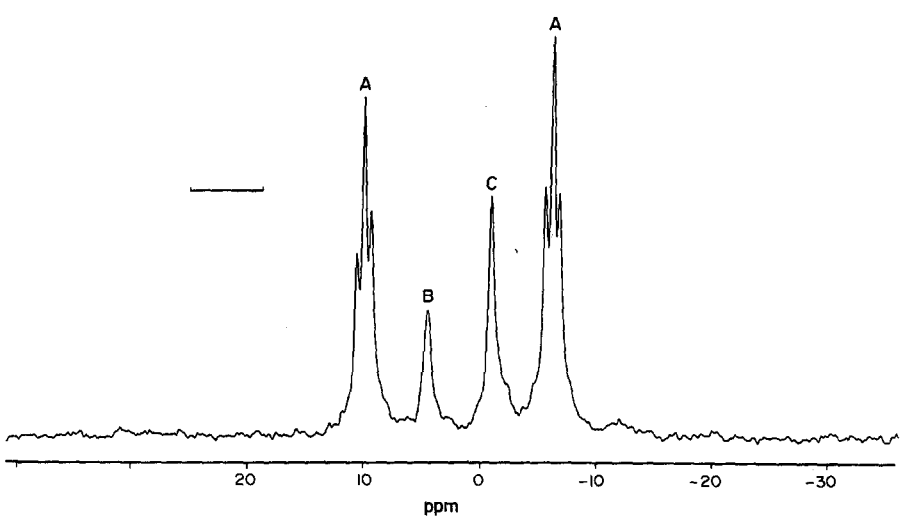

Fig. 1. ^{31}P (32.44 MHz) NMR spectrum of the product obtained on reacting $[Pd(C_2H_4)(dppp)]$ with dmpe in THF at 213 K. (A) [Pd(dmpe)(dppp)]; (B) $[Pd(dppp)_2]$; and (C) $[Pd(dmpe)_2]$. The bar represents 200 Hz.

Reactions of $[Pd(C_2H_4)(dppb)]$ *with biphosphines*

The addition of 1 molar equivalent of dppp to $[Pd(C_2H_4)(dppb)]$ at 203 K gave a mixture with a ^{31}P NMR spectrum showing a signal only for $[Pd(dppp)_2]$. Free dppb is rather insoluble in THF at this temperature, but the appropriate signal was observed on warming. No mixed complex was obtained, in contrast with the reaction in the platinum series.[1] In that case disproportionation was significant, but some [Pt(dppb)(dppp)] could be observed. Complete disproportionation was also noted in the reaction of $[Pd(C_2H_4)(dppb)]$ with dcpe.

Reactions of $[Pd(C_2H_4)(dppf)]$ *with biphosphines*

The addition of 1 molar equivalent of dcpe to $[Pd(C_2H_4)(dppf)]$ at 203 K resulted in the formation of $[Pd(dcpe)_2]$ as the major product, although some [Pd(dcpe)(dppf)] and $[Pd(dppf)_2]$ were also present. The proportions of the components of the mixture did not vary significantly with temperature and at 263 K the signals due to $[Pd(dppf)_2]$ and dppf were broadened by an exchange process. At 283 K there was also evidence that the dppf ligand in the mixed complex is in exchange with free dppf.

The reaction of $[Pd(C_2H_4)(dppf)]$ with dppb gave only $[Pd(dppf)_2]$ and $[Pd(dppb)_2]$.

Reactions to form dmpe complexes

The reactions of $[Pd(C_2H_4)(dppe)]$ and $[Pd(C_2H_4)(dppp)]$ with dmpe gave the expected mixed complexes, together with disproportionation products, as previously noted. The mixed complex [Pd(dmpe)(dppf)] is also a significant product in the reaction of $[Pd(C_2H_4)(dppf)]$ with dmpe (Fig. 2). Signals in the ^{31}P NMR spectrum due to both free phosphines were readily assigned, but assignment of two doublets [δ 0.0, -46.0, $J(PP) = 25$ Hz] was more problematic. That the signals might be due to partial oxidation of dmpe to $Me_2P(=O)CH_2CH_2PMe_2$ was ruled out by the independent preparation (*in situ*, by addition of H_2O_2 to a THF solution of dmpe in an NMR tube) of this monoxide [δ -47.7, 38.5, $^3J(PP) = 38.2$ Hz]. It was noted that the chemical shift of one of the signals from the unknown complex was similar to that for free dmpe and the other similar to $[Pd(dmpe)_2]$. We therefore suggest that the unknown material is $[Pd(\eta^1\text{-dmpe})_n]$. This is supported by NMR spectroscopic studies from the work of Connor on $[M(CO)_5(dmpe)]$ (M = Cr, Mo or W).[6] On warming the sample to 243 K disproportionation of the mixed complex leads to an increase in the concentration of $[Pd(\eta^1\text{-dmpe})_n]$ and at 263 K broadening of the signals gives evidence for an exchange process between free and coordinated dmpe.

Addition of $Li[Et_3BH]$ to a mixture of palladium (II) chloride and dmpe in THF gave a pale yellow solution, the ^{31}P NMR spectrum of which showed two doublets at δ 0 and -46 ppm [$^3J(PP) = 25$ Hz], assigned to $[Pd(\eta^1\text{-dmpe})_n]$, a singlet for $[Pd(dmpe)_2]$ and two triplets centred at δ -3.0 and -10.0 ppm ($^2J = 30$ Hz). We tentatively propose structure **1a** to account for the latter signals, in which there are two non-equivalent sets of phos-

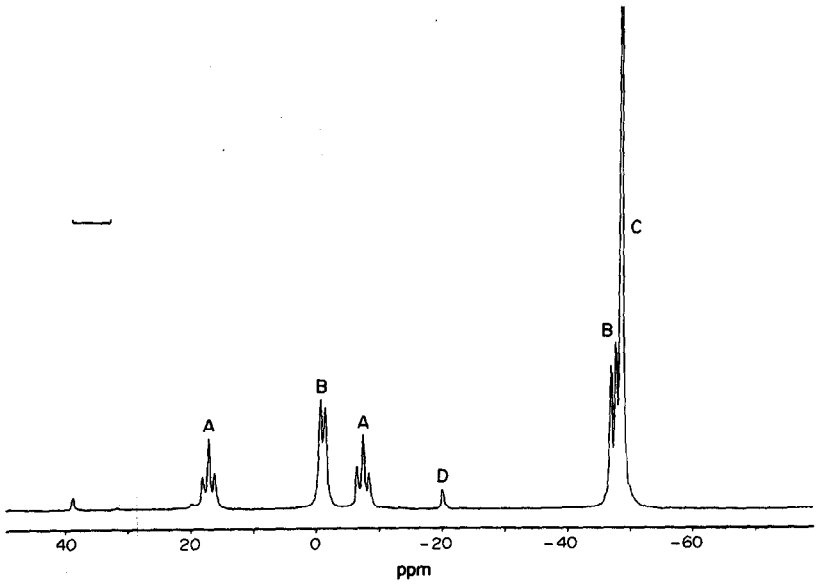

Fig. 2. ^{31}P (32.44 MHz) NMR spectrum of the products from reacting $[Pd(C_2H_4)(dppf)]$ with dmpe in THF at 203 K. (A) [Pd(dmpe)(dppf)]; (B) $[Pd(\eta^1\text{-dmpe})_n]$; (C) dmpe; and (D) dppf. The bar represents 200 Hz.

phorus atoms. The addition of dmpe to $[PtCl_2(dmpe)]$ in the presence of $Li[Et_3BH]$ also gave a pale yellow solution. The ^{31}P NMR spectrum of the mixture showed an intense singlet assigned to $[Pt(dmpe)_2]$ [$\delta = -7.0$, $^1J(PPt) = 3710$ Hz]. A pair of doublets [$\delta = 0.0, -46.0$, $^3J(PP) = 26$ Hz] was assigned to $[Pt(\eta^1\text{-dmpe})_n]$. No platinum satellites were observed. They would not be expected for the pendant phosphines and we may postulate that the two phosphorus sites are in rapid exchange on the NMR spectroscopic time scale. A pair of triplets [$\delta = -11.0$, $^1J(PPt) = 3412$ Hz; $\delta = -28.0$, $^1J(PPt) = 4110$ Hz, $^2J(PP) = 60$ Hz] were assigned to **1b**. On warming the signals assigned to $[Pt(dmpe)_2]$ remained sharp, but those due to $[Pt(\eta^1\text{-dmpe})_n]$ were broadened by exchange. We are investigating conditions for the isolation of **1** or of $[M(\eta^1\text{-dmpe})_n]$.

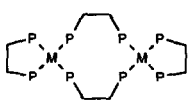

1a M = Pd
1b M = Pt

Reaction of $[Pd(C_2H_4)(dcpe)]$ with dmpe at 203 K gave a mixture of [Pd(dcpe)(dmpe)], $[Pd(\eta^1\text{-dmpe})_n]$ and $[Pd(dmpe)_2]$. On warming there is exchange between free dmpe and $[Pd(\eta^1\text{-dmpe})_n]$ and $[Pd(dcpe)_2]$ is formed by disproportionation.

When $[Pd(C_2H_4)(dppb)]$ was reacted with dmpe at 203 K, the main products were **1a** and $[Pd(\eta^1\text{-dmpe})_n]$, together with a very small amount of the mixed complex. Further evidence for the formation of the mixed complex was obtained by FAB mass spectrometry (*vide infra*).

Reaction of $[Pd(C_2H_4)(dcpe)]$ *with dppm*

Reaction of $[Pd(C_2H_4)(dcpe)]$ with 1 molar equivalent of dppm [dppm = 1,1-bis(diphenylphosphino)methane] at 203 K gave [Pd(dcpe)(dppm)] and a species which we postulate to be $[Pd(\eta^1\text{-dppm})_2]$ [$\delta = 35.0, -29.0$ ppm; $^2J(PP) = 56$ Hz]. We confirmed that the latter signals were not attributable to partially oxidized dppm by independent synthesis (*in situ*, by addition of H_2O_2 to a THF solution of dppm in an NMR tube) of $Ph_2PCH_2P(=O)Ph_2$ [$\delta = 24.2, -27.0$ ppm; $^2J(PP) = 51.8$ Hz]. It could also not be due to the known compound $[Pd_2(\mu\text{-dppm})_3]$, since this has high symmetry and its ^{31}P NMR spectrum shows only a singlet at δ 12.4.[7] As with the derivatives of dmpe, the chemical shift of the phosphine, which we suppose to be pendant, is similar to that of the free ligand and the data are quite similar to those reported for chromium, molybdenum or tungsten complexes of monodentate dppm.[6] Disproportionation of the mixed complex occurred irreversibly on warming.

Reactions involving triphos, $[MeC(CH_2CH_2PPh_2)_3]$

Reaction of $[Pd(C_2H_4)(dppe)]$ with triphos at 203 K gave the mixed complex [Pd(dppe)(triphos)], together with substantial amounts of $[Pd(dppe)_2]$ and $[Pd(triphos)_2]$ (**2**). The complex $[Pd(triphos)_2]$ was identified by independent preparation from $[Pd(C_2H_4)(triphos)]$ and triphos. The resonance due to the uncoordinated phosphine was observed with δ −27.0, essentially the same as for the free phosphine. The coordinated phosphines give rise to an AA′BB′ system (all the AA′BB″ systems approximate to A_2B_2, as the couplings are very similar), which could be readily simulated. This lack of symmetry is not unexpected and mirrors the data reported for $[Pt(triphos)_2]$, for which the structure has been determined.[6] The ^{31}P NMR spectrum of [Pd(dppe)(triphos)] showed a singlet assigned to the pendant phosphine ($\delta = -25.0$) and an AA′BB′ multiplet for the coordinated phosphines [$\delta = 3.0, -6.5$ ppm; $^2J(PP) = 14$ Hz].

The reaction of triphos with $[Pd(C_2H_4)(dcpe)]$ at 203 K gave only disproportionation products.

Crystal and molecular structure of [Pd(dcpe)(dppe)]

Relatively few palladium(0) complexes have been characterized crystallographically. The monomeric two-coordinated complexes $[PdL_2]$ (L = PCy_3[9] or PBu^t_2Ph[10]) both exhibit C_2 symmetry, but the tricyclohexylphosphine complex is bent whilst the derivative of PBu^t_2Ph is almost linear. Two three-coordinate palladium(0) phosphine complexes, $[Pd(PPh_3)_3]$[11] and $[Pd\{Ph_2P(C_6H_4\text{-}3\text{-}SO_3K)\}_3]$,[12] have been characterized, as have the four-coordinate species $[Pd(PPh_3)_4]\cdot 0.5C_6H_6$,[13] $[Pd(PCH_2OH)_4]\cdot MeOH$[14] and $[Pd\{P(C{\equiv}CPh)_3\}_4]$.[15] Related structurally characterized platinum complexes include $[Pt\{P(CMe_3)_3\}_2]$.[16] $[Pt\{PPh(CMe_3)_2\}_2]$,[10] $[Pt(PCy_3)_2]$,[17] $[Pt(PCy_3)_3]$,[18] $[Pt(PPh_3)_3]$[19,20] and $[Pt_2(\mu\text{-dppm})_3]$.[21] Two platinum derivatives of chelating phosphines have been studied. $[Pt(triphos)_2]$ is four-coordinate at platinum, with two pendant phosphines.[8] There have been two reports on the structure of $[Pt(dppp)_2]$, but in one of these the space group is wrongly assigned,[22] giving rise to some anomalies in the bond length and angle data. The correctly refined structure[23] is rather more symmetrical, which

is slightly surprising in view of the non-equivalence of the phosphines in the low-temperature NMR spectrum. The structure of [Pd(dcpe)(dppe)] is the first example of a mixed biphosphine complex of either platinum or palladium to be structurally characterized.

The crystal was monoclinic, space group $P2_1/n$, $Mr = 923.4$, $a = 20.138(4)$, $b = 11.901(2)$, $c = 22.515(5)$ Å, $\beta = 114.37(2)°$, $U = 4915.1$ Å, $Z = 4$, $D_{calc} = 1.25$ g cm^{-1}, $F(000) = 1944$. Selected bond lengths and angles are given in Table 3 and the structure is shown in Fig. 3. The geometry at palladium is approximately tetrahedral, but the distortions are quite large. The angles P(1)—Pd—P(2) (85.7°) and P(3)—Pd—P(4) (86.9°), within each phosphine chelate, are considerably reduced from tetrahedral, whilst the others range from 119.1(2) to 124.8(2)°. The Pd—P bond lengths are slightly longer for the phosphorus atoms of the dcpe ligand [2.352(5), 2.360 Å] than for the dppe [2.324(5), 2.334(5) Å], but the difference is barely statistically significant. These may be compared with a mean Pd—P distance of 2.451(5) Å for $[Pd(PPh_3)_4]$ and 2.319(2) Å for $[Pd\{P(CH_2OH)_3\}_4]$, suggesting that steric demand has some influence on bond length. There is little evidence for the high steric demand of the cyclohexyl rings from the angles at phosphorus with C(33)—P(3)—C(27) = 99.9(8)° and C(41)—P(4)—C(47) = 103.9°. The related angles for the phenyl bearing phosphorus atoms are 100.2(8)° and 102.5(8)°. The P—C_{aryl} and P—C_{alkyl} bond lengths differ a little.

FAB mass spectra of $[Pd(LL)_2]$

FAB mass spectrometry has, over the last decade, proved to be an invaluable tool in the characterization of organometallic and coordination complexes.[24,25] It is especially valuable for species which are not particularly stable, because it is not necessary to subject the complex to thermal shock.[26] FAB mass spectra were obtained for the complexes $[Pd(LL)_2]$ (LL = dppe, dcpe, or dppf) and the mixed complexes [Pd(dcpe)(dppe)] and [Pd(dmpe)(dppb)]. Palladium has several naturally occurring isotopes of rather similar abundance and for the purposes of this discussion we will consider only the peaks arising from ^{106}Pd. In all cases the isotope pattern observed could be correctly simulated and remained essentially unchanged throughout the fragmentation.

The first fragmentation from the molecular ion observed for $[Pd(dppe)_2]^+$ ($m/z = 902$) was a loss of $\{Ph_2PCH_2CH_2\}$ to give a peak at m/z 689. A

Table 3. Selected intramolecular distances (Å) and angles (°) with estimated standard deviations in parentheses

Pd—P(1)	2.324(5)	Pd—P(2)	2.334(5)
Pd—P(3)	2.352(5)	Pd—P(4)	2.360(6)
P(1)—C(1)	1.84(2)	P(1)—C(7)	1.86(2)
P(1)—C(13)	1.87(2)	P(2)—C(14)	1.81(2)
P(2)—C(15)	1.82(2)	P(2)—C(21)	1.91(2)
P(3)—C(27)	1.85(1)	P(3)—C(33)	1.90(2)
P(3)—C(39)	1.83(2)	P(4)—C(40)	1.78(2)
P(4)—C(41)	1.88(2)	P(4)—C(47)	1.86(2)

P(1)—Pd—P(2)	85.7(2)	P(1)—Pd—P(3)	123.0(2)
P(1)—Pd—P(4)	119.1(2)	P(2)—Pd—P(3)	121.7(2)
P(2)—Pd—P(4)	124.8(2)	P(3)—Pd—P(4)	86.9(2)
Pd—P(1)—C(1)	128.9(8)	Pd—P(1)—C(7)	117.1(6)
Pd—P(1)—C(13)	108.5(6)	C(1)—P(1)—C(7)	100.2(8)
C(1)—P(1)—C(13)	100(1)	C(7)—P(1)—C(13)	96.3(9)
Pd—P(2)—C(14)	106.0(5)	Pd—P(2)—C(15)	124.5(7)
Pd—P(2)—C(21)	117.7(7)	C(14)—P(2)—C(15)	102.3(9)
C(14)—P(2)—C(21)	100(1)	C(15)—P(2)—C(21)	102.5(8)
Pd—P(3)—C(27)	121.8(6)	Pd—P(3)—C(33)	120.5(6)
Pd—P(3)—C(39)	107.8(6)	C(27)—P(3)—C(33)	99.9(8)
C(27)—P(3)—C(39)	102.9(8)	C(33)—P(3)—C(39)	100.9(9)
Pd—P(4)—C(40)	104.3(8)	Pd—P(4)—C(41)	119.1(7)
Pd—P(4)—C(47)	122.4(6)	C(40)—P(4)—C(41)	99.3(9)
C(40)—P(4)—C(47)	104(1)	C(41)—P(4)—C(47)	103.9(9)

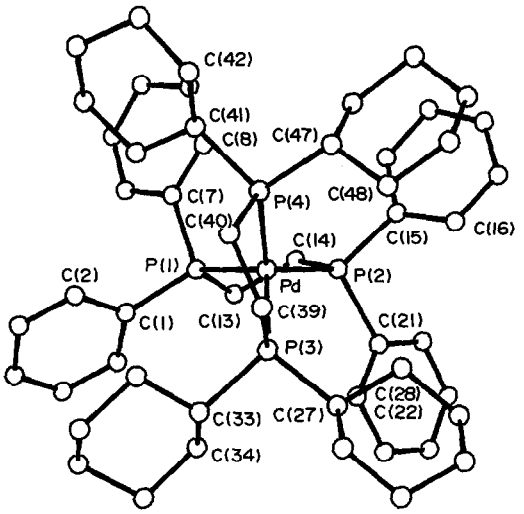

Fig. 3. Structure of [Pd(dcpe)(dppe)] showing atom numbering scheme.

further loss of $\{PPh_2\}$ gives a peak at m/z 504, for $\{Pd(dppe)\}^+$. Loss of a further $\{Ph_2PCH_2CH_2\}$ fragment gave a peak at m/z 291. By contrast, the mass spectrum of $[Pd(dcpe)_2]$ is characterized by the loss of cyclohexyl groups. The first fragmentation of the molecular ion ($m/z = 950$) is the loss of C_6H_{11} to give a peak at m/z 867. Loss of successive C_6H_{12} and C_6H_{11} units gave peaks at m/z 783 and 701, respectively. A strong peak at m/z 590 is difficult to assign. The mass would correspond to $\{Pd(dcpe)P_2\}^+$. Whilst it is possible to envisage a rearrangement which might give rise to this, we are aware of no precedents. An alternative possibility is $\{Pd(dcpe)(PH_2CH_2CH_3)\}^+$. This seems a bit more likely, although it is difficult to envisage the source of the hydrogen atoms. There is also a peak at m/z 528 for the fragment $\{Pd(dcpe)\}^+$.

In the FAB mass spectrum of $[Pd(dppf)_2]$ there is no peak corresponding to the molecular ion at m/z 1214, but the peak for $\{Pd(dppf)\}^+$ (m/z 660) is quite clear.

The spectrum of [Pd(dcpe)(dppe)] ($m/z = 926$) shows the features which one might have expected from those of the homoleptic complexes. The fragments $\{Pd(dppe)\}^+$ and $\{Pd(dcpe)\}^+$ are prominent, as are peaks arising from the loss of either a cyclohexyl group or a $Ph_2CH_2CH_2$ unit.

The FAB mass spectrum was obtained for the mixture obtained on reacting $[Pd(C_2H_4)(dppb)]$ with dmpe. The molecular ion for the mixed complex (m/z 682) was observed, confirming its presence in the reaction mixture. There was also a strong peak for $\{Pd(dppb)\}^+$, presumably formed by loss of dmpe from the mixed complex or dppb from $[Pd(dppb)_2]$. We believe that FAB mass spectrometry may have considerable potential for establishing the composition of such mixtures under ambient conditions. ^{31}P NMR spectroscopy of these species is not generally useful at room temperature, since many of the complexes show dynamic behaviour.

CONCLUSIONS

Complexes of the type [Pd(LL)(LL′)], where LL and LL′ are bidentate chelating phosphines, may generally be prepared by the reaction of LL′ with $[Pd(C_2H_4)(LL)]$ at low temperature. On warming disproportionation occurs in many cases, especially when one of the products, $[Pd(LL)_2]$, has LL as a biphosphine which forms a five-membered chelate ring. Rather few of the complexes are stable towards disproportionation at room temperature, and a number also display exchange processes involving the free phosphine. It is noteworthy that replacement of ethene is not as facile as has been previously assumed; a number of ethene complexes have been observed as stable species, even in the presence of uncoordinated chelating biphosphines. Complexes of dmpe and dppm were anomalous and it is believed that some monodentate and/or bimetallic species were involved in the equilibria. It is intended to study these reactions further. Preliminary experiments by FAB mass spectrometry indicated that this will prove a useful method of complex characterization.

EXPERIMENTAL

Apparatus

All manipulations involving air-sensitive complexes were carried out under dry nitrogen using standard Schlenk-line techniques. ^{31}P NMR spectra were recorded on a Bruker WM360 or Bruker WP80SY spectrometer and are referenced to external 85% H_3PO_4. Mass spectra were recorded using a Kratos MS80RF double focussing spectrometer using a Kratos DS55M data system.

Reagents

Cyclooctadiene palladium(II) dichloride was prepared as described by Frye and co-workers.[27] Biphosphines were purchased from Aldrich and were used as received.

Preparation of $[PdCl_2(dppe)]$

To a solution of dppe (0.721 g, 1.81 mmol) in CH_2Cl_2 (10 cm^3) was added a solution of

$[PdCl_2(cod)]$ (0.491 g, 1.72 mmol) in CH_2Cl_2. After stirring at 25°C for 2 h a white precipitate was formed and the solvent was removed under reduced pressure. Toluene was added to the off-white solid and the mixture heated under reflux for 4 h. On cooling a pale yellow solid was precipitated, collected by filtration and dried *in vacuo* to give $[PdCl_2(dppe)]$ as a pale yellow powder (0.8 g, 86%). The complexes $[PdCl_2(dppp)]$, $[PdCl_2(dppb)]$, $[PdCl_2(dppm)]$ and $[PdCl_2(dppf)]$ were prepared similarly.

Preparation of [Pd(dppe)(dppp)]

$[PdCl_2(dppe)]$ (0.053 g, 0.092 mmol) was weighed into an 8 mm NMR tube, which was evacuated and flushed with dry nitrogen. The solid was dissolved in THF (1 cm^3) and ethene was bubbled through the solution until the mixture was saturated. An excess of $Li[Et_3BH]$ (0.5 cm^3) was transferred to the tube by syringe and the mixture became deep red in colour. Ethene was bubbled through the mixture for a further 5 min. The tube was cooled to −78°C and dppp (0.038 g, 0.092 mmol) was added as a solid. The tube was gently warmed by hand until the solid dissolved and the solution became yellow–brown in colour. ^{31}P NMR spectra were recorded at various temperatures.

A range of mixed-chelating bisphosphine complexes were similarly prepared and their spectra recorded.

Structure of [Pd(dcpe)(dppe)]

Suitable crystals were obtained by slow evaporation of a THF solution and are stable in air. A crystal of dimensions 0.30 × 0.20 × 0.08 mm was used for data collection. Enraf–Nonius CAD-4 diffractometer, graphite monochromated Mo-K_α radiation, $\lambda = 0.71069$ Å, $\mu = 5.3$ cm^{-1}, θ–2θ scan, $\Delta\theta = (0.8 + 0.35 \tan\theta)°$, maximum scan time 1 min, 6379 unique measured reflections for $2 < \theta < 22°$ and $h\ 0 \rightarrow 21$, $k\ 0 \rightarrow 12$, $l\ -23 \rightarrow 23$, 3742 observed reflections with $|F^2| > \sigma(F^2)$, $\sigma(F^2) = \{\sigma^2(I) + (0.04I)^2\}^{1/2}/Lp$. There was no crystal decay. Lorentz and polarization corrections, no absorption or extinction corrections. The structure was solved by routine heavy-atom methods with non-hydrogen atoms refined anisotropically by full-matrix least-squares. Hydrogen atoms were held fixed at calculated positions with $U_{iso} = 1.3U_{eq}$ for the parent atom. Within the ring C(33)–C(38) the carbon atom temperature factors were high, with C(35) non-positive definite, suggestive of partial disorder, although no alternative atom sites were identifiable. With a weighting scheme of $w = 1/\sigma^2(F)$, $\Sigma w(|F_o| - |F_c|)^2$ minimized, the final residuals were $R = 0.079$, $wR = 0.142$ for 514 variables, $S = 3.9$, $(\Delta/\sigma)_{max} = 0.01$, $(\Delta\rho)_{max,min} = +1.1, -1.6$ e Å^{-3} on a final difference map. Programs from the Enraf–Nonius SDP-Plus package (Frenz, 1984) were run on a microVAX II computer. Atomic scattering factors were from the International Tables for X-ray Crystallography (1974). Drawings were by PLUTO.[28]

Acknowledgements—We thank the SERC for financial support (to GTLB-S) and Johnson Matthey plc for a generous loan of palladium and platinum salts. We also thank Dr K. R. Seddon for useful discussions.

REFERENCES

1. H. C. Clark, P. N. Kapoor and I. J. McMahon, *J. Organomet. Chem.* 1984, **265**, 107.
2. R. O. De Jongh, R. van de Linde and A. Viser, *Inorg. Synth.* 1976, **16**, 127.
3. S. O. Grim and R. C. Barth, *J. Organomet. Chem.* 1975, **94**, 327.
4. We thank Dr D. Carmichael for a gift of this compound.
5. F. C. March, R. Mason, D. W. Meek and G. R. Scollary, *Inorg. Chim. Acta* 1976, **19**, L25.
6. J. A. Connor, J. P. Day, E. M. Jones and G. K. McEwan, *J. Chem. Soc., Dalton Trans.* 1973, 347.
7. A. L. Balch, *Adv. Chem. Ser.* 1980, **196**, 243.
8. F. C. March, R. Mason and G. R. Scollary, *Aust. J. Chem.* 1977, **30**, 2407.
9. A. Immirzi and A. Musco, *J. Chem. Soc., Chem. Commun.* 1974, 400.
10. S. Otsuka, T. Yoshida, M. Matsumoto and K. Nakatsu, *J. Am. Chem. Soc.* 1976, **98**, 5850.
11. V. S. Sergienko and M. A. Porai-Koshits, *Zh. Strukt. Khim.* 1987, **28**, 103.
12. A. L. Casalnuovo and J. C. Calabrese, *J. Am. Chem. Soc.* 1990, **112**, 4324.
13. V. G. Andrianov, I. S. Akhrem, N. M. Chistovalova and Yu. T. Struchkov, *Zh. Strukt. Khim.* 1976, **17**, 135.
14. K. N. Harrison, P. T. A. Hoye, A. G. Orpen, P. G. Pringle and M. B. Smith, *J. Chem. Soc., Chem. Commun.* 1989, 1096.
15. L. G. Kuz'mina, Yu. T. Struchkov, L. Yu. Ukhin and N. A. Dolgoplova, *Koord. Khim.* 1985, **11**, 1694.
16. K. J. Moynihan, C. Chieh and R. G. Goel, *Acta Cryst., Sect. B* 1979, **35**, 3060.
17. I. I. Immirzi, A. Musco, P. Zambelli and G. Carturan, *Inorg. Chim. Acta* 1975, **13**, L13.
18. A. Immirzi, A. Musco and B. E. Mann, *Inorg. Chim. Acta* 1977, **21**, L37.
19. V. Albano, P. L. Bellon and V. Scatturin, *J. Chem. Soc., Chem. Commun.* 1966, 507.
20. P. A. Chaloner, P. B. Hitchcock and G. T. L. Broadwood-Strong, *Acta Cryst., Sect. C* 1989, **C45**, 1309.
21. L. Manojlović-Muir and K. W. Muir, *J. Chem. Soc., Chem. Commun.* 1982, 1155.

22. P. D. Harvey, W. P. Schaefer and H. B. Gray, *Inorg. Chem.* 1988, **27**, 1101.
23. K. A. Asker, P. B. Hitchcock, R. P. Moulding and K. R. Seddon, *Inorg. Chem.* 1990, **29**. 4146.
24. D. J. Surman and J. C. Vickerman, *J. Chem. Soc., Chem. Commun.* 1981, 324.
25. M. Barber, R. S. Bordeli, R. D. Sedgwick and A. N. Tyler, *J. Chem. Soc., Chem. Commun.* 1981, 325.
26. K. A. Asker, A. M. Greenway, K. R. Seddon and A. A. Shimran, *J. Organomet. Chem.* 1988, **354**, 257.
27. H. Frye, E. Kuljian and J. Viebrock, *Inorg. Chem.* 1965, **4**, 1499.
28. W. D. S. Motherwell, Pluto Program for Plotting Molecular and Crystal Structures. University of Cambridge, U.K. (1976).

Polyhedron Vol. 12, No. 7, pp. 731–737, 1993
Printed in Great Britain

0277–5387/93 $6.00+.00
© 1993 Pergamon Press Ltd

SYNTHESES AND SPECTROSCOPIC STUDIES OF $X_4Al_2(\mu\text{-}NR_2)_2$ [X = Br, CH_3, C_2H_5; R = C_2H_5, $C^i{}_3H_7$]. X-RAY CRYSTAL STRUCTURES OF $Br_4Al_2[\mu\text{-}N(Et)_2]_2$ AND $Et_4Al_2[\mu\text{-}N(C^i{}_3H_7)_2]_2$

T. Y. HER, C. C. CHANG,* J. O. TSAI and Y. Y. LAI

Department of Chemistry, National Sun Yat-Sen University, Kaohsiung, Taiwan, R.O.C.

and

L. K. LIU

Institute of Chemistry, Academia Sinica, Taipei, Taiwan, R.O.C.

and

H. C. CHANG

Chun Shan Institute of Science and Technology, Lung-Tan, Taiwan, R.O.C.

and

J. H. CHEN

Department of Chemistry, National Kaohsiung Normal University, Kaohsiung, Taiwan, R.O.C.

(*Received* 1 *October* 1991; *accepted* 2 *December* 1992)

Abstract—The reactions of bis(dialkylamino)magnesium [$Mg(NR_2)_2$; R = C_2H_5, $C^i{}_3H_7$] with either diethylaluminum chloride or aluminum bromide yielded the following compounds: $Me_4Al_2[\mu\text{-}N(C^i{}_3H_7)_2]_2$ (**1**), $Et_4Al_2[\mu\text{-}N(Et)_2]_2$ (**2**), $Et_4Al_2[\mu\text{-}N(C^i{}_3H_7)_2]_2$ (**3**) and $Br_4Al_2[\mu\text{-}N(Et)_2]_2$ (**4**). The products were characterized on the basis of their elemental analyses, mass spectra, IR spectra and ^1H, ^{13}C and ^{27}Al nuclear magnetic resonance spectra. The X-ray crystal structures of compounds **3** and **4** were also determined. In addition, ^1H NMR studies of the solvent effect on the dialuminum complexes were explored and a spectroscopic investigation of benzene interaction with these dialuminum complexes was undertaken.

The reactions of organoaluminum compounds with reagents containing one acidic hydrogen may lead to the formation of dimeric or trimeric species.[1–7] Coates assessed the relative importance of entropy, ring strain and steric hindrance on the formation of these dimeric and trimeric molecules.[2a,8] Smith also found that the degree of aggregation of the isopropylimido compound ($[AlMe_2(NH(C^i{}_3H_7))]_2$) depended on the preparation route.[3] Recently, Interrante and co-workers reported that the Me_2AlNH_2 trimer is thermodynamically favoured in the following equilibrium:[4]

$$2(Me_2AlNH_2)_3 \underset{T=40\text{–}800^\circ C,\ \Delta H=38\ Kj}{\overset{K=1\times10^{-5}}{\rightleftharpoons}} 3(Me_2AlNH_2)_2 \quad (1)$$

The area of organoaluminum compounds possessing Al_2N_2 fragments has attracted considerable attention.[1] Furthermore, aluminum nitride has

* Author to whom correspondence should be addressed.

found application as a ceramic material,[4,9] resulting in increased attention being paid to the syntheses of the precursors $R_4Al_2(NR_2)_2$ and $X_4Al_2(NR_2)_2$ in high yield.

In our laboratory, the reactions of aluminum alkyl with bis(dialkylamino)magnesium in a 1:1 molar ratio produced the following aluminum–magnesium complexes: $[(CH_3)_2Al(\mu\text{-}NR_2)_2Mg(CH_3)]_n$ [$R = C_2H_5$, $n = 2$; $R = C^iH_7$, $n = 4$] and $(CH_3)_4Al_2(\mu\text{-}NR_2)_2$ [$R = C_2H_5$, C^iH_7].[10] This paper reports the formation of organoaluminum dimers in quantitative yield from the reaction of bis(dialkylamino)magnesium with either dialkylaluminum chloride or aluminum bromide. Crystal data and solvent effects of these products are also presented.

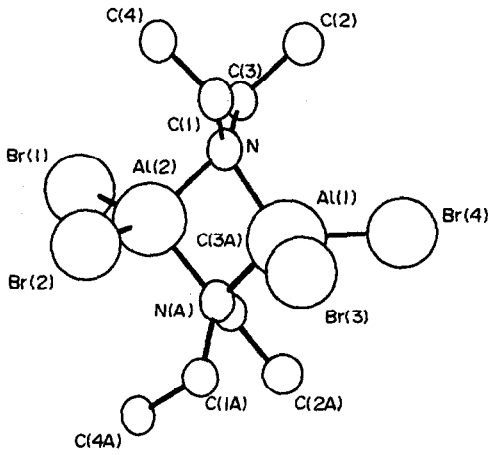

Fig. 2. Molecular structure of $Br_4Al_2[\mu\text{-}N(C_2H_5)_2]_2$.

RESULTS AND DISCUSSION

X-ray structural data

The reactions of bis(dialkylamino)magnesium with either dialkylaluminum chloride or aluminum bromide in diethyl ether gave $X_4Al_2(\mu\text{-}NR_2)_2$, according to the following equation:

$$2AlX_2Y + Mg(NR_2)_2 \xrightarrow{\text{diethyl ether}} X_4Al_2(\mu\text{-}NR_2)_2 + MgY_2. \quad (2)$$

The products were purified by sublimation or crystallization from hexane.

The X-ray crystal structures of compounds **3** and **4** are shown in Figs 1 and 2, respectively; selected bond distances and angles are listed in Table 1. Note that in compound **3** the central Al_2N_2 moiety is non-planar, with the following distorted tetrahedral coordination geometry existing about the aluminum atoms: N(1a)—Al(1)—N(1) = 88.0(1)°, N(1a)—Al(1)—C(1) = 110.2(2)°, N(1a)—Al(1)—C(3) = 119.9(2)° and C(1)—Al(1)—C(3) = 109.7(2)°. The distance between the aluminum atoms [Al···Al distance; 2.784(2) Å] is much shorter than the sum of their van der Waals radii. A comparison of the bridging ligands of $Al_2(CH_3)_6$ and compound **3** reveals that, not surprisingly, since the nitrogen atom in an NR_2 group possesses a lone pair, it differs from a CH_3 group. According to Mason and Mingos,[11] since the NR_2 bridging ligand possesses a filled *p* orbital parallel to the metal–metal vector, it can overlap with antibonding metal orbital combinations, whereas the CH_3 bridging ligand's filled σ-bonding orbitals cannot. Furthermore, metal–metal bond order decreases as orbitals in electron-precise bridged compounds become filled. With the above in mind, the relatively short distance between the two aluminum atoms is mostly likely attributable to $d\pi$–$p\pi$ interactions between aluminum and nitrogen atoms, i.e. overlap between the metal and bridging ligand orbitals. The Al—N distance [1.996(3) Å] is slightly longer than in other amino-bridged aluminum

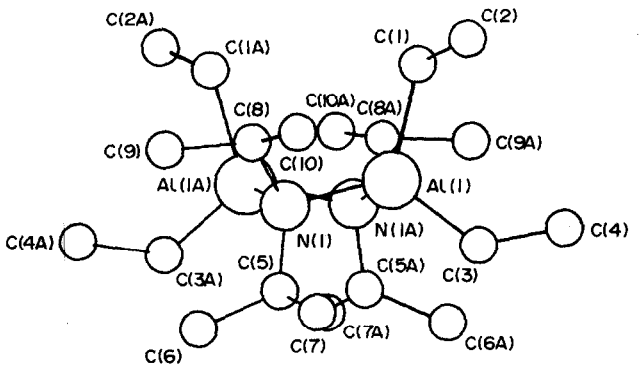

Fig. 1. Molecular structure of $(C_2H_5)_4Al_2[\mu\text{-}N(C^iH_7)_2]_2$.

Table 1. Selected bond distances (Å) and angles (°)

$(C_2H_5)_4Al_2[\mu\text{-}N(C^i{}_3H_7)_2]_2$			
Al(1)—N(1)	1.996(3)	C(1)—C(2)	1.531(9)
Al(1)—N(1a)	2.018(3)	C(3)—C(4)	1.533(7)
Al(1)—C(1)	1.987(5)	C(5)—C(6)	1.519(9)
Al(1)—C(3)	1.972(5)	C(5)—C(7)	1.536(8)
N(1)—C(5)	1.508(5)	C(8)—C(9)	1.517(8)
N(1)—C(8)	1.539(4)	C(8)—C(10)	1.525(8)
Al(1)···Al(1a)	2.784(2)		
N(1a)—Al(1)—N(1)	88.0(1)	Al(1)—N(1)—C(8)	112.9(2)
N(1a)—Al(1)—C(1)	110.2(2)	C(5)—N(1)—C(8)	116.4(2)
N(1a)—Al(1)—C(3)	119.9(2)	Al(1)—C(1)—C(2)	117.2(3)
N(1)—Al(1)—C(1)	113.1(2)	Al(1)—C(3)—C(4)	117.4(4)
N(1)—Al(1)—C(3)	114.7(2)	N(1)—C(5)—C(6)	116.9(4)
C(1)—Al(1)—C(3)	109.7(2)	N(1)—C(5)—C(7)	116.1(4)
Al(1a)—N(1)—Al(1)	87.8(1)	C(6)—C(5)—C(7)	108.0(4)
Al(1a)—N(1)—C(5)	115.0(3)	N(1)—C(8)—C(9)	114.4(4)
Al(1a)—N(1)—C(8)	109.9(2)	N(1)—C(8)—C(10)	115.9(4)
Al(1)—N(1)—C(5)	122.5(2)	C(9)—C(8)—C(10)	110.1(4)
$Br_4Al_2[\mu\text{-}N(Et)_2]_2$			
Br(1)—Al(2)	2.259(4)	Al(2)—N	1.936(8)
Br(2)—Al(2)	2.268(4)	N—C(1)	1.50(1)
Br(3)—Al(1)	2.276(4)	N—C(3)	1.51(1)
Br(4)—Al(1)	2.255(4)	C(1)—C(4)	1.51(2)
Al(1)···Al(2)	2.709(6)	C(2)—C(3)	1.53(1)
Al(1)—N	1.935(7)		
Br(3)—Al(1)—Br(4)	111.0(2)	Al(1)—N—Al(2)	88.8(3)
Br(3)—Al(1)—N	110.6(3)	Al(1)—N—C(1)	117.3(5)
Br(4)—Al(1)—N	116.9(3)	Al(1)—N—C(3)	111.9(5)
N—Al(1)—N(a)	89.1(3)	Al(2)—N—C(1)	114.6(6)
Br(1)—Al(2)—Br(2)	112.6(2)	Al(2)—N—C(3)	111.5(5)
Br(1)—Al(2)—N	115.3(2)	C(1)—N—C(3)	111.0(7)
Br(2)—Al(2)—N	111.3(3)	N—C(1)—C(4)	113.4(8)
N—Al(2)—N(a)	89.1(3)	N—C(3)—C(2)	116.5(7)

dimers and it may be due to steric hindrance imposed by the isopropyl group. In compound **4** the Al_2N_2 core is similar to that in $Et_4Al_2[\mu\text{-}N(C^i{}_3H_7)_2]_2$. Note that the Al—Br distance [2.259(4) Å] is shorter than the bridged Al—Br bond in $AlBr_3$, but longer than the terminal Al—Br bond in $AlBr_3$.

A comparison of the X-ray structural data of $Al_2(CH_3)_6$, $(CH_3)_5Al_2NPh_2$ and $[(CH_3)_2AlN(CH_3)_2]_2$ reveals that the Al···Al distance as well as the Al—N—Al angle increases as the number of bridging amino groups increase.[1,2b,5,12] The stability of these compounds had been previously studied and it was suggested that an increase in the metal–metal distance across the $(AlX)_2$ or $(AlY)_2$ rings does not necessarily imply that the bridge itself progressively weakens. The propensity for these compounds to dissociate into monomers increases according to the following sequence: $Al_2(CH_3)_6 < Al_2(CH_3)_5(NPh_2) < Al_2(CH_3)_4[N(CH_3)_2]_2$. At this point it is interesting to compare the structural data of $[(CH_3)_2AlN(CH_3)_2]_2$, $[Cl_2AlN(C_2H_5)_2]_2$,[13] $[Br_2AlN(C_2H_5)_2]_2$ and $[(C_2H_5)_2AlN(C^i{}_3H_7)_2]_2$, in which $[Cl_2AlN(C_2H_5)_2]_2$ and $[Br_2AlN(C_2H_5)_2]_2$ have almost the same structural parameters. The Al···Al distances are 2.700(3) Å in $[Cl_2AlN(C_2H_5)_2]_2$, 2.709(6) Å in $[Br_2AlN(C_2H_5)_2]_2$ and 2.784(2) Å in $[(C_2H_5)_2AlN(C^i{}_3H_7)_2]_2$. They are shorter than the Al···Al distance (2.815 Å) in $[(CH_3)_2AlN(CH_3)_2]_2$; the expected tendency is due to the bulky amino groups. However, the angle Al—N—Al did not

correlate with the Al···Al distance, which is not an unreasonable result because the Al(1), N(1), Al(1a) and N(1a) atoms do not remain in a plane as in $[(CH_3)_2AlN(CH_3)_2]_2$. The deviations from the best plane of these four atoms in $[(C_2H_5)_2AlN(C^iH_7)_2]_2$ are 0.1922, −0.1921, 0.1921 and −0.1922 Å, respectively, so the Al_2N_2 ring in $[(C_2H_5)_2AlN(C^iH_7)_2]_2$ has the cyclobutane-like structure. Similarly, the Al(1), N, Al(2) and N(a) atoms of $[Br_2AlN(C_2H_5)_2]_2$ do not remain in the plane; the deviations from the best plane of these four atoms in $[Br_2AlN(C_2H_5)_2]_2$ are −0.055(5), 0.196(9), −0.064(6) and 0.21(1) Å.

The X-ray structural data of $In_2(CH_3)_4[NR_2]_2$ (R = Me, Et and C^iH_7)[14] and $Al_2(CH_3)_4[N(CH_3)_2]_2$ reveals that all the In_2N_2 and Al_2N_2 rings are planar; however, compound **3** has a cyclobutane-like structure. This is an unusual and interesting result. It is reasonable to believe that the aluminum atom is smaller than the indium atom, so the aluminum cannot accept more steric hindrance of the isopropyl group, such as the indium, to keep in the plane.

Spectroscopic studies

The ^1H NMR spectra of $(C_2H_5)_4Al_2[\mu\text{-}N(C^iH_7)_2]_2$ in $CDCl_3$ show the chemical shift of methyl in the ethyl group is upfield from the methyl in the isopropyl group; however, in benzene-d_6 the chemical shift of methyl in the ethyl group is downfield from the methyl of the isopropyl group.[15] According to these results a strong solvation effect between benzene and the dimer was suspected. In the course of investigating this effect, several solvents were used to determine the solvent effect, as shown in Table 2. It was found that the specific aromatic solvation effect does indeed exist. It depends on the orientation of approach of the aromatic solvent molecules on solute molecules. The solvent molecules' ring current induces a strong anisotropic effect which affects the chemical shift of the solute.

EXPERIMENTAL

Apparatus and materials

All operations were carried out in a nitrogen-flushed glove-bag, dry-box or vacuum system. All solvents were distilled prior to use. IR, mass, nuclear magnetic resonance, electronic absorption and X-ray single-crystal spectral data were obtained using a Perkin–Elmer 1320 IR spectrophotometer, VG 70-250S GC/MS spectrophotometer, Varian VXR-300 MHz FT-NMR spectrometer, Perkin–Elmer Lambda 3B UV spectrophotometer and an Enraf–Nonius CAD-4 automatic diffractometer, respectively. Elemental analyses were carried out at the Galbraith Laboratory, U.S.A.

Reaction of bis(dialkylamino)magnesium (R = C_2H_5, C^iH_7) *with dialkylaluminum chloride* (R = CH_3, C_2H_5)

Bis(dialkylamino)magnesium was prepared by following the literature method.[16] Dialkylaluminum chloride (0.090 mol) in 2 M toluene solution was added to a round-bottomed flask containing bis(dialkylamino) magnesium (0.045 mol) in ether solution (100 cm^3) under nitrogen. The reaction mixture was stirred for 12 h at room temperature and the magnesium chloride precipitate was isolated by centrifuging. The filtrate was evaporated *in vacuo* to give the product, $R_4Al_2(NR_2)_2$.

(1) $(C_2H_5)_4Al_2[\mu\text{-}N(C_2H_5)_2]_2$ (liquid) was purified by distillation at *ca* 140°C. ^1H NMR (C_6D_6): δ 2.614 (q, 8H, CH_2), 1.267 (t, 12H, CH_3), 0.865 (t, 12H, CH_3), 0.444 (q, 8H, CH_2). ^{13}C NMR (C_6D_6): δ 39.541, 12.244, 9.666, 0.532. ^{27}Al NMR (C_6D_6): δ 156. Mass spectrum (EI, 70 eV): the 10 most intense *m/z* peaks at 285 (base peak), 199, 156, 128, 100, 286, 257, 98, 57, 313 ($M^+ - 1$). Found: C, 60.3; H, 12.4; N, 9.9. Calc.: C, 61.1; H, 12.7; N, 8.9%. Note that this is a known compound and the above data is consistent with that in the literature.[1f]

Table 2. ^1H NMR chemical shifts for $Et_4Al_2[\mu\text{-}N(C^iH_7)_2]_2$ in different solvents

Solvent	Heptet	Triplet	Doublet	Quartet	Standard (TMS)
C_6D_6	3.575	1.371	1.214	0.337	0.000
C_7D_8	3.570	1.327	1.218	0.307	0.000
$C_{12}D_{12}$	3.665	1.133	1.371	0.189	0.000
$CDCl_3$	3.605	1.097	1.353	0.126	0.000
CD_2Cl_2	3.612	1.101	1.355	0.137	0.000

(2) $(CH_3)_4Al_2[\mu\text{-}N(C^iH_7)_2]_2$ (solid) was purified by sublimation at 60°C. M.p. 125–128°C. ^{1}H NMR (C_6D_6): δ 3.632 (sept, 4H, CH), 1.194 (d, 24H, CH_3), −0.260 (s, 12H, CH_3). ^{13}C NMR (C_6D_6): δ 51.194, 26.898, −4.0. ^{27}Al NMR (C_6D_6): δ 160. IR (Nujol): 3020(w), 3000(m), 2965(s), 2922(s), 2855(s), 1460(s), 1408(s), 1378(s), 1305(w), 1260(w), 1202(s), 1165(s), 1135(s), 960(s), 920(m), 840(m), 764(s), 685(s), 648(w), 578(m), 447(w), 410(w). Mass spectrum (EI, 70 eV): the 10 most intense m/z peaks at 142 (base peak), 299, 214, 86, 57, 314 (M^+), 156, 98, 126, 241. Found: C, 62.0; H, 13.1; N, 9.3. Calc.: C, 61.1; H, 12.8; N, 8.9%.

(3) $(C_2H_5)_4Al_2[\mu\text{-}N(C^iH_7)_2]_2$ (solid) was obtained by crystallization from hexane. M.p.$_{dec}$ > 100°C. ^{1}H NMR (C_6D_6): δ 3.575 (sept, 4H, CH), 1.371 (t, 12H, CH_3), 1.214 (d, 24H, CH_3), 0.337 (q, 8H, CH_2). ^{13}C NMR (C_6D_6): δ 51.165, 27.085, 10.293, −4.451. ^{27}Al NMR (C_6D_6): δ 152. IR (KBr): 2990(w), 2940(s), 2910(s), 2880(s), 2840(s), 2780(w), 1445(m), 1405(w), 1390(m), 1380(m), 1360(m), 1320(w), 1295(w), 1250(m), 1225(w), 1185(w), 1165(w), 1150(m), 1120(m), 1090(w), 1010(w), 975(m), 945(m), 900(m), 825(m), 790(m), 765(w), 745(s), 630(s), 585(m), 550(w), 515(m), 435(m), 320(s). Mass spectrum (EI, 70 eV): the 10 most intense m/z peaks at 86 (base peak), 58, 341 ($M^+ - 29$), 156, 101, 128, 70, 170, 227, 269. Found: C, 62.6; H, 12.8; N, 7.8. Calc.: C, 64.8; H, 13.0; N, 7.6%.

*Crystallographic structure determination.** Single crystals were grown by crystallization from hexane. A colourless $Et_4Al_2[\mu\text{-}N(C^iH_7)_2]_2$ crystal with the dimensions 0.65 × 0.52 × 0.45 mm was sealed into a glass capillary for X-ray measurements. During data collection, three standard reflections, $0\bar{4}2$, $04\bar{2}$ and $1\bar{2}7$, were measured every 7200 s; their intensities dropped gradually by 21% at the end of measurement. A decay correction was applied. The correction factors on the intensities of the measured reflections ranged from 1.000 to 1.2075 with an average value of 1.0985. The crystallographic data and refinement details are listed in Table 3. The structure was solved by direct methods. The hydrogen atoms were located from a difference Fourier synthesis. The positional parameters of all hydro-

Table 3. Crystallographic data and refinement details for $(C_2H_5)_4Al_2[\mu\text{-}N(C^iH_7)_2]_2$ and $Br_4Al_2[\mu\text{-}NEt_2]_2$

Molecular formula	$C_{20}H_{48}Al_2N_2$	$C_8H_{20}Al_2Br_4N_2$
Crystal system	Monoclinic	Orthorhombic
Space group	*I2/a*	*Pnma*
Cell dimensions:		
a (Å)	18.159(7)	13.437(2)
b (Å)	7.512(2)	10.732(2)
c (Å)	19.064(7)	12.206(2)
β (°)	115.12(3)	
Cell volume (Å^3)	2353.6	1760.2(5)
Molecular weight	370.58	517.84
Z	4	4
F(000)	831.95	991.77
D_{calc} (g cm^{-3})	1.045	1.954
μ (mm^{-1})	7.63	9.14
λ (Å)	1.54051	0.70930
2θ (max)	130	45
Crystal dimensions (mm)	0.65 × 0.52 × 0.45	0.50 × 0.19 × 0.26
Diffractometer	Nonius CAD-4	Nonius CAD-4
Scan mode	$\omega/2\theta$	$\theta/2\theta$
Measured reflections	3978	1224
Unique reflections	2326	1224
Observations [$I > 2.0\sigma(I)$]		738
[$I > 2.5\sigma(I)$]	2227	
Last least-squares cycle		
Atoms	36	21
Parameters	191	82
Weights	$1.0/[\sigma^2(F_o)+0.0254F_o^2]$	$1.0/[\sigma^2(F_o)+0.00015F_o^2]$
R	0.081	0.040
Rw	0.108	0.041
Highest peak in D-map (e Å^{-3})	0.42	0.380

* See footnote to p. 736.

gen atoms were constrained during the refinement to those of the carbon atoms to which they were bonded [d(C—H) = 0.95 Å]. Full matrix least-squares refinement with anisotropic temperature factors for non-hydrogen atoms and with isotropic temperature factors for hydrogen atoms gave final $R = 0.081$ and $Rw = 0.108$ with $w = 1.0/[\sigma^2(F_o)+0.0254F_o^2]$ for all the observed reflections. The relatively high R values are attributed to the crystal property which is extremely hygroscopic and air-sensitive. During data collection the intensities dropped gradually. Atomic scattering factors were taken from the International Tables for X-ray Crystallography (1974). All crystallographic computations were performed on a VAX 11/780 computer using the SHELX76, MULTAN77 and GEOM78 programs.[17–19]

Synthesis of $Br_4Al_2[\mu\text{-}N(C_2H_5)_2]_2$

The reaction of bis(diethylamino)magnesium with aluminum bromide was carried out by the same procedure as described previously. The compound was purified by sublimation at 72°C in a vacuum system. M.p. 61–62°C. ^{1}H NMR (C_6D_6): δ 2.978 (q, 8H, CH_2), 0.817 (t, 12H, CH_3). ^{13}C NMR (C_6D_6): δ 42.674, 12.426. ^{27}Al NMR (C_6D_6): δ 115.631. IR (KBr): 2970(s), 1470(s), 1380(s), 1310(m), 1285(m), 1220(m), 1168(s), 1120(w), 1090(m), 1032(m), 993(w), 895(m), 880(m), 780(m), 723(w), 620(w). Mass spectrum (EI, 70 eV): the 10 most intense m/z peaks at 244 (base peak), 502, 72, 235, 58, 504, 237, 178, 180, 56. Found: C, 18.2; H, 4.1. Calc.: C, 18.4; H, 3.9%.

*Crystallographic structure determination.** Single crystals were grown by sublimation. A colourless $Br_4Al_2[\mu\text{-}N(Et)_2]_2$ crystal with the dimensions $0.50 \times 0.19 \times 0.26$ mm was sealed into a glass capillary for X-ray measurements. During data collection, three standard reflections, $0.3\bar{5}$, 024 and 060, were measured every 7200 s; their intensities dropped gradually by 20% at the end of measurement. A decay correction was applied. The correction factors on the intensities of the measured reflections ranged from 1.000 to 1.2048 with average value of refinement listed in Table 3. The structure was solved by direct methods. The hydrogen atoms were calculated at anisotropic convergence. The positional parameters of all hydrogen atoms were constrained during the refinement to those of the carbon atoms to which they were bonded [d(C—H) = 1.00 Å]. Full-matrix least-squares refinement with anisotropic temperature factors for non-hydrogen atoms gave final $R = 0.040$ and $Rw = 0.041$ with $w = 1.0/[\sigma^2(F_o)+0.00015F_o^2]$ for all the observed reflections. Atomic scattering factors were taken from the International Tables for X-ray Crystallography (1974). All crystallographic computations were performed on the Micro VAX 3600 computers using the NRCC package programs.[20]

Spectroscopic studies

The chemical shifts of the NMR spectral data of dialuminum complexes were measured in different deuterated solvents, listed in Table 1, and the chemical shifts of $(C_2H_5)_4Al_2[\mu\text{-}N(C^i{}_3H_7)_2]_2$ were observed in different molar ratios between benzene(d_6) and cyclohexane(d_{12}).

Acknowledgement—We thank the National Science Council for financial support.

REFERENCES

1. (a) J. C. Huffman and W. E. Streib, *J. Chem. Soc., Chem. Commun.* 1971, 911; (b) J. F. Malone and W. S. McDonald, *J. Chem. Soc., Dalton Trans.* 1972, 2646; (c) R. G. Vranka and E. L. Amma, *J. Am. Chem. Soc.* 1967, **89**, 3121; (d) J. W. Moore, D. A. Sanders, P. A. Scherr, M. D. Glick and J. P. Oliver, *J. Am. Chem. Soc.* 1971, **93**, 1035; (e) G. H. Robinson and S. A. Sangokoya, *Polyhedron* 1988, **7**, 24, 2727; (f) L. Cocco and D. P. Eyman, *J. Organomet. Chem.* 1979, **179**, 1.
2. (a) G. M. McLaughlin, G. A. Sim and J. D. Smith, *J. Chem. Soc., Dalton Trans.* 1972, 2197; (b) V. H. Hess, A. Hinderer and S. Steinhauser, *Z. Anorg. Allg. Chem.* 1970, **377**, 1; (c) K. J. Alford, K. Gosling and J. D. Smith, *J. Chem. Soc., Dalton Trans.* 1972, 2203; (d) O. T. Beachley Jr and T. Y. Claire, *Inorg. Chem.* 1979, **18**, 3188.
3. S. Amirkhalili, P. B. Hitchcock, A. D. Jenkins, J. Z. Nyathi and J. D. Smith, *J. Chem. Soc., Dalton Trans.* 1981, 377.
4. (a) F. C. Sauls, L. V. Interrante and Z. Jiang, *Inorg. Chem.* 1990, **29**, 2989; (b) L. V. Interrante, G. A. Sigel, M. Garbauskas, C. Hejna and G. A. Slack, *Inorg. Chem.* 1989, **28**, 252.
5. (a) V. R. Magnuson and G. D. Stucky, *J. Am. Chem. Soc.* 1969, **91**, 2544; (b) V. R. Magnuson and G. D. Stucky, *J. Am. Chem. Soc.* 1968, **90**, 3269.
6. J. K. Gilbert and J. D. Smith, *J. Chem. Soc.* (*A*) 1968, 233.
7. (a) P. B. Hitchcock, J. D. Smith and K. M. Thomas,

* Supplementary material available: Tables of crystal data, distances and angles, final fractional coordinates, torsional angles and thermal parameters (12 pages); a listing of observed and calculated structure factors (19 pages).

J. Chem. Soc., Dalton Trans. 1976, 1433; (b) S. Amirkhalili, P. B. Hitchcock and J. D. Smith, *J. Chem. Soc., Dalton Trans.* 1979, 1206.
8. O. T. Beachley Jr and G. E. Coates, *J. Chem. Soc.* 1965, 3241.
9. (a) G. A. Slack, R. A. Tanzilli, R. O. Pohl and J. W. Vandersande, *J. Phys. Chem. Solids* 1987, **48**, 641; (b) N. Kuramato and H. Taniguchi, *J. Mater. Sci. Lett.* 1984, **3**, 471; (c) G. A. Slack and T. F. McNelly, *J. Cryst. Growth* 1976, **34**, 263.
10. C. C. Chang, T. Y. Her and L. K. Liu, *Inorg. Chem.* 1992, **31**, 2292.
11. R. Mason and D. M. Mingos, *J. Organomet. Chem.* 1973, **50**, 53.
12. M. E. O'Neill and K. Wade, in *Comprehensive Organometallic Chemistry* (Edited by F. G. A. Stone, G. Wilkinson, and E. W. Abel), Vol. 1, Chs 1 and 12. Pergamon Press, Oxford (1982).
13. C. C. Chang, S. C. Lin and J. O. Tsai, *J. Chin. Chem. Soc.* 1992, **39**, 55.
14. K. A. Aitchison, J. D. Julius Backer-Dirks, D. C. Bradley, M. M. Faktor, D. M. Frigo, M. B. Hursthouse, B. Hussain and R. L. Short, *J. Organomet. Chem.* 1989, **366**, 11.
15. S. J. Dzugan and V. L. Goedken, *Inorg. Chem.* 1986, **25**, 2858.
16. G. E. Coates and D. Ridley, *J. Chem. Soc.* (*A*) 1967, 56.
17. G. M. Sheldrick, SHELX76, Program for Crystal Structure Determination. University of Cambridge, U.K. (1976).
18. P. Main, L. Lessinger, G. Germain and M. M. Woolfson, MULTAN77, A System of Computer Programs for the Automatic Solution of Crystal Structures from X-ray Diffraction Data. Universities of York, U.K., and Louvain, Belgium (1977).
19. S. Motherwell, GEOM78, Program for Molecular Geometry Calculation. University Chemical Laboratory, Cambridge, U.K. (1983).
20. E. J. Gabe, F. L. Lee and Y. Le Page, in *Crystallographic Computing 3: Data Collection, Structure Determination, Proteins, and Databases* (Edited by G. M. Sheldrick, C. Krueger and R. Goddard), p. 167. Clarendon Press, Oxford (1985).

Polyhedron Vol. 12, No. 7, pp. 739–743, 1993
Printed in Great Britain

0277–5387/93 $6.00+.00
© 1993 Pergamon Press Ltd

AN ASED-MO CALCULATION OF A SIDE-ON BOUND DIMER MODEL OF OXYHAEMOCYANIN

MUNIME LUNDEEN†

Division of Chemistry, Atatürk Eğitim Fakültesi, Marmara University, Fikirtepe 81040, Istanbul, Turkey

and

ALFRED B. ANDERSON

Department of Chemistry, Millis Science Center, Case Western Reserve University, Cleveland, Ohio, U.S.A.

(*Received* 30 *September* 1992; *accepted* 30 *November* 1992)

Abstract—The molecular orbitals of a non-planar side-on bound μ-η^2:η^2-peroxodi-(diamminecopper(II))$^{2+}$ model of the active site of oxyhaemocyanin have been calculated. The σ_{O-O} orbital, the two σ_{Cu-O} orbitals, a bonding and a non-bonding π_V orbital were assigned to −4.693, −4.215, −5.183, −4.849 and −1.505 eV, respectively. The absorption bands which were observed in the absorption or CD spectra of oxyhaemocyanin appear to be transitions from molecular orbitals with large 3*d*(Cu) character to the LUMO orbital, which has *ca* 30.4% $3d_{xy}$(Cu) and 55.6% $2p_x$(O) character. The oscillator strengths of the transitions allowed in the C_{2v} point group were calculated. The singlet–triplet separation corresponds to the difference in energy of the asymmetric and symmetric combinations of the $3d_{xy}$(Cu) atomic orbitals and is large (2.060 eV). These molecular orbitals have B_2 and A_1 symmetry, respectively, and, therefore, the electronic transition is allowed in the model compound. The singlet–triplet transition may not be spin-forbidden in all molecules.

Haemocyanin is an oxygen-carrying copper protein which is found in arthropods and molluscs.[1] Each subunit of haemocyanin has a dicopper(I) site in the deoxy form of the protein which, when the protein binds dioxygen, is transformed into a μ-peroxo-bound dicopper(II) site with a very strong absorption band at $\sim$ 350 nm (ε = 20,000 M^{-1} cm^{-1}) and a less intense absorption band at $\sim$ 580 nm (ε = 1000 M^{-1} cm^{-1}).[2] These absorption bands, which are also found in the CD spectrum of oxyhaemocyanin, are explained as two $\pi_V \rightarrow 3d$(Cu) ligand-to-metal charge-transfer bands from the anti-bonding π lone-pair orbitals on the peroxide, which are no longer degenerate to the $3d_{xy}$ (or $3d_{x^2-y^2}$) orbitals on the copper(II) ions which have formed an empty molecular orbital in this strongly anti-ferromagnetically-coupled dicopper(II) site.[2] Various geometries have been considered for this dicopper(II) site bridged by a peroxide ligand: (1) an end-on bound symmetric planar *trans*-μ-peroxodicopper(II) site; (2) an end-on bound symmetric non-planar *trans*-μ-peroxodicopper(II) site; (3) an end-on bound symmetric planar *cis*-μ-peroxodicopper(II) site, which has an endogenous bridging ligand in addition to the peroxo bridge; (4) a side-on bound planar μ-η^2:η^2-peroxodicopper(II) site; and (5) an end-on bound μ-O,O-peroxodicopper(II) site which may have a non-planar dangling oxygen atom. The copper–oxygen bonds in these geometries have been discussed by Freedman, Loehr and Loehr[3] and by Ross and Solomon.[4] This paper is a report of the calculated molecular orbitals of a non-planar side-on bound symmetric μ-η^2:η^2-peroxodi(diamminecopper(II))$^{2+}$ site, in which the oxygen atoms of the peroxo ligand are about 18° above and below the *xy*-equatorial plane which contains $Cu_A(\uparrow)$ and $Cu_B(\downarrow)$ along the axis.

† Author to whom correspondence should be addressed.

EXPERIMENTAL

The method of calculation was the semi-empirical "Atom Superposition and Electron Delocalization Molecular Orbital Method" (ASED-MO), which has been described previously.[5,6] The atomic parameters which were used in the calculation were taken from Mehandru and Anderson[7] and Anderson *et al.*[8] 3*d* orbital exponents were used only for the copper atom.[7,8]

RESULTS AND DISCUSSION

The absorption bands of oxyhaemocyanin consist of two major bands in the near-UV to near-IR region and are noticeably intense.[1,2] Two intense absorption bands are found in this region in models of oxyhaemocyanin also,[9–16] but some models have a third major band which also occurs in the spectrum of the non-oxygenated compound.[12–16]

The compound chosen for this study as a model of oxyhaemocyanin is very similar to the planar μ-η^2:η^2-peroxo-bridged side-on bound dimer compound (**5**) of Ross and Solomon,[4] but the oxygen atoms of the peroxo ligand have been lifted and lowered symmetrically *ca* 18° off the equatorial plane of the two copper(II) ions (Fig. 1). Thus, this non-planar side-on bound model compound bears a resemblance to the non-planar symmetric *trans*-μ-O,O′-peroxo-bridged dicopper(II) model of Freedman *et al.*[3] and to a proposed more or less planar side-on bound dimer model by Larrabee and Spiro,[17] which has no endogenous bridging ligand. Very briefly, the model compound has two nitrogen donors at the bond length of 1.997 Å per copper(II) ion. There are two symmetric and equal copper–oxygen bonds to each oxygen of the peroxo group at 1.914 Å. The oxygen–oxygen bond length is 1.410 Å and the copper(II)–copper(II) distance is 3.560 Å

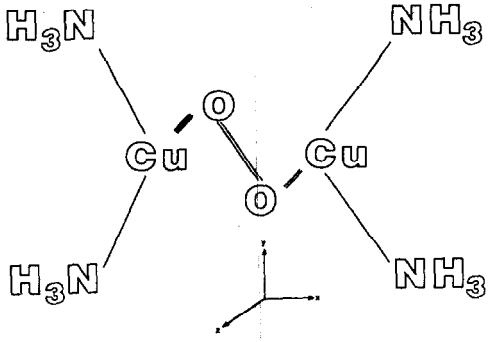

Fig. 1. The model of a peroxodicopper site which may be found in haemocyanin: μ-η^2:η^2-peroxodi(diamminecopper(II))$^{2+}$.

in the model. These distances are similar to the observed bond lengths and copper(I)–copper(I) distances in the structures of the six subunits of *Panulirus interruptus* haemocyanin in the crystal structure reported by Volbeda and Hol[18,19] and are also similar to the reported copper–nitrogen and copper–copper distances in the structures of deoxy- and oxyhaemocyanin determined by the EXAFS method.[20] The non-planar side-on bound model leaves out the two nitrogen donors at long bond distances of 2.77 and 2.66 Å, respectively, each of which is bound to a different copper(II) ion.[18,19]

The molecular orbitals of the model which are shown in Table 1 are for 15 higher-energy orbitals. The symmetry was assigned as the C_{2v} point group (which has a C_2 axis, two symmetry planes, σ_{xz} and σ_{yz}, and no inversion symmetry) rather than the C_{2h} point group (which has a C_2 axis, the inversion operator, and a σ_h plane).[21] At first glance C_{2h} might appear to be the appropriate point group as the geometry of the model has an inversion centre, an equatorial symmetry plane (xy) about the copper(II) ions and a $C_2(z)$ axis. However, if this point group is used, all magnetic dipole-allowed electronic transitions are expected to show resonance enhancement of Raman bands and each electronic transition is allowed by either the magnetic dipole mechanism or the electric dipole mechanism.[22] The assumption was made that the portion of the geometry of the model which might be most useful in determining which electronic transitions are allowed was the central Cu_2O_2 chromophore. The Cu_2O_2 chromophore can be assigned the C_{2v} point group [or, if the model and the dicopper(II) site of haemocyanin are considered to be not strictly planar, the D_2 point group is satisfactory].

The lowest energy unoccupied molecular orbital, assigned zero energy arbitrarily, is a molecular orbital which has mostly $3d_{xy}$(Cu) character and some $3d_{xz}$, $4p_y$ and $4p_z$(Cu) character (Fig. 2). This orbital has a larger percentage of $2p_x$(O) character than copper atomic orbital character and shows antibonding sigma interactions of the $2p_x$(O) atomic orbitals with the $3d_{xy}$ and $3d_{xz}$ atomic orbitals on the copper(II) ions. The symmetry of this orbital is A_1. It is 1.505 eV above the doubly filled HOMO orbital, which is a lone-pair molecular orbital π_V* of the peroxo ligand which has 96.2% oxygen character and some copper character. This molecular orbital has A_2 symmetry and a transition from this orbital, which is non-bonding towards the copper(II) ions, is allowed in the CD spectrum but not in the absorption spectrum.[22] This transition would occur at 824 nm and is close in location to the 930 nm electronic Raman band in oxyhaemocyanin, which was thought to correspond to the singlet–

Table 1. The molecular orbitals of the non-planar side-on bound μ-η^2:η^2-peroxodi(diammine-copper(II))$^{2+}$ model compound calculated by the ASED-MO program are shown. The last column shows the calculated oscillator strength, f, of an electronic transition to the LUMO (top orbital)

Symmetry of MO	Energy (eV)	%Copper	%Oxygen	%Nitrogen	MO composed of (mostly)	$10^2 \times f$
A_1	0.0	33.85	55.59	8.48	$(xy)+(xy)$	—
A_2	−1.505	3.74	96.24	0.01	π_V	2.6×10^{-2}
B_2	−2.060	65.42	12.88	21.62	$(xy)-(xy)$	2.3
A_2	−3.082	57.92	40.95	0.71	$(xz)-(xz)$	2.7×10^{1}
B_2	−3.365	69.52	27.15	2.65	$(x^2-y^2)+(x^2-y^2)$	5.2×10^{-5}
A_2	−3.390	80.82	16.26	2.03	$(x^2-y^2)-(x^2-y^2)$	2.3
A_2	−3.728	70.67	14.71	14.41	$(xz)-(xz)$	5.3×10^{-3}
A_2	−3.910	97.40	0.01	2.54	$(z^2)-(z^2)$	0.15
A_1	−3.929	38.79	1.91	9.02	$(z^2)+(z^2)$	1.6×10^{1}
A_2	−4.038	99.69	1.09	0.08	$(yz)-(yz)$	5.0×10^{-3}
A_1	−4.071	95.07	3.63	0.68	$(yz)+(yz)$	0.26
B_1	−4.215	79.80	13.74	6.12	π_{Cu-O}	5.8×10^{-2}
A_1	−4.693	35.05	64.26	0.14	σ_{O-O}	2.9
A_1	−4.849	51.34	46.46	1.08	π_{Cu-O}	1.1×10^{1}
B_2	−5.183	38.60	50.07	11.08	σ_{Cu-O}	4.0

triplet transition by Larrabee and Spiro.[17] The oxyhaemocyanin molecule is known to exhibit strong antiferromagnetism and the value of $-2J$ has been estimated to be 550 cm^{-1} for *Limulus polyphemus* haemocyanin.[23] The reported minimum value of $-2J$ would correspond to a separation of 0.068 eV between the singlet and triplet states and no molecular orbital was calculated at this distance from the lowest unoccupied molecular orbital. However, if the value of $-2J$ can be much larger than the reported minimum value, the molecular orbital, which is below the HOMO orbital which was identified as a π_V*(peroxo) orbital above and which has B_2 symmetry, can give an electric dipole allowed transition to the LUMO orbital. This molecular orbital has 64.5% $3d_{xy}$(Cu) and some $3d_{xz}$, $4p_y$ and $4p_z$(Cu) character and it corresponds to the asymmetric combination of the $3d_{xy}$(Cu) atomic orbitals (Fig. 3). The singlet–triplet transition may not be spin-forbidden in a dimeric molecule such as the present non-planar side-on bound model of the active site of oxyhaemocyanin. The electronic transition from the molecular orbital, which has the asymmetric combination of the $3d_{xy}$(Cu) atomic orbitals, to the LUMO orbital, which has the symmetric combination of the $3d_{xy}$(Cu) atomic orbitals, is expected to occur at 601 nm based on Koopman's theorem[24] and, therefore, this transition appears to correspond to the

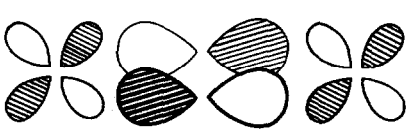

Fig. 2. A schematic diagram of the LUMO of the side-on bound peroxodicopper(II) compound shown in Fig. 1, which has mostly $3d_{xy}$(Cu) and $2p_x$(O) atomic orbital character. The composition of the LUMO is: 30.4% $3d_{xy}$(Cu), 2.0% $4p_z$(Cu), 1.4% $3d_{xz}$(Cu), $\approx$ 0.04% $4p_y$(Cu) and 55.6% $2p_x$(O).

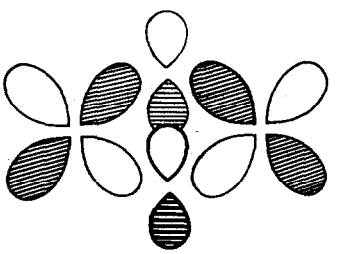

Fig. 3. A schematic diagram of the highest occupied molecular orbital of the side-on bound peroxodicopper(II) compound shown in Fig. 1, which has mostly 3*d*(Cu) atomic orbital character. The composition of this molecular orbital is: 64.5% $3d_{xy}$(Cu), 0.9% $4p_y$(Cu), 0.3% $4p_z$(Cu), $\approx$ 0.4% $3d_{xz}$(Cu), 10.0% $2p_y$(O), 2.1% $2s$(O) and 0.8% $2p_z$(O) atomic orbital character. This molecular orbital is just below the HOMO which has: 87.3% $2p_z$(O), 8.9% $2p_y$(O), $\approx$ 0.001% $2s$(O), 2.4% $3d_{yz}$(Cu), 0.9% $3d_{z^2}$(Cu), 0.4% $3d_{x^2-y^2}$(Cu), 0.03% $4s$(Cu) and $\approx$ 0.01% $4p_x$(Cu).

observed 580 nm absorption band in oxyhaemocyanin, which has an extinction coefficient of *ca* 1000 M^{-1} cm^{-1} and which had been assigned previously as the $\pi_V^* \rightarrow Cu^{2+}$ charge transfer band.[1-4,17] Similar bands were observed in the visible region of the absorption spectrum of model compounds and these bands were also assigned as ligand-to-metal charge-transfer bands from the peroxo ligand to the copper(II) ions.[9-11,13-16] The nature of the absorption band, which is at about 350 nm and which exists in the deoxygenated model compounds, was left unexplained by the authors.[13-16] If the $4p_z$ and $4p_x$ atomic orbitals on the coppers are considered to be distorting portions of a total $3d$ wavefunction f in the formulation of Griffith[25] so that $f = f_g + f_u$, and if approximate molecular orbitals consisting of the $2p_z$ atomic orbitals on the oxygens and the $4p_z$ or $4p_x$ atomic orbitals on the coppers are employed, the oscillator strength, f, of an electronic transition which is electric dipole allowed may be calculated. The value of f is 2.3×10^{-2} for the electronic transition expected at 601 nm. This transition is allowed by the magnetic dipole mechanism as well. Its intensity may be due to the presence of σ Cu—O character in the lower-energy orbital and σ^* Cu—O character in the higher-energy orbital.

The remaining eight $3d$ atomic orbitals of the two copper(II) ions make large contributions to the eight molecular orbitals which follow the top two doubly filled molecular orbitals. The first of these is a mostly $3d_{xz}$(Cu) orbital which has large π_V lone-pair contributions in it. This molecular orbital is the asymmetric combination of the $3d_{xz}$(Cu) atomic orbitals and, although it is calculated to have high oscillator strength, it has A_2 symmetry and a transition from this orbital to the LUMO orbital is expected to be observed in the CD spectrum in the C_{2v} point group. In fact, the CD spectrum of oxyhaemocyanin has a band at *ca* 480 nm, which is not observed in the absorption spectrum.[2]

The region in oxyhaemocyanin in the neighbourhood of 350 nm has very intense absorptions, which are also seen in the CD spectrum.[2] Molecular orbitals which may give rise to transitions in this region appear to have mostly $3d_{x^2-y^2}$(Cu) but also some $3d_{z^2}$(Cu) and $3d_{yz}$(Cu) atomic orbital character, in addition to σ_{O-O} and π_V^* lone-pair character from the π_V^* orbitals which were degenerate in the peroxo ligand. Electronic transitions from the higher-energy molecular orbital, which has the symmetric combination of the $3d_{x^2-y^2}$(Cu) atomic orbitals to the LUMO orbital, are calculated to have low oscillator strength ($f = 5.2 \times 10^{-7}$).

Very high oscillator strength is calculated for an electronic transition from a lower-energy molecular orbital which is mostly made up of the symmetric combination of the $3d_{z^2}$(Cu) atomic orbitals. This molecular orbital includes considerable amounts of $3d_{x^2-y^2}$, $3d_{yz}$ and $4s$(Cu) atomic orbitals, in addition to $3d_{z^2}$ character, and is calculated to give an electronic transition to the LUMO orbital at 317 nm ($f = 0.159$).

Similarly, only one combination of the $3d_{yz}$(Cu) atomic orbitals which follow the symmetric combination, is expected to show an electronic transition to the LUMO orbital in the C_{2v} point group ($f = 2.6 \times 10^{-3}$ for this transition).

The molecular orbital which is next may be described as a σ copper–oxygen orbital. An electronic transition to the LUMO orbital is expected at 294 nm ($f = 6 \times 10^{-4}$). The molecular orbital below it has σ_{O-O} character. An electronic transition from this molecular orbital to the LUMO orbital is calculated to occur at 264 nm and to have much higher oscillator strength ($f = 2.87 \times 10^{-2}$). The π_{Cu-O} molecular orbital follows this orbital and it is followed by the second σ_{Cu-O} molecular orbital. A transition from this σ_{Cu-O} molecular orbital to the LUMO orbital is calculated to have high oscillator strength ($f = 1.05 \times 10^{-2}$).

Molecular orbitals of σ_{Cu-N} character are calculated to give rise to electronic transitions below 200 nm in this calculation. However, contributions from atomic orbitals on the nitrogen donors appear to enter into the σ_{Cu-O} molecular orbitals, which have been assigned B_1 and A_1 symmetry. Thus, these σ_{Cu-O} molecular orbitals may have electric dipole allowed electronic transitions, which are x-polarized and z-polarized, respectively. These electronic transitions to the LUMO orbital are calculated to occur at 294 and 239 nm, respectively, and are expected to show resonance-enhanced-Raman lines in the C_{2v} point group.[22]

CONCLUSIONS

The allowed electronic transitions at *ca* 600 nm and 370 nm in the non-planar side-on bound peroxodi(diamminecopper(II))$^{2+}$ model are calculated to have high oscillator strengths. These electronic transitions may correspond to the major absorption bands observed in oxyhaemocyanin at *ca* 580 and 350 nm. These molecular orbitals appear to contain a great deal of $3d$(Cu) atomic orbital character in addition to lone-pair character from the peroxo ligand. Thus, this description differs substantially from the description given by Ross and Solomon,[4] Solomon *et al.*,[2] Freedman *et al.*[3] and Larrabee and Spiro.[17] Of the 15 molecular orbitals which are reported in Table 1, only the HOMO level and four others have essentially lone-pair character or may

be considered to be a peroxo ligand bond orbital. The calculation appears to explain the intensities of the observed electronic transitions in oxyhaemocyanin satisfactorily in a semi-quantitative way.

The singlet–triplet transition in the model is calculated to correspond to more than 2 eV and to occur at about 600 nm. A singlet–triplet transition is spin-forbidden in a compound,[26] but it may not be forbidden in the antiferromagnetically coupled ground state of the dicopper(II) site in the model.

Acknowledgement—The NATO Collaborative Research Grant award (CRG. 900137) is gratefully acknowledged. The ASED-MO calculations were carried out at the Department of Chemistry of Case Western Reserve University.

REFERENCES

1. R. Lontie and C. Gielens, in *Metalloproteins* (Edited by U. Weser), pp. 62–72. Thieme, Stuttgart (1979).
2. E. I. Solomon, M. J. Baldwin and M. D. Lowery, *Chem. Rev.* 1992, **92**, 521.
3. T. B. Freedman, J. S. Loehr and T. M. Loehr, *J. Am. Chem. Soc.* 1976, **98**, 2809.
4. P. K. Ross and E. I. Solomon, *J. Am. Chem. Soc.* 1991, **113**, 3246.
5. S. F. Jen, A. B. Anderson and C. L. Hill, *J. Phys. Chem.* 1992, **96**, 5658.
6. S. F. Jen and A. B. Anderson, *Inorg. Chem.* 1992, **31**, 2651.
7. S. P. Mehandru and A. B. Anderson, *Sur. Sci.* 1989, **216**, 105.
8. A. B. Anderson, R. W. Grimes and S. Y. Hong, *J. Phys. Chem.* 1987, **91**, 4245.
9. J. E. Pate, R. W. Cruse, K. D. Karlin and E. I. Solomon, *J. Am. Chem. Soc.* 1987, **109**, 2624.
10. K. D. Karlin and Y. Gutneh, *J. Chem. Educ.* 1985, **62**, 983.
11. N. Kitajima, T. Koda, S. Hashimoto, T. Kitagawa and Y. Moro-oka, *J. Chem. Soc., Chem. Commun.* 1988, 151.
12. N. Kitajima, K. Fujisawa and Y. Moro-oka, *J. Am. Chem. Soc.* 1989, **111**, 8975.
13. K. D. Karlin, Z. Tyeklar, A. Farooq, M. S. Haka, P. Ghosh, R. W. Cruse, Y. Gultneh, J. C. Hayes, P. J. Toscano and J. Zubieta, *Inorg. Chem.* 1992, **31**, 1436.
14. K. D. Karlin, M. S. Haka, R. W. Cruse, G. J. Meyer, A. Farooq, Y. Gultneh, J. C. Hayes and J. Zubieta, *J. Am. Chem. Soc.* 1988, **110**, 1196.
15. K. D. Karlin, R. W. Cruse, Y. Gultneh, J. C. Hayes and J. Zubieta, *J. Am. Chem. Soc.* 1984, **106**, 3372.
16. K. D. Karlin, R. W. Cruse, Y. Gultneh, A. Farooq, J. C. Hayes and J. Zubieta, *J. Am. Chem. Soc.* 1987, **109**, 2679.
17. J. A. Larrabee and T. G. Spiro, *J. Am. Chem. Soc.* 1980, **102**, 4217.
18. A. Volbeda and W. G. J. Hol, *J. Molec. Biol.* 1989, **209**, 249.
19. A. Volbeda and W. G. J. Hol, *J. Molec. Biol.* 1989, **206**, 531.
20. T. G. Spiro, G. L. Woolery, J. M. Brown, L. Powers, M. E. Winkler and E. I. Solomon, in *Copper Coordination Chemistry: Biochemical and Inorganic Perspectives* (Edited by K. D. Karlin and J. Zubieta), pp. 23–41. Adenine Press, New York (1982).
21. G. Davidson, *Introductory Group Theory for Chemists*, p. 132. Applied Science Publishers Ltd, London (1971).
22. A. B. P. Lever, *Inorganic Electronic Spectroscopy*, p. 124. Elsevier Publishing Co., Amsterdam (1968).
23. D. M. Dooley, R. A. Scott, J. Ellinghaus, E. I. Solomon and H. B. Gray, *Proc. Natl. Acad. Sci. U.S.A.* 1978, **75**, 3019.
24. J. N. Murrell, S. F. Kettle and J. M. Tedder, *The Chemical Bond*, 2nd edn, p. 62. John Wiley, New York (1985).
25. J. S. Griffith, *The Theory of Transition-Metal Ions*, p. 289. Cambridge University Press, Cambridge (1961).
26. F. L. Pilar, *Elementary Quantum Chemistry*, p. 325. McGraw-Hill, New York (1990, 1968).

Polyhedron Vol. 12, No. 7, pp. 745–748, 1993
Printed in Great Britain

0277–5387/93 $6.00+.00
© 1993 Pergamon Press Ltd

PREPARATION AND CHARACTERIZATION OF Mn^{II}, Co^{II}, Ni^{II}, Cu^{II} AND Zn^{II} KANAMYCIN COMPLEXES

A. MASHALY

Chemistry Department, Faculty of Science, Menoufia University, Shebin El-Kom, Egypt

(*Received* 13 *July* 1992; *accepted* 25 *November* 1992)

Abstract—Binuclear complexes of manganese(II), cobalt(II), nickel(II), copper(II) and zinc(II) with kanamycin sulphate have been synthesized and characterized by elemental analysis, IR, ^{1}H NMR, electronic and ESR spectra in order to throw more light on their structures. The spectral results obtained indicate octahedral geometry around manganese(II), cobalt(II) and nickel(II), distorted octahedral geometry around copper(II) and tetrahedral geometry around zinc (II) ions.

Kanamycin, 0-(3-amino-3-deoxy-α-D-glucopyranosyl)-(1→6)-0-(6-amino-6-deoxy-α-D-glucopyranosyl)-(1→4)-2-deoxy-D-streptamine,[1] has found worldwide use in the treatment of serious gram-negative infections.[2] Despite the importance of aminoglucosides and their metal chelates, little attention has been paid to them by previous authors.[3–6] In addition, no systematic studies are present in the literature concerning complex formation between kanamycin and transition metal ions. The aim of the present investigation was to synthesize the complexes of manganese(II), cobalt (II), nickel(II), copper(II) and zinc(II) with kanamycin and to characterize them in a systematic way using elemental analysis, IR, electronic, ^{1}H NMR and ESR spectra and magnetic moments in order to throw more light on their structure.

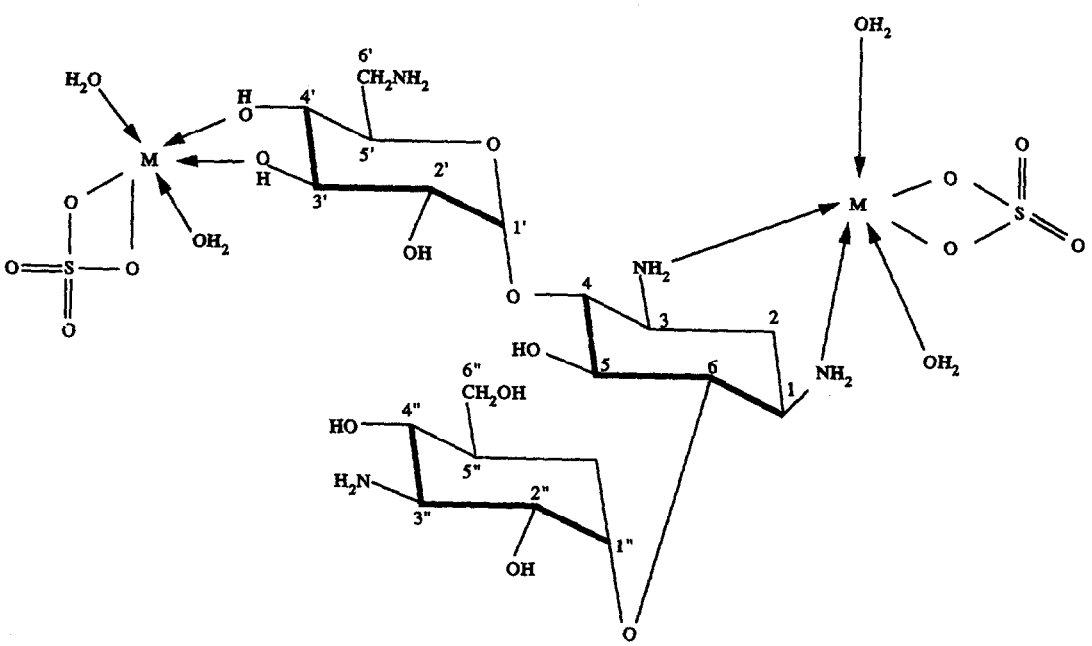

I

where M = Mn^{II}, Co^{II}, Ni^{II}, Cu^{II}, in Zn^{II}. Axial water molecules are absent.

EXPERIMENTAL

All the compounds used in the present investigation were pure laboratory grade chemicals from BDH. Kanamycin sulphate was an A.R. product supplied by the Memphies Company, Egypt.

Preparation of the complexes

Kanamycin sulphate (0.001 mol) was dissolved in twice distilled water (10 cm^3). After complete dissolution of the ligand an ethanolic solution of the metal chloride (0.001 mol dissolved in 15 cm^3 of ethanol) was added dropwise. The addition of KOH (0.0019 mol) dissolved in ethanol (75 cm^3) to the solution mixture caused various colour changes and the formation of coloured precipitates, the colours depending on the nature of the metal(II) ion used; buff in the case of manganese(II), pink for cobalt(II), blue–grey for nickel(II), blue for copper(II) and white for zinc(II). After stirring the reaction mixture for 6 h the complexes thus obtained were separated by centrifugation, washed with ethanol and then ether and dried *in vacuo*. The apparatus and working procedures were as described previously.[7,8]

RESULTS AND DISCUSSION

On the basis of the analytical data obtained (Table 1) the complexes prepared can be formulated as $[M_2(Kan.)(H_2O)_n(SO_4)_2]$, where M = Mn, Co, Ni, Cu, and Zn; n = 0–4 and Kan. is kanamycin. The molar conductances of all complexes in DMF were less than 12 Ω^{-1} cm^2 mol^{-1}, indicating that they are non-electrolytes.[9] This indicates the coordinated nature of $[SO_4]^{2-}$ and also that kanamycin behaves as a neutral ligand. The mode of bonding between kanamycin and the metal ions was deduced from the results of the following investigations (Table 2).

(a) On comparing the IR spectra of the solid complexes with that of kanamycin sulphate, the following can be pointed out. The existence of water molecules (lattice or coordinated) in the complexes is gathered from the appearance of the new broad band at 3450–3420 cm^{-1}, corresponding to γ_{sym} of coordinated water. The presence of a new band at 805–810 cm^{-1}, especially in the spectra of copper(II) and manganese(II) complexes, not present in the spectra of free kanamycin, can be assigned to the out-of-plane deformation vibrations of coordinated water[10,11] and supports the presence of coordinated water molecules in copper(II) and manganese(II) complexes. The IR spectra of metal (II)-kanamycin complexes display interesting changes in comparison to that of the free kanamycin molecule.

The bands observed at 3320 and 3200 cm^{-1} in the spectra of the free ligand due to ν(OH) and ν(NH), respectively, are shifted by 100–150 cm^{-1} to lower wave numbers in the spectra of the metal(II)-kanamycin complexes with the same intensity. This denotes that two NH_2 and two OH alcoholic groups contribute to chelation, which is in accordance with the results of conductance measurements. Based on the information gained, kanamycin behaves as a neutral bidentate chelate ligand on reaction with metal(II) ions.

The presence of ν_3(S—O) and ν_1(S—O) in the spectra of kanamycin complexes, not present in the spectra of the free kanamycin located at 1080–1070

Table 1. Analytical data of some transition metal(II)-kanamycin complexes

Complex	Colour	Microanalysis results[a] %C	%H	%N	%M	%S	Λ^b (Ω^{-1} cm^2 mol^{-1})
$[Mn_2(Kan.)(H_2O)_4(SO_4)_2]\cdot 3H_2O$	Buff	23.9 (23.9)	5.0 (5.5)	6.7 (6.2)	11.3 (11.0)	7.1 (7.1)	11.9
$[CO_2(Kan.)(SO_4)_2(H_2O)_2]\cdot 2H_2O$	Pink	25.6 (25.2)	4.8 (5.1)	6.7 (6.5)	12.8 (12.6)	7.8 (7.5)	11.3
$[Ni_2(Kan.)(SO_4)_2(H_2O)_2]\cdot 2H_2O$	Blue–grey	25.4 (25.1)	4.9 (5.1)	6.8 (6.5)	12.6 (13.1)	7.0 (7.4)	9.6
$[Cu_2(Kan.)(H_2O)_4(SO_4)_2]\cdot 6H_2O$	Blue	22.2 (22.0)	5.4 (5.7)	6.2 (5.7)	13.0 (12.9)	7.0 (6.5)	10
$[Zn_2(Kan.)(SO_4)_2]\cdot 4H_2O$	White	25.3 (24.9)	5.5 (5.1)	7.0 (6.4)	13.4 (13.8)	7.6 (7.4)	7.8

[a] % Found (% Calc.).
[b] 10^{-3} M in DMF solution; Kan. = kanamycin.

Table 2. IR and electronic spectra data of some transition metal(II)-kanamycin complexes

Complex	IR (cm^{-1})						Electronic
	$\nu(H_2O)$	$\nu_s(S—O)$	$\nu(S—O)$	$\gamma_{sym}(H_2O)$	$\nu(M—O)$	$\nu(M—N)$	λ_{max} (nm)
$[Mn_2(Kan.)(H_2O)_4(SO_4)_2]\cdot 3H_2O$	3450–3420	1080	980	805	490	375	150, 460
$[CO_2(Kan.)(SO_4)_2(H_2O)_2]\cdot 2H_2O$	3450–3420	1070	960	810	480	380	530, 960
$[Ni_2(Kan.)(SO_4)_2(H_2O)_2]\cdot 2H_2O$	3450–3420	1080	950	805	490	390	415, 620, 1135
$[Cu_2(Kan.)(H_2O)_4(SO_4)_2]\cdot 6H_2O$	3450–3420	1070	970	810	480	375	810, 650
$[Zn_2(Kan.)(SO_4)_2]\cdot 4H_2O$	3450–3420	1070	950	805	490	385	380

and 980–950 cm^{-1}, indicates the chelating bidentate nature of the $[SO_4]^{2-}$ ion. This is in line with earlier studies on the coordinated nature of sulphate complexes.[10,12,13] The two new bands observed at 490–480 and 390–375 cm^{-1} in the spectra of the kanamycin complexes can be assigned to ν(M—O) and ν(M—N), respectively, hence confirming the mode of bonding suggested through the oxygen of the —OH and nitrogen of the NH groups.

(b) The ^1H NMR spectra for nickel(II) and zinc (II) complexes in DMSO (d_6) display a shift of 0.6–0.8 ppm downfield in the spectra of the complexes: δ(2-Ha) (1.65), δ(2-He) (2.45), δ(3″-H) (3.50), δ(2″-H) (3.89), δ(2′-H) (4.20), δ(3′-H) (4.50) and δ(1′-H) (6.20 ppm).

The shift of the signals downfield is due to the deshielding effect of the central metal ion on the kanamycin protons as a result of coordination. The presence of a new signal at $\delta(H_2O)$ (4.0 ppm) in the spectra of these complexes, not present in the spectrum of free kanamycin, can be assigned to H_2O and supports the coordinated nature of the water molecules in these complexes.

The bulk magnetic susceptibility measurements for all the solid complexes under investigation at room temperature, 300 K, are indicative of: five unpaired electrons per manganese(II) ion, $\mu_{eff} = 5.8$, three unpaired electrons per cobalt(II) ion, $\mu_{eff} = 4.04$, two unpaired electrons per nickel (II) ion, $\mu_{eff} = 3.21$ and one unpaired electron per copper(II) ion, $\mu_{eff} = 1.7$ B.M. (Table 2). The magnetic moments are close to the spin-only moments of the free ions, which indicates the absence of metal–metal interactions within the binuclear complexes under investigation.

(c) The reflectance spectra of the complexes under investigation exhibit broad maxima with λ_{max} at 510 and 460 nm for manganese(II), 530 and 960 nm for cobalt(II), 415, 620 and 1135 nm for nickel(II), 810 and 650 nm for copper(II) and 380 nm for zinc(II) complexes. These bands can be assigned to: $^6A_{1g} \rightarrow {}^4T_{2g}(G)$, $^6A_{1g} \rightarrow {}^4T_{1g}(G)$; $^4T_{1g} \rightarrow {}^4T_{1g}(P)$, $^4T_{1g} \rightarrow {}^4T_{2g}$; $^3A_{2g} \rightarrow {}^3T_{1g}(P)(\nu_3)$, $^3A_{2g} \rightarrow {}^3T_{1g}(\nu_2)$, $^3A_{2g} \rightarrow {}^3T_{2g}(\nu_1)$, $^2B_{1g} \rightarrow {}^2B_{2g}$; $^2B_{1g} \rightarrow {}^2E_g$ transitions, as well as charge-transfer interactions within the whole molecule, respectively. These spectral patterns are characteristic of octahedral geometry around manganese(II), cobalt(II) and nickel(III) ions, distorted octahedral geometry around copper(II) ions and tetrahedral symmetry around zinc(II) ions.[14]

(d) *X*-band ESR spectra of the manganese(II)- and copper(II)-kanamycin complexes under investigation (Fig. 1) were measured at room temperature in order to elucidate the nature of the coordination around the manganese(II) and copper(II) ions. The spectra show an intense broad signal and no obvious hyperfine splitting for manganese(II), $g_{eff} = 1.9417$; the pattern of the g_{eff} value, together with the shape of the ESR spectra, indicate octahedral geometry around the manganese(II) ion. For the copper(II)-kanamycin complex the spectrum exhibits an intense broad signal with two lines at $g_{\parallel} = 2.1217$ and $g_{\perp} = 2.0954$, with no obvious hyperfine structure. The calculated value $[g_{iso} = 1/3(2g_{\perp} + g_{\parallel})]$ for the copper-kanamycin com-

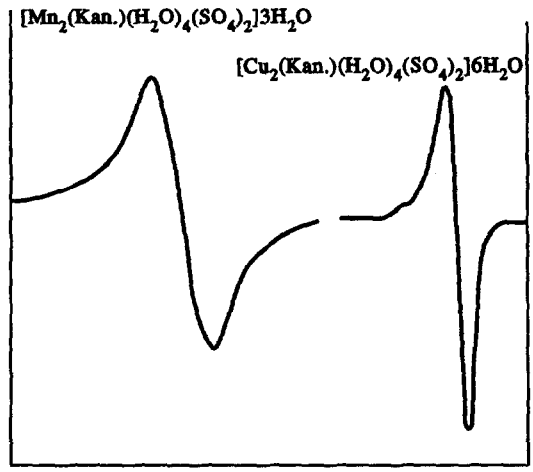

Fig. 1. *X*-band ESR spectra of copper(II)- and manganese(II)-kanamycin complexes at 298 K.

plex amounts to 2.1058, which is in reasonable agreement with the observed value for g_{iso} of copper(II) in similar axial symmetry.[15,16] The values of $G = (g_{\parallel}^{-2}/g_{\perp}^{-2}) < 4$ reveal that exchange is taking place and the local tetragonal axes are misaligned.[17,18]

Based on the knowledge gained from the present investigation, the bonding of metal(II) ions to kanamycin can be formulated as shown in **I**.

REFERENCES

1. British pharmacopoeia, Addendum (1975).
2. H. Umezawa, M. Ueda, K. Maeda, K. Yagishita, S. Kondo, Y. Okami, R. Utahra, Y. Osata, K. Nitta and T. Takeuchi, *J. Antibiot. (Tokyo)* 1957, **10**, 181.
3. J. R. J. Sorenson, *Metal Ions in Biological Systems*, Vol. 14, II edn. Marcel Dekker, New York (1982).
4. M. A. El-Ries, S. M. Abu El-Wafa, F. A. Aly and M. El-Behairy, *Anal. Lett.* 1981, **18**, 1905.
5. S. M. Abu-El-Wafa, M. A. El-Ries and R. M. Issa, *Inorg. Chim. Acta* 1988, **151**, 197.
6. S. M. Abu-El-Wafa, M. A. El-Ries, F. M. Abou-Attia and R. M. Issa, *Anal. Lett.* 1989, **22**, 2703.
7. M. I. Ayad, A. Mashaly and M. M. Ayad, *Thermochim. Acta* 1991, **184**, 173.
8. M. Gaber and A. Mashaly, *Egypt. J. Chem.*, in press.
9. W. J. Geary, *J. Coord. Chem. Rev.* 1971, **7**, 81.
10. K. Nakamoto, *Infrared Spectra of Inorganic and Coordination Compounds*. John Wiley, New York (1977).
11. S. M. Abou El-Wafa, M. A. El-Ries and F. H. Ahmed, *Inorg. Chim. Acta* 1987, **136**, 127.
12. R. Eskenazi, J. Rasonvan and R. Levitus, *J. Inorg. Nucl. Chem.* 1966, **28**, 521.
13. R. Ugo, F. Conti, S. Cenimi, R. Mason and G. B. Robertson, *J. Chem. Soc., Chem. Commun.* 1968, 1498.
14. F. E. Lewis and H. Weigeld, *J. Chem. Soc. A* 1968, 1699.
15. B. J. Hathaway and A. A. G. Tomlinson, *Coord. Chem. Rev.* 1970, **5**, 1.
16. M. Hassanien and S. M. Abu-El-Wafa, *Z. Anorg. Allg. Chem.* 1989, **570**, 145.
17. B. J. Hathaway and D. E. Billing, *Coord. Chem. Rev.* 1970, **5**, 143.
18. Y. Nishida and S. Kida, *Coord. Chem. Rev.* 1979, **27**, 275.

Polyhedron Vol. 12, No. 7, pp. 749–757, 1993
Printed in Great Britain

0277–5387/93 $6.00+.00
© 1993 Pergamon Press Ltd

PREPARATION, CHARACTERIZATION, ELECTROCHEMICAL PROPERTIES AND SINGLE-CRYSTAL STRUCTURAL ANALYSIS OF $[Tc(SCP)_2(DMPE)_2](PF_6)_3$, WHERE SCP IS THE ZWITTER-IONIC LIGAND $^-SCH_2P^+(CH_3)_2(CH_2)_2P(S)(CH_3)_2$ AND DMPE IS 1,2-BIS(DIMETHYLPHOSPHINO)ETHANE

KEN-ICHI OKAMOTO,† JON R. KIRCHHOFF,† WILLIAM R. HEINEMAN and EDWARD DEUTSCH†‡

Biomedical Chemistry Research Center, Department of Chemistry, University of Cincinnati, Cincinnati, OH 45221-0172, U.S.A.

and

MARY JANE HEEG‡

Department of Chemistry, Wayne State University, Detroit, MI 48202-3489, U.S.A.

(*Received* 27 *August* 1992; *accepted* 23 *November* 1992)

Abstract—Dithiocarbamates react with excess 1,2-bis(dimethylphosphino)ethane (DMPE) in acid conditions in the presence of $[Tc(OH)(O)(DMPE)_2]^{2+}$ to generate the novel zwitter-ionic ligand $^-SCH_2P^+(CH_3)_2(CH_2)_2P(S)(CH_3)_2$ (abbreviated SCP). The technetium(III) complex $[Tc(SCP)_2(DMPE)_2](PF_6)_3$ has been isolated and characterized by elemental analysis, UV–vis spectroscopy and X-ray crystallography. Bond lengths around the octahedrally coordinated technetium(III) ion are Tc—S = 2.299(2) and Tc—P (average) = 2.437(8) Å. Electrochemical and spectroelectrochemical measurements are reported for the reversible technetium(III/II) couple; $E^{0\prime}$ has been determined to be −0.113 V vs Ag/AgCl (0.5 M TEAP/DMF). In addition, a chemically irreversible technetium(II/I) couple is observed at −1.310 V. The properties of $[Tc^{III/II}(SCP)_2(DMPE)_2]^{3+/2+}$ are compared to those observed previously for the related *cis*- and *trans*-$[Tc^{III/II}(SR)_2(DMPE)_2]^{+/0}$ complexes.

We[1–4] and others[5] are currently engaged in the exploration of six-coordinate cationic technetium-bis(thiolato) complexes with bidentate phosphine ligands. The technetium 3+ oxidation state is most stable in this series of compounds, although solids containing technetium in the 2+ oxidation state can be isolated. Technetium(III)/(II) redox potentials span a range of values (~ −0.2 to −0.6 V vs Ag/AgCl) as a result of manipulation of the R group on the thiolato ligand. A study of *cis* vs *trans* isomer formation in these complexes has been evolving and a reasonable explanation for observed isomer ratios has recently been proposed.[6] A number of crystallographic studies have shown little variability within a specific technetium oxidation state, i.e. all the technetium(III) complexes tend to have identical structural parameters and likewise for the technetium(II) complexes. The visible absorption spectra of these complexes contain sulphur-to-technetium charge-transfer bands and the energies of these bands can be related to their reduction potentials. In turn, the reduction potentials are related to the nucleophilicity of the thiolato ligand.

Most recently, the tris chelate complex [Tc(tdt)

† Present addresses: Dr Ken-Ichi Okamoto, Department of Chemistry, The University of Tsukuba, Tsukuba, Ibaraki 305, Japan. Dr Jon R. Kirchhoff, Department of Chemistry, University of Toledo, Toledo, OH 43606, U.S.A. Dr Edward Deutsch, Mallinckrodt Medical, Inc., 675 McDonnell Blvd, P.O. Box 5840, St Louis, MO 63134, U.S.A.

‡ Authors to whom correspondence should be addressed.

$(DMPE)_2]^+$ [where tdt is 3,4-toluenedithiolate and DMPE is 1,2-bis(dimethylphosphino)ethane] has been prepared and examined.[7] The trigonal prismatic distortion induced by the tdt ligand is accompanied by unusual properties which suggest that the technetium(III) centre in $[Tc(tdt)(DMPE)_2]^+$ is displaying some "technetium(II) character". This has encouraged further studies of other complexes containing bidentate sulphur ligands.

Dithiocarbamates are an interesting group of ligands that can stabilize unusual oxidation states, have multiple bonding properties and bridging modes of coordination.[8] The preparation and study of technetium complexes of dithiocarbamates, also known as 1,1-dithiolato ligands,† would allow important comparisons to $[Tc(tdt)(DMPE)_2]^+$ since tdt is a member of the class of 1,2-dithiolato ligands. The following is a preliminary report of our dithiocarbamate studies, wherein under the reaction conditions utilized the intact dithiocarbamate anion does not function as a ligand to technetium. Rather, a novel zwitter-ionic thiolato ligand is formed by the reaction of dithiocarbamate with DMPE. Since the product so formed contains a new thiolato ligand, we have characterized it fully and have related it to previously studied $[Tc(SR)_2(DMPE)_2]^{+/0}$ complexes.

EXPERIMENTAL

CAUTION! Technetium-99 emits a low energy (0.292 MeV) β particle with a half-life of 2.12×10^5 years. When handled in milligram amounts ^{99}Tc does not present a serious health hazard since common laboratory materials provide adequate shielding. Bremsstrahlung is not a significant problem due to the low energy of the β particle emission, but normal radiation safety procedures must be used at all times, especially when dealing with solid samples, to prevent contamination and inadvertent inhalation. In this paper the symbol Tc refers only to technetium-99; the metastable isotope ^{99m}Tc was not used in these studies.

Reagents

Unless otherwise noted, all chemicals were of reagent grade. Technetium-99, in the form of solid ammonium pertechnetate, was obtained from Oak Ridge National Laboratory and purified.[9] The DMPE ligand was purchased from Strem Chemical Co. and used without further purification. DMF and propylene carbonate were obtained from Burdick and Jackson Lab., Inc. Polarographic grade TEAP from G. F. Smith Chemicals was used in the electrochemical measurements. Prior to use the TEAP was dried at 60°C *in vacuo* over P_2O_5. No significant electroactive impurities were detected in either the solvent or supporting electrolyte. Na(dedc)·$3H_2O$ was purchased from Fisher Scientific and Na(dmdc)·$2H_2O$ from Aldrich Chemicals.

Synthesis of $[Tc(SCP)_2(DMPE)_2](PF_6)_3$

The starting complex, *trans*-$[Tc(OH)(O)(DMPE)_2](PF_6)_2$, was prepared by a method similar to that described in a previous paper,[1] using NH_4TcO_4 (200 mg, 1.1×10^{-3} mol) and DMPE (0.8 cm^3, 4.8×10^{-3} mol). To the orange–brown reaction mixture was added dropwise a solution of NH_4PF_6 (4 g) dissolved in a small amount of 1:1 methanol–water (v/v). The brown precipitate which appeared was kept at room temperature for 1 h and then refrigerated overnight. The precipitate was collected by filtration, washed with a methanol–water (1:1) solution, washed with pure water and then dried in air. Yield: 1.34 g. This material is a mixture of *trans*-$[Tc(OH)(O)(DMPE)_2](PF_6)_2$ and $H_2DMPE \cdot 2PF_6$.

To a suspension containing the above material (150 mg) in degassed ethanol (5 cm^3) was added Na(dedc)·H_2O (340 mg) in degassed ethanol (10 cm^3). This mixture was stirred at *ca* 50°C for 10 min, whereupon it became deep brown in colour. To this solution was added concentrated CF_3SO_3H (0.4 cm^3). The solution was kept at 50°C and continuously stirred for 40 min. The colour of the solution changed gradually from deep brown to dark brown to dark yellowish green and then to deep bluish green. The solution was then cooled to *ca* 30°C and solid NH_4PF_6 (0.2 g) was added. After standing at room temperature for *ca* 30 min a blue precipitate appeared which was collected by filtration, washed with ethanol and dried in a vacuum desiccator. Yield: 15–17 mg. This blue product was recrystallized as a powder from propylene carbonate/ethanol. Found: C, 26.2; H, 5.4; N,

† Acronyms and abbreviations: The following acronyms and abbreviations are used in this article: tdt = 3,4-toluenedithiolate; dedc = diethyldithiocarbamate; DEPE = 1,2-bis(diethylphosphino)ethane; dmdc = dimethyldithiocarbamate; DMF = N,N-dimethylformamide; DMPE = 1,2-bis(dimethylphosphino)ethane; DMSO = dimethylsulphoxide; OTTLE = optically transparent thin-layer electrode; PDE = platinum disk electrode; Ph = phenyl; pmdc = pentamethylenedithiocarbamate; ppmdc = 3-piperidino-pentamethylenedithiocarbamate; SCP = $^-SCH_2P^+(CH_3)_2(CH_2)_2P(S)(CH_3)_2$; STTCT = sulphur-to-technetium charge transfer; TEAP = tetraethylammonium perchlorate.

< 0.1; F, 24.2; P, 24.1; S, 7.7. Calc. for $[Tc(SCH_2P(CH_3)_2CH_2CH_2P(CH_3)_2S_{0.71})_2(DMPE)_2](PF_6)_3 \cdot 1.75(C_4H_6O_3) = C_{33}H_{78.5}O_{4.75}F_{18}P_{11}S_{3.4}Tc$: C, 26.6; H, 5.4; F, 24.4; P, 24.4; S, 7.8%. The non-stoichiometric amount of sulphur in the formulation is discussed in the crystallography sections below.

Single crystals suitable for X-ray analysis were obtained by dissolving the blue product at *ca* 38°C in a solution of 1:7 (v/v) propylene carbonate/ethanol. The solution was filtered to remove insoluble materials. The filtrate, which was preserved under an argon atmosphere, was held at room temperature for 4 h and then placed in a refrigerator for 4 days. The deep blue–black, diamond-plate shaped crystals which appeared were collected by filtration, washed with ethanol and dried in air.

Similar blue products were obtained by the above procedure using dmdc, pmdc and ppmdc instead of the dedc. The pmdc and ppmdc ligands were prepared by literature methods.[10]

Table 1. Crystallographic data for $[Tc(SCP)_2(DMPE)_2](PF_6)_3 \cdot 2(C_4H_6O_3)$

Formula	$Tc_1S_{3.4}P_{11}F_{18}O_6C_{34}H_{80}$
a (Å)	13.237(3)
b (Å)	21.709(6)
c (Å)	12.409(4)
β (°)	112.77(2)
V (Å^3)	3288(2)
Z	2
R^a	0.056
wR^a	0.056
Formula weight (amu)	1475.71
Space group	$P2_1/c$ (No. 14)
T (°C)	20
λ (Å)	0.71073
ρ(calc) (g cm^{-3})	1.490
μ (cm^{-1})	6.84
Transmission coefficients	1.000–0.692

$^a R = (\Sigma|\Delta F|)/\Sigma|F_o|$; w$R = [(\Sigma w|\Delta F|^2)/\Sigma w F_o^2]^{1/2}$.

Measurements

Elemental analysis was performed by Galbraith Laboratories, Knoxville, TN, U.S.A. UV–vis spectra were recorded in acetonitrile on a Cary 210 spectrophotometer (Varian) at ambient temperature. Electrochemical measurements were made with a Bioanalytical Systems, Inc. (BAS) CV-1B voltammograph. Potentials were monitored with a Keithley 178 digital multimeter and voltammograms were recorded on a Hewlett–Packard 7015B *X–Y* recorder. The visible spectra in the spectroelectrochemical experiment were also recorded on a Cary 210 spectrophotometer; the cell compartment was modified to accommodate electrical leads and an inert gas inlet. The working electrode for conventional cyclic voltammetry was a PDE (BAS). OTTLEs were constructed as previously described with 100 wires per inch gold minigrid.[11] An aqueous Ag/AgCl (3 M NaCl) electrode (BAS) and a platinum wire were used as reference and auxiliary electrodes, respectively. The reference electrode was isolated from the solution by a porous Vycor plug. All potentials are reported vs the Ag/AgCl (3 M NaCl) electrode.[12] In general, electrochemical experiments were performed as previously described.[13–17]

Crystallography. Single-crystal X-ray diffraction experiments were performed on a Nicolet R3 automated diffractometer with a graphite monochromator. Data are summarized in Table 1. All non-hydrogen atoms are refined anisotropically. Hydrogen atoms are placed in calculated positions with U defined as $\sim$ 1.5 times the equivalent isotropic U of the carbon atom to which they are bound. Absorption corrections were empirically derived from psi scans with the program SHELXTL.[18] Structure solutions by Patterson methods and refinements used the programs of SHELX-76.[19] Neutral atom scattering factors and corrections for anomalous dispersion were from the International Tables for X-ray Crystallography, Vol. 4.[20]

RESULTS AND DISCUSSION

Synthesis

Excess amounts of a dithiocarbamate, such as dmdc, dedc, pmdc or ppmdc, added to a suspension of *trans*-$[Tc(OH)(O)(DMPE)_2](PF_6)_2$ and $H_2DMPE \cdot 2PF_6$ under anaerobic conditions yield deep brown solutions. Acidification of these solutions produces gradual colour changes through dark brown to dark yellowish green and finally to a deep bluish green, ultimately yielding the title complex. These reactions do not proceed without the dithiocarbamate. Dithiocarbamates are known[8,10,21] to undergo an acid induced C—N cleavage to produce an amine and carbon disulphide.

$$H^+ + R_2NCS_2^- \rightleftharpoons HNR_2 + CS_2$$

The carbon atom of CS_2 is susceptible to nucleophilic attack by the DMPE phosphorus lone pair,

yielding a positively charged phosphonium ion and a negatively charged thiol:

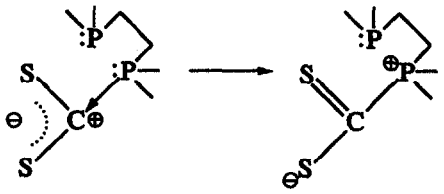

The final step in the formation of SCP involves a two-equivalent oxidation and the transfer of a sulphido group to the terminal phosphine. This process may or may not be assisted by coordination to technetium; it is unclear at what stage in the reaction sequence the thiol ligates to technetium. Reduction of the technetium(V) ion can be accomplished by excess dithiocarbamate or excess DMPE.

Under anaerobic conditions, a small amount of 1 M NaOH aqueous solution added to an aqueous solution of *trans*-$[Tc(SCP)_2(DMPE)_2]^{3+}$ yields a brown precipitate. When dissolved in acetonitrile this brown precipitate exhibits the identical absorption spectrum as that obtained at −0.500 V in the spectroelectrochemistry experiment (*vide infra*, spectrum B in Fig. 4). This suggests that the brown precipitate is the technetium(II) complex *trans*-$[Tc(SCP)_2(DMPE)_2]^{2+}$. When a small amount of concentrated HCl is added to an acetonitrile solution of the brown precipitate under an argon atmosphere, the colour of the solution changes to greenish blue and its spectrum coincides with that of the starting technetium(III) complex. Apparently the pH controlled interconversion between the technetium(III) and (II) complexes *trans*-$[Tc(SCP)_2(DMPE)_2]^{2+/3+}$ under anaerobic conditions is reversible; this pH induced redox interconversion is a general feature of *trans*-$[Tc^{III}(SR)_2(DMPE)_2]^{+/0}$ (R = alkyl or benzyl) complexes.[1,2]

The *trans*-$[Tc(SCP)_2(DMPE)_2](PF_6)_3$ salt is soluble in water, methanol, acetone, acetonitrile, propylene carbonate, DMF and DMSO, but is insoluble in 2-propanol, dichloromethane, chloroform, carbon tetrachloride and hexane. The complex is slightly soluble in ethanol and *p*-dioxane. These observations are consistent with the presence of a 3+ charged cation.

The synthesis of the novel ligand SCP has its basis in the acid induced C—N cleavage of dithiocarbamates. Consequently, reactions intending to preserve the dithiocarbamate ligand for intact coordination to technetium must be conducted in alkaline conditions. Even so, the zwitter-ionic ligand SCP is interesting in its own right. For one thing, the negatively charged ligating thiol is α to a positively charged phosphonium group and this is expected to significantly decrease the nucleophilicity of the thiol. Nucleophilicity, or σ-donating ability, of the thiol has been one of the properties we have been tracking through a series of technetium and rhenium thiolato complexes, in order to explore how changes in R are expressed in the redox potentials and spectral energies of the complexes.[1-4,6,22,23] Further interest in SCP might come from its potential use for bidentate coordination. In addition, modification of the terminal sulphido group could make SCP a valuable starting material.

UV–vis spectrum

The absorption spectrum of *trans*-$[Tc(SCP)_2(DMPE)_2]^{3+}$ exhibits three bands at 15.88 ($\varepsilon = 15.8 \times 10^3$ M^{-1} cm^{-1}), 26.60 ($\varepsilon = 4.6 \times 10^3$ M^{-1} cm^{-1}) and 36.90 kK ($\varepsilon = 7.2 \times 10^3$ M^{-1} cm^{-1}). The spectrum of the complex in acetonitrile is shown in Fig. 1. The absorption pattern over the entire region is similar to those of the corresponding bis-thiolato-DMPE complexes, *trans*-$[Tc(SR)_2(DMPE)_2]^+$, where R = methyl, ethyl, n-propyl, benzyl and *p*-methoxybenzyl.[2] By analogy,[4] the two lower energy bands are assigned to be sulphur (π) → Tc(π*) transitions. The higher energy UV absorption at 36.9 kK represents a P → Tc charge transfer band arising from the DMPE ligand.

Crystallography of trans-$[Tc(SCP)_2(DMPE)_2](PF_6)_3 \cdot 2(C_4H_6O_3)$

The independent portion of the structure consists of a half-cation, half-anion, complete PF_6 anion and a loosely held solvent molecule. The technetium atom and the phosphorus atom [P(5)] from the half-anion each occupy crystallographic inversion

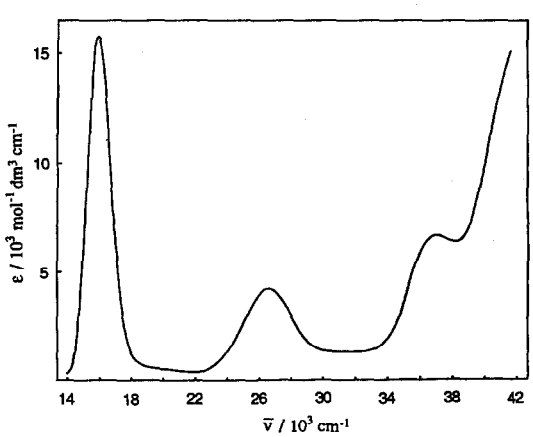

Fig. 1. The absorption spectrum of *trans*-$[Tc(SCP)_2(DMPE)_2]^{3+}$ recorded in acetonitrile.

centres. The general position PF_6 anion shows obvious disorder, so the six fluorine atoms around P(6) are described by 12 partial fluorine atoms. F(4)–F(9) are at 0.65 occupancy and F(10)–F(15) are at 0.35 occupancy. The assignment of these partial fluorine atoms makes little difference in the *R* value, but does improve the final ΔF map. Bond lengths and angles for the cation are presented in Table 2. Figure 2 illustrates the geometry and assigned labelling scheme for the cation.

The technetium atom is coordinated in *trans* octahedral geometry. The DMPE ligand bite angle is the largest distortion from ideal geometry and is normal for this ligand; P(3)—Tc—P(4) = 80.81(7)°. The zwitter-ionic ligand SCP is formally neutral, carrying a formal negative charge on the coordinated sulphur atom [S(1)] and a formal positive charge on the atom P(1). The terminal $R_3P{=}S$ fragment is neutral since the phosphorus–sulphur bond is best described as a double bond [S(2)—P(2) = 1.920(4) Å]. For comparison, the molecule $(2,4,6\text{-}Me_3C_6H_2PS_2)_2$ has a terminal P=S length of 1.917(1) Å.[24] P—S linkages are often found in dithiophosphate molecules wherein the phosphorus atom binds to two terminal sulphur atoms, theoretically in one double bond and one single bond. In these dithiophosphate molecules there is some delocalization and the average P—S length is approximately 1.97 Å,[25] significantly longer than that observed in the title complex.

The terminal sulphur atom [S(2)] has been assigned an occupancy factor less than unity (0.71) based on a comparison of thermal parameters with the other terminal atoms [C(6) and C(7)] and based on the knowledge that the elemental analysis implies the presence of a sulphur atom in about 71% of these sites in a bulk sample. The remaining sites might be occupied by either the phosphorus lone pair electrons or possibly a doubly-bound oxygen atom, neither of which would disturb the overall charge of the complex or lead to serious lattice disruptions. Disorders of the sulphido/oxo type have been noted in other structures.[26]

The solvated propylene carbonate molecule is disordered and probably exists at partial occupancy in the crystal lattice, although the solvent was assigned full occupancy in the model leading to a technetium/solvent ratio of 1/2. In fact, the elemental analysis results agree best with 1.75 solvent molecules per technetium (*vide supra*).

Table 2. Bond lengths (Å) and angles (°) in the cation $[Tc(SCP)_2(DMPE)_2]^{3+}$

Tc(1)—S(1)	2.299(2)	P(2)—C(6)	1.82(1)
Tc(1)—P(3)	2.442(2)	P(2)—C(7)	1.80(1)
Tc(1)—P(4)	2.431(2)	P(3)—C(8)	1.79(1)
S(1)—C(1)	1.842(7)	P(3)—C(9)	1.805(7)
S(2)—P(2)	1.920(4)	P(3)—C(10)	1.82(1)
P(1)—C(1)	1.809(7)	P(4)—C(11)	1.84(1)
P(1)—C(2)	1.787(7)	P(4)—C(12)	1.794(9)
P(1)—C(3)	1.772(6)	P(4)—C(13)	1.82(1)
P(1)—C(4)	1.783(6)	C(4)—C(5)	1.55(1)
P(2)—C(5)	1.802(8)	C(10)—C(11)	1.37(1)

Tc(1)—S(1)—C(1)	122.7(2)	P(4)—C(11)—C(10)	117(1)
Tc(1)—P(3)—C(8)	118.1(2)	C(1)—P(1)—C(2)	107.7(3)
Tc(1)—P(3)—C(9)	119.9(3)	C(1)—P(1)—C(3)	109.3(3)
Tc(1)—P(3)—C(10)	108.9(3)	C(1)—P(1)—C(4)	110.8(3)
Tc(1)—P(4)—C(11)	108.3(4)	C(2)—P(1)—C(3)	109.1(3)
Tc(1)—P(4)—C(12)	119.1(3)	C(2)—P(1)—C(4)	108.7(3)
Tc(1)—P(4)—C(13)	122.7(4)	C(3)—P(1)—C(4)	111.2(3)
S(1)—Tc(1)—P(3)	85.73(6)	C(5)—P(2)—C(6)	102.3(4)
S(1)—Tc(1)—P(4)	83.20(7)	C(5)—P(2)—C(7)	106.4(4)
S(1)—C(1)—P(1)	109.3(4)	C(6)—P(2)—C(7)	105.6(5)
S(2)—P(2)—C(5)	113.6(3)	C(8)—P(3)—C(9)	103.6(4)
S(2)—P(2)—C(6)	113.8(4)	C(8)—P(3)—C(10)	103.4(5)
S(2)—P(2)—C(7)	114.0(3)	C(9)—P(3)—C(10)	100.5(5)
P(1)—C(4)—C(5)	111.9(4)	C(11)—P(4)—C(12)	103.0(5)
P(2)—C(5)—C(4)	115.7(4)	C(11)—P(4)—C(13)	102.6(6)
P(3)—Tc(1)—P(4)	80.81(7)	C(12)—P(4)—C(13)	98.6(4)
P(3)—C(10)—C(11)	116.0(9)		

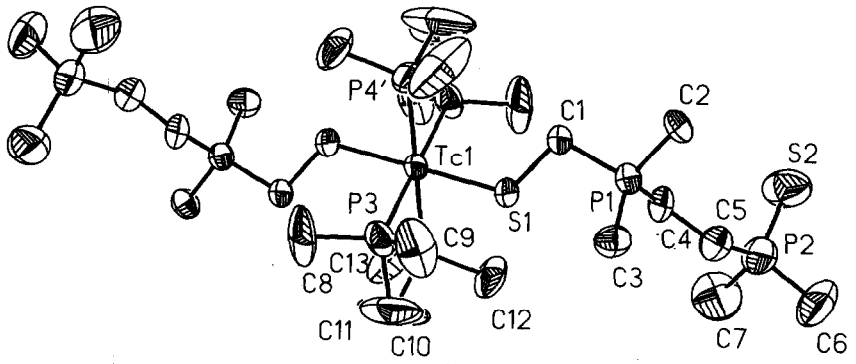

Fig. 2. A perspective view of *trans*-$[Tc(SCP)_2(DMPE)_2]^{3+}$ showing the assigned atom labels. The technetium atom occupies a crystallographic inversion centre. Ellipsoids represent 50% probability.

Structural analyses have been published previously for *trans*-$[Tc^{III}(SCH_3)_2(D)_2]^+$, where D = DMPE and DEPE,[1] and correspond closely with the structural parameters measured herein, cf. Tc—P = 2.428(6), Tc—S = 2.300(3) Å, Tc—S—C = 122.3(8)° and S—C = 1.842(7) Å for *trans*-$[Tc^{III}(SCH_3)_2(DMPE)_2]^+$; Tc—P = 2.45(1), Tc—S = 2.3025(5) Å, Tc—S—C = 121.2(1)° and S—C = 1.821(4) Å for *trans*-$[Tc^{III}(SCH_3)_2(DEPE)_2]^+$; and Tc—P = 2.437(8), Tc—S = 2.299(2) Å, Tc—S—C = 122.7(2)° and S—C = 1.842(7) Å for *trans*-$[Tc^{III}(SCP)_2(DMPE)_2]^{3+}$. Both Tc—S and Tc—P lengths in these complexes are sensitive to the technetium oxidation state and support the assignment of technetium(III) in the title complex. It should be noted that there is a substantial formal charge difference between the +1 complex $[Tc(SCH_3)_2(DMPE)_2]^+$ and the +3 complex $[Tc(SCP)_2(DMPE)_2]^{3+}$, but the coordination distances around technetium remain constant. A summary table presented previously[4] shows that Tc^{III}—SR distances are relatively insensitive to the nature of the R group.

Cyclic voltammetry

Figure 3 shows the cyclic voltammogram at a PDE for a 0.6 mM solution of *trans*-$[Tc(SCP)_2(DMPE)_2]^{3+}$, wherein two major redox couples are observed. A negative potential scan initiated at +0.400 V gives a reduction wave with a peak potential (E_{pc}) at −0.150 V, and upon switching the potential at −0.500 V the coupled oxidation wave (E_{pa}) is observed at −0.076 V on the positive scan. The separation between the cathodic and anodic peaks is 74 mV, which is typical for the one-electron reduction of *trans*-$[Tc(SR)_2(DMPE)_2]^{+/0}$ complexes[1] in TEAP/DMF. The ratio of the anodic/cathodic peak current is nearly unity. These facts indicate that the redox couple can be identified with the following one-electron reversible reaction:

$$trans\text{-}[Tc^{III}(SCP)_2(DMPE)_2]^{3+} + e^- \rightleftharpoons trans\text{-}[Tc^{II}(SCP)_2(DMPE)_2]^{2+}.$$

The formal reduction potential, $E^{0\prime}$, is determined to be −0.113 V and is recorded in Table 3. If the voltammogram is continued for a second cycle with an extension of the negative potential window to −1.55 V, a second reduction wave is observed with E_{pc} = −1.345 V. On the subsequent positive scan the corresponding oxidation is observed at E_{pa} = −1.275 V ($E^{0\prime}$ = −1.310 V). The second process is attributed to the technetium(II/I) redox couple. A close examination of the second cyclic voltammogram indicates that i_{pa} for the oxidation of technetium(II) to technetium(III) is reduced relative to i_{pc} for the reduction of technetium(III) to technetium(II) (i_{pc}/i_{pa} is approximately 1.85) and i_{pa} for the oxidation peak at +0.28 V is increased. This behaviour in the cyclic voltammogram can

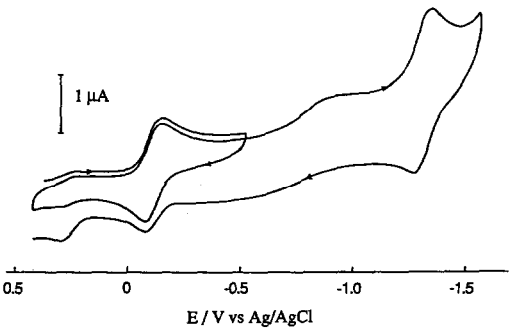

Fig. 3. Cyclic voltammograms of 0.6 mM *trans*-$[Tc(SCP)_2(DMPE)_2]^{3+}$ in 0.5 M TEAP/DMF at a PDE and room temperature; scan rate = 100 mV s^{-1}.

Table 3. Comparison redox potentials[a,b]

	Technetium(III/II), $E^{0\prime}$	Technetium(II/I), E^c
Trans-$[Tc(SCP)_2(DMPE)_2]^{3+}$	−0.113	−1.31[d]
Trans-$[Tc(SCH_3)_2(DMPE)_2]^{+}$ [1]	−0.550	−1.72
Cis-$[Tc(SPh)_2(DMPE)_2]^{+}$ [4]	−0.299	−1.11[d]
Trans-$[Tc(Cl)_2(DMPE)_2]^{+}$ [13]	−0.231	−1.41
Trans-$[Tc(Br)_2(DMPE)_2]^{+}$ [13]	−0.098	−1.27

[a] 25°C; PDE working electrode; scan rate 100 mV s^{-1}; 0.5 M TEAP/DMF; all values in V.
[b] $E^{0\prime} = (E_{pc}+E_{pa})/2$ vs Ag/AgCl (3 M NaCl) from cyclic voltammetry.
[c] Either E_p or $E^{0\prime}$, as specified.
[d] Irreversible at 25°C.

be ascribed to the instability of the technetium(I) species on the cyclic voltammetry time-scale, which results in a chemically irreversible technetium(II/I) redox couple.

Spectroelectrochemistry

In the thin-layer cyclic voltammogram in propylene carbonate *trans*-$[Tc^{III}(SCP)_2(DMPE)_2]^{3+}$ exhibits a reduction wave at −0.250 V and a coupled oxidation wave at −0.106 V ($E^{0\prime} = -0.178$ V). The large peak separation, $E_{pc} - E_{pa} = 0.144$ V, is typical for OTTLEs used with non-aqueous solvents, because of the large solution resistance inherent to the cell arrangement.[14,15] A similar thin-layer cyclic voltammogram was observed in DMF ($E^{0\prime} = -0.138$ V), but spectra could not be recorded because the complex decomposes in DMF on the time-scale of the OTTLE spectroelectrochemical experiment.

The spectra recorded for the technetium(III)/(II) couple during a potential step experiment are shown in Fig. 4. The initial spectrum recorded in the OTTLE after a potential application of +0.400 or +0.075 V is identical with that of the conventional UV–vis measurement for *trans*-$[Tc^{III}(SCP)_2(DMPE)_2]^{3+}$ (*vide supra*). The potential was subsequently moved in the negative direction from +0.075 to −0.500 V. In the spectrum recorded at −0.500 V a new absorption band appears at 513 nm and the band at 630 nm disappears, i.e. the reduction of technetium(III) to technetium(II) causes a large blue shift, consistent with its assignment as an S → Tc CT band. The spectrum at −0.500 V does not change for 2 h in propylene carbonate under these conditions. This supports the synthetic observation that the brown technetium(II) complex obtained from alkaline solution is stable over several hours in polar or non-polar solvents under argon. Apparently the technetium(II) complex is stable under anaerobic conditions. The potential was then moved in the positive direction from −0.500 to +0.075 V and the spectrum was scanned again. In this spectrum, a new absorption band appears at 497 nm along with the original band of the technetium(III) complex at 630 nm, although the band at 630 nm has only 30% of the initial absorbance. The spectrum at +0.400 V shows an increase in intensity of the band at 630 nm and a decrease in intensity of the band at 497 nm.

Similar spectral changes were observed during aerobic oxidation of bulk amounts of the brown technetium(II) complex obtained from the alkaline solution. That is, when the acetonitrile solution of

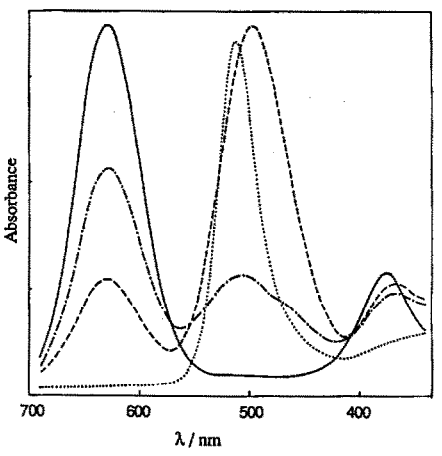

Fig. 4. The absorption spectra obtained during an OTTLE potential step experiment of 0.6 mM *trans*-$[Tc(SCP)_2(DMPE)_2]^{3+}$ in 0.5 M TEAP/propylene carbonate. Applied potentials vs Ag/AgCl are: original, −0.400 and +0.075 V (——); −0.500 V (· · ·); +0.075 V (– – –); and final scan +0.400 V (– · –).

the technetium(II) complex stands in air, it changes to the technetium(III) complex plus some other species; the spectrum of this solution is similar to that of the final scan in Fig. 4 in that it contains the additional peak at 497 nm which is not present in the original technetium(III) solution. Taking the stability of the technetium(II) species into consideration, these facts suggest that part of the *trans*-$[Tc^{II}(SCP)_2(DMPE)_2]^{2+}$ complex reverts to the original technetium(III) complex, but another fraction converts to a different species during oxidation.

The technetium(III/II) $E^{0\prime}$ values are solvent dependent, *viz.* the value obtained in propylene carbonate is more negative than that obtained in DMF. A similar trend was also observed for the technetium(II/I) couple of $[Tc(DMPE)_3]^{2+/+}$.[13] These data suggest that the variation of $E^{0\prime}$ in DMF and propylene carbonate follows the basicity of these solvents.

Electronic properties

The bis(thiolato)-bis(DMPE)-technetium(III) complexes hitherto examined have naturally separated into two classes. When the carbon atom bound to sulphur is saturated, $[Tc^{III}(SR)_2(DMPE)_2]^+$ (R = alkyl or benzyl) complexes have the following characteristics: (1) their geometry tends to be *trans*, (2) reversible couples are observed at *ca* −0.5 to −0.6 V for technetium (III/II) in TEAP/DMF vs Ag/AgCl, and (3) there are two visible STTCT bands *ca* 17 and 28 kK in acetonitrile. When the R group in $[Tc^{III}(SR)_2(DMPE)_2]^+$ is phenyl or a phenyl derivative the following characteristics are observed: (1) the geometry tends to be *cis*, (2) reversible technetium(III/II) couples are in the range −0.19 to −0.38 V, and (3) there are three visible STTCT bands at *ca* 17, 22 and 29 kK. The complex $[Tc(SCP)_2(DMPE)_2]^{3+}$ newly presented here has properties that transcend those of the two classes outlined above. As with an alkylthiolato complex it has *trans* geometry and this is expected since it is thought that the driving force which determines *cis*/*trans* isomerism in these complexes is primarily steric. However, unlike the other alkylthiolato complexes $[Tc(SCP)_2(DMPE)_2]^{3+}$ exhibits an uncommon ease of reduction. The technetium(III/II) reduction potential of this complex is −0.113 V, which is 437 mV more positive than that of *trans*-$[Tc(SCH_3)_2(DMPE)_2]^+$ and even 186 mV more positive than that of *cis*-$[Tc(SPh)_2(DMPE)_2]^+$ (see Table 3). The technetium(III/II) redox potential is strongly linked to the nature of the thiolato R group and as such is inversely related to the σ-donor ability at the thiol.[4] This suggests that the nucleophilicity of the SCP ligand is weaker than those of the other thiolato ligands examined since this complex is the easiest to reduce. Apparently this arises from the positively charged phosphonium group α to the sulphur donor atom in SCP. Orbital mixing between the sulphur donor and the P^+ atoms is also implied by the energies of the two STTCT bands, which are substantially lower than those found in *trans*-$[Tc(SCH_3)_2(DMPE)_2]^+$.

Speculation as to the identity of the intermediate species in the spectroelectrochemical reoxidation experiment leads to the possibility that the electron may be lost first from the terminal sulphido atom, temporarily forming an $S^\bullet$ radical or a disulphide linked dinuclear technetium(II) species. Internal reorganization could then restore the SCP ligand and yield the original technetium(III) species.

Acknowledgement—Financial support by the National Institute of Health grants nos HL-21276 and CA-42179 (E.D.), by the Department of Energy grant DE-FG02-86ER60487 (W.R.H.) and by Mallinckrodt, Inc. (E.D.) is gratefully acknowledged. The diffractometer used herein was purchased through an NSF equipment grant to Wayne State University.

REFERENCES

1. T. Konno, M. J. Heeg and E. Deutsch, *Inorg. Chem.* 1988, **27**, 4113.
2. T. Konno, J. R. Kirchhoff, W. R. Heineman and E. Deutsch, *Inorg. Chem.* 1989, **28**, 1174.
3. T. Konno, M. J. Heeg and E. Deutsch, *Inorg. Chem.* 1989, **28**, 1694.
4. T. Konno, M. J. Heeg, R. Seeber, J. R. Kirchhoff, W. R. Heineman and E. Deutsch, *Trans. Met. Chem.* 1993, in press.
5. For example, R. Münze, U. Abram, J. Stach and W. Hiller, *Inorg. Chim. Acta* 1991, **186**, 151; U. Abram, R. Beyer, P. Mading, I. Hoffman, R. Münze and J. Stach, *Z. Anorg. Allg. Chem.* 1989, **578**, 229; J. Stach, U. Abram and R. Münze, *Z. Chem.* 1989, **29**, 249.
6. L. Chang, M. J. Heeg and E. Deutsch, *Trans. Met. Chem.* 1993, in press.
7. T. Konno, M. J. Heeg, J. R. Kirchhoff, W. R. Heineman and E. Deutsch, *J. Chem. Soc., Dalton Trans.* 1992, 3069.
8. D. Coucouvanis, *Prog. Inorg. Chem.* 1970, **11**, 233.
9. K. Libson, B. L. Barnett and E. Deutsch, *Inorg. Chem.* 1983, **22**, 1695
10. D. DeFilippo, P. Deplano, F. Devillanova, E. F. Trogu and G. J. Verani, *Org. Chem.* 1973, **38**, 560.
11. T. P. DeAngelis and W. R. Heineman, *J. Chem. Ed.* 1976, **53**, 594.
12. The potential of this electrode is 0.201 V to the NHE.
13. A. Ichimura, W. R. Heineman, J.-L. Venderheyden and E. Deutsch, *Inorg. Chem.* 1984, **23**, 1272.

14. D. F. Rohrbach, W. R. Heineman and E. Deutsch, *Inorg. Chem.* 1979, **18**, 2536.
15. R. W. Hurst, W. R. Heineman and E. Deutsch, *Inorg. Chem.* 1981, **20**, 3298.
16. J. R. Kirchhoff, W. R. Heineman and E. Deutsch, *Inorg. Chem.* 1987, **26**, 3108.
17. A. Ichimura, W. R. Heineman and E. Deutsch, *Inorg. Chem.* 1985, **24**, 2134.
18. G. M. Sheldrick, SHELXTL. University of Göttingen, F.R.G. (1978).
19. G. M. Sheldrick, SHELX-76. University Chemical Laboratory, Cambridge (1976).
20. *International Tables for X-ray Crystallography*, Vol. 4. Kynoch Press, Birmingham (1974).
21. S. P. Ewing, D. Lockshon and W. P. Jencks, *J. Am. Chem. Soc.* 1980, **102**, 3072.
22. T. Konno, M. J. Heeg, J. A. Stuckey, J. R. Kirchhoff, W. R. Heineman and E. Deutsch, *Inorg. Chem.* 1992, **31**, 1173.
23. L. Chang, S.-I. Aizawa, M. J. Heeg and E. Deutsch, *Inorg. Chem.* 1991, **30**, 4920.
24. C. Lensch and G. M. Sheldrick, *J. Chem. Soc., Dalton Trans.* 1984, 2855.
25. J.-E. Andersson and C. Stalhadske, *Acta Cryst.* 1976, **B32**, 587 and refs therein.
26. For example, S. Bernès, F. Sécheresse and Y. Jeannin, *Inorg. Chim. Acta* 1992, **194**, 105.

Polyhedron Vol. 12, No. 7, pp. 759–763, 1993
Printed in Great Britain

0277–5387/93 $6.00+.00
© 1993 Pergamon Press Ltd

SUBSTITUTION REACTIONS OF $[Cu^{I}(AsPh_3)_3X]$ (X = Cl, Br OR I) WITH 3-PHENYL-2-THIOXOIMIDAZOLIDIN-4-ONE (ptiH) AND 5-MERCAPTO-1-PHENYL-1,2,3,4-TETRAZOLE (mptH)

RAMSHARAN SINGH and S. K. DIKSHIT*

Department of Chemistry, Indian Institute of Technology Kanpur, Kanpur 208 016, India

(*Received* 10 *August* 1992; *accepted* 20 *November* 1992)

Abstract—Reactions of $[Cu(AsPh_3)_3X]$ with the title ligands yield $[Cu(AsPh_3)_2(LH)X]$

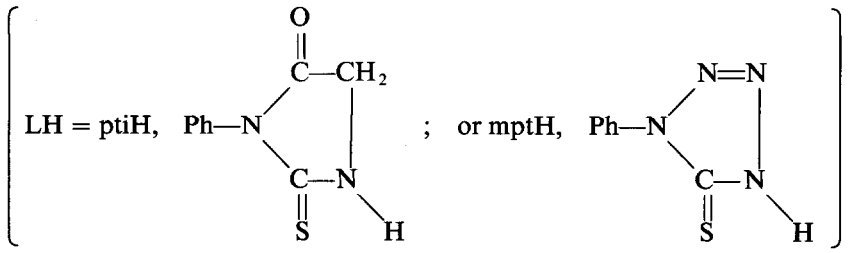

These complexes have been characterized on the basis of analytical, IR, electronic (UV–vis), ^1H NMR, conductivity and magnetic measurements. In all cases there is a distorted tetrahedral environment around copper(I), and the ligands (LH) bind through the thione sulphur atom to copper(I).

The application of heterocyclic thioamides in corrosion protection[1] and the biological importance of copper–sulphur interactions[2,3] have stimulated much of the research efforts exemplified by reports on the ligating behaviour of heterocyclic thiones.[4–16] Moreover, the copper(I) complexes may adopt di-,[17] tri-,[18] tetra-[2,19] and penta-coordination,[20] which basically depends upon the bulk as well as the electronic properties of the ligands. This has stimulated many workers to study the ligating behaviour of heterocyclic thiones, possessing an α-nitrogen heteroatom. Specifically, in this field of research the group of Karagiannidis has characterized structurally a number of mixed-ligand coordination compounds of copper(I) with heterocyclic thiones, possessing an α-nitrogen heteroatom and triaryl-phosphines[7–14] and -arsines.[15,16] The properties of triphenylphosphine, heterocyclic thione mixed-ligand complexes are fairly well known, but their arsine, stibine and bismuthine analogues are not well studied.

Following our interest in coordination properties of the ligands having the H—N—C=S group,[5,6,21–23] we have recently reported the phosphine counterpart[6] of the complexes. For the sake of comparison and in view of the unique properties of copper coordinated triphenylarsine,[24,25] we describe the syntheses and characterization of novel copper(I) distorted tetrahedral complexes, $[Cu(AsPh_3)_2(LH)X]$, with the title ligands, which behave as monodentate thione sulphur donors.

EXPERIMENTAL

Starting materials

All the chemicals used were either of Analar or chemically pure grade. Complexes of the type $[Cu(AsPh_3)_3X]$,[26] (X = Cl, Br or I) and the ligands 3-phenyl-2-thioxoimidazolidin-4-one[6] (ptiH) and 5-mercapto-1-phenyl-1,2,3,4-tetrazole[6] (mptH) were prepared by literature methods.

Physical methods

Sulphur, halide and copper were determined gravimetrically. The carbon, hydrogen and nitrogen analyses were performed at the Microanalytical

* Author to whom correspondence should be addressed.

Table 1. Analytical data of the complexes with colours, melting points (M.p.) and yields

Compound	Colour	Analytical data: Found (Calc.) (%) C	H	N	Cu	S	Halide	M.p.[a] (°C)	Yield (%)
$[Cu(AsPh_3)_2(ptiH)Cl]$	Maroon	54.5 (54.3)	3.6 (3.9)	4.6 (4.7)	10.8 (10.6)	5.3 (5.4)	6.0 (5.9)	95d	82
$[Cu(AsPh_3)_2(ptiH)Br]$	White	50.6 (50.5)	3.5 (3.6)	4.2 (4.4)	9.7 (9.9)	5.2 (5.0)	12.3 (12.5)	140d	85
$[Cu(AsPh_3)_2(ptiH)I]$	White	47.2 (47.1)	3.3 (3.4)	4.2 (4.1)	9.5 (9.2)	4.9 (4.7)	18.6 (18.4)	135d	80
$[Cu(AsPh_3)_2(mptH)Cl]$	White	51.2 (51.5)	3.7 (3.6)	9.9 (9.6)	10.7 (10.9)	5.3 (5.5)	5.9 (6.1)	158d	45
$[Cu(AsPh_3)_2(mptH)Br]$	White	47.2 (47.8)	3.2 (3.4)	8.7 (8.9)	10.3 (10.1)	5.3 (5.1)	12.9 (12.7)	158d	58
$[Cu(AsPh_3)_2(mptH)I]$	Orange	44.3 (44.5)	3.2 (3.1)	8.6 (8.3)	9.6 (9.4)	4.8 (4.8)	18.7 (18.8)	160d	46

[a] d = decomposed.

Laboratory, I.I.T. Kanpur, India. The IR spectra were recorded in KBr in the range 4000–400 cm^{-1} on Perkin–Elmer and Shimadzu IR-420 spectrophotometers. The electronic (UV–vis) spectra were recorded on a Shimadzu double beam UV-160 spectrophotometer. The ^1H NMR spectra were recorded on a JEOL JNM-PMX 60 SI NMR spectrometer in the range 0–20 ppm in $CDCl_3$ using TMS as an internal calibrant at room temperature. Conductivity measurements were performed on an Elico conductivity bridge type CM 82T in acetonitrile solution. Magnetic measurements were performed using a parallel-field vibrating sample magnetometer (VSM), model-150A (Princeton Applied Research Corporation, Princeton, NJ). Melting points of the complexes were recorded on a Fisher–John melting point apparatus and are uncorrected.

Preparation of compounds

Preparation of $[Cu(AsPh_3)_2(ptiH)X]$. To a benzene solution (30 cm^3) of the air-stable compound $[Cu(AsPh_3)_3X]$ (0.2 mmol) was added an equivalent amount (0.2 mmol) of the ligand ptiH and the solution/suspension was heated under reflux for *ca* 2 h. During refluxing the reaction mixture became almost clear. After cooling, the solution was filtered through a Whatman No. 1 filter paper to remove any insoluble particles. The resulting solution was concentrated under reduced pressure to half its volume. The addition of petroleum ether (60–80°C) (50 cm^3) resulted in the precipitation of the microcrystalline products on standing for 2–3 h. The complexes were centrifuged and washed several times with petroleum ether and dried *in vacuo*.

Preparation of $[Cu(AsPh_3)_2(mptH)X]$. To a benzene solution (30 cm^3) of $[Cu(AsPh_3)_3X]$ (0.2 mmol) was added an equivalent amount (0.2 mmol) of the ligand mptH and the resulting clear solution was stirred for *ca* 3 h. During the stirring some crystals of the complex were separated. The volume of the reaction mixture was reduced to *ca* 5 cm^3 under vacuum and excess petroleum ether (60–80°C) (50 cm^3) was added to ensure the maximum precipitation of the complexes. These complexes were centrifuged and washed several times with petroleum ether and dried *in vacuo*.

All these compounds are stable in air for several days but a few complexes are susceptible to air oxidation when left in air for more than a week. The air-oxidized products were not further studied. Melting points, yields and colours of the complexes are given in Table 1 along with the analytical data.

RESULTS AND DISCUSSION

The analytical data are in good agreement with the stoichiometry proposed as $[Cu(AsPh_3)_2(LH)X]$ (Table 1). These compounds are soluble in most of the organic solvents like C_6H_6, $CHCl_3$, CH_2Cl_2, DMSO, DMF, CH_3CN, etc. All the compounds are diamagnetic at room temperature. The conductivity of the complexes was found in the range 50–65 Ω^{-1} cm^2 mol^{-1} in acetonitrile and, consequently, were interpreted according to Geary[27] as being non-electrolytes.

The IR spectra of the ligands and complexes are summarized in Table 2. All the ligands adopt the thione form both in the free state and in their complexes. This is evident by the absence of the ν(SH) band in the 2500 cm^{-1} region in each, and by

Table 2. Major IR bands of the ligands and complexes (cm^{-1})

Compound	ν(NH)	ν(C=O)	ν(C=S)	Thioamide bands I	II	III	IV
Ligand (ptiH)	3180	1770	1165	1530	1300	1020	780
$[Cu(AsPh_3)_2(ptiH)Cl]$	3177	1771	1080	1532	1324	1140	745sh
$[Cu(AsPh_3)_2(ptiH)Br]$	3180	1776	1077	1530	1320	1139	746sh
$[Cu(AsPh_3)_2(ptiH)I]$	3240	1775	1075	1525	1320	1145	760
Ligand (mptH)	3023, 2904, 2745	—	1050	1492	1279, 1298	1002, 993	751, 793
$[Cu(AsPh_3)_2(mptH)Cl]$	2900	—	1040	1495	1300	995	754
$[Cu(AsPh_3)_2(mptH)Br]$	2900	—	1045	1495	1300	995	752
$[Cu(AsPh_3)_2(mptH)I]$	2950	—	1050	1505	1310	1000	751

sh = shoulder.

the presence of ν(NH) in the 2900–3300 cm^{-1} region.[28] The ligands contain a thioamide group (H—N—C=S) and give rise to four characteristic thioamide bands, namely, I, II, III and IV, in the regions 1500, 1300, 1000 and 800 cm^{-1} and have contributions from δ(N—H)+ν(C—N), ν(C=S)+ν(C=N)+ν(C—H), ν(C—N)+ν(C—S) and ν(C—S) modes of vibrations, respectively[6,29–31] (Table 2).

All complexes exhibited the characteristic bands of triphenylarsine.[32] In the case of coordination of the ligand with a carbonyl group, namely ptiH, through the carbonyl oxygen atom the ν(C=O) band should shift to a lower wave number and the thioamide band I [δ(N—H)+ν(C—N)] should shift to a higher wave number. However, if coordination is through the nitrogen atom the thioamide band I will shift to a lower wave number. However, the position of the band at *ca* 1770 cm^{-1}, assigned to ν(C=O), remains almost unaffected or slightly shifts to the higher wave number (*ca* $\Delta\nu = 1$–6 cm^{-1}) in the complexes, ruling out coordination through the carbonyl group. The band at *ca* 1165 cm^{-1}, assigned to ν(C=S) in the spectra of the ligand ptiH, either splits or shifts to a lower wave number (*ca* $\Delta\nu = 10$–15 cm^{-1}) on coordination. The thioamide band IV, which contains a major contribution from ν(C=S), splits or shifts to the lower region by *ca* $\Delta\nu = 41$–42 cm^{-1}, which indicates the involvement of the C=S group in the coordination (Fig. 1).

On complexation ν(C=S) of the ligand mptH (Fig. 2) at 1050 cm^{-1} splits. The thioamide band I at 1492 cm^{-1} undergoes a blue shift by 3–16 cm^{-1}. The thioamide band IV at 793 cm^{-1} undergoes a red shift (lit.[33] value 785 cm^{-1}). These observations support the bond formation between the metal and thione sulphur.

The band at 3180 cm^{-1}, assigned to ν(N—H), for the ligand ptiH becomes weak in the IR spectra of the complexes. The discernible ν(N—H) bands of the ligand mptH (Table 2) shift a little on complexation, indicating the non-involvement of the N—H group in the coordination.

Bonding via sulphur is also favoured in the complexes because copper(I), being a soft acid, should prefer to interact with a soft base such as sulphur and, indeed, the presence of a sulphur–copper(I) bond was confirmed by X-ray single-crystal structure of many complexes having a heterocyclic thione ligand possessing an α-nitrogen heteroatom.[7–16,34] Very recently the mixed-ligand coordination compounds of copper(I) with heterocyclic thiones and triphenylarsine[19] have been synthesized and their X-ray crystal structural characterization

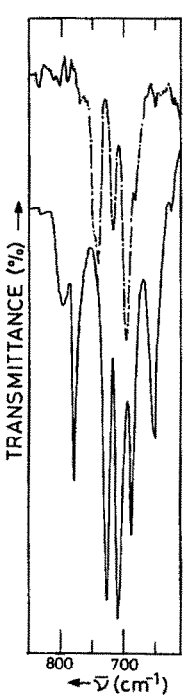

Fig. 1. The IR spectra of the ligand ptiH (——) and the complex $[Cu(AsPh_3)_2(ptiH)Br]$ (— - —).

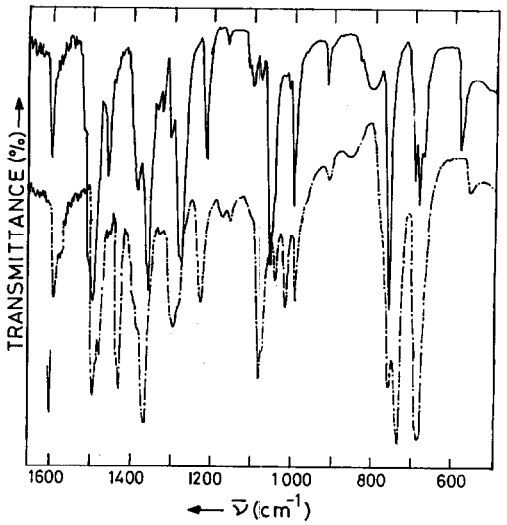

Fig. 2. The IR spectra of the ligand mptH (——) and the complex $[Cu(AsPh_3)_2(mptH)Cl]$ (— · —).

has been performed, in which exactly the same type of coordination environment and stoichiometry have been observed.

The ^1H NMR and electronic (UV–vis) spectra of the complexes and free ligands are given in Table 3, with assignments. The ^1H NMR spectra of the complexes clearly show peaks due to the ligands and triphenylarsines. The NMR signal of the >NH

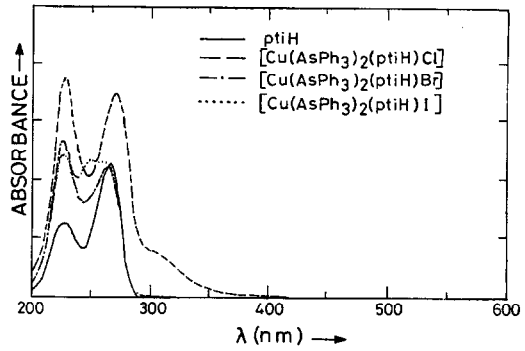

Fig. 3. The electronic (UV–vis) spectra of the ligand ptiH and its complexes.

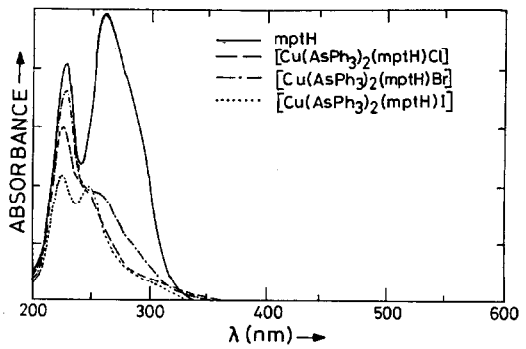

Fig. 4. The electronic (UV–vis) spectra of the ligand mptH and its complexes

Table 3. Electronic spectra of the ligands and the complexes in CH_3CN and ^1H NMR spectra of the ligands and complexes in $CDCl_3$

Compound	Band position λ_{max} (nm)	Assignment	^1H NMR signal with assignments (δ)
Ligand (ptiH)	227.0		4.30 (s, 2H, $>CH_2$ ring); 7.28 (m, 3H, *ortho*-H of $—C_6H_5$);
	265.0		*ca* 7.46 (m, *meta*- and *para*-H of $—C_6H_5$); 10.37 (s, 1H, >NH group)[a]
$[Cu(AsPh_3)_2(ptiH)Cl]$	226.5	IL	4.00 (s, 2H, $>CH_2$ ring); 6.83–7.67 (m, 35H, $—C_6H_5$ groups);
	270.0	IL	
	305.0sh	IL	
$[Cu(AsPh_3)_2(ptiH)Br]$	225.0	IL	4.10 (s, 2H, $>CH_2$ ring); 7.00–7.67 (m, 35H, $—C_6H_5$ groups);
	263.0	IL	10.27 [s(broad), 1H, >NH group]
$[Cu(AsPh_3)_2(ptiH)I]$	225.0	IL	4.00 (s, 2H, $>CH_2$ ring); 6.83–7.67 (m, 35H, $—C_6H_5$ groups);
	249.5	IL	9.47 [s(broad), 1H, >NH group]
Ligand (mptH)	227.0		7.63 (m, 3H, *ortho*- and *para*-H of $—C_6H_5$); 7.89 (m, 2H, *meta*-H of $—C_6H_5$); 10.50–13.50 (s, 1H, —SH)[b]
	259.5		
$[Cu(AsPh_3)_2(mptH)Cl]$	225.0	IL	6.83–7.67 (m, $—C_6H_5$ groups)
	245.0sh	IL	
$[Cu(AsPh_3)_2(mptH)Br]$	226.5	IL	6.83–7.67 (m, $—C_6H_5$ groups)
	251.5	IL	
$[Cu(AsPh_3)_2(mptH)I]$	224.0	IL	7.00–7.67 (m, 35H, $—C_6H_5$ groups); 9.37 [s(broad), 1H, >NH
	247.0	IL	group]

[a] These are the literature values from ref. 35, in DMSO-d_6; sh = shoulder.
[b] These are the literature values from ref. 36, in DMSO-d_6.

proton of the complexes appeared as a broad signal. The broadening of the signals may be due to hydrogen bonding.[8,15,16] The δ values become lower as the halogen atomic radius increases (10.27 and 9.47 in the bromine and iodine complexes of the ligand ptiH, respectively).[16] The proportions of the protons, observed by integration, exactly match the proposed stoichiometry of the complexes. As expected, only UV absorption bands are observed, which are assigned as intraligand (IL) transitions (Figs 3 and 4).

REFERENCES

1. B. Donnelly, T. C. Downine, R. Grzeskowiak, H. R. Hamburg and D. Short, *Corros. Sci.* 1978, **18**, 109.
2. P. J. Colman, H. C. Freeman, J. M. Gun, M. Murata, V. A. Norris, J. A. M. Ramshow and M. P. Venkatappe, *Nature (London)* 1978, **272**, 319.
3. K. D. Karlin and J. Zubieta (Editors), *Copper Coordination Chemistry: Biochemical and Inorganic Perspectives*. Adenine Press, Guilderland, NY (1983).
4. E. S. Raper, *Coord. Chem. Rev.* 1985, **61**, 115.
5. R. Singh and S. K. Dikshit, *Polyhedron* 1992, **11**, 2099.
6. R. Singh and S. K. Dikshit, *Synth. React. Inorg. Met.-Org. Chem.* 1992, **22**, 1141 and refs therein.
7. P. Karagiannidis, P. Aslanidis, S. Papastefanou, D. Mentzafos, A. Hountas and A. Terzis, *Inorg. Chim. Acta* 1989, **156**, 265.
8. P. Karagiannidis, P. Aslanidis, D. P. Kessissoglon, B. Krebs and M. Dartmann, *Inorg. Chim. Acta* 1989, **156**, 47 and refs therein.
9. S. Skoulika, A. Aubry, P. Karagiannidis, P. Aslanidis and S. Papastefanou, *Inorg. Chim. Acta* 1991, **183**, 207.
10. C. Leconite, St. Skoulika, P. Aslanides, P. Karagiannidis and S. Papastefanou, *Polyhedron* 1989, **8**, 1103.
11. S. K. Hadjikakou, P. Aslanidis, P. Karagiannidis, A. Hountas and A. Terzis, *Inorg. Chim. Acta* 1991, **184**, 161.
12. P. Karagiannidis, S. K. Hadjikakau, P. Aslanidis and A. Hountas, *Inorg. Chim. Acta* 1990, **178**, 27.
13. S. K. Hadjikakou, P. Aslanidis, P. Karagiannidis, D. Mentzafos and A. Terzis, *Polyhedron* 1991, **10**, 935.
14. P. Karagiannidis, P. Aslanidis, S. Papastefanou, D. Mentzafos, A. Hountas and A. Terzis, *Polyhedron* 1990, **9**, 981.
15. P. Karagiannidis, P. Akrivos, A. Aubry and S. Skoulika, *Inorg. Chim. Acta* 1991, **188**, 79.
16. P. Karagiannidis, P. Akrivos, D. Mentzafos and A. Terzis, *Inorg. Chim. Acta* 1991, **181**, 263.
17. T. N. Sarrel and D. L. Jameson, *J. Am. Chem. Soc.* 1983, **105**, 6013.
18. J. C. Dyason, P. C. Healy, C. Pakawatchai, V. A. Patrick and A. H. White, *Inorg. Chem.* 1985, **24**, 1957 and refs therein.
19. L. M. Engelhardt, C. Pakawatchai, A. H. White and P. C. Healy, *J. Chem. Soc., Dalton Trans.* 1985, 125 and refs therein.
20. B. C. Green, C. H. L. Kennard, G. Smith, M. M. Elcombe, F. H. Moore, B. D. James and A. H. White, *Inorg. Chim. Acta* 1984, **83**, 117.
21. S. K. Dikshit and V. Chauhan, *Trans. Met. Chem.* 1986, **11**, 223.
22. S. K. Dikshit and V. Chauhan, *Trans. Met. Chem.* 1986, **11**, 403.
23. S. K. Dikshit and V. Chauhan, *Bull. Chem. Soc. Japan* 1987, **60**, 3005.
24. S. J. Lippard and P. S. Welcker, *Inorg. Chem.* 1972, **11**, 6.
25. S. Sakaki, K. Ohkubo, H. Fujiwara and A. Ohyoshi, *J. Molec. Catal.* 1982, **16**, 181.
26. S. J. Lippard and D. A. Ucko, *Inorg. Chem.* 1968, **7**, 1051.
27. W. J. Geary, *Coord. Chem. Rev.* 1971, **7**, 81.
28. L. K. Ramachandran, E. P. P. Agues and W. B. McConnel, *Analyt. Chem.* 1955, **27**, 1734.
29. C. N. R. Rao and R. Venkataraghvan, *Spectrochim. Acta* 1962, **18**, 541.
30. C. N. R. Rao, R. Venkataraghvan and T. R. Kartruri, *Can. J. Chem.* 1964, **42**, 36.
31. I. Suzuki, *Bull. Chem. Soc. Japan* 1962, **35**, 1286, 1449, 1456.
32. J. C. Sheldon and S. Y. Tyree Jr, *J. Am. Chem. Soc.* 1958, **80**, 2120.
33. B. Singh and R. D. Singh, *J. Inorg. Nucl. Chem.* 1977, **39**, 25.
34. E. S. Raper, J. R. Creighton, J. D. Wilson, W. Clegg and A. Milne, *Inorg. Chim. Acta* 1989, **115**, 77.
35. *Hand book of Proton—NMR Spectra and Data* (Edited by Asahi Research Center Co., Ltd, Tokyo, Japan), Vol. 3, Spectra No. 2153. Supervised by Shin-ichi Sasaki, Academic Press, Tokyo (1985).
36. *Hand book of Proton—NMR Spectra and Data* (Edited by Asahi Research Center Co., Ltd, Tokyo, Japan). Vol. 3, Spectra No. 1315. Supervised by Shin-ichi Sasaki, Academic Press, Tokyo (1985).

Polyhedron Vol. 12, No. 7, pp. 765–770, 1993
Printed in Great Britain

0277–5387/93 $6.00+.00
© 1993 Pergamon Press Ltd

CATIONIC DERIVATIVES OF NIOBOCENE(IV). CRYSTAL STRUCTURES OF $[Cp_2NbL_2][BF_4]_2$ (L = CNMe, NCMe)

MARIA A. A. F. DE C. T. CARRONDO, JOSÉ MORAIS, CARLOS C. ROMÃO* and MARIA J. ROMÃO

Centro de Tecnologia Química e Biológica and Instituto Superior Técnico, R. da Quinta Grande 6, 2780 Oeiras, Portugal

and

LUÍS F. VEIROS

Centro de Química Estrutural, I.S.T., Av. Rovisco Pais, 1096 Lisboa Codex, Portugal

(*Received* 31 *July* 1992; *accepted* 20 *November* 1992)

Abstract—The isomeric cationic derivatives of niobocene, $[Cp_2Nb(NCMe)_2][BF_4]_2$ and $[Cp_2Nb(CNMe)_2][BF_4]_2$, were prepared from $[Cp_2NbCl_2]$ and the ligands in the presence of $TlBF_4$. The crystal structure determination made on both complexes shows that the cations are isostructural, with pseudo-tetrahedral symmetry and linear ligands. Although the C≡N distances are normal, the Nb—N and Nb—C distances are at the short end of the range found for niobium complexes of these ligands.

In the course of our work on group 6 metallocene chemistry we have prepared a number of d^2 cationic complexes of types $[Cp_2MXL]^+$ and $[Cp_2ML_2]^{2+}$ (M = Mo, W; L = two-electron donor). Some of these 18-electron cations are rather stable to substitution and addition of nucleophiles at the η^5-Cp ring[1] or at the unsaturated ligand L. In the case where L = NCR or CNR, amidines[2] or the iminocarbenes[3] are formed.

No similar chemistry has been performed for the group 5 metallocene complexes and very few cationic complexes of these metallocenes have been reported.[4] In this group three consecutive oxidation states (+3, +4, +5) are easily available and, therefore, the possibility of tuning ligand reactivity by changes in complex charge and electronic configuration (d^2, d^1, d^0) is to be expected.

As an entry into this field resulting from our interest in nitrile and isonitrile activation, we describe, in this paper, the preparation and structural characterization of the isomeric complexes $[Cp_2NbL_2][BF_4]_2$ (L = NCMe, CNMe).

*Author to whom correspondence should be addressed.

RESULTS AND DISCUSSION

Chemical studies

Treatment of a suspension of $[Cp_2NbCl_2]$ with $TlBF_4$ in acetonitrile gives a smooth reaction and a red–brown solution. After filtration, concentration and addition of diethyl ether a crystalline orange precipitate of $[Cp_2Nb(NCMe)_2][BF_4]_2$ (**1**) is isolated in 80% yield. When the same reaction is performed in the presence of excess CNMe, also in acetonitrile solvent, the yellow complex $[Cp_2Nb(CNMe)_2][BF_4]_2$ (**2**) is isolated in 70% yield.

Both complexes **1** and **2** are very air-sensitive and the analytical results obtained were rather poor. Their paramagnetism precluded NMR measurements and, therefore, the characterization is based on IR and single-crystal X-ray diffraction analysis (see below). The IR spectrum of **1**, in KBr pellets prepared and measured under an argon atmosphere, shows two weak absorptions at 2280 and 2245 cm^{-1}, assignable to the NCMe ligands. These values are shifted *ca* 50 cm^{-1} to lower wave numbers relative to the isostructural $[Cp_2Mo(NCMe)_2][PF_6]_2$,[1] but still have a positive shift relative to free NCMe (2220 cm^{-1}).

The values of the ν(C≡NMe) stretching vibrations in **2** appear at 2250 and 2240 cm^{-1}, which is the same value observed for the isostructural $[Cp_2Mo(CNMe)_2][PF_6]_2$.[3]

Attempts to produce the d^0 cation $[Cp_2Nb(NCMe)_3]^{3+}$ through reaction of $[Cp_2NbCl_2]^{2+}$[5] with $TlBF_4$ were unsuccessful and, even in refluxing acetonitrile, no reaction was observed.

Preliminary reactions show that the dications **1** and **2** are very reactive towards nucleophiles, but the paramagnetic products have not yet been unequivocally characterized. Nevertheless, **1** does not undergo simple nitrile substitution with bipyridyl since the known $[Cp_2Nb(bipy)]^{2+}$[4c] complex is not formed in the reaction of **1** with this chelating ligand.

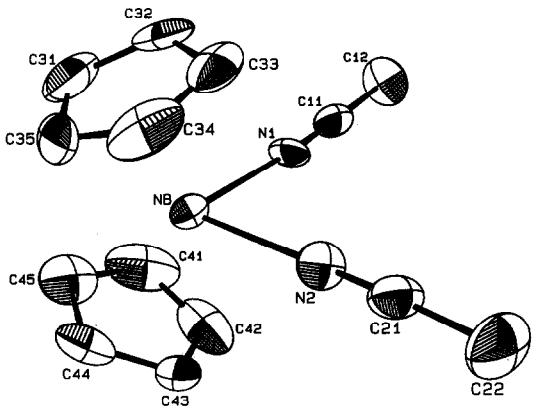

Fig. 1. ORTEP diagram of $[Cp_2Nb(NCMe)_2][BF_4]_2$ showing 30% thermal ellipsoids.

Crystallographic studies

Complexes **1** and **2** are isostructural; molecular diagrams with atom numbering schemes are represented in Figs 1 and 2, respectively. Bond lengths and angles are given in Tables 1 and 2, respectively. The crystal structures consist of discrete $[Cp_2Nb(NCMe)_2]^{2+}$ and $[Cp_2Nb(CNMe)_2]^{2+}$ cations and two $[BF_4]^-$ anions in each case. The cations show the usual bent metallocene coordination with a pseudo-tetrahedral arrangement about the metal atom, if the coordination is considered to the centre of the η^5-cyclopentadienyl rings. However, this type of ligand can also be described as occupying three coordination positions, giving the central metal atom a formal eight-fold coordination.[6] The Cp—Nb—Cp angles defined by the ring normals are 136.6(6)° for **1** and 139.2(5)° for **2**. The bonding angles at the metal atom, N(1)—Nb—N(2)

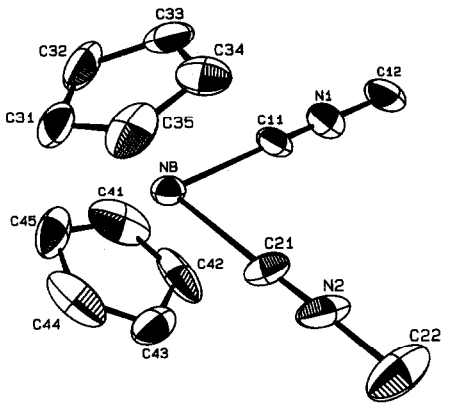

Fig. 2. ORTEP diagram of $[Cp_2Nb(CNMe)_2][BF_4]_2$ showing 30% thermal ellipsoids.

Table 1. Selected bond lengths (Å) and angles (°) for $[Cp_2Nb(NCMe)_2][BF_4]_2$ (**1**)

Nb—N(1)	2.165(5)	Nb—Cp(1)	2.11(1)[a]
Nb—N(2)	2.159(4)	Nb—Cp(2)	1.99(1)
N(1)—C(11)	1.111(6)		
N(2)—C(21)	1.124(7)	B—F range	1.23(2)–1.43(2)
C(11)—C(12)	1.463(8)		
C(21)—C(22)	1.449(8)	Cp rings	
		C—C range	1.37(1)–1.42(1)
N(2)—Nb—N(1)	83.8(2)	Cp(1)—Nb—Cp(2)	136.6(6)[b]
C(11)—N(1)—Nb	175.9(12)		
C(21)—N(2)—Nb	177.3(10)	F—B—F range	82(2)–132(2)
C(12)—C(11)—N(1)	178.7(6)		
C(22)—C(21)—N(2)	177.5(10)	Cp rings	
		C—C—C range	103(1)–112(1)

[a] Ring normal lengths.
[b] Angle between the ring normals at the niobium atom.

Table 2. Selected bond lengths (Å) and angles (°) for $[Cp_2Nb(CNMe)_2][BF_4]_2$ (**2**)

Nb—C(11)	2.164(6)	Nb—Cp(1)	2.07(1)[a]
Nb—C(21)	2.179(5)	Nb—Cp(2)	2.02(1)
C(11)—N(1)	1.133(6)		
C(21)—N(2)	1.122(6)	B—F range	1.28(1)–1.41(1)
N(1)—C(12)	1.479(7)		
N(2)—C(22)	1.451(7)	Cp rings	
		C—C range	1.32(1)–1.46(1)
C(21)—Nb—C(11)	84.6(2)	Cp(1)—Nb—Cp(2)	139.2(5)[b]
N(1)—C(11)—Nb	179.4(16)		
N(2)—C(21)—Nb	178.5(15)	F—B—F range	100(1)–120(1)
C(12)—N(1)—C(11)	173.8(16)		
C(22)—N(2)—C(21)	176.6(9)	Cp rings	
		C—C—C range	101(1)–114(1)

[a] Ring normal lengths.
[b] Angle between the ring normals at the niobium atom.

83.8(2)° and C(11)—Nb—C(21) 84.6(2)°, are comparable to the theoretical value 85°, calculated by Lauher and Hoffmann[7] for bis-cyclopentadienyl d^1 complexes.

The Nb—N bond distances are 2.165(5) and 2.159(4) Å in **1** and the Nb—C bond distances are 2.164(6) and 2.179(5) Å in **2**. The C≡N bond distances are comparable in both complexes (see Table 3) and the acetonitrile and methyl-isonitrile ligands are both linear.

Most of the structurally characterized niobium complexes with nitrile and isonitrile ligands have octahedral and pentagonal bipyramidal coordinations with linear terminal ligands. A comparison between Nb—N, Nb—C and C≡N bond lengths in some of these and the title complexes is presented in Table 3. From these data it is clear that the metal–ligand bonds in complexes **1** and **2** lie in the short range of distances normally observed. A similar shortened W—CNMe bond [1.15(3) Å] is observed in the related cation $[Cp_2WBr(CNMe)]^+$, which shows ν(C≡N) at wavelengths similar to **2** (2210 cm^{-1}).[3]

This effect cannot be rationalized on the basis of back-donation from the metal to the ligands, as this would imply longer C≡N distances and bent ligands as reported for the strongly bent CN^{t}Bu ligand of complex $[Cp_2MoCN^tBu]$, which has a C≡N distance of 1.193(4) Å and shows ν(C≡N) at very low wave numbers in the IR spectrum.[12]

Table 3. Comparison of structural parameters within alkyl isonitrile/acetonitrile niobium complexes

Complex	Nb—C (Å)	Nb—N (Å)	C≡N (Å)	Ref.
$[Cp_2Nb(CNMe)_2][BF_4]_2$	2.164(6) 2.179(5)		1.133(6) 1.122(6)	This work
$[CpNb(CNCMe_3)_4Cl]^+$	2.203(9) 2.211(10)		1.13(1) 1.14(1)	6
$[Nb_2Cl_6(CNCMe_3)_6]$	2.226(13)–2.299(14)		1.12(2)–1.15(2)	8
$[Nb_3Cl_8(CNCMe_3)_5]$	2.202(12)–2.266(13)		1.12(1)–1.17(1)	9
$[Cp_2Nb(NCMe)_2][BF_4]_2$		2.165(5) 2.159(4)	1.111(6) 1.124(7)	This work
$[Nb_2Cl_4(OMe)_4(NCMe)_2]$		2.215(15) 2.242(14)	1.14(2) 1.15(2)	10
$[NbCl_4(NCMe)_2]\cdot CH_3CN$		2.220(13)	1.17(2)	11
$[\{NbCl_2S(NCMe)_2\}_2]\cdot 2CH_3CN$		2.312(12) 2.322(16)	1.12(2) 1.13(2)	11
$[\{NbCl_2S(NCMe)_2\}_2]\cdot CH_3CN$		2.286(26)–2.334(22)	1.10(4)–1.15(4)	11

Furthermore, according to EHMO calculations, π-back-donation from the Cp_2Mo^{IV} fragment to nitriles is negligible.[2] Thus, the observed contraction of the M—NCMe and M—CNMe bonds in metallocene cationic derivatives probably results from a set of circumstances: namely (1) a very favourable σ-donation overlap between these ligands and the cationic $[Cp_2M]^{n+}$ fragment and (2) a rather sterically undemanding coordination environment on the C—M—C plane.

CONCLUSIONS

From the IR and structural data reported, both nitrile and isonitrile ligands seem to be activated towards nucleophilic addition reactions in the complexes $[Cp_2Nb(NCMe)_2][BF_4]_2$ (**1**) and $[Cp_2Nb(CNMe)_2][BF_4]_2$ (**2**). Failure to observe the simple substitution reaction of bipy for NCMe in complex **1** supports this suggestion, which is currently under investigation.

EXPERIMENTAL

All preparations and manipulations were performed under argon, using standard Schlenk techniques and an MBraun glove-box. Acetonitrile was dried by refluxing CaH_2, followed by distillation and was kept over 3 Å molecular sieves. Et_2O was distilled over Na/benzophenone and kept over 4 Å molecular sieves. IR samples were prepared in a glove-box and measured in an argon purged compartment of a Mattson Polaris FTIR spectrometer. Literature procedures were followed for the preparation of Cp_2NbCl_2[13] and CNMe.[14]

Preparation of **1**

A suspension of Cp_2NbCl_2 (0.120 g, 0.41 mmol) in dry acetonitrile (15 cm^3) was treated with $TlBF_4$ (0.262 g, 0.90 mmol) with rapid magnetic stirring at room temperature. After 2 h the mixture was filtered and the red–brown solution concentrated. Addition of Et_2O gave an orange precipitate, which was collected by filtration and recrystallized from acetonitrile/Et_2O. Yield 151 mg, 80%. IR (cm^{-1}; KBr): 2280 (vw); 2245 (w).

Preparation of **2**

A suspension of Cp_2NbCl_2 (0.280 g, 0.98 mmol) in dry acetonitrile (15 cm^3) was successively treated with excess CNMe (0.1 cm^3) and $TlBF_4$ (0.584 g, 2.00 mmol). A red solution and a white suspension were promptly formed and after 2 h stirring at room temperature the mixture was filtered and the resulting red solution concentrated. The slow addition of Et_2O formed yellow needles of **2**, which were collected by filtration and dried *in vacuo*. Yield 328 mg, 70%. IR (cm^{-1}; Nujol mull): 2250 (m); 2240 (m).

X-ray data of **1** *and* **2**

Suitable crystals of the complexes were obtained by slow diffusion of Et_2O in concentrated solutions of the complexes in NCMe. A single crystal of each compound was mounted in Lindemann capillaries under an argon atmosphere and the intensity data were measured on an Enraf–Nonius CAD-4 diffractometer using graphite monochromatized Mo-K_α radiation ($\lambda = 0.71069$ Å). Cell dimensions and an orientation matrix were obtained by least-squares refinement of setting angles for 25 automatically centred reflections, in the range $13.0° < \theta < 16.0°$ for **1** and $10.4° < \theta < 15.3°$ for **2**. Crystallographic and data collection parameters are presented in Table 4.

Structure determination and refinement

The structures were solved by a combination of Patterson and electron density difference-Fourier syntheses. From the systematic absences, both space groups *Pnma* (No. 62) and $Pna2_1$ (No. 33) were possible. Refinement on each structure was performed in both space groups up to a complete isotropic model. In the space group *Pnma* both ligands L and the metal atom were sitting in crystallographic mirror planes, but disordered models with constrained distances had to be considered for the BF_4^- anions. However, while in the acentric space group a reasonable geometric definition with inverted tetrahedra could be achieved for each structure, in the centric space group this was only possible for one of the anionic positions. Consequently, the R factors were not so good, $R = 0.12$ and $R = 0.11$ for **1** and **2** in space group *Pnma*, while in the space group $Pna2_1$, R was 0.09 for **1** and 0.08 for **2**. Refinement was thus continued in $Pna2_1$, for both structures, and constraints were applied to the C—C bonds in the Cp rings.

As compound **2** was prepared and crystallized in the presence of acetonitrile the correct assignment of the type of atom bonded to the metal had to be confirmed. When both ligands were considered as isonitriles the isotropic thermal parameters gradually increased from the niobium atom to the methyl group. However, when carbon and nitrogen atoms from the C≡N moiety were interchanged abnormal thermal parameters resulted, indicating that the initial assignment was the correct one.

Table 4. Crystallographic and data collection parameters

	$[Cp_2Nb(NCMe)_2][BF_4]_2$	$[Cp_2Nb(CNMe)_2][BF_4]_2$
Crystal data		
Formula	$C_{14}H_{16}N_2B_2F_8Nb$	$C_{14}H_{16}N_2B_2F_8Nb$
M	478.807	478.807
Space group	$Pna2_1$	$Pna2_1$
a (Å)	17.925(2)	17.829(3)
b (Å)	13.436(2)	13.404(3)
c (Å)	7.9467(7)	7.994(1)
V (Å^3)	1913.9	1910.4
Z	4	4
D_c (g cm^{-3})	1.661	1.665
μ(Mo-K_α) (cm^{-1})	6.40	6.42
F(000)	948	948
Data collection		
No. of measured reflections	3174 ($\pm h, k, l$)	3703 ($\pm h, k, l$)
2θ range (°)	$3.0 \leqslant 2\theta \leqslant 60.0$	$3.0 \leqslant 2\theta \leqslant 54.0$
Scan type	ω–2θ	ω–2θ
Scan width	$0.80+0.35\tan\theta$	$0.80+0.35\tan\theta$
No. of unique reflections	2433	2777
No. of reflections with $F > 3.0\sigma(F)$	1791	2112
No. of parameters	333	331
Largest shift (e.s.d.)	1.423	0.884
Residual electron density (e Å^{-3})	0.36	0.51
R	0.039	0.038
Rw[a]	0.039	0.035

[a] $Rw = (\Sigma w|F_o - F_c|^2/\Sigma wF_o^2)^{1/2}$; with $w = 1.8907/\sigma^2(F)+0.000319F^2$ for **1** and $w = 1.5880/\sigma^2(F)+0.000202F^2$ for **2**.

Anisotropic refinement for all the non-hydrogen atoms gave $R = 0.043$ for **1** and $R = 0.046$ for **2**. Subsequent difference-Fourier syntheses revealed the positions of three methyl hydrogen atoms for both compounds; all other hydrogen atoms were included at calculated positions. Further refinement was continued keeping the hydrogen atoms at a fixed distance to the parent carbon atoms, but allowing individual refinement of the thermal parameters.

Some of the Cp ring carbon atoms show, for both compounds, high thermal ellipsoids; attempts were made to find a disordered model for the rings, but did not lead to any reasonable solution. The Cp rings adopt an almost eclipsed configuration in both complexes. A weighting scheme was introduced to give final $R = 0.039$ and $Rw = 0.039$ for **1** and $R = 0.038$ and $Rw = 0.035$ for **2**.

Final atomic coordinates and anisotropic thermal parameters for non-hydrogen atoms, hydrogen atomic coordinates and isotropic thermal parameters are available from the Cambridge Crystallographic Data Centre. Lists of observed and calculated structure factors have been submitted as supplementary material. All computations required to solve and refine the structures were made with SHELX76,[15] while drawings were made with ORTEP.[16] Atomic scattering values were taken from the International Tables.[17]

REFERENCES

1. T. Aviles, M. L. H. Green, A. R. Dias and C. C. Romão, *J. Chem. Soc., Dalton Trans.* 1979, 1367.
2. M. J. Calhorda, M. A. A. F. de C. T. Carrondo, A. R. Dias, A. M. T. Domingos, M. T. L. S. Duarte, M. H. Garcia and C. C. Romão, *J. Organomet. Chem.* 1987, **320**, 63.
3. M. J. Calhorda, A. R. Dias, M. T. Duarte, A. M. Martins, P. M. Matias and C. C. Romão, *J. Organomet. Chem.* 1992, **440**, 119.
4. (a) F. A. Urbanos, M. Mena, P. Royo and A. Antiñolo, *J. Organomet. Chem.* 1984, **276**, 185; (b) G. Fachinetti, S. del Nero and C. Floriani, *J. Chem. Soc., Dalton Trans.* 1976, 1046; (c) M. J. Calhorda,

M. A. A. F. de C. T. Carrondo, S. A. Bram, P. N. Olsen, A. R. Dias, A. M. Freitas, M. H. Garcia and M. F. M. Piedade, *J. Organomet. Chem.* 1992, **426**, 195; (d) L. Roullier, D. Lucas, Y. Mugnier, A. Antiñolo, M. Fajardo and A. Otero, *J. Organomet. Chem.* 1990, **396**, C12.

5. J. Arnold, T. D. Tilley, A. L. Rheinfold and S. J. Geib, *Organometallics* 1987, **6**, 473.
6. H. C. Aspinall, M. M. Roberts and S. J. Lippard, *Inorg. Chem.* 1984, **23**, 1782.
7. J. W. Lauher and R. Hoffmann, *J. Am. Chem. Soc.* 1976, **98**, 1729.
8. F. A. Cotton, S. A. Duraj and W. J. Roth, *J. Am. Chem. Soc.* 1984, **106**, 6987.
9. F. A. Cotton and W. J. Roth, *Inorg. Chim. Acta* 1987, **126**, 161.
10. F. A. Cotton, M. P. Diebold and W. J. Roth, *Inorg. Chem.* 1987, **26**, 3319.
11. A. J. Benton, M. G. B. Drew, R. J. Hobson and D. A. Rice, *J. Chem. Soc., Dalton Trans.* 1981, 1304.
12. A. M. Martins, M. J. Calhorda, C. C. Romão, C. Völkl, P. Kiprof and A. C. Filippou, *J. Organomet. Chem.* 1992, **423**, 367.
13. P. B. Hitchcock, M. F. Lappert and C. R. C. Milne, *J. Chem. Soc., Dalton Trans.* 1981, 180.
14. R. E. Schuster, J. E. Scott and J. Casanova Jr, *Org. Synth. Coll.* 1973, **5**, 772.
15. G. M. Sheldrick, SHELX Crystallographic Calculation Program. University of Cambridge (1976).
16. C. K. Johnson, ORTEP-II, Report ORNL-5138. Oak Ridge National Laboratory, Oak Ridge, TN (1976).
17. *International Tables for X-ray Crystallography*, Vol. IV. Kynoch Press, Birmingham (1974).

Polyhedron Vol. 12, No. 7, pp. 771–782, 1993
Printed in Great Britain

0277–5387/93 $6.00+.00
© 1993 Pergamon Press Ltd

CHARACTERIZATION OF VAPOUR COMPLEXES OVER MOLTEN $POCl_3$–MCl_3 (M = Al, Ga) MIXTURES: RAMAN SPECTRA AND THERMODYNAMICS

S. BOGHOSIAN,* D. A. KARYDIS and G. A. VOYIATZIS

Institute of Chemical Engineering and High Temperature Chemical Processes and Department of Chemical Engineering, University of Patras, GR-26110 Patras, Greece

(*Received* 1 *October* 1992; *accepted* 16 *November* 1992)

Abstract—Raman spectra were obtained at temperatures up to 800 K and pressures up to 6 atm. for vapours over $POCl_3$–$AlCl_3$ and $POCl_3$–$GaCl_3$ molten mixtures under static equilibrium conditions. Spectra are also measured for molten $POCl_3$–$AlCl_3$ and $POCl_3$–$GaCl_3$ salt mixtures. A comparison of the spectral features in the $POCl_3$–MCl_3 (M = Al, Ga) vapours with the spectra of the 1 : 1 and 1 : 2 $POCl_3$–MCl_3 molten mixtures indicates that the vapour complexes have a 1 : 1 stoichiometry and that complexing occurs through oxygen bridging. Gaseous $POCl_3 \cdot AlCl_3$ remains stable with no sign of decomposition at temperatures up to 825 K, while the $POCl_3 \cdot GaCl_3$ vapour complex vaporizes dissociatively. The spectra are interpreted in terms of a C_s symmetry for $POCl_3 \cdot AlCl_3$ with a bent P—O—Al bridge (nine polarized and eight depolarized bands assigned) and C_{3v} symmetry for $POCl_3 \cdot GaCl_3$, with a straight P—O—Ga bridge (five polarized and six depolarized bands assigned). In the spectra of $POCl_3$–MCl_3 (M = Al, Ga) melts several bands are interpreted to account for $POCl_3(AlCl_3)_2$(l) (four polarized and six depolarized bands assigned) and $POCl_3(GaCl_3)_2$(l) (two polarized and three depolarized bands assigned) species. Accurate relative Raman intensity measurements are used for determining the thermodynamic functions of the reactions: (a) $POCl_3(g)+nGa_2Cl_6(g) = POCl_3(GaCl_3)_{2n}(g)$, in the temperature range 600–800 K and pressures up to 6 atm.; it is shown that the predominant vapour complex formed has $n = 0.5$ ($POCl_3 \cdot GaCl_3$) and the thermodynamic functions according to this reaction ($n = 0.5$) are determined from the Raman experiments as $\Delta H^\circ = -37 \pm 0.8$ kJ mol^{-1} and $\Delta S^\circ = -44 \pm 1.1$ J mol^{-1} K^{-1}. (b) $Ga_2Cl_6(g) = 2GaCl_3(g)$ in the temperature range 400–800 K and pressures up to 2.5 atm., where the thermodynamic functions are determined as $\Delta H^\circ = 83 \pm 1.3$ kJ mol^{-1} and $\Delta S^\circ = 131 \pm 2.2$ J mol^{-1} K^{-1}.

A wide range of liquid complex compounds with low melting points, in which phosphoryl chloride acts as a donor molecule towards other inorganic metal halides, has been studied and a detailed summary of their chemistry is available.[1] The chlorides of aluminium and gallium as Lewis acids undergo complex formation with $POCl_3$ and such a complexation has been proposed a few decades ago for the removal of aluminium chloride from Friedel Crafts mixtures.[1].

The phase diagram of the $POCl_3$–$AlCl_3$ system[2] shows a clear and sharp maximum at 186.5°C, corresponding to the 1 : 1 compound and a second compound, $AlCl_3 \cdot 2POCl_3$, with m.p. 164°C (or $2AlCl_3 \cdot 3POCl_3$ with m.p. 166°C[3]) very close to a eutectic at 160°C with 64 mol% $POCl_3$. A mass spectrometric investigation[4] of the vapours over the $POCl_3 \cdot AlCl_3$ compound showed a high stability of this complex and provides confirmation of a bond through the oxygen atom of $POCl_3$ (P—O—Al bridge), as also indicated from a Raman study of the compounds $POCl_3 \cdot AlCl_3$ and $POCl_3 \cdot GaCl_3$ in the liquid state.[5] Results of a vapour pressure study of the $POCl_3$–$AlCl_3$ system in the range 50–64 mol% $AlCl_3$ indicate the formation of

* Author to whom correspondence should be addressed.

$POCl_3 \cdot AlCl_3$ and $POCl_3 \cdot 2AlCl_3$ in the liquid state and point to $POCl_3 \cdot AlCl_3$ as the stable and predominant vapour species.[6] In the $POCl_3$–$GaCl_3$ system 1 : 1 and 2 : 1 compounds (m.p.s 185°C and 77°C, respectively) occur[7] and a high percentage of adduct in the vapour is reported as a result of sublimation of the $POCl_3 \cdot GaCl_3$ compound.[8]

The aim of the present work is to characterize the vapour complexes over molten mixtures of $POCl_3$ and MCl_3 (M = Al, Ga) under equilibrium conditions by Raman spectroscopy. It has been demonstrated that in certain cases Raman spectroscopy can be used to study the vibrational and structural properties of vapour complexes[9,10] and "adduct" vapour compounds,[11,12] as well as for establishing the stoichiometry and thermodynamics of formation of gas phase reactions.[13] In the present work the vapours over molten $POCl_3$–MCl_3 (M = Al, Ga) mixtures are studied by Raman spectroscopy at temperatures up to 800 K. The vibrational band frequencies of the complexes formed in the vapour as well as in the liquid state are determined and possible complex structures are considered and discussed. Finally, for the $POCl_3$–$GaCl_3$ system the data obtained are shown to be capable for an accurate determination of the stoichiometry, n, and of the thermodynamic functions ($\Delta H°$, $\Delta S°$) of the reaction:

$$POCl_3(g) + nGa_2Cl_6(g) \rightleftharpoons POCl_3 \cdot (GaCl_3)_{2n}(g) \quad 600\,K < T < 800\,K, \quad 2\,atm. < P < 6\,atm. \tag{1}$$

EXPERIMENTAL

High purity anhydrous $AlCl_3$ and $GaCl_3$ were prepared from the corresponding Cerac/Pure Inc. reagents by repeated slow sublimations in fused silica tubes under vacuum. All handling of these chemicals took place in a nitrogen-filled glove-box with a water vapour content of less than 1 ppm. Liquid $POCl_3$ was purchased from Fluka.

The Raman (optical) cells containing the salt vapours consisted of fused silica tubing (20 ± 0.2 mm o.d., 18 ± 0.2 mm i.d., 3–4 cm long). In the case of melts containing molten salt mixtures silica tubing with 4 ± 0.1 mm o.d. and 2 ± 0.1 mm i.d. was used. Preweighed amounts of $AlCl_3$ or $GaCl_3$ were transferred into a clean, dry, flamed and degassed optical cell of known volume, which was attached to an all-glass vacuum line for feeding the $POCl_3$. In the same line a container with $POCl_3$ was attached. Phosphoryl chloride was then allowed to vaporize and occupy a confined bulb of known volume and it was afterwards transferred by distillation and condensed in the bottom of the optical cell which was immersed in liquid nitrogen. The optical cell was then sealed off, the salt mixtures were reacted inside a side tube (6 ± 0.1 mm o.d., 4 ± 0.1 mm i.d.), vapour transported into the main cell compartment and finally the side tube was sealed off. In this way transparent liquids and colourless vapours could be obtained, indicating a high degree of sample purity.

For the study of the $POCl_3$–$AlCl_3$ system stoichiometric amounts of the two components were heated carefully, yielding a clear colourless liquid with m.p. ~185°C, which could be vapour transported over a temperature gradient with no sign of decomposition. Mixtures having excess $POCl_3$ or $AlCl_3$ showed similar behaviour and the distillate could be isolated by sealing away (into the side tube) the excess chemicals. The so-collected 1 : 1 mixture was transferred into optical cells and the vapour Raman spectra recorded thereafter showed no bands due to $POCl_3$ or $Al_2Cl_6/AlCl_3$, even at temperatures up to 800 K, indicating a high thermal stability of the formed complex. During cooling in ice-water or liquid nitrogen no glass formation could be observed.

In the $POCl_3$–$GaCl_3$ system the two components in stoichiometric amounts were mixed as described before at 77 K and while attaining room temperature reacted vigorously, yielding a white solid which gave a clear colourless liquid upon melting at *ca* 120°C. The solid could be sublimed giving needle-shape crystals and preliminary studies of the temperature dependence of its vapour Raman spectra indicated a decomposition to $POCl_3$ and $Ga_2Cl_6/GaCl_3$. Thus, in this system the procedure and method described in ref. 13 could be applied for establishing the stoichiometry and thermodynamics of the vapour complex formed. The "ideal gas" pressure ($P_{0,D}$) of undissociated and non-reacted Ga_2Cl_6 at temperature t was calculated from the number of moles (n_D) added to the cell. Three different cells were made for studying the Ga_2Cl_6–$GaCl_3$ system. The first column in Table A (supplementary material, deposited with the Editor) gives the characteristics of each cell. Measurements from these cells were used to establish the thermodynamics of the Ga_2Cl_6 dissociation and to calculate the equilibrium partial pressures of Ga_2Cl_6, P_D, in $POCl_3$–$GaCl_3$ vapours. Furthermore, seven different cells for the study of the $POCl_3$–$GaCl_3$ system were prepared. The characteristics of these cells are listed in the first column of Table B (supplementary material). An additional cell containing pure $POCl_3$ was prepared and used as a reference standard for calculating the equilibrium partial pressures of $POCl_3$, P_P, in the $POCl_3$–$GaCl_3$ vapour system. The first column in Table B (supplementary material) shows the characteristics of the $POCl_3$ reference cell.

Raman spectra were excited with the 514.5 and/or 488.0 nm lines of a 4 W Spectra Physics argon laser. The scattered light was collected at an angle of 90° (vertical scattering plane) and analysed with a Spex 1403, 0.85-m double monochromator equipped with a −20°C cooled RCA photomultiplier and Eg & G/ORTEC rate meter and photon counting electronics. The optical furnace for obtaining the high-temperature Raman spectra was similar to that described in detail elsewhere.[14]

During the present investigation, the optical geometry, the spectral slit width and the laser power measured before and after the entrance and exit windows of the furnace were maintained constant. The Raman cells were placed inside the mechanically stable metal core of the furnace and were always in a fixed position relative to the collecting lens and entrance slit. The intensity of the scattered light was "maximized" by positioning the focusing and collecting lenses with two x, y, z micropositioners. After the spectra were obtained the cell could be removed and cooled to room temperature and then reintroduced into the optical furnace, yielding always with no further micropositioner adjustments the same Raman intensities. Thus, by the use of the same experimental conditions the Raman intensities could be reproduced to within less than 2% and the relative Raman intensities of gases at different temperatures and pressures could be obtained within the same error.

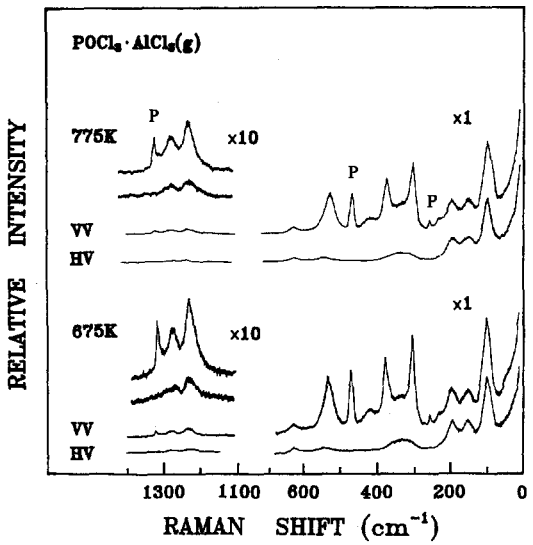

Fig. 1. Raman spectra of $POCl_3 \cdot AlCl_3$(g) at 675 and 775 K. Bands due to $POCl_3$(g) are marked by "P". $\lambda_o = 488$ nm; laser power, w = 280 mW; spectral slit width, ssw = 6 cm^{-1}; time constant, $\tau = 0.3$ s; scan speed, ss = 60 cm^{-1} min^{-1}. Inserts show the high frequency bands; $\tau = 3$ s; ss = 10 cm^{-1} min^{-1}.

RESULTS AND DISCUSSION

The $POCl_3$–$AlCl_3$ *system*

Figure 1 shows representative Raman spectra of $POCl_3$–Al_2Cl_6 vapours at 675 and 775 K. Identical spectra were obtained from samples prepared by either reacting stoichiometric amounts of $POCl_3$ and $AlCl_3$ or reacting aluminium chloride with excess $POCl_3$ and sealing away the excess $POCl_3$ vapours after condensing them in a side-tube by cooling in liquid nitrogen. None of the well-known[15] characteristic Al_2Cl_6(g) bands can be observed in Fig. 1, while three out of 16 totally observed bands can be assigned as the $\nu_1(A_1)$, $\nu_2(A_1)$ and $\nu_3(A_1)$ $POCl_3$(g) bands[16] (see bands in Fig. 1 marked by "P"). These bands could be either due to a slight dissociation of a vapour complex or due to the dissociative vaporization of initially formed $2AlCl_3 \cdot 3POCl_3$ compound.[3] Thus, seven polarized and six depolarized bands (see Table 1 for wave numbers and polarization characteristics) were assigned to the 1 : 1 $POCl_3 \cdot AlCl_3$ vapour complex, which seems to be the one and only stable vapour complex over $POCl_3$–$AlCl_3$ molten mixtures. This is in agreement with Brockner *et al.*,[6] who from vapour pressure measurements deduced that $POCl_3 \cdot AlCl_3$ was the predominant vapour species. The temperature dependence of the spectra in Fig. 1 shows that $POCl_3 \cdot AlCl_3$(g) exhibits a high thermal stability, as postulated earlier.[4] No sign of decomposition could be observed at temperatures up to 800 K. This is quite unusual behaviour, since around this temperature most of the to-date studied inorganic halide vapour complexes[9,10,12–14,16–18] are present in low percentages in equilibrium with the vapours of their component gases.

The structural properties of the vapour complex are better clarified by also studying the Raman spectra of some $POCl_3$–$AlCl_3$ melt mixtures. Figure 2 shows Raman spectra from melts with 1 : 1 ($X_{AlCl_3} = 0.50$) and 1 : 2 ($X_{AlCl_3} = 0.67$) compositions at 500 K. In the case of the 1 : 1 composition none of the 17 observed bands could be assigned to $POCl_3$(l)[19] or Al_2Cl_6(l).[15] Furthermore, the spectrum resembles closely the vapour Raman spectrum of Fig. 1. All 17 bands (nine polarized and eight depolarized) are assigned to the liquid $POCl_3 \cdot AlCl_3$ compound. The observed wave numbers due to $POCl_3 \cdot AlCl_3$(l) are listed in Table 1 and compare well with those of the vapour molecule. Four weak extra bands due to the liquid compound at wave numbers 130, 349, 457 and 480 could not be observed in the vapour Raman spectrum, presumably due to their low intensities. Wave numbers

Table 1. Observed vibrational Raman wave numbers (cm^{-1}) of gaseous $POCl_3 \cdot AlCl_3$ and $AlCl_3$–$POCl_3$ molten mixtures[a]

$POCl_3 \cdot AlCl_3$(g) 775 K		Liquid mixture with $X_{AlCl_3} = 0.50$ 500 K $[POCl_3 \cdot AlCl_3$(l)]			Liquid mixture with $X_{AlCl_3} = 0.67$ 500 K				
					$POCl_3 \cdot AlCl_3$(l)		$POCl_3(AlCl_3)_2$(l)		Al_2Cl_6(l)
ν (cm^{-1})	Assignment[b]	ν (cm^{-1})	Assignment[b]	Ref. 5 (485 K)	ν (cm^{-1})	Assignment[b]	ν (cm^{-1})	Assignment[b]	ν (cm^{-1})
							95 sh, dp	A''	
				95					103 m, dp
111 s, dp	A'	115 s, dp	A''	105					120 m, dp
		130 sh, dp	A''						
							145 w, dp	A''	
160 m, dp	A''	170 m, dp	A''	171					165 m, dp
205 m, dp	A''	207 s, dp	A''	208			209 m, dp	A''	
									219 sh, p
242 w, p	A'	244 m, dp	A''	250			238 w, dp	A''	
265 w, p	$\nu_3(POCl_3)$, A_1						312 sh, p	A'	
313 s, p	A'	324 vs, p	A'	323	324 m, p	A'			342 s, p
		349 w, p	A'						
345 w, dp	A''	354 w, dp	A''	365			366 w, dp	A''	
383 s, p	A'	391 s, p	A'	389	391 m, p	A'			
425 m, p	A'	445 m, p	A'	449			437 m, p	A'	
		457 m, p	A'						
478 m, p	$\nu_3(POCl_3)$, A_1	480 w, p	A'	497			481 w, p	A'	
		532 w, dp	A''						510 sh, p
537 s, p	A'	573 s, p	A'	576	573 sh, p	A'	601 m, p	A'	
550 w, dp	A''								
633 w, dp	A''	646 m, dp	A''	637			650 w, dp	A''	(606 sh)
				701					
				830					
1231 m, p	A'	1208 m, p	A'		1208 w, br, p	A'			
1279 w, p	A'	1265 w, p	A'						
1321 w, p	$\nu_1(POCl_3)$, A_1								

[a] Abbreviations: s: strong, m: medium, w: weak, v: very, sh: shoulder, br: broad, p: polarized, dp: depolarized.
[b] Assignments based on assumed C_s symmetry (see text).

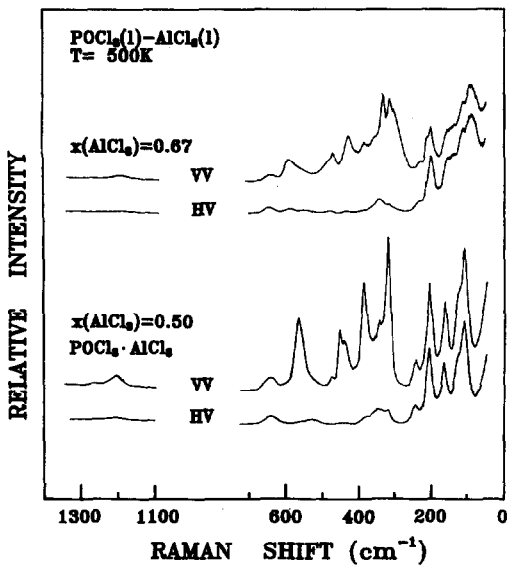

Fig. 2. Raman spectra of molten $POCl_3 \cdot AlCl_3$ mixtures with $X_{AlCl_3} = 0.50$ [i.e. $POCl_3 \cdot AlCl_3$(l)] and $X_{AlCl_3} = 0.67$ at 500 K. $\lambda_o = 488$ nm; w = 250 mW; ssw = 4 cm^{-1}; $\tau = 0.03$ s; ss = 60 cm^{-1} min^{-1}.

reported in ref. 5 for $POCl_3 \cdot AlCl_3$(l) are also included in Table 1 for comparison.

Bonding in the vapour and liquid $POCl_3 \cdot AlCl_3$ complex presumably occurs by bridging the oxygen from $POCl_3$ with the aluminium atom to form a P—O—Al bridge, as in a series of known $POCl_3$ addition compounds.[1] Figure 3 shows two possible structures for the $POCl_3 \cdot AlCl_3$ complex in the vapour or in the liquid state. Structure **A** possesses a three-fold axis along a straight P—O—Al bridge and three vertical symmetry planes (C_{3v} symmetry),

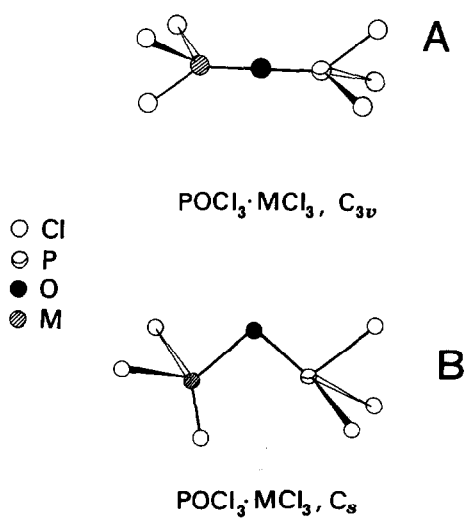

Fig. 3. Molecular models for $POCl_3 \cdot MCl_3$ (M = Al or Ga) vapour complexes with C_{3v} (**A**) and C_s (**B**) symmetry.

while structure **B** possesses a single symmetry plane containing a bent P—O—Al bridge (C_s symmetry). The 21 vibrational modes of the complex for the molecular configurations shown in Fig. 3 can be classified as follows:

$$\Gamma_{C_{3v}} = 6A_1(\mathrm{R,IR}) + A_2 + 7E(\mathrm{R,IR}) \quad (2)$$

$$\Gamma_{C_s} = 13A'(\mathrm{R,IR}) + 8A''(\mathrm{R,IR}) \quad (3)$$

One can exclude the C_{3v} structure on the basis of the nine polarized and eight depolarized Raman bands observed (see Table 1) and thus C_s remains as the most probable structure, but no definite conclusion can be made on this basis. It is assumed here that all the symmetric vibrational modes observed (assigned as A' in Table 1) are fundamentals. Simple combinations and/or first overtones of antisymmetric or symmetric fundamentals do not seem to give rise to any of the nine totally symmetric vibrations observed. The only exception is the 457 cm^{-1} polarized band which may arise from a combination between the 207 and 244 cm^{-1} depolarized bands. However, it is quite unusual for the intensity of a combination band to be so strong and not even a Fermi resonance with a neighbouring symmetric mode (i.e. 445 cm^{-1}) could account for such a high intensity (Fig. 2). Therefore, all bands are assigned in Table 1 as due to fundamentals.

The formation of the ionic $POCl_2^+AlCl_4^-$ liquid compound by chlorine ion transfer from $POCl_3$ to the acceptor molecule "$AlCl_3$" is excluded on the basis of the observed 17 Raman bands due to $POCl_3 \cdot AlCl_3$(l), contrary to the totally expected 10 bands if $POCl_2^+$ (plane symmetry, C_{2v} with six bands) and $AlCl_4^-$ (T_d symmetry with four bands) moities were formed. Furthermore, no observation of the characteristic $AlCl_4^-$ band at 351 cm^{-1} [20] was made.

Addition of aluminium chloride up to $X_{AlCl_3} = 0.67$ causes drastic changes in the liquid Raman spectra (see the upper part of Fig. 2 and list of observed wave numbers, Table 1). The following observations can be made: (1) Six bands emerge at wave numbers 103, 120, 165, 219, 342, 510 and maybe a shoulder at 606 cm^{-1} with relative intensities and polarization characteristics as expected for Al_2Cl_6(l);[15] (2) four of the more characteristic bands due to $POCl_3 \cdot AlCl_3$(l) at wave numbers 324, 391, 573 and 1208 can still be observed indicating the presence of this compound in mixtures with 67 mol% $AlCl_3$; (3) no bands of the spectrum with 50 mol% $AlCl_3$ (Fig. 3, lower part), previously assigned to $POCl_3 \cdot AlCl_3$(l), appear to grow; and (4) 10 new bands (four polarized and six depolarized) appear and are assigned to a higher species [presumably $POCl_3(AlCl_3)_2$[6]].

Thus, while at 50 mol% $AlCl_3$ the mixture can be looked upon as a molecular compound, $POCl_3 \cdot AlCl_3$, at 67 mol% $AlCl_3$ composition the system can most probably be considered as a molecular liquid mixture consisting of Al_2Cl_6(l), $POCl_3 \cdot AlCl_3$(l) and $POCl_3(AlCl_3)_2$(l) participating in the equilibrium:

$$POCl_3 \cdot AlCl_3(l) + \tfrac{1}{2}Al_2Cl_6(l) \Leftrightarrow POCl_3(AlCl_3)_2(l).$$

This statement confirms a recent observation reported in ref. 6. From a structural point of view the $POCl_3(AlCl_3)_2$ liquid complex probably possesses a single symmetry plane with the oxygen coordinated three-fold (C_s symmetry). Such a configuration was also essentially proposed by Brockner *et al.*[6]

The $POCl_3$–$GaCl_3$ *system*

Figure 4 shows representative vapour Raman spectra obtained for $POCl_3$(g) ($POCl_3$ reference cell), for gallium chloride vapours (Cell G3) at 635 K and for vapour mixtures from cell I at 635 and 790 K. Spectral band positions and polarization properties for gaseous phosphorus oxychloride and gallium chloride vapours were in agreement with those previously reported in refs 16 and 21. The spectra of the vapour mixtures consist of superpositions of bands due to the component gases plus eight new bands at wave numbers listed in Table 2 (first column), which are attributed to a vapour complex formed according to reaction (1). The intensities of the bands assigned to the vapour complex are decreasing with increasing temperature, probably due to thermal decomposition. It should be pointed out here that a temperature rise shifts the dissociation equilibrium

$$Ga_2Cl_6(g) \Leftrightarrow 2GaCl_3(g) \qquad (4)$$

to the right. This is illustrated in Fig. 5, which shows the temperature-dependent features of the gallium chloride vapour Raman spectra. Bands due to the dimer (marked by D in Fig. 5) lose intensity with increasing temperature, while bands due to the monomer (marked by M) become progressively stronger.

Consequently, several bands due to the vapour

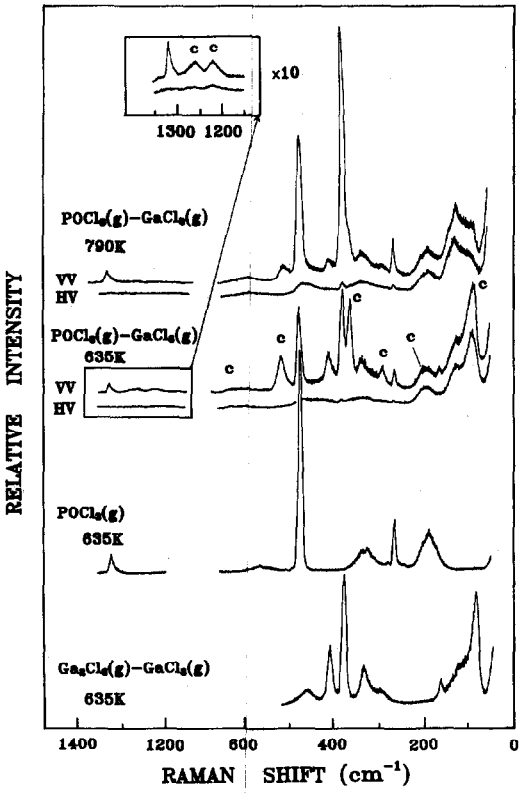

Fig. 4. Raman spectra of Ga_2Cl_6–$GaCl_3$ vapours from cell G3, $POCl_3$(g) from the $POCl_3$ reference cell at 635 K and mixtures from cell I at 635 and 790 K. Bands due to the vapour complex are marked by "c". $\lambda_o = 488$ nm; w = 220 mW; ssw = 6 cm^{-1}; $\tau = 0.2$ s; ss = 15 cm^{-1} min^{-1}.

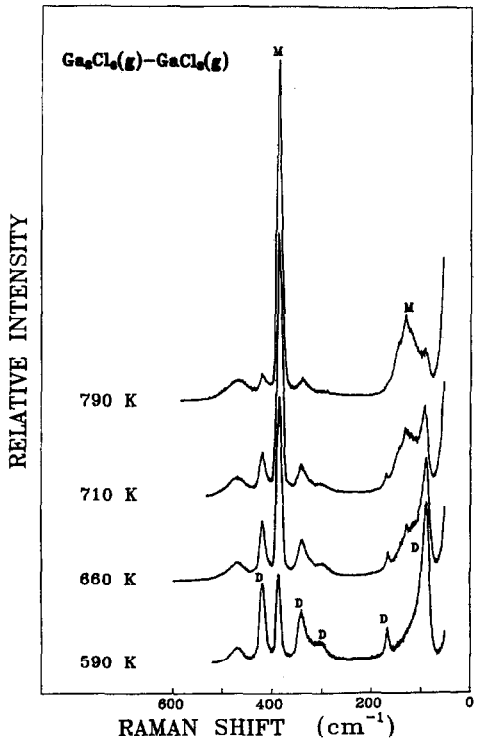

Fig. 5. Temperature dependence of the Raman spectra of Ga_2Cl_6–$GaCl_3$ vapours from cell G3. Bands due to Ga_2Cl_6 and $GaCl_3$ are marked by "D" and "M", respectively. $\lambda_o = 488$ nm; w = 220 mW; ssw = 6 cm^{-1}; $\tau = 0.2$ s; ss = 15 cm^{-1} min^{-1}.

complex might have been obscured by bands due to $POCl_3$(g) and Ga_2Cl_6–$GaCl_3$ vapours in the vapour Raman spectra (Fig. 4). More information about the number of bands due to the complex can be obtained by also considering some liquid state spectra.

Figure 6 shows Raman spectra from melts with 1:1 ($x_{GaCl_3} = 0.50$) and 1:2 ($x_{GaCl_3} = 0.66$) compositions at 500 K. There are 13 bands appearing in the lower spectrum with $x_{GaCl_3} = 0.50$ that *cannot* be assigned to $POCl_3$(l) or Ga_2Cl_6(l). Nevertheless, the strongest Raman line of $POCl_3$(l)[17] at 485 cm^{-1} is observed as a weak polarized band, a fact excluding the possibility of any other band to be assigned as due to $POCl_3$(l). An increase in the $GaCl_3$ concentration to $x_{GaCl_3} = 0.66$ results in the disappearance of this band. Furthermore, two bands in the spectrum with $X_{GaCl_3} = 0.50$ at 165 and 410 cm^{-1} can be assigned as due to Ga_2Cl_6(l). Increasing the $GaCl_3$ concentration results in an intensity increase of these two bands and the appearance of two more bands due to Ga_2Cl_6(l) at 96 and 462 cm^{-1}. All four bands behave as expected for Ga_2Cl_6(l)[22] in terms of positions in the spectrum, relative intensities and polarization properties. The 11 bands dominating the spectrum with $x_{GaCl_3} = 0.50$ (see Table 2 for a list of their wave numbers) can be assigned to a single species, most probably $POCl_3 \cdot GaCl_3$ attaining its maximum concentration at $x_{GaCl_3} = 0.50$, while two shoulder bands at 129 and 400 cm^{-1} probably have to be assigned to a higher complex. The intensities of these two bands increase drastically on going from $x_{GaCl_3} = 0.50$ to 0.66, while the 11 bands assigned to 1:1 $POCl_3 \cdot GaCl_3$ become weaker and four of them even disappear, being obscured by other bands. Moreover, three more bands appear in the spectrum with $x_{GaCl_3} = 0.66$ and are assigned to the higher complex, which could probably be the $POCl_3(GaCl_3)_2$ compound although no definite conclusion can be made on this issue. Table 2 summarizes the vibrational wave numbers of all the bands resolved in the spectra of Fig. 6. Wave numbers reported in ref. 5 for $POCl_3 \cdot GaCl_3$(l) are also included for comparison. Bands assigned as due to the vapour complex in the spectra of $POCl_3$–$GaCl_3$ vapours (Fig. 4) are closely related to certain respective bands in the 1:1 molten mixture (Fig. 5), a fact indicating that the predominant vapour complex species is 1:1 $POCl_3 \cdot GaCl_3$. The determination of the stoichiometric coefficient, n, of reaction (1) which is presented in the next section will show that this is indeed the case.

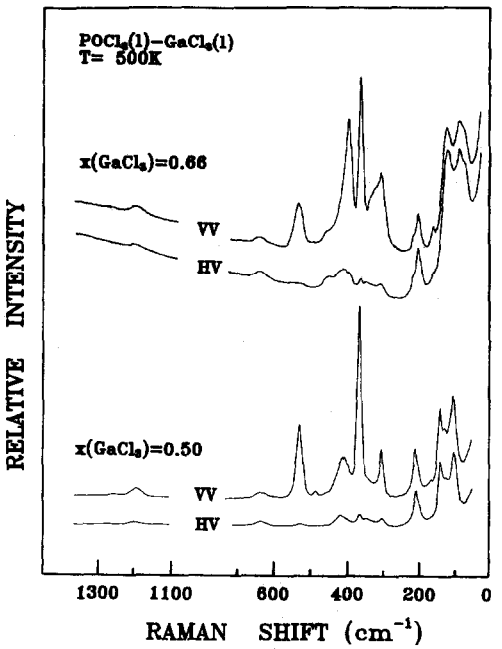

Fig. 6. Raman spectra of molten $POCl_3$–$GaCl_3$ mixtures with $X_{GaCl_3} = 0.50$ and 0.66. $\lambda_o = 488$ nm; w = 250 mW; ssw = 6 cm^{-1}; $\tau = 0.03$ s; ss = 180 cm^{-1} min^{-1}.

The bonding in the vapour and liquid adduct $POCl_3 \cdot GaCl_3$ complex presumably occurs by coordination of the oxygen with the gallium atom, leading to $Cl_3POGaCl_3$. In this way deformation of the $GaCl_3$ group from planar to pyramidal occurs through the addition of an oxygen to the gallium atom, giving rise to four-coordination for both gallium and phosphorus atoms, in agreement with the coordination generally found for these atoms.

Figure 3 shows the possible structures for the vapour or liquid $POCl_3 \cdot GaCl_3$ complex, while relations (2) and (3) represent the classification of the 21 vibrational degrees of freedom for the C_{3v} and C_s configurations. Assignment of five polarized and six depolarized bands to $POCl_3 \cdot GaCl_3$ (see Table 2) points to C_{3v} rather than C_s as the most plausible structure. None of the bands seems to be due to simple combinations or first overtones of other states.

Based on the same arguments put forward in the above discussion concerning the $POCl_3$–$AlCl_3$ molten mixtures one can exclude the formation of the ionic $POCl_2^+GaCl_4^-$ liquid compound by chloride atom transfer. Consequently, the molten $POCl_3$–$GaCl_3$ mixtures in the composition range studied can be considered as molecular liquids consisting of $POCl_3 \cdot GaCl_3$, $POCl_3$, Ga_2Cl_6 and probably $POCl_3(GaCl_3)_2$ linked by the equilibria:

$$POCl_3 \cdot GaCl_3(l) + \tfrac{1}{2}Ga_2Cl_6(l) = POCl_3(GaCl_3)_2(l)$$

$$2POCl_3 \cdot GaCl_3(l) = POCl_3(GaCl_3)_2(l) + POCl_3(l).$$

Table 2. Observed vibrational Raman wave numbers (cm^{-1}) of gaseous $POCl_3 \cdot GaCl_3$ and $GaCl_3$–$POCl_3$ molten mixtures[a]

$POCl_3 \cdot GaCl_3$(g)		Liquid mixture with $X_{GaCl_3} = 0.50$ 450 K					
		$POCl_3 \cdot GaCl_3$(l)		$POCl_3$(l)	Ga_2Cl_6(l)	$POCl_3(GaCl_3)_2$(l)	
ν (cm^{-1})	Assignment[b]	ν (cm^{-1})	Assignment[b]			ν (cm^{-1})	Assignment[b]
94 s, dp	E	108 s, dp	E				
						129 w, dp	A''
		144 s, dp	E				
					165 w, p		
202 sh, dp	E	210 s, dp	E				
293 m, p	A_1	306 s, p	A_1				
		348 w, dp	E				
366 vs, p	A_1	367 vs, p	A_1				
						400 sh, p	A'
					410 w, p		
		423 m, dp	E				
				485 w, p			
513 s, p	A_1	532 s, p	A_1				
617 w, dp	E	640 w, dp	E				
1220 w, p	A_1	1198 m, p	A_1				
1263 w, p	A_1	1260 vw, p	A_1				

[a] Abbreviations: see Table 1.

[b] Assignments based on C_{3v} symmetry for $POCl_3 \cdot GaCl_3$ and C_s for $POCl_3(GaCl_3)_2$ (see text).

Considering the second complex formed in $GaCl_3$-rich melts no definite suggestions can be made from a structural point of view, due to the small number of bands (five) assigned to this species. Nevertheless, as for the $POCl_3$–$AlCl_3$ system a C_s configuration with three-fold coordination for the oxygen atom is possible for a $POCl_3(GaCl_3)_2$ compound.

Stoichiometry and thermodynamics of the vapour complex in the $POCl_3$–$GaCl_3$ *system*

Recently it has been pointed out[13] that the correct formalism for correlating Raman band intensities with equilibrium constants of gaseous reactions should include a temperature factor which depends on the stoichiometric coefficients. Following the procedure derived in ref. 13 the stoichiometry and thermodynamic functions ($\Delta H°$, $\Delta S°$) of reaction (1) are established as follows. (For further details concerning limitations, breadth of applicability and derivation of the procedure, see ref. 13.)

Determination of stoichiometry. This requires measurements at the same temperature from two Raman cells, *a* and *b*, containing the reacting gases at different pressures. If the experiments are conducted with "identical" cells maintaining the optical geometry and the laser power constant, then the following relation can be used for calculating the stoichiometric coefficient, *n*, of reaction (1)

$$\left.\frac{I_C}{I_P I_D^n}\right|_a = \left.\frac{I_C}{I_P I_D^n}\right|_b \quad \text{at constant } T, \tag{5}$$

where I_C, I_P and I_D are the integrated Raman intensities of representative bands due to the vapour complex, phosphoryl chloride and gallium chloride dimer, respectively.

Table B lists the relative integrated Raman intensities of the 265 cm^{-1} $POCl_3$ band (I_P), the 413 cm^{-1} Ga_2Cl_6 band (I_D) and the 512 cm^{-1} complex

Table 2.—*continued*

	Liquid mixture with $X_{GaCl_3} = 0.66$ 450 K				
$POCl_3 \cdot GaCl_3$(l) Ref. 5 (400 K)	$POCl_3 \cdot GaCl_3$(l) ν (cm^{-1})	Assignment[b]	$POCl_3(GaCl_3)_2$(l) ν (cm^{-1})	Assignment[b]	Ga_2Cl_6(l)
			81 sh, dp	A''	
97					96 s, dp
107					
			129 s, dp	A''	
143					
					165 w, p
207	210 s, dp	E			
221			220 sh, p	A''	
283					
302	306 s, p	A_1			
			328 sh, p	A'	
333					
363	367 vs, p	A_1			
406			400 s, p	A'	
					410 sh, p
422	423 sh, p	E			
					462 w, dp
527	532 s, p	A_1			
623	640 w, dp	E			
692					
858					
	1198 m, p	A_1			
	1260 vw, p	A_1			

band (I_C), measured from the different cells used. The stoichiometry of reaction (1) is calculated from eq. (5) and the Raman intensities I_P, I_D and I_C listed in Table B. Combinations of measurements from the seven different cells constructed allowed for 104 calculations of n over the studied temperature range, 610–789 K, with an average value

$$n_{\text{av., reaction (1)}} = 0.54 \pm 0.06,$$

which shows that the predominant vapour complex formed is 1:1 $POCl_3 \cdot GaCl_3$. Thus, the temperature-dependent features of the spectra (e.g. Fig. 4) can be interpreted in terms of shifts in the equilibria:

$$POCl_3 \cdot GaCl_3(g) \Leftrightarrow POCl_3(g) + \tfrac{1}{2}Ga_2Cl_6(g)$$

$$Ga_2Cl_6(g) \Leftrightarrow 2GaCl_3(g).$$

Enthalpy. The calculation of the "second law" enthalpy is based on the following equation:[13]

$$R \ln K = R \ln [T^{\Delta n} K_f K_I]$$

$$= -\Delta H^\circ (1/T) + (\Delta S^\circ - R \ln K_L), \quad (6)$$

where K_I is the quotient of the terms $I_i(\nu_i)$ (with ν_i being the vibrational wave number) due to the gaseous species participating in reaction (1), K_f is the quotient of the terms $1 - \exp(-hc\nu_i/kT)$ and K_L is a temperature-independent parameter involving the intensity of the excitation laser line, the molecular scattering properties and the sensitivity of the spectrometric system used.[13]

For the enthalpy of reaction (1) ($n = 0.5$) a plot [Fig. 7(a)] of $R \ln K$, where $K = 1/T^{0.5} K_f K_I$ vs $1/T$ [i.e. eq. (4), $\Delta n = -0.5$], for all seven cells used gives:

$$\Delta H^\circ_{1, n=0.5} = -36.7 \pm 0.8 \text{ kJ mol}^{-1}.$$

Entropy. The entropy ΔS° is determined from the intercept of an $R \ln K_P$ vs $1/T$ plot. This requires measurements of the partial pressures and the equi-

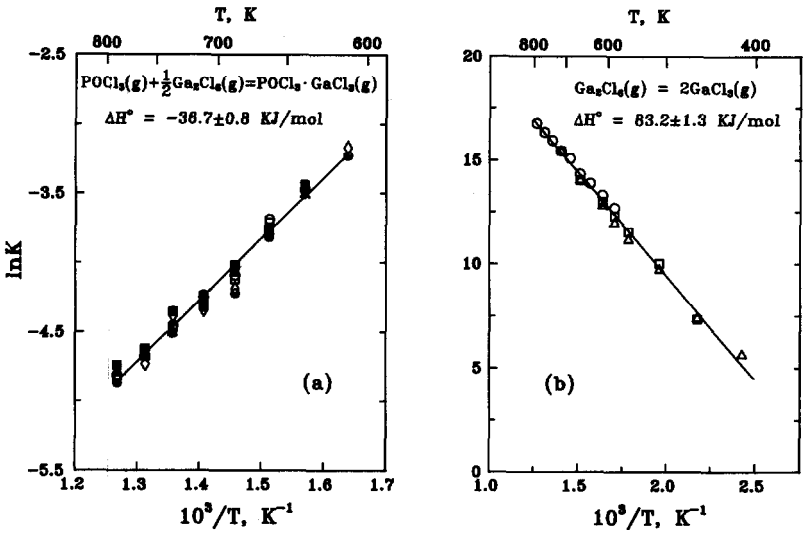

Fig. 7. Plots of $\ln K$ vs $1/T$ for the reactions: (a) $POCl_3(g)+\frac{1}{2}Ga_2Cl_6(g) \Leftrightarrow POCl_3\cdot GaCl_3(g)$, $K=(1/T^{0.5})K_fK_I$ and (b) $Ga_2Cl_6(g) \Leftrightarrow 2GaCl_3(g)$, $K=TK_fK_I$. Points indicate measurements from the different cells as follows: (a) cell I, ○; cell II, ◒; cell III, ●; cell IV, □; cell V, ▲; cell VI, ◇; cell VII, ■. (b) Cell G1, △; cell G2, □; cell G3, ○.

librium constants for the gaseous reaction at different temperatures. Raman experiments can be used for measuring partial pressures by comparing the Raman intensity I_i of a representative band of a species in the reacting mixture in a cell x at temperature T_x, with the Raman intensity of the same band in a reference cell R containing only this species with a known pressure P_R at temperature T_R. If cells x and R are "identical" and if the spectra are obtained under identical conditions, then the unknown partial pressure P_i in cell x is determined[13] by:

$$[P_i]_{\text{cell x}} = [I_i]_{\text{cell x}} \frac{[P_i]_{\text{cell R}}}{[I_i]_{\text{cell R}}} \frac{T_x}{T_R} \frac{f_i(v_i, T_x)}{f_i(v_i, T_R)}. \qquad (7)$$

The partial pressures determined according to the above equation are subject to uncertainties, which are related to the error associated with the measurements of the Raman intensities $[I_i]_{\text{cell x}}$ and $[I_i]_{\text{cell R}}$ (i.e. ±2%, see Experimental). The calculation of the equilibrium partial pressures of $POCl_3$ (P_P) and Ga_2Cl_6 (P_D) in cells I–VII is based on eq. (7) using the pure substance reference cells. An internal reference standard for the complex could be established by considering the gallium mole balance equation $P_C = 2(P_{0,D} - P_D) - P_M$, where $P_{0,D}$ is the expected pressure from the moles of undissociated and unreacted Ga_2Cl_6 added originally in each cell and P_M is the equilibrium partial pressure of the $GaCl_3$ monomer. The intensity of the complex band at 762 K from cell I was selected arbitrarily as a reference standard. The reference state was chosen from high temperature measurements so as to ensure that no other (higher) complexes should be involved in the gallium mole balance equation. Values of P_C listed in Table B are thus calculated using eq. (7) and the complex reference standard.

The last column of Table B lists the equilibrium constants calculated from the P_P, P_D and P_C values. The entropy is calculated from the intercept of a $R\ln K_P$ vs $1/T$ plot, where the slope of the least-squares line corresponds to the $\Delta H^\circ_{1,n=0.5}$ value given above. The result is:

$$\Delta S^\circ_{1,n=0.5} = -43.6 \pm 1.1\ \text{J mol}^{-1}\ \text{K}^{-1}.$$

Furthermore, the data obtained from the cells containing pure gallium chloride (e.g. Fig. 5, Table A) are adequate for establishing the thermodynamics of reaction (4). Table A lists the relative integrated Raman intensities of the 382 cm^{-1} monomer band, I_M, and the 413 cm^{-1} dimer band, I_D. The second law enthalpy, ΔH°, for reaction (4) ($\Delta n = 1$) can be calculated from the data I_M, I_D (Table A) and eq. (6). A linear least-squares fitting of $R\ln K$ ($K = TK_fK_I$) vs $1/T$ for all three cells used determines the enthalpy as the slope of the line shown in Fig. 7b. The measured value is:

$$\Delta H^\circ_4 = 83.2 \pm 1.3\ \text{kJ mol}^{-1}.$$

The calculation of the partial pressures of $GaCl_3$, P_M, is based on eq. (7) using as a reference standard the I_M value from cell G1 at 737 K. An internal reference standard for the dimer was established (cell G1, 510 K) by considering the mole balance

equation $P_D = P_0 - 1/2P_M$. Thus, the calculation of the partial pressures of Ga_2Cl_6, P_D, is based on eq. (7) using as a reference standard the I_D value from cell G1 at 510 K. The last column of Table A lists the equilibrium constants calculated from the P_M and P_D values. As in the case of the vapour complex the entropy was determined from the intercept of a $R\ln K_P$ vs $1/T$ plot, where the slope of the least-squares line corresponds to the ΔH_4° value calculated above. The result is:

$$\Delta S_4^\circ = 130.6 \pm 2.2\,\text{J mol}^{-1}\,\text{K}^{-1}.$$

By combining the thermodynamic functions of reactions (1) and (4) one obtains values for ΔH° and ΔS° for the following reaction:

$$POCl_3(g) + GaCl_3(g) \Leftrightarrow POCl_3 \cdot GaCl_3(g) \quad (8)$$

$$\Delta H_8^\circ = -73.8 \pm 0.8\,\text{kJ mol}^{-1}$$

$$\Delta S_8^\circ = -108.9 \pm 1.1\,\text{J mol}^{-1}\,\text{K}^{-1}.$$

Table 3 summarizes the thermodynamic functions calculated in this work from Raman spectral data. In the case of reaction (4) the measured ΔH° and ΔS° values are in good agreement with earlier reported values.[23,24]

Table 3. Thermodynamic functions of reactions

Temperature range (K)	Reaction	ΔH° (kJ mol^{-1}) This work	ΔH° (kJ mol^{-1}) Lit.	Ref.	ΔS° (J mol^{-1} K^{-1}) This work	ΔS° (J mol^{-1} K^{-1}) Lit.	Ref.
400–800	$Ga_2Cl_6(g) \Leftrightarrow 2GaCl_3(g)$	83.2 ± 1.3			130.6 ± 2.2		
			90.3	24			
			85.8	23		135.4	23
640–690							
600–800	$POCl_3(g) + \frac{1}{2}Ga_2Cl_6(g) = POCl_3 \cdot GaCl_3(g)$	−36.7 ± 0.8			−43.6 ± 1.1		
600–800	$POCl_3(g) + GaCl_3(g) = POCl_3 \cdot GaCl_3(g)$	−78.3 ± 0.8			−108.9 ± 1.1		

Acknowledgement—The authors are indebted to Professor G. N. Papatheodorou for helpful discussions during the course of the present investigation and for valuable comments on the manuscript.

REFERENCES

1. R. H. Tomlinson, in *Mellor's Comprehensive Treatise on Inorganic and Theoretical Chemistry*, Vol. 8, Supplement 3, p. 496. Longmans, London (1971).
2. W. L. Groeneveld and A. P. Zuur, *Rec. Trav. Chim.* 1957, **76**, 1005.
3. A. S. Barabanova and B. A. Voitorich, *Russ. J. Inorg. Chem.* 1964, **9**, 1455.
4. V. L. Shubaev, A. V. Suvorov and G. A. Semenov, *Russ. J. Inorg. Chem.* 1970, **15**, 479.
5. H. Gerding, J. A. Koningstein and E. R. van der Worm, *Spectrochim. Acta* 1960, **16**, 881.
6. W. Brockner, K. Grande and H. A. Øye, *Ber. Bunsenges. Phys. Chem.* 1987, **91**, 561.
7. N. N. Greenwood and K. Wade, *J. Chem. Soc.* 1957, 1516.
8. A. V. Suvorov, *Zh. Koord. Khim.* 1977, **3**, 1141.
9. M. Brooker and G. N. Papatheodorou, in *Advances in Molten Salt Chemistry* (Edited by G. Mamantov), Vol. 5, pp. 27–165 Elsevier, New York (1983).
10. G. N. Papatheodorou, *Curr. Top. Mater. Sci.* 1982, **10**, 249.
11. (a) G. N. Papatheodorou, L. A. Curtiss and V. A. Maroni, *J. Chem. Phys.* 1983, **78**, 3303; (b) T. Østvold, E. Rytter and G. N. Papatheodorou, *Polyhedron* 1986, **5**, 821.

12. S. Boghosian, G. N. Papatheodorou, R. W. Berg and N. J. Bjerrum, *Polyhedron* 1986, **5**, 1393.
13. S. Boghosian and G. N. Papatheodorou, *J. Phys. Chem.* 1989, **93**, 415.
14. G. N. Papatheodorou, in *Proceedings of the 10th Materials Research Symposium on Characterization of High Temperature Vapors and Gases* (Edited by J. W. Hastie), NBS Publication 561. National Bureau of Standards, Washington, DC (1979).
15. T. Tomita, C. E. Sjogren, P. Klaeboe, G. N. Papatheodorou and E. Rytter, *J. Raman Spectrosc.* 1983, **14**, 415.
16. G. N. Papatheodorou, in *Metal Bonding and Interactions in High Temperature Systems* (Edited by J. L. Cole and W. C. Stwalley), ACS Symposium Series No. 179, p. 309. American Chemical Society, Washington, DC (1982).
17. J. W. Hastie (Editor), *Proceedings of the 10th Materials Research Symposium on Characterization of High Temperature Vapors and Gases*, NBS Publication 561. National Bureau of Standards, Washington, DC (1979).
18. H. Schäfer, *Adv. Inorg. Chem. Radiochem.* 1983, **26**, 201.
19. K. Olie and D. J. Stufkens, *Spectrochim. Acta* 1976, **32A**, 469.
20. B. Gilbert, G. Mamantov and G. M. Begun, *Inorg. Nucl. Chem. Lett.* 1974, **10**, 1123.
21. I. R. Beattie and J. R. Horder, *J. Chem. Soc. A.* 1969, 2655.
22. E. Rytter, PhD thesis, Norwegian Institute of Technology (1974).
23. W. Ficher and O. Z. Jubermann, *Anorg. Allg. Chem.* 1936, **227**, 227.
24. H. Schäfer, *Ang. Chem.* 1976, **15**, 713.

Polyhedron Vol. 12, No. 7, pp. 783–789, 1993
Printed in Great Britain

0277–5387/93 $6.00+.00
© 1993 Pergamon Press Ltd

ISOMERIC DITHIOCYANATE COMPLEXES OF RUTHENIUM(II), SYNTHESIS, CHARACTERIZATION OF ALL POSSIBLE BOND ISOMERS OF *TRANS,CIS*-$Ru(CNS)_2L_2$ [L = 2-(ARYLAZO)PYRIDINE] AND STUDIES OF ISOMERIZATION

MAUSHUMI KAKOTI, SUBRATA CHAUDHURY, ALOK K. DEB and SREEBRATA GOSWAMI†

Department of Chemistry, North-Eastern Hill University, Shillong 793 003, India

(*Received* 10 *November* 1992; *accepted* 16 *November* 1992)

Abstract—A series of isomeric new dithiocyanate ruthenium(II) complexes of the type *trans,cis*-$Ru(CNS)_2L_2$ [L = 2-(arylazo)pyridine] have been synthesized by a stereoretentive substitution reaction from the known diaquo cationic complex *trans,cis*-$[Ru(OH_2)_2L_2]^{2+}$. All possible linkage isomers have been separated on a silica gel column and investigated for linkage isomerism. These isomers have been thoroughly characterized from physical properties, ^1H NMR, IR and UV–vis spectroscopy. It has been shown that the most stable linkage isomer in this case is S,S bonded. Two (S,N and N,N) out of three isomers of *trans,cis*-$Ru(CNS)_2L_2$ are converted into the third (S,S) isomer on boiling in xylene. Similar transformations have also been observed in the solid state. Factors influencing the population of the various isomers are noted.

Thiocyanate (SCN^-) is a potential ambidentate[1–5] ligand for metal ions. Much effort has been expanded towards understanding the role of co-ligands[2,6–13] in relation to the thiocyanate bonding mode in mixed-ligand transition metal thiocyanate complexes. It has now been established that both electronic as well as steric factors in metal thiocyanates largely influence the bonding modes of the pseudo-halide. In an attempt to sort out the effect of a strong π-acceptor co-ligand on the bonding mode of the thiocyanate ion to a ruthenium(II) centre we report here the synthesis, characterization and isomerization of isomeric dithiocyanates of the type *trans,cis*-$Ru(CNS)_2L_2$ [L = 2-(arylazo)-pyridine]. The *trans,cis* designation refers to the relative positions of the coordinated pyridine and azo nitrogens of the ligand L, respectively. Besides the fact that examples of ruthenium(II) thiocyanates are scarce,[14–20] no systematic approach on the isomerization of such complexes have been reported. It may be relevant to add here that in most cases only one (most stable) of the possible isomers is formed, which probably precludes the possible studies on the isomerization in such complexes. The two ligands used are abbreviated as L^1 and L^2.

RESULTS AND DISCUSSION

Stereochemistry of the starting material and synthesis

The cationic diaquo complex $[Ru(OH_2)_2L_2]^{2+}$ exists[21] in two geometrical isomeric forms; both have the *cis*-$Ru(OH_2)_2$ moiety. The stereochemistries of isomers having the RuL_2 moiety have been defined.[22] Thus, isomer **1** of $[Ru(OH_2)_2L_2]^{2+}$ is *trans,cis* or simply *t,c*. This diaquo complex (**1**) was used as the starting material for the synthesis of the desired dithiocyanate complex.

An ethanolic solution of **1** reacts smoothly with a large excess of aqueous NH_4SCN (1:>20) to yield [eq. (1)] an isomeric mixture of $Ru(CNS)_2L_2$ (CNS does not imply the bonding mode).

$$t,c\text{-}Ru(H_2O)_2L_2^{2+} \xrightarrow[C_2H_5OH/H_2O]{NH_4SCN} t,c\text{-}Ru(CNS)_2L_2 \quad (1)$$

† Author to whom correspondence should be addressed.

The compound is moderately soluble in the reaction mixture. On concentration of the solution, followed by cooling to 273 K, the crystalline product precipitates. The crude product was then subjected to column chromatography for isomer purification. Three pure isomers were eluted from the column, which on evaporation and further crystallization yielded crystalline compounds. Formulations of the compounds are made on the basis of elemental analyses (Table 1). The solution colours of the three isomers are: first band, greenish blue (**2**); second band, blue (**3**); and third band, violet (**4**). The overall yield of $Ru(CNS)_2L_2$ is quite high (>80%). The relative yields of the isomers vary with the temperature of the reaction. If the anation reaction is performed by boiling the reaction mixture the relative yields of the three isomers **2**:**3**:**4** are 6:3:1, and when the reaction is carried out at room temperature (300 K) the observed relative yields of **2**:**3**:**4** are 3:3:1. Furthermore, we note here that in refluxing xylene (1) both **3** and **4** or a mixture of **3** and **4** isomerizes to **2** and (2) **4** isomerizes to **3**. Similar transformations have also been observed in the solid state. From the above observations it may be concluded that of the three isomers, bluish green **2** is thermally the most stable. It may also be noted here that a very large excess of NH_4SCN is required for the completion of reaction (1). At a lower concentration of NH_4SCN the reaction was incomplete, even after 20 h boiling of the reaction mixture.

Geometry of $Ru(CNS)_2L_2$

It has now been well established that the *t,c* geometry of the RuL_2^{n+} moiety is thermally the most stable[23–25] and **1** undergoes[26,27] stereoretentive nucleophilic substitution reactions with several monodentate and bidentate ligands. Thus, it is reasonable to assume that the anation reaction under consideration occurs without change in the RuL_2 moiety. This assumption is further strengthened by the product of the reaction of crude

$$t,c\text{-}Ru(OH_2)_2L_2^{2+} \underset{Ag^+}{\overset{SCN^-}{\rightleftharpoons}} t,c\text{-}Ru(CNS)_2L_2$$

Scheme 1.

$Ru(CNS)_2L_2$ with 2 mol of $AgNO_3$. The optical spectra of the diaquo compound obtained from the above reaction were indistinguishable from those of authentic $t,c\text{-}Ru(OH_2)_2L_2^{2+}$. Thus, we have the stereoretentive interconversion Scheme 1.

Spectra and identification of linkage isomers of t,c-$Ru(CNS)_2L_2$

The stereoretentive anation reaction of **1** should in principle produce three linkage isomers of *t,c*-$Ru(CNS)_2L_2$ (Scheme 2). Of the three possible isomers two (S,S and N,N) are symmetrical, whereas S,N is unsymmetrical. The geometry and bonding mode of the thiocyanates have been clearly revealed by ^1H NMR and optical spectral data.

^1H *NMR spectra.* The ^1H NMR spectral data of the complexes were used to determine the symmetry of the complexes and thus the bonding mode of CNS in the isomers. Assignment of individual pyridyl proton resonances was made[28,29] on the basis of relative intensity, chemical shifts and by comparison of the spectra with those of analogous complexes of L. Unfortunately, we could not obtain resolvable signals for aryl protons under our experimental conditions. Chemical shifts, along with the *J* values of the proton resonances in the complexes, are listed in Table 2 and a set of representative spectra are displayed in Fig. 1.

Examination of the data in Table 2 reveals that: (1) the methyl and pyridyl proton resonances of **4** are in general upfield to those of **3** and **2**, (2) two (**2** and **4**) of the three isomers exhibited only one signal (singlet or multiplet) both for the pyridyl and methyl protons, whereas the same signals split in the case of the blue isomer (**3**) (Fig. 1). Therefore,

Table 1. Analytical data[a] of the complexes

Compound	%C	%H	%N
(**2**) *t,c*-$Ru(SCN)_2(L^1)_2$	49.2(49.4)	3.0(3.1)	19.1(19.2)
(**3**) *t,c*-$Ru(SCN)(NCS)(L^1)_2$	49.5(49.4)	3.1(3.1)	19.3(19.2)
(**4**) *t,c*-$Ru(NCS)_2(L^1)_2$	49.3(49.4)	3.1(3.1)	19.2(19.2)
(**2**) *t,c*-$Ru(SCN)_2(L^2)_2$	50.8(51.1)	3.6(3.6)	18.2(18.3)
(**3**) *t,c*-$Ru(SCN)(NCS)(L^2)_2$	51.1(51.1)	3.6(3.6)	18.0(18.3)
(**4**) *t,c*-$Ru(NCS)_2(L^2)_2$	50.7(51.1)	3.6(3.6)	18.3(18.3)

[a] Calculated values are in parentheses.

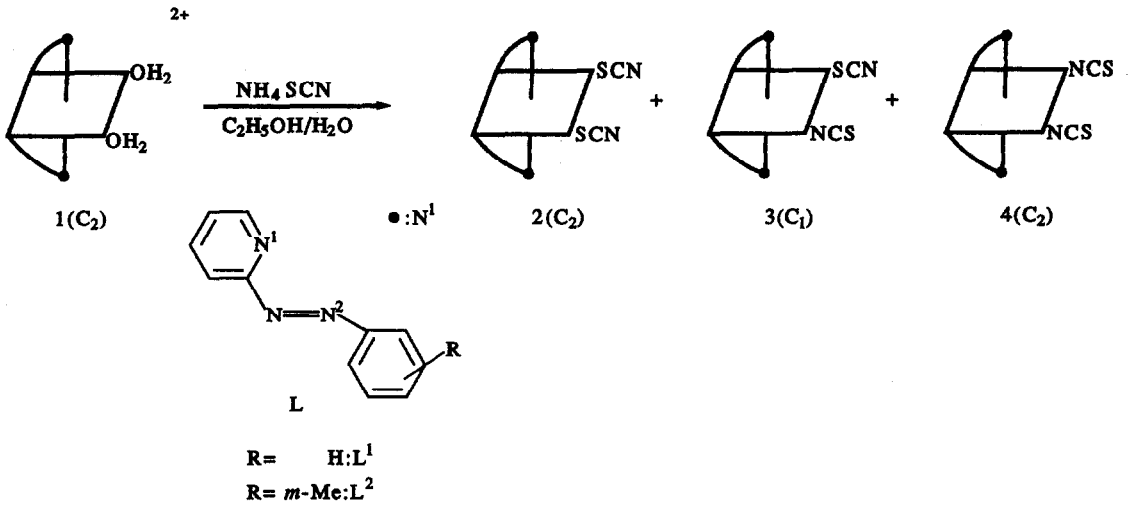

Scheme 2.

in isomer **3** two ligands are magnetically inequivalent and the other two isomers are symmetrical. It has already been noted that the t,c geometry of the RuL_2 moiety is symmetrical and the loss of symmetry in **3** must arise from the unsymmetrical coordination of the two CNS groups. Clearly, isomer **3** is S,N bonded, t,c-$Ru(SCN)(NCS)L_2$. The other two isomers are S,S and N,N bonded and each of them retains the symmetry axis as expected. This ambiguity regarding the S,S and N,N coordination modes could not be settled by ^1H NMR data, however, this problem has been solved by the use of optical spectral data (*vide infra*). (3) Each of the three isomers exhibit resonance(s) due to the orthopyridyl proton at *ca* 9.15 ppm. We note that this proton is shielded in *trans* geometry and the resonance appears at a higher field[28] in the analogous complexes. This further confirms the *cis* geometry of $Ru(CNS)_2L_2$ complexes.

UV–vis spectra. The solution spectra of all three isomers, t,c-$Ru(CNS)_2L_2$, show highly intense allowed transitions in the visible region. UV–vis spectral data of the complexes are collected in Table 3 and representative spectra are displayed in Fig. 2. The lowest energy transition in each case has been attributed[21–27] to metal-to-ligand charge transfer [$Ru(t_2) \rightarrow \pi^*(L)$] MLCT transitions. We note here that the MLCT transition in each case is associated with a shoulder at a higher energy. This spectral

Table 2. ^1H NMR[a] spectral data of complexes

Compound	δ, ppm (J, Hz) Pyridyl protons 6-H[c]	3-H[c]	4-H[d]	5-H[d]	Phenyl/tolyl protons[b]	Methyl protons 9-Me
(**2**) t,c-$Ru(SCN)_2(L^1)_2$	9.10(6.3)	8.65(8.9)	8.25(8.1)	7.70(6.5)	7.37–6.77	
(**3**) t,c-$Ru(SCN)(NCS)(L^1)_2$	9.17(5.8) 9.00(6.5)	8.70–8.60	8.27–8.03	7.76–7.58	7.28–6.85	
(**4**) t,c-$Ru(NCS)_2(L^1)_2$	9.00(5.9)	8.61(8.9)	8.04(8.0)	7.60(6.3)	7.25–6.83	
(**2**) t,c-$Ru(SCN)_2(L^2)_2$	9.12(6.3)	8.69(9.0)	8.28(8.1)	7.77(6.3)	7.27–6.67	2.19
(**3**) t,c-$Ru(SCN)(NCS)(L^2)_2$	9.20(6.3) 9.07(6.3)	8.80–8.65	8.35–8.10	7.82–7.65	7.30–6.67	2.20, 2.17
(**4**) t,c-$Ru(NCS)_2(L^2)_2$	9.17(6.0)	8.73(9.0)	8.17(8.1)	7.69(5.9)	7.30–6.67	2.07

[a] In $CDCl_3$; $SiMe_4$ is used as an internal standard.
[b] Resolved spectra could not be obtained.
[c] Doublet.
[d] Triplet.

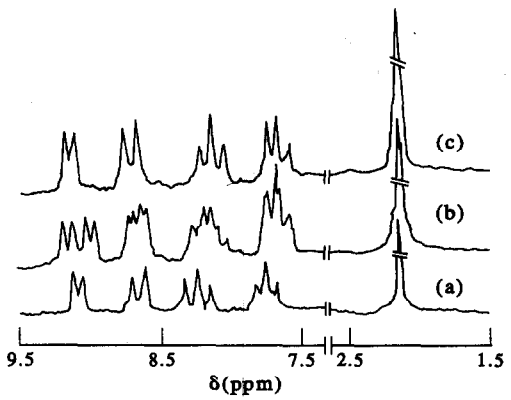

Fig. 1. Segmented ^{1}H NMR spectra of (a) *t,c*-Ru(SCN)$_2$(L^2)$_2$ (**2**), (b) *t,c*-Ru(SCN)(NCS)(L^2)$_2$ (**3**), and (c) *t,c*-Ru(NCS)$_2$(L^2)$_2$ (**4**) in $CDCl_3$.

feature has only been observed[22,30] in the *cis* geometry of bis-ligated ruthenium(II) complexes of L. It is significant to note that the trend of MLCT energies in this triad (**2**–**4**) is mutually consistent with the shift of ν(N=N) of coordinated L. In the spectrochemical series the position of isothiocyanate (N-bonded) is higher[31] than that of the thiocyanate (S-bonded) ligand. Thus, it is expected that N-coordination would stabilize the Ru(t_2) level better than that in the case of S-coordination. If it is assumed that the energies of the acceptor π^* (L) levels are more or less unaffected by a change in the coordination mode of CNS, the order of ν(MLCT) would be S,S < S,N < N,N and a parallel shift of ν(N=N) is also expected. This is exactly what is observed in the spectra of the three-bond isomers of *t,c*-Ru(CNS)$_2$L$_2$. Therefore, based on the spectral data it may be concluded with certainty that the greenish-blue isomer (**2**) is S,S-bonded *t,c*-Ru(SCN)$_2$L$_2$, the blue isomer (**3**) is S,N-bonded *t,c*-Ru(SCN)(NCS)L$_2$ and the violet isomer (**4**) is N,N-bonded *t,c*-Ru(NCS)$_2$L$_2$. This conclusion has been further proven by the examination of IR data.

IR spectra. IR spectral data were collected in the range 4000–250 cm^{-1} using KBr discs. Characteristic group frequencies are given in Table 3.

One of the significant observations in the IR spectrum of each of the isomers of *t,c*-Ru(CNS)$_2$L$_2$ is the consistent and systematic appearance of a strong band at *ca* 2100 cm^{-1}, which was assigned[6,16,31,32] to ν(CN) of coordinated CNS. Interestingly, the intensity of this band of **4** in DMF solution (0.011 g cm^{-3} of DMF) is most intense in this triad (**2**–**4**).

The three isomers of L^1 were chosen for the examination of IR spectra in the range 500–250 cm^{-1}. The violet isomer (**4**) showed two absorptions of almost equal intensity at 330 and 320 cm^{-1}. These bands are absent in the greenish-blue isomer (**2**)—

Table 3. Optical spectral data of complexes

Compound	IR[a,b] ν_{max} (cm^{-1}) N=N	C≡N	C—S	Ru—NCS	Ru—SCN	UV–vis[c,d] λ_{max} (nm) ($10^{-3}\times\varepsilon$, M^{-1}cm^{-1})
(**2**) *t,c*-Ru(SCN)$_2$(L^1)$_2$	1315	2081	826		305, 298	602(4.563), 495[e](2.309), 365[e](8.970), 320(11.360)
(**3**) *t,c*-Ru(SCN)(NCS)(L^1)$_2$	1328	2085	824	320	305	575(4.595), 465[e](2.240), 360[e](11.360), 325(13.230)
(**4**) *t,c*-Ru(NCS)$_2$(L^1)$_2$	1335	2104	845	330, 320		535(5.765), 442[e](2.060), 350[e](14.350), 322(17.580)
(**2**) *t,c*-Ru(SCN)$_2$(L^2)$_2$	1314	2080–2097[f]	829	[g]	[g]	602(5.670), 500[e](2.920), 370[e](11.490), 323(13.935)
(**3**) *t,c*-Ru(SCN)(NCS)(L^2)$_2$	1324	2086	826	[g]	[g]	575(4.255), 470[e](3.100), 375[e](12.695), 325(11.940)
(**4**) *t,c*-Ru(NCS)$_2$(L^2)$_2$	1334	2112	883	[g]	[g]	538(4.635), 450[e](2.035), 380(9.100), 326(14.295)

[a] In KBr discs (4000–250 cm^{-1}).
[b] All bands are sharp and strong unless otherwise stated.
[c] Solvent, $CHCl_3$.
[d] Solute concentration *ca* 10^{-3} M.
[e] Shoulder.
[f] Broad.
[g] Not examined.

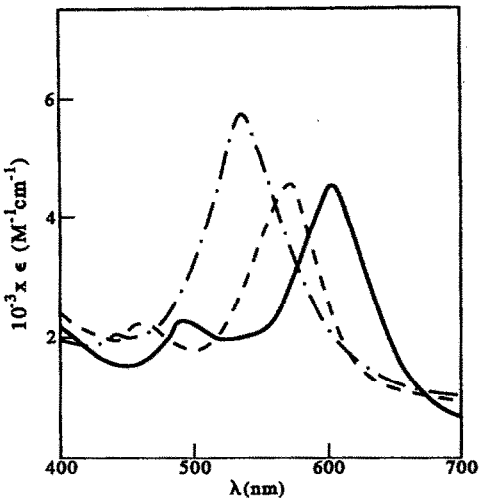

Fig. 2. Visible spectra of *t,c*-$Ru(SCN)_2(L^1)_2$ (**2**) (——), *t,c*-$Ru(SCN)(NCS)_2(L^1)_2$ (**3**) (-----) and *t,c*-$Ru(NCS)_2(L^2)_2$[4] (–·–·–) in $CHCl_3$.

instead, a two-band structure (relatively weak) at 305 and 298 cm^{-1} was observed. The blue isomer (**3**) showed a moderately strong absorption at 320 cm^{-1}, together with a weak absorption at 305 cm^{-1}. To explain the origin of these bands (500–250 cm^{-1}) in our complexes we note that M—NCS complexes give rise to strong bands at values comparable to M—Cl stretches of the corresponding chloro complexes, whereas thiocyanate linkages (M—SCN) give weaker bands occurring[33] inbetween the metal halide stretches of the corresponding chloro and bromo complexes. In the spectra[30] of the dichloride and dibromide analogues of the present complexes the frequencies corresponding to valence vibrations at ν(Ru—Cl), 336 and 310, and ν(Ru—Br), 275 and 250 cm^{-1}, were observed. Thus, we conclude that the absorptions at 330 and 320 cm^{-1} in isomer **4** are due to ν(Ru—NCS); the absorptions at 320 and 305 cm^{-1} in **3** are respectively due to ν(Ru—NCS) and ν(Ru—SCN); and the absorptions at 305 and 298 cm^{-1} are due to ν(Ru—SCN). The two-band structure of ν(Ru—NCS) in **4** and ν(Ru—SCN) in **2** once again confirms[23] the *cis* coordination of the two CNS ligands.

The IR spectral data of the complexes strengthen our conclusion regarding the modes of bonding of the pseudo-halide in the three linkage isomers of *t,c*-$Ru(CNS)_2L_2$ (**2–4**).

CONCLUSIONS

The spectral properties of the complexes, discussed above, clearly establish the bonding mode of the coordinated thiocyanate ligands in all three isomers, *t,c*-$Ru(CNS)_2L_2$. From statistical considerations the distribution of isomers in *t,c*-$Ru(CNS)_2L_2$ should be S,S (**2**): S,N (**3**): N,N (**4**) = 1 : 2 : 1. We find that the relative populations of **4** and **3** decrease with a rise in temperature of the reaction mixture. Thus, in boiling ethanol the yield of **4** is very poor. This result, together with the results of the thermal isomerizations of **4** → **3** and **3** → **2**, suggest that isomer **2** of the present complex is thermally the most stable. The isomerizations in the present case are surely controlled by the electronic factor alone, since the geometry and thus the steric factor arising from the two L ligands in the RuL_2 framework in all three linkage isomers remain identical. It may be relevant to mention here that the 2,2′-bipyridine (bpy) analogue of *t,c*-$Ru(CNS)_2L_2$ exists only as an N,N isomer, *cis*-$Ru(NCS)_2(bpy)_2$. These results may be interpreted as indicating that —SCN acts[31] as both a σ- and π-donor but a poor π-acceptor. In the present complex two azo groups, which are much better π-acceptors than the two pyridines, are *trans* to two thiocyanate ligands and thus promote S-bonding. In other words the symbiotic theory proposed by Jørgensen[34] is applicable in explaining the linkage preference of —SCN in the present case.

EXPERIMENTAL

Materials

The complexes *t,c*-$[Ru(OH_2)_2L_2](ClO_4)_2 \cdot H_2O$ were prepared as before.[21] Ammonium thiocyanate was obtained from Sarabhai M. Chemicals, Baroda. Spectrograde solvents were used for spectrochemical work. All other chemicals and solvents for preparative work were of reagent grade and used without further purification.

Measurements

Electronic spectra were recorded with a Hitachi 330 spectrophotometer; IR spectra (KBr disc, 4000–250 cm^{-1}) were obtained with a Perkin–Elmer 983 spectrophotometer; and solution IR spectra were measured using DMF solutions. ^1H NMR data were collected in $CDCl_3$ solvent with a Varian EM 390 spectrometer and chemical shifts were referenced to tetramethylsilane.

Preparation of the complexes

t, c- *Dithiocyanatobis* [2- (*arylazo*) *pyridine*] *ruthenium*(II), t,c-$Ru(CNS)_2L_2$. The complexes are prepared by following a general procedure. Specific details are given for *t,c*-$Ru(CNS)_2(L^1)_2$:

A sample of *t,c*-$[Ru(OH_2)_2(L^1)_2](ClO_4)_2 \cdot H_2O$ (0.720 g, 1 mmol) was dissolved in ethanol (25 cm^3) and to it an aqueous solution of NH_4SCN (1.5 g, 20 mmol) in water (5 cm^3) was added and stirred at room temperature (300 K) for 10 h. The ethanolic solution was concentrated *in vacuo* when a dark crystalline compound was obtained. It was filtered, dried and subjected to column chromatography on a silica gel column (60–120 mesh). The first moving greenish-blue band was eluted with a 1:50 acetonitrile: chloroform mixture. Two other fractions, viz. blue and violet bands, were eluted with 1:20 and 1:10 acetonitrile: chloroform mixtures, respectively. The solution of each fraction was evaporated *in vacuo*, each were crystallized from a 1:1 chloroform: hexane mixture. Yields are as follows: First band: *t,c*-$Ru(SCN)_2(L^1)_2$, bluish-green (**2**), 0.200 g (34%); second band: *t,c*-$Ru(SCN)(NCS)(L^1)_2$, blue (**3**), 0.200 g (34%); third band: *t,c*-$Ru(NCS)_2(L^1)_2$, violet (**4**), 0.067 g (12%).

A similar reaction was performed in boiling ethanol. The yields of the three isomers in this case are as follows: **2**, 0.300 g (51%); **3**, 0.150 g (25%); **4**, 0.050 g (9%). Yields of the analogous complexes of L^2: Room temperature (295 K): **2**, 0.205 g (34%); **3**, 0.200 g (33%); **4**, 0.070 g (12%). Boiling ethanol: **2**, 0.330 g (54%); **3**, 0.170 g (27%); **4**, 0.060g (10%).

Conversion of t,c-$Ru(SCN)(NCS)(L^1)_2$ (**3**) *to* t,c-$Ru(SCN)_2(L^1)_2$ (**2**). A solution of **3** (0.583 g, 1 mmol) was suspended in xylene (500 cm^3) and heated to reflux for 12 h. TLC showed only one spot due to the bluish-green isomer (**2**). The solution was concentrated to half volume and the bluish-green crystalline compound was obtained. It was filtered and dried *in vacuo*. Yield, 90%.

Conversion of t,c-$Ru(NCS)_2(L^1)_2$ (**4**) *to* t,c-$Ru(SCN)_2(L^1)_2$ (**2**). This was done similarly to above with the exception that **4** was heated to reflux for 20 h. The solution colour gradually turned blue due to the formation of the second isomer (**3**), and finally it became bluish-green (isomer **2**). Yield, 90%.

Solid-state thermal isomerization

$[t,c\text{-}Ru(SCN)(NCS)(L^2)_2]$ (**3**)→t,c-$Ru(SCN)(L^2)_2$ (**2**). A sample of **3** (0.583 g, 1 mmol) was heated slowly using an oil-bath. The temperature was raised to 150°C and maintained for 5 min. The solid mass was extracted with $CHCl_3$ (50 cm^3). The volume was then reduced to 25 cm^3 and on the addition of hexane dark crystals were obtained. On the TLC plate it showed only one spot due to isomer (**2**). The crystals were collected by filtration and dried *in vacuo*. Yield, 80%. The conversion process **4** → **2** was performed similarly. The temperature required for this transformation was *ca* 200°C. Yield, 80%.

Acknowledgements—Financial assistance received from the Council of Scientific and Industrial Research, New Delhi, is gratefully acknowledged. We thank Professor S. N. Bhat for allowing us to use the UV–vis spectrophotometer. Thanks are also due to Ms M. Bhattacharjee for carrying out preliminary experiments.

REFERENCES

1. A. M. Golub, H. Köhler and V. V. Skopenko, *Chemistry of Pseudohalides*, p. 239. Elsevier, Amsterdam (1986).
2. J. L. Burmeister, *Coord. Chem. Rev.* 1990, **105**, 77.
3. F. Basalo, *Coord. Chem. Rev.* 1990, **100**, 47.
4. J. L. Burmeister, *Coord. Chem. Rev.* 1968, **3**, 225.
5. J. E. Huheey, *Inorganic Chemistry*, p. 384. Harper and Row, New York (1983).
6. J. L. Burmeister, *Inorg. Chem.* 1964, **3**, 919.
7. L. A. Epps and L. G. Marzilli, *Inorg. Chem.* 1973, **12**, 1514.
8. J. A. Kargol, K. D. Lavin, R. W. Crecely and J. L. Burmeister, *Inorg. Chem.* 1980, **19**, 1515.
9. C. T. Hunt and A. L. Balch, *Inorg. Chem.* 1982, **21**, 1242.
10. G. J. Palenik, M. Mathew, W. L. Steffen and G. Beran, *J. Am. Chem. Soc.* 1975, **97**, 1059.
11. A. L. Paviglianiti, D. J. Minn, W. C. Fultz and J. L. Burmeister, *Inorg. Chim. Acta* 1989, **159**, 65.
12. D. W. Meek, P. E. Nicpon and V. I. Meek, *J. Am. Chem. Soc.* 1970, **92**, 5351.
13. J. J. MacDougall, A. W. Verstuyft, L. W. Cary and J. H. Nelson, *Inorg. Chem.* 1980, **19**, 1036.
14. A. R. M. Abbadi, M. A. Shehadeh and J. V. Kingston, *J. Inorg. Nucl. Chem.* 1974, **36**, 1173.
15. F. P. Dwyer, H. A. Goodwin and E. C. Gyarfas, *Aust. J. Chem.* 1963, **16**, 42.
16. S. Wajda and K. Rachlewicz, *Inorg. Chim. Acta* 1978, **31**, 35.
17. (a) H. J. Schwerdtfeger and W. Preetz, *Angew. Chem., Int. Edn Engl.* 1977, **16**, 108; (b) H. H. Fricke and W. Preetz, *Z. Naturforsch.* 1983, **38b**, 917.
18. (a) P. E. Hoggard and G. B. Porter, *J. Inorg. Nucl. Chem.* 1981, **43**, 185; (b) K. S. De Haas, *J. Inorg. Nucl. Chem.* 1973, **35**, 3231.
19. R. H. Harber, G. Nan, J. A. Potenga, H. J. Schugar and A. Bino, *Inorg. Chem.* 1989, **28**, 938.
20. B. Durham, J. L. Walsh, C. L. Carter and T. J. Meyer, *Inorg. Chem.* 1980, **19**, 860.
21. S. Goswami, A. R. Chakravarty and A. Chakravorty, *Inorg. Chem.* 1983, **22**, 602.
22. S. Goswami, A. R. Chakravarty and A. Chakravorty, *Inorg. Chem.* 1982, **21**, 2737.
23. R. A. Krause and K. Krause, *Inorg. Chem.* 1980, **19**, 2600.
24. A. K. Deb, M. Kakoti and S. Goswami, *J. Chem. Soc., Dalton Trans.* 1991, 3249.

25. T. Bao, K. Krause and R. A. Krause, *Inorg. Chem.* 1988, **27**, 759.
26. S. Goswami, R. N. Mukherjee and A. Chakravorty, *Inorg. Chem.* 1983, **22**, 2825.
27. R. A. Krause and K. Krause, *Inorg. Chem.* 1982, **21**, 1714.
28. A. K. Mahapatra, B. K. Ghosh, S. Goswami and A. Chakravorty, *J. Ind. Chem. Soc.* 1986, **63**, 101.
29. M. N. Ackermann, C. R. Barton, C. J. Deodene, E. M. Specht, S. C. Keill, W. E. Schreiber and H. Kim, *Inorg. Chem.* 1989, **28**, 397.
30. S. Goswami, A. R. Chakravarty and A. Chakravorty, *Inorg. Chem.* 1981, **20**, 2246.
31. D. F. Gutterman and H. B. Gray, *J. Am. Chem. Soc.* 1971, **93**, 3364.
32. K. Nakamoto, *Infrared and Raman Spectra of Inorganic and Coordination Compounds*, p. 283. Wiley Interscience, New York (1986).
33. D. Forster and D. M. L. Goodgame, *Inorg. Chem.* 1965, **4**, 715.
34. C. K. Jørgensen, *Inorg. Chem.* 1964, **3**, 1201.

Polyhedron Vol. 12, No. 7, pp. 791–794, 1993
Printed in Great Britain

0277–5387/93 $6.00+.00
© 1993 Pergamon Press Ltd

SEPARATION OF TIN ISOTOPES USING REDOX ION-EXCHANGE CHROMATOGRAPHY

A. K. NAJJAR and M. F. ORAYTH

Tajura Nuclear Research Centre, P.O. Box 30878, Tripoli, Libya

and

S. I. NIKITENKO*

Institute of Physical Chemistry of Russian Academy of Sciences, Leninsky pr. 31, 117915 Moscow, Russia

(*Received* 15 *October* 1992 ; *accepted* 26 *October* 1992)

Abstract—The equilibrium isotope effect in tin(II)–tin(IV) electron-exchange systems has been studied by a redox chromatography method using an anion-exchange resin. It was shown that the light isotopes are concentrated in tin(II) preferably. The values of the isotope separation coefficient (α) for ^{112}Sn and heavy isotopes were determined at 82°C and 5.5 mol dm^{-3} HCl. The dependence of α on isotopic mass ratio was found to be defined by the curve reaching top values of α for isotopes heavier than ^{120}Sn.

Redox chromatography in adsorption columns has been used successfully for the separation of uranium isotopes.[1,2] The same approach seems to be available for isotope fractionation of other elements. The aim of our work was to study the isotope effect in tin(II)–tin(IV) electron-exchange systems by means of redox ion-exchange chromatography. The isotope separation was accomplished through the isotopic exchange between tin(IV) adsorbed by a strongly basic anion-exchange resin and tin(II) in hydrochloric acid solution. Iron(III) adsorbed by anion-exchange resin was used as the oxidizing agent for tin(II).

EXPERIMENTAL

All the chemicals used were analytical grade reagents. Solutions were prepared with de-ionized distilled water. The anion-exchange resin Dowex 2 (50–100 mesh, Cl^- form, supplied by Fluka AG) was pretreated with HCl (5.5 mol dm^{-3}) in a hot water bath and packed in a water-jacket glass column (1.6 cm I.D. and 115 cm long). A solution of $FeCl_3$ (0.5 mol dm^{-3}) in HCl (5.5 mol dm^{-3}) at 82 ± 2°C was fed into the column until the resin was saturated by iron(III). The adsorbed iron(III) was then eluted by tin(II) (0.44 mol dm^{-3}) in HCl (5.5 mol dm^{-3}) at the same temperature. Tin(IV), produced by a redox reaction, was adsorbed by the anion-exchange resin.

The temperature of the column was controlled by a LKB 2209 thermostat. The eluant was fed into the column from the thermostated closed vessel to prevent contact with air. The effluent, which emerged from the column, was sampled and iron(III), iron(II) and tin(II) concentrations were then determined.

The concentration of iron(III) was determined spectrophotometrically with potassium thiocyanate.[3] Iron(II) was oxidized with a small excess of H_2O_2 and determined as iron(III). The concentration of tin(II) was determined by iodometric titration.[3]

After the determination of concentrations the samples which were to be analysed mass spectrometrically were treated to separate tin and iron. The separation was carried out by solvent extraction using 30% tri-n-butylphosphate solution in dodecane as an extractant.[4] Tin(II) and tin(IV) in the effluent were oxidized by H_2O_2 and then tin(IV) was extracted from HCl (3 mol dm^{-3}). Equal vol-

* Author to whom correspondence should be addressed.

umes of water and organic phases were shaken mechanically in stoppered glass tubes over 5 min and subsequently the tubes were centrifuged. Tin(IV) in the organic phase was stripped from an aliquot by HCl (0.1 mol dm^{-3}) and used for mass spectrometric analysis.

The abundances of the tin isotopes were measured using an MI-1201 mass spectrometer. The mass range from 112 to 124 was repeatedly scanned and the isotopic abundances were determined from the heights of the corresponding peaks. The statistical error of ^{112}Sn, ^{116}Sn, ^{117}Sn, ^{118}Sn, ^{119}Sn, ^{120}Sn, ^{122}Sn and ^{124}Sn abundance determination was found to be 4–6%. The absolute error for natural tin determination did not exceed the statistical error. For ^{114}Sn and ^{115}Sn the statistical error was found to be more than 15% and satisfactory accuracy (error *ca* 10–15%) of isotope separation coefficient values for these isotopes could not be provided. For this reason ^{114}Sn and ^{115}Sn were excluded from further consideration.

RESULTS AND DISCUSSION

It is known[5] that in hydrochloric acid solutions tin(II) is oxidized rapidly by iron(III). However, in our preliminary experiments it was found that iron(III) adsorbed by Dowex 2 resin can react with tin(II) rapidly only when the temperature is more than 70°C. In order to provide high rates of tin(II) oxidation and tin(II)–tin(IV) isotopic exchange the redox chromatographic experiment was performed at temperatures above 80°C.

In passing through the iron(III) adsorption zone tin(II) is oxidized in accordance with the following scheme:

$$Sn^{II}_{sol} + 2Fe^{III}_{res} \rightarrow Sn^{IV}_{res} + 2Fe^{II}_{sol}, \quad (1)$$

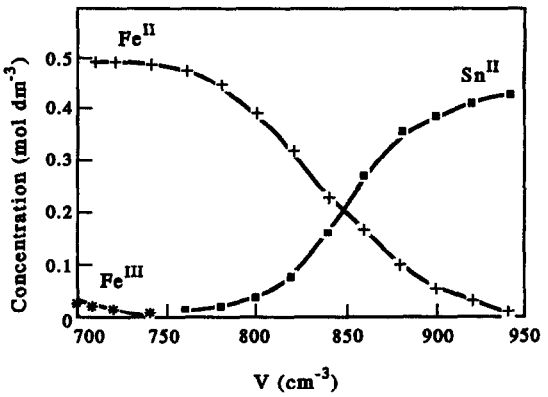

Fig. 1. Concentration profiles of tin(II), iron(II) and iron(III) at the rear boundary of the iron elution zone. Elution rate = 5 $cm^3\ h^{-1}\ cm^{-2}$.

where the terms "sol" and "res" refer to solution and resin, respectively. Since in our experimental conditions tin(II) and iron(II) are adsorbed by the anion-exchange resin more weakly than tin(IV) and iron(III), most of the iron(III) adsorbed by resin was eluted and replaced by tin(IV).

The concentration profiles of tin and iron chromatograms obtained are shown in Fig. 1. The concentration of tin(IV) in the first fractions of effluent did not exceed 5×10^{-4} mol dm^{-3}.

The values of tin isotopic abundances in samples at the front boundary of the tin(II) elution zone are presented in Fig. 2 and Table 1.

The results obtained show that the first portions of tin(II) emerged from the column are enriched by light isotopes. The values of the single stage separation coefficient (α), calculated by the Spedding method,[6] for ^{112}Sn and heavy tin isotopes are presented in Table 2. The values of α are expected

Table 1. The values of tin isotopic abundances (R_i) at the front boundary of the tin(II) elution zone. R_0 = natural isotopic abundance

Volume of effluent (cm^3)	R_i[a] ^{112}Sn	^{116}Sn	^{117}Sn	^{118}Sn	^{119}Sn	^{120}Sn	^{122}Sn	^{124}Sn
740	0.0622	0.134	0.0650	0.216	0.0770	0.295	0.0405	0.0580
760	0.0450	0.137	0.0700	0.228	0.0794	0.301	0.0430	0.0530
780	0.0340	0.139	0.0720	0.238	0.0823	0.310	0.0442	0.0559
800	0.0221	0.140	0.0735	0.243	0.0840	0.316	0.0460	0.0580
820	0.0160	0.142	0.0738	0.246	0.0855	0.324	0.0468	0.0588
840	0.0100	0.141	0.0740	0.245	0.0860	0.328	0.0475	0.0593
R_0[a]	0.0096	0.141	0.0739	0.244	0.0861	0.329	0.0472	0.0594

[a] Values of standard deviation (σ) were found to be in the limits 4–6%.

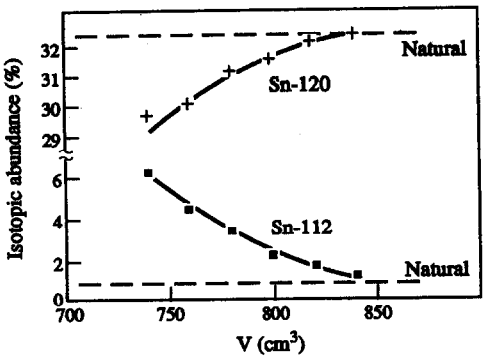

Fig. 2. Isotopic abundances of ^{112}Sn and ^{120}Sn at the front boundary of the tin elution zone.

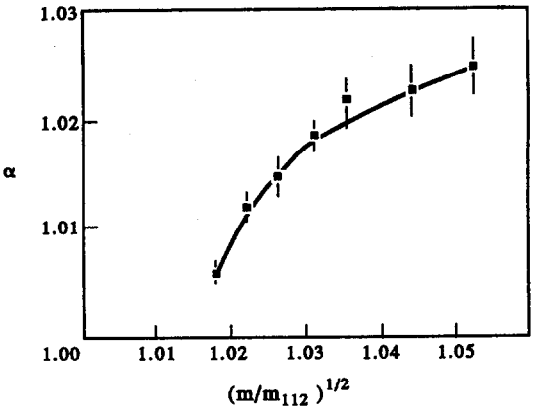

Fig. 3. Values of α plotted as a function of $(m/m_{112})^{1/2}$.

to be linearly proportional to $(m/m_{112})^{1/2}$, where m refers to the masses of the considered tin isotopes, as a first approximation. However, as shown in Fig. 3, such dependence is defined by the curve, reaching top values of α at $m > 120$.

It can be assumed that the magnitude of the isotope separation coefficient is determined by the fine structure of the complexes involved in the isotopic exchange. When tin(II) solution passes through the tin(IV) adsorption zone the following sorption–desorption and isotopic exchange processes are possible:

$$Sn^{IV}_{res} \rightarrow Sn^{IV}_{sol} \quad (2)$$

$$Sn^{II}_{sol} \rightarrow Sn^{II}_{res} \quad (3)$$

$$*Sn^{II}_{sol} + **Sn^{IV}_{res} \rightarrow **Sn^{II}_{sol} + *Sn^{IV}_{res} \quad (4)$$

$$*Sn^{II}_{res} + **Sn^{IV}_{res} \rightarrow **Sn^{II}_{res} + *Sn^{IV}_{res} \quad (5)$$

$$*Sn^{II}_{sol} + **Sn^{IV}_{sol} \rightarrow **Sn^{II}_{sol} + *Sn^{IV}_{sol} \quad (6)$$

$$*Sn^{II}_{res} + **Sn^{IV}_{sol} \rightarrow **Sn^{II}_{res} + *Sn^{IV}_{sol}, \quad (7)$$

where *Sn and **Sn refer to any pair of tin isotopes. During reactions (2)–(7) a little of one tin isotope is transferred from the solution to the resin and other isotopes from the resin to the solution. If isotopic exchange between the different chemical species of tin(II) and tin(IV) is sufficiently fast the multistage separation of tin isotopes occurs.

As predicted from the theoretical treatments[7] the equilibrium isotope effects in the exchange processes of mass transfer are significantly smaller than in the reactions of electron transfer. For this reason the observed isotope effect can be defined by reactions (2) or (3). Since the concentration of tin(IV) in the aqueous phase is sufficiently low the contribution of isotope effects on states (6) and (7) is supposed to be neglected. Thus, the observed isotope effect may be assigned to the isotopic exchange processes in accordance with eqs (4) and (5).

Under our experimental conditions tin(II) and tin(IV) in the resin phase and in the aqueous phase are known[8] to exist in the forms of $SnCl_3^-$ and $SnCl_6^{2-}$ complexes, respectively. Therefore, in order to explain the dependence of α on isotopic mass ratio a detailed investigation of tin isotopic mass influence on zero-point energies of Sn–Cl bond vibrations in $SnCl_3^-$ and $SnCl_6^{2-}$ complexes is required.

Table 2. Values of the single stage isotope separation coefficient

Isotopic pair	$\alpha \pm \sigma$
$^{112}Sn/^{116}Sn$	1.0058 ± 0.0009
$^{112}Sn/^{117}Sn$	1.0115 ± 0.0017
$^{112}Sn/^{118}Sn$	1.0150 ± 0.0021
$^{112}Sn/^{119}Sn$	1.0190 ± 0.0018
$^{112}Sn/^{120}Sn$	1.0246 ± 0.0028
$^{112}Sn/^{122}Sn$	1.0230 ± 0.0025
$^{112}Sn/^{124}Sn$	1.0251 ± 0.0030

Acknowledgements—The authors are grateful to Mr W. M. Abdulhafid and Mr A. M. Alhemmali for the mass spectrometric analysis reported in this work.

REFERENCES

1. M. Seko, T. Miyake, K. Inada and K. Takeda, *Nucl. Technol.* 1980, **50**, 178.
2. T. Miyake, K. Takeda, K. Imamura and H. Obanawa, *Nucl. Technol.* 1984, **64**, 237.
3. *Treatise on Analytical Chemistry* (Edited by I. M. Kolthoff and P. J. Elving), Part 2, Vols 2–3. Interscience Publishers, New York (1962).

4. A. K. De, S. M. Khopkar and R. A. Chalmers, *Solvent Extraction of Metals*. VNR Ltd, London (1970).
5. F. R. Duke and R. C. Pinkerton, *J. Am. Chem. Soc.* 1951, **73**, 3045.
6. F. H. Spedding, J. E. Powel and H. J. Svec, *J. Am. Chem. Soc.* 1955, **77**, 6125.
7. D. A. Knyazev and G. D. Klinskii, *Isotopenpraxis* 1978, **14**, 41.
8. *Comprehensive Inorganic Chemistry* (Edited by A. F. Trotman-Dickenson), Vol. 2, p. 43. Pergamon Press, Oxford (1975).

Polyhedron Vol. 12, No. 7, pp. 795–800, 1993
Printed in Great Britain

0277–5387/93 $6.00+.00
© 1993 Pergamon Press Ltd

SYNTHESIS AND CRYSTAL STRUCTURE OF MONOCYCLOPENTADIENYL HOLMIUM DICHLORIDE TRIS(TETRAHYDROFURAN)

ZHONGZHI WU,* ZHENG XU and XIAOZENG YOU

Coordination Chemistry Institute, Nanjing University, Nanjing 210008, P.R.C.

and

XIGEN ZHOU

Institute of Organic Chemistry, Anhui Normal University, Wuhu 241000, P.R.C.

and

HUAQING WANG and YAO YANG

The Analytical Center of Nanjing University, Nanjing 210008, P.R.C.

(*Received* 10 *September* 1992; *accepted* 22 *October* 1992)

Abstract—The one-pot reaction of $HoCl_3$ with C_5H_6 and sodium (1 : 5 : 1 molar ratio) in THF resulted in the formation of the compound η^5-$CpHoCl_2 \cdot 3THF$ ($Cp = C_5H_5$), which was characterized by elemental analysis, IR and MS spectra, and X-ray crystallography, showing that it is monomeric in both the vapour and solid states. The holmium atom has a distorted octahedral geometry coordinated by one Cp ring centroid, three THF molecules and two chloride atoms. The Ho—C(Cp) bond lengths range from 2.656(11) to 2.674(11) Å and average 2.668(11) Å. The three THF molecules coordinate to the holmium atom at the Ho—O bond distances of 2.366(6), 2.376(6) and 2.454(7) Å, respectively. A comparison of some significant structural parameters along with the isostructural series $CpLnCl_2 \cdot 3THF$ (Ln = Nd, Gd, Ho, Er and Yb) was made.

The investigation of the structures of organolanthanide compounds has been of interest for many years, because it is important to interpret the bond nature and chemical properties of lanthanide compounds. Crystal structures of monocyclopentadienyl lanthanide dichlorides, such as $CpNdCl_2 \cdot 3THF$,[1] $CpErCl_2 \cdot 3THF$,[2] $CpGdCl_2 \cdot 3THF$[3] and $CpYbCl_2 \cdot 3THF$,[4] have been reported. To our knowledge, however, the study of the crystal structure of $CpHoCl_2 \cdot 3THF$ has not yet been reported. In order to characterize the Ho—C bond and to learn about the strength of coordination of the THF molecules, we herein report the synthesis of $CpHoCl_2 \cdot 3THF$ by using a one-pot method and its crystal structure by single-crystal X-ray diffraction investigations. At the same time we compare some significant structural parameters along the isostructural series $CpLnCl_2 \cdot 3THF$ (Ln = Nd, Gd, Ho, Er and Yb).

EXPERIMENTAL

General

The title compound is extremely air- and moisture-sensitive. Therefore, both the synthesis and subsequent manipulations of the compound were conducted under purified argon with rigorous exclusion of air and water using Schlenk or glovebox techniques. THF and n-hexane solvents were refluxed and distilled over fine $LiAlH_4$ or the sodium ketyl of benzophenone under argon immediately before use. Anhydrous $HoCl_3$ was prepared according to the literature method.[5]

* Author to whom correspondence should be addressed.

Measurements

Carbon and hydrogen analyses were performed on a Perkin–Elmer 240C microanalyser. The IR spectra were recorded over the 200–4000 cm^{-1} range on a Perkin–Elmer 983G spectrometer using Nujol and fluorolobe mulls and examined between disc-shaped CsI crystals. Mass spectra were recorded on a Shimadzu QP-1000A spectrometer using crystal samples; EI mode; the sample was introduced by direct inlet techniques. Mass data are based on ^{165}Ho, ^{35}Cl, ^{16}O, ^{12}C and ^{1}H. The analysis of holmium was accomplished using a literature procedure with disodium EDTA.[6]

Preparation of $CpHoCl_2 \cdot 3THF$, Cp_2HoCl *and* Cp_3Ho *by the one-pot method*

$CpHoCl_2 \cdot 3THF$. Freshly distilled cyclopentadiene (1.7 cm^3, 20 mmol) and anhydrous $HoCl_3$ (1.1 g, 4 mmol) were dissolved together in THF (40 cm^3). To this suspension was added dispersed sodium metal (0.1 g, 4 mmol) and the reaction mixture was allowed to stir overnight. After the reaction was complete the solution/suspension was centrifuged to remove the precipitate. The solution thus separated out was concentrated by reducing the pressure to *ca* 10 cm^3. n-Hexane (30 cm^3) was then added and a yellow solid was precipitated out, which was purified by recrystallization from THF/n-hexane. Crystals suitable for X-ray diffraction were grown by cooling the saturated THF solution at −25°C for 2 weeks. Yield: 65.3%. Found: C, 39.1; H, 5.4; Ho, 32.2. Calc. for $CpHoCl_2 \cdot 3THF$ ($C_{17}H_{29}O_3Cl_2Ho$): C, 39.5; H, 5.6; Ho, 31.9%. IR (cm^{-1}): 3081m, 2953s, 2878m, 1602s, 1443s, 1046s, 1012s, 914s, 862m, 780s, 762s, 438s, 365m, 238s, 212s. MS: *m/z* (relative intensity %) and fragment: 516(11.2), M; 481(2.5), M−Cl; 451(43.5), M−Cp; 416(8.9), M−Cp−Cl; 381(5.6), M−Cp−2Cl; 66(100.0), HCp; 65(42.3), Cp.

Cp_2HoCl. Freshly distilled cyclopentadiene (3.0 cm^3, 36 mmol) and anhydrous $HoCl_3$ (1.1 g, 4 mmol) were dissolved in THF (40 cm^3). To this suspension was added dispersed sodium metal (0.18 g, 8 mmol) and the reaction mixture was allowed to stir overnight. After the reaction was complete the resulting mixture was dried by reduced pressure. The dried mixture was purified by vacuum sublimation above 160°C, 10^{-3} torr, to afford a yellow crystal product. Yield: 78.3%. The results of elemental, IR and MS spectra are consistent with those reported for Cp_2HoCl in the literature.[7]

Cp_3Ho can be obtained by a procedure similar to that for Cp_2HoCl, using the molar ratio of C_5H_6 : $HoCl_3$: Na as 5 : 1 : 3.

Crystal structure determination

A yellow crystal of the title compound was sealed in a thin-walled glass capillary under argon for X-ray diffraction determination. Intensities were collected on an Enraf–Nonius CAD4 four-circle diffractometer using graphite monochromated Mo-K_α radiation at room temperature and ω–2θ techniques. Lattice parameters were determined by the least-squares refinement of setting angles of 25 computer-centred reflections in the range $10° \leqslant \theta \leqslant 15°$. Three standard reflections were monitored every 200 reflections to check crystal stability. No decrease of intensity during data collection was observed. The intensities were corrected for Lorentz–polarization effects and empirical absorption. A summary of crystallographic data is given in Table 1.

The structure was solved by direct methods and Fourier syntheses using the MULTAN system. Refinement was performed by blocked full-matrix least-squares techniques, converged to a conventional R factor of 0.036 using 2242 reflections with $I \geqslant 3\sigma(I)$. The positions of the hydrogen atoms were calculated with a C—H bond length of 0.95 Å. Non-hydrogen atoms were refined using anisotropic temperature factors and hydrogen atoms isotropic temperature factors. All calculations were performed on a PDP 11/44 computer (Digital Equipment Corporation) using the SDP program system. Atom scattering factors were taken from the International Tables for X-ray Crystallography.[8] Fractional atomic coordinates and thermal parameters, together with observed and calculated structure factors, have been deposited with the Editor.

RESULTS AND DISCUSSION

Discussion of the one-pot reaction for the preparation of cyclopentadienyl lanthanide derivatives

The previous method for preparing the cyclopentadienyl lanthanide derivatives, such as $CpLnCl_2 \cdot 3THF$, Cp_2LnCl and Cp_3Ln (Ln = La − Lu), involves two steps, as shown in the following equations.[7,9–11]

$$2C_5H_6 + 2Na \xrightarrow{THF} 2NaC_5H_5 + H_2 \quad (1)$$

$$LnCl_3 + nNaC_5H_5 \xrightarrow{THF} Cp_nLnCl_{3-n} + NaCl$$
$$n = 1, 2 \text{ or } 3. \quad (2)$$

Due to NaCp being extremely sensitive to air and moisture, the preparation of a good quality solution of NaCp is usually difficult. Therefore, this method

Table 1. Summary of crystallographic data and data collection parameters

Formula	$(C_5H_5)HoCl_2 \cdot 3(C_4H_8O)$
*M*w	517.25
Crystal dimensions (mm)	$0.32 \times 0.34 \times 0.45$
Crystal system	Monoclinic
Cell parameters	
a (Å)	7.8039(2)
b (Å)	17.1068(4)
c (Å)	15.1707(3)
α (°)	90.00
β (°)	95.79
γ (°)	90.00
V (Å^3)	2015
D_c (g cm^{-3})	1.705
Z	4
Space group	$P2_1/n$
μ_c (cm^{-1})	42.5
F(000)	1024
Radiation (Å)	Mo-K_α ($\lambda = 0.71073$)
Scan mode	ω–2θ
Scan rate (° min^{-1})	4
Scan width	$0.9 + 0.35 \tan\theta$
2θ range (°)	$1 \leqslant 2\theta \leqslant 50$
h, *k*, *l* range	$0 \rightarrow 9$, $0 \rightarrow 20$, $-18 \rightarrow 18$
Total reflections measured	3967
Unique reflections observed	2248
Data used in refinement with $I \geqslant 3\sigma(I)$	2242
Transmission coefficients (max., min.)	1.08, 0.86
Max. shift/error	0.01
Variables in last cycle	324
ρ factor in weight[a]	0.04
R[b]	0.036
Rw[c]	0.040
GOF[d]	2.7

[a] The weighting scheme for the final refinement was $w = 1/(\sigma_F)^2$, where $\sigma_F = \sigma_{F^2}/2F$ and $\sigma_{F^2} = [(\sigma_I)^2 + (\rho F^2)^2]^{1/2}$.

[b] $R = \Sigma \| F_o | - | F_c \| / \Sigma F_o$.

[c] $Rw = [w(F_o - |F_c|)^2 / \Sigma w(F_o)^2]^{1/2}$.

[d] $GOF = [\Sigma w(F_o - |F_c|)^2 / (N_o - N_v)]^{1/2}$ (N_o, N_v are the number of observations and variables, respectively).

is not convenient due to the overelaborate procedure of the preparation and purification of NaCp. Thus, we suggest a modified procedure, namely, the one-pot method for the preparation of lanthanide metallocenes, as shown in the following equation:

$$n C_5H_6 + n Na + LnCl_3 \xrightarrow{THF} (C_5H_5)_n LnCl_{3-n} + NaCl + H_2$$

$$n = 1, 2 \text{ or } 3.$$

The above one-pot reaction is suitable for preparing Cp_3Ln, Cp_2LnCl and $CpLnCl_2 \cdot 3THF$ (see Experimental). However, it must be noted that compounds of Eu^{3+}, Sm^{3+} and Yb^{3+} could not be prepared using the one-pot reaction because of the formation of divalent compounds at the same time. Due to omitting the preparation of NaCp, our new method for the syntheses of cyclopentadienyl lanthanide derivatives is simple and economical compared to the traditional method.

Spectroscopic characterization of $CpHoCl_2 \cdot 3THF$

The compound $CpHoCl_2 \cdot 3THF$ was characterized by elemental analysis, IR and MS spectra. The IR spectra show characteristic absorptions of the η^5-Cp group at *ca* 250, 780, 1010, 1440 and 3080 cm^{-1} and the coordinated THF molecule near 890

and 1046 cm^{-1}.[12-14] The ν(Ho—O) and ν(Ho—Cl) vibrations appear at 438 and 365 cm^{-1}, respectively.[15,16] Mass spectra clearly show the molecular ion and main fragments of the compound $CpHoCl_2 \cdot 3THF$. The molecular ion is characterized by the ready loss of a Cp group with a strong peak, $[M—Cp]^+$, in the spectra. It is interesting to note that in the mass spectra the ion peak of $[M—Cl]^+$ is weaker than that of $[M—Cp]^+$, and no ion peak due to $[M—THF]^+$ formed by the direct loss of coordinated THF from the molecular ion. This indicates that the bond strength is of the order Ho—C < Ho—Cl < Ho—O, the Ho—C bond easily breaking under electron impact.

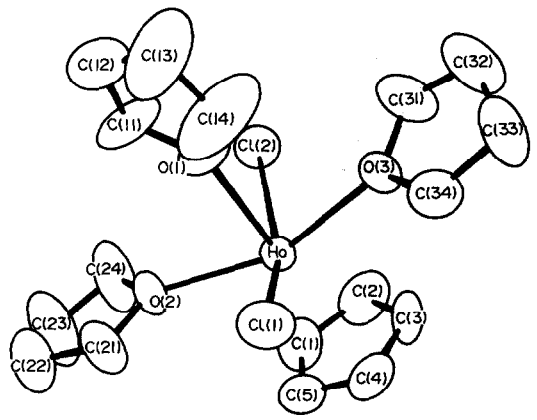

Fig. 1. The structure of the compound $CpHoCl_2 \cdot 3THF$ with the hydrogen atoms omitted for clarity.

Description of the stucture of $CpHoCl_2 \cdot 3THF$

The molecular structure with atomic numbering scheme is shown in Fig. 1. Selected bond distances and angles are listed in Table 2. The compound is monomeric and isostructural with the known

Table 2. Main bond distances (Å) and angles (°)

Ho—Cl(1)	2.618(3)	C(1)—C(2)	1.42(2)
Ho—Cl(2)	2.623(3)	C(2)—C(3)	1.39(2)
Ho—O(1)	2.454(7)	C(3)—C(4)	1.37(2)
Ho—O(2)	2.367(6)	C(4)—C(5)	1.42(2)
Ho—O(3)	2.366(6)	C(5)—C(1)	1.36(2)
Ho—C(1)	2.656(11)	C(11)—C(12)	1.51(2)
Ho—C(2)	2.673(12)	C(12)—C(13)	1.34(2)
Ho—C(3)	2.669(10)	C(13)—C(14)	1.41(3)
Ho—C(4)	2.674(11)	C(21)—C(22)	1.48(2)
Ho—C(5)	2.663(11)	C(22)—C(23)	1.40(2)
O(1)—C(11)	1.44(2)	C(23)—C(24)	1.43(2)
O(1)—C(14)	1.38(2)	C(31)—C(32)	1.44(2)
O(2)—C(24)	1.435(15)	C(32)—C(33)	1.48(2)
O(2)—C(21)	1.436(14)	C(33)—C(34)	1.47(2)
O(3)—C(31)	1.440(15)	Ho—Cav.(Cp)	2.668(11)
O(3)—C(34)	1.435(14)	Ho—Cent[a]	2.390

Cl(1)—Ho—Cl(2)	154.71(9)	Cl(1)—Ho—O(1)	77.1(2)
Cl(1)—Ho—O(2)	87.5(2)	Cl(1)—Ho—O(3)	86.3(2)
Cl(2)—Ho—O(1)	77.6(2)	Cl(2)—Ho—O(2)	87.1(2)
Cl(2)—Ho—O(3)	88.2(2)	O(1)—Ho—O(2)	78.3(2)
O(1)—Ho—O(3)	76.6(2)	O(2)—Ho—O(3)	154.9(2)
C(11)—O(1)—C(14)	107.0(1)	C(21)—O(2)—C(24)	109.0(9)
C(31)—O(3)—C(34)	108.8(9)	O(1)—C(11)—C(12)	106.0(1)
C(11)—C(12)—C(13)	105.0(1)	C(12)—C(13)—C(14)	111.0(2)
C(13)—C(14)—O(1)	110.0(1)	O(2)—C(21)—C(22)	107.0(1)
C(21)—C(22)—C(23)	104.0(1)	C(22)—C(23)—C(24)	111.0(1)
C(23)—C(24)—O(2)	105.0(1)	O(3)—C(31)—C(32)	109.0(1)
C(31)—C(32)—C(33)	105.0(1)	C(32)—C(33)—C(34)	107.0(1)
C(33)—C(34)—O(3)	106.0(1)	C(1)—C(2)—C(3)	107.0(1)
C(2)—C(3)—C(4)	108.0(1)	C(3)—C(4)—C(5)	108.0(1)
C(4)—C(5)—C(1)	108.0(1)	C(5)—C(1)—C(2)	109.0(1)
O(1)—Ho—Cent	179.1(3)	O(2)—Ho—Cent	102.4(3)
O(3)—Ho—Cent	102.7(3)	Cl(1)—Ho—Cent	102.3(4)
Cl(2)—Ho—Cent	103.0(4)		

[a] The Cent is defined as the centroid of the C(1)—C(5) ring.

Table 3. Significant structural parameters in the isostructural series $CpLnCl_2 \cdot 3THF$

Compound	Ln^{3+} radii (Å)[22]	Ln—Cav. (Cp) (Å)	Ln—Cent (Å)	Ln—Cl(1) (Å)	Ln—Cl(2) (Å)	Ln—O(1) (Å)	Ln—O(2) (Å)	Ln—O(3) (Å)	Ref.
$CpNdCl_2 \cdot 3THF$	0.995	2.799	2.503	2.712	2.719	2.529	2.448	2.445	1
$CpGdCl_2 \cdot 3THF$	0.938	2.683	2.404	2.633	2.638	2.458	2.370	2.364	2
$CpHoCl_2 \cdot 3THF$	0.894	2.668	2.390	2.618	2.623	2.454	2.367	2.366	3
$CpErCl_2 \cdot 3THF$	0.881	2.667	2.383	2.613	2.620	2.452	2.365	2.350	This work
$CpYbCl_2 \cdot 3THF$	0.858	2.641		2.591	2.598	2.417	2.365	2.335	4

derivatives of Nd, Gd, Er and Yb.[1–4] The holmium atom is coordinated by a η^5-Cp ring centroid, three THF molecules and two chloride atoms to form distorted octahedral geometry.

The Ho—C(Cp) bond distances range from 2.656(11) to 2.674(11) Å, and average 2.668(11) Å. The Ho—O(2) and Ho—O(3) bond lengths are similar, which are 2.367(6) and 2.366(6) Å, respectively. The Ho—O(1) bond distance of 2.454(7) Å is significantly longer than both Ho—O(2) and Ho—O(3) bonds. This deviation indicates that the steric repulsion around the THF1 ring [O(1)–C(14)] is larger than that existing about THF(2) [O(2)–C(22)] and THF(3) [O(3)–C(33)] rings. The Ho—Cl(1) and Ho—Cl(2) bond distances are also similar, which are 2.618(3) and 2.623(3) Å, respectively. The average Ho—Cl bond length [2.621(5) Å] is shorter than that found in the corresponding dimeric compound $[Cp_2HoCl]_2$ [2.674(5) Å].[17] This difference is normal for monomeric and dimeric compounds and is in agreement with the results reported for organolanthanide alkoxides.[18–20] This correlation is especially evident in the compound $(C_5Me_5)_2Y(\mu\text{-Cl})ClY(C_5Me_5)_2$,[21] which contains both bridging and terminal chloride atoms. The bond angle of O(1)—Ho—Cent [179.1(3)°] indicates that the O(1), Ho and the centroid of the Cp ring are almost on one line. The O(2)—Ho—Cent, O(3)—Ho—Cent, Cl(1)—Ho—Cent and Cl(2)—Ho—Cent angles are almost same and are *ca* 102°, which is larger than that (90°) in an octahedron, due to the steric repulsion of the Cp group. It was also found that the order of Ho—C, Ho—Cl and Ho—O bond distances was Ho—C > Ho—Cl > Ho—O.

All the bond distances in the title compound are reasonable in comparison with the corresponding values in the isostructural compounds $CpLnCl_2 \cdot 3THF$ (Ln = Nd, Gd, Er and Yb) (see Table 3).[1–4] It is obvious that all the bond lengths of Ln—C(Cp), Ln—O(THF), Ln—Cl and Ln—Cent(Cp) decrease with increasing atomic numbers of the lanthanide elements. This result is in agreement with the effect of the "lanthanide contraction". The "gadolinium break" phenomenon reported in the structural series $Cp_3Ln \cdot THF$[23] does not occur in the structural series $CpLnCl_2 \cdot 3THF$.

Acknowledgement—This work was supported by the National Natural Science Foundation of China.

REFERENCES

1. G. Yang, Y. Fan, Z. Jin, Y. Xing and W. Chen, *J. Organomet. Chem.* 1987, **322**, 57.
2. Z. Wu, Z. Xu, X. You, X. Zhou and L. Shi, *J. Coord. Chem.* 1992, **26**, 329.

3. C. S. Day, V. W. Day, R. D. Ernst and S. H. Vollmer, *Organometallics* 1982, **1**, 998.
4. M. Adam, X. F. Li, W. Oroschin and R. D. Fischer, *J. Organomet. Chem.* 1985, **296**, C19.
5. M. D. Taylor and C. P. Carter, *J. Inorg. Nucl. Chem.* 1962, **24**, 387.
6. C. Ye and Y. Li, *Youji Hua Xue* 1981, 210.
7. R. E. Maginn, S. Manastyrskyj and M. Dubeck, *J. Am. Chem. Soc.* 1963, **85**, 672.
8. *International Tables for X-ray Crystallography*, Vol. IV. Kynoch Press, Birmingham (1974).
9. G. Wilkinson and J. M. Birmingham, *J. Am. Chem. Soc.* 1956, **78**, 42.
10. S. Manastyrskyj, R. E. Maginn and M. Dubeck, *Inorg. Chem.* 1963, **2**, 904.
11. F. G. A. Stone, *Advances in Organometallic Chemistry*, Vol. 2, p. 365. Academic Press, New York (1964).
12. N. M. Ely and M. Tsutsui, *Inorg. Chem.* 1975, **14**, 2680.
13. C. Qian, C. Ye, H. Lu, Y. Li, J. Zhou, Y. Ge and M. Tsutsui, *J. Organomet. Chem.* 1983, **247**, 161.
14. C. Qian, X. Wang, Y. Li and C. Ye, *Polyhedron* 1990, **9**, 479.
15. Z. Wu and Z. Ye, *Polyhedron* 1991, **10**, 27.
16. K. Nakamoto, *Infrared and Raman Spectra of Inorganic and Coordination Compounds*, 4th edn, p. 152. Wiley-Interscience, New York (1986).
17. Z. Wu, Z. Xu, X. You, H. Wang and X. Zhou, *Polyhedron* 1993, **12**, 677.
18. Z. Wu, Z. Xu, X. You, X. Zhou and Z. Jin, *Polyhedron* 1992, **11**, 2673.
19. Z. Wu, Z. Xu, X. You, X. Zhou and Z. Jin, *Inorg. Chim. Acta*, in press.
20. X. Zhou, Z. Wu and Z. Jin, *J. Organomet. Chem.* 1992, **431**, 289.
21. W. J. Evans, T. T. Peterson, M. D. Raush, W. E. Hunter and J. L. Atwood, *Organometallics* 1985, **5**, 554.
22. H. Shumann and W. Genthe, *Handbook on the Physics and Chemistry of Rare Earth* (Edited by K. A. Gschneidner and L. Eyring), Vol. 7, Ch. 53. Elsevier, Amsterdam (1985).
23. Z. Ye, S. Wang, Y. Yu and L. Shi, *Inorg. Chim. Acta* 1990, **177**, 97.

Polyhedron Vol. 12, No. 7, pp. 801–806, 1993
Printed in Great Britain

0277–5387/93 $6.00+.00
© 1993 Pergamon Press Ltd

SYNTHESES AND CRYSTAL STRUCTURES OF THREE POLYMERIC CLUSTER COMPOUNDS $+AgMoS_4 \cdot \alpha$-MePyH$+_n$, $+AgMoS_4 \cdot \gamma$-MePyH$+_n$ AND $+AgWS_4 \cdot \gamma$-MePyH$+_n$

LANG JIANPING, LI JIGUO, BAO SHIAN and XIN XINQUAN*

Coordination Chemistry Institute, Nanjing University, Nanjing 210008, China

and

YU KAIBEI

Chengdu Center of Analysis and Measurement, Academic Sinica, Chengdu 610015, China

(*Received* 30 *June* 1992; *accepted* 22 *October* 1992)

Abstract—The title compounds were obtained by reacting $(NH_4)_2MS_4$ (M = Mo, W) and AgI with excess α-methylpyridine or γ-methylpyridine. The structures can be described as extended networks of —AgS_2M— (M = Mo, W) as four-membered rhombs which are alternately parallel and perpendicular all along the polymer chain composed of continuous metal–metal bonds.

It is still a challenge to prepare polymeric species containing different metals. One elegant method is the use of thiometallates as adducts. The number of species of this type is still small and those reported are mostly copper containing compounds of thiometallates, such as MoS_4^{2-}, WS_4^{2-} and ReS_4^{1-}.[1–6] Early in 1982 Müller *et al.* discovered that there was a strong absorption in the Mo—S absorption bands from the resonance Raman spectrum of $[(C_6H_5)_4P]AgMoS_4$, and supposed that it may have a polymeric structure.[7,8] However, no report on the crystal structure of such a compound has been published so far. In this context we report the syntheses and crystal structures of the title compounds. In addition, a comparison is given on the generation of different types of polynuclear compounds by thiometallates containing Cu^+ and Ag^+ in the presence of basic ligands such as pyridine and its derivatives.

EXPERIMENTAL

All manipulations were carried out in air. IR spectra (KBr discs) between 4000 and 400 cm^{-1} were recorded on a Nicolet FT-170SX spectrophotometer. Carbon, hydrogen and nitrogen analyses were performed on a PE-240C elemental analyser. Molybdenum, tungsten and silver analyses were performed on a JA-1100 ICP spectrophotometer. $(NH_4)_2MS_4$ (M = Mo, W) was prepared by literature methods.[9] The other chemicals were used as purchased.

Preparation of $+AgMoS_4 \cdot \alpha$-MePyH$+_n$ (1)

To α-methylpyridine (60 cm^3) were added $(NH_4)_2MoS_4$ (0.26 g, 1.0 mmol) and AgI (0.94 g, 4.0 mmol). The mixture was stirred for 1 h at room temperature and then filtered. The resultant filtrate was allowed to stand at ambient temperature for 4 days whereupon dark red crystals of **1** formed, which were filtered off and washed with a mixture (20 cm^3) of acetone and α-methylpyridine (4:1). Yield: 0.20 g (46.93%). In the course of crystal growth a silver mirror appeared on the surface of the glass vessel. Found: C, 16.8; H, 1.8; N, 3.4; Ag, 25.6; Mo, 22.0. Calc. for $C_6H_8NS_4AgMo$: C, 16.9; H, 1.9; N, 3.3; Ag, 25.3; Mo, 22.5%. IR spectrum: ν(Mo—S_{br}) 439.0 cm^{-1}.

Preparation of $+AgWS_4 \cdot \alpha$-MePyH$+_n$ (2)

Compound **2** was prepared as above starting from $(NH_4)_2WS_4$ (0.35 g, 1.0 mmol). Yield: 0.18 g

* Author to whom correspondence should be addressed.

(35.01%) of yellow crystals of **2**. Found: C, 14.0; H, 1.5; N, 2.8; Ag, 21.1; W, 35.0. Calc. for $C_6H_8NS_4AgW$: C, 14.0; H, 1.6; N, 2.7; Ag, 21.0; W, 35.8%. IR spectrum: ν(W—S_{br}), 430.0 cm^{-1}.

Preparation of $+AgMoS_4 \cdot \gamma\text{-MePyH}+_n$ (**3**)

Compound **3** was prepared in the same way as **1** with excess γ-methylpyridine instead of α-methylpyridine. Yield: 0.29 g (68.04%) of dark red crystals of **3**. Found: C, 16.9; H, 1.9; N, 3.3; Ag, 25.5; Mo, 22.1. Calc. for $C_6H_8NS_4AgMo$: C, 16.9; H, 1.9; N, 3.3; Ag, 25.3; Mo, 22.5%. IR spectrum: ν(Mo—S_{br}) 445.0 cm^{-1}.

Preparation of $+AgWS_4 \cdot \gamma\text{-MePyH}+_n$ (**4**)

Compound **4** was prepared by the same route as **3** with $(NH_4)_2WS_4$ (0.36 g, 1.0 mmol). Yield: 0.39 g (75.86%) of yellow crystals of **4**. Found: C, 14.0; H, 1.6; N, 2.8; Ag, 21.1; W, 35.3. Calc. for $C_6H_8NS_4AgW$: C, 14.0; H, 1.6; N, 2.7; Ag, 21.0; W, 35.8%. IR spectrum: ν(W—S_{br}) 437.3 cm^{-1}.

X-ray crystallography

The crystals obtained directly from the preparations were suitable for single-crystal X-ray work. All measurements were made on samples mounted on the tip of a glass fibre with epoxy resin using a Nicolet R3m four-circle diffractometer operating in the θ–2θ scan mode with graphite monochromated Mo-K_α radiation source at 293 K. The cell constants and orientation matrix for the data collection of the three compounds were based on 25 carefully centred reflections in the range $7° < 2\theta < 24°$ for **1** and **4** and $6° < 2\theta < 24°$ for **3**. Data were corrected for Lorentz–polarization effects and an empirical absorption correction (except for **3**) was applied. Structures were solved by a combination of direct methods and the heavy-atom Fourier technique. Full-matrix least-squares refinement was carried out with anisotropic thermal parameters for all the non-hydrogen atoms. Hydrogen atoms were not included in the calculations. Scattering factors with anomalous-dispersion corrections were taken from ref. 10. All calculations for the solution and refinement of the structures were performed on an Eclipse S/140 computer using the SHELXTL program package (Nicolet corporation, 1986). Specific parameters to the data collections are reported in Table 1. Selected bond lengths and angles are listed in Tables 2, 3 and 4, respectively.

RESULTS AND DISCUSSION

The reaction of MS_4^{2-} (M = Mo, W) with Cu^+ in the presence of basic ligands such as pyridine and its derivatives leads to the formation of two types of polynuclear compounds: (1) trinuclear cluster compounds, $(Py)_4Cu_2MS_4$ (M = Mo, W);[11,12] and (2) species with the formula $[Cu_4MS_4X_2Y_6]$ (M = Mo, W; X = Cl, Br, I, CN, SCN; Y = pyridine and its derivatives).[13,14] The similar reaction of MS_4^{2-} and Ag^+ only produces the polymeric cluster compounds with the formula $[AgMS_4 \cdot RPyH]_n$ (M = Mo, W; R = H, α-Me, β-Me, γ-Me). The different reactions between these two metal ions may be explained by the fact that the soft acid Ag^+ has more difficulty accepting the electrons donated from the harder basic ligands such as pyridine than Cu^+, therefore, it preferably accepts electrons from the soft basic ligand MS_4^{2-}. The following reaction may partly reflect this difference:

$$(NH_4)_2WS_4 + CuBr + AgBr + \gamma\text{-MePy} \longrightarrow [Cu_4WS_4(\gamma\text{-MePy})_8][W_6O_{19}].^{15}$$

Although the formation mechanism of this compound and the role of Ag^+ are unclear, the formation of the cation $[Cu_4WS_4(\gamma\text{-MePy})_8]^{2+}$ shows that Cu^+ prefers to form compounds of the type **2**.

Figure 1 shows a view of a short section of $[MoS_2AgS_2]_2$ and the cell packing of $[AgMoS_4 \cdot \alpha\text{-MePyH}]_n$. Figure 2 shows a view of the fragment $[MoS_2AgS_2]_2$ and the cell packing of $[AgMoS_4 \cdot \gamma\text{-MePyH}]_n$. Evidently, compound **1** is crystallographically different from the isomorphous **3** and **4**. From Figs 1(b) and 2(b) it can be found that because of the C_2 axis running along a direction parallel to b in the cell packing of crystals **3** and **4**, they have higher symmetry than **1**. However, in terms of the coordination mode the structures of the three compounds are remarkably similar. In the structures of **1**, **3** and **4** the asymmetric unit contains one $[AgMS_4]^-$ and one $[RPyH]^+$ unit (**1**: M = Mo, R = α-Me; **3**: M = Mo, R = γ-Me; **4**: M = W, R = γ-Me) [see Figs 1(a) and 2(a)]. The nearest four-membered MS_2Ag rings are not quite planar, but are essentially perpendicular to each other. The $MS_2Ag_2M(a)S_2Ag(a)$ moiety approaches linearity with M—Ag—M(a) and Ag—M(a)—Ag(a) close to 180°. The structures can be described as extended networks of AgS_2Mo rhombs, which are alternately parallel and perpendicular all along the polymer chain. In the anion $[AgMS_4]^-$ (M = Mo or W) the geometry of the molybdenum or tungsten atom displays a slightly distorted tetrahedron. The lengthening of the M—S bonds, from 2.178 Å in

Table 1. Summary of crystallographic data for **1**, **3** and **4**

Compound	$+AgMoS_4 \cdot \alpha$-MePyH$+_n$	$+AgMoS_4 \cdot \gamma$-MePyH$+_n$	$+AgWS_4 \cdot \gamma$-MePyH$+_n$
Formula	$[C_6H_8NS_4AgMo]_n$	$[C_6H_8NS_4AgMo]_n$	$[C_6H_8NS_4AgW]_n$
Formula weight	426.2 (for the monomer)	426.2 (for the monomer)	514.11 (for the monomer)
Crystal system	Monoclinic	Monoclinic	Monoclinic
Space group	*Pc*	*C*2/*c*	*C*2/*c*
a (Å)	7.778(1)	24.388(16)	24.357(10)
b (Å)	5.819(1)	5.835(3)	5.897(2)
c (Å)	19.442(3)	20.398(11)	20.415(10)
β (°)	100.97(1)	92.06(2)	92.02(2)
V (Å^3)	863.8(2)	2901(2)	2930(2)
Z	2	8	8
$d_{calc.}$ (g cm^{-3})	1.99	1.61	1.80
F(000)	506	1412	1540
μ (Mo-K_α) (cm^{-1})	22.89	13.87	49.62
Crystal size (mm)	0.10 × 0.40 × 0.60	0.30 × 0.30 × 0.40	0.20 × 0.28 × 0.40
Radiation	Mo-K_α (λ = 0.71073 Å)	Mo-K_α (λ = 0.71073 Å)	Mo-K_α (λ = 0.71073 Å)
Transmission factors (max., min.)	0.642, 0.987	—	0.902, 0.725
Scan type	θ–2θ	θ–2θ	θ–2θ
Scan rate (° min^{-1})	8	8	8
Scan range (°)	2.0 + ($2\theta_{K\alpha2}$–$2\theta_{K\alpha1}$)	2.3 + ($2\theta_{K\alpha2}$–$2\theta_{K\alpha1}$)	2.0 + ($2\theta_{K\alpha2}$–$2\theta_{K\alpha1}$)
θ limits	1–25	1–22.5	1–22.5
Range of *h*, *k*, *l*	*h* 0–10, *k* 0–7, *l* 24–24	*h* 0–27, *k* 0–7, *l* 22–22	*h* 0–27, *k* 0–7, *l* 22–22
No. of data collected	1866	2202	2235
Unique data [$I > 1.5\sigma(I)$]	1407	1631	1766
No. of parameters	179	156	156
$(\Delta\sigma)_{max}$	0.341	0.025	0.011
R^a	0.035	0.0656	0.0630
$R_w{}^b$	0.035	0.0580	0.0521
Goof (or *S*)	1.681	1.761	2.715
$\Delta\rho$ (e Å^{-3}) in final difference map	0.703, −0.486	3.105, −2.116	2.656, −0.961

[a] $R = \Sigma\|F_o| - |F_c\|/\Sigma|F_o|$.

[b] $R_w = [\Sigma w(|F_o| - |F_c|)^2/\Sigma w|F_o|^2]^{1/2}$. w = 1 for **1**: w = $1/\sigma^2(|F_o| + 0.0001(|F_o|^2)$ for **3** and **4**.

Table 2. Selected bond lengths (Å) and angles (°) for **1**

Mo—S(1)	2.225(5)	Mo—S(2)	2.187(5)	Mo—S(3a)	2.217(5)
Mo—S(4a)	2.218(4)	Mo(a)—S(4)	2.218(4)	Mo(a)—S(3)	2.217(5)
Mo—Ag	2.908(1)	Mo(a)—Ag	2.911(1)	Mo—Ag(a)	2.911(1)
Ag—S(1)	2.488(4)	Ag—S(2)	2.573(3)	Ag—S(3)	2.495(3)
Ag—S(4)	2.548(3)				
Mo—Ag—S(1)	47.9(1)	Mo—Ag—S(2)	46.5(1)	S(1)—Ag—S(2)	94.4(1)
Mo—Ag—S(3)	132.2(1)	S(1)—Ag—S(3)	117.5(1)	S(2)—Ag—S(3)	115.8(1)
Mo—Ag—S(4)	132.7(1)	S(1)—Ag—S(4)	119.1(1)	S(2)—Ag—S(4)	116.8(1)
S(3)—Ag—S(4)	95.0(1)	Mo—Ag—Mo(a)	179.3(2)	S(1)—Ag—Mo(a)	132.8(1)
S(2)—Ag—Mo(a)	132.8(1)	S(3)—Ag—Mo(a)	47.7(1)	S(4)—Ag—Mo(a)	47.4(1)
Ag—Mo—S(1)	56.1(1)	Ag—Mo—S(2)	58.7(1)	S(1)—Mo—S(2)	114.7(1)
Ag—Mo—Ag(a)	179.3(2)	S(1)—Mo—Ag(a)	123.2(2)	S(2)—Mo—Ag(a)	122.1(2)
Ag—Mo—S(3a)	123.9(2)	S(1)—Mo—S(3a)	108.2(2)	S(2)—Mo—S(3a)	105.6(2)
Ag—Mo—S(4a)	122.2(1)	S(1)—Mo—S(4a)	108.9(2)	S(2)—Mo—S(4a)	105.6(2)
Ag—S(1)—Mo	76.0(1)	Ag—S(2)—Mo	74.8(1)	Ag—S(3)—Mo(a)	76.1(1)
Ag—S(4)—Mo(a)	74.9(1)				

Table 3. Selected bond lengths (Å) and angles (°) for **3**

Mo—S(1)	2.200(3)	Mo—S(2)	2.204(3)	Mo—S(1b)	2.200(3)
Mo—S(2b)	2.204(3)	Mo—Ag	2.920(1)	Mo(a)—Ag(a)	2.915(1)
Mo(a)—Ag	2.915(1)	Ag—S(2)	2.518(3)	Ag—S(1a)	2.523(3)
Ag—S(2b)	2.518(3)	Ag—S(1c)	2.523(3)		
Ag—Mo—S(1)	122.9(1)	Ag—Mo—S(2)	56.8(1)	S(1)—Mo—S(2)	106.9(1)
Ag—Mo(a)—Ag(a)	180.0(1)	Ag—Mo—S(1b)	122.9(1)	S(1)—Mo—S(1b)	114.2(1)
S(2)—Mo—S(1b)	107.8(1)	Ag—Mo—S(2b)	56.8(1)	S(1)—Mo—S(2b)	107.8(1)
S(2)—Mo—S(2b)	113.7(1)	Mo—Ag—S(2)	47.1(1)	Mo—Ag—Mo(a)	180.0(1)
S(2)—Ag—Mo(a)	132.9(1)	Mo—Ag—S(1a)	133.0(1)	S(2)—Ag—S(1a)	117.3(1)
Mo—Ag—S(1c)	133.0(1)	S(2)—Ag—S(1c)	118.0(1)	Mo—Ag—S(2b)	47.1(1)
S(2)—Ag—S(2b)	94.2(1)	Mo(a)—S(1a)—Ag	75.9(1)	Mo—S(2)—Ag	76.1(1)

Table 4. Selected bond lengths (Å) and angles (°) for **4**

W—S(1)	2.203(4)	W—S(2)	2.209(4)	W—S(2b)	2.209(4)
W—S(1b)	2.203(4)	W—Ag	2.951(1)	W(a)—Ag(a)	2.946(1)
W(a)—Ag	2.946(1)	Ag—S(2)	2.533(4)	Ag—S(1a)	2.533(4)
Ag—S(1c)	2.533(4)	Ag—S(2b)	2.533(4)		
Ag—W—S(1)	123.3(1)	Ag—W—S(2)	56.6(1)	S(1)—W—S(2)	107.3(1)
Ag—W(a)—Ag(a)	180.0(1)	Ag—W—S(1b)	123.2(1)	S(1)—W—S(1b)	113.5(2)
S(2)—W—S(1b)	107.8(1)	Ag—W—S(2b)	56.6(1)	S(1)—W—S(2b)	107.8(1)
S(2)—W—S(2b)	113.3(2)	W—Ag—S(2)	46.7(1)	W—Ag—W(a)	180.0(1)
S(2)—Ag—S(1a)	133.3(1)	W—Ag—S(1a)	133.3(1)	S(2)—Ag—S(1a)	117.9(1)
W—Ag—S(1c)	133.3(1)	S(2)—Ag—S(1c)	118.2(1)	W—Ag—S(2b)	46.7(1)
S(2)—Ag—S(2b)	93.5(2)	W(a)—S(1a)—Ag	76.6(1)	W—S(2)—Ag	76.6(1)

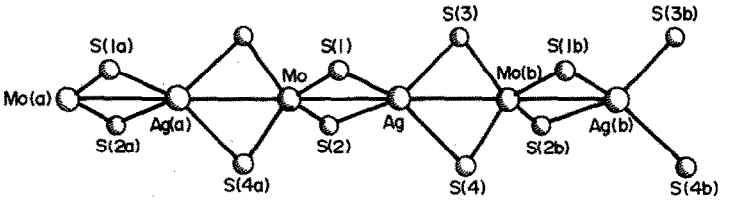

Fig. 1(a). View of a short section of $[MoS_2AgS_2]_2$.

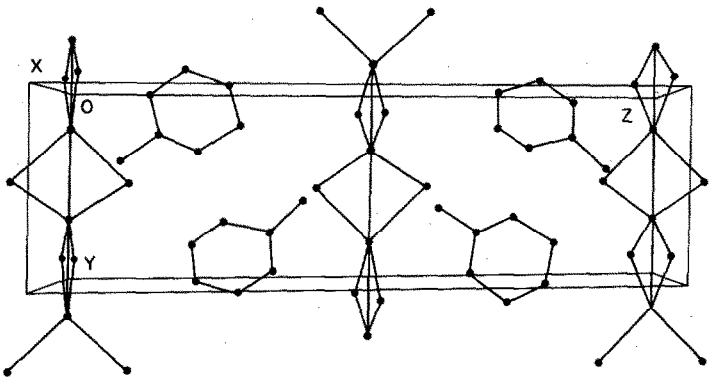

Fig. 1(b). Cell packing of $[AgMoS_4 \cdot \alpha\text{-MePyH}]_n$ viewed down *b*.

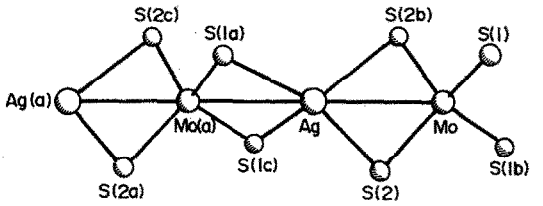

Fig. 2(a). View of a short section of $[MoS_2AgS_2]_2$.

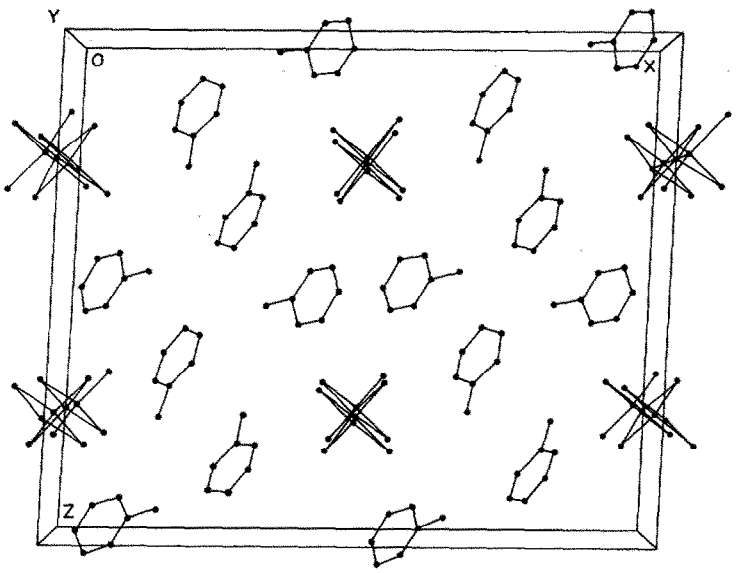

Fig. 2(b). Cell packing of $[AgMoS_4 \cdot \gamma\text{-MePyH}]_n$ viewed down *b*.

$[MoS_4]^{2-}$ to 2.187(5)–2.225(5) Å in **1**, or to 2.200(3)–2.204(3) Å in **3**, or from 2.165 Å in $[WS_4]^{2-}$ to 2.203(4)–2.209(4) Å in **4**, is due to the sulphur-coordinated silver and is reflected in the change of the $\nu(M—S_{br})$ IR stretching frequency from 472 cm^{-1} in $[MoS_4]^{2-}$ to 439 cm^{-1} in **1** or to 445 cm^{-1} in **3**, or from 455 cm^{-1} in $[WS_4]^{2-}$ to 437 cm^{-1} in **4**. The silver ion is also four-coordinated with approximate tetrahedral coordination geometry. The mean Ag—S distance (2.526 Å in **1**, 2.520 Å in **3**, 2.533 Å in **4**) is of the same order of magnitude as those observed in compounds containing tetrahedrally coordinated silver [e.g. in $[Ag_2MoS_4](PPh_3)_3 \cdot 0.8CH_2Cl_2$ ($Ag—S_{av} = 2.515$ Å)[16] or $[Ag_2WS_4](PPh_3)_3 \cdot 0.8CH_2Cl_2$ ($Ag—S_{av} = 2.624$ Å)[17]]. The M—Ag distances [2.908(1)–2.911(1) Å in **1**, 2.915(1)–2.920(1) Å in **3** and 2.946(1)–2.951(1) Å in **4**] are much shorter than the values found in other M—Ag—S compounds (e.g. 2.945 Å in $[(PPh_3)_3Ag_2MoS_4 \cdot 0.8CH_2Cl_2]$,[16] 2.975 Å in $[Ag_4Mo_2S_6](PPh_3)_4S_2$,[18] 2.971 Å in $[(PPh_3)_3Ag_2WS_4 \cdot 0.8CH_2Cl_2]$[17] or 2.997 Å in $[Ag_4W_2S_6](PPh_3)_4S_2$).[19] Although these lengths are only slightly greater (*ca* 0.1–0.15 Å) than the sum of reasonable estimates of the atomic radii of M (Mo or W) and Ag in these environments, significant M—Ag bonding [$Ag^I(d^{10}) \rightarrow M^{VI}(d^0)$ charge delocalization] is a possibility. Because of the continuous metal–metal interaction in this type of polymeric heterometallic compound, they may display some potentially unusual electrical properties. This aspect of the work is worth further investigation.

Acknowledgements—This research was supported by the National Natural Science Foundation of China and the State Education Commission Foundation of China.

REFERENCES

1. A. Müller, D. Dartmann, C. Romer, W. Clegg and G. M. Sheldrich, *Angew. Chem., Int. Edn Engl.* 1981, **20**, 1060.
2. A. Müller, W. Hellmann, J. Schneider, U. Schimanski, U. Demmer, A. Trautwein and U. Bender, *Inorg. Chim. Acta* 1982, **65**, L41.
3. J. R. Nicholson, A. C. Flood, C. D. Garner and W. Clegg, *J. Chem. Soc., Chem. Commun.* 1983, 1179.
4. J. M. Manoli, C. Potvin, F. Secheresse and S. Marzak, *Inorg. Chim. Acta* 1988, **150**, 257.
5. A. Müller, E. Krickemeyer, A. Hildebrand, H. Bögge, K. Schncider and M. Lemke, *J. Chem. Soc., Chem. Commun.* 1991, 1685.
6. L. Jianping, B. Shian, X. Xinquan and Y. Kaibei, *J. Chem. Soc., Chem. Commun.*, submitted.
7. A. Müller, W. Jaegermann and W. Hellmann, *J. Molec. Struct.* 1983, **100**, 559.
8. A. Müller and W. Hellmann, *Spectrochim. Acta* 1985, **41A**, 359.
9. J. W. McDonald. G. D. Friesen, L. D. RosenHein and W. E. Newton, *Inorg. Chim. Acta* 1983, **72**, 205.
10. *International Tables for X-ray Crystallography*, Vol. IV, pp. 72–98. Kynoch Press, Birmingham (1974).
11. J. Xiangling, T. Kaluo, T. Liang and T. Youqi, *ZIRAN* 1984, **7**, 314.
12. G. Fengjun, Z. Huizhen, X. Xinquan, D. Anbang, L. WangXi, W. Boyi and Z. Peiju, *Chem. J. Chin. Univ.* 1990, **11**, 1045.
13. Z. Gongdu, G. Yan, Z. Shiwei and T. Youqi, *Acta Chim. Sin.* 1984, **43**, 107.
14. J. Guoxin, PhD Thesis, Nanjing University, Nanjing (1987).
15. L. Jianping and X. Xinquan, unpublished results.
16. A. Müller, H. Bögge and U. Schimanski, *Inorg. Chim. Acta* 1983, **69**, 5.
17. A. Müller, H. Bögge and E. Koniger-Ahlborn, *Z. Naturforsch.* 1979, **34b**, 1698.
18. A. Müller, H. Bögge, E. Koniger-Ahlborn and W. Hellmann, *Inorg. Chem.* 1979, **18**, 2301.
19. A. Müller, H. Bögge and E. Koniger-Ahlborn, *J. Chem. Soc., Chem. Commun.* 1978, 739.

Polyhedron Vol. 12, No. 7, pp. 807–819, 1993
Printed in Great Britain

0277–5387/93 $6.00+.00
© 1993 Pergamon Press Ltd

INVESTIGATION OF THE INTERMEDIATES IN THE OXIDATION OF A BULKY ARYLPHOSPHINE LIGAND WITH FERRIC CHLORIDE

KIM R. DUNBAR*† and ANNE QUILLEVÉRÉ

Department of Chemistry, Michigan State University, East Lansing, MI 48824, U.S.A.

(*Received* 10 *July* 1992; *accepted* 22 *October* 1992)

Abstract—The syntheses, spectroscopic properties and structures of iron(II) and iron(III) complexes prepared by reactions of ferric chloride with the tertiary phosphine ligand tris(2,4,6-trimethoxyphenyl)phosphine (TMPP) are described. The novel diferrous chloride salt $[H\text{-}TMPP]_2[Fe_2Cl_6]$ (**1**) was prepared by the reaction of anhydrous ferric chloride with 1 equivalent of TMPP in benzene or diethyl ether. This redox reaction also produces $[TMPP\text{-}Cl][FeCl_4]$ (**2**) as the oxidized by-product. The structure of **1**, determined by single-crystal X-ray diffraction, revealed that the $[Fe_2Cl_6]^{2-}$ anion consists of two edge-sharing tetrahedra with two terminal and two bridging chlorides per metal atom. Dissolution of complex **1** in ethanol produces $[H\text{-}TMPP]_2[Fe^{II}Cl_4]$ (**3**), which was identified on the basis of a preliminary X-ray investigation. Compound **3**, independently prepared by the reaction of $[Fe(NCCH_3)_6][AlCl_4]_2$ with 2 equivalents of TMPP in methanol, reacts with molecular oxygen to initially form $[H\text{-}TMPP][Fe^{III}Cl_4]$ (**4**) and finally the phosphine oxide species $FeCl_3$(O=TMPP) (**5**). The structure of **4** was determined by single-crystal X-ray diffraction. To test the importance of compound **4** as an intermediate in the production of TMPP=O, it was prepared directly by reaction of $[Fe(NCCH_3)_6][SbCl_6]_2$ with 2 equivalents of TMPP in methanol and reacted with oxygen to give **5** in high yield. Compounds **1–5** were further characterized by IR and electronic spectroscopies, as well as by elemental analyses. The reactions of the salts **1**, **3** and **4** suggest that the oxidation of tertiary arylphosphines with $FeCl_3$ in alcohols does not proceed via the formation of dioxygen complexes, but rather via quaternarization of the phosphine ligand.

Phosphine oxides are important reagents for a variety of applications, including the extraction of transition elements and lanthanides from acidic solutions.[1] A considerable body of research has been devoted to the study of the catalytic oxidation of triphenylphosphine to triphenylphosphine oxide by a variety of transition metal complexes including those containing iron, ruthenium, cobalt, iridium, nickel and palladium.[2–7] Recently, Ondrejovic and co-workers investigated the catalytic oxidation of triphenylphosphine by $FeCl_3$ and the phosphine complex $FeCl_3(PPh_3)_2$, and in the course of their investigation isolated bis-phosphine oxide adducts of the type $FeX_3(Ph_3P{=}O)_2$ (X = Br, Cl, NCS), which are themselves catalysts for the reaction.[8] The reaction proceeds too rapidly to allow for the detection of intermediates, thus it is not possible to obtain detailed mechanistic information. One way to approach this dilemma is to use bulkier arylphosphine ligands to lend kinetic stability to compounds along the reaction pathway. To this end, we undertook an investigation of the ferric chloride chemistry of the bulky triphenylphosphine derivative tris(2,4,6-trimethoxyphenyl)phosphine (TMPP).[9] This phosphine ligand has a cone angle of 184° as compared to that of 145° for triphenylphosphine. In the course of this work we were successful at isolating three key intermediates in the pathway leading to the thermodynamically stable product $FeCl_3$(O=TMPP), which is a catalyst for the production of O=TMPP. Our results suggest that O_2 adducts of transition metal phosphine complexes are not responsible for catalytic oxidation of

* Author to whom correspondence should be addressed.

† Camille and Henry Dreyfus Teacher–Scholar 1991–1995 and Fellow of the Alfred P. Sloan Foundation 1992–1994.

this particular phosphine ligand. A portion of this work was the subject of a previous report.[10]

EXPERIMENTAL

Starting materials

Anhydrous $FeCl_3$ was purchased from Strem Chemicals and used as received. The starting materials $[Fe(NCCH_3)_6][AlCl_4]_2$ and $[Fe(NCCH_3)_6][SbCl_6]_2$ were prepared as described in the literature.[11] Tris(2,4,6-trimethoxyphenyl)phosphine (TMPP) was prepared by a modification of the reported method; the corresponding phosphine oxide was synthesized in our laboratories.[12] All solvents were dried over 4 Å molecular sieves. Benzene, diethyl ether and THF were distilled from sodium/potassium benzophenone ketyl radical, whereas methylene chloride, acetonitrile and methanol were distilled under nitrogen from P_2O_5, CaH_2 and $Mg(OCH_3)_2$, respectively.

Reaction procedures

All reactions were carried out under argon using standard Schlenk and dry-box techniques, unless otherwise specified.

(a) *Preparation of* $[H\text{-}TMPP]_2[Fe_2^{II,II}Cl_6]$ (**1**).

(i) Preparation of $[H\text{-}TMPP]_2[Fe_2^{II,II}Cl_6]$ (**1**) in benzene. A quantity (0.162 g, 0.999 mmol) of anhydrous $FeCl_3$ was added to 1 equivalent of TMPP (0.532 g, 0.999 mmol) in deoxygenated benzene (30 cm^3). The resulting suspension was stirred at room temperature for 24 h, after which time the solvent was decanted from a yellow solid. The product was washed with several aliquots of benzene (3×10 cm^3) and THF (3×10 cm^3) until the washings were colourless. The resulting pale yellow product was dried *in vacuo*; yield: 0.456 g (65% relative to $FeCl_3$). Found: Cl, 15.3; C, 46.0; H, 4.9. Calc. for $Fe_2Cl_6PC_{54}O_{18}H_{68}$: Cl, 15.3; C, 46.6; H, 4.9%. Slow diffusion of hexanes into an acetone solution of **1** resulted in the formation of X-ray quality yellow crystals of **1**. Four ν(Fe—Cl) stretches were observed in the far-IR spectrum at 360(s), 300(m), 280(m) and 230(w) cm^{-1}. The ^1H NMR spectrum exhibited the characteristic resonances attributed to the protonated phosphine ligand $[H\text{-}TMPP]^+$ (CD_3CN, δ ppm): 3.67 (s, 18, *o*-OCH_3), 3.85 (s, 9, *p*-OCH_3), 6.24 (d, 6, *m*-*H*), 8.37 (d, 1, P—*H*). The electronic spectrum consists of three features [$CHCl_3$, λ_{max} (nm); ε M^{-1} cm^{-1}]: 377(1.80×10^3), 287(sh) and 260(6.80×10^4). The decanted brown–red reaction solution was evaporated to dryness; yield of $[TMPP\text{-}Cl][FeCl_4]$ (**2**): 0.078 g (11% relative to $FeCl_3$). ^1H NMR (CD_3CN, δ ppm): 3.35 (s, 18H), 3.64 (s, 9H), 5.95 (d, 6H). ^{31}P NMR (CD_3CN, δ ppm): −1.56. IR (CsI, Nujol): ν(Fe—Cl) = 380 cm^{-1}. FAB mass spectrum: m/z = 567 (corresponding to $[TMPP\text{-}Cl]^+$).

(ii) Preparation of $[H\text{-}TMPP]_2[Fe_2^{II,II}Cl_6]$ (**1**) in diethyl ether. A quantity of $FeCl_3$ (0.062 g, 0.380 mmol) was dissolved in diethyl ether (15 cm^3) and filtered into a diethyl ether solution (25 cm^3) of TMPP (0.203 g, 0.380 mmol). The resulting yellow suspension was stirred at room temperature for 24 h. The reaction was treated in a manner identical to that described in (i) above; yield: 0.148 g (56%).

(b) *Preparation of* $[H\text{-}TMPP]_2[Fe^{II}Cl_4]$ (**3**).

(i) From decomposition of $[H\text{-}TMPP]_2[Fe_2Cl_6]$ (**1**) in alcohols. An amount of **1** (0.050 g, 0.036 mmol) was dissolved in EtOH or MeOH (40 cm^3). The resulting yellow solution slowly became colourless over the period of 1 week under an argon atmosphere. Careful evaporation of the solvent by purging the solution with a strong flow of argon yielded a crop of pale yellow crystals suitable for a single-crystal X-ray study.

(ii) From reaction of $[Fe^{II}(NCCH_3)_6][AlCl_4]_2$ with TMPP. An amount of $[Fe(NCCH_3)_6][AlCl_4]_2$ (0.303 g, 0.474 mmol) was reacted with 2 equivalents of TMPP (0.505 g, 0.949 mmol) in MeOH (20 cm^3). The bright yellow solution was stirred at room temperature for 0.5 h. A pale yellow solid, isolated after reduction of the volume, was dried under a dynamic vacuum and recrystallized from an acetone/hexanes mixture (v/v 1 : 1); yield: 0.240 g (40%). Found: C, 51.9; H, 4.9. Calc. for $FeCl_4P_2C_{54}O_{18}H_{68}$: C, 51.3; H, 5.4%. Pale yellow microcrystals were grown by slow diffusion of diethyl ether into a THF solution of **3**, or by diffusion of toluene into a CH_2Cl_2 solution. IR (CsI, Nujol, cm^{-1}): ν(Fe—Cl) = 280(s). UV–vis [$CHCl_3$, λ_{max} (nm); ε (M^{-1} cm^{-1})]: 361(4.6×10^3), 309(4.9×10^3), 287(sh), 261(7.2×10^4). ^1H NMR (CD_3CN, δ ppm): 3.68(s, 18), 3.88(s, 9), 6.25(d, 6), 8.40(d, 1). Cyclic voltammetry: $(E_{1/2})_{ox}$ = +0.04 V; μ_{eff} = 5.29 μ_B.

(c) *Preparation of* $[H\text{-}TMPP][Fe^{III}Cl_4]$ (**4**).

(i) From oxidation of $[H\text{-}TMPP]_2[Fe^{II}Cl_4]$ (**3**) with molecular oxygen. An amount of **3** (0.050 g, 0.039 mmol) was dissolved in MeOH (20 cm^3). Upon bubbling dry oxygen into the solution the colour changed from yellow to orange. Evaporation of the solution produced long orange needles that were of a quality suitable for an X-ray study. Found: C, 44.3; H, 4.7. Calc. for $FeCl_4PC_{27}O_9H_{34}$: C, 44.3; H, 4.6%. IR (CsI, Nujol, cm^{-1}): ν(Fe—Cl) = 380(s). ^1H NMR (CD_3CN, δ ppm): 3.70(s, 18), 3.88(s, 9), 6.26(d, 6), 8.38(d, 1). UV–vis [$CHCl_3$, λ_{max} (nm); ε (M^{-1} cm^{-1})]: 365(5.05×10^3), 315(4.9×10^3), 289(sh) and 261(7.54×10^4). Cyclic voltammetry: $(E_{1/2})_{red}$ = +0.03 V; μ_{eff} = 6.11 μ_B.

(ii) From reaction of $[Fe^{II}(NCCH_3)_6][SbCl_6]_2$ with TMPP. A quantity of $[Fe(NCCH_3)_6][SbCl_6]_2$ (0.173 g, 0.179 mmol) was added to 2 equivalents of TMPP (0.190 g, 0.357 mmol) in MeOH (10 cm^3). Upon addition of the solvent a bright yellow solid rapidly precipitated from an orange solution. The orange filtrate was decanted from the solid and subjected to a dynamic vacuum to yield a residue which was washed with diethyl ether (2×10 cm^3) and dried *in vacuo*; yield: 0.0642 g (51% relative to Fe^{2+}). The resulting orange compound was identified by a comparison of its IR and ^1H NMR properties to those of an authentic, structurally characterized sample of $[H\text{-}TMPP][Fe^{III}Cl_4]$. The yellow solid was characterized as $[H\text{-}TMPP][SbCl_6]$; yield: 0.089 g (40% relative to TMPP). Found: Cl, 24.5; C, 37.3; H, 3.9. Calc. for $SbCl_6P C_{27}O_9H_{34}$: Cl, 24.1; C, 36.7; H, 3.9%. IR (CsI, Nujol): ν(Sb—Cl) = 345 cm^{-1}. ^1H NMR ($CDCl_3$, δ ppm): 3.69(s, 18), 3.87(s, 9), 6.11(d, 6) and 8.33(d, 1). The identical compound was independently prepared from the reaction of $Na^+SbCl_6^-$ with 1 equivalent of TMPP in MeOH.

(d) *Oxygen reactions to yield* $Fe^{III}Cl_3$(O=TMPP) (**5**).

(i) From $[H\text{-}TMPP]_2[Fe_2Cl_6]$ (**1**). An amount of **1** (0.050 g, 0.036 mmol) was dissolved in EtOH (30 cm^3). The resulting yellow solution was bubbled with dry oxygen for 10 min, during which time it turned to a dark orange colour. The reaction solution was then left to evaporate under a purge of oxygen gas which produced red–orange crystals of **5**; yield: 0.041 g (80% relative to **1**). Found: C, 45.9; H, 4.7. Calc. for $FeCl_3PO_{10}C_{27}H_{33}$: C, 45.6; H, 4.6%. IR (CsI, Nujol, cm^{-1}): 380(s) and 320(w). Electronic spectrum [$CHCl_3$, λ_{max} (nm); ε (M^{-1} cm^{-1})]: 342(4.3×10^3), 287(sh), 258(4.0×10^4). FAB-mass spectrum: m/z = 548 (corresponding to TMPP=O); ^1H NMR (CD_3CN): very broad. Cyclic voltammetry: $(E_{1/2})_{red} = -0.02$ V, $\mu_{eff} = 6.31$ μ_B.

An anaerobic EtOH solution of **1**, as described above, became colourless during a period of standing for 1 week. After bubbling oxygen through this solution for 5 min, a yellow colour ensued, which converted to dark orange within 10 min. Red–orange crystals of **5** formed under an oxygen atmosphere after several days.

An amount of **1** (0.050 g, 0.036 mmol) was dissolved in acetonitrile (20 cm^3) and a stream of oxygen gas was passed through the solution for *ca* 1 h. The resulting orange solution was layered with hexanes and diethyl ether. Crystals of **5** were isolated from this solvent mixture after 1 day; yield 0.040 g (78% relative to **1**).

(ii) From $[H\text{-}TMPP]_2[Fe^{II}Cl_4]$ (**3**) with molecular oxygen. An amount of **3** (0.100 g, 0.079 mmol) was dissolved in MeOH (20 cm^3), treated with oxygen for 4 h and layered with hexanes and diethyl ether. Red–orange crystals of **5** were isolated after 1 day; yield: 0.030 g (53% relative to **3**).

(iii) From $[H\text{-}TMPP][Fe^{III}Cl_4]$ (**4**). A quantity of **4** (0.100 g, 0.137 mmol) was dissolved in MeOH (30 cm^3), whereupon the solution was bubbled with oxygen for 3–4 days. During this time, the solvent was replenished regularly to avoid complete evaporation. Red–orange crystals of **5** were eventually deposited at the bottom of the flask; yield: 0.058 g (60% relative to **4**).

(iv) From $FeCl_3$, TMPP and O_2 mixtures. An amount of $FeCl_3$ (0.142 g, 0.874 mmol) was treated with 1 equivalent of TMPP (0.465 g, 0.874 mmol) in EtOH (20 cm^3) under a slow stream of oxygen for 3 h. The resulting orange solution was evaporated under reduced pressure to yield a dark orange solid, which was then recrystallized from EtOH and diethyl ether; yield: 0.345 g (54%).

(v) From $FeCl_3$ and TMPP=O. A quantity of $FeCl_3$ (0.119 g, 0.736 mmol) was treated with 1 equivalent of TMPP oxide (0.404 g, 0.736 mmol) in EtOH (12 cm^3). The resulting orange suspension was stirred at room temperature for *ca* 1 h until all of the $FeCl_3$ had dissolved. The suspension was then filtered in air and washed with EtOH (3×10 cm^3), followed by diethyl ether (1×10 cm^3) and finally dried *in vacuo*; yield: 0.423 g (81% relative to $FeCl_3$).

(e) *Preparation of* TMPP=O. A quantity of $FeCl_3$(O=TMPP) (**5**) (0.067 g, 0.094 mmol) was reacted with a 10-fold excess of TMPP (0.500 g, 0.939 mmol) in acetone (20 cm^3) under a stream of dry oxygen. The solution was stirred at room temperature for 1–2 h, during which time a significant quantity of white solid precipitated from solution. The orange solution was decanted from the solid, which was washed with diethyl ether (3×10 cm^3) and dried *in vacuo*. Chilling the orange filtrate produced more white product, characterized as TMPP=O; yield: 0.325 g (63% relative to TMPP). Work-up of the remaining orange solution consisted of successive extractions by CH_2Cl_2 and EtOH, which yielded crystals of $FeCl_3$(O=TMPP); total recovered yield: 0.062 g (93% of the initial mass). ^1H NMR of TMPP=O (CD_3CN, δ ppm): 3.48(s, 18), 3.79(s, 9), 6.10(d, 6).

(f) *Reaction of* [TMPP-Cl]Cl *with* $FeCl_3$. A solution of TMPP (0.461 g, 0.867 mmol) in benzene (20 cm^3) was bubbled with chlorine gas for 1–2 min until it had turned bright yellow, thereby signifying the formation of the oxidized compound TMPP-Cl^+Cl^-. The reaction solution was then pumped down to a sticky residue, but since no solid could be isolated it was redissolved in benzene (20 cm^3)

and added to $FeCl_3$ (0.141 g, 0.867 mmol). A colour change from yellow to dark brown–red immediately ensued. The solvent was removed under dynamic vacuum to produce a brown residue that was recrystallized from an acetone/hexanes mixture (v/v 1:1); yield: 0.020 g. The properties of this solid were identical to those described for [TMPP-Cl][$FeCl_4$] (**2**) (*vide supra*).

Physical measurements

IR spectra were recorded on a Perkin–Elmer 599 or a Nicolet 740 FT-IR spectrophotometer. ^{1}H NMR spectra were measured on a Varian–Gemini 300 MHz spectrometer. Chemical shifts were referenced relative to the residual proton impurity of d_3-acetonitrile (1.93 ppm with respect to TMS). Electronic absorption spectra were measured on a Hitachi U-2000 spectrophotometer. Electrochemical measurements were performed using an EG&G Princeton Applied Research Model 362 scanning potentiostat in conjunction with a BAS Model RXY recorder. Cyclic voltammetry experiments were carried out at 22 ± 2°C in methylene chloride containing 0.1 M tetra-*n*-butylammonium tetrafluoroborate ($TBABF_4$) as the supporting electrolyte. $E_{1/2}$ values, determined as $(E_{p,a}+E_{p,c})/2$, were referenced to the Ag/AgCl electrode and are uncorrected for junction potentials. The Cp_2Fe/Cp_2Fe^+ couple occurs at $E_{1/2} = +0.51$ V under the same experimental conditions. Variable-temperature magnetic susceptibility measurements were carried out on a Quantum Design MPMS susceptometer in the Physics and Astronomy Department at Michigan State University. Data points were collected over a temperature range from 5 to 300 K at 20° intervals in a field of 500 G. Elemental analyses were performed at Galbraith Laboratories, Inc.

X-ray crystallographic procedures

The structures of complexes **1**, **3** and **4** were determined by applications of general procedures described elsewhere.[13] Geometric and intensity data were collected on a Nicolet P3/F diffractometer for **3** and on a Rigaku AFC6S diffractometer for **1** and **4**; both instruments were equipped with graphite monochromated Mo-K_α ($\lambda_{\bar{\alpha}} = 0.71073$ and 0.71069 Å, respectively) radiation. The data were corrected for Lorentz and polarization effects. Calculations for **1**, **3** and **4** were performed on a VAXSTATION 2000 computer using programs from the TEXSAN Crystallographic Package of the Molecular Structure Corporation.[14] A summary of crystallographic data for compounds **1** and **4** is listed in Table 1, whereas data for compound **3** have been deposited as supplementary material.

[H-TMPP]$_2$[Fe_2Cl_6] (**1**). A yellow parallelepiped of approximate dimensions $0.31\times0.47\times0.52$ mm^3 was mounted at the end of a glass fibre with Dow Corning silicone grease and placed into a nitrogen cold stream at -100 ± 2°C. A preliminary monoclinic cell was determined by centring and indexing 20 reflections. The cell was then refined by a least-squares fit of 21 reflections in the range $23 \leqslant 2\theta \leqslant 30°$. Intensity data were collected from 4 to 47° in 2θ, by using the θ–2θ scan mode. Three standard reflections were measured at regular intervals during data collection and showed no significant decay in crystal quality. After averaging equivalent reflections, 4952 unique data remained, of which 3440 were observed with $F_o^2 \geqslant 3\sigma(F_o)^2$.

The position of the metal atom was determined by a solution provided by the direct methods program in SHELXS-86.[15] The positions of the remaining non-hydrogen atoms and of H(1) bound to the phosphorus atom were located by use of the program DIRDIF.[16] An empirical absorption correction based on the program DIFABS was applied after isotropic convergence had been achieved.[17] The positions of the hydrogen atoms that were not directly located were generated by a program in the TEXSAN package. These were included in the structure factor calculation but not refined. The final full-matrix refinement involved 3440 data and 370 parameters and converged with residuals $R(R_w) = 0.046(0.079)$ and a quality-of-fit of 2.84. The final difference-Fourier map showed a highest peak of 0.96 e Å^{-3}.

[H-TMPP]$_2$[$Fe^{II}Cl_4$] (**3**). The structure of this compound is of a poor quality and is mentioned only in a preliminary form to confirm the identity of the salt as an intermediate in the chemistry of $FeCl_3$ with TMPP. Lack of data and problems with refining the solvent molecule precluded a full refinement of the structure to a satisfactory point. A full listing of data and a description of the structure solution have been deposited in the supplementary material.

[H-TMPP][$Fe^{III}Cl_4$] (**4**). An orange platelet of approximate dimensions $0.10\times0.21\times0.52$ mm^3 was selected and mounted on the end of a glass fibre with epoxy cement. Intensity and geometric data were collected at room temperature. A preliminary orthorhombic unit cell was determined by centring and indexing on 20 reflections. The cell was then refined by a least-squares determination of 24 reflections with $9 \leqslant 2\theta \leqslant 23$. Intensity data were collected by the θ–2θ scan mode over the range 4–45° in 2θ. Three standard reflections were measured at regular intervals during data collection and

Table 1. Crystallographic data for $[H\text{-}TMPP]_2[Fe_2Cl_6]$ (1) and $[H\text{-}TMPP][FeCl_4]$ (4)

Formula	$Fe_2Cl_6P_2C_{54}O_{18}H_{68}$	$FeCl_4PO_9C_{27}H_{34}$
Formula weight	1391.48	731.19
Space group	$P2_1/n$	$Pbca$
Systematic absences	$h0l: h+l \neq 2n$; $0k0: k \neq 2n$	$0kl: k = 2n$; $h0l: l = 2n$; $hk0: h = 2n$
a (Å)	14.294(8)	19.952(5)
b (Å)	10.140(9)	19.352(7)
c (Å)	22.543(8)	17.821(4)
α (°)	90.0	90.0
β (°)	105.76(4)	90.0
γ (°)	90.0	90.0
V (Å^3)	3144(3)	6881(6)
Z	2	8
d_{calc} (g cm^{-3})	1.469	1.411
Crystal size (mm)	$0.31 \times 0.47 \times 0.52$	$0.10 \times 0.21 \times 0.52$
μ (Mo-K_α) (cm^{-1})	8.32	8.40
Data collection instrument	Rigaku AFC6S	Rigaku AFC6S
Radiation (monochromated in incident beam)	Mo-K_α ($\lambda_{\bar{\alpha}} = 0.71073$ Å) Graphite monochromated	Mo-K_α ($\lambda_{\bar{\alpha}} = 0.71073$ Å) Graphite monochromated
Orientation reflections number, range (2θ)	21, 23–30	25, 8–25
Temperature (°C)	−100	23 ± 2
Scan method	θ–2θ	θ–2θ
Data collection, 2θ (°)	4–47	4–45
No. of unique data	4952	3612
Total with $F_o^2 > 3\sigma(F_o^2)$	3440	1472
Number of parameters refined	370	379
Transmission factors, max., min.	0.82–1.26	0.79–1.00
R^a	0.046	0.051
$R_w{}^b$	0.079	0.066
Quality-of-fit indicator^c	2.84	1.457
Largest shift/e.s.d. final cycle	0.00	0.066
Largest peak (e Å^{-3})	0.96	0.494

$^a R = \Sigma\|F_o| - |F_c\|/\Sigma|F_o|$.
$^b R_w = [\Sigma(w|F_o| - |F_c|)^2/\Sigma w|F_o|^2]^{1/2}$; $w = 1/\sigma^2(|F_o|)$.
^{c} Quality-of-fit $= [\Sigma(w|F_o| - |F_c|)^2/(N_{obs} - N_{para})]^{1/2}$.

showed no decay over time. An empirical absorption correction was applied using the PSI-scan program within the TEXSAN package. After averaging equivalent reflections 3612 unique data remained, of which 1472 were observed with $F_o^2 \geqslant 3\sigma(F_o)^2$. The position of the metal atom was determined from a solution provided by the direct methods program MITHRIL.[18] The positions of the remaining non-hydrogen atoms and of H(1) were located by the program DIRDIF. All of the non-hydrogen atoms were refined anisotropically. The hydrogen atoms were placed in calculated positions and were included in the structure factor calculations, but not refined. The final full-matrix refinement involved 1472 data and 379 parameters. The refinement converged with residuals R and R_w of 0.051 and 0.066, respectively, and a quality-of-fit indicator of 1.457. The final difference-Fourier map showed a highest peak of 0.49 e Å^{-3}.

RESULTS

Synthesis

Several years ago we reported that the reaction of anhydrous $FeCl_3$ with 1 equivalent of tris(2,4,6-trimethoxyphenyl)phosphine in benzene yields a pale yellow compound, formulated as $Fe^{III}Cl_3(\eta^3\text{-TMPP})$ on the basis of elemental analyses. Although no X-ray study of the compound was available at the time, its structure was proposed to be octahedral from the number of observed ν(Fe—Cl) modes in the IR spectrum.[10] Although we realized that hard first-row transition metals are not particularly compatible with a soft donor atom such as phosphorus,[19] we argued that this particular phosphine would be rendered more compatible with a hard Lewis acid such as $FeCl_3$ by the presence of the oxygen donors, which we expected to participate

in the bonding to the iron centre. Precedence for the assignment of a tridentate mode for the phosphine (i.e. η^3-TMPP) existed in the form of the structurally characterized species $Mo(CO)_3(\eta^3$-TMPP)[9c] and $[Rh(\eta^3\text{-TMPP})_2][BF_4]_x$ ($x = 2, 3$),[9a,b] wherein the ligand is coordinated to the metal centre through the phosphorus atom and two oxygen atoms from the pendent methoxy groups on the phenyl rings. At the time, this picture was the most reasonable structure that fit the available data for the iron compound.

Since the earlier report Mössbauer and EPR studies were performed, the results of which did not support this formulation.[20] Most importantly, we finally managed to crystallize compound **1** from acetone and the single-crystal X-ray study revealed that the complex is actually $[H\text{-TMPP}]_2[Fe_2Cl_6]$, in which Fe^{III} has been reduced to Fe^{II} and the tertiary phosphine has become protonated. The empirical formula for this salt differs by only one H^+ from the earlier molecule, thus it was not possible to distinguish between the two designations on the basis of elemental composition. Three ν(Fe—Cl) bands are observed in the IR spectrum of $[H\text{-TMPP}]_2[Fe_2Cl_6]$, one of which is split which accounts for the four bands expected for a D_{2h} symmetry.

Facile reduction of $FeCl_3$ is not uncommon, as in the synthesis of $Fe^{II}Cl_2(HPyS)_2$ from the reaction of $FeCl_3$ and HPyS (HPyS = 2-mercaptopyridine),[21] furthermore, TMPP is known to be quite sensitive to quaternarization in the presence of metal halides. In fact, similar chemistry was seen to occur earlier, with alcoholic cobalt(II) solutions giving rise to $[H\text{-TMPP}]_2[Co^{II}Cl_4]$ and TMPP reactions of $CoCl_2$ in benzene yielding $[CH_3\text{-TMPP}]_2[Co_2Cl_6]$.[22a,b] To our knowledge, however, there is no documentation in the literature of the $[Fe_2Cl_6]^{2-}$ moiety,[22d] although the cobalt(II) and copper(II) analogues are known and $[Fe_2I_6]^{2-}$ has been documented.[22b,c] It is interesting to note that when the reaction is carried out in acetonitrile small amounts of **1** are isolated, but if other solvents such as chloroform or ethanol are used $[H\text{-TMPP}][FeCl_4]$ is obtained, indicating that no reduction of the metal centre occurs in these solvents.

Upon slow dissolution of $[H\text{-TMPP}]_2[Fe_2Cl_6]$ in ethanol under anaerobic conditions, the phosphonium salt $[H\text{-TMPP}]_2[Fe^{II}Cl_4]$ (**3**) is observed to form. In an effort to study the reactions of this salt as they pertain to the overall reaction to form TMPP=O, the compound was prepared deliberately by the reaction of $[Fe^{II}(NCCH_3)_6][AlCl_4]_2$ with 2 equivalents of TMPP in methanol. Redissolution of **3** in methanol followed by rapid evaporation in air or treatment with a stream of oxygen gas yields the oxidized form of the anion, viz. $[H\text{-TMPP}][Fe^{III}Cl_4]$ (**4**). The conversion of Fe^{II} to Fe^{III} was monitored by IR spectroscopy in the far-IR region, according to the Fe—Cl stretching frequency which occurs at 280 cm^{-1} for $\nu(Fe^{II}$—Cl) and 380 cm^{-1} for $\nu(Fe^{III}$—Cl). Compound **4** was, in turn, independently prepared by the reaction of $[Fe^{II}(NCCH_3)_6][SbCl_6]_2$ with 2 equivalents of TMPP in methanol. Approximately 50% of the original phosphine is consumed to form $[H\text{-TMPP}][SbCl_6]$, as determined by NMR and IR spectroscopies as well as elemental analysis. Antimony(V) is a good oxidizing agent[23] and, therefore, it is not surprising to observe a conversion from Fe^{II} to Fe^{III} in this reaction. In a similar fashion as for **3** protonation of the phosphine occurs with the formation of the very stable $[Fe^{III}Cl_4]^-$ anion, which is quite a common phenomenon.[24,25] The spectroscopic and electrochemical properties of **3** and **4** are in excellent agreement with the reported literature values for various salts of $[Fe^{III}Cl_4]^-$ and $[Fe^{II}Cl_4]^{2-}$.[26]

Lastly, $FeCl_3$(O=TMPP) (**5**) can be obtained quantitatively, *inter alia*, from the reaction of **4** with oxygen in methanol over a period of 1–2 days. The stability of $FeCl_3$(O=TMPP) is evidenced by the extreme facility with which this compound is formed from **1**, **3** or **4**. Scheme 1 summarizes the different synthetic routes to **5** that we have encountered in this work.

Molecular structures

$[H\text{-TMPP}]_2[Fe_2Cl_6]$ (**1**). The X-ray structure unequivocally established the identity of **1** as an $[Fe_2Cl_6]^{2-}$ salt, for which two protonated phosphines serve as counter-ions. An ORTEP representation of $[H\text{-TMPP}]_2[Fe_2Cl_6]$ is shown in Fig. 1, while pertinent bond distances and angles are summarized in Table 2. The $[Fe_2Cl_6]^{2-}$ anion consists of two edge-sharing tetrahedra, with two bridging and two terminal chlorides per metal atom, and an inversion centre situated at the mid-point of the $Fe(1)\cdots Fe(1)'$ axis, as was previously observed in the isomorphous structure of $[CH_3\text{-TMPP}]_2[Co_2Cl_6]$.[22b] The $Fe(1)\cdots Fe(1)'$ separation of 3.350(4) Å, much larger than the sum of the covalent radii, precludes the assignment of a direct metal–metal bond, and is comparable to the distances of 3.32 Å found in $[Fe_2(\mu\text{-OH})(OAc)_2(Me_3TACN)_2](ClO_4)$[27] and 3.35 Å in $[Fe_2(BPMP)_2]$ (BPh_4),[28] but considerably longer than the corresponding distances reported for the two closely related structures $[Fe_2(SEt)_6]^{2-}$ and $[Fe_2Cl_4(OPh)_2]^{2-}$, these being 2.978(1) and 3.177(3) Å, respectively.[29] The average Fe^{II}—Cl bond distance for the terminal chloride

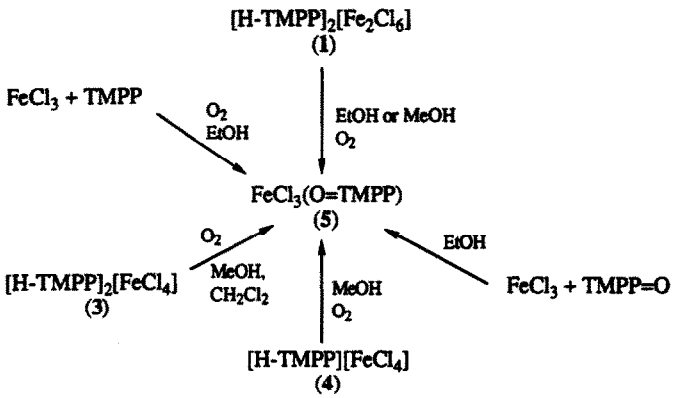

Scheme 1. Synthetic routes to $FeCl_3$(O=TMPP) (**5**).

[2.231(2) Å] is somewhat intermediate between the reported range for Fe^{II}—Cl (2.25–2.35 Å)[30] and Fe^{III}—Cl (2.15–2.20 Å).[31] As expected, the average distance for the bridging chlorides is longer [2.397(2) Å] than the terminal chlorides. The Cl—Fe—Cl bond angles fall in the range expected for tetrahedral geometry [108.02(9)–120.5(1)°], but the Cl(2)—Fe(1)—Cl(2)′ and the Fe(1)—Cl(2)—Fe(1)′ angles of 91.36(8) and 88.64(8)°, respectively, are considerably distorted from ideal geometry. A three-dimensional packing diagram of $[H\text{-}TMPP]_2[Fe_2Cl_6]$ is presented in Fig. 2 and clearly shows the segregated packing of cations and anions when viewed down the *b*-axis. The structural features of the protonated phosphine are similar to those of previously reported examples. Related polynuclear iron chloride salts are $[Fe_2Cl_9]^{3-}$, $[Fe_2Cl_6(\mu\text{-}O)]^{2-}$, $[Fe_2Cl_6(\mu\text{-}OR)_2]^{2-}$ and $Fe_4Cl_8(THF)_6$.[26,32]

$[H\text{-}TMPP]_2[Fe^{II}Cl_4]$ (**3**). The structure of this salt is reported only for the purpose of positively identifying the species and is without remarkable

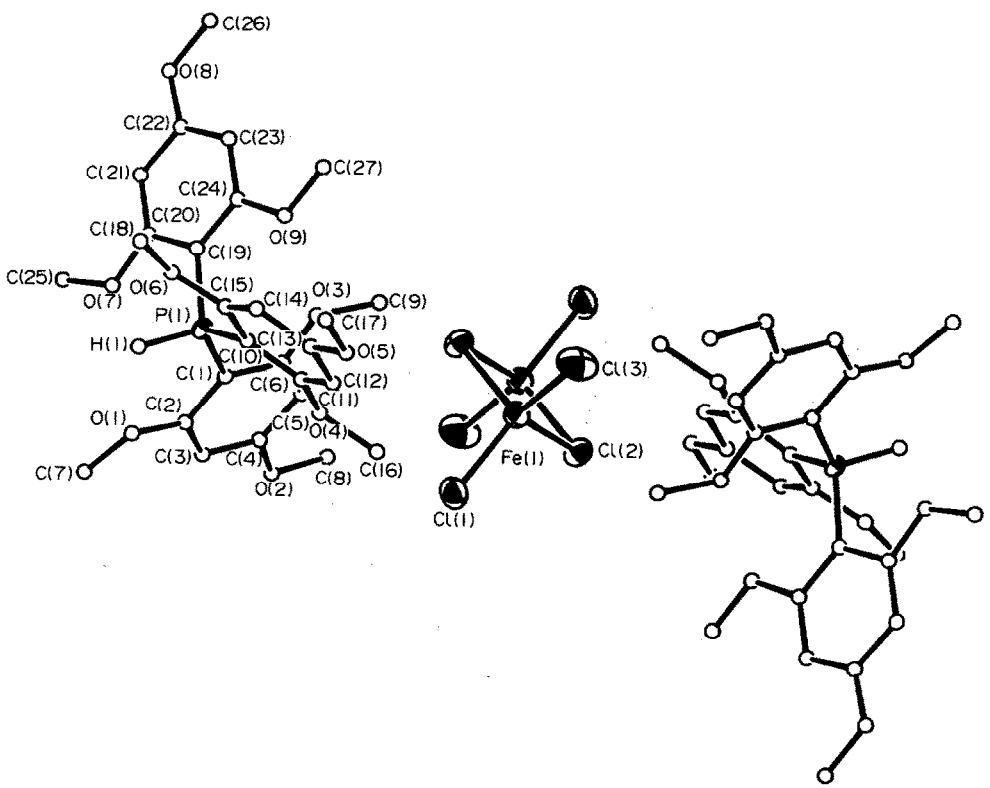

Fig. 1. ORTEP diagram showing the constituent ions in the salt $[H\text{-}TMPP]_2[Fe_2Cl_6]$ (**1**). Phenyl group atoms are represented as small circles for clarity, whereas all other atoms are represented as their 50% probability thermal ellipsoids.

Table 2. Selected bond distances (Å) and angles (°) for compounds **1** and **4**

Compound	1		4	
Fe—Cl	Fe(1)—Cl(1)	2.235(2)	Fe(1)—Cl(1)	2.161(4)
	Fe(1)—Cl(2)	2.385(2)	Fe(1)—Cl(2)	2.155(4)
	Fe(1)—Cl(3)	2.227(2)	Fe(1)—Cl(3)	2.168(4)
	Fe(1)—Cl(2)′	2.409(2)	Fe(1)—Cl(4)	2.182(5)
	Fe(1)—Fe(1)′	3.350(4)		
P—C	P(1)—C(1)	1.773(6)	P(1)—C(1)	1.76(1)
	P(1)—C(10)	1.782(6)	P(1)—C(10)	1.76(1)
	P(1)—C(19)	1.793(6)	P(1)—C(19)	1.79(1)
Cl—Fe—Cl	Cl(1)—Fe(1)—Cl(2)	108.02(9)	Cl(1)—Fe(1)—Cl(2)	112.6(2)
	Cl(1)—Fe(1)—Cl(2)′	110.57(8)	Cl(1)—Fe(1)—Cl(3)	106.2(2)
	Cl(1)—Fe(1)—Cl(3)	120.5(1)	Cl(1)—Fe(1)—Cl(3)	109.8(2)
	Cl(2)—Fe(1)—Cl(2)′	91.36(8)	Cl(2)—Fe(1)—Cl(3)	106.9(2)
	Cl(2)—Fe(1)—Cl(3)	110.96(9)	Cl(2)—Fe(1)—Cl(4)	110.0(2)
	Cl(3)—Fe(1)—Cl(2)′	111.50(8)	Cl(3)—Fe(1)—Cl(4)	111.2(2)
	Fe(1)—Cl(2)—Fe(1)′	88.64(8)		
C—P—C	C(1)—P(1)—C(10)	115.3(3)	C(1)—P(1)—C(10)	114.5(7)
	C(1)—P(1)—C(19)	109.2(3)	C(1)—P(1)—C(19)	116.0(6)
	C(10)—P(1)—C(19)	114.4(3)	C(10)—P(1)—C(19)	112.4(7)

features. The metal atom lies on a two-fold axis and is ligated by four chlorine atoms to form the $[FeCl_4]^{2-}$ anion. Two protonated phosphines, [H-TMPP]$^+$, serve as the cations in this structure. The structural features of the cation are similar to those of the free phosphine and other phosphonium salts.[24] It is noteworthy that the $[FeCl_4]^{2-}$ anion has been observed to crystallize only with very large cations, such as quaternary ammonium or phosphonium ions.[26]

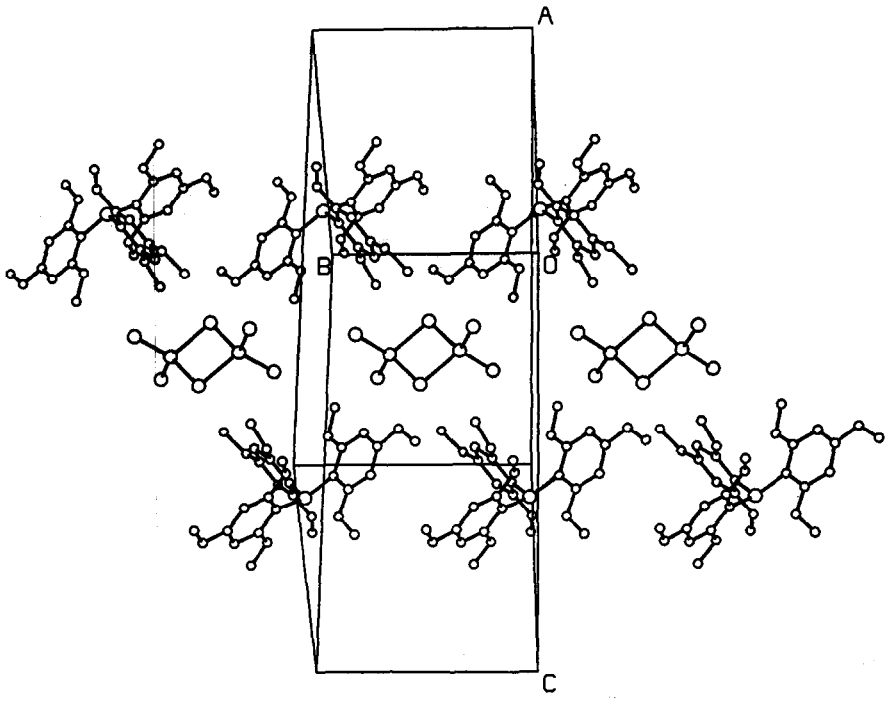

Fig. 2. Packing diagram of $[H\text{-}TMPP]_2[Fe_2Cl_6]$ (**1**) viewed down the *b*-axis.

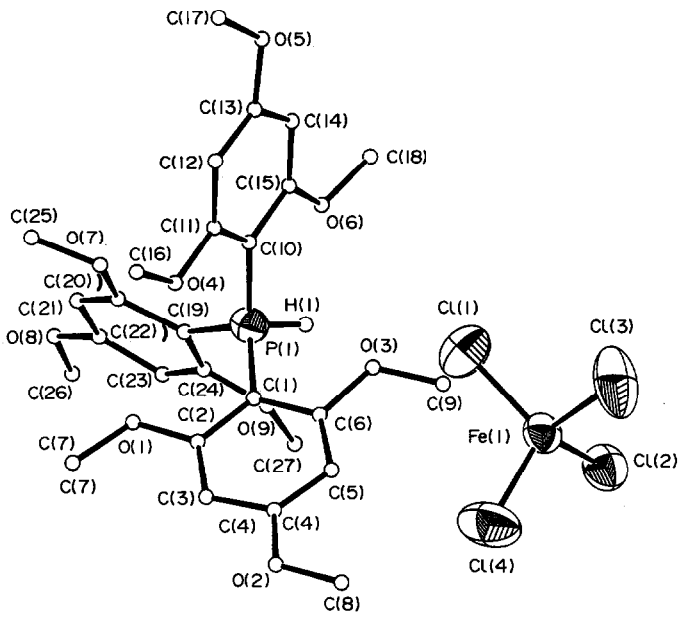

Fig. 3. ORTEP diagram for [H-TMPP][$FeCl_4$] (**4**). Phenyl group atoms are represented as small circles for clarity, whereas all other atoms are represented as their 50% probability thermal ellipsoids.

[H-TMPP][$Fe^{III}Cl_4$] (**4**). An ORTEP diagram of the two constituent ions in the asymmetric unit of **3** is shown in Fig. 3. Pertinent bond angles and distances are summarized in Table 2. The metal atom is surrounded by four chlorine atoms to form the well-known [$FeCl_4$]$^-$ anion. The Fe—Cl bond distances are in the range 2.161(4)–2.182(5) Å, which is in excellent agreement with the literature.[31,32] The Cl—Fe—Cl bond angles fall between 106.2(2) and 112.6(2)°, which deviates very little from ideal tetrahedral geometry. The phosphonium cation is similar to that found in other structures.[24]

DISCUSSION

Chemistry of $FeCl_3$ *with* TMPP.

The compound [H-TMPP]$_2$[Fe_2Cl_6] is the first reported example of a compound containing the unit [Fe_2Cl_6]$^{2-}$.[22d,33] Whereas the molecule Fe_2Cl_6 is known to be the stable form of $FeCl_3$ in the gas phase, and similar di-Fe^{III} compounds of the type [Fe_2Cl_9]$^{3-}$ or [$Fe_2Cl_6(\mu$-O)]$^{2-}$, [$Fe_2Cl_6(\mu$-OEt)$_2$]$^{2-}$ and $Fe_4Cl_8(THF)_6$ have been structurally characterized,[26,32] no such analogous di-ferrous chloride complexes have been reported. There are more examples of the [M_2X_6]$^{2-}$ unit with the heavier halogens, for example the anions [Fe_2I_6]$^{2-}$ and [Mn_2X_6]$^{2-}$ (X = Br, I) are known.[34] The isolation of [H-TMPP]$_2$[Fe_2Cl_6] from the 1 : 1 stoichiometric reaction of $FeCl_3$ with TMPP casts some doubt on the proposed formulations of stable *yellow* compounds, such as $FeCl_3(PCy_3)$[35] and $FeCl_3(PPh_3)$.[36] Actually, neutral four-coordinate adducts of $FeCl_3$ are quite rare in general; among them only $FeCl_3(S_4N_4)$[37] and $FeCl_3(THF)$[31d] have been structurally characterized. Most neutral "FeX_3L" species have actually proven to be of the type [$FeCl_4$][$FeCl_2L_2$]. A more common stoichiometry for this type of complex is $FeCl_3(PR_3)_2$ (R = Me, Ph),[38] as in the recently reported $FeBr_3(PMePh_2)_2$.[39] Further supporting our contention that the mono-adducts $FeCl_3(PR_3)$ are not likely to be particularly stable is the work of Poli *et al.*, who report the synthesis and isolation of $FeCl_3(PCy_3)$ and crystallization of $FeCl_3(PBu^t_3)$,[32a] but only the detection of $FeCl_3(PMe_3)$ and $FeCl_3(PPh_3)$ as elusive dark *red* species by low-temperature EPR experiments.[38] In the same work, the eventual formation of unidentified iron(II) species from the $FeCl_3/PPh_3$ reaction in toluene was noted, along with the concomitant production of chloro-substituted toluene as the oxidized by-product. In the present case, work-up of the benzene reaction filtrate produced a red–brown solid, whose mass-spectrometry, ^{1}H and ^{31}P NMR and IR data collectively point to the salt [Cl-TMPP][$FeCl_4$]. A rational synthesis of this species involved the use of [Cl-TMPP]$^+Cl^-$, prepared by reacting TMPP with chlorine gas in benzene, which was then reacted with $FeCl_3$ to give a compound whose properties are in agreement with those of the by-product. Consequently, we propose the following mechanism for the formation of **1**:

$$3FeCl_3 + 3TMPP \xrightarrow{2HCl} [H\text{-}TMPP]_2[Fe_2Cl_6] + [Cl\text{-}TMPP][FeCl_4]$$

Fe^{III} P^{III} Fe^{II}, P^{III} Fe^{III}, P^{V}

As the equation clearly indicates, the source of the protons and the extra chloride ions is postulated to be adventitious HCl, which is a ubiquitous contaminant in metal halides. In order to test the general nature of this reaction, and to isolate the iron(II) species previously mentioned by Poli *et al.*, we set out to re-investigate the chemistry of PPh_3 and $FeCl_3$. The reactions of $FeCl_3$ with 1 equivalent of PR_3(R = Cy, Ph) in benzene produce dark red solutions instantaneously, from which red solids can be isolated. The spectroscopic properties of the products are in agreement with those of the reported mononuclear $FeCl_3(PR_3)$ complexes.[32a,38] However, if the reaction is allowed to progress further, the solution turns yellow. The yellow solids isolated from these solutions exhibit far-IR spectra that are very similar to that of **1** [ν(Fe—Cl) = 380(s), 360(m), 315(m), 300(w) cm^{-1} for R = Cy and 380(s), 330(m), 320(m), 300(w) cm^{-1} for R = Ph]. In addition, the highest peaks in the FAB mass spectrum of these complexes are $m/z = 281$ and $m/z = 263$, corresponding to $[H\text{-}PCy_3]^+$ and $[H\text{-}PPh_3]^+$, respectively, and in the case of the tricyclohexylphosphonium compound, the characteristic P—H stretch at 2400 cm^{-1} was observed in the IR spectrum.

The final oxidized product $FeCl_3$(O=TMPP) (**5**) is a very stable compound and quite unique in itself, since it is atypical for a mono-phosphine oxide adduct of $FeCl_3$ to be more stable than the corresponding bis-adduct. To date, only two analogous compounds have been reported to our knowledge; these are $FeCl_3(O{=}PPh_3)$ by Lindner *et al.* in 1967[40] and $FeCl_3(O{=}PCy_3)$ by Issleib *et al.* in 1954,[35] but neither have been structurally characterized. A much more commonly encountered stoichiometry is FeX_3L_2 or FeL_4^{n+}, where L is a phosphine oxide ligand.[41]

Oxidation chemistry of $[Fe_2Cl_6]^{2-}$

We now discuss the reaction pathway that leads to the formation of complex **5**, summarized in Scheme 2. In order to understand the present results, one must first take note of previous work in this area, particularly with respect to the solvent dependence of this chemistry. Let us first consider the reactions of $FeCl_3$ and PR_3 ligands that have been performed in CH_3CN. In this solvent the oxidation of triphenylphosphine to triphenylphosphine oxide by iron(III) complexes in the presence of molecular oxygen was reported by Ondrejovic and co-workers to yield complexes of empirical formula $FeX_3(O{=}PPh_3)_2$ (X = Cl, NCS, Br),[8a] among which "$FeCl_3(O{=}PPh_3)_2$" was structurally characterized and proven to actually be $[FeCl_4][FeCl_2(O{=}PPh_3)_4]$.[42] When identical chemistry was performed in a protic solvent such as methanol, the compound $[CH_3\text{-}PPh_3][FeCl_4]$ was isolated.[31a] Ondrejovic proposes that protic solvents induce the quaternarization of the phosphine, by methylation in this case, which is then oxidized to $Ph_3P{=}O$.[31a] In the 1970s Sutin *et al.* also investigated the oxidation of PPh_3 in the presence of iron(III) and iron(IV) dithiolate complexes of the type $[Fe(mnt)_2]^-$, where $[mnt]^{2-}$ is maleonitriledithiolate.[43] In this work, only the stable bis-phosphine oxide complex $[Fe(mnt)_2(O{=}PPh_3)_2]^-$ was observed, however, with no evidence of intermediate species such as the previously postulated dioxygen adducts.[5,44] Recently, McAuliffe and coworkers reported that oxygen decomposes $FeBr_3(PMePh_2)_2$ to an orange product that exhibits a strong P=O stretching frequency in the IR spectrum, but no molecular oxygen species were detected or isolated. These results, like ours, disfavour the hypothesis that stable dioxygen complexes are important intermediates in the oxidation of PR_3 to $O{=}PR_3$.[39]

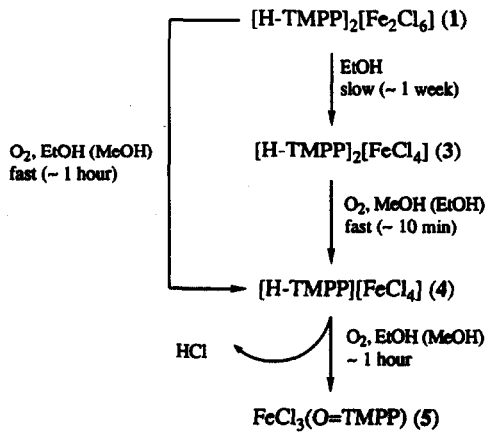

Scheme 2. Major products isolated from the reaction of $[H\text{-}TMPP]_2[Fe_2Cl_6]$ with O_2 in alcohols.

As in the aforementioned chemistry, the reaction between $FeCl_3$/TMPP and oxygen is also solvent-dependent. The reaction of $[H\text{-}TMPP]_2[Fe_2Cl_6]$ (**1**) with oxygen in CH_3CN leads to the rapid formation of $FeCl_3$(O=TMPP) (**5**) with no detection of phosphonium intermediates. The reaction pathway is dramatically different in alcohol solvents in which protic phosphonium salts of tetrachloroferrate(II)

and (III) are formed. A suspension of $[H\text{-}TMPP]_2[Fe_2Cl_6]$ (**1**) reacts with molecular oxygen in ethanol or methanol to form [H-TMPP][$FeCl_4$] (**4**), as determined by IR spectroscopy and confirmed by X-ray crystallography. One must bear in mind, however, that this reaction is not quantitative, since some $[H\text{-}TMPP]_2[Fe_2Cl_6]$ must be sacrificed to yield extra chloride ions for $[FeCl_4]^-$. The salt [H-TMPP][$FeCl_4$] further reacts with oxygen in alcohols to form $FeCl_3$(O=TMPP) (**5**). Scheme 2 also points out that if $[H\text{-}TMPP]_2[Fe_2Cl_6]$ is suspended in ethanol (but without the addition of oxygen) for a period of time in excess of 1 week, the compound eventually dissolves, with reaction, to yield the iron(II) species $[H\text{-}TMPP]_2[FeCl_4]$ (**3**). Compound **3** can, in turn, be reacted with oxygen in methanol or ethanol to form compound **4**, and subsequently, compound **5**. We have independently prepared complexes **3** and **4** and demonstrated that they indeed react as proposed in the scheme.

Two years ago we reported the formation of a green intermediate during the reaction of $[H\text{-}TMPP]_2[Fe_2Cl_6]$ (**1**) with molecular oxygen in CH_2Cl_2.[10] At that time we hypothesized that the species was a dioxygen adduct, but subsequent IR studies of the behaviour of **1** in CH_2Cl_2 revealed only the appearance of $[FeCl_4]^-$ and $[ClCH_2\text{-}TMPP]^+$ ions over time. Facile decomposition of free TMPP in CH_2Cl_2 to give $[ClCH_2\text{-}TMPP]Cl$ is well-known.[12a] Thus, we conclude that the TMPP ligand in $[H\text{-}TMPP]_2[Fe_2Cl_6]$ is reacting with CH_2Cl_2. We note that photochemically induced reactions of similar $FeCl_3/PR_3$ compounds in chlorinated solvents are documented as in the formation of $[FeCl_4][FeCl_2(dmpe)_2]$ from the photochemical oxidation of $FeCl_2(dmpe)_2$ in chlorinated solvents such as CH_2Cl_2, $CHCl_3$ or CCl_4.[45]

Catalytic formation of TMPP=O

Finally, in view of Ondrejovic's work and the demonstrated catalytic nature of the $FeCl_3/PR_3/O_2$ systems, it was relevant to ask whether $FeCl_3$ (O=TMPP) (**5**) could act as a catalyst for the oxidation of TMPP to TMPP=O. Indeed, when $FeCl_3$(O=TMPP) is reacted with an excess of the phosphine (from 10- to 100-fold) in acetone, acetonitrile or ethanol in the presence of oxygen, TMPP=O is formed in high yield with essentially complete recovery of $FeCl_3$(O=TMPP).

CONCLUSIONS

In summary, the chemistry of 1:1 mixtures of $FeCl_3$/TMPP with oxygen appears to be dominated by the formation of $[Fe^{II}Cl_4]^{2-}$, $[Fe^{III}Cl_4]^-$ and $[H\text{-}TMPP]^+$ species. In accord with this observation is the demonstrated role of quaternary onium tetrachloroferrate salts in numerous catalysed reactions such as hydrosilylation,[46] polymerization of ε-caprolactone[47] and polymerization of α-oxides.[48] The present work has also established the existence of a hitherto unknown di-ferrous chloride, namely $[Fe_2Cl_6]^{2-}$.[22d] Collectively, the results of this investigation support the conclusion that the stable and unprecedented mono-phosphine oxide adduct $FeCl_3$(O=TMPP) does not form via the formation of metal–oxygen adducts, but via quaternarization of the phosphine. Finally, we did not observe the formation of bis-phosphine oxide complexes, a result that is in contrast to previously reported work.

Acknowledgements—We gratefully acknowledge the National Science Foundation (Grant CHE-8914915 to K.R.D.) and the Camille and Henry Dreyfus Foundation for financial support. The X-ray equipment was purchased with grants provided by the National Science Foundation (Grants CHE-8403823 and CHE-8908088). The NMR equipment was supported by grants from the National Science Foundation (Grant CHE-88-00770) and the National Institutes of Health (Grant No. 1-510-RR04750-01). The SQUID instrument is housed in the Physics and Astronomy Department and was purchased by The Center for Fundamental Materials Research, Michigan State University. The authors would like to thank Dr Sue-Jane Chen for help with the data collection of compound **3** and Dr Steven C. Haefner for assistance with the crystallographic procedures and helpful discussions.

REFERENCES

1. T. S. Lobana and S. S. Sandhu, *Coord. Chem. Rev.* 1982, **47**, 283.
2. (a) G. Wilke, H. Schott and P. Heimbach, *Angew. Chem., Int. Edn Engl.* 1967, **6**, 92; (b) A. Sen and J. Halpern, *J. Am. Chem. Soc.* 1977, **99**, 8337.
3. S. Cenini, A. Fusi and G. Capparella, *Inorg. Nucl. Chem. Lett.* 1972, **8**, 127.
4. K. Takao, Y. Fujiwara, T. Imanaka and S. Teranishi, *Bull. Chem. Soc. Japan* 1970, **43**, 1153.
5. J. Halpern, B. L. Goodall, G. P. Khare, H. S. Lim and J. J. Pluth, *J. Am. Chem. Soc.* 1975, **97**, 2301.
6. D.-H. Chin, G. N. La Mar and A. L. Balch, *J. Am. Chem. Soc.* 1980, **102**, 5945.
7. (a) E. F. Epstein, I. Bernal and A. L. Balch, *Chem. Commun.* 1970, **136**; (b) J. P. Birk, J. Halpern and A. L. Pickard, *J. Am. Chem. Soc.* 1968, **90**, 4491.
8. (a) I. Ondrejkovicova, V. Vancova and G. Ondrejovic, *Coll. Czech. Chem. Commun.* 1983, **48**, 254; (b) I. Ondrejkovicova, V. Vancova and G. Ondrejovic, *Proc. Conf. Coord. Chem.* 1983, **9**, 321; (b) I. Ondrejkovicova and G. Ondrejovic, *Proc. Conf. Coord.*

Chem. 1985, **10**, 303; (c) V. Vancova, I. Ondrejkovicova and G. Ondrejovic, *Chem. Zvesti* 1984, **38**, 363; (d) I. Ondrejkovicova, V. Vancova and G. Ondrejovic, *Proc. Conf. Coord. Chem.* 1989, **12**, 263; (e) I. Ondrejkovicova, M. Melnik, K. Smolander and M. Ahlgrén, Book of abstracts, 29th International Conference on Coordination Chemistry. Lausanne, Switzerland; 19–24 July 1992, Paper P688.

9. (a) K. R. Dunbar, S. C. Haefner and L. E. Pence, *J. Am. Chem. Soc.* 1989, **111**, 5504; (b) K. R. Dunbar, S. C. Haefner and C. Bender, *J. Am. Chem. Soc.* 1991, **113**, 9540; (c) K. R. Dunbar, S. C. Haefner and D. J. Burzynski, *Organometallics* 1990, **9**, 1347; (d) S.-J. Chen and K. R. Dunbar, *Inorg. Chem.* 1990, **29**, 588; (e) S.-J. Chen and K. R. Dunbar, *Inorg. Chem.* 1991, **30**, 2018.
10. K. R. Dunbar, S. C. Haefner and A. Quillevéré, *Polyhedron* 1990, **9**, 1695 and refs therein.
11. (a) A. P. Zuur and W. L. Groeneveld, *Rec. Trav. Chim. Pays Bas* 1967, **86**, 1089; (b) J. Reedijk and W. L. Groeneveld, *Rec. Trav. Chim. Pays Bas* 1968, **87**, 513.
12. (a) M. Wada, *J. Chem. Res.* 1985, (S), 38; (M), 0467; (b) K. R. Dunbar and S. C. Haefner, in preparation.
13. (a) A. Bino, F. A. Cotton and P. E. Fanwick, *Inorg. Chem.* 1979, **18**, 3558; (b) F. A. Cotton, B. A. Frenz, G. Deganello and A. Shaver, *J. Organomet. Chem.* 1973, 227.
14. TEXSAN-TEXRAY Structure Analysis Package, Molecular Structure Corporation (1985).
15. G. M. Sheldrick, SHELXS, in *Crystallographic Computing 3* (Edited by G. M. Sheldrick, C. Krüger and R. Goddard), p. 175. Oxford University Press, Oxford (1984).
16. DIRDIF, Direct Methods for Difference Structures, An Automatic Procedure for Phase Extension; Refinement of Difference Structure Factors. Technical Report 1984/1. Crystallography Laboratory, Toernooivelt, 6525 Ed Nijmegen, The Netherlands.
17. N. Walker and D. Stuart, *Acta Cryst.* 1983, **A39**, 158.
18. C. J. Gilmore, *J. Appl. Cryst.* 1984, **17**, 42.
19. W. Levason, *Comm. Inorg. Chem.* 1990, **9**, 331.
20. K. R. Dunbar, A. Quillevéré and W. R. Dunham, in preparation.
21. D. C. Povey, G. W. Smith, T. S. Lobana and P. K. Bhatia, *J. Cryst. Spect. Res.* 1991, **21**, 9.
22. (a) K. R. Dunbar and A. Quillevéré, unpublished results; (b) K. R. Dunbar, A. Quillevére and S. C. Haefner, *Acta Cryst.* 1991, **C47**, 2319 and refs therein; (c) O. K. Kireeva, B. M. Bulychev, N. R. Streitsova, V. K. Belsky, A. G. Dunin, *Polyhedron* 1992, **11**, 1801; since the submission of this manuscript, an independent report of a salt containing $[Fe_2Cl_6]^{2-}$ has appeared. U. Ruhlandt-Senge and U. Müller, *Z. Naturforsch.* 1992, **47b**, 1095.
23. C. A. McAuliffe, in *Comprehensive Coordination Chemistry* (Edited by G. Wilkinson), Vol. 3, Ch. 28, pp. 275–276. Pergamon Press, Oxford (1987).
24. K. R. Dunbar and L. E. Pence, *Acta Cryst.* 1991, **C47**, 23.
25. L. Naldini, *Gazz. Chim. Ital.* 1960, **90**, 1231.
26. F. A. Cotton and G. Wilkinson, *Advanced Inorganic Chemistry*, 5th edn. John Wiley, New York (1988).
27. (a) J. R. Hartman, R. L. Rardin, P. Chaudhuri, K. Pohl, K. Wieghardt, B. Nuber, J. Weiss, G. C. Papaefthymiou, R. B. Frankel and S. J. Lippard, *J. Am. Chem. Soc.* 1987, **109**, 7387; (b) P. Chaudhuri and K. Wieghardt, *Angew. Chem., Int. Edn Engl.* 1985, **24**, 778.
28. (a) A. S. Borovik and L. Que Jr, *J. Am. Chem. Soc.* 1988, **110**, 2345; (b) A. S. Borovik, M. P. Hendrich, T. R. Holman, E. Münck, V. Papaefthymiou and L. Que Jr, *J. Am. Chem. Soc.* 1990, **112**, 6031.
29. (a) K. S. Hagen and R. H. Holm, *Inorg. Chem.* 1984, **23**, 418; (b) D. Coucouvanis, K. Greiwe, A. Salifoglou, P. Challen, A. Simopoulos and A. Kostikas, *Inorg. Chem.* 1988, **27**, 593.
30. (a) J. W. Lauher and J. A. Ibers, *Inorg. Chem.* 1975, **14**, 348; (b) T. Toan and L. F. Dahl, *J. Am. Chem. Soc.* 1971, **93**, 2654; (c) H. C. Freeman, G. H. W. Milburn and C. E. Nockolds, *Chem. Commun.* 1969, 55; (d) R. Mason, E. D. McKenzie, G. B. Robertson and G. A. Rusholme, *Chem. Commun.* 1968, 1673.
31. (a) T. Glowiak, E. Durcanska, I. Ondrejkovicova and G. Ondrejovic, *Acta Cryst.* 1986, **C42**, 1331; (b) F. A. Cotton and C. A. Murillo, *Inorg. Chem.* 1975, **14**, 2467; (c) G. Constant, J.-C. Daran and Y. Jeannin, *J. Organomet. Chem.* 1972, **44**, 353; (d) F. A. Cotton, R. L. Luck and K.-A. Son, *Acta Cryst.* 1990, **C46**, 1424 and refs therein; (e) J. D. Walker and R. Poli, *Polyhedron* 1989, **8**, 1293.
32. (a) J. D. Walker and R. Poli, *Inorg. Chem.* 1990, **29**, 756; (b) F. A. Cotton, R. L. Luck and K.-A. Son, *Inorg. Chim. Acta* 1991, **179**, 11.
33. K. R. Dunbar and A. Quillevéré, *Angew. Chem.* 1993, in press.
34. (a) S. Pohl, W. Saak and P. Stolz, *Z. Naturforsch.* 1988, **43b**, 289; (b) S. Pohl, W. Saak and P. Stolz, *Z. Naturforsch.* 1988, **43b**, 171.
35. K. Issleib and A. Brack, *Z. Anorg. Allg. Chem.* 1954, **277**, 258.
36. (a) P. P. Singh and R. Rivest, *Can. J. Chem.* 1968, **46**, 1733; (b) T. Birchall, *Can. J. Chem.* 1969, **47**, 1351.
37. (a) U. Thewalt, *Z. Naturforsch.* 1980, **35b**, 855; (b) U. Thewalt, *Z. Anorg. Allg. Chem.* 1981, **476**, 105.
38. J. D. Walker and R. Poli, *Inorg. Chem.* 1989, **28**, 1793.
39. S. M. Godfrey, D. G. Kelly, A. G. Mackie, P. P. MacRory, C. A. McAuliffe, R. G. Pritchard and S. M. Watson, *J. Chem. Soc., Chem. Commun.* 1991, 1447.
40. E. Lindner, R. Lehner and H. Scheer, *Chem. Ber.* 1967, **100**, 1331.
41. (a) T. S. Lobana, H. S. Cheema and S. S. Sandhu, *J. Chem. Soc., Dalton Trans.* 1983, 2039; (b) S. A. Cotton and J. F. Gibson, *J. Chem. Soc. (A)* 1971, 859; (c) E. Bannister and F. A. Cotton, *J. Chem. Soc.* 1960, 1878, (d) D. C. Povey, T. S. Lobana and P. K. Bhatia, *J. Cryst. Spect. Res.* 1991, **21**, 13;

(e) B. Beagley, D. G. Kelly, P. P. MacRory, C. A. McAuliffe and R. G. Pritchard, *J. Chem. Soc., Dalton Trans.* 1991, 2657.
42. E. Durcanska, T. Glowiak, J. Kozisek, I. Ondrejkovicova and G. Ondrejovic, *Acta Cryst.* 1989, **C45**, 410.
43. N. Sutin and J. K. Yandell, *J. Am. Chem. Soc.* 1973, **95**, 4847.
44. A. L. Balch, *Inorg. Chem.* 1971, **10**, 276.
45. L. D. Field, A. V. George and T. W. Hambley, *Polyhedron* 1990, **9**, 2139.
46. I. Iovel, Y. Goldberg, M. Shymanska and E. Lukevics, *Appl. Organomet. Chem.* 1987, **1**, 371.
47. Z. G. Aliev and A. M. Karateev, *Koord. Khim.* 1988, **14**, 111.
48. A. M. Karateev, P. P. Kushch, Ye. N. Frolov, N. S. Ovanesyan, E. A. Dzhavadyan and B. A. Rozenberg, *Vysokomol. Soyed.* 1988, **A30**, 1075.

Polyhedron Vol. 12, No. 7, pp. 821–829, 1993
Printed in Great Britain

0277–5387/93 $6.00+.00
© 1993 Pergamon Press Ltd

SYNTHESIS, CHARACTERIZATION AND REACTIVITY OF RUTHENIUM TETRAPHENYLPORPHYRIN COMPLEXES CONTAINING THE THIOCARBONYL LIGANDS

KRYSTYNA RACHLEWICZ, MARIA GRZESZCZUK and LECHOSŁAW LATOS-GRAŻYŃSKI*

Institute of Chemistry, University of Wrocław, 14 F. Joliot-Curie St, Wrocław 50 383, Poland

(*Received* 10 *August* 1992; *accepted* 12 *October* 1992

Abstract—A new synthetic route to generate tetraphenylporphyrin ruthenium(II) thiocarbonyl complexes of the general formula Ru^{II}(Por)(CS)L has been developed and the chemistry and electrochemistry of these complexes have been studied. $[Ru^{IV}(Por)(EtO)]_2O$ has been applied as a convenient starting material for ligand incorporation using carbon disulphide, thiophosgene and benzyl trichloromethyl thioether as thiocarbonyl precursors in the reducing medium. The Ru—CS bond is very strong and resistant to nucleophilic replacement. Thiocarbonyl and carbonyl ruthenium(II) porphyrin complexes reveal essential similarity as far as chemical and electrochemical properties are concerned, with the exception of the internal reactivity of the thiocarbonyl ligand. One-electron oxidation of [Ru(Por)(CS)(EtOH)] led to the formation of the respective π-cation radical characterized by visible, IR and ^{1}H NMR spectroscopy.

The novel features of ruthenium porphyrins, including their versatile redox behaviour,[1] the formation of the reactive Ru=O,[2] Ru—H_2,[3] Ru—N_2,[4] Ru—C,[5] Ru=C[6] and Ru—Ru[7] bonds and their relation to naturally occurring metalloporphyrins, have attracted considerable attention. In particular, high-valent oxoruthenium porphyrin complexes have been established to be competent catalysts for the aerobic expoxidation of olefins.[2a] Unusual rupture and repair of the porphyrin inner core in ruthenium complexes of a N,N′-bridged porphyrin have been also described.[8]

Ruthenium organometallic chemistry seems to be of special interest in light of the implication of metal–carbon species in reactions of cytochrome P-450 with polyhalogenated compounds, widely used as solvents, insecticides and fungicides.[9] Various organic compounds containing the SCl_3 moiety display fungicidal activity.[10a] The SCl_3 group can be metabolized into thiophosgene and carbon disulphide, which may account for the activity.[10] Iron porphyrin thiocarbonyl complexes can also be formed in the course of biochemical processes.[11b]

Chemical and electrochemical properties of iron porphyrin thiocarbonyl complexes have been studied in detail.[11,12] The studies on ruthenium porphyrin thiocarbonyl complexes have been limited to the particular case of [Ru(OP)(CS)(py)] species.[13] The similarity of carbon monosulphide (CS) to carbon monoxide has stimulated much interest in the synthesis and reactivity of thiocarbonyl complexes in general.[14] The crucial step of the synthetic route to the thiocarbonyl system elaborated by James and Dolphin[13] involves an oxidative decarbonylation of [Ru(OEP)(CO)(py)] by bromine in the presence of excess cyanide to produce $[Ru^{III}(OEP)(CN)_2]^-$, which is treated with pyridine to give [Ru^{III}(OEP)(CN)(py)]. Reduction of this species in the presence of thiophosgene gives the thiocarbonyl complex $[Ru^{II}(OEP)(CS)(py)]$. Because of the reaction procedure the pyridine ligand occupies one of the axial positions.

In order to probe the influence of axial ligation we have developed a new synthetic route to general ruthenium thiocarbonyl complexes of the general formula $[Ru^{II}(TPP)(CS)L]$, where L is a ligand of choice. $[Ru^{IV}(TPP)(EtO)]_2O$ has been used as a convenient, already decarbonylated starting material to form $[Ru^{II}(TPP)(CS)(EtOH)]$. Here we report on

* Author to whom correspondence should be addressed.

the synthesis and properties of ruthenium porphyrin thiocarbonyl complexes. In particular, the paper extends our previous effort[15] to describe the spectroscopy and reactivity of ruthenium porphyrin cation radicals.

EXPERIMENTAL

Materials

Carbon disulphide (Fluka) and thiophosgene (Aldrich) were used as received. Tetraphenylporphyrin ($TPPH_2$), tetra-*p*-tolylporphyrin (TT PH_2),[16] pyrrole-d_8-tetra-*p*-tolylporphyrin (d_8-TT PH_2)[17] and [Ru^{II}(TPP)(CO)(EtOH)][18] were prepared by reported procedures.

Synthesis of the compounds

μ-oxo-bis(ethoxo)(tetraphenylporphyrinato)ruthenium(IV), [Ru^{IV}(TPP)(OEt)]$_2$O·2H_2O. Ru^{II}(TPP)(CO)(EtOH) (100 mg, 0.12 mmol) was dissolved in dichloromethane–ethanol (100 cm^3, 1:1 vv), vigorously stirred and 30% H_2O_2 (3 cm^3) was added gradually. When the starting material was totally consumed in the reaction, as determined by the disappearance of the ν(C=O) band at the IR spectrum, a 5% solution of sodium cyanate in water was added to precipitate the product. The solid material was collected, dried and purified by column chromatography (neutral alumina, dichloromethane as an eluant). The electronic and ^{1}H NMR spectra of [Ru^{IV}(TPP)(OEt)]$_2$O·2H_2O corresponded to those previously reported.[2,19] This product was used to synthesize the thiocarbonyl complexes. Benzyl trichloromethyl thioether was prepared from benzyl thiocyanates by Makosza's procedure.[20]

Synthesis of ruthenium(II) *porphyrin thiocarbonyl complexes*

Method A. Direct reduction of thiophosgene: [Ru^{IV}(TPP)(OEt)]$_2$O·2H_2O (100 mg, 0.06 mmol) was dissolved in dry dichloromethane (60 cm^3; purged with nitrogen for 10 min) and zinc amalgam (100 mg) was added as a powder at 298 K. The solution was energetically stirred for 30 min and a degassed solution of thiophosgene (0.12 mol) in dichloromethane was added. The reaction mixture was stirred for 4 h. The solution was then filtered to remove an excess of zinc amalgam, ethyl alcohol (10 cm^3) was added and the solution was evaporated to dryness on the rotary evaporator. The progress of the reaction was monitored by product electronic (530 nm) and IR [ν(C=S) band at 1295 cm^{-1}] spectra. The sample was subjected to column chromatography (neutral alumina). The red band of the thiocarbonyl complex was eluted with a mixture of dichloromethane and carbon tetrachloride (2:98 vv). The solution of [Ru^{II}(TPP)(CS)(EtOH)] was evaporated to dryness and crystallized from the dichloromethane/ethanol/n-hexane mixture (1:1:10). Yield 90%.

Method B. Sulphur abstraction from carbon disulphide: [Ru^{IV}(TPP)(OEt)]$_2$O·2H_2O (100 mg, 0.06 mmol) was dissolved in dried THF (60 cm^3; purged with nitrogen for 15 min). The sodium amalgam was added. The solution was stirred for 30 min and degassed carbon disulphide (0.2 cm^3) was added. The reaction mixture was stirred under nitrogen for 48 h and the solution was then filtered through Celite. The volume was reduced on a rotary evaporator and the sample was subjected to chromatography on a 5 × 30 cm column of neutral alumina. The thiocarbonyl complex was then eluted with toluene. The chromatography was repeated to remove the side-products of the reactions. Yield 30%.

Method C. Reductive dehalogenation of benzyl trichloromethyl thioether: [Ru^{IV}(TPP)(OEt)]$_2$O·2H_2O (100 mg, 0.06 mmol) in toluene (100 cm^3) under nitrogen was reduced for 30 min. Benzyl trichloromethyl thioether in toluene (0.02 mg, 0.12 mmol) was then added. The progress of the reaction was followed by absorption spectroscopy. The Q band at 520 nm and the Soret band at 430 nm were tentatively assigned to the intermediate, i.e. the ruthenium porphyrin carbene compound [Ru(TPP)(C(Cl)(SR))]. A solution of $FeCl_2$ in ethanol (2 cm^3) was added to catalyse the decomposition of the intermediate carbene complex and to form the ruthenium tetraphenylporphyrin thiocarbonyl complex (530 and 410 nm). Usually this step required 48 h. The reaction mixture was filtered through Celite and dried on a rotary evaporator. Further purification as in Method A. Yield 60%. Each method gave identical products after recrystallization. Found: C, 69.8; H, 3.5; N, 6.8. Calc. for [Ru^{II}(TPP)(CS)(EtOH)] ($C_{47}H_{30}N_4OSRu$): C, 70.6; H, 3.7; N, 7.0%. Found: C, 70.7; H, 4.7; N, 6.3. Calc. for [Ru^{II}(TTP)(CS)(EtOH)]($C_{51}H_{42}N_4OSRu$): C, 71.2; H, 4.9; N, 6.51.

Hexa-coordinate ruthenium(II) *tetraphenylporphyrin thiocarbonyl complexes*, [Ru^{II}(TPP)(CS)L]

A general procedure was used to generate [Ru^{II}(TPP)(CS)L] in solutions.

[Ru^{II}(TPP)(CS)(EtOH)] was dissolved in dichloromethane and the ligand of interest was added (1:1.5 molar ratio). The coordination of axial ligands was followed by electronic and IR spectra.

Pyridine, chloropyridine, bromopyridine, 4,3-phenylpropylpyridine, 4-methylpyridine, imidazole, 1-methyimidazole, 1-benzylimidazole, triphenylphosphine, toluidine and acetonitrile was used as received. The cyanide source was bis(triphenylphosphine)imminium cyanide. The samples for IR spectra were prepared as a film on KBr or CaF_2 plates.

Chemical oxidation of $[Ru^{II}(TTP)(CS)(EtOH)]$ *and* $[Ru^{II}(TTP)(CO)(EtOH)]$

Method A. $[Ru^{II}(TTP)(CS)(EtOH)]$ (20 mg, 0.023 mmol) was dissolved in dichloromethane (10 cm^3) and 1.5 equivalents of phenoxanthiinylium hexachloroantimonate were added. The solution was stirred for 30 min until the red solution turned green. π-Cation radical formation was followed by electronic and ^1H NMR spectra.[21] The π-cation radical was precipitated with n-hexane. Phenoxanthiinylium hexachloroantimonate was obtained from phenoxanthiin and antimony pentachloride as previously described.[21g]

Method B. $[Ru^{II}(TTP)(CS)(EtOH)]$ in dichloromethane was stirred with a four-fold excess of $Fe(ClO_4)_3 \cdot 9H_2O$ until the colour changed from red to green. π-Cation radical formation was followed by electronic and NMR spectra.[21] After filtration, the π-cation radical $[Ru^{II}(TTP^{+\bullet})(CS)(ClO_4)]$ was used for further investigation. The same procedures were used to generate the π-cation radical of carbonyl tetratolylporphyrin ruthenium(II).

Method C. The oxidation of $[Ru^{II}(TTP)(EtOH)]$ to the π-cation radical was also performed by NMR titration with Br_2 in $CDCl_3$. The titration was stopped before bromination of the pyrrole or the phenyl positions could be observed in the respective ^1H NMR spectrum.[15]

Instrumentation

^1H NMR spectra were recorded on Bruker AMX 300 MHz and Tesla 100 MHz spectrometers. UV–vis spectra in dichloromethane, chloroform and toluene solutions were recorded on a Specord M40 and IR on a Specord M42 spectrophotometer, respectively. The samples for IR measurements were prepared as films on CaF_2 or KBr plates, or as chloroform solution KBr cells. Cyclic voltammetry measurements were carried out as previously described.[22]

RESULTS AND DISCUSSION

Properties and characterization of ruthenium porphyrinthiocarbonyl complexes

Three synthetic routes have been established for the incorporation of the thiocarbonyl ligand into metalloporphyrins: (1) reduction of thiophosgene,[23] (2) sulphur abstraction from carbon disulphide,[24] and (3) conversion of CCl(SR) carbene complexes to thiocarbonyl[16] complexes.

Each method requires metalloporphyrin reduction as a prerequisite condition of the reaction. The dinuclear μ-oxo ruthenium(IV) porphyrin complex $[Ru^{IV}(Por)(OEt)]_2O$ can be reduced to monomeric ruthenium(II) porphyrins.[19] This seems to be the most convenient route to generate ruthenium (II) porphyrins bearing a wide variety of axial ligands. We have established that it is convenient to form thiocarbonyl complexes as well. The three routes listed above have been explored (Scheme 1). The best results have been obtained in the case of thiophosgene reduction. The catalytic decomposition of the ruthenium carbene intermediate is

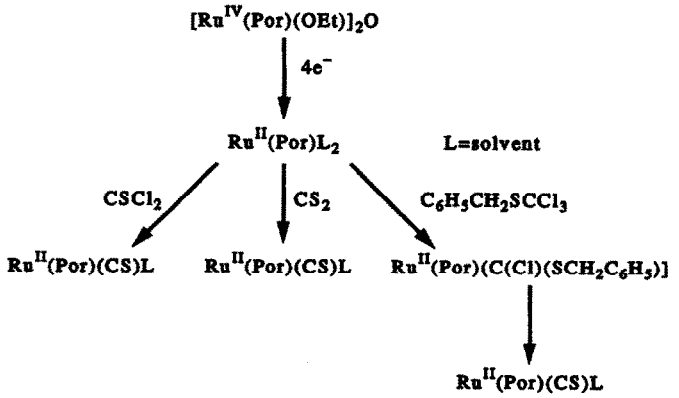

Scheme 1.

Table 1. ν(C=S) frequency for [Ru(TTP)(CS)L] complexes

Ligand L	ν(C=S) (cm^{-1})
CS free in CS_2 matrix[25]	1274
Cyanide	1249
Imidazole	1274
Benzimidazole	1275
Acetonitrile	1277
Pyridine	1290
4-Methylpyridine	1281
Toluidine	1282
4,3-Phenylpropylpyridine	1283
3-Chloropyridine	1283
4-Chloropyridine	1285
1-Methylimidazole	1286
Triphenylphosphine	1286
2-Chloropyridine	1288
5,5-Diacyanoimidazole	1290

slow and not quantitative. The [Ru^{II}(Por)(C(Cl)($SCH_2C_6H_5$))] intermediate can be postulated based upon the characteristic changes observed in the electronic spectra and by analogy with the formation of the corresponding iron analogues.[11b]

As determined by electronic and IR spectrocopy the product, [Ru^{II}(Por)(CS)(EtOH)], can be converted into derivatives containing strongly coordinating ligands, e.g. pyridine, imidazole, cyanide or phosphine. The electronic spectra of [Ru^{II}(TTP)(CS)(EtOH)] and [Ru^{II}(TTP)(CO)(EtOH)] are almost superimposable with a small bathochromic shift determined for the Soret band, in spite of the greater π-acceptor capacity of the thiocarbonyl ligand. It has been shown that the C=S stretching frequency for [Ru^{II}(TTP)(CS)L] is dependent upon the identity of the axial ligand L (Table 1). Generally, the frequency shifts to a lower wave number as the basicity of the ligand increases. However, all frequencies observed are higher than those of the CS molecule in the carbon disulphide matrix,[25] which occurs at 1274 cm^{-1}. One has to consider the fact that the CS stretching mode is considerably mixed with the M—C(S) mode.[26] The observed dependency is not interpreted in a straightforward manner in terms of π-back bonding.[27] Iron porphyrin thiocarbonyl complexes demonstrate a similar relationship.[11,12]

Reactivity of [Ru^{II}(TPP)(CS)L]

The [Ru^{II}(TPP)(CS)L] complexes are stable in the presence of dioxygen and all operations including chromatography could be carried out in the presence of air. The Ru—CS bond has not dissociated in diluted solution or during heating at 180°C. The thiocarbonyl complex is resistant to the nucleophilic replacement by pyridine or benzonitrile, even after refluxing for 60 h. However, triphenylphosphine refluxed in toluene (10-fold excess) reacted with [Ru^{II}(TPP)(CS)(EtOH)] to form the previously characterized [Ru^{II}(TPP)(PPh_3)$_2$], as confirmed by IR and ^{1}H NMR spectra.[28] [Ru^{II}(TTP)(CS)] reacted with butylamine to form the isocyanide complex. The formation of the isocyanide ligand was easy followed by IR spectra, where the disappearance of the ν(C—S) band at 1295 cm^{-1} was accompanied by an increase in intensity of ν(C—N) at 2050 cm^{-1}, which is typical for the isocyanide group. The formation of isocyanide-metal complexes from thiocarbonyl complexes has been established for the thiocarbonyl iron porphyrins[11b] and for other non-porphyrin transition metal complexes.[29]

One-electron chemical oxidation of [Ru^{II}(TTP)(CS)(EtOH)] with phenoxanthiinylium hexachloroantimonate leads to the formation of the respective cation radical [Ru^{II}($TTP^{+\cdot}$)(CS)]($SbCl_6$). Other oxidants such as $Fe(ClO_4)_3$ or Br_2 have also been applied. The coordination of thiocarbonyl in the cation radical form has been confirmed by the characteristic frequency of the CS stretching, ν(CS) = 1295.4 cm^{-1}, which is very close to that established for [Ru^{II}(TTP)(CS)(EtOH)]. This fact clearly confirms that the oxidation state of ruthenium is not changed in the course of the oxidation. The electronic and NMR spectra of the cation radical are presented in Figs 1 and 2, respectively.

The assignment of porphyrin resonances in the ^{1}H NMR spectrum has been carried out based upon selective methyl and deuterium substitution. The respective data are collected in Table 2. The pattern of tetraphenylporphyrin resonances can be used as a well-accepted criterion of paramagnetic metalloporphyrin electronic structure. In particular, clear distinction between metal- and ligand-centred oxidation can be made.[15,21] The pattern of phenyl resonances (*p*-methyl, *meta* proton downfield, *ortho*, *para* protons upfield) is expected for the cation radical in the electronic ground state dominated by the A_{2u} molecular orbital of the porphyrin ligand. In this structure the spin density is located to a large extent at the *meso* carbons, which is reflected in the considerable π-spin density delocalization on phenyl rings.[21f].

The [Ru^{II}($TTP^{+\cdot}$)(CS)]($SbCl_6$) cation radical undergoes a one-electron reduction in the presence of excess zinc powder, pyridine or triphenylphosphine. The [Ru^{II}(TTP)(CS)(EtOH)] complex is

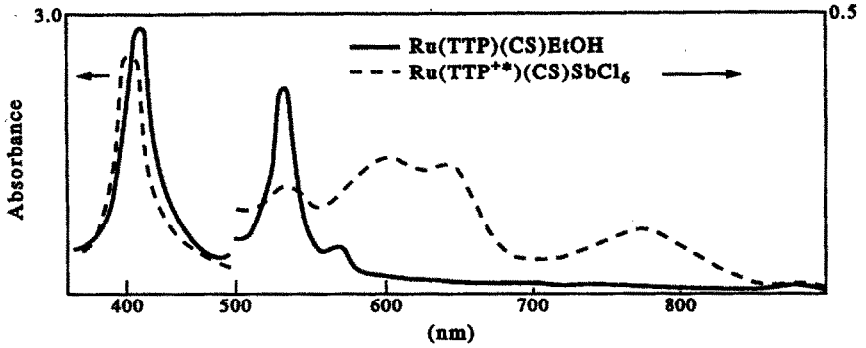

Fig. 1. Electronic spectra of [Ru(TTP)(CS)EtOH] and its π-cation radical in chloroform solution at 25°C.

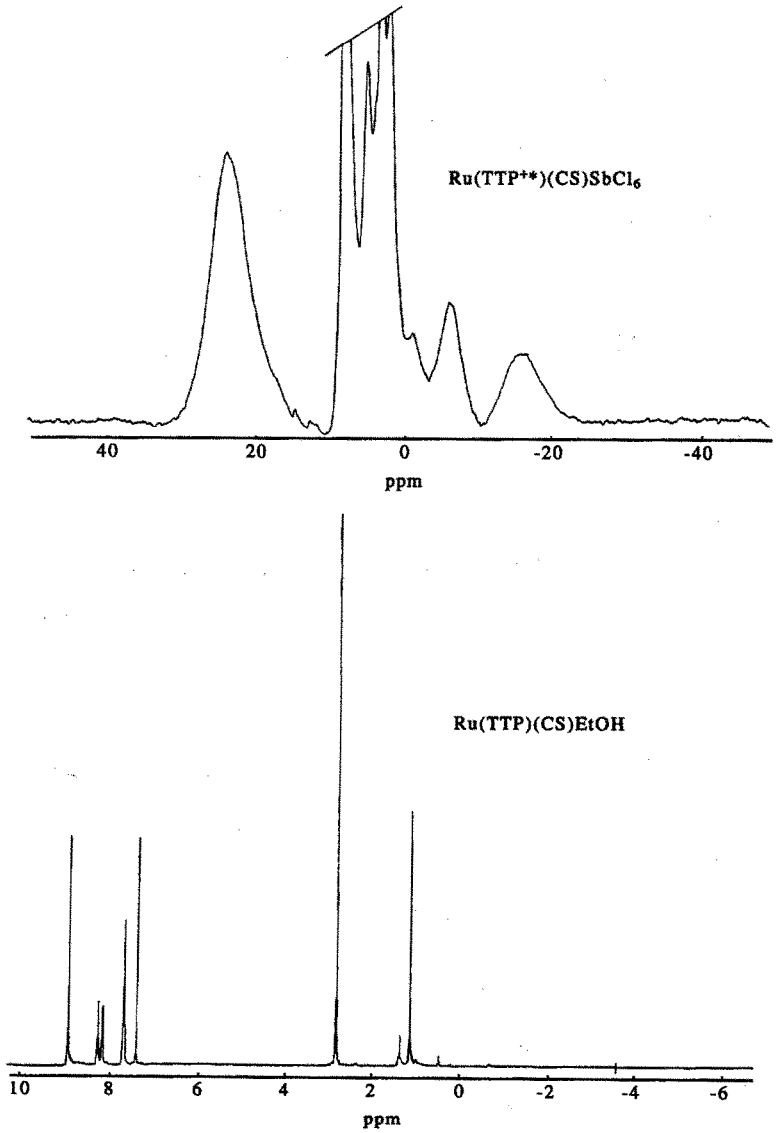

Fig. 2. 300 MHz ^{1}H NMR spectra of [Ru(TTP)(CS)(EtOH)] and its π-cation radical [Ru(TTP)(CS)($SbCl_6$)] in $CDCl_3$ at 25°C.

Table 2. ^{1}H NMR chemical shift of ruthenium complexes (ppm vs TMS in $CDCl_3$, 25°C)

Compound	Position			
	Pyrrole	*Ortho*	*Meta*	*Para*
[Ru(CS)(TTP)(EtOH)]	8.84	8.05	7.53	2.69
[Ru(CO)(TTP)(EtOH)][15]	8.75	8.07	7.56	2.70
[Ru(CS)(TTP)$^{+\cdot}$($SbCl_6$)]	−6.69	−17.04	23.89	23.89
[Ru(CO)(TTP)$^{+\cdot}$($SbCl_6$)]	−8.75	−16.75	25.25	25.25
[Ru(CS)(TTP)$^{+\cdot}$Br]	−5.35	−15.77	25.66	22.60
[Ru(CO)(TTP)$^{+\cdot}$Br][15]	2.60	−15.60	23.40	20.20

recovered in the case of the zinc reduction, as confirmed by ^{1}H NMR and electronic spectra. Two other reagents generate the starting compound and β-substituted derivatives analogously as other diamagnetic[30a] and paramagnetic cation radicals.[30b]

The reaction of [Ru^{II}(TTP$^{+\cdot}$)(CS)]($SbCl_6$) with pyridine and triphenylphosphine has been followed by ^{1}H NMR. The conversion of the paramagnetic π-cation radical into the diamagnetic compound has been determined. The complex resonance pattern at the pyrrole region has been established as the β-substitution markedly lowers the symmetry of the ruthenium tetraphenylporphyrin. A number of organic cation radicals react with pyridine forming pyridinium analogues.[31] ^{1}H NMR investigation on the reaction of [(TTP$^{+\cdot}$)Fe^{III}](ClO_4)$_2$ with pyridine showed also the nucleophilic attack and β-pyridinium derivative formation.[32]

Electrochemistry of [Ru^{II}(TTP)(CS)(EtOH)]

The electrochemistry of [Ru^{II}(TTP)(CS)(EtOH)] was studied with a platinum electrode in dichloroethane (DCE) or dimethylformamide (DMF). The cyclic voltammetric response of [Ru^{II}(TTP)(CS(DMF)] is shown in Fig. 3 (for the sake of simplicity the coordinated DMF molecule is not presented directly in Scheme 2). Two separate quasi-reversible electron-transfer processes were observed during the reduction of [Ru^{II}(TTP)(CS)(DMF)] in DMF solution. The proposed mechanism of reduction is described in Scheme 2.

The reaction mechanism involves the conversion of the initial ruthenium thiocarbonyl complex into a thioformyl [Ru^{II}(TTP)(CHS)]$^-$ complex by a $2e^- + H^+$ process as the second reduction step presents characteristic features of a follow-up chemical reaction. The protonation of [Ru(TTP)(CS)]$^{2-}$ is apparent in Fig. 3. The stability of the dianion decreased as the water concentration has been gradually increased. The reversibility is smaller even for sweep rates five times higher in the second case than in the first one. The irreversible oxidation of [Ru(TTP)(CHS)] occurs at a potential more positive than that of the first reduction potential of the parent thiocarbonyl complex according to eq. (1):

$$[Ru(TTP)(CS)] \underset{-e^-,\,-H^+,\,-e^-}{\overset{e^-,e^-,H^+}{\rightleftharpoons}} [Ru(TTP)(CHS)]^- . \quad (1)$$

The thioformyl species undergoes one electron reduction at potentials of its generation. Its re-

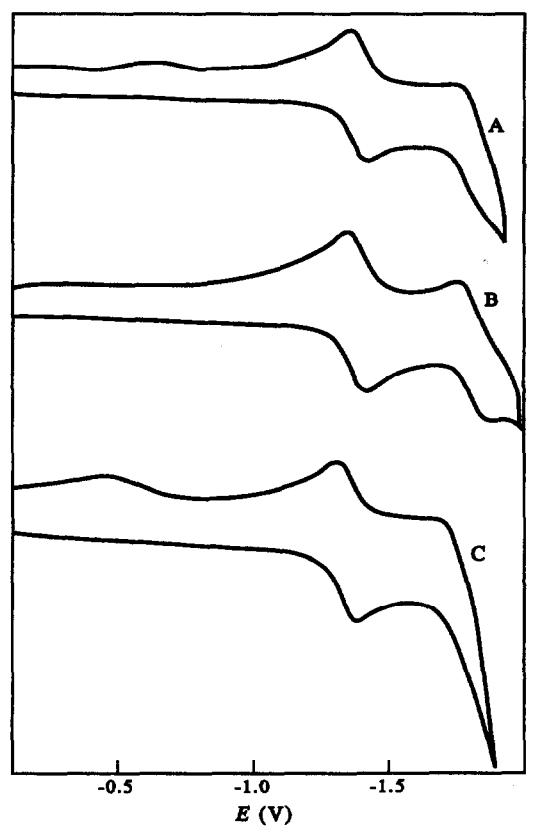

Fig. 3. Cyclic voltammograms of [Ru(TTP)(CS)] in 0.1 M TBAP–DMF; (A) V = 100 (DMF), (B) V = 500 (DMF), and (C) V = 500 mV s^{-1} (DMF with water added).

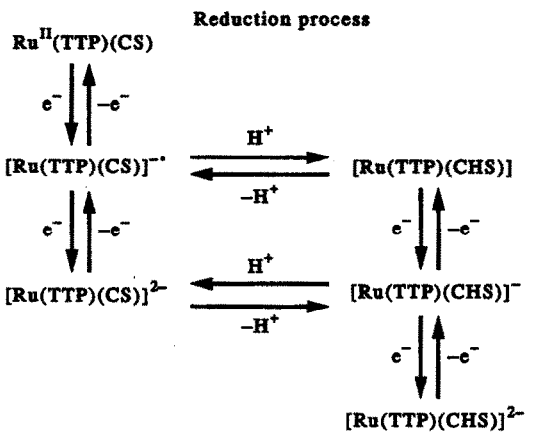

Scheme 2.

oxidation wave ($[Ru(TTP)(CHS)]^{-\cdot}/[Ru(TTP)(CHS)]^{2-}$) is visible at potentials positive to the second electron transfer of the thiocarbonyl species. Potentials for the reduction process of [Ru^{II}(TTP)(CS)(DMF)] and the related complexes are displayed in Table 3. The dependence of the first reduction potential on the nature of the axial ligand (C_2H_5OH, CN^-, pyridine) is presented in Table 4.

Cyclic voltammetry reveals that the reduction mechanism of [Ru(TTP)(CS)] is similar to that of [Fe(TPP)(CS)].[12] It was established that divalent metals present a linear relationship between either the first oxidation or first reduction potential at the ring and the electronegativity of the central metal ion.[33] Since electronegativities of iron and ruthenium are quite close the half-wave potentials for the ring centred process should be the same within 0.1 V for the ruthenium and iron species, as observed. The porphyrin macrocycle of [Ru(TPP)(CS)] is the centre of the first electron addition.

Table 3. Characteristic potentials for the reduction processes in DMF (0.1 TBAP)[a]

System[b]	$a/a^{-\cdot}$	$a^{-\cdot}/a^{2-}$	$b/b^{-\cdot}$	$b^{-\cdot}/b^{2-}$
[Ru(TTP)(CS)]	−1.32	−1.69	−0.55[c]	−1.52[c]
[Fe(TTP)(CS)][d]	−1.31	−1.69	−0.43	−1.79
[Ru(TTP)(CO)]	−1.44	−1.69[e]		

[a] In V vs S.C.E.; values represent $E_{1/2} = (E_{pk} + E_{pa})/2$, unless indicated differently.
[b] a = [M(TTP)(CS)]; b = [M(TTP)(CHS)].
[c] The anodic peak potential at $V = 100$ mV s^{-1}.
[d] From ref. 12.
[e] The cathodic peak potential at $V = 100$ mV s^{-1}.

Table 4. Characteristic potentials of [Ru^{II}(TTP)(CS)L][a]

	Reduction step I	Oxidation step I	Oxidation step II
[Ru^{II}(TTP)(CS)(EtOH)]	−1.40	0.85	1.22
[Ru^{II}(TTP)(CS)(CN)]$^-$	−1.43	0.66	1.12[b]
			1.36[b]
[Ru^{II}(TTP)(CS)(Im)]	−1.47	0.78	1.23[b]
[Ru^{II}(TTP)(CS)(py)]	−1.52	0.82	1.32[b]
[Ru^{II}(TTP)(CO)(EtOH)]	−1.44	0.78	1.19

[a] $E_{1/2}$, in D.C.E. (0.1 M TBAP) vs S.C.E.
[b] Irreversible, $E_{p/2}$ given.

[Ru^{II}(TTP)(CS)] is oxidized in two well separated quasi-reversible electron-transfer steps (Table 4). The product of the first oxidation, [Ru^{II}($TTP^{+\cdot}$)(CS)], is stable and has been characterized chemically and spectroscopically in this paper as the π-cation radical. The mechanism of the oxidation is proposed in the following equations:

$$[Ru^{II}(TTP)(CS)L] \underset{e^-}{\rightleftharpoons} [Ru^{II}(TTP^{+\cdot})(CS)L] \quad (2)$$

$$[Ru^{II}(TTP^{+\cdot})(CS)L] \underset{-e^-}{\overset{e^-}{\rightleftharpoons}}$$

$$[Ru^{III}(TTP^{+\cdot})(CS)L]\{Ru^{II}(TTP^{2+})(CS)L\}. \quad (3)$$

The second oxidation step is chemically irreversible in the presence of CN^-, pyridine or imidazole. The follow-up chemical reaction results in the appearance of an irreversible reduction wave at potentials (0.5–0 V) depending on the ligand. The formation of β-substituted forms or isoporphyrins can be considered to account for this phenomenon[30,34] as typical for porphyrin dications.

As established by Fuhrop *et al.*[35] the difference in $E_{1/2}$ potentials between the first ring oxidation and the first ring reduction is always equal to 2.25 ∓ 0.15 V. The corresponding values for [Ru^{II}(TTP)(CS)L] systems presented in Table 4 are entirely consistent with the proposed electronic structure of the one-electron reduction and one-electron oxidation products, i.e. [Ru^{II}($TTP^{+\cdot}$)(CS)L] and [Ru^{II}($TTP^{-\cdot}$)(CS)L], respectively.

CONCLUSION

Thiocarbonyl and carbonyl ruthenium(II) porphyrin complexes reveal essential similarity as far as chemical and electrochemical properties are concerned, with the exception of internal reactivity of

the thiocarbonyl ligand. We intend to probe the influence of the thiocarbonyl ligand on the formation of highly-oxidized ruthenium porphyrins.

REFERENCES

1. (a) J. P. Collman, J. W. Prodolliet and C. R. Leidner, *J. Am. Chem. Soc.* 1986, **108**, 2916; (b) J. W. Sejler and C. R. Leidner, *Inorg. Chem.* 1990, **29**, 3636.
2. (a) J. T. Groves and R. Quinn, *Inorg. Chem.* 1984, **23**, 3844; (b) J. T. Groves and R. Quinn, *J. Am. Chem. Soc.* 1985, **107**, 5790; (c) J. T. Groves and K.-H. Ahn, *Inorg. Chem.* 1987, **26**, 3831; (d) W.-H. Leung and C.-M. Che, *J. Am. Chem. Soc.* 1989, **111**, 28812.
3. (a) J. P. Collman, P. S. Wagenknecht, R. T. Hembre and N. S. Lewis, *J. Am. Chem. Soc.* 1990, **112**, 1294; (b) J. P. Collman, J. E. Hutchison, P. S. Wagenknecht, N. S. Lewis, M. A. Lopez and R. Guilard, *J. Am. Chem. Soc.* 1990, **112**, 8206.
4. (a) R. F. Hopf and D. G. Whitten, *J. Am. Chem. Soc.* 1976, **98**, 7422; (b) M. J. Camenzind, B. R. James and D. Dolphin, *J. Chem. Soc., Chem. Commun.* 1986, 1137; (c) M. J. Camenzind, B. R. James, D. Dolphin, J. W. Sparapany and J. A. Ibers, *Inorg. Chem.* 1988, **27**, 3054.
5. (a) Ch. Sishta, M. Ke, B. R. James and D. Dolphin, *J. Chem. Soc., Chem. Commun.* 1986, 787; (b) M. Ke, S. J. Rettig, B. R. James and D. Dolphin, *J. Chem. Soc., Chem. Commun.* 1987, 1110; (c) M. Ke, Ch. Sishta, B. R. James, D. Dolphin and J. W. Sparapany, *Inorg. Chem.* 1991, **30**, 4766.
6. N. Rajapakse, B. R. James and D. Dolphin, *Can. J. Chem.* 1990, **68**, 2274.
7. (a) F. R. Hopf, T. P. O'Brien, W. R. Scheidt and D. G. Whitten, *J. Am. Chem. Soc.* 1975, **97**, 277; (b) J. P. Collman, T. J. Barnes, T. J. Collins and P. J. Brothers, *J. Am. Chem. Soc.* 1981, **103**, 7030.
8. A. L. Balch, Y.-W. Chan, M. M. Olmstead, M. W. Renner and F. E. Wood, *J. Am. Chem. Soc.* 1988, **110**, 3897.
9. (a) C. R. Volf, D. Mansuy, W. Nastainczyk, G. Deutschman and V. Ullrich, *Molec. Pharmacol.* 1977, **13**, 698; (b) D. Mansuy, D. Fontecave and J.-C. Chottard, *Biochem. Biophys. Res. Commun.* 1980, **95**, 1536; (c) M. J. Arch, J. K. King, W. Nastainczyk and V. Ullrich, *Biochem. Pharmacol.* 1980, **29**, 2885.
10. (a) R. J. Lukens, *J. Agricult. Food. Chem.* 1966, **16**, 365; (b) R. J. Lukens and H. D. Sisler, *Science* (Washington, DC) 1958, **127**, 650; (c) J. R. De Braun, J. B. Miaullis, J. Knarr, A. Mihailovski and J.-J. Menn, *Xenobiotica* 1974, **4**, 101; (d) A. Peeples and R. R. Dalvi, *Toxicology* 1978, **9**, 341.
11. (a) D. Mansuy, J.-P. Battioni and J.-C. Chottard, *J. Am. Chem. Soc.* 1978, **100**, 4311; (b) J.-P. Battioni, J.-C. Chottard and D. Mansuy, *Inorg. Chem.* 1982, **21**, 2056.
12. (a) J.-P. Battioni, D. Lexa, D. Mansuy and J.-M. Saveant, *J. Am. Chem. Soc.* 1983, **105**, 207; (b) L. A. Bottomley, M. R. Deakin and J.-N. Gorce, *Inorg. Chem.* 1984, **23**, 3563.
13. P. D. Smith, D. Dolphin and B. R. James, *J. Organomet. Chem.* 1981, **208**, 239.
14. R. A. Doyle, L. M. Daniels, R. J. Angelici and F. G. A. Stone, *J. Am. Chem. Soc.* 1989, **111**, 4995.
15. K. Rachlewicz and L. Latos-Grażyński, *Inorg. Chim. Acta* 1988, **144**, 213.
16. A. D. Adler, F. R. Longo, F. Karplus and J. Kim, *J. Inorg. Nucl. Chem.* 1970, **32**, 2443.
17. A. D. Boersma and H. M. Goff, *Inorg. Chem.* 1982, **21**, 581.
18. J. J. Bonnet, S. S. Eaton, G. R. Eaton, R. H. Holm and J. A. Ibers, *J. Am. Chem. Soc.* 1973, **95**, 2141.
19. J. P. Collman, C. E. Barnes, P. J. Brothers, T. J. Collins, T. Ozawa, J. C. Gallucci and J. A. Ibers, *J. Am. Chem. Soc.* 1984, **106**, 5151.
20. M. Mąkosza and M. Fedoryński, *Synthesis* 1974, 274.
21. (a) P. Gans, J.-C. Marchon, C. A. Reed and J.-R. Regnard, *Nouv. J. Chim.* 1981, **5**, 203; (b) W. F. Scholtz, C. A. Reed, Y.-J. Lee, W. R. Scheidt and G. Lang, *J. Am. Chem. Soc.* 1982, **104**, 6791; (c) G. Buisson, A. Deronzier, E. Duee, P. Gans, J.-C. Marchon and J.-R. Regnard, *J. Am. Chem. Soc.* 1982, **103**, 6793; (d) M. A. Phillippi and M. H. Goff, *J. Am. Chem. Soc.* 1982, **104**, 6026; (e) M. H. Goff and M. A. Phillippi, *J. Am. Chem. Soc.* 1983, **105**, 7567; (f) A. L. Balch, L. Latos-Grażyński and M. W. Renner, *J. Am. Chem. Soc.* 1985, **107**, 2983; (g) P. Ganz, G. Buisson, E. Duee, J.-C. Marchon, B. C. Erler, W. F. Scholz and Ch. A. Reed, *J. Am. Chem. Soc.* 1986, **108**, 1223; (h) I. Morishima, Y. Shiro and K. Nakijama, *Biochemistry* 1986, **25**, 3576; (i) I. Morishima, Y. Shiro and Y. Takamuki, *J. Am. Chem. Soc.* 1983, **105**, 6168; (j) 1984, **106**, 7666.
22. J. Lisowski, M. Grzeszczuk and L. Latos-Grażyński, *Inorg. Chim. Acta* 1989, **161**, 153.
23. (a) D. Mansuy, J.-P. Bationi and J.-C. Chottard, *J. Am. Chem. Soc.* 1978, **100**, 4311; (b) J. W. Buchler, W. Kokisch, P. D. Smith and B. Tonn, *Z. Naturforsch. B* 1978, **33B**, 1371.
24. (a) M. C. Baird, G. Hartwell and G. Wilkinson, *J. Chem. Soc. A* 1967, 2037; (b) M. Yagupsky and G. Wilkinson, *J. Chem. Soc. A* 1968, 2813; (c) A. E. Fenster and I. S. Butler, *Can. J. Chem.* 1972, **30**, 598; (d) G. Jauoen and R. Dabard, *J. Organomet. Chem.* 1974, **72**, 598; (e) M. Herberhold and M. Suess-Fink, *Chem. Ber.* 1978, **111**, 2273; (f) M. Herberhold and P. D. Smith, *Angew. Chem., Int. Edn Engl.* 1979, **18**, 63.
25. R. Steudel, *Z. Naturforsch. B* 1966, **21**, 1106.
26. L. S. Butler, A. Garcia-Rodriguez, K. R. Plowman and C. F. Shaw III, *Inorg. Chem.* 1976, **15**, 2602.
27. J. W. Buchler, W. KoKisch and P. D. Smith, *Struct. Bonding* 1978, **34**, 79.
28. S. Ariel, D. Dolphin, G. Domazetis, B. R. James, T. W. Leung, S. J. Rettig, J. Trotter and G. M. Williams, *Can. J. Chem.* 1984, **62**, 755.
29. (a) L. Busetto and A. Palazzi, *Inorg. Chim. Acta*

1976, **19**, 233; (b) B. D. Dombek and R. J. Angelici, *Inorg. Chem.* 1976, **15**, 2403; (c) B. D. Dombek and R. J. Angelici, *J. Am. Chem. Soc.* 1976, **98**, 4110.

30. (a) H. J. Schine, A. G. Padilla and S.-M. Wu, *J. Org. Chem.* 1979, **44**, 4069; (b) A. Małek, L. Latos-Grażyński, T. J. Bartczak and A. Żadło, *Inorg. Chem.* 1991, **30**, 3222.
31. Kunihisa Yoshida, in *Electrooxidation in Organic Chemistry*, p. 85. John Wiley and Sons, New York (1984).
32. K. Rachlewicz and L. Latos-Grażyński, *Inorg. Chem.*, submitted.
33. L. Pauling, in *The Nature of the Chemical Bond*, 3rd edn, p. 93. Cornell University, New York (1960).
34. K. M. Kadish and R. K. Rhodes, *Inorg. Chem.* 1981, **20**, 2961.
35. (a) K. M. Kadish, D. G. Davis and J.-H. Fuhrfop, *Angew. Chem.* 1972, **84**, 1072; (b) J.-H. Fuhrfop, K. M. Kadish and D. G. Davis, *J. Am. Chem. Soc.* 1973, **95**, 5140.

Polyhedron Vol. 12, No. 7, pp. 831–834, 1993
Printed in Great Britain

0277-5387/93 $6.00+.00
© 1993 Pergamon Press Ltd

COMPLEX OF COPPER(II) WITH 5,5,7,12,14-HEXAMETHYL-1,4,8,11-TETRAAZACYCLOTETRADECANE-1,8-DIACETIC ACID: SYNTHESIS, STRUCTURE AND KINETICS OF FORMATION

V. K. BELSKY and N. R. STRELTSOVA

Karpov Physico-Chemical Institute, 103064 Moscow, Russia

and

E. N. KUZMINA and A. Y. NAZARENKO*

Shevchenko University, 252017 Kiev, Ukraine

(*Received* 5 *April* 1991; *accepted* 12 *October* 1992)

Abstract—The molecular structure of the copper complex with title ligand has been determined by X-ray diffraction. It shows a slightly distorted tetragonal bipyramidal coordination of the copper ion. The macrocycle is coordinated in a planar configuration and two carboxylic groups are in a *trans* arrangement. The unusually high activation energy (*ca* 200 kJ mol^{-1}) was measured for second-order complex formation reactions in aqueous solution.

In recent years the metal ion reactions with macrocyclic ligands containing additional ligating groups have been widely studied.[1–5] The kinetics of metal complex formation with such ligands have also been measured.[3–5] Nevertheless, the rate constants and activation energies are known only for a few complexes. The goal of this work is the study of the structure and kinetics of the synthesis of a copper complex with disubstituted tetraazacycloalkane-5,5,7,12,12,14-hexamethyl-1,4,8,11-tetraazacyclotetradecane-1,8-diacetatic acid (H_2TEDA). Metal complexes of TEDA with Cu^{2+}, Co^{2+} and Ni^{2+} solvated with HBr molecules were synthesized and the structure of the NiTEDA · HBr · H_2O complex has been investigated by X-ray diffractometry.[6]

EXPERIMENTAL

IR spectra were recorded as Nujol mulls or potassium bromide pellets on a UR-10 spectrometer. Magnetic susceptibility was measured by Gouy's method.

The free ligand was prepared by standard procedures[6] as H_2TEDA · 2HBr · $8H_2O$ and characterized using IR and NMR spectra.

* Author to whom correspondence should be addressed.

Preparation of CuTEDA · $4H_2O$

Copper acetate, $Cu(CH_3COO)_2 \cdot 2H_2O$ (0.185 g, 1.3 mmol) and H_2TEDA · 2HBr · $8H_2O$ (0.708 g, 1.0 mmol) were dissolved in methanol. The pH was increased to 3 by the addition of sodium acetate and the solution was heated for 2–3 h under reflux. The dark blue solution was acidified by the dropwise addition of trichloroacetic acid until the light blue precipitate appeared. The resulting blue crystals were crystallized from methanol (IR: 1705 cm^{-1}). After heating under reflux for 5 h in ethanol–water solution, for the decomposition of the trichloroacetic acid, blue crystals of tetrahydrate were obtained (IR: 1608 cm^{-1}). Found: Cu, 12.8; N, 11.1. Calc. for $CuC_{20}H_{38}N_4O_4 \cdot 4H_2O$: Cu, 12.8; N, 11.2%. μ_{eff} = 1.93 B.M.

Preparation of CuTEDA · $2CCl_3COOH$

This compound was prepared using the procedure above, but in aqueous solution. A light blue precipitate formed after trichloroacetic acid addition and was filtered and dried in air. Found: Cu, 8.4; N, 7.4; Cl, 28.1. Calc. for $CuC_{20}H_{38}N_4O_4 \cdot 2CCl_3COOH$: Cu, 8.1; N, 7.1; Cl, 27.1%.

Kinetic measurements

The kinetics of H_2TEDA reaction with Cu^{2+} ions were measured spectrophotometrically ($\lambda = 602$ nm) in a thermostated cell. Sodium acetate buffer solutions (pH = 5–6.8) were used. The reactions were made with equal initial concentrations of copper ions and ligand (C = 3–6 mM).

Crystallography

A blue crystal suitable for X-ray study was grown from acetonitrile–ethanol. The complex crystallizes in the triclinic space group with the unit cell parameters $a = 9.009(2)$, $b = 8.936(2)$, $c = 9.846(2)$ Å, $\alpha = 101.86(2)$, $\beta = 101.86(2)$, $\gamma = 116.63(2)°$; $V = 629.1(4)$ Å^3; $\rho_{calc} = 1.40$ g cm^{-3}; structural class $\bar{P}_1$, $z = 1$ ($\bar{1}$; 1; 1).

Experimenal data were collected on a four-circle Nicolet P3 diffractometer using Mo-K_α radiation with a β-filter and θ–2θ scan technique. 1628 independent reflections were collected to $2\theta_{max} = 45°$. No absorption correction was made ($\mu = 9.6$ cm^{-1}). The structure was solved by the heavy-atom method with further refinement using full-matrix least-squares using 1511 reflections with $I \geqslant 3\sigma(I)$. All non-hydrogen atom positions were refined in the anisotropic approximation. Hydrogen atoms of the macrocycle and water molecules were localized from the difference-Fourier map and refined in the isotropic approximation. The final values of R factors are $R = 0.029$, $R_w = 0.033$ ($S = 1.97$).

RESULTS AND DISCUSSION

Formation of CuTEDA *complexes*

The experimental data confirm the second-order rate equation:

$$\frac{d[CuTEDA]}{dt} = k_{eff}[Cu][TEDA];$$

where k_{eff} is an effective rate constant (Fig. 1). The k_{eff} value slightly increases with pH over the range 5–7. The observed k_{eff} values (*ca* 3×10^{-3} M^{-1} s^{-1}, 25°C, pH 6) are much lower than those for *meso*-Me_6[14]aneN$_4$ under similar conditions (2×10^{-2} M^{-1} s^{-1}, 25°C, pH 4.7[7]). This observation contradicts the previously observed phenomenon[1,5] that the rate constants of functionalized macrocycles are 10^3–10^4 times larger than those of the unsubstituted macrocycles.

The temperature dependence of the effective rate constants is shown in Fig. 2 as an Arrhenius plot. The activation energy calculated from the least-squares fit to the data is 200 kJ mol^{-1}. This value

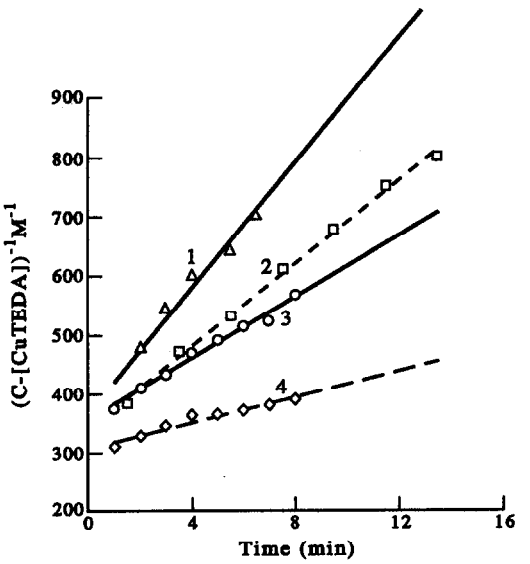

Fig. 1. The typical kinetic data. $C_{Cu} = C_{TEDA} = 3.35$ mM. (1) pH = 6.3, T = 48°C; (2) pH = 6.4, T = 40°C; (3) pH = 5.4, T = 40°C; and (4) pH = 5.1, T = 38°C.

is twice as high as that for the *meso*-Me_6[14]aneN$_4$ complex (93 kJ mol^{-1}).[8] An unusually high activation energy may be explained by the superposition of several effects: (1) The multistage nature of the complex formation reaction. The total activation energy is the sum of several contributions. (2) The ligand deprotonation reaction. An active form of the ligand is probably partly deprotonated (ΔH value for the deprotonation reaction is *ca* 30–50 kJ mol^{-1}). (3) The significant steric effects: the distortion of ligand geometry increases the energy of the transition state for the ligands with a large number of substituents.

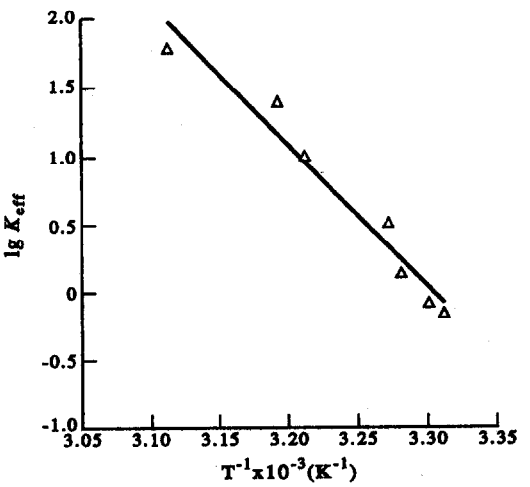

Fig. 2. The temperature dependence of the second-order formation rate constant k_{eff} as an Arrhenius plot.

Table 1. Hydrogen bond distances (Å) and angles (°)

D—H···A	D—H	H—A	D—A	∠DHA
O(W1)—H(11)···O(1)	0.86	1.98	2.83	167
O(W1)—H(W12)···O(2)	0.92	1.90	2.82	174
O(W2)—H(W1)···O(W1)	0.85	2.18	2.96	153
O(W2)—H(W22)···O(1)	0.82	2.02	2.81	166

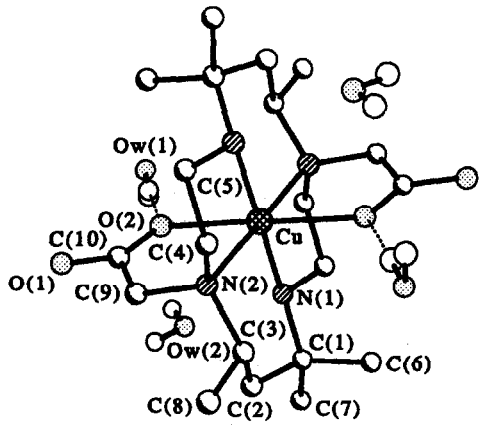

Fig. 3. The molecular structure of the copper complex with 5,5,7,12,12,14-hexamethyl-1,4,8,11-tetraazacyclotetradecane-1,8-diacetic acid.

Description of the structure

In the crystal cell the molecular complex CuTEDA is connected by a system of hydrogen bonds via water molecules. The hydrogen bond parameters are collected in Table 1.

The copper ion has a slightly distorted tetragonal bipyramidal coordination (Fig. 3). Unlike the nickel complex with the same ligand, the carboxylic groups are coordinated in a *trans* arrangement. This fact contradicts the suggestion[6] that the *cis* structure is attributed to the stereochemical pattern of the ligand. The Cu—N distances (Table 2) are typical for copper complexes with secondary (2.00–2.05) and tertiary (2.05–2.10) amines.[9] The Cu—N (secondary) distance is shorter than that of Cu—N (tertiary), unlike the NiTEDA complex. The Jahn–

Table 2. Main bond lengths (Å) and bond angles (°) in the complex CuTEDA·$2H_2O$

Bond	*d* (Å)	Angle	w (°)
Cu—N(1)	2.070(3)	N(1)—Cu—N(2)	93.6(1)
Cu—N(2)	2.094(3)	N(2)—Cu—N(1a)	86.4(1)
O(1)—C(10)	1.257(6)	O(2)—Cu—N(1)	84.9(1)
O(2)—C(10)	1.249(6)	O(2)—Cu—N(2)	79.4(1)
N(1)—C(1)	1.513(5)	C(1)—N(1)—C(5a)	114.5(4)
N(2)—C(3)	1.514(5)	C(3)—N(2)—C(4)	109.6(3)
N(2)—C(4)	1.498(5)	C(3)—N(2)—C(9)	112.0(2)
N(2)—C(9)	1.496(5)	C(4)—N(2)—C(9)	109.9(3)
C(1)—C(2)	1.522(7)	N(1)—C(1)—C(2)	107.5(3)
C(1)—C(6)	1.530(6)	N(1)—C(1)—C(6)	112.0(2)
C(1)—C(7)	1.531(5)	C(2)—C(1)—C(6)	110.7(4)
C(2)—C(3)	1.530(6)	N(1)—C(1)—C(7)	109.8(3)
C(3)—C(8)	1.531(8)	C(2)—C(1)—C(7)	108.2(3)
C(4)—C(5)	1.506(6)	C(6)—C(1)—C(7)	108.5(4)
C(9)—C(10)	1.524(7)	C(1)—C(2)—C(3)	118.7(3)
		N(2)—C(3)—C(2)	112.0(4)
		N(2)—C(3)—C(8)	112.3(4)
		C(2)—C(3)—C(8)	110.5(3)
		N(2)—C(4)—C(5)	110.1(4)
		O(1)—C(10)—O(2)	126.4(5)
		O(1)—C(10)—C(9)	113.7(4)
		O(2)—C(10)—C(9)	119.9(4)
		N(2)—C(9)—C(10)	116.1(3)

Table 3. Main torsion angles in the macrocycle of the complex CuTEDA · $2H_2O$

N(1a)—C(5)—C(4)—N(2)	−59.4	C(5)—C(4)—N(2)—C(3)	166.8
C(4)—N(2)—C(3)—C(2)	172.3	N(2)—C(3)—C(2)—C(1)	76.4
C(3)—C(2)—C(1)—N(1)	−65.2	C(2)—C(1)—N(1)—C(5a)	179.2
C(1)—N(1)—C(5a)—C(4a)	173.0		

Teller effect probably causes the increase in the Cu—O distance to 2.31 Å; Ni—O distances in the same complex are 2.19 and 2.07 Å. The *d*(Cu—O) value is consistent with those observed for copper alkylcarboxylates with "long" Cu—O bonds (2.30–2.40 Å).[9] The average interatomic distances and angles in the macrocycle ring are also similar to those for copper macrocyclic complexes:[10–12] *d*(C—C) = 1.526, *d*(C—N) = 1.513 Å.

The torsion angles of the C—C bonds correspond to a *gauche* conformation and C—N bonds to *trans* (Table 3).

The five-membered ring formed by the ethylenediamine residue and the copper atom has an envelope conformation with a C_4 atom in the flap and with a flap angle equal to 51° ($\Delta_{max} = \pm 0.05$ Å, $\Delta C_4 = -0.66$ Å). The six-membered ring $CuN_1N_2C_1C_2C_3$ has a chair conformation. The maximum deviation of atoms from the plane $N_1N_2C_1C_3$ is 0.05 Å, while the deviations of Cu and C_2 atoms are −0.83 and 0.69 Å, respectively. The C—O bond lengths in the acetate fragment are the same within experimental error. The aminoacetate five-membered chelate ring is nearly planar, the maximum deviation of atoms from the plane is less than 0.04 Å.

IR spectra

The *v*(C=O) band position is similar to those in copper glycinate (1593 and 1607 cm^{-1}).[13] The hydrogen bonding N—H···O causes a slight shift of the N—H band (3190 cm^{-1}) from the usual position for *meso*-Me_6[14]aneN_4 complexes (*ca* 3200 cm^{-1}).

REFERENCES

1. T. A. Kaden, *Top. Curr. Chem.* 1984, **121**, 157.
2. P. V. Bernhardt and G. A. Lawrance, *Coord. Chem. Rev.* 1990, **104**, 297.
3. T. A. Kaden, *Helv. Chim. Acta* 1971, **57**, 2307.
4. D. A. Buckingham, C. R. Clark and W. S. Webley, *J. Chem. Soc., Chem. Commun.* 1981, 192.
5. S. P. Kasprzyk and R. G. Wilkins, *Inorg. Chem.* 1982, **21**, 3349.
6. X. Ji-De, N. Shi-Sheng and L. Yu-Juan, *Inorg. Chim. Acta* 1986, **111**, 61.
7. D. K. Cabbiness and D. W. Margerum, *J. Am. Chem. Soc.* 1970, **92**, 2151.
8. R. W. Hay and C. R. Clark, *J. Chem. Soc., Dalton. Trans.* 1977, 1148.
9. A. G. Orpen, L. Brammer, F. H. Allen, O. Kennard, D. G. Watson and R. Taylor, *J. Chem. Soc., Dalton Trans.* 1989, S1.
10. R. Clay, J. Murray-Rust and P. Murray-Rust, *J. Chem. Soc., Dalton Trans.* 1979, 1135.
11. E. Ochiai, S. J. Rettig and J. Troffer, *Can. J. Chem.* 1978, **56**, 267.
12. T. J. Lee, H. Y. Lee, C. S. Lee and C. S. Chung, *Acta Cryst.* 1984, **C40**, 641.
13. K. Nakamoto, Y. Murito and A. E. Martell, *J. Am. Chem. Soc.* 1961, **83**, 4528.

Polyhedron Vol. 12, No. 7, pp. 835–845, 1993
Printed in Great Britain

0277–5387/93 $6.00+.00
© 1993 Pergamon Press Ltd

REACTIONS OF A DINUCLEAR COPPER(I) COMPLEX DERIVED FROM A HEXADENTATE LIGAND HAVING N_2As_4 DONOR SITES. CRYSTAL STRUCTURE OF $[Cu_2(BDAE)(PPh_3)_2Cl_2]$

PARIMAL PAUL* and K. VENKATASUBRAMANIAN

Discipline of Coordination Chemistry and Homogeneous Catalysis,
Central Salt and Marine Chemicals Research Institute, Bhavnagar 364 002, India

(*Received* 11 *June* 1992; *accepted* 1 *October* 1992)

Abstract—The reactions of a tri-coordinate dinuclear copper(I) complex of the composition $[Cu_2(BDAE)](ClO_4)_2$ (where BDAE = α,α′-bis{bis[2-(diphenylarsino)ethyl]amino}ethane) with some mono- and bidentate species having different donor atoms were studied. The reaction of the complex with anionic species such as LiCl, NaN_3, NH_4NCS and $NaBH_4$ resulted in the formation of tetra-coordinate complexes of compositions $[Cu_2(BDAE)Cl_2]$, $[Cu_2(BDAE)(N_3)](ClO_4)$, $[Cu_2(BDAE)(NCS)](ClO_4)$ and $[Cu_2(BDAE)(BH_4)_2]$, respectively. The reactions of CS_2 and thiourea gave the products $[Cu_2(BDAE)(CS_2)_2](ClO_4)_2$ and $[Cu_2(BDAE)(H_2NCSNH_2)_2](ClO_2)_2$, respectively. The reactions of monodentate neutral molecules B (B = PPh_3, $AsPh_3$ and imidazole) yielded complexes of the composition $[Cu_2(BDAE)(B)_2](ClO_4)_2$. The reaction with pyridine in a 1:4 molar ratio gave a complex of composition $[Cu_2(BDAE)(C_5H_5N)_4](ClO_4)_2$. The bidentate ligands 1,2-bis(diphenylphosphino)methane/ethane (dppm/dppe) react with the complex to yield complexes of the composition $[Cu_2(BDAE)(dppm)](ClO_4)_2$/$[Cu_2(BDAE)(dppe)](ClO_4)_2$, in which dppm/dppe acts as a bridge between two metal centres. The reaction with bipyridine gave a tetra-coordinate complex of the composition $[Cu_2(BDAE)(C_{10}H_8N_2)_2](ClO_4)_2$. The molecular structure of the complex $[Cu_2(BDAE)(PPh_3)_2Cl_2]$ was established by single-crystal X-ray diffraction. The cyclic voltammetric behaviour of all of these complexes was investigated.

The chemistry of copper(I) with tertiary phosphine and arsine donors has gained much importance because of their interesting structural properties,[1–5] photochemistry,[6–8] reactions with small molecules[9–11] and catalytic activity.[12–14] In most of these studies tertiary phosphine is mainly used as the ligand, whereas the chemistry of copper(I) with tertiary arsine is less extensive. Although some examples are available in the literature,[1,15–18] they are mainly concerned with monodentate tertiary arsine and their chemistry is restricted to structural investigation.

We were interested to explore copper(I) chemistry with binucleating ligands having tertiary phosphine and arsine donors and some of these studies have been reported recently.[19–22] These ligands have some advantages: due to the π-acidic nature of the donors stable complexes with copper(I) can be formed, and because of the chelating effect they prevent the dissociation of the M—P/As bonds thus limiting the number of available coordination sites for reactivity studies.

We report herein the reactions of a tri-coordinate dinuclear copper(I) complex of the ligand α,α′-bis{bis[2-(diphenylarsino)ethyl]amino}ethane (BDAE) with a variety of mono- and bidentate nucleophiles, which resulted in the formation of tetra-coordinate mixed-ligand dinuclear complexes. The crystal structure of the complex $[Cu_2(BDAE)(PPh_3)_2Cl_2]$ is reported. The cyclic voltammetric behaviour of these complexes is also reported.

EXPERIMENTAL

Physical measurements

Elemental analyses were performed on a Carlo-Erba Elemental Analyser Model 1106. A digisun

* Author to whom correspondence should be addressed.

electronics digital conductivity meter model D1-909 was used for the conductivity measurements. IR spectra were recorded on a Carl Zeiss Specord M80 spectrometer as KBr pellets. ^1H and $^{31}P\{^1H\}$ NMR spectra were recorded on a Jeol FX-100 FT NMR spectrometer. For ^1H tetramethylsilane was used as an external reference and the instrument operated at 99.55 MHz. The $^{31}P\{^1H\}$ NMR spectra were recorded at 40.27 MHz using 10 mm tubes with a capillary of deuterium oxide for the internal lock and 85% H_3PO_4 as an external standard. A Princeton Applied Research (PAR) electrochemical instrument equipped with a precision *X–Y* recorder and a PAR-175 universal programmer coupled with the PAR-174A analyser was used along with a glassy carbon working electrode for recording the cyclic voltammograms. All potentials were measured against a standard calomel electrode (S.C.E.) at 25 ± 1°C using tetrabutylammoniumperchlorate as the supporting electrolyte with scan rates from 50 to 200 mV s^{-1}.

Materials

The ligand BDAE was synthesized by a procedure described previously.[19] The compounds $[Cu(PPh_3)_3Cl]$[23] and $[Cu(NCCH_3)_4](ClO_4)$[24] were prepared by published procedures. Lithium chloride, sodium azide, ammonium thiocyanate, sodium tetrahydroborate, triphenylphosphine, triphenylarsine, 1,2-bis(diphenylphosphino)ethane/methane, bipyridine and imidazole were obtained from Aldrich Chemical Co. Pyridine and carbon disulphide were purchased from S.D. Fine Chemicals and thiourea from Sarabhai M. Chemicals (India).

All organic solvents used were of reagent grade and were purified and dried before use. All the preparations were carried out under dry nitrogen or argon.

Synthesis of the complexes

$[Cu_2(BDAE)(PPh_3)_2Cl_2]$ (**1**). To a boiling solution of $[Cu(PPh_3)_3Cl]$ (0.5 mmol) in dry acetone (40 cm^3) BDAE (0.25 mmol) dissolved in benzene (10 cm^3) was added dropwise and refluxing continued for 4 h. The white compound which separated during reflux was isolated by filtration, washed with benzene and acetone and recrystallized from a chloroform–ethanol (2 : 1) mixture; yield 75%.

$[Cu_2(BDAE)](ClO_4)_2$ (**2**). To a refluxing solution of $[Cu(NCCH_3)_4]$ (0.5 mmol) in acetone (25 cm^3) BDAE (0.25 mmol) dissolved in benzene (5 cm^3) was added dropwise and refluxing continued for 3 h. The volume of the solution thus obtained was reduced to *ca* 10 cm^3 by rotary evaporation and after adding diethyl ether (15 cm^3) the white compound which precipitated was isolated by filtration and recrystallized from acetonitrile–ethanol (2 : 1); yield 70%.

$[Cu_2(BDAE)Cl_2]$ (**3**), $[Cu_2(BDAE)(N_3)](ClO_4)$ (**4**), $[Cu_2(BDAE)(NCS)](ClO_4)$ (**5**) *and* $[Cu_2(BDAE)(BH_4)_2]$ (**6**). To a solution of complex **2** (0.62 g, 0.5 mmol) in acetone (30 cm^3) was added solid LiCl (0.085 g, 2 mmol)/NaN_3 (0.033 g, 0.5 mmol)/NH_4NCS (0.038 g, 0.5 mmol), or an ethanolic solution (5 cm^3) of $NaBH_4$ (0.15 g, 4 mmol), and the reaction mixture was refluxed for 4 h, except in the case of $NaBH_4$ where it was stirred for 2 h at room temperature. For complexes **3** and **6** during the reactions the white compounds were precipitated and were isolated by filtration, washed with water and acetone. For complexes **4** and **5** the volume of the solution was reduced to 10 cm^3 and white compounds separated after the addition of diethyl ether. Compounds **3** and **6** were recrystallized from DMF–ethanol (1 : 5) and **4** and **5** from a dichloromethane–ethanol (3 : 1) mixture; yield 70–80%.

$[Cu_2(BDAE)(CS_2)_2](ClO_4)_2$ (**7**). To a solution of complex **2** (0.62 g, 0.5 mmol) in acetone (30 cm^3) was added carbon disulphide (5 cm^3) and the mixture stirred for 10 h at room temperature. The solution was then concentrated to 0.5 cm^3 and diethyl ether was added. The light yellow solid which separated was isolated by filtration and recrystallized from dichloromethane–n-hexane; yield 90%.

$[Cu_2(BDAE)(H_2NCSNH_2)_2](ClO_4)_2$ (**8**). An aqueous solution (2 cm^3) of thiourea (0.11 g, 1.5 mmol) was added dropwise to a solution of complex **2** (0.62 g, 0.5 mmol) in acetone (30 cm^3) with stirring at room temperature. After complete addition stirring was continued for 2 h, during which time a white compound was deposited. The compound was isolated by filtration, washed with water and acetone and finally recrystallized from hot DMF; yield 75%.

$[Cu_2(BDAE)(PPh_3)_2](ClO_4)_2$ (**9**), $[Cu_2(BDAE)(AsPh_3)_2](ClO_4)_2$ (**10**), $[Cu_2(BDAE)(dppm)](ClO_4)_2$ (**11**) *and* $[Cu_2(BDAE)(dppe)](ClO_4)_2$ (**12**). To a solution of complex **2** (0.31 g, 0.25 mmol) in acetone (20 cm^3) was slowly added $PPh_3/AsPh_3$ (0.5 mmol) or dppm/dppe (0.25 mmol) dissolved in dichloromethane (10 cm^3) through a pressure equalizer and the solution was refluxed for 4 h. The solvent of the reaction mixture was removed by rotary evaporation and the white solid washed with diethyl ether, dissolved in dichloromethane (5 cm^3), filtered and to the filtrate n-hexane was added slowly with stirring. The white compound which deposited was

isolated by filtration and dried *in vacuo*; yield 75–80%.

$[Cu_2(BDAE)(C_3H_4N_2)_2](ClO_4)_2$ (**13**) *and* $[Cu_2(BDAE)(C_{10}H_8N_2)_2](ClO_4)_2$ (**14**). Complexes **13** and **14** were prepared following the same procedures as described for complexes **9–12**. In this case complexes were recrystallized from dichloromethane–ethanol; yield 80–85%.

$[Cu_2(BDAE)(C_5H_5N)_4](ClO_4)_2$ (**15**). An alcoholic solution (10 cm^3) of pyridine (0.24 g, 3 mmol, obtained by dilution of a concentrate solution) was added slowly through a pressure equalizer to a solution of **2** (0.62 g, 0.5 mmol) in acetone (25 cm^3) and the solution was refluxed for 2 h. The assembly was then connected to a vacuum line and the solution was concentrated to *ca* 5 cm^3, allowed to reach room temperature and then deaerated diethyl ether (25 cm^3) was added slowly with stirring. The pale yellow compound which separated was isolated by filtration, washed with diethyl ether and dried *in vacuo*; yield 70%.

X-ray structure determination of $[Cu_2(BDAE)(PPh_3)_2Cl_2]$ (**1**)

Preliminary data on space group and unit cell dimensions, as well as intensity data, were collected using a crystal of suitable size on an Enraf–Nonius CAD4/PDP-11/73 system with graphite monochromatized Cu-K_α radiation in the 2θ range 4–130°. Accurate cell dimensions were obtained by a least-squares fit of 25 arbitrarily chosen higher-order reflections ($30° \leqslant 2\theta \leqslant 32°$). Data were collected using the $\omega/2\theta$ scan method and monitoring two sets of three control reflections to correct for decay and alignment during the entire data collection process. The intensities were corrected for Lorentz and polarization factors. An empirical absorption correction method[25] was employed using three reflections near $\chi = 90°$. The structure was solved by the heavy atom method. An origin-removed sharpened three-dimensional Patterson map gave the positions of both the arsenic atoms in the molecule. The cycle of isotropic least-squares refinement, followed by a difference map gave the locations of the copper, chlorine and phosphorus atoms. All the non-hydrogen atoms could be located from a difference map, phased on the other heavy-atoms. Hydrogen atoms were either generated by stereochemical constraints or from a difference map, after the complete convergence of anisotropic refinement of non-hydrogen atoms. Anisotropic refinement of the non-hydrogen atoms was by full-matrix refinement using ORFLS with two blocks with hydrogen fixed. A unit-weighting scheme with a Dunitz–Seiler factor[26] resulted in convergence. At the end of the refinement the shifts-to-error ratio was less than 0.10. The scattering factors for copper, arsenic, chlorine, phosphorus, oxygen, carbon and nitrogen were taken from the International Tables of Crystallography[27] while those of hydrogen were from Stewart *et al.*[28] All the computations were carried out using the SDP package of the Enraf–Nonius system with a PDP-11/73.[29] The final R and Rw values were calculated using the equations $R = \Sigma||F_o|-|F_c||/|F_o|$ and $Rw = [\Sigma w(|F_o|-|F_c|)^2/wF_o^2]^{1/2}$. For relevant crystallographic data and structure solution parameters, see later.

RESULTS AND DISCUSSION

Complex **1**, $[Cu_2(BDAE)(PPh_3)_2Cl_2]$, obtained by the reaction of $Cu(PPh_3)_3Cl$ with BDAE was characterized by single-crystal X-ray diffraction (discussed later). The reaction of $[Cu(NCCH_3)_4](ClO_4)$ with BDAE resulted in the formation of a dinuclear complex of composition $[Cu_2(BDAE)](ClO_4)_2$ (**2**), in which copper(I) is tricoordinate with ligation to two arsine and a nitrogen of the ligand (Scheme 1).[19] The reactions of this coordinately unsaturated complex (**2**) were studied with various nucleophiles in different molar ratios.

The reactions of complex **2** with LiCl and $NaBH_4$ in a 1:2 molar ratio resulted in the complete displacement of perchlorate with the formation of tetra-coordinate dinuclear complexes of compositions $[Cu_2(BDAE)Cl_2]$ (**3**) and $[Cu_2(BDAE)(BH_4)_2]$ (**6**), respectively. The reactions of **2** with NaN_3 and NH_4NCS in a 1:1 molar ratio gave the products $[Cu_2(BDAE)(X)](ClO_4)$ [X = N_3 (**4**) and NCS (**5**)]. The reaction of **2** with excess CS_2 yielded a complex of composition $[Cu_2(BDAE)(CS_2)_2](ClO_4)_2$ (**7**). The reaction of thiourea, PPh_3, $AsPh_3$, imidazole and bipyridine (B) with **2** in the 1:2 molar ratio yielded complexes of the composition $[Cu_2(BDAE)(B)](ClO_4)_2$ (**8–10**, **13** and **14**). The reactions with the bidentate ligands dppm and dppe in a 1:2 molar ratio resulted in the partial displacement of the ligand DBAE, but with a 1:1 molar ratio yielded complexes of composition $[Cu_2(BDAE)(Z)](ClO_4)_2$ [where Z = dppm (**11**) and dppe (**12**)]. This difference can be attributed to the steric effect; with a 1:2 molar ratio two PPh_2 groups of dppm/dppe have to coordinate to a single copper(I) atom and such a situation creates severe steric overcrowding with either phenyl rings of the two AsP_2 and two PPh_2 groups around the metal ion. Therefore, Cu—As bond dissociation takes place as the Cu—P bond is stronger than the Cu—As bond. In the case of a 1:1 molar ratio dppm/dppe can act as a bridge between two

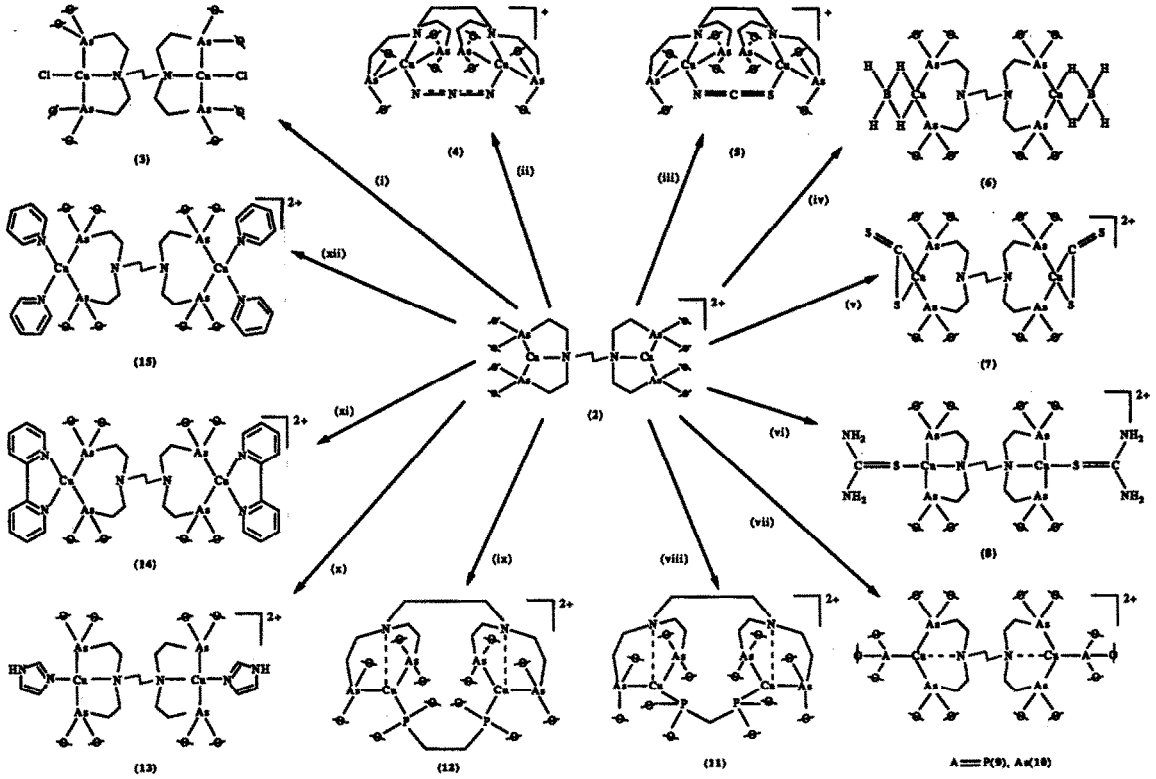

Scheme 1. (i) LiCl; (ii) NaN_3; (iii) NH_4NCS; (iv) $NaBH_4$; (v) CS_2; (vi) $(NH_2)_2CS$; (vii) $PPh_3/AsPh_3$; (viii) dppm; (ix) dppe; (x) imidazole; (xi) bipyridine; (xii) pyridine.

copper(I) centres, as found in many other cases.[30,31] Here, only one PPh_2 of dppm/dppe coordinates to copper(I), which decreases steric overcrowding and stable complexes are formed. In the case of pyridine with a 1 : 2 molar ratio a pure compound could not be isolated, but with a 1 : 4 molar ratio the complex $[Cu_2(BDAE)(C_5H_5N)_4](ClO_4)_2$ was obtained. All these reactions are summarized in Scheme 1. The compositions of all the complexes were confirmed by elemental analyses (Table 1). They are dia-

Table 1. Analytical data for the complexes[a]

Complex	Analysis (%) C	H	N
$[Cu_2(BDAE)(PPh_3)_2Cl_2]$ (1)	62.1(62.4)	5.1(5.0)	1.4(1.6)
$[Cu_2(BDAE)](ClO_4)_2$ (2)	49.7(49.4)	4.2(4.3)	1.9(2.0)
$[Cu_2(BDAE)Cl_2]$ (3)	54.6(54.3)	4.8(4.7)	2.0(2.2)
$[Cu_2(BDAE)(N_3)](ClO_4)$ (4)	51.3(51.5)	4.5(4.4)	5.0(5.2)
$[Cu_2(BDAE)(NCS)](ClO_4)$ (5)	51.6(51.8)	4.3(4.4)	2.9(3.1)
$[Cu_2(BDAE)(BH_4)_2]$ (6)	56.4(56.1)	5.2(5.5)	2.1(2.3)
$[Cu_2(BDAE)(CS_2)_2](ClO_4)_2$ (7)	46.3(46.1)	3.7(3.8)	1.6(1.8)
$[Cu_2(BDAE)(H_2NCSNH_2)_2](ClO_4)_2$ (8)	46.2(46.1)	4.5(4.3)	5.2(5.4)
$[Cu_2(BDAE)(PPh_3)_2](ClO_4)_2$ (9)	58.0(58.3)	4.7(4.6)	1.3(1.6)
$[Cu_2(BDAE)(AsPh_3)_2](ClO_4)_2$ (10)	55.5(55.8)	4.3(4.5)	1.3(1.4)
$[Cu_2(BDAE)(dppm)](ClO_4)_2$ (11)	55.7(55.5)	4.7(4.6)	1.4(1.6)
$[Cu_2(BDAE)(dppe)](ClO_4)_2$ (12)	55.8(55.7)	4.4(4.7)	1.4(1.6)
$[Cu_2(BDAE)(C_3H_4N_2)_2](ClO_4)_2$ (13)	49.5(49.7)	4.3(4.4)	5.2(5.4)
$[Cu_2(BDAE)(C_{10}H_8N_2)_2](ClO_4)_2$ (14)	54.7(54.4)	4.3(4.4)	4.3(4.5)
$[Cu_2(BDAE)(C_5H_5N)_4](ClO_4)_2$ (15)	54.0(54.2)	4.8(4.6)	4.6(4.9)

[a] Calculated values are given in parentheses.

Table 2. Selected IR bands and conductivity data for copper(I) complexes[a]

Complex	IR data (cm^{-1})[b]	Solvent	Conductivity Λ_M ($\Omega^{-1}\,cm^2\,mol^{-1}$)	Comment
1	465(ν(Cu—As)); 232(ν(Cu—Cl))	DMF	8	Non-electrolyte
2	460(ν(Cu—As))	CH_3CN	235	1:2 electrolyte
3	466(ν(Cu—As)); 270(ν(Cu—Cl))	DMF	6	Non-electrolyte
4	468(ν(Cu—As)); 2085($\nu_{as}(N_3)$)	CH_3CN	128	1:1 electrolyte
5	465(ν(Cu—As)); 2110(ν_{as}(NCS))	CH_3CN	124	1:1 electrolyte
6	460(ν(Cu—As)); 2370(ν(B—H_t)); 1990(ν(B—He)); 1125(BH_2)	DMF	6	Non-electrolyte
7	465(ν(Cu—As)); 1160(ν(C=S)); 630(ν(C—S))	CH_3CN	240	1:2 electrolyte
8	462(ν(Cu—As)); 3405, 3300, 3200(NH_2); 355(ν(Cu—S))	DMF	136	1:2 electrolyte
9	465(ν(Cu—As))	DMF	147	1:2 electrolyte
10	464, 468(ν(Cu—As))	DMF	135	1:2 electrolyte
11	462(ν(Cu—As))	DMF	152	1:2 electrolyte
12	460(ν(Cu—As))	DMF	130	1:2 electrolyte
13	464(ν(Cu—As)); 3150(ν(N—H))	DMF	144	1:2 electrolyte
14	468(ν(Cu—As))	DMF	138	1:2 electrolyte
15	462(ν(Cu—As))	DMF	134	1:2 electrolyte

[a] Complexes **2**, **4**, **5** and **7–15** exhibit a broad band centring at 1100 cm^{-1} and a sharp band at 620 cm^{-1} due to ν_3 and ν_4 frequencies of ClO_4^-.

[b] KBr pellets.

magnetic and show no *d–d* bands in the visible region of their electronic spectra.

Conductivity measurements in DMF show that complexes **2** and **7–15** correspond to 1:2 electrolytes (Table 2), **4** and **5** correspond to 1:1 electrolytes and complexes **1**, **3** and **6** are non-electrolytes. This shows that the perchlorate anion in all of these complexes is not coordinated to the metal ion, but other anionic species (Cl^-, N_3^-, NCS^- and BH_4^-) do coordinate to copper(I).

Some selected IR bands of the complexes are shown in Table 2. The IR spectra of all the complexes containing the perchlorate anion exhibit a broad band centring at 1100 cm^{-1} and a sharp band at 620 cm^{-1} due to ν_3 and ν_4 frequencies, respectively, for the isolated ClO_4^-.[32] Complex **4** exhibits $\nu_{as}(N_3)$ at 2085 cm^{-1}, shifted to a higher frequency by 35 cm^{-1} compared to that of other azido complexes of copper(I) with similar ligands (2050 cm^{-1}).[19] The $\nu_s(N_3)$ band which is expected to appear around 1350 cm^{-1} [33] could not be observed. It has been reported that $\nu_s(N_3)$ in 1,3-bridged azides is either IR inactive or of low intensity.[33] These data, therefore, suggest that the azide in complex **4** is bridged between two copper(I) centres.[34] A similar observation has also been noted in **5** where a ν_{as}(NCS) band appears at 2110 cm^{-1}, a higher frequency shift by 30 cm^{-1} compared to that of monodentate thiocyanato complexes of copper(I) with similar ligands, indicating that thiocyanate has formed a bridge between the two metal centres. The IR spectrum of **6** shows two broad bands at 2370 and 1990 cm^{-1} and a sharp band at 1125 cm^{-1}, which are assigned to ν(B—H_t), ν(B—H_b) and BH_2 deformations, respectively, of bidentate BH_4^- [19,21,35] (H_b = hydrogen bonded to copper and H_t = hydrogen not bonded to copper). The IR spectrum of **7** exhibits two new bands at 1160 and 630 cm^{-1}, which can be assigned to ν(C=S) (out-of-ring) and ν(C—S) (in-ring), respectively, for bidentate CS_2 (bonding through carbon and one of the sulphur atoms as shown in Scheme 1).[36,37] Complex **8** shows new bands at 3405, 3300 and 3200 cm^{-1} due to NH_2 groups of coordinated thiourea. Complex **8** also exhibits a strong band at 1610 cm^{-1} and a medium intensity band at 355 cm^{-1}, which can be assigned to $\delta(NH_2)$ and ν(Cu—S), respectively. Complexes **13** and **14** exhibit a number of new bands in the range 1600–600 cm^{-1} due to the coordination of imidazole, bipyridine and pyridine to the metal ion.

The ^1H and $^{31}P\{^1H\}$ NMR data of the complexes are shown in Table 3. All the ^1H NMR spectra exhibit distinct resonances due to the principal ligand BDAE. The aromatic protons appear in the range 7.17–7.30 ppm. The *x*-, *y*- and *z*-CH_2 (see footnote to Table 3 for labelling) of the ligand BDAE appeared in the ranges 2.09–2.29, 2.62–2.81 and 2.32–2.58 ppm, respectively. The resonances of *x*-CH_2 and *y*-CH_2 were deshielded significantly

Table 3. ^1H and $^{31}P\{^1H\}$ NMR data of the copper(I) complexes[a]

Compound	^1H and $^{31}P\{^1H\}$ NMR data, chemical shifts (δ)[b]					$^{31}P\{^1H\}$ NMR data, chemical shift (δ)
	x-CH_2[c]	y-CH_2	z-CH_2	Ph	Others	
BDAE	1.94t	2.44t	2.26s	7.28		
1	2.18	2.41	2.32	7.12; 7.21		−3.63s
2	2.27	2.55	2.41s	7.28		
3	2.28	2.67	2.37s	7.17		
4	2.23	2.75	2.56s	7.23		
5	2.25	2.80	2.58s	7.28		
6	2.18	2.67	2.35s	7.27	1.15s[d]	
7	2.18	2.65	2.32s	7.26		
8	2.09	2.71	2.35s	7.30	2.89s[e]	
9	2.17	2.78	2.40s	7.25		1.45s
10	2.15	2.73	2.42s	7.18		
11	2.16	2.62	2.50s	7.05; 7.26	3.20s[f]	−16.71s
12	2.18	2.72	2.45s	7.12; 7.20	2.45s[g]	−2.78s
13	2.16	2.81	2.57s	7.18; 7.26	14.10s[h]	
14	2.18	2.78	2.45s	7.26; 8.66		
15	2.18	2.80	2.50s	7.19; 8.70		

[a] Except complexes **1** and **2** all other spectra were recorded in $CDCl_3$; **1** and **2** were recorded in DMSO-d_6.
[b] The multiplicity of x- and y-CH_2 and that of Ph were not well resolved.
[c] See below for labelling CH_2 groups.
[d] Due to BH_4^-.
[e] Due to NH_2 of thiourea.
[f] Due to CH_2 of dppm.
[g] Due to CH_2 of dppe.
[h] Due to NH of imidazole.

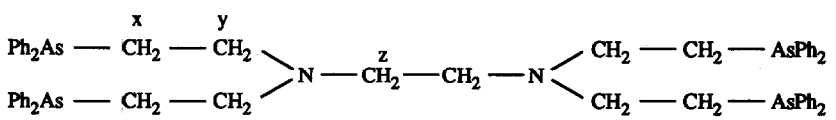

(BDAE)

compared with that of the free ligand due to the coordination of $AsPh_2$ to copper(I). In the case of z-CH_2 deshielding is significant in the complexes where the nitrogen atom is coordinated to the metal ion, otherwise it appears very close to the position found for the free ligand. Complexes **6**, **8** and **11**–**13** show an addition signal at 1.15, 2.89, 3.20, 2.45 and 14.30 ppm, respectively. This additional peak can be attributed to protons of BH_4^- (**6**),[38] NH_2 of thiourea (**8**), CH_2 of dppm (**11**), and dppe (**12**) and NH of imidazole (**13**). The resonances due to the CH_2 of dppm/dppe are shifted significantly downfield compared to that of free dppm (2.82 ppm) and dppe (2.11 ppm) and are definitely due to the coordination of PPh_2 to copper(I). However, the resonances of NH_2 and NH of thiourea and imidazole in complexes **8** and **13**, respectively, appear almost at the same positions as found for the free moieties in the same solvent, indicating that the NH_2 of thiourea and NH of imidazole are not involved in coordination. Complexes **14** and **15** show resonances at 8.66 and 8.70 ppm, due in part to the protons of coordinated bipyridine and pyridine molecules, respectively.

Structures

Complex **I** is tetra-coordinate and shows distorted tetrahedral geometry around copper, as established from single-crystal X-ray data. The copper atom in complex **2** is tri-coordinate with a trigonal-planar geometry.[19] In complex **3**, as Cl^- is coordinated to copper(I), a tetrahedral geometry is therefore proposed; however, a significant distortion cannot be ruled out due to different coordinating atoms (As, N, Cl) around copper(I). For complexes **4** and **5** as conductivity measurements show perchlorate is not involved in coordination and IR data indicates that N_3^- (**4**) and NCS^- (**5**) form bridges between two copper(I) centres, there-

fore, a distorted tetrahedral geometry around each copper as shown in Scheme 1 (**4** and **5**) is proposed. In the case of complex **6** it is clear from the IR data that two hydrogen atoms of BH_4^- interact with the copper, therefore, a tetrahedral geometry with an As_2H_2 core is suggested. The geometry of a similar compound with the phosphine analogue of BDAE was established by single-crystal X-ray study and reported recently.[21] For complex **7**, on the basis of IR absorption bands due to CS_2 and comparing with others reported with metal ion d^{10} configuration,[36,37] a triangular bonding of CS_2 with copper(I) (**7**, Scheme 1) is proposed. In the case of **8** from IR and NMR data it is clear that the NH_2 of thiourea is not involved in bonding, consistent with other reports of crystal structures for copper(I);[39,40] therefore, a tetrahedral geometry of the metal ion with ligation to two arsene, nitrogen and sulphur atoms of thiourea is suggested. For complex **9** $^{31}P\{^1H\}$ NMR data exhibit a singlet at 1.45 ppm, indicating that both the PPh_3 molecules are magnetically equivalent and coordinated to copper(I). Therefore, a tetrahedral geometry is expected. However, due to steric overcrowding of a number of phenyl rings around copper, there is the possibility of the elongation of the copper–nitrogen distance. For complex **10**, where $AsPh_3$ is coordinated, a similar geometry to that assigned for **9** is proposed. $^{31}P\{^1H\}$ NMR spectra of complexes **11** and **12** show a singlet at −16.71 (**11**) and −2.78 (**12**), respectively, indicating that in each compound both the phosphorus atoms of dppm/dppe are bound symmetrically to the copper, and presumably the dppm/dppe ligands form bridges between the copper centres, as shown in Scheme 1 (**11** and **12**). In this case, also due to the steric overcrowding of phenyl groups, elongation of the Cu—N distance is possible. For complex **13** IR and ^1H NMR data indicate that the NH of imidazole is not involved in coordination and, therefore, a tetrahedral geometry of copper with the coordination of nitrogen atoms of imidazole is suggested. In the case of **14** two nitrogen atoms of the bipyridine molecule are bonded to copper(I), resulting in a tetrahedral geometry with an As_2N_2 core. For complex **15** a similar geometry is expected with the coordination of two pyridine molecules to each copper(I), as shown in Scheme 1.

Structure of complex **1**

An ORTEP[41] view of complex **1** is shown in Fig. 1. A summary of crystal and refinement data is given in Table 4. Some selected bond lengths and angles are presented in Table 5.

The crystal structure of **1** contains a crystallographic centre of inversion, located at the midpoint of the C(34)—C(34*) bond, thus dividing the molecule into identical halves. The copper atom is ligated to two arsine atoms of the $AsPh_2$ groups,

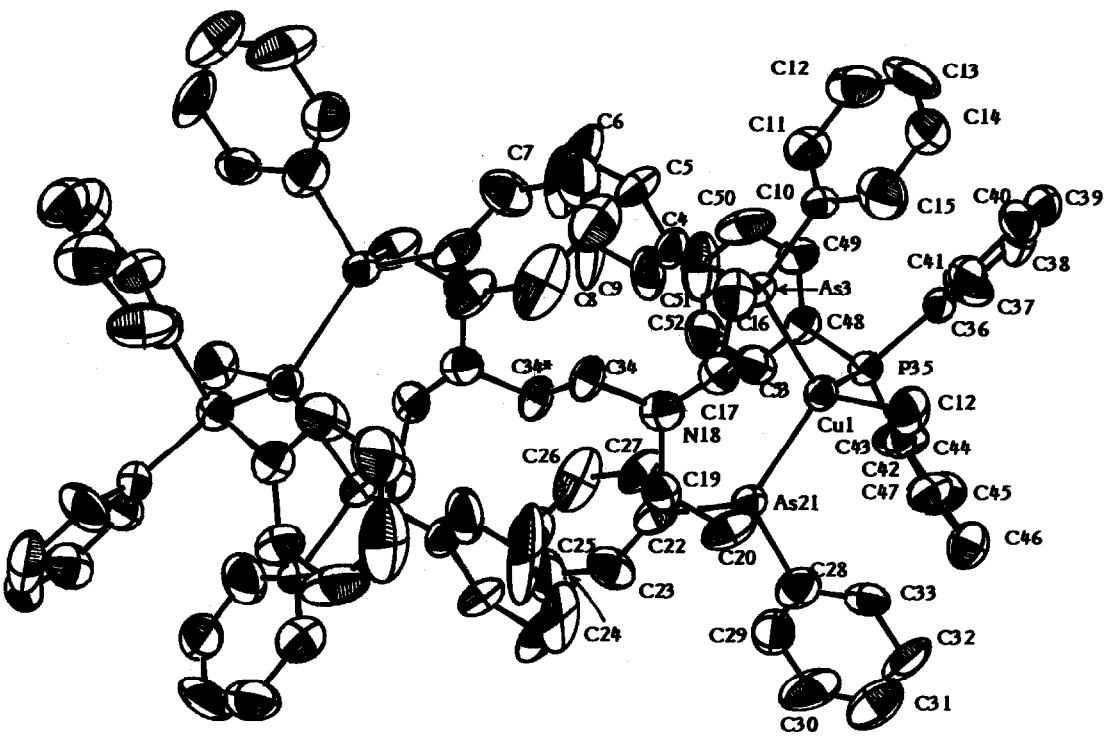

Fig. 1. ORTEP diagram of complex **1**, $[Cu_2(BDAE)(PPh_3)_2Cl_2]$, showing the atom labelling scheme.

Table 4. Crystallographic data for complex **1**

Empirical formula	$C_{94}H_{90}Cl_2Cu_2N_2P_2As_4$
Formula weight	1807.40
Space group	$P2_1/c$ (monoclinic)
a (Å)	10.149(1)
b (Å)	23.319(1)
c (Å)	17.977(1)
β (°)	99.413(1)
V (Å^3)	4197.4(5)
Z	2
D_{calc} (g cm^{-3})	1.430
Crystal dimension (mm)	$0.14 \times 0.26 \times 0.34$
Radiation (λ, Å)	Cu-K_α (1.54184)
μ (cm^{-1})	36.99
Temperature (°C)	25 ± 1
Reflections collected	6149
Reflections used in refinement ($I > 3\sigma(I)$)	3013
R	0.056
Rw	0.066

phosphorus atom of PPh_3 and a chloride ion and shows a distorted tetrahedral geometry. The angles in the coordination sphere involving the metal are in the range 97.3(2)–120.04(9)° (Table 5), a notable deviation from the idealized value of 109.5°, indicating distortion is significant. This distortion is a consequence of the differing Cu—As, Cu—P and Cu—Cl bond lengths (Table 5) as well as steric overcrowding of seven phenyl rings around each copper atom. The dihedral angles in the coordination sphere are Cu(1)—As(3)—As(21)/Cu(1)—P(35)—Cl(2), 89.75(9); Cu(1)—As(21)—P(35)/Cu(1)—As(3)—Cl(2), 84.46(8); and Cu(1)—As(3)—P(35)/Cu(1)—As(21)—Cl(2), 85.02(9)°. The copper atom lies 0.810(1) Å above the As(3)—P(35)—Cl(2) plane, 0.690(1) Å above the As(21)—P(35)—Cl(2) plane and 0.586(1) Å below the As(3)—As(21)—P(35) plane. The Cu···N distance is 3.840(3) Å and the Cu···Cu separation is 9.680(1) Å.

The Cu—As distances of 2.431(2) and 2.426(2) Å, Cu—P distance of 2.262(3) Å and Cu—Cl distance of 2.328(3) Å compare well with other reported values for tetra-coordinate copper(I).[1,15–18] An inspectrion of the intermolecular distances between the phenyl rings show that they tend to pack in a random fashion. The molecule has no intermolecular short contact less than 3.745 Å and hence the structure is held in space by van der Waals contacts.

Electrochemical study

The cyclic voltammograms of all these copper(I) complexes were studied in DMF in the potential range −0.4 to +1.6 V (vs SCE), in which the free ligand does not show any electrochemical response. The cyclic voltammograms of $[Cu_2(BDAE)(PPh_3)_2](ClO_4)_2$ (**9**) and $[Cu_2(BDAE)(C_5H_5N)_4](ClO_4)_2$ (**15**) are shown in Figs 2 and 3, respectively. The electrochemical data are presented in Table 6. The electrochemical behaviour of the complexes **1–6** and **9–12** are similar and exhibited two quasi-reversible oxidation–reduction couples in the ranges +0.40 to +0.70 V and +0.85 to +1.08 V. For complexes **7** and **13–15** the first couple, however, shifted significantly towards the negative side (+0.15 to +0.06 V) and the second couples are in the range +0.80 to +0.84 V. Complex **8** shows two couples at +0.26 and +0.76 V. The notable points in these experiments are the facts that the $E_{1/2}$ values were independent of scan rates (50 to 200 mV s^{-1}), the ratio of the peak currents due to cathodic and anodic sweeps were close to unity at different scan rates and the difference in potential due to anodic and cathodic peaks (ΔE_p) are in the range 80–120 mV. The above observations are consistent with a quasi-reversible one-electron transfer process. The observed two couples, therefore, can be attributed to the sequential one-electron transfer reactions. Similar observations have also been noted for a series of dinuclear copper(I)[22] and ruthenium(II)[42] complexes of hexadentate ligands having N_2P_4 donor sites and also dinuclear complexes of different transition metal ions with various ligands.[43–47] This type of stepwise electron transfer process for a dinuclear system is often used for determining the stabilities of the mixed-valence intermediate species.[43–47] Thus, the stabilities of the mixed-valence copper(II)–copper(I) species can be expressed in terms of the comproportionation constant (K_{com}) as:

Table 5. Bond distances (Å) and angles (°) in the coordination sphere of complex **1**

Cu(I)—As(3)	2.431(2)	Cu(I)—P(35)	2.262(3)
Cu(I)—As(21)	2.426(2)	Cu(I)—Cl(2)	2.328(3)
As(3)—Cu(1)—As(21)	109.5(6)	As(21)—Cu(1)—Cl(2)	99.0(1)
As(3)—Cu(1)—Cl(2)	97.3(2)	As(21)—Cu(1)—P(35)	120.04(9)
As(3)—Cu(1)—P(35)	112.5(8)	P(35)—Cu(1)—Cl(2)	115.3(1)

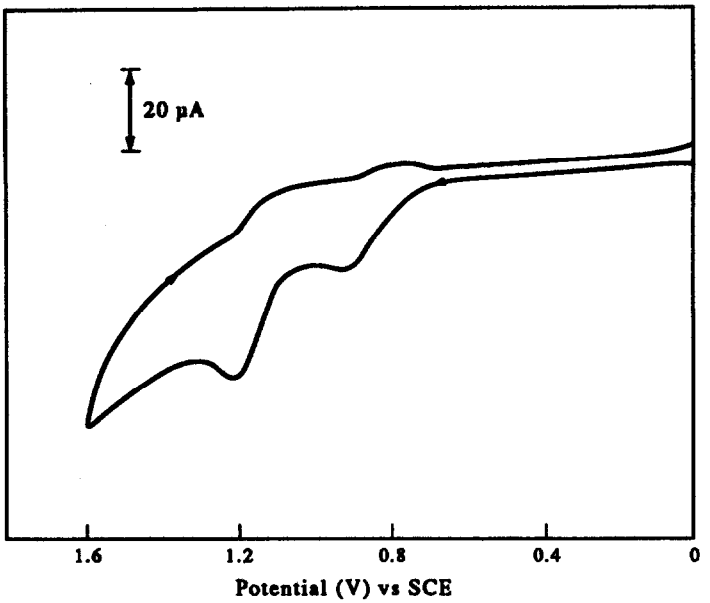

Fig. 2. Cyclic voltammogram of $[Cu_2(BDAE)(PPh_3)_2](ClO_4)_2$, 2.4×10^{-3} M solution in DMF at 25 ± 1°C.

$$K_{com} = \exp(nF\Delta E/RT);$$

where ΔE is the difference between the $E_{1/2}$ values of two oxidation–reduction couples in volts. The K_{com} values thus calculated are given in Table 6.

The K_{com} values found in the range 1.19×10^{5}–3.32×10^{12} indicate that the intermediate species are moderately stable. The interesting observation noted in this study is that in complexes **7** and **13**–**15**, where CS_2, imidazole, bipyridine and pyridine molecules are coordinated to copper(I), the first $E_{1/2}$ values decrease significantly and the K_{com} values are considerably higher compared with those of other compounds. This is definitely due to the fact that the attachment of the σ-donor moiety to copper(I) increases the electron density on the metal ion which caused easy removal of an electron from copper(I) to form copper(II). Secondly, the presence of both a σ-donor and π-acceptor in the coordination sphere provides a balanced electron density on the metal ion, which resulted in extra stability of the mixed-valence intermediate species.

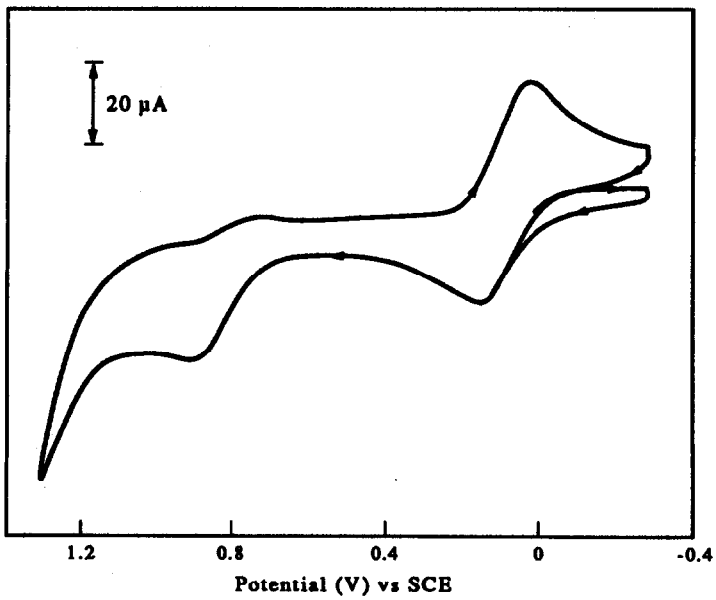

Fig. 3. Cyclic voltammogram of $[Cu_2(BDAE)(C_5H_5N)_4](ClO_4)_2$, 2.2×10^{-3} M solution in DMF at 25 ± 1°C.

Table 6. Comparison of cyclic voltammetric data for copper(I) complexes in DMF

Complex	$E_{1/2}$ (V)[a] Cu^{I}–Cu^{I}/ Cu^{II}–Cu^{I}	$E_{1/2}$ (V) Cu^{II}–Cu^{I}/ Cu^{II}–Cu^{II}	K_{com}
$[Cu_2(BDAE)(PPh_3)_2Cl_2]$ (**1**)	0.60	1.05	4.11×10^{7}
$[Cu_2(BDAE)](ClO_4)_2$ (**2**)	0.58	1.00	1.28×10^{7}
$[Cu_2(BDAE)Cl_2]$ (**3**)	0.47	0.92	4.11×10^{7}
$[Cu_2(BDAE)(N_3)](ClO_4)$ (**4**)	0.42	0.88	6.07×10^{7}
$[Cu_2(BDAE)(NCS)](ClO_4)$ (**5**)	0.52	1.00	1.32×10^{8}
$[Cu_2(BDAE)(BH_4)_2]$ (**6**)	0.50	0.94	2.79×10^{7}
$[Cu_2(BDAE)(CS_2)_2]$ (**7**)	0.06	0.80	3.32×10^{12}
$[Cu_2(BDAE)(H_2NCSNH_2)_2](ClO_4)_2$ (**8**)	0.26	0.76	2.89×10^{8}
$[Cu_2(BDAE)(PPh_3)_2](ClO_4)_2$ (**9**)	0.74	1.08	5.66×10^{5}
$[Cu_2(BDAE)(AsPh_3)_2](ClO_4)_2$ (**10**)	0.40	0.85	4.11×10^{7}
$[Cu_2(BDAE)(dppm)](ClO_4)_2$ (**11**)	0.70	1.02	2.60×10^{5}
$[Cu_2(BDAE)(dppe)](ClO_4)_2$ (**12**)	0.64	0.96	1.19×10^{5}
$[Cu_2(BDAE)(C_3H_4N_2)_2](ClO_4)_2$ (**13**)	0.15	0.84	4.73×10^{11}
$[Cu_2(BDAE)(C_{10}H_8N_2)_2](ClO_4)_2$ (**14**)	0.09	0.82	2.25×10^{12}
$[Cu_2(BDAE)(C_5H_5N)_4](ClO_4)_2$ (**15**)	0.08	0.82	3.32×10^{11}

[a] $E_{1/2} = 0.5(E_{pa}+E_{pc})$.

REFERENCES

1. J. T. Gill, J. J. Mayerle, P. S. Welcker, D. F. Lewis, D. A. Ucko, D. J. Barton, D. Stowens and S. J. Lippard, *Inorg. Chem.* 1976, **15**, 1155.
2. G. A. Bowmaker, J. C. Dyason, P. C. Healy, L. M. Engelhardt, C. Pakawatchai and A. H. White, *J. Chem. Soc., Dalton Trans.* 1987, 1089.
3. P. F. Barron, J. C. Dyason and P. C. Healy, *J. Chem. Soc., Dalton Trans.* 1987, 1099.
4. G. A. Bowmaker, B. W. Skelton, A. H. White and P. C. Healy, *J. Chem. Soc., Dalton Trans.* 1988, 2825.
5. G. A. Bowmaker, J. D. Cotton, P. C. Healy, J. D. Kildea, S. B. Silong, B. W. Skelton and A. H. White, *Inorg. Chem.* 1989, **28**, 1462.
6. D. J. Fife, W. M. Moore and K. W. Morse, *J. Am. Chem. Soc.* 1985, **107**, 7077.
7. S. Sakaki, K. S. Hinokuma, S. Hashimoto and K. Ohkubo, *Inorg. Chem.* 1987, **26**, 1817.
8. B. Liaw, S. W. Orchard and C. Kutal, *Inorg. Chem.* 1988, **27**, 1311.
9. C. Bianchini, C. A. Ghilardi, A. Meli, S. Midollini and A. Orlandini, *Inorg. Chem.* 1985, **24**, 924.
10. C. Bianchini, C. A. Ghilardi, A. Meli, S. Midollini and A. Orlandini, *Inorg. Chem.* 1985, **24**, 932.
11. S. Sakaki and K. Ohkubo, *Inorg. Chem.* 1988, **27**, 2020.
12. G. V. Goeden and K. G. Caulton, *J. Am. Chem. Soc.* 1981, **103**, 7354.
13. W. S. Mahoney, D. M. Brestensky and J. M. Stryker, *J. Am. Chem. Soc.* 1988, **110**, 291.
14. W. S. Mahoney and J. M. Stryker, *J. Am. Chem. Soc.* 1989, **111**, 8818.
15. M. R. Churchill and K. L. Kalra, *Inorg. Chem.* 1974, **13**, 1899.
16. M. R. Churchill and J. R. Missert, *Inorg. Chem.* 1981, **20**, 619.
17. P. Karagiannidis, P. S. Akrivos, D. Mentzafos and A. Terzis, *Inorg. Chim. Acta* 1991, **181**, 263.
18. P. Karagiannidis, P. D. Akrivos, A. Aubry and S. Skoulika, *Inorg. Chim. Acta* 1991, **188**, 79.
19. M. M. Taqui Khan, P. Paul, K. Venkatasubramanian and S. Purohit, *J. Chem. Soc., Dalton Trans.* 1991, **3405**.
20. M. M. Taqui Khan, P. Paul, K. Venkatasubramanian and S. Purohit, *Inorg. Chim. Acta* 1991, **183**, 229.
21. M. M. Taqui Khan, P. Paul and K. Venkatasubramanian, *Polyhedron* 1991, **10**, 1827.
22. M. M. Taqui Khan and P. Paul, *Polyhedron* 1992, **11**, 805.
23. S. J. Lippard and D. A. Ucko, *Inorg. Chem.* 1968, **7**, 1051.
24. P. Hemmerich and C. Sigwart, *Experientia* 1963, **19**, 488.
25. A. C. T. North, D. C. Philips and F. S. Mathews, *Acta. Cryst., Sect. A.* 1968, **24**, 351.
26. J. D. Dunitz and P. Seiler, *Acta. Cryst., Sect. B* 1973, **29**, 589.
27. *International Tables for Crystallography*, Vol. IV. Reidel, Dordrecht, The Netherlands (1983).
28. R. F. Stewart, E. R. Davidson and W. T. Simpson, *J. Chem. Phys.* 1965, **42**, 3175.
29. S.D.P. Structure Determination Package. Enraf–Nonius, Delft, The Netherlands (1986).
30. V. G. Albano, P. L. Bellon and G. Ciani, *J. Chem. Soc., Dalton Trans.* 1972, 1938.
31. J. Diez, M. P. Gamasa, J. Gimeno, A. Tiripicchio and M. T. Camellini, *J. Chem. Soc., Dalton Trans.* 1987, 1275.

32. K. Nakamoto, *Infrared Spectra of Inorganic and Coordination Compounds*, p. 161. John Wiley, New York (1963).
33. Y. Nako, M. Yamazaki, S. Suzuki, W. Mori, A. Nakahara, K. Matsumoto and S. Ooi, *Inorg. Chim. Acta* 1983, **159**, 74.
34. P. Paul and K. Nag, *Inorg. Chem.* 1987, **26**, 2969.
35. C. Kutal, P. Grutsch, J. L. Atwood and R. D. Rogers, *Inorg. Chem.* 1978, **17**, 3558.
36. C. Bianchini, C. A. Ghilardi, A. Meli and A. Orlandini, *J. Organomet. Chem.* 1984, **270**, 251.
37. C. Bianchini, D. Masi, C. Mealli and A. Meli, *Inorg. Chem.* 1984, **23**, 2838.
38. T. J. Marks and J. R. Kolb, *Chem. Rev.* 1977, 77, 263.
39. R. G. Vranka and E. L. Amma, *J. Am. Chem. Soc.* 1966, **88**, 4270.
40. I. F. Taylor Jr, M. S. Weininger and E. L. Amma, *Inorg. Chem.* 1974, **13**, 2835.
41. C. K. Johnson, ORTEP II, Oak Ridge National Laboratory, Tennessee (1971).
42. M. M. Taqui Khan, P. Paul and S. Purohit, *Inorg. Chim. Acta* 1991, **189**, 165.
43. P. Zanello, S. Tamburini, P. A. Vigato and G. A. Mazzocchin, *Coord. Chem. Rev.* 1987, **77**, 165.
44. D. V. Richardson and H. Taube, *Coord. Chem. Rev.* 1984, **60**, 107.
45. J. Chatt, *Coord. Chem. Rev.* 1982, **43**, 337.
46. P. Paul, R. Das, S. K. Mandal and K. Nag, *Ind. J. Chem.* 1990, **29A**, 335.
47. B. Adhikary, S. K. Mandal and K. Nag, *J. Chem. Soc., Dalton Trans.* 1988, 935.

Polyhedron Vol. 12, No. 7, pp. 847–849, 1993
Printed in Great Britain

0277–5387/93 $6.00+.00
© 1993 Pergamon Press Ltd

COMMUNICATION

^{183}W NUCLEAR MAGNETIC RESONANCE OF α-$[H_2W_{11}VO_{40}]^{7-}$ AND α-$[H_2W_{11}MoO_{40}]^{6-}$

J. J. HASTINGS and O. W. HOWARTH*

Department of Chemistry, University of Warwick, Coventry CV4 7AL, U.K.

(*Received* 4 *December* 1992; *accepted* 4 *January* 1993)

Abstract—The anions $[H_2W_{11}VO_{40}]^{7-}$ and $[H_2W_{11}MoO_{40}]^{6-}$ have been identified in aqueous solution by ^{183}W, ^{51}V and ^{1}H NMR. They almost certainly both have the α-Keggin structure.

Although many examples are known of the substitution of metal atoms such as vanadium into heteropolytungstates, there is at present only one known case of such substitution into isopolytungstates with the Keggin structure. Pope[1] has reported the substitution of a vanadium(V) atom into α-$[H_2W_{12}O_{40}]^{6-}$ and he argues from both the single, broad vanadium resonance and the proton shift of the two encapsulated protons that this yields $[H_2W_{11}VO_{40}]^{7-}$. The proposed 7- anionic charge is consistent with the observation that this anion has its maximum stability at somewhat higher pH than the α-Keggin species.[2,3] We now confirm Pope's proposal and also report the corresponding molybdenum-substituted anion, $[H_2W_{11}MoO_{40}]^{6-}$.

The $W_{11}V$ anion was prepared between pH 2.5 and 5 in aqueous solution typically containing vanadate (0.333 mol dm^{-3}) and tungstate (1.667 mol dm^{-3}). These solutions typically take several weeks to reach equilibrium. The $W_{11}V$ anion is present at *ca* 0.026 mol dm^{-3}, along with paratungstate B (0.0485 mol dm^{-3})[3] and the dominant $[W_4V_2O_{19}]^{4-}$ species.[1] Other anions are also present in smaller quantities, but have not yet been fully analysed. The ^{51}V and ^{1}H NMR shifts of $W_{11}V$ are -543 and 6.05 ppm, respectively. These agree with Pope's report.[1] A ^{183}W NMR spectrum [Fig. 1(a)] showed six resonances that correspond to $W_{11}V$ by having the correct relative area both to each other and to $[W_4V_2O_{19}]^{4-}$, as predicted from the areas in the ^{51}V spectrum. The peaks are in the area ratio 2:2:(2+1):2:2, where the + sign indicates partial overlap. These ratios show that the anion retains a plane of symmetry. The shifts are listed in Table 1. No broadenings are apparent from coupling to V, but these would not in fact be expected with such a broad V resonance. The peak ratios probably show that the species retains the α-Keggin structure, because the β-isomer would have to be substituted solely at just one of its two sets of three equivalent tungsten atoms, in order to retain a plane of symmetry and also to remain a single species. Even if it did this, rather different tungsten shifts would be expected, for the shifts in the mixed-metal species range from -114.1 to -127.6 ppm (the unsubstituted α-Keggin resonates at -123 ppm), whereas the unsubstituted β-Keggin anion has resonances between -112 and -136 ppm.[3] One would expect a substituted β-Keggin anion to have a larger shift range than an unsubstituted one.

The above range of shifts is surprisingly small in comparison with the corresponding shifts reported by Domaille[4] for mono-substituted heteropolytungstates with the α-Keggin structure. These typically extend from -70 to -140 ppm, with the tungsten nearest to vanadium often having the highest shift. One possible reason for this difference is that the present species have two internal protons. These may move so as to correct any imbalance of charge resulting from the metal substitution. Internal protonation certainly affects the tungsten shifts. We have already shown that the removal of just one internal proton decreases the isopolytungstate shift by 21 ppm.[3]

* Author to whom correspondence should be addressed.

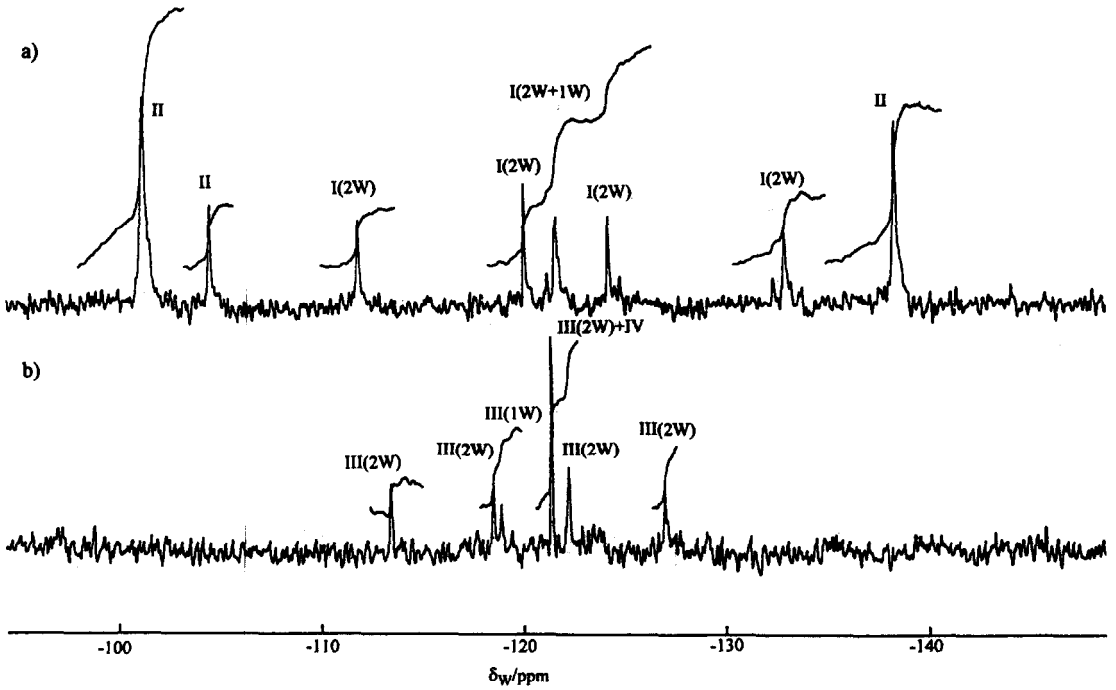

Fig. 1. (a) 16.65 MHz ^{183}W NMR spectrum of 0.333 mol dm^{-3} [V], 1.667 mol dm^{-3} [W] aqueous solution at 295 K, pH 4.9. Species I α-$[H_2W_{11}VO_{40}]^{7-}$, II paratungstate-B $[H_2W_{12}O_{42}]^{10-}$ (with two peaks 2W+4W overlapping at −101 ppm). (b) 16.65 MHz ^{183}W NMR spectrum of 0.1667 mol dm^{-3} [Mo], 1.833 mol dm^{-3} [W] aqueous solution at 295 K, pH 2.2. Species III α-$[H_2W_{11}MoO_{40}]^{6-}$, IV α-$[H_2W_{12}O_{40}]^{6-}$ overlapping one of the 2W resonances of α-$[H_2W_{11}MoO_{40}]^{6-}$.

The corresponding tungstomolybdate species $[H_2W_{11}MoO_{40}]^{6-}$ was prepared in aqueous solution at pH 2–4, with [Mo] = 0.1667 and [W] = 1.833 mol dm^{-3}, along with a complex range of heptametallate species that will be reported separately. It is present at *ca* 0.132 mol dm^{-3}. Its spectrum is shown in Fig. 1(b), and its shifts are also listed in Table 1. They show a close correspondence with those of the $W_{11}V$ anion, but although they also centre approximately at the shift of the unsubstituted α-Keggin isopolytungstate, their spread of shifts is only *ca* 60% of $W_{11}V$. One may deduce that the structure of the $W_{11}Mo$ anion is also probably α-Keggin, and that the substitution of molybdenum perturbs the remaining tungsten atoms even less than does that of vanadium. However, we

Table 1. Tungsten chemical shifts and relative integrals

α-$[H_2W_{11}VO_{40}]^{7-}$	α-$[H_2W_{11}MoO_{40}]^{6-}$	α$[H_2W_{12}O_{40}]^{6-}$
−111.6[a] (2W)[b]	−114.1 (2W)	−123 (12W)
−119.8 (2W)	−119.0 (2W)	
−121.3 (2W)	−119.5 (1W)	
−121.5 (1W)	−122.0[c] (2W)	
−124.0 (2W)	−122.8 (2W)	
−132.7 (2W)	−127.6 (2W)	

[a] Tungsten chemical shift in ppm from external 2 mol dm^{-3} aqueous $Na_2[WO_4]^{2-}$.

[b] Relative tungsten integral.

[c] Obscured by α-$[H_2W_{12}O_{40}]^{6-}$.

have so far been unable to detect the resonances of the presumed central protons or to perform the tungsten homonuclear shift correlation experiments[4] that could in principle permit a more detailed assignment of the resonances. We also have no evidence at present for the substitution of more than one molybdenum or vanadium atom into the isopolytungstate.

REFERENCES

1. C. M. Flynn Jr, M. T. Pope and S. O'Donnell, *Inorg. Chem.* 1974, **13**, 831.
2. O. W. Howarth, L. Pettersson and I. Andersson, *J. Chem. Soc., Dalton Trans.* 1991, 1799.
3. J. J. Hastings and O. W. Howarth, *J. Chem. Soc., Dalton Trans.* 1992, 209.
4. P. J. Domaille, *J. Am. Chem. Soc.* 1984, **106**, 7677,

Polyhedron Vol. 12, No. 7, pp. 851–853, 1993
Printed in Great Britain

0277–5387/93 $6.00+.00
© 1993 Pergamon Press Ltd

COMMUNICATION

METAL-DIRECTED SYNTHESIS OF A PENDENT-ARM N_2S_2-MACROCYCLE INCORPORATING AN *ORTHO*-XYLENE UNIT

ANTHONY J. ELLIOTT, GEOFFREY A. LAWRANCE* and GANG WEI

Department of Chemistry, The University of Newcastle, Callaghan 2308, Australia

(*Received* 27 *October* 1992; *accepted* 21 *December* 1992)

Abstract—Reaction of (2,2′-[*o*-phenylenebis(methylenethio)]bis[ethanamine])copper(II) in alcoholic base with formaldehyde and nitroethane yields the macrocycle (8-methyl-8-nitro-6,10-diaza-3,13-dithia-1,15,16,17,18,19-dehydrobicyclo[13.4.0]nonadecane)copper (II), which incorporates an *ortho*-xylene unit as part of a 15-membered macrocylic ring with *cis*-N_2S_2 donors which also carry pendent nitro and methyl groups. Zinc–acid reduction of the complex permits isolation of a potentially quinquedentate N_3S_2-donor ligand.

Despite the fairly detailed study of the metal-directed reaction involving copper(II) complexes with *cis*-disposed primary amines, formaldehyde and the carbon acid nitroethane,[1,2] only one example of a simple mononuclear macrocyclic complex with mixed nitrogen and sulphur donors has been reported to date[3] and, in general, the study of mixed-donor ligands resulting from this reaction has been neglected. Further, all metal-directed nitroethane/formaldehyde condensation reactions reported to date have involved the synthesis of fully saturated molecules, with the incorporation of aromatic groups in the resultant macrocyclic compounds not attempted previously. To explore some aspects of both the above areas we have examined the facility of a nitroethane/formaldehyde condensation reaction involving the copper(II) complex of **1**. This reaction is directed towards the synthesis of **2**, which incorporates an *ortho*-xylene unit in the macrocycle skeleton. Reduction of the nitro group in **2** yields **3**, which carries an additional potential donor pendent to the macrocycle ring. Details of this chemistry are described herein.

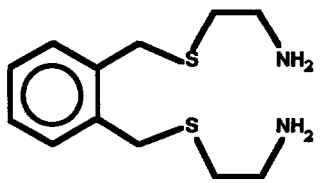

(1)

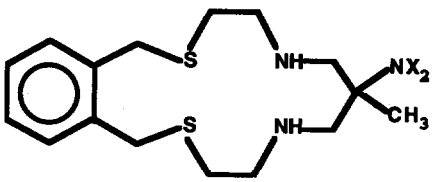

(2) X = O
(3) X = H

EXPERIMENTAL

Syntheses

The precursor **1** was prepared essentially as described previously from *ortho*-dibromoxylene and 2-aminoethanethiol.[4]

(2,2′ - [o - *Phenylenebis(methylenethio)]bis[ethanamine])copper*(II) *perchlorate*, $[Cu(\mathbf{1})](ClO_4)_2$. To a warm solution of $Cu(NO_3)_2 \cdot 2.5H_2O$ (30.2 g) in methanol (100 cm^3) was added **1** (24.7 g) in meth-

* Author to whom correspondence should be addressed.

anol (100 cm^3) with stirring. The dark purple solution was allowed to stand overnight and the dark purple solid was collected and air dried (39 g, 67%). Part was reprecipitated from a minimum volume of warm water by the addition of solid $NaClO_4$ in excess. The purple product was collected from the chilled solution, washed well with ethanol and air dried. Found: C, 26.9; H, 4.1; N, 5.6. Calc. for $C_{12}H_{20}Cl_2CuN_2O_8S_2 \cdot H_2O$: C, 26.8; H, 4.1; N, 5.2%. Electronic spectrum (water): λ_{max} 570 (ε 325), 320 nm (ε 3740 M^{-1} cm^{-1}). IR spectrum (KBr disc): 3240, 3115, 1588 (—NH_2), 780 (*ortho*-Ar), 1115, 620 cm^{-1} (ClO_4^-).

(8 - *Methyl* - 8 - *nitro* - 6,10 - *diaza* - 3,13 - *dithia* - 1,15,16,17,18,19 - *dehydrobicyclo*[13.4.0]*nonadecane*) *copper*(II) *perchlorate*, [Cu(**2**)]$(ClO_4)_2$. To a warm solution of [Cu(**1**)]$(NO_3)_2$ (5.1 g) in a mixture of ethanol (50 cm^3) and water (350 cm^3) were added, with stirring, triethylamine (3 cm^3), nitroethane (5 cm^3) and formaldehyde (37% aq., 11 cm^3). The mixture was heated at 60°C for 2 h and then stirred at room temperature for 1 day. The filtered solution was treated with $HClO_4$ (10 cm^3, conc.) and solid $NaClO_4$ (2 g) and the pink–purple solution was chilled to produce a pink precipitate, which was collected, washed with ethanol and air dried (1.1 g, 15%). Further crops were collected after extended standing. Found: C, 28.5; H, 3.7; N, 6.1. Calc. for $C_{16}H_{25}Cl_2CuN_3O_{10}S_2 \cdot 0.5NaClO_4$: C, 28.3; H, 3.7; N, 6.2%. Electronic spectrum (water): λ_{max} 560 (ε 490), 339 (ε 4860), 262 cm^{-1} (ε 3060 M^{-1} cm^{-1}). Magnetic moment (300 K): 1.7 μ_B (d^9 spin-only value is 1.73). IR spectrum (KBr disc): 1540, 1340 (—NO_2), 770 (*ortho*-Ar), 1115, 620 cm^{-1} (ClO_4^-).

8 - *Methyl* - 6,10 - *diaza* - 3,13 - *dithia* - 1,15,16,17,18,19 - *dehydrobicyclo*[13.4.0]*nonadecan* - 8 - *amine hydrochloride*, (**3**)·3HCl. Equal volumes of [Cu(**2**)]$(ClO_4)_2$ (2.0 g) dissolved in water and 3 M HCl were added dropwise at equal rates to constantly stirred excess zinc dust, with the temperature of the mixture adjusted to *ca* 50°C. The final colourless solution was filtered to remove excess zinc dust and copper metal, diluted eight-fold with water and loaded onto a column (20 × 4 cm) of Dowex 50W × 2 (H^+-form) cation exchange resin. The column was washed with 1 M HCl to remove the zinc ions and then eluted with 5 M HCl. The eluate was taken to dryness, twice stirred with a small volume of ethanol and taken to dryness to yield an off-white powder (1.2 g, 85%). Found: C, 37.6; H, 6.9; N, 8.15. Calc. for $C_{16}H_{30}Cl_3N_3S_2 \cdot 4H_2O$: C, 37.9; H, 7.5; N, 8.3%. ^1H NMR spectrum (D_2O): δ 1.35 (s, —CH_3), 2.7–3.4 (m, —CH_2—), 4.1 (s, Ar—CH_2—S), 7.4 (m, Ar—) ppm. ^{13}C NMR spectrum (D_2O): δ 22.5 (—CH_3), 32.4, 35.7 (—NH—CH_2—), 41.3 (tert. C), 50.6, 56.5 (—S—CH_2—), 130.9, 133.7 (Ar—) ppm.

Physical methods

Electronic (in water), IR (KBr discs) and NMR spectra (in D_2O) and cyclic voltammetry (aqueous 0.1 M $NaClO_4$ solution, glassy carbon working electrode) were performed as previously described.[3,5] Magnetic moments were determined by the Evans method.[6]

RESULTS AND DISCUSSION

The metal-directed synthesis of the macrocycle **2** proceeds with reasonable facility in a one-step process, the mechanism of which has been described previously.[2] The macrocycle is characterized readily by a number of physical properties: the introduced nitro group is readily identified by IR spectroscopy (asymmetric and symmetric stretching vibrations at 1540 and 1340 cm^{-1}) and voltammetry (irreversible multielectron reduction at −1.08 V vs Ag/AgCl), while the resistance of the product to dissociation even in strong acid is indicative of macrocyclization. The strong primary amine bands (3240, 3115 and 1588 cm^{-1}) in the IR spectrum of the open-chain precursor are replaced by weaker secondary amine resonances (3227, 3181 and 1600 cm^{-1}) in the macrocycle, whereas a vibration associated with the characteristic *ortho*-disubstituted benzene ring near 770 cm^{-1} is preserved.

The copper(II)/(I) couple for $[Cu(2)]^{2+}$ is observed at −0.20 V vs Ag/AgCl and is quasi-reversible (ΔE 80 mV at 100 mV s^{-1} scan rate, i_{pc}/i_{pa} 1.05). The shift to more negative potential vs the precursor $[Cu(1)]^{2+}$ ($E_{1/2}$ −0.04 V, ΔE 70 mV) is the same as that observed with the saturated analogues **4** and **5**,[3] where a shift from $E_{1/2}$ −0.09 (ΔE 138 mV) to −0.245 V (ΔE 140 mV) is observed. A more negative potential for the macrocycle compared with the acycle for tetraamine analogues is ascribed to the reduced flexibility in the former case,[7] with the macrocycle less able to accommodate the larger copper(I) ion and its preferred tetrahedral geometry, but this is relaxed somewhat in the case of the N_2S_2 system as a result of the longer C—S and Cu—S bond lengths. The relatively large chelate ring incorporating the benzene unit in $[Cu(2)]^{2+}$ does not appear to influence accommodation of the change in ion size and geometry upon reduction compared with $[Cu(5)]^{2+}$, as $E_{1/2}$ values are very similar. However, electronic effects from the incorporation of the aromatic group may play some role in the present case.

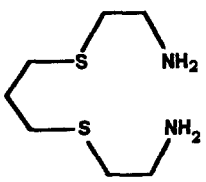

(4)

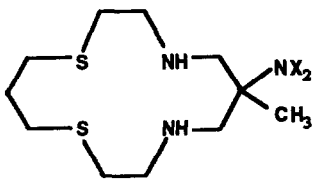

(5) X=O

(6) X=H

Reversibility of the couple is enhanced in $[Cu(2)]^{2+}$ compared with $[Cu(5)]^{2+}$.

The electronic spectra of all acyclic and cyclic species are similar, with an absorbance near 330 nm characteristic of the presence of thioether donors.[8] An additional absorbance at 262 nm in the case of the macrocyclic complex can be assigned to the nitro group. A number of CuN_2S_2 complexes with different macrocycle ring sizes have been reported, the *d–d* transition varying with the 12-membered (620 nm), 14-membered (534 nm) and 16-membered (607 nm) ring size.[3,8] The maximum in the present case, which is a 15-membered ring, is observed at 560 nm. This fits into the general trend with ring size, suggesting that $[Cu(2)]^{2+}$ adopts the approximately square-planar geometry of the 14- and 16-membered analogues, despite the incorporation of the benzene ring in the framework.

The present example, $[Cu(2)]^{2+}$, is the first of a macrocycle incorporating an aromatic ring produced by the metal-directed carbon acid/formaldehyde process. Other examples of N_2S_2-macrocycles with benzene rings in the framework have been produced by condensations of dialdehydes and diamines followed by borohydride reduction of the cyclic diimine intermediate,[9] or by condensation of the nickel(II) complex of **1** with acetone.[10] Reduction of $[Cu(2)]^{2+}$ with Zn/HCl produces a macrocycle (**3**) with a pendent primary amine capable of coordination, and the chemistry of this potential N_3S_2-ligand, analogous to the known **6**,[11] is being pursued.

Acknowledgements—Financial assistance by the Australian Research Council and the Research Management Committee of the University of Newcastle is gratefully acknowledged.

REFERENCES

1. P. V. Bernhardt and G. A. Lawrance, *Coord. Chem. Rev.* 1990, **104**, 297.
2. G. A. Lawrance and M. A. O'Leary, *Polyhedron* 1987, **6**, 1291.
3. P. Comba, G. A. Lawrance, M. Rossignoli, B. W. Skelton and A. H. White, *Aust. J. Chem.* 1988, **41**, 773.
4. R. W. Hay, P. M. Gidney and G. A. Lawrance, *J. Chem. Soc., Dalton Trans.* 1975, 799.
5. T. W. Hambley, G. A. Lawrance, M. Maeder and E. N. Wilkes, *J. Chem. Soc., Dalton Trans.* 1992, 1283.
6. J. Löliger and R. Scheffold, *J. Chem. Ed.* 1972, **49**, 646.
7. P. Comba, N. F. Curtis, G. A. Lawrance, A. M. Sargeson, B. W. Skelton and A. H. White, *Inorg. Chem.* 1986, **25**, 4260; G. A. Lawrance, M. Rossignoli, B. W. Skelton and A. H. White, *Aust. J. Chem.* 1987, **40**, 1441.
8. L. Siegfried and T. A. Kaden, *Helv. Chim. Acta* 1984, **67**, 29.
9. L. F. Lindoy and R. J. Smith, *Inorg. Chem.* 1981, **20**, 1314.
10. M. C. Thompson and D. H. Busch, *J. Am. Chem. Soc.* 1964, **86**, 3651.
11. G. A. Lawrance, M. Martinez, B. W. Skelton and A. H. White, *Aust. J. Chem.* 1991, **44**, 113.

Polyhedron Vol. 12, No. 8, pp. 855–858, 1993
Printed in Great Britain

0277–5387/93 $6.00+.00
© 1993 Pergamon Press Ltd

POLYMERIZATION OF ACRYLAMIDE PHOTOSENSITIZED BY THE TRIS(2,2′-BIPYRIDINE)CHROMIUM(III) ION IN AQUEOUS SOLUTION

CHRISTINE PIZZOCARO and MICHÈLE BOLTE†

Laboratoire de Photochimie Moléculaire at Macromoléculaire, URA CNRS 433, UFR de Recherche Scientifique et Technique, Université Blaise Pascal, 63177-Aubière Cedex, France

and

MORTON Z. HOFFMAN

Department of Chemistry, Boston University, Boston, MA 02215, U.S.A.

(*Received* 23 *November* 1992; *accepted* 6 *January* 1993)

Abstract—The 365 nm continuous irradiation of acidic aqueous solutions of $Cr(bpy)_3^{3+}$ and acrylamide yields polyacrylamide; the $Cr(bpy)_2(OH_2)_2^{3+}$ aquation product is also produced. Upon pulsed-laser excitation, no chromium(II) product is observed, likely due to the low rate constant for the quenching of thermally-equilibrated $^2T_1/^2E$ excited states of the photosensitizer by acrylamide and the low-cage escape yield of redox products. Nevertheless, $Cr(bpy)_3^{3+}$ is a suitable photosensitizer even for excitation with visible light up to 450 nm. The positive dependence of the rate of polymerization on the intensity of absorbed light and [monomer]^2 and the inverse dependence on $[Cr(bpy)_3^{3+}]$ suggest that the termination step of the chain reaction involves the oxidative scavenging of the macroradicals by the photosensitizer.

The use of light to initiate the generation of free radicals has been extensively used in polymerization processes. In addition to providing on–off control at ambient temperature, the photochemical method permits the selection of the wavelength of light, and thus the nature of the excited states and radicals to be generated. Unfortunately, monomeric species generally absorb at short wavelengths and their polymerizations only occur with the excitation of high energy ($\lambda < 270$ nm). Through the use of a photosensitizer the selective formation of radicals can be achieved with light of lower energy.

The polymerizations of vinyl monomers photoinitiated by coordination complexes, such as those of iron(III),[1,2] cobalt(III),[3–6] ruthenium(II)[7] and chromium(VI),[8–10] have already been reported. Chromium(III) as $Cr(H_2O)_6^{3+}$ also appears to be an efficient photoinitiator of vinyl monomer polymerization.[11] In order to elucidate the mechanism of the photoinitiation process, and because of our previous work on the photochemistry and photophysics of polypyridyl complexes of chromium (III),[12] we chose to investigate the polymerization of acrylamide (AA) photosensitized by $Cr(bpy)_3^{3+}$ (bpy = 2,2′-bipyridine), the thermally-equilibrated $^2T_1/^2E$ excited states of which are luminescent, long-lived ($\tau = 70$ μs) in the absence of O_2 and strongly oxidizing ($^*E^\circ = 1.44$ V).[13]

EXPERIMENTAL

Materials

$Cr(bpy)_3^{3+}$ (as the ClO_4^- salt) was synthesized according to literature procedures.[14] Acrylamide (Fluka puriss) was used without further purification. The solutions were prepared with doubly-

† Author to whom correspondence should be addressed.

distilled water and deaerated by bubbling with argon for 45 min. The pH of the solutions was adjusted with HCIO4 to +0.02 units; the ionic strength was not controlled.

Procedures

The irradiations at 365 nm were performed with a high pressure mercury lamp (Osram HBO 200W) equipped with a grating monochromator (Bausch and Lomb). The beam was parallel and the reactor was a square cuvette with a 1 cm pathlength. The incident light intensity was determined by ferrioxalate actinometry (Io~ 1-2x1015 photon cm 2 s--l). In order to study the effect of the absorbed light intensity on the polymerization rate neutral density filters were placed in front of the cell.

Absorption spectra were recorded on a Cary 118C spectrophotometer; emission spectra were obtained with a Jobin Yvon JY 3C spectrofluorimeter equipped with a red-sensitive Hamamatsu detector. The extent of quenching of *Cr(bpy)33+ by acrylamide was determined by monitoring the emission intensity at 727 nm as a function of *[AA]*. The polymer was precipitated by pouring the irradiated solution into methanol; the polymer was separated and weighed, which offered a measure of the fractional conversion of acrylamide into polymer. The rate of polymerization, Rp, was taken from the slope of the linear part of the plot of per cent of monomer conversion vs irradiation time ; the precision of the values of Rp is estimated to be _ 10%.

RESULTS

Quenching and photochemistry

A linear Stern-Volmer plot from emission intensity measurements *(Io/Ivs* [AA]) yields kq = 3 × 103 M-~ s-1 in the presence and absence of air. Irradiation of a deaerated solution at 365 nm, containing 0.11 mM Cr(bpy)33+ and 1 M AA at pH 2.24, resulted in spectral changes that indicated the formation of the aquation product Cr(bpy)2 (OH2)23+ (Fig. 1). The quantum yields of photoaquation (~pa) were virtually the same in the absence (7.0x 10-4) and presence (8.0x 10-4) of 1 MAA.

Rate of polymerization

All experiments were performed on carefully deaerated solutions ; in aerated solutions only traces of polymer were observed. Figure 2 shows a plot of the per cent of monomer conversion vs irradiation

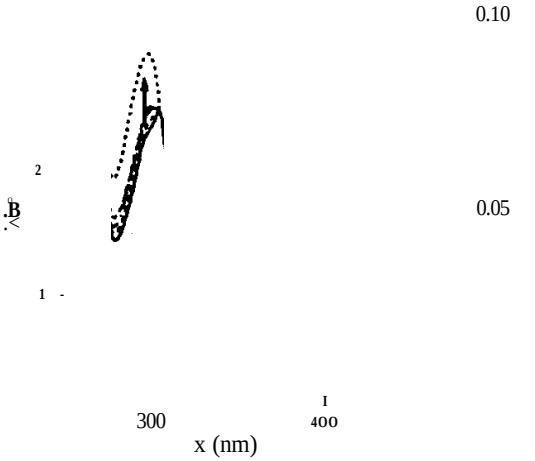

Fig. 1. Spectral changes upon irradiation at 365 nm m the absence of air at pH 2.24. [Cr(bpy)33+] = 0.11 raM; [AA] = 1 M.

time; a steady state was attained without any detectable induction period and the polymerization rate was constant over a large extent of the photoreaction. Since the formation of a gel at high conversion (> 50%) made the solution difficult to handle, the influence of the various parameters on Rp was studied at conversions usually lower than 25%.

Influence of [Cr(bpy)33+]. The variation of Rp as a function of [Cr(bpy)33+] is shown in Fig. 3. In the studied domain the rate of polymerization decreased with an increase in the concentration of the complex.

Influence of pH. The variation of Rp with pH is complex (Fig. 4), with Rp first rising to a plateau with increasing pH, then falling off around pH 4. Due to the pH dependence all other experiments were performed at a pH in the plateau range.

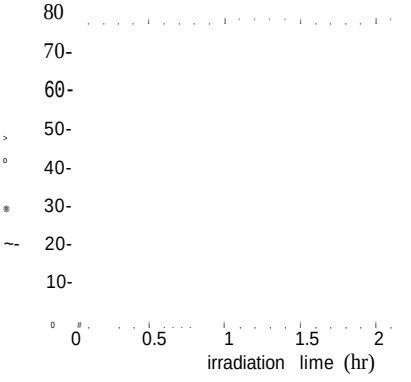

Fig. 2. Plot of per cent conversion of monomer vs irradiation time in the absence of air at pH 2.70. [Cr(bpy)33+1 = 0.12 mM ; [AA] = 1 M.

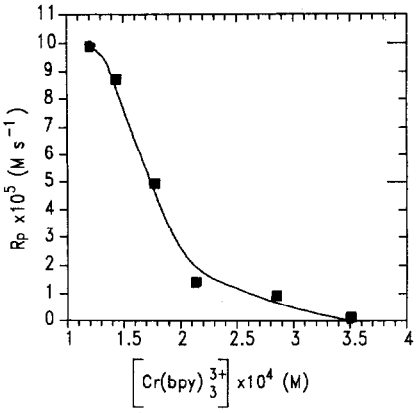

Fig. 3. Plot of R_p vs $[Cr(bpy)_3^{3+}]$ at pH 2.75. [AA] = 1 M.

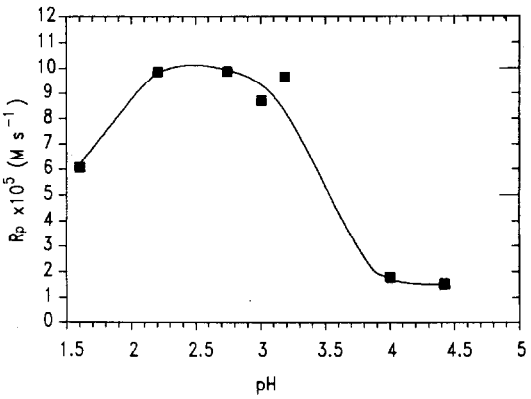

Fig. 4. Plot of R_p vs pH. $[Cr(bpy)_3^{3+}] = 0.12$ mM; [AA] = 1 M.

Influence of absorbed light intensity and [AA]. R_p is directly proportional to I_a (Fig. 5) and shows a square dependence on [AA] (Fig. 6).

Influence of excitation wavelength. A few experiments were performed at 400, 425 and 450 nm. Polymerization was observed with values of R_p of the order 10^{-5} mol dm^{-3} s^{-1}.

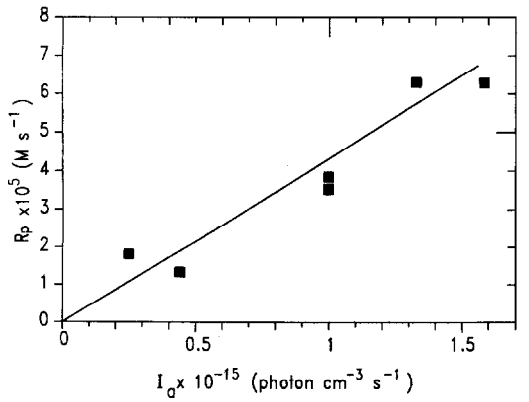

Fig. 5. Plot of R_p vs I_o at pH 2.93. $[Cr(bpy)_3^{3+}]$ = 0.14 mM; [AA] = 1 M.

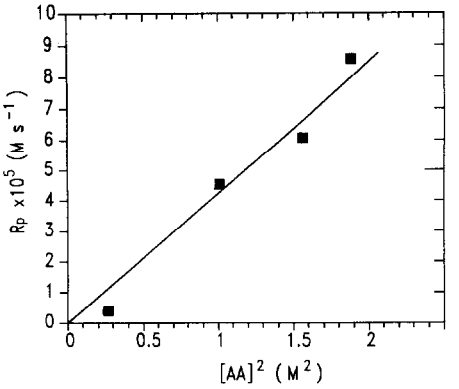

Fig. 6. Plot of R_p vs $[AA]^2$ at pH 2.20. $[Cr(bpy)_3^{3+}]$ = 0.14 mM.

DISCUSSION

From the results we can propose the following simplified scheme of acrylamide polymerization photosensitized by $Cr(bpy)_3^{3+}$.

(1) *Photophysics and photochemistry*

Reactions (1)–(3) describe the formation and disappearance of $*Cr(bpy)_3^{3+}$. The lifetime of the excited state in the absence of quencher is determined by the rates of the various decay modes; $\tau_o = 1/(k_o + k_{pa})$. Reaction (3) is a complex multistep process, presumably involving the formation of a seven-coordinate intermediate from the attack of H_2O at the metal centre and subsequent ligand loss and solvent substitution.

$$Cr(bpy)_3^{3+} \xrightarrow{h\nu} *Cr(bpy)_3^{3+} \quad (1)$$

$$*Cr(bpy)_3^{3+} \xrightarrow{k_o} Cr(bpy)_3^{3+} (+h\nu') \quad (2)$$

$$*Cr(bpy)_3^{3+} + 2H_2O \xrightarrow{k_{pa}} Cr(bpy)_2(OH_2)_2^{3+} + bpy \quad (3)$$

(2) *Initiation*

Reaction (4) describes the electron-transfer quenching of $*Cr(bpy)_3^{3+}$ by acrylamide:

$$*Cr(bpy)_3^{3+} + AA \xrightarrow{k_q} Cr(bpy)_3^{2+} + M^{\cdot}, \quad (4)$$

where $M^{\cdot}$ is the radical arising from the oxidation of the monomer. Due to the value of k_q, the extent of quenching, even with 1 M AA, is quite low. Furthermore, the formation of $Cr(bpy)_3^{2+}$ is not observed in pulsed-laser flash photolysis; the quantum yield of redox products is estimated to be <0.01.

The rate of initiation (R_i) is equal to ΦI_a, where

@ is the quantum yield of M" formation in reaction (4); qb is given as $kq[AA]/(ka+kq[AA])$ with kd = ko+kp~. Due to the low extent of quenching and the low value of ~p,, Ri = $(kq/ko)[AA]Ia$.

(3) *Propagation*

$$M'+AA \xrightarrow{k1} M2"$$

$$M2"+AA \xrightarrow{k2} M3"$$

$$M._{}l"+AA \xrightarrow{4r,} M,"$$

The rate of propagation (Rpr) is equal to kpr[P'][AA], where [P'] is the total concentration of radicals.

(4) *Termination*

It is proposed that in the presence of the photosensitizer the radicals (probably carbon-centred radicals adjacent to an amide moiety) react with Cr(bpy)33+ ($E°= -0.25$ V), according to redox reaction (5); the rate of termination (Rt) is equal to kt[P'][Cr(bpy)33+].

$$p.+Cr(bpy)33+ \xrightarrow{k,} polymer+Cr(bpy)32+ \quad (5)$$

(5) *Overall kinetics*

For the overall process, [P'] = $(kq/kokt)[AA]I~/$ [Cr(bpy)33+]; the rate of polymerization is given by equation (6), where Rp = Rpr.

$$Rp = \frac{Fkqkpr]\ [nA]2Ia}{L\ kokt\ _][Cr(bpy)33+]} \quad (6)$$

Thus, the proposed mechanism accounts for a first-order dependence of Rp on/~ (Fig. 5), a second-order dependence on [AA] (Fig. 6) and predicts an inverse first-order dependence on Cr(bpy)33+ at constant [AA] and Ia.

Inasmuch as Ia is a function of [Cr(bpy)33+] via Beer's Law, a plot of *Rp/I*, vs 1/[Cr(bpy)33+] from the data in Fig. 3 should be linear with a y-intercept of zero. Such a plot is shown in Fig. 7, although we are at a loss to account for the non-zero intercept. Nevertheless, we feel that linear behavior demonstrates, in a general way, the efficacy of the mechanism.

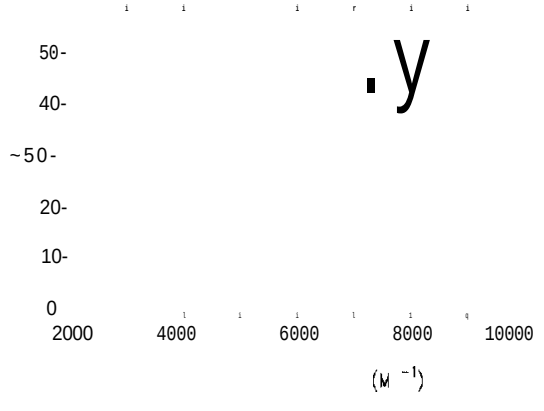

Fig. 7. Plot of *Rp/I~* vs 1/[Cr(bpy)33+].

CONCLUSION

Cr(bpy)3 3+ is a suitable photosensitizer for the polymerization of acrylamide in acidic aqueous solution by near-UV and visible light. However, the low value of the rate constant for the quenching of *Cr(bpy)33+ by acrylamide and the low cage escape of the redox products are features that severely limit the overall efficiency of the process.

Acknowledgements--This research was supported in part by the Office of Basic Energy Sciences, Division of Chemical Sciences, U.S. Department of Energy. M.B. and M.Z.H. also acknowledge support from the NATO Collaborative Research Grants Programme (CRG 900037). The authors thank Hai Sun for assistance with the pulsed-laser flash photolysis experiments.

REFERENCES

1. T. Okimoto, Y. Inaki and K. Takemoto, *J. Macromolec. Sci. Chem.* 1973, A7(8), 1537.
2. A. Abbas and I. Tadjudin, *J. Photochem.* 1986, 35, 87.
3. H. Kothandaraman and M. Santappa, *J. Polym. Sci. Polym. Chem. Ed.* 1971, 9, 1351.
4. K. Kaeriyama and Y. Shimura, *Makromolec. Chem.* 1973, 167, 129.
5. R. Bhaduri and S. Aditya, *Makromolec. Chem.* 1977, 178, 1385.
6. G. A. Delzenne, *J. Polym. Sci. Part C.* 1967, 16, 1027.
7. K. Iwai, M. Uesugi and F. Takemura, *Polym. J.* 1985, 17, 1005.
8. P. Fageol, M. Bolte and J. Lemaire, *J. Phys. Chem.* 1988, 92, 239.
9. P. Fageol and M. Bolte, *Makromolee. Chem.* 1989, 190, 367.
10. P. Fageol and M. Bolte, *Makromolec. Chem. Rapid Commun.* 1989, 10, 533.
11. T. Galcera, X. Jouan and M. Bolte, *J. Photochem. Photobiol. A Chem.* 1988, 45, 249.
12. G. Neshvad, M. Z. Hoffman, M. Bolte, R. Sriram and N. Serpone, *Inorg. Chem.* 1987, 26, 2984 and refs therein.
13. M. A. Jamieson, N. Serpone and M. Z. Hoffman, *Coord. Chem. Rev.* 1981, 39, 121.
14. B. R. Baker and B. D. Hehta, *Inorg. Chem.* 1965, 4, 848.

Polyhedron Vol. 12, No. 8, pp. 859–864, 1993
Printed in Great Britain

0277–5387/93 $6.00+.00
© 1993 Pergamon Press Ltd

BOROSILICATE COMPOUNDS OF THE TYPE $H_2N(CH_2)_3OB(R)(OSiR'_3)$; THE STRUCTURE OF 2-(DIMETHYLPHENYLSILOXY)-2-PHENYL-1,3,2-OXAZABORINANE

GEORGE FERGUSON* and JOHN F. GALLAGHER

Chemistry Department, University of Guelph, Guelph, Ontario, Canada N1G 2W1

and

DENIS MURPHY, JAMES P. SHEEHAN and TREVOR R. SPALDING*

Chemistry Department, University College, Cork, Ireland

(*Received* 11 *November* 1992; *accepted* 18 *December* 1992)

Abstract—The syntheses of compounds of the types $H_2N(CH_2)_3OB(Ph)(OSiR'_3)$ [$R'_3 = Me_3$ (**1**), Me_2Ph (**2**), $MePh_2$ (**3**), Ph_3 (**4**)] and $H_2N(CH_2)_3OB(Bu)(OSiR'_3)$ [$R'_3 = Me_2Ph$ (**5**), $MePh_2$ (**6**), Ph_3 (**7**)] are reported. The structure of **2** was determined by X-ray crystallography. There are two independent molecules in the unit cell. Both molecules contain tetrahedral $BCNO_2$— and SiC_3O— units joined by B—O—Si bridges with angles of 145.7(3)° and 150.5(3)°, respectively. In solution compounds **1–7** are involved in intramolecular equilibrium reactions between four- and three-coordinate boron species with the latter formed by scission of the B—N bond.

The work described in this paper continues our studies on borosilicate chemistry.[1,2] Previously we have reported the solid state structure of $H_2N(CH_2)_3OB(Ph)(OSiMePh_2)$ (**3**),[1] which contained two tetrahedrally coordinated $BCNO_2$— and R_3SiO— units linked through an oxygen atom. Notable features in the structure of **3** included the large B—O—Si angle, 152.2(2)°, and short Si—O bond length, 1.585(2) Å.[1] In chloroform solution the ^{11}B NMR spectrum of **3** contained two peaks at 28.7 and 2.5 ppm in the ratio of 1 : 2.5.[2] Compound **1** was also reported to exhibit two peaks in its ^{11}B spectrum, at 28.9 and 3.5 ppm, in the ratio of 1 : 1.3.[2] The peaks at *ca* 29 ppm are consistent with a trigonally coordinated boron atom, while those at *ca* 3 ppm correspond to a tetrahedrally coordinated boron.[3] Hence, it was suggested that an equilibrium reaction involving the cleavage of the intramolecular B—N bond occurs in solution, eq. (1).[2]

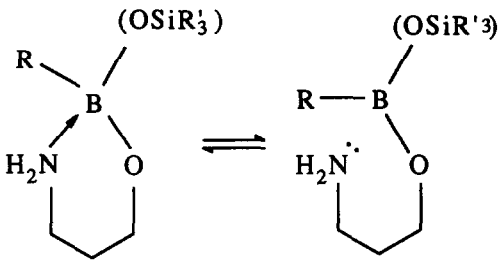

RESULTS AND DISCUSSION

Compounds **1–7** were obtained from the reactions between $PhB(OSiR'_3)_2$ or $BuB(OSiR'_3)_2$ and $NH_2(CH_2)_3OH$ in dichloromethane at room temperature. Reaction times were either 0.5 h (**1** and **3** only) or 24 h and yields varied between 27% (**3**) and 76% (**2**). These borosilicate compounds are relatively stable in air in the solid state and dissolve readily in non-reacting organic solvents. We decided to determine the solid state structure of a typical member of the series and chose compound **2**, 2-(dimethylphenylsiloxy)-2-phenyl-1,3,2-oxazaborinane.

* Authors to whom correspondence should be addressed.

Crystals of **2** suitable for X-ray crystallographic analysis were grown from a toluene/heptane solution. The unit cell of **2** contains two independent molecules [(A) and (B)] with very similar geometries and conformations. Fig. 1 is a view of molecule (A). Selected bond angles and distances for both (A) and (B) are listed in Table 1. Each molecule contains tetrahedral $BCNO_2$— and Me_2PhSiO— units. The boron atom is part of a six-membered BOC_3N ring which has a chair conformation. The deviation of the atoms C(3) and B from the O(1), N(1), C(2), C(4)-containing mean-plane for molecule (A) are −0.684(7) and 0.637(6) Å, and for molecule (B), −0.689(7) and 0.656(6) Å, respectively.

As can be seen from Table 1 there are only small differences between the two molecules. The largest difference between them is the difference of 4.8° in the B—O—Si angles, which are 145.7(3)° and 150.5(3)° in (A) and (B), respectively. In the compound $H_2\overline{N(CH_2)_3OB(Ph)(OSiMePh_2)}$ (**3**) the B—O—Si angle was 152.2(3)°.[2] For comparison the mean value of the B—O—Si angle in the borosilicate mineral datolite, $CaBSiO_4(OH)$,[4] which contains BO_3OH sites, is 124.3°. In the mineral homilite $Ca_{2.00}(Fe_{0.90}Mn_{0.03})B_{2.0}Si_{2.0}O_{9.86}(OH)_{0.14}$, which also contains tetrahedral boron sites, there are three independent B—O—Si angles which are between 119.2(1)° and 125.7(1)°.[5]

The mean Si—O bond length in **2** is 1.601(2) Å, significantly shorter than the value in $(Ph_3Si)_2O$, 1.616(1) Å,[6] but longer than that in **3**, 1.585(2) Å. The mean B—O(1) and B—O(2) bond lengths in **2** are 1.454 and 1.443 Å, respectively, which may be compared with the B—O(1) and B—O(2) distances in **3** of 1.461(3) and 1.439(4) Å, respectively.[1,2]

The mean B—N bond length of 1.641(6) Å in **2** is comparable with B—N distances of 1.639(4) in **3** and 1.638(3) Å in $Ph_2\overline{BO(CH_2)_3N}H_2$.[7(a)]

None of the B—C, C—O, C—N and C—C bond lengths in **2** are unusual. For each molecule there is an intermolecular hydrogen bond between one of the N—H hydrogens and the oxygen atom in the BOC_3N ring of an adjacent molecule [see Fig. 2, NA···OA 2.883(4) and NB···OB 2.927(4) Å], which leads to infinite hydrogen bonded chains of (A) and (B) molecules. Similar hydrogen bonding occurs in compound **3**.[1,2]

All the ^{11}B NMR spectra of compounds **1**–**7** in

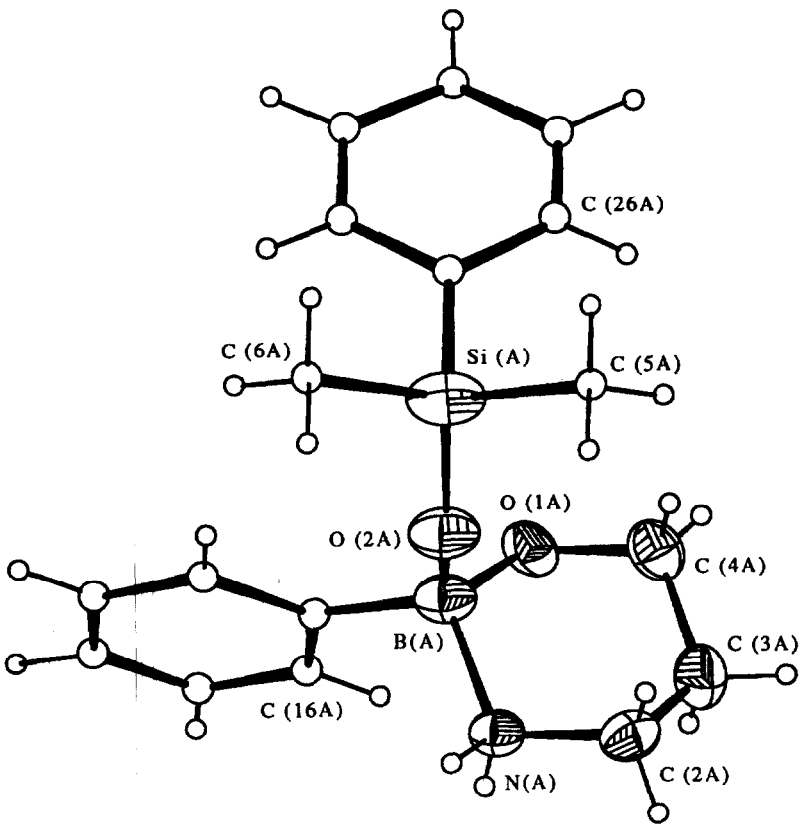

Fig. 1. A view of one of the two independent molecules of **2**, showing conformation and the numbering scheme.

Table 1. Selected bond lengths (Å) and bond angles (°) in $H_2N(CH_2)_3OB(Ph)(OSiMe_2Ph)$ (**2**)

	Molecule (A)	Molecule (B)
Si—O(2)	1.602(3)	1.599(3)
Si—C(5)	1.846(6)	1.844(5)
Si—C(6)	1.860(6)	1.848(5)
Si—C(21)	1.866(4)	1.876(4)
B—O(1)	1.455(6)	1.452(6)
B—O(2)	1.443(6)	1.442(6)
O(1)—C(4)	1.420(5)	1.424(6)
N—C(2)	1.485(5)	1.483(5)
N—B	1.639(6)	1.642(6)
C(2)—C(3)	1.516(7)	1.520(7)
C(3)—C(4)	1.506(7)	1.502(8)
C(11)—B	1.611(7)	1.598(6)
Si—O(2)—B	145.7(3)	150.5(3)
O(2)—Si—C(5)	109.8(2)	110.8(2)
O(2)—Si—C(6)	109.6(2)	108.2(2)
O(2)—Si—C(21)	112.1(2)	111.6(2)
C(5)—Si—C(6)	107.8(3)	108.1(3)
C(5)—Si—C(21)	108.5(2)	109.6(2)
C(6)—Si—C(21)	108.9(2)	108.4(2)
O(1)—B—O(2)	114.9(4)	115.3(4)
O(1)—B—N	106.6(3)	106.5(3)
O(1)—B—C(11)	108.7(4)	108.7(4)
O(2)—B—N	103.1(3)	102.4(3)
O(2)—B—C(11)	114.9(4)	115.4(4)
N—B—C(11)	108.1(3)	107.6(3)

either chloroform or dichloromethane at ambient temperature contain two broad singlet peaks (Table 2). Generally, it can be seen that for each set of compounds (R = Ph or Bu) the tetrahedral species becomes more favourable with increasing number of phenyl groups on the silicon atom; compound **2** is the only exception.

The tetrahedrally coordinated phenylboron compounds are relatively more stable than the corresponding butylboron compounds. Indeed, it is noteworthy that for $H_2N(CH_2)_3OB(Bu)(OSiMe_2Ph)$ the trigonally coordinated boron species is more stable in solution at ambient temperature. The underlying causes of the observed sequence are not clear at this time and we are continuing our study of this phenomenon with a view to determining if it can be rationalized on the basis of electronic and/or steric arguments.

There appear to be no previous reports in the literature of any reactions such as (1) which involve boron-containing compounds analogous to **1**–**7**. Rettig and Trotter have determined the structures (by X-ray analysis) of compounds such as $H_2N(CH_2)_3OBPh_2$ and $H_2N(CH_2)_2OBR_2$ (R = Ph, MeC_6H_4, FC_6H_4),[7] which contain intramolecular B—N bonds and are broadly similar to **1**–**7**, but they did not report any ^{11}B NMR data. However, ring rearrangement–isomerization reactions of compounds of the types **8** and **9**, which occur with the cleavage of the B—N bonds, have been studied by Contreras, Wrackmeyer and coworkers using ^{11}B, ^1H and ^{13}C NMR techniques.[8a,b] Activation energies for the ring inversion reactions of **8a** and **b** were 59.6 ± 1 and 49.2 ± 1 kJ M^{-1}, respectively, and for isomerization reactions which occur at the nitrogen atom in four compounds of type **9** the activation energies ranged from 61 ± 4 to > 80 kJ M^{-1}.

Table 2. ^{11}B NMR data on compounds of the type $H_2N(CH_2)_3OB(R)(OSiR'_3)$

Compound	R	R_3	$\delta(^{11}B)$ ppm	Relative intensity
1[a]	Ph	Me_3	28.5	(1.0)
			3.5	(1.3)
2[a]	Ph	Me_2Ph	28.5	(1.0)
			2.3	(3.4)
3[a]	Ph	$MePh_2$	28.7	(1.0)
			2.5	(2.5)
4[b]	Ph	Ph_3	27.9	(1.0)
			4.1	(2.7)
5[b]	Bu	Me_2Ph	31.8	(1.0)
			6.0	(0.7)
6[b]	Bu	$MePh_2$	31.6	(1.0)
			4.8	(1.2)
7[b]	Bu	Ph_3	31.7	(1.0)
			4.7	(1.4)

[a] Solvent $CHCl_3$.
[b] Solvent CH_2Cl_2.

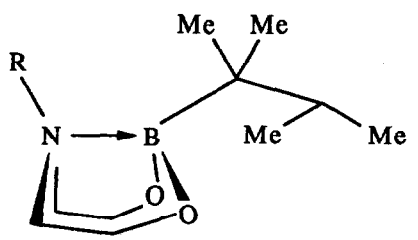

8; R = H (**a**), Me (**b**)

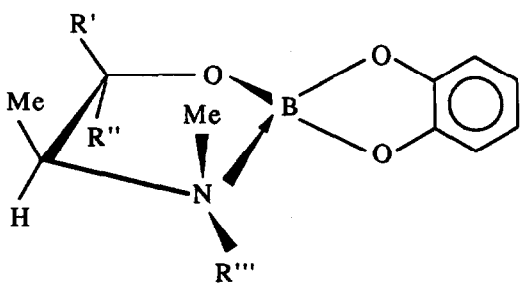

9

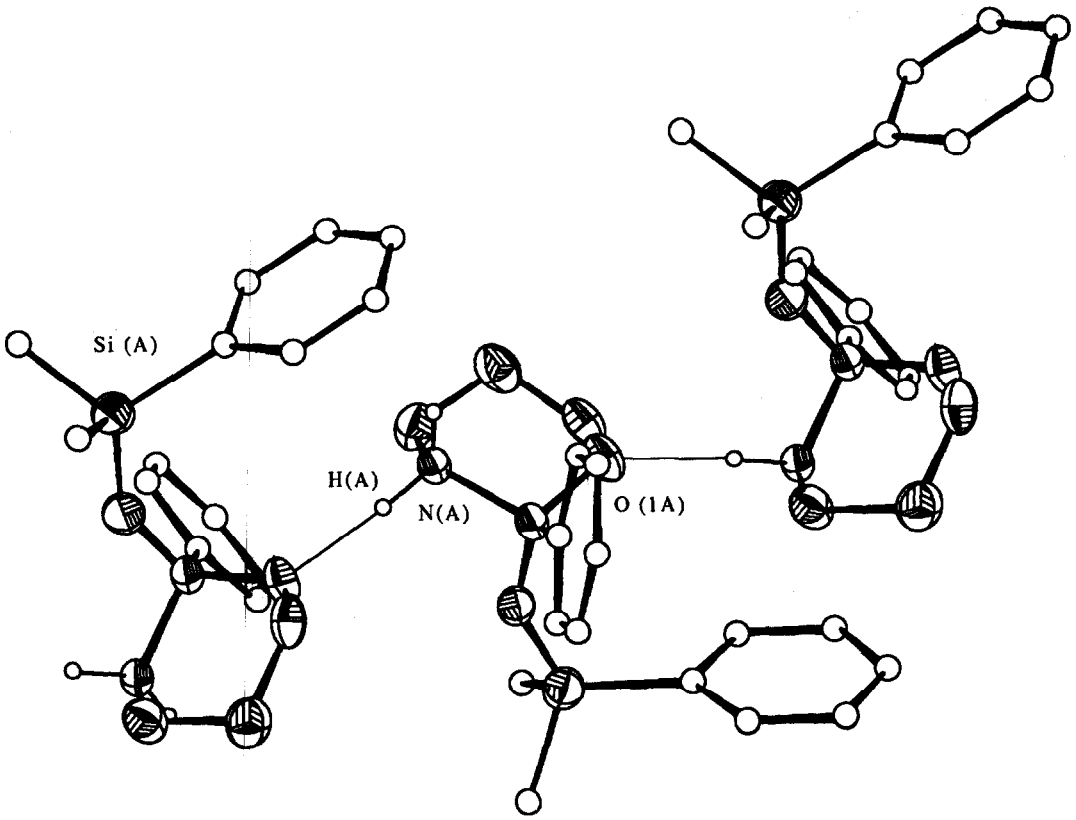

Fig. 2. Part of a hydrogen-bonded chain in **2**.

EXPERIMENTAL

General

Elemental analyses were carried out at UCC. Melting points are uncorrected. IR spectra were recorded, as KBr discs, on a Perkin–Elmer 682 IR spectrometer. The ^{1}H NMR spectra were recorded on a JEOL FX60 FT NMR spectrometer operating at 33°C, while the ^{11}B NMR spectra were recorded on a JEOL FT GSX-270 series NMR spectrometer at 25°C. Chemical shifts, δ ppm, are reported relative to $SiMe_4$ (^{1}H) and BF_3OEt_2 (external) (^{11}B) and positive values represent shifts to higher frequencies of the standards. All reactions were carried out under inert atmospheres. Solvents were distilled under an inert atmosphere from the appropriate drying agents prior to use.

The 3-aminopropanol was used as supplied by Aldrich, $PhB(OSiPh_3)_2$ was synthesized by reacting 2 equivalents of Ph_3SiOH with 1 equivalent of $PhB(OH)_2$ in refluxing toluene.[1] The water produced was removed azeotropically and collected in a Dean–Stark apparatus. The compounds $PhB(OSiR'_3)_2$ ($R = Me_3$, Me_2Ph, $MePh_2$) and $BuB(OSiR'_3)_2$ ($R = Me_2Ph$, $MePh_2$, Ph_3) were synthesized by reacting $PhB(OH)_2$ or $BuB(OH)_2$ with the appropriate organosilylchloride in the presence of base (Et_3N).[1]

Preparation of compounds **1–7**

1 - (*Trimethylsiloxy*) - 2 - *phenyl* - 1,3,2 - *oxazaborinane* (**1**). To a dichloromethane solution (20 cm^3) of $PhB(OSiMe_3)_2$ (0.810 g, 3.042 mmol) was added dropwise a dichloromethane solution (20 cm^3) of $NH_2(CH_2)_3OH$ (0.233 cm^3, 3.042 mmol) at room temperature. The clear solution was stirred for 0.5 h, after which time the solvent was removed under reduced pressure to leave a white solid. Recrystallization from dichloromethane/heptane solution afforded colourless microcrystals of **1** in 34% yield (0.260 g, 1.034 mmol); m.p. = 80–81°C. Found: C, 57.6; H, 8.4; N, 6.3. Calc. for $C_{12}H_{22}BNO_2Si$: C, 57.4; H, 8.8; N, 5.6%. ^{1}H NMR ($CDCl_3$): 7.54–7.06 (m, 5H, C_6H_5), 3.80 (t, 2H, CH_2O), 3.22 (s, 2H, NH_2), 2.86 (t, 2H, CH_2N), 1.54 (m, 2H, CH_2—CH_2—CH_2—), 0.26 [s, 9H, $(CH_3)_3$—Si]. IR, ν_{max} cm^{-1}: 3318m, 3282m, 3046s, 3020s, 2962s, 2925m, 2858s, 1615s, 1432m, 1406m, 1376m, 1335s, 1310m, 1276m, 1242s, 1266vs, 1195vs, 1114s, 1102vs, 1081s, 1072vs, 1064s, 1050m, 1005s, 1005s, 954m, 948m, 903s, 891m, 857m, 835s, 802m, 752s, 723s, 706vs.

2-(*Dimethylphenylsiloxy*)-2-*phenyl*-1,3,2-*oxazaborinane* (**2**) $PhB(OSiMe_2Ph)_2$ (0.677 g, 1.774 mmol) and $NH_2(CH_2)_3OH$ (0.133 cm^3, 1.774 mmol) were reacted as dichloromethane solutions in a procedure similar to the preparation of **1** for 24 h. Compound **2** was obtained in 76% yield (0.413 g, 1.319 mmol), m.p. = 101–102°C, on recrystallization from dichloromethane/heptane solution. Found: C, 65.2; H, 7.8; N, 4.0. Calc. for $C_{17}H_{24}BNO_2Si$: C, 65.2; H, 7.7; N, 4.5%. ^1H NMR ($CDCl_3$): 7.88–7.10 (m, 10H, BC_6H_5 and SiC_6H_5), 3.76 (t, 2H, CH_2O), 3.28–2.60 (m, 4H, H_2NCH_2), 2.10–1.30 (m, 2H, CH_2—CH_2—CH_2), 0.23 [s, 6H, $Si(CH_3)_2$]. IR, ν_{max} cm^{-1}: 3260m, 3060m, 3045m, 3000m, 2985m, 2965m, 2935m, 2910m, 1422m, 1415m, 1365m, 1338m, 1325m, 1245m, 1235m, 1223m, 1190m, 1110vs, 1090m, 1066s, 1054m, 1038m, 995m, 948m, 890m, 815m, 790m, 768m, 735m, 720s, 695s, 648s, 635m.

Structural analysis of **2**. Table 3 gives a concise summary of data collection, structure solution and refinement details of the X-ray analysis of **2**. Selected bond lengths and angles are given in Table 1. Figures 1 and 2 are views of a molecule prepared using ORTEP II.[9] A complete list of final fractional coordinates, dimensions, thermal parameters and structure factors has been deposited as supplementary material with the Editor, from whom copies are available on request.

2-(*Diphenylmethylsiloxy*)-2-*phenyl*-1,3,2-*oxazaborinane* (**3**). $PhB(OSiMePh_2)_2$ (1.089 g, 2.099 mmol) and $NH_2(CH_2)_3OH$ (0.161 cm^3, 2.099 mmol) were reacted as dichloromethane solutions using the procedure employed in the preparation of **1**. Compound **3** was obtained in 27% yield (0.210 g, 0.567 mmol); m.p. = 108–111.5°C. Found: C, 70.5; H, 6.7; N, 3.6. Calc. for $C_{22}H_{26}BNO_2Si$: C, 70.4; H, 7.0; N, 3.7%. ^1H NMR ($CDCl_3$): 7.65–6.98 [m, 15H, BC_6H_5 and $Si(C_6H_5)_2$], 3.64 (t, 2H, OCH_2), 3.29 (s, 2H, NH_2), 2.82 (t, 2H, NCH_2), 1.47 (m, 2H, CH_2—CH_2—CH_2), 0.40 (s, 3H, CH_3Si). IR, ν_{max} cm^{-1}: 3286m, 3076s, 3054m, 3001m, 2867m, 1594m, 1432m, 1334m, 1252m, 1233s, 1198s, 1125vs, 1118vs, 1096s, 1078s, 1064s, 1032w, 998m, 897m, 786s, 759m, 730vs, 712s, 704s.

2-(*Triphenylsiloxy*)-2-*phenyl*-1,3,2-*oxazaborinane* (**4**). $PhB(OSiPh_3)_2$ (2.000 g, 3.131 mmol) and $NH_2(CH_2)_3OH$ (0.234 cm^3, 3.131 mmol) were reacted as dichloromethane solutions using the procedure employed in the preparation of **2**. Compound **4** was obtained in 74% yield (1.048 g, 2.396 mmol), m.p. = 138–140°C, on recrystallization from dichloromethane/heptane solution. Found: C, 73.9; H, 6.2; N, 3.1. Calc. for $C_{27}H_{28}BNO_2Si$: C, 74.1; H, 6.5; N, 3.2%. ^1H NMR ($CDCl_3$): 7.80–7.03 [m, 20H, BC_6H_5 and $Si(C_6H_3)_3$], 3.78 (t, 2H, OCH_2), 3.20 (s, 2H, NH_2), 2.87 (t, 2H, NCH_2), 1.55–1.22 (m, 2H, CH_2—CH_2—CH_2). IR, ν_{max} cm^{-1}: 3040m, 3020m, 2970m, 2940m, 1586m, 1419s, 1324m, 1239m, 1190m, 1110vs, 1072m, 1060m, 890m, 740m, 730m, 698vs.

2-(*Dimethylphenylsiloxy*)-2-*butyl*-1,3,2-*oxazaborinane* (**5**). $BuB(OSiMe_2Ph)_2$ (1.142 g, 3.082 mmol) and $NH_2(CH_2)_3OH$ (0.236 cm^3, 3.082 mmol) were reacted as dichloromethane solutions using the procedure employed in the preparation of **2**. On evaporation of the solvent under reduced pressure a liquid was obtained, which became an oil after being pumped *in vacuo* overnight. On the addition of ice-cold heptane (20 cm^3) compound **5** was produced as a colourless solid in 33% yield (0.296 g, 1.009 mmol); m.p. = 62–64°C. Found: C, 61.1; H, 9.6; N, 4.3. Calc. for $C_{15}H_{28}BNO_2Si$: C, 61.4; H, 9.6; N, 4.8%. ^1H NMR ($CDCl_3$): 7.70–

Table 3. Summary of data collection, structure solution and refinement details

Formula	$C_{17}H_{24}BNO_2Si$
fw	313.3
Colour, habit	Colourless, block
Crystal size (mm)	0.35, 0.40, 0.35
Crystal system	Monoclinic
a (Å)	19.560(4)
b (Å)	9.880(2)
c (Å)	19.697(6)
β (°)	107.88(2)
V (Å^3)	3623(2)
Space group	$P2_1/c$
Z	8
F(000)	1344
d_{calc} (g cm^{-3})	1.15
μ (cm^{-1})	0.8
Diffractometer	Enraf–Nonius, CAD4
Radiation	Mo-K_α (λ = 0.7093 Å)
Monochromator	Graphite
2θ range (°)	4–48
Temperature (°C)	20
hkl range of reflections	0–22, 0–11, −22 to 21
Reflections measured	5822
Unique reflections	5647
R_{int}	0.015
Reflections with $I > 3\sigma(I)$	2344
Computer programs	NRCVAX[10] on Silicon Graphics 4D-380
No. of variables in LS	397
k in $w = 1/(\sigma^2 F_o + kF_o^2)$	0.001
R, R_w, g.o.f.	0.041, 0.051, 1.16
Density range in final Δ-map (e Å^{-3})	−0.16 to 0.16
Final shift/error ratio	0.003

7.17 (m, 5H, SiC_6H_5), 3.80 (t, 2H, OCH_2), 3.23–2.57 (m, 4H, NH_2CH_2), 1.95–1.50 (m, 2H, CH_2—CH_2—CH_2), 1.45–1.07 (m, 4H, BCH_2CH_2), 1.00–0.70 (m, 5H, CH_3CH_2), 0.40 [s, 6H, $Si(CH_3)_2$]. IR, ν_{max} cm^{-1}: 3270m, 3045m, 3020m, 2935s, 2960s, 1590m, 1450m, 1315s, 1405m, 1365m, 1340m, 1325s, 1259m, 1242s, 1110vs, 1090s, 1060s, 1030m, 918m, 885m, 822s, 775s, 735s, 698s, 640m.

2-(*Diphenylmethylsiloxy*)-2-*butyl*-1,3,2-*oxazaborinane* (**6**). $BuB(OSiMePh_2)_2$ (2.248 g, 4.545 mmol) and $NH_2(CH_2)_3OH$ (0.348 cm^3, 4.545 mmol) were reacted as dichloromethane solutions. Compound **6** was obtained in a procedure similar to **2** in 37% yield (0.581 g, 1.634 mmol); m.p. = 61–62°C. Found: C, 67.7; H, 8.9; N, 4.0. Calc. for $C_{20}H_{30}BNO_2Si$: C, 67.6; H, 8.5; N, 3.9%. ^1H NMR ($CDCl_3$): 7.66–7.07 [m, 10H, $Si(C_6H_5)_2$], 3.80 (t, 2H, OCH_2), 3.15–2.66 (m, 4H, NH_2CH_2), 1.90–1.45 (m, 2H, CH_2—CH_2—CH_2), 1.40–0.63 (m, 12H, BC_4H_9 and $SiCH_3$). IR, ν_{max} cm^{-1}: 3270m, 3040m, 3020m, 3000m, 2970m, 2930s, 2890m, 2850m, 1590m, 1475m, 1445m, 1418s, 1365m, 1349m, 1325m, 1271m, 1230m, 1180m, 1106vs, 1089s, 1050s, 1050s, 1020s, 992m, 971m, 945m, 915m, 875m, 860m, 780vs, 750s, 731s, 710s, 698vs, 659m.

2-(*Triphenylsiloxy*)-2-*butyl*-1,3,2-*oxazaborinane* (**7**). $BuB(OSiPh_3)_2$ (1.232 g, 1.891 mmol) and $NH_2(CH_2)_3OH$ (0.152 cm^3, 1.991 mmol) were reacted as dichloromethane solutions in a procedure similar to the preparation of compound **2**. Compound **7** was obtained in 73% yield (0.611 g, 1.463 mmol) on recrystallization from dichloromethane/heptane solution; m.p. = 97–98°C. Found: C, 72.5; H, 7.7; N, 2.9. Calc. for $C_{25}H_{32}BNO_2Si$: C, 72.9; H, 7.7; N, 3.4%. ^1H NMR ($CDCl_3$): 7.73–7.10 [m, 15H, $Si(C_6H_5)_3$], 3.78 (t, 2H, OCH_2), 3.43–2.66 (m, 4H, NH_2CH_2), 1.95–1.43 (m, 2H, CH_2—CH_2—CH_2), 1.40–0.40 (m, 9H, C_4H_9B). IR, ν_{max} cm^{-1}: 3044m, 3024m, 2902m, 2856m, 1590m, 1578m, 1475m, 1419s, 1370m, 1362m, 1295m, 1270m, 1226m, 1110vs, 1090m, 1062s, 1021m, 992m, 915m, 740m, 700vs.

Acknowledgement—G.F. thanks NSERC Canada for Grants in Aid of Research.

REFERENCES

1. G. Ferguson, A. J. Lough, J. P. Sheehan and T. R. Spalding, *Acta Cryst.* 1991, **C47**, 379.
2. J. P. Sheehan, MSc Thesis, U.C.C. (1989).
3. *Nuclear Magnetic Resonance Spectroscopy of Boron Compounds* (Edited by H. Nöth and B. Wrackmeyer). Springer-Verlag, Berlin (1978).
4. F. F. Forts, M. W. Philips and G. V. Gibbs, *Am. Min.* 1973, **58**, 909.
5. R. Miyawaki, I. Nakai and K. Nagashima, *Acta Cryst.* 1985, **C41**, 13.
6. C. Glidewell and D. C. Liles, *Acta Cryst.* 1978, **B34**, 124.
7. (a) S. J. Rettig and J. Trotter, *Can. J. Chem.* 1983, **61**, 2334; (b) 1973, **51**, 1288; (c) 1976, **54**, 3130; (d) S. J. Rettig and J. Trotter, *Acta Cryst.* 1974, **B30**, 2139.
8. (a) R. Contreras, C. Garcia, T. Mancilla and B. Wrackmeyer, *J. Organomet. Chem.* 1983, **246**, 213; (b) F. Santiesteban, M. A. Campos, H. Morales and R. Contreras, *Polyhedron* 1984, **3**, 589; (c) T. Mancilla, R. Contreras and B. Wrackmeyer, *J. Organomet. Chem.* 1986, **307**, 1; (d) T. Mancilla and R. Contreras, *J. Organomet. Chem.* 1987, **321**, 191; (e) N. Farfan, P. Joseph-Nathan, L. M. Chiquete and R. Contreras, *J. Organomet. Chem.* 1988, **34**, 149; (f) N. Frafan, T. Mancilla, D. Dastillo, G. Unibe, L. Carnillo, P. Joseph-Nathan and R. Contreras, *J. Organomet. Chem.* 1990, **381**, 1.
9. C. K. Johnson, ORTEP II, Report ORNL-5138. Oak Ridge National Laboratory, Tennessee (1976).
10. E. J. Gabe, Y. Le Page, J.-P. Charland, F. L. Lee and P. S. White, *J. Appl. Cryst.* 1989, **22**, 384.

Polyhedron Vol. 12, No. 8, pp. 865–870, 1993
Printed in Great Britain

0277–5387/93 $6.00+.00
© 1993 Pergamon Press Ltd

EFFECT OF COPPER(II), NICKEL(II) AND ALUMINUM(III) IONS ON THE HYDROLYSIS RATES OF INORGANIC CONDENSED PHOSPHATE OLIGOMERS

GENICHIRO KURA* and TOMOKI TSUKUDA

Department of Chemistry, Fukuoka University of Education, Akama, Munakata, Fukuoka 811-41, Japan

(*Received* 27 *October* 1992; *accepted* 18 *December* 1992)

Abstract—The effects of Cu^{2+}, Ni^{2+} and Al^{3+} on the hydrolysis rates of cyclic and linear condensed phosphate oligomers have been investigated. Al^{3+} ions affected the hydrolysis rate most strongly, except for the Al^{3+}-cyclo-octaphosphate system at pH 3. Cu^{2+} ions accelerated the rate more strongly than Ni^{2+} ions. The hydrolysis rate is influenced not only by the degree of complex formation with the cations, but also by the nature of the cation bonding in the complexes.

As the major components of condensed phosphates produced by the dehydration of the oxoacid of phosphorus(V), linear phosphates with linear chain structures and cyclophosphates with cyclic structures are well known. They have the general formula $M^{I}_{2n+1}P_nO_{3n+1}$ and $M^{I}_n(PO_3)_n$, respectively. The chemical properties of condensed phosphates having a relatively low degree of polymerization have been investigated because of the biochemical importance of ATP and ADP; however, the properties of the phosphates above the tetramer have not been studied because of the difficulty involved in their preparation and isolation. These oligomers are very important and interesting materials for electrolyte solution chemistry.[1]

When using these compounds for various purposes, for example, as water conditioners, detergent builders, food additives, etc., their hydrolysis properties must be known clearly. Cyclic phosphates are degraded to linear phosphates with the same degree of polymerization and they are also hydrolysed to linear and cyclic phosphates. It has been reported that the hydrolysis rate is significantly affected by experimental conditions such as temperature, H^+ and OH^- ion concentration and the presence of other cations.[2,3]

In this study, the effects of copper(II), nickel(II) and aluminum(III) ions on the hydrolysis reactions of the condensed phosphate oligomers with degrees of polymerization between 3 and 8 have been investigated. These three cations are known to have different rate constants for solvent exchange: the exchange rate for Cu^{2+} is fastest, for Ni^{2+} moderately slow and for Al^{3+} very slow, therefore, different catalytic effects can be expected. Moreover, for the Al^{3+} systems the investigation of the interaction with the phosphate anions is made possible by the ^{31}P and ^{27}Al NMR measurements and the effect of complexation on the hydrolysis rates can be discussed.

Aluminum(III) ions affected most strongly the degradation rate of the phosphates and copper(II) ions catalysed hydrolysis more strongly than nickel (II) ions.

In this paper cyclic and linear oligomers are abbreviated as P_{nm} and P_n, respectively; in both cases n indicates the degree of polymerization.

EXPERIMENTAL

Chemicals

Sodium salts of cyclo-tri-($Na_3P_3O_9 \cdot 6H_2O$), cyclo-tetra-($Na_4P_4O_{12} \cdot 4H_2O$) and cyclo-hexaphosphate ($Na_6P_6O_{18} \cdot 6H_2O$) were prepared following the methods described in the literature.[1,4,5] Sodium cyclo-octaphosphate ($Na_8P_8O_{24} \cdot 6H_2O$) and guanidinium tetraphosphate ($[NH_2]_2[C{=}NH_2]_6P_4O_{13} \cdot H_2O$) were prepared using modified methods of Schülke and Quimby, respectively.[6,7] Cyclo-penta- and -heptaphos-

* Author to whom correspondence should be addressed.

phate were isolated from the fractionated solution of Graham's salts, a high molecular weight polyphosphate [(NaPO3),, r7 = 100], using a QAE-Sephadex A-25 column. 8 Aluminum chloride, nickel nitrate and cupric perchlorate were used as metal ions. Cupric perchlorate was prepared by mixing perchloric acid and cupric carbonate. Other chemicals were reagent grade and commercially available.

The concentrations of metal ions were determined complexiметrically. The concentration of AI3+ was also determined by spectrophotometry with 5-sulpho-4'-diethylamino-2',-2-dihydroxyazobenzene (DDB). 9 The acidity of cupric perchlorate and aluminum chloride stock solutions was maintained at 0.1 M with perchloric acid and hydrochloric acid, respectively, to prevent hydrolysis.

Hydrolysis

The concentrations of condensed phosphate oligomers to be hydrolysed were 10-4-2.5 × 10-3 M and those of the metal ions added were 2.5 × 10 4_ 2.5 x 10 3 M. The pH of the test solutions was adjusted to pH 5 for the Ni 2÷ and Cu 2+ systems and to pH 3 for the A13+ systems with HNO3, HC104, HC1 or (CH3)4NOH. The pH of the test solutions was measured with a Horiba pH meter M8-S. The hydrolysis reaction was performed in an oil bath, whose temperature was maintained within _ 0.1°C. The phosphates were degraded at 50, 60 or 70°C. However, for the very slow rate systems, the hydrolysis temperature was increased to 90°C. At measured time intervals an aliquot of the test solutions was withdrawn and the reaction was stopped by a rapid neutralization or by the addition of EDTA, followed in either case by cooling.

Hydrolysis products were analysed with a Hitachi high-performance liquid chromatograph. 10

RESULTS AND DISCUSSION

Cyclic oligomers can be hydrolysed to linear oligomers having the same degree of polymerization and the linear oligomers can be similarly hydrolysed to lower linear and cyclic oligomers. The degradation rate constants are defined as :

$$P,m \quad km\ p, \quad k.\ pn_l,pn_2,...,p1,P3m.$$

The hydrolysis reactions of the condensed phosphates are known to be first-order under various experimental conditions and, therefore, if the concentration of cyclic and linear phosphates with the same degree of polymerization at time t are denoted as x and y, the rate can be expressed as :

$$-\frac{dx}{dt} = k,.x \qquad (1)$$

$$\frac{dy}{dt} - k, y-- kmx. \qquad (2)$$

Solving these differential equations by substituting a and b for the initial concentration of the cyclic and linear oligomers, respectively, yields the following equations :

$$x = a \exp(-kmt) \qquad (3)$$

$$Y - \left(k2\sim,,\right)^{kma} \exp(- kmt)$$

$$+\{b \quad (k-\sim m)^{kma}\}exp(-knt). \qquad (4)$$

The value of km was determined by the time dependence of the cyclic oligomer concentration and kn was calculated by the least-squares procedure substituting x, y and k,,, which are experimentally determined from the chromatograms of hydrolysis samples, for eq. (4).

In order to investigate the effect of metal ions on the hydrolysis reaction of condensed phosphates Ni 2+, Cu 2+ and A13+ were added to each phosphate solution and then the respective rates were determined. The pH of the solutions was adjusted to pH 5 for the Ni 2÷ and Cu e+ systems and to pH 3 for the A13÷ systems to avoid the hydrolysis of the metal ions. For the A13+ systems the concentration of H ÷ had to be kept relatively high and thus the effect of H ÷ on the hydrolysis rate was not negligible.

The rate constants determined for Ni 2– systems are summarized in Table 1. The rate constant for the Ni2+-Ps,, system at 90°C was calculated from its Arrhenius plots. The rate constants for these systems are also illustrated in Fig. 1. The rate constants of cyclic oligomers decreased with the degree of polymerization from 3 to 5 and then increased again. This trend can be explained in a similar manner to their hydrolysis in acidic solutions. 2'll The increasing flexibility in the ring structure of larger cyclic phosphates caused a strong affinity for Ni 2+, while the rate constant of linear oligomers slightly increased with the degree of polymerization, which is also similar to their behaviour in acidic media.

In the case of the Cu 2+ systems the rate data are shown in Fig. 2. The rate constants at 90°C for cyclo-tri-, tri- and tetraphosphate were obtained from their Arrhenius plots. The rates were extremely enhanced by the addition of Cu 2+ and the rate constants for cyclic oligomers had a minimum at a degree of polymerization near 5. For

Table 1. Rate constants of the condensed phosphate oligomers at 90°C in the presence and absence of Cu^{2+} and Ni^{2+}

		$10^2 k$ (h^{-1})					
	n	3	4	5	6	7	8
no M^{2+}	Cyclic	0.718	0.195	0.176	0.393		2.92
	Linear	52.0	58.7	173			
Cu^{2+}	Cyclic	112	9.20	94.0	1.30		49.1
	Linear	204	222	998			
Ni^{2+}	Cyclic	9.72	0.615	1.44	0.910		6.99
	Linear	35.3	117	493			

the linear oligomers, the rate constants gradually increased with the degree of polymerization.

The rate constants determined for the Al^{3+} systems are summarized in Table 2 and are also illustrated in Figs 3 and 4. Aluminum(III) ions also accelerated the hydrolysis rate of the oligomers, except for cyclo-octaphosphate. The reason why the rate did not change so much for cyclo-octaphosphate can be explained by a substitution reaction of Al^{3+} with H^+, which strongly affects the hydrolysis rate. At higher pH the enhancement of the rate of cyclo-octaphosphate by Al^{3+} might be expected. The degradation rates of linear oligomers were only slightly affected by Al^{3+}, probably because of the disturbance of bond formation of H^+ with terminal PO^- groups caused by the substitution of Al^{3+}.

The catalytic effect increased in the order: $Ni^{2+} < Cu^{2+} < Al^{3+} \ll H^+$. The hydrolysis reactions of condensed phosphate oligomers depended strongly on the cations present.[12] The catalytic effect of Al^{3+}, stronger than that of Ni^{2+} and Cu^{2+}, might be due to its stronger complex formation with the oligomers.[13,14] Ni^{2+} and Cu^{2+} complexes with cyclic phosphate anions were expected to have the same degree of stability constants;[13,15] therefore,

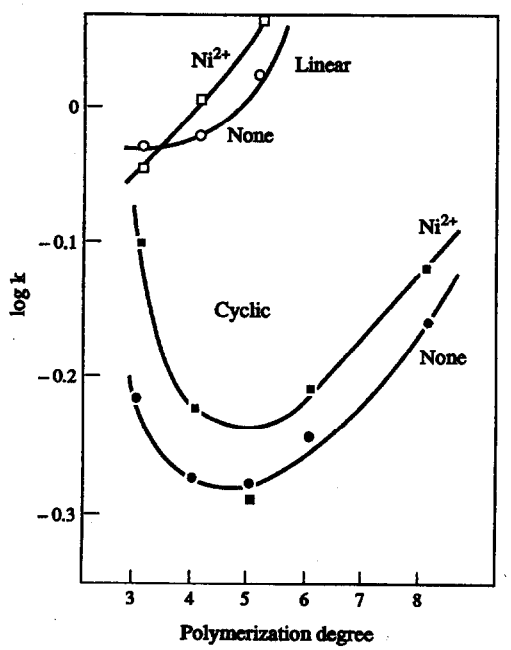

Fig. 1. Hydrolysis rate constants of the condensed phosphate oligomers in the presence and absence of Ni^{2+} at 90°C.

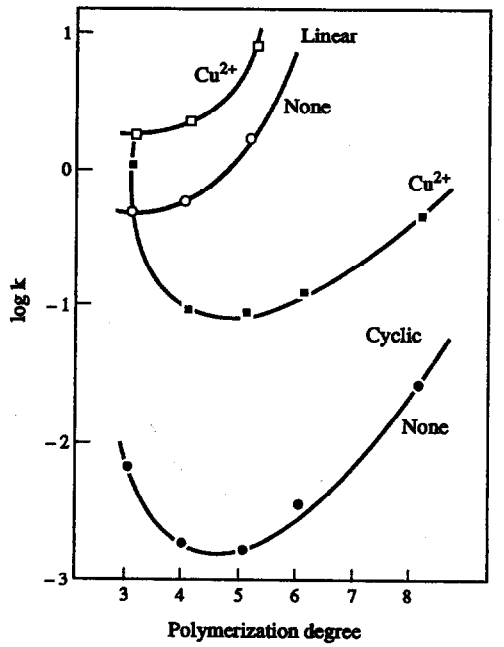

Fig. 2. Hydrolysis rate constants of the condensed phosphate oligomers in the presence and absence of Cu^{2+} at 90°C.

Table 2. Rate constants of the condensed phosphate oligomers at 70°C in the presence and absence of Al^{3+}

		$10^2 k$ (h^{-1})					
	n	3	4	5	6	7	8
no M^{3+}	Cyclic	4.63	1.94	1.10	5.19	3.63	57.4
	Linear	12.9	15.7	37.4	116	201	280
Al^{3+}	Cyclic	54.5	24.1	216	17.1	49.1	32.0
	Linear	11.8	13.0	195	388	617	269

the stronger catalytic effect of Cu^{2+} observed is presumed to be due to the difference in the M^{2+}—$^{-}$OP bond length in the complexes.

The activation energies of cyclic and linear oligomers in the presence of Al^{3+} were determined. Typical Arrhenius plots are shown in Fig. 5. Good linear relations were obtained and the activation energies are given in Table 3. The activation energies of cyclo-tri- and -tetraphosphate, which have a weak affinity with H^+, were decreased by *ca* 6–9 kcal mol^{-1} by the addition of Al^{3+}. However, a significant decrease in the activation energy for the other cyclic oligomers was not observed. The decrease in activation energies for linear hexa-, hepta- and octaphosphate systems can be also explained by their relatively weak affinity for H^+.

The rate depends not only on the type of cations present but also on their concentration. It has been thought that the rate acceleration in the presence of the cations might be due to complex formation between the cations and phosphate anions. If so, the rate equation, when complex forming cations are present, can be expressed as:

$$-\frac{dc}{dt} = k_0[P]+k_1[MP]+k_2[M_2P]+\cdots \quad (5)$$

where M and P denote cation and phosphate, respectively, and k_0, k_1 and k_2 denote the individual rate constants of the free phosphate, the 1 : 1 (M : P) complex and the 2 : 1 complex, respectively. If the formation of only the 1 : 1 and 2 : 1 complexes (or

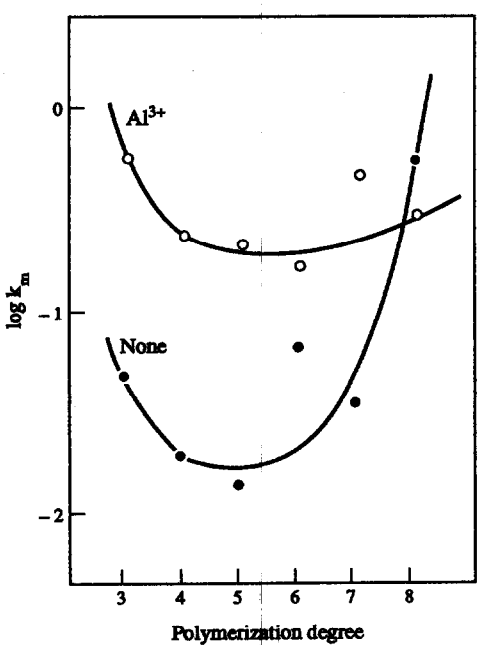

Fig. 3. Hydrolysis rate constants of the cyclic phosphate oligomers in the presence and absence of Al^{3+} at 70°C.

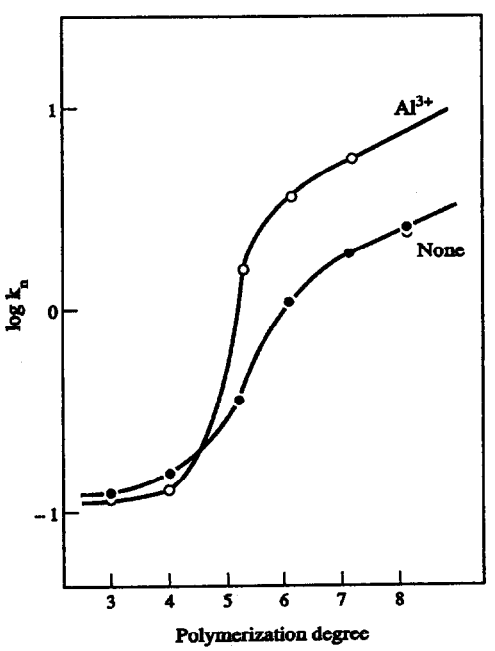

Fig. 4. Hydrolysis rate constants of the linear phosphate oligomers in the presence and absence of Al^{3+} at 70°C.

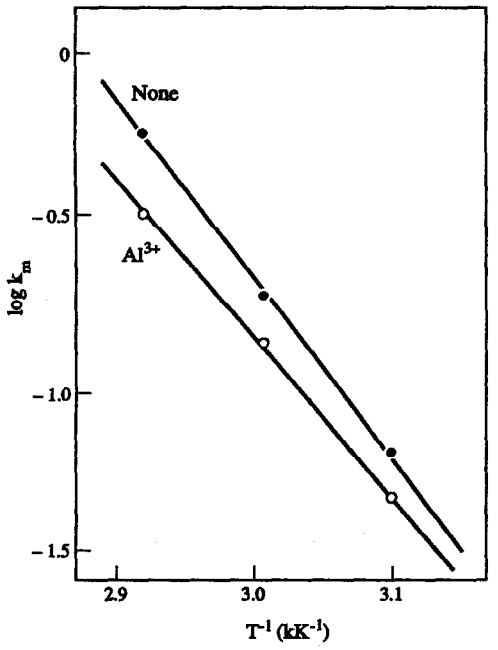

Fig. 5. Arrhenius plots for the Al^{3+}-cyclo-octaphosphate system.

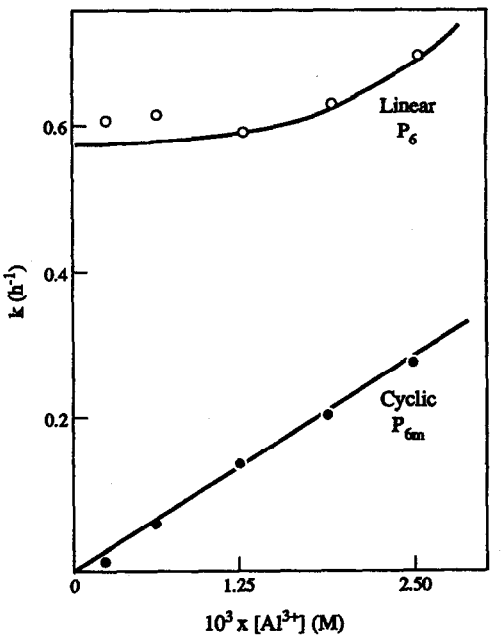

Fig. 6. Effect of Al^{3+} concentration on the rate constants of cyclo-hexa- and linear hexaphosphate at 50°C.

ion pairs) can be assumed and their stability constants are defined as:

$$\beta_1 = \frac{[MP]}{[M][P]} \quad \text{and} \quad \beta_2 = \frac{[M_2P]}{[M]^2[P]},$$

respectively, eq. (5) can be written as:

$$-\frac{dc}{dt} = k_0[P] + k_1\beta_1[M][P] + k_2\beta_2[M]^2[P] + \cdots. \tag{6}$$

The molar fraction of the free phosphate against the total phosphate concentration c can be written as:

$$\frac{[P]}{c} = \frac{1}{1+\beta_1[M]+\beta_2[M]^2},$$

and eq. (7) can be rewritten as:

$$-\frac{dc}{dt} = \frac{k_0 + k_1\beta_1[M] + k_2\beta_2[M]^2}{1+\beta_1[M]+\beta_2[M]^2}c. \tag{7}$$

The apparent rate constants can be expressed as:

$$k_{obs} = \frac{k_0 + k_1\beta_1[M] + k_2\beta_2[M]^2}{1+\beta_1[M]+\beta_2[M]^2}. \tag{8}$$

This concentration dependence of the rate was investigated for the Al^{3+}-cyclo-hexaphosphate system. The concentration of cyclo-hexaphosphate had to be fixed at 1.25×10^{-4} M to prevent precipitate formation, and the Al^{3+} concentration was varied from 2.5×10^{-4} to 2.5×10^{-3} M. The rate constant variation with the concentration of Al^{3+} for cyclo-hexa- and hexaphosphate is shown in Fig. 6. The rate constant for the cyclic hexamer nearly

Table 3. Activation energies (kcal mol^{-1}) of cyclic and linear phosphate oligomers in the presence and absence of Al^{3+}

	n	3	4	5	6	7	8
Cyclic	no M^{3+}	24.1	27.4	28.4	24.6	25.1	25.3
	Al^{3+}	18.7	18.6	27.3	25.4	23.9	22.5
Linear	no M^{3+}	25.8	26.3	24.0	26.6	21.9	22.9
	Al^{3+}	23.6	21.8	23.6	17.6	17.9	18.3

linearly varied with the Al^{3+} concentration. Assuming that $\beta_1[M] \gg \beta_2[M]^2$, 1 and $k_1\beta_1[M]$, $k_2\beta_2[M]^2 \gg k_0$, eq. (8) can be rewritten as:

$$k_{obs} = k_1 + \frac{k_2\beta_2}{\beta_1}[M]. \quad (9)$$

The linear relation between the rate constant observed and Al^{3+} ion concentration can be qualitatively explained by these assumptions. By contrast the rate for linear hexaphosphate did not vary much with Al^{3+} concentration. In an acidic solution, such as pH 3 for example, the complex formation between Al^{3+} and terminal PO^- groups may be difficult.

Acknowledgements—The authors are indebted to Miss Itsuko Nakamura and Miss Yumi Maeda for their help with the experiments and also gratefully acknowledge Professor Hirohiko Waki for his useful suggestions.

REFERENCES

1. J. R. van Wazer, *Phosphorus and its Compounds*, Vol. I. Interscience, New York (1958).
2. G. Kura, *Polyhedron* 1987, **6**, 531.
3. G. Kura, *Polyhedron* 1991, **10**, 697.
4. K. R. Andress, K. Fischer and W. Gehring, *Z. Anorg. Allg. Chem.* 1949, **260**, 331.
5. E. J. Griffith and R. L. Buxton, *Inorg. Chem.* 1965, **4**, 549.
6. U. Schülke, *Z. Anorg. Allg. Chem.* 1968, **360**, 231.
7. O. T. Quimby, *J. Phys. Chem.* 1954, **58**, 603.
8. G. Kura and S. Ohashi, *J. Chromatogr.* 1971, **56**, 111.
9. T. M. Florence, *Analyt. Chem.* 1965, **37**, 704.
10. G. Kura, *J. Chromatogr.* 1988, **447**, 91.
11. G. Kura, *Bull. Chem. Soc. Japan* 1983, **56**, 3769.
12. G. Kura, *Polyhedron* 1987, **6**, 1863.
13. G. Kura and S. Ohashi, *J. Inorg. Nucl. Chem.* 1976, **38**, 1151.
14. QI. Feng, H. Waki and G. Kura, *Polyhedron* 1991, **10**, 1537.
15. G. Kura and H. Waki, *Polyhedron* 1990, **9**, 511.

Polyhedron Vol. 12, No. 8, pp. 871–878, 1993
Printed in Great Britain

0277–5387/93 $6.00+.00
© 1993 Pergamon Press Ltd

COBALT COMPLEXES WITH PNICOGEN (PHOSPHINE OR PYRIDINE) AND THIOLATO LIGANDS. SYNTHESES, X-RAY CRYSTAL STRUCTURES AND SPECTROSCOPIC CHARACTERIZATION

BEI-SHENG KANG,* YONG-JIN XU, JING-HAI PENG, DA-XU WU, XUE-TAI CHEN, YONG-HAN HU, MAO-CHUN HONG and JIA-XI LU

State Key Laboratory of Structural Chemistry and Fujian Institute of Research on the Structure of Matter, Chinese Academy of Sciences, Fuzhou, Fujian 350002, P.R.C.

(*Received* 1 *October* 1992; *accepted* 18 *December* 1992)

Abstract—Mixed pnicogen and thiolato mononuclear cobalt complexes, $Co(SR)_2(PBu^n_3)_2$ [R = Ph (**1**); R = Stolyl-*p* (**2**)] and $Co(mpo)_2L$ [L = PBu^n_3 (**3**); L = Py (**4**)], have been synthesized and studied spectroscopically. The complexes **1** and **2** are tetrahedral, as determined by magnetic susceptibility studies. The structures of **3** and **4** were determined by X-ray diffraction. The cobalt(II) ions in both **3** and **4** are in a square-pyramidal environment with the two *trans*-oriented mpo ligands in the basal plane and the pnicogen group in the axial position.

Cobalt complexes with mixed pnicogen (phosphine or pyridine) and dithiolene ligands were studied 20 years ago for their interesting spectroscopic features and electron transfer properties.[1–5] Balch[3,4] and Schrauzer[5] have studied the magnetic, electronic and ligand exchange properties of a series of mononuclear dithiolene cobalt complexes containing phosphine ligands PPh_3, PBu^n_3 or $P(OEt)_3$. Some cobalt complexes with a combination of mono-, bi- or tridentate phosphine and mono- or bidentate thiolate ligands have been identified structurally, such as mononuclear $[Co(SPh)_3(PPh_3)]^-$ and $[Co(Stolyl\text{-}m)_2(dppep)]$,[6] $[Co(SPh)_2(dppp)]$ and $[Co(SPh)_2(dppep)]$,[7] $[Co(bdt)_2(PBu^n_3)]^-$,[8] binuclear $[Co_2(SR)_2(\mu\text{-}SR)_2(dppm)]$[9] (R = Ph, tolyl-*m*, -*p*, $C_6H_4Bu^t$-*p*) and $[Co_2(SPh)(\mu\text{-}SPh)_3(dppe)]$,[9,10] and trinuclear $[Co_3(bdt)_3(PBu^n_3)_3]$.[8] In our continuing investigation on the coordination chemistry of cobalt complexes containing mono- or bidentate thiolate and monodentate phosphine ligands, a series of mononuclear complexes (**1–3**) was obtained and the X-ray structure, magnetic and electrochemical properties and ^1H NMR spectra studied. The isolation of complex **4** is an indication that pyridine is a much stronger coordinating ligand than phosphine.

EXPERIMENTAL

Materials and methods

All reactions were performed under an atmosphere of dinitrogen in Schlenk-type apparatus on a vacuum-line. Solvents were dried over molecular sieves, distilled and degassed before use. The reagents $CoCl_2$ (Merck), $Co(OAc)_2 \cdot 4H_2O$ (Merck), PBu^n_3 (Merck), sodium *o*-mercaptopyridine N-oxide (Nampo, Aldrich), PhSH (Fluka) and HStolyl-*p* (Merck) are commercially available. Sodium thiolates were prepared by mixing sodium metal and thiol in dry benzene and isolating the white powder obtained.

Physical measurements were performed on the following instruments: IR, Digilab FTS40 spectrophotometer; ^1H NMR, Varian FT-80A spectrometer; magnetic susceptibility, Gouy-Faraday magnetic balance by the Faraday method; CV, Longjin Model 8511B potentiostat (a platinum-inlay working electrode, platinum-wire auxiliary electrode, S.C.E. reference electrode).

* Author to whom correspondence should be addressed.

Abbreviations: Hmpo: *o*-mercaptopyridine N-oxide; dtpo: 2,2′-dithiobis(pyridine N-oxide); dppep: $\{Ph_2P(CH_2)_2\}_2PPh$; dppp: $Ph_2P(CH_2)_3PPh_2$; dppe: $Ph_2P(CH_2)_2PPh_2$; dppm: $Ph_2PCH_2PPh_2$; H_2bdt: *o*-benzenedithiol; H_2mnt: maleonitriledithiol.

Preparations

Co(SPh)z(PBun3)2 (1). To an MeCN (50 cm3) solution of CoC12 (0.82 g, 6.32 mmol) and NaSPh (1.67 g, 12.64 mmol) was added PBun3 (3 cm3, 12.64 mmol, d = 0.85 g cm- 3) with stirring at room temperature. After 20 h the solution was filtered and the purple filtrate gave 2.3 g (53%) of dark crystals of 1 on standing at 5°C overnight. Found : C, 61.3 ; H, 9.6; Co, 8.5; P, 9.6; S, 9.8. Calc. for C36H64CoP2S2 : C, 63.4; H, 9.4; Co, 8.7; P, 9.1 ; S, 9.4%. IR (KBr): 3050, 2960, 2940, 2870, 1575, 1465, 1080, 1025, 970, 910, 740, 695, 480, 425, 360 cm- 1.

Co(Stolyl-p)2(PBun3)2 (2). To an MeCN (50 cm3) solution of COC12 (0.82 g, 6.32 mmol) and NaStolyl-p (1.83 g, 12.64 mmol) was added PBun3 (3 cm3, 12.64 mmol) slowly with stirring at room temperature. After stirring for 20 h and filtration the purple solution gave 2.1 g (46.9%) of dark crystals of 2 on standing at 5°C overnight. Found : C, 64.3 ; H, 9.8; Co, 8.0; P, 8.8; S, 9.8. Calc. for C38H68CoP252 : C, 64.3 ; H, 9.7 ; Co, 8.3 ; P, 8.7 ; S, 9.0%. IR (KBr): 3040, 2960, 2940, 2870, 1590, 1485, 1460, 1090, 1020, 970, 910, 810, 720, 630, 490, 395, 340 cm- 1.

Co(mpo)EPBun3 (3). To an EtOH (40 cm3) solution of COC12 (0.09 g, 0.69 mmol) was added, with stirring at room temperature, a mixture of dtpo (0.175 g, 0.69 mmol), sodium metal (0.032 g, 1.39 mmol) and PBun3 (0.32 cm3, 1.28 mmol) in EtOH (10 cm3). The solution turned reddish-brown immediately, which was filtered and the filtrate gave block-shaped dark crystals of 3 (yield 63%) on standing at 5QC for several days. After isolation of 3 the mother liquor on prolonged standing gave plate-shaped dark red crystals of Co(mpo)3, which was identified by comparison of its IR spectrum with the known compound, 11 showing the oxidation ofcobalt(II) to cobalt(III). Found: C, 50.9 ; H, 7.1; Co, 11.5; N, 5.3; P, 6.1. Calc. for C22H35CoNzO2PS2: C, 51.5 ; H, 6.9; Co, 11.5 ; N, 5.5; P, 6.0%. IR (KBr): 3089, 3066, 3022, 2955, 2928, 2866, 1598, 1538, 1455, 1414, 1187, 1156, 1144, 1086, 824, 781,705,602, 569, 457, 350 cm-1.

Co(mpo)aPy (4). To a stirred MeCN (40 cm3) solution of Co(OAc)2 •4H20 (0.25 g, 1.0 mmol) was added first pyridine (0.08 cm3, 1.0 mmol) and then an MeOH (10 cm3) solution of Nampo (0.30 g, 2.0 mmol) at room temperature. After standing at 5°C for 2 weeks the dark plate-like crystalline product of 4 separated, together with some unreacted Co(OAc)2 which was detected from its red colour. This crude product was filtered and washed with MeOH twice (10 cm3) to give the pure complex 4 (yield 10%). Found: C, 45.9; H, 2.9; Co, 15.7; N, 10.0. Calc. for C15H13CoN3OzS2: C, 46.2; H, 3.4; Co, 15.1; N, 10.8%. IR (KBr): 3097-3012 (six peaks), 1596, 1538, 1456, 1441, 1411, 1216, 1182, 1159, 1136, 1088, 1066, 824, 767, 748, 705,635,611, 571,520, 447, 429, 353 cm- 1.

Crystal structure determinations

The crystallographic data and data collection parameters for complexes 3 and 4 are summarized in Table 1. Single crystals were coated with epoxy resin and mounted on the Rigaku AFC5R diffractometer for data collection with Mo-K, radiation. After data reduction, including correction for Lorentz and polarization effects, the remaining unique reflections with I > 3o-(1)were used for subsequent structure solution and refinement. The structures were solved by direct methods and successive Fourier syntheses and refined by full-matrix least-squares procedures with anisotropic thermal parameters for all the non-hydrogen atoms. The hydrogen atoms were added only to the structure-factor calculations but not refined. All calculations were performed on a VAX 11/785 computer with the SDP program package.

RESULTS AND DISCUSSION

Synthesis

It was found that monodentate thiolate substituted mononuclear cobalt(II) complexes with bi- or tridentate phosphine ligands are more stable than those with monodentate phosphines, since many complexes6.7.9,10 of the former type have been characterized structurally while only one complex of the latter type has been reported. 6This unique complex, (Et4N)[Co(SPh)3(PPh3)], was obtained by reaction of CoC12 with NaSPh and PPh3 in the ratio 1 : 3 : 1.6 When a ratio of 1:2:2 for CoC12:NaSPh (or NaStolyl-p) :PBun3 was employed the reaction in MeCN led to the complex Co(SPh)2(PBun3)2 (1) or Co(Stolyl-p)ffPBun3)2 (2), which was identified by elemental analysis, IR and 1H NMR. Due to the extreme air-sensitivity of the single crystals of 1 and 2 for X-ray diffraction study the bidentate ligalad o-mercaptopyridine-N-oxide was employed and complexes ofpenta-coordination can be obtained which are much more stable than the tetra-coordinated ones. With a molar ratio of 1: 1:2 for the starting materials Co2+:dtpo:PBun3 the complex Co(mpo)aPBun3 (3) was obtained, where dtpo was decomposed heterolytically by the neocleophilic attack of the methoxide ion present in solution on the S--S bond to give the anionic ligand mpo-. The complex Co(mpo)2Py (4) was isolated instead when

Table 1. Summary of crystallographic data and data collection parameters for complexes **3** and **4**

	3	**4**
Formula	$CoC_{22}H_{35}N_2O_2PS_2$	$CoC_{15}H_{13}N_3O_2S_2$
Mol. wt	513.57	390.35
Space group	$P\bar{1}$	$P\bar{1}$
a (Å)	9.947(2)	12.091(2)
b (Å)	15.740(5)	14.435(3)
c (Å)	8.444(2)	9.675(2)
α (°)	94.63(2)	103.68(2)
β (°)	99.47(2)	99.76(2)
γ (°)	96.12(2)	83.66(2)
V (Å^3)	1290.0	1612.6
Z	2	4
d_{calc} (g cm^{-3})	1.32	1.61
Crystal dimensions (mm)	$0.30 \times 0.25 \times 0.20$	$0.25 \times 0.25 \times 0.15$
Temperature (°C)	23	23
Radiation (wavelength)	Mo-K_α (0.71069 Å)	Mo-K_α (0.71069 Å)
Monochromator	Graphite	Graphite
Linear absorbance coefficient (cm^{-1})	9.0	13.2
Scan method	ω–2θ	ω–2θ
2θ range (°)	50.0	46.1
Scan width (°)	0.47	0.46
F(000)	542	796
Number of reflections collected	4448	4768
Number of data for refinement[a]	3809	2237
Number of variables	271	415
Largest residue (e Å^{-3})	0.48	0.51
R	0.053	0.065
Rw	0.055[b]	0.075[c]

[a] $I > 3.0\sigma(I)$.
[b] $w = 1.0$.
[c] $w = 1/[\sigma^2(F_o)^2 + 0.020(F_o)^2 + 1.0]$.

Table 2. Selected bond distances (Å) and angles (°) for the complex $Co(mpo)_2PBu^n_3$ (**3**)

Co—S(1)	2.355(2)	Co—S(2)	2.375(2)
Co—P	2.424(3)	Co—O(1)	1.997(3)
Co—O(2)	2.018(4)	S(1)—C(11)	1.702(5)
S(2)—C(21)	1.701(6)	P—C(31)	1.827(8)
P—C(35)	1.832(7)	P—C(39)	1.833(7)
O(1)—N(1)	1.352(6)	O(2)—N(2)	1.346(6)
N(1)—C(11)	1.355(7)	N(1)—C(15)	1.359(6)
N(2)—C(21)	1.350(7)	N(2)—C(25)	1.359(5)

S(1)—Co—S(2)	153.78(6)	S(1)—Co—P	104.24(9)
S(1)—Co—O(1)	83.8(1)	S(1)—Co—O(2)	92.0(1)
S(2)—Co—P	101.75(9)	S(2)—Co—O(1)	91.4(1)
S(2)—Co—O(2)	82.3(1)	P—Co—O(1)	108.3(1)
P—Co—O(2)	95.2(1)	O(1)—Co—O(2)	156.6(1)
Co—S(1)—C(11)	96.4(2)	Co—S(2)—C(21)	95.4(2)
Co—P—C(31)	116.7(3)	Co—P—C(35)	118.1(3)
Co—P—C(39)	110.9(2)	Co—O(1)—N(1)	118.4(3)
Co—O(2)—N(2)	117.0(3)		

Table 3. Selected bond distances (/~) and angles (°) for the complex Co(mpo)2Py (4)

Co(I)--S(I 1)	2.401(2)	Co(2)--S(21)	2.364(2)
Co(1)--S(12)	2.366(2)	Co(2)--S(22)	2.398(2)
Co(1)--O(11)	1.967(4)	Co(2)--O(21)	1.961(4)
Co(1)--O(12)	1.955(4)	Co(2)--O(22)	1.990(4)
Co(1)--N(1B)	2.090(4)	Co(2)--N(201)	2.101(4)
S(11)--C(111)	1.733(6)	S(21)--C(211)	1.681(6)
S(12)--C(121)	1.708(6)	S(22)--C(221)	1.694(6)
O(11)--N(11)	1.363(6)	O(21)--N(21)	1.334(5)
O(12)--N(12)	1.339(5)	O(22)--N(22)	1.334(6)

S(11)--Co(1)--S(12)	157.26(7)	S(21)--Co(2)--S(22)	155.97(7)
S(I 1)--Co(1)--O(11)	82.9(2)	S(21)--Co(2)--O(21)	84.0(1)
S(I 1)--Co(1)--O(12)	92.5(1)	S(21)--Co(2)~O(22)	91.8(1)
S(11)--Co(1)--N(I B)	98.3(1)	S(21)--Co(2)--N(201)	104.8(1)
S(12)--Co(1)--O(11)	90.4(1)	S(22)--Co(2)--O(21)	91.1(1)
S(12)--Co(1)--O(12)	83.5(1)	S(22)--Co(2)--O(22)	82.3(2)
S(12)--Co(I)--N(1 B)	104.5(1)	S(22)--Co(2)--N(201)	99.3(1)
O(11)--Co(1)--O(12)	153.1(2)	O(21)--Co(2)--O(22)	153.8(2)
O(11)--Co(I)--N(1B)	104.8(2)	O(21)--Co(2)--N(201)	101.1(2)
O(12)--Co(I)--N(1B)	102.2(2)	O(22)--Co(2)--N(201)	105.0(2)
Co(1)--S(! 1)--C(111)	95.4(2)	Co(2)--S(21)--C(211)	94.6(2)
Co(1)--S(12)--C(121)	95.7(2)	Co(2)--S(22)--C(221)	95.0(2)
Co(1)--O(11)--N(11)	119.6(3)	Co(2)---O(21)--N(21)	119.3(4)
Co(1)--O(12)--N(12)	119.2(3)	Co(2)--O(22)--N(22)	120.3(4)
Co(1)--N(1B)--C(IB)	122.6(4)	Co(2)--N(201)--C(201)	120.7(4)
Co(1)--N(1B)--C(3B)	118.0(4)	Co(2)--N(201)--C(205)	119.1(4)

under the same reaction conditions a trace of pyridine was added, showing the stronger coordination ability of the pyridine molecule. Complex 4 can also be prepared with a Co 2+ : dtpo : Py ratio of 1 : 2 : 1. The amount ofpyridine has to be limited to less than 1mol since if an excess ofpyridine was employed the complex Co(mpo)2Py2 forms immediately, which can be identified by the appearance of proton peaks corresponding to mpo and py in the ratio of 1 : **1 in** the ~H NMR spectrum. Facile formation of the mono- and bis-pyridine adducts of [Co(mnt)2] 1 ,2 has been reported.

Structure

Single-crystal X-ray diffraction studies have been performed on complexes 3 and 4. Tables 2 and 3 give the selected atomic distances and bond angles for complexes 3 and 4, respectively. Figures 1 and 2 depict the ORTEP structures of 3 and 4, respectively. A comparison of related structural data with other mpo substituted complexes ~-~3 is shown in Table 4. There are two discrete molecules of 4 in an asymmetric unit.

Molecules of both 3 and 4 contain a square-pyramidally coordinated cobalt atom chelated by two *trans-oriented* mpo ligands in the basal plane and a neutral pnicogen molecule, PBUn3 or Py, in the axial position. The Co--S and Co--O bonds in both complexes 3 and 4 are in the ranges 2.36-2.40 and 1.96-2.02 ~, respectively, which are all longer than those in the six-coordinate Co(mpo)3 (average 2.194 and 1.933 /~).11 The N--O bond changes neither with the coordination number nor with the type of central atom of the complexes and is maintained in the range 1.34-1.35 ~, whilst the average S--C bonds are in the range 1.70-1.72/~ for the complexes listed in Table 4 with the shortest values for complexes 3 and 4, agreeing with the fact that the thione form is the predominant coordination mode of mpo :~3

0 **OH**

Thiol **Thione**

Thus, this results in the shortening of the C--S bond compared to the normal covalent distance (1.81 /~)14 for a single bond. The Co--P distance of 2.424 A in 3 is so far the longest observed in cobalt-phosphine complexes,6-10,~5,~6 implying the weak bonding and easy dissociation of PBun3,

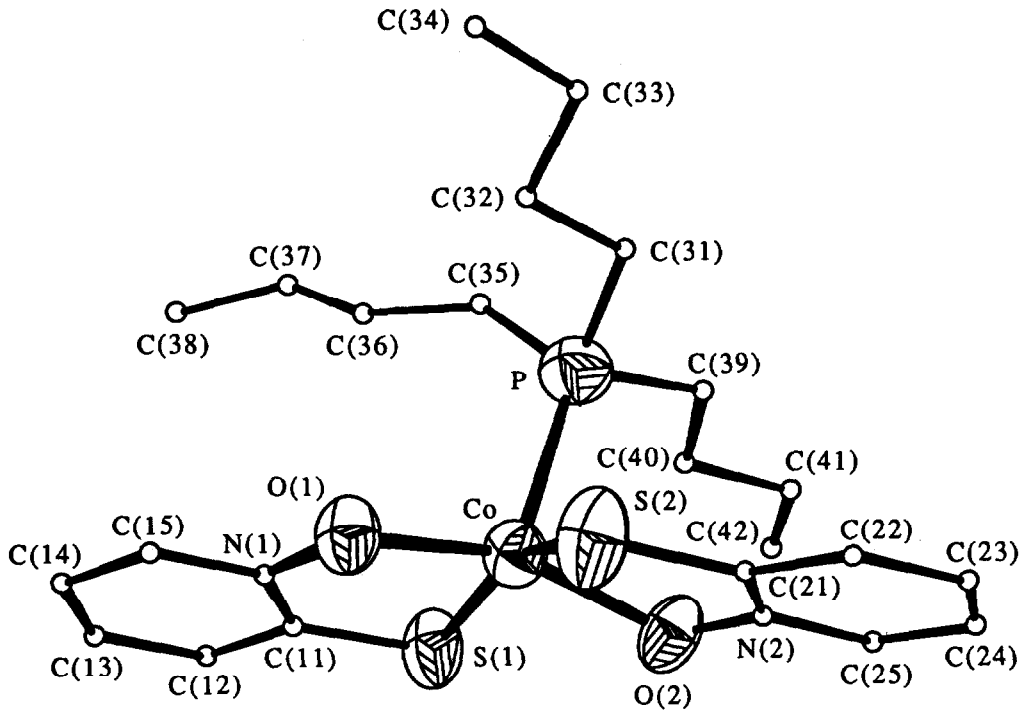

Fig. 1. ORTEP structure of the complex $Co(mpo)_2PBu^n_3$ (**3**) with the carbon atoms represented by arbitrary spheres for clarity.

which agrees well with the ^1H NMR data (see below).

The bite angles S_n—Co—O_n (average 83.2°) for the *trans*-coordinated mpo ligands in complexes **3** and **4** are obviously smaller than those in $Co(mpo)_3$[11] (88.0°) or $Ni(mpo)_2$[13] (89.6°), where the mpos are in *facial* (S_n—Co—S_m 91.2°) or *cis* conformations (S_n—Co—S_m 92.8°), respectively, but comparable to that in $Fe(mpo)_3$[12] (S_n—Co—O_n 81.1°; S_n—Co—S_m 167.7°) in which the mpo ligands are *meridionally* oriented. This result may indicate the fact that the S···S interaction, when

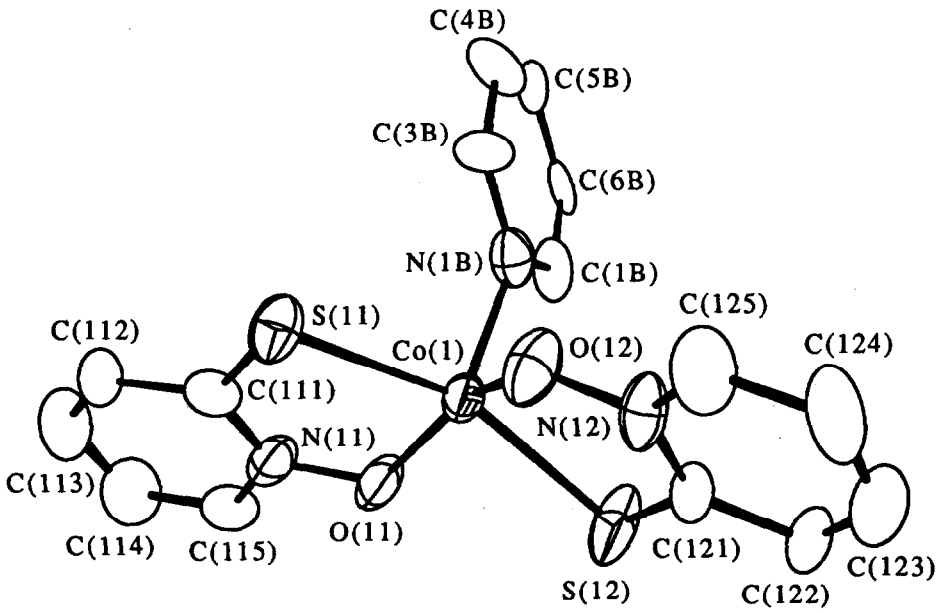

Fig. 2. ORTEP structure of the complex $Co(mpo)_2Py$ (**4**).

Table 4. Comparison of average atomic distances (/~) and bond angles (°) of some complexes containing o-mercaptopyridine N-oxide

Parameter	3	4	Fe(mpo)31:	Co(mpo)311	Ni(mpo)213
Co--S	2.365	2.382	2.419	2.194	2.133
Co--O	2.008	1.968	2.009	1.933	1.866
O~N	1.349	1.343	1.340	1.348	1.350
S--C	1.702	1.704	1.716	1.716	1.712
Co--S--C	95.9	95.2	96.7	96.8	
Co--O---N	117.7	119.6	121.3	116.0	
S,--Co---On	83.1	83.2	81.1	88.0	89.6
Sn--Co----O m	153.8	156.6	167.74	91.15	92.81
			100.37		
			89.10		
On--Co--Om	156.6	153.5	167.7	86.9	88.1
			97.6		
			88.3		
Coordination	5	5	6a	6b	4

aMeridional.
bFacial.

the sulphur atoms are in nearby positions, expands the bite angle by drawing electrons away from the chelate ring. Both Co--S--C (average 95.6°) and Co--O--N (average 118.7°) angles within the five-membered chelate ring Co--O--N--C--S are within the normal ranges 13for the sulphur and oxygen donor atoms to employ mainly p and *sp2*hybrid orbitals for bonding, respectively.

Spectroscopic studies

The IR spectra of complexes 1 and 2 are quite similar to each other, except for the C--H out-of-plane bending absorptions of the benzene ring. Two peaks at 740 and 698 cm- ~are characteristic for the mono-substituted phenyl group in complex 1, while the p-tolyl group in complex 2 gave only one absorption at 810 cm ~for the 1,4-disubstituted phenyl ring. Complex 3 showed an absorption at 1144 cm- ~with a shoulder at 1156 cm- ~for S--C bonds, which appeared as two strong bands at 1136 and 1159 cm-1 for complex 4. These absorptions are indications of partial kS double bond character, as compared with the free ligand Hmpo (1142 cm-1) which has been established by Jones t7 to be predominantly in the thione form. The appearance of a set of three peaks in the region 2960-2870 cm- in complexes 1-3 is a clear indication of the presence of the PBun3 group. The C--H stretching vibrations of the mpo ligand appear in the range 3100-3020 cm- ~in complexes 3 and 4 and the Co--S absorptions appear at 457 and 350 cm- ~(3) and 447 and 353 cm i (4).

The 1H NMR data at room temperature of complexes 1~4 are listed in Table 5, where the paramagnetism of the complexes is clearly shown by the large chemical shifts. Contact contributions to the chemical shifts are shown by signals with alternating signs for the *meta-* and *para-protons* of the phenyl groups: 29.74 and -48.88 ppm, respectively, in the ratio 2:1 for complex 1, while the *ortho-proton* signals are too broad to be detected. In the meantime, complex 2 showed the same result of contact interaction where methyl substitution in the *para-position* for the tolyl-p group alternates the sign of the p-proton to give a signal at 52.92 ppm, with the m-protons appearing at 29.89 ppm. Complexes 3 and 4 showed very similar chemical shifts for the mpo ligands, yet the fate of the pnicogen ligands is quite different in the solvent DMSO. The spectrum showed the dissociation of PBun3 for 3 as the chemical shifts of 0.98 and 1.50 ppm are close to those for the free ligand. 8 The pyridine ligand in 4 showed completely different chemical shifts as compared with the free molecule (8.5, 7.35 and 7.0 for ~-, r- and ~-H, respectively)~ 18 with the signal for a-protons near 20 ppm buried under the peaks of Hc of mpo (see Table 5 for proton assignment). These data indicate the strong affinity of pyridine with the central Co 2÷ ion as compared to phosphine.

Physical-chemical properties

All the complexes are paramagnetic. The magnetic moments of I and 2 at room temperature are

Table 5. ^1H NMR data (ppm) of the complexes **1–4** at room temperature

Complex	Solvent	SR			mpo[a]				PBu^n_3		
		m-H	*p*-H	*p*-CH_3	H_A	H_B	H_C	H_D	α-CH_2	β-CH_2	Other
$Co(SPh)_2(PBu^n_3)_2$	CD_2Cl_2	29.74	−48.88	/	/	/	/	/	90.08	3.62	1.74
$Co(Stolyl\text{-}p)_2(PBu^n_3)_2$	CD_2Cl_2	29.89	/	52.92	/	/	/	/	89.5	3.62	1.69
$Co(mpo)_2PBu^n_3$	DMSO-d_6	/	/	/	65.5	18.7	19.9	24.7	0.98–1.50[b]		
$Co(mpo)_2Py$	DMSO-d_6	/	/	/	65.5	18.3	19.8	24.5	12.3 (β-H)[c]		
									8.0 (Γ-H)[c]		

[a] The assignment for protons of mpo:

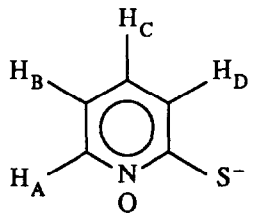

[b] Data indicate dissociation of Bu^n_3.
[c] Data for the pyridine ligand.

4.40 and 4.54 μ_B, respectively. These values being higher than the calculated spin-only value of 3.87 μ_B for a high spin state $S = 3/2$ for cobalt(II) show that there is a certain degree of orbital contribution to the magnetic moment.[19–21] Knowing that tetrahedral $[Co(SR)_4]^{2-}$[22] possesses a solid moment of 4.6 μ_B[23] and comparing with a series of reported phosphine substituted cobalt(II) complexes with tetrahedral structures and magnetic moments in the range 4.41–4.63 μB,[21] the tetrahedral geometry

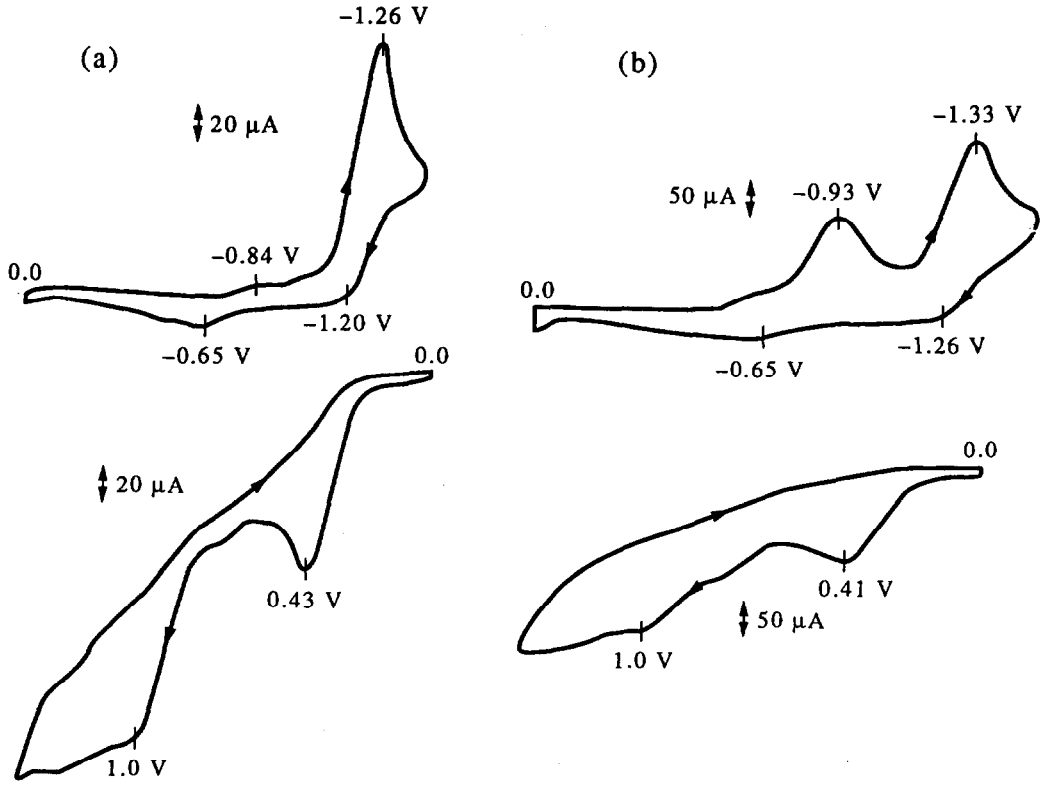

Fig. 3. Cyclic voltammograms of (a) complex **1** and (b) complex **2** in MeCN vs S.C.E. at a scan rate of 100 mV s^{-1} at room temperature.

of the cobalt atom in complexes 1 and 2 can be deduced. Their X-ray single-crystal structure determinations await low temperature facilities. The effective magnetic moment of 3.77 #~ for complex 3 corresponds to a spin-only state of S = 3/2 for the cobalt(II) ion.

The cyclic voltammograms of complexes 1 and 2 were measured in MeCN in the range 1.5 to - 1.5 V, either reductively or oxidatively. Both complexes showed two quasi-reversible reduction waves and two irreversible oxidation waves, as shown in Fig. 3. It is believed that in addition to the reduction (- 1.26 and - 1.33 V) or oxidation (0.43 and 0.41 V) of the complexes (3 and 4, respectively), the ligands also engaged in redox processes within the applied potentials. The waves near 1.0 V account for the oxidation of the thiolates.

Acknowledgement--This work was supported by NNSF, NSFCAS and FNSF.

REFERENCES

1. I. G. Dance, *Inorg. Chem.* 1973, 12, 2381.
2. I. G. Dance and T. R. Miller, *Inorg. Chem.* 1974, 13, 525.
3. A. L. Balch, *Inorg. Chem.* 1967, 6, 2158.
4. A. L. Balch, *Inorg. Chem.* 1971, 10, 388.
5. G. N. Schrauzer, V. P'. Mayweg, H. W. Finck and W. Heinrich, J. *Am. Chem. Soc.* 1966, 88, 4604.
6. F. L. Jiang, G. W. Wei, Z. Y. Huang, X. J. Lei, M. C. Hong, B. S. Kang and H. Q. Liu, J. *Coord. Chem.* 1992, 25, 183.
7. G. W. Wei, M. C. Hong, Z. Y. Huang and H. Q. Liu, *J. Chem. Soc., Dalton Trans.* 1991, 3145.
8. B. S. Kang, J. H. Peng, M. C. Hong, D. X. Wu, X. T. Chen, L. H. Weng, X. J. Lei and H. Q. Liu, J. *Chem. Soc., Dalton Trans.* 1991, 2897.
9. G. W. Wei, H. Q. Liu, Z. Y. Huang, M. C. Hong, L. R. Huang and B. S. Kang, *Polyhedron* 1991, 10, 553.
10. G. W. Wei, H. Q. Liu, Z. Y. Huang, L. R. Huang and B. S. Kang, J. *Chem. Soc., Chem. Commun.* 1989, 1839.
11. Y. H. Hu, L. H. Weng, L. R. Huang, X. T. Chen, D. X. Wu and B. S. Kang, *Acta Cryst.* 1991, C47, 2655.
12. Y. H. Hu, X. T. Chen, L. Dai, L. H. Weng and B. S. Kang, *Jeigou Huaxue* 1993, 12, 38.
13. X. T. Chen, Y. H. Hu, D. X. Wu, L. H. Weng and B. S. Kang, *Polyhedron* 1991, 10, 2651.
14. J. D. Lydon, R. C. Elder and E. Deutsch, *Inorg. Chem.* 1982, 21, 3186.
15. P. B. Hitchcock and G. M. McLanghlin, J. *Chem. Soc., Dalton Trans.* 1976, 1929.
16. W. Levason, J. S. Ogden and M. D. Spicer, *Inorg. Chem.* 1989, 28, 2128.
17. R. A. Jones and A. R. Katritzsky, J. *Chem. Soc.*, 1960, 2937.
18. R. M. Silverstein and G. C. Bassler, *Spectrometric Identification of Organic Compounds,* p. 85. John Wiley and Sons, New York (1964).
19. R. H. Holm and F. A. Cotton, J. *Chem. Phys.* 1960, 32, 1168.
20. F. A. Cotton and M. Goodgame, J. *Am. Chem. Soc.* 1961, 83, 1177.
21. F. A. Cotton, O. D. Faut, D. M. L. Goodgame and R. H. Holm, J. *Am. Chem. Soc.* 1961, 83, 1780.
22. R. W. Lane, J. A. Ibers, R. B. Frankel, G. C. Papaefthymiou and R. H. Holm, J. *Am. Chem. Soc.* 1977, 99, 84,
23. J. R. Dorfman, Ch. P. Rao and R. H. Holm, *Inorg. Chem.* 1985, 24, 453.

Polyhedron Vol. 12, No. 8, pp. 879–882, 1993
Printed in Great Britain

0277–5387/93 $6.00+.00
© 1993 Pergamon Press Ltd

LITHIUM COMPLEXES OF 1,2-NAPHTHAQUINONE MONO-OXIMES. THE X-RAY CRYSTAL STRUCTURE OF (1,2-NAPHTHAQUINONE-1-OXIME)(1,2-NAPHTHAQUINONE-1-OXIMATO)LITHIUM(I)·ETHANOL

JOHN CHARALAMBOUS,* PETER G. T. FOGG, PARASKEVI GAGANATSOU and KIM HENDRICK

School of Applied Chemistry, University of North London, Holloway Road, London N7 8DB, U.K.

(*Received* 30 *September* 1992; *accepted* 18 *December* 1992)

Abstract—The complexes Li(1-nqo)·1/2EtOH, Li(1-nqo)(1-nqoH)·EtOH (1-nqoH = 1,2-naphthaquinone-1-oxime), and Li(2-nqo)·1/2EtOH, Li(2-nqo)(2-nqoH)·EtOH (2-nqoH = 1,2-naphthaquinone-2-oxime), were prepared by the interaction of the quinone oxime with lithium hydroxide. The structure of Li(1-nqo)(1-nqoH)·EtOH was determined by single-crystal X-ray diffraction techniques. The lithium atom is penta-coordinated in a distorted square pyramidal environment.

The study of the synthesis, structure and applications of transition and actinide metal complexes derived from the mono-oximes of 1,2-naphthaquinone and several 1,2-benzoquinone mono-oximes has attracted considerable attention.[1–7] The preparation of the complexes Li(1-nqo) (1-nqoH = 1,2-naphthaquinone-1-oxime), Li(2-nqo)(2-nqoH) (2-nqoH = 1,2-naphthaquinone-2-oxime) and of related sodium, potassium, caesium and rubidium complexes has been described, but there is only limited information on their properties and structure.[8–11] As a continuation of our interest in quinoneoximato complexes we now report on the synthesis, properties and structure of several naphthaquinoneoximato complexes of lithium and on the X-ray crystallographic study of Li(1-nqo)(1-nqoH)·EtOH.

EXPERIMENTAL

Elemental analyses were performed by the Microanalytical Laboratory of the University of North London. IR spectra were recorded as KBr discs on a Perkin–Elmer 781 spectrophotometer.

* Author to whom correspondence should be addressed.

Preparation of the lithium complexes

[Li(1-nqo)·1/2EtOH]. To a suspension of $LiOH \cdot H_2O$ (1.30 g, 31.0 mmol) in ethanol (40 cm^3) was added a solution of 1-nqoH (5.35 g, 31.0 mmol) in ethanol (125 cm^3) portionwise. The reaction mixture was heated on a water bath for 0.5 h and then filtered hot. After slow evaporation of the filtrate the dark green crystalline product was filtered off, washed with ethanol and light petroleum and dried at 40°C/1.0 mm Hg. Yield: 5.15 g, 82%. Found: C, 64.9; H, 5.1; Li, 3.6; N, 6.7. Calc. for $C_{22}H_{18}Li_2N_2O_5$: C, 65.4; H, 4.5; Li, 3.4; N, 6.9%.

[Li(2-nqo)·1/2EtOH]. Similarly, and by using 2-nqoH, the brown complex resulted in 93% yield. Found: C, 64.8; H, 5.0; Li, 3.5; N, 6.2. Calc. for $C_{22}H_{18}Li_2N_2O_5$: C, 65.4; H, 4.5; Li, 3.4; N, 6.9%.

[Li(1-nqo)(1-nqoH)·EtOH]. To a suspension of LiOH (0.30 g, 12.5 mmol) in ethanol (45 cm^3) was added solid 1-nqoH (4.30 g, 25 mmol) portionwise and the resultant mixture was heated on a water bath for 0.5 h and then filtered hot. After slow evaporation of the filtrate the green crystalline product was filtered off, washed with ethanol and dried at 40°C/1.0 mm Hg. Yield: 2.27 g, 45%. Found: C, 65.9; H, 5.0; Li, 1.8; N, 7.4. Calc. for $C_{22}H_{19}LiN_2O_5$: C, 66.3; H, 4.8; Li, 1.7; N, 7.0%.

[Li(2-nqo)(2-nqoH)·EtOH]. Similarly and by using 2-nqoH the light brown complex resulted in 78% yield and was recrystallized from methanol. Found: C, 66.3; H, 4.2; Li, 1.8; N, 7.4. Calc. for $C_{22}H_{19}LiN_2O_5$: C, 66.3; H, 4.8; Li, 1.7; N, 7.0%.

Pyrolysis of the lithium complexes

Li(1-nqo)·1/2EtOH (4.0814 g) was heated at 110–120°C/1.0 mm Hg for 30 h to give green Li(1-nqo) (3.5603 g, 98%). Found: C, 66.9; H, 3.8; Li, 3.9; N, 7.5. Calc. for $C_{10}H_6LiNO_2$: C, 66.1; H, 3.4; Li, 3.9; N, 7.8%. Using the same method Li(2-nqo)·1/2EtOH (6.1440 g) gave light brown Li(2-nqo) (5.3849 g, 99%). Found: C, 66.8; H, 3.7; Li, 3.7; N, 7.6. Calc. for $C_{10}H_6LiNO_2$: C, 67.1; H, 3.4; Li, 3.9; N, 7.8%. Similarly Li(1-nqo)(1-nqoH)·EtOH (4.9929 g) gave light green Li(1-nqo)(1-nqoH) (4.4020 g, 99%). Found: C, 68.4; H, 4.0; Li, 1.9; N, 7.5. Calc. for $C_{20}H_{13}LiN_2O_4$: C, 68.2; H, 3.4; Li, 2.0; N, 7.9%. Li(2-nqo)(2-nqoH)·EtOH (6.3449 g) gave brown Li(2-nqo)(2-nqoH) (5.5784 g, 99%). Found: C, 68.0; H, 4.0; Li, 1.8; N, 7.6. Calc. for $C_{20}H_{13}LiN_2O_4$: C, 68.2; H, 3.4; Li, 1.9; N, 7.9%.

Crystal data

$C_{22}H_{19}LiN_2O_5$, $M = 398.35$. Orthorhombic, $a = 18.839(3)$, $b = 14.170(3)$, $c = 7.390(2)$ Å, $\alpha = \beta = \gamma = 90°$, $V = 1972.75$ cm^3, $\lambda = 0.71069$ Å, space group $P2_12_12_1$, $Z = 4$, $D_c = 1.34$ g cm^{-3}. Green, rhombic-like crystals. Crystal dimensions $0.32 \times 0.12 \times 0.12$ mm, μ(Mo-K_α) = 0.50 cm^{-1}.

Data collection and processing

A Phillips PW1100 four-circle diffractometer with a graphite monochromator, using Mo-K_α radiation, was employed; θ–2θ scan, 0.05° s^{-1}, $2\theta_{max} = 50°$ for the range $0 \leqslant h \leqslant 24$, $0 \leqslant k \leqslant 18$, $0 \leqslant l \leqslant 10$; three reflections monitored every 200 min with no significant variation. 1998 unique reflections, 716 observed with $I > 3\sigma(I)$. Corrections were made for Lorentz–polarization factors, but not for absorption.

Structure analysis and refinement

The structure was solved by direct methods and all non-hydrogen atoms were located. All the hydrogen atoms were included in structure-factor calculations with fixed isotropic thermal parameters of 0.08 Å^2, but were not refined. The nitrogen and oxygen atoms were assigned anisotropic thermal parameters in the refinement of the structure by a full-matrix least-squares procedure, which converged to $R = 0.056$ ($R = \Sigma|F_o - F_c|/\Sigma|F_o|$). $R_w = 0.053$ ($R_w = \Sigma|F_o - F_c|w^{1/2}/\Sigma|F_o|w^{1/2}$), with a weight of $w = 1/\sigma^2(F_o)$, applied to individual reflections. A final difference-Fourier showed a maximum height of 0.18 e Å^{-3}. Neutral atomic scattering factors and anomalous dispersion corrections were from the International Tables for X-ray Crystallography (1974); all calculations were performed using the SHELX76 Crystallographic Package (Sheldrick 1976).

RESULTS AND DISCUSSION

The reactions of 1,2-naphthaquinone-1-oxime with lithium hydroxide in 1 : 1 and 2 : 1 molar ratios were investigated in ethanol under reflux. The 1 : 1 reaction afforded the complex Li(1-nqo)·1/2EtOH, while the 2 : 1 reaction gave Li(1-nqo)(1-nqoH)·EtOH. Similarly, the reactions of 1,2-naphthaquinone-2-oxime with lithium hydroxide in 1 : 1 and 2 : 1 molar ratios gave Li(2-nqo)·1/2EtOH and Li(2-nqo)(2-nqoH)·EtOH, respectively.

Macro-scale pyrolysis showed that ethanol (1/2 mol mol^{-1} adduct; 1 mol mol^{-1} adduct) was lost between 80 and 130°C for the complexes Li(1-nqo)·1/2EtOH and Li(1-nqo)(1-nqoH)·EtOH, respectively, to give the unsolvated species Li(1-nqo) and Li(1-nqo)(1-nqoH).

All the complexes are highly coloured, involatile solids, fairly soluble in acetone, pyridine and ethanol but insoluble in toluene. They are stable in air, in the solid state and in solution (both in water and organic solvents), but decompose in aqueous acids.

Table 1. Selected bond lengths (Å) for Li(1-nqo)(1-nqoH)·EtOH

Li—N(1a)	2.19(2)	Li—O(2a)	2.03(2)
Li—N(1b)	2.15(2)	Li—O(2b)	2.04(2)
Li—O(1e)	1.92(2)	C(1a)—N(1a)	1.33(1)
C(1a)—C(2a)	1.45(1)	C(1a)—C(9a)	1.44(1)
N(1a)—O(1a)	1.30(1)	C(2a)—O(2a)	1.25(1)
C(2a)—C(1a)	1.47(1)	C(3a)—C(4a)	1.33(2)
C(4a)—C(1a)	1.44(2)	C(5a)—C(6a)	1.40(1)
C(5a)—C(10a)	1.40(1)	C(6a)—C(7a)	1.37(2)
C(7a)—C(8a)	1.38(1)	C(8a)—C(9a)	1.41(1)
C(9a)—C(10a)	1.39(1)	C(1b)—N(1b)	1.27(1)
C(1b)—C(2b)	1.51(1)	C(1b)—C(9b)	1.46(1)
N(1b)—O(1b)	1.34(1)	C(2b)—O(2b)	1.23(1)
C(2b)—C(3b)	1.45(1)	C(3b)—C(4b)	1.31(2)
C(4b)—C(10b)	1.44(2)	C(5b)—C(6b)	1.33(2)
C(5b)—C(10b)	1.38(2)	C(6b)—C(7b)	1.38(2)
C(7b)—C(8b)	1.39(2)	C(8b)—C(9b)	1.40(1)
C(9b)—C(10b)	1.42(1)	C(1e)—C(2e)	1.47(3)
C(2e)—C(1e)	1.39(2)		

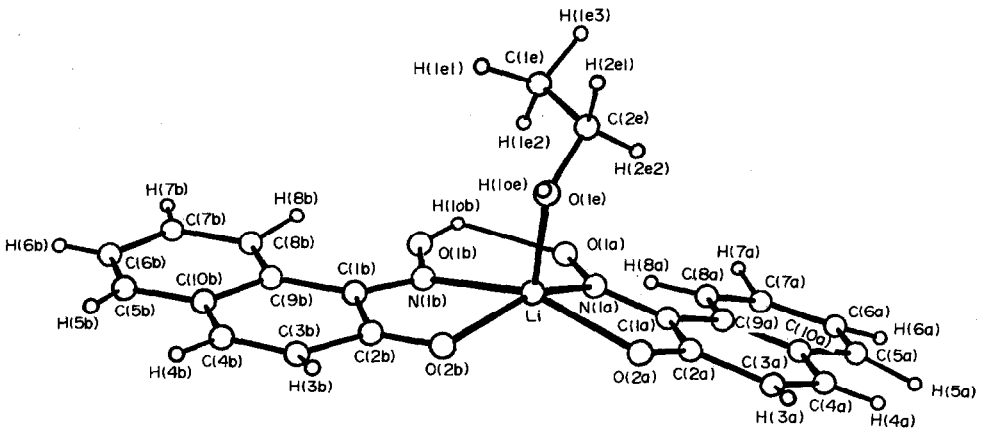

Fig. 1. A view of Li(1-nqo)(1-nqoH)·EtOH, with the atomic numbering scheme.

In all cases the IR spectra exhibit strong bands at 1618–1500 cm^{-1}, which are characteristic of chelated quinoneoximato ligands. Conductance measurements at 25°C in ethanol indicate that dissociation is inappreciable and suggest covalent character. In the case of Li(1-nqo)(1-nqoH)·EtOH the suggested covalent character and the mode of bonding in the ligands has been confirmed by an X-ray crystallographic study.

Crystal structure of Li(1-nqo)(1-nqoH)·EtOH

The lithium atom is penta-coordinated in a distorted square-pyramidal environment with two chelating ligands at the base and an ethanol molecule at the apex. A view of the molecule with the atomic numbering scheme is shown in Fig. 1. Selected bond lengths and angles are given in Tables 1 and 2, respectively.

In this complex both the 1-nqo and protonated 1-nqoH ligands are quinoneoximic in character and are chelated to the metal via the NO and CO groups. The quinoneoximic character of these ligands is indicated by the short C(3)—C(4) and long C(1)—C(2) bond distances. An analogous situation has been found in the free 1,2-naphthaquinone-2-oxime [C(3)—C(4) 1.327(6), C(1)—C(2) 1.484(6) Å][12] and in transition metal quinone-oximato complexes in general.[1,2,5] As in the case of transition complexes the chelate ring is five-membered and the NO group is bonded to the metal via the nitrogen. Both the metal–oxygen and metal–nitrogen bond lengths in Li(1-nqo)(1-nqoH)·EtOH are short [2.033(22)–2.198(23) Å] and compare well to those found in other covalently chelated transition metal complexes [1.951(4)–2.100(3) Å].[1,2,5] In contrast, in K(Clqo)·1/2H_2O (ClqoH = 4-chloro-1,2-benzoquinone-2-oxime) the ligand is bidentate but non-chelating and the NO group bonds to the metal via the oxygen atom.[11] In this compound the metal–

Table 2. Selected bond angles (°) for Li(1-nqo)(1-nqoH)·EtOH

O(2a)—Li—N(1a)	75.5(8)	N(1b)—Li—N(1a)	85.8(8)
N(1b)—Li—O(2a)	148(1)	O(2b)—Li—N(1a)	148(1)
O(2b)—Li—O(2a)	108(1)	O(2b)—Li—N(1b)	75.0(8)
O(1e)—Li—N(1a)	110(1)	O(1e)—Li—O(2a)	105(1)
O(1e)—Li—N(1b)	105(1)	O(1e)—Li—O(2b)	100(1)
C(2a)—C(1a)—N(1a)	110(1)	C(9a)—C(1a)—N(1a)	128(1)
O(1a)—N(1a)—Li	125.3(9)	C(1a)—N(1a)—Li	114.9(9)
O(2a)—C(2a)—C(1a)	122(1)	O(1a)—N(1a)—C(1a)	120(1)
C(3a)—C(2a)—O(2a)	121(1)	C(3a)—C(2a)—C(1a)	116(1)
C(2b)—C(1b)—N(1b)	109(1)	C(2a)—O(2a)—Li	117(1)
O(1b)—N(1b)—Li	124(1)	C(9b)—C(1b)—N(1b)	131(1)
O(2b)—C(2b)—C(1b)	120(1)	C(1b)—N(1b)—Li	117(1)
C(3b)—C(2b)—O(2b)	124(1)	O(1b)—N(1b)—C(1b)	118(1)
C(2e)—O(1e)—Li	126(1)	C(3b)—C(2b)—C(1b)	116(1)
		C(2b)—O(2b)—Li	116(1)

oxygen bond lengths are rather long [2.728(4)-2.859(3) A] and it has been suggested that this is due to the presence of considerable ionic character.

In Li(1-nqo)(1-nqoH)-EtOH the NO groups of the two chelating ligands are in a *cis* arrangement. This contrasts the *trans* arrangement, which is shown by other chelated quinoneoximato complexes, 13,14 and can be correlated to the formation of an asymmetrical hydrogen bond between the neutral and anionic ligands of the lithium complex. The hydrogen atom is positioned 0.84 ~ from the oxygen of the neutral ligand and 1.90 A from the oxygen of the formally anionic ligand. Such an asymmetrical hydrogen bridge at 0.72(6) ,~ from the NO oxygen and at 1.88(6)/~ from the carbonyl oxygen is also found in the protonated free ligand. ~2 A similar hydrogen bridge has also been suggested for bis(salicylaldoximato)nickel(II). 15

In Li(1-nqo)(1-nqoH)" EtOH the ~netal attains a coordination number of five and a distorted square-pyramidal geometry through the attachment of an ethanol molecule. Penta-coordinated lithium has been found in several other complexes, mainly those of crown ethers. 16In Li(1-nqo)(1-nqoH) •EtOH the distance of lithium from the oxygen atom of the ethanol molecule is 1.923(24) ~ and compares well with those found in other penta-coordinate/square-pyramidal lithium solvated complexes *(ca* 1.91-1.96 **A). 16**

Acknowledgement--Thanks are due to N.P.L. (National Physical Laboratory) for financial support to P.G.

REFERENCES

1. J. Charalambous, W. C. Stoten and K. Hendrick, *Polyhedron* 1989, 8, 103.
2. O. Carugo, C. B. Castellani and K. Djinovic, J. *Chem. Soc., Dalton Trans.* 1991, 1255.
3. G. Graziani, U. Casellato, P. A. Vigato, S. Tamburini and M. Vidali, *J. Chem. Soc., Dalton Trans.* 1983, 697.
4. A. McKillop and T. S. B. Sayer, *J. Or9. Chem.* 1976, 41, 1079.
5. C. B. Castellani, G. Gatti and R. Millini, *Inor#. Chem.* 1984, 23, 4004.
6. J. Charalambous, M. J. Kensett and J. M. Jenkins, *J. Chem. Res. (S)* 1982, 306.
7. D. Baluch, J. Charalambous and L. I. B. Haines, J. *Chem. Soc., Chem. Commun.* 1988, 1178.
8. A. K. Banerjee, A. J. Layton, R. S. Nyholm and M. R. Truter, *J. Chem. Soc. A* 1969, 2536.
9. S. V. Patil and J. R. Raju, *Ind. J. Chem.* 1974, 12, 770.
10. A. K. Banerjee, D. Prakash and S. K. Roy, *J. Ind. Chem. Soc.* 1976, 53, 773.
11. C. B. Castellani, O. Carugo and A. Coda, *Acta Cryst., Sect. C* 1988, 44, 265.
12. H. Saarinen and J. Korvanranta, *Finn. Chem. Lett.* 1978, 223.
13. H. Saarinen and J. Korvanranta, *Acta Chem. Scand., Set. A* 1975, 29, 409.
14. J. Korvanranta and H. Saarinen, *Acta Chem. Scand., Ser. A.* 1975, 29, 861.
15. L. L. Merritt, J. C. Guare and A. E. Lessor, *Acta Cryst.* 1956, 9, 253.
16. V. Olsher, R. M. Izatt, J. S. Bradshaw and N. K. Dulley, *Chem. Rev.* 1991, 91, 137.

Polyhedron Vol. 12, No. 8, pp. 883–889, 1993
Printed in Great Britain

0277–5387/93 $6.00+.00
© 1993 Pergamon Press Ltd

COMPLEXES OF MANGANESE(III), COBALT(III), IRON(II), NICKEL(II) AND COPPER(II) WITH 5-ACETYLAMINO-1,2-BENZOQUINONE-2-OXIME

HENGAMEH BARJESTEH, JOHN CHARALAMBOUS* and NAVIN D. PATHIRANA

School of Applied Chemistry, University of North London, Holloway Road, London N7 8DB, U.K.

(*Received* 23 *November* 1992; *accepted* 30 *November* 1992)

Abstract—Nitrosation of 3-acetylaminophenol in the presence of the appropriate metal(II) chloride or $Na_3[Co(NO_2)_6]$ has led to the complexes $M(5\text{-Acqo})_2 \cdot nH_2O$ (M = Ni, $n = 6$; Cu, $n = 0$), $Mn(5\text{-Acqo})_3 \cdot H_2O$, $Na[Fe(5\text{-Acqo})_3]$ and $Na[Co(5\text{-Acqo})_2(NO_2)_2]$ (AcqoH = 5-acetylamino-1,2-benzoquinone-2-oxime). $Co(5\text{-Acqo})_3$ resulted from the reaction of 5-AcqoH with $CoCl_2 \cdot 6H_2O$. The reaction of $M(5\text{-Acqo})_2$ with pyridine and 2,2′-dipyridine afforded the adducts $M(5\text{-Acqo})_2(py)_2$ and $M(5\text{-Acqo})_2(dipy)$, respectively. Solution electronic spectra and magnetochemical studies indicated octahedral geometries for all complexes prepared, except $Cu(5\text{-Acqo})_2$. ^1H NMR and/or ^{13}C NMR studies indicated that $Co(5\text{-Acqo})_3$ exists as a mixture of the *meridional* and *facial* isomers, whereas the anion in $Na[Fe(5\text{-Acqo})_3]$ is entirely in the *meridional* form.

The study of quinone mono-oximes and especially of their metal complexes is currently receiving much attention.[1–3] Our continuing interest in such compounds is related to their potential in organic synthesis and their application in metal extraction and the treatment of metal overload. Here we report on the preparation and characterization of copper(II), nickel(II), iron(II), cobalt(III) and manganese(III) complexes of 5-acetylamino-1,2-benzoquinone-2-oxime.

EXPERIMENTAL

Elemental analyses were performed on a Carlo–Erba 1106 microanalytical instrument at the Polytechnic of North London. Metals were determined by atomic absorption using a Pye–Unicam SP9 atomic absorption spectrometer. Wet oxidation of the complex was achieved by heating the complex in concentrated nitric acid and 30% hydrogen peroxide. IR spectra in the 4000–400 cm^{-1} region were recorded on a BIO-RAD FTS40 spectrometer and the samples were prepared as pressed potassium discs. Fourier-transform ^1H and ^{13}C NMR spectra were recorded on a Bruker AM250 or a Joel 270 and 500 MHz spectrometer. Trimethylsilane was used as a reference standard for the spectra recorded in d_6-dimethylsulphoxide. UV–vis spectra in the 900–190 nm region were obtained using a Shimadzu UV-2100 spectrometer. Magnetic susceptibilities were recorded at room temperature using a Johnson–Matthey magnetic susceptibility balance. The instrument was calibrated using a solution of manganese(II) chloride. The magnetic susceptibility values were corrected for the diamagnetic effects of the metal and the ligands. A thermal gravimetric analysis was carried out on a Stanton HT-SM thermobalance. The mass spectra were obtained using a Kratos Profile spectrometer.

Preparation of copper(II), *nickel*(II), *manganese*(III) *and cobalt*(III) *complexes of 5-acetylamino*-1,2-*benzoquinone 2-oxime by nitrosation of 3-acetylaminophenol*

3-Acetylaminophenol (8 g, 50 mmol) in methanol (50 cm^3) was added to a solution of the hydrated metal(II) chloride or sodium hexanitrocobaltate (III) (25 mmol), acetic acid (15 cm^3) and sodium acetate trihydrate (15.0 g) in water (75 cm^3).

* Author to whom correspondence should be addressed.

Table 1. Analytical data and yields of products arising from the nitrosation of 3-acetylaminophenol in the presence of metal salts

Metal salt	Complex	Product Yield (%)	Found (%) (Calc.) C	H	M	N	3-AcqoHa yield (%)
CuC12"2H20	Cu(5-Acqo)2h	90	45.7 (45.6)	3.4 (3.3)	14.9 (15.0)	13.2 (13.3)	8
NiC12"6H:O	Ni(5-Acqo)•6H20b	87	36.1 (36.6)	4.9 (5.0)	11.2 (11.2)	10.5 (10.7)	l0
MnC12"4H:O	Mn(5-Acqo)3" H20c	20	46.6 (47.2)	3.9 (3.8)	8.9 (9.0)	13.6 (13.8)	15
COC12"6H20	„*a*	54	45.9 (45.9)	3.3 (3.3)	11.2 (10.2)	13.4 (13.4)	43
Na3[Co(NO2)6]	Na[Co(~Acqo) 2(NO 2)2]"	81	36.8 (36.1)	3.3 (2.6)	11.3e (ll.1)	15.1f (15.8)	5

3-AcqoH = 3-acetylamino-l,4-benzoquinone-4-oxime.
bPurified by extracting with ethyl acetate.
' Purified by extracting with diethyl ether.
dNot formulated.
e CO (O/0),
JNa (Found = 4.5 ; Calc. = 4.3%).

Sodium nitrite (125 mmol) in water (50 cm3) was added dropwise and the mixture was stirred for 24 h. Concentration followed by filtration gave a solid, which was washed with water and methanol. Extraction of the crude product with ethyl acetate or diethyl ether gave the metal complex as a residue. Concentration of the extract gave 3-acetylamino-1,4-benzoquinone-4-oxime ; m.p. 190°C (decomposition). Found: M÷, 179; C, 52.9; H, 4.4; N, 15.7. Calc. for CsH8NzO2 : M÷, 179 ; C, 53.0 ; H, 4.4 ; N, 15.6%. See Table 1 for yield and analytical data.

Pyrolysis of bis(5-acetylarnino-1,2-benzoquinone-2-oximato)nickel(II) hexahydrate

Bis(5-acetylamino-1,2-benzoquinone-2-oximato)nickel(II) hexahydrate (1.1176 g) was heated at 0.1 mm/100-120°C (2 h) to give bis(5-acetylamino-1,2-benzoquinone-2-oximato)nickel (II) (0.8876 g, 100%); m.p. 250-260°C (decomposition). Found: C, 45.5; H, 4.0; N, 14.0; Ni, 14.1. Calc. for CI6HlaNaNiO6 : C, 46.0; H, 3.4; Ni, 14.0; N, 13.5%.

Nitrosation of 3-acetylaminophenol in the presence of ammonium iron(II) sulphate hexahydrate

Sodium nitrite (1.4 g, 20 mmol) in water (20 cm3) was added dropwise with stirring to a solution of ammonium iron(ll) sulphate hexahydrate (3.0 g, 7.5 mmol), 3-acetylaminophenol (2.3 g, 15 mmol), acetic acid (4.5 cm3) and sodium acetate in ethanol/water (1:1) (60 cm3) at 0°C. The mixture was set aside at 20°C for 72 h and then filtered to obtain a dark green solid (2.5 g), which was chromatographed on silica gel. Elution with ethyl acetate gave 3-acetylamino-l,4-benzoquinone-4-oxime (0.3 g, 10%). Elution with methanol gave sodium tris(5-acetylamino-1,2-benzoquinone-2-oximato)-ferrate(II) tetrahydrate (1.4 g, 50%). Found: C, 41.7; H, 4.3; Fe, 8.2; Na, 3.1; N, 12.0. Calc. for C24H29FeNaN6OI3 : C, 41.9; H, 4.2; Fe, 8.1 ; Na, 3.3; N, 12.2%. Pyridine was then added to the chromatography column. Elution with methanol after 1 h yielded bis(5-acetylamino-l,2-benzoquinone-2-oximato)(dipyridine)iron(II) (0.7 g, 20%). Found: C, 54.9; H, 4.3; Fe, 9.6; N, 14.7. Calc. for C26H24FeN606 : C, 54.6 ; H, 4.2 ; Fe, 9.8 ; N, 14.7%.

Direct reaction of 5-acetylamino-l,2-benzoquinone-2-oxime with cobalt(II) chloride hexahydrate in aqueous acetic acid

To a solution of cobalt(II) chloride hexahydrate (1.6 g, 5 mmol) in acetic acid-water (50 cm3, 1 : 1) was added 5-acetylamino-l,2-benzoquinone-2-oxime (3.2 g, 18 mmol) with stirring (3 h). Filtration of the mixture afforded red tris(5-acetylamino-1,2-benzoquinone-2-oximato)cobalt(III) (2.5 g, 85%);

Table 2. Analytical data and yields for pyridine and 2,2′-dipyridine adducts

Adduct	Yield (%)	Found (%) (Calc.) C	H	M	N
$Ni(5\text{-}Acqo)_2(py)_2$	90	54.2 (54.3)	4.3 (4.2)	9.8 (10.3)	14.5 (14.6)
$Ni(5\text{-}Acqo)_2(dipy)$	95	54.7 (54.5)	3.9 (3.8)	10.1 (10.3)	14.7 (14.7)
$Cu(5\text{-}Acqo)_2(py)_2$	90	53.9 (53.8)	4.1 (4.1)	10.8 (11.0)	14.8 (14.5)
$Cu(5\text{-}Acqo)(dipy)_2$	95	54.0 (54.0)	3.8 (3.8)	10.4 (11.1)	14.6 (14.6)

m.p. 290–300°C (decomposition). Found: M^+, 597; C, 47.9; H, 3.9; Co, 9.9; N, 14.0. Calc. for $C_{24}H_{21}CoN_6O_9$: M, 597; C, 48.3; H, 3.5; Co, 9.9; N, 14.1%. The filtrate was washed with water (4×100 cm^3), diethyl ether (4×100 cm^3) and then dried at 0.1 mm/20°C.

Interaction of $M(5\text{-}Acqo)_2 \cdot nH_2O$ *with pyridine*

$M(5\text{-}Acqo)_2 \cdot nH_2O$ (M = Ni, $n = 6$; M = Cu, $n = 0$) (1.2 mmol) and pyridine (0.6 mmol) were stirred in acetone (40 cm^3) (24 h). Dropwise addition of the resultant viscous solution to light petroleum (b.p. 30–40°C; 100 cm^3), followed by filtration gave bis(5-acetylamino-1,2-benzoquinone-2-oximato)bis(pyridine)metal(II), which was washed with light petroleum (b.p. 30–40°C; 3×50 cm^3) and dried at 20°C/0.1 mm (see Table 2 for yield and analytical data).

Interaction of $M(5\text{-}Acqo)_2 \cdot nH_2O$ *with 2,2′-dipyridine*

$M(5\text{-}Acqo)_2O \cdot nH_2O$ (M = Ni, $n = 6$; M = Cu, $n = 0$) (10 mmol) and 2,2′-dipyridine (5 mmol) were stirred in acetone (70 cm^3) (24 h). Filtration gave a solid residue, which was washed with acetone (3×25 cm^3) and dried at 0.1 mm/20°C to give bis-(5-acetylamino-1,2-benzoquinone-2-oximato)(2,2′-dipyridine)metal(II) (see Table 2 for yield and analytical data).

RESULTS AND DISCUSSION

The complexes $M(5\text{-}Acqo)_2 \cdot nH_2O$ (M = Cu, $n = 0$; Ni, $n = 6$) listed in Table 1 have been obtained in high yield by nitrosating 3-acetylaminophenol with sodium nitrite/acetic acid in the presence of the respective metal chloride. The analogous reaction involving manganese(II) chloride afforded the manganese(III) complex $Mn(5\text{-}Acqo)_3 \cdot H_2O$. Nitrosation reactions performed in the presence of ammonium iron(II) sulphate led to the formation of a mixture of the iron(II) complexes, $Fe(5\text{-}Acqo)_2$ and $Na[Fe(5\text{-}Acqo)_3]$, the former of which was separated from the mixture in the form of its dipyridine adduct $Fe(5\text{-}Acqo)_2(py)_2$.

Previous studies have indicated that nitrosation of 1-naphthol or 2-naphthol in the presence of cobalt(II) chloride leads to the formation of a mixture of cobalt(III) complexes of the type $Co(nqo)_3$ and $Na[Co(nqo)_2(NO_2)_2]$ [nqoH = 1-nqoH (1,2-naphthoquinone-1-oxime) or 2-nqoH (1,2-naphthoquinone-2-oxime)].[4] In contrast this study has shown that the analogous reaction with 3-acetylaminophenol leads to a mixture of 3-acetylamino-1,4-benzoquinone-4-oxime and a black diamagnetic cobalt containing product which could not be characterized. However, the complex $Co(5\text{-}Acqo)_3$ was successfully prepared by the direct reaction of 5-acetylamino-1,2-benzoquinone-2-oxime with cobalt(II) chloride hexahydrate in aqueous acetic acid. The synthesis of $Na[Co(5\text{-}Acqo)_2(NO_2)_2]$ was achieved by the nitrosation of 3-acetylaminophenol in the presence of sodium hexanitrocobaltate(III).

The complexes $Cu(5\text{-}Acqo)_2$ and $Ni(5\text{-}Acqo)_2 \cdot 6H_2O$ reacted readily with pyridine to give adducts of the type $M(5\text{-}Acqo)_2(py)_2$ (Table 2). In the case of the copper complex the formation of the di-adduct is novel, as in all previous reactions involving complexes of the type $Cu(qo)_2$ and pyridine only the formation of the monoadduct has been reported.[5] The complexes also reacted readily with 2,2′-dipyridine to give adducts of the type $M(5\text{-}Acqo)_2(dipy)$ (Table 2).

Thermal gravimetric analyses (Table 3) of $Ni(5\text{-}Acqo)_2 \cdot 6H_2O$ and $M(5\text{-}Acqo)_2(py)_2$ (M = Cu or Ni) and macroscale pyrolysis of the former showed that quantitative loss of water or pyridine occurs

Table 3. Thermal gravimetric analysis

Compound	Weight of sample (mg)	T a'b (°C)	Weight loss (mg) Found	Calc.	Decomposition temperature (°C) of M(5-Acqo)2
Ni(5-Acqo)2 •6H20	156	100-120	32	31c	250-260
Ni(5-Acqo)2(py)2	172	150-180	47	47a	240-250
Cu(5-Acqo)E(PY)2	136	140-220	18	19a	250-260

"Temperature of the loss of water or pyridine.
bMaxima on the rate of weight loss against temperature curve.
"Calculated for the loss of water.
dCalculated for the loss of pyridine.

below 200°C, followed by decomposition of the resultant M(5-Acqo)2 at *ca* 250°C.

In the protonated ligand, 5-AcqoH, v(CO) of the ring quinone group appears at *ca* 1640 cm-t whereas a strong band at *ca* 1600 cm- 1, assignable to v(CO) of the ring quinone group, is shown by all complexes (Table 4). The observed shift to lower frequency in the complexes suggests that the ring CO group is involved in bonding to the metal.

The solution electronic spectra of all complexes reported are similar and as with other quinone oximic complexes show intense ~tbsorptions in the UV region, which tail into the visible region (Table 4). 6As a consequence bands due to *d-d* transitions appear as broad shoulders and their unambiguous assignment is not always possible. For the nickel(II) and cobalt(III) complexes some assignments indicative of octahedral geometry can be made. The spectra of the cobalt complex show two bands in the 17,000-18,000 and 24,300-24,700 cm-J ranges, as expected for low-spin six-coordinated cobalt(III) complexes. 7 The first band can be assigned to a lT~g~ lAlg transition and the other to a IT2g-"~ 'A lg transition. All nickel(II) complexes show two bands in the 20,000-21,500 and 26,000-27,000 cm- 1ranges, which are assignable to the transitions 3Tlg(F) --o 3A2g(F) and 3TI#(P) --~ 3A2a(F), respectively. 7 In addition in the case of Ni(5-Acqo)2"6H20 a band is observed at *ca* 11,000 cm-~, which is assignable to the transition 3T2g(F) ~ 3A2g(F).7

The proposed octahedral geometry of the nickel (II) complexes Ni(5-Acqo)2"6H20, Ni(5-Acqo)z (PY)2 and Ni(5-Acqo)2(dipy) is further supported by room-temperature magnetic moments, which, as expected for such geometry, are in the range 3.0-3.3/lB.

The room-temperature magnetic moment of the complex Mn(5-Acqo)3"H20 was found to be 2.88 #B, which is close to the spin-only magnetic

Table 4. Selected IR and electronic spectroscopic data and magnetic moments for 5-acetylamino-l,2-benzoquinone-2-oximeand its complexes

Compound	v(CO)a (cm-1)	Electronic spectra (cm-t)			PB (B.M.)
5-AcqoH	1642				
Ni(5-Acqo)2"6H20	1605	26,596	20,619	11,111	3.00
Ni(5-Acqo)2	1601				1.11
Cu(5-Acqo)2	1601	20,367			2.00
Co(5-Acqo)3	1598	24,272			Diamagnetic
Na[Co(5-Acqo)2(NO2)2]	1598	24,991	17,391		Diamagnetic
[Co(5-Acqo) 5]O2	1598	24,691	17,857		Diamagnetic
Mn(5-Acqo)3-H20	1591	18,315	14,493	13,315	2.89
Ni(5-Acqo)2(py)2	1605	26,667	21,368		3.00
Ni(5-Acqo)2(dipy)	1604	26,667	21,505		2.98
Cu(5-Acqo) 2(py)2	1605	19,646			1.90
Cu(5-Acqo) ffdipy)	1604	20,000			1.79

Ring carbonyl group.

moment expected for spin-paired manganese(III) in an octahedral environment. So far only a few examples of spin-paired manganese(III) complexes have been reported. These include $Mn(1\text{-nqo})_3$, $Mn(2\text{-nqo})_3$[8] and tris(dimethylaminotroponiminato) manganese(III).[9]

The complexes $Co(5\text{-Acqo})_3$, $Na[Co(5\text{-Acqo})_3(NO_2)_2]$, $Na[Fe(5\text{-Acqo})_3]$ and $Fe(5\text{-Acqo})_2(py)_2$ were found to be diamagnetic, which is in accordance with octahedral geometry and spin-paired configurations. The Mössbauer parameters for the iron complexes $Na[Fe(5\text{-Acqo})_3]\cdot 4H_2O$ ($\delta = 0.10$ mm s^{-1}, $\Delta = 0.67$ mm s^{-1}) and $Fe(5\text{-Acqo})_2(py)_2$ ($\delta = 0.22$ mm s^{-1}, $\Delta = 0.62$ mm s^{-1}) are similar to those reported for other octahedral quinone oximato iron(II) complexes.[6,10] The diamagnetism of these complexes, as well as the low-spin d^4 configuration of $Mn(5\text{-Acqo})_3$, are indicative of the strong field character of the 5-acetylamino-1,2-benzoquinone 2-oximato ligand, a feature which has also been observed for other quinone oximic ligands.[4,6]

The room-temperature magnetic moments of the complex $Cu(5\text{-Acqo})_2$ and its adducts were found to be in the range 1.79–1.94 μ_B, which indicates that the compounds are magnetically dilute and hence monomeric. Previously, similar magnetic moments have been obtained for other copper(II) quinone oximic complexes.[5]

The magnetic moment of the anhydrous complex, $Ni(5\text{-Acqo})_2$, was found to be 1.1 μ_B. The subnormal magnetic moment of the complex can be accounted for in terms of association and antiferromagnetic interaction between adjacent nickel atoms, as suggested previously for the related complexes $Ni(1\text{-nqo})_2$ and $Ni(2\text{-nqo})_2$.[11]

Previous studies of the complexes $Co(1\text{-nqo})_3$ and $Co(2\text{-nqo})_3$ have indicated that the compounds exist as a mixture of isomers.[12] The isomeric forms were subsequently separated by chromatography and characterized as *facial* and *meridional* geometric isomers by NMR studies.[12] Their formation reflects the unsymmetric nature of the ligand and as expected the *facial* isomer, which has a three-fold rotation axis, showed a simpler spectrum than the *meridional* isomer, which has no symmetry. Due to the unsymmetrical nature of the 5-Acqo^- ligand in the complexes $Co(5\text{-Acqo})_3$ and $[Fe(5\text{-Acqo})_3]^-$ a similar type of isomerism could also be exhibited. The ^1H NMR spectra of both $Co(5\text{-Acqo})_3$ and $Na[Fe(5\text{-Acqo})_3]\cdot 4H_2O$ in d_6-dimethylsulphoxide were recorded. At 270 MHz the spectrum of the iron complex (Fig. 1) indicated the presence of three aromatic proton environments. Each signal inte-

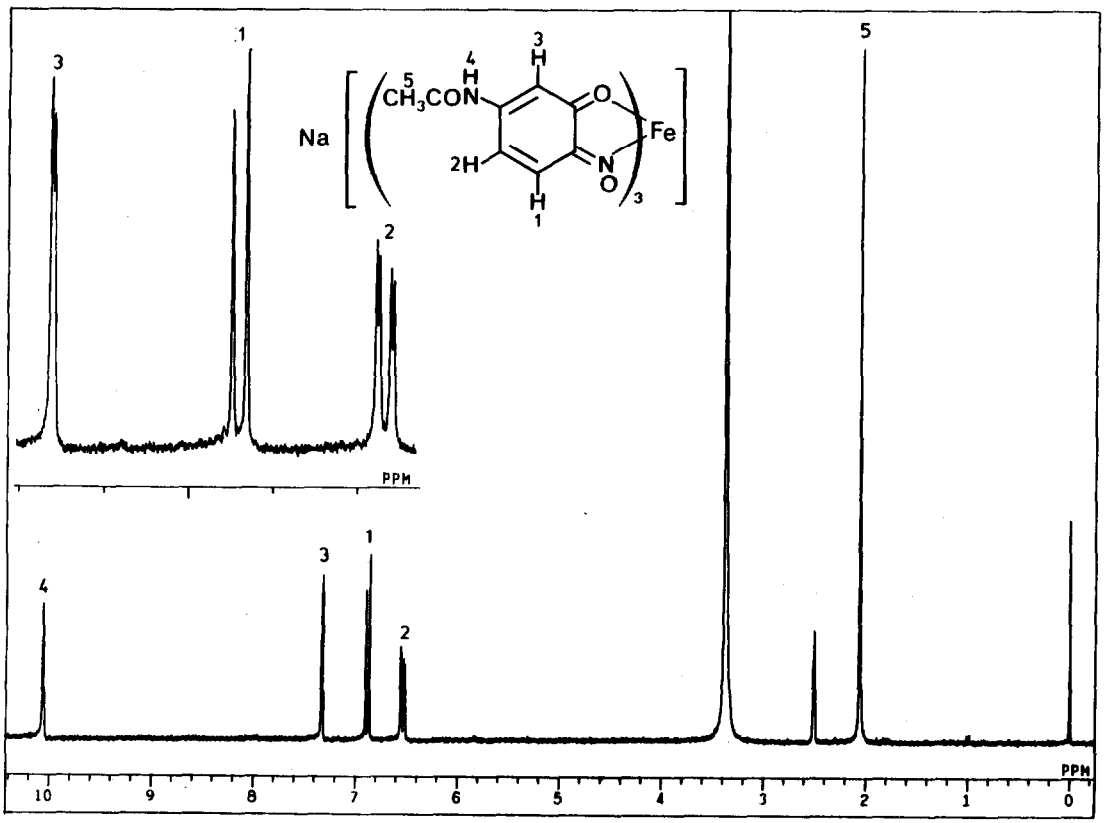

Fig. 1. ^1H NMR spectrum of $Na[Fe(5\text{-Acqo})_3]$ in d_6-DMSO at 270 MHz.

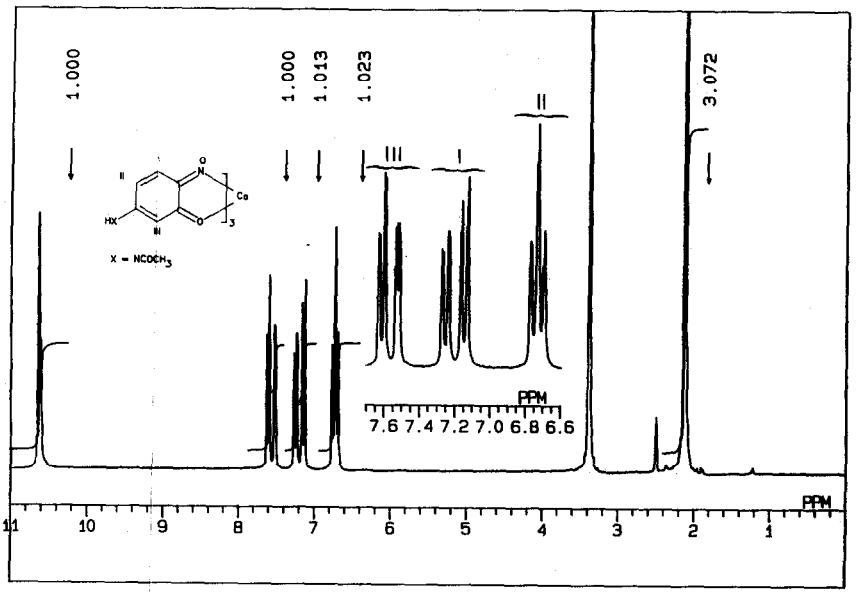

Fig. 2. ^{1}H NMR spectrum of Co(5-Acqo)$_3$ in d_6-DMSO at 270 MHz.

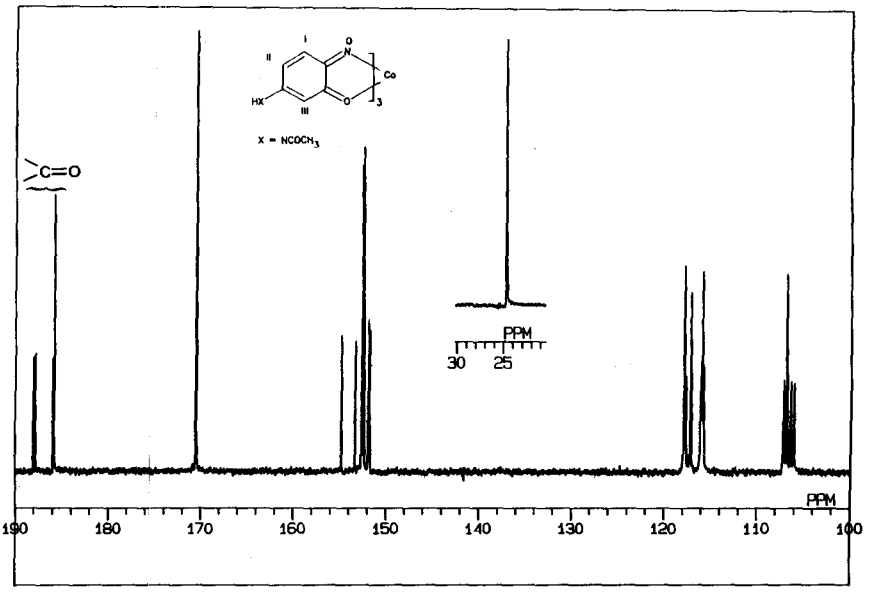

Fig. 3. ^{13}C NMR spectrum of Co(5-Acqo)$_3$ in d_6-DMSO at 270 MHz.

grated for three equivalent protons and showed the expected *ortho* and *meta* couplings, thus indicating the presence of the *facial* isomer only. The ^{1}H NMR spectrum of Co(5-Acqo)$_3$ (Fig. 2) measured at 270 MHz was not well defined, although the presence of four different aromatic proton environments was observed. This suggested that the complex was a mixture of *facial* and *meridional* isomers.

The broad-band decoupled ^{13}C NMR of Co(5-Acqo)$_3$ (Fig. 3) also confirms the presence of *facial* and *meridional* isomers, as it shows peaks corresponding to four different quinonoid (>C=O) carbons. The peaks for the quinonoid carbons were assigned by comparison with chemical shift data for similar compounds.[13]

Acknowledgement—The support of The A.G. Leventis Foundation is gratefully acknowledged.

REFERENCES

1. J. Charalambous, W. C. Stoten and K. Henrick, *Polyhedron* **1989**, **8**, 103.

2. C. Bisi Castellani, O. Carugo and A. Coda, *Acta Cryst.* 1988, **C44**, 265.
3. P. C. Christidis, A. Dodd, N. D. Pathirana, J. Charalambous, M. McPartlin and N. Talee, *Acta Cryst.* 1991, **C47**, 2640.
4. J. Charalambous, G. Soobramanien, A. Betts and J. Bailey, *Inorg. Chim. Acta* 1982, **60**, 151.
5. J. Charalambous, M. J. Frazer and F. B. Taylor, *J. Chem. Soc.* (*A*) 1969, 2787.
6. J. Charalambous, M. J. Frazer and R. Sims, *Inorg. Chim. Acta* 1976, **18**, 247.
7. K. Nakamoto and P. J. McCarthy, *Spectroscopy and Strucure of Metal Chelate Compounds*. John Wiley and Sons Inc., New York (1968).
8. D. Baluch, J. Charalambous and L. I. B. Haines, unpublished data.
9. D. R. Eaton, W. R. McClellan and J. F. Weiher, *Inorg. Chem.* 1968, **7**, 2040.
10. J. Charalambous, L. I. B. Haines, J. S. Morgan, D. S. Peat, M. J. M. Campbell and J. Bailey, *Polyhedron* 1987, **6**, 1027.
11. J. Charalambous, P. Maple, N. A. Nassef and F. B. Taylor, *Inorg. Chim. Acta* 1978, **26**, 107.
12. S. I. Tyukhtenko, V. I. Kofanov and T. L. Vrubel, *J. Liq. Chrom.* 1988, **11**, 3103.
13. A. Arnone, G. Fronza and R. Mondalli, *J. Magnet. Reson.* 1977, **28**, 69.

Polyhedron Vol. 12, No. 8, pp. 891–895, 1993
Printed in Great Britain

0277–5387/93 $6.00+.00
© 1993 Pergamon Press Ltd

CRYSTAL AND MOLECULAR STRUCTURE AND SPECTRAL PROPERTIES OF DIISOTHIOCYANATO-(1,10-PHENANTHROLINE)COPPER(II)

GARY L. BRENEMAN and O. JERRY PARKER*

Department of Chemistry and Biochemistry, Eastern Washington University, Cheney, WA 99004, U.S.A.

(*Received* 5 *October* 1992; *accepted* 11 *December* 1992)

Abstract—Adding solid NH_4SCN to a light blue solution which contains a pale green precipitate of $Cu(phen)Cl_2$ produces a green solid that can be recrystallized to produce single crystals. The IR spectrum indicates that both ends of the thiocyanate ion bond to the copper. An X-ray structure determination verifies this conclusion. The structure of this complex has a four-coordinated distorted square-planar arrangement of nitrogen atoms with one nitrogen-bonded thiocyanate twisted above the plane described by copper and phen, and another thiocyanate twisted below the plane. The sulphur ends of the two thiocyanates form longer fifth and sixth bonds to copper atoms in adjacent molecules, forming a linear infinite chain of SCN^- bridged copper atoms. The copper is thus six-coordinated with distorted tetragonal symmetry.

The composition of complexes formed from copper(II), 1,10-phenanthroline and thiocyanate is very sensitive to the nature of the solvent system. The compound $Cu(phen)_2(NCS)_2$ can be prepared from a pyridine solution,[1] which contains phenanthroline, thiocyanate and copper(II) in the appropriate ratios. The five-coordinate compound $[Cu(phen)_2(NCS)]NCS$ can be prepared in aqueous acetone solutions.[2] The addition of this compound to nitrobenzene[2] produces $Cu(phen)(NCS)_2$. The IR and electronic spectra suggested that this complex[3] has a distorted planar or distorted octahedral stereochemistry in the solid state. Previous work on the interpretation of IR data has suggested that $Cu(phen)(NCS)_2$ contains nitrogen-bonded bridging thiocyanate ligands.[3] Copper as a borderline class b metal[4] has the possibility of bonding with either end of the ambidentate thiocyanate ligand. It is difficult to predict whether the electronic factor or the steric factor associated with this ambidentate ligand will predominate. It has been suggested that steric pressure produces a conjunctive response which mandates both a nitrogen- and a sulphur-bonded thiocyanate when two ambidentate ligands reside in a complex that provides steric pressure.[5] We have determined the crystal structure of this complex in order to understand the nature of the thiocyanate linkage.

RESULTS AND DISCUSSION

Synthesis

The procedure for the preparation of the 2,2′-bipyridine complex[3] was slightly modified for the synthesis of $Cu(phen)(NCS)_2$. The compound is extremely insoluble in water and ethanol. The complex is soluble in dimethylsulphoxide and this solubility is very temperature dependent. Dark green crystals were produced when the light green complex was recrystallized in DMSO. A single parallelepiped crystal was selected for the crystal structure determination.

Crystal and molecular structure of $Cu(phen)(NCS)_2$

A summary of crystal data is given in Table 1.

A drawing of the $Cu(phen)(NCS)_2$ molecule, showing thermal ellipsoids, is shown in Fig. 1. Another angle is presented in Fig. 2, showing the lack of planarity of the nitrogen atoms coordinated

* Author to whom correspondence should be addressed.

Table 1. Crystallographic data for the molecule Cu(phen)(NCS)$_2$

Empirical formula	$CuS_2N_4C_{14}H_8$
Cell dimensions	
a (Å)	8.1986(8)
b (Å)	16.235(2)
c (Å)	10.609(1)
β (°)	97.11(1)
V (Å^3)	1401.3(3)
Z (molecule/cell)	4
Mol. wt	359.91
Space group	$C2/c$
T (°C)	22
Wavelength (Å)	0.71073
d_{calc} (g cm^{-3})	1.706
Linear absorption coefficient (cm^{-1})	18.87
$R(F)$	0.041
$R_w(F)$	0.046

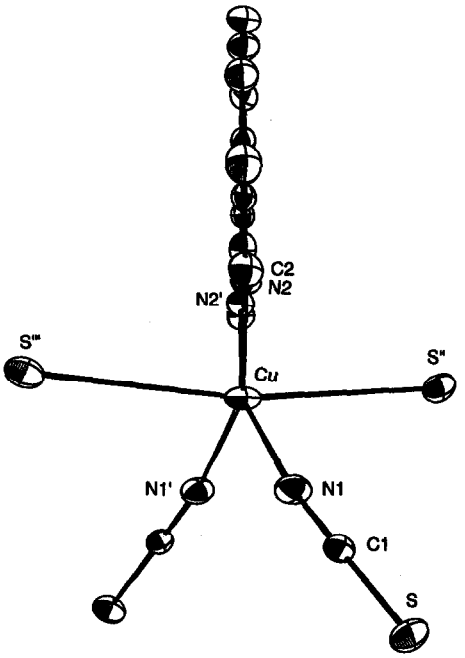

Fig. 2. ORTEP drawing showing the SCN$^-$ ions being non-planar with the phenanthroline and coordination of sulphur atoms from other molecules (S″ and S‴) to the copper atom.

to the copper atom. Also shown are the sulphur atoms on other molecules weakly coordinated to the copper in the fifth and sixth positions. Bond distances and angles are given in Tables 2 and 3.

The structure consists of one 1,10-phenanthroline molecule and two thiocyanate ions coordinated to a copper(II) ion, all through nitrogen atoms. The resulting four-coordinate geometry is not square planar, as can be clearly seen in Fig. 2 looking edge on to the 1,10-phenanthroline. The thiocyanate ions are clearly splayed out at a significant angle. The N(1)—Cu—N(2)—C(2) torsion angle is 21.9(4)°. This distortion, from more nearly square-planar geometry, appears to be due to the significant bridging interactions of the sulphur atoms on the ends of the SCN$^-$ ions with neighbouring copper atoms, forming an infinite linear chain along the c-axis. Figure 3 shows a stereoscopic drawing of the unit cell packing in this compound, including the sulphur interactions with the copper atoms. This Cu—S(SCN) distance is 3.163(2) Å. The sulphur atoms are in the fifth and sixth positions of a fairly distorted octahedral geometry. The angles around the copper atom vary from 73.8(1)° to 99.1(1)°. The SCN$^-$ ions are essentially linear [178.5(4)°], but are not quite co-linear with the copper atom [the

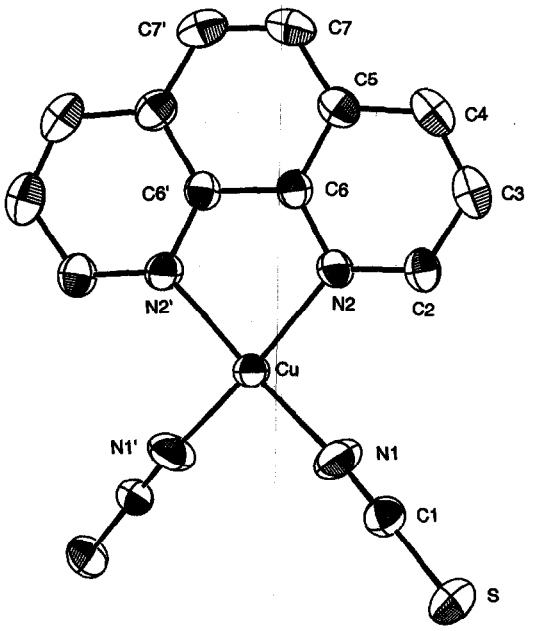

Fig. 1. ORTEP drawing for the Cu(phen)(NCS)$_2$ molecule showing the atom numbering scheme. Primed atoms are related to unprimed atoms by the two-fold axis through the copper atom. Hydrogen atoms have been omitted.

Table 2. Selected bond distances (Å) for the Cu(phen)(NCS)$_2$ molecule (S″ is the sulphur atom from another molecule weakly coordinated to the copper)

Cu—N(1)	1.945(4)
Cu—N(2)	2.011(4)
S—C(1)	1.628(5)
N(1)—C(1)	1.148(6)
Cu—S″	3.163(2)

Table 3. Selected bond angles (°) for the Cu(phen) $(NCS)_2$ molecule

S″—Cu—S‴	170.86(6)
S″—Cu—N(1)′	98.1(1)
S″—Cu—N(2)′	73.8(1)
N(1)—Cu—N(1)′	96.0(2)
N(1)—Cu—N(2)	93.8(2)
Cu—N(1)—C(1)	168.1(5)
S—C(1)—N(1)	178.5(4)
S″—Cu—N(1)	88.0(1)
S″—Cu—N(2)	99.1(1)
N(1)—Cu—N(2)′	160.4(2)
N(2)—Cu—N(2)′	82.2(2)
Cu—S″—C(1)″	103.3(2)

Cu—N(1)—C(1) angle is 168.1(5)°] apparently also from the distortion caused by the Cu—S(SCN) interactions. The Cu—S—C(1) angle between molecules is 103.3(2)°.

UV–vis spectroscopy

The absorption spectrum of $Cu(phen)(NCS)_2$ in dimethylsulphoxide displayed two maxima with a molar absorptivity that agreed with previous work.[3] Our work: 373 ($\varepsilon = 689\ M^{-1}\ cm^{-1}$) and 704 nm ($\varepsilon = 61.8\ M^{-1}\ cm^{-1}$); ref. 3: 370–380 ($\varepsilon = 704\ M^{-1}\ cm^{-1}$) and 690–710 nm ($\varepsilon = 76.5\ M^{-1}\ cm^{-1}$).

IR spectroscopy

The diffuse reflectance spectra of Cu(phen) $(NCS)_2$ shows two very strong bands at 2094 and 2118 cm^{-1}. The conventional interpretation of ν(C—N) at 2094 cm^{-1} is that the thiocyanate ligand is sulphur-bonded, but exceptions to this [chromium(III) near 2090 cm^{-1}] are known.[6] The band at 2118 cm^{-1} is usually indicative of thiocyanate bridging. The presence of 1,10-phenanthroline produces medium bands at 718 and 852 cm^{-1}, which precludes the use of ν(C—S) for structural diagnosis. There are weak bands at 424 and 476 cm^{-1} in the spectrum of 1,10-phenanthroline, but the complex shows a very strong band at 424 and a strong band at 474 cm^{-1}. These δ(N—C—S) bands, respectively, would imply a sulphur-bonded and nitrogen-bonded thiocyanate.

Concluding remarks

The IR diffuse reflectance spectra of Cu $(phen)(NCS)_2$ indicates a bridged thiocyanate ligand and a subtle suggestion of both nitrogen- and sulphur-bonded thiocyanate from the δ(N—C—S) bands. Neither provide a clear indication of the polymeric nature of the crystalline solid. The low solubility of the solid in several solvents is the clearest indication of the nature of the linkage in the crystal. The solubility of the compound in DMSO and its temperature dependence is likely the result of the fifth- and six-coordination positions of copper being occupied by the solvent, DMSO.

Bonding distances of 1.945(4) for Cu—N(phen) and 2.011(4) Å for Cu—N(NCS) in Cu(phen) $(NCS)_2$ are normal distances for the short bonds with copper(II) ions. An average bond distance of 2.041 Å for Cu—N(phen) has been observed in $Cu(phen)Br_2$.[7] Bond distances of 1.99 and 2.00 Å have been reported for Cu—N(NCS) in [Cu(bimtp)$(NCS)_2$], where bimtp = (1,5-bis(4-imidazolyl)-3-thiapentane).[8] A distance of 2.60

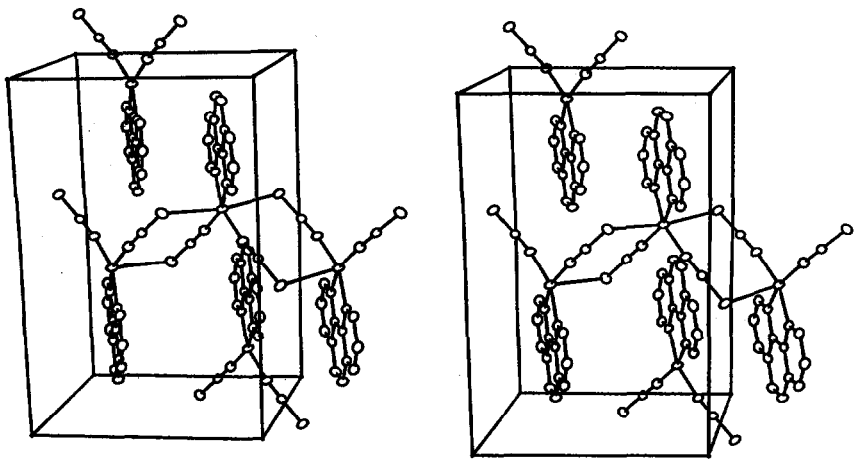

Fig. 3. Stereoscopic picture of the unit cell looking down the *a*-axis with the *b*-axis vertical and the *c*-axis horizontal, showing the linear chain of weakly bridged copper atoms.

/~ has been reported 8 for Cu--S(bimtp) in [Cu(bimtp)(NCS)2], which is representative of a short bond distance in a copper(II) ion. A bonding distance of 3.163(2) /~ for Cu--S(SCN) in Cu (phen)(NCS): is indicative of a long bond distance in copper(II) complexes. Using 2.07 and 2.62 .~ for the short and long bonds 9in Cu(NH 3)6C12and 0.71 ,~ for the ionic radius ~° of the short distance in copper(II) predicts a value of 1.26 A for the ionic radius of the long distance in copper(II). The value of 1.26 A in conjunction with the calculated ionic radius of 1.89 ,~ for sulphur from the Cu--S (bimtp) distance of 2.60/~ estimates a value of 3.15

for Cu--S(SCN), the long distance in the crystal lattice of Cu(phen)(NCS)2. This is in close agreement with the observed value of 3.163(2) ,~. The reported Cu--S(SCN) distance is 3.27 /~ in Cu (en) 2(SCN) 2.1l

The nitrogen-bonded thiocyanate ligands are not coordinated linearly to the central copper(II) ion. The Cu--N(1)--C(1) angle is 168.1 (5)°, which may be a result of the sulphur end of the ligand interacting with a neighbouring copper or it may just represent the normal bonding pattern for thiocyanate. This deviation from 180° is very common with angles of 161.8° and 152.6° observed in [Cu(bimtp)(NCS)2]. 8 The sulphur end of the thiocyanate ion forms a bond with a neighbouring copper(II) at an angle of 103.3(2)°, which is approximately the usual tetrahedral angle. The crystal packing of Cu(phen)(NCS)2 shows that both the nitrogen and sulphur ends of the thiocyanate ligand interact with copper(II) ions and the atoms that surround copper approximate tetragonal coordination. The fact that the thiocyanate ligands are splayed out at a significant angle may vitiate a conjunctive response from the pair of thiocyanate ligands, with the result that both are nitrogen-bonded. 5The smaller size ofcopper(II) as compared to palladium(II) would presumably produce more steric pressure in the copper(II) complex, but this may be effectivelyrelieved by the twisting of the two thiocyanate ligands which significantly removes these ligands from the plane of the complex which is occupied by copper(II) and the phenanthroline ligand.

EXPERIMENTAL

General procedures for the preparation of 1,10-phenanthroline and 2,2'-bipyridine complexes of copper(II) have been described. 3

Preparation of Cu(phen)(NCS) 2

A solution (25 cm 3) of 1,10-phenanthroline monohydrate (1.98 g, 10.0 mmol) in ethanol was slowly added to a 20 cm 3 solution of CuC12" 2H20 (1.71 g, 10.0 mmol) dissolved in water. To the resulting light blue solution which contained a pale green precipitate of Cu(phen)C12, solid NH4SCN (1.52 g, 20.0 mmol) was slowly added with continuous stirring. The product was a very light green solid, which was washed with a small volume of ethanol and anhydrous ether. The light green solid was dissolved in DMSO at *ca* 40°C and allowed to stand overnight. A single crop of dark green crystals was filtered and air-dried.

Single-crystal X-ray determination

Cu(phen)(NCS)2. A summary of crystal data is given in Table 1. The unit cell was determined on an Enraf-Nonius CAD4-diffractometer using Mo-K~ radiation. Symmetry and systematic extinctions *(hkl, h + k* odd and *hOl, l* odd) indicated monoclinic *Cc* or *C2/c* as the choices for the space group. Successful refinement in the centrosymmetric *C2/c* proved this to be the correct space group. An approximate 0.12x0.12x0.30 mm crystal was mounted with epoxy cement on a glass fibre for data collection on the CAD4 diffractometer using a 1.6° 0-20 scan with monochromated Mo-K, radiation. Cell dimensions were determined by least-squares refinement of 25 reflections in the range $34 < 20 < 43°$. One standard reflection was monitored periodically and showed no systematic variation. Psi scan absorption corrections were made. The structure was solved using direct methods and subsequent cycles of structure-factor calculations and difference synthesis. The non-hydrogen atoms were refined anisotropically. Hydrogen atom positions were calculated and refined isotropically to R=0.041 and wR=0.046 using w-1= ~rffFo)+0.00041Fol^2, Yw(IFol- IFcl)2 minimized. All data reduction, structure solution, refinement and graphics were executed using MolEN 12 on a VAX 6410 computer.

Supplementary data. Final values of all refined atomic coordinates, thermal parameters, bond lengths and angles have been deposited.

REFERENCES

1. A. A. Schilt and K. Fritsch, *J. Inorg. Nucl. Chem.* 1966, 28, 2677.
2. C. M. Harris, T. N. Lockyer and H. Waterman, *Nature* 1961, 192, 424.
3. R. L. Dutta and D. Dhrubananda, *J. Ind. Chem. Soc.* 1969, 46, 1.
4. S. Ahrland, J. Chatt and N. R. Davies, *Q. Rev.* 1958, 11,265.

5. A. J. Paviglianiti, D. J. Minn, W. C. Fultz and J. L. Burmeister, *Inorg. Chim. Acta* 1989, **159**, 65.
6. R. A. Bailey, S. L. Kozak, T. W. Michelsen and W. N. Mills, *Coord. Chem. Rev.* 1971, **6**, 407.
7. M. T. Garland, D. Grandjean, E. Spodine, A. M. Atria and J. Manzur, *Acta Cryst.* 1988, **C44**, 1547.
8. M. Zoeteman, E. Bouwman, R. A. G. de Graaff, W. L. Driessen, J. Reedijk and P. Zanello, *Inorg. Chem.* 1990, **29**, 3487.
9. T. Distler and P. A. Vaughan, *Inorg. Chem.* 1967, **6**, 126.
10. J. E. Huheey, *Inorganic Chemistry*, 3rd edn. Harper and Row, New York (1983).
11. B. W. Brown and E. C. Lingafelter, *Acta Cryst.* 1964, **17**, 254.
12. Enraf–Nonius, MolEN Structure Determination System. Delft, The Netherlands (1990).

Polyhedron Vol. 12, No. 8, pp. 897–901, 1993
Printed in Great Britain

0277–5387/93 $6.00+.00
© 1993 Pergamon Press Ltd

STEREOCHEMICAL CHANGES IN MONONUCLEAR COMPLEXES ML_n ($n = 10$–12)

BRIAN F. G. JOHNSON,* RUTH MALLORS, EMILIO PARISINI† and YVONNE V. ROBERTS

Department of Chemistry, The University of Edinburgh, West Mains Road, Edinburgh EH9 3JJ, U.K.

(*Received* 2 *December* 1992; *accepted* 11 *December* 1992)

Abstract—The process of edge-cleavage (simple and multiple), recently applied to generate complementary geometries for complexes ML_n ($n = 4$–9), has been extended to include values of $n = 10$–12.

Molecules are not rigid, even in the solid state. If a species has a low frequency vibrational mode (i.e. one with a large amplitude) it is likely that any structural distortion will occur along the pathway described by that vibration. In an earlier paper[1] we explored the possibility of a unifying approach to the many mechanisms of fluxionality and isomerization that coordination complexes of the generic formula ML_n might undergo. In that work, because of the more complex nature of polyhedra with greater than 10 vertices, we restricted our attention to values of n from 4 to 9. We concluded that such processes could be *systematized* and that, irrespective of the coordination number, the mechanism of polyhedral interconversion *may* be viewed as being essentially the same, corresponding to the sequential edge-breaking in the parent or ground-state polyhedron until an appropriate complementary polyhedron for the transformation is produced. For coordination numbers 4–9 at least, this process corresponded to the pathway of low frequency, edge-breaking modes and thus Scheme 1 was derived.

In this paper we report the results of our investigations of the sequential formation of polyhedra for coordination numbers 10–12 via the same edge-breaking procedure. These coordination numbers do not appear to have been explored in such detail previously and the geometries associated with them are of relevance mainly for complexes of the heaviest transition metals, e.g. the lanthanide elements.

Rearrangement of the 10*-vertex polyhedron*

The minimum energy polyhedron for 10-coordination is generally accepted as being the bicapped square antiprism, {10},‡ which in Föppl notation corresponds to the 1 : 4 : (4) : 1 arrangement. This is shown in Fig. 1. Apart from this well-established form the only other 10-vertex polyhedron commonly described is the close relative, the bicapped square prism 1 : 4 : 4 : 1, {14−4}.

Within the bicapped square antiprism are edges of three different types: a, b and c. Edge a is associated with the two caps and links vertices with connectivities of four and five, whereas both edges b and c link vertices with the same connectivity of five. Following the rule established previously[1] that edges connecting vertices of maximum connectivity are preferentially broken,§ we shall consider the cleavage of edges b or c only. Thus, in our consideration of polyhedral expansion by sequential cleavage, we have for the first time a polyhedron which offers a choice of two distinct possibilities.

(1) Cleavage of the single edge 2–3 leads directly to the *nido*-undecahedron {11−1}. This is not a

* Author to whom correspondence should be addressed.
† Università Degli Studi di Bologna, Dipartimento di Chimica, G. Ciamician, 40126 Bologna, Italy.

‡ Throughout this paper {n} denotes the most commonly observed n-vertex polyhedron, while {$n-x$} denotes the same polyhedron with x vertices missing.

§ For example, in the trigonal bipyramid {5} edges connecting vertices of four in the equatorial plane are broken, and in the pentagonal bipyramid {7} edges connecting vertices with connectivities of four and five.

$\{5\} \rightleftarrows \{6-1\}$

$\{6\} \rightleftarrows \{7-1\} \rightleftarrows \{8-2\} \rightleftarrows \{9-3\}$

$\{7\} \rightleftarrows \{8-1\} \rightleftarrows \{9-2\}$

$\{8\} \rightleftarrows \{9-1\}$

$\{9\} \rightleftarrows \{10-1\}$

{n} denotes a *closo*–polyhedron with n vertices

{n–1} denotes a *nido* n–polyhedron with n–1 vertices

{n–2} denotes an *arachno* n–polyhedron with n–2 vertices

{n–3} denotes a *hypo* n–polyhedron with n–3 vertices

Scheme 1. The postulated general mechanism for structural variation in polyhedra ML_n (n = 4–9).

suitable complementary geometry for the interconversion process since a diamond → square → diamond operation does not lead to a "new" bicapped square antiprism (see Scheme 2), but rather to a close-packed, polytetrahedral arrangement corresponding to a 3 : 7 Föppl arrangement (Fig. 2). If the edge cleavage process is continued, however, with the cleavage of a second edge 6–7, a $\{12^A-2\}$* polyhedron is produced. This is a perfectly satisfactory complementary geometry and the formation of a "new" bicapped square antiprism follows from the reformation of two "new" edges following typical diamond → square → diamond operations by closing 1–7 and 2–10. Thus, interconversion of the bicapped square antiprism may follow the four-step process in which two square faces are generated in the complementary polyhedron $\{12^A-2\}$. This is shown in Scheme 2(A).

$$\{10\} \rightarrow \{11-1\} \rightarrow \{12^A-2\} \rightarrow \{11^A-1\}' \rightarrow \{10\}'.$$

The collapse of the bicapped square antiprism to the 3 : 7 close-packed arrangement is clearly of some significance. Although unsuitable for a ligated system of the type ML_{10} and of no immediate interest in the context of this paper, it is of some importance in consideration of M_{10} cluster systems (M = metal ion), indicating a surprisingly simple and direct transfer from a polyhedral to close-packed form. The 3 : 7 arrangement here corresponds to a fragment of ptcp (3 : 7 : 3).

(2) In contrast, cleavage of an edge of type c leads to a different process [see Scheme 2(B)]. In this case sequential cleavage of four edges, 2–6, 3–7, 4–8 and 5–9, must occur before a suitable complementary geometry, viz. the bicapped cube (1 : 4 : 4 : 1), is produced. This corresponds to the overall process:

$$\{10\} \rightarrow \{11^B-1\} \rightarrow \{12^B-2\} \rightarrow \{13^B-3\} \rightarrow \{14^B-4\} \rightarrow \{13^B-3\}' \rightarrow \{12^B-2\}' \rightarrow \{11^B-1\}' \rightarrow \{10\}'.$$

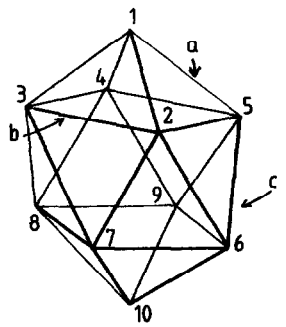

Fig. 1. The bicapped square antiprism.

* The icosahedron is deemed to be {12}; the bicapped cuneane arrangement 12^A.

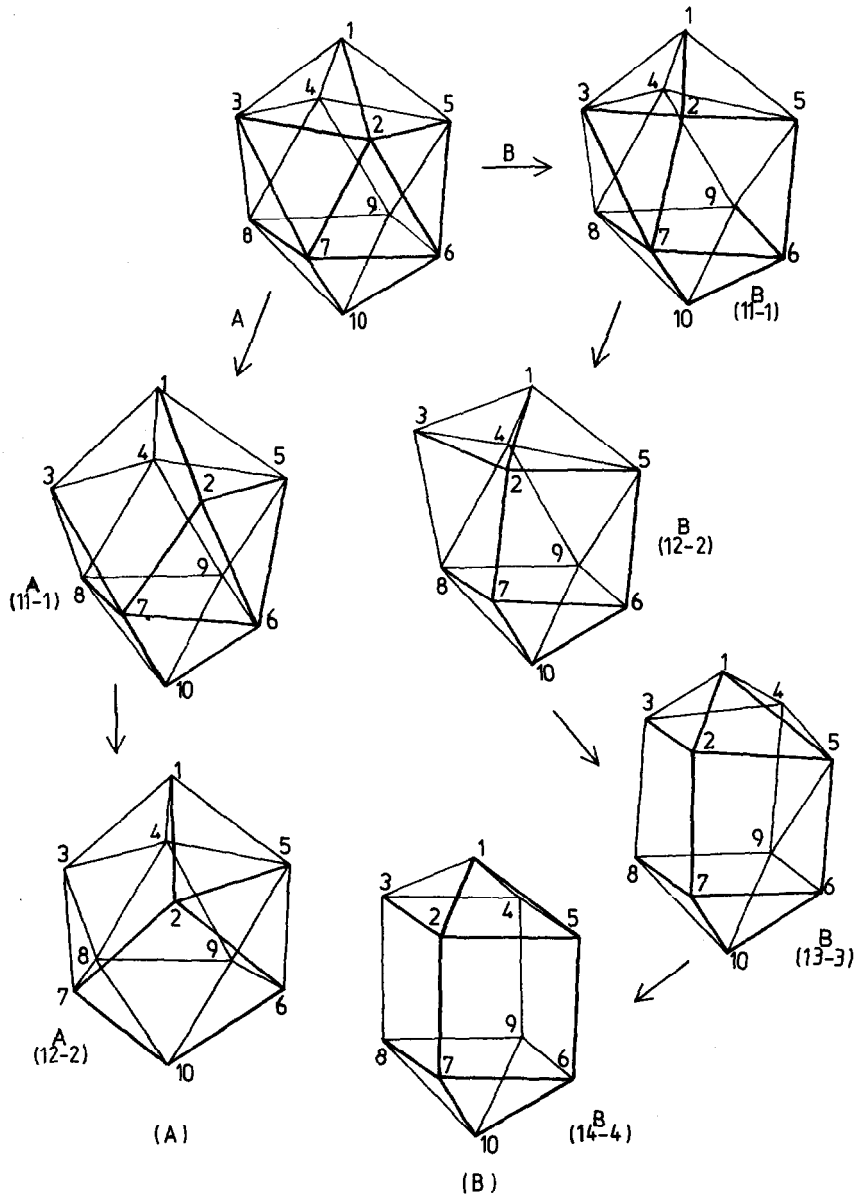

Scheme 2. Sequential edge-cleavage mechanisms for a bicapped square antiprism.

This process, with eight steps, would appear to be less favourable than that given in Scheme 2(A), which requires four steps. Within this sequence, the first intermediate polyhedron, $\{11^{B}-1\}$, appears to be very strained and moving towards a close-packed array of ligands, but beyond that surprisingly reasonable polyhedral forms appear, formally corresponding to the gradual conversion of the central unit from a square antiprism to a cube. Thus, as the process is continued more and more square faces are generated, from one initially to a maximum of four in $\{14-4\}$.

In the above rearrangements, Schemes 2(A) and 2(B), we have chosen the most reasonable of several alternatives. It is important to note that neither process (A) nor (B) (Scheme 2) leads to an *arachno*-icosahedron $\{12-2\}$. However, in process (A) the cuneane complementary geometry may be easily converted to the *arachno*-icosahedron $\{12-2\}$ form by the migration of a single edge.

Rearrangement of an 11*-vertex polyhedron*

It follows from our discussion of the bicapped square antiprism that the rearrangement of the undecahedron $\{11\}$ may be expected to proceed via a monocapped cuneane complementary geometry with a single edge cleavage [see Scheme 3(A)] in two

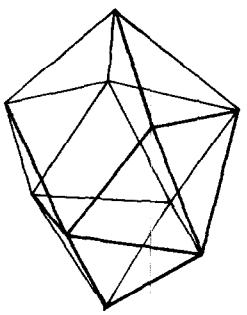

Fig. 2. The polytetrahedral 3 : 7 fragment.

steps:

$$\{11\} \rightarrow \{12^{A}-1\} \rightarrow \{11\}'.$$

Similarly, rearrangement of the alternative 11-vertex polyhedron, related to that established in Scheme 2(B), proceeds via a tricapped cube complementary geometry, viz.

$$\{11^{B}\} \rightarrow \{12^{B}-1\} \rightarrow \{13^{B}-2\} \rightarrow \{14-3\} \rightarrow$$

$$\{13^{B}-2\}' \rightarrow \{12^{B}-1\}' \rightarrow \{11^{B}\}' \text{ [see Scheme 3(B)]}.$$

Clearly, since there is a large increase in the number of steps involved, the former two-step process is expected to be preferable.

Rearrangement of the 12*-vertex polyhedron*

For the "best" 12-vertex polyhedron, viz. the icosahedron {12}, the process of rearrangement is not simple and has been examined extensively.[2-7] A suitable complementary geometry is not found until at least five edges have been broken and the bicapped right pentagonal prism, strictly {17−5},

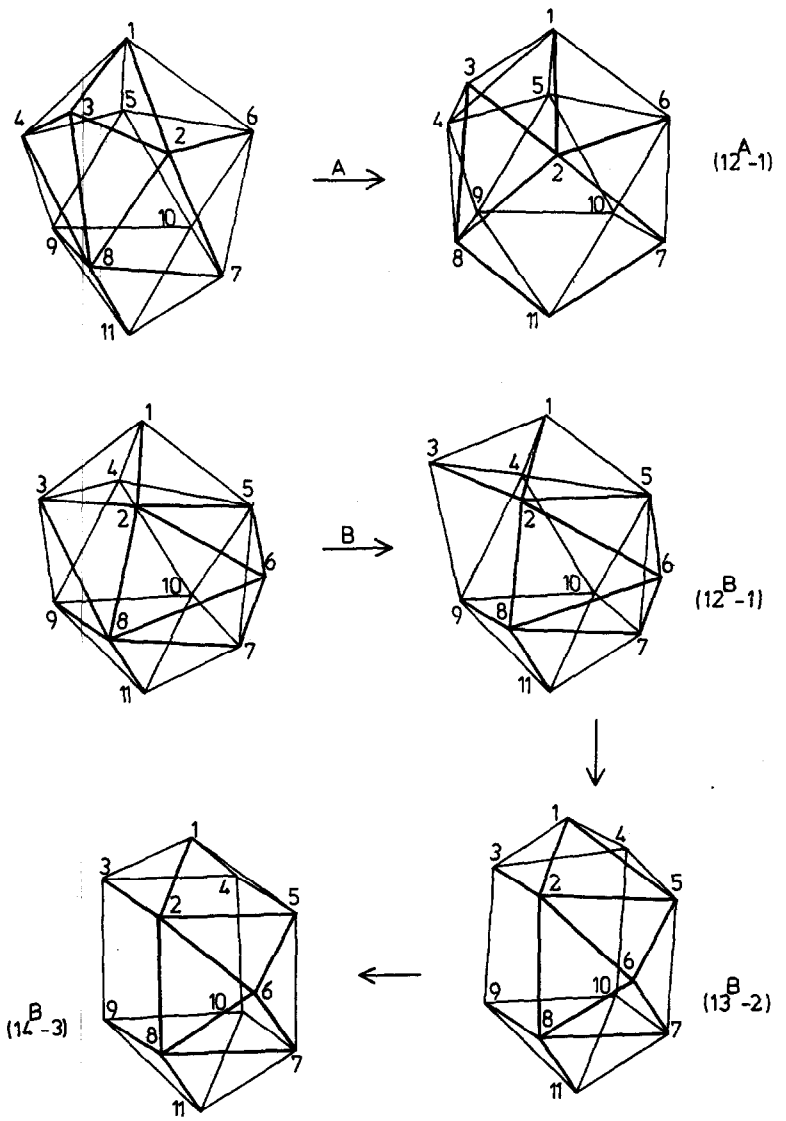

Scheme 3. Sequential edge-cleavage mechanisms for 11-vertex polyhedra.

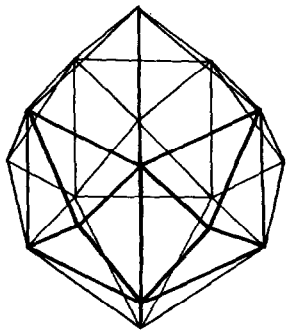

Fig. 3. A 17-vertex polyhedron.

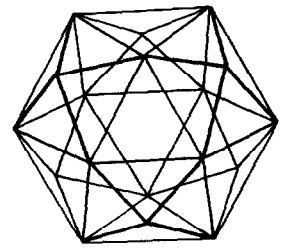

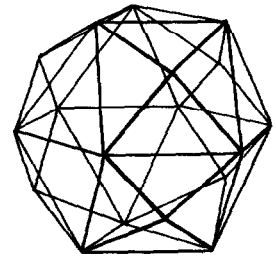

Fig. 4. 18-vertex polyhedra derived from both cubeoctahedron and anticubeoctahedron forms.

has been produced (see Fig. 3):

$$\{12\} \rightarrow \{13-1\} \rightarrow \{14-2\} \rightarrow \{15-3\} \rightarrow$$
$$\{16-4\} \rightarrow \{17-5\} \rightarrow \{16-4\}' \rightarrow \{15-3\}' \rightarrow$$
$$\{14-2\}' \rightarrow \{13-1\}' \rightarrow \{12\}'.$$

Cleavage of six edges leads to either the cubeoctahedron or the anticubeoctahedron $\{18-6\}$ (see Fig. 4) and provides a 12-step interconversion process.

$$\{12\} \rightarrow \{13-1\} \rightarrow \{14-2\} \rightarrow \{15-3\} \rightarrow$$
$$\{16-4\} \rightarrow \{17-5\} \rightarrow \{18-6\} \rightarrow \{17-5\}' \rightarrow$$
$$\{16-4\}' \rightarrow \{15-3\}' \rightarrow \{14-2\}' \rightarrow$$
$$\{13-1\}' \rightarrow \{12\}'.$$

Nevertheless, the same process is adopted, viz. the sequential cleavage of edges to provide complementary geometries. It is interesting to note, however, that the icosahedron is unique amongst the low energy polyhedra studied, which have been grown from forms with 4–10 vertices. Neither the icosahedron itself nor any of its derivatives can be directly produced from the edge-cleavage processes described earlier. If the usual method of polyhedral growth is applied, i.e. edge cleavage, followed by the capping of the square face so produced, the ultimate low energy shape produced is $\{14\}$, the omni-capped cube. The 12-vertex polyhedron derived by this route is the bicapped cuneane form, i.e. the growth sequence follows the path to cubic or hexagonal packing and not pentagonal symmetry, as found in the isosahedron.

CONCLUSIONS

This work has revealed that, as with lower coordination numbers (4–9), the process of sequential edge-cleavage provides a convenient mechanism to suitable complementary geometries for polyhedral interconversion. However, in contrast to those lower coordination numbers for which the process generates only one possible complementary geometry, for coordination numbers 10–12 at least two complementary geometries are available. Significantly, no complementary geometries based on the icosahedron may be derived by this route. Of considerable significance is the observation that cleavage of the appropriate adjacent edges of the bicapped square antiprism leads to a close-packed arrangement of ligands. This is of no use in the ligated systems, but clearly of importance when applied to polyhedra of metal atoms, since it demonstrates a facile movement from polyhedral to close-packed arrays of metal atoms.

REFERENCES

1. B. F. G. Johnson, J. Cook, D. Ellis, S. Hefford and A. Whittaker, *Polyhedron* 1990, **9**, 2221.
2. S. H. Wu and M. Jones, *J. Am. Chem. Soc.* 1989, **111**, 5373 and refs therein.

Polyhedron Vol. 12, No. 8, pp. 903–910, 1993
Printed in Great Britain

0277–5387/93 $6.00+.00
© 1993 Pergamon Press Ltd

DISPROPORTIONATION REACTION OF $Ru_2Cl(\mu\text{-}O_2CCH_3)_4$ WITH bbtp [bbtp = TERT-BUTYLBIS(2-THIENYL)PHOSPHINE]. X-RAY CRYSTAL STRUCTURES OF $Ru_2(\mu\text{-}O)(\mu\text{-}O_2CCH_3)_2(O_2CCH_3)_2(bbtp)_2$ AND *CIS*-$Ru(O_2CCH_3)_2(bbtp)_2 \cdot CH_2Cl_2$

M. C. BARRAL and R. JIMÉNEZ-APARICIO*

Departamento de Química Inorgánica, Facultad de Ciencias Químicas, Universidad Complutense, Ciudad Universitaria, 28040 Madrid, Spain

and

R. KRAMOLOWSKY and I. WAGNER

Institut für Anorganische und Angewandte Chemie, Universität Hamburg, Martin-Luther-King Platz 6, D-2000 Hamburg 13, F.R.G.

(*Received* 21 *October* 1992; *accepted* 11 *December* 1992)

Abstract—The reaction of $Ru_2Cl(\mu\text{-}O_2CCH_3)_4$ with bbtp [bbtp = tert-butylbis(2-thienyl)-phosphine] in methanol under nitrogen leads to a disproportionation process with the formation of $Ru_2(\mu\text{-}O)(\mu\text{-}O_2CCH_3)_2(O_2CCH_3)_2(bbtp)_2$ (**1**) and *cis*-$Ru(O_2CCH_3)_2(bbtp)_2$ (**2**). In the presence of air compound **2** is very unstable in solution, giving compound **1**. The X-ray crystal structures of **1** and the CH_2Cl_2 solvate of **2** have been determined. Compound **1** contains two ruthenium(III) atoms linked by two bridging acetate groups and one bridging oxo ligand; the pseudo-octahedral environment of each ruthenium atom is completed by one bidentate chelating acetate and one monodentate phosphine ligand. Compound $\mathbf{2} \cdot CH_2Cl_2$ also has a pseudo-octahedral environment, with two monodentate bbtp ligands and two bidentate chelating acetate ligands giving a *cis* arrangement.

The reactions of $Ru_2Cl(\mu\text{-}O_2CR)_4$ (R = alkyl or aryl) with phosphines have attracted much interest in recent years.[1–14] Earlier studies,[4] performed on the reactivity of $Ru_2Cl(\mu\text{-}O_2CCH_3)_4$ with PPh_3, have shown that in methanol the compound $Ru_2(\mu\text{-}O)(\mu\text{-}O_2CCH_3)_2(O_2CCH_3)_2(PPh_3)_2$ is obtained in a yield of *ca* 100%. More recently,[5,6] it has been described that the reactions of $Ru_2Cl(\mu\text{-}O_2CR)_4$ (R = Ph, *p*-C_6H_4—OMe) with PPh_3 in acetonitrile also lead to the formation of similar oxodimer compounds. In all these reactions the initial ruthenium(II)–ruthenium(III) complex gives only ruthenium(III) compounds, indicating that some oxidation process has occurred. Although in these reactions the oxidizing agent was not mentioned, atmospheric oxygen is the most probable agent.

In some cases only ruthenium(II) complexes were obtained from $Ru_2Cl(\mu\text{-}O_2CCH_3)_4$.[7–10] For example, in the reaction with chelating diphosphines, $Ph_2P(CH_2)_nPPh_2$ (n = 1–3), in cold or refluxing benzene, *cis*- and *trans*-$Ru(O_2CCH_3)_2[PPh_2(CH_2)_nPPh_2]_2$ were obtained. In these cases the phosphine is the most likely reducing agent, which is very usual in the synthesis of phosphine complexes of ruthenium(II) from ruthenium (III).[15]

In contrast to the results described for $Ru_2Cl(\mu\text{-}O_2CCH_3)_4$, we have found previously[11,12] that the reaction of $[Ru_2(\mu\text{-}O_2CCH_3)_4(thf)_2]BF_4$ with PPh_3 leads to a disproportionation process in which, in addition to an oxodimer of ruthenium(III), a yellow ruthenium(II) compound was obtained. Furthermore, in the reactions of $Ru_2Cl(\mu\text{-}O_2CR)_4$ (R = Me, Et, *cyclo*-C_6H_{11}, Ph, *o*-C_6H_4OH) with PPh_3 in 2-methoxyethanol only ruthenium(II) compounds have been obtained, but the existence of a previous disproportionation process has been proposed.[13]

* Author to whom correspondence should be addressed.

Due to the differences observed in the reactivity of Rtl2CI(#-O2CCH3) 4 and [Ru2(I/-O2CCH3) 4 (thf) 2]BF4, and because we think that many of these reactions occur via a disproportionation process, we have decided to investigate the reaction of Ru2CI(#-O2CCH3) 4 with bbtp [bbtp = tert-butyl-bis(2-thienyl)phosphine]. This new ligand is a functional tertiary phosphine containing two different donor centres, separated by a single atom bridge, and is supposed to be able to stabilize some intermediate compounds. However, previous investigations of mercury(II), palladium(II), platinum(II) and rhodium(I) complexes of tris(2-thienyl)phosphines and aryl(2-thienyl)phosphines have shown only a monodentate coordination of the phosphines via the phosphorus atom.16]9

I

RESULTS AND DISCUSSION

Under an atmosphere of dinitrogen the reaction of Ru2CI(#-O 2CCH 3)4with bbtp in methanol leads to the formation of Ru2(#-O)(~-O2CCH3) 2 (OzCCH3)2(bbtp)2 (1) and Ru(OzCCH3)2(bbtp)2 (2). Compound 1 is stable to air and moisture in the solid state and is soluble with a violet colour in most of the usual organic solvents like CHC13, tetrahydrofuran and toluene. Compound 2 has been obtained from CH2C12/petroleum ether (40-60°C) as dichloromethanc solvate, which is only stable in a dichloromethane atmosphere. Compound 2 is soluble with a brown colour in CH2C12, toluene, tetrahydrofuran and other polar organic solvents and the colour of its solutions changes in air to violet, giving the oxodimer 1. In accordance with these results, in the presence of air the reaction of RuzCI(#-O2CCH3)4 with bbtp yields only 1 (Scheme 1). The similar oxidation of Ru(O2CCHa)2(PPh3)2 with oxygen to give Ru2(#-O)(#-OzCCH3)2 (O2CCHa)E(PPh3) 2 has also been previously observed. 4

IR, IH and 31p(1H} NMR spectroscopic data for 1 are listed in Table 1.

The IH NMR spectrum shows only one doublet for the tert-butyl groups, but two singlets for the methyl groups, in accordance with two types of acetate groups. In contrast to Ru2(/~-O)(#-O2CCH3)a(O2CCHa)2(PPh3)2 (A6 0.05 ppm) 12 the A6 separation between the signals corresponding to the acetate methyl groups of 1 (A6 0.199 ppm) is greater.

The region of the thienyl protons (6-8 ppm) shows six groups of signals, indicating two different types of thienyl groups (Table 2).

The reason for the pronounced downfield shift for H' may be a certain type of interaction between these protons and the metal caused by the spatial proximity, as seen in the crystal structure (see Fig. 1).

The 31p{~H} NMR spectrum only shows a singlet at 52.14 ppm, indicating that the two phosphine ligands are in equivalent positions.

The IR spectra of 1 in trichloromethane solution and in the solid state are very similar in the carboxylate region. The marked differences between the spectrum of 1 in the solid state and in CHCI3 solution in the region of the v(C--H) stretching vibrations may be rationalized in terms of different rotational conformers caused by the positions of the tert-butyl and thienyl groups of the phosphine ligands. Thus, the observed pronounced separation, A6, of the ~H NMR signals of the acetate methyl groups of 1 also must be due to the nature of the phosphine.

A PLUTON view of 1 is shown in Fig. 1. The most important distances and angles are summarized in Table 3. The Ru2(#-O)(p-O2CCH3)2 (O2CCH3)2(bbtp)2 molecule is formed by two ruthenium(Ill) atoms finked by two bridging acetate ligands and a bridging oxo group; the hexa-coordination of each ruthenium atom is completed by a chelating bidentate acetate group and a monodentate bbtp ligand which coordinates via the phosphorus atom in the *trans* position to one of the bridging acetates. The structure of this compound is very similar to that found in Ru2(g-O)(#-O 2CCH 3)2(O 2CCH 3)2(PPh 3)2.~2The Ru--Ooxo distances and the Ru--O--Ru angle are similar to those found for other oxodimer compounds.6122w23

IR, IH and 31p{ill} NMR spectroscopic data for 2 are summarized in Table 1.

The existence of only one singlet for the methyl protons and only three groups of signals for the thienyl protons in the IH NMR spectrum of 2 indicates the equivalence of the two acetate groups, as well as of the two phosphine ligands. In accordance with this the 31p{IH} NMR spectrum only shows

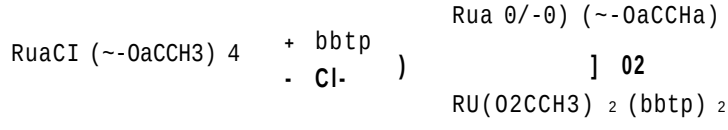

Scheme I.

Table 1. IR, ^1H and $^{31}P\{^1H\}$ NMR data for the ruthenium complexes **1** and **2**

IR (cm^{-1})[a]	Compound **1**	Compound **2**
ν(CH) (Thienyl ring)		
KBr disc	3152 sh	3100 m
	3081 m	
$CHCl_3$ solution	3026 sh	
	3021 sh	
	3018 m	
ν(CH)(CH_3)		
KBr disc	2981–2867 m	2975–2878 m
$CHCl_3$ solution	2965–2868 m	
$\nu_a(COO)-\nu_s(COO)$		
KBr disc	1469–1345 vs	1460–1380 vs
$CHCl_3$ solution	1469–1345 vs	
^1H NMR data (ppm)[b]		
CH_3 (Bu^t)	1.35 d	1.20 d
J(P—H) (Hz)	21.6	14.4
$CH_3(O_2CCH_3)$	1.97 s	1.86 s
	1.77 s	
C_4H_3S	6.88 t 6.94 t	6.78 t
	7.09 q 7.52 d	7.00 q
	7.44 d 7.64 q	7.30 d
$^{31}P\{^1H\}$ NMR data (ppm)[b]		
bbtp	52.14 s	67.83 s

[a] sh: shoulder; m: medium; vs: very strong.
[b] s: singlet; d: doublet; t: triplet; q: quartet.

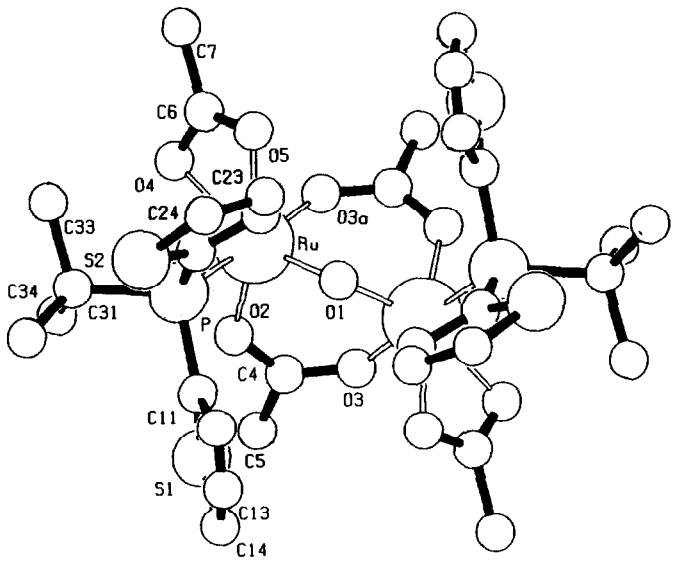

Fig. 1. PLUTON view of $Ru_2(\mu\text{-}O)(\mu\text{-}O_2CCH_3)_2(O_2CCH_3)_2(bbtp)_2$ (**1**). The hydrogen atoms are omitted for clarity.

Table 2. ^{1}H NMR data of **1** in the thienyl protons region[a]

Proton	δ (ppm)[b]
H^3	7.09 q
$H^{3'}$	7.64 q
H^4	6.88 t
$H^{4'}$	6.94 t
H^5	7.44 d
$H^{5'}$	7.52 d

[a] The protons $H^{x'}$ correspond to ring 2 of the molecular structure.

[b] d: doublet; t; triplet; q: quartet.

one singlet at 67.83 ppm, indicating that only one isomer exists in solution. The spectral data alone are not sufficient to decide whether this is the *cis* or the *trans* isomer. Therefore, we have undertaken a single-crystal X-ray diffraction analysis of $\mathbf{2}\cdot CH_2Cl_2$, showing that the *cis* isomer is formed. A PLUTON view of $\mathbf{2}\cdot CH_2Cl_2$ is shown in Fig. 2. Selected bond lengths and angles are given in Table 4. In the crystal molecules of complex **2** and dichloromethane molecules of solvation are present and linked by van der Waals forces. The ruthenium atom is six-coordinated in a distorted octahedral geometry by two chelating acetate groups and two monodentate phosphine ligands in *cis* positions to each other. The Ru—O(2) and Ru—O(4) bond lengths, which are *trans* to the phosphine ligands, are longer than the Ru—O(1) and Ru—O(3) bond distances. The differences in these bond lengths are probably a consequence of the high *trans*-influence of the phosphine ligand. The Ru—P distances are similar to those found for other *cis*-phosphine complexes.[24,25]

Since the starting material, $Ru_2Cl(\mu\text{-}O_2CCH_3)_4$, is a diruthenium(II,III) compound and the reaction products are **1** and **2**, which are ruthenium(III) and ruthenium(II) compounds, respectively, a disproportionation process has been produced. Some disproportionation reactions of the $[Ru_2(\mu\text{-}O_2CCH_3)_4]^+$ unit have been previously observed.[12,26-28] Thus, the results obtained in the reaction of $Ru_2Cl(\mu\text{-}O_2CCH_3)_4$ with bbtp are con-

Table 3. Selected bond lengths (Å) and angles (°) with e.s.d.s in parentheses for $Ru_2(\mu\text{-}O)(\mu\text{-}O_2CCH_3)_2(O_2CCH_3)_2(bbtp)_2$ (**1**)

Ru—P	2.292(1)	Ru—O(1)	1.864(3)
Ru—O(2)	2.009(4)	Ru—O(3)	2.148(4)
Ru—O(4)	2.178(4)	Ru—O(5)	2.101(4)
Ru—C(6)	2.474(9)	S(2)—C(21)	1.721(6)
S(2)—C(24)	1.697(8)	P—C(21)	1.780(5)
P—C(31)	1.872(6)	O(2)—C(4)	1.261(9)
O(3)—C(4)	1.263(7)	O(4)—C(6)	1.247(9)
O(5)—C(6)	1.270(9)	C(4)—C(5)	1.50(1)
C(6)—C(7)	1.51(1)	C(21)—C(22)	1.363(8)
C(22)—C(23)	1.46(1)	C(23)—C(24)	1.30(1)
P—Ru—O(1)	88.2(1)	P—Ru—O(2)	91.3(1)
P—Ru—O(3)	176.8(1)	P—Ru—O(4)	98.4(1)
P—Ru—O(5)	94.3(1)	P—Ru—C(6)	99.5(1)
O(1)—Ru—O(2)	99.6(1)	O(1)—Ru—O(3)	94.8(1)
O(1)—Ru—O(4)	158.5(1)	O(1)—Ru—O(5)	98.2(1)
O(1)—Ru—C(6)	128.6(1)	O(2)—Ru—O(3)	89.2(1)
O(2)—Ru—O(4)	100.7(1)	O(2)—Ru—O(5)	161.4(1)
O(2)—Ru—C(6)	130.6(2)	O(3)—Ru—O(4)	78.3(1)
O(3)—Ru—O(5)	84.2(1)	O(4)—Ru—O(5)	61.0(1)
O(5)—Ru—C(6)	30.9(2)	Ru—P—C(21)	113.7(2)
Ru—P—C(31)	116.1(2)	Ru—P—>C(112)	109.8(3)
C(21)—P—C(31)	107.2(3)	C(21)—P—<C(111)	100.9(4)
C(31)—P—<C(111)	106.0(4)	Ru—O(1)—Ru	119.2(3)
Ru—O(2)—C(4)	124.3(4)	Ru—O(3)—C(4)	132.1(4)
Ru—O(4)—C(6)	88.1(5)	Ru—O(5)—C(6)	91.0(4)
O(2)—C(4)—O(3)	126.4(6)	Ru—C(6)—O(4)	61.6(4)
Ru—C(6)—C(7)	174.1(6)	O(4)—C(6)—O(5)	119.4(7)

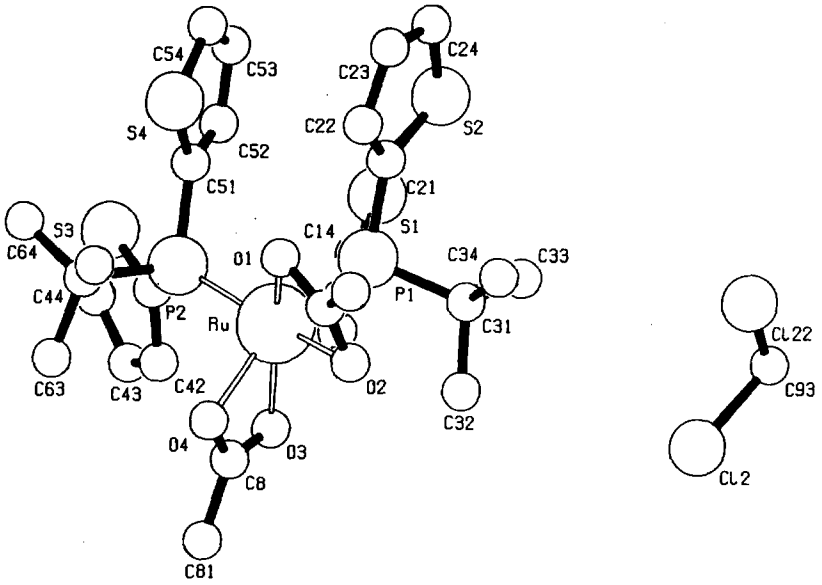

Fig. 2. PLUTON view of *cis*-$Ru(O_2CCH_3)_2(bbtp)_2 \cdot CH_2Cl_2$, $2 \cdot CH_2Cl_2$. The hydrogen atoms are omitted for clarity.

sistent with those observed in the reaction of $[Ru_2(O_2CCH_3)_4(thf)_2]BF_4$ with PPh_3[12] and with the proposed disproportionations in the reactions of $Ru_2Cl(O_2CR)_4$ (R = Me, Et, Ph, *cyclo*-C_6H_{11}, *o*-C_6H_4OH) with PPh_3 in 2-methoxyethanol.[13] However, these results are in contrast to the reactions of $Ru_2Cl(O_2CR)_4$ (R = Me, Ph, *p*-C_6H_4—OMe) with PPh_3 in MeOH[4] or MeCN,[5,6] which give only ruthenium(III) complexes. The ease of oxidation of $Ru(O_2CR)_2(PPh_3)_2$ in air could explain why in these last mentioned reactions, which are carried out in air, ruthenium(III) compounds were obtained.

In conclusion, the results obtained in the reaction of $Ru_2Cl(\mu\text{-}O_2CCH_3)_4$ with bbtp show that in an atmosphere of dinitrogen a disproportionation process has occurred with the formation of **1** and **2**, whereas in air only **1** is formed. Thus, we believe that other similar reactions, described in the literature as oxidation reactions of the Ru_2^{5+} unit to give the unstable Ru_2^{6+} unit, are better described as reactions of disproportionation with posterior oxidation of the ruthenium(II) compound. Finally, the presence of a sulphur atom in the bbtp ligand does not have any important influence in the reactivity towards $Ru_2Cl(\mu\text{-}O_2CCH_3)_4$.

EXPERIMENTAL

All manipulations were carried out in an inert atmosphere of dinitrogen, using standard Schlenk techniques. $RuCl_3 \cdot 3H_2O$ (Engelhard) was purchased from commercial sources; $Ru_2Cl(\mu\text{-}O_2CCH_3)_4$ was prepared by the literature procedure;[4] bbtp was synthesized in analogy to the method of Allen and Ashford.[29] The exact procedure will be published elsewhere.[30]

The ^1H and $^{31}P\{^1H\}$ NMR spectra were recorded with a Varian VXR-300 or a WP 80 Fa.Bruker spectrophotometer using $CDCl_3$ as the solvent; ^1H chemical shifts are relative to $SiMe_4$; ^{31}P chemical shifts are relative to external 85% H_3PO_4 (positive values = downfield shifts). IR spectra were recorded on a Philips PU 9712 spectrophotometer or a Perkin–Elmer 1720 FT-IR spectrometer. Elemental analyses were performed by the Analytical Service of the Complutense University of Madrid.

Synthesis of $Ru_2(\mu\text{-}O)(\mu\text{-}O_2CCH_3)_2(O_2CCH_3)_2(bbtp)_2$ *and* cis-$Ru(O_2CCH_3)_2(bbtp)_2$

To the red solution of $Ru_2Cl(\mu\text{-}O_2CCH_3)_4$ (0.50 g, 1.05 mmol) in methanol (15 cm^3) was added a solution of bbtp (0.55 g, 2.1 mmol) in methanol (15 cm^3) with stirring. The mixture was stirred for 5 h at room temperature. During this time the colour of the solution changed to violet and compound **2** deposited as a brown precipitate, which was filtered off, washed with methanol and reprecipitated by dissolving in dichloromethane (1 cm^3) and adding petroleum ether (30 cm^3; b.p. 40–60°C). A brown power was obtained (**2**) (yield: 0.17 g,

Table 4. Selected bond lengths (Å) and angles (°) with e.s.d.s in parentheses for *cis*-$Ru(O_2CCH_3)_2(bbtp)_2 \cdot CH_2Cl_2$, $2 \cdot CH_2Cl_2$

Ru—P(1)	2.281(3)	Ru—P(2)	2.270(3)
Ru—O(1)	2.124(6)	Ru—O(2)	2.233(7)
Ru—O(3)	2.144(6)	Ru—O(4)	2.210(7)
S(1)—C(11)	1.71(1)	S(1)—C(14)	1.71(1)
S(2)—C(21)	1.73(1)	S(2)—C(24)	1.71(1)
S(4)—C(51)	1.73(1)	S(4)—C(54)	1.69(1)
P(1)—C(11)	1.85(1)	P(1)—C(21)	1.82(1)
P(1)—C(31)	1.89(1)	P(2)—C(51)	1.83(1)
P(2)—C(61)	1.89(1)	O(1)—C(7)	1.28(1)
O(2)—C(7)	1.25(1)	O(3)—C(8)	1.26(1)
O(4)—C(8)	1.26(1)	C(7)—C(71)	1.55(1)
C(8)—C(81)	1.52(1)	C(11)—C(12)	1.38(1)
C(12)—C(13)	1.39(1)	C(13)—C(14)	1.35(1)
C(21)—C(22)	1.36(1)	C(22)—C(23)	1.42(1)
C(23)—C(24)	1.32(2)	C(31)—C(32)	1.57(1)
C(31)—C(33)	1.53(1)	C(31)—C(34)	1.53(1)
C(51)—C(52)	1.35(1)	C(52)—C(53)	1.40(1)
C(53)—C(54)	1.33(1)	C(61)—C(62)	1.57(1)
C(61)—C(63)	1.52(1)	C(61)—C(64)	1.52(1)

P(1)—Ru—P(2)	95.3(1)	P(1)—Ru—O(1)	96.7(2)
P(1)—Ru—O(2)	96.1(1)	P(1)—Ru—O(3)	101.5(2)
P(1)—Ru—O(4)	159.7(2)	P(2)—Ru—O(1)	99.8(2)
P(2)—Ru—O(2)	158.9(1)	P(2)—Ru—O(3)	96.8(1)
P(2)—Ru—O(4)	95.7(2)	O(1)—Ru—O(2)	61.1(3)
O(1)—Ru—O(3)	154.0(3)	O(1)—Ru—O(4)	98.2(3)
O(2)—Ru—O(3)	98.4(2)	O(2)—Ru—O(4)	79.3(2)
O(3)—Ru—O(4)	60.3(2)	C(21)—S(2)—C(24)	93.1(6)
Ru—P(1)—C(11)	113.4(3)	Ru—P(1)—C(21)	120.5(4)
Ru—P(1)—C(31)	112.6(3)	C(11)—P(1)—C(21)	104.9(5)
C(11)—P(1)—C(31)	101.3(4)	C(21)—P(1)—C(31)	101.7(5)
Ru—P(2)—C(51)	112.6(3)	Ru—P(2)—C(61)	114.3(3)
C(51)—P(2)—C(61)	104.8(5)	O(1)—C(7)—O(2)	122.0(1)
O(3)—C(8)—O(4)	119.6(9)	S(2)—C(21)—C(22)	108.8(8)
C(21)—C(22)—C(23)	113.0(1)	C(22)—C(23)—C(24)	114.0(1)
S(2)—C(24)—C(23)	111.0(1)		

22%). Found: C, 45.7; H, 4.9. Calc. for $C_{28}H_{36}O_4P_2RuS_4$: C, 46.2; H, 5.0%.

A dichloromethane solvate of **2** can be obtained by dissolving the powder in dichloromethane, followed by layering with petroleum ether.

Compound **1** was obtained from the violet filtrate by removing the solvent *in vacuo* and by reprecipitating the residue from dichloromethane/petroleum ether (b.p. 40–60°C). A violet powder was obtained (**1**) (yield: 0.54 g, 53%); m.p. 228°C. Found: C, 40.2; H, 4.5. Calc. for $C_{32}H_{42}O_9P_2Ru_2S_4$: C, 39.9; H, 4.4%.

Crystal structure determination of complexes **1** *and* $2 \cdot CH_2Cl_2$

Suitable crystals of complexes **1** and $2 \cdot CH_2Cl_2$ were grown from dichloromethane–petroleum ether by slow layer diffusion at room temperature.

Crystal data. **1**: $C_{32}H_{42}O_9P_2Ru_2S_4$, $M = 963.0$, monoclinic, space group $I2/a$, $a = 20.485(3)$, $b = 9.947(1)$, $c = 21.016(2)$ Å, $\beta = 108.15(1)°$, $U = 4069.2(9)$ Å^3, $Z = 4$, $D_c = 1.562$ g cm^{-3}, $F(000) = 1928$, μ(Mo-K_α) = 10.5 cm^{-1}.

$2 \cdot CH_2Cl_2$: $C_{28}H_{36}O_4P_2RuS_4 \cdot CH_2Cl_2$, $M = 812.8$, monoclinic, space group $P2_1/c$, $a = 11.411(1)$, $b = 10.029(1)$, $c = 31.157(5)$ Å, $\beta = 93.39(1)°$, $U = 3559(1)$ Å^3, $Z = 4$, $D_c = 1.507$ g cm^{-3}, $F(000) = 1644$, μ(Mo-K_α) = 9.3 cm^{-1}.

Data collection. Unique data sets were measured within the limit $2\theta_{max} = 55°$ using a four-circle diffractometer (Syntex $P2_1$) by the $2\theta/\omega$-scan technique; monochromatic Mo-K_α radiation, $\lambda = 0.71069$ Å.

For crystal **1** of the approximate dimensions $0.2 \times 0.3 \times 0.4$ mm 5210 reflections were collected, of which 4330 symmetry-independent reflections

were recorded and 3456 had $F_o > 5\sigma(F_o)$. For crystal $2 \cdot CH_2Cl_2$ (dimensions $0.1 \times 0.2 \times 0.4$ mm) 7288 reflections were collected, of which 5333 symmetry-independent reflections were recorded and 3227 had $F_o > 5\sigma(F_o)$. Both data sets were corrected for Lorentz–polarization effects and absorption (empirical absorption correction).

Determination and refinement of the structure. The structures were solved by the Patterson method[31–33] and refined by full-matrix least-squares calculations.[34]

In **1** the bridging oxygen atom occupies a special position (1/4, y, 1/2) and, therefore, the asymmetric unit consists only of half a molecule.

One of two 2-thienyl units shows disorder by rotation around a two-fold axis defined by the P—C(11) bond. The disordered 2-thienyl entity was given ideal geometry and included in the least-squares refinement with common isotropic temperature factors applied to atoms related by pseudo-symmetry. The population parameters applied to each pair of thienyl units were refined, the final values giving occupancies of 45% [C(111), C(121), C(131), C(141), S(11)] and 55% [C(112), C(122), C(132), C(142), S(12)]. Hydrogen atoms were introduced at idealized positions with fixed thermal parameters only for the ordered 2-thienyl group and the methyl groups. All non-hydrogen atoms were given anisotropic temperature factors and refinement converged at $R = 0.053$, $R_w = 0.043$. A weighting scheme, $w = 1/[\sigma^2(F_o)]$, was adopted. Selected bond distances and angles are given in Table 3 (taken from the program PLATON[35]).

In $2 \cdot CH_2Cl_2$ the S(3) atom had very large temperature factors, while those for C(42) were very small. This suggests that there also is a disorder about the P—C bond. The site occupation factor for position 1 is 0.70 and for position 2 0.30. The refinement was carried out by the same procedure as for **1**. In the final cycles of refinement the weighting scheme $w = 1/[\sigma^2(F_o) + 0.0001(F_o)^2]$ was adopted. The final value of R (R_w) was 0.063 (0.053). Selected bond lengths and angles are listed in Table 4 (taken from the program PLATON[35]).

Acknowledgements—We are grateful to the Dirección General de Investigación Científica y Técnica (DGYCIT, project PB90-0020) (Spain) and the Fonds der Chemischen Industrie (FRG) for financial support. I. Wagner is indebted to the D.A.A.D. (Deutscher Akademischer Austauschdienst) for financial support.

REFERENCES

1. P. Legzdins, R. W. Mitchell, G. L. Rempel, J. D. Ruddick and G. Wilkinson, *J. Chem. Soc. A* 1970, 3322.
2. F. A. Cotton and J. G. Norman Jr, *Inorg. Chim. Acta* 1972, **6**, 411.
3. S. K. Mandal and A. R. Chakravarty, *Inorg. Chim. Acta* 1987, **132**, 157.
4. R. W. Mitchell, A. Spencer and G. Wilkinson, *J. Chem. Soc., Dalton Trans.* 1973, 846.
5. B. K. Das and A. R. Chakravarty, *Inorg. Chem.* 1990, **29**, 1783.
6. B. K. Das and A. R. Chakravarty, *Inorg. Chem.* 1990, **29**, 2078.
7. R. A. Andersen, R. A. Jones and G. Wilkinson, *J. Chem. Soc., Dalton Trans.* 1978, 446.
8. R. A. Jones and G. Wilkinson, *J. Chem. Soc., Dalton Trans.* 1979, 472.
9. E. B. Boyar, P. A. Harding, S. D. Robinson and C. P. Brock, *J. Chem. Soc., Dalton Trans.* 1986, 1771.
10. F. A. Cotton, M. P. Diebold and M. Matusz, *Polyhedron* 1987, **6**, 1131.
11. F. A. Urbanos, M. C. Barral and R. Jiménez-Aparicio, *Polyhedron* 1988, **7**, 2597.
12. M. C. Barral, R. Jiménez-Aparicio, E. C. Royer, F. A. Urbanos, A. Monge and C. Ruíz-Valero, *Polyhedron* 1991, **10**, 113.
13. M. C. Barral, R. Jiménez-Aparicio, M. J. Larrubia, E. C. Royer and F.A. Urbanos, *Inorg. Chim. Acta* 1991, **186**, 239.
14. B. K. Das and A. R. Chakravarty, *Inorg. Chem.* 1992, **31**, 1395.
15. M. I. Bruce, in *Comprehensive Organometallic Chemistry* (Edited by G. Wilkinson), Vol. 4, p. 651. Pergamon Press, Oxford (1982).
16. D. W. Allen, N. A. Bell, S. T. Fong, L. A. March and I. W. Nowell, *Inorg. Chim. Acta* 1985, **99**, 157.
17. L. Gold'farb, A. A. Dudinov, V. P. Litvinov, D. S. Yurit and Yu. T. Struchkov, *Khim. Geterotsikl. Soedin* 1982, **10**, 1326, C.A. 98 : 89625b.
18. D. W. Allen and B. F. Taylor, *J. Chem. Soc., Dalton Trans.* 1982, 51.
19. D. G. Dick and D. W. Stephan, *Can. J. Chem.* 1986, **64**, 1870.
20. Y. Sasaki, M. Suzuki, A. Tokiwa, M. Ebihara, T. Yamaguchi and T. Ito, *J. Am. Chem. Soc.* 1988, **110**, 6251.
21. P. Neubold, K. Wieghardt, B. Nuber and J. Weis, *Inorg. Chem.* 1989, **28**, 459.
22. A. Llovet, M. E. Curry, H. T. Evans and T. J. Meyer, *Inorg. Chem.* 1989, **28**, 3131.
23. A. Syamala, B. K. Das and A. R. Chakravarty, *Polyhedron* 1992, **11**, 335.
24. S. R. Fletcher and A. C. Skapski, *J. Chem. Soc., Dalton Trans.* 1972, 635.
25. J. D. Owen and D. J. Cole-Hamilton, *J. Chem. Soc., Dalton Trans.* 1974, 1867.
26. R. P. Tooze, G. Wilkinson, M. Motevalli and M. B. Hursthouse, *J. Chem. Soc., Dalton Trans.* 1986, 2711.
27. F. A. Cotton, V. M. Miskowski and B. Zhong, *J. Am. Chem. Soc.* 1989, **111**, 6177.
28. M. C. Barral, R. Jiménez-Aparicio, E. C. Royer, M. J. Saucedo, F. A. Urbanos, E. Gutiérrez-Puebla and C. Ruíz-Valero, *J. Chem. Soc., Dalton Trans.* 1991, 1609.

29. D. W. Allen and D. F. Ashford, *J. Inorg. Nucl. Chem.* 1976, **38**, 1953.
30. I. Wagner and R. Kramolowsky, unpublished work.
31. G. M. Sheldrick, SHELX-76, Programs for Crystal Structure Determination. University of Cambridge, U.K. (1976).
32. D. T. Cromer and J. B. Mann, *Acta Cryst.* 1968, **A24**, 321.
33. D. T. Cromer and D. Liberman, *J. Chem. Phys.* 1970, **53**, 1891.
34. G. M. Sheldrick, SHELXS-86, Programs for Crystal Structure Solution. Universität Göttingen, F.R.G. (1986).
35. A. L. Spek, PLATON, *Computational Crystallography*. Clarendon Press, Oxford (1982).

Polyhedron Vol. 12, No. 8, pp. 911–914, 1993
Printed in Great Britain

0277–5387/93 $6.00+.00
© 1993 Pergamon Press Ltd

STUDIES ON THE STRUCTURE OF MOLYBDENUM(VI) IN ACIDIC SOLUTION BY XANES AND EXAFS

KUNIHIKO YOKOI*

Department of Natural Science, Osaka Kyoiku University, Kashiwara, Osaka 582, Japan

and

NOBUYUKI MATSUBAYASHI

National Chemical Laboratory for Industry, Tsukuba, Ibaraki 305, Japan

and

TAKAFUMI MIYANAGA

Department of Physics, Faculty of Science, Hirosaki University, Hirosaki, Aomori 036, Japan

and

IWAO WATANABE

Department of Chemistry, Faculty of Science, Osaka University, Toyonaka, Osaka 560, Japan

and

SHIGERO IKEDA

Department of Material Chemistry, Faculty of Science and Technology, Ryukoku University, Otsu, Shiga 520-21, Japan

(*Received* 14 *April* 1992; *accepted* 9 *December* 1992)

Abstract—X-ray absorption spectra for molybdenum(VI) in acidic solutions were measured and their XANES and EXAFS were analysed. The cationic monomer MoO_2^{2+} is present in $HClO_4$, H_2SO_4 and HNO_3. In HCl the coordination of chloride ions to MoO_2^{2+} was observed. Diethyl ether extracts MoO_2Cl_2 selectively from a HCl solution of molybdenum(VI).

Hexavalent molybdenum exists in the monomeric form of MoO_4^{2-} in neutral or alkaline solution, while in weakly acidic solutions polymeric anions such as $Mo_7O_{24}^{6-}$, $Mo_8O_{26}^{4-}$ and $Mo_6O_{19}^{2-}$ are present.[1–3] A previous spectroscopic investigation has clarified the structures of these anions.[3] In strongly acidic solutions cationic monomers and dimers are present,[4,5] however, their structures have not been elucidated [for example, Cruywagen *et al.*[4] have considered the existence of $Mo(OH)_5H_2O^+$ and Burclova *et al.*[5] proposed MoO_2^{2+}].

In recent years XANES (X-ray absorption near edge structure) and EXAFS (extended X-ray absorption fine structure) have been proved to be useful for the study of the short range order of atoms

* Author to whom correspondence should be addressed.

in polynuclear compounds.[6-10] In our previous paper[7] the structure of the μ-oxo dimeric cation, $Mo_2O_5^{2+}$, in acid solution (2 M) was studied and it was shown that its Mo—O—Mo bond angle is *ca* 125° by analysing XANES and EXAFS. In this work the structure of molybdenum(VI) in further acidic solutions and of the species extracted by ether are investigated.

EXPERIMENTAL

Molybdenum(VI) solutions were prepared from $Na_2MoO_4 \cdot 2H_2O$ and their concentrations were determined gravimetrically with 8-hydroxyquinoline and volumetrically with lead nitrate.[11] The concentration of molybdenum(VI) was adjusted to 0.1 M unless otherwise noted. Other chemicals were of guaranteed reagent grade and were used without further purification. X-ray absorption spectra were obtained with the EXAFS apparatus at beam line 10B of the 2.5 GeV storage ring from the Photon Factory at Tsukuba. Photon energy was calibrated by using the pre-edge peak of sodium molybdate, $Na_2MoO_4 \cdot 2H_2O$, at 20,007 eV. Other conditions were the same as those reported previously.[7]

RESULTS AND DISCUSSION

K-edge XANES spectra of molybdenum(VI) taken in hydrochloric acid solutions are shown in Fig. 1. When c_{HCl}, the concentration of HCl, is less than 3 M a pre-edge peak is observed clearly at *ca* 20,008.8 eV, while in further acidic solutions the peak is obscured by the red shift of the absorption edge. This pre-edge peak is assigned to the $1s$–$4d$ transition.[12] It is known that the intensity of the peak correlates with the number of Mo=O bonds per molybdenum atom,[7,12] and in HCl solution of less than 3 M the intensity corresponds to two Mo=O bonds. This is in agreement with the structure of MoO_2^{2+}, proposed by Burclova.[5] The intensity of the pre-edge peak is slightly decreased in HCl solutions of more than 3 M. The coordination of chloride ion may cause the shift of the edge, which is shown by the result of EXAFS analysis described later in this paper. The threshold energy, E_0 (which was determined from the position of the half height of the absorption edge at around 20040 eV; in this method experimental errors for E_0 are within about ± 0.2 eV), for various molybdenum(VI) samples are listed in Table 1. The spectra and E_0 obtained for 1–6 M perchloric, 1–3 M sulphuric and 1–8 M nitric acid solutions are almost the same as those obtained in less than 3 M HCl. This means that the coordination of perchlorate, sulphate and nitrate is not important.

EXAFS Fourier transforms for molybdenum(VI) in HCl solutions are shown in Fig. 2. In the Fourier transforms the corrections for the phase shift and the backscattering amplitude were performed using the theoretical parameters for the Mo—O bond, given by Teo and Lee[13] (in this method experimental errors for bond distances are

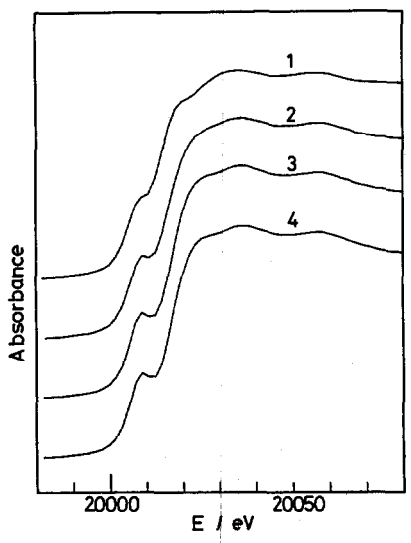

Fig. 1. Molybdenum K-edge XANES spectra for 0.1 M molybdenum(VI) in HCl solutions. c_{HCl}: (1) 6 M, (2) 4 M, (3) 2 M, (4) 1 M.

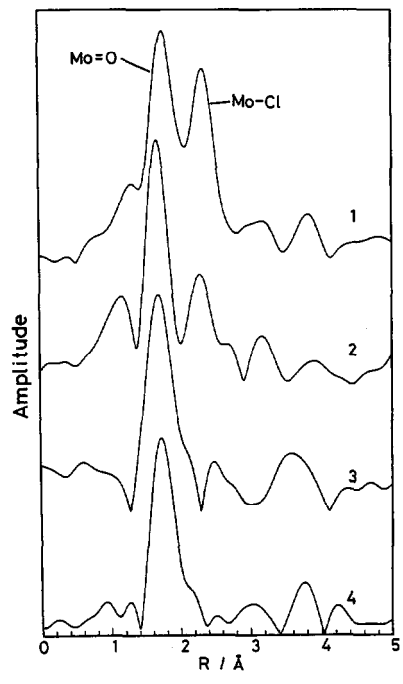

Fig. 2. EXAFS Fourier transforms for 0.1 M molybdenum(VI) in HCl solutions. c_{HCl}: (1) 6 M, (2) 4 M, (3) 2 M, (4) 1 M. k: 4.5–19 Å^{-1}.

Table 1. Results of EXAFS analyses for various sample solutions

	R_O (Å)	N_O	E_0 (eV)		R_O (Å)	N_O	R_{Cl} (Å)	N_{Cl}	E_0 (eV)
c_{HClO_4} (M)				c_{HCl} (M)					
1.0	1.71	1.8	20,015.7	1.0	1.74	1.7	—	—	20,015.5
3.0	1.72	2.0	20,015.3	2.0	1.70	1.8	—	—	20,015.4
6.0	1.75	1.8	20,015.1	3.0	1.69	2.2	2.39	0.4	20,015.2
c_{HNO_3} (M)				4.0	1.68	2.0	2.32	1.1	20,014.6
1.0	1.71	2.0	20,015.4	5.0	1.70	2.0	2.34	1.6	20,013.6
3.0	1.70	1.9	20,015.6	6.0	1.77	2.1	2.38	1.9	20,012.5
8.0	1.73	2.1	20,016.1	7.0	1.74	2.2	2.31	2.4	20,012.1
$c_{H_2SO_4}$ (M)				c_{HCl} (M)[a]					
1.0	1.71	1.8	20,016.3	5.0	1.72	1.8	2.38	2.4	20,012.5
3.0	1.72	2.0	20,015.6	6.0	1.73	1.8	2.37	2.2	20,012.9
				7.0	1.72	1.8	2.37	2.2	20,012.6

[a] The R and N values are for molybdenum(VI) complexes extracted into diethyl ether from HCl aqueous solutions.

within *ca* ±0.02 Å). In HCl solutions of less than 3 M only one distinct peak is observed around 1.7 Å, corresponding to the distance of the Mo=O bond, and no peak due to the Mo—O bond (*ca* 1.9 Å) is observed. For the monomeric cation of molybdenum(VI) Cruywagen *et al.*[4] have considered the existence of $Mo(OH)_5H_2O^+$ and Burclova *et al.*[5] proposed the presence of MoO_2^{2+}. As described above the results of XANES support the existence of MoO_2^{2+} and the results of EXAFS Fourier transforms are also in agreement with this conclusion. This species must be hydrated, such as $MoO_2(H_2O)_4^{2+}$ (molybdenum centre should be coordinated octahedrally because the pre-edge peak is observed at 20,008.8 eV in XANES spectra; if it is surrounded tetrahedrally the peak should be at 20,007 eV[7]), however, coordinated oxygen atoms of water molecules which should appear at *ca* 2.2–2.3 Å in Fourier transforms could not be observed clearly. This may be due to rapid exchange of coordinated water molecules, i.e. the labile character of molybdenum(VI).[14] For 0.4 M molybdenum(VI) solutions a dimeric cation can be detected by EXAFS (the peak at 3.37 Å corresponding to Mo—Mo was observed[7]), while for 0.1 M molybdenum(VI) solutions the dimeric cation cannot be detected clearly. In HCl solutions of more than 3 M the peak at *ca* 2.3 Å, corresponding to the distance of the Mo—Cl bond, increases with c_{HCl}, indicating that the number of coordinated chloride ions increases. The numbers of coordinating oxygen and chlorine atoms, N_O and N_{Cl}, in the cationic species of molybdenum(VI) are estimated using the relation $hR^2 = PN$, where h is the peak height in Fourier transform, R is the bond length and P is the proportional constant. In this case the root-mean-square relative deviation (RMSRD) of R is assumed to be constant.[7,15] This assumption leads to the experimental errors for N within *ca* ±7%. The reference samples used to determine the value of P were MoO_4^{2-} (in pH 7.28) for N_O and $MoOCl_5^{2-}$ (in 8 M HCl) for N_{Cl}.[16] The values of R_O, N_O, R_{Cl} and N_{Cl} determined are listed in Table 1 (in these analyses values for N are averaged ones for each molybdenum atom and, therefore, not for each species). In perchloric, sulphuric and nitric acid solutions the values of R_O are almost constant and N_O values are around two, and no coordination of the anion is observed. The structure of the cationic species MoO_2^{2+} seems to be the same in these acid solutions, which is also in agreement with the results of XANES. In HCl solution of less than 3 M coordination of the chloride ion is not observed clearly. Above 3 M N_{Cl} increases steadily, while N_O remains almost two. Thus, the unit of MoO_2^{2+} does not change when the chlorine atom coordinates.

It is well known that molybdenum(VI) is extracted into diethyl ether from 6 M HCl solution. Nelidow and Diamond[17] concluded from chemical analysis that the extracted species in diethyl ether is MoO_2Cl_2, while Zharovskii[18] and others[19] claimed that $HMoO_2Cl_3$ was extracted. EXAFS results are listed in Table 1 for the organic phase after extraction from HCl solution. While N_{Cl} in aqueous solution depends on c_{HCl}, both N_O and N_{Cl} for the organic phase are constantly two, indicating that the species extracted is MoO_2Cl_2. N_{Cl} in diethyl ether is somewhat larger than in aqueous solutions, which is probably due to the small RMSRD resulting from solvation by ether molecules to produce the stable structure of MoO_2Cl_2. The result in Table 1 indicates that the composition of the molyb-

denum(VI) species in 6 M HCl solution is almost the same as that in the organic phase. This result is in agreement with that reported by Griffith and Wickins[20] that the Raman spectrum of an ether solution of $MoO_2Cl_2(OEt_2)_2$ is very similar to that of molybdate in 6 M HCl solution. The distribution ratio, D_{Mo}, is largest at *ca* 6 M HCl[13] (D_{Mo} determined in this work was 0.50, 1.62, 2.15 and 1.88 in 4, 5, 6 and 7 M HCl, respectively). Further, even if c_{HCl} for aqueous solutions are different (4–7 M) E_0 values for the organic phase after extraction are almost the same as those in 6 M HCl aqueous solution. That is, a few kinds of species having the same MoO_2^{2+} unit but having different numbers of coordinating chlorine atom, such as MoO_2Cl^+, MoO_2Cl_2 and $MoO_2Cl_3^-$, are present in aqueous HCl solutions.[17,21] However, the species of MoO_2Cl_2 seems to be extracted selectively into diethyl ether.

Recently, Coddington and Taylor[22] reported a ^{95}Mo NMR investigation and concluded that MoO_2Cl_2 is present in HCl solution and is extracted into the ether phase. These observations are in agreement with the results of our work.

Acknowledgements—The authors thank Dr Tadashi Matsushita and Dr Masaharu Nomura, the National Laboratory for High Energy Physics (KEK), for their help with X-ray absorption measurements.

REFERENCES

1. Y. Sasaki and L. G. Sillen, *Arkiv Kemi* 1968, **29**, 253.
2. E. Pungor and A. Halasz, *J. Inorg. Nucl. Chem.* 1970, **32**, 1187.
3. K. Murata and S. Ikeda, *Spectrochim. Acta A* 1983, **39**, 787.
4. J. J. Cruywagen, J. B. B. Heyns and E. F. C. H. Rohwer, *J. Inorg. Nucl. Chem.* 1976, **38**, 2033.
5. J. Burclova, J. Prasilova and P. Benes, *J. Inorg. Nucl. Chem.* 1973, **35**, 909.
6. S. P. Cramer, P. K. Eidem, M. T. Paffett, J. R. Winkler, Z. Dori and H. B. Gray, *J. Am. Chem. Soc.* 1983, **105**, 799.
7. K. Yokoi, N. Matsubayashi, T. Miyanaga, I. Watanabe, K. Murata and S. Ikeda, *Chem. Lett.* 1987, 1453.
8. T. Miyanaga, N. Matsubayashi, T. Fukumoto, K. Yokoi, I. Watanabe, K. Murata and S. Ikeda, *Chem. Lett.* 1988, 487.
9. T. Miyanage, T. Fukikawa, N. Matsubayashi, T. Fukumoto, K. Yokoi, I. Watanabe and S. Ikeda, *Bull. Chem. Soc. Japan* 1989, **62**, 1791.
10. K. Yokoi, N. Matsubayashi, T. Miyanaga, I. Watanabe, S. Ikeda and K. Murata, *Polyhedron* 1989, **8**, 45.
11. G. A. Parker, *Analytical Chemistry of Molybdenum*, pp. 26 and 34. Springer Verlag, New York (1983).
12. S. P. Cramer, K. O. Hodgson, W. O. Gillum and L. E. Mortenson, *J. Am. Chem. Soc.* 1978, **100**, 3398.
13. B. K. Teo and P. A. Lee, *J. Am. Chem. Soc.* 1979, **101**, 2815.
14. T. K. Sham, *Accts Chem. Res.* 1986, **19**, 99.
15. E. A. Stern, D. E. Sayers and F. W. Lytle, *Phys. Rev. B* 1975, **11**, 4836.
16. $MoOCl_5^{2-}$ is a compound of molybdenum(V), however, the difference between RMSRD for molybdenum(VI) and that for molybdenum(V) can be small.
17. I. Nelidow and R. M. Diamond, *J. Phys. Chem.* 1955, **59**, 710.
18. F. G. Zharovskii, *Zh. Neorg. Khim.* 1957, **2**, 623.
19. I. P. Alimarin and V. M. Polyansky, *J. Anal. Chem., USSR* 1953, **8**, 253.
20. W. P. Griffith and T. D. Wickins, *J. Chem. Soc. (A)* 1967, 675.
21. S. Himeno and S. Hasegawa, *Inorg. Chim. Acta* 1983, **73**, 255.
22. J. M. Coddington and T. J. Taylor, *J. Chem. Soc., Dalton Trans.* 1990, 41.

Polyhedron Vol. 12, No. 8, pp. 915–919, 1993
Printed in Great Britain

0277–5387/93 $6.00+.00
© 1993 Pergamon Press Ltd

THE REACTIONS OF $[WI_2(CO)(NCMe)(\eta^2\text{-}RC_2R)_2]$ (R = Me OR Ph) WITH $OPPh_3$ AND $SPPh_3$

PAUL K. BAKER* and STEPHEN D. RIDYARD

Department of Chemistry, University of Wales, Bangor, Gwynedd LL57 2UW, U.K.

(*Received* 30 *September* 1992; *accepted* 4 *December* 1992)

Abstract—Equimolar quantities of $[WI_2(CO)(NCMe)(\eta^2\text{-}RC_2R)_2]$ (R = Me or Ph) and L (L = $OPPh_3$ or $SPPh_3$) react in CH_2Cl_2 at room temperature to give $[WI_2(CO)L(\eta^2\text{-}RC_2R)_2]$ (**1–4**). The reaction of $[WI_2(CO)(NCMe)(\eta^2\text{-}RC_2R)_2]$ (R = Me or Ph) with 2 equivalents of L (L = $OPPh_3$ or $SPPh_3$) eventually affords the cationic complexes $[WI(CO)L_2(\eta^2\text{-}RC_2R)_2]I$ (**5–8**). The complexes $[WI_2(CO)(NCMe)(\eta^2\text{-}RC_2R)_2]$ (R = Me or Ph) react with 3 equivalents of L (L = $OPPh_3$ or $SPPh_3$) to yield the dicationic complexes $[W(CO)L_3(\eta^2\text{-}RC_2R)_2]2I$ (**9–12**). The mono- and dicationic nature of **5–8** and **9–12** was established by preparing the tetraphenylborate complexes $[WI(CO)(OPPh_3)_2(\eta^2\text{-}MeC_2Me)_2][BPh_4]$ (**13**) and $[W(CO)(OPPh_3)_3(\eta^2\text{-}MeC_2Me)_2][BPh_4]_2$ (**14**), respectively.

Since the discovery of the tris(alkyne) tungsten complex $[W(CO)(\eta^2\text{-hex-3-yne})_3]$ in 1963,[1] a considerable number of alkyne complexes of molybdenum and tungsten have been reported.[2] Although a large number of alkyne complexes of molybdenum or tungsten containing neutral phosphorus donor ligands have been reported,[2–9] hitherto very few alkyne complexes containing neutral oxygen or sulphur donor ligands have been made. We have previously described the reactions of $[WI_2(CO)(NCMe)(\eta^2\text{-}RC_2R)_2]$ (R = Me or Ph)[10] or $[WI(CO)(NCMe)(dppm)(\eta^2\text{-}MeC_2Me)][BF_4]$[11] with thiourea and related ligands. In this paper we describe the reactions of $[WI_2(CO)(NCMe)(\eta^2\text{-}RC_2R)_2]$ (R = Me or Ph) with $OPPh_3$ or $SPPh_3$.

EXPERIMENTAL

All the new complexes described in this paper were prepared using standard Schlenk-line techniques. The starting materials, $[WI_2(CO)(NCMe)(\eta^2\text{-}RC_2R)_2]$ (R = Me or Ph), were prepared by the published method.[12] All chemicals used were purchased from commercial sources. The solvent CH_2Cl_2 was dried and distilled before use.

Elemental analyses (carbon, hydrogen and nitrogen) were determined using a Carlo–Erba Elemental Analyser MOD 1106 (using helium as a carrier gas). IR spectra were recorded on a Perkin–Elmer 1430 ratio recording IR spectrophotometer. The ^1H NMR spectra reported in this paper were recorded on either a Bruker AC 250 CP/MAS NMR spectrometer or a Bruker WH 400 MHz NMR spectrometer. All spectra were referenced to tetramethylsilane.

Preparation of $[WI_2(CO)(OPPh_3)(\eta^2\text{-}MeC_2Me)_2]$ (**1**)

To $[WI_2(CO)(NCMe)(\eta^2\text{-}MeC_2Me)_2]$ (0.5 g, 0.813 mmol) dissolved in CH_2Cl_2 under a stream of dry nitrogen with continuous stirring was added $OPPh_3$ (0.23 g, 0.813 mmol). After stirring the solution for 3 h, filtration followed by removal of the solvent *in vacuo* gave yellow crystals of $[WI_2(CO)(OPPh_3)(\eta^2\text{-}MeC_2Me)_2]$ (**1**), which were recrystallized from CH_2Cl_2/Et_2O; yield = 0.56 g, 81%.

Similar reactions of $[WI_2(CO)(NCMe)(\eta^2\text{-}RC_2R)_2]$ (R = Me or Ph) with an equimolar quantity of L (L = $OPPh_3$ or $SPPh_3$) gave $[WI_2(CO)L(\eta^2\text{-}RC_2R)_2]$ (**2–4**) (see Table 1 for physical and analytical data).

* Author to whom correspondence should be addressed.

Preparation of $[WI(CO)(OPPh_3)_2(\eta^2\text{-}MeC_2Me)_2]I$ **(5)**

To $[WI_2(CO)(NCMe)(\eta^2\text{-}MeC_2Me)_2]$ (0.5 g, 0.813 mmol) dissolved in CH_2Cl_2 (20 cm^3) under a stream of dry nitrogen with continuous stirring was added $OPPh_3$ (0.45 g, 1.626 mmol). After stirring the solution for 4 h, filtration followed by removal of the solvent *in vacuo* gave orange/yellow crystals of $[WI(CO)(OPPh_3)_2(\eta^2\text{-}MeC_2Me)_2]I$ **(5)**, which were recrystallized from CH_2Cl_2/Et_2O; yield = 0.86 g, 94%.

Similar reactions of $[WI_2(CO)(NCMe)(\eta^2\text{-}RC_2R)_2]$ (R = Me or Ph) with 2 equivalents of L (L = $OPPh_3$ or $SPPh_3$) gave $[WI(CO)L_2(\eta^2\text{-}RC_2R)_2]I$ **(6–8)** (see Table 1 for physical and analytical data).

Preparation of $[W(CO)(SPPh_3)_3(\eta^2\text{-}MeC_2Me)_2]2I$ **(11)**

To $[WI_2(CO)(NCMe)(\eta^2\text{-}MeC_2Me)_2]$ (0.5 g, 0.813 mmol) dissolved in CH_2Cl_2 (20 cm^3) under a stream of dry nitrogen with continuous stirring was added $SPPh_3$ (0.72 g, 2.439 mmol). After stirring the solution for 18 h, filtration followed by removal of the solvent *in vacuo* gave yellow/brown crystals of $[W(CO)(SPPh_3)_3(\eta^2\text{-}MeC_2Me)_2]2I$ **(11)**, which were recrystallized from CH_2Cl_2/Et_2O; yield = 0.94 g, 80%.

Similar reactions of $[WI_2(CO)(NCMe)(\eta^2\text{-}RC_2R)_2]$ with 3 equivalents of L (L = $OPPh_3$ or $SPPh_3$) gave $[W(CO)L_3(\eta^2\text{-}RC_2R)_2]2I$ **(9, 10, 12)** (see Table 1 for physical and analytical data).

Preparation of $[WI(CO)(OPPh_3)_2(\eta^2\text{-}MeC_2Me)_2][BPh_4]$ **(13)**

To $[WI_2(CO)(NCMe)(\eta^2\text{-}MeC_2Me)_2]$ (0.5 g, 0.813 mmol) suspended in acetonitrile (25 cm^3) was added $OPPh_3$ (0.45 g, 1.626 mmol), followed by $Na[BPh_4]$ (0.28 g, 0.813 mmol) under a stream of dry nitrogen. After stirring the solution at room temperature for 18 h removal of the solvent *in vacuo* afforded an orange/white slurry, which was redis-

Table 1. Physical and analytical data[a] for the $OPPh_3$ and $SPPh_3$ alkyne complexes of tungsten(II)

Complex	Colour	Yield (%)	Analysis[a] C (%)	H (%)
$[WI_2(CO)(OPPh_3)(\eta^2\text{-}MeC_2Me)_2]$ **(1)**	Yellow	81	37.7 (38.1)	3.3 (3.2)
$[WI_2(CO)(OPPh_3)(\eta^2\text{-}PhC_2Ph)_2]$ **(2)**	Orange–brown	48	50.6 (51.3)	3.4 (3.2)
$[WI_2(CO)(SPPh_3)(\eta^2\text{-}MeC_2Me)_2]$ **(3)**	Yellow–orange	61	37.5 (37.4)	3.3 (3.1)
$[WI_2(CO)(SPPh_3)(\eta^2\text{-}PhC_2Ph)_2]$ **(4)**	Orange–brown	48	50.2 (50.6)	3.5 (3.2)
$[WI(CO)(OPPh_3)_2(\eta^2\text{-}MeC_2Me)_2]I$ **(5)**	Orange–yellow	94	48.0 (47.8)	3.9 (3.7)
$[WI(CO)(OPPh_3)_2(\eta^2\text{-}PhC_2Ph)_2]I$ **(6)**	Orange–yellow	53	56.8 (56.6)	4.1 (3.7)
$[WI(CO)(SPPh_3)_2(\eta^2\text{-}MeC_2Me)_2]I$ **(7)**	Brown	88	48.0 (48.6)	3.8 (3.6)
$[WI(CO)(SPPh_3)_2(\eta^2\text{-}PhC_2Ph)_2]I$ **(8)**	Brown	72	56.0 (55.3)	3.9 (3.8)
$[W(CO)(OPPh_3)_3(\eta^2\text{-}MeC_2Me)_2]2I$ **(9)**	Yellow	86	53.7 (53.7)	4.1 (4.1)
$[W(CO)(OPPh_3)_3(\eta^2\text{-}PhC_2Ph)_2]2I$ **(10)**	Orange–brown	85	59.8 (60.2)	4.4 (4.0)
$[W(CO)(SPPh_3)_3(\eta^2\text{-}MeC_2Me)_2]2I$ **(11)**	Yellow–brown	80	52.3 (51.9)	4.5 (3.9)
$[W(CO)(SPPh_3)_3(\eta^2\text{-}PhC_2Ph)_2]2I$ **(12)**	Brown	79	58.5 (58.5)	3.9 (3.8)
$[WI(CO)(OPPh_3)_2(\eta^2\text{-}MeC_2Me)_2][BPh_4]$ **(13)**	Orange	46	63.0 (62.7)	4.7 (4.7)
$[W(CO)(OPPh_3)_3(\eta^2\text{-}MeC_2Me)_2][BPh_4]_2$ **(14)**	Orange	30	72.6 (74.3)	5.5 (5.5)

[a] Calculated values in parentheses.

solved in CH_2Cl_2 (20 cm^3) and filtered twice. Removal of the solvent *in vacuo* gave orange crystals of $[WI(CO)(OPPh_3)_2(\eta^2\text{-}MeC_2Me)_2][BPh_4]$ (**13**), which were recrystallized from CH_2Cl_2/Et_2O; yield = 0.49 g, 46%.

Preparation of $[W(CO)(OPPh_3)_3(\eta^2\text{-}MeC_2Me)_2][BPh_4]_2$ (**14**)

To $[WI_2(CO)(NCMe)(\eta^2\text{-}MeC_2Me)_2]$ (0.5 g, 0.813 mmol) suspended in acetonitrile (25 cm^3) was added $OPPh_3$ (0.68 g, 2.439 mmol) followed by $Na[BPh_4]$ (0.56 g, 1.626 mmol) under a stream of nitrogen. After stirring at room temperature for 18 h removal of the solvent *in vacuo* afforded an orange/white slurry, which was redissolved in CH_2Cl_2 (20 cm^3) and filtered twice. Removal of the solvent *in vacuo* afforded orange crystals of $[W(CO)(OPPh_3)_3(\eta^2\text{-}MeC_2Me)_2][BPh_4]_2$ (**14**), which were recrystallized from CH_2Cl_2/Et_2O; yield = 0.43 g, 30%.

RESULTS AND DISCUSSION

The starting materials used in this research, namely $[WI_2(CO)(NCMe)(\eta^2\text{-}RC_2R)_2]$ (R = Me or Ph), were prepared by reacting the seven-coordinate complex $[WI_2(CO)_3(NCMe)_2]$ with an excess of RC_2R in CH_2Cl_2 at 0°C.[12] The reactions of $[WI_2(CO)(NCMe)(\eta^2\text{-}RC_2R)_2]$ (R = Me or Ph) with 1, 2 or 3 equivalents of L (L = $OPPh_3$ or $SPPh_3$) in CH_2Cl_2 at room temperature afford the new alkyne complexes $[WI_2(CO)L(\eta^2\text{-}RC_2R)_2]$ (**1–4**), $[WI(CO)L_2(\eta^2\text{-}RC_2R)_2]I$ (**5–8**) and $[W(CO)L_3(\eta^2\text{-}RC_2R)_2]2I$ (**9–12**), respectively. The cationic nature of complexes **5–8** was confirmed by reacting $[WI(CO)(OPPh_3)_2(\eta^2\text{-}MeC_2Me)_2]I$ (**5**) with 1 equivalent of $Na[BPh_4]$ in acetonitrile, which gave the iodide exchanged product $[WI(CO)(OPPh_3)_2(\eta^2\text{-}MeC_2Me)_2][BPh_4]$ (**13**). Similarly, the dicationic nature of **9–12** was established by treating $[W(CO)(OPPh_3)_3(\eta^2\text{-}MeC_2Me)_2]2I$ with 2 equivalents of $Na[BPh_4]$ in acetonitrile to yield the bis(tetraphenylborate) product $[W(CO)(OPPh_3)_3(\eta^2\text{-}MeC_2Me)_2][BPh_4]_2$ (**14**). Complexes **1–14** have all been characterized by elemental analysis (carbon, hydrogen and nitrogen) (Table 1) and IR and ^1H NMR spectroscopy (Table 2). All the complexes (**1–14**) are soluble in chlorinated solvents such as CH_2Cl_2 and $CHCl_3$ and also in acetone. However, they are only partially soluble (**1–4**) or totally insoluble in hydrocarbon solvents and diethyl ether. The complexes (**1–14**) are all air-sensitive in the solid state and very air-sensitive in solution. The more L (L = $OPPh_3$ or $SPPh_3$) groups which are attached to the metal, the more sensitive and less stable the complexes were found to be.

Table 2. IR[a] and ^1H NMR data[b,c] for the $OPPh_3$ and $SPPh_3$ alkyne complexes of tungsten(II)

Complex	$\nu(C{\equiv}O)$ (cm^{-1})	^1H (δ, ppm)
1[b]	2010(s)	2.91 (s, 6H, *Me*), 3.03 (s, 6H, *Me*), 7.50–7.70 (m, 15H, *Ph*)
2[b]	2070(s)	7.30–7.70 (brm, *Ph*)
3[b]	2050(s)	2.86 (s, 6H, *Me*), 2.89 (s, 6H, *Me*), 7.49–7.76 (m, 15H, *Ph*)
4[b]	2070(s)	7.45–7.76 (m, *Ph*)
5[b]	2060(s)	2.72 (s, 6H, *Me*), 3.09 (s, 6H, *Me*), 7.09–7.60 (m, 30H, *Ph*)
6[b]	2080(s)	7.42–7.78 (m, *Ph*)
7[c]	2020(s)	2.91 (s, 6H, *Me*), 3.03 (s, 6H, *Me*), 7.53–7.66 (m, 30H, *Ph*)
8[b]	2080(s)	7.45–7.72 (m, *Ph*)
9[b]	2040(s)	2.68 (s, 6H, *Me*), 3.11 (s, 6H, *Me*), 7.53–7.73 (m, 45H, *Ph*)
10[b]	2050(s)	7.05–7.56 (m, *Ph*)
11[c]	2060(s)	2.84 (s, 6H, *Me*), 2.90 (s, 6H, *Me*), 7.12–7.32 (m, 45H, *Ph*)
12[b]	2050(s)	7.10–7.61 (m, *Ph*)
13[c]	2039(s)	2.74 (s, 6H, *Me*), 3.08 (s, 6H, *Me*), 7.09–7.60 (m, 50H, *Ph*+B*Ph*)
14[c]	2010(s)	2.91 (s, 6H, *Me*), 3.03 (s, 6H, *Me*), 7.52–7.64 (m, 85H, *Ph*+B*Ph*)

[a] Spectra recorded in $CHCl_3$ as thin films between NaCl plates; s, strong.

[b] Spectra recorded in $CDCl_3$ (+25°C) on a Bruker AC250 CP/MAS NMR spectrometer and referenced to Me_4Si.

[c] Spectra recorded in CD_2Cl_2 (+32°C) on a Bruker WH 400 NMR spectrometer and referenced to Me_4Si.

It is likely that the reactions of $[WI_2(CO)(NCMe)(\eta^2\text{-}RC_2R)_2]$ with 1 equivalent of L (L = $OPPh_3$ or $SPPh_3$) to give the acetonitrile displaced products $[WI_2(CO)L(\eta^2\text{-}RC_2R)_2]$ (**1–4**) proceed via an associative mechanism, since alkyne ligands can rearrange their mode of bonding from a "three-electron" donor to a two-electron donor and hence incorporate the donor ligand, L, before expelling the acetonitrile and reverting to being a four-electron donor. Other workers[3,13] have proposed these associative mechanisms for reactions of neutral donor ligands with alkyne complexes of molybdenum(II) and tungsten(II). It is interesting to note that the IR spectra of **1–4** all show carbonyl bands at similar wave-numbers compared with the starting materials $[WI_2(CO)(NCMe)(\eta^2\text{-}RC_2R)_2]$ [for R = Me, $\nu(CO)$ = 2050; for R = Ph, $\nu(CO)$ = 2090 cm^{-1}],[12] hence it is likely that $OPPh_3$ and

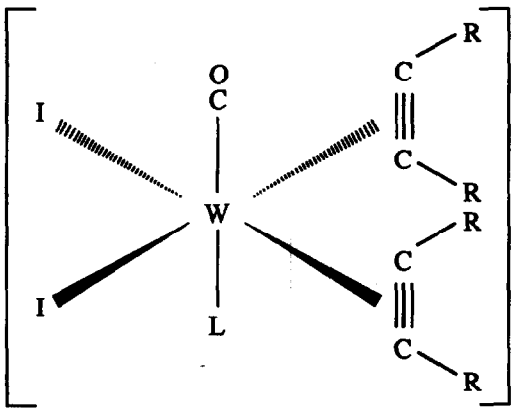

Fig. 1. Proposed structure for $[WI_2(CO)L(\eta^2\text{-}RC_2R)_2]$ (**1–4**).

$SPPh_3$ are acting mainly as σ-donor ligands in these complexes. Unfortunately, the $\nu(C{\equiv}C)$ bands were masked by the phenyl overtones in complexes **1–14**. Since the molecular structures of $[WI_2(CO)(NCMe)(\eta^2\text{-}RC_2R)_2]$ (R = Me or Ph),[12] $[WI_2(CO)_2(\eta^2\text{-}MeC_2Me)_2]$[14] and $[WI_2(CO)\{NCCH_2(C_4H_3S)\}(\eta^2\text{-}MeC_2Me)_2][NCCH_2(C_4H_3S)$ = thiophene-3-acetonitrile][15] have been determined crystallographically, it is likely that complexes **1–4** will have a similar structure, as shown in Fig. 1. The ^1H NMR data (Table 2) conform with the structure shown in Fig. 1.

The reaction of $[WI_2(CO)(NCMe)(\eta^2\text{-}PhC_2Ph)_2]$ with 2 equivalents of $OPPh_3$ in $CHCl_3$ was followed by IR spectroscopy. After 1 h the spectrum showed a broad band at 2085 cm^{-1} due to $[WI_2(CO)(NCMe)(\eta^2\text{-}PhC_2Ph)_2]$ and **2**, and a very weak band at 1970 cm^{-1} which is likely to be due to the mono(diphenylacetylene) complex $[WI_2(CO)(OPPh_3)_2(\eta^2\text{-}PhC_2Ph)]$. After 2 h the solution became darker green and the band at 1970 cm^{-1} had reached a maximum intensity. We have previously reported the preparation of bis(phosphine) complexes of the type $[WI_2(CO)L'_2(\eta^2\text{-}MeC_2Me)]$ (L′ = monodentate phosphine),[7] and many of these four-electron alkyne complexes are dark green in colour. After 4 h the colour of the solution became orange/yellow and the band at 1970 cm^{-1} had disappeared in the IR spectrum, leaving only a band at 2080 cm^{-1} due to $[WI(CO)(OPPh_3)_2(\eta^2\text{-}PhC_2Ph)_2]I$ (**6**). Many unsuccessful attempts were made to isolate the dark green intermediate $[WI_2(CO)(OPPh_3)_2(\eta^2\text{-}PhC_2Ph)]$ and also the analogous $SPPh_3$ complex. The proposed mechanism of the reaction of $[WI_2(CO)(NCMe)(\eta^2\text{-}PhC_2Ph)_2]$ with 2 equivalents of $OPPh_3$ is shown in Scheme 1. Further evidence to support this proposed mechanism comes from the reaction of $[WI_2(CO)(OPPh_3)(\eta^2\text{-}PhC_2Ph)_2]$ (**2**) with an equimolar amount of $OPPh_3$ in CH_2Cl_2 at room temperature, which eventually gives the cationic complex $[WI(CO)(OPPh_3)_2(\eta^2\text{-}PhC_2Ph)_2]I$ (**6**). It is interesting to note that the reaction of $[WI_2(CO)(NCMe)(\eta^2\text{-}MeC_2Me)_2]$ with 2 equivalents of L [L = $SC(NH_2)_2$ or $SC(NMe_2)_2$] in acetone gave the purple mono(but-2-yne) complexes $[WI_2(CO)L_2(\eta^2\text{-}MeC_2Me)]$.[10] This behaviour is likely to be due to the stronger π-acceptor properties of $SC(NH_2)_2$ and $SC(NMe_2)_2$ compared to $OPPh_3$ and $SPPh_3$.

The X-ray crystal structure of the 2,2-bipyridyl complex $[WI(CO)(2,2'\text{-bipy})(\eta^2\text{-}MeC_2Me)_2][BPh_4]$ has been determined[16] and shows the two *cis*-but-2-yne ligands are parallel and have the 2,2′-bipyridyl ligand in the equatorial plane with the carbonyl and iodide ligands in the axial positions. Hence, it is very likely that the structure of **5–8** will be similar and as shown in Fig. 2. The ^1H NMR data (Table 2) of **5–8** conform with the structure which is shown in Fig. 2.

Surprisingly, the reactions of $[WI_2(CO)(NCMe)(\eta^2\text{-}RC_2R)_2]$ with 3 equivalents of L (L = $OPPh_3$ or $SPPh_3$) apparently give the bis(alkyne) complexes $[W(CO)L_3(\eta^2\text{-}RC_2R)_2]2I$ (**9–12**) rather than the mono(alkyne) complexes $[WI(CO)L_3(\eta^2\text{-}RC_2R)]I$. This may be due to the electron-rich nature of $OPPh_3$ and $SPPh_3$. It should also be noted that reaction of $[WI(CO)(OPPh_3)_2(\eta^2\text{-}PhC_2Ph)_2]I$ (**6**) with an equimolar quantity of $OPPh_3$ in CH_2Cl_2 at room temperature affords the expected dicationic complex $[W(CO)(OPPh_3)_3(\eta^2\text{-}PhC_2Ph)_2]2I$ (**10**).

In summary, the reactions of $[WI_2(CO)(NCMe)(\eta^2\text{-}RC_2R)_2]$ with 1 equivalent of $OPPh_3$ or $SPPh_3$ are similar to other reactions with electron-rich neutral nitrogen, oxygen and sulphur donor ligands. However, for reactions with 2 or more

(i) $[WI_2(CO)(NCMe)(\eta^2\text{-}PhC_2Ph)_2] \xrightarrow{OPPh_3} [WI_2(CO)(OPPh_3)(\eta^2\text{-}PhC_2Ph)_2] + NCMe$

(ii) $[WI_2(CO)(OPPh_3)(\eta^2\text{-}PhC_2Ph)_2] \xrightarrow{OPPh_3} [WI_2(CO)(OPPh_3)_2(\eta^2\text{-}PhC_2Ph)] + PhC_2Ph$

(iii) $[WI_2(CO)(OPPh_3)_2(\eta^2\text{-}PhC_2Ph)] \xrightarrow{PhC_2Ph} [WI(CO)(OPPh_3)_2(\eta^2\text{-}PhC_2Ph)_2]I$

Scheme 1.

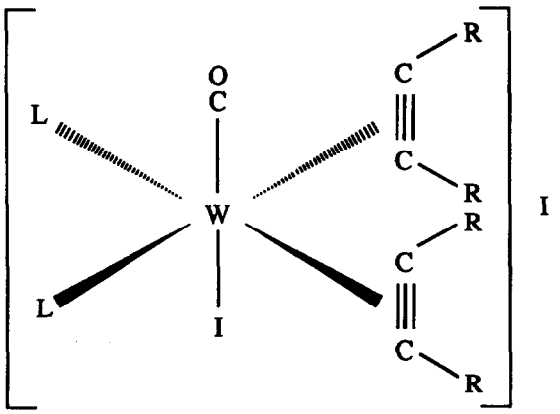

Fig. 2. Proposed structure for [$WI(CO)L_2(\eta^2\text{-}RC_2R)_2$]I (**5–8**).

equivalents of L different products are obtained, which must depend on the electronic and steric properties of L.

Acknowledgements—We thank the European Social Fund (S.D.R.) for support. We also wish to thank Dr O. W. Howarth for obtaining several ^1H NMR spectra at the University of Warwick on the SERC NMR service. We also thank Mr Michael P. Shaw for performing the two mechanistic experiments suggested by the referee.

REFERENCES

1. D. P. Tate and J. M. Augl, *J. Am. Chem. Soc.* 1963, **85**, 2174.
2. J. L. Templeton, *Adv. Organomet. Chem.* 1989, **29**, 1.
3. S. R. Allen, P. K. Baker, S. G. Barnes, M. Green, L. Trollope, L. M. Muir and K. W. Muir, *J. Chem. Soc., Dalton Trans.* 1981, 873.
4. S. R. Allen, T. H. Glauert, M. Green, K. A. Mead, N. C. Norman, A. G. Orpen, C. J. Schaverien and P. Woodward, *J. Chem. Soc., Dalton Trans.* 1984, 2747.
5. J. L. Davidson and G. Vasapollo, *J. Chem. Soc., Dalton Trans.* 1985, 2239.
6. P. B. Winston, S. J. N. Burgmayer, T. L. Tonker and J. L. Templeton, *Organometallics* 1986, **5**, 1707.
7. E. M. Armstrong, P. K. Baker, M. E. Harman and M. B. Hursthouse, *J. Chem. Soc., Dalton Trans.* 1989, 295.
8. P. K. Baker, E. M. Armstrong and M. G. B. Drew, *Inorg. Chem.* 1989, **28**, 2406.
9. P. K. Baker, K. R. Flower, M. G. B. Drew and G. Forsyth, *J. Chem. Soc., Dalton Trans.* 1989, 1903.
10. P. K. Baker and E. M. Armstrong, *Polyhedron* 1989, **8**, 351.
11. P. K. Baker, K. R. Flower, P. A. Bates and M. B. Hursthouse, *J. Organomet. Chem.* 1989, **372**, 263.
12. E. M. Armstrong, P. K. Baker and M. G. B. Drew, *Organometallics* 1988, **7**, 319.
13. R. J. Herrick, D. M. Leazer and J. L. Templeton, *Organometallics* 1983, **2**, 834.
14. E. M. Armstrong, P. K. Baker and M. G. B. Drew, *J. Organomet. Chem.* 1987, **336**, 377.
15. P. K. Baker, M. G. B. Drew, S. Edge and S. D. Ridyard, *J. Organomet. Chem.* 1991, **409**, 207.
16. P. K. Baker, E. M. Armstrong and M. G. B. Drew, *Inorg. Chem.* 1988, **27**, 2287.

Polyhedron Vol. 12, No. 8, pp. 921–924, 1993
Printed in Great Britain

0277–5387/93 $6.00+.00
© 1993 Pergamon Press Ltd

CRYSTAL STRUCTURE AND MASS SPECTRA OF A COPPER(I) COMPLEX WITH A CHAIN ARRANGEMENT: $[\mu$-4,4′-bipy-Cu(TTA)$]_n$

MINGXING LI, ZHENG XU* and XIAOZENG YOU

Coordination Chemistry Institute, Coordination Chemistry State Key Laboratory, Nanjing University, Nanjing 210008, Jiangsu, P.R.C.

and

ZHENCHAO DONG and GUOCONG GUO

Fujing Institute of Research on the Structure of Matter, Fuzhou 350002, Fujian, P.R.C.

(*Received* 8 *October* 1992; *accepted* 2 *December* 1992)

Abstract—The first chain copper(I) complex with 4,4′-bipyridine as the bridging ligand, of the formula $[\mu$-4,4′-bipy-Cu(TTA)$]_n$ (TTA = 2-thienoyltrifluoroacetone), has been prepared and characterized by elemental analysis, IR and FAB mass spectra. Its X-ray crystal structure determination reveals that the local coordination geometry around copper(I) is a distorted tetrahedron. Cu(TTA) units are bridged by 4,4′-bipyridine to form an infinite zigzag chain with an N—Cu—N angle of 143.3(7)°. The short Cu—N distance (1.98 Å) indicates that quite strong molecular chains have been formed in the crystal.

One-dimensional transition metal complexes bridged by bidentate π-electron-containing ligands, such as pyrazine and 4,4′-bipyridine, have gained more importance with respect to their properties as organic conductors. Many polymers, most containing metallomacrocycles, have been synthesized and extensively investigated.[1–3] After partial oxidation or reduction of the polymers mixed-valence solids can be obtained and show good conducting or semiconducting properties. Recently we have reported a one-dimensional β-diketonate complex with copper(II) as the central metal ion and 4,4′-bipyridine as the bridging ligand.[4] In the partial reduction process of the copper(II) complex with ascorbic acid a novel copper(I) complex with an infinite zigzag chain structure appeared unexpectedly. Although copper(II) complexes of β-diketonate have been extensively investigated, there are few reports of copper(I) β-diketonate compounds.[5] To our knowledge, the title complex is the first structurally characterized copper(I) complex with a chain arrangement. Here we report the synthesis, mass spectra and X-ray single crystal structure of the copper(I) complex, $[\mu$-4,4′-bipy-Cu(TTA)$]_n$.

EXPERIMENTAL

Synthesis

Analytical grade copper(II) chloride, 2-thienoyltrifluoroacetone, 4,4′-bipyridine and ascorbic acid were used without further purification. Solvents were refluxed and distilled over $MgSO_4$ for DMF and NaH for methanol under nitrogen. $Cu(TTA)_2$ was prepared according to the literature method.[6] The title complex was prepared by mixing ascorbic acid (1 mmol), 4,4′-bipyridine (2 mmol) and $Cu(TTA)_2$ (0.5 mmol) in DMF (10 cm^3). The solution was stirred for 2 h at room temperature and filtered to leave a red–brown filtrate. The filtrate was then poured into methanol (50 cm^3) and red crystals precipitated out. The crystals were collected by filtration, washed with methanol and dried *in vacuo*; yield 0.10 g (45%). Found: C, 49.2; H, 2.7; N, 6.3. Calc. for $C_{18}H_{12}N_2F_3O_2SCu$: C, 49.0; H, 2.7; N, 6.3%. The red plate-like crystals suitable for X-ray structure analysis were grown from the

* Author to whom correspondence should be addressed.

filtrate by diffusion with methanol vapour for 2 weeks. Each process was performed under nitrogen. The pure solid complex is relatively stable in dry air, but the copper(I) can be oxidized slowly in moist air.

Physical measurements

Elemental analyses for carbon, hydrogen and nitrogen were performed on a Perkin–Elmer 240C analyser. IR spectra were obtained with KBr pellets in the 4000–400 cm^{-1} region, using a Nicolet 170SX FTIR spectrophotometer. Fast atom bombardment (FAB) mass spectra were obtained on a VG-ZAB-HS spectrometer with thioglycerol as a matrix. Xenon was used to produce the primary beam. A primary current of 1 mA at an energy of 8 KeV provided good sample ion intensities.

Crystallographic structure determination

A single crystal with the dimensions $0.1 \times 0.2 \times 0.2$ mm was selected for X-ray diffraction analysis. Diffraction data were collected on a Rigaku AFC5R diffractometer using graphite-monochromated Mo-K_α ($\lambda = 0.71069$ Å) radiation. During the course of the intensity data collection the crystal showed no loss in intensity. A summary of crystallographic data is given in Table 1. The crystal structure was solved using direct methods and difference-Fourier syntheses, and refined by the full-matrix least-squares technique using anisotropic temperature factors. Hydrogen atoms were calculated as riding on carbon atoms at 0.95 Å and refined using isotropic temperature factors. The intensity data were corrected for Lorentz–polarization effects and empirical absorption. All the calculations were performed on a micro VAXII computer using the TEXSAN program system. Complete tables of atomic coordinates and thermal parameters, together with observed and calculated structure factors, have been deposited with the Editor, from whom copies are available on request. Atomic coordinates have also been deposited with the Cambridge Crystallographic Data Center.

Table 1. Summary of crystal and intensity collection data

Empirical formula	$C_{18}H_{12}N_2F_3O_2SCu$
F_w	440.91
Crystal dimensions (mm)	$0.1 \times 0.2 \times 0.2$
Crystal system	Monoclinic
Space group	$C2/c$
a (Å)	9.640(5)
b (Å)	24.97(1)
c (Å)	16.032(7)
β (°)	106.76(3)
V (Å^3)	3695(3)
Z	8
D_c (g cm^{-3})	1.58
$F(000)$	1776
Radiation	Mo-K_α ($\lambda = 0.71069$ Å)
μ (cm^{-1})	13.35
Scan method	ω–2θ
$2\theta_{max}$ (°)	50.0
$(h, k, l)_{min}$, $(h, k, l)_{max}$	(0, 0, −19), (11, 30, 19)
No. of data collected	3558
No. of unique data	3344
No. of data with $I > 3\sigma(I)$	669
R	0.062
R_w [w = $1/\sigma^2(F_o)$]	0.069
Goodness of fit	1.24
Maximum shift in final cycle	0.01
Largest peak in final difference map (e Å^{-3})	0.60

RESULTS AND DISCUSSION

By reaction of $Cu(TTA)_2$ and 4,4′-bipyridine with ascorbic acid, we have synthesized a novel copper(I) complex. Elemental analysis has confirmed the formula $[Cu(C_8H_4F_3O_2S)(C_{10}H_8N_2)]_n$.

When 4,4′-bipyridine is the bridging ligand IR spectroscopy is a useful tool for distinguishing monomers from polymers.[7] The monomeric derivatives give rise to new bands at 800, 1070, 1215, 1402, 1483 and 1589 cm^{-1}. These absorptions are caused by the ligand and agree with the bands exhibited by the free 4,4′-bipyridine. The predominant spectral difference observed for the 4,4′-bipyridine bridging compounds, compared with monomeric compounds containing terminal 4,4′-bipyridine, is the disappearance of absorptions at *ca* 1215, 1402 and 1589 cm^{-1}. The IR spectra of the title complex display three characteristic absorptions of 4,4′-bipyridine at 808, 1055 and 1470 cm^{-1}. The disappearance of in-plane vibrations around 1215, 1402 and 1589 cm^{-1} indicates that the copper(I) complex is a polymer with 4,4′-bipyridine as the bridging group.

FAB mass spectra, developed rapidly during the last few years, promise to be extremely valuable in characterizing polar involatile compounds. Table 2 summarizes the results obtained for the FAB-MS analysis on the copper(I) complex. The most intense peak corresponds to the fragment ion $(4,4'\text{-bipy}+H)^+$. Every original cation peak is bound with two peaks corresponding to the addition of one and two hydrogen atoms.[8] Peak a is assigned to two fragment ions, $[(C_4H_3S)CO]^+$ ($m/z = 111$) and $(CH_2COCF_3)^+$ ($m/z = 111$), due to the cleavage of the TTA ligand at the carbonyl carbon.[9] The

Table 2. FAB mass spectral data

Peak	Fragment (+nH)	m/z (relative intensity I, %) $n=0$	$n=1$	$n=2$	$n=3$
a	TTA/2	111(98.7)	112(8.5)	113(6.3)	—
b	4,4′-bipy	—	157(100)	158(45.9)	159(10.2)
c	TTA	—	223(82.2)	224(11.8)	225(5.4)
d	bipy-Cu-TTA/2	—	331(5.4)	332(1.1)	333(0.7)
e	Cu-bipy-Cu-TTA/2	393(1.6)	394(0.3)	395(0.9)	—
f	bipy-Cu(bipy)-TTA/2	—	487(1.1)	488(0.4)	489(0.3)

Table 3. Selected bond distances (Å) and angles (°) in [μ-4,4′-bipy-Cu(TTA)]$_n$

Cu—N(1)	1.98(2)	Cu—N(2)	1.97(2)
Cu—O(1)	2.20(1)	Cu—O(2)	2.15(2)
O(1)—C(13)	1.29(2)	O(2)—C(11)	1.23(3)
C(3)—C(8)	1.50(3)	C(11)—C(12)	1.40(3)
C(12)—C(13)	1.35(3)	C(13)—C(14)	1.44(3)
N(1)—Cu—N(2)	143.3(7)	O(1)—Cu—O(2)	83.3(6)
N(1)—Cu—O(1)	100.6(7)	N(1)—Cu—O(2)	107.9(7)
N(2)—Cu—O(1)	104.5(7)	N(2)—Cu—O(2)	101.4(7)

presence of peak e indicates that the complex is polymeric with 4,4′-bipyridine as bridging groups. According to the relative intensity I the ligand ratio of TTA and 4,4′-bipyridine can be calculated. $I_{4,4'\text{-bipy}} = I_b+I_d+I_e+2I_f = 169.7\, I_{TTA} = I_c+1/2(I_a+I_d+I_e+I_f) = 162.1$ $I_{4,4'\text{-bipy}}$ is nearly equal to I_{TTA}, indicating that the ligand ratio is 1 : 1. This is exactly in agreement with the result of elemental analysis.

The molecular structure of the copper(I) complex is shown in Fig. 1. Selected bond distances and angles are listed in Table 3. The local coordination geometry around the copper(I) ion is distorted tetrahedral. Cu(TTA) units are linked by 4,4′-bipyridine in a zigzag fashion with an N(1)—Cu—N(2) angle of 143.3(7)°, forming an infinite chain in the crystal. Eight of these chains pass through a cell in a parallel fashion.

The average Cu—O bond length (2.18 Å) is longer, whereas Cu—N (1.98 Å) is shorter than those found in the related known β-diketonate complexes, such as trigonal planar Cu^{I}(tfacac)(PMe_3), Cu—O 1.986;[5] square planar Cu^{II}(TTA)$_2$, Cu—O 1.914;[10] square-pyramidal μ-4,4′-bipy-

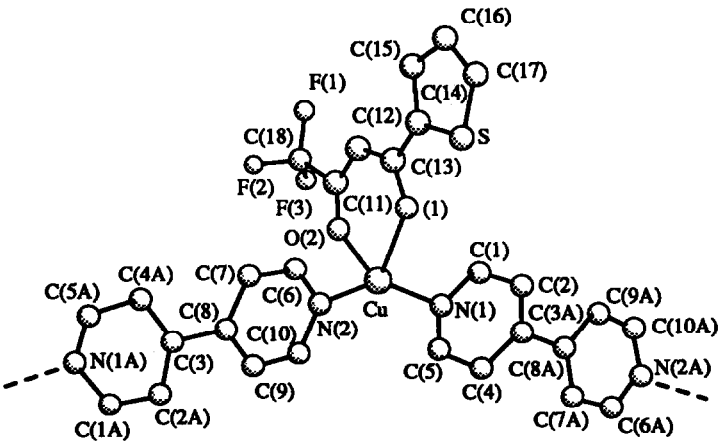

Fig. 1. Structure of the complex [μ-4,4′-bipy-Cu(TTA)]$_n$.

cun2(TTA)4, Cu--O 1.934, Cu--N 2.262; 11 and octahedral [#-4,4'-bipy-Cu~(TTA)2]n,Cu--O 2.039, Cu--N 2.201/~.4 The unusually short Cu--N distance, taking into consideration the difference in metallic ion radii (Cu ÷ 0.96, Cu 2÷ 0.72 A), indicates that strong bonds and quite firm molecular chains have been formed. The bond angle of O(1)---Cu--O(2) is 83.3°. The chelate ring between O(1) and 0(2) with the copper atom is basically planar. The dihedral angle between the thiophene ring and the chelate ring is rather small (4.47°), indicating some kind of conjugation effect. This leads to the fact that the bond length of 1.44 /~ between C(13) and C(14) is shorter than the usual *sp2-sp 2* C--C single bond length of 1.50 ~.

Acknowledgements--This work is supported by a grant for a key research project from the State Science and Technology Commission and National Nature Science Foundation of China.

REFERENCES

1. M. Hanack, S. Deger and A. Lange, *Coord. Chem.* Rev. 1988, 83, 115.
2. B. N. Diel, T. Inabl, N. K. Jaggi, J. W. Lyding, O. Schneider, M. Hanack, C. R. Kannewurf, T. J. Marks and L. H. Schwartz, *J. Am. Chem. Soc.* 1984, 106, 3207.
3. J. Strahle, F. Kubel, W. Hiller and R. Dantona, *Molee. Cryst. Liq. Cryst.* 1982, 81,265.
4. S. H. Gou, X. Z. You, Z. Xu, Z. Y. Zhou, K. B. Yu, Y. P. Yu and D. L. Zhu, *Acta Cryst.* 1991, C47, 1303.
5. H. K. Shin, M. J. Hampden-Smith, E. N. Duesler and T. T. Kodas, *Polyhedron* 1991, 10, 645.
6. W. B. Eugene and T. T. Joseph, J. *Phys. Chem.* 1960, 64, 487.
7. J. Metz, O. Schneider and M. Hanack, *Spectrochim. Acta* 1982, 38A, 1265.
8. B. Divisia-Blohorn, G. Kyriakakou and J. Ulrich, *Or9. Mass Spectrom.* 1985, 20, 463.
9. J. D. B. Smith, D. C. Phillips and T. D. Kaczmarck, *Microchem.* J. 1976, 21, 424.
10. Y. P. Yu, Z. Xu, X. Z. You, J. N. Lu, S. Shi, S. X. Liu and C. C. Lin, J. *lnor9. Chem. (Chinese)* 1988, **4,** 30.
11. M. X. Li, Z. Xu, X. Z. You and C. G. Chen, *Acta Cryst.,* to be published.

Polyhedron Vol. 12, No. 8, pp. 925–930, 1993
Printed in Great Britain

0277–5387/93 $6.00+.00
© 1993 Pergamon Press Ltd

SYNTHESIS AND STRUCTURAL CHARACTERIZATION OF DIMERIC DIORGANOTIN(IV) N-2-HYDROXYNAPHTHALIDENE-β-AMINO ACID COMPLEXES: X-RAY STRUCTURE OF $[Me_2Sn(OC_{10}H_6CH{=}NCH_2CH_2COO)]_2$

NGOH KHANG GOH and LIAN EE KHOO*

School of Science, Nanyang Technological University, 469 Bukit Timah Road, Singapore 1025

and

THOMAS C. W. MAK*

Department of Chemistry, The Chinese University of Hong Kong, Shatin, New Territories, Hong Kong

(*Received* 8 *October* 1992; *accepted* 2 *December* 1992)

Abstract—Two new compounds with the formula $[R_2Sn(OC_{10}H_6CH{=}NCH_2CH_2COO)]_2$ where R = CH_3 or n-C_4H_9, have been synthesized. The crystal structure of the dimethyltin compound is reported along with ^1H, ^{13}C and IR spectroscopic data for both compounds. The centrosymmetric dimethyltin complex exhibits octahedral coordination for each tin atom. The tridentate ligand chelates meridionally via the phenolate oxygen, the imino nitrogen and one carboxylate oxygen atom. Two further *trans* positions in the tin coordination sphere are taken up by the two methyl groups while the apical (sixth) position is filled by a shared carboxylate oxygen atom from the other organotin unit.

Many organotin compounds are active *in vitro* and *in vivo* against P388 leukemia.[1,2] Some are characterized by a bicyclic structure such as the dibutyltin derivative of glycylglycine[3] and the diorganotin 2,6-pyridine dicarboxylates.[4] Although extensive biological[5] and structural[6,7] studies have been conducted on these eight- and nine-membered bicyclic compounds, there is to-date no structural characterization of 10-membered bicyclic diorganotin complexes with two six-membered chelate rings resulting from a 1,6-intramolecular Sn—N interaction. As a continuation of our studies on the eight- and nine-membered bicyclic diorganotin compounds,[8,9] we now report the results of our investigation into the synthesis and characterization of diorganotin(IV) N-2-hydroxynaphthalidene-β-amino acid complexes: $R_2Sn(OC_{10}H_6CH{=}NCH_2CH_2COO)$ (R = CH_3 and Bu^n). A full X-ray structural analysis of the dimethyltin complex of the N-2-hydroxynaphthalidene-β-alanine ligand has been performed and the results are reported along with a variety of spectroscopic data for both the dimethyltin and dibutyltin derivatives of the ligand.

* Authors to whom correspondence should be addressed.

RESULTS AND DISCUSSION

Diorganotin complexes of bis-chelating tridentate ligands capable of forming two chelate rings frequently have trigonal bipyramidal geometry with the ligand occupying the axial–equatorial–axial sites.[6,9] It was anticipated that the ligand, 2-$HOC_{10}H_6CH{=}NCH_2CH_2COOH$, which forms two six-membered chelate rings upon complexation, would behave likewise. However, the X-ray structural investigation of $Me_2Sn(OC_{10}H_6CH{=}NCH_2CH_2COO)$ confirms that the complex crystallized as a centrosymmetric dimer. The six-coordinate geometry of the complex organotin moiety and the atomic numbering scheme are shown in

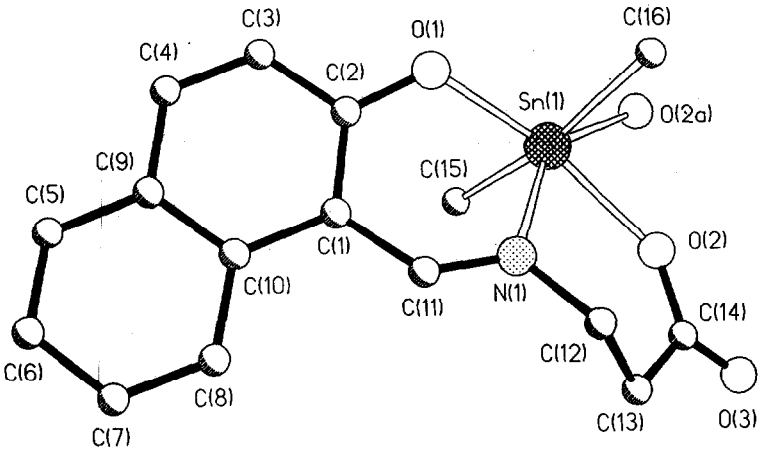

Fig. 1. Molecular structure and crystallographic numbering scheme employed for $[Me_2Sn(OC_{10}H_6CH{=}NCH_2CH_2COO)]_2$.

Fig. 1, while packing of the dimeric units is illustrated in Fig. 2. Table 1 lists the bond distances and bond angles. The ^1H and ^{13}C NMR data for both the dimethyl and di-n-butyl compounds are listed in Table 2, together with those of the ligand, while the IR, physical and analytical data are included in the Experimental.

Each tin atom is in a distorted octahedral environment and coordinated meridionally by the tridentate ligand via the phenolate oxygen, imino nitrogen and one-carboxylate oxygen atom. Two further *trans* positions in the coordination sphere are taken up by the two methyl groups, while the apical (sixth) position is filled by a shared carboxylate oxygen (O2a) from the other organotin unit, resulting in a dimer consolidated by a centrosymmetric, planar, four-membered Sn_2O_2 ring (Fig. 2).

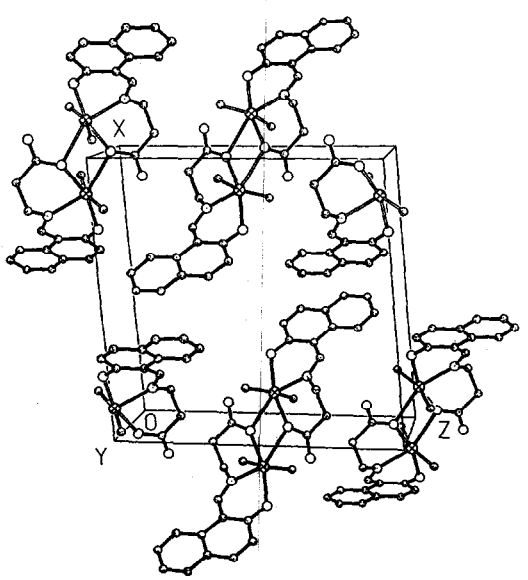

Fig. 2. Molecular packing in the dimeric crystal structure of $[Me_2Sn(OC_{10}H_6CH{=}NCH_2CH_2COO)]_2$.

In this configuration the three *trans* angles around the tin atom, 163.2° [C(15)—Sn—C(16)], 161.6° [O(1)—Sn—O(2)] and 146.9° [N(1)—Sn—O(2a)], are normal for octahedral tin(IV) complexes.[10,11] However, the *trans* angle of 161.6°, formed between the two terminal oxygen donors of the ligand and the tin atom, [O(1)—Sn—O(2)], is 5.7° wider than that reported for the pentacoordinate dibutyltin complex[9] $Bu_2Sn[OC_6H_4CH{=}NCH(Pr^i)COO]$, which contained a six-membered and a five-membered chelate ring. This is further reflected by the lengthening of the intramolecular Sn—N bond from 2.158 Å for $Bu_2Sn[OC_6H_4CH{=}NCH(Pr^i)COO]$ to 2.224 Å in the title complex, which now has two six-membered chelate rings. In spite of this, the two six-membered chelate rings are puckered into a boat and a half-chair conformation. The atoms forming the floor of the boat, Sn, N(1), C(13) and C(14), are co-planar to within 0.022 Å, while the prow atoms, O(2) and C(12), are displaced from this plane in the same direction by 0.087 amnd 0.672 Å, respectively. In the half-chair conformation N(1), C(11), C(1), C(2) and O(1) are co-planar to within 0.121 Å, while the remaining tin atom is displaced from this plane by a distance of 1.006 Å.

The similarities of the spectroscopic data indicate that the six-coordinate dimeric structure should be proposed for the dibutyltin derivative. The IR carbonyl stretching vibrations for the two diorganotin derivatives are normal in the range 1630–1610 cm^{-1}. However, the absence of a symmetric and the presence of an asymmetric Sn—Me stretching vibration at 580 cm^{-1} indicate a linear C—Sn—C

Table 1. Selected interatomic parameters (Å, °) for $[Me_2Sn(OC_{10}H_6CH{=}NCH_2CH_2COO)]_2$

Sn(1)—N(1)	2.224(3)	Sn(1)—O(1)	2.148(3)
Sn(1)—O(2)	2.221(3)	Sn(1)—O(2a)	2.587(4)
Sn(1)—C(15)	2.101(4)	Sn(1)—C(16)	2.105(4)
N(1)—C(11)	1.293(5)	N(1)—C(12)	1.471(5)
O(1)—C(2)	1.303(5)	O(2)—C(14)	1.291(5)
O(3)—C(14)	1.224(5)	C(1)—C(2)	1.421(6)
C(1)—C(10)	1.442(6)	C(1)—C(11)	1.449(6)
C(2)—C(3)	1.422(7)	C(3)—C(4)	1.359(7)
C(4)—C(9)	1.414(7)	C(5)—C(6)	1.358(8)
C(5)—C(9)	1.417(7)	C(6)—C(7)	1.405(8)
C(7)—C(8)	1.371(7)	C(8)—C(10)	1.418(6)
C(9)—C(10)	1.427(6)	C(12)—C(13)	1.528(6)
C(13)—C(14)	1.513(6)		
N(1)—Sn(1)—O(1)	80.2(1)	N(1)—Sn(1)—O(2)	81.5(1)
O(1)—Sn(1)—O(2)	161.6(1)	N(1)—Sn(1)—C(15)	96.0(2)
O(1)—Sn(1)—C(15)	91.0(2)	O(2)—Sn(1)—C(15)	92.9(1)
N(1)—Sn(1)—C(16)	100.5(1)	O(1)—Sn(1)—C(16)	89.1(1)
O(2)—Sn(1)—C(16)	92.3(1)	C(15)—Sn(1)—C(16)	163.2(2)
N(1)—Sn(1)—O(2a)	146.9(1)	O(1)—Sn(1)—O(2a)	132.8(1)
O(2)—Sn(1)—O(2a)	65.6(1)	C(15)—Sn(1)—O(2a)	82.9(2)
C(15)—Sn(1)—O(2a)	84.7(2)		
Sn(1)—N(1)—C(11)	122.6(3)	Sn(1)—N(1)—C(12)	118.8(2)
C(11)—N(1)—C(12)	118.5(3)	Sn(1)—O(1)—C(2)	123.5(3)
Sn(1)—O(2)—C(14)	138.2(2)		
C(2)—C(1)—C(10)	119.4(4)	C(2)—C(1)—C(11)	120.7(4)
C(10)—C(1)—C(11)	119.5(4)	O(1)—C(2)—C(1)	123.3(4)
O(1)—C(2)—C(3)	117.7(4)	C(1)—C(2)—C(3)	119.0(4)
C(2)—C(3)—C(4)	121.8(4)	C(3)—C(4)—C(9)	121.1(4)
C(6)—C(5)—C(9)	121.2(5)	C(5)—C(6)—C(7)	119.5(5)
C(6)—C(7)—C(8)	120.9(5)	C(7)—C(8)—C(10)	121.3(4)
C(4)—C(9)—C(5)	120.8(4)	C(4)—C(9)—C(10)	119.4(4)
C(5)—C(9)—C(10)	119.7(4)	C(1)—C(10)—C(8)	123.4(4)
C(1)—C(10)—C(9)	119.3(4)	C(8)—C(10)—C(9)	117.2(4)
N(1)—C(11)—C(1)	127.5(4)	N(1)—C(12)—C(13)	113.7(3)
C(12)—C(13)—C(14)	116.1(3)	O(2)—C(14)—O(3)	120.9(4)
O(2)—C(14)—C(13)	118.1(4)	O(3)—C(14)—C(13)	120.9(4)

Symmetry transformation: a $(-x, -y, -z)$.

moiety in the methyl groups. This would be consistent with an octahedral configuration for the tin atom with the methyl groups in the *trans* positions. Table 2 gives the proton and ^{13}C NMR data for the complexes and the ligand. A downfield shift for the proton and ^{13}C signals was observed for the ligand upon complexation. This downfield shift was also observed in the diorganotin complex formed with 2-hydroxynaphthalidene-α-amino acid.[9] The spin–spin coupling between the azomethine proton and the tin nucleus, ^3J(SnN=CH), was detected in the two complexes. This type of spin–spin coupling, where the tin nuclei are located in a *trans* position to the azomethine proton, has previously been reported.[12,13] It thus confirms the presence of nitrogen–tin coordination in the complexes. In addition the values of the coupling constant (50–54 Hz) for ^3J(SnN=CH) (Table 2) are smaller than those (53–58 Hz) reported for the $[R_2Sn(OC_{10}H_6CH{=}NCH_2COO)]$ complexes.[9] This is attributed to the longer bond distance of the intramolecular Sn—N interaction in the present complexes.

EXPERIMENTAL

Chemicals and reagents

Dimethyltin and dibutyltin oxides were purchased from Alfa Inorganics and other chemicals

Table 2. NMR data for N-2-hydroxynaphthalidene-β-amino acid and its diorganotin derivatives

Chemical shifts (δ)	2-$HOC_{10}H_6CH{=}NCH_2CH_2COOH$[a]	$Me_2Sn(OC_{10}H_6CH{=}NCH_2CH_2COO)$	$Bu_2Sn(OC_{10}H_6CH{=}NCH_2CH_2COO)$
^{1}H NMR (ppm) [Hz]			
—CH=N— [^3J(SnN=CH)]	8.27(s)	8.99(s) [54.2]	8.99(s) [50.4]
—NCH_2CH_2COO—	3.13(t); 1.93(t)	4.04(t); 2.82(t)	4.00(t); 2.82(t)
Aromatic	6.0–7.3	6.9–7.9	6.9–7.9
—OH/—COOH	13.40 (br)	—	—
R_2Sn— [$^2J(SnCH_3)$]		0.9(s) [79]	0.8–1.7
^{13}C NMR (ppm) [Hz]			
—C=O	176.14	174.00	174.66
—C—O—	172.51	172.00	172.00
—CH=N—	159.33	167.97	167.84
Aromatic	105.96–136.80	117.94–133.79	118.58–139.35
—NCH_2CH_2—	47.77; 35.00	58.18; 38.12	58.75; 38.28
R_2Sn—	—	1.41	13.53; 22.45; 26.60; 27.03

[a] M.p. 198–200°C.[18]

The symbols s, t, and br have their usual meanings.

from the Aldrich Chemical Company. All were used without further purification, except salicylaldehyde which was distilled before use.

Microanalyses were performed at the School of Chemical Sciences, Universiti Sains Malaysia, using an elemental analyser (Model 240-XA).

NMR spectra

The proton and ^{13}C NMR spectra were recorded in $CDCl_3$:DMSO-d_6 on a CFT-20 Varian or Bruker AC-P300 spectrometer. NMR results are summarized in Table 2.

IR spectra

These were obtained on a Nicolet 5MX instrument with the samples as Nujol mulls or in KBr discs.

Preparation of diorganotin N-2-hydroxynaphthalidene-β-amino acid complexes

To a suspension of β-alanine (20 mmol) in absolute ethanol (120 cm^3) was added R_2SnO (20 mmol) (R = CH_3; Bu^n), followed by 2-hydroxynaphthaldehyde (3.4 g, 20 mmol). The mixture was stirred under nitrogen and refluxed for 10–12 h. After cooling in the refrigerator a crystalline precipitate formed, which was filtered, dried and recrystallized from methanol to give the pure product. Analytical data, melting points, along with the yields obtained, and the IR stretching vibrations data are as follows:

(a) $Me_2Sn(OC_{10}H_6CH{=}NCH_2CH_2COO)$: m.p. 232–234°C; yield 72%. Found: C, 49.1; H, 4.5; N, 3.4. Calc. for $C_{16}H_{17}NO_3Sn$: C, 49.3; H, 4.4; N, 3.6%. IR (cm^{-1}): ν(C=O): 1610; $\nu(Sn{-}Me)_{asym}$: 580. (b) $Bu_2Sn(OC_{10}H_6CH{=}NCH_2CH_2COO)$: m.p. 138–140°C; yield 88%. Found: C, 54.4; H, 6.5; N, 2.7. Calc. for $C_{22}H_{29}NO_3Sn$: C, 55.7; H, 6.2; N, 2.9%. IR (cm^{-1}): ν(C=O): 1630.

X-ray crystallography

$(C_{16}H_{17}NO_3Sn)_2$, $M_r = 780$, monoclinic, space group $P2_1/c$ (No. 14), $a = 14.891(4)$, $b = 6.764(1)$, $c = 15.070(3)$ Å, $\beta = 94.01(2)°$, $V = 1514.2(6)$ $Å^3$, $Z = 2$, $F(000) = 776$, $\lambda = 0.71073$ Å, $\mu(Mo\text{-}K_\alpha) = 1.70$ mm^{-1}.

A selected crystal of the dimensions $0.10 \times 0.16 \times 0.28$ mm was used. Diffraction data (2771 unique reflections) were collected up to $2\theta_{max} = 50°$ on Siemens P4 diffractometer using the ω-scan mode (2.96–15.64° min^{-1}), processed with a profile-fitting procedure[14] and corrected for absorption using ψ-scan data ($\mu r = 0.10$, transmission factors 0.751–0.812).[15] A total of 2215 independent reflections with $I > 3\sigma(I)$ were considered as observed data and used in the structure analysis. The structure was solved by Patterson superposition and subsequent Fourier synthesis. Non-hydrogen atoms were refined anisotropically. All hydrogen atoms were generated geometrically (C—H = 0.96 Å) and included in structure–factor calculations with assigned isotropic thermal parameters. Final R_F and R_{WF_2} values are 0.028 and 0.030 for 190 variables with the weighting scheme $w = [\sigma^2(|F^0|) + 0.00002|F^0|^2]^{-1}$. The residual extrema in the final difference map are in the range +0.37 to −0.52 e $Å^{-3}$. Computations were performed using the SHELXTL-PC program package.[16] Analytical expressions of neutral atomic scattering factors were used and anomalous dispersion corrections were incorporated.[17]

Acknowledgements—Financial support from Nanyang Technological University, (RP9/92KLE), and Hong Kong Research Grants Council (A/C 221600010) is gratefully acknowledged.

REFERENCES

1. A. K. Saxena and F. Huber, *Coord. Chem. Rev.* 1989, **95**, 109.
2. M. Gielen, *Tin as a Vital Nutrient* (Edited by N. F. Cardarelli), Ch. 13. CRC Press, Cleveland, OH (1986).
3. G. Ruisi, A. Silvestri, M. T. Lo Giudice, R. Barbieri, G. Atassi, F. Huber, K. Grätz and L. Lamartina, *J. Inorg. Biochem.* 1985, **25**, 229.
4. M. Gielen, E. Joosen, T. Mancilla, K. Jurkschat, C. Roobol, J. Bernheim, G. Atassi, F. Huber, E. Hoffmann, H. Perut and B. Mahieu, *Main Group Met. Chem.* 1987, **10**, 148.
5. A. J. Crowe, *Drugs Future* 1987, **12**, 255.
6. J. Wang, F. Liu, Y. Zhang, R. Wang, H. Wang and X.Yao, *J. Organomet. Chem.* 1989, **375**, 173.
7. O. Jung, J. H. Jeong and Y. S. Sohn, *Organometallics* 1991, **10**, 761.
8. F. L. Lee, E. J. Gabe, L. E. Khoo, W. H. Leong, G. Eng and F. E. Smith, *Inorg. Chim. Acta* 1989, **166**, 257.
9. F. E. Smith, R. C. Hynes, T. T. Ang, L. E. Khoo and G. Eng, *Can. J. Chem.* 1992, **70**, 1114.
10. E. Labisbal, A. Deblas, J. A. Vazquez, J. Romero, M. L. Duran, A. Sosusa, N. A. Bailey, D. E. Fenton, P. B. Leeston and R. V. Parish, *Polyhedron* 1992, **11**, 227.
11. M. Calligaris, G. Nardin and L. Randaccio, *J. Chem. Soc., Dalton Trans.* 1972, 2003.
12. K. Kawkami and T. Tanaka, *J. Organomet. Chem.* 1973, **49**, 409.
13. G. Matsubayashi, T. Tanaka, S. Nisbigigaki and K.

Nakatsu, *J. Chem. Soc., Dalton Trans.* 1979, 501.
14. R. Diamond, *Acta Cryst.* 1969, **25A**, 43.
15. G. Kopfmann and R. Huber, *Acta Cryst.* 1968, **24A**, 348.
16. G. M. Sheldrick, *Crystallographic Computing 3: Data Collection, Structure Determination, Proteins, and Databases* (Edited by G. M. Sheldrick, C. Krüger and R. Goddard), p. 175. Oxford University Press, New York (1985).
17. *International Tables for X-Ray Crystallography*, Vol. IV, pp. 55, 99, 149. Kynoch Press, Birmingham (1974).
18. L. E. Khoo, Z. H. Zhou and T. C. W. Mak, *J. Cryst. Spectrosc. Reson.* 1993, **23**, 153.

Polyhedron Vol. 12, No. 8, pp. 931–937, 1993
Printed in Great Britain

0277–5387/93 $6.00+.00
© 1993 Pergamon Press Ltd

SYNTHESIS, ELECTROCHEMICAL BEHAVIOUR AND STRUCTURAL CHARACTERIZATION OF THE MERCURY COMPLEX [Hg([18]aneN$_6$)]·(HgCl$_4$)

MARIA A. A. F. DE C. T. CARRONDO* and VITOR FÉLIX

Centro de Tecnologia Química Biológica, I.S.T., 2780 Oeiras, Portugal

and

M. TERESA DUARTE and M. AMÉLIA SANTOS†‡

Centro de Química Estrutural, Instituto Superior Técnico, 1096 Lisboa Codex, Portugal

(*Received* 1 *October* 1992; *accepted* 30 *November* 1992)

Abstract—Reaction of $HgCl_2$, in slight excess of 1 molar equivalent of the ligand ([18]aneN$_6$) in water, produces a colourless solution containing [Hg([18]aneN$_6$)](HgCl$_4$). The X-ray structure of this complex shows that the six nitrogen donor atoms of the macrocycle surround the mercury(II) atom in a distorted trigonal prismatic coordination. Cyclic voltammetry of [Hg([18]ane)]$^{2+}$ shows a chemically reversible reduction at a HDM electrode, with $E_{1/2} = -0.293$ V vs S.C.E. at pH 9.37 and a scan rate of 200 mV s^{-1}. The global oxidation–reduction process involves two electrons and two protons.

The coordination chemistry of potentially hexadentate macrocycles containing 18-membered rings (namely [18]aneX$_m$Y$_n$; X,Y = O,N,S; $m+n = 6$) is of particular interest, since these large ring systems have high flexibility and, therefore, can encapsulate and readily bind to a range of transition metal atoms, with the resulting complexes adopting different geometries.[1,2]

The macrocycle 1,4,7,10,13,16-hexaazacyclooctadecane (18-azacrown-6 or [18]aneN$_6$) is a ligand known to have great ability to form 1:1 complexes with several different metal cations, such as Co^{3+}, Ni^{2+}, Cu^{2+}, Cd^{2+}, Hg^{2+}, Pb^{2+}, Ca^{2+}, Sr^{2+}, La^{3+} and K^+ (as has been demonstrated by potentiometric techniques[3]), and also, as a triprotonated species, with some anions.[4] However, only two metal complexes with this ligand have been characterized by single-crystal X-ray analysis, *meso*-[Co([18]aneN$_6$)]Cl$_3$[5] and *rac*-[Co([18]aneN$_6$)](ClO$_4$)$_3$.[6] They both present an octahedral coordination involving all six nitrogen atoms of the ligand, but adopt different configurations.

Most properties exhibited by macrocyclic complexes appear to be controlled by the size of the cavity of the ligand.[7] According to previous molecular mechanics calculations[8] on metal 18-azacrown-6 complexes, it was concluded that for small metal ions (M—N ≈ 2.1, 2.2 Å) an octahedral geometry in two different isomeric structures, *rac* and *meso* (**I** and **II** on diagram), was preferred, while for larger metal ions (M—N ≈ 3.1 Å) a hexagonal bipyramidal geometry (**III**) was more probable.

Studies of the stability constants of different metal complexes with this ligand have shown that the highest values found were for copper [log K(CuL) = 21.6] and mercury [log K(HgL) = 29.1] complexes.[3]

We thus decided to synthesize both complexes. However, crystals of good quality were only obtained for the mercury complex. We report here the synthesis, characterization, electrochemical behaviour and crystal structure of the [Hg(18-azacrown-6)](HgCl$_4$) complex.

* Author responsible for the crystallographic analysis.
† Author responsible for the chemical and electrochemical results.
‡ Author to whom correspondence should be addressed.

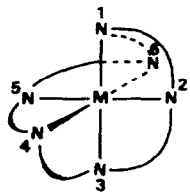

I

rac

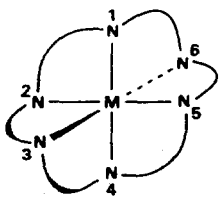

II

meso

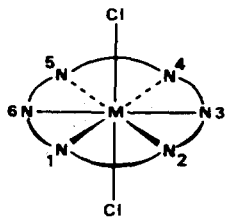

III

RESULTS AND DISCUSSION

Synthesis and characterization

Reaction of $HgCl_2$ with 1 molar equivalent of [18]aneN$_6$·HCl and an equivalent amount of base gave a colourless solution, which upon slow evaporation afforded white crystals of a mercury complex. Spectroscopic data and elemental analysis are indicative of the compound [Hg([18]aneN$_6$)] ($HgCl_4$). IR spectra showed peaks at *ca* 3400 and 1630 cm^{-1}, corresponding to N—H stretching and bending vibrations, respectively. The absence of any amine salt stretching vibration band, as has been found for the corresponding hexaamine ligand [as its 6 HCl adduct, ν(NH) $\approx$ 2700 cm^{-1}], was noticed. A strong sharp band was also observed at $\nu = 570$ cm^{-1}, which was attributed to the ν(Hg—N) stretching vibration. According to Adams[9] ν(M—N) in ethylenediamine metal complexes appears in the range 590–606 cm^{-1}; also, the IR frequency of ν(Hg—N) in amidomercury(II) chlorides is 573 cm^{-1}. The band corresponding to ν(Hg—Cl) stretching may be present in the far-IR regions [$(HgCl_4)^{2-}$, as a mull of NEt_4N^+ salts, presents $\nu = 223$ cm^{-1}], but the weakness of all far-IR bands makes it impossible to identify that vibration.

The ^{1}H NMR spectrum of [Hg([18]aneN$_6$)] ($HgCl_4$) showed a very thin multiplet at 2.61–2.63 ppm, which is characteristic of methylene protons, but it is shifted to a higher field relative to the free ligand ($\delta = 3.59$ ppm), as a consequence of the electrophilic character of the bonded Hg^{2+} ion. Moreover, an identical behaviour was observed for the ^{13}C NMR spectra of the complex and ligand, both presenting only one single resonance at $\delta = 43.22$ and $\delta = 44.39$ ppm, respectively. These data probably indicate the presence of a single product in solution, all the protons and carbons being magnetically equivalent but quite different from the free ligand.

The cyclic voltammetric behaviour observed for [Hg([18]aneN$_6$)]$^{2+}$ in water (0.1 M KNO_3 supporting electrolyte) is consistent with that expected for a reversible redox process,[10] namely $ip^c/ip^a \approx 1$ for all ranges of scan rates (v = 200–1000 mV s^{-1}), Ep^c and Ep^a are independent of scan rate and the plot of ip^c against $v^{1/2}$ gave a straight line. A peak potential separation of 30 mV is indicative of a two-electron transfer process, where $\Delta E_p = 59/n$ mV is expected for a reversible n-electron couple.

The half-wave potential, $E_{1/2}$, is -0.293 V vs S.C.E. at pH = 9.37 and a scan rate $v = 200$ mV s^{-1} (Fig. 1). No other waves appear within the limits of the solvent.

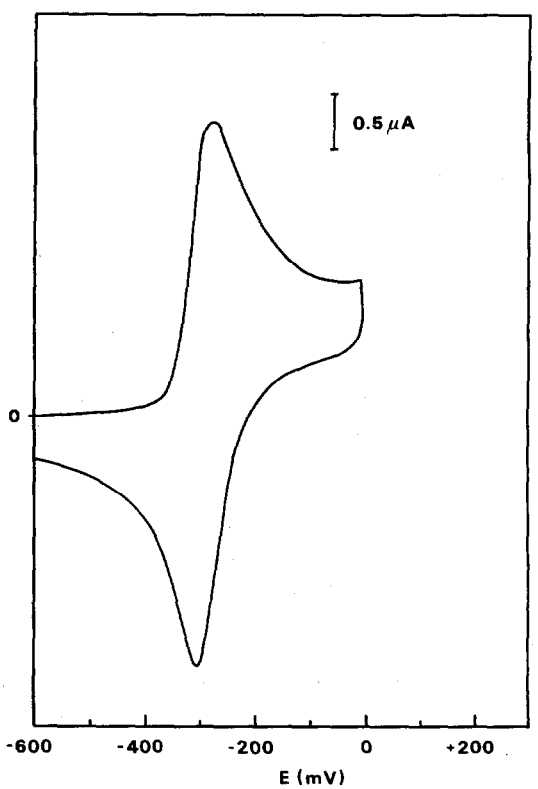

Fig. 1. Cyclic voltammogram of [Hg([18]aneN$_6$)]$^{2+}$ in water (0.1 M KNO_3) at HME. Scan rate = 200 mV s^{-1}, $T = 25 \pm 1$°C, pH = 9.37, $C_L = 5 \times 10^{-4}$ M.

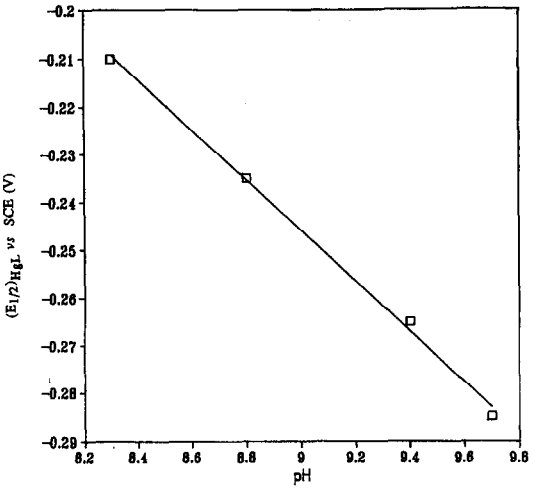

Fig. 2. Effect of pH on $(E_{1/2})_{HgL}$ at $I = 0.1$ M (KNO_3), 25°C, $C_L = 5 \times 10^{-4}$ M.

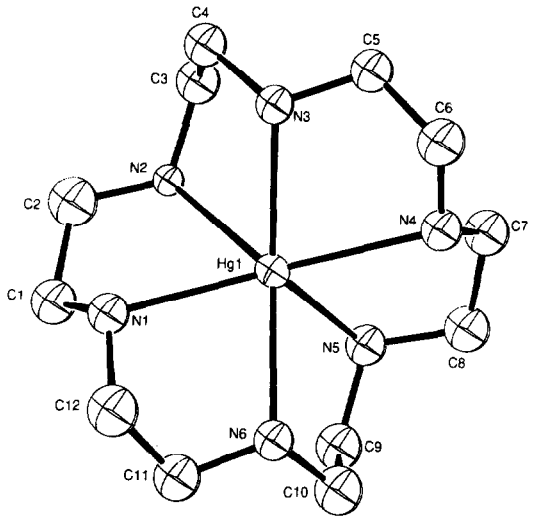

Fig. 3. Molecular structure of $[Hg([18]aneN_6)]^{2+}$ with 30% probability thermal ellipsoids showing the atom labelling scheme.

$E_{1/2}$ is independent of the macrocycle concentration in solution, but shifted linearly to a more negative value, with an increase in pH and a slope of $\Delta E_{1/2}/\Delta pH = -53$ mV (Fig. 2). These findings suggest that in the experimental conditions used in this work Hg^{2+} forms a 1:1 complex with the macrocycle ligand $[18]aneN_6$, the oxidation being easier in less acidic conditions. In the pH range studied (pH = 8.0–9.7) the global oxi-reduction process should involve two electrons and two protons, as expressed by eq. (1):

$$Hg + H_2L^{2+} \rightleftharpoons [HgL]^{2+} + 2H^+ + 2e^- \quad (1)$$

These results seem to indicate that the only complex formed in solution is $[Hg^{II}L]^{2+}$. The corresponding mercury(I) complex has not been found in the time scale of our experiment (0.025–0.25 s).[11]

The Ep^a value now determined (−0.235 V, at pH 8.8) is comparable to that found in the literature[12] for the half-wave potential, $E_{1/2}$, for the DC polarographic anodic wave of a solution of the same polyamine at D.M.E. (dropping mercury electrode).

Further comparisons of redox potentials with values from related azacrown complexes[13] (namely, *rac*-$[Hg([18]aneN_2S_4)]^{2+}$, $Ep^c = -0.85$ V at a platinum electrode in acetonitrile) are not valid because different solvents and different working and reference electrodes have been used. Furthermore, the effect of donor atom substitution on the macrocycle[14] and other structural effects can, in some way, influence the ratio of stability for oxidized and reduced species, and consequently the peak potentials. Also, in contrast to azacrown complexes thio-aza analogues present irreversible reductions, which might be indicative of a slow large stereochemical change occurring at the metal centre.

X-ray structural analysis

A molecular diagram presenting the numbering scheme is shown in Fig. 3. Relevant bond lengths and angles are listed in Tables 1 and 2, respectively.

The metal atom is coordinated to the six nitrogen donor atoms of the macrocycle, with an average Hg—N bonding distance of 2.44(2) Å. Other complexes also containing a HgN_6 central core have similar Hg—N bond lengths, 2.46(2) Å in $[Hg(pyridine)_6]^{2+}$[15] and 2.400(6) Å in $[Hg(1,10\text{-phenanthroline})_3]^{2+}$.[16] Complexes with related macrocyclic ligands show comparable metal-to-nitrogen distances, e.g. 2.47(1) Å in $[Hg([18]aneN_2S_4)]$.[13]

The C—N and C—C bonding distances, within the macrocycle skeleton, ranging from 1.37(3) to

Table 1. Bond lengths (Å) for the complex $[Hg([18]aneN_6)](HgCl_4)$

N(1)—Hg(1)	2.416(22)	N(2)—Hg(1)	2.425(17)
N(3)—Hg(1)	2.426(20)	N(4)—Hg(1)	2.497(22)
N(5)—Hg(1)	2.416(22)	N(6)—Hg(1)	2.435(21)
C(1)—N(1)	1.482(34)	C(12)—N(1)	1.479(36)
C(2)—N(2)	1.367(32)	C(3)—N(2)	1.430(30)
C(4)—N(3)	1.449(32)	C(5)—N(3)	1.441(30)
C(6)—N(4)	1.386(33)	C(7)—N(4)	1.466(32)
C(8)—N(5)	1.449(32)	C(9)—N(5)	1.460(33)
C(10)—N(6)	1.451(34)	C(11)—N(6)	1.443(34)
C(2)—C(1)	1.537(38)	C(4)—C(3)	1.546(35)
C(6)—C(5)	1.500(40)	C(8)—C(7)	1.553(38)
C(10)—C(9)	1.548(39)	C(12)—C(11)	1.412(39)
Cl(1)—Hg(2)	2.518(9)	Cl(2)—Hg(2)	2.492(9)
Cl(3)—Hg(2)	2.447(9)	Cl(4)—Hg(2)	2.476(9)

Table 2. Bond angles (°) for [Hg([18]aneN$_6$)](HgCl$_4$)

N(2)—Hg(1)—N(1)	71.5(7)	N(3)—Hg(1)—N(1)	100.7(8)
N(3)—Hg(1)—N(2)	72.8(7)	N(4)—Hg(1)—N(1)	155.4(7)
N(4)—Hg(1)—N(2)	126.2(7)	N(4)—Hg(1)—N(3)	73.0(8)
N(5)—Hg(1)—N(1)	123.4(8)	N(5)—Hg(1)—N(2)	96.3(7)
N(5)—Hg(1)—N(3)	128.9(7)	N(5)—Hg(1)—N(4)	75.1(7)
N(6)—Hg(1)—N(1)	73.5(8)	N(6)—Hg(1)—N(2)	130.7(6)
N(6)—Hg(1)—N(3)	148.1(7)	N(6)—Hg(1)—N(4)	99.0(8)
N(6)—Hg(1)—N(5)	75.5(7)	C(1)—N(1)—Hg(1)	107.0(16)
C(12)—N(1)—Hg(1)	105.4(18)	C(12)—N(1)—C(1)	117.4(23)
C(2)—N(2)—Hg(1)	114.7(17)	C(3)—N(2)—Hg(1)	107.2(15)
C(3)—N(2)—C(2)	118.7(22)	C(4)—N(3)—Hg(1)	112.2(16)
C(5)—N(3)—Hg(1)	106.9(15)	C(5)—N(3)—C(4)	114.8(21)
C(7)—N(4)—C(6)	117.2(23)	C(8)—N(5)—Hg(1)	109.8(16)
C(9)—N(5)—Hg(1)	105.7(17)	C(9)—N(5)—C(8)	113.9(23)
C(2)—C(1)—N(1)	109.5(23)	C(1)—C(2)—N(2)	113.7(26)
C(4)—C(3)—N(2)	112.0(22)	C(3)—C(4)—N(3)	109.1(22)
C(10)—N(6)—Hg(1)	108.5(17)	C(11)—N(6)—Hg(1)	108.8(17)
C(11)—N(6)—C(10)	112.0(23)	C(6)—C(5)—N(3)	112.5(23)
C(5)—C(6)—N(4)	113.3(26)	C(8)—C(7)—N(4)	111.6(23)
C(7)—C(8)—N(5)	112.8(23)	C(10)—C(9)—N(5)	112.0(25)
C(9)—C(10)—N(6)	112.3(25)	C(12)—C(11)—N(6)	109.0(26)
C(11)—C(12)—N(1)	117.5(28)		
Cl(3)—Hg(2)—Cl(1)	105.5(3)	Cl(2)—Hg(2)—Cl(1)	109.0(4)
Cl(4)—Hg(2)—Cl(1)	109.2(4)	Cl(3)—Hg(2)—Cl(2)	116.6(4)
Cl(4)—Hg(2)—Cl(3)	116.9(4)	Cl(4)—Hg(2)—Cl(2)	99.5(3)

1.48(3) and 1.41(4) to 1.55(4) Å, respectively, are close to the values found in the cobalt complexes of the same ligand. In the *meso* cobalt complex[5] the average distances are 1.498(2) and 1.515(2) Å, while in the *rac* isomer[6] they are 1.47(2) and 1.47(3) Å, respectively.

The geometry of the $(HgCl_4)^{2-}$ anion is a distorted tetrahedron, with Hg—Cl distances ranging from 2.447(9) to 2.518(9) Å and Cl—Hg—Cl angles between 99.5(3) and 116.9(4)°. The overall geometry of this anion is comparable to that observed in the complex $[Hg([14]aneN_4)Cl]_2(HgCl_4)$.[17]

In a survey of the CSD Cambridge Crystallographic Database,[18] on macrocyclic complexes of the type (M([18]aneX$_m$X$_n$), with M = transition metal and X = O, S, N, $m+n=6$, the coordination geometry found for the MX$_m$X$_n$ centre is mainly octahedral in *meso* and *rac* isomers.[19,20]

There are, however, some exceptions, e.g. the hexagonal bipyramidal geometry in some [M([18]aneO$_6$)X$_2$] (M = Cd, X = Cl, Br; M = Hg, X = Cl, SCN)[21] and [M([18]aneN$_2$O$_4$)I$_2$] (M = Hg, Cd)[22] complexes and the square planar geometry in the N-methylated [18]aneN$_2$S$_4$ complex of palladium.[23]

The coordination geometry obtained for the title complex is of a different type: a distorted trigonal prism, with the two bases of the prism defined by the nitrogen atoms N(1), N(2), N(3) and N(4), N(5), N(6), respectively. The different N···N intramolecular distances [2.88(2)–3.75(3) Å] between the nitrogen atoms on the triangular bases and the values of the angles made between the planes defined by the metal atom and the lateral edges of the prism, 107.1(6), 108.1(5) and 144.1(5)°, are a measure of the distortion on the trigonal prism. Additionally, a third criterion based on the angle of rotation, θ, of one triangular base relative to the other has been used to quantify this distortion.[23] It is 0° for an ideal trigonal prism and at the other extreme 30° for an ideal octahedron. In the title complex this parameter is 11.5(2)°.

Recent molecular mechanics calculations[2] performed for a trigonal prismatic configuration of M[18]aneN$_6$ complexes indicated an ideal M—N distance of 2.4 Å, with a minimized steric energy 20.8 kcal mol^{-1} lower than the *meso* and 22.4 kcal mol^{-1} lower than the *rac* octahedral configurations. These calculations are, therefore, in agreement with the observed coordination geometry now reported for the $[Hg([18]aneN_6)]^{2+}$ complex. Additionally, the molecular parameters in the metal coordination sphere obtained with this conformational analysis,

Table 3. Comparison between structural parameters obtained by X-ray diffraction and calculated by molecular mechanics[2] for the coordination sphere of the $[Hg([18]aneN_6)]^{2+}$ complex

	Observed values[a]	Calculated values[a]
Bond distances (Å)		
Hg—N	2.44(2)	2.44
Bonding angles (°)		
	72.8(7)	74.3
	128.5(7)	130.5
N—Hg—N	99.5(8)	96.9
	152.1(7)	146.3

[a] Mean values.

listed in Table 3, show a reasonable agreement with those found in the X-ray determination.

It is noteworthy that the geometry adopted by the $[(Hg[18]aneO_6)Cl_2]$[21b] complex is hexagonal bipyramidal, which also agrees with theoretical calculations. In fact the best hole size for this geometry (ideal M—O = 2.85 Å)[24] is very close to the Hg—O bond distance observed in the X-ray analysis, 2.825(4) Å. Therefore, the coordination geometries preferred for the two $[Hg([18]aneX_6)]$, X = N, O, complexes seem to result mainly from the ligand preferences, in particular the fit of the metal ion into the cavity of the macrocycle.

EXPERIMENTAL

Materials and synthesis

All chemical reagents were analytical grade and used as supplied.

1,4,7,10,13,16-*Hexaazacyclooctadecane hexahydrochloride*. A suspension of commercial 1,4,7,10,13,16-hexaazacyclooctadecane trisulphate salt, purchased from Aldrich (2.763 g, 5 mmol), in water (100 cm^3) was treated with an equivalent amount of $BaCO_3$. After the resulting slurry was kept at 80°C with stirring for 2 h, the filtered solution was concentrated with a rotary evaporator. The addition of a large excess of hydrochloric acid and concentration of the resulting solution gave a white solid. Recrystallization from 6 M hydrochloric acid/methanol and vacuum drying gave 1.884 g (79%) of white crystals; m.p. 309–311°C (dec). ^1H NMR (D_2O) δ: 3.59 (s). ^{13}C NMR (D_2O) δ: 44.39. IR ν(KBr, cm^{-1}): 3360–3540 (N—H); 2600–2750 (N—H). Found: C, 30.3; H, 7.6; N, 17.4. Calc. for $C_{12}N_6H_{36}Cl_6$: C, 30.2; H, 7.5; N, 17.6%.

$[Hg(18\text{-azacrown-}6)](HgCl_4)$ *complex*. To a solution of 18-azacrown-6·6HCl (111 mg, 0.25 mmol) in water (20 cm^3) was added a solution of $HgCl_2$ in a slight excess (80 mg, 0.29 mmol) in water (20 cm^3). After adjustment of pH at 6 with 1 M sodium hydroxide solution, this reaction mixture was kept at 60°C with stirring for 2 h. This solution was then concentrated until about one fifth of the initial volume and left in the cool for several days. Slow evaporation gave colourless crystals that were air-dried. ^1H NMR (D_2O) δ: 2.62 (m). ^{13}C NMR (D_2O) δ: 43.22 (s). Found: C, 16.0; H, 4.3; N, 9.3. Calc. for $[(HgC_{12}N_6H_{30})(HgCl_4)]\cdot 2H_2O$: C, 16.5; H, 4.4; N, 9.6%.

Measurements

Melting points were taken on a Buchi 530 apparatus. IR spectra were measured as KBr pellets using a Perkin–Elmer 683 spectrometer over the range 200–400 cm^{-1}. ^1H NMR and ^{13}C NMR spectra were measured on a Varian–Unity 300 spectrophotometer. Elemental analyses were obtained using a Perkin–Elmer 240B elemental analyser.

The electrochemical measurements were performed with a Princeton Applied Research PAR 173 potentiostat coupled with the universal programmer PAR 175. Cyclic voltammetry was conducted at a hanging mercury-drop working electrode (H.M.E.) with a platinum auxiliary electrode and a saturated calomel electrode (S.C.E.) as references. All potentials were referred to the saturated calomel electrode. The supporting electrolyte was KNO_3 (0.1 M). All solutions were thermostated at 25±1°C and degassed with nitrogen.

X-ray analysis

Crystal data. $[Hg([18]aneN_6)](HgCl_4)$, $C_{12}H_{30}Cl_4Hg_2N_6$, $M = 801.4$, orthorhombic system, space group *Pbca* (No. 61), $a = 14.20(1)$, $b = 14.37(2)$, $c = 21.323(9)$ Å, $V = 4.352(6)$ $Å^3$, $Z = 8$, $D_c = 2.45$ g cm^{-3}, $F(000) = 2976$, λ(Mo-K_α) = 0.71069 Å, mosaic spread = 0.61(4)°, μ(Mo-K_α) = 145.98 cm^{-1}.

Data was collected "on line" at 273 K on an Enraf–Nonius FAST diffractometer equipped with a molybdenum rotating anode using SADNESS, a modified version of MADNESS,[25] for small molecule data collection. The detector was kept at a distance of 40 mm from the crystal and at a θ angle of 25°.

Unit cell parameters and orientation matrix were

obtained by auto-indexing 50 intense reflections collected by the ω-scan mode in two narrow ($\approx 5°$), almost orthogonal zones in reciprocal space. Both the cell parameters and orientation matrix were refined every 10° of measured data.

PROCOR[26] was used in the data reduction of the measured intensities applying the Kabsch method of profile fitting. Data was corrected from polarization and Lorentz effects and then it was merged using SHELX76,[27] with $R_{merge} = 0.074$.

Structure analysis and refinement

The positions of the heavy atoms were obtained from a three-dimensional Patterson map, while the positions for the remaining non-hydrogen atoms were obtained from successive difference-Fourier syntheses.

The isotropic refinement (without hydrogen atoms) converged to $R = 0.1103$. At this point an absorption correction was applied using a version of DIFABS,[28] modified for the FAST geometry. The maximum and minimum correction factors applied were 1.030 and 0.440, respectively, and the R factor then lowered to 0.1022.

The anisotropic refinement of the mercury and chlorine atoms lowered the final R value that converged to 0.0739.

No weighting scheme was used in the final refinement of 127 parameters with 5953 unique reflections with $|F_o| > 3\sigma|F_o|$.

The final electron density in the difference Fourier map was -1.08 and 3.36 e $Å^{-3}$, situated near the mercury atom of the cation.

A drawing was made with the ORTEP-II program.[29] Atomic scattering factors were taken from the international tables.[30]

Tables listing fractional atomic coordinates and anisotropic displacement parameters and tables of observed and calculated structure factors have been deposited as supplementary material.

Acknowledgements—The authors thank Prof. J. J. Fraústo da Silva for fruitful discussions and the Junta Nacional de Investigação Científica e Tecnológica for financial support to V. Félix.

REFERENCES

1. R. M. Izaat, K. Pawlak and J. S. Bradshaw, *Chem. Rev.* 1991, **91**, 1721.
2. M. G. B. Drew and M. A. Santos, *Struct. Chem.* 1993, **4**, 5.
3. M. Kodama, E. Kimura and S. Yamagushi, *J. Chem. Soc., Dalton Trans.* 1980, 2537.
4. M. A. Santos and M. G. B. Drew, *J. Chem. Soc., Faraday Trans.* 1991, **87**, 1321.
5. Y. Yoshikawa, K. Toriumi, T. Ito and H. Yamatera, *Bull. Chem. Soc. Japan* 1982, **55**, 1422.
6. D. J. Royer, G. J. Grant, D. G. Van der Derveer and M. J. Castillo, *Inorg. Chem.* 1982, **21**, 1902.
7. R. D. Hancock and A. E. Martell, *Chem. Rev.* 1989, **89**, 1875.
8. M. A. Santos and M. G. B. Drew, I Italian–Portuguese–Spanish Meeting in Inorganic Chemistry. Valencia, Spain (1990).
9. David M. Adams, *Metal–Ligand and Related Vibrations*. Spottiswood, London (1967).
10. R. S. Nicholson and I. Shain, *Analyt. Chem.* 1964, **36**, 706.
11. A. J. Bard and L. R. Faulkner, in *Electrochemical Methods*. John Wiley & Sons, Inc., New York (1980).
12. E. Kimura, A. Sakonara, T. Yatsunami and M. Kodama, *J. Am. Chem. Soc.* 1981, **103**, 3041.
13. A. J. Blake, G. Reid and M. Schroder, *Polyhedron* 1990, **9**, 2931.
14. G. S. Patterson and R. H. Holm, *Bioinorg. Chem.* 1975, **4**, 257.
15. R. Akesson, M. Sandstrom, C. Stalhandske and I. Person, *Acta Chem. Scand.* 1991, **45**, 1165.
16. G. B. Deacon, C. L. Raston, D. Tunaley and A. H. White, *Aust. J. Chem.* 1979, **32**, 2195.
17. N. W. Alcock, E. H. Curson, N. Herron and P. Moore, *J. Chem. Soc., Dalton Trans.* 1979, 1987.
18. Cambridge Crystallographic Database, July 1992 update.
19. (a) A. J. Blake, G. Reid and M. Schröder, *Polyhedron* 1990, **9**, 2925; (b) N. Atkinson, A. J. Blake, M. G. B. Drew, G. Forsyth, A. J. Lavery, G. Reid and M. Schröder, *J. Chem. Soc., Chem. Commun.* 1989, 984; (c) A. J. Blake, G. Reid and M. Schröder, *J. Chem. Soc., Dalton Trans.* 1990, 3363; (e) A. J. Blake, T. H. Hyde and M. Schröder, *J. Chem. Soc., Chem. Commun.* 1988, 1397; (f) A. S. Craig, R. Kataky, D. Parker, H. Adams, N. Bailey and H. Schneider, *J. Chem. Soc., Chem. Commun.* 1989, 870; (g) A. S. Craig, R. Kataky, R. C. Matthews, D. Parker, G. Ferguson, A. Lough, H. Adams, N. Bailey and H. Schneider, *J. Chem. Soc., Perkin Trans. 2* 1990, 1523; (h) N. Atkinson, A. J. Lavery, A. J. Blake, G. Reid and M. Schröder, *Polyhedron* 1990, **9**, 2641.
20. (a) J. R. Hartman, E. J. Hintsa and S. R. Cooper, *J. Am. Chem. Soc.* 1986, **108**, 1208; (b) S. R. Cooper, S. C. Rawle, J. R. Hartman, E. J. Hintsa and G. Admans, *Inorg. Chem.* 1988, **27**, 1209; (c) J. R. Hartman and S. R. Cooper, *J. Am. Chem. Soc.* 1986, **108**, 1202; (d) M. N. Bell, A. J. Blake, A. J. Holder, T. H. Hyde and M. Schröder, *J. Chem. Soc., Dalton Trans.* 1990, 3841; (e) A. J. Blake, R. O. Gould, A. J. Holder, T. H. Hyde and M. Schröder, *Polyhedron* 1989, **8**, 513; (f) A. J. Blake, R. O. Gould, A. J. Lavery and M. Schröder, *Angew. Chem., Int. Edn Engl.* 1986, **25**, 274.
21. (a) M. G. Drew, K. C. Lee and K. F. Mok, *Inorg. Chim. Acta* 1989, **155**, 39; (b) C. R. Paige and M. F. Richardson, *Can. J. Chem.* 1983, **62**, 332; (c) A.

Hazell, *Acta Cryst.* 1988, **C44**, 88; L. Malmsten, *Acta Cryst.* 1979, **B35**, 1702.
22. N. W. Alcock, M. Ravindran and G. R. Wiley, *J. Chem. Soc., Chem. Commun.* 1989, 1063.
23. (a) A. J. Blake, G. Reid and M. Schröder, *J. Chem. Soc., Dalton Trans.* 1990, 3363; (b) A. J. Blake, T. H. Hyde and M. Schröder, *J. Chem. Soc., Chem. Commun.* 1988, 1397.
24. M. G. B. Drew, S. Hollis and P. C. Yates, *J. Chem. Soc., Dalton Trans.* 1985, 1820.
25. J. W. Pflugraph and A. Messerchmidt, *Crystallography in Molecular Biology*, Meeting, Abstracts. Bischenberg, France (1985); A. Messerschmidt and J. W. Pflugraph, *J. Appl. Cryst.* 1987, **20**, 306.
26. W. Kabsch, *J. Appl. Cryst.* 1988, **21**, 916.
27. G. M. Sheldrick, SHELX76, Crystallographic Calculation Program. University of Cambridge (1979).
28. N. Walker and D. Stuart, "DIFABS", An Empirical Method for Correcting Diffractometer Data for Absorption Effects, *Acta Cryst., Sect. A.* 1983, **39**, 158.
29. C. K. Johnson, "ORTEP-II", Report ORNL-5138. Oak Ridge National Laboratory, Tennessee (1976).
30. *International Tables for X-Ray Crystallography*, Vol. IV. Kynoch Press, Birmingham (1974).

Polyhedron Vol. 12, No. 8, pp. 939–944, 1993
Printed in Great Britain

0277–5387/93 $6.00+.00
© 1993 Pergamon Press Ltd

X-RAY CRYSTAL STRUCTURE OF THE 1:1 COMPLEX BETWEEN LANTHANUM NITRATE AND N,N,N′,N′-TETRAPHENYL-3,6-DIOXAOCTANEDIOIC DIAMIDE

YING ZHU*

Instrumental Analysis and Research Centre, Lanzhou University, Lanzhou 730000, P.R.C.

and

WEI SHENG LIU, MINYU TAN **and** TIANQUAN JIAO

Department of Chemistry, Lanzhou University, Lanzhou 730000, P.R.C.

and

GANZU TAN

Lanzhou Institute of Chemical Physics, Chinese Academy of Sciences, Lanzhou 730000, P.R.C.

(*Received* 9 *April* 1992; *accepted* 25 *November* 1992)

Abstract—The crystalline compound $[La(C_{30}H_{28}N_2O_4)_2(H_2O)_2][La(NO_3)_6]\cdot 2H_2O\cdot 2CH_3CN$ has been structurally characterized by X-ray crystallography. The compound contains a complex cation, $[La(C_{30}H_{28}N_2O_4)_2(H_2O)_2]^{3+}$, with a 10-coordinate lanthanum ion and a hexanitrato anion, $[La(NO_3)_6]^{3-}$, with a 12-coordinate lanthanum(III) ion. The coordination polyhedra of lanthanum in the cation and anion are distorted bicapped dodecahedron and eicosahedron, respectively. The La—O bond lengths in the cation lie in the range 2.503(3)–2.771(3) Å and the ether oxygens have weaker bonding than the amide oxygens; La—O distances in the anion range between 2.618(4) and 2.749(4) Å. There are also two lattice water molecules and two acetonitrile solvent molecules in the asymmetric unit cell, which form hydrogen bonds with the complex cations and anions.

Although macrocyclic and non-cyclic polyethers, especially those containing CH_2CH_2O units, can react with rare earths to form stable solid complexes, the ligands which are composed of CH_2CH_2O and amide oxygens are superior. Previous research work has mainly focused on the polyethylene glycols,[1–7] while rare earth complexes with derivatives of glycol-O,O′-diacetoamide have been little reported. We report here the synthesis of the lanthanum complex with the ligand N,N,N′,N′-tetraphenyl-3,6-dioxaoctanedioic diamide and an investigation of the crystal structure of this new lanthanum complex. As previously reported, rare earth salts react with crown ethers in organic solvents to yield stable complexes with different metal/ligand ratios, both 1:1 and 4:3 complexes form with lanthanide nitrates. The present complex is an example of a 1:1 complex with lanthanide nitrate.

EXPERIMENTAL

Preparation

A solution of lanthanum nitrate (0.5 mmol) in anhydrous ethanol (20 cm^3) was added dropwise to a solution of N,N,N′,N′-tetraphenyl-3,6-dioxaoctanedioic diamide[8] (0.5 mmol) in chloroform (15 cm^3). The mixture was stirred at room temperature for 24 h and the solution was then partially evaporated. The precipitated solid complex was filtered, washed with anhydrous ethanol and ether and dried

* Author to whom correspondence should be addressed.

in a desiccator (0.1 mm Hg) over P_4O_{10}. The single crystals for the X-ray study were prepared by dissolving the solid complex in acetonitrile and by allowing the resulting solution to stand for 4 weeks.

Crystal structure determination

Crystal data. $[C_{30}H_{32}N_2O_6La][N_6O_{18}La]\cdot 2[H_2O]\cdot 2[C_2H_3N]$, $Mr = 1765.15$, monoclinic, $a = 16.463(2)$, $b = 23.231(4)$, $c = 19.914(2)$ Å, $\beta = 96.58(1)°$, $V = 7566$ Å^3, space group $P2_1/n$, $Z = 4$, $D_c = 1.55$ g cm^{-3}, μ(Mo-K_α) = 12.04 cm^{-1}. A crystal of the dimensions $0.5 \times 0.5 \times 0.8$ mm^3 was sealed with some mother liquor in a capillary tube and mounted on an Enraf–Nonius CAD4 diffractometer. The unit-cell parameters were determined by least-squares calculations based on the angular setting of 25 automatically centred reflections with 2θ between 24° and 34°. Intensities were measured in the ω–2θ scan mode (scan width: $0.6+0.35\tan\theta$) with graphite-monochromated Mo-K_α radiation, θ range $1 \leqslant \theta \leqslant 24°$ ($h = -18$ to 18; $k = 0$–26; $l = 0$–22). 13,957 reflections were collected, 13,109 independent reflections ($R_{int} = 0.017$), of which 11,004 were considered observed [$I > 3\sigma(I)$]. Lorentz and polarization, but no absorption, corrections were made.

Two lanthanum atoms were located from a Patterson synthesis and the remaining non-hydrogen atoms from Fourier syntheses. 108 Non-hydrogen atoms were refined anisotropically by full-matrix least-squares. The function minimized was $\Sigma w(|F_o|-|F_c|)^2$, where w = 1. All hydrogen atoms were located from a difference synthesis and were included in the structure–factor calculation, but not refined. The final R factor was 0.040 ($R_w = 0.042$), $(\Delta/\sigma)_{max} = 0.37$ and the final difference synthesis-Fourier map showed peaks less than 0.631 e Å^{-3}.

Atomic scattering factors were taken from ref. 9. All calculations were performed on an PDP 11/44 computer using the SDP package.[10]

RESULTS AND DISCUSSION

As shown in Figs 1 and 2 the crystal structure of this lanthanum complex is composed of a complex cation, $[La(A)(C_{30}H_{28}N_2O_4)_2(H_2O_2)_2]^{3+}$, and a hexanitrato anion, $[La(B)(NO_3)_6]^{3-}$, and the two different moieties are found in the ratio 1 : 1. Lattice water molecules and two acetonitrile solvent molecules are also found in the asymmetric unit. Selected bond distances and angles for $[La(C_{30}O_{28}N_2O_4)(H_2O)_2]^{3+}$ and $[La(NO_3)_6]^{3-}$ are listed in Tables 1 and 2, respectively.

The lanthanum ion is 10-coordinate being

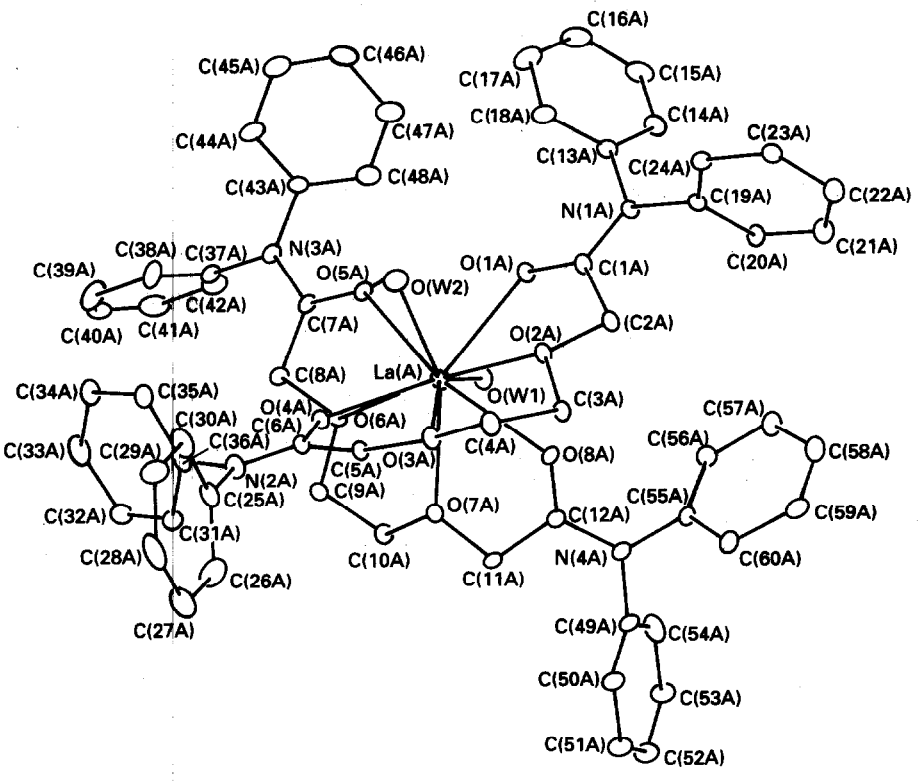

Fig. 1. View of the $[La(C_{30}H_{28}N_2O_4)_2(H_2O)_2]^{3+}$ cation.

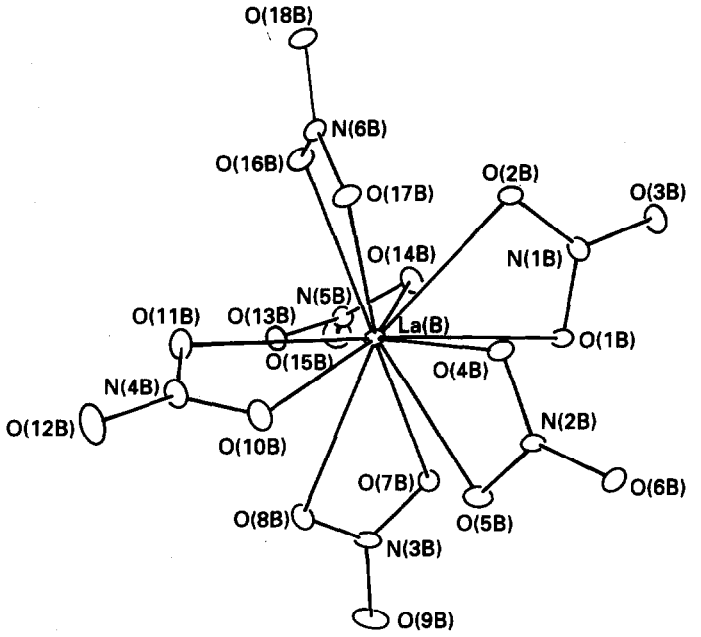

Fig. 2. View of the $[La(NO_3)_6]^{3-}$ anion.

bonded to oxygen atoms of two water molecules and to the eight oxygen atoms of two ligands in the cation. The coordination polyhedron is a bicapped dodecahedron (BCDod) with D_2 symmetry.[12-14] The framework diagram illustrating the coordination polyhedron in the lanthanum(A) complex cation described here is given in Fig. 3. For the D_2 polyhedron atoms O(W1), O(8A), O(5A) and O(3A) would define the first trapezoidal plane, then O(W2), O(4A), O(1A) and O(7A) the second. The two planes are no longer perpendicular; the dihedral angle listed in Table 5 is 74.86°. Atoms O(W1), O(8A), O(W2) and O(4A) are (A) type atoms and O(1A), O(7A), O(5A) and O(3A) are (B) type. The two capping atoms, O(2A) and O(6A), occupy ligand sites (C) and O(2A)—La(A)—O(6A) is 172.34(9)°. The angular parameters θ_A and θ_B are 36.2(2) and 67.5(1)°, respectively, which are similar to those structure parameters in the compounds with BCDod reported in the literature.[12,13] There are seven types of edges in BCDod and the values of these edges in the polyhedron of the complex cation are listed in Table 3. The La(A)—O(water) bond lengths are 2.522(3) and 2.541(3) Å. The La(A)—O(L) distances are of two types: as expected, the four La(A)—O(ether) distances [mean 2.729(3) Å] are significantly longer than the four La(A)—O(amide) distances [mean 2.546(3) Å]. The

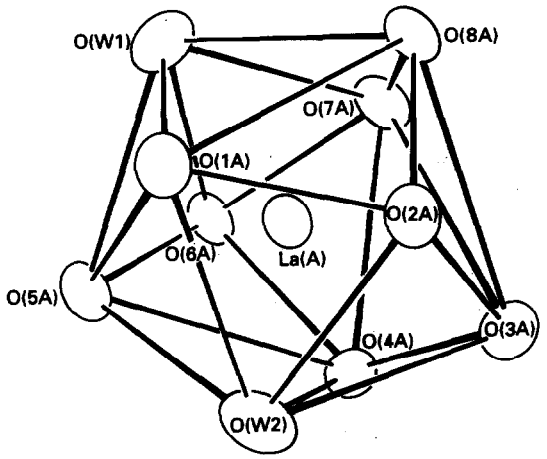

Fig. 3. Coordination polyhedron of lanthanum(A) in $[La(C_{30}H_{28}N_2O_4)_2(H_2O)_2]^{3+}$.

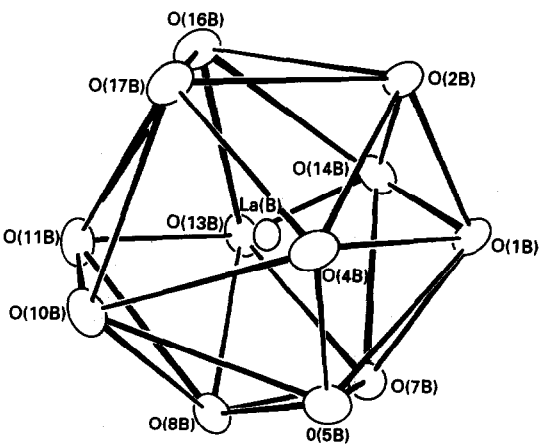

Fig. 4. Coordination polyhedron of lanthanum(B) in $[La(NO_3)_6]^{3-}$.

Table 1. Selected bond distances (Å) and angles (°) for $[La(C_{30}H_{28}N_2O_4)_2(H_2O)_2]^{3+}$ with e.s.d.s in parentheses

Coordination			
La(A)—O(1A)	2.581(3)	La(A)—O(2A)	2.697(3)
La(A)—O(4A)	2.503(3)	La(A)—O(3A)	2.771(3)
La(A)—O(5A)	2.571(3)	La(A)—O(6A)	2.722(3)
La(A)—O(8A)	2.529(3)	La(A)—O(7A)	2.724(3)
La(A)—O(W1)	2.522(3)	La(A)—O(W2)	2.541(3)
O(W1)—La(A)—O(1A)	72.8(1)	O(8A)—La(A)—O(7A)	58.26(9)
O(W1)—La(A)—O(5A)	73.4(2)	O(8A)—La(A)—O(3A)	80.79(9)
O(W1)—La(A)—O(7A)	71.8(1)	O(8A)—La(A)—O(1A)	86.0(1)
O(W1)—La(A)—O(6A)	68.4(1)	O(8A)—La(A)—O(2A)	63.16(9)
O(W2)—La(A)—O(1A)	73.0(1)	O(4A)—La(A)—O(7A)	79.25(9)
O(W2)—La(A)—O(3A)	70.54(9)	O(4A)—La(A)—O(3A)	58.38(9)
O(W2)—La(A)—O(5A)	73.0(1)	O(4A)—La(A)—O(5A)	85.2(1)
O(W2)—La(A)—O(2A)	69.30(9)	O(4A)—La(A)—O(6A)	63.7(1)
O(1A)—La(A)—O(5A)	79.14(9)	O(7A)—La(A)—O(3A)	86.98(8)
O(1A)—La(A)—O(2A)	58.59(9)	O(7A)—La(A)—O(6A)	57.90(8)
O(5A)—La(A)—O(6A)	58.06(9)	O(3A)—La(A)—O(2A)	58.06(8)
O(W1)—La(A)—O(8A)	72.0(1)[a]	O(1A)—La(A)—O(7A)	135.7(1)[a]
O(W2)—La(A)—O(4A)	72.7(2)[a]	O(2A)—La(A)—O(6A)	172.34(9)[a]
O(3A)—La(A)—O(5A)	134.27(9)[a]		
Organic ligand			
O(1A)—C(1A)	1.236(5)	N(1A)—C(1A)	1.344(6)
O(4A)—C(6A)	1.237(5)	N(2A)—C(6A)	1.334(7)
O(5A)—C(7A)	1.237(6)	N(3A)—C(7A)	1.353(6)
O(8A)—C(12A)	1.234(6)	N(4A)—C(12A)	1.341(6)
O(2A)—C(2A)	1.432(6)	N(1A)—C(13A)	1.437(6)
O(2A)—C(3A)	1.445(5)	N(1A)—C(19A)	1.455(6)
O(3A)—C(4A)	1.446(6)	N(2A)—C(25A)	1.457(6)
O(3A)—C(5A)	1.428(6)	N(2A)—C(36A)	1.446(6)
O(6A)—C(8A)	1.430(6)	N(3A)—C(37A)	1.453(7)
O(6A)—C(9A)	1.425(7)	N(3A)—C(43A)	1.443(6)
O(7A)—C(10A)	1.445(6)	N(4A)—C(49A)	1.451(6)
O(7A)—C(11A)	1.424(6)	N(4A)—C(55A)	1.450(6)

[a] These angles correspond to the trapezoidal plane angles $2\theta_A$ and $2\theta_B$ of dodecahedral geometry.[11]

Table 2. Selected bond distances (Å) and angles (°) for $[La(NO_3)_6]^{3-}$ with e.s.d.s in parentheses

La(B)—O(1B)	2.652(5)	La(B)—O(10B)	2.626(4)
La(B)—O(2B)	2.687(5)	La(B)—O(11B)	2.625(4)
La(B)—O(4B)	2.627(4)	La(B)—O(13B)	2.645(5)
La(B)—O(5B)	2.691(4)	La(B)—O(14B)	2.749(4)
La(B)—O(7B)	2.693(4)	La(B)—O(16B)	2.630(4)
La(B)—O(8B)	2.678(4)	La(B)—O(17B)	2.618(4)
O(1B)—La(B)—O(11B)	171.3(1)	O(2B)—La(B)—O(8B)	155.4(1)
O(4B)—La(B)—O(13B)	173.3(1)	O(5B)—La(B)—O(16B)	155.6(1)
O(7B)—La(B)—O(17B)	170.4(1)	O(10B)—La(B)—O(14B)	154.8(1)

Table 3. Non-bonded contact distances of the coordination polyhedron in $[La(C_{30}H_{28}N_2O_4)_2(H_2O)_2]^{3+}$

a	O(W1)—O(8A)	2.967(4)	O(W2)—O(4A)	2.990(4)
m	O(W1)—O(5A)	3.042(4)	O(8A)—O(3A)	3.439(4)
m	O(W2)—O(1A)	3.043(5)	O(4A)—O(7A)	3.338(4)
g	O(W1)—O(1A)	3.027(4)	O(8A)—O(7A)	2.563(5)
g	O(W2)—O(5A)	3.037(4)	O(4A)—O(3A)	2.582(4)
g′	O(W1)—O(7A)	3.079(4)	O(1A)—O(8A)	3.484(4)
g′	O(W2)—O(3A)	3.073(5)	O(4A)—O(5A)	3.434(4)
b	O(5A)—O(1A)	3.281(5)	O(3A)—O(7A)	3.781(4)
b′	O(5A)—O(6A)	2.571(4)	O(3A)—O(2A)	2.654(4)
b′	O(1A)—O(2A)	2.585(4)	O(7A)—O(6A)	2.637(4)
c	O(W1)—O(6A)	2.952(4)	O(8A)—O(2A)	2.740(4)
c	O(W2)—O(2A)	2.981(4)	O(4A)—O(6A)	2.760(4)

The intramolecular distances are classified according to the polyhedron edges of D_2 10-coordinate geometry.[12]

Table 4. Selected mean planes

Plane	Defining atoms	Max. deviation from plane (Å)	Plane	Defining atoms	Max. deviation from plane (Å)
1	O(W1), O(8A), O(5A), O(3A)	0.142	9	C(13A)–C(18A)(Ph)	0.010
2	O(W2), O(4A), O(1A), O(7A)	0.160	10	C(19A)–C(24A)(Ph)	0.005
3	O(1A), O(2A), O(3A), O(4A)	0.010	11	C(25A)–C(30A)(Ph)	0.009
4	O(5A), O(6A), O(7A), O(8A)	0.069	12	C(31A)–C(36A)(Ph)	0.002
5	O(1A), C(1A), C(2A), N(1A)	0.009	13	C(37A)–C(42A)(Ph)	0.015
6	O(4A), C(5A), C(6A), N(2A)	0.001	14	C(43A)–C(48A)(Ph)	0.010
7	O(5A), C(7A), C(8A), N(3A)	0.005	15	C(49A)–C(54A)(Ph)	0.007
8	O(8A), C(11A), C(12A), N(4A)	0.001	16	C(55A)–C(60A)(Ph)	0.002

Interplanar angles (°)

1–2	74.86	6–11	87.50	8–15	103.63	13–14	83.01
3–4	50.22	6–12	87.24	8–16	63.76	15–16	77.56
5–9	52.57	7–13	100.32	9–10	102.28		
5–10	86.01	7–14	46.96	11–12	66.64		

Table 5. Distances (Å) and angles (°) associated with hydrogen bonds

O—H···O	O—H	H···O	O···O	O—H···O
O(W1)—H(OW1)···O(W4)	0.829	1.965	2.766[a]	162.2
O(W1)—H(OW1′)···O(1B)	0.963	2.179	2.889[a]	129.5
O(W1)—H(OW1′)···O(3B)	0.963	2.295	3.232[a]	164.4
O(W2)—H(OW2)···O(13B)	6.844	2.258	2.951[b]	139.4
O(W2)—H(OW2)···O(15B)	0.844	2.362	3.173[b]	161.2
O(W2)—H(OW2′)···O(W3)	0.983	1.947	2.772[b]	139.9
O(W3)—H(OW3)···N(2)	1.228	1.945	3.154[c]	167.1
O(W4)—H(OW4′)···O(5B)	1.057	2.127	3.021[c]	140.9

Symmetry codes:

[a] $1-x, 1-y, 1-z$.

[b] $\frac{1}{2}+x, 1\frac{1}{2}-y, \frac{1}{2}+z$.

[c] x, y, z.

former are close to the value in another open-chain crown ether complex of lanthanum, $[La(NO_3)_3(C_8H_{18}O_5)]$, La—O(ether) 2.70 Å, where La—O (alcohol) = 2.58 Å.[7] According to expectations the latter are longer than the distances of La—O (ketonic), 2.473 Å.[15] The data of bond distances in two types of oxygens show that amide oxygens are more strongly bonded than ether oxygens.

The N,N,N′,N′-tetraphenyl-3,6-dioxaoctanedioic diamide ligand coordinated to lanthanum is a type of open-chain crown ether. The co-planarity of O(1A), O(2A), O(3A) and O(4A) atoms in one ligand is better than that of O(5A), O(6A), O(7A) and O(8A) atoms in the other ligand (see Table 4). The N—C bond distances [mean 1.343(6) Å] connected with the ketone group are shorter than that [mean 1.449(6) Å] connected to the phenyl rings. The phenyl rings and planes containing nitrogen atoms have dihedral angles which are listed in Table 4.

The lanthanum(B) ion is 12-coordinate surrounded by six bidentate nitrate ions (Fig. 2). The geometry of the hexanitratolanthanate ion is a distorted eicosahedron and is similar to that previously found.[7,14,16] The coordination polyhedron of lanthanum (B) is shown in Fig. 4.

As shown in Table 5 four water molecules form hydrogen bonds with the oxygen atoms in the hexanitrato lanthanum ion and the nitrogen atom in one acetonitrile solvent molecule, just as the complex cation and the anion are interconnected with lattice water and solvent molecules by hydrogen bonds.

Additional crystallographic data, bond lengths and angles are available from the Editor on request. Atomic coordinates have also been deposited with the Cambridge Crystallographic Data Centre.

Acknowledgement—This work was supported by the National Natural Science Foundation of China.

REFERENCES

1. Y. Hirashima, K. Kanetsaki, J. Shiokawa and N. Tanaka, *Bull. Chem. Soc. Japan* 1981, **54**, 1567.
2. H. Sieger and F. Voegtle, *Tetrahedron Lett.* 1978, 2709.
3. U. Casellato, G. Tomat, P. Di Bernardo and R. Grziani, *Inorg. Chim. Acta* 1982, **61**, 181.
4. Y. Hirashima, K. Kanetsaki, I. Yonezu, K. Kamakura and J. Shiokawa, *Bull. Chem. Soc. Japan* 1983, **56**, 738.
5. Y. Hirashima, K. Ito and J. Shiokawa, *Chem. Lett.* 1983, 9.
6. Y. Hirashima and J. Shiokawa, *Chem. Lett.* 1979, 463.
7. J.-C. Buenzli, J.-M. Prefferle, B. Ammann, G. Chapuis and F.-J. Zuniga, *Helv. Chim. Acta* 1984, **67**, 1121.
8. G. Z. Tan, G. Z. Xu, Z. Q. Yao and F. S. Zhang, *HUAXUE, SHI JI* 1983, **5**, 100.
9. *International Tables for X-ray Crystallography*, Vol. IV. Kynoch Press, Birmingham (1974).
10. Enraf–Nonius Structure Determination Package. Enraf–Nonius, Delft, The Netherlands (1981).
11. J. L. Hoard and J. V. Silveton, *Inorg. Chem.* 1963, **22**, 235.
12. A. R. Al-Karghouli and J. S. Wood, *Inorg. Chem.* 1972, **11**, 229.
13. M. G. B. Drew, *Coord. Chem. Rev.* 1977, **24**, 179.
14. A. Zalkin, J. D. Forrester and D. H. Templeton, *J. Chem. Phys.* 1963, **39**, 2881.
15. T. Phillips, D. E. Sands and W. F. Wanger, *Inorg. Chem.* 1968, **7**, 2295.
16. F. A. Hart, M. B. Hursthouse, K. M. A. Malik and S. Moorhouse, *J. Chem. Soc., Chem. Commun.* 1978, 549.

Polyhedron Vol. 12, No. 8, pp. 945–948, 1993
Printed in Great Britain

0277–5387/93 $6.00+.00
© 1993 Pergamon Press Ltd

SYNTHESIS AND CHARACTERIZATION OF LIGHT LANTHANIDE PIPERIDINOCARBODITHIOATE COMPLEXES

ZHU HAILIANG, TANG NING,† GAN XINMIN, ZHANG WEIGUANG, TAN MINYU and WANG AILI

Department of Chemistry, Lanzhou University, Lanzhou 730000, China

(*Received* 10 *September* 1992; *accepted* 20 *November* 1992)

Abstract—The light lanthanide piperidinocarbodithioate complexes with the general formula $(PipH_2)[Ln(PipCS_2)_4]$ (Pip = piperidino, Ln = La, Pr, Nd, Sm, Eu and Gd) have been prepared using anhydrous lanthanide chloride and piperidinium piperidinocarbodithioate as reactants. They have been characterized by chemical analyses, IR spectra, electronic spectra, conductivity measurement and TG–DTA techniques. In all the complexes the carbodithioate ligands show bidentate behaviour.

In recent years complexes of transition metal elements with dithiocarbamates have not only been studied thoroughly, but also have been widely used in the rubber industry, inorganic analyses and agriculture.[1] However, much less has been reported on similar complexes of the lanthanides. As an extension of our previous research studies on the complexes of lanthanides with sulphur containing ligands,[2,3] we have recently synthesized the solid complexes of light lanthanides with piperidinocarbodithioate and investigated the composition and properties of these new complexes.

EXPERIMENTAL

Preparation of anhydrous lanthanide chlorides

Anhydrous lanthanide chlorides were prepared by the literature[4] method with sulphinyl chloride as the dehydrating agent.

Preparation of the ligand

Piperidinium piperidinocarbodithioate ($[\overline{CH_2CH_2CH_2CH_2CH_2}\overline{NH_2}]\cdot[\overline{CH_2CH_2CH_2CH_2CH_2}\overline{NCS_2}]$) was obtained according to the literature[5] by the reaction of piperidine and carbon disulphide (molar ratio 2 : 1) in petroleum ether medium. The product was purified by sublimation and then verified by elemental analysis, IR and ^1H NMR spectroscopy.

Preparation of the complexes

Piperidinium piperidinocarbodithioate (0.4 mmol) was dissolved in absolute ethanol (10 cm^3). To this solution was slowly added a solution (10 cm^3) of anhydrous lanthanide chloride (0.1 mmol) in absolute ethanol. The complex precipitated slowly. Prior to isolating the complex by filtration, the solution was continually stirred at room temperature for 10 h. The product was washed with anhydrous ethyl ether and dried *in vacuo* with P_4O_{10} for 1 week. All the complexes obtained were solid yellow powders and unstable in moist air. The whole process of synthesis of the complexes was carried out in a glove-box filled with dry nitrogen gas.

Analyses

The metal ions were determined by EDTA titration using xylenol-orange as an indicator. Carbon, nitrogen and hydrogen were determined using a Carlo–Erba 1106 elemental analyser.

IR measurements

The IR spectra were recorded on a 170 SX FTIR spectrometer in the 4000–200 cm^{-1} region using KBr pellets.

† Author to whom correspondence should be addressed.

Table 1. Analytical data

Compound[a]	%N Found (Calc.)	%C Found (Calc.)	%H Found (Calc.)	%M Found (Calc.)
$PipH_2[La(PipCS_2)_4]$	7.7 (8.1)	40.4 (40.2)	6.1 (6.1)	15.9 (16.0)
$PipH_2[Pr(PipCS_2)_4]$	7.9 (8.1)	39.6 (40.1)	6.0 (6.0)	15.9 (16.2)
$PipH_2[Nd(PipCS_2)_4]$	8.0 (8.0)	39.6 (40.0)	5.9 (6.0)	16.1 (16.6)
$PipH_2[Sm(PipCS_2)_4]$	8.1 (8.0)	40.2 (39.7)	6.0 (6.0)	16.6 (17.1)
$PipH_2[Eu(PipCS_2)_4]$	7.8 (8.0)	40.0 (39.6)	6.0 (6.0)	16.8 (17.3)
$PipH_2[Gd(PipCS_2)_4]$	8.0 (7.9)	39.7 (39.4)	5.6 (5.9)	17.0 (17.8)

[a] Pip = piperidino ($\overline{CH_2CH_2CH_2CH_2CH_2N}$—).

Electronic spectra

The electronic spectra were recorded with a Shimadzu UV-240 spectrophotometer in the acetonitrile solution in the 190–400 nm range.

Thermal analyses

Thermal analyses (TG and DTA) were performed on a Dupont 1090 thermobalance. The heating rate was 10°C min^{-1}.

Conductivity measurements

These measurements were performed with a DDS-11A type conductivity bridge for freshly prepared solutions in acetonitrile at 25°C.

RESULTS AND DISCUSSION

The composition of the complexes

The analytical data for the newly synthesized complexes listed in Table 1 indicate that there are one piperidinium ion, one lanthanide ion and four piperidinocarbodithioate groups in each of the complex molecules.

IR spectra

The most important IR peaks of the ligand salt and of the complexes are reported in Table 2. The presence of a single strong band due to a ν(CSS) mode in the range 984–996 cm^{-1} in the spectra of the complexes is strongly indicative of the bidentate behaviour of the dithio ligand in the complexes,[6,7] otherwise a doublet is expected in the 1000 ± 70 cm^{-1} region in the case of monodentate coordination.[8,9] The analysis of the position of the ν(C···N) mode, in the range 1469–1476 cm^{-1}, gives further confirmation of the above suggested behaviour: this band, in fact, undergoes a blue shift in all the complexes, while for unidentate coordination this stretching mode would be shifted towards lower wave numbers or would remain unchanged at the value of the free carbodithioate sodium salt.[10]

In the far-IR region the bands of the ligand

Table 2. Significant IR bands (cm^{-1})

Compound	ν(CSS)	ν(C—N)	ν(M—S)	ν(N—H)
$PipH_2(PipCS_2)$	971s	1449s		3428w
$PipH_2[La(PipCS_2)_4]$	984s	1469s	332w	3373w
$PipH_2[Pr(PipCS_2)_4]$	991s	1476s	336w	3374w
$PipH_2[Nd(PipCS_2)_4]$	991s	1469s	333w	3365w
$PipH_2[Sm(PipCS_2)_4]$	991s	1469s	331w	3372w
$PipH_2[Eu(PipCS_2)_4]$	996s	1476s	332w	3372w
$PipH_2[Gd(PipCS_2)_4]$	996s	1476s	330w	3361w

Table 3. The electronic spectra (nm)

Compound	Band 1	Band 2	Band 3
$PipH_2(PipCS_2)$	220	260	295
$PipH_2[La(PipCS_2)_4]$	220	242	277
$PipH_2[Pr(PipCS_2)_4]$	220	243	273
$PipH_2[Nd(PipCS_2)_4]$	220	243	277
$PipH_2[Sm(PipCS_2)_4]$	219	240	275
$PipH_2[Eu(PipCS_2)_4]$	219	240	275
$PipH_2[Gd(PipCS_2)_4]$	218	241	274

appear unchanged in the spectra of the complexes; in addition, new bands, absent in the spectra of the starting material, are present in the 330–336 cm^{-1} range, which may be assigned as the ν(M—S) stretching frequency.[6,11]

Electronic spectra

The electronic spectra are given in Table 3. All the complexes show three absorption bands due to the chromophore group NCS_2[12] (these absorptions are indicated as Band 1, Band 2 and Band 3).

Band 1 is assigned to an intramolecular charge transfer in the ligand, i.e. a $\pi \rightarrow \pi^*$ transition located mainly in the N···C···S group.[13,14] Band 2 is attributed to the $\pi \rightarrow \pi^*$ transition of the S···C···S group.[15] This band does not undergo splitting and this fact clearly indicates the equivalence of the C···S bonds in the complexes. Band 3 is a low-intensity band assigned to an $n \rightarrow \pi^*$ transition, i.e. the transition of an electron of the lone pair on the sulphur atom to an antibonding π-orbital.[16] It can be seen from Table 3 that Bands 2 and 3, not Band 1, undergo a considerable violent shift upon complexation. This change can be attributed to the formation of M—S bonds and the deviation of the electron cloud around the sulphur atoms, the electron donors, towards the lanthanide ions, which is bound to decrease the π–π and p–π conjugate effects in the chromophore group and to increase the energy needed for the $\pi \rightarrow \pi^*$ and $n \rightarrow \pi^*$ transition, and results in the absorption bands to shift towards the short wavelength direction.

Thermal analyses

The thermal analyses studies were performed by means of TG and DTA techniques.

The processes of thermal decomposition for all the complexes were almost the same. The complexes decomposed very rapidly in the 206–213°C range. Continuous weight loss was then detected up to 850°C. At this temperature Ln_2O_3 (Pr_6O_{11} for the praseodymium complex) was formed.

Solubility and molar conductance

All the complexes are sparingly soluble in ethyl ether and cyclohexane, but are soluble in methanol, ethanol, acetone and THF and readily soluble in acetonitrile and methylene dichloride. The molar conductance values of the complexes measured in acetonitrile at 25°C lie in the range 146.7–152.8 Ω^{-1} cm^2 mol^{-1}, which indicates that all the complexes are 1 : 1 electrolytes and denotes that each of the complex molecules dissociate as one cation and one anion in the solution.[17]

From the above discussion it can be concluded that the new complexes reported in this paper are ion-association type coordination compounds. In

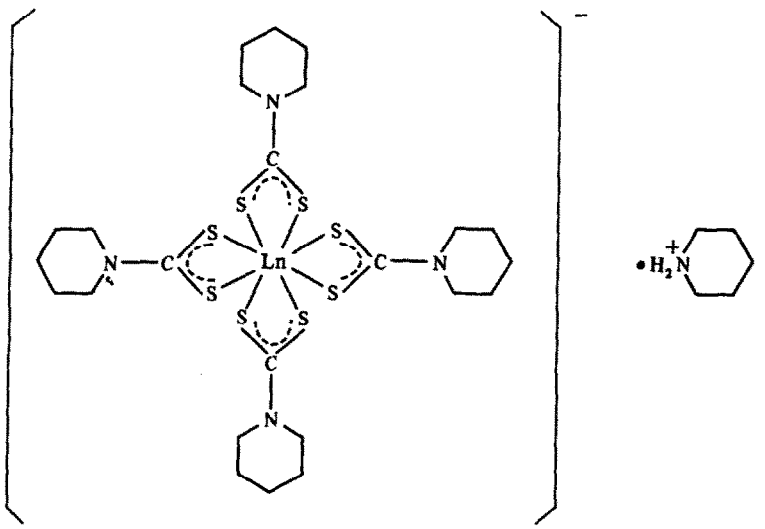

Fig. 1. Proposed structure of the complexes.

each of the complex molecules four carbodithioate groups, as uninegative bidentate ligands, are coordinated to a lanthanide ion through eight sulphur atoms to form a complex anion, and a cation, piperidinium, lies out of the coordination shell (see Fig. 1). This coordination state was also found in some other types of lanthanide carbodithioate complexes.[18–20]

REFERENCES

1. M. B. Hursthouse, M. A. Malik, M. Motevalli and P. O'Brien, *Polyhedron* 1992, **11**, 45.
2. T. Ning, G. Xinmin, Z. Hailiang and T. Minyu, *Polyhedron* 1990, **9**, 859.
3. T. Ning, Z. Hailiang, T. Minyu, G. Xinmin and W. Xin, *Acta Chim. Sin.* 1991, **49**, 42.
4. A. R. Pray, *Inorganic Synthesis*, Vol. 5, p. 153. McGraw-Hill, New York (1957).
5. G. G. R. Nair, V. R. S. Rao and A. R. V. Murthy, *Mikrochim. Acta* 1961, 741.
6. C. Preti, G. Tosi and P. Zannini, *J. Molec. Struct.* 1980, **65**, 283.
7. R. C. Aggarwal, R. Bala and R. L. Prasad, *Spectrochim. Acta* 1986, **42A**, 725.
8. F. Bonati and R. Ugo, *J. Organomet. Chem.* 1967, **10**, 257.
9. T. N. Srivastava and V. Kumar, *J. Organomet. Chem.* 1976, **107**, 55.
10. C. O'Connor, J. D. Gilbert and G. Wilkinson, *J. Chem. Soc. (A)* 1969, 84.
11. D. Perry and R. A. Geanangel, *Inorg. Chim. Acta* 1975, **13**, 185.
12. C. K. Jorgensen, *Inorganic Complexes*. Academic Press, London (1963).
13. C. K. Jorgensen, *J. Inorg. Nucl. Chem.* 1962, **24**, 1571.
14. F. Takami, S. Wakahara and T. Maeda, *Tetrahedron Lett.* 1971, 2645.
15. M. J. Janssen, *Rec. Trav. Chim.* 1960, **79**, 1066.
16. M. J. Janssen, *Rec. Trav. Chim.* 1960, **79**, 454.
17. W. J. Geary, *Coord. Chem. Rev.* 1971, **7**, 81.
18. T. Yongchi, Z. Fengyun, L. Juzheng and L. Yingqiu, *J. Struct. Chem.* 1985, **4**, 115.
19. M. Ciampolini, N. Nardi, P. Colamarino and P. Orioli, *J. Chem. Soc., Dalton Trans.* 1977, 379.
20. A. A. Pinkerton and D. Schwarzenbach, *J. Chem. Soc., Dalton Trans.* 1976, 2464.

Polyhedron Vol. 12, No. 8, pp. 949–953, 1993
Printed in Great Britain

0277–5387/93 $6.00+.00
© 1993 Pergamon Press Ltd

A TRANSITION METAL COMPLEX AS A LIGAND IN THE CHEMISTRY OF GROUP (IV) ELEMENTS

K. S. SIDDIQI,* FATHI M. A. M. AQRA, S. A. SHAH and S. A. A. ZAIDI

Division of Inorganic Chemistry, Department of Chemistry, Aligarh Muslim University, Aligarh 202 002, India

and

J. CASABO

Department de Química, Universitat Autonoma de Barcelona, Bellaterra, 08193 Barcelona, Spain

and

F. TEIXIDOR

Institut de Ciencia de Materials C.S.I.C. Barcelona, C/Marti i Franques s/n, 08028 Barcelona, Spain

(*Received* 1 *October* 1992; *accepted* 20 *November* 1992)

Abstract—Heterobimetallic complexes of the type $[Cu(TETA)Cl_2MCl_2]$ (M = Si, Ge, Sn, Ti and Zr; TETA = triethylene tetramine) have been synthesized and characterized by elemental analyses, ESR, electronic and IR spectra and conductivity measurements. The complex $[Cu(TETA)Cl_2SnPh_2]$ has also been prepared. The results indicate that $[Cu(TETA)]Cl_2$ is square planar and ionic in nature, while its bimetallic complexes, $[Cu(TETA)Cl_2MCl_2]$ and $[Cu(TETA)Cl_2SnPh_2]$, are covalent with an octahedral environment around the copper(II) ion.

The development of binuclear systems has arisen from the idea that two metal atoms in close proximity could react in a cooperative manner with substrate molecules.[1,2] A major role in the building of binuclear complexes has been played by tertiary diphosphines, bis(diphenylphosphino)methane (dppm) being particularly efficient for this purpose.[3,4] Substitution of one of the donor atoms in the dppm skeleton for a softer (As) or harder (N) centre has been introduced to create heterobinuclear complexes of the platinum group metals. Such ligand systems studied by Balch are (diphenylarsino)(diphenylphosphino)methane (dapm)[5,6] and 2-(diphenylphosphino)pyridine (Ph_2PPY),[7–15] which have led to a controlled synthesis of platinum–rhodium complexes having two bridging ligands.[16]

The growing interest in electrochemical, magnetic and spectroscopic studies on multimetallic complexes is due to their great importance in biology.[17–24] They are ubiquitous in nature as active sites in a variety of metalloenzymes and are playing a significant role in industrial catalysis. Furthermore, they provide interesting cases for the study of magnetic interaction and may also serve as models in certain cases for some metalloproteins, for which the biological function is associated with the occurrence of metals centres in pairs.

By a judicious choice of the two metals, it is possible to synthesize a large number of multimetallic compounds. Since the heterobimetallic chelates containing group (IV) elements seem to be scarce, it was considered worthwhile to synthesize a number of new heterobimetallic complexes of the type $[Cu(TETA)Cl_2MCl_2]$ (M = Si, Ge, Sn, Ti and Zr).

* Author to whom correspondence should be addressed.

EXPERIMENTAL

Triethylene tetramine (Koch Light), cupric chloride, $SiCl_4$, $GeCl_4$, $SnCl_4$, $TiCl_4$, $ZrCl_4$ (BDH) and Ph_2SnCl_2 (Fluka) were used as received. Ethanol and DMSO were distilled before use. Microanalyses of the complexes were obtained on a Carlo–Erba Analyser Model 1106. Molar conductance was measured at room temperature on a Digisun electronic conductivity bridge. The IR spectra (200–4000 cm^{-1}) were recorded on a Carl–Zeiss Specord M-80 spectrophotometer in Nujol mulls. The electronic spectra were recorded on a Shimadzu UV–vis recording spectrophotometer Model 60. The EPR spectrum was recorded on a Bruker Scientific *X*-band spectrometer (ESP-300) using a 100 kHz field modulation and quartz sample tubes and the values determined calibrated with DPPA powder, $g = 2.0036$. The estimation of chlorine was determined by the usual gravimetric method.

Synthesis of $[Cu(TETA)]Cl_2$

This complex was prepared by dissolving cupric chloride (0.01 mol, 2.42 g) in ethanol (30 cm^3) with dropwise addition of triethylene tetramine (0.01 mol, 1.46 cm^3). The dark blue product was formed after keeping the mixture overnight and was washed, recrystallized from ethanol and dried *in vacuo*.

Synthesis of $[Cu(TETA)Cl_2MCl_2]$ *and* $[Cu(TETA)Cl_2SnPh_2]$

A hot ethanolic solution (15 cm^3) of $[Cu(TETA)]Cl_2$ (0.01 mol, 2.8 g) was treated with group (IV) metal tetrachlorides or diphenyltindichloride (0.01 mol). In each case an immediate precipitate appeared, which was washed with ethanol and dried *in vacuo*. All the synthesized complexes are soluble only in DMSO.

RESULTS AND DISCUSSION

The analytical data (Table 1) conform to the compositions $[Cu(TETA)]Cl_2$, $[Cu(TETA)Cl_2MCl_2]$ and $[Cu(TETA)Cl_2SnPh_2]$ (M = Si, Ge, Sn, Ti and Zr; TETA = triethylenetetramine). The reaction of copper(II) chloride with TETA in ethanol yields $[Cu(TETA)]Cl_2$. Further reaction of this complex with group(IV) metal tetrachlorides and diphenyltin(IV) dichloride gives high yields of the heterobimetallic chelates $[Cu(TETA)Cl_2MCl_2]$ and $[Cu(TETA)Cl_2SnPh_2]$, respectively. The conductivity measurements in DMSO[25] show that the ligand $[Cu(TETA)]Cl_2$ is ionic, while the heterobimetallic chelates are covalent. Therefore, the complexes are formed by the replacement of amine hydrogens by group (IV) metals and the removal of 2HCl molecules, which has also been confirmed by the quantitative estimation of chlorine as AgCl. The reactions followed are represented in Scheme 1.

A room-temperature ESR spectrum of the powdered sample of $[Cu(TETA)]Cl_2$ gives approximate g values with $g_{\parallel} = 2.09$ and $g_{\perp} = 2.06$, which favours the square planar geometry around the copper(II) ion.[26,27] The apparent g values of the bimetallic polycrystalline samples are $g_{\parallel} = 1.99$ and $g_{\perp} = 2.07$, with the average g values $\langle g \rangle = (2g_{\parallel} + g_{\perp}/3 = 2.04)$ being in accordance with those

Table 1. Analytical data, melting point, colour and % yield of the ligand, $[Cu(TETA)]Cl_2$, and its heterobimetallic complexes

Complex	Yield (%)	Colour	Melting point (°C)	Analysis (%) [Found (Calc.)] C	H	N	Cl
$[C_6H_{18}N_4CuCl_2]$	90	Blue	200	25.7 (25.7)	6.4 (6.4)	20.0 (20.0)	25.3 (25.4)
$[C_6H_{16}N_4CuSiCl_4]$	80	Yellow	175	19.0 (19.0)	4.2 (4.2)	14.8 (14.8)	37.6 (37.5)
$[C_6H_{16}N_4CuGeCl_4]$	80	Yellow	154	17.0 (17.1)	3.8 (3.7)	13.2 (13.3)	33.6 (33.6)
$[C_6H_{16}N_4CuSnCl_4]$	80	Yellow	172	15.4 (15.3)	3.4 (3.4)	11.9 (11.9)	30.4 (30.3)
$[C_6H_{16}N_4CuTiCl_4]$	80	Yellow	155	18.1 (18.1)	4.0 (4.1)	14.1 (14.0)	35.8 (35.7)
$[C_6H_{16}N_4CuZrCl_4]$	80	Yellow	160	16.2 (16.3)	3.6 (3.7)	12.6 (12.7)	32.1 (32.1)
$[C_6H_{16}N_4CuSnCl_2(C_6H_5)_2]$	70	Yellow	120	39.2 (39.3)	4.7 (4.7)	10.1 (10.1)	12.9 (12.8)

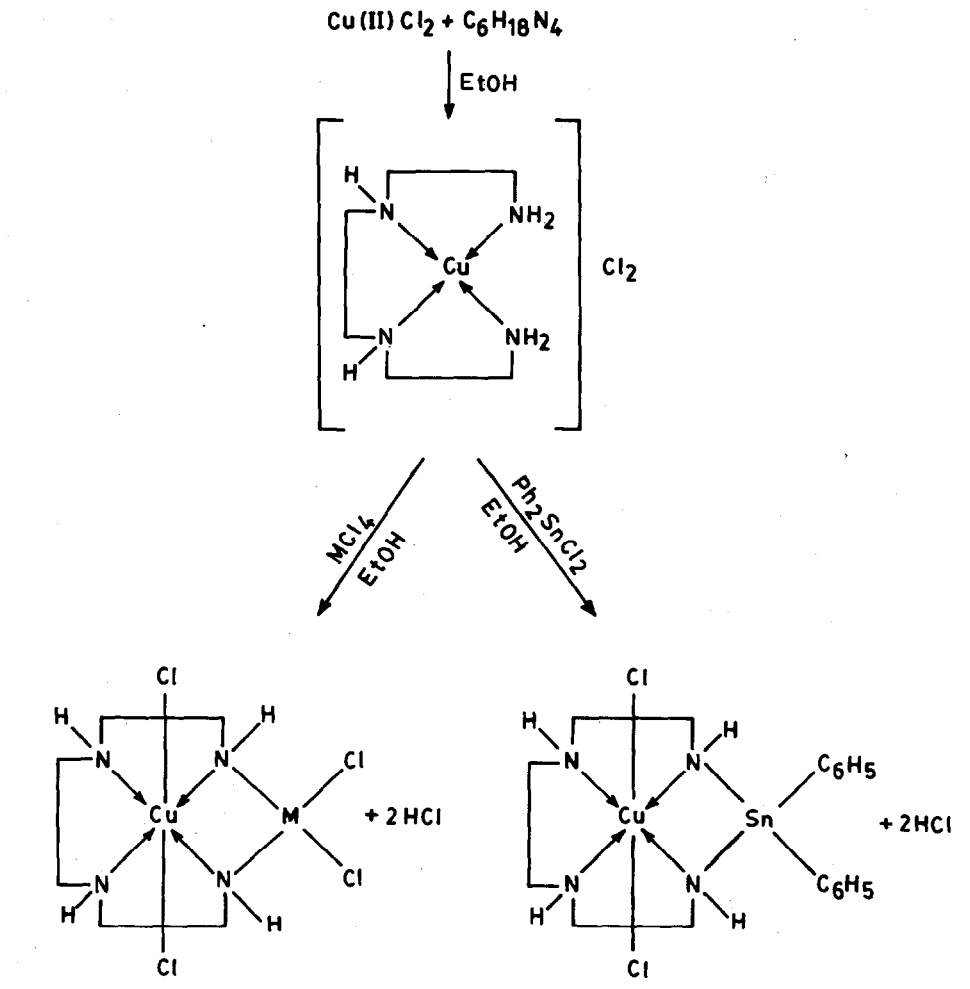

Scheme 1.

of typical octahedral copper(II) complexes.[28] On this basis we suggest that the chloride ions present in $[Cu(TETA)]Cl_2$ coordinate with copper(II) ions upon complexation with group(IV) metal tetrachlorides to produce an octahedral environment around the copper(II) ion. It is to be noted that the chloride ions present in $[Cu(TETA)]Cl_2$ coordinate to the copper(II) ion and not the group (IV) metal chlorine. This may be due to (a) the easy availability of the anionic chlorine of $[Cu(TETA)]Cl_2$, which should in any case be a better ligand than the covalently bonded chlorine of group (IV) metals and (b) since copper(II) achieves an octahedral geometry only after complexation with MCl_4, it is thought that the removal of aminohydrogen occurs due to the group (IV) metal chlorine. Otherwise, the chloride ions present in $[Cu(TETA)]Cl_2$ would have gone as HCl before its reaction with MCl_4.

The electronic spectra of the mononuclear complex in methanol, $[Cu(TETA)]Cl_2$, shows a high intensity charge-transfer band at 247 nm, along with the ligand–metal charge-transfer band at 304 nm. A strong *d–d* band at 596 nm is also observed, which is characteristic of square planar complexes.[29] The bimetallic complexes in DMSO also show strong bands at 275 nm, along with the shoulders assignable to intra-ligand transitions and ligand–metal charge-transfer, which is in agreement with the observation reported.[30,31] The *d–d* band maxima, one at 930 and another at 882 nm, are due to octahedral bimetallic copper(II) complexes. It is known that octahedral distortion in copper(II) complexes leads to the displacement of *d–d* bands to lower energies.[32]

It is possible to assign some of the important IR bands which are helpful in determining the structures of the synthesized complexes. In $[Cu(TETA)]Cl_2$ the band at 3270 cm^{-1} is characteristic of the N—H stretching frequency, while the peak at 1584 cm^{-1} is assigned to δ(N—H). In the bimetallic

Table 2. IR and far-IR absorption bands of the ligand, $[Cu(TETA)]Cl_2$, and its heterobimetallic complexes

Complex	Peak positions (cm^{-1})				
	ν(N—H)	ν(Cu—N)	ν(Cu—Cl)	ν(M—N)	ν(M—Cl)
$[C_6H_{18}N_4CuCl_2]$	3270m	405s	—	—	—
$[C_6H_{16}N_4CuSiCl_4]$	3110m	403s	315m	430s	300s
$[C_6H_{16}N_4CuGeCl_4]$	3112m	403s	315m	485s	305s
$[C_6H_{16}N_4CuSnCl_4]$	3112m	403s	315m	455s	300s
$[C_6H_{16}N_4CuTiCl_4]$	3110m	403s	315m	520s	290s
$[C_6H_{16}N_4CuZrCl_4]$	3110m	403s	315m	525s	290s
$[C_6H_{16}N_4CuSnCl_2(C_6H_5)_2]$	3108m	403s	310m	472s	300s

chelates ν(N—H) appears at a lower wave number (3110 cm^{-1}), suggesting the formation of a group (IV) metal–nitrogen covalent bond, and δ(N—H) remains unaffected. Two sharp absorption bands appear at 1060 and 1384 cm^{-1} in both the mono- and binuclear complexes, assigned to ν(C—C) and ν(C—N) modes, respectively. Another two distinct bands appear at 2962 and 751 cm^{-1}, assigned to ν(C—H) and CH_2 rocking modes, respectively.

The far-IR region of the spectra is very significant as it includes the M—N and M—X stretches. The M—X absorption bands are stronger and appear at lower wave numbers compared to M—N absorption bands. New bands of medium intensity in the range 430–525 cm^{-1} in the complexes have been assigned to ν(M—N). A distinct band appeared in the ligand and the heterobimetallic complexes at 405 cm^{-1}, assigned to a Cu—N stretching frequency. A band appeared in the complexes at 315 cm^{-1}, assigned to ν(Cu—Cl), which was absent in the spectra of the free ligand, $[Cu(TETA)]Cl_2$. Sharp bands appeared in the complexes in the range 290–305 cm^{-1} and are attributed to ν(M—Cl). The characteristic IR bands are given in Table 2.

In further communications our interest lies in reporting the results of the reaction between $[Cu(TETA)](BF_4)_2$ and $[Cu(TETA)]Br_2$ with group (IV) metal tetrachlorides and organotin(IV) chlorides.

Acknowledgement—We thank Rasheed Jamhour for his immense assistance throughout the work.

REFERENCES

1. E. L. Muetterties, *Bull. Soc. Chem. Belg.* 1975, **84**, 959.
2. E. L. Muetterties and J. Stein, *J. Chem. Rev.* 1979, **79**, 479.
3. R. Puddephatt, *Chem. Soc. Rev.* 1983, **12**, 98.
4. B. Chaudret, B. Delavuse and R. Poilblanc, *Coord. Chem. Rev.* 1988, **86**, 191.
5. A. L. Balch, R. R. Guimerans, J. Linehan and F. E. Wood, *Inorg. Chem.* 1985, **24**, 2021.
6. A. L. Balch, R. R. Guimerans, J. Linehan, M. M. Olmstead and D. E. Oram, *Organometallics* 1985, **4**, 1445.
7. J. P. Farr, M. M. Olmstead and A. L. Balch, *J. Am. Chem. Soc.* 1980, **102**, 6654.
8. J. P. Farr, M. M. Olmstead, C. H. Hunt and A. L. Balch, *Inorg. Chem.* 1981, **20**, 1182.
9. A. Maisonnat, J. P. Farr and A. L. Balch, *Inorg. Chim. Acta* 1981, **53**, L217.
10. A. Maisonnat, J. P. Farr, M. M. Olmstead, C. H. Hunt and A. L. Balch, *Inorg. Chem.* 1982, **21**, 3961.
11. J. P. Farr, M. M. Olmstead, F. E. Wood and A. L. Balch, *J. Am. Chem. Soc.* 1983, **105**, 792.
12. J. P. Farr, M. M. Olmstead and A. L. Balch, *Inorg. Chem.* 1983, **22**, 1229.
13. J. P. Farr, F. E. Wood and A. L. Balch, *Inorg. Chem.* 1983, **22**, 3387.
14. J. P. Farr, M. M. Olmstead, F. E. Wood, N. M. Rutherford and A. L. Balch, *Organometallics* 1983, **2**, 1758.
15. G. Bruno, S. Lo Schiavo, E. Rotondo, C. G. Arena and F. Faraone, *Organometallics* 1989, **8**, 886.
16. M. A. Ciriano, J. J. Perez-Torrente, F. J. Lahoz and L. A. Oro, *Inorg. Chem.* 1992, **31**, 969.
17. S. Wang, G. Garzon, C. King, J. Wang and J. P. Fackler Jr, *Inorg. Chem.* 1989, **28**, 4623.
18. D. Cunningham and J. McGintey, *J. Chem. Soc., Dalton Trans.* 1992, 1387.
19. N. Torihara, H. Okawa and S. Kida, *Chem. Lett.* 1978, 185.
20. C. J. O'Connor, D. P. Freberg and E. Sinn, *Inorg. Chem.* 1979, **18**, 1077.
21. P. J. Hay, J. C. Thibeault and R. Hoffmann, *J. Am. Chem. Soc.* 1975, **97**, 4884.
22. R. R. Gange, C. L. Spiro, T. J. Smith, C. A. Hammann, W. R. Thies and A. K. Sheimke, *J. Am. Chem. Soc.* 1981, **103**, 4073.
23. R. C. Long and D. N. Hendrickson, *J. Am. Chem. Soc.* 1983, **105**, 1513.
24. S. L. Lambert, C. L. Spiro, R. R. Gangne and D. N. Hendrickson, *Inorg. Chem.* 1982, **21**, 68.
25. W. J. Geary, *Coord. Chem. Rev.* 1971, **7**, 81.
26. R. K. Ray and G. B. Kauffman, *Inorg. Chim. Acta* 1990, **174**, 257.

27. D. Kivelson and R. Neiman, *J. Chem. Phys.* 1961, **35**, 149.
28. D. D. Brown, J. R. Wason, J. W. Hall and W. E. Hatfield, *Inorg. Chem.* 1977, **16**, 2526.
29. R. K. Ray, M. K. Baudyopadhyay and G. B. Kauffman, *Polyhedron* 1989, **8**, 757.
30. N. A. Ahmad and F. Kalili, *Synth. React. Inorg. Met.-Org. Chem.* 1988, **18**, 919.
31. W. Vrengdenhil, J. G. Haasnoot and J. Reedijk, *Inorg. Chim. Acta* 1990, **167**, 109.
32. E. I. Solomon, J. W. Hare and H. B. Gray, *Proc. Natn. Acta Sci.* (U.S.A.) 1976, **73**, 1389.

Polyhedron Vol. 12, No. 8, pp. 955–960, 1993
Printed in Great Britain

0277–5387/93 $6.00+.00
© 1993 Pergamon Press Ltd

CYANO-BRIDGED COMPLEXES OF BIS(2,2′-BIPYRIDINE)(PYRIDINE)RUTHENIUM(II)†

EDGARDO H. CUTIN and NÉSTOR E. KATZ‡

Instituto de Química Física, Facultad de Bioquímica, Química y Farmacia, Universidad Nacional de Tucumán, Ayacucho 491, 4000 San Miguel de Tucumán, Argentina

(*Received* 30 *September* 1992; *accepted* 20 *November* 1992)

Abstract—New complexes with the $Ru(bpy)_2(py)^{2+}$ moiety (bpy = 2,2′-bipyridine, py = pyridine) connected through a cyano group to $Ru(NH_3)_5^{3+}$ and $Fe(CN)_5^{2-}$ as electron acceptors have been prepared and their spectroscopic, electrochemical and photophysical properties investigated. Cyano-bridging is disclosed by changes in the shape and position of the cyanide stretching vibration, $\nu(C{\equiv}N)$, in the IR spectrum of the dinuclear ruthenium species, as compared with the mononuclear parent complex. Blue shifts in the lowest energy $d_\pi \rightarrow \pi^*$ (Ru → bpy) metal-to-ligand charge transfer (MLCT) transition occur when going from $[Ru(bpy)_2(py)(CN)]^+$ (**A**) to $[(bpy)_2(py)Ru^{II}{-}CN{-}Ru^{III}(NH_3)_5]^{4+}$ (**B**) and to $[(bpy)_2(py)Ru^{II}{-}CN{-}Fe^{III}(CN)_5]^-$ (**C**), thus pointing to the existence of nitrile-bound pentaammineruthenium(III) and pentacyanoferrate(II) capping groups in the mixed-valence species **B** and **C**. Besides, new intense and broad absorptions at 697 (in HCl 0.01 M) and 700 nm (in H_2O/Me_2CO, 1 : 1 v/v) appear in **B** and **C**, respectively, and can be assigned to metal-to-metal charge transfer (MMCT) or "intervalence" transitions. The luminescence of **A** is completely quenched in **B**, even at 77 K, a fact which can be explained on the basis of efficient excited-state electron transfer to form the electronic mixed-valence isomer of **B**. The strong asymmetric nature of **B**, as deduced from cyclic voltammetry data (the difference in redox potentials between both ruthenium sites amounts to 1.30 V), together with a strong electronic coupling [$H_{AB} = 2200\ cm^{-1}$, calculated from the "intervalence" absorption data] indicate that the back electron transfer (or charge recombination) from the MMCT excited state of **B** probably lies in the "inverted" region.

Cyano-bridged transition metal complexes are interesting systems in the field of mixed-valence chemistry,[1] because of the relatively strong metal–metal interaction mediated by the short cyanide group, which gives rise to intense metal-to-metal charge transfer (MMCT) or "intervalence" transitions in the visible or near-IR spectra. We have recently reported[2–5] a new series of asymmetric mixed-valence complexes with $Ru(bpy)_2(py)^{2+}$ and $Ru(trpy)(bpy)^{2+}$ (bpy = 2,2′-bipyridine, trpy = 2,2′:6′,2″-terpyridine) as photosensitizing moieties connected through different bridging ligands to $Ru(NH_3)_5^{2+/3+}$ and $Fe(CN)_5^{3-/2-}$ groups that can act as electron "relays". These dinuclear compounds can be useful as models for energy conversion devices and molecular electronics.[6]

We report here the syntheses and spectroscopic, electrochemical and photophysical properties of new dinuclear complexes derived from the mononuclear species $[Ru(bpy)_2(py)(CN)]^+$ (**A**), first reported by Calvert and Meyer,[7] and which has been separated in this work from its main impurity, $Ru(bpy)_2(CN)_2$, using a chromatographic procedure. The new species, $[(bpy)_2(py)Ru^{II}{-}CN{-}Ru^{III}(NH_3)_5]^{4+}$ (**B**) and $[(bpy)_2(py)Ru^{II}{-}CN{-}Fe^{III}(CN)_5]^-$ (**C**), have been characterized in the solid state and in solution. Intense MMCT tran-

† Presented, in part, at the XIX Congreso Latinoamericano de Química, Buenos Aires, Argentina, 1990.

‡ Author to whom correspondence should be addressed.

Dedicated to Dr Pedro J. Aymonino on the occasion of his 65th birthday.

sitions have been detected in the visible region for both mixed-valence ions. In contrast to **A** complex **B** does not emit, even at 77 K, thus evidencing an efficient oxidative quenching process, probably due to the presence of low-lying MMCT excited states.

EXPERIMENTAL

Syntheses

$[Ru(bpy)_2(py)(CN)](PF_6)\cdot 11H_2O$. $[Ru(bpy)_2(py)Cl]Cl$ (0.60 g, 1.1 mmol), prepared as in ref. 8, and KCN (0.07 g, 1.1 mmol) were refluxed for 2 h in a solution of water (8 cm^3) and ethanol (2 cm^3). After filtering and evaporating to a volume of 5 cm^3 the solution was sorbed onto a CM-Sephadex C-25 column. Elution with pure H_2O was performed first in order to remove the undesired complex $Ru(bpy)_2(CN)_2$. Then, 0.1 M LiCl was used to elute a second orange fraction containing the ion **A**. This fraction was rotoevaporated to a minimum volume and precipitation was achieved by adding a concentrated aqueous solution of NH_4PF_6. The solid was filtered, washed with cold water and ether and dried *in vacuo* over KOH. Yield: 15%. Found: C, 36.4; H, 3.3; N, 9.1. Calc.: C, 36.5; H, 4.1; N, 9.8%.

$[(bpy)_2(py)Ru^{II}—CN—Ru^{III}(NH_3)_5](PF_6)_4\cdot 12H_2O$. $[Ru(NH_3)_5Cl]Cl_2$ (20 mg, 0.07 mmol) dissolved in 0.01 M HCl (6 cm^3) was added to $[Ru(bpy)_2(py)(CN)](PF_6)\cdot 11H_2O$ (50 mg, 0.05 mmol) in an H_2O/Me_2CO (5 cm^3; 1:1 v/v) solution under argon. After 0.5 h Zn(Hg) was added and the mixture was stirred for 5 h with continuous argon bubbling at room temperature. After removal of the Zn(Hg) a few drops of H_2O_2 35% were added. The colour of the solution changed from red to green after a few minutes. After evaporating to a minimum volume, the solution was sorbed onto an SP-Sephadex C-25 column (3 × 50 cm). After eluting with 0.3 M HCl to remove unreacted species a dark green solution was collected with 0.5 M HCl as an eluant. This solution was rotoevaporated to a small volume, and excess NH_4PF_6 was added to precipitate the product, which was redissolved in H_2O and reprecipitated with NH_4PF_6, washed with cold water and ether and dried *in vacuo*. Yield: 39%. Found. C, 19.1; H, 3.3; N, 11.0. Calc.: C, 20.9; H, 3.5; N, 10.3%.

$[(bpy)_2(py)Ru^{II}—CN—Fe^{III}(CN)_5]^-$. This complex was prepared in solution by mixing stoichiometric amounts of $[Ru(bpy)_2(py)(CN)](PF_6)\cdot 11H_2O$ and $Na_3[Fe(CN)_5(NH_3)]\cdot 3H_2O$ in H_2O/Me_2CO (10 cm^3; 1:1 v/v). After stirring under argon for 1 h Br_2 vapour was added and visible spectra were recorded.

Instrumentation and techniques

Analytical reagent chemicals were used throughout this work. IR spectra were recorded (as KBr pellets) on a Perkin–Elmer 983G spectrophotometer (wave-number precision: ± 2 cm^{-1}). UV–vis spectra were obtained with Perkin–Elmer Coleman 124 and Shimadzu UV-160A spectrophotometers at 22°C (errors in λ_{max} and ε_{max} were ± 2 nm and $\pm 5\%$, respectively). Cyclic voltammetry data were obtained as described before.[3] Luminescence measurements were performed on a Perkin–Elmer LS5 spectrophotometer at room temperature and 77 K. Microanalyses were performed at UMYMFOR, Universidad de Buenos Aires, Argentina.

RESULTS AND DISCUSSION

Syntheses

The mononuclear complex **A** can be separated from its main impurity, $Ru(bpy)_2(CN)_2$ (cf. ref. 7), by a chromatographic exchange on a Sephadex C-25 column. The dinuclear mixed-valence species **B** has been prepared as a solid PF_6^- salt using a method similar to that reported[9] for the dinuclear compound $[(NH_3)_5Ru^{III}—NC—Ru^{II}(bpy)_2(CN)](PF_6)_3$. The corresponding dinuclear iron species **C** can be detected in an H_2O/Me_2CO (1:1 v/v) solution.

IR spectra

Figure 1 shows the IR spectra (as KBr pellets) of the PF_6^- salts of **A** and **B**. Assignments can be made by comparison to analogous complexes.[2] For the mononuclear species **A**, the sharp absorption at 2071 cm^{-1} can be attributed to the cyanide stretching vibration $\nu(C\equiv N)$. In the dinuclear mixed-valence complex **B** this band is much broader and appears at 2024 cm^{-1}. The broadening effect in $\nu(C\equiv N)$ has already been observed in the mixed-valence species $(NH_3)_5Ru—NC—Ru(CN)_5$ when compared to $Ru(CN)_6^{4-}$.[10] The negative shift in $\nu(C\equiv N)$ of **B** with respect to **A** contrasts to the increase observed in $[(trpy)(bpy)Ru^{II}—CN—Ru^{II}(NH_3)_5](PF_6)_3\cdot 3Me_2CO$,[4] when compared with the mononuclear parent complex. This difference can be accounted for by the different inductive effects of a capping pentaammineruthenium group when the oxidation state of ruthenium is changed from (II) to (III). The wave-numbers of the ammonia stretching and deformation vibrations in the PF_6^- salt of **B** [$\nu(N—H) = 3300–3150$ cm^{-1}

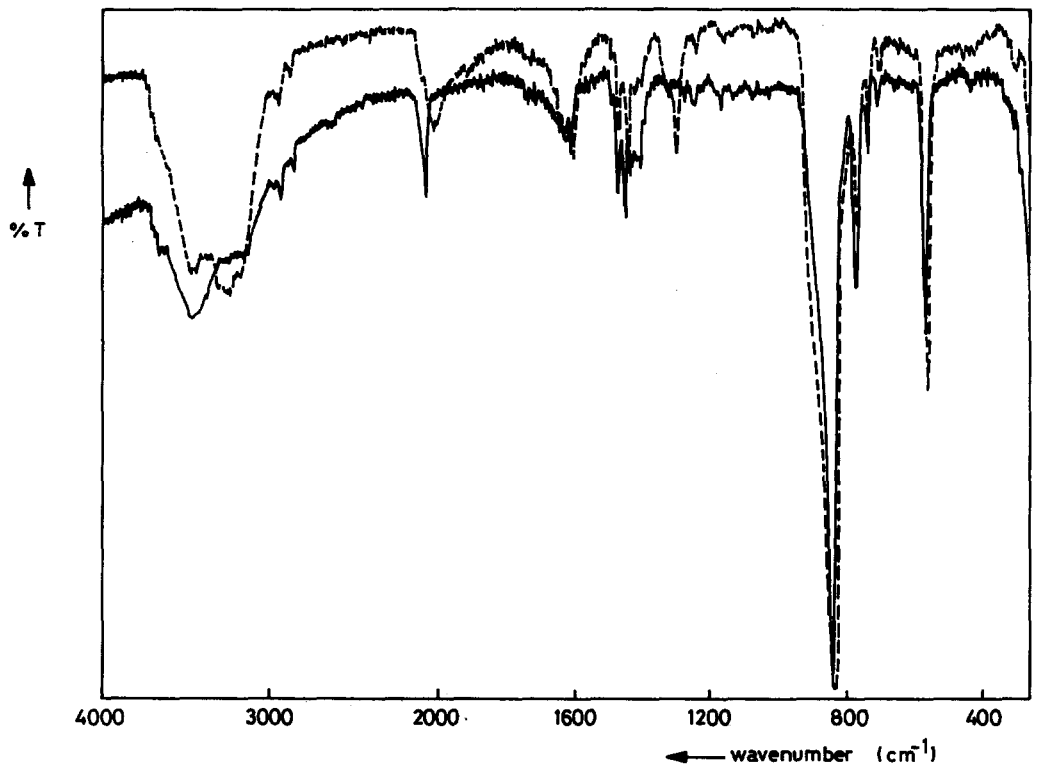

Fig. 1. IR spectra (as KBr pellets) of: (——) $[Ru(bpy)_2(py)(CN)](PF_6)\cdot 11H_2O$ and (– – –) $[(bpy)_2(py)Ru—CN—Ru(NH_3)_5](PF_6)_4\cdot 12H_2O$.

and $\delta(NH_3) = 1312\ cm^{-1}$] are typical of pentaammineruthenium(III) moieties.[11]

UV–vis spectra

Table 1 shows the observed absorption maxima in the UV–vis region for complexes **A** (in CH_3CN) and **B** (in 0.01 M HCl). For the former ion the lowest-energy band appears at $\lambda_{max} = 470$ nm, in agreement with the value previously reported,[7] and can be assigned to the metal-to-ligand charge transfer (MLCT) transition $d_\pi(Ru) \rightarrow \pi_1^*(bpy)$. The following absorption band at $\lambda_{max} = 346$ nm has contributions from $d_\pi(Ru) \rightarrow \pi_2^*(bpy)$ and $d_\pi(Ru) \rightarrow \pi^*(py)$ MLCT transitions, as discussed before.[12] These two low-energy bands are shifted in H_2O to 442 and 330 nm, respectively, as shown in Fig. 2. This strong solvatochromic effect can be explained by considering the higher electron-accepting abilities of H_2O with respect to CH_3CN.[13] When comparing the lowest-energy absorption maximum of this ion in aqueous solution to the corresponding values of $Ru(bpy)_2(CN)_2$ ($\lambda_{max} = 431$ nm)[14] and $[Ru(bpy)_2(py)_2]^{2+}$ ($\lambda_{max} = 455$ nm),[14] we infer that increasing the number of CN^- ligands attached to a ruthenium bipyridil moiety causes a noticeable

Table 1. Electronic absorption spectra

Complex	λ_{max} (nm) ($10^{-4} \times \varepsilon_{max}$, $M^{-1}\,cm^{-1}$)
$[Ru(bpy)_2(py)(CN)]^+$ (**A**)[a]	470 (0.9), 346 (1.1), 288 (5.3), 244 (2.3), 208 (2.9)
$[(bpy)_2(py)Ru^{II}—CN—Ru^{III}(NH_3)_5]^{4+}$ (**B**)[b]	697 (0.2), 423 (0.6), 285 (4.0), 243 (2.2)
$[(bpy)_2(py)Ru^{II}—CN—Fe^{III}(CN)_5]^-$ (**C**)[c]	700 (0.2), 440 (1.2)

[a] In CH_3CN.
[b] In 0.01 M HCl.
[c] In H_2O/Me_2CO (1 : 1 v/v).

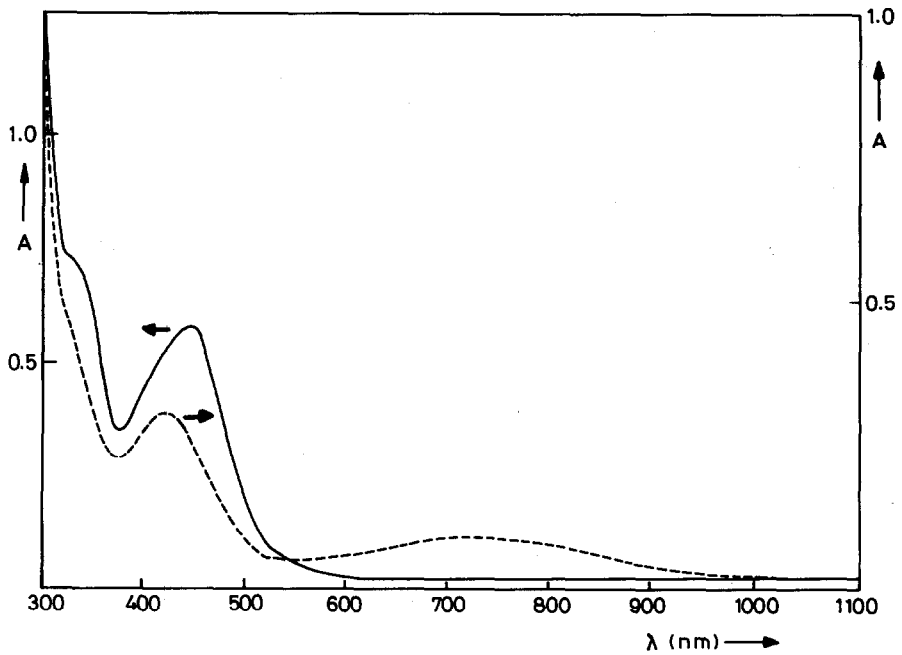

Fig. 2. Visible spectra in aqueous solutions of: (——) $[Ru(bpy)_2(py)(CN)]^+$ ($C = 9 \times 10^{-5}$ M) and (– – –) $[(bpy)_2(py)Ru^{II}—CN—Ru^{III}(NH_3)_5]^{4+}$ ($C = 4.8 \times 10^{-5}$ M).

decrease in Ru → bpy π-backbonding, with a concomitant increase in the energy of the MLCT band. The bands at 288 and 244 nm in **A** are assigned to $\pi \rightarrow \pi^*$ intraligand transitions, while the band at 208 nm is due to a $d_\pi(Ru) \rightarrow \pi^*(CN^-)$ MLCT transition.

The UV–vis absorption spectrum of **B** in aqueous solution is also shown in Fig. 2. The bands at 285 and 243 nm are again assigned to $\pi \rightarrow \pi^*$ intraligand transitions. The $d \rightarrow \pi^*$ ($Ru^{II} \rightarrow$ bpy) CT band at 442 nm in **A** is shifted to 423 nm in **B**, as expected for dinuclear complexes with metal binding through cyanide bridges.[9] A new intense and broad absorption band at $\lambda_{max} = 697$ nm can be confidently assigned to an MMCT transition, $Ru_b^{II} \rightarrow Ru_a^{III}$ (Ru_b = Ru bonded to bpy, Ru_a = Ru bonded to NH_3), since it disappears in the corresponding $Ru_b^{II}—CN—Ru_a^{II}$ and $Ru_b^{III}—CN—Ru_a^{III}$ species (obtained by adding solid $S_2O_4^{2-}$ and Ce^{IV} salts, respectively, to aqueous solutions of **B**). This band is shifted to 690 nm in CH_3CN, typical of this type of asymmetric system.[9] Besides, it compares reasonably well in shape and position to the MMCT bands of the complexes $[(trpy)(bpy)Ru^{II}—CN—Ru^{III}(NH_3)_5]^{4+}$ ($\lambda_{max} = 700$ nm in CH_3CN)[4] and $[(NH_3)_5Ru^{III}—NC—Ru^{II}(bpy)_2(CN)]^{3+}$ ($\lambda_{max} = 694$ nm in H_2O).[9] For the $Ru^{II}—CN—Fe^{III}$ complex **C** the MMCT band is observed at 700 nm in H_2O/Me_2CO (1 : 1 v/v) solution.

Electrochemistry

The redox potentials for the ruthenium-based and two bpy-based couples have already been determined for complex **A**: 1.04, −1.48 and −1.72 V, respectively, in CH_3CN, vs S.C.E.[15] In complex **B** $E_{1/2}$ (Ru_b^{III}/Ru_b^{II}), as determined by cyclic voltammetry, appears at 1.28 V (in CH_3CN, vs S.C.E.), as expected for its higher charge with respect to **A**. The value for $E_{1/2}$ (Ru_a^{III}/Ru_a^{II}) = −0.02 V (in CH_3CN, vs S.C.E.) is consistent with those values observed for nitrile-bound pentaammineruthenium complexes.[9] The energy difference between both mixed-valence isomers of **B** thus amounts to 1.30 eV. The reduction waves were somewhat irreversible, with peak potentials at −1.46 and −1.74 V due to bpy reduction processes. Due to the narrow electrochemical window for aqueous solutions, $E_{1/2}$ values for both metallic couples could not be determined for the ion **C**, but we expect them to be very similar to **B**, the ruthenium analogue.

Luminescence

Complex **A** emits at room temperature ($\lambda_{em} = 620$ nm in H_2O).[7] Figure 3 shows the emission spectrum of **A** at 77 K as an EtOH/MeOH glass (4 : 1 v/v; the solution had to be filtered). At $\lambda_{ex} = 466$ nm there is an emission maximum at 585

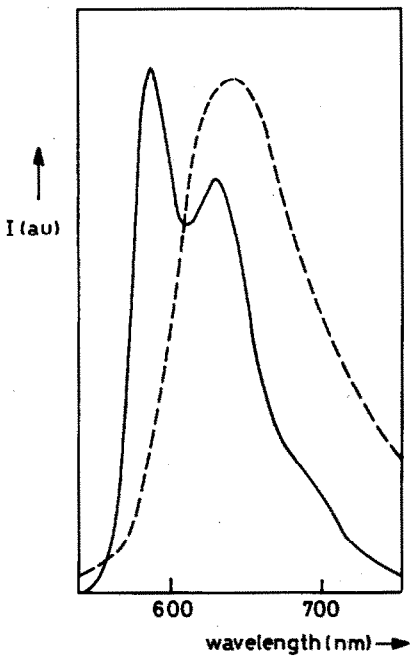

Fig. 3. Emission spectrum ($\lambda_{ex} = 466$ nm) of $[Ru(bpy)_2(py)(CN)]^+$ in EtOH/MeOH (4:1 v/v): (——) at 77 K and (– – –) at room temperature.

nm and a shoulder at 623 nm, characteristic of $Ru(bpy)_2(L)_2^{n+}$ complexes which decay from an ^{3}MLCT excited state.[16] The excitation and absorption spectra were almost identical. At room temperature this alcoholic solution emits at 636 nm, as also shown in Fig. 3. Complex **B** does not emit at room temperature or 77 K. This lack of emission may be due to an efficient oxidative quenching process, such as those proposed[17] for similar cyano-bridged systems:

$$[(bpy)_2(py)Ru^{II}CNRu^{III}(NH_3)_5]^{4+} \xrightarrow{h\nu} [(bpy)(bpy^-)(py)Ru^{III}CNRu^{III}(NH_3)_5]^{4+}$$

$$[(bpy)(bpy^-)(py)Ru^{III}CNRu^{III}(NH_3)_5]^{4+} \xrightarrow{k_q} [(bpy)_2(py)Ru^{III}CNRu^{II}(NH_3)_5]^{4+*}$$

$$[(bpy)_2(py)Ru^{III}CNRu^{II}(NH_3)_5]^{4+*} \xrightarrow{k_b} [(bpy)_2(py)Ru^{II}CNRu^{III}(NH_3)_5]^{4+}.$$

The "unstable" isomer of **B** is involved in the quenching step k_q, i.e. the MMCT excited state can quench the radiative decay from the ^{3}MLCT excited state.

Electronic coupling

By using the Marcus–Hush formalism[1] it is possible to calculate the electronic metal-to-metal coupling in the mixed-valence species **B** from spectroscopic data. Indeed, from values of $\nu_{max} = 1.45 \times 10^4$ cm^{-1}, $\varepsilon_{max} = 3.4 \times 10^3$ M^{-1} cm^{-1} and $\Delta\nu_{1/2} = 6.0 \times 10^3$ cm^{-1}, obtained by analysing the MMCT band of **B**, a value of $H_{AB} = 2200$ cm^{-1} (0.27 eV) results, typical for cyano-bridged mixed-valence complexes.[9,18]

The reorganization barrier for the optical electron transfer, λ, can be calculated from the following equation:[16]

$$E_{op} = \lambda + \Delta G^0 + \Delta E_{ex},$$

where E_{op} is the maximum of the MMCT band, ΔG^0 is the free energy difference between both metal sites and ΔE_{ex} is a correction for excited state/ground state differences. Since, for ion **B**, $E_{op} = 1.80$ eV, $\Delta G^0 = 1.30$ eV and $\Delta E_{ex} = 0.15$ eV,[19] a value of $\lambda = 0.35$ eV is obtained. For the ion $[(py)(NH_3)_5 Ru^{III}—NC—Ru^{II}(bpy)_2(CN)]^{3+}$, for which ΔG^0 is lower by $\cong 0.3$ eV, a concomitant decrease of $\cong 0.2$ eV in E_{op} is observed.[20] Values for λ and ΔG^0 are very similar for analogous cyano-bridged complexes[4,9] and thus E_{op} appears at almost the same value ($\cong 1.8$ eV). For the thermal back electron transfer $Ru_b^{III} \rightarrow Ru_a^{II}$ $\Delta G^0 = -1.30$ eV and $\lambda < -\Delta G^0$, so that an "inverted" behaviour is predicted.[4] A non-adiabatic treatment[21] gives the reverse rate constant $k_{th,r} \cong 7 \times 10^8$ s^{-1}. However, recent picosecond IR experiments[22] performed on the mixed-valence dimer $[(NC)_5Ru^{II}—CN—Ru^{III}(NH_3)_5]^{-*}$ have shown that an ultrafast ($\tau < 0.5$ ps) back electron transfer, followed by vibrational relaxation, occurs in this system from the MMCT excited state, suggesting that a theory considering vibrational equilibrium is not adequate for this process. Besides, it has been pointed out that electronic coupling elements for optical electron transfers are not necessarily equal to those for thermal electron transfers.[23]

To conclude, strong coupling in cyano-bridged asymmetric mixed-valence complexes, such as **B** or **C**, gives rise to intense MMCT bands in the visible region. The complete lack of emission, even at 77 K, of dimer **B** points to efficient quenching of the MLCT (Ru → bpy) excited state, probably through crossing to the MMCT excited state. Increasing the metal-to-metal separation, such as in the complex $[(trpy)(bpy)Ru^{II}(4,4'\text{-bpy})Ru^{III}(NH_3)_5]^{5+}$ (with 4,4′-bpy = 4,4′-bipyridine),[5] causes a higher reorganization barrier λ, which may result in longer-lived MMCT excited states.

Acknowledgements—We thank CONICET and CIUNT for financial support, Dr C. Catalán for permission to use the UV–vis spectrophotometers and Dr C. Colombano for helping in the luminescence experiments. The

authors are Members of the Research Career, CONICET, Argentina.

REFERENCES

1. C. Creutz, *Prog. Inorg. Chem.* 1983, **30**, 1.
2. E. H. Cutin and N. E. Katz, *Polyhedron* 1991, **10**, 653.
3. A. Ben Altabef, S. D. Ribotta de Gallo, M. E. Folquer and N. E. Katz, *Inorg. Chim. Acta* 1991, **188**, 67.
4. A. Ben Altabef, S. B. Ribotta de Gallo, M. E. Folquer and N. E. Katz, *Trans. Met. Chem.* 1993, in press.
5. F. Fagalde and N. E. Katz, *J. Chem. Soc., Dalton Trans.* 1993, in press.
6. V. Balzani and F. Scandola, *Supramolecular Photochemistry*. Ellis Horwood, U.K. (1991).
7. J. M. Calvert and T. J. Meyer, *Inorg. Chem.* 1982, **21**, 3978.
8. B. Bosnich and F. P. Dwyer, *Aust. J. Chem.* 1966, **19**, 2229.
9. C. A. Bignozzi, S. Roffia and F. Scandola, *J. Am. Chem. Soc.* 1985, **107**, 1644.
10. S. Siddiqui, W. W. Henderson and R. E. Shepherd, *Inorg. Chem.* 1987, **26**, 3101.
11. R. E. Clarke and P. C. Ford, *Inorg. Chem.* 1970, **9**, 227.
12. G. M. Bryant, J. E. Fergusson and H. K. J. Powell, *Aust. J. Chem.* 1971, **24**, 257.
13. N. Kitamura, M. Sato, H.-B. Kim, R. Obata and S. Tazuke, *Inorg. Chem.* 1988, **27**, 651.
14. A. Juris, V. Balzani, F. Barigelletti, S. Campagna, P. Belser and A. Von Zelewsky, *Coord. Chem. Rev.* 1988, **84**, 85.
15. B. P. Sullivan, D. Conrad and T. J. Meyer, *Inorg. Chem.* 1985, **24**, 3640.
16. N. E. Katz, C. Creutz and N. Sutin, *Inorg. Chem.* 1988, **27**, 1687.
17. V. Balzani, N. Sabbatini and F. Scandola, *Chem. Rev.* 1986, **86**, 319.
18. A. Burewicz and A. Haim, *Inorg. Chem.* 1988, **27**, 1611.
19. B. S. Brunschwig, S. Ehrenson and N. Sutin, *J. Phys. Chem.* 1986, **90**, 3657.
20. C. A. Bignozzi, C. Paradisi, S. Roffia and F. Scandola, *Inorg. Chem.* 1988, **27**, 408.
21. R. A. Marcus and N. Sutin, *Biochim. Biophys. Acta* 1985, **811**, 265.
22. S. K. Doorn, P. O. Stoutland, R. B. Dyer and W. H. Woodruff, *J. Am. Chem. Soc.* 1992, **114**, 3133.
23. M. H. Chou, C. Creutz and N. Sutin, *Inorg. Chem.* 1992, **31**, 2318.

Polyhedron Vol. 12, No. 8, pp. 961–965, 1993
Printed in Great Britain

0277-5387/93 $6.00+.00
© 1993 Pergamon Press Ltd

SYNTHESIS AND CHARACTERIZATION OF $M_2(EPh_3)_2(NMe_2)_4$ COMPOUNDS (E = C, Si, Ge, Sn; M = Mo, W)

MALCOLM H. CHISHOLM,* GENNARO J. GAMA and IVAN P. PARKIN

Department of Chemistry, Indiana University, Bloomington, IN 47405, U.S.A.

(*Received* 10 *November* 1992; *accepted* 16 *November* 1992)

Abstract—The reaction between $M_2Cl_2(NMe_2)_4$ and $LiEPh_3$ (2 equivalents) (M = W; E = C, Si, Ge, Sn; M = Mo; E = Si, Ge, Sn) in toluene/THF at room temperature produces a precipitate of $M_2(EPh_3)_2(NMe_2)_4$ in 35–65% isolated yield. The compounds are air-, water- and light-stable for prolonged periods in the solid state (except when E = C). All are soluble in aromatic hydrocarbon solvents and decompose on heating at 161–270°C. They were characterized by IR, UV, mass spectrometry and VT ^{1}H NMR. The latter revealed only the *anti* isomer in solution with $T_c \geqslant 115$°C and $\Delta G^{\dagger} \geqslant 74$ kJ mol^{-1} for the amide rotation (M = W, Mo; E = Si, Ge). For $W_2(SnPh_3)_2(NMe_2)_4$ a coalescence point of $T_c = 75$°C ($\Delta G^{\dagger} = 70$ kJ mol^{-1}) was observed and the compound slowly isomerizes to a mixture of the *gauche* and *anti* configurations.

Compounds of the type $M(R)_2(NMe_2)_4$ [M = Mo, W; R = Cl, $Si(SiMe_3)_3$, CR'_3, $Sn(SnMe_3)_3$, $SeC_6H_2Me_3$, PR'_2][1] have been synthesized by metathesis reactions involving LiR and substitutionally labile $M_2Cl_2(NMe_2)_4$ compounds.[2] More recently compounds of the formula $W_2(OCPh_3)_2(NMe_2)_4$,[3] $W_2(OSiPh_3)_2(NMe_2)_4$[3] and $W_2(OC(CF_3)_2NMe_2)_2(NMe_2)_4$[4] has been formed by reaction of $W_2(NMe_2)_6$ with the appropriate alcohol. Presumably steric hindrance prevents further substitution. Despite the synthesis of a number of $W_2(ER_3)_2(NMe_2)_4$ complexes, where E is a group 14 element, no systematic synthesis for the same R group has been obtained. This is important as it may give information about trends and reactivity within the homologous series.[5] Here we describe the formation of complexes of the form $M_2(EPh_3)_2(NMe_2)_4$ (E is a group 14 element and M = Mo, W).[6]

EXPERIMENTAL

All reactions were performed in oven-dried glassware, under dry nirogen, by Schlenk or glove-box techniques. All non-deuterated solvents were distilled from Na/benzophenone ketyl and stored over molecular sieves or metallic sodium, under dry nitrogen. ^{1}H NMR spectra were recorded on a Varian XL 300 spectrometer at 299.66 MHz in C_6D_6 or $C_6D_5CD_3$ and referenced to residual proton impurities at 7.16 and 2.09 ppm, respectively. Variable-temperature ^{1}H NMR were calibrated by an external methanol curve. IR spectra were obtained on a Perkin–Elmer PE 283B spectrophotometer as pressed KBr pellets. Ditungsten dichloride tetrakis(dimethylamide) and the dimolybdenum analogue were made by standard procedures.[2] Lithium powder, sodium and Ph_3ECl were purchased from Aldrich Chemical Co. and used as supplied.

Synthesis of Ph_3ELi *compounds*[7]

A solution of Ph_3ECl (1.66×10^{-3} mol) in THF (5 cm^3) was added to an eight-fold excess of lithium powder (containing 2% of Na) (0.090 g, 1.30×10^{-2} mol) and vigorously stirred in THF (5 cm^3). During the addition the original solution changed colour from colourless to pale yellow and to deep green after all the Ph_3ECl had been added. The only exception was the compound where E = carbon, whose solution turned brownish-red. The reaction was allowed to stand for 3 h and the volume reduced *in vacuo* to precipitate LiCl. The resulting solution was filtered through a fine glass frit and used directly in the subsequent reactions.

The lead congener was prepared according to the procedures below: (a) From the reaction between Ph_3PbCl and lithium (containing from 5 up to 10%

* Author to whom correspondence should be addressed.

of sodium) in THF, which resulted in a canary green solution of the salt; (b) from the reaction between the Pb_2Ph_6 dimer and lithium in liquid ammonia, which resulted in a bright yellow solution which was evaporated under vacuum and the yellow solid redissolved in THF.

Preparation of $M_2(EPh_3)_2(NMe_2)_4$ (M = Mo; E = Si, Ge, Sn; M = W, E = C, Si, Fe, Sn)

To $M_2Cl_2(NMe_2)_4$ (7.20×10^{-4} mol) in toluene (5 cm^3) was added Ph_3ELi (1.66×10^{-3} mol) in THF (3 cm^3) at room temperature. The resulting solution was vigorously stirred for 30 min with the generation of a white precipitate. The precipitate was removed by filtration and the resulting filtrate was reduced to 1/4 of the volume *in vacuo*. The resulting solution precipitated an orange solid. The solvent was filtered off and the solid washed with toluene (1 cm^3) and THF (1 cm^3) and dried for 7 h *in vacuo*. The physical characterization data and yields of the solids obtained are given in Table 1. All solids were air stable for prolonged periods, but their solutions quickly showed some decomposition after a few seconds of exposure to air. The tin derivatives decompose, in the solid state, after 2–3 h. Attempts to prepare the lead derivatives, following the same procedures, led always to the formation of a black intractable precipitate upon addition of the Ph_3PbLi solution to Mo or the W substrate solution in toluene.

The IR spectra for all the $M_2(EPh_3)_2(NMe_2)_4$ compounds were similar with the following main bands (cm^{-1}): 3040, 2980, 2840, 2790, 1570, 1430, 1410, 1245, 1145, 845, 720, 685, 475, 315.

RESULTS AND DISCUSSION

Synthesis

Reaction of $LiEPh_3$ with $M_2Cl_2(NMe_2)_4$ in toluene/THF produces $M_2(EPh_3)_2(NMe_2)_4$ in reasonable yields (35–65%), according to eq. (1).

$$M_2Cl_2(NMe_2)_4 + 2LiEPh_3 \longrightarrow M_2(EPh_3)_2(NMe_2)_4 + 2LiCl \quad (1)$$

The reactions were extremely rapid with LiCl being immediately precipitated on mixing the reagents. This precluded monitoring the reaction by ^1H NMR. The $M_2(EPh_3)_2(NMe_2)_4$ compounds precipitated from the reaction solution after reducing the volume of the solution to between a quarter or half of its original amount. A constant problem in the isolation of the $M_2(EPh_3)_2(NMe_2)_4$ compounds is the removal of the remaining LiCl, which co-precipitates with the product. Washing the final product with THF, or extracting the product with a benzene/hexane mixture or washing the solid with small amounts of degassed water (followed by washing with small amounts of THF) and drying the product for several hours helps to remove the LiCl contaminant. $Mo_2(SiPh_3)_2(NMe_2)_4$ was washed with degassed water (1.5 cm^3) at 10°C for approximately 30 s and then washed with THF (1 cm^3). Only a small decomposition was observed. The yields obtained in these reactions were comparable to other alkylation reactions of $M_2Cl_2(NMe_2)_4$.

It is not clear whether our failure to obtain the lead containing compound is a reflection of thermodynamic factors (weak W—Pb bonds) or is

Table 1. Microanalytical and other characterization data for $M_2(EPh_3)_2(NMe_2)_4$

M	E	Colour	Yield (%)	M.p. (°C)[a]	Found (Calc.) (%) C	H	N
W	C	Red–orange	35	270	53.9 (53.4)	5.2 (5.3)	5.5 (5.4)
W	Si	Orange	36	203	48.0 (48.6)	4.9 (5.4)	4.7 (5.3)
W	Ge	Orange	48	209	46.3 (45.8)	4.6 (4.7)	4.8 (4.7)
W	Sn	Light orange	38	161			
Mo	Si	Orange	49	140	58.8 (59.3)	5.8 (6.1)	5.9 (6.3)
Mo	Ge	Red–orange	54	226			
Mo	Sn	Light orange	51	176			

[a] All compounds decompose without melting.

merely a kinetic problem in that $LiPbPh_3$ is highly reducing.

Characterization

All the $M_2(EPh_3)_2(NMe_2)_4$ compounds are air-stable, relatively inert to alcoholysis by PrOH, EtOH and MeOH, and in the case of the germanium derivatives, the compounds are inert to 6 M KOH in EtOH and react only slowly with 1 M HNO_3. These remarkable properties are likely steric in origin as $M_2R_2(NMe_2)_4$ (M = Mo, W; R = alkyl or aryl) undergo ready alcoholysis to form $M_2R_2(OR)_4$ compounds.[8] The steric protection is almost certainly afforded by the large "propeller-like" hydrophobic EPh_3 groups. The $M_2(EPh_3)_2$ containing complexes are all orange or orange–red in colour and have decomposition points in the range 161–270°C, dependent on the nature of E.

The IR spectra of $M_2(EPh_3)_2(NMe_2)_4$ are all virtually identical within the range 3000–300 cm^{-1}, with the same general shape and shift of individual bands by no more than 5–15 cm^{-1}, dependent on the sample. No M—E vibrations were identified; for E = Si, Ge and Sn they likely occur below 300 cm^{-1}. The C—E vibrations in the EPh_3 groups are weak and no definitive assignment was possible.

The ^1H NMR spectra of the $M_2(EPh_3)_2(NMe_2)_4$ complexes at room temperature showed only two resonances in the amide region. This observation is consistent with the *anti*-isomer in solution. The observed spectra show two types of dimethylamide resonances at room temperature and below, both with equal intensities. It is in agreement with the staggered ethane-like geometry adopted. For $M_2(R)_2(NMe_2)_4$ complexes, the R groups can be oriented in a *gauche* or *anti* fashion. For the *anti* isomer all the dimethylamide groups are equivalent, being related by a mirror plane and a C_2 axis, however, the methyl groups on each dimethylamido ligand are proximal and distal with respect to the metal–metal multiple bond.[9] The M—N bond is formally a multiple bond in the $M_2(EPh_3)_2(NMe_2)_4$ complexes. The barrier to free rotation about the M—N bond can be observed in the NMR timescale by measuring the coalescence of the proximal and distal resonances. In the *gauche* isomer either two or four resonances are observed, depending on the temperature, as two sets of dimethylamide groups are present.

In the series $M_2(EPh_3)_2(NMe_2)_4$ all the compounds showed only two resonances in the amide region from −70 to 25°C in d_8-toluene, indicating that only the anti-isomer is formed in the reaction. Heating the solutions of $M_2(EPh_3)_2(NMe_2)_4$ up to 105°C in d_8-toluene showed a marked broadening of the amide resonances for M = Mo, W, E = C, Si, Ge, but no coalescence. The estimated coalescence temperature for these compounds is above 120°C. For M = Mo, W; E = Sn, a coalescence point at 70°C is observed for the free amide rotation. Further in this case the appearance of the gauche isomer occurs at $T \geqslant 65$°C, until the equilibrium distribution of rotamers (66.7% *gauche*: 33.3% *anti*) is obtained after prolonged heating. This indicates that the *anti* rotamer is the kinetic product in eq. (1). Figure 1 shows the spectra of $W_2(NMe_2)_4(CPh_3)_2$. Pertinent ^1H NMR data are presented in Table 2.

At high temperatures ($T \geqslant 65$°C) $W_2(SnPh_3)_2(NMe_2)_4$ rotation about the metal–metal bond occurs at a significant rate, such that on cooling a sample heated to 75°C for 15 min six resonances of equal intensity are observed in the amide region, indicative of a statistical distribution of *anti* and *gauche* rotamers. In the case of the latter compound the estimated M—E distance, based on the atomic radii, is the largest for the homologous series, thus restriction of rotation about the M—M bond due to the cogging of the EPh_3 group is lower in energy than in the other compounds.

The structure of *anti*-$W_2(GePh_3)_2(NMe_2)_4$ has been previously reported, but is shown again here in Fig. 2 since it is instructive to consider the consequences of the M—E distances within this series.

The freedom of the amide rotation in W_2^{6+} complexes has been ascribed to electronic and steric contributions. In the $M_2(EPh_3)_2(NMe_2)_4$ series the electronic nature of the ligands is almost constant as there is little change in the electronegativity between silicon and tin; however, the steric effects change

Table 2. ^1H NMR data (δ) and coalescence temperature for amide rotation in $M_2(EPh_3)_2(NMe_2)_4$ compounds

M	E	Me_d[a] (ppm)	Me_p[a] (ppm)	T_c[b] (°C)	$\Delta G^{\dagger}$[c] (kJ mol^{-1})
W	C	1.37	3.36	> 150	> 81
W	Si	2.11	3.63	125	77
W	Ge	2.18	3.73	115	74
W	Sn	2.37	3.87	75	67[d]
Mo	Si	2.22	3.64	125	77
Mo	Ge	2.28	3.73	120	77
Mo	Sn	2.40	3.86	105	73[d]

[a] $Me_{p,d}$ denote the proximal and distal Me groups, respectively.

[b] Values for T_c were estimated by line shape analysis for free amide rotation.

[c] $\Delta G^{\dagger}$ values calculated by $\Delta G^{\dagger} = -\ln(K_{ex}h/KT_c)RT_c$.

[d] Equilibrium between the *anti* and *gauche* rotamers was observed.

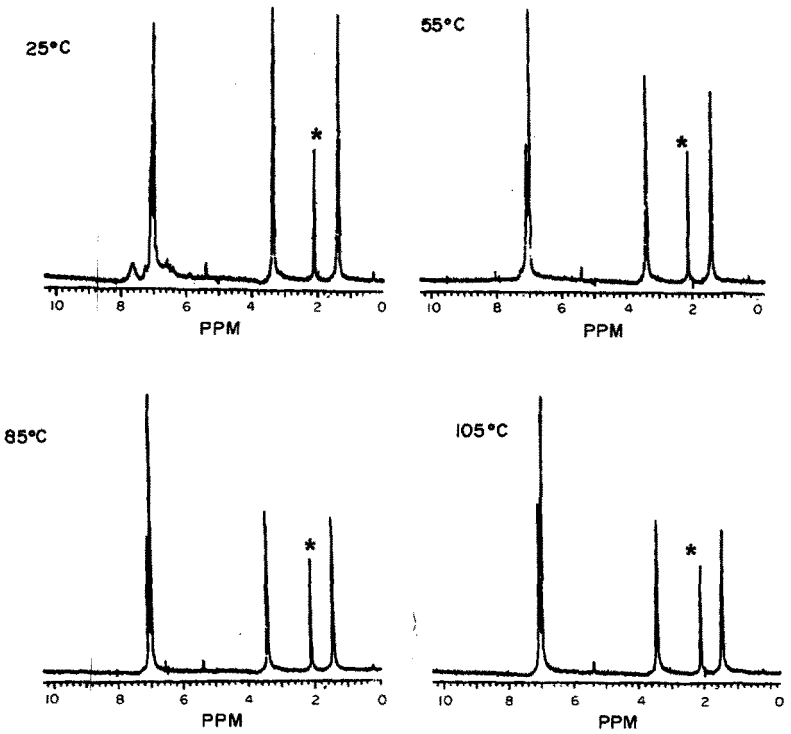

Fig. 1. Variable-temperature ^1H NMR spectra for $W_2(CPh_3)_2(NMe_2)_4$ in d_8-toluene. * = protio-toluene.

quite dramatically ($\simeq$ 2.20 for W—C and $\simeq$ 2.70 Å for W—Sn). Here we observe the estimated coalescence temperature for the free amide rotation following the order C $\gg$ Si > Ge > Sn. This indicates that the steric interaction between the EPh_3 and NMe_2 groups across the M—M bond decreases as the M—E bond increases. A small electronic component to the amide rotation barrier caused by differences in electronegativity of E would work in parallel with the steric effects. The higher the electronegativity of E, the stronger the $M_{d\pi}$–$N_{p\pi}$ interaction and the higher the rotational energy.

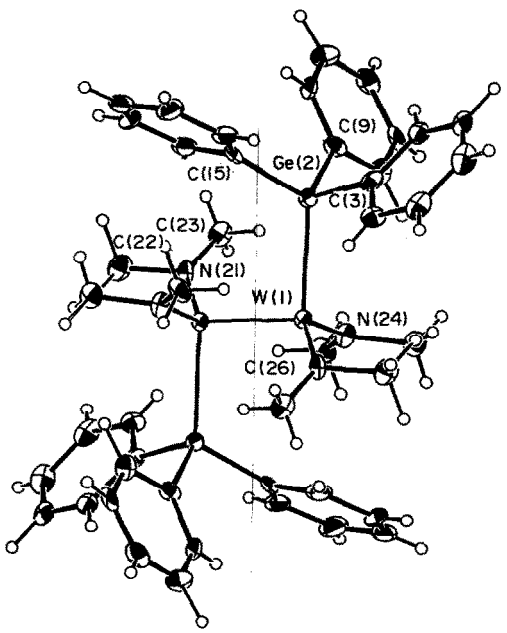

Fig. 2. An ORTEP view of the centrosymmetry *anti*-$W_2(GePh_3)_2(NMe_2)_4$. Pertinent distances (Å) and angles (°) are W—W = 2.297(1), W—Ge = 2.625(1), W—N = 1.95(1), W—W—Ge = 95.9(1), W—W—N = 106.9(1).

CONCLUSIONS

The analysis of the ^1H NMR data suggests that the $M_2(EPh_3)_2(NMe_2)_4$ compounds form a structurally homologous series with an *anti* ethane-like staggered configuration. The rotational barrier for M—N free rotation depends on the steric hindrance afforded by the EPh_3 groups which decrease with the length of the M—E bond. An electronic component due to the electronegativity of the EPh_3 groups plays a minor role in the rotational process. The partial conversion of the kinetically formed *anti* isomer to the *gauche* form is facilitated at high temperatures ($T > 75$°C), only for E = Sn. This is mainly a consequence of the lower barrier to rotation about the W≡W bond afforded by the longer M—E bond.

Acknowledgements—The authors thank the National Science Foundation for financial support, NATO for a post-

doctoral fellowship to IPP and CNPq/Brazil for a doctoral fellowship to GJG.

REFERENCES

1. M. H. Chisholm, *Accts Chem. Res.* 1990, **23**, 419.
2. M. Akiyama, M. H. Chisholm, F. A. Cotton, M. W. Extine and C. A. Murillo, *Inorg. Chem.* 1977, **16**, 2407.
3. M. H. Chisholm, I. P. Parkin, J. C. Huffman, E. M. Lobkovsky and K. Folting, *Polyhedron* 1991, **10**, 2839.
4. H. W. Roesky, N. Berte, F. Edelman, R. Herbst, E. Egert and G. M. Sheldrick, *Z. Naturforsch, B: Anorg. Chem. Org. Chem.* 1986, **41B**, 1506.
5. The compounds where $R = Si(SiMe_3)_3$ and $Sn(SnMe_3)_3$ are the closest related compounds to this series: M. H. Chisholm, H. T. Chiu, K. Folting and J. C. Huffman, *Inorg. Chem.* 1984, **23**, 4097.
6. A preliminary report on the synthesis of $W_2(GePh_3)_2(NMe_2)_4$ has appeared: M. H. Chisholm, I. P. Parkin and J. C. Huffman, *Polyhedron* 1991, **10**, 1215.
7. E. G. Rochow, in *Comprehensive Coordination Chemistry* (Edited by J. C. Bailar, H. J. Emeleus, R. Nyholm and A. F. Trotman-Dickenson), Vol. 1, pp. 1323–1468; Vol. 2, pp. 1–42; Vol. 2, pp. 43–104. Pergamon Press, New York (1973).
8. (a) M = Mo: M. H. Chisholm and R. J. Tatz, *Organometallics* 1986, **5**, 1590; (b) M = W: M. H. Chisholm, B. W. Eichhorn, K. Folting and J. C. Huffman, *Organometallics* 1986, **5**, 1599.
9. M. H. Chisholm and F. A. Cotton, *Accts Chem. Res.* 1978, **11**, 356.

Polyhedron Vol. 12, No. 8, pp. 967–970, 1993
Printed in Great Britain

0277–5387/93 $6.00+.00
© 1993 Pergamon Press Ltd

SYNTHESIS OF (3-METHOXYPROPYL)-CYCLOPENTADIENYLTITANIUM AND ZIRCONIUM COMPLEXES

YANLONG QIAN* and GUISHENG LI

Shanghai Institute of Organic Chemistry, Academia Sinica, 345 Lingling Lu, Shanghai 200032, China

(*Received* 4 *November* 1992; *accepted* 13 *November* 1992)

Abstract—Four titanium and zirconium complexes of (3-methoxypropyl)cyclopentadienyl, Cp'_2MCl_2 (M = Ti, Zr), $Cp'CpTiCl_2$ and $Cp'Cp''TiCl_2$ (Cp = C_5H_5, Cp′ = $MeOCH_2CH_2C_5H_4$, Cp″ = $MeOCH_2CH_2C_5H_4$), have been synthesized in good yields by reacting the potassium salt Cp′K with MCl_4 (M = Ti, Zr), $CpTiCl_3$ and $Cp''TiCl_3$, respectively. Their IR spectra show that the oxygen atom in the side-chain does not coordinate with the central metals, while mass specta imply the coordination of oxygen with the metals is possible, in particular in some low-valent species.

Investigation of synthesis, structure and reactivity of metal complexes with cyclopentadienyl ligands remains an active research field in organometallic chemistry. A number of interests are related to the introduction of various kinds of substituents onto the cyclopentadienyl ligand, aimed at studying the structures of metal complexes and adjusting their properties.[1] Among them, great attention has been paid to group IV element complexes.[2–6] We have synthesized several kinds of ring-substituted cyclopentadienyl titanium and zirconium complexes[7–11] and found remarkable substituent effects upon the catalytic properties of the titanium complexes toward olefin isomerizations.[12–14] For example, the isomerization of 1,5-hexadiene catalysed by $(RC_5H_4)_2TiCl_2/Pr^iMgBr$ afforded 90% methylenecyclopentane, when R is 2-methoxyethyl, while 95% 2,4-hexadiene was obtained, when R is an allyl.[13] We recognized and confirmed that the methoxy in the side-chain on the cyclopentadienyl ring can chelate with titanium, thus regulating the structure and reactivity of the complex. In this paper we further present the synthesis of the 3-methoxypropylcyclopentadienyl ligand and its titanium and zirconium complexes.

* Author to whom correspondence should be addressed at the new address: Prof. Yanlong Qian, East China University of Chemical Technology, Box 421, 130 Meilong Road, Shanghai 200237, China.

RESULTS AND DISCUSSION

3-Methoxypropylcyclopentadiene (**1**), prepared from 3-methoxypropyl chloride and sodium cyclopentadienide in THF, was converted immediately into the corresponding potassium salt in 86% yield on treatment with metal potassium in THF.

$Cp'H$ $Cp'K$ Cp'_2TiCl_2
(**1**) (**2**) (**3**)

Cp'_2ZrCl_2 $Cp'CpTiCl_2$ $Cp'Cp''TiCl_2$
(**4**) (**5**) (**6**)

(Cp = C_5H_5, Cp′ = $MeOCH_2CH_2CH_2C_5H_4$,
Cp″ = $MeOCH_2CCH_2C_5H_4$)

The potassium salt of 3-methoxypropylcyclopentadiene (**2**) reacted with $TiCl_4$, giving rise to bis(3-methoxypropyl-cyclopentadienyl)titanium dichloride (**3**) as purple needle crystals in 71% yield. A similar reaction between **2** and $ZrCl_4$ afforded bis-(3-methoxypropyl-cyclopentadienyl)zirconium dichloride (**4**) in 87% yield. The mono-substituted cyclopentadienyl titanium complex (**5**) was obtained in 88% yield by reacting **2** with cyclopentadienyltitanium trichloride. In order to compare the effect of different lengths of the side-chain, with 2-methoxyethyl on one cyclopentadienyl and 3-methoxypropyl on another, complex **6**

was also successfully synthesized from the reaction of **2** with (2-methoxyethyl-cyclopentadienyl)-titanium trichloride ($Cp''TiCl_3$). Complex **6** is much more soluble than complexes **3** and **5** in ordinary organic solvents, such as ether, acetone, THF, etc. Attempts to synthesize bis(3-methoxypropyl-cyclopentadienyl)titanium chloride (Cp'_2TiCl) via reaction between **2** and $TiCl_3 \cdot 3THF$ or reduction of **3** by aluminium foil were unsuccessful. The target compound should be a solid, but these two synthetic routes led to a green viscous oily substance, which could not be crystallized or solidified by the usual methods available.

Introduction of 3-methoxypropyl and 2-methoxyethyl into the cyclopentadienyl rings caused the ^1H NMR signals of the ring hydrogens to move towards a higher magnetic field in comparison with that of dicyclopentadienyltitanium dichloride. The ring protons on the Cp′ moiety are split into two groups of muliplets, with an equal integrated area, centred at 6.40 and 6.33 ppm, respectively, for complexes **3**, **5** and **6**. The ring protons of Cp″ appeared as a broad singlet, falling into the multiplet around 6.40 of Cp′. The ring protons in the zirconium complex were also found to be two groups of multiplets, centred at 6.30 and 6.22 ppm, approximately 0.1 ppm higher field than those in the corresponding titanium complexes.

In the IR spectra the stretching vibration frequencies of C—O in these complexes are around 1120 cm^{-1}, almost identical to that in the ligand (**1**). This fact indicates that the oxygen atom is not coordinated with the metals in these quadrivalent metal complexes. The mass spectra of these complexes have regular types of fragmentation. The molecular ion peaks are usually weak and the main fragments are M—Cl, M—Cp′ and M—Cp″, etc. For complexes **3** and **4** the base peaks are attributed to M—Cp′ species. In the case of complex **5** the peak of M—Cp ($Cp'TiCl_2$) is much stronger than that of M—Cp′ ($CpTiCl_2$), indicating that the M—Cp species is more stable than M—Cp′ species under gas phase conditions, possibly due to intramolecular coordination between the oxygen and titanium in M—Cp species. For complex **6**, with two different oxygen-containing substituents on the cyclopentadienyls, the relative intensity for the peak due to M—Cp″ is only 35% of that for M—Cp′. A similar case is found for the peaks of M—Cp″—HCl and M—Cp′—HCl. These results reveal that the oxygen atom in 2-methoxyethyl is more favourable towards chelation to the titanium than for the 3-methoxypropyl analogue. This kind of interaction between the substituent and the central metal may be an important factor in controlling the structure and reactivity of the metal complex.

EXPERIMENTAL

All experiments were carried out under purified argon using standard Schlenk techniques. Melting points were not corrected. Solvents (THF, Et_2O, n-hexane and toluene) were refluxed over sodium Ph_2CO and distilled prior to use. The ^1H NMR spectra of **1** and **3–6** were recorded on Varian 360A and Varian XL-200 NMR spectrometers, respectively. IR were measured on a Shimadzu IR-40 spectrometer and MS were obtained on a Finnigan 4021 mass spectrometer. Compound $Cp''TiCl_3$ was prepared according to ref. 10. Commercially available $ZrCl_4$ was purified by sublimation before use.

Synthesis of **1**

Sodium cyclopentadienide, prepared from sodium sand (3.0 g, 0.13 mol), cyclopentadiene (18 cm^3, 0.22 mol) and THF (150 cm^3), was added to $CH_3OCH_2CH_2CH_2Cl$ (14.0 g, 0.13 mol) under magnetic stirring. The mixture was stirred at room temperature overnight, accompanied by the formation of a white solid (NaCl) precipitate. Solvents were removed under reduced pressure, and then the solid was dissolved with water. The organic layer was separated and the water-phase was extracted with petroleum ether (30–60°C) (3×30 cm^3). The combined organic phase was washed with saturated NaCl solution until neutral and dried over $CaCl_2$ for 2 h. After filtration and removal of the solvents, the residue was distilled. A colourless liquid (12.8 g, b.p. 34–36°C/1.0 mmHg) was obtained in 71% yield. Found: C, 78.3; H, 9.7. Calc. for $C_9H_{14}O$: C, 78.2; H, 10.2%. ^1H NMR (CCl_4, ppm): 6.0 (m, 3H), 3.06 (m, 5H), 2.68 (m, 2H), 2.26 (m, 2H), 1.60 (m, 2H). IR (neat, cm^{-1}): 3080m, 1618m, 1605m, 1120s, 900s, 680s.

Synthesis of **2**

3-Methoxypropylcyclopentadiene (**1**) (12 g, 87 mmol) was added to metal potassium (3.6 g, 92 mmol) in THF (190 cm^3). The mixture was stirred until almost no hydrogen was released (*ca* 12 h). The reddish solution was transferred through a stainless steel tube and washed twice with THF (60 cm^3). The concentration of the combined THF solution (*ca* 250 cm^3) was determined by titration with standard HCl solution to be 0.2985 mmol cm^{-3}, corresponding to approximately 86% yield based on **1**.

Synthesis of **3**

A solution of $MeOCH_2CH_2CH_2C_5H_4K$ in THF (134 cm^3, 40.0 mmol) was added dropwise to $TiCl_4$

(2.19 cm^3, 20.0 mmol) with stirring. After completing the addition, the reaction mixture was stirred for another 5 h. Removal of the solvents gave a red solid, which was extracted in a Soxhlet extractor with Et_2O and purple needles (5.56 g) were isolated in 71%; m.p. 92–93°C. Found: C, 54.8; H, 6.6; Ti, 12.1. Calc. for $C_{18}H_{26}Cl_2O_2Ti$: C, 5.5; H, 6.7; Ti, 12.2%. ^1H NMR ($CDCl_3$, ppm): 6.40 (m, 1H), 6.33 (m, 1H), 3.39 (t, 2H, $J = 6.4$ Hz), 3.33 (s, 3H), 2.78 (t, 2H, $J = 8.0$ Hz), 1.86 (m, 2H). IR (KBr, cm^{-1}): 3100m, 1500m, 1460m, 1440m, 1385m, 1215w, 1150m, 1118s, 1010m, 840s. MS (*m/z*, %): 357 (M—Cl, 2), 255 (M—Cp′, 100), 219 (M − Cp′ − HCl, 28), 187 (M − Cp′ − HCl − MeOH, 15), 105 (Cp′ − MeOH, 11), 91 (Cp′ − MeOME, 22), 78 ($CH_2C_5H_4$, 25), 45 ($MeOCH_2$, 59).

Synthesis of **4**

A solution of $MeOCH_2CH_2CH_2C_5H_4K$ in THF (40 cm^3, 12 mmol) was added to a mixture of sublimated $ZrCl_4$ (1.405 g, 6 mmol) and THF (15 cm^3) with stirring for 0.5 h. A yellowish solution was obtained and stirred overnight. KCl formed in the reaction was separated by centrifuging. The clear solution was transferred and concentrated, followed by the addition of n-hexane. A white solid (2.28 g) (**4**) was obtained in 87%. Sublimation at 90°C (oil bath)/3×10^{-4} mmHg) gave an analytical sample; m.p. 94°C. Found: C, 49.1; H, 5.9; Zr, 20.5. Calc. for $C_{18}H_{26}Cl_2O_2Zr$: C, 49.5; H, 6.0; Zr, 20.9%. ^1H NMR ($CDCl_3$, ppm): 6.30 (m, 1H), 6.22 (m, 1H), 3.38 (t, 2H, $J = 6.5$ Hz), 3.30 (s, 3H), 2.71 (t, 2H, $J = 7.4$ Hz), 1.83 (m, 2H). IR (KBr, cm^{-1}): 3100m, 1496m, 1480m, 1455s, 1390s, 1210m, 1135m, 1120s, 1010s, 810s. MS (*m/z*, %): 399 (M − Cl), 297 (M − Cp′, 95), 261 (M − Cp′ − HCl, 41), 91 (Cp′ − MeOMe, 49), 57 (C_3H_6O, 100), 42 (C_2H_4O, 82).

Synthesis of **5**

A solution of $MeOCH_2CH_2CH_2C_5H_4K$ in THF (38.15 cm^3, 11.4 mmol) was added to $CpTiCl_3$ (2.498 g, 11.4 mmol) in THF (20 cm^3). The reaction mixture was stirred at room temperature for 5 h. The red solid remaining after removal of the solvent was extracted in a Soxhlet extractor with Et_2O. The crude product **5** (3.22 g, 88%) was obtained. Recrystallization from PhMe–n-hexane provided an analytical sample; m.p. 78–79°C. Found: C, 51.9; H, 5.4; Ti, 15.3. Calc. for $C_{14}H_{18}Cl_2OTi$: C, 52.4; H, 5.6; Ti, 14.9%. ^1H NMR ($CDCl_3$, ppm): 6.55 (s, 5H), 6.33–6.44 (m, 4H), 3.39 (t, 2H, $J = 6.5$ Hz), 3.33 (s, 3H), 2.78 (m, 2H), 1.85 (m, 2H). IR (KBr, cm^{-1}): 3150m, 1460s, 1125s, 1030m, 840s. MS (*m/z*, %): 285 (M − Cl, 5), 255 (M − Cp, 100), 219 (M − Cp − HCl, 39), 187 (M − Cp′, 16), 151 (M − Cp′ − HCl, 2), 105 (Cp′ − MeOH, 20), 91 ($CH_2{=}CHC_5H_4$, 26), 78 ($CH_2C_5H_4$, 34), 45 ($MeOCH_2$, 77).

Synthesis of **6**

A solution of $MeOCH_2CH_2CH_2C_5H_4K$ in THF (31.4 cm^3, 9.38 mmol) was added to $MeOCH_2CH_2C_5H_4TiCl_3$ (2.60 g, 9.38 mmol) with stirring for 20 min. The resulting red solution was stirred for another 5 h. The solvent was then removed and the residue was extracted in a Soxhlet extractor with Et_2O. Concentration of the extract and washing with petroleum ether gave a red solid (3.25 g) in 91% yield; m.p. 48–50°C. Found: C, 53.8; H, 6.0; Ti, 12.7. Calc. for $C_{17}H_{24}Cl_2O_2Ti$: C, 53.8; H, 6.4; Ti, 12.6%. ^1H NMR ($CDCl_3$, ppm): 6.40 (m, 6H), 6.34 (m, 2H), 3.62 (t, 2H, $J = 6.0$ Hz), 3.39 (t, 2H, $J = 6.4$ Hz), 3.35 (s, 3H), 3.33 (s, 3H), 2.99 (t, 2H, $J = 6.0$ Hz), 2.78 (t, 2H), 1.86 (m, 2H, $J = 7.8$ Hz). IR (KBr, cm^{-1}): 3100m, 1500m, 1120s, 840s. MS (*m/z*, %): 343 (M − Cl, 22), 255 (M − Cp″, 35), 241 (M − Cp′, 100), 219 (M − Cp″ − HCl, 13), 205 (M − Cp′ − HCl, 39), 91 ($CH_2{=}CHC_5H_4$, 37), 78 ($CH_2C_5H_4$, 28), 45 ($MeOCH_2$, 69).

Acknowledgement—We thank the National Natural Science Foundation for financial support of this work.

REFERENCES

1. D. W. Macomber, W. P. Hart and M. D. Rausch, *Adv. Organomet. Chem.* 1982, **21**, 1.
2. B. G. Conway and M. D. Rausch, *J. Organomet. Chem.* 1984, **277**, 13.
3. P. G. Gassman and C. H. Winter, *J. Am. Chem. Soc.* 1986, **108**, 4228.
4. M. D. Rausch, J. F. Lewison and W. P. Hart, *J. Organomet. Chem.* 1988, **358**, 161.
5. M. F. Lappert, C. J. Pickett, P. I. Riley and R. I. W. Yarrow, *J. Chem. Soc., Dalton Trans.* 1981, 805.
6. K.-P. Stahl, G. Boche and W. Massa, *J. Organomet. Chem.* 1984, **277**, 113.
7. Q. Huang, Y. Qian and Y. Tang, *J. Organomet. Chem.* 1989, **368**, 277.
8. Q. Huang, Y. Qian and Y. Tang, *Trans. Met. Chem.* 1989, **14**, 315.

9. Y. Qian, G. Li, W. Chen, B. Li and X. Jin, *J. Organomet. Chem.* 1989, **373**, 185.
10. Q. Huang, Y. Qian, G. Li and Y. Tang, *Trans. Met. Chem.* 1990, **15**, 483.
11. Y. Qian, G. Li, W. Chen, B. Li and X. Jin, *Trans. Met. Chem.* 1990, **15**, 478.
12. Y. Qian, J. Zhuang, J. Lu, Q. Huang, W. Xu and S. Chen, *J. Molec. Catal.* 1986, **38**, 331.
13. Y. Qian, G. Li, Y. He, W. Chen, B. Li and S. Chen, *J. Molec. Catal.* 1990, **60**, 19.
14. G. Li, Y. Qian and Y.-Z. Huang, *J. Molec. Catal.* 1992, **72**, L15.

Polyhedron Vol. 12, No. 8, pp. 971–975, 1993
Printed in Great Britain

0277–5387/93 $6.00+.00
© 1993 Pergamon Press Ltd

SYNTHESIS, CHARACTERIZATION AND REACTIVITY OF *TRANS*-$[Ru(NH_3)_4\{P(OEt)_3\}_2]^{3+}$ IONS

S. E. MAZZETTO, E. RODRIGUES and D. W. FRANCO*

Universidade de São Paulo, Instituto de Física e Química de São Carlos, Cx. Postal 369, 13560-970 São Carlos, SP, Brazil

(*Received* 18 *August* 1992; *accepted* 2 *November* 1992)

Abstract—*Trans*-$[Ru(NH_3)_4\{P(OEt)_3\}_2]^{3+}$ ions were generated by electrochemical oxidation of the corresponding *trans*-$[Ru(NH_3)_4\{P(OEt)_3\}_2]^{2+}$ ions. The oxidation is quantitative and reversible and the resulting complex absorbs at 292 nm ($\varepsilon = 5.9 \times 10^2$ M^{-1} cm^{-1}). ESR spectra of frozen solutions are compatible with axial symmetry D_{4h}, with $g_{\parallel} = 1.83$ and $g_{\perp} = 2.36$. Aqueous solutions of the ruthenium(III) complex yield *trans*-$[Ru(NH_3)_4\{P(OEt)_3\}(H_2O)]^{2+}$ as the main product upon ageing.

The chemistry of phosphite complexes of ruthenium(II) tetraamines has been the subject of research in our laboratory for many years.[1–6]

The synthesis, characterization and reactivity of *trans*-$[Ru(NH_3)_4\{P(OR)_3\}(H_2O)]^{2+}$ type complexes have been reported,[1–6] and provide information regarding the degree of back-bonding in $Ru^{II} \rightarrow P^{III}$ and the influence on the chemical properties of the metal centre and the ligand upon coordination. Extending our investigation to d^5 low-spin systems, we recently reported similar results for the *trans*-$[Ru(NH_3)_4\{P(OEt)_3\}(H_2O)]^{3+}$ system.[7]

In the present paper we describe the synthesis, characterization and stability of the *trans*-$[Ru(NH_3)_4\{P(OEt)_3\}_2]^{3+}$ ion in aqueous solution.

EXPERIMENTAL

Reagents

Doubly distilled water was used throughout. All reagents were of analytical grade purity. Ethanol, acetone and diethyl ether were purified as described in the literature.[8]

The ruthenium compounds $[Ru(NH_3)_5Cl]Cl_2$, $[Ru(NH_3)_5(H_2O)](PF_6)_2$ and *trans*-$[Ru(NH_3)_4\{P(OEt)_3\}_2](PF_6)_2$ were prepared and characterized as described in the literature.[1,9,10]

The ruthenium(III) compound was generated in solution by the electrochemical oxidation of the corresponding ruthenium(II) salt. In a typical preparation *trans*-$[Ru(NH_3)_4\{P(OEt)_3\}_2]^{2+}$ was dissolved in a 1.0×10^{-3} M aqueous solution of trifluoroacetic acid. Electrochemical oxidation was performed at +0.85 V (vs S.C.E.) and the oxidation was monitored through coulometric and spectrophotometric measurements.

Apparatus and techniques

All manipulations were performed under pure argon. All the complexes were stored *in vacuo* and protected from light. The purity of the complexes was always checked by means of cyclic voltammetry and spectrophotometric measurements. CF_3COONa/CF_3COOH aqueous solutions were used to control the ionic strength. During the spectrophotometric and electrochemical measurements the temperature was controlled at 25.0± 0.2°C using a Superohm thermostat.

The controlled potential electrolysis, coulometric and cyclic voltammetric measurements were performed in a multifunctional PARC system consisting of a model 175 Universal Programmer, a model 173 potentiostat–galvanostat, a model 379 digital coulometer, a model 376 voltage-current convertor and a model Re-0074 *X–Y* recorder.

For cyclic voltammetric measurements a glassy carbon, platinum wire and S.C.E. were used as the working, auxiliary and reference electrodes, respectively. During the electrolysis a platinum net (area 13.6 cm^2) was used as the working electrode.

All absorbance measurements were performed

* Author to whom correspondence should be addressed.

using a Hewlett–Packard 8450A diode-array spectrophotometer and the λ_{max} values found in the electronic spectra were determined by deconvolution.

Frozen solutions of the *trans*-$[Ru(NH_3)_4\{P(OEt)_3\}_2]^{3+}$ salt in aqueous medium, produced immediately after electrolysis, were used for ESR measurements on a Varian E-109 spectrometer at (153 ± 5 K).

Kinetic measurements

The decay of the *trans*-$[Ru(NH_3)_4\{P(OEt)_3\}_2]^{3+}$ species was monitored following the changes in absorbance at 316 nm and changes in peak current (i_{pa}) at 0.54 and 0.50 V, respectively.

Good agreement was observed for first-order rate constants, determined graphically from plots of $\log(A_\infty - A_t)$ vs t, and those obtained from the electrochemical measurements.

RESULTS AND DISCUSSION

Two absorption bands can be observed in the electronic spectra of solutions containing *trans*-$[Ru(NH_3)_4\{P(OEt)_3\}_2]^{2+}$, $\lambda_1 = 262\ M^{-1}\ cm^{-1}$ ($\varepsilon_1 = 4.3 \times 10^2$) and $\lambda_2 = 294$ nm ($\varepsilon_2 = 2.3 \times 10^2\ M^{-1}\ cm^{-1}$), both attributed to *d–d* transitions.

During oxidation of the metal centre in acidic medium, $C_{H^+} = 10^{-3}$ M, the resulting solutions strongly absorb light below 260 nm, without defining a peak or shoulder in this region, whereas a shoulder can be observed at 292 nm ($\varepsilon = 5.9 \times 10^2\ M^{-1}\ cm^{-1}$) which we attribute tentatively to a ligand field transition (see Fig. 1). As expected the voltammetric spectra did not change during the oxidation, since the coordination sphere was not altered. The coulometric measurements indicate that in acidic media, C_{H^+}, the electrochemical oxidation:

$$trans\text{-}[Ru(NH_3)_4\{P(OEt)_3\}_2]^{2+} \longrightarrow trans\text{-}[Ru(NH_3)_4\{P(OEt)_3\}_2]^{3+} + e^-$$

occurs quantitatively and is reversible.

The number of electrons per *trans*-$[Ru(NH_3)_4\{P(OEt)_3\}_2]^{2+}$ ion becomes significantly higher than 1 as the hydrogen ion concentration of the medium decreases. Furthermore, the solution develops a blue colour and the original *trans*-$[Ru(NH_3)_3\{P(OEt)_3\}_2]^{2+}$ species are not regenerated by reversion of the current direction or by addition of a chemical reductor.

The thermal decay of the *trans*-$[Ru(NH_3)_4\{P(OEt)_3\}_2]^{3+}$ species was followed using UV–vis and ESR spectroscopy and cyclic voltammetry.

As shown in Fig. 2(a) only two systems can be observed in the voltammetric spectra of the aged acidic solutions originally containing the *trans*-$[Ru(NH_3)_4\{P(OEt)_3\}_2]^{3+}$ species. The couple whose peak current decreases with time, $E_{1/2} = +0.64$ V, corresponds to the *trans*-$[Ru(NH_3)_4\{P(OEt)_3\}_2]^{3+/2+}$ system. The second process exhibits $E_{1/2} = +0.50$ V and its peak currents (i_{pa} and I_{pc}) increase as the peak currents for the first process decrease. The process with $E_{1/2} = +0.50$ V has been assigned to the Ru^{III}/Ru^{II} couple in the *trans*-$[Ru(NH_3)_4\{P(OEt)_3\}(H_2O)]^{3+/2+}$ system and is the only one present in the voltammogram of the ruthenium(III) solution following 70 h of storage, see curve (b) in Fig. 2.

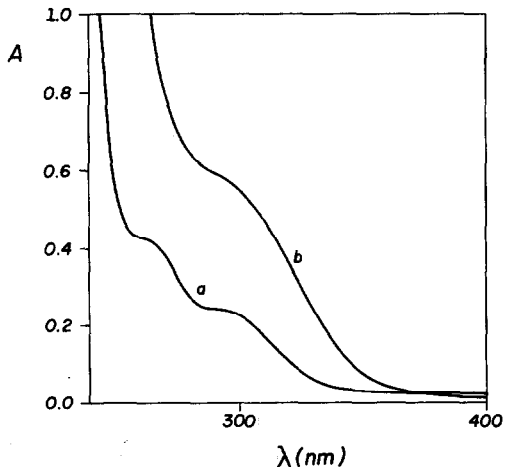

Fig. 1. Changes in electronic spectra associated with the oxidation in aqueous solutions of the ion *trans*-$[Ru(NH_3)_4\{P(OEt)_3\}_2]^{2+}$: (a) before oxidation and (b) after oxidation is completed. $C_{Ru} = 1.0 \times 10^{-3}$ M, $\mu = 0.10$ $NaCF_3COO$; pH = 3.0.

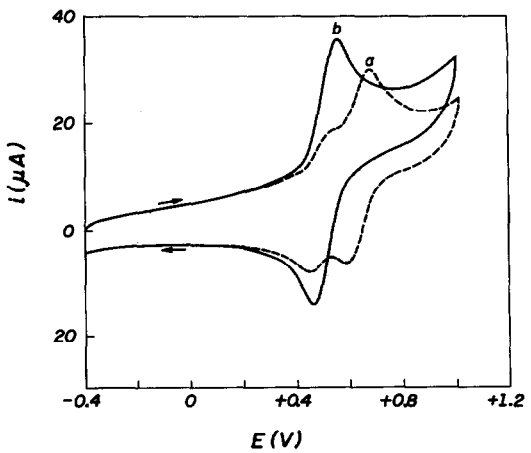

Fig. 2. Cyclic voltammogram containing the complex ions *rans*-$[Ru(NH_3)_4\{P(OEt)_3\}_2]^{2+}$: (a) 6 h after the oxidation and (b) after 70 h. $C_{Ru} = 1.0 \times 10^{-3}$ M, $\mu = 0.10$ $NaCF_3COO$, 25°C, scan rate = 200 mV s^{-1}.

From i_{pa} and i_{pc} data obtained from the voltammogram of the starting ruthenium(III) solution and the same solution after ageing for 50 h, it is possible to estimate that *ca* 80% of the original ruthenium(III) complex is still present in the mixture of the *trans*-$[Ru(NH_3)_4\{P(OEt)_3\}[H_2O)]^{3+/2+}$ ions.

From potentiometric measurements it was possible to estimate that the concentration of *trans*-$[Ru(NH_3)_4\{P(OEt)_3\}(H_2O)]^{3+}$ is less than 10% of the total ruthenium monophosphite complex present.

Similarly to the voltammetry, the electronic spectra of acidic solutions containing the *trans*-$[Ru(NH_3)_4\{P(OEt)_3\}_2]^{3+}$ complex ions also change with time. The absorbance at 292 nm decreases with the simultaneous increase of absorbance at 265 and 316 nm. After ageing for 70 h only one absorption maximum at 316 nm can be observed in the electronic spectrum. Therefore, in agreement with the voltammetric and potentiometric data the electronic spectra strongly suggest that *trans*-$[Ru(NH_3)_4\{P(OEt)_3\}(H_2O)]^{2+}$ is the final product.

Additional support for the above hypothesis was obtained by monitoring the decay of the *trans*-$[Ru(NH_3)_4\{P(OEt)_3\}_2]^{3+}$ species through ESR spectroscopy.

Frozen aqueous solutions of *trans*-$[Ru(NH_3)_4\{P(OEt)_3\}_2](PF_6)_3$ exhibit well-defined axial spectra with $g_\perp = 2.36$ and $g_\parallel = 1.83$ and without any hyperfine interaction (see Fig. 3).

Considering that ruthenium(III) is a low-spin $4d^5$ ion and that the experimental g-factors found are far from spin-only values and such that $g_\perp > g_\parallel$, we suppose the ion is subjected to a strong octahedral crystal field with tetragonal distortion. This is consistent with the observed absorption band at 292 nm, which points to a crystal field splitting of *ca* 34,000 cm^{-1} for the ^2D level. A low-spin $4d^5$ ion may be regarded as having a hole in the t_{2g} shell and an effective spin of $S = 1/2$. As a consequence we have an orbital triplet for the ground state and a negative spin orbit coupling constant. Under the combined action of the spin-orbit interaction and the crystal field distortion three Kramers' doublets may be considered.

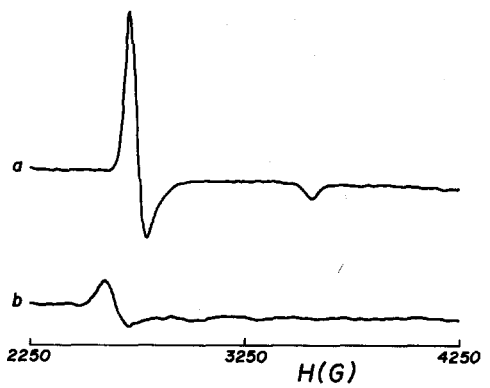

Fig. 3. EPR spectra of frozen solutions containing the complex ions *trans*-$[Ru(NH_3)_4\{P(OEt)_3\}_2]^{3+}$: (a) immediately after electrolysis and (b) 50 h after electrolysis. $C_{Ru} = 1.0\times10^{-3}$ M, $\mu = 0.10$ $NaCF_3COO$; gain = 5×10^3; scan time 2 min; scan range 2000 G; $t = 153$ K.

For the ground doublet the g values are given by the following expressions.[11-14]

$$g_\parallel = |(2+k)\cos 2\alpha + k| \quad (1)$$

$$g_\perp = |1+\sqrt{2}k\sin 2\alpha - \cos 2\alpha|, \quad (2)$$

where k is the orbital reduction factor for the magnetic electron and α is a parameter connected to the states of the ground doublet.

The axial splitting of the energy levels, δ, and the spin-orbit coupling parameter λ are related by the expression

$$\delta/\lambda = \sqrt{2}\cot 2\alpha - 1/2. \quad (3)$$

An exact fit to the experimental g values is obtained from eqs (1) and (2) with $k = 0.875$ and $\alpha = 1.398$. For a hole in the t_{2g} shell we take a value of $\lambda = -1000$ cm^{-1} for Ru^{3+} complexes,[15] which when taken in eq. (3) results in a value of $\delta = 4428$ cm^{-1}.

These results are similar to those found in a number of Ru^{3+} complexes studied in ESR experiments.[16-18]

After 50 h of ageing only a small concentration of paramagnetic species could be detected. This remaining paramagnetic species exhibited $g_\perp = 2.44$, a value very close to that of 2.429 reported for the *trans*-$[Ru(NH_3)_4\{P(OEt)_3\}(H_2O)]^{3+}$ ions.

As reported[7] for the *trans*-$[Ru(NH_3)_4\{P(OEt)_3\}(H_2O)]^{3+}$ ion, the stability of the *trans*-$[Ru(NH_3)_4\{P(OEt)_3\}_2]^{3+}$ species also depends on the hydrogen ion concentration of the solution. Table 1 summarizes the kinetic data for the *trans*-$[Ru(NH_3)_4\{P(OEt)_3\}_2]^{3+}$ ion decay in acidic media.

Table 1. Kinetic data for the *trans*-$[Ru(NH_3)_4\{P(OEt)_3\}_2]^{3+}$ ion decay

C_{H^+} (M)	k_{obs} (s^{-1})
0.0	2.3×10^{-5}
1.0	6.9×10^{-5}
2.0	1.1×10^{-4}
3.0	1.5×10^{-4}

Each value is the mean of at least three independent determinations with better than 90% agreement. $\mu = 0.1$ ($NaCF_3COO$), $C_{Ru} = 1.0\times10^{-3}$ M (25.0±0.2°C).

For the decay of *trans*-$[Ru(NH_3)_4\{P(OEt)_3\}(H_2O)]^{3+}$ experimental evidence supports[7] the disproportionation of the ruthenium(III) species, yielding ruthenium(II) and the mixture of ruthenium(IV) and ruthenium(VI) with a predominance of the latter. However, for the *trans*-$[Ru(NH_3)_4\{P(OEt)_3\}_2]^{3+}$ complex ions, as far as our experiments in acidic media are concerned, it is unlikely that a disproportionation reaction takes place.

Based on the experimental data and accumulated experience[1-7] in the chemistry of phosphorus as the ligand in ruthenium(II) and ruthenium(III) complexes, the tentative scheme below was suggested to explain the conversion of the *trans*-$[Ru(NH_3)_4\{P(OEt)_3\}_2]^{3+}$ ions into the *trans*-$[Ru(NH_3)_4\{P(OEt)_3\}_2]^{3+/2+}$ mixture.

$$\textit{trans}\text{-}[Ru(NH_3)_4\{P(OEt)_3\}_2]^{3+} \xrightarrow{\text{slow}} \textit{trans}\text{-}[Ru(NH_3)_4\{P(OEt)_3 \ldots P(OEt)_3\}]^{3+}$$

$$\textit{trans}\text{-}[Ru(NH_3)_4\{P(OEt)_3\}_2]^{3+} + \textit{trans}\text{-}[Ru(NH_3)_4\{P(OEt)_3 \ldots P(OEt)_3\}]^{3+} + H_2O \longrightarrow$$
$$\textit{trans}\text{-}[Ru(NH_3)_4\{P(OEt)_3\}(H_2O)]^{2+} + \textit{trans}\text{-}[Ru(NH_3)_4\{P(PEt)_3\}_2]^{2+} + (O)P(OEt)_3 + 2H^+$$

$$\textit{trans}\text{-}[Ru(NH_3)_4\{P(OEt)_3\}_2]^{2+} + H_2O \longrightarrow \textit{trans}\text{-}[Ru(NH_3)_4\{P(OEt)_3\}(H_2O)]^{2+} + P(OEt)_3$$

$$2\,\textit{trans}\text{-}[Ru(NH_3)_4\{P(OEt)_3\}(H_2O)]^{3+} + P(OEt)_3 + H_2O \longrightarrow$$
$$2\,\textit{trans}\text{-}[Ru(NH_3)_4\{P(OEt)_3\}(H_2O)]^{2+} + (O)P(OEt)_2 + 2H^+$$

$$\textit{trans}\text{-}[Ru(NH_3)_4\{P(OEt)_3\}_2]^{3+} + \textit{trans}\text{-}[Ru(NH_3)_4\{P(OEt)_3\}(H_2O)]^{2+} \longrightarrow$$
$$\textit{trans}\text{-}[Ru(NH_3)_4\{P(OEt)_3\}_2]^{2+} + \textit{trans}\text{-}[Ru(NH_3)_4\{P(OEt)_3\}(H_2O)]^{3+}$$

It is well known that the $P(OEt)_3$ molecule in acidic solution hydrolyses fast yielding $P(O)(H)(OEt)_2$, which is quite resistant to oxidation under these experimental conditions. On the other hand, it has been shown[1,3,7] that the coordinated phosphite molecule does not hydrolyse nor undergo oxidation as long as it is coordinated to a ruthenium(II) or ruthenium(III) centre.

Therefore, the $P(OEt)_3$ ligand needs to be activated to become reactive. This activation could be achieved when the phosphite molecule is in a semi-coordination position. In such a situation the $P(OEt)_3$ ligand would be positioned far from the ruthenium(III) centre at a distance between that of the coordinated phosphite and that of the free $P(OEt)_3$ molecule. Under these conditions the Ru^{III}—P^{III} bond is weakened and the ester becomes susceptible to oxidation by the collision of these excited ruthenium(III) complexes with other ruthenium(III) species.

Work is in progress in this laboratory aiming at improving the understanding of the mechanism of *trans*-$[Ru(NH_3)_4\{P(OEt)_3\}_2]^{3+}$ and *trans*-$[Ru(NH_3)_4\{P(OEt)_3\}(H_2O)]^{2+}$ decays. Results on this subject will be reported soon.

Acknowledgements—The authors are thankful to the Brazilian agencies FAPESP, CNPq and PRONACCAT for financial support and to Prof. Marcel Tabak for recording the ESR spectra.

REFERENCES

1. D. W. Franco and H. Taube, *Inorg. Chem.* 1978, **17**, 571.
2. D. W. Franco, *Inorg. Chim. Acta* 1979, **32**, 273.
3. D. W. Franco, *Inorg. Chim. Acta* 1981, **48**, 1.
4. S. M. C. Neiva, L. S. Santos, S. B. Araujo, J. C. Nascimento Filho and D. W. Franco, *Can. J. Chem.* 1987, **65**, 372.
5. R. L. Sernaglia and D. W. Franco, *Inorg. Chem.* 1988, **28**, 3485.
6. J. C. Nascimento Filho, J. M. Rezende, B. S. Lima Neto and D. W. Franco, *Inorg. Chim. Acta* 1988, **145**, 111.
7. J. M. Rezende, S. C. Martins, L. A. Marinho, J. A. V. Santos, M. Tabak, J. R. Perussi and D. W. Franco, *Inorg. Chim. Acta* 1991, **182**, 87.
8. D. D. Perrin, W. L. F. Almarengo and D. R. Perin, *Purification of Laboratories Chemicals*, 2nd edn. Pergamon Press, New York (1980).
9. L. H. Vogt, J. L. Katz and S. E. Wiberley, *Inorg. Chem.* 1965, **4**, 115.
10. C. G. Kvenk and H. Taube, *J. Am. Chem. Soc.* 1976, **98**, 689.
11. B. Bleaney and M. C. M. O'Brien, *Proc. Phys. Soc.* 1956, **1369**, 1216.
12. J. E. Wertz and J. R. Botton, *Electron Spin Resonance Elementary Theory and Practical Applications*, pp. 109, 324 and 335. McGraw-Hill Book Co., New York (1972).
13. A. Abragam and B. Bleaney, *Electron Paramagnetic Resonance of Transiton Ions*, Ch. XVIII. Clarendon Press, Oxford (1970).

14. J. H. E. Griffiths, J. Owen and I. M. Ward, *Proc. Roy. Soc.* (*A*) 1953, **219**, 526.
15. B. N. Figgs, J. Lewis, F. E. Mabbs and G. A. Webb, *J. Chem. Soc.* (*A*) 1966, 422.
16. R. E. De Simone and R. S. Drago, *J. Am. Chem. Soc.* 1970, **92**, 2343.
17. O. K. Medhi and U. Agarwala, *Inorg. Chem.* 1980, **19**, 1381.
18. S. Sakaki, Y. Yanase, N. Hagiwara, T. Takeshita, H. Naganuma, A. Ohyoshi and K. Ohkubo, *J. Phys. Chem.* 1982, **86**, 1038.

Polyhedron Vol. 12, No. 9, pp. 977–990, 1993
Printed in Great Britain

0277–5387/93 $6.00+.00
Pergamon Press Ltd

POLYHEDRON REPORT NUMBER 47

THE LIGAND POLYHEDRAL MODEL AND ITS APPLICATION TO THE BINARY CARBONYLS

BRIAN F. G. JOHNSON* and YVONNE V. ROBERTS

Department of Chemistry, The University of Edinburgh, West Mains Road, Edinburgh EH9 3JJ, U.K.

CONTENTS

1. INTRODUCTION 977
2. THE LIGAND POLYHEDRAL MODEL 980
3. ISOMERS 982
4. FLUXIONAL BEHAVIOUR 984
5. CARBONYL SUBSTITUTION 986
6. CONCLUSIONS 989

1. INTRODUCTION

This review gives an up-to-date account of the ligand polyhedral model (LPM) and its application to the binary carbonyls. The model not only offers a satisfactory explanation of the wide variety of structures observed for the binary carbonyls, but also offers an alternative view of their fluxionality and chemical reactivity.

Following the initial discovery of binary carbonyls[1] much effort, inspired by the pioneering work of Hieber,[2] was put into establishing and rationalizing their structures. For simple monometal systems, such as $Cr(CO)_6$, $Fe(CO)_5$ and $Ni(CO)_4$, this proved to be a relatively straightforward matter. Following the ideas of Sidgewick[3] on the effective atomic number (or 18-electron rule) led to a simple understanding of the metal : CO ratios and furthermore, the valence bond approach provided a clear understanding of the geometries of octahedral $Cr(CO)_6$ (d^2sp^3), trigonal bipyramidal $Fe(CO)_5$ (dsp^3) and tetrahedral $Ni(CO)_4$ (sp^3) (Fig. 1). Although the basic tenets of Gillespie and

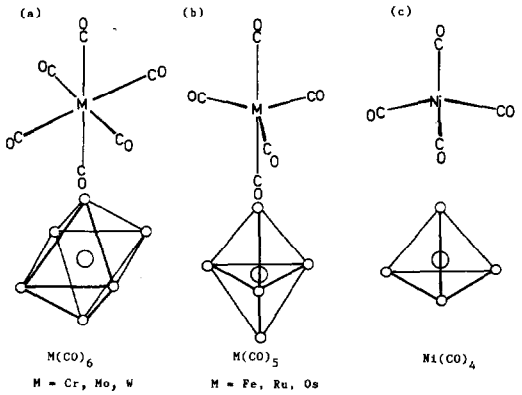

Fig. 1. The molecular structures of the simple mononuclear binary carbonyls.

* Author to whom correspondence should be addressed.

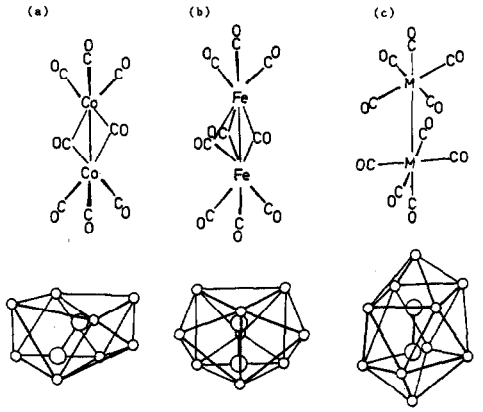

Fig. 2. The molecular structures of the binuclear carbonyls: (a) $Co_2(CO)_8$, (b) $Fe_2(CO)_9$ and (c) $M_2(CO)_{10}$ (M = Mn, Tc or Re).

Nyholm[4] are not strictly applicable to transition metal complexes, because of problems in deciding upon the location or effect of lone pairs in such systems, the observed geometrical forms fitted nicely with the overall picture of coordination geometry at that time.

Nor did the elucidation of the structures of $Co_2(CO)_8$,[5] $Fe_2(CO)_9$[6] and $Mn_2(CO)_{10}$[7] by X-ray diffraction present any major problems and, indeed, $Co_2(CO)_8$ [Fig. 2(a)] provided an early but classic illustration of the enormous value of X-ray diffraction methods in structural chemistry. Here was a structure which was special in that the molecule appeared bent or "book-shaped"; a description which persists to this day. It presented an early example of both μ_2-bridging CO ligands (i.e. one CO ligand bridging two metal atoms) and a "bent" or "banana-shaped" metal–metal bond. Equally intriguing was di-iron nonacarbonyl, $Fe_2(CO)_9$ [Fig. 2(b)], providing the first and only example of a dinuclear compound spanned by three CO bridges. This led to much speculation about whether or not an Fe—Fe bond was present in the molecule. As far as electron counting goes we assume there is, and this is supported by the observed diamagnetism and the Fe—Fe distance (2.56 Å) in the crystal state.

Dimanganese dodecacarbonyl was synthesized much later, but again its structure elucidation posed no major experimental problem and in another classic paper Dahl and Rundle described the structure shown in Fig. 2(c). The structure of $Mn_2(CO)_{12}$ was considered to be unusual in that the Mn—Mn bond was found to be considerably longer than anticipated (3.02 Å). No CO bridges were located and the 10 carbonyl ligands were shown to adopt a bicapped square-bipyramidal arrangement. Other binary carbonyls such as $Fe_3(CO)_{12}$[8] and $Co_4(CO)_{12}$[9] provided far more serious experimental difficulties but, after considerable effort, their molecular structures were also established. Tri-iron dodecacarbonyl, $Fe_3(CO)_{12}$, was considered extremely unusual in that it adopted

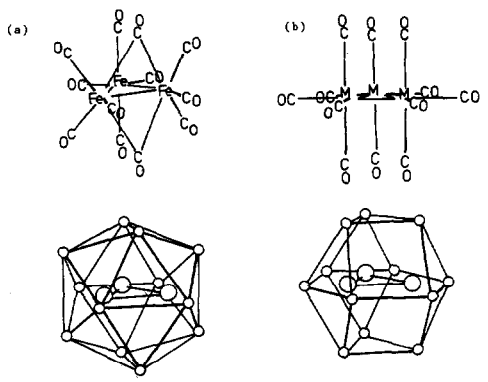

Fig. 3. The molecular structures of the trinuclear carbonyls: (a) $Fe_2(CO)_{12}$ and (b) $M_3(CO)_{12}$ (M = Ru or Os).

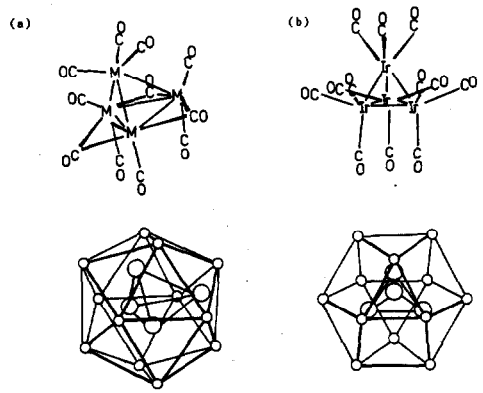

Fig. 4. The molecular structures of the tetranuclear carbonyls: (a) $M_4(CO)_{12}$ (M = Co or Rh) and (b) $Ir_4(CO)_{12}$.

what appeared to be a highly asymmetric structure, which resembled $Fe_2(CO)_9$ with one carbonyl bridge replaced by an $Fe(CO)_4$ unit [Fig. 3(a)]. In the paper reporting the correct structure of $Fe_3(CO)_{12}$, which had followed a series of erroneous predictions, Dahl commented on the apparent icosahedral arrangement of the 12 carbonyl ligands. The structural history of $Co_4(CO)_{12}$ closely paralleled that of $Fe_3(CO)_{12}$. Despite the employment of a wide range of physicochemical techniques, the correct structure was finally established much later and again by single-crystal X-ray diffraction analysis. The structure of $Co_4(CO)_{12}$ is remarkable in that, contrary to expectation, it is asymmetric with one unique cobalt atom [Fig. 4(a)]. The completion of the X-ray diffraction analysis of both $Fe_3(CO)_{12}$ and $Co_4(CO)_{12}$ was, and remains, a triumph for Dahl and his co-workers. The two structures show certain similarities. Both are more asymmetric than expected and both contain CO bridges supporting some (but not all) metal–metal vectors. In each case the 12 CO ligands adopt the same highly symmetric icosahedral form and this accounts for some of the problems encountered in the X-ray diffraction analysis.

The close relatives of $Fe_3(CO)_{12}$, viz. $Ru_3(CO)_{12}$ and $Os_3(CO)_{12}$, are quite different from $Fe_3(CO)_{12}$ itself. Both have virtually identical structures [Fig. 3(b)]. Triruthenium dodecacarbonyl shows a slight but significant distortion of carbonyl ligands, which may be taken as indicating a shift from an icosahedral towards an anticubeoctahedral arrangement,[10] whereas $Os_3(CO)_{12}$ adopts a more regular D_{3h} symmetry.[11] There are no bridges in either case and whereas there is considerable evidence to support a second, non-carbonyl bridged isomer of $Fe_3(CO)_{12}$,[12] no evidence for a bridged form of either $Ru_3(CO)_{12}$ or $Os_3(CO)_{12}$ exists.

In the cobalt series $Rh_4(CO)_{12}$ is very similar to the cobalt compound, although the X-ray data is not totally reliable because of the difficulties in growing a crystal suitable for analysis,[9,13] but $Ir_4(CO)_{12}$[14] has a tetrahedral M_4 core, with 12 terminally bonded CO ligands [Fig. 4(b)] forming a cubeoctahedron. With all these molecules the 18-electron rule may be applied satisfactorily, but beyond four metals the rule fails to reliably rationalize the observed cluster geometries and alternative methods of electron-counting must be applied.

Thus, the carbonyls have provided a remarkably interesting area for study. Many have highly useful catalytic activity[15] and all have proved to be invaluable precursors in organometallic chemistry.[15–17] Their physicochemical properties have proved an exceptionally fertile area of study and the fundamental questions raised by their unpredictable structures have provoked much theoretical debate.[17] Many are photosensitive[18] and the mechanism by which they undergo chemical reactions continues to provide a substantial challenge to chemists.

Several years ago[19] we developed ideas which we believe have been successful in permitting a better understanding of the structures and chemical behaviour of these apparently complicated compounds. These ideas also go a long way towards rationalizing the variety of isomeric forms and fluxional behaviour they frequently exhibit and help to explain the substitution chemistry they undergo. These ideas and, more especially, the development of the ligand polyhedral model (LPM) over the last 5 years[20] form the basis of this article.

2. THE LIGAND POLYHEDRAL MODEL

As we mentioned in the introduction workers in the area of cluster chemistry have often commented on the structural form or ligand geometry that the binary carbonyls adopt. For coordination compounds Gillespie, Nyholm and others regard the minimum energy ligand polyhedra as being the tetrahedron ($n = 4$), trigonal bipyramid ($n = 5$), octahedron ($n = 6$), pentagonal bipyramid ($n = 7$), square antiprism (or possibly dodecahedron) ($n = 8$), tricapped trigonal prism ($n = 9$), bicapped square antiprism ($n = 10$) and for 12-coordination the icosahedron (Fig. 5). In the main, but with notable exceptions for $n = 7$ or 8, these correspond to the polyhedra found for $Ni(CO)_4$, $Fe(CO)_5$, $Co(CO)_6$, $Fe_2(CO)_9$, $Mn_2(CO)_{10}$, $Fe_3(CO)_{12}$ and $Co_4(CO)_{12}$. These observations led us to consider the possibility that, just as in mononuclear coordination complexes, the geometry of the ligand shell in metal carbonyl clusters is determined not by the major bonding forces, but rather by the interaction between the ligands themselves. We argued that, at least for moderately spherical metal cluster units, such as the triangle or tetrahedron, the same principles employed for mononuclear systems might be extended to include the carbonyl clusters. This model, when applied to mononuclear systems, is frequently referred to as a ligand repulsion model,[21] a term we do not fully accept but which does give a reliable guide to ligand geometries. If our proposals are valid then we might expect the same regular or semi-regular geometries to be found in cluster systems. We further postulated that the number and type of CO ligands (i.e. terminal or bridging) present would then depend upon the possible arrangements of one polyhedron or polygon (the metal cluster unit) within the other (the CO envelope). Thus, for the 12 CO ligands of $Fe_3(CO)_{12}$ we predicted that optimum geometry to be an icosahedron and that the formation of two CO bridges along one Fe—Fe vector would be a direct result of packing an Fe_3 triangle within that CO icosahedron. This corresponds exactly with the observed structure. The icosahedron is also observed for $Co_4(CO)_{12}$ and $Rh_4(CO)_{12}$ and the three O bridges spanning the basal M—M vectors are again a consequence of inserting the M_4 tetrahedron into that icosahedron. Thus, our argument is based purely on geometric arrangements and there is no need to consider directed valence bonds.

The same logic clearly applies to $Fe_2(CO)_9$ and $Mn_2(CO)_{10}$. In each case the optimum CO geometry, viz. the tricapped trigonal prism and the bicapped square antiprism, respectively, are found. The insertion of the linear M—M unit into the tricapped trigonal bipyramid naturally leads to a structure with three CO bridges, where insertion into a bicapped square antiprism leads to a form in which no bridges are generated. Thus, for many of the simpler binary carbonyls, their structures are readily understood on a straightforward geometric basis.

Problems arise, however, when we consider $Co_2(CO)_8$, $Ru_3(CO)_{12}$, $Os_3(CO)_{12}$ or $Ir_4(CO)_{12}$. Here the *optimum* CO geometry is not found. Again, the problem may be resolved within the terms of the ligand polyhedral model. If we assume that the CO ligand is *quasi*-spherical with a centre

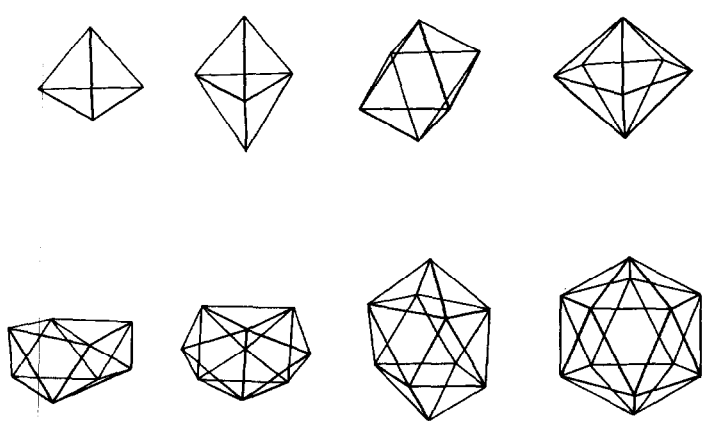

Fig. 5. The "low energy" polyhedral forms found in coordination compounds ML_n (for $n = 4$–10 and 12).

localized on the oxygen atom, then a radius of 3.0 Å may be estimated (or derived empirically)[19] and stems from the synergic nature of the M—C—O bond. As the M—C bond strengthens (or shortens) the C—O bond weakens (or lengthens), hence the M···O distance remains more-or-less constant. This is fortunate since it allows the estimated radius of the CO to be transferred from one binary carbonyl to another, almost irrespective of the metal concerned. However, it must be remembered that this is an estimated value (although it may be derived empirically from a study of the multitude of structures now available) and puts a severe limitation on the model. Taking this value of *ca* 3.0 Å we can, using the sample radius ratio ideas applied to infinite solid-state structures (especially ionic solids), compute the size of the interstitial holes within the polyhedra described by the CO ligands. Thus, for eight CO ligands we can easily establish that a dodecahedron has a hole of radius 2.4 Å. This is too small for a Co_2 unit with a predicted bond length of 2.5 Å and a square antiprism would lead to a Co—Co distance of *ca* 3.0 Å [cf. $Mn_2(CO)_{10}$], which is too long. However, for the intermediate polyhedron, the tricapped trigonal prism, a Co—Co bond length of 2.50 Å is generated, in line with the predicted requirements. Hence, for $Co_2(CO)_8$ the second most favourable geometry, viz. the bicapped trigonal bipyramid, is observed. It is now easier to appreciate the unusual bent-shape of the molecule. The "hole" in the structure corresponds to the missing vertex of a tricapped trigonal prism [i.e. $Co_2(CO)_8$ has an *arachno* nine-vertex structure]. Nevertheless, we must expect that closely related structures based on a dodecahedron or square antiprismatic arrangement of CO groups will lie in additional potential energy wells. Thus, we might anticipate that under the right conditions (e.g. on interaction with solvent) these alternative forms might also exist and it is noteworthy that several isomeric forms of $Co_2(CO)_8$ have been reported. We would argue that these isomers correspond (in part) to the different geometries available for eight carbonyl ligands.

The same explanation may be used to account for the change in structure observed in going from $Fe_3(CO)_{12}$ to $Ru_3(CO)_{12}$ or $Os_3(CO)_{12}$. For a CO icosahedron with a radius ratio of 0.95 Å it can be shown that an Fe_3 triangle with Fe—Fe bond lengths similar to those found in the bulk metal (2.5 Å) can be accommodated, whereas the larger Ru_3 or Os_3 unit (Ru—Ru 2.75, Os—Os 2.75 Å) cannot. These larger triangles will, however, fit into an anticubeoctahedron with a radius ratio of 1.00 Å and consequently a larger interstitial site. Placement of an M_3 triangle within an anticubeoctahedron leads to the observed all-terminal structure. Precisely the same arguments may be applied to the change in structure (or polyhedral form) on going from $Co_4(CO)_{12}$ (icosahedron) to $Ir_4(CO)_{12}$ (cubeoctahedron).

Thus, the model works well in attempts to rationalize the structures of the simpler binary carbonyls. It may be easily extended to embrace more complicated systems such as $Rh_6(CO)_{16}$ (an Rh_6 octahedron within the best 16-vertex polyhedron; the tetracapped truncated tetrahedron)[22] or $Co_6(CO)_{14}^{4-}$ (a Co_6 octahedron within the optimum 14-vertex polyhedron; the *omni*-capped cube).[23] These structures are illustrated in Fig. 6.

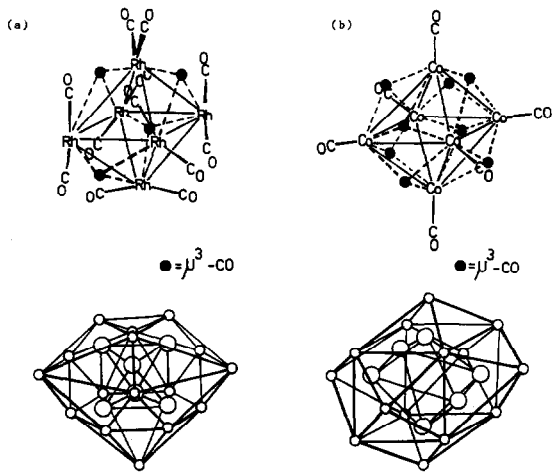

Fig. 6. The molecular structures of: (a) $Rh_6(CO)_{16}$ and (b) $Co_6(CO)_{14}^{4-}$.

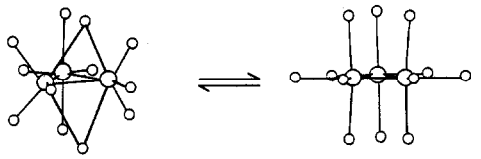

Fig. 7. A postulated rearrangement for the interconversion of the bridged form (C_{2v}) and the non-bridged (D_{3h}) form of $Fe_3(CO)_{12}$.

3. ISOMERS

A common feature of many of these compounds is the apparent ease with which they undergo structural change with a change in the environment. The classic example in this regard must be $Fe_3(CO)_{12}$, which in solvents changes structure from the bis-μ_2 form (C_{2v}) to a non-bridged form (D_3).[24] At one time it was assumed, for obvious reasons, that this non-bridged form corresponded to an $Ru_3(CO)_{12}$ structural type.[25] It has been argued that the two CO bridges simply opened out to give the non-bridged $Ru_3(CO)_{12}$ form (see Fig. 7). However, detailed examination of the observed IR spectrum of the new species [in the ν(CO) stretching region] revealed that the spectrum is not compatible with a *pseudo*-$Ru_3(CO)_{12}$ arrangement.[19]

In 1976 we offered an alternative view. Given that the 12 CO ligands adopted an icosahedral arrangement, we recognized that within this polyhedron three orientations of the Fe_3 triangle were possible and that they were related by a simple librational motion. These orientations correspond to the solid state (C_{2v}) μ_2-bridged form [Fig. 8(a)], a new all-terminal form (D_3) [Fig. 8(b)] and a C_2 μ_3-bridged form [Fig. 8(c)]. The ease by which interconversion might occur, combined with the observation that the IR spectrum of a D_3-form corresponded closely to that recorded, led us to suggest that the existence of a second isomeric form based on the same icosahedron of carbonyl ligands was preferable to the D_{3h} anticubeoctahedral form.[19] Nevertheless, we would emphasize that the possibility of conversion to an anticubeoctahedral or cubeoctahedral ligand envelope, both of which are expected to occupy potential energy wells, cannot be entirely discounted.

Similar arguments have also been applied to explain the several isomers of $Co_2(CO)_8$ which apparently exist.[26] In our discussion of this molecule above, we pointed out that several closely related carbonyl polyhedra could exist and that interconversion between these forms would be a relatively facile process. This process is illustrated in Fig. 9, where it can be seen that the sequential cleavage of single polyhedral edges would lead progressively from the dodecahedron [Fig. 9(a)], through the bicapped trigonal prism observed in the solid [Fig. 9(b)] to the square antiprism, which is clearly based on the non-bridged arrangement of carbonyls found for $Mn_2(CO)_{10}$ [Fig. 9(c)].

In addition, and just as with $Fe_3(CO)_{12}$, we might anticipate that the Co—Co dimer will undergo libration within the various carbonyl polyhedra. This librational motion, which will be synchronized with a Co—Co bond stretch, will not be independent of the polyhedral interconversion. Indeed, the

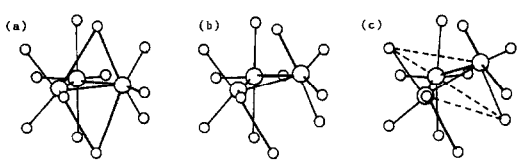

Fig. 8. The three isomeric forms of $Fe_3(CO)_{12}$, based on the icosahedral distribution of carbonyl ligands: (a) C_{2v}, (b) D_3 and (c) $C_{2v}(2)$.

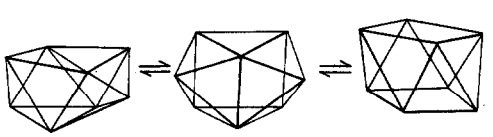

Fig. 9. The carbonyl polyhedra expected for $Co_2(O)_8$.

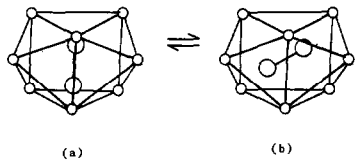

Fig. 10. The interconversion of two possible isomeric forms of $Co_2(CO)_8$ by libration of the Co—Co vector through a two-fold axis within the bicapped trigonal prism and carbonyl ligands.

two processes will occur simultaneously, although the contribution of each to the rearrangement will be dependent on phase and temperature. It is apparent that the same librational motion can occur within the dodecahedron or square antiprism, as in Fig. 10, leading to a variety of bridged and non-bridged isomeric forms of $Co_2(CO)_8$, or indeed any $M_2(CO)_8$ species.

Related to these observations are the isomeric forms observed for $Ir_6(CO)_{16}$.[22] We have commented on the molecular structure of $Rh_6(CO)_{16}$ above. One form of $Ir_6(CO)_{16}$ is isostructural with the Rh_6 analogue, with two terminal CO groups per metal atom and four face-bridging CO groups occupying the corners of a tetrahedron (corresponding to the four caps of the tetracapped truncated tetrahedron). The second isomeric form has a very similar structure, except that the four bridges now span four metal–metal edges of the Ir_6 octahedron but still occupy the four corners of a tetrahedron within the same tetracapped truncated tetrahedron. In other words, the CO polyhedron is the same in each case. The two isomers are related by the simple rotation of the metal octahedron about an octahedral (Ir_6) C_4 axis. This rotation simply changes μ_3-bridges into μ_2-bridges and back again. These observations emphasize the importance of similar motions to those employed to account for the formation of different isomers of $Fe_3(CO)_{12}$, except in that case they cannot be characterized independently in the solid.

Similar arguments can be applied to $Co_4(CO)_{12}$. Again, there is more than one orientation of the metal tetrahedron within the icosahedron. The two most obvious possibilities are shown in Fig. 11 and are related by rotation about the C_3 axis through the unique cobalt atom in this Co_4 tetrahedron. Other possibilities exist. These are derived either by rotation about the other available *pseudo*-C_3 axis (of the Co_4 tetrahedron) through a basal cobalt atom or by rotation through a *pseudo*-C_2 axis of the Co_4 tetrahedron. Circumstantial evidence derived from an examination of the a.d.p.s[19] would favour rotation about the primary C_2 axis, according to Fig. 11.

Further possibilities exist. Given that $Ir_4(CO)_{12}$ adopts a cubeoctahedral distribution of carbonyl groups, $Co_4(CO)_{12}$ could do the same. However, another possibility is that the CO groups could rearrange into another closely related polyhedron, viz. the anticubeoctahedron, as observed with $Ru_3(CO)_{12}$ (see Fig. 12). All are related by a comparatively small motion, either of the Co_4 tetrahedron by libration or the polyhedral rearrangement of the carbonyl envelope.

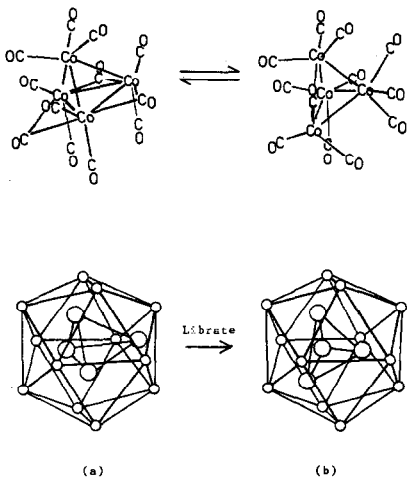

Fig. 11. Interconversion of C_{3v} and T forms of $Co_4(CO)_{12}$ by libration about the unique C_3 axis of the Co_4 tetrahedron in the $(CO)_{12}$ icosahedron.

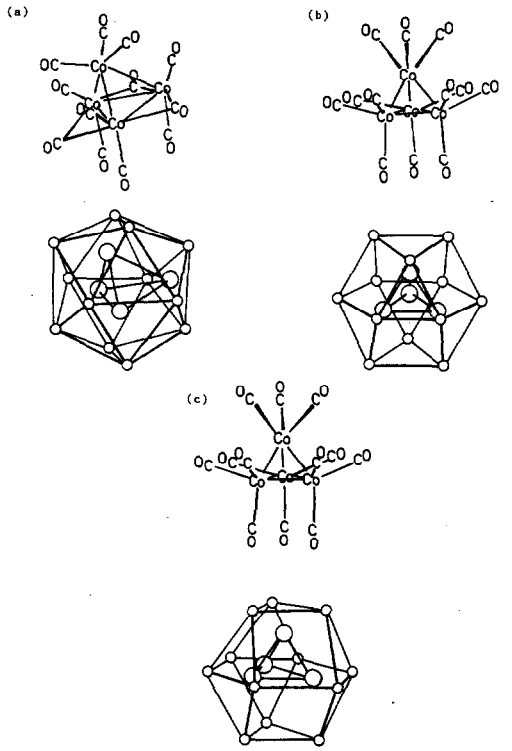

Fig. 12. The three possible polyhedral forms for $M_4(CO)_{12}$ (M = Co, Rh or Ir): (a) icosahedron, (b) cubeoctahedron and (c) anticubeoctahedron.

There has been some confusion as to the true nature of these librational motions. First, it is difficult to obtain direct evidence for such movement, but examination of the a.d.p.s in both $Fe_3(CO)_{12}$[19] and $Co_4(CO)_{12}$ provides some support for the proposals offered. However, it must be appreciated that such evidence must, at best, be tentative given the unreliability of the structural data currently available. Secondly, there has been some confusion with regard to the motion itself. Clearly, in solution it does not matter whether the motion is regarded as that of the metal unit with a stationary carbonyl polyhedron or *vice versa*. In the solid the movement of the metal unit must dominate. Obviously, movement of the carbonyls within a crystalline lattice will be severely restricted unless there are special circumstances as with $Co_2(CO)_8$. Major movement will lead first to phase transition and ultimately to the complete degradation of the lattice. It is important to appreciate that the relative masses of the cluster units and CO polyhedra in question are not that different, e.g. Fe_3 168, Co_4 236, $(CO)_{12}$ 336. As the relative mass increases (as, for example, with Os_3 588), then librational motion of the metal unit will be restricted accordingly and here it is more reasonable to consider that the motion corresponds to that of the CO polyhedron about the metal unit. This will be discussed in more detail in the section below devoted to fluxional behaviour.

The main advantages of the approach offered here are clear to see. First, the frequent observation of isomeric forms of many of the binary carbonyls is easily understood. The model allows us to appreciate more fully how these different forms or isomers might arise. In this sense it is no different from mononuclear coordination chemistry where such phenomena are frequently encountered as, for example, with five-coordinate species which exhibit both trigonal bipyramidal and square-based pyramidal forms and seven-coordinate complexes with bicapped pentagonal and monocapped octahedral geometries. The ideas put forward here are a natural extension of the geometric isomers observed in monometal coordination systems.

4. FLUXIONAL BEHAVIOUR

The carbonyls have a unique place in studies of fluxional behaviour.[25,27] The observation that they are able to undergo structural rearrangement on the NMR timescale, combined with their

relative ease of study, has made them ideal examples of this fundamentally important and interesting phenomenon. Fluxional behaviour simply tells us that the molecule has a number of closely related structures accessible by relatively low energy barriers. In that sense it is immediately clear why the LPM may be so easily applied. Fluxional behaviour also tells us that the precise direction of the chemical bonds coming out of the central cluster unit is not important (just as with mononuclear systems). In mononuclear systems it is usual to describe intermolecular rearrangements in terms of polyhedral interconversions. The classic example must be the Berry *pseudo*-rotation mechanism[28] for the fluxional behaviour exhibited by five-coordinate ML_5 systems, in which the scrambling of the five ligands (two axial, three equatorial) is envisaged as occurring through a square-pyramidal *complementary geometry*. This view is widely taught at the undergraduate level. This approach is easily extendable to higher polyhedra and we have suggested that a simple methodology involving successive edge cleavage may be applied in order to understand the motion of ML_n ligand polyhedra for values of n from 4 to 12. It may also be extended to embrace clusters. Provided that the central cluster unit is spherical (or nearly so), there is little difference between mononuclear systems of the type ML_n and polynuclear systems of the type M_mL_n. For carbonyl clusters with two to four metal atoms the problem is slightly more complicated because of the larger values of n involved and less is known of the rearrangement patterns of these larger polyhedra ($n > 12$). Nevertheless, in principle, the same rules apply and the only difficulty lies in establishing or deciding upon the correct complementary geometry. This is an alternative way of looking at carbonyl fluxionality and differs from that developed historically[29] (and still widely applied) which considers only localized carbonyl migrations. We believe this localized view cannot be correct and believe that the motion of carbonyl ligands about a central metal unit must be concerted.

Unlike the mononuclear systems, however, there is a further contribution to fluxionality which is extremely important and certainly of great significance to motion in the solid state. This is the idea that the cluster metal core may librate without the motion of the carbonyl polyhedron and *vice versa*. In this case the carbonyl polyhedron retains its integrity throughout and individual CO ligands do not undergo interchange within the total polyhedron. Thus, for an icosahedral arrangement, the antipodal relationships are constant, no matter how the relationship they have with the internal metal unit may change (terminal, edge-bridging-μ_2 or face-bridging-μ_3).

If we consider, for example, the fluxional behaviour of $Fe_3(CO)_{12}$. This is a particularly surprizing example in that even at the very lowest accessible temperatures the process cannot be stopped and the ground-state structure revealed by ^{13}CO NMR spectroscopy. The conventional explanation has been a bridge open $\rightleftarrows$ close motion of the sort outlined in Fig. 7. More recently, it has been suggested that this is incorrect and that the motion may be viewed as being totally concerted,[30,33] and as bridges open along one edge bridges close along another. In our view, as expressed in 1976, the low energy fluxional pathway exhibited by $Fe_3(CO)_{12}$ involves the simple libration of the Fe_3 triangle about its unique C_2 axis in the carbonyl icosahedron; or, as an alternative which we gave at the time, the motion of the "totally preserved" icosahedron about the central metal triangular unit (Fig. 13). This we believe to be exactly the same as the concerted motion discussed above.[30,33]

Very similar arguments may be applied to $Co_4(CO)_{12}$ or $Rh_4(CO)_{12}$. Again, migration of the "preserved icosahedron" about the central metal tetrahedron is exactly the same as saying that as one set of bridges open a new set are formed. There is no difference in outcome.

So much for the lowest energy process. For higher energy processes we must now invoke, in addition to metal libration, the idea of polyhderal interconversion of the type outlined above. However, it is important to reiterate at the outset that the two motions, libration and polyhedral interconversion, are not independent but are closely related. The contribution each makes to the

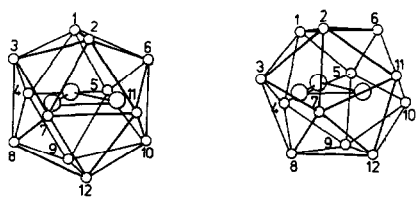

Fig. 13. Rotation of CO icosahedron about the internal Fe_3 triangle.

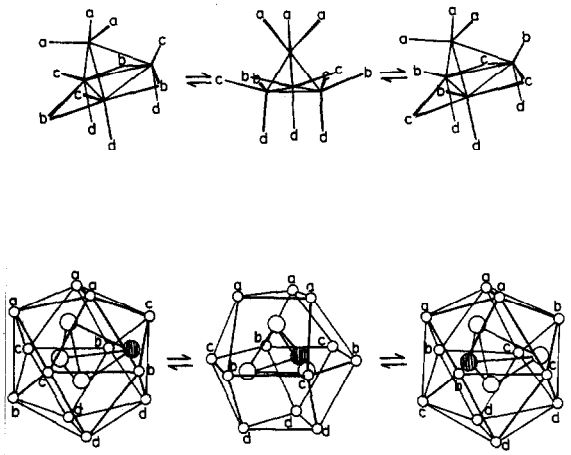

Fig. 14. (a) One of the five modes of polyhedral interconversion for $M_4(CO)_{12}$. The three original bridges (b) move to basal axial positions (c).

overall fluxional process will depend not only on the phase and temperature but also, as we indicated above, on the relative masses of the M_m and $(CO)_n$ units. Thus, libration may be more important in one instance and polyhedral interconversion in another. Irrespective of the circumstances, we would argue that the motions will be *symmetry controlled* and, as such, generally predictable.

If we apply these arguments to $Fe_3(CO)_{12}$ and its derivatives we would expect librational motion to dominate any fluxionality observed in the solid, while a combination of libration and polyhedral interconversion would take place in solution. Following the procedures laid down by Dunitz and Burgi[31] it has been possible to show, from an examination of a number of crystallographic structure determinations for a wide range of $M_3(CO)_{12-n}L_n$ systems (M = Fe, Ru, Os; L = ligand), that the most likely complementary geometry for the fluxional process is the anticubeoctahedron[32] and that libration or reorientation of the M_m and $(CO)_n$ polyhedra does occur.

Similarly, the same ideas may be applied to $M_4(CO)_{12}$ compounds and their derivatives. Again, the rotation of one polyhedron relative to the other is sufficient to bring about the observed low energy process and similar polyhedral conversion will apply to additional processes at higher temperatures. It is difficult to establish these processes by direct experimental means, but examination of the molecular structures of substituted derivatives of the type $M_4(CO)_{11}L$ and $RhCo_3(CO)_{12}$ has given support to the overall mechanism suggested. A special advantage of the LPM, and the fact that it is symmetry governed, is that the number of potential (although not necessarily observable) mechanistic pathways may be predicted. Put simply, for the icosahedron there are five degenerate pathways to the cubeoctahedron or the anticubeoctahedron. Substitution of a carbonyl group in the CO polyhedron by, for example, a tertiary phosphine ligand L will remove this degeneracy in a manner totally predictable from symmetry arguments. Similarly, exchange of one metal within the tetrahedron, for example forming $RhCo_3(CO)_{12}$, will also lift the degeneracy in a predictable way. By this means both the number and type of fluxional processes may be predicted.

A feature of the polyhedron interconversion process is that it does not exclude the conventional terminal $\rightleftarrows$ bridge mechanisms previously suggested, but argues that these correspond to one of the five degenerate modes. This is illustrated in Fig. 14 for $Co_4(CO)_{12}$. Other modes lead to movements which involve, apparently, highly unusual migration. Thus, for $M_4(CO)_{12}$ one mode leads to the prediction that a μ_2-CO bridge around the basal plane migrates to the apical metal atom across a tetrahedral face. This is in accord with recent suggestions based on detailed NMR structures of $Ir_4(CO)_{10}$(diars).[33]

5. CARBONYL SUBSTITUTION

The application of the LPM relies upon the use of a CO radius of *ca* 3.0 Å. Clearly, if a CO ligand is replaced by a ligand L, with a different cone angle, then the radius ratio will change and the size of the interstitial hole will vary accordingly. Thus, substitution of CO by large, bulky

phosphines will lead to larger interstitial holes for the ligand polyhedron. As a consequence, conversion of the polyhedron from a less favourable to a more favourable geometry may occur. This is best illustrated by the series of substituted derivatives of $Ir_4(CO)_{12}$, viz. $Ir_4(CO)_{12-n}L_n$ (n = 1–3).[34] As the larger ligand L is inserted into the molecule the ligand arrangement is modified from the less favourable cubeoctahedron towards the lower energy and thus more favourable icosahedron. This change will bring about the modification of the structure from the T_d ground state to the C_{3v} ground state and the formation of three basal bridging ligands, as is observed experimentally.

For those systems for which the minimum energy polyhedron, e.g. the icosahedron, is already present, as in $Fe_3(CO)_{12}$, the insertion of bulkier ligands will bring about a lengthening and hence weakening of the M—M bond. Thus, rather than simple structural modification, the tendency to undergo fragmentation will be enhanced.

Since the lowest energy polyhedron is more readily accessible to the smaller metal ions of the first transition metal series, which are known to have the lowest metal–metal bond energies, it follows that the first series are the most susceptible to fragmentation. Although, for all metal cluster compounds, the insertion of several bulky ligands will lead first to the lower energy polyhedron and then subsequently to fragmentation.

The substitution reactions of the cluster carbonyls of the iron and cobalt triads have been explored in some detail, but the mechanism(s) by which these reactions occur remains a matter of some debate.[35] The higher cluster carbonyls containing greater than four metal atoms have been investigated far less extensively. In general, two mechanisms have emerged for the fragmentation of small clusters. The original proposal considered that the reaction of, for example, $Ru_3(CO)_{12}$ with PBu^n_3 occurs via a radical pathway in which the triangular metal unit undergoes complete fragmentation into three radical species. These 17-electron radicals are then considered to undergo substitution, followed by recombination to produce the substituted trimer.

The alternative suggestion, that the important step is CO-dissociation generating the coordinatively unsaturated (46-electron) system $M_3(CO)_{11}$, is very attractive, especially when one recalls the similar behaviour shown by a range of the simpler carbonyl systems.[36] Certainly, it ties in well with much of the reported kinetic data. Nevertheless, it fails to explain much of the more detailed aspects of the substitution reactions described by several groups of independent workers (see ref. 35). If we consider this approach in detail we must also examine the geometrical implications of the carbonyl envelope or polyhedron. It is interesting to note in this connection that whereas the geometry of the complex is regarded as important in kinetic studies of mononuclear systems, as far as we are aware the implications of ligand geometry are completely ignored in considerations of cluster systems. As described above, in the parent molecule, $Fe_3(CO)_{12}$, the carbonyl ligands described an icosahedron, whereas in both $Ru_3(CO)_{12}$ and $Os_3(CO)_{12}$ the polyhedron is found to be the less favourable anticubeoctahedron. The dissociation of CO from $Fe_3(CO)_{12}$ would lead therefore to a *nido*-icosahedral array, which, contrary to current opinion, leads to a remarkably open array of CO groups with a very spacious pentagonal face open to incoming substrate (Fig. 15). In this case steric effects, i.e. the bulk of the entering nucleophile, would be minimized and less restrictive than an attack on, for example, a square pyramidal intermediate in the substitution of an octahedral complex. With the corresponding derivatives of ruthenium and osmium, CO dissociation would lead to an even more open polyhedron of CO ligands in the *nido*-anticubeoctahedron. On these grounds it is difficult to understand the observed change in the k_2 term and particularly difficult to appreciate the main difference in behaviour between the compounds of ruthenium and osmium, given the similarity of both their ligand polyhedral shells and the metal–metal bond distance, for the dissociative process.

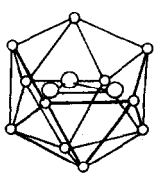

Fig. 15. The *nido*-icosahedral array of 11 ligands in the intermediate $M_3(CO)_{11}$ (M = Fe, Ru or Os).

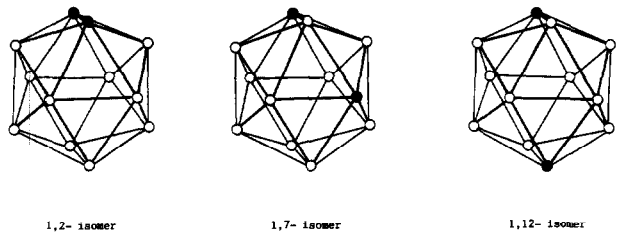

Fig. 16. Icosahedral 1,2-, 1,7- and 1,12-isomers.

Further substitution of CO by L in $M_3(CO)_{11}L$ to give first $M_3(CO)_{10}L_2$ and eventually $M_3(CO)_9L_3$ also requires a more detailed assessment. Firstly, we must again consider the geometry of the ligand envelope and take note of the fact that as substitution of CO by L occurs (for Ru and Os), there is a concomitant change in the geometry of the ligand shell from basically anticubeoctahedron towards quasi-icosahedral. The reasons for this fundamental change have been discussed in detail above, but the important point as far as we are concerned here is that in our consideration of the substitution reactions of $M_3(CO)_{12}$ and $M_3(CO)_{12-n}L_n$ we must remember that we are not strictly comparing substitution patterns of compounds with the same ligand geometry.

Consideration of the ligand polyhedral shell also reveals that for the bis-substituted derivatives, $Fe_3(CO)_{10}L_2$, we have three potential ligand distributions within the icosahedron, viz. the 1,2-, 1,7- and 1,12- forms (Fig. 16). Clearly the 1,2-disubstituted form requires the two ligands L to occupy adjacent positions and unless these ligands are smaller than CO, on steric grounds this will be unfavourable. The 1,7-form is more desirable since the two ligands will not be isolated from each other and, finally, in the 1,12-form we might argue that we have the most favourable arrangement, which minimizes any L—L interaction.

Finally, for the tris-substituted complex a 1,7,9-tri-substituted ligand icosahedron is expected if all ligands L are to occupy positions which minimize their interaction. If we accept the CO-

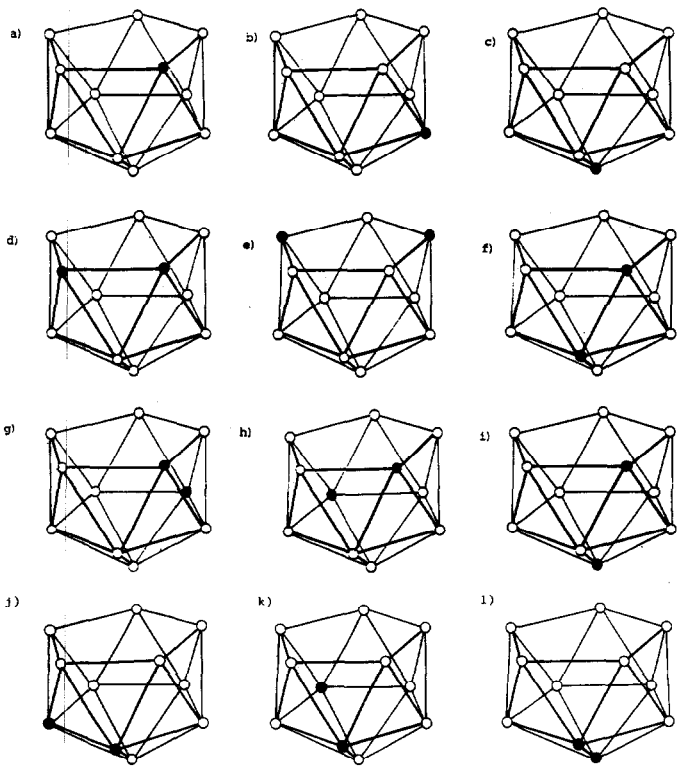

Fig. 17. The various isomeric forms of the *nido*-icosahedral ligand shell in $Fe(CO)_{10}L$ and $Fe_3(CO)_9L_2$.

dissociation mechanism we can imagine that dissociation of CO from $Fe_3(CO)_{11}L$ to produce the reactive intermediate $Fe_3(CO)_{10}L$ may occur in at least two distinct ways. First to produce a pentagonal ligand face containing L as in Fig. 17(a), or without L as in Figs 17(b) or (c). Further substitution to generate $M_3(CO)_9L_3$ would require L addition to the unsaturated intermediate $M_3(CO)_9L_2$, for which it is also possible to present vacant or occupied pentagonal faces [Figs 17(d)–(l)]. The presentation of L onto the open face (17k) would appear to present the least steric problems and would lead to the tris-substituted product, with significantly an equally disposed set of three L ligands (1,7,9).

Thus, we must conclude that although the CO dissociation mechanism is clearly attractive, little attention appears to have been paid to the more detailed geometric aspects of this route. It certainly fits the data far better than complete homolytic fission and is in line with current thought on simpler carbonyl systems. Neverthelesss, we have recently put forward another and, to us, more attractive explanation, which we have described elsewhere[37–39] and which we believe accounts more satisfactorily for the diverse set of observations made on these systems and outlined above. This approach differs from those described above in that the process of substitution is regarded as associative and requires the initial fragmentation of the metal–metal bond. Since our original suggestion,[37] similar ideas have been proposed[38] and a variety of structures having a cleaved metal–metal bond have been proposed to describe possible intermediates formed by ligand addition. Significantly, the cleavage and re-formation of metal–metal bonds by the addition and elimination of nucleophiles has been observed for some high nuclearity clusters and for other small clusters with bridging ligands.[40–46] Very recently, Adams and his co-workers have observed the formation of the two addition products $Os_3(CO)_{11}(\mu\text{-}CNCF_3)_2$ and $Os_3(CO)_{10}(NCMe)(\mu\text{-}CNCF_3)_2$ as the products of the reaction of $Os_3(CO)_{12-n}(NCMe)_n$ ($n = 1$ or 2) with $CNCF_3$. These may be regarded as stabilized derivatives of the unknown binary carbonyl $Os_3(CO)_{13}$ and a possible structural model for the intermediate addition product of the type described above. Thus, direct evidence for the cleavage of a metal–metal bond during the reaction sequence leading to a bis-substituted derivative has been found, providing direct experimental support for this new approach.[47]

6. CONCLUSIONS

In this account we have attempted to illustrate the usefulness of the ligand polyhedral model in the rationalization of cluster carbonyl structures. We hope we have also demonstrated its versatility in its application to the fluxional behaviour, isomeric formation and reaction mechanisms and kinetics of these fascinating systems. It is clear that there remains much more to do. More experimental evidence is required to support much of the work reported here and we are aware of some of the criticism levelled at this approach. Nevertheless, we are convinced that this method, which considers the molecular structure as a whole, offers a more understandable and more general view of these truly beautiful compounds.

Acknowledgements—We wish to thank our colleagues at Cambridge and elsewhere for their many helpful comments over the years. We would especially like to acknowledge our many helpful and vigorous discussions with Professor Lord Lewis (Cambridge), Professor Ken Wade (Durham) and our energetic co-workers Professor Dario Braga and Fabrizia Grepioni (Bologna).

REFERENCES

1. J. Dewar and H. O. Jones, *Proc. Roy. Soc.* 1906, **A79**, 66.
2. W. Hieber, *Adv. Organomet. Chem.* 1970, **8**, 1.
3. (a) N. V. Sidgwick, *The Electronic Theory of Valency*. Oxford University Press, Oxford (1928); (b) N. V. Sidgwick and N. Powell, *Proc. Roy. Soc. (London)* 1940, **A176**, 153.
4. R. J. Gillespie and R. S. Nyholm, *Q. Rev. London* 1957, **11**, 339.
5. G. G. Sumner, H. P. Klug and L. E. Alexander, *Acta. Cryst.* 1974, **17**, 732; P. C. Leung and P. Coffens, *Acta Cryst.* 1983, **B39**, 535.
6. F. A. Cotton and J. M. Troup, *J. Chem. Soc., Dalton Trans.* 1974, 800.
7. (a) L. F. Dahl and R. E. Rundle, *Acta Cryst.* 1963, **16**, 419; (b) M. Martin, B. Rees and A. Mitschler, *Acta Cryst.* 1982, **B38**, 6.

8. (a) L. F. Dahl and R. E. Rundle, *J. Chem. Phys.* 1957, **26**, 175; (b) C.-H. Wei and L. F. Dahl, *J. Am. Chem. Soc.* 1969, **91**, 1351; (c) F. A. Cotton and J. M. Troup, *J. Am. Chem. Soc.* 1974, **96**, 4155.
9. C.-H. Wei, *Inorg. Chem.* 1969, **8**, 2384.
10. M. R. Churchill, F. J. Hollander and J. P. Hutchinson, *Inorg. Chem.* 1977, **16**, 2655.
11. J. J. DeBoer, J. A. Van Downs and C. Masters, *J. Chem. Soc., Chem. Commun.* 1978, 1005.
12. B. E. Hanson, E. C. Lisic, J. T. Perry and G. Lannoconne, *Inorg. Chem.* 1986, **25**, 4062.
13. C.-H. Wei, G. R. Wilkes and L. F. Dahl, *J. Am. Chem. Soc.* 1967, **89**, 4792.
14. M. R. Churchill and J. P. Hutchinson, *Inorg. Chem.* 1978, **17**, 3528.
15. M. I. Bruce, in *Comprehensive Organometallic Chemistry* (Edited by G. Wilkinson, F. G. A. Stone and E. W. Abel), Vol. 4, Ch. 32, p. 943. Pergamon Press, Oxford (1982).
16. (a) R. D. Adams and J. P. Selegue, in *Comprehensive Organometallic Chemistry* (Edited by G. Wilkinson, F. G. A. Stone and E. W. Abel), Vol. 4, Ch. 33. Pergamon Press, Oxford (1982); (b) G. J. Leigh and R. L. Richards, Vol. 5, p. 617 and refs therein.
17. D. F. Schriver and K. H. Whitmire, in *Comprehensive Coordination Chemistry* (Edited by G. Wilkinson, F. G. A. Stone and E. W. Abel), Vol. 4, Ch. 31, p. 261. Pergamon Press, Oxford (1982).
18. B. F. G. Johnson, J. Lewis and M. V. Twigg, *J. Organomet. Chem.* 1974, **67**, C75.
19. B. F. G. Johnson, *J. Chem. Soc., Chem. Commun.* 1976, 211.
20. (a) D. Braga, A. Rodger and B. F. G. Johnson, *Inorg. Chim. Acta* 1990, **174**, 185; (b) B. F. G. Johnson and E. Parisini, *Inorg. Chim. Acta* 1992, **198**, 345.
21. D. L. Kepert, *Prog. Inorg. Chem.* 1979, **23**, 1 and refs therein.
22. E. R. Corey, L. F. Dahl and W. Beck, *J. Am. Chem. Soc.* 1963, **85**, 1202.
23. V. G. Albano, P. L. Bellon, P. Chini and V. Scatturin, *J. Organomet. Chem.* 1969, **16**, 461.
24. J. M. Knight and M. J. Mays, *J. Chem. Soc., Chem. Commun.* 1976, 703.
25. F. A. Cotton and D. L. Hunter, *Inorg. Chim. Acta* 1974, **11**, L9.
26. R. L. Sweany and T. L. Brown, *Inorg. Chem.* 1977, **17**, 415; D. L. Lichtenburger and T. L. Brown, *Inorg. Chem.* 1978, **17**, 1381.
27. F. A. Cotton, *Inorg. Chem.* 1966, **5**, 1083; B. F. G. Johnson, J. Lewis and J. W. Matheson, *J. Chem. Soc., Chem. Commun.* 1974, 441.
28. R. S. Berry, *J. Chem. Phys.* 1960, **32**, 933.
29. R. D. Adams and F. A. Cotton, in *Dynamic Nuclear Magnetic Resonance Spectroscopy* (Edited by L. M. Jackman and F. A. Cotton). Academic Press, New York (1975).
30. A. Bott and B. F. G. Johnson, *J. Chem. Soc., Dalton Trans.* 1990, 2437; C. E. Anson, R. E. Benfield, A. Bott, D. Braga, B. F. G. Johnson and E. A. Marseglia, *J. Chem. Soc., Chem. Commun.* 1988, 889; *J. Chem. Soc., Dalton Trans.* 1990, 3517.
31. J. D. Dunitz and H.-B. Burgi, *Accts Chem. Rev.* 1983, **16**, 153.
32. B. F. G. Johnson, Y. V. Roberts and E. Parisini, *J. Chem. Soc., Dalton Trans.* 1992, 2573.
33. J. R. Shapley, G. F. Stuntz, M. R. Churchill and J. P. Hutchinson, *J. Am. Chem. Soc.* 1979, **101**, 7425.
34. V. Albano, P. Bellon and V. Scatturin, *J. Chem. Soc., Chem. Commun.* 1969, 730.
35. For general reviews see J. D. Atwood, *Inorganic and Organometallic Reaction Mechanisms*. Brooks/Cole Publishers, Monterey, California (1985); N. M. J. Brodie, L. Chen and A. J. Poë, *Int. J. Chem. Kinet.* 1988, **20**, 467.
36. A. J. Poë and M. V. Twigg, *J. Chem. Soc., Dalton Trans.* 1974, 1860.
37. B. F. G. Johnson, *Inorg. Chim. Acta* 1986, **115**, L39.
38. B. F. G. Johnson, *J. Organomet. Chem.* 1991, **415**, 109.
39. B. F. G. Johnson and Y. V. Roberts, *Inorg. Chim. Acta* 1993, **205**, 175.
40. N. M. J. Brodie and A. J. Poë, *Inorg. Chem.* 1988, **27**, 3156.
41. D. H. Farrar, B. F. G. Johnson, J. Lewis, P. R. Raithby and M. J. Rosales, *J. Chem. Soc., Dalton Trans.* 1982, 2051.
42. G. John, B. F. G. Johnson and J. Lewis, *J. Organomet. Chem.* 1979, **181**, 143.
43. R. J. Goudsmit, B. F. G. Johnson, J. Lewis, P. R. Raithby and K. H. Whitmire, *J. Chem. Soc., Chem. Commun.* 1982, 640.
44. R. D. Adams and I. T. Horvath, *Prog. Inorg. Chem.* 1985, **33**, 127 and refs therein.
45. R. K. Pomeroy, *J. Organomet. Chem.* 1990, **383**, 387 and refs therein.
46. H. Vahrenkamp, *Adv. Organomet. Chem.* 1983, **22**, 169 and refs therein.
47. R. D. Adams, D. D. DesMarteau, D. Lentz and R. Marshall, *J. Am. Chem. Soc.* 1992, **114**, 1909; R. D. Adams, D. D. DesMarteau, D. Lentz, R. Marshall and A. Scherrman, private communication.

Polyhedron Vol. 12, No. 9, pp. 991–1001, 1993
Printed in Great Britain

0277–5387/93 $6.00+.00
Pergamon Press Ltd

MECHANISTIC INSIGHTS INTO CATALYTIC CYCLOPROPANATION BY COPPER(I) PHOSPHINE COMPLEXES. X-RAY CRYSTAL STRUCTURES OF $[Cu(F—BF_3)(PCy_3)_2]$ (Cy = cyclo-C_6H_{11}) AND $[Cu(MeCN)_2\{1,2\text{-}C_6H_4CH_2NMe_2(PPh_2)\}]BF_4$

JASON GREEN, EKKHARD SINN and SIMON WOODWARD*

School of Chemistry, University of Hull, Kingston-upon-Hull HU6 7RX, U.K.

and

RAYMOND BUTCHER

Department of Chemistry, Howard University, Washington, DC 20059, U.S.A.

(*Received* 11 *December* 1992; *accepted* 27 *January* 1993)

Abstract—The complexes $[Cu(PPh_3)_n(MeCN)_{4-n}]BF_4$ (n = 0, 2–3), $[Cu(F—BF_3)(PCy_3)_2]$, $[Cu(MeCN)_2\{1,2\text{-}C_6H_4CH_2NMe_2(PPh_2)\}]BF_4$ and species formed by *in situ* addition of various ligands to $[Cu(MeCN)_4]BF_4$ are all active catalysts for cyclopropanation reactions using N_2=CH(CO_2Et). With styrene as a substrate the *trans/cis* selectivity in the product cyclopropane may be somewhat controlled by the appropriate choice of phosphine ligand. Catalysis by $[Cu(MeCN)_2(PPh_3)_2]BF_4$ and $[Cu(MeCN)_2\{1,2\text{-}C_6H_4CH_2NMe_2(PPh_2)\}]BF_4$ is proposed to involve alkene coordination, while that by $[Cu(MeCN)(PPh_3)_3]BF_4$ and $[Cu(F—BF_3)(PCy_3)_2]$ is not. The structures of the catalysts showing the highest selectivity have been determined. For monoclinic $[Cu(F—BF_3)(PCy_3)_2]$ the molecule contains an unusually large P—Cu—P angle (*ca* 160°).

Cyclopropanes constitute important structural fragments in many pharmaceutical and insecticidal molecules of economic importance.[1] One attractive cyclopropanation route to these targets is the decomposition of a diazo compound in the presence of an alkene.[2,3] Although many transition metals, in one form or another, show activity for this reaction, traditionally copper species are recognized as pre-eminent catalysts. A wide variety of copper sources, including activated copper powders,[4] simple copper(I) or copper(II) salts[5] and complexes such as $[CuCl\{P(OR)_3\}]_4$ (R = alkyl),[6,7] are active pre-catalysts. Recent studies have concentrated on reactions employing chiral ligands in the presence of labile copper(I) sources to fashion highly enantioselective (> 95% enantiomeric excess, e.e.) cyclopropanation reactions.[8–10]

It is popularly assumed, generally without proof, that in all these reactions unstable copper(I) carbenoid intermediates form and that these are trapped by substrate alkene resulting in cyclopropanation (Scheme 1). Alternatively, two carbene complexes may undergo binuclear C—C coupling to yield a substituted alkene, a commonly observed reaction by-product in catalytic cyclopropanation reactions. One reason for assuming copper(I) intermediates is that many diazo compounds show appreciable reductive ability and reduction of copper(II) sources to the lower oxidation state is facile under these conditions. Relatively few mechanistic studies in copper(I) catalysed cyclopropanation have been reported.[5,11] Whether a single reaction coordinate and set of common intermediates is responsible is unclear. These vagaries piqued our interest in the mechanism of catalytic cyclopropanation and led us to begin an investigation into the possibility of designing a cyclo-

* Author to whom correspondence should be addressed.

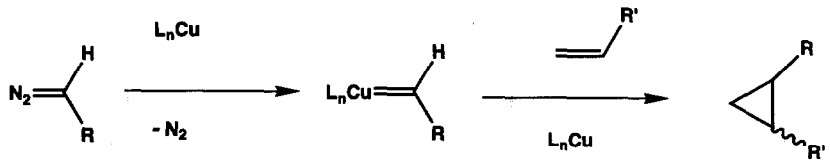

Scheme 1.

propanation reaction with well-defined catalytic intermediates, the preliminary results of which are the subject of this paper.

We selected the complex $[Cu(MeCN)_4]BF_4$ (**1**) as a versatile candidate with which to probe catalytic cyclopropanation for a number of reasons: complex **I** is easily prepared, fairly air-stable and the $[BF_4]^-$ anion can be systematically varied if necessary.[12] The cations $[Cu(MeCN)_4]^+$ are known to be active cyclopropanation catalysts.[10] The acetonitrile ligands in **1** are rather labile. For example, partial displacement with EPh_3 (E = P, Sb) forms the family of complexes $[Cu(MeCN)_{4-n}(EPh_3)_n]^+$ (n = 2–4).[13] Thus, steric and electronic modification of the copper(I) environment is possible. The presence of phosphine ligands also allows ^{31}P NMR reaction monitoring of such species on exposure to the catalytic reaction conditions.

RESULTS AND DISCUSSION

Preparation of the copper complexes

The preparation of $[Cu(MeCN)_4]BF_4$ (**1**), $[Cu(MeCN)_2(PPh_3)_2]BF_4$ (**2**) and $[Cu(MeCN)(PPh_3)_3]BF_4$ (**3**) follows the routine literature preparations used for the related ClO_4 and PF_6 salts.[12,13] Attempts to prepare $[Cu(MeCN)_3(PPh_3)]BF_4$ deserve special comment. Addition of 1 equivalent of PPh_3 to **1** results in mixtures containing variable Cu:PPh_3 ratios. Fractional crystallization of the mixture from CH_2Cl_2–Et_2O leads to well-formed needles with a PPh_3:MeCN ratio of 3:5, as judged by ^1H NMR spectroscopy. However, crystallographic investigation of these needles reveal them to be $[Cu(MeCN)_2(PPh_3)_2]BF_4$ (**2**).* The hexafluorophosphate salt $[Cu(MeCN)_3(PPh_3)]PF_6$ is suggested on the basis of ^{31}P NMR spectroscopic evidence, but these claims are not yet substantiated crystallographically.[14] The versatility of acetonitrile replacement in **1** is further demonstrated by its reactions with PCy_3 (Cy = cyclo-C_6H_{11}), the nitrogen–phosphorus chelate **4** and other ligands in Scheme 2.

Reaction of PCy_3 and **1** in a 2:1 ratio affords colourless crystals. The toluene solubility of this material is inconsistent with the properties of a salt, suggesting the formula $[Cu(F—BF_3)(PCy_3)_2]$ (**5**). Consistent with this idea the ν(B—F) stretch observed in the solid-state IR spectrum is sharper than that observed for $[Cu(MeCN)_2(PPh_3)_2]BF_4$ (**2**) and $[Cu(MeCN)(PPh_3)_3]BF_4$ (**3**) but different from that of $[Cu(F—BF_3)(PPh_3)_3]$ (**6**) prepared by pyrolysis of **3** under vacuum and subsequent recrystallization. The formation of **5** is confirmed by the absence of an MeCN signal in the ^1H NMR spectrum and by the results of an X-ray crystallographic study (see later).

The nature of tetrafluoroborate coordination in solutions of **5** is apparent from ^{19}F NMR studies. Two signals are seen for solutions of **5** in C_6D_6, acetone-d_6 or DMSO-d_6 in the range δ_F −145 to −150. The exact chemical shifts depend on the solvent, however, the integral ratio of the two signals shows the larger signal to be due to ^{10}B—F environments while the smaller signal represents ^{11}B—F. While the smaller signal remains a featureless envelope in all solvents the larger signal, in DMSO-d_6, shows the four-line multiplet [$J(^{10}BF)$ = 1.2 Hz] expected for an uncoordinated $[BF_4]^-$ anion. For comparison, the $J(^{10}BF)$ coupling for $NaBF_4$ (δ_F −152.10) in D_2O is 2.2 Hz. These results indicate that the salt $[Cu(PCy_3)_2]BF_4$ is exclusively present in DMSO-d_6. In less polar solvents an equilibrium between **5** and $[Cu(PCy_3)_2]BF_4$ probably exists. A related anion exchange process has recently been characterized by ^{27}Al NMR spectroscopy for the complex Ti$(CH_2SiMe_3)(Cl—AlCl_3)(\eta$-$C_5H_5)_2$.[15]

The reaction of **4** with $[Cu(MeCN)_4]BF_4$ (**1**) affords a moderate yield (66%) of the complex $[Cu(MeCN)_2\{1,2\text{-}(Me_2NCH_2)(PPh_2)C_6H_4\}]BF_4$ (**7**) (Scheme 2). The purification procedure is complicated by the presence of yellow impurities and by the higher air-sensitivity of **7** compared to the bis-

* $[Cu(MeCN)_2(PPh_3)_2]BF_4$ crystallizes from CH_2Cl_2–Et_2O as monoclinic colourless prisms. Space group $P2_1/n$, a = 9.211(3), b = 26.864(9), c = 15.397(4) Å, β = 94.60(2)°, V = 3798(2) Å^3, Z = 8. Full details are deposited in the Cambridge crystallographic database. The structure of the copper cation is essentially identical to the known perchlorate salt. See also ref. 20.

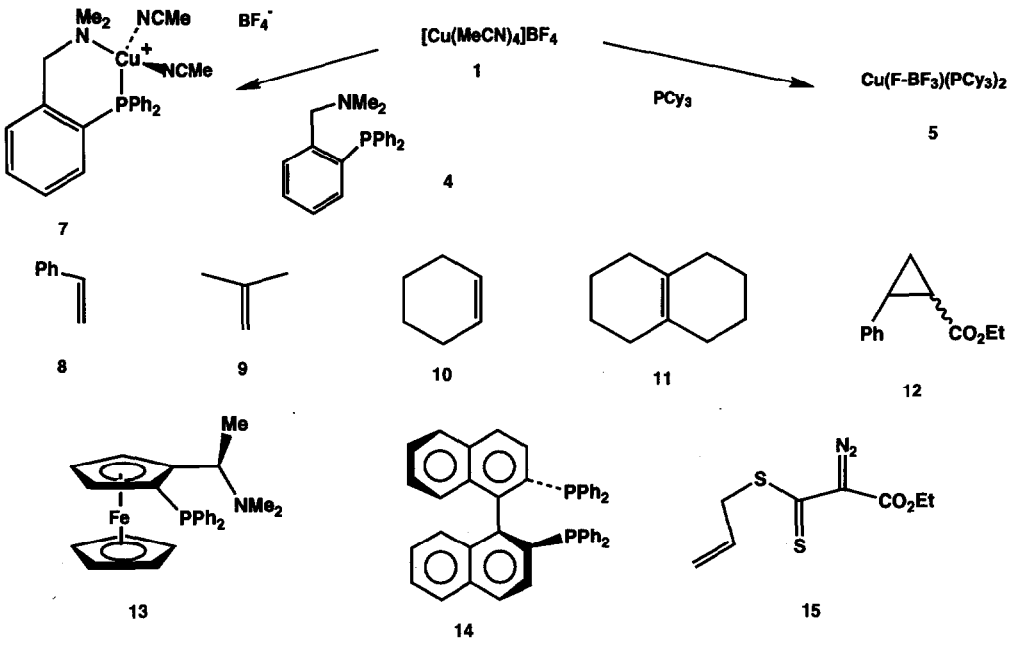

Scheme 2.

phosphine complexes. The spectroscopic properties of **7** and the results of a crystallographic study (see later) are fully consistent with the formula proposed.

Catalytic and mechanistic studies

At the outset of this project information regarding cyclopropanation reactions using **1** was rather limited. We, therefore, undertook some initial screening reactions to identify the catalytic activity of **1** and the related phosphine complexes **2**, **3**, **5** and **7** for cyclopropanations using ethyl diazoacetate and the alkenes **8**–**11** (Scheme 2). In addition cyclopropanation reactions of **1** in the presence of added ligands were performed. Ethyl diazoacetate is an excellent test compound as known literature compounds are formed in most cases. In all cases, after a short induction period (*ca* 10–30 s), prompt decomposition of N_2=CH(CO_2Et) at room temperature is observed (Table 1). The complexes are highly active compared to traditional catalysts.

Table 1. Catalytic cyclopropanation results

Catalyst[a]	Alkene [Conc.]	Reaction time	Cyclopropane[b] yield	Isomer[c] ratio	Alkene[b] yield	*E*/*Z*[c] ratio
$[Cu(MeCN)_4]^+$	**8** [1.5 M]	10 min	60%	1.65	30%	1.35
$[Cu(MeCN)_4]^+$	**8** [0.35 M]	20 min	34%	1.95	43%	1.55
$[Cu(MeCN)_2(PPh_3)_2]^+$	**8** [1.5 M]	2.25 h	55%	2.50	31%	1.80
$[Cu(MeCN)(PPh_3)_3]^+$	**8** [1.5 M]	16 h	27%	2.38	34%	1.75
$[Cu(MeCN)_2(\mathbf{4})]^+$	**8** [1.5 M]	15 h (at 4°C)	65%	2.75	32%	1.60
$[Cu(MeCN)_2(\mathbf{13})]^+$[d]	**8** [1.3 M]	45 min	47%	2.50	34%	4.10
$[Cu(F{-}BF_3)(PCy_3)_2]$	**8** [1.5 M]	4.5 h	29%	4.00	49%	4.20
$[Cu(MeCN)_4]^+$	**9** [3.5 M]	20 min	71%	—	30%	1.25
$[Cu(MeCN)_4]^+$	**10** [1.5 M]	10 min	30%	5.50[e]	44%	3.90
$[Cu(MeCN)_4]^+$	**11** [1.5 M]	10 min	7%	—	46%	1.35

[a] Reactions performed on a 1–2 mmol scale in CH_2Cl_2 using 2 mol% catalyst ($[BF_4]^-$ counter-anion) at ambient temperature.

[b] Isolated by column or preparative TLC.

[c] *Trans*/*cis* ratio (cyclopropane) or *E*/*Z* ratio (alkene) determined by GC on the crude reaction mixture, error ±0.05.

[d] Prepared *in situ*.

[e] *Exo*/*endo* value.

However, for high yields of cyclopropanes the effective concentration of the alkene must be above 1.0 molar. Terminal alkenes, especially styrene, are the most reactive. Although various enantioselective routes to the styrene derived product **12** are available, catalyst control of the relative *trans*/*cis* stereochemistry by a family of complexes is rarely demonstrated. Selective formation of cyclopropanes related to *trans*-**12** using sterically hindered diazoacetates is known,[16] but catalyst-based *trans*/*cis* control is rare.

In the PPh_3 substituted catalysts the *trans*/*cis*-**12** selectivity and rate is influenced by the number of phosphine ligands coordinated to the catalyst, maximizing for $[Cu(MeCN)_2(PPh_3)_2]BF_4$ (**2**). Different PPh_3:Cu ratios result in inferior selectivity and rates, the 3 : 1 ratio of **3** gives a *trans*/*cis* value of 2.38 after 16 h, while the complex $[Cu(PPh_3)_4]BF_4$ shows only feeble catalytic activity. Complex **5** catalyses the reaction rather slowly, but in this case with high *trans*/*cis*-**12** selectivity (4.00). Crystallographic studies show that $M(PCy_3)_2$ (M = Cu, Ag) based complexes often attain a maximum coordination number of only three.[17] The above results indicate although only one free coordination site is required for these catalysts, significant rate enhancements are attained where at least two are present. In support of this notion is the observation that the rate of $N_2{=}CH(CO_2Et)$ decomposition by **2** is faster in the presence of styrene than in its absence. The *trans*/*cis*-**12** selectivity of the nitrogen–phosphorus chelate complex **7** is also relatively high (2.75), but the reaction proceeds much faster than that catalysed by **5**. Attempts at chiral catalysis using the *in situ* complex $[Cu(MeCN)_2(\mathbf{13})]BF_4$ results in a modest yield of essentially racemic **12**. Similarly, racemic **12** is isolated from very low activity catalysts prepared by (*S*)-BINAP (**14**) addition to $[Cu(MeCN)_4]BF_4$ (**1**) in a 1 : 1 ratio. The low cyclopropane yields obtained from **11** are due to steric factors. Attempts at intramolecular cyclopropanation using **15** are unsuccessful due to the high stability of the diazo-species.

Mechanistically the two most probable transition states for copper-catalysed cyclopropanation involve alkene coordination (**16**) or attack on the coordinated carbene ligand by an outer-sphere alkene (**17**) (Scheme 3). As kinetic regimes often cannot distinguish between these two possibilities[5] we sought for alternative evidence for alkene and carbene coordination. No MeCN exchange with

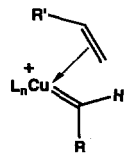

16

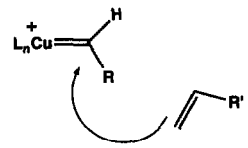

17

Scheme 3.

styrene in **2** could be detected by ^{31}P NMR spectroscopy at room temperature or −30°C. Further, no MeCN liberation from **2** is detected by IR or ^{31}P NMR spectroscopy for the related π-acid CO. These results suggest rather small equilibrium constants for MeCN dissociation. In the catalytic systems MeCN is removed by degradation with ethyl diazoacetate during the short induction period, thus preventing equilibrium back reactions. Supporting this idea reactions in acetonitrile alone give small variable yields of $MeC{=}NCH(CO_2Et)$, together with *E*/*Z* alkene and polymeric material. The catalytic species *do* coordinate π-acids, admission of CO totally inhibits the catalysis but the activity returns once a nitrogen atmosphere is readmitted. The lowest temperature at which our catalysts are active is *ca* 4°C, precluding NMR investigations by low-temperature mixing. However, prompt cooling of the active reaction mixtures using a $[Cu(MeCN)_2(PPh_3)_2]BF_4$ (**2**) pre-catalyst allows the catalytic rest state to be interrogated by ^{31}P NMR spectroscopy. Under these conditions the signal for the starting material [δ_P (109.25 MHz, $CDCl_3$, −30°C) −0.3 ($W_{1/2}$ = 48 Hz)] is replaced by a broad resonance at δ_P −0.8 ($W_{1/2}$ = 180 Hz) and a smaller sharp signal at δ_P 20.7. This signal is identified as $Ph_3P{-}N_2{=}CHCO_2Et$ by comparison with an authentic sample.[18] However, attempts to probe the structure of the active copper species are thwarted by the quadrupolar nature of copper (I = 3/2 for both ^{63}Cu and ^{65}Cu).

Crystallographic studies

In order to gain some further insights into the origins of the higher *trans*/*cis* selectivity shown by complexes **5** and **7** the crystal structures of these molecules were investigated.* ORTEP views of the molecules are shown in Figs 1 and 2, while selected bond length and angle data are presented in Tables 2 and 3. Details of the crystal and structure refinement data for both compounds are summarized in Table 4.

The $[Cu(F{-}BF_3)(PCy_3)_2]$ (**5**) molecule exhibits positional disorder in one of the cyclohexyl groups (designated "6") and in the three BF_4 fluorine atoms

* Full details for **5** and **7** are deposited at the Cambridge Crystallographic database.

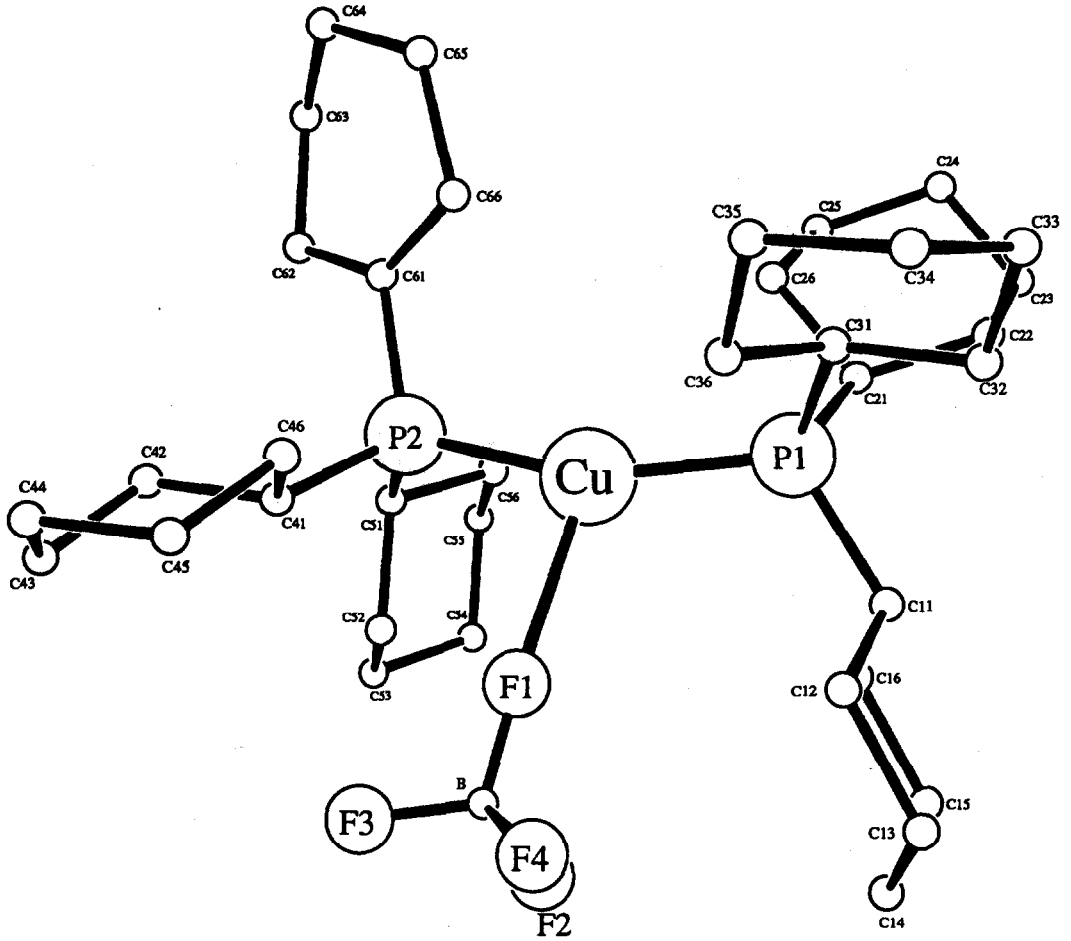

Fig. 1. An ORTEP view of $Cu(F—BF_3)(PCy_3)_2$ (**5**); hydrogen atoms are omitted for clarity.

which are not coordinated to the metal. However, the disorder is not of great consequence to the discussion and for this reason and to eliminate clutter the multiple occupancy positions are not shown; the figure shows the primary fluorine atom positions. The semi-coordinated BF_4 group is anchored at the coordinated fluorine atom, which is uniquely positioned and shows no disorder. Overall three-coordinate copper is observed in **5** with a Cu—F contact distance of 2.420(6) Å. The second nearest fluorine of the coordinated BF_4 group [F(2), 70% occupancy] at *ca* 4.2 Å is effectively non-bonded. Coordination of the anion results in a slight shortening of the coordinated B—F bond B—F(1) to 1.29(2) Å, while the uncoordinated B—F bonds are in the range expected [1.33(2)–1.39(2) Å]. Similar features are seen in the structure of $Cu(F—BF_3)(PPh_3)_3$ (**6**), where the principal Cu—F contact is 2.306 Å,[19] but in this case no B—F contraction is observed. Commensurate with the high steric bulk of PCy_3, a large P—Cu—P angle of 159.98(8)° is observed. This is the largest angle observed in $M(PR_3)_2$ (M = Cu, Ag) systems, some 13–15° greater than those in $M(X)(PCy_3)_2$ (M = Cu, Ag; X = NO_3, ClO_4)[17] at 139.0–147.3° and considerably greater than those at 127.6(1)° and 127.1(1)° in the structures $[Cu(MeCN)_2(PPh_3)_2]X$ (X = ClO_4, BF_4).[20] The bulky phosphines offer considerable steric protection to the metal, however, due to disorder in one of the cyclohexyl rings extensive discussion of the ring geometries is not profitable.

The coordination geometry about copper in **7** is approximately tetrahedral. The most significant deviation is the P—Cu—N angle of 98.3(1)° due to the chelate ligand. Direct comparison with related phosphorus nitrogen chelates on copper(I) is difficult as apparently no other is crystallographically characterized. The Cu—P distance at 2.195(2) Å is in the range expected by comparison with the structures of $Cu(MeCN)_n(PPh_3)_{4-n}$ (n = 0–2).[13] The Cu—NMe_2 distance at 2.179 Å is somewhat longer than Cu^I—N bond distances observed in coordinated acetonitrile complexes,

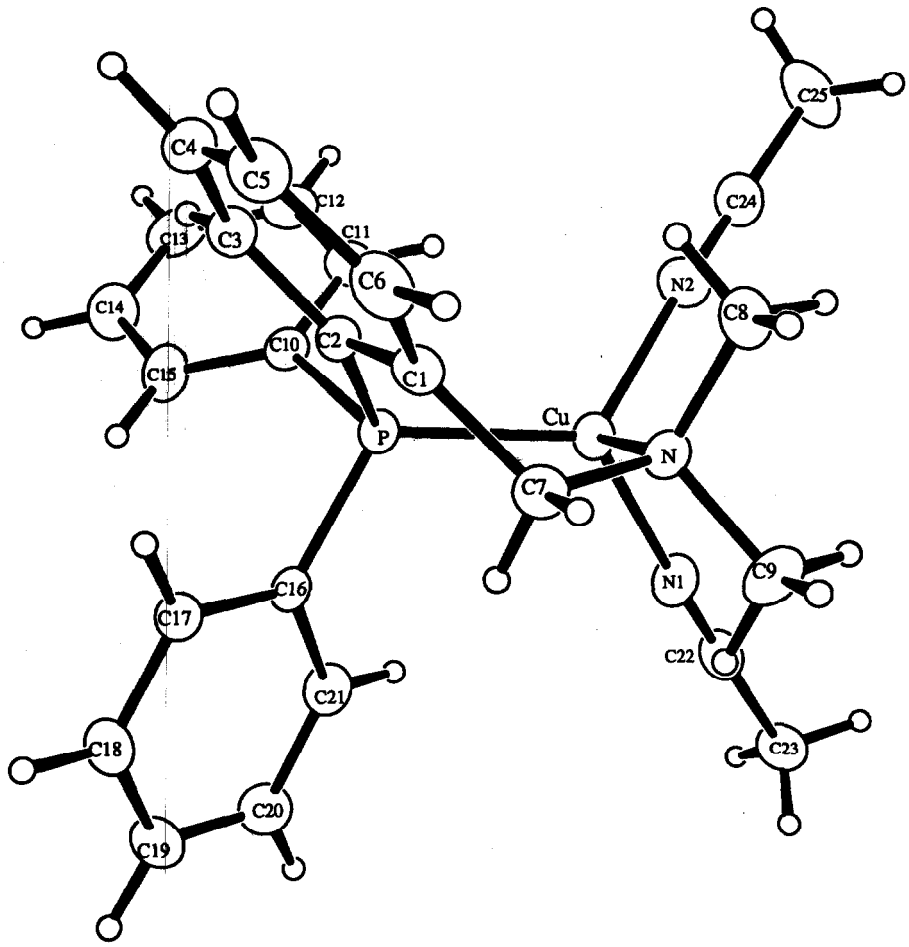

Fig. 2. An ORTEP view of $[Cu(MeCN)_2\{1,2\text{-}(Me_2NCH_2)(PPh_2)C_6H_4\}]BF_4$ (**7**).

2.02–2.12 Å.[13] Solution ^1H NMR studies suggest that the chelate ring is flat, but in the solid state the ring is kinked about the methylene linkage of the chelate ligand. This is most clearly seen in the N—C(7)—C(1) and Cu—P—C(2) angles, which are 114.9(5)° and 105.7(2)°, respectively. Rapid ring deformation must occur in solution rendering the CH_2 and NMe_2 groups equivalent in the ^1H NMR spectra. The $[BF_4]^-$ counter-anion in $[Cu(MeCN)_2\{1,2\text{-}(Me_2NCH_2)(PPh_2)C_6H_4\}]BF_4$ (**7**) exhibits positional disorder, hence, additional positions are tabulated with the other data.

CONCLUSIONS

The observed rate differences and selectivities shown by these complexes indicate that alkene coordination and a transition state similar to **16** is important in cyclopropanation catalysis by **2**, **7** and related sterically unencumbering ligands. For the species **3** and **5** no alkene coordination is proposed to occur due to steric blocking of the fourth coordination site at the copper. In these cases direct attack on the coordinated carbene $[L_nCu{=}CH(CO_2Et)]$ (viz. **17**) is likely.

EXPERIMENTAL

General

All manipulations involving nitrogen ligated copper complexes, together with catalytic reactions, were performed under nitrogen atmospheres using standard Schlenk techniques. All alkenes and ethyl diazoacetate were commercial products (Aldrich), used after drying over 4 Å molecular sieves. Commercial PCy_3 was used as supplied. Carbon disulphide and dichloromethane were distilled from CaH_2 immediately prior to use; hexane, light petroleum (b.p. 40–60°C) and Et_2O were dried

Table 2. Selected bond length and angle data for $Cu(F—BF_3)(PCy_3)_2$ (5)

(a) Distances (Å)			
Cu—P(1)	2.235(2)	P(2)—C(51)	1.857(6)
Cu—P(2)	2.237(2)	P(2)—C(61)	1.843(8)
Cu—F(1)	2.420(6)	B—F(1)	1.29(2)
P(1)—C(11)	1.841(8)	B—F(2)	1.39(2)
P(1)—C(21)	1.859(7)	B—F(3)	1.33(2)
P(1)—C(31)	1.851(6)	B—F(4)	1.38(2)
P(2)—C(41)	1.854(7)		
Nearest interionic distances			
C(33)—F(7)	3.22(2) (a)	C(65)—F(6)	3.25(3) (a)
C(41)—F(1)	3.27(1) (b)		
Symmetry operators: (a) $x, y, z-1$; (b) x, y, z			
(b) Angles (°)			
P(1)—Cu—P(2)	159.98(8)	C(11)—P(1)—C(31)	108.4(3)
P(1)—Cu—F(1)	108.5(2)	C(21)—P(1)—C(31)	105.1(3)
P(2)—Cu—F(1)	91.5(2)	Cu—P(2)—C(41)	110.3(2)
Cu—F(1)—B	176(1)	Cu—P(2)—C(51)	111.7(2)
Cu—P(1)—C(11)	115.7(2)	Cu—P(2)—C(61)	113.1(3)
Cu—P(1)—C(21)	109.3(2)	C(41)—P(2)—C(51)	106.1(3)
Cu—P(1)—C(31)	111.3(2)	C(41)—P(2)—C(61)	110.5(4)
C(11)—P(1)—C(21)	106.4(3)	C(51)—P(2)—C(61)	104.6(3)

over sodium wire. Column chromatography and preparative TLC were run on activated silica gel; Fisons S/0780/60 and Merck Kieselgel 60 $HF_{254+366}$, respectively. IR spectra were recorded using a Perkin–Elmer 983G instrument. Proton NMR spectra were recorded on Jeol-270 (270 MHz) or Bruker WH-400 (400 MHz) spectrometers. ^{13}C NMR (67.8 MHz), ^{31}P NMR (109.3 MHz) and ^{19}F NMR (254.1 MHz) spectra were recorded on the Jeol-270. Mass spectra were obtained on Finnigan 1020 (electron impact ionization, EI) or VG–ZAB (fast atom bombardment ionization, FAB) machines. Optical activities were assayed by polarimetry on a Optical Activity Ltd AA-10 instrument. Catalytic reaction mixtures were investigated with a Sigma-3 GC using a Carbowax-20M column, a carrier gas flow of 30 $cm^3\ min^{-1}$ (N_2) and either a temperature program (8 min at

Table 3. Selected bond length and angle data for $[Cu(MeCN)_2\{1,2\text{-}(Me_2NCH_2)(PPh_2)C_6H_4\}]BF_4$ (7)

(a) Distances (Å)			
Cu—P	2.195(2)	Cu—N(1)	2.020(7)
Cu—N	2.179(5)	Cu—N(2)	1.974(7)
Nearest interionic distances			
F(2)—C(22)	3.13(1) (a)	F(6)—C(23)	3.09(2) (b)
Symmetry operators: (a) $1+x, y, z$; (b) $1/2+x, 1/2-y, z-1/2$			
(b) Angles (°)			
P—Cu—N	98.3(1)	Cu—P—C(2)	105.7(2)
N—Cu—N(1)	105.9(3)	Cu—P—C(10)	120.5(2)
N—Cu—N(2)	103.1(2)	Cu—P—C(16)	117.9(2)
N(1)—Cu—N(2)	105.7(3)	C(2)—C(1)—C(7)	123.0(6)
P—Cu—N(1)	120.8(2)	P—C(2)—C(1)	119.1(5)
P—Cu—N(2)	120.2(2)	N—C(7)—C(1)	114.9(5)

Table 4. Crystal and structure refinement data

Compound	$[Cu(c\text{-}hex_3P)_2F{-}BF_3]$	$[Cu(Ph_2PC_6H_4CH_2NMe_2)MeCN_2]BF_4$
Mol. wt	711.2	551.8
a (Å)	16.102(3)	13.772(3)
b (Å)	24.931(9)	14.468(3)
c (Å)	9.563(2)	15.067(5)
β (°)	93.61(3)	115.70(2)
V (Å^3)	3831(3)	2705(2)
Space group	$P21/n$ (No. 14)	Cc (No. 9)
Z	4	4
D_{calc} (g cm^{-3})	1.233	1.355
μ (cm^{-1})	6.94	9.10
Crystal dimensions (mm)	$0.65\times0.40\times0.22$	$0.40\times0.30\times0.22$
Transmission coefficients	0.607, 0.403	0.922, 0.650
Scan mode	$\theta/2\theta$	$\theta/2\theta$
Scan width (°)	$(0.7+0.35\tan\theta)$	$(0.6+0.35\tan\theta)$
2θ range (°)	3.0–50.0	3.0–50.0
Unique data measured	6970	2576
Unique data used	3545 ($>3\sigma$)	2043 ($>3\sigma$)
No. of variables	381	315
R ($\Sigma\|\|F_o\|-\|F_c\|\|/\Sigma\|F_o\|$) (%)	6.5	4.3
R_w ($[(\Sigma w(\|F_o\|-\|F_c\|)^2/\Sigma wF_o^2)]^{1/2}$ (%)	7.3	4.8
Shift/error	0.02	0.02
$\Delta\rho_{max}$ (e Å^{-3})	0.62	0.44

145°C/ramp to 185°C over 5 min/12 min at 185°C) or an isothermal run at 100°C. The complex $[Cu(MeCN)_4]BF_4$ (**1**) was prepared in an identical manner to $[Cu(MeCN)_4]PF_6$ using HBF_4 (48%wt in water) and recrystallized from MeCN before use.[12] The species $[Cu(MeCN)_2(PPh_3)_2]BF_4$ (**2**)[13] and the ligand **4**[21] are literature compounds.

Preparations and catalysis

Preparation of $Cu(F{-}BF_3)(PCy_3)_2$ (**5**). Solid PCy_3 (0.60 g, 2.14 mmol) was added to a suspension of $[Cu(MeCN)_4]BF_4$ (**1**) (0.33 g, 1.07 mmol) in CH_2Cl_2 (30 cm^3) at room temperature. The reaction was stirred for 1 h, during which time the mixture became homogeneous. The colourless solution was filtered, concentrated to a minimal volume and crystallized by addition of Et_2O and cooling, resulting in two crops of colourless plates; 0.57 g (75%); m.p. 218–219°C. Found: C, 60.5; H, 9.1; M(cation)$^+$, 623. Calc. for $C_{36}H_{66}BCuF_4P_2$: C, 60.8; H, 9.35%; M(cation), 623. ν_{max} (cm^{-1}) (KBr disc): 2919s, 2842s (CH) and 1080s (BF). δ_H (400 MHz, $CDCl_3$): 1.13–1.46 (30 H, m, axial H), 1.68–1.95 (30 H, m, equatorial H) and 1.95–2.06 [6 H, m, H—C(1)]; δ_C (67.8 MHz, $CDCl_3$): 25.9 [6 C, s, C(4)], 27.0 [12 C, t, J(PC) = 6 Hz, C(2)], 31.0 [12 C, s, C(3)] and 31.6 [6 C, t, J(PC) = 11 Hz, C(1)]; δ_P (109.3 MHz, $CDCl_3$): 21.3 (PCy_3); δ_F (254.1 MHz, C_6D_6): 148.96, 149.00; δ_F (254.1 MHz, acetone-d_6): 149.47, 149.51; δ_F (254.1 MHz, DMSO-d_6): 146.80, 146.85.

Preparation of $[Cu(F{-}BF_3)(PPh_3)_3]$ (**6**). Addition of PPh_3 (0.62 g, 2.40 mmol) to $[Cu(MeCN)_4]BF_4$ (**1**) (0.25 g, 0.80 mmol) in CH_2Cl_2 (50 cm^3), followed by crystallization from CH_2Cl_2–Et_2O afforded colourless cubes of $[Cu(MeCN)(PPh_3)_3]BF_4$ (**3**); 0.72 g (92%). The complex had properties closely related to the known ClO_4 salts;[13] m.p. 225–226°C. Found: C, 68.3; H, 4.8; N, 1.7; M(cation-MeCN)$^+$, 849. Calc. for $C_{56}H_{48}BCuF_4NP_3$: C, 68.8; H, 4.95; N, 1.4%; M(cation), 890. ν_{max} (cm^{-1}) (KBr disc): 3062m (CH), 2282w, 2244w (CN), 1485s, 1434s (CC) and 1050s br (BF). δ_H (270 MHz, $CDCl_3$): 2.03 (3 H, s, Me), 7.00–7.12 (18 H, m, Ph-*o*), 7.12–7.23 (18 H, m, Ph-*m*) and 7.32–7.41 [9 H, m, Ph-*p*]; δ_P (109.3 MHz, $CDCl_3$): 1.4 (PPh_3). Heating the solid under vacuum (0.05 mm Hg) at 90°C (2 h) followed by recrystallization from CH_2Cl_2–Et_2O yielded colourless needles of $[Cu(F{-}BF_3)(PPh_3)_3]$, 0.57 g (82%), with literature properties;[19] m.p. 219–220°C. Found: C, 68.9; H, 4.75. Calc. for $C_{54}H_{45}BCuF_4P_3$: C, 69.2; H, 4.8. ν_{max} (cm^{-1}) (KBr disc): 3062m (CH), 1482s, 1437s (CC) and 1060s br (BF). δ_H (270 MHz, $CDCl_3$): 6.95–7.10 (18 H, m, Ph-*o*), 7.10–7.23 (18 H, m, Ph-*m*) and 7.32–7.42 [9 H, m, Ph-*p*]; δ_P (109.3 MHz, $CDCl_3$): 1.8 (PPh_3).

Preparation of $[Cu(MeCN)_2\{1,2\text{-}(Me_2NCH_2)$

$(PPh_2)C_6H_4\}]BF_4$ (**7**). A degassed solution of 1,2-$(Me_2NCH_2)(PPh_2)C_6H_4$ (**4**) (0.34 g, 1.05 mmol) in CH_2Cl_2 (5 cm^3) was added by cannula to a suspension of $[Cu(MeCN)_4]BF_4$ (**1**) (0.33 g, 1.03 mmol) in CH_2Cl_2 (10 cm^3) at ambient temperature and stirred (30 min). The resulting deep yellow solution was filtered under nitrogen and concentrated to *ca* 4 cm^3. An equal volume of degassed Et_2O was added and the yellow by-products removed by filtration under nitrogen. Further Et_2O addition and slow cooling afforded two crops of colourless rhomboid crystals; 0.37 g (66%); m.p. 128–130°C (dec.). Found: C, 54.1; H, 5.0; N, 7.2; M(cation)$^+$, 464. Calc. for $C_{25}H_{28}BCuF_4N_3P$: C, 54.1; H, 5.1; N, 7.6%; M(cation), 464. ν_{max} (cm^{-1}) (KBr disc): 3044w, 2999w, 2960w, 2940w, 2875w, 2837w, 2795w (CH), 2300w, 2267w, 2243w (CN), 1478m, 1454m, 1430m (CC), and 1060s br (BF); δ_H (270 MHz, $CDCl_3$): 2.28 (6 H, s, MeCN), 2.44 (6 H, s, NMe_2), 6.84–6.90 (1 H, m, phenylene), 7.26–7.59 (13 H, m, Ph + phenylene); δ_P (109.3 MHz, $CDCl_3$): 1.3 (PPh_2).

Typical procedure for catalytic cyclopropanation. Neat N_2=CH(CO_2Et) (0.2 cm^3, 1.90 mmol) was added by microlitre syringe to a solution containing styrene (1.1 cm^3, 9.5 mmol) and $[Cu(MeCN)_4]BF_4$ (**1**) (12 mg, 0.04 mmol, 2 mol%) in CH_2Cl_2 (5 cm^3) and the reaction stirred at room temperature until nitrogen evolution ceased. The cyclopropane *trans/cis* and alkene *E/Z* ratios were determined by GC; the relevant response factors were checked at regular intervals. Chromatography in 1:1 CH_2Cl_2: light petroleum afforded styrene followed by the cyclopropane *trans/cis*-**12**.[10] *Trans*-**12**: TLC (1:1 CH_2Cl_2: hexane), $R_f = 0.57$; GC retention time = 18.7 min (program). δ_H (400 MHz, $CDCl_3$): 1.23 [3 H, t, J(HH) = 7.2 Hz, Me], 1.30 [1 H, ddd, J(HH) = 8.4, 6.5, 4.5 Hz, H—C(3)], 1.59 [1 H, ddd, J(HH) = 9.2, 5.4, 4.5 Hz, H—C(3)], 1.89 [1 H, ddd, J(HH) = 8.4, 5.4, 4.2 Hz, H—C(1)], 2.51 [1 H, ddd, J(HH) = 9.2, 6.5, 4.2 Hz + unresolved long range couplings to Ph, H—C(2)], 4.16 [2 H, q, J(HH) = 7.2 Hz, OCH_2], 7.08–7.10 (2 H, m, Ph-*o*) and 7.10–7.29 (3 H, m, Ph-*m* + *p*). *Cis*-**12**: TLC (1:1 CH_2Cl_2: hexane), $R_f = 0.35$; GC retention time = 16.9 min (program). δ_H (400 MHz, $CDCl_3$): 0.96 [3 H, t, J(HH) = 7.2 Hz, Me], 1.32 [1 H, ddd, J(HH) = 9.1, 7.8, 5.1 Hz, H—C(3)], 2.07 [1 H, ddd, J(HH) = 9.1, 7.8, 5.6 Hz, H—C(1)], 2.57 [1 H, dt, J(HH) = 9.1, 9.1, 7.5 Hz + unresolved long range couplings to Ph, H—C(2)], 3.86 [2 H, q, J(HH) = 7.2 Hz, OCH_2] and 7.10–7.29 (5 H, m, Ph). The diastereomers could be separated by preparative TLC (10:1 light petroleum: EtOAc); complete resolution was only achieved at low plate loadings. Optical activities were assessed by use of literature optical rotations.[22] Continued elution with 1:1 CH_2Cl_2: EtOAc afforded a mixture of diethyl fumarate/maleate. Fumarate (*E*-alkene): TLC (1:1 CH_2Cl_2: hexane), $R_f = 0.11$–0.28; GC retention time = 8.2 min (program). δ_H (270 MHz, $CDCl_3$): 1.30 [3 H, t, J(HH) = 7.2 Hz, Me], 4.23 [2 H, q, J(HH) = 7.2 Hz, OCH_2] and 6.80 (2 H, s, =CH). Maleate (*Z*-alkene): TLC (1:1 CH_2Cl_2: hexane), $R_f = 0.11$–0.28; GC retention time = 10.3 min (program). δ_H (270 MHz, $CDCl_3$): 1.29 [3 H, t, J(HH) = 7.2 Hz, Me], 4.23 [2 H, q, J(HH) = 7.2 Hz, OCH_2] and 6.42 (2 H, s, =CH).

Cyclopropanation of 1,1-*dimethylethene* (**9**). Application of the above procedure afforded the cyclopropane having literature properties.[8] TLC (1:1 CH_2Cl_2: hexane): $R_f = 0.37$; GC retention time = 4.9 min (100°C). ν_{max} (cm^{-1}) (thin film): 2960s, 2925s, 2858m (CH) and 1732s (CO). δ_H (270 MHz, $CDCl_3$): 0.84 [1 H, dd, J(HH) = 8, 4 Hz, H—C(3)], 1.08 [1 H, dd, J(HH) = 5, 4 Hz, H—C(3)], 1.15 (3H, s, Me), 1.21 (3 H, s, Me), 1.27 [3 H, t, J(HH) = 7 Hz, OCH_2*Me*), 1.48 [1 H, dd, J(HH) = 8, 5 Hz, H—C(1)] and 4.07–4.19 (2 H, m, OCH_2). MS (EI): 142 (M^+).

Cyclopropanation of cyclohexane (**10**). Using the standard method afforded the cyclopropane having literature properties.[6] TLC (1:1 CH_2Cl_2: hexane), $R_f = 0.44$; GC retention time = 9.3 min (program). ν_{max} (cm^{-1}) (thin film): 2930s, 2861s (CH) and 1725s (CO). δ_H (270 MHz, $CDCl_3$): 1.28 [3 H, t, J(HH) = 7 Hz, Me-*exo*], 1.29 [3 H, t, J(HH) = 7 Hz, Me-*endo*], 1.20–1.99 (11 H, m, ring protons), 4.10 [2 H, q, J(HH) = 7 Hz, OCH_2-*exo*] and 4.12 [2 H, q, J(HH) = 7 Hz, OCH_2-*endo*]. MS (EI): 168 (M^+).

Cyclopropanation of 1,2,3,4,5,6,7,8-*octahydronaphthylene* (**11**). Using the above protocol yielded the cyclopropane as a clear oil. TLC (1:1 CH_2Cl_2: hexane), $R_f = 0.50$; GC retention time = 17.9 min (program). ν_{max} (cm^{-1}) (thin film): 2920s, 2849s, (CH) and 1725s (CO). δ_H (270 MHz, $CDCl_3$): 1.28 [3 H, t, J(HH) = 7 Hz, Me], 1.30–2.28 (17 H, m, ring protons) and 4.13 [2 H, q, J(HH) = 7 Hz, OCH_2]. MS (EI): 222 (M^+).

Decomposition of N_2=CH(CO_2Et) *in* MeCN. A solution of N_2=CH(CO_2Et) (0.2 cm^3, 1.90 mmol) in MeCN (1 cm^3) was decomposed by $[Cu(MeCN)_4]BF_4$ (**1**) (12 mg, 0.04 mmol, 2 mol%) over 3 h. Preparative TLC afforded 39 mg (23%) of *E/Z*-(EtO_2C)CH=CH(CO_2Et), $R_f = 0.20$–0.40, and a slow moving band, $R_f = 0.09$–0.16, containing variable amounts of MeC=NCH(CO_2Et), *ca* 11 mg (9%) as a yellow oil with literature properties.[23] TLC (3:2 hexane: EtOAc), $R_f = 0.35$. ν_{max} (cm^{-1}) (thin film): 1784s (C=N) and 1709s (CO). δ_H (270 MHz, $CDCl_3$): 1.41 [3 H, t, J(HH) = 7 Hz,

CH_2Me), 2.34 (3 H, s, CMe), 4.08 [2 H, q, J(HH) = 7 Hz, OCH_2]. MS (EI): 127 (M^+).

Preparation of $N_2{=}C(CO_2Et)(CS_2CH_2CH{=}CH_2)$ **(15)** *and attempted intramolecular cyclopropanation.* Freshly prepared $LiNPr^i_2$ (LDA) (10.00 mmol) in THF (10 cm^3) was added slowly by cannula to a mixture of $N_2{=}CH(CO_2Et)$ (1.09 g, 9.51 mmol) and CS_2 (0.76 g, 9.98 mmol) in THF (40 cm^3) at −78°C, causing a darkening to orange. Allyl bromide (0.85 cm^3, 1.19 g, 9.82 mmol) was then added by syringe. The solution was allowed to come to room temperature (2 h), during which time its colour darkened to brown. The solution was stirred at ambient temperature, concentrated and quenched (NH_4Cl solution, 20 cm^3). Extraction with CH_2Cl_2 and water afforded on drying (Na_2SO_4) a yellow oil. Chromatography on SiO_2 (115 × 30 mm), eluting with 10:1 (light petroleum:CH_2Cl_2), afforded small amounts of an uncharacterized species. TLC (4:1 hexane:CH_2Cl_2), R_f = 0.75. Continued elution with 4:1 (light petroleum:CH_2Cl_2) yielded **15** as a yellow oil, 0.53 g (24%). TLC (4:1 hexane:CH_2Cl_2), R_f = 0.38. ν_{max} (cm^{-1}) (thin film): 2985m, 2938w, 2910w (CH), 2105w, (NN), 1706s (CO) and 1063s (CS). δ_H (270 MHz, $CDCl_3$): 1.47 [3 H, t, J(HH) = 7.1 Hz, Me], 3.72 [2 H, dt, J(HH) = 6.6, 1.3, 1.3 Hz, CH_2CH], 4.52 [2 H, q, J(HH) = 7.1 Hz, OCH_2], 5.38 [1 H, ddt, J(HH) = 10.0, 1.3, 1.3, 1.0 Hz, $=CH_2$], 5.50 [1 H, ddt, J(HH) = 16.9, 1.3, 1.3, 1.0 Hz, $=CH_2$] and 5.90 [1 H, m, J(HH) = 16.9, 10.0, 6.6, 6.6 Hz, =CH]. δ_C (67.8 MHz, $CDCl_3$): 14.1 (Me), 40.3 (OCH_2), 61.9 (SCH_2), 121.4 (=CH), 129.7 ($=CH_2$), 146.4, 160.5, 164.2 ($C{=}N_2$, C=O, C=S). MS (EI): 230 (M^+). Attempted intramolecular cyclopropanation using **1** in CH_2Cl_2 at ambient temperature or 1,2-dichloroethane at 65°C led only to the recovery of the starting material.

Crystallographic studies

Colourless crystals of $Cu(F{-}BF_3)(PCy_3)_2$ **(5)** were grown from an Et_2O solution containing traces of CH_2Cl_2 at −20°C. Greenish tinged crystals of $[Cu(MeCN)_2\{1,2\text{-}(Me_2NCH_2)(PPh_2)C_6H_4\}]BF_4$ **(7)** were grown from a CH_2Cl_2–Et_2O mixture at 0°C. For each complex a colourless crystal was mounted on a glass fibre with epoxy resin. In each case cell dimensions and space group data were obtained by standard methods on an Enraf–Nonius CAD4 four-circle diffractometer with graphite-monochromated Mo-K_α radiation. The θ–2θ technique was used, as previously described,[24] to record the intensities of all non-equivalent reflections, for which $3° < 2\theta < 50°$. Scan widths were calculated as $A + B \tan\theta$, where A is estimated from the mosaicity of the crystal and B allows for the increase in peak width due to $K\alpha_1$–$K\alpha_2$ splitting. Scan speeds were varied depending on the prescan reflection intensity. Data were collected as previously described on the Enraf–Nonius CAD4 diffractometer.[24]

Solution and refinement of the structures. Computations were carried out using the data with $F^2_o > 3\sigma(F^2_o)$, where $\sigma(F^2_o)$ was estimated from counting statistics.[25] Corrections were applied for Lorentz and polarization effects and for absorption.[26] In each case the positions of the metal and one phosphorus atom were determined using a Patterson map. Other atoms were located from Fourier-difference syntheses. The initial calculations were made with the MolEN program set,[27] while the final full-matrix least-squares refinement was performed using the TEXRAY program set.[28] Full-matrix least-squares refinement was based on F. The function minimized was $\Sigma w(|F_o| - |F_c|)^2$, where $w = 4F_o^2/\sigma^2(F_o^2)$, $\sigma^2(F_o^2) = [S^2\{(C + R^2B) + 0.03F_o^2\}^2]/Lp^2$; S = scan rate, C = total integrated peak count, R = ratio of scan time to background counting time, B = total background count and Lp = Lorentz polarization factor. Atomic scattering factors for both non-hydrogen[29] and hydrogen[30] atoms were taken from literature values. The effects of anomalous dispersion were included using literature values for $\Delta f'$ and $\Delta f''$.[31]

Acknowledgements—We thank the SmithKline (1982) Foundation, Great Lakes Chemical (Europe) Ltd, and Rhône-Poulenc Ltd for financial support. We are grateful to SERC for FAB mass spectra and for a studentship (to JG). We are grateful to Dr D. F. Ewing for help with ^{19}F NMR spectroscopy and to Prof. D. Beltran for access to a CAD4 diffractometer.

REFERENCES

1. General review: J. Solaün, *Chem. Rev.* 1989, **89**, 1247.
2. H. M. L. Davies, in *Comprehensive Organic Synthesis* (Edited by B. M. Trost and I. Fleming), Vol. 4, Ch. 4.8, pp. 1031–1067. Pergamon Press, Oxford (1991).
3. M. P. Doyle, *Recl. Trav. Chim. Pays-Bas* 1991, **110**, 305.
4. G. Maas, *Top. Curr. Chem.* 1987, **137**, 75.
5. R. G. Solomon and J. K. Kochi, *J. Am. Chem. Soc.* 1973, **95**, 3300.
6. W. R. Moser, *J. Am. Chem. Soc.* 1969, **91**, 1135.
7. W. R. Moser, *J. Am. Chem. Soc.* 1969, **91**, 1141.
8. Chiral schiff bases: T. Aratani, Y. Yoneyoshi and T. Nagase, *Tetrahedron Lett.* 1977, 2599; T. Arantani, *Pure Appl. Chem.* 1985, **57**, 1839.
9. Chiral semicorrins: A. Pfaltz, in *Modern Synthetic Methods 1989* (Edited by R. Scheffold), pp. 199–248. Springer-Verlag, Berlin (1989); H. Fritschi, U.

Leutenegger and A. Pfaltz, *Angew. Chem., Int. Edn Engl.* 1986, **25**, 1005; H. Fritschi, U. Leutenegger and A. Pfaltz, *Helv. Chim. Acta* 1988, **71**, 1541; H. Fritschi, U. Leutenegger and A. Pfaltz, *Helv. Chim. Acta* 1988, **71**, 1553.

10. Bis-tetrahydrooxazoles: D. A. Evans, K. A. Woerpel and M. J. Scott, *Angew. Chem., Int. Edn Engl.* 1992, **31**, 430; D. A. Evans, M. M. Faul and M. T. Bilodeau, *J. Org. Chem.* 1991, **56**, 6744; D. A. Evans, K. A. Woerpel, M. M. Hindman and M. M. Faul, *J. Am. Chem. Soc.* 1991, **113**, 726; J. Hall, J.-M. Lehn, A. DeCian and J. Fischer, *Helv. Chim. Acta* 1991, **74**, 1; D. Müller, G. Umbricht, B. Weber and A. Pfaltz, *Helv. Chim. Acta* 1991, **74**, 232; R. E. Lowenthal, A. Abiko and S. Masamune, *Tetrahedron Lett.* 1990, **31**, 6005.
11. M. P. Doyle, *Chem. Rev.* 1986, **86**, 919; M. P. Doyle, R. L. Dorow, W. E. Buhro, J. H. Griffin, W. H. Tamblyn and M. L. Trudell, *Organometallics* 1984, **3**, 44.
12. G. J. Kubas, B. Monzyk and A. L. Crumbliss, *Inorg. Synth.* 1991, **28**, 68.
13. J. Diez, S. Falagan, P. Gamasa and J. Gimeno, *Polyhedron* 1988, **7**, 37; P. F. Barron, J. C. Dyason, L. M. Engelhardt, P. C. Healy and A. H. White, *Aust. J. Chem.* 1985, **38**, 261; A. Hetherington, W. Levason and M. D. Spicer, *Polyhedron* 1990, **9**, 1609.
14. A. M. Leiva, L. Rivera and B. Loeb, *Polyhedron* 1991, **10**, 347.
15. J. J. Eisch, K. R. Caldwell, S. Werner and C. Kruger, *Organometallics* 1991, **10**, 3417.
16. M. P. Doyle, V. Bagheri, T. J. Wandless, N. K. Harn, D. A. Brinker, C. T. Eagle and K.-L. Loh, *J. Am. Chem. Soc.* 1990, **112**, 1906.
17. R. J. Restivo, A. Costin, G. Ferguson and A. J. Carty, *Can. J. Chem.* 1975, **53**, 1949; W. A. Anderson, A. J. Carty, G. J. Palenik and G. Schreiber, *Can. J. Chem.* 1971, **49**, 761; M. Camalli and F. Caruso, *Inorg. Chim. Acta* 1988, **144**, 205.
18. H. J. Bestmann, F. M. Solimann and K. Geibel, *J. Organomet. Chem.* 1980, **192**, 177.
19. A. P. Gaughan, Z. Dori and J. A. Ibers, *Inorg. Chem.* 1974. **13**, 1657.
20. P. F. Barron, J. C. Dyason, L. M. Engelhardt, P. C. Healy and A. H. White, *Aust. J. Chem.* 1985, **38**, 261; see also footnote on p. 992.
21. T. B. Rauchfuss, T. B. Patino and D. M. Roundhill, *Inorg. Chem.* 1975, **14**, 652.
22. Supplementary material to D. A. Evans, K. A. Woerpel, M. M. Hindman and M. M. Faul, *J. Am. Chem. Soc.* 1991, **113**, 726; B. Scholl and H. J. Hansen, *Helv. Chim. Acta* 1986, **69**, 1936.
23. G. R. Harvey and K. W. Ratts, *J. Org. Chem.* 1966, **31**, 3907.
24. D. P. Freyberg, G. M. Mockler and E. Sinn, *J. Chem. Soc., Dalton Trans.* 1976, 447.
25. P. W. P. Corfield, R. J. Doedens and J. A. Ibers, *Inorg. Chem.* 1967, **6**, 197.
26. N. Walker and D. Stuart, *Acta Cryst.* 1983, **A39**, 158.
27. MolEN 19901, Enraf–Nonius Co., Delft, Holland.
28. TEXRAY Structure Analysis Package, Molecular Structure Corporation, Houston, Texas (1985).
29. D. T. Cromer and J. T. Waber, *Acta Cryst.* 1965, **18**, 511.
30. R. F. Stewart and E. R. Davidson, *J. Chem. Phys.* 1965, **45**, 3175.
31. D. T. Cromer, *Acta Cryst.* 1965, **18**, 17.

Polyhedron Vol. 12, No. 9, pp. 1003–1006, 1993
Printed in Great Britain

0277-5387/93 $6.00+.00
© 1993 Pergamon Press Ltd

BIS-AMINOPHENYLFERROCENES: SYNTHESIS AND ELECTROCHEMISTRY

IAN R. BUTLER,* MAHER KALAJI,* LOUISE NEHRLICH and DENIS J. WILLIAMS

Chemistry Department, University of Wales, Bangor, Gwynedd LL57 2UW, U.K.

(*Received* 27 *November* 1992; *accepted* 26 *January* 1993)

Abstract—The synthesis and electrochemistry of bis-2-aminophenylferrocene is described and the synthesis and characterization of the co-polymer formed by reaction of bis-2-aminophenylferrocene with *p*-terephthaloyl chloride is discussed.

There is currently an enormous interest in the synthesis of redox active polymers in the general area of new material science.[1] A large proportion of the work in this area has focussed on the polyaniline system, which is one of the most promising as far as material development in electrochromic applications is concerned.[2] Coupled with this is a resurgence in the similar area of metallocene chemistry because of the ability to use the fine tuning of the redox couple of the metal centre in a metallocene as a probe for chemical sensing.[3] It was decided to examine the electrochemical behaviour of bis-2-aminophenylferrocene to see if the combination of the two redox active systems might be useful in material development.

EXPERIMENTAL

All reaction organic solvents were distilled prior to use. ^{1}H NMR spectra were recorded using either a Bruker WH-250 or a WH-400 instrument, in $CDCl_3$ unless otherwise stated. Sulphuric acid was reagent grade and was used as supplied.

Preparation of bis-4-nitrophenylferrocene,[4] *general procedure*

Ferrocene (50.0 g, 0.27 mol) was added to 96% sulphuric acid (250 cm^3), while allowing the temperature to rise to 50°C. The solution was then stirred at room temperature overnight and then poured into an ice/water mixture. 4-Nitroaniline was diazotised as follows: 4-nitroaniline (80.0 g, 0.59 mol) was dissolved in 20% v/v H_2SO_4 (250 cm^3) solution and the mixture cooled to < 4°C. This solution was then added slowly to a solution of sodium nitrite (40 g, 0.58 mol) in water (250 cm^3), maintaining the temperature below 4°C throughout. The diazonium salt was then added to the ferrocenium solution and foaming began with the concomitant formation of a finely divided precipitate. The reaction was allowed to proceed for a further 20 h. The reaction mixture was then filtered and the filtrate extracted several times with dichloromethane. The combined dichloromethane fractions were then evaporated to dryness and the solid residue was extracted in a Soxhlet with the following solvents: (1) petroleum ether (b.p. 40–60°C): evaporation of the extract and crystallization gives pure mono 4-nitrophenylferrocene; (2) dichloromethane: evaporation gives a red oil, which on crystallization gives pure bis-4-nitrophenylferrocene (**1**); and (3) acetone: evaporation of the solvent gives a brown powder, identified by ^{1}H NMR to be primarily a tri-substituted ferrocene compound. An insoluble (organic solvents) residue remained, which was bright purple. Found: C, 46.7; H, 4.2; N, 8.4%. The latter material dissolves in concentrated sulphuric acid to give a pink solution which turns blue on neutralization with sodium hydroxide solution.

4-Nitrophenylferrocene:[4] ^{1}H NMR ($CDCl_3$), 250 MHz: 4.08 (s, 5H), 4.50 (t, 2H), 4.70 (t, 2H), 7.51 (d, 2H), 8.13 (d, 2H); yield 6.4 g, 7.7%.

Bis-4-nitrophenylferrocene: ^{1}H NMR ($CDCl_3$), 250 MHz: 4.03 (t, 4H), 4.63 (t, 4H), 7.34 (d, 4H), 8.01 (d, 4H); yield 28.6 g, 24.7%.

* Authors to whom correspondence should be addressed.

Tris-1,3,1′-(4-*nitrophenyl*)*ferrocene*: ^{1}H NMR ($CDCl_3$), 250 MHz: 4.26 (bs, 2H), 4.6 (bs, 2H), 4.96 (bs, 2H), 5.19 (bs, 1H), 8.14 (m, 4H), 7.90 (bm, 2H), 7.45 (m, 4H), 7.07–7.26 (ms, 2H). Combined yield for trisubstituted derivatives 4 g.

Preparation of bis-2-nitrophenylferrocene (**1**)

An identical procedure to that for 4-nitrophenylferrocene was followed using petroleum ether and diethyl ether for the product extraction. Only two fractions were crystallized, the mono-substituted ferrocene from the petroleum ether fraction (4.3 g, 5.2%) and the di-substituted derivative from the ether fraction (36.1 g, 31.2%).

Bis-2-nitrophenylferrocene (**1**). Found: C, 61.6; H, 3.8; N, 7.2. Calc. for $C_{22}H_{16}FeN_2O_4$: C, 61.7; H, 3.7; N, 6.5. ^{1}H NMR ($CDCl_3$), 250 MHz: 4.35 (t, 4H), 4.50 (t, 4H), 7.25 (td, 2H), 7.33 (td, 2H), 7.45 (dd, 2H), 7.51 (dd, 2H). Mass spectrum, *m/z* (rel. intensity): 428(100), M^+, 412(6), 224(12), 212(13), 184(20), 170(15), 158(16), 139(27), 130(32). IR: 3054 (aryl C—H str.), 2986 (Fc C—H str.), 1526 (asymm. N=O str.), 14,222 (symm. N=O str.), 896 cm^{-1} (aryl deform.).

Compound **1** was reduced almost quantitatively using Zn/HCl using standard methodology to give the product amine **2**.

Bis-2-aminophenylferrocene (**2**). Found: C, 69.2; H, 5.3; N, 7.3. Calc. for $C_{22}H_{20}FeN_2$: C, 71.7; H, 5.4; N, 7.6. ^{1}H NMR ($CDCl_3$), 250 MHz: 4.14 (bs, 4H, N*H*), 4.32 (t, 4H, C_5H_4—β-H), 4.55 (t, 4H, C_5H_4—α-H), 6.57 (d, 2H), 6.65 (t, 2H), 7.02 (t, 2H), 7.21 (d, 2H). Mass spectrum, *m/z* (rel. intensity): 368(86), M^+, 211(100), 184(9), 156(15), 155(33), 154(40), 139(9), 130(13), 129(26), 128(23), 126(20). 121(24). IR: 3045 (C—H str.), 2986 (Fc C—H str.).

Preparation of the polymer from **2** *and* p-*terephthaloyl chloride*

Bis-2-aminophenylferrocene and *p*-terephthaloyl chloride were reacted in equimolar quantities with stirring in dry diethyl ether. The polymeric product which precipitated was filtered off and washed with acetone and vacuum dried. ^{1}H NMR (d^6-DMSO): (a) 4.12 (t), (b) 4.37 (t), ratio (a):(b) $\cong$ 1:7, total integral 4H, (c) 4.48 (t), (d) 4.94 (t), ratio (c):(d) $\cong$ 1:7, total integral 4H, 7.10–7.40 (2 ms, 3H), 7.68 (bd, 1H), 8.01–8.08 (2bs, 4H), 9.93 (bs, 1H).

Electrochemical characterization

Cyclic voltammetry experiments were performed using a Hi-Tek potentiostat (type DT2101) and waveform generator (type PPR1). The working electrode was a platinum disc (2 mm diameter) polished to a mirror finish on successively finer grade alumina (Buehler 3.0, 0.3 and 0.05 μm). A platinum mesh served as a counter electrode. All potentials are quoted with respect to the saturated calomel electrode (S.C.E.). The measurements were performed in either aqueous solutions containing HCl (1 mol dm^{-3}) or acetonitrile solutions containing tetrabutylammonium tetrafluoroborate (0.1 mol dm^{-3}) (Aldrich). All solutions were degassed with nitrogen prior to any measurement.

RESULTS AND DISCUSSION

There are a variety of different synthetic routes which would give the desired ferrocenylaniline compounds, such as Heck coupling of a haloferrocene with iodoaniline or nickel or palladium catalysed arylation; however, we decided to adopt the simplest approach possible using a diazonium salt coupling reaction.

The reaction of aryldiazonium salts with ferrocenium ion in the presence of ferrocene in acidic media is one of the oldest established reactions of ferrocene.[5–8] The mechanism of this reaction has not been fully elucidated, but has been the subject of intense scrutiny and free aryl radicals are known to be key intermediates in the reaction.[9] As a test the diazonium salt of *p*-nitroaniline was reacted initially with the ferrocenium salt derived from the reaction of ferrocene with sulphuric acid to prepare the known *p*-nitrophenylferrocene. In this reaction a complex mixture of ferrocenyl products was obtained including mono-, di-, tri- and tetra-substituted ferrocenes. In all 10 products were observed by TLC, however, the major components identified by NMR were the known mono- and di-substituted ferrocene derivatives. When the reaction was repeated with *o*-nitroaniline only two predominant products were obtained, the mono- and di-substituted products. The desired di-substituted compound, bis-2-nitrophenylferrocene (**1**), was then reduced with zinc in aqueous HCl to give the bis-2-aminophenylferrocene (**2**).

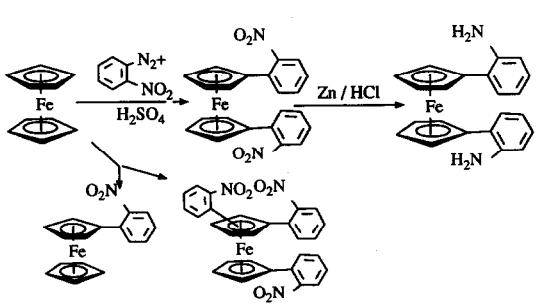

The reaction of bis-2-aminophenylferrocene with *p*-terephthaloyl chloride results in the formation of a polymer (**3**), which is soluble in DMSO. The ^1H NMR spectrum is surprisingly simple with only two predominantly different ferrocenyl environments discernable. The ratio of these is approximately 1:7, with the low intensity cyclopentadienyl resonances lying downfield of the higher intensity resonances by 0.25 and 0.43 ppm, respectively, which would indicate that the latter resonances may be associated with ferrocenyl carboxylic acid termini. This and similar polymers may be useful in the development of redox active polymers in their own right. The electrochemistry of the monomeric pro-

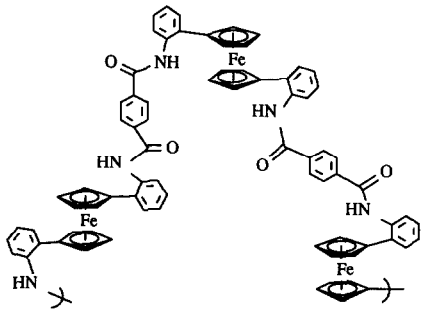

ducts was then investigated. Table 1 shows a summary of the results obtained. Compound **2** exhibits similar electrochemical behaviour to ferrocene. However, $E_{1/2}$ is shifted anodically by 71 mV ($E_{1/2}$ for ferrocene is 435 mV vs S.C.E.) (Fig. 1). The nitro substitution (compound **1**) results in an even bigger shift ($E_{1/2}$ = 575 mV), indicating the presence of the electron withdrawing group with ΔE = 150 mV. The dianilinium tetrafluoroborate salt (**4**) exhibits an even larger anodic shift. However, when the dianilinium hydrochloride salt **5** was studied in aqueous HCl the oxidation and reduction potentials were very similar to that of ferrocene.

Attempts were made to electropolymerize the bis-2-aminophenylferrocene and its dihydrochloride salt potentiodynamically[10] to form the equivalent polyaniline (Fig. 2). However, as the anodic limit was increased above that of the first oxidation the

Table 1.

Compound	E_{ox} (mV)	E_{red} (mV)	ΔE (mV)	$E_{1/2}$ (mV)
Ferrocene	465	405	60	435
1	650	500	150	575
2	552	460	92	506
4	690	560	130	625
5	443	378	65	410

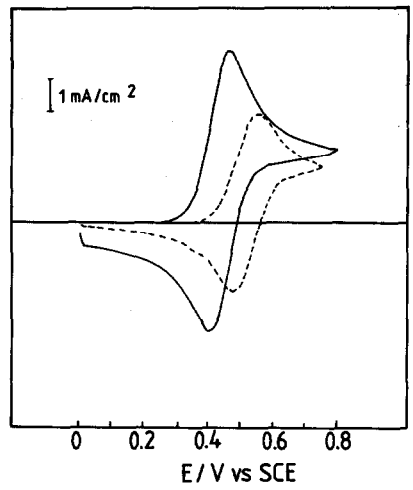

Fig. 1. Cyclic voltammograms for solutions (0.01 mol dm^{-3}) of —— ferrocene and ---- bis-2-aminophenylferrocene in tetrabutylammonium tetrafluoroborate (0.1 mol dm^{-3}) in MeCN on a platinum disc. Note that the latter is for the unprotonated form of compound **4**.

peak heights decreased and the peak separation increased on every cycle until eventually no peaks were observed. It is clear that an insulating layer forms on the surface. If the electrode is polished then the peaks appear again. The insulating film is transparent even though a species with a deep-red colour diffuses away from the electrode at the high anodic limits. Such behaviour has recently been observed for ferrocenylpyrrole.[11,12]

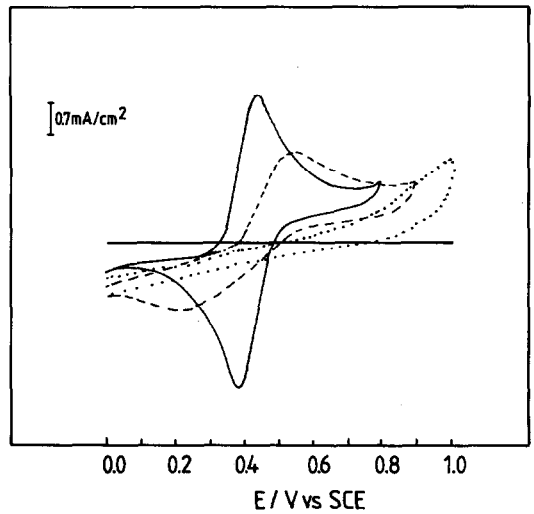

Fig. 2. Cyclic voltammograms for a solution of bis-2-aminophenylferrocene (0.01 mol dm^{-3}) in HCl (1 M) on a platinum disc electrode. Each CV is the second cycle taken at increasing anodic limits.

Our investigations are continuing into the nature of the thin insulating film deposited on the electrode surface and we are currently investigating the effect of a range of spacers between the ferrocene and the anilinium group. It should be noticed that Horowitz and Dailey has previously investigated the complementary system[13] with a methylene space. Our results in this area will be published in due course.

REFERENCES

1. J. Heinze, in *Topics in Current Chemistry* (Edited by E. Steckman), Vol. 152, p. 1. Springer, Heidelberg (1990).
2. A. MacDiarmid and A. J. Epstein, *Faraday Discuss., Chem. Soc.* 1989, **88**, 317.
3. I. R. Butler, in *Organometllic Chemistry* (Edited by E. Abel), Vol. 21, pp. 338–341. Royal Society of Chemistry Specialist Periodic Reports (1992).
4. W. F. Little and A. K. Clark, *J. Org. Chem.* 1960, **25**, 1979.
5. G. D. Broadhead and P. L. Pauson, *J. Chem. Soc.* 1955, 367.
6. V. Weinmayer, *J. Am. Chem. Soc.* 1955, **77**, 3012.
7. J. G. Mason and M. J. Rosenblum, *J. Am. Chem. Soc.* 1960, **82**, 406.
8. W. F. Little, K. N. Lynn and R. Williams, *J. Am. Chem. Soc.* 1963, **85**, 3055.
9. A. L. H. Beckwith, R. A. Jackson and R. W. Longmore, *Aust. J. Chem.* 1992, **45**, 857.
10. R. Greef, M. Kalaji and L. Peter, *Faraday Discuss., Chem. Soc.* 1989, **88**, 277.
11. T. Rose, A. Kon and J. Foos, 204th ACS Meeting, Washington, DC, Abstract No. 114 (1992).
12. I. R. Butler, M. Kalaji and V. W. Jones, unpublished results.
13. C. P. Horowitz and G. C. Dailey, *Chem. Mat.* 1990, **2**, 343.

Polyhedron Vol. 12, No. 9, pp. 1007–1017, 1993
Printed in Great Britain

0277–5387/93 $6.00+.00
© 1993 Pergamon Press Ltd

A MECHANISM OF HYDROXYALUMINOSILICATE FORMATION

C. EXLEY* and J. D. BIRCHALL

Unit for Inorganic Chemistry and Materials Science, Department of Chemistry, Keele University, Staffordshire ST5 5BG, U.K.

(*Received* 17 *November* 1992; *accepted* 26 *January* 1993)

Abstract—The simple fractionation procedure membrane filtration was successfully applied to the identification of the formation of hydroxyaluminosilicates. The mechanism of formation was shown to proceed through the inhibition of the nucleation of aluminium hydroxide. The inhibition was the result of silicic acid replacing hydroxylated aluminium at growth sites on aluminium hydroxide lattices. The ability of silicic acid to poison the growth of aluminium hydroxide lattices was dependent upon solution pH and the silicic acid concentration. This may be the first fully supported observation of a reaction of this ilk involving the neutral silicic acid molecule.

The biological availability and toxicity of aluminium is of increasing concern in biology and medicine.[1] The observation that silicic acid protected against the toxicity of aluminium in fish[2] was explained as being due to the reduction in the biological availability of aluminium through the formation of stable hydroxyaluminosilicates (HAS).[3] A recent experiment has confirmed the formation of HAS in solutions containing a "biologically relevant" total aluminium concentration and a mechanism to describe their formation was proposed.[4] Silicic acid was suggested to poison the nucleation of aluminium hydroxide, an effect which could be observed in solution by determining the size distribution profile (SDP) of aluminium particles using membrane filtration. In the experiments described herein the proposed mechanism of HAS formation was thoroughly tested using membrane filtration and an additional technique in which the base neutralizing capacities (BNC) of aluminium hydroxide and HAS solutions were compared.

EXPERIMENTAL

Materials and method

Membrane filtration was used to investigate changes in the size distribution profile of aluminium particles in solutions of known silicic acid concentration. In an additional experiment solutions of aluminium and aluminium and silicic acid were titrated against a base and their pH response recorded. Solutions were prepared in a medium of $NaHCO_3$ (10 mmol dm^{-3}; Sigma Chem. Co.) with the exception of the titration studies when solutions were additionally made up in ultra-pure water, the conductivity of which was consistently below 0.5 μS cm^{-1} (Russel CD800). Solution pH values in the range 3.0–9.0 were measured using a laboratory pH meter (Phillips PW 9420) and any pH adjustments were achieved through manual additions of microlitre aliquots of 0.1 M NaOH or HNO_3 (both BDH Aristar). Magnetic stirrers set at a constant speed were used to agitate the solution both during pH adjustment and final measurement. Aluminium was added to treatments from a stock solution (2 mmol dm^{-3}) of $Al(NO_3)_3 \cdot 9H_2O$ (Aldrich Chem. Co.) to give a nominal concentration in the treatment solutions of 4 μmol dm^{-3}. Silicic acid was used in the concentration range 0–2000 μmol dm^{-3} and was added as a stock solution (2 mmol dm^{-3}) of $Si(OH)_4$, prepared freshly as required using Na_4SiO_4 (Alfa Prod.). The contamination of solutions was reduced through the use of polypropylene, polythene and polycarbonate laboratoryware pre-washed in 5% nitric acid solution and rinsed in ultra-pure water for 24 h prior to use. All experiments were performed at a laboratory temperature recorded as 20 ± 2°C.

* Author to whom correspondence should be addressed.

The method of preparation of treatment solutions is critical to the efficacy with which membrane filtration can be used to discriminate changes in the size distribution profile of aluminium particles.[4] With this in mind the following experimental protocol was adopted for all preparations of treatment solutions unless otherwise specifically stated.

(1) The required silicic acid solution was made up in the appropriate medium (either 10 mmol dm^{-3} $NaHCO_3$ or ultra-pure water) and the solution pH adjusted to 3.0.
(2) Aluminium was added from the stock solution to give a treatment solution of 4 μmol dm^{-3} and, if necessary, the solution pH readjusted to 3.0.
(3) The treatment solution was then left to equilibrate for 24 h.
(4) If necessary the treatment solution pH was readjusted to 3.0 and thereafter base was added to effect the required treatment solution pH.
(5) The treatment solution was then left to equilibrate for a pre-determined time; in these studies anything from 300 s to 12 weeks.

At the appropriate time solutions were filtered under reduced pressure through 0.04 μm membrane filters (Ultipor, Pall UK Ltd.) in closed polycarbonate filtration vessels (Sterifil, 47 mm, Millipore) using protocol described in detail elsewhere.[4]

Four separate experiments comprized the present study.

(i) *The influence of* $[Si(OH)_4]$ *on HAS formation.* Treatment solutions containing silicic acid (0, 50, 100, 1000 and 2000 μmol dm^{-3}) and Al (4 μmol dm^{-3}) were adjusted to pH in the range 3.0–9.0 and thereafter equilibrated for 24 h before filtation. The total aluminium concentration ($[Al_t]$) in the filrate was expressed as a proportion of the total aluminium in solution at each recorded pH.

(ii) *Solution age and the size distribution profile of aluminium particles.* Solutions containing $Si(OH)_4$ (0 or 2000 μmol dm^{-3}) and Al (4 μmol dm^{-3}) were adjusted to pH in the range 5.0–9.0 and thereafter equilibrated for 300 s, 24 h, 1, 2, 3, 4 or 12 weeks, at which point the solutions were filtered and the total aluminium ($[Al_t]$) in the filtrate determined. Any change in the pH of solutions during their equilibration was not adjusted and the recorded pH values refer to solution pH immediately prior to their filtration. Results were plotted as $-\log_{10}[Al_t]$ against the solution pH.

(iii) *The effect of initial solution pH on the size distribution profile of aluminium particles in pH-adjusted solutions.* In this experiment modifications to the protocol of solution preparation were made. Solutions containing $Si(OH)_4$ (0 or 2000 μmol dm^{-3}) and Al (4 μmol dm^{-3}) were made up as detailed above, except that they were initially adjusted to either pH 3.0, 6.0 or 9.0. After the initial aging for 24 h the solution pH values were then adjusted, using microlitre additions of acid or base as appropriate, in the range 3.0–9.0 and then left to equilibrate for a further 24 h at their adjusted pH. Solutions were then filtered and $[Al_t]$ in the filtrate determined. Again, $[At_t]$ was expressed as a proportion of the total aluminium in solution at each recorded pH.

(iv) *The influence of silicic acid on the base neutralizing capacity (BNC) of aluminium solutions.* Four treatment solutions were prepared, as in the general solution preparation protocol, in both $NaHCO_3$ (10 mmol dm^{-3}) and ultra-pure water only.

1. Medium only, i.e. $NaHCO_3$ (10 mmol dm^{-3}) or ultra-pure water.
2. Medium + $Si(OH)_4$ (2000 μmol dm^{-3}).
3. Medium + $Si(OH)_4$ (2000 μmol dm^{-3}) + Al (4 μmol dm^{-3}).

Each treatment solution was equilibrated for 24 h at pH 3.0 before known volumes of NaOH (0.1 M) were added to 100 cm^3 aliquots of each. These aliquots were then left to equilibrate for either 24 h or 2 weeks, at which time their solution pH values were recorded. The results for each treatment solution in each medium were recorded as a final pH for each discrete volume of base added.

Total aluminium and total silicon were measured by graphite furnace atomic absorption spectroscopy (Perkin–Elmer 2280, HGA 400) using previously developed programmes.[5]

RESULTS AND DISCUSSION

The experiments were designed to test the hypothesis that hydroxyaluminosilicate (HAS) formation, as identified by changes in the size distribution profile (SDP) of aluminium-containing particles, was dependent upon the interaction of silicic acid ($Si(OH)_4$) with polymers of aluminium hydroxide ($\{Al(OH)_3\}_n$). Membrane filtration was the chosen method of fractionation, whilst the additional method of titration was used to elucidate further on the chemical nature of HAS in solution.

1. *The influence of* $[Si(OH)_4]$ *on HAS formation*

In the first experiment the fractionation procedure, membrane filtration, was evaluated. It was important to determine the $[Si(OH)_4]$ that in comparatively young (24 h) solutions would effect an observable change in the SDP of aluminium

particles. The SDP of aluminium particles formed in solutions aged for 24 h and containing $Si(OH)_4$ (0, 50, 100, 1000 and 2000 μmol dm^{-3}) were compared in the pH range 3.0–9.0. The results are shown in Figs 1(a)–(f). In the absence of silicic acid the SDP of aluminium particles assumed a characteristic V-shaped curve with the maximum growth and aggregation of particles to a filterable size occurring at *ca* pH 6.5 [Fig. 1(a)]. This profile remained largely unchanged for 50, 100 and 500 μmol dm^{-3} [Figs 1(b), (c) and (d)], except for a gradual widening, with increasing $[Si(OH)_4]$, of the pH regime in which these effects on aluminium particle size were enhanced. A more definitive response to the presence of silicic acid was seen in solutions containing 1000 and 2000 μmol dm^{-3} $Si(OH)_4$ [Figs 1(e) and (f)]. The mean particle size (MPS) was significantly reduced in the pH regime 5.5–7.5 and the pH at which the maximal growth and aggregation of particles to a filterable size occurred had moved from 6.5 to 5.5.

These results confirm silicic acid as a poison of the growth and aggregation of aluminium hydroxide. The kinetics were dependent upon both the pH ($5.5 < pH < 7.5$) and the silicic acid concentration ($[Si(OH)_4] > 500$ μmol dm^{-3}) in solution. The results do not preclude the possibility that HAS were formed in solutions of pH and $[Si(OH)_4]$ outside these limits (both chemical[4] and biological studies[2,6,7] have either identified or implied the formation of HAS at $[Si(OH)_4] \leqslant 500$ μmol dm^{-3}), only that their growth and aggregation to a filterable size (> 40 nm) could not be distinguished from that of aluminium hydroxide alone. If the size distribution profiles shown in Figs 1(a)–(f) were inverted they might be re-interpreted as the influence of solution pH on the tendency of aluminium particles to reach a filterable size, which in these experiments was *ca* 40 nm. The processes that contributed towards these tendencies were (1) the attainment of a critical nucleus, (2) the growth of critical nuclei of aluminium atoms, and (3) the aggregation of these growing nuclei. Which of these events were influenced by the formation of HAS cannot be easily determined from the results of these experiments. At the lower silicic acid concentrations ($[Si(OH)_4] \leqslant 500$ μmol dm^{-3}) the reaction kinetics of HAS formation were not sufficiently rapid in the time-scale available (24 h) to affect any of these processes relative to those of aluminium hydroxide alone; however, the higher concentrations of silicic acid ($[Si(OH)_4] \geqslant 1000$ μmol dm^{-3}) might alternatively be interpreted as influencing each of these mechanisms. (The identification in a previous study[4] of HAS $\leqslant$ 14 Å in size might lend support towards the formation of HAS involving critical nuclei containing fewer aluminium atoms than for aluminium hydroxide alone.) Certainly the tendency for HAS to form more easily at pH 5.5 than 6.5 was evidence of competition between silicic acid and hydroxylated aluminium for addition onto critical nuclei.

The influence of the aging of solutions might help to clarify which of the processes that determine the size distribution profiles of aluminium particles were in fact influenced by HAS formation. This was tested in the next experiment.

To make the most of the method of membrane filtration to identify the formation of HAS a silicic acid concentration of 2000 μmol dm^{-3} was used in all the remaining experiments.

2. *Solution age and the size distribution profile of aluminium particles*

HAS formation in young solutions changed the tendancy of aluminium particles to achieve a filterable size. Whether this was an effect on particle growth, aggregation or both was not clear. In this experiment the contribution of the age of the solution to the SDP of aluminium particles was determined.

The influence of equilibration time or solution age on the SDP of aluminium particles was ascertained for solutions of initial pH between 5.0 and 7.0 and containing $Si(OH)_4$ (0 or 2000 μmol dm^{-3}). Solutions were aged for up to 12 weeks, at which time their aluminium particle SDP was determined by membrane filtration. The results are shown in Figs 2(a)–(g).

The influence of silicic acid was immediate with an inhibition of nucleation, relative to aluminium hydroxide alone, occurring within 300 s of equilibration [Fig. 2(a)]. The further aging of the solutions produced the now characteristic V-shaped SDP of both aluminium hydroxide and HAS. In solutions aged for 12 weeks the growth and aggregation of particles in both aluminium only and HAS solutions reached an apparent steady-state [Fig. 2(g)]. At the respective solution pH where the growth of aluminium particles to a filterable size was greatest the concentration of aluminium particles not retained by membrane filtration was reduced, relative to the 24 h solutions, for both the aluminium only (*ca* 0.6–0.1 μmol dm^{-3}) and the HAS (*ca* 1.6–0.6 μmol dm^{-3}) treatments. Thus, aggregation of aluminium particles was occurring in both aluminium hydroxide and HAS solutions. The extent, however, to which aggregation occurred was reduced by HAS formation and this might be explained as a difference between the surface properties of HAS and aluminium hydroxide.

These results further support the hypothesis of silicic acid poisoning the nucleation of aluminium hydroxide through the substitution of silicic acid for hydroxylated aluminium at growth points on an aluminium hydroxide lattice. This hypothesis was further tested in the following experiment.

3. *The effect of the initial solution pH on the SDP of aluminium particles in pH-adjusted solutions*

In the aforementioned experiments all solutions were made up via the pH adjustment of solutions that had been previously equilibrated for 24 h at pH 3.0. In this way silicic acid would be able to influence the critical nucleus size and both the growth and subsequent aggregation of the critical nuclei of aluminium particles. How then might silicic acid influence the SDP of aluminium particles in solutions in which either (1) a variety of aluminium hydroxide lattices were preformed or (2) the tendancy to form aluminium hydroxide lattices was aproached from solutions containing predominantly tetrahedral anionic aluminium, i.e. the aluminate anion, $Al(OH)_4^-$. The effect of these

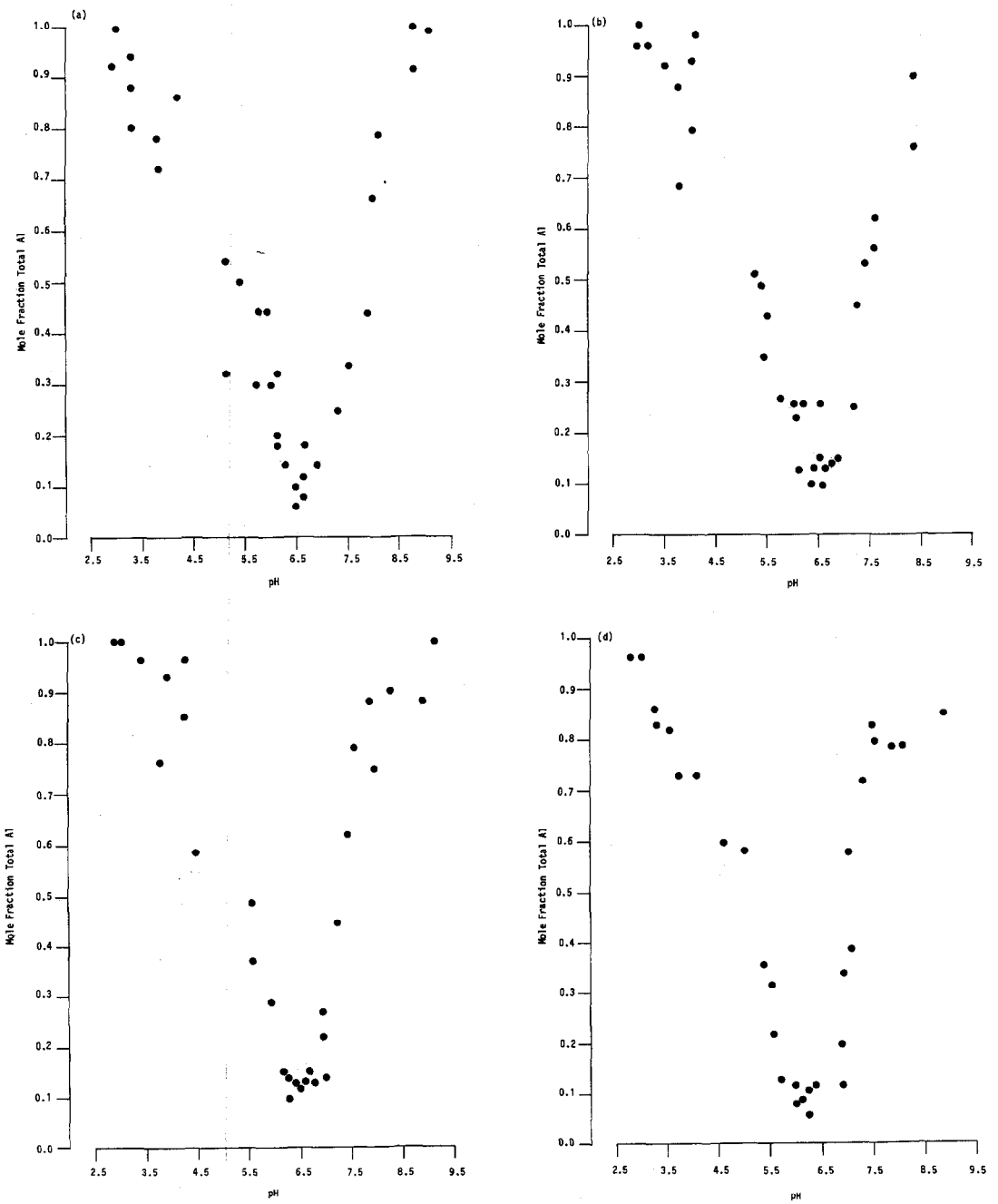

Fig. 1. (a)–(d)

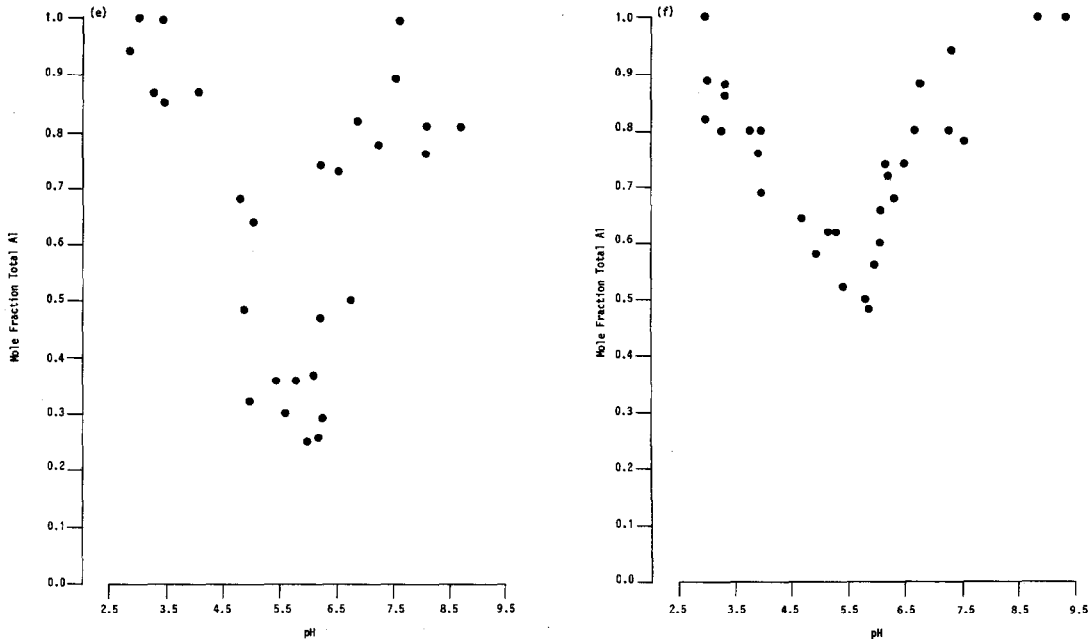

Fig. 1. The influence of: (a) 0, (b) 50, (c) 100, (d) 500, (e) 1000 and (f) 2000 μmol dm^{-3} [Si(OH)$_4$] on the SDP of aluminium particles in solutions in the pH range 3.0–9.0; $n = 36$.

differences in treatment solution preparation and the species composition of the solutions prior to pH adjustments on the SDP of aluminium particles was tested in young solutions in which pH adjustments were made in the range 3.0–9.0. The results are shown in Figs 3(a)–(c). The SDP of aluminium particles originally equilibrated at pH 3.0 [cf. Figs 1(a) and (f)] is shown in Fig. 3(a) for comparison. For solutions originally equilibrated at pH 6.0 the SDPs of aluminium hydroxide and HAS were only marginally different [Fig. 3(b)]. The MPS for HAS solutions was reduced slightly in the circumneutral pH regime and the pH at which the maximum particle size occurred had moved from 6.5 to 5.5. These effects, however, were much reduced when compared to the solutions that had been prepared from an original pH of 3.0 [cf. Figs 3(a) and (b)]. In this experiment the influence of HAS formation on the size stability of preformed aluminium hydroxide lattices was tested. The subsequent adjustments in solution pH from 6.0 towards both 3.0 and 9.0 tested the further stabilities of the complexes formed at pH 6.0 to both acid and base attack. The results confirmed an interaction between silicic acid

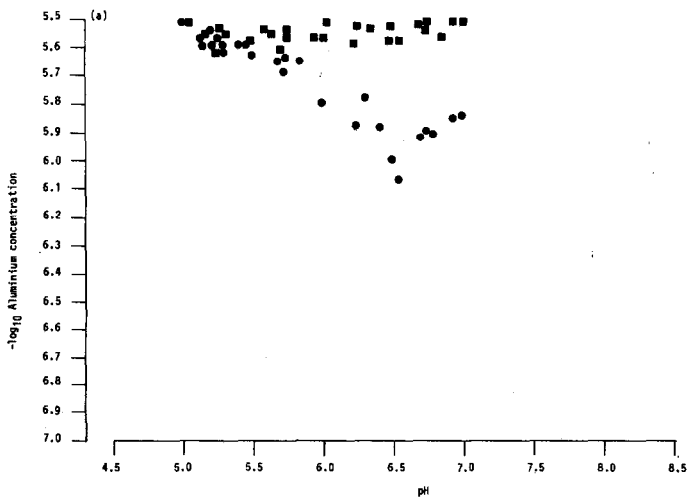

Fig. 2. (a)

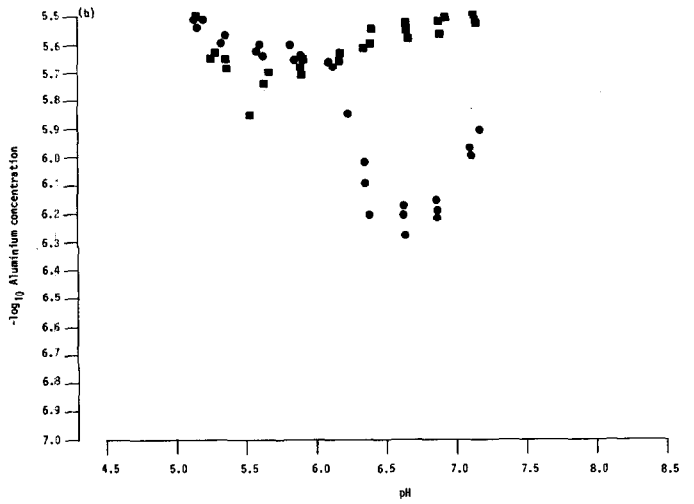
(b)
-log10 Aluminium concentration
pH

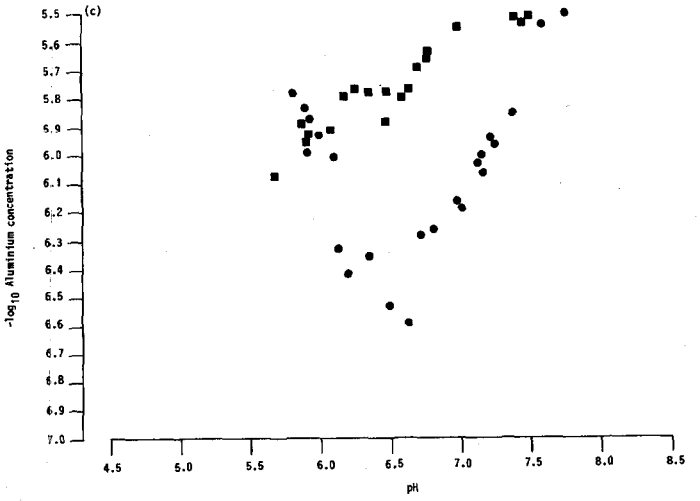
(c)
-log10 Aluminium concentration
pH

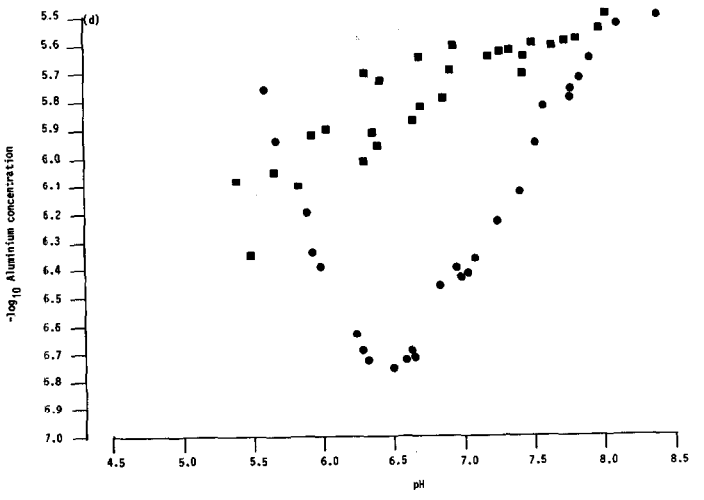
(d)
-log10 Aluminium concentration
pH

Fig. 2. (b)–(d)

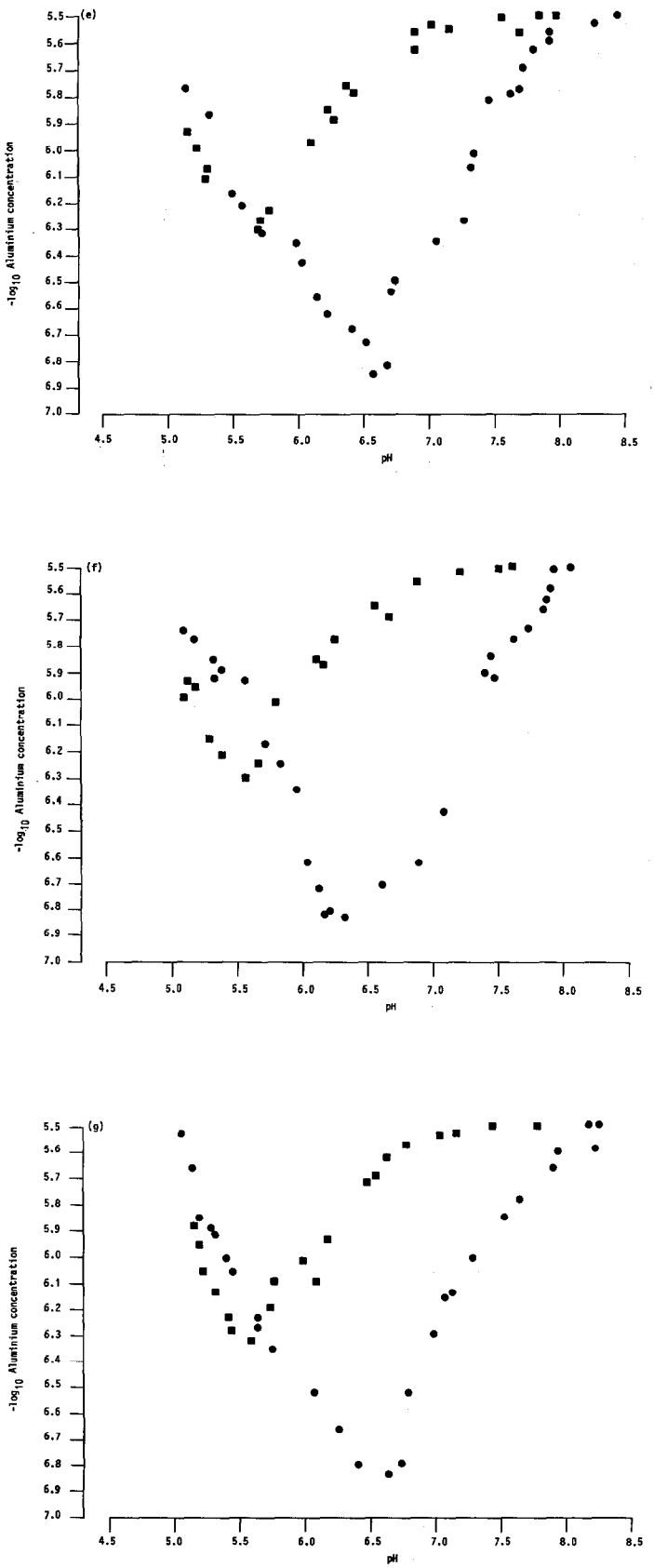

Fig. 2. The influence of solution age: (a) < 300 s, (b) 24 h, (c) 1, (d) 2, (e) 3, (f) 4 and (g) 12 weeks on the SDP of aluminium hydroxide (●) and hydroxyaluminosilicate (■) particles in solutions in the pH range 4.5–8.5; $n = 30$.

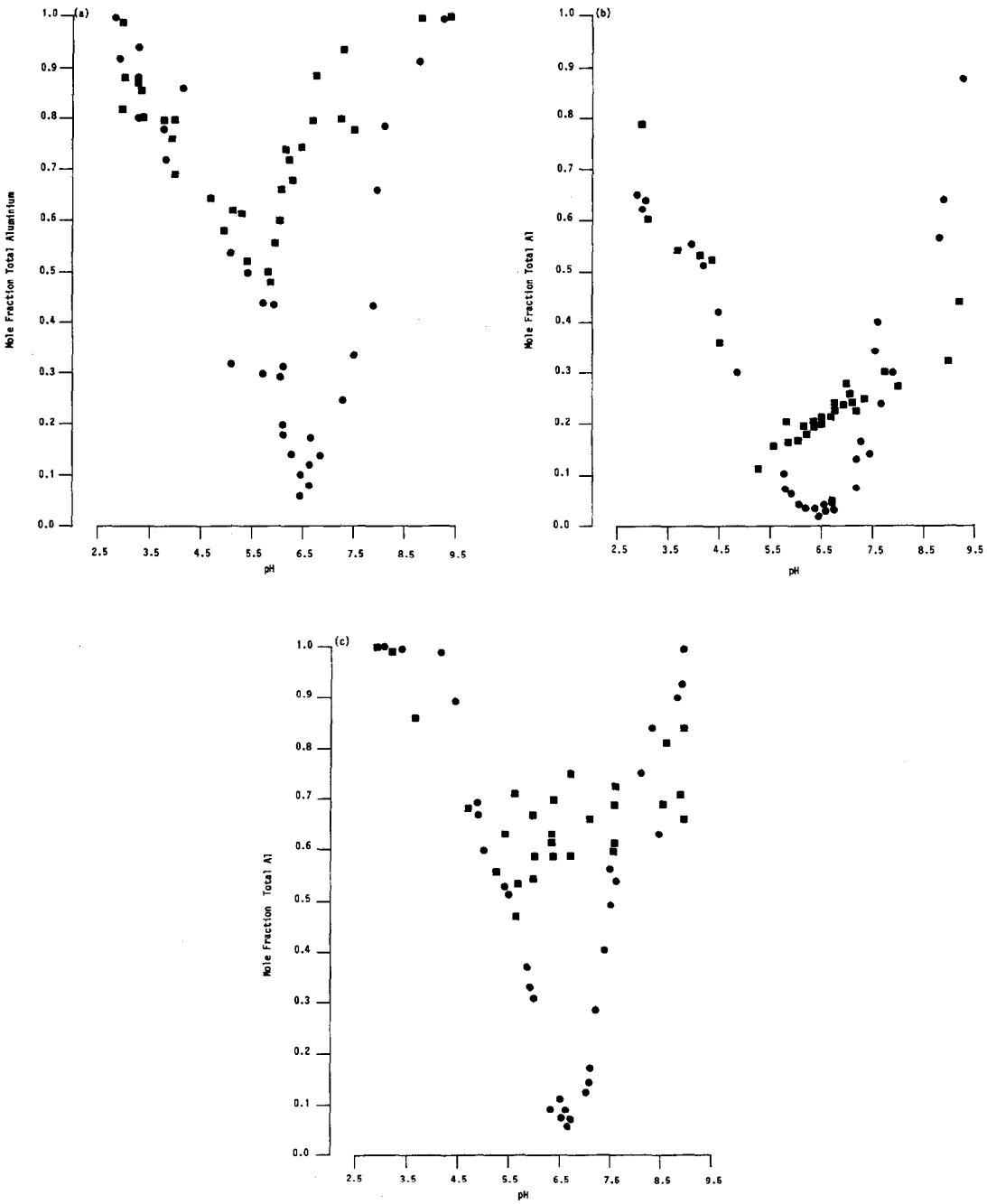

Fig. 3. The influence of the initial solution pH: (a) pH 3.0, (b) pH 6.0 and (c) pH 9.0 on the SDP of aluminium hydroxide (●) and hydroxyaluminosilicate (■) particles in solutions in the pH range 3.0–9.0; $n = 36$.

and the preformed aluminium hydroxide polymers with the formation of HAS producing a diminution of their size in the expected pH range 5.5–7.5. These changes might be interpreted as HAS solutions approaching the steady-state characteristics of particle size distribution seen in aged solutions [Fig. 2(g)], although in the present experimental conditions the solutions were undersaturated (as opposed to oversaturated for solutions originally equilibrated at pH 3.0) with respect to their SDP of HAS. Thus, the extended HAS lattices formed at pH 6.0 were subject to pH-induced changes in their size. The response to pH changes of solutions of aluminium and silicic acid originally equilibrated at pH 9.0 was again different, although the final SDP was similar to that of solutions of an initial pH of

3.0 [Fig. 3(c)]. The SDP was largely ambiguous, although it gave some indication that HAS were formed at and around pH 9.0 and that the growth and aggregation of these HAS was relatively insensitive to pH adjustments in alkaline solution. Whether these HAS formed in alkaline solution were of similar structure and stoichiometry to those identified in acidic milieu cannot be ascertained from these results. There is evidence, although not from comparative studies in the laboratory, that they may not be.[8–11] Our own studies have indicated an increased silicon content of HAS formed in alkaline solutions.[4]

The results to-date suggest that HAS formation and the subsequent poisoning of the growth and aggregation of aluminium hydroxide may influence the hydrolytic reactions of aluminium in solution. In a final experiment the influence of silicic acid on the base neutralizing capacity (BNC) of aluminium solutions was determined.

4. *The influence of silicic acid on the BNC of aluminium solutions*

The change in pH of solutions of aluminium only and aluminium and silicic acid, which had previously been equilibrated for 24 h at pH 3.0, after the addition of known volumes of NaOH (0.1 M) were measured after either 24 h or 14 days equilibration. The experiment was first conducted using the standard bicarbonate medium [Fig. 4(a) and (b)]. Equilibrium with respect to the solution pH was aproached only very slowly and this phenomenon was directly attributable to the effect of bicarbonate *per se*. For this reason the pH response of the younger solutions (although largely vindicating the effects seen in the aged solutions) were largely discounted. Aluminium improved the BNC of solutions relative to bicarbonate alone only within the pH regime 4.0–7.0. The presence of silicic acid reduced this improvement of BNC. A closer examination of the results revealed that aluminium could be discerned as a contributor to the BNC in the pH range 4.1–5.9, whilst in the presence of silicic acid its efficacy was only evident up to a pH of 5.2. Below pH 4.0 and above pH 7.0 any effect of aluminium on BNC was not discernable from the effect of bicarbonate alone. The response of solution BNC to the presence of silicic acid corresponded closely to the pH regime in which the formation of HAS produced identifiable changes in the SDP of aluminium particles. For solutions of pH above *ca* 5.2 (the approximate pH range in which the MPS of aluminium particles was reduced in the presence of silicic acid) the presence of silicic acid abolished any significant addition of the presence of aluminium to the BNC of solutions. Whilst these results suggest that HAS formed at pH 5.2 and above were stable towards further hydrolysis they cannot totally preclude the possibility that further proton release was occurring, but that any effects of such on solution pH were masked by the burgeoning buffering potential of bicarbonate at these circumneutral pH. To look at the possible effects of bicarbonate on these results the experiment was repeated, making up the solutions in pure water as opposed to $NaHCO_3$ (10 mmol dm^{-3}). The results are shown in Figs 4(c) and (d). The results were surprizing and apparently contrary to those found for the bicarbonate medium. Above pH 4.0 aluminium significantly improved the BNC of the pure water medium. This was most significant in the pH range 4.2–6.6 and was evident in both young and aged solutions. The presence of silicic acid did not reduce aluminium's contribution to the BNC of solutions, as might have been predicted from the previous experiment, but actually increased the BNC over the entire pH range at which aluminium *per se* was effective. Although only preliminary and prone to the vagaries of pH measurements in solutions of different ionic potential these results were indicative of the possible influence of media on the fate of chemical reactions. Bicarbonate will bind aluminium[12] and bicarbonate was implicated in the reaction of aluminium with silicic acid in a previous experiment.[13] The importance of any such interactions of bicarbonate with aluminium on HAS formation will be investigated in future experiments.

CONCLUSIONS

Membrane filtration was successfully applied to the identification of HAS formation in solutions of low total aluminium concentration. The formation of hydroxyaluminosilicates was identified as changes in the tendancy of aluminium-containing particles to achieve a filterable size. The pH-dependency of these changes in SDP of aluminium-containing particles supported the interaction of silicic acid with both the growth and aggregation of critical nuclei of aluminium atoms. The mechanism of HAS formation and thus the inhibition of the nucleation of aluminium hydroxide included both steric and kinetic components. Silicic acid blocked growth sites on aluminium hydroxide lattices, possibly in the same way as the dimeric silicate anion inhibits the growth of calcium hydroxide crystals.[14] The rate of HAS formation was dependent upon both the solution pH and the silicic acid concentration. The poisoning of the nucleation of aluminium hydroxide was rapid at high silicic acid concentrations (> 500 μmol dm^{-3}) and was iden-

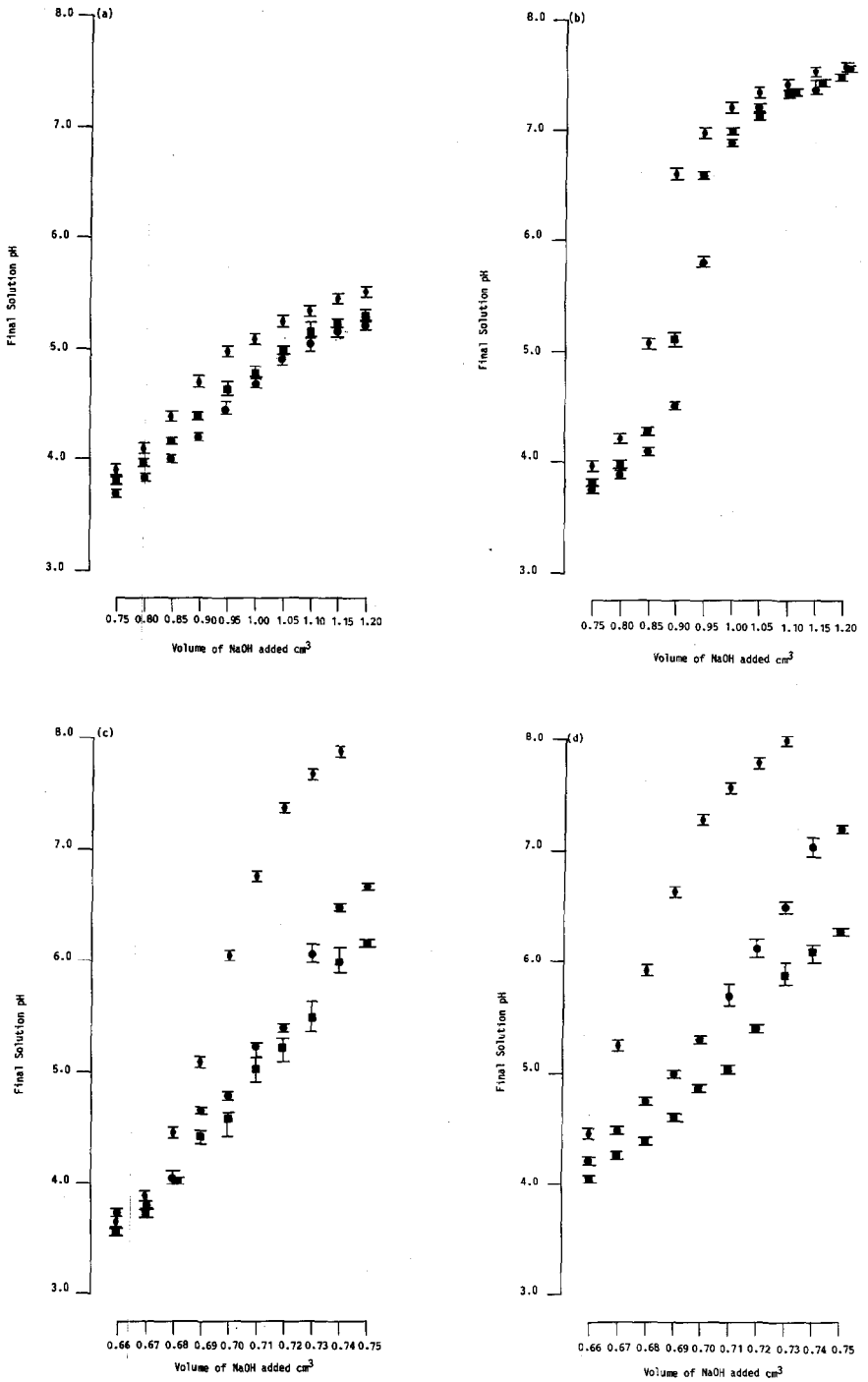

Fig. 4. The base neutralizing capacity of different solutions aged for: (a) and (c) 1 day and (b) and (d) 14 days and made up in either a medium of (a) and (b) 10 mmol dm^{-3} $NaHCO_3$ or (c) and (d) pure water only. Key: ◆ medium $\pm$ 2000 μmol dm^{-3} $Si(OH)_4$, ● medium + 4 μmol dm^{-3} Al, ■ medium + 4 μmol dm^{-3} Al + 2000 μmol dm^{-3} $Si(OH)_4$. Mean and the range is plotted; $n = 9$.

tified by membrane filtration. At lower concentrations of silicic acid the formation of HAS has been observed,[4] although in these studies, as in the previous study, it was not identified by membrane filtration. These experiments do not preclude the existence of soluble aluminosilicates such as those postulated in a recent publication.[15] The formation of HAS of this type through the substitution of silicic acid for water in the inner coordination sphere of the hexa-aqua aluminium species has a precedent, although unproven, in iron–silicon chemistry.[16] If such species do form they are, how-

Table 1. The influence of pH on the ratio of Si:Al retained on sulphonic acid and acetate functional groups after the cation exchange of solutions aged for 1 week and containing Al (4 μmol dm^{-3}) and $Si(OH)_4$ (250 μmol dm^{-3}). Mean (S.D.) $n = 9$ (see ref. 4 for details of experimental method)

pH	Sulphonic acid	Acetate
4.0	0.02 (0.00)	0.02 (0.00)
4.5	0.01 (0.00)	0.02 (0.01)
5.0	1.66 (0.19)	0.47 (0.09)
5.5	1.61 (0.31)	0.44 (0.05)
6.0	2.00 (0.36)	0.67 (0.11)

ever, expected to be only weak complexes. Resin elution studies (including those detailed in Table 1) have consistently failed to identify Al/Si complexes below pH 5.0.[4,13,17] Where aluminium and silicon were co-localized on resins, they were of varying stoichiometry and not the 1:1 stoichiometry postulated by Browne and Driscoll.[15]

Acknowledgement—CE acknowledges the support of the ICI Watercare.

REFERENCES

1. D. J. Chadwick (Editor), *Aluminium in Biology and Medicine*, Ciba Found. Symp. 169, p. 316. Wiley-Interscience, New York (1992).
2. J. D. Birchall, C. Exley, J. S. Chappell and M. J. Phillips, *Nature* 1989, **338**, 146.
3. J. D. Birchall, C. Exley and J. S. Chappell, *J. Inorg. Biochem.* 1989, **36**, 347.
4. C. Exley and J. D. Birchall, *Polyhedron* 1992, **11**, 1901.
5. C. Exley, PhD Thesis, p. 282. University of Stirling, Scotland (1989).
6. C. Exley, A. Tollervey, G. Gray, S. Roberts and J. D. Birchall, *Proc. Roy Soc. London Biol. Sci.*, submitted.
7. C. Exley, N. Price and J. D. Birchall, manuscript in preparation.
8. H. Bilinski, L. Horváth, N. Ingri and S. Sjöberg, *J. Soil Sci.* 1990, **41**, 119.
9. V. C. Farmer, F. Palmieri, A. Violante and P. Violante, *Clay Mins.* 1991, **26**, 281.
10. S. D. Kinrade and T. W. Swaddle, *Inorg. Chem.* 1989, **28**, 1952.
11. V. C. Farmer, W. J. McHardy, F. Palmieri, A. Violante and P. Violante, *Soil Sci. Soc. Am. J.* 1991, **55**, 1162.
12. T. Hedlund, S. Sjöberg and L.-O. Öhman, *Acta Chem. Scand.* 1987, **A41**, 197.
13. J. S. Chappell and J. D. Birchall, *Inorg. Chim. Acta* 1988, **153**, 1.
14. J. D. Birchall and N. L. Thomas, *Brit. Ceram. Proc.* 1984, **35**, 305.
15. B. A. Browne and C. R. Driscoll, *Science* 1992, **256**, 1667.
16. W. J. Weber and W. Stumm, *J. Inorg. Nucl. Chem.* 1965, **27**, 237.
17. J. D. Birchall and J. S. Chappell, *Clin. Chem.* 1988, **34**, 265.

Polyhedron Vol. 12, No. 9, pp. 1019–1026, 1993
Printed in Great Britain

0277–5387/93 $6.00+.00
© 1993 Pergamon Press Ltd

SYNTHESIS, STRUCTURE AND MAGNETIC STUDIES OF COPPER(II) AND COPPER(I) COMPLEXES OF METHYLPYRAZINES

CARLOS NAVAS and MARK M. TURNBULL*

Department of Chemistry, Clark University, 950 Main St, Worcester, MA 01610, U.S.A.

and

CHRISTOS GIOGAS, CHRISTOPHER P. LANDEE* and WANRU ZHANG

Department of Physics, Clark University, 950 Main St, Worcester, MA 01610, U.S.A.

and

GEORGE PON and ROGER WILLETT

Department of Chemistry, Washington State University, Pullman, WA 99164, U.S.A.

(*Received* 14 *August* 1992; *accepted* 19 *January* 1993)

Abstract—Reaction of $Cu(ClO_4)_2$ with 2-methylpyrazine (mepz), 2,5-dimethylpyrazine (2,5-dmpz) or 2,6-dimethylpyrazine (2,6-dmpz) in aqueous solution yields the corresponding $CuL_n(ClO_4)_2(H_2O)_m$ ($n = 2,4$; $m = 1,2,4$). Single-crystal X-ray diffraction of $Cu(mepz)_2(ClO_4)_2(H_2O)_2$ (**1**) reveals a roughly octahedral geometry with all ligands *trans*. Similarly, $Cu(mepz)_4(ClO_4)_2(H_2O)$ (**2**) is pseudo-octahedral with one coordinated perchlorate and one H_2O in the axial sites. The pyrazines are coordinated through the N(4) nitrogen atom in both **1** and **2**. The magnetic susceptibilities of these compounds have been measured in the range 2–300 K. All the compounds behave as paramagnets. Conversely, reaction of $Cu(ClO_4)_2$ with 2,3-dimethylpyrazine in aqueous solution, or with mepz, 2,3-dmpz or 2,5-dmpz and $NaBH_4$ or NaSCN in aqueous solution yields complexes of the type $Cu_2(L)_3(ClO_4)_2$ or $Cu_2(L)(SCN)_2$, respectively. IR analysis suggests that the complexes are polymeric lattices of tri-coordinate copper(I) atoms bridged by the pyrazine ligands or the pyrazine and thiocyanate ligands, similar to the known structure of Cu_2(2,3-dimethylpyrazine)$_3(ClO_4)_2$.

Through our interest in magnetic interactions between metals mediated by organic ligands we began a study of complexes of bidentate heterocyclic ligands. Pyrazine is known to bridge metal ions and form coordination polymers such as the 2D-Heisenberg antiferromagnetic system $Cu(pz)_2(ClO_4)_2$ (pz = pyrazine).[1] In the crystalline state this complex is described as a two-dimensional array of Cu^{2+} atoms with bridging pyrazines, such that each copper atom is bonded to four pyrazine molecules in a pseudo-square planar array (the perchlorate ions are loosely coordinated in the axial sites). The material exhibits typical antiferromagnetic behaviour with a rounded maximum in the magnetic susceptibility versus temperature curve around 12 K.[1a] The pyrazine rings are rotated out of the plane described by the copper and nitrogen atoms by 66°, presumably to relieve steric crowding. We hoped that modification of the pyrazine ligand to increase the steric interactions between the rings would increase the angle between the pyrazine rings and the coordination plane and so examined the effect of methyl substitution on the structure and magnetism of the compounds in the series $Cu(mepz)_n^{2+}$, $Cu(2,3\text{-dmpz})_n^{2+}$, Cu(2,5-

* Authors to whom correspondence should be addressed.

dmpz)$_n^{2+}$ and Cu(2,6-dmpz)$_n^{2+}$, along with their related diamagnetic Cu^+ equivalents (2-methylpyrazine = *mepz*; 2,3-dimethylpyrazine = 2,3-dmpz; 2,5-dimethylpyrazine = 2,5-dmpz and 2,6-dimethylpyrazine = 2,6-dmpz; $n = 2, 4$). Under the synthetic conditions employed, only the copper(I) compounds proved to be coordination polymers.

RESULTS

Synthesis and structure of copper(II) *complexes*

Addition of one or more methyl substituents to the pyrazine ring disrupted the two-dimensional lattice and no Cu^{2+} coordination polymers were isolated. Two Cu^{2+} complexes of 2-methylpyrazine were isolated with the formulae $Cu(mepz)_2(ClO_4)_2(H_2O)_2$ (**1**) and $Cu(mepz)_4(ClO_4)_2(H_2O)$ (**2**).

The major product of the reaction between $Cu(ClO_4)_2$ and 2,3-dimethylpyrazine was the previously reported Cu^+ complex $Cu_2(2,3\text{-dmpz})_3(ClO_4)_2$ (**10**).[2] Only one Cu^{2+} complex of 2,5-dimethylpyrazine was obtained, $[Cu(2,5\text{-dmpz})_2(H_2O)_4](ClO_4)_2$ (**3**). Trace amounts of minute yellow crystals were also recovered and characterized as $Cu_2(2,5\text{-dmpz})_3(ClO_4)_2$ (**11**) by combustion analysis.

Similar to mepz, reaction of Cu^{2+} with 2,6-dimethylpyrazine gave two Cu^{2+} complexes, $Cu(2,6\text{-dmpz})_2(ClO_4)_2(H_2O)_2$ (**4**), as the major product and trace amounts of $Cu(2,6\text{-dmpz})_4(ClO_4)_2(H_2O)$ (**5**). Compound **5** co-crystallized with **4** and could be recovered only in trace amounts by physical separation under a stereomicroscope. Sufficient material for IR, EPR and combustion analysis was obtained. Magnetic susceptibility data were not collected.

Single-crystal X-ray diffraction studies of compounds **1** and **2** were completed. Figures 1 and 2 show ORTEP drawings of **1** and **2**, respectively. Compound **1** crystallizes in the orthorhombic space group $Pna2_1$. The geometry about the metal ion is roughly octahedral with the ligated pairs of mepz, H_2O and ClO_4 groups mutually *trans* (L—Cu—L bond angles 175–180°). The mepz rings are coordinated through the nitrogen atom distal to the methyl substituent and the rings are nearly coplanar with the methyl groups oriented *anti* to each other. Compound **2** occurs as triclinic crystals, space group $P\bar{1}$. The metal coordination sphere is again roughly octahedral with the four mepz ligands occupying the equatorial positions and a water molecule and one of the perchlorate ions in the axial sites. The CuL_4 species assumes a propellor structure with the pyrazine rings twisted out of the CuN_4 plane by an average of 53° (range 46.6–56.5°).

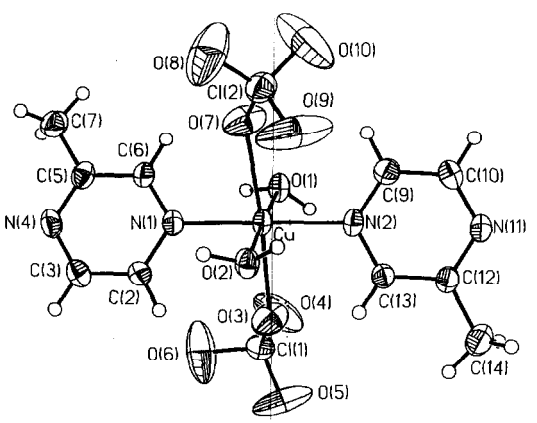

Fig. 1. ORTEP picture of Cu(2-methylpyrazine)$_2$ $(H_2O)_2(ClO_4)_2$ (**1**).

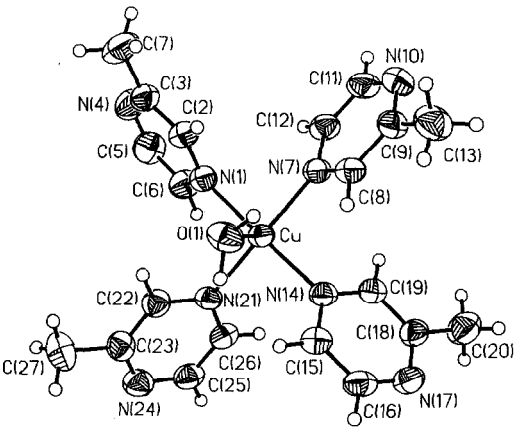

Fig. 2. ORTEP picture of [Cu(2-methylpyrazine)$_4$ $(H_2O)(ClO_4)]ClO_4$ (**2**) (ClO_4 ions have been removed for clarity).

EPR and magnetic data for copper(II) *complexes*

The magnetic susceptibility data of polycrystalline samples of compounds **1**–**4** have been measured between 2 and 300 K. All four of the data sets are similar with temperature intercepts close to zero, indicating the absence of any significant interactions. Least-squares fits to the data have been made to the Curie–Weiss equation $\chi^{-1} = (T-\theta)/C$, where C is the Curie constant $= Ng^2mb2S(S+1)/3kB = 0.375(g/2)^2$ cgs K mol^{-1} for the $S = 1/2$ Cu^{2+} ion. Both C and the Weiss parameter θ were adjusted for the best fit. The parameters (C, θ) were found to be **1**: 0.42(1) emu K mol^{-1}; −0.3(1) K; **2**: 0.43(1) emu K mol^{-1}; −0.2(1) K; **3**: 0.43(1) emu K mol^{-1}; −0.2(1) K; **4**: 0.42(1) emu K mol^{-1}; −0.3(1) K.

EPR spectra of samples **1**–**5** were collected at room temperature. The average g values (and the

corresponding Curie constant) for each compound were determined to be: **1** and **2**: 2.067 (0.40 emu K mol^{-1}, line width = 49.5 and 47.5 G, respectively); **3**: 2.084 (0.41 emu K mol^{-1}, line width = 47.5 G); **4**: 2.085 (0.41 emu K mol^{-1}, line width = 35.1 G); **5**: 2.065 (0.41 emu K mol^{-1}, linewidth = 80.5 G). Although the Curie constants determined by magnetic susceptibilities are higher than those determined by the EPR measurements, the differences are within experimental error.

Synthesis of copper(I) complexes

We recently reported the serendipitous preparation of $Cu_2(2,3\text{-dmpz})_3(ClO_4)_2$ (**10**)[2] and a related report appeared shortly thereafter.[3] Compound **10** formed spontaneously from an aqueous solution of $Cu(ClO_4)_2$ and 2,3-dmpz. Single-crystal X-ray diffraction showed the material to be a polymeric sheet of tri-coordinate copper(I) ions, bridged by the 2,3-dmpz ligands. Reaction with other pz ligands gave no copper(I) products under these conditions.

Previous work by Davies[4] showed that $Cu^{I}L_nClO_4$ complexes could be prepared by treatment of the corresponding copper(II) compounds with SCN^- ions in aqueous solution. Reaction of mepz, 2,3-dmpz or 2,5-dmpz with NaSCN in aqueous solution gave good yields of $Cu_2(mepz)(SCN)_2$ (**6**), $Cu_2(2,3\text{-dmpz})(SCN)_2$ (**7**) and $Cu_2(2,5\text{-dmpz})(SCN)_2$ (**8**). Under the same reaction conditions 2,6-dmpz and tetramethylpyrazine gave CuSCN in nearly quantitative yield.

A second attempt to prepare the complexes $Cu_2(L)_3(ClO_4)_2$ was made using $NaBH_4$ as the reducing agent. $Cu_2(mepz)_3(ClO_4)_2$ (**9**), $Cu_2(2,3\text{-dmpz})_3(ClO_4)_2$ (**10**) and $Cu_2(2,5\text{-dmpz})_3(ClO_4)_2$ (**11**) were recovered in good yields and $Cu_2(2,6\text{-dmpz})_3(ClO_4)_2$ (**12**) was recovered in trace amounts when excess $NaBH_4$ was used. All the copper(I) complexes appear to be stable to air indefinitely in the solid state.

DISCUSSION

Structure of the ligands and reactions with copper(II)

The stoichiometry and stability of the complexes varied substantially with the ligand. 2-Mepz and 2,6-dmpz are similar in differentiating the ring nitrogens based on steric effects. The difference between 2,3-dmpz and 2,5-dmpz is more subtle and is best seen by looking at 2,3-dmpz. The adjacent methyl groups on C(2) and C(3) will exert a steric pressure on each other, bending them towards the nitrogens. Thus, there should be slightly more steric crowding around the nitrogens in 2,3-dmpz than in 2,5-dmpz. Molecular mechanics calculations[5] show the N(1)—C(2)—CH^3 bond angle in 2,3-dmpz (116.3°) to be *ca* 3° smaller than the equivalent angle in 2,5-dmpz (119.3°).

In the copper complexes these steric differences are obvious. Both isolated complexes of mepz, **1** and **2**, show coordination of the Cu^{2+} ion only to the distal nitrogen. Combustion analysis of **4** and **5**, the two complexes of 2,6-dmpz, indicates that they have the same composition as the mepz compounds **1** and **2**, respectively.

In the case of the 2,3- and 2,5-dimethylpyrazines the difference in reactivity with copper(II) is much more dramatic. Reaction of 2,3-dmpz with $Cu(ClO_4)_2$, even in the absence of an added reducing agent, gave the copper(I) complex $Cu_2(2,3\text{-dmpz})_3(ClO_4)_2$ (**10**) as the major product. Traces (20 mg) of an unidentified Cu^{2+} complex were isolated during one attempt, but this could not be reproduced. Conversely, reaction of 2,5-dmpz with $Cu(ClO_4)_2$ produced $[Cu(2,5\text{-dmpz})_2(H_2O)_4](ClO_4)_2$ (**3**) in 69% yield and only traces of **11**, the copper(I) complex analogous to **10**.

For both of these ligands coordination can only occur through a nitrogen adjacent to a methyl substituent. The slight increase in crowding provided by the 2,3-dmpz ligand, relative to 2,5-dmpz, is sufficient to dissociate the perchlorate groups and distort the geometry of the complex towards tetrahedral, whereupon it is reduced to copper(I) and **10** forms. Copper reductions of this type are well documented.[6] For 2,5-dmpz the crowding of the methyl substituents appears to be sufficient to dissociate the perchlorates and replace them with water molecules, but must not cause the degree of distortion that 2,3-dmpz does, as evidenced by the minute amounts of **11** recovered. We note that we are presuming the structure of **3** is $[Cu(2,5\text{-dmpz})_2(H_2O)_4](ClO_4)_2$. The alternative structure $[Cu(2,5\text{-dmpz})_2(H_2O)_2(ClO_4)_2]\cdot 2H_2O$, where the coordination sphere about the metal is similar to **1**, would have the same composition and would also contain only unidentate pyrazine ligands.

IR spectra and structure of the copper(I) complexes

Work by Lever[7] and Ahuja[8] has shown that IR spectra are useful in determining the coordination mode, bridging or unidentate, of pyrazines. Compounds **1**, **2**, **4** and **5** all exhibit the characteristic IR absorbances for unidentate pyrazines. These bands occur at 1256 cm^{-1} in the bis-methylpyrazine complex **1** and as a doublet (1258 and 1250 cm^{-1}) in the tetrakismethylpyrazine complex **2**.[9] This method for determining the coordination mode of

the methylpyrazine ligand may also be demonstrated in the related $Mn(mepz)Cl_2$ (**13**) and $Zn(mepz)_2Br_2$ (**14**) compounds. Compound **13** does not exhibit an absorbance near 1250 cm^{-1}, in agreement with a structure similar to the analogous cobalt(II)[7a] and nickel(II)[7c] complexes, while **14** shows a medium intensity band at 1254 cm^{-1}, suggesting unidentate coordination as is observed for $Zn(mepz)_2Cl_2$ and $Zn(mepz)_2I_2$.[8] For 2,6-dimethylpyrazine compounds the band that characterizes unidentate coordination occurs near 1160 cm^{-1}. Bands are observed at 1165 and 1164 cm^{-1} for **4** and **5**, respectively, but not for the copper(I) complex **12**. All are in agreement with monomeric copper(II) compounds and bridged copper(I) compounds.

The steric differences between 2-methylpyrazine and 2,6-dimethylpyrazine are more pronounced in the copper(I) complexes. 2-Methylpyrazine forms bridging complexes with copper(I) in both the SCN complex **6** and the perchlorate **10**. No IR absorption is seen near 1250 cm^{-1} for either compound. In the thiocyanate complex (**6**) the SCN absorbances at 2110 and 770 cm^{-1} are indicative of bridging SCN groups as well,[6c,7,10] suggesting that these complexes have structures similar to **10** with trigonal coordination spheres for the copper(I) ions. The coordination geometry about the copper atoms in $KCu_2(CN)_3 \cdot H_2O$ is similar.[11]

Reaction of 2,6-dmpz with $Cu(ClO_4)_2$ and $NaBH_4$ gave poor yields of $Cu_2(2,6\text{-dmpz})_3(ClO_4)_2$ (**12**). No absorbance was observed in the IR spectrum of **12** near 1160 cm^{-1}, suggesting bridging pyrazines. As seen in **4** this ligand does form stable complexes in less crowded systems such as $Zn(2,6\text{-dmpz})_2Br_2$ (**15**), where bridging is not required. The strong absorbance at 1162 cm^{-1} in the IR spectrum of **15** confirms the unidentate nature of the 2,6-dmpz.

Only copper(I) complexes of 2,3-dmpz were obtained. In **7** the SCN bands appear at 2100 and 770 cm^{-1}, indicating bridging thiocyanates. The IR bands arising from the ligand resemble those of the crystals of **10**, which contains bridging 2,3-dmpzs and thus we conclude the ligand is bridging in **7** as well. A weak IR band is observed at 1250 cm^{-1} in all our 2,3-dmpz compounds, indicating that although the absence of this band may characterize a bridging 2,3-dmpz, its presence does not exclude bridging, as suggested earlier.[12]

Of greater interest is the observation that the IR spectrum of **10**, as prepared via addition of $NaBH_4$, does not match the spectrum of the crystals of **10** that grew spontaneously, although they have the same composition according to combustion analysis. The differences are most obviously in the perchlorate regions where the hydride reduction product shows bands at 1140s, 1110s, 1080s, 632mw, 622m cm^{-1}, while the spontaneously generated material shows only two bands, a strong broad absorbance centred at 1090 cm^{-1} and a sharp medium intensity peak at 622 cm^{-1}. The existence of two phases of this material was confirmed by powder X-ray diffraction. The observed low-angle lines in a powder spectrum of **10**, from hydride reduction, did not match the values calculated based on the crystal structure of the spontaneous product.[13]

The copper(I) thiocyanate of 2,5-dmpz (**8**) also contains bridging thiocyanate groups, as indicated by the IR spectrum (2105 and 765 cm^{-1}). The presence of a bridging 2,5-dmpz in **8** is also indicated by the presence of only a single absorbance (at 1068 cm^{-1}) in the 1050–1080 cm^{-1} range.[7] In the perchlorate complex (**11**) it also appears that only one absorbance is presented (at 1060 cm^{-1}), but a second band could be obscured by the strong ClO_4 peak at 1090 cm^{-1}. This is also true for $[Cu(2,5\text{-dmpz})(H_2O)_4](ClO_4)_2$ (**3**). However, a different change in the IR spectrum is readily detected. A single peak is observed in both **8** and **11** at 1375 and 1382 cm^{-1}, respectively, which we assign to the symmetric bending mode of the methyl C—H bonds. In **3** this band is split into two peaks at 1372 and 1382 cm^{-1}. If the 2,5-dmpz is indeed unidentate in **3**, then the two methyl groups would be inequivalent and two absorbances would be expected. Unfortunately, the absorbances in this region for the tetrahedral zinc compound $Zn(2,5\text{-dmpz})_2Br_2$ (**16**) do not resemble those of the copper complexes and cannot be used to confirm or deny this means of distinguishing the unidentate and bridging modes of 2,5-dmpz.

Magnetic properties

The magnetic susceptibility data for the copper(II) compounds show the absence of significant magnetic interactions. This result is not unexpected, given the known structures. The closest metal–metal distances in **1** and **2** correspond to unit cell translations of 4.8 and 10.1 Å, respectively. Long metal–metal distances by themselves do not imply weak magnetic interactions. A copper dimer has recently been reported in which the exchange interaction has a strength of 70 cm^{-1}, although the copper ions are separated by 11.3 Å.[14] The extended conjugated network provided excellent overlap between the magnetic *d*-orbitals. In the present compounds the only possible conjugated pathways would be through the methyl-substituted pyrazines. The copper ions are monomeric units, with only weak dipolar interactions to couple them.

CONCLUSIONS

Addition of one or more methyl group to the pyrazine ring provides sufficient steric hindrance to prevent formation of the desired two-dimensional copper(II) coordination polymer when isolated from aqueous solution. A variety of monomeric compounds are formed containing either two or four pyrazine ligands and all are paramagnetic. The methylpyrazines do form bridging coordination polymers with copper(I) ions and these compounds may be readily produced by the addition of reducing agents such as SCN^- or H^-. The bridged complexes most likely result from the reduced steric requirements of the tri-coordinate copper(I) ions. Further work in this area is in progress involving the use of anhydrous conditions and alternate geganions.

EXPERIMENTAL

2-Methylpyrazine, 2,5-dimethylpyrazine, 2,6-dimethylpyrazine and 2,3,5,6-tetramethylpyrazine were purchased from Aldrich Co. and used without further purification. $Cu(ClO_4)_2 \cdot 6H_2O$ was purchased from Aesar and dried under vacuum prior to use. IR spectra were taken on a Perkin–Elmer 467 spectrophotometer in a KBr or KCl matrix[15] and calibrated against polystyrene (br = broad, sh = shoulder, d = doublet, s = strong, w = weak). Elemental analyses were performed by the University Instrumentation Centre, University of New Hampshire, Durham, NH. All compounds gave acceptable analyses ($\pm 0.4\%$).

Diaquobis(2-methylpyrazine)bisperchloratocopper(II) (**1**)

$Cu(ClO_4)_2 \cdot 6H_2O$ (3.70 g, 10 mmol) was dissolved in H_2O (8 cm^3) and added to a solution of 2-methylpyrazine (1.88 g, 20 mmol) dissolved in H_2O (5 cm^3). The mixture was allowed to stand at room temperature. After 1–2 days blue crystals formed, which were collected by filtration, washed briefly with cold H_2O, followed by acetone and air-dried to give 0.82 g of compound **2** (25%). Further evaporation at room temperature over 2 weeks gave blue crystals of **1**, which were isolated as above to give 1.46 g (55%, corrected for isolated **2**). IR (KCl): 3400m br, 1592m, 1520w br, 1480m, 1440m, 1400m, 1375w, 1300m, 1256w, 1175s, 1110vs br, 1025s, 940w, 910w, 830s, 735m, 625s, 445w, 415m cm^{-1}.

Aquotetrakis(2-methylpyrazine)perchloratocopper(II) *perchlorate* (**2**)

$Cu(ClO_4)_2 \cdot 6H_2O$ (1.85 g, 5.0 mmol) was dissolved in H_2O (10 cm^3) and added to a solution of 2-methylpyrazine (1.88 g, 20 mmol) dissolved in H_2O (5 cm^3). After standing at room temperature for 10 days, blue crystals of **2** were recovered, as described above; yield 1.2 g (37%). Further evaporation gave an additional 1.6 g (49%) of somewhat less pure material. IR (KCl): 3400m br, 1650vw br, 1595w, 1525w, 1480m, 1445m, 1400m, 1375w, 1300m, 1260w, 1250w, 1175m-s, 1140s, 1100vs br, 1080sh, 1025m, 940w, 910w, 830s, 735m-w, 635sh, 625s, 495w, 415m, 400m cm^{-1}.

Tetraaquobis(2,5-dimethylpyrazine)copper(II) *bisperchlorate* (**3**) *and tris(2,5-dimethylpyrazine)-dicopper*(II) *bisperchlorate* (**11**)

$Cu(ClO_4)_2 \cdot 6H_2O$ (3.70 g, 10.0 mmol) was dissolved in H_2O (5 cm^3) and added to a solution of 2,5-dimethylpyrazine (2.16 g, 20 mmol) dissolved in H_2O (5 cm^3). After standing at room temperature for 2 weeks large blue crystals were deposited on the bottom of the beaker and trace amounts of tiny yellow crystals were observed floating in the supernatant liquid. The supernate was decanted away from the blue solid and filtered to give a yellow solid (**11**); yield 0.018 g (< 1%), which will be described below. The blue crystals of **4** were recorded as described above; yield 3.82 g (69%). IR (KCl): 3400w br, 3040w, 1500m, 1480sh, 1460w, 1435w, 1382w, 1372w, 1350m, 1140–1080vs br, 1040m, 990m, 940w, 878m, 622s, 435m cm^{-1}

Diaquobis(2,6-dimethylpyrazine)bisperchloratocopper(II) (**4**) *and aquotetrakis(2,6-di-methylpyrazine)-perchloroatecopper*(II) *perchlorate* (**5**)

$Cu(ClO_4)_2 \cdot 6H_2O$ (3.70 g, 10.0 mmol) was dissolved in H_2O (5 cm^3) and added to a solution of 2,6-dimethylpyrazine (2.16 g, 20 mmol) dissolved in H_2O (10 cm^3) The solution immediately became a very dark blue and crystals formed within 7 min after the addition was complete. After 10 min the solution was filtered and the precipitate was washed with cold water, followed by acetone and allowed to air dry to give **4** as a blue solid; yield 1.31 g (25%). The filtrate and the aqueous wash were combined and left to evaporate. After standing at room temperature for 1 week blue crystals were recovered as described above; yield 2.91 g (57%, based on **4**). Upon examination under a stereomicroscope, this material proved to be a mixture of two different substances, greater than 95% (estimated visually), blue crystals of **4** and deep violet crystals of **5**. Sufficient crystals of **5** for IR and combustion analysis were carefully separated by hand under the microscope. Data for **4**: IR (KBr): 3450br, 3090w, 1600w, 1530m, 1460sh, 1450m, 1425m, 1410m,

1380m, 1290w, 1255m, 1165s, 1125s br, 1100sh, 1050m-s, 1035m-s, 950w, 932w, 927w, 875w, 868m, 760w, 735m, 635sh, 625m-s, 490m cm^{-1}. For **5**: IR (KBr): 3450br w, 3090w, 1590w, 1530m, 1455m br, 1425m, 1410m, 1380m, 1365w, 1290w, 1255m, 1165s, 1140s, 1100vs br, 1025m, 940w d, 865m, 760w, 735m-w, 635sh, 625m-s, 490m-w cm^{-1}.

2-*Methylpyrazinobisthiocyanatodicopper*(I) (**6**)

$Cu(ClO_4)_2 \cdot 6H_2O$ (1.85 g, 5.00 mmol) was dissolved in H_2O (5.0 cm^3) and added to a stirred solution of 2-methylpyrazine (1.88 g, 20.0 mmol) in H_2O (5.0 cm^3). A solution of NaSCN (0.40 g, 5.0 mmol) in H_2O (5 cm^3) was then added, generating an immediate dark green–brown precipitate. The mixture was stirred for 2 h and then filtered to yield a dirty brown solid. Repeated washing with water and acetone gave an orange–red solid; yield 0.65 g (77%). IR (KBr): 2110vs, 1510w, 1470m, 1442m, 1385w, 1300m, 1175m, 1150m, 1110m, 1080m-s, 1035m, 990w, 960w, 835m, 770w, 625w, 500w, 420m cm^{-1}.

2,3-*Dimethylpyrazinobisthiocyanatodicopper*(I) (**7**)

Prepared as in **6** to give a dark yellow solid; yield 0.80 g (91%). IR (KBr): 2100vs, 1465w, 1432w, 1402m, 1372w, 1257w, 1190m, 1182m, 1012w, 972w, 812w, 770m, 485m cm^{-1}.

2,5-*Dimethylpyrazinobisthiocyanatodicopper*(I) (**8**)

Prepared as in **6** to give a yellow solid; yield 0.77 g (87%). IR (KBr): 2105s, 1480m, 1430w br, 1375w, 1330w, 1160w, 1068w, 1035vw, 765m-w, 430w cm^{-1}

Tris(2-*methylpyrazino*)*dicopper*(I) *perchlorate* (**9**)

$Cu(ClO_4)_2 \cdot 6H_2O$ (1.85 g, 5.00 mmol) was dissolved in H_2O (5.0 cm^3) and added to a stirred solution of 2-methylpyrazine (0.70 g, 7.5 mmol) in H_2O (5.0 cm^3). $NaBH_4$ (0.19 g, 5.0 mmol) was added in portions to the mixture. The originally green mixture turned brown and a precipitate formed. The mixture was stirred overnight and the resulting solid was collected by vacuum filtration, washed with H_2O and acetone and then air-dried to give a yellow solid; yield 0.84 g (62%). IR (KBr): 3115vw, 3080vw, 3045vw, 1605w, 1510w, 1485m, 1480sh, 1450m, 1402m, 1380w, 1310m, 1180m, 1167m, 1155m, 1100vs br, 1050s br, 925w, 845w, 830w, 730vw, 620s, 695vw, 475vw, 437m, 412w cm^{-1}.

Tris(2,3-*dimethylpyrazino*)*dicopper*(I) *perchlorate* (**10**)

Prepared as in **9** to give a yellow solid; yield 0.79 g (54%). IR (KBr): 3080w, 1435m br, 1405s, 1255w, 1175m-s, 1142s, 1100vs br, 1018m, 990m, 972m, 942w, 862w, 638m, 630s, 480w, 440w cm^{-1}. IR of spontaneously formed product (KBr): 3080w, 1437s, 1408s, 1262w, 1255w, 1190sh, 1180s, 1090vs br, 1010m-s br, 675s, 858m, 840m, 750w br, 620s, 490m, 470w cm^{-1}.

Tris(2,5-*dimethylpyrazino*)*dicopper*(I) *perchlorate* (**11**)

Prepared as in **9** to give a yellow solid; yield 0.34 g (23%). This compound also crystallizes in very low yield as a by-product in the synthesis of **3**. IR (KBr): 1500m, 1490sh, 1440w br, 1382w, 1340w, 1162m, 1140m, 1105s, 1095s, 1060m-s, 1045m, 970w, 930w, 620m, 420w br cm^{-1}. Found: C, 33.23; H, 3.71; N, 13.08%.

Tris(2,6-*dimethylpyrazino*)*dicopper*(I) *perchlorate* (**12**)

Prepared as in **9**. A substantial amount of the material dissolved in the H_2O wash and only traces of the product were recovered. IR (KBr): 1535m, 1450w br, 1412m, 1380w, 1280vw, 1250m, 1140m-s, 1105s, 1095s, 1020m-w, 940w, 870w, 735w, 632w, 625m, 462w cm^{-1}.

Dichloro(2-*methylpyrazine*)*manganese*(II) (**13**)

$MnCl_2 \cdot 4H_2O$ (2.69 g, 10.0 mmol) was dissolved in absolute ethanol (13 cm^3) and added to a stirred solution of 2-methylpyrazine (1.88 g, 20.0 mmol) in absolute ethanol (3.0 cm^3) generating an immediate precipitate. The mixture was filtered, the precipitate was washed with ethanol and air dried to give a white solid; yield 2.57 g (36%). IR: 3100w, 1600w, 1510w, 1475m, 1440m, 1405m, 1385m, 1305w, 1180m, 1160s, 1080s, 1035s, 820s, 740w, 480m, 420s cm^{-1}. Found: C, 27.50; H, 2.78; N, 12.69%.

Dibromobis(2-*methylpyrazine*)*zinc*(II) (**14**)

Prepared as in **13** and recrystallized from THF/Et_2O to give a white solid; yield 0.30 g (36%). IR: 3050w br, 1595w, 1515m br, 1477s, 1440s, 1490s, 1375s, 1297m, 1254m, 1165s br, 1077s, 1040sh, 1022s, 980m, 920w, 835s, 737m, 660w, 495w, 475m, 405s br cm^{-1}.

Table 1. Crystallographic data

Compound	$Cu(mepz)_2(ClO_4)_2(H_2O)_2$ (**1**)	$Cu(mepz)_4(ClO_4)_2(H_2O)$ (**2**)
Chemical formula	$C_{10}H_{16}Cl_2CuN_4O_{10}$	$C_{20}H_{26}Cl_2CuN_8O_9$
Formula weight	486.71	656.92
Crystal size (mm)	$0.5 \times 0.5 \times 0.4$	$0.5 \times 0.5 \times 0.5$
Crystal class	Orthorhombic	Triclinic
Space group	$Pna2_1$	$P\bar{1}$
T (°C)	22	22
a (Å)	15.947(1)	8.766(3)
b (Å)	7.276(2)	12.645(2)
c (Å)	15.092(2)	13.123(2)
α (°)	90	91.67(1)
β (°)	90	106.14(2)
γ (°)	90	89.94(2)
V (Å^3)	1751.1(5)	1396.7(6)
Z	4	2
λ (Å)	0.71069	0.71069
ρ_{calc} (g cm^{-3})	1.85	1.56
μ (cm^{-1})	16.2	10.4
Transmission coefficient	0.687–0.939	0.683–0.858
$R(F_o)$	0.0332	0.0497
$R_w(F_o)$	0.0461	0.0673

Table 2(a). Selected bond distances (Å) and angles (°) for $Cu(mepz)_2(ClO_4)_2(H_2O)_2$ (**1**)

Cu—N(1)	2.021(3)	Cu—N(2)	2.019(3)
Cu—O(1)	1.970(3)	Cu—O(2)	1.964(3)
Cu—O(3)	2.443(4)	Cu—O(7)	2.419(4)
N(1)—Cu—N(2)	178.1(1)	N(1)—Cu—O(1)	92.2(1)
N(1)—Cu—O(2)	90.4(1)	N(1)—Cu—O(3)	89.1(1)
N(1)—Cu—O(7)	86.4(1)	N(2)—Cu—O(1)	86.8(1)
N(2)—Cu—O(2)	90.6(1)	N(2)—Cu—O(3)	89.0(1)
N(2)—Cu—O(7)	95.3(1)	O(1)—Cu—O(2)	177.0(1)
O(1)—Cu—O(3)	89.6(1)	O(1)—Cu—O(7)	91.0(1)
O(2)—Cu—O(3)	89.0(1)	O(2)—Cu—O(7)	90.7(1)
O(3)—Cu—O(7)	175.4(2)		

Table 2(b). Selected bond distances (Å) and angles (°) for $[Cu(mepz)_4(ClO_4)(H_2O)]ClO_4$ (**2**)

Cu—N(1)	2.044(3)	Cu—N(7)	2.027(2)
Cu—N(14)	2.024(3)	Cu—N(21)	2.035(3)
Cu—O(1)	2.310(3)	Cu—O(2)	2.721(4)
N(1)—Cu—N(7)	92.1(1)	N(1)—Cu—N(14)	171.9(1)
N(1)—Cu—N(21)	88.4(1)	N(1)—Cu—O(1)	94.0(1)
N(1)—Cu—O(2)	84.4(1)	N(7)—Cu—N(14)	89.4(1)
N(7)—Cu—N(21)	177.9(1)	N(7)—Cu—O(1)	90.2(1)
N(7)—Cu—O(2)	82.6(1)	N(14)—Cu—N(21)	89.8(1)
N(14)—Cu—O(1)	94.0(1)	N(14)—Cu—O(2)	87.9(1)
N(21)—Cu—O(1)	91.8(1)	N(21)—Cu—O(2)	95.4(1)
O(1)—Cu—O(2)	172.6(1)		

Dibromobis(2,6-*dimethylpyrazine*)*zinc*(II) (**15**)

Prepared as in **13** to give a white solid; yield 0.125 g (14%). Additional material of slightly lower purity can be recovered by further evaporation of the filtrate. IR: 3050w, 2960w, 2920w, 1530m, 1420s br, 1400sh, 1370m, 1288m, 1255m, 1175sh, 1162vs, 1020s, 942w, 870m, 755m, 735m, 555w, 470m, 460m cm^{-1}.

Dibromobis(2,5-*dimethylpyrazine*)*zinc*(II) (**16**)

Prepared as in **13** to give a white solid; yield 0.248 g (27%). IR: 1645m, 1585m, 1535sh, 1525w, 1485s, 1415m, 1305m, 1222s, 1180m, 1040w, 665w, 652w, 580m, 565m, 480w br cm^{-1}.

Magnetic data collection

Measurements of magnetic susceptibility were made using a Foner-type vibrating sample magnetometer (EG&G PAR Model 155) using a custom Helium cryostat.[16] Temperatures were measured with a Ga—Al—As diode, which had been calibrated *in situ* against magnetic standards. Magnetic field measurements were performed with a calibrated Hall probe. All data were corrected for diamagnetism and the temperature-independent paramagnetism of copper(II), taken as 60×10^{-6} cgs mol^{-1}. The EPR spectra were performed using a Varian E-9 spectrometer operating at 9.3 GHz. DPPH was used as an internal standard.

X-ray structure determination

The data collections were performed on an upgraded Syntex $P2_1$ diffractometer, employing Mo-K_α radiation ($\lambda = 0.71069$) and a graphite monochromator. The orientation matrix and lattice parameters were optimized from a least-squares calculation on 25 centred reflections with high Bragg angles (35–40° (**1**), 33–35° for **2**). Two standard reflections were monitored every 96 reflections. All data reduction, structure solution and refinement and graphics were performed using SHELXTL 5.1 software.[17] Crystallographic data may be found in Table 1. Selected bond distances and angles are given in Table 2. Additional structural details may be found in the supplementary material and details of the refinement procedure are available from the authors.

Acknowledgements—This work was supported in part by a grant from the National Science Foundation (DMR-9006470), an NSF-REU Supplement Award (CG, CN) and by the Chemistry Department at Clark University through a Summer Undergraduate Research Fellowship (CN). We also thank Mr Jeffrey Weisberg and Mr Elliot Jones for technical assistance.

REFERENCES

1. (a) J. Darriet, M. S. Haddad, E. N. Duesler and D. N. Hendrickson, *Inorg. Chem.* 1979, **18**, 2679; (b) M. S. Haddad, D. N. Hendrickson, J. P. Cannady, R. S. Drago and D. S. Bieksza, *J. Am. Chem. Soc.* 1979, **101**, 898.
2. M. M. Turnbull, G. Pon and R. D. Willett, *Polyhedron* 1991, **10**, 1835.
3. S. Kitagawa, M. Munakata and T. Tanimura, *Inorg. Chem.* 1992, **31**, 1714.
4. G. Davies and D. J. Loose, *Inorg. Chem.* 1976, **15**, 694.
5. Molecular mechanics calculations were preformed using MMX86 from Serena Software, Bloomington, IN.
6. F. H. Jardine, *Adv. Inorg. Chem. Radiochem.* 1975, **17**, 115 and refs therein.
7. (a) A. B. P. Lever, J. Lewis and R. S. Nyholm, *J. Chem. Soc.* 1962, 1235; (b) A. B. P. Lever, J. Lewis and R. S. Nyholm, *J. Chem. Soc.* 1963, 3156; (c) A. B. P. Lever, J. Lewis and R. S. Nyholm, *J. Chem. Soc.* 1963, 5042.
8. I. S. Ahuja and P. Rastogi, *J. Chem. Soc. A* 1970, 2161.
9. We have also prepared the analogous tetrafluoroborate complex, $Cu(mepz)_2(BF_4)_2(H_2O)_2$, which also shows an absorption at 1258 cm^{-1}.
10. B. W. Dockum, G. A. Eisman, E. H. Witten and W. M. Reiff, *Inorg. Chem.* 1983, **22**, 150.
11. D. T. Cromer and A. C. Larson, *Acta Cryst.* 1962, **15**, 397.
12. A. Shamin, A. Adeyemo, M. T. Shamin, J. Wheeler, A. Turner and A. B. Hussein, *Inorg. Chim. Acta* 1984, **91**, 179.
13. Theoretical values for the X-ray powder diffraction pattern of **10** were calculated from the crystal data using PPPROG, J. S. Miller and S. Z. Goldberg, *J. Chem. Ed.* 1976, **53**. Calculated *d* spacings from crystal structure (first six): 12.688, 9.640, 8.445, 8.067, 6.012, 4.912; observed *d* spacings from hydride reduction product (first five lines): 10.490, 8.656, 7.824, 6.130, 4.948.
14. P. Chaudhuri, K. Oder, K. Wieghardt, S. Gehring, W. Haase, B. Nuber and J. Weiss, *J. Am. Chem. Soc.* 1988, **110**, 3657.
15. Many of these compounds react with KBr in the solid state. The reaction is noted by colour changes from the blue of the starting material to anywhere from green to yellow, dependent upon the compound. No such changes are observed using KCl as the window material. Changes in the spectra between KBr and KCl matrix are most easily seen in the range between 1550 and 1300 cm^{-1}. Spectra reported in KCl matrix showed significant changes when recorded in KBr.
16. C. P. Landee, R. E. Greeney and A. C. Lamas, *Rev. Sci. Inst.* 1987, **58**, 1957.
17. Sheldrick, G. SHELXTL, Nicolet Analytical Instruments, Madison, WI (1986).

Polyhedron Vol. 12, No. 9, pp. 1027–1030, 1993
Printed in Great Britain

0277–5387/93 $6.00+.00
© 1993 Pergamon Press Ltd

CHARACTERIZATION OF REACTION PRODUCTS OF 2-THIENYLAMINE AND 2-FURFURYLAMINE WITH BIS(ACETYLACETONATO)PALLADIUM(II)

MASAKAZU KITA and MATSUO NONOYAMA*

Department of Chemistry, Faculty of Science, Nagoya University, Chikusa, Nagoya 464-01, Japan

(*Received* 11 *December* 1992; *accepted* 8 *January* 1993)

Abstract—2-Thienylamine (Hata) and 2-furfurylamine (Hafa) reacted with bis(acetylacetonato)palladium(II) [Pd(acac)$_2$] in dichloromethane at room temperature to give Pd(acac)$_2$(Hata) and Pd(acac)$_2$(Hafa), respectively. In refluxing toluene the former amine gave [Pd(acac)(ata)]$_2$, while with the latter no further reaction took place. In Pd(acac)$_2$(Hata) and Pd(acac)$_2$(Hafa) the amines were coordinated through the amino group, with one acac ligand as an O—O chelate and the other γ-carbon bonded. X-ray analysis revealed that [Pd(acac)(ata)]$_2$ was a dimer where the palladium atoms were bridged by deprotonated amino groups and coordinated with O—O chelating acac ligands.

A large number of cyclometallated benzene derivatives have been reported.[1] Benzene derivatives containing a tertiary amino group are easily cyclopalladated, but those containing a primary amino group are far more difficult.[1] Bis(acetylacetonato)-palladium(II) [Pd(acac)$_2$] has been reported[2] to be capable of cyclopalladating a primary amine, benzylamine, which is not cyclopalladated with palladium(II) chloride. This fact stimulated us to attempt the cyclopalladation of 2-thienylamine (abbreviated as Hata) and 2-furfurylamine (Hafa), which are the heteroaromatic equivalents of benzylamine, since we have been interested in cyclometallation of heteroaromatic compounds.[3] The two heteroaromatic amines are not cyclopalladated, contrary to our expectation, coordinating only through amino groups. Cyclopalladation of Hafa and Hata with Pd(acac)$_2$ is hence more difficult than that of benzylamine.

RESULTS AND DISCUSSION

Pd(acac)$_2$ reacted with Hata and Hafa at room temperature to give Pd(acac)$_2$(Hata) and Pd(acac)$_2$(Hafa), respectively. The IR spectra show the presence of O—O chelated acac and γ-carbon bonded acac ligands: 1517, 1551, 1675 cm^{-1} for the former complex and 1518, 1565, 1673 cm^{-1} for the latter. The bands of the amino group are at 3225, 3145 [ν(NH)], 1633 [$\delta(NH_2)$] for the former and 3217, 3150, 1620 cm^{-1} for the latter. These bands are close to those of Pd(acac)$_2$(Hbza) (Hbza = benzylamine).[4] Structure **I** is thus proposed (E = S and O), where one acac is O—O chelated and the other γ-carbon bonded. The ^{1}H and ^{13}C NMR spectra of the two complexes (Table 1) are reasonably explained on the basis of structure **I**: the signals of

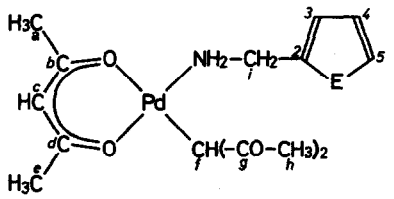

I(E = O, S)

both O—O chelated and γ-carbon bonded acacs are observed and their chemical shifts similar to those of the corresponding signals of Pd(acac)$_2$(Hbza). All the signals of the heteroaromatic amines remain intact with changes in chemical shift.

The reaction of Pd(acac)$_2$ with Hata in refluxing toluene gave [Pd(acac)(ata)]$_2$, in which Hata was deprotonated but the reaction with Hafa did not lead to deprotonation. Under these reaction con-

* Author to whom correspondence should be addressed.

ditions benzylamine (Hbza) was reported to be cyclopalladated to form Pd(acac)(bza)[2]. No ^{13}C NMR spectrum of $[Pd(acac)(ata)]_2$ was available because of its low solubility. The IR spectrum reveals the presence of only an O—O chelated acac (1510, 1570 cm^{-1}) and an N—H group (3210 cm^{-1}). The ^1H NMR spectrum (Table 1) is consistent with the result, but no N—H signal is detected. The doublet of the CH_2 signal ($J = 4.4$ Hz) may result from coupling with the N—H group. All the thiophene ring signals remain: there is no possibility of thiophene-ring cyclopalladation. Structure **II** was proposed and confirmed by X-ray analsyis: the conformation (*syn* or *anti*) of the bridging part, $Pd_2(\mu\text{-}NHR)_2$, was determined (R = 2-thienyl). A similar dimer has been obtained by the reaction of $Pd(acac)_2$ with aniline, but no structural details were reported.[5]

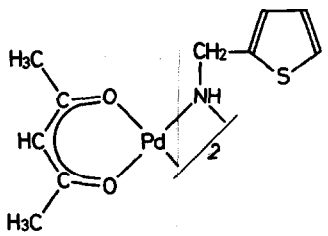

II

The bond distances and angles of $[Pd(acac)(ata)]_2$ are given in Table 2 and the molecular structure, with atom-numbering scheme, is shown in Fig. 1. Two square-planar four-coordinated palladium atoms are bridged by deprotonated amino groups and the mid-point of the two palladium atoms is a centre of symmetry. There is nothing unusual on coordination of the acac ligands (Table 2). The bridging nitrogen atom is significantly flattened [Pd—N—C(5) angles, 119.6(6) and 118.5(5)°, are larger than the tetrahedral angle 109.5°] and the conformation of the $Pd_2(NHR)_2$ ring is *anti*: the two R groups are on different sides of the rhombic Pd_2N_2 plane (R = 2-thienyl group). The Pd—N bond distances are in the normal range found for aliphatic amine palladium(II) complexes.[6] The dihedral angle of the thiophene ring with respect to

Table 1. ^1H and $^{13}C\{^1H\}$ NMR spectra of the free amines and the complexes (in $CDCl_3$, δ ppm against tetramethylsilane)

^1H NMR [figures in parentheses are J(H—H) in Hz][a]

Compound	acac (O—O) CH_3	acac (O—O) CH	acac (γ-C) CH_3	acac (γ-C) CH	NH_2	CH_2	Amine 3-H	Amine 4-H	Amine 5-H
Hafa					1.44	3.78	6.10dd (3.1, 0.8)	6.28dd (3.1, 1.8)	7.31dd (1.8, 0.8)
$Pd(acac)_2$(Hafa)	1.99 1.98	5.37	2.19	4.46	3.4br	3.71m	6.32m[b]		7.37t (1.3)
Hata					1.60	4.02d (0.7)	6.87m[b]		7.17dd (4.6, 1.8)
$Pd(acac)_2$(Hata)	2.00	5.38	2.15	4.45	3.4br	3.86m	7.12dd (3.5, 1.3)	6.97dd (5.1, 3.5)	7.25dd (5.1, 1.3)
$[Pd(acac)(ata)]_2$	1.90	5.25			[c]	3.32d (4.4)	7.01dd (3.5, 1.3)	6.91dd (4.8, 3.5)	7.21dd (4.8, 1.3)

$^{13}C\{^1H\}$ NMR

Compound	acac (O—O) CH_3	acac (O—O) CH	acac (O—O) C=O	acac (γ-C) CH_3	acac (γ-C) CH	acac (γ-C) C=O	CH_2	Amine 2-C	Amine 3-C	Amine 4-C	Amine 5-C
Hafa							39.3	156.7	104.8	110.0	141.3
$Pd(acac)_2$(Hafa)	26.9 26.7	100.3	186.6 185.8	31.4	48.1	202.5	40.2	150.8	108.2	110.4	142.4
Hata							41.3	147.3	(123.4,	126.6)[d]	123.7
$Pd(acac)_2$(Hata)	27.0 26.8	100.3	186.5 185.9	31.3	48.0	202.5	41.6	139.6	(125.6,	127.1,	127.3)[d]

[a] Signals are singlets unless otherwise noted. d = doublet, t = triplet, m = multiplet, br = broad.
[b] Overlapped signal of 3-H and 4-H.
[c] Not detected.
[d] Not assigned individually.

Table 2. Selected bond lengths (Å) and angles (°) of [Pd(acac)(ata)]$_2$

Pd—O(1)	2.015(6)	Pd—O(2)	2.043(6)	Pd—N	2.023(6)	Pd—N′	2.013(7)
O(1)—C(7)	1.30(1)	C(7)—C(8)	1.42(1)	C(8)—C(9)	1.38(2)	C(9)—O(2)	1.27(1)
N—C(5)	1.47(1)	C(5)—C(1)	1.47(2)				
Pd···Pd	3.0633(9)	N···N′	2.627(9)	Pd···S	3.641(6)		

O(1)—Pd—O(2)	93.7(3)	O(1)—Pd—N	92.6(3)	O(2)—Pd—N′	92.9(3)
N—Pd—N′	81.2(3)	Pd—N—Pd′	98.8(3)	Pd—N—C(5)	118.5(5)
C(5)—N—Pd′	119.6(6)	Pd—O(1)—C(7)	123.9(6)	Pd—O(2)—C(9)	121.5(7)
O(1)—C(7)—C(8)	123.3(9)	C(7)—C(8)—C(9)	128.3(8)	C(8)—C(9)—O(2)	128.1(8)
N—C(5)—C(1)	114.5(8)	C(5)—C(1)—S	124.4(8)	C(5)—C(1)—C(2)	124.7(9)

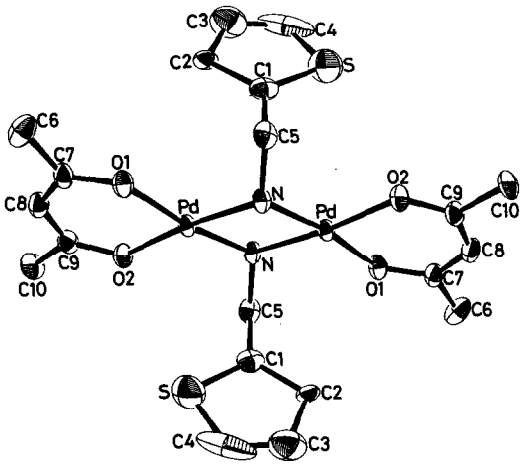

Fig. 1. ORTEP drawing and atomic numbering scheme of [Pd(acac)(ata)]$_2$.

the coordination plane is 77.8(3)° and there is no interaction between the palladium and sulphur atoms [the distance is 3.641(6) Å]. The Pd—Pd separation is 3.0633(9) Å, suggesting no bonding between the two palladium atoms.

EXPERIMENTAL

Measurements

Measurements were performed using the methods reported previously.[3]

Preparation

Pd(acac)$_2$(Hafa) *and* Pd(acac)$_2$(Hata). A mixture of Pd(acac)$_2$(305 mg, 1 mmol) and Hafa (117 mg, 1.2 mmol) or Hata (136 mg) in dichloromethane (20 cm^3) was stirred for a few hours at room temperature and mixed with hexane (30 cm^3). The filtered mixture was evaporated to a small volume to precipitate yellow crystals, which were collected, washed with hexane and dried in air. Pd(acac)$_2$(Hafa): yield 85% and m.p. 123°C (decomposed). Found: C, 44.7; H, 5.3; N, 3.4. Calc. for $C_{15}H_{21}NO_5Pd$: C, 44.8; H, 5.3; N, 3.5%. Pd(acac)$_2$(Hata): yield 60% and m.p. 133°C (decomposed). Found: C, 43.0; H, 5.0; N, 3.2. Calc. for $C_{15}H_{21}NO_4SPd$: C, 43.1; H, 5.1; N, 3.4%.

Pd(acac)(ata). A mixture of Pd(acac)$_2$ (305 mg, 1 mmol) and Hata (113 mg, 1 mmol) in toluene (15 cm^3) was refluxed for 5 h with stirring and allowed to cool. A yellow product crystallized, which was collected, washed with toluene and dried in air. The product was recrystallized from dichloromethane. Crystals suitable for X-ray diffraction were obtained upon slow evaporation of a dichloromethane solution. Yield 38% and m.p. 179°C (decomposed). Found: C, 37.8; H, 4.1; N, 4.3. Calc. for $C_{10}H_{13}NO_2SPd$: C, 37.8; H, 4.1; N, 4.4%.

X-ray analysis of [Pd(acac)(ata)]$_2$

Diffraction data of a crystal with approximate dimensions 0.1 × 0.2 × 0.3 mm^3 were collected on a Rigaku AFC-5R diffractometer with graphite Mo-K_α radiation (λ = 0.71069 Å). Crystal data: monoclinic, $P2_1/n$, a = 10.934(2), b = 5.611(1), c = 19.565(2) Å, β = 95.99(1)°, V = 1193.8(3) Å^3, Z = 2, D_x = 1.77 g cm^{-3}, μ(Mo-K_α) = 16.8 cm^{-1}. Within the range $2\theta < 60°$, 2341 independent reflections with $|F_o| > 3\sigma(|F_o|)$ were obtained. A ψ scan empirical absorption correction was applied. All the computations were performed on a HITAC M-680H computer at the Computer Center of the Institute for Molecular Science, using the Universal Crystallographic Computation Program System UNICS III.[7] The structure was solved by the usual heavy-atom method. The positions of all the non-hydrogen atoms were identified in subsequent Fourier maps. The hydrogen atoms could not be located by the difference Fourier synthesis. The final R was 0.051 for 1496 unique reflections. The bond lengths and angles, atomic parameters and anisotropic tem-

perature factors are given as supplementary material.

Acknowledgement—We wish to thank the Institute for Molecular Science (Okazaki) for the use of X-ray measurement and computation facilities.

REFERENCES

1. I. Omae, *Organometallic Intramolecular Coordination Compounds* (J. Organomet. Chem. Library, Vol. 18). Elsevier, Amsterdam (1986).
2. S. Baba and S. Kawaguchi, *Inorg. Nucl. Chem. Lett.* 1975, **11**, 415.
3. H. Mizuno, M. Kita, M. Nonoyama and J. Fujita, *Inorg. Chim. Acta* 1992, **202**, 183.
4. S. Okeya, H. Sazaki, M. Ogita, T. Takemoto, Y. Onuki, Y. Nakamura, B. K. Mohapatra and S. Kawaguchi, *Bull. Chem. Soc. Japan* 1981, **54**, 1978.
5. S. Okeya, H. Yoshimatsu, Y. Nakamura and S. Kawaguchi, *Bull. Chem. Soc. Japan* 1982, **55**, 483.
6. F. Hori, K. Matsumoto, S. Ooi and H. Kuroya, *Bull. Chem. Soc. Japan* 1977, **50**, 138.
7. T. Sakurai and K. Kobayashi, *Rikagaku Kenkyusho Hokoku* 1979, **55**, 69.

Polyhedron Vol. 12, No. 9, pp. 1031–1037, 1993
Printed in Great Britain

0277–5387/93 $6.00+.00
© 1993 Pergamon Press Ltd

CRYSTAL STRUCTURE AND MÖSSBAUER STUDY OF TETRALITHIUM IRON(III) TRIOXALATE CHLORIDE NONAHYDRATE

J. P. DECLERCQ* and J. FENEAU-DUPONT

Laboratoire de Chimie Physique et de Cristallographie, Université Catholique de Louvain, 1 Place Louis Pasteur, B-1348 Louvain la Neuve, Belgium

and

J. LADRIERE

Laboratoire de Chimie Inorganique et Nucléaire, Université Catholique de Louvain, 1 Place Louis Pasteur, 1348 Louvain la Neuve, Belgium

(*Received* 27 *November* 1992; *accepted* 8 *January* 1993)

Abstract—The crystal structure of the complex $Li_4[Fe(C_2O_4)_3]Cl \cdot 9H_2O$ has been determined by X-ray diffraction analysis. It is composed of sheets perpendicular to the *c*-axis of the hexagonal cell. In the direction of *c*, short and long intervals, occupied by hydrated lithium ions, alternate between the sheets. The coordination is distorted octahedral for the iron ion, the chlorine ion and one of the lithium ions. It is nearly tetrahedral for the other lithium ions. The Mössbauer spectra are characterized by an asymmetric quadrupole doublet arising from a local distorsion of the iron octahedral coordination and the presence of a relatively fast spin–spin relaxation process.

The tris oxalato complexes, $[M(C_2O_4)_3]^{3-}$ (M = Al, Fe, Cr, Co, Rh, Ir), have played an important role in coordination chemistry for a long time. Since the discovery of the Mössbauer effect, particular interest has been devoted to tris(oxalato)ferrate(III) complexes, but, although Mössbauer spectroscopy has been widely applied in numerous radiolysis, photolysis and thermal decomposition studies,[1–14] little attention has been paid to chemical bond and structural problems. This is presumably due to the fact that the spectra of these complexes are subject to electronic paramagnetic relaxation[15–17] and need, therefore, for their interpretation knowledge of the iron interionic distances, which are well established only for few compounds.[18,19]

In this paper the detailed crystallographic structure of a novel tris(oxalato)ferrate(III) complex, $Li_4[Fe(Ox)_3]Cl \cdot 9H_2O$, is determined by X-ray diffraction analysis (XRD) and the Mössbauer absorption spectra of ^{57}Fe in this compound are interpreted in connection with the crystallographic data.

EXPERIMENTAL

Synthesis and chemical analysis

The green complex of lithium tris(oxalato) ferrate(III) has been prepared by mixing equal volumes of a 3 M lithium oxalate solution and 1 M iron(III) chloride solution. The slow evaporation of this solution in the dark gives rise to the formation of two different hydrates of the complex $Li_4[Fe(Ox)_3]Cl$, depending on the crystallization temperature. A dodecahydrate crystallizes below 18°C, whereas the nonahydrate is formed at *ca* 28°C. The crystals of both compounds are emerald green and present a triangular prismatic shape. The dodecahydrated crystals are not stable at room temperature and transform readily in a few days into the nonahydrate, without apparent change of external morphology, but an apparition of opacity. The crystals of nonahydrate obtained in this way present

* Author to whom correspondence should be addressed.

a flake-like texture parallel to the triangular plane and become very easy to cleave along this direction. As a result of this transformation very thin single crystals can be obtained, which are suitable for XRD and Mössbauer measurements.

The chemical composition of $Li_4[Fe(Ox)_3]Cl \cdot 9H_2O$ was determined by elemental analysis of iron, oxalate and chloride ions and are in good agreement with the above formula (W%, Fe, Cl^-, $C_2O_4^{2-}$; th. 10.2, 6.5 and 48.4; obs. 10.1, 6.6 and 47.9).

The water of crystallization was determined by thermogravimetric analysis and the observed weight loss corresponding to the dehydration (29.5%) is consistent with the theoretical value (29.7%).

Crystal structure determination of $Li_4[Fe(C_2O_4)_3]Cl \cdot 9H_2O$

The crystal used had the shape of a triangular base prism with the dimensions 0.65 (edge of the triangle) × 0.2 mm (height of the prism). Lattice parameters were refined using 16 reflections in the range $9° \leqslant 2\theta \leqslant 28°$. Intensity data were collected at room temperature on a Huber four-circle diffractometer, using graphite monochromatized Mo-K_α radiation ($\lambda = 0.71069$ Å). A standard reflection (4, 1, 6) was checked every 50 reflections and showed no significant deviation. 2918 reflections were collected with $\sin\theta/\lambda \leqslant 0.617$ Å^{-1}, providing 1616 unique reflections ($R_{merge} = 0.023$), of which 1360 with $I \geqslant 2.5\sigma(I)$ were considered as observed and used in further calculations. The crystal data are given in Table 1.

It is worth remarking that according to the compilation of Padmaja *et al.*,[20] this is a unique occurrence of the space group (*P*-6*c*2) among organo carbon compounds. It appears that in the meantime the 1992 release of the Cambridge Structural Database[21] contains only two structures belonging to this space group.

The structure was solved by heavy atom and Patterson methods using SHELXS86.[22] An anisotropic least-squares refinement (SHELX76[23]) using *F* converged to $R = 0.046$, $Rw = 0.052$ for 1360 observed reflections. The maximum and minimum heights in final difference-Fourier synthesis are 1.04 (close to Cl^- ion) and −0.53 e Å^{-3}. The atomic scattering factors are from the International Tables for X-ray Crystallography (1974, Vol. IV). The atomic parameters, lists of anisotropic thermal parameters and observed and calculated structure factors have been deposited as supplementary material with the Editor, from whom copies are available on request.

Table 1. Crystal data and structure refinement of $Li_4[Fe(C_2O_4)_3]Cl \cdot 9H_2O$

Formula	$C_6H_{18}O_{21}Li_4FeCl$
Formula weight	545.25
Crystal system	Hexagonal
Space group	*P*-6*c*2
a (Å)	9.465(5)
c (Å)	26.72(2)
V (Å^3)	2073(2)
Z	4
D_c (g cm^{-3})	1.747
D_m (g cm^{-3})	1.726
F(000)	1108
Wavelength (Å)	0.71069
$(\sin\theta/\lambda)_{max}$ (Å^{-1})	0.617
μ (cm^{-1})	9.78
Data collected	2918
Unique data	1616
R_{merge}	0.023
Data with $I \geqslant 2.5\sigma(I)$	1360
R	0.046
*R*w	0.052
w	$1/[\sigma^2(F_o)+0.0076F_o^2]$
$(\Delta\rho)_{max}$ (e Å^{-3}) (close to Cl^-)	1.04

Mössbauer measurements

Mössbauer spectra of $Li_4[Fe(OX)_3]Cl \cdot 9H_2O$ were obtained with a polycrystalline sample, as well as with single crystals and in the latter case they were recorded as a function of the angle θ between the gamma ray beam and the principal crystallographic axis *c*. The thickness of the samples was of the order 0.5 mm in order to have an effective thickness of 9 mg of natural iron per square centimeter. The measurements were performed at room temperature with an ordinary constant-acceleration spectrometer using a ^{57}Co(Rh) source. Experimental data were resolved into Lorentzian lines using a conventional iterative least-square fit program.

RESULTS AND DISCUSSION

Description of the structure

The structure can be described as a succession along the *c*-axis of two-dimensional sheets extending infinitely in the *a*,*b*-plane. The approximate *z*-coordinate of the sheets in one unit-cell are successively 0.10, 0.40, 0.60 and 0.90. The separations between the sheets alternate between a short distance (*ca* $0.2 \times c \approx 5.3$ Å) and a long distance (*ca* $0.3 \times c \approx 8.0$ Å).

Each sheet corresponds to the chemical com-

position $Li^+[Fe(C_2O_4)_3]^{3-}Cl^- \cdot 6H_2O$. The Fe^{3+}, Li^+(1) and Cl^- ions lie on the three different three-fold axes present in the space group, respectively, at (1/3,2/3,z), (0,0,z) and (2/3,1/3,z). The cohesion inside the sheets is principally secured by the oxalate ions. For each of them two oxygen atoms belonging to two different carboxylate groups are bound to the iron ion, and the two remaining ones to the lithium ion. Schematically this could be compared to an assembly of hexagonal tiles in which the vertices are alternatively occupied by iron and lithium ions and the edges by the oxalate ions. A hexahydrated chlorine atom lies on the centre of the hexagon according to the following scheme.

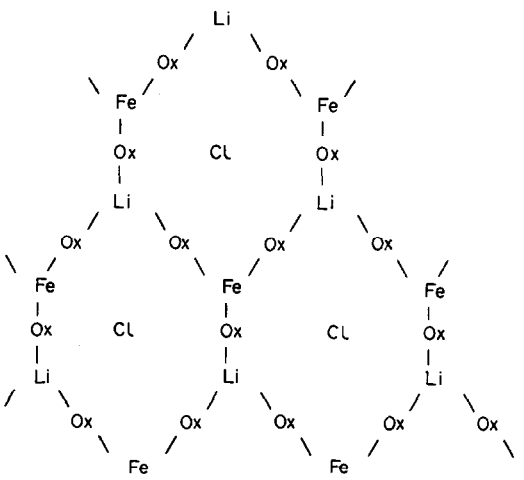

Fig. 1. presents one of these sheets with the numbering of the atoms (Program ORTEP[24]).

Such an arrangement in two-dimensional sheets has been described, for example in hexaaquatris(oxalato)dipraseodymium(III) pentahydrate[25] and in hexaaquatris(oxalato)dineodymium(III) 4.5 hydrate,[26] where both sides of the oxalate ions are bound to the same metal. It differs markedly from the situation observed in other tris(oxalato)ferrate (III) compounds of monovalent cations, $(NH_4)_3[Fe(C_2O_4)_3]3H_2O$[19] and $K_3[Fe(C_2O_4)_3]3H_2O$,[18] where discrete complex anions, $[Fe(C_2O_4)_3]^{-3}$, are observed. The latter situation is also usually found in similar complexes with other M^{III} atoms such as Cr,[27-29] Mn,[30] Al[29] and Ti.[31]

The coordination of Fe^{3+} is a distorded octahedron composed of the oxygen atoms O(1) and O(4) of three oxalate ions related by a three-fold axis through the central ion. A very similar coordination is observed around Li^+(1) with the two other oxygen atoms of the oxalate ion O(2) and O(3). The distances and angles are given in Table 2. It is worth noting that the two oxygen atoms coordinating the iron ion correspond to the longest C—O bonds in the oxalate ion. The oxalate ions are planar within experimental error (largest deviation from mean plane < 0.008 Å). The Fe^{3+}—O values (2.020 and 2.023 Å) are comparable to the mean distance observed in potassium tris(oxalato)ferrate trihydrate (2.037 Å) by Herpin[18] and in ammonium tris(oxalato)ferrate trihydrate (2.002 Å) by Merrachi *et al.*[19] The deformation of the octahedra can be related to the constraints imposed on the distance between the two oxygen atoms belonging to the same oxalate ion. In a regular octahedron the length of the edges should be the mean metal–oxygen dis-

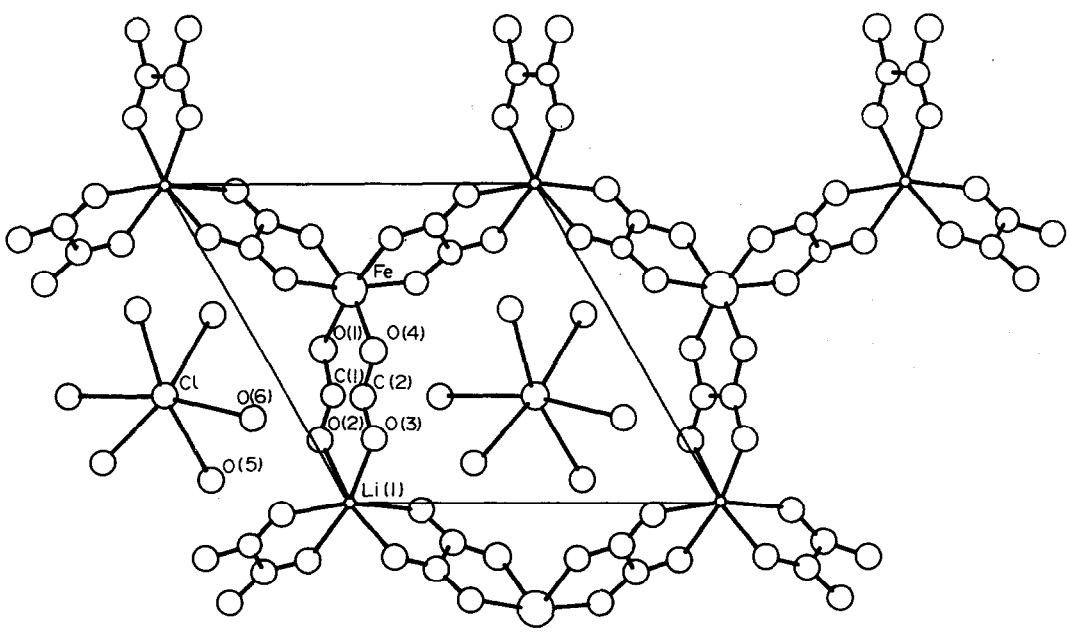

Fig. 1. Disposition and numbering of the atoms belonging to one sheet.

Table 2. Distances (Å) and angles (°)

		The oxalate ion	
C(2)—C(1)	1.554(4)	O(1)—C(1)—C(2)	114.9(2)
O(1)—C(1)	1.282(4)	O(2)—C(1)—C(2)	118.3(3)
O(2)—C(1)	1.251(4)	O(2)—C(1)—O(1)	126.7(2)
O(3)—C(2)	1.214(4)	O(3)—C(2)—C(1)	118.8(3)
O(4)—C(2)	1.281(4)	O(4)—C(2)—C(1)	113.7(2)
		O(4)—C(2)—O(3)	127.4(2)
		Octahedral coordination of Fe^{3+}	
Fe^{3+}—O(1)	2.023(2)	O(1)—Fe^{3+}—O(1)	92.3(1)
Fe^{3+}—O(4)	2.020(2)	O(4)—Fe^{3+}—O(4)	91.4(1)
		O(1)—Fe^{3+}—O(4)	80.4(1)
			97.0(1)
			168.3(1)
		Octahedral coordination of $Li^{+}(1)$	
$Li^{+}(1)$—O(2)	2.193(5)	O(2)—$Li^{+}(1)$—O(2)	92.6(1)
$Li^{+}(1)$—O(3)	2.127(5)	O(3)—$Li^{+}(1)$—O(3)	93.3(1)
		O(2)—$Li^{+}(1)$—O(3)	78.5(3)
			97.0(1)
			167.1(1)
		Octahedral coordination of Cl^{-}	
Cl^{-}—O(5)	3.104(3)	O(5)—Cl^{-}—O(5)	86.0(1)
Cl^{-}—O(6)	3.063(3)	O(6)—Cl^{-}—O(6)	81.8(1)
		O(5)—Cl^{-}—O(6)	89.9(1)
			103.2(1)
			169.7(1)
		Tetrahedral coordination of $Li^{+}(2)$	
$Li^{+}(2)$—O(2)	1.993(5)	O(2)—$Li^{+}(2)$—O(2)	134.5(1)
$Li^{+}(2)$—O(5)	1.948(6)	O(5)—$Li^{+}(2)$—O(5)	111.1(1)
		O(2)—$Li^{+}(2)$—O(5)	99.6(1)
			105.8(1)
		Tetrahedral coordination of $Li^{+}(3)$	
$Li^{+}(3)$—O(6)	1.942(6)	O(6)—$Li^{+}(3)$—O(6)	126.9(1)
$Li^{+}(3)$—O(7)	1.936(10)	O(6)—$Li^{+}(3)$—O(7)	98.7(1)
$Li^{+}(3)$—O(8)	1.895(10)	O(6)—$Li^{+}(3)$—O(8)	108.2(1)
		O(7)—$Li^{+}(3)$—O(8)	116.0(2)

tance multiplied by $\sqrt{2}$, i.e. 2.86 and 3.05 Å for the iron and lithium ions, respectively. The corresponding observed distances are O(1)···O(4) 2.61 and O(2)···O(3) 2.73 Å. The coordination of the chloride ions is also octahedral, composed of the water molecules O(5) and O(6) and four symmetry-related water molecules. Hydrogen bonds exist between these water molecules and the oxalate oxygens: O(5)—O(1) = 2.99, O(5)—O(2) = 3.01 and O(6)—O(3) = 2.82 Å, improving the intra-sheet cohesion. As will be described in the next paragraphs, these water molecules also take part in the connections between the sheets.

A quantitative description of the deformation of the octahedra has been proposed by Muetterties and Guggenberger.[32] As shown in Table 3 this description includes a dihedral angle (ϕ), describing the relative twist of opposed triangular faces of the octahedron and angles (δ) between the normal to the faces. In this way the coordination figure is described as an intermediate between $O_h(D_{3d})$ and D_{3h}. The values describing the polyhedron around the iron atom can be compared to the values computed by Merrachi *et al.*[28] in tris(oxalato)-ferrate(III) and -chromate(III) of monovalent cations. Interestingly, the values observed by these authors around chromium [$48 \leqslant \phi \leqslant 50$; $60 \leqslant \delta(b_1) \leqslant 63$; $78 \leqslant \delta(b_2) \leqslant 81$] resemble much more our observations than the values given around iron [$\phi = 40$; $51 \leqslant \delta(b_1) \leqslant 53$; $85 \leqslant \delta(b_2) \leqslant 86$].

Table 3. Description of the deformations of (a) the octahedra and (b) the tetrahedra using the symbolism proposed by Muetterties and Guggenberger.[32] For comparison, the extreme situations, regular octahedron (O_h) and trigonal prism (D_{3h}) for (a), regular tetrahedron (T_d) and square planar (D_{4h}) for (b), are indicated

(a)	Φ	$\delta(b1)$	$\delta(b2)$	δ(remaining)
O_h	60.0	70.5	70.5	70.5
Fe	46.0	59.3	82.2	70.5; 71.0
Li(1)	−44.7	58.7	83.5	69.7; 71.1
Cl	47.0	56.6	78.7	75.2; 72.7
D_{3h}	0	0	120.0	90.0
(b)	δ'			δ(remaining)
T_d	109.5			109.5
Li(2)	81.8; 88.8			114.65; 114.65; 119.5; 119.5
Li(3)	81.9; 86.0			115.0; 115.0; 118.1; 118.1
D_{4h}	0			180

The space between two adjacent sheets corresponding to a short distance (5.3 Å) is occupied by a lithium ion, $Li^+(2)$, lying on a two-fold axis $(x,-x,0)$, The distorted tetrahedral coordination (see Table 3) of this ion includes O(2), an oxygen atom of the oxalate ion, O(5), a water molecule around the chlorine ion, and two symmetry related oxygen atoms. This lithium ion is thus directly bound to four oxygen atoms belonging to two different sheets, justifying the short distance observed.

The remaining lithium ion, $Li^+(3)$, is located in the gap corresponding to a long distance between sheets (8.0 Å), lying on a mirror plane at $z = 1/4$. Its coordination is also approximately tetrahedral (Table 3): two symmetry related oxygen atoms [O(6)] belonging to the hydration sphere of the chlorine ions in two different sheets and two additional water molecules, O(7) and O(8), in the mirror plane. There is only one direct bond with the adjacent sheets and some hydrogen bonds, including the water molecules: O(7)—O(3) = 2.93 and O(8)—O(4) = 3.05 Å.

Figure 2 is a schematic representation of the stacking of the sheets in the unit cell.

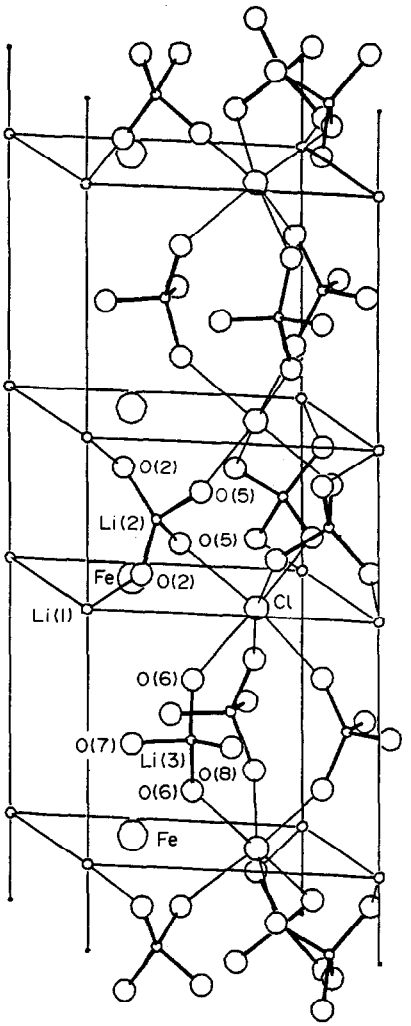

Fig. 2. Schematic representation of the stacking of the sheets in the unit cell. Horizontal planes are drawn at the positions of the sheets. The short gaps contain $Li^+(2)$ and the long ones $Li^+(3)$, both with a tetrahedral coordination.

Mössbauer spectroscopy

Figure 3 shows the Mössbauer spectrum of a polycrystalline sample [Fig. 3(a)], as well as the spectra obtained with single crystals for different values of the angle θ between the gamma ray beam and the crystallographic axis c [Fig. 3(b), $\Theta = 0°$; Fig. 3(c), $\Theta = 54.73°$; Fig. 3(d), $\Theta = 90°$].

All these spectra exhibit a badly resolved and asymmetric quadrupole pattern consisting of two lines with different line-widths and different relative areas (intensities). The apparent quadrupole splitting is 0.60 ± 0.05 mm s^{-1} and the centre of the lines indicates an isomer shift of 0.33 ± 0.05 mm s^{-1} relative to natural iron. Both values are characteristic of a high spin Fe^{3+} ion in a non-cubic environment. The presence of a quadrupolar interaction is consistent with the above described deformation of the octahedral coordination of the iron atom from O_h to D_{3h} symmetry. Furthermore, as the ternary symmetry axis of the distorted octahedra is parallel to the c-axis, one can assume that the quadrupole interaction results from an axially symmetric electric field gradient (EFG) oriented in the

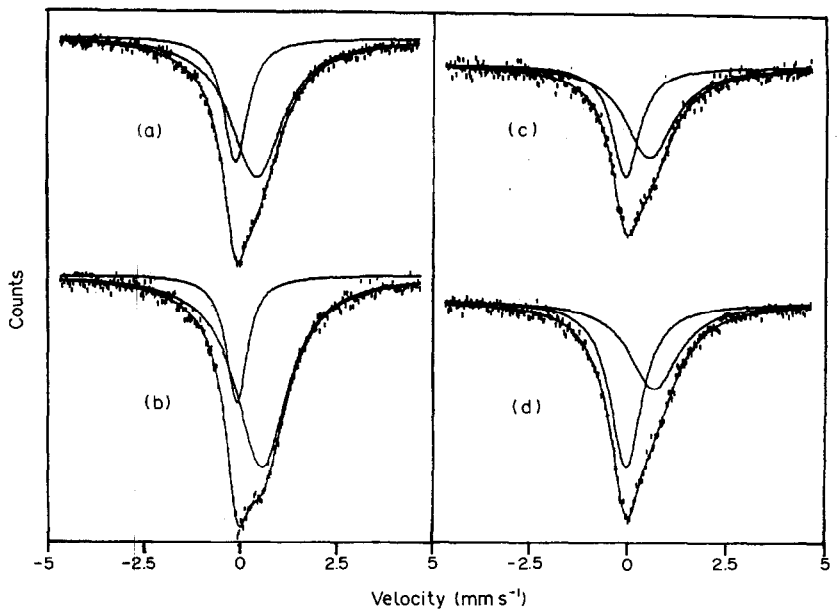

Fig. 3. Mössbauer spectra at room temperature of (a) a polycrystalline sample and of a single crystal with the *c*-axis oriented at (b) 0°, (c) 54.73° and (d) 90°, with respect to the gamma ray beam.

same direction. Neglecting for the moment the problem of the origin of the line-width asymmetry, this result seems in relatively good agreement with the observed values of the intensities ratio of the two lines for the different orientations of the single crystal with respect to the gamma ray beam.

The intensities ratios I^+/I^- of the highest energy line (I^+) to the lowest energy one (I^-) were found to be equal to 3.46 ± 0.3, 1.42 ± 0.2 and 0.78 ± 0.1 for $\Theta = 0°$, 54.73° and 90°, respectively. These values are indeed close to the corresponding theoretical values 3, 1 and 0.66 calculated from the formula $I^+/I^- = 3(1+\cos^2\Theta)/(5-3\cos^2\Theta)$, considering that the highest energy line corresponds to the $|\pm3/2\rangle \rightarrow |\pm1/2\rangle$ nuclear transition and that the EFG is parallel to the *c*-axis.

In the case of a randomly distributed polycrystalline sample this ratio should also be equal to one, but the observed value is larger: 2.2 ± 0.3. The asymmetry observed here could be due to a Goldanskii–Karyagin effect, which is based on the anisotropy of the Debye–Waller factor *f* in connection with the angular distribution of the gamma radiation, but this effect is usually small. The *f* factor can be related to the mean square vibrational amplitudes of the nucleus in the direction of the gamma rays. From XRD analysis we find that the root mean square amplitudes of the iron atoms along the principal axes *x,y,z* of the thermal vibration ellipsoid are 0.129, 0.129 and 0.179 Å, respectively, and that the *z*-axis of the ellipsoid coincides with the crystallographic *c*-axis. This result is of course in agreement with an axially symmetric EFG along this direction. This means that, at room temperature, the Debye–Waller factors in the *a,b*-plane and along the *c*-axis are 0.71 and 0.52, respectively. These values correspond (according to ref. 33) to an intensity ratio I^+/I^- of only 0.96, which cannot explain the observed difference. It is likely that this difference is to be attributed to a residual orientation of the crystallites with respect to the gamma ray beam, an effect which can be quite large and difficult to eliminate in plate-like materials.

The asymmetry in the line-width of the lines can be attributed to relaxation of paramagnetic ions, causing fluctuating magnetic fields, rather than to a Goldanskii–Karyagin effect because the former effect gave lines with different shapes and equal areas while the latter results in lines with different areas and equal shapes.

A broadening of a line will result when the relaxation time of the magnetic field is comparable to or larger than the nuclear Larmor period. For *S*-state ions such as high spin Fe^{3+} the orbital angular momentum is rigorously zero and the spin-lattice mechanism is, therefore, negligible compared to the spin–spin relaxation process, which depends on the distance *r* between the dipoles as $\langle r^{-3}\rangle$. Hence, in iron(III) compounds with a small Fe—Fe distance ($\sim$ 5 Å) the relaxation is fast and the lines are comparatively sharp, whereas compounds with larger iron interionic distances ($\sim$ 10 Å) tend to show definite magnetic structure.

According to the structure of $Li_4[Fe(Ox)_3]$

$Cl \cdot 9H_2O$, each iron ion has at least one nearest neighbour iron located (on the *c*-axis) at a considerably shorter distance (5.356 Å) than the other adjacent ions (8.004 Å on the *c*-axis, 9.465 Å in the *a*,*b*-plane) and, therefore, the spin–spin relaxation between the closest iron ions will be predominant and relatively fast. If the fluctuating magnetic field is parallel to the electric field gradient Blume and Tjon[34] have shown that the $|\pm 3/2\rangle \rightarrow |\pm 1/2\rangle$ nuclear transitions, which make up one of the lines (I^+) of the quadrupole doublet, have a larger splitting than do the $|\pm 1/2 \rightarrow |\pm 1/2\rangle$ transitions, which make up the other line (I^-). This is in agreement with the observation that the line-width of the highest energy line (I^+) is larger (1.58 ± 0.07 mm s^{-1}) than that of the lowest one (I^-) (0.80 ± 0.15 mm s^{-1}). In this particular compound we may expect to find, as in the case of $FeCl_3 \cdot 6H_2O$,[35] a relaxation time for which the I^- line is narrowed while the I^+ line is still broad. Furthermore, the temperature and the external magnetic field dependences of the Mössbauer spectra of both compounds should be similar, but these results will be presented separately.

REFERENCES

1. A. A. Temperley, *Bull. Am. Phys. Soc.* 1967, **12**, 924.
2. K. G. Dharmawardena and G. H. Bancroft, *J. Chem. Soc.* (*A*) 1968, 2655.
3. G. H. Bancroft, K. G. Dharmawardena and A. G. Maddock, *J. Chem. Soc.* (*A*) 1969, 2914.
4. A. A. Temperley and D. W. Pumplin, *J. Inorg. Nucl. Chem.* 1969, **31**, 2711.
5. W. Heidrich, *Z. Phyzik.* 1970, **230**, 418.
6. J. Ladrière, *Hyp. Int.* 1988, **42**, 993.
7. J. Ladrière, V. Senterre and D. Apers, *Hyp. Int.* 1992, **70**, 917.
8. B. S. Randhawa, A. S. Brar and T. K. Bansal, *Radiochem. Radioanal. Lett.* 1982, **53**, 359.
9. P. K. Gallagher and C. R. Kurkjian, *Inorg. Chem.* 1966, **5**, 214.
10. H. Sato and T. Sano, *Bull. Chem. Soc. Japan* 1979, **52**, 1402.
11. A. S. Brar and B. S. Randhawa, *Bull. Chem. Soc. Japan* 1981, **54**, 3166.
12. J. Ladrière and D. Apers, *Hyp. Int.* 1988, **42**, 1055.
13. J. Ladrière, *Hyp. Int.* 1992, **70**, 1091.
14. J. Ladrière, *Hyp. Int.* 1992, **70**, 1095.
15. D. Barb, L. Diamandescu and D. Tarabasan, *J. Phys C*1 1980, **41**, 227.
16. D. Barb, L. Diamandescu and D. Tarabasan, *J. Phys C*6 1976, **12**, 113.
17. S. Yamauchi, Y. Sakai and T. Tominaga, *J. Radioanal. Nucl. Chem. Lett.* 1990, **146**, 185.
18. P. Herpin, *Bull. Soc. Fr. Min. Crist.* 1958, **81**, 245.
19. E. H. Merrachi, B. F. Mentzen, F. Chassagneux and J. Bouix, *Rev. Chim. Min.* 1987, **24**, 56.
20. N. Padmaja, S. Ramakumar and M. A. Viswamitra, *Acta Cryst.* 1990, **A46**, 725.
21. F. H. Allen, S. Bellard, M. D. Brice, B. A. Cartwright, A. Doubleday, H. Higgs, T. Hummelink, B. G. Hummelink-Peters, O. Kennard, W. D. S. Motherwell, J. R. Rodgers and D. G. Watson, *Acta Cryst.* 1979, **B35**, 2331.
22. G. M. Sheldrick, in *Crystallographic Computing 3* (Edited by G. M. Sheldrick, C. Kruger and R. Goddard), pp. 175–189. Oxford University Press, Oxford (1985).
23. G. M. Sheldrick, SHELX76, Program for Crystal Structure Determination. University of Cambridge, U.K. (1976).
24. C. K. Johnson, ORTEP, A Fortran Thermal-Ellipsoid Plot Program for Crystal Structure Illustrations. Oak Ridge National Laboratory, ORNL-3974 (1971).
25. B. Beagley, R. G. Pritchard, N. P. Evmiridis, A. Michailides and S. Skoulika, *Acta Cryst.* 1988, **C44**, 174.
26. E. Hansson, *Acta Chem. Scand.* 1973, **27**, 2852.
27. E. H. Merrachi, B. F. Mentzen and F. Chassagneux, *Rev. Chim. Min.* 1986, **23**, 329.
28. E. H. Merrachi, B. F. Mentzen and F. Chassagneux, *Rev. Chim. Min.* 1987, **24**, 427.
29. D. Taylor, *Aust. J. Chem.* 1978, **31**, 1455.
30. T. Lis and J. Matuszenwski, *Acta Cryst.* 1980, **B36**, 1938.
31. D. J. Eve and M. L. Niven, *Inorg. Chim. Acta* 1990, **174**, 205.
32. E. L. Muetterties and L. J. Guggenberger, *J. Am. Chem. Soc.* 1974, **96**, 1748.
33. V. I. Goldanskii and E. F. Makarov, in *Chemical Applications of Mössbauer Spectroscopy* (R. H. Herber and V. I. Goldanskii), p. 105. Academic Press, London (1968).
34. M. Blume and J. A. Tjon, *Phys. Rev.* 1968, **165**, 446.
35. N. Thrane and G. Trumpy, *Phys. Rev. B* 1970, **1**, 153.

Polyhedron Vol. 12, No. 9, pp. 1039–1041, 1993
Printed in Great Britain

0277–5387/93 $6.00+.00
© 1993 Pergamon Press Ltd

A CONVENIENT METHOD FOR THE SYNTHESIS OF DINITROSYLMOLYBDENUM(0) COMPLEXES OF HETEROCYCLIC ACIDS†

MANNAR R. MAURYA‡ and C. GOPINATHAN

Inorganic Chemistry Division, National Chemical Laboratory, Pune 411 008, India

(*Received* 21 *October* 1992; *accepted* 7 *January* 1993)

Abstract—A simple procedure is described for the synthesis of dinitrosylmolybdenum(0) complexes of picolinic acid and its derivatives by the reaction of $Mo(NO)_2(acac)_2$ (where acacH = acetylacetone) with the respective ligand in methanol under aerobic conditions.

Ligand exchange reactions are a very common method in coordination chemistry to design and synthesize metal complexes with deliberately tailored properties. In the chemistry of dioxo-metal cations, such as dioxomolybdenum(VI),[1] dioxotungsten(VI),[2] dioxouranium(VI),[3] etc., such reactions have been studied extensively using $MO_2(acac)_2$ (where M = Mo, W or U) as a starting precursor. Only acetylacetone exchanges with the ligand during the chemical reaction and the strongly bound oxygens of the oxometal group remain intact. With this background we have recently studied the exchange ability of the acetylacetone group in $Mo(NO)_2(acac)_2$ with the Schiff bases and have shown that similar dinitrosylmolybdenum(0) complexes can be prepared in aerobic conditions using $Mo(NO)_2(acac)_2$ as a starting precursor.[4] We have now extended the reactivity of this precursor towards simple heterocylic acids (**1**), where X = H, 3-COOH or 5-COOH, and report that $Mo(NO)_2(acac)_2$ can be readily used to prepare dinitrosylmolybdenum(0) complexes of these ligands.

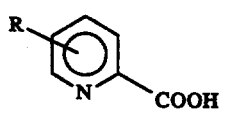

1

R	Abbreviations
H	2-pic
3-COOH	2, 3-pydc
5-COOH	2, 5-pydc

† NCL communication No. 5640.

‡ Author to whom correspondence should be addressed.

EXPERIMENTAL

Reagents

All chemicals used were of analytical grade. $Mo(NO)_2(acac)_2$ was prepared following the method described by Sarkar and Subramanian.[5]

Preparation of the complexes

$Mo(NO)(2\text{-pic})_3$ (**1**) *and* $Mo(NO)_2(2\text{-pic})_2$ (**2**). A mixture of $Mo(NO)_2(acac)_2$ (0.354 g, 0.001 mol) and 2-picolinic acid (0.246 g, 0.002 mol) in methanol (15 cm^3) was refluxed on a water bath for 15 h. After cooling the reaction mixture for 2 h the yellow complex (**1**) separated was filtered, washed with methanol and dried *in vacuo*. The combined washings and filtrate were evaporated to *ca* 3 cm^3 under a current of air. The green complex (**2**) separated was filtered, washed with cold methanol and dried. Finally compound **2** was recrystallized from CH_2Cl_2. Yield: $Mo(NO)(2\text{-pic})_3$ = 0.025 g (7.6%); $Mo(NO)_2(2\text{-pic})_2$ = 0.21 g (52.5%).

$Mo(NO)_2(2,3\text{-pydc})_2$(**3**) *and* $Mo(NO)_2(2,5\text{-pydc})_2$ (**4**). 2,3-Pyridine dicarboxylic acid or 2,5-pyridine dicarboxylic acid (0.334 g, 0.002 mol) was added to a methanolic solution of $Mo(NO)_2(acac)_2$ (0.354 g, 0.001 mol in 15 cm^3) and the reaction mixture was refluxed on a water bath for 15 h. After removal of the solvent under reduced pressure the crude product was suspended in methanol (5 cm^3) and heated at reflux for 5 min. The green solid was filtered after cooling, washed with methanol and dried *in vacuo*. Yield: $Mo(NO)_2(2,3\text{-pydc})_2$ = 0.19 g (39%); $Mo(NO)_2(2,5\text{-pydc})_2$ = 0.22 g (43%).

Table 1. Analytical, IR and electronic spectral data of the complexes

Complex/ stoichiometry	Found (Calc.) % C	H	N	Mo	ν(NO) (cm^{-1})	λ_{max} (ε)[a] (nm)
$Mo(NO)(2\text{-pic})_3$	43.8	2.5	11.2	19.2	1655	—
$C_{18}H_{12}N_4O_7Mo$	(43.9)	(2.4)	(11.4)	(19.5)		
$Mo(NO)_2(2\text{-pic})_2$	35.8	2.1	14.2	24.4	1783, 1665	656(95), 434(1540)
$C_{12}N_8N_4O_6Mo$	(36.0)	(2.0)	(14.0)	(24.0)		
$Mo(NO)_2(2,3\text{-pydc})_2$	34.2	1.9	10.9	20.0	1801, 1675	657(82), 440(1681)
$C_{14}H_8N_4O_{10}Mo$	(34.4)	(1.8)	(11.3)	(19.7)		
$Mo(NO)_2(2,5\text{-pydc})_2$	34.7	1.6	11.5	19.3	1818, 1642	657(78), 439(1528)
$C_{14}H_8N_4O_{10}Mo$	(34.4)	(1.8)	(11.3)	(19.7)		

[a] ε in $dm^3\ mol^{-1}\ cm^{-1}$.

The analytical and physicochemical data of the complexes are presented in Table 1.

Measurements

Molybdenum was estimated gravimetrically as bis(8-hydroxyquinolinato)dioxomolybdenum(VI) after decomposing the complexes with concentrated HNO_3. Other elemental analyses were performed by the microanalytical section of this laboratory. The electrical conductance measurements were performed in 1×10^{-3} M DMF solutions using a Toshniwal conductivity bridge (Type CLO1-02A) and a dip-type cell calibrated with KCl solution. IR spectra were recorded as KBr discs on a Perkin–Elmer model 1620 FT-IR spectrophotometer. Electronic spectra were recorded in DMF on a Shimadzu UV-160A UV–vis spectrophotometer.

RESULTS AND DISCUSSION

Although $Mo(NO)_2(2\text{-pic})_2$ and $Mo(NO)(2\text{-pic})_3$ have already been reported by reductive nitrosylation of dioxomolybdenum(VI) by hydroxylamine hydrochloride in the presence of 2-picolinic acid under aqueous-aerobic conditions,[6] all the complexes reported here have been prepared by a single-step ligand exchange process using $Mo(NO)_2(acac)_2$ as the starting material. Thus, $Mo(NO)_2(acac)_2$ undergoes ligand exchange reactions with **1** in methanol to give complexes of the type $Mo(NO)_2L_2$ (where LH = **1**; R = H, 3-COOH and 5-COOH). Under the reaction conditions both molecules of acetylacetone are replaced by the heterocyclic acids as follows:

$$Mo(NO)_2(acac)_2 + 2LH \xrightarrow{MeOH} Mo(NO)_2L_2 + 2acacH.$$

Analytical data support the above formulation of the complexes. Some unidentified minor secondary products were also formed which were neglected. Only in the case of 2-picolinic acid was a secondary product of the composition $Mo(NO)(2\text{-pic})_3$ isolated in reasonably good yield (see Experimental) and characterized. Perpinan *et al.*[6] have also noticed the formation of such minor secondary products in the case of some bidentate ligands. However, they were also unable to characterize these, except that obtained by us in the case of 2-picolinic acid.

All the dinitrosyl complexes are non-electrolytes ($\Lambda_M = 3.5-7.8\ \Omega\ mol^{-1}\ cm^2$) in DMF. They are soluble in coordinating solvents like pyridine, DMF and DMSO, but $Mo(NO)(2\text{-pic})_3$ is insoluble in most solvents. The high decomposition temperature (>250°C) indicates the increased stability of the complexes.

IR spectra

The IR spectra of the dinitrosyl complexes exhibit two well-separated bands in the 1800 and 1650 cm^{-1} regions, indicating the presence of a *cis*-$Mo(NO)_2$ structure; the *trans*-$Mo(NO)_2$ structure would only show one band. The frequencies of the bands suggest that NO is coordinated as NO^+. In fact, the NO^+ character of the nitrosyl group in the complex $Mo(NO)_2(2\text{-pic})_2$ has been confirmed by X-ray crystal study, in which the Mo—N—O bond angles of 173.9° and 194.9° are characteristic of linear coordination of the NO^+ group.[6] The mononitrosyl complex $Mo(NO)(2\text{-pic})_3$ shows only one band at 1655 cm^{-1}.

The $\nu_a(COO^-)$ and $\nu_s(COO^-)$ bands of free 2,3-pydc and 2,5-pydc appear at 1670 and 1469, and

1694 and 1492 cm^{-1}, respectively. These bands are still present in the complexes together with two new bands. In complex **3** these new bands are at 1693 and 1455 cm^{-1}, whereas in **4** they are at 1731 and 1460 cm^{-1} and are assigned to ν(C=O) and ν(C—O) modes, respectively. The mode of shifting and magnitude of separation between the two ν(CO) bands clearly indicate the unidentate coordination of the carboxylate ion.[7] The other two bands which are present in the ligands and the complexes suggest the non-participation of the other carboxylic acid group. The position of the ν(C=O) and ν(C—O) bands in **1** and **2** are also in-line with the unidentate coordination of the carboxylate ion. The ν(C=N) bands due to coordinated nitrogen could not be located unequivocally due to complexity of the spectra. However, in the light of the X-ray crystal structure of $Mo(NO)_2(2\text{-pic})_2$[6] it is suggested that pyridinic nitrogen is coordinated to molybdenum in all complexes.

Electronic spectra

The electronic spectra of the dinitrosyl complexes are dominated by two strong bands centred at *ca* 657 and 440 nm. These bands are tentatively assigned to the transitions from a_2 [d_{xy}, π^*(NO)] or b_2 [d_{yz}, π^*(NO)] to the lowest empty molecular orbital b_1 [π^*(NO)] and a_1 [d_{z^2}, π^*(NO)] to b_1 [π^*(NO)] within the $\{Mo(NO)_2\}^6$ group. The values obtained here agree well with the values reported for the majority of the *cis*-dinitrosylmolybdenum(0) complexes.[6,8]

CONCLUSION

On the basis of physicochemical and spectroscopic results an octahedral structure has been suggested for the dinitrosyl complexes, in which the two nitrosyl groups are *cis* to each other. We believe that the synthetic route described here can be generalized to the other dinitrosylmolybdenum(0) complexes.

Acknowledgement—One of the authors (MRM) is thankful to the Council of Scientific and Industrial Research New Delhi 110 012 for the award of Pool Officership.

REFERENCES

1. A. Syamal and M. R. Maurya, *Coord. Chem. Rev.* 1989, **95**, 183.
2. S.-B. Yu and R. H. Holm, *Inorg. Chem.* 1989, **28**, 4385.
3. R. L. Dutta and A. K. Pal, *Ind. J. Chem.* 1985, **24A**, 76.
4. M. R. Maurya, S. Gopinathan, C. Gopinathan and R. C. Maurya, *Polyhedron* 1993, **12**, 159.
5. S. Sarkar and P. Subramanian, *Inorg. Chim. Acta* 1979, **35**, L 357.
6. M. F. Perpinan, L. Ballester, A. Stones, A. Monge, C. Ruiz-Valero and E. G. Puebla, *Polyhedron* 1987, **6**, 1523.
7. K. Nakamoto, *Infrared and Raman Spectra of Inorganic and Coordination Compounds*, 3rd edn, p. 232. John Wiley & Sons, New York (1978).
8. M. Minelli, J. L. Hubbard and J. H. Enemark, *Inorg. Chem.* 1984, **23**, 970.

Polyhedron Vol. 12, No. 9, pp. 1043–1046, 1993
Printed in Great Britain

0277–5387/93 $6.00+.00
© 1993 Pergamon Press Ltd

LANTHANIDE ION COMPLEXES OF A LIGAND DERIVED FROM SALICYLALDEHYDE AND MALONYL DIHYDRAZONE

LIANG YONGMIN, HUANG GUOSHENG and MA YONGXIANG†

Department of Chemistry, Lanzhou University, Lanzhou 730000, P.R.C.

and

ZHAO GANG

Department of Chemistry, Chengdu University of Science and Technology, Chengdu 610065, P.R.C.

(*Received* 4 *November* 1992; *accepted* 4 *January* 1993)

Abstract—The chelates $Na_2[Ln(C_{34}H_{28}N_8O_8)Cl]\cdot nH_2O$ of the malonyl dihydrazone of salicylaldehyde with the lanthanides have been prepared and characterized by elemental analysis, IR, UV, molar conductance and TGA. It is shown that the ligand coordinates to the central ion with one hydrazone unit in the keto form and one chloride ion participates in coordination to the metal ion. These chelates are 1 : 2 electrolytes in DMF and are more thermostable than their ligand due to the formation of chelate rings.

Since Sacconi[1] first reported the complexes of nickel (II) with dihydrazones a large number of transition metal complexes of acid dihydrazides have been studied.[2–4] However, no work has been performed on the complexes of the lanthanides with dihydrazones. In the present work the reaction of N-salicylidene derivatives of malonic dihydrazides (H_2L) with 11 lanthanide(III) chlorides in anhydrous ethanol in the presence of sodium hydroxide have been investigated, and the IR, UV, molar conductance and thermal analysis (TGA) of the complexes are discussed.

EXPERIMENTAL

All the solvents were dried by the reported method.[5] Lanthanide(III) chlorides were prepared from their oxides and hydrochloric acid. The ligand was prepared by the literature method.[6]

Preparation of the lanthanide chelates

H_2L (1 mmol) was dissolved in warm ethanol (25 cm^3) containing NaOH (2 mmol). This solution was added to the hydrated lanthanide(III) chloride (0.5 mmol) in anhydrous ethanol (20 cm^3). The mixture was refluxed for 2–3 h until the reaction was complete. The product was separated, washed with warm water, ethanol and diethyl ether, respectively, and dried *in vacuo*. Yields were 75%. Elemental analyses and some physical properties of the products obtained are listed in Table 1.

Measurements

The IR spectra were obtained with a Nicolet 5-DX spectrophotometer using KBr discs in the 4000–400 cm^{-1} region. UV spectra were recorded on a UV-240 spectrometer in the 190–600 nm region using a solution in DMF. Electrolytic conductivities were obtained using a DDS-II A molar conductometer and DMF as the solvent at room temperature. TGA analyses were carried out with a thermal analyser (Japan) between room temperature and 850°C in a nitrogen atmosphere.

RESULTS AND DISCUSSION

These chelates of malonyl dihydrazone of salicylaldehyde with lanthanide are insoluble in non-polar

† Author to whom correspondence should be addressed.

Table 1. Analytical and physical data of the compounds

Compound	Formula	Colour	Yield (%)	Decomposed temperature (°C)	Elemental analysis Found (Calc. %)[a] C	H	N
I	$(C_{17}H_{16}N_4O_4)$	White	88	242	60.2 (60.0)	4.7 (4.7)	16.5 (16.4)
II	$Na_2[LaL_2Cl]\cdot 3H_2O$	Yellow	87	321	42.7 (42.9)	3.7 (3.6)	11.8 (11.8)
III	$Na_2[PrL_2Cl]\cdot 3H_2O$	Yellow	89	312	43.0 (42.9)	3.2 (3.6)	11.4 (11.8)
IV	$Na_2[EuL_2Cl]\cdot 3H_2O$	Yellow	75	310	42.5 (42.4)	3.3 (3.6)	11.2 (11.6)
V	$Na_2[YL_2Cl]\cdot 3H_2O$	Pale yellow	81	286	45.6 (45.3)	3.9 (3.8)	12.2 (12.4)
VI	$Na_2[ErL_2Cl]\cdot H_2O$	Light yellow	78	284	43.6 (43.3)	3.3 (3.2)	11.4 (11.9)
VII	$Na_2[HoL_2Cl]\cdot 5H_2O$	Light red	85	264	40.5 (40.3)	3.7 (3.8)	10.6 (11.0)
VIII	$Na_2[TbL_2Cl]$	Pale red	91	286	44.8 (44.5)	3.4 (3.1)	11.9 (12.2)
IX	$Na_2[CeL_2Cl]\cdot 3H_2O$	Red–brown	84	276	43.1 (42.9)	3.3 (3.6)	11.4 (11.8)
X	$Na_2[LuL_2Cl]\cdot 2H_2O$	Pale yellow	89	264	42.3 (42.1)	3.3 (3.3)	11.4 (11.6)
XI	$Na_2[NdL_2Cl]\cdot 3H_2O$	Yellow	92	284	42.2 (42.7)	3.2 (3.6)	11.2 (11.7)
XII	$Na_2[DyL_2Cl]\cdot 3H_2O$	Yellow	78	285	42.6 (42.9)	3.3 (3.5)	11.2 (11.5)

[a] Calculated values are given in parentheses.

solvents, such as pentane and benzene, but soluble in DMF, warm methanol, warm ethanol and hot water. These chelates are hygroscopic. Their elemental analyses, molar conductance, IR and UV spectra and TGA measurements show that $LnCl_3\cdot nH_2O$ (Ln = lanthanide) forms chelates with the loss of two chloride ions and they conform to the formula $Ln(NaL)_2Cl\cdot nH_2O$.

Table 2. IR spectra of the ligand and its complexes

Compound	$\gamma(H_2O)$	γ(N—H)	Amide I γ(C=O)		γ(C=N)		γ(N—N)		γ(M—O)
H_2L	—	3283ms	1679vs		1602s		969m		—
II	3414vb	3206b	1673s[a]	1631s	1609s[a]	1546s	1011m	969w[a]	583m
III	3440vb	3240b	1673s	1627s	1608s	1546s	1011m	969w	583m
IV	3440vb	3220s	1673s	1630s	1609s	1546s	1009m	969w	589w
V	3380b	3282m	1673s	1633s	1609s	1567s	1012w	969w	596w
VI	3410b	3282m	1673s	1634s	1609s	1567s	1011w	969w	596w
VII	3472b	3171vb	1673s	1635s	1603s	1560s	1012m	963w	589m
VIII	—	3282s	1673s	1632s	1609s	1546s	1012w	969m	589m
IX	3418b	3220m	1673s	1634s	1609s	1546s	1011w	966w	589m
X	3427b	3282s	1679s	1635s	1616s	1547s	1012m	969m	596m
XI	3392b	3281s	1673s	1632s	1608s	1546s	1011m	968w	589m
XII	3417b	3282s	1673s	1630s	1609s	1547s	1011m	968w	584w

[a] Another hydrazone unit of the ligand which is uncoordinated to the central ions.
b = broad; m = medium; w = weak; s = strong.

Table 3. Molar conductivities and UV spectra of the ligand and its complexes in DMF at room temperature

Compound	Molar conductance (Ω^{-1} cm^2 mol^{-1})	UV absorption spectra λ (nm)		
		1	2	3
H_2L	—	280.0	322.0	
II	124.1	287.0	315.5	371.2
III	131.8	292.0	315.2	374.5
IV	139.8	289.0	315.5	371.5
V	169.2	286.3	315.8	370.8
VI	158.6	287.0	315.5	372.5
VII	122.8	292.5	315.6	376.5
VIII	117.4	287.3	318.5	372.5
IX	134.6	288.0	316.0	371.2
X	175.8	287.1	320.5	382.0
XI	125.4	286.0	315.0	377.0
XII	139.0	289.0	315.5	373.4

IR spectra

The IR spectra of the ligand and its complexes are shown in Table 2. The IR spectra of H_2L show bands at 3283, 1679, 1602, 969 and 2700–2800 cm^{-1}, assigned to ν(N—H), ν(C=O), ν(C=N), ν(N—N) and ν(O—H) (phenolic), respectively.[7] In contrast to the parent ligand the IR spectra of these complexes, $Ln(NaL)_2Cl\cdot nH_2O$, show two bands at *ca* 1673 and 1630 cm^{-1} due to uncoordinated and coordinated ν(C=O). In addition, the corresponding band of ν(C=N) appears at 1609 and 1560 cm^{-1} and that of ν(N—N) at 1011 and 969 cm^{-1}, respectively. The presence of both the free and coordinated ν(C=O), ν(C=N) and ν(N—N), and also a band due to ν(N—H) at *ca* 3250 cm^{-1}, suggests that only one of the hydrazone units is coordinated to the lanthanide(III) ion in the keto form.[4] A broad medium band in the region 2700–2800 cm^{-1} of the ligand, assigned to ν(O—H) of salicylaldehyde, disappeared in the complexes. This suggests that one of the hydrogens is replaced by a sodium ion and another by a lanthanide ion, which was confirmed by a new single band at 589 cm^{-1} due to ν(M—O).[8]

Electrolytic conductance

Dissolving the lanthanide chelates in DMF obtained a light yellow to red–brown solution. The molar conductances (Table 3) of these solutions

Table 4. TGA data of the ligand and its complexes

Compound	Temperature (°C)	Loss of groups	Loss of weight (%)[a]
H_2L	242.3(dec.)		
	254.2–271.2	$2HOC_6H_4CH{=}NNH$	78.10 (79.4)
	402.7–437.4	$—COCH_2CO—$	21.2 (20.6)
	Up to 850	No residue	
$Na_2[La(C_{34}H_{28}N_8O_8)Cl]\cdot 3H_2O$	84.3	$4H_2O$	7.3 (7.6)
	322.3–459.7	$—OC_6H_4—CH{=}NNH—COCh_2—C—ONH—$, Cl	48.5 (49.8)
	459.7–576.2	2-$C_6H_4—CH{=}N—$	20.6 (21.7)
	Up to 850	Residue, $\frac{1}{2}La_2O_3+Na_2O$	23.7 (23.6)
$Na_2[Pr(C_{34}H_{28}N_8O_8)Cl]\cdot 3H_2O$	86.1	$4H_2O$	7.95 (7.56)
	311.9–494.5	$—OC_6H_4—CH{=}NNHCOCH_2CO—NH—$, Cl	49.36 (49.72)
	494.5–541.5	2-$C_6H_4—CH{=}N—$	20.08 (21.63)
	Up to 850	Residue, $\frac{1}{2}Pr_2O_3+Na_2O$	23.95 (23.80)

[a] Calculated values are given in parentheses.

approach those reported for 1:2 electrolytes,[9] showing that the chloride ion participates in coordination. The complexes are, therefore, formulated as $Na_2[Ln(C_{34}H_{28}N_8O_8)Cl]\cdot nH_2O$.

UV spectra

Important bands in the UV spectra of the ligand and its complexes in DMF are shown in Table 3. It can be seen that the K absorption band ($\pi \rightarrow \pi^*$ transition) of the ligand appears at 280 nm, but is shifted to a longer wavelength by 6–12 nm in the complexes. This may be attributed to the interaction between ligands and metal ions when complexing. The absorption band at 322 nm in the ligand is shifted to a lower wavelength, 315–321 nm, after chelating, which can be assignable to the $\pi \rightarrow \pi^*$ transition on azomethine. This indicates that in the complexes the nitrogen in the imino group participated in coordination to the metal ion. In addition, there is a new broad band at *ca* 372 nm, which is due to the ligand–metal charge-transfer band.[3]

Thermal analysis

The thermal analysis data of the ligand and its complexes are listed in Table 4; thermal analyses shows that the ligand decomposes exothermically at 242.3–271.2°C and loses *ca* 78.1% of its weight. Perhaps this is due to two $HOC_6H_4CH{=}NNH$— groups breaking away from the molecule. The exothermic peak at 427.4°C is due to the loss of another part of the molecule. The decomposition of the ligand is complete and there is no residue. The thermal analysis diagrams of all complexes are different from that of the ligand. The diagram of $Na_2[PrL_2Cl]\cdot 3H_2O$ shows that it loses water at 86.1°C, but the water content is more than that resulting from the elemental analysis which can be due to their hygroscopic properties. Two $-OC_6H_4CH{=}NNHCOCH_2CONH-$ groups and two $-C_6H_4CH{=}N-$ groups are then released at 311.9–494.5°C and 494.5–541.5°C, respectively. It seems the molecules of the chelates are thermally more stable than its ligand.

These results show that the ligand has the following structure:

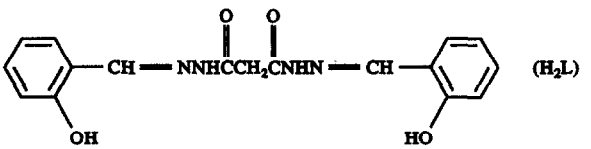

(H_2L)

and forms the complexes with some lanthanide ions, $Na_2[LnL_2Cl]\cdot nH_2O$.

Acknowledgement—This research has been supported by the National Science Foundation of China.

REFERENCES

1. L. Sacconi, *J. Chem. Soc.* 1954, 1326.
2. R. A. Lal and N. Kailash, *Synth. React. Inorg. Met.-Org. Chem.* 1988, **18**, 837.
3. G. H. Havanur, V. K. Revenkar and V. B. Mahale, *Ind. J. Chem.* 1988, **27A**, 803.
4. M. F. Iskander, I. El. Sayed, A. F. M. Hefry and S. E. Zayan, *J. Inorg. Nucl. Chem.* 1976, **38**, 2209.
5. A. I. Vogel, *A Text Book of Organic Chemistry*. Longmans, London (1974).
6. J. J. Blanksma and H. A. Bakels, *Rec. Trav. Chim.* 1939, **58**, 497.
7. M. Mashima, *Bull. Chem. Soc. Japan* 1962, **35**, 1882; 1962, **35**, 202; 1963, **36**, 210.
8. C. Natarajan and P. Tharmaraj, *Synth. React. Inorg. Met.-Org. Chem.* 1990, **20**, 151.
9. W. J. Geary, *Coord. Chem. Rev.* 1971, **71**, 81.

Polyhedron Vol. 12, No. 9, pp. 1047–1053, 1993
Printed in Great Britain

0277–5387/93 $6.00+.00
© 1993 Pergamon Press Ltd

REACTIVITY OF P_2N_2 AND $P_2N_2H_4$ TOWARDS $C_7H_8M(CO)_4$ (M = Cr, Mo). X-RAY STRUCTURE OF *FAC*-$(CO)_3Mo[PN_2P(O)]$

WAI-KWOK WONG*

Department of Chemistry, Hong Kong Baptist College, Kowloon, Hong Kong

and

JING-XING GAO

Department of Chemistry, Xiamen University, Xiamen 361005, Fujian, P.R.C.

and

WING-TAK WONG*

Department of Chemistry, The University of Hong Kong, Pokfulam Road, Hong Kong

(*Received* 10 *November* 1992; *accepted* 18 *December* 1992)

Abstract—The interaction of $C_7H_8M(CO)_4$ (M = Cr, Mo) with half an equivalent of P_2N_2 (P_2N_2 = N,N′-bis[*o*-(diphenylphosphino)benzylidene]ethylenediamine) in THF at ambient temperature gives [*cis*-$(CO)_4M]_2(P_2N_2)$ (**I**, M = Cr; **II**, M = Mo) in high yield. The interaction of $C_7H_8M(CO)_4$ with 1 equivalent of P_2N_2 in refluxed THF gives [*cis*-$(CO)_4M]_2(P_2N_2)$, *fac*-$(CO)_3M(PN_2P)$ (**III**, M = Cr; **IV**, M = Mo) and *fac*-$(CO)_3M[PN_2P(O)]$ (**V**, M = Mo). The yield of the products depends on the length of the reaction time. For a short reaction time the major product is [*cis*-$(CO)_4M]_2(P_2N_2)$, whereas for a long reaction time *fac*-$(CO)_3M(PN_2P)$ is the major product. However, the interaction of $C_7H_8Cr(CO)_4$ with 1 equivalent of $P_2N_2H_4$ ($P_2N_2H_4$ = N,N′-bis[*o*-(diphenylphosphino)benzyl]ethylenediamine) in refluxed THF produces [*cis*-$(CO)_4Cr]_2(P_2N_2H_4)$ (**VI**) as the only isolated product in high yield. Prolonged refluxing of [*cis*-$(CO)_4M]_2(P_2N_2)$ with P_2N_2 in THF does not give *fac*-$(CO)_3M(PN_2P)$. In solution **IV** slowly oxidizes to **V**, whose structure has been determined by X-ray crystallography.

The potential of polydentate ligands having both soft and hard base donor atoms as good bridging ligands for the preparation of heterobimetallic complexes containing an oxophilic metal and a late transition metal has led to extensive studies on the synthesis and reactivities of polydentate ligands containing both phosphine and nitrogen donor groups.[1–3] N-N′-bis[*o*-(diphenylphosphino)benzylidene]ethylenediamine (P_2N_2), a tetradentate ligand containing both imino and phosphino groups, has been synthesized for some time; however, its reactivity towards transition metals has only been briefly explored.[4] We are interested in examining whether transition metals of low oxidation state will preferentially interact with the phosphino groups of the P_2N_2 ligand, leaving the imino groups uncoordinated. Recently, we have briefly described the interaction of P_2N_2 with $C_7H_8Cr(CO)_4$, which gave the centrosymmetric dimeric species [*cis*-$(CO)_4Cr]_2(P_2N_2)$ in high yield.[5] In this paper we report the detailed study of the reactivity of P_2N_2 towards $C_7H_8M(CO)_4$ (M = Cr, Mo) and the X-ray diffraction analysis of the complex *fac*-$(CO)_3Mo[PN_2P(O)]$.

* Authors to whom correspondence should be addressed.

RESULTS AND DISCUSSION

Preparation of $[cis\text{-}(CO)_4M]_2(P_2N_2)$ (M = Cr, Mo)

(1) M = Cr (**I**). When $C_7H_8Cr(CO)_4$ was treated with half an equivalent of P_2N_2 in THF at ambient temperature for 16 h dark orange crystals of stoichiometry $[(CO)_4Cr]_2(P_2N_2)$ (**I**) were isolated in high yield (90%). The IR spectrum (KBr) of **I** exhibits three absorptions at 1996m, 1876vs and 1832s cm^{-1}. The absorption pattern is indicative of a *cis* configuration for the four terminal carbonyl groups of the two $Cr(CO)_4$ moieties. The $^{31}P\{^1H\}$ NMR spectrum of **I** exhibits only a singlet at δ50.3 ppm. This suggests that the two phosphorus centres of the P_2N_2 ligand were coordinated and equivalent. The ^1H NMR spectrum of **I** exhibits a broad singlet, a broad multiplet and a singlet of relative intensity 1/14/2 at δ8.26, 7.45 and 4.04 ppm, respectively. The spectroscopic data suggest that the dimeric species should be symmetrical and that an imino group and a phosphino group of the P_2N_2 ligand should be coordinated to each individual $Cr(CO)_4$ moiety. This is confirmed by an X-ray diffraction study[5] which shows that the P_2N_2 ligand acts as a bidentate ligand with an imino group and a phosphino group coordinated to each of the two $Cr(CO)_4$ moieties, which adopt a *cis* configuration for the four terminal carbonyl groups, and the dimeric species has a centro-symmetrical structure (**A**).

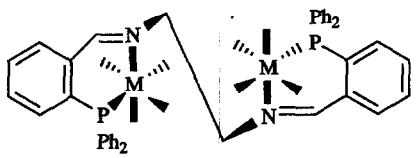

A

(2) M = Mo (**II**). Similar to chromium orange crystals of stoichiometry $[(CO)_4Mo]_2(P_2N_2)$ (**II**) were isolated in high yield (90%) when $C_7H_8Mo(CO)_4$ was treated with half an equivalent of P_2N_2 in THF at ambient temperature for 16 h. The IR spectrum (KBr) of **II** exhibits three absorptions at 2000m, 1878vs and 1838s cm^{-1}. The absorption pattern is indicative of a *cis* configuration for the four terminal carbonyl groups of the two $Mo(CO)_4$ moieties. The $^{31}P\{^1H\}$ NMR spectrum of **II** exhibits only a singlet at δ32.5 ppm. This suggests that the two phosphorus centres of the P_2N_2 ligand were coordinated and equivalent. The ^1H NMR spectrum of **II** exhibits a broad singlet, a broad multiplet and a singlet of relative intensities 1/14/2 at δ8.15, 7.49 and 4.13 ppm, respectively. The spectroscopic data of **II** are very similr to **I**. This suggest that the structure of **II** is similar to that of **I** and thus, structure **A** is assigned to **II**.

Compound **II** can also be prepared in good yield (72%) by the interaction of $(CO)_3Mo(CH_3CN)_3$ with 1 equivalent of P_2N_2 in THF at ambient temperature for 4–5 h.

Interaction of $C_7H_8M(CO)_4$ *with* 1 *equivalent of* P_2N_2

(1) M = Cr. When $C_7H_8Cr(CO)_4$ was treated with 1 equivalent of P_2N_2 in refluxing THF **I** and dark red crystals of stoichiometry $[(CO)_3Cr](PN_2P)$ (**III**) were isolated. The yields of **I** and **III** depended on the length of the reaction time. When refluxed for 4 h **I** and **III** were isolated in 86 and 5% yields, respectively. However, when the reaction was refluxed for 16 h **I** and **III** were isolated in 12 and 76% yields, respectively. The $^{31}P\{^1H\}$ NMR spectrum of **III** exhibits two singlets of relative intensities 1/1 at δ49.5 and -17.0 ppm, respectively. The resonance at δ49.5 ppm corresponds to a coordinated phosphorus and the resonance at $\delta -17.0$ ppm corresponds to an uncoordinated phosphorus. This suggests that the P_2N_2 ligand acts as a tridentate ligand with one of its phosphino groups remaining uncoordinated. This is further supported by the ^1H NMR spectrum which exhibits a broad singlet at δ9.3 ppm, which corresponds to the proton of the uncoordinated benzylidene, and a broad multiplet at δ8.4 ppm, which corresponds to the proton of the coordinated benzylidene. There are two possible structures for **III**. These are the *fac* and *mer* isomers as shown below.

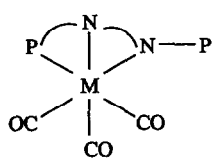

fac
B

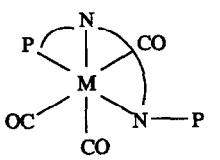

mer
C

The IR spectrum (KBr) of **III** exhibits two absorptions at 1900s and 1780vs cm^{-1}, which is indicative of a *fac* configuration for the three terminal carbonyl groups.[6] Thus, structure **B**, the *fac* isomer, is assigned to **III**.

(2) M = Mo. Similar to chromium **II** and dark red crystals of stoichiometry $[(CO)_3Mo](PN_2P)$ (**IV**) and $[(CO)_3Mo][PN_2P(O)]$ (**V**) were isolated when $C_7H_8Mo(CO)_4$ was treated with 1 equivalent of P_2N_2 in refluxing THF. The yields of **II**, **IV** and **V** depended on the length of the reaction time. When refluxed for 4 h **II** and **IV** were the products isolated in 85 and 5% yields, respectively. However, when the reaction was refluxed for 24 h **II**, **IV** and **V** were isolated in 13, 45 and 15% yields, respectively. The $^{31}P\{^1H\}$ NMR spectrum of **IV** exhibits

two singlets of relative intensities 1/1 at δ34.1 and -17.4 ppm, respectively. The resonance at δ34.1 ppm corresponds to a coordinated phosphorus and the resonance at $\delta-17.4$ ppm corresponds to an uncoordinated phosphorus. This suggests that the P_2N_2 ligand acts as a tridentate ligand with one of its phosphino groups remaining uncoordinated. This is further supported by the ^1H NMR spectrum which exhibits a broad singlet at δ9.5 ppm, which corresponds to the proton of the uncoordinated benzylidene, and a broad multiplet at δ8.5 ppm which corresponds to the proton of the coordinated benzylidene. The IR spectrum (KBr) of **IV** exhibits two absorptions at 1902s and 1778vs cm^{-1}, which is indicative of a *fac* configuration for the three terminal carbonyl groups. Thus, structure **B** is assigned to **IV** as well.

The IR spectrum (KBr) of **V** exhibits two absorptions at 1902s and 1778vs cm^{-1}, which is indicative of a *fac* configuration for the three terminal carbonyl groups. The $^{31}P\{^1H\}$ NMR spectrum exhibits two singlets of relative intensities 1/1 at δ33.3 and 31.9 ppm, respectively. The chemical shift of the resonance at δ33.3 ppm corresponds to that of coordinated phosphorus as in **II** and **IV**, and the resonance at δ31.9 ppm corresponds to that of phosphine oxides.[7] This suggests that the uncoordinated phosphorus of **IV** has been oxidized to phosphine oxide. Thus, based on the spectroscopic data, structure **D** is assigned to **V**.

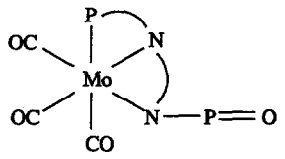

D

The structure of **V** was confirmed by X-ray crystallography. Crystals suitable for the diffraction study were grown from a mixture of CH_2Cl_2/hexane. The structure consists of two independent but structurally very similar molecules of **V** and a partially occupying molecule of dichloromethane, all separated by normal van der Waals distances. There are only small conformational differences between the two chelated ring systems. A perspective drawing of **V** is shown in Fig. 1. Selected bond lengths and angles are listed in Table 1. The structure can be described as a distorted octahedral with the three carbonyl groups in a *fac* configuration and the uncoordinated phosphine oxidized to the corresponding phosphine oxide.

In solution **IV** was slowly oxidized to **V** when exposed to air. The oxidation process is conveniently monitored by $^{31}P\{^1H\}$ NMR spectroscopy. $^{31}P\{^1H\}$ NMR study shows that **IV**, when dissolved in an undeaerated solution of $CDCl_3$, decomposed completely within 6 h to give a complex mixture from which the oxidized product **V** was observed in 30% yield. Unlike **IV** the chromium analogue (**III**) did not undergo oxidation as readily as **IV**. In a similar study **III** was found to be unchanged after leaving it in an undeaerated solution of $CDCl_3$ for 48 h.

Attempts to synthesize *fac*-$(CO)_3M(P_2N_2)$ via the interaction of $(CO)_3M(CH_3CN)_3$ with 1 equivalent of P_2N_2 were unsuccessful. The interaction of $(CO)_3M(CH_3CN)_3$ with 1 equivalent of P_2N_2 gave [*cis*-$(CO)_4M]_2(P_2N_2)$ as the only isolated product in 75% yield.

Interaction of [cis-$(CO)_4M]_2(P_2N_2)$ *with* P_2N_2 (M = Cr, Mo)

Attempts to synthesize *fac*-$(CO)_3M(P_2N_2)$ from the dimeric species [*cis*-$(CO)_4M](P_2N_2)$ were unsuccessful. When [*cis*-$(CO)_4M]_2(P_2N_2)$ (**I**, M = Cr; **II**, M = Mo) was treated with excess P_2N_2 in refluxed THF for 24 h [*cis*-$(CO)_4M](P_2N_2)$ was recovered almost quantitatively. The formation of *fac*-$(CO)_3M(P_2N_2)$ was not observed. This suggests that the formation of *fac*-$(CO)_3M(P_2N_2)$ is not derived

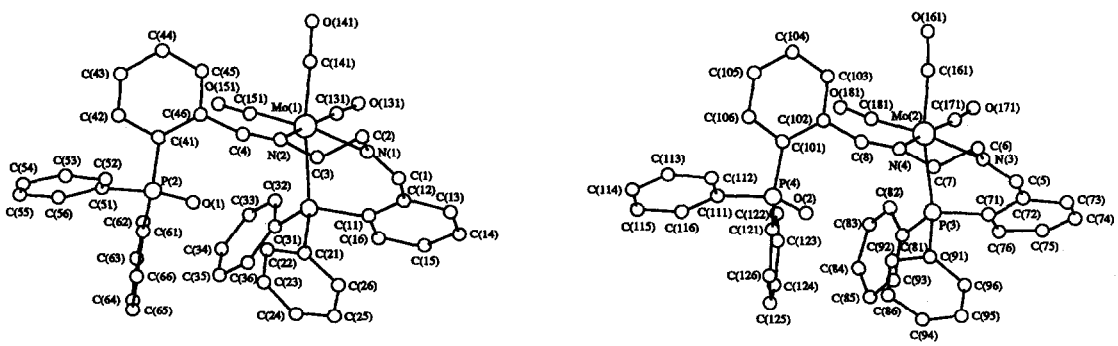

Fig. 1. A perspective view of the molecular structure of **V**. Both independent molecules are shown.

Table 1. Selected bond lengths (Å) and angles (°) for **V**. The values for the second molecules are in square brackets

Mo(1)—P(1)	2.485(3)	[2.512(3)]
Mo(1)—N(1)	2.247(3)	[2.254(3)]
Mo(1)—N(2)	2.325(7)	[2.306(8)]
Mo(1)—C(131)	1.92(2)	[1.95(2)]
Mo(1)—C(141)	1.96(2)	[1.96(2)]
Mo(1)—C(151)	1.94(2)	[1.93(2)]
P(2)—O(1)	1.484(9)	[1.473(8)]
C(1)—N(1)	1.26(1)	[1.26(1)]
C(2)—N(1)	1.47(1)	[1.48(1)]
C(2)—C(3)	1.52(1)	[1.54(1)]
C(3)—N(2)	1.48(1)	[1.48(1)]
C(4)—N(2)	1.27(1)	[1.28(1)]
P(1)—Mo(1)—N(1)	78.4(3)	[76.5(2)]
P(1)—Mo(1)—N(2)	97.8(2)	[96.9(2)]
P(1)—Mo(1)—C(131)	85.5(3)	[85.2(3)]
P(1)—Mo(1)—C(141)	169.1(3)	[169.2(3)]
P(1)—Mo(1)—C(151)	95.3(3)	[98.5(4)]
N(1)—Mo(1)—N(2)	74.6(3)	[74.6(3)]
N(1)—Mo(1)—C(131)	95.4(3)	[97.6(4)]
N(1)—Mo(1)—C(141)	100.0(4)	[100.7(3)]
N(1)—Mo(1)—C(151)	172.7(4)	[173.7(3)]
N(2)—Mo(1)—C(131)	168.5(4)	[171.1(4)]
N(2)—Mo(1)—C(141)	92.3(4)	[92.3(3)]
N(2)—Mo(1)—C(151)	103.1(4)	[102.5(3)]
C(131)—Mo(1)—C(141)	83.8(4)	[84.8(4)]
C(131)—Mo(1)—C(151)	87.6(4)	[85.8(4)]
C(141)—Mo(1)—C(151)	86.9(4)	[85.0(4)]
O(1)—P(2)—C(41)	112.8(5)	[113.0(4)]
O(1)—P(2)—C(51)	111.4(5)	[113.2(5)]
O(1)—P(2)—C(61)	113.5(5)	[112.2(5)]
C(41)—P(2)—C(51)	106.7(5)	[103.6(5)]
C(41)—P(2)—C(61)	106.5(5)	[107.8(5)]
C(51)—P(2)—C(61)	105.2(6)	[106.4(5)]

from [*cis*-$(CO)_4M](P_2N_2)$. The origin of the formation of the monomeric species *fac*-$(CO)_3M(P_2N_2)$ is still unknown.

Preparation of [cis-$(CO)_4Cr]_2(P_2N_2H_4)$ **(VI)**

When $C_7H_8Cr(CO)_4$ was treated with 1 equivalent of $P_2N_2H_4$ in refluxed THF overnight yellow crystals of stoichiometry $[(CO)_4Cr]_2(P_2N_2H_4)$ **(VI)** were isolated in good yield (78%). Compound **VI** exhibits three absorptions at 1992w, 1856s and 1832vs cm^{-1} in the IR spectrum (KBr), indicative of a *cis* configuration for the four terminal carbonyl groups and a singlet at δ43.2 ppm in the $^{31}P\{^1H\}$ NMR spectrum, indicating that the two phosphorus atoms of the $P_2N_2H_4$ ligand are coordinated and equivalent. The absorption pattern of the IR and $^{31}P\{^1H\}$ spectra of **VI** is very similar to that of **I**, indicating that **I** and **VI** have similar structures. Thus, based on the above spectroscopic data, structure **E**, shown below, is assigned to **VI**.

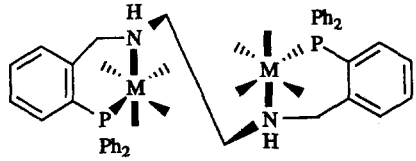

E

EXPERIMENTAL

Microanalysis were performed by the Shanghai Institute of Organic Chemistry, Chinese Academy of Sciences, China. IR spectra (KBr pellets) were recorded on a Hitachi 270-30 IR spectrometer; data are given in cm^{-1}. NMR spectra were recorded on a JEOL FX90Q spectrometer. Chemical shifts of ^1H NMR spectra were referenced to internal deuterated solvents and then recalculated to TMS = δ0.0 ppm. ^{31}P NMR spectra were referenced to external 85% H_3PO_4.

All operations were performed under nitrogen or *in vacuo*. All chemicals used were of reagent grade. Solvents were dried by standard procedures, distilled and deaerated prior to use. Melting points were taken in sealed capillaries and are uncorrected.

$C_7H_8Cr(CO)_4$,[8] $C_7H_8Mo(CO)_4$,[8] $Mo(CO)_3(CH_3CN)_3$,[8] P_2N_2[4] and $P_2N_2H_4$[4] were prepared according to literature methods. ^1H and $^{31}P\{^1H\}$ NMR data are given in Table 2.

Preparation of [cis-$(CO)_4M](P_2N_2)$ (M = Cr, Mo)

(1) M = Cr **(I)**. A solution of $C_7H_8Cr(CO)_4$ (0.13 g, 0.5 mmol) and P_2N_2 (0.15 g, 0.25 mmol) in THF (15 cm^3) was stirred at room temperature for 16 h. A deep red colour solution was obtained. The solvent was removed *in vacuo* to give a dark red residue. The residue was redissolved in a minimum amount of CH_2Cl_2 and chromatographed on a silica gel column (2 × 15 cm) using CH_2Cl_2 as an eluant. The orange–red band obtained was concentrated to *ca* 5 cm^3 and then diethyl ether was added until the solution turned cloudy. The CH_2Cl_2/diethyl ether mixture was then cooled to −20°C to give orange–red crystals, which were filtered and dried *in vacuo*. Yield: 0.21 g, 90%; m.p. 192–195°C (decomposed). Found: C, 60.1; H, 3.3; N, 2.9. Calc. for $C_{48}H_{34}O_8N_2P_2Cr_2 \cdot \frac{1}{2}CH_2Cl_2$: C, 59.7; H, 3.6; N, 2.9%. IR (KBr): ν(CO): 1996m, 1876vs, 1832s cm^{-1}.

(2) M = Mo **(II)**. The procedure was similar to that of **I**, except $C_7H_8Mo(CO)_4$ (0.15 g, 0.5 mmol) and P_2N_2 (0.15 g, 0.25 mmol) were used. An orange

Table 2. ^1H and $^{31}P\{^1H\}$ NMR data

Compound	^1H[a]	Assignment	^{31}P[b]	Assignment
I	8.26br, s(2)	N=C*H*—	50.3s	P_2N_2
	7.45m(28)	Phenyl		
	4.04s(4)	$N(CH_2)_2N$		
II	8.11br, s(2)	N=C*H*—	32.4s	P_2N_2
	7.45m(28)	Phenyl		
	4.09s(4)	$N(CH_2)_2N$		
III	9.20br, s(1)	N=C*H*— of P[c]	49.4s	PN_2P^c
	8.33br, m(1)	N=C*H*— of P	−17.0s	PN_2P^c
	6.60–7.45br, m(28)	Phenyl		
	4.23br, m(1)			
	3.52br, m(2)	$N(CH_2)_2N$		
	2.40br, m(1)			
IV	9.15br, s(1)	N=C*H*— of P[c]	34.1s	PN_2P^c
	8.23br, s(1)	N=C*H*— of P	−17.3	PN_2P^c
	6.62–7.60br, m(28)	Phenyl		
	4.18br, m(1)			
	3.55br, m(2)			
	2.58br, m(1)			
V	9.47br, s(1)	N=C*H*— of P(O)	33.3s	$PN_2P(O)$
	8.23br, s(1)	N=C*H*— of P	31.9s	$PN_2P(O)$
	6.62–7.56br, m(28)	Phenyl		
	4.18br, m(1)			
	3.55br, m(2)	$N(H_2)_2N$		
	2.58br, m(1)			
IV	7.47br, m(28)	Phenyl	43.2s	$P_2N_2H_4$
	3.76br, m(4)	$N(CH_2)_2N$		
	2.82br, m(4)	$PhCH_2N$		
	1.86br, m(2)	N*H*		

[a] In $CDCl_3$ at 30°C, referenced to Me_4Si (δ0.00).

[b] In $CDCl_3$ at 30°C, referenced to external 85% H_3PO_4 (δ0.00), negative for upfield shift.

Abbreviations: s, singlet; m, multiplet; br, broad.

[c] Uncoordinated phosphorus.

band was obtained using CH_2Cl_2 as an eluant. Orange crystals were obtained from a mixture of CH_2Cl_2/diethyl ether. Yield: 0.23 g, 90%; m.p. 203–206°C (decomposed). Found: C, 49.1; H, 3.1; N, 2.3. Calc. for $C_{48}H_{34}O_8N_2P_2Mo_2 \cdot 2CH_2Cl_2$: C, 50.4; H, 3.2; N, 2.4%. IR (KBr): ν(CO): 2000m, 1878vs, 1838vs cm^{-1}.

Interaction of $C_7H_8M(CO)_4$ *with* 1 *equivalent of* P_2N_2

(1) M = Cr. A solution of $C_7H_8Cr(CO)_4$ (0.13 g, 0.5 mmol) and P_2N_2 (0.32 g, 0.53 mmol) in THF (15 cm^3) was refluxed for 16 h. A violet–red coloured solution was obtained. The solvent was removed *in vacuo* to give a dark purple residue. The residue was redissolved in a minimum amount of CH_2Cl_2 and chromatographed on a silica gel column (2 × 15 cm). An orange–red band and a violet–red band were obtained when the column was eluted with CH_2Cl_2 and CH_2Cl_2/acetone (1 : 1) solutions, respectively. Work-up of the orange–red band gave orange–red crystals, which were identical to the dimeric species **I**. Yield: 0.03 g, 12%. The violet–red band was evaporated to dryness *in vacuo* and redissolved in *ca* 5 cm^3 of CH_2Cl_2. Diethyl ether was added slowly to the CH_2Cl_2 solution until it turned cloudy. The CH_2Cl_2/diethyl ether mixture was then cooled to −20°C to give violet–red crystals of stoichiometry $(CO)_3Cr(P_2N_2) \cdot H_2O$ (**III**). Yield: 0.28 g, 76%; m.p. 175–178°C (decomposed). Found: C, 67.9; H, 4.9; N, 3.6. Calc. for $C_{43}H_{34}O_3N_2P_2Cr \cdot H_2O$: C, 68.1; H, 4.8; N, 3.7%. IR (KBr): ν(CO): 1900s, 1780vs cm^{-1}.

When a solution of $C_7H_8Cr(CO)_4$ (0.13 g, 0.5 mmol) and P_2N_2 (0.32 g, 0.53 mmol) in THF (15 cm^3) was refluxed for 4 h, work-up of the solution following the above procedure gave **I** and **III** in

86% (0.22 g) and 5% (0.02 g) yields, respectively.

(2) M = Mo. A solution of $C_7H_8Mo(CO)_4$ (0.09 g, 0.3 mmol) and P_2N_2 (0.19 g, 0.3 mmol) in THF (15 cm^3) was refluxed for 16 h. A deep red solution was obtained. The solvent was removed *in vacuo* to give a dark red residue. The residue was redissolved in a minimum amount of CH_2Cl_2 and chromatographed on a silica gel column (2 × 15 cm). An orange band and a deep red band were obtained when the column was eluted with CH_2Cl_2 and acetone solution, respectively. Work-up of the orange band gave orange crystals, whose IR, ^1H and $^{31}P\{^1H\}$ spectra were identical to that of **II**. Yield: 0.02 g, 13%. Removal of the solvent from the deep red band gave a deep red residue, which was redissolved in *ca* 5 cm^3 of CH_2Cl_2. Diethyl ether was added to the CH_2Cl_2 solution slowly until it turned cloudy. The CH_2Cl_2/diethyl ether mixture was then cooled to −20°C to give 0.15 g deep red crystals. The $^{31}P\{^1H\}$ NMR spectrum of the red crystals indicated that they were a 3:1 mixture of $(CO)_3Mo(P_2N_2)\cdot H_2O$ (**IV**) and $(CO)_3Mo[PN_2P(O)]\cdot \frac{1}{2}CH_2Cl_2$ (**V**). Recrystallization of the crude mixture in CH_2Cl_2/diethyl ether solution gave **V** first then **IV**. Yield of **IV** (based on the $^{31}P\{^{31}H\}$ spectrum of the crude mixture): 0.11 g, 45%; m.p. 173–176°C (decomposed). Found: C, 64.2; H, 4.4; N, 3.4. Calc. for $C_{43}H_{34}O_3N_2P_2Mo\cdot H_2O$: C, 64.3; H, 4.5; N, 3.5%. IR (KBr): ν(CO): 1900s, 1780vs cm^{-1}. Yield of **V** (based on $^{31}P\{^1H\}$ spectrum of the crude mixture): 0.04 g, 15%; m.p. 180–184°C (decomposed). Found: C, 61.7; H, 4.4; N, 3.2. Calc. for $C_{43}H_{34}O_4N_2P_2Mo\cdot \frac{1}{2}CH_2Cl_2$: C, 62.0; H, 4.2; N, 3.3%. IR (KBr): ν(CO): 1900s, 1780vs cm^{-1}.

Preparation of $[cis\text{-}(CO)_4Cr]_2(P_2N_2)$ **(VI)**

A solution of $C_7H_8Cr(CO)_4$ (0.26 g, 1.0 mmol) and P_2N_2 (0.64 g, 1.06 mmol) in THF (20 cm^3) was refluxed for 20 h. A yellow solid precipitate was obtained. The precipitate was filtered, washed with hexane (2 × 10 cm^3) and redissolved in CH_2Cl_2 (20 cm^3) to give a yellow solution. Hexane was added slowly to the CH_2Cl_2 solution until it turned cloudy. The CH_2Cl_2/hexane mixture was then cooled to −20°C to give yellow crystals of stoichiometry $[(CO)_4Cr]_2(P_2N_2)$ (**VI**). Yield: 0.36 g, 77%; m.p. 207–210°C (decomposed). Found: C, 61.4; H, 4.3; N, 2.8. Calc. for $C_{48}H_{38}O_8N_2P_2Cr_2$: C, 61.5; H, 4.1; N, 3.0%. IR (KBr): ν(CO): 1992w, 1856s, 1832vs cm^{-1}.

Interaction of **I** *with* P_2N_2

A solution of **I** (0.1 g, 0.1 mmol) and P_2N_2 (0.08 g, 0.13 mmol) was stirred and refluxed in THF (15 cm^3) for 20 h. The resultant solution was evaporated to dryness, redissolved in a minimum amount of CH_2Cl_2 and chromatographed on a silica gel column (2 × 15 cm). An orange–red band was obtained using CH_2Cl_2 as an eluant. No other colour band was obtained. Removal of the solvent from the orange–red band gave an orange–red residue, whose IR spectrum was identical to that of **I**.

Interaction of $(CO)_3Mo(CH_3CN)_3$ *with* P_2N_2

A solution of $(CO)_3Mo(CH_3CN)_3$ (0.23 g, 0.76 mmol) and P_2N_2 (0.46 g, 0.76 mmol) in THF (15 cm^{-1}) was stirred at room temperature for 4 h. A red solution was obtained. The solution was evaporated to dryness *in vacuo*, redissolved in a minimum amount of CH_2Cl_2 and chromatographed on a silica gel column (2 × 15 cm) using CH_2Cl_2 as an eluant. The orange band obtained was concentrated to *ca* 5 cm^3 and then diethyl ether was added until the solution turned cloudy. The CH_2Cl_2/diethyl ether mixture was then cooled to −20°C to give orange crystals, whose IR spectrum was identical to that of **II**. Yield: 0.29 g, 75%.

X-ray diffraction studies

Crystals of **V** suitable for X-ray diffraction study were grown from CH_2Cl_2/n-hexane as a solvate of stoichiometry $\mathbf{V}\cdot\frac{1}{4}CH_2Cl_2$. A dark red crystal of dimensions 0.17 × 0.22 × 0.25 mm^3 was mounted on a glass fibre with an epoxy resin. Intensity data were collected on an Enraf–Nonius CAD-4 diffractometer at room temperature, using graphite monochromated Mo-K_α radiation (λ = 0.71073 Å). 11,385 reflections ($2\theta \leqslant 45°$) were measured; 10,993 were unique, R_{int} = 0.024, and of these 7406 had $I \geqslant 3\sigma(I)$ and were considered to be observed. The data were collected for Lorentz and polarization factors, but no absorption correction was applied. Crystal data, data collection parameters and results of the analysis are given in Table 3. The structure was solved by a combination of Patterson and direct methods (DIRDIF).[9] Two crystallographic independent molecules of **V** and a partially occupying solvent molecule of CH_2Cl_2 were located in the asymmetric unit. All non-carbon, non-hydrogen atoms, except for the solvent molecule, were refined anisotropically. The hydrogen atoms were generated in their idealized positions (C—H bond fixed at 0.96 Å) and included in structure-factor calculations, but not in refinement. Refinement was by full-matrix least-squares. All calculations were carried out on a MicroVAC-II computer using the Enraf–Nonius SDP program.[10] Final atomic coordinates, thermal parameters and structure factors

Table 3. Data collection and processing parameters

Molecular formula	$[Mo(C_{40}H_{34}N_2OP_2)(CO)_3]\cdot 0.25CH_2Cl_2$
Molecular weight	821.89
Colour and habit	Dark red block
Unit cell parameters	
a (A°)	18.689(4)
b (A°)	21.935(4)
c (A°)	19.954(8)
V (A°)	8170(2)
β (°)	92.65(2)
Z	8
Density (calc.) (g cm^{-3})	1.336
Space group	$P2_1/c$ (No. 14)
Radiation	Graphite-monochromatized Mo-K_α, $\lambda = 0.71073$ Å
Absorption coefficient (cm^{-1})	4.3
Crystal size (mm^3)	$0.17\times0.22\times0.25$
Scan type and rate (° min^{-1})	ω–2θ; 1.08–8.24
Scan range	$0.50+0.34\tan\theta$
Collection range	$h, k, \pm1$; $2\theta_{max} = 45°$
Unique data measured	10,993
Observed data with $I \geqslant 3\sigma(I)$, n	7406
Number of variables, p	507
$R = \Sigma\|\|F_o\|-\|F_c\|\|/\Sigma\|F_o\|$	0.065
$R_w = [\Sigma(\|F_o\|-\|F_c\|)^2/\Sigma w\|F_o\|^2]^{1/2}$	0.084
Weighting scheme	$w = 1/\{1+[(F_o-23.8)/111.9]^2\}$
$S = [\Sigma w(\|F_o\|-\|F_c\|)^2/(n-p)]^{1/2}$	3.287
Residual extrema in final difference map (e Å^{-3})	+1.70 to −0.66

have been deposited with the Editor as supplementary data. Atomic coordinates have also been deposited with the Cambridge Crystallography Data Centre.

Acknowledgements—W.-K. W. thanks the Hong Kong Baptist College and the UPGC (Hong Kong) for financial support. W.-T. W. thanks the Hong Kong Research Grant Council and the University of Hong Kong for financial support.

REFERENCES

1. J. Powell, A. Kuksis, C. J. May, P. E. Meindl and S. J. Smith, *Organometallics* 1989, **8**, 2933.
2. L. Wei, A. Bell, K.-H. Ahn, M. M. Holl, S. Warner, I. D. Williams and S. L. Lippard, *Inorg. Chem.* 1990, **29**, 825.
3. A. Balch, F. Neve and M. M. Olmstead, *J. Am. Chem. Soc.* 1991, **113**, 2995.
4. J. C. Jeffrey, T. B. Rauchfuss and P. A. Tucker, *Inorg. Chem.* 1980, **19**, 3306.
5. W. K. Wong, J.-X. Gao, Z.-Y. Zhou and T. C. W. Mak, *Polyhedron* 1992, **11**, 2965.
6. D. F. Shriver, P. W. Atkins and C. H. Langford, *Inorganic Chemistry*, p. 509. Oxford University Press, Oxford (1990).
7. J. G. Verkade and L. D. Quin (Editors), *Phosphorus-31 NMR Spectroscopy in Stereochemical Analysis*. VCH Publishers, Inc., New York (1987).
8. J. J. Eisch and R. B. King, *Organometallic Synthesis*, Vol. 1, pp. 124–125, Academic Press, New York (1965).
9. P. T. Beurskens, W. P. Bosman, H. M. Doesberg, R. O. Gould, Th. E. M. Van Den Hark, P. A. J. Prick, J. H. Noordik, M. Beurskens and J. M. M. Smith (1984), DIRDIF, Technical Report 1984/1. Crystallography Laboratory, Toernooiveld, 6525 ED Nijmegen, The Netherlands.
10. Enraf–Nonius, Structure Determination Package. Enraf–Nonius, Delft, The Netherlands (1985).

Polyhedron Vol. 12, No. 9, pp. 1055–1059, 1993
Printed in Great Britain

0277–5387/93 $6.00+.00
© 1993 Pergamon Press Ltd

STUDIES ON CROWN ETHER COMPLEXES—XXIX. SYNTHESIS AND CHARACTERIZATION OF THE COMPLEXES OF LANTHANIDE ISOTHIOCYANATES WITH 13-CROWN-4

TONGBU LU and MINYU TAN*

Department of Chemistry, Lanzhou University, Lanzhou 730000, P.R.C.

and

HAISONG SU

Xiaogan University of Television Broadcasting, Xiaogan 432100, Hubei, P.R.C.

and

YU LIU

Lanzhou Institute of Chemical Physics, Academia Sinica, Lanzhou 730000, P.R.C.

(*Received* 10 *September* 1992; *accepted* 18 *December* 1992)

Abstract—The lanthanide isothiocyanate complexes with 13C4 have been prepared in ethyl acetate medium. These new complexes with the general formula $[Ln(NCS)_3(13C4)2H_2O]$ (Ln = La, Pr–Tb, Er–Yb) have been characterized by elemental analysis, IR spectra, *f–f* hypersensitive transitions spectra, ^1H NMR spectra, conductivity measurements and TG–DTA techniques. In the complexes the ligand 13C4, isothiocyanate groups and water molecules are all coordinated to the metal ions.

Many lanthanide-crown ether complexes have been investigated in recent years.[1,2] Most attention has been concentrated on the crown ethers containing ethylene groups, while the lanthanide complexes with the crown ethers containing a trimethylene unit have been studied less. Recent studies have demonstrated that the crown ethers containing trimethylene units have a lower coordination power towards most metal ions, but they have a selectivity to the best-fit metal ions[3,4] due to their enlarged cavity size and the favourable orientation of donor atoms. In order to study more deeply the selectivity and coordination pattern of these crown ethers to lanthanide ions, we have synthesized the solid complexes of 13C4 with lanthanide isothiocyanates in anhydrous medium and investigated the composition and properties of these new complexes.

EXPERIMENTAL

Reagents

Hydrated lanthanide isothiocyanates were prepared as follows:[5] NH_4SCN (0.5 mol) was added to a solution of $LnCl_3 \cdot nH_2O$ (0.04 mol) in water (1000 cm^3). The mixture was shaken with TBP (500 cm^3) for 20 min and then separated. The organic phase was then washed twice with cold water (15°C). The product was obtained by extracting the TBP solution with hot water (40–50°C) three times. After moving the water under reduced pressure the pure product was obtained as crystals in 35% yield.

The ligand 13C4 was prepared as reported previously.[3] All other chemicals used were AnalaR grade.

Chemical and physical measurements

The metal ion contents were determined by EDTA titration using Xylenol orange as an indi-

* Author to whom correspondence should be addressed.

cator. Carbon, nitrogen and hydrogen contents were determined using a Carlo–Erba 1106 elemental analyser. The IR spectra were recorded in the 4000–200 cm^{-1} region using KBr pellets and a 170SX FTIR spectrometer. A Shimadzu UV-240 spectrophotometer was used to obtain the electronic absorption spectra. The ^1H NMR spectra were recorded on a FT-80A spectrophotometer using acetone-d_6 as a solvent and TMS as an internal standard. Thermal analyses (TG and DTA) were performed on a Beijing PcT-2 thermobalance. The heating rate was 10°C min^{-1}. Conductivity measurements were carried out with a DDS-11A type conductivity bridge for a freshly prepared solution in acetone at 25°C.

Preparation of the complexes

A solution of lanthanide isothiocyanate (0.2 mmol) in ethyl acetate (2 cm^3) was added dropwise to a solution of the ligand (0.2 mmol) in ethyl acetate (2 cm^3). The mixture was stirred at room temperature for over 24 h. The precipitated solid complex was filtered, washed with ethyl acetate and dried in a desiccator (0.1 mm Hg) over P_4O_{10} for 2 days. All the complexes are powdered solids and air stable with the characteristic colour of the corresponding lanthanide isothiocyanates.

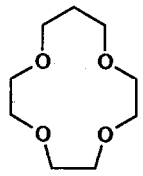

Fig. 1. The structure of the ligand.

RESULTS AND DISCUSSION

The composition of the complexes

The analytical data for the newly synthesized complexes, listed in Table 1, indicate that all of the complexes conform to a 1 : 1 stoichiometry of the metal ion and crown ether.

IR spectra

The most important IR peaks of the ligand and the complexes are reported in Table 2.

Compared with those of the free ligand, the absorptions of ν(R—O—R) of the complexes showed shifts of 64–76 cm^{-1} towards lower wave numbers. This provides evidence for the coordination of the crown ether with the metal ions. In addition, in the far-IR region new bands, absent in the spectrum of the free ligand, are found in the

Table 1. Elemental analysis and molar conductance data

M in $[M(NCS)_3(13C4)(H_2O)_2]$	N% Found (Calc.)	C% Found (Calc.)	H% Found (Calc.)	Ln% Found (Calc.)	Molar conductance (Ω^{-1} cm^2 mol^{-1})
La	7.5 (7.8)	26.4 (26.7)	3.9 (4.1)	25.4 (25.8)	17.5
Pr	7.4 (7.8)	26.3 (26.7)	3.8 (4.1)	25.7 (25.9)	19.5
Nd	7.4 (7.7)	26.6 (26.5)	3.8 (4.0)	26.3 (26.5)	12.0
Sm	7.3 (7.6)	26.5 (26.2)	3.8 (4.0)	27.1 (27.3)	12.4
Eu	7.3 (7.6)	26.6 (26.1)	3.7 (4.0)	27.3 (27.5)	9.8
Gd	7.4 (7.5)	26.1 (25.8)	3.7 (4.0)	28.0 (28.2)	13.5
Tb	7.3 (7.5)	26.4 (25.8)	3.6 (3.9)	28.0 (28.4)	10.7
Er	7.2 (7.4)	25.6 (25.4)	3.6 (3.9)	29.3 (29.5)	12.3
Tm	6.8 (7.4)	25.8 (25.3)	3.6 (3.9)	29.4 (29.7)	7.4
Yb	7.4 (7.3)	25.5 (25.1)	3.6 (3.8)	29.9 (30.2)	9.0

Table 2. The most important IR bands (cm^{-1})

M in $[M(NCS)_3(13C4)(H_2O)_2]$	ν(R—O—R)	ν(CN)	ν(CS)	δ(NCS)	ν(OH)	δ(HOH)	ρ(rHOH)	ν(Ln—O)	ν(Ln—N)
13C4	1126s								
La	1062s	2055s	835w	480m	3379s	1630m	553w	373w	349w
Pr	1055s	2068s 2049s	838w	481m	3400s	1649m	553w	378w	324w
Nd	1051s	2069s 2030s	839w	481m	3223s	1603m	551w	381w	335w
Sm	1052s	2077s 2033s	841w	482m	3255s	1603m	551w	385w	338w
Eu	1051s	2075s 2038s	842w	482m	3227s	1604m	551w	386w	343w
Gd	1051s	2078s 2042s	843w	482m	3229s	1604m	552w	387w	344w
Tb	1051s	2079s 2042s	844w	482m	3228s	1604m	552w	388w	343w
Er	1051s	2082s 2049s	845w	483m	3243s	1609m	554w	390w	346w
Tm	1050s	2074s 2057s	843w	484m	3327s	1614m	555w	387w	335w
Yb	1051s	2076s 2045s	844w	484m	3296s	1610m	553w	387w	348w

373–388 cm^{-1} region, which may be assigned to the $\nu(Ln—O_{crown})$ stretching frequency.[6] The wave numbers of the $\nu(Ln—O_{crown})$ stretching frequency rise with increasing atomic number due to the lanthanide contraction.

The IR absorptions of ν(CN), ν(CS) and δ(NCS) of the isothiocyanate groups are present in the 2030–2082, 835–845 and 480–484 cm^{-1} regions, respectively, which suggests that the isothiocyanate groups in the complexes are coordinated to the metal ions through the nitrogen atoms,[7] while the absence of absorptions near 2100, 700 and 420 cm^{-1} indicates that the sulphur atoms in the isothiocyanate groups are not bonded to the metal ions. Moreover, weak bands assigned to $\nu(Ln—N_{NCS})$[8] are found in the 324–349 cm^{-1} region, further supporting the above assignment.

^{1}H *NMR spectra*

After formation of the lanthanum complex the proton chemical shifts of $\delta(—CH_2—O)$ (3.45–3.66, 16H, m) and $\delta(R—CH_2—R)$ (1.58–1.71 ppm, 2H, m) of the ligand show significant downfield shifts [$\Delta\ \delta(CH_2—O) = 0.12$, $\Delta\ \delta(R—CH_2—R) = 0.15$ ppm], indicating metal–ligand complex formation. Moreover, the chemical shift of water, which appears at 3.08 ppm, suggests that water molecules exist in the lanthanum complex. This result agrees with those of the elemental analysis and IR spectra.

Electronic absorption spectra

The electronic absorption spectra of lanthanide ions have been the subject of several investigations.[9] We measured the *f–f* electronic hypersensitive transitions of Pr^{III}, Nd^{III} and Er^{III} isothiocyanates and their corresponding complexes in acetone. The spectral data along with various calculated parameters are given in Table 3. The nephelauxetic ratio β, the Sinha's covalency parameter δ and the bonding parameter $b^{1/2}$ are expressed as follows:[10,11]

$$\beta = n^{-1}\sum_{1}^{n} \nu_{comp}/\nu_{aq}, \quad \delta(\%) = [(1-\beta)/\beta] \times 100,$$

$$b^{1/2} = [1/2(1-\beta)]^{1/2}.$$

The positive and negative values of δ and $b^{1/2}$ for a complex correspond to covalent and ionic characters, respectively.

From Table 3 it can be found that the positive values of $\delta(\%)$ and $b^{1/2}$ indicate the covalency existing in the metal–ligand bonding, and the small $\delta(\%)$ values of the complexes indicate weak covalent bonding in the complexes.

Thermal analyses

The thermal analyses studies were performed by means of TG and DTA techniques. The thermal analytical data for the ligand and some of the complexes are summarized in Table 4.

The DTA curve of the ligand shows an exothermic peak at 186°C, then an endothermic peak appears at 312°C. The ligand decomposes completely when heated up to 630°C.

The processes of thermal decomposition for all the complexes are almost the same and are different from that of the ligand. For example, the lanthanum complex loses two water molecules when heated to 223°C; the weight loss found in this process is 7.14% (calc. 6.68%). After the loss of two water molecules the lanthanum complex decomposes exo-

Table 3. Electronic spectral data (cm^{-1})

Compound	ν(complex)	ν(salt)	Levels	Parameter values
Pr^{III}	16,877	16,889	$^3H_4 \rightarrow {}^1D_2$	$\beta = 0.9995$
	20,717	20,725	$^3H_4 \rightarrow {}^3P_0$	$\delta = 0.05000$
	21,272	21,276	$^3H_4 \rightarrow {}^3P_1$	$b^{1/2} = 0.01581$
	22,432	22,447	$^3H_4 \rightarrow {}^3P_2$	
Nd^{III}	17,178	17,181	$^4I_{9/2} \rightarrow {}^2G_{7/2}$	$\beta = 0.9994$
	19,069	19,084	$^4I_{9/2} \rightarrow {}^2G_{7/2}$	$\delta = 0.06107$
	19,512	19,529	$^4I_{9/2} \rightarrow {}^2G_{9/2}$	$b^{1/2} = 0.01747$
Er^{III}	19,231	19,249	$^4I_{15/2} \rightarrow {}^2H_{11/2}$	$\beta = 0.9990$
	20,513	20,534	$^4I_{15/2} \rightarrow {}^4F_{7/2}$	$\delta = 0.1001$
	22,198	22,222	$^4I_{15/2} \rightarrow {}^4F_{5/2}$	$b^{1/2} = 0.02236$

Table 4. Thermal analytical data of some of the complexes

M in $[M(NCS)_3(13C4)(H_2O)_2]$	Endothermic peaks (°C)	Exothermic peaks (°C)	Total weight loss (%) Found	Calc.[a]
13C4	312	186	100	
La	223	297, 449, 468, 516	63.78	62.35
Nd	175, 279	309, 472, 482, 551	62.95	61.74
Eu	184	276, 487, 501, 510	62.37	60.87

[a] Calculated weight loss for the change from the complexes to $Ln_2O_2SO_4$.

thermically at 297°C. After this other exothermic peaks and continuous weight loss are detected up to 850°C. At this temperature $La_2O_2SO_4$ is formed.[6] The total weight loss found was approximately consistent with that calculated (Table 4).

By comparing the first exothermic peaks of the $Ln(NCS)_3(13C4)2H_2O$ complexes with those of $Ln(NO_3)_3(12C4)$ complexes[1] we find that the $[Ln(NCS)_3(13C4)2H_2O]$ complexes are thermally less stable than the $Ln(NO_3)_3(12C4)$ complexes due to the existence of trimethylene units, indicating that the lanthanide ions are bound more weakly with less symmetrical 13C4.

Solubility and molar conductance

All the complexes are sparingly soluble in diethyl ether and benzene, slightly soluble in acetonitrile, ethyl acetate and THF and much more soluble in acetone, methanol and dimethyl sulphoxide. The molar conductance values of the complexes measured in acetone at 25°C lie in the range 7.4–19.5 Ω^{-1} cm^2 mol^{-1} (Table 1), indicating that all the complexes are non-electrolytes.[12] This indicates that all the isothiocyanate groups in the complexes are coordinated to the metal ions.

REFERENCES

1. J.-C. G. Bünzli, in *Handbook on the Physics and Chemistry of Rare Earths* (Edited by K. A. Gschneidner Jr and L. Eyring), Ch. 60. North Holland Publishing Co., Amsterdam (1987).
2. Y. Inoue and G. W. Gokel, *Cation Binding by Macrocycle Complexation of Cationic Species by Crown Ethers*. Marcel Dekker, Inc., New York (1990).
3. Y. Liu, Y. Inoue and T. Hakushi, *Bull. Chem. Soc. Japan* 1990, **63**, 3044.
4. M. Ouchi, Y. Inoue, K. Wada, S. Iketani, T. Hakushi and E. Weber, *J. Org. Chem.* 1987, **52**, 2420.
5. Z. Yuehua and Y. Xinkan, *Hua Xue Shi Ji.* 1982, **4**, 30.
6. T. Lu, X. Gan, N. Tang and M. Tan, *Polyhedron* 1990, **9**, 2371.
7. K. Nakamoto, *Infrared and Raman Spectra of Inorganic and Coordination Compounds*, 3rd edn. John Wiley, New York (1978).
8. D. J. Olszanski and G. A. Melson, *Inorg. Chim. Acta* 1978, **26**, 263.
9. S. S. L. Surana, M. Singh and S. N. Misra, *J. Inorg. Nucl. Chem.* 1980, **42**, 610.
10. S. P. Sinha, *Spectrochim. Acta* 1966, **22**, 57.
11. K. Iftikhar, M. Sayeed and N. Ahmad, *Bull. Chem. Soc. Japan* 1982, **55**, 2258.
12. W. J. Geary, *Coord. Chem. Rev.* 1971, **7**, 81.

Polyhedron Vol. 12, No. 9, pp. 1061–1071, 1993
Printed in Great Britain

0277–5387/93 $6.00+.00
Pergamon Press Ltd

ORGANOIMIDO COMPLEXES OF TUNGSTEN. X-RAY CRYSTAL STRUCTURES OF $W(NC_6H_{11})Cl_2(PMe_3)_3$, $[W(NC_6H_{11})Cl_2(PMe_3)_3]O_3SCF_3$, $[W(NC_6H_{11})Cl(PMe_3)_4]BPh_4$, $W[NSi(o\text{-}MeC_6H_4)_3]Cl_2(PMe_3)_3$, $W[NB(mes_2)]_2Cl_2(PMe_3)_2$, $\{W(NPh)Cl[O_2C_2(CF_3)_4]_2\}Li$ AND $WCl_4(PMe_2Ph)_3$

ANDREAS A. DANOPOULOS, CARL REDSHAW, ALAIN VANICHE and GEOFFREY WILKINSON†

Johnson Matthey Laboratory, Chemistry Department, Imperial College, London SW7 2AY, U.K.

and

BILQUIS HUSSAIN-BATES and MICHAEL B. HURSTHOUSE†

Department of Chemistry and Applied Chemistry, University of Wales Cardiff, P.O. Box 912, Cardiff CF1 3TB, U.K.

(*Received* 2 *December* 1992; *accepted* 11 *December* 1992)

Abstract—The cyclohexylimido complex of tungsten(VI), $[W(NCy)Cl_4]_2$ (**1**), is reduced by Na/Hg in the presence of PMe_3 to give *cis,mer*-$W^{IV}(NCy)Cl_2(PMe_3)_3$ (**2**). Interaction of **2** with AgO_3SCF_3 in THF gives the tungsten(V) complex $[W(NCy)Cl_2(PMe_3)_3]O_3SCF_3$ (**3**); with $NaBPh_4$ in the presence of PMe_3 $[W(NCy)Cl(PMe_3)_4]BPh_4$ (**4**) is obtained. Interaction of $WCl_2(PMe_3)_4$ with the new organoazide $(o\text{-tolyl})_3Si(N_3)$ produced $W[NSi(o\text{-tolyl})_3]Cl_2(PMe_3)_3$ (**5**), while with $(mesityl)_2B(N_3)$, *cis,cis,trans*-$W[NB(mes)_2]_2Cl_2(PMe_3)_2$ (**6**) is obtained. Interaction of $[W(NPh)Cl_4]_2$ with dilithium perfluoropinacolate gives $Li\{W(NPh)Cl[O_2C_2(CF_3)_4]_2\}$ (**7**). The structures listed in the title have been determined by X-ray crystallographic study. In complexes **2**–**7** the metal has octahedral geometry. The W—N(imido) distances vary from 1.69(1) Å in complex **4**, a tungsten(IV) species, to 1.78(1) Å in the tungsten(VI) bis-imido complex **6**, with no simple correlation with the oxidation state of the metal. The *trans*-lengthening effect of the imido function also varies, with the greatest effect generally in the tungsten(V) complex **3**. No lengthening seems to occur in the tungsten(IV) complexes **2** and **4**, but there is a slight effect in complex **5**. The complex $WCl_4(PMe_2Ph)_3$ has a capped octahedral geometry.

The synthesis of several new organoimido complexes of tungsten in oxidation states IV, V and VI together with their X-ray crystal structures are reported.

Analytical and physical data for new compounds are collected in Table 1.

RESULTS AND DISCUSSION

Cyclohexylimido compounds

The starting material, $WOCl_4$, has been previously used for the synthesis of organoimido compounds.[1] While some examples are known,[2] the use of the cyclohexyl group is not common; cyclohexylimido species can often be more easily isolated and crystallized than other imido species with e.g. NBu^t groups.

The interaction of CyNCO and $WOCl_4$ in refluxing toluene readily gives multigram quantities of $[W(NCy)Cl_4]_2$ (**1**) as orange–red needles. The compound doubtless has the same chlorine-bridged structure as in similar compounds where other imido groups (e.g. NEt) are present.[3] The reduction of **1** with sodium amalgam or sodium naphthalenide in toluene in the presence of excess PMe_3 gives red–purple crystals of the diamagnetic tungsten(IV)

† Authors to whom correspondence should be addressed.

Table 1. Analytical[a] and physical data for new compounds

	Compound	Colour	M.p. (°C)	Analysis (%) C	H	N
1	$[W(NCy)Cl_4]_2$	Orange–red	198	18.0 (17.6)	2.8 (2.6)	3.4 (3.3)
2	$W(NCy)Cl_2(PMe_3)_3$[b]	Red	*ca* 218	31.2 (31.1)	6.7 (6.6)	2.2 (2.4)
3	$[W(NCy)Cl_2(PMe_3)_3]CF_3SO_3$	Orange	> 240	25.3 (25.3)	5.1 (5.1)	1.8 (1.9)
4	$[W(NCy)Cl(PMe_3)_4]BPh_4$	Yellow–orange	238 (dec.)	52.5 (52.9)	7.2 (7.8)	1.5 (1.7)
5	$W[NSi(o\text{-tol})_3]Cl_2(PMe_3)_3$	Purple–blue	248 (dec.)	45.7 (45.3)	5.7 (6.0)	1.6 (1.7)
6	$W[NB(mes)_2]_2Cl_2(PMe_3)_2$	Yellow	235–238	53.4 (54.0)	7.0 (6.7)	2.9 (3.0)
7	$Li\{W(NPh)Cl[O_2C_2(CF_3)_4]_2\}$[c]	Red	*ca* 220	36.8 (26.4)	1.3 (1.5)	2.0 (1.9)

[a] Calculated values in parentheses.
[b] Cl 11.6 (12.2%).
[c] 0.5 toluene solvate.

complex, $W(NCy)Cl_2(PMe_3)_3$ (**2**), in high yield. The structure of **2** is shown in Fig. 1; selected bond lengths and angles are given in Table 2. The molecule has approximate octahedral geometry with a *mer* arrangement of PMe_3 ligands that are *cis* to the near-linear imido function [$\angle WNC = 172.5(8)°$]. A similar *cis,mer* configuration was found for the analogous $Mo(N\text{-}p\text{-tolyl})Cl_2(PMe_3)_3$[4] and for $W(NPh)Cl_2(PMe_3)_3$.[1a] The ^1H NMR data show the presence of two magnetically inequivalent PMe_3 groups in a 1 : 2 ratio coupled to each other and one C_6H_{11} group. The $^{31}P\{^1H\}$ spectrum (100 MHz) consists of a singlet, which suggests coincidence of the two types of PMe_3 groups, a fact supported by the presence of two pairs of tungsten–phosphorus satellites, $^1J(W—P) = 20.0$ Hz (*trans* to Cl), $^1J(W—P) = 152.6$ Hz. The data favour *cis*-chlorine atoms, but the distinction between *mer* and *fac* arrangements of PMe_3 groups it not unequivocal on spectroscopic data.

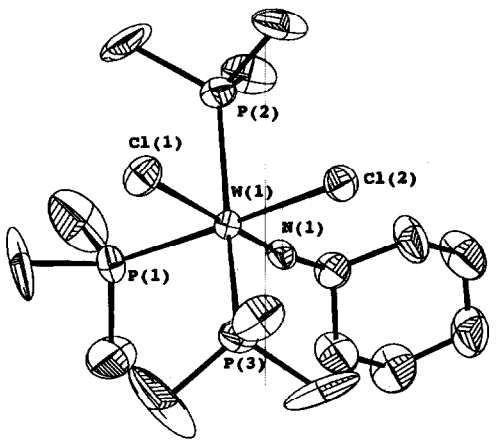

Fig. 1. The structure of $W(NC_6H_{11})Cl_2(PMe_3)_3$ (**2**).

Complex **2** is oxidized by silver trifluoromethanesulphonate in THF to give the W^V complex $[W(NCy)Cl_2(PMe_3)_3]CF_3SO_3$ (**3**), which is paramagnetic (d^1) but which gives only slightly broadened ^1H NMR spectra. These have a C_6H_{11} peak and two singlets (1 : 2) for the inequivalent PMe_3 ligands [$^2J(P—H)$ or $^4J(P—H)$ coupling is not resolved]. The $^{31}P\{^1H\}$ spectrum has a sharp singlet [−28 ppm, $^1J(W—P) = 142.4$ Hz] assigned to the *trans*-equatorial phosphines, while the third PMe_3 resonance is broad (*ca* 0 ppm: no coupling was observed). NMR data on paramagnetic W^V compounds have been obtained previously, e.g. for Cp^*WMe_4.[5a] Cationic tungsten(V) compounds are quite rare.[5b] The spectroscopic data is consistent with a *cis,mer* arrangement of Cl and PMe_3 groups, as found via an X-ray structure determination. A diagram of cation **3** is shown in Fig. 2; bond lengths and angles are given in Table 3.

Complexes **2** and **3** thus have the same structural configuration, but bond length and angle differences are more complex than would be expected from the simple difference in the metal oxidation state. In complex **3** the W—Cl bond *trans* to the imido function is *ca* 0.07 Å longer than that which is *trans* to one of the phosphines. The W—P distances are very similar, but with that *trans* to the chlorine the shorter of the three. In the W^{IV} d^2 complex **2** the imido function seems to exert little

Table 2. Selected bond lengths and angles for $W(NC_6H_{11})Cl_2(PMe_3)_3$ (**2**)

Cl(1)—W(1)	2.507(6)	Cl(2)—W(1)	2.522(6)
P(1)—C(1)	2.448(5)	P(2)—W(1)	2.491(5)
P(3)—W(1)	2.500(6)	N(1)—W(1)	1.702(12)
C(11)—P(1)	1.798(18)	C(12)—P(1)	1.789(18)
C(13)—P(1)	1.763(19)	C(21)—P(2)	1.797(17)
Cl(2)—W(1)—Cl(1)	87.8(2)	P(1)—W(1)—Cl(1)	88.1(2)
P(1)—W(1)—Cl(2)	175.6(1)	P(2)—W(1)—Cl(1)	82.8(2)
P(2)—W(1)—Cl(2)	87.0(2)	P(2)—W(1)—P(1)	94.0(2)
P(3)—W(1)—Cl(1)	83.7(2)	P(3)—W(1)—Cl(2)	82.1(2)
P(3)—W(1)—P(1)	95.9(2)	P(3)—W(1)—P(2)	162.9(1)
N(1)—W(1)—Cl(1)	176.8(3)	N(1)—W(1)—Cl(2)	94.2(4)
N(1)—W(1)—P(1)	90.0(4)	N(1)—W(1)—P(2)	94.8(4)
N(1)—W(1)—P(3)	99.1(4)	C(11)—P(1)—W(1)	115.1(7)
C(12)—P(1)—W(1)	118.1(9)	C(13)—P(1)—W(1)	119.6(8)
C(21)—P(2)—W(1)	118.8(6)	C(22)—P(2)—W(1)	116.1(7)
C(23)—P(2)—W(1)	116.1(6)	C(31)—P(3)—W(1)	115.2(7)
C(32)—P(3)—W(1)	110.5(7)	C(33)—P(3)—W(1)	124.8(9)
C(1)—N(1)—W(1)	172.5(8)		

Table 3. Selected bond lengths and angles for $[W(NC_6H_{11})Cl_2(PMe_3)_3]^+$ in **3**

Cl(1)—W(1)	2.480(4)	Cl(2)—W(1)	2.411(6)
P(1)—W(1)	2.549(9)	P(2)—W(1)	2.563(7)
P(3)—W(1)	2.557(9)	N(1)—W(1)	1.728(10)
Cl(2)—W(1)—Cl(1)	89.0(3)	P(1)—W(1)—Cl(1)	84.1(3)
P(1)—W(1)—Cl(2)	171.6(2)	P(2)—W(1)—Cl(1)	85.9(2)
P(2)—W(1)—Cl(2)	79.9(2)	P(2)—W(1)—P(1)	94.9(2)
P(3)—W(1)—Cl(1)	81.5(3)	P(3)—W(1)—Cl(2)	85.6(3)
P(3)—W(1)—P(1)	98.0(2)	P(3)—W(1)—P(2)	160.9(2)
N(1)—W(1)—Cl(1)	171.2(4)	N(1)—W(1)—Cl(2)	99.8(5)
N(1)—W(1)—P(1)	87.2(5)	N(1)—W(1)—P(2)	96.2(4)
N(1)—W(1)—P(3)	98.4(5)	C(11)—P(1)—W(1)	111.8(6)
C(12)—P(1)—W(1)	118.4(6)	C(13)—P(1)—W(1)	114.3(6)
C(21)—P(2)—W(1)	109.6(5)	C(22)—P(2)—W(1)	121.1(5)
C(23)—P(2)—W(1)	112.1(5)	C(31)—P(3)—W(1)	114.2(7)
C(32)—P(3)—W(1)	115.0(7)	C(33)—P(3)—W(1)	118.8(7)
C(1)—N(1)—W(1)	174.7(10)		

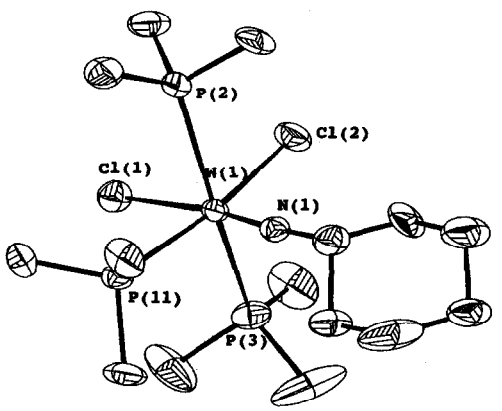

Fig. 2. The structure of the cation $[W(NC_6H_{11})Cl_2(PMe_3)_3]^+$ in the trifluoromethanesulphonate (**3**).

trans influence, and indeed, the *trans*-W—Cl bond is actually shorter, by 0.015 Å, than the W—Cl bond *trans* to a phosphine. This phosphine has a W—P bond *ca* 0.05 Å shorter than the other two, which are mutually *trans*. It is also surprising to find that the W—N (imido) bond in the W^V complex (**3**), at 1.73(1) Å, is slightly longer than that in the W^{IV} complex (**2**), which is 1.70(1) Å.

However, the results found for the molecule of **2** are very similar to those previously found for the phenylimido complex $WCl_2(PMe_3)_3(NPh)$.[1a] Although a configuration analogous to the W^V complex **3** has not previously been structurally characterized, a strong imido *trans* influence has in fact been noted for another W^V complex, WCl_3

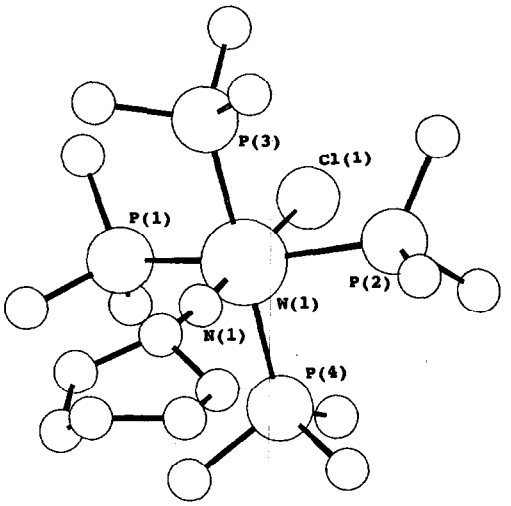

Fig. 3. The structure of the cation $[W(NC_6H_{11})Cl(PMe_3)_4]^+$ in the tetraphenylborate (**4**).

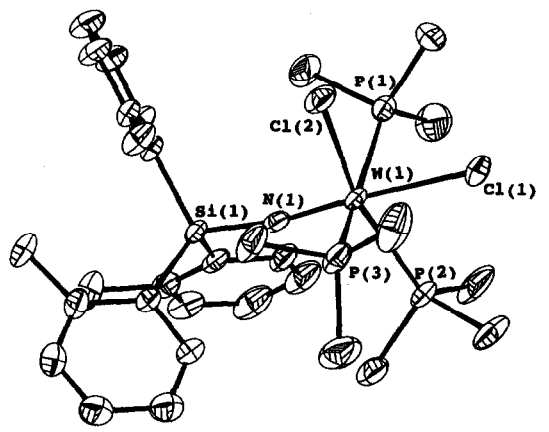

Fig. 4. The structure of $W[NSi(o\text{-tol})_3]Cl_2(PMe_3)_3$ (**5**).

$(PMe_3)_2NPh$,[1a] where the *trans* bond length is 2.443(7) and the *cis* lengths are 2.368–2.405(3) Å.

The interaction of **2** with the $NaBPh_4$ in THF containing PMe_3 gives a tungsten(IV) cation, $[W(NCy)Cl(PMe_3)_4]^+$, as the BPh_4^- salt **4**, whose structure is shown in Fig. 3; bond lengths and angles are in Table 4.

In this W^{IV} complex the single Cl atom is *trans* to the imido function and gives a similar W—Cl distance to that in complex **2**. The four W—P bonds, which form an "equatorial" plane are, not unexpectedly, all very similar. The W—N distance, at 1.69(1) Å, is short, as in complex **2**.

The cyclohexyl groups in all three complexes show varying degrees of conformational thermal motion/disorder, most extreme in the last structure.

The ^1H and $^{31}P\{^1H\}$ NMR spectra of **4** show the presence of a single type of PMe_3 group, showing that in solution the structure formed in the solid is maintained.

Triarylsilyl- and bis(aryl)boryl-imido species

The interaction of $Me_3Si(N_3)$ with $WCl_2(PR_3)_4$, R = Me and Me_2Ph, gives the corresponding tungsten(IV) species, $W(NSiMe_3)Cl_2(PR_3)_3$,[6] in oxidative-addition reactions.

The interaction of $WCl_2(PMe_3)_4$ with the new azide $(2\text{-}MeC_6H_4)_3Si(N_3)$ leads to the similar air-stable, crystalline $W[NSi(o\text{-tol})_3]Cl_2(PMe_3)_3$ (**5**). Both NMR and X-ray data indicate again the *cis,mer* configuration; the structure is shown in Fig. 4 with bond lengths and angles in Table 5. In this

Table 4. Selected bond lengths and angles for $[W(NC_6H_{11})Cl(PMe_3)_4]^+$ in **4**

P(1)—W(1)	2.521(7)	P(2)—W(1)	2.517(6)
P(3)—W(1)	2.525(7)	P(4)—W(1)	2.525(7)
Cl(1)—W(1)	2.514(6)	N(1)—W(1)	1.688(13)
P(2)—W(1)—P(1)	156.2(1)	P(3)—W(1)—P(1)	91.1(2)
P(3)—W(1)—P(2)	90.8(2)	P(4)—W(1)—P(1)	89.1(2)
P(4)—W(1)—P(2)	89.9(2)	P(4)—W(1)—P(3)	177.7(1)
Cl(1)—W(1)—P(1)	78.3(2)	Cl(1)—W(1)—P(2)	77.9(2)
Cl(1)—W(1)—P(3)	90.9(2)	Cl(1)—W(1)—P(4)	91.4(2)
N(1)—W(1)—P(1)	101.3(5)	N(1)—W(1)—P(2)	102.4(5)
N(1)—W(1)—P(3)	89.5(5)	N(1)—W(1)—P(4)	88.2(5)
N(1)—W(1)—Cl(1)	179.5(3)	C(11)—P(1)—W(1)	119.7(7)
C(12)—P(1)—W(1)	117.3(8)	C(13)—P(1)—W(1)	114.8(8)
C(21)—P(2)—W(1)	115.4(7)	C(22)—P(2)—W(1)	118.4(7)
C(23)—P(2)—W(1)	118.0(7)	C(31)—P(3)—W(1)	119.5(7)
C(32)—P(3)—W(1)	114.7(7)	C(33)—P(3)—W(1)	115.3(7)
C(41)—P(4)—W(1)	115.7(7)	C(42)—P(4)—W(1)	115.8(7)
C(43)—P(4)—W(1)	117.2(7)	C(10)—N(1)—W(1)	174.4(12)

Table 5. Selected bond lengths and angles for $W[NSi(o\text{-tol})_3]Cl_2(PMe_3)_3$ (**5**)

Cl(1)—W(1)	2.537(4)	Cl(2)—W(1)	2.498(3)
P(1)—W(1)	2.535(4)	P(2)—W(1)	2.477(4)
P(3)—W(1)	2.512(5)	N(1)—W(1)	1.758(6)
C(101)—P(1)	1.837(9)	C(102)—P(1)	1.824(8)
C(103)—P(1)	1.852(9)	C(201)—P(2)	1.838(9)
C(202)—P(2)	1.828(8)	C(203)—P(2)	1.830(9)
C(301)—P(3)	1.786(9)	C(302)—P(3)	1.837(9)
C(303)—P(3)	1.791(9)	Si(1)—N(1)	1.766(6)

Cl(1)—W(1)—Cl(1)	85.3(2)	P(1)—W(1)—Cl(1)	80.6(1)
P(1)—W(1)—Cl(2)	81.5(2)	P(2)—W(1)—Cl(1)	77.7(1)
P(2)—W(1)—Cl(2)	162.3(1)	P(2)—W(1)—P(1)	100.4(2)
P(3)—W(1)—Cl(1)	89.0(1)	P(3)—W(1)—Cl(2)	82.2(2)
P(3)—W(1)—P(1)	161.3(1)	P(3)—W(1)—P(2)	91.5(2)
N(1)—W(1)—Cl(1)	172.1(1)	N(1)—W(1)—Cl(2)	101.1(2)
N(1)—W(1)—P(1)	95.7(2)	N(1)—W(1)—P(2)	96.3(2)
N(1)—W(1)—P(3)	96.3(2)	Si(1)—N(1)—W(1)	171.4(3)
C(101)—P(1)—W(1)	111.1(3)	C(102)—P(1)—W(1)	114.2(4)
C(103)—P(1)—W(1)	125.1(4)	C(201)—P(2)—W(1)	117.6(3)
C(202)—P(2)—W(1)	115.2(3)	C(203)—P(2)—W(1)	121.1(4)
C(301)—P(3)—W(1)	112.7(3)	C(302)—P(3)—W(1)	124.3(4)
C(303)—P(3)—W(1)	113.3(4)		

complex the W—Cl bond *trans* to the imido group is the longer of the two and the W—P bonds *trans* to chlorine is again the shortest of the three. The W—N (imido) bond length at 1.758(6) Å is longer than any of these in the three complexes described above. An additional factor here is the presence of the Ar_3Si group on the imide. The Si—N distance of 1.766(6) Å indicates some π-interaction between these two atoms, which could weaken the W—N interaction.

Interaction of $WCl_2(PMe_3)_4$ with $mes_2B(N_3)$ at 60° leads to the relatively air stable 4e tungsten (VI) oxidative-addition, bis-imido product, $W[NB(mes)_2]_2Cl_2(PMe_3)_2$ (**6**). The ^1H NMR spectrum indicates the presence of two equivalent *trans*-PMe_3 groups and two borylimido groups, each possessing magnetically inequivalent mesityls at 25°C. On heating the four upfield *o*-methyl bands start to broaden at 55°C and collapse to a single band at 70°C, while the two downfield *p*-methyls start to broaden at 65°C and collapse at 90°C. The fast exchange limit could not be reached at 120°C. The inequivalence of mesityl groups is a result of hindered rotation around aryl—B, B—N and N—W bonds. Collapse of the *o*-methyls at 70°C reveals the first dynamic process ($\sim$ 68 kJ mol^{-1}), rotation around the B—aryl bond, while collapse of *p*-methyls a second one (140 kJ mol^{-1}), e.g. rotation around B—N and/or W—N bonds, although we consider that W—N rotation is less likely than B—N in view of the high π-bond character of W—N.

The solid state structure of **6** is given in Fig. 5; important bond lengths and angles are given in Table 6. The molecular geometry is octahedral with *trans* phosphines, but *cis* chloride and *cis* imido groups. The N—W—N angle has opened up to 100.0(4)° and the Cl—W—Cl angle has reduced to 79.9(2)°. The *cis*-P—W—Cl and *trans*-P—W—P angles are also all less than the ideal 90° or 180°. The W—N distances are equal within the limits of error at 1.78(1) Å, but the pairs of formally chemically equivalent W—P and W—Cl bonds each show small differences. It would seem that steric

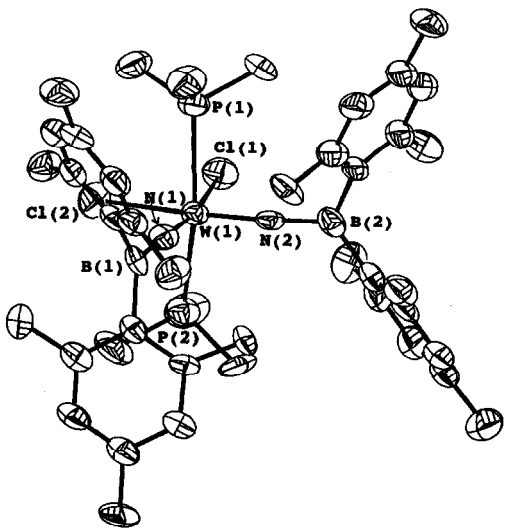

Fig. 5. The structure of $W[NB(mes)_2]_2Cl_2(PMe_3)_2$ (**6**).

Table 6. Selected bond lengths and angles for $W[NB(mes)_2]_2Cl_2(PMe_3)_2$ (**6**)

Cl(1)—W(1)	2.524(5)	Cl(2)—W(1)	2.508(6)
P(1)—W(1)	2.574(6)	P(2)—W(1)	2.559(6)
N(1)—W(1)	1.775(9)	N(2)—W(1)	1.783(10)
Cl(1)—W(1)—Cl(1)	79.9(2)	P(1)—W(1)—Cl(1)	78.4(2)
P(1)—W(1)—Cl(2)	86.6(2)	P(2)—W(1)—Cl(1)	86.7(2)
P(2)—W(1)—Cl(2)	80.6(2)	P(2)—W(1)—P(1)	161.9(1)
N(1)—W(1)—Cl(1)	168.8(2)	N(1)—W(1)—Cl(2)	89.2(4)
N(1)—W(1)—P(1)	98.7(3)	N(1)—W(1)—P(2)	93.9(3)
N(2)—W(1)—Cl(1)	91.0(3)	N(2)—W(1)—Cl(2)	170.8(2)
N(2)—W(1)—P(1)	93.0(3)	N(2)—W(1)—P(2)	97.6(3)
N(2)—W(1)—N(1)	100.0(4)	C(10)—P(1)—W(1)	114.3(6)
C(20)—P(1)—W(1)	113.9(5)	C(30)—P(1)—W(1)	115.4(5)
C(40)—P(2)—W(1)	113.8(5)	C(50)—P(2)—W(1)	114.5(5)
C(60)—P(2)—W(1)	116.2(5)	B(1)—N(1)—W(1)	175.9(6)
B(2)—N(2)—W(1)	176.4(7)		

factors may be affecting bond lengths, as well as angles. The W—N(imido) lengths of 1.78(1) Å are long, but a similar value was found for the anionic W^{VI} species $[WCl_5(NPr^i)]^-$,[1b] where the distance is 1.76(2) Å.

The geometries of the compounds described above show that the origins of a structural *trans* effect, generally quite common in octahedral or other "axial" stereochemistries, containing multiply bonded ligands such as imide, nitride or oxide, are complex. Previous discussions[1a,b] have considered the possibility that steric effects may be partly responsible, with compression from the equatorial ligands which are repelled by the high concentration of charge in the M—L multiple bond "squeezing out" the *trans* ligand. The results obtained for the structurally analogous complexes **2** and **3** do not agree with this model. An electronic explanation is also possible, with the strongly multiply-bonding ligand causing a weakening of the bonding to the *trans* ligand. A recent *ab initio* study of transition metal–imido bonding, in which mainly tetrahedral complexes are studied,[7] showed that a number of canonicals contribute to the M—N bonding. However, the study did not seem to model experimentally found structural *trans* effects for the only octahedral complexes investigated, of rhenium and technetium.

It may be noted that while the octahedral *bis* imido compound **6** is obtained with the borylimido group, Doherty *et al.*[6] found that $WCl_2(PMePh_2)_4$ with 2 equivalents of $Me_3Si(N_3)$ gave the five-coordinate $W(NSiMe_3)_2Cl_2(PMePh_2)$; they also reported that with excess $Me_3Si(N_3)$ at elevated temperature $W(NSiMe_3)Cl_2(PMe_3)_3$ underwent elimination of Me_3SiCl. The reluctance of $W(NSiMe_3)Cl_2(PMe_3)_3$ to be oxidized to tungsten(VI) is ascribed to the non-lability of PMe_3 ligands, making Me_3SiCl elimination competitive.

The different behaviour of the $(mes)_2BN$ system can be attributed to (a) the greater electrophilic nature of the nitrogen atom in $(mes)_2B(N_3)$ and the greater reactivity due to the presence of the electron-withdrawing B atom in the α-position, (b) the fact that mes_2BCl will be a poorer leaving group than Me_3SiCl. We have been unable to observe any tungsten(IV) monoimido intermediate, even when using a deficiency of $mes_2B(N_3)$.

Phenylimido species

Interaction of $[W(NCy)Cl_4]_2$ with lithium perfluoropinacolate gave intractable mixtures, but using $[W(NPh)Cl_4]_2$ in Et_2O gave red prisms of what proved to be the salt $Li[W(NPh)Cl\{OC(CF_3)_2C(CF_3)_2O\}_2]$ (**7**) which is a 1:1 electrolyte in THF. The anion is shown in Fig. 6; bond lengths and angles are given in Table 7. The tungsten has close to octahedral coordination with a bent WNPh group, ∠W—N—C = 158.5°. This angle is slightly smaller than the angles found in the related monomeric pinacolato (L) tungsten(VI) complexes[8] $W(NBu^t)_2(L)(NH_2Bu^t)$ and $W(NBu^t)(L)(NH_2Bu^t)_2$ of 161–166°; other bond distances and angles are similar. The Cl atom is *cis* to NPh, with the shortest W—Cl bond found in any of the complexes described here. The distance is 2.22(1) Å and compares with a value of 2.24 Å in WCl_6.[9] The Li^+ atom has close contacts with CF_3 fluorine atoms and with the phenyl group on the imido ligand. Unlike other reactions involving replacement of Cl by LiOR (R = ^{i}Pr, Cy),[10] lithium chloride does not appear in the crystals.

Table 7. Selected bond lengths and angles for Li[W(NPh)Cl{OC(CF_3)$_2$C(CF_3)$_2$O}$_2$] (7)

Cl(1)—W(1)	2.220(9)	O(1)—W(1)	1.945(13)
O(2)—W(1)	2.053(16)	O(3)—W(1)	1.929(13)
O(4)—W(1)	2.021(16)	N(1)—W(1)	1.718(21)
O(1)—W(1)—Cl(1)	155.6(4)	O(2)—W(1)—Cl(1)	80.0(5)
O(2)—W(1)—O(1)	101.5(6)	O(3)—W(1)—Cl(1)	114.9(5)
O(3)—W(1)—O(1)	88.6(6)	O(3)—W(1)—O(2)	74.9(7)
O(4)—W(1)—Cl(1)	81.4(5)	O(4)—W(1)—O(1)	74.4(6)
O(4)—W(1)—O(2)	99.0(7)	O(4)—W(1)—O(3)	160.5(5)
N(1)—W(1)—Cl(1)	88.3(6)	N(1)—W(1)—O(1)	99.5(7)
N(1)—W(1)—O(2)	152.2(6)	N(1)—W(1)—O(3)	87.7(7)
N(1)—W(1)—O(4)	104.0(8)	C(1)—O(1)—W(1)	125.1(9)
C(2)—O(2)—W(1)	119.8(15)	C(3)—O(3)—W(1)	124.2(15)
C(4)—O(4)—W(1)	121.7(11)	C(101)—N(1)—W(1)	158.5(13)

Table 8. Selected bond lengths and angles for $WCl_4(PMe_2Ph)_3$ (8)

Cl(1)—W(1)	2.411(5)	Cl(2)—W(1)	2.435(5)
Cl(3)—W(1)	2.433(5)	Cl(4)—W(1)	2.434(5)
P(1)—W(1)	2.559(6)	P(2)—W(1)	2.554(6)
P(3)—W(1)	2.561(6)		
Cl(1)—W(1)—Cl(1)	127.2(2)	Cl(3)—W(1)—Cl(1)	127.4(2)
Cl(3)—W(1)—Cl(2)	87.1(2)	Cl(4)—W(1)—Cl(4)	128.4(2)
Cl(4)—W(1)—Cl(2)	86.1(2)	Cl(4)—W(1)—Cl(3)	86.5(2)
P(1)—W(1)—Cl(1)	74.4(2)	P(1)—W(1)—Cl(2)	76.8(2)
P(1)—W(1)—Cl(3)	77.7(2)	P(1)—W(1)—Cl(4)	157.2(1)
P(2)—W(1)—Cl(1)	74.1(2)	P(2)—W(1)—Cl(2)	78.6(2)
P(2)—W(1)—Cl(3)	158.5(1)	P(2)—W(1)—Cl(4)	76.6(2)
P(2)—W(1)—P(1)	113.9(2)	P(3)—W(1)—Cl(1)	74.8(2)
P(3)—W(1)—Cl(2)	158.0(1)	P(3)—W(1)—Cl(3)	77.0(2)
P(3)—W(1)—Cl(4)	78.0(2)	P(3)—W(1)—P(1)	113.7(2)
P(3)—W(1)—P(2)	111.6(2)	C(12)—P(1)—W(1)	116.8(5)
C(13)—P(1)—W(1)	114.4(5)	C(101)—P(1)—W(1)	115.3(4)
C(22)—P(2)—W(1)	116.1(5)	C(23)—P(2)—W(1)	113.5(5)
C(201)—P(2)—W(1)	116.1(4)	C(32)—P(3)—W(1)	116.8(6)
C(33)—P(3)—W(1)	114.7(5)	C(301)—P(3)—W(1)	115.1(4)

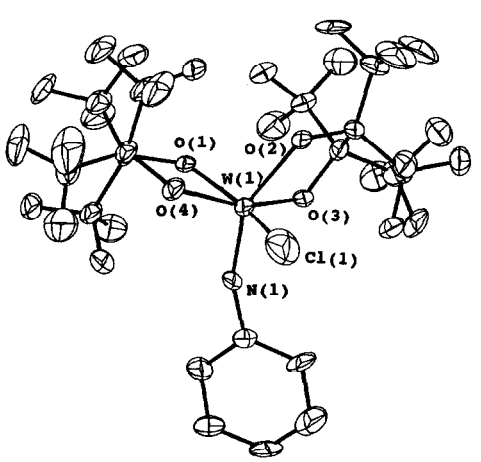

Fig. 6. The structure of Li[W(NPh)Cl{OC(CF_3)$_2$C(CF_3)$_2$O}$_2$] (7).

Other tungsten(IV) *species*

The paucity of X-ray structural information for seven-coordinate W^{IV} complexes, available only for $WCl_4(PMe_3)_3$,[11] prompted the study of compounds with bulkier PR_3 groups, since considerable variation of stereochemistry has been observed for tertiary phosphine adducts of Nb^{IV} and Ta^{V} chlorides.[12]

The structure of $WCl_4(PMe_2Ph)_3$[13] is shown in Fig. 7; bond lengths and angles are given in Table 8. The molecule has a capped octahedral geometry with C_{3v} symmetry: thus Cl(1) occupies the unique capping position surrounded by the more sterically demanding phosphorus ligands and gives the shortest W—Cl bond. The atoms Cl(1), (3) and (4) form the non-capped face. There is no distortion in the

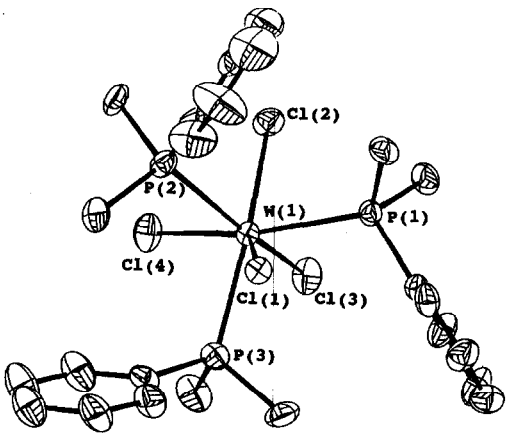

Fig. 7. The structure of $WCl_4(PMe_2Ph)_3$.

uncapped face as was reported for $WCl_4(PMe_3)_3$. Otherwise, there are no marked structural differences. The W—P bond lengths [2.554(6)–2.561(6) Å] are closer together and similar to the longer bonds in $WCl_3(PMe_2Ph)_3$[14a] [2.514(1)–2.555(1) Å] and the facial W—Cl bonds [2.433(5)–2.435(5) Å] are also similar to two of those in $WCl_3(PMe_2Ph)_3$ [2.437(1) and 2.441(1) Å]; the third W—Cl bond was somewhat shorter [2.295(2) Å], a fact suggested[14b] as being due to co-crystallization with $WOCl_2(PMe_2Ph)_3$.

EXPERIMENTAL

Microanalyses were performed by MEDAC Ltd, Brunel University, and Imperial College laboratories. The general techniques and instrumentation have been described.[15] NMR: JEOL EX-270 (270 MHz, ^1H; 100 MHz, ^{31}P); δ ppm (vs Me_4Si); referenced internally on residual proton impurity in the solvent (7.15 ppm, C_6D_6; 7.26 ppm, $CDCl_3$) and external H_3PO_4. IR spectra were obtained (cm^{-1}) in Nujol mulls unless otherwise specified. Commercial chemicals were from Aldrich. Published procedures were used for $WCl_2(PMe_3)_4$,[16] $LiO_2C_2(CF_3)_4$,[17] (*o*-tolyl)$_3$SiCl[18] and (mesityl)$_2$B(N_3).[19]

Table 9. Crystal data and details of refinement

Compound	**2**	**3**	**4**
Formula	$[C_{15}H_{38}Cl_2NP_3W]$	$[C_{15}H_{38}Cl_2NW][CF_3O_3S]$	$[C_{18}H_{47}ClNP_4W][BC_{24}H_{20}]$
M	566.14	636.30	940.01
Crystal system	Orthorhombic	Monoclinic	Orthorhombic
Space group	$P2_12_12_1$	$P2_1$	$P2_12_12_1$
a (Å)	9.370(1)	9.000(2)	17.350(3)
b (Å)	13.920(1)	10.014(2)	13.183(1)
c (Å)	18.548(1)	16.134(8)	22.170(10)
α (°)	90	90	90
β (°)	90	105.30(3)	90
γ (°)	90	90	90
U (Å^3)	2419.28	1402.56	5071.06
Z	4	2	4
D_c (g cm^{-1})	1.554	1.507	1.231
F(000)	1124	632	1928
μ (cm^{-1})	94.57	45.03	25.29
Total no. of reflections	13,905	6739	17,563
No. of unique reflections	3572	5414	8201
No. of observed reflections ($F_o > 3\sigma(F_o)$)	3079	3786	7763
No. of refined parameters	236	313	449
Weighting scheme parameter g in $w = 1/[\sigma^2(F)+gF^2]$	0	0	Unit weight
Final R	0.0331	0.0361	0.0478
Final Rw	0.0318	0.0367	0.0478

Tris(2-methylphenyl)silylazide

Tris(2-methylphenyl)silylchloride (3.3 g, 9.9 mmol) and a 10-fold excess of NaN_3 (6.5 g, 99 mmol) in MeCN (50 cm^3) were refluxed for 24 h, when the solution was evaporated in vacuum. The residue was extracted with toluene (3×50 cm^3) and the solution filtered and evaporated under reduced pressure, affording a white powder which is sufficiently pure to use in syntheses. Yield: 2.2 g, 65%; 105–108°C. IR: 2145 (N_3). ^1H NMR ($CDCl_3$): δ 7.45–7.05 (m, 12H, aromatic); 2.35 ppm (s, 9H, *o*-$CH_3C_6H_4$).

Tetrachloro(cyclohexylimido)tungsten(VI) (**1**)

To $WOCl_4$ (6.2 g, 18.2 mmol) in toluene (80 cm^3) was added CyNCO (2.5 cm^3, 19.6 mmol). After refluxing (*ca* 12 h) and cooling (−20°C) the orange precipitate was washed with hexane (2×20 cm^3) and dried *in vacuo*. Yield: typically 70–80%. IR: 2662w, 2195w, 1668m, 1593m, 1558w, 1346s, 1306s, 1281s, 1261s, 1144s, 1108s, 1030m, 1009s, 924s, 891m, 862s, 856s, 815m, 799s, 777m, 723s, 715s, 570s, 537w, 479w, 422w, 390s, 341bs, 284s, 233m. ^{13}C NMR (CD_2Cl_2): δ_α 78.7, δ_β 33.8 ($\Delta = 45$, cf. 48.4 for $[W(NPr^i)Cl_4]_2$.[20]

Cis-*dichloro(cyclohexylimido)*mer-*tris(trimethylphosphine)tungsten*(IV) (**2**)

(a) *By sodium naphthalenide reaction.* To a solution of **1** (1.05 g, 2.45 mmol) and PMe_3 (1.3 cm^3, 14.6 mmol) in THF (40 cm^3) at −78°C was added a solution of $NaC_{10}H_8$ in THF (37 cm^3 of 0.265 M solution; 9.85 mmol). After stirring for 12 h the volatiles were removed in vacuum, the residue washed with hexane (30 cm^3) and extracted into toluene (40 cm^3). Filtration, concentration (to *ca* 20 cm^3) and cooling (−20°C, 12 h) gave red crystals. Yield: *ca* 20%.

(b) *By Na/Hg reduction.* A solution of **1** (2.0 g, 4.75 mmol) in toluene (50 cm^3) was added to toluene

5	**6**	**7**	**8**
$[C_{30}H_{49}Cl_2NP_3SiW][CF_3O_3S]$	$[C_{54}H_{106}B_4Cl_2N_2P_2W]$	$[C_{18}H_5ClF_{24}NO_4W][Li]\cdot OEt_2\cdot C_7H_8$	$[C_{24}H_{33}Cl_4P_3W](C_4H_8O)$
799.49	1143.40	1131.71	812.22
Triclinic	Monoclinic	Triclinic	Monoclinic
$P\bar{1}$	$P2_1/c$	$P\bar{1}$	$P2_1/n$
9.359(2)	16.773(66)	12.023(2)	11.747(3)
11.735(4)	11.695(17)	12.316(1)	12.042(2)
18.363(3)	24.544(62)	13.648(1)	24.396(4)
72.52(1)	90	90.65(1)	90
76.48(1)	107.52(16)	110.90(1)	103.57(2)
67.44(2)	90	108.67(1)	90
1760.28	4591.05	1770.53	3354.66
2	4	2	4
1.508	1.651	2.12	1.608
806	2408	1092	1616
36.93	27.99	35.69	40.01
9277	10,068	5768	5195
7408	4624	3686	4650
5829	3865	2936	3156
392	174	524	319
0	0	0	0.00002
0.0291	0.0364	0.0505	0.0490
0.0300	0.0361	0.0507	0.0391

($30\ cm^3$) at 0°C containing PMe_3 (2 cm^3, 20 mmol) and Na/Hg (1.0 g Na and 60 g Hg). On stirring, the colour changed to orange, then green, blue and finally purple: after 24 h the mercury was separated and the mixture worked up as above. Yield: 1.7 g, 62% in two crops. ^1H NMR (C_6D_6): δ 1.5 [t, 18H, P_AMe_3]; 1.4 [d, 9H, P_BMe_3]; 2.4, 1.8, 1.2–0.8 [m, 11H, $C_6H_{11}N$]. $^{31}P\{^1H\}$ NMR: −23.2 [s, $^1J(W—P_A) = 152.6$ Hz, $J(W—P_B) = 200$ Hz].

Cis-*dichloro*(*cyclohexylimido*)mer-*tris*(*trimethylphosphine*)*tungsten*(V)*trifluoromethanesulphonate* (**3**)

To a solution of **2** (0.57 g, 0.98 mmol) in THF ($20\ cm^3$) was added AgO_3SCF_3 (0.26 g, *ca* 1 mmol) when a black precipitate of silver appeared. After stirring (2 h) the solution was filtered, evaporated and the residue washed with toluene ($2 \times 20\ cm^3$): this was then dissolved in THF ($20\ cm^3$) and the filtered solution layered with hexane. After 3–4 days the orange crystals were collected. Yield: 0.6 g, 85%. ^1H NMR (CD_2Cl_2): δ 1.7 (s, 18H, $w_{1/2} = 15$ Hz, PMe_3); 1.6 (s, 9H, $w_{1/2} = 10$ Hz, PMe_3); 2.0–2.2 and 0.8–1.2 (br.m., $C_6H_{11}N$). $^{31}P\{^1H\}$: δ −28.2 [s, $J(W—P) = 142.5$ Hz]; *ca* 0 (br.s., $w_{1/2} = 450$ Hz). No ^{19}F NMR spectrum could be obtained.

Chloro(*cyclohexylimido*)*tetrakis*(*trimethylphosphine*)-*tungsten*(IV) *tetraphenylborate* (**4**)

Solid **2** (0.56 g, 1 mmol) was added to a THF (30 cm^3) solution of $NaBPh_4$ (0.37 g, 1.1 mmol). The mixture was stirred for 5 h, filtered, the solution concentrated (*ca* 15 cm^3) and layered with hexane. After several hours the yellow–orange, moisture-sensitive crystals were collected. Yield: *ca* 55%. IR: 1579m, 1287m, 1263m, 946s, 851m, 614m. ^1H NMR (CD_2Cl_2): δ 6.95–7.22 [m, 20H, $B(C_6H_5)_4$]; 1.7 [s, 36H, PMe_3]; 0.9–1.15 (m, 11H, $C_6H_{11}N$). ^{31}P NMR: δ −28.6, $^1J(W—P) = 142.6$ Hz.

Cis-*dichloro*[*tris*(2-*methylphenyl*)*silylimido*]mer-*tris*(*trimethylphosphine*)*tungsten*(IV) (**5**)

$WCl_2(PMe_3)_4$ (0.56 g, 1 mmol) and tritolylsilylazide (0.4 g, 1.17 mmol) were mixed in the dry box, then dissolved in toluene ($30\ cm^3$) and stirred for 24 h at 45–50°C. The green–brown mixture was filtered and layered with hexane to give purple–blue crystals after 2 days. Yield: 0.15 g, *ca* 20%. ^1H NMR (C_6D_6): δ 6.95–7.95 (m, 12H, C_6H_4Me); 2.2 (s, 9H, *o*-MeC_6H_4); 1.4 [virtual t, 27H, PMe_3]. $^{31}P\{^1H\}$ NMR: δ −26 [$^1J(W—P) = 156$ Hz, *trans*-PMe_3]; −29.4 [$^1J(W—P) = 204$ Hz].

Cis,cis,trans-*dichlorobis*[*bis*(2,4,6-*trimethylphenyl*)-*borylimido*]*bis*(*trimethylphosphine*)*tungsten*(VI) (**6**)

To a mixture of $WCl_2(PMe_3)_4$ (0.59 g, 0.9 mmol) and $(mes)_2B(N_3)$ (0.53 g, 1.8 mmol) was added toluene ($30\ cm^3$); after 12 h at 55–60°C volatiles were removed and the residue crystallized from Et_2O as yellow plates. Yield: 0.21 g, 25%. X-ray quality crystals were grown from Bu^n_2O. ^1H NMR (C_6D_6): δ 6.8–7.1 (4s, 8H, $C_6H_2Me_3$); 3.15, 2.75, 2.3, 2.2, 2.12, 2.0 (s, each 6H, $C_6H_2Me_3$); 1.1 (t, 18H, PMe_3). ^{31}P NMR: −8.7 [s, $^1J(W—P) = 152$ Hz].

Lithiumchlorobis(*perfluoropinacolato*)*phenylimido-tungstate*(VI) (**7**)

To $W(NPh)Cl_4 \cdot OEt_2$ (0.86 g, 1.75 mmol) in Et_2O ($30\ cm^3$) at −78°C was added dropwise a solution of $LiO_2C_2(CF_3)_4$ (1.21 g, 3.5 mmol) in Et_2O (30 cm^3). After warming and stirring for 12 h volatiles were removed and the residue extracted with toluene ($30\ cm^3$), which was concentrated (to $20\ cm^3$) and cooled (−20°C) to give red prisms. Yield: *ca* 30%. Λ_M (THF, 21°C) = 70.7 $\Omega^{-1}\ cm^2\ mol^{-1}$. ^1H NMR (d_6-acetone): 7.59–7.65 (m, 5H, aromatic); additional bands due to *ca* 0.1 and 0.2 molecules of toluene and Et_2O of solvation. X-ray quality crystals with 0.5 toluene per W were grown from toluene.

X-ray crystallography

Crystals of all complexes were sealed under argon in thin-walled glass capillaries. Cell dimensions and intensity data were recorded using a FAST TV area detector diffractometer as previously described.[21] The structures were solved and developed via the heavy atom method and refined via full-matrix least-squares. An absorption correction was applied in each case using the DIFABS method. Most non-hydrogen atoms were refined anisotropically and hydrogens included in idealized positions and refined in the "riding" mode. However, for complex **4** the carbons of the cyclohexyl ligand were refined isotropically and hydrogens in this group were not included. Crystal data and experimental details are given in Table 9. Tables of atomic coordinates and other data have been deposited as supplementary material with the Editor, from whom copies are available on request. Atomic coordinates have also been deposited with the Cambridge Crystallographic data centre.

Acknowledgements—We thank the SERC for support and provision of X-ray facilities.

REFERENCES

1. (a) D. C. Bradley, M. B. Hursthouse, K. M. A. Malik, A. J. Nielson and R. I. Short, *J. Chem. Soc., Dalton Trans.* 1983, 2651; (b) B. R. Ascroft, G. R. Clark, A. J. Nielson and C. F. Rickard, *Polyhedron* 1987, **5**, 2081.
2. See, e.g. C. Redshaw, W. Clegg and G. Wilkinson, *J. Chem. Soc., Dalton Trans.* 1992, 2059; R. R. Schrock, U. Schubert and K. Weiss, *Organometallics* 1986, **5**, 397.
3. D. C. Bradley, R. J. Errington, M. B. Hursthouse and R. L. Short, *J. Chem. Soc., Dalton Trans.* 1990, 1043.
4. C. Y. Chan, J. C. Huffman and E. A. Maata, *Inorg. Chem.* 1986, **25**, 822.
5. (a) A. H. Liu, R. C. Murray, J. C. Dewan, B. D. Santarsiero and R. R. Schrock, *J. Am. Chem. Soc.* 1987, **109**, 4282; (b) for references, see V. Saboonchian, G. Wilkinson, B. Hussain-Bates and M. B. Hursthouse, *Polyhedron* 1991, **10**, 595.
6. J. D. Lichtenstein, S. C. Critchlow and N. M. Dougherty, *Inorg. Chem.* 1990, **29**, 439.
7. T. R. Cundari, *J. Am. Chem. Soc.* 1992, **114**, 7879.
8. D. M. T. Chan, W. C. Fultz, W. A. Nugent, D. C. Roe and T. H. Tulip, *J. Am. Chem. Soc.* 1985, **107**, 251.
9. J. A. A. Katelaar and G. W. Oosterhout, *Recl. Trav. Chim. Pays-Bas* 1943, **62**, 197.
10. (a) P. G. Edwards, G. Wilkinson, M. B. Hursthouse and K. M. A. Malik, *J. Chem. Soc., Dalton Trans.* 1980, 2467; (b) W. Clegg, R. J. Errington and C. Redshaw, *J. Chem. Soc., Dalton Trans.* 1992, 3189.
11. R. D. Rogers, E. Carmona, A. Cralindo, J. L. Atwood and L. G. Canada, *J. Organomet. Chem.* 1984, **277**, 403.
12. F. A. Cotton, M. P. Diebold and W. J. Roth, *Polyhedron* 1985, **4**, 1103 and refs therein.
13. J. R. Moss and B. L. Shaw, *J. Chem. Soc.* (*A*) 1970, 595.
14. (a) A. Hills, D. L. Hughes, G. L. Leigh and R. Prieto-Alcon, *J. Chem. Soc., Dalton Trans.* 1991, 1515; (b) K. Yoan, G. Parkin, D. L. Hughes and G. J. Leigh, *J. Chem. Soc., Dalton Trans.* 1992, 769.
15. A. A. Danopoulos, A. C. C. Wong, G. Wilkinson, B. Hussain-Bates and M. B. Hursthouse, *J. Chem. Soc., Dalton Trans.* 1990, 315.
16. P. R. Sharp, J. C. Bryan and J. M. Mayer, *Inorg. Chem.* 1990, **28**, 329.
17. A. P. Conroy and R. D. Dresdner, *Inorg. Chem.* 1970, **9**, 2739.
18. H. Gilman and G. N. Smart, *J. Org. Chem.* 1950, **15**, 720.
19. P. Paetzold and R. Truppat, *Chem. Ber.* 1983, **116**, 1531.
20. B. R. Ashcroft, G. R. Clark, A. J. Nielson and C. E. F. Rickard, *Polyhedron* 1986, **5**, 2081.
21. A. A. Danopoulos, G. Wilkinson, B. Hussain-Bates and M. B. Hursthouse, *J. Chem. Soc., Dalton Trans.* 1991, 1855.

Polyhedron Vol. 12, No. 9, pp. 1073–1077, 1993
Printed in Great Britain

0277–5387/93 $6.00+.00
© 1993 Pergamon Press Ltd

SYNTHESIS AND CHARACTERIZATION OF THE FIRST HETEROLEPTIC TIN(II) ISOPROPOXOMETALLATES

SANJAY MATHUR, ANIRUDH SINGH* and RAM C. MEHROTRA†

Department of Chemistry, University of Rajasthan, Jaipur 302004, India

(*Received* 10 *September* 1992; *accepted* 9 *December* 1992)

Abstract—Tin(II) isopropoxometallates of the types $XSn\{Al(OPr^i)_4\}$, $XSn\{Zr_2(OPr^i)_9\}$, $XSn\{M(OPr^i)_6\}$, $\{Al(OPr^i)_4\}Sn\{Zr_2(OPr^i)_9\}$ and $\{Nb(OPr^i)_6\}Sn\{Ta(OPr^i)_6\}$ (where X = Cl, OPr^i/OBu^t; M = Nb/Ta) have been synthesized and characterized by elemental analyses, molecular weight measurements and multinuclear (^1H, ^{13}C, ^{27}Al and ^{119}Sn) NMR studies.

Although the chemistry of organic compounds of subvalent group 14 elements[1–10] has been extensively investigated during the last two decades, comparatively scant attention has been focused on the development[5,11–13] of the chemistry of compounds with M—O—C functionalities. Amongst the latter classes of compounds examples of heterometal alkoxide systems[14–17] are limited to $Sn\{Al(OPr^i)_4\}_2$, $Sb\{Sn(OR)_3\}_3$, $Tl\{Sn(OBu^t)_3\}$ and $Sr\{Sn(OBu^t)_3\}_2$. In this paper we report the synthesis of novel alkoxo- and (chloro)isopropoxometallatotin(II) complexes, of which the latter complexes have been used as starting materials for the preparation of two trimetallic alkoxides of tin(II) for the first time.

EXPERIMENTAL

All manipulations have been performed under a dry and oxygen-free nitrogen atmosphere. The glass apparatus used was oven-dried (140–150°C) after rinsing with ethyl alcohol and cooled in dry nitrogen prior to use.

Aluminium, zirconium, niobium and tantalum alkoxides were prepared by the literature methods.[18] Anhydrous tin(II) chloride was prepared by the interaction of $SnCl_2 \cdot 2H_2O$(BDH) with acetic anhydride, followed by washing of the solid product with n-hexane and drying under reduced pressure (~ 1 mm). Found: Sn, 62.5; Cl, 37.1. Calc. for $SnCl_2$: Sn, 62.6; Cl, 37.4%.

Tin was determined as SnO_2 after precipitation as cupferrate followed by ignition. The aluminium content in the filtrate was determined gravimetrically as oxinate. Niobium and tantalum were estimated as oxides. In the case of zirconium-containing derivatives tin was determined as cupferrate in the filtrate obtained after the removal of zirconium as mandelate. Isopropoxy contents in isopropoxide derivatives were estimated by an oxidimetric method,[19] using M/6 $K_2Cr_2O_7$ solution in 12.5% H_2SO_4. Chloride was estimated volumetrically by Volhard's method.[20]

IR (4000–200 cm^{-1}) spectra were recorded as Nujol mulls on a Carl Zeiss Jena specord M-80 spectrophotometer. Multinuclear NMR studies were performed on a JEOL FX 90Q spectrometer. ^{27}Al and ^{119}Sn NMR chemical shifts were measured using $Al(NO_3)_3 \cdot xH_2O$ and $SnMe_4$ as external references, respectively. ^1H and ^{13}C NMR chemical shifts were measured using $SiMe_4$ as an internal reference.

Molecular weights were determined ebullioscopically in benzene using a Gallenkamp ebulliometer with a thermistor sensing device.

Preparation of heterometal isopropoxides of tin(II)

In view of the similarity of the procedures for the syntheses of a number of derivatives, only typical preparations are described below:

(1) $ClSn\{Al(OPr^i)_4\}$ (**Ia**). A solution of $K\{Al(OPr^i)_4\}$ [freshly prepared by the reaction of potassium (0.94 g, 24.23 mmol) and $Al(OPr^i)_3$ (4.95 g, 24.24 mmol) with isopropyl alcohol (~ 5 cm^3) in benzene

* Author to whom correspondence should be addressed.
† Present address: Vice-Chancellor, University of Allahabad, Allahabad 211002 (U.P.), India.

($\sim$ 15 cm^3)] was slowly added to $SnCl_2$(4.59 g, 24.23 mmol) dispersed as a suspension in benzene ($\sim$ 15 cm^3). After the addition was complete the reaction mixture was stirred for $\sim$ 4 h at room temperature. The precipitated KCl (1.78 g, 23.86 mmol) was filtered; removal of volatiles from the filtrate under reduced pressure ($\sim$ 1 mm) at room temperature (33°C) yielded the viscous product $ClSn\{Al(OPr^i)_4\}$ (9.88 g, 98%), which on heating under reduced pressure (0.1 mm) disproportionated, giving a volatile product which closely corresponded to the composition $Sn\{Al(OPr^i)_4\}_2$ (b.p. 140°C/0.1 mm).

A similar procedure was followed to prepare **1c** and **1d** in quantitative yields by the equimolar reactions of $SnCl_2$ with $KNb(OPr^i)_6$ and $KTa(OPr^i)_6$, respectively.

(2) $ClSn\{Zr_2(OPr^i)_9\}$ (**1b**). The method was slightly modified in the synthesis of $ClSn\{Zr_2(OPr^i)_9\}$ as the reaction of a solution of $KZr_2(OPr^i)_9$ in isopropyl alcohol with $SnCl_2$ led to partial crystallization of $Zr(OPr^i)_4 \cdot Pr^iOH$. However, the reaction went smoothly as in the above case when a benzene solution of $KZr_2(OPr^i)_9$ [obtained by reacting potassium (0.16 g, 4.12 mmol) with $Zr(OPr^i)_4 \cdot Pr^iOH$ (3.21 g, 4.14 mmol) in a mixture of isopropyl alcohol ($\sim$ 5 cm^3) and benzene ($\sim$ 15 cm^3), followed by removal of volatiles] was added slowly to a suspension of $SnCl_2$ (0.79 g, 4.16 mmol) in benzene ($\sim$ 15 cm^3). After stirring the reaction mixture for 4 h the precipitated KCl (0.29 g, 3.99 mmol) was filtered off. Removal of volatiles from the filtrate under reduced pressure yielded a white sticky solid, $ClSn\{Zr_2(OPr^i)_9\}$ (3.51 g, 97%). The compound was purified by sublimation (140°/0.1 mm) in 70% yield.

(3) $(Pr^iO)Sn\{Zr_2(OPr^i)_9\}$ (**3a**). To a benzene ($\sim$ 20 cm^3) solution of $ClSn\{Zr_2(OPr^i)_9\}$ (3.9 g, 4.38 mmol) was added slowly a suspension of $KOPr^i$ [prepared by reacting potassium (0.17 g, 4.40 mmol) with isopropyl alcohol ($\sim$ 5 cm^3), followed by removal of volatiles]. The reaction mixture was stirred at 70°C for $\sim$ 4 h. The precipitated KCl (0.31 g, 4.15 mmol) was removed by filtration. The volatiles were stripped from the filtrate under reduced pressure ($\sim$ 1 mm) to yield the title product (3.95 g, 96%) as a sticky solid, which was purified by sublimation at 141°C/0.1 mm in 60% yield.

In a similar manner the equimolar reaction of $KOBu^t$ with $ClSn\{Zr_2(OPr^i)_9\}$ afforded $(OBu^t)Sn\{Zr_2(OPr^i)_9\}$ as a sticky solid (b.p. 146°C/0.1 mm).

(4) $\{Al(OPr^i)_4\}Sn\{Zr_2(OPr^i)_9\}$ (**3c**). To a benzene ($\sim$ 20 cm^3) solution of $ClSn\{Zr_2(OPr^i)_9\}$ (7.38 g, 9.79 mmol) was added $KAl(OPr^i)_4$ [freshly pepared from potassium (0.38 g, 9.87 mmol) and $Al(OPr^i)_3$ (2.01 g, 9.86 mmol) in isopropyl alcohol ($\sim$ 5 cm^3) and benzene ($\sim$ 15 cm^3), followed by removal of the volatiles]. The reaction mixture after stirring for $\sim$ 3 h was refluxed for *ca* 1 h. The precipitated KCl (1.40 g, 18.76 mmol) was filtered off. Removal of the volatiles from the filtrate yielded the title product (10.5 g, 97%) as a viscous mass, which could be volatilized at 180°C/0.1 mm, unchanged in 60% yield.

Details of analytical and physical data for all the derivatives are listed in Table 1.

RESULTS AND DISCUSSION

Heterometal chloride alkoxides of tin(II) can be synthesized readily in quantitative yields by the equimolar reaction of the appropriate potassium alkoxometallate with $SnCl_2$ in a suitable solvent, according to the following equation [eq. (1)]:

$$SnCl_2 + KM_x(OR)_y \longrightarrow ClSn(M_x(OPr^i)_y) + KCl\downarrow \quad (1)$$

(**1a**): M = Al, $x = 1, y = 4$

(**1b**): M = Zr, $x = 2, y = 9$

(**1c**): M = Nb, $x = 1, y = 6$

(**1d**): M = Ta, $x = 1, y = 6$.

These chloro derivatives (**1a** and **1b**) have been shown to be convenient precursors for the synthesis of many interesting hetero- (bi- or tri-)metal alkoxides via chloride–alkoxide (or alkoxometallate) exchange reactions [eqs (2)–(4)], as shown below:

$$\mathbf{1a} + Kx \longrightarrow \mathbf{2} + KCl\downarrow \quad (2)$$

2a: x = OPr^i, **2b**: x = OBu^t

$$\mathbf{1b} + Kx \longrightarrow \mathbf{3} + KCl\downarrow \quad (3)$$

3a: x = OPr^i, **3b**: x = OBu^t,
3c: x = $\{Al(OPr^i)_4\}$

$$\mathbf{1c} + Kx \longrightarrow \mathbf{4} + KCl\downarrow \quad (4)$$

4a: x = OPr^i, **4b**: x = OBu^t,
4c: x = $\{Ta(OPr^i)_6\}$.

Most of these derivatives are colourless viscous materials and attain a yellowish tinge on storage. They are highly susceptible to moisture and air. The compounds are readily soluble in common organic solvents and show molecular complexities in the range 1.4–1.7 in boiling benzene, indicating the existence of an equilibrium between monomeric and dimeric species. The derivatives $\{Al(OPr^i)_4\}Sn\{Zr_2(OPr^i)_9\}$ and $\{Nb(OPr^i)_6\}Sn\{Ta(OPr^i)_6\}$ are monomeric.

These derivatives could be volatilized unchanged under reduced pressure, except the compounds containing hexaisopropoxoniobate and -tantalate units

Table 1. Analytical, some physical and NMR (^{27}Al and ^{119}Sn) data for new heterometal alkoxides of tin(II)

Compound[a]	Yield (%)	Analysis (%), Found (Calc.) Sn	Al	M (Zr/Nb/Ta)	OPr^i	Cl	Mol. wt Found (Calc.)	NMR (in benzene, δ ppm) ^{119}Sn	^{27}Al
1a	55	28.3 (28.4)	6.4 (6.5)	—	56.3 (56.6)	8.2 (8.5)	743 (417)	−229.75, −326.69	59.74
1b	70	13.2 (13.7)	—	21.2 (21.0)	61.0 (61.2)	3.9 (4.1)	1354 (868)	−190.16, −322.30	—
1c	95[b]	19.3 (19.7)	—	15.2 (15.4)	58.1 (58.9)	5.7 (5.9)	914 (602)	−191.04, −297.82	—
1d	98[b]	17.1 (17.2)	—	26.1 (26.2)	50.4 (51.4)	5.0 (5.2)	1034 (689)	—	—
2a	60	26.7 (26.9)	6.2 (6.1)	—	66.7 (66.2)	—	728 (441)	—	65.37
2b	95[b]	25.8 (26.1)	5.8 (5.9)	—	51.3 (51.9)	—	(455)	—	61.20
3a	65	13.2 (13.3)	—	20.6 (20.5)	65.9 (66.3)	—	1463 (892)	−235.08, −341.71	—
3b	55	13.0 (13.1)	—	20.3 (20.1)	58.2 (58.7)	—	1449 (906)	−233.70, −347.50	—
4a	90[b]	18.7 (19.0)	—	14.8 (14.9)	65.8 (66.2)	—	—	−207.55, −296.87	—
4b	95[b]	18.3 (18.5)	—	14.4 (14.5)	55.0 (55.5)	—	—	−204.34, −296.02	—
3c	70	10.7 (10.8)	2.5 (2.5)	16.4 (16.6)	69.4 (70.1)	—	1041 (1096)	−234.30, −328.15	64.30
4c	95[b]	10.6[c] (10.8)	—	32.1[c] (32.2) (Nb+Ta) as mixed oxide	64.0[c] (64.4)	—	980 (1102)	−329.75	—

[a] These are either colourless viscous (**1a**, **1c**, **1d**, **2a**, **2b**, **4a**, **4b** and **4c**) or soft solids (**1b**, **3a**, **3b** and **3c**).

[b] Yield refers to the undistilled product, except **1b**, **2a**, **3a**, **3b** and **3c** which are volatile; others tend to disproportionate on heating *in vacuo*.

[c] Refers to undistilled product.

which disproportionated at higher temperatures into the volatile $[M(OPr^i)_5$ (M = Nb or Ta)] and non-volatile components $[ClSn(OPr^i)]$.

IR spectral studies

Following published data[21–23] on metal alkoxides and metal halide complexes,[24] these new derivatives have been characterized by absorption bands in the region 1170–300 cm^{-1}. The ν(C—O) absorptions due to terminal and bridging isopropoxy groups appear at 1160–950 and 935–900 cm^{-1}, respectively. Absorptions in the range 720–430 cm^{-1} have been observed for ν(Al—O), 750–675, ν(Zr—O), 585–510, and ν(M′—O) [M = Nb or Ta], 610–540 cm^{-1}. The ν(Sn—O) stretching frequencies have been observed in the range 705–535 cm^{-1}. The chloro complexes exhibit additional bands in the 335–305 cm^{-1} region due to Sn—Cl stretching frequencies.

NMR studies

The ^{1}H NMR spectrum of **1a** exhibits two overlapping doublets at δ 1.09 and 1.15 ppm, arising from terminal isopropoxy methyl protons. The two doublets at δ 1.32 (J = 6 Hz) and 1.40 (J = 6 Hz) may be assigned to methyl protons of bridging isopropoxy groups. The integrated intensity ratio of terminal and bridging methyl protons is approximately 1 : 1. The methine protons are observed as overlapping septets at δ 4.44 ppm (J = 6 Hz). The ^{13}C NMR spectrum of **1a** shows peaks at δ 25.27, 26.65, 28.22 and 63.60, 65.49, 66.41 ppm for β- and α-carbon atoms, respectively.

The ^{1}H NMR spectrum of **1b** displays two overlapping doublets at δ 1.27 and 1.18 ppm due to the methyl protons of terminal and bridging isopropoxy groups. The methine protons of terminal and bridging isopropoxy groups appear as a complex multiplet in the range δ 4.62–3.24 ppm (J = 6

Hz), in which 11 peaks can be distinguished. The above observation is supported by ^{13}C NMR data: δ 25.84, 25.05 (β-carbons) and 75.08, 75.57 (α-carbons). It is noteworthy that the nature of the ^{1}H NMR spectrum of **1b** remains unaltered even at $-65°C$.

The ^{1}H NMR spectrum of **1d** shows: (1) peaks due to methine protons as two multiplets at δ 3.95 and 4.88 ppm, wherein 10 and seven peaks, respectively, can be distinguished arising from terminal and bridging isopropoxy groups; and (2) two doublets centred at δ 1.37 and 1.44 ppm ($J = 6$ Hz), assignable to bridging isopropoxy groups, while the upfield signals at δ 1.21, 1.26 and 1.32 ppm may be due to two overlapping doublets of terminal isopropoxy groups. Interestingly, the ^{13}C NMR spectrum in benzene exhibits a simpler pattern with peaks at δ 25.13 and 71.56 ppm, ascribable to β- and α-carbons of the isopropoxy groups, respectively.

The ^{1}H NMR spectrum of **4a** shows two overlapping doublets at δ 1.17 and 1.25 ppm, arising from $OCHMe_2$ groups present in bridging and terminal positions. The methine protons appear as an average septet centred at δ 4.53 ppm ($J = 6$ Hz). The derivative **4b** displays four peaks (δ 1.14, 1.23, 1.27 and 1.34 ppm) in the form of two doublets ($J = 6$ Hz) centred at δ 1.19 and 1.31 ppm, due to *gem*-dimethyl protons. Out of the above the peaks at δ 1.34 and 1.27 appear to be mixed respectively with the singlets arising from CH_3 protons of the OBu^t group of the two types, i.e. terminal and bridging in the monomeric and dimeric forms of **4b**.

The ^{1}H NMR spectra of the complexes **2a**, **3a**, **3b** and **3c** exhibit doublets ($J = 6$ Hz) centred at δ 1.26, 1.21, 1.21 and 1.21 ppm due to *gem*-dimethyl protons, respectively, while the septets ($J = 6$ Hz) due to methine protons from the corresponding complexes have been observed, respectively, at δ 4.22, 4.46, 4.18 and 4.15 ppm, indicating a rapid interchange between terminal and bridging isopropoxy groups at room temperature. In the case of **3b** the peaks for tert-butoxy protons appear to merge in the peak due to isopropoxy methyl protons at δ 1.24 ppm. The ^{13}C NMR spectrum of **3c** exhibits a single peak at δ 27.34 ppm for β-carbons and two peaks at δ 68.69 and 69.18 ppm for α-carbons. The appearance of two peaks at δ -234.3 and -327.15 ppm in the ^{119}Sn NMR spectrum is indicative of the presence of two species in solution, probably in three- and four-coordinated environments around tin(II). The appearance of a broad signal centred at δ 64.3 ppm in the ^{27}Al NMR spectrum is indicative[25,26] of a pseudo-tetrahedral environment around aluminium. Further, the high-temperature ($+71°C$) ^{119}Sn NMR spectrum shows a relative decrease in intensity of the peak at δ -327.15 ppm, favouring the shifting of the equilibrium towards the formation of species in a lower coordination state.

The ^{1}H NMR spectrum of **4c** displays two doublets ($J = 6$ Hz) in the integrated intensity ratio 1 : 2, centred at δ 1.16 and 1.30 ppm, assignable to bridging and terminal *gem*-dimethyl groups. The methine protons appear as two septets centred at δ 4.20 and 4.70 ppm in the ratio indicated above. The ^{13}C NMR spectrum exhibits resonances at δ 25.11, 25.74 and 73.82, 75.08 ppm due to β- and α-carbons, respectively. The ^{119}Sn NMR spectrum shows a sharp signal at δ -329.75 ppm, possibly due to a tetra-coordinated tin atom with a stereochemically active lone pair.

The ^{119}Sn NMR spectra of chloro- and alkoxo-bimetallic derivatives (**1a**, **1b**, **1c**, **3a**, **3b**, **4a** and **4b**) exhibit two signals in the ranges δ -190 to -236 and -296 to -350 ppm, characteristic of three- and four-coordinated tin atoms, respectively, which could be interpreted in terms of an equilibrium between the three-coordinated monomer and the four-coordinated dimer, as indicated below:

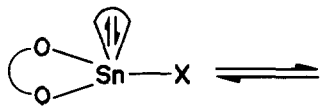

(A)

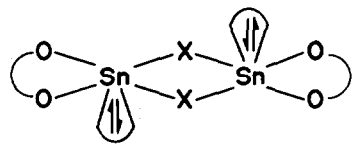

(B)

where, X = Cl, OPr^i, OBu^t; = $Al(OPr^i)_4$,

$Zr_2(OPr^i)_9$, $M(OPr^i)_6$; M = Nb or Ta.

The above equilibrium is consistent with the observed molecular complexity in benzene (Table 1).

Acknowledgements—The authors are grateful to the CSIR, New Delhi, for financial assistance and the award of a Senior Research Fellowship to (S.M.), and to Mr Suman K. Gupta for recording the NMR spectra.

REFERENCES

1. P. G. Harrison, *Coord. Chem. Rev.* 1976, **20**, 1.
2. O. M. Nefedow, S. P. Kolesnikov and I. A. Ioffe, *Organomet. Chem. Rev.* 1977, **5**, 181.
3. J. W. Commolly and C. Hoff, *Prog. Inorg. Chem.* 1981, **19**, 123.
4. (a) A. G. Davies and P. J. Smith, in *Comprehensive*

Organometallic Chemistry (Edited by G. Wilkinson, F. G. A. Stone and E. W. Abel), Vol. 2, pp. 597–598. Pergamon Press, New York (1982); (b) P. G. Harrison, in *Comprehensive Organometallic Chemistry* (Edited by G. Wilkinson, F. G. A. Stone and E. W. Abel), Vol. 2, pp. 670–672. Pergamon Press, New York (1982).

5. P. G. Harrison, in *Comprehensive Coordination Chemistry* (Edited by G. Wilkinson, R. D. Gillard and J. A. McCleverty), Vol. 3, pp. 188–199, 216–233. Pergamon Press, New York (1987).
6. R. West, *Angew. Chem., Int. Edn Engl.* 1987, **26**, 1201.
7. S. Masamune, *Angew. Chem., Int. Edn Engl.* 1991, **30**, 920.
8. P. Jutzi, *Chem. Ber.* 1989, **122**, 1629.
9. D. L. Regar, S. J. Knox, M. F. Huff, A. L. Rheingold and B. S. Haggerty, *Inorg. Chem.* 1991, **30**, 1754.
10. M. N. Hansen, K. Niedenzu, J. Serwatowski and K. R. Woodrum, *Inorg. Chem.* 1991, **30**, 866.
11. M. Veith and F. Tollner, *J. Organomet. Chem.* 1983, **246**, 219.
12. T. Tjeldberg. P. B. Hitchcock, M. F. Lappert, S. J. Smith and A. J. Thorne, *J. Chem. Soc., Chem. Commun.* 1985, 939 and refs therein.
13. R. Jain, A. K. Rai and R. C. Mehrotra, *Polyhedron* 1991, **10**, 1103.
14. N. C. Jain, R. R. Goel and R. C. Mehrotra, *Synth. React.-Inorg. Met.-Org. Chem.* 1981, **11**, 345.
15. T. Athar, R. Bohra and R. C. Mehrotra, *Synth. React. Inorg. Met.-Org. Chem.* 1989, **19**, 195.
16. R. C. Mehrotra, *Alkoxy and Acyloxy Derivatives of Silicon and Tin*, Ch. 6, p. 92. Oxford University Press, Oxford (1991).
17. M. Veith and R. Rosler, *Angew. Chem., Int. Edn Engl.* 1982, **21**, 858.
18. D. C. Bradley, R. C. Mehrotra and D. P. Gaur, *Metal Alkoxides*. Academic Press, London (1978).
19. R. C. Mehrotra, *J. Ind. Chem. Soc.* 1953, **30**, 585.
20. A. I. Vogel, *A Text Book of Quantitative Inorganic Analysis*. Longmans, London (1978).
21. C. G. Barraclough, D. C. Bradley, J. Lewis and I. M. Thomas, *J. Chem. Soc.* 1961, 2601.
22. (a) L. J. Bellamy, *The Infrared Spectra of Complex Molecules*. Methuen, London (1958); (b) L. J. Bellamy, *Advances in Infrared Group Frequencies*. Methuen, London (1968).
23. C. N. R. Rao, *Chemical Applications of Infrared Spectroscopy*, p. 188. Academic Press, New York/London (1963).
24. J. R. Ferraro, *Low Frequency Vibrations of Inorganic and Coordination Compounds*. Plenum Press, New York (1971).
25. D. Dakternicks, R. W. Gable and G. Winter, *Inorg. Chim. Acta* 1983, **75**, 185 and refs therein.
26. J. W. Akitt and W. Gessner, *J. Chem. Soc., Dalton Trans.* 1984, 147 and refs therein.

Polyhedron Vol. 12, No. 9, pp. 1079–1081, 1993
Printed in Great Britain

0277–5387/93 $6.00+.00
© 1993 Pergamon Press Ltd

REACTIVITY OF (dtc)$BiCl_2$ (dtc = DIETHYLDITHIOCARBAMATE) TOWARDS PHENYLLITHIUM: SYNTHESIS AND CHARACTERIZATION OF NOVEL ORGANOMETALLIC TETRADENTATE BISMUTH(III) COMPLEXES

R. SHUKLA and P. K. BHARADWAJ*

Department of Chemistry, Indian Institute of Technology, Kanpur 208016, India

(*Received* 10 *September* 1992; *accepted* 9 *December* 1992)

Abstract—Two tetradentate organometallic complexes of bismuth(III) have been synthesized in high yields from the reactions of (dtc)$BiCl_2$ with phenyllithium in 1:1 and 1:2.5 molar ratios. These complexes were characterized by elemental analysis, IR and NMR spectroscopy. In Bi(dtc)PhCl (**1**) the bismuth(III) ion is coordinated to a dtc, a chloride and a phenyl group, thus providing the first example of a bismuth(III) complex having three different types of ligation. The other complex has ligation from two phenyl groups in addition to one dtc.

The dithiocarbamate anion (dtc) can bind strongly to transition as well as non-transition metal ions and a large number of dithiocarbamato complexes are known.[1–3] Our interest in bismuth chemistry stems from the facts that it is a relatively unexplored area and some bismuth compounds are used as heterogeneous catalysts.[4,5] We have initiated[6] a research program to explore the chemistry of bismuth in the +3 oxidation state with the ultimate goal of preparing catalytically active compounds. The difficulty in isolating pure bismuth compounds lies in the facile formation of BiO^+ in the presence of moisture unless the solutions are very acidic.[7] However, bismuth(III) being a heavy metal has a very strong affinity towards sulphur donor ligands. Thus, an aqueous solution of sodium dialkyldithiocarbamate reacts readily with an alcoholic solution of $BiCl_3$ to form $Bi(dtc)_3$ in high yields.[3] Even when BiOCl is allowed to react with an excess of dtc, the $Bi(dtc)_3$ can be isolated in good yields,[8] indicating the high stability of such bonding. In studying the reactivity of (dtc)$BiCl_2$ our assumption was that the bonding between dtc and bismuth(III) being quite stable should remain intact during cleavage of Bi—Cl bonds by various reagents, giving rise to the formation of new compounds.[8] When the (dtc)$BiCl_2$ complex was allowed to react with phenyllithium different bismuth(III) complexes could be isolated, depending upon the ratio of the reactants used. In the present paper we describe the facile syntheses of two such new bismuth(III) complexes and their characterization in the solid state.

EXPERIMENTAL

Materials

Bismuth trichloride and tetraethylthiuram disulphide were purchased from Aldrich, while carbon disulphide, diethylamine, sodium hydroxide, phenyl bromide and the solvents were obtained from SD Fine Chemicals, India. Lithium metal in the form of wire was acquired from Fisher Scientific. All the solvents, phenyl bromide and diethylamine were purified using standard procedures[9] prior to use. The reactions were carried out under dry nitrogen unless otherwise mentioned.

Proton NMR spectra were recorded on a Bruker WP-80 FT instrument using TMS as the internal standard. IR spectra were recorded on an Acculab-10 IR spectrophotometer. Conductivity data in acetonitrile were obtained using an all-glass model 82-CT conductivity bridge. Microanalyses were performed at the Central Drug Research Institute, Lucknow, India.

* Author to whom correspondence should be addressed.

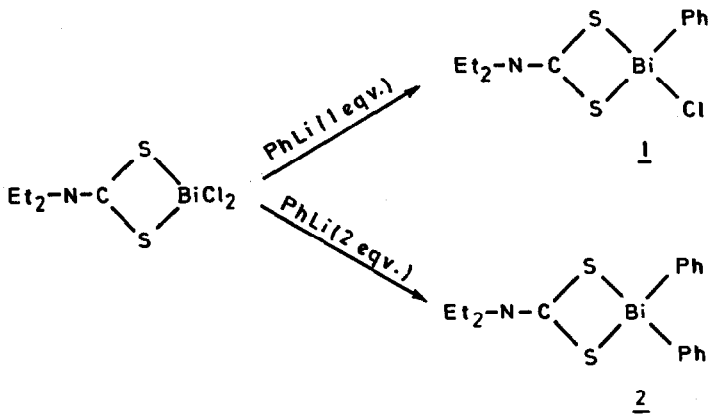

Fig. 1. Synthetic scheme for complexes **1** and **2**.

Synthesis of the complexes

Syntheses of the complexes are shown schematically in Fig. 1.

$Bi(dtc)Cl_2$. This compound was prepared[8] by reacting $BiCl_3$ with $Bi(dtc)_3$ in a 2 : 1 molar ratio in an acetonitrile–chloroform mixed solvent system at room temperature. The crystal structure of this compound has been determined.[10] It forms an extended chloride-bridged species in the solid state.

Bi(dtc)PhCl (**1**). This compound could be prepared by allowing phenyllithium to react with $Bi(dtc)Cl_2$ in a 1 : 1 molar ratio in THF medium at 0°C. Lithium metal (0.16 g, 0.023 mol) was added to THF (50 cm^3), followed by freshly distilled bromobenzene (0.37 g, 0.023 mol) dropwise with constant stirring. All the lithium dissolved in *ca* 1 h. At this point solid $Bi(dtc)Cl_2$ (1.0 g, 0.023 mol) was added to the solution in small portions. After the addition was complete, in 0.5 h, the resulting yellow solution was kept at room temperature for another 2 h and then filtered. The filtrate evaporated to dryness and the yellow residual solid was dissolved in acetone and allowed to evaporate at room temperature. A light yellow microcrystalline solid deposited, which was collected by filtration and air-dried. Yield 52% ; m.p. 125–127°C.

$Bi(dtc)Ph_2$ (**2**). When phenyllithium and $Bi(dtc)Cl_2$ was allowed to react in a 2.5 : 1 molar ratio under warm conditions (50–60°C) both the chloride groups were replaced by the phenyl groups to give the title compound in 66% yield. Elemental analyses and ^1H NMR data for the two complexes are given in Table 1.

RESULTS AND DISCUSSION

Both of the complexes are stable in air in the solid state, as well as in solvents like acetone, acetonitrile, etc. Both behave as non-electrolytes in the above two solvents, signifying that the integrity of the complexes remains intact in these solvents. Selective IR spectral data for **1** and **2** and related complexes are collected in Table 1. Both **1** and **2**, as well as other dithiocarbamato complexes of bismuth(III), show two strong peaks in the region 1450–1550 cm^{-1}. However, triphenyl bismuthine does not absorb appreciably in this region and hence, these two peaks are associated with carbon–nitrogen stretching vibrations. Transition metal complexes of dialkyldithiocarbamato ligands are reported to show absorption in this region due to C—N stretching vibrations.[3] Positions of these absorptions fall between C—N single and C=N double bonds,[11] signifying partial double-bond character for this bond. The 950–1050 cm^{-1} region is associated with ν(CSS) vibrations. However, the phenyl group absorbs strongly in this region and hence, no comment can be made regarding the ν(CSS) vibrations. The complexes $(dtc)BiCl_2$ and **1** show three sharp peaks in the 400–300 cm^{-1} region, which are not present either in the spectrum of **2** or in the spectrum of the $(dtc)_3Bi$ complex. These vibrations are assigned as the Bi—Cl stretching vibrations. Bi—Cl stretching vibrations are reported[12] to occur in this region.

The NMR spectral data for the complexes are also given in Table 1. For complex **1** the ratio of integration of the aliphatic and the aromatic protons is 1 : 1, indicating the formation of the complex as shown in Fig. 1. An alternative structure of **1** can be a chloride-bridged dimer or polymer. However, in the absence of an X-ray structure, it cannot be said with certainty whether the structure is monomeric or dimeric. However, the FAB-mass data showed a peak at 434, which is attributable to the cation $[(Ph)Bi(dtc)]^+$. The NMR spectrum of complex **2** shows the ratio of integration of the aliphatic and aromatic protons as 1 : 2 and it is most likely a discrete monomeric complex, as shown in Fig. 1.

Table 1. Selective IR spectral bands of **1**, **2** and some related bismuth(III) compounds and analytical data[a] for **1** and **2**

Compound	IR bands (cm^{-1}) (selective)	^1H NMR peaks (80 MHz, $CDCl_3$, $SiMe_4$)	Analysis (%) C	H	N	S
1	1480(sb) 1420(sb) 380(w) 345(m) 300(m)	1.2(t, 6H, $2CH_3$) 3.7(q, 4H, $2CH_2$) 7.3(m, 5H, aromatic)	27.9(28.1)	3.3(3.2)	3.0(3.0)	13.8(13.6)
2	1485(sb) 1430(sb)	1.3(t, 6H, $2CH_3$) 3.8(q, 4H, $2CH_2$) 7.4(m, 10H, aromatic)	39.5(39.9)	3.7(3.9)	2.6(2.7)	12.2(12.5)
$(dtc)BiCl_2$	1515(sb) 1440(sb) 390(w) 365(s) 305(w)					
$(dtc)_3Bi$	1500(sb) 1490(s) 1430(s)					

[a] Values in parentheses are calculated.

The electronic spectra of the complexes do not show any LMCT or MLCT transitions involving bismuth(III) and are not discussed here.

Acknowledgement—We thank the Council of Scientific and Industrial Research, New Delhi, India, for financial support of this work.

REFERENCES

1. J. Willemse, J. A. Cras, J. J. Steggerda and C. P. Keijzers, *Struct. Bonding (Berlin)* 1976, **28**, 83.
2. L. H. Pignolet, *Top. Curr. Chem.* 1975, **56**, 91.
3. D. Coucouvanis, *Prog. Inorg. Chem.* 1970, **11**, 233; D. Coucouvanis, *Prog. Inorg. Chem.* 1979, **26**, 301.
4. R. K. Grasselli and J. D. Burrington, *Adv. Catal.* 1981, **30**, 133.
5. R. K. Grasselli, *J. Chem. Educ.* 1986, **63**, 216.
6. B. R. Srinivasan and P. K. Bharadwaj, *Inorg. Chim. Acta* 1990, **178**, 165; S. Mandal, G. Mandal, R. Shukla and P. K. Bharadwaj, *Ind. J. Chem.* 1992, **31A**, 128.
7. C. F. Baes and R. E. Mesmer, *The Hydrolysis of Cations*, p. 377. John Wiley, New York (1976).
8. P. K. Bharadwaj and W. K. Musker, *Inorg. Chem.* 1987, **26**, 1453.
9. D. D. Perin, W. L. F. Armarego and D. R. Perrin, *Purification of Laboratory Chemicals*. Pergamon Press, Oxford (1980).
10. B. R. Srinivasan, P. K. Bharadwaj and A. H. White, unpublished results.
11. K. Nakamoto, *Infrared and Raman Spectra of Inorganic and Coordination Compounds*, 4th edn, p. 346. John Wiley, New York (1986) and refs cited therein.
12. J. D. Smith, in *Comprehensive Inorganic Chemistry* (Edited by A. F. Trotman-Dickerson), Vol. 2, pp. 591–592. Pergamon Press, Oxford (1973).

Polyhedron Vol. 12, No. 9, pp. 1083–1092, 1993
Printed in Great Britain

0277-5387/93 $6.00+.00
© 1993 Pergamon Press Ltd

NICKEL(II) COMPLEXES OF 1,7-BIS(BENZIMIDAZOL-2-YL)-2,6-DITHIAHEPTANE (BBDHP). CRYSTAL AND MOLECULAR STRUCTURE OF $[Ni_2(BBDHP)_2(\mu\text{-}Cl)_2]Cl_2 \cdot 5H_2O \cdot 2EtOH$ AND $Ni(BBDHP)Br_2 \cdot EtOH \cdot 1/2Bu^tOH$

R. CARBALLO* and A. CASTIÑEIRAS†

Departamento de Química Inorgánica, Universidad de Santiago de Compostela, E-15706 Santiago de Compostela, Spain

and

W. HILLER‡ and J. STRÄHLE

Institut für Anorganische Chemie der Universität Tübingen, Auf der Morgenstelle 18, D-7400 Tübingen, Germany

(*Received* 15 *October* 1992; *accepted* 2 *December* 1992)

Abstract—The synthesis and characterization by elemental analyses, mass, IR and electronic spectrometry and conductance and magnetic measurements of compounds with the general formula $Ni(BBDHP)X_2 \cdot n$Solv. is reported [X = Cl, Br, I, ClO_4 or NO_3; Solv. = H_2O, EtOH or Bu^tOH; n = 2–5; BBDHP = 1,7-bis(benzimidazol-2-yl)-2,6-dithiaheptane]. The structures of $[Ni(BBDHP)(\mu\text{-}Cl)]_2Cl_2 \cdot 5H_2O \cdot 2EtOH$ (**II**) and $Ni(BBDHP)Br_2 \cdot EtOH \cdot 1/2Bu^tOH$ (**IV**) were determined by single-crystal X-ray diffraction. A molecule of **II** exhibits a dimeric structure involving two approximately symmetrical chlorine bridges. In both complexes the nickel atom has an octahedral environment with *cis* coordination of the two halide ligands [av. Ni—Cl = 241.6(1), av. Ni—Br = 256.9(9) pm] and the BBDHP in a symmetrical-*cis* arrangement [av. Ni—S = 243.6(2), av. Ni—N = 207.1(4) pm]. In both compounds the crystal packing is governed mainly by hydrogen bonds involving benzimidazole groups, halide atoms and water molecules.

Metal complexes of sulphur–nitrogen chelating ligands have attracted considerable attention because of their interesting physicochemical properties, pronounced biological activities[1–3] and as models of the metalloprotein and metalloenzyme active sites, since it is well known that histidine imidazole nitrogen atoms and methionine thioether sulphur atoms play key roles in the coordination of metals at the active sites of numerous metallobiomolecules,[4] whereby linear tetradentate chelating ligands with an NSSN-donor system are some of the most utilized.[5]

As part of our comprehensive research into compounds formed by transition and post-transition metal(II) ions and polydentate ligands,[6–14] this paper describes the synthesis and structural characterization of nickel(II) complexes of the ligand 1,7-bis(benzimidazole-2-yl)-2,6-dithiaheptane (BBDHP), which also has an N_2S_2 donor system via two benzimidazole nitrogen atoms and two thioether sulphur atoms.[15,16] These complexes, with chlorine and bromine as counter-ions, have already been partially studied,[16] but we have now completed that study and also have determined the crystal and molecular structure.

* Present address: Departamento de Química Pura y Aplicada, Universidad de Vigo, Spain.

† Author to whom correspondence should be addressed.

‡ Actual address: Anorganisch-chemisches Institut der Technischen Universität München, Lichtenbergstr. 4, D-8046 Garching, Germany.

Table 1. Analytical and physical data for the complexes

Compound	Colour	M.p. (°C)	Analytical data[a] C	H	N
$[Ni(BBDHP)Cl_2]\cdot 4H_2O$ (I)	Green	300	39.7(40.0)	4.0(4.9)	9.1(9.8)
$[Ni_2(BBDHP)_2(\mu\text{-}Cl)_2]Cl_2\cdot 5H_2O\cdot 2EtOH$ (II)	Green	255	42.3(42.8)	4.9(5.3)	8.9(9.1)
$[Ni(BBDHP)Br_2]\cdot 2H_2O$ (III)	Green	300	36.8(36.6)	3.7(3.8)	8.1(9.0)
$[Ni(BBDHP)Br_2]\cdot EtOH\cdot \frac{1}{2}Bu^tOH$ (IV)	Green	300	40.7(41.1)	4.1(4.6)	8.1(8.4)
$[Ni(BBDHP)I_2]\cdot 2Bu^tOH$ (V)	Green	190	40.3(39.1)	4.4(4.8)	7.1(6.3)
$[Ni(BBDHP)(H_2O)_2](ClO_4)_2$ (VI)	Green	120	35.2(34.5)	4.3(3.6)	7.3(8.4)
$[Ni(BBDHP)(NO_3)_2]\cdot 4EtOH$ (VII)	Green	100	45.1(44.1)	6.2(6.0)	12.1(11.4)

[a] Calculated values are given in parentheses.

EXPERIMENTAL

Materials

The ligand BBDHP was prepared according to the method described in the literature.[17] Nickel(II) salts and solvents were reagent-grade chemicals.

Metal complexes

All the complexes were isolated by the following general procedure. To a solution of nickel(II) salt (1 mmol) in a minimum amount of EtOH was added a solution of BBDHP (1 mmol) in hot EtOH and the mixture was left with constant stirring for several days. The solid products were filtered off, washed with EtOH and dried over $CaCl_2$ (yield 60–90%). Crystals of $[Ni(BBDHP)(\mu\text{-}Cl)]_2Cl_2\cdot 5H_2O\cdot 2EtOH$ (**II**) were grown by slow evaporation of the EtOH solution and $Ni(BBDHP)Br_2\cdot EtOH\cdot 1/2Bu^tOH$ (**IV**) crystals were obtained after recrystallization from Bu^tOH. The analytical data are reported in Table 1.

Physical measurements

Microanalyses for carbon, hydrogen and nitrogen were determined on a Perkin–Elmer 240B microanalyser. Positive ion FAB mass spectra were obtained on a Kratos MS-50 mass spectrometer retrofitted with a Kratos FAB source and interfaced to a Kratos DS-90 data system. Xenon was used as the bombarding gas with atom gun energies of 8 kV. The source was operated at 250°C. The liquid matrix used was 3-nitrobenzyl alcohol (NBA). IR spectra in the range 4000–200 cm^{-1} were measured in KBr pellets on a Perkin–Elmer 1330 spectrometer. Conductance measurements in acetonitrile at *ca* 10^3 M were made with a WTW conductivity bridge type LF-3. Magnetic measurements in the temperature range 70–300 K were obtained by the Faraday method with a DSM-5 susceptometer calibrated with $HgCo(NSC)_4$. Diamagnetic corrections were applied using Pascal's constants.[18] Diffuse reflectance spectra were recorded on Perkin–Elmer Lambda 15 and Lambda 9 spectrophotometers equipped with a reflectance accessory, using MgO as the reference.

Data collection and structure analyses for II *and* IV

Prismatic crystals of **II** ($0.55\times0.55\times0.65$ mm) and **IV** ($0.50\times0.40\times0.40$ mm) were mounted on glass fibres and placed on an Enraf–Nonius CAD-4 automatic diffractometer. Cell parameters were determined on the diffractometer and were refined by least-squares fit of the parameters to 25 reflections for both **II** and **IV**. Crystal data are summarized in Table 2.*

Data for both compounds were collected with graphite-monochromatized Mo-K_α radiation ($\lambda = 0.71073$ Å) using the ω/θ scan technique ($3 < \theta < 25°$). 5705 (**II**) and 3517 (**IV**) independent reflections with $I > 3\sigma(I)$ were used for the structure refinement. The intensities were corrected for Lorentz–polarization effects and absorption.[19]

The structures were solved by direct methods,[20] which revealed the positions of all non-hydrogen atoms, and refined by the full-matrix least-squares method based on F with a weighting scheme of $w = 1/\sigma^2(F)$.[21] The positions of the hydrogen atoms were obtained by a difference-Fourier synthesis and included in the structure-factor calculation with B_{iso} fixed, but not refined.

In the last cycle of the refinement, in **II** with anisotropic displacement factors for all non-hydro-

* Further details of the structure determination have been deposited as supplementary publication No. CDS 56700. Copies may be obtained through the Fachinformationszentrum Karlsruhe, D-7514 Eggenstein-Leopoldschafen 2, Germany.

Table 2. Crystal data for **II** and **IV**

	II	**IV**
Formula	$C_{42}H_{62}Cl_4N_8Ni_2O_7S_4$	$C_{23}H_{31}Br_2N_4NiO_{1.5}S_2$
Mr	1177.76	670.17
Space group	Monoclinic, $P2_1/c$	Orthorhombic, *Pbcn*
a (pm)	1615.4(5)	2047.8(4)
b (pm)	1522.5(3)	1605.0(3)
c (pm)	2221.7(4)	3111.6(5)
α (°)	90.00	90.00
β (°)	95.88(2)	90.00
γ (°)	90.00	90.00
V ($\times 10^6$ pm^3)	5435.7	10,227.0
D_c (g cm^{-3})	1.440	1.741
μ(Mo-K_α) (cm^{-1})	10.925	40.416
Z	4	16
F(000)	2456	5424
Temperature (K)	293	233

gen atoms and in **IV** with anisotropic displacement factors for nickel, sulphur, bromine and four nitrogen atoms and isotropic factors for the remaining non-hydrogen atoms, including a secondary extinction correction,[22] no parameters shifted by more than 0.001. The final values of R and R_w were 0.050 and 0.054 (**II**) and 0.063 and 0.076 (**IV**), respectively. A final difference-Fourier contained no peak higher than 0.78 for **II** and 0.87 e Å^{-3} for **IV**, respectively. All the calculations were performed on a DEC MicroVAXII. The atomic scattering factors were taken from the International Tables.[23]

RESULTS AND DISCUSSION

The metal complexes are quite stable at room temperature and do not show any decomposition after a long period, but were found to be insoluble in most common polar and non-polar organic solvents. Solutions in acetonitrile (*ca* 10^{-3} M) could only be obtained with the complexes [Ni(BBDHP)I_2] $\cdot$ 2Bu^{t}OH (**V**) and [Ni(BBDHP)$(H_2O)_2$]$(ClO_4)_2$ (**VI**). The molar conductance of 39 Ω^{-1} cm^2 mol^{-1} for complex **V** in acetonitrile is consistent with its non-electrolytic nature,[24] showing that the iodine atom is coordinated to the nickel. The value of 285 Ω^{-1} cm^2 mol^{-1} found for compound **VI** proves this complex to behave as a uni-univalent electrolyte,[24] indicating the dissociation of bonds between nickel and anions and shows the presence of perchlorate anions inside the coordination sphere.

The mass spectra of the complexes, summarized in Table 3, have two peaks. That of greater m/z can be assigned to the $[Ni(BBDHP)X]^+$ species and another of $m/z = 426$ to the $[Ni(BBDHP)]^+$ species. Both these species are common in the mass spectra of similar complexes with the metal in oxidation states of II or III.[14,25,26] The spectra also show some peaks at lower m/z values that are due to the ligand and its fragmentation products. At

Table 3. Positive ion FAB spectra of the complexes in NBA[a]

Compound	$[Ni(BBDHP)]^+$ m/z (RA)	$[Ni(BBDHP)X]^+$ m/z (RA)	Others
I	426(58)	461(75)	
II	426(35)	461(60)	923(50) $[Ni_2(BBDHP)_2Cl_2]^+$
III	426(6)	507(20)	
IV	426(15)	507(36)	1013(3) $[Ni_2(BBDHP)_2Br_2]^+$
V	426(25)	556(11)	
VI	426(25)	525(32)	
VII	426(100)	488(73)	

[a] Relative abundances (RA) normalized to a value of 100 units for the most abundant ion, after removal of ions arising from the matrix.

higher *m/z* values the spectra of compounds **II** and **IV** contain peaks assigned to the dimeric species $[Ni_2(BBDHP)_2X_2]^+$, which in complex **II** appear with high relative abundance, thus indicating their stability.

Description of the structure of **II**

In this compound the asymmetric unit is formed by an $[Ni_2(BBDHP)_2(\mu\text{-}Cl)_2]^{2+}$ cation, two chloride anions, five water molecules, three of them being disordered, and also two disordered ethanol molecules.

The cation consists of dichloro-bridged dimeric units. A view of a single dimer is given in Fig. 1. The geometry at the nickel(II) centres is octahedral with the BBDHP ligand in a symmetrical-*cis* disposition, in which the axial positions around both metals are occupied by nitrogen donor atoms of the two benzimidazolyl groups and two of the equatorial positions by the thioether sulphur atoms. The remaining equatorial positions are occupied by the two bridging chlorine atoms.

The geometry at the nickel centre is highly distorted. The bond lengths and angles in the coordination sphere are given in Table 4. The *cis* angles in the equatorial planes range from 86.90(5) to 97.73(4)° for Ni(1) and 86.22(4) to 99.95(4)° for Ni(2), while the *trans* angles are between 173.13(4) and 174.44(4)° and the N—Ni—N axial angles are 171.70(1) and 170.30(1)° for Ni(1) and Ni(2), respectively. Some distortion may be introduced because of the four five-membered and two six-membered chelate rings present in the molecule. Least-squares planes were calculated for all four chelate rings, and in all cases the rings were not planar. The deviations from planes range from −27.4 to 24.8 pm.

The nickel–sulphur bond lengths between 240.9(1) and 246.3(1) pm are in the lower range of 240–260 pm, generally observed for Ni—S distances in octahedral molecules. The nickel–nitrogen bond lengths of 205.8(3)–206.2(3) pm are within the range found in other octahedral nickel complexes with NSSN-type ligands and benzimidazolyl groups,[9,16] but significantly different from the nickel to nitro-

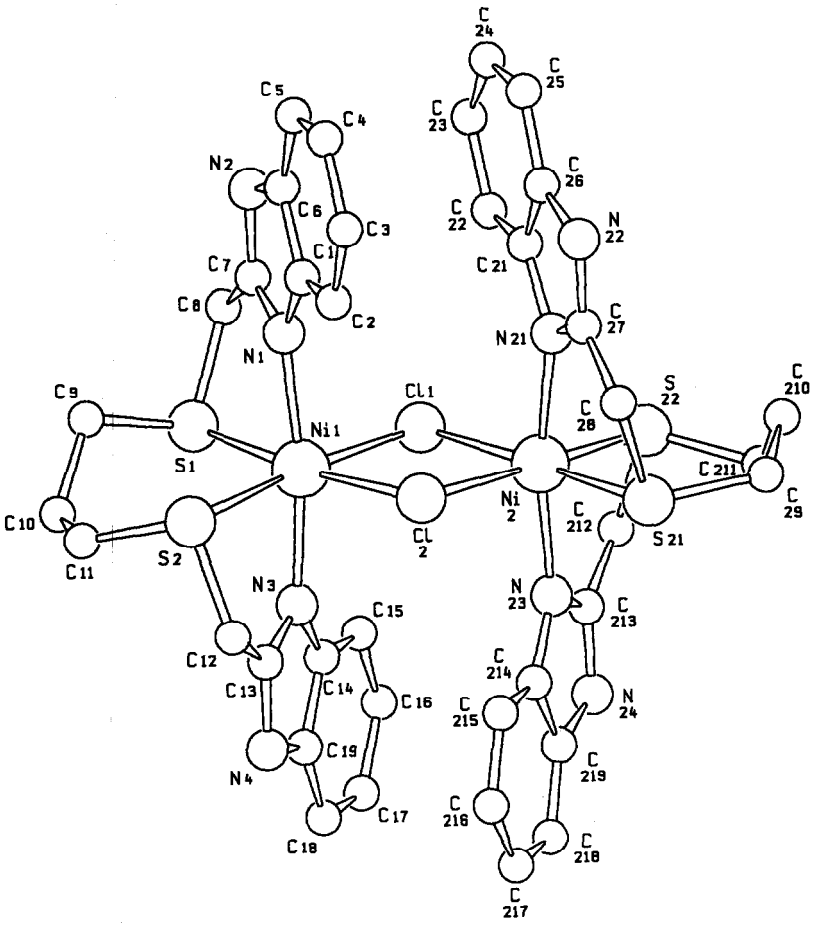

Fig. 1. Perspective drawing of the $[Ni_2(BBDHP)_2(\mu\text{-}Cl)_2]^{2+}$ cation and the numbering scheme.

Table 4. Selected bond distances (pm) and angles (°) for **II**

Ni(1)—Cl(1)	243.0(1)	Ni(2)—Cl(1)	240.9(1)
Ni(1)—Cl(2)	241.0(2)	Ni(2)—Cl(2)	241.5(1)
Ni(1)—S(1)	240.9(1)	Ni(2)—S(21)	244.8(2)
Ni(1)—S(2)	246.3(1)	Ni(2)—S(22)	242.5(1)
Ni(1)—N(1)	206.2(3)	Ni(2)—N(21)	206.1(3)
Ni(1)—N(3)	205.8(3)	Ni(2)—N(23)	205.8(3)
Cl(1)—Ni(1)—Cl(2)	86.90(3)	Cl(1)—Ni(2)—Cl(2)	87.29(3)
Cl(1)—Ni(1)—S(1)	86.97(3)	Cl(1)—Ni(2)—S(21)	173.72(4)
Cl(1)—Ni(1)—S(2)	174.44(4)	Cl(1)—Ni(2)—S(22)	86.22(4)
Cl(1)—Ni(1)—N(1)	90.89(8)	Cl(1)—Ni(2)—N(21)	95.70(8)
Cl(1)—Ni(1)—N(3)	95.03(8)	Cl(1)—Ni(2)—N(23)	92.32(9)
Cl(2)—Ni(1)—S(1)	173.13(4)	Cl(2)—Ni(2)—S(21)	86.59(4)
Cl(2)—Ni(1)—S(2)	88.57(5)	Cl(2)—Ni(2)—S(22)	173.20(4)
Cl(2)—Ni(1)—N(1)	94.95(8)	Cl(2)—Ni(2)—N(21)	90.42(8)
Cl(2)—Ni(1)—N(3)	91.16(9)	Cl(2)—Ni(2)—N(23)	95.49(9)
S(1)—Ni(1)—S(2)	97.73(4)	S(21)—Ni(2)—S(22)	99.95(4)
S(1)—Ni(1)—N(1)	82.03(8)	S(21)—Ni(2)—N(21)	82.98(8)
S(1)—Ni(1)—N(3)	92.48(9)	S(21)—Ni(2)—N(23)	89.63(9)
S(2)—Ni(1)—N(1)	92.73(8)	S(22)—Ni(2)—N(21)	92.21(8)
S(2)—Ni(1)—N(3)	81.81(9)	S(22)—Ni(2)—N(23)	82.79(9)
N(1)—Ni(1)—N(3)	171.70(1)	N(21)—Ni(2)—N(23)	170.30(1)

gen distances of 210–214 pm found in complexes with similar ligands with pyridyl groups.[27] The question if the difference is related to the basicity of the two types of heterocycle nitrogen atoms cannot be answered at present.

The Ni(1)—Cl—Ni(2) bridges are quite symmetrical and the Ni—Cl distances of 240.9(1)–243.0(1) pm compare well with the mean distance of 243.6 pm, calculated on the basis of the structures of 20 six-coordinate nickel(II) complexes.[28] The angles within the bridge Ni(1)—Cl—Ni(2) of 92.67(3) and 93.04(3)° are also comparable with those in other octahedral dichloro-bridged nickel(II) dimers. The large Ni(1)···Ni(2) distance of 350.08(7) pm indicates the absence of orbital interactions between the metal atoms. The Cl(1)···Cl(2) distance is 332.9(1) pm.

The bond distances and angles in the BBDHP ligand are within the expected range, except the C(10)—C(11) bond which is 137.0(9) pm. This is a result of the disorder of these atoms. The benzimidazolyl rings are planar with deviations from the mean plane less than 5 pm.

The two Cl^- counter-ions are associated with two water molecules (Fig. 2). From the H···Cl and O···Cl distances and O—H···Cl angles there is evidence of hydrogen bond interactions.[29] The resulting $[Cl_2(H_2O)_2]^{2-}$ units also form hydrogen bonds with N—H of the benzimidazolyl groups of neighbouring cations. A summary of the dimensions of the hydrogen bonds is given in Table 5 and a stereoview of the packing of the molecules in the unit cell in Fig. 3.

Discussion of the structure of **IV**

The asymmetric unit consists of two Ni(BBDHP)Br_2 molecules, two ethanol molecules and a disordered n-butanol molecule. The perspective drawing of the two independent [Ni(BBDHP)Br_2] molecules and the numbering scheme of the atoms are shown in Fig. 4. As can be seen in this figure, and as is expected, the complex exhibits an octahedral geometry and the BBDHP ligand molecules have a very similar symmetrical-*cis* arrangement to that of the $[Ni_2(BBDHP)_2(\mu\text{-}Cl)_2]^{2+}$ cation, with Ni—S distances between 240.9(2) and 246.1(2) pm and average Ni—N distances of 208.3(4) pm being also comparable with those of compound **II**. The selected interatomic distances and angles are listed in Table 6.

The observed Ni—Br distances from 254.3(9) to 257.8(9) pm are in the range normally observed for octahedrally coordinated nickel(II)[28] and are similar to those found in Ni(BBDH)Br_2 [BBDH = 1,6-bis(benzimidazol-2-yl)-2,5-dithiahexane].[16]

The most obvious deviations from the ideal octahedral coordination polyhedron are the Br—Ni—N angles between 99.00(1) and 101.60(1)° and the angles N(1)—Ni(1)—N(3) and N(21)—Ni(2)—N(23) of 162.00(2) and 162.20(2)°, respectively.

The geometry of the BBDHP ligand does not

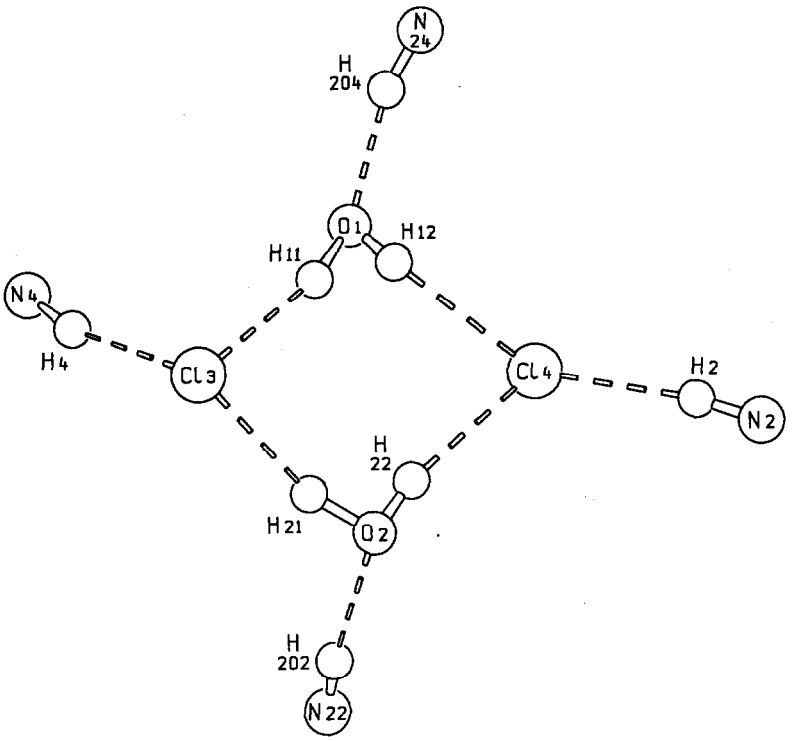

Fig. 2. Perspective drawing of the associated chloride anions in **II** showing the inter- and intramolecular hydrogen bond.

show any dissimilarity with that observed in compound **II**.

The symmetrically independent molecules appear to be joined by a pair of hydrogen bonds between the benzimidazole N—H group of one complex and a bromide ligand of the other complex (Table 5). The N···Br and H···Br distances and associated N—H···Br angles are well within the range observed for other N—H···Br hydrogen bonds.[30] A stereoview of the unit cell is shown in Fig. 5.

IR spectra

The assignments of some of the IR spectral bands of free BBDHP and its nickel(II) complexes are

Table 5. Hydrogen bonds in compounds **II** and **IV**

A—H···B	A—H (pm)	H···B (pm)	A···B (pm)	A—H···B (°)
Compound **II**				
O(1)—H(011)—Cl(3)	105(6)	214(5)	314.6(5)	158(5)
O(1)—H(012)—Cl(4)	80(6)	240(5)	310.3(5)	146(5)
O(2)—H(021)—Cl(3)	100(5)	226(5)	320.6(5)	159(4)
O(2)—H(022)—Cl(4)	87(5)	229(5)	313.6(4)	167(5)
N(2)—H(02)—Cl(4)a	91(5)	222(5)	311.4(4)	170(4)
N(4)—H(04)—Cl(3)	104(5)	212(5)	313.2(4)	162(4)
N(22)—H(202)—O(2)b	81(6)	200(6)	279.9(5)	170(6)
N(24)—H(204)—O(1)c	91(6)	186(6)	273.4(5)	160(5)
Symmetry code: (a) $1-x, y, z$; (b) $1-x, -\frac{1}{2}+y, \frac{1}{2}-z$; (c) $1-x, \frac{1}{2}+y, \frac{1}{2}-z$.				
Compound **IV**				
N(2)—H(20)—Br(21)	97(5)	240(4)	334.5(4)	164(2)
N(22)—H(220)—Br(1)d	96(5)	243(4)	334.5(4)	159(3)
Symmetry code: (d) $x, 1-y, -\frac{1}{2}+z$.				

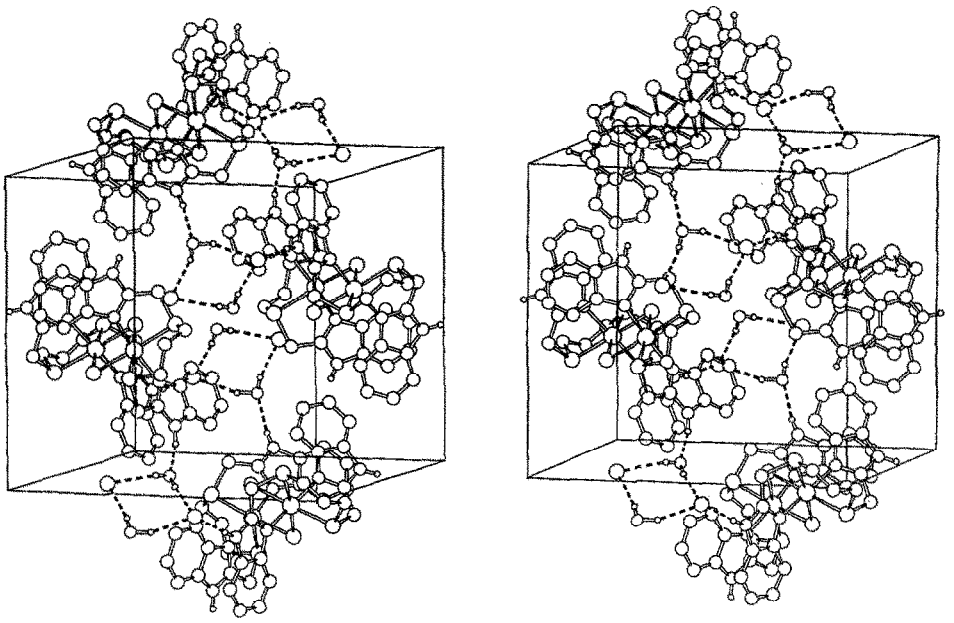

Fig. 3. Stereoview diagram of the unit-cell packing of **II**; dotted lines indicate hydrogen bonds.

reported in Table 7. The IR spectra of the compounds are very similar to one another and to BBDHP itself. The most significant differences are in the NH stretching region. The ν(NH) frequency on coordination is raised by *ca* 200 cm^{-1} relative to that of the free ligand, and in the 1450–1400 cm^{-1} region the low frequency shift of the deformations δ(NH) shifts from 1430 cm^{-1} in BBDHP to *ca* 1400 cm^{-1} in the complexes. This indicates that there are direct bonds between the pyridine nitrogen atoms of the benzimidazolyl groups and the nickel atoms. A weak band observed at 690 cm^{-1} is assigned mainly to the ν(CS) stretching vibration[31] and on coordination is irregularly displaced.

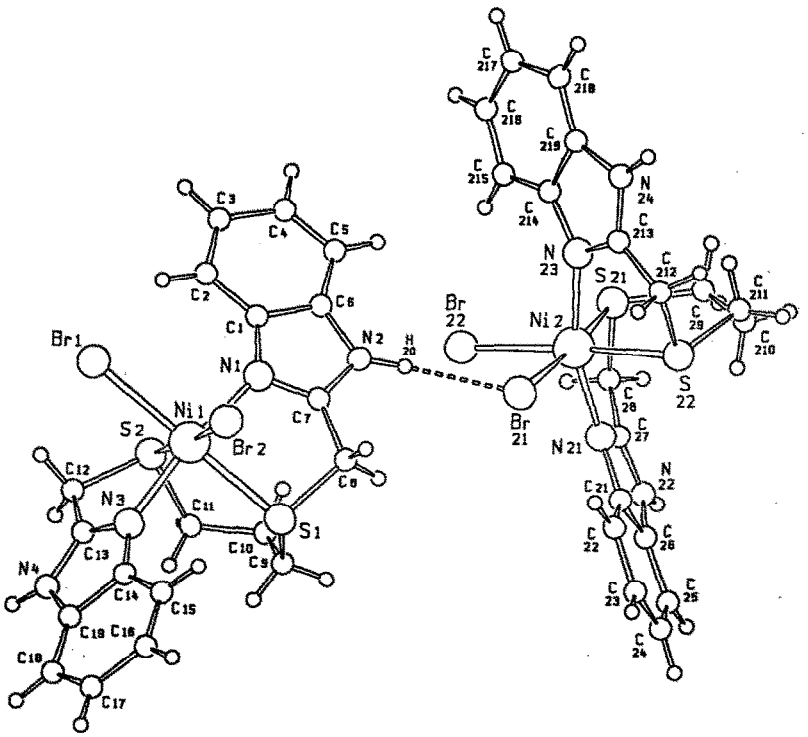

Fig. 4. Perspective view of the asymmetric unit in **IV**.

Table 6. Selected bond distances (pm) and angles (°) for **IV**

Ni(1)—Br(1)	257.8(9)	Ni(2)—Br(21)	257.8(9)
Ni(1)—Br(2)	257.6(9)	Ni(2)—Br(22)	254.3(9)
Ni(1)—S(1)	240.9(2)	Ni(2)—S(21)	246.1(2)
Ni(1)—S(2)	243.9(2)	Ni(2)—S(22)	243.6(2)
Ni(1)—N(1)	209.8(5)	Ni(2)—N(21)	206.4(4)
Ni(1)—N(3)	208.9(4)	Ni(2)—N(23)	208.0(4)
Br(1)—Ni(1)—Br(2)	89.25(3)	Br(21)—Ni(2)—Br(22)	89.15(3)
Br(1)—Ni(1)—S(1)	172.45(5)	Br(21)—Ni(2)—S(21)	173.63(5)
Br(1)—Ni(1)—S(2)	86.60(4)	Br(21)—Ni(2)—S(22)	86.98(4)
Br(1)—Ni(1)—N(1)	99.00(1)	Br(21)—Ni(2)—N(21)	99.80(1)
Br(1)—Ni(1)—N(3)	91.80(1)	Br(21)—Ni(2)—N(23)	91.20(1)
Br(2)—Ni(1)—S(1)	83.69(4)	Br(22)—Ni(2)—S(21)	84.70(4)
Br(2)—Ni(1)—S(2)	175.54(5)	Br(22)—Ni(2)—S(22)	175.63(5)
Br(2)—Ni(1)—N(1)	93.60(1)	Br(22)—Ni(2)—N(21)	92.70(1)
Br(2)—Ni(1)—N(3)	101.10(1)	Br(22)—Ni(2)—N(23)	101.60(1)
S(1)—Ni(1)—S(2)	100.54(5)	S(21)—Ni(2)—S(22)	99.23(6)
S(1)—Ni(1)—N(1)	84.20(1)	S(21)—Ni(2)—N(21)	82.10(1)
S(1)—Ni(1)—N(3)	86.90(1)	S(21)—Ni(2)—N(23)	88.40(1)
S(2)—Ni(1)—N(1)	85.40(1)	S(22)—Ni(2)—N(21)	86.10(1)
S(2)—Ni(1)—N(3)	80.80(1)	S(22)—Ni(2)—N(23)	80.50(1)
N(1)—Ni(1)—N(3)	162.00(2)	N(21)—Ni(2)—N(23)	162.20(2)

The IR spectrum of the nitrate derivative exhibits bands around 1530, 1278 and 1005 cm^{-1}, assigned to ν_4, ν_1 and ν_2 modes associated with a monodentate nitrate group.[32] In the case of the perchlorate derivative strong singlets at 1100 and 625 cm^{-1} are observed, which are assigned to the ν_3 stretching vibration and ν_4 deformations in an ionic perchlorate group.[32]

In the far-IR region the complexes exhibit bands at 320 and 285 cm^{-1}, which are assigned to ν(NiN) and ν(NiS) vibrations, respectively.[33] In compounds **I** and **II** ν(NiCl) appear at 260 (Ni—Cl_t) and 220 cm^{-1} (Ni—Cl_b), and in compounds **VI** and **VII** ν(NiO) appear at *ca* 405 cm^{-1}, which are in good agreement with the reported values.[33]

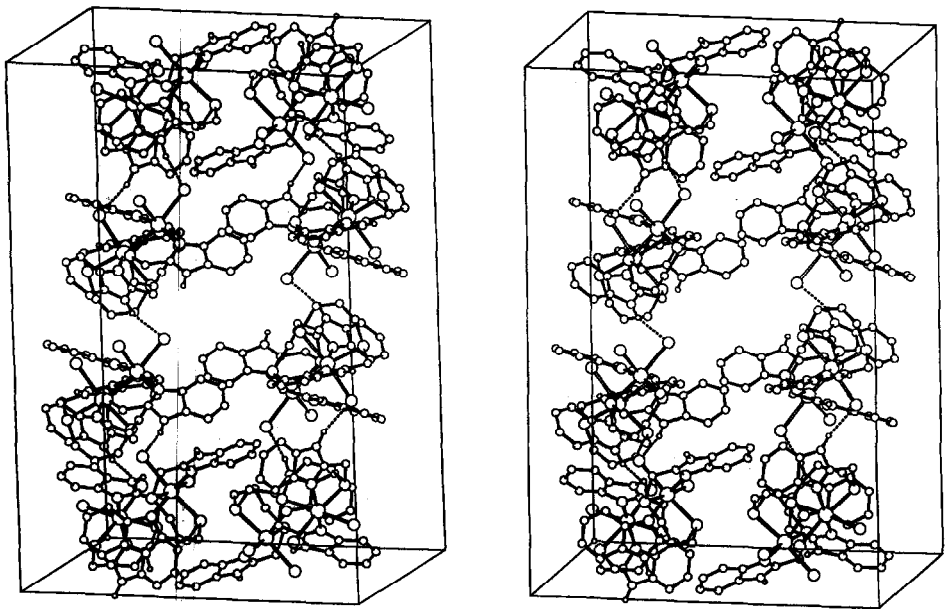

Fig. 5. Stereodrawing of the unit cell of **IV** showing the hydrogen bonding scheme.

Table 7. Selected IR vibrations for BBDHP and its nickel(II) complexes

BBDHP	I	II	III	IV	V	VI	VII	Assignment
—	3400sh	3380sh	3400sh	3500sh	3400sh	3500sh	3400sh	ν(OH)
3060s,b	3150s,b	3120s,b	3180s,b	3300s,b	3100s,b	3300s,b	3100s,b	ν(NH)
1430s	1398m	1396m	1395m	1393m	1393s	1395s	1387s	δ(NH)
690w	690w	698w	675w	690w	700w	680w	700w	ν(CS)
—	—	—	—	—	—	410sh	405sh	ν(NiO)
—	320m	315w	320w	320w	318w	320w	320w	ν(NiN)
—	285m	285m	290m	285m	289m	285m	290m	ν(NiS)
—	260m	220sh	—	—	—	—	—	ν(NiCl)

Table 8. Electronic spectral data and crystal field parameters (cm^{-1}) calculated for the complexes[a]

Compound	$^3A_{2g}(F) \rightarrow {}^3T_{2g}(F)$	$\rightarrow {}^3T_{1g}(F)$	$\rightarrow {}^3T_{1g}(P)$	B	10 Dq	β
I	9730	15,625	25,700	811	9730	0.79
II	9230	15,430	25,060	854	9230	0.83
III	8895	14,945	24,570	855	8900	0.83
IV	8880	14,835	24,450	843	8880	0.82
V	9600	16,365	25,700	888	9605	0.86
VI	9600	16,285	25,640	857	9690	0.83
VII	9680	16,420	25,640	868	9680	0.84

[a] $B(Ni^{2+}) = 1030\ cm^{-1}$; $\beta = B/1030$.

Electronic spectra

The reflectance spectra of the nickel(II) complexes (Table 8) display three sets of low-intensity absorption bands at 8880–9730 [ν_1, $^3A_{2g}(F) \rightarrow {}^3T_{2g}(F)$], 14,830–16,420 [$\nu_2$, $^3A_{2g}(F) \rightarrow {}^3T_{1g}(F)$] and 24,450–25,700 cm^{-1} [ν_3, $^3A_{2g}(F) \rightarrow {}^3T_{1g}(P)$]. The position of those bands and the calculated $10Dq$, B and β values are analogous to other octahedral nickel(II) complexes.[34]

Magnetic moments

The μ_{eff} values at room temperature and in the range 70–300 K with Curie–Weiss, θ, and Curie, c, constants are reported in Table 9. The magnitude and slight temperature dependence of the μ_{eff} values betweem 2.7 and 3.2 B.M. are in the range expected for distorted octahedral complexes of nickel(II).[35]

Table 9. Magnetic properties of the nickel(II) complexes

Compound	μ'_{eff} (M.B.)	μ_{eff} (M.B.)	θ (K)	c
I	2.90	—	—	—
II	2.86	2.92	13.0	1.1
III	2.97	—	—	—
IV	3.11	3.08	2.5	1.2
V	2.72	2.68	10.2	0.9
VI	2.95	2.79	16.0	1.0
VII	2.81	—	—	—

μ'_{eff} at room temperature; θ: Curie–Weiss constant; c: Curie constant.

Acknowledgement—This work was supported by a grant from Direccion General de Investigación Científica y Técnica (Spain) (PS88-0051).

REFERENCES

1. M. Akbar Ali and S. E. Livingstone, *Coord. Chem. Rev.* 1974, **13**, 101.
2. M. J. M. Campbell, *Coord. Chem. Rev.* 1975, **15**, 279.
3. S. Padhye and G. B. Kauffman, *Coord. Chem. Rev.* 1985, **63**, 127.
4. K. D. Karlin and J. Zubieta (Editors), *Biological and Inorganic Copper Chemistry*. Adenine Press, New York (1983); L. Quee Jr (Editor), *Metal Clusters in Proteins*. ACS Symposium Series, 372. American Chemical Society, Washington (1988).
5. E. Bouwman, W. L. Driessen and J. Reedijk, *Coord. Chem. Rev.* 1990, **104**, 143.
6. A. Castiñeiras, G. Diaz, F. Florencio, S. García-Blanco and S. Martínez-Carrera, *Z. Anorg. Allg. Chem.* 1988, **567**, 101.
7. A. Castiñeiras, R. Carballo, W. Hiller and J. Strähle, *Acta Cryst.* 1990, **C46**, 1739.

8. W. Hiller, J. Strähle, A. Castiñeiras, R. Carballo, M. R. Bermejo and M. Gayoso, *An. Quím.* 1990, **86**, 506.
9. A. Castiñeiras, W. Hiller, J. Strähle, R. Carballo, M. R. Bermejo and M. Gayoso, *Z. Naturforsch.* 1990, **45b**, 1267.
10. A. Castiñeiras, R. Carballo, W. Hiller and J. Strähle, *Z. Krystallogr.* 1990, **193**, 251.
11. A. Castiñeiras, R. Carballo, W. Hiller and J. Strähle, *Acta Cryst.* 1991, 1725.
12. R. Carballo, A. Castiñeiras, W. Hiller and J. Strähle, *Acta Cryst.* 1991, 1736.
13. E. Bermejo, R. Carballo, A. Castiñeiras, A. Lombao, W. Hiller and J. Strähle, *Polyhedron* 1991, **10**, 1579.
14. A. Castiñeiras, R. Carballo and C. Vázquez, *Polyhedron* 1991, **10**, 1675.
15. M. J. Schilstra, P. J. M. W. L. Birker, G. C. Verschoor and J. Reedijk, *Inorg. Chem.* 1982, **21**, 2637.
16. J. M. M. Smits, R. Janssen, P. T. Beurskens, J. van Rijn and J. Reedijk, *Polyhedron* 1987, **6**, 1843.
17. A. W. Addison and P. J. Burke, *J. Heterocyc. Chem.* 1981, **18**, 803.
18. F. E. Mabbs and D. J. Machin, *Magnetism and Transition Metal Complexes.* Chapman and Hall, London (1973).
19. N. Walker and D. Stuart, *Acta Cryst.* 1983, **A39**, 158.
20. G. M. Sheldrick, SHELXS86, Program for the Solution of Crystal Structures. University of Göttingen, Germany (1986).
21. B. A. Frenz, in *Computing in Crystallography* (Edited by H. Schenk, R. Olthof-Hazekamp, H. van Koningsveld and G. C. Bassi). Delft University Press, Delft (1978).
22. W. H. Zachariazen, *Acta Cryst.* 1963, **16**, 1139.
23. *International Tables for X-ray Crystallography*, Vol. IV, Table 2.2A. Kynoch Press, Birmingham (1974).
24. W. J. Geary, *Coord. Chem. Rev.* 1971, **7**, 81.
25. G. Bojesen, *Org. Mass Spectrom.* 1985, **20**, 413.
26. M. R. Malachowski and M. G. Davidson, *Inorg. Chem. Acta* 1989, **162**, 199.
27. E. Bermejo, A. Castiñeiras, R. Dominguez, W. Hiller and J. Strähle, *Fourteenth European Crystallographic Meeting.* Enschede, The Netherlands (1992).
28. A. G. Orpen, L. Brammer, F. H. Allen, O. Kennal, D. G. Watson and R. Taylor, *J. Chem. Soc., Dalton Trans.* 1989, S1.
29. S. C. Wallwork, *Acta Cryst.* 1962, **15**, 758.
30. G. C. Pimentel and A. L. McClelland, *The Hydrogen Bond.* Freeman, San Francisco (1960).
31. M. Ohsaku, *Bull. Chem. Soc. Japan* 1975, **48**, 707.
32. K. Nakamoto, *Infrared Spectra of Inorganic and Coordination Compounds*, 2nd edn. Willey Interscience, New York (1971).
33. J. R. Ferraro, *Low-Frequency Vibrations of Inorganic and Coordination Compounds.* Plenum Press, New York (1971).
34. A. B. P. Lever, *Inorganic Electronic Spectroscopy*, 2nd edn. Elsevier, Amsterdam (1984).
35. R. L. Carlin, *Magnetochemistry.* Springer-Verlag, Berlin (1986).

Polyhedron Vol. 12, No. 9, pp. 1093–1096, 1993
Printed in Great Britain

0277–5387/93 $6.00+.00
© 1993 Pergamon Press Ltd

SYNTHESIS, CHARACTERIZATION AND SCAVENGER EFFECTS ON OH$^{\cdot}$ AND $O_2^{-\cdot}$ RADICALS OF LANTHANIDE(III) COMPLEXES WITH PYRUVIC ACID SEMICARBAZONE

SHUYAN YU, SHUANGXI WANG and QINHUI LUO

Coordination Chemistry Institute, Nanjing University, Nanjing 210008, P.R.C.

and

LIUFANG WANG,* ZHOUREN PENG and XING GAO

Department of Chemistry, Lanzhou University, Lanzhou 730000, P.R.C.

(*Received* 1 *October* 1992; *accepted* 20 *November* 1992)

Abstract—Complexes of lanthanide chlorides with pyruvic acid semicarbazone (PASH), having the general formula $Ln(PAS)_3 \cdot nH_2O$ (where Ln = La–Nd, Sm–Dy, Er, Yb; n = 1–3), have been synthesized and characterized on the basis of elemental analyses, IR spectra and thermal analyses. It has been found that the ligand and its complexes possess scavenger effects on OH$^{\cdot}$ and $O_2^{-\cdot}$ radicals.

Thiosemicarbazones, semicarbazones and their metal complexes have aroused great interest due to their possession of a broad spectrum of biological activity.[1–7] Moreover, in many cases it has been suggested that the biological activities of thiosemicarbazones and semicarbazones can be increased on being coordinated or mixed with suitable metal ions.[8–10] This idea led us to prepare thiosemicarbazones[11] and semicarbazone-metal complexes with a view to evaluate their biological properties.

Although some transition metal complexes with pyruvic acid semicarbazone (= PASH) have been reported,[12–14] no paper concerning the study of lanthanide(III) complexes with this ligand has yet appeared. Therefore, we now wish to report the synthesis characterization of lanthanide(III) complexes with PASH and discuss their biological properties.

EXPERIMENTAL

All chemicals used were of reagent grade. All biochemicals were obtained from Sigma Chemical Co. The hydrated lanthanide(III) chlorides were prepared by dissolving the respective oxides (99.95%) in concentrated HCl. The ligand pyruvic acid semicarbazone was prepared according to the literature method.[15] The purity of the ligand was confirmed by elemental analysis and ^{1}H NMR spectroscopy. δH: 2.05 (3H, s, —CH_3), 7.04 (2H, s, —NH_2), 9.92 (1H, s, —NH), 11.15 (1H, s, —COOH).

Preparation of the complexes

A solution of an appropriate lanthanide(III) chloride (1 mmol) in water (20 cm^3) was added dropwise to a solution of NaOH (3 mmol) and PASH (3 mmol) in water (20 cm^3). After stirring for 4 h at room temperature a precipitate was collected by filtration, washed with water until the Cl^- ions disappeared and dried in a vacuum desiccator over P_4O_{10}. The elemental analyses of the complexes are given in Table 1.

Physical measurements

Carbon, hydrogen and nitrogen were determined using a Carlo-Erba 1106 elemental analyser. The metal contents of the complexes were estimated by titration with EDTA. The IR spectra were recorded on a Nicolet-170SX FT-IR spectrophotometer using KBr discs in the range 4000–200 cm^{-1}. ^{1}H NMR spectra were obtained using a

* Author to whom correspondence should be addressed.

Table 1. Colours and analytical data of the ligand and its complexes

Compound	Colour	Calc. (%) C	H	N	M	Found (%) C	H	N	M
PASH	White	33.1	4.8	28.9	—	33.3	4.8	28.6	—
$La(PAS)_3 \cdot H_2O$	White	24.5	3.4	21.4	23.6	24.6	3.5	21.3	23.4
$Ce(PAS)_3 \cdot H_2O$	Yellow	24.4	3.4	21.4	23.7	24.6	3.1	21.6	23.8
$Pr(PAS)_3 \cdot H_2O$	Light green	24.4	3.4	21.3	23.7	24.5	3.5	21.3	23.9
$Nd(PAS)_3 \cdot H_2O$	Light violet	24.2	3.4	21.2	24.3	24.4	3.3	21.2	24.4
$Sm(PAS)_3 \cdot H_2O$	White	24.0	3.3	21.0	25.0	24.1	3.2	20.9	25.2
$Eu(PAS)_3 \cdot H_2O$	White	23.9	3.3	21.0	25.3	23.8	3.4	20.8	25.4
$Gd(PAS)_3 \cdot 3H_2O$	White	22.4	3.7	20.6	24.5	22.2	3.7	19.4	24.5
$Tb(PAS)_3 \cdot 3H_2O$	White	22.3	3.7	19.5	24.5	22.3	3.7	19.4	24.7
$Dy(PAS)_3 \cdot 3H_2O$	White	22.2	3.7	19.4	25.1	22.1	3.6	19.4	25.0
$Er(PAS)_3 \cdot 3H_2O$	Light red	22.0	3.7	19.3	25.6	22.5	4.0	18.4	25.5
$Yb(PAS)_3 \cdot 2H_2O$	White	22.5	3.4	19.7	27.0	22.8	3.6	19.8	27.1

Varian FT-80A spectrometer with $CDCl_3$ as the solvent and TMS as the internal reference. Thermal analyses were performed using a Du Pont 1090 thermal analyser. Gas chromatography was performed using a Shimadzu GC-8A gas chromatograph spectrometer. Absorbances were determined on a 751-spectrophotometer at 560 nm.

Tests for scavenger effects on $OH^{\bullet}$ *and* $O_2^{-\bullet}$

The hydroxyl radicals ($OH^{\bullet}$) were produced by the H_2O_2/Fe^{2+}-EDTA/ascorbic acid[16] system and determined by their reaction with 3-methylthiopropionaldehyde to give ethylene. The reaction mixture (5 cm^3) contained Fe^{2+}-EDTA (0.1 mM), 3-methylthiopropionaldehyde (0.1 mM), L-ascorbic acid (0.20 mM), H_2O_2 (0.40 mM), the tested compound (0.3 mM) and NaH_2PO_4–K_2HPO_4 buffer (0.01 M) (pH = 7.4). The reaction was left for 0.5 h at a constant 37°C. The amount of ethylene produced was detected by gas chromatography. The suppression ratio for $OH^{\bullet}$ was calculated from the following expression:

$$\text{Suppression ratio} = 100 \times \frac{M_0 - M}{M_0},$$

where M = ethylene content in the presence of the ligand or its complexes and M_0 = ethylene content in the absence of the ligand or its complexes.

The superoxide radicals ($O_2^{-\bullet}$) were produced by a system of NADH/PMS (phenazine methosulphate)/NBT (nitro blue tetrazolium)[17] and measured by the amount of NBT reduced by $O_2^{-\bullet}$. The reaction mixture (5 cm^3) contained NADH (79 μM), PMS (30 μM), NBT (75 μM), tris-HCl buffer (0.01 M) (pH = 8.0) and the tested compound (3 μM). The reaction was left for 5 min at room temperature. The amount of reduced NBT was detected by the absorbance at 560 nm, since the reduced product, blue formazan, absorbs at this wavelength. The suppression ratio for $O_2^{-\bullet}$ was calculated from the following expression:

$$\text{Suppression ratio} = 100 \times \frac{A_0 - A}{A_0}$$

where A = the absorbance in the presence of the ligand or its complexes and A_0 = the absorbance in the absence of the ligand or its complexes.

RESULTS AND DISCUSSION

The elemental analyses of the lanthanide(III) complexes (see Table 1) show that the lanthanide(III) ions form 1:3 (metal:ligand) complexes having the general formula $Ln(PAS)_3 \cdot nH_2O$ (where Ln = La–Nd, Sm–Dy, Er, Yb; n = 1–3). These data also show that all the complexes contain water molecules, which was also confirmed by the thermal studies and IR spectra of the complexes. The complexes are stable at room temperature and insoluble in most common organic solvents, but they are slightly soluble in DMF and DMSO.

Thermal analysis

The TG curves of the complexes show a weight loss between 35 and 150°C. The weight loss corresponds to one water molecule for La–Eu (except Pm) complexes; two water molecules for the Yb complex and three water molecules for Gd–Dy and Er complexes. These results are in accordance with the compositions of the complexes determined by elemental analyses. Although the dehydration temperature for some complexes is relatively high (over

Table 2. Thermal studies for dehydration and decomposition process of typical complexes

Thermal reaction	Temperature (°C)	Process	% Weight loss Found	Calc.
$La(PAS)_3 \cdot H_2O \rightarrow La(PAS)_3 + H_2O$	35–80	Endothermic	3.4	3.0
$La(PAS)_3 \rightarrow La_2O_3 +$ products	320–700	Exothermic	72.1	71.5
$Nd(PAS)_3 \cdot H_2O \rightarrow Nd(PAS)_3 + H_2O$	35–85	Endothermic	3.2	3.0
$Nd(PAS)_3 \rightarrow Nd_2O_3 +$ products	320–709	Exothermic	71.4	70.9
$Tb(PAS)_3 \cdot 3H_2O \rightarrow Tb(PAS)_3 + 3H_2O$	51–121	Endothermic	8.1	8.3
$Tb(PAS)_3 \rightarrow Tb_4O_7 +$ products	353–618	Exothermic	69.0	68.5
$Er(PAS)_3 \cdot 3H_2O \rightarrow Er(PAS)_3 + 3H_2O$	50–140	Endothermic	8.6	8.2
$Er(PAS)_3 \rightarrow Er_2O_3 +$ products	260–633	Exothermic	68.4	68.2
$Yb(PAS)_3 \cdot 2H_2O \rightarrow Yb(PAS)_3 + 2H_2O$	50–148	Endothermic	6.0	5.6
$Yb(PAS)_3 \rightarrow Yb_2O_3 +$ products	320–637	Exothermic	68.1	67.6

100°C), it appears that the water molecules in these complexes are present as crystal water, since no characteristic band due to coordinated water is observed in the far-IR spectra of the complexes. The higher dehydration temperature for some complexes may be due to the existence of relatively strong hydrogen bonds between water molecules and the ligand in the complexes in the solid state, as was observed in the manganese complex with PASH whose crystal structure was determined by single-crystal X-ray diffraction.[18] The complexes undergo decomposition over the range 260–710°C. The final products are metal oxides in all cases. The thermal analytical data of typical complexes are given in Table 2.

IR spectra

The important data for the ligand and its complexes are listed in Table 3. In the IR spectra of the complexes the bands at 3567–3518 cm^{-1} assigned to $\nu(OH)(H_2O)$, which are absent in the free ligand, are weak and broad, indicating that the water in all of these complexes is crystal water.[19] This is further supported by the absence of any modes of coordinated water.[20] The strong band at ~ 3440 in the free ligand assigned to $\nu(NH_2)$ vibrations of the terminal $-NH_2$ group is unchanged or slightly shifted towards the higher side in all the complexes, suggesting that the $-NH_2$ group is not involved in bonding. The bands at 1750, 1679 and 1620 cm^{-1} in

Table 3. Some characteristic IR data (cm^{-1}) and their assignments for the ligand and its complexes

Complex	ν(O—H)	ν(C=O) carboxyl group	ν(C=O) semicarbazide moiety	ν(C=N)
PASH	—	1750s	1679s	1620s
$La(PAS)_3 \cdot H_2O$	3567wb	1663s	1617s	1545s
$Ce(PAS)_3 \cdot H_2O$	3565wb	1681s	1618s	1544s
$Pr(PAS)_3 \cdot H_2O$	3542wb	1657s	1618s	1546s
$Nd(PAS)_3 \cdot H_2O$	3562wb	1656s	1619s	1545s
$Sm(PAS)_3 \cdot H_2O$	3541wb	1679s	1625s	1554s
$Eu(PAS)_3 \cdot H_2O$	3532w	1679s	1626s	1556s
$Gd(PAS)_3 \cdot 3H_2O$	3556wb	1679s	1625s	1555s
$Tb(PAS)_3 \cdot 3H_2O$	3529w	1681s	1625s	1556s
$Dy(PAS)_3 \cdot 3H_2O$	3546wb	1680s	1625s	1557s
$Er(PAS)_3 \cdot 3H_2O$	3532w	1683s	1625s	1556s
$Yb(PAS)_3 \cdot 2H_2O$	3518w	1681s	1625s	1556s

s: strong; m: medium; w: weak; b: broad; sh: shoulder.

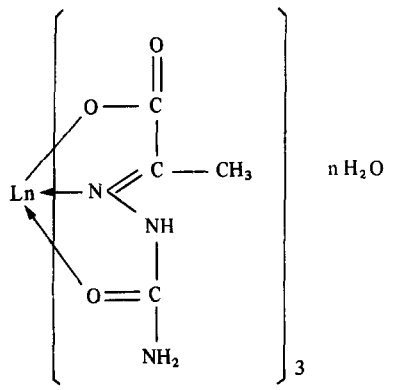

Ln = La - Nd, Sm - Dy, Er, Yb; n = 1-3

Fig. 1.

Table 4. Data of scavenging effects on $OH^{\cdot}$ and $O_2^{-\cdot}$ of the ligand and its complexes

Compound	Average suppression ratio for $OH^{\cdot}$ (%)	Average suppression ratio for $O_2^{-\cdot}$ (%)
PASH	46	61
Ce	88	97
Er	87	64
Yb	71	66

the free ligand, assigned to ν(C=O) of the carboxyl group, ν(C=O) of the semicarbazide moiety and ν(C=N) vibrations, respectively, shift towards lower wave numbers in all the complexes. This indicates that the pyruvic acid semicarbazone behaves as a tridentate ligand,[12] i.e. the ligand coordinates to the metal ion through the C=N nitrogen, the oxygen of the semicarbazone and the oxygen of the carboxylic group, forming two five-membered rings around the metal ion. The metal ion seems to be nine-coordinated. On the basis of the above discussion, the probable structure of the complexes is proposed and shown in Fig. 1.

The scavenger effects on $OH^{\cdot}$ *and* $O_2^{-\cdot}$

The suppression ratios of the ligand and its complexes for $OH^{\cdot}$ and $O_2^{-\cdot}$ radicals are summarized in Table 4. The results show that the ligand and its complexes possess scavenging effects on $OH^{\cdot}$ and $O_2^{-\cdot}$.

The suppression ratios of the complexes for $OH^{\cdot}$ and $O_2^{-\cdot}$ are mostly higher than that of the ligand. Also, it has been observed that the scavenging effects on $OH^{\cdot}$ and $O_2^{-\cdot}$ of the cerium complex are stronger than the other complexes. This may be due to the variable valency (III, IV) of the cerium ion.

Acknowledgement—This research was supported by grants from the State Key Laboratory of Applied Organic Chemistry, Lanzhou University.

REFERENCES

1. G. Domagk, R. Behnisch, F. Mietzsch and H. Schmidt, *Naturwissenschaften* 1946, **33**, 315.
2. J. D. Garber, U.S. Patent 2749270, 5 June 1956.
3. S. Padhy and G. B. Kauffman, *Coord. Chem. Rev.* 1985, **63**, 127.
4. R. W. Brockman, J. R. Thomson, M. J. Bell and H. E. Skipper, *Cancer Res.* 1956, **16**, 167.
5. D. H. Jones, R. Slack, S. Squares and K. R. H. Wooldridge, *J. Med. Chem.* 1965, **8**, 676.
6. Z. Xinde, W. Chenggang, L. Zhifeng, M. Shangyun, Y. Zhenhuan and W. Zishen, *Synth. React. Inorg. Met.-Org. Chem.* 1991, **21**, 1365.
7. W. Zishen, G. Ziqi and Y. Zhenhuan, *Synth. React. Inorg. Met.-Org. Chem.* 1990, **20**, 335.
8. K. N. Thimmaiah, W. D. Lloyd and G. T. Chandrappa, *Trans. Met. Chem.* 1985, **10**, 94.
9. Y. Okada, Japan Patent. 7017189 (1970); *Chem. Abstr.* 1970, **73**, 77252y.
10. R. S. Srivastava, *J. Inorg. Nucl. Chem.* 1980, **42**, 1526.
11. S. Y. Yu, Q. H. Lou, L. F. Wang and Z. R. Peng, unpublished results.
12. G. L. Sauhney, J. S. Bcijal, S. Chandra and K. B. Pandeya, *Acta Chim. Acad. Scient., Hung. Tomus* 1981, **108**, 325.
13. S. Chandra and K. K. Sharma, *Trans. Met. Chem.* 1984, **9**, 1.
14. V. M. Leovac, V. I. Cesljevic, D. Z. Obadovic, D. M. Petrovic and S. Y. Chundak, *Z. Anorg. Allg. Chem.* 1989, **570**, 177.
15. M. Pankaskie and M. M. Abdel-Monem, *J. Pharm. Sci.* 1980, **69**, 1000.
16. C. C. Winterbourm, *Biochem. J.* 1981, **198**, 125.
17. V. Ponti, *Chem-Biol. Interact.* 1978, **23**, 281.
18. L. F. Wang, X. Wang, Z. R. Peng, S. Y. Yu, Q. H. Lou and Q. Wang, *Polyhedron*, submitted.
19. G. Ertem and X. West, *Trans. Met. Chem.* 1985, **10**, 131.
20. K. Nakamato, *Infrared and Raman Spectra of Inorganic and Coordination Compounds*, 3rd edn, Wiley, New York (1978).

Polyhedron Vol. 12, No. 9, pp. 1097–1099, 1993
Printed in Great Britain

0277–5387/93 $6.00+.00
© 1993 Pergamon Press Ltd

SYNTHESIS AND CRYSTAL STRUCTURE OF PYRIDINE[NN′-ETHYLENEBIS(SALICYLIDENEIMINATO)](ISO-BUTYL)COBALT(III)

HUILAN CHEN,* DEYAN HAN, HONG YAN and WENXIA TANG

Department of Chemistry and Coordination Chemistry State Key Laboratory, Nanjing University, Nanjing 210008, P.R.C.

and

YAO YANG and HUAQIN WANG

Centre of Materials Analysis, Nanjing University, Nanjing 210008, P.R.C.

(*Received* 31 *July* 1992; *accepted* 2 *November* 1992)

Abstract—The title complex pyridine[NN′-ethylenebis(salicylideneiminato)](iso-butyl)-cobalt(III) [$C_4^iH_9Co(salen)(py)$] has been synthesized and characterized and its crystal structure has been determined by X-ray diffraction methods. The crystal consists of discrete molecules with distorted octahedral stereochemistry around the cobalt(III) ion. The tetradentate "salen" ligand is in the equatorial plane and $C_4^iH_9$ and pyridine occupy the two axial positions. The lengths of axial Co—C and Co—N bonds are 2.003(4) and 2.184(3) Å, respectively.

As is well known, co-enzyme B_{12} (5′-deoxyadenosylcobalamin) was the first reported example of a naturally occurring organometallic compound. It serves as a co-factor for various rearrangement reactions in biological systems.[1] It is important to prepare the related organocobalt compounds containing Co—C σ-bonds as co-enzyme B_{12} models and to study the crystal structure of these compounds. Unfortunately, among the number of B_{12} model compounds only a few organocobalt(III) Schiff base complexes have undergone crystal structure determinations and there is a lack of X-ray diffraction data for those salen Schiff base complexes with both secondary alkyl and pyridine axial ligands.[2,3] Recently we prepared a new alkylcobalt(III) Schiff base complex [$C_4^iH_9Co(salen)(py)$] and in this paper we describe its synthesis and structure determination.

EXPERIMENTAL

Preparation

The title complex was prepared by dissolving 60 mg of $C_4^iH_9Co(salen)(H_2O)$[4] in pyridine (10 cm^3), after the addition of light petroleum/ether (5 cm^3), allowing the solvents to evaporate slowly at room temperature. All manipulations were performed in the dark. The purple crystal can be obtained in 15 days. Found: C, 64.8; H, 6.1; N, 9.2; Co, 12.9. Calc. for $C_{25}H_{28}CoN_3O_2$: C, 65.1; H, 6.1; N, 9.1; Co, 12.8%.

Characterization

IR spectra were recorded on a Shimadzu IR-440 spectrophotometer with KBr pellets. UV–vis spectra were performed on a Shimadzu UV-240 spectrophotometer. All manipulations for preparing the solutions were performed in the dark. TG and DTA analyses were determined on a ZRY-1 Thermal Analyser under a nitrogen flow at a heating rate of 10°C min^{-1}.

Crystal data

$C_{25}H_{28}CoN_3O_2$, $M = 461.45$; monoclinic, $a = 9.476(9)$, $b = 19.621(9)$, $c = 12.383(3)$ Å; $\beta = 106.5(4)°$, $V = 2288.6$ Å^3, $Z = 4$, $D_c = 1.339$ g cm^{-3}, Mo-K_α radiation, $\lambda = 0.71073$ Å, μ(Mo-K_α) = 7.7 cm^{-1}, $F(000) = 968e$, space group $P2_1/c$.

* Author to whom correspondence should be addressed.

Data collection, structure solution and refinement

Data were collected at room temperature from a specimen measuring $0.4 \times 0.3 \times 0.3$ mm^3 on an Enraf–Nonius CAD4 four-circle diffractometer. 4922 reflections were collected by the $\omega/2\theta$ scan mode within the range $2° \leqslant 2\theta \leqslant 50°$, giving 4354 unique reflections, of which 3356 with $I > 3\sigma(I)$ were used in the structure refinement. Crystal monochromatized Mo-K_α radation ($\lambda = 0.71073$ Å) was used. Intensity data were corrected for Lorentz and polarization effects and empirically for absorption. The position of the cobalt atom was found by direct methods. Several cycles of difference-Fourier syntheses revealed all the non-hydrogen atoms. Full-matrix least-squares refined anisotropic thermal parameters on all the non-hydrogen atoms. All hydrogen atoms were located on difference-Fourier maps and refined isotropically. The final R and Rw [$w = 1/\sigma^2(F_o)$] factors are 0.038 and 0.043, respectively. The maximum peak in the final difference-Fourier analysis was 0.212 e Å^{-3}. All calculations were performed on a PDP11/44 computer using the SDP-PLUS program package.

Atomic fractional coordinates, anisotropic thermal parameters, bond lengths and bond angles, important equations of least-square planes and interplanar angles are deposited with the Editor as supplementary material. Atomic coordinates have also been deposited with the Cambridge Crystallographic Data Centre.

DISCUSSION

The structure of the alkylcobalt(III) complex and the packing diagram of the unit cell are shown in Figs 1 and 2, respectively.

The crystal contains discrete molecules with distorted octahedral stereochemistry around the cobalt(III) ion. The salen ligand occupies the four equatorial positions, whereas the $C_4^iH_9$ group and the pyridine molecule occupy the two axial positions. The structure determination shows that the cobalt atom is almost in the plane of the equatorial donors $N_1N_2O_2O_1$ (which are co-planar within ± 0.080 Å). The two salicylaldimine residues are bent towards the $C_4^iH_9$ group and assume an umbrella shape ($\alpha = 4.1$, $\beta = 12.1$, $\gamma = +16.1°$), with a slight twist between the planes of the aromatic rings. The pyridine plane is nearly perpendicular to the salicylaldimine plane (98.1°). The ethylene bridge atoms were not co-planar with $N_1N_2O_2O_1$ and the carbon atoms are asymmetrically displaced from the coordination plane leading to a "half-chair" (*gauche*) conformation of the ring. This conformation is preferred for asymmetric umbrella-shape molecules of salen derivatives.[2]

Important bond lengths and angles are given in Table 1. The distances for the Co-salen ligand are consistent with the average values reported for a series of salen compounds (Co—N 1.884, Co—O 1.904 Å).[2] The Co—C bond length (2.003 Å) of the title compound is not significantly different compared with the organometallic derivatives, but somewhat longer than in the vinyl analogue. [CH_2=CHCo(salen)py] shows a significantly shorter Co—C bond (1.930 Å), even after correction from an sp^2 to sp^3 carbon σ-covalent radius (1.950 Å).[5] On the other hand the Co—N(31) bond length is 2.184 Å. This is comparable with reported Co—N bond lengths *trans* to —CH=CH_2 (2.190 Å), —CH_2CN (2.092 Å) and —OCH_3 (2.031 Å) in octahedral salen compounds.

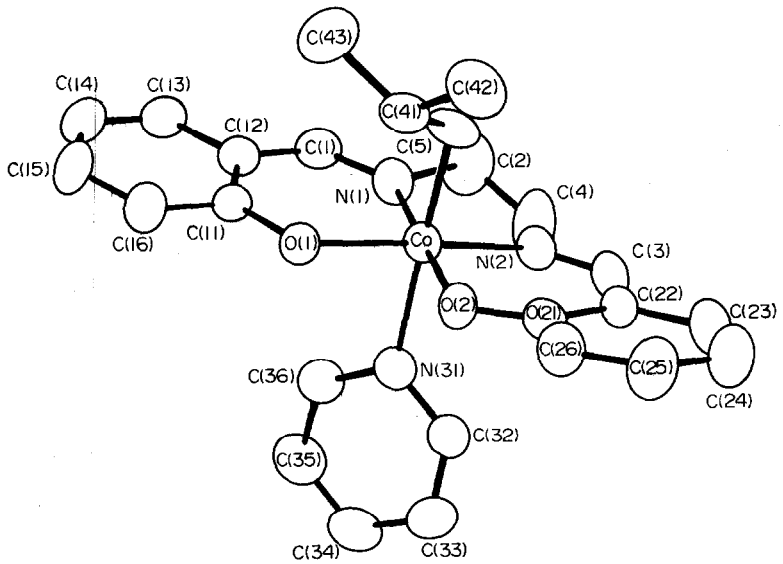

Fig. 1. Crystal structure of the molecule.

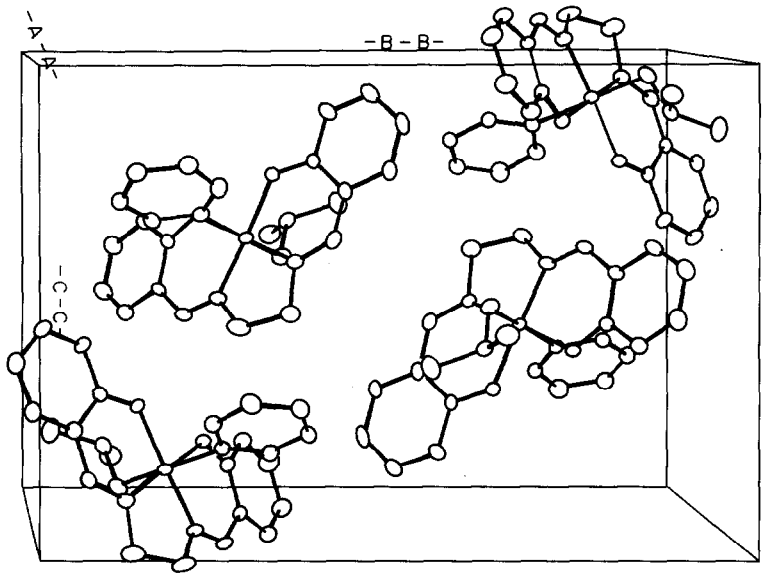

Fig. 2. Unit cell packing diagram.

Table 1. Important bond lengths (Å) and angles (°)

Co—N(1)	1.881(3)	Co—N(2)	1.878(3)
Co—O(1)	1.908(2)	Co—O(2)	1.901(2)
Co—O(5)	2.003(4)	Co—N(31)	2.184(3)
O(1)—Co—N(1)	93.5(1)	O(1)—Co—O(2)	87.6(1)
O(1)—Co—N(2)	175.8(1)	N(1)—Co—N(2)	85.5(1)
N(1)—Co—O(2)	178.8(1)	O(2)—Co—N(2)	93.5(1)
O(1)—Co—C(5)	92.6(1)	O(1)—Co—N(31)	87.2(1)
N(1)—Co—C(5)	91.8(2)	N(1)—Co—N(31)	92.8(1)
N(2)—Co—C(5)	91.5(1)	N(2)—Co—N(31)	88.7(1)
O(2)—Co—C(5)	87.6(1)	O(2)—Co—N(31)	87.8(1)
C(5)—Co—N(31)	175.3(2)	Co—N(31)—C(32)	120.0(2)
Co—N(31)—C(36)	122.7(3)	Co—C(5)—C(41)	115.2(3)

Acknowledgements—This research was supported by grants from the Natural Science Foundation of China and the Foundation of Centre of Material Analysis of Nanjing University.

REFERENCES

1. D. Dolphin (Editor), B_{12}, Vols 1 and 2. Wiley, New York (1982).
2. M. Calligaris, G. Nardin and L. Randaccio, *Coord. Chem. Rev.* 1972, **7**, 385.
3. L. Randaccio, N. Bresciani Pahor and E. Zangrando, *Chem. Soc. Rev.* 1989, **18**, 225.
4. G. N. Schrauzer, J. W. Sibert and R. J. Windgassen, *J. Am. Chem. Soc.* 1968, **90**, 6691.
5. M. Calligaris, G. Nardin and L. Randaccio, *J. Chem. Soc., Dalton Trans.* 1972, 1433.

Polyhedron Vol. 12, No. 9, pp. 1101–1102, 1993
Printed in Great Britain

0277–5387/93 $6.00+.00
© 1993 Pergamon Press Ltd

COMMUNICATION

A RAPID COBALT CARBONYL MEDIATED CLEAVAGE OF BOTH PHOSPHORUS–CARBON BONDS IN BIS(DIPHENYLPHOSPHINO)METHANE UNDER VERY MILD CONDITIONS: EXTRUSION OF METHYLENE AS KETENE

SHAMSUDDIN AHMED, DAVID G. HOLAH, ALAN N. HUGHES* and ROBERT T. MARKEWICH

Department of Chemistry, Lakehead University, Thunder Bay, Ontario, Canada P7B 5E1

(*Received* 29 *July* 1992; *accepted* 5 *February* 1993)

Abstract—In cobalt(II)/{bis(diphenylphosphino)methane}/$NaBH_4$/CO reactions, in which the $NaBH_4$ is added very rapidly, both P—C bonds of the phosphine are cleaved with extrusion of the methylene group as ketene.

It has been established[1] that the ease of transition-metal mediated phosphorus–carbon bond cleavage in tertiary phosphines is in the order P—C_{sp} > P—C_{sp^2} > P—C_{sp^3} and, therefore, the great majority of such reactions in the literature involve phosphorus bound to *sp* or sp^2 carbon.[2] While P—C_{sp^3} cleavage is the least common and normally requires more forcing conditions, several recent reports of this type of bond scission in bis(diphenylphosphino)methane (dppm) in the presence of di-iron,[3] platinum,[4] cobalt[5] or nickel[5] centres under comparatively mild conditions have appeared. These reactions normally result in the formation of products containing both the Ph_2P— and Ph_2PCH_2— fragments (or derivatives thereof) arising from a single P—C cleavage.[3a,4] However, products containing bridging Ph_2P— groups as in **1** and **2**, but with no trace of the Ph_2PCH_2— fragment, have also been reported;[5] there is one very recent report of a product containing both Ph_2P— fragments arising from a double P—C cleavage.[3b] In this last reaction (described as being unprecedented) $[Fe_2(CO)_6(\mu\text{-}CHCO_2Et)(\mu\text{-dppm})]$ under reflux in toluene generates[3b] ethyl acrylate and $[Fe_2(CO)_6(\mu\text{-}PPh_2)_2]$, probably via the formation of an $Fe_2(\mu\text{-}CH_2)$ unit followed by the intramolecular linking of the —CH_2— and —$CHCO_2Et$ bridges in the manner observed[6] for some other di-μ-alkylidene species. We report here evidence for another such double scission which occurs very rapidly under extraordinarily mild conditions and with the extrusion of methylene as ketene.

Examination of the filtrates obtained from reactions in which $NaBH_4$ is added very rapidly (< 1 min) to cobalt(II) and nickel(II) salts in ethanol/benzene under CO in the presence of dppm at room temperature (or below), giving[5] systems of types **1** and **2**, showed no traces of Ph_2PMe or

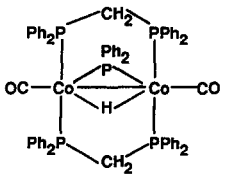

(1)

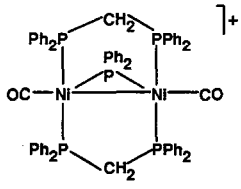

(2)

any other derivative of the Ph_2PCH_2— fragment. However, filtrates obtained from the cobalt(II) system (the cleanest of these reactions) always showed

* Author to whom correspondence should be addressed.

(GLC, MS)* the presence of ethyl acetate. Similar reactions performed in the absence of dppm showed no evidence of ethyl acetate formation. The $-CH_2-$ bridge in dppm is therefore extruded, together with CO, as ketene which then reacts[7] with the ethanol in the solvent mixture to give ethyl acetate with the entire reaction, starting from cobalt(II), being complete in *ca* 1 min at room temperature.

Clearly, there are important differences between the di-iron case[3] noted above and the cobalt(II) reactions leading to **1** in that the final product in the di-iron case contains two bridging phosphido units, while for **1** the second bridging species is hydride. Also, in the di-iron case the reaction requires more rigorous conditions (reflux) than pertain in the cobalt case (room temperature) and it is possible that the two reactions are mechanistically quite different. Mechanistic studies are in progress and the results of these studies will be the subject of a separate report.

Acknowledgement—We thank the Natural Sciences and Engineering Research Council of Canada for financial support.

REFERENCES

1. For a review, see P. E. Garrou, *Chem. Rev.* 1985, **85**, 171.
2. For some recent examples, see (a) B. J. Bobbie, N. J. Taylor and A. J. Carty, *J. Chem. Soc., Chem. Commun.* 1991, 1511; (b) V. V. Grushin, A. B. Vymenits, A. J. Yanovsky, Y. T. Struchkov and M. E. Vol'pin, *Organometallics* 1991, **10**, 48; (c) J. M. McFarland, M. R. Churchill, R. F. See, C. H. Lake and J. D. Atwood, *Organometallics* 1991, **10**, 3530.
3. (a) N. M. Doherty, G. Hogarth, S. A. R. Knox, K. A. Macpherson, F. Melchior and A. G. Orpen, *J. Chem. Soc., Chem. Commun.* 1986, 540; (b) G. Hogarth, S. A. R. Knox and M. L. Turner, *J. Chem. Soc., Chem. Commun.* 1990, 145.
4. (a) N. W. Alcock, P. Bergamini, T. J. Kemp and P. G. Pringle, *J. Chem. Soc., Chem. Commun.* 1987, 235; (b) P. Bergamini, S. Sostero, O. Traverso, T. J. Kemp and P. G. Pringle, *J. Chem. Soc., Dalton Trans.* 1989, 2017; (c) I. J. B. Lin, J. S. Lai and C. W. Liu, *Organometallics* 1990, **9**, 530.
5. D. J. Elliot, D. G. Holah, A. N. Hughes, H. A. Mirza and E. Zawada, *J. Chem. Soc., Chem. Commun.* 1990, 32.
6. R. E. Colborn, D. L. Davies, A. F. Dyke, S. A. R. Knox, K. A. Mead, A. G. Orpen, J. E. Guerchais and J. Roué, *J. Chem. Soc., Dalton Trans.* 1989, 1799.
7. *The Chemistry of Ketenes, Allenes and Related Compounds* (Edited by S. Patai). John Wiley, New York (1980).

* In a typical experiment, a solution of $CoCl_2 \cdot 6H_2O$ (0.22 g) and dppm (0.70 g) in degassed $EtOH/C_6H_6$ (1 : 1, 4 cm^3) was saturated with CO for 5 min and solid $NaBH_4$ (0.10 g) was added in one portion. After 1 min the mixture was filtered to remove **1** and some $[Co_2(\mu\text{-dppm})_2(CO)_4]$ and the filtrate was distilled to low volume. The metal- and phosphine-free distillate was examined by GLC on both Poropak Q and Chromosorb 101 columns. In each case ethyl acetate (not present in either of the solvents used for the reaction and not formed if dppm is absent from the reaction mixture) was detected. The retention times observed for each stationary phase were found to be identical to those observed for a standard sample of 1 : 1 $EtOH/C_6H_6$ containing 0.1% ethyl acetate, which, given the quantities of reagents and solvents used and the measured[5] yield of **1**, is representative of the low concentration which should be, and was, observed. Ethyl acetate formation was confirmed by low-voltage electron-impact mass spectrometric studies on the distillate. At 14 eV a weak peak assigned to the low concentration of ethyl acetate was observed at m/z 88. This peak decreased in intensity with increasing voltage, while a new peak at m/z 60 ($M-C_2H_4$, McLafferty elimination of ethylene) grew. This trend is clearer for the solvent system THF/C_6H_6, which, however, is not suitable for GLC studies since THF and ethyl acetate have similar retention times.

Polyhedron Vol. 12, No. 9, pp. 1103–1106, 1993
Printed in Great Britain

0277–5387/93 $6.00+.00
© 1993 Pergamon Press Ltd

COMMUNICATION

THE PREPARATION AND X-RAY STRUCTURE OF A SEVEN-COORDINATE TRIS(CATECHOLAMIDE)NIOBIUM(V) COMPLEX

DENNIS F. EVANS,✠ ALEXANDRA M. Z. SLAWIN, DAVID J. WILLIAMS,* CHIH Y. WONG and J. DEREK WOOLLINS*

The Evans and Chemical Crystallography Laboratories, Department of Chemistry, Imperial College, London SW7 2AY, U.K.

(*Received* 18 *December* 1992; *accepted* 1 *February* 1993)

Abstract—The preparation and crystal structure of the Nb^{V}(Htrencam)·DMSO complex is reported [where H_6trencam is the hexadentate tris(catecholamide) ligand and DMSO is dimethylsulphoxide], revealing a cavitand-like arrangement of the three catecholamide groups with the protonated non-binding nitrogen atom directed inwards to the niobium atom.

Biological metal encapsulation of iron(III) has been dominated by a group of low molecular weight macromolecules, the siderophores.[1] These are complexing agents that have a very high affinity for iron(III) and solubilize this otherwise insoluble ion, facilitating its transport into microbes such as bacteria and fungi. The synthetic analogue, H_6trencam [Fig. 1(a)], described by Raymond and co-workers,[2] has been well characterized for its ability to mimic the naturally occurring siderophore enterobactin [Fig. 1(b)]. The X-ray crystal structures of both K_3[Fe(trencam)]·CH_3OH·H_2O[3] and K_3[V(trencam)]·$4CH_3OH$·$2H_2O$[4] have been recently reported. Both anions show six-coordination by phenolic oxygen donors to form a distorted octahedral environment around the M^{3+} cation (M = Fe or V). An analogous ligand, H_6tripace [Fig. 1(c)], has been reported to chelate to titanium(IV) to form [NEt_3H][Ti(Htripace)], where the hexadentate chelate was protonated at the central nitrogen atom.[5]

Here, we describe the complex formed from the reaction between H_6trencam and $NbCl_5$ in refluxing ethanol, according to eq. (1).† This is the first neutral "trencam"-like bound metal complex.

The X-ray crystal structure‡ of Nb^{V}(Htrencam)·DMSO (Fig. 2) shows the niobium to be seven-coordinate. The "trencam" ligand binds to the niobium atom in a highly symmetric fashion via all six phenolic oxygen atoms. The C_3 sym-

* Authors to whom correspondence should be addressed.

† Preparation of Nb(Htrencam)·DMSO. $NbCl_5$ (0.35 g, 1.30 mmol) was added to H_6trencam·HBr·H_2O (0.85 g, 1.30 mmol) in ethanol (15 cm^3) under argon. The mixture was refluxed for 48 h and the orange solid filtered off. Nb^{V}(Htrencam)·DMSO recrystallized by slow diffusion of a DMSO solution layered with an ethanol/ether mixture. Mass spectrum (FAB$^-$, *m*-nitrobenzyl alcohol matrix): $m/z = 641$, corresponds to [Nb^{V}(trencam)]$^-$.

‡ Crystals of Nb^{V}(Htrencam)·DMSO suitable for X-ray diffraction measurements were obtained by slow diffusion (*ca* 2 months) from a DMSO solution layered with an ethanol/ether mixture. The resulting crystal quality was still extremely poor, the crystals giving diffuse diffraction patterns. Full data sets on two different crystals were obtained and we report that of the better crystal. *Crystal data.* Nb^{V}(Htrencam)·DMSO: $C_{29}H_{31}N_4O_{10}SNb$, $M = 720.6$, triclinic, $a = 9.798(6)$, $b = 12.136(6)$, $c = 12.860(11)$ Å, $\alpha = 91.64(5)$, $\beta = 99.61(6)$, $\gamma = 100.11(5)°$, $U = 1482$ Å^3, space group $P\bar{1}$, $Z = 2$, $D_c = 1.615$ Mg m^{-3}, μ(Mo-K_α) = 0.54 mm^{-1}, $\lambda = 0.71073$ Å, $F(000) = 740$. Siemens P4/PC diffractometer, room temperature, ω-scan method (2θ range 3.0–50.0°), graphite monochromated Mo-K_α radiation; 2955 observed reflections, [$|F_o| > 5.0\sigma(|F_o|)$], corrected for Lorentz and polarization factors. Refinement was by full-matrix least-squares to $R = 0.0765$, $R_w = 0.0744$. Computations were carried out on an IBM 386/70 using SHELXTL PC.[6] Atomic coordinates, and bond lengths and angles have been deposited at the Cambridge Crystallographic Data Centre.

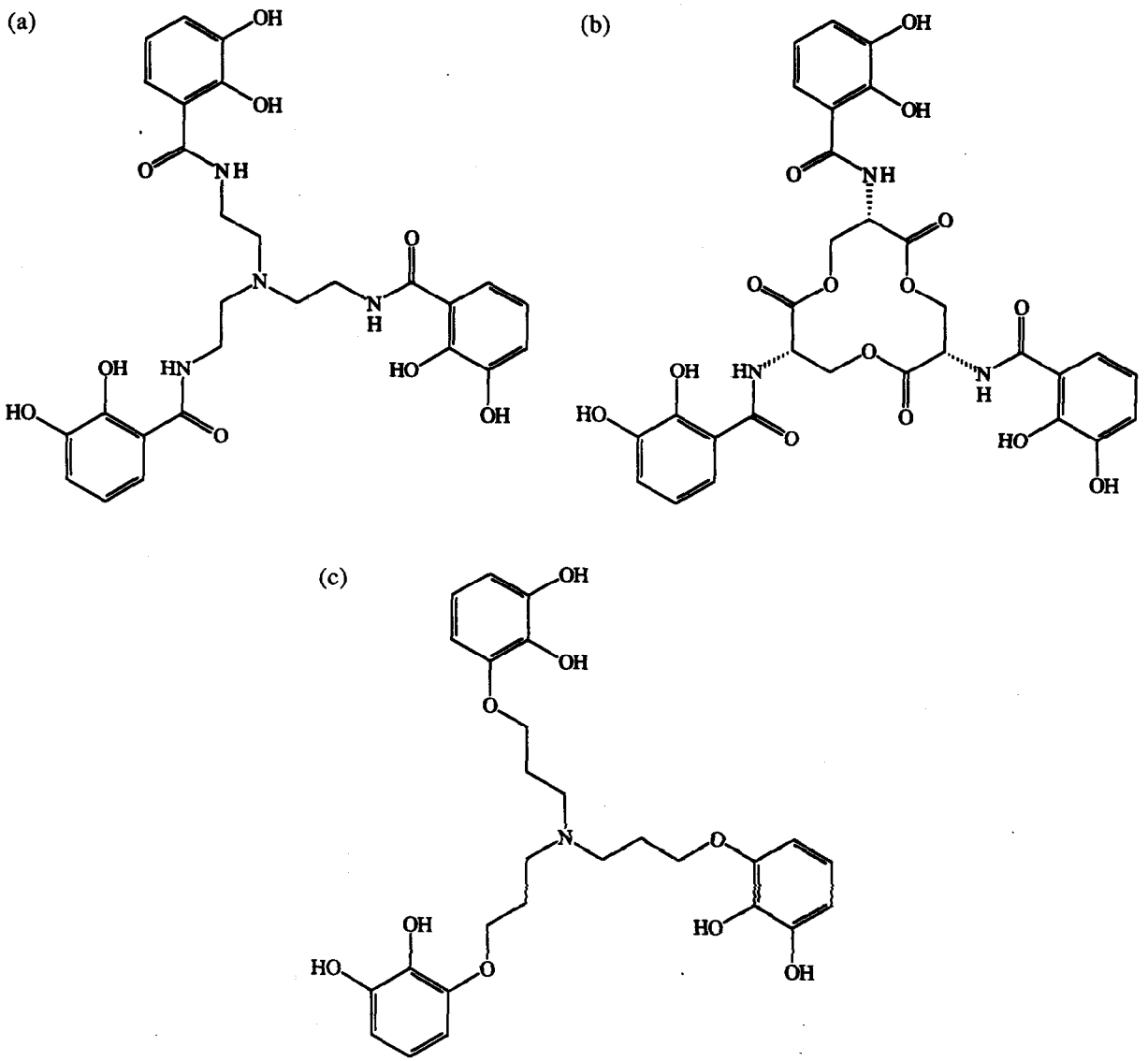

Fig. 1. Structure of (a) H_6trencam, (b) enterobactin and (c) H_6tripace.

Table 1. Selected bond lengths and angles with e.s.d.s in parentheses

Nb—O(1)	1.999(6)	Nb—O(2)	2.063(8)
Nb—O(1′)	1.967(8)	Nb—O(2′)	2.073(7)
Nb—O(1#)	1.997(7)	Nb—O(2#)	2.067(6)
Nb—O(11)	2.155(8)		

O(1)—Nb—O(2)	75.1(3)	O(1)—Nb—O(1′)	110.7(3)
O(2)—Nb—O(1′)	151.0(3)	O(1)—Nb—O(2′)	84.0(3)
O(2)—Nb—O(2′)	77.2(3)	O(1′)—Nb—O(2′)	75.2(3)
O(1)—Nb—O(1#)	117.8(3)	O(2)—Nb—O(1#)	87.0(3)
O(1′)—Nb—O(1#)	112.6(3)	O(2′)—Nb—O(1#)	149.0(3)
O(1)—Nb—O(2#)	149.4(3)	O(2)—Nb—O(2#)	78.0(3)
O(1′)—Nb—O(2#)	86.6(3)	O(2′)—Nb—O(2#)	75.9(2)
O(1#)—Nb—O(2#)	74.7(3)	O(1)—Nb—O(11)	74.3(3)
O(2)—Nb—O(11)	131.8(3)	O(1′)—Nb—O(11)	75.6(4)
O(2′)—Nb—O(11)	134.3(3)	O(1#)—Nb—O(11)	75.6(3)
O(2#)—Nb—O(11)			

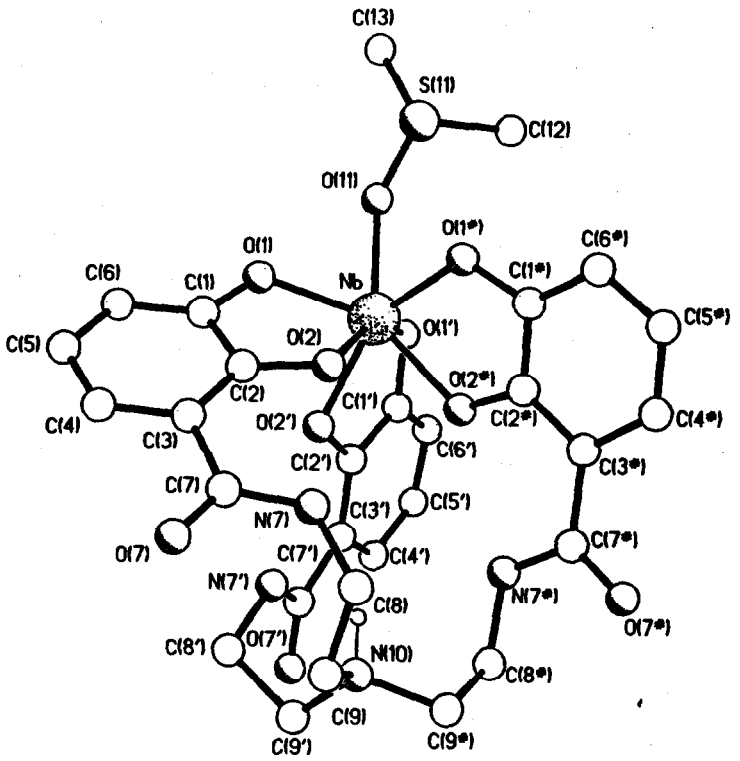

Fig. 2. The crystal structure of Nb^{V}(Htrencam)·DMSO.

metry [about the N(10)···Nb vector, Fig. 3] is broken only by the coordinated DMSO molecule.

$$Nb_5Cl + H_6trencam \xrightarrow[48\ h\ reflux]{EtOH}$$

$$\text{'Nb(Htrencam)'} \xrightarrow[DMSO/ethanol/ether]{Recryst.} \text{Nb(Htrencam)·DMSO} \quad (1)$$

The coordination polyhedron is a distorted monocapped trigonal prism (Fig. 4) with O(1)···O(1')···O(11) and O(1#)···O(2)···O(2#) forming the prism with O(2') as the capping atom. The Nb—O bond distances are slightly longer for the oxygen atoms O(2), O(2') and O(2#) (mean Nb—O 2.07 Å), cf. O(1), O(1') and O(1#) (mean Nb—O 1.99 Å, Table 1). All three amide groups are held co-planar with their associated catechol units by intramolecular N(7)—H···O(2) hydrogen bonds, thus stabilizing the macrobicyclic framework. The Nb—O(11) bond distance is longest at 2.155(8) Å, which reflects the weaker dative

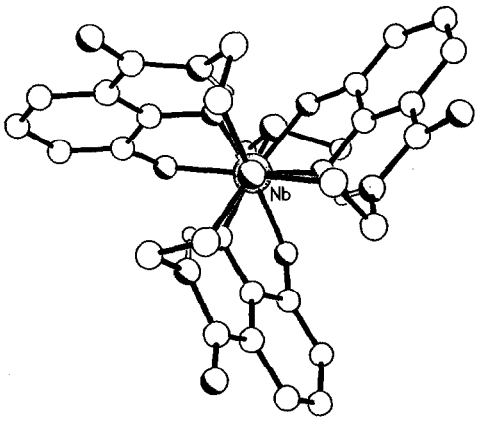

Fig. 3. The crystal structure of Nb^{V}(Htrencam)·DMSO, viewed down the C_3 axis.

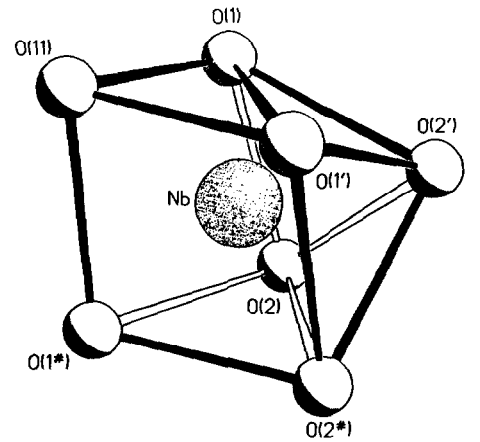

Fig. 4. Distorted monocapped trigonal prismatic representation of the coordination sphere of niobium in Nb^{V}(Htrencam)·DMSO.

bonding nature of DMSO. The central nitrogen [N(10)] is protonated in the "in" conformation [Nb···N(10) 5.91, Nb···H(10) 4.93 Å and N(10)—H(10)···Nb 176°]. The protonated "in" conformation is probably favoured by the three weak, equidistant (2.45 Å), intramolecular N(10)—H(10)···N(7) interactions. This protonation has not previously been observed for "trencam" complexes derived from vanadium(III) and iron(III), which also possess an "in" conformation.[3,4] The protonation of the central nitrogen may be dependent on a number of factors, including the experimental conditions and the metal ion involved. The structure reported here with protonation within the cavitand-like framework raises the possibility of the formation of bimetallic cavitand systems.

Acknowledgements—We are grateful to the SERC for an equipment grant. One of us (C.Y.W.) thanks the SERC for a grant.

REFERENCES

1. K. N. Raymond, *Coord. Chem. Rev.* 1990, **105**, 135.
2. S. J. Rodgers, C. W. Lee, C. Y. Ng and K. N. Raymond, *Inorg. Chem.* 1987, **26**, 1622.
3. T. D. P. Stark, T. B. Karpishin and K. N. Raymond, *J. Am. Chem. Soc.* 1992, **114**, 1512.
4. A. R. Bulls, C. G. Pippin, F. E. Hahn and K. N. Raymond, *J. Am. Chem. Soc.* 1990, **112**, 2627.
5. F. E. Hahn, S. Rupprecht and K. H. Moock, *J. Chem. Soc., Chem. Commun.* 1991, 224.
6. SHELXTL PC, Version 4.2, Siemens X-Ray Analytical Instruments (1991).

Polyhedron Vol. 12, No. 9, pp. 1107–1113, 1993
Printed in Great Britain

0277–5387/93 $6.00+.00
© 1993 Pergamon Press Ltd

COMMUNICATION

SIMULATION OF COPPER(II) COORDINATION POLYHEDRON DISTORTION: AN IMPROVEMENT OF THE MOLECULAR MECHANICS MODEL BASED ON COULOMBIC INTERACTIONS

J. SABOLOVIĆ*

Chemistry Department A, The Technical University of Denmark,
DK-2800 Lyngby, Denmark

(*Received* 11 *December* 1992; *accepted* 1 *February* 1993)

Abstract—In order to reproduce the shapes of distorted coordination polyhedra of tetra-coordinated copper(II) complexes by means of a molecular mechanics method, an electrostatic model was proposed (J. Sabolović and N. Raos, *Polyhedron* 1990, **9**, 2419). With the model a square-planar complex was defined as an octahedron consisting of four charges situated in the coordination plane, and two charges (denoted as X and X′) above and below the plane. The model proved good in reproducing the geometry of both planar and non-planar copper(II)-aminoacidates. The analysis of the potential energy surface for the coordination polyhedron distortion showed, however, that besides two "real" (*trans*- and *cis*-planar) minima, a large series of "false" minima (distorted pyramids, trigonal bipyramids) appeared with a lower conformational energy than the "real" ones. The reason for their occurrence was the lack of a repulsive potential between apically placed charges, so the system was able to degenerate easily to the "penta-coordinated" complex (X—M—X′ = 0°). The repulsive coulombic interaction between the apically placed charges is now introduced. The empirical parameters used are the same except the bond-stretching parameter $k_{b,MX}$ is chosen in such a way as to give the same M—X value as before. The new model reproduces the copper(II)-aminoacidato geometries in the same manner as the old model or slightly better. From the shape of the potential energy surface in the space of *trans*-valence angles for the "complex" $CuX_2N_2O_2$ it can be concluded that: the degeneracy to the "penta-coordinated" complex is suppressed but three "false" minima that correspond to three distorted pyramids (X—M—X = 105°) are left; while in the previous model the energy difference between the *trans*-planar minimum and the pyramid with the lowest conformational energy was 70.61 kJ mol^{-1}, in the new model the corresponding difference is 0.78 kJ mol^{-1}. Tetrahedral configuration would be possible to achieve only by choosing a very small value of $k_{b,MX}$. The appearance of the distorted pyramid minima opens a possibility of the application of the new model to penta-coordinated copper(II) complexes.

In order to reproduce and predict geometrical and thermodynamical properties of tetra-coordinated copper(II)-aminoacidates three kinds of molecular mechanics models were proposed: a "dummy" atom model,[1,2] models with a distortion potential[3–5] and a model based on coulombic interactions.[6] The models differ with respect to the choice of empirical potentials for the description of interactions inside the copper(II) coordination sphere. The reason for their development was a need for a model that could reproduce, not only the chelate rings geometries, but also the shapes of copper(II) coordination polyhedra (usually an irregular square-planar or a flattened tetrahedron).

* On leave from the Institute for Medical Research and Occupational Health, University of Zagreb, Zagreb, Croatia.

Among the six available models the model based on coulombic interactions, Model 6, gave the best agreement with the X-ray structures of copper(II) complexes with amino acids and their N-alkylated derivatives.[6] Therefore, the electrostatic model was selected for further development in an attempt to determine a force field suitable for dealing with the class of compounds of our interest.

The model was termed electrostatic because of the assumption that repulsive coulombic interactions among the non-bonded atoms of the coordination polyhedron determine its shape.* The coordination polyhedron was defined with five "real" atoms (M, N, N′, O and O′), situated in the plane of the chelate rings, and two "dummy" ligand atoms (denoted as X and X′), imagined to represent an electron pair placed half above and half below the plane. As a counterbalance to these coulombic interactions (between all non-bonded atoms, except between X and X′) only harmonic bond-stretching interactions with the metal atom were calculated.

It was shown,[6] however, that the absence of any interaction between apically placed charges was a short-coming of the model. Namely, the checking of the model on the $CuX_2N_2O_2$ "molecule", in order to analyse its ability to simulate the plasticity† of copper(II) coordination without "additional" sterical influences of the rest of the molecule, showed that besides two "real" (*trans*- and *cis*-planar) minima, a large series of "false" minima (distorted pyramids, trigonal bipyramids, even linear molecules) appeared, some of them with a lower conformational energy than the "real" ones. The model appeared to be reliable for not too great deviations from planarity (15–30° for *trans*-valence angles around copper), otherwise the system could degenerate easily to the "penta-coordinated" complex, i.e. the "dummy" atoms came on top of each other (X—M—X′ = 0°). Since the deviation from planarity in the real molecules was not so high, the model was able to reproduce the geometry of the coordination polyhedra in a proper way. However, the change of coordination from "octahedral" into the "penta-coordinated" complex might cause problems during the process of empirical parameters' optimization with respect to experimental data. Therefore, a repulsive coulombic interaction between the "dummy" atoms has to be introduced.

The influence of this particular interaction on the reproduction of the copper(II)-aminoacidato geometries, as well as on the potential energy surface for coordination polyhedron distortion, in comparison with the results of Model 6, have been investigated. For this reason all the empirical parameter values are left the same as in Model 6, except for the bond-stretching parameter $k_{b,MX}$. The parameter for the M—X bond is calculated in such a way as to give the same b_{MX} distance as before,[6] from the condition that at the distance b_{MX} from the central metal atom there is an equilibrium of attractive bonding (between M and X, $b_{0,MX} = 0$) and the repulsive coulombic forces (between X and other ligated atoms):

$$k_{b,MX} = \frac{qq_X}{\varepsilon_r} k'_b; \qquad (1)$$

where q is the charge parameter for atom O or N (it is taken to be equal), q_X is the charge parameter for the "dummy" atom X, ε_r is the effective dielectric constant and k'_b is a sterical parameter dependent on the geometry of the system (appropriate bond lengths, b, valence angles, θ, and non-bonded distances, r, between atoms in coordination polyhedron). By introducing the interaction between apically placed charge k'_b becomes dependent also on the ratio between two charges' parameters:

$$k'_b = \sum_Y \frac{b_{MX} - b_{MY}\cos\theta_{XMY}}{r^3_{XY} b_{MX}} + \frac{q_X}{q}\frac{b_{MX} - b_{MX'}\cos\theta_{XMX'}}{r^3_{XX'} b_{MX}}; \qquad (2)$$

where Y is O or N. It was shown before[6] that by plotting the dependence of k'_b on b_{MX} for a regular coordination (square-planar, pyramidal and tetrahedral) it was possible to deduce semi-quantitatively the distance from M at which X would be in the equilibrium for a certain k'_b. In order to obtain the same b_{MX} distance as in Model 6, q and q_X values were left the same and the new value of the sterical parameter was calculated (it was assumed that $b_{MX} = b_{MX'}$ and X—M—X′ = 180°) (see Table 1, footnotes d and e).

The first step in checking the new model, Model 7, was the calculation of the root-mean-square deviations between crystal and theoretical structures for all tetra-coordinated copper(II) bis-complexes with α-amino acids and their N-alkylated derivatives, which showed no pronounced intermolecular interactions, and their comparison with the results of Model 6. Calculations were performed with the

* No charge was supposed to reside on the atoms outside the coordination sphere.

† The plasticity means that copper seldom forms "regular" planar, tetrahedral or octahedral coordination polyhedra. Due to plasticity, copper compounds form crystal modifications with differently distorted coordination polyhedra and show less pronounced stereoselectivity effects than corresponding complexes of nickel and cobalt, metals with rigid coordination.

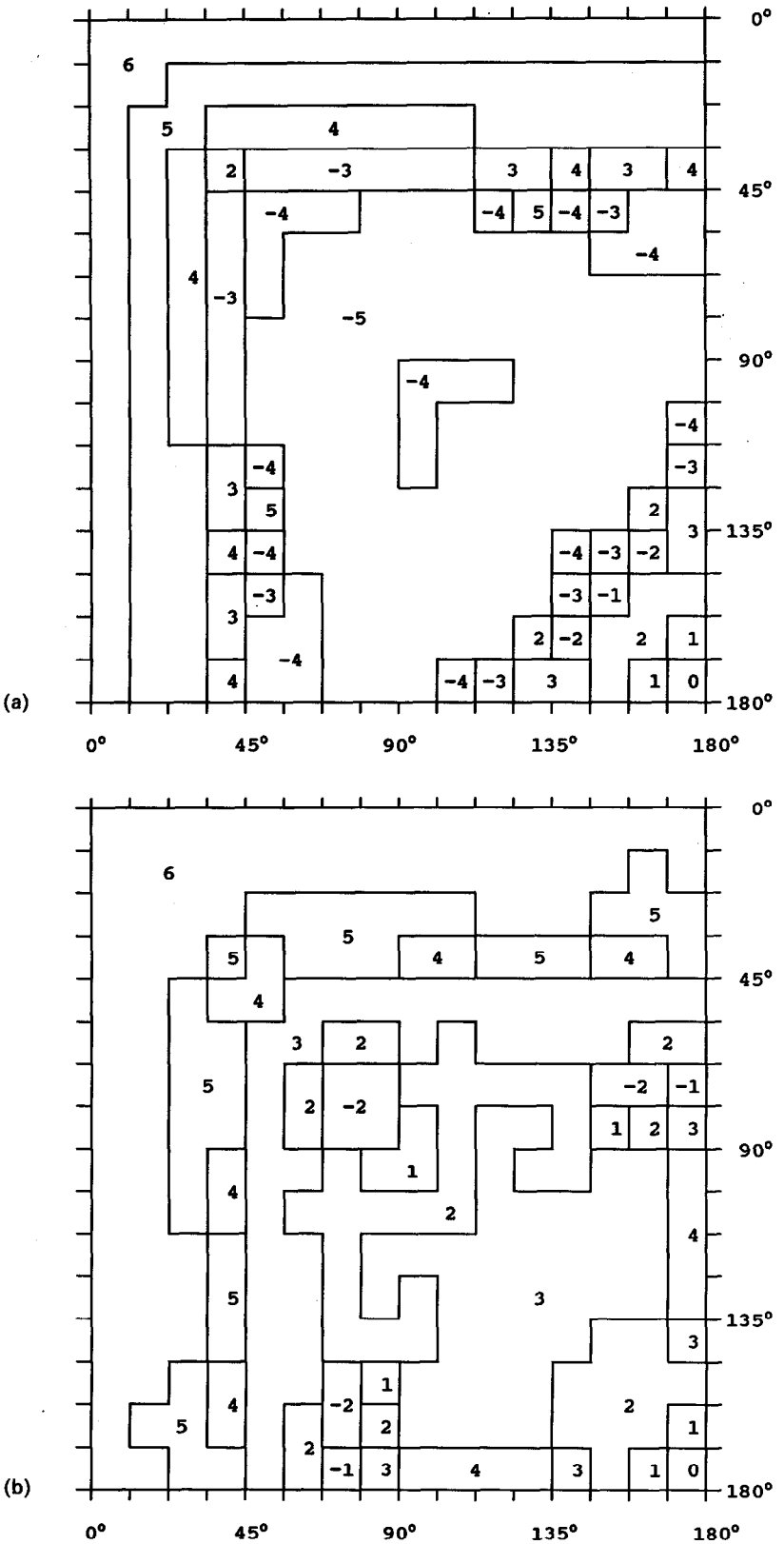

Fig. 1. Diagrams of potential (conformational) energy of the $CuX_2N_2O_2$ "complex" in the frame of coordinates N—M—N′ and O—M—O′ for (a) Model 6 and (b) Model 7. The energy ranges (in kcal mol^{-1}) are expressed by the numbers (absolute values): 0 (< 0.001), 1 (0.001–0.1), 2 (0.1–1), 3 (1–5), 4(5–10), 5 (10–50) and 6 (> 50). Zero values correspond to *trans*-planar minima: (a) $V = 204.298$ kcal mol^{-1} and (b) $V = 236.139$ kcal mol^{-1}.

Table 1. Comparison of experimental and theoretical geometries of non-planar copper(II) bis-aminoacidates by means of root-mean-square deviations[a,b]

Angle	Crystal structure[c]	Model 6[d]	Model 7[e]
Bis-(L-N,N-dimethylvalinato)copper(II)[9]			
N—Cu—N′	161.5	160.1	160.1
N—Cu—O	84.3	82.1	82.1
N—Cu—O′	97.2	98.6	98.6
N′—Cu—O	95.3	98.6	98.6
N′—Cu—O′	84.5	82.1	82.1
O—Cu—O′	175.7	176.3	176.1
O′—N′—N—O	156.3	156.1	156.0
β	170.3	169.3	169.4
$\varepsilon_{r.m.s.}(\Delta\theta)$		2.1	2.1
$\varepsilon_{r.m.s.}(\Delta\theta,\Delta\phi,\Delta\beta)$		1.8	1.8
$\varepsilon_{r.m.s}(\Delta r)$		0.118	0.118
X—Cu—X′		180.0	180.0
Bis-(L-N-benzylprolinato)copper(II)[10]			
N—Cu—N′	172.7	178.6	178.7
N—Cu—O	85.6	84.0	84.0
N—Cu—O′	96.2	95.1	95.2
N′—Cu—O	93.4	96.8	96.7
N′—Cu—O′	85.7	83.9	83.9
O—Cu—O′	173.3	171.3	171.4
O′—N′—N—O	−165.5	172.4	172.4
β	−178.6	−173.4	−173.5
$\varepsilon_{r.m.s.}(\Delta\theta)$		3.1	3.1
$\varepsilon_{r.m.s.}(\Delta\theta,\Delta\phi,\Delta\beta)$		8.4	8.4
$\varepsilon_{r.m.s}(\Delta r)$		0.309	0.309
X—Cu—X′		179.1	179.4
Bis-(L-leucinato)copper(II)[11]			
N—Cu—N′	174.6	177.1	178.7
N—Cu—O	84.2	82.7	82.7
N—Cu—O′	95.7	99.6	97.8

Angle	Crystal structure[c]	Model 6[d]	Model 7[e]
Bis-(L-phenylalaninato)copper(II)[13]			
N—Cu—N′	175.9	171.7	176.7
N—Cu—O	84.8	82.3	82.4
N—Cu—O′	96.4	88.8	93.8
N′—Cu—O	94.6	105.9	100.5
N′—Cu—O′	83.9	83.0	83.2
O—Cu—O′	176.9	170.7	175.5
O′—N′—N—O	178.6	178.5	178.8
β	175.2	−171.1	−175.2
$\varepsilon_{r.m.s.}(\Delta\theta)$		6.4	2.9
$\varepsilon_{r.m.s.}(\Delta\theta,\Delta\phi,\Delta\beta)$		7.4	4.2
$\varepsilon_{r.m.s}(\Delta r)$		0.843	0.785
X—Cu—X′		170.0	177.5
(L-serinato)(glycinato)copper(II)[14]			
N—Cu—N′	175.2	179.0	179.4
N—Cu—O	82.9	82.8	82.8
N—Cu—O′	94.4	96.1	96.8
N′—Cu—O	101.1	98.1	97.4
N′—Cu—O′	81.5	83.0	83.0
O—Cu—O′	177.3	178.8	179.4
O′—N′—N—O	177.5	179.9	179.9
β	176.2	178.8	179.2
$\varepsilon_{r.m.s.}(\Delta\theta)$		2.3	2.7
$\varepsilon_{r.m.s.}(\Delta\theta,\Delta\phi,\Delta\beta)$		2.3	2.7
$\varepsilon_{r.m.s}(\Delta r)$		0.175	0.174
X—Cu—X′		178.9	179.8
Bis-(L-N,N-dimethylisoleucinato)copper(II)[15]			
N—Cu—N′	166.0	160.2	160.2
N—Cu—O	84.4	82.1	82.1
N—Cu—O′	95.8	98.9	98.9

N′—Cu—O	96.0	94.6	96.4
N′—Cu—O′	84.2	83.0	83.0
O—Cu—O′	179.7	177.6	179.3
O′—N′—N—O	174.7	−179.6	−179.5
β	176.2	−177.3	−178.8
$\varepsilon_{r.m.s.}(\Delta\theta)$		2.3	2.1
$\varepsilon_{r.m.s.}(\Delta\theta,\Delta\phi,\Delta\beta)$		3.7	3.3
$\varepsilon_{r.m.s}(\Delta r)$		0.242	0.232
X—Cu—X′		177.1	179.5
Bis-(L-alaninato)copper(II)[12]			
N—Cu—N′	175.5	179.3	179.4
N—Cu—O	83.8	83.1	83.1
N—Cu—O′	95.5	96.8	97.0
N′—Cu—O	96.2	97.3	97.1
N′—Cu—O′	84.4	82.8	82.8
O—Cu—O′	179.3	179.6	179.6
O′—N′—N—O	175.8	−179.8	−179.8
β	176.7	−179.3	−179.3
$\varepsilon_{r.m.s.}(\Delta\theta)$		1.9	1.9
$\varepsilon_{r.m.s.}(\Delta\theta,\Delta\phi,\Delta\beta)$		2.7	2.7
$\varepsilon_{r.m.s}(\Delta r)$		0.161	0.162
X—Cu—X′		179.7	179.9
N′—Cu—O	96.3	98.4	98.5
N′—Cu—O′	84.0	82.0	82.0
O—Cu—O′	178.3	175.5	175.4
O′—N′—N—O	163.5	155.5	155.4
β	171.8	169.9	170.0
$\varepsilon_{r.m.s.}(\Delta\theta)$		3.3	3.3
$\varepsilon_{r.m.s.}(\Delta\theta,\Delta\phi,\Delta\beta)$		4.1	4.1
$\varepsilon_{r.m.s}(\Delta r)$		0.088	0.088
X—Cu—X′		179.7	179.8
Bis-(L-2-aminobutyrato)copper(II)[16]			
N—Cu—N′	174.6	178.8	179.3
N—Cu—O	83.6	83.1	83.2
N—Cu—O′	95.9	98.4	97.5
N′—Cu—O	96.0	95.9	96.8
N′—Cu—O′	84.4	82.6	82.6
O—Cu—O′	178.6	178.4	179.1
O′—N′—N—O	175.9	−179.8	−179.9
β	175.5	−178.5	−179.0
$\varepsilon_{r.m.s.}(\Delta\theta)$		2.1	2.2
$\varepsilon_{r.m.s.}(\Delta\theta,\Delta\phi,\Delta\beta)$		3.2	3.1
$\varepsilon_{r.m.s}(\Delta r)$		0.265	0.261
X—Cu—X′		178.6	179.7

[a] The root-mean-square deviation was calculated from:

$$\varepsilon_{r.m.s.} = \left(\frac{1}{N}\sum_{i=1}^{N}(\Delta X_i)^2\right)^{1/2};$$

where X are the angles around copper (valence angles θ, "torsional" angle ϕ_{ONNO} and distortion angle β[3,4]) when comparing the copper coordination geometry, or for interatomic distance, r, when comparing the overall similarity (only distances between non-hydrogen atoms were taken into account). The symbol Δ denotes the difference between the values of observable X in two structures.

[b] All angles are expressed in degrees and $\varepsilon_{r.m.s.}(\Delta r)$ values in Å.

[c] References correspond to crystal structures.

[d] Force-field parameters: $q = -0.375$ e, $q_X = -0.750$ e, $\varepsilon_r = 2$, $k'_b = 0.150$ Å^{-3}, $k_{b,MX} = 7.005$ kcal mol^{-1} Å^{-2}, $b_{0,MX} = 0$.

[e] Force-field parameters: $q = -0.375$ e, $q_X = -0.750$ e, $\varepsilon_r = 2$, $k'_b = 0.197$ Å^{-3}, $k_{b,MX} = 9.198$ kcal mol^{-1} Å^{-2}, $b_{0,MX} = 0$.

Table 2. Statistical analysis (mean and standard deviation) of the differences between the experimental and theoretical values, Δ, of the angles around copper (data from Table 1)[a]

Angle	Model 6	Model 7
Δ N—Cu—N′	−1.1 (4.3)	−2.1 (3.9)
Δ N—Cu—O	1.4 (0.9)	1.4 (0.9)
Δ N—Cu—O′	−0.7 (3.6)	−1.1 (1.9)
Δ N′—Cu—O	−2.1 (4.3)	−1.6 (2.8)
Δ N′—Cu—O′	1.3 (1.2)	1.3 (1.2)
Δ O—Cu—O′	1.4 (2.5)	0.4 (1.6)
Δ O′—N′—N—O	1.7 (9.3)	1.7 (9.3)
Δ β	−4.4 (4.9)	−3.7 (3.7)

[a] All values are expressed in degrees. Standard deviations are given in parentheses.

CFF programme for conformational analysis,[7,8] which was further modified to cope with the electrostatic models. For the planar molecules Model 7 yielded the same values as Model 6.[6] For the distorted non-planar molecules the results were slightly different (Table 1): for the complexes with L-phenylalanine and L-leucine the new electrostatic model gave lower root-mean-square deviations, for (glycinato)(L-serinato)copper(II) the coordination polyhedron geometry was reproduced almost as well as with Model 6, while for the other molecules the results were the same as with the old model. The comparison of the differences between experimental and theoretical values of the individual angles around copper (Table 2) showed that: N—Cu—O, N′—Cu—O′ and O′—N′—N—O angles were equally well reproduced by both models; for O—Cu—O′, N′—Cu—O and β angles Model 7 gave better results than Model 6, while for N—Cu—N′ and N—Cu—O′ angle differences the new model yielded numerically larger mean values but lower standard deviations than the old electrostatic model.

The checking of the new model on the $CuX_2N_2O_2$ "complex" revealed that it yields five minima (Table 3): *trans*- and *cis*-planar and three distorted pyramids (X—M—X′ = 105°), with conformational energy differences lower than 1 kJ mol^{-1}. The degeneracy to a "penta-coordinate" complex was suppressed but three "false" minima were left. These five minima were those which fulfilled the condition of equilibrium of the attractive and repulsive forces (each of them has a C_2-symmetry axis as a bisector of the all valence angles, while in the old model all the minima had a C_2-symmetry axis with X atoms placed on it). The atoms tend to be as far apart as possible and at the same time as close as possible to their equilibrium bond lengths. Our initial intention was to find a model that could give only two minima: a planar and a tetrahedral.[3–6] The tetrahedral configuration would be possible to achieve with the electrostatic models only when the X atoms are so far away that their influence is very weak, i.e. when the value of $k_{b,MX}$ is small enough not to hold the "dummy" atoms close to the central metal atom. Otherwise, the tetrahedral minimum is energetically unfavourable—this configuration imposes too close contacts between real and "dummy" atoms. On the other hand, the appearance of

Table 3. The five minima of conformational energy for the "complex" $CuX_2N_2O_2$[a]

	Trans-planar	*Cis*-planar	Pyramid 1	Pyramid 2	Pyramid 3
N—M—N′	180.0	89.8	162.5	74.8	82.9
N—M—O	90.0	179.7	83.1	83.0	82.9
N—M—O′	90.0	90.0	83.1	83.0	162.5
N′—M—O	90.0	90.0	83.1	83.0	74.9
N′—M—O′	90.0	179.7	83.1	83.0	83.1
O—M—O′	180.0	90.3	75.1	162.3	83.2
O′—N′—N—O	180.0	0.0	−87.4	−112.3	54.0
β	180.0	90.0	101.7	−101.5	101.6
X—M—X′	180.0	179.8	105.3	105.5	105.4
M—X	2.199	2.199	2.181	2.181	2.179
M—X′	2.199	2.199	2.181	2.181	2.184
V	988.008	988.016	987.333	987.225	987.282

[a] All angles are expressed in degrees, M—X bond lengths in Å and conformational potential (*V*) in kJ mol^{-1}.

the distorted pyramid minima makes possible the application of Model 7 to penta-coordinated copper(II) complexes too.

The influence of the introduction of the "dummy" atom interaction on the shape of the potential energy surface can be studied by means of the energy diagrams in the frame of *trans*-valence angles (details of their construction were given elsewhere[4,6]) (Figs 1 and 2). Around the planar minimum both models have similar behaviour. That is the reason for essentially the same reproduction of copper(II)-aminoacidato geometries. A very flat region in the vicinity of the planar minimum points out that the $CuX_2N_2O_2$ "molecule" is very flexible there, so the plasticity of the copper(II) coordination sphere is evident. While in Model 6 upon larger distortions (> 15–30° for N—M—N′ and O—M—O′ angles) the $CuX_2N_2O_2$ "complex" was placed in the lower regions of the potential energy surface yielding the "false" minima (the energy difference between the planar minima and the pyramid with the lowest conformational energy is 70.6 kJ mol^{-1}), in Model 7 there is a potential barrier (up to 42 kJ mol^{-1}) that separates the "real" minimum from the "false" minima regions.

As a conclusion it can be stated that Model 7 is an improved version of Model 6 because the new electrostatic model reproduces the geometries of the real molecules in the same manner or better than the old electrostatic model; it does not allow for the "dummy" atoms to fold over and alleviates the "false" minima problem. As such, it is more suitable for further force field development.

Acknowledgements—I would like to thank Professor Kjeld Rasmussen for encouragement and helpful discussion and to the Danish Research Academy for supporting my work in Denmark.

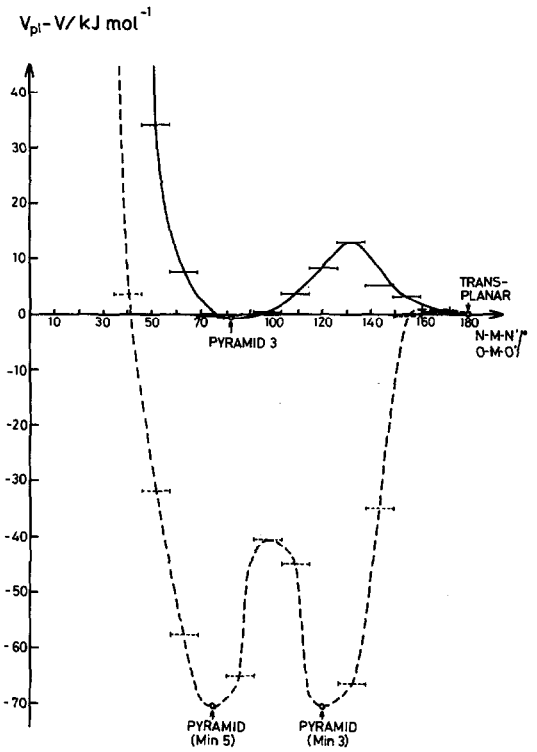

Fig. 2. Plot of conformational energy of the "complex" $CuX_2N_2O_2$ in the frame of the *trans*-valence angles for the points (obtained for Model 7 from Fig. 1 and Table 2 and for Model 6 from ref. 6) where N—M—N′ ≈ O—M—O′. Heavy line: Model 7; broken line: Model 6.

REFERENCES

1. N. Raos, S. R. Niketić and Vl. Simeon, *J. Inorg. Biochem.* 1982, **16**, 1.
2. N. Raos and Vl. Simeon, *Croat. Chem. Acta* 1985, **58**, 127.
3. J. Sabolović, N. Raos and Kj. Rasmussen, *Croat. Chem. Acta* 1989, **62**, 495.
4. J. Sabolović and N. Raos, *Polyhedron* 1990, **9**, 1277.
5. J. Sabolović, N. Raos and Kj. Rasmussen, *Polyhedron* 1991, **10**, 2079.
6. J. Sabolović and N. Raos, *Polyhedron* 1990, **9**, 2419.
7. S. R. Niketić and Kj. Rasmussen, *The Consistent Force Field: A Documentation, Lecture Notes in Chemistry*, Vol. 3. Springer, Berlin (1977).
8. Kj. Rasmussen, *Potential Energy Functions in Conformational Analysis, Lecture Notes in Chemistry*, Vol. 37. Springer, Berlin (1985).
9. B. Kaitner, B. Kamenar, N. Paulić, N. Raos and Vl. Simeon, *J. Coord. Chem.* 1987, **15**, 373.
10. G. G. Aleksandrov, Yu. T. Struchkov and A. A. Kuganov, *Zh. Strukt. Khim.* 1973, **14**, 492.
11. T. G. Fewcett, M. Ushay, J. P. Rose, R. A. Lalancette, J. A. Potenza and H. J. Schugar, *Inorg. Chem.* 1979, **18**, 327.
12. M. A. Hitchman, L. Kwan, L. M. Engelhardt and A. H. White, *J. Chem. Soc., Dalton Trans.* 1987, 457.
13. D. van der Helm, M. B. Lawson and E. L. Enwall, *Acta Cryst.* 1971, **B27**, 2411.
14. I. A. Dyakov, S. V. Donu, L. F. Chapurina and A. S. Avilov, *Kristallografiya* 1984, **29**, 384.
15. B. Kaitner, N. Paulić and N. Raos, *J. Coord. Chem.* 1991, **22**, 269.
16. P. R. Levstein, R. Calvo, E. E. Castellano, O. E. Piro and B. E. Rivero, *Inorg. Chem.* 1990, **29**, 3918.

Polyhedron Vol. 12, No. 9, pp. 1115–1117, 1993
Printed in Great Britain

0277–5387/93 $6.00+.00
© 1993 Pergamon Press Ltd

COMMUNICATION

COMPLEXATION OF A TRIS-BIPYRIDINE CRYPTAND WITH AMERICIUM(III)

V. K. MANCHANDA* and P. K. MOHAPATRA

Radiochemistry Division, B.A.R.C., Bombay 400085, India

(*Received* 17 *November* 1992; *accepted* 25 *January* 1993)

Abstract—Extraction studies on the americium(III) tris-bipyridine cryptate revealed acid-assisted slow dissociation of the complex and improved separation from europium(III) under non-equilibrium conditions.

Due to their large hydration energies trivalent actinides and lanthanides form weak complexes with crown ethers[1] and diaza-crown ethers[2] in the aqueous phase. On the other hand the ionizable macrocyclic as well as macrobicyclic ligands (cryptands) form thermodynamically stable and substitutionally inert complexes in aqueous medium.[3–8] The efficiency of these ionophores depends largely on the protection of the encapsulated lanthanide ions from solvent (water) molecules. The hydrophobic nature of the cryptand and the simultaneous decrease in the number of associated water molecules is expected to facilitate the cation transfer towards the organic phase. The present work is the first attempt to understand the complexation behaviour of americium(III) with tris-bipyridine cryptand, L (Fig. 1), employing the solvent extraction tracer technique.

EXPERIMENTAL

Reagents

^{241}Am and $^{152-154}$Eu were used as tracers after ascertaining their purity by alpha and gamma spectrometry, respectively.[9] Dinonylnaphthalenesulphonic acid (HD) was obtained from R. T. Vanderbilt Co., U.S.A. The tris-bipyridyl cryptand in the NaBr form was provided by Prof. J.-M. Lehn. All other reagents are of A.R. Grade.

Procedure

HD solutions were made in toluene and used as the organic phase. For the experiments performed with controlled pH pre-equilibration of the HD solution was done with a 4 M solution of $N(CH_3)_4Cl$ for 24 h to convert it quantitatively into the $N(CH_3)_4D$ form.

The tris-bipyridine cryptate complex of americium was prepared in a 1:1 mixture of CH_3CN and $CHCl_3$ by refluxing the mixture at 70°C for 12 hours[10] ($[L] = 5 \times 10^{-5}$ M). The solvent was then removed at room temperature and the complex extracted into the organic phase containing HD or $N(CH_3)_4D$ as the case may be. Distribution studies were performed by equilibrating the complex-loaded organic phase with dilute HCl solutions of known concentrations. The assays of the two phases were obtained using an 80CC Ge detector coupled to a multichannel analyser by monitoring ^{241}Am at 60 keV and $^{152-154}$Eu at 122 keV.

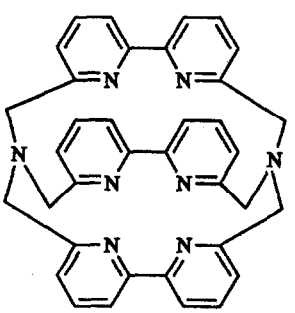

Fig. 1. Ligand L.

* Author to whom correspondence should be addressed.

Table 1. Distribution data for the americium(III)-tris-bipyridine cryptand-HD system as a function of aqueous acidities and time. Organic phase: 5×10^{-3} M HD (experiments 1–5); 1×10^{-3} M $(CH_3)_4D$ (experiments 6 and 7)

[HCl]/pH	D_o	D_t (h) $t = 2$	96	384	552	912	1272	D_2/D_{1272}
1.0	0.19	2.64	1.36	0.78	0.68	0.56	0.49	5.4
0.8	0.45	3.28	1.69	1.05	0.93	0.79	0.69	4.8
0.6	1.06	5.11	2.85	1.89	1.73	1.46	1.32	3.5
0.4	4.00	13.38	8.13	5.95	5.52	5.01	4.35	3.1
0.2	33.27	71.21	57.09	45.17	39.38	32.78	32.23	2.2
3.0	12.29	35.50	31.96	30.33	30.40	—	—	—
6.0	17.76	77.24	87.82	71.44	79.15	—	—	—

RESULTS AND DISCUSSION

Experiments in the absence of L

The behaviour of HD depends on the size and composition of the micelle formed on aggregation, which in turn is a function of the nature of the diluent.[11] The variation of log D_o* with log [HD] (in the concentration range 2×10^{-3}–1×10^{-2} M) showed a dependence of 1. Figure 2(a) shows that in the absence of L the slope of the plot of log D_o vs log a_{H^+} is approximately −3. These observations lead to the following two-phase equilibrium:

$$M^{3+}_{(a)} + (HD)_{n(o)} \rightleftharpoons M(H_{3-n}D_n)_{(o)} + 3H^+_{(a)}, \quad (1)$$

where M = Am and $(HD)_n$ represents the micelles of the extractant with n being the aggregation number.

Experiments in the presence of L

As in the above case the complex also extracts by the micelle mechanism in the $[H^+]$ range 0.2–0.5 M as follows:

$$ML^{3+}_{(a)} + (HD)_{n(o)} \rightleftharpoons ML(H_{n-3}D_n)_{(o)} + 3H^+_{(a)}. \quad (2)$$

Figure 2(b) shows that in the presence of L the plot of log D vs log a_{H^+} deviates from linearity beyond 0.5 M. This is explained due to the fact that the D values in the presence of L do not refer to the states of equilibrium, even though the two phases are in contact for 2 h. The enhancement in the D value appears to be due to the increased hydrophobic nature of the cryptate with respect to the uncomplexed metal ion. It is interesting that the enhancement, represented as D/D_o, observed in the present work is much larger at 1 M acidity (14 times) compared with that observed at 0.2 M. This is a consequence of the kinetic inert nature of the cryptate formed. The macrobicyclic complex originally present in the organic phase has to undergo dissociation several folds, more at 1 M $[H^+]$ compared with lower acidities, to attain the blank distribution ratio (D_o) values.

The distribution data at different time intervals are listed in Table 1 up to 1272 h. Data obtained with pH 3.0 and 6.0 are also included for better interpretation of the results. The data indicate that although there is no change in the D values in the pH range studied, an acid-dependent decrease in these values is observed in the HCl concentration range 0.2–1.0 M. It is clearly seen from the last column of Table 1 that whereas the drop in D value

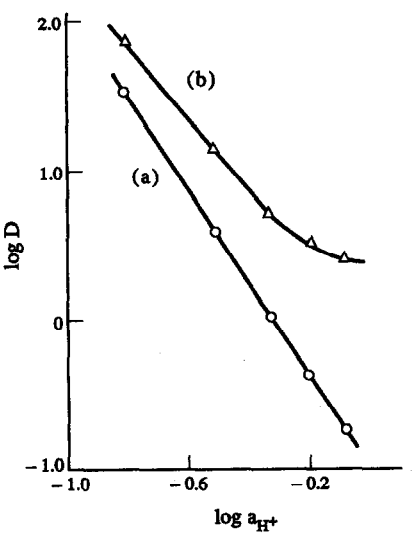

Fig. 2. Variation of log D with log a_{H^+}; (a): [HD] = 5×10^{-3} M; no L present; (b): [HD] = 5×10^{-3} M; [L] = 5×10^{-5} M.

* D_o is the distribution ratio in the absence of L and D is that in the presence of L.

is 5.4 times at 1 M acidity, it is only 2.2 times at 0.2 M $[H^+]$ under identical experimental conditions. It can also be observed from Table 1 that whereas the D value after 912 h has already approached the D_0 value in the case of 0.2 M HCl, the corresponding value is quite close for 0.4 M HCl. In other cases also the D values are expected to drop to their respective D_0 values after prolonged contact periods of the two phases. The continuous drop in D value is related to the dissociation of the cryptate in the presence of $[H^+]$, as shown by the following probable aqueous phase equilibrium:

$$ML^{3+} + 2H^+ \rightleftharpoons M^{3+} + LH_2^{2+}. \quad (3)$$

There is no enhancement in the D value if L is replaced by 18-crown-6, Kryptofix 22 or 2,2′-bipyridyl, even though other experimental conditions are identical. It seems that these ligands interact weakly (outer sphere complexes), as compared with the cryptates by L, with the metal ion and dissociate readily on contact with the aqueous phase (1 M HCl). This is supported by the structural studies on lanthanide-cryptates by Walksman *et al.*[12] and lanthanide-crown ether complexes by Rogers *et al.*[13]

To explore the possible application of cryptands for the separation of lanthanides and actinides experiments were conducted on a synthetic mixture of americium(III) and europium(III). Employing 1 M HCl as the aqueous phase and a phase contact time of 2 h the distribution data were obtained as a function of refluxation time for the two cations. The separation factor of 2.2 ± 0.2 thus obtained was distinctly larger than the corresponding value of 1.1 ± 0.1 in the absence of L. The separation factor was, however, not as high as one expects for a cryptate system. However, a non-equilibrium system like this needs the optimization of the equilibration time which could yield improved results.[14]

Acknowledgements—The authors are grateful to Prof. Jean-Marie Lehn, Institut Le Bel, Université Louis Pasteur, Strasbourg (France), for providing a sample of the tris-bipyridyl cryptand in the NaBr form, which was used throughout this work. Thanks are also due to Dr R. H. Iyer, Head, Radiochemistry Division, for his constant encouragement.

REFERENCES

1. P. K. Mohapatra and V. K. Manchanda, *Radiochim. Acta* 1991, **55**, 193.
2. P. K. Mohapatra and V. K. Manchandra, communicated.
3. X. Wang, T. Jin, V. Comblin, A. Lopez-mut, E. Merciny and J. F. Desreux, *Inorg. Chem.* 1992, **31**, 1095.
4. M. F. Loncin, J. F. Desreux and E. Merciny, *Inorg. Chem.* 1986, **25**, 2646.
5. V. K. Manchanda and P. K. Mohapatra, *Inorg. Chim. Acta* 1990, **170**, 141.
6. C. A. Chang, V. K. Manchanda and J. Peng, *Inorg. Chim. Acta* 1987, **130**, 117.
7. J. H. Burns and C. F. Baes, *Inorg. Chem.* 1981, **20**, 616.
8. E. L. Yee, O. A. Gansow and M. J. Weaver, *J. Am. Chem. Soc.* 1980, **102**, 2278.
9. V. K. Manchanda and P. K. Mohapatra, *Polyhedron* 1990, **9**, 2455.
10. B. Alpha, J.-M. Lehn and G. Mathis, *Angew. Chem., Int. Edn Engl.* 1987, **26**, 266.
11. E. O. Otu and A. W. Westland, *Solv. Ext. Ion Ex.* 1991, **9**, 875.
12. I. B. Walksman, J. Guilhem, C. Pascard, B. Alpha, R. Deschenaux and J.-M. Lehn, *Helv. Chim. Acta* 1991, **74**, 1163.
13. R. D. Rogers and L. K. Kurihara, *Inorg. Chim. Acta* 1986, **116**, 171.
14. V. K. Manchanda and P. K. Mohapatra, work in progress.

Polyhedron Vol. 12, No. 10, pp. 1119–1122, 1993
Printed in Great Britain

0277–5387/93 $6.00+.00
Pergamon Press Ltd

THE PREPARATION AND CRYSTAL STRUCTURE OF μ,μ'-DICHLORO-BIS[(DI-*p*-TOLYLMETHYLAMIDO)-(TRIPHENYLPHOSPHINE)COPPER(II)] FORMED BY AMIDE TRANSFER FROM RHODIUM

S. C. NYBURG, A. W. PARKINS* and M. SIDI-BOUMEDINE

Department of Chemistry, King's College London, Strand, London WC2R 2LS, U.K.

(*Received* 4 *January* 1993; *accepted* 18 *February* 1993)

Abstract—The addition of $HRh(CO)(PPh_3)_3$ to di-*p*-tolyl ketimine has been shown to give a metal amide rather than a metal alkyl. The initial rhodium amide product could not be characterized, but reaction with CuCl gave the title compound which has been characterized by X-ray crystallography. The copper complex has terminal amide and triphenylphosphine ligands coordinated to a Cu_2Cl_2 core, in which the copper atoms have pseudo-tetrahedral geometry.

There is considerable current interest in the hydrogenation of imines catalysed by homogeneous transition metal catalysts.[1] The mechanism proposed for the reduction involves the addition of a metal hydride to the carbon–nitrogen double bond. In principle this addition could give either a metal amide or a metal alkyl [eq. (1)]:

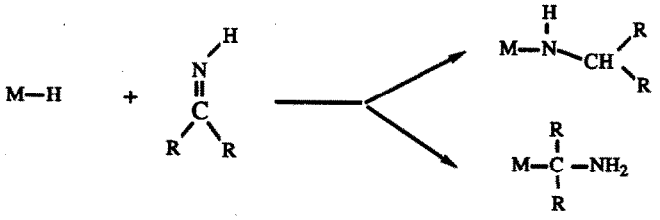

(1)

Fryzuk and Piers[2] have shown that dinuclear rhodium hydrides add to diphenyl ketimine to give a bridging amide complex, although no crystal structure was reported. We describe here the reaction of the mononuclear hydride $HRh(CO)(PPh_3)_3$ with di-*p*-tolyl ketimine and the structural characterization of a copper amide, obtained by transfer of the amide initially formed on rhodium to copper. The crystal and molecular structures have been established by X-ray diffraction and show unequivocally that the product is an amide, the hydrogen atom of the hydride having become attached to the β-carbon atom.

* Author to whom correspondence should be addressed.

EXPERIMENTAL

Materials and methods

$HRh(CO)(PPh_3)_3$ was prepared by a modification[3] of the procedure described in Inorganic Syntheses.[4] Di-*p*-tolyl ketimine, which has previously been reported by Pickard and Vaughan,[5] was prepared using the procedure described by Pickard and Tolbert[6] for diphenyl ketimine. CuCl was prepared by the method of Keller and Wycoff.[7] The preparation of the amide complex (**I**) was performed under nitrogen.

Rhodium on silica catalyst

Chromatographic silica (Merck 7734) (3 g) was stirred at room temperature in a solution of rhodium trichloride trihydrate (0.25 g) in methanol (50 cm^3). Addition of sodium borohydride (0.2 g) caused immediate reduction to the metal. After 10

min the solid was filtered off, washed with methanol and dried *in vacuo*.

μ,μ′-Dichloro-bis[(di-p-tolylmethylamido)(triphenylphosphine)copper(II)] (I)

$HRh(CO)(PPh_3)_3$ (1.0 g, 1.09 mmol), di-*p*-tolyl ketimine (0.6 g, 2.87 mmol) and rhodium on silica (0.2 g) were heated under reflux in THF (40 cm^3) for 2 h. The mixture was cooled to room temperature and treated with CuCl (0.2 g, 2.02 mmol) and heated under reflux for a further 30 min. The mixture was then cooled, filtered through celite, concentrated to *ca* 10 cm^3 and set aside in the refrigerator (42 h at 5°C). The product was isolated by decanting off the very dark mother liquor and washing the orange solid with THF. Crude yield 0.60 g, 97%. The analytical sample was obtained by recrystallization from THF. As the main impurity is the less soluble $(PPh_3)_2Rh(CO)Cl$ it was found helpful to avoid dissolving up the last few crystals of the crude product, before decantation and cooling; m.p. 164–165°C. Found: C, 69.1; H, 4.9; Cl, 7.1; Cu, 11.2; N, 2.4: Calc. for $C_{66}H_{62}Cl_2Cu_2N_2P_2$: C, 69.3; H, 5.5; Cl, 6.2; Cu, 11.1; N, 2.5%.

Crystallography

$C_{66}H_{62}Cl_2Cu_2N_2P_2$, $Mr = 1143.20$, triclinic, $P\bar{1}$ $a = 9.395(15)$, $b = 13.587(6)$, $c = 13.659(8)$ Å, $\alpha = 116.07(4)$, $\beta = 70.76(7)$, $\gamma = 106.46(8)°$, $V = 1459(2)$ $Å^3$, $Z = 1$, $D_{calc} = 1.30$ g cm^{-3}, $D_{obs} = 1.28$ g cm^{-3}; $\lambda(Mo\text{-}K_\alpha) = 0.7107$ Å, $\mu = 9.2$ cm^{-1}; $F(000) = 594$. Temperature = 298 K, $R = 0.039$, $Rw = 0.041$, 68 atoms, 346 parameters. Quality-of-fit 2.17 for 3015 reflections with $I_{net} > 2.5\sigma(I_{net})$ out of a total of 3809 reflections in the range $3° < 2\theta < 45°$.

A crystal of **I** (0.65 × 0.38 × 0.22 mm), crystallized from THF was X-ray photographed to establish quality and the cell dimensions were obtained from 24 reflections ($37° < 2\theta < 41°$) on a Picker four-circle diffractometer interfaced to an AT TURBO 286 IBM-compatible micro computer, using Zr-filtered Mo-K_α radiation with pulse height analysis. A standard reflection was measured every 50 reflections and showed no significant change during the data collection. An absorption correction was applied and the maximum and minimum transmission factors were 0.812 and 0.721. The structure was solved by direct methods and difference-Fourier synthesis using the NRCVAX program package.[8] The positions of the amide hydrogen and of two methyl hydrogen atoms were found from the difference map; the remaining hydrogen atoms were placed in calculated positions with temperature factors related to the atoms to which they are attached. The positions of all non-hydrogen atoms and the three experimentally determined hydrogen atoms were refined by full-matrix least-squares, together with anisotropic temperature factors for the non-hydrogen atoms and isotropic temperature factors for the three hydrogens. The refinement was performed with unit weighting of the *F*s and converged to a final *R* of 0.039.

RESULTS AND DISCUSSION

On warming a solution of $HRh(CO)(PPh_3)_3$ with diphenyl or di-*p*-tolyl ketimine in THF a colour change from yellow to deep red occurs within minutes. We were able to isolate a red solid from this reaction, but we were unable to characterize it. As one of the problems appeared to be removing triphenylphosphine from the product, we decided to add CuCl, which is known[9] to form an adduct with triphenylphosphine. The addition of CuCl to the red solution causes the mixture to become brown and allows the isolation of an orange crystalline material, which was shown to contain both copper and chloride. The structural investigation subsequently showed that the rhodium amide intermediate had acted as an amidating agent on the copper producing a copper amide (**I**) [eq. (2)].

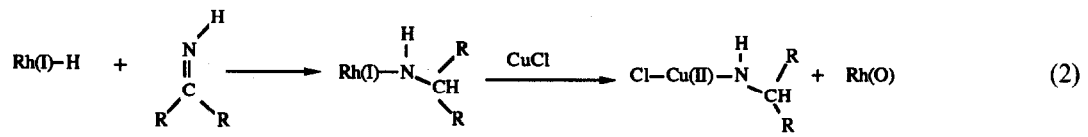

(2)

During the development of the preparation it was found that the desired product was not obtained reproducibly and that sometimes the main product was the well known chloride complex, $(PPh_3)_2Rh(CO)Cl$. After considerable experimentation it was found that the formation of $(PPh_3)_2Rh(CO)Cl$ could be minimized if the reaction is performed in the presence of rhodium deposited on silica. The catalysis of the displacement of carbonyl groups by supported transition metals or zero-valent complexes has been reported by several groups,[10] but usually the reactants employed are well-defined compounds rather than the intractable intermediate described here.

The molecular structure of the copper amide is

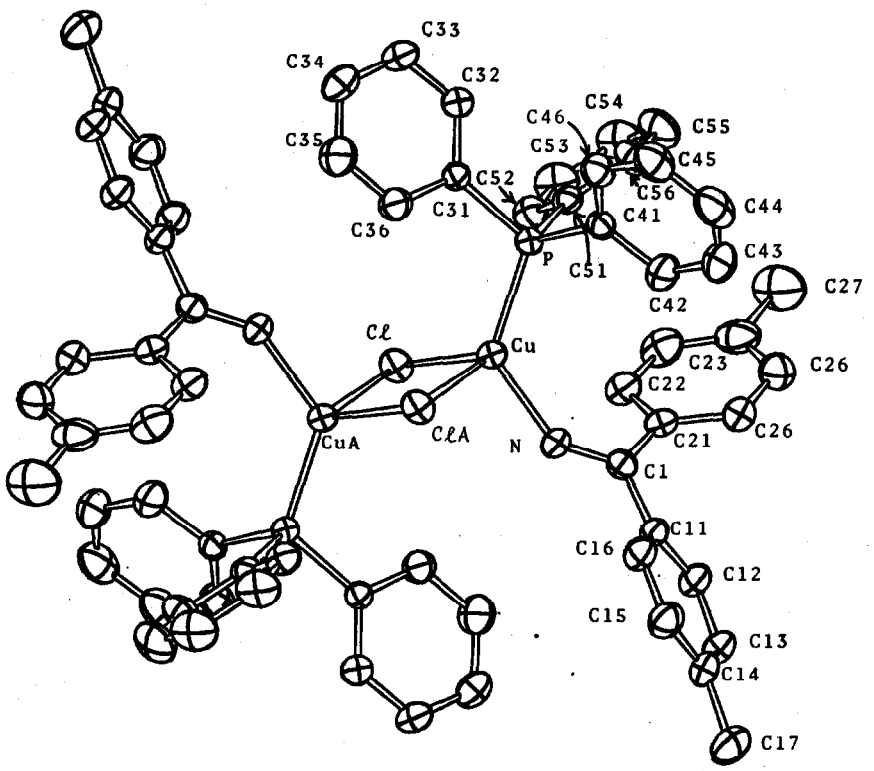

Fig. 1. ORTEP plot of **I**, showing the atomic numbering scheme. The molecule is centrosymmetric and so numbers are not shown for all atoms.

shown in Fig. 1 and selected bond distances and angles are given in Table 1. The molecule consists of two identical pseudo-tetrahedrally coordinated copper atoms linked by a planar Cu_2Cl_2 bridge. This is a common structural unit and compounds of this type have been reviewed recently.[11] The molecule has a crystallographically imposed centre of symmetry and the Cu—Cu distance is 3.268(3) Å. The evidence points clearly to the complex being an amide complex of copper(II), rather than an amine complex of copper(I). Only one hydrogen atom could be seen in the difference map and the N—H stretching vibration is a very sharp peak at 3265 cm^{-1}. Cooper and Downes[12] have previously remarked upon the sharpness of the N—H bands in platinum amides. The sum of the bond angles at the nitrogen atom [139.1(4)+96(4)+124(4)] is 359.1, which indicates planarity at nitrogen as required for an amide. Two recent reports[13] of amide structures have discussed the planarity of the substituents bonded to amide nitrogen atoms. The structure of a compound of similar coordination geometry has been reported by White and coworkers,[14] although the complex they studied, $[(Ph_3P)(py)CuCl_2Cu(py)(PPh_3)]$, has a shorter Cu—Cu distance [2.915(2) Å] and being a complex

Table 1. Selected bond distances (Å) and angles (°) for **I**

Cu—Cu	3.268(3)	Cu—N	1.993(4)
Cu—Cl	2.349(2)	N—C(1)	1.300(6)
Cu—Cl(a)	2.558(4)	N—H	0.97(6)
Cu—P	2.190(2)		
Cl—Cu—Cl(a)	96.60(10)	Cl(a)—Cu—N	87.32(16)
Cu—Cl—Cu(a)	83.40(10)	Cu—N—C(1)	139.1(4)
Cl—Cu—P	113.06(7)	Cu—N—H	96(4)
Cl—Cu—N	112.32(15)	C(1)—N—H	124(4)
Cl(a)—Cu—P	114.51(9)		

of copper(I) is colourless. The amide complex (**I**) is orange and paramagnetic. The Cu—N distance in the amide 1.993(4) Å is slightly longer than the value reported[15] for bridging copper amide [1.904(3) Å] groups, but we were unable to find any report of a terminal copper amide bond. The Cu—P bond length [2.190(2) Å] is shorter than the mean value (2.252 Å) given by Orpen *et al.*[16] but the latter value is derived mainly if not exclusively from complexes of copper(I). The Cu—Cl distances in **I** are slightly longer than average, but White and co-workers have pointed out that there is a large range of distances within Cu_2Cl_2 units.

The results of the magnetic measurements we made were erratic. We attribute this, in view of the method of preparation, to the presence of rhodium metal impurities. We are trying to prepare **I** without the intervention of rhodium, and, if successful, this will enable us to carry out an investigation of the magnetic properties of the copper amide.

Supplementary material available. Tables of positional and thermal parameters for **I** (Table 2), together with all bond distances and angles (Table 3) and listings of observed and calculated structure factors.

Acknowledgement—We thank Johnson Matthey plc for a loan of rhodium trichloride.

REFERENCES

1. C. J. Longley, T. J. Goodwin and G. Wilkinson, *Polyhedron* 1986, **5**, 1625; A. G. Becalski, W. R. Cullen, M. D. Fryzuk, B. R. James, G. J. Kang and S. J. Rettig, *Inorg. Chem.* 1991, **30**, 5002; H. A. Brune, J. Unsin, R. Hemmer and M. Reichhardt, *J. Organomet. Chem.* 1989, **369**, 335; F. Spindler, B. Pugin and H. U. Blaser, *Angew. Chem., Int. Edn Engl.* 1990, **29**, 558; Y. Ng Cheong Chan, D. Meyer and J. A. Osborn, *J. Chem. Soc., Chem. Commun.* 1990, 869; G. Z. Wang and J. E. Bäckvall, *J. Chem. Soc., Chem. Commun.* 1992, 980; J. Bakos, A. Orosz, B. Heil, M. Laghmari, P. Lhoste and D. Simon, *J. Chem. Soc., Chem. Commun.* 1991, 1684; M. J. Burk and J. E. Feaster, *J. Am. Chem. Soc.* 1992, **114**, 6266.
2. M. D. Fryzuk and W. E. Piers, *Organometallics* 1990, **9**, 986.
3. I. S. Babra, L. S. Morley, S. C. Nyburg and A. W. Perkins, submitted.
4. N. Ahmad, J. J. Levison, S. D. Robinson and M. F. Uttley, *Inorg. Syn.* 1974, **15**, 59.
5. P. L. Pickard and D. J. Vaughan, *J. Am. Chem. Soc.* 1950, **72**, 5017.
6. P. L. Pickard and T. L. Tolbert, *Organic Syntheses*, Collective Vol. 5, p. 520. Wiley, New York (1973).
7. R. N. Keller and H. D. Wycoff, *Inorg. Syn.* 1946, **2**, 1.
8. E. J. Gabe, Y. Le Page, P. F. Charland, F. L. Lee and P. S. White, *J. Appl. Cryst.* 1989, **22**, 384.
9. D. F. Fife, W. M. Moore and K. W. Morse, *Inorg. Chem.* 1984, **23**, 1684.
10. M. O. Albers and N. J. Coville, *Coord. Chem. Rev.* 1984, **53**, 227; M. O. Albers, N. J. Coville and E. Singleton, *J. Chem. Soc., Chem. Commun.* 1982, 96; S. J. Wang and R. J. Angelici, *Inorg. Chem.* 1988, **27**, 3233.
11. R. D. Willet, *Coord. Chem. Rev.* 1991, **109**, 181.
12. M. K. Cooper and J. M. Downes, *Inorg. Chem.* 1978, **17**, 880.
13. M. A. Dewey, A. M. Arif and J. A. Gladysz, *J. Chem. Soc., Chem. Commun.* 1991, 713; J. Feldman and J. C. Calabrese, *J. Chem. Soc., Chem. Commun.* 1991, 1042.
14. L. M. Engelhardt, P. C. Healy, J. D. Kildea and A. H. White, *Aust. J. Chem.* 1989, **42**, 913.
15. H. Hope and P. Power, *Inorg. Chem.* 1984, **23**, 936.
16. A. G. Orpen, L. Brammer, F. H. Allen, O. Kennard, D. G. Watson and R. Taylor, *J. Chem. Soc., Dalton Trans.* 1989, S1.

Polyhedron Vol. 12, No. 10, pp. 1123–1128, 1993
Printed in Great Britain

0277-5387/93 $6.00+.00
© 1993 Pergamon Press Ltd

REACTIONS OF AMINES WITH ARENE–RUTHENIUM COMPLEXES: CRYSTAL STRUCTURES OF [(1,3,5-$Me_3C_6H_3$)$RuCl_2(HNC_5H_{10})$] AND [(1,3,5-$Me_3C_6H_3$)$RuCl_2(NC_5H_5)$]

LEE CARTER, DAVID L. DAVIES,* JOHN FAWCETT and DAVID R. RUSSELL

Chemistry Department, University of Leicester, Leicester LE1 7RH, U.K.

(*Received* 10 *November* 1992; *accepted* 10 *February* 1993)

Abstract—A range of primary and secondary amines have been reacted with the dimers [(arene)$RuCl_2]_2$ to give simple adducts [(arene)$RuCl_2(NHRR^1)$]. We have structurally characterized the complexes [(1,3,5-$Me_3C_6H_3$)$RuCl_2(HNC_5H_{10})$] and [(1,3,5-$Me_3C_6H_3$)$RuCl_2(NC_5H_5)$]. Amine exchange reactions have been performed to assess the relative stabilities of these adducts. With certain ligands complex cations, [(1,3,5-$Me_3C_6H_3$)RuCl$(NHRR^1)_2]^+$, can form, although these are more easily prepared by reaction in the presence of $AgBF_4$.

The reactions of the dimers [(arene)$RuCl_2]_2$ with tertiary phosphines, phosphites and nitrogen bases such as pyridine, hydrazines and ammonia have been well studied.[1] However, the reactions with simple amines are much less well investigated and are limited to complexes with primary amines.[2,3] In particular, a previous study using ultrasound promoted reactions found no reactions with secondary or tertiary amines.[3] This is unlikely to be due to steric crowding since tertiary phosphines will coordinate easily.

The recent publication[3] of the use of ultrasound to promote the reactions of the dimers [(arene)$RuCl_2]_2$ with amines prompted us to report our work in this area. We have established that such reactions are just as easily performed thermally. Thus, heating a suspension of [(1,3,5-$Me_3C_6H_3$)$RuCl_2]_2$ with a slight excess of amine in dichloromethane or chloroform leads after a few hours to a red–orange solution from which the adducts [(1,3,5-$Me_3C_6H_3$)$RuCl_2(NHRR^1)$] (**1a–e**) can be isolated. An analogous product (**1f**) can be isolated starting from a solution of [(*p*-cymene)$RuCl_2]_2$ (Scheme 1). Of particular note is the formation of secondary amine adducts **1c–f**.

The complexes were characterized by ^{1}H NMR, microanalysis and FAB mass spectroscopy. In most cases molecular ions were observed in the FAB mass spectra (see Experimental), although in a number of samples ions due to dimeric species were also observed. These may have been formed in the matrix, or possibly by reactions in the spectrometer. All the complexes show the expected signals due to coordinated arene and the amine in their ^{1}H NMR spectra. The coordinated mesitylene signals occur at *ca* δ 2.0–2.2 and δ 4.8–5.0. It is noticeable that for **1c** and **1d** the methylene groups attached to nitrogen contain inequivalent hydrogens, i.e. NCHH,[1] as expected for diastereotopic protons. This shows that dissociation of the amine is slow, at least on the NMR time-scale, since these hydrogens are equivalent in the free amines. However, complexes **1c** and **1d** are unstable in solution with some loss of amine occurring, thus free amine is always observed in the NMR spectra of these products. Complex **1c** also decomposes in the solid state over a period of several days and hence the analysis results are inaccurate.

In the reactions with benzylamine the products formed depend on the reaction time or the solvent used. The adduct **1b** can be made without contamination by the cationic product by reacting [(1,3,5-$Me_3C_6H_3$)$RuCl_2]_2$ with excess benzylamine in refluxing hexane or by using exactly 1 equivalent per ruthenium atom in dichloromethane. If excess benzylamine is used in chloroform then a mixture of the adduct [(1,3,5-$Me_3C_6H_3$)$RuCl_2(NHRR^1)$] and the salt [(1,3,5-$Me_3C_6H_3$)RuCl$(NHRR^1)_2$][Cl] is formed, which cannot be separated easily. This sol-

* Author to whom correspondence should be addressed.

$$[(\eta\text{-arene})RuCl_2]_2 \xrightarrow{RR^1NH} [(\eta\text{-arene})RuCl_2(RR^1NH)]$$

1a - f

arene	R	R^1	
1,3,5-$Me_3C_6H_3$	H	Ph	a
1,3,5-$Me_3C_6H_3$	H	CH_2Ph	b
1,3,5-$Me_3C_6H_3$	Et	Et	c
1,3,5-$Me_3C_6H_3$	Bu	Bu	d
p-cymene	Et	Et	f

1e arene = 1,3,5-$Me_3C_6H_3$; RR^1NH = piperidine

$$[(1,3,5\text{-}Me_3C_6H_3)RuCl_2(RR^1NH)] \xrightarrow[AgBF_4]{RR^1NH} [(1,3,5\text{-}Me_3C_6H_3)RuCl(RR^1NH)_2][BF_4]$$

2a,b

R	R^1	
H	Ph	a
H	CH_2Ph	b

Scheme 1.

vent dependence has been observed previously in the reaction of pyrazoles with $[(benzene)RuCl_2]_2$.[4]

Although steric factors do not prevent the formation of complexes of secondary amines they may influence their relative stability. In order to try and assess the degree of steric crowding in these complexes we determined the crystal structure of the piperidine adduct **1e**. For comparison purposes we also determined the structure of the related pyridine complex $[(1,3,5\text{-}Me_3C_6H_3)RuCl_2(NC_5H_5)]$, which has been made previously.[1a] The structures of the complexes are shown in Figs 1 and 2, respectively, and selected bond lengths and angles are listed in Table 1. The most notable feature of the structures is the orientation of the piperidine, with the N—H pointing away from the arene and the sterically more demanding CH_2 groups pointing towards the arene. This may be due to attractive forces between the alkyl groups on the arene and the piperidine ring and also the possibility of hydrogen bonding between the N—H and the two chlorine atoms. The HN–chlorine distances [2.588 to Cl(1) and 2.712 Å to Cl(2)] are consistent with hydrogen bonding, although it should be remembered that this hydrogen atom has been included in a calculated position and was not found in the difference-Fourier map. The Ru—N bond in the piperidine complex, 2.153(4) Å, is longer than in the pyridine complex, 2.127(7) Å, as expected. The average Ru—Cl bond lengths and Cl—Ru—Cl bond angle are the same in the two complexes. The mesitylene ring is essentially planar in both structures and the distances from the ring to the metal are 1.673 and 1.676 Å for the piperidine and pyridine complex, respectively.

We thought it might also be possible to assess the role of steric factors in determining the relative stability of these amine complexes by attempting amine exchange reactions.

$$[(1,3,5\text{-}Me_3C_6H_3)RuCl_2L] + L^1 \rightleftharpoons [(1,3,5\text{-}Me_3C_6H_3)RuCl_2L^1] + L$$

This has resulted in the following series of stabilities: **1e** > **1a** > **1d**. Qualitatively we have observed that the primary amine complexes are more stable than the secondary amine ones, however, piperidine seems to be a special case. The use of this amine exchange reaction is limited by the occurrence of competing side reactions in certain cases. For example, the reaction of the piperidine complex **1e** with

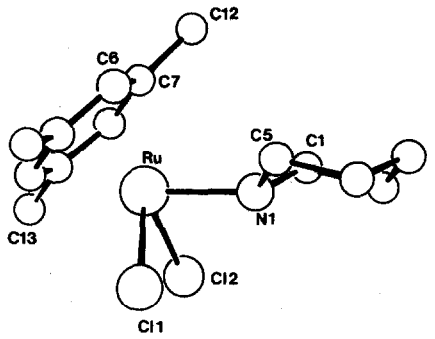

Fig. 1. Molecular structure of $[(1,3,5\text{-}Me_3C_6H_3)RuCl_2(HNC_5H_{10})]$ (**1e**).

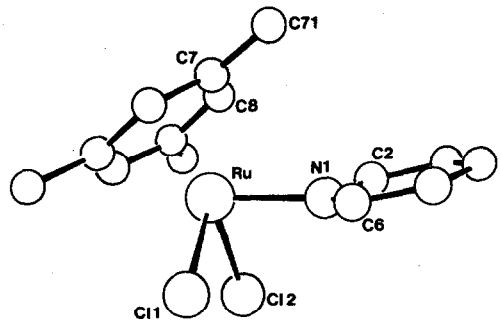

Fig. 2. Molecular structure of $[(1,3,5\text{-}Me_3C_6H_3)RuCl_2(NC_5H_5)]$.

Table 1. Selected bond lengths (Å) and angles (°) for the complexes $[(1,3,5\text{-}Me_3C_6H_3)RuCl_2(HNC_5H_{10})]$ and $[(1,3,5\text{-}Me_3C_6H_3)RuCl_2(NC_5H_5)]$

$[(1,3,5\text{-}Me_3C_6H_3)RuCl_2(HNC_5H_{10})]$		$[(1,3,5\text{-}Me_3C_6H_3)RuCl_2(NC_5H_5)]$	
Ru—Cl(1)	2.409(2)	Ru—Cl(1)	2.419(2)
Ru—Cl(2)	2.422(1)	Ru—Cl(2)	2.415(2)
Ru—N(1)	2.153(4)	Ru—N(1)	2.127(7)
Cl(1)—Ru—Cl(2)	88.4(1)	Cl(1)—Ru—Cl(2)	88.4(1)
N(1)—Ru—Cl(1)	80.4(1)	N(1)—Ru—Cl(1)	87.4(2)
N(1)—Ru—Cl(2)	82.4(1)	N(1)—Ru—Cl(2)	85.4(2)

1 equivalent of benzylamine when monitored by ^1H NMR shows the presence of some starting complex **1e**, some **1b** and some species, which judging by the chemical shift of the mesitylene protons are due to cationic species containing two amines. During the course of our work a report has been published on amine exchange reactions of the complex cations $[(dppe)PdMe(NRR'RR'')]^+$, which concluded that both steric and electronic factors were important in determining the relative stability of the various cations.[5]

As mentioned above with benzylamine it is possible to form the cation $[(1,3,5\text{-}Me_3C_6H_3)RuCl(NHRR^1)_2]^+$ by direct reaction of $[(1,3,5\text{-}Me_3C_6H_3)RuCl_2]_2$ with benzylamine. Similar behaviour has been observed previously for aromatic amines.[3] An alternative is to react the amine adducts $[(1,3,5\text{-}Me_3C_6H_3)RuCl_2(NHRR^1)]$ with 1 equivalent of amine and $AgBF_4$. Using this method we have isolated the compounds **2a** and **2b**.

The ^1H NMR spectra of the cations showed peaks in the expected regions. However, the mesitylene signals for **2a** are shifted to higher field than in **1a**, while for **2b** they are to lower field than in **1b**. Since complexes **2** contain cationic ruthenium fragments one might expect a shift to lower field, as is observed with **2b**. Thus, the upfield shift for **2a** may be due to the ring current effects of the phenyl rings. It is noteworthy that for **1a** the methyl groups of the mesitylene ring are *ca* 0.2 ppm upfield from the complexes **1b–e**, which may also be a consequence of a ring current effect.

EXPERIMENTAL

Petroleum ether and diethyl ether were dried by refluxing over purple sodium/benzophenone under nitrogen, while dichloromethane was purified by refluxing over calcium hydride. The compounds $[(p\text{-cymene})RuCl_2]_2$[6] and $[(1,3,5\text{-}Me_3C_6H_3)RuCl_2]_2$[7] were prepared using literature procedures. The reactions described were performed in deoxygenated solvents under nitrogen; however, once isolated as pure solids the compounds are relatively air-stable and precautions for their storage are unnecessary.

^1H NMR spectra were recorded on a Bruker AM300 or a Varian EM390 spectrometer. Microanalyses were performed by Butterworth Labor-

atories Ltd, Middlesex. FAB mass spectra were performed at the SERC Mass Spectroscopy service centre at University College Swansea.

Preparation of [(1,3,5-$Me_3C_6H_3$)$RuCl_2(NH_2Ph)$] (**1a**)

Aniline (114 mg, 1.55 mmol) was added to a suspension of [(1,3,5-$Me_3C_6H_3$)$RuCl_2]_2$ (301 mg, 0.52 mmol) in dichloromethane (50 cm^3) and the mixture was refluxed for 2.5 h. The solvent was removed and the solid was washed with petroleum ether. Recrystallization from dichloromethane/diethyl ether gave [(1,3,5-$Me_3C_6H_3$)$RuCl_2(NH_2$ Ph)] as a yellow solid (338 mg, 85%). Found: C, 47.2; H, 4.8; N, 3.5. Calc. for $C_{15}H_{19}Cl_2NRu$: C, 46.8; H, 5.0; N, 3.6%. ^1H NMR ($CDCl_3$): 2.00 (s, 9H, Me), 4.83 (s, 3H, C_6H_3), 7.25 (m, 5H, Ph).

Preparation of [(1,3,5-$Me_3C_6H_3$)$RuCl_2(NH_2CH_2$ Ph)] (**1b**)

Benzylamine (90 mg, 0.84 mmol) was added to a suspension of [(1,3,5-$Me_3C_6H_3$)$RuCl_2]_2$ (245 mg, 0.42 mmol) in dichloromethane (50 cm^3) and the mixture was refluxed for 2.5 h. The solvent was removed and the solid was washed with petroleum ether. Recrystallization from dichloromethane/diethyl ether gave [(1,3,5-$Me_3C_6H_3$)$RuCl_2(NH_2$ CH_2Ph)] as orange crystals (287 mg, 86%). Found: C, 48.2; H, 5.6; N, 3.4. Calc. for $C_{16}H_{21}Cl_2NRu$: C, 48.1; H, 5.3; N, 3.5%. ^1H NMR ($CDCl_3$): 2.21 (s, 9H, Me), 3.22 (br, 2H, NH), 4.12 (m, 2H, CH_2), 4.92 (s, 3H, C_6H_3), 7.30 (m, 5H, Ph). Mass spectrum: *m/z* 399 $(M)^+$, 364 $(M-Cl)^+$.

Preparation of [(1,3,5-$Me_3C_6H_3$)$RuCl_2(NHEt_2)$] (**1c**)

Diethylamine (94 mg, 1.2 mmol) was added to a suspension of [(1,3,5-$Me_3C_6H_3$)$RuCl_2]_2$ (251 mg, 0.43 mmol) in chloroform (50 cm^3) and the mixture was refluxed for 2 h. The solvent was removed and the solid was washed with petroleum ether to leave [(1,3,5-$Me_3C_6H_3$)$RuCl_2(NHEt_2)$] as a yellow solid (232 mg, 74%). Found: C, 33.4; H, 4.3; N, 1.3. Calc. for $C_{13}H_{23}Cl_2NRu$: C, 42.7; H, 6.3; N, 3.8%. ^1H NMR ($CDCl_3$): 1.22 [t, 6H, CH_3CH_2, *J*(7)], 2.26 (s, 9H, C_6Me_3), 3.13 (m, 2H, CHH^1), 3.63 (m, 2H, CHH^1), 4.91 (s, 3H, C_6H_3). Mass spectrum: *m/z* 378 $(M+H)^+$.

Preparation of [(1,3,5-$Me_3C_6H_3$)$RuCl_2(NHBu_2)$] (**1d**)

Dibutylamine (278 mg, 2.15 mmol) was added to a suspension of [(1,3,5-$Me_3C_6H_3$)$RuCl_2]_2$ (252 mg, 0.43 mmol) in chloroform (75 cm^3) and the mixture was refluxed for 1.5 h. The solvent was removed and the solid was washed with petroleum ether. Recrystallization from dichloromethane/petroleum ether gave [(1,3,5-$Me_3C_6H_3$)$RuCl_2(NHBu_2)$] as a yellow solid (363 mg, 100%). Found: C, 48.6; H, 7.6; N, 3.6. Calc. for $C_{17}H_{31}Cl_2NRu$: C, 48.4; H, 7.4; N, 3.3%. ^1H NMR ($CDCl_3$): 0.90 [t, 6H, CH_3, *J*(7)], 1.28 (m, 4H, CH_2), 1.55 (m, 4H, CH_2), 2.26 (s, 9H, C_6Me_3), 3.01 (m, 2H, $NCHH^1$), 3.47 (m, 2H, $NCHH^1$), 4.90 (s, 3H, C_6H_3). Mass spectrum: *m/z* 422 $(M+H)^+$.

Preparation of [(1,3,5-$Me_3C_6H_3$)$RuCl_2(HNC_5$ H_{10})] (**1e**)

Piperidine (183 mg, 2.15 mmol) was added to a suspension of [(1,3,5-$Me_3C_6H_3$)$RuCl_2]_2$ (252 mg, 0.43 mmol) in chloroform (50 cm^3) and the mixture was refluxed for 3 h. The solvent was removed and the solid was washed with petroleum ether. Recrystallization from dichloromethane/petroleum ether gave [(1,3,5-$Me_3C_6H_3$)$RuCl_2(HNC_5H_{10})$] as an orange solid (281 mg, 86%). Found: C, 44.5; H, 5.9; N, 3.7. Calc. for $C_{14}H_{23}Cl_2NRu$: C, 44.5; H, 6.1; N, 3.7%. ^1H NMR ($CDCl_3$): 1.40–1.90 (m, 6H, various piperidine), 2.26 (s, 9H, C_6Me_3), 2.93 [dt, 2H, NCH, *J*(12,12)], 3.75 [d, 2H, $NCHH^1$, *J*(12)], 4.97 (s, 3H, C_6H_3). Mass spectrum: *m/z* 378 $(M+H)^+$, 342 $(M+H-Cl)^+$.

Preparation of [(p-cymene)$RuCl_2(NHEt_2)$] (**1f**)

Diethylamine (39 mg, 0.53 mmol) was added to a solution of [(*p*-cymene)$RuCl_2]_2$ (108 mg, 0.176 mmol) in chloroform (50 cm^3). The mixture was refluxed for 3 h, during which time the solution became orange. The solvent was removed and the solid was washed with petroleum ether. Recrystallization from dichloromethane/petroleum ether gave [(*p*-cymene)$RuCl_2(NHEt_2)$] as a bright yellow solid (66 mg, 50%). Found: C, 43.6; H, 6.5; N, 3.5. Calc. for $C_{14}H_{25}Cl_2NRu$: C, 44.3; H, 6.6; N, 3.7%. ^1H NMR ($CDCl_3$): 1.22 [t, 6H, CH_2CH_3, *J*(7)], 1.31 [d, 6H, $CHMe_2$, *J*(7)], 2.23 (s, 3H, C_6H_4Me), 3.03 [sep, 1H, $CHMe_2$, *J*(7)], 3.16 (m, 2H, CHH^1), 3.50 (m, 2H, CHH^1), 5.33, 5.38 [$(AB)_2$, 4H, C_6H_4, *J*(AB)6].

Amine exchange reactions

Complex **1d** (250 mg, 0.59 mmol) and aniline (166 mg, 1.78 mmol) were refluxed in chloroform (50 cm^3) for 2.5 h. The solvent was removed and the oily solid was washed with petroleum ether to give

a yellow solid, identified as complex **1a** on the basis of its ^1H NMR spectrum (157 mg, 70%).

The same general procedure was used for the reaction of complex **1a** with piperidine in equimolar amounts to give complex **1e** in 71% yield. Using the same method refluxing of complex **1e** with aniline gave no reaction.

Preparation of [(1,3,5-$Me_3C_6H_3$)$RuCl(NH_2Ph)_2$][BF_4] (**2a**)

Aniline (48 mg, 0.52 mmol) and $AgBF_4$ (101 mg, 0.52 mmol) were added to a solution of [(1,3,5-$Me_3C_6H_3$)$RuCl_2(NH_2Ph)$] (20 mg, 0.52 mmol) in dichloromethane (50 cm^3) and the mixture was stirred for 0.5 h. The AgCl was removed by filtration through celite and the solvent was rotary evaporated. Recrystallization from dichloromethane/diethylether gave [(1,3,5-$Me_3C_6H_3$)$RuCl(NH_2Ph)_2$][BF_4] as an orange crystalline solid (259 mg, 94%). Found: C, 47.2; H, 4.9; N, 5.0. Calc. for $C_{21}H_{26}BClF_4N_2Ru$: C, 47.6; H, 4.9; N, 5.3%. ^1H NMR ($CDCl_3$): 1.69 (s, 9H, C_6Me_3), 4.48 (br, 2H, NH), 4.76 (s, 3H, C_6H_3), 5.83 (br, 2H, NH), 7.35 (m, 10H, Ph).

Preparation of [(1,3,5-$Me_3C_6H_3$)$RuCl(NH_2CH_2Ph)_2$][BF_4] (**2b**)

Benzylamine (47 mg, 0.44 mmol) and $AgBF_4$ (86 mg, 0.44 mmol) were added to a solution of [(1,3,5-$Me_3C_6H_3$)$RuCl_2(NH_2CH_2Ph)$] (177 mg, 0.44 mmol) in dichloromethane (60 cm^3) and the mixture was stirred for 0.5 h. The AgCl was removed by filtration through celite and the solvent was rotary evaporated. Recrystallization from dichloromethane/diethylether gave [(1,3,5-$Me_3C_6H_3$)$RuCl(NH_2CH_2Ph)_2$][BF_4] as an orange crystalline solid (170 mg, 68%). Found: C, 49.7; H, 5.4; N, 4.9. Calc. for $C_{23}H_{30}BClF_4N_2Ru$: C, 49.5; H, 5.4; N, 5.0%. ^1H NMR (CD_2Cl_2): 2.30 (s, 9H, C_6Me_3), 2.50 (br, 2H, NH), 4.01 (m, 4H, CH_2), 4.42 (br, 2H, NH), 5.10 (s, 3H, C_6H_3), 7.34 (m, 10H, Ph). Mass spectrum: m/z 471 $[M]^+$, 364 $[M-NH_2CH_2Ph]^+$ (M refers to the complex cation).

X-ray structure determinations

Crystals of [(1,3,5-$Me_3C_6H_3$)$RuCl_2(HNC_5H_{10})$] were grown from dichloromethane/mesitylene, while those of [(1,3,5-$Me_3C_6H_3$)$RuCl_2(NC_5H_5)$] were grown from dichloromethane/diethylether. The crystals used for data collection were mounted in air and the unit cell parameters were determined by least-squares refinement of ω-measurements of different layers.[8] Data were collected on a Stoe STADI-2 diffractometer with an ω-scan technique in the range $7 < 2\theta < 54°$. Scattering factors were taken from ref. 9.

Crystal data for [$C_{14}H_{23}Cl_2NRu$] (**1e**). $M = 377.3$; monoclinic, space group $P2_1/c$, $a = 11.573(9)$, $b = 9.341(8)$, $c = 15.100(14)$ Å, $\beta = 107.3(1)°$, $U = 1558.3$ Å^3, $Z = 4$, $\mu = 12.09$ cm^{-1}, λ(Mo-K_α) = 0.7107 Å, $F(000) = 768$, $D_c = 1.61$ g cm^{-3}. Crystal dimensions $0.48 \times 0.28 \times 0.155$ mm.

The intensities of 3178 unique reflections were measured and these data were corrected for Lorentz and polarization effects to give 2098 unique reflections with $I > 3\sigma(I)$. The structure was solved using the PATT option of SHELXS-86; all subsequent calculations were performed with the computer programme SHELX-76.[10] All hydrogen atoms were included in calculated positions (C—H = 1.08 Å) and all non-hydrogen atoms were refined anisotropically. Final cycles of least-squares refinement used a weighting parameter $w = 1/(\sigma^2F+gF^2)$, where $g = 0.0007$, and gave final residual indices of $R = 0.038$ and $R_w = 0.041$.

Crystal data for [$C_{14}H_{17}Cl_2NRu$]. $M = 371.3$; orthorhombic space group $P2_12_12_1$, $a = 13.623(14)$, $b = 13.928(14)$, $c = 7.633(2)$ Å, $U = 1448.27$ Å^3, $z = 4$, $\mu = 13.01$ cm^{-1}, λ(Mo-K_α) = 0.7107 Å, $F(000) = 744$, $D_c = 1.70$ g cm^3. Crystal dimensions $0.38 \times 0.12 \times 0.06$ mm.

The intensities of 1740 reflections were measured and these data were corrected for Lorentz and polarization effects to give 1411 unique reflections with $I > 3\sigma(I)$. The structure was solved by direct methods using SHELXS-86; all subsequent calculations were carried out with the computer program SHELX-76.[10] All hydrogen atoms were put in calculated positions (C—H = 1.08 Å) and all non-hydrogen atoms were refined anisotropically. Final cycles of least-squares refinement used a weighting parameter $w = 1.1827/(\sigma^2F+gF^2)$, where $g = 0.0007$, and gave final residual indices of $R = 0.0416$ and $R_w = 0.0422$.

Acknowledgements—We thank the S.E.R.C. for a studentship (L.C) and for use of the Mass Spectroscopy Service Centre at University College Swansea and Leicester University Computer Centre who provided support and facilities for X-ray single-crystal calculations.

REFERENCES

1. (a) M. A. Bennett and A. K. Smith, *J. Chem. Soc., Dalton Trans.* 1974, 233; (b) R. A. Zelonka and M. C. Baird, *Can. J. Chem.* 1972, **50**, 3063; (c) R. H. Crabtree and A. J. Pearson, *J. Organomet.*

Chem. 1977, **141**, 325; (d) W. Weber and P. C. Ford, *Inorg. Chem.* 1986, **25**, 1088.
2. P. Pertici, P. Salvadori, A. Biasci, G. Vitulli, M. A. Bennett and L. A. P. Kane-Maguire, *J. Chem. Soc., Dalton Trans.* 1988, 315.
3. R. S. Bates, M. J. Begley and A. H. Wright, *Polyhedron* 1990, **9**, 1113.
4. C. J. Jones, J. A. McCleverty and A. S. Rothin, *J. Chem. Soc., Dalton Trans.* 1986, 109.
5. A. L. Seligson and W. C. Trogler, *J. Am. Chem. Soc.* 1991, **113**, 2520.
6. M. A. Bennett and A. K. Smith, *Inorg. Synth.* 1982, **21**, 74.
7. J. W. Hull Jr and W. L. Gladfelter, *Organometallics* 1984, **3**, 605.
8. W. Clegg and G. M. Sheldrick, *Z. Krist.* 1984, **167**, 23.
9. *International Tables for X-ray Crystallography*, Vol. 4. Kynoch Press, Birmingham (1975).
10. G. M. Sheldrick, SHELX-76, Program for Crystal Structure Determination. University of Cambridge, U.K. (1976), updated Göttingen (1986).

Polyhedron Vol. 12, No. 10, pp. 1129–1133, 1993
Printed in Great Britain

0277–5387/93 $6.00+.00
© 1993 Pergamon Press Ltd

THE REACTIVITY OF Se_4N_4 IN LIQUID AMMONIA

PAUL F. KELLY and J. DEREK WOOLLINS*

Department of Chemistry, Imperial College, London SW7 2AY, U.K.

(*Received* 27 *January* 1993; *accepted* 5 *February* 1993)

Abstract—Tetraselenium-tetranitride, Se_4N_4, dissolves in liquid ammonia at high pressure (*ca* 50 atm.) and reacts with $PtCl_2(PMe_2Ph)_2$ to give $Pt(Se_2N_2)(PMe_2Ph)_2$ in quantitative yield. If the reaction is performed using $Se_4{}^{15}N_4$ the product is obtained with a low (<20%) degree of ^{15}N labelling; in contrast $Se_4{}^{15}N_4$ may be recrystallized from ammonia with no loss of ^{15}N content, indicating that, unlike S_4N_4, it does not react with ammonia as it dissolves.

After many years in the role of "poor-relation" to their sulphur–nitrogen counterparts, selenium–nitrogen compounds have recently become the focus of much attention.[1] One of the main catalysts for this upsurge of interest was the realization that although Se_4N_4 is undoubtedly less reactive (and substantially more hazardous) than S_4N_4, it can, in the right circumstances, act as a source of novel Se—N compounds and ligands. Thus, reaction with $[Se_4]^{2+}$ generates cations of the type $[Se_3N_2]^{n+}$,[2] while a number of different metal species have been shown to react to give complexes of [NSeCl],[3] Se_3N^-,[4] $Se_2N_2{}^{2-}$ [5] and $Se_2N_2N^-$.[6] Although recent work has resulted in a number of less explosive species such as $[Me_3SiN]_4Se$,[7] which clearly have great potential as synthons, it is likely that Se_4N_4 will remain an extremely important source of new Se—N systems.

A major hindrance to the advancement of the chemistry of Se_4N_4 is its extreme insolubility in common solvents. By way of illustration we have found that the solubility in xylene is so low that even at temperatures greater than 150°C there is only a very slight colouration of the solvent; clearly the solubility is many orders of magnitude less than S_4N_4. In contrast, previous work by Street *et al.* revealed that a new phase of Se_4N_4 crystallizes from ammonia after heating to 70°C,[8] implying that the compound has a reasonable solubility at this temperature. Here we report on investigations into the use of ammonia as a solvent for Se_4N_4 reactions.

* Author to whom correspondence should be addressed.

EXPERIMENTAL

High-pressure reactions were performed in a Bergfhof pressure reactor (HR 100) equipped with a 70 cm^3 Teflon insert. The compounds Se_4N_4[9] and $Se_4{}^{15}N_4$[10] were pepared by the literature methods. **NOTE!** Se_4N_4 is a powerful explosive which is extremely shock sensitive and should not be handled with a metal spatula; residues should be destroyed by slurrying with water followed by cautious addition of hypochlorite solution.

Dissolution of $Se_4{}^{15}N_4$ *in ammonia*

A suspension of $Se_4{}^{15}N_4$ (17 mg, 0.045 mmol) in liquid ammonia (50 cm^3) was slowly heated over a period of 30 min until the internal pressure reached 50 atm. (external heating temperature 135°C, internal temperature measured as *ca* 90°C). After 10 min at this pressure the system was cooled and the ammonia decanted from the pressure tube; the latter was thoroughly rinsed with CH_2Cl_2 and these washings added to the ammonia, which was allowed to evaporate. The resulting solid Se_4N_4 was transferred, as a suspension, to a Schlenk tube and allowed to settle. CH_2Cl_2 was decanted and the solid dried *in vacuo*; it was then treated with a solution of $Pt(PPh_3)_3$ (40 mg, 0.04 mmol) in dried, degassed CH_2Cl_2 (20 cm^3) with stirring. The resulting dark solution was allowed to stand for a few hours to precipitate all the resulting insoluble green $[Pt(Se_2N_2)(PPh_3)]_2$ and then filtered. After removal of the solvent *in vacuo* $CDCl_3$ was added to dissolve the $Pt(Se_2N_2)(PPh_3)_2$ present, the resulting solution

treated with a drop of the base DBU (to remove any protonation effects of residual HCl) and the ^{31}P NMR spectrum recorded. The splitting pattern obtained for both phosphorus atoms was identical to that obtained for analogous products formed from unrecrystallized $Se_4{}^{15}N_4$, indicating that no exchange with nitrogen from the ammonia had occurred and that the Se_4N_4 was, therefore, still fully labelled.

Reaction of $PtCl_2(PMe_2Ph)_2$ *with* Se_4N_4

A mixture of Se_4N_4 (46 mg, 0.12 mmol) and $PtCl_2(PMe_2Ph)_2$ (70 mg, 0.13 mmol) in liquid ammonia (50 cm^3) was heated and cooled as above and the ammonia allowed to evaporate. After extraction into CH_2Cl_2 (50 cm^3), filtration and removal of the solvent *in vacuo* the resulting yellow oily residue was dissolved in $CDCl_3$, treated with one drop of DBU and then the ^{31}P NMR spectrum of the solution recorded. This revealed that complete conversion of the starting material to $Pt(Se_2N_2)(PMe_2Ph)_2$ had taken place, the latter being characterized by an AX pair of doublets at δ −2.6 ($^1J\{^{195}Pt—^{31}P\}$ 2814 Hz) and δ −28.4 ($^1J\{^{195}Pt—^{31}P\}$ 2565 Hz).

The reaction involving $Se_4{}^{15}N_4$ was performed in an identical manner using 13 mg (0.03 mmol) of the latter and 20 mg (0.04 mmol) of the platinum complex.

RESULTS AND DISCUSSION

When Se_4N_4 [Fig. 1(a)] is prepared by the action of ammonia gas upon a toluene solution of diethylselenite,[9] $[EtO]_2SeO$, it forms as an amorphous orange solid with no evidence of crystallinity. If this material is then suspended in liquid ammonia in a high-pressure system, the temperature raised (internal temperature *ca* 90°C ≡ 50 atm.), then after 10 min the mixture re-cooled, the resulting Se_4N_4 is obtained as dark-orange, well-formed microcrystals. From this observation it is clear that Se_4N_4 is actually soluble in the ammonia at this temperature.

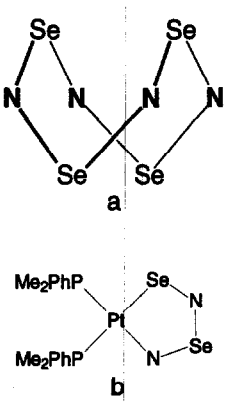

Fig. 1. The structures of (a) Se_4N_4 and (b) $Pt(Se_2N_2)(PMe_2Ph)_2$.

If the above experiment is repeated in the presence of *cis*-$PtCl_2(PMe_2Ph)_2$ and the ammonia removed from the resulting orange solution ^{31}P NMR spectroscopy reveals that complete conversion of the platinum complex to $Pt(Se_2N_2)(PMe_2Ph)_2$ [Fig. 1(b)] takes place. This reaction, therefore, mirrors that of the platinum species with $[S_3N_2Cl]Cl$, $[S_4N_3]Cl$ or S_4N_4 in ammonia (at −78°C), all of which generate $Pt(S_2N_2)(PMe_2Ph)_2$.[11] In the latter cases the reactions proceed via S—N anions such as $[S_3N_3]^-$, which we have observed in solution using ^{14}N NMR. Clearly, it is possible that so-far unknown selenium analogues, such as $[Se_3N_3]^-$, may be responsible for the reactivity of Se_4N_4 in ammonia.

Previous work showed that when a solution of a fully ^{15}N labelled species, such as $[S_4{}^{15}N_3]Cl$, in ammonia is used to generate $Pt(S_2N_2)(PMe_2Ph)_2$ the latter is obtained with a degree of ^{15}N labelling substantially less than 100%. This intermixing with the nitrogens of the ammonia is brought about by two different processes: (1) incorporation of ammoniacal nitrogens into the S—N systems during the initial formation of the reactive anions (e.g. $S_3N_3{}^-$) and (2) a slow exchange between the nitrogens in the latter and those in the ammonia. This was illustrated by analysis of S_4N_4 recovered from ammonia solutions of $[S_4{}^{15}N_3]Cl$; work-up after a few minutes yields the product with a degree of labelling of *ca* 60%—in contrast if the ammoniacal solution is left overnight this figure drops to only 20%.[12]

We have recently reported the preparation of $Se_4{}^{15}N_4$ by reaction of $[EtO]_2SeO$ with stoichiometric amounts of $^{15}NH_3$ in xylene.[12] Access to the labelled compound allows us to use NMR techniques to investigate the Se_4N_4/NH_3 system. If the reaction between $Se_4{}^{15}N_4$ and $PtCl_2(PMe_2Ph)_2$ is performed as above, and the ^{31}P NMR spectrum of the resulting $Pt(Se_2N_2)(PMe_2Ph)_2$ measured (Fig. 2), it indicates that a very large percentage of the ^{15}N has been washed from the system, leaving a degree of labelling of *ca* 20%. There are three possible explanations for this decrease in ^{15}N content: (1) that Se_4N_4 actually reacts with the ammonia as it dissolves, in the same manner as S_4N_4; (2) that Se_4N_4 reacts with the platinum compound to give a species such as $[Se_3N_3]^-$, which then undergoes nitrogen exchange with the ammonia *before* generation of the final complex;

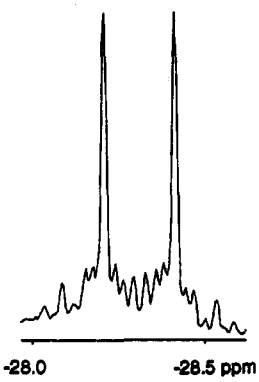

Fig. 2. $^{31}P\{^1H\}$ NMR of the phosphorus *trans* to nitrogen in $Pt(Se_2N_2)(PMe_2Ph)_2$, prepared by the reaction of $Se_4{}^{15}N_4$ with $PtCl_2(PMe_2Ph)_2$ in ammonia. The simplicity of the spectrum shows that there is a low degree of ^{15}N in the product.

or (3) that fully labelled $Pt(Se_2N_2)(PMe_2Ph)_2$ is produced and this then undergoes nitrogen exchange with the ammonia. Obviously a combination of the latter two could occur but the conclusion would still be that there was no initial reaction of Se_4N_4 with ammonia.

Given the fact that the high temperature of the system would undoubtedly increase the rate of the slow exchange between the nitrogen atoms in the ammonia and any Se—N anions present, the degree of labelling in the products obtained in this manner lends credance to explanation (1). In such a situation it is possible that the anions produced would be relatively unstable and would revert to Se_4N_4 upon cooling and evaporation of the ammonia. This would explain why only Se_4N_4 (together with some residual red selenium) is obtained during recrystallization. However, if spontaneous reaction of Se_4N_4 with ammonia, to give reactive anionic species, was occurring then this would mean that the ^{15}N content of a solution of $S_4{}^{15}N_4$ in ammonia would slowly diminish.

Monitoring the decrease in ^{15}N content of Se_4N_4 presents more of a challenge than in the case of S_4N_4. The latter is more amenable to mass spectrometry, both in terms of the ease in obtaining parent ion peaks and in calculating ^{15}N content from such peaks, and to ^{15}N NMR spectroscopy. In the latter case we have found that there is a small but measurable isotope effect giving rise to individual peaks for $S_4{}^{15}N^{14}N_3$, $S_4{}^{15}N_2N_2$, $S_4{}^{15}N_3N$ and $S_4{}^{15}N_4$ separated by *ca* 0.04 ppm. This is illustrated by Fig. 3, which shows the high resolution ^{15}N

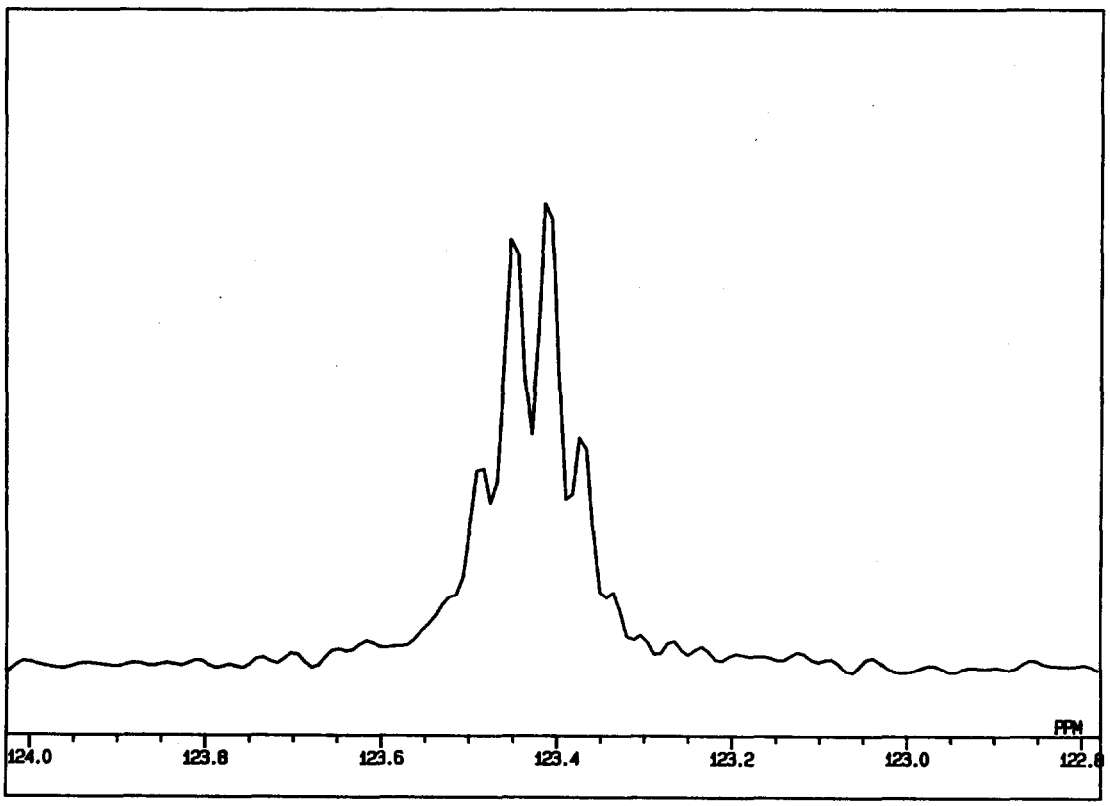

Fig. 3. Resolution-enhanced ^{15}N NMR spectrum of 50% ^{15}N labelled S_4N_4; each resonance is due to a different isotopomer.

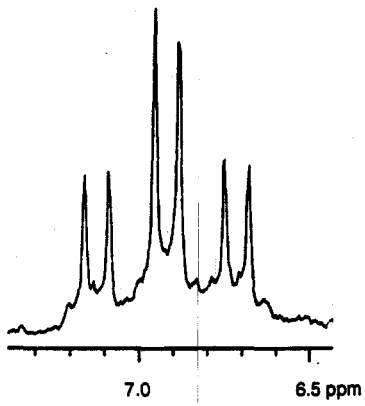

Fig. 4. $^{31}P\{^{1}H\}$ NMR of the phosphorus *trans* to nitrogen in $Pt(Se_2N_2)(PPh_3)_2$ prepared by the reaction of $Se_4{}^{15}N_4$ with $Pt(PPh_3)_3$. An identical spectrum is obtained from the reaction of $Se_4{}^{15}N_4$, which has been recrystallized from liquid ammonia.

NMR spectrum of 50% labelled Se_4N_4; the four lines for the four different isotopomers are seen in the predicted 1:3:3:1 intensity ratio. Obviously the extreme insolubility of Se_4N_4 in common solvents precludes analogous studies; however, a convenient technique which can be employed utilizes its reactivity towards the platinum(0) species $Pt(PPh_3)_3$. This reaction generates $Pt(Se_2N_2)(PPh_3)_2$,[5] which is soluble and shows characteristic splitting patterns in the ^{31}P NMR spectrum, which are indicative of the degree of labelling. Particularly informative is the resonance for phosphorus *trans* to nitrogen, which, in the fully labelled case, shows a pattern due to two $^{15}N—^{31}P$ interactions of magnitude 24 and 8 Hz (Fig. 4). If $Se_4{}^{15}N_4$, which has been recrystallized from ammonia, is used to generate the latter species the splitting pattern obtained is identical to that in Fig. 4. In other words *there is no incorporation of nitrogen from the ammonia into* Se_4N_4 *during recrystallization* and thus we can conclude that, unlike S_4N_4, Se_4N_4 does not spontaneously react with the ammonia.

If fully labelled $Pt(Se_2{}^{15}N_2)(PMe_2Ph)_2$ is dissolved in ammonia and the temperature raised as before the ^{31}P NMR spectrum of the product obtained after cooling is identical to that of the starting material. From this observation we can conclude that the third possibility listed above, namely that there may be slow exchange between the nitrogens of the ammonia and of $Pt(Se_2{}^{15}N_2)(PMe_2Ph)_2$, can be ruled out.

The above results, summarized in Scheme 1, lead to the conclusion that a reactive Se—N intermediate must be the first product of the reaction with the platinum compound and that this intermediate can then undergo nitrogen exchange with ammonia prior to ultimately generating $Pt(Se_2N_2)(PMe_2Ph)_2$. It is difficult to speculate upon the exact nature of this intermediate, especially as we do not know what form the platinum species takes in this situation; preliminary studies indicate that when $PtCl_2(PMe_2Ph)_2$ is dissolved in ammonia under similar conditions to the above reactions there is at least some degree of conversion to substituted species (which we speculate are of the type $[Pt(PMe_2Ph)_2(NH_3)Cl]^+$ and $[Pt(PMe_2Ph)_2(NH_3)_2]^{2+}$). If these solutions are allowed to cool and the ammonia evaporated off under a steam of nitrogen a white solid is left. Extraction of this solid with CH_2Cl_2 yields $PtCl_2(PMe_2Ph)_2$ (as shown by ^{31}P NMR); we have yet to characterize the white, CH_2Cl_2-insoluble residue. Interestingly, if CH_2Cl_2 is added to the ammonia before it has been evaporated then a new soluble product is obtained, which is seen as a singlet in the ^{31}P NMR spectrum (δ −13.9; $^{1}J\{^{195}Pt—^{31}P\}$ 2825 Hz). This product appears to decompose slowly to the dichloride in solution and thus any attempt to crystallize it by slow diffusion simply yields colourless crystals of the latter.

In conclusion it is clear that liquid ammonia at high, but relatively easily handled pressure is an excellent solvent for Se_4N_4. The latter does not appear to undergo significant reaction with the

$$PtCl_2(PMe_2Ph)_2 + Se_4N_4\ (98\%\ {}^{15}N) \xrightarrow[50\ Atm.]{NH_3(liq.)} Pt(Se_2N_2)(PMe_2Ph)_2\ (<20\%\ {}^{15}N)$$

$$Se_4N_4\ (98\%\ {}^{15}N) \xrightarrow[50\ Atm.]{NH_3(liq.)} Se_4N_4\ (98\%\ {}^{15}N)$$

$$Pt(Se_2N_2)(PMe_2Ph)_2\ (98\%\ {}^{15}N) \xrightarrow[50\ Atm.]{NH_3(liq.)} Pt(Se_2N_2)(PMe_2Ph)_2\ (98\%\ {}^{15}N)$$

Scheme 1.

ammonia and should therefore be amenable to reaction with a wide range of species. Of course the latter must be compatible with the ammonia but even allowing for this *caveat* it is likely that this system will be a valuable tool in the advancement of selenium–nitrogen chemistry.

REFERENCES

1. P. F. Kelly, A. M. Z. Slawin, D. J. Williams and J. D. Woolins, *Chem. Soc. Rev.* 1992, **21**, 245.
2. E. G. Awere, J. Passmore, P. S. White and T. Klapotke, *J. Chem. Soc., Chem. Commun.* 1989, 1415.
3. J. Adel, A. El-Kholi, W. Willing, U. Muller and K. Dehnicke, *Chimia* 1988, **42**, 70.
4. P. F. Kelly, I. P. Parkin, A. M. Z. Slawin, D. J. Williams and J. D. Woollins, *J. Chem. Soc., Chem. Commun.* 1989, 408.
5. P. F. Kelly, A. M. Z. Slawin, D. J. Williams and J. D. Woollins, *Polyhedron* 1990, **9**, 1567.
6. P. F. Kelly, I. P. Parkin, A. M. Z. Slawin, D. J. Williams and J. D. Woollins, *Angew. Chem., Int. Edn Engl.* 1989, **28**, 1047.
7. A. Haas, J. Kasprowski, K. Angermund, P. Betz, C. Kruger, Y. Tsay and S. Werner, *Chem. Ber.* 1991, **124**, 1895.
8. G. Wolmershauser, G. R. Brulet and G. B. Street, *Inorg. Chem.* 1978, **17**, 3586.
9. J. Adel, C. Ergezinger, R. Figge and K. Dehnicke, *Z. Naturforsch.* 1988, **B43**, 639.
10. V. C. Ginn, P. F. Kelly and J. D. Woollins, *J. Chem. Soc., Dalton Trans.* 1992, 2129.
11. P. F. Kelly, Sulphur–nitrogen compounds of platinum and palladium, PhD Thesis, Imperial College (1987).
12. I. P. Parkin, Reactions in liquid ammonia, PhD Thesis, Imperial College (1989).

Polyhedron Vol. 12, No. 10, pp. 1135–1139, 1993
Printed in Great Britain

0277-5387/93 $6.00+.00
© 1993 Pergamon Press Ltd

THE PREPARATION AND X-RAY STRUCTURE OF [NBu$_4$][*fac*-PtBr$_3$(S$_4$N$_4$)]

VANESSA C. GINN, PAUL F. KELLY, ALEXANDRA M. Z. SLAWIN, DAVID J. WILLIAMS and J. DEREK WOOLLINS*

Department of Chemistry, Imperial College, London SW7 2AY, U.K.

(*Received* 23 *November* 1992; *accepted* 27 *January* 1993)

Abstract—Reaction of [NBu$_4$][Pt$_2$Br$_6$] with S$_4$N$_4$ gives the title compound, which has been characterized by ^{15}N/^{195}Pt NMR and X-ray crystallography. The anion consists of fused PtS$_2$N$_2$ and PtS$_3$N$_2$ rings with coordination to the platinum via two sulphur atoms and one nitrogen. The five-membered ring is essentially planar, whereas the six-membered ring is planar with the exception of the coordinated sulphur atom which is common to both rings. The N—S—N angles can be related to the magnitude of the $^2J\{^{15}N—^{15}N\}$ coupling constants.

Metalla-sulphur–nitrogen chemistry continues to excite interest,[1,2] in part because of the ability of the metal to stabilize unknown S—N anions and because of the diversity of the structural types which are observed. Thus, although S$_4$N$_4^{2-}$ has not been isolated in any simple salts three configurations have been observed when it behaves as a ligand in metal complexes. Reaction of S$_4$N$_4$ with Ir(CO)Cl(PPh$_3$)$_2$ gives[3,4] *fac*-Ir(CO)Cl(S$_4$N$_4$)(PPh$_3$) (**1**), whereas reaction with [PtCl$_2$(PMe$_2$Ph)]$_2$ gives[5,6] *mer*-PtCl$_2$(PMe$_2$Ph)(S$_4$N$_4$) (**2**), which can (from NMR studies) adopt two different coordination modes. Recently, we have reported on the formation of [PPh$_4$][PtX$_3$(S$_4$N$_4$)] (**3**) from the oxidative addition reaction of S$_4$N$_4$ with [PPh$_4$]$_2$[Pt$_2$X$_6$]. The facial coordination of the S$_4$N$_4^{2-}$ ligand in **3** was postulated[7] on the basis of ^{15}N and ^{195}Pt NMR, but could not be substantiated by X-ray crystallography because of disorder problems. Here we report the preparation and X-ray structure of [Bu$_4$N][PtBr$_3$(S$_4$N$_4$)] (**4**). ^{15}N and ^{195}Pt NMR studies indicate that **4** is isostructural with **3**.

EXPERIMENTAL

[Bu$_4$N]$_2$[Pt$_2$Br$_6$]

To K$_2$PtBr$_4$ (0.49 g, 0.8 mmol) in water (100 cm^3) was added [Bu$_4$N]Br (0.26 g, 0.8 mmol) in water (200 cm^3). The resulting sage green precipitate was filtered off, washed with water (250 cm^3) and Et$_2$O (100 cm^3) and recrystallized from CH$_2$Cl$_2$/toluene (yield 0.13 g, 24%). Found: C, 27.8; H, 5.1; N, 2.0. Calc.: C, 28.4; H, 5.4; N, 2.1%. The ^{195}Pt NMR spectrum consists of a singlet at δ −2293.

[Bu$_4$N][PtBr$_3$(S$_4$N$_4$)] (4)

[Bu$_4$N]$_2$[Pt$_2$Br$_6$] (0.134 g, 0.1 mmol) and S$_4$N$_4$ (37 mg, 0.2 mmol) were dissolved in CH$_2$Cl$_2$ (30 cm^3) and the resulting dark solution stirred for 3 days. The volume of the solution was then reduced to 2–3 cm^3 *in vacuo* and slow diffusion of Et$_2$O resulted in dark crystals. X-ray crystallography showed these to be [Bu$_4$N][PtBr$_3$(S$_4$N$_4$)] (yield 70 mg, 40%). Found: C, 22.3; H, 4.3; N, 7.5. Calc.: C, 22.3; H, 4.2; N, 8.1%. The ^{195}Pt NMR spectrum consisted of a singlet at δ −2272.

For the ^{15}N labelled sample of **4** S$_4$^{15}N$_4$ was prepared by the literature method from 98% ^{15}N enriched NH$_4$Cl (Aldrich). [Bu$_4$N]$_2$[Pt$_2$Br$_6$] (59 mg, 0.04 mmol) with S$_4$^{15}N$_4$ (16 mg, 0.08 mmol) were mixed as solids and then CH$_2$Cl$_2$ (30 cm^3) was added with stirring. After stirring for 4 h the dark red solution was reduced to 2–3 cm^3 in volume and the ^{15}N{^{1}H} and ^{195}Pt NMR spectra (CD$_2$Cl$_2$) of the solution recorded.

Attempted preparation of fac-[PtCl$_2$(PMe$_2$Ph)(S$_4$N$_4$)]

A solution of [PPh$_4$][PtCl$_3$(S$_4$N$_4$)] (0.115 g, 0.14 mmol) in CH$_2$Cl$_2$ (20 cm^3) was placed in an ice bath

* Author to whom correspondence should be addressed.

and treated with a dilute solution of PMe_2Ph (0.02 cm^3, 0.14 mmol) in the same solvent (1.0 cm^3). The orange red solution did not change colour after addition of the phosphine and was maintained at 0°C for $\frac{1}{2}$ h; on warming to room temperature the solution darkened to orange–brown. The volume of the solution was reduced to 3 cm^3 *in vacuo* and its $^{31}P\{^1H\}$ NMR spectrum recorded ($CDCl_3$). This revealed two singlets at δ −14.5 ($^1J\{^{31}P—^{195}Pt\}$ 3550 Hz) [*cis*-$PtCl_2(PR_3)_2$] and δ −21.8, attributable to $PtCl(S_2N_2H)(PMe_2Ph)$; the presence of the latter was further confirmed by TLC, which gave identical results to an authentic sample (yellow spot at $R_f = 0.37$, eluant CH_2Cl_2).

X-ray crystallography

Crystal data. $C_{16}H_{36}Br_3N_5PtS_4$, $M = 861.6$, monoclinic, $a = 11.540(2)$, $b = 11.955(2)$, $c = 21.646(5)$ Å, $\beta = 104.45(2)°$, $U = 2892$ Å^3, space group $P2_1/c$, $Z = 4$, $D_c = 1.979$ g cm^{-3}. Red plates, dimensions $0.025 \times 0.283 \times 0.300$ mm, μ(Mo-K_α) = 93.0 cm^{-1}, $\bar{\lambda} = 0.71073$ Å, $F(000) = 1656$.

Data collection and processing. Siemens *P*4 diffractometer, ω-scan method ($3 \leqslant 2\theta \leqslant 50°$) graphite monochromated Mo-K_α radiation; 4084 independent measured reflections, 1904 observed [$|F_o| > 4\sigma(|F_o|)$], corrected for Lorentz and polarization factors; empirical absorption correction, maximum and minimum transmission factors 0.783 and 0.100, respectively.

Structure analysis and refinement. The structure was solved by the heavy atom method and all the non-hydrogen atoms refined anisotropically. The hydrogen atoms were idealized (C—H = 0.96 Å), assigned isotropic thermal parameters $U(H) = 1.2U_{eq}(C)$ and allowed to ride on their parent carbons. Refinement was by full-matrix least-squares to $R = 0.0552$ ($R = \Sigma[|F_o| - |F_c|]/\Sigma|F_o|$), $R_w = 0.0446$ [$w^{-1} = \sigma^2(F) + 0.0007F^2$]. The maximum and minimum residual electron densities in the final ΔF map were 1.56 and −0.79 e Å^{-3} and the mean and maximum shifts/error in the final refinement cycle were 0.021 and 0.224, respectively. Computations were carried out on an IBM 386 computer using the SHELXTL/PC program system.[8]

RESULTS AND DISCUSSION

Reaction of $[Bu_4N]_2[Pt_2Br_6]$ with S_4N_4 in CH_2Cl_2 proceeds at room temperature according to eq. (1) to give **4** in 40% yield. Compound **4** is air-stable, soluble in common organic solvents and appears to be insensitive to shock or heat.

$$[Bu_4N]_2[Pt_2Br_6] + S_4N_4 \longrightarrow [Bu_4N][PtBr_3(S_4N_4)] \quad (1)$$

After reaction for 3 days the product was crystallized by slow diffusion of Et_2O into a solution in CH_2Cl_2. The resulting species was more amenable to X-ray crystallography than its $[PPh_4]^+$ counterpart. The X-ray structure of $[Bu_4N][PtBr_3(S_4N_4)]$ (Fig. 1, Table 1) reveals that the

Table 1. Selected bond lengths (Å) and angles (°) in **4**. Values in square brackets are those cited[4] for the related iridium compound **1**

Pt(1)—N(1)	2.028(18)	Pt(1)—S(2)	2.304(7)
Pt(1)—S(4)	2.292(6)	Pt(1)—Br(1)	2.476(3)
Pt(1)—Br(2)	2.482(3)	Pt(1)—Br(3)	2.508(2)
N(1)—S(1)	1.496(21) [1.528(6)]	S(1)—N(2)	1.572(20) [1.581(6)]
N(2)—S(2)	1.700(22) [1.692(6)]	S(2)—N(3)	1.547(17) [1.646(7)]
N(3)—S(3)	1.605(19) [1.575(7)]	S(3)—N(4)	1.503(21) [1.560(6)]
N(4)—S(4)	1.611(19) [1.608(6)]		
N(1)—Pt(1)—S(2)	89.9(5)	N(1)—Pt(1)—S(4)	87.3(5)
S(2)—Pt(1)—S(4)	98.8(2)	N(1)—Pt(1)—Br(1)	176.8(4)
S(2)—Pt(1)—Br(1)	88.9(2)	S(4)—Pt(1)—Br(1)	89.9(2)
N(1)—Pt(1)—Br(2)	88.5(5)	S(2)—Pt(1)—Br(2)	177.4(2)
S(4)—Pt(1)—Br(2)	83.2(2)	Br(1)—Pt(1)—Br(2)	92.8(1)
N(1)—Pt(1)—Br(3)	88.1(4)	S(2)—Pt(1)—Br(3)	84.2(2)
S(4)—Pt(1)—Br(3)	174.5(2)	Br(1)—Pt(1)—Br(3)	94.8(1)
Br(2)—Pt(1)—Br(3)	93.7(1)	Pt(1)—N(1)—S(1)	113.1(9)
N(1)—S(1)—N(2)	120.0(11)	S(1)—N(2)—S(2)	115.6(13)
Pt(1)—S(2)—N(2)	101.2(7)	Pt(1)—S(2)—N(3)	113.6(8)
Pt(1)—S(4)—N(4)	111.5(7)	S(2)—N(3)—S(3)	130.3(11)
N(3)—S(3)—N(4)	118.7(10)	S(3)—N(4)—S(4)	138.4(11)
N(2)—S(2)—N(3)	105.8(10) [103.4(3)]		

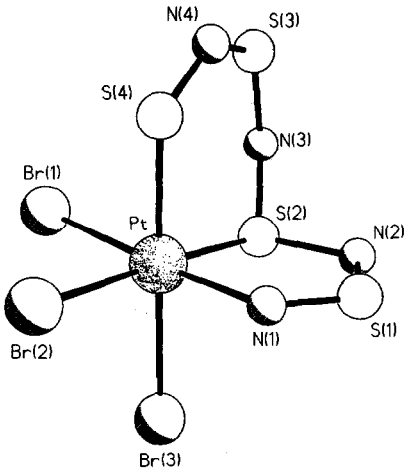

Fig. 1. The X-ray structure of the anion in **4**.

geometry around the platinum in the anion is slightly distorted from octahedral, with angles at platinum in the ranges 83.2(2)–98.8(2)° and 174.5(2)–177.4(2)°. The platinum atom is facially coordinated by three bromine atoms, together with two sulphur atoms and one nitrogen of the $S_4N_4^{2-}$ ligand. The coordination bond lengths are normal and in the range expected for platinum(IV).[9] The PtS_2N_2 ring is essentially planar [maximum deviation from the mean plane 0.04 Å for N(2)], whereas the PtS_3N_2 ring is puckered. Pt, S(4), N(4), S(3) and N(3) are co-planar to within 0.02 Å, with S(2) and Br(3) being 0.49 and 0.11 Å, respectively, from this plane (Fig. 2). The five- and six-membered rings are essentially orthogonal to each other. The gross structure of the MS_4N_4 unit is comparable to that

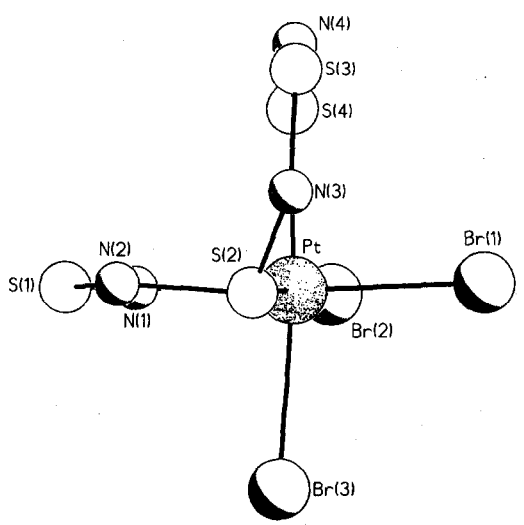

Fig. 2. View of the anion in **4** illustrating the puckering of the PtS_3N_2 ring at S(2) and the orthogonal relationship of the two fused rings.

reported for **1**, the only other structurally characterized *fac*-$S_4N_4^{2-}$ metal complex.

Although there is a superficial similarity between the aforementioned PtS_2N_2/PtS_3N_2 rings in **4** and the rings in the structures of species such as $Pt(S_2N_2)(PR_3)_2$ and $[Pd_2Cl_4(S_3N_2)]^{2-}$, there are also subtle differences between them. In the $S_2N_2^{2-}$ complexes there are two short (*ca* 1.55 Å) and one long (*ca* 1.7 Å) S—N bond lengths, which is mirrored in the PtS_2N_2 unit of $[PtBr_3(S_4N_4)]^-$. However, the planarity of the $S_3N_2^{2-}$ ligand in the binuclear palladium species contrasts with the puckered unit in the $S_4N_4^{2-}$ ligand in **4**. By comparing the geometry of the $S_4N_4^{2-}$ ligand to that of free S_4N_4 it can be seen that the S···S distances S(1)—S(3) and S(2)—S(4) correspond to two of the weak S···S interactions observed in the latter. The distances in the coordinated ligand are much larger, however, at 4.3 and 3.5 Å, respectively (cf. 2.6 Å in S_4N_4).

In **4** there is an absence of significant intermolecular S···S or S···N contacts of the type that have been observed in other S—N systems.[2] The closest inter-anion contact is S(3)···S(3′) (3.8 Å), although there is a fairly short Br(1)···Br(1′) contact of 4.0 Å. The bulk of the $[NBu_4]^+$ cation mitigates against good interanion interactions.

The ^{15}N NMR parameters for **4** are essentially identical (Table 2) to those of **3**, indicating that our previous NMR analysis was correct and that the anions in **3** and **4** are isostructural. The ^{195}Pt NMR spectra of ^{15}N labelled and normal **4** are compared in Fig. 3; the relative magnitudes of the two $\{^{15}N—^{195}Pt\}$ couplings are quite apparent from these spectra. It is possible to relate the geometry within the $S_4N_4^{2-}$ ligand to the $^2J\{^{15}N—^{15}N\}$ coupling constants measured from the ^{15}N NMR spectrum. As noted earlier the largest such interaction is between N(3) and N(4) (5.6 Hz), with a smaller interaction between N(1) and N(2) (3 Hz) and no observable interaction between N(2) and N(3). The angles at the sulphur atoms bridging these pairs of atoms are 119, 120 and 106° at S(3), S(1) and S(2), respectively. Thus, we postulate that the presence of an angle close to tetrahedral at S(2) results in poor orbital overlap (especially via any π-system) and consequent lack of interaction between nitrogen atoms. It should be remembered, however, that the couplings in question are only a few Hz in magnitude and thus any rationalization of their precise magnitude must be treated with some caution.

Mechanistically the formation of **3** and **4** is interesting. During the course of these reactions the halo-bridged dimeric starting materials are, as predicted, acting as a source of the coordinatively unsaturated $[PtX_3]^-$ unit. It is tempting to suggest

Table 2. Comparison of the ^{15}N NMR parameters for $[Bu_4N]^+$ and $[PPh_4]^+$ salts of $[PtBr_3(S_4N_4)]^-$ (* indicates coupling not resolved)

Compound	Nitrogen	δ (ppm)	$^2J\{^{15}N—^{15}N\}$ (Hz)	$^{15}N—^{195}Pt$ (Hz)
$[Bu_4N][PtBr_3(S_4N_4)]$	N(1)	433	2.6	152
	N(2)	284	2.6	*
	N(3)	164	6.0	*
	N(4)	345	6.0	*
$[PPh_4][PtBr_3(S_4N_4)]$	N(1)	433	3.0	150
	N(2)	283	3.0	6
	N(3)	164	5.6	16
	N(4)	343	5.6	*

that the initial stage of the reaction involves the formation of a simple σ-bonded platinum(II) species of the type $PtX_3(S_4N_4)^-$, which then undergoes an internal rearrangement to the final platinum(IV) species. There is, however, no unequivocal evidence for such an intermediate.

As noted earlier it is possible to prepare *mer*-$PtCl_2(S_4N_4)(PMe_2Ph)$ by reaction of S_4N_4 with $[PtCl_2(PMe_2Ph)]_2$. We attempted to generate its *facial* analogue by addition of a stoichiometric amount of the free phosphine to **3**. An ice-cold solution of $[PPh_4][PtCl_3(S_4N_4)]$ in CH_2Cl_2 was treated with a dilute solution of PMe_2Ph and the resulting orange–red solution maintained at this temperature for $\frac{1}{2}$ h. After warming to room temperature the $^{31}P\{^1H\}$ NMR spectrum of the concentrated solution was recorded. This showed that most of the compound had been converted to $PtCl_2(PMe_2Ph)_2$, together with a small amount of a species characterized by a singlet at δ −22 ppm; this chemical shift is similar to that of $PtCl(S_2N_2H)(PMe_2Ph)$ (reported value[10] −21 ppm), although the spectrum was too weak for $^1J\{^{31}P—^{195}Pt\}$ satellites to be resolved. Confirmation that this was indeed the compound present came from the TLC of the solution (CH_2Cl_2), which revealed a yellow band at $R_f = 0.37$, identical to that for $PtCl(S_2N_2H)(PMe_2Ph)$. Although disappointing this result was not entirely unexpected. Earlier work in our group has shown that any attempts to involve *mer*-$PtCl_2(S_4N_4)(PMe_2Ph)$ in further reactions inevitably result in massive decomposition to mixtures of the two species mentioned above. Thus, despite its relative stability once formed, the $S_4N_4^{2-}$ unit does not appear to be robust enough to be retained during these types of reactions. Further studies into its reactivity (e.g. protonation) are in progress.

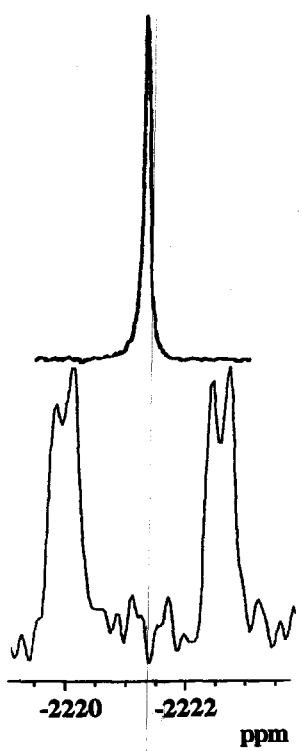

Fig. 3. ^{195}Pt NMR spectra of (a) normal and (b) ^{15}N labelled **4**.

Acknowledgements—We are grateful to the Wolfson Foundation for support and to the SERC for the provision of the diffractometer.

REFERENCES

1. P. F. Kelly and J. D. Woollins, *Polyhedron* 1986, **5**, 607; T. Chivers and F. Edelmann, *Polyhedron* 1986, **5**, 1661.
2. P. F. Kelly, A. M. Z. Slawin, D. J. Williams and J. D. Woollins, *Chem. Soc. Rev.* 1992, 245.
3. B. J. McCormick and B. Anderson, *J. Inorg. Nucl. Chem.* 1970, **32**, 3414.
4. F. Edelmann, H. W. Roesky, C. Spang, M. Nolte-

meyer and G. M. Sheldrick, *Angew. Chem. Int. Edn Engl.* 1986, **25**, 931.
5. M. B. Hursthouse, P. F. Kelly, M. Motevalli and J. D. Woollins, *Polyhedron* 1989, **8**, 997.
6. P. F. Kelly, R. N. Sheppard and J. D. Woollins, *Polyhedron* 1992, **11**, 2605.
7. P. S. Belton, V. C. Ginn, P. F. Kelly and J. D. Woollins, *J. Chem. Soc., Dalton Trans.* 1992, 1135.
8. SHELXTL PC Version 4.2. Siemens X-Ray Analytical Instruments (1991).
9. A. G. Orpen, L. Brammer, F. H. Allen, O. Kennard, D. G. Watson and R. Taylor, *J. Chem. Soc., Dalton Trans.* 1989, S1.
10. J. M. Joliffe, P. F. Kelly and J. D. Woollins, *J. Chem. Soc., Dalton Trans.* 1989, 2179.

Polyhedron Vol. 12, No. 10, pp. 1141–1143, 1993
Printed in Great Britain

0277–5387/93 $6.00+.00
© 1993 Pergamon Press Ltd

SYNTHESIS AND STRUCTURAL STUDIES OF (3,5-DINITROBENZOATE)BIS(TRIPHENYLPHOSPHINE)COPPER(I)

A. E. MAURO* and C. C. PORTA

Instituto de Química de Araraquara, UNESP C.P. 355, 14800-900 Araraquara, SP, Brazil

and

C. A. DE SIMONE, J. ZUKERMAN-SCHPECTOR and E. E. CASTELLANO

Instituto de Física e Química de São Carlos, USP, C.P. 369, 13560 São Carlos, SP, Brazil

(*Received* 11 *December* 1992; *accepted* 1 *February* 1993)

Abstract—The compound (3,5-dinitrobenzoate)bis(triphenylphosphine)copper(I) was synthesized and studied by IR spectroscopy and X-ray diffraction techniques. It is monomeric with the carboxylato acting as a monodentate ligand. The copper atom shows a trigonal planar coordination geometry.

The study of copper(I) complexes is a topic currently being investigated in many laboratories. Among the reasons for carrying out the investigation of such species are their structural features,[1,2] the usefulness of copper(I) compounds in organic syntheses[3] and the well-documented importance of copper(I) centres at the active sites of a number of proteins.[4] Concerning copper(I) carboxylates a further interest exists, stemming from their use in homogeneous catalysed hydrogenation.[5] In continuation of our research on copper compounds[2,6–8] we prepared [Cu(3,5-$NO_2C_6H_3CO_2$)(PPh_3)$_2$], which was subjected to a full IR and X-ray crystallographic characterization.

EXPERIMENTAL

Synthesis of [Cu(3,5-$NO_2C_6H_3CO_2$)(PPh_3)$_2$]

All operations described herein, except the weighings, were performed in an atmosphere of purified nitrogen in a Schlenk apparatus. To a solution containing [Cu(BH_4)(PPh_3)$_2$] (0.2 g, 0.33 mmol) in chloroform (10 cm^3) was added a tetrahydrofuran solution (5 cm^3) containing 3,5-dinitrobenzoic acid (0.071 g, 0.33 mmol). The mixture was stirred for 5 h at room temperature. The solution was concentrated under reduced pressure and by adding pentane an orange solid was formed. Recrystallization from ether gave orange crystals suitable for X-ray analysis. The elemental analysis results were in agreement with the proposed formula.

IR spectrum

The IR spectrum was recorded as KBr pellets on a Nicolet 730-FT spectrophotometer.

Crystal structure determination

$C_{43}H_{33}N_2O_6P_2Cu$, *crystal data.* $M = 799.24$, monoclinic, $a = 14.839(2)$, $b = 13.771(2)$, $c = 18.745(3)$ Å, $\beta = 101.21(1)°$, $U = 3757(2)$ Å^3 (by least-squares refinement on diffractometer angles for 25 automatically centred reflections, $9 < \theta < 26°$, $\lambda = 0.71073$ Å), space group $P2_1/n$, $Z = 4$, $D_c = 1.413$ g cm^{-3}. An irregular shaped crystal was used of maximum and minimum linear dimensions 0.55 and 0.25 mm, μ(Mo-K_α) = 7.15 cm^{-1}.

Data collection and processing. CAD4 diffractometer, $\omega/2\theta$ mode with ω scan width = 0.85+0.15 tan θ, graphite monochromated Mo-K_α radiation, 5904 unique reflections measured ($0 < \theta < 25°$, $-17 \leqslant h \leqslant 17$, $0 \leqslant k \leqslant 16$, $0 \leqslant l \leqslant 22$), 4278 with $I > 3\sigma(I)$; Lorentz and polarization corrections were applied. Absorption corrections were applied

* Author to whom correspondence should be addressed.

at a later stage in the refinement[9] (max., min. transmission factors = 1.609, 0.504). The intensity of a standard reflection was essentially constant throughout the experiment.

Structure analysis and refinement. Standard direct methods followed by normal difference Fourier techniques. Blocked-matrix least-squares refinement with all non-hydrogen atoms anisotropic and hydrogens included, as fixed contributors, at positions found in difference synthesis, with one overall isotropic temperature factor which was refined to $U_{iso} = 0.082(2)$ Å^2. The function minimized was $\Sigma w(|F_o|-|F_c|)^2$, with the weighting scheme $w = 1/[\sigma^2(F_o)+0.003F_o^2]$, gave satisfactory agreement analysis. Final $R = [\Sigma(|F_o|-|F_c|)/\Sigma|F_o|]$ and $R' = \{[\Sigma w(|F_o|-|F_c|)^2/\Sigma w|F_o|^2]^{1/2}\}$ values were 0.041 and 0.042, respectively. Programs used: SHELX76,[10] ORTEP;[11] scattering factors for non-hydrogen atoms were from Cromer and Mann[12] (with corrections for anomalous dispersion from Cromer and Liberman)[13] and for hydrogen atoms from Stewart *et al.*[14] The atomic positions, full lists of bond lengths and angles and other crystallographic data have been deposited as supplementary material.

RESULTS AND DISCUSSION

It is a well known fact that cuprous carboxylates, that in general are sensitive to moisture, can be effectively stabilized by ligands such as triphenylphosphine, affording compounds of the type [Cu(RCOO)$(PPh_3)_2$]. These complexes can be synthesized by reducing cupric carboxylates with the phosphorus ligand[15] or through the reaction of tetrahydroborato-bis(triphenylphosphine)copper(I), [Cu$(BH_4)(PPh_3)_2$], with carboxylic acids, as was used to obtain the title compound. The IR spectrum of [Cu(3,5-$NO_2C_6H_3CO_2$)$(PPh_3)_2$] showed a number of absorption bands, but the most characteristic ones[16,17] were those assigned to stretching modes of the carboxylato and nitro groups, respectively, at 1617s, $\nu_{as}(CO_2)$; 1341vs, $\nu_s(CO_2)$; 1537s, $\nu_{as}(NO_2)$; 1374s, $\nu_s(NO_2)$ cm^{-1}.

An important feature to be noted is the separation between the two stretching modes, $\Delta\nu = \nu_{as}(CO_2)-\nu_s(CO_2) = 276$ cm^{-1}, which suggests that the 3,5-dinitrobenzoate acts as a monodentate ligand to the copper atom. Moreover, this conclusion is further supported by the lower differences, 247 and 214 cm^{-1}, respectively, found in similar compounds[18] such as [Cu(2-$NO_2C_6H_4CO_2$)$(PPh_3)_2$] and [Cu(4-$NO_2C_6H_4CO_2$)$(PPh_3)_2$], where the anions are bidentate.

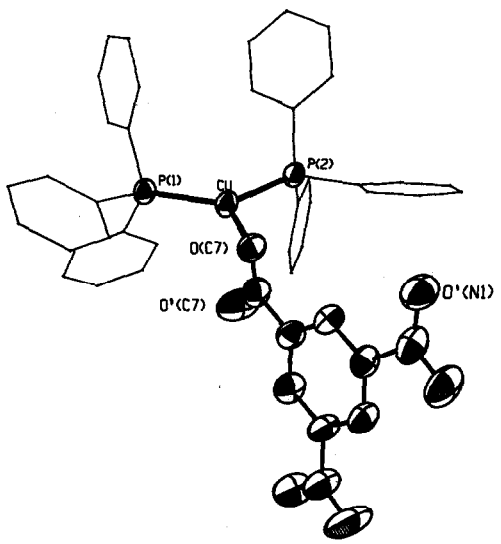

Fig. 1. Molecular structure of [Cu(3,5-$NO_2C_6H_3CO_2$)$(PPh_3)_2$].

The monomeric nature of the compound and the important structural features of the carboxylate group suggested by IR spectroscopy were definitively proved by the crystal and molecular structural X-ray analyses. The structure of the compound with the labelling scheme is presented in Fig. 1. Selected bond lengths and angles are given in Table 1. The molecular structure shows that the copper atom is bonded to the phosphorus atoms of the two triphenylphosphine ligands and to one oxygen atom of the carboxylate group, giving rise to a nearly trigonal planar coordination. In fact the copper atom is only 0.026(3) Å out of the plane through P(1)—P(2)—O(C7). The other copper contacts are: Cu···O'(C7) = 2.643(3), Cu···O'(N1) [$1-x$, $-y$, $1-z$] = 3.009(3) Å.

The 3,5-dinitrobenzoate anion behaves as a monodentate carboxylate ligand making the shortest interaction with the metal atom [Cu—C

Table 1. Selected distances (Å) and angles (°) for [Cu(3,5-$NO_2C_6H_3CO_2$)$(PPh_3)_2$]

Cu—P(1)	2.221(1)	P(1)—Cu—P(2)	129.24(4)
Cu—P(2)	2.243(1)	P(1)—Cu—O(C7)	121.76(8)
Cu—O(C7)	2.051(3)	P(2)—Cu—O(C7)	108.95(8)

(C7) = 2.051(3) Å]. The dihedral angles between the phenyl ring and the carboxylate and nitro groups [N(1) and N(2)] are 16.7(7), 9.0(9) and 8.2(9)°, respectively.

Finally, the important structural differences related to the coordination polyhedra (trigonal planar) and the Cu—O bond length, 2.051(3) Å, for $[Cu(3,5\text{-}NO_2C_6H_3CO_2)(PPh_3)_2]$ and those of the related compounds $[Cu(2\text{-}NO_2C_6H_4CO_2)(PPh_3)_2]$ and $[Cu(4\text{-}NO_2C_6H_4CO_2)(PPh_3)_2]$, both tetrahedral with Cu—O distances in the range 2.145(3)–2.304(3) Å, are probably of electronic origin caused by the presence of two nitro groups in the present compound.

Acknowledgements—We thank CNPq, FAPESP and FINEP for financial support.

REFERENCES

1. F. H. Jardine, *Adv. Inorg. Chem. Radiochem.* 1975, **17**, 115.
2. J. Zukerman-Schpector, E. E. Castellano, A. E. Mauro and M. Roveri, *Acta Cryst.* 1986, **C42**, 302.
3. T. Tsuda, T. Fujii, K. Kawasaki and T. Saegusa, *J. Chem. Soc., Chem. Commun.* 1980, 1013.
4. R. Lontie and R. Witter, *Inorganic Biochemistry*, Vol. 1. Elsevier, New York (1973).
5. A. Toth, C. Floriani, A. C. Villa and C. Guastini, *Inorg. Chem.* 1987, **26**, 236.
6. O. L. Casagrande, S. I. Klein, A. E. Mauro and K. Tomita, *Trans. Met. Chem.* 1989, **14**, 45.
7. A. E. Mauro, S. I. Klein, J. S. Saldaña, C. A. Simone, J. Zukerman-Schpector and E. E. Castellano, *Polyhedron* 1990, **9**, 2937.
8. J. Zukerman-Schpector, E. E. Castellano, C. A. Simone and A. E. Mauro, *Acta Cryst.* 1991, **C47**, 957.
9. N. Walker and D. Stuart, *Acta Cryst.* 1983, **A39**, 158.
10. G. M. Sheldrick, SHELX76, Program for Crystal Structure Determination. University of Cambridge, U.K. (1976).
11. C. K. Johnson, ORTEP, Report ORNL-3794. Oak Ridge National Laboratory, Tennessee (1965).
12. D. T. Cromer and J. B. Mann, *Acta Cryst.* 1968, **A24**, 321.
13. D. T. Cromer and D. Liberman, *J. Chem. Phys.* 1970, **53**, 1891.
14. R. F. Stewart, E. R. Davidson and W. T. Simpson, *J. Chem. Phys.* 1965, **42**, 3175.
15. B. Hammond, F. H. Jardine and A. G. Vohra, *J. Inorg. Nucl. Chem.* 1971, **33**, 1017.
16. G. B. Deacon and R. J. Phillips, *Coord. Chem. Rev.* 1980, **33**, 227.
17. K. Nakamoto, *Infrared Spectra of Inorganic and Coordination Compounds*. Wiley Interscience, New York (1970).
18. M. A. Cabras, L. Naldini, M. A. Zoroddu, F. Cariati, F. Demartin, N. Masciocchi and M. Sansoni, *Inorg. Chim. Acta* 1985, **104**, L19.

Polyhedron Vol. 12, No. 10, pp. 1145–1148, 1993
Printed in Great Britain

0277–5387/93 $6.00+.00
© 1993 Pergamon Press Ltd

SOLVATION OF INORGANIC COMPLEXES IN OCTANOL-WATER, HEXANOL-WATER, AND RELATED MICROEMULSIONS

SUADA AHMED,* JOHN BURGESS,† GLEN CAPPER, NICOLA C. FELLOWES and MARTTAND S. PATEL

Department of Chemistry, University of Leicester, Leicester LE1 7RH, U.K.

(*Received* 7 *January* 1993; *accepted* 27 *January* 1993)

Abstract—Solubilities of tris(ethylmaltolato)iron(III) have been determined in dry 1-octanol, 1-hexanol and isobutanol and in the limited ranges of alcohol–water binary mixtures accessible for these alcohols. The observed pattern is discussed in terms of particularly favourable synergic solvation in the mixed solvents and is compared with solvation patterns indicated by the solvatochromic iron(II) complex $Fe(CN)_2(bipy)_2$.

Inorganic complexes are becoming increasingly relevant to pharmacology.[1,2] Their solvation properties are important in this connection, especially if they are to be administered orally. There is a requirement for an appropriate hydrophilic–lipophilic balance (HLB)[3] so that they can cross the various membranes and barriers—the gut wall, blood–brain barrier, cell walls—between the dosage site and the site of action. It is conventional to assess the HLB through partition coefficients, generally between water and 1-octanol.[4] Partition coefficients have been obtained for a very large number of organic compounds, but for relatively few inorganic species. The determination of partition coefficients for methylmercury(II)-thiol[5] and methylmercury(II)-antidote[6] complexes provided useful information in relation to the treatment of alkylmercury poisoning, but the determination of reliable partition coefficients for such complexes as tris-maltolatoaluminium(III) proved unexpectedly difficult.[7] The widely-used and valuable partition coefficient approach does not, however, give any indication of possible synergic solvation in a binary medium, of which a membrane/aqueous medium interface may be considered a special case. The process of transport across a membrane may be split into *pre-equilibrium siting of the substrate at* the interface, followed by passage through the membrane.[8] The partition coefficient is the key parameter in relation to the first step, favourable interaction at the interface. It seems likely that a substrate which is favourably solvated *both* by water and by octanol would be most stable at a membrane surface. In a sense the water–octanol partition coefficient is particularly relevant in that the octanol contains up to about 6% water,[9] which limited solubility arises from favourable solvent–solvent hydrogen-bonding interactions.[10] It has long been recognized that the solubility of a species in wet octanol in a partition experiment may be considerably different from its solubility in dry octanol,[11] but quantitative data seem to be sparse. We have recently demonstrated that a number of inorganic complexes of pharmacological relevance, including a number of pyrone (**1**) and pyridinone (**2**)

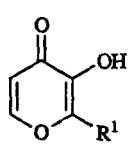

1

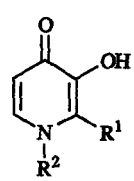

2

complexes of iron(III), aluminium(III), gallium(III) and indium(III)[12–14] and classical inorganic complexes, such as $[Fe(bipy)_2(CN)_2]$,[15] are more soluble in alcohol–water mixtures than in either separate component. These results were obtained mainly with methanol or t-butyl alcohol as the co-solvent, so that solubilities could be established over the

* Present address: Department of Chemistry, School of Applied Sciences, De Montfort University, Leicester LE1 9BH, U.K.

† Author to whom correspondence should be addressed.

complete solvent composition range and solubility maxima corresponding to favourable synergic solvation by both components readily identified. We now report an extension of these studies to alcohols which are not fully miscible with water, especially to 1-hexanol and 1-octanol, and to "organized aqueous media" in which the addition of surfactants solubilizes these alcohols in water. The main aim has been to monitor the effects of adding small quantities of water to the organic components. This we have done through solubility measurements, with derived transfer chemical potentials to give an idea of energy changes, and through solvatochromism. This latter phenomenon is valuable in providing an easy indication of preferential solvation, but is restricted to a small number of inorganic compounds, of which ternary iron(II)-diimine-cyanide complexes have suitable sensitivity and solubility characteristics to use here. Solubility determinations are of much more general applicability. Here we have used tris-ethylmaltolatoiron(III) [ethylmaltol = etmaH = pyrone (1) with R = Et] as a typical substrate of pharmacological relevance—pyrones and pyridinones are proving of actual and potential value in the control of iron and aluminium levels in the body,[16] may provide suitable vehicles for the introduction of radioisotopes such as those of gallium, indium, or yttrium into the body for diagnostic or therapeutic purposes,[2,17] or gadolinium for MRI,[2] and, in the form of the maltol-vanadyl complex, may be valuable in the control of diabetes.[18]

The solubility of $Fe(etma)_3$ in dry 1-octanol (4.6×10^{-4} mol dm^{-3}) is only slightly higher than in water (3.7×10^{-4} mol dm^{-3}), but it is over eight times more soluble in 1-octanol containing 6.3% water (solubility 38×10^{-4} mol dm^{-3}) than in 1-octanol itself. The situation is similar with respect to 1-hexanol, where the solubilities of $Fe(etma)_3$ are 8.2×10^{-4}, 36×10^{-4} and 68×10^{-4} mol dm^{-3} in 1-hexanol containing 0%, 3.3% and 9.1% water, respectively. These effects of addition of small amounts of water to these alcohols are shown in terms of transfer chemical potentials [$\delta_m\mu^0$ = (solubility in medium 2)/(solubility in medium 1)] in Fig. 1. This figure also shows the effects on $Fe(etma)_3$ solubility of adding water to isobutanol, and of isobutanol to water, and, for comparison, the transfer chemical potential trend for this complex in methanol–water mixtures.[13] It is interesting that the transfer chemical potential minimum (solubility maximum) is obtained within the limited mutual miscibility range[19] in the case of iso-butanol, and that $Fe(etma)_3$ has a large salting-in effect on the isobutanol (solubility of isobutanol in water is 19%[20]). In this its behaviour parallels that of a

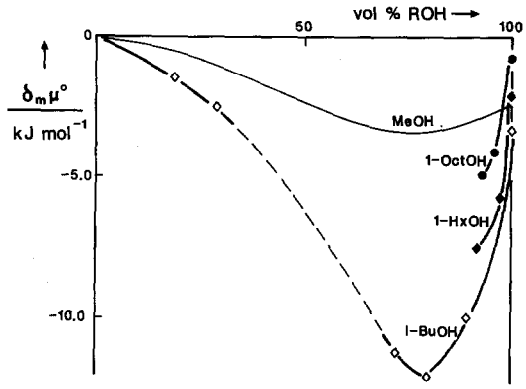

Fig. 1. Transfer chemical potentials for $Fe(etma)_3$ to water–alcohol media, at 298.2 K.

range of organic solutes in water/di-n-butylether[21] and transition metal(II) perchlorates in 1-butanol/water.[22] Figure 1 shows clearly the considerable increase in overall solvation caused by hydration of hydrophilic areas on the periphery of the complex when water is added to 1-octanol, 1-hexanol, isobutanol or methanol.

Our observations in the 1-octanol–water system can be related to the partition coefficient. We have measured this, by the shaking method, finding a value of 8.2. This may be compared with the value of 0.08 reported for the rather more lipophilic tris-maltolatoaluminium(III)[23] and a range of values from 0.03 to 7.7 for tris-pyridinatoiron(III) complexes containing various alkyl substitutents.[24] A partition coefficient of 8.2 corresponds to a chemical potential change of -5.2 kJ mol^{-1} for transfer

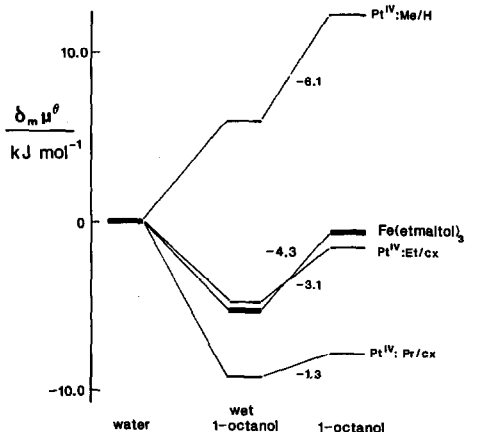

Fig. 2. Chemical potentials for $Fe(etma)_3$ and for three platinum(IV) complexes of formula 3 in water–1-octanol. The values given on the diagram are for transfer from dry 1-octanol to water-saturated 1-octanol, in kJ mol^{-1} at 298.2 K.

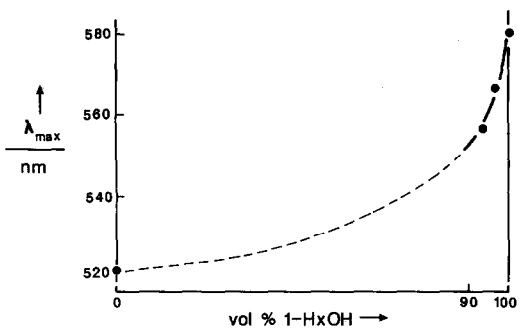

Fig. 3. Solvatochromic behaviour of the MLCT band of $Fe(CN)_2(bipy)_2$ in water–1-hexanol.

from the water layer into the wet octanol layer. The transfer chemical potential of $Fe(etma)_3$ from water into dry 1-octanol is only -0.7 kJ mol^{-1} from our solubility measurements, but the transfer chemical potential from dry octanol to wet octanol (6.3% water) is -4.3 kJ mol^{-1}. Significant changes in solubility or chemical potential between dry and wet octanol have been noted before,[11] but do not seem to have been systematized and rationalized.[25] A recent inorganic example has been provided by a series of platinum(IV) complexes (**3**). The transfer chemical potentials for such compounds with R = Me, R′ = H; R = Et, R′ = cyclohexyl; R = Pr, R′ = cyclohexyl from dry octanol into water-saturated octanol are -6.1, -3.1 and -1.3 kJ mol^{-1}, respectively.[26] Solvational stabilization decreases as ligand hydrophilicity decreases. These results are included in Fig. 2, where they are compared with our estimates for $Fe(etma)_3$.

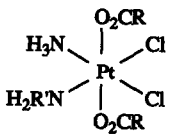

3

An alternative approach to demonstrating the importance of hydration of hydrophilic areas on adding a little water to organic solvents is offered by solvatochromism, at least in those few cases where the solute exhibits this phenomenon. Pyrone and pyridinone complexes are only very slightly solvatochromic, so we have had to turn to iron(II) complexes of the $[Fe(CN)_2(bipy)_2]$ and $[Fe(CN)_4(bipy)]^{2-}$ type. Figure 3 shows λ_{max} values for $[Fe(CN)_2(bipy)_2]$ in 1-hexanol–water mixtures, with a rapid decrease in λ_{max} towards the value for pure water on adding relatively small amounts of water to 1-hexanol. Solubilities of 1-hexanol or 1-octanol in water can be significantly increased by the use of appropriate surfactants. Figure 4 shows the dependence of λ_{max} on water content for three such systems. The patterns are similar and indeed are very similar to Fig. 3. In all cases the strong preferential hydration of the cyanide ligands in the

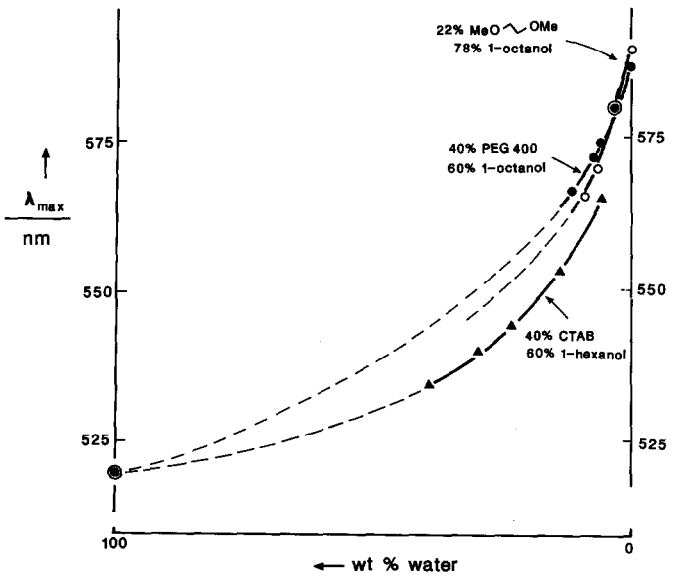

Fig. 4. Solvatochromic behaviour of the MLCT band of $Fe(CN)_2(bipy)_2$ in water–alcohol–surfactant systems. The compositions specified against the three curves are those corresponding to the 0% water axis.

complex by the added water cause marked shifts of λ_{max} towards its value in pure water.

Acknowledgements—We are grateful to Dr C. F. J. Barnard (Johnson Matthey) for providing information on the platinum(IV) complexes.

REFERENCES

1. P. J. Sadler, *Adv. Inorg. Chem.* 1991, **36**, 1.
2. J. Burgess, *Trans. Met. Chem.* 1992, **17**, in press.
3. W. C. Griffin, *J. Soc. Cosmet. Chem.* 1954, **5**, 249; C. Hansch and A. Leo, *Substitution Constants for Correlation Analysis in Chemistry and Biology*, pp. 49–54. John Wiley, New York (1979); R. F. Rekker and R. Mannhold (Editors), *Calculation of Drug Lipophilicity*. VCH, Weinheim (1992).
4. A. Leo, C. Hansch and D. Elkins, *Chem. Rev.* 1971, **71**, 525.
5. A. P. Arnold, A. J. Canty, P. W. Moors and G. B. Deacon, *J. Inorg. Biochem.* 1983, **19**, 319.
6. A. J. Canty, P. W. Moors and G. B. Deacon, *J. Inorg. Biochem.* 1984, **22**, 65.
7. M. M. Finnegan, T. G. Lutz, W. O. Nelson, A. Smith and C. Orvig, *Inorg. Chem.* 1987, **26**, 2171.
8. W. R. Stein, *Transport and Diffusion Across Cell Membranes*. Academic Press, New York (1986).
9. Y. Marcus, *J. Soln Chem.* 1990, **19**, 507.
10. B. C. Lippold and M. S. Adel, *Arch. Pharm.* 1972, **305**, 417.
11. I. Kojima and S. S. Davis, *Sep. Sci. Technol.* 1985, **20**, 131; A. Radzicka and R. Wolfenden, *Biochemistry* 1989, **27**, 1664; P. R. Gibbs, A. Radzicka and R. Wolfenden, *J. Am. Chem. Soc.* 1991, **113**, 4714.
12. J. Burgess and M. S. Patel, *Inorg. Chim. Acta* 1990, **170**, 241.
13. J. Burgess, M. S. Patel and R. C. Hider, *J. Pharm. Pharmacol.*, submitted.
14. E. Beatty, J. Burgess and M. S. Patel, *Can. J. Chem.*, submitted.
15. J. Burgess, S. Radulović and F. Sanchez, *Trans. Met. Chem.* 1987, **12**, 529.
16. For example: J. B. Porter, R. C. Hider and E. R. Huehns, *Sem. Haematol.* 1990, **27**, 95; A. Aito, A. Aro, J. Järvisalo and H. Vainio (Editors), *Trace Elements in Health and Disease*. Royal Society of Chemistry, Cambridge (1991).
17. D. J. Clevette, D. M. Lyster, W. O. Nelson, T. Rihela, G. A. Webb and C. Orvig, *Inorg. Chem.* 1990, **29**, 667 and refs therein.
18. C. Orvig, J. McNeill, V. Yuen and H. Hoveyda, *J. Med. Chem.* 1992, **35**, 1489.
19. A. Apelblat and E. Manzurola, *Ber. Bunsenges. Phys. Chem.* 1990, **94**, 653; A. Apelblat, *Ber. Bunsenges. Phys. Chem.* 1990, **94**, 1128.
20. G. T. Hefter, A. F. M. Barton and A. Chand, *J. Chem. Soc., Faraday Trans.* 1991, **87**, 591.
21. For example: W. Fan, N. El Tayar, B. Testa and L. B. Kier, *J. Phys. Chem.* 1990, **94**, 4764 and refs therein.
22. M. Mahr and K. G. Weil, *Ber. Bunsenges. Phys. Chem.* 1991, **95**, 787.
23. A. Tapparo and M. Perazzolo, *Int. J. Environ. Anal. Chem.* 1989, **36**, 13.
24. J. B. Porter, M. Gyparaki, L. C. Burke, E. R. Heuhns, P. Sarpong, V. Saez and R. C. Hider, *Blood* 1988, **72**, 1497.
25. P. J. Taylor, in *Comprehensive Medicinal Chemistry*, Vol. 4, Ch. 18.6.3.3.4. Pergamon Press, Oxford (1989).
26. L. R. Kelland, B. A. Murrer, G. Abel, C. M. Giandomenico, P. Mistry and K. R. Harrap, *Cancer Res.* 1992, **52**, 822; C. M. Giandomenico, M. J. Abrams, B. A. Murrer, J. F. Vollano, K. R. Harrap, P. M. Goddard, L. R. Kelland and S. E. Morgan, *Proceedings of the 6th International Symposium on Platinum and Other Metal Coordination Complexes in Cancer Chemotherapy*, in press.

Polyhedron Vol. 12, No. 10, pp. 1149–1155, 1993
Printed in Great Britain

0277–5387/93 $6.00+.00
Pergamon Press Ltd

THE PHENOMENON OF CONGLOMERATE CRYSTALLIZATION—XXXII. THE CRYSTALLIZATION BEHAVIOUR OF [*cis*-$Co(en)_2(NO_2)_2$]I (I). COUNTER-ION EFFECTS ON CRYSTALLIZATION PATHWAY OF RACEMATE SOLUTIONS—III

IVAN BERNAL,* JOZEF MYRCZEK†‡ and JIWEN CAI†

Chemistry Department, University of Houston, Houston, TX 77204-5641, U.S.A.

(*Received* 10 *November* 1992; *accepted* 26 *January* 1993)

Abstract—[*Cis*-$Co(en)_2(NO_2)_2$]I (**I**), $ICoO_4N_6C_4H_{16}$, crystallizes from water at 18°C as both a racemate and a conglomerate. The structure of the latter was determined in this study. Unlike its chloride and bromide brethren, which crystallize exclusively as conglomerates, in the space group $P2_1$, the iodide crystallizes in the tetragonal space group $P4_1$ (No. 76). The absolute configuration was determined by comparison with that of the parent compound, $(-)_{589}$-[$\Lambda(\delta\lambda)$-*cis*-$Co(en)_2(NO_2)_2$]Br (**III**), from which it was made by metathesis. Unlike the chloride and parent bromide, whose chiroptical symbols are [*cis*-$(-)_{589}$-$\Lambda(\delta\lambda)$-$Co(en)_2(NO_2)_2$]Cl (**II**) and [*cis*-$(-)_{589}$-$\Lambda(\delta\lambda)$-$Co(en)_2(NO_2)_2$]Br (**III**), in the solid state that of [*cis*-$(-)_{589}$-$Co(en)_2(NO_2)_2$]I (**I**) is $\Lambda(\lambda\lambda)$. The cations of **I** form infinitely hydrogen-bonded, homochiral, helical strings about the four-fold screw axis of the crystals. In turn, adjacent helical strings are held together by hydrogen bonds between the iodides and $-NH_2$ hydrogens of the amine ligands. Such an arrangement is also present in the isomorphous chloride and bromide derivatives; however, in those compounds the infinite spirals are wound about the two-fold screw axis of the space group $P2_1$.

In previous studies[1–9] we reported conglomerate crystallization[10] of Werner coordination compounds belonging to a class characterized by having *clavic* (from the Latin word for paddle or tiller) ligands, such as $-NO_2$, which can be anchored into specific dissymmetric arrangements by hydrogen bonds to adjacent amine ligands, all of which have a pronounced tendency to crystallize as conglomerates—mechanical mixtures of pure homochiral crystals derived from a solution of a racemate. Examples of compounds of such class, crystallizing as conglomerates and whose structures and absolute configurations have been determined, are the series [*cis*-α-$Co(trien)_2(NO_2)_2]\cdot H_2O$ (X = Cl,[1] I[2]), the series [*cis*-$Co(en)_2(NO_2)_2$]X (X = Cl,[1] Br[3]) and [*cis*-$Rh(en)_2(NO_2)_2$]Cl.[4]

We have recently explored[5] in some detail the effect of the counter-ion on the crystallization pathway selected by a series of ionic species in which either the cation or the anion was retained while varying the nature of the counter-ion, a topic which had been mentioned since the beginning of our studies.[1] The conclusions reached[5] were that (a) in substituted cobalt amine series hydrogen bonding plays an important role in selecting the crystallization pathway, (b) in *cis*-dinitro cobalt amines strong intramolecular bonds are formed by the axial amine $-NH_2$ hydrogens with the $-NO_2$ oxygens and the presence of these bonds seems to be a necessary condition for conglomerate crystallization, and (c) that counter-anions capable of forming strong hydrogen bonds with the cation $-NH_2$ hydrogens can often compete for the formation of hydrogen bonds, and, thus, block the formation of intramolecular ones. When this happens cations which crystallize as conglomerates with halide counter-ions now crystallize as racemates. However, anions

* Author to whom correspondence should be addressed.
† Fellow of the Robert A. Welch Foundation.
‡ On leave from the Technical University of Wrocław, 1-5 Wrocław, Poland.

capable of forming strong hydrogen bonds with the metal amine hydrogens can function in different ways depending on the nature of the cation: (1) in a positive manner (conglomerate crystallization results, i.e. in $[Ni(en)_3]NO_3$[6,7]), or (2) in a negative fashion (racemates result, e.g. [*cis*-$Co(en)_2(NO_2)_2]NO_2$).[8] (d) It appears that in the [*cis*-metal $(en)_2(NO_2)_2$] series a sign of the intramolecular hydrogen-bonded interactions is the fact that the two en rings have opposite torsional chirality (e.g. one is δ, the other one λ).[9] For more details the interested reader is directed to our arguments and examples in the published literature.[1-9]

With respect to compounds such as **I** the following information was known prior to this study:

Compound	Space group	Ref.
[*cis*-$Co(en)_2(NO_2)_2$]Cl (**II**)	$P2_1$	1
[*cis*-$Co(en)_2(NO_2)_2$]Br (**III**)	$P2_1$	3
[*cis*-$Co(en)_2(NO_2)_2]NO_3$ (**IV**)	$P2_1/c$	11
[*cis*-$Co(en)_2(NO_2)_2]NO_2$(**V**)	Cc	8

Thus, it seemed interesting to document whether or not the pattern noted in the ethylenediamine derivatives could be observed with additional charge compensating anions. This is particularly interesting for the iodide (**I**) in view of the observation, by Yamanari *et al.*,[12(a)] that **II** and **III** crystallize as conglomerates, whereas **I** crystallizes as both a racemate and a conglomerate. It seems then that the iodide (**I**) provides a golden opportunity for exploring the differences in intra- and intermolecular interactions during the course of one or the other crystallization mode. Our results of such exploration are given below.

EXPERIMENTAL

Preparation of the compounds and crystal growth

Racemic [cis-$Co(en)_2(NO_2)_2$]I (**I**). [*Cis*-$Co(en)_2(NO_2)_2$]Br was prepared as described before.[13] Compound **I** was obtained by the addition of solid NaI to a stirred, warm (60°C), saturated solution of [*cis*-$Co(en)_2(NO_2)_2$]Br until precipitation. We already knew[1,3,12(a)] that in the *cis*-dinitro series (both trien and en) the solubility order is Cl > Br > I. The solution was cooled overnight in a refrigerator and filtered. The dried solid was used to prepare a room-temperature, saturated solution which was allowed to slowly crystallize at room temperature. Crystals obtained in this fashion were completely useless for single-crystal X-ray diffraction work. We tried for 5 years to obtain useful crystals but without success.

Eventually, we decided to use pure, chiral [*cis*-$Co(en)_2(NO_2)_2$]I derived from our previously prepared $(-)_{589}$-[$\Lambda(\delta\lambda)$-*cis*-$Co(en)_2(NO_2)_2$]Br and grow crystals in the dark, since we had observed that $[Co(en)_2$oxalato]I decomposes when in solution and exposed to laboratory lights.[13]

$(-)_{589}$-[*Cis*-$Co(en)_2(NO_2)_2$]I (**I**) was prepared by metathesis with NaI, as described above, but using $(-)_{589}$-{$\Lambda(\delta\lambda)$-*cis*-$Co(en)_2(NO_2)_2$]Br. Crystals grown in the dark are of varying quality. The worst ones are as bad as those obtained from racemic solutions. However, after several crystallization batches were sampled, one produced a very good crystal, which was used in the current study.

Elemental analyses for **I** were unnecessary since this is a known compound [12(a)] prepared from another known compound.[13,2(a)]

Collection of X-ray diffraction data

All data collection and processing were performed with the Molecular Structure Corporation TEXRAY-230 Modification[14] of the SDP-Plus[15] programs. The reader is referred to this manual for the details of the various routines mentioned and for the procedures recommended by them.

Nearly cubic, amber-brown crystals (**I**) were formed on slow evaporation of a water solution (*ca* 18°C) of the optically active compound, kept in the dark. The crystal was mounted on a translation head and onto an Enraf–Nonius CAD-4 diffractometer. A set of 25 reflections were centred and used to define the orientation and Niggli[16] matrices. The cell is primitive, tetragonal; the only systematic absences are those for which $011 \neq 4n$, which suggest the space groups $P4_1$, $P4_3$, $P4_122$ or $P4_322$ since the compound was known to be a pure enantiomorph.

Mo-K_α radiation was used throughout. Data for **I** were collected over the range $4° \leqslant 2\theta \leqslant 60°$. Two reflections were used as intensity standards in order to monitor crystal orientation and electronic stability. Intensity standards were collected every 2 h and an absorption correction was applied to the structure factors. No decay or systematic variation were observed and details of data collection and processing are listed in Table 1. The scattering curves of Cromer and Waber[17] were used throughout.

The phase problem was solved using a Patterson summation, from which the position of **I** was readily extracted. Heavy atoms were refined anisotropically and every five cycles of refinement new positions were calculated for the hydrogen atoms of the cation (C—H = N—H = 0.95 Å), added to the list and the structure refined until convergence.

Table 1. Summary of data collection and processing parameters for $(-)_{589}$-[*cis*-$Co(en)_2(NO_2)_2$]I (I)

Space group	$P4_1$
Cell constants	
a (Å)	7.721(3)
b (Å)	7.721(3)
c (Å)	20.087(14)
Cell volume (Å^3)	1197.39
Molecular formula	$C_4H_{16}N_6O_4CoI$
Molecular weight (g mol^{-1})	398.05
Density (calc; $z = 4$ mol/cell) (g cm^{-3})	2.208
Radiation employed	Mo-K_α ($\lambda = 0.71073$ Å)
Absorption coefficient, μ (cm^{-1})	39.930
Transmission coefficients	0.8874–0.9993
Data collection range	$4° \leqslant 2\theta \leqslant 60°$
Scan width	$\Delta\theta = 0.90+0.35 \tan\theta$
Total data collected	2036
Data used in refinement	1574
$R = \Sigma\|\|F_o\|-\|F_c\|\|/\Sigma\|F_o\|$	0.0475
$R_w = [\Sigma w^2(\|F_o\|-\|F_c\|)^2/\Sigma\|F_o\|^2]^{1/2}$	0.0561
Weights used	$w = [\sigma(F_o)]^{-2}$

Bond lengths, angles, torsional angles and hydrogen bonds for I are listed in Table 2.

The absolute configuration of (I) was determined by refinement of the coordinates of the two enantiomorphs. The original coordinates (space group $P4_1$) gave the known absolute configuration of the cation of the parent bromide, namely Λ; consequently, it was assumed to be the correct one inasmuch as there is no reason to expect inversion at the cobalt centre; moreover, the sign of the rotation (−) of the solution of I used to grow the crystals matches that of the parent bromide.

RESULTS

The absolute configuration of the cation is shown in Fig. 1, which displays the contents of the asymmetric unit. As expected from the prepara-

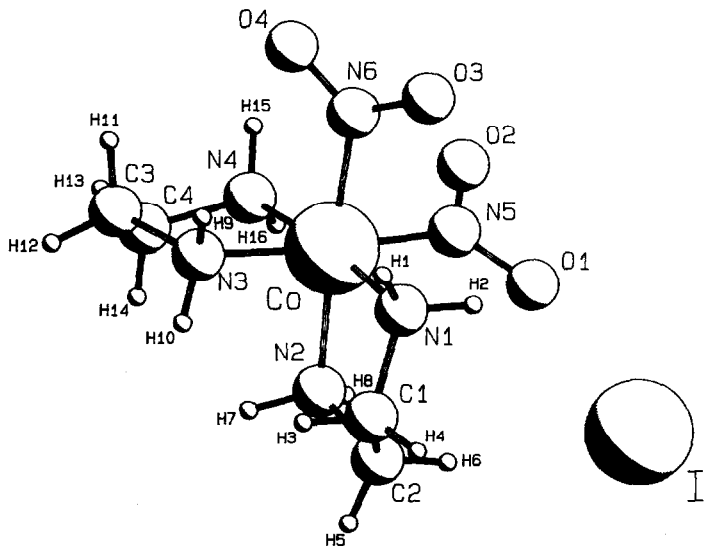

Fig. 1. The contents of the asymmetric unit. Note that the configuration about cobalt is Λ while the conformations of N(1)—C(1)—C(2)—N(2) and N(3)—C(3)—C(4)—N(4) are λ and λ. Also the hydrogen bonds between O(1) and H(2) and between O(4) and H(15) are evident from this view. For details of the bond lengths see Table 2(D).

Table 2. Bond distances (Å) and angles (°) for **I**

(A) Distances[a]

Co—N(1)	1.950	O(1)—N(5)	1.265	N(3)—C(3)	1.505
Co—N(2)	2.014	O(2)—N(5)	1.229	N(4)—C(4)	1.437
Co—N(3)	1.981	O(3)—N(6)	1.224	C(1)—C(2)	1.540
Co—N(4)	1.946	O(4)—N(6)	1.215	C(3)—C(4)	1.466
Co—N(5)	1.877	N(1)—C(1)	1.480		
Co—N(6)	1.930	N(2)—C(2)	1.474		

(B) Angles[b]

N(1)—Co—N(2)	84.32	N(3)—Co—N(5)	174.84	Co—N(5)—O(2)	122.13
N(1)—Co—N(3)	90.70	N(3)—Co—N(6)	90.37	O(1)—N(5)—O(2)	115.95
N(1)—Co—N(4)	173.51	N(4)—Co—N(5)	91.37	Co—N(6)—O(3)	117.92
N(1)—Co—N(5)	93.65	N(4)—Co—N(6)	91.41	Co—N(6)—O(4)	121.98
N(1)—Co—N(6)	92.99	N(5)—Co—N(6)	86.63	O(3)—N(6)—O(4)	119.93
N(2)—Co—N(3)	92.47	Co—N(1)—C(1)	109.65	N(1)—C(1)—C(2)	105.25
N(2)—Co—N(4)	91.51	Co—N(2)—C(2)	110.09	N(2)—C(2)—C(1)	106.84
N(2)—Co—N(5)	90.73	Co—N(3)—C(3)	108.71	N(3)—C(3)—C(4)	108.69
N(2)—Co—N(6)	176.11	Co—N(4)—C(4)	110.02	N(4)—C(4)—C(3)	107.33
N(3)—Co—N(4)	84.50	Co—N(5)—O(1)	121.87		

(C) Torsional angles

N(2)—Co—N(1)—C(1)	−22.7	N(2)—Co—N(5)—O(2)	121.0
N(4)—Co—N(1)—C(1)	27.5	N(3)—Co—N(5)—O(2)	−7.3
N(5)—Co—N(1)—C(1)	−113.1	N(4)—Co—N(5)—O(1)	−153.1
N(6)—Co—N(1)—C(1)	160.1	N(4)—Co—N(5)—O(2)	29.4
N(1)—Co—N(2)—C(2)	−7.1	N(6)—Co—N(5)—O(1)	115.6
N(3)—Co—N(2)—C(2)	−97.6	N(6)—Co—N(5)—O(2)	−61.9
N(4)—Co—N(2)—C(2)	177.8	N(1)—Co—N(6)—O(3)	28.1
N(5)—Co—N(2)—C(2)	86.5	N(1)—Co—N(6)—O(4)	−147.0
N(6)—Co—N(2)—C(2)	39.2	N(2)—Co—N(6)—O(3)	−18.0
N(1)—Co—N(3)—C(3)	179.4	N(2)—Co—N(6)—O(4)	166.8
N(2)—Co—N(3)—C(3)	−96.3	N(3)—Co—N(6)—O(3)	118.9
N(4)—Co—N(3)—C(3)	−5.0	N(3)—Co—N(6)—O(4)	−56.3
N(5)—Co—N(3)—C(3)	32.0	N(4)—Co—N(6)—O(3)	−156.6
N(6)—Co—N(3)—C(3)	86.4	N(4)—Co—N(6)—O(4)	28.2
N(1)—Co—N(4)—C(4)	20.5	N(5)—Co—N(6)—O(3)	−65.3
N(2)—Co—N(4)—C(4)	70.4	N(5)—Co—N(6)—O(4)	119.5
N(3)—Co—N(4)—C(4)	−21.9	Co—N(1)—C(1)—C(2)	46.2
N(5)—Co—N(4)—C(4)	161.2	Co—N(2)—C(2)—C(1)	33.8
N(6)—Co—N(4)—C(4)	−112.2	Co—N(3)—C(3)—C(4)	30.4
N(1)—Co—N(5)—O(1)	22.8	Co—N(4)—C(4)—C(3)	44.5
N(1)—Co—N(5)—O(2)	−154.7	N(1)—C(1)—C(2)—N(2)	−51.6
N(2)—Co—N(5)—O(1)	−61.6	N(3)—C(3)—C(4)—N(4)	−48.6

(D) Selected list of hydrogen bonds

O(1)—H(2)	2.298	N(1)—H(2)···O(1)	117.6	
O(4)—H(15)	2.301	N(4)—H(15)···O(4)	117.1	
O(1)—H(1)	2.267	N(1)—H(1)···O(1)	145.5	N(1) at $1-y, x, 1/4+z$
O(4)—H(16)	2.291	N(4)—H(16)···O(4)	143.4	N(4) at $y, -x, z-1/4$
O(3)—H(16)	2.333	N(4)—H(16)···O(3)	141.4	N(4) at $y, -x, z-1/4$
O(2)—H(1)	2.364	N(1)—H(1)···O(2)	138.6	N(1) at $1-y, x, 1/4+z$

[a] Estimated errors in distances range from 0.005 to 0.01 Å.

[b] Estimated errors in angles range from 0.02 to 0.05°.

No e.s.d.s are shown since hydrogen atoms were not refined.

Numbers in parentheses are estimated standard deviations in the least significant digits.

tion the cation has the configuration Λ; however, the helical chiralities of the two en rings are λ[<N(1)—C(1)—C(2)—N(2) = −51.6°] and λ[< N(3)—C(3)—C(4)—N(4) = −48.6°], which is an interesting solid state result since that of the bromide **III**, from which **I** was prepared, was Λ($\delta\lambda$), implying that intra- or intermolecular interactions, or both, are responsible for a change which increases the conformational energy of the system.[18]

The packing of the molecules in the unit cell is shown in Fig. 2, which illustrates the fact that the cations form infinite spiral strings, propagating along the four-fold screw axis, and held together by hydrogen bonds between the —NO_2 oxygens and the —NH_2 hydrogens, typical of which are those listed in Table 3(D). The spiral strings are made up of homochiral cations inasmuch as we used a resolved species.

In **I** the helical strings are, in turn, held together by hydrogen bonds between the iodide and hydrogens of the —NH_2 moieties. The strings have the same helical chirality and, in that regard, resemble the helical strings of a polypeptide derived from homochiral amino acids.

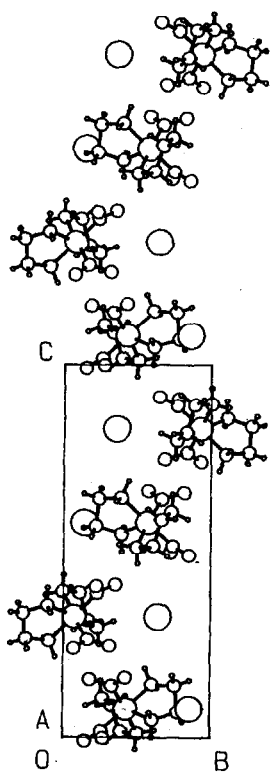

Fig. 2. A portion of the unit cell. Note the infinite spirals of hydrogen-bonded cations into pockets of which fit the iodide anions which link adjacent spiral strings.

Table 3. Torsional angles for [*cis*-Co(en)$_2$(NO$_2$)$_2$]Cl, bromide and iodide (**I**)

Chiroptical symbol	Chloride Λ($\delta\lambda$)	Bromide Δ($\delta\lambda$)	Iodide[a] Λ($\lambda\lambda$)
N(1)—Co—N(5)—O(1)	−137.3	−135.0	−154.7
N(1)—Co—N(5)—O(2)	39.9	44.9	22.8
N(1)—Co—N(6)—O(3)	−165.5	−169.2	−147.0
N(1)—Co—N(6)—O(4)	15.86	12.6	28.1
N(4)—Co—N(5)—O(1)	41.63	42.8	29.4
N(4)—Co—N(5)—O(2)	−141.2	−137.3	−153.1
N(4)—Co—N(6)—O(3)	16.41	13.4	28.2
N(4)—Co—N(6)—O(3)	−162.3	−164.8	−156.6

[a] Angle labels were rearranged to correspond to those of the lower halides, since in the labelling for the —NO_2 oxygens O(1) and O(2) and O(3) and O(4) for the iodide were reversed compared with the labels for the other two.

DISCUSSION

Racemic [*cis*-Co(en)$_2$(NO$_2$)$_2$]I (**I**) crystallizes either as a racemate[12(a)] or in the enantiomorphic space group $P4_1$, whose contents ($z = 4$) are homochiral, as shown above. Thus far, we have not been able to isolate X-ray quality crystals of the racemate, and, as stated above, the enantiomorphic ones were obtained from pre-resolved material. However, we know that they should be the same as those precipitating during conglomerate crystallization since Aoki *et al.*[19] studied the structure of resolved $(-)_{589}$-[*cis*-[Λ($\delta\lambda$)-Co(en)$_2$oxalato] Br·H_2O while we[5(b)] determined its structure using crystals from a conglomerate crystallization. The results are identical. The interested reader is referred to our previous paper on this subject.[5(b)]

It is noteworthy that the iodide (**I**) is not isomorphous with its chloride (**II**) or bromide (**III**) analogues, which is in line with the observation that it is capable of crystallizing as both a racemate and a conglomerate[12(a)] from the same racemic solution, while **II** and **III** crystallize as conglomerates. The same observations apply to the oxalato series, [*cis*-Co(en)$_2$Ox]X·nH$_2$O (X = Cl, $n = 4$; X = Br, $n = 1$; X = I, $n = 0$). in which the chloride and bromide crystallize as conglomerates, while the iodide crystallizes as both.[5(b),12(b),(c)] In that series one could argue that space group changes would not be surprising inasmuch as the degree of hydration varies; however, such is not the case with the current series. Finally, in the oxalato series similar difficulties arise from the quality of the crystals of the iodide salt, as we have demonstrated earlier.[5(b)]

A pertinent fact is that while **I** winds its cations on a four-fold spiral screw, **II** and **III** crystallize in

the space group $P2_1$ and their cations pack in helical strings also, but the order of the screw axis is two. However, they all wrap themselves about a screw axis, in a helical arrangement internally held by $—NO_2 \cdots H_2N—$ hydrogen bonds. In turn, strings of the same helical chirality are held together in a three-dimensional array by hydrogen bonds between the counter-anion and the $—NH_2$ hydrogens of the cations. This feature is shared by the three homochiral crystalline forms of **I**, **II** and **III**.

The following observations concerning the crystallization characteristics of the three halides of the $[cis\text{-}[Co(en)_2(NO_2)_2]^+$ cation are useful to understand the reasons for their crystallization behaviour:

(1) The ionic radii of six-coordinate Cl^-, Br^- and I^- are, respectively,[20] 1.67, 1.82 and 2.06 Å. Therefore, their respective volumes are 19.41, 25.25 and 36.62 Å^3. The differences between **I** and **III**, between **I** and **II** and between **III** and **II** are, respectively, 17.11, 11.37 and 5.74 Å^3. The experimental volume per molecule of **I** is 299.35 Å^3. The chloride (**II**) is characterized by a molecular volume of 288.17 Å^3, while the molecular volume of the bromide (**III**) is 292.67 Å^3. The experimental volume differences between **I** and **III** and between **I** and **II** are, respectively, 6.68 and 11.18 Å^3; the difference in volume between **II** and **III** is 4.50 Å^3. These differences are too small to be due to the radius differences of the halide counter-anion, which means expansion of the lattices is less than expected from a simple, linear, additive model. Here we note that (see Fig. 2) the anions lie in cages formed by the cationic strings, which it helps stitch together. The same feature has been observed[5(b)] in the packing of **II** and **III**, despite the difference in space groups. Apparently the chloride fits well in the cage, which needs to expand only slightly to accommodate the larger bromide anion. This is not a trivial observation since in the current series, as well as in the series $[Co(en)_2Ox]X$, with X = Cl, Br and I, the radius of the anion plays a crucial role in the crystallization pathway. Shimura *et al.* have shown, from phase diagrams, that *cis*-dinitro[12(a)] and the oxalato chlorides and bromides crystallize as conglomerates, while the iodides can crystallize as both a conglomerate and a racemate.[12(b),(c)] In separate papers of ours,[3,13] we have shown that the reason for this behaviour is that the cations form infinite hydrogen-bonded helical strings which extend throughout the length of the crystal. Between these strings are cavities into which the anions and the waters of crystallization fit; in turn, they link the strings by hydrogen bonds. The iodide anion is apparently large enough to force the cations apart and disrupts, or otherwise modifies, the spiral formation. Furthermore, given the fact[12] that the iodide derivative crystallizes as a racemate as well as a conglomerate, it appears that this anion loses the ability to differentiate between joining homochiral strings vs joining heterochiral strings, which is probably due to (a) the formation of much weaker hydrogen bonds than the chloride and bromide anions due to its inherently lower basicity and (b) its larger radius, which mechanically disrupts the cages formed by the cationic spiral strings present in the lower halides, and the result is apathy to the form of packing of the spiral strings. (c) Finally, when forced to form an enantiomorphic lattice (as happened here) the pitch of the screw axis is changed from 2_1 to 4_1 in order to better accommodate the bulkier iodide anion.

(2) The conformation and configuration of the cation in **I** is $\Lambda(\lambda\lambda)$; e.g. given the conformational symbol Λ both en rings have been coerced into the highest energy conformation ($\lambda\lambda$) in order to form stronger intramolecular hydrogen bonds between the $—NO_2$ oxygen and the $—NH_2$ hydrogens now that in **I** there is a weaker hydrogen bonding network between cations and anions (see Figs 1 and 2). We have pointed out before[1,21-23] that for a $\Lambda(\delta\delta)$-$[cis\text{-}Co(en)_2(NO_2)_2]^+$ cation, if through torsional motion about the $Co—NO_2$ bond one $—NO_2$ orients itself at the most advantageous position for hydrogen bonding with a δ ring, it is impossible for the second $—NO_2$ ligand to achieve an equally effective hydrogen bonding with another δ ring while a proper interligand $O \cdots O$ distance (*ca* 3.1 Å) is achieved. However, if the second en ring acquires the λ conformation, a much more effective intramolecular hydrogen bonding scheme is achieved by the second $—NO_2$ ligand. This appears to be the reason for the occurrence of $\Lambda(\delta\lambda)$, $\Delta(\lambda\delta)$, $\Lambda(\lambda\lambda)$ and $\Delta(\delta\delta)$ $[cis\text{-}Co(en)_2(NO_2)_2]^+$ cations in the crystalline state. This phenomenon can best be demonstrated by comparison of the torsional angles defined by (axial nitrogen)—Co—(NO_2 nitrogen)—(NO_2 oxygen), as listed below (Table 3). For more details of these arguments, the reader is referred to the original papers.[1,21-23]

(3) The energy associated with en ring inversion has been recently measured[24] to be 24.7 ± 4.5 KJ mol^{-1} in the anion $[Fe(CN)_4(en)]^-$, implying that the intramolecular hydrogen bonds present in the cation must exceed that barrier in order to be effective. Thus, we have an appropriate value of the strength of these hydrogen bonds.

(4) Finally, we should point out that the helical nature of the strings is not the result of packing forces in crystals belonging to space groups containing such symmetry elements. We know this

is so because such strings are also found in compounds crystallizing in the space groups $P1$ and $P\bar{1}$, where no such symmetry element is found. The point will be discussed in a separate paper[25] on the structure of K[Co(edda)$(NO_2)_2$] and K[Co(edda)$(NO_2)_2$]·H_2O (edda = ethylenediamine-diacetic acid), which crystallize, respectively, in space groups $P2_12_12_1$ and $P\bar{1}$. Such helical strings are found in both; however, in the latter compound pairs of adjacent strings are of opposite helical chirality, while the anionic members of each string are homochiral.

CONCLUSIONS

We have previously[1,21-23] emphasized that in order for cations of the two series [*cis*-Co$(en)_2$$(NO_2)_2$]X to crystallize as conglomerates the counter-anions (and/or waters of crystallization) must not compete for the hydrogen bonds of the —NH_2 ligands. In the conglomerate halide series the anion is always hydrogen-bonded to the equatorial —NH_2 hydrogens and leaves the —NO_2 oxygens free to form relatively strong hydrogen bonds with axial hydrogens and with the hydrogens of adjacent cations within that string, thus increasing the rigidity of the molecule and destroying the potential two-fold axis which these cations could have if the —NO_2 ligands were properly oriented. We find the current results gratifying since the consistency in crystallization mode indicates our suggestions for the origin of conglomerate crystallization are reasonable and consistent with experimental facts obtained with a wide range of compounds of the *cis*-dinitro and oxalato series.

Supplementary material available. Compound **I**: anisotropic thermal parameters (1 page), structure factor tables (18 pages). The latter are available in PC diskette form from Ivan Bernal.

Acknowledgements—We thank the Robert A. Welch Foundation for a research grant (E-594 to IB) and for Fellowships to Jozef Myrczek and Jiwen Cai. The National Science Foundation provided the funds for purchasing the X-ray diffractometer.

REFERENCES

1. I. Bernal, *Inorg. Chim. Acta* 1985, **96**, 99.
2. I. Bernal and J. Cetrullo, *Inorg. Chim. Acta* 1987, **134**, 105.
3. I. Bernal, J. Cetrullo, J. Myrczek and S. Massoud, [Co(trien)$(NO_2)_2$]NO_3 and [Co$(en)_2$$(NO_2)_2$]Br—Clearfield Symposium.
4. I. Bernal and J. Cetrullo, *Inorg. Chim. Acta* 1988, **150**, 75.
5. (a) I. Bernal and J. Cetrulo, *J. Coord. Chem.* 1989, **20**, 259; (b) I. Bernal, J. Cetrullo, J. Myrczek and S. S. Massoud, *J. Coord. Chem.*, submitted for publication. [Co$(en)_2$oxalato]X paper.
6. J. D. Korp, I. Bernal, R. A. Palmer and J. C. Robinson, *Acta Cryst.* 1980, **B36**, 560.
7. I. Bernal and R. A. Palmer, *Inorg. Chem.* 1981, **20**, 295.
8. I. Bernal, J. Cetrullo and S. Berhane, *Struct. Chem.* 1990, **1**, 361.
9. I. Bernal, *Inorg. Chim. Acta* 1988, **142**, 21.
10. J. Jacques, A. Collet and S. H. Wilen, *Enantiomers, Racemates and Resolutions.* Wiley-Interscience, New York (1981).
11. O. Bortin, *Acta Chem. Scand.* 1976, **A30**, 657.
12. (a) For [Co$(en)_2$$(NO_2)_2$]X phase diagrams see: K. Yamanari, J. Hidaka and Y. Shimura, *Bull. Chem. Soc. Japan* 1972, **46**, 3724. For [Co$(en)_2$oxalato]X phase diagrams see: (b) A. Fuyuhiro, K. Yamanari and Y. Shimura, *Bull. Chem. Soc. Japan* 1981, **54**, 2531; (c) Y. Shimura and K. Tsutsui, *Bull. Chem. Soc. Japan* 1977, **50**, 145.
13. I. Bernal, J. Cetrullo, J. Myrczek and S. Massoud, unpublished results on [Co$(en)_2$oxalato]I. Submitted for publication to *J. Coord. Chem.*
14. TEXRAY-230 is a modification of the SDP-Plus[15] set of X-ray crystallographic programs distributed by the Molecular Structure Corporation, 3200 Research Forest Dr, The Woodlands, TX 77386, for use with their automation of the CAD-4 diffractometer.
15. SDP-Plus is the Enraf–Nonius Coroporation X-ray diffraction data processing programs distributed by B. A. Frenz & Associates, 209 University Dr. East, College Station, TX 77840.
16. R. B. Roof, *A Theoretical Extension of the Reduced Cell Concept in Crystallography.* Report LA-4038, Los Alamos Scientific Laboratory, Los Alamos (1969).
17. D. T. Cromer and J. T. Waber, *International Tables for X-ray Crystallography*, Vol. IV, Tables 2.2.B and 2.3.1, respectively, for the scattering factor curves and the anomalous dispersion values. Kynoch Press, Birmingham (1975).
18. T. Saito, in *Stereochemistry of Optically Active Transition Metal Complexes* (Edited by B. E. Douglas and Y. Saito), ACS Symposium Series 119, pp. 13–42. American Chemical Society, Washington, DC (1985).
19. T. Aoki, K. Matsumoto, S. Ooi and H. Kuroya, *Bull. Chem. Soc. Japan* 1973, **46**, 159.
20. R. D. Shannon, *Acta Cryst.* 1976, **A32**, 751.
21. I. Bernal, J. Cetrullo and S. Berhane, *Struct. Chem.* 1990, **1**, 361.
22. I. Bernal and J. Cetrullo, *Inorg. Chim. Acta* 1985, **101**, 175.
23. I. Bernal and J. Cetrullo, *Inorg. Chim. Acta* 1988, **150**, 75.
24. Y. Kuroda, N. Tanaka, M. Goto and T. Sakai, *Inorg. Chem.* 1989, **28**, 997.
25. I. Bernal, J. Cetrullo, J. Myrczek, J. Cai and W. T. Jordan, unpublished work.

Polyhedron Vol. 12, No. 10, pp. 1157–1162, 1993
Printed in Great Britain

0277–5387/93 $6.00+.00
Pergamon Press Ltd

THE PHENOMENON OF CONGLOMERATE CRYSTALLIZATION—XXXIII. COUNTER-ION EFFECTS ON CRYSTALLIZATION PATHWAY OF RACEMATE SOLUTIONS—IV. THE CRYSTAL AND MOLECULAR STRUCTURE OF RACEMIC $(H_3O^+)[Co(en)_2ox]Cl_2 \cdot H_2O$ (I)

IVAN BERNAL,* JIWEN CAI† and JOZEF MYRCZEK†‡

Chemistry Department, University of Houston, Houston, TX 77024-5641, U.S.A.

(*Received* 10 *November* 1992; *accepted* 27 *January* 1993)

Abstract—$(H_3O^+)[Co(en)_2ox]Cl_2 \cdot H_2O$ (I), $CoCl_2O_6N_4C_6H_{21}$, crystallizes as a racemate in the monoclinic space group $P2_1/c$ (No. 14). Infinitely hydrogen-bonded spiral strings of homochiral $[Co(en)_2ox]^+$ cations are formed which are wrapped about the two-fold screw axis of the crystals. Adjacent spirals are held together by hydrogen bonds between the waters and chlorides and the $—NH_2$ hydrogens of the cations. Such an arrangement is also present in the conglomerate crystals of the $[Co(en)_2ox]Cl \cdot 4H_2O$ (II) and $[Co(en)_2ox]Br \cdot H_2O$ (III) derivatives; however, unlike II and III, which crystallize as conglomerates and all spiral strings are of the same helicity, in I adjacent spirals are of opposite helical chirality and related to one another by the inversion operation of the space group.

It has been known for some time[1–3] that the series $[M(en)_2ox]X$ (M = Co, Cr, Rh; X = Cl^-, Br^-) crystallize as conglomerates, whereas $[Co(en)_2ox]I$ crystallizes both as a conglomerate and as a racemate.[1(c)] In fact, this observation was used by Shimura *et al.*[1(c)] as evidence of the success of the thermodynamic formulation of the condition $S_r > 1.414S_e$ (where S_r is the solubility of the racemate and S_e that of the enantiomer), which defines what crystallization pathway will a given substance prefer—racemate or conglomerate. Relevant crystallization data on these systems are summarized below:

Compound	Space group	Ref.
$[Co(en)_2ox]Cl \cdot 4H_2O$ (III)	$P2_12_12_1$	1(c), 2
$[Co(en)_2ox]Br \cdot H_2O$ (IV)	$P2_12_12_1$	2, 3
$[Co(en)_2ox]I$ (V)	?§	1(c)
$[Cr(en)_2ox]Br$	?§	1(a), 4
$[Rh(en)_2ox]Br$	?§	4
$[Rh(en)_2ox]Cl \cdot H_2O$	?§	4

Our crystallization and structural studies of III[2] and IV[2] demonstrated that, in both compounds, homochiral cations are present in spiral strings linked by hydrogen bonds spanning from the terminal oxalato oxygens of one cation to the basal plane amines of an adjacent one, each string being an infinite polymer running along the length of the *b*-direction of the crystal.[2] Adjacent strings are also homochiral with respect to their helical sense and in III and IV are held together by halide anions which are bonded to hydrogens of an axial $—NH_2$ and to a water of crystallization, the latter being bonded to an axial $—NH_2$ hydrogen of a cation belonging to the adjacent string. This stitching to-

* Author to whom correspondence should be addressed.

† Fellow of the Robert A. Welch Foundation.

‡ On leave from the Technical University of Wroclaw, 1-5, Wroclaw, Poland.

§ These substances were identified as forming conglomerates either from solubility measurements, by seeding experiments or by measuring the CD spectra of resulting crystalline material. No structural data were reported. See refs 1(a), 1(c) and 5 for details of the crystallization, seeding and spectroscopic experiments performed on these compounds.

gether of the strings occurs across the entire length of adjacent spirals.

At the time we published ref. 2 we suggested that anything that interfered with the orderly formation of the spiral string and/or of the stitching pattern found in **III** and **IV** would probably result in the formation of heterochiral crystals (racemates). Sometime later we were able to prepare $NH_4[Cr(en)_2ox]Cl_2 \cdot H_2O$ (**VI**)[5] and found that the ammonium cation hydrogen bonds to the terminal oxalato oxygens and, thus, disrupts the formation of the spiral strings mentioned above. It is, therefore, noteworthy that **VI** crystallizes as a racemate in the space group $P2_1/c$, as suggested earlier.[2] We have been unable to prepare the cobalt analogue to **VI**, despite repeated efforts, as discussed in our report[5] on the crystallization behaviour of **VI**. The similarity of **I** and **VI** suggested they should crystallize similarly and made it possible to, once more, test our hypothesis[2] since it was reasonable to expect that, as in **VI**, the hydronium cation would also alter drastically the hydrogen bond pattern observed in **III** and **IV**.

Finally, **I** was prepared by accident while attempting to grow crystals of $[Co(en)_2ox]Pb_2Cl_5 \cdot 2H_2O$, the analogue of $[Co(N\text{-}Me\text{-}ethylenediamine)_2ox]Pb_2Cl_5 \cdot 2H_2O$—a compound previously studied here.[6] That effort was unsuccessful, but the product obtained easily compensated for our failure to produce the lead compound we were seeking.

EXPERIMENTAL

Synthesis

Compound **I** was prepared as follows: $PbCl_2$ was slurried with distilled water, at 60°C, and concentrated HCl was added until all the solid had dissolved. A solution of $[Co(en)_2ox]Cl \cdot 4H_2O$[2,7,8] in water was stirred at 60°C with enough of the acidified lead chloride so that the Co : Pb ratio was 1 : 2. The solution was allowed to cool, filtered and set aside to crystallize (*ca* 18°C). Approximately equilateral crystals of the reddish-orange substance were formed, filtered and washed with ethanol. One was selected for single-crystal X-ray data collection.

Elemental analysis.[9] For $(H_3O^+)[Co(en)_2ox]Cl_2 \cdot H_2O$, $CoCl_2O_6N_4C_6H_{21}$: Mol. wt = 375.10. Found: C, 19.4; H, 5.6; N, 16.1. Calc.: C, 19.2; H, 5.6; N, 14.9%.

X-ray diffraction

Data for **I** were collected with an Enraf–Nonius CAD-4 diffractometer operating with a Molecular Structure Corporation TEXRAY-230 modification[10] of the SDP-Plus software package (see Table 1).[11] The crystal was centred with data in the $22° \leqslant 2\theta \leqslant 34°$ range and examination of the cell constants and Niggli matrix[12] clearly showed it to crystallize in a primitive, monoclinic lattice whose

Table 1. Summary of data collection and processing parameters for racemic $(H_3O^+)[Co(en)_2ox]Cl_2 \cdot H_2O$

Space group	$P2_1/c$
Cell constants	
a (Å)	7.397(2)
b (Å)	12.137(3)
c (Å)	17.011(3)
β (°)	100.66(4)
Cell volume (Å^3)	1400.97
Molecular formula	$CoCl_2O_6N_4C_6H_{21}$
Molecular weight (g mol^{-1})	375.10
Density (calc; $z = 4$ mol cell^{-1}) (g cm^{-3})	1.660
Radiation employed	Mo-K_α ($\lambda = 0.71073$ Å)
Absorption coefficient, μ (cm^{-1})	15.237
Transmission coefficients	0.9247–0.9995
Data collection range	$4° \leqslant 2\theta \leqslant 60°$
Scan width	$\Delta\theta = 1.00 + 0.35 \tan\theta$
Total data collected	3139
Data used in refinement	2543
$R = \Sigma\|\|F_o\| - \|F_c\|\|/\Sigma\|F_o\|$	0.0449
$Rw = [\Sigma w^2(\|F_o\| - \|F_c\|)^2/\Sigma\|F_o\|^2]^{1/2}$	0.0458
Weights used	$w = [\sigma(F_o)]^{-2}$

Laue symmetry and systematic absences belong to those of the space group $P2_1/c$ (No. 14). The intensity data set was corrected for absorption using empirical curves derived from Psi scans[10,11] of five reflections. The scattering curves were taken from Cromer and Waber's compilation.[13]

RESULTS

The contents of the asymmetric unit are shown in Fig. 1, which shows that there is a cobalt cation, a hydronium cation and a water of crystallization which is hydrogen bonded to a terminal oxalato oxygen [O(3)] and to the chloride anion [Cl(2)], which in turn is hydrogen bonded to a terminal —NH_2 hydrogen (H1). The hydronium cation is weakly hydrogen bonded to O(4), but it also blocks access to a non-bonded pair of O(4). Finally, Cl(1) is hydrogen bonded to H(8) and H(9), thus blocking some of the hydrogens needed by the terminal oxalato oxygens to form the helical strings observed in the conglomerate crystallization of **III** and **IV**.

Figure 2 is a packing diagram in which the centre of the cell is one of the inversion centres, as readily ascertained by the relationship of the chloride and waters of crystallization clustered about that point. Note also that there are strings of cations running along the *b*-axis, as expected from the space group; however, given the position of the inversion centre, the cations of adjacent strings are of opposite chirality, as is the sense of the helical chirality of adjacent spiral strings. Thus, not only does the lattice contain racemic pairs of $[Co(en)_2ox]^+$ cations, but an enantiomorphic relationship exists also between the helicities of the entire sets of adjacent strings.

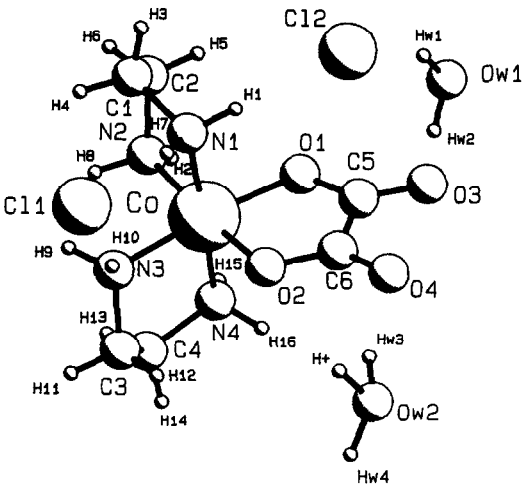

Fig. 1. A view of the contents of the asymmetric unit. Note the position of the (H_3O^+) cation, blocking access to O(4) and of the water of crystallization blocking access to O(3) of the oxalato ligand. Also note the position of the chloride anions, which effectively block access to the —NH_2 hydrogens. These hydrogen-bonded interactions effectively eliminate all chances of forming the spiral strings of cobalt cations found (see refs 2 and 5) in the series of $[Co(en)_2ox]X$ (X = Cl, Br, I) and whose formation was postulated as the origin of conglomerate crystallization.

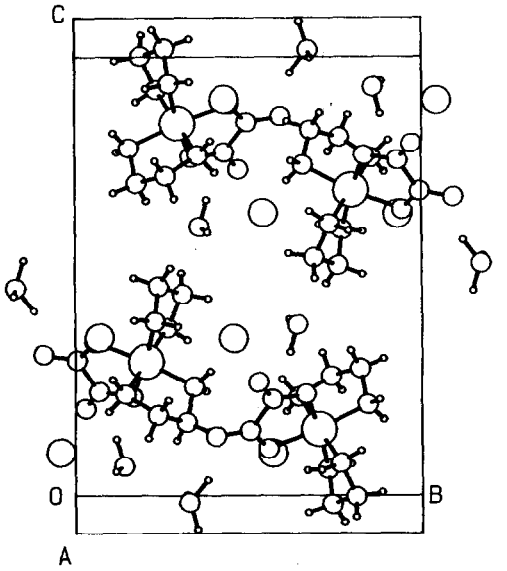

Fig. 2. A view of the unit cell contents. Here, the viewer can see the approach between cobalt cations blocked by the water, the (H_3O^+) cation and the chlorides. Note the inversion centre located at the centre of the cell. This centre relates enantiomorphic pairs of cations as well as spiral strings of opposite helicity.

Table 2(D) shows that the shortest hydrogen bond in the entire lattice is between O(4) and Hw(3) and the next shortest is between O(3) and Hw(2). Therefore, the two terminal oxalato oxygens are engaged in hydrogen bonding which preclude the formation of the spiral strings observed in the case of the chloride (**III**) and the bromide (**IV**). Such was precisely the case with the double salt $NH_4[Cr(en)_2ox]Cl_2 \cdot H_2O$ (**VI**),[5] with which compound **I** is nearly isomorphous. Given that fact, we refer the interested reader to the original paper on **VI**[5] for details of the hydrogen bonding present there.

Finally, the hydronium cation is very far from the water of crystallization (nearest contact, see Table 2(D), is 2.21 Å). Therefore, the correct formulation of this hydrated cation is H_3O^+ and not $H_5O_2^+$.

DISCUSSION

It was our good fortune to accidentally obtain **I** since it is chemically different, yet nearly iso-

Table 2. Bond distances (Å) and angles (°) for **I**

(A) Distances

Co—O(1)	1.915(1)	O(1)—C(5)	1.284(2)	N(3)—C(3)	1.466(2)
Co—O(2)	1.920(1)	O(2)—C(6)	1.276(2)	N(4)—C(4)	1.480(2)
Co—N(1)	1.941(1)	O(3)—C(5)	1.232(2)	C(1)—C(2)	1.506(2)
Co—N(2)	1.941(1)	O(4)—C(6)	1.239(2)	C(3)—C(4)	1.485(3)
Co—N(3)	1.925(1)	N(1)—C(1)	1.485(2)	C(5)—C(6)	1.531(2)
Co—N(4)	1.955(1)	N(2)—C(2)	1.478(2)		

(B) Angles

O(1)—Co—O(2)	85.8(4)	N(1)—Co—N(4)	177.2(5)	N(2)—C(2)—C(1)	107.1(2)
O(1)—Co—N(1)	91.8(5)	N(2)—Co—N(3)	95.3(5)	N(3)—C(3)—C(4)	107.2(2)
O(1)—Co—N(2)	90.5(5)	N(2)—Co—N(4)	92.3(5)	N(4)—C(4)—C(3)	108.2(2)
O(1)—Co—N(3)	173.3(5)	N(3)—Co—N(4)	86.1(6)	O(1)—C(5)—O(3)	125.7(2)
O(1)—Co—N(4)	90.3(5)	Co—O(1)—C(5)	112.3(1)	O(1)—C(5)—C(6)	114.4(1)
O(2)—Co—N(1)	89.4(5)	Co—O(2)—C(6)	111.8(1)	O(3)—C(5)—C(6)	119.9(1)
O(2)—Co—N(2)	173.9(5)	Co—N(1)—C(1)	110.5(9)	O(2)—C(6)—O(4)	125.0(2)
O(2)—Co—N(3)	88.6(5)	Co—N(2)—C(2)	108.2(9)	O(2)—C(6)—C(5)	115.4(1)
O(2)—Co—N(4)	92.6(5)	Co—N(3)—C(3)	108.8(1)	O(4)—C(6)—C(5)	119.6(1)
N(1)—Co—N(2)	85.9(5)	Co—N(4)—C(4)	109.1(1)		
N(1)—Co—N(3)	92.0(6)	N(1)—C(1)—C(2)	106.1(1)		

(C) Torsional angles

O(2)—Co—O(1)—C(5)	2.2	N(1)—Co—N(3)—C(3)	−162.0
N(1)—Co—O(1)—C(5)	91.5	N(2)—Co—N(3)—C(3)	111.9
N(2)—Co—O(1)—C(5)	177.4	N(4)—Co—N(3)—C(3)	20.0
N(3)—Co—O(1)—C(5)	−32.8	O(1)—Co—N(4)—C(4)	−178.5
N(4)—Co—O(1)—C(5)	−90.3	O(2)—Co—N(4)—C(4)	95.6
O(1)—Co—O(2)—C(6)	0.6	N(1)—Co—N(4)—C(4)	−38.4
N(1)—Co—O(2)—C(6)	−91.2	N(2)—Co—N(4)—C(4)	−88.1
N(2)—Co—O(2)—C(6)	−52.1	N(3)—Co—N(4)—C(4)	7.1
N(3)—Co—O(2)—C(6)	176.8	Co—O(1)—C(5)—O(3)	174.4
N(4)—Co—O(2)—C(6)	90.8	Co—O(1)—C(5)—C(6)	−4.2
O(1)—Co—N(1)—C(1)	99.5	Co—O(2)—C(6)—O(4)	176.7
O(2)—Co—N(1)—C(1)	−174.7	Co—O(2)—C(6)—C(5)	−2.9
N(2)—Co—N(1)—C(1)	9.2	Co—N(1)—C(1)—C(2)	−34.6
N(3)—Co—N(1)—C(1)	−86.1	Co—N(2)—C(2)—C(1)	−43.1
N(4)—Co—N(1)—C(1)	−40.6	Co—N(3)—C(3)—C(4)	−42.7
O(1)—Co—N(2)—C(2)	−72.6	Co—N(4)—C(4)—C(3)	−32.4
O(2)—Co—N(2)—C(2)	−20.1	N(1)—C(1)—C(2)—N(2)	50.3
N(1)—Co—N(2)—C(2)	19.2	N(3)—C(3)—C(4)—N(4)	48.9
N(3)—Co—N(2)—C(2)	110.8	O(1)—C(5)—C(6)—O(2)	5.0
N(4)—Co—N(2)—C(2)	−162.9	O(1)—C(5)—C(6)—O(4)	−174.7
O(1)—Co—N(3)—C(3)	−37.7	O(3)—C(5)—C(6)—O(2)	−173.7
O(2)—Co—N(3)—C(3)	−72.7	O(3)—C(5)—C(6)—O(4)	6.6

(D) Selected list of hydrogen bonds

Cl(1)—H(2)	2.38	N(1)—H(2)···Cl(1)	162.4	
Cl(1)—H(10)	2.39	N(3)—H(10)···Cl(1)	153.2	
Cl(2)—H(1)	2.32	N(1)—H(1)···Cl(2)	170.7	
O(3)—Hw(1)	2.48	Ow(1)—Hw(1)···O(3)	86.1	
O(3)—Hw(2)	1.66	Ow(1)—Hw(2)···O(3)	149.4	
O(4)—Hw(3)	1.59	Ow(2)—Hw(3)···O(4)	151.9	
Cl(1)—H(16)	2.39	N(4)—H(16)···Cl(1)	177.1	N(4) at $x+1, y, z$
Cl(1)—Hw(4)	2.03	Ow(2)—Hw(4)···Cl(1)	152.5	Ow(2) at $1-x, -y, z$
Cl(2)—H(8)	2.48	N(2)—H(8)···Cl(2)	158.4	N(2) at $1-x, y-1/2, 1/2-z$
Cl(2)—H(9)	2.31	N(3)—H(9)···Cl(2)	178.1	N(3) at $1-x, y-1/2, 1/2-z$
O(4)—H(7)	2.10	N(2)—H(7)···O(4)	162.6	N(2) at $-x, y-1/2, 1/2-z$
O(4)—H(15)	2.42	N(4)—H(15)···O(4)	150.1	N(4) at $-x, y-1/2, 1/2-z$
Ow(1)—H+	2.21	Ow(2)—H+···Ow(1)	85.5	Ow(2) at $x-1, y, z$

No e.s.d.s are shown since hydrogen atoms were not refined.
Numbers in parentheses are estimated standard deviations in the least significant digits.

morphous with the ammonium salt **VI**[5] and provided us with an additional piece of the puzzle mentioned in the Introduction; namely, the ammonium cation of **VI** was bound to form hydrogen bonds with the oxalato oxygens, with the anions and with the water of crystallization. Therefore, it would be expected to alter the nature of the packing by (a) intercalating between cobalt cations and modifying or destroying the spiral strings, or by (b) upsetting the nature of the bridges between adjacent strings, or both. The same comments would apply to the hydrogen bonding scheme expected for **I** if our previous statements[5] were correct and general.

Figure 1, together with the hydrogen bonding data in Table 2(D), shows that $Cl(1)^-$ and $Cl(2)^-$ are busily enagaged in hydrogen bonds with both axial and equatorial $-NH_2$ hydrogens and that irrespective of the strength or weakness of their hydrogen bonds, they present a steric barrier to the approach of a second cobalt cation. Consequently, the onset of the formation of a spiral string is obviously hopelessly compromised. Second, on the other side of the cobalt cation, terminal oxygens [O(3) and O(4)] are hydrogen bonded to the hydronium cation and to the water of crystallization, Ow(1). Consequently, the presence of such hydrogen bonds would force additional hydrogen bonds between oxalato terminal oxygens and $-NH_2$ hydrogens to be bifurcated bonds insofar as the oxygens are concerned. Such bonds would be expected to be weaker, if they took place. Moreover, the chlorides, waters and hydronium cations are sterically demanding fragments which would effectively hinder access by another cobalt cation to the amino hydrogens. Again, the possibility of retaining the spiral string geometry observed in previous cases is seriously impaired on the both sides of cobalt cation.

These observations strengthen our previously derived conclusions as to why and how the halides of the $[Co(trien)_2(NO_2)_2]^+$, $[Co(en)_2(NO_2)_2]^+$ and $[Co(en)_2ox]^+$ cations undergo conglomerate crystallization.[2,14–17] Therefore, there appears to be consistency in our crystallization mechanistic conclusions, even when we compare members of different series of cations—a fact which is greatly satisfying.

Supplementary material available. Compound **1**: anisotropic thermal parameters (1 page), structure factor table (28 pages).

Acknowledgements—We thank the Robert A. Welch Foundation for a grant (E-594; to IB) and for a fellowship to J. Cai and J. Myrczek. The structural work was carried out with diffractometer purchased with funds provided by the National Science Foundation, whom we also thank.

REFERENCES

1. (a) Alfred Werner was the first to establish a large solubility difference between the racemate and the enantiomers of the cobalt and chromium compounds, see A. Werner, *Chem. Ber.* 1914, **47**, 2171; (b) further work in this area was done by K. Yamasaki, H. Igarishi and Y. Yoshikawa, *Inorg. Nucl. Chem. Lett.* 1968, **4**, 491; (c) for a more quantitative description of the phase diagram of this substance see K. Yamanari, J. Hidaka and Y. Shimura, *Bull. Chem. Soc. Japan* 1973, **46**, 3724; (d) for the crystal structure of $[Co(en)_2ox]Br \cdot H_2O$, determined from crystals of pre-resolved material, see ref. 3. However, that structural study (ref. 3) was carried out with a very limited set of film data; consequently, it lacks precision and no hydrogen atom positions were given for either the cation or the water of crystallization.
2. Using crystals from conglomerate crystallization experiments we have determined the crystals structures of $[Co(en)_2ox]Br \cdot H_2O$ and $[Co(en)_2ox]Cl \cdot 4H_2O$. In general, the former agrees with the results given in ref. 3; the latter is a new structural analysis. A detailed description and comparison of both will be published elsewhere: I. Bernal, J. Cetrullo, J. Myrczek and S. S. Massoud, *J. Coord. Chem.*, submitted. Both compounds crystallize in the enantiomorphic space group $P2_12_12_1$, with $z = 4$.
3. T. Aoki, K. Matsumoto, S. Ooi and H. Kuroya, *Bull. Chem. Soc. Japan* 1973, **46**, 159.
4. R. D. Gillard and L. H. R. Tipping, *J. Chem. Soc., Dalton Trans.* 1977, 1241.
5. I. Bernal, J. Myrczek and J. Cai, *J. Coord. Chem.*, in press.
6. J. Cai, J. Myrczek and I. Bernal, *J. Chem. Soc., Chem. Commun.* 1992, 1147.
7. J. C. Bailar Jr, *Inorganic Syntheses*, Vol. 2, p. 222. McGraw-Hill, New York (1949).
8. W. T. Jordan and L. R. Froebe, *Inorganic Syntheses*, Vol. XVII, p. 96. McGraw-Hill, New York (1978).
9. Galbraith Laboratories, Inc., P.O. Box 51610, Knoxville, TN 37950-1610.
10. TEXRAY-230 is a modification of the SDP-Plus[11] set of X-ray crystallographic programs distributed by Molecular Structure Corporation, 3200 Research Forest Dr, The Woodlands, TX 77386, for use with their automation of the CAD-4 diffractometer.
11. SDP-Plus is the Enraf–Nonius Corporation X-ray diffraction data processing programs distributed by B. A. Frenz & Associates, 209 University Dr. East, College Station, TX 77840.
12. R. B. Roof, *A Theoretical Extension of the Reduced Cell Concept in Crystallography*, Report LA-4038, Los Alamos Scientific Laboratory (1969).
13. D. T. Cromer and J. T. Waber, *International Tables for X-Ray Crystallography*, Vol. IV, Tables 2.2.8 and 2.3.1, respectively, for the scattering factor curves

and the anomalous dispersion values. Kynoch Press, Birmingham (1975).
14. I. Bernal, *Inorg. Chim. Acta* 1985, **96**, 99.
15. I. Bernal and J. Cetrullo, *Inorg. Chim. Acta* 1988, **144**, 227.
16. I. Bernal and J. Cetrullo, *Inorg. Chim. Acta* 1988, **150**, 75.
17. I. Bernal, S. Berhane and J. Cetrullo, *Struct. Chem.* 1990, **1**, 361.

Polyhedron Vol. 12, No. 10, pp. 1163–1169, 1993
Printed in Great Britain

0277–5387/93 $6.00+.00
© 1993 Pergamon Press Ltd

SYNTHESIS OF WATER-SOLUBLE AND ETHER-SOLUBLE TETRA-μ-ACETATODIRUTHENIUM(II,III) COMPLEXES AND X-RAY CRYSTAL STRUCTURE OF $[Ru_2(\mu\text{-}O_2CC_6H_5)_4(C_2H_5OH)_2][Ru_2(\mu\text{-}O_2CC_6H_5)_4(HSO_4)_2]$

MALACHY McCANN* and ANDREW CARVILL

Chemistry Department, St Patrick's College, Maynooth, Co. Kildare, Ireland

and

CHRISTINE CARDIN and MAIRE CONVERY

Chemistry Department, Trinity College, Dublin, Ireland

(*Received* 27 *October* 1992; *accepted* 26 *January* 1993)

Abstract—$[Ru_2(\mu\text{-}O_2CCH_3)_4Cl]$ reacts readily with aqueous Ag_2SO_4 (2:1 molar ratio) to give the sulphate salt $[Ru_2(\mu\text{-}O_2CCH_3)_4(H_2O)_2]_2(SO_4)$ (**1**). Addition of $NaBPh_4$ to an aqueous solution of **1** produces the ether-soluble tetraphenylborate salt $[Ru_2(\mu\text{-}O_2CCH_3)_4(H_2O)_2][BPh_4]$ (**2**). A methanolic solution of **1** reacts with $Ba(C_6H_5C{\equiv}CCO_2)_2\cdot H_2O$ to give the tetraacetatemonophenylpropynoate complex $[Ru_2(\mu\text{-}O_2CCH_3)_4(O_2CC{\equiv}CC_6H_5)]\cdot H_2O$ (**3**). The reaction of an ethanolic suspension of $[Ru_2(\mu\text{-}O_2CC_6H_5)_4Cl]$ with Ag_2SO_4 and H_2SO_4 (2:1:1 molar ratio) leads to the tetra-μ-benzoatodiruthenium(II,III) double complex salt $[Ru_2(\mu\text{-}O_2CC_6H_5)_4(C_2H_5OH)_2][Ru_2(\mu\text{-}O_2CC_6H_5)_4(HSO_4)_2]$ (**4**). Complex **4** is also obtained by reacting an ethanolic solution of **1** with an excess of benzoic acid in the presence of H_2SO_4. The X-ray crystal structure of **4** shows it to consist of $[Ru_2(\mu\text{-}O_2CC_6H_5)_4(C_2H_5OH)_2]^+$ and $[Ru_2(\mu\text{-}O_2CC_6H_5)_4(HSO_4)_2]^-$ ions, which are linked together by hydrogen bonds into an infinite polymeric chain. The Ru—Ru distances in the cation and anion are very similar [2.265(2) and 2.272(2) Å, respectively]. Spectroscopic, magnetic, conductivity and cyclic voltammetry data are given for the complexes.

As part of our continuing interest in the synthesis and applications of bimetallic carboxylates[1] we have been seeking to develop complexes with potentially useful solubility properties. Herein, we outline the preparation and properties of water-soluble and ether-soluble tetra-μ-acetatodiruthenium(II,III) complexes. In addition, the synthesis and X-ray crystal structure of a novel tetra-μ-benzoatodiruthenium(II,III) double complex salt is given.

RESULTS AND DISCUSSION

Routes to the four new diruthenium(II,III) complexes are summarized in Scheme 1 and, in general, their spectroscopic and magnetic properties were similar to those reported for other Ru_2^{5+} carboxylates.[2–4] $[Ru_2(\mu\text{-}O_2CCH_3)_4Cl]$ dissolved readily in water containing Ag_2SO_4 (2:1 molar ratio) to give the sulphate salt $[Ru_2(\mu\text{-}O_2CCH_3)_4(H_2O)_2]_2(SO_4)$ (**1**). Complex **1** was very soluble in a wide range of solvents (see Experimental), its extreme solubility in water (it is also slightly hygroscopic) being unique among complexes of the $[Ru_2(\mu\text{-}O_2CCH_3)_4]^+$ cation. The large molar conductivity of an aqueous solution of **1** [Λ_M (H_2O) = 186 S cm^2 mol^{-1}] suggests that the complex behaves as a 2:1-type electrolyte in water.[3]

The water-solubility of **1**, together with the presence of sulphate in the complex, proved useful for synthetic purposes. For example, addition of $NaBPh_4$ to a cooled solution of **1** caused the

* Author to whom correspondence should be addressed.

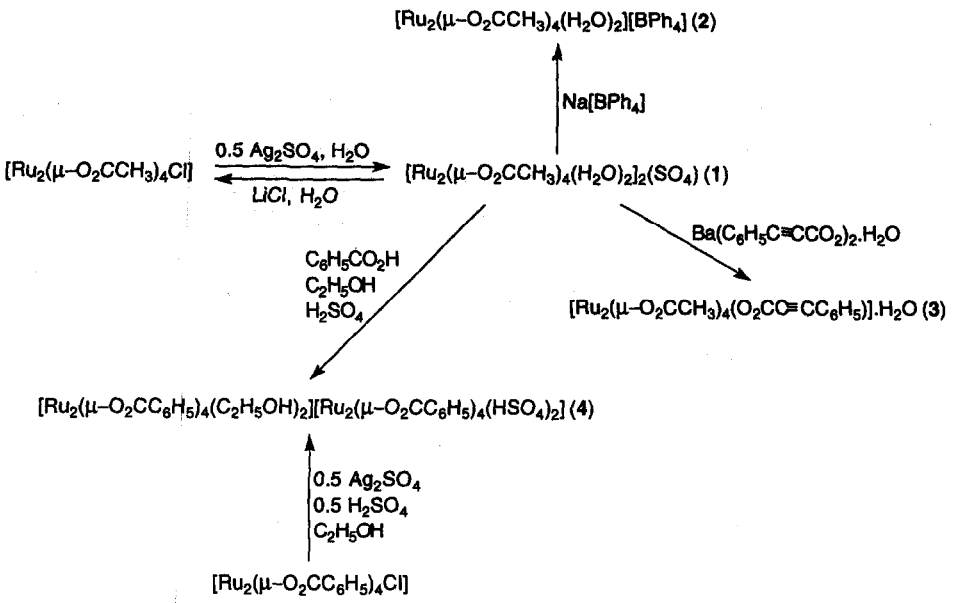

Scheme 1.

immediate precipitation of the orange–brown solid $[Ru_2(\mu\text{-}O_2CCH_3)_4(H_2O)_2][BPh_4]$ (**2**). This result differs with that reported[2] for the reaction of $[Ru_2(\mu\text{-}O_2CCH_3)_4Cl]$ with $NaBPh_4$ in water, which apparently gave a partially hydrolysed product, formulated as $[Ru_2(\mu\text{-}O_2CCH_3)_3(OH)(H_2O)][BPh_4]$. Like the latter complex **2** decomposed on heating in water and it also slowly darkened in the solid state. Complex **2** was a 1 : 1-type electrolyte in methanol [Λ_M (MeOH) = 59 S cm^2 mol^{-1}].

The presence of the SO_4^{2-} ion in **1** was exploited in order to bring about precipitation reactions in the presence of barium salts, particularly in cases where the corresponding silver salts were unsuitable for reaction with $[Ru_2(\mu\text{-}O_2CR)_4Cl]$ complexes. Thus, on reacting a methanolic solution of **1** with barium phenylpropyonate, $Ba(C_6H_5C{\equiv}CCO_2)_2\cdot H_2O$, a white precipitate of $BaSO_4$ was formed and subsequent concentration of the filtrate gave $[Ru_2(\mu\text{-}O_2CCH_3)_4(O_2CC{\equiv}CC_6H_5)]\cdot H_2O$ (**3**) in high yield. Efforts to prepare **3** by reacting $[Ru_2(\mu\text{-}O_2CCH_3)_4Cl]$ with silver phenylpropynoate were unsuccessful due to the extreme insolubility of the silver salt.

Attempts to prepare a sulphate salt of the tetra-μ-benzoate cation $[Ru_2(\mu\text{-}O_2CC_6H_5)_4]^+$, by the method employed for the synthesis of the acetate **1**, were unsuccessful, presumably because of the extreme insolubility of $[Ru_2(\mu\text{-}O_2CC_6H_5)_4Cl]$ in water, and the insolubility of Ag_2SO_4 in other solvents. On refluxing $[Ru_2(\mu\text{-}O_2CC_6H_5)_4Cl]$ with Ag_2SO_4 (Ag : Cl = 1 : 1) in ethanol dissolution was minimal. However, upon the addition of an equivalent amount of H_2SO_4 to the reaction mixture the complex rapidly dissolved. After removing the AgCl precipitate crystals of $[Ru_2(\mu\text{-}O_2CC_6H_5)_4(C_2H_5OH)_2][Ru_2(\mu\text{-}O_2CC_6H_5)_4(HSO_4)_2]$ (**4**) formed in the filtrate. Thus, the overall stoichiometry of the reaction is:

$$2[Ru_2(\mu\text{-}O_2CC_6H_5)_4Cl] + Ag_2SO_4 + H_2SO_4 + 2C_2H_5OH \rightarrow [Ru_2(\mu\text{-}O_2CC_6H_5)_4(C_2H_5OH)_2][Ru_2(\mu\text{-}O_2CC_6H_5)_4(HSO_4)_2]\ (\mathbf{4}) + 2AgCl.$$

Complex **4** was also prepared by reacting an ethanolic solution of **1** with excess benzoic acid in the presence of H_2SO_4.

The X-ray crystal structure of **4** (Figs 1 and 2) showed that it was a double complex salt of the type $[Ru_2(\mu\text{-}O_2CC_6H_5)_4(C_2H_5OH)_2]^+[Ru_2(\mu\text{-}O_2CC_6H_5)_4(HSO_4)_2]^-$. Although individual cationic $[Ru_2^{5+}]^+$ and anionic $[Ru_2^{5+}]^-$ tetra-μ-carboxylato species have previously been structurally characterized (e.g. $[Ru_2(\mu\text{-}O_2CCH_3)_4(H_2O)_2]^+$ and $[Ru_2(\mu\text{-}O_2CCH_3)_4Cl_2]^-$ ions[5]), complex **4** is the first example in which both ions have formed a single crystalline salt together. However, it should be mentioned that in the course of electrochemical studies on a solution of the butyrate complex $[Ru_2(\mu\text{-}O_2CC_3H_7)_4Cl]$ (discussed below) Cotton and Pedersen[6] detected the presence of both $[Ru_2(\mu\text{-}O_2CC_3H_7)_4]^+$ and $[Ru_2(\mu\text{-}O_2CC_3H_7)_4Cl_n]^{(n-1)-}$ ions.

Figure 2 illustrates how the $[Ru_2(\mu\text{-}O_2CC_6H_5)_4$

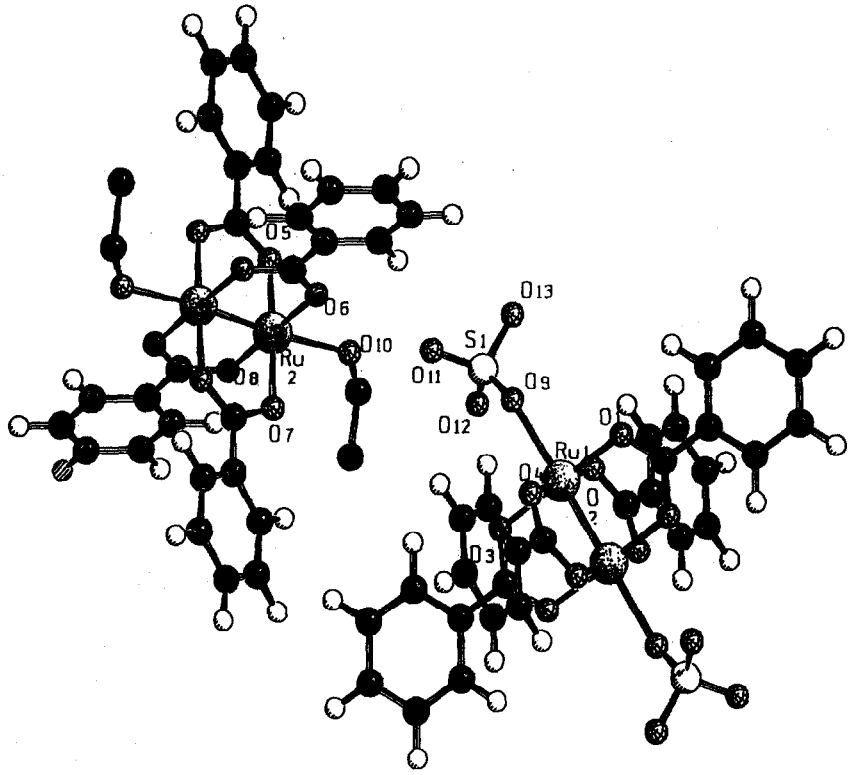

Fig. 1. The $[Ru_2(\mu\text{-}O_2CC_6H_5)_4(C_2H_5OH)_2]^+$ and $[Ru_2(\mu\text{-}O_2CC_6H_5)_4(HSO_4)_2]^-$ ions as they occur in **4**.

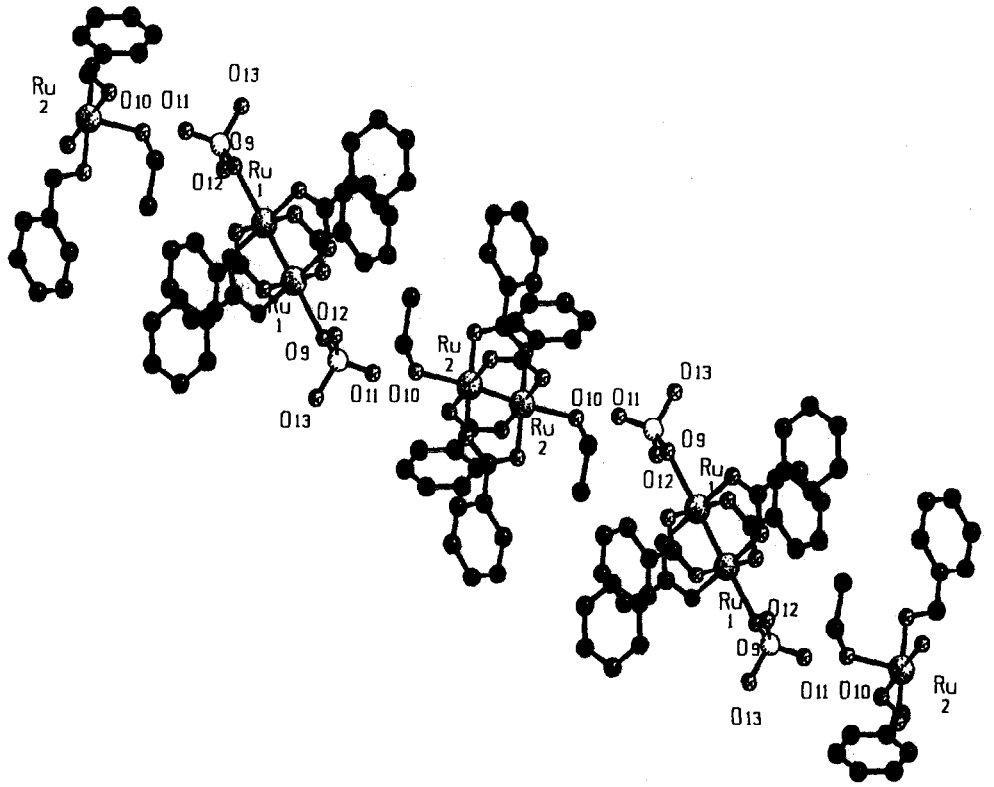

Fig. 2. Infinite chain structure of **4** in the solid state.

$(C_2H_5OH)_2]^+$ cations alternate with the $[Ru_2(\mu\text{-}O_2CC_6H_5)_4(HSO_4)_2]^-$ anions to form extended chains in the solid state. The Ru—Ru distances in the cation and anion (Table 1) are very similar [2.265(2) and 2.272(2) Å, respectively], that in the anion being very slightly longer. These metal–metal distances compare closely with the values found for other Ru_2^{5+} carboxylates[5,7,8] and in particular with the Ru—Ru distance of 2.277(1) Å in the benzoate $[Ru_2(\mu\text{-}O_2CC_6H_5)_4(O_2CC_6H_5)(HO_2CC_6H_5)]$.[9] The Ru—O (bridging benzoate) distances in **4** range from 2.00(1) to 2.014(9) Å in the cation and from 2.005(8) to 2.024(8) Å in the anion. Thus, there is no real distinction between the Ru—O(benzoate) bond lengths in the cation and the anion. The Ru—O(ethanol) bond length [2.234(9) Å] also compares closely with the Ru—O(water) distance [mean = 2.31(1) Å] found in $[Ru_2(\mu\text{-}O_2CCH_3)_4(H_2O)_2][BF_4]$.[5]

The short non-bonded distance (2.77 Å) between the ethanol oxygen O(10) and the hydrogensulphate oxygen O(11) indicates the presence of a hydrogen bond (incorporating the hydroxyl hydrogen of ethanol) between these two atoms. Thus, it appears that in the solid state the alternating anionic and cationic dimeric units are linked together by these hydrogen bonds into infinite linear arrays. This is a similar situation to that found in $[Ru_2(\mu\text{-}O_2CCH_3)_4(O_2CCH_3)_2H]$.[8,10]

The relatively low value obtained for the molar conductivity of **4** in ethanol [Λ_M (EtOH) = 52 S cm^2 mol^{-1}] suggests that the large complex anion and cation are dissociated from each other in solution, and that further dissociation of the hydrogen sulphate ligands from the complex anion $[Ru_2(\mu\text{-}O_2CC_6H_5)_4(HSO_4)_2]^-$ is minimal. This means that the anionic and cationic moieties of **4** retain their identities in solution, instead of the anion dissociating to become equivalent to the cation as follows:

$$[Ru_2(\mu\text{-}O_2CC_6H_5)_4(HSO_4)_2]^- + 2C_2H_5OH \rightarrow [Ru_2(\mu\text{-}O_2CC_6H_5)_4(C_2H_5OH)_2]^+ + 2HSO_4^-.$$

Electrochemistry

The cyclic voltammogram of $[Ru_2(\mu\text{-}O_2CCH_3)_4(H_2O)_2]_2(SO_4)$ (**1**) in aqueous Na_2SO_4 showed a single reversible wave for the Ru_5^{5+}/Ru_2^{4+} couple with $E_{1/2} = +189$ mV [vs Ag/AgCl]. The voltammogram of the tetraphenylborate salt $[Ru_2(\mu\text{-}O_2CCH_3)_4(H_2O)_2][BPh_4]$ (**2**) in methanolic $LiClO_4$ (Fig. 3) contained a reversible Ru_2^{5+}/Ru_2^{4+} couple with $E_{1/2} = +78$ mV, together with an irreversible oxidation wave ($Ea = +810$ mV) for the $[BPh_4]^-$ ion. The potential for the $[BPh_4]^-$ oxidation was close to that found for $Na[BPh_4]$ in methanol/$LiClO_4$. For a solution of the double

Table 1. Selected molecular dimensions for **4**

(a) Bond lengths (Å)

Ru(1)—O(1)	2.005(8)	Ru(1)—O(2)	2.024(8)
Ru(1)—O(3)	2.017(8)	Ru(1)—O(4)	2.107(8)
Ru(1)—O(9)	2.270(9)	Ru(1)—Ru(1)	2.272(2)
Ru(2)—O(5)	2.01(1)	Ru(2)—O(6)	2.014(9)
Ru(2)—O(7)	2.00(1)	Ru(2)—O(8)	2.012(9)
Ru(2)—O(10)	2.234(9)	Ru(2)—Ru(2)	2.265(2)
S(1)—O(9)	1.38(1)	S(1)—O(11)	1.39(1)
S(1)—O(12)	1.57(3)	S(1)—O(13)	1.43(3)
O(10)—O(11)	2.77		

(b) Bond angles (°)

O(2)—Ru(1)—O(1)	88.3(3)	O(3)—Ru(1)—O(1)	179.6(2)
O(3)—Ru(1)—O(2)	92.0(3)	O(4)—Ru(1)—O(1)	90.8(3)
O(4)—Ru(1)—O(2)	178.5(3)	O(4)—Ru(1)—O(3)	89.0(3)
O(9)—Ru(1)—O(1)	89.3(4)	O(9)—Ru(1)—O(2)	92.2(4)
O(9)—Ru(1)—O(3)	91.0(4)	O(9)—Ru(1)—O(4)	88.9(4)
O(6)—Ru(2)—O(5)	90.4(4)	O(7)—Ru(2)—O(5)	177.3(4)
O(7)—Ru(2)—O(6)	91.2(4)	O(8)—Ru(2)—O(5)	89.3(4)
O(8)—Ru(2)—O(6)	179.6(2)	O(8)—Ru(2)—O(7)	89.1(4)
O(10)—Ru(2)—O(5)	90.1(4)	O(10)—Ru(2)—O(6)	85.2(4)
O(10)—Ru(2)—O(7)	92.1(4)	O(10)—Ru(2)—O(8)	94.6(4)
O(11)—S(1)—O(9)	120.0(1)	O(12)—S(1)—O(9)	105.?(1)
O(12)—S(1)—O(11)	118.0(1)	O(13)—S(1)—O(9)	108.?(1)
O(13)—S(1)—O(11)	101.0(2)	O(13)—S(1)—O(12)	103.?(2)

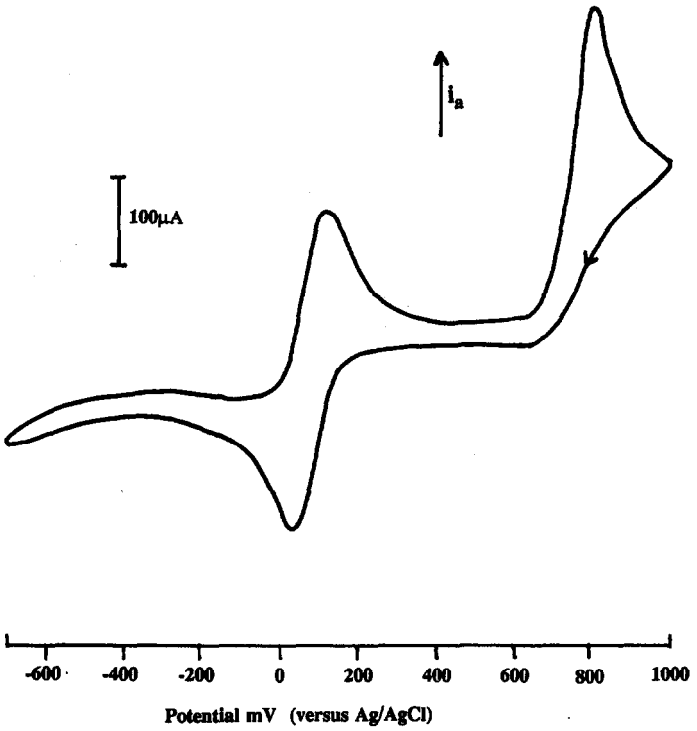

Fig. 3. Cyclic voltammogram of complex **2**.

complex salt $[Ru_2(\mu\text{-}O_2CC_6H_5)_4(C_2H_5OH)_2][Ru_2(\mu\text{-}O_2CC_6H_5)_4(HSO_4)_2]$ (**4**) in ethanol/tetrabutylammonium perchlorate (TBAP) only a single, quasi-reversible Ru_2^{5+}/Ru_2^{4+} couple was detected, with $E_{1/2} = +159$ mV. This is somewhat surprising since two separate Ru_2^{5+}/Ru_2^{4+} couples might have been expected, one for the $[Ru_2(\mu\text{-}O_2CC_6H_5)_4(C_2H_5OH)_2]^+$ ion and the other for the $[Ru_2(\mu\text{-}O_2CC_6H_5)_4(HSO_4)_2]^-$ ion, the latter couple occurring at the more negative potential. This indeed is what was found in the voltammogram of $[Ru_2(\mu\text{-}O_2CC_3H_7)_4Cl]$ when the experiment was run in a CH_2Cl_2/TBAP solvent/supporting electrolyte systems.[6] In that particular case separate quasi-reversible Ru_2^{5+}/Ru_2^{4+} couples were observed for the $[Ru_2(\mu\text{-}O_2CC_3H_7)_4]^+$ cation and the $[Ru_2(\mu\text{-}O_2CC_3H_7)_4Cl_n]^{(n-1)-}$ anion, the two ions originating from the equilibrium outlined in Scheme 2. One possible explanation for the presence of only a single Ru_2^{5+}/Ru_2^{4+} couple in the voltammogram of **4** is that there may be a surface effect operating at the platinum working electrode that causes the $[Ru_2(\mu\text{-}O_2CC_6H_5)_4(HSO_4)_2]^-$ ion to dissociate to give a second $[Ru_2(\mu\text{-}O_2CC_6H_5)_4(C_2H_5OH)_2]^+$ ion and two HSO_4^- ions.

EXPERIMENTAL

Literature methods were used to prepare $[Ru_2(\mu\text{-}O_2CCH_3)_4Cl]$[11] and $[Ru_2(\mu\text{-}O_2CC_6H_5)_4Cl]$.[12] $Ba(C_6H_5C{\equiv}CCO_2)_2 \cdot H_2O$ was prepared by reacting phenylpropynoic acid with barium carbonate (2:1 molar ratio) in a mixture of methanol and water. A satisfactory microanalysis was obtained for this compound. IR spectra for the solids (as KBr discs) were recorded in the 4000–200 cm^{-1}

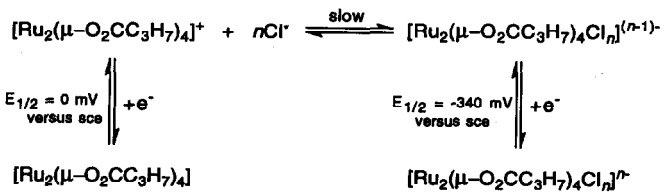

Scheme 2. See ref. 6.

region on a Perkin–Elmer 783 grating spectrometer and UV–vis spectra were run on a Milton Roy spectronic 3000 array. Room-temperature magnetic susceptibility measurements on the solids were made on a Johnson–Matthey magnetic susceptibility balance. Cyclic voltammograms were recorded (*ca* 20°C and under nitrogen) using an EG & G Model 264A polarographic analyser and the data were analysed using the EG & G Condecon software package. A platinum bead and a platinum wire were used as the working and counter electrodes, respectively, and potentials were recorded with respect to a silver–silver chloride (aqueous KCl) reference electrode. Sample concentrations were 8.0×10^{-3} M with respect to ruthenium and the scan rate was 50 mV s^{-1}. For complex **1** the solvent/supporting electrolyte was H_2O/Na_2SO_4 (0.1 M), against which the $[Fe(CN)_6]^{2+}/[Fe(CN)_6]^{3+}$ couple had $E_{1/2} = +329$ mV [vs Ag/AgCl]. For **2** the solvent/supporting electrolyte was $MeOH/LiClO_4$ (0.1 M), against which the ferrocene/ferrocenium(1+) couple (Fc/Fc^+) had $E_{1/2} = +497$ mV [vs Ag/AgCl]. For **3** the solvent/supporting electrolyte was EtOH/TBAP (0.1 M), against which the Fc/Fc^+ couple had $E_{1/2} = +529$ mV [vs Ag/AgCl]. Conductivity readings were taken with an AGB model 10 conductivity meter and elemental analyses were performed by the Microanalytical Laboratory, University College Cork, Ireland.

Crystallography

Crystal data for $[Ru_2(\mu\text{-}O_2CC_6H_5)_4(C_2H_5OH)_2][Ru_2(\mu\text{-}O_2CC_6H_5)_4(HSO_4)_2]$ (**4**). Formula: $C_{30}H_{27}O_{13}Ru_2S_1$, $M_r = 829.733$; triclinic, $P-1$ (no. 2), $a = 10.530(5)$, $b = 11.667(5)$, $c = 13.883(6)$ Å, $\alpha = 80.60(3)$, $\beta = 84.20(3)$, $\gamma = 87.82(3)°$, $U = 1673(1)$ Å^3, $D_c = 1.647$ g cm^{-3}, $Z = 2$, $F(000) = 830$, $\lambda = 0.71069$, $\mu(\text{Mo-}K_\alpha) = 9.73$ cm^{-1}.

A brown crystal was mounted on an Enraf–Nonius CAD4 diffractometer. Accurate cell dimensions were established by refining the setting angles of 25 reflections ($14° < \theta < 16°$). The intensities of 4327 reflections in the range $0° < \theta < 22°$ were measured using graphite monochromated Mo-K_α radiation. These were reduced to give 3759 unique reflections (merging R of 0.0118), of which 3265 had $|F_{obs}| > 4\sigma|F_{obs}|$ and were used in the structure solution and refinement.

The structure was solved by both the Patterson and direct methods of SHELXS and refined by full-matrix least-squares. There were two half molecules in the asymmetric unit, the central ruthenium portion being the same for both, but the coordinated terminal groups being different, one C_2H_5OH and the other HSO_4^-. The non-hydrogen atoms, with the exception of two of the oxygen atoms attached to the sulphur, were refined with anisotropic temperature factors. These two oxygens were found to have high temperature factors and along with the carbons in the ethyl group were thought to be slightly disordered. The hydrogen atoms were placed geometrically and refined with common temperature factors. Due to the short contact distance a hydrogen bond was inferred[8] to exist between the ethanolic hydrogen and one of the oxygens attached to the sulphur (the hydrogen itself could not be located because of the reasons outlined above). The refinement was weighted to give a flat analysis of variance with final $R = 0.0800$ and $R_w = 0.0937$. The final difference-Fourier had highest peaks of 1.9 e Å^{-1}, which were in the areas of disorder of the sulphur oxygens and the ethyl group. SHELXS-86 and SHELX-76 were used by kind permission of G. M. Sheldrick (Universität Göttingen).

$[Ru_2(\mu\text{-}O_2CCH_3)_4(H_2O)_2]_2(SO_4)$ (**1**)

$[Ru_2(\mu\text{-}O_2CCH_3)_4Cl]$ (0.48 g, 1.0 mmol) and silver(I) sulphate (0.16 g, 0.5 mmol) were stirred in water (20 cm^3) at *ca* 40°C for 10 min. The ruthenium complex rapidly dissolved to give a deep orange solution and a white precipitate of AgCl formed. The AgCl was filtered off and the aqueous solution was then evaporated under reduced pressure to give a brown tar. The tar was redissolved by adding methanol (10 cm^3) and ethyl acetate (40 cm^3) was then added. The solution was evaporated to low volume and more ethyl acetate (30 cm^3) was added. When this solution was concentrated to low volume the product precipitated as a yellow–brown solid. The solid was filtered off, washed with dry ethyl acetate (5 cm^3) and then dried *in vacuo*. The complex was slightly hygroscopic and was very soluble in water, methanol and ethanol, slightly soluble in acetone and was insoluble in THF, dichloromethane, ethyl acetate and diethyl ether; yield: 0.36 g (69%). Found: C, 18.7; H, 3.1; S, 2.7. Calc.: C, 18.4; H, 3.1; S, 3.1%. IR: 3440 (OH), 2940 (CH), 1400, 1395 (OCO), 1115 cm^{-1} (SO_4). λ_{max} (H_2O) = 426 nm ($\varepsilon = 1414$ dm^3 mol^{-1} cm^{-1}). $\mu = 4.1$ B.M. per Ru_2.

$[Ru_2(\mu\text{-}O_2CCH_3)_4(H_2O)_2][BPh_4]$ (**2**)

$[Ru_2(\mu\text{-}O_2CCH_3)_4Cl]$ (0.48 g, 1.0 mmol) and silver(I) sulphate (0.16 g, 0.5 mmol) were stirred in water (20 cm^3) at *ca* 40°C for 10 min. The AgCl was filtered off and the solution was chilled to 0°C. An aqueous solution of sodium tetraphenylborate (0.4 g, 1.2 mmol) was added dropwise with stirring

and the orange–brown product precipitated immediately. The solid was filtered off, washed with cold water (3×2 cm^3) and then dried *in vacuo* at 30°C. The complex was *very* soluble in acetone, THF, ethanol and cold methanol (decomposes in hot methanol), soluble in dichloromethane, ethyl acetate and diethyl ether and was slightly soluble in water; yield: 0.67 g (84%). Found: C, 48.3; H, 4.6. Calc.: C, 48.4; H, 4.6%; IR: 3440 (OH), 2930 (CH), 1440, 1395 (OCO), 740, 708 cm^{-1} (BPh_4). λ_{max} (MeOH) = 426 nm (ε = 726 dm^3 mol^{-1} cm^{-1}). μ = 3.9 B.M. per Ru_2.

$[Ru_2(\mu\text{-}O_2CCH_3)_4(O_2CC{\equiv}CC_6H_5)]\cdot H_2O$ (**3**)

Complex **1** (0.12 g, 0.25 mmol) and $Ba(C_6H_5C{\equiv}CCO_2)_2\cdot H_2O$ (0.056 g, 0.125 mmol) were stirred in methanol (20 cm^3) at 20°C for 0.5 h. The fine white precipitate of $BaSO_4$ was removed by centrifugation and the reddish-brown solution was evaporated to low volume under reduced pressure (not heated above 30°C). On addition of ethyl acetate and further evaporation under reduced pressure the product appeared as an orange–brown precipitate. The solid was washed with diethyl ether and dried *in vacuo*; yield: 0.10 g (66%). Found: C, 33.9; H, 3.0. Calc.: C, 33.9; H, 3.2%; IR: 3430 (OH), 2930 (CH), 2210 (C≡C), 1440, 1440 cm^{-1} (OCO). Note: the IR spectrum of $Ba(C_6H_5C{\equiv}CCO_2)_2\cdot H_2O$ had ν(C≡C) at 2210 cm^{-1} and in phenylpropyonic acid there were ν(C≡C) bands at 2200 and 2260 cm^{-1}.

$[Ru_2(\mu\text{-}O_2CC_6H_5)_4(C_2H_5OH)_2][Ru_2(\mu\text{-}O_2CC_6H_5)_4(HSO_4)_2]$ (**4**)

Method (*a*). A suspension of $[Ru_2(\mu\text{-}O_2CC_6H_5)_4Cl]$ (0.29 g, 0.4 mmol), silver(I) sulphate (0.063 g, 0.2 mmol) and H_2SO_4 (0.98 g of a 2% weight solution in ethanol, 0.2 mmol) in ethanol (40 cm^3) was refluxed for 2 h. During this time the ruthenium complex slowly dissolved to give a bright red–brown solution. The AgCl was then filtered off and the filtrate was concentrated *in vacuo* to *ca* 5 cm^3. After standing for several days the product formed as deep red crystals. Addition of ethyl acetate to the mother liquor gave a further crop of microcrystalline product; yield: 0.26 g (78%).

Method (*b*). Complex **1** (0.42 g, 0.4 mmol), benzoic acid (2.44 g, 20 mmol) and H_2SO_4 (0.98 g of a 2% weight solution in ethanol, 0.2 mmol) were dissolved in ethanol (20 cm^3) and the mixture was stirred for 72 h. n-Hexane (20 cm^3) was then added. The solution was filtered and sat aside in a sealed tube for several months, during which time deep-red single crystals of the product formed. Found: C, 43.3; H, 3.6; S, 3.4. Calc.: C, 43.4; H, 3.3; S, 3.9%. IR: 3380, 3220 (OH), 2980 (CH), 1465, 1400 (OCO), 1175 cm^{-1} (SO_4). λ_{max} (EtOH) = 437 nm (ε = 1310 dm^3 mol^{-1} cm^{-1}). μ = 3.8 B.M. per Ru_2.

Acknowledgement—We thank Johnson Matthey plc for the loan of ruthenium trichloride.

REFERENCES

1. For example: M. McCann, A. Carvill, P. Guinan, P. Higgins, J. Campbell, H. Ryan, M. Walsh, G. Ferguson and J. Gallagher, *Polyhedron* 1991, **10**, 2273; M. McCann and P. Guinan, *Polyhedron* 1991, **10**, 2283; J. G. Hamilton, K. J. Ivin, M. McCann and J. J. Rooney, *Makromol. Chem.* 1985, **186**, 1477.
2. T. A. Stephenson and G. Wilkinson, *J. Inorg. Nucl. Chem.* 1966, **28**, 2285.
3. M. Mukaida, T. Nomura and T. Ishimori, *Bull. Chem. Soc. Japan* 1972, **45**, 2143.
4. J. G. Norman Jr, G. E. Renzoni and D. A. Case, *J. Am. Chem. Soc.* 1979, **101**, 5256.
5. A. Bino, F. A. Cotton and T. R. Felthouse, *Inorg. Chem.* 1979, **18**, 2599.
6. F. A. Cotton and E. Pedersen, *Inorg. Chem.* 1975, **14**, 388.
7. M. J. Bennett, K. G. Caulton and F. A. Cotton, *Inorg. Chem.* 1969, **8**, 1.
8. F. A. Cotton, M. A. Matusz and B. Zhong, *Inorg. Chem.* 1988, **27**, 4368.
9. M. Spohn, J. Straehle and W. Hiller, *Z. Naturforsch.* (*B*) 1986, **41**, 541.
10. M. G. B. Drew, P. Higgins and M. McCann, *J. Chem. Soc., Chem. Commun.* 1987, 1385.
11. R. W. Mitchell, A. Spencer and G. Wilkinson, *J. Chem. Soc., Dalton Trans.* 1973, 846.
12. P. Higgins and M. McCann, *J. Chem. Soc., Dalton Trans.* 1988, 661.

Polyhedron Vol. 12, No. 10, pp. 1171–1177, 1993
Printed in Great Britain

0277-5387/93 $6.00+.00
© 1993 Pergamon Press Ltd

SYNTHESIS AND CHARACTERIZATION OF TRIAZENIDO AND AMIDINO COMPLEXES OF NICKEL AND PALLADIUM

MONTSERRAT GÓMEZ, GUILLERMO MULLER* and JOAQUIM SALES*

Departament de Química Inorgànica, Universitat de Barcelona,
Diagonal 647, 08028 Barcelona, Spain

(*Received* 4 *December* 1992; *accepted* 26 *January* 1993)

Abstract—The reaction of LiPhN(Y)NPh [Y = N or C(Ph)] with $[MX_2L_2]$ (M = Ni, Pd; X = Cl, Br, mesityl; L = PEt_3, **a**; PMe_2Ph, **b**; PPh_3, **c**; PBz_3, **d**) has been studied. With Y = N complexes containing the triazenido ligand as monodentate $[MX(NNN)L_2]$ (Ni: **1**; Pd: **2**), bidentate [MX(NNN)L] (Ni: **3**; Pd: **4**) and bridging two metal atoms $[M(\mu\text{-}NNN)L_2]_2(ClO_4)_2$ (Ni: **5**; Pd: **6**) have been prepared. However, when Y = C(Ph) only palladium derivatives having the bridging amidino group $[Pd(\mu\text{-}NCN)XL]_2$ (**7**) can be obtained. These complexes have been characterized by IR, ^1H and ^{31}P NMR spectroscopy.

The study of transition metal complexes containing triazenido $[RN{=}N{-}NR]^-$ and amidino $[RN{-}CR'{=}NR]^-$ ligands has increased greatly in the past few years, because of their potential reactivity in relation to their several modes of coordination.[1] As these ligands are isoelectronic with allyl and carboxylato anions, their complexes can be very active catalytic species. Moreover, the nitrogen ligands are more versatile, since the ligating properties are influenced by both the electronic and steric properties of the substituents R and R'.

These anionic ligands (NNN and NCN) may act as a monodentate group [I], a bidentate ligand [II] or a bridging ligand between two metal centres [III], and examples of the three types have been reported[1] (see Fig. 1).

Several complexes, mainly of nickel, palladium and platinum, with monodentate bonded triazenido ligands have been reported.[2] However, no complex derivative of the monodentate amidino group has been prepared so far, although some formamidine complexes are known.[2a,b,f,g] Several years ago[3] it was proposed that 1,3-diphenyltriazenido complexes of nickel contained bidentate triazenido ligands, but subsequent structural studies confirmed that the ligand actually bridges the metal centres.[4] Some complexes containing bridging amidino groups are known.[5] The chelating bonding mode is less common for these ligands than the bridging mode. One factor may be the steric bulk of the ligand, but another is clearly the strain involved in the formation of a four-membered ring, which is clear from the acute NYN angle of *ca* 102–105°. Some structurally characterized complexes with chelating triazenido ligands of several transition metals[5a,6] have been reported, but, to the best of our knowledge no derivative of nickel, palladium or platinum has been obtained. As for amidino derivatives, complexes of these metals are known.[7] Recently, triazenido complexes of indium (chelate ones) and rhodium (bridging ones) have been reported.[8]

We describe here the preparation and structural characterization of a series of nickel and palladium complexes containing 1,3-diphenyltriazenido or 1,3-diphenylbenzamidino ligands. These ligands

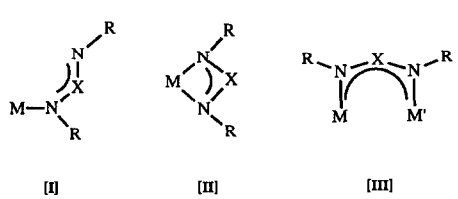

(X = CR, N; R = aril, alquil)

Fig. 1.

* Authors to whom correspondence should be addressed.

adopt the three modes of coordination indicated. The catalytic activity of these complexes has also been tested in the oligomerization of ethylene, but in no case have satisfactory results been obtained.

RESULTS AND DISCUSSION

The general method used in the preparation of the new complexes is the reaction of the lithium salts LiNYN (NYN = PhNNNPh or PhNC(Ph)NPh], which were prepared *in situ* from the neutral ligand, with metallic complexes. Depending on the experimental conditions and the metallic complex used, compounds containing the triazenido ligand in the different modes of coordination are obtained (see Scheme 1).

With $[NiX_2L_2]$ (X = Cl, Br) compounds of type [I], containing the monodentate ligand [NiX(NNN)L_2] (**1a**, X = Br, L = PEt_3; **1b**, X = Cl, L = PMe_2Ph), are obtained, but when L = PPh_3 only decomposition is observed. With the organonickel complex [NiX(mesityl)L_2] the compound with the monodentate triazenido [Ni(mesityl)(NNN)$(PMe_2Ph)_2$] (**1'b**) and the complexes with the bidentate ligand [Ni(mesityl)(NNN)L], when L = PPh_3 or PBz_3 (**3c,d**), are obtained. With the bulkier phosphines the M—P bond is weaker and the easy decoordination of the phosphine ligand favours the action of the triazenido ligand as a chelate.

The palladium derivatives of type [I] [PdCl(NNN)L_2] (**2a,b**) and [Pd(mesityl)(NNN)$(PPh_3)_2$] (**2c**) are easily obtained from $[PdCl_2L_2]$ and [PdBr(mesityl)$(PPh_3)_2$], respectively. It should be noted, that the addition of LiNNN, at 10°C, to *trans*-$[PdCl_2(PEt_3)_2]$ gives *cis*-[PdCl(NNN)$(PEt_3)_2$] (*cis*-**2a**); when the solution is heated to 40°C the more stable *trans*-[PdCl(NNN)$(PEt_3)_2$] (*trans*-**2a**) is formed. This *trans*-isomer can be obtained directly by reaction of the neutral ligand and the metallic complex, at 50°C, in the presence of a base such as NaOH.

The bidentate [II] complex of palladium, [Pd(mesityl)(NNN)(PPh_3)] (**4c**), has been obtained from the dinuclear compound [Pd(μ-Cl)(mesityl)$(PPh_3)]_2$ by reaction with the neutral ligand (HNNN) and subsequent addition of DBU [1,8-diazabicyclo[5.4.0]undec-7-en(1,5-5)]. Initially the HNNN ligand breaks the chlorine-bridge, giving [PdCl(mesityl)(HNNN)(PPh_3)]. The subsequent addition of DBU deprotonates the ligand and as it is very bulky, does not prevent the coordination of the second nitrogen atom and the triazenido ligand can act as a chelate ligand. The complex **4c** can also be obtained by abstraction of one PPh_3 ligand by silver salts from **2c**. Therefore, it is possible to prepare complexes of type [I] or [II] with the same phosphine ligand.

Complexes of type [III], M = Ni (**5a**) or Pd (**6a**), are obtained by reaction of $[MX(NNN)(PEt_3)_2]$ with silver salts.

With the 1,3-diphenylbenzamidino ligand different results have been obtained and only complexes of palladium of type [III] (**7**), with the ligand as a bridge, have been isolated (see Scheme 2). These compounds, [Pd(μ-NCN)ClL]$_2$ (**7b,c**; L = PMe_2

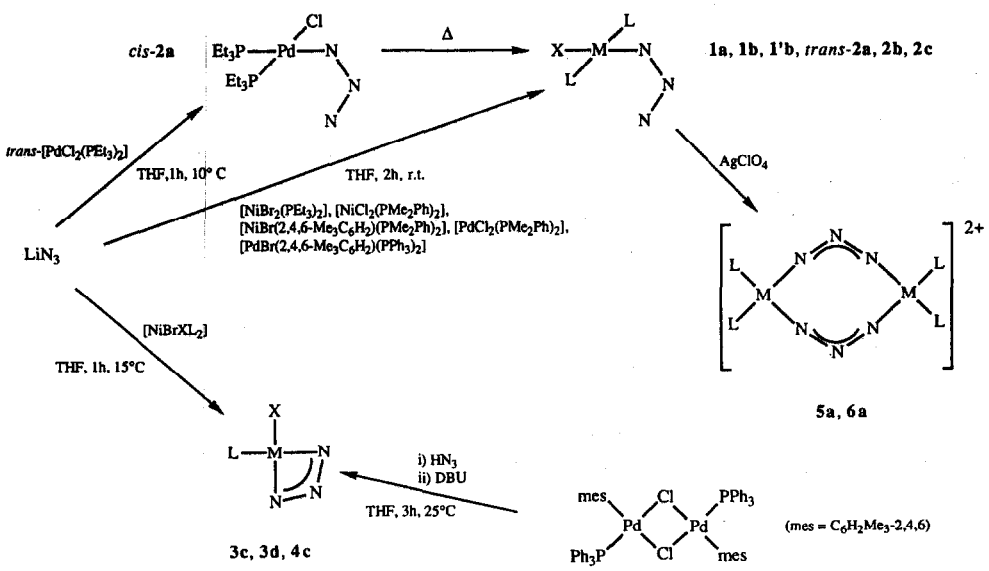

Scheme 1.

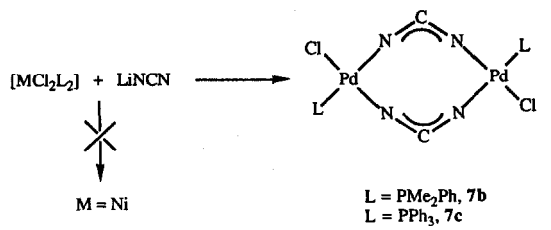

Scheme 2.

Ph, PPh_3), are prepared by the general method from $[PdCl_2L_2]$ and LiNCN. Their insolubility suggests that they are not mononuclear species. The EM–FAB studies show that they are dimeric complexes and that the amidino ligand acts as a bridge between the two palladium atoms. Table 1 shows the fragments detected for the compound **7b**.

The reaction of LiNCN with the nickel complexes $[NiX_2L_2]$, [NiX(mesityl)L_2] or [Ni(mesityl)L_2]$^+$ does not give any isolable complex. The addition of the neutral ligand PhNC(Ph)NPh(H) on nickel(0) complexes, such as $[Ni(cod)_2]$, does not give any complex either. Probably, the amidino group is not able to replace the cod ligand.

It has been reported[9] that complexes of type [I] insert CO, CN^-, etc. giving five-membered metallocycles. However, in our case the action of CO in a solution (at room temperature and 1 atm.) on $[NiCl(NNN)(PMe_2Ph)_2]$ produces only the substitution of one molecule of phosphine, as can be observed by ^{31}P NMR spectroscopy. After concentration of the solution the starting nickel complex was recovered.

Table 1. Mass fragments (FAB) obtained for $[Pd(\mu\text{-NCN})Cl(PMe_2Ph)]_2$ (**7b**)

Ion	*m/z*
$[Pd_2(NCN)_2Cl(PMe_2Ph)_2]^+$	1067
$[Pd_2(NCN)_2(PMe_2Ph)_2]^+$	1030
$[Pd_2(NCN)_2Cl(PMe_2Ph)]^+$	930
$[Pd_2(NCN)(Cl)_2(PMe_2Ph)_2]^+$	831
$[Pd_2(NCN)_2Cl]^+$	795
$[Pd(NCN)(PMe_2Ph)]^+$	788
$[Pd_2(NCN)_2]^+$	757
$[Pd(NCN)_2]^+$	650
$[Pd_2(NCN)(PMe_2Ph)]^+$	623
$[Pd(NCN)Cl(PMe_2Ph)]^+$	552
$[Pd(NCN)(PMe_2Ph)]^+$	516
$[Pd_2(NCN)]^+$	485
$PhNCPh^+$	182
PMe_2Ph^+	138
Pd^+	106

The catalytic activities of the monodentate and bidentate complexes have been tested in the oligomerization of ethylene at 40 bar and 95°C in toluene. The organometallic compounds containing the mesityl group (**1'b**, **2c**, **3c**, **3d** and **4c**) were used solely as precursors, because the insertion of ethylene and subsequent β-elimination produces the hydrido complex that is the catalytic active species. With the other complexes $AlEt_3$ was added ($M/AlEt_3$: 1/2) in order to promote the formation of the hydrido complex, but oligomers were not detected in any case.

These results and those obtained from the analogous nickel and palladium compounds of bis(diphenylphosphino)methanide ($Ph_2PCHPPh_2$ = PCP) and bis(diphenylphosphino)amide (Ph_2PNPPh_2 = PNP) ligands[10] show that the formation of four-membered metallocycle complexes of type [II] depends on the lability of the M–phosphine bond. The nickel compounds and/or the largest phosphines make it easier for the ligand to act as a chelate. On the other hand, the ligands containing one central carbon atom (PCP and NCN) do not stabilize the nickel derivatives, although these derivatives can be obtained when the central atom is nitrogen (PNP and NNN).

Characterization

The new compounds obtained are air-stable solids, but in solution they decompose slowly, even under nitrogen.

Table 2 shows the ^1H and ^{31}P NMR data and Table 3 shows the most significant IR bands. The main stretching bands arising from the triazenido ligand have been classified into three groups. Bands at *ca* 1300–1260 and 1600–1580 cm^{-1} are indicative of the ligand acting as a chelate;[3a,3b,11] in compounds **3** and **4** a very strong band at 1250–1260 cm^{-1} is observed. In compounds **5** and **6** the strong band at 1350–1375 cm^{-1} indicates that the ligand acts as a bridge between the two metal atoms.[12] When the ligand acts as a monodentate ligand the number and intensity of the bands increase. The most significant absorptions are observed at 1190–1210, 1250–1280, 1300–1350 and 1580–1600 cm^{-1}. In contrast, the bands due to the amidino ligands (**7b, c**) do not allow unambiguous deduction of the mode of coordination of the ligand. By comparison with the IR spectrum of *trans*-$[PtCl(NCN)(PPh_3)_2]$ [1370(vs), 1470(vs), 1520(vs) and 1620(s) cm^{-1}] the monodentate coordination can be ruled out. Data obtained from other benzamidino complexes[8] suggest a bidentate form of bonding, but it is not possible to differentiate between chelating and bridging modes. As indicated above the mass spectra con-

Table 2. ^1H and $^{31}P\{^1H\}$ NMR data for 1,3-diphenyltriazenido derivatives

Complexes	$\delta(^{31}P)^a$	$\delta(^1H)^b$
[NiBr(NNN)(PEt_3)$_2$] (**1a**)	2.8[c]	1.1(q); 1.4(m)[d]
[Ni(mesityl)(NNN)(PMe_2Ph)$_2$] (**1b'**)	−9.7	2.2(*p*); 2.5(*o*); 6.4(arom.)[e] 1.1(m)[f]
[NiCl(NNN)(PMe_2Ph)$_2$] (**1b**)	−13.4[c]	1.4(s)[f]
[Ni(mesityl)(NNN)(PPh_3)] (**3c**)	25.4	2.9(*p*); 2.1(*o*); 6.1(arom.)[e]
[Ni(mesityl)(NNN)(PBz_3)] (**3d**)	11.0	—[g]
[Ni(μ-NNN)(PEt_3)$_2$]$_2$(ClO_4)$_2$ (**5a**)	5.0	0.9(q); 1.6(m)
Cis-[PdCl(NNN)(PEt_3)$_2$] (*cis*-**2a**)	26.7(d); 22.0(d)[b] ^2J(P—P) = 19.7 Hz	0.9(q); 1.2(m)[d]
Trans-[PdCl(NNN)(PEt_3)$_2$] (*trans*-**2a**)	18.7[h]	1.1(q); 1.6(m)[d]
[PdCl(NNN)(PMe_2Ph)$_2$] (**2b**)	−1.0	—[g]
[Pd(mesityl)(NNN)(PPh_3)$_2$] (**2c**)	23.0	2.1(*p*); 2.3(*o*); 6.4(arom.)[e]
[Pd(mesityl(NNN)(PPh_3)] (**4c**)	27.1	2.1(*p*); 2.4(*o*); 6.3(arom.)[e]
[Pd(μ-NNN)(PEt_3)$_2$]$_2$(ClO_4)$_2$ (**6a**)	15.0	1.0(q); 1.6(m)

[a] δ in ppm; solvent: THF; NMR temperature: 308 K.
[b] δ in ppm; solvent: $CHCl_3$; NMR temperature: 308 K.
[c] NMR temperature: 220 K.
[d] δ for the protons of CH_3 and CH_2 of PEt_3.
[e] δ for the protons of mesityl: *o* = ortho; *p* = para; arom. = aromatics; all these signals are singlets.
[f] δ for the protons of methyl of phosphine.
[g] Non-defined signals.
[h] Solvent: CH_2Cl_2.

firmed that the ligand bridges the two palladium atoms.

EXPERIMENTAL

IR spectra were recorded as KBr pellets on a Perkin–Elmer 1330 spectrophotometer over the range 4000–200 cm^{-1}. $^{31}P\{^1H\}$ NMR spectra were recorded on a Bruker FT-80 SY spectrophotometer at 32.4 MHz with 85% H_3PO_4 as an external standard. ^1H spectra were recorded on a Varian XL-200 or a Varian XL-500 instrument with $SiMe_4$ as an internal standard. Positive chemical shifts indicate shifts to lower fields relative to the standard. Chemical analyses (carbon, hydrogen and nitrogen) were performed at the Institut de Química Biorgànica de Barcelona (C.S.I.C.). FAB (fast atom bombardment) mass spectra were obtained with a HP CG/Ms 5988A instrument.

Materials and syntheses

N,N'-diphenylbenzamidine[13] and diazoaminobenzene[14] were prepared by published methods. The following complexes were prepared by the methods reported: [MX_2L_2] (M = Ni; X = Cl, Br; L = PEt_3, PMe_2Ph, PPh_3, PBz_3;[15] M = Pd; X = Cl; L = PEt_3, PMe_2Ph, PPh_3[16]) and [$MXR(PPh_3)_2$] (M = Ni, R = mesityl;[17] M = Pd, R = mesityl[18]). All new compounds were prepared in a dry nitrogen atmosphere using conventional Schlenk techniques. The solvents used were dried and freshly distilled under nitrogen. Lithiotriazenido, Li^+NNN^-,[11] and lithiobenzamido, Li^+NCN^-,[19] were prepared by reaction of the nitrogenated ligand with Bu^nLi in THF at −15°C for 1 h. These solutions were used immediately after preparation.

Preparation of [MX(NNN)L_2] (M = Ni, Pd; X = Cl, Br, mesityl; L = PEt_3, PMe_2Ph, PPh_3) (**1a,b**; **1'b**; **2a, b, c**)

Li^+NNN^- (1 mmol, 0.20 g of diazoaminobenzene in 10 cm^3 of THF was treated with 0.63 cm^3 of Bu^nLi—*ca* 1.6 M—at −15°C for 1 h) was added to [MX_2L_2] (1 mmol; 0.45 g for [$NiBr_2$(PEt_3)$_2$]; 0.40 g for [$NiCl_2$(PMe_2Ph)$_2$]; 0.53 g for [NiBr(mesityl)(PMe_2Ph)$_2$]; 0.41 g for [$PdCl_2$(PEt_3)$_2$]; 0.45 g for [$PdCl_2$(PMe_2Ph)$_2$]; 0.85 g for [PdBr(mesityl)(PPh_3)$_2$]) in THF (25 cm^3) at −25°C. The mixture was slowly warmed and after 1 h at room temperature (for [PdBr(mesityl)(PPh_3)$_2$] 2 h at room temperature) the orange solid was filtered off and recrystallized from CH_2Cl_2/hexane. Yields: 0.25 g (55%) for [NiBr(NNN)

Table 3. IR absorption data for the 1,3-diphenyltriazenido complexes

Complexes	ν (cm^{-1})[a]
[NiBr(NNN)(PEt_3)$_2$] (**1a**)	1195 s; 1275 s; 1210 w; 1350 s; 1580 m
[NiCl(NNN)(PMe_2Ph)$_2$] (**1b**)	1200 m; 1260 vs; 1300 s; 1350 m; 1470 m; 1580 m
[Ni(mesityl)(NNN)(PMe_2Ph)$_2$] (**1'b**)	1200 m; 1260 s; 1300 s; 1350 m; 1580 m
[Ni(mesityl)(NNN)(PPh_3)] (**3c**)	1260 vs; 1590 m
[Ni(mesityl)(NNN)(PBz_3)] (**3d**)	1250 vs; 1590 m
[Ni(μ-NNN)(PEt_3)$_2$]$_2$(ClO_4)$_2$ (**5a**)	1205 vw; 1360 vs; 1590 w
[PdCl(NNN)(PEt_3)$_2$] (**2a**)	1190 s; 1280 s; 1290 s; 1360 vs; 1590 m
[PdCl(NNN)(PMe_2Ph)$_2$] (**2b**)	1200 s; 1280 vs; 1300 s; 1370 s; 1590 m
[Pd(mesityl)(NNN)(PPh_3)$_2$] (**2c**)	1180 s; 1280 vs; 1290 s; 1360 s; 1580 m
[Pd(mesityl)(NNN)(PPh_3)] (**4c**)	1265 vs; 1590 m
[Pd(μ-NNN)(PEt_3)$_2$]$_2$(ClO_4)$_2$ (**6a**)	1205 m; 1350 vs; 1590 w

[a] Intensity absorptions: vs = very strong; s = strong; m = medium; w = weak; vw = very weak.

(PEt_3)$_2$] (**1a**); 0.22 g (55%) for [NiCl(NNN)(PMe_2Ph)$_2$] (**1b**); 0.32 g (50%) for [Ni(mesityl)(NNN)(PMe_2Ph)$_2$] (**1'b**); 0.25 g (60%) for [PdCl(NNN)(PEt_3)$_2$] (**2a**); 0.37 g (60%) for [PdCl(NNN)(PMe_2Ph)$_2$] (**2b**); 0.55 g (65%) for [Pd(mesityl)(NNN)(PPh_3)$_2$] (**2c**). Found: C, 50.1; H, 7.0; N, 7.2. Calc. for $C_{24}H_{40}BrN_3P_2Ni$ (**1a**): C, 50.5; H, 7.1; N, 7.4%. Found: C, 59.3; H, 5.7; N, 7.4. Calc. for $C_{28}H_{32}ClN_3P_2Ni$ (**1b**): C, 59.4; H, 5.7; N, 7.4% Found: C, 68.5; H, 6.7; N, 6.2. Calc. for $C_{37}H_{43}N_3P_2Ni$ (**1'b**): C, 68.3; H, 6.7; N, 6.5. Found: C, 50.1; H, 7.0; N, 7.3. Calc. for $C_{24}H_{40}ClN_3P_2Pd$ (**2a**): C, 50.2; H, 7.0; N, 7.3%. Found: C, 54.6; H, 5.1; N, 6.8. Calc. for $C_{28}H_{32}ClN_3P_2Pd$ (**2b**): C, 54.7; H, 5.3; N, 6.8%. Found: C, 72.1; H, 5.3; N, 4.6. Calc. for $C_{57}H_{51}N_3P_2Pd$ (**2c**): C, 72.3; H, 5.4; N, 4.4%. M.p.s (decomposition): 130, 163, 95, 142, 110 and 95°C, respectively.

Preparation of [M(mesityl)(NNN)L] (M = Ni, Pd)

[Ni(mesityl)(NNN)L] (**3c, d**). Li^+NNN^- (1 mmol) was added to [NiBr(mesityl)L_2] (1 mmol; 0.74 g for [NiBr(mesityl)(PPh_3)$_2$]; 0.86 g for [NiBr(mesityl)(PBz_3)$_2$]) in THF (20 cm^3) at −25°C. The mixture was warmed to −5°C for 1 h and the solvent then removed under reduced pressure. After adding hexane (20 cm^3) an orange solid was obtained, which was recrystallized from toluene/hexane. Yields: 0.41 g (55%) for [Ni(mesityl)(NNN)(PPh_3)] (**3c**); 0.31 g (45%) for [Ni(mesityl)(NNN)(PBz_3)] (**3d**). Found: C, 73.8; H, 5.9; N, 6.3. Calc. for $C_{39}H_{36}N_3PNi$ (**3c**): C, 73.6; H, 5.7; N, 6.6%. Found: C, 74.1; H, 6.1; N, 6.0. Calc. for $C_{42}H_{42}N_3PNi$ (**3d**): C, 74.4; H, 6.2; N, 6.2%. M.p.s (decomposition): 135 and 100°C, respectively.

[Pd(mesityl)(NNN)(PPh_3)] (**4c**).

From [Pd(μ-Cl)(mesityl)(PPh_3)]$_2$. [Pd(μ-Cl)(mesityl)(PPh_3)]$_2$ (1.05 g, 1 mmol) and diazoaminobenzene (0.40 g, 2 mmol) in THF (30 cm^3) were warmed to 50°C for 2 h. The mixture was cooled to room temperature and DBU (0.3 cm^3) (*ca* d = 1.022) was added. The solution was warmed to 50°C for 2 h. The solvent was removed at room temperature under reduced pressure and an orange solid was obtained after the addition of ethanol (20 cm^3). This was filtered off and recrystallized from THF/ethanol. Yield: 0.53 g (50%) (**4c**). Found: C, 68.4; H, 5.3; N, 6.0. Calc. for $C_{39}H_{36}N_3PPd$ (**4c**): C, 68.5; H, 5.3; N, 6.1%. M.p. (decomposition): 105°C.

From [Pd(mesityl)(NNN)(PPh_3)$_2$]. [Pd(mesityl)(NNN)(PPh_3)$_2$] (0.95 g, 1 mmol) in toluene (20 cm^3) was treated with $AgClO_4 \cdot H_2O$ (0.21 g, 1 mmol) at room temperature for 45 min. The mixture was filtered off and the solvent was removed under reduced pressure. The yellow solid obtained (**4c**)

was recrystallized from toluene/hexane. Yield: 0.67 g (70%).

Preparation of $[M(\mu\text{-NNN})(PEt_3)_2]_2(ClO_4)_2$ (M = Ni, Pd) (**5a**, **6a**)

$[MX(NNN)(PEt_3)_2]$ (1 mmol; 0.52 g for $[NiBr(NNN)(PEt_3)_2]$; 0.57 g for $[PdCl(NNN)(PEt_3)_2]$) in THF (40 cm^3) was treated with $AgClO_4 \cdot H_2O$ (0.21 g, 1 mmol) at 0°C for 30 min. The mixture was warmed at room temperature for 30 min more and the solution was then filtered off with celite in order to separate the AgCl formed. The solvent was removed under reduced pressure and the residue was treated with toluene (20 cm^3), giving a yellow precipitate after cooling. Yield: 0.21 g (40%) for (**5a**); 0.31 g (55%) for (**6a**). Found: C, 48.2; H, 6.5; N, 6.9. Calc. for $C_{36}H_{25}ClN_3OPNi$ (**5a**): C, 48.8; H, 6.8; N, 7.1%. Found: C, 45.0; H, 3.8; N, 6.1. Calc. for $C_{36}H_{25}ClN_3OPPd$ (**6a**): C, 45.2; H, 3.9; N, 6.5%. M.p.s (decomposition): 120 and 155°C, respectively.

Preparation of $[Pd(\mu\text{-NCN})ClL]_2$ (L = PMe_2Ph, PPh_3; **7b**, **7c**)

Li^+NCN^- (1 mmol, 0.27 g of N,N′-diphenylbenzamidine in 10 cm^3 of THF was treated with 0.63 cm^3 of Bu^nLi—*ca* 1.6 M—at −15°C for 1.5 h) was added to $[PdCl_2L_2]$ (1 mmol, 0.45 g for L = PMe_2Ph; 0.70 g for L = PPh_3) in THF (25 cm^3) at −30°C. The mixture was warmed to room temperature for 16 h. The solvent was removed under reduced pressure and a red oil was formed, which when treated with hexane gave a very insoluble red solid. The solid was filtered off and washed with THF and ether. Yields: 0.38 g (70%) for $[Pd(\mu\text{-NCN})Cl(PMe_2Ph)]_2$ (**7b**); 0.51 g (75%) for $[Pd(\mu\text{-NCN})Cl(PPh_3)]_2$ (**7c**). Found: C, 59.0; H, 4.9; N, 4.9. Calc. for $C_{54}H_{52}Cl_2N_4P_2Pd_2$ (**7b**): C, 58.8; H, 4.8; N, 5.0%. Found: C, 66.0; H, 4.6; N, 3.9. Calc. for $C_{74}H_{60}Cl_2N_4P_2Pd_2$ (**7c**): C, 68.5; H, 4.5; N, 4.1%. M.p.s (decomposition): 120 and 130°C, respectively.

Preparation of trans-$[PtCl(NCN)(PPh_3)_2]$

N,N′-Diphenylbenzamidine (0.27 g, 1 mmol) in THF (10 cm^3) was treated with Bu^nLi (0.63 cm^3) (*ca* 1.6 M) at −15°C for 1.5 h. To this solution was added *cis*-$PtCl_2(PPh_3)_2$ (0.79 g, 1 mmol) in THF (25 cm^3) at −25°C. The mixture was warmed to room temperature for 2 h. The solvent was removed under reduced pressure. The yellow solid obtained was recrystallized from toluene/hexane. Yield: 0.60 g (58%). Found: C, 64.1; H, 4.2; N, 2.5. Calc. for $C_{55}H_{45}ClN_2P_2Pd$: C, 64.3; H, 4.4; N, 2.7%. M.p. (decomposition): 105°C. $^{31}P\{^1H\}$ NMR: δ = 10.8 ppm; $^1J(^{31}P—^{195}Pt)$ = 1733 Hz.

Acknowledgements—We thank the Dirección General de Investigación Científica y Técnica (Grant PB88-0186) for financial support and to Johnson and Matthey Inc. for a loan of palladium chloride.

REFERENCES

1. K. Vrieze and G. Van Koten, *Comprehensive Coordination Chemistry* (Edited by G. Wilkinson), Vol. 2, pp. 189–244. Pergamon Press, Oxford (1987).
2. (a) S. D. Robinson and M. F. Uttley, *J. Chem. Soc., Chem. Commun.* 1971, 315; (b) K. R. Laing, S. D. Robinson and M. F. Uttley, *J. Chem. Soc., Dalton Trans.* 1974, 1205; (c) C. M. Harris, B. F. Hoskins and R. L. Martin, *J. Chem. Soc.* 1959, 3728; (d) G. Bombieri, A. Immirzi and L. Toniolo, *Inorg. Chem.* 1976, **15**, 2428; (e) G. Bombieri, A. Immirzi and L. Toniolo, *Trans. Met. Chem.* 1976, **1**, 130; (f) D. M. Grove, G. van Koten, H. J. C. Ubbels and K. Vrieze, *J. Chem. Soc., Dalton Trans.* 1986, 717; (g) L. Toniolo, A. Immirzi, U. Croato and G. Bombieri, *Inorg. Chim. Acta* 1976, **19**, 209.
3. (a) F. P. Dwyer, *J. Am. Chem. Soc.* 1941, **63**, 78; (b) F. P. Dwyer and D. P. Mellor, *J. Am. Chem. Soc.* 1941, **63**, 81.
4. M. Corbett, B. F. Hoskins, N. J. McLeod and B. P. O'Day, *Aust. J. Chem.* 1975, **28**, 2377.
5. (a) T. Inglis, M. Kilner, T. Reynoldson and E. E. Robertson, *J. Chem. Soc., Dalton Trans.* 1975, 930; (b) F. J. Lahoz, A. Tiripicchio, M. Tiripicchio, L. A. Oro and M. T. Pinillos, *J. Chem. Soc., Dalton Trans.* 1985, 1487.
6. (a) M. Corbett and B. F. Hoskins, *J. Am. Chem. Soc.* 1967, **89**, 1530; (b) D. Brown and J. A. Ibers, *Inorg. Chem.* 1976, **15**, 2788; (c) R. Rossi, A. Duatti, L. Magon, U. Cassellato, R. Graziani and L. Toniolo, *J. Chem. Soc., Dalton Trans.* 1982, 1949.
7. (a) J. Barker, N. Cameron, M. Kilner, M. M. Mahoud and S. C. Wallwork, *J. Chem. Soc., Dalton Trans.* 1986, 1359; (b) J. Barker, M. Kilner and R. O. Gould, *J. Chem. Soc., Dalton Trans.* 1987, 2687.
8. (a) J. T. Leman, H. A. Roman and A. R. Barron, *J. Chem. Soc., Dalton Trans.* 1992, 2183; (b) N. G. Connelly, T. Einig, G. Garcia Herbosa, P. M. Hopkins, C. Meali, A. G. Orpen and G. M. Rosair, *J. Chem. Soc., Chem. Commun.* 1992, 143.
9. (a) E. Pfeiffer, A. Oskan and K. Vrieze, *Trans. Met. Chem.* 1977, **2**, 240; (b) R. Rossi, A. Duatti, L. Margon and L. Toniolo, *Inorg. Chim. Acta* 1981, **48**, 243.
10. M. Gómez, G. Muller, J. Sales and X. Solans, *J. Chem. Soc., Dalton Trans.* 1993, 221.
11. W. H. Knoth, *Inorg. Chem.* 1973, **12**, 38.
12. (a) E. Pfeiffer, J. Kuyper and K. Vrieze, *J. Organomet. Chem.* 1976, **105**, 371; (b) J. Kuyper, P. I. van

Vliet and K. Vrieze, *J. Organomet. Chem.* 1976, **105**, 379; (c) J. Kuyper, P. I. van Vliet and K. Vrieze, *J. Organomet. Chem.* 1975, **96**, 289.
13. A. C. Hontz and E. C. Wagner, *Org. Synth.* 1951, **31**, 48.
14. W. W. Hartman and J. B. Dickey, *Org. Synth., Coll.* 1943, 163.
15. E. C. Aleya and D. W. Meek, *J. Am. Chem. Soc.* 1969, **91**, 5761.
16. (a) D. A. Redfield, L. W. Cary and J. H. Nelson, *Inorg. Chem.* 1975, **14**, 50; (b) A. J. Carty, P. C. C. Chieh, N. J. Taylor and Y. S. Wong, *J. Chem. Soc., Dalton Trans.* 1976, 572.
17. J. Chatt and B. L. Shaw, *J. Chem. Soc.* 1960, 1718.
18. P. Fitton, *J. Chem. Soc., Chem. Commun.* 1968, 6.
19. L. Toniolo, G. Deganello, P. L. Sandrini and G. Bombieri, *Inorg. Chim. Acta* 1975, **15**, 11.

Polyhedron Vol. 12, No. 10, pp. 1179–1185, 1993
Printed in Great Britain

0277–5387/93 $6.00+.00
© 1993 Pergamon Press Ltd

THE CRYSTAL AND MOLECULAR STRUCTURES OF A TETRAAZAANNULENE AND ITS COBALT(II) COMPLEX AND THE PREPARATION OF THE CHROMIUM(II) COMPLEX

JAYNE JUBB, LESLIE F. LARKWORTHY,* DAVID C. POVEY and GALLIENUS W. SMITH

Department of Chemistry, University of Surrey, Guildford GU2 5XH, U.K.

(*Received* 4 *November* 1992; *accepted* 26 *January* 1993)

Abstract—The structures of the diphenyl-substituted tetraazaannulene dptaaH_2 (**1**) and its cobalt(II) complex Co(dptaa) (**2**) have been determined by X-ray diffraction. The cobalt(II) complex is low spin (μ_{eff} = 2.5 B.M. at 291 K) and except for the two phenyl groups, which are rotated by 30.0° and 38.1° with respect to the CoN_4 plane, the molecule shows less deviation from planarity than the ligand. The chromium(II) complex is low spin (μ_{eff} = 2.85 at 292 K and 2.72 B.M. at 87 K) and could not be obtained as a crystalline form. It is believed to be structurally analogous to Co(dptaa) and not to the related chromium(II) complex Cr_2(tmtaa)$_4$ of the tetramethyldibenzotetraaza[14]annulene tmtaaH_2, which is essentially diamagnetic and contains an unsupported quadruple bond.

The cobalt(II) complexes of the unsaturated diphenyl-substituted tetraazaannulene (**1**), 6,13-diphenyl-1,8-dihydro-2,3:9,10-dibenzo-1,4,8,11-tetraazacyclotetradecane-4,6,11,13-tetraene (dptaa H_2) and various substituted derivatives have been considered as catalysts for the reduction of oxygen in fuel cells.[1] Since absorption of the complex on the cathode surface may be important in the electrochemical process the structures of the cobalt complex and the ligand have been determined by single-crystal X-ray methods. The preparation of the chromium(II) complex Cr(dptaa) is also reported. There are brief accounts of the complexes Ni(dptaa),[2–4] Pd(dptaa),[3] Cu(dptaa)[2] and Zn(dptaa)[2] and of some iron(III) complexes[4] of uncertain structure; when doped with I_2 the nickel and palladium complexes exhibit metallic conductivity.

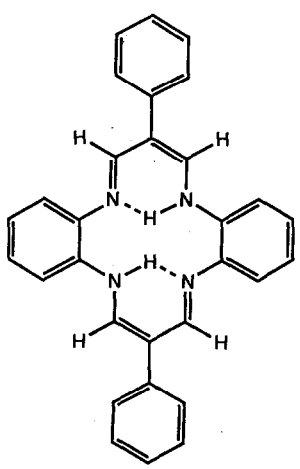

(1)

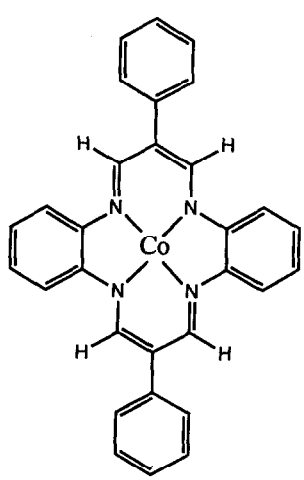

(2)

*Author to whom correspondence should be addressed.

EXPERIMENTAL

Unless otherwise stated below, the reagents and solvents were obtained from commercial sources and used as received.

Preparation of the ligand

The ligand (**1**) was prepared[1] by heating a solution of α-phenyl-β-dimethylaminoacraldehyde[5] (9.0 g, 0.05 mol) and *o*-phenylenediamine (5.55 g, 0.05 mol) in dimethylformamide (100 cm^3) under reflux for 5 h. The brown needle-like crystals which separated were filtered off, washed with methanol and dried *in vacuo* at 50°C (4.4 g, 40%). Found: C, 81.1; H, 5.7; N, 12.85. Calc. for $C_{30}H_{24}N_4$: C, 81.8; H, 5.5; N, 12.7%. δ_H ($CDCl_3$): 14.27 (2H, t, NH), 8.07, 8.05 (4H, d, CH), 7.40, 7.38 (10H, C_6H_5), 6.97–7.18 (8H, C_6H_4).

Preparation of the cobalt(II) *complex*

The cobalt(II) complex was prepared[1] by a template synthesis. *o*-Phenylenediamine (1.08 g, 0.01 mol) and cobalt(II) acetate tetrahydrate (1.24 g, 0.005 mol) were heated in dimethylformamide (40 cm^3) at 120°C for 4 h, α-phenyl-β-dimethylaminoacraldehyde (1.75 g, 0.01 mol) was added and the mixture was heated under reflux for 3 h. It was then cooled in ice, the dark purple solid filtered off, washed with methanol, air-dried and dried at 50°C *in vacuo*. The complex was recrystallized from dimethylformamide (1.28 g, 52%). Found: C, 71.7; H, 4.6; N, 11.3. Calc. for $C_{30}H_{22}N_4Co$: C, 72.4; H, 4.6; N, 11.3%. The complex was also prepared by heating the ligand (0.39 g, 0.0009 mol) and $Co(O_2CCH_3)_2 \cdot 4H_2O$ (0.23 g, 0.0009 mol) in dimethylformamide (4 cm^3) under reflux for 5 h. The product was treated as above (0.39 g, 87%). Found: C, 72.0; H, 4.5; N, 11.2%. μ_{eff} = 2.5 B.M. at 291 K (Gouy method).

Preparation of the chromium(II) *complex*

The ligand dptaaH_2 (1.05 g, 2.38 mmol) was suspended in freshly distilled THF (50 cm^3) under nitrogen and the solution was cooled to −40°C. Butyllithium in hexane (1.90 cm^3, 4.80 mmol) was added to the vigorously stirred solution to give a solution of Li_2dptaa (2.38 mmol). Anhydrous chromium(II) acetate (0.41 g, 2.38 mmol), prepared by heating the monohydrate[6] at 120°C under oil-pump vacuum, was added to the cold solution. After being stirred and allowed to warm to room temperature overnight the purple–black mixture was taken to dryness, the residue extracted with hot anhydrous toluene (200 cm^3) and filtered while hot to remove the lithium acetate. The filtrate was left at −18°C overnight and the purple–black powder which separated was filtered off and dried *in vacuo*. It could not be recrystallized from dimethylformamide or toluene and the microanalysis indicates the inclusion of toluene. Found: C, 76.3; H, 6.1; N, 8.6. Calc. for $C_{30}H_{22}CrN_4 \cdot 1.5C_7H_8$: C, 77.4; H, 5.5; N, 8.9%. IR spectrum (Nujol): 1580 m, br, 1560 m, br, 1540 sh, 1535 sh, 1310 s, vbr, 1275 s, 1205 m, 1175 m, 1020 w, br, 970 w, 830 w, 765 sh, 760 m, 740 s, 730 m, sh, 700 m, 670 w. Magnetic measurements: μ_{eff} = 2.85 (292 K), μ_{eff} = 2.72 B.M. (87 K), θ = 11° (Gouy method).

X-ray crystal structure analysis of 6,13-*diphenyl*-1,8-*dihydro*-2,3:9,10-*dibenzo*-1,4,8,11-*tetraaza*-*cyclotetradecane*-4,6,11,13-*tetraene*

The crystals prepared as described were suitable for X-ray study and one of approximate dimensions 0.3 × 0.2 × 0.1 mm was mounted on a glass fibre.

Crystal data. $C_{30}H_{24}N_4$, M = 440.55, monoclinic, space group $P2_1/c$, a = 11.402(5), b = 7.088(4), c = 27.069(8) Å, β = 90.24(03)°, U = 2187.6(2.0) Å^3, Z = 4, D_c = 1.338 g cm^{-3}, $F(000)$ = 928, graphite-monochromated Mo-K_α radiation (λ = 0.71073 Å), μ(Mo-K_α) = 0.75 cm^{-1}.

Data collection. Cell parameters were determined on an Enraf–Nonius CAD4 diffractometer by measurement of 25 accurately centred reflections. Intensity data were collected by the ω–2θ scan mode in the range $1° \leqslant \theta \leqslant 22°$ ($0 \leqslant h \leqslant 12$, $0 \leqslant k \leqslant 7$, $-28 \leqslant l \leqslant 28$); in all 3015 reflections were measured, which after the usual Lp correction and removal of systematic absences yielded 873 having $I \geqslant 3\sigma(I)$.

Structure solution and refinement. In the absence of the cobalt complex ready to hand the structure determination of the ligand itself proved difficult. Many runs of the direct methods program MULTAN[7] were made using a wide range of options available. In all cases the top 5–8 solutions were of the chicken-wire type, consistent with a multi-ring system, but in solutions lower down the list there appeared structures containing 29–31 atoms having the desired molecular arrangement. However, none of these trial structures proved correct, R being in the range 0.32–0.38, and none produced the missing atoms in the subsequent electron density maps. The molecule has many atoms lying close to the 0 0 22 and 10 0 $\bar{10}$ planes and it was obvious that the signs of these two reflections were not being correctly determined by MULTAN. Attempts with the four possible sign combinations gave similar results as before. It was surmised that

the orientation of the molecule was probably correct, but that it required small shifts in the *ac* plane to obtain the correct position. The program DIRDIF,[8] which has a translation function as part of its routines, is ideally suited for such a problem. One of the trial structures initially input into DIRDIF did not produce sensible shifts, but a second trial structure produced shifts of 0.029 in the x direction and -0.022 in the z direction. The resulting E map also produced the missing three atoms of the trial structure. Thereafter, refinement went smoothly. Isotropic full-matrix least-squares refinement converged at $R = 0.078$ with hydrogen atoms in fixed calculated positions ($d_H = 1.0$ Å). Anisotropic refinement of non-hydrogen atoms converged at $R = 0.058$ and from a difference map the two hydrogens attached to N(1) and N(3) were found. Including these two hydrogen atoms in the refinement the final value of R was 0.055, $R_w = 0.061$ and $S = 1.045$, using the weighting scheme[9] $w^{-1} = [\sigma(F^2)+0.07F]$. The largest peak in the difference map was 0.2 electrons.

Selected bond distances and angles are given in Table 1, and the atom numbering scheme in Fig. 1. All calculations were performed with the Enraf–Nonius Structure Determination Package.[10]

X-ray crystal structure analysis of Co(dptaa). A crystal of the cobalt(II) complex, obtained by slow recrystallization from hot dimethylformamide and of approximate dimensions $0.4 \times 0.3 \times 0.1$ mm, was mounted on a glass fibre for the crystal structure determination.

Crystal data. $C_{30}H_{22}N_4Co$, $M = 497.5$, monoclinic, space group $P2_1/c$, $a = 11.470(2)$, $b = 7.061(4)$, $c = 27.045(5)$ Å, $\beta = 90.82(01)°$, $U = 2190.1(2.0)$ Å^3, $Z = 4$, $D_c = 1.509$ g cm^{-3}, $F(000) = 1028$, graphite-monochromated Mo-K_α radiation ($\lambda = 0.71073$ Å), μ(Mo-K_α) = 8.08 cm^{-1}.

Data collection. The unit cell was obtained by the measurement of 25 accurately centred reflections on an Enraf–Nonius CAD4 diffractometer. Intensity data were collected by the ω–2θ scan mode in the range $1 \leqslant \theta \leqslant 24°$ ($0 \leqslant h \leqslant 13$, $0 \leqslant k \leqslant 8$, $-31 \leqslant l \leqslant 31$); in all 3954 reflections were measured, which after the usual Lp correction and removal of systematic absences yielded 2256 reflections having $I \geqslant 3\sigma(I)$.

Structure solution and refinement. Comparison of this unit cell with that of the ligand shows that the two compounds are isostructural and that atomic coordinates would be closely similar. The coordinates of the cobalt atom were derived from the Patterson synthesis and were found to be very close to the centre of gravity of the ligand molecule. An F_o map based upon the phases of the cobalt atom revealed all but one atom of the ligand and a subsequent structure–factor/Fourier cycle produced the complete molecule. With the inclusion of hydrogen atoms in fixed calculated positions ($d_H = 1.0$ Å) R fell to 0.061. An absorption correction by the program DIFABS[11] gave maximum and minimum absorption corrections of 0.86 and 1.11. Anisotropic full-matrix refinement, initially with cobalt alone and then with all non-hydrogen atoms, con-

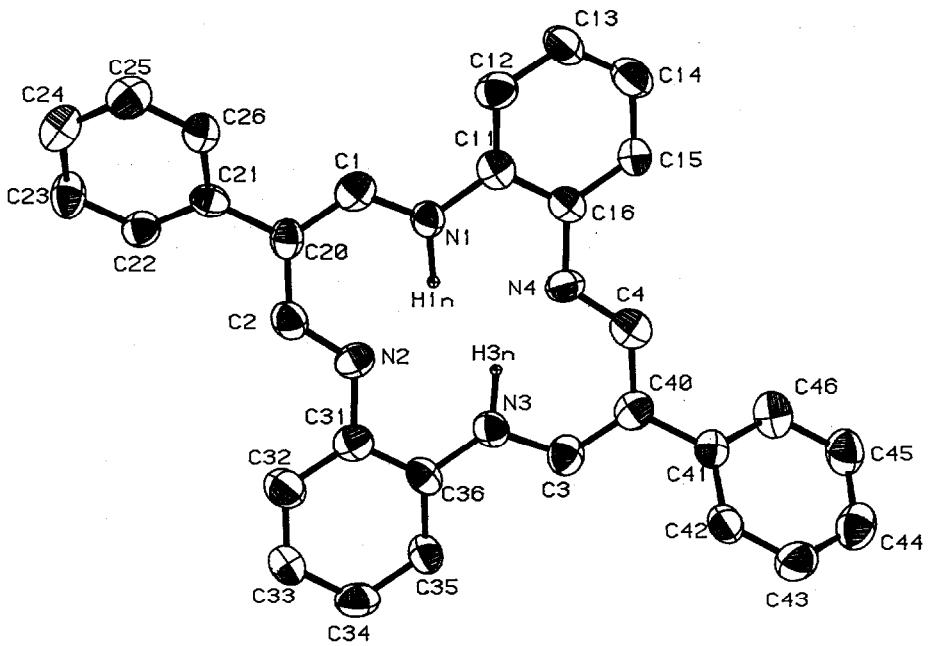

Fig. 1. Atom numbering scheme for the ligand dptaaH$_2$.

Table 1. Selected bond lengths (Å) and angles (°) in dptaaH_2 and Co(dptaa) with e.s.d.s in parentheses

dptaaH_2		Co(dptaa)	
		Co—N(1)	1.861(3)
		Co—N(2)	1.863(3)
		Co—N(3)	1.866(3)
		Co—N(4)	1.869(3)
N(1)—C(1)	1.321(8)	N(1)—C(1)	1.326(5)
N(1)—C(11)	1.420(8)	N(1)—C(11)	1.427(5)
N(1)—H(1n)	1.11(7)		
N(2)—C(2)	1.305(8)	N(2)—C(2)	1.328(5)
N(2)—C(31)	1.420(8)	N(2)—C(31)	1.409(5)
N(3)—C(3)	1.337(8)	N(3)—C(3)	1.328(5)
N(3)—C(36)	1.391(8)	N(3)—C(36)	1.415(5)
N(3)—H(3n)	1.04(7)		
N(4)—C(4)	1.333(8)	N(4)—C(4)	1.324(5)
N(4)—C(16)	1.398(7)	N(4)—C(16)	1.413(5)
C(1)—C(20)	1.397(9)	C(1)—C(20)	1.404(6)
C(2)—C(20)	1.406(9)	C(2)—C(20)	1.385(6)
C(3)—C(40)	1.383(9)	C(3)—C(40)	1.382(6)
C(4)—C(40)	1.399(9)	C(4)—C(40)	1.389(6)
C(20)—C(21)	1.471(8)	C(20)—C(21)	1.489(6)
C(40)—C(41)	1.475(9)	C(40)—C(41)	1.496(6)
		N(1)—Co—N(2)	94.2(1)
		N(1)—Co—N(3)	179.7(6)
		N(1)—Co—N(4)	86.1(1)
		N(2)—Co—N(3)	85.8(1)
		N(2)—Co—N(4)	179.7(8)
		N(3)—Co—N(4)	93.9(1)
C(1)—N(1)—C(11)	123.9(5)	C(1)—N(1)—C(11)	119.9(3)
C(1)—N(1)—H(1n)	116(3)		
C(11)—N(1)—H(1n)	118(3)		
C(2)—N(2)—C(31)	122.4(5)	C(2)—N(2)—C(31)	120.2(3)
C(3)—N(3)—C(36)	124.6(5)	C(3)—N(3)—C(36)	120.4(3)
C(3)—N(3)—H(3n)	106(4)		
C(36)—N(3)—H(3n)	128(4)		
C(4)—N(4)—C(16)	121.9(5)	C(4)—N(4)—C(16)	120.5(3)
N(1)—C(1)—C(20)	124.7(6)	N(1)—C(1)—C(20)	124.7(4)
N(2)—C(2)—C(20)	124.8(6)	N(2)—C(2)—C(20)	126.0(4)
N(3)—C(3)—C(40)	126.0(6)	N(3)—C(3)—C(40)	125.3(4)
N(4)—C(4)—C(40)	125.7(6)	N(4)—C(4)—C(40)	124.9(4)
N(1)—C(11)—C(16)	117.3(5)		
N(4)—C(16)—C(11)	117.0(5)	N(4)—C(16)—C(11)	114.5(3)
C(1)—C(20)—C(2)	122.2(6)	C(1)—C(20)—C(2)	121.8(4)
C(1)—C(20)—C(21)	118.9(6)	C(1)—C(20)—C(21)	119.4(4)
C(2)—C(20)—C(21)	118.8(5)	C(2)—C(20)—C(21)	118.8(4)
N(2)—C(31)—C(36)	116.6(5)	N(2)—C(31)—C(36)	113.7(3)
N(3)—C(36)—C(31)	118.1(5)	N(3)—C(36)—C(31)	113.6(4)
C(3)—C(40)—C(4)	121.7(6)	C(3)—C(40)—C(4)	122.7(4)
C(3)—C(40)—C(41)	119.1(6)	C(3)—C(40)—C(41)	118.3(4)
C(4)—C(40)—C(41)	119.2(6)	C(4)—C(40)—C(41)	119.0(4)

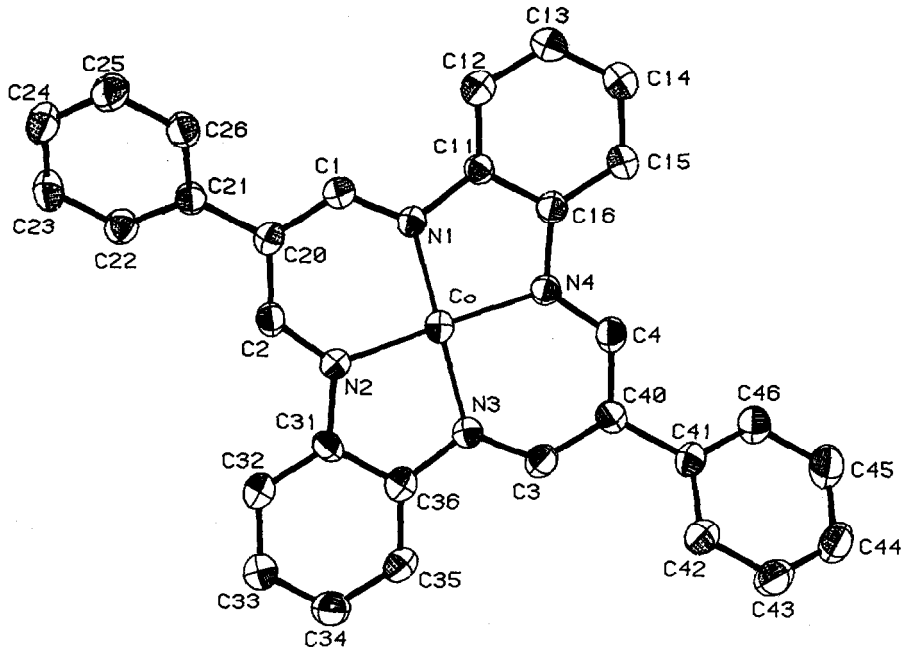

Fig. 2. Atom-numbering scheme for the cobalt(II) complex Co(dptaa).

verged at $R = 0.042$, $R_w = 0.053$ and $S = 1.073$, using the weighting scheme $w^{-1} = [\sigma(F^2) + (0.025F)^2 + 2.5]$. The largest peak in the difference map was 0.3 electrons. Selected bond distances and angles are listed in Table 1 and the atom numbering scheme is given in Fig. 2.

RESULTS AND DISCUSSION

Structure of the ligand

The nitrogen atoms of the ligand are almost coplanar. Atoms N(2) and N(4) (Fig. 1) are, respectively, 0.020 and 0.019 Å above the mean plane of the four nitrogen atoms, whereas N(1) and N(3) lie the same distances below the plane. The two benzenoid rings are at angles of 3.2° [C(11)—C(16)] and 2.3° [C(31)—C(36)] to the plane of the four nitrogen atoms and the phenyl groups are rotated at 29.8° [C(21)—C(22)/C(2)—C(20)] and 38.2° [C(41)—C(42)/C(4)—C(40)] in opposite directions. The sideways representation of the molecule in Fig. 3 shows clearly the planarity of all except the phenyl groups. Hydrogen bonds bridge adjacent nitrogen atoms of the 2-phenyl-1,3-propanediimine bridges.

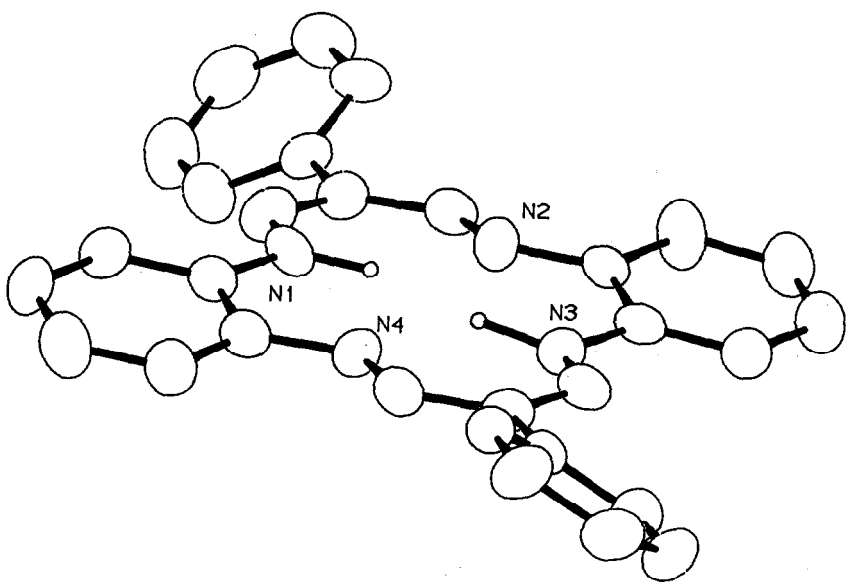

Fig. 3. Sideways representation of the ligand molecule.

The hydrogen bond distances are 1.906 [H(1n)—N(2)] and 1.843 Å [H(3n)—N(4)]. These are much shorter than the non-bonded N—H distances across the *o*-phenylenediamine rings, which average 2.343 Å. There is considerable delocalization in the 2-phenyl-1,3-propenediimine bridges since the C—C distances are similar [1.383(9)–1.406(9) Å] and close to those in benzene (1.39 Å). The N—H bonds lie in the N_4 plane so each nitrogen atom can be considered sp^2-hybridized with a *p*-orbital freed for delocalization. Also, the C—N bonds in the bridges (mean 1.324 Å) are much shorter than the C—N bonds to benzo groups (mean 1.407 Å), which might be considered closer to single C—N bonds. The diagonally opposed nitrogen atoms have separations of 3.852 [N(1)—N(3)] and 3.800 Å [N(2)—N(4)]. Thus, the nitrogen-to-centre distance of the neutral ligand is approximately 1.913 Å. The cavity is, therefore, slightly larger than that of the related neutral ligand tmtaaH_2 (1.902 Å). Consequently, it is not surprising that a cobalt(II) complex can be prepared easily.

Structure of the cobalt(II) *complex*

The structure of the cobalt(II) complex (Figs 2 and 4) is very similar to that of the free ligand, except that the nitrogen atoms in the complex are exactly planar and the cobalt is at the centre equidistant from the four donor atoms (mean Co—N = 1.865 Å). Thus, the nitrogen lone pairs are positioned directly in the plane. As expected for a planar N_4 coordination sphere the cobalt(II) is low spin (μ_{eff} = 2.5 B.M. at 291 K). The radius of low-spin cobalt(II) is estimated to be 0.63 Å[12] so that the macrocycle cavity can clearly accommodate the metal ion without strain in the ligand; in fact, corresponding bond distances in the 14-membered macrocycle are more nearly equal in the complex than in the free ligand, and except for the phenyl groups the molecule is nearly planar and shows less deviation from planarity than the (neutral) uncomplexed ligand. The phenyl groups are rotated with respect to the macrocycle plane (30.0° and 38.1°) as in the free ligand.

Chromium(II) *complex*

The chromium(II) complex is low spin. The magnetic moment is 2.85 B.M. at room temperature, close to the spin-only value for the t_{2g}^4 configuration of 2.83 B.M. The magnetic moment decreases only slightly to 2.72 B.M. at 87 K. The chromium(II) complex Cr_2(tmtaa)$_4$ of the analogous tetraazannulene ligand is dinuclear,[13] with an unsupported metal–metal bond and is only weakly paramagnetic (μ_{eff} = 0.49 B.M.). It is difficult to know whether this weak paramagnetism is due to traces of paramagnetic impurity, temperature-independent paramagnetism, slight population of the triplet state or a combination of all three effects, but the magnetic behaviour is clearly different from that of Cr(dptaa). This suggests that Cr(dptaa) has a planar structure more analogous to that of Co(dptaa).

The radius of low-spin chromium(II) is estimated to be 0.75 Å.[12] This is 0.1 Å greater than the value for low-spin cobalt(II) and since the nitrogen-to-centre distance in the ligand is 1.913 Å and the Co—N distance in the planar Co(dptaa) is 1.86 Å, it is likely that the Cr^{2+} can be accommodated in the ligand cavity without great distortion to give a planar complex (except for the twist of the phenyl substituents).

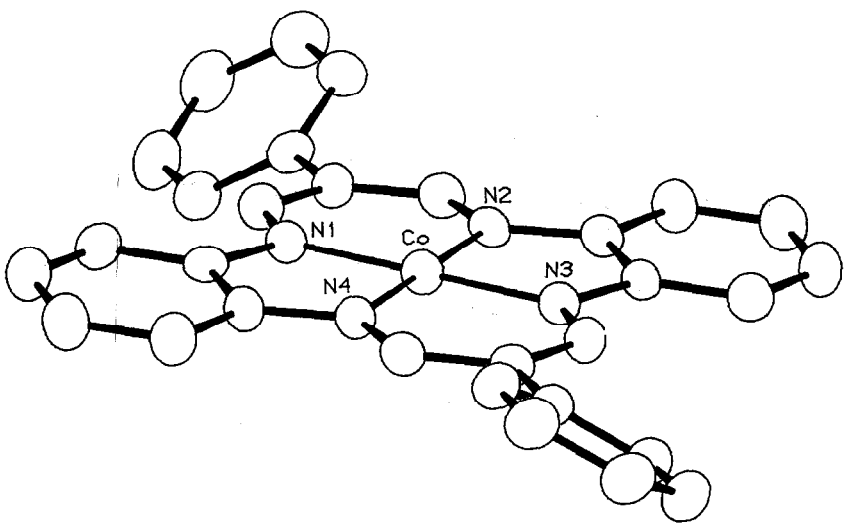

Fig. 4. Sideways representation of the molecule of the cobalt(II) complex.

Acknowledgements—We thank Paul Morton for some experimental assistance, the Catalysis Group at the Johnson Matthey Technology Centre for their help and encouragement and the SERC for a studentship (JJ).

REFERENCES

1. K. Akashi and N. Suga, EP 0073456, 1983, CA 99, 88241.
2. A. Abelleira and F. Walsh, *Electrochim. Acta* 1986, **31**, 113.
3. M. Hunziker, B. Hilti and G. Rihs, *Helv. Chim. Acta* 1981, **62**, 82.
4. Y. Nishida, A. Sumita, K. Hayashida, H. Ohshima, S. Kida and Y. Maeda, *J. Coord. Chem.* 1979, **9**, 161.
5. Z. Arnold and F. Sorm, *Collect. Czech Chem. Commun.* 1958, **23**, 452; Z. Arnold and A. Holy, *Collect. Czech Chem. Commun.* 1961, **26**, 3051.
6. L. R. Ocone and B. P. Block, *Inorg. Synth.* 1966, **8**, 130.
7. P. Main, S. E. Hull, L. Lessinger, G. Germain, J. P. Declerqc and M. M. Woolfson, MULTAN 78, A System of Computer Programs for the Automatic Solution of Crystal Structures from X-ray Diffraction Data, Universities of York, England and Louvain, Belgium (1978).
8. H. M. Doesburg and P. T. Beurskens, *Acta Cryst., Sect. A* 1983, **39**, 368.
9. R. C. G. Killean and J. L. Lawrence, *Acta Cryst., Sect B* 1969, **25**, 1750.
10. Structure Determination Package. B. A. Frenz and Associates, College Station, TX (1985).
11. N. Walker and D. Stuart, *Acta Cryst., Sect. A* 1983, **39**, 158.
12. N. N. Greenwood and A. Earnshaw, *Chemistry of the Elements*, p. 1497. Pergamon Press, Oxford (1984).
13. J. J. Edema, S. Gambarotta, P. van der Sluis, W. J. J. Smeets and A. L. Spek, *Inorg. Chem.* 1989, **28**, 3782.

Polyhedron Vol. 12, No. 10, pp. 1187–1192, 1993
Printed in Great Britain

0277-5387/93 $6.00+.00
© 1993 Pergamon Press Ltd

STRUCTURAL AND ANTITUMOUR STUDIES OF METAL COMPLEXES WITH THIOSEMICARBAZONES OF β-DIKETOESTERS

S. JAYASREE and K. K. ARAVINDAKSHAN*

Department of Chemistry, University of Calicut, Kerala 673 635, India

(*Received* 1 *September* 1992; *accepted* 26 *January* 1993)

Abstract—The reactions of thiosemicarbazones of methyl- and ethylacetoacetates ($MatH_2$ and $EatH_2$, respectively) with the acetates of manganese(II), cobalt(II), nickel(II), copper(II), zinc(II) and cadmium(II) gave solid complexes, which were characterized by various physicochemical methods such as microanalyses, magnetic measurements and ESR, UV–vis, IR and NMR spectral studies. They were found to be of the following general formulae: $[M(LH)_2]$, where M = Mn^{II}, Co^{II}, Ni^{II} or Cd^{II} and LH = monoanions, MatH or EatH; [Cu(L)] and $[Zn(L)(H_2O)]$, where L = dianions, Mat or Eat. The thiosemicarbazones and their cobalt(II) and copper(II) complexes were screened for their possible antitumour activity.

In continuation of our work on biologically important transition metal complexes[1] of thiosemicarbazones derived from β-diketones, we herein report the complexes with methyl- and ethylacetoacetate thiosemicarbazones. Apart from one report[2] on the complexes of certain metal chlorides with $EatH_2$, no systematic investigations have been reported on the donor properties of thiosemicarbazones of β-diketoesters and hence it was considered worthwhile and interesting to investigate the reactions of $MatH_2$ and $EatH_2$ towards various transition metal acetates so as to isolate and characterize the solid complexes formed. The inhibitory activity of these compounds against tumour cells were also studied.

EXPERIMENTAL

Materials

Methyl- and ethylacetoacetates and the metal acetates were bought from BDH. The solvents were of reagent grade and were purified before use by the standard methods.[3] The chemicals used for the antitumour screening tests were of E. Merck's reagent grade. Minimum Essential Medium (MEM) and trypsin were purchased from Hi-Media Laboratories Pvt. Ltd, Bombay. Ehrlich ascites and Chinese Hamster Ovary (CHO) tumour cells were obtained from Tata Memorial Hospital, Bombay, and the National Faculty for Cell and Tissue Culture, Pune, respectively. Swiss Albino mice were bought from C.M.C. Vellore.

Synthetic procedures

(a) *Preparation of ligands.* β-Diketoester (1.17–1.36 g, 0.01 mol) and thiosemicarbazide (0.90 g, 0.01 mol) were mixed in EtOH (25 cm^3) and refluxed on a steam bath for 1 h. Partial evaporation of the solvent yielded the crystalline compound, which was suction filtered, washed with EtOH and dried under reduced pressure over P_4O_{10} [Figs 1(a) and (b)].

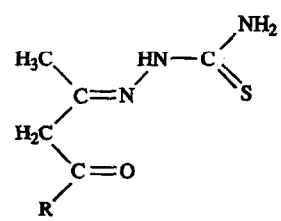

Fig. 1. (a) Where R = OCH_3($MatH_2$) and (b) where R = OC_2H_5($EatH_2$).

*Author to whom correspondence should be addressed.

(b) *Preparation of complexes.* The complexes were prepared by refluxing methanolic solutions of the ligands (0.005 mol in 15 cm^3) and metal acetates (0.005 mol in 20 cm^3) for 2 to 3 h. The solid complexes which separated out on keeping the reaction mixtures overnight were filtered off, washed with methanol and dried under reduced pressure over P_4O_{10}.

Analyses and physical measurements

Metals present in the complexes were estimated as per the standard procedure of Vogel.[3] Microanalyses were performed using a Heraues CHN-O rapid analyser. Magnetic measurements were performed at room temperature using a Gouy type magnetic balance with $Hg[Co(NCS)_4]$ as the calibrant. ESR spectra of the copper(II) complexes were recorded on a Varian E-109 EPR spectrophotometer using DPPH as the internal standard. Electronic spectra of the complexes in the solid state were recorded on a Hitachi 3200 UV–vis spectrophotometer. The IR spectra in the range 4000–200 cm^{-1} were recorded using KBr discs on a Perkin–Elmer 580 IR spectrophotometer. NMR spectra of the ligands and the zinc(II) complexes were recorded on a Bruker ACF 200 MHz NMR spectrometer.

(a) In vitro *cytotoxicity*. The *in vitro* cytotoxicity was performed using Ehrlich ascites tumour cells. The drugs were incubated with 1×10^5 cells at 37°C for 3 h. After incubation the percentage of dead cells was determined by the trypan blue exclusion method.[4]

(b) *Effect on cultured cells.* CHO cells were grown in culture flasks with MEM (10 cm^3) containing 10% heat inactivated serum and some antibiotics. Drugs were added in different concentrations and incubated for 7 days at 37°C. After the incubation period the medium was removed, trypsinized and the number of cells counted using a haemocytometer.

(c) In vivo *experiment.* The tumour cells were transplanted in the peritoneal cavity of 12 female Swiss Albino mice (two groups of six each) so that they may develop ascites tumour. After 24 h 100 μg of the lyposomally encapsulated drug was administered intraperitoneally to one group and continued for 5 alternate days and the survival of the animals was watched. The other group was kept as a control. The percentage increase in life span (ILS) was determined using the formula $(T-C)$ 100/C, where T is the average number of days survived by the test animals and C is the number of days survived by the control animals.

RESULTS AND DISCUSSION

The data obtained from chemical analyses and physicochemical measurements can be correlated so as to explain the properties, structure and geometries of the ligands and the complexes. All the complexes are coloured. They are air and light stable non-hygroscopic amorphous powders and they decompose above 200°C. They are sparingly soluble in common organic solvents, but are appreciably soluble in DMSO. The microanalytical data of the complexes correspond to $[M(LH)_2]$, where M = Mn^{II}, Co^{II}, Ni^{II} or Cd^{II} and LH = monoanions, MatH or EatH, [Cu(L)] and $[Zn(L)(H_2O)]$, where L = dianions, Mat or Eat (Table 1).

Magnetic susceptibility measurements

The room-temperature magnetic moment value of $[Mn(EatH)_2]$ is 5.88 B.M., which suggests octahedral geometry for the manganese(II) complex.[5] $[Co(MatH)_2]$ and $[Co(EatH)_2]$ exhibit μ_{eff} values of 4.98 and 4.86 B.M., respectively, which suggest octahedral coordination around the cobalt(II) ions. The two nickel(II) chelates had magnetic moments of 3.17 and 3.29 B.M., respectively, which are as expected for a nickel(II) complex with octahedral geometry. The copper(II) complexes of $MatH_2$ and $EatH_2$ exhibit magnetic moments of 1.58 and 1.24 B.M., respectively. These values are significantly lower than expected for copper(II) complexes and may be due to some exchange interactions between the neighbouring molecules, as the dibasic tridentate ligand forces the molecule to dimerize or polymerize.

ESR spectra

The ESR spectra of the copper(II) chelates of $MatH_2$ and $EatH_2$ in polycrystalline samples at room temperature and liquid nitrogen temperature show broad intense signals with isotropic g values of 2.12 and 2.13, respectively. These values indicate considerable covalent character of the metal–ligand bonds in the complexes.[6]

Electronic spectra

The manganese(II) complex with a high-spin d^5 state registers no characteristic bands in the visible region. However, in the present complex the two broad bands at 29,500 and 24,200 cm^{-1} are typical charge-transfer transitions, as expected for an octahedral manganese(II) complex[7] (Table 2).

For an octahedral cobalt(II) complex the visible spectrum will be dominated by the highest energy

Table 1. Colour, analytical results and magnetic moments of the ligands and their complexes

Compound	Colour	Analysis: % Found (Calc.) M	N	S	μ_{eff} (B.M.)
$MatH_2$	—	—	22.1	16.2	—
			(22.2)	(16.9)	
$[Co(MatH)_2]$	Pale pink	13.3	19.3	14.4	4.98
		(13.5)	(19.3)	(14.7)	
$[Ni(MatH)_2]$	Light blue	13.6	19.0	14.2	3.17
		(13.5)	(19.3)	(14.7)	
[Cu(Mat)]	Brown	25.7	16.2	12.1	1.58
		(25.4)	(16.8)	(12.8)	
$[Zn(Mat)(H_2O)]$	White	23.7	15.2	11.6	
		(24.3)	(15.5)	(11.7)	
$EatH_2$			20.2	15.6	
			(20.7)	(15.7)	
$[Mn(EatH)_2]$	Pale pink	12.1	17.9	14.1	5.88
		(12.0)	(18.3)	(13.9)	
$[Co(EatH)_2]$	Pale rose	12.1	19.1	13.0	4.86
		(12.8)	(18.2)	(13.9)	
$[Ni(EatH)_2]$	Green	12.2	18.0	13.7	3.29
		(12.7)	(18.2)	(13.9)	
[Cu(Eat)]	Dark green	24.6	15.2	12.0	1.24
		(24.0)	(15.9)	(12.1)	
$[Zn(Eat)(H_2O)]$	White	22.0	14.6	11.5	
		(23.0)	(14.8)	(11.3)	
$[Cd(EatH)_2]$	Pale yellow	20.9	16.1	12.8	
		(21.9)	(16.3)	(12.4)	

transition, $^4T_{1g}(F) \rightarrow {}^4T_{2g}(P)$. The next possible transition, $^4T_{1g}(F) \rightarrow {}^4T_{1g}(P)$, which is also spin-allowed, occurs in the near-IR region. The third transition, $^4T_{1g}(F) \rightarrow {}^4A_{2g}(F)$ is a two-electron transition and, therefore, is much weaker than the other two transitions. In the spectra of the present cobalt(II) complexes only the first two bands are present in the expected regions, whereas the third

Table 2. Spectral data (cm^{-1})

Compound	IR ν(C=O)	ν(C=S)	ν(C=N)	Electronic Bands	Assignments
$MatH_2$	1745	1070	1580	—	
				17,890	$^4T_{1g} \rightarrow {}^4T_{2g}(F)(\nu_2)$
$[Co(MatH)_2]$	1690	738	1490	24,330	$^4T_{1g} \rightarrow {}^4T_{1g}(P)(\nu_3)$
$[Ni(MatH)_2]$	1685	750	1495	24,300	$^1A_{1g} \rightarrow {}^1A_{2g}$
Cu(Mat)	1120	750	1500	18,580	$^1B_{1g} \rightarrow {}^2B_{2g}$
$[Zn(Mat)(H_2O)]$	1105	745	1490	—	
$EatH_2$	1738	1075	1600	—	
$[Mn(EatH)_2]$	1700	725	1550	24,200	$C-T$ transitions
				29,500	
$[Co(EatH)_2]$	1690	730	1555	16,210	$^4T_{1g} \rightarrow {}^4A_{2g}(F)(\nu_2)$
				23,040	$^4T_{1g} \rightarrow {}^4T_{1g}(P)(\nu_3)$
$[Ni(EatH)_2]$	1690	750	1545	10,240	$^3A_{2g} \rightarrow {}^3A_{2g}(F)(\nu_1)$
				18,283	$^3A_{2g} \rightarrow {}^3T_{1g}(F)(\nu_2)$
				22,880	$^3A_{2g} \rightarrow {}^3T_{1g}(P)(\nu_3)$
[Cu(Eat)]	1130	735	1550	19,250	$^2B_{1g} \rightarrow {}^2B_{2g}$
$[Zn(Eat)(H_2O)]$	1110	750	1550	—	
$[Cd(EatH)_2]$	1695	745	1545	—	

one is absent. Similar situations occur in the electronic spectra of several octahedral cobalt(II) complexes.[7]

[Ni(MatH)$_2$] and [Ni(EatH)$_2$] register bands in the regions 22,880–24,390, 19,283–18,200 and 10,240 cm^{-1}. These may arise from $^3A_{2g} \rightarrow {}^3T_{1g}$(P), $^3A_{2g} \rightarrow {}^3T_{1g}$(F) and $^3A_{2g} \rightarrow {}^3T_{2g}$(F) transitions, respectively, of a six-coordinate octahedral nickel(II) ion.[8]

The bands observed around 19,200 cm^{-1} for the copper(II) chelates may be assigned to the transition $^2B_{1g} \rightarrow {}^2B_{2g}$, typical of square-planar geometry.[8]

IR spectra

The IR spectra of the ligands exhibit bands due to NH vibrations at 3400, 3340, 3200 and 3120 cm^{-1}. Out of these, the first two bands are attributed to the asymmetric stretching modes and the other two are assigned to the symmetric NH of the terminal NH_2 and NH groups.[9] The lower frequency bands suffer a series of changes in the spectra of the complexes. In the spectra of the chelates there are fewer bands in this region and they are found to be broad in nature. This may be due to the participation of the hydrazine nitrogen of the system N—NH—C=S in chelate formation (Table 2).

The absence of bands in the region 2600–2450 cm^{-1} in the spectra of the ligands indicate that there are no S—H groups in these free ligands in the solid state.[10]

The bands of strong intensities in the spectra of the ligands around 1750–1720 cm^{-1} may be attributed to the carbonyl stretching vibration of the ester group.[2] In the spectra of complexes of manganese(II), cobalt(II), nickel(II) and cadmium(II) this band has undergone a shift to a lower frequency region, i.e. 1700–1690 cm^{-1}, which demonstrates the involvement of the carbonyl group in coordination. However, in the spectra of the copper(II) and zinc(II) complexes this ester carbonyl frequency band is absent and a new band is observed around 1000 cm^{-1}, which may be attributed to the enolization and subseqeunt coordination through the deprotonated oxygen atom of the system CH_2—C=O.

The strong bands at 1600–1580 cm^{-1} in the spectra of the ligands are assigned to ν(C=N). In the spectra of all the complexes a shift, by *ca* 30–40 cm^{-1}, for this band indicates the coordination of azomethine nitrogen to the metal ions.

The band of medium intensity at 1070 cm^{-1} in the spectra of all the ligands may be assigned to the (C=S) stretch. In the spectra of the complexes this band disappears and a new band simultaneously appears in the 750–700 cm^{-1} region. All these observations may be attributed to the enolization of C=S and subsequent coordination through the thiolate (S$^-$).[11,12]

The broad bands of medium intensities due to ν(O—H) around 3550 cm^{-1} in the spectra of the zinc(II) complexes indicate the presence of water molecules. In addition, a band of strong intensity at 940–890 cm^{-1} suggests that these water molecules are coordinated.

Further evidence for the nature of the metal–ligand bonding is given by the ν(M—S), ν(M—N) and ν(M—O) bands observed in the spectra of the complexes at 300–270, 390–360 and 450–430 cm^{-1}, respectively.[2]

NMR spectra

The ^{1}H NMR spectra of $MatH_2$ and $EatH_2$ in DMSO-d_6 register signals at 2.13–2.01 and 3.39–3.32 ppm due to CH_3 and CH_2 protons, respectively. The ethoxy group (O—CH_2—CH_3) proton signals of $EatH_2$ are observed as a triplet at 1.31 ppm due to CH_3 and as a quartet at 4.24 ppm due to O—CH_2. The —OCH_3 signal of $MatH_2$ is observed around 3.89 ppm. The NH proton signals are observed at 6.68–6.58 ppm and the broad signal in the range 8.87–8.68 ppm may be attributed to the NH_2 group.

In the spectra of the zinc(II) chelates the CH_2

Table 3. Cytotoxic action of compounds on Ehrlich ascites tumour cells

Compound	% Dead cells				
	5 μg cm^{-3}	10 μg cm^{-3}	20 μg cm^{-3}	50 μg cm^{-3}	100 μg cm^{-3}
$MatH_2$	—	—	—	17	38
[Co(MatH)$_2$]	—	—	—	48	59
[Cu(Mat)]	—	—	31	52	68
$EatH_2$	18	35	48	66	100
[Co(EatH)$_2$]	—	—	—	48	63
[Cu(Eat)]	48	93	95	100	100

Table 4. Effect of [Cu(Eat)] in Ehrlich ascites tumour-bearing animals

Compound	Tumour model	Dose and mode of therapy	No. of mice survived after (days) 10	15	20	25	30	% ILS
[Cu(Eat)]	Ehrlich ascites	20 mg kg^{-1} b.wt Intraperitoneally	6	6	6	3	1	61.18
Control			6	6	0	0	0	—

proton signals are not present and new signals are observed at 4.39–4.87 ppm, due to the CH proton. This may be due to the enolization of the CH_2—C=O group to CH=C—OH during coordination. The NH proton signals are also not observed in the spectra of the zinc(II) complexes. This may be as a consequence of enolization of N—NH—C=S to N—N=C—SH. The other main characteristic features in the spectra of the ligands are retained in those of the complexes.

Antitumour studies

Of all the compounds tested *in vitro* (Table 3) $MatH_2$ alone was found to be the least active or effective, while others produced $\geqslant 50\%$ cell death. The more active compounds, namely $EatH_2$ and [Cu(Eat)], were then placed in culture medium. A concentration of 1 $\mu g\ cm^{-3}$ of [Cu(Eat)] produced 100% growth inhibition of CHO cells (Fig. 2), whereas the same concentration of $EatH_2$ produced only 73%. Thus, from the preliminary studies it was found that chelates are more active than their respective free ligands, which is consistent with earlier observations.[13] Further, *in vivo* studies were conducted with [Cu(Eat)], administration of which could considerably delay the onset of tumour development and increase the life-span of the treated animals to 61.18% (Table 4).

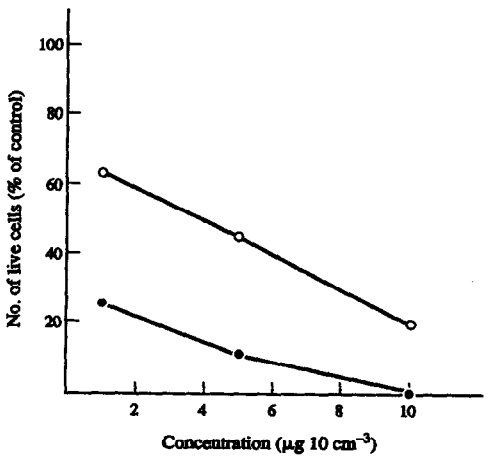

Fig. 2. Effect of ($EatH_2$) and [Cu(Eat)] on tissue cultured cells (CHO): O——O ($EatH_2$); ●——● [Cu(Eat)].

From all these observations it is inferred that [Cu(Eat)] possesses appreciable tumour reducing action. Even though remarkable progress in understanding the antitumour activities of related compounds has been made by biological methods, the chemistry behind them still remains rather obscure. It has been suggested that similar compounds interfere with the incorporation of thymine in DNA and also interact with cellular thiols,[14–16] diminishing their concentration. Metal coordination increases the lipophilicity, which may be a contributing factor to the enhanced activity of the metal chelates. However, it requires more detailed investigation to ascertain their actual mode of action.

Acknowledgement—We wish to thank Dr N. Thankarajan, Head, Department of Chemistry, for facilities, Dr Ramadas Kuttan, Research Director, and Dr Girija Kuttan, Amala Cancer Research Centre, for their help in the antitumour screening tests.

REFERENCES

1. S. Jayasree and K. K. Aravindakshan, *Trans. Met. Chem.* 1993, **18**, 85.
2. N. C. Mishra, B. B. Mohapatra and S. Guru, *J. Inorg. Nucl. Chem.* 1979, **41**, 408.
3. A. I. Vogel, *A Text Book of Practical Organic Chemistry*, 3rd edn, pp. 163–179. Longmans, London (1956).
4. G. Kuttan, D. M. Vasudevan and R. Kuttan, *Cancer Lett.* 1988, **41**, 307.
5. B. N. Figgis and J. Lewis, *Progress in Inorganic Chemistry* (Edited by F. A. Cotton), Vol. 6. Interscience, New York (1964).
6. D. Kivelson and R. Neiman, *J. Chem. Phys.* 1961, **35**, 149.
7. F. A. Cotton and G. Wilkinson, *Advanced Inorganic Chemistry*. Wiley Interscience, New York (1980).
8. A. B. P. Lever, *Inorganic Electron Spectroscopy*. Elsevier, Amsterdam (1968).
9. B. A. Gingras, R. W. Hornal and C. H. Bayley, *Can. J. Chem.* 1960, **38**, 712.
10. K. K. Aravindakshan and C. G. R. Nair, *Proc. Ind. Acad. Sci. (Chem. Sci.)* 1984, **93**, 111.

11. A. Syamal, S. Ahmed and M. A. Bari Niazi, *J. Ind. Chem. Soc.* 1983, **60**, 493.
12. M. M. Mostafa, A. El-Hammid, M. Shallaby and A. A. El-Asmy, *Trans. Met. Chem.* 1981, **6**, 303.
13. R. S. Srivastava, *J. Inorg. Nucl. Chem.* 1980, **42**, 1526.
14. B. A. Booth and A. C. Sartorelli, *Molec. Pharmacol.* 1967, **3**, 290.
15. G. J. Vangiessen, J. A. Crim, D. H. Petering and H. G. Petering, *J. Natl. Cancer Inst.* 1973, **51**, 139.
16. D. H. Petering, *Bioinorg. Chem.* 1972, **1**, 255.

Polyhedron Vol. 12, No. 10, pp. 1193–1199, 1993
Printed in Great Britain

0277–5387/93 $6.00+.00
© 1993 Pergamon Press Ltd

SOME HYDRIDOTRIS(3,5-DIMETHYLPYRAZOLYL)BORATE COMPLEXES OF ZINC, CADMIUM AND MERCURY—SYNTHETIC, STRUCTURAL AND NMR INVESTIGATIONS

WILLIAM R. McWHINNIE,† ZAHRA MONSEF-MIRZAI, MICHAEL C. PERRY and NIRMALA SHAIKH

Department of Chemical Engineering and Applied Chemistry, Aston University, Aston Triangle, Birmingham B4 7ET, U.K.

and

THOMAS A. HAMOR

School of Chemistry, University of Birmingham, PO Box 363, Edgbaston, Birmingham B15 2TT, U.K.

(*Received* 2 *December* 1992; *accepted* 8 *January* 1993)

Abstract—Attempts to prepare 1 : 1 complexes, L*CdX, where L* = hydridotris(3,5-dimethylpyrazolyl)borate and X = Cl, I, met with limited success. Thus, with X = Cl, CdL^*_2 was a usual product, although the reactions were not always clean. An L*CdI compound was prepared. By contrast, reactions of KL* with $HgCl_2$ gave L*HgCl cleanly. The reactions of $[(Ph_3P)_2CdCl_2]$ or [(di-2-pyridylamine)$CdCl_2$] with KL* gave "L*Cd(OH)·H_2O" in alcoholic media, whereas [(1,2-phenylenediamine)CdI_2] on reaction with KL* in CH_2Cl_2 gave CdL^*_2. KL* removed 18-crown-6 from [(18-crown-6)$CdCl_2$] as [(18-crown-6)K]L*. PhHgCl reacted with KL* in THF to give a product of stoichiometry "PhHgL*·0.5KCl". Variable-temperature ^1H and ^{199}Hg NMR studies in $CDCl_3$ gave data consistent with the equilibrium

$$PhHg^+ + L^{*-} \rightleftharpoons PhHgL^*$$

with low temperatures favouring the covalent form. Other NMR data are presented and discussed. The crystal structure of CdL^*_2 is reported, but severe disorder, with the molecule taking up two orientations about a $\bar{3}$ axis, reduced the accuracy of the structure determination. The environment around cadmium is essentially octahedral with a slight trigonal distortion in one molecule (**A**), but not in the other (**B**). The Cd—N distances [2.36(1) in **A**, 2.43(2) Å in **B**] are in good agreement with those found in analogous cadmium complexes.

Since the first report of their use in 1966[1] the pyrazolylborates, $[R_nB(pz)_{4-n}]^-$ (R = H, alkyl or aryl; pz = pyrazolyl),[2,3] and related ligands[3] have established themselves as an important weapon in the armory of the coordination chemist. The hydridotris(pyrazolyl)borate $[HB(pz)_3]^-$[2] in particular is of great interest and the parent ligand readily gives uncharged bis-ligand complexes with bipositive metal ions, e.g. $[ZnL_2]$ and $[CdL_2]$.[4] Modified ligands carrying substituents on the 3- and 5- (or solely 3-) carbon atoms of the pyrazolyl ring are now well known, e.g. [HB(3,5-dimethylpyrazolyl)borate](L*);[3] other examples include the presence of more sterically demanding substituents in the 3-position,[3] e.g. Ph and Bu^t.[5,6] The 3-tertiarybutyl and 3-phenyl derivatives have recently been shown to give monomeric zinc complexes, "L^1ZnX", where X = NO_3, NCS, NCO, N_3[5] or groups such as SEt.[6] The large pendant-like substituents in the 3-position of the ring are considered to form a hydrophobic cage around the metal. Also,

† Author to whom correspondence should be addressed.

in a similar fashion the sterically demanding ligands have been used to prepare important organomagnesium derivatives of the type LMgR where L is the substituted pyrazolylborate and R an organic moiety.[7,8]

Compounds of stoichiometry "LMER" (L = anionic ligand; M = Zn, Cd, Hg; E = Se, Te; R = organic group) may be of interest as semi-conductor precursors in MOCVD experiments and the hydridotris(pyrazolyl)borates are an attractive choice of L for preliminary studies. This paper reports observations made during efforts to obtain monomeric cadmium complexes of the type L*CdX(ligand)$_2$, where L* is hydridotris(3,5-dimethylpyrazolyl)borate and ligand is a nitrogen, oxygen or phosphorus donor. The desired compounds were not in fact formed but some new results were obtained and these are briefly communicated.

EXPERIMENTAL AND RESULTS

Syntheses

Bis[hydrido(3,5 - dimethylpyrazolyl)borate]cadmium(II). A solution of K[HB(3,5-Me$_2$pz)] (0.34 g, 1 mmol) in water (15 cm^3) was added dropwise to a stirred solution of $CdCl_2$ (0.19 g, 1 mmol) in water (20 cm^3). The mixture was stirred for 1 h at room temperature and filtered. The white solid was recrystallized from carbon tetrachloride and dried *in vacuo*; m.p. 350°C (dec.). Found: C, 49.5; H, 6.1; N, 22.9. Calc. for $C_{30}H_{44}B_2CdN_{12}$: C, 50.9; H, 6.2; N, 23.8%.

If the above preparation is performed using $Cd(ClO_4)_2$ in water an impure product was obtained. Contamination of the bis complex with the species L*Cd(OH) (see below) occurred (IR, analysis). Also, the use of ethanol rather than water as the solvent for $CdCl_2$ gave a less pure product. Found: C, 48.6; H, 6.0; N, 22.1%. In this case ^{1}H and ^{13}C NMR showed contamination with a small quantity of another species, but microscopic examination of the material showed that the bulk of the crystals were CdL*$_2$ [L* = hydridotris-(3,5-dimethylpyrazolyl)borate], which could readily be hand separated. Similar problems were found when the corresponding zinc(II) complex was prepared by reaction of KL* (1 mmol) in ethanol (10 cm^3) with $ZnCl_2$ (1 mmol) in ethanol (10 cm^3). The white product obtained after the mixture was stirred for $\frac{1}{2}$ h gave a poor analysis. Found: C, 51.4; H, 6.4; N, 23.8. Calc. for $C_{30}H_{44}B_2N_{12}Zn$: C, 54.6; H, 6.7; N, 25.5%. In this case also crystals of pure ZnL*$_2$ could be hand picked (X-ray crystallography, see below).

Reactions of KL* *with cadmium chloride complexes.* The following complexes were prepared from $CdCl_2$ and the appropriate ligand: (a) [(Et_2N, $CH_2CH_2 \cdot NEt_2$)$CdCl_2$]. Found: C, 33.8; H, 6.90; N, 7.9. Calc. for $C_{10}H_{24}CdCl_2N_2$: C, 33.8; H, 6.7; N, 7.87%. (b) [$(Ph_3P)_2CdCl_2$]. Found: C, 60.7; H, 4.1. Calc. for $C_{36}H_{30}CdCl_2P_2$: C, 61.1; H, 4.3%. (c) [(18-crown-6)$CdCl_2$]. Found: C, 66.2; H, 6.9. Calc. for $C_{12}H_{24}CdCl_2O_6$: C, 66.7; H, 6.7%.

Both [$(Et_2NCH_2CH_2NEt_2)CdCl_2$] and [$(Ph_3P)_2$ $CdCl_2$] gave the same product when reacted with KL* under the following conditions. A solution of KL* (0.334 g, 1 mmol) in acetone (20 cm^3) was added dropwise to a solution of [$(Et_2NCH_2CH_2$ $NEt_2)CdCl_2$] (0.36 g, 1 mmol) in acetone (15 cm^3). The mixture was stirred for 1 h at room temperature, after which a white solid was filtered, washed and dried *in vacuo*. The rather intractable material analysed as L*Cd(OH) $\cdot$ H_2O [m.p. = 320°C (dec), ν(OH) = 3440 cm^{-1}). Found: C, 41.1; H, 5.1; N, 18.5. Calc. for $C_{15}H_{25}BCdN_6O_2$: C, 40.5; H, 5.6; N, 18.9%. The IR spectra showed the absence of N,N'-tetraethyl-1,2-diamine and similarly the absence of Ph_3P when the phosphine complex was used in the synthesis.

Another ligand to be considered was 1,2-phenylenediamine(pd), thus [(pd)CdI_2] was prepared by the direct reaction of CdI_2 and 1,2-phenylenediamine in CH_2Cl_2. When this complex was reacted with KL* in a 1 : 1 mole ratio in CH_2Cl_2, a sample of pure CdL*$_2$ was isolated. Found: C, 50.3; H, 6.2; N, 23.5%.

Different behaviour was observed for [(18-crown-6)]$CdCl_2$, thus, a solution of KL* (0.34 g, 1 mmol) in acetone (20 cm^3) was added dropwise to a stirred solution of [(18-crown-6)$CdCl_2$] (0.45 g, 1 mmol) in acetone (25 cm^3). The mixture was stirred for 5 h at room temperature, over which period a white precipitate shown to be [(18-crown-6)K]L* separated; m.p. = 100°C. Found: C, 54.5; H, 7.1; N, 14.9. Calc. for $C_{27}H_{46}BKN_6O_6$: C, 54.0; H, 7.7; N, 14.0%.

Reaction of KL* *with cadmium*(II) *iodide and mercury*(II) *chloride.* (a) CdI_2: A solution of CdI_2 (3.35 g, 9.2 mmol) in dichloromethane (30 cm^3) was heated under reflux and to the hot solution was added dropwise a solution of KL* (1.54 g, 4.6 mmol) in dichloromethane (60 cm^3). The combined solution was heated under reflux for 1 h and the solid product was filtered hot; m.p. 280°C. Found: C, 33.6; H, 4.1; N, 15.2. Calc. for $C_{15}H_{22}CdIN_6$: C, 33.6; H, 4.1; N, 15.7%.

(b) $HgCl_2$: A solution of KL* (0.34 g, 1 mmol) in acetone (20 cm^3) was added dropwise to a stirred solution of $HgCl_2$ (0.28 g, 1 mmol) in acetone (20 cm^3). The mixture was stirred for 5 h at room tem-

perature, after which the solid product was filtered, washed with acetone and dried *in vacuo*; m.p. = 200°C (dec.). Found: C, 34.0; H, 4.2; N, 15.1. Calc. for $C_{15}H_{22}BClHgN_6$: C, 33.8; H, 4.1; N, 15.8%.

Reaction of PhHgCl *with* KL*. A solution of KL* (0.34 g, 1 mmol) in dry THF (30 cm^3) was added dropwise to a solution of PhHgCl (0.32 g, 1 mmol) in dry THF (30 cm^3). The mixture was stirred for 1.5 h at room temperature and the separated solid was filtered. The material was recrystallized from THF. Found: C, 42.2; H, 4.6; N, 13.5. Calc. for $C_{21}H_{27}BN_6Hg \cdot 0.5KCl$: C, 41.9; H, 4.5; N, 13.9%. A flame test was positive for potassium.

Physical measurements

IR spectra were measured as KBr discs or Nujol mulls with a Perkin–Elmer 1710 FTIR spectrometer. ^1H and ^{13}C NMR spectra were recorded with a Bruker AC(E) 300 MHz spectrometer. Both spectra were referenced to tetramethylsilane. ^{199}Hg spectra were also determined and referenced to aqueous $HgCl_2$. Fast atom bombardment mass spectra (FABMS) were obtained via the SERC service at Swansea.

X-ray crystallography

Cadmium complex—crystal data. $C_{30}H_{44}B_2CdN_{12}$, $M_r = 706.8$, trigonal, space group $R\bar{3}$, $a = 10.423(4)$ Å, $\alpha = 63.71(4)°$, $V = 866.3$ Å^3, $Z = 2$, $D_c = 2.710$ g cm^{-3}, $F(000) = 732$, μ(MO-K_α) = 1.339 mm^{-1}, $\lambda = 0.71069$ Å.

A colourless crystal was mounted on an Enraf–Nonius CAD-4 diffractometer; cell dimensions and intensities were measured by ω–2θ scans with graphite monochromated Mo-K_α radiation. 4212 reflections were scanned in the range $2 < \theta < 27.5°$ and of these 1338 were independent ($R_{int} = 0.034$) and 1206 having $I > 2.5\sigma(I)$ were considered observed and used in the analysis. Three standard reflections measured every 2 h showed no significant variation in intensity.

The structure was determined by Patterson and Fourier methods and refined by least-squares using anisotropic thermal parameters for non-hydrogen atoms. Hydrogen atoms were placed in calculated positions riding on their respective bonded atoms. Weights, $w = 1/[\sigma^2(F) + 0.002F^2)]$, were used in the least-squares refinement. The molecule possesses crystallographic $\bar{3}$ (C_{3i}) symmetry, cadmium and boron lying on special positions with point symmetry $\bar{3}$ (C_{3i}) and 3 (C_3), respectively. The organic ligand is disordered, occupying two sites rotated through *ca* 30° with respect to each other. The two half molecules were refined in separate blocks. The calculations were terminated when all shift/e.s.d. ratios were < 0.1 and $R = 0.0632$, $R_w = 0.0893$ for 1206 observed reflections. The residual electron density in a final difference map was within the range −1.07 to +1.02 e Å^{-3}.

Computations were performed on the IBM 3090 computer at the University of Birmingham and on the Ahdahl 5890 at the Manchester Computing Centre with the SHELXS 86[9] and SHELX 76[10] programs. The molecular diagram was drawn using PLUTO.[11] A crystal of the related zinc(II) complex $C_{30}H_{44}B_2N_{12}Zn$ was shown to be isomorphous (same space group, unit cell). Atomic coordinates and thermal parameters for the cadmium complex have been deposited with the Cambridge Crystallographic Data Centre. Bond lengths and angles are listed in Table 1.

Table 1. Bond lengths (Å) and angles (°) with e.s.d.s in parentheses

	Molecule A	Molecule B
Cd—N(1)	2.36(1)	2.43(2)
N(2)—B	1.53(1)	1.54(1)
N(2)—N(1)	1.35(2)	1.57(3)
C(2)—N(2)	1.37(1)	1.39(2)
C(4)—N(1)	1.41(1)	1.19(2)
C(2)—C(1)	1.51(3)	1.49(3)
C(3)—C(2)	1.35(2)	1.30(3)
C(4)—C(3)	1.40(2)	1.43(3)
C(5)—C(4)	1.52(3)	1.50(4)
N(1)—Cd—N(11)	180	180
N(1)—Cd—N(21)	80.1(3)	89.7(8)
N(1)—Cd—N(31)	99.9(3)	90.3(8)
N(2)—B—N(22)	110(1)	111(1)
N(2)—N(1)—Cd	116(1)	104(1)
C(4)—N(1)—Cd	129(1)	139(2)
C(4)—N(1)—N(2)	104(1)	103(2)
N(1)—N(2)—B	119(1)	125(1)
C(2)—N(2)—B	130(1)	129(1)
C(2)—N(2)—N(1)	111(1)	105(1)
C(1)—C(2)—N(2)	121(1)	121(1)
C(3)—C(2)—N(2)	108(1)	107(1)
C(3)—C(2)—C(1)	130(1)	131(1)
C(4)—C(3)—C(2)	106(1)	109(1)
C(3)—C(4)—N(1)	109(1)	114(2)
C(5)—C(4)—N(1)	122(1)	116(2)
C(5)—C(4)—C(3)	129(1)	129(1)

N(11) is related to N(1) by symmetry operation $-x, -y, -z$.

N(21) is related to N(1) by symmetry operation z, x, y.

N(31) is related to N(1) by symmetry operation $-z, -x, -y$.

N(22) is related to N(2) by symmetry operation z, x, y.

DISCUSSION

Despite the fact that the ligand [HB(3,5-dimethylpyrazolyl)borate] (L*) may reduce the accessibility of the metal to which it is coordinated[12] (cone angle estimated to be 225°) and that, in consequence, novel molybdenum and tungsten derivatives have been stabilized, e.g. $L^*Mo(NO)X_2$ (X = halogen),[13,14] the readiness with which both zinc(II) and cadmium(II) ions gave bis complexes[4] with $[HB(pz)_3]^-$ made it unlikely that mono-ligand complexes would be easily prepared on reaction of L* with these ions. The reactions between KL* and cadmium(II) salts were, in general, not clean. Similar problems were encountered by Trofimenko *et al.*[15] when hydridotris(3-iso-propylpyrazolyl)-borate, a ligand of intermediate steric demand, was reacted with zinc(II) salts. Even when KL* and cadmium(II) salts were reacted in a 1:1 metal: ligand ratio, the bis complex CdL^*_2 was the dominant product. The best procedure was to use water as a solvent for $CdCl_2$ and to recrystallize the product from CCl_4. Use of ethanol as a solvent for $CdCl_2$ and KL* gave products of variable analysis, microscopic examination of which revealed crystalline CdL^*_2 (X-ray analysis) with small quantities of a second product. When $Cd(ClO_4)_2$ was used there was IR evidence that the contaminant may be a hydroxo species, possibly the intractable material "$L^*Cd(OH)\cdot H_2O$" formed under other circumstances (see below). This material contains strong broad features in the IR spectrum, which are characteristic of strongly hydrogen-bonded species. Confirmation of the preparation of CdL^*_2 (and similarly, ZnL^*_2) was obtained from FABMS which showed the parent ion; the base peak was, however, derived from the loss of one 3,5-dimethylpyrazolyl moiety. Also, the crystal structure was solved by X-ray methods (see below).

It was speculated that other ligands might be able to reduce the Lewis acidity of cadmium(II) and encourage the formation of 1:1 Cd:L* complexes. Thus, as detailed in the Experimental $[Cd(Et_2NCH_2CH_2NEt_2)Cl_2]$, $[Cd(PPh_3)_2Cl_2]$[16] and [Cd(18-crown-6)Cl_2][17] were reacted, in turn, with KL* in a 1:1 molar ratio. The first two complexes afforded the intractable "$L^*Cd(OH)\cdot H_2O$", referred to above. The product which precipitated from the reaction involving the cadmium(II)-crown ether complex was in fact [K(18-crown-6)][L*]. Thus, whilst in two cases the presence of the second ligand has influenced the stoichiometry of the product complex, the material is of limited value for our ultimate purpose. No greater success was achieved using complexes of cadmium(II) iodide. Thus, $[(pd)CdI_2]$ (pd = 1,2-phenylenediamine) in reaction with KL* in CH_2Cl_2 afforded pure CdL^*_2. The problem of hydrolysis had been overcome but six-coordinate cadmium products still resulted.

The failure to obtain clean preparations of 1:1 complexes, L*CdX, with X = Cl led to the consideration of a larger halogen, iodine. A compound of stoichiometry L*CdI was obtained, but in this case also replicate syntheses gave some products of variable (usually high) carbon percentages. ^1H NMR spectroscopy indicated contamination with greater or smaller amounts of CdL^*_2. By contrast, the reaction with $HgCl_2$ to give L*HgCl was clean. An interesting reaction was that of PhHgCl with KL* in THF. The product, on repeated recrystallization, was of stoichiometry "$PhHgL^*\cdot 0.5$ KCl" and gave a positive qualitative test for potassium. The IR spectrum showed L* and Ph to be the only organic moieties present.

The IR spectra of the compounds CdL^*_2, ZnL^*_2, L*CdI, L*HgCl and "$PhHgL^*\cdot 0.5$ KCl" are all extremely similar with respect to the contributions of L*. Given the known (see below) bis-terdentate mode of coordination for the ligands in CdL^*_2, the IR spectra provide circumstantial evidence that the terdentate mode of bonding is adopted for all the listed compounds in the solid state. It is not, however, possible to comment at this juncture on the metal coordination number for L*CdI or L*HgCl.

NMR studies

There is evidence in the literature of fluxional behaviour for complexes of L* with both transition metal[18] and main group[19] elements. It was prudent to explore that possibility for the present compounds, although it is known that ligand exchange reactions may be very rapid for cadmium(II) and mercury(II) species—for example, MeHgL [L = $HB(pz)_3$] underwent such rapid exchange even at −90°C that it was not possible to determine the mode of attachment (mono-, bi- or terdentate) with ^1H NMR spectroscopy.[20] In the case of the complexes studied here the ^1H NMR data showed the three pyrazolyl rings to be equivalent over the temperature range considered (300–220 K), thus a choice between fluxional bidentate and terdentate behaviour is not possible. However, the NMR data which are gathered into Table 2 are useful in other respects and a brief discussion follows.

Whilst ^1H NMR data for CdL^*_2 are certainly consistent with the presence of terdentate ligands the data cannot eliminate the possibility of lower coordination numbers in solution. Cooling a $CDCl_3$ solution of CdL^*_2 to 263 K did allow direct observation of the rarely reported resonance of the pro-

Table 2. ^{1}H and ^{199}Hg NMR data for cadmium and mercury complexes in $CDCl_3$ solution

Compound		^{1}H data[a] Ph	4-H	5-CH_3, 3-CH_3	B—H	^{199}Hg data[b]
CdL^*_2	295 K	—	5.63	2.40, 1.67		—
	263 K	—	5.73	2.39, 1.67	4.8	—
L*CdI	295 K	—	5.77	2.38, 2.32		—
	253 K	—	5.75	2.35, 2.30	4.7	—
L*HgCl	297 K	— [$J(^{1}H–^{199}Hg) = 15$ Hz]	5.80	2.36, 2.29		—
	253 K	—	5.79	2.34, 2.27	4.5	—
PhHgL*·0.5 KCl						
	278 K	7.57–7.23(m)	5.84 5.77	2.39, 2.28 2.23		815.8, 614.4
	223 K	7.63–7.23(m)	5.88 5.80	2.33, 2.27 2.24	4.7	
	220 K	7.62–7.23(m)	5.88 5.80	2.39, 2.32 2.24	4.7	v.w, 621.2
	295 K	7.58–7.24(m)	5.84 5.76	2.37, 2.26 2.21		
	243 K					815.1, 618.8
	228 K					812.8, 620.8
	213 K					812.6 (v.w.) 662.0
PhHgCl	278 K					420.4
KL*	297 K		5.80	2.21, 2.16	4.6	

[a] Standard $(CH_3)_4Si$, 300.13 MHz.
[b] vs aqueous $HgCl_2$, 53.673 MHz.

ton attached to boron as a broad band at $\delta = 4.8$ ppm (N.B. both ^{10}B and ^{11}B are quadrupolar). The spectrum of the product obtained from the reaction of KL* with $CdCl_2$ in ethanol clearly shows the presence of CdL^*_2 and another species, possibly L*CdCl. CdL^*_2 was also detected as a minor contaminant in preparations of L*CdI (see above), the integrals were constant with temperature and hence, the material is an impurity rather than arising from a redistribution reaction of L*CdI in $CDCl_3$. The presence of CdL^*_2 is also apparent in the ^{13}C NMR spectrum, another feature of interest in which is the observation of a 14 Hz coupling of $^{111,113}Cd$ with C(3).

The ^{1}H NMR spectrum of L*HgCl confirms the clean preparation of this compound and also shows a 15 Hz $^{1}H(4)–^{199}Hg$ coupling. Cooling effects produce no spectral changes. The most interesting data were obtained for the material "PhHgL*·0.5 KCl". The ^{1}H data confirmed the 1:1 Ph:L* ratio, but strongly suggested that two phenyl environments were present (overlapping multiplets). The data also suggested that free and coordinated L* co-existed in the solution ($CDCl_3$). The temperature dependence of the ^{199}Hg NMR spectrum was determined (Table 2) and two mercury resonances were observed. At higher temperatures a sharp resonance at 815.8 ppm (278 K) dominated a broad resonance at 614.4 ppm (both relative to aqueous $HgCl_2$). However, on cooling ultimately to the point of freezing (213 K) the broad resonance becomes dominant (622 ppm at 213 K) and the sharp resonance becomes almost vanishingly weak. It is sensible to assign the broad resonance of the mercury species carrying the L* ligand since the quadrupolar ^{14}N ligand atoms are likely to reduce the relaxation time of the ^{199}Hg nucleus. The other resonance does not arise from PhHgCl, which gives a peak at 420.4 ppm at 278 K.

The significant deshielding of the mercury nucleus is consistent with a positively charged species and hence, an explanation which is consistent

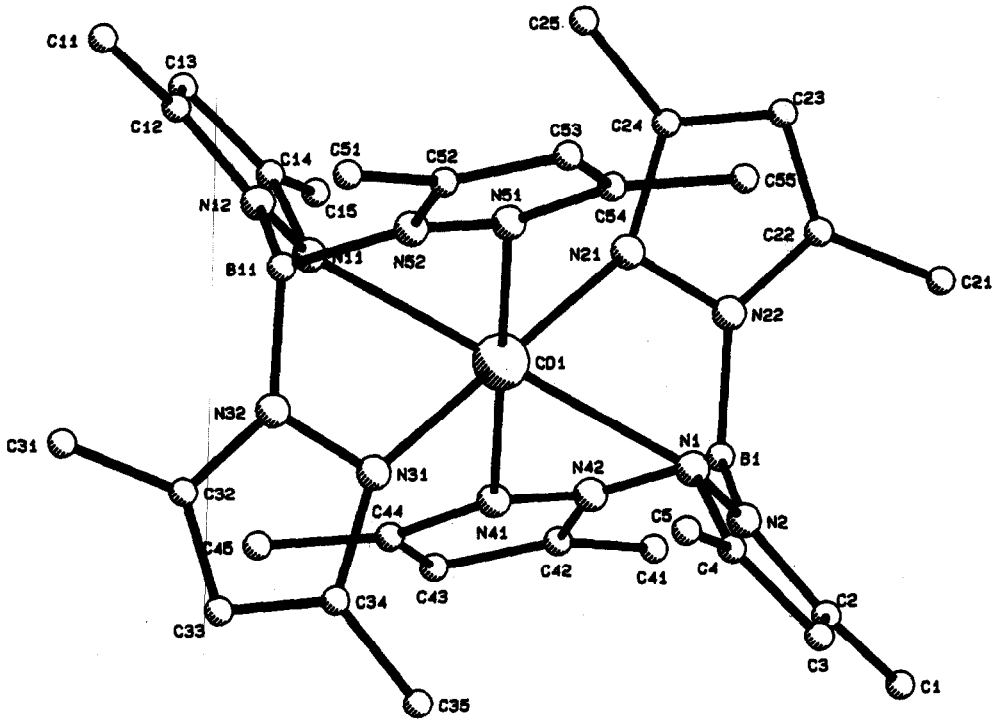

Fig. 1. View of molecule A. Hydrogen atoms have been omitted for the sake of clarity. Atoms labelled 11–15, 21–25, 31–35, 41–45 and 51–55 are related to those labelled 1–5 by the symmetry operations $-x, -y, -z; z, x, y; -z, -x, -y; y, z, x$; and $-y, -z, -x$, respectively.

with all ^{1}H and ^{199}Hg data involves the following equilibrium:

$$\underset{614.4\ \text{ppm (278 K)}}{\text{PhHgL*}} \overset{CDCl_3}{\rightleftharpoons} \underset{815.8\ \text{ppm (278 K)}}{\text{PhHg}^{+}} + \text{L*}^{-}. \quad (1)$$

It seems likely that PhHgL* is present in the solid state also. If $CDCl_3$ solutions of PhHgL*·0.5KCl are allowed to stand overnight some mercury is deposited together with some small quantities of a white solid; however, the ^{1}H and ^{199}Hg spectra of the decanted supernatant solution show the continued presence of the species in eq. (1). If the solution is left several days a very simple ^{1}H NMR spectrum is obtained, which consists of resonances from the phenyl-group, the 4-hydrogen atom of the pyrazolyl ring and a single methyl resonance in the ratio 2.5:1.6. It would seem that the ligand has decomposed with the rupture of B—N bonds by a mechanism as yet unknown.

Structural studies

A view of one of the "half molecules" (molecule **A**) is displayed in Fig. 1. Due to the disorder in the crystal structure accurate molecular parameters could not be obtained. The coordination geometry around cadmium is essentially octahedral with some trigonal distortion in molecule **A**, but not in molecule **B**. The Cd—N bond distances are greater than previously found in analogous complexes. Thus, in the copper,[21] high-spin iron(II)[22] and magnesium[23] analogues metal—N bond distances are in the ranges 2.04–2.32, 2.15–2.19 and 2.17–2.20 Å, respectively. Our results are, however, in good agreement with previous determinations of Cd—N(pyrazolyl) bond distances in complexes of different ligands; 2.43 in dichloro[2,5-dimethyl-1,6-bis(3,5-dimethyl-1-pyrazolyl)-2,5-diazahexane-N,N′,N″,N‴]cadmium(II),[24] 2.35 in Cd_2(bddo)(NCS)$_4$ [bddo = 1,8-bis(3,5-dimethyl-1-pyrazolyl)-3,6-dithiaoctane],[25] 2.26 (mean) in [bis(2-(3,5-dimethyl-1-pyrazolyl)ethyl)oxide]bis(nitrato-O,O′)cadmium (II)[26] and 2.31 Å (mean) in the amine analogue.[26]

Acknowledgements—The authors thank the SERC for support. N.S. thanks the SERC and RSRE (Malvern) for a CASE award.

REFERENCES

1. S. Trofimenko, *J. Am. Chem. Soc.* 1966, **88**, 1842.
2. S. Trofimenko, *Chem. Rev.* 1972, **72**, 497.

3. S. Trofimenko, *Prog. Inorg. Chem.* 1986, **34**, 115.
4. S. Trofimenko, *J. Am. Chem. Soc.* 1967, **89**, 3170.
5. S. Trofimenko, J. C. Calabrese and J. S. Thompson, *Inorg. Chem.* 1987, **26**, 1507.
6. R. Alsfasser, A. K. Powell and H. Vahrenkamp, *Angew. Chem., Int. Edn Engl.* 1990, **29**, 898.
7. R. Han and G. Parkin, *Organometallics* 1991, **10**, 1010.
8. R. Han and G. Parkin, *J. Am. Chem. Soc.* 1992, **114**, 748.
9. G. M. Sheldrick, SHELXS 86, Program for the Solution of Crystal Structures. University of Göttingen, F.R.G. (1987).
10. G. M. Sheldrick, SHELX 76, Program for Crystal Structure Determination. University of Cambridge, U.K. (1976).
11. W. D. S. Motherwell and W. Clegg, PLUTO 88, Program for Plotting Crystal and Molecular Structures, Cambridge Structural Database System Users Manual (1988). Implemented at the Manchester Computing Centre.
12. E. Frauendorfer and H. Brunner, *J. Organomet. Chem.* 1982, **240**, 371.
13. A. S. Drane and J. A. McCleverty, *Polyhedron* 1983, **2**, 53.
14. J. A. McCleverty, D. Seddon, N. A. Bailey and N. W. J. Walker, *J. Chem. Soc., Dalton Trans.* 1976, 898.
15. S. Trofimenko, J. C. Calabrese, P. J. Domaille and J. S. Thompson, *Inorg. Chem.* 1989, **28**, 1091.
16. J. R. Blackburn, R. Nordberg, F. Stevie, R. G. Albridge and M. M. Jones, *Inorg. Chem.* 1970, **9**, 2374.
17. C. R. Paige and M. F. Richardson, *Can. J. Chem.* 1984, **62**, 332.
18. For example: D. L. Reger and M. E. Tarquini, *Inorg. Chem.* 1983, **22**, 1064.
19. For example: D. L. Reger, M. F. Huff, A. L. Reingold and B. S. Haggerty, *J. Am. Chem. Soc.* 1992, **114**, 579.
20. A. J. Canty, N. J. Minchin, J. M. Patrick and A. M. White, *Aust. J. Chem.* 1983, **36**, 1107.
21. N. Kitajima, Y. Moro-Oka, A. Uchida, Y. Sasada and Y. Ohashi, *Acta Cryst.* 1988, **C44**, 1876.
22. J. D. Oliver, D. F. Mullica, B. D. Hutchinson and W. O. Milligan, *Inorg. Chem.* 1980, **19**, 165.
23. R. Han and G. Parkin, *J. Organomet. Chem.* 1990, **393**, C43.
24. F. Paap, A. Erdonmez, W. L. Driessen and J. Reedijk, *Acta Cryst.* 1986, **C42**, 783.
25. W. G. Haanstra, W. L. Driessen, J. Reedijk, U. Turpeinen and R. Hamalainen, *J. Chem. Soc., Dalton Trans.* 1989, 2309.
26. E. A. H. Griffith, N. G. Charles, K. Lewinski, E. L. Amma and P. F. Rodesiler, *Inorg. Chem.* 1987, **26**, 3983.

Polyhedron Vol. 12, No. 10, pp. 1201–1207, 1993
Printed in Great Britain

0277–5387/93 $6.00+.00
© 1993 Pergamon Press Ltd

X-RAY STRUCTURE AND SPECTROSCOPIC PROPERTIES OF PLATINUM(II) COMPLEXES OF 1,1′-BIISOQUINOLINE

LUK-KI CHENG, KAP-SUN YEUNG and CHI-MING CHE†

Department of Chemistry, The University of Hong Kong, Pokfulam Road, Hong Kong

and

MING-CHU CHENG and YU WANG

Department of Chemistry, National Taiwan University, Taipei, Taiwan, R.O.C.

(*Received* 11 *December* 1992; *accepted* 8 *January* 1993)

Abstract—Three platinum(II) complexes of biq (biq = 1,1′-biisoquinoline), $[Pt(biq)Cl_2]$, $[Pt(biq)(py)_3](ClO_4)_2$ (py = pyridine) and $[Pt(biq)(dapy)_3](ClO_4)_2$ [dapy = 4-(dimethylamino)pyridine] were prepared. Using ^1H NMR spectroscopy and X-ray crystallography, biq in the former complex was found to be bidentate and in the two latter complexes monodentate. Dihedral angles between the two isoquinoline rings were determined to be 35.18° and 41.12° in $[Pt(biq)Cl_2]$ and 77.61° in $[Pt(biq)(dapy)_3](ClO_4)_2$. The crystal structure of $[Pt(biq)Cl_2]$ is the first example of η^2-μ_1 biq complexes with a five-membered chelating ring. Weak intramolecular π–π stacking occurs in the solid phase of $[Pt(biq)(dapy)_3](ClO_4)_2$.

Ligands incorporating a 1,1′-binaphthyl unit have been receiving current interest because of their application in catalytic asymmetric reactions.[1] In our search for new metal catalysts for asymmetric organic oxidation the ligand 1,1′-biisoquinoline (biq), which possesses the combined structural features of 2,2′-bipyridine (bpy) and 2,2′-bis(diphenylphosphino)-1,1′-binaphthyl, has attracted our interest. Dai *et al.* first reported the X-ray crystal structure of a chiral palladium complex of biq, in which the ligand acts as a bridging ligand.[2] Here we describe three mononuclear platinum(II)-biq complexes, $[Pt(biq)Cl_2]$, $[Pt(biq)(py)_3](ClO_4)_2$ and $[Pt(biq)(dapy)_3](ClO_4)_2$, with the crystal structures of $[Pt(biq)Cl_2]$ and $[Pt(biq)(dapy)_3](ClO_4)_2$ determined.

EXPERIMENTAL

Physical measurements

UV–vis absorption spectra were recorded with a Shimadzu UV-240 spectrophotometer or a Milton Roy Spectronic 3000 Array spectrophotometer in acetonitrile. NMR spectra were run on a Jeol GSX 270 spectrometer. Chemical shifts (δ/ppm) were reported relative to tetramethylsilane (TMS).

X-ray structure determination

Crystals of $[Pt(biq)Cl_2]$ were obtained by the addition of diethyl ether to a dimethyl formamide solution of $[Pt(biq)Cl_2]$. Yellow crystals of $[Pt(dapy)(dapy)_3](ClO_4)_2$ were obtained by diffusion of diethyl ether into acetonitrile solution. X-ray diffraction data were collected on an Enraf–Nonius CAD4 diffractometer with graphite-monochromated Mo-K_α radiation ($\lambda = 0.71069$ Å) using the $\omega/2\theta$ scan mode. Details of crystal parameters, data collection and structure refinement are given in Table 1. Cell dimensions were obtained from 24 reflections with 2θ in the ranges 18.90–23.60° and 18.84–29.16° for $[Pt(biq)Cl_2]$ and $[Pt(biq)(dapy)_3](ClO_4)_2$, respectively. All reflections were corrected for Lorentz, polarization and absorption effects. All data reduction and structure refinement were performed using the NRCC-SDP-VAX packages.[3] The structure was solved by the Patterson method

† Author to whom correspondence should be addressed.

Table 1. Crystallographic data for $[Pt(biq)Cl_2]$ and $[Pt(biq)(dapy)_3](ClO_4)_2$

	$[Pt(biq)Cl_2]$	$[Pt(biq)(dapy)_3](ClO_4)_2 \cdot 0.5(C_2H_5)_2O$
Crystal data		
Empirical formula	$C_{18}H_{12}N_2Cl_2Pt$	$C_{41}H_{47}N_8O_{8.5}Cl_2Pt$
Formula weight	522.29	1053.86
System	Monoclinic	Triclinic
Space group	$P2_1/c$	$P\bar{1}$
a (Å)	14.644(4)	11.553(5)
b (Å)	19.973(4)	14.208(2)
c (Å)	11.127(2)	14.378(5)
α (°)		85.96(2)
β (°)	101.93(2)	97.70(3)
γ (°)		100.07(3)
V (Å^3)	3184(1)	2300(1)
Z	8	2
$\rho_{calc.}$ (g cm^{-3})	2.179	1.52
μ (cm^{-1})	92.4	32.5
$F(000)$	1968	1058
Temperature (K)	297	297
Data collection, reduction, solution and refinement		
Scan range	$0.8+0.35\tan\theta$	$0.9+0.35\tan\theta$
Scan speed (° min^{-1})	2.06–8.24	2.35–8.24
Crystal dimensions (mm)	$0.20\times0.20\times0.30$	$0.50\times0.50\times0.40$
Range h, k, l	−17–17 0–23 0–13	−13–13 0–16 −16–17
Total no. of reflections	5594	8078
No. of observed reflections ($I > 2\sigma(I)$)	3271	6639
No. of atoms and parameters refined	70, 415	106, 504
Residual electron density (e Å^{-3})	−0.970–1.290	−1.350–2.220
R^a	0.040	0.053
$R_w{}^b$	0.032	0.050
S^c	1.77	4.45

[a] $R_f = \Sigma(|F_o|-|F_c|)/\Sigma|F_o|$.
[b] $R_w = [\Sigma(w||F_o|-|F_c||^2)/\Sigma w|F_o|^2]^{1/2}$.
[c] $S = [\Sigma(w||F_o|-|F_c||^2)/(n-p)]^{1/2}$; n is the number of observed reflections, p is the number of parameters used.

and refined by least-squares. Selected bond distances and angles for $[Pt(biq)Cl_2]$ and $[Pt(biq)(dapy)_3](ClO_4)_2$ are given in Tables 2 and 3, respectively.

Materials

Potassium tetrachloroplatinate(II) (K_2PtCl_4) and isocarbostyril were purchased from Aldrich Chemical Company, Inc. Nickel chloride (GPR) ($NiCl_2 \cdot 6H_2O$) and zinc powder (LR) were purchased from BDH. 4-(Dimethylamino)pyridine (dapy) and triphenylphosphine (PPh_3) were purchased from Merck. All chemicals and solvents were used without further purification.

Syntheses

The ligand biq was prepared by homo-coupling of 1-bromoisoquinoline catalysed by $NiCl_2$–PPh_3–Zn in 20% yield.[4] 1-Bromoisoquinoline was prepared by bromination of isocarbostyril with phosphorus tribromide (PBr_3).

$[Pt(biq)Cl_2]$ was prepared in a similar manner to [Pt(substituted 2,2′-bipyridine)Cl_2].[5] In a typical reaction a mixture of K_2PtCl_4 (0.10 g) and biq (0.07

Table 2. Selected bond distances (Å) and angles (°) for $[Pt(biq)Cl_2]$

Type I		Type II	
Pt(1)—Cl(1)	2.295(4)	Pt(2)—Cl(3)	2.293(4)
Pt(1)—Cl(2)	2.278(4)	Pt(2)—Cl(4)	2.276(4)
Pt(1)—N(1)	1.99(1)	Pt(2)—N(21)	1.99(1)
Pt(1)—N(11)	2.00(1)	Pt(2)—N(31)	2.00(1)
Cl(1)—Pt(1)—Cl(2)	88.7(2)	Cl(3)—Pt(2)—Cl(4)	89.8(2)
Cl(1)—Pt(1)—N(1)	95.5(3)	Cl(3)—Pt(2)—N(21)	95.4(3)
Cl(2)—Pt(1)—N(11)	96.1(3)	Cl(4)—Pt(2)—N(31)	94.7(4)
N(1)—Pt(1)—N(11)	79.7(4)	N(21)—Pt(2)—N(31)	80.3(5)
C(2)—N(1)—C(10)	117(1)	C(22)—N(21)—C(30)	119(1)
C(12)—N(11)—C(20)	118(1)	C(32)—N(31)—C(40)	120(1)

g) in water (20 cm^3) was heated to boiling for ½–1 h. The solid precipitate was filtered and washed with dilute hydrochloric acid, water and finally ethanol. The orange solid product yielded 88%. UV–vis spectral data in acetonitrile [λ/nm ($\varepsilon/\times 10^4$ mol^{-1} dm^3 cm^{-1})]: 245 (3.10), 302 (1.20), 385 (1.06), 404 (1.19), 446 (0.50).

The complexes $[Pt(biq)(py)_3](ClO_4)_2$ and $[Pt(biq)(dapy)_3](ClO_4)_2$ were prepared in a similar manner to that for $[Pt(bpy)(py)_2]^{2+}$ by Bielli *et al.*[5] In a typical reaction a mixture of $[Pt(biq)Cl_2]$ (0.13 g) and pyridines (py, dapy; 1 cm^3) in ethanol was warmed at *ca* 50°C for *ca* 10 min until the orange suspension turned to a clear pale-yellow solution. The reaction mixture was filtered and excess $LiClO_4$ was added to the filtrate to give a pale yellow solid, which was filtered and washed with ethanol and diethyl ether. Anal. for $[Pt(biq)(py)_3](ClO_4)_2(PtC_{33}H_{27}N_5O_8Cl_2)$: Found: C, 44.0; H, 2.7; N, 7.8. Calc.: C, 44.7; H, 3.1; N, 7.9%. UV–vis spectral data in acetonitrile [λ/nm ($\varepsilon/\times 10^4$ mol^{-1} dm^3 cm^{-1})]: $[Pt(biq)(py)_3](ClO_4)_2$: 251 (3.02), 325 (2.10), 339 (shoulder); $[Pt(biq)(dapy)_3](ClO_4)_2$: 288 (0.47), 325 (shoulder).

RESULTS AND DISCUSSION

The UV–vis spectral data of $[Pt(biq)(py)_3](ClO_4)_2$ and $[Pt(biq)(dapy)_3](ClO_4)_2$ show two allowed transition bands between 200 and 400 nm, which are assigned to intraligand π–π^* transitions. The UV–vis absorption spectrum of $[Pt(biq)Cl_2]$ is similar to that of $[Pt(LL)Cl_2]$ reported by Gidney *et al.*[6]

Perspective drawings of the molecule and unit cell of $[Pt(biq)Cl_2]$ are given in Figs 1 and 2, respectively. In $[Pt(biq)Cl_2]$ two kinds of configuration were found and they are principally different in the dihedral angles between the two isoquinoline planes. The one with smaller dihedral angle is designated type I (35.18°) and another one type II (41.12°). In both types the platinum atom is in a slightly distorted square-planar coordination geometry. The two isoquinoline moieties are bent away from the coordination plane in opposite directions as a result of mutual repulsion between protons 8 and 8′ on the biq moiety. Similar to $[Pt(bpy)Cl_2]$,[5,7] dimorphism occurs in $[Pt(biq)Cl_2]$. The freshly prepared $[Pt(biq)Cl_2]$ was orange in colour, but after recrystallization from dimethyl formamide dark brown crystals were obtained. An orange solid was precipitated when recrystallization was attempted in a water–acetone mixture. The difference in crystal colour is believed to be due to a change in the degree of hydration. Although $[Pt(biq)Cl_2]$ is similar to $[Pt(bpy)Cl_2]$ in exhibiting dimorphism, no superimposition of molecules is found in the crystal structure of $[Pt(biq)Cl_2]$, as shown in $[Pt(bpy)Cl_2]$.[7] The intermolecular Pt—Pt

Table 3. Selected bond distances (Å) and angles (°) for $[Pt(biq)(dapy)_3](ClO_4)_2$

Pt—N(1)	2.038(7)	Pt—N(31)	1.997(7)
Pt—N(21)	2.022(8)	Pt—N(41)	2.021(8)
N(1)—Pt—N(21)	91.9(3)	N(31)—Pt—N(41)	87.0(3)
N(1)—Pt—N(41)	89.1(3)	C(2)—N(1)—C(10)	119.7(7)
N(21)—Pt—N(31)	92.0(3)	C(11)—N(12)—C(13)	116.3(9)

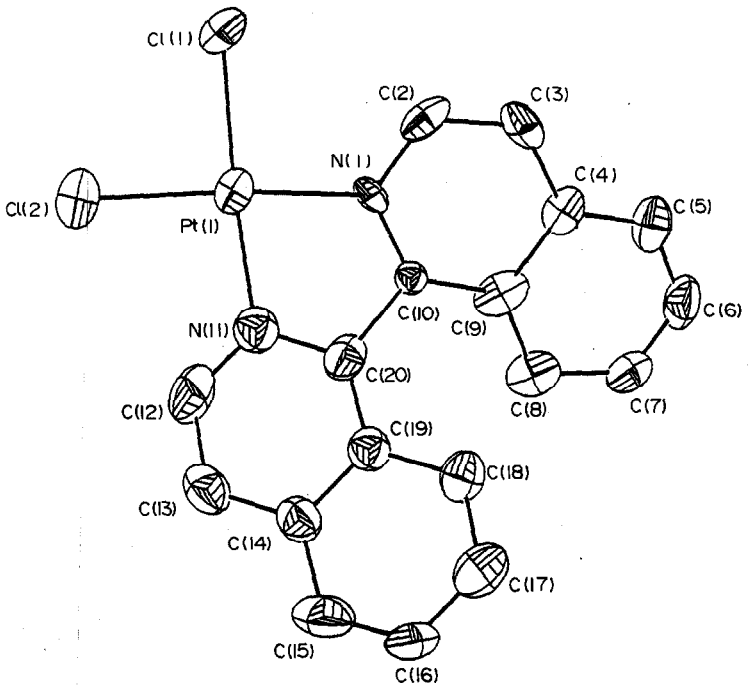

Fig. 1. Perspective drawing of $[Pt(biq)Cl_2]$.

distances are 6.221, 5.128 and 6.414 Å for Pt(1)—Pt(1), Pt(2)—Pt(2) and Pt(1)—Pt(2), respectively, indicating no Pt—Pt interaction. The reason why two forms exist in the crystal is not fully understood. From the unit cell diagam (Fig. 2) it can be seen that the twisted biq moiety in the type II complexes is interlocking with other biq units, hence, reasonably giving an enlarged dihedral angle.

A perspective drawing of the $[Pt(biq)(dapy)_3]^{2+}$ cation is given in Fig. 3. The platinum atom is in a distorted square-planar configuration with Pt, N(1), N(21), N(31) and N(41) all on the same plane. Three dapys are more or less perpendicular to the coordination plane. For the coordinated biq ligand the two isoquinoline moieties are almost planar, in which the deviation of atoms from the least-squares planes is within 0.072 Å. The biq ligand is in an η^1 coordination mode, despite it also being a bidentate chelating ligand. The dihedral angle between the two isoquinoline rings is 77.61°, which is substantially larger than the related values of 35.18° and 41.12° for the $[Pt(biq)Cl_2]$ complex described above. The isoquinoline moiety with the non-coordinated nitrogen atom [N(12)] is weakly stacked adjacent to its neighbouring dapy ring. The interplane distance between the isoquinoline and dapy plane is *ca* 3.5 Å. Such intramolecular π–π stacking is absent in solution, as revealed by ^1H NMR study (*vide infra*). The angle C(2)—N(1)—C(10) [119.7(7)°] [N(1) is coordinated to platinum] is greater than the angle C(11)—N(12)—C(13) [116.3(9)°] [N(12) is uncoordinated]. The former value is similar to those in $[Pt(biq)Cl_2]$, while the latter is typical of non-coordinated sp^2-hybridized nitrogen.

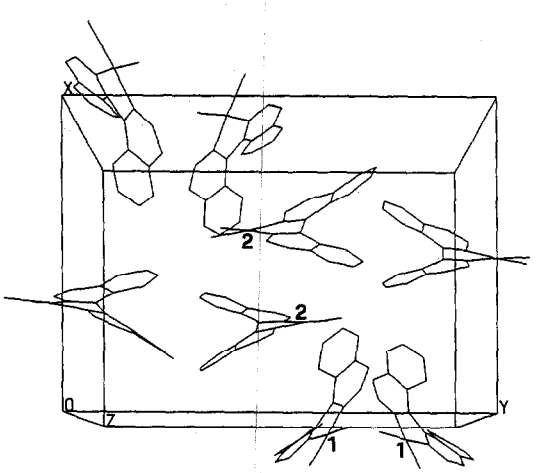

Fig. 2. The unit cell of $[Pt(biq)Cl_2]$.

The ^1H NMR spectroscopic data are listed in Table 4. The ^1H NMR spectrum of $[Pt(biq)Cl_2]$ in $CDCl_3$, with the atomic numbering scheme, is shown in Fig. 4. Figure 5 shows the numbering schemes of $[Pt(biq)(dapy)_3]^{2+}$ and $[Pt(biq)(py)_3]^{2+}$. As discussed above, in the solid form the

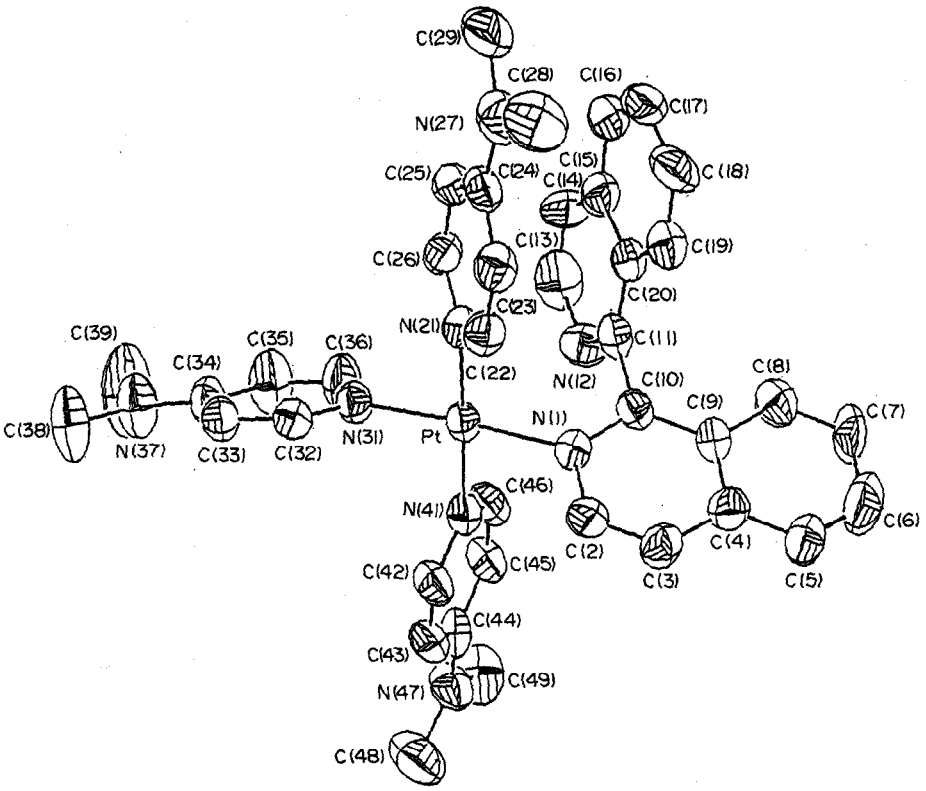

Fig. 3. Perspective drawing of $[Pt(biq)(dapy)_3]^{2+}$.

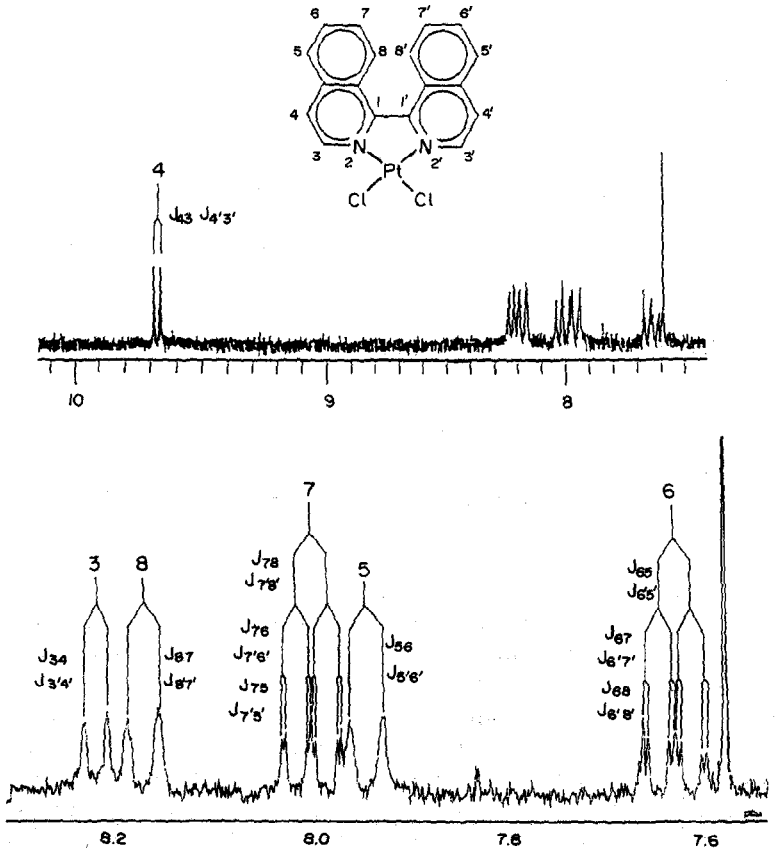

Fig. 4. ^1H NMR spectrum and numbering scheme of $[Pt(biq)Cl_2]$ in $CDCl_3$.

Table 4. Chemical shifts (δ, ppm) and coupling constants (Hz) in ^{1}H NMR spectra of platinum(II)-biq complexes; designation of protons is given in Figs 4 and 5

		Free biq	$[Pt(biq)Cl_2]$	$[Pt(biq)(py)_3]^{2+}$	$[Pt(biq)(dapy)_3]^{2+}$
Chemical shifts and multiplicity					
biq	3	8.72(d)	9.67(d)	9.08(d)	9.04(d)
	3′			9.32(d)	9.20(d)
	4	7.82(d)	8.22(d)	8.20(d)	8.14(d)
	4′			8.32(d)	8.23(d)
	5	7.75(d)	7.95(d)	8.20(d)	8.19(d)
	5′			7.37(d)	7.33(d)
	6	7.71(dd)	7.64(dd)	7.59(dd)	7.56(dd)
	6′			6.96(dd)	7.01(dd)
	7	7.48(dd)	8.00(dd)	8.00(dd)	7.95(dd)
	7′			7.64(dd)	7.62(dd)
	8	7.95(d)	8.17(d)	8.06(d)	8.06(d)
	8′			6.40(d)	6.51(d)
py_t, $dapy_t$	2,6			9.28(d)	8.50(d)
	3,5			7.42(dd)	6.55(d)
	4			7.94(t)	
py_c, $dapy_c$	2			7.42(d)	6.73(d)
	3			6.73(dd)	5.70(d)
	4			7.47(t)	
	5			7.42(dd)	6.44(d)
	6			8.39(d)	7.69(d)
Me_N[a]	c				2.79(s)
	c′				2.96(s)
	t				2.99(s)
Coupling constants					
biq	J_{34}	5.62	6.59	6.59	6.60
	$J_{3'4'}$			5.62	5.62
	J_{56}	8.54	8.79	8.54	8.54
	$= J_{5'6'}$				
	J_{67}	7.08	6.83	6.83	6.83
	$= J_{6'7'}$				
	J_{78}	8.05	8.30	8.30	8.30
	$= J_{7'8'}$				
py, dapy	J_{23}			5.13	7.32
	$= J_{56}$				
	J_{34}			7.81	
	$= J_{45}$				

[a] Me_N = N-methyl protons.
s = singlet, d = doublet, dd = double doublet, t = triplet.

Pt—N(biq) bond of $[Pt(biq)(dapy)_3](ClO_4)_2$ is not free to rotate as it is restricted by two dapys *cis* to it and the π–π stacking (*vide supra*). However, the ^{1}H NMR spectrum in acetonitrile solution reveals no π–π stacking in solution. This is evidenced by the magnetic equivalence of two dapys *cis* to the biq ligand. The change in coordination mode of biq from η^2 to η^1 upon treatment of $[Pt(biq)Cl_2]$ with nitrogen base is likely due to the ring strain of the five-membered ring in the η^2-μ_1 coordination mode and the regain of the planarity of the isoquinoline rings in the η^1-μ_1 geometry.

Similar to rhodium(I) and palladium(II), four-coordinated platinum(II)-biq complexes are coordinatively unsaturated. The availability of vacant coordination sites and the C—H bond activating property of platinum(II) should be useful in platinum(II)-biq complexes in asymmetric C—H

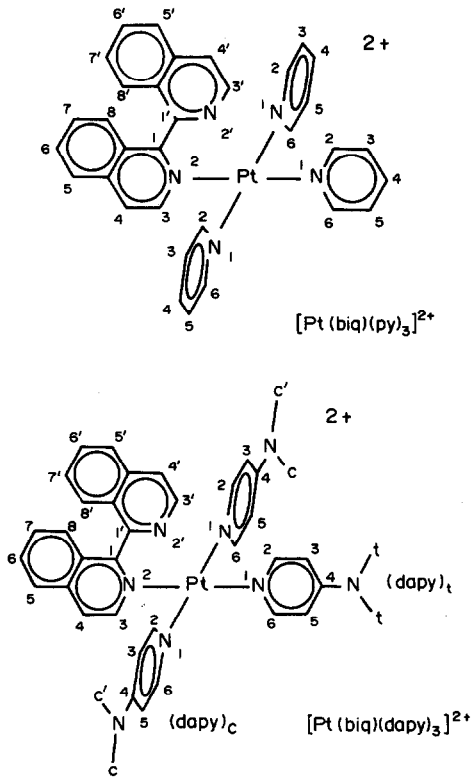

Fig. 5. Numbering schemes of $[Pt(biq)(dapy)_3]^{2+}$ and $[Pt(biq)(py)_3]^{2+}$.

bond oxidation. On the other hand, Calladine's rule is present in DNA. The base pairs have a propeller twist, 11° for dG–DC and 17° for dA–dT pairs.[8] The small twist angles of $[Pt(biq)Cl_2]$ compared with that of Toriumin's complex [77.4(2)°][9] may make chiral recognition binding to DNA possible.

Acknowledgements—We acknowledge support from the University of Hong Kong, the Hong Kong Research Grant Council and the National Science Council of Taiwan. CMC is grateful for the award of a visiting professorship, administered by the National Taiwain University.

REFERENCES

1. C. Rosini, L. Franzini, A. Raffaelli and P. Salvadori, *Synthesis* 1992, 503.
2. L. X. Dai, Z. H. Zhou, Y. Z. Zhang, C. I. Ni, Z. M. Zhang and Y. F. Zhou, *J. Chem. Soc., Chem. Commun.* 1987, 1760.
3. E. J. Gabe, Y. LePage, J.-P. Charland, F. L. Lee and P. S. White, *J. Appl. Cryst.* 1989, **22**, 384.
4. M. Tiecco, L. Testaferri, M. Tingoli, D. Chianell and M. Montanucci, *Synthesis* 1984, 736.
5. E. Bielli, P. M. Gillard and B. T. Heaton, *J. Chem. Soc., Dalton Trans.* 1974, 2133.
6. P. M. Gidney, R. D. Gillard and B. T. Heaton, *J. Chem. Soc., Dalton Trans.* 1973, 132.
7. R. S. Osborn and D. Rogers, *J. Chem. Soc., Dalton Trans.* 1974, **9**, 1002.
8. W. Saenger, *Principles of Nucleic Acid Structure*, Springer Advanced Texts in Chemistry (Edited by C. R. Cantor), p. 254. Springer-Verlag, New York (1984).
9. K. Toriumin, T. Ito and H. Takaya, *Acta. Cryst., Sect. B* 1982, **38**, 807.

Polyhedron Vol. 12, No. 10, pp. 1209–1214, 1993
Printed in Great Britain

0277–5387/93 $6.00+.00
© 1993 Pergamon Press Ltd

CHARACTERIZATION OF BIS(β-DIIMINO-TETRACYANO-PYRROLIZINIDO)COPPER(II) COMPLEX. X-RAY CRYSTAL STRUCTURE OF THE ACETONITRILE ADDUCT AND STRUCTURAL COMPARISON WITH THE TETRAHYDROFURAN DERIVATIVE

MARIO BONAMICO, VINCENZO FARES,† ALBERTO FLAMINI† and NICOLA POLI

Istituto di Chimica dei Materiali del CNR, Area della Ricerca di Roma, P.O. Box 10, 00016 Monterotondo Stazione, Italy

and

GIORGIO MATTEI

Istituto di Metodologie Avanzate Inorganiche del CNR, Area della Ricerca di Roma, P.O. Box 10, 00016 Monterotondo Stazione, Italy

(*Received* 11 *December* 1992; *accepted* 8 *January* 1993)

Abstract—The X-ray crystal structure of the bis(1,2,6,7-tetracyano-3,5-diimino-3,5-dihydro-pyrrolizinido)copper(II) complex, as an adduct with acetonitrile, $CuL_2 \cdot 2CH_3CN$ (**1a**), is described and compared with that of the analogous tetrahydrofuran derivative $CuL_2 \cdot 2THF$ (**1b**), previously reported. The molecular structure of both complexes is almost the same (the copper atom is centrosymmetrically surrounded by four chelating imino groups in a square planar configuration), whereas the spatial arrangement is totally different: in **1a** the molecular units are slipped stacked, while in **1b** they are mutually orthogonal. The results of a number of physical measurements on both **1a** and **1b** are reported and correlated with the structures. The solution electronic spectrum is also reported and compared with that, extraordinarily similar, of copper-phthalocyanine.

Our current investigations are concerned with the bis(1,2,6,7-tetracyano-3,5-diimino-3,5-dihydro-pyrrolizinodo)metal(II), ML_2, complexes (**1**), resulting from a metal-assisted intramolecular cyclization of the corresponding pyrrolenine anion (**2**), as outlined in the scheme below.

We have already reported preliminary information on copper(II)[1] and more extensively discussed nickel(II),[2] iron(II)[3] and cobalt(II)[3] derivatives. The interest in such compounds is due to their electronic structure, which is very similar to that of metal-phthalocyanines (MPc),[4] and, therefore, they might

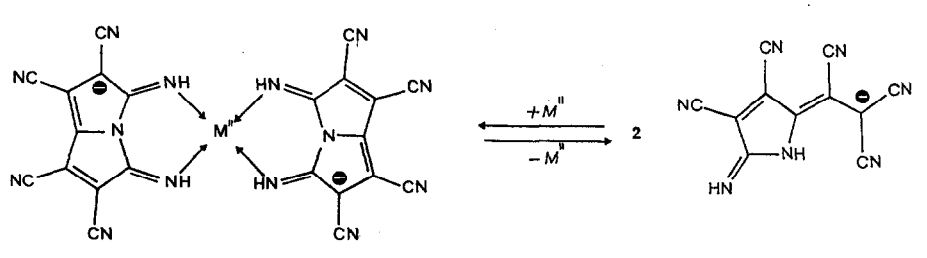

Scheme 1.

† Authors to whom correspondence should be addressed.

be technologically important as an analogy.[5]

As far as the solid state structure is concerned systems **1** differ considerably from MPc. In fact, while MPc adopt the classical herring-bone structure,[6] **1** display a variety of crystal packing depending on the cystallization solvent, usually laterally adducted to the chelating imino groups in the molecular plane via hydrogen bonds. Sometimes the difference in packing arrangement is remarkable, due to the variation in the crystallization solvent. This is the case for the title complex, which shows either slipped-stacked interacting molecular units when crystallized from acetonitrile, CH_3CN, or mutually orthogonal units when crystallized from tetrahydrofuran. The X-ray crystal structure of $Cu(C_{11}N_7H_2)_2 \cdot 2CH_3CN$ (**1a**) is presented here and compared with that of $Cu(C_{11}N_7H_2)_2 \cdot 2THF$ (**1b**), previously reported;[1] the results of a number of physical measurements on both compounds are also reported and discussed.

EXPERIMENTAL

All manipulations were performed under dinitrogen on a vacuum line using standard Schlenk techniques or in a dry-box; solvents were dried and freshly distilled before use.

Preparations

CuPc was purified by sublimation. $Cu(C_{11}N_7H_2)_2 \cdot 2THF$ (**1b**) was prepared as described previously.[1]

$Cu(C_{11}N_7H_2)_2 \cdot 2CH_3CN$ (**1a**). By solvent substitution: a suspension of **1b** (0.50 g, 0.74 mmol) in CH_3CN (50 cm^3) was refluxed for 3 h. After cooling to room temperature and filtering **1a** was collected in a quantitative yield as bronze microcrystals. Crystals suitable for X-ray determinations were obtained after crystallization of crude **1a** in CH_3CN, as follows: a hot saturated acetonitrile solution was filtered and sealed in a vial under vacuum. On very slow cooling from 80°C to room temperature over 7 days needle-like crystals of **1a** separated. The elemental analysis data of **1a** from several analyses were not reproducible, due to the partial loss of the solvent when **1a** was dried; however, the experimental X-ray powder diffraction pattern from a freshly prepared sample of **1a** was in excellent agreement with the diffraction pattern generated from X-ray diffraction studies of a single crystal sample.[7]

Physical measurements

A Cary 5 instrument was used to record diffuse relectance spectra on MgO-diluted samples. The solution electronic spectra were recorded with a Perkin–Elmer 330 spectrometer. A Biorad FTS40 FTIR spectrometer was used to measure the IR spectra in Nujol mulls; CsI windows were used in the spectral range 4000–180 cm^{-1} and polyethylene windows in the range 500–50 cm^{-1}; the reproducibility was 0.3 cm^{-1} or better. Magnetic measurements were performed on a commercial SQUID magnetometer (Quantum Design, H_{max} = 5 T); molar susceptibilities were corrected for intrinsic diamagnetism, estimated from Pascal's constants.

X-ray analysis

An irregularly shaped crystal of approximate dimensions $0.60 \times 0.25 \times 0.20$ mm was sealed in a capillary in the presence of the mother liquor and used for data collection on a Nicolet $P2_1$ four-circle diffractometer. Unit cell parameters were determined from 25 accurately centred reflections ($23° \leqslant 2\theta \leqslant 37°$). Intensity data were collected at room temperature using graphite crystal monochromated Mo-K_α radiation ($\lambda = 0.71069$ Å) by the θ–2θ scan technique and corrected for Lorentz and polarization effects. No absorption correction was applied, given the low value of μ and the crystal dimensions. Furthermore, a ψ-scan on two reflections showed a maximum deviation of less than 4%.

The structure was solved by conventional Patterson and Fourier methods and refined by full-

Table 1. Crystal data and main experimental and processing details

Compound	$Cu(C_{11}N_7H_2)_2 \cdot 2CH_3CN$
Molecular formula	$C_{26}H_{10}CuN_{16}$
Molecular weight	610.018
Crystal system	Monoclinic
a (Å)	6.918(2)
b (Å)	12.248(3)
c (Å)	15.452(4)
β (°)	95.85(2)
V (Å^3)	1302.5(6)
Space group	$P2_1/n$
D_{calc} (g cm^{-3})	1.556
$F(000)$	614
Z	2
μ (cm^{-1})	9.281
2θ collection limit (°)	55
Number of observed reflections [$I \geqslant 3\sigma(I)$]	2357
Least-squares parameters	196
R	0.039
R_w	0.043
Weighting scheme w^{-1}	$\sigma^2(F_o)$

matrix least-squares methods, with neutral scattering factors calculated using the data from ref. 8. The final refinements were made with anisotropic temperature factors for non-hydrogen atoms; hydrogens were placed in calculated positions with fixed isotropic thermal parameters.

All calculations were performed using the SIR-CAOS Crystallograhic Program System.[9] Crystallographic and processing data are given in Table 1. Positional and anisotropic thermal parameters, a full list of bond lengths and angles and observed and calculated structure factors have been deposited with the Editor as supplementary material.

RESULTS AND DISCUSSION

Crystal structure of $CuL_2 \cdot 2CH_3CN$ (**1a**)

The molecular geometry and relative orientation of the two symmetry-related formula units, comprised in the unit cell, are shown in Fig. 1. The main interatomic distances and angles are given in Table 2: they are strictly comparable with those found in **1b** which have already been discussed.[1-3] The copper atom is centrosymmetrically surrounded by four chelating imino groups in a square planar arrangement with Cu(1)—N(8) and Cu(1)—N(14) distances of 1.986 and 2.005 Å, respectively, and completes its tetragonally elongated octahedral geometry with two axial cyano groups at 2.900 Å. These latter groups do not belong to almost orthogonal equivalent complex units, as in the case of **1b**,[1,3] but to parallel *a*-shifted units (Fig. 2), giving rise to symmetry-related, differently oriented slipped stacks of planar molecules, with an interplanar distance of 3.09 Å. Although no degree of π-superposition is present within the stack, such packing resembles that of the β-phase of CuPc,[10] thus enhancing its similarity with Mpc discussed below.

The adducted acetonitrile molecules act as bridging groups between the stacks via weak hydrogen interactions (Fig. 1), with the coordinated imino groups on one side and peripheral cyano groups on the other ($N_{acetonitrile}$—N_{imino} and $C_{acetonitrile}$—N_{cyano} mean distances: 3.15 and 3.45 Å, respectively).

In conclusion it is worth noting that, probably owing to its small dimensions and strong polarized character, the acetonitrile molecule causes a Cu $L_2 \cdot 2CH_3CN$ crystal packing completely different from the analogous dimethoxyethane (DME) com-

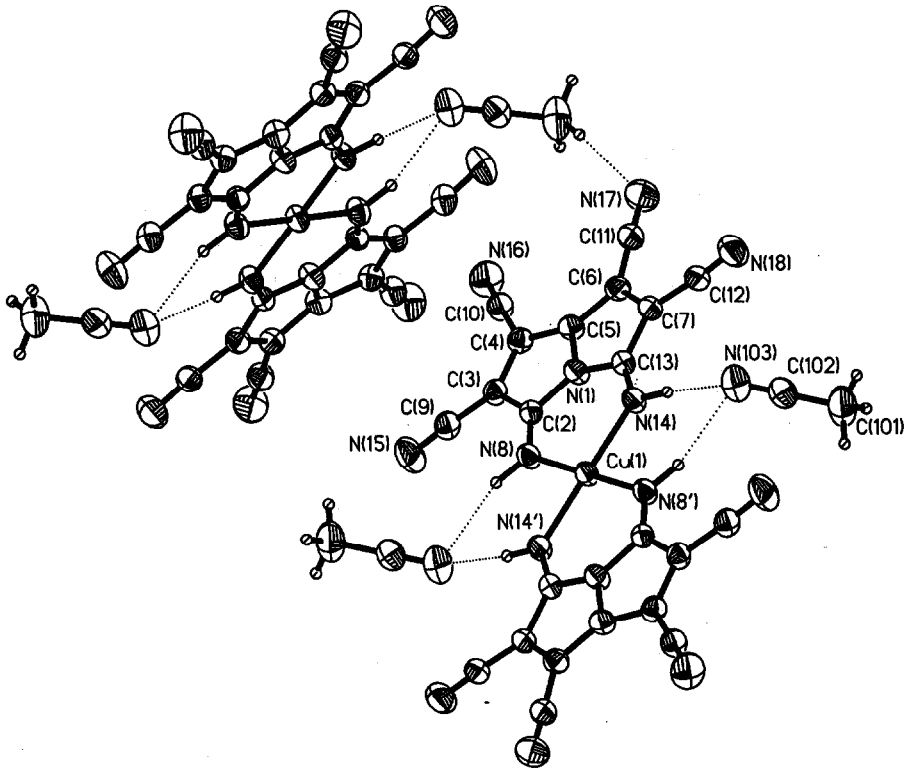

Fig. 1. A perspective view of the unit cell content, showing the two symmetry-related complex molecules and the labelling of the atoms. The laterally adducted acetonitrile solvent molecules act as bridging groups between them via weak hydrogen bonds (dotted lines).

Table 2. Bond lengths (Å) and angles (°), with e.s.d.s in parentheses

Cu(1)—N(8)	1.986(3)	C(5)—C(6)	1.396(3)
Cu(1)—N(14)	2.005(2)	C(6)—C(7)	1.403(4)
Cu(1)—N(18)^{I}	2.900(3)	C(6)—C(11)	1.424(4)
N(1)—C(2)	1.380(3)	C(7)—C(12)	1.415(4)
N(1)—C(5)	1.386(3)	C(7)—C(13)	1.458(3)
N(1)—C(13)	1.383(3)	C(9)—N(15)	1.139(4)
C(2)—C(3)	1.452(4)	C(10)—N(16)	1.141(4)
C(2)—N(8)	1.287(3)	C(11)—N(17)	1.132(4)
C(3)—C(4)	1.402(4)	C(12)—N(18)	1.139(4)
C(3)—C(9)	1.418(4)	C(13)—N(14)	1.286(3)
C(4)—C(5)	1.413(4)	C(101)—C(102)	1.436(5)
C(4)—C(10)	1.429(4)	C(102)—N(103)	1.128(4)

N(14)—Cu(1)—N(8)	92.64(9)	C(7)—C(6)—C(5)	108.5(2)
N(18)^{I}—Cu(1)—N(8)	86.5(1)	C(11)—C(6)—C(5)	125.8(2)
N(18)^{I}—Cu(1)—N(14)	91.6(1)	C(11)—C(6)—C(7)	125.7(2)
C(5)—N(1)—C(2)	112.8(2)	C(12)—C(7)—C(6)	125.9(2)
C(13)—N(1)—C(2)	133.7(2)	C(13)—C(7)—C(6)	108.6(2)
C(13)—N(1)—C(5)	113.3(2)	C(13)—C(7)—C(12)	125.3(2)
C(3)—C(2)—N(1)	104.2(2)	C(2)—N(8)—Cu(1)	126.1(2)
N(8)—C(2)—N(1)	120.8(2)	N(15)—C(9)—C(3)	176.1(3)
C(4)—C(3)—C(2)	108.7(2)	N(16)—C(10)—C(4)	177.5(3)
C(9)—C(3)—C(2)	122.6(2)	N(17)—C(11)—C(6)	178.8(3)
C(9)—C(3)—C(4)	128.4(2)	N(18)—C(12)—C(7)	176.2(3)
C(5)—C(4)—C(3)	107.9(2)	C(7)—C(13)—N(1)	103.4(2)
C(10)—C(4)—C(3)	128.2(2)	N(14)—C(13)—N(1)	120.7(2)
C(10)—C(4)—C(5)	123.8(2)	C(13)—N(14)—Cu(1)	125.7(2)
C(4)—C(5)—N(1)	106.4(2)	N(103)—C(102)—C(101)	178.8(3)
C(6)—C(5)—N(1)	106.2(2)		

Symmetry code: I $x-1, y, z$.

plexes $FeL_2 \cdot 2DME$,[3] $CoL_2 \cdot 2DME$[3] and $CuL_2 \cdot 2THF$,[1] and more similar to that of the β-phase of MPc. Tuning of the metal β-diiminopyrrolizinido solid-state features can, therefore, be envisaged by varying the crystallization solvent and/or the metal atom.

Solution behaviour

The copper complex, like the other first-row transition metal derivatives, is sparingly soluble in donor solvents (solubility in THF $\approx 4.32 \times 10^{-4}$); in solution it does not obey Beer's law; water labilizes the coordination bond, shifting the dissociation equilibrium (see Scheme 1) to the right [ν_{max} (**2**) = 546 nm]. By increasing the amounts of Cu^{2+}, as $CuCl_2 \cdot 2H_2O$, it is possible to reverse the equilibrium to the left so that a large excess (≈ 100 times) is needed in order to observe the intrinsic visible spectrum of the undissociated species. Such a spectrum is reported in Fig. 3, together with that of CuPc for comparison. The spectra in Fig. 3 are very similar, exhibiting two major bands (the characteristic Q and Soret bands of MPc), spaced by a window in the 500 nm region. The key to this extraordinary similarity has been found for the analogous nickel(II) complex, based on semi-empirical MO calculations.[4] It follows from these calculations and the observed overall similarity that also in the copper complex the Q-like band arises from two allowed, accidentally degenerate, electronic $\pi \rightarrow \pi^*$ intraligand transitions between HOMO and LUMO orbitals.

Solid state properties: electronic and IR spectroscopy and magnetic measurements

The reflectance spectrum of **1b** is dominated by the very intense Q-like band centred at 660 nm; in **1a** this band is broadened and split into two components with maxima at 670 and 717 nm. According to the Davydov theory[11] this splitting (≈ 970 cm^{-1}) is caused by the interaction between molecules of differing site symmetry in the unit cell and, as in CuPc,[12] it can be correlated with the interaction between equivalent molecules along the

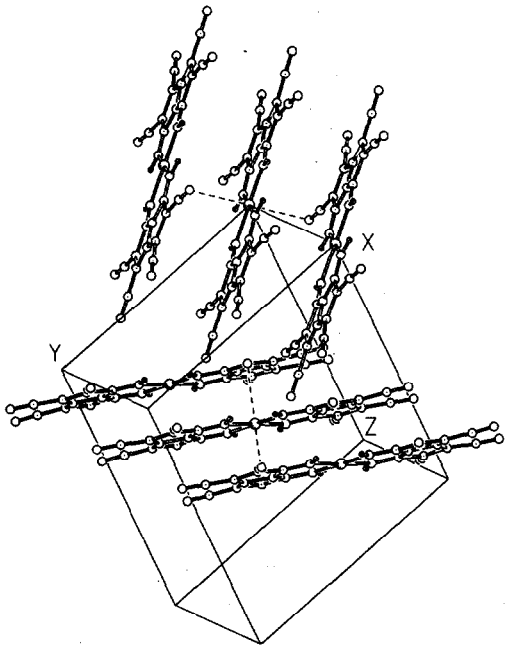

Fig. 2. Crystal packing of **1a**, showing the two differently oriented slipped stacks of *a*-spaced complex molecules. The axial copper–nitrogen interactions within each stack are drawn as dashed lines. Acetonitrile groups have been omitted for clarity.

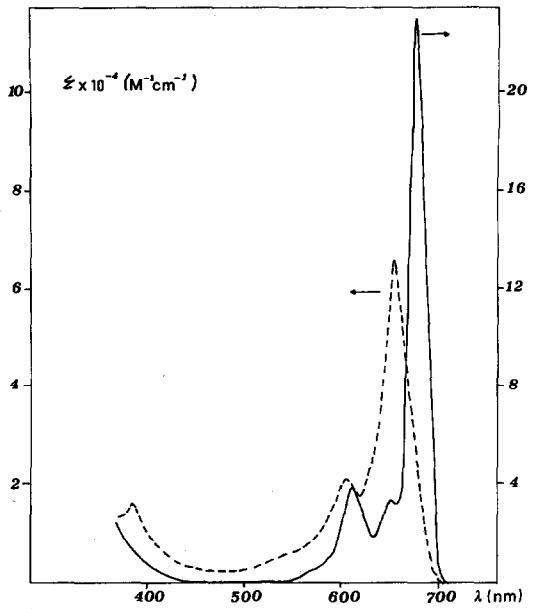

Fig. 3. Solution electronic spectra of CuPc (——) (α-chloro-naphthalene) and CuL_2 (– – – –) (THF+0.11 M $CuCl_2 \cdot 2H_2O$).

stacks. It is worthwhile noting that in CuPc, in spite of a larger intermolecular separation (3.28 Å),[10a] such an interaction appears to be greater than in **1a**, being almost double the size of the Davydov splitting (1890–1960 cm^{-1}).[12] Moreover, both **1a** and **1b** show a weak band at low energy (1070 and 1060 nm, respectively), which can be correlated with the weak intermolecular Cu···N bonds (2.90 and 2.82 Å, respectively) and probably due to the metal $d_{z^2} \rightarrow d_{x^2-y^2}$ electronic transition, confined within the axially distorted octahedral $CuN_4N'_2$ chromophore. The energy of such a band is clearly due to the difference in the out-of-plane bond length.[13] In addition, **1b** shows another band, appearing as a shoulder at 970 nm, probably due to the second metal $d \rightarrow d$ transition, as previously assigned.[1]

As far as the IR spectra are concerned, most interest is associated with the N—H and Cu—N stretching vibrations (Fig. 4); the first giving bands in the higher energy region, diagnostic of the hydrogen bond involving the imino groups. Such bands are in effect red-shifted, split (**1a**) and broadened (**1b**), compared with the band attributable to the imino group, when not involved in a hydrogen bond as in the tetraphenylarsonium salt of the pyrrolenine anion **2** [ν(N—H) = 3360 cm^{-1}].[14] The peak energy values [Fig. 4(a)] in **1a** (3258 and 3295 cm^{-1}) and **1b** (3165 and 3258 cm^{-1}) parallel the corresponding hydrogen bond distances (2.158 and 2.239 Å for **1a** and 1.953 and 2.298 Å for **1b**). The Cu—N stretching absorptions [Fig. 4(b)] fall in the lower energy region. In D_{2h} these IR-allowed vibrations have the symmetry B_{2u} and B_{3u} (in-plane) and A_u (out-of-plane).[15] The first two symmetries can be assigned at 232.5 and 256 cm^{-1} in both materials. Such an assignment is supported by the observation that in the analogous zinc complex, adducted with THF, these bands (224.6 and 200 cm^{-1}) are red-shifted as a consequence of the mass effect and the longer Zn—N bond distance (2.016 Å).[16] However, note that the similarities of the frequencies of the two in-plane Cu—N stretching vibrations in **1a** and in **1b** are consistent with the fact that in-plane distances between copper and nitrogen atoms are almost equal in these materials. The frequency of the A_u mode should fall at lower energy (probably < 200 cm^{-1});[13] unfortunately, this energy region is very rich in weak absorptions so that no reliable assignment can be made at present without further carefully designed IR experiments.

Finally, we wondered whether **1a** exhibits any linear-chain behaviour, given that its intermolecular separation is much lower than the characteristic van der Waals distance (3.4 Å). Surprisingly enough, it does not show any cooperative property: it is an electrical insulator ($\sigma < 10^{-7}$ S) and the temperature dependence of the corrected

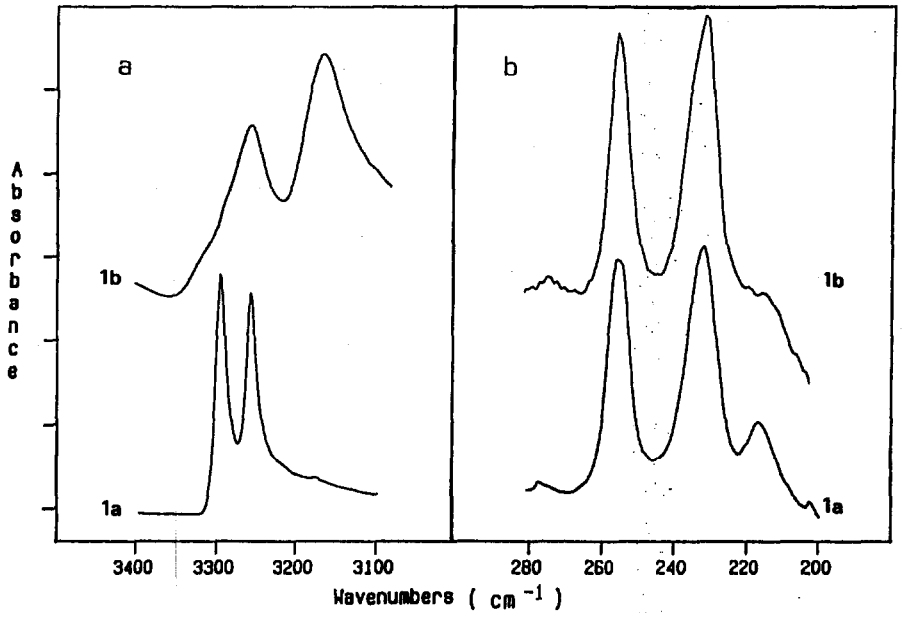

Fig. 4. IR absorption spectra in (a) the 3400–3100 cm^{-1} region and (b) the 280–200 cm^{-1} region. The upper curves are relative to compound **1b**, the bottom ones to **1a**.

molar susceptibility follows the Curie law within the temperature range investigated (6–300 K). The copper ions are magnetically isolated as they are in the compound **1b** (μ_{eff} = 1.73 and 1.77 B.M., respectively).

REFERENCES

1. M. Bonamico, V. Fares, A. Flamini and N. Poli, *Angew. Chem., Int. Edn Engl.* 1989, **28**, 1049.
2. M. Bonamico, V. Fares, A. Flamini and N. Poli, *Inorg. Chem.* 1991, **30**, 3081.
3. M. Bonamico, V. Fares, A. Flamini and N. Poli, *J. Chem. Soc., Dalton Trans.* 1992, 3273.
4. S. Nakamura, A. Flamini, V. Fares and M. Adachi, *J. Phys. Chem.* 1992, **96**, 8351.
5. A. L. Thomas, *Phthalocyanines Research & Applications*. CRC Press, Baton Rouge, FL (1990).
6. J. A. Ibers, L. J. Pace, J. Martinsen and B. M. Hoffman, in *Structure and Bonding*, Vol. 50, p. 1. Springer-Verlag, Heidelberg (1982).
7. SHELXTL PC, Siemens Crystallographic Research System (1990).
8. *International Tables for X-ray Crystallography*, Vol. IV. Kynoch Press, Birmingham (1974).
9. M. Camalli, D. Capitani, G. Cascarano, S. Cerrini, C. Giacovazzo and R. Spagna, Italian Patent 35403/86 (1986).
10. (a) C. J. Brown, *J. Chem. Soc.* (*A*) 1968, 2488; (b) S. E. Harrison and J. M. Assour, *J. Chem. Phys.* 1963, **40**, 365.
11. M. Pope and C. E. Swenberg, *Electronic Process in Organic Crystals*, p. 59. Clarendon Press, New York (1982).
12. P. Day and R. J. P. Williams, *J. Chem. Phys.* 1962, **37**, 567.
13. B. J. Hathaway, in *Structure and Bonding*, Vol. 14, p. 49. Springer-Verlag, Heidelberg (1973).
14. M. Bonamico, V. Fares, A. Flamini, A. M. Giuliani and P. Imperatori, *J. Chem. Soc., Perkin Trans. II* 1988, 1447.
15. J. N. Murrel, *J. Chem. Soc.* (*A*) 1969, 297.
16. M. Bonamico, V. Fares, A. Flamini and N. Poli, to be submitted.

Polyhedron Vol. 12, No. 10, pp. 1215–1225, 1993
Printed in Great Britain

0277–5387/93 $6.00+.00
© 1993 Pergamon Press Ltd

PREPARATION, X-RAY CRYSTAL STRUCTURE AND THEORETICAL STUDY OF THE BONDING IN $[Mo_2O_4I_2L_3]$ (L = $OPPh_3$), AN EXAMPLE OF AN UNSYMMETRICAL DINUCLEAR MOLYBDENUM COMPLEX

P. RABE, J. E. GUERCHAIS* and J. SALA PALA*

Laboratoire de Chimie, Electrochimie Moléculaires et Chimie Analytique, URA CNRS 322, Equipe de Chimie Inorganique Moléculaire, Université de Bretagne Occidentale, 29275 Brest Cédex, France

and

M. EL KHALIFA and J.-Y. SAILLARD

Laboratoire de Chimie du Solide et Inorganique Moléculaire, URA CNRS 1495, Université de Rennes I, 35042 Rennes Cédex, France

and

L. TOUPET

Groupe Matière Condensée et Matériaux, URA CNRS 804, Université de Rennes I, 35042 Rennes Cédex, France

(*Received* 2 *December* 1992; *accepted* 8 *January* 1993)

Abstract—The reaction between the oxomolybdenum(V) complex $Et_4N[MoOI_4(H_2O)]$ and triphenylphosphine oxide (L = $OPPh_3$) produces the mononuclear complex $[MoOI_3L_2]$ and the dinuclear complex **1** $[Mo_2O_4I_2L_3]$, the crystal structure of which has been studied by X-ray. Each metal centre is bound to a terminal and two bridging oxygen atoms; the Mo_2O_2 central fragment appears slightly disymmetric with a short Mo—Mo distance [2.557(1) Å], in agreement with a single metal–metal bond. The whole structure is strongly asymmetric, with the three phosphorus ligands bound to a first molybdenum atom with a distorted octahedral MoO_6 coordination and the two iodo ligands bound to a second molybdenum atom which has a *cis*-$MoOO_2I_2$ square-pyramidal coordination. Extended Hückel calculations on the model $[Mo_2O_4I_2L_3]$ (L = OPH_3), the structure of which was derived from the averaged structure of **1**, have been performed to understand the structure and bonding in this unsymmetrical dimer. They show a HOMO–LUMO gap of 1.06 eV and indicate that **1** can be considered unambiguously as an Mo^V–Mo^V [and not an Mo^{IV}–Mo^{VI}] dinuclear complex. An orbital explanation is provided to rationalize why the *cis* conformation is generally preferred for Mo^V–Mo^V dinuclear species: such a conformation allows a stronger Mo—Mo bond. Some predictions are made, concerning the reactivity of the Mo—Mo bond with respect to nucleophilic and electrophilic attacks.

At the end of the 70s most of the known dinuclear complexes were symmetrical homodinuclear species, but in the last two decades much attention has been focused upon heterodimetallic complexes.[1,2] Such complexes obviously present a richer reactivity than mono- and homodinuclear complexes and much effort has been particularly directed towards the use of early/late transition metal combinations as catalysts themselves, catalyst precursors or as model compounds for catalytic intermediates.[3] Unsymmetrical homodinuclear complexes con-

* Authors to whom correspondence should be addressed.

stitute an interesting intermediate class which has been relatively little studied up to date; the two metallic centres, of the same chemical nature, differ only in their coordination sphere and the subtle differences in the properties and reactivities of the two metal sites can only arise from the different ligands bound to each of them.

In the specific case of molybdenum, examples of dinuclear compounds with non-equivalent metal sites are very diverse: various oxidation states and various coordination numbers of both metallic cations, as well as various overall geometries and various charges of the complexes are seen. The large range of unambiguously X-ray characterized, unsymmetrical molybdenum complexes includes mono-bridged complexes such as $[O_3Mo^{VI}(\mu\text{-}O)Mo^{VI}O_3(en)]^{2-}$ [4] and $[LCl(O)Mo^{V}(\mu\text{-}O)Mo^{VI}O_2L]$ $[L = \{HB(Me_2pz)_3\}^-]$,[5] doubly-bridged complexes such as $[L_2ClMo^{III}(\mu\text{-}Cl)(\mu\text{-}S)Mo^{III}Cl_2L_n]$ $[L = PMe_3;\ n = 1,2]$,[6] $[(RCp)_2Mo(\mu\text{-}S)_2MoO_2]$[7] and $[L_2Mo(\mu\text{-}OPr^i)_2Mo(OPr^i)_2L]$ (L = 9,10-phenanthrenequinone),[8] and triply-bridged complexes such as $[LX_2Mo^{III}(\mu\text{-}X)_3Mo^{III}L_2X]$ $(X = Cl, Br;\ L = PMe_2Ph)$[9] and $[L(NR)Mo(\mu\text{-}S)_2(\mu\text{-}O_2CR)Mo(NR)L']$ $[L = \{PS_2(OR)_2\}^-;\ L' = dppe]$.[10] It also includes, however, unbridged complexes such as $[L_2Mo{\equiv}Mo(OPr^i)_4]$ (L = dmpe),[11] which contains a triple metal–metal bond associating d^6-Mo^0 and d^2-Mo^{IV} centres.

In the course of our study on iodooxomolybdenum complexes we obtained a dinuclear complex, $[Mo_2O_4I_2L_3]$ $(L = OPPh_3)$, for which a crystal structure determination by X-ray diffraction clearly showed a strongly unsymmetrical structure. This strong asymmetry and the availability of precise structural data prompted us to examine the electronic properties of this compound. The synthesis, structural results and the theoretical calculations are presented in this paper.

EXPERIMENTAL

All reactions were performed in Schlenk tubes in a dry oxygen-free nitrogen atmosphere. Solvents were distilled by standard techniques and thoroughly deoxygenated before use. Elemental analyses were performed by Service Central d'Analyse du CNRS, Vernaison, France. IR spectra were obtained with a Perkin–Elmer 1430 spectrometer (KBr pellets). The starting molybdenum complex $Et_4N[MoOI_4(H_2O)]$ was synthesized as previously described.[12]

Synthesis

$Et_4N[MoOI_4(H_2O)]$ (1 mmol, 0.75 g) was dissolved at room temperature in the minimum amount of acetonitrile. This solution was then transferred into a concentrated solution of $OPPh_3 \cdot 0.5H_2O$ (2 mmol, 0.56 g) in acetonitrile. The solution, which was stirred for *ca* 15 min, became violet. Upon standing a purple precipitate appeared; it was filtered, washed and dried under reduced pressure (yield *ca* 65%). Found: Mo, 8.7; C, 41.7; H, 2.9; I, 35.9; P, 5.8. Calc. for $MoC_{36}H_{30}I_3O_3P_2$: Mo, 9.1; C, 41.2; H, 2.9; I, 36.3; P, 5.9%. IR (KBr, cm^{-1}): 970, ν(MoO). The resulting filtrate was kept under nitrogen at −20°C. The solution slowly became brown and reddish microcrystals of complex **1** precipitated. They were filtered, washed and dried under reduced pressure (yield *ca* 10%). Found: C, 47.8; H, 3.7; I, 19.6; P, 5.8. Calc. for $Mo_2C_{54}H_{45}I_2O_7P_3$: C, 48.5; H, 3.5; I, 18.3; P, 6.7%. IR (KBr, cm^{-1}): 975 and 940, ν(MoO).

Crystal and molecular structure of **1**, $[Mo_2O_4I_2L_3]$ $(L = OPPh_3)$

Crystal data. $Mo_2C_{54}H_{45}I_2O_7P_3$, $M = 1344.6$, triclinic, space group $P\bar{1}$, $a = 10.717(5)$, $b = 11.631(2)$, $c = 12.336(4)$ Å, $\alpha = 69.49(3)$, $\beta = 74.76(3)$, $\gamma = 66.46(4)°$, $V = 1306.8(9)$ Å^3, $Z = 1$, $Dx = 1.708$ g cm^{-3}, $F(000) = 660$, λ(Mo-K_α) = 0.71069 Å, $\mu = 17.76$ cm^{-1}.

A reddish translucent crystal (approximate dimensions $0.20 \times 0.22 \times 0.28$ mm) with well-developed faces was used for the data collection. No problems were encountered collecting the data on an Enraf–Nonius CAD4 four-circle diffractometer at room temperature using graphite-monochromated Mo-K_α radiation (0.71069 Å) and employing the ω–2θ scan technique. There was no decomposition of the sample during the experiment (intensity variation <0.2%). Unit cell parameters were obtained from least-squares refinement on the setting angles of 25 reflections. No symmetry higher than triclinic was found. Of 6002 reflections collected up to $2\theta = 50°$ (hkl range: h 0,13; k −14,14; l −15,15) only 3415 independent reflections ($R_{int} = 0.028$) with $I > 3\sigma(I)$ were used to solve and refine the structure. After Lorentz and polarization corrections the structure was solved with direct methods which reveal the iodine, phosphorus and molybdenum atoms of the asymmetric unit. The remaining non-hydrogen atoms of the structure were found after successive scale factor refinements and Fourier differences. After isotropic refinement an absorption correction was made with Difabs.[13a] The whole structure was refined by the full-matrix least-squares techniques (use of F magnitude; x, y, z, β_{ij} for I, Mo, P, O and C atoms and x, y, z fixed for hydrogen atoms; 611 variables

Table 1. Parameters and exponents used in the calculations

Atom	Orbital	H_{ii} (eV)	ζ_1	ζ_2	$C_1{}^a$	$C_2{}^a$
H	1*s*	−13.60	1.300			
O	2*s*	−32.30	2.275			
	2*p*	−14.80	2.275			
P	3*s*	−18.60	1.600			
	3*p*	−14.00	1.600			
I	5*s*	−17.80	2.680			
	5*p*	−12.00	2.320			
Mo	5*s*	−8.34	1.956			
	5*p*	−5.24	1.921			
	4*d*	−10.50	4.540	1.900	0.5899	0.5899

[a] Contraction coefficients used in the double-ζ expansion.

and 3415 observations; $w = 1/\sigma^2(F_o) = [\sigma^2(I) + (0.04F_o^2)^2]^{-1/2}$) with the resulting $R = 0.031$ and $R_w = 0.029$ and $S_w = 1.32$ (residual $\Delta\rho < 0.32$ e Å^{-3}). The scattering factors were taken from the International Tables.[14] All calculations were made with the MolEN program[13b] using a Digital MicroVAX 3100 computer.

Computational details for MO calculations

All the calculations were made within the extended Hückel formalism,[15] using the weighted H_{ij} formula.[16] The atomic parameters, listed in Table 1, are taken from the literature.[17] A double-ζ expansion was used for the metallic 4*d* AOs. The molecular structures of the models used in the calculations are derived from the averaged idealized experimental structure of **1** with the following bond distances in Å (unless specified in the text): Mo—Mo = 2.56; Mo=O = 1.68; Mo—OPH_3 = 2.19; Mo—O(bridge) = 1.93; Mo—I = 2.77; P—O = 1.49; P—H = 1.42; O—H = 0.96. The C_s symmetry was assumed for **2**, **2′**, **3** and **4**, and the C_{2v} symmetry for **5** and **6**.

RESULTS AND DISCUSSION

Preparation and crystal structure

Reaction of $Et_4N[MoOI_4(H_2O)]$ with 2 mole equivalents of L = $OPPh_3$ in acetonitrile at room temperature quickly resulted in the precipitation of a purple compound. The resulting filtrate, kept under nitrogen at −20°C, slowly gave reproducible reddish microcrystals of complex **1**. The purple compound, formed in *ca* 65% yield, analysed as $[MoOI_3L_2]$ and seemed likely to be a pseudo-octahedral mononuclear oxomolybdenum(V) complex [ν(MoO) = 970 cm^{-1}]. Elemental analyses for complex **1**, which indicated an unusual L/Mo ratio of 3/2, were in agreement with the $[Mo_2O_4I_2L_3]$ stoichiometry, i.e. with the presence of nine ligands for two metallic centres. For such a stoichiometry, and since examples of $OAsPh_3$ bridging ligands have been unambiguously found,[18] the symmetrical confacial bioctahedral structure shown below, in which

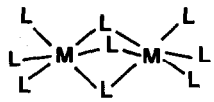

the ligand atoms define two octahedra with a common face, as in $[Mo_2Cl_9]^{3-}$ and various other molybdenum complexes,[2,9,19] was possible. However, since a careful examination of the IR spectra showed two absorptions assignable to ν(MoO) (975 and 940 cm^{-1}), in disagreement with such a symmetrical structure, a single-crystal structure determination for complex **1** was performed. This study unequivocally shows that **1** may be formulated as an unsymmetrical dinuclear oxomolybdenum complex (Figs 1 and 2). While the discrete dimeric molecule possesses no crystallographically imposed geometry, it has virtual C_s symmetry with the mirror plane encompassing the two molybdenum and the two terminal oxygen atoms, as well as the oxygen atom O(5) of one of the triphenylphosphine oxide ligands.

The main structural features shown by the structure determination (Figs 1 and 2; Table 2) are the following: (1) the three phosphorus ligands are bound to the first molybdenum atom Mo(1), while the two iodo ligands are coordinated to the second molybdenum atom Mo(2); (2) each metal atom is bound to a terminal oxygen atom [Mo(1)—O(2) = 1.692(8); Mo(2)—O(7) = 1.677(8) Å], in

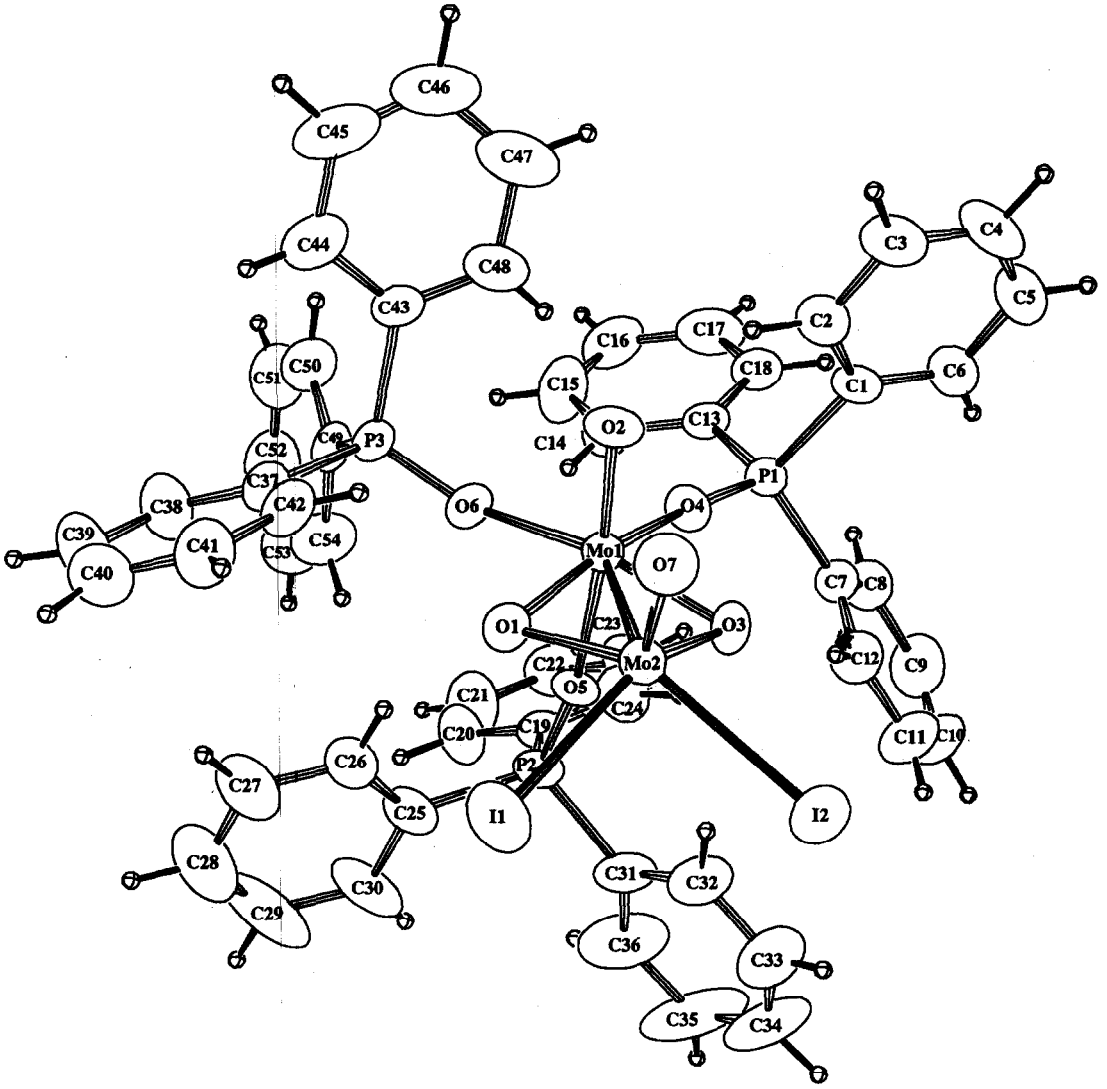

Fig. 1. Structure and labelling of the $[Mo_2O_4I_2L_3]$ complex **1** (L = $OPPh_3$).

agreement with the IR spectra, and also to two bridging oxygen atoms; and (3) the Mo_2O_2 central fragment appears puckered and slightly unsymmetric [Mo(1)—O(1) = 1.888(5); Mo(1)—O(3) = 1.919(5); Mo(2)—O(1) = 1.950(5); Mo(2)—O(3) = 1.956(5) Å] with a short Mo(1)—Mo(2) distance [2.557(1) Å], indicating a single metal–metal bond. Disregarding the metal–metal bond, (1) Mo(1) presents a distorted octahedral MoO_6 coordination with an O(1)O(3)O(4)O(6) fragment planar within ±0.0007 Å and with the metal atom displaced by 0.321 Å from this mean plane, and (2) Mo(2) has a *cis*-$MoOO_2I_2$ square pyramidal coordination with an O(1)O(3)I(1)I(2) fragment planar within ±0.004 Å and the metal atom displaced by 0.646 Å from this mean plane.

It is noteworthy that the terminal oxo groups are located in a *cis* arrangement (*vide infra*) and that, as expected, the terminal oxo group on Mo(1) exerts a *trans* influence on Mo—O(P) bond lengths [2.241(7) for the phosphorus ligand *trans* to the terminal oxo ligand vs 2.155(5) and 2.182(5) Å for the phosphorus ligands *trans* to oxo bridges].

The main structural features of the di-μ-oxo complex **1**, $[X_2MoO(\mu\text{-}O)_2MoOL_3]$, with X = I and L = $OPPh_3$, are similar to those of the recently reported di-μ-sulphido complex $[X_2MoO(\mu\text{-}S)_2MoOL_3]$, with $X_2 = S_2$ and L = DMF.[20]

Theoretical calculations

A question which arises from the dissymmetry of the dinuclear complex **1** concerns the nature of its metal–metal bond: can it be considered as a simple

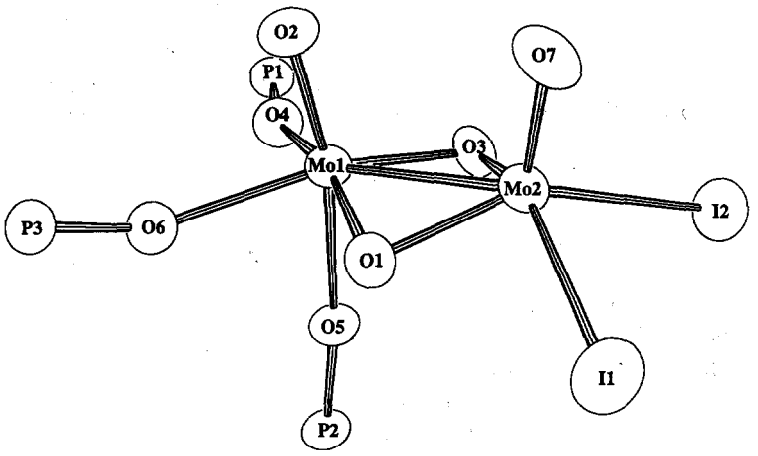

Fig. 2. The $Mo_2O_7I_2$ central unit of the $[Mo_2O_4I_2L_3]$ complex **1** (L = $OPPh_3$).

covalent bond between two Mo^V atoms, or is it better viewed as a dative bond from an Mo^{IV} to an Mo^{VI} centre? In order to answer this question, to understand the general structural features of **I** and to explore the reactivity of the Mo—Mo bond, we have undertaken extended Hückel calculations on the model $Mo_2O_4I_2(OPH_3)_3$ (**2**), the structure of which is derived from the averaged experimental structure of **1**. Other related models were also investigated (*vide infra*). All the structural and computational details are given in the experimental section.

(a) *The nature of the* Mo—Mo *bond.* Conceptually, one can consider the Mo—Mo bonding in

Table 2. Interatomic distances (Å) and bond angles (°) in **1**[a]

Mo(1)—Mo(2)	2.557(1)		
Mo(1)—O(1)	1.888(5)	Mo(1)—O(2)	1.692(8)
Mo(1)—O(3)	1.919(5)	Mo(1)—O(4)	2.155(5)
Mo(1)—O(5)	2.241(7)	Mo(1)—O(6)	2.182(5)
Mo(2)—O(1)	1.950(5)	Mo(2)—O(3)	1.956(5)
Mo(2)—O(7)	1.677(8)		
Mo(2)—I(1)	2.756(1)	Mo(2)—I(2)	2.792(1)
O(4)—P(1)	1.476(5)	O(5)—P(2)	1.493(8)
O(6)—P(3)	1.494(6)		
O(1)—Mo(1)—O(2)	105.0(3)	O(1)—Mo(1)—O(3)	94.6(2)
O(1)—Mo(1)—O(4)	161.3(3)	O(1)—Mo(1)—O(5)	82.2(3)
O(1)—Mo(1)—O(6)	89.2(2)	O(2)—Mo(1)—O(3)	106.5(3)
O(2)—Mo(1)—O(4)	92.2(3)	O(2)—Mo(1)—O(5)	166.3(2)
O(2)—Mo(1)—O(6)	91.1(3)	O(3)—Mo(1)—O(4)	87.4(2)
O(3)—Mo(1)—O(5)	84.2(3)	O(3)—Mo(1)—O(6)	160.2(3)
O(4)—Mo(1)—O(5)	79.5(2)	O(4)—Mo(1)—O(6)	83.0(2)
O(5)—Mo(1)—O(6)	77.1(2)		
O(1)—Mo(2)—O(3)	91.5(2)	O(1)—Mo(2)—O(7)	109.5(3)
O(1)—Mo(2)—I(1)	81.6(1)	O(1)—Mo(2)—I(2)	147.3(2)
O(3)—Mo(2)—O(7)	110.1(3)	O(3)—Mo(2)—I(1)	146.6(2)
O(3)—Mo(2)—I(2)	81.6(2)	O(7)—Mo(2)—I(1)	103.0(2)
O(7)—Mo(2)—I(2)	102.8(2)	I(1)—Mo(2)—I(2)	86.74(3)
O(1)—Mo(1)—Mo(2)	49.3(1)	O(1)—Mo(2)—Mo(1)	47.2(1)
O(3)—Mo(1)—Mo(2)	49.3(2)	O(3)—Mo(2)—Mo(1)	48.1(1)

[a] Numbers in parentheses are estimated standard deviations in the least significant digits.

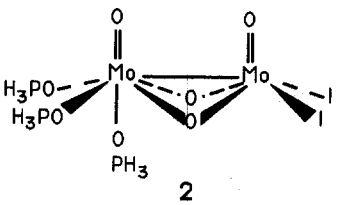

2

2 as resulting from the interaction between two mononuclear units, namely the six-coordinated $MoO(OPH_3)_3(1/2O)_2$ and the five-coordinated $MoOI_2(1/2O)_2$ fragments. Before entering into the bonding analysis of **2**, we shall start by discussing the electronic structure of these two mononuclear subunits. In order to avoid π-type interactions which are not present in the dinuclear species hydrogen atoms have been placed on the two oxygen atoms which are bridging in **2**. The two resulting models considered in the calculations, $[MoO(OPH_3)_3(OH)_2]^+$ and $[MoOI_2(OH)_2]^-$, are shown in **3** and **4**, respectively. Their charges have been chosen in order to have arbitrary Mo^V (d^1) oxidation states on both units.

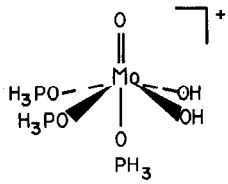

3

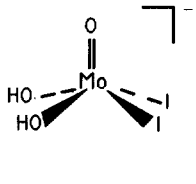

4

To understand simply the MO pattern of fragment **3**, shown on the left-hand side of Fig. 3, it is useful to consider it as a distorted octahedron, i.e. as being, at a zero-order approximation, structurally related to the class of ML_6 complexes of O_h symmetry. It exhibits the general 4*d* splitting of a

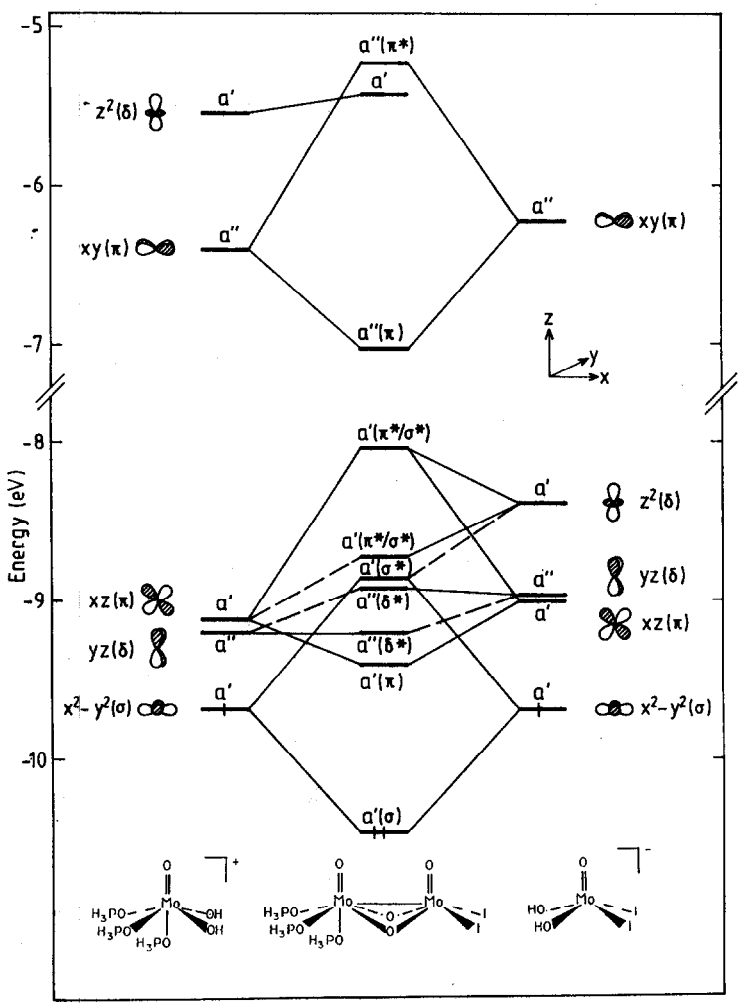

Fig. 3. The metallic MO diagram of the dinuclear compound **2**, based on the interaction of the two mononuclear units **3** and **4**.

group of three low-lying orbitals, the "t_{2g}" set (xz, yz and x^2-y^2 in our coordinate system), lying below two antibonding "e_g" orbitals (xy, z^2). However, one can see that the degeneracy inside each of the so-called "t_{2g}" and "e_g" groups of levels is far from being reached for **3**. This level splitting is principally due to the presence of a metal-oxo formal double bond, which reduces the O_h pseudo-symmetry to four-fold (C_{4v}) pseudo-symmetry. The shorter Mo=O bond induces a destabilization of the metallic levels, which have the proper symmetry to interact with the apical oxo ligand AOs. Indeed, the overlap between the atomic orbitals of the molybdenum and the apical oxygen is larger. As a result, the apical oxygen AOs are stabilized, while their molybdenum counterpart 4*d* AOs are destabilized, becoming somewhat antibonding. This effect is particularly noticeable for the z^2 level, which is much more destabilized by the σ-oxo lone pair than the other component of the "e_g" group (the xy level) by the lone pairs of the equatorial ligands. A similar but weaker destabilization is afforded by the xz and yz MOs, due to their interaction with the π-type oxo lone pairs. This π-type interaction, which splits the "t_{2g}" group, is responsible for the existence of the Mo=O formal double bond.

Another distortion from ideal O_h symmetry is present in fragment **3** (as well as in **1**). The molybdenum atom does not lie exactly in the plane of the four equatorial oxygen atoms, but slightly above, on the same side as the doubly bonded oxygen (*vide supra*). This distortion allows the xz and yz metallic orbitals to mix in a bonding way with the occupied metal–ligand bonding MOs of the same e pseudo-symmetry (assuming a near C_{4v} symmetry group). These levels, which have some molybdenum x and y character, are stabilized upon hybridation with the xz and yz AOs. This interaction, which is not possible when the molybdenum valence bond angles are equal to 90°, contributes to the destabilization of the empty xz and yz levels.

From the above analysis it results that the lowest 4*d* level in **3** is of x^2-y^2 dominant character. This MO, situated at −9.69 eV, has a large metallic character (93%) and is the frontier orbital which will be involved in the building of the Mo—Mo bond in the dinuclear species.

The MO diagram of fragment **4**, shown on the right-hand side of Fig. 3, can be understood in the same way as that used for fragment **3**. At the zero-order approximation it can be considered as belonging to the class of pseudo-octahedral ML_5 units, i.e. deriving from an O_h ML_6 complex by the removal of one ligand. The ordering of the metallic levels in such a fragment is well known.[21] There is a block of three low-lying levels derived from the t_{2g} set of the octahedron, lying below a hybridized z^2-type level which is antibonding with respect to the apical ligand. Significantly above this z^2 level, there is an in-plane antibonding level (xy in our coordinate system).[21] The presence of the metal–oxo double bond slightly perturbes this general MO pattern. The z^2 level appears more antibonding than usually found in related pseudo-octahedral ML_5 fragments because of the dominant interaction with the oxo atom; nevertheless, it remains far below the xy level which is antibonding on four Mo—L bonds. As found for **3**, the oxo π-type lone pairs split the "t_{2g}" set by destabilizing the xz and yz MOs. Similarly, the position of the metal atom above the plane of the equatorial ligands reinforces the four equatorial Mo—L bonds and contributes to the destabilization of the xz and yz levels. As a result, and as for **3**, the lowest metallic level, situated at −9.69 eV, is of x^2-y^2 parentage. Its localization on the metal atom is large (90%). This level can be identified as being the σ-type frontier orbital of **4** responsible for the Mo—Mo bond in the dinuclear species. From the comparison of the nature, energy and occupation of the σ-type frontier orbitals of the two Mo^V units **3** and **4**, it can be concluded that these two units have the same bonding properties and can be considered as being isolobal.[21]

The MO diagram for **2** is represented in the middle of Fig. 3, where it can be seen that each mononuclear level generates in **2** a pair of in-phase and out-of-phase combinations. Although the low symmetry (C_s) of **2** allows some $\sigma/\pi/\delta$ mixing, its HOMO can be clearly identified as being the bonding combination of the x^2-y^2 σ-type frontier orbitals of fragments **3** and **4**. Since these two frontier orbitals are very similar in energy and composition the HOMO of **2** is symmetrically distributed on both metal atoms (46% on the six-coordinated molybdenum and 43% on five-coordinated). A plot of this HOMO is shown in Fig. 4. The Mo—Mo bonding overlap population in this MO is large (0.169), reflecting a strong σ-bond. This value is very close to the total Mo—Mo overlap population (0.173), indicating that the HOMO is the only occupied level of significant metal–metal bonding character. Since the Mo—Mo bonding electron pair is equally shared by the metal atoms, complex **2** can be considered without any ambiguity as an Mo^V–Mo^V compound. However, it should be noted that the net atomic charges of the molybdenum atoms are not strictly equal. They are 2.96 for the six-coordinated atom and 2.48 for five-coordinated. In fact, this difference does not reflect any significant electron transfer between the metal atoms, but different metal–ligand charge polarization inside the mononuclear units. Indeed, the

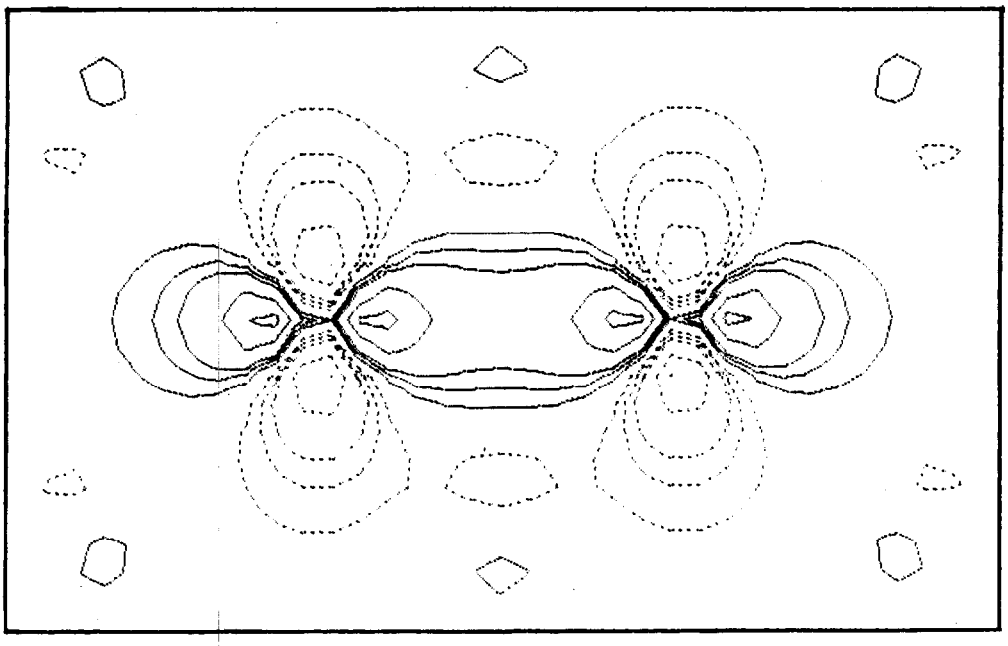

Fig. 4. Contour plots of the HOMO of **2**.

molybdenum net charges calculated for the monomers **3** and **4** (i.e. before the making of the Mo—Mo bond) are very close that found in **2** (3.05 and 2.59, respectively).

The calculated HOMO/LUMO gap is 1.06 eV. This is a rather large value, in full agreement with the stability, colour and diamagnetism of **1**. The LUMO is plotted in Fig. 5. It is a π-type bonding orbital, derived from the xz mononuclear levels. Due to some σ-type molybdenum atomic orbital

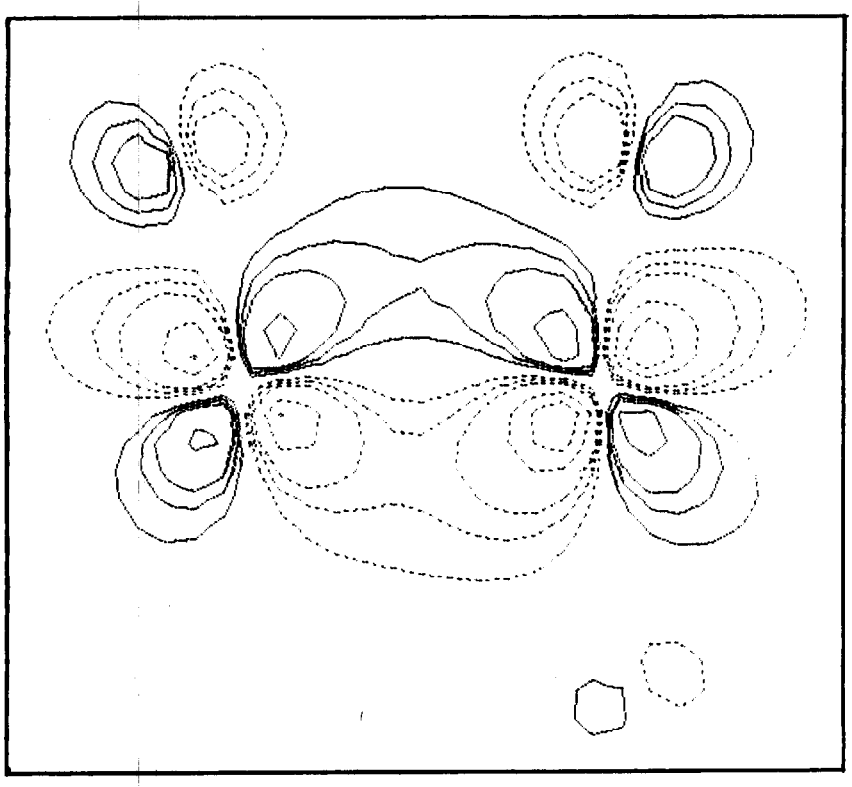

Fig. 5. Contour plots of the LUMO of **2**.

admixture, this level is strongly bonding, as shown in its Mo—Mo overlap population (0.164). Therefore, the reduction of **1** is expected to cause a significant shortening of the Mo—Mo bond.

Another way to show that fragments **3** and **4** have similar bonding abilities is to perform calculations on the hypothetical symmetrical d^1–d^1 dinuclear species **5** and **6**, the structures of which are generated by duplication of **3** and **4**, respectively, with the same metal–ligand environment and the same Mo—Mo bond distance (2.56 Å) as in **2**. Therefore, **5** and **6** can be considered as prototypical models for a number of symmetrical Mo^V μ-oxo dinuclear compounds.[2] Their MO diagrams appear to be very similar to that of **2**, with a σ(Mo—Mo) HOMO and a π(Mo—Mo) LUMO. The HOMO/LUMO gap is 0.99 and 1.14 eV for **5** and **6**, respectively. The Mo—Mo overlap populations in the HOMO are 0.164 and 0.168, respectively. These values compare well with the corresponding values found in **2**. The calculations on **2**, **5** and **6** are in qualitative agreement with previous calculations on related μ-oxo and μ-sulphido molybdenum(V) dinuclear complexes.[22]

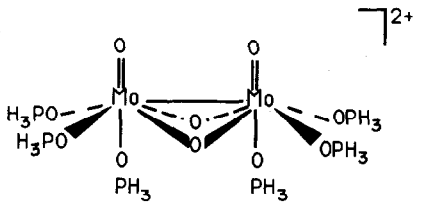

5

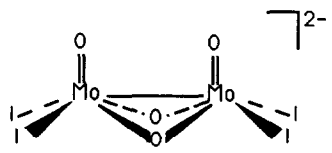

6

(b) Cis/trans *isomerism in dibridged* Mo^V–Mo^V *complexes*. At this stage of the discussion, it is interesting to consider the possibility of the existence of a *trans* isomer of **2**, namely **2′**. It should be noted that most of the dibridged dimolybdenum(V) compounds with an Mo_2O_2 core have been characterized as having the *cis* conformation and only a few examples of *trans* conformers exist.[2] It has been shown by Wieghardt and co-workers,[23] who have structurally characterized two conformers, that the environment of the molybdenum atoms is the same in both isomers. The only significant difference lies in the structure of the Mo_2O_2 ring, which is puckered in the *cis* isomer and planar in the *trans* form.

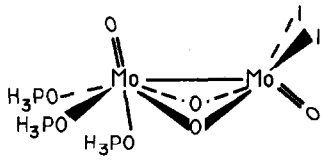

2′

The structure of **2′** has been modelled using exactly the same metal–ligand environment as in **2**. Keeping this environment frozen, the puckering (and, therefore, the Mo—Mo distance) of the Mo_2O_2 butterfly has been varied. The lowest energy was found for the puckering shown in the diagram of **2′**, the bending angle (Mo—Mo—middle of the O···O vector) is small (10°) and the Mo—Mo distance is 2.61 Å. The energy difference between this energy minimum and the structure corresponding to a planar Mo_2O_2 core is very small (0.02 eV), a value not significant at our level of calculations. The optimized structure of **2′** is found to be less stable than its *cis* conformer **2** by 0.4 eV. Consistently, the Mo—Mo overlap population is lower (0.154). This conformational preference for the *cis* structure can be easily understood if it is assumed that it is driven by the Mo—Mo interaction, i.e. by the overlap between the two σ-type frontier orbitals of the mononuclear units. In the *cis* conformation, the maximum overlap can be reached for the puckered structure which allows both overlapping lobes to be lined up with the Mo—Mo vector, as shown in **7a**. This ideal σ-type overlap cannot be reached for the *trans* conformation, which provides its best (but not so strong) overlap when the Mo_2O_2 core is planar, as shown in **7b**. In that situation, both overlapping lobes are parallel, but not lined up. The fact that the calculations on **2′** very slightly favour a puckered structure arises from some participation of the z^2-type level of the five-coordinated molybdenum atom (see Fig. 3). Indeed, when the Mo_2O_2 core is bent this MO can to a degree overlap and consequently mixes in a bonding fashion with the occupied σ(Mo—Mo) bonding orbital. This mixing is disfavoured when the puckering is made in the other direction. Moreover, steric repulsion between ligands occurs also in that case, causing this puckering to be significantly disfavoured.

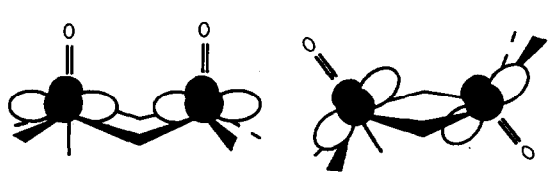

7a **7b**

In the absence of steric hindrance, the above results can be generalized to the whole series of

dibridged dimolybdenum(V) compounds with an Mo_2O_2 core. Thus, the preference for the *cis* conformation is rationalized on the basis that this geometry allows a stronger Mo—Mo σ-bond.

(c) MO *investigations of the reactivity of the metal–metal bond in* **1**. In order to model the reactivity of the metal–metal bond of **1** toward acids we have undertaken calculations on the $[2+H^+]$ system, with the proton attacking at different sites. At our level of calculations (which does not consider ionic interactions) the attack of the Mo—Mo bond does not appear strongly disfavoured with respect to attack on oxygen or iodine atoms. The more attractive approach of the bond is when H^+ attacks on the same side as the terminal oxo ligands. The proton 1*s* AO interacts mainly with the HOMO and the LUMO of **2**, so that the $[2+H^+]$ system can be considered as a two-electron three-orbital system. When the Mo—H distances are set to 1.8 Å, the occupation of these two metallic orbitals in the $[2+H^+]$ system is 0.30 and 0.96, respectively. The Mo—H overlap populations are 0.190 for the six-coordinated molybdenum atom and 0.262 for the five-coordinated one. These values indicate a strong bonding interaction. The presence of the bridging proton considerably reduces the Mo—Mo overlap population (0.057), suggesting that the attack of the Mo—Mo bond by H^+ would ultimately lead to the formation of mononuclear species.

Replacing H^+ by H^- provides us with the opportunity to model the reactivity of **1** with respect to a nucleophilic attack. The best site of attack for **2** is found to be the vacant site on the five-coordinated molybdenum atom. Indeed, the unoccupied z^2-type MO of this metal atom (Fig. 3) can overlap significantly with the nucleophile lone pair. The attack of the Mo—Mo bond is found repulsive. This result suggests that a hydride attack of the Mo—Mo bond would better lead to electron transfer rather than to Mo—H bond formation. Indeed, the reduction of **2** is expected to reinforce the metal–metal bond by occupying the Mo—Mo π-bonding LUMO (*vide supra*).

Acknowledgements—CNRS, Université de Bretagne Occidentale, and Université de Rennes I are acknowledged for financial support.

REFERENCES

1. For recent reviews, see for example: (a) R. H. Holm, *Chem. Rev.* 1987, **87**, 1401; (b) P. Braunstein, *New J. Chem.* 1988, **12**, 307; (c) P. A. Vigato, S. Tamburini and D. E. Fenton, *Coord. Chem. Rev.* 1990, **106**, 25.
2. For specific examples in molybdenum chemistry, see for instance: (a) C. D. Garner, *Comprehensive Coordination Chemistry* (Edited by G. Wilkinson), Vol. 3, p. 1301. Pergamon Press, Oxford (1987); (b) C. D. Garner and J. M. Charnock, *Comprehensive Coordination Chemistry* (Edited by G. Wilkinson), Vol. 3, p. 1329. Pergamon Press, Oxford (1987); (c) E. I. Stiefel, *Comprehensive Coordination Chemistry* (Edited by G. Wilkinson), Vol. 3, p. 1375. Pergamon Press, Oxford (1987); (d) J. Corfield, *Comprehensive Coordination Chemistry* (Edited by G. Wilkinson), Vol. 7, p. 255. Pergamon Press, Oxford (1987); (e) S. Ikari, Y. Sasaki, A. Nagasawa, C. Kabuto and T. Ito, *Inorg. Chem.* 1989, **28**, 1248; (f) R. S. Pilato, D. Rubin, G. L. Geoffroy and A. L. Rheingold, *Inorg. Chem.* 1990, **29**, 1986; (g) M. T. Pope, *Prog. Inorg. Chem.* 1991, **39**, 181.
3. See for example: (a) J. H. Sinfelt, *Bimetallic Catalysts: Discoveries, Concepts and Applications*. Wiley, New York (1983) and refs therein; (b) R. M. Bullock and C. P. Casey, *Accts Chem. Res.* 1987, **20**, 167 and refs therein; (c) A. Fukuoka, T. Kimura and M. Ichikawa, *J. Chem. Soc., Chem. Commun.* 1988, 428; (d) E. N. Jacobsen, K. I. Goldberg and R. G. Bergman, *J. Am. Chem. Soc.* 1988, **110**, 3706; (e) F. Ozawa, J. W. Park, P. B. Mackenzie, W. P. Schaefer, L. M. Henling and R. H. Grubbs, *J. Am. Chem. Soc.* 1989, **111**, 1319; (f) D. W. Stephan, *Coord. Chem. Rev.* 1989, **95**, 41 and refs therein.
4. P. Roman, A. Luque, J. M. Gutierrez-Zorrilla and S. Garcia-Granda, *Polyhedron* 1991, **10**, 2057.
5. A. A. Eagle, M. F. Mackay and C. G. Young, *Inorg. Chem.* 1991, **30**, 1425.
6. K. A. Hall, S. C. Critchlow and J. M. Mayer, *Inorg. Chem.* 1991, **30**, 3593.
7. J. Cl. Daran, K. Prout, G. J. S. Adam, M. L. H. Green and J. Sala Pala, *J. Organomet. Chem.* 1977, **131**, C40.
8. T. P. Blatchford, M. H. Chisholm and J. C. Huffman, *Inorg. Chem.* 1988, **27**, 2059.
9. (a) R. Poli and H. D. Mui, *Inorg. Chem.* 1991, **30**, 65; (b) J. C. Gordon, H. D. Mui, R. Poli and K. J. Ahmed, *Polyhedron* 1991, **10**, 1667.
10. A. C. Lizano, J. F. Richardson and M. E. Noble, *Inorg. Chem.* 1989, **28**, 1451.
11. M. H. Chisholm, J. C. Huffman and W. G. Van Der Sluys, *J. Am. Chem. Soc.* 1987, **109**, 2514.
12. A. Bino and F. A. Cotton, *Inorg. Chem.* 1979, **18**, 2710.
13. (a) N. Walker and D. Stuart, *Acta Cryst.* 1983, **A39**, 159; (b) Enraf–Nonius Molecular Structure Determination Package, MolEN Version 1990. Enraf–Nonius, Delft, The Netherlands (1990).
14. *International Tables for X-ray Crystallography*, Vol. IV. Kynoch Press, Birmingham (1974).
15. (a) R. Hoffmann and W. N. Lipscomb, *J. Chem. Phys.* 1962, **36**, 2179; (b) R. Hoffmann, *J. Chem. Phys.* 1963, **39**, 1397.
16. J. M. Ammeter, H. B. Bürgi, J. C. Thibeault and R. Hoffmann, *J. Am. Chem. Soc.* 1978, **100**, 3686.
17. (a) S. Y. Chu and R. Hoffmann, *J. Phys. Chem.* 1982, **86**, 1289; (b) G. Trinquier and G. Bertrand, *Inorg. Chem.* 1985, **24**, 3842.

18. P. L. Goggin, *Comprehensive Coordination Chemistry* (Edited by G. Wikinson), Vol. 2, p. 487. Pergamon Press, Oxford (1987).
19. F. A. Cotton and G. Wilkinson, *Advanced Inorganic Chemistry*, 5th edn. Wiley, New York (1988).
20. D. Coucouvanis, A. Toupadakis, J. D. Lane, S. M. Koo, C. G. Kim and A. Hadjikyriacou, *J. Am. Chem. Soc.* 1991, **113**, 5271.
21. R. Hoffmann, *Angew. Chem., Int. Edn Engl.* 1982, **21**, 711.
22. See for example: (a) D. H. Brown, P. G. Perkins and J. J. Stewart, *J. Chem. Soc., Dalton Trans.* 1972, 1105; (b) L. Natkaniec, M. F. Rudolf and B Jezowska-Trzebiatowska, *Theoret. Chim. Acta* 1973, **28**, 193; (c) B. Jezowska-Trzebiatowska, M. F. Rudolf, L. Natkaniec and H. Sabat, *Inorg. Chem.* 1974, **13**, 617; (d) T. Chandler, D. L. Lichtenberger and J. H. Enemark, *Inorg. Chem.* 1981, **20**, 75; (e) J. Bernholc and N. A. W. Holzwarth, *J. Phys. Chem.* 1984, **81**, 3897; (f) L. Junqian and C. Wendan, *J. Molec. Struct.* 1987, **151**, 19.
23. (a) K. Wieghardt, M. Hahn, W. Swiridoff and J. Weiss, *Angew. Chem., Int. Edn Engl.* 1983, **22**, 491; (b) K. Wieghardt, M. Hahn, W. Swiridoff and J. Weiss, *Inorg. Chem.* 1984, **23**, 94; (c) K. Wieghardt, M. Guttmann, P. Chaudhuri, W. Gebert, M. Minelli, C. G. Young and J. H. Enemark, *Inorg. Chem.* 1985, **24**, 3151.

Polyhedron Vol. 12, No. 10, pp. 1227–1230, 1993
Printed in Great Britain

0277–5387/93 $6.00+.00
© 1993 Pergamon Press Ltd

COMPLEXES OF YTTRIUM AND LANTHANIDE NITRATES WITH 4-N-(4′-ANTIPYRYLMETHYLIDENE)AMINOANTIPYRINE

M. K. MURALEEDHARAN NAIR and P. K. RADHAKRISHNAN†

School of Chemical Sciences, Mahatma Gandhi University, Ettumanoor, Kottayam, Kerala 686 631, India

(*Received* 4 *November* 1992; *accepted* 7 *January* 1993)

Abstract—Yttrium and lanthanide nitrate complexes with the Schiff base 4-N-(4′-antipyrylmethylidene)aminoantipyrine (AA) of the composition of $[Ln(AA)_2(NO_3)_2]NO_3$ (where Ln = Y, La, Pr, Nd, Sm, Eu, Gd, Dy, Ho and Er) have been synthesized and characterized by elemental analyses, electrical conductance in non-aqueous solvents, magnetic susceptibility measurements, IR, electronic and proton NMR spectra and thermogravimetric analyses. The Schiff base AA acts as a tridentate ligand in all these complexes, coordinating through the oxygens of both carbonyl groups and the azomethine nitrogen. Only two of the nitrate ions are coordinated monodentately to the central metal ion, while the third remains uncoordinated.

As part of our studies on the Schiff base complexes of yttrium and the lanthanides[1–4] a new series of complexes of the nitrates with AA were synthesized and characterized. The present complexes includes Y^{III} and the lanthanides La^{III}, Pr^{III}, Nd^{III}, Sm^{III}, Eu^{III}, Gd^{III}, Dy^{III}, Ho^{III} and Er^{III}. The ligand possessing two antipyrine groups and an azomethine group may act as a terdentate ligand, forming two chelate rings imparting considerable stability for the resulting complexes. Also, the Schiff base being an antipyrine derivative possessing antibacterial and anti-inflammatory properties,[5] the complexes would be expected to be of physiological importance.

EXPERIMENTAL

Reagents

The Schiff base AA was prepared from 4-aminoantipyrine and 4-antipyrine carboxaldehyde by condensation in ethanolic medium. The nitrates of Y, La, Pr, Nd, Sm, Eu, Gd, Dy, Ho and Er were prepared as reported previously.[3]

Preparation and analysis of the complexes

Solutions of the Schiff base (2.5 mmol) in acetonitrile (100 cm^3) and the metal nitrate (1 mmol) in acetonitrile (20 cm^3) were mixed and refluxed for *ca* 2 h. The resulting mixture was cooled, filtered and evaporated to dryness. The residue obtained was repeatedly washed with hot chloroform to remove excess ligand and finally recrystallized from methanol. The purified complexes were dried *in vacuo* over phosphorus(V) oxide and were analysed for metal content by conventional methods.[6]

Measurements

Molar conductivities of the complexes in DMF and methanol (*ca* 10^{-3} M solution) were measured at room temperature using a Toshniwal conductivity bridge with a dip-type conductance cell and platinum electrode (cell constant = 0.9588 cm^{-1}). Elemental analyses were obtained with a Heraeus CHNO rapid analyser. The IR spectra of the ligand and complexes were recorded in the range 4000–400 cm^{-1} on a Shimadzu IR-470 spectrophotometer using the KBr disc technique. Electronic spectra of the ligand and complexes in acetonitrile (10^{-4} M solution) were recorded in the 200–1100 nm range on a Shimadzu UV-160A spectro-

† Author to whom correspondence should be addressed.

photometer. Proton NMR spectral studies were performed using an NMR-GSX-400 instrument. Thermal studies were performed on a Shimadzu DT-40 thermal analyser (sample: 10 mg; heating rate: 10°C min^{-1}; atmosphere: nitrogen). Magnetic moments were measured at room temperature by the Gouy method using mercury(II) tetrathiocyanatocobaltate(II) as the calibrant.

RESULTS AND DISCUSSION

The analytical data (Table 1) indicate that all the complexes have the general formula $Ln(AA)_2(NO_3)_3$, where Ln = Y, La, Pr, Nd, Sm, Eu, Gd, Dy, Ho and Er. All these complexes are soluble in acetonitrile, DMF, DMSO, ethanol and methanol and insoluble in acetone, benzene, chloroform, ethyl acetate and toluene.

Electrical conductance

The molar conductance data of the complexes are presented in Table 1. The conductance values in DMF and methanol are in the range expected for 1 : 1 electrolytes.[7] Hence, the present complexes may be formulated as $[Ln(AA)_2(NO_3)_2]NO_3$.

Magnetic behaviour

The magnetic susceptibility data given in Table 1 show that all complexes, except those of Y and La, are paramagnetic, as expected. The measured magnetic moments of the complexes agree well with the theoretical values calculated from the Van Vleck formula,[8] which suggest that the 4*f* electrons play a negligible role in bonding.

IR spectra

The important IR frequencies of the Schiff base ligand and the complexes are presented in Table 2. The strong band at 1658 cm^{-1}, due to ν(C=O) in AA, is shifted to 1625 cm^{-1} in the complexes, suggesting that both carbonyl oxygens are coordinated.[4] The IR spectrum of the Schiff base shows a strong band at 1596 cm^{-1}, attributable to the C=N stretching vibration. On complexation this band shifts to the 1586 cm^{-1} region, showing that the nitrogen of the azomethine group is also coordinated to the metal ion.[4] The spectra of the complexes show three bands at *ca* 1425, 1382 and 1320 cm^{-1}, which are not present in the spectrum of AA. These bands are assigned to ν_4(coordinated),

Table 1. Analytical[a] and molar conductance[b] data of rare earth nitrate complexes of AA

	Complex	Ln %	C %	H %	N %	Molar conductance DMF	Molar conductance MeOH	μ_{eff} (B.M.)
1	$[Y(AA)_2(NO_3)_2]NO_3$	8.3 (8.3)	51.4 (51.3)	4.2 (4.3)	16.9 (16.9)	102.7	87.5	—
2	$[La(AA)_2(NO_3)_2]NO_3$	12.2 (12.3)	48.6 (49.0)	3.9 (4.0)	16.0 (16.2)	101.4	89.6	—
3	$[Pr(AA)_2(NO_3)_2]NO_3$	12.7 (12.5)	48.7 (48.9)	4.0 (4.1)	16.0 (16.1)	98.9	84.2	3.40
4	$[Nd(AA)_2(NO_3)_2]NO_3$	12.7 (12.7)	48.5 (48.6)	4.0 (4.1)	15.9 (16.1)	93.4	84.9	3.65
5	$[Sm(AA)_2(NO_3)_2]NO_3$	13.2 (13.2)	48.4 (48.4)	4.0 (4.0)	15.9 (15.9)	99.0	82.3	1.85
6	$[Eu(AA)_2(NO_3)_2]NO_3$	13.3 (13.3)	48.6 (48.8)	4.0 (4.0)	15.8 (15.9)	98.0	99.0	3.37
7	$[Gd(AA)_2(NO_3)_2]NO_3$	13.6 (13.7)	48.0 (48.2)	4.0 (4.0)	15.8 (15.9)	100.2	77.0	8.33
8	$[Dy(AA)_2(NO_3)_2]NO_3$	14.2 (14.1)	48.0 (48.0)	3.9 (4.0)	15.8 (15.8)	99.2	94.2	10.47
9	$[Ho(AA)_2(NO_3)_2]NO_3$	14.3 (14.3)	47.7 (47.9)	3.9 (4.0)	15.7 (15.8)	95.2	97.2	10.51
10	$[Er(AA)_2(NO_3)_2]NO_3$	14.5 (14.5)	47.7 (47.8)	3.8 (4.0)	15.7 (15.8)	98.5	89.6	9.69

[a] Calculated values in parentheses.
[b] 10^{-3} M solutions used; Ω^{-1} cm^2 mol^{-1}.

Table 2. Important IR absorptions (cm^{-1}) of rare earth nitrate complexes of AA

	Compound	ν(C=O)	ν(C=N)	$\nu_4(NO_3)$	$\nu_3(NO_3)$	$\nu_2(NO_3)$	ν(M—O)	ν(M—N)
1	AA	1658s	1596s	—	—	—	—	—
2	$[Y(AA)_2(NO_3)_2]NO_3$	1625s	1586s	1430m	1382s	1320m	540m	455m
3	$[La(AA)_2(NO_3)_2]NO_3$	1625s	1586s	1430w	1382s	1320w	540m	460m
4	$[Pr(AA)_2(NO_3)_2]NO_3$	1625s	1586s	1435w	1382s	1320w	540m	460m
5	$[Nd(AA)_2(NO_3)_2]NO_3$	1625s	1586s	1435w	1380s	1320w	542m	460m
6	$[Sm(AA)_2(NO_3)_2]NO_3$	1625s	1586s	1430w	1382s	1320m	542m	460m
7	$[Eu(AA)_2(NO_3)_2]NO_3$	1625s	1586s	1435m	1382s	1320m	540m	460m
8	$[Gd(AA)_2(NO_3)_2]NO_3$	1625s	1586s	1430w	1382s	1320m	542m	460m
9	$[Dy(AA)_2(NO_3)_2]NO_3$	1625s	1586s	1435w	1382s	1320m	542m	460m
10	$[Ho(AA)_2(NO_3)_2]NO_3$	1625s	1586s	1430m	1380s	1320m	542m	460m
11	$[Er(AA)_2(NO_3)_2]NO_3$	1625s	1586s	1430m	1380s	1320m	542m	460m

s = strong; m = medium; w = weak.

ν_3(uncoordinated) and ν_1(coordinated) vibrations of the nitrate groups.[9] The magnitude of $\nu_4-\nu_1$ is 105 cm^{-1}, indicating that the nitrate ions are coordinated in a monodentate fashion.[10] This conforms with the conductance data, which shows that only two of the nitrate groups are coordinated. The ν(M—O) and ν(M—N) stretching vibrations are observed at *ca* 540 and 460 cm^{-1}, respectively, in the spectra of the complexes.[11]

Proton NMR spectra

The proton NMR spectrum of the ligand AA shows the —CH=N— proton resonance at 8.35δ and it is shifted to 8.6 and 8.45δ in the yttrium and lanthanum complexes, respectively, with respect to TMS, suggesting coordination of the azomethine nitrogen.[12] The spectra of the ligand and its complexes show the following bands: phenyl multiplet

Table 3. Important *f–f* bands and their tentative assignments

Complex	Band (nm)	Tentative assignments	Covalency parameters calculated
Pr	446	$^3H_4 \rightarrow {}^3P_2$	$\beta = 0.9963$
	471	$^3H_4 \rightarrow {}^3P_1$	$\delta = 0.3714$
	485	$^3H_4 \rightarrow {}^3P_0$	$b^{1/2} = 0.0304$
	592	$^3H_4 \rightarrow {}^1D_2$	$\eta = 0.0019$
Nd	513	$^4I_{9/2} \rightarrow {}^2G_{9/2}$	$\beta = 0.9961$
	525	$^4I_{9/2} \rightarrow {}^2G_{7/2}$	$\delta = 0.3915$
	581	$^4I_{9/2} \rightarrow {}^4G_{5/2}, {}^2G_{7/2}$	
	682	$^4I_{9/2} \rightarrow {}^4F_{9/2}$	$b^{1/2} = 0.0312$
	745	$^4I_{9/2} \rightarrow {}^4F_{7/2}$	$\eta = 0.0020$
	800	$^4I_{9/2} \rightarrow {}^4F_{5/2}$	
	872	$^4I_{9/2} \rightarrow {}^4F_{3/2}$	
Ho	451	$^5I_8 \rightarrow {}^5G_5$	$\beta = 0.9966$
	538	$^5I_8 \rightarrow {}^5S_2, {}^5S_4$	$\delta = 0.3412$
	645	$^5I_8 \rightarrow {}^5F_5$	$b^{1/2} = 0.0292$
			$\eta = 0.0017$
Er	521	$^5I_{15/2} \rightarrow {}^2H_{11/2}$	$\beta = 0.9972$
	543	$^5I_{15/2} \rightarrow {}^5S_{3/2}$	$\delta = 0.2808$
	653	$^4I_{15/2} \rightarrow {}^4F_{9/2}$	$b^{1/2} = 0.0265$
			$\eta = 0.0014$

at 7.52δ, =C—CH_3 at 2.5δ and —N—CH_3 at 2.7 and 3.35δ.

Electronic spectra

The electronic spectrum of the ligand shows the following maxima: $n \rightarrow \pi^*$ transition at 347.9 nm and $\pi \rightarrow \pi^*$ at 247 nm. In the complexes the $n \rightarrow \pi^*$ band is red-shifted to 345–342 nm and $\pi \rightarrow \pi^*$ to 227–222 nm, respectively. The complexes of Pr, Nd, Ho and Er show *f–f* bands, the tentative assignments of which are given[13,14] in Table 3. The inter-electronic repulsion parameter (β), percentage covalency (δ), the bonding parameter ($b^{1/2}$) and the covalency angular overlap parameter (η) calculated[13] for these complexes are also included in Table 3. The values of β are found to be less than unity and also $b^{1/2}$ and η are positive, suggesting covalency in the metal–ligand bonding. The "δ" values less than 1.5 in all these complexes indicate weak covalent character in the metal–ligand bond. Also, from the shape of the hypersensitive $^4I_{9/2} \rightarrow {}^2G_{5/2}$, $^2G_{7/2}$ transition of Nd^{III}, a coordination number of eight may be assigned[14] to the complex $[Nd(AA)_2(NO_3)_2]NO_3$.

Thermal behaviour

The thermogravimetric data of the complexes show that they are stable up to 220°C. The TG and DTG curves do not have stages or peaks up to 220°C, therefore, the complexes do not contain small molecules (water or solvent). The complexes undergo two-stage decomposition with DTG peaks at 275 and 330°C. The complexes undergo complete decomposition in the 800–850°C region, forming the corresponding metal oxides.

Acknowledgements—We are thankful to Prof. V. N. Rajasekharan Pillai, Director of this School, and the Head, RSIC, IIT, Madras, for providing experimental facilities and to the authorities of the University Grants Commission, New Delhi, India, for the award of a Senior Research Fellowship to one of us (MKM).

REFERENCES

1. P. K. Radhakrishnan, P. Indrasenan and C. G. R. Nair, *Polyhedron* 1984, **3**, 67.
2. P. K. Radhakrishnan, *J. Ind. Chem. Soc.* 1984, **61**, 838.
3. P. K. Radhakrishnan, *Inorg. Chim. Acta* 1985, **110**, 211.
4. P. K. Radhakrishnan, *Polyhedron* 1986, **5**, 995.
5. L. Singh, G. Mohan, R. K. Parashar, S. P. Tripathi and R. C. Sharma, *Curr. Sci.* 1986, **55**, 846.
6. M. R. G. Nair, M. J. Kurian and C. P. Prabhakaran, *Talanta* 1981, **28**, 395.
7. W. J. Geary, *Coord. Chem. Rev.* 1971, **7**, 81.
8. J. H. Van Vleck and N. Frank, *Phys. Rev.* 1929, **34**, 1494.
9. K. Nakamoto, *Infrared and Raman Spectra of Inorganic and Coordination Compounds*, p. 251. Wiley, New York (1986).
10. B. J. Hathaway, D. G. Holah and M. Hudson, *J. Chem. Soc.* 1963, 4586.
11. S. K. Agarwal and J. P. Tandon, *Monatshefte Chem.* 1979, **110**, 401.
12. R. Jagannathan and S. Soundararajan, *Inorg. Nucl. Chem. Lett.* 1981, **17**, 65.
13. S. P. Sinha, *Spectrochim. Acta* 1966, **22**, 57.
14. D. G. Karraker, *Inorg. Chem.* 1967, **6**, 1863.

Polyhedron Vol. 12, No. 10, pp. 1231–1237, 1993
Printed in Great Britain

0277–5387/93 $6.00+.00
© 1993 Pergamon Press Ltd

SYNTHESIS AND STRUCTURAL CHARACTERIZATION OF A POLYOXOVANADATE COORDINATION COMPLEX $[V_4O_8(CH_3O)_4(bipy)_2]$ WITH A TETRAMETALLATE CORE

ISABEL CAVACO, JOÃO COSTA PESSOA* and M. TERESA DUARTE

Centro de Química Estrutural, Complexo I, Instituto Superior Técnico, 1096 Lisboa Codex, Portugal

and

PEDRO M. MATIAS

Centro de Tecnologia Química e Biológica, 2780 Oeiras, Portugal

and

RUI T. HENRIQUES

ICEN-LNETI, Departamento de Química, 2686 Sacavém Codex, Portugal

(*Received* 21 *October* 1992; *accepted* 6 *January* 1993)

Abstract—A vanadium(V) tetramer, $[V_4O_8(CH_3O)_4(bipy)_2]$ (**1**), has been isolated from a solution of $[V^{IV}O(sal\text{-}gly)(H_2O)]$ (**2**) (sal-gly = N-salicylideneglycinate) and bipyridyl. Its structure has been determined by X-ray diffraction analysis. There is one molecule per unit cell and its centre lies at a crystallographic inversion centre. The vanadium atoms lie on the corners of a diamond-shaped planar unit and each of the two independent vanadium atoms V(1) and V(2) are octahedrally coordinated. The tetramer contains a V_4O_8 core, two μ_3-OCH_3, two CH_3O^- and two bipy ligands. The magnetic susceptibility was measured and data could be fitted to a $\chi_p = A + C/T$ function with $A = 9.087 \times 10^{-5}$ emu mol^{-1} and $C = 1.809 \times 10^{-3}$ emu K mol^{-1}.

Vanadium is receiving considerable attention as a biologically important metal since the discovery of the first two vanadoenzymes (bromoperoxidase from marine algae[1,2] and nitrogenase from *Azotobacter vinelandii*[3]). In order to understand how the uptake of vanadium from living organisms occurs and how it might function in a complex biomolecule it is necessary to study its basic coordination chemistry and the oxidation–reduction reactivity of vanadium complexes.

Polynulcear μ-oxo and μ-hydroxo vanadyl (d^0 and/or d^1) are interesting classes of compounds. Decavanadates are perhaps the best characterized and current research interest for these and other polyoxometallates has been increased due to the wide field of applications that has been found for these compounds, including analytical and clinical chemistry, catalysis, biochemistry, medicine and solid-state devices.[4,5] Other types of polyoxovanadates and their structural characteristics were also recently reviewed.[6] Mixed-valence metal oxygen clusters that exist with different electron populations are of importance for understanding electron-transfer and electron-storage systems in nature and in materials science. Mixed-valence vanadium–oxygen clusters have recently received much interest.[5,7,8] The simplest of these involve complexes with the $V_2O_3^{3+}$ unit, whose stability is now quite well established.[9–11]

Several examples of simple organic units incorporated into polyoxovanadate frameworks have

*Author to whom correspondence should be addressed.

been structurally characterized (see, e.g. refs 7, 8 and 12–18). (Alkoxo)oxovanadium complexes ("vanadate esters") are receiving increased attention, on one hand because of their potential in generating thin metal-oxide and -carbide layers by gas-phase deposition[19] and on the other because of the biological importance of vanadium ester compounds.[20] The present paper describes the synthesis, X-ray crystallographic and magnetic characterization of a vanadium tetramer containing a V_4O_8 core, two μ_3-OCH_3 ligands, two CH_3O^- and two bipy ligands.

EXPERIMENTAL

Reagents and apparatus

Reagent grade salicylaldehyde (Carlo Erba), glycine (BDH), vanadium sulphate pentahydrate (Merck), bipyridyl (Merck) and methanol (Merck) were used without further purification.

The IR spectra of KBr discs were recorded on a Perkin–Elmer 683 spectrometer and magnetic susceptibilities were measured using a Faraday balance down to 5 K.

Preparation of complex **1**

[VO(sal-gly)(H_2O)] (**2**) (0.0622 g, 0.24 mmol) was prepared by standard procedures[21,22] and dissolved in methanol (20 cm^3). Bipyridyl (0.0335 g, 0.21 mmol) was dissolved in methanol (5 cm^3) and slowly added to the solution of **2** by diffusion through a strip of filter paper until green/brownish crystals of the title compound were obtained. No recrystallization was needed. The compound is reasonably stable when exposed to the atmosphere.

X-ray crystal structure determination of complex **1**

Crystal data. $V_4O_8(CH_3O)_4(C_{10}H_8N_2)_2$, M_r = 768.27, triclinic, space group $P\bar{1}$, a = 8.1240(7), b = 9.0857(7), c = 11.1945(9) Å, α = 104.83(1), β = 105.78(1), γ = 103.78(1)°, V = 725(3) $Å^3$, Z = 1, $F(000)$ = 388, D_c = 1.76 g cm^{-3}, μ(Mo-K_α) = 2.73 cm^{-1}.

Data collection. X-ray measurements were made with an Enraf–Nonius CAD-4 diffractometer and graphite monochromatized Mo-K_α radiation (λ = 0.71069 Å). Cell dimensions were determined from the measured θ-values for 25 intense reflections with $14 \leqslant \theta \leqslant 16°$. The intensities of 4438 observations of 4347 independent reflections in the range $2.0 \leqslant \theta \leqslant 27.0°$ were measured by the ω–2θ scan mode. Data was corrected for Lorentz, polarization and absorption effects.

Structure determination and refinement. The 3679 reflections with $F_o \geqslant 3\sigma(F_o)$ were used in the structure solution and refinement. The non-hydrogen atomic positions were determined by a direct method with the SHELXS-86 program[23] and refined to convergence with anisotropic thermal motion parameters using the SHELX-76 program.[23] At this stage the positions of the hydrogen atoms were obtained from a difference-Fourier map and were included in the refinement process with isotropic thermal motion parameters. The final refinement was carried out with a weighting scheme of $w = 1/(\sigma^2(F_o)+0.0006F_o^2)$ and converged to $R(F) = 0.038$ and $R_w(F) = 0.040$ for 3783 reflections with $F_o \geqslant 2\sigma(F_o)$ and 255 refined parameters. The largest negative and positive peaks in the final difference map were 0.82 and −0.68 e $Å^{-3}$ and were located near the vanadium atoms. Data for atomic scattering factors were taken from the International Tables.[24]

Additional material is available from the Cambridge Crystallographic Data Centre, which comprises hydrogen atom coordinates, atomic thermal motion parameters, remaining bond lengths and angles and a list of observed and calculated structure factors.

RESULTS AND DISCUSSION

The solid tetramer **1** was isolated from methanolic solutions. The formation of a vanadium(V) compound may be explained by the slow diffusion of atmospheric oxygen into the solution and reaction with oxovanadium(IV).

A molecular diagram[25] presenting the numbering scheme is shown in Fig. 1; bond distances and bond angles are listed in Tables 1 and 2, respectively.

Table 1. Bond lengths (Å) for $V_4O_8(CH_3O)_4(C_{10}H_8N_2)_2$

V(1)—O(1)	1.597(1)	V(1)—O(3)	2.299(1)
V(1)—O(3)[a]	2.039(1)	V(1)—O(4)	1.802(1)
V(1)—O(5)	1.822(1)	V(1)—O(6)[a]	2.000(1)
V(2)—O(2)	1.610(1)	V(2)—O(3)	2.274(1)
V(2)—O(5)	1.818(1)	V(2)—O(6)	1.719(1)
V(2)—N(11)	2.189(1)	V(2)—N(21)	2.168(1)
C(3)—O(3)	1.422(1)	C(4)—O(4)	1.384(4)
N(11)—C(12)	1.339(2)	N(11)—C(16)	1.344(2)
C(12)—C(13)	1.378(2)	C(13)—C(14)	1.375(2)
C(14)—C(15)	1.369(3)	C(15)—C(16)	1.389(1)
N(21)—C(22)	1.338(2)	N(21)—C(26)	1.344(1)
C(22)—C(23)	1.386(3)	C(23)—C(24)	1.367(3)
C(24)—C(25)	1.379(3)	C(25)—C(26)	1.386(3)
C(16)—C(26)	1.468(2)		

[a] Symmetry related atom by $-x, 1-y, 1-z$.

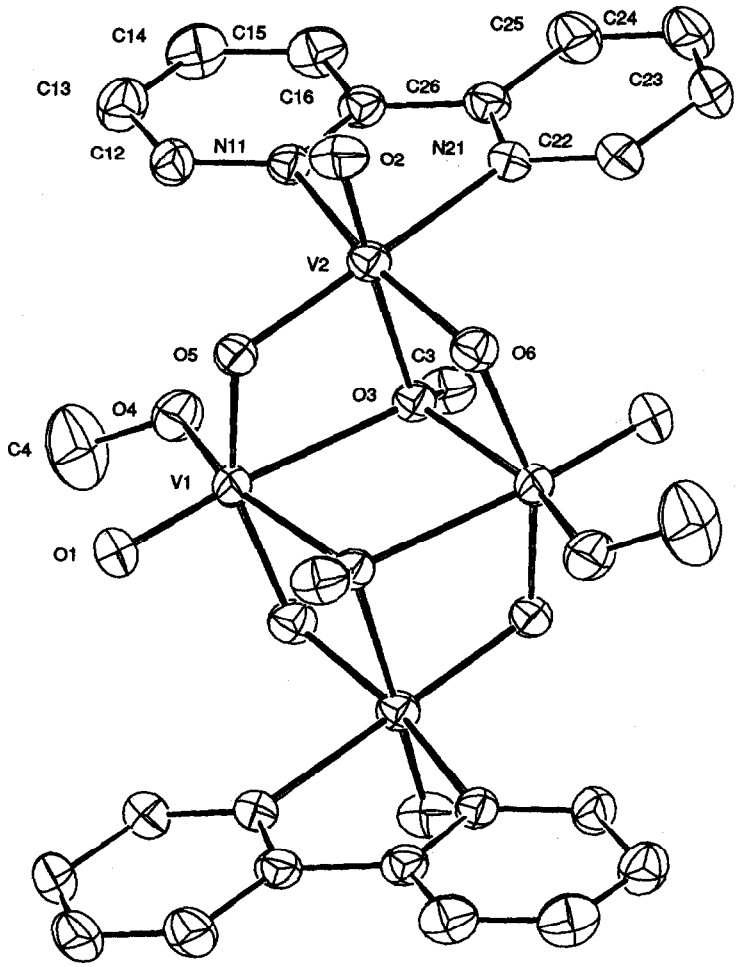

Fig. 1. ORTEP[25] diagram of $[V_4O_8(CH_3O)_4(bipy)_2]$ (1). There are two independent types of vanadium atoms: V(1) and V(2). The four vanadium atoms form a planar unit and its centre lies on a crystallographic inversion centre.

There is one molecule per unit cell and its centre lies at a crystallographic inversion centre. The vanadium atoms lie on the corners of a diamond-shaped planar unit, with nearly identical V(1)—V(2) distances [3.1212(4) and 3.1225(3) Å]. The shortest diagonal is defined by the two V(1) atoms [3.4633(4) Å] and the longest by the two V(2) atoms [5.1951(4) Å]. The μ-oxo groups are alternately above and below the plane of the four vanadium atoms (see Fig. 2) and all coordinated groups above this plane have their symmetry-related counterparts as required by the existence of an inversion centre.

Each of the two independent vanadium atoms V(1) and V(2) are octahedrally coordinated. The V(1) atom is coordinated to vanadyl oxygen (O1) [1.597(1) Å] and there are two other relatively short bonds: to the methoxy oxygen O(4) [1.802(1) Å] and to the bridging oxygen μ_2-O(5) [1.822(1) Å]. The bond distance [2.299(1) Å] between V(1) and the methoxy oxygen O(3), *trans* to the vanadyl bond, is relatively long, as expected, while the V(1)—O(3a) distance [2.039(1) Å] is again in the expected range for an oxygen atom coordinated *cis* to the vanadyl group. The V(2) atom is coordinated to the vanadyl oxygen O(2) [1.610(1) Å] and there are also two other short bonds, namely to the bridging μ_2-oxo atoms O(5) [1.818(1) Å] and O(6) [1.719(1) Å]. The bond distance between V(2) and the methoxy oxygen μ_3-O(3) [2.274(1) Å], *trans* to the vanadyl bond, is also in the expected range. The six-fold coordination of V(2) is completed by the two nitrogen atoms of the bipy moiety [V(2)—N(11), 2.189(1); V(2)—N(21), 2.168(1) Å].

The IR spectrum exhibits two bands at 940 and 955 cm^{-1}, which can be associated with ν(V=O) of the two unequivalent vanadyl groups. A band at 2800 cm^{-1} might be associated with the C—H stretching modes of the methoxy groups. The absorp-

Table 2. Bond angles (°) for $V_4O_8(CH_3O)_4(C_{10}H_8N_2)_2$

O(1)—V(1)—O(3)	171.92(9)	O(1)—V(1)—O(3)[a]	97.95(6)
O(1)—V(1)—O(4)	101.25(7)	O(1)—V(1)—O(5)	100.84(8)
O(1)—V(1)—O(6)[a]	96.98(7)	O(3)—V(1)—O(3)[a]	74.19(5)
O(3)—V(1)—O(4)	86.83(6)	O(3)—V(1)—O(5)	77.55(6)
O(3)—V(1)—O(6)[a]	83.23(6)	O(3)[a]—V(1)—O(4)	156.96(6)
O(3)[a]—V(1)—O(5)	89.48(5)	O(3)[a]—V(1)—O(6)[a]	76.90(5)
O(4)—V(1)—O(5)	99.23(6)	O(4)—V(1)—O(6)[a]	88.18(6)
O(5)—V(1)—O(6)[a]	158.92(9)		
O(2)—V(2)—O(3)	177.48(9)	O(2)—V(2)—O(5)	103.67(8)
O(2)—V(2)—O(6)	104.40(8)	O(2)—V(2)—N(11)	94.51(6)
O(2)—V(2)—N(21)	94.72(7)	O(3)—V(2)—O(5)	78.28(6)
O(3)—V(2)—O(6)	76.55(6)	O(3)—V(2)—N(11)	83.93(5)
O(3)—V(2)—N(21)	82.92(5)	O(5)—V(2)—O(6)	103.37(7)
O(5)—V(2)—N(11)	87.66(6)	O(5)—V(2)—N(21)	153.79(9)
O(6)—V(2)—N(11)	154.91(6)	O(6)—V(2)—N(21)	89.66(5)
N(11)—V(2)—N(21)	72.23(5)		
V(1)—O(3)—V(1)[a]	105.81(2)	V(1)—O(3)—V(2)	86.07(3)
V(1)—O(3)—C(3)	118.4(1)	V(1)[a]—O(3)—V(2)	92.60(3)
V(1)[a]—O(3)—C(3)	116.17(7)	V(2)—O(3)—C(3)	131.6(1)
V(1)—O(4)—C(4)	127.3(2)	V(1)—O(5)—V(2)	118.05(5)
V(1)[a]—O(6)—V(2)	113.95(4)		
C(12)—N(11)—C(16)	118.7(2)	C(22)—N(21)—C(26)	119.0(2)
N(11)—C(12)—C(13)	122.4(2)	C(12)—C(13)—C(14)	118.7(2)
C(13)—C(14)—C(15)	119.6(2)	C(14)—C(15)—C(16)	119.0(2)
N(11)—C(16)—C(15)	121.5(1)	N(11)—C(16)—C(26)	114.0(1)
C(15)—C(16)—C(26)	124.5(2)	N(21)—C(22)—C(23)	121.9(2)
C(22)—C(23)—C(24)	119.0(2)	C(23)—C(24)—C(25)	119.5(2)
C(24)—C(25)—C(26)	118.9(2)	N(21)—C(26)—C(25)	121.6(1)
N(21)—C(26)—C(16)	114.3(1)	C(25)—C(26)—C(16)	124.0(2)

[a] Symmetry related atom by $-x, 1-y, 1-z$.

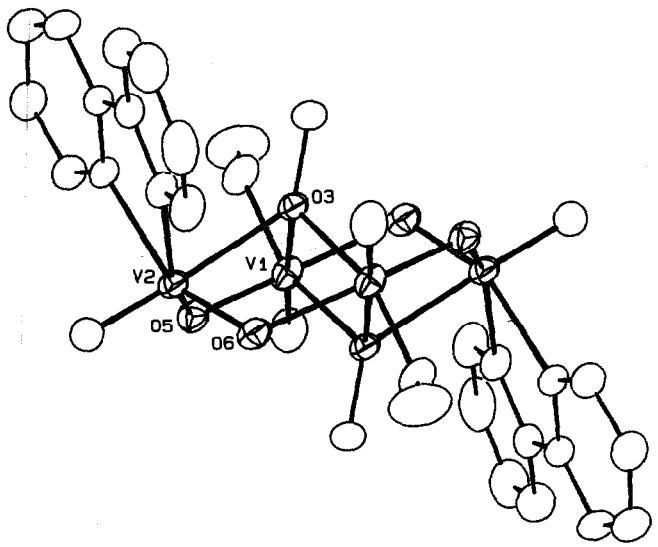

Fig. 2. ORTEP[25] diagram of **1** illustrating the bridging through oxo and alkoxo oxygen atoms and emphasizing the alternating position of the ligands above and below the plane of the four vanadium atoms.

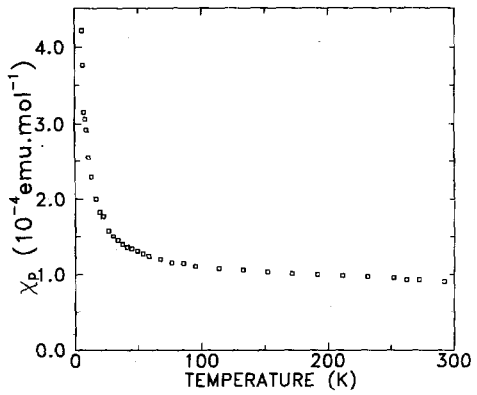

Fig. 3. Temperature dependence of the magnetic susceptibility of **1** per vanadium atom at 5 Tesla. The data were corrected from the diamagnetic contribution ($\chi_d = -9.97 \times 10^{-5}$ emu mol^{-1}).

tions in the 850–900 cm^{-1} range might be associated to bridging oxo groups, as well as some of the more sharp bands in the 650–780 cm^{-1} and 500–580 cm^{-1} range. Some of the bands observed in the 700–770 cm^{-1} range might be associated with the bipy moiety.

Having started with a vanadium(IV) compound, the possibility of tetramer **1** being a mixed-valence product existed; in this case the methoxy oxygens O(4) and/or O(4′) [or bridging oxygens O(5) and/or O(6)] would be protonated. As there is no safe way to assess this from the IR, X-ray or analytical data, the magnetic susceptibility was measured by the Faraday method at 5 Tesla between 5 and 290 K and was corrected for the diamagnetic contribution. Data in Fig. 3 can be fitted to a $\chi_p = A + C/T$ function with $A = 9.087 \times 10^{-5}$ emu mol^{-1} and $C = 1.809 \times 10^{-3}$ emu K mol^{-1}. The C term corresponds to a paramagnetic $S = 1/2$ impurity of $\sim 0.5\%$ per vanadium atom. The temperature-independent paramagnetic term A is within the values commonly found in vanadium(V) compounds (10^{-5}–10^{-4} emu mol^{-1}).[26] Therefore, tetramer **1** is definitely a vanadium(V) cluster.

The bond lengths to vanadium atoms for bridging [O(3)] and non-bridging [O(4)] methoxy oxygens are within the values found in other structurally characterized vanadium complexes (see e.g. refs 8, 12–15, 18, 20 and 27). The μ_2-(V—O) bond lengths are also within the normal range, but they are shorter for the V(2) atoms. The V—N bond lengths are of the order of magnitude (but in the higher range) of the values found in many other vanadium(IV) and (V) complexes containing the bipy moiety (see e.g. refs 28–35). The V—O bond lengths are distributed over a relatively wide range of values. The shortest bonds correspond to the four vanadyl bonds. The bonds corresponding to V—O—V (oxo) bridges lie between 1.719 and 1.822 Å and those corresponding to V—O—V (alkoxo) bridges, including the oxygens located in *trans* positions to vanadyl bonds, vary between 2.039 and 2.299 Å. The presence of differentiated V—O linkages indicates the possibility of a variety of internal vibrations, although some of them could be expected to superimpose or to fall in restricted spectral ranges, as observed.

Cyclic vanadate tetramers containing V_4O_4 rings have been structurally characterized,[16] including the *meta*-vanadates $[N(C_4H_9)_4]_3HV_4O_{12}$[36] and $[HC_4H_{11}N]_4[V_4O_{12}]$,[37] and were suggested as intermediates in water exchange and depolymerization reactions of the polyanion $V_{10}O_{28}^{6-}$,[38] as "constituents" of the decavanadate framework[39] and of clusters $[(C_4H_9)_4N]_2[V_6O_{13}\{(OCH_2)_3CR\}_2]$ (R = NO_2, CH_2OH, CH_3), $[V_6O_{11}(OH)_2\{CH_3C(CH_2O)_3\}_2]$, $[(C_4H_9)_4N]_2[V_4^{IV}V_2^{V}O_9(OH)_4\{(OCH_2)_3CCH_3\}_2]$ and $[(C_4H_9)_4N][V_6^{IV}O_7(OH)_6\{(OCH_2)_3CCH_3\}_2]\cdot 2CH_2Cl_2\cdot 0.5C_6H_5NNC_6H_5$.[18] The observation of the V_4O_4 rings for both coordination complexes and the metavanadate ion suggests that this core may have a relevant role in the chemistry of oxovanadates, and that significant variations in the structural parameters associated with the core may be tolerated.

The vanadium tetramer **1** is structurally similar to $[Mo_4O_8(OPr^i)_4(py)_4]$ (**3**), characterized by Chisholm and co-workers,[40] and to other molybdenum and tungsten compounds containing M_4O_{16} units. It also confirms Chisholm's suggestion[40] of a large class of structurally related compounds of the formula $M_4X_aY_bZ_c$, where $a+b+c = 16$, having 0–12 cluster electrons. Tetramer **1** has zero cluster electrons and to our knowledge the structure of **1** is the first of this type in vanadium chemistry; it is similar to compound **3**,[40] but the triply bridging oxygen atoms are from methoxy groups and not from oxo groups; the μ_2-(OPr^i) groups are here replaced by μ_2-oxo groups and only V(2) atoms are bonded to nitrogens.

Although [VO(sal-gly)(H_2O)] (**2**) can be used as a starting material for the preparation of several monomeric vanadium(IV) complexes,[22,41] we do not expect that we have found a useful general route to substituted vanadium(IV) and/or vanadium(V) clusters when making changes in reagents. In fact when trying the reaction with pyridine we isolated green, brown and pink complexes. The brown complex is [VO(sal-gly)($py)_2$], characterized by X-ray diffraction.[42] Elemental analyses for the pink and green products were not satisfactory, but suggest the presence of the Schiff base ligand and of water,

pyridine and eventually methanol in the compounds. When reacting [VO(sal-ala)(H_2O)] with bipy, crystals of a compound with an elemental analysis consistent with [VO(sal-ala)(bipy)] were easily obtained[43] and we are presently collecting X-ray data for this compound. Nothing similar to Chisholm's complex **3** or our tetramer **1** was isolated in these reactions.

The vanadate tetramer characterized constitutes a remarkable example of a complex containing the bipy moiety, so commonly found in vanadium(IV) and vanadium(V) complexes with known molecular structures. It also constitutes one more example of the incorporation of simple organic units into polyoxovanadate frameworks. When trying to get solids out of solutions containing vanadium salts and organic ligands this phenomenon is probably much more common than one would expect, but the difficulty in obtaining suitable crystals normally precludes their structural characterization.

Acknowledgement—The authors thank INIC and JNICT (Project PMCT/C/CEN/367/90 and Programa STRIDE—Medida A, N. STRDA/P/CEN/436/92) for financial support.

REFERENCES

1. H. Vilter, *Phytochemistry* 1984, **23**, 1387.
2. E. de Boer, Y. van Kooyk, M. G. M. Tromp, H. Plat and R. Wever, *Biochim. Biophys. Acta* 1986, **869**, 48.
3. R. L. Robson, R. R. Eady, T. H. Richardson, R. W. Miller, M. Hawkins and J. R. Postgate, *Nature (London)* 1986, **322**, 388.
4. (a) M. T. Pope, in *Comprehensive Coordination Chemistry* (Edited by G. Wilkinson, R. D. Gillard and J. A. McCleverty), Vol. 3, pp. 1023. Pergamon Press, Oxford (1987); (b) W. P. Griffith, *Trans. Met. Chem.* 1991, **16**, 548 and refs therein.
5. M. T. Pope and A. Müller, *Angew. Chem., Int. Edn Engl.* 1991, **30**, 34 and refs therein.
6. W. G. Klemperer, T. A. Marquart and O. M. Yaghi, *Angew. Chem., Int. Edn Engl.* 1992, **31**, 49 and refs therein.
7. A. Müller, J. Döring and H. Bögge, *J. Chem. Soc., Chem. Commun.* 1991, 273.
8. Q. Chen, D. P. Goshorn, C. P. Scholes, X. Tan and J. Zubieta, *J. Am. Chem. Soc.* 1992, **114**, 4667 and refs therein.
9. L. F. Vilas Boas and J. Costa Pessoa, in *Comprehensive Coordination Chemistry* (Edited by G. Wilkinson, R. D. Gillard and J. A. McCleverty), Vol. 3, p. 453. Pergamon Press, Oxford (1987).
10. C. G. Young, *Coord. Chem. Rev.* 1989, **96**, 89 and refs therein.
11. J. Costa Pessoa, J. A. L. Silva, A. L. Vieira, L. F. Vilas Boas, P. O'Brien and P. Thornton, *J. Chem. Soc., Dalton Trans.* 1992, 1745.
12. Q. Chen, S. Liu and J. Zubieta, *Inorg. Chem.* 1989, **28**, 4433.
13. D. Rehder, W. Priesch and M. von Oeynhausen, *Angew. Chem., Int. Edn Engl.* 1989, **28**, 1221.
14. Q. Chen and J. Zubieta, *Inorg. Chem.* 1990, **29**, 1456.
15. M. I. Khan, Q. Chen and J. Zubieta, *J. Chem. Soc., Chem. Commun.* 1992, 305.
16. W. Priebsch, D. Rehder and M. von Oeynhausen, *Chem. Ber.* 1991, **124**, 761.
17. G. Christou, D. Heinrich, J. K. Money, J. C. Huffman and K. Folting, *Polyhedron* 1989, **89**, 1723.
18. M. I. Khan, Q. Chen, D. P. Goshorn, H. Hope, S. Parkin and J. Zubieta, *J. Am. Chem. Soc.* 1992, **114**, 3341 and refs therein.
19. D. C. Bradley, *Chem. Rev.* 1989, **89**, 1317.
20. F. Hillerns, F. Olbrich, U. Behrens and D. Rehder, *Angew. Chem., Int. Edn Engl.* 1992, **31**, 447 and refs therein.
21. L. J. Theriot, G. O. Carlisle and H. J. Hu, *J. Inorg. Nucl. Chem.* 1969, **31**, 3303.
22. J. J. R. Fraústo da Silva, R. Wootton and R. D. Gillard, *J. Chem. Soc. A* 1970, 3369.
23. (a) G. M. Sheldrick, in *Crystallographic Computing* (Edited by G. M. Sheldrick, C. Kruger and R. Goddard), Vol. 3, p. 175. Oxford University Press, Oxford (1985); (b) G. M. Sheldrick, SHEL Crystallographic Calculation Program. University of Cambridge (1976).
24. *International Tables for X-Ray Crystallography*, Vol. IV. Kynoch Press, Birmingham (1974).
25. C. K. Johnson, ORTEP-II, Report ORNL-5138. Oak Ridge National Laboratory, Oak Ridge, Tennessee (1976).
26. J. H. Van Vleck, *The Theory of Electrical and Magnetic Susceptibilities*, pp. 302–303. Oxford University Press, Oxford (1932).
27. C. N. Caughlan, H. M. Smith and K. Watenpaugh, *Inorg. Chem.* 1966, **5**, 2131.
28. M. A. A. F. de C. T. Carrondo, M. T. Leal S. Duarte, J. A. L. Silva and J. J. R. Fraústo da Silva, *Polyhedron* 1991, **10**, 1991.
29. M. Ghosh and S. Ray, *Acta Cryst.* 1983, **C39**, 1367.
30. H. Szentivanyi and R. Stomberg, *Acta Chem. Scand.* 1983, **A37**, 553.
31. H. Szentivanyi and R. Stomberg, *Acta Chem. Scand.* 1983, **A37**, 709.
32. H. Szentivanyi and R. Stomberg, *Acta Chem. Scand.* 1984, **A38**, 101.
33. R. Stomberg and H. Szentivanyi, *Acta Chem. Scand.* 1984, **A38**, 121.
34. N. J. Campbell, M. V. Capparelli, W. P. Griffith and A. C. Skapski, *Inorg. Chim. Acta* 1983, **77**, L215.
35. P. Basu, S. Pal and A. Chakravorty, *J. Chem. Soc., Dalton Trans.* 1991, 3217.
36. J. Fuchs, S. Mahjour and J. Pickardt, *Angew. Chem., Int. Edn Engl.* 1976, **15**, 374.
37. P. Román, A. San José, A. Luque and J. M. Gutiérrez-Zorrila, 14th European Crystallographic

Meeting ECM-14, Poster 164. University of Twente, Enschede, The Netherlands, August (1992).
38. R. K. Murmann and K. C. Giese, *Inorg. Chem.* 1978, **17**, 1160.
39. V. W. Day, W. G. Klemperer and D. J. Maltbie, *J. Am. Chem. Soc.* 1987, **109**, 2991.
40. M. H. Chisholm, J. C. Huffman, C. C. Kirkpatrick, J. Leonelli and K. Folting, *J. Am. Chem. Soc.* 1981, **103**, 6093 and refs therein.
41. J. Costa Pessoa, D. C. Costa, I. Cavaco and L. F. Vilas Boas, Proceedings of the Second Italian–Portuguese–Spanish Meeting in Inorganic Chemistry, Commun. MS12-3. Alfa Mar, Portugal, March (1992).
42. I. Cavaco, J. Costa Pessoa, M. T. Duarte, S. M. Luz and P. M. Matias, Proceedings of the Third International Conference on the Chemistry of the Early Transition Metals, Commun. P15. Brighton, U.K., July (1992).
43. I. Cavaco, J. Costa Pessoa, M. T. Duarte, R. D. Gillard and P. M. Matias, manuscript in preparation.

Polyhedron Vol. 12, No. 10, pp. 1239–1244, 1993
Printed in Great Britain

0277–5387/93 $6.00+.00
© 1993 Pergamon Press Ltd

NMR STUDY OF THE CONFORMATIONAL CHANGES OF DIBENZO-22-CROWN-6 ETHER BY COMPLEXATION WITH THALLIUM(I) AND POTASSIUM(I) IONS IN SOLUTION

MANABU FUJIWARA* and TAKAYUKI MATSUSHITA

Department of Materials Chemistry, Faculty of Science and Technology, Ryukoku University, Seta, Otsu 520-21, Japan

and

YUKO YAMASHOJI and MINORU TANAKA

Department of Applied Chemistry, Faculty of Engineering, Osaka University, Yamada-oka, Suita, Osaka 565, Japan

and

MIKIO OUCHI and TADAO HAKUSHI

Department of Applied Chemistry, Faculty of Engineering, Himeji Institute of Technology, Shosha, Himeji, Hyogo 671-22, Japan

(*Received* 4 *September* 1992; *accepted* 6 *January* 1993)

Abstract—The higher selectivity towards a thallium(I) ion of dibenzo-22-crown-6 (DB22C6) compared with dibenzo-18-crown-6 (DB18C6) and dibenzo-20-crown-6 (DB20C6) was investigated by ^{1}H and ^{13}C NMR spectroscopy and ^{13}C relaxation time (T_1) measurements. The results indicate that DB22C6 has a much larger cavity than the ionic radii of univalent metal ions such as thallium(I) and potassium(I). Therefore, its conformational change by complexation with the metal ions should be larger than those of DB18C6 and DB20C6, and the conformational change in DB22C6 by complexation with a potassium(I) ion is larger than with a thallium(I) ion.

Crown ethers have been extensively investigated as host compounds in host–guest chemistry and many analogues of various numbers of ring size, donor set and so on have been synthesized.[1] Since these compounds exhibit a high selectivity towards a certain metal ion or cationic compounds, their applications to analytical chemistry fields such as ion-selective electrode,[2] solvent extraction,[3] ion-pair chromatography,[4] etc. have been accomplished. In previous papers[5,6] solvent extraction and ion selective electrode studies revealed that dibenzo-22-crown-6 ether (DB22C6) exhibits higher selectivity for the thallium(I) ion than dibenzo-18-crown-6 ether (DB18C6) and dibenzo-20-crown-6 ether (DB20C6) against other univalent metal ions, such as potassium(I), sodium(I) and lithium(I), although its complexing ability is lower. In this paper we describe the conformational changes of these crown ethers caused by complexation with the above metal ions in acetonitrile-d_3, which were determined by ^{1}H and ^{13}C NMR spectroscopies. In addition, ^{13}C relaxation time (T_1) measurements were obtained to reveal the changes in molecular motion for the dibenzocrown ethers.

* Author to whom correspondence should be addressed.

EXPERIMENTAL

Materials

DB22C6 and DB20C6 ethers were prepared by literature methods.[5] DB18C6 was obtained from a commercial source.

Measurements

The ^{1}H NMR, ^{13}C NMR and ^{13}C relaxation time (T_1) measurements were recorded on a Bruker CX-600 spectrometer at 600 MHz for ^{1}H and at 150 MHz for ^{13}C nuclei, using TMS as an internal standard. Each sample solution was almost saturated with the respective compounds in CD_3CN.

Metal picrates were used for complexation of the crown ethers with metal ions.

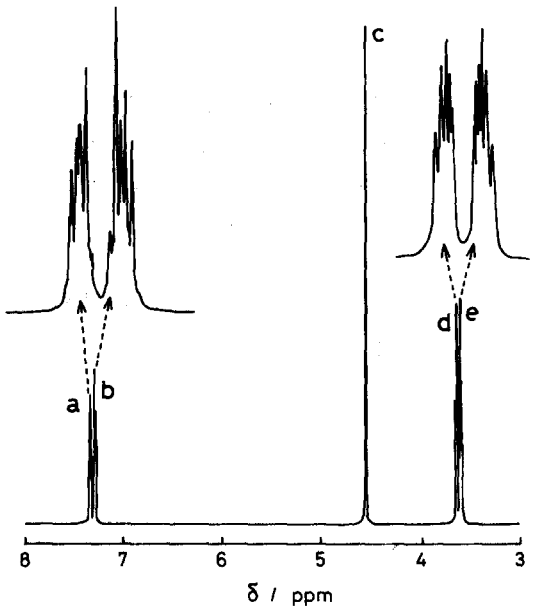

Fig. 2. ^{1}H spectrum of DB22C6 in CD_3CN.

RESULTS AND DISCUSSION

^{1}H *NMR spectra of crown ethers*

Figure 2 shows the ^{1}H NMR spectrum of DB22C6 in CD_3CN. The spectrum has four multiplet resonance peaks centred at 3.605, 3.611, 7.276 and 7.340 ppm and a singlet resonance peak at 4.632 ppm. These resonance peaks can be assigned to methylene protons (e) and (d), phenyl protons (b) and (a) and methylene protons (c) as shown in Fig. 1. Similarly the ^{1}H NMR spectra of DB18C6 and DB20C6 have four and nine resonance peaks, respectively, as shown in Table 1.

^{13}C *NMR spectra of crown ethers*

The ^{13}C NMR spectrum of DB22C6 exhibits six resonance peaks at 70.22, 70.97, 71.09, 128.09, 129.14 and 137.77 ppm due to methylene carbons (e), (d) and (c), phenyl carbons (b) and (a) and quarternary carbons (f), respectively. Similarly the ^{13}C NMR spectra of DB18C6 and DB20C6 have five and 11 resonance peaks, respectively, as shown in Table 1.

Changes in chemical shifts caused by the addition of thallium(I)

Figures 3–5 show the chemical shift changes on ^{1}H and ^{13}C NMR signals of BD18C6, DB20C6 and DB22C6 ligands caused by the addition of thallium(I) picrate, where positive and negative values represent the changes to higher and lower fields, respectively.

As shown in Fig. 3 all ^{1}H NMR signals for DB18C6 shifted to lower fields by the addition of a thallium(I) picrate and the shift values increased with increasing concentrations of thallium(I) ions. This behaviour can be interpreted in terms of a decrease in the electron density on all protons of DB18C6 by the thallium(I) ion. On the other hand the signals of (b), (c) and (e) carbons of DB18C6 are shifted to higher fields, without any significant change in (a) and (d) carbons. By the addition of thallium(I) a conformational change of DB18C6 may occur to allow coordination with the metal ion through six oxygen donor atoms of DB18C6. Thus,

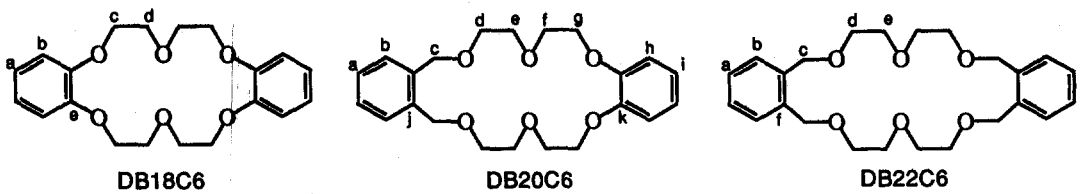

Fig. 1. Chemical structure of dibenzocrown-6-ethers.

Table 1. ^{1}H and ^{13}C NMR spectral data (ppm) for DB18C6, DB20C6 and DB22C6 in CD_3CN

	DB18C6	DB20C6	DB22C6
^{1}H	3.848(d)	3.653(e)	3.605(e)
	4.092(c)	3.686(d)	3.611(d)
	6.895(b)	3.786(f)	4.632(c)
	6.907(a)	4.086(g)	7.276(b)
		4.619(c)	73.40(a)
		6.896(i)	
		6.908(h)	
		7.286(b)	
		7.343(a)	
^{13}C	68.14(c)	69.39(g)	70.22(e)
	69.80(d)	70.12(f)	70.97(d)
	112.45(a)	70.55(e)	71.09(c)
	121.34(b)	71.09(d)	128.09(b)
	148.68(e)	71.18(c)	129.14(a)
		114.75(i)	137.77(f)
		121.95(h)	
		128.28(b)	
		129.60(a)	
		137.80(j)	
		149.49(k)	

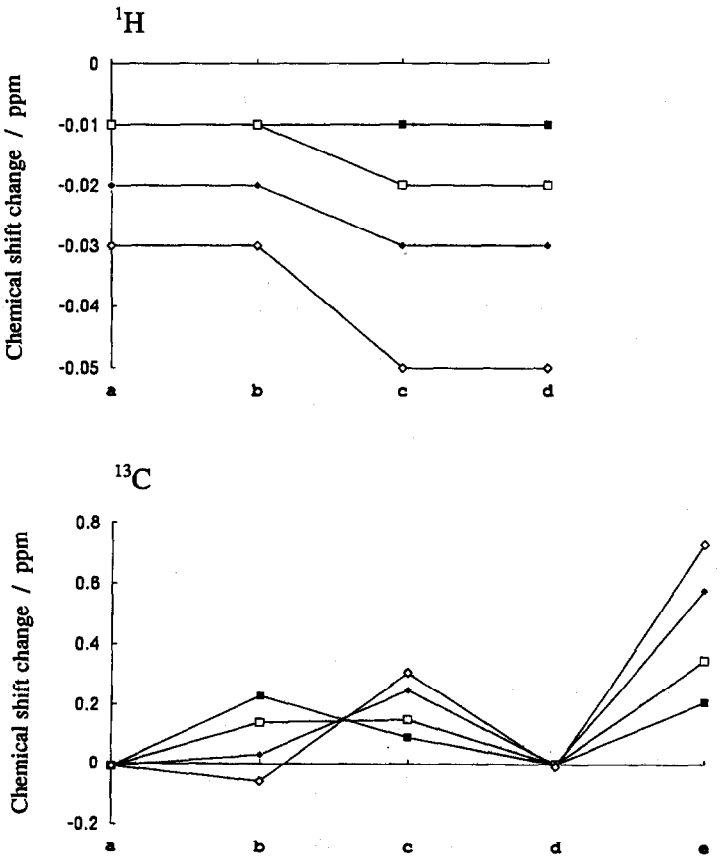

Fig. 3. Chemical shift changes of NMR signals of DB18C6 caused by the addition of thallium(I) ions. The molar ratios of thallium(I)-to-DB18C6 are 0.12 (■), 0.19 (□), 0.30 (◆) and 0.39 (◇).

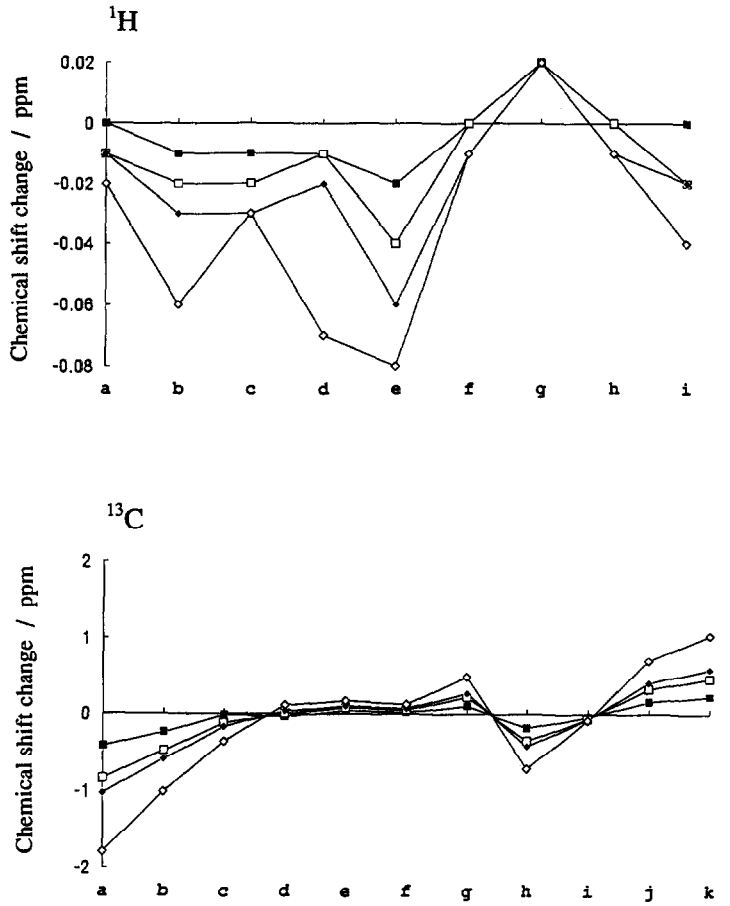

Fig. 4. Chemical shift changes of NMR signals of DB20C6 caused by the addition of thallium(I) ions. The molar ratios of thallium(I)-to-DB18C6 are 0.20 (■), 0.35 (□), 0.44 (◆) and 0.73 (◇).

the C—C and C—O bonds in the DB18C6 molecule should accept distortional stress, compared with those under the metal-free conditions which may shift ^{13}C NMR signals to higher field due to the steric compression effect,[7] especially on the quaternary (e) carbons.

As shown in Fig. 4 all ^{1}H NMR signals for DB20C6 are shifted to lower fields, except (g) protons. These shift values are similar to those observed for the DB18C6 system. However, a very different behaviour was observed for DB22C6, as shown in Fig. 5. The (a) and (c) proton signals are shifted to higher fields by 0.07 ppm at a thallium(I)-to-ligand molar ratio of 0.84; further addition of the thallium(I) salt was not possible due to its poor solubility in CD_3CN. The opposite shifts of the (a) and (c) protons, compared with DB18C6 and DB20C6, can be explained as follows. Since the cavity size of DB22C6 is much larger than the ionic radius of the thallium(I) ion, the ligand molecule must change its conformation in order to coordinate with the metal ion through the oxygen donor atoms. This conformational change may induce the rising of the (c) carbons [with (c) protons] out of the planes of the benzo groups. In such circumstances the (c) protons may suffer a reverse magnetic anisotropic effect from the benzene ring current. Thus, relatively large and higher field shifts on the (c) protons are observed. If this consideration is true a shift value for the (a) protons may reflect the extent of interaction between the metal ion and crown ethers, and a shift value for the (c) protons may reflect the extent of the conformational change of the ligand molecule.

On the other hand, higher field shifts of the (a) and (c) protons of DB22C6 were observed in complexation with potassium(I) ions; at the metal-to-ligand molar ratio of 0.81 the shift values are 0.04 and 0.09 ppm for the (a) and (c) protons, respectively. The shift value for the (c) protons is larger with potassium(I) than with the thallium(I) ion, although that for the (a) protons is smaller, which means that a larger conformational change for DB22C6 may occur in the former case.

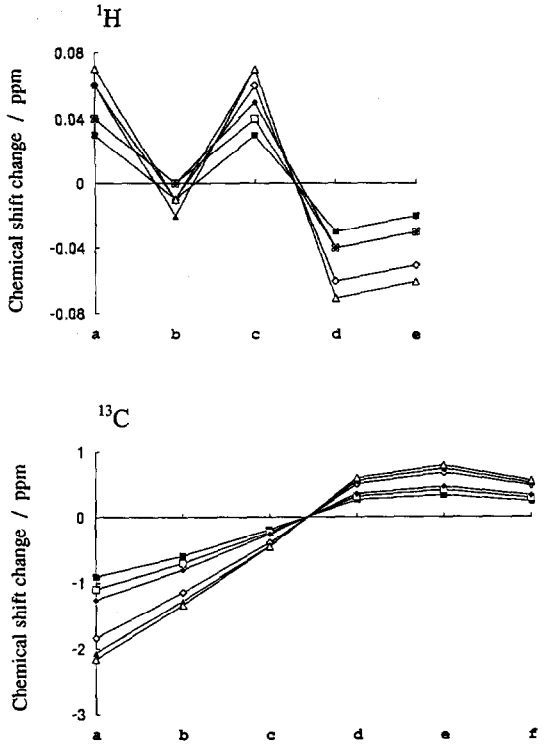

Fig. 5. Chemical shift changes of NMR signals of DB22C6 caused by the addition of thallium(I) ions. The molar ratios of thallium(I)-to-DB18C6 are 0.34 (■), 0.44 (□), 0.51 (◆), 0.72 (◇), 0.75 (▲) and 0.84 (△).

T_1 *measurements*

The T_1 measurements were obtained using the inversion recovery method for DB18C6,[8] DB20C6 and DB22C6 ligands in the presence and absence of thallium(I) in CD_3CN. The T_1 data for three systems are listed in Table 2. From these data only it is difficult to discuss intramolecular motion such as distortion of the ligand, dissociation and formation of the coordination bond between oxygen donor atoms in the ligand molecule and the thallium(I) ion, and conformational changes. However, the relative difference in intramolecular motion between DB18C6, DB20C6 and DB22C6 ligands, or between a ligand and its thallium(I) complex, can be discussed qualitatively based on T_1 data. It can be said that the larger the T_1 value for a ^{13}C atom the faster its motion becomes, if the number of hydrogen atoms bonded to the ^{13}C atom is the same.

For DB18C6 the crown ether ligand has been found to undergo intramolecular motion such as the conversion between the *syn-* and *anti-gauche* rotamers on its ethylene moieties.[9] In the presence of thallium(I) the T_1 values of all the carbon atoms of the DB18C6 molecules were found to decrease, which indicates that the ligand molecule interacts with the metal ion and its molecular motion is restricted considerably. The largest decrease in the T_1 values was observed for the (c) carbon atoms; the ratio of T_1 values on the (c) carbons for Tl^+ complex-to-uncoordinated ligand is 0.57 and those on other carbons are *ca* 0.8. The results may suggest that the oxygen donor atoms interposed between the benzene ring and (c) carbons play an important role in the complexation with metal(I) ions. For the DB20C6 ligand all the T_1 values are larger than for DB18C6, in spite of a large molecular weight. This result can be interpreted as the intramolecular motion in DB20C6, especially the conversion between *syn-* and *anti-gauche* rotamers on its

Table 2. T_1 data for DB18C6, DB20C6 and DB22C6 and their thallium(I) complexes

	DB18C6		DB20C6		DB22C6	
^{13}C	Ligand	Complex[a]	Ligand	Complex[b]	Ligand	Complex[c]
(a)	1.9	1.4	2.2	1.5	3.1	1.5
(b)	1.5	1.2	1.9	1.3	3.0	1.5
(c)	1.0	0.6	1.8	1.2	2.6	1.2
(d)	1.1	0.9	1.9	1.1	2.6	1.1
(e)	(11.2)	(8.6)	1.8	1.1	2.7	1.4
(f)			1.7	1.0	(10.0)	(6.1)
(g)			1.5	1.0		
(h)			1.8	1.3		
(i)			1.9	1.4		
(j)			(8.0)	(5.6)		
(k)			(15.2)	(11.3)		

[a] Molar ratio of thallium(I)-to-ligand is 0.22.
[b] Molar ratio of thallium(I)-to-ligand is 0.63.
[c] Molar ratio of thallium(I)-to-ligand is 0.70.

ethylene moieties, becoming more vigorous due to the increase from an 18- to a 20-membered ring. The interaction of DB20C6 with the thallium(I) ion was also responsible for the decrease in T_1 values of all the carbon atoms in DB20C6, especially those of the ethylene carbons.

Similarly, as mentioned above, all the T_1 values on DB22C6 increase steadily, indicating that its intramolecular movements become most vigorous among three dibenzocrown-6-ethers. By complex formation with the thallium(I) ion each T_1 value for DB22C6 is decreased to approximately one half. Relatively large decreases in the T_1 values on (c) and (d) carbons suggest that the oxygen donor atoms interposed between (c) and (d) carbons play an important role in the complexation with metal(I) ions.

CONCLUSIONS

The results obtained from ^{1}H and ^{13}C NMR spectral data and relaxation time (T_1) measurements for DB18C6, DB20C6 and DB22C6 ligands and their thallium(I) and potassium(I) complexes may clarify the reason why DB22C6 possesses a higher ion-selectivity towards thallium(I) over potassium(I). Since DB22C6 has a much larger cavity than the ionic size of thallium(I) and potassium (I), a considerable conformational change should occur when all the six oxygen donor atoms in DB22C6 interact with the metal(I) ion; that is, DB22C6 should adopt a distorted or strained conformation. The evidence for this can be deduced from large higher field shifts on (c) protons observed only for DB22C6 among the three crown ethers. On the other hand, the effective ionic radii of six-coordinated thallium(I) and potassium(I) ions are 150 and 138 pm, respectively.[10] Therefore, when DB22C6 interacts with potassium(I) to form the complex ion it should adopt a more highly strained form than that with the thallium(I) ion. This consideration is supported by the fact that the higher field shift value for the (c) protons of DB22C6 is much larger with potassium(I) than that with thallium(I). This may be taken into account for the higher ion-selectivity of DB22C6 towards the thallium(I) ion in spite of its lower complexing ability compared with DB18C6 and DB20C6, which is revealed by the solvent extraction and ion-selective electrode studies.

Acknowledgements—The authors thank Professor Yoshikane Kawasaki of Osaka Institute of Technology for his helpful comments and discussion. The authors are also indebted to Professor E. Weber and Dr K. Stobridis of Bonn University for their invaluable assistance on the preparation of dibenzo-20-crown-6 and dibenzo-22-crown-6 ethers.

REFERENCES

1. R. M. Izatt, J. S. Bradshaw, S. A. Nielsen, J. D. Lamb, J. J. Christensen and D. Sen, *Chem. Rev.* 1985, **85**, 271.
2. G. A. Rechnitz and E. Eyal, *Analyt. Chem.* 1972, **44**, 370.
3. H. K. Frensdorff, *J. Am. Chem. Soc.* 1971, **93**, 4684.
4. E. Blassius, W. Adrian, K.-P. Janzen and G. Klautke, *J. Chromatogr.* 1974, **96**, 89.
5. E. Weber, K. Skobridis, M. Ouchi, T. Hakushi and Y. Inoue, *Bull. Chem. Soc. Japan* 1990, **63**, 3670.
6. Y. Yamashoji, M. Tanaka, S. Nagamune, M. Ouchi, T. Hakushi and T. Shono, *Anal. Sci.* 1991, **7**, 485.
7. J. B. Stohers, *Carbon-13 NMR Spectroscopy*. Academic Press, New York (1972).
8. M.-C. Fedarko, *J. Magn. Reson.* 1973, **12**, 30.
9. D. Live and S. I. Chan, *J. Am. Chem. Soc.* 1976, **98**, 1976.
10. W. L. Tolly, *Modern Inorganic Chemistry*. McGraw-Hill, New York (1984).

Polyhedron Vol. 12, No. 10, pp. 1245–1249, 1993
Printed in Great Britain

0277–5387/93 $6.00+.00
© 1993 Pergamon Press Ltd

A NEW SYNTHETIC ROUTE FOR MONO- AND POLY-TIN(IV) OXALATE ADDUCTS: IR AND MÖSSBAUER STUDY

O. GUEYE, H. QAMAR, L. DIOP and C. A. DIOP

Département de Chimie, Faculté des Sciences, Université C.A. Diop, Dakar, Senegal

and

U. RUSSO*

Dipartimento di Chimica Inorganica, Metallorganica e Analitica, Università di Padova, Via Loredan 4, I-35131 Padova, Italy

(*Received* 11 *November* 1992; *accepted* 4 *January* 1993)

Abstract—A new synthetic route to prepare mono- and poly-tin(IV) complexes with the oxalate anion is reported. It behaves either as a mono- or bichelating terminal ligand, or as a bi- or tetra-unidentate bridging ligand, according to the experimental conditions. Possible structures for these complexes are proposed on the basis of IR and Mössbauer spectroscopic data.

The coordination ability of the oxalate anion has been widely investigated in the past. X-ray crystal structures of binuclear inorganic tin(IV) adducts with the general formula $(SnX_4)_2C_2O_4(R_4N)_2$ (X = Cl, Br, I; R = Et, Bu) have been reported[1] and a subsequent detailed spectroscopic investigation based on the X-ray results was performed.[2] Bi-, tri- and tetranuclear cobalt(III) complexes have been described[3] and some oxalate amine complexes with transition metals such as nickel(II), copper(II) and zinc(II) have also been reported.[4]

The aim of this paper, that is the continuation of our research on oxyanionic ligands,[5–7] is to describe a new and facile way to synthesize inorganic and metallorganic mono- and poly-tin(IV) adducts with the oxalate anion, to suggest possible structures on the basis of IR and Mössbauer data and to check the influence of the cation dimensions on the products.

EXPERIMENTAL

All the starting materials were used as purchased, without any further purification.

$(R_4N)_2C_2O_4 \cdot nH_2O$ (R = Me, $n = 2$; R = Et, $n = 4$) was prepared by mixing water solutions of the appropriate tetraalkyl ammonium hydroxide with oxalic acid. A white powder was obtained by solvent evaporation; it was recrystallized from absolute ethanol.

All the products were obtained in a similar way: an ethanolic solution of the appropriate oxalate was added to a solution in benzene of SnX_4 (X = Cl or Br), in ethanol of $SnPh_2Cl_2$ or in diethyl ether of $SnPh_3Br$ in the defined metal-to-ligand ratio reported in Table 1. A white solid was immediately formed; however, the suspensions were stirred for several hours. The solid was then filtered off, washed with the solvent and dried *in vacuo*.

The analytical data are reported in Table 1. Elemental analyses were performed by the analytical laboratory of the Department of Inorganic Chemistry (University of Padua, Italy) and the "Service central d'analyses", Vernaison, France. IR spectra were recorded as KBr pellets and Nujol mulls on a 580 Perkin–Elmer or a Bruker FTIR model FS 113 V spectrophotometer. Mössbauer spectra were collected in a liquid nitrogen cryostat at 80.0 K. The $Ca^{119}SnO_3$ source (15 mCi, New England Nuclear) was kept at room temperature and moved at constant acceleration with a triangular wave form. Suitable computer programs have been employed in the fitting procedure of the experimental spectra to Lorentzian line shapes by using standard least-squares computer minimization techniques.

*Author to whom correspondence should be addressed.

Table 1. Elemental analyses and metal-to-ligand ratios for the compounds

No.	Compound		C (%)	H (%)	N (%)	X (%)	Ratio
1	$SnCl_4 \cdot C_2O_4(Me_4N)_2$	Calc.	24.1	4.8	5.6	28.6	1:1
		Found	24.2	5.1	5.5	28.3	
2	$SnBr_4 \cdot C_2O_4(Me_4N)_2$	Calc.	17.8	3.5	4.2	47.4	1:1
		Found	17.2	3.5	4.2	48.1	
3	$(SnCl_5)_2 \cdot C_2O_4(Me_4N)_4 \cdot 2H_2O$	Calc.	21.3	5.1	5.5	35.1	2:1
		Found	21.5	5.2	5.6	34.5	
4	$(SnBr_5)_2 \cdot C_2O_4(Me_4N)_4 \cdot 2H_2O$	Calc.	14.8	3.5	3.8	54.9	2:1
		Found	14.8	3.4	3.8	55.2	
5	$(SnCl_4)_2 \cdot C_2O_4(Et_4N)_2$	Calc.	24.8	4.6	3.2	32.6	2:1
		Found	25.1	4.6	3.2	32.8	
6	$(SnBr_4)_2 \cdot C_2O_4(Et_4N)_2$	Calc.	17.6	3.3	2.3	52.2	2:1
		Found	17.6	3.4	2.1	52.1	
7	$(SnPh_2Cl_2) \cdot C_2O_4(Me_4N)_2$	Calc.	44.2	4.7	3.0	15.3	2:1
		Found	44.2	4.9	3.0	15.8	
8	$(Et_4N)_2C_2O_4 \cdot 2(SnPh_3)_2C_2O_4$	Calc.	59.2	6.2	2.4	—	1:1
		Found	58.4	6.1	2.5	—	

RESULTS AND DISCUSSION

IR study

The most relevant IR absorption bands are listed in Table 2, together with their assignments. The data for compounds **5** and **6** are virtually the same as those already known[2] and so are not reported.

The tetra-halo adducts **1**, **2** and **5**, **6** present in the far-IR region three bands that are attributable to $\nu_{as}(SnX_4)$ $(A_1+B_1+B_2)$; the triplet is indicative of *cis* coordination of the halide within an octahedral environment with C_{2v} symmetry around the tin centre.[8-10] In the two pentahalo complexes **3** and **4** $\nu(SnX_5^-)$ exhibits only two absorption bands; it is important to note the constant value of the halogen shift for the two bands: $335/234 = 302/211 = 1.431$. In all the inorganic derivatives the carboxylate groups present four bands; this set is consistent with a C_{2v}, C_s or C_1 symmetry for the oxalate anion. The presence in the far-IR region of a band due to ν(SnO) indicates an oxygen coordination of the ligand.

In the spectrum of the diphenyl derivative **7** two bands, one at 1630 and the second at 1346 cm^{-1}, are due to $\nu_{as}(COO^-)$ $(B_{1u}$ and $B_{2u})$ and point to a centrosymmetrical geometry for the oxalate anion, which behaves as a bichelating oxygen-donor

Table 2. Main IR data for the compounds with relative assignments

Compounds					Assignment
1	**2**	**3**	**4**	**7**	
1706s	1702s	1713s	1710s		ν(C=O)
1684s	1682s	1682s	1680s	1630s	$\nu_{as}(COO^-)$
1357s	1353s	1357s	1345s	1346m	$\nu_s(COO^-)$
1226s	1221s	1222m	1219m	—	ν(C—O)
885m	879w	884w	877w	857w	ν(C—C)
791s	791s	794s	791s	795s	$\delta(COO^-)$
545	538	545	536	481s	$\rho(COO^-)$
359	356	—	352	398m	$\omega(COO^-)$
335s	216s	335	234	289m	ν(Sn—X)
330s	205sh	302	211	260m	
308s	199sh	—	—	—	
—	—	—	—	316m	$\nu_{as}(SnC_2)$
229m	279m	231	234	213m	ν(Sn—O)

ligand. On the basis of the assignments already reported for $SeO_4(Me_4N)_2 \cdot 2SnPh_2Cl_2$,[5] the bands at 316, 289 and 260 cm^{-1} have been attributed to $\nu_{as}(SnC_2)$, $\nu_{as}(SnCl_2)$ and $\nu_s(SnCl_2)$, respectively. This attribution indicates the presence of *cis* coordination geometry for $SnPh_2Cl_2$, with the phenyl groups occupying the apical positions of the octahedron.

The important role of the size of the cation is noteworthy: with large cations such as tetraethyl and tetrabutyl ammonium, the only type of adduct that was obtained with SnX_4 was $(R_4N)_2 \cdot C_2O_4 \cdot (SnX_4)_2$,[1,2] while with a smaller cation such as tetramethyl ammonium new types of adducts have been isolated: $SnX_4 \cdot C_2O_4(Me_4N)_2$ and $(SnX_5)_2 \cdot C_2O_4(Me_4N)_4 \cdot 2H_2O$. This last compound can be considered as $(SnX_4)_2 \cdot C_2O_4(Me_4N)_2$ (that has not yet been isolated probably because of the small size of the cation) reacting with two more Me_4NX molecules. The formation of R_4NX (R = Me, Et) *in situ* in a mixture of ethanolic solutions of tetraalkyl ammonium salts of oxyacids and of metal halides has been reported recently.[11]

The triphenyl compound **8** represents the first adduct of $(SnPh_3)_2C_2O_4$[7] with a polybasic anion. In fact it can be considered as the coordination of an oxalate anion to the triphenyl tin(IV) oxalate derivative. Its IR spectrum exhibits a strong absorption at 1663 cm^{-1} with shoulders at 1680 and 1655 cm^{-1}, all of which are assigned to $\nu_{as}(COO^-)$. The relative symmetric stretching can be found at 1297 and 1248 cm^{-1} with shoulders at 1262 and 1235 cm^{-1}. The presence of several bands due to these stretching vibrations is indicative of the presence of more than one type of oxalate ligand; $\nu_s(SnC_3)$ can be found as a weak band at 224 cm^{-1}, in the same position as in the $(SnPh_3)_2C_2O_4$ derivative,[7] and indicates an almost planar SnC_3 moiety, as in $(SnPh_3)_2SO_4$;[7] the weak intensity of the band is characteristic of a flat SnC_3 group.[12]

Mössbauer study

The Mössbauer effect spectral data are reported in Table 3. The parameters of compounds **1–6** are typical for inorganic tin(IV) derivatives: in fact they present a virtually zero quadrupole splitting, indicating nearly regular geometries around the tin centre. The isomer shift values for all the complexes are lower than for the respective hexahalo compounds, as a consequence of the substitution of one or two halogen atoms with the more electronegative oxygens of the oxalic anion. This effect is much more evident in the bromo than in the chloro complexes, probably because of the much larger difference in the electronegativity values. So, while δ for $SnBr_6^{2-}$ is around 0.87 mm s^{-1},[13] it decreases to 0.71 mm s^{-1} for the $SnBr_5O$ adduct (sample **4** in Table 3) and to 0.58 and 0.34 mm s^{-1} for the two $SnBr_4O_2$ derivatives (samples **2** and **6** in Table 3). The different δ values for compounds **2** and **6** indicate different donating behaviour for the oxalate ligand. In fact the involvement of all the four oxygens in bonding, that is likely to occur in the 2:1 compound **6**, should decrease the electron density on the Sn—O bonds with respect to the 1:1 compound **2**, in which only two oxygens are bonded to the tin centre. As a consequence the δ value for the latter compound should be lower than that for the former one, as is actually the case. As expected, the δ values for the chloro derivatives are generally lower than for the bromo complexes, but are insensitive to the variations in the coordination sphere.

The high value for the quadrupole splitting of the diphenyl derivative **7** is a clear indication of an octahedral coordination with the phenyl groups in apical positions. In the case of the triphenyl tin derivative **8**, the increase in the ΔE_Q value with respect to $SnPh_3Cl$ (2.54 mm s^{-1}), which presents tetrahedral coordination, seems to indicate an increase in the coordination number and so the

Table 3. ^{119m}Sn Mössbauer effect parameters for the compounds recorded at 80.0 K

No.	Compound	δ^a (mm s^{-1})	ΔE_Q (mm s^{-1})	Γ (mm s^{-1})
1	$SnCl_4 \cdot C_2O_4(Me_4N)_2$	0.40	—	1.01
2	$SnBr_4 \cdot C_2O_4(Me_4N)_2$	0.58	—	1.01
3	$(SnCl_5)_2 \cdot C_2O_4(Me_4N)_4 \cdot 2H_2O$	0.38	—	0.98
4	$(SnBr_5)_2 \cdot C_2O_4(Me_4N)_4 \cdot 2H_2O$	0.71	—	0.98
5	$(SnCl_4)_2 \cdot C_2O_4(Et_4N)_2$	0.42	—	1.04
6	$(SnBr_4)_2 \cdot C_2O_4(Et_4N)_2$	0.34	—	1.03
7	$(SnPh_2Cl_2)_2 \cdot C_2O_4(Me_4N)_2$	1.29	3.69	0.94
8	$(Et_4N)_2C_2O_4 \cdot 2(SnPh_3)_2C_2O_4$	1.27	3.01	0.92

[a] Referenced to room temperature SnO_2.

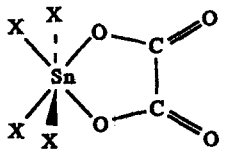

Fig. 1. Proposed schematic structure for the compounds $SnX_4 \cdot C_2O_4(Me_4N)_2$, X = Cl or Br.

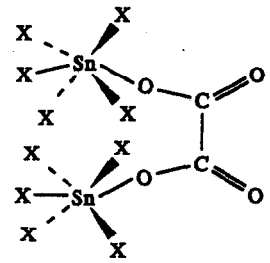

Fig. 2. Proposed schematic structure for the compounds $(SnX_5)_2 \cdot C_2O_4(Me_4N)_4$, X = Cl or Br.

presence of a penta-coordinated tin centre. Point charge calculations give a ΔE_Q value of 3.07 mm s^{-1} for a penta-coordinated compound with bridging oxalate anions in apical positions, in good agreement with the experimental value and the δ value reported for $CH_3COOSnPh_3$,[14] for which the same type of coordination around tin is considered.

Proposed structures

From all the above considerations on the IR and the Mössbauer spectroscopic data it is possible to obtain some clues to hypothesize the geometrical structures for these complexes. Therefore, for the 1:1 adducts **1** and **2** a discrete structure can be proposed in which the oxalate anion behaves as a monochelating ligand and the tin atom assumes an octahedral coordination geometry with the oxygen atoms in *cis* positions (see Fig. 1). Also, in the pentahalo complexes **3** and **4** the tin atoms present an octahedral geometry, the sixth position of which is occupied by an oxygen of the oxalate ion which behaves as a bi-unidentate ligand connecting two SnX_5^- moieties (see Fig. 2). The 2:1 tetrahalo derivatives **5** and **6** and the diphenyl tin adduct **7** should present the same structure: the oxalate

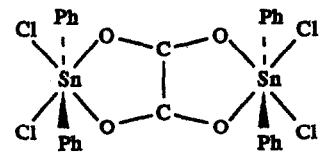

Fig. 3. Proposed schematic structure for the compound $(SnPh_2Cl_2)_2 \cdot C_2O_4(Me_4N)_2$.

anion behaves as a bichelating ligand with all the oxygens involved in bonds to the tin centre, which is octahedrally surrounded by two oxygen atoms in *cis* positions and either by the four halogens or by two apical phenyl groups and the two chlorine atoms again in *cis* positions (see Fig. 3). For the triphenyl tin derivative **8** two structures are equally possible. In both cases the tin atom is penta-coordinated with a trigonal bipyramidal geometry, in which the phenyl groups occupy the three planar positions and two oxygens from the oxalate anion the apical positions. The difference between the two

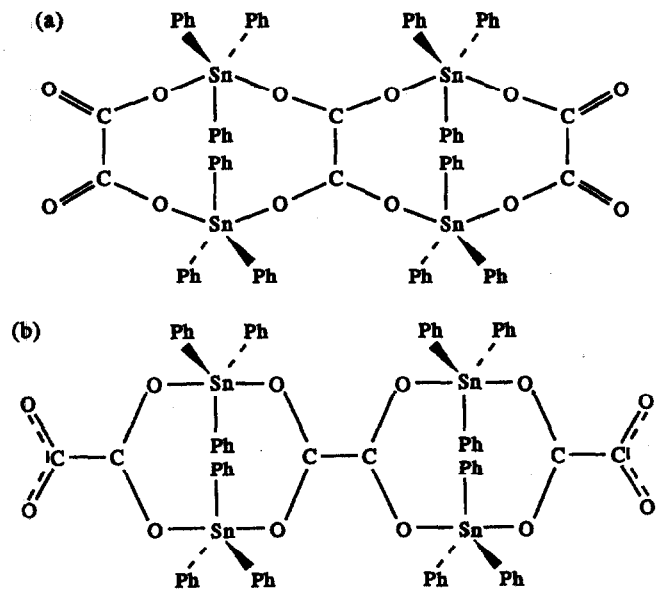

Fig. 4. Proposed schematic structures for the compound $(Et_4N)_2C_2O_4 \cdot 2(SnPh_3)_2C_2O_4$.

structures is due to the different arrangements of the oxalate ions (see Fig. 4).

CONCLUSIONS

In this series of compounds the variety of coordination possibilities typical for the oxalate anion is widely demonstrated. Therefore, compounds in which it behaves as a mono- or bichelating or as a bridging poly-unidentate ligand have been obtained and characterized. The results of Mössbauer and IR spectroscopic techniques allowed the proposal of suitable structures for each compound.

The important role of the size of the cation has been discussed: with large cations such as tetraethyl and tetrabutyl ammonium only a binuclear bichelating oxalate ligand-containing adduct was obtained with SnX_4, while with a smaller cation such as tetramethyl ammonium two new compounds (a mononuclear monochelating oxalate ligand-containing adduct and a binuclear bridging oxalate ligand-containing adduct) were isolated. The first adduct of $(SnPh_3)_2C_2O_4$ has also been reported in this paper.

Acknowledgements—Support for the Senegalese group from Professors M. Vidali, A. Cassol and C. Pecile (University of Padua, Italy) is gratefully acknowledged.

REFERENCES

1. A. C. Skapski, J. E. Guerchais and J. Y. Calves, *C.R. Acad. Sci.* 1974, **278**, 1377.
2. F. LeFloch, J. Sala-Pala and J. E. Guerchais, *Bull. Soc. Chim.* 1975, **1–2**, 120.
3. K. L. Scott, K. Wieghardt and A. G. Sykes, *Inorg. Chem.* 1973, **12**, 655.
4. N. F. Curtis, *J. Chem. Soc.* 1963, 4109; *J. Chem. Soc. A* 1968, 1584.
5. O. Sarr and L. Diop, *Spectrochim. Acta* 1990, **46A**, 1239.
6. A. S. Sall and L. Diop, *Inorg. Chim. Acta* 1990, **171**, 53.
7. M. Lahlou and L. Diop, *Spectrochim. Acta* 1991, **47A**, 1775.
8. I. R. Beattie and G. P. McQuillan, *J. Chem. Soc.* 1963, 1523.
9. I. R. Beattie and L. Rule, *J. Chem. Soc.* 1965, 2995.
10. N. Ohkaru and K. Nakamoto, *Inorg. Chem.* 1973, **12**, 2440.
11. A. S. Sall, A. Diasse, O. Sarr and L. Diop, *Main Group Met. Chem.* 1992, in press.
12. A. S. Sall and L. Diop, *Spectrochim. Acta* 1990, **46A**, 793.
13. P. A. Flinn, in *Mössbauer Isomer Shifts* (Edited by G. K. Shenoy and F. E. Wagner), p. 593. North Holland Publishers, Amsterdam (1978).
14. K. C. Molloy, T. G. Purcell, K. Quill and I. W. Nowell, *J. Organomet. Chem.* 1984, **267**, 237.

Polyhedron Vol. 12, No. 10, pp. 1251–1252, 1993
Printed in Great Britain

0277–5387/93 $6.00+.00
© 1993 Pergamon Press Ltd

COMMUNICATION

SYNTHESIS AND STRUCTURE OF $[SMe_3]_2[Bi_2I_8(SMe_2)_2]$: A DIMETHYLSULPHIDE COMPLEX OF BISMUTH(III)

WILLIAM CLEGG, NICHOLAS C. NORMAN* and NIGEL L. PICKETT

Department of Chemistry, The University of Newcastle upon Tyne, Newcastle upon Tyne NE1 7RU, U.K.

(*Received* 22 *February* 1993; *accepted* 4 *March* 1993)

Abstract—The synthesis and X-ray crystal structure of the ionic compound $[SMe_3]_2[Bi_2I_8(SMe_2)_2]$ is described. The bismuth-containing dianion can be considered as a complex of $[Bi_2I_8]^{2-}$ and two molecules of SMe_2, with an edge-shared bioctahedral structure in which the weakly bound SMe_2 ligands are in axial sites and *trans*.

We have recently described the preparation and structural characterization of some phosphine (PR_3) complexes of bismuth(III) halides and halogenoanions,[1] which were the first such compounds to be described and also the first structurally characterized examples of bismuth–phosphorus bonds. Analogous chemistry with organosulphide ligands (SR_2) is still undeveloped and we report herein the synthesis and X-ray crystal structure of the first compound of this type, namely the ionic species $[SMe_3]_2[Bi_2I_8(SMe_2)_2]$ (**1**), which contains an iodobismuthate anion in which the bismuth centres are each coordinated by a dimethylsulphide (SMe_2) ligand.

Bismuth tri-iodide was found to dissolve readily in SMe_2 to give dark red solutions, but subsequent crystallization procedures (solvent diffusion from an overlayer of hexane) afforded a dark crystalline material which was found to be mostly unsolvated BiI_3.† However, small quantities of dark red crystals were also present and these were examined by X-ray crystallography,‡ the results of which revealed an ionic compound with the formula $[SMe_3]_2[Bi_2I_8(SMe_2)_2]$ (**1**).

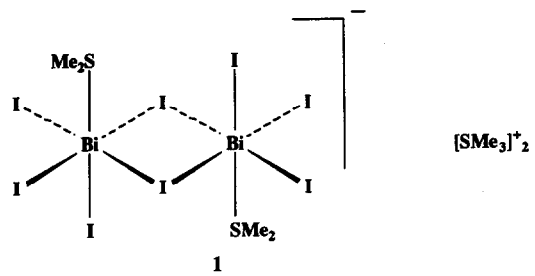

1

* Author to whom correspondence should be addressed.

† SMe_2 (20 cm^3) was condensed onto a sample of BiI_3 (0.85 g, 1.44 mmol) in a nitrogen atmosphere and the mixture stirred and allowed to warm to room temperature. Most of the BiI_3 dissolved to give a deep red solution, over which hexane (20 cm^3) was then layered. Solvent diffusion over a period of days resulted in the formation of a crop of dark crystals, most of which were BiI_3 (assumed on the basis of colour and the fact that elemental analysis showed only traces of carbon and hydrogen), but which also included a small yield of red crystals of **1**. These crystals were suitable for X-ray diffraction, but satisfactory microanalytical data could not be obtained since it was not possible to separate a pure sample from an intimate mixture of **1** and BiI_3.

‡ Crystal data for **1**: $C_{10}H_{30}Bi_2I_8S_2$, $M = 1711.74$, monoclinic, $P2_1/c$, $a = 9.403(5)$, $b = 16.177(6)$, $c = 12.884(13)$ Å, $\beta = 106.21°$, $V = 1882(2)$ $Å^3$, $Z = 2$, $D_c = 3.021$ g cm^{-3}, λ(Mo-K_α) = 0.71073 Å, $\mu = 16.12$ mm^{-1}, $F(000) = 1488$, $T = 293$ K. The structure was determined by direct methods and difference syntheses and refined by full-matrix least-squares methods on 3302 unique F^2 values (2θ max 50°) measured on a Stoe–Siemens diffractometer and corrected for 40% intensity decay and for absorption (semi-empirically; transmission 0.058–0.143). Anisotropic displacement parameters were refined; hydrogen atoms were not included; extinction effects were negligible. $R' = [\Sigma w(F_o^2 - F_c^2)^2/\Sigma w(F_o^2)^2]^{1/2} = 0.1983$ for all data, conventional $R = 0.0597$ for F values of 1147° "observed" [$F^2 > 2\sigma(F^2)$] reflections only, goodness of fit = 1.028. All features in a final difference map were within the range −0.95–1.11 e $Å^{-3}$. Programs: SHELXS-86 and SHELXL-92 (G. M. Sheldrick, University of Göttingen, Germany). Atomic coordinates, bond lengths and angles and atomic displacement parameters have been deposited as supplementary material at the Cambridge Crystallographic Data Centre.

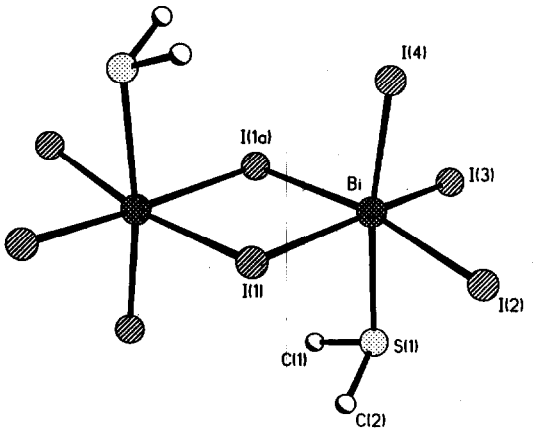

Fig. 1. A view of the anionic part of the structure of **1** showing the atom numbering scheme. Important bond lengths (Å) and angles (°): Bi—I(1) 3.234(3), Bi—I(1a) 3.229(3), Bi—I(2) 2.955(3), Bi—I(3) 2.954(3), Bi—I(4) 2.934(3), Bi—S(1) 3.054(8); I(1)—Bi—I(1a) 84.04(7), I(1)—Bi—I(2) 91.65(9), I(1)—Bi—I(3) 169.79(7), I(1)—Bi—I(4) 92.31(9), I(1)—Bi—S(1) 90.4(2), I(2)—Bi—I(1a) 170.43(7), I(2)—Bi—I(3) 94.95(9), I(2)—Bi—I(4) 93.94(9), I(2)—Bi—S(1) 77.8(2), I(3)—Bi—I(1a) 88.24(8), I(3)—Bi—I(4) 94.98(9), I(3)—Bi—S(1) 83.4(2), I(4)—Bi—I(1a) 94.76(9), I(4)—Bi—S(1) 171.4(2), I(1a)—Bi—S(1) 93.7(2), Bi—I(1)—Bi(a) 95.96(7).

The anionic part of **1** is shown in Fig. 1 and may be viewed as a complex of the dimeric dianion $[Bi_2I_8]^{2-}$ and two SMe_2 ligands with an overall edge-shared, crystallographically centrosymmetric, bioctahedral geometry. Specifically, the SMe_2 ligands are mutually *trans* and occupy axial sites *cis* to both bridging iodides. The terminal Bi—I bond lengths (av. 2.948 Å) and the bond lengths to the two symmetrically bridging iodides [3.234(3) and 3.229(3) Å] are normal and very similar to the corresponding distances found in the dianion $[Bi_2Ph_2I_6]^{2-}$.[2] Bismuth–sulphur bonds, in contrast to those involving phosphorus, are well established and fall within the range 2.6–3.2 Å, as exemplified by a number of bismuth complexes of thioureas,[3] thiosemicarbazides,[4] imidazolidine-2-thiones,[3b,5] xanthates[6] and dithiocarbamates,[7] particular distances depending on the nature of the sulphur donor (e.g. monodentate or bidentate), the nature of the other ligands and the coordination number around the bismuth centre. Complex **1**, however, is the first example of a bismuth complex of a dialkylsulphide and the Bi—S distance [Bi—S(1) 3.054(8) Å] is towards the long end of this range which indicates that the SMe_2 ligand is only weakly bound to the bismuth centre. A further and informative comparison is between **1** and the related ionic phosphine complex $[PMe_3H][Bi_2Br_7(PMe_3)_2]$ (**2**),[1a] which contains a polymeric anion, the essential dibismuth unit of which is very similar to the structure of the dianion in **1**. The Bi—P distance in **2** [2.762(3) Å] is considerably shorter than the Bi—S distance in **1**, indicating that PMe_3 is probably a much better ligand than SMe_2 in this type of complex.

The formation of **1** under the reaction conditions employed is most likely due to a small degree of hydrolysis resulting from adventitious water, as was also considered likely with regard to the formation of **2**,[1a] and it is interesting to note also that whilst a crystalline SMe_2 complex of an iodobismuthate anion is formed we have been unable to isolate a neutral complex.

Acknowledgement—We thank the SERC for financial support and for a studentship (N. L. P.). N. C. N. also thanks the Royal Society for additional supporting funds.

REFERENCES

1. (a) W. Clegg, R. J. Errington, G. A. Fisher, M. E. Green, D. C. R. Hockless and N. C. Norman, *Chem. Ber.* 1991, **124**, 2457; (b) W. Clegg, R. J. Errington, R. J. Flynn, M. E. Green, D. C. R. Hockless, N. C. Norman, V. C. Gibson and K. Tavakkoli, *J. Chem. Soc., Dalton Trans.* 1992, 1753.
2. W. Clegg, R. J. Errington, G. A. Fisher, D. C. R. Hockless, N. C. Norman, A. G. Orpen and S. E. Stratford, *J. Chem. Soc., Dalton Trans.* 1992, 1967.
3. (a) L. P. Battaglia, A. B. Corradi, G. Pelizzi and M. E. V. Tani, *J. Chem. Soc., Dalton Trans.* 1977, 1141; (b) L. P. Battaglia and A. B. Corradi, *J. Chem. Soc., Dalton Trans.* 1983, 2425; (c) L. P. Battaglia and A. B. Corradi, *J. Chem. Soc., Dalton Trans.* 1981, 23; (d) G. B. Jameson, E. Blazso and H. R. Oswald, *Acta Cryst., Sect. C* 1984, **40**, 350; (e) W. Bensch, E. Blazso, E. Dubler and H. R. Oswald, *Acta Cryst., Sect. C* 1987, **43**, 1699.
4. L. P. Battaglia, A. B. Corradi, N. Nardelli and M. E. V. Tani, *J. Chem. Soc., Dalton Trans.* 1978, 583.
5. L. P. Battaglia, A. B. Corradi and G. Pelosi, *J. Cryst. Spectrosc. Res.* 1992, **22**, 275.
6. E. R. T. Tiekink, *J. Cryst. Spectrosc. Res.* 1992, **22**, 231.
7. (a) C. L. Raston and A. H. White, *J. Chem. Soc., Dalton Trans.* 1976, 791; (b) C. L. Raston, G. L. Rowbottom and A. H. White, *J. Chem. Soc., Dalton Trans.* 1981, 1379.

Polyhedron Vol. 12, No. 10, pp. 1253–1256, 1993
Printed in Great Britain

0277-5387/93 $6.00+.00
© 1993 Pergamon Press Ltd

COMMUNICATION

HYDROGEN BONDING OF H_2O TO THE HYDROXO LIGANDS OF $Cp^*_2Zr(OH)_2$: IMPLICATIONS FOR PROTON AND OXYGEN EXCHANGE PROCESSES. THE CRYSTAL AND MOLECULAR STRUCTURE OF THE HYDRATE $Cp^*_2Zr(OH)_2 \cdot (H_2O)$

WILLIAM A. HOWARD and GERARD PARKIN†

Department of Chemistry, Columbia University, New York, NY 10027, U.S.A.

(*Received* 31 *November* 1992; *accepted* 25 *February* 1993)

Abstract—The molecular structure of $Cp^*_2Zr(OH)_2 \cdot (H_2O)$ ($Cp^* = \eta^5$-C_5Me_5) has been determined by single-crystal X-ray diffraction. The asymmetric unit of $Cp^*_2Zr(OH)_2 \cdot (H_2O)$ consists of a hydrogen-bonded dimeric structure in which two water molecules serve to link two $Cp^*_2Zr(OH)_2$ moieties together. The hydrogen bonding of H_2O to the hydroxo ligands of $Cp^*_2Zr(OH)_2$, rather than the direct coordination of H_2O to the zirconium centre, provides support for the mechanisms proposed previously to rationalize the fact that proton exchange between $Cp^*_2Zr(OH)_2$ and labelled H_2O is more facile than that for oxygen exchange.

Monomeric, unbridged terminal metal-hydroxo complexes of the early transition metals are relatively uncommon, possibly due to the tendency of such groups either (1) to bridge two or more metal centres or (2) to eliminate water with the concomitant formation of an oxo derivative.[1] In the course of a study of the reactivity of bis(pentamethylcyclopentadienyl)zirconium complexes towards H_2O, Hillhouse and Bercaw successfully utilized the steric demands of the pentamethylcyclopentadienyl ligand to stabilize $Cp^*_2Zr(OH)_2$ ($Cp^* = \eta^5$-C_5Me_5).[2] $Cp^*_2Zr(OH)_2$ is a rare example of an early transition metal bis(hydroxo) complex and its stability contrasts with that of the corresponding tungsten derivative, $[Cp^*_2W(OH)_2]$, which is unstable with respect to loss of water and formation of the terminal oxo complex $Cp^*_2W{=}O$.[3] In this regard it is also noteworthy that $Cp^*_2Zr(OH)_2$ has been independently synthesized by Carty *et al.* with the aim of utilizing this complex as a precursor for the formation of a monomeric terminal zirconium oxo derivative.[4]

In addition to the synthesis of $Cp^*_2Zr(OH)_2$ Hillhouse and Bercaw also reported that the bis(hydroxo) complex could be isolated as a monohydrate derivative, $Cp^*_2Zr(OH)_2 \cdot (H_2O)$.[2] The structure of the monohydrate derivative is of some interest, especially in view of the role that it may play in both proton and oxygen exchange between $Cp^*_2Zr(OH)_2$ and labelled water ($H_2{}^{17}O$ and D_2O).[2] Here we report (1) the structure of the monohydrate $Cp^*_2Zr(OH)_2 \cdot (H_2O)$, as determined by single-crystal X-ray diffraction, (2) its relationship to the structure of $Cp^*_2Zr(OH)_2$ and (3) the implications for proton and oxygen exchange between $Cp^*_2Zr(OH)_2$ and H_2O.

The molecular structure of $Cp^*_2Zr(OH)_2 \cdot (H_2O)$ was determined by a single-crystal X-ray diffraction study. The asymmetric unit of $Cp^*_2Zr(OH)_2 \cdot (H_2O)$ consists of a hydrogen-bonded dimeric structure in which two water molecules serve to link two $Cp^*_2Zr(OH)_2$ moieties together,

† Author to whom correspondence should be addressed.

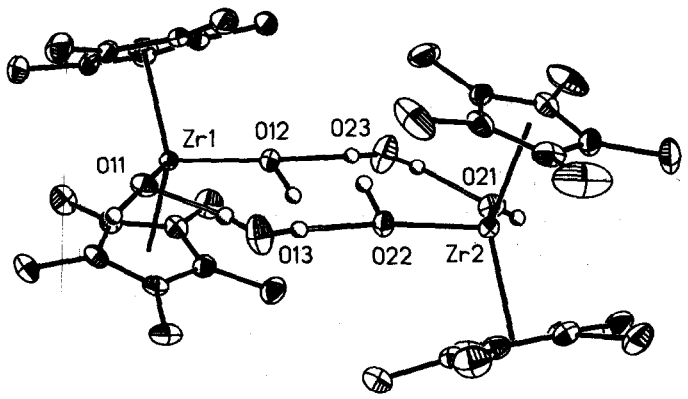

Fig. 1. The asymmetric unit of $Cp^*_2Zr(OH)_2 \cdot (H_2O)$. Hydrogen-bonding interactions are represented by open bonds. Hydrogen-bonding separations (e.s.d.s *ca* 0.005–0.01 Å): O(11)···O(13) 2.828, O(13)···O(22) 2.879, O(21)···O(23) 2.787 and O(23)···O(12) = 2.974 Å. In view of the location of the hydrogen atoms attached to O(12) and O(22) a hydrogen bond is not considered to be present between these atoms, even though the O(12)···O(22) separation is 2.994 Å.

as shown in Fig. 1.† The four O···O separations involved in the hydrogen bonding are in the range 2.79–2.97 Å, so that the interactions are best characterized as weak hydrogen bonds.[5] Furthermore, the hydrogen-bonding network extends beyond this dimeric assembly, so that the units are linked together into an infinite chain-type structure, a portion of which is illustrated in Fig. 2.

The coordination environments about each zirconium centre are very similar, as summarized in Table 1. For comparative purposes Table 1 also includes metrical data for $Cp^*_2Zr(OH)_2$, which indicate that the coordination environment about zirconium in the monohydrate $Cp^*_2Zr(OH)_2 \cdot (H_2O)$ is relatively unperturbed from that observed for $Cp^*_2Zr(OH)_2$. For example, the average Zr—O bond length in $Cp^*_2Zr(OH)_2 \cdot (H_2O)$ is 2.00(2) Å, very similar to that of 1.98(1) Å in $Cp^*_2Zr(OH)_2$.

† Crystal data for $Cp^*_2Zr(OH)_2 \cdot (H_2O)$ at room temperature: Triclinic $P\bar{1}$, $a = 10.501(1)$, $b = 13.160(2)$, $c = 16.927(2)$ Å, $\alpha = 111.58(1)°$, $\beta = 106.86(1)°$, $\gamma = 91.03(1)°$, $V = 2061.2(5)$ Å^3, $Z = 4$, $R = 0.0368$, $R_w = 0.0474$. All hydrogen atoms attached to oxygen atoms were located, but their positional parameters were refined subject to constraints to limit the O—H bond lengths to chemically reasonable values (see refs 5 and 9). A complete set of tables of crystal and intensity collection data, atomic coordinates, bond distances and angles, anisotropic displacement parameters, observed and calculated structure factors and an ORTEP drawing for $Cp^*_2Zr(OH)_2 \cdot (H_2O)$ have been deposited with the Editor as supplementary material. The atomic coordinates have also been deposited with the Cambridge Crystallographic Data Center.

Perhaps the most significant feature of the structure of the monohydrate $Cp^*_2Zr(OH)_2 \cdot (H_2O)$ is that the water molecule is *not* coordinated to the zirconium centre. As such, the structure contrasts with those of the cationic bis(cyclopentadienyl)-zirconium aqua complexes $[Cp_2Zr(H_2O)_3]^{2+}$ and $[Cp_2Zr(H_2O)_2(OTs)]^+$,[6,7] in which there are three substituents in the equatorial plane, compared with two for $Cp^*_2Zr(OH)_2 \cdot (H_2O)$. Moreover, the Zr—O interactions in $Cp^*_2Zr(OH)_2 \cdot (H_2O)$ [see Table 1] are also shorter than those in $[Cp_2Zr(H_2O)_3]^{2+}$ [$d(Zr—OH_2)_{(lateral)} = 2.261(7)$ and 2.239(7), $d(Zr—OH_2)_{(central)} = 2.195(7)$ Å][7] and $[Cp_2Zr(H_2O)_2(OTs)]^+$ [$d(Zr—OH_2)_{(lateral)} = 2.276(5)$ and 2.242(5), $d(Zr—OTs) = 2.169(5)$ Å].[6,8]

Hillhouse and Bercaw's exchange studies between (1) $Cp^*_2Zr(OH)_2$ and D_2O and (2) $Cp^*_2Zr(OH)_2$ and $H_2{}^{17}O$ have elegantly demonstrated that the rate of $^{16}O/^{17}O$ exchange is dramatically slower than the rate of H/D exchange.[2] These results clearly indicated that the two exchange processes do not involve a common mechanism and the two pathways illustrated in Scheme 1 were suggested to account for the results of the exchange studies.[2] $^{16}O/^{17}O$ exchange was proposed to require the presence of an intermediate in which water was bound to the zirconium centre (mechanism A), a pathway that would also result in proton exchange. In contrast, the more facile H/D exchange (to the exclusion of oxygen exchange) could be achieved by an intermediate in which water was *not* involved in the first coordination sphere of the metal, i.e. an intermediate in which the water molecule and the hydroxo ligands of $Cp^*_2Zr(OH)_2$ are involved in hydrogen bonding. Therefore, our observation that the ground state structure of the monohydrate

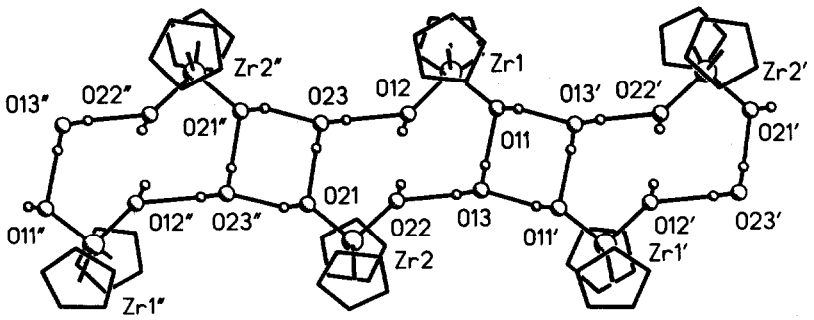

Fig. 2. A portion of the extended chain-type structure of $Cp^*_2Zr(OH)_2 \cdot (H_2O)$. For clarity the Cp* ligands are represented by pentagons. Hydrogen-bonding separations that are not included in Fig. 1 (e.s.d.s *ca* 0.005–0.01 Å): O(11)···O(13′) 2.821 and O(23)···O(21″) 2.800 Å.

Table 1. Selected bond lengths and angles for $Cp^*_2Zr(OH)_2 \cdot (H_2O)$

	$Cp^*_2Zr(OH)_2 \cdot (H_2O)$		
	Zr(1)	Zr(2)	$Cp^*_2Zr(OH)_2$[a]
Zr(X)—O(X1)	1.976(2)	1.978(2)	1.975(8)
Zr(X)—O(X2)	2.028(3)	2.026(3)	1.982(7)
Zr(X)—C $[Cp^*]_{av}$	2.57	2.57	2.55
O(X1)···O(X2)	3.011(5)	3.001(5)	3.025(12)
O(X1)—Zr(X)—O(X2)	97.5(1)	97.1(1)	99.7(3)

[a] Data taken from ref. 4.

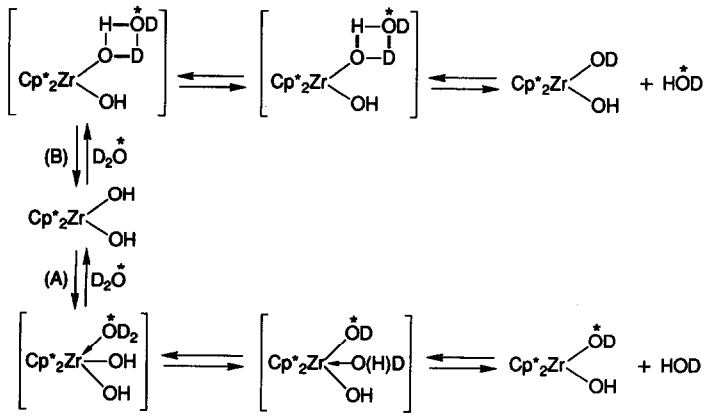

Scheme 1. Two pathways for proton and oxygen exchange between $Cp^*_2Zr(OH)_2$ and labelled water ($D_2{}^*O = D_2O$ or $H_2{}^{17}O$). Adapted from ref. 2.

$Cp^*_2Zr(OH)_2 \cdot (H_2O)$ does *not* involve coordination of the water molecule to the zirconium centre provides good support for Hillhouse and Bercaw's mechanistic proposals concerning H/D and $^{16}O/^{17}O$ exchange processes in this system.

Acknowledgement—We thank the donors of the Petroleum Research Fund, administered by the ACS, for support of this research. G. P. is the recipient of an A. P. Sloan Research Fellowship (1991–1993), a Camille and Henry Dreyfus Teacher–Scholar Award (1991–1996) and a Presidential Faculty Fellowship Award (1992–1997).

REFERENCES

1. For some leading references on monomeric metal hydroxo complexes see: (a) H. E. Bryndza and W. Tam, *Chem. Rev.* 1988, **88**, 1163; (b) G. J. Kubas, C. J. Burns, G. R. K. Khalsa, L. S. Van Der Sluys, G. Kiss and C. D. Hoff, *Organometallics* 1992, **11**, 3390.
2. G. L. Hillhouse and J. E. Bercaw, *J. Am. Chem. Soc.* 1984, **106**, 5472.
3. (a) G. Parkin and J. E. Bercaw, *Polyhedron* 1988, **7**, 2053; (b) G. Parkin and J. E. Bercaw, *J. Am. Chem. Soc.* 1989, **111**, 391.
4. R. Bortolin, V. Patel, I. Munday, N. J. Taylor and A. J. Carty, *J. Chem. Soc., Chem. Commun.* 1985, 456.
5. (a) J. Emsley, *Chem. Soc. Rev.* 1980, **9**, 91; (b) W. C. Hamilton and J. A. Ibers, *Hydrogen Bonding in Solids*. W. A. Benjamin, New York (1968).
6. W. Lasser and U. Thewalt, *J. Organomet. Chem.* 1986, **302**, 201.
7. U. Thewalt and W. Lasser, *J. Organomet. Chem.* 1984, **276**, 341.
8. For the structures of some mono Cp and Cp* zirconium hydroxo complexes see: (a) W. Lasser and U. Thewalt, *J. Organomet. Chem.* 1986, **311**, 69; (b) G. Hidalgo, M. A. Pellinghelli, P. Royo, R. Serrano and A. Tiripicchio, *J. Chem. Soc., Chem. Commun.* 1990, 1118.
9. M. R. Churchill, *Inorg. Chem.* 1973, **12**, 1213.

Polyhedron Vol. 12, No. 10, pp. 1257–1260, 1993
Printed in Great Britain

0277–5387/93 $6.00+.00
© 1993 Pergamon Press Ltd

COMMUNICATION

STEPWISE SYNTHESIS AND REACTIVITY OF A CHLORINE-FUNCTIONALIZED σ^3,λ^4-PHOSPHANEDIYL COMPLEX; X-RAY CRYSTAL STRUCTURE OF (2,4,6-$Bu^t_3C_6H_2O$)(Cl)P—$MoCp(CO)_3$

MICHAEL LEISE, LASZLO ZSOLNAI and HEINRICH LANG*

Anorganisch-Chemisches Institut der Universität, Im Neuenheimer Feld 270, W-6900 Heidelberg 1, F.R.G.

(*Received* 4 *November* 1992; *accepted* 10 *February* 1993)

Abstract—The stepwise formation of the bifunctional σ^3,λ^4-phosphanediyl complex (2,4,6-$Bu^t_3C_6H_2O$)(Cl)P=$MoCp(CO)_2$ (**4**) (R = 2,4,6-$Bu^t_3C_6H_2O$) is reported. The primary metallo-chlorophosphine (R)(Cl)P—$MoCp(CO)_3$ (**3**) is isolated in almost quantitative yield from the reaction of $RPCl_2$ (**1**) with $Na[MoCp(CO)_3]$ (**2**). Decarbonylation of **3** affords **4**. The reactivity of **4** towards different nucleophiles is discussed. The identities of all new compounds are documented by analytical as well as spectroscopic (IR, MS, ^1H, ^{13}C and ^{31}P NMR) data; the X-ray structure of (R)(Cl)P—$MoCp(CO)_3$ (**3**) is reported.

Complexes of the type (R)(R′)P=ML_n [R,R′ = single-bonded organic ligand; ML_n = $Co(CO)_3$,[1] $Mn(CO)_4$,[2] $MoCp(CO)_2$, $WCp(CO)_2$[3–6]], which each contain an sp^2-hybridized phosphorus atom in a trigonal planar environment, can be prepared either via reductive dehalogenation of (R)(R′)PCl with $Co_2(CO)_8$[1a,c] or dehydrochlorination of R_2XP—$MCp(CO)_2Y$ (M = Mo, W; X = H, Y = Cl; X = Cl, Y = H).[3]

However, another possibility for preparing this type of compound is given in the reaction of (R)(R′)PCl with $Na[ML_{n+1}]$ [ML_{n+1} = $Co(CO)_4$,[1] $Mn(CO)_5$,[2] $MoCp(CO)_3$, $WCp(CO)_3$[3–6]]. The sodium-chloride metathesis reaction affords first the appropriate metallo-phosphine intermediates (R)(R′)P—ML_{n+1}, which then readily eliminate CO to yield (R)(R′)P=ML_n [ML_n = $Co(CO)_3$,[1] Mn $(CO)_4$,[2] $MoCp(CO)_2$, $WCp(CO)_2$[3–6]]. To our knowledge the intermediates (R)(R′)P—ML_{n+1} have never been isolated in crystalline form and converted to neutral phosphenium-ion complexes, which contain a formal phosphorus–metal double bond.

We report here the selective synthesis of the stable metallo-phosphine (R)(Cl)P—$MoCp(CO)_3$ (**3**) and its controlled decarbonylation to the σ^3,λ^4-phosphanediyl complex (R)(Cl)P=$MoCp(CO)_2$ (**4**). Some aspects of the reactivity of **4** are discussed.

RESULTS AND DISCUSSION

The complex (R)(Cl)P—$MoCp(CO)_3$ (R = 2,4,6-$Bu^t_3C_6H_2O$) is easily accessible in high yields via the reaction of equimolar amounts of $RPCl_2$[7] (**1**)

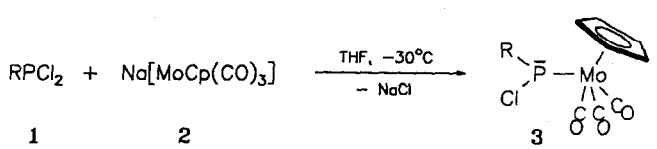

1 2 3

R = 2,4,6-^{t}Bu$_3$C$_6$H$_2$O

* Author to whom correspondence should be addressed.

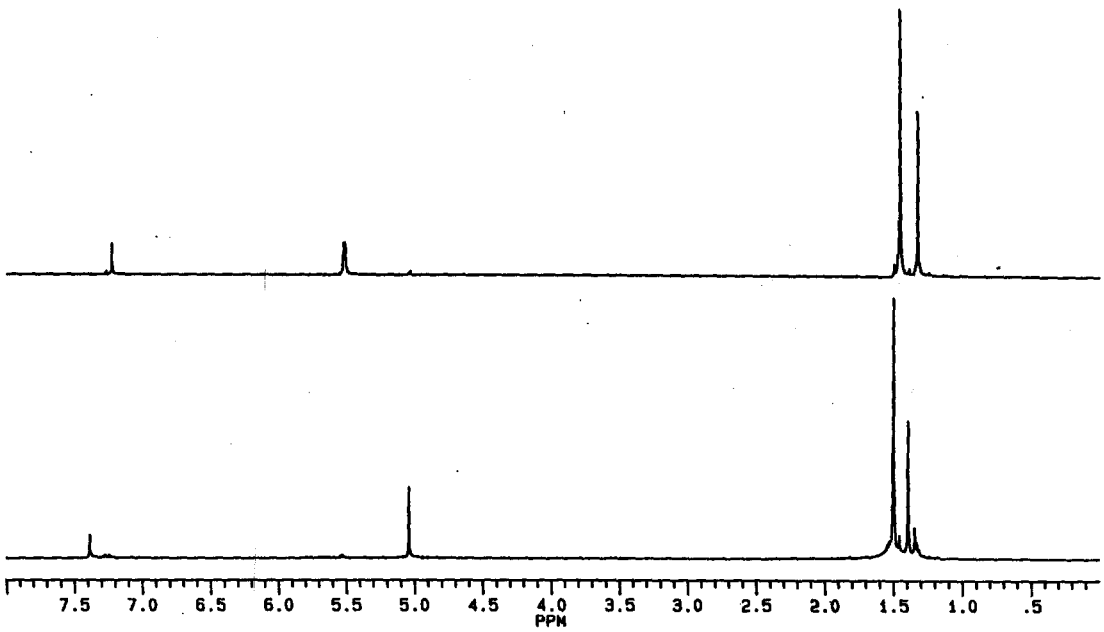

Fig. 1. ^{1}H NMR; thermal conversion of **3** to **4** (**3** top: recorded at −15°C; **4** bottom: same sample recorded after 90 min at 25°C.

and Na[MoCp(CO)$_3$][8] (**2**) in THF at −20°C.* The yellow metallo-phosphine **3** is best purified by column chromatography at −20°C.*

On warming this compound up to *ca* 25°C in methylenechloride for 5 h decarbonylation occurs and the orange-coloured σ^3,λ^4-phosphanediyl complex (R)(Cl)P=MoCp(CO)$_2$ (**4**) is formed in almost quantitative yields.*

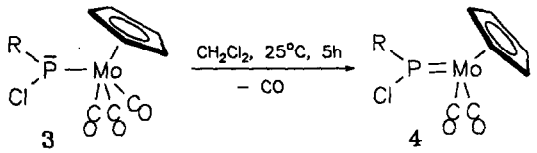

R = 2,4,6-^{t}Bu$_3$C$_6$H$_2$O

Compound **4** is the only isolated product obtained upon extraction of the reaction residue with n-pentane, followed by filration through Celite. Recrystallization from n-pentane yields analytically pure **4**. The most characteristic features in the IR spectrum of **4** is the ν(CO) pattern of the MoCp(CO)$_2$ moiety, with two strong absorption bands at 1975 and 1946 cm^{-1}, which is typical for neutral phosphenium ion complexes containing an MoCp(CO)$_2$ unit.[3-6]

The decarbonylation of **3** to **4** is best followed by ^{31}P and ^{1}H NMR experiments.* The most significant observation in the ^{1}H NMR spectra of **3** and **4** (Fig. 1) is the high-field shift of the cyclopentadienyl resonance signal, which moves from $\delta = 5.5$ (**3**) to $\delta = 5.0$ (**4**). In addition the typical PH coupling constant of J(PC) = 2.6 Hz in **3**, which is typical for this class of compounds,[9] disappears in **4**.

* The composition and constitution of compounds **3** and **4** were given by satisfactory elemental analysis and spectroscopic (IR, MS, ^{1}H, ^{13}C and ^{31}P NMR) data.

3: ^{1}H NMR ($CDCl_3$, −15°C): 1.32 (s, 9H, *p*-Bu^t), 1.45 (s, 18H, *o*-Bu^t), 5.52 [d, J(PH) = 2.6 Hz, 5H, Cp], 7.23 (s, 2H, C_6H_2) ppm. ^{13}C{^{1}H} NMR ($CDCl_3$, −15°C): 31.5 (s, 3C, *p*-Bu^t), 33.3 (s, 3C, *o*-Bu^t), 33.4 (s, 3C, *o*-Bu^t), 34.4 (s, 1C, *p*-C^i/Bu^t), 36.2 (s, 2C, *o*-C^i/Bu^t), 95.4 [d, J(PC) = 6.5 Hz, 5C, Cp], 123.8 (s, 2C, C_6H_2), 141.0 [d, J(PC) = 3.5 Hz, 2C, C_6H_2], 144.4 [d, J(PC) = 2 Hz, 1C, C_6H_2], 152.1 (s, 1C, C_6H_2), 224.0 [d, J(PC) = 6 Hz, 1C, CO], 224.3 [d, J(PC) = 25.5 Hz, 1C, CO], 232.4 [d, J(PC) = 11 Hz, 1C, CO] ppm. ^{31}P{^{1}H} NMR ($CDCl_3$, −15°C): 358.6 (s) ppm. IR (n-pentane; CaF_2 cells): 2022 vs, 1957 s, 1946 s [ν(CO)], 1592 w [ν(C=C)] cm^{-1}. M.p. 112°C (decomposition).

4: ^{1}H NMR ($CDCl_3$): 1.38 (s, 9H, *p*-Bu^t), 1.49 (s, 18H, *o*-Bu^t), 5.03 (s, 5H, Cp), 7.38 (s, 2H, C_6H_2) ppm. ^{13}C{^{1}H} NMR ($CDCl_3$): 31.5 (s, 3C, *p*-Bu^t), 32.7 (s, 6C, *o*-Bu^t), 34.7 (s, 1C, *p*-C^i/Bu^t), 36.0 (s, *o*-C^i/Bu^t, 2C), 91.1 [d, J(PC) = 6.5 Hz, 5C, Cp], 123.9 (s, 2C, C_6H_2), 142.1 [d, J(PC) = 4.5 Hz, 2C, C_6H_2], 147.4 (s, 1C, C_6H_2), 147.5 (s, 1C, C_6H_2), 231.9 [d, J(PC) = 23 Hz, 2C, CO] ppm. ^{31}P{^{1}H} NMR ($CDCl_3$): 197.1 (s), EI MS [m/z (rel. int.)]: M^+ 546(6), $M^+ - 2CO$ 490(25), $M^+ - 2CO - Bu^t$ 433(9), $M^+ - 2CO - Bu^t - Cl$ 398(8), $Bu^t{}_3C_6H_2OH^+$ 262(24), $Bu^t{}_3C_6H_2OH^+ - Me$ 247(100), Bu^{t+} 57(28). IR (n-pentane, CaF_2 cells): 1975 s, 1946 s [ν(CO)], 1592 w [ν(C=C)] cm^{-1}.

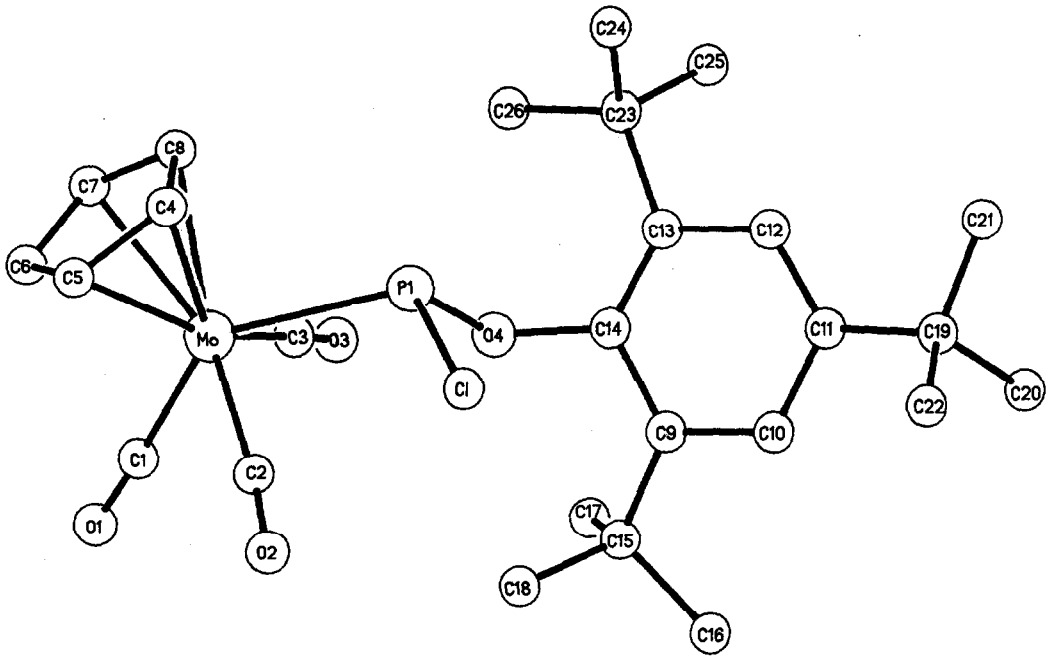

Fig. 2. Molecular geometry and atom labelling scheme for **3**; selected interatomic distances (Å) and angles (°) are: P—Mo 2.584(4), P—O(4) 1.654(6), P—Cl 2.118(4), O(4)—P—Mo 106.4(2), Mo—P—Cl 111.8(1), Cl—P—O(4) 101.1(2).

Conspicuous in the ^{31}P NMR spectra of **3** and **4** is the observed high-field shift of the appropriate resonance signal from $\delta = 359$ (**3**) to $\delta = 197$ (**4**). This shielding is attributed to a change of hybridization of the phosphorus atom (sp^3 (**3**) $\rightarrow sp^2$ (**4**)), as well as to a transfer of electron density from the molybdenum centre to the phosphorus atom in **4**. The spectroscopic data for **4** confirm the notion that the phosphorus atom possesses a trigonal planar environment and is part of a formal phosphorus–molybdenum doubly bonded system.

The structure of **3** is related to structures of other metallo-phosphines, in which the phosphorus atom is σ-bonded to 17-electron complex fragments such as $MoCp(CO)_3$.[10] A representation of the solid state structure of **3**, as determined by single-crystal X-ray diffraction, is shown in Fig. 2.*

The molecule consists of a single molybdenum atom bonded to a cyclopentadienyl group, three terminal carbonyls and a terminal phosphino ligand P(Cl)(R). Figure 2 shows that the phosphorus atom possesses a tetrahedral environment with a chemically reactive lone pair of electrons. Indicative of the absence of π-character between the phosphorus and molybdenum atoms in compound **3**, as compared to compounds of type **4**, is the elongated phosphorus–molybdenum bond length [2.584(4) Å] (Fig. 2). The other interatomic distances and angles are in the range for the usual values.[11]

An overview of the reactivity of **4** is given in Scheme 1. As demonstrated by the reactions depicted in Scheme 1 compound **4** has been shown to be useful for the synthesis of multi-functionalized σ^3,λ^4-phosphanediyl complexes containing a formal phosphorus–molybdenum double bond, as well as an organic π-system. With this in mind **4** is a promising building block for the synthesis of various functionalized complexes of the type (R)(R′)P=$MoCp(CO)_2$ [R = 2,4,6-$Bu^t_3C_6H_2O$; R′ = CH=C(H)(Ph) (**5**), C≡CPh (**6**), $CH_2C{\equiv}CH$ (**7**), NEt_2 (**8**)].[8]

* Crystal data for **3**: $C_{26}H_{34}ClMoO_4P$, $M = 572.9$, monoclinic, space group $P2_1/c$, $a = 11.34(1)$, $b = 11.41(2)$, $c = 20.99(3)$ Å, $\beta = 97.2(1)°$, $V = 2693(2)$ Å^3, $Z = 4$, $D_c = 1.41$ g cm^{-3}.

Diffraction data were collected on a Siemens (Nicolet Syntex) R3m/V diffractometer using the ω-scan technique [2θ limits 2–47°, scan range 0.75°, scan speed $2.3 \leqslant \dot{\omega} \leqslant 29.3°$ min^{-1} (in 2θ)] and Mo-K_α radiation ($\lambda = 0.71069$ Å).

The structure was solved by direct methods [SHELXTL-PLUS on 3386 unique reflections with $F \geqslant 4\sigma(F)$]. An empirical absorption correction was applied. The functional discrepancy indices were $R_F = 0.065$, $R_w = 0.071$.

Atomic coordinates, interatomic distances and angles and atomic thermal parameters have been deposited at the Cambridge Crystallographic Data Center.

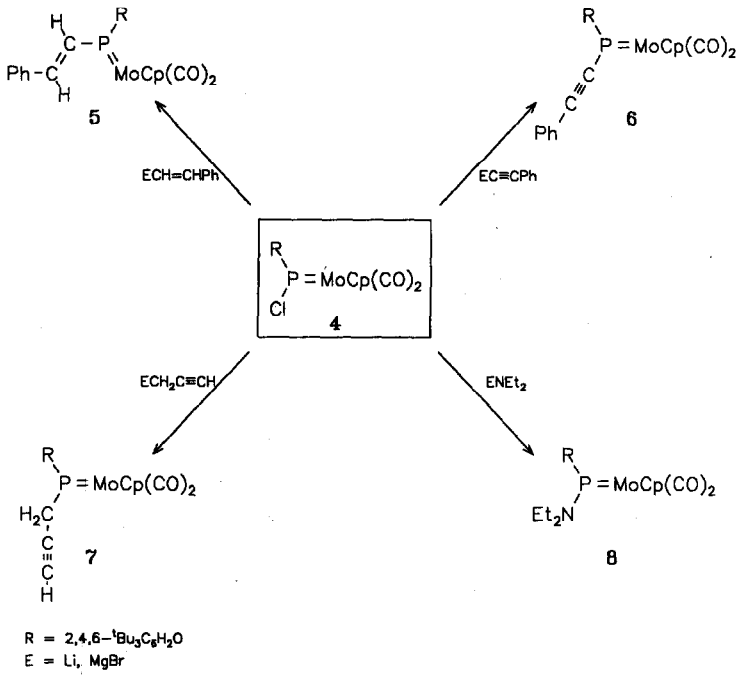

Scheme 1. Reactivity of (R)(Cl)P=MoCp(CO)$_2$ (**4**).

Acknowledgements—We thank the "Deutsche Forschungsgemeinschaft", the "Sonderforschungsbereich SFB 247" and the "Fonds der Chemischen Industrie" for financial support.

REFERENCES

1. (a) H. Lang, M. Leise and L. Zsolnai, *J. Organomet. Chem.* 1991, **410**, 379; (b) H. Lang and M. Leise, *J. Organomet. Chem.* 1990, **393**, C17; (c) H. Lang and O. Orama, *J. Organomet. Chem.* 1989, **371**, C48.
2. H. Lang, M. Leise and Chr. Emmerich, *J. Organomet. Chem.* 1991, **418**, C9.
3. For example: (a) E. Groß, K. Jörg, K. Fiederling, A. Göttlein, W. Malisch and R. Boese, *Angew. Chem.* 1984, **96**, 705; *Angew. Chem., Int. Edn Engl.* 1984, **23**, 738; (b) K. Jörg, W. Malisch, W. Reich, A. Meyer and U. Schubert, *Angew. Chem.* 1986, **98**, 103; *Angew. Chem., Int. Edn Engl.* 1986, **25**, 92; (c) W. Malisch, K. Jörg, U. Hofmockel, M. Schmeusser, R. Schemm and W. S. Sheldrick, *Phosphorus, Sulfur* 1987, **30**, 205 and refs therein.
4. For example: (a) R. W. Light and R. T. Paine, *J. Am. Chem. Soc.* 1978, **100**, 2230; (b) L. D. Hutchins, R. T. Paine and C. F. Campana, *J. Am. Chem. Soc.* 1980, **102**, 4521; (c) L. D. Hutchins, H.-U. Reissacher, G. L. Wood, E. N. Duessler and R. T. Paine, *J. Organomet. Chem.* 1987, **335**, 229 and refs therein.
5. For example: (a) A. H. Cowley, D. M. Giolando, C. M. Nunn, M. Pakulski, D. Westmoreland and N. C. Norman, *J. Chem. Soc., Dalton Trans.* 1988, 2127; (b) A. M. Arif, A. H. Cowley, C. M. Nunn, S. Quashie, N. C. Norman and A. G. Orpen, *Organometallics* 1989, **8**, 1878 and refs therein.
6. (a) H. Lang, M. Leise and L. Zsolnai, *Polyhedron* 1992, **11**, 1281; (b) H. Lang, M. Leise and W. Imhof, *Z. Naturforsch.* 1991, **46b**, 1650; (c) H. Lang, M. Leise, L. Zsolnai and M. Fritz, *J. Organomet. Chem.* 1990, **395**, C30; (d) H. Lang, M. Leise and L. Zsolnai, *J. Organomet. Chem.* 1990, **389**, 325.
7. P. P. Power, R. A. Bartlett, H. V. R. Dias, K. M. Flynn and M. M. Olmstead, *J. Am. Chem. Soc.* 1987, **109**, 5699.
8. G. Brauer, *Handbuch der Präparativen Anorganischen Chemie*, Vol. 3, p. 1969. Ferdinand Enke Verlag, F.R.G. (1987) and refs therein.
9. H. Lang, G. Mohr, O. Scheidsteger and G. Huttner, *Chem. Ber.* 1985, **118**, 574 and refs therein.
10. D. Gudat, E. Niecke, W. Malisch, U. Hofmockel, S. Quashie, A. Cowley, A. A. Arif, B. Krebs and M. Dartmann, *J. Chem. Soc., Chem. Commun.* 1985, 1687 and refs therein.
11. (a) S. W. Kirtley, in *Comprehensive Organometallic Chemistry* (Edited by G. Wilkinson and E. W. Abel), p. 1079. Pergamon Press, Oxford (1982); (b) D. E. C. Corbridge, in *The Structural Chemistry of Phosphorus*. Elsevier, Amsterdam (1974).

Polyhedron Vol. 12, No. 10, pp. 1261–1263, 1993
Printed in Great Britain

0277–5387/93 $6.00+.00
© 1993 Pergamon Press Ltd

COMMUNICATION

FURTHER ON THE CHEMICAL REDUCTION OF $Fe_2(NO)_4(\mu\text{-SR})_2$

CHUNG-NIN CHAU and ANDREW WOJCICKI*

Department of Chemistry, The Ohio State University, Columbus, OH 43210, U.S.A.

(*Received* 27 *January* 1993; *accepted* 5 *February* 1993)

Abstract—Reduction of $Fe_2(NO)_4(\mu\text{-SR})_2$ (R = Me, Et or Bu^t) with 2 equivalents of sodium, KH or MBR_3H (M = Li, Na or K; R = Et or Bu^s) in THF affords $[Fe_2(NO)_4(\mu\text{-SR})_2]^{2-}$, as evidenced by quantitative analysis of evolved hydrogen, conductivity measurements in MeOH and ^1H and ^2H NMR and IR ν(NO) spectroscopic data of the products. In contrast, reduction of $Fe_2(NO)_4(\mu\text{-SR})_2$ with 1 equivalent of MBR_3H yields products that differ from the foregoing dianions by the presence of hydrogen derived from the borohydride. The combined product characterization data do not support the formulation $[Fe_2(NO)_4(\mu\text{-SR})_2]^-$.

For approximately a decade we have been engaged in investigations on the chemical reduction of complexes of the type $M_2L_x(\mu\text{-Y})_2$ (L = CO or NO; L = a three-electron donor ligand) and the chemistry of resultant reduced species.[1,2] Although most of our studies have been concerned with phosphido complexes (Y = PR_2), we have also investigated thiolato complexes (Y = SR) of the composition $Fe_2(NO)_4(\mu\text{-SR})_2$. In a recent paper we reported[3] some details of the previously mentioned by us[4,5] chemical reduction of $Fe_2(NO)_4(\mu\text{-SR})_2$ (R = Me or Et) and of the conversion of the resultant anions by alkyl iodides (R'I) to $Fe_2(NO)_4(\mu\text{-SR})(\mu\text{-NHR}')$. Regrettably, in the preparation of this manuscript we overlooked a relevant publication by Glidewell and co-workers.[6] This omission and our formulation of the products of reduction with 2 equivalents of sodium or hydride as $[Fe_2(NO)_4(\mu\text{-SR})_2]^{2-}$ came under criticism by Glidewell and Lambert,[7] who apparently were unaware of our ongoing researches in this area since the 1980s[4,5] and who have formulated these products as the monoanions $[Fe_2(NO)_4(\mu\text{-SR})_2]^-$.[6] The purpose of the present communication is not only to set straight the chronology of these events, but also to point out that the chemical reduction of $Fe_2(NO)_4(\mu\text{-SR})_2$ is more complex than that which Glidewell and coworkers have reported.

In our hands reduction of $Fe_2(NO)_4(\mu\text{-SR})_2$ (R = Me, Et or Bu^t) with 1 and 2 equivalents of hydride (as MBR_3H: M = Li, Na or K; R = Et or Bu^s) affords different products, **A** and **B**, respectively. [The reaction with 2 equivalents of sodium yields **B**; with 4 equivalents of sodium an uncharacterized product showing no IR ν(NO) bands is obtained.] Compound **B** is formulated as $[Fe_2(NO)_4(\mu\text{-SR})_2]^{2-}$, while **A** may be $[HFe_2(NO)_4(\mu\text{-SR})_2]^-$ on the basis of the following evidence.

(1) Probably the most compelling evidence for the credibility of the proposed formula of **B** comes from quantitative analysis of the gas evolved in the reaction of $Fe_2(NO)_4(\mu\text{-SMe})_2$ with $LiBEt_3H$ in THF. When 2 equivalents of $LiBEt_3H$ were used 92% of all hydrogen derived from the hydridic H in $LiBEt_3H$ was collected. Thus, this reaction proceeds according to the stoichiometry:

$$Fe_2(NO)_4(\mu\text{-SMe})_2 + 2LiBEt_3H \longrightarrow Li_2[Fe_2(NO)_4(\mu\text{-SMe})_2] + 2BEt_3 + H_2.$$

In contrast, when 1 equivalent of $LiBEt_3H$ was employed under similar conditions, only 3% of the hydridic hydrogen was collected. At the conclusion of each experiment the IR ν(NO) spectrum of the reaction solution revealed that all of the $Fe_2(NO)_4(\mu\text{-SMe})_2$ had reacted. Thus, the unex-

* Author to whom correspondence should be addressed.

pelled hydridic hydrogen must be part of the product **A**. In both reactions hydrogen was analysed by mass spectrometry. The presence of BR_3 (R = Et or Bu^s) in solution was observed by ^{11}B NMR spectroscopy at the conclusion of these and related experiments. Apparently the role of the second equivalent of $LiBEt_3H$ is that of a scavenger of the hydrogen (as H^+) acquired as H^- in the formation of **A**, to give **B** and H_2. If $[Fe_2(NO)_4(\mu\text{-SMe})_2]^-$ had formed in these reduction reactions then 50% of the hydridic hydrogen of $LiBEt_3H$ would have been evolved for both 1 : 1 and 1 : 2 ratios of reactants.

(2) The formulation of **B** as $[Fe_2(NO)_4(\mu\text{-SR})_2]^{2-}$ receives further support from a series of conductivity measurements on MeOH solutions of a solid that was isolated from the reaction of $Fe_2(NO)_4(\mu\text{-SMe})_2$ with 2 equivalents of KH in diethyl ether. The resulting Onsager plot[8] is shown in Fig. 1. Also shown, for comparison, is the corresponding plot for the structurally characterized[9] $Na_2[Fe_2(CO)_6(\mu\text{-PPh}_2)_2]$. Clearly, both compounds are of the same electrolyte type (i.e. 2 : 1[8]).

(3) The ^1H NMR spectrum of $K_2[Fe_2(NO)_4(\mu\text{-SEt})_2]$ [isolated from the reaction of $Fe_2(NO)_4(\mu\text{-SEt})_2$ with 2 equivalents of KH in diethyl ether] in acetone-d_6 shows resonances at δ 1.8 (q) and 0.9 (t) ($J = ca$ 7 Hz). These resonances are shifted to higher field compared to those of the uncharged $Fe_2(NO)_4(\mu\text{-SEt})_2$ [δ 3.05 (q) and 1.55 (t)]. Similarly, $Na_2[Fe_2(NO)_4(\mu\text{-SCD}_3)_2]$, from $Fe_2(NO)_4(\mu\text{-SCD}_3)_2$ and 2 equivalents of $LiBEt_3H$ in THF, shows one ^2H NMR resonance at δ 2.57; neutral $Fe_2(NO)_4(\mu\text{-SCD}_3)_2$ gives a signal at δ 3.42. All of these resonances are sharp, occur in the region expected for diamagnetic compounds and experience, as predicted, upfield shifts when compared to those of the uncharged counterparts.

(4) Rather unexpectedly, **A** and **B** exhibit very similar IR spectra in the ν(NO) region: two absorptions at 1670–1675 and 1650–1660 cm^{-1} in THF. Under favourable resolution both bands show shoulders at *ca* 1680 and 1645 cm^{-1}, indicating the presence of another, minor iron nitrosyl species. For comparison, neutral precursors $Fe_2(NO)_4(\mu\text{-SR})_2$ absorb at 1785–1790 and 1750–1760 cm^{-1} in $CHCl_3$. Similar IR ν(NO) spectra of complexes such as **A** and **B** are not unprecedented, however; e.g. $[Fe_2(NO)_3(PPh_2H)(\mu\text{-NO})(\mu\text{-PPh}_2)]^-$ and $[Fe_2(NO)_4(\mu\text{-PPh}_2)_2]^{2-}$ display ν(NO) bands at comparable average frequencies.[10] It is more difficult to reconcile IR ν(NO) spectral trends with the formulation $[Fe_2(NO)_4(\mu\text{-SR})_2]^-$. On going from $Fe_2(NO)_4(\mu\text{-PPh}_2)_2$ [ν(NO) 1762, 1748 cm^{-1}] to $[Fe_2(NO)_4(\mu\text{-PPh}_2)_2]^{2-}$ [ν(NO) 1673 (br, unresolved) cm^{-1}][10] ν(NO) decreases by *ca* 80 cm^{-1}. On this basis the observed decrease in ν(NO) by $\gtrsim$ 100 cm^{-1} upon reduction of $Fe_2(NO)_4(\mu\text{-SR})_2$ to $[Fe_2(NO)_4(\mu\text{-SR})_2]^{n-}$ is more consistent with n being 2 rather than 1.

(5) Complexes **A** and **B** from $Fe_2(NO)_4(\mu\text{-SMe})_2$ and $LiBEt_3H$ also differ in their UV–vis spectra in THF. For example, the former shows an absorption band at 360 nm, which is missing in the spectrum of **B**.

The foregoing results notwithstanding, we do not dispute that Glidewell and co-workers generated and correctly characterized the ESR-active $[Fe_2(NO)_4(\mu\text{-SR})_2]^-$ in their studies. However, evidence obtained in our investigations on *bulk* reaction and product solutions for the reduction of $Fe_2(NO)_4(\mu\text{-SR})_2$ with 2 equivalents of sodium or hydride clearly implicates $[Fe_2(NO)_4(\mu\text{-SR})_2]^{2-}$ as the major species. (In our work freshly opened hydride reagents obtained from Aldrich Chemical Co. were employed, solvents were dried and freshly distilled and experiments were conducted under purified argon by the use of Schlenk, dry-box and vacuum-line techniques.)

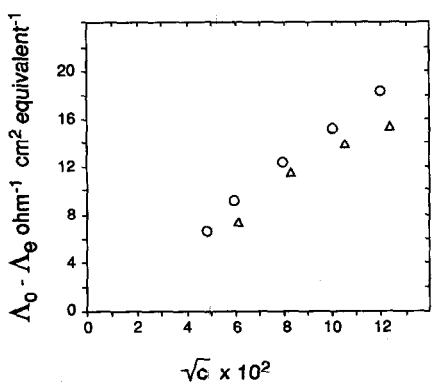

Fig. 1. Onsager plots for solutions of $K_2[Fe_2(NO)_4(\mu\text{-SMe})_2]$ (Δ) and $Na_2[Fe_2(NO)_4(\mu\text{-PPh}_2)_2]$ (○) in MeOH.

Acknowledgement—We thank the National Science Foundation for financial support.

REFERENCES

1. Y.-F. Yu, J. Gallucci and A. Wojcicki, *J. Am. Chem. Soc.* 1983, **105**, 4826.
2. M. R. Adams, J. Gallucci, A. Wojcicki and G. J. Long, *Inorg. Chem.* 1992, **31**, 2.
3. C.-N. Chau and A. Wojcicki, *Polyhedron* 1992, **11**, 851.
4. C.-N. Chau, *Diss. Abstr. Int.* 1986, **46**, 3434-B; C.-N. Chau, *Chem. Abstr.* 1986, **105**, 17124c.
5. A. Wojcicki, in *Coordination Chemistry and Catalysis*

(Edited by J. J. Ziółkowski), p. 3. World Scientific Publishing Co., Teaneck, NJ (1988).
6. J. A. Crayston, C. Glidewell and R. J. Lambert, *Polyhedron* 1990, **9**, 1741.
7. C. Glidewell and R. J. Lambert, *Polyhedron* 1992, **11**, 2803.
8. W. J. Geary, *Coord. Chem. Rev.* 1971, **7**, 81.
9. R. E. Ginsburg, R. K. Rothrock, R. G. Finke, J. P. Collman and L. F. Dahl, *J. Am. Chem. Soc.* 1979, **101**, 6550.
10. Y.-F. Yu, C.-N. Chau and A. Wojcicki, *Inorg. Chem.* 1986, **25**, 4098.

Polyhedron Vol. 12, No. 10, pp. 1265–1267, 1993
Printed in Great Britain

0277–5387/93 $6.00+.00
© 1993 Pergamon Press Ltd

COMMUNICATION

REACTIONS OF COORDINATED β-KETOESTERS. A NEW ROUTE FOR THE SYNTHESIS OF 4-SUBSTITUTED-3-METHYL/PHENYL-1-PHENYL PYRAZOL-5-ONES VIA A METAL CHELATED STABLE INTERMEDIATE

S. ABDUL SAMATH,* K. JEYASUBRAMANIAN, S. THAMBIDURAI, S. KAMARDEEN and S. K. RAMALINGAM

Department of Inorganic Chemistry, School of Chemistry, Madurai Kamaraj University, Madurai 625 021, India

(*Received* 23 *November* 1992; *accepted* 27 *January* 1993)

Abstract—Unsubstituted and γ-substituted copper(II) complexes of β-ketoesters on treatment with phenylhydrazine give ring-rearranged chelate intermediates, which on subsequent demetallation afford the new 4-halo/phenylamido-3-methyl/phenyl-1-phenyl pyrazol-5-ones.

Pyrazolone compounds have a wide variety of applications in biological,[1] clinical,[2] pharmacological[3,4] and analytical areas.[5,6] The synthesis of their 4-substituted derivatives involves more than one reaction step. As part of our interest in the reactions of coordinated β-diketonates,[7] we have investigated the reaction of phenylhydrazine with β-ketoester complexes of copper(II) in an attempt to synthesize 4-substituted pyrazolones in one step. This also serves to test the potential of the reaction for preparing analogous compounds starting from the metal chelates. We briefly report here the reactions involving copper(II) complexes of ethylacetoacetate (EAA), methylacctoacetate (MAA), benzoylacetate ethylester (BZAE) and their 3-bromo and 3-phenylamido products.

Reaction of phenylhydrazine with copper(II) complexes of β-ketoesters gives the ring-rearranged product **I**. The formation of the chelates is indicated by their elemental analyses and their IR spectra which exhibit ring-rearrangement features as reported in our earlier studies.[7–9]

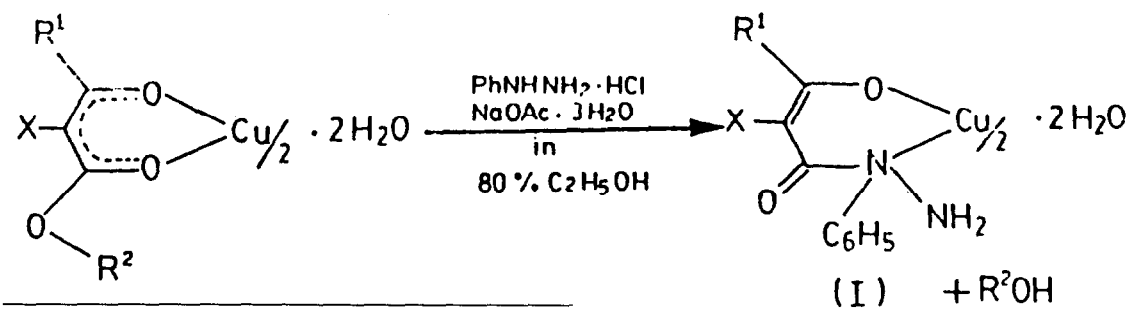

Subsequent demetallation of complex **I** by treatment with H_2S affords 2 mol of 4-X-pyrazolones (X = H, Br or C_6H_5NHCO—) per mole of complex, which on further treatment with dimethyl sulphate gives the corresponding 4-X-3-methyl/phenyl-N-methyl-1-phenyl pyrazolones (**IIIa–f**).

The analytical data (Table 1) along with the spectral features of compounds **II(a–f)** and **III(a–f)** indi-

*Author to whom correspondence should be addressed.

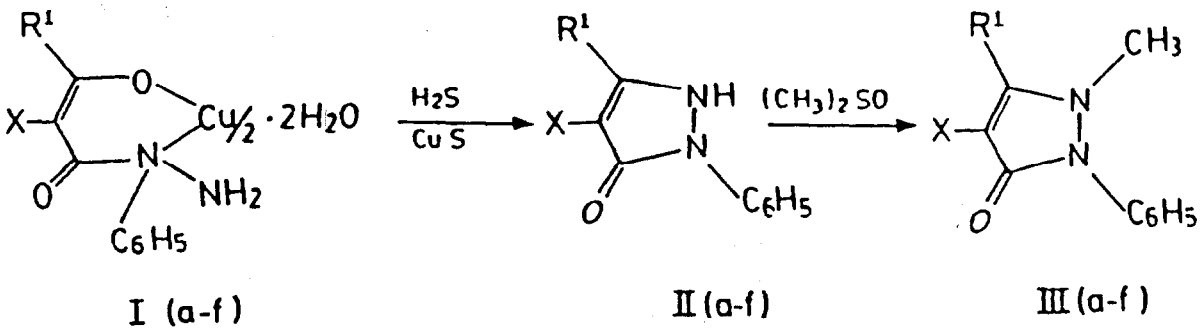

I (a-f) II (a-f) III (a-f)

Table 1. Analytical data for the intermediate complexes and pyrazolone compounds

No.	Composition	X	% Yield	% Found (Calc.) Cu	C	H	N
I—Intermediate complexes							
Ia	$[Cu(C_{10}H_{11}N_2O_2)_2 \cdot 2H_2O]$	H	90	13.1 (13.2)	49.9 (49.8)	5.4 (5.4)	11.7 (11.6)
Ib	$[Cu(C_{10}H_{10}N_2O_2Br)_2 \cdot 2H_2O]$	Br	75	11.5 (11.4)	43.1 (42.9)	4.4 (4.3)	10.2 (10.0)
Ic	$[Cu(C_{17}H_{16}N_3O_3)_2 \cdot 2H_2O]$	C_6H_5NHCO	85	8.9 (8.8)	56.7 (56.7)	5.1 (5.0)	12.0 (11.7)
Id	$[Cu(C_{15}H_{13}N_2O_2)_2 \cdot 2H_2O]$	H	85	10.6 (10.5)	60.1 (59.5)	4.9 (5.0)	9.6 (9.3)
Ie	$[Cu(C_{15}H_{12}N_2O_2Br)_2 \cdot 2H_2O]$	Br	75	9.4 (9.3)	53.1 (52.7)	4.3 (4.1)	8.4 (8.2)
If	$[Cu(C_{22}H_{18}N_3O_3)_2 \cdot 2H_2O]$	C_6H_5NHCO	80	7.3	63.0	4.8	10.2
II—4-X-NH-3-Methyl/phenyl-1-phenyl pyrazol-5-one				M.p. (°C)			
IIa	$C_{10}H_{10}N_2O$	H	70	129	69.2 (69.0)	5.9 (5.8)	16.3 (16.1)
IIb	$C_{10}H_9N_2OBr$	Br	65	132	47.6 (47.4)	3.6 (3.7)	11.3 (11.1)
IIc	$C_{17}H_{15}N_3O_2$	C_6H_5NHCO	70	127	70.2 (69.6)	5.0 (5.1)	14.2 (14.3)
IId	$C_{15}H_{12}N_2O$	H	75	109	76.5 (76.3)	5.0 (5.1)	12.1 (11.9)
IIe	$C_{15}H_{11}N_2OBr$	Br	70	141	57.2 (57.1)	3.5 (3.5)	9.1 (8.9)
IIf	$C_{22}H_{17}N_3O_2$	C_6H_5NHCO	70	121	74.2 (74.4)	4.9 (4.8)	12.0 (11.8)
III—4-X-N-Methyl-3-methyl/phenyl pyrazol-5-ones							
IIIa	$C_{11}H_{12}N_2O$	H	80	112	70.5 (70.2)	6.5 (6.4)	15.3 (14.9)
IIIb	$C_{11}H_{11}N_2OBr$	Br	60	121	49.4 (49.4)	4.2 (4.1)	10.5 (10.5)
IIIc	$C_{18}H_{17}N_3O_2$	C_6H_5NHCO	70	141	70.8 (70.4)	5.6 (5.5)	14.1 (13.7)
IIId	$C_{16}H_{14}N_2O$	H	85	122	77.1 (76.8)	5.5 (5.6)	11.7 (11.2)
IIIe	$C_{16}H_{13}N_2OBr$	Br	65	129	58.3 (58.4)	4.1 (4.0)	9.1 (8.5)
IIIf	$C_{23}H_{19}N_3O_2$	C_6H_5NHCO	75	132	74.6 (74.8)	5.1 (5.1)	11.6 (11.4)

cate that the cyclization has occurred upon demetallation between the $—NH_2$ group (of the phenyl hydrazine) and the carbonyl oxygen (adjacent to the R^1 group). It can, therefore, be inferred that this new ring-rearranged chelate **I** acts as a probable stable intermediate and is vital in the synthesis of the pyrazolone compounds **II** and **III**. In the reported synthesis[10] of such compounds from the direct reaction of β-ketoesters and phenylhydrazine the probable intermediate must be the one represented as below, although it has not been isolated.

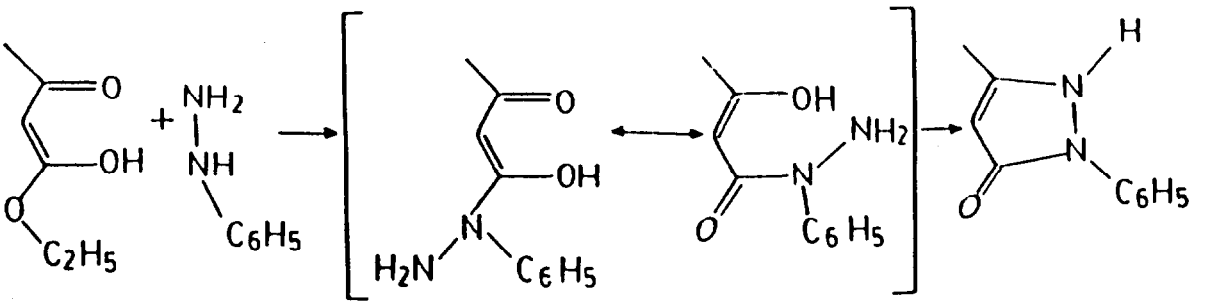

Unstable intermediate

The 4-bromo [**II(b,e)** and **III(b,e)**] and 4-phenylamido [**II(c,f)** and **III(c,f)**] pyrazolones and the intermediate complexes [**I(a–f)**] reported in this communication are new. Not only are these intermediates becoming increasingly important in the synthesis of substances of scientific appeal, but they are also significant in the study of new pathways in reaction mechanisms.

EXPERIMENTAL

Action of phenylhydrazine on copper(II) chelates

Phenylhydrazine (10 mmol) and an ethanolic suspension (80%) of copper(X-β-ketoester)$_2 \cdot 2H_2O$ (X = H, Br or $C_6H_5NHCO—$; 5 mmol) were stirred together at 60–80°C for 2 h. The solid intermediate complex **I** was filtered off, washed with ethanol and dried *in vacuo*. IR (KBr): ν(C=O); 1695 and ν(NH)$_2$ 3280–3360 cm^{-1}.

Demetallation and cyclization reactions

A stream of H_2S was bubbled through complex **I** suspended in 50% (v/v) ethanol for 30–45 min. The precipitated CuS was filtered off and excess H_2S was expelled by boiling. The solution on concentration gave the solid 4X-3-methyl/phenyl-1-phenyl pyrazol-5-ones. On further treatment with dimethyl sulphate this yielded the corresponding N-methyl pyrazolones. IR (KBr): ν(C=O) (amide) 1660 and ν(NH) 3130–3210 cm^{-1}. ^1H NMR (δ ppm): 7.36–7.20 (5H, m, C_5H_5), 5.10–5.30 (1H, s, 4-H), 3.12–3.22 (3H, s, N—CH_3), 2.30–2.05 (3H, s, 2-CH_3).

Acknowledgements—The authors thank the USIC, Madurai Kamaraj University, for providing spectral facilities. SAS thanks the CSIR, New Delhi, for the award of a Research Associateship.

REFERENCES

1. D. G. Craciunescu, *An. R. Acad. Farm.* 1977, **43**, 265.
2. J. Hosler, C. Tschanz, C. E. Hignite and D. L. Azarnoff, *J. Invest. Dermatol.* 1986, **74**, 51.
3. P. J. Meffin, R. L. Williams, T. K. Blaschke and M. Rowland, *J. Pharm. Sci.* 1977, **66**, 135.
4. M. M. Shoukry, A. Kh. Ghoneim, E. M. Shourkry and M. H. El. Nagdi, *Synth. React. Inorg. Met.-Org. Chem.* 1982, **12**, 815.
5. N. L. Olenovich and L. I. Koval Chuk, *Zh. Anal. Khim.* 1975, **28**, 2162.
6. B. Janik and S. Sawicki, *Mikro. Chim. Acta* 1970, 1050.
7. G. Shankar and S. K. Ramalingam, *Trans. Met. Chem.* 1984, **9**, 449.
8. S. K. Ramalingam and S. Abdul Samath, *Trans. Met. Chem.* 1990, **15**, 374.
9. S. Abdul Samath, N. Raman, K. Jeyasubramanaian and S. K. Ramalingam, *Polyhedron* 1992, **11**, 33.
10. A. I. Vogel, *A Text Book of Practical Organic Chemistry*, p. 882, 4th edn. Longmans, London (1978).

Polyhedron Vol. 12, No. 10, p. 1269, 1993
Pergamon Press Ltd. Printed in Great Britain

CORRIGENDUM

Fluorine NMR study of the two *cis*-β-configurations of a hexafluoro-2,4-pentanedionatocobalt(III) complex. Y. Kitamura and A. Shibata (*Polyhedron* Vol. 11, No. 19, pp. 2441–2446, 1992).

The authors regret that the isomeric designations Δ-β-*SR* and Δ-β-*SS* are incorrect. They should read *rel*-Δ-β-*RR* and *rel*-Δ-β-*RS*. The conclusions of the paper are not affected by this change.

Polyhedron Vol. 12, No. 11, pp. 1271–1275, 1993
Printed in Great Britain

0277–5387/93 $6.00+.00
© 1993 Pergamon Press Ltd

OXIDATIONS WITH SOLUBLE MANGANESE(IV) PHOSPHATE

MIKLÓS JÁKY*

Central Research Institute for Chemistry, Hungarian Academy of Sciences, H-1525 Budapest, P.O. Box 17, Hungary

and

MIKLÓS ZRINYI

Department of Physical Chemistry, Technical University, 1521 Budapest, P.O. Box 91, Hungary

(*Received* 7 *January* 1991; *accepted* 19 *February* 1993)

Abstract—Manganese(IV) phosphate was prepared in 3 M phosphoric acid. Ultracentrifugal and electron microscopic studies did not indicate colloid properties. Manganese(IV) phosphate oxidizes mainly oxygen-containing bifunctional substrates in an autocatalytic way. Its reactivity was found to be higher in every case than that of manganese(III) phosphate.

In our investigations performed with dissolved manganese(IV) we had two aims in view. Solid MnO_2 is an oxidant which has been known for a long time and is still used today in some interesting preparation methods.[1] As can be seen, however, the kinetics and mechanism of these reactions have not been satisfactorily clarified, due not only to the heterogeneity of the reactions but also to the fact that the reactivity of MnO_2 is highly affected by precipitation and special pre-treatments. Therefore, we strived to transfer manganese(IV) in the dissolved state in the hope that these questions may be clarified in the homogeneous phase and the results may—at least partly—be applied under heterogeneous conditions.

In the course of permanganate oxidation a soluble brownish-yellow manganese species usually appears,[2–10] with the oxidation state +4, determined iodometrically, and which in many cases accelerates permanganate oxidation autocatalytically.[5–10] For the sake of detailed clarification of the mechanism of permanganate oxidation, it is important to determine what substrates or intermediate products can be attacked by the manganese(IV) intermediate. This was the other goal of our investigations.

Although manganese(IV) forms water soluble complexes with several inorganic[11–15] and organic[16–24] ligands, Perez-Benito[25–27] and recently Freeman[28,29] verified that in the reduction of permanganate at pH 6.8 a fine colloid dispersion of MnO_2 appears, which is stabilized by anions, predominantly by phosphate ions adsorbed on the surface. We performed our kinetic investigations in phosphoric acid since in this case, owing to the lower pH value, there is no danger of disproportionation of manganese(III).

EXPERIMENTAL

The permanganate used was Merck analytical grade, phosphoric acid was Rudipont electronic grade and the substrates were Fluka purest grade products. Special stress was laid on the purity of the water used, which was distilled three times, once from permanganate.

The active MnO_2, which is actually a mixture of oxides and hydroxides containing various amounts of water, was prepared by the reduction of permanganate. The sample taken was dissolved in

* Author to whom correspondence should be addressed.

phosphoric acid of an appropriate concentration, using a shaking device, then the excess was removed by filtration on a filter of G5 porosity. The first filtrate usually shows some Tyndall effect, therefore, the filtration was repeated through the precipitate on the same filter. The solution thus obtained showed no Tyndall effect and lost from its iodometrically determined titre no more than 1% per day.

The reduction of permanganate can be performed most suitably with excess sodium formate, when the permanganate is reduced quantitatively to manganese(IV). Reduction with Mn^{2+} is the least advisable since its excess cannot be removed from the precipitate by washing and when dissolved in phosphoric acid it reduces some of the manganese(IV) immediately into manganese(III). Only freshly prepared MnO_2 stored in an aqueous suspension should be used. The solubility equilibrium is practically established after half an hour's shaking. Figure 1 shows the amount of soluble manganese(IV) against the concentration of phosphoric acid.

Kinetic investigations were performed with a Hewlett–Packard 8432 A type spectrophotometer. For reactions with half-times less than 1 min a stopped-flow stirring system built in our laboratory was used. Manganese(IV) consumption was followed at 390 nm ($\varepsilon_{390} = 2130$) since manganese(III) has practically no absorption here. Manganese(III) consumption, on the other hand, was measured at its absorption maximum, 505 nm ($\varepsilon_{505} = 93$).

Electron microphotographs were taken with a Zeiss EM 902 transmission electron microscope. The sample was placed on the 1 μ density sieve of the microscope and dried for 1 day at room temperature in high vacuum as completely as possible. The ultracentrifuge used was a MOM device, type 3180 (r.p.m.: 45,000).

RESULTS AND DISCUSSION

The experiments were performed in 3 M phosphoric acid. The spectrum of the brown coloured,

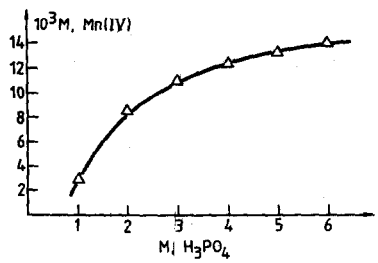

Fig. 1. Total concentrations of dissolved manganese(IV) plotted against phosphoric acid concentration; $T = 25°C$.

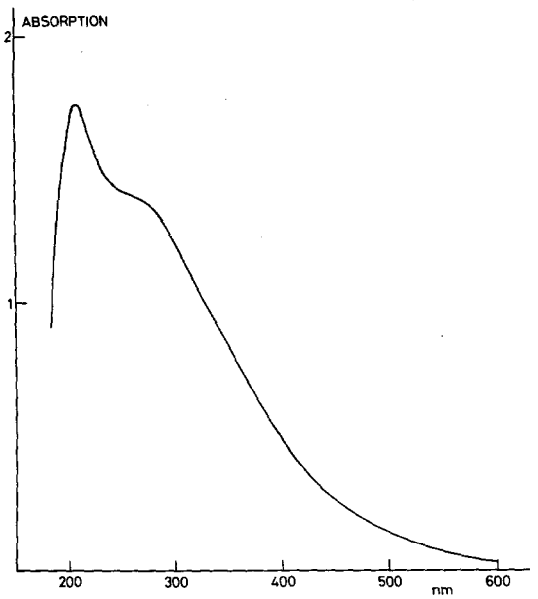

Fig. 2. The spectrum of manganese(IV) phosphate; $[Mn^{IV}] = 1.00 \times 10^{-3}$ M, $[H_3PO_4] = 3.0$ M.

clearly transparent manganese(IV) species is shown in Fig. 2. The characterless, monotonous curve is in agreement with spectra obtained by Selim and Lingane[30] in sulphuric acid and in a phosphate buffer of pH 6.8.[25,28,29] If a solution of a manganese(II) salt is added in excess the brown colour turns immediately into pale pink, but the oxidation titre of the solution does not change. The spectrum of the pink solution is practically identical to that of manganese(III) pyrophosphate.[31] The absorption of both the manganese(IV) and manganese(III) solutions strictly obeys the Beer–Lambert law.

The question is whether manganese(IV) is present in dissolved or in colloidal form. It should be noted that in such a high electrolyte concentration (3 M), generally no stable colloid can be expected, even if the anion happens to be the phosphate ion which can be well adsorbed on the surface of MnO_2. At any rate the investigations performed with an ultracentrifuge and an electron microscope did not indicate any colloid. The solutions containing manganese(IV) in 6×10^{-3} and 10×10^{-3} M concentrations did not show sedimentation in the ultracentrifuge at 45,000 r.p.m. This means that the particle size must be below 50 nm. In the case of electron microscope studies the starting solution was 6×10^{-3} M manganese(IV). This was diluted five times to half its concentration and photographs were taken for each. In no case have we obtained a picture indicating a particle. At the same time, known colloids [SiO_2–sol, FeO(OH)–sol] gave excellent pictures. In our experience,[32,33] particles larger than 2 nm are easily detected by this method.

Thus, in the case of a colloid particle size cannot exceed 2 nm. In any case, our species will be subsequently referred to as manganese(IV) phosphate.

Manganese(IV) phosphate is a strong oxidizing agent. In order to determine what kind of compound or functional group it can attack we performed comparative kinetic measurements under identical reaction conditions. Since the reactions, except in the case of some substrates, do not show simple kinetics, but an accelerating trend, the half-time of consumption of the oxidizing agent was measured and these values are listed in Table 1. Thus, $t_{1/2} = \infty$ indicates that the reduction of manganese(IV) is not much faster than the blind test in the absence of the substrate. In Table 1 virtual reaction rates determined by the tangent-method at half time are also indicated: ($w = \Delta[Mn^{IV}]/\Delta t$).

The intermediate product in the reduction of manganese(IV) is in each case manganese(III). The reduction can proceed in one electron step or in a very rapid

$$Mn^{IV} + Mn^{II} \longrightarrow 2Mn^{III}$$

process following a two-electron step.

The appearance of manganese(III) justified the investigation of its reactivity with the same substrates, in order to obtain at least a qualitative picture of the difference between the reactivities of

Table 1. (A) Half-times of the reactions of manganese(IV) phosphate and the reaction rate at half-time and (B) half-times of the reactions of manganese(III) phosphate; $[H_3PO_4] = 3.0$ M, [substrate] = 0.10 M, $[Mn^{IV}] = 1.0 \times 10^{-3}$ M or $[Mn^{III}] = 1.0 \times 10^{-3}$ M, $T = 25°C$

	(A) Mn^{IV}		(B) Mn^{III}
	$t_{1/2}$ (min)	$10^5 \times W_{1/2}$ (M min^{-1})	$t_{1/2}$ (min)
Methanol	∞	0	∞
Ethanol	∞	0	∞
Ethylene glycol	36.5	2.5	∞
n-Propanol	∞	0	∞
Propane-1,2-diol	31.5	3.8	∞
Propane-1,3-diol	52.0	1.1	∞
n-Butanol	∞	0	∞
Butane-2,3-diol	16.5	3.3	∞
Butane-1,3-diol	67	0.81	∞
1,4-Butanediol	∞	0	∞
Formaldehyde[a]	73	0.46	∞
Acetaldehyde	4.4	19	20.3
Glycolaldehyde	1.9	16.9	12.7
Glyoxal	0.30	130	0.83
Glycollic acid	3.4	15.1	∞
Glyoxylic acid	0.12	432	0.21
Acetone	400	0.36	∞
Hydroxy-acetone	3.9	8.7	11.2
Lactic acid	2.6	32	72
Pyruvic acid	0.11	514	0.23
Formic acid[a]	595	0.058	∞
Acetic acid	∞	0	∞
Oxalic acid	0.33	65	1.7
Malonic acid	0.78	66	14.4
Succinic acid	450	0.12	∞
Allyl alcohol[a]	5.5	6.3	220
1,4-Butenediol[a]	3.4	10.2	72
Propargyl alcohol[a]	43	0.80	∞
1,4-Butinediol[a]	13.8	2.5	∞
Maleic acid	34	1.6	∞
Chloro-maleic acid	24	2.1	∞
Dichloro-maleic acid	7.1	4.9	∞
Brom-maleic acid	31	1.8	∞

[a] First-order related to both manganese(IV) phosphate and the substrate; zero-order to manganese(III).

the two manganese species. As can be seen from the comparison of half-times the reaction of manganese(III) with each substrate studied by us proved to be slower than that of manganese(IV).

Among the substrates listed in Table 1 only formic acid, formaldehyde and α,β-unsaturated alcohols show virtual first-order kinetics; in each other case the reaction was accelerating and a sigmoid-shape kinetic curve was obtained. In the case of the latter substrates, if manganese(III) is added to the system so that $[Mn^{III}]_0 = [Mn^{IV}]_0 = 1 \times 10^{-3}$ M, the induction period is considerably shorter and the sigmoid character decreases. This points to autocatalytic reactions, where manganese(III) plays a decisive role even in the case of substrates which are not oxidized by manganese(III) alone.

The half-times and the reaction rates measured at half-times do not show exactly the same reactivity sequence of substrates, but similar tendencies can be observed in both cases. Due to the kinetic relationships, which are generally not of first-order, this reactivity sequence only presents a rather qualitative picture; nevertheless, certain conclusions may automatically present themselves. Thus, it is at once evident that manganese(IV) attacks mainly those bifunctional substrates which allow the formation of a complex of chelate character. Thus, it practically does not oxidize primary alcohols, but it does oxidize glycols. The vicinal position seems to be somewhat more favourable than the 1,3-position. However, it does not oxidize 1,4-butenediol, presumably because of the great distance no chelate complex can be formed here. The same tendency can be observed with carboxylic acids. Although it undergoes a slow reaction with the markedly reducing formic acid, it cannot attack acetic acid. At the same time it oxidizes oxalic acid and malonic acid rapidly, while succinic acid, presumably again for steric reasons, is oxidized very slowly. The situation is practically the same with carbonyl compounds as well, since although their monofunctional derivatives can be oxidized, bifunctional derivatives show a considerable increase in reactivity. A particularly convincing example, from this aspect, is the weak oxidation tendency of acetone compared with hydroxyacetone. The highest reactivity was observed with compounds having a carbonyl group in the proximity of the carboxyl group (pyruvic acid, glyoxylic acid).

Column B in Table 1 indicates that manganese(III) phosphate also oxidizes those substrates which are capable of chelate complex formation, but its reactivity is much lower than that of the manganese(IV) phosphate, as manifested also by its inactivity towards glycols.

Although it could not be verified unambiguously that the manganese(IV) phosphate prepared by us is a real solution and not a finely dispersed colloid, as with the species observed by Perez-Benito and Freeman under totally different conditions, these investigations may offer some information on its behaviour towards various groups of compounds.

Acknowledgement—This work has been supported by the Hungarian Research Fund (Grant No. 1778).

REFERENCES

1. A. J. Fatiadi, *Synthesis* 1976, **65**, 133.
2. K. B. Wiberg, C. J. Deutsch and J. Rocek, *J. Am. Chem. Soc.* 1973, **95**, 3034.
3. L. I. Simándi, M. Jáky, F. Freeman, C. O. Fuselier and E. M. Karchefski, *Inorg. Chim. Acta* 1978, **31**, L457.
4. F. Freeman and J. C. Kappos, *J. Org. Chem.* 1989, **54**, 2730.
5. J. F. Perez-Benito, F. Mata-Perez and E. Brillas, *Can. J. Chem.* 1987, **65**, 2329.
6. F. Mata-Perez and J. F. Perez-Benito, *Can. J. Chem.* 1987, **65**, 2373.
7. J. Andres, E. Brillas, J. A. Garzido and J. F. Perez-Benito, *J. Chem. Soc., Perkin Trans. II* 1988, 107.
8. J. F. Perez-Benito, R. M. Rodriquez, J. Andres, E. Brillas and J. A. Garzolo, *Int. J. Chem. Kinet.* 1989, **21**, 71.
9. J. F. Perez-Benito, C. Arias and E. Brillas, *Int. J. Chem. Kinet.* 1990, **22**, 261.
10. J. F. Perez-Benito and C. Arias, *Int. J. Chem. Kinet.* 1991, **23**, 717.
11. M. W. Lister, *Can. J. Chem.* 1961, **39**, 2330.
12. C. M. Flynn and G. D. Stucky, *Inorg. Chem.* 1969, **8**, 332.
13. C. M. Flynn and M. T. Pope, *Inorg. Chem.* 1970, **9**, 2009.
14. T. S. Dzzhaliev, V. Y. Shafirovich and A. E. Shilov, *React. Kinet. Catal. Lett.* 1976, **4**, 11.
15. V. Y. Shafirovich, N. K. Khannanov and A. E. Shilov, *J. Inorg. Biochem.* 1981, **15**, 113.
16. Z. Marchenko, *Bull. Soc. Chem. France* 1964, 939.
17. S. R. Cooper, E. C. Dismukes, M. P. Klein and M. Calvin, *J. Am. Chem. Soc.* 1978, **100**, 7248.
18. B. L. Velikov and J. Dolezal, *J. Electroanalyt. Chem.* 1976, **71**, 91.
19. E. Bodini and D. T. Sawyer, *J. Am. Chem. Soc.* 1976, **98**, 8367.
20. K. D. Magers, C. G. Smith and D. T. Sawyer, *Inorg. Chem.* 1978, **17**, 515.
21. D. T. Richens, C. G. Smith and D. T. Sawyer, *Inorg. Chem.* 1979, **18**, 706.
22. K. D. Magers, C. G. Smith and D. T. Sawyer, *Inorg. Chem.* 1980, **19**, 492.
23. T. Matsushita, L. Spencer and D. T. Sawyer, *Inorg. Chem.* 1988, **27**, 1167.
24. L. Nagy, T. Gajda, T. Páli and K. Burger, *Acta Chim. Acad. Sci. Hung.* 1988, **125**, 403.
25. F. Mata-Perez and J. F. Perez-Benito, *Can. J. Chem.* 1985, **63**, 988.

26. J. F. Perez-Benito and D. G. Lee, *Can. J. Chem.* 1985, **63**, 3545.
27. J. F. Perez-Benito, E. Brillas and R. Pouplana, *Inorg. Chem.* 1989, **28**, 390.
28. F. Freeman and J. C. Kappos, *J. Am. Chem. Soc.* 1985, **107**, 6628.
29. F. Freeman, L. Y. Chang, J. C. Kappos and L. Sumarta, *J. Org. Chem.* 1987, **52**, 1460.
30. R. Selim and J. Lingane, *Analyt. Chim. Acta* 1959, **21**, 536.
31. G. Davies, *Coord. Chem. Rev.* 1969, **4**, 199.
32. M. Zrinyi, H. G. Kilian, K. Dierksen and F. Horkay, *Makromol. Chem. Macromol. Symp.* 1991, **45**, 205.
33. W. Haas, M. Zrinyi, H. G. Kilian and B. Heise, *Colloid Polym. Sci.*, in press.

Polyhedron Vol. 12, No. 11, pp. 1277–1288, 1993
Printed in Great Britain

0277–5387/93 $6.00+.00
© 1993 Pergamon Press Ltd

EFFECT OF PHYSICO-CHEMICAL PROPERTIES OF BINARY LIQUID MEMBRANES ON STEADY-STATE TRANSPORT OF COPPER(II) IONS

MARIOLA SZPAKOWSKA

Katedra Chemii Fizycznej, Wydział Chemii, Politechnika Gdańska, Ul. Majakowskiego 11/12, 80-952 Gdańsk, Poland

and

OTTÓ B.NAGY*

Laboratoire de Chimie Organique Physique, Université Catholique de Louvain, Bâtiment Lavoisier, Pl. Pasteur 1,1348 Louvain-la-Neuve, Belgium

(*Received* 27 *January* 1993; *accepted* 18 *February* 1993)

Abstract—The coupled transport of copper(II) ions by the carrier Acorga P-50 through mono and binary liquid membranes has been analysed in the steady-state approximation. The membranes were composed of C_8–C_{14} normal chain paraffins and their mixtures. It was found that the total ion fluxes are the most appropriate kinetic parameters for asymmetric membranes in the steady-state approximation. The results obtained for single component (mono) membranes have shown the importance of the physicochemical nature of membrane material. In all cases transport rates were diminished by increasing viscosity and by increased copper(II)–carrier-membrane interactions, as governed by general solvent effects (polarity and polarizability). Using binary solvent mixtures as the membrane a surprising variety of substitution profiles have been obtained, despite the very similar chemical character of the membrane components. The regular substitution profile obtained for the n-octane (*S*)–n-tetradecane (*Z*) solvent pair could be analysed successfully by COPS theory. The results confirmed quantitatively the decisive role played by molecular interactions in transport kinetics. A simple molecular model is proposed to explain the dominating role played by membrane polarity in determining transport rates. The general conclusions support fully those obtained previously for non-steady state kinetic conditions.

Liquid membranes represent a very efficient means for the removal of various impurities, including metal ions, from aqueous solutions (e.g. industrial waste waters).[1–4] Therefore, scientific research to obtain more information is important from both the fundamental[1,5] and technological[3,4,6,7] viewpoints. Surprisingly, not many reports have been published which are based on the use of different membrane systems[8] or multicomponent membranes.[9] However, our previous papers[10–13] have shown the importance of the nature of the membrane material and its composition in metal ion transport through liquid membranes. The behaviour of organic solvents belonging to different solvent classes has been examined in detail.[12] It was found that some solvents were very efficient (paraffins), but others have even stopped the transport flux completely. It was also shown that physicochemical properties of membrane material and solute–solvent interactions inside the membrane have substantial influence on process efficiency.[12,13]

In the present paper the influence of the membrane solvent composition (binary mixtures of C_8–C_{14} normal chain paraffins) on process efficiency is investigated in order to check whether binary membranes are more efficient than single component ones. For this purpose the kinetics of coupled transport of copper(II) ions through

* Author to whom correspondence should be addressed.

different pure liquid paraffin membranes and their mixtures of variable compositions are studied in the steady-state approximation. The purpose of using this latter approximation in the present study is to verify the general validity of the conclusions obtained in non-steady-state conditions.[12]

EXPERIMENTAL

Materials

Copper(II) sulphate pentahydrate (Aldrich > 99.999%), acorga P50 (Acorga Ltd, 94% in kerosene) and fresh solvents (Aldrich > 99%) were used without further purification. The aqueous solutions were made up using demineralized water.

Measurement of membrane properties

Viscosity (η), refractive index (n_D^{20}) and dielectric constant (ε) of the various pure paraffins and their mixtures were determined by standard methods.[14]

Kinetic procedure

All transport experiments were conducted at $T = 25 \pm 0.1$°C using an apparatus described previously,[12] containing asymmetric membranes. The ratio of interphase surfaces between donor phase/membrane (S_d) and acceptor phase/membrane (S_a) was $S_d/S_a = 2$. The organic solvents used as membrane material were pure open-chain paraffins (n-octane, n-decane, n-dodecane, n-tetradecane) or their mixtures, immiscible with water (weight % solubilities in water $< 1 \times 10^{-4}$). For every solvent pair (see Tables 1 and 2) the initial compositions of the three phases were as follows: Donor phase: $C_{do}(CuSO_4) = 0.1175$ M, pH = 3.64, in water; membrane: carrier acorga P-50 ($C_{AC} = 0.01$ M) dissolved in pure or binary solvents S–Z of variable compositions; acceptor phase: 2 M H_2SO_4 in water (experimental conditions I). For the n-octane–n-tetradecane system a second series of experiments has also been realized (experimental conditions II): donor phase: $CuSO_4$, $C_{do} = 0.1166$ M, pH = 3.71 in H_2O; membrane: acorga P-50, $C_{AC} = 0.0094$ M; acceptor phase: 1 M H_2SO_4 in H_2O. Stirring speeds for donor, membrane and acceptor phases, 400, 250 and 400 rpm, respectively, were the highest possible ones at which hydrodynamic complications (whirls, interface deformations) were still absent. Samples (0.5 cm^3) were taken from both water phases at regular time intervals and analysed by EDTA titration using murexide as an indicator. Each

Table 1. Steady-state kinetic parameters for the coupled transport of copper(II) through binary liquid membranes (experimental conditions I)

No.	Y_Z[a]	$-J_d \times 10^4$[b] (M h^{-1})	$J_a \times 10^4$[b] (M h^{-1})	r_d[c]	r_a[c]	R_d[d]	R_a[d]	R_m[d]	Δt[e] (h)
			n-dodecane(S)–n-decane(Z)						
1	0	6.52±0.35	6.67±0.32	0.9905	0.9919	0.801	0.152	0.047	48.0
2	0.3	6.76±0.28	7.04±0.25	0.9931	0.9948	0.784	0.165	0.051	48.3
3	0.9	6.51±0.24	6.47±0.09	0.9953	0.9996	0.735	0.204	0.061	47.8
4	1.0	6.76±0.14	6.87±0.21	0.9983	0.9955	0.778	0.168	0.054	50.0
			n-dodecane(S)–n-tetradecane(Z)						
5	0.45	3.18±0.25	2.85±0.02	0.9877	0.9895	0.875	0.067	0.058	36.7
6	0.9	2.52±0.48	2.46±0.20	0.9185	0.9821	0.879	0.056	0.065	31.0
7	1.0	3.21±0.19	3.23±0.10	0.9897	0.9972	0.883	0.067	0.050	47.0
			n-dodecane(S)–n-octane(Z)						
8	0.3	6.25±0.44	6.77±0.42	0.9832	0.9884	0.800	0.147	0.053	47.5
9	0.6	10.41±0.17	10.98±0.27	0.9993	0.9984	0.694	0.267	0.039	33.1
10	0.9	12.16±0.15	12.08±0.20	0.9995	0.9993	0.637	0.312	0.051	31.0
11	1.0	12.34±0.17	12.65±0.15	0.9995	0.9996	0.624	0.326	0.050	55.0

[a] Volume fraction of membrane Z component.
[b] Steady-state membrane permeation (J_d) and stripping (J_a) rates.
[c] Correlation coefficients for the zero-order straight lines of steady-state kinetics.
[d] Relative concentrations of copper in the donor (R_d) and acceptor (R_a) phases and in the membrane (R_m).
[e] Total process time length.

Table 2. Steady-state kinetic parameters for coupled transport of copper(II) through n-octane(S)–n-tetradecane(Z) binary liquid membranes in two different experimental conditions[a]

No.	Y_Z	$-J_d \times 10^4$ (M h^{-1})	$J_a \times 10^4$ (M h^{-1})	r_d	r_a	R_d	R_a	R_m	Δt (h)
Experimental conditions I[b]									
1	0	12.34±0.17	12.65±0.15	0.9995	0.9996	0.624	0.326	0.050	55.0
2	0.3	7.18±0.22	7.43±0.15	0.9971	0.9987	0.770	0.172	0.058	36.0
3	0.4	6.52±0.23	6.56±0.35	0.9969	0.9926	0.787	0.156	0.057	32.0
4	0.6	4.72±0.25	4.89±0.29	0.9898	0.9878	0.821	0.112	0.067	47.0
5	0.8	3.37±0.20	3.26±0.15	0.9895	0.9936	0.862	0.078	0.060	37.0
6	1.0	3.21±0.19	3.23±0.10	0.9897	0.9972	0.883	0.067	0.050	47.0
Experimental conditions II[b]									
7	0	9.94±0.53	10.35±0.39	0.9956	0.9979	0.692	0.270	0.038	38.5
8	0.3	6.12±0.36	5.81±0.13	0.9948	0.9992	0.815[c]	0.150[c]	0.035[c]	28.4
9	0.4	5.19±0.06	5.53±0.11	0.9998	0.9993	0.827	0.140	0.023	41.2
10	0.5	5.39±0.19	5.22±0.17	0.9987	0.9988	0.843[c]	0.137[c]	0.020[c]	26.3
11	0.6	4.30±0.16	4.29±0.18	0.9978	0.9972	0.848	0.103	0.049	40.4
12	0.8	3.86±0.30	3.97±0.11	0.9907	0.9986	0.853	0.098	0.049	32.3
13	1.0	3.23±0.35	3.35±0.10	0.9773	0.9979	0.871	0.080	0.049	38.6

[a] Same symbols as in Table 1.
[b] See Experimental.
[c] Extrapolated values.

experimental result reported is the arithmetic mean of two independent titrations (error < 2%). The reproducibility of the kinetic curves is fairly good.

RESULTS AND DISCUSSION

For the systems investigated using either pure or mixed membranes all kinetic measurements were performed in exactly the same experimental conditions, except for the variable membrane composition (from $Y_Z = 0$ to $Y_Z = 1$, with Y_Z = volume fraction of membrane component Z, see below). Steady-state conditions were established using a large excess of copper in the donor phase (concentration C_{do} in M) compared to the amount of carrier (acorga P-50: AC) in the membrane (concentration C_{AC} in M units): $C_{do}/C_{AC} = 11.75$.[10,22] The change in copper concentration with time was measured directly in both the donor (C_d in M) and acceptor (C_a in M) aqueous phases. The corresponding copper concentration changes in the membrane (C_m in M) were established from material balance. It was found useful to use reduced concentrations in all kinetic analyses: $R_d = C_d/C_{do}$ for the donor phase, $R_m = C_m/C_{do}$ for the membrane and $R_a = C_a/C_{do}$ for the acceptor phase.[12] Obviously, $R_d + R_m + R_a = 1$.

Figure 1 represents typical concentration vs time diagrams obtained for n-octane(S)–n-tetradecane(Z) mixtures used as membranes. It can be seen (see also Tables 1 and 2) that fairly good straight lines have been obtained throughout the full kinetic run with correlation coefficients $r_i > 0.99$ in the majority of cases. Tables 1 and 2 also show that R_m values are rather low and remain fairly constant during the entire transport process time interval, as indicated in Fig. 1. These two important criteria, i.e. linear concentration vs time relationships (zero-order kinetics) and constancy and low levels of copper concentration in the membrane, show that the kinetic behaviour of metal ion transport through liquid membranes described by a general scheme involving two consecutive irreversible first-order reactions[12] can also be analysed in the steady-state approximation. Therefore, the straight lines of Fig. 1 obey the following equations:[12]

$$R_d = -k_o t + R_{do} \quad (1)$$

$$R_a = +k_o t + R_{ao}, \quad (2)$$

with $R_{ao} = 0$ and k_o in time^{-1} units (here h^{-1}). The corresponding copper ion fluxes are:

$$J_d = \frac{dR_d}{dt} C_{do} = -k_o C_{do} \quad (3)$$

and

$$J_a = \frac{dR_a}{dt} C_{do} = +k_o C_{do}. \quad (4)$$

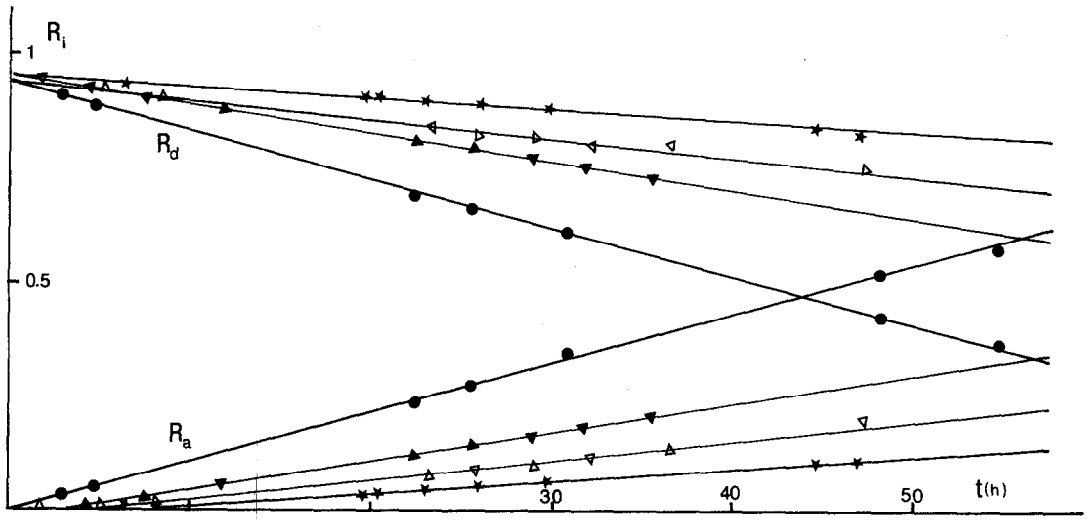

Fig. 1. Steady-state zero-order kinetics of copper(II) ion transport through n-octane(S)–n-tetradecane(Z) binary liquid membranes. R_d and R_a are the relative concentrations of copper(II) ions in the donor and acceptor aqueous phases, respectively. Volume fraction of Z component: $Y_Z = 0$ (●), $Y_Z = 0.3$ (▲), $Y_Z = 0.6$ (△), $Y_Z = 1$ (★).

J_d and J_a are actually the membrane permeation and membrane exit fluxes, respectively. They are given in M h^{-1} units. Since they are standardized to the donor phase volume (V_d), because of the requirements of material balance, they can be obtained also in mol h^{-1} units by simple multiplication by the factor V_d (in L units). Both J_d and J_a are in reality total fluxes crossing the appropriate interface surface area [donor phase/membrane (S_d) and membrane/acceptor phase (S_a), respectively]. Their values in M h^{-1} units are collected in Tables 1 and 2. It can be seen that in each case the two fluxes are identical (i.e. $-J_d = +J_a$) within experimental error, in full agreement with steady-state requirements. It is important to realize that this identity could never have been obtained using the traditional fluxes per unit area (in M h^{-1} cm^{-2} units) on account of the asymmetry of the membranes used (i.e. $S_d \neq S_a$). Fluxes reported to the unit area can satisfy steady-state requirements only in the case of symmetrical membranes.

Tables 1 and 2 also show the relative amounts of copper(II) ions present after 30 h of transport in the donor phase (R_d), membrane phase (R_m) and acceptor phase (R_a). The R_a values show clearly that copper ion transport is rather slow in the investigated systems. In the most favourable cases only *ca* 30% of the copper is transported from the donor to the acceptor phase during the time interval considered. This seems to be due to the high C_{do}/C_{AC} ratio which is necessary to obtain and to maintain zero-order kinetics during the experiments (see above).

(a) *Transport through single component membranes*

Steady-state transport rates were measured through the following pure membranes: n-octane (OC), n-decane (DC), n-dodecane (DD) and n-tetradecane (TD). They are given by the entries of Table 1 corresponding to either $Y_Z = 0$ or $Y_Z = 1$. It can be seen from this table that steady-state fluxes are quite sensitive to the nature of the membrane material, despite the fact that the organic solvents used have similar chemical character. They all belong to the same homologous series of normal chain paraffins.

When the actual flux values in the acceptor phase (J_a) are compared the different solvents can be put into the following order of decreasing transport efficiency: OC > DC > DD > TD. Due to the steady-state conditions the analysis of J_d values leads to the same conclusions as expected. It should be noted that the observed order of transport efficiency is identical to the sequence that was established previously[12] using non-steady-state kinetic analyses. This confirmation raises the question as to the nature of the physicochemical properties which decide transport efficiency. It might be expected that if the rate limiting step of the transport process is diffusion through a thin membrane layer situated between the interface and the bulk of the membrane

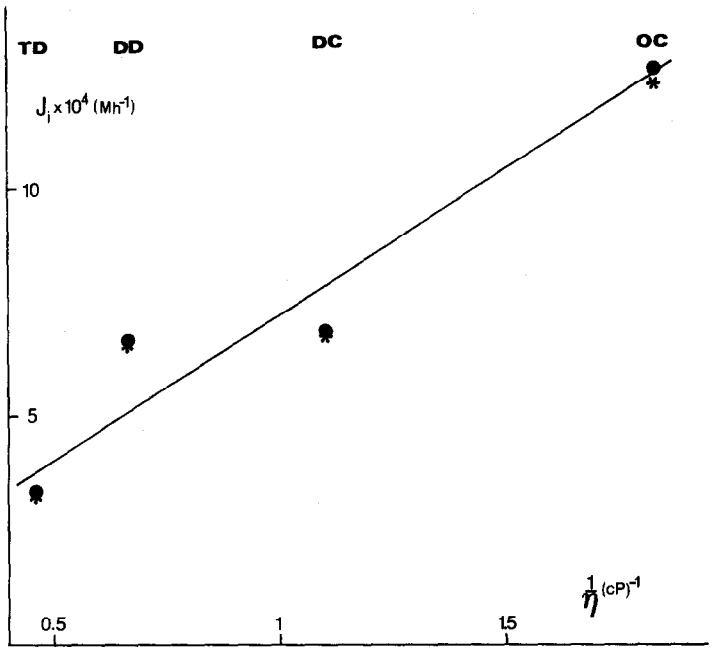

Fig. 2. Variation of membrane permeation, J_d (*), and membrane exit, J_a (●), fluxes with membrane viscosity. OC: n-octane; DC: n-decane; DD: n-dodecane; TD: n-tetradecane.

(as previously, see ref. 12), fluxes should be inversely proportional to the membrane viscosity. Figure 2 shows that this is indeed the case (Tables 1–3). The straight line obtained obeys the following equation:

$$J_a = -(0.077 \pm 0.25)10^{-4} + (0.148 \pm 0.031)10^{-4}\eta^{-1}, \quad (5)$$

with the correlation coefficient $r = 0.9577$ and standard deviation $\sigma = 0.213 \times 10^{-4}$. Therefore, increasing membrane viscosity slows down the transport rate.

Furthermore, molecular interactions between the diffusing metal ion–carrier complex and the membrane molecules, as expressed by membrane material polarity [Kirkwood function $(\varepsilon-1)/(2\varepsilon+1)$] and polarizability $[(n^2-1)/(n^2+2)]$ parameters, should also have a strong influence on transport kinetics. The reason for using the Kirkwood function was explained in a previous paper.[12] When the interaction between the diffusing species and the membrane molecules increases, i.e. when membrane polarity and polarizability increase, the transport rate should decrease if these general solvent effects stabilize the initial state more than the transition state of diffusion. This expectation is fully borne out by the following relationships obtained for the present steady-state kinetics data (Tables 1–3):

$$\ln J_a = (14.242 \pm 1.425) - (0.783 \pm 0.194)[(\varepsilon-1)/(2\varepsilon+1)] \quad (6)$$

with $r = 0.9437$; $\sigma = 0.187$

and

$$\ln J_a = (17.784 \pm 2.78) - (0.979 \pm 0.378)[(n^2-1)/(n^2+2)] \quad (7)$$

with $r = 0.8775$; $\sigma = 0.366$.

However, it should be noted that these relationships are valid only in the first approximation since J_a values are composite quantities[12] and each of their components may be influenced differently by membrane properties.

When the same analysis is made for the permeation flux J_d the same conclusions are obtained as for J_a. This is due, of course, to the steady-state conditions: $|J_d| = |J_a|$ within experimental error.

It is important to emphasize that the conclusions concerning membrane material effects are the same as those obtained for non-steady-state kinetic conditions.[12] This confirms the validity of both approaches to the same transport process. However, non-steady-state analysis appears to be superior to steady-state at the molecular level. As a matter of fact, it was shown previously[12] that permeation rates and membrane exit rates are

Table 3. Physicochemical properties of membrane materials

Y_Z	n_D^{20} [a]	ε [a]	$\frac{n^2-1}{n^2+2}10^2$	$\frac{\varepsilon-1}{2\varepsilon+1}10^2$	Y_Z	d^{20}	η^{20} [a]
			n-dodecane(S)–n-decane(Z)				
1.0	1.4120	2.009	24.88	20.11	1.0	0.7305	0.874
	(1.4120)[b]	(1.993)				(0.7301)	(0.907)
0.8	1.4140	2.000	24.99	20.00	0.705	0.7370	1.003
0.6	1.4159	2.007	25.09	20.08	0.545	0.7401	1.076
0.5	1.4165	2.006	25.12	20.07	0.375	0.7433	1.172
0.4	1.4178	2.033	25.19	20.39	0.286	0.7449	1.220
0.2	1.4198	2.040	25.30	20.47	0.255	0.7455	1.246
0	1.4214	2.037	25.38	20.44	0.155	0.7474	1.311
	(1.4215)	(2.016)			0	0.7498	1.430
						(0.7511)	(1.504)
			n-dodecane(S)–n-tetradecane(Z)				
1.0	1.4289	2.064	25.77	20.75	1.0	0.7678	2.195
	(1.4291)	(2.037)				(0.7624)	(2.180)
0.8	1.4271	2.063	25.68	20.74	0.705	0.7623	1.931
0.6	1.4259	2.063	25.62	20.74	0.545	0.7597	1.793
0.4	1.4242	2.057	25.52	20.67	0.375	0.7566	1.668
0.2	1.4230	2.044	25.46	20.52	0.286	0.7550	1.600
					0.166	0.7528	1.509
			n-dodecane(S)–n-octane(Z)				
1.0	1.3975	1.936	24.11	19.21	1.0	0.7036	0.550
	(1.3975)	(1.948)				(0.7027)	(0.548)
0.8	1.4026	2.009	24.38	20.11	0.660	0.7190	0.708
0.6	1.4071	2.021	24.62	20.25	0.500	0.7260	0.827
0.5	1.4093	2.023	24.74	20.27	0.330	0.7340	0.978
0.4	1.4120	2.035	24.88	20.41	0.250	0.7380	1.070
0.2	1.4165	2.049	25.12	20.58	0.166	0.7417	1.177
			n-octane(S)–n-tetradecane(Z)				
0.8	1.4219	2.054	25.41	20.63	0.705	0.7489	1.373
0.6	1.4167	2.045	25.13	20.53	0.545	0.7385	1.082
0.4	1.4100	2.030	24.78	20.36	0.375	0.7278	0.858
0.2	1.4040	2.007	24.46	20.08	0.286	0.7220	0.760
					0.166	0.7143	0.655

[a] n_D^{20} refractive index; ε dielectric constant; η viscosity (cP); all at $T = 20°C$.
[b] In parentheses literature data; see ref. 12 and references therein.

influenced differently by membrane material effects. This fact could be exploited as a useful diagnosis for the molecular mechanism of the transport process. The very identity of J_d and J_a in steady-state conditions obviously precludes such a possibility.

(b) *Transport through binary membranes*

By mixing different membrane solvents a great variety of physicochemical conditions could be realized with the aim of optimizing transport efficiency. Namely, when one membrane component is gradually replaced by another one the transport rate can be varied in a systematic way (Fig. 1, Table 1). Figures 3–6 represent the variation of steady-state fluxes in the acceptor phase (J_a) with composition of the binary membrane (Y_Z). The volume fraction of the Z membrane component (Y_Z) was determined by the actual membrane composition used in the various experiments.

It can be seen that when the starting membrane material (S) is gradually replaced by another one (Z), different kinds of substitution or stripping profiles are obtained. Adding n-decane (Z) to n-dodecane (S) (Fig. 3) almost no change of kinetic flux is observed, even at complete substitution

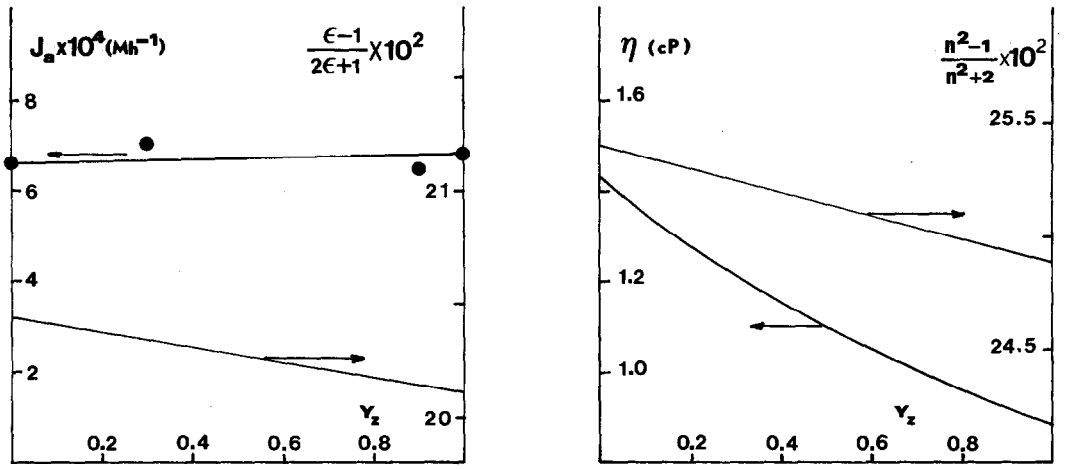

Fig. 3. Stripping profile of membrane exit rate J_a and membrane properties for the system n-dodecane(S)–n-decane(Z).

($Y_Z = 1$). On the other hand, when n-octane is added to the same initial solvent (Fig. 4) a sizeable increase in J_a is observed, while the presence of n-tetradecane brings about a slowing down of the transport process (Fig. 5). In the latter case even a minimum appears on the stripping profile. The greatest decrease of J_a appears when n-octane is substituted by n-tetradecane (Fig. 6).

This great variety of stripping profiles appears rather surprising in the light of the very similar chemical character of the membrane components. It was shown in the case of single component membranes (see above) that increasing membrane viscosity and/or the membrane–metal-carrier complex interactions, as expressed by polarity and polarizability, brings about a decrease in transport rate. Unfortunately, the different linear relationships obtained [eqs (5)–(7)] do not allow us to conclude definitively which property is the dominating factor. In the case of binary membranes the same regularities may be observed. When the stepwise replacement of one membrane component (S) by another (Z) increases the resulting membrane viscosity and the corresponding membrane–metal-carrier interactions, the steady-state fluxes are systematically decreased (Figs 3–6). Furthermore, the comparison of stripping profiles obtained for viscosity, polarizability and polarity (Figs 3–6) shows

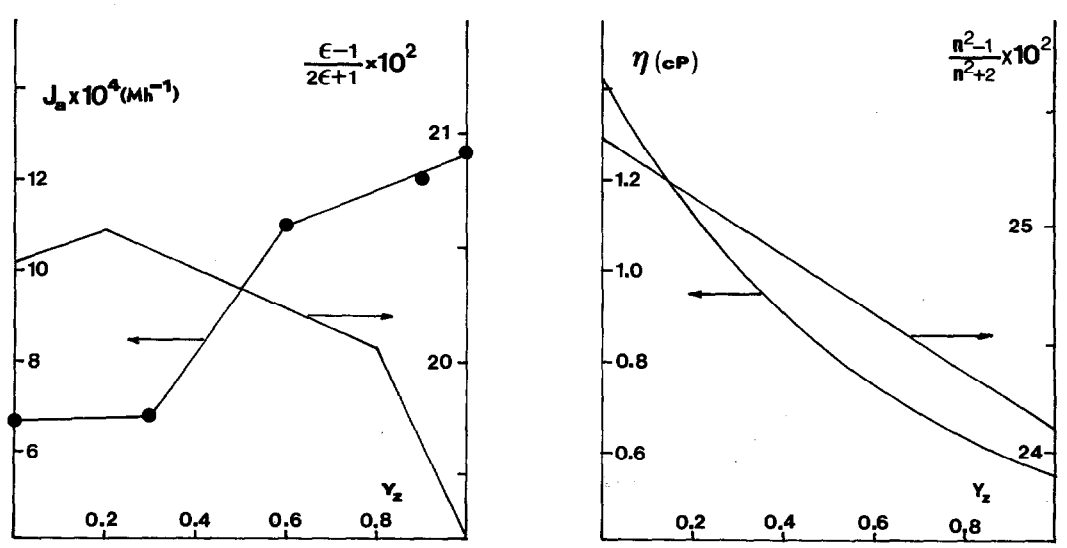

Fig. 4. Stripping profile of membrane exit rate J_a and membrane properties for the system n-dodecane(S)–n-octane(Z).

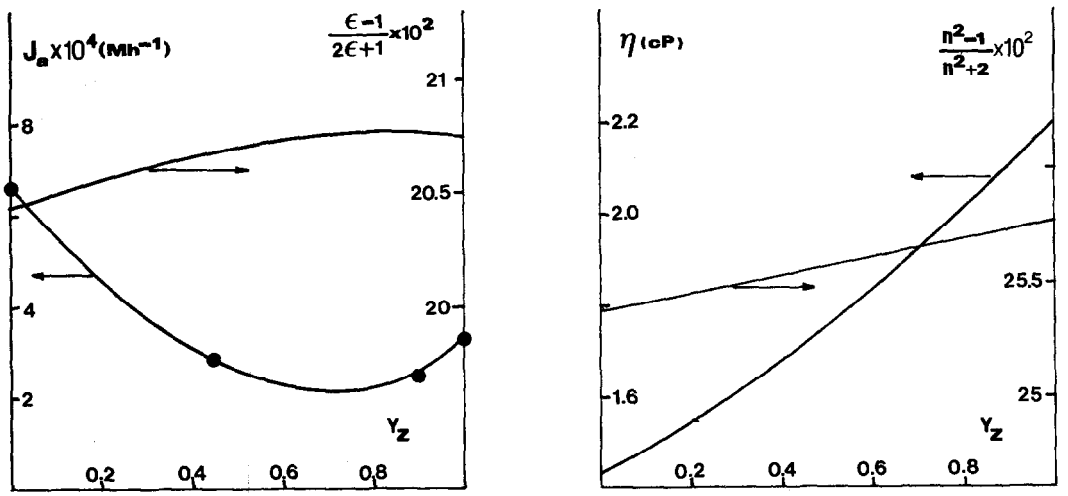

Fig. 5. Stripping profile of membrane exit rate J_a and membrane properties for the system n-dodecane(S)–n-tetradecane(Z).

clearly that only the latter has a profile, the shape of which is roughly the mirror image of the stripping profile obtained for the transport flux J_a. This suggests that the dominating membrane property may be its polarity in determining transport efficiency. This important observation may be interpreted using the following simple model.

It is assumed, in agreement with reaction field theory,[15] that the membrane constitutes a homogeneous, isotropic medium having a bulk dielectric

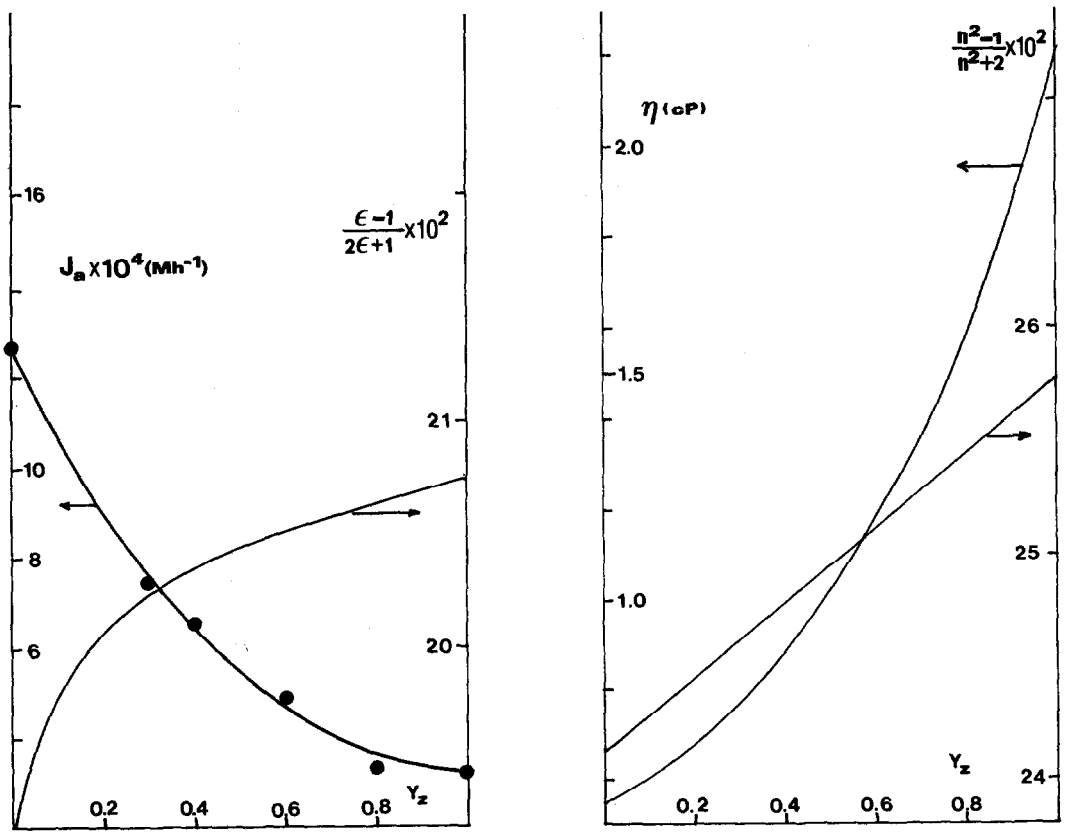

Fig. 6. Stripping profile of membrane exit rate J_a and membrane properties for the system n-octane(S)–n-tetradecane.

constant ε. The solute A, characterized by a permanent (point) dipole μ_A and by a polarizability α_A, sits in the middle of a solvent cavity of radius r. The solute molecule polarizes the solvent cage and as a consequence a reaction field F is produced by the polarized solvent. This reaction field depends directly on solvent polarity through the Kirkwood function (see above). Furthermore, F is composed of an electronic part depending on solvent polarizability[16] and a nuclear part depending on position and orientation of the atoms in the solvent molecules. The actual value of the reaction field is not constant. It is fluctuating in a random way due to the Brownian motion of the solute and solvent molecules. Such a motion may be described by the Langevin equation.[17] When this latter is combined with stochastic considerations (random walk), the following expression may be derived for the translational diffusion coefficient D: $D = kT/f$, where k is the Boltzmann constant, T is the absolute temperature and f represents the so-called friction coefficient opposing the diffusional movement.[18] It can be shown by hydrodynamic considerations[19] that $f = 6\pi r\eta$, where η is the solvent viscosity, leading to the well known Stokes–Einstein formula of the diffusion coefficient: $D = kT/6\pi\eta r$. This formula shows clearly why transport flux diminishes with increasing membrane viscosity. At the molecular level the friction coefficient is nothing other than the time integral of the auto-correlation function of the fluctuating force acting on the solute molecule.[17] We propose that in the present case such a force is created by the fluctuating reaction field F. Recalling that the transport flux J (either steady or non-steady state) is directly proportional to the diffusion coefficient D (Fick's laws), the observed medium dependence of transport fluxes may be easily explained. If the membrane dielectric constant increases the reaction field F also increases and the friction coefficient f becomes greater. However, increasing f decreases the diffusion coefficient D and this brings about a corresponding decrease of the transport flux J in full agreement with the experiment.

Our model also makes clear why polarity is a more important factor than polarizability in defining membrane medium effect on transport rate: polarizability is only part of the total reaction field, determined completely by polarity, and it cannot give a full description of the observed phenomena.

All these considerations confirm our previous hypotheses[12] that the rate determining step of the studied transport kinetics implies a diffusion process across a thin membrane layer situated between the water–membrane interface and the bulk membrane interior.

The regularity of the stripping profile obtained for the n-octane(S)–n-tetradecane(Z) binary membrane system (Fig. 6) suggests that it may be analysed in the light of the competitive preferential solvation (COPS) theory.[10,13,20]

It should be recalled that COPS theory is very useful in evaluating quantitatively solute–solvent interactions.[20] It is based essentially on a virtual microscopic partitioning of the solute in homogeneous media. It is admitted that the components S and Z of a binary solvent mixture compete for solvating the solute A to the extent of their electronic-geometric affinity, $\kappa_{A(S)}$ and $\kappa_{A(Z)}$, respectively. When solvent–solvent interactions may be neglected compared with solute–solvent interactions the solute can be considered as partitioned between the solvent components. Since the latter act independently, the steady-state transport flux J_i through a binary membrane may be written as:

$$J_i = P_{A(S)}J_{i(S)} + P_{A(Z)}J_{i(Z)}. \tag{8}$$

$J_{i(S)}$ and $J_{i(Z)}$ represent membrane permeation (i = d) or membrane exit (i = a) fluxes measured through pure S and pure Z membranes, respectively. $P_{A(S)}$ and $P_{A(Z)}$ are the respective generalized partitioning factors:

$$P_{A(j)} = \frac{\kappa_{A(j)}C_j}{\sum_k \kappa_{A(k)}C_k}, \tag{9}$$

where j = S or Z, k = S and Z, and C_j and C_k are concentrations of components j and k in M units.

Therefore, the COPS equation for the membrane exit flux, J_a, will have the form

$$J_a = \frac{J_{a(S)}\kappa_{A(S)}C_S + J_{a(Z)}\kappa_{A(Z)}C_Z}{\kappa_{A(S)}C_S + \kappa_{A(Z)}C_Z}. \tag{10}$$

Neglecting the eventual volume change of mixing and using the relationship between volume fraction (Y_i) and concentration ($C_i = Y_i v_i^{-1}$, where v_i is the molar volume of component i), the following useful relationship between C_S and C_Z can be obtained:

$$C_S = (1 - v_Z C_Z)/v_S. \tag{11}$$

Substitution of this relationship into eq. (10) leads to the following equation:

$$J_a = \frac{J_{a(S)} + \left[J_{a(Z)}\dfrac{\kappa_{A(Z)}}{\kappa_{A(S)}}v_S - J_{a(S)}v_Z\right]C_Z}{1 + \left[\dfrac{\kappa_{A(Z)}}{\kappa_{A(S)}}v_S - v_Z\right]C_Z}, \tag{12}$$

which may be used to describe the substitution (or stripping) profiles.

The quantity $\kappa_{A(Z)}/\kappa_{A(S)}$ appearing in this equation

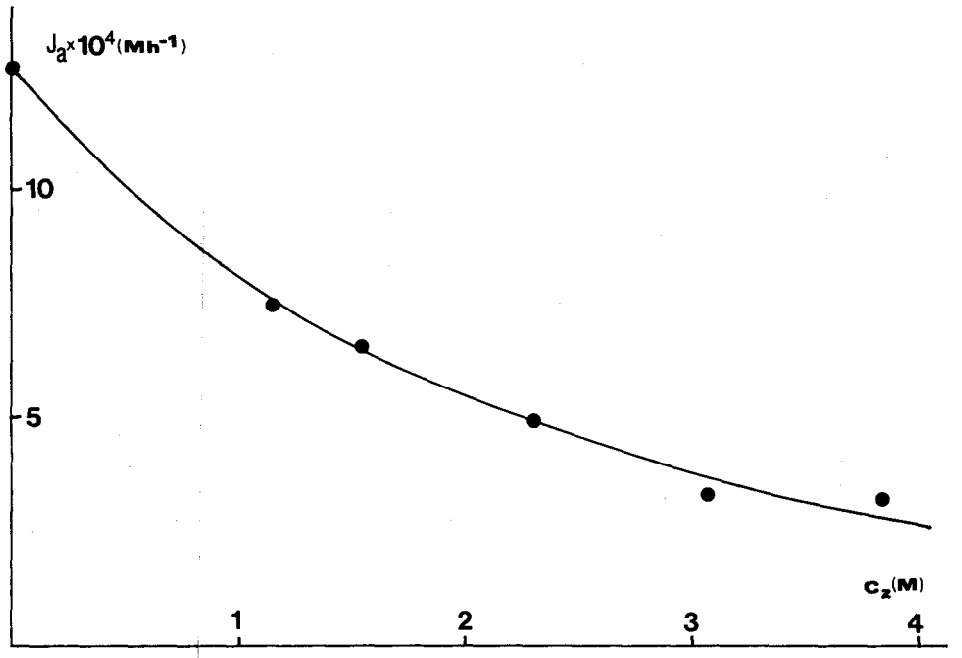

Fig. 7. Stripping profile for membrane exit flux J_a in the case of n-octane(S)–n-tetradecane(Z) binary membrane (experimental conditions I). The theoretical curve was calculated from the data of Tables 2 and 5 using eq. (12).

is the affinity constant ratio.[20] It accounts quantitatively for the solute (A = copper(II)–carrier complex)–solvent (membrane components S and Z) interactions. Its graphical determination may be realized using a Scatchard-type linearized form of eq. (12):

$$\frac{J_{a(S)}-J_a}{C_Z} = (J_{a(S)}-J_{a(Z)})\frac{\kappa_{A(Z)}}{\kappa_{A(S)}}v_S - \left[\frac{\kappa_{A(Z)}}{\kappa_{A(S)}}v_S - v_Z\right](J_{a(S)}-J_a). \quad (13)$$

The results of the stripping experiments realized for the n-octane(S)–n-tetradecane(Z) binary membrane in two different experimental conditions are collected in Table 2 and Fig. 7. Details of COPS theory calculations are given in Table 4. As an example, Table 5 and Fig. 8 show that the linear equation [eq. (13)] is obeyed in the full concentration range, in agreement with all the previous results.[10,13,20] The final results obtained from the COPS theoretical analysis are given in Table 6. It can be seen from the obtained affinity constant ratios that n-tetradecane interacts with the copper(II)–carrier complex about four times stronger than n-octane, independently of the exper-

Table 4. Application of COPS theory to copper(II) ion transport through n-octane(S)–n-tetradecane(Z) binary liquid membranes of variable compositions (steady-state kinetics; experimental conditions I of Table 2). Molar volumes of membrane components:[12] $v_S = 0.1625\ M^{-1}$ and $v_Z = 0.2602\ M^{-1}$

No.	Y_Z	C_Z (M)	$(J_{d(S)}-J_d)\times 10^4$ (M h^{-1})	$\frac{J_{d(S)}-J_d}{C_Z}\times 10^4$ (h^{-1})	$(J_{a(S)}-J_a)\times 10^4$ (M h^{-1})	$\frac{J_{a(S)}-J_a}{C_Z}\times 10^4$ (h^{-1})
2	0.3	1.1529	5.16	4.48	5.22	4.53
3	0.4	1.5373	5.82	3.79	6.09	3.96
4	0.6	2.3059	7.62	3.30	7.76	3.36
5	0.8	3.0745	8.97	2.92	9.39	3.05
6	1.0	3.8432	9.13	2.38	9.42	2.45

Table 5. Analytical equations obtained for the Scatchard linearization of stripping profiles of the n-octane(S)–n-tetradecane(Z) binary liquid membrane: $y = ax+b$ [eq. (17)]

y	x	Experimental conditions	a	$b\times10^4$	r^a	$\sigma\times10^{4b}$
$\frac{J_{d(S)}-J_d}{C_Z}\times10^4$	$(J_{d(S)}-J_d)\times10^4$	I	-0.429 ± 0.071	6.521 ± 0.538	0.9606	0.258
		II	-0.504 ± 0.131	5.136 ± 0.698	0.8877	0.314
$\frac{J_{a(S)}-J_a}{C_Z}\times10^4$	$(J_{a(S)}-J_a)\times10^4$	I	-0.406 ± 0.067	6.545 ± 0.526	0.9606	0.258
		II	-0.718 ± 0.155	6.769 ± 0.886	0.9182	0.336

[a] Correlation coefficient.
[b] Standard deviation.

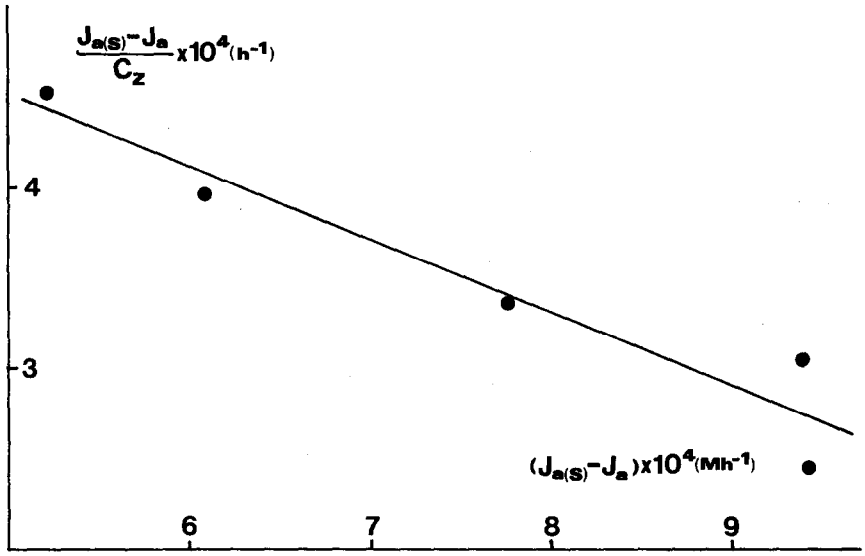

Fig. 8. Linearization by COPS theory of the stripping profile of membrane exit flux J_a in the case of n-octane(S)–n-tetradecane(Z) binary liquid membrane (experimental conditions I). Least-squares analysis by eq. (13).

Table 6. Steady-state transport kinetic parameters obtained from COPS theory for the n-octane(S)–n-tetradecane(Z) binary liquid membrane system

Flux	Experimental conditions[a]	$\frac{\kappa_{A(Z)}}{\kappa_{A(S)}}$	$(J_{d(S)}-J_{d(Z)})\times10^{4b}$ ($M\,h^{-1}$)	$(J_{a(S)}-J_{a(Z)})\times10^{4b}$ ($M\,h^{-1}$)	v_Z (M^{-1})
J_d	I	4.2	9.46(9.13)[c]	—	0.2852
	II	4.7	6.72(6.71)[c]	—	0.2614
J_a	I	4.1	—	9.83(9.42)[c]	0.2891
	II	6.0	—	6.92(6.99)[c]	0.2493
					(0.2602)[d]

[a] See Experimental.
[b] $J_{i(S)}$ and $J_{i(Z)}$ are fluxes J_i in pure S (n-octane) and in pure Z (n-tetradecane) membrane components, respectively.
[c] Directly measured values in pure S and Z.
[d] Literature value for Z component molar volume.[12]

imental conditions and the transport fluxes (J_d or J_a) used for their determination. This confirms and supports the conclusion above that more strongly interacting membranes slow down the transport rate [eqs (6) and (7)].

The validity of the COPS equation can also be firmly established from the fact that the calculated differences between fluxes characterizing pure membrane components (e.g. $J_{a(S)}-J_{a(Z)}$) are identical, within experimental errors, to the directly measured values. Furthermore, COPS theory can also be used to determine the molar volume of the component $Z(v_Z)$. As a matter of fact, if the linear COPS equation [eq. (13)] is valid the following formula can be used to predict v_Z values:

$$v_Z = \frac{\text{intercept of eq. (13)}}{J_{a(S)}-J_{a(Z)}} - \text{slope of eq. (13)}. \quad (14)$$

Here $(J_{a(S)}-J_{a(Z)})$ represents the directly measured flux difference. Table 6 shows that the calculated v_Z values are in fairly good agreement with the official values reported in the literature. Let us note finally that the coherence of COPS parameters (Table 6) is demonstrated by the fact that when they are substituted into eq. (12) they allow the correct reproduction of the experimental stripping profile (Fig. 7).

CONCLUSIONS

The present study allows us to draw the important conclusion that, notwithstanding the approach (steady state or non-steady state) used to analyse the transport kinetics,[21] the same general conclusions can be obtained for the physicochemical mechanism of action and transport efficiency of mono and binary liquid membranes.

Acknowledgements—This work was produced within the Belgian–Polish Cultural and Scientific Exchange Programme and was supported by funds from Politechnika Gdańska and partially by a grant from KBN, Warsaw. We thank Acorga Ltd for the generous gift of the carrier acorga P50 used in the transport experiments.

REFERENCES

1. M. Mulder, *Basic Principles of Membrane Technology*. Kluwer Academic Publishers, London (1991).
2. R. D. Noble and J. D. Way, in *Liquid Membranes* (Edited by R. D. Noble and J. D. Way). American Chemical Society Symposium Series, No. 347, Washington, DC (1987).
3. B. M. Kim, *AIChE Symp. Series* 1985, **81**, 127.
4. L. L. Tavlarides, J. H. Bae and C. K. Lee, *Sep. Sci. Tech.* 1987, **22**, 581.
5. E. L. Cussler, *AIChE* 1971, **17**, 1300.
6. R. Schügerl, A. Mohrmann, W. Gutknecht and H. B. Hanertmann, *Desalination* 1985, **53**, 197.
7. M. Ruppert, J. Draxler and R. Marr, *Sep. Sci. Tech.* 1988, **23**, 1659.
8. A. Narebska, R. Wódzki and A. Wyszyńska, *Makromol. Chem.* 1989, **190**, 1501.
9. P. R. Danesi, L. Reichley-Yinger and P. G. Rickert, *J. Membrane Sci.* 1987, **31**, 117.
10. M. Szpakowska and O. B.Nagy, *J. Phys. Chem.* 1989, **93**, 3851.
11. M. Szpakowska and O. B.Nagy, *Bull. Soc. Chim. Belg.* 1990, **99**, 243.
12. M. Szpakowska and O. B.Nagy, *J. Membrane Sci.* 1991, **64**, 129.
13. M. Szpakowska and O. B.Nagy, *Bull. Soc. Chim. Belg.* 1990, **99**, 889.
14. H. Strzelecki (Editor), *Ćwiczenia Laboratoryjne z Chemii Fizycznej*. PWN, Gdańsk (1985).
15. L. Onsager, *J. Am. Chem. Soc.* 1936, **58**, 1486.
16. W. Liptay, in *Modern Quantum Chemistry* (Edited by O. Sinanoglu), Vol. II, p. 173. Academic Press, New York (1965).
17. C. A. Croxton, *Liquid State Physics*, p. 289. Cambridge University Press, Cambridge (1974).
18. W. H. Flygare, *Molecular Structure and Dynamics*, p. 532. Prentice-Hall, Englewood Cliffs, NJ (1978).
19. R. S. Berry, S. A. Rice and J. Ross, *Physical Chemistry*, p. 1104. Wiley, New York (1980).
20. O. B.Nagy, M. waMuanda and J. B.Nagy, *J. Chem. Soc., Faraday Trans. 1* 1978, **74**, 2210.
21. M. Szpakowska and O. B.Nagy, *J. Membrane Sci.* 1993, **76**, 27.
22. T. M. Fyles, V. A. Malik-Diemer and D. M. Whitfield, *Can. J. Chem.* 1981, **59**, 1734.

Polyhedron Vol. 12, No. 11, pp. 1289–1294, 1993
Printed in Great Britain

0277–5387/93 $6.00+.00
© 1993 Pergamon Press Ltd

ORGANOAMIDO- AND ARYLOXO-LANTHANIDES—VII.* THE X-RAY STRUCTURE OF FIVE-COORDINATE $[La(OC_6H_3Ph_2\text{-}2,6)_3(THF)_2]\cdot THF$

G. B. DEACON,† B. M. GATEHOUSE, Q. SHEN‡ and G. N. WARD

Chemistry Department, Monash University, Clayton, Victoria 3168, Australia

and

E. R. T. TIEKINK

Jordan Laboratories, Department of Physical and Inorganic Chemistry, University of Adelaide, Adelaide, South Australia 5001, Australia

(*Received* 4 *January* 1993; *accepted* 18 *February* 1993)

Abstract—The X-ray crystal structure of $[La(Odpp)_3(THF)_2]\cdot THF$ (Odpp = $OC_6H_3Ph_2$-2,6), prepared by reaction of lanthanum metal, bis(pentafluorophenyl)mercury and 2,6-diphenylphenol in THF, shows distorted trigonal-bipyramidal stereochemistry for lanthanum. A phenolate oxygen [La—O 2.25(1) Å] and a THF oxygen [La—O 2.68(2) Å] occupy apical positions [O—La—O 165.9(4)°], whilst two phenolate oxygens [La—O 2.25(1), 2.234(9) Å] and a THF oxygen [La—O 2.52(1) Å] occupy trigonal positions [O—La—O 122.1(4), 124.8(5), 96.5(6)°]. The apical La—O(THF) distance is exceptionally and unexpectedly long. Unit cell data for $[Nd(Odpp)_3(THF)_2]\cdot THF$ suggest that it is isostructural with the lanthanum compound.

The effect of lanthanide ion contraction (*ca* 0.2 Å from La^{3+} to Lu^{3+})[1] on the coordination number and stereochemistry of lanthanide complexes is of considerable interest.[2] Although the larger lanthanides might be expected to favour higher coordination numbers than the smaller elements, the observed effects are quite variable. Thus, determination of the structures of 10 $LnCp_3(THF)$ ($Cp = \eta^5$-cyclopentadienyl, Ln = Y,[3] La,[3] Ce,[4] Pr,[5] Nd,[5,6] Sm,[7] Gd,[8] Dy,[9] Yb,[10] Lu[11]) complexes has shown all to be isostructural with pseudo-tetrahedral 10-coordination for the lanthanide. By contrast, $LnCp_3$ structures show a gradation from 11-coordination (Ln = La,[12] Pr[13]) through 10-(Ln = Er, Tm[14]) and nine-coordination (Ln = Yb[15]) to eight-coordination (Ln = Lu[16]). We recently reported the structure of $[Yb(Odpp)_3(THF)_2]\cdot THF$ (Odpp = $OC_6H_3Ph_2$-2,6), which shows distorted square pyramidal, five-coordination for ytterbium,[17] the unusually low coordination number for the lanthanide[2] being stabilized by the bulky 2,6-diphenylphenolate ligands. To examine the effect of lanthanide ion size on structures of complexes of this ligand we have now determined the X-ray structure of the THF complex of lanthanum 2,6-diphenylphenolate.

RESULTS AND DISCUSSION

The reaction of lanthanum metal with bis(pentafluorophenyl)mercury and 2,6-diphenylphenol in THF yielded the THF complex of lanthanum 2,6-diphenylphenolate.

$$2La + 3Hg(C_6F_5)_2 + 6HOdpp \longrightarrow 2La(Odpp)_3 + 3Hg\downarrow + 6C_6F_5H \quad (1)$$

This synthetic route has previously been used for heavier lanthanide 2,6-diphenylphenolates.[17] It can be rationalized as a redox transmetallation (2)

* Part VI, *Angew. Chem.*, in press.

† Author to whom correspondence should be addressed.

‡ Present address: Changchun Institute of Applied Chemistry, Chinese Academy of Sciences, Changchun 130022, P.R.C.

between the metal and $Hg(C_6F_5)_2$, giving $La(C_6F_5)_3$ which is trapped by protolytic ligand exchange (3) with the phenol.

$$2La + 3Hg(C_6F_5)_2 \longrightarrow 2La(C_6F_5)_3 + 3Hg\downarrow \quad (2)$$

$$La(C_6F_5)_3 + 3HOdpp \longrightarrow La(Odpp)_3 + 3C_6F_5H \quad (3)$$

Alternatively, initial redox transmetallation giving $La(C_6F_5)$ may be followed by a rapid series of ligand exchange and redox reactions through e.g. La(Odpp), $La(Odpp)C_6F_5$, $La(Odpp)_2$, etc. Protolytic ligand exchange is favoured by the greater acidity of 2,6-diphenylphenol (phenols have pK *ca* 10)[18] than pentafluorobenzene (pK 25.6 in THF, derived[19] from the value in cyclohexylamine[20] by the method of Streitwieser[21]).

The IR spectrum of the product showed no ν(OH) absorptions, consistent with the formation of a phenolato complex, and was similar to spectra of reported 2,6-diphenylphenolates.[17] No unambiguous information concerning coordination of THF can be derived from the IR spectrum owing to significant absorption of the phenolate ligand in the relevant regions. Although single crystals of the complex had the composition $[La(Odpp)_3(THF)_2]\cdot THF$, the ^1H NMR spectrum of the crystals gave a THF:Odpp ratio of 4:3. Preservation of the crystals for X-ray crystallography precluded drying and it is possible that some free THF was retained, and it is of interest that a microanalysis was marginally closer to the calculated figures for $La(Odpp)_3\cdot 4THF$ than $La(Odpp)_3\cdot 3THF$. Alternatively, the use of d_8-toluene as an NMR solvent may have led to the slight precipitation of a species with a THF:Odpp ratio $< 1:1$, leaving a higher ratio in solution. Dissolution of $Yb(C_5H_4PPh_2)_2(THF)_2$ in toluene is followed by deposition of $Yb(C_5H_4PPh_2)_2(THF)$.[22]

X-ray crystal structure

The structure of the complex $[La(Odpp)_3(THF)_2]\cdot THF$ is displayed in Fig. 1. Selected bond distances and angles are given in Table 1, together with analogous data[17] for $[Yb(Odpp)_3(THF)_2]\cdot THF$. Lanthanum is five-coordinate with distorted trigonal bipyramidal stereochemistry, in contrast to the distorted square pyramidal arrangement in the ytterbium complex. In particular, there is only one near linear O—La—O angle [165.9(4)°, next nearest 124.8(5)°], whereas there are O—Yb—O angles of 147.8(3)° and 151.8(3)° for $[Yb(Odpp)_3(THF)_2]\cdot THF$. The lanthanum complex has apical phenolate and THF ligands, with two phenolates and one THF in the trigonal plane (Fig. 1). There is no significant difference in the La—Odpp distances, despite the different environments for the Odpp ligands. By contrast, the apical La—O(THF) distance is appreciably lengthened (0.16 Å) over the equatorial La—O(THF) bond. In the ytterbium complex the O(THF) donor atoms are *trans* and the

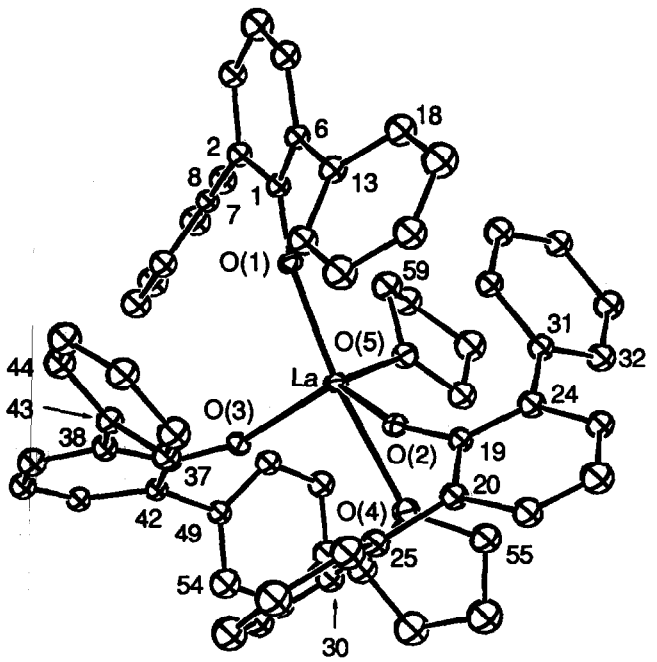

Fig. 1. Crystal structure of $[La(Odpp)_3(THF)_2]\cdot THF$.

Table 1. Selected bond distances (Å) and angles (°) for $[Ln(Odpp)_3(THF)_2]\cdot THF$ (Ln = La or Yb)

$[La(Odpp)_3(THF)_2]\cdot THF$		$[Yb(Odpp)_3(THF)_2]\cdot THF$[17]	
La—O(1)	2.25(1)	Yb—O(1)	2.038(7)
La—O(2)	2.25(1)	Yb—O(2)	2.111(8)
La—O(3)	2.234(9)	Yb—O(3)	2.084(9)
La—O(4)	2.68(2)	Yb—O(4)	2.305(7)
La—O(5)	2.52(1)	Yb—O(5)	2.305(8)
O(1)—C(1)	1.34(2)[a]	O(1)—C(1)	1.34(1)[a]
O(2)—C(19)	1.33(2)[a]	O(2)—C(7)	1.33(2)[a]
O(3)—C(37)	1.27(2)[a]	O(3)—C(13)	1.32(2)[a]
O(1)—La—O(2)	114.7(5)	O(1)—Yb—O(2)	108.6(3)
O(1)—La—O(3)	101.0(7)	O(1)—Yb—O(3)	103.5(3)
O(1)—La—O(4)	165.9(4)	O(1)—Yb—O(4)	110.2(3)
O(1)—La—O(5)	91.5(5)	O(1)—Yb—O(5)	98.0(3)
O(2)—La—O(3)	122.1(4)	O(2)—Yb—O(3)	147.8(3)
O(2)—La—O(4)	75.1(4)	O(2)—Yb—O(4)	87.7(3)
O(2)—La—O(5)	124.8(5)	O(2)—Yb—O(5)	82.1(3)
O(3)—La—O(4)	80.5(7)	O(3)—Yb—O(4)	83.2(3)
O(3)—La—O(5)	96.5(6)	O(3)—Yb—O(5)	91.6(3)
O(4)—La—O(5)	74.4(5)	O(4)—Yb—O(5)	151.8(3)
C(1)—O(1)—La	169(1)[a]	C(1)—O(1)—Yb	168.2(7)[a]
C(19)—O(2)—La	154(1)[a]	C(7)—O(2)—Yb	167.9(7)[a]
C(37)—O(3)—La	164(2)[a]	C(13)—O(3)—Yb	164.4(7)[a]

[a] Beyond the donor atoms, the numbering scheme is different for the two compounds.

Yb—O(THF) bond lengths are equal, whereas there is some variation (0.07 Å) in the Yb—Odpp lengths (Table 1) with the longer bonds in the square plane. The stereochemical arrangement in $[La(Odpp)_3(THF)_2]\cdot THF$ is similar to that of distorted trigonal bipyramidal $[Ce(OC_6H_3Bu^t_2\text{-}2,6)_3(CNBu^t)_2]$, which has apical aryloxide and t-butyl isocyanide ligands.[23] In particular, the O—Ce—C angle for the apical donor atoms is 161.4(3)°. However, there is much less variation between apical and planar Ce—C distances (0.045 Å) than between corresponding La—O(THF) distances. The average La—O(Ar) distance (2.24 Å) corresponds closely to ⟨Ce—O(Ar)⟩ (2.23 Å). This is consistent with the small difference (0.02 Å)[1] in ionic radii for La^{3+} and Ce^{3+} with the same coordination number. Further, ⟨La—Odpp⟩ exceeds ⟨La—$OCPh_3$⟩ (2.18 Å) for the terminal La—O bonds of $La_2(OCPh_3)_6$[24] by an amount (0.06 Å) reasonable (see ref. 1) for the difference in ionic radii between five- and four-coordinate La^{3+}.

Subtraction of an ionic radius for five-coordinate La^{3+} (0.96 Å) (derived from extrapolation of data for higher coordination numbers[1]) from ⟨La—O(Ar)⟩ gives 1.28 Å, a value consistent with 1.27 Å similarly derived from ⟨Yb—O(Ar)⟩ of $[Yb(Odpp)_3(THF)_2]\cdot THF$,[17] and with values from analogous subtractions for a variety of low-coordinate lanthanide(II or III) aryloxides.[25] The distance (1.56 Å) from subtraction of the lanthanum five-coordinate radius from La—O(5) is much larger than usual values [1.34(5) Å] for lanthanide-ether complexes,[26] but is within the range (1.48–1.59 Å) for THF complexes of bulky lanthanide phenolates.[25] However, a similar subtraction for La—O(4) gives the exceptionally large 1.72 Å, indicating that the apical THF is very weakly bound. Indeed, without this THF ligand there is a plausible distorted tetrahedral $[La(Odpp)_3(THF)]$ species, in which the bond distances are only slightly longer (*ca* 0.03–0.05 Å) than reasonable values for four-coordinate lanthanum. The abnormal length of La—O(4), in contrast to the Yb—O(THF) bonds of $[Yb(Odpp)_3(THF)_2]\cdot THF$, is surprising since steric repulsion should be lower for La^{3+} than the smaller Yb^{3+}. Possibly, the apical 2,6-diphenylphenolate strongly repels (electronically and sterically) the transoid THF ligand, whereas no THF is *trans* to Odpp in the ytterbium complex.[17] It is of interest that the two mutually *trans* Odpp ligands of $[Yb(Odpp)_3(THF)_2]\cdot THF$ are bound more weakly than the apical Odpp (Table 1). In $[Ce(OC_6H_3Bu^t_2\text{-}$

$2,6)_3(CNBu^t)_2]$ elongation of the apical Ce—C bond is far less marked (above). Steric repulsion by THF is likely to be greater than by an isonitrile, even one with a bulky alkyl group, because of the spear-like nature of the latter.

The steric coordination number[27]* of Odpp (1.9), determined from X-ray data for $[Yb(Odpp)_3(THF)_2]\cdot THF$, is intermediate between those of 2,6-di-i-propylphenolate (1.7) and 2,6-di-t-butylphenolate (2.4). Thus, the sum of the steric coordination numbers of the ligands in $[La(Odpp)_3(THF)_2]\cdot THF$ is 8.1, indicative[25] of a high degree of crowding.

The C—O distances of the phenolate ligands are substantially reduced from single bond lengths, reflecting substantial delocalization from oxygen into the aromatic rings; this effect being enhanced by the essentially ionic character of the lanthanum–oxygen bonds. In addition, these bonds are consistently shorter [⟨C—O(Ar)⟩ 1.31 Å], as are those of the Yb analogue [⟨C—O(Ar)⟩ 1.33 Å], than ⟨C—O(Ar)⟩ (1.38 Å) of $[Yb(OC_6H_2Bu^t_3\text{-}2,4,6)_3 THF]$.[17] This can be attributed to the electron-withdrawing effect of the phenyl substituents.

Unit cell data for $[Nd(Odpp)_3(THF)_2]\cdot THF$ (see Experimental) are similar to those of the title lanthanum complex and very different from those of the Yb analogue, hence the Nd and La complexes are probably isostructural. Similarities between the properties of complexes of lighter lanthanides, e.g. La and Nd, are common.[28]

Thus, increasing the lanthanide ion size in $Ln(Odpp)_3(THF)_n$ complexes does not result in an increase in coordination number. Rather, there is a change from square-pyramidal stereochemistry to a trigonal bipyramidal arrangement with one elongated bond.

EXPERIMENTAL

General

The lanthanide phenolates are air- and moisture-sensitive and were handled under purified nitrogen or argon. Handling methods, gas and solvent purification and analytical methods were as reported previously.[19,29–32] IR spectra are of Nujol mulls for the region 4000–650 cm^{-1}. The ^1H NMR spectrum was recorded for a solution in C_7D_8 and chemical shifts are in ppm downfield from internal tetramethylsilane. Lanthanum metal (REACTON Grade) was from Johnson–Matthey Rare Earth Products. Bis(pentafluorophenyl)mercury was obtained by the reported method.[33] 2,6-Diphenylphenol was from Aldrich.

Tris(2,6-diphenylphenolato)bis(tetrahydrofuran)lanthanum(III)-tetrahydrofuran (1/1)

Lanthanum powder (0.52 g, 3.7 mmol), 2,6-diphenylphenol (0.38 g, 1.5 mmol) and bis(pentafluorophenyl)mercury (0.40 g, 0.75 mmol) were stirred in dry THF at room temperature under purified nitrogen. After 1 day, two drops of mercury metal were added to promote the reaction. Following stirring for 4 days the reaction mixture was filtered through a celite pad. The yellow filtrate was concentrated *in vacuo*. Cooling at −20°C for several days gave elongated tubular, light yellow–gold crystals of the title compound (yield 60%). Found: C, 71.5; H, 6.1. Calc. for $C_{66}H_{63}LaO_6$: C, 72.6; H, 5.8%. Calc. for $C_{70}H_{71}LaO_7$ ($La(Odpp)_3(THF)_4$): C, 72.2; H, 6.2%. IR: 1595m, 1495m, 1404m, 1307m, 1281m, 1260s, 1174w, 1086m, 1064m, 1025m, 966w, 914w, 855s, 753s and 703s cm^{-1}. ^1H NMR: 1.13, m, 16H, CH_2C; 3.09, m, 16H, CH_2O; 6.73, m, 11H aromatic; 6.93, m, 22H, aromatic; 7.13, d, 6H, aromatic. Single crystals of the complex were present in the isolated crystalline product. Crystals suitable for X-ray study were sealed in Lindeman glass capillaries under argon in a recirculating atmosphere dry-box.

Tris(2,6-diphenylphenolato)bis(tetrahydrofuran)neodymium(III)-tetrahydrofuran (1/1)

The complex was prepared by the method reported for $[Nd(Odpp)_3(THF)_2]$,[17] but crystals obtained from cooling the filtered, partly evaporated reaction mixture were not dried under vacuum (which gives $[Nd(Odpp)_3(THF)_2]$ as a powder[17]). Suitable crystals were mounted for X-ray examination as for the La analogue.

X-ray crystallography

Intensity data for a multifaceted transparent crystal of $[La(Odpp)_3(THF)_2]\cdot THF$, with the dimensions $0.1\times0.1\times0.3$ mm mounted in a glass capillary, were measured at room temperature on an Enraf–Nonius CAD4F diffractometer fitted with Mo-K_α radiation, $\lambda = 0.7107$ Å (graphite monochromator). The ω–2θ scan technique was employed to measure 4225 data to a maximum Bragg angle of 22.5°. Significant decomposition of the crystal occurred during the data collection, as

* This provides an estimate of the steric demands of a ligand relative to chloride as 1.0, and is based on the solid angle comprising the van der Waals radii of all atoms of the ligand.[27]

evidenced by the linear decrease in the net values (to *ca* 90% of their original values) of two intensity standards monitored every 7600 s of X-ray exposure time. The data set was corrected for this intensity variation, Lorentz and polarization effects, but not for absorption. Of the reflections measured 3994 were unique and 2007 satisfied the $I \geqslant 2.5\sigma(I)$ criterion and were used in the subsequent analysis. $[La(Odpp)_3(THF)_2]\cdot THF$, $C_{66}H_{63}LaO_6$, $M = 1091.1$, monoclinic, space group $P2_1$, $a = 10.231(3)$, $b = 22.000(3)$, $c = 13.390(4)$ Å, $\beta = 100.76(3)°$, $V = 2960.9$ Å^3, $Z = 2$, $D_c = 1.224$ g cm^{-3}, $F(000) = 1128$, $\mu = 7.43$ cm^{-1}.

The structure was solved by the interpretation of the Patterson synthesis and refined by a full-matrix least-squares procedure based on F.[34] The lanthanum and oxygen atoms were refined with anisotropic thermal parameters and the C_6H_5 groups were refined as hexagonal rigid groups; hydrogen atoms were included in the model at their calculated positions (C—H 0.97 Å). After the inclusion of a weighting scheme of the form $w = [\sigma^2(F)+gF^2]^{-1}$ the refinement was continued until convergence, when $R = 0.061$, $g = 0.0093$ and $R_w = 0.063$. The analysis of variance showed no special features and the maximum residual electron density peak in the final difference map was 0.69 e Å^{-3}. The absolute configuration of the structure was determined on the basis of differences in high-angle Friedel pairs included in the data set. The molecular structure and numbering scheme are shown in Fig. 1, which was drawn with ORTEP[35] at 15% probability ellipsoids. Structure solution and refinement were performed with the SHELX76 program installed on a SUN 4/280 computer. Scattering factors (corrected for f' and f'') for neutral lanthanum were from ref. 36 and those for the remaining atoms were as incorporated in SHELX76.[34] Fractional atomic coordinates, complete lists of bond distances, bond angles, thermal parameters, hydrogen atom parameters and structure–factor tables are available from the Editor and the atomic coordinates have also been deposited with the Cambridge Crystallographic Data Centre.

Unit cell data for $[Nd(Odpp)_3(THF)_2]\cdot THF$

$a = 10.149$, $b = 21.839$, $c = 13.192$ Å, $\beta = 100.51°$, measured with a Philips PW1100 diffractometer.

Acknowledgements—We are grateful to the Australian Research Council for support, to the Australian Academy of Science for an exchange visit by Q.S. and to Prof. J. Marçalo, ICEN-LNETI, Portugal, for calculation of the steric coordination number of Odpp.

REFERENCES

1. R. D. Shannon, *Acta Cryst., Sect. A* 1976, **32**, 751.
2. F. A. Hart, in *Comprehensive Coordination Chemistry* (Edited by G. Wilkinson, R. D. Gillard and J. A. McCleverty), Vol. 3, Ch. 39. Pergamon Press, Oxford (1987).
3. R. D. Rogers, J. L. Atwood, A. Emad, D. J. Sikora and M. D. Rausch, *J. Organomet. Chem.* 1981, **216**, 383.
4. P. S. Gradeff, K. Yunlu, T. J. Deming, J. M. Olofson, J. W. Ziller and W. J. Evans, *Inorg. Chem.* 1989, **28**, 2600.
5. Y. Fan, P. Lu, Z. Jin and W. Chen, *Sci. Sin., Ser. B. (Engl. Ed.)* 1984, **27**, 993.
6. F. Benetollo, G. Bombieri, C. B. Castellani, W. Jahn and R. D. Fischer, *Inorg. Chim. Acta* 1984, **95**, L7.
7. G. B. Deacon, A. J. Koplick and T. D. Tuong, *Aust. J. Chem.* 1984, **37**, 517.
8. R. D. Rogers, R. Vann Bynum and J. L. Atwood, *J. Organomet. Chem.* 1980, **192**, 65.
9. R. Maier, B. Kanellakopulos, C. Apostolidis and B. Nuber, *J. Organomet. Chem.* 1992, **435**, 275.
10. W. J. Evans, D. K. Drummond, L. R. Chamberlain, R. J. Doedens, S. G. Bott, H. Zhang and J. L. Atwood, *J. Am. Chem. Soc.* 1988, **110**, 4983.
11. C. Ni, D. Deng and C. Qian, *Inorg. Chim. Acta* 1985, **110**, L7.
12. S. H. Eggers, J. Kopf and R. D. Fischer, *Organometallics* 1986, **5**, 383.
13. W. Hinrichs, D. Melzer, M. Rewoldt, W. Jahn and R. D. Fischer, *J. Organomet. Chem.* 1983, **251**, 299.
14. S. H. Eggers, W. Hinrichs, J. Kopf, W. Jahn and R. D. Fischer, *J. Organomet. Chem.* 1986, **311**, 313.
15. S. H. Eggers, J. Kopf and R. D. Fischer, *Acta Cryst.* 1987, **C43**, 2288.
16. S. H. Eggers, H. Schultze, J. Kopf and R. D. Fischer, *Angew. Chem., Int. Edn Engl.* 1986, **25**, 656.
17. G. B. Deacon, S. Nickel, P. MacKinnon and E. R. T. Tiekink, *Aust. J. Chem.* 1990, **43**, 1245.
18. G. Kortüm, W. Vogel and K. Andrussow, *Dissociation Constants of Organic Acids in Aqueous Solution.* Butterworths, London (1961).
19. G. B. Deacon and R. H. Newnham, *Aust. J. Chem.* 1985, **38**, 1757.
20. A. Streitwieser, P. J. Scannon and H. M. Niemeyer, *J. Am. Chem. Soc.* 1972, **94**, 7936.
21. A. Streitwieser, D. A. Bors and M. J. Kaufman, *J. Chem. Soc., Chem. Commun.* 1983, 1394.
22. G. B. Deacon, C. M. Forsyth, W. C. Patalinghug, A. H. White, A. Dietrich and H. Schumann, *Aust. J. Chem.* 1992, **45**, 567.
23. H. A. Stecher, A. Sen and A. L. Rheingold, *Inorg. Chem.* 1988, **27**, 1130.
24. W. J. Evans, R. E. Golden and J. W. Ziller, *Inorg. Chem.* 1991, **30**, 4963.
25. G. B. Deacon, T. Feng, S. Nickel, M. I. Ogden and A. H. White, *Aust. J. Chem.* 1992, **45**, 671.
26. G. B. Deacon, P. I. MacKinnon, T. W. Hambley and J. C. Taylor, *J. Organomet. Chem.* 1983, **259**, 91.

27. J. Marçalo and A. Pires de Matos, *Polyhedron* 1989, **8**, 2431.
28. L. C. Thompson, in *Handbook on the Physics and Chemistry of Rare Earths* (Edited by K. A. Gschneidner and L. Eyring), Vol. 3, Ch. 25. North Holland, Amsterdam (1979).
29. G. B. Deacon, W. D. Raverty and D. G. Vince, *J. Organomet. Chem.* 1977, **135**, 103.
30. G. B. Deacon, A. J. Koplick, W. D. Raverty and D. G. Vince, *J. Organomet. Chem.* 1979, **182**, 121.
31. G. B. Deacon, C. M. Forsyth, R. H. Newnham and T. D. Tuong, *Aust. J. Chem.* 1987, **40**, 895.
32. G. B. Deacon, C. M. Forsyth, B. M. Gatehouse and P. A. White, *Aust. J. Chem.* 1990, **43**, 795.
33. G. B. Deacon and R. N. M. Smith, *J. Org. Chem., U.S.S.R.* 1992, **18**, 1584.
34. G. M. Sheldrick, SHELX76, Program for Crystal Structure Determination. University of Cambridge, U.K. (1976).
35. C. K. Johnson, ORTEPII, Report ORNL-5138. Oak Ridge National Laboratory, Tennessee, U.S.A. (1976).
36. J. A. Ibers and W. C. Hamilton, *International Tables for X-ray Crystallography*, Vol. 4. Kynoch Press, Birmingham (1974).

Polyhedron Vol. 12, No. 11, pp. 1295–1300, 1993
Printed in Great Britain

0277–5387/93 $6.00+.00
© 1993 Pergamon Press Ltd

RAPID SYNTHESIS OF TiN, HfN AND ZrN FROM SOLID-STATE PRECURSORS

J. C. FITZMAURICE, A. HECTOR and I. P. PARKIN*

Department of Chemistry, The Open University, Milton Keynes MK7 6AA, U.K.

(*Received* 10 *February* 1993; *accepted* 16 *February* 1993)

Abstract—Microwave or conventional oven initiation of the reaction between lithium nitride and anhydrous metal chloride (M = Ti, Zr, Hf) produces metal nitride MN, dinitrogen and lithium chloride via a metathesis reaction. The metal nitrides were characterized by X-ray powder diffraction, SEM, EDAX, IR, magnetic moment measurement and microanalysis.

Titanium nitride is a hard, durable refractory material with reflectance properties similar to that of gold.[1] It has been used as a hardness coating[2] for drill bits, as an abrasive and for microelectronic applications.[3] Conventionally titanium, zirconium and hafnium nitrides have been made by either high-temperature combination of the metal or metal hydride with ammonia/dinitrogen[4] or by reaction of metal tetrachloride with ammonia[5] at 800°C.

Current interest in finding low-energy "chemical molecular precursor routes" to ceramic nitrides has led to the study of facile unimolecular or ammonia-initiated bimolecular degradation of homoleptic metal amides.[6] This has been studied for thin film deposition[7] and for bulk solid synthesis.[8] Unfortunately, these routes ofen suffer from sample contamination either in the form of an oxide (from the reactor walls) or a carbide—the latter being formed from competitive decomposition pathways within the amide precursor.[9] Solid state routes to metal sulphides and phosphides have been developed by Kaner *et al.* by reaction of anhydrous metal halides with alkali metal pnictides[10] or chalcogenides.[11] Such reactions provide a facile method of producing low-impurity ceramic materials,[12] often with the reaction once initiated being highly exothermic.

We report here an alternative solid-state route to crystalline TiN, ZrN and HfN via a rapid, low-temperature initiated precursor approach.

EXPERIMENTAL

All reactions and preparations were carried out *in vacuo* or in a dinitrogen filled dry-box. Glass ampoules were made out of either pyrex, borosilicates or quartz glass and were either flame-dried under vacuum or heated to 400°C for 6 h prior to reaction. All solvents were degassed; THF was distilled from sodium/benzophenone and stored over 4 Å molecular sieves prior to use. Metal halides and lithium nitride were purchased from Aldrich Chemical Co. and Strem Chemicals and used as supplied. X-ray powder diffraction patterns were obtained using a Siemens D5000 diffractometer using Cu-K_α radiation, SEM and EDAX analysis on a Jeol JSM 820 equipped with Kevex program,[13] FT-IR as pressed KBr pellets on a Nicolet 205 (CsI), GC on a Pye–Unicam 204 with a 5 Å sieve column using a thermal conductivity detector and helium carrier gas, and magnetic moment measurements were determined by an Oxford Instruments resistive Faraday balance. Nitrogen microanalyses were measured by fierce condition combustion (powdered tin and maximum oxygen flow at 1800°C) by MEDAC Ltd, Brunel University. Thermal initiation of the reactions was performed in a 750 W industrial microwave oven with a ceramic brick support or a Lenton Thermal Designs Tube furnace.

Transition metal nitride preparation (M = Hf, Zr)

Lithium nitride (50–100 mg) and anhydrous metal chloride, MCl_4 (such quantities needed to

* Author to whom correspondence should be addressed.

achieve a 1 : 1 molar ratio of chlorine to lithium), were ground together using an agate pestle and mortar in a nitrogen filled dry-box. The powder was added to a thick-walled glass ampoule, sealed under vacuum and sonicated with an ultrasonic gun for 10 min. The ampoule was then wrapped in glass wool and placed in a conventional oven at 400°C for 5–10 min. After a variable induction time of a few seconds to 5 min (dependent on the sample) a red glow eminated from the ampoule for 2–3 s, during which time a white solid sublimed onto the reactor walls, whilst the main bulk of the product was contained in a grey–black solid-fused lump. The ampoule was removed from the oven, allowed to cool to room temperature and then broken open in a nitrogen filled glove-box. Trituration of the grey–black solid with THF ($3 \times 20\ cm^3$) for 10 h produced a fine black precipitate and a cloudy THF layer. Evaporation of the THF filtrate produces crystals of a white solid identified as LiCl by X-ray powder diffraction, lithium flame test and EDAX analysis (only chlorine present). The black powders were identified as transition metal nitrides by X-ray powder diffraction, EDAX analysis, magnetic moment measurements and nitrogen microanalysis. Ceramic yields, based on the metal after THF trituration, varied from 60% ZrN to 90% HfN. Microanalysis for HfN; Observed (%): $C < 0.2$, $H < 0.2$, $N = 6.41$, $Li < 0.25$, $Cl < 0.25$; required (%) $N = 7.25$. Magnetic moment measurements (0.4 T, 298 K), HfN: $\mu = 1.73$ B.M.

The same general procedure was followed for M = Ti; however, the product was not contained in a fused black lump but was uniformly distributed on the walls of the ampoule—typically the yield of crystalline TiN was less than 50%.

Alternative processes

(1) An identical procedure to that outlined above can be performed by initiating the reaction using a microwave oven with a variable induction period of 1–5 min depending on the sample. The work-up and properties of the materials obtained were identical to those initiated in a conventional oven.

(2) The metal nitrides produced can also be washed free of the lithium chloride by-product by triturating with degassed water for 10 min.

Mixed metal nitrides

Attempts at making mixed metal nitrides were investigated under the same conditions and work-up conditions as above, except equimolar quantities of the starting metal halide powders were ground together before adding lithium nitride.

Detection of evolved dinitrogen

These reactions were identical to those described above, except that evacuated glass ampoules sealable with Teflon taps and an adaptor suitable for use with a GC were used. After the reaction had been initiated (by the conventional oven technique) and allowed to cool to room temperature the ampoule was opened to an argon line for a few seconds to equalize the pressure and the gases in the ampoule run on a GC. This showed the presence of dinitrogen in excess of that of the initial argon and quantified as at least 20% of the nitrogen in the initial lithium nitride.

CAUTION! The reaction of hydrated metal halides with lithium nitride invariably leads to an uncontrollable exothermic reaction, which results in explosion of the ampoule. The reaction of anhydrous halides with lithium nitride is also extremely exothermic and approximately one in 20 of the ampoules explodes if poorly annealed. **The use of a safety screen around the oven and suitable tongs to handle the ampoule is advisable.** No reaction was observed between the anhydrous metal halides and lithium nitride on manually grinding the reagents together.

RESULTS AND DISCUSSION

Thermal initiation of the reaction of an anhydrous group IVA metal chloride ($TiCl_4$, $ZrCl_4$, $HfCl_4$) with lithium nitride (Li_3N) produces crystalline powders of the metal nitride, MN, in seconds via a metathesis reaction [eq. (1)]:

$$3MCl_4 + 4Li_3N \xrightarrow{\text{initiation}} 12LiCl + 3MN + \tfrac{1}{2}N_2. \quad (1)$$

The reactions were performed by placing preground Li_3N and the metal halide into a glass ampoule that was sealed under vacuum and initiated by either heating in a conventional (400°C) or a microwave oven. After a variable induction period ranging from a few seconds to a few minutes in either oven the ampoules glowed red for 2–3 s as the reaction proceeded. This glow was accompanied, in the reactions containing Zr and Hf, by sublimation of a white solid onto the walls of the ampoule and the formation of a black fused solid. In the reaction using $TiCl_{4(l)}$ as a starting material a black particulate solid was spread over the walls of the ampoule. This is probably due to the fact that $TiCl_4$ is a liquid/gas at the initiation temperature. The sublimed white solid was confirmed as LiCl by the lithium flame test, EDAX analysis (only chloride detected) and

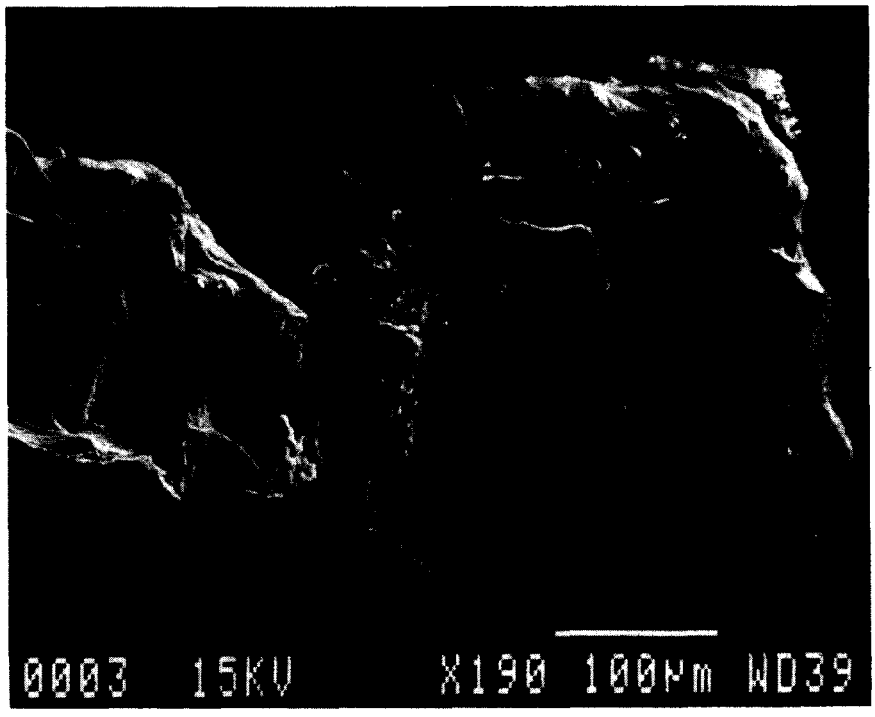

Fig. 1(a). SEM photograph of HfN, unwashed sample.

powder X-ray diffraction (XRD). The black solids were analysed by SEM, which indicated only smooth lines consistent with a lithium chloride coating [Fig. 1(a)]. Triturating the black solid with THF removed the lithium chloride coating and left (as assessed by SEM) small, uniform, micron-sized particles with sharp angles and faces [Fig. 1(b)]. The THF washings were allowed to evaporate in air and produced crystalline lithium chloride, in agreement with eq. (1). The formation of dinitrogen in the

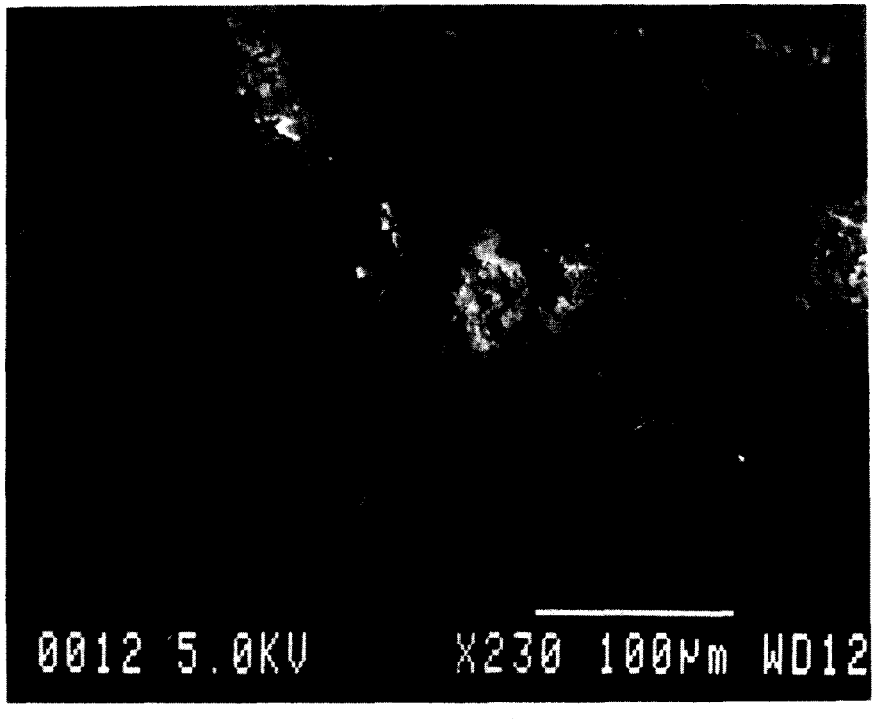

Fig. 1(b). SEM photograph of HfN, THF washed sample.

reaction of MCl_4 (M = Ti, Zr, Hf) and Li_3N was confirmed by performing the reaction in a glass ampoule sealed with a Young's Teflon tap, back filling the ampoule with argon and determining the concentration of dinitrogen by GC analysis. Quantification indicated that approximately 20% of the initial nitrogen in the lithium nitride forms dinitrogen in the ampoule [also in good agreement with eq. (1)].

The reactions are dependent on the quantities of Li_3N and the metal halide used. When performed on a small scale (50 mg of metal halide) some unreacted metal halide was observed by XRD; on a larger scale (500 mg of metal halide) no unreacted starting material was observed and the SEM and EDAX analysis of the fused lump indicated homogeneity across the surface. It is probable that larger scale reactions are better insulated against heat loss.

The THF-washed black powders were characterized as binary metal nitrides, MN, by X-ray powder diffraction, FT-IR, magnetic moment measurement, EDAX analysis and nitrogen microanalysis. Powder X-ray diffraction (XRD) shows that the materials are phase pure after THF washing and assume the NaCl-type structure (Fm3m) with lattice constants a (Å) = 4.23, 4.57 and 4.52 for TiN, ZrN and HfN, respectively, compared to literature values[14] of a (Å) = 4.24, 4.56 and 4.51. The X-ray powder diffraction patterns of HfN and TiN are shown in Figs 2(a) and (b). The Scherrer equation[15] based on the XRD line-widths indicates crystallite sizes of 200–250 Å for the TiN and HfN powders. Analysis of the black powders by FT-IR showed only a broad band at *ca* 450 cm^{-1}, probably due to M—N stretches. The observed room-temperature magnetic moment measurement of HfN ($\mu = 1.73$ B.M., 0.4 T) is consistent with one unpaired electron on the hafnium. The material displays an interesting field-dependent magnetism, which is currently being investigated.

The EDAX analysis of the THF triturated black powders showed only the metal and nitrogen are present. If the nitrides were exposed to air an oxygen peak was additionally detected, consistent with surface oxidation. This oxygen peak could be reduced by polishing the air-exposed sample and handling under an inert atmosphere. No peak due to chlorine was detected for the triturated powders by EDAX analysis. The microanalysis of the THF triturated powder from reaction of $HfCl_4$ and Li_3N showed no carbon or hydrogen and 6.41% nitrogen. This is approximately 90% of all the nitrogen expected for HfN (7.25%); the analysis was performed using a maximum oxygen flow and powdered tin to raise the temperature of the combustion. The refractory nature of the product HfN (m.p. = 3300°C) and its resistance to chemical attack, including oxidation even at high temperatures,[4] probably accounts for the incomplete nitrogen analysis; a residue was left after combustion analysis. Negligible values for lithium (< 0.25%) and chloride (< 0.25%) were observed for the HfN powder, indicating that THF

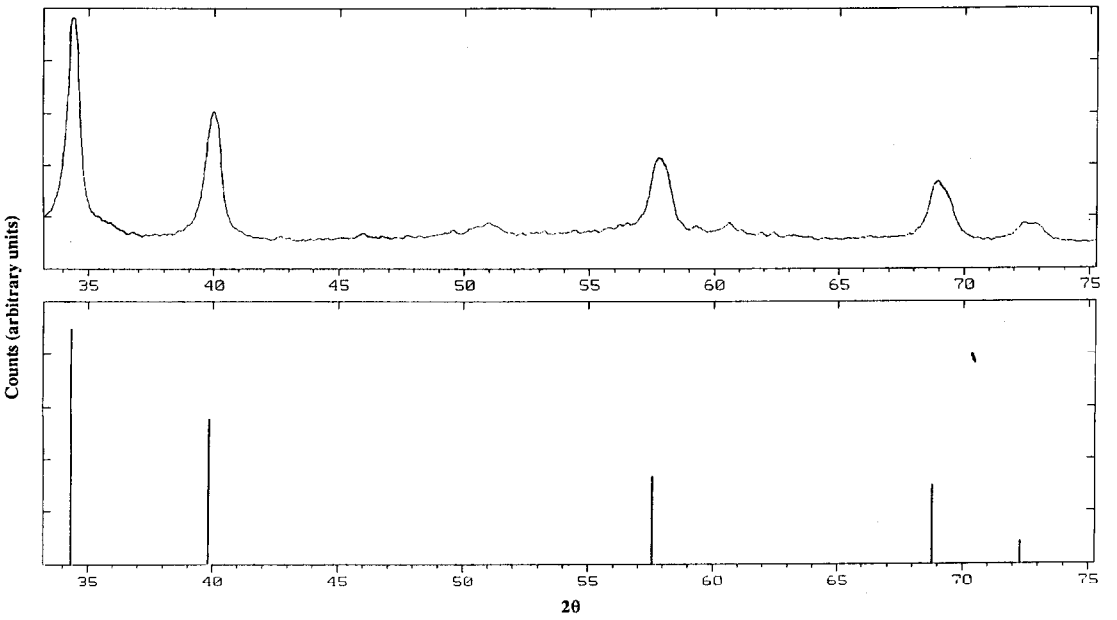

Fig. 2(a). Upper trace: X-ray powder diffraction pattern of the reaction product from $HfCl_4$ and Li_3N. Lower trace: standard HfN X-ray powder diffraction pattern.

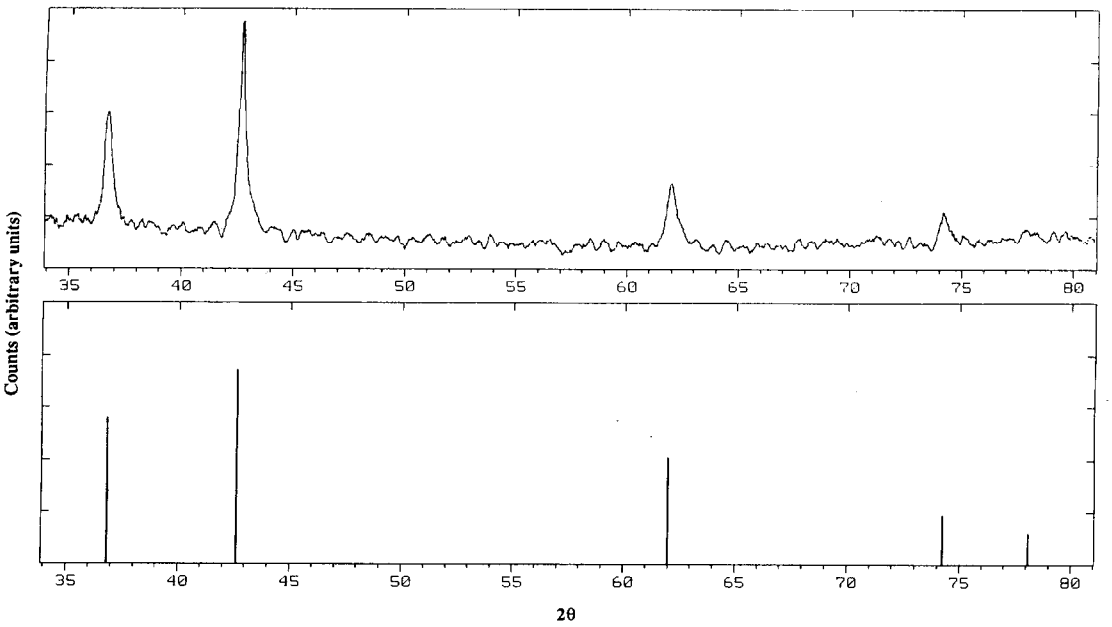

Fig. 2(b). Upper trace: X-ray powder diffraction pattern of the reaction product $TiCl_4$ and Li_3N. Lower trace: standard TiN X-ray powder diffraction pattern.

trituration removes the lithium chloride co-product.

The reaction of lithium nitride with a group IVA chloride is highly exothermic (as judged by the red glow and sublimation of LiCl) and once initiated is extremely rapid. The enthalpy of formation for the precursor reaction used to produce TiN is $\Delta H_f^{\ominus} = -900$ kJ mol^{-1}, from Hess law calculations.[16] The temperature reached could be as much as 1100°C, because metal nitrides often require annealing at 900°C for 12–24 h to induce sufficient crystallinity to be characterized by powder XRD.[4] Previous TGA studies of metal amide precursor routes to metal nitrides have generated metal nitrides with small crystallite size (80–150 Å) when rapidly heated to 1000°C in a platinum crucible and allowed to slowly cool to room temperature over an hour.[17] Optical pyrometry[10] studies of analogous solid state reactions to form GaP have indicated temperatures in excess of 850°C.

The sublimation of LiCl (b.p. = 1300°C) in the reaction of metal halides and Li_3N indicates that the high temperatures generated in the reactions are sufficient to overcome the solid-state diffusion barrier. Initiation, by heating in a conventional oven at temperatures up to 300°C, did not induce any reaction in the samples under observation, indicating that a critical temperature (assessed as 375–400°C) is required for sufficient localized reaction to proliferate throughout the whole material. The co-formation of LiCl and metal nitride may be advantageous in the formation of crystalline metal nitrides because the addition of both LiCl and $LiNH_2$ was found to decrease both the temperature and annealing time required to form lanthanide nitrides by a molecular precursor route.[18]

The initial process in the formation of hafnium and zirconium nitrides is likely to be the breakdown of the metal halide lattice, although notably no change in induction period or temperature was observed for the reaction involving $TiCl_{4(l)}$. The breakdown of the transition-metal halide lattice is accompanied by the formation of $LiCl_{(s)}$, which provides the driving force for the reaction and accounts for 80% of the energy produced in the reaction. However, initiation of these reactions was more difficult than for the formation of MoS_2 and GaAs[11] using a similar solid-state metathesis reaction, where grinding the reagents together was sufficient to stimulate reaction.

It is possible that intermixed Hf_xZr_yN compounds may be made by combination of suitable proportions of metal halide and lithium nitride. This is illustrated by the powder X-ray diffraction pattern for the reaction of equimolar quantities of $ZrCl_4$ and $HfCl_4$ with lithium nitride (Fig. 3). This shows diffraction lines which are slightly broader and intermediate in position between the individual diffraction lines for ZrN and HfN,[13] indicating that the same lattice (NaCl type Fm3m) is adopted for the mixed nitrides. The degree of actual intermixing is difficult to discern, however, because there is only a small difference in the pattern observed to that of overlapping two individual ZrN and HfN patterns. The EDAX step analysis of the mixed nitride

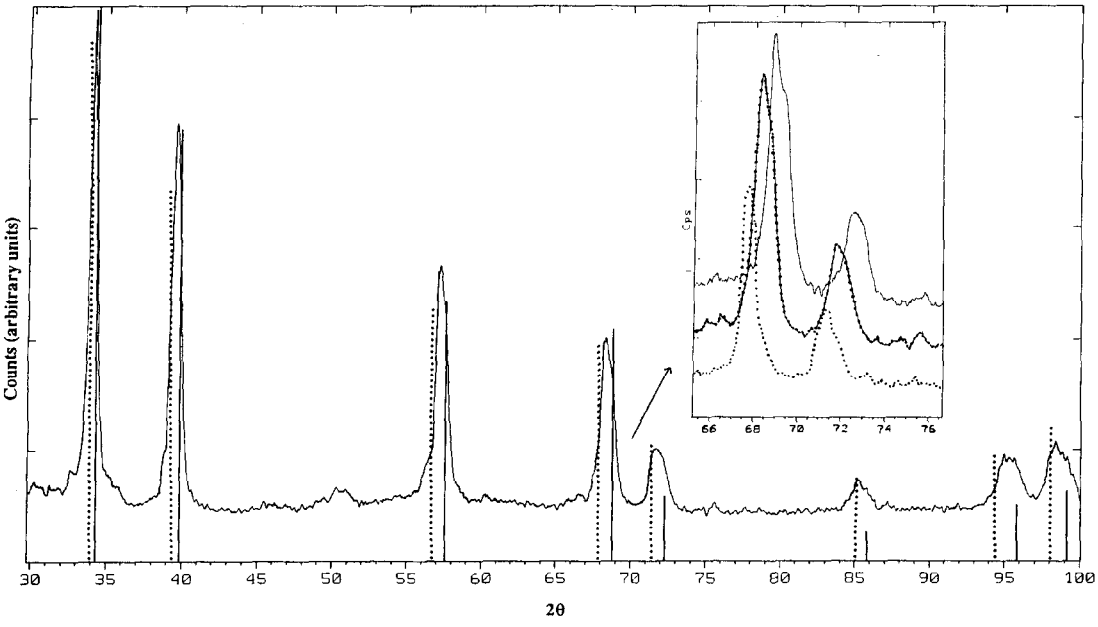

Fig. 3. X-ray powder diffraction pattern of the reaction of equimolar quantities of $HfCl_4$ and $ZrCl_4$ with Li_3N. Standard patterns for ZrN (· · ·) and HfN (——). Insert shows an expanded superposition of ZrN (· · ·) and HfN (——) made in this study and the mixed species obtained by reaction of equimolar quantities of $HfCl_4$, $ZrCl_4$ and Li_3N (–·–·–).

showed approximately equal concentrations for Zr and Hf, in agreement with the formation of an intermixed species.

Crystalline products are invariably produced by these metathesis reactions; however, by incorporation of a suitable inert heat sink (NaCl) it may be possible to control particle size and produce more amorphous materials.

Acknowledgements—Leverhulme Trust (Fellowship to J.C.F.), Nuffield Trust, Royal Society, SERC. Dr C. Harding is thanked for assistance in determiming the magnetic moment measurements.

REFERENCES

1. *Comprehensive Inorganic Chemistry* (Edited by J. C. Bailar, H. J. Emeleus, R. Nyholm and A. F. Trotman), Vol. 2. Pergamon Press, Oxford (1973).
2. S. Koichi, T. Masashi, O. Takuji and S. Susumu, Japan Kokai Tokkyo Koho JP 01, 308, 848 [89, 308, 848].
3. N. Nobuhiro, M. Kazvo, M. Atsushi, F. Sakae, T. Toshiyuki and A. Kelichi, *KenkuHokoky. Tokyotoritsu Kogyo Gitjutsu Sentra* 1990, **19**, 33.
4. L. Toth, *Transition Metal Carbides and Nitrides*, p. 176. Academic Press, New York (1971).
5. A. V. Vikar, T. B. Jackson and R. A. Cutler, *J. Am. Ceram. Soc.* 1989, **72**, 2031.
6. R. M. Fix, R. G. Gordon and D. M. Hoffman, *J. Am. Chem. Soc.* 1990, **112**, 7833; R. G. Gordon and D. M. Hoffman, *Chem. Mat.* 1992, **4**, 68.
7. L. V. Interrante, W. Lee, M. McConnell, N. Lewis and E. Hall, *J. Electrochem. Soc.* 1989, **136**, 472.
8. C. B. Ross, T. Wade and R. M. Crooks, *Chem. Mat.* 1991, **3**, 768,
9. C. Russel, *Chem. Mat.* 1990, **2**, 241; C. Russel and M. M. Seibold, *J. Am. Ceram. Soc.* 1989, **72**, 1503.
10. R. E. Treece, G. S. Macala and R. B. Kaner, *Chem. Mat.* 1992, **4**, 9.
11. P. R. Bonneau, R. F. Jarvis and R. B. Kaner, *Inorg. Chem.* 1992, **31**, 2127.
12. P. R. Bonneau, R. F. Jarvis and R. B. Kaner, *Nature* 1991, **349**, 510.
13. Quantex 6.2, with quantum detector Kevex delta 4.
14. Values obtained from PDF-2 data base on CD-ROM, International Centre for Diffraction Data, Warthmore, PA (1989).
15. H. P. Klug and L. E. Alexander, *X-Ray Diffraction Procedure for Polycrystalline and Amorphous Materials*, 2nd edn. J. Wiley & Sons, New York (1974).
16. D. D. Wayman, W. H. Evans, V. B. Parker, R. H. Schumm, J. Halow, S. M. Bailey, K. C. Chumey and R. L. Nuttal, *The NBS Tables of Chemical Thermodynamics Properties*. American Chemical Society, Washington, DC (1982).
17. M. H. Chisholm, G. Gamma, V. Distasi, D. Baxter and I. P. Parkin, *Inorg. Chem.*, manuscript in preparation.
18. R. L. LaDuca and P. T. Wolczanski, *Inorg. Chem.* 1992, **31**, 1312.

Polyhedron Vol. 12, No. 11, pp. 1301–1310, 1993
Printed in Great Britain

0277–5387/93 $6.00+.00
© 1993 Pergamon Press Ltd

ELECTRONIC STRUCTURE OF HETEROBORANES DERIVED FROM THE ICOSAHEDRAL SKELETON. UV PHOTOELECTRON AND MNDO STUDY

TOMÁŠ VONDRÁK*

J. Heyrovský Institute of Physical Chemistry and Electrochemistry, Academy of Sciences of the Czech Republic, Dolejškova 3, 182 23 Prague 8, Czech Republic

and

STANISLAV HEŘMÁNEK **and** JAROMÍR PLEŠEK

Institute of Inorganic Chemistry, Academy of Sciences of the Czech Republic, 250 68 Řež near Prague, Czech Republic

(*Received* 27 *January* 1993; *accepted* 10 *February* 1993)

Abstract—The HeI photoelectron spectra of the 12-vertex *closo*-1-$SB_{11}H_{11}$, 11-vertex *nido*-7-$SB_{10}H_{12}$ and *nido*-7,8,10-$C_2SB_8H_{10}$, 10-vertex *arachno*-6,9-CSB_8H_{12} and nine-vertex *arachno*-4-CB_8H_{14} and *arachno*-4,6-$C_2B_7H_{13}$ species are reported. The highest symmetry 1-thia *closo* species has the simplest spectrum: The five well-resolved band systems are assigned to F(surface), D(surface + B—H), F(surface), P(B—H) and F(B—H) orbitals in the limit of spherical symmetry. The decrease of the symmetry in the open-face systems manifests itself in a greater complexity of photoelectron spectra and in the decrease of the first ionization energy by approximately 1 eV, due to the appearance of a new well-resolved band. The HOMO has a cluster surface bonding character in the open face systems. Going from *closo* to *arachno* clusters the contribution of hydrogen *s* functions in HOMO increases. For the *arachno* species a large H 1*s* contribution is found in low energy valence orbitals.

The bonding in deltahedral borane hydrides attracts considerable attention.[1,2] The interest of theoretical chemists is concentrated mainly on the high symmetry *closo* molecules where all vertices of the deltahedron are occupied.[3–11] These systems form an appealing paradigm for bonding in transition metal clusters through the isolobal principle.[12–14] The electronic structure of the *closo* species and the Wade–Williams–Rudolph electron counting rules[13,15–18] were rationalized in a straightforward way by the Stone's tensor surface harmonics (TSH) approach.[19–22] A reasonable agreement of the TSH method with the MNDO method was found.[8] The photoelectron (PE) spectral data on the cluster borane hydrides are rather scarce. Fehlner *et al.* published PE spectra of thiaboranes,[23] *closo*-1,2- and 1,4-dicarba-hexaboranes[24,25] and pentaborane.[26] The PE spectra of icosahedral carboranes were interpreted making use of MNDO orbital energies.[27–30] The electronic structures of *closo*-1-$SB_{11}H_{11}$ and especially *closo*-1-SB_9H_9 were described by Brint *et al.* in terms of the capping of the $B_{11}H_{11}$ and B_9H_9 fragments by the sulphur atom,[31] respectively. The recent *ab initio* results[32] for the *closo* species $C_2B_{10}H_{12}$ support the assignment of the lowest ionization energy (IE) band system to surface bonding orbitals. To our knowledge the only PE spectral data available for the low symmetry heteroboranes derived from an icosahedral skeleton are for the *nido*-6-SB_9H_{12} species.[23] The NMR chemical shifts in the nine-vertex *arachno* heteroboranes were correlated with the STO-3G and CNDO/2 density matrix properties, but the orbital energies were not published.[33] Understanding the bonding situation and the nature of the highest MOs of the low symmetry cluster boranes may contribute to the rationalization of the structural patterns of polyhedral metallaboranes.[34–36]

* Author to whom correspondence should be addressed.

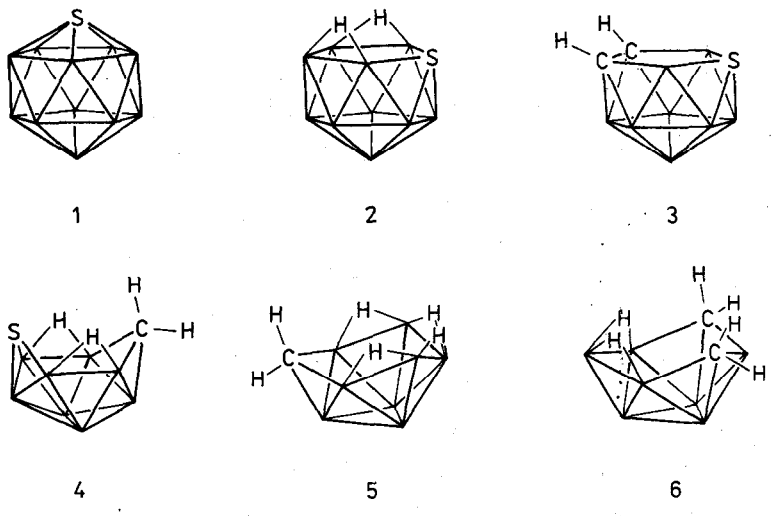

Fig. 1. Structures of studied boranes: *closo*-1-$SB_{11}H_{11}$ (**1**), *nido*-7-$SB_{10}H_{12}$ (**2**), *nido*-7,8,10-$C_2SB_8H_{10}$ (**3**), *arachno*-6,9-CSB_8H_{12} (**4**), *arachno*-4-CB_8H_{14} (**5**) and *arachno*-4,6-$C_2B_7H_{13}$ (**6**).

We report here the PE spectra of thia and carba cluster boranes derived from the icosahedron (12-vertex regular deltahedron) *closo*-1-$SB_{11}H_{11}$ (**1**), *nido* structures (one vacant vertex) 7-$SB_{10}H_{12}$ (**2**) and 7,8,10-$C_2SB_8H_{10}$ (**3**), *arachno* species (two vacant vertices) 6,9-CSB_8H_{12} (**4**), as well as nine-vertex *arachno* species 4-CB_8H_{14} (**5**) and 4,6-$C_2B_7H_{13}$ (**6**), derived from an 11-vertex *closo* precursor (two vacant vertices) (Fig. 1). The MNDO MO energies are used for the assignment of the PE spectra features.

EXPERIMENTAL

HeI photoelectron spectra were recorded using the VG Scientific UVG 3 instrument. The working resolution was 30–40 meV (full width at half maximum, FWHM). Spectra were calibrated by an Ar/Xe mixture. The temperature for the measurements was in the 120–140°C range.

The MNDO calculations were performed by the MOPAC 5.0 program. The standard parametrization for hydrogen and carbon was used.[37] The parameters for boron and sulphur were taken from refs 38 and 39, respectively. All internal coordinates were the subject of the optimization procedure.

The compounds were prepared by published methods: **1**,[40] **2**,[41], **3**,[42] **4**,[43] **5**[44] and **6**.[45,46]

RESULTS AND DISCUSSION

Closo-1-$SB_{11}H_{11}$ (1)

The PE spectrum of **1** is in general agreement with that already published by Fehlner *et al.*[23] The spectrum can be divided into three regions, analogous to the PE spectra of the isoelectronic $C_2B_{10}H_{12}$ species[28,29] (Fig. 2). Four overlapping ionizations between 10.67 and 11.56 eV (a–d) and a well-resolved band at 12.36 eV are found within the region A. Two maxima are resolved in the region B at 13.40 and 13.68 eV (f, g). In the deepest region C three bands lie below the HeI ionization edge.

Before discussing the assignment of the particular photoelectron bands it is feasible to introduce Stone's tensor surface harmonics formalism.[18] According to this theory the molecular orbitals

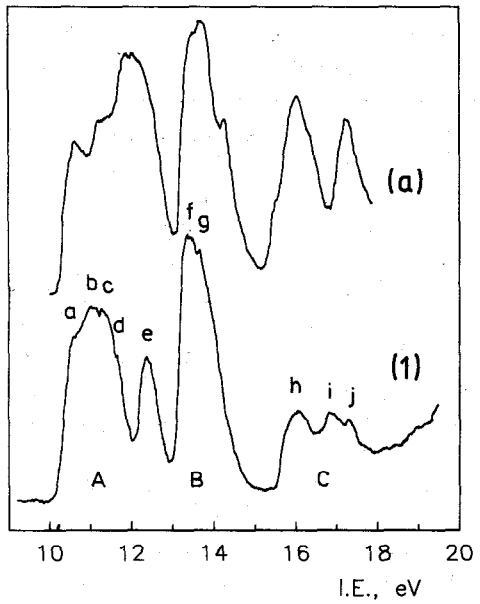

Fig. 2. HeI PE spectrum of *closo*-1-$SB_{11}H_{11}$ (**1**) and *closo*-1,12-$C_2B_{10}H_{12}$ (**a**).[29]

Table 1. Descent in symmetry. Correlation of some irreducible representations of the full rotation group (R_3) and its subgroups I_h and C_{5v}

R_3	I_h	C_{5v}
S	A_g	A_1
P	T_{1u}	A_1+E_1
D	H_g	$A_1+E_1+E_2$
F	$T_{2u}+G_u$	$T_{2u}\rightarrow A_1+E_2$
		$G_u\rightarrow E_1+E_2$

(MOs) of a *closo* system are classified in the spherical limit by the atomic orbital labels, and the $2n+1$ (n = number of vertices) occupied MOs can be separated into two groups. nMOs are B—H bonding and have a large outward pointing boron $2p$ composition (labelled S^x, P^x, D^x). The $n+1$ cluster bonding orbitals can be divided into two groups: (1) the MOs composed predominantly of the boron $2s$ orbitals have the properties of regular surface harmonic functions and are labelled S^σ, P^σ, D^σ; (2) the MOs composed of boron $2p$ orbitals oriented tangentially to the cluster surface. These orbitals have the properties of vector surface harmonic functions and are labelled P^π, D^π, F^π.

The inspection of the eigenvectors and the small average deviation of the p lobes from the tangent to the cluster surface shows that the highest occupied MO (HOMO) is the e_2 symmetry species, which is a component of the g_u level in the I_h symmetry (Table 1). The HOMO is composed mainly of the boron $2p$ orbitals, which are oriented nearly tangentially to the sphere encircling the icosahedron. Thus, the HOMO can be labelled F^π. The HOMO has no sulphur contribution. The s,p basis orbitals of the atoms located on the rotation axis cannot generate the e_2 representation. Thus, the calculated zero contribution of sulphur orbitals in the upper component of the F^π level may be a basis-dependent phenomenon due to the absence of the sulphur d-functions. The following three levels, namely $5e_1$, $7a_1$ and $3e_2$, correlate with the h_g representation of the I_h group. These orbitals have a 25–35% localization on the hydrogen atoms (Table 2). The p orbitals are more deviated from the tangential direction in comparison to HOMO. The weighted average (the p-localization is taken as the weight) is in the interval 22–54°. Brint and coworkers recently assigned the $2h_g$ orbitals to the B—H bonding D^x level, making use of the results of a localization procedure.[47] The $7a_1$ orbital has a 24% contribution from the sulphur p orbitals. It is equal to the hydrogen s participation in this orbital. The deviation of the p lobes from the cluster surface in these orbitals is lower than for the deeper lying levels of t_{1u} and t_{2u} symmetry, which can be un-

Table 2. Vertical ionization energies, orbital energies and composition of occupied MOs for *closo*-1-$SB_{11}H_{11}$ (1)

IE	$-\varepsilon$ (eV)	Composition S	B (%)	H	C_{5v}	I_h	Assignment[a]
10.67 a	12.40	0	98 (98[b], 11[c])	2	$4e_2$	$1g_u$	F^π endo
11.00 b	12.47	0	76 (76, 22)	24	$5e_1$		
11.30 c	12.56	24	52 (71, 54)	24	$7a_1$	$2h_g$	D B—H+endo
11.58 d	12.85	0	65 (64, 38)	35	$3e_2$		
12.36 e	13.90	39	49 (82, 19)	12	$4e_1$	$1g_u$	F^π endo
13.40 f	14.60	30	41 (61, 81)	29	$6a_1$	$2t_{1u}$	P^x B—H
13.67 g	15.15	4	56 (59, 72)	40	$3e_1$		
15.90 h	16.54	0	58 (18, 60)	42	$2e_2$	$1t_{2u}$	F^x B—H
16.87 i	16.92	19	51 (21, 54)	30	$5a_1$		
17.25 j	18.47	7	58 (55, 79)	35	$4a_1$	$2a_g$	S^x B—H
	21.30	0	86 (33, 9)	14	$1e_2$		
	21.50	14	72 (42, 5)	14	$2e_1$	$1h_g$	D endo
	22.07	34	59 (25, 12)	7	$3a_1$		
	29.17	3	91 (21, 16)	6	$1e_1$	$1t_{1u}$	P^σ endo
	29.31	32	64 (22, 28)	4	$2a_1$		
	39.16	8	90 (22, 80)	2	$1a_1$	$1a_g$	S^σ endo

[a] Endo: cluster bonding character.

[b] p function contribution; sum for all heavy atoms.

[c] Weighted average of the deviation of the p direction from the tangent to the cluster surface. The weight is the p density at the atom.

equivocally assigned to the B—H bonding interaction. The *p* orbital orientations (with the exception of the $7a_1$ orbital) tend to favour assignment to the D^{π} level, whereas the high hydrogen contribution clearly indicates the exo-bonding feature. The endo–exo mixing within the *D* level is symmetrically allowed as the 12 hydrogen *s* orbitals generate the a_g, t_{1u}, t_{2u} and h_g representations in the I_h group. The $2h_g$ orbitals cannot be assigned in a straightforward way to the endo or exo bonding.

The first four occupied orbitals are found in the 0.5 eV interval. Four overlapping bands are resolved within the first band system between 10.5 and 11.5 eV. Thus, bands a–d are assigned to the $4e_2$, $5e_1$, $7a_1$ and $3e_2$ orbitals ($1g_u$ and $2h_g$ species in the I_h symmetry). The next level is calculated approximately 1 eV deeper. It has the e_1 symmetry and has a 12% hydrogen 1*s* composition. The weighted average of the *p* orbitals' deviation from the cluster surface is lower in comparison to the $2h_g$ orbitals. Detailed inspection of the nodal properties indicate that the $4e_1$ level adheres to the $1g_u$ level in the I_h limit. Thus, this orbital can be labelled F^{π}. This level has its counterpart in the well-resolved band e, peaking at 12.36 eV. The appearance of band *e* forms a significant difference between the PE spectrum of **1** and that of the *closo*-$C_2B_{10}H_{12}$[29] species (Fig. 2). From the calculation it follows that the appearance of this band is due both to a higher splitting of the F^{π} level brought about by the perturbation of the I_h symmetry and by a decrease in the width of the group of *D* orbitals.

The B region of the PE spectrum, where two band maxima at 13.40 and 13.67 eV are found, can be assigned to the $6a_1$ and $3e_1$ orbitals which correlate with the $2t_{1u}$ level. The boron *p* orbitals point outward and the hydrogen 1*s* contributions are 29% and 40%, respectively, indicating unequivocally the B—H bonding character. Thus, these orbitals can be labelled as P^x.

In the deepest region C three maxima are resolved. They can be tentatively assigned to the $2e_2$, $5a_1$ and $4a_1$ orbitals. The $2e_2$ and $5a_1$ orbitals correlate with the $1t_{2u}$ level and the $4a_1$ orbital corresponds to the $2a_g$ species in the I_h group. These levels have hydrogen localizations of 30–42% and a prevailing outward pointing *p* orbital. The $1t_{2u}$ orbitals can be labelled as F^x and the $4a_1$ orbital corresponds to the S^x level.

The second set of occupied orbitals of *D* symmetry ($1h_g$) lies above the HeI ionization edge. The deviation of the *p* orbitals from the tangential direction and the hydrogen 1*s* contribution is lower than for the upper *D* level. The main contribution from the heavy atoms comes from the *s* orbitals. The $1h_g$ level has clearly a cluster bonding character, but it cannot be labelled as D^{π} due to the prevailing *s* composition. Brint *et al.* recently assigned the upper *D* level to B—H bonding and the lower *D* level to π-endo bonding.[46] It seems that a large exo/endo mixing and the *s*/*p* mixing occur in the *D* symmetry species, thus preventing the straightforward Stone's labelling.

Table 3. MNDO optimized internal coordinates for *closo*-1-$SB_{11}H_{11}$ (**1**)

	MNDO	Experimental values[a]
	Bond lengths (Å)	
S—B	2.004	2.007
B(2)—B(3)	1.892	1.905
B(3)—B(7)	1.794	1.781
B(7)—B(8)	1.840	1.778
B(7)—B(12)	1.824	1.775
B—H[b]	1.166	1.187
	Bond angles (°)	
S—B—H	109.2	120.4
B(12)—B(7)—H	124.8	125.4

[a] Electron diffraction results from ref. 48.
[b] Mean values.

The deepest three levels, $1e_2$, $2a_1$ and $1a_1$, correlate with the t_{1u} and a_g representations. They have a predominant heavy atoms *s* composition and clearly adhere to Stone's P^{σ} and S^{σ} levels.

The MNDO optimized geometry is in a good agreement with the electron diffraction results.[48] The sulphur atom is pulled slightly out of the deltahedron and the B—B distances in the pentagon neighbouring the sulphur are elongated in comparison with the more distant B—B bonds (Table 3).

Nido-7-$SB_{10}H_{12}$ (**2**) *and* nido-7,8,10-$C_2SB_8H_{10}$ (**3**)

The decrease in symmetry of the *nido* species results in higher complexity of their photoelectron spectra (Fig. 3). The low ionization energy (IE) region A of the PE spectra of the *nido* compounds differs significantly from the spectra of the *closo* species. A new isolated band appears before the onset of the broad band envelope. Due to the appearance of this band the first IE is 0.86 eV for **2** and 1.37 eV for **3**, which is lower in comparison to **1**. The calculations for both *nido* structures show that the HOMO is separated by nearly 1 eV from the second highest occupied orbital (HOMO-1). The HOMO has a negligible contribution from the hydrogen atoms and the direction of the *p* lobes is close to the cluster surface tangent (Tables 4 and 5). Thus, the first band (a) in the PE spectra of the

Table 4. Vertical ionization energies, orbital energies and composition of occupied MOs detected in the HeI PE spectrum of *nido*-7-$SB_{10}H_{12}$ (2)

IE (eV)	MO	$-\varepsilon$ (eV)	Composition S	B (%)	H	*p* function[b]	Angle[c] (°)	Assignment[a]
9.81 a	24	11.46	10	84	6	92	11	π-endo
10.70 b	23	12.12	14	64	22	76	37	π-endo + B—H
11.13 c	22	12.14	11	68	21	77	35	π-endo + B—H
11.34 d	21	12.52	3	74	23	76	26	π-endo + B—H
12.01 e	20	12.72	4	67	29	69	38	π-endo + B—H
	19	12.84	8	51	40	58	31	π-endo + B—H
	18	13.49	40	48	13	84	11	π-endo
12.96 f	17	13.66	10	59	31	63	45	B—H
13.40 g	16	14.27	25	44	31	63	77	B—H
13.77 h	15	14.40	19	56	25	70	21	π-endo
14.14 i	14	14.80	6	54	40	56	64	B—H
	13	14.91	7	53	40	57	63	B—H
15.44 j	12	16.48	12	53	36	19	75	B—H
	11	16.63	2	41	57	18	68	B—H
16.62 k	10	18.05	6	58	36	55	84	B—H
17.50 l	9	19.44	7	70	23	41	10	σ-endo

[a] Endo: cluster bonding character.
[b] Sum of the *p* density for all heavy atoms.
[c] Weighted average of the deviation of the *p* direction from the tangent to the cluster surface. The weight is the *p* density at the atom.

Table 5. Vertical ionization energies, orbital energies and composition of occupied MOs detected in the HeI PE spectrum of *nido*-7,8,10-$C_2SB_8H_{10}$ (3)

IE (eV)	MO	$-\varepsilon$ (eV)	Composition S	C	B (%)	H	*p* function[b]	Angle[c] (°)	Assignment[a]
9.30 a	24	10.96	2	20	75	3	95	12	π-endo
10.45 b	23	11.80	22	25	48	5	94	18	π-endo
10.98 c	22	12.36	1	15	59	25	75	30	π-endo + B—H
11.22 d	21	12.39	14	15	51	20	80	25	π-endo + B—H
11.46 e	20	12.65	22	4	57	17	79	37	π-endo + B—H
11.73 f	19	13.08	1	12	56	31	69	36	π-endo + B—H
12:63 g	18	13.42	17	10	45	28	68	38	π-endo + B—H
13.02 h	17	13.96	16	37	37	10	86	18	π-endo
	16	14.01	33	11	43	13	83	14	π-endo
13.65 i	15	14.63	17	11	41	31	65	68	B—H
13.95 j	14	15.07	0	15	46	39	60	75	B—H
14.41 k	13	15.26	3	20	31	36	60	73	B—H
15.23 l	12	16.49	13	2	49	36	18	71	B—H
16.25 m	11	16.84	0	11	48	41	20	73	B—H
17.64 n	10	18.40	7	20	40	33	54	81	B—H
	9	18.98	8	10	62	20	43	21	σ-endo

[a] Endo: cluster bonding character.
[b] Sum of the *p* density for all heavy atoms.
[c] Weighted average of the deviation of the *p* direction from the tangent to the cluster surface. The *p* density at the atom is the weight.

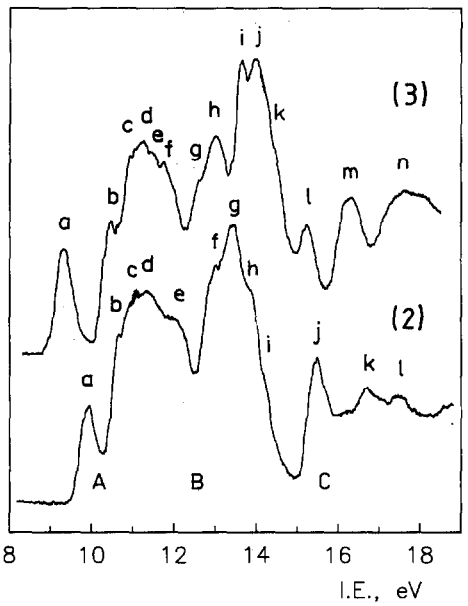

Fig. 3. HeI PE spectrum of *nido*-7-$SB_{10}H_{12}$ (**2**) and *nido*-7,8,10-$C_2SB_8H_{10}$ (**3**).

nido structures can be assigned to a surface bonding cluster MO.

In the PE spectrum of **2** four maxima are found within the broad band system in region A. In region B four observed ionization features (f–i) coalesce in an intense band system, peaking at 13.5 eV with an FWHM of 1.6 eV. In the high energy region C three bands (j–l) at 15.44, 16.62 and 17.5 eV are resolved. The calculation predicts a similar grouping of MOs. Five MOs below the HOMO lie within the 12.12–12.84 eV interval. The contribution from the hydrogen 1*s* orbitals is 20–40%. The sulphur *p* orbitals deviate more from the cluster surface in comparison to the HOMO. These orbitals can be described as cluster bonding MOs mixed with B—H orbitals. The band system between 10.7 and 12.01 eV can, therefore, be assigned to these orbitals. The following group of orbitals (18th MO to 13th MO in Table 4) can be assigned to the ionizations f–i in region B. The 18th MO has a 40% contribution from the sulphur atom. The sulphur *p* density is directed to the vacant vertex in the icosahedral skeleton. The deviation angle of the *p* lobes from the tangential direction indicates the *endo* bonding character of the 15th MO. The remaining levels within this band system have B—H bonding character. The *p* lobes of the skeletal atoms are pointed outwards and the contribution of hydrogen 1*s* orbitals exceeds 30%. In the high IE region the bands j and k can be tentatively assigned to three orbitals (12th MO to 10th MO) having the B—H character. The deepest ionization observed at 17.5 (**1**) may originate from the 9th MO, which has a considerable boron 2*s* contribution and can be labelled as σ-endo bonding.

In the spectrum of *nido*-7,8,10-$C_2SB_8H_{10}$ (**3**) band b at 10.45 eV is resolved on the onset of the broad band system in region A. According to the MNDO calculation the HOMO-1 has a low contribution from hydrogen 1*s* orbitals and the π-endo bonding character. In the following four MOs the hydrogen 1*s* composition varies from 17% to 31%. The inspection of the eigenvectors shows that these MOs have, analogous to **2**, endo bonding character with a B—H contribution. The band system between 10.98 and 11.73 eV (c–g) can be assigned to these orbitals. A new band system with two resolved maxima (g, h) appears between 12.6 and 13.0 eV. The shoulder at 12.63 can be assigned to the 18th MO, having predominantly π-endo character. Feature h can have its counterpart in the 17th and the 16th MO, which are calculated to be close in energy. These MOs have a cluster bonding character as follows from the 10–13% hydrogen 1*s* contribution. The 16th MO has the highest sulphur 2*p* composition. Contrary to **2** the sulphur *p* density is in the plane of the pentagonal face. The band system i–k, peaking at 14 eV, is attributed to the B—H bonding orbitals (15th and 13th MOs). The B—H bonding 12th and 11th MOs can be assigned to the bands l and m at 15.23 and 16.25 eV, respectively. The highest ionization energy feature observed at 17.64 eV (n) may come from the exo bonding MO and the uppermost σ-endo level.

Arachno-6,9-CSB_8H_{12} (**4**)

The absence of two atoms in the icosahedral cage makes the PE spectrum more complex (Fig. 4). In the low IE region three bands are observed before the steep onset of broad band envelopes. The calculation predicts the highest three occupied MOs to

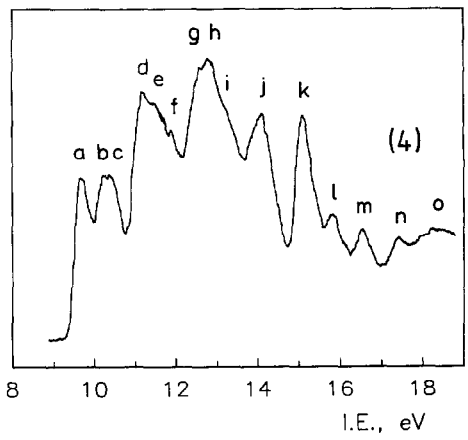

Fig. 4. HeI PE spectrum of *arachno*-6,9-CSB_8H_{12} (**4**).

Table 6. Vertical ionization energies, orbital energies and composition of occupied MOs detected in the HeI PE spectrum of *arachno*-6,9-CSB_8H_{12} (**4**)

IE (eV)	MO	$-\varepsilon$ (eV)	Composition S	C	B (%)	H	*p* function[b]	Angle[c] (°)	Assignment[a]
9.74 a	23	11.26	28	4	38	29	68	23	π-endo
10.28 b	22	11.81	5	4	88	3	97	11	π-endo
10.44 c	21	11.91	44	0	46	10	81	50	π-endo + *p*(S)
11.27 d	20	12.29	8	20	40	32	67	25	
11.50 e	19	12.41	11	6	58	25	72	36	
11.59 f	18	12.81	1	7	53	39	60	29	
	17	13.00	3	15	50	32	63	58	
12.59 g	16	13.79	20	21	23	36	62	15	
12.85 h	15	13.84	9	3	37	51	62	54	
13.26 i	14	14.58	14	11	40	35	60	72	
14.08 j	13	14.94	17	8	53	22	73	14	
15.12 k	12	15.50	1	17	39	43	46	37	
15.83 l	11	16.40	1	2	47	34	27	53	
16.55 m	10	17.34	8	10	51	31	43	58	
17.48 n	9	17.85	6	4	56	35	46	58	
18.34 o	8	19.18	1	2	69	28	29	22	

[a] Endo: cluster bonding character.

[b] Sum of the *p* density for all heavy atoms.

[c] Weighted average of the deviation of the *p* direction from the tangent to the cluster surface. The weight is the *p* density at the atom.

be separated from the deeper lying levels (Table 6). The HOMO has a π-endo bonding character. The exo contribution to the HOMO is from the bridging hydrogen atoms and the C—H bonds. The following two MOs lie close in energy. This agrees with the presence of the two overlapping bands b and c. The HOMO-1 has unequivocally π-endo bonding character. The HOMO-2 has a large contribution from the sulphur atom. Inspection of the atomic orbital coefficients indicates that the sulphur *p* density is directed radially. As the hydrogen 1*s* composition is 10%, the HOMO-2 can be described as π-endo bonding.

In the deeper lying MOs a large endo–exo mixing occurs. The properties of the *p* orbitals of heavy atoms and the hydrogen 1*s* localization do not allow us to distinguish unequivocally the cluster bonding and the B—H bonding orbitals. The calculated grouping of MOs finds its counterpart in the observed IE band envelopes. The ionization features d–f can be assigned to the group of four MOs (20th to 17th MO). The band system within the 12.53 and 13.5 eV interval (g–i) can be assigned to MOs between 13.79 and 14.58 eV. The following bands can be tentatively assigned to single MOs. The highest IE band observed at 18.34 eV may correspond to the highest σ-endo level.

Arachno-4-CB_4H_{14} (**5**) *and* arachno-4,6-$C_2B_7H_{13}$ (**6**)

In the spectrum of **5** a resolved low IE band is found (Fig. 5). The corresponding HOMO has only a 13% hydrogen 1*s* composition (Table 7). The main hydrogen contribution comes from the bridge atoms more distant from the carbon atom. The average direction of the *p* lobes is very close to the surface tangent. The HOMO has unequivocally a π-endo bonding character. Band b at 10.71 eV can be assigned to the HOMO-1. The calculation provides a higher hydrogen 1*s* composition in comparison to HOMO. Thus, HOMO-1 can be classified as π-endo bonding with some contribution from B—H bonding. The successive bands observed in the PE spectrum are tentatively assigned to MOs, as depicted in Table 7. The MNDO calculation predicts a strong mixing of the hydrogen 1*s* orbitals with the cluster orbitals. It prevents any conclusion on the nature of the observed bands.

For the isoelectronic *arachno*-4,6-$C_2B_7H_{13}$ (**6**) a decrease in the first IE is observed (Table 8). Carbon atoms have a higher electronegativity than boron. The destabilization of the HOMO is obviously due to the decrease in the number of hydrogen atoms rather than due to the substitution of boron by

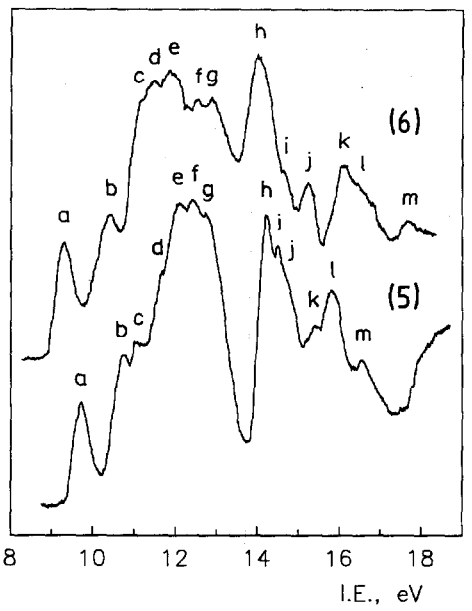

Fig. 5. HeI PE spectrum of *arachno*-4-CB_8H_{14} (**5**) and *arachno*-4,6-$C_2B_7H_{13}$ (**6**).

carbon. The same effect is observed for the *nido* species. The HOMO has a 10% contribution from the 1*s* orbitals of the bridging and carbon-bonded hydrogen atoms. This indicates the cluster bonding character. The directional properties of the *p* orbitals also corroborate the π-endo bonding character of the HOMO. Band b at 10.41 can be assigned to HOMO-1. The hydrogen 1*s* composition and nearly surface orientation of the *p* orbitals indicate the π-endo character of HOMO-1. The deeper MOs have large contributions from hydrogen 1*s* orbitals. It does not allow us to distinguish between the exo or endo bonding character of the observed spectral features. The MOs are tentatively assigned to the spectral bands, as shown in Table 8.

CONCLUSIONS

The PE spectra show a significant destabilization of the HOMO if one or more vertices are vacant in the icosahedral skeleton. The MNDO calculated orbital energies qualitatively agree with the observed PE band envelopes. In all species studied the HOMO has cluster bonding character. With the departure from icosahedral symmetry the endo bonding levels mix to a higher extent with B—H bonding orbitals. For the *arachno* species the endo/exo character of the particular levels cannot be distinguished. Thus, it seems that the endo/exo bonding separation cannot be applied if two or more vertices are vacant in the deltahedral cluster. In the *arachno* clusters derived from the 11-vertex *closo* species there is a significant contribution of the bridge hydrogen atoms to the cluster bonding

Table 7. Vertical ionization energies, orbital energies and composition of occupied MOs detected in the HeI PE spectrum of *arachno*-4-CB_8H_{14} (**5**)

IE (eV)	MO	$-\varepsilon$ (eV)	Composition C (%)	B (%)	H (%)	*p* function[b]	Angle[c] (°)	Assignment[a]
9.73 a	21	11.88	7	80	13	87	6	π-endo
10.71 b	20	11.96	2	70	28	68	31	π-endo
11.11 c	19	12.49	21	43	36	64	32	
11.72 d	18	12.65	13	42	45	54	41	
12.13 e	17	12.81	1	56	43	55	39	
12.47 f	16	12.96	16	43	41	57	44	
12.70 g	15	13.36	3	54	46	51	33	
14.22 h	14	14.02	11	52	37	62	17	
14.51 i	13	14.14	0	53	47	50	57	
14.74 j	12	14.43	13	45	42	57	59	
15.40 k	11	15.23	24	33	43	52	26	
15.83 l	10	17.03	2	40	58	15	65	
16.57 m	9	17.41	10	52	38	58	80	
18.2 n	8	18.45	8	55	37	33	25	
	7	18.99	1	67	32	27	21	

[a] Endo : cluster bonding character.

[b] Sum of the *p* density for all heavy atoms.

[c] Weighted average of the deviation of the *p* direction from the tangent to the cluster surface. The weight is the *p* density at the atom.

Table 8. Vertical ionization energies, orbital energies and composition of occupied MOs detected in the HeI PE spectrum of *arachno*-4,6-$C_2B_7H_{13}$ (**6**)

IE (eV)	MO	$-\varepsilon$ (eV)	Composition C	B (%)	H	*p* function[b]	Angle[c] (°)	Assignment[a]
9.31 a	21	10.73	19	71	10	88	6	π-endo
10.41 b	20	11.65	16	69	15	85	16	π-endo
11.25 c, 11.48 d, 11.83 e	19	12.26	19	49	33	67	42	
	18	12.34	34	34	32	68	32	
	17	12.64	7	45	48	49	51	
	16	13.24	57	8	35	66	43	
12.52 f	15	13.84	35	31	34	64	9	
12.91 g	14	14.00	43	18	39	53	35	
14.03 h	13	14.34	42	14	44	55	77	
14.60 i	12	14.56	22	33	45	54	70	
15.22 j	11	15.17	32	28	40	54	26	
16.16 k	10	16.60	56	6	38	25	43	
16.63 l	9	17.65	46	16	38	56	82	
17.72 m	8	18.54	61	10	29	29	22	
	7	19.01	54	13	33	33	15	

[a] Endo: cluster bonding character.
[b] Sum of the *p* density for all heavy atoms.
[c] Weighted average of the deviation of the *p* direction from the tangent to the cluster surface. The weight is the *p* density at the atom.

HOMO. This implies that the bridge hydrogen atoms in the open face of the deltahedron are involved in the cluster bonding. This is in an agreement with the earlier published idea by Rudolph[13] that the electrons of endo hydrogens contribute to the framework electron count.

REFERENCES

1. W. N. Lipscomb, *Boron Hydrides*. Benjamin, New York (1963).
2. E. L. Muetterties (Editor), *Boron Hydride Chemistry*. Academic Press, New York (1975).
3. R. Hoffman and W. N. Lipscomb, *J. Chem. Phys.* 1962, **36**, 2179.
4. R. B. King and D. H. Rowray, *J. Am. Chem. Soc.* 1977, **99**, 7834.
5. D. A. Dixon, D. A. Klier, T. A. Halgren, J. H. Hall and W. N. Lipscomb, *J. Am. Chem. Soc.* 1977, **99**, 6226.
6. J. Bicerano, D. S. Marinick and W. N. Lipscomb, *Inorg. Chem.* 1978, **17**, 3442.
7. D. M. P. Mingos, T. Slee and L. Zhenyang, *Chem. Rev.* 1990, **90**, 383.
8. P. Brint, J. P. Cronin, E. Seward and T. Whelan, *J. Chem. Soc., Dalton Trans.* 1983, 975.
9. M. J. S. Dewar and M. L. McKee, *Inorg. Chem.* 1978, **17**, 1569.
10. M. J. S. Dewar and M. L. McKee, *Inorg. Chem.* 1980, **19**, 2662.
11. T. Whelan, P. Brint, T. R. Spalding, W. S. McDonald and D. R. Lloyd, *J. Chem. Soc., Dalton Trans.* 1982, 2469.
12. B. F. G. Johnson (Editor), *Transition Metal Clusters*. Wiley, New York (1980).
13. R. W. Rudolph, *Accts Chem. Res.* 1979, **9**, 446.
14. M. Elian, M. M. L. Chen, D. M. P. Mingos and R. Hoffmann, *Inorg. Chem.* 1976, **15**, 1148.
15. R. E. Williams, *Inorg. Chem.* 1971, **10**, 210.
16. R. E. Williams, *Adv. Inorg. Chem. Radiochem.* 1976, **18**, 67.
17. K. Wade, *Adv. Inorg. Chem. Radiochem.* 1976, **18**, 1.
18. K. Wade, *J. Chem. Soc., Chem. Commun.* 1971, 792.
19. A. J. Stone, *Molec. Phys.* 1980, **41**, 1339.
20. A. J. Stone, *Inorg. Chem.* 1981, **20**, 563.
21. A. J. Stone and M. J. Alderton, *Inorg. Chem.* 1982, **21**, 2297.
22. A. J. Stone, *Polyhedron* 1984, **3**, 1299.
23. T. P. Fehlner, M. Wu, B. J. Menengheli and R. W. Rudolph, *Inorg. Chem.* 1980, **19**, 49.
24. J. A. Ulman and T. P. Fehlner, *J. Am. Chem. Soc.* 1978, **100**, 449.
25. J. A. Ulman, E. L. Andersen and T. P. Fehlner, *J. Am. Chem. Soc.* 1978, **100**, 456.
26. J. A. Ulman and T. P. Fehlner, *J. Am. Chem. Soc.* 1976, **98**, 1119.
27. P. Brint, J. P. Cronin, E. Seward and T. Whelan, *J. Chem. Soc., Dalton Trans.* 1983, 975.
28. T. Vondrák, *Polyhedron* 1987, **6**, 1559.
29. T. Vondrák, J. Plešek, S. Heřmánek and B. Štíbr, *Polyhedron* 1989, **8**, 805.
30. P. Brint, B. Sangkchakr, M. McGrath, T. R. Spalding and R. J. Suffolk, *Inorg. Chem.* 1990, **29**, 47.

31. J. MacCurtain, P. Brint and T. R. Spalding, *J. Chem. Soc., Dalton Trans.* 1985, 2591.
32. T. A. Green, A. C. Switendick and D. Emin, *J. Chem. Phys.* 1988, **89**, 6815.
33. J. Dolanský, S. Heřmánek and R. Zahradník, *Coll. Czech. Chem. Commun.* 1981, **46**, 2479.
34. J. D. Kennedy, *Prog. Inorg. Chem.* 1984, **32**, 512.
35. J. D. Kennedy, *Prog. Inorg. Chem.* 1986, **34**, 211.
36. N. N. Greenwood, *Chem. Soc. Rev.* 1984, **13**, 353.
37. M. J. S. Dewar and W. Thiel, *J. Am. Chem. Soc.* 1977, **99**, 4899.
38. M. J. S. Dewar and M. L. McKee, *J. Am. Chem. Soc.* 1977, **99**, 5231.
39. M. J. S. Dewar and C. H. Reynolds, *J. Comput. Chem.* 1986, **7**, 140.
40. J. Plešek and S. Heřmánek, *J. Chem. Soc., Chem. Commun.* 1975, 127.
41. W. R. Hertler, F. Klanberg and E. L. Muetterties, *Inorg. Chem.* 1967, **6**, 1696.
42. J. Plešek, S. Heřmánek and Z. Janoušek, *Collect. Czech. Chem. Commun.* 1977, **42**, 785.
43. J. Holub, T. Jelínek, J. Plešek, B. Štíbr, S. Heřmánek and J. D. Kennedy, *J. Chem. Soc., Chem. Commun.* 1991, 1389.
44. K. Baše, B. Štíbr, J. Dolanský and J. Duben, *Collect. Czech. Chem. Commun.* 1981, **46**, 2345.
45. F. N. Tebbe, P. M. Garrett and M. F. Hawthorne, *J. Am. Chem. Soc.* 1968, **90**, 869.
46. J. Plešek, B. Štíbr and S. Heřmánek, *Chem. Ind. (London)* 1980, 626.
47. P. Brint, B. Sangchakr, M. McGruth, T. R. Spalding and R. J. Suffolk, *Inorg. Chem.* 1990, **29**, 47.
48. D. Hnyk, unpublished results.

Polyhedron Vol. 12, No. 11, pp. 1311–1317, 1993
Printed in Great Britain

0277–5387/93 $6.00+.00
© 1993 Pergamon Press Ltd

THERMOCHROMISM IN COPPER(II) COMPLEXES: THERMAL, SPECTROSCOPIC, SOLID-STATE BROAD-LINE ^{1}H NMR AND ROOM-TEMPERATURE SINGLE-CRYSTAL X-RAY ANALYSIS OF BIS(N,N′-DIMETHYL-1,2-ETHANEDIAMINE)COPPER(II) DINITRATE

SUBRATANATH KONER, ASHUTOSH GHOSH* and NIRMALENDU RAY CHAUDHURI†

Department of Inorganic Chemistry, Indian Association for the Cultivation of Science, Calcutta 700 032, India

and

ALOK K. MUKHERJEE

Department of Physics, Jadavpur University, Calcutta 700 032, India

and

MONIKA MUKHERJEE

Department of Solid State Physics, Indian Association for the Cultivation of Science, Calcutta 700 032, India

and

RYUICHI IKEDA

Department of Chemistry, University of Tsukuba, Tsukuba, Ibaraki 305, Japan

(*Received* 10 *August* 1992; *accepted* 10 *February* 1993)

Abstract—The complex bis(N,N′-dimethyl-1,2-ethanediamine)copper(II) dinitrate, Cu(NN′-dmen)$_2$(NO$_3$)$_2$, undergoes a first-order thermochromic phase transition at *ca* 148°C, changing from blue–violet to blue. The low-temperature phase has been characterized by X-ray crystallography. The copper ion possesses distorted (4+2) octahedral geometry with two five-membered chelate rings, in the $\delta\lambda$ conformation, forming the CuN$_4$ plane [Cu—N = 2.000(6) and 2.033(7) Å] and oxygens from the two nitrate groups weakly coordinated in the two axial coordination sites [Cu—O = 2.506(8) Å]. The broad-line ^{1}H NMR indicates the onset of a dynamic disorder of diamine chelate rings at the phase transition temperature region. The electronic spectrum broadens on phase transition.

The thermochromic phenomena of copper(II) and nickel(II) salts with N,N-diethyl-1,2-ethanediamine (dieten) have been thoroughly investigated by several workers.[1–4] It is now well established that the discontinuous thermochromism exhibited by M(dieten)$_2$X$_2$ [where M = copper(II) or nickel(II) and X = ClO$_4$ or BF$_4$] is due to a weakening of the in-plane ligand field strength, resulting from the onset of dynamic disorder of the chelate rings, while the anions remain uncoordinated in both the low-

*Present address: Department of Chemistry, Jhargram Raj College, Jhargram 721507, West Bengal, India.

†Author to whom correspondence should be addressed.

Non-S.I. units employed: B.M. $\simeq 9.27 \times 10^{-24}$ Am^2; $S = 10^{-4}$ T.

and high-temperature phases.[5,6] Single-crystal X-ray analysis as well as temperature-variable ^{1}H NMR second-moment data have been found to be very useful to understand this type of thermochromic behaviour properly.

The same phenomena with other diamines are not well documented. The following factors are likely to play very important and crucial roles for this type of thermochromic phase transition: (1) steric effect of the alkyl group, (2) nature of the anions, (3) hydrogen-bonding network in the molecule, (4) decomposition temperature, etc. Amongst them, the role of the anion, especially that of nitrate, appears to be interesting in this connection. For example, in the complex $Cu(dicten)_2(NO_3)_2$[1,7] an increased axial interaction of the nitrate ions is taken into account to explain the drastic change in colour in addition to the dynamic disorder of the chelate rings. However, $Cu(dmpd)_2(NO_3)_2$[8] (dmpd = 2,2-dimethyl-1,3-propanediamine) and $Cu(daco)(NO_3)_2$[9] (daco = 1,5 diazocyclooctane) show similar but less drastic thermochromic transitions, which is explained to be due to the decrease in the axial interaction of the semi-coordinated nitrate ions. To generalize this it is necessary to search for similar systems.

We noticed for the first time that the complex $Cu(N,N'\text{-dmen})_2(NO_3)_2$ (where N,N'-dmen = N,N'-dimethyl-1,2-ethanediamine) is discontinuously thermochromic. Here we report the preparation, characterization and ^{1}H NMR second moment study of this complex. The crystal structure of the title complex was reported[10] to an R value of 0.072, without the hydrogen atom positions. However, to calculate the ^{1}H NMR second moment the positions of the hydrogen atoms are essential. Therefore, we have redetermined the crystal structure of the complex with hydrogen atom positions.

EXPERIMENTAL

Materials

N,N'-dimethyl-1,2-ethanediamine(NN'-dmen) was purchased from Fluka AG in high purity grade and used as received. All other chemicals used were of AR grade.

Synthesis of $Cu(NN'\text{-dmen})_2(NO_3)_2$

This was prepared by adding diamine (NN'-dmen) (2 mmol) dropwise to copper(II) nitrate (1 mmol) dissolved in methanol (10 cm^3). The resultant solution was stirred for 1 h. The desired blue–violet complex was separated and washed with methanol and dried in a desiccator. Found: C, 23.0; H, 6.7; N, 26.3; Cu, 17.6. Calc. for $C_8H_{24}N_6CuO_6$: C, 23.1; H, 6.6; N, 26.4; Cu, 17.4%. $\mu_{eff} = 1.83$ B.M.; $\lambda_{max} = 547, 742$ (sh) nm.

A crystal suitable for X-ray analysis was obtained from a methanolic solution kept at room temperature.

Physical measurements

The solid-state thermal measurements, elemental analyses, IR spectra (KBr discs, at ambient and above ambient), electronic spectra (mulls, at ambient and above ambient) and effective magnetic moments at room temperature were recorded using apparatus reported earlier.[11,12] The second moments of ^{1}H NMR absorptions were determined on a JEOL-MW-40S spectrometer at several temperatures, with an accuracy of ± 3 K, and X-ray powder patterns were recorded at 25°C and 155°C using a Rigaku Denki D-3F diffractometer equipped with a copper anticathode at Nagoya University, Japan. The visual colour change associated with phase transition was monitored by keeping the complex in the desired temperature range in an air oven.

Crystal data

$C_8H_{24}N_6CuO_6$, $M = 363.9$, monoclinic, $a = 7.425(2)$, $b = 8.533(2)$, $c = 13.072(3)$ Å, $\beta = 105.56(3)°$, $U = 797.86(4)$ Å^3 (by least-squares refinement on diffractometer angles for 20 automatically centred reflections, $\lambda = 0.71069$ Å), space group $P2_1/c$, $Z = 2$, $D_c = 1.51$ g cm^{-3}, $F(000) = 382$, blue–violet crystals, dimensions $0.35 \times 0.25 \times 0.15$ mm, $\mu(\text{Mo-}K_\alpha) = 14.04$ cm^{-1}, $T = 293$ K.

Data collection, structure solution and refinement

A Hilger–Watts diffractometer was used in the ω–2θ mode, with graphite-monochromated Mo-K_α radiation, and 1175 unique reflections measured ($1.5 \leqslant \theta \leqslant 25°$; $\pm h, k, l$) giving 726 with $I > 3\sigma(I)$. No significant decay of intensity controls occurred during data collection. Absorption corrections (max., min. transmission factors 0.941, 0.715) were performed following ref. 13.

The heavy-atom method was followed by a successive difference-Fourier analysis. The copper atom was located at a crystallographic inversion centre, so that only one chelated ligand (L) and one nitrate group are independent. A full-matrix least-squares refinement was performed, with all non-hydrogen atoms anisotropic and hydrogen atoms (methyl hydrogen atoms were kept fixed with $U_{iso} = 0.05$ Å^2) isotropic. The weighting scheme

$w = 1/[\sigma^2(F_o)+0.004F_o^2]$ with $\sigma(F_o)$ from counting statistics gave satisfactory analyses. Final R and R' values are 0.053 and 0.054. Programs, computers used and sources of scattering factor data are given in ref. 14.

Supplementary material. Tables of positional and thermal parameters, interatomic distances and angles, prominent lines in the X-ray powder patterns recorded below and above transition temperature and structure factors have been deposited with the Editor.

RESULTS AND DISCUSSION

Description of the structure

An ORTEP[15] view of the complex with the atom labelling scheme is shown in Fig. 1. Selected bond lengths and bond angles are listed in Table 1. The structure consists of $[CuL_2]^{2+}$ cations and two NO_3 anions. The copper atom at the inversion centre is co-planar with four ligand nitrogen atoms [N(1), N(2) and their centrosymmetrically related ones]. The geometry around copper is distorted square-planar, with an in-plane distortion introduced by the ligand bite angle N(1)—Cu—N(2) = 84.8(3)°. The two five-membered chelate rings are in the $\delta\lambda$ conformation. Weak coordinations, Cu—O(1) = 2.506(8) Å, of two symmetry-related oxygen atoms [O(1) at x, y, z and O(1)′ at $-x$, $-y$, $-z$] of the NO_3^- ion complete a distorted octahedron. O(2) of the nitrate ion is hydrogen bonded to one of the amino nitrogen atoms [N(1)] of the cation: O(2)···N(1) 3.02, O(2)···H(N1) 2.27 Å; N(1)—H(N1)—O(2) 148.5°. Similar weak hydrogen bonding between NO_3^- and nitrogen atoms in the ligand was reported for bis(1,5-diazacyclooctane)copper(II) nitrate.[9] The nitrate ion is essentially planar [displacement of N(3) from the weighted least-squares plane through O(1), O(2), O(3) being 0.007(7) Å] and inclined to the CuN_4 chelate plane by 66.4(3)°. The observed C(2)—C(3) bond, 1.441(16) Å (Table 1), is short but a similar

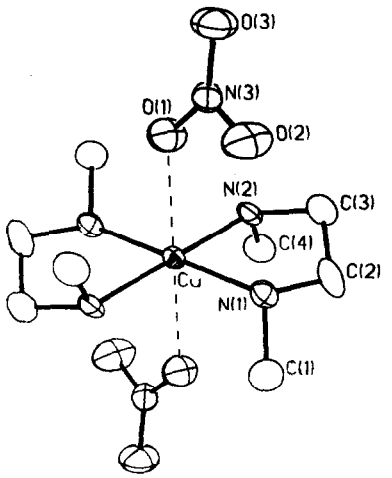

Fig. 1. ORTEP plot of $Cu(NN'\text{-dmen})_2(NO_3)_2$, showing the atom numbering scheme and the semi-coordination of the nitrate ions.

shortening of the C—C bond [1.41(1)–1.47(1) Å] in the 1,2-diaminoethane fragment is reported in the literature.[16] The Cu—N distances 2.000(6) and 2.033(7) Å are comparable to those observed in similar systems.[10,17,18] The small difference between the Cu—N(1) and Cu—N(2) distance is a consequence of an unsymmetrical interaction of the anion to the ligand.

Thermal analysis

The result of the simultaneous TG–DTA measurement of the title complex is shown in Fig. 2. The DTA curve shows a sharp endothermic peak associated with a colour change from blue–violet to blue in the temperature range 145–155°C, where the corresponding TG curve remains flat. The enthalpy change for this transformation was calculated from the DSC curve (ΔH = 12.1 kJ mol^{-1}). The transformation is reversible and on cooling the blue species reverts to its original form in the temperature range 90–120°C (ΔH = −12.4 kJ mol^{-1}).

Table 1. Selected bond lengths (Å) and angles (°)

Cu—N(1)	2.033(7)	Cu—N(2)	2.000(6)
Cu—O(1)	2.506(8)	N(1)—C(2)	1.455(12)
N(2)—C(3)	1.522(12)	N(3)—O(1)	1.243(11)
N(3)—O(2)	1.229(11)	N(3)—O(3)	1.204(12)
C(2)—C(3)	1.441(16)		
N(1)—Cu—N(2)	84.8(3)	N(1)—Cu—O(1)	94.2(3)
N(2)—Cu—O(1)	85.5(3)	O(1)—N(3)—O(2)	119.0(8)
O(1)—N(3)—O(3)	120.6(8)	O(2)—N(3)—O(3)	120.4(9)

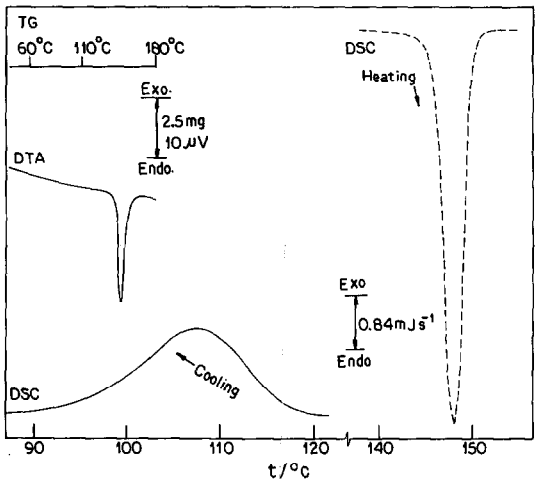

Fig. 2. Simultaneous TG–DTA (weight taken = 14.50 mg) and DSC (weight taken = 5.85 mg) (broken line for heating and solid line for cooling) curves for Cu(NN′-dmen)$_2$(NO$_3$)$_2$, showing the endothermic phase transformation.

Therefore, the transformation is associated with some amount of hysteresis.

IR and electronic spectra and X-ray powder diffraction

The IR spectra of the complex recorded at room temperature and at the temperature where phase transformation is assumed to be completed do not differ much. Only the combination band of the nitrate ion,[7,19] appearing at *ca* 1750 cm^{-1}, broadens on heating and a small change in the relative intensities of some of the bands is also observed in the fingerprint region,[12] although these changes are not so significant. Therefore, it is very difficult to draw any conclusion from the IR spectral change.

The colour change from blue–violet to blue, associated with reversible thermochromism, can be visually observed as mentioned earlier (*vide supra*). The visible absorption spectrum of the copper(II) complex recorded at room temperature (Fig. 3) shows a broad band at 547 nm with a shoulder at 742 nm. Gaussian resolution of the spectra has not been performed in this study but such a study has been published recently in a similar type of complex.[4] On phase transformations the absorption bands become broader and thereby none of the transitions can be assigned. However, the broadening of the spectrum was reported in a similar thermochromic complex.[8]

X-ray powder diffraction patterns of the complex were recorded below (at 25°C) and above (at 155°C) the transition temperature. The two powder patterns appear to be almost identical with respect to the positions of the lines, although some changes in the intensities of the corresponding diffraction maxima for the two phases are observed. This indicates that the unit cell dimensions of the two phases are almost the same, while the internal structures are different.

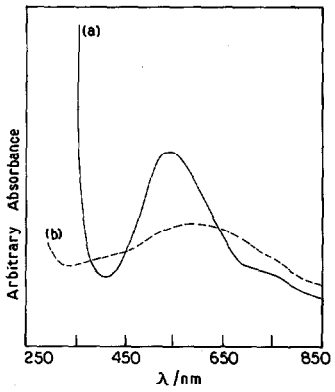

Fig. 3. Electronic spectra of Cu(NN′-dmen)$_2$(NO$_3$)$_2$: (a) at room temperature (25°C); (b) above the phase transition temperature (150°C).

Solid-state broad-line ^{1}H *NMR*

A broad-line ^{1}H NMR spectrum in the solid state of the complex Cu(NN′-dmen)$_2$(NO$_3$)$_2$ was taken from room temperature to its phase transformation temperature range. The second moment (M_2) of the resonance line was obtained by integration of the observed spectrum, as given in eq. (1),[20,21] where H_0 is the field at the centre of the peak and $I(H-H_0)$ is the intensity at a given field H. The results are shown in Fig. 4.

$$M_2 = \frac{\int [I(H-H_0)](H-H_0)^2 \, dH}{\int [I(H-H_0)] \, dH} \qquad (1)$$

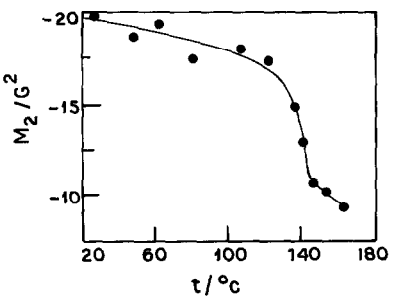

Fig. 4. Plot of ^{1}H NMR second moments vs temperature for Cu(NN′-dmen)$_2$(NO$_3$)$_2$.

Theoretical values of M_2 for possible motional states of the complex ion below and above the phase transition temperture are evaluated as follows: in the low-temperature phase, for example at room temperature, the reorientation of the two CH_3 groups about the C—N bonds in the complex ion is the only allowed motion and the rest of the complex ion is expected to be rigid. The M_2 calculation in a powder sample for this model was performed using Van Vleck's equation:[20]

$$M_2(\text{static})_{jk} = (9/10)g^2u_0^2N^{-1}\Sigma r_{jk}^{-6}, \qquad (2)$$

for the interacting protons j and k. Here g, N, u_0 and r_{jk} denote the proton g-factors, the number of interacting protons considered in the calculation, nuclear magneton and the distance between the protons, respectively. The contribution from the rotating CH_3 groups[21] was calculated assuming that the three protons are concentrated at the centre of gravity. The calculated values for this motional state, $M_2(\text{static})_{jk}$, are shown in Table 2 for the respective interproton interactions. The interproton distances used in this calculation were evaluated using the atomic coordinates from the X-ray structural analysis.

The total values of the theoretical M_2 can be given by the summation of the contributions from intramolecular interactions (20.4 G^2) and intermolecular origin (roughly estimated to be 2–3 G^2). The resultant value is close to the observed M_2 [19.5 G^2]. This small difference in these two values is attributable to the effects of thermal vibrations, which is also corroborated from the experimental observation that M_2 at low temperature is not constant but increases with lowering of the temperature.

We can also expect a contribution to line-width from the magnetic dipolar field due to the unpaired electrons in paramagnetic copper(II) atoms. In isolated paramagnetic systems like the present com-

Table 2. ^1H NMR second moment calculations for $Cu(NN'\text{-dmen})_2(NO_3)_2$

Atoms[a]	θ''_{jk} (°)	r_{jk}^{-6} (Å^{-6})	M_2 (static)[b] (G^2)	M_2 (dynamic)[c] (G^2)
$CH_3(1)$—H(N1)	85.1319	0.0274	1.6378	0.8917
$CH_3(1)$—H1(C2)	60.2357	0.0066	0.3953	0.2510
$CH_3(1)$—H2(C2)	44.9586	0.0071	0.4218	0.3141
H(N1)—H1(C2)	63.6224	0.0027	0.1615	0.0994
H(N1)—H2(C2)	29.5909	0.0148	0.8851	0.7689
H(N1)—H1(C3)	62.4496	0.0032	0.1882	0.1171
H(N1)—H2(C3)	56.7747	0.0004	0.0241	0.0158
H(N1)—H(N2)	91.1884	0.0004	0.0226	0.0122
H1(C2)—H2(C2)	68.1001	0.0835	4.9843	2.9554
H1(C2)—H1(C3)	89.6334	0.0023	0.1352	0.0733
H1(C2)—H2(C3)	70.1092	0.0049	0.2933	0.1713
H1(C2)—H(N2)	112.2127	0.0007	0.0421	0.0250
H1(C2)—CH_3(10)	111.5628	0.0046	0.2738	0.1619
H2(C2)—H1(C3)	103.8298	0.0070	0.4179	0.2350
H2(C2)—H2(C3)	84.0769	0.0038	0.2280	0.1244
H2(C2)—H(N2)	119.2133	0.0004	0.0214	0.0135
H1(C3)—H2(C3)	59.2905	0.0640	3.8185	2.4474
H1(C3)—H(N2)	128.5873	0.0131	0.7805	0.5424
H1(C3)—CH_3(10)	108.4295	0.0017	0.1007	0.0582
H2(C3)—H(N2)	158.4487	0.0077	0.4603	0.4261
H2(C3)—CH_3(10)	134.4505	0.0073	0.4378	0.3240
H(N2)—CH_3(10)	85.0955	0.0297	1.7699	0.9637
$CH_3(1)$	115.9500	0.0242	1.4408	0.8838
CH_3(10)	113.7500	0.0242	1.4408	0.8674
Total			20.3817	12.7430

[a] $CH_3(1)$ and CH_3(10) denote the average position of the three protons attached to the carbon atoms C(1) and C(4), respectively (Fig. 1), assuming that the protons are concentrated at the centre of gravity of the methyl group.

[b] Static molecule with rotating methyl groups.

[c] $\phi_0 = 25.7°$.

plex it is generally accepted[22] that the electron spin states are interconverting so rapidly that the time-average magnetic moments of electrons produce a constant local magnetic field at each proton. This results in a paramagnetic shift of the whole spectrum and/or an asymmetric line-shape caused by the superposition of various shifts at different proton sites in a molecule.[23] The latter contribution may change the line-width. In the present measurements, however, we could not observe either detectable shifts of spectra or any sign of anisotropic line-shapes in the whole temperature range studied. These results imply that effects from the paramagnetic electrons on the line-width are, if any, smaller than those from the interproton dipolar interactions.

Short relaxation times of unpaired electrons sometimes broaden the proton line-width and this effect can also be operative in the present system. To estimate this contribution we measured proton M_2 values in diamagnetic thermochromic nickel(II) complexes with N,N-diethyl-1,2-ethanediamine ligands[24] and compared the observed values with the reported data on paramagnetic copper(II) complexes[2] having the isomorphous crystal structure with the nickel(II) complexes. The M_2 values of these two kinds of complexes observed around the thermochromic phase transition temperatures appear to be quite similar to each other, suggesting that the broadening due to the paramagnetic electron spins in copper(II) atoms is much smaller than the interproton contribution. In the present complex the fact that the M_2 observed at room temperature is very close to the value calculated without paramagnetic contribution indicates the adequacy of this expectation. For these reasons we simplified the calculation and roughly evaluated the M_2 values without including contributions from the electron spins. An analogous treatment has been reported in the M_2 calculation for copper(II) complexes with N,N-diethyl-1,2-ethanediamine ligands.[2]

In the high-temperature phase the dynamic disorder of the chelate rings is the most probable motion for explaining the marked decrease of M_2 observed around 140°C, as is reported in the thermochromic $[Cu(dieten)_2]^{2+}$ complexes.[2] The theoretical M_2 value reduced by the puckering of the chelate rings was calculated by employing the same assumptions reported earlier[2] to simplify the calculation. The puckering motion was approximated by the jumps between the two equivalent orientations of the ligand molecules superimposed by rotating the molecules about the axis connecting the central metal and the mid-point of the CH_2—CH_2 bond by an angle of $51.5°(2\phi_0)$. This motion affords the reducing factor R_{jk} for the M_2 contribution from the dipolar interaction between protons j and k which is given by:

$$R_{jk} = [1+3(\sin^2\theta''_{jk}\cos 2\phi_0+\cos^2\theta''_{jk})^2]/4; \quad (3)$$

where θ''_{jk} is the angle between the rotation axis and the interproton vector r_{jk}. The values of M_2 which contributed by the interaction between protons j and k averaged by this motion can be given by:

$$M_d(\text{dynamic})_{jk} = M_2(\text{static})_{jk}\, R_{jk}. \quad (4)$$

The calculated values of $M_2(\text{dynamic})_{jk}$ are listed in Table 2 using the θ''_{jk} values evaluated from the X-ray data. Summation of these values gives M_2 (dynamic) of 12.74 G^2. This value is close to M_2 of 9.5 G^2 observed at 142°C. The difference between the calculated and observed values is attributable to the rough approximation of the puckering motion by two-fold rotation.

CONCLUSIONS

It is evident from the above discussion that a weakening of the in-plane ligand field strength due to the onset of dynamic disorder of the chelate rings (evident from the substantial drop of the second moment) is responsible for the thermochromic phase transition of the $Cu(NN'\text{-dmen})_2(NO_3)_2$ complex. Semi-coordination of the nitrate ion in the room-temperature phase and a slight change in colour upon phase transition lead to the conclusion that the thermochromic behaviour of the complex resembles that of bis(2,2-dimethyl-1,3-propanediamine)copper(II) dinitrate rather than that of bis(N,N-diethyl-1,2-ethanediamine)copper(II) dinitrate.

Acknowledgements—The authors are grateful to the Referee for pointing out ref. 10. We are also grateful to the Department of Physics, University of York, U.K., for allowing two of the authors (AKM, MM) to use the X-ray diffractometer facility. We thank S. Bhanja Chowdhury, National Single Crystal Diffractometer Facility, IACS, for the ORTEP plot and to the Ministry of Education, Science and Culture, Japan Government, for the award of a Fellowship (to AG).

REFERENCES

1. D. R. Bloomquist and R. D. Willett, *Coord. Chem. Rev.* 1982, **47**, 125 and refs therein.
2. R. J. Pylkii, R. D. Willett and H. W. Dodgen, *Inorg. Chem.* 1984, **23**, 594.
3. H. Yokoi, M. Sai and T. Isobe, *Bull. Chem. Soc. Japan* 1969, **42**, 2232.

4. K. L. Bray, H. G. Drickamer, E. A. Schmitt and D. Hendrickson, *J. Am. Chem. Soc.* 1989, **111**, 2849.
5. M. M. Andino, J. D. Curet and M. M. Muir, *Acta Cryst.* 1976, **B32**, 3185.
6. I. Grenthe, P. Paoletti, M. Sandstrom and S. Glikberg, *Inorg. Chem.* 1979, **18**, 2687.
7. A. B. P. Lever, E. Mantovani and J. C. Donini, *Inorg. Chem.* 1971, **10**, 2424.
8. L. Menabue, G. C. Pellacani, L. P. Battaglia, A. B. Corradi, F. Sandrolini, A. Motori, R. J. Pylkki and R. D. Willett, *J. Chem. Soc., Dalton Trans.* 1984, 2187.
9. N. Hoshino, Y. Fukuda, K. Sone, K. Tanaka and F. Marumo, *Bull. Chem. Soc. Japan* 1989, **62**, 1822.
10. A. Pajunen, *Suom. Kemistil.* 1969, **B42**, 261.
11. S. Koner and N. Ray Chaudhuri, *Thermochim. Acta* 1991, **180**, 177.
12. A. K. Mukherjee, M. Mukherjee, A. J. Welch, A. Ghosh, G. De and N. Ray Chaudhuri, *J. Chem. Soc., Dalton Trans.* 1987, 997.
13. A. C. T. North, D. Philips and F. S. Mathews, *Acta Cryst.* 1968, **A24**, 351.
14. (a) G. M. Sheldrick, SHELX 76, Program for Crystal Structure Determination. University of Cambridge, U.K. (1976); (b) M. Nardelli, PARST, A System of Computer Programs for Calculating Molecular Parameters from Results of Crystal Structure Analyses. University of Parma (1982); (c) Vax Cluster System at the University of York, U.K.; (d) *International Tables for X-ray Crystallography*, Vol. 4. Kynoch Press, Birmingham (1974).
15. C. K. Johnson, ORTEP, Report ORNL-5138. Oak Ridge National Laboratory, Tennessee (1976).
16. A. J. Finney, M. A. Hitchman, C. L. Raston, G. L. Rowbottom and A. White, *Aust. J. Chem.* 1981, **34**, 2085.
17. P. Murray-Rust, J. Murray-Rust and R. M. Clay, *Acta Cryst.* 1980, **B36**, 452.
18. J. M. Latour, S. S. Tandon and D. C. Povey, *Acta Cryst.* 1989, **C45**, 7.
19. A. B. P. Lever, E. Mantovani and B. S. Ramaswamy, *Can. J. Chem.* 1971, **49**, 1975.
20. J. H. Van Vleck, *Phys. Rev.* 1948, **74**, 1168.
21. H. S. Gutowsky and G. E. Pake, *J. Chem. Phys.* 1950, **18**, 162.
22. R. G. Shulman and V. Jaccarino, *Phys. Rev.* 1957, **108**, 1219.
23. M. Inoue, *J. Magnet. Reson.* 1977, **27**, 159.
24. A. Ghosh, D. Nakamura and R. Ikeda, *Ber. Bunsenges. Phys. Chem.* 1992, **96**, 919.

Polyhedron Vol. 12, No. 11, pp. 1319–1328, 1993
Printed in Great Britain

0277–5387/93 $6.00+.00
© 1993 Pergamon Press Ltd

KINETICS AND MECHANISM OF COMPLEX FORMATION REACTION OF IRON(III) WITH 4-METHYL-8-(CARBOXYMETHYL)AMINOMETHYL UMBELLIFERRONE AND RELATED LIGANDS: ROLE OF SUBSTITUENT GROUPS ON NITROGEN DONOR ATOMS ON THE REACTION

HIROTO YOSHIDA, TOMOHIRO OZAWA, KOICHIRO JITSUKAWA and HISAHIKO EINAGA†

Department of Applied Chemistry, Faculty of Engineering, Nagoya Institute of Technology, Gokiso-cho, Showa-ku, Nagoya 466, Japan

(*Received* 23 *November* 1992; *accepted* 8 *February* 1993)

Abstract—The formation of the iron(III) complex of 4-methyl-8-(carboxymethyl)aminomethyl umbelliferrone (**1**, H_2mug) and its N-methyl (**2**, H_2mugm) and N-carboxymethyl (**3**, H_3muia) derivatives has been investigated spectrophotometrically in an aqueous sodium nitrate solution (0.10 mol dm^{-3}) at 25°C. A 1 : 1 (metal : ligand) complex forms uniquely for all three ligands, indicating a steric interference between the coordinated and a coordinating ligand. The stability constant [log β_{11}/(mol^{-1} dm^3)] is 15.74 ± 0.20 for **4** [Fe(mug)$^+$], 15.69 ± 0.20 for **5** [Fe(mugm)$^+$] and18.67 ± 0.20 for **6** [Fe(muia)]. The complex formation reaction proceeds through two parallel pathways of Fe^{3+} and $Fe(OH)^{2+}$ with diprotonated ligand species of **1**, **2** and **3**; a slow coordination of the phenolato oxygen, followed by rapid donations of the amino nitrogen and carboxylato oxygen(s) to form a mono(terdentato- and tetradentato)iron(III) complex was deduced as the reaction mechanism. The possibility of changing the thermodynamic stability with no variation in the reaction mechanism by the introduction of substituent groups on the amino nitrogen of **1** is suggested.

The design and development of functional chelating agents for metal cations are some of our recent concerns. More specifically, we are now interested in the synthesis and the coordination characteristics of those multidentate ligands capable of forming fused chelate rings with metal ions, in which their aromatic groups are incorporated. As such a ligand, 4-methyl-8-(carboxymethyl)aminomethyl umbelliferrone (**1**, H_2mug) was designed and synthesized and its metal–chelate complex formation characteristics were studied with iron(III) from thermodynamic and kinetic aspects. Futhermore, they were compared with the related ligands 4-methyl-8-(N-carboxymethyl-N-methyl)aminomethyl umbelliferrone (**2**, H_2mugm) and 4-methyl-8-di(carboxymethyl)aminomethyl umbelliferrone (**3**, H_3muia) in order to elucidate the role of substituent groups on the amino nitrogen on these characteristics (cf. Scheme 1). Iron(III) was chosen here for the coordinated central metal atom because the iron(III) complex of aminocarboxylato ligating groups generally takes a high-spin d^5-state in octahedral coordination, being comparable with the aminocarboxylato metal(III) complexes of d^0- and d^{10}-electronic configurations of the same coordination structure, and because the former usually exhibits a characteristic charge-transfer (CT) band in the visible wavelength region, which is convenient for the spectrophotometric investigation of metal complex systems.

The present paper describes the thermodynamic stability and the formation reaction mechanism of the iron(III) complexes of **1**, **2** and **3**; attention was paid to the possibility of changing the thermodynamic stability with no variation in the formation reaction mechanism by introducing substituent groups on the amino nitrogen attached via a methylene group to the skeletal umbelliferrone.

† Author to whom correspondence should be addressed.

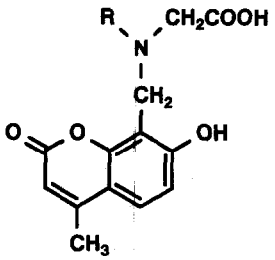

1 (H_2mug), R = H
2 (H_2mugm), R = CH_3
3 (H_2muia), R = CH_2COOH

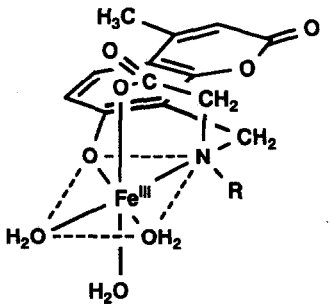

4 ($Fe(mug)^+$), R = H
5 ($Fe(mugm)^+$), R = CH_3

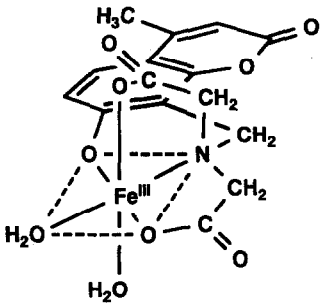

6 (Fe(muia))

Scheme 1.

EXPERIMENTAL

Materials

The ligand **1** was synthesized using a Mannich reaction with 4-methyl umbelliferrone, glycine and formaldehyde in acetic acid, according in principle to a procedure given in the literature.[1] The ligand was purified by recrystallization from water. Found: C, 58.8; H, 5.0; N, 5.3. Calc. for $C_{13}H_{13}NO_5 \cdot (1/5)H_2O$: C, 58.7; H, 5.1; N, 5.2%.

The ligands **2** and **3** were synthesized by the same procedure as **1**, but using sarcosine and iminodiacetic acid in place of glycine, respectively. **2**: Found: C, 57.9; H, 5.9; N, 4.6. Calc. for $C_{14}H_{15}NO_5 \cdot (2/3)H_2O$: C, 58.1; H, 5.6; N, 4.8%. **3**: Found: C, 54.4; H, 4.7; N, 4.3. Calc. for $C_{15}H_{15}NO_7 \cdot (1/2)H_2O$: C, 54.5; H, 4.9; N, 4.2%.

An aqueous iron(III) solution was prepared as described elsewhere.[2] All the other chemicals used were of an analytical or equivalent grade.

Measurements

Electronic absorption spectra were recorded on JASCO spectrophotometers, models UVIDEC-1M and -660. Absorbance change with time at a fixed wavelength was followed with a JASCO spectrophotometer, model SS-25, equipped with a stopped-flow attachment, model SFC-5, and a data processor, model DP-500.[3]

Other apparatus and the general procedures for the determination of protonation, stability and observed rate constants have been given in a previous paper,[3] except that the ionic strength was kept constant at 0.10 mol dm^{-3} $NaNO_3$. The formation of the iron(III) complex was monitored spectrophotometrically at 510 nm. Kinetic runs were performed under the pseudo-first-order conditions of an excess and constant ligand concentration. Temperature was maintained constant at 25.0 ± 0.2°C throughout the experiments.

RESULTS

Absorption spectral characteristics

The iron(III) complex of **1** shows an electronic absorption spectrum, which is given in Fig. 1. Figure 1 also depicts the absorption spectra of the iron(III) complexes of **2** and **3** and of the free ligands. Besides the maxima and shoulders due to intraligand charge-transfer transitions in the higher wave-number region, the iron(III) complex of **1** exhibits a characteristic spectral feature giving a maximum at 18.0×10^3 cm^{-1} with a molar absorption coefficient [log ε/(mol^{-1} dm^3 cm^{-1})] of 3.2 and a

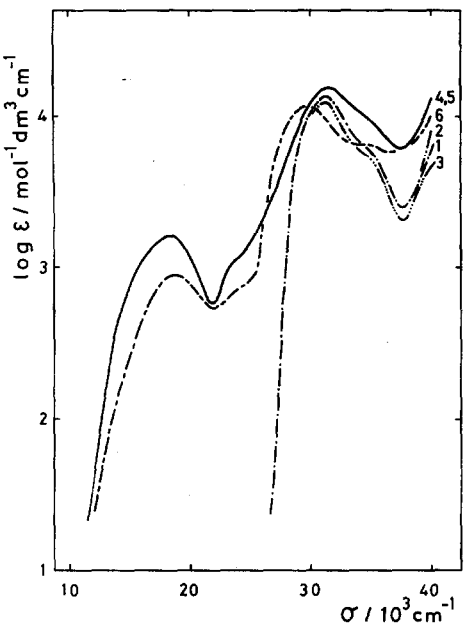

Fig. 1. Absorption spectra of the ligands and their iron (III) complexes. **1**: H_2mug (pH 2.50); **2**: H_2mugm (pH 2.50); **3**: H_2muia$^-$ (pH 2.50); **4**: Fe(mug)$^+$ (pH 2.50); **5**: Fe(mugm)$^+$ (pH 2.50); and **6**: Fe(muia) (pH 2.50).

shoulder around 24×10^3 cm^{-1}, with the coefficient slightly smaller in magnitude than the former; assignable to the $t_{2g}(O_h) \leftarrow \pi$ and $\pi^* \leftarrow e_g(O_h)$ charge-transfer transitions, respectively.[2] This spectral feature remains unchanged on going from the coordinated ligand of **1** to **2** and principally unchanged from **1** and **2** to **3**, although a slightly hypsochromic shift and a slight decrease in the molar absorption coefficient are noticed; this fact indicates that these iron(III) complexes equally have a metal-centred chromophore of the $[Fe^{III}(N)(O)_5]$-type.

The phenolate-oxygen protonated species of **1**, **2** and **3** gave characteristic fluorescence spectra of the same form with an excitation spectral maximum around 336 nm and an emission spectral maximum around 448 nm. However, this fluorescence disappeared completely in the iron(III) complexes of these ligands. Radiative $\pi^* \rightarrow \pi$ transition processes in the coumarin chromophore must have been replaced by an energy-transfer process, which accompanies an electron-transfer from the coordinated, excited coumarin chromophore to the central metal atom, followed by radiationless transitions via many intermediate *d*-electronic energy levels to the ground state in the metal-centred chromophore of the complex.

These results suggest that the ligand-to-metal charge-transfer band $[t_{2g}(O_h) \leftarrow \pi]$ is suitable for the thermodynamic and kinetic investigations of the iron(III) complexes of **1** and related ligands.

Thermodynamic stability

The protonation constants of **1** were determined spectrophotometrically, according in principle to a literature procedure.[3] The values of $K_{a(phOH)}$ and $K_{a(amNH)}$, corresponding to protonations at the phenolate oxygen and amino nitrogen atoms, were obtained from the experimental absorbance vs hydrogen-ion concentration plots by assignment based on comparison with related compounds (given in Table 1). Table 1 also summarizes $K_{a(phOH)}$ and $K_{a(amNH)}$ of **2** and $K_{a(phOH)}$, $K_{a(amNH)}$ and $K_{a(COOH)}$ of **3**, the latter corresponds to the protonation at the carboxylate oxygen atom.

Ligand **1** is potentially terdentate, capable of coordinating with two oxygen atoms and a nitrogen donor. The method of continuous variations[4] revealed the coordination of one ligand molecule to a central metal atom capable of taking an octahedral coordination, which indicates that a steric interference exists between the coordinated and a coordinating ligand in the iron(III) complex of **1** [**4**, Fe(mug)$^+$]. The same result was obtained for the iron(III) complex of **2** [**5**, Fe(mugm)$^+$]. The potentially tetradentate ligand **3** afforded a 1 : 1 (metal : ligand) complex of iron(III) [**6**, Fe(muia)].

Stability constants (β_{11}) were determined spectrophotometrically under the conditions $C_M \gg C_L$ and $C_L \gg C_M$ for complexes of **1** and **2** and $C_M \gg C_L$ for the complex of **3**, on the basis of a procedure given elsewhere:[2]

For complexes of **1** and **2**:

$$\beta_{11} = [\mathrm{Fe(mu)^+}]/[\mathrm{Fe^{3+}}] \times [\mathrm{mu^{2-}}] \quad (\mathrm{mu} = \mathrm{mug\ or\ mugm})$$

$$\log (A_{max} - A)/(A - A_{min}) = \log \{K_{a(amNH)}K_{a(phOH)}[H^+]^2 + K_{a(amNH)}[H^+] + 1\} + \log (1 + K^{11}_{OH}/[H^+]) - \log C_M - \log \beta_{11} \quad (C_M \gg C_L)$$

$$= \log \{K_{a(amNH)}K_{a(phOH)}[H^+]^2 + K_{a(amNH)}[H^+] + 1\} + \log (1 + K^{11}_{OH}/[H^+]) - \log C_L - \log \beta_{11} \quad (C_L \gg C_M); \qquad (1)$$

and for the complex of **3**:

$$\beta_{11} = [\mathrm{Fe(muia)}]/[\mathrm{Fe^{3+}}][\mathrm{muia^{3-}}]$$

$$\log (A_{max} - A)/(A - A_{min}) = \log \{K_{a(amNH)}K_{a(phOH)}K_{a(COOH)}[H^+]^3 + K_{a(amNH)}K_{a(phOH)}[H^+]^2 + K_{a(amNH)}[H^+] + 1\} + \log (1 + K^{11}_{OH}/[H^+]) - \log C_M - \log \beta_{11} \quad (C_M \gg C_L). \qquad (2)$$

Table 1. Protonation and stability constants

Ligand	log $K_{a(COOH)}$ (mol^{-1} dm^3)	log $k_{a(phOH)}$ (mol^{-1} dm^3)	log $K_{a(amNH)}$ (mol^{-1} dm^3)	Ref.
1 (H_2mug)	—	6.89±0.10	10.28±0.10	This work[a]
2 (H_2mugm)	—	6.51±0.10	10.94±0.10	This work[a]
3 (H_3muia)	1.90±0.10	6.78±0.10	11.50±0.10	This work[a]
	2.97	6.92	11.26	1b[b]
	—	7.2	12.2	8[c]
Hmu[d]	—	6.82±0.10	—	This work[d]
H_3hbida[e]	2.34	8.07	11.71	9[e]

Complex	log β_{11} (mol^{-1} dm^3)	
4 ($Fe(mug)^+$)	15.74±0.20	This work[a]
5 ($Fe(mugm)^+$)	15.69±0.20	This work[a]
6 (Fe(muia))	18.67±0.20	This work[a]
Fe(hbida)	22.4	9[e]

[a] 0.10 mol dm^{-3} ($NaNO_3$), 25°C. $K_{a(amNH)}$ = [Hmug$^-$]/[H$^+$][mug^{2-}] (at 358 nm) = [Hmugm$^-$]/[H$^+$][mugm^{2-}] (at 360 nm) = [Hmuia^{2-}]/[H$^+$][muia^{3-}] (at 362 nm). $K_{a(phOH)}$ = [H_2mug]/[H$^+$][Hmug$^-$] (at 358 nm) = [H_2mugm]/[H$^+$][Hmugm$^-$] (at 360 nm) = [H_2muia$^-$]/[H$^+$][Hmuia^{2-}] (at 362 nm). $K_{a(COOH)}$ = [H_3muia]/[H$^+$][H_2muia$^-$] (at 320 nm).

[b] 0.10 mol dm^{-3} (KCl), no specification on temperature.

[c] No specifications on ionic strength and temperature.

[d] Hmu: 4-methyl umbelliferrone. $K_{a(phOH)}$ = [Hmu]/[H$^+$][mu$^-$] (at 355 nm); 0.10 mol dm^{-3} ($NaNO_3$), 25°C.

[e] H_3hbida: N-(2-hydroxybenzyl)iminodiacetic acid; 0.10 mol dm^{-3}, 25°C.

Here A_{max}, A_{min} and A represent the absorbance of the iron(III) complex, the free ligand and the complex and the free ligand co-existing at the hydrogen ion concentration of [H$^+$]; K_{OH}^{11} is the hydrolysis constant of iron(III) forming $Fe(OH)^{2+}$ [K_{OH}^{11} = [$Fe(OH)^{2+}$][H$^+$]/[Fe^{3+}], log K_{OH}^{11} (mol dm^{-3}) = −2.78 [0.10 mol dm^{-3} ($NaClO_4$), 25°C)];[5] and C_L and C_M are the total concentrations of iron(III) and the ligand, respectively. Linear relations were obtained for all the complexes between the absorbance and the hydrogen ion concentration terms in eqs (1) and (2) (cf. Fig. 2), with a slope of unity, which substantiates the formation of only the complex species of a 1 : 1 (metal : ligand) composition, i.e. **4**, **5** and **6**. The values of β_{11} for these complexes were calculated from the experimental data plots on the relation between these terms (summarized in Table 1).

Kinetics and mechanism

Stopped-flow spectrophotometric kinetic measurements at 510 nm of the iron(III)–**1** system allowed us to deduce that, under the conditions of $C_L \gg C_M$ and constant [H$^+$], a single exponential curve fits the experimental absorbance vs time plots well for more than 3.5 half-life periods. The same evidence was obtained for the iron(III)–**2** and –**3** systems. Hence, it is inferred that the formation reactions of the iron(III) complexes of these multidentate ligands proceed equally with a single rate-determining step.

The rate equation for the formation of the iron (III) complex of **1** was derived in an analogous way to that previously described,[2] with the consideration that the protonation/deprotonation processes are much faster than the coordination process[3] [cf. Scheme 2(a)].

$$k_{obsd}\{K_{a(amNH)}K_{a(phOH)}[H^+]^2 + K_{a(amNH)}[H^+] + 1\}(1 + K_{OH}^{11}/[H^+])/C_L = k_{32}K_{a(amNH)}K_{a(phOH)}[H^+]^2 + \{k_{31} + k_{22}K_{OH}^{11}K_{a(phOH)}\}K_{a(amNH)}[H^+] + k_{30} + k_{21}K_{OH}^{11}K_{a(amNH)} + k_{20}K_{OH}^{11}/[H^+] \quad (3)$$

Here k_{ij} (i = 2 and 3, and j = 0–2) is the rate constant for the formation reaction pathway of $Fe(OH)_{3-i}^{i+}$ and $H_jmug^{(2-j)-}$ species. Equation (3) also holds for the iron(III) complex of **2**, but eq. (4) should be applicable to the iron(III) complex of **3** [cf. Scheme 2(b)].

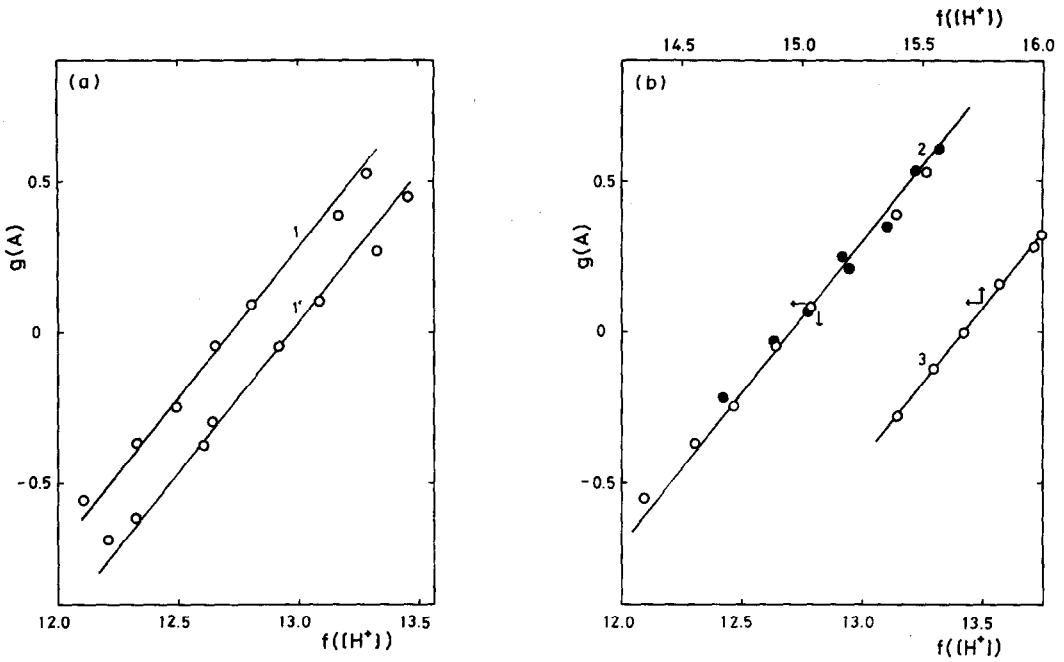

Fig. 2. Relation between the absorbance term, $g(A)$, and the hydrogen-ion concentration term, $f([H^+])$, of the iron(III)–ligand systems. $g(A) \equiv \log (A_{max}-A)/(A-A_{min})$; 0.10 mol dm^{-3} ($NaNO_3$), 25°C. Wavelength: 510 nm. (a) Iron(III)–**1** system. $f([H^+]) \equiv \log \{K_{a(amNH)}K_{a(phOH)}[H^+]^2 + K_{a(amNH)}[H^+]+1\} + \log (1+K_{OH}^{II}/[H^+])$. **1**: $C_M \gg C_L$, $C_M = 1.00\times10^{-3}$ mol dm^{-3}; $C_L = 1.00\times10^{-4}$ mol dm^{-3}. **1'**: $C_L \gg C_M$, $C_M = 1.62\times10^{-3}$ mol dm^{-3}; $C_L = 1.00\times10^{-4}$ mol dm^{-3}. Bold lines are theoretical lines drawn using the values of log $K_{a(amNH)}$/(mol^{-1} dm^3) = 10.28, log $K_{a(phOH)}$/(mol^{-1} dm^3) = 6.89, log β_{11}/(mol^{-1} dm^3) = 15.74 and log K_{OH}^{II}/(mol dm^{-3}) = −2.78. (b) Iron(III)–**2** and –**3** systems. Fe^{III}–**2** system: $f([H^+]) \equiv \log \{K_{a(amNH)}K_{a(phOH)}[H^+]^2+K_{a(amNH)}[H^+]+1\} + \log (1+K_{OH}^{II}/[H^+])$. ○: $C_M \gg C_L$, $C_M = 1.00\times10^{-3}$ mol dm^{-3}; $C_L = 1.00\times10^{-4}$ mol dm^{-3}. ●: $C_L \gg C_M$, $C_L = 1.59\times10^{-3}$ mol dm^{-3}; $C_M = 1.00\times10^{-4}$ mol dm^{-3}. The bold line is theoretically drawn using the values of log $K_{a(amNH)}$/(mol^{-1} dm^3) = 10.94, log $K_{a(phOH)}$/(mol^{-1} dm^3) = 6.51, log β_{11}/(mol^{-1} dm^3) = 15.69 and log K_{OH}^{II} given above. Fe^{III}–**3** system: $f([H^+]) \equiv \log \{K_{a(amNH)}K_{a(phOH)}K_{a(COOH)}[H^+]^3 + K_{a(amNH)}K_{a(phOH)}[H^+]^2 + K_{a(amNH)}[H^+]+1\} + \log (1+K_{OH}^{II}/[H^+])$. $C_M \gg C_L$, $C_M = 1.00\times10^{-3}$ mol dm^{-3}, $C_L = 1.00\times10^{-4}$ mol dm^{-3}. The bold line is theoretically drawn using the values of log $K_{a(amNH)}$/(mol^{-1} dm^3) = 11.50, log $K_{a(phOH)}$/(mol^{-1} dm^3) = 6.79, log $K_{a(COOH)}$/(mol^{-1} dm^3) = 1.90, log β_{11}/(mol^{-1} dm^3) = 18.67 and log K_{OH}^{II} given above.

$$
\begin{aligned}
&k_{obsd}\{K_{a(amNH)}K_{a(phOH)}K_{a(COOH)}[H^+]^3 \\
&\quad + K_{a(amNH)}K_{a(phOH)}[H^+]^2 \\
&\quad + K_{a(amNH)}[H^+]+1\}(1+K_{OH}^{II}/[H^+])/C_L \\
&\quad = k_{33}K_{a(amNH)}K_{a(phOH)}K_{a(COOH)}[H^+]^3 \\
&\quad + \{k_{32}+k_{23}K_{OH}^{II}K_{a(COOH)}\} \\
&\quad \times K_{a(amNH)}K_{a(phOH)}[H^+]^2 \\
&\quad + \{k_{31}+k_{22}K_{OH}^{II}K_{a(phOH)}\}K_{a(amNH)}[H^+] \\
&\quad + k_{30}+k_{21}K_{OH}^{II}K_{a(amNH)} \\
&\quad + k_{20}K_{OH}^{II}/[H^+] \qquad (4)
\end{aligned}
$$

In eq. (4) k_{ij}(i = 2 and 3, and j = 0–3) is the rate constant for the formation reaction pathway of $Fe(OH)_{3-i}^{i+}$ and $H_jmuia^{(3-j)-}$.

Kinetic experimental data are plotted in Fig. 3 in the form of a relation between the left-hand side of eqs (3) and (4) as a function of $[H^+]$. A quadratic curve of the form:

$$y = ax^2 + bx,$$

with y of an ordinate and x of an abscissa fit best the experimental data plots for the iron(III) complex of **1**, as well as the complexes of **2** and **3**. These results, together with a general kinetic characteristic of the iron(III) ion,[6a] indicate that the pathways of Fe^{3+} and $Fe(OH)^{2+}$ with diprotonated ligand species, which proceed in a parallel pathway, are universal among the complexes of **1**, **2** and **3**. A contribution of the pathways of Fe^{3+} with mono-protonated ligand species for **1**, **2** and **3** and the pathway of $Fe(OH)^{2+}$ with H_3muia species was ruled out because the estimated magnitude of each rate con-

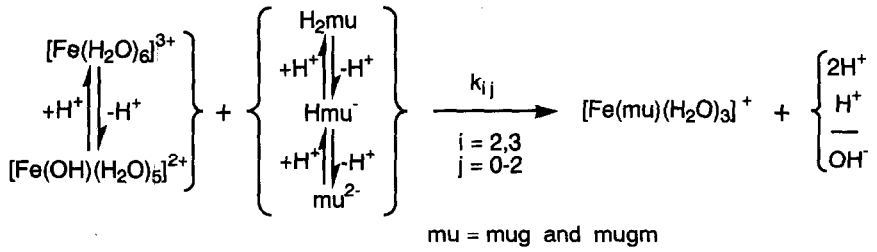

Scheme 2(a).

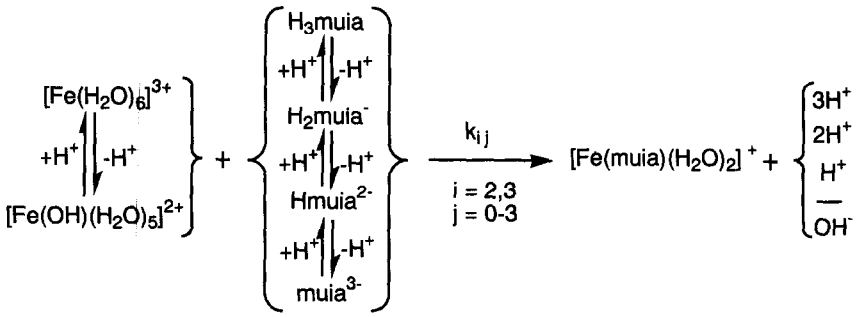

Scheme 2(b).

stant was abnormally large in comparison with the reported rate constants of known reaction mechanisms[6a] (*vide infra*). The values of the single and composite rate constants determined experimentally are summarized in Table 2, together with those of the iron(III) complexes of concern.

DISCUSSION

Formation

The terdentate ligands **1** and **2** are anticipated, forming bis(ligand)- as well as mono(ligand)iron (III) complexes (cf. Scheme 1). However, no formation of the former was noticed. A molecular model consideraion indicated the possible configurations of *fac*(O,N,O) and *mer*(O,N,O) around the octahedral central metal atom, with the former more intraligand- and less interligand-crowded than the latter. The formation of the bis(ligand) iron(III) complex was due to a mutual repulsive interaction between the coordinated and a coordinating ligand because no thermodynamic reason could be found (cf. log $\beta_{11} = ca$ 12 mol^{-1} dm^3; Table 1).

Substitution of a methyl group for the hydrogen atom on the nitrogen donor atom in **1** causes a slight decrease in the stability constant, β_{11}, in contrast to the protonation constant, $K_{a(amNH)}$, related to the nitrogen atom [and the sum of $K_{a(amNH)}$ and $K_{a(phOH)}$], which increases as is expected from the electron-donating nature of the methyl group. This contrary change in the stability and protonation constants on substitution may be due to the steric restriction of a chelate ring conformation by the methyl group on the nitrogen rather than the thermodynamic consequence of changes in the basicity of the nitrogen by the substitution. A marked increase in the stability constant was confirmed when the coordinating carboxymethyl group was introduced on the nitrogen donor atom (cf. **4** and **6**).

Kinetics and mechanism

There have been many papers concerning the kinetics and mechanism of the formation of iron (III) complexes with ligands containing N and/or O donor atoms;[6] e.g. α-hydroxycarboxylic acids,[6b] substituted salicyclic acids,[6c] hydroxamic acid and derivatives,[6d–h] 4-isopropyltropolone,[6i] 2,4-pentanedione derivatives,[6j–l] 2-carboxy (and 2,6-dicarboxy)pyridines,[6m] etc.,[6a] excluding those ligands cited in Table 2 which are of direct concern to the present discussion.

A general kinetic feature of the formation of these iron(III) complexes lies in the fact that they form usually through more than one reaction pathway,[6] i.e. formation accompanies the proton ambiguity. This is also the case for the iron(III) complexes of **1**, **2** and **3**. Therefore, the composite rate constants are assigned to the constant of the individual pathway by taking its characteristic magnitude, existing

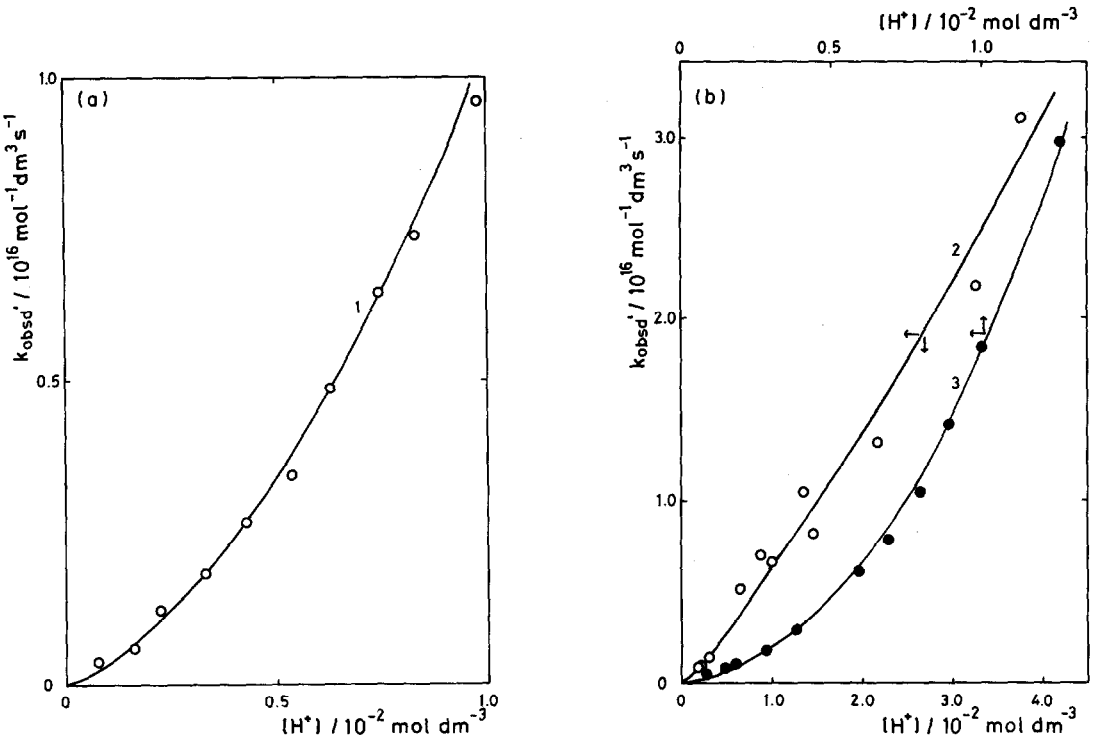

Fig. 3. Dependence of k_{obsd}' on [H$^+$] of the iron(III)–ligand systems. 0.10 mol dm^{-3} ($NaNO_3$), 25°C. Wavelength: 510 nm. $C_L \gg C_M$. (a) Iron(III)–**1** system. $k_{obsd}' \equiv k_{obsd}\{K_{a(amNH)}K_{a(phOH)}[H^+]^2+K_{a(amNH)}[H^+]+1\}(1+K_{OH}^{II}/[H^+])/C_L$. $C_L = 2.00\times10^{-3}$ mol dm^{-3}; $C_M = 1.00\times10^{-4}$ mol dm^{-3}. The bold line is theoretically drawn using the values of $K_{a(amNH)}$ and $K_{a(phOH)}$, of **1** given in Fig. 2, k_{32}/(mol^{-1} dm^3 s^{-1}) = 5.25×10^2, $k_{31}+k_{22}K_{OH}^{II}K_{a(phOH)}$/(mol^{-1} dm^3 s^{-1}) = 1.47×10^7. (b) Iron(III)–**2** and –**3** systems. Iron(III)–**2** system: $k_{obsd}' \equiv k_{obsd}\{K_{a(amNH)}K_{a(phOH)}[H^+]^2+K_{a(amNH)}[H^+]+1\}(1+K_{OH}^{II}/[H^+])/C_L$. $C_L = 2.00\times10^{-3}$ mol dm^{-3}; $C_M = 1.00\times10^{-4}$ mol dm^{-3}. The bold line is theoretically drawn using the values of $K_{a(amNH)}$ and $K_{a(phOH)}$ of **2** given in Fig. 2, k_{32}/(mol^{-1} dm^3 s^{-1}) = 6.17×10^2, $k_{31}+k_{22}K_{OH}^{II}K_{a(phOH)}$/(mol^{-1} dm^3 s^{-1}) = 1.03×10^6. Iron(III)–**3** system: $k_{obsd}' \equiv k_{obsd}\{K_{a(amNH)}K_{a(phOH)}K_{a(COOH)}[H^+]^3+K_{a(amNH)}K_{a(phOH)}[H^+]^2+K_{a(amNH)}[H^+]+1\}(1+K_{OH}^{II}/[H^+])/C_L$. $C_L = 0.50_0\times10^{-3}$ mol dm^{-3}; $C_M = 0.50_0\times10^{-4}$ mol dm^{-3}. The bold line is theoretically drawn using the values of $K_{a(amNH)}$, $K_{a(phOH)}$ and $K_{a(COOH)}$ of **3** given in Fig. 2, $k_{32}+k_{23}K_{OH}^{II}K_{a(COOH)}$/(mol^{-1} dm^3 s^{-1}) = 2.42, $k_{31}+k_{22}K_{OH}^{II}K_{a(phOH)}$/(mol^{-1} dm^3 s^{-1}) = 1.87×10^6.

metal and ligand species and the nature of the metal–donor atom bonds before discussing the reaction mechanism.

The rate constants for the formation of the iron(III) complex of **1** are $(5.25\pm0.20)\times10^2$ for k_{32} and $(1.47\pm0.20)\times10^7$ mol^{-1} dm^3 s^{-1} for $k_{31}+k_{22}K_{OH}^{II}K_{a(phOH)}$. The former may be of a reasonable magnitude for the iron(III) complex of a zwitter-ionic H_2mug ligand species. The latter, on the contrary, is too high for the iron(III) complex of singly protonated $Hmug^-$ ligand species. A tentative estimation of k_{22} from this composite rate constant value using K_{OH}^{II} and $K_{a(phOH)}$, by neglecting the pathway of k_{31} afforded k_{22} as $(1.14\pm0.30)\times10^3$ mol^{-1} dm^3 s^{-1}. This is quite a reasonable magnitude for the pathway of $Fe(OH)^{2+}$ with the H_2mug species. Accordingly, the iron(III) complex of **1** is expected to form via two parallel pathways of Fe^{3+} and $Fe(OH)^{2+}$ with H_2mug. The same consideration holds for the iron(III) complex of **2**: The estimated rate constant is $(1.92\pm0.30)\times10^2$ mol^{-1} dm^3 s^{-1}.

The tetradentate ligand **3** experimentally gave two composite rate constants of $k_{32}+k_{23}K_{OH}^{II}K_{a(COOH)} = 2.42\pm0.20$ and $k_{31}+k_{22}K_{OH}^{II}K_{a(phOH)} = (1.87\pm0.20)\times10^6$ mol^{-1} dm^3 s^{-1}. The same consideration afforded $k_{22} = (1.87\pm0.30)\times10^2$ mol^{-1} dm^3 s^{-1} from the latter. Likewise, an estimation of k_{23} from the former using K_{OH}^{II} and $K_{a(COOH)}$ gave k_{23} as $(1.84\pm0.30)\times10^{-1}$ dm^3 s^{-1}. This value is rather small compared with the rate constant of the $Fe(OH)^{2+}$ species.[6a] Hence, it may be safe to state that the pathway of k_{32} is with a rate constant 2.42 ± 0.20, and that of k_{23} may be of little contribution to the composite rate constants.

Table 2. Reaction rate constants

Ligand	Pathway	k_{ij} ($mol^{-1}\,dm^3\,s^{-1}$)	Ref.
1 (H_2mug)	$Fe^{3+}+H_2mug$ (k_{32})	k_{32}: $(5.25\pm0.20)\times10^2$	This work[a]
	$Fe^{3+}+Hmug^-$ (k_{31}) and $Fe(OH)^{2+}+H_2mug$ (k_{22})	k_{22}: $(1.14\pm0.30)\times10^3$	
		$[k_{31}+k_{22}K_{OH}^{II}K_{a(phOH)}$: $(1.47\pm0.20)\times10^7]$	
2 (H_2mugm)	$Fe^{3+}+H_2mugm$ (k_{32})	k_{32}: $(6.17\pm0.20)\times10^2$	This work[a]
	$Fe^{3+}+Hmugm^-$ (k_{31}) and $Fe(OH)^{2+}+H_2mugm$ (k_{22})	k_{22}: $(1.92\pm0.30)\times10^2$	
		$[k_{31}+k_{22}K_{OH}^{II}K_{a(phOH)}$: $(1.03\pm0.20)\times10^6]$	
3 (H_3muia)	$Fe^{3+}+H_2muia^-$ (k_{32}) and $Fe(OH)^{2+}+H_3muia$ (K_{23})	$k_{32}+k_{23}K_{OH}^{II}K_{a(COOH)}$: 2.42 ± 0.20	This work[a]
	$Fe^{3+}+Hmuia^{2-}$ (k_{31}) and $Fe(OH)^{2+}+H_2muia^-$ (k_{22})	k_{22}: $(1.87\pm0.30)\times10^2$	
		$[k_{31}+k_{22}K_{OH}^{II}K_{a(phOH)}$: $(1.87\pm0.20)\times10^6]$	
Hpdx-L-Htrp[b]	$Fe^{3+}+H_2$pdx-L-trp (k_{32}) and $Fe(OH)^{2+}+H_2$pdx-L-Htrp (k_{23})	$k_{32}+k_{23}K_{OH}^{II}K_{a(COOH)}$: $(2.13\pm0.06)\times10^1$	2[b]
HClac[c]	$Fe^{3+}+HClac$ (k_{31})	k_{31}: 2.1 ± 1.7	10[c]
	$Fe^{3+}+Clac^-$ (k_{30}) and $Fe(OH)^{2+}+HClac$ (k_{21})	$k_{30}+k_{21}K_{OH}^{II}K_{a(COOH)}$: $(6.8\pm0.1)\times10^3$	
Hac[d]	$Fe^{3+}+Hac$ (k_{31})	k_{31}: 4.8 ± 0.8	11[d]
	$Fe^{3+}+ac^-$ (k_{30}) and $Fe(OH)^{2+}+Hac$ (k_{21})	$k_{30}+k_{21}K_{OH}^{II}K_{a(COOH)}$: $(3.4\pm0.2)\times10^5$	
Hsalal[e]	$Fe^{3+}+Hsalal$ (k_{31})	k_{31}: 2.46×10^1	12[e]
	$Fe^{3+}+salal^-$ (k_{30}) and $Fe(OH)^{2+}+Hsalal$ (k_{21})	$k_{30}+k_{21}K_{OH}^{II}K_{a(phOH)}$: 2.12×10^6	
Hphe[f]	$Fe^{3+}+Hphe$ (k_{31})	k_{31}: 2.5×10^1	13[f]
	$Fe^{3+}+phe^-$ (k_{30}) and $Fe(OH)^{2+}+Hphe$ (k_{21})	$k_{30}+k_{21}K_{OH}^{II}K_{a(phOH)}$: 7.2×10^2	

[a] 0.10 mol dm^{-3} ($NaNO_3$), 25°C.
[b] Hpdx-L-Htrp: N-pyridoxylidene-L-tryptophan; 0.50 mol dm^{-3} (NaCl), 25°C.
[c] HClac: chloroacetic acid; 1.0 mol dm^{-3} ($NaClO_4$), 25°C. $\log K_a(COOH)/(mol^{-1}\,dm^3) = 2.86$.
[d] Hac: acetic acid. 1.0 mol dm^{-3} ($NaClO_4$), 20°C. $\log K_{a(COOH)}/(mol^{-1}\,dm^3) = 4.53$.
[e] Hsalal: salicylaldehyde; 0.2 mol dm^{-3} ($LiClO_4$), 20°C. $\log K_{a(phOH)}/(mol^{-1}\,dm^3) = 8.13$.
[f] Hphe: phenol. 0.1 mol dm^{-3} (KNO_3), 25°C. $\log K_{a(phOH)}/(mol^{-1}\,dm^3) = 9.82$.

The fact that these three ligands take universal pathways for Fe^{3+} and $Fe(OH)^{2+}$ with the diprotonated ligand species suggests the formation reaction mechanism is based on the dependence of each rate constant on the basicity of the donor atoms and the molecular structure of the ligands.

The reaction mechanism of Fe^{3+} with H_2mug, H_2mugm and H_2muia$^-$, where Fe^{3+} has been accepted to have an associative or associative interchange characteristic,[7] can be explained in terms of a mechanistic rate-determining coordination of phenolato oxygen to iron(III). This is because the deprotonated carboxymethyl group on the nitrogen of **3**, which is expected to form an intramolecular hydrogen bond with the phenolic hydroxyl group, markedly decreases the formation rate constant k_{32}. In fact, the rate constant for the coordination of the (protonated) carboxylate group to Fe^{3+} is substantially smaller than that for the coordination of the (protonated) phenolate group (cf. Table 2); the latter being similar to k_{32} of H_2mug and H_2mugm. Contrary to the carboxymethyl group, the methyl group on the nitrogen donor atom of **2** influences very little the coordination reaction kinetics of Fe^{3+} species.

The mechanism of reaction of $Fe(OH)^{2+}$ with H_2mug, H_2mugm and H_2muia$^-$, where $Fe(OH)^{2+}$ has been accepted to have a dissociative interchange characteristic,[7] can also be explained by the mechanistic rate-determining interchange of a coordinated water molecule of $Fe(OH)^{2+}$ ($[Fe(OH)(H_2O)_5]^{2+}$) with a phenolato oxygen of the ligand species. The rather narrow range of k_{22} for the three ligand species of different molecular structure substantiates the dissociative interchange mechanism of $Fe(OH)^{2+}$. It is interesting to note that the substitution of the methyl or carboxymethyl group for hydrogen on the nitrogen causes a decrease in the magnitude of k_{22}.

An increase in the rate constant on going from Fe^{3+} to $Fe(OH)^{2+}$ was noticed for **1** and **3**, which is in line with those reported as a general feature of the iron(III) ion.[6a] Ligand **2** is an exception; no enhancement of the rate constant by the hydroxylation of iron(III) was noticed. This has already been reported for the iron(III) complex of salicylaldehyde [Hsalal; cf. Table 2: the rate constant for the pathway of $Fe(OH)^{2+}$ with Hsalal, k_{21}, estimated from the composite rate constant of 2.12×10^6 mol^{-1} dm^3 s^{-1}, K_{OH}^{11}, and the protonation constant (K_a) of the ligand ($\log K_a/(\text{mol}^{-1}\ \text{dm}^3) = 8.13$) is *ca* 8.5, which is smaller than the rate constant for the pathway of Fe^{3+} with Hsalal, $k_{31} = 2.46 \times 10$ mol^{-1} dm^3 s^{-1}]. The coordination reaction mechanism is shown in Scheme 3.

In conclusion, the formation of iron(III) complexes of **1** and the related terdentate (**2**) and tetradentate (**3**) ligands proceeds through pathways of Fe^{3+} and $Fe(OH)^{2+}$ with the diprotonated ligand species. They coordinate to iron(III) by the associative donation of and the dissociative interchange of a coordinated water molecule with phenolato oxygen as the mechanistic rate-determining step, which is followed by rapid donation of the amino nitrogen and carboxylato oxygen(s) to complete mono(terdentato- and tetradentato)iron(III) complexes. Steric repulsive interactions between the coordinated and coordinating ligand molecule may

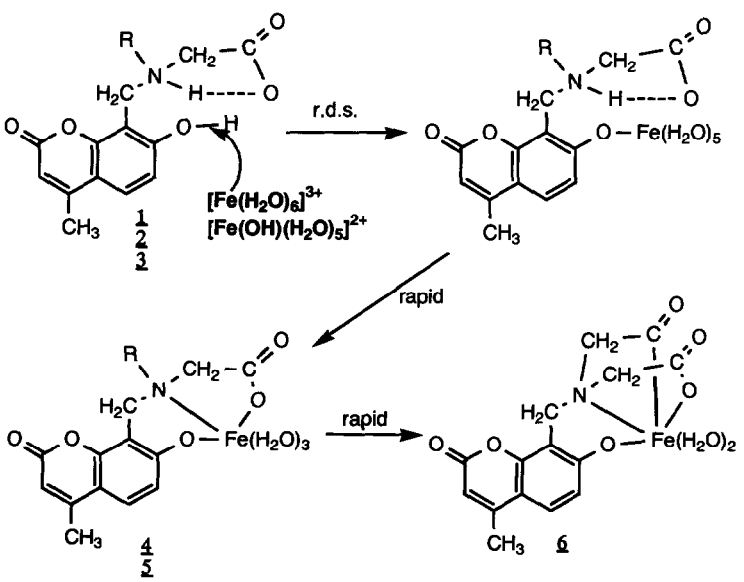

Scheme 3.

be the reason why bis(terdentato)iron(III) complexes are not formed.

REFERENCES

1. (a) M. A. S. Khan and W. I. Stephen, *Anal. Chim. Acta* 1970, **49**, 255; (b) G. M. Huitink, D. P. Poe and H. Diehl, *Talanta* 1974, **21**, 1221.
2. H. Kuno, K. Okamoto, J. Hidaka and H. Einaga, *Bull. Chem. Soc. Japan* 1989, **62**, 2824.
3. M. Noritake, K. Okamoto, J. Hidaka and H. Einaga, *Bull. Chem. Soc. Japan* 1990, **63**, 353.
4. H. L. Schläfer, *Komplexbildung in Lösung*, Ch. 8. Springer, Berlin (1961).
5. L. G. Sillén and A. E. Martell, *Stability Constants of Metal-Ion Complexes*, Special Publication No. 17, p. 53. Chemical Society, London (1964).
6. For example: (a) D. W. Margerum, G. R. Cayley, D. C. Weatherburn and G. K. Pagenkopf, *Coordination Chemistry* (Edited by A. E. Martell), Vol. 2, Ch. 1. American Chemical Society, Washington, DC (1978); (b) E. Mentasti, *Inorg. Chem.* 1979, **18**, 1512; (c) E. Mentasti, F. Secco and M. Venturini, *Inorg. Chem.* 1982, **21**, 602; (d) B. Monzyk and A. L. Crumbliss, *J. Am. Chem. Soc.* 1979, **101**, 6203; (e) S. Funahashi, K. Ishihara and M. Tanaka *Inorg. Chem.* 1983, **22**, 2070; (f) C. P. Brink and A. L. Crumbliss, *Inorg. Chem.* 1984, **23**, 4708; (g) M. S. El-Ezaby and M. M. Hassan, *Polyhedron* 1985, **4**, 429; (h) M. Biruš and R. van Eldik, *Inorg. Chem.* 1991, **30**, 4559; (i) K. Ishihara, S. Funahashi and M. Tanaka, *Inorg. Chem.* 1983, **22**, 194; (j) D. P. Fay, A. R. Nichols Jr and N. Sutin, *Inorg. Chem.* 1971, **10**, 2096; (k) M. R. Jaffe, D. P. Fay, M. Cefola and N. Sutin, *J. Am. Chem. Soc.* 1971, **93**, 2878; (l) M. J. Hynes and M. T. O'Shea, *J. Chem. Soc., Dalton Trans.* 1983, 331; (m) K. Bridger, R. C. Patel and E. Matijević, *Polyhedron* 1982, **1**, 269.
7. A. E. Merbach, *Pure Appl. Chem.* 1982, **54**, 1479; 1987, **59**, 161.
8. T. Imasaka, T. Ogawa and N. Ishibashi, *Bull. Chem. Soc. Japan* 1976, **49**, 2687.
9. W. R. Harris, R. J. Motekaitis and A. E. Martell, *Inorg. Chem.* 1975, **14**, 974.
10. B. Perlmutter-Hayman and E. Tapuhi, *J. Coord. Chem.* 1976, **6**, 31.
11. F. A. Accascina, F. P. Cavasino and E. D. Dio, *Trans. Faraday Soc.* 1969, **65**, 489.
12. P. G. T. Fogg and R. J. Hall, *J. Chem. Soc. A* 1971, 1365.
13. S. Gouder and J. Stuehr, *Inorg. Chem.* 1974, **13**, 379.

Polyhedron Vol. 12, No. 11, pp. 1329–1333, 1993
Printed in Great Britain

0277–5387/93 $6.00+.00
© 1993 Pergamon Press Ltd

THE REDOX BEHAVIOUR OF FERROCENE DERIVATIVES—V.* 5,5′-FERROCENEDIYLDI(5-FLUORO-1,3-DIPHENYL-1-λ^6,3-λ^6,2,4,6,5-λ^5-DITHIATRIAZAPHOSPHORINE-1,3-DIOXIDE)

PIERO ZANELLO† and GIULIANA OPROMOLLA

Dipartimento di Chimica dell'Università di Siena, Pian dei Mantellini 44, 53100 Siena, Italy

and

GIANLUCA GIORGI

Centro Interdipartimentale di Analisi e Determinazioni Strutturali dell'Università di Siena, Via Mattioli 10, 53100 Siena, Italy

and

JOHAN C. VAN DE GRAMPEL and HERMAN F. M. SCHOO‡

Department of Polymer Chemistry, University of Groningen, Nijenborgh 4, 9747 AG Groningen, The Netherlands

(*Received* 27 *January* 1993; *accepted* 5 *February* 1993)

Abstract—Preparation of the title compound (**1**) is reported together with its detailed mass spectrometric investigations, which revealed the high stability of the molecular ion under electron impact and allow its fragmentation pathways to be rationalized. In dichloroethane solution the one-electron oxidation of **1** occurs at the highest potential value so far known for ferrocene molecules ($E^{\circ\prime} = +1.19$ V, vs S.C.E.).

Interest in metallocenes linked to cyclo(thia) phosphazenes arises from the fact that such small molecules can function as structural models for their open-chain high polymeric analogues, which should display physical properties quite different from those of conventional organic macromolecules.[2]

Chemical and electrochemical properties of metallocenes linked to some cyclophosphazene rings have been reported.[2,3] Here we present the chemical, mass spectrometric and electrochemical characterization of the ferrocene title compound **1**, in which each cyclopentadienyl ring bears one cyclophosphadithiazene unit. The crystal structure of such a species has been previously reported.[4]

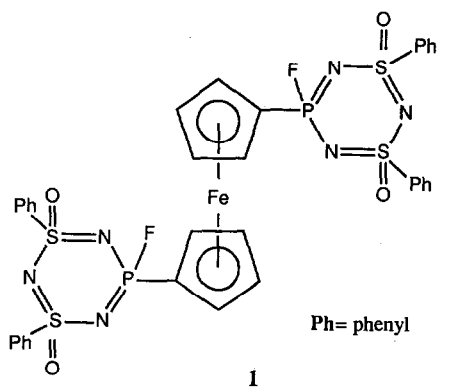

1

EXPERIMENTAL

Materials and apparatus for electrochemistry have been described elsewhere.[5] All potential values

* For Part IV see Ref. 1.

† Author to whom correspondence should be addressed.

‡ Present address: Philips Research Laboratories, Eindhoven, The Netherlands.

are referred to the saturated calomel electrode (S.C.E.).

All synthetic experiments were performed in an atmosphere of dry, oxygen-free nitrogen, applying gas vacuum techniques in combination with Schlenk-type glassware. THF was distilled from a Na/K-melt prior to use. All other solvents were dried and distilled by conventional methods. *Cis*-$NPF_2(NSOPh)_2$ was synthesized using the method described in ref. 6. Ferrocene was sublimed prior to use. $Fe(C_5H_4Li)_2 \cdot TMEDA$ was prepared according to the method of Bishop *et al.*[7]

^1H NMR spectra ($CDCl_3$ solutions) were measured on a Bruker WH90 spectrometer (90 MHz), using TMS as an internal reference. ^{31}P and ^{19}F NMR spectra ($CDCl_3$ solutions) were recorded on a Nicolet NT200 spectrometer, operating at 81.0 and 188.2 Hz, respectively; $(NPCl_2)_3$ (19.9 ppm, $CDCl_3$ solution) and $CFCl_3$ (0.0 ppm, $CDCl_3$ solution) were used as external references. Chemical shifts are positive in the low-field direction.

Mass spectra were obtained by a double focusing VG 70-250S mass spectrometer operating in the electron ionization mode at 70 eV, emission current 0.2 mA, with a source temperature of 220°C and an accelerating voltage of 8 KV. The resolution was 2000 $M/\Delta M$ (10% of valley def.). The samples were introduced via the direct inlet system at room temperature. Metastable ions were measured by computer-controlled B/E and B^2/E linked scans performed in the first free region. Acquisition and analysis of the data were performed with a VG 11-250J data system equipped with a Digital PDP 11/83 minicomputer. High-resolution mass measurements were performed at resolution 10,000 $M/\Delta M$ against at perfluorokerosene standard (Fluka) under the control of the data system.

Preparation of $[(NSOPh)_2NPF]_2(C_5H_4)_2Fe$

To a mixture of $(\eta^5\text{-}C_5H_4Li)_2Fe \cdot TMEDA$ (0.52 g, 1.66 mmol) and $NPF_2(NSOPh)_2$ (1.20 g, 3.32 mmol) was added THF (10 cm^3) at −50°C. After stirring for 24 h the mixture was allowed to warm up to room temperature during 8 h. After filtration the residue was recrystallized from a $CHCl_3$–pentane mixture, yielding 0.570 g of orange crystals of $[(NSOPh)_2NPF]_2(C_5H_4)_2Fe$. The THF filtrate was subjected to column chromatography on silica gel-60 (Merck). Using successively pentane, CH_2Cl_2 and a mixture of CH_2Cl_2/THF as eluants, ferrocene, small amounts of a mono-substituted ferrocene derivative and an additional amount (0.200 g) of $[(NSOPh)_2NPF]_2(C_5H_4)_2Fe$ were obtained. The yield of $[(NSOPh)_2NPF]_2(C_5H_4)_2Fe$ was 0.770 g (0.89 mmol = 54%); m.p. ≈ 250°C. ^1H NMR: δ 5.2 (8H, m), 7.7 (10H, m). ^{19}F NMR: δ −49.4 [d, $^1J(PF) = 987$ Hz]. ^{31}P NMR: δ 35.8 [d, $^1J(PF) = 987$ Hz]. MS: Found: 867.9849. Calc. for $C_{34}H_{28}F_2FeN_6O_4P_2S_4$: m/z 867.9848.

RESULTS AND DISCUSSION

Synthesis of 1

Under the conditions illustrated in the Experimental the reaction of $(\eta^5\text{-}C_5H_4Li)_2Fe \cdot TMEDA$ with *cis*-$NPF_2(NSOPh)_2$ in a 1 : 2 ratio afforded the di-substituted ferrocenyl complex $[(NSOPh)_2NPF]_2(C_5H_4)_2Fe$ (**1**), which crystallized in two forms, one of which has been described previously.[4]

Mass spectrometric studies

In analogy with other ferrocene compounds[8] the mass spectrum of **1** (Table 1) is dominated by the molecular ion (m/z 868), which is responsible for 25% of the total ion current.

High-resolution mass data with the assignments of the elemental compositions of the molecular ion and main fragmentation ions are reported in Table 2. The main fragmentation pathways for the molecular ion obtained by B/E spectra are reported in Scheme 1.

A metal–ligand bond cleavage is observed and it produces the ion $[FeC_5H_4(NSOPh)_2NPF]^+$ at m/z 462. This ion is the more intense fragment ion in the spectra (23.8%), indicating that this fragmentation pathway is highly favoured.

In the crystal structure of **1** the average distance for Fe···N(—P) is 3.90 Å.[4] This structural arrangement also seems to be present in the gas

Table 1. Significant mass spectra data for **1**

m/z (relatve abundances, %)					
872(2.6)	871(8.5)	870(24.3)	869(41.2)	868(100)	
866(5.6)	464(2.7)	463(5.3)	462(23.8)	434(3.5)	
407(4.2)	278(2.8)	256(2.6)	200(2.9)	165(2.4)	
125(10.4)	110(8.6)	109(6.4)	97(7.1)	78(3.8)	77(12.7)

Table 2. High-resolution mass data

Ion	Observed mass (μ)	Error (μ^{-3})
$[C_{34}H_{28}F_2FeN_6O_4P_2S_4]^{+\cdot}$	867.9849	−0.1
$[C_{17}H_{14}FFeN_3O_2PS_2]^{+\cdot}$	461.9612	−1.3
$[C_{17}H_{15}FN_3O_2PS_2]^{+\cdot}$	407.0323	0.5
$[C_6H_5OS]^+$	125.0050	1.1

phase and the direct interaction of the electron-deficient metal atom lacking one coordination site with one nitrogen atom of the $(NSOPh)_2NPF$ substituent can be responsible for the high stability of such an ion.

This type of fragmentation is also present in other ferrocenyl derivatives, in which an interaction of the metal ion with electronegatives groups, such as a double bond or an heteroatom possessing a lone pair, is allowed.[9]

All other fragmentations of the molecular ion involve the NSOPh group yielding the ions at *m/z* 729 and 604 (Scheme 1).

An interesting feature in the behaviour of **1** under electron impact ionization is the presence of doubly charged ions. The molecular ion itself is present as M^{2+} at *m/z* 434, which in turn fragments to doubly-charged ions at *m/z* 302.0, 364.5 and 371.5, corresponding to the mono-charged species at *m/z* 604, 729 and 743. To the best of our knowledge this is the first case in which doubly-charged ions are described in the mass spectra of ferrocene molecules. It is likely that the stabilization of these ions comes from the aromatic character of the peripheral cyclophosphadithiazene rings.

Electrochemistry

As ferrocene molecules usually lose one electron to give the corresponding ferrocenium cations we decided to test the electrochemical behaviour of **1**. Unfortunately, the very low solubility of this complex in solvents useful for electrochemistry (insoluble in acetonitrile and dimethyl sulphoxide, very slightly soluble in dichloromethane, 1,2-dichloroethane and THF) prevented an accurate study.

Figure 1 shows the cyclic voltammogram exhibited by a saturated solution of **1** in 1,2-dichloroethane. As a result of the low concentrations caused by the poor solubility controlled potential coulometry ($Ew = +1.3$ V) showed no effective current. Therefore, it is not possible to calculate the number of electrons involved in the oxidation process. However, it is most likely that the observed redox change is attributable to the ferrocene/

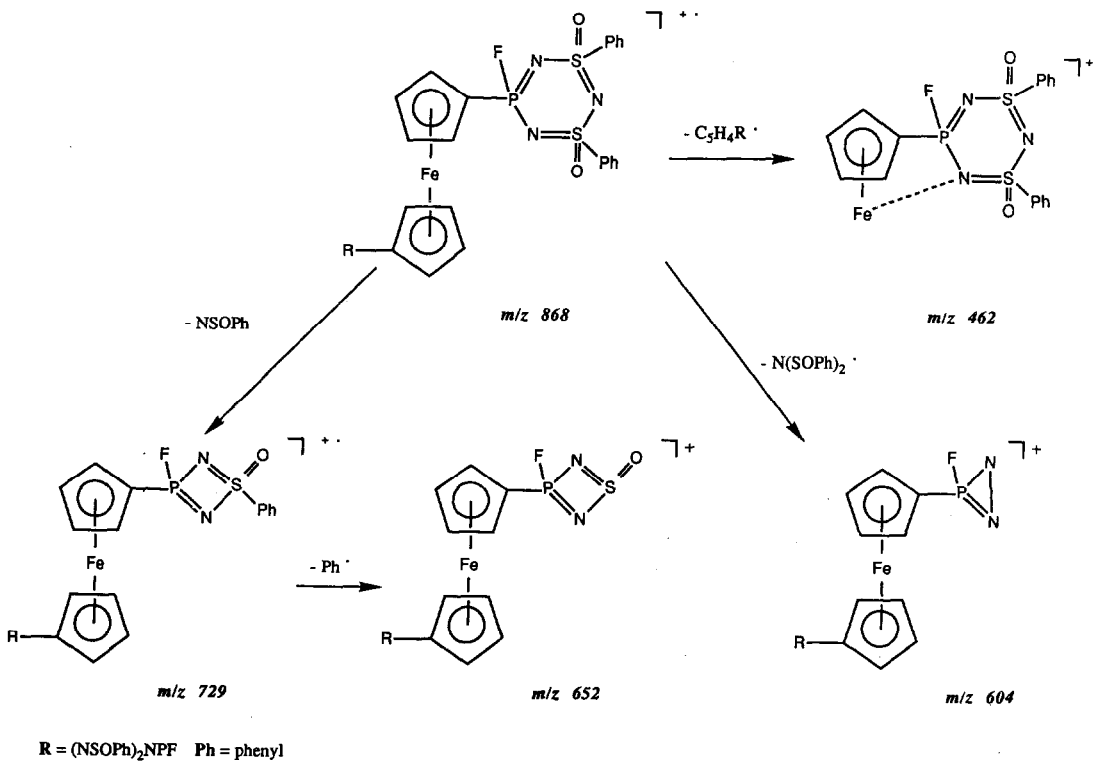

Scheme 1.

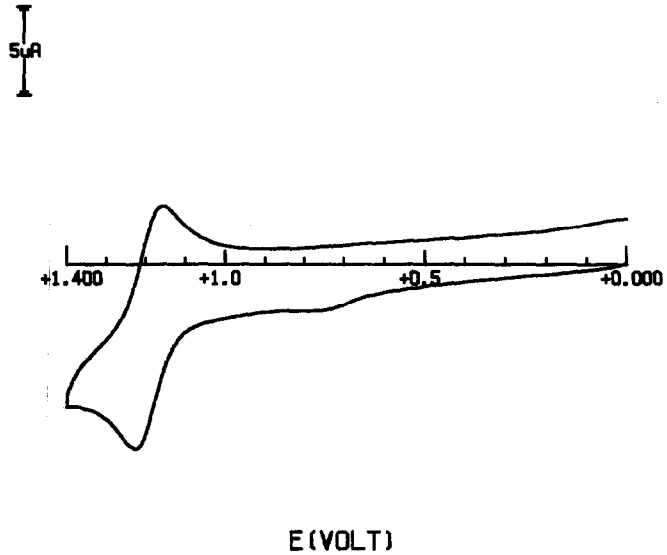

Fig. 1. Cyclic voltammogram recorded at a platinum electrode on a 1,2-$C_2H_4Cl_2$ solution containing $[NBu_4][ClO_4]$ (0.2 mol dm^{-3}) and saturated with **1** (4.5 mg in 25 cm^3). Scan rate = 0.5 V s^{-1}.

Table 3. Redox potentials (in V, vs S.C.E.) for the one-electron oxidation of some disubstituted ferrocene molecules, (X—C_5H_4)Fe(C_5H_4—X)

X	$E^{\circ\prime}$	Solvent	Ref.
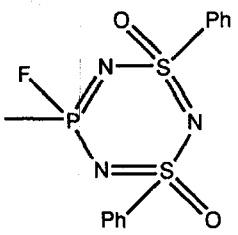	+1.19	1,2-$C_2H_4Cl_2$	Present work
	+1.18	CH_2Cl_2	Present work
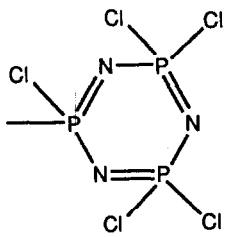	+1.16[a]	MeCN	3
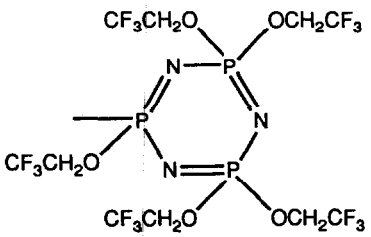	+1.04	MeCN	3
CF_3	+1.09	CH_2Cl_2	11
H	+0.46	1,2-$C_2H_4Cl_2$	Present work
	+0.45	CH_2Cl_2	Present work
	+0.38	MeCN	Present work

[a] Peak potential value for an irreversible oxidation.

ferrocenium couple. Such an anodic step displays all the features of an uncomplicated electron transfer, substantially reversible in character; in fact, analysis[10] of the response with scan rate v varying from 0.02 to 10.24 V s^{-1} shows that the current ratio i_{pc}/i_{pa} is constantly equal to 1, the current function $i_{pa}\ v^{-1/2}$ remains constant and the peak-to-peak separation progressively increases from 68 to 130 mV (likely because of some uncompensated solution resistances).

Table 3 compares the redox potentials of the **1**/[**1**]$^+$ process with that of some related molecules. The strong electron-withdrawing effect of the two cyclophosphadithiazene rings is clearly evident when the formal electrode potential of **1**/[**1**]$^+$ is compared with that of unsubstituted ferrocene. Furthermore, the redox potential of the title compound is even higher than that of 1,1′-trifluoromethyl-substituted ferrocene.

REFERENCES

1. J. C. Gallucci, G. Opromolla, L. A. Paquette, L. Pardi, P. F. T. Schirch, M. R. Sivik and P. Zanello, *Inorg. Chem.*, in press.
2. H. R. Allcock, K. D. Lavin, G. H. Riding, P. R. Suszko and R. R. White, *J. Am. Chem. Soc.* 1984, **106**, 2337.
3. R. A. Saraceno, G. H. Riding, H. R. Allcock and A. G. Ewing, *J. Am. Chem. Soc.* 1988, **110**, 980.
4. A. Meetsma, H. F. M. Schoo, J. C. Van de Grampel and W. P. Bosman, *Acta Cryst.* 1987, **C43**, 2314.
5. P. Zanello, G. Opromolla, M. Casarin, M. Herberhold and P. Leitner, *J. Organomet. Chem.* 1993, **443**, 199.
6. H. Winter, PhD Thesis, University of Groningen, The Netherlands (1986).
7. J. J. Bishop, A. Davison, D. W. Lichtenberg, R. E. Merrill and J. C. Smart, *J. Organomet. Chem.* 1971, **27**, 241.
8. J. Mirek, S. Rachval, T. Gorecki, B. Kawalek, P. Milart and E. Szneler, *J. Organomet. Chem.* 1988, **344**, 363.
9. Yu. S. Nekrasov and D. V. Zagorevskii, *Org. Mass. Spectrom.* 1991, **26**, 733 and refs therein.
10. E. R. Brown and J. R. Sandifer, in *Physical Methods of Chemistry. Electrochemical Methods* (Edited by B. W. Rossiter and J. F. Hamilton), Vol. 2, Ch. 4. Wiley, New York (1986).
11. P. G. Gassman and C. H. Winter, *J. Am. Chem. Soc.* 1986, **108**, 4228.

Polyhedron Vol. 12, No. 11, pp. 1335–1343, 1993
Printed in Great Britain

0277–5387/93 $6.00+.00
© 1993 Pergamon Press Ltd

REACTIONS OF $[WO_2Cl_2(dme)]$ WITH TERT.BUTYLTRIMETHYLSILYLAMINE— X-RAY STRUCTURE OF $[W(NBu^t)_2Cl_2(Bu^t\text{-dab})]$ (Bu^t-dab = N,N′-di-t-butyl-1,4-diaza-1,3-butadiene)

KLAUS DREISCH,* CARLAXEL ANDERSSON and CLAES STÅLHANDSKE

Department of Inorganic Chemistry, Chemical Centre, University of Lund, P.O. Box 124, S 22100 Lund, Sweden

(*Received* 18 *December* 1992; *accepted* 1 *February* 1993)

Abstract—$[WO_2Cl_2(dme)]$ (dme = dimethoxyethane) reacts with 4 equivalents of $Me_3SiNH(Bu^t)$ to give different products depending on the solvent used. In n-hexane and dme as solvents the known complex $\{[W(NBu^t)_2Cl_2(NH_2Bu^t)]_2\}$ was obtained, a monomeric derivative of which, $[W(NBu^t)_2Cl_2(Bu^t\text{-dab})]$ (Bu^t-dab = N,N′-di-t-butyl-1,4-diaza-1,3-butadiene), has been characterized by X-ray structure determination. The molecule has a distorted octahedral geometry with *cis*-butylimido ligands [W—N distances: 1.756(8) and 1.758(8) Å; N—W—N angle: 105.9(4)°] and *trans*-dichloro ligands [W—Cl distances: 2.389(2) and 2.394(3) Å; Cl—W—Cl angle: 154.1(1)°]. The bidentate Bu^t-dab ligand is *trans* to the bisimido function; the W—N distances of Bu^t-dab are 2.507(7) and 2.533(7) Å and the N—W—N bite angle is 67.0(2)°. In dimethylformamide (dmf) as a solvent a binuclear tungsten(VI) compound is formed. A structure with a linear N═W—O—W═N arrangement and three terminal trimethylsilanolato ligands at each tungsten atom, $\{[W_2(NBu^t)_2(\mu\text{-}O)(OSiMe_3)_6]\cdot dmf\}$, is suggested for this complex. This suggestion is based on elemental analysis, molecular weight determination, FAB mass spectroscopy, ^1H, ^{13}C, ^{14}N, ^{17}O and ^{29}Si NMR, IR and Raman spectroscopy.

Much research activity is currently focused on high valent imido complexes of molybdenum and tungsten. Such compounds with M = NR functions can be used as catalysts or catalyst models of industrially important processes as ammoxidation[1–3] and olefin metathesis.[4–7] One of the preparative methods[8] by which an imido group, =N—R, can be introduced is the reaction of chloro, oxo or chloro-oxo metal complexes with monosilylated primary amines, as exemplified by different trimethylsilylamines Me_3SiNHR, R = 2,6 Pr^iPh[4–7] and R = Bu^t.[9–13] WCl_6[9–11] and $WOCl_4$[13] have been used as starting materials for the preparation of t-butylimido complexes of tungsten(VI), while WO_2Cl_2 has been found to be too unreactive to undergo reactions with $Me_3SiNH(Bu^t)$.[10,11]

The synthesis of monomeric $[WO_2Cl_2(dme)]$ (dme = dimethoxyethane) has recently been described.[14] This compound is highly soluble in organic solvents and more reactive than WO_2Cl_2. With this complex at hand we thought it worthwhile investigating its reactions with $Me_3SiNH(Bu^t)$. As the reactions of MoO_2Cl_2[10] and its 2,2′ bipyridyl adduct[15] with $Me_3SiNH(Bu^t)$ give different kinds of products depending partly on the solvents used it was considered necessary to perform the reactions of $[WO_2Cl_2(dme)]$ and $Me_3SiNH(Bu^t)$ in different solvents, viz. n-heptane, dme and dimethylformamide (dmf). The results of these experiments and the crystal structure of one of the compounds obtained, $[W(NBu^t)_2Cl_2(Bu^t\text{-dab})]$ (Bu^t-dab = N,N′-di-t-butyl-1,4-diaza-1,3-butadiene), are presented here.

RESULTS AND DISCUSSION

Reaction of $[WO_2Cl_2(dme)]$ *with* $Me_3SiNH(Bu^t)$ *in n-heptane and dme*

A yellow solution and a white precipitate were obtained from the reaction of $[WO_2Cl_2(dme)]$ with

* Author to whom correspondence should be addressed.

4 equivalents of $Me_3SiNH(Bu^t)$, either in dimethoxyethane homogeneously or in n-heptane heterogeneously. After 24 h reaction time at room temperature the reaction mixture was filtered to remove the white precipitate, identified by vibrational spectroscopy as pure $(Bu^tNH_3)Cl$. Approximately 0.25 mol equivalents of $(Bu^tNH_3)Cl$ relative to $[WO_2Cl_2(dme)]$ were formed at room temperature, but in reactions performed at 70°C for 6 h the relative amount of $(Bu^tNH_3)Cl$ increased substantially to approximately 0.5 mol equivalents. By cooling the filtrate at −30°C a yellow compound crystallized; IR and ^1H, $^{13}C\{^1H\}$ NMR data of this compound are in accordance with those of the well-known bisimido complex $\{[W(NBu^t)_2Cl_2(H_2NBu^t)]_2\}$[9] (**1**). Isolated yields of compound **1** were low, not exceeding 30% in the room-temperature reactions. The formation of **1** in the above reaction can be formulated as:

$$2[WO_2Cl_2(dme)] + 8Me_3SiNH(Bu^t) \longrightarrow [\mathbf{1}] + 4O(SiMe_3)_2 + 2H_2NBu^t + 2dme. \quad (1)$$

GLC analysis of the filtrate obtained after isolation of complex **1** revealed two of the reaction products, viz. dme and $O(SiMe_3)_2$. The third product of eq. (1), H_2NBu^t, has been consumed in aminolysis reactions of tungsten chlorine bonds, as indicated by the isolation of $(Bu^tNH_3)Cl$. The reaction of WO_2Cl_2 with primary amines, RNH_2, has been reported to give polymeric $[WO_2(NR)]_n$ and RNH_3Cl.[16] Brief experiments in the present study in which $[WO_2Cl_2(dme)]$ was reacted with 4 equivalents of H_2NBu^t in n-heptane gave 2 equivalents of $(Bu^tNH_3)Cl$ and a compound analysing to approximately $[WO_2(NBu^t)\cdot 0.5(H_2NBu^t)]$, which was highly soluble in common organic solvents. Found: C, 22.1; H; 4.7; N, 5.9; W, 55.9. Calc: C, 22.2; H, 4.5; N, 6.5; W, 56.8%.

The solution remaining after separation of $(Bu^tNH_3)Cl$ and the dimer **1** was evaporated at room temperature to give a yellow oil. The ^{13}C NMR spectrum of this oil showed the presence of traces of **1**, some $Me_3SiNH(Bu^t)$ and additional resonances between 60–70, 30–35 and 0.8–3.1 ppm, characteristic of the tertiary carbon atoms of t-butylimido groups and the methyl carbons of $NCMe_3$ and of $SiMe_3$, respectively. Aminolysis reactions leading to these imido species of unknown constitution and $(Bu^tNH_3)Cl$ are most likely the competitive reactions limiting the yield of complex **1**. Higher temperatures seem to accelerate aminolysis more than the complicated multistep reaction [eq. (1)] leading to the formation of complex **1**. Aminolysis of complex **1** by H_2NBu^t, which has been observed previously,[9] does not interfere under the reaction conditions used in the present study because no NMR signals of the reaction product, $[W(NBu^t)_2(HNBu^t)_2]$,[9,11] were observed in the filtrate. Due to easily accessible starting materials, WCl_6 and H_2NBu^t [or $Me_3SiNH(Bu^t)$], and higher yields it can be concluded that the original method of synthesizing the dimer **1**[9] is the superior one.

A derivative prepared by the reaction of complex **1** with 2 equivalents of Bu^t-dab in toluene provides further evidence of the nature of **1**. The crystal structure of this derivative, $[W(NBu^t)_2Cl_2(Bu^t\text{-dab})]$ (**2**), is discussed below. In analogy to the synthesis of $[Mo(NBu^t)_2Cl_2(bipy)]$ from $[MoO_2Cl_2(bipy)]$[15] it should be possible to prepare complex **2** by a different reaction path. $[WO_2Cl_2(Bu^t\text{-dab})]$[17] was, therefore, heated with 4 equivalents of $Me_3SiNH(Bu^t)$ in n-heptane; at room temperature the starting materials were left unchanged despite stirring the suspension for several weeks, while at 70°C a reaction occurred within 6 h. Unexpectedly, no $[W(NBu^t)_2Cl_2(Bu^t\text{-dab})]$ (**2**) was formed. By concentrating, filtering and cooling the reaction mixture yellow crystals and a white powder were isolated. The yellow crystals and the white substance were identified by vibrational spectroscopy as complex **1** and $(Bu^tNH_3)Cl$, respectively. The imido bridges of the dimer **1** are cleaved by reaction with Bu^t-dab or other nitrogen donors[9,18] to give monomeric bisimido complexes, such as complex **2**. The outcome of the reaction between $[WO_2Cl_2(Bu^t\text{-dab})]$ and $Me_3SiNH(Bu^t)$ is, therefore, unexpected and no straightfoward explanation can be given.

Finally, some further remarks on the reaction under discussion are noteworthy. Firstly, there is a clear reactivity difference between uncomplexed WO_2Cl_2 and $[WO_2Cl_2(dme)]$; the former does not react with $Me_3SiNH(Bu^t)$ in refluxing hexane,[10,11] while the latter reacts readily at room temperature. The reactivity difference is most likely related to the strong oxo-bridges in the polymeric structure of WO_2Cl_2,[19] which are not present in monomeric $[WO_2Cl_2(dme)]$ with the labile dme ligand.[14] Secondly, it has been observed that the reaction of MoO_2Cl_2 with $Me_3SiNH(Bu^t)$ in n-heptane leads to monomeric $[(Bu^tN)_2Mo(OSiMe_3)_2]$,[10,11] where chlorine has been removed and oxygen has been retained. Experiments in the present study using dme instead of n-heptane as the solvent confirm the same reaction product in that solvent. The opposite behaviour, i.e. retaining the chloro ligands and oxo/imido exchange, is observed in the case of $[WO_2Cl_2(dme)]$, where the dimeric complex **1** is formed. Thirdly, ethers cannot substitute the terminal amino ligand or break the imido bridges of complex **1**, because complex **1** is also formed in dme as the solvent.

Reaction of $[WO_2Cl_2(dme)]$ *with* $Me_3SiNH(Bu^t)$ *in dmf*

As can be observed by ^1H NMR and ^{13}C NMR dmf is immediately and quantitatively liberated upon dissolving $[WO_2Cl_2(dme)]$ in dmf. Due to a fast dme exchange at the tungsten centre which averages the NMR resonances no extra signals of the complex $[WO_2Cl_2(dmf)_2]$ can be observed. The addition of 2 equivalents of $Me_3SiNH(Bu^t)$ to $[WO_2Cl_2(dme)]$, dissolved in dmf, gave a solution which, according to its NMR spectrum, after stirring for 4 days at room temperature contained nothing but unreacted $Me_3SiNH(Bu^t)$, free dme and solvated WO_2Cl_2. The addition of 4 equivalents of $Me_3SiNH(Bu^t)$ to $[WO_2Cl_2(dme)]$ in dmf, however, gave a clear yellow solution from which a white solid began to precipitate after 2 h stirring. This substance could be sublimed easily at 70°C/0.01 torr to give a white diamagnetic and chlorine-free powder containing dmf and analysing as $C_{29}H_{79}N_3O_8Si_6W_2$ (**3**). A molecular weight determination (osmometry in dmf, 75°C) established that in solution compound **3** is a dimer and not a monomer (Mol. wt: found: 1030; (3-dmf) calc.: 1061). Further evidence of a dimeric species **3** was provided by its FAB mass spectrum. Although no molecular ion peak was detectable the fragment ions are larger than those expected from a monomer. Moreover, the solution and solid-state Raman spectra of compound **3** (see below) are similar, indicating that complex **3** is a dimer in the solid state. The compound is highly soluble in common organic solvents such as ethers, nitriles, aromatic, aliphatic and chlorinated hydrocarbons, while the solubility in dmf at room temperature is low. Dissolving the sublimed compound in heptane, precipitation by cooling and repeated sublimation did not remove dmf. GLC of the filtrate obtained after isolation of complex **3** showed the presence of dme, traces of $O(SiMe_3)_2$ and *ca* 10% of unreacted $Me_3SiNH(Bu^t)$; no Me_3SiCl was detected. Besides GLC no attempts were made to trace the fate of the reaction products not containing tungsten. The O/W ratio of ionic oxygen in the product is higher than that in the adducts (7:4). As the experiments were performed under rigorous exclusion of water/oxygen there are three sources for the additional oxygen atoms available, viz. those of dme, the oxo groups of the starting complex $[WO_2Cl_2(dme)]$ and the solvent dmf. Even if oxygen abstraction from complexed dme is known to occur in tungsten(VI) complexes,[20] dme is a weaker donor to tungsten(VI) than dmf. It is, therefore, unlikely that dme should re-enter the coordination sphere of tungsten during the reaction in dmf as the solvent. Furthermore, no deoxygenation products of dme such as methylchloride, 1,2-dichloroethane or 1-chloro-2-methoxyethane were detected by GLC. As complex **3** is formed in approximately 80% yield, the oxo groups of yet unreacted solvated WO_2Cl_2 cannot be the only source of the extra oxygen atoms. This leaves dmf as the most likely source of oxygen in the reaction.

No details of the reaction mechanism leading to complex **3** are known. One feature of the reaction, viz. the formation of the silanolato ligands in complex **3** (see below) by the migration of the trimethylsilyl group in complexed $Me_3SiNH(Bu^t)$ to some metal bound oxygen, is well known: the formation of silanolato ligands from metal oxo M=O bonds and $Me_3SiNH(Bu^t)$ has been ascribed to a rearrangement reaction from an intermediate oxo-amido complex $\{M(=O)[-N(Bu^t)(SiMe_3)]\}$ to an imido-silanolato complex $[M(=NBu^t)(-OSiMe_3)]$, M = V,[10,21,22] W.[13] Also, the reactions of $MOCl_3$ (M = Nb, Ta) with $Li[N(SiMe_3)_2]$ to form complexes $\{M(NSiMe_3)(OSiMe_3)[N(SiMe_3)_2]\}$[23] represent this reaction type. Attempts to obtain single crystals of **3** have until now been unsuccessful. Suggestions concerning the structure of **3** must, therefore, be based on the information from ^1H, ^{13}C, ^{14}N, ^{17}O, ^{29}Si NMR, IR and Raman spectra given in the Experimental.

Characterization of complex **3** *by spectroscopic methods*

The collected spectroscopic information prove the presence of a terminal monoimido function, W = NBu^t, in molecule **3**. The ^{14}N NMR spectrum shows, besides the ^{14}N resonance signal of free dmf, one resonance at 5.6 ppm. Only one ^{13}C NMR resonance, at 68.4 ppm, in the range of tertiary carbons is observed. The position of this resonance is characteristic of a tertiary carbon in a t-butylimido ligand.[24] Molecule **3** does not, therefore, contain amino or amido ligands, a conclusion strengthened by the absence of IR and Raman peaks at wave numbers higher than 3100 cm^{-1}, where N—H stretching vibrations occur.[25] Furthermore, a strong peak at 1298 cm^{-1} in the Raman spectrum, which is polarized in the CH_2Cl_2-solution Raman spectrum, can be assigned to ν_s(W=N—C) of a terminal imido function;[26] ν_{as}(W=N—C) appears with medium intensity at 958 and 954 cm^{-1} in the IR spectrum and the solution Raman spectrum (solvent: CH_2Cl_2), respectively; the Raman band at 954 cm^{-1} is not observed in the solid state spectrum. The deformation mode, δ(W=N—C), expected[26] between 600 and 700 cm^{-1}, is probably obscured by the vibrations of the trimethylsilyl group,[27]

$\nu_{as}(SiC_3)$ and $\nu_s(SiC_3)$, which are centred around 680 and 630 cm^{-1}, respectively.

The C—O stretching vibration of dmf in molecule **3** at 1662 (IR) and 1661 (Raman) cm^{-1} is not significantly shifted to lower wave numbers relative to neat dmf [measurements on dmf in the present study: 1668 (IR, Nujol, CsI), 1661 cm^{-1} (Raman)]; dmf is, therefore, not coordinated to tungsten in the solid state.

No spectroscopic evidence for terminally-bound oxo functions is found in the spectrum of molecule **3**. The W=O stretching vibrations of mono- and dioxo tungsten(VI) complexes[28] usually give rise to very intense Raman and IR bands between 850 and 1000 cm^{-1}; no intense Raman bands are found in this region. The intense IR bands at 921 and 898 cm^{-1} can be assigned to silicon–oxygen stretching vibrations,[29] which have low Raman and high IR intensities.[30]

The ^1H and ^{13}C NMR spectra of complex **3** reveal the presence of $OSiMe_3$ groups. By integration of the ^1H NMR signals the ratio 1:3:3 (dmf):18 (the two t-butyl signals):54 (all $OSiMe_3$ signals) is obtained. A formulation of complex **3** as $\{[W_2(NBu^t)_2(O)(OSiMe_3)_6]\cdot dmf\}$ is, therefore, reasonable.

For reasons of charge compensation one oxygen atom has been included in this formula to obtain tungsten(VI) and as no terminal oxo functions are present in complex **3**, this oxygen atom must be a bridging one. Based on the observation of a single ^{29}Si NMR resonance and provided no fast exchange between potentially bridging and terminal $OSiMe_3$ groups proceed at the ambient temperature at which the ^{29}Si NMR spectrum has been run, the six trimethylsilanolato ligands ought to be terminal ones; a conclusion supported by the ^{17}O NMR spectrum reported below. The tungsten–oxygen stretching vibrations ν(W—$OSiMe_3$) are assigned to the bands of highest intensity both in the IR and the solid-state Raman spectra between 400 and 620 cm^{-1}; they occur at 430 cm^{-1} and are very broad, with no fine structure discernable; this broad band is polarized in the CH_2Cl_2-solution Raman spectrum. Compared to the metal–oxygen stretching frequencies of terminal silanolato ligands in other metal complexes,[29,30] this band is shifted to the red and is in the region of bridging silanolato ligands (400–500 cm^{-1}).[31] However, it is very unlikely that all six silanolato ligands are bridging ones and it is not reasonable that a molecule with both terminal and bridging silanolato groups should have tungsten–oxygen stretchings ν(W—O_t) and ν(W—O_b) at similar wave numbers. Consequently, all $OSiMe_3$ ligands are of one kind, i.e. terminal ones. The ^{17}O NMR spectrum from −100 to 1100 ppm [$\delta(H_2{}^{17}O) = 0$ ppm] shows signals at 293 ppm, assignable to dmf (measurement on dmf in $CDCl_3$ in the present study: 307 pm), and at 199 ppm. As ^{17}O NMR signals of terminal $OSiMe_3$ ligands in a niobium and a tantalum complex[23] occur at 243 and 229 ppm the resonance at 199 ppm in the spectrum of **3** is due to terminally bound silanolate ligands. No signals of terminal or bridging oxo groups, which are expected at much lower fields[32] than those observed, are found. A low-field ^{17}O NMR signal of an isotope enriched compound **3** synthesized from $[W^{17}O_2Cl_2(dme)]$ in $HC(^{17}O)NMe_2$ as a solvent would, with no X-ray structure determination, confirm the presence of a bridging oxo ligand in complex **3**. The structure $\{[W_2(NBu^t)_2(\mu\text{-}O)(OSiMe_3)_6]\cdot dmf\}$ could also be indicated by the appearance of the symmetric and antisymmetric W—O—W stretching bands of a linear or bent W—O—W linkage. In a tungsten complex with a non-linear W—O—W bridge $\nu_{as}(W_2O)$ and $\nu_s(W_2O)$ have been assigned to bands at 700 (IR, Raman), 530 (IR) and 556 cm^{-1} (Raman), respectively;[33] intensities are high for $\nu_{as}(W_2O)$ in IR and $\nu_s(W_2O)$ in Raman. In the Raman spectrum of molecule **3** only two weak bands between 430 and 630 cm^{-1} appear, and thus no bent W—O—W group is present in molecule **3**.

In the complex $[W_2O_2(\mu\text{-}O)(CH_2CMe_3)_6]$,[34] with a linear O=W—O—W=O arrangement, $\nu_{as}(W_2O)$ and $\nu_s(W_2O)$ occur at 693 (IR) and 205 (Raman) cm^{-1}, respectively, while in other linear oxygen-bridged transition metal complexes $\nu_{as}(M_2O)$ and $\nu_s(M_2O)$ have been found between 840–890 (IR) and 200–250 cm^{-1} (Raman), respectively.[35] Vibrational spectroscopic studies in this laboratory on complexes of the type $W_2O_3Cl_4(L_2)_2$ (L_2 = dme and bidentate nitrogen donors)[36] showed $\nu_{as}(W_2O)$ with medium to low intensity in the range 815–850 cm^{-1} (IR); low-quality Raman spectra precluded the assignments of $\nu_s(W_2O)$ for these complexes. In the IR spectrum of molecule **3** three bands at 839, 748 and 681 cm^{-1} appear in the range 650–850 cm^{-1}. Due to the $SiMe_3$ groups present they are assigned to the rocking and stretching modes $\rho(CH_3Si)$ and $\nu_{as}(SiC_3)$,[27] respectively. If a linear W—O—W linkage exists in molecule **3** $\nu_{as}(W_2O)$ should appear in this spectral range or, if not observed separately from these three IR bands which is the case here, coincide with one of them. The Raman spectrum of the CH_2Cl_2 solution of complex **3** between 250 and 125 cm^{-1} shows (Fig. 1) that only one band in this region, at 186 cm^{-1}, is polarized. This observation is a strong indication that there is indeed a linear W—O—W linkage present in molecule **3** with $\nu_s(W_2O) = 186$ cm^{-1}. Molecule **3** could then, by analogy to $[W_2O_2(\mu\text{-}O)(CH_2CMe_3)_6]$,[34] consist of

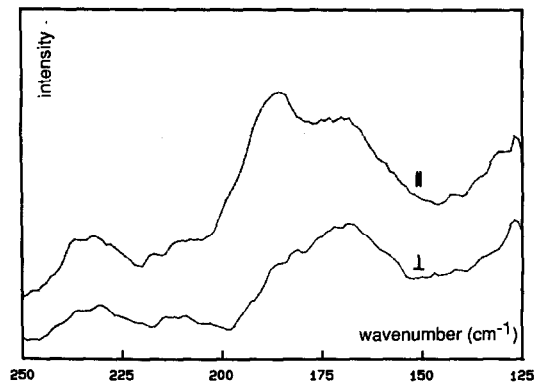

Fig. 1. Raman spectrum of compound **3** between 125 and 250 cm^{-1} in CH_2Cl_2 solution.

a linear N=W—O—W=N frame and three silanolato ligands about each tungsten atom, thus giving two apex-sharing trigonal bipyramids. In this context it is noteworthy that the size of the ^{14}N chemical shift of the imido nitrogen atom in complex **3** is consistent with data on tetra- and penta-coordinated terminal imido complexes with nitrogen and oxygen donors as co-ligands.[37]

The rhenium compound $[\{Re(NBu^t)_2(OSiMe_3)\}_2(\mu\text{-}O)(\mu\text{-}OReO_3)(\mu\text{-}OSiMe_3)]$[38] is another complex to which complex **3** could bear a structural resemblance. By analogy to the structure of this rhenium complex molecule **3** could be formulated as $\{[\{W(NBu^t)(OSiMe_3)_2\}_2(\mu\text{-}O)(\mu\text{-}OSiMe_3)_2] \cdot dmf\}$, but the spectroscopic data on the tungsten–oxygen stretchings of the silanolato groups are, as discussed above, not in accordance with such a structure.

Summarizing all the results molecule **3** has most probably a linear W—O—W arrangement and is best described as $\{[W_2(NBu^t)_2(\mu\text{-}O)(OSiMe_3)_6] \cdot dmf\}$.

One more complication concerning the ^1H and ^{13}C NMR spectra of complex **3**, not accounted for in the discussion above, cannot be left without comment. There are two resonances of the t-butyl methyl groups, one major at 1.33 and one minor at 1.23 ppm (integrals 9 : 1) in the ^1H NMR. This is matched by two methyl carbon resonances at 31.47 and 31.04 ppm in ^{13}C NMR. Furthermore, centred around the main resonances of the $OSiMe_3$ groups at 0.08 ppm in ^1H NMR and at 2.09 ppm in ^{13}C NMR small additional peaks appear at 0.15, 0.14, 0.09, 0.07, 0.06 and 0.03 ppm (^1H NMR) and at 1.69, 1.63 and 1.52 ppm (^{13}C NMR). The spectra obtained from different preparations are reproducible and these additional peaks are, therefore, not due to impurities of hydrolysis products. At present nothing but a proposal that these NMR peaks are due to some kind of isomerism can be given.

Structure of $[W(NBu^t)_2Cl_2(Bu^t\text{-}dab)]$ (**2**)

The structure of molecule **2** with atomic numbering is depicted in Fig. 2; selected bond distances and angles are given in Table 1. The tungsten atom in molecule **2** exhibits a distorted octahedral geometry, with *cis*-orientated t-butylimido and *trans*-dichloro ligands. The nitrogen atoms of Bu^t-dab are coordinated *trans* to the imido ligands. The tertiary carbon atoms of the two t-butylimido ligands are placed 0.12 Å above [C(11)] and 0.12 Å below [C(15)] and those of the Bu^t-dab ligand 0.29 Å below [C(7)] and 0.19 Å above [C(3)] the plane defined by the atoms N(3), W and N(4). The distance from the chlorine atoms to this plane is the same, 2.32 Å. Thus, the overall symmetry of molecule **2** is close to C_2 with the C_2 axis intersecting the N(3)—W—N(4) and Cl(1)—W—Cl(2) angles.

The tungsten–nitrogen bond lengths of the two imido ligands are very similar, 1.758(8) and 1.756(8) Å, respectively, and the corresponding W—N—C angles are far from linear, 161.8(7)° and 160.8(7)°. The two nitrogen atoms of these bent imido ligands have been described as six-electron donors, thus enabling an 18-electron count at the six-coordinate tungsten centre.[39] As can be seen from Table 2 the structural data of the $W(NBu^t)_2$ moiety of molecule **2** agree well with those of other known tungsten complexes with terminal bisimido ligands (see Table 2). The deviations from regular octahedral geometry comprise the wide N(3)—W—N(4) bond angle of 105.9(4)° and the small Cl(1)—W—Cl(2) bond angle of 154.1(1)°, whereby the chloro ligands are tilted away from the bisimido ligands. The tungsten chlorine bonds, 2.389(2) and 2.394(3) Å, indicate minimal or no participation of π-bonding in these bonds.[39]

The tungsten–nitrogen bond lengths of Bu^t-dab are 2.507(7) and 2.533(7) Å, respectively. They are

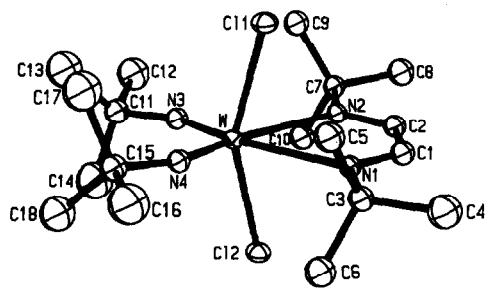

Fig. 2. A perspective view of the $[W(NBu^t)_2Cl_2(Bu^t\text{-}dab)]$ (**2**) molecule.

Table 1. Selected bond distances (Å) and angles (°) for $[W(NBu^t)_2Cl_2(Bu^t\text{-dab})]$ (**2**)

W—N(4)	1.756(8)	N(1)—C(1)	1.24(1)	N(3)—C(11)	1.46(1)
W—N(3)	1.758(8)	N(1)—C(3)	1.53(1)	C(11)—C(12)	1.52(2)
W—Cl(2)	2.389(2)	C(3)—C(4)	1.52(2)	C(11)—C(13)	1.47(2)
W—Cl(1)	2.394(3)	C(3)—C(5)	1.55(2)	C(11)—C(14)	1.52(2)
W—N(1)	2.507(7)	C(3)—C(6)	1.50(2)	N(4)—C(15)	1.44(1)
W—N(2)	2.533(7)	C(1)—C(2)	1.45(1)	C(15)—C(16)	1.50(2)
		C(2)—N(2)	1.27(1)	C(15)—C(17)	1.51(2)
		N(2)—C(7)	1.49(1)	C(15)—C(18)	1.52(2)
		C(7)—C(8)	1.54(2)		
		C(7)—C(9)	1.49(2)		
		C(7)—C(10)	1.51(2)		

N(1)—W—N(2)	67.0(2)	W—N(1)—C(1)	115.0(7)
N(3)—W—N(4)	105.9(4)	N(1)—C(1)—C(2)	122.6(9)
Cl(1)—W—Cl(2)	154.1(1)	C(1)—C(2)—N(2)	121.6(9)
W—N(3)—C(11)	161.8(7)	C(2)—N(2)—W	113.7(6)
W—N(4)—C(15)	160.8(7)		

significantly longer than the bonds between tungsten and the nitrogen atoms of 2,2′-bipyridyl in $[W(NPh)_2Cl_2(bipy)]$,[39,40] 2.309(12) and 2.319(13) Å. Such large differences in metal–N(sp^2) bond lengths between Bu^t-dab complexes and their analogues containing aromatic dinitrogen ligands have been observed earlier, e.g. $[MoO_2Cl_2(Bu^t\text{-dab})]$[17] and $[MoO_2Cl_2(o\text{-phen})]$.[42] An interplay of electronic effects, viz. more electron donation from *o*-phen or bipy than from Bu^t-dab into empty metal *d*-orbitals and of steric effects, viz. the bulkiness of t-butyl in Bu^t-dab, can explain the shorter metal–nitrogen bonds in bipy and *o*-phen complexes.

In complexed Bu^t-dab the orientation of the three methyl groups of each t-butyl group is such that two carbon atoms are directed towards the other ligands with about the same distance to the tungsten atom, thus leading to four close carbon–nitrogen contacts with the two t-butyl imido nitrogen atoms in the range 3.41–3.49 Å (sum of the van der Waals radii of C and N: 3.39 Å[43]). Any rotation of the methyl groups around the N(1)—C(3) or N(2)—C(7) bond of Bu^t-dab should, therefore, lead to stronger methyl carbon/imido nitrogen repulsion. Similar conformations of Bu^t-dab methyl groups were earlier observed in $[MoO_2Cl_2(Bu^t\text{-dab})]$,[17] in which methyl carbon/oxo repulsions determine the t-butyl conformations.

In each t-butyl imido ligand only one methyl carbon is orientated towards the metal atom giving four short carbon–carbon contacts to the Bu^t-dab methyl carbons with an average C···C distance of 3.67 Å (van der Waals radius of C: 1.85 Å[43]). Any other orientations of the imido methyl groups will

Table 2. Tungsten–nitrogen distances (Å) and WNC and NWN angles (°) of the imido ligands in monomeric bisimido tungsten(VI) complexes

Complex	*d*(W—N)	W—N—C	N—W—N	Ref.
$[W(NPh)_2(Cl_2)(bipy)]$[a]	1.789(6)	165.9(6)	104.3(4)	39, 40
$[W(NBu^t)_2Cl_2(Bu^t\text{-dab})]$	1.756(8)	160.8(7)	105.9(4)	This work
	1.758(8)	161.8(7)		
$[(PFP)W(NBu^t)_2(NH_2Bu^t)]$[b]	1.741(4)	166.6(3)	[c]	3
	1.743(3)	164.0(3)		
$[Cis\text{-}(\eta^1\text{-}CF_3SO_3)_2W(NBu^t)_2(NH_2Bu^t)_2]$	1.73(1)	167.2(8)	106.4(5)	41
	1.75(1)	169.5(7)		

[a] Mean values.
[b] PFP = perfluoropinacole.
[c] Not given.

introduce additional close contacts to the Bu^t-dab methyl groups and increase steric strain. The distances between the methyl carbon atoms of the two imido ligands are outside the double van der Waals radius of carbon.

EXPERIMENTAL

All manipulations were performed under argon as an inert gas using standard Schlenk techniques. n-Heptane and toluene were dried over activated molecular sieves, dimethylformamide was stirred with CaH_2 at 70°C for several hours and distilled under reduced pressure. $[WO_2Cl_2(dme)]$,[14] N,N'-di-t-butyl-1,4-diaza-1,3-butadiene (Bu^t-dab),[44] $[WO_2Cl_2(Bu^t\text{-dab})]$[17] and $Me_3SiNH(Bu^t)$[45] were prepared according to the literature. Elemental analyses and molecular weight determination were performed by Analytische Laboratorien Malissa und Reuter, Gummersbach, F.R.G. IR spectra (Nujol mulls between CsI plates) and Raman spectra were recorded with a Nicolet 20SXC and a Bruker FRA 106 spectrometer (excitation radiation 1064 nm, resolution 4 cm^{-1}, 1000–3000 scans), respectively. Polarization measurements were performed in CH_2Cl_2 solution with a Dilor Z 24 (excitation radiation 514.5 nm, resolution 4 cm^{-1}, laser power 400 mW). ^1H NMR, ^{13}C NMR ($SiMe_4$ as an internal standard with $\delta = 0$ ppm), ^{29}Si NMR [$SiMe_4$ as an external standard with $\delta(^{29}Si) = 0$ ppm] and ^{14}N NMR [CD_3NO_2 as an external standard with $\delta(^{14}N) = 0$ ppm] were recorded with a Varian XL 300 spectrometer. ^{17}O NMR [H_2O/D_2O (1/1) as an external standard with $\delta(^{17}O) = 0$ ppm] was recorded with a Varian–Unity 300 MHz spectrometer.

X-ray crystallography

Orange crystals of $[W(NBu^t)_2Cl_2(Bu^t\text{-dab})]$ (**2**) were obtained from toluene solution by cooling at −30°C for 2 weeks. A prismatic crystal of complex **2** was enclosed in a Lindemann capillary to protect it from air. Unit-cell parameters were derived from least-squares fitting of angular settings of 50 reflections. The data were corrected for a decrease of 10% during the data collection and for Lorentz, polarization and absorption effects, the latter by an empirical method.[46] Some crystal data are collected in Table 3.

The structure was solved by direct methods (MULTAN87), which gave the tungsten and chlorine positions, followed by subsequent difference-Fourier syntheses. In the final refinements the tungsten and chlorine atoms were refined with anisotropic and the other non-hydrogen atoms with isotropic temperature factors. The hydrogen atoms were included with fixed positional parameters at calculated positions with C—H = 0.95 Å.

Table 3. Crystal and data collection parameters for $[W(NBu^t)_2Cl_2(Bu^t\text{-dab})]$ (**2**)

Crystal data	
Formula	$WC_{18}H_{38}Cl_2N_4$
Molecular weight	565.3
Size	$0.30 \times 0.14 \times 0.08$
Space group	$P2_1/c$
a (Å)	12.592(2)
b (Å)	12.134(2)
c (Å)	16.060(3)
β (°)	99.76(2)
V (Å^3)	2418.5(7)
z	4
D_c (g cm^{-3})	1.55
μ(Mo-K_α) (cm^{-1})	51.1
Temperature (°C)	23
Data collection and structure refinement	
Diffractometer	HUBER
Radiation	Mo-K_α (λ = 0.71073 Å)
Data collection ($2\theta_{max}$)	50
Monochromator	Graphite
Scan mode	ω–2θ
Independent reflections	4444
Observed reflections ($I > 3\sigma(I)$)	2867
Weighting scheme (w^{-1})	$\sigma^2(F_o)+(0.030F_o)^2+3.0$
R	0.042
R_w	0.056
$\Delta(\rho_{max})$ (e Å^{-3})	0.96

Syntheses

$\{[W(NBu^t)_2Cl_2(NH_2Bu^t)]_2\}$ (**1**). To $[WO_2Cl_2(dme)]$ (1.90 g, 5.0 mmol), suspended in n-heptane (30 cm^3) was slowly added $Me_3SiNH(Bu^t)$ (2.92 g, 20.1 mmol) in n-heptane (10 cm^3) with stirring. The suspension immediately turned yellow. After 1 day stirring a white precipitate, $Bu^t(NH_3)Cl$ (0.13 g, 1.2 mmol), was separated by filtration and the yellow filtrate concentrated to approximately half the volume. The solution was kept at −30°C for 2 days and **1** collected on a filter and dried *in vacuo*. Yield: 0.67 g, 29%. The purity and identity of compound **1** was checked by comparison of its NMR and IR spectra with the spectra of a sample synthesized according to the published preparation of **1**.[9] Raman bands at: 3295w, 3175w, 3099w, 2979vs, 2920vs, 2794w, 2761w, 2731w, 2699vw, 2601vw, 2500vw, 1471m, 1448m, 1383vw, 1337vw, 1304m, 1283vs, 1237m, 1217m, 1151m, 1138m,

1105vw, 1075w, 1025w, 996w, 935w, 917w, 887w, 808m, 752w, 731m, 696vw, 635vw, 605w, 559w, 536w, 453m, 380vw, 350vw, 307w, 283m, 252m, 237m, 212m, 193m cm^{-1}.

$[W(NBu^t)_2Cl_2(Bu^t\text{-dab})]$ (**2**). Compound **1** (0.46 g, 0.5 mmol) was dissolved in toluene (10 cm^3) and solid Bu^t-dab (0.19 g, 1.1 mmol) was added with stirring. The solution was heated at 70°C for 5 h. The orange solution was then kept at −30°C for 2 weeks. Orange crystals of **2**, which contained single crystals suitable for an X ray structure determination, were collected, washed with a small amount of cooled ether and dried *in vacuo*. Yield: 0.32 g, 56.6%. Found: C, 37.3; H, 6.6; N, 9.5; Cl, 12.1. Calc. for $C_{18}H_{38}Cl_2N_4W$: C, 38.2; H, 6.8; N, 9.9; Cl, 12.5%. IR and *Raman* data (in cm^{-1}); 1630vw, 1609vw, *1631w*, *1613s* [*v*(C=N)]; 1260s, 1208s, *1262vs*, *1212m* [*v*(W=N—C)]; 318vs, 311s, 290sh, *317m*, *295m* [*v*(W—Cl)]. NMR data (CD_2Cl_2, $T = 293$ K); ^1H: 8.13 (s, 2H, —C*H*=N—), 1.58 [s, 18H, W=NC(CH_3)$_3$], 1.44 [s, 18H, CH=NC(CH_3)$_3$]. $^{13}C\{^1H\}$: 153.2 (—*C*H=N—), 69.2 [W=N*C*(CH_3)$_3$], 68.2 [CH=N*C*(CH_3)$_3$], 32.3 [W=NC(*C*H_3)$_3$], 29.4 [CH=NC(*C*H_3)$_3$].

$\{[W_2(NBu^t)_2(\mu\text{-O})(OSiMe_3)_6]\cdot dmf\}$ (**3**). $[WO_2Cl_2(dme)]$ (1.21 g, 3.2 mmol) was dissolved in dmf (13 cm^3); to the stirred solution was slowly added neat $Me_3SiNH(Bu^t)$ (1.86 g, 12.8 mmol). The colourless solution became yellow immediately and after approximately 2 h a white substance began to precipitate. After stirring for 24 h at room temperature and cooling at −30°C for 1 day the white precipitate was filtered and dried *in vacuo* for 5 h to give 1.55 g (84%) of raw product (**3**), which was sublimed at 70°C bath temperature and 10^{-2} torr. Yield of sublimed **3**: 1.24 g, 68.1%. Found: C, 31.3; H, 6.8; N, 3.4; W, 30.3. Calc. for $C_{29}H_{79}N_3O_8Si_6W_2$: C, 30.7; H, 7.0; N, 3.7; W, 32.4%. Mol. wt (osmometric, dmf, 75°C): calc. for $C_{26}H_{72}N_2O_7Si_6W_2$ (**3**-dmf): 1061; found: 1030. Mass spectrum (FAB): $[\{NBu^tW(OSiMe_3)_3\}_2O—(Me_3Si)_2O]^+$; 899 (1%), $[NBu^tW(OSiMe_3)_2((Me_3Si)_2O)H]^+$; 596 (35%), $[NBu^tW(OSiMe_3)_3]^+$; 522 (78%), $[NBu^tW(OSiMe_3)_2(O)_2H]^+$; 466 (40%), $[NBu^tW(OSiMe_3)_2(O)_2H]^+$; 450 (35%), $[NBu^tW(OSiMe_3)_2H]^+$; 434 (28%). IR (Nujol) bands at: 1661s, 1338vw, 1297m, 1263w,sh, 1246s, 1218w, 1169vw, 1105w, 1052w, 958m, 930vs, 911vs, 839s, 749m, 681m, 630vw, 593vw, 545vw, 433m,b, 374w, 337w, 322w cm^{-1}. Raman bands at: 2976vs, 2957vs, 2925vs, 2898vs, 1662vw, 1475w, 1442m, 1419m, 1410m, 1298vs, 1246w, 1218w, 1169w, 1106vw, 921m,b, 872w, 842w, 807w, 749w, 682s, 631vs, 584vw, 546vw, 428m,b, 376vw, 341vw, 278m, 231m, 208m, 181m, 170m cm^{-1}. NMR data ($CDCl_3$, $T = 293$ K): ^1H (see text): 8.04 [s, *H*—C(O)N(CH_3)$_2$], 2.99 and 2.91 [s, H—C(O)N(CH_3)$_2$], 1.33 and 1.23 [s, =N—C(CH_3)$_3$], 0.08 [s, OSi(CH_3)$_3$]. $^{13}C\{^1H\}$: 164.54 [H—*C*(O)N(CH_3)$_2$], 68.49 [N—*C*(CH_3)$_3$], 36.93 and 32.05 [H—C(O)N(*C*H_3)$_2$], 31.47 and 31.04 [=N—C(*C*H_3)$_3$], 2.09 [—OSi(*C*H_3)$_3$] and 1.69, 1.63, 1.52 [—OSi(*C*H_3)$_3$]. ^{29}Si: 9.2, $^2J(^{29}Si–^1H) = 6.7$ Hz. ^{15}N: 5.6 (half width: 100 Hz) (=*N*CMe_3). ^{17}O: 293 [H—C(*O*)N(CH_3)$_2$], 199 (*O*$SiMe_3$).

Acknowledgements—Financial support from TFR (Swedish Research Council for Engineering Sciences) and NUTEK (Swedish National Board for Industrial and Technical Development) is gratefully acknowledged. We thank Dr L. Bengtsson for running the ^{17}O NMR spectra and Dr O. Faurskov-Nielsen for performing the Raman polarization measurements.

REFERENCES

1. J. D. Burrington and R. K. Grasselli, *J. Cat.* 1979, **59**, 79.
2. D. M. T. Chan and W. A. Nugent, *Inorg. Chem.* 1985, **24**, 1422.
3. D. M. T. Chan, W. C. Fultz, W. A. Nugent, D. C. Roe and T. H. Tulip, *J. Am. Chem. Soc.* 1985, **107**, 251.
4. C. J. Schaverien, J. C. Dewan and R. R. Schrock, *J. Am. Chem. Soc.* 1986, **108**, 2771.
5. J. S. Murdzek and R. R. Schrock, *Organometallics* 1987, **6**, 1373.
6. R. R. Schrock, R. T. DePue, J. Feldman, K. B. Yap, D. C. Yang, W. M. Davis, L. Park, M. DiMare, M. Schofield, J. Anhaus, E. Walborsky, E. Evitt, C. Krüger and P. Betz, *Organometallics* 1990, **9**, 2262.
7. R. R. Schrock, J. S. Murdzek, G. C. Bazan, J. Robbins, M. DiMare and M. O'Regan, *J. Am. Chem. Soc.* 1990, **112**, 3875.
8. W. A. Nugent and B. L. Haymore, *Coord. Chem. Rev.* 1980, **31**, 123.
9. A. J. Neilson, *Polyhedron* 1987, **6**, 1657.
10. W. A. Nugent, *Inorg. Chem.* 1983, **22**, 965.
11. W. A. Nugent and R. L. Harlow, *Inorg. Chem.* 1980, **19**, 777.
12. B. R. Ashcroft, A. Nielson, D. C. Bradley, R. J. Errington, M. B. Hursthouse and R. L. Short, *J. Chem. Soc., Dalton Trans.* 1987, 2059.
13. D. C. Bradley, A. J. Howes, M. B. Hursthouse and J. D. Runnacles, *Polyhedron* 1991, **10**, 477.
14. K. Dreisch, C. Andersson and C. Stålhandske, *Polyhedron* 1991, **10**, 2417.
15. W. A. Herrmann, W. R. Thiel and E. Herdtweck, *Chem. Ber.* 1990, **123**, 271.
16. A. A. Kuznetsova, Y. G. Podzolko and Y. A. Buslaev, *Russ. J. Inorg. Chem.* 1969, **14**, 393.
17. K. Dreisch, C. Andersson and C. Stålhandske, *Polyhedron* 1993, **12**, 303.
18. J. Sundermeyer, *Chem. Ber.* 1991, **124**, 1977.

19. O. Jarchow, F. Schröder and H. Schulz, *Z. Anorg. Allg. Chem.* 1968, **363**, 58.
20. G. A. Fowles, D. A. Rice and K. J. Shanton, *J. Chem. Soc., Dalton Trans.* 1978, 1658.
21. W. A. Nugent and R. L. Harlow, *J. Chem. Soc., Chem. Commun.* 1979, 342.
22. F. Preuss, E. Fuchslocher, E. Leber and W. Towae, *Z. Naturforsch.* 1989, **44b**, 271.
23. W. A. Herrmann, M. Denk, F. Dyckhoff and J. Behm, *Chem. Ber.* 1991, **124**, 2401.
24. W. A. Nugent, R. J. MaKinney, R. V. Kasowski and F. A. Van-Catledge, *Inorg. Chim. Acta* 1982, **65**, L91.
25. K. Nakamoto, *Infrared and Raman Spectra of Inorganic and Coordination Compounds*, 4th edn, p. 191. Wiley, New York (1986).
26. W. P. Griffith, A. J. Nielson and M. J. Taylor, *J. Chem. Soc., Dalton Trans.* 1988, 647.
27. H. Bürger, *Organomet. Chem. Rev. A* 1968, **3**, 425.
28. W. A. Nugent and J. M. Mayer, in *Metal Ligand Multiple Bonds*. Wiley, New York (1988).
29. C. G. Barraclough, D. C. Bradley , J. Lewis and I. M. Thomas, *J. Chem. Soc.* 1961, 2601.
30. H. Kriegsmann and K. Licht, *Z. Elektrochem.* 1958, **62**, 1163.
31. F. Schindler and H. Schmidbaur, *Angew. Chem.* 1967, **79**, 697.
32. A. D. English, J. P. Jesson, W. G. Klemperer, T. Mamouneas, L. Messerle, W. Shum and A. Tramontano, *J. Am. Chem. Soc.* 1975, **97**, 4785.
33. W. P. Griffith, *J. Chem. Soc.* 1963, 5345.
34. I. Feinstein-Jaffe, D. Gibson, S. J. Lippard, R. R. Schrock and A. Spool, *J. Am. Chem. Soc.* 1984, **106**, 6305.
35. W. P. Griffith, *J. Chem. Soc. (A)* 1969, 211.
36. C. Persson, K. Dreisch and C. Andersson, unpublished results.
37. D. C. Bradley, S. R. Hodge, J. D. Runnacles, M. Hughes, J. Mason and R. L. Richards, *J. Chem. Soc., Dalton Trans.* 1992, 1663.
38. W. A. Nugent and R. L. Harlow, *J. Chem. Soc., Chem. Commun.* 1979, 1105.
39. D. C. Bradley, R. J. Errington, M. B. Hursthouse, R. L. Short, B. R. Ashcroft, G. R. Clark, A. J. Nielson and C. E. F. Rickard, *J. Chem. Soc., Dalton Trans.* 1987, 2067.
40. B. R. Ashcroft, D. C. Bradley, G. R. Clark, R. J. Errington, A. J. Nielson and C. E. F. Rickard, *J. Chem. Soc., Chem. Commun.* 1987, 170.
41. A. A. Danopoulos, G. Wilkinson, M. B. Hursthouse and B. Hussain, *Polyhedron* 1989, **8**, 2947.
42. P. B. Viossat and N. Rodier, *Acta Cryst.* 1979, **B35**, 2715.
43. J. Emsley, *The Elements*. Clarendon Press, Oxford (1991).
44. J. M. Klirgman and R. K. Barnes, *Tetrahedron* 1970, **26**, 2555.
45. R. M. Pieke, *J. Org. Chem.* 1961, **26**, 232.
46. N. Walker and D. Stuart, *Acta Cryst.* 1983, **A39**, 158.

Polyhedron Vol. 12, No. 11, pp. 1345–1352, 1993
Printed in Great Britain

0277-5387/93 $6.00+.00
© 1993 Pergamon Press Ltd

SYNTHESIS AND CHEMICAL CHARACTERIZATION OF 2-METHYLPYRIDINIUM SALTS OF PLANAR NICKEL(II), PALLADIUM(II) AND PLATINUM(II) 1,2-DITHIOOXALATO-S,S′ COMPLEXES. CRYSTAL AND MOLECULAR STRUCTURE OF BIS(2-METHYLPYRIDINIUM) BIS(1,2-DITHIOOXALATO-S,S′)NICKELATE(II)

PASCUAL ROMÁN,† JAVIER I. BEITIA, ANTONIO LUQUE and ANA ARANZABE

Departamento de Química Inorgánica, Universidad del País Vasco, Apartado 644, 48080 Bilbao, Spain

(*Received* 18 *December* 1992; *accepted* 1 *February* 1993)

Abstract—Microcrystalline powders of the complexes $(HC_6H_7N)_2[Ni(S_2C_2O_2)_2]$ (**1**), $(HC_6H_7N)_2[Pd(S_2C_2O_2)_2]$ (**2**) and $(HC_6H_7N)_2[Pt(S_2C_2O_2)_2]$ (**3**) were obtained by reaction of 2-methylpyridinium hydrochloride and the corresponding $K_2[M(S_2C_2O_2)_2]$ salts in aqueous solution. These compounds were characterized by elemental analysis, IR and UV–vis spectroscopies, thermal analysis (TG, DTG and DTA) and X-ray diffraction techniques. Single crystals of compound **1** were obtained by recrystallization in N,N-dimethylformamide and its crystal structure was determined from single-crystal X-ray diffraction. The crystal structure consists of mixed layers of quasi-planar complex $[Ni(S_2C_2O_2)_2]^{2-}$ anions and 2-methylpyridinium cations held together by electrostatic interactions, an extensive network of hydrogen bonds of the types N—H···O and C—H···O and anion–cation π–π interactions.

Interest in square-planar d^8 metal complexes involving sulphur donor ligands has received increased attention in recent years because of their crystal structures, based on columnar stacked structures of square co-planar metal complexes and their electronic properties.[1–11] The presence of four donor atoms in the dithiooxalate dianion and the possibilities of charge delocalization on its atoms result in a multifunctional ligand with unique coordination properties.[12] X-ray structure determinations demonstrate the ability of the dithiooxalate ligand to coordinate to the central metal ion by two sulphur or two oxygen donor atoms, respectively; furthermore, dithiooxalate may coordinate simultaneously to more than one metal ion in polynuclear complexes.[2,4]

Previous X-ray reports on the structures containing $[M(S_2C_2O_2)_2]^{2-}$ anions[7–11] have demonstrated that the nature and size of the counter-ions play an important role in the crystal packing of this kind of compound. The almost planarity of the most inorganic dithiooxalato anions leads to a more compact crystal packing in compounds containing organic planar cations than those observed for compounds of large and bulky cations.[8,11]

In this context we decided to study the reaction between aromatic organoammonium molecules and several square-planar inorganic metal(II) 1,2-dithiooxalato-S,S′ anions, in order to obtain a deeper insight into the cation and metal effects on the crystal packing and the strength of the intramolecular interactions in this type of compound. On the other hand, oxidative thermal decompositions of various nickel, palladium and platinum complexes are used for the production of metal and metal oxides, which are extensively applied as catalysts in a variety of important chemical processes.[13]

In the light of the recent interest in the bio-

† Author to whom correspondence should be addressed.

inorganic chemistry of nickel[14] the present paper reports the syntheses, the chemical characterization and the thermal behaviour of 2-methylpyridinium salts of 1,2-dithiooxalate-S,S′ metalate anions, $[M(S_2C_2O_2)_2]^{2-}$, where M is nickel(II), palladium (II) or platinum(II), as well as the crystal and molecular structure of the compound bis(2-methylpyridinium) bis(1,2-dithiooxalate-S,S′)nickelate(II) (**1**).

EXPERIMENTAL

General and instrumental

The dithiooxalate ligand was used as purchased from Eastman Kodak. Elemental analyses were performed on a Perkin–Elmer 240 C, H and N analyser. The metal was determined using atomic absorption. IR spectra were recorded in the 4000–350 cm^{-1} range on an IR Beckman 4240 spectrophotometer using KBr discs. A Bausch–Lomb Spectronic 2000 spectrophotometer was used to record the UV–vis spectra (650–220 nm) of ethanol solutions (2×10^{-5} M) in 1 cm silica cells. Density values were measured by flotation in a mixture of $CCl_4/CHBr_3$. The differential thermal analysis (DTA) and thermogravimetric analysis (TG and DTG) curves were obtained, simultaneously, in argon and argon–oxygen atmospheres on a SETARAM TAG 24 S16 thermobalance, with a heating rate of 5°C min^{-1}. X-ray powder diffraction patterns of **2**, **3** and the final products from thermal decompositions of compounds **1–3** were obtained on a Philips PW 1710 instrument with nickel-filtered Cu-K_α radiation. Diffraction patterns of thermal decomposition residues were compared with those obtained from the ASTM powder diffraction files of the Joint Committee on Powder Diffraction Standards.

Synthesis of complexes

The potassium salts of the complex anions $[M(S_2C_2O_2)_2]^{2-}$ were prepared following the procedure described by Cox[15] and the purity checked by elemental analysis.

Bis(2-*methylpyridinium*) *bis*(*dithiooxalato*)*nickelate* (II), $(HC_6H_7N)_2[Ni(S_2C_2O_2)_2]$ (**1**). A sample of 2-methylpyridinium hydrochloride (0.60 g, 4.63 mmol) was dissolved in water (25 cm^3) and an aqueous solution (25 cm^3) of $K_2[Ni(S_2C_2O_2)_2]$ (0.80 g, 2.12 mmol) was added with stirring at room temperature. Immediately an insoluble microcrystalline powder of **1** was obtained. Dark-purple single crystals suitable for X-ray investigations were obtained by recrystallization in an H_2O/DMF (3/1, v/v) mixture, after 3 weeks. Yield: 0.75 g, 1.53 mmol, 72% based on nickel. Found: C, 39.2; H, 3.4; N, 5.7; Ni, 12.2. Calc. for $C_{16}H_{16}N_2NiO_4S_4$: C, 39.4; H, 3.3; N, 5.8; Ni, 12.1%. Selected IR data (KBr, cm^{-1}): 1590vs, 1535vs, 1440s [ν(C=O)]; 1080vs [ν(C—C)+ν(C—S)]; 945s [δ(C—O)+ν_a(C—S)]; 580w, 520w, 435w [ν_s(C—S)]; 410m [ν_a(Ni—S)]; 360w [ν_s(Ni—S)]. UV–vis [EtOH, nm (ε, M^{-1} cm^{-1})]: 563.4 (2805), 511.3 (3471), 298.3 (22,089), 260.9 (23,843).

Bis(2-*methylpyridinium*) *bis*(*dithiooxalato*)*paladate*(II), $(HC_6H_7N)_2[Pd(S_2C_2O_2)_2]$ (**2**). This compound was synthesized from $K_2(Pd(S_2C_2O_2)_2]$ (0.25 g, 0.59 mmol) and 2-methylpyridinium hydrochloride (0.20 g, 1.54 mmol) in water (30 cm^3) following the general method described for **1**. The resultant yellow precipitate was isolated by vacuum filtration, washed with EtOH and Me_2O and recrystallized from DMF. Unfortunately, yellow dark crystals were twinned and were not suitable for single-crystal X-ray diffraction. Yield: 0.228 g, 0.54 mmol, 91% based on palladium. Found: C, 35.8; H, 3.2; N, 5.1; Pd, 19.8%. Calc. for $C_{16}H_{16}N_2O_4PdS_4$: C, 35.9; H, 3.0; N, 5.2; Pd, 19.9%. Selected IR data (KBr, cm^{-1}): 1585vs, 1440m [ν(C=O)]; 1080vs [ν(C—C)+ν(C—S)]; 940s [δ(C—O)+ν_a(C—S)]; 540w [ν_s(C—S)]; 410m [ν_a(Pd—S)]; 365m [ν_s(Pd—S)]. UV–vis [EtOH, nm (ε, M^{-1} cm^{-1})]: 388.7 (8498), 276.5 (39,504), 244.9 (22,996).

Bis(2-*methylpyridium*) *bis*(*dithiooxalato*)*platinate* (II), $(HC_6H_7N)_2[Pt(S_2C_2O_2)_2]$ (**3**). Red crystals of this compound were prepared from $K_2[Pd(S_2C_2O_2)_2]$ (0.10 g, 0.19 mmol) and 2-methylpyridinium hydrochloride (0.05 g, 0.42 mmol) in water (15 cm^3) by a similar procedure to above. Yield: 0.230 g, 0.37 mmol, 63% based on platinum. Found: C, 30.9; H, 2.6; N, 4.4; Pt, 31.1. Calc. for $C_{16}H_{16}N_2O_4PtS_4$: C, 30.8; H, 2.6; N, 4.5; Pt, 31.3%. Selected IR data (KBr, cm^{-1}): 1580vs, 1435m [ν(C=O)]; 1080vs [ν(C—C)+ν(C—S)]; 945s [δ(C—O)+ν_a(C—S)]; 575w, 520w, 435w [ν_s(C—S)]; 415m [ν_a(Pt—S)]; 390w [ν_s(Pt—S)]. UV–vis [EtOH, nm (ε, M^{-1} cm^{-1})]: 466.3 (4968), 433.3 (6062), 413.5 (5594), 332.7 (4156), 266.3 (9156), 260.5 (11,718), 239.9 (20,875).

Crystallographic data collection and structural refinement of **1**

A dark purple, prismatic, single crystal of **1** with the approximate dimensions $0.25 \times 0.30 \times 0.15$ mm was mounted on an Enraf–Nonius CAD4 four-circle diffractometer. X-ray data were collected with graphite-monochromated Mo-K_α radiation ($\lambda = 0.71069$ Å) at 295 K using the ω–2θ scan technique. Accurate unit-cell parameters and an orien-

tation matrix for data collection were obtained from least-squares refinement, using the setting angles of 25 reflections in the range $8 < \theta < 15°$. A total of 4389 independent reflections were measured in the range $2 \leqslant \theta \leqslant 35$ ($0 \leqslant h \leqslant 16$; $0 \leqslant k \leqslant 12$; $-22 \leqslant l \leqslant 22$), 1648 of which, with $I > 3\sigma(I)$, were used in the development and refinement of the structure. No significant decay of intensity of three standard reflections recorded after every 100 reflections was observed. The intensity data were corrected for Lorentz and polarization effects. An empirical absorption correction ($\mu = 13.954\ cm^{-1}$) following the procedure DIFABS[16] with minimum and maximum correction coefficients 0.551–1.263 was applied. The atomic scattering factors and anomalous dispersion corrections were taken from the International Tables for X-ray Crystallography (1974).[17] The structure was solved by a combination of Patterson and difference-Fourier methods and refined by full-matrix least-squares. Non-hydrogen atoms were refined anisotropically. A convenient weighting scheme[18] was used to obtain flat dependence in $\langle w\Delta^2F \rangle$ vs $\langle F_o \rangle$ and $\langle \sin\theta/\lambda \rangle$. All aromatic hydrogen atoms were clearly visible in a difference-Fourier synthesis and were refined isotropically. The hydrogens of the methyl groups were introduced in the final refinement in calculated positions as fixed isotropic contributors ($U = 0.07\ Å^2$). Last cycles of refinement led to the discrepancy indices $R = 0.038$ and $wR = 0.047$ for 144 parameters; goodness of fit = 1.23; maximum shift/error in the final cycle = 0.09 and the highest peak in the final difference-Fourier map was 0.21 e $Å^{-3}$. Most calculations were performed using the X-RAY76 system[19] running on a MicroVAX II computer. Final atomic positional and thermal parameters, together with anisotropic thermal parameters for non-hydrogen atoms, full list of bond distances and angles, dihedral angles, and a list of observed and calculated structure factors have been deposited as supplementary material with the Editor, from whom copies are available on request. Atomic coordinates have also been submitted to the Cambridge Crystallographic Data Centre.

Compounds **2** and **3** crystallize in insufficient quality to be studied as single crystals, but their cell parameters have been obtained by powder diffraction data. The powder diffraction pattern was recorded on a Philips PW 1710 diffractometer; 2θ values were corrected using the GUINIER program[20] with an α-SiO_2 standard pattern. Accurate cell parameters were obtained by least-squares refinement using the LSUCRE program.[21] Table 1 summarizes the crystal data for the three compounds and shows that all of them are isostructural.

RESULTS AND DISCUSSION

Spectroscopic characterization

The IR spectra certify the presence of the 2-methylpyridinium cations; giving evidence of this point are the corresponding bands at *ca* 3000 cm^{-1} for the C—H groups and 2700 cm^{-1} for N—H^+ groups. The characteristic and very strong bands of 2-methylpyridinium cations were obtained between 1650 and 600 cm^{-1}.[22] IR assignments of the bis(dithiooxalato)metallate(II) anions have been made in the 1600–350 cm^{-1} region and a comparison of the results with the observed spectra of the reported compounds[9–11] led to the assignments described in the Experimental.

The UV–vis spectra of the compounds exhibit two strong absorption bands in the UV range, at

Table 1. Crystal data for compounds **1**, **2** and **3**

Compound	**1**[a]	**2**[b]	**3**[b]
Formula	$C_{16}H_{16}N_2NiO_4S_4$	$C_{16}H_{16}N_2O_4PdS_4$	$C_{16}H_{16}N_2O_4PtS_4$
Formula weight	487.24	534.97	623.63
Space group	$P2_1/c$	$P2_1/c$	$P2_1/c$
a (Å)	10.141(3)	10.296(9)	10.211(2)
b (Å)	7.639(2)	7.623(3)	7.621(2)
c (Å)	13.747(2)	13.72(2)	13.537(3)
β (°)	109.74(1)	110.09(8)	109.60(2)
V ($Å^3$)	1002.4(4)	1011(1)	992.5(3)
Z	2	2	2
D_x (g cm^{-3})	1.61	1.76	2.09
D_o (g cm^{-3})	1.62(1)	1.77(1)	2.08(1)

[a] X-ray single-crystal diffraction data.
[b] X-ray powder diffraction data.

Table 2. Thermal analysis data for compounds **1–3**

	Ar+O_2					Ar			
Step	T_i	T_f	T_m[a]	Δm[b]	Step	T_i	T_f	T_m[a]	Δm[b]
				1					
1	185	230	227(+)	49.44	1	179	265	239(−)	81.20
2[c]	230	275		3.03					(81.20)
3	275	294	285(+)	28.85					
				(81.32)					
				2					
1	195	251	241(+)	63.25	1	193	283	233(−)	67.27
2[c]	251	293		2.25	2[c]	283	675		2.83
3	293	315	308(+)	2.34	3	675	820	750(−)	5.50
4	315	350	330(+)	7.36					(75.60)
				(75.20)					
				3					
1	202	255	251(+)	53.15	1	165	351	248(−)	55.55
2[c]	255	282		3.05	2[c]	351	602		1.42
3	282	311	292(+)	11.30	3	602	780	675(−)	10.43
				(67.50)					(67.40)

[a] Endothermic (−) or exothermic (+) process.
[b] Total mass losses are shown between parentheses.
[c] Progressive mass loss without clear peaks in DTG and/or DTA curves.

ca 240 and 290 nm, which may be due to the $\pi^* \leftarrow n$ and $\pi^* \leftarrow \pi$ transitions of the aromatic cations and the dithiooxalate ligands. The less intensive bands in the visible region, which do not appear in the cation spectra, are attributable to metal–ligand charge transfer absorption and they are shifted as a function of the metal nature.[12,23–25]

Thermal analysis

Table 2 presents the thermoanalytical results of thermal decompositions of the three compounds in an argon–oxygen and argon atmospheres.

The TG–DTA curves for the compounds in the oxidative atmosphere are shown in Fig. 1. The compounds are anhydrous and stable up to approximately 185°C, beyond which a first abrupt weight loss takes place corresponding to an exothermic peak in the DTA curve. The thermal decompositions are quite similar and the first abrupt weight loss step is followed by a lower weight loss, which is accompanied by a stronger exothermic peak in the DTA curves. Final residues from the thermal decompositions at 600°C depend on the starting compound. For compound **1** the solid stable residue was identified as nickel(II) sulphide by its X-ray

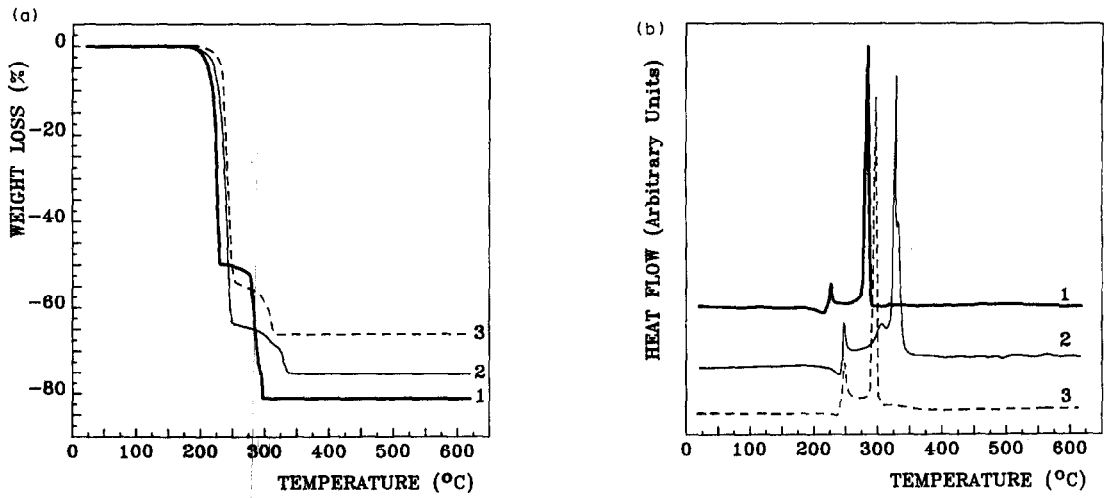

Fig. 1. (a) TG and (b) DTA curves for compounds **1–3** in an argon–oxygen atmosphere.

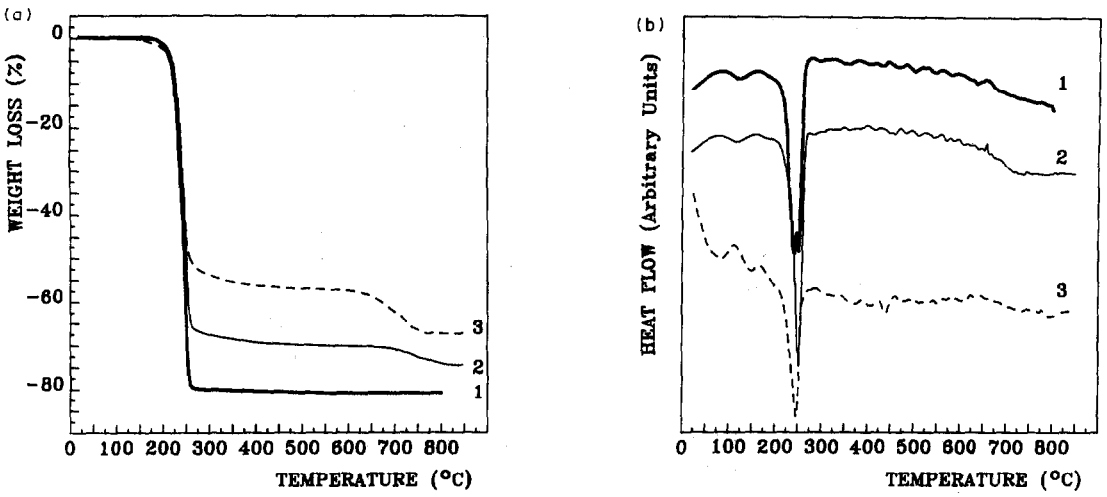

Fig. 2. (a) TG and (b) DTA curves for compounds **1–3** in an argon atmosphere.

powder diffractogram. The thermal decomposition of compound **2** yields a mixture of palladium(0) and palladium(II) oxide, whereas the final residue of **3** is platinum(0).

In an argon atmosphere (Fig. 2) most of the mass is lost in the first step with a high endothermic peak in the DTA curve around 240°C. For the nickel complex the solid residue at 265°C is stable and was identified as nickel(II) sulphide. No peaks belonging to nickel or other nickel compounds were found in the X-ray powder diffraction patterns. For **2** and **3** the first thermal decomposition step is followed by a progressive weight loss without clear peaks in the DTA curve and a constant mass was reached at 850°C. The final residues were identified as PdS and platinum for **2** and **3**, respectively.

X-ray structure determination

The asymmetric unit of **1** consists of one 2-methylpyridinium cation and one half of a complex anion, $[Ni(S_2C_2O_2)_2]^{2-}$, with the nickel atom lying on a centre of symmetry. Figure 3 shows the structure of the complex dianion and the cation with the atomic numbering scheme. Selected bond lengths, angles and the hydrogen contacts are listed in Table 3. The cation 2-methylpyridinium is almost planar and the bond lengths and angles are within the normal range reported in the bibliography.[22] The complex dianion is almost planar with a dihedral angle between the strictly planar NiS_4 group and the $S_2C_2O_2$ ligand mean plane of 1.83(5)°. This angle is in the lower end of the range previously

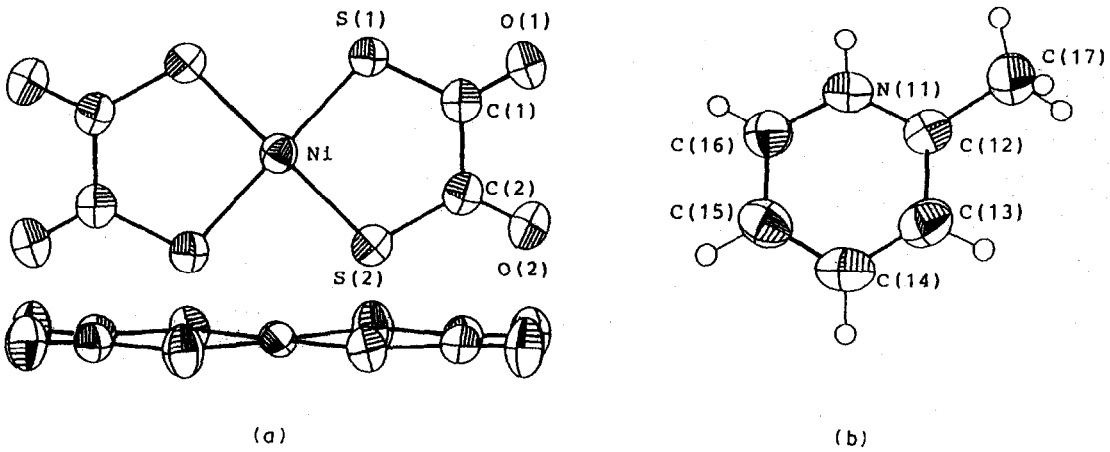

Fig. 3. ORTEP view of the structure of (a) the $[Ni(S_2C_2O_2)_2]^{2-}$ anion and (b) the 2-methylpyridinium cation, showing the atom labelling scheme.

Table 3. Selected bond lengths (Å), bond angles (°) and hydrogen contacts for **1**

		Anion	
Ni—S(1)	2.1879(9)	S(1)—Ni—S(2)	92.59(4)
Ni—S(2)	2.1803(11)	Ni—S(1)—C(1)	105.6(1)
S(1)—C(1)	1.712(4)	Ni—S(2)—C(2)	105.4(1)
S(2)—C(2)	1.713(3)	S(1)—C(1)—C(2)	117.9(3)
C(1)—C(2)	1.539(4)	S(2)—C(2)—C(1)	118.5(3)
C(1)—O(1)	1.224(4)	S(1)—C(1)—O(1)	124.0(3)
C(2)—O(2)	1.221(5)	S(2)—C(2)—O(2)	124.3(3)
		C(1)—C(2)—O(2)	117.2(3)
		C(2)—C(1)—O(1)	118.1(3)
		Cation	
N(11)—C(12)	1.345(4)	N(11)—C(12)—C(13)	117.1(3)
C(12)—C(13)	1.383(6)	C(12)—C(13)—C(14)	120.5(4)
C(13)—C(14)	1.380(6)	C(13)—C(14)—C(15)	120.2(4)
C(14)—C(15)	1.380(5)	C(14)—C(15)—C(16)	118.7(4)
C(15)—C(16)	1.368(6)	C(15)—C(16)—N(11)	119.6(4)
N(11)—C(16)	1.350(5)	C(16)—N(11)—C(12)	123.9(3)
C(12)—C(17)	1.500(5)	N(11)—C(12)—C(17)	119.4(3)
		C(13)—C(12)—C(17)	123.5(3)

Hydrogen contacts

	X—H	X···O	H···O	<X—H···O
N(11)—H(11)···O(1)	0.82(6)	2.905(5)	2.13(6)	160(5)
N(11)—H(11)···O(2)	0.82(6)	2.983(4)	2.41(5)	128(4)
C(16)—H(16)···O(2)	0.87(4)	2.972(5)	2.41(5)	123(4)
C(15)—H(15)···O(1) (1)	1.00(8)	3.383(4)	2.59(7)	135(6)
C(15)—H(15)···O(2) (2)	1.00(8)	3.315(5)	2.67(8)	122(6)

Symmetry codes

(1) $x, \frac{1}{2}-y, -\frac{1}{2}+z$ (2) $1-x, \frac{1}{2}+y, -\frac{1}{2}-z$

observed for similar bis(dithiooxalato)metallate(II) anions in compounds also containing aromatic cations[3,7] and is considerably lower than those observed in analogous complexes containing large and bulky cations.[8,11] The value of this angle is affected by a combination of factors, including the hydrogen contacts between the oxygen atoms and the hydrogen atoms of cations, as well as the π–π interactions between the aromatic cations and the dithiooxalate groups where a significant degree of electronic delocalization is present. Both of them may produce a displacement of the ligand atoms and a higher value of the dihedral angle between the MS_4 and the dithiooxalate groups. The short average C—S bond distance of 1.71 Å and the long average C=O bond distance of 1.22 Å are consistent with the existence of a significant degree of delocalization throughout the S—C—O units in the dianion, with a single C—C bond of 1.539(4) Å.

A stereoscopic view of the unit cell is shown in Fig. 4 (hydrogen contacts: dotted lines). The anions and cations are stacked in mixed sheets (at $z = 0$ and 1/2) along the [210] direction following the sequence ...accacc... (where a = anion and c = cation). Anion and cation best planes are almost parallel to each other, with a dihedral angle of 7.77(8)°. The crystal structure is stabilized by electrostatic attractions, an extensive network of hydrogen bonds of the type N—H···O and C—H···O is present (Table 3) and weak anion–cation π–π interactions. The ions situated in the same z-level are linked by a bifurcated hydrogen contact between the hydrogen atom of the pyridine ring nitrogen atom and two oxygen atoms of the same dithiooxalate ligand, and a monofurcated hydrogen contact between C(16) and O(2). The sheets placed in different z-levels are connected by hydrogen contacts among C(15) atoms of the cation and the anions. On the other hand, the stacking of cations and anions may suggest the existence of a significant interaction between the dithiooxalate groups and the π-systems of the aromatic cations, as found in other $[Ni(S_2C_2O_2)_2]^{2-}$ salts.[9,10] Each anion is placed between four 2-methylpyridinium

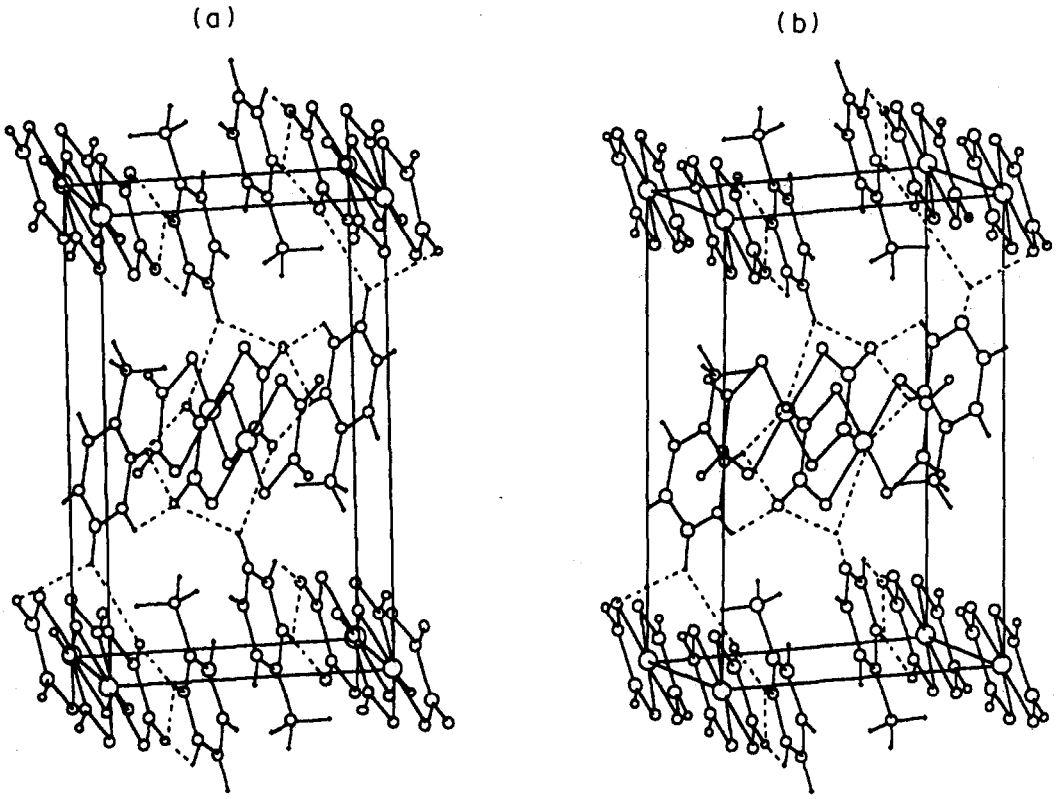

Fig. 4. Stereo packing diagram for $(HC_6H_7N)_2[Ni(C_2S_2O_2)_2]$ (hydrogen contacts: dotted line). (a) is out of the paper plane, (b) is horizontal and (c) is vertical.

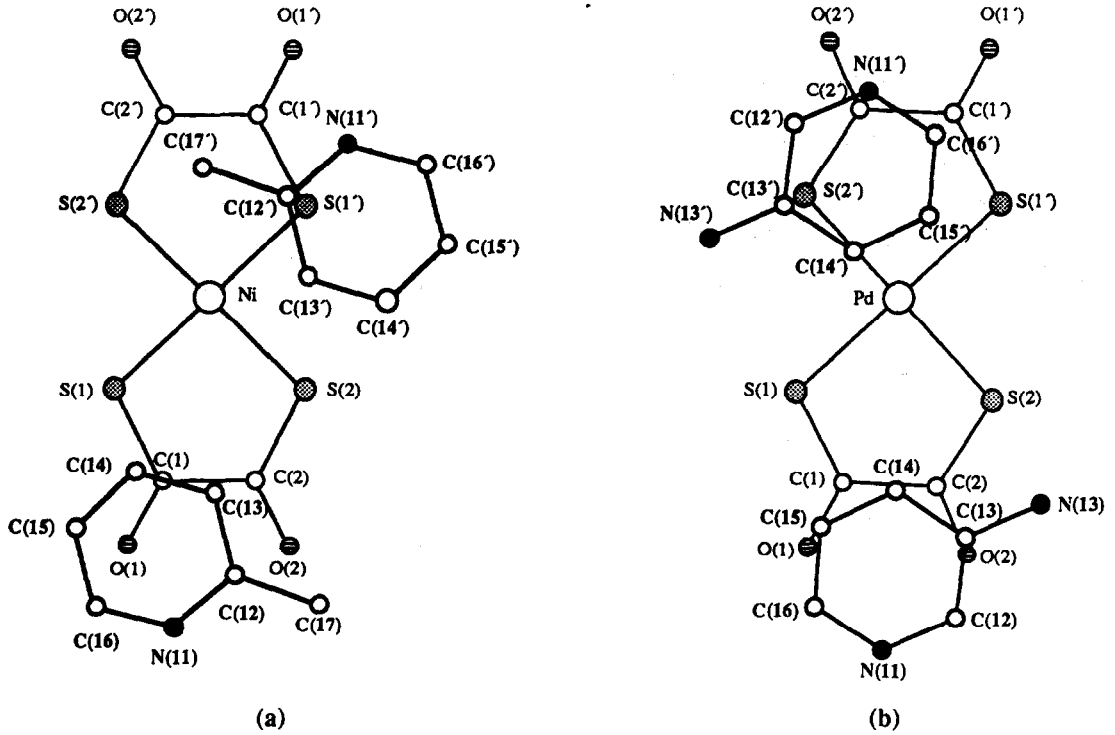

Fig. 5. Overlapping of anions and cations in the crystal structure of (a) compound 1 and (b) bis(3-aminopyridinium) bis(dithiooxalato)palladate(II).

cations of two neighbour sheets, which are disposed above and below the dithiooxalate ligands. The interstack distances range from 3.30 to 3.70 Å and the shortest contacts between C(1) and C(13) and C(2) and C(13) are 3.39 Å. These values are comparable to interplanar distances found in aromatic π-systems (3.2–3.6 Å) with strong π–π interactions.[26] In these salts there is no evidence of π–π interactions between dithiooxalate groups belonging to neighbour anions or between aromatic cations, which have been observed previously.[9,10] Figure 5 shows the similar anion–cation overlapping in **1** and in the previously reported crystal structure of bis(3-aminopyridinium) bis(dithiooxalato)palladate(II).[9] Both arrangements are different to that found in the bis(4-aminopyridinium) bis(dithiooxalato)palladate(II) structure,[10] in which the anion is placed between two 4-aminopyridinium cations which lie up and down the PdS_4 plane. This arrangement suggests the existence of a significant interaction between the d_{z^2} orbital of the metal and the π-systems of the aromatic cations. Therefore, the nature and size of the cation play an important role in this type of interaction.

Acknowledgements—The authors would like to thank Iberdrola, S.A. and UPV/EHU (Grant No. 169.310-E180/91) for financial support.

REFERENCES

1. A. Gleizes, F. Maury, P. Cassoux and J. Galy, *Z. Krist.* 1981, **155**, 293.
2. A. Gleizes and M. Verdaguer, *J. Am. Chem. Soc.* 1984, **106**, 3727.
3. R. Enjalbert, A. Gleizes, J.-C. Trombe, M. L. Gutiérrez-Campo and P. Román, *J. Molec. Struct.* 1985, **131**, 1.
4. C. Frasse, J.-C. Trombe, A. Gleizes and J. Galy, *C.R. Acad. Sci. Paris* 1985, **300**, 403.
5. J.-C. Trombe, A. Gleizes and J. Glay, *C.R. Acad. Sci. Paris* 1985, **300**, 5.
6. J. M. Gutiérrez-Zorrilla, P. Román and A. Gleizes, *C.R. Acad. Sci. Paris* 1987, **305**, 1353.
7. P. Román, C. Bao, J. M. Gutiérrez-Zorrilla and A. Vegas, *J. Cryst. Spect. Res.* 1988, **18**, 207.
8. P. Román, J. M. Gutiérrez-Zorrilla, A. Luque, J. I. Beitia and C. Guzmán-Miralles, *Acta Cryst.* 1991, **C47**, 48.
9. P. Román, J. I. Beitia, A. Luque and J. M. Gutiérrez-Zorrilla, *Polyhedron* 1992, **11**, 1883.
10. P. Román, A. Luque, J. I. Beitia and C. Guzmán-Miralles, *Mat. Res. Bull.* 1992, **27**, 339.
11. P. Román, A. Luque, J. M. Gutiérrez-Zorrilla and J. I. Beitia, *Z. Krist.* 1992, **198**, 213.
12. D. Coucouvanis, N. C. Baezinger and S. M. Johnson, *J. Am. Chem. Soc.* 1973, **95**, 3875.
13. P. A. Chaloner, *Coord. Chem. Rev.* 1990, **101**, 1.
14. R. Cammack, *Adv. Inorg. Chem.* 1988, **32**, 297.
15. E. G. Cox, W. Wardlaw and K. C. Webster, *J. Chem. Soc.* 1935, 1475.
16. N. Walker and D. Stuart, *Acta Cryst.* 1983, **A39**, 158.
17. D. T. Cromer and J. T. Waber, *International Tables for X-ray Crystallography*, Vol. 4, pp. 72–102. Kynoch Press, Birmingham (1974).
18. M. Martínez-Ripoll and F. H. Cano, PESOS, A Program for the Automatic Treatment of Weighting Schemes for Least-Squares Refinement. Instituto Rocasolano, CSIC, Madrid, Spain (1975).
19. J. M. Stewart, P. A. Machin, C. W. Dickinson, H. L. Ammon, H. Heck and H. Flack, The XRAY76 System. Technical Report TR-446. Computer Science Center, University of Maryland, College Park, Maryland, U.S.A. (1976).
20. C. D. Carpentier, GUINIER, Kristallographisches Institut Freiburg, Freiburg, Germany (1972).
21. D. E. Appleman and H. T. Evans Jr, LSUCRE, Report PB 216188. U.S. Department of Commerce, National Technical Information Service, 5285 Port Royal Rd, Springfield, VA 22151, U.S.A. (1973).
22. P. Román, J. M. Gutiérrez-Zorrilla, M. Martínez-Ripoll and S. García-Blanco, *Acta Cryst.* 1986, **C42**, 956.
23. R. Czernuszewick, D. P. Strommen and K. Nakamoto, *Inorg. Chim. Acta* 1979, **34**, L211.
24. J. A. McCleverty, in *Progress in Inorganic Chemistry* (Edited by F. A. Cotton), Vol. 10, pp. 49–221. Wiley, New York (1968).
25. A. R. Latham, V. C. Hascall and H. B. Gray, *Inorg. Chem.* 1965, **6**, 788.
26. C. A. Hunter and J. K. M. Sanders, *J. Am. Chem. Soc.* 1990, **112**, 5525.

Polyhedron Vol. 12, No. 11, pp. 1353–1360, 1993
Printed in Great Britain

0277–5387/93 $6.00+.00
© 1993 Pergamon Press Ltd

CRYSTAL AND MOLECULAR STRUCTURE OF A FIVE-COORDINATE ZINC COMPLEX OF *MESO*-TETRAPHENYLTETRABENZOPORPHYRIN

RU-JEN CHENG* and YU-REN CHEN

Department of Chemistry, National Chung-Hsing University, Taichung, Taiwan 40227, R.O.C.

and

S. L. WANG and C. Y. CHENG

National Tsing Hua University, Hsinchu, Taiwan 30043, R.O.C.

(*Received* 18 *December* 1992; *accepted* 1 *February* 1993)

Abstract—The crystal and molecular structure of a five-coordinate zinc tetrabenzoporphyrin, (tetrahydrofuran)(*meso*-tetraphenyltetrabenzoporphyrin)zinc(II), [(TPTBP)Zn(THF)], has been determined. The molecule is severely non-planar and assumes a saddle shape. The average absolute displacement of C_b from the mean plane is 0.7652 Å. The predominant feature of the crystal structure is layers of three saddle-shaped macrocycles stacked with infinite cylindrical channels along the crystallographic *c*-axes. The results of this study indicate that extension of the π-electron system of the porphyrinato core results in significant effects for both molecular and crystal structure.

Porphyrins continue to attract research interest, not only for well-established biological importance, but also for the good opportunities they offer to study structure–bonding–reactivity inter-relationships.[1] Within the whole spectrum of closely controlled variations of the basic porphyrin structure, tetrabenzoporphyrin (TBP) happens to be an exception. Tetrabenzoporphyrin has been claimed as a structural intermediate between porphyrin and phthalocyanine.[2] The extension of the π-electron system of porphyrin has the effect of a drastic decrease in the redox potential.[3] However, details of the coordination chemistry are limited by the poor solubility in most innocent organic solvents.[4] *Meso*-tetraphenyltetrabenzoporphyrin (TPTBP) is the *meso*-tetraphenylporphyrin (TPP) analogue of the tetrabenzoporphyrin system. Due to the enhanced solubility we have been able to make (TPTBP)Zn pure enough for some basic spectroscopic characterization.[5] In this paper we report the molecular and crystal structure of a five-coordinate *meso*-tetraphenyltetrabenzoporphyrin zinc complex, [(TPTBP)Zn(THF)], determined by single-crystal X-ray diffraction. To the best of our knowledge, other than the partially oxidized nickel complexes of octamethyltetrabenzoporphyrin (OMTBP) and tetrabenzoporphyrin,[6,7] this will be the first structural data for a TBP system.

EXPERIMENTAL

Synthesis

(TPTBP)Zn was prepared as previously reported by Remy.[8] The condensation of isoindole and two-fold benzaldehyde in the presence of zinc acetate as a template was fused at 375°C for 40 min. The product mixture was first purified through silica gel using CH_2Cl_2/hexane (2 : 1) as the eluant, then followed by repeated recrystallization from THF and hexane. Crystals suitable for diffraction studies were obtained by a combination of diffusion and evaporation of a layer of hexane floated on a THF

* Author to whom correspondence should be addressed.

solution of (TPTBP)Zn. The solution was left in the dark until half of the liquid had evaporated. All crystals collected were small thin cubes with the same crystalline phase under microscopic examination.

X-ray structure determination

Crystal data for [(TPTBP)Zn(THF)], together with details of the X-ray diffraction experiment, are reported in Table 1. A small blue crystal of approximate dimensions $0.025 \times 0.10 \times 0.20$ mm was mounted on a Nicolet R3m/V diffractometer equipped with a graphite monochromator (Mo-K_α radiation). Unit cell constants were determined from a least-squares fit to the automatically centred settings of 25 reflections with $14.73° < 2\theta < 24.74°$. The space group $R\bar{3}$ was determined from the systematic absences hkl, $-h+k+l = 3n$, and then confirmed by refinement. $\theta/2\theta$ scan data were collected at room temperature (23°C). The data were corrected for Lorentz and polarization effects.

The structure was solved by direct methods using SHELXTL PLUS.[9] Full-matrix least-squares refinement based on F with anomalous dispersion corrections for atoms with atomic numbers greater than 16 was used. Neutral-atom scattering factors were taken from the International Tables for X-ray Crystallography.[10] The weights had the form $w = [\Sigma^2(F)+gF^2]^{-1}$ with $g = 0.1196$. Carbon atoms which form phenyl substituents were confined to a rigid group (C—C = 1.395 Å, C—C—C = 120.0°) and refined isotropically. All of the hydrogen atoms included in the refinement were placed in idealized positions (C—H = 0.96 Å, H—C—H = 109.4°) and refined with a fixed U of

Table 1. Crystal data, data collection and refinement of [(TPTBP)Zn(THF)]

Empirical formula	$C_{64}H_{44}N_4OZn$
Colour; habit	Blue; plate
Crystal size (mm)	$0.2 \times 0.1 \times 0.025$
Space group	Trigonal; $R\bar{3}$
Unit cell dimensions (hexagonal axes)	
a (Å)	34.15(5)
c (Å)	23.44(5)
Volume (Å^3)	23674(66)
Z	18
Formula weight	950.4
Density (calc.) (g cm^{-3})	1.200
Absorption coefficient (mm^{-1})	0.520
$F(000)$	8892
Diffractometer	Nicolet R3m/V
Radiation	Mo-K_α ($\lambda = 0.71073$ Å)
Temperature (K)	296
Monochromator	Highly oriented graphite crystal
2θ range (°)	2.0–45.0
Scan type	$\theta/2\theta$
Scan speed (° min^{-1})	Variable; 2.93–14.65 in ω
Scan range (ω) (°)	1.00 plus K_α-separation
Background measurement	Stationary crystal and stationary counter at beginning and end of scan, each for 50.0% of total scan time
Standard reflections	3 measured every 50 reflections
Index ranges	$-36 \leqslant h \leqslant 0$, $0 \leqslant k \leqslant 36$, $0 \leqslant l \leqslant 22$
Reflections collected	7368 ($2667 > 3.0\sigma(I)$)
Independent reflections	6066 ($2091 > 3.0\sigma(I)$)
Extinction correction	$\chi = 0.00007(2)$, where $F^* = F[1+0.002\kappa F^2/\sin(2\theta)]^{-1/4}$
Hydrogen atoms	Riding model, fixed isotropic U
Weighting scheme	$w-1 = \sigma^2(F)+0.1196F^2$
R	0.0854
R_w	0.0905
Goodness-of-fit	0.38
Largest and mean Δ/σ	0.042, 0.000
Data-to-parameter ratio	6.1 : 1

Table 2. Average bond distances and bond angles in [(TPTBP)Zn(THF)]

Zn—N	2.077(17)	Ca—Cb	1.465(28)
Zn—O	2.211(13)	Cb—Cb	1.396(29)
N—Ca	1.367(26)	Cb—Cc	1.403(29)
Cm—Ca	1.388(29)	Cc—Cd	1.388(32)
Cm—Cf	1.491(24)	Cd—Cd	1.372(35)
N—Zn—N	89.5(7)	Ca—Cb—Cc	133.2(19)
Zn—N—Ca	123.8(11)	Cb—Cb—Cc	119.8(18)
N—Ca—Cm	125.3(18)	Cb—Cc—Cd	119.4(20)
N—Ca—Cb	107.5(17)	Cb—Ca—Cm	126.9(19)
Ca—N—Ca	110.7(16)	Cc—Cd—Cd	120.6(22)
Ca—Cm—Ca	125.8(19)	O—Zn—N	96.6(6)
Ca—Cb—Cb	106.9(18)		

0.08 Å^2. All calculations were performed on a MicroVAX II-based Nicolet SHELXTL PLUS system.

The average bond lengths and angles involving the tetrabenzoporphyrin core and the zinc atom may be found in Table 2. Tables of final fractional atomic coordinates and anisotropic thermal parameters for the non-hydrogen atoms, final positional parameters for the hydrogen atoms and complete bond distances and angles have been included as supplementary material.

RESULTS

Molecular structure

A projection of the structure and the atom-labelling scheme of [(TPTBP)Zn(THF)] is shown in Fig. 1. The extreme non-planar nature of the tetrabenzoporphyrin core is evident in the perspective view of an isolated molecule shown in Fig. 2. A formal diagram of the tetrabenzoporphyrin core is given in Fig. 3, in which we display the perpendicular displacement of each atom from the mean plane of the 40 atom core. As is readily observed in Figs 2 and 3 the isoindole rings are displaced, alternatively, above and below the mean plane of the tetrabenzoporphyrin core. The average absolute displacement of C_b from the mean plane is 0.7652 Å and that of C_d is 1.6647 Å. Although departures of the tetrabenzoporphyrin ring from planarity are large, individually the isoindole rings are planar to within 0.03 Å and the four *meso*-carbons are planar to within 0.071 Å. The dihedral angles between the mean tetrabenzoporphyrin

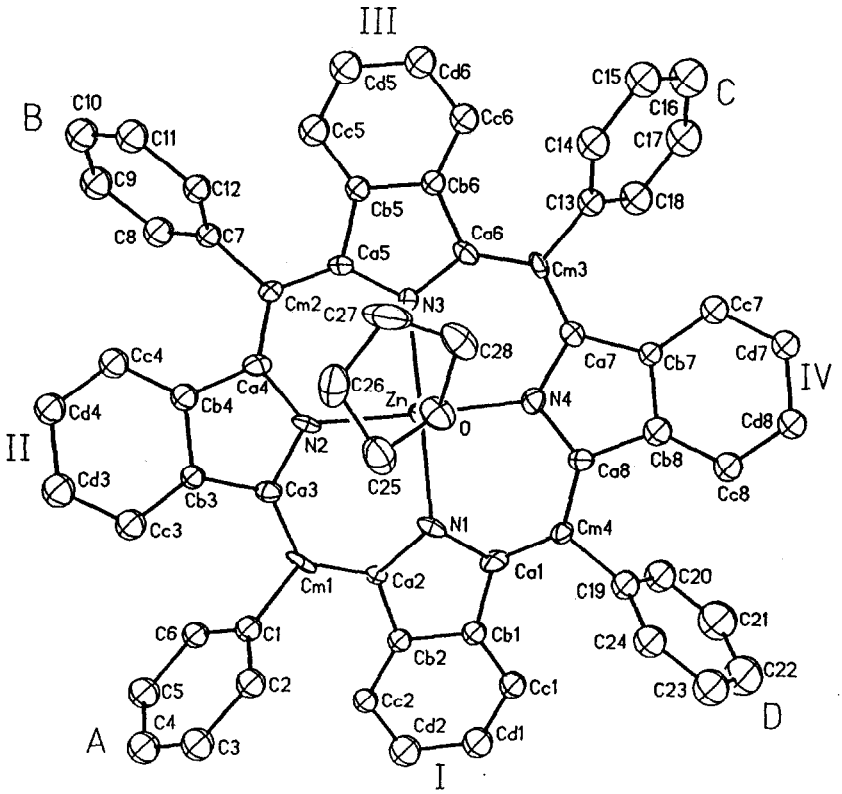

Fig. 1. Projection of the molecular structure in the porphyrin plane, including the atom-labelling scheme of [(TPTBP)Zn(THF)]. Hydrogens are omitted for clarity.

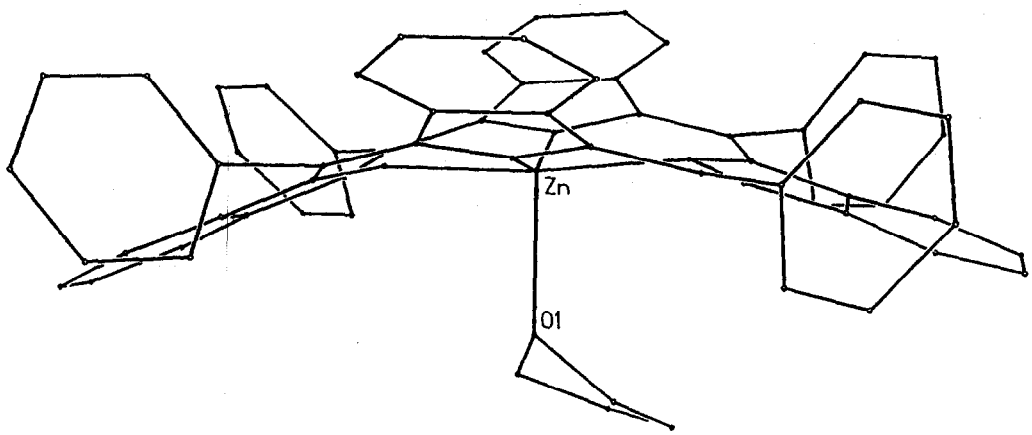

Fig. 2. Perspective view of [(TPTBP)Zn(HF)] that illustrates the saddle-deformation of the tetrabenzoporphyrin skeleton.

plane and isoindole rings I, II, III and IV are 24.1, 21.1, 21.2 and 22.2°, respectively.

The approximate D_{2d}-type ruffled geometry of this species, while differing from most of the corresponding *meso*-tetraphenylporphyrin analogues, can find similar trends for all π-cation-radical metalloporphyrin complexes[11] and sterically crowded zinc(II) octaethyltetraphenylporphyrinate (OETPPZn).[12] In agreement with previous studies of metalloporphyrins with a saddle core conformation the phenyl ring dihedral angles of 62.8, 66.1, 55.3 and 63.6° for rings A–D with the mean tetrabenzoporphyrin plane are toward the small end of other values of reported data. The orientations of the phenyl groups appear to depend upon interactions of the *ortho*-phenyl hydrogens with the adjacent isoindole hydrogens (the average contact distance between the hydrogens attached to benzo-

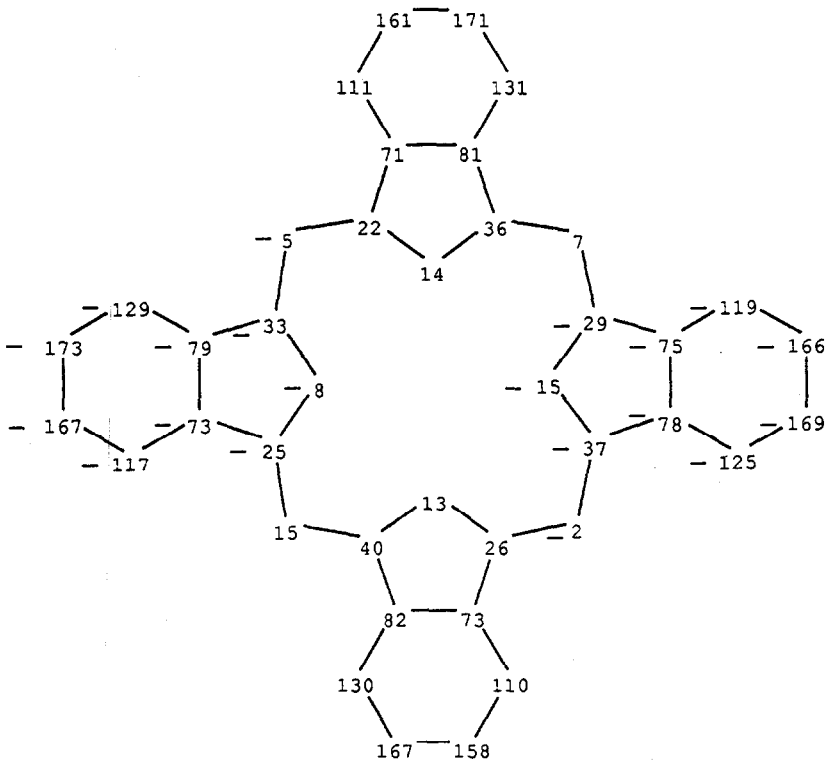

Fig. 3. Formal diagram of the tetrabenzoporphyrin core of [(TPTBP)Zn(THF)], showing displacements of the 40 atoms from the mean plane in units of 0.01 Å.

C_c and *ortho*-phenyl-carbon is 3.166 Å); they all tilt towards the troughs of the saddle. It is clear that the vertical tilt of the isoindole rings is important in maximizing phenyl and core atom contacts for phenyls with small dihedral angles.

The THF molecule is bound quite strongly to the zinc atom [Zn—O = 2.212(13) Å], as demonstrated by comparison with the much longer distance of 2.380(2) Å reported for the six-coordinate $[(TPP)Zn(THF)_2]$,[13] but compares well with that observed in the five-coordinate $[(TPP)Zn(H_2O)]$.[14] The coordinated THF molecule exhibits the commonly observed envelope conformation, with the pocket fold towards the porphyrin plane. It is also clear from Fig. 2 that the oxygen atom lies along the normal to the porphyrin plane instead of forming a tilt angle, as observed in the six-coordinate case.

The geometry about the zinc atom is close to square pyramid with zinc situated 0.240 Å above the base of the four-nitrogen plane, significantly smaller than the 0.347 and 0.33 Å out-of-plane displacements observed in $[(TPP)ZnClO_4]$ and [(TPyP)ZnPy].[15] Nevertheless, the average Zn—N distance (2.077 Å) is close to similar bonds in $[(TPP)ZnClO_4]$.

Other than the partially oxidized TBP system[6,7] there are no appropriate structural data available for comparison to reflect the major changes of the bond distances and angles caused by the macrocycle deformation. Comparison with average porphyrin values[12] illustrates that C_a—N—C_a, C_a—C_m—C_a and C_b—C_a—C_m angles increase with a concomitant decrease in N—C_a—C_b and Zn—N—C_a angles as a result of the saddle deformation. These bond angle changes do not parallel completely with those in (OETPP)Zn. The major difference in bond distances is the increase of C_b—C_b by 0.042 Å. However, this bond elongation should be ascribed mostly to the fused benzene ring in isoindole.

Crystal packing

Other than the unusual saddle-shaped molecular structure these molecules are also packed in a very special way in the crystals. The most pronounced feature is the extremely large unit cell with volume 23,674 $Å^3$ and $Z = 18$. Six of them form a "ball" around the inversion centre (Fig. 4) and a C_3 axis (Fig. 5). All the coordinated THF ligands point outwards with a cavity inside the ball. Along *c*-axes the cavities link into infinite channels (Fig. 6). This type of framework makes the density of the crystal (1.200 g cm^{-3}) lower than usual. Also there seems to be some extra electron densities inside the channels. These may be caused by the crystallographically disordered solvent molecules

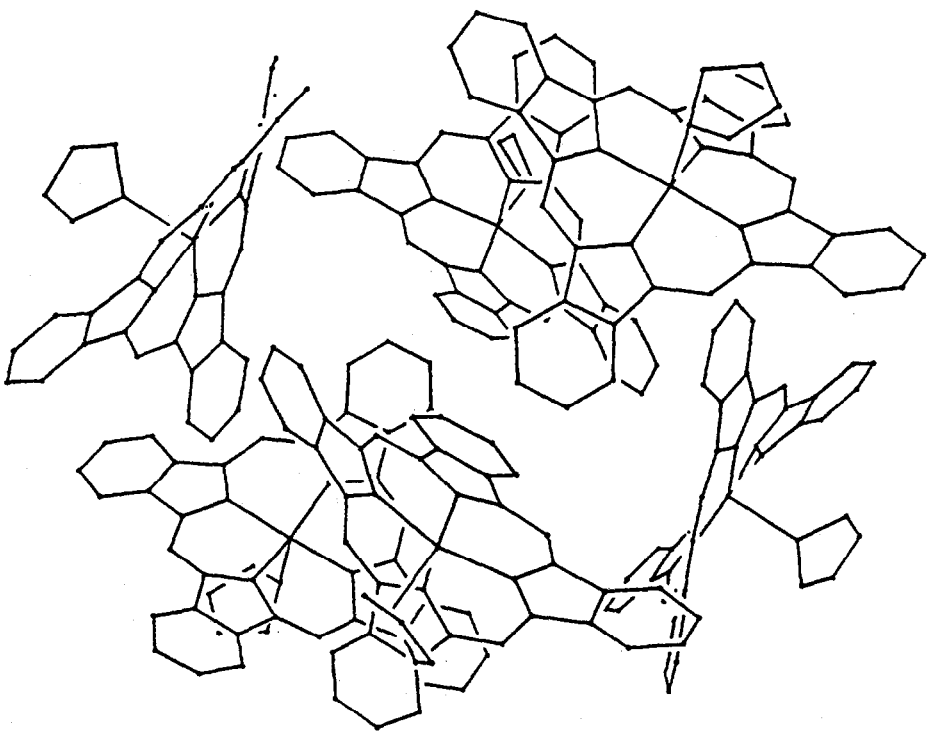

Fig. 4. Illustration of the packing of a six-molecules unit into a ball with an inversion centre and cavity inside. Phenyl substituents have been removed for clarity.

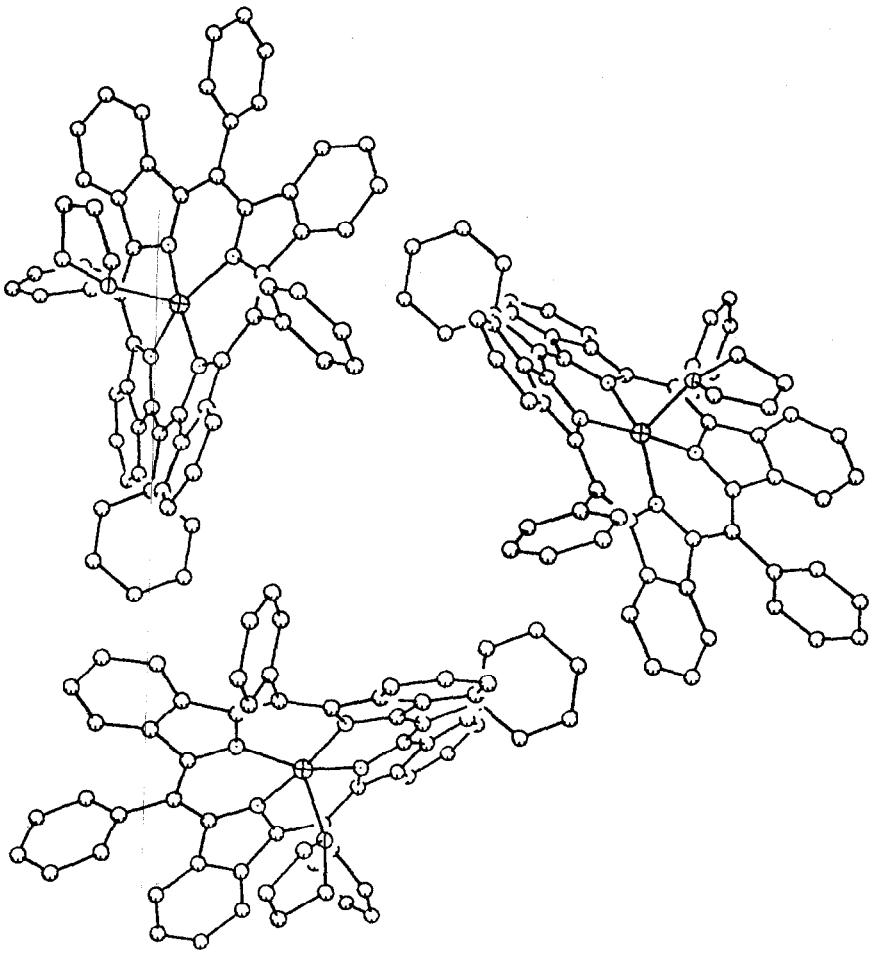

Fig. 5. Illustration of the arrangement of a three-molecules unit with C_3 axis.

residing in the channels. A similar phenomenon has recently been reported for a polynuclear copper complex, $[Cu_8(dmpz)_8(OH)_8]_2C_6H_5NO_2$ (Hdmpz = 3,5-dimethylpyrazole).[16] However, to the best of our knowledge this is the first example of this special crystal packing pattern reported for a porphyrin system. Most other saddle-shaped porphyrins tend to be dimerized with the porphinato core having similar orientation with respect to the unit cell axes.

DISCUSSION

The quality of the structure determination is not very good, however, this is presumably because residual electron density due to solvent molecules residing in the channels was not accounted for. Nevertheless, the severe distortion of the tetrabenzoporphyrin ring and the unique crystal packing pattern are noteworthy. Prior to the structural determination of this complex it was expected that the aromaticity of the extended π-electron system is the most crucial factor that should dictate the structure of the macrocycle. Based on the available structural data a large number of tetraarylporphyrin complexes can be described as planar, while some of them have been reported to be "ruffled" or "saddle-shaped".[11] The origin of the unusual distorted conformation can be traced to either internal strain within a contracted or an expanded core, or the steric requirements of face-to-face dimer formation. Solid-dimer formation has been proved to lead to antiferromagnetic coupling between the ring radicals of the π-cation–radical metalloporphyrin complexes. It is obvious that in our case of [(TPTBP)Zn(THF)] the saddle deformation is not due to either the size of the metal or dimerization. Actually, other than the extended π-system, (TPTBP)Zn and (OETPP)Zn have similar carbon skeletons and should suffer similar steric hindrances which would prevent them from forming planar macrocycles. Based on the red-shifted

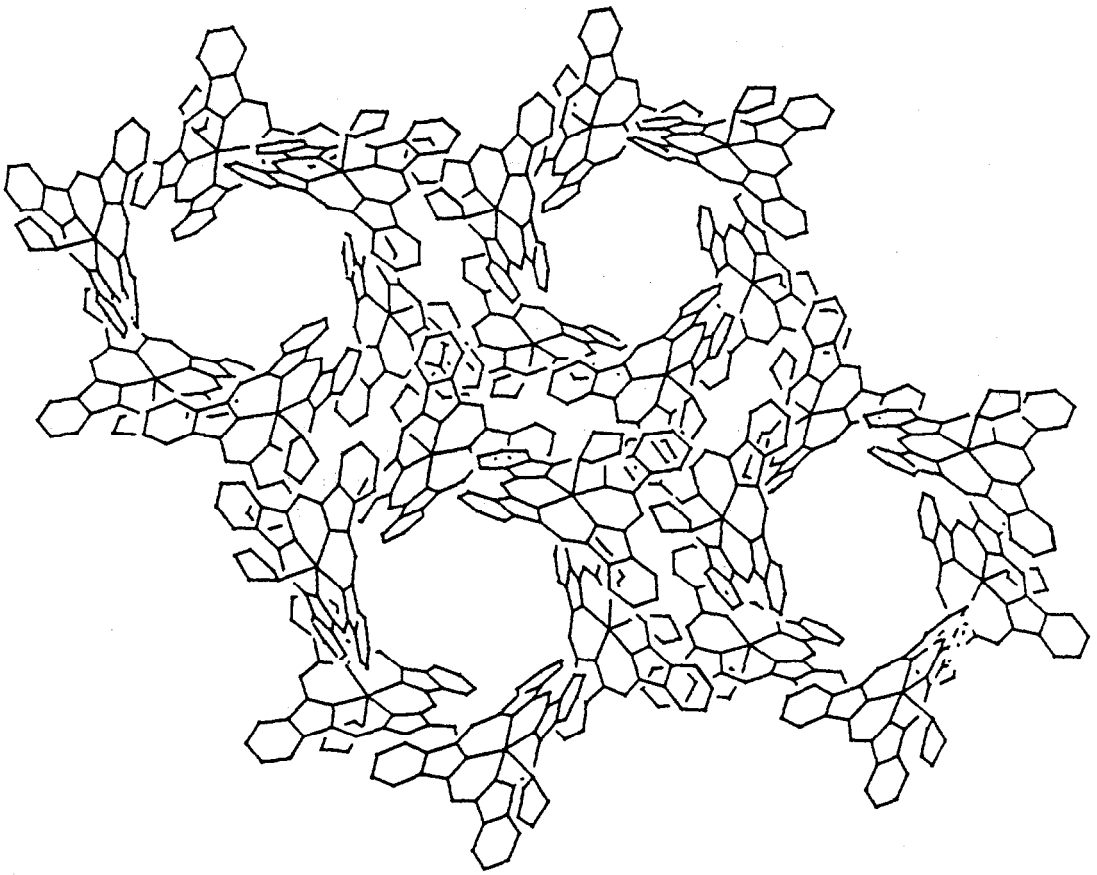

Fig. 6. Illustration of the packing in [(TPTBP)Zn(THF)] along c-axes; the cavities link into infinite hallow channels. Phenyl substituents have been removed for clarity.

electronic absorption spectra and molecular mechanics calculations another two TPP derivatives with peripheral steric strain were also claimed to adopt non-planar conformations.[17] While partially oxidized TBPNi maintains a planar structure partially oxidized (OMTBP)Ni assumes a ruffled conformation, presumably for the same steric reasoning. More structural data for the TBP system are expected to appear in the near future for detailed comparison.

The consequences of saddle deformation on the properties of the non-planar tetrabenzoporphyrin are significant. As reported previously the cumulative effects of conformational changes and substituent addition are reflected in the red-shifted optical spectrum, diminished fluorescence, increased basicity[5] and ease of oxidation of the neutral compound, and in a shift of unpaired spin density from a_{1u} (TBPZn) to a_{2u} (TPTBPZn) character in the cation radical.[18] The increased basicity also results in decreased axial coordination ability, i.e. five-coordinate [(TPTBP)Zn(THF)] instead of six-coordinate [(TPTBP)Zn(THF)$_2$]. Similar effects on optical, redox, basicity and excited-state properties have also been noticed in (OETPP)Zn and related systems.[12]

The results of this study indicate that, compared with TPP and TBP, extension of the π-electron system of the porphyrinato core or introduction of the *meso*-phenyl substituents results in tremendous effects for both molecular and crystal structure, and the properties following them. Therefore, TPTBP may not be a more soluble model for TBP, but it offers a good chance to study the conformational effect. Further studies of this conformational effect on the bonding of transition metal complexes of TPTBP are underway in our laboratory.

Acknowledgement—This work was supported by the National Science Council of the Republic of China, Grant no. NSC76-0208-M005-10.

REFERENCES

1. A. D. Adler, *Ann. N.Y. Acad. Sci.* 1971, **206**, 7.
2. N. Kobayashi, M. Koshiyama and T. Osa, *Chem. Lett.* 1983, 163.

3. A. Vogler, B. Rethwisch, H. Kunkely, J. Hüttermann and J. O. Besenhard, *Angew. Chem., Int. Edn Engl.* 1978, **17**, 951.
4. N. Kobayashi, M. Koshiyama and T. Osa, *Inorg. Chem.* 1985, **24**, 2502.
5. R.-J. Cheng, Y.-R. Chen and C.-E. Huang, *Heterocycles* 1993, **34**, 1.
6. T. E. Phillips, R. P. Scaringe, B. M. Hoffman and J. A. Ibers, *J. Am. Chem. Soc.* 1980, **102**, 3435.
7. K. Yakushi, M. Yoshitake, H. Kuroda, A. Kawamoto, J. Tanaka, T. Sugano and M. Kinoshita, *Bull. Chem. Soc. Japan* 1988, **61**, 1571.
8. D. E. Remy, *Tetrahedron Lett.* 1983, **24**, 1451.
9. G. M. Sheldrick, SHELXTL PLUS User Manual. Nicolet XRD Corporation, Madison, Wisconsin (1986).
10. *International Tables for X-ray Crystallography*, Vol. IV. Kynoch Press, Birmingham (1974) (present distributor: Kluwer Academic Publishers, Dordrecht).
11. W. R. Scheidt and Y. J. Lee, *Struct. Bonding* 1987, **64**, 1.
12. K. M. Barkigia, M. D. Berber, J. Faber, C. J. Medforth, M. W. Renner and K. M. Smith, *J. Am. Chem. Soc.* 1990, **112**, 8851.
13. C. K. Schauer, O. P. Anderson, S. S. Eaton and G. R. Eaton, *Inorg. Chem.* 1985, **24**, 4082.
14. M. D. Glick, G. H. Cohen and J. L. Hoard, *J. Am. Chem. Soc.* 1967, **89**, 1996.
15. L. D. Spaulding, P. G. Eller, J. A. Bertrand and R. H. Felton, *J. Am. Chem. Soc.* 1974, **96**, 95.
16. G. A. Ardizzoia, M. A. Angaroni, G. L. Monica, F. Cariati, S. Cenini, M. Moret and N. Masciocchi, *Inorg. Chem.* 1991, **30**, 4347.
17. (a) C. J. Medforth and K. M. Smith, *Tetrahedron Lett.* 1990, **33**, 5583; (b) C. J. Medforth, M. D. Berber, K. M. Smith and J. A. Shelnutt, *Tetrahedron Lett.* 1990, **31**, 3719; (c) J. A. Shelnutt, C. J. Medforth, M. D. Berber, K. M. Barkigia and K. M. Smith, *J. Am. Chem. Soc.* 1991, **113**, 4077.
18. M. W. Renner, R.-J. Cheng, C. K. Chang and J. Fajor, *J. Phys. Chem.* 1990, **94**, 8508.

Polyhedron Vol. 12, No. 11, pp. 1361–1370, 1993
Printed in Great Britain

0277–5387/93 $6.00+.00
© 1993 Pergamon Press Ltd

METAL COMPLEXES OF THE ANTI-INFLAMMATORY DRUG SODIUM [2-[(2,6-DICHLOROPHENYL)AMINO]PHENYL]ACETATE (DICLOFENAC SODIUM). MOLECULAR AND CRYSTAL STRUCTURE OF CADMIUM DICLOFENAC

DIMITRA KOVALA-DEMERTZI*

Inorganic Chemistry Department, University of Ioannina, Ioannina 45110, Greece

and

DIMITRIS MENTZAFOS and ARISTIDIS TERZIS

NRC "Demokritos" Institute of Materials Science, 15310 Aghia Paraskevi Attikis, Greece

(*Received* 11 *December* 1992; *accepted* 1 *February* 1993)

Abstract—The reactions of $ZnCl_2$, $CdCl_2$ and $Hg(NO_3)_2 \cdot H_2O$ with deprotonated diclofenac (L) were studied in aqueous solutions. Complexes of the formulae $[Zn(L)_2(H_2O)]$, $[Cd(L)_2(H_2O)]$, $[HgL_2]$ and $[Cd_2(H_2O)(C_2H_5OH)_2(L)_4]_n$ were isolated and characterized as solid products by elemental analyses and spectral (IR, ^1H NMR) and thermal studies. The crystal structure of the complex $[Cd_2(H_2O)(C_2H_5OH)_2L_4]_n$ was also solved. The central feature of the macromolecule is a dinuclear moiety. Distorted octahedral coordination at Cd(1) is completed by oxygen atoms from one molecule of water, two molecules of C_2H_5OH, two oxygen atoms from one chelating ligand with a monoatomic bridging oxygen that bridges the atoms Cd(2)—Cd(I) = 4.490(1) Å and one oxygen from a bidentate bridging carboxylato group that bridges the atoms Cd(1)—Cd(2) = 4.300(1) Å. The geometry at Cd(2) is that of a distorted square pyramid with oxygen atoms from one chelating and one monodentate carboxylato group and the monoatomic bridging oxygen atom occupying equatorial positions. The apical site of the square pyramid is occupied by the oxygen atom of the bidentate bridging carboxylato group. The crystal structure of the diclofenac acid is also reported.

Diclofenac sodium [2-[(2,6-dichlorophenyl)amino]-phenyl]acetate is a potent non-steroidal anti-inflammatory drug (NSAID), therapeutically used in inflammatory and painful diseases of rheumatic and non-rheumatic origin. The anti-inflammatory activity of diclofenac and most of its other pharmacological effects are thought to be related to the inhibition of the conversion of arachidonic acid to prostaglandins, which are the mediators of the inflammatory process.[1,2] Diclofenac is a potent inhibitor of cyclo-oxygenase *in vitro* and *in vivo*, thereby decreasing the synthesis of prostaglandins, prostacyclin and thromboxane products. Also diclofenac is a potent reversible inhibitor of the secondary phase of induced platelet aggregation. Like other NSAIDs, diclofenac is highly (> 95%) protein bound.[1]

The importance of zinc to biochemistry, biology, pathology and clinical and veterinary medicine is now generally recognized. In the cells it is incorporated into more than 200 metalloenzymes involved in nucleic acid, protein, carbohydrate and lipid metabolism. Although zinc belongs to the "essential" metal ions, it becomes hazardous when present in excess. As a result there are metabolic disorders connected with both deficiencies and excess amounts of the metal ion. Cadmium and mercury have been found to be environmental pollutants. The toxicity of metals such as cadmium and

* Author to whom correspondence should be addressed.

mercury on a biological system may result from blocking the essential functional group of the biomolecules and inhibiting or enhancing their enzymatic activities or from displacing the essential metal ion in biomolecules. Cadmium appears to compete with zinc at the active sites of enzymes; isolation in the kidney and liver of a cadmium-containing metalloprotein, metallothionein, suggest that the protein is involved in detoxification processes.[3]

The interaction of these metal ions with drugs administered for therapeutic reasons is a subject of considerable interest. It is known that the drugs act via chelation or by inhibiting the activity of metalloenzymes, but for most of the drugs such as diclofenac little is known about how metal binding influences their activity.

As part of our research on understanding drug–metal interactions[4] we have been studying the complexing ability of diclofenac with d^{10} metal ions and transition metal ions.[4c]

RESULTS AND DISCUSSION

The complexes $[Zn(L)_2(H_2O)]$ (**1**), $[Cd(L)_2(H_2O)]$ (**2**) and $[Hg(L)_2]$ (**3**) were formed according to eqs (1)–(3) in aqueous solution in the pH range 5.0–7.0. Diclofenac has a dissociation constant near 4; at a physiological pH of 7.4 the molecules dissociate to more than 99% and thus are essentially confined to plasma in intra- and extracellular water.[2]

$$ZnCl_2 + 2LNa + H_2O \longrightarrow [ZnL_2H_2O] + 2NaCl \quad (1)$$

$$CdCl_2 + 2LNa + H_2O \longrightarrow [CdL_2H_2O] + 2NaCl \quad (2)$$

$$Hg(NO_3)_2 \cdot H_2O + 2LNa + H_2O \longrightarrow [HgL_2] + 2NaNO_3 + 2H_2O \quad (3)$$

Crystals of the complex $[Cd_2L_4Et_2H_2O]_n$ (**4**) suitable for X-ray analysis were formed by slow evaporation of an ethanolic solution of complex **2**. The

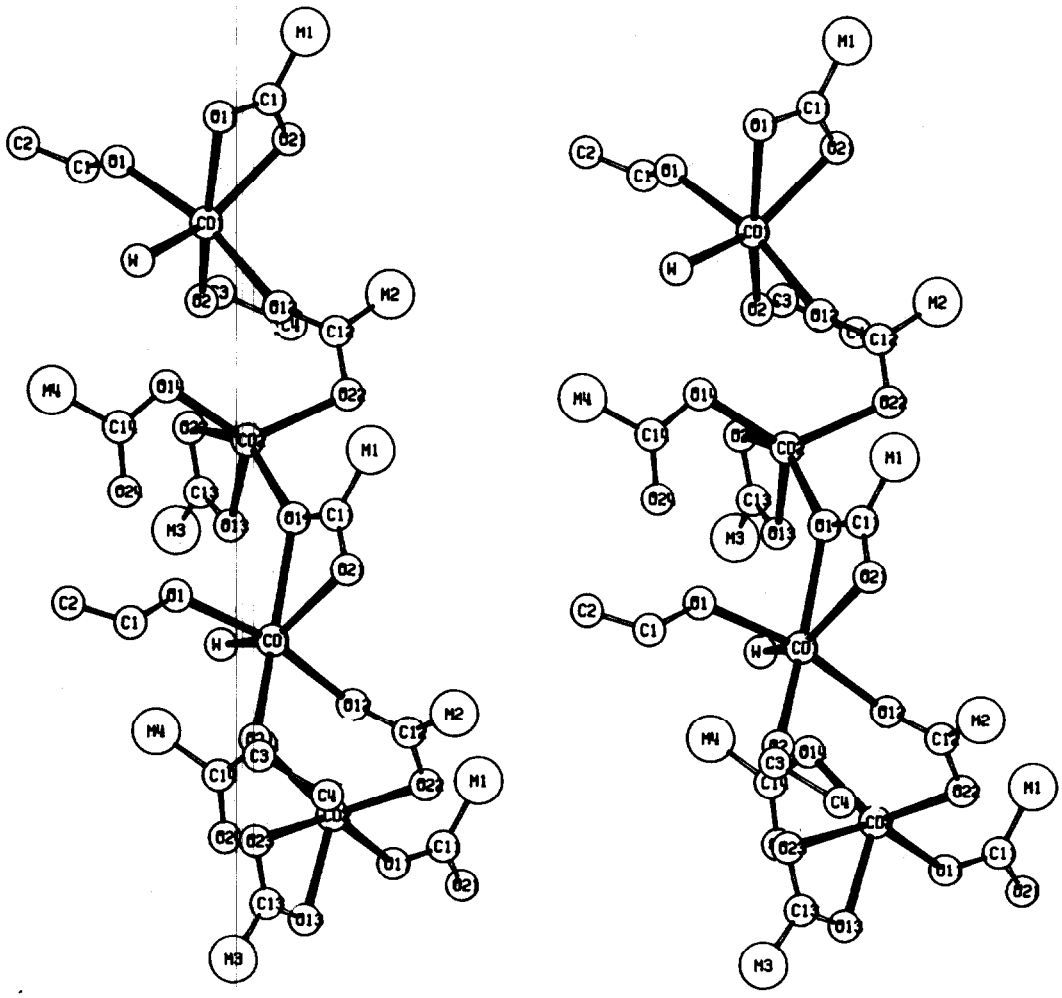

Fig. 1. Structure of compound **4**.

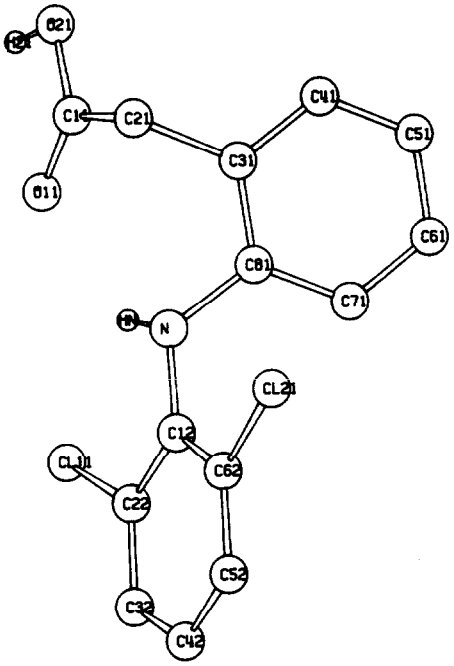

Fig. 2. Structure of diclofenac acid.

compounds are white, microcrystalline, diamagnetic solids that appear to be air- and moisture-stable. They are soluble in CH_3OH, C_2H_5OH, C_6H_{12} and are insoluble in water.

Description of the structures

An ORTEP plot of the inner coordination sphere about the Cd(1) and Cd(2) core for complex **4** is depicted in Fig. 1. The structure of diclofenac acid is shown in Fig. 2. A crystal packing diagram for the same complex (**4**) is shown in Fig. 3. Complete crystal data and parameters for data collection for diclofenac acid and complex **4** are reported in Table 1. Selected bond distances and angles are given in Table 2.

The formation of the compound only took place in ethanolic solution; during crystallization two molecules of EtOH are incorporated into the coordination sphere of Cd(1). The coordination geometry around each metal ion is severely distorted by the bulky ligand L. The compound is polymeric, consisting of hexa-coordinated Cd(1) atoms connected by oxygens O(12) and O(22) of a bridging carboxylato group to the Cd(2) atom, which is penta-coordinated and connected by the monoatomic bridging oxygen O(11) to Cd(1). The Cd(2) atom is, however, subjected to a sixth weaker interaction in the form of a carboxylato oxygen atom, O(12), approaching the Cd(2) atom. The distance Cd(2)—O(12) is 2.76(8) Å, long enough to be considered as a bond distance. When only the bonding interactions are considered Cd(2) is penta-coordinated. The Cd(1)—O(12)—O(22)—Cd(2) bridge is nearly symmetrical with bond distances Cd(1)—O(12) = 2.249(9) and Cd(2)—O(22) = 2.216(1) Å, $\Delta\delta$ = 0.031 Å, while the Cd(2)—O(11)—Cd(1) bridge is asymmetrical with the two Cd—O distances, Cd(2)—O(11) = 2.278(8) and Cd(1)—O(11) = 2.407(7) Å, being significantly different. This bonding mode is probably responsible for the distortion of the coordination polyhedron.

In the complex molecule the ligands surround the Cd(1) atom in a propeller-like arrangement. The resulting coordination about the Cd(1) atom assumes distorted octahedral geometry with the

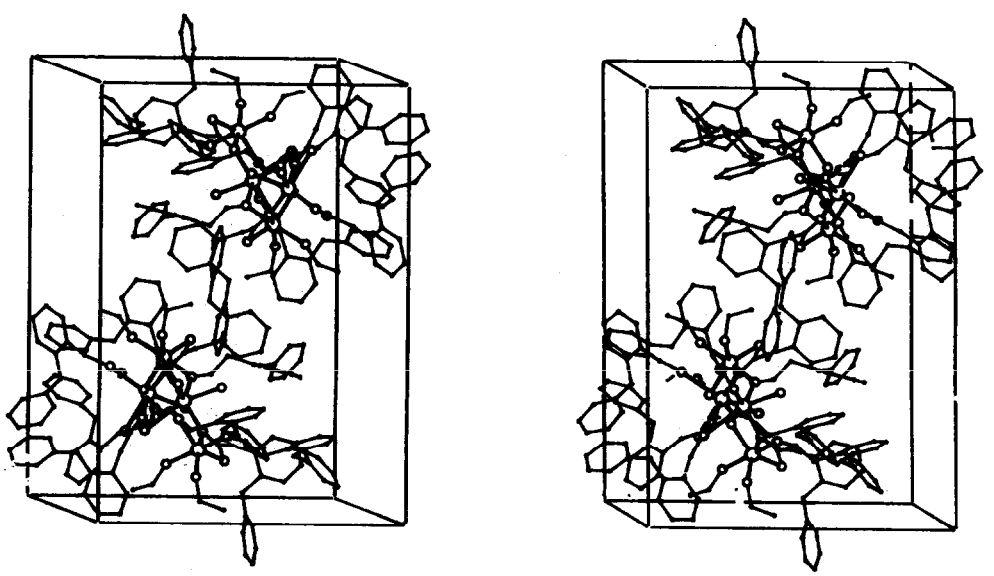

Fig. 3. Packing diagram of compound **4**.

Table 1. Summary of crystal and intensity collection data

Compound	Ligand	Complex
Formula	$C_{14}H_{11}NO_2Cl_2$	$Cd_2(C_{14}H_{10}NO_2Cl_2)_4(C_2H_5O)_2H_2O$
fw	296.15	1513.52
a (Å)	20.263(1)	17.467(2)
b (Å)	7.0050(3)	25.187(3)
c (Å)	20.111(1)	15.000(2)
β (°)	109.578(2)	102.59(1)
V (Å^3)	2689.51(7)	6440(1)
Z	8	4
D_{calc} (Mg m^{-3})	1.462	1.560
D_{meas} (Mg m^{-3})	1.45	1.54
Space group	*C2/c*	$P2_1/c$
Radiation	Cu-K_α (λ = 1.5418)	
μ (cm^{-1})	41.65	87.94
Scan speed (° min^{-1})	3.0	5.0–18.0
Scan range (°)	1.7 plus α_1-α_2	
Background counting (s)	0.5 of scan time	
2θ limit (°)	130.0	100.0
Data unique	2267	6623
Data used	2087	6615
	$F_o > 4.0\sigma(F_o)$	All data
Range of *h*	−23–23	−17–17
Range of *k*	0–8	0–25
Range of *l*	−22–22	0–14
Weighting scheme	$1/w = \sigma^2(F_o)+gF^2_o$	
g	0.0003	0.0028
F(000)	1216	3040
Nr[a]	216	780
$\lvert\Delta/\sigma\rvert_{max}$	0.351	0.249
$(\Delta\rho)_{max}$ (e Å^{-3})	0.304	1.906
$(\Delta\rho)_{min}$ (e Å^{-3})	−0.321	−0.855
R_{obsd}[b]	0.0517	0.1000
$R_{all\ data}$[b]	0.0549	0.1007
$R_{w\ obsd}$[c]	0.0763	0.1119
$R_{w\ all\ data}$[c]	0.0771	0.1125

[a] *Nr* = number of refined parameters.
[b] $R = \Sigma|\Delta F|/\Sigma|F_o|$.
[c] $R_w = [\Sigma w(\Delta F)^2/\Sigma w|F_o|^2]^{1/2}$.

Cd(1)—O distances showing rather wide ranges of values. Cd(1) is surrounded by one water molecule, two EtOH molecules and three oxygen atoms from two carboxylato groups of the ligands M_1 and M_2. The penta-coordinate Cd(2) atom assumes square pyramidal geometry, with one apical bond, Cd(2)—O(22), from the bidentate bridging carboxylato group of the ligand M_2 and four equatorial bonds, two from the chelating carboxylate group O(13), O(23) of the ligand M_3, one from the monodentate carboxylate group O(14) of the ligand M_4 and one from the monoatomic bridging oxygen O(11) of the chelated carboxylato monoinion M_1. The cadmium-to-EtOH oxygen distances are Cd(1)—O(1) = 2.27(1) and Cd(1)—O(2) = 2.253(8) Å. The cadmium-to-H_2O oxygen distance is Cd(1)—O = 2.213(8) Å. One Cd—$O_{(carb.)}$ bond length, Cd(2)—O(23) = 2.5051(8) Å, is longer than the others. The Cd(2)—$O(14)_{(carb.monod.)}$ bond distance is 2.173(8) Å. The Cd—$O_{(carb.chel.)}$ bonds range from 2.282(8) to 2.505(8) Å. Although bidentate chelating carboxylates are known,[5–10] the formation of a four-membered M—O—C—O ring with the high angular strain involved is not expected to be energetically favourable. The distortion as well as the significant difference between Cd(2)—O(14) and Cd(2)—O(23) distances, 2.173 and 2.505 Å, respectively, could be due to intraligand steric interactions and a different coordination mode.

A comparison of the cadmium–oxygen bond distances in the present compound with those in other

Table 2. Coordination of the Cd atoms of the complex

Cd(1)—O(11)	2.407(7)	Cd(2)—O(11)	2.278(8)
Cd(1)—O(12)	2.249(9)	Cd(2)—O(12)	2.760(8)
Cd(1)—O(21)	2.321(7)	Cd(2)—O(22)	2.216(1)
Cd(1)—O(1)	2.27(1)	Cd(2)—O(13)	2.282(8)
Cd(1)—O(2)	2.253(8)	Cd(2)—O(23)	2.505(8)
Cd(1)—W	2.213(8)	Cd(2)—O(14)	2.173(8)
O(11)—Cd(1)—O(12)	109.5(3)	O(11)—Cd(2)—O(12)	133.8(3)
O(11)—Cd(1)—O(21)	54.6(3)	O(11)—Cd(2)—O(22)	93.6(3)
O(11)—Cd(1)—W	87.9(3)	O(11)—Cd(2)—O(13)	90.2(3)
O(11)—Cd(1)—O(1)	81.2(3)	O(11)—Cd(2)—O(14)	105.8(3)
O(11)—Cd(1)—O(2)	161.6(3)	O(11)—Cd(2)—O(23)	143.5(3)
O(12)—Cd(1)—O(21)	96.5(3)	O(13)—Cd(2)—O(23)	53.6(3)
O(12)—Cd(1)—O(2)	81.1(3)	O(13)—Cd(2)—O(14)	125.4(3)
O(12)—Cd(1)—W	83.0(3)	O(12)—Cd(2)—O(22)	51.4(3)
O(12)—Cd(1)—O(1)	167.8(3)	O(13)—Cd(2)—O(22)	105.6(3)
O(21)—Cd(1)—W	140.3(3)	O(22)—Cd(2)—O(23)	99.6(3)
O(21)—Cd(1)—O(1)	94.6(3)	O(23)—Cd(2)—O(14)	94.4(3)
O(21)—Cd(1)—O(2)	110.4(3)	O(22)—Cd(2)—O(14)	124.3(4)
O(1)—Cd(1)—O(2)	90.2(3)	O(12)—Cd(2)—O(23)	78.8(3)
W—Cd(1)—O(2)	108.7(3)	O(12)—Cd(2)—O(13)	124.5(3)
W—Cd(1)—O(1)	91.7(3)	O(12)—Cd(2)—O(14)	79.7(3)
		O(12)—Cd(2)—O(24)	127.7(3)

cadmium–carboxylate and cadmium–oxygen species are presented in Table 3.

The C—O bond lengths range from 1.22 to 1.30 Å and the C—C bonds of the C_6H_5 ring from 1.36 to 1.42 Å, while the $C_6H_3Cl_2$ ring ranges from 1.32 to 1.42 Å. The shorter C—O bond of each carboxylato group is held to the cadmium atom, indicating that the doubly-bonded oxygen is coordinated.

The relative orientation of the two phenyl rings depends upon the torsional angles. The observed values of the ligands M_1, M_2, M_3 and M_4 in the present crystal structure, compared with those of diclofenac acid are given in Table 4. The two torsion angles C(7j)—C(8j)—N(j)—C(1i) and C(8j)—N(j)—C(1i)—C(2i), between the two phenyl rings and the nitrogen, and the angle of twist C(8j)—N(j)—C(1i)—C(6i), between the planes of the phenyl rings, show that diclofenac acid and the ligands of complex **4**, M_1, M_3 and M_4, show very similar preferred conformations.

Moser *et al.*[2] studied for 36 congeners of diclofenac the inhibition of cyclooxygenase at the enzyme level and the *in vivo* inhibition of rat adjuvant arthritis and found that both activities can be explained by the lipophilicity and the twisting of the two aromatic rings (angle of twist = 58–69°). These findings allowed the rationalization of the high activity of diclofenac.

Spectral and thermal studies

Table 5 presents some diagnostic IR bands. In the $\nu(OH)_{water}$ region the spectra of complexes **1**, **2** and **4** show a broad absorption at 3500 cm^{-1}, attributed to the presence of coordinated water. As the carboxylic hydrogen is more acidic than the amino hydrogen the deprotonation occurs in the carboxylic group. This is confirmed by the IR spectra of the complexes, showing the characteristic bands for the secondary amino groups and for the coordinated carboxylate group.[11–13] The strong band at 3388 cm^{-1}, which appears in diclofenac, is assigned to the NH stretching motion and the broad band at 3260 cm^{-1} is taken to represent the ν(NH---O) mode, due to intramolecular hydrogen bonding.[2] The absence of large systematic shifts of the ν(NH) and δ(NH) bands in the spectra of the complexes compared with those of the ligand indicates that there is no interaction between the NH group and the metal ions, which is also confirmed by X-ray analysis. Assignment of the type of carboxylate group coordination was based on both the position of the ν_s and ν_{as} bands and the values of Δ_ν.[11–13] The separations between ν_{as} and ν_s, Δ_ν, in a bidentate (chelate) complex will be significantly smaller than in the free ion; in the bridging complex the Δ_ν value is closer to the free ion, while in the monodentate complex it will be

Table 3. Comparison of cadmium–oxygen bond distances (Å) in various cadmium(II) derivatives

Compound	Coordination number	Geometry	Coordination site	Distance ν(Cd—O) (Å)	Ref.
$Cd[C_6H_4(COO)_2]\cdot H_2O$	7		$O_{(H_2O)}$	2.338(4)	5
			$O_{(carb.chel.)}$	2.368(4)–2.436(4)	
			$O_{(carb.bridg.)}$	2.254(3)	
			$O_{(C=O.\ ketonic)}$	2.489.9–2.571(8)	
$Sr[Cd(EGTA)]\cdot 7H_2O$	8	Dodecahedral	$O_{(ether)}$	2.580(8)	6
			$O_{(carb.chel.)}$	2.325(3)–2.585(3)	
$K[Cd(ClC_6H_4SO_2NCONH_nPr)_3]$	6	Trigonal prismatic	$O_{(C=O,\ ketonic)}$	2.489(9)–2.581(8)	7
$[(C_6H_4OHCOO)_2Cd\cdot H_2O]_2$	7	Pentagonal bipyramid	$O_{(H_2O)}$	2.300(2), 2.243(2)	8
			$O_{(carb.chel.)}$	2.322(2), 2.429(1); 2.314(1), 2.535(2)	
			$O_{(carb.monoatom.bridg.)}$	2.271(2), 2.535(2)	
$[(C_6H_5N)_3(C_6H_4OHCOO)_2Cd]$	7	Pentagonal bipyramid	$O_{(carb.chel.)}$	2.375(2), 2.497(2); 2.424(2), 2.481(2)	8
$[(H_2O)_6Mg(EDTA)H_2OCd]_n\cdot 3nH_2O$	7	Pentagonal bipyramid	$O_{(H_2O}$	2.246(9)	9
			$O_{(carb.chel.)}$	2.336(6)–2.457(7)	
$2CdO(CH_2COO)_2\cdot 7H_2O$	7	Pentagonal bipyramid	$O_{(carb.chel.)}$	2.278(15)–2.491(14)	10
$[Cd_2C_{14}H_{10}NC_2Cl_2)_4(C_2H_5OH)_2H_2O]_n$	6	Cd(1) distorted-octahedral	$O_{(H_2O)}$	2.213(8)	Present work
	5	Cd(2) tetragonal-pyramid	$O_{(C_2H_5OH)}$	2.253(8), 2.27(1)	
			$O_{(carb.chel.)}$	2.321(7)–2.505(8)	
			$O_{(carb.bridg.)}$	2.216(1), 2.249(9)	
			$O_{(carb.monod.)}$	2.173(8)	
			$O_{(carb.oxyg.monoat.bridg.)}$	2.278(8), 2.407(7)	

Table 4. Torsion angles of the ligands

Angles	Ligand[a] $j=1, i=2$	Complex[b] $j=1, i=5$	Complex[c] $j=2, i=6$	Complex[d] $j=3, i=7$	Complex[e] $j=4, i=8$
O(1j)—C(1j)—C(2j)—C(3j)	70	−151	−136	−162	−172
O(2j)—C(1j)—C(2j)—C(3j)	−109	33	49	22	13
C(1j)—C(2j)—C(3j)—C(4j)	98	103	111	105	116
C(1j)—C(2j)—C(3j)—C(8j)	−82	−75	−72	−76	−67
C(2j)—C(3j)—C(8j)—N(j)	2	2	1	2	3
C(3j)—C(8j)—N(j)—C(1i)	−166	−166	−166	−174	−162
C(7j)—C(8j)—N(j)—C(1i)	15	10	12	6	14
C(8j)—N(j)—C(1i)—C(2i)	−123	−118	62	−122	−125
C(8j)—N(j)—C(1i)—C(6i)	62	60	−127	62	60

[a] See fig. 2; *j* is referred to the phenyl acetate ring and *i* is referred to the 2,6-dichloro-phenyl-amino ring.

[b,c,d,e] Referred to the ligand molecules M_1, M_2, M_3 and M_4, respectively.

Table 5. Diagnostic IR and far-IR bands (cm^{-1}) of dichlofenac and its complexes

Assignments	Diclofenac	1	2	3	4
ν(OH)		3550br	3550br		3550–32000br
ν(NH)	3388s 3260br	3380s 3314s	3300br	3330br	
ν(CH)	3085m 3040m	3070w 3040w	3078w 3030w	3070m 3030m	
$\nu(CH_2)$	2980m 2920w	2980w 2915vw	2990vw 2930vw	2970w 2920vw	2980w 2920w
$\nu_s(COO^-)$	1572vs	1630vs 1545vs	1545vs 1565vs	1707s 1565vs	1610m 1580s 1540vs
δ(OH)		1610mw	1610mw		1620sh
δ(NH) + ring stretch	1590s	1592s	1590mw	1590s	1592ms
Ring stretch	1558s 1510sh	1580s 1568s 1510sh 1508s	1580s 1570ms 1508s	1577s 1500s	1577s 1560sh 1500sh
$\delta(CH_2)$	1456vs	1458vs	1453vs	1452vs	1458vs
$\nu_{as}(COO^-)$	1402s	1436s 1395s	1410s	1350ms	1420s 1400vs 1320m
δ(CH)	767vs 748vs	766vs 742vs	768vs 745vs	769vs 742vs	761s 741vs
ν(M—O)$_{(HO)}$		405mw	390mw		390m
ν(M—O)$_{(carb.monod.)}$		392m		402m	400m
ν(M—O)$_{(carb.bid.chel.)}$		312w 299ms 280m	315w 305m 250m		312w 291m 279mw

Table 6. Chemical shifts and coupling constants obtained from ^{1}H NMR spectra of diclofenac and its complexes

	NH	N—C(3i) H—C(5i)	H—C(4i)	H—C(4*j*)	H—C(6*j*)	H—C(5*j*)	H—C(7*j*)	CH_2	$H_2O_{coor.}$
Diclofenac	10.24s	7.43; 7.46 $^3J = 8.0$	7.03; 7.06; 7.09 $^3J = 8.0$	7.05; 7.08 $^3J = 7.8$ $^4J = 1.5$	6.89; 6.92; 6.95 $^3J = 7.8$ $^4J = 1.6$	6.70; 6.73; 6.76 $^3J = 7.3$ $^4J = 1.2$	6.23; 6.26 $^3J = 8.0$ $^4J = 0.8$	3.44s	
1	8.29s	7.42; 7.45 $^3J = 8.0$ $\Delta\delta = -0.01$	7.06; 7.09; 7.12 $^3J = 7.8$ $\Delta\delta = +0.03$	7.15; 7.18 $^3J = 6.4$ $^4J = 1.5$ $\Delta\delta = +0.10$	6.99; 7.01; 7.04 $^3J = 7.3$ $^4J = 1.2$ $\Delta\delta = +0.10$	6.79; 6.82; 6.85 $^3J = 6.49$ $^4J = 1.4$ $\Delta\delta = +0.09$	6.29; 6.32 $^3J = 7.5$ $^4J = 0.9$ $\Delta\delta = +0.06$	3.59s	3.36s
2	8.61s	7.42; 7.45 $^3J = 8.0$ $\Delta\delta = -0.1$	7.05; 7.08; 7.11 $^3J = 8.0$ $\Delta\delta = +0.02$	7.15; 7.18 $^3J = 7.5$ $\Delta\delta = +0.10$	6.98; 7.01; 7.04 $^3J = 7.5$ $^3J = 7.9$ $^4J = 1.5$ $\Delta\delta = +0.11$	6.79; 6.82; 6.85 $^3J = 7.5$ $^3J = 7.9$ $^4J = 1.5$ $\Delta\delta = +0.09$	6.28; 6.31 $^3J = 7.9$ $^4J = 0.7$ $\Delta\delta = +0.05$	3.59s	3.37
3	7.66br	7.49; 7.52 $^3J = 8.1$ $\Delta\delta = +0.04$	7.13; 7.15; 7.18 $^3J = 8.1$ $\Delta\delta = +0.10$	7.21; 7.24 $^3J = 8.3$ $^4J = 1.4$ $\Delta\delta = +0.16$	7.03; 7.06; 7.09 $^3J = 7.4$ $^4J = 1.2$ $\Delta\delta = 0.14$	6.84; 6.87; 6.89 $^3J = 7.10$ $\Delta\delta = +0.14$	6.28; 6.30; 6.33 $^3J = 8.2$ $\Delta\delta = +0.05$	3.71	

higher.[11,12] The $\nu_{as}(COO^-)$ and $\nu_s(COO^-)$ bands of complex **2** are observed at 1545 and 1410 cm^{-1}, respectively; the difference, $\Delta_\nu = 135\ cm^{-1}$, is less than that of the free ion (sodium salt diclofenac), $\Delta_\nu = 1572–1402 = 170\ cm^{-1}$, as expected for bidentate coordination. Two $\nu_{as}(COO^-)$ bands at 1630 and 1545 cm^{-1} and two $\nu_s(COO^-)$ bands at 1436 and 1395 cm^{-1} are observed for complex **1**. The bands at 1630 and 1395 cm^{-1}, $\Delta_\nu = 235\ cm^{-1}$, are assigned to the stretching mode for monodentate carboxylate ligation, while the bands at 1545 and 1436 cm^{-1}, $\Delta_\nu = 109\ cm^{-1}$, are assigned to the stretching mode for bidentate chelate carboxylate ligation. The $\nu_{as}(COO^-)$ and $\nu_s(COO^-)$ bands are observed at 1577 and 1350 cm^{-1} for complex **3**; the difference, $\Delta_\nu = 227\ cm^{-1}$, is consistent with monodentate coordination. The new bands in the region 400–200 cm^{-1} are assigned to $\nu(M—O)(H_2O)$ and $\nu(M—O)(COO^-)$ modes.[11–14] The metal–ligand vibrations are important in determining the structures of the complexes and are included in Table 5.

Table 6 gives the ^1H NMR chemical shifts of diclofenac and its complexes in DMSO-d_6. The study was based on comparisons with a number of related ligands and complexes.[2,15,16]

Coordination of a metal centre to NH or a carboxylato group causes a downfield shift in the proton resonances. These metal ions deshield the CH_2 protons attracting electron density; the CH_2 protons are affected more, while the phenyl ring protons, away from the coordination site, are less affected. The above data show that all the δ values move to lower fields on complex formation. The $\Delta\delta$ values ($\delta_{complex}$-$\delta_{free\ ligand}$) depend on the proximity of the proton in question to the metal centres. The H—C(7j) signal of diclofenac appears at the rather high field 6.26 ppm, due to the shielding effect of the aryl ring (2,6-dichlorophenyl).[2] The proton on the nitrogen atom undergoes rapid exchange and is decoupled from the nitrogen atom and from protons on adjacent carbon atoms. The NH peak is, therefore, a sharp singlet. A deshielding effect is exerted on this NH proton via intramolecular or intermolecular hydrogen bonding, with the resonance occurring at low fields[15,16] from 7.66 to 10.24 ppm.

Complexes **1** and **2** show that a similar decomposition occurs in two steps. The complex CdL_2H_2O was decomposed at 194°C. This reaction appears to be completed at 265°C. Two endothermic and one exothermic effect are observed at 199, 229 and 240°C, respectively. The first inflection in the mass loss curve corresponds to a loss of $H_2O \cdot 1\frac{1}{2}L$ molecules. The thermal decomposition of the complex is completed in the 465–605°C temperature range. The final residue of pyrolysis was the corresponding carbonate salt and metallic oxide.

From the overall study presented above it is concluded that in all the new complexes prepared diclofenac behaves as a monodentate or bidentate ligand, bonding through the carboxylate oxygen atoms. Several stereochemistries are assigned for the diclofenac complexes in the solid state. Synthetic and spectroscopic data suggests that **1** consists of the pseudo-tetrahedral ZnO_4 entity, formed by one bidentate chelate ligand, one monodentate ligand and one coordinated water molecule. For complex **2** two ligands are coordinated to one cadmium(II) atom in a bidentate chelate mode, with both the oxygens of the carobylato group bound to the metal centre. Complex **2** consists of the $CdO_{2(carb.chel.)}O_{2(carb.chel.)}O_{(H_2O)}$ coordination sphere. In complex **3** the coordination environment around the Hg^{2+} atom is linear and the ligands are bound in a monodentate fashion. Complex **4** has a polymeric structure with both the monodentate and bidentate ligands chelating and bridging. One M_2 ligand is in the familiar bidentate bridging mode and another M_1 ligand is in the rare monoatomic bridging mode.

EXPERIMENTAL

All the solvents and chemicals used were of high purity and purchased from Fluka. Diclofenac was a gift from "HELP EPE". Physicochemical measurements and spectroscopic techniques were performed using published methods.[4,17,18] Proton NMR spectra were obtained on a Bruker AC 250 MH FT-NMR spectrophotometer with Me_4Si as an internal standard. Chemical shifts are reported in parts per million (ppm).

Preparation of the complexes

The complexes were prepared by mixing aqueous solutions of the ligand diclofenac (sodium salt) and aqueous solutions of the metal salts (4 : 2 ligand-to-metal molar ratio). The pH of the reaction mixture was adjusted to 5.5–7.5 by the addition of small quantities of 0.1 N KOH. The reaction mixture was stirred for 4–6 h at room temperature. The resulting powders were filtered, washed with water and dried *in vacuo* over silica gel. They were further dried at 90°C *in vacuo* over P_4O_{10}. The yields of the products were 82% for complex **3** and *ca* 100% for complexes **1** and **2**. The elemental analyses agreed very well with the assigned formulae.

X-ray analysis

The crystal system and space group (Table 1) were determined from preliminary oscillation and

Weissenberg photographs. Unit cell dimensions were derived from least-squares refinement of the setting angles of 15 automatically centred reflections in the range $50° < 2\theta < 52°$ on a Syntex $P2_1$ diffractometer using nickel filtered Cu-K_α radiation. The crystal was of very low quality. The intensities of three standard reflections monitored after every 67 reflections showed $<3\%$ intensity fluctuation. Lorentz, polarization and ψ-scan absorption corrections were applied.

The structure was solved by direct methods using the SHELX86 program.[19] Refinement was performed by blocked full-matrix least-squares, in which $\Sigma w\Delta^2$ was minimized with SHELX76.[20] All hydrogen atoms were calculated as riding on carbon atoms at 0.96 Å. All non-hydrogen atoms were refined using anisotropic and hydrogen atoms using isotropic temperature factors. Atomic scattering factors were taken from the International Tables of X-ray Crystallography.[21]

Supplementary material. Tables of positional parameters and anisotropic temperatures factors, observed and calculated structure factors and a list of bond distances and angles of the ligand have been deposited.

Acknowledgement—Our work is supported by the G.S.E.T. and by "HELP EPE".

REFERENCES

1. P. A. Todd and E. M. Sorkin, *Drugs* 1988, **35**, 244.
2. P. Moser, A. Sallmann and I. Wiesenberg, *J. Med. Chem.* 1990, **33**, 2358.
3. (a) E. Ochiai, *Bioinorganic Chemistry. An Introduction*, p. 468. Allyn and Bacon, Inc., Boston (1977); (b) A. V. Xavier, *Frontiers in Bioinorganic Chemistry*, p. 356. VCH, Weinheim (1986).
4. (a) D. Kovala-Demertzi, N. Hadjiliadis and J. M. Tsangaris, *J. Less-Common Met.* 1986, **115**, 1; (b) D. Kovala-Demertzi and J. M. Tsangaris, *Inorg. Chim. Acta* 1986, **125**, L31; (c) D. Kovala-Demertzi and A. Theodorou, unpublished results.
5. C. Robl, *Z. Anorg. Allg. Chem.* 1988, **566**, 144.
6. C. K. Schauer and O. P. Anderson, *J. Am. Chem. Soc.* 1987, **109**, 3646.
7. D. P. Kessisoglou, G. E. Manoussakis, A. G. Hatjidimitriou and M. G. Kanatzidis, *Inorg. Chem.* 1987, **26**, 1395.
8. N. G. Charles, E. A. H. Griffith, P. F. Rosesiler and E. L. Amma, *Inorg. Chem.* 1983, **22**, 2717.
9. X. Solans, S. Gali and M. Fout-Altaba, *Acta Cryst.* 1981, **C39**, 438.
10. C. E. Boman, *Acta Cryst.* 1977, **B33**, 838.
11. G. Maistralis, N. Katsaros, S. P. Perlepes and D. Kovala-Demertzi, *J. Inorg. Biochem.* 1992, **45**, 1 and refs therein.
12. G. B. Deacon and R. J. Phillips, *Coord. Chem. Rev.* 1980, **33**, 227.
13. K. Nakamoto, *Infrared Spectra of Inorganic and Coordination Compounds*, 2nd edn. Wiley Interscience, New York (1970).
14. J. R. Ferraro, *Low-Frequency Vibrations of Inorganic and Coordination Compounds*. Plenum Press, New York (1971).
15. D. Kovala-Demertzi, S. P. Perlepes and G. Lazaras, *Bull. Soc., Chim. Belg.* 1989, **8**, 503.
16. R. M. Silverstein, C. G. Bassler and T. C. Morrill, *Spectrometric Identification of Organic Compounds*. J. Wiley & Sons, U.S.A. (1974).
17. D. Kovala-Demertzi, J. M. Tsangaris, H. O. Desseyn and B. J. Van der Veken, *Bull. Soc. Chim. Belg.* 1987, **1**, 7.
18. D. Kovala-Demertzi, P. Kurkou and I. Zakharoba, *Polyhedron* 1991, **10**, 1507.
19. G. M. Sheldrick, SHELX86. Universität Göttingen, F.R.G. (1986).
20. G. M. Sheldrick, SHELX76, Program for Crystal Structure Determination. University of Cambridge, U.K. (1976).
21. International Tables of X-ray Crystallography, Vol. IV. Kynoch Press, Birmingham (1974).

Polyhedron Vol. 12, No. 11, pp. 1371–1376, 1993
Printed in Great Britain

0277–5387/93 $6.00+.00
© 1993 Pergamon Press Ltd

SYNTHESIS AND CHARACTERIZATION OF MONO- AND BIS-AZIRIDINE BIS-DIMETHYLGLYOXIMATO COBALT(III) COMPLEXES

D. C. WARE,* D. S. MACKIE, P. J. BROTHERS and W. A. DENNY

Department of Chemistry and Cancer Research Laboratory (School of Medicine), University of Auckland, Private Bag 92019, Auckland, New Zealand

(*Received* 7 *January* 1993; *accepted* 27 *January* 1993)

Abstract—The syntheses of the neutral bis-dimethylglyoximato [$(DH)_2$] dimethylsulphide (DMS) cobalt(III) complexes, [$Co(DH)_2(DMS)X$] (X = Cl, Br, I, SeCN), are described. Substitution of the DMS ligand in these complexes by aziridine (Az) produces the neutral complexes [$Co(DH)_2(Az)X$] (X = Cl, Br, I, SeCN), containing one aziridine ligand. The syntheses of the cationic bis-aziridine complex [$Co(DH)_2(Az)_2$]Cl and its bis-diphenylglyoximato (DpgH) analogue [$Co(DpgH)_2(Az)_2$]Cl are also described.

As part of our interest in the preparation of cobalt (III) complexes containing cytotoxic ligands[1,2] we made a series of cobalt(III) aziridine complexes containing ammine and amine ancilliary ligands.[3] We have now extended this chemistry to the synthesis of a new series of cobalt(III) aziridine complexes containing the bis-dimethylglyoximato pseudo-macrocycle, [$(DH)_2$].

We wished to prepare a series of bis-dimethylglyoximato complexes containing only one aziridine ligand and one other ligand which could be varied in order to tailor the properties of the complexes. The choice of a synthetic route for the preparation of such aziridine complexes required careful consideration. Aziridine is a volatile and highly reactive molecule that readily undergoes ring-opening reactions, particularly under acid conditions. In addition the preparation of neutral cobalt(III) complexes of the form [$Co(DH)_2LX$] is often impeded by symmetrization reactions, leading to complex salts of the formula [$Co(DH)_2L_2$]$^+$ [$Co(DH)_2X_2$]$^-$. Substitution of aziridine for the labile neutral ligand dimethylsulphide (DMS) in suitable precursor complexes proved to be successful for the preparation of neutral complexes containing one aziridine ligand. A cationic complex containing two aziridine ligands, [$Co(DH)_2(Az)_2$]Cl, has been reported in the literature, but was characterized only by elemental analysis. We have reinvestigated this chemistry and fully characterized both this complex and its bis-diphenylglyoximato [$(DpgH)_2$] analogue. The synthesis, characterization and spectroscopic data for the cationic bis-aziridine complexes, neutral DMS precursor complexes and neutral mono-aziridine complexes all containing cobalt(III) are detailed below.

EXPERIMENTAL

IR spectra were recorded on a Perkin–Elmer Model 597 spectrometer using Nujol mulls between KBr discs. ^1H and $^{13}C\{^1H\}$ NMR spectra were recorded on a Bruker AM400 spectrometer operating at 400 and 100 MHz, respectively. Microanalyses were performed by Dr R. Cunninghame and associates at the Department of Chemistry, University of Otago. Aziridine, prepared by published procedures,[4,5] was purified by repeated distillation from NaOH and was stored under nitrogen over NaOH at 5°C. **CAUTION:** Aziridine is a highly toxic and volatile substance. All reactions involving aziridine were performed under nitrogen using Schlenk techniques in a well-ventilated fumehood. All aziridine residues were decomposed by treatment with aqueous HCl. [$Co(DH)_2(DMS)Br$] (**1b**),[6] [$Co(DH)_2(Az)_2$]Cl (**3**)[7] and [$Co(DH)(DH_2)Cl_2$][8] were prepared by modifications of literature methods.

* Author to whom correspondence should be addressed.

Synthesis of [Co(DH)$_2$(DMS)Cl] (**1a**)

(a) A solution of DH$_2$ (3.02 g, 0.026 mol) in hot 95% ethanol (75 cm^3) was added to a solution of Co(NO$_3$)$_2$·6H$_2$O (3.79 g, 0.013 mol) in hot 95% ethanol (75 cm^3). After heating the resulting red–brown suspension for 5 min a solution of NaCl (1.18 g, 0.020 mol) in water (4 cm^3) was added. The mixture was cooled to 35°C, dimethylsulphide (1.5 cm^3, 1.27 g, 0.020 mol) was added and air oxidation was achieved by stirring the mixture vigorously in air for 8 h. A fine gelatinous precipitate formed during this time, which was isolated by filtration, washed with water, ethanol and diethyl ether and dried in air to give a brown solid. This was extracted into CH_2Cl_2, filtered and CH_2Cl_2 removed under reduced pressure to produce a brown powder. Yield 0.48 g, 9.5%.

(b) A green suspension of [Co(DH)(DH$_2$)Cl$_2$] (1.65 g, 0.005 mol) in $CHCl_3$ (45 cm^3) was shaken with dimethylsulphide (0.84 cm^3, 0.71 g, 0.011 mol) and left to stand for 5 min. Water (15 cm^3) was added and the mixture was shaken vigorously to give a two-phase system, an upper aqueous layer containing flocculant green material and a lower $CHCl_3$ layer as an orange–brown suspension. After stirring the two-phase system for several hours the $CHCl_3$ layer was collected and washed with water several times until the washings were colourless. The aqueous layer was extracted with $CHCl_3$ (45 cm^3) and the two $CHCl_3$ portions were combined and concentrated by removal of the solvent under reduced pressure. The product was precipitated by the addition of ethanol and dried in air. Yield 0.30 g, 18%.

Synthesis of [Co(DH)$_2$(DMS)I] (**1c**)

This complex was prepared as described for **1a**, method (a), using DH$_2$ (3.02 g, 0.026 mol), Co(NO$_3$)$_2$·6H$_2$O (3.79 g, 0.013 mol), NaI (3.00 g, 0.020 mol) and dimethylsulphide (1.5 cm^3, 1.27 g, 0.020 mol). The product was recrystallized from $CHCl_2$/hexane. Yield 0.97 g, 16%.

Synthesis of [Co(DH)$_2$(DMS)(SeCN)] (**1d**)

To a hot solution of DH$_2$ (6.40 g, 0.055 mol) in methanol (150 cm^3) was added solid Co(OAc)$_2$·4H$_2$O (6.23 g, 0.025 mol) with stirring to form a dark brown solution. The solution was cooled to room temperature and dimethylsulphide (1.90 cm^3, 1.60 g, 0.026 mol) was added to the reaction mixture with stirring, followed by an aqueous solution of KSeCN (3.60 g, 0.025 mol) in water (20 cm^3). After passing a stream of air through the solution for 90 min the light brown solid which had precipitated out was filtered and washed with water, methanol, hexane and diethyl ether. The tan powder was dried over P_2O_5 and dissolved in CH_2Cl_2, filtered and crystallized by the addition of hexane. Yield 4.75 g, 40%.

Synthesis of [Co(DH)$_2$(Az)Cl] (**2a**)

The DMS complex **1a** (1.80 g, 4.65 mmol) was dissolved in CH_2Cl_2 (20 cm^3) and aziridine (0.23 cm^3, 0.19 g, 4.44 mmol) was slowly added to the solution with stirring. The solution was stirred for 20 min, during which time a light brown solid precipitated, which was isolated by filtration and washed with diethyl ether. The solid was suspended in water and stirred for 10 min, filtered, dried in air and recrystallized from CH_2Cl_2/hexane. Yield 0.431 g, 25%. Found: C, 32.0; H, 4.9; N, 18.1. Calc. for $C_{10}H_{19}ClCoN_5O_4$·0.5H$_2$O: C, 31.9; H, 5.2; N, 18.6%.

Synthesis of [Co(DH)$_2$(Az)Br] (**2b**)

This complex was prepared as described for **2a** using complex **1b** (1.20 g, 2.78 mmol) and aziridine (0.14 cm^3, 0.12 g, 2.70 mmol). Yield 0.69 g, 60%. Found: C, 29.1; H, 4.5; N, 17.1. Calc. for $C_{10}H_{19}BrCoN_5O_4$: C, 29.1; H, 4.7; N, 17.0%.

Synthesis of [Co(DH)$_2$(Az)I] (**2c**)

This complex was prepared as described for **2a** using complex **1c** (1.50 g, 3.14 mmol) and aziridine (0.17 cm^3, 0.14 g, 3.28 mmol). Yield 1.07 g, 74%. Found: C, 25.9; H, 4.1; N, 15.4. Calc. for $C_{10}H_{19}CoIN_5O_4$: C, 26.2; H, 4.2; N, 15.3%.

Synthesis of [Co(DH)$_2$(Az)(SeCN)] (**2d**)

This complex was prepared as described for **2a** using complex **1d** (1.50 g, 3.29 mmol) and aziridine (0.18 cm^3, 0.15 g, 3.48 mmol). Yield 1.17 g, 81%. Found: C, 30.6; H, 4.0; N, 19.7. Calc. for $C_{11}H_{19}CoN_6O_4Se$: C, 30.2; H, 4.4; N, 19.2%.

Synthesis of [Co(DH)$_2$(Az)$_2$]Cl (**3**)

CoCl$_2$·6H$_2$O (0.50 g, 2.10 mmol) and DH$_2$ (0.50 g, 4.31 mmol) were dissolved in 95% ethanol (12 cm^3), resulting in a dark red–brown solution to which aziridine (1.0 cm^3, 0.83 g, 19.3 mmol) in 95% ethanol (3 cm^3) was added. A stream of air was passed through the solution for 1 h, during which time the colour lightened. The solution was cooled on ice and orange–brown crystals of the product

deposited. These were filtered, washed with ethanol and diethyl ether and dried. Yield 0.42 g, 49%. Found: C, 32.9; H, 6.3; N, 19.2. Calc. for $C_{12}H_{24}ClCoN_6O_4 \cdot 1.5H_2O$: C, 32.9; H, 6.2; N, 19.2%.

Synthesis of $[Co(DpgH)_2(Az)_2]Cl$ (**4**)

$CoCl_2 \cdot 6H_2O$ (0.48 g, 2.02 mmol) and $DpgH_2$ (0.96 g, 4.01 mmol) were dissolved in hot 95% ethanol (100 cm^3). The initially green solution changed to brown as it was cooled to room temperature and aziridine (1.0 cm^3, 0.83 g, 19.3 mmol) was added. The solution was bubbled with a stream of air for 30 min and was then allowed to stand for a further 90 min, resulting in the precipitation of a mustard–brown solid. This was filtered, washed with ethanol and diethyl ether and dried. Yield 0.67 g, 50%. Found: C, 56.1; H, 5.3; N, 11.5. Calc. for $C_{32}H_{32}ClCoN_6O_4 \cdot C_2H_6O \cdot H_2O$: C, 56.5; H, 5.6; N, 11.6%.

RESULTS AND DISCUSSION

The complex $[Co(DH)_2(DMS)Br]$ is readily prepared from a cobalt(II) salt in the presence of DH_2, Br^- and DMS by air oxidation in ethanol.[6] This complex was chosen as a potential precursor to a neutral monoaziridine complex because the labile DMS ligand is known to be readily substituted by amines.[6] We have prepared this complex using the published method and we have extended this chemistry by preparing new complexes containing Cl^-, I^- and $SeCN^-$ in place of Br^-, by substituting the appropriate sodium salt for NaBr in the reaction to give the series of complexes $[Co(DH)_2(DMS)X]$ (X = Cl, **1a**; Br, **1b**; I, **1c**; SeCN, **1d**). The use of $Co(OAc)_2 \cdot 4H_2O$ rather than $Co(NO_3)_2 \cdot 6H_2O$ as the source of Co^{2+} ions for the preparation of the $SeCN^-$ complex **1d** resulted in an improvement in the yield. Attempts to prepare complexes containing F^-, NO_2^-, CN^-, OCN^- and SCN^- were unsuccessful. Reactions for the preparation of neutral complexes $[Co(DH)_2LX]$ (L = neutral ligand) often give, in addition to the desired product, significant yields of the complex salt $[Co(DH)_2L_2]^+$ $[Co(DH)_2X_2]^-$.[9,10] The low yields reported for the preparations of **1a** and **1c** were presumed to be a consequence of the formation of such salts (L = DMS), based on the formation of significant amounts of water-soluble material which could not be extracted into CH_2Cl_2. An alternative synthesis of the chloro complex **1a** in better yield was by substitution of DMS on the preformed complex $[Co(DH)(DH_2)Cl_2]$ with concomitant elimination of HCl.

Table 1. IR data for complexes **1–4**[a]

	Compound	ν(C=N)		ν(NO)		δ((DH)$_2$)	ν(CoN)	ν(NH)	δ(Az)	ν(SeCN)
1a	$[Co(DH)_2(DMS)Cl]$	1550s	1240vs	1090vs	973m	723m, br	515m			
1b	$[Co(DH)_2(DMS)Br]$	1545s	1238vs	1088s	975m	730m, br	515m			
1c	$[Co(DH)_2(DMS)I]$	1560s	1233s	1080vs	980s	725m, br	510m			
1d	$[Co(DH)_2(DMS)SeCN]$	1555s	1240vs	1095s	980s	723m, br	518m			2120w, 2160w
2a	$[Co(DH)_2(Az)Cl]$	1565s	1247vs	1098m	980m	735m, br	513m	3250m	890m	
2b	$[Co(DH)_2(Az)Br]$	1565s	1242vs	1092m	975m	735m, br	535m	3125m, br	884m	
2c	$[Co(DH)_2(Az)I]$	1575s	1238vs	1080s	978s	728m, br	510m	3135m, br	890m	
2d	$[Co(DH)_2(Az)SeCN]$	1563s	1240vs	1088vs	980m	742m, br	518m	3135m, br	888m	2120m
3	$[Co(DH)_2(Az)_2]Cl$	1568s	1245vs	1095s	980w	725m, br	518s	3105m	890s	
4	$[Co(DpgH)_2(Az)_2]Cl$	1445s	1235m	1075m	987vs	715m, br		3275m	878s	

[a] All data recorded as Nujol mulls. Intensity: w, weak; m, medium; s, strong; vs, very strong; br, broad.

Table 2. ^{1}H and $^{13}C\{^{1}H\}$ NMR data for complexes **1–4**[a]

	Compound	Solvent	^{1}H NMR CH_3	DMS	Az_{syn}	Az_{anti}	NH	Solvent	^{13}C NMR CH_3	C=N	DMS	Az
1a	$[Co(DH)_2(DMS)Cl]$	$CDCl_3$	2.49	1.54								
1b	$[Co(DH)_2(DMS)Br]$	$CDCl_3$	2.50	1.53				DMSO-d_6	12.64	152.75	17.48	
1c	$[Co(DH)_2(DMS)Cl$	$CDCl_3$	2.49	1.48								
1d	$[Co(DH)_2(DMS)SeCN]$	$CDCl_3$	2.49	1.65								
2a	$[Co(DH)_2(Az)Cl]$	DMSO-d_6	2.37		0.63	1.26	2.63	DMSO-d_6	12.32	151.25		19.46
2b	$[Co(DH)_2(Az)Br]$	DMSO-d_6	2.38		0.62	1.27	2.67	DMSO-d_6	12.42	151.65		19.19
2c	$[Co(DH)_2(Az)I]$	DMSO-d_6	2.37		0.59	1.30	2.73	DMSO-d_6	12.52	152.27		18.66
2d	$[Co(DH)_2(Az)SeCN]$	DMSO-d_6	2.37		0.78	1.43	3.11	DMSO-d_6	12.66	151.97		19.28
3	$[Co(DH)_2(Az)_2]Cl$	D_2O[b]	2.51		1.01	1.65		D_2O[c]	12.74	156.92		20.85
4	$[Co(DpgH)_2(Az)_2]Cl$	DMSO-d_6	[d]		1.24	1.84	4.37	DMSO-d_6	[e]	152.06		20.39

[a] Data recorded in $CDCl_3$ or DMSO-d_6 (except where specified) and referenced to internal TMS (tetramethylsilane). ^{1}H data recorded at 400 MHz, $^{13}C\{^{1}H\}$ data at 100 MHz.

[b] Referenced to internal DSS (3-(trimethylsilyl)-1-propanesulphonic acid, sodium salt).

[c] Referenced using internal dioxane (66.6 ppm downfield from TMS).

[d] Phenyl protons at 7.40 ppm.

[e] Phenyl resonances at 127.90 (*ortho*), 129.48 (*para*), 129.66 (*meta*) and 132.75 (*ipso*) ppm.

The series of complexes $[Co(DH)_2(DMS)X]$ (X = Cl, **1a**; Br, **1b**; I, **1c**; SeCN, **1d**) was characterized by ^1H NMR and IR spectroscopy, ^{13}C NMR spectroscopy for **1b** and by comparison of the spectroscopic data with that published for **1b**.[6] The presence of one DMS ligand and two dimethylglyoximato ligands was confirmed by the 1 : 2 ratio of the corresponding methyl resonances in the ^1H NMR spectra of **1a–d**. The chemical shift of the DMS methyl resonance (1.48 ppm for **1c**) shifts progressively downfield in the order X = I, Br, Cl, SeCN. The $(DH)_2$ methyl group resonances are almost invariant across the series. IR and NMR spectroscopic data are collected in Tables 1 and 2, respectively.

The reactions of **1a–d** with 1 equivalent of aziridine in chloroform at room temperature served both to complete the characterization of **1a–d** by substitution of the DMS ligand by aziridine and to prepare the new aziridine complexes $[Co(DH)_2(Az)X]$ (X = Cl, **2a**; Br, **2b**; I, **2c**; SeCN, **2d**). These complexes precipitated from solution as brown solids, which were recrystallized from dichloromethane/hexane. Although the preparation of the precursor complexes **1a–d** gave low yields in some cases, the substitution of aziridine for coordinated DMS proceeded in good yield, an important consideration since it is desirable to minimize the preparation and handling of the toxic and reactive aziridine.

The cationic bis-aziridine complexes $[Co(DH)_2(Az)_2]Cl$ (**3**) and $[Co(DpgH)_2(Az)_2]Cl$ (**4**) were prepared by air oxidation of $CoCl_2$ in ethanol in the presence of the glyoxime and excess aziridine, and were isolated as red–brown crystalline species. The use of excess aziridine is required because, in addition to coordinating to cobalt, the aziridine acts as a base towards the two protons released upon coordination of the two glyoximato ligands. Complexes **2–4** were characterized by IR, ^1H NMR and ^{13}C NMR spectroscopy (Tables 1 and 2) and by elemental analysis.

The presence of the intact aziridine ligand in **2–4** was confirmed by a characteristic medium strong band near 890 cm^{-1} in the IR spectra, which is assigned to a deformation of the coordinated aziridine ring.[11] The $SeCN^-$ ligand in **2d** gives rise to a ν(CN) stretch at 2120 cm^{-1}, consistent with the expected coordination of selenocyanate through the nitrogen atom to the hard cobalt(III) centre.[12]

The two pairs of chemically equivalent protons on the aziridine ring are defined as H_{syn} and H_{anti} (where H_{syn} is on the same side of the aziridine ring as the cobalt atom). Inversion at nitrogen is suppressed on coordination of aziridine to cobalt.[3] The H_{syn} and H_{anti} protons exhibit non-first-order coupling and appear as two multiplets with different splitting patterns, primarily due to the different NH—H_{syn} and NH—H_{anti} coupling constants in the AA′MM′X spin system. Exchange of the NH proton of **3** or **4** in D_2O results in simplification of the H_{syn} and H_{anti} multiplets, which become identical in form. The aziridine CH resonances are assigned by comparison with those in the cobalt(III) aziridine complexes containing amine ligands, with the H_{syn} resonance appearing upfield of the H_{anti} resonance.[3] In the $(DH)_2$ series of complexes the chemical shift difference between the H_{syn} and H_{anti} resonances is generally greater than that observed in the amine series, with the H_{syn} resonances shifted markedly upfield (0.59–0.77 ppm for **2a–d**) as a result of shielding of these protons due to their proximity to the π-electron clouds on the dimethylglyoximato ligands.

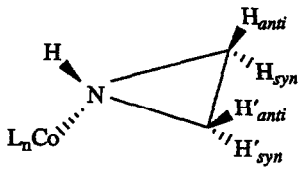

The two aziridine carbon atoms give rise to only one resonance in the ^{13}C NMR spectrum as a result of the symmetric nature of the complexes and free rotation about the Co—N_{Az} bond. This resonance moves downfield in the order I < Br < SeCN ~ Cl, consistent with increasing inductive electron withdrawal by the *trans* ligand. A similar progression is observed for the imine carbon resonance of the $(DH)_2$ ligand. Both the ^1H and ^{13}C NMR spectra of the cationic bis-aziridine complexes **3** and **4** show downfield shifts of the aziridine resonances relative to the neutral mononaziridine complexes. For example, the mid-point position of the H_{anti} and H_{syn} aziridine proton resonance in **3** (1.33 ppm) is closer to the free ligand value of 1.48 ppm than in the neutral complex **2a** (0.95 ppm). This may be ascribed to the greater deshielding of the aziridine hydrogen atoms in the cationic relative to the neutral complexes.

A further series of cationic cobalt(III) bis-aziridine complexes containing Schiff base ligands is the subject of a separate report.[13]

Acknowledgement—D.C.W. is grateful to the Cancer Society of New Zealand for financial support.

REFERENCES

1. D. C. Ware, W. R. Wilson, W. A. Denny and C. E. F. Rickard, *J. Chem. Soc., Chem. Commun.* 1991, 1171.

2. D. C. Ware, B. D. Palmer, W. R. Wilson and W. A. Denny, *J. Med. Chem.*, in press.
3. D. C. Ware, B. G. Siim, K. J. Robinson, W. A. Denny, P. J. Brothers and G. R. Clark, *Inorg. Chem.* 1991, **30**, 3750.
4. T. C. Owen, *J. Chem. Soc.* 1967, 1373.
5. W. A. Reeves, G. L. Drake Jr and C. L. Hoffpauir, *J. Am. Chem. Soc.* 1951, **73**, 3522.
6. J. Bulkowski, A. Cutler, D. Dolphin and R. B. Silverman, *Inorg. Synth.* 1980, **20**, 127.
7. T. B. Jackson and J. O. Edwards, *Inorg. Chem.* 1962, **1**, 398.
8. W. C. Trogler, R. C. Stewart, L. A. Epps and L. G. Marzilli, *Inorg. Chem.* 1974, **13**, 1564.
9. G. Costa, G. Tauzher and A. Puxeddu, *Inorg. Chim. Acta* 1969, **3**, 45.
10. L. G. Marzilli, J. G. Salerno and L. A. Epps, *Inorg. Chem.* 1972, **11**, 2050.
11. H. T. Hoffman Jr, G. E. Evans and G. Glocker, *J. Am. Chem. Soc.* 1951, **73**, 3028.
12. K. Nakamoto, *Infrared and Raman Spectra of Inorganic and Coordination Compounds*, 4th edn. Wiley, New York (1986).
13. D. C. Ware, D. S. Mackie, P. J. Brothers and W. A. Denny, *Polyhedron*, submitted.

Polyhedron Vol. 12, No. 11, pp. 1377–1382, 1993
Printed in Great Britain

0277–5387/93 $6.00+.00
© 1993 Pergamon Press Ltd

AN ^{15}N NMR SPECTROSCOPIC STUDY OF SOME RHODIUM COMPLEXES OF 3,5-DICARBOMETHOXY-4-PHENYLPYRIDINE-^{15}N

LAURENCE CARLTON* and GINA DE SOUSA

Centre for Molecular Design, Department of Chemistry, University of the Witwatersrand, Johannesburg, Republic of South Africa

(*Received* 21 *December* 1992; *accepted* 27 *January* 1993)

Abstract—^{15}N NMR data are reported for the complexes [*cis*-$RhX(PPh_3)_2$(dcpp-^{15}N)], [$Rh(H)_2X(PPh_3)_2$(dcpp-^{15}N)] (X = Cl, SC_6F_5; dcpp-^{15}N = 3,5-dicarbomethoxy-4-phenylpyridine-^{15}N), [$RhCl(PPh_3)(L)$(dcpp-^{15}N)] (L = C_2H_4, CO) and [$Rh(H)(C_2Ph)(X)(PPh_3)_2$(dcpp-^{15}N)] (X = Cl, OCN, N_3, C_2Ph), prepared *in situ* from [$RhX(PPh_3)_3$], [$Rh_2Cl_2(C_2H_4)_4$] and [$Rh_2(SC_6F_5)_2(PPh_3)_4$].

Pyridines and related compounds serve as ligands in a wide range of metal complexes. Where the metal in these complexes exists to a significant extent as an isotope of spin 1/2 and/or where other ligands that bind via a spin 1/2 nucleus are present ^{15}N NMR spectroscopy can provide valuable structural information. In an earlier study[1] natural-abundance ^{15}N NMR data (obtained using the INEPT[2] method) were reported for a series of complexes [$Rh(H)_2(PPh_3)_2(O_2CArN)$][3] ($O_2CArN$ = e.g. pyridine-2-carboxylate): here the value of the ^{15}N—^1H *trans* coupling constant, required to optimize delay times in the INEPT pulse sequence, was measured from a partially ^1H-decoupled ^{15}N spectrum to an accuracy no greater than 10%. The use of an ^{15}N-enriched ligand, in addition to greatly increasing the ^{15}N sensitivity, allows the relevant ^{15}N—^1H coupling constants to be measured directly from the ^1H spectrum. In the present study the ^{15}N-enriched (~ 99%) compound 3,5-dicarbomethoxy-4-phenylpyridine-^{15}N (dcpp-^{15}N) (Fig. 1) was prepared by a method described by Chennat and Eisner[4] for the synthesis of substituted pyridines and incorporated into a number of complexes of rhodium.

EXPERIMENTAL

The ligand dcpp-^{15}N was prepared by the method of Chennat and Eisner.[4] A mixture of ammonium-^{15}N acetate, methyl propiolate, benzaldehyde and acetic acid (in a 0.4 : 1 : 1 : 1 molar ratio) was first heated (100°C, 2 h) and then cooled to −20°C for 3 days to give crystals of 3,5-dicarbomethoxy-5-phenyl-1,4-dihydropyridine-^{15}N, which was subsequently oxidized with 20% nitric acid to give dcpp-^{15}N. Ammonium-^{15}N acetate was obtained from ammonium-^{15}N chloride by exchange with silver acetate. The overall yield (based on ^{15}N) was 20%; in our hands the step by which the dihydropyridine was formed gave yields no better than 25% (the authors quote 79%). [$Rh(OCN)(PPh_3)_3$][5] and [$Rh(N_3)(PPh_3)_3$][5] were prepared from [$RhCl(PPh_3)_3$];[6] [$Rh_2(SC_6F_5)_2(PPh_3)_4$][7] was prepared from [$RhH(PPh_3)_4$]; [$Rh_2Cl_2(C_2H_4)_4$], ammonium-^{15}N chloride, methyl propiolate and phenylacetylene were purchased from Aldrich. Benzaldehyde was distilled before use.

Spectra were recorded on a Bruker AC200 FT spectrometer operating at 200.13 (^1H), 20.29 (^{15}N) and 81.01 (^{31}P) MHz. Solutions in toluene-d_8 or toluene/toluene-d_8 in tubes of diameter 5 mm (*ca* 0.06 M complex, *ca* 0.2 M dcpp-^{15}N, 0.5 cm^3) or 10 mm (*ca* 0.015 M complex, *ca* 0.03 M dcpp-^{15}N,

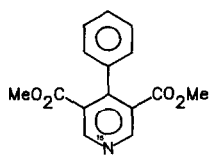

Fig. 1. dcpp-^{15}N.

* Author to whom correspondence should be addressed.

3.0 cm^3) were prepared under nitrogen. Reagents {$[Rh_2Cl_2(C_2H_4)_4]$, 0.25–1.0 equivalents; PhC_2H *ca* 5 equivalents with respect to Rh; H_2, CO, bubbled through the solution for 1–2 min at room temperature} were then added as required. Spectra (1000–25,000 scans) were obtained using a spectral width of 7000 Hz and an acquisition time of 1.16 s; after zero-filling this gave a digital resolution of 0.2 Hz/pt. INEPT delay times were based on ^{15}N—^1H coupling constants measured from the ^1H spectrum of free dcpp-^{15}N or, where appropriate, from the ^1H spectrum of the complex. Chemical shifts were measured relative to CH_3NO_2 (external standard).

RESULTS AND DISCUSSION

In the ^1H spectrum of the ^{15}N-enriched ligand dcpp-^{15}N the two equivalent hydrogens in the 2 and 6 positions appear as a doublet (δ 9.09 ppm, J = 10.6 Hz, solution in $CDCl_3$) as a result of spin-coupling to ^{15}N. INEPT delay times derived from this coupling constant were used in a number of the experiments described below. However, it is generally found that where more than one spin-coupling interaction (^{15}N—^1H) exists, as in the case where the nitrogen dcpp and a hydride are positioned *trans* to each other in a complex, the results obtained using polarization transfer from the hydrogen exhibiting the larger coupling are the more satisfactory. The value of $J(^{15}N$—^1H-*trans*) in the rhodium hydride complexes of dcpp-^{15}N, measured directly from the ^1H spectrum (Fig. 2), has a value of *ca* 22 Hz (Table 1): accordingly, in acquiring ^{15}N spectra from these compounds polarization was transferred from the hydride rather than from the dcpp ring protons.

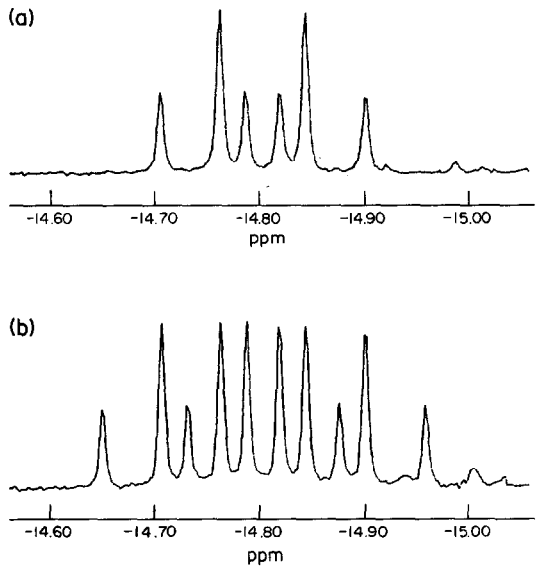

Fig. 2. Highfield signal in the ^1H spectrum of $[Rh(H)(N_3)(C_2Ph)(PPh_3)_2(dcpp)]$ (a) dcpp unenriched and (b) dcpp-^{15}N (99% ^{15}N-enriched).

^1H, ^{15}N and ^{31}P spectral data for the dcpp-^{15}N complexes are shown in Tables 1–3, respectively.

The complexes described in this study are analogues of known compounds containing pyridine[5,7,8] or 2,6-dimethylpyridine.[9] [*cis*-$RhX(PPh_3)_2(py)$] (X = Cl, SC_6F_5; py = pyridine) [Fig. 3(a)] is readily prepared *in situ* from $[RhCl(PPh_3)_3]$ or $[Rh_2(SC_6F_5)_2(PPh_3)_4]$ in the presence of excess pyridine. Where the pyridine carries substituent groups (as with dcpp) the formation of the pyridine-substituted compound is less favoured and a higher concentration of ligand

Table 1. ^1H spectral data for the dcpp-^{15}N complexes[a]

Complex	Signal	δ^1H[b]	$J(^{103}Rh$—$^1H)$[c]	$J(^{31}P$—$^1H)$	$J(^{15}N$—^1H *trans*)
$[Rh(H)_2Cl(PPh_3)_2(dcpp\text{-}^{15}N)]$[d]	mult	−16.37			
	dddt[e]	−16.93	*ca* 15	*ca* 15	22.6
$[Rh(H)_2(SC_6F_5)(PPh_3)_2(dcpp\text{-}^{15}N)]$[f]	mult	−13.61			
	mult	−16.72			*ca* 23
$[Rh(H)(C_2Ph)Cl(PPh_3)_2(dcpp\text{-}^{15}N)]$	ddt	−14.93	15.1	11.0	22.5
$[Rh(H)(C_2Ph)(OCN)(PPh_3)_2(dcpp\text{-}^{15}N)]$	ddt	−14.81	16.1	10.8	22.8
$[Rh(H)(C_2Ph)(N_3)(PPh_3)_2(dcpp\text{-}^{15}N)]$	ddt	−14.80	16.4	11.4	22.6
$[Rh(H)(C_2Ph)_2(PPh_3)_2(dcpp\text{-}^{15}N)]$	ddt	−15.28	17.6	11.4	21.8

[a] Solution in toluene-d_8 at 22°C unless otherwise specified.
[b] In ppm from TMS.
[c] Coupling constants (absolute magnitude) in Hz.
[d] −25°C.
[e] $J(^1H$—$^1H)$ = 10.8 Hz.
[f] −40°C.

Table 2. ^{15}N spectral data for the dcpp-^{15}N complexes[a]

Complex	Signal	$\delta^{15}N$[b]	$J(^{31}P—^{15}N\ trans)$[c]	$J(^{31}P—^{15}N\ cis)$	$J(^{103}Rh—^{15}N)$
[*cis*-RhCl(PPh$_3$)$_2$(dcpp-^{15}N)][d]	ddd	−110.6	42.4	2.6	13.8
[*cis*-Rh(SC$_6$F$_5$)(PPh$_3$)$_2$(dcpp-^{15}N)]	ddd	−111.2	38.2	2.5	14.5
[RhCl(PPh$_3$)(C$_2$H$_4$)(dcpp-^{15}N)][d]	dd	−114.0	47.5		12.2
[RhCl(PPh$_3$)(CO)(dcpp-^{15}N)][d]	dd	−128.9	43.5		13.2
[Rh(H)$_2$Cl(PPh$_3$)$_2$(dcpp-^{15}N)][d]	d	−113.6			8.0
[Rh(H)$_2$(SC$_6$F$_5$)(PPh$_3$)$_2$(dcpp-^{15}N)][e]	d	−118			8.4
[Rh(H)(C$_2$Ph)Cl(PPh$_3$)$_2$(dcpp-^{15}N)]	dt	−114.8		1.7	6.9
[Rh(H)(C$_2$Ph)(OCN)(PPh$_3$)$_2$(dcpp-^{15}N)]	dt	−115.8		1.1	7.5
[Rh(H)(C$_2$Ph)(N$_3$)(PPh$_3$)$_2$(dcpp-^{15}N)]	dt	−116.8		1.2	7.8
[Rh(H)(C$_2$Ph)$_2$(PPh$_3$)$_2$(dcpp-^{15}N)]	dt	−117.3		1.1	7.4

[a] Solution in toluene at 22°C unless otherwise specified. The free ligand has $\delta^{15}N = -66.7$ ppm.
[b] In ppm from CH_3NO_2 (external standard), negative values to high field. Values are uncorrected for bulk susceptibility effects.
[c] Coupling constants (absolute magnitude) in Hz.
[d] −25°C.
[e] −50°C.

is required to achieve full (> 95%) conversion.

$$[RhCl(PPh_3)_3] \underset{-dcpp+PPh_3}{\overset{-PPh_3+dcpp}{\rightleftharpoons}} [cis\text{-}RhCl(PPh_3)_2(dcpp)] \quad (1)$$

$$[Rh_2(SC_6F_5)_2(PPh_3)_4] \underset{-dcpp}{\overset{+dcpp}{\rightleftharpoons}} [cis\text{-}Rh(SC_6F_5)(PPh_3)_2(dcpp)] \quad (2)$$

In the case where X = SC_6F_5 [eq. (2)] a 0.2 M concentration of dcpp is sufficient to convert a 0.05 M solution of [Rh$_2$(SC$_6$F$_5$)$_2$(PPh$_3$)$_4$] almost quantitatively to [*cis*-Rh(SC$_6$F$_5$)(PPh$_3$)$_2$(dcpp)], but with X = Cl [eq. (1)] the conversion is *ca* 25% and with [RhX(PPh$_3$)$_3$] (X = OCN, N$_3$) ⩽ 5%. Clearly the position of the equilibrium in eq. (1) can be forced to the right if a means can be found to remove free PPh$_3$ from solution without causing other major changes. A reagent which performs this task admirably is [Rh$_2$Cl$_2$(C$_2$H$_4$)$_4$]. In solution in the presence of PPh$_3$ it releases ethylene and forms [*trans*-RhCl(PPh$_3$)$_2$(C$_2$H$_4$)][6,10] and [RhCl(PPh$_3$)$_3$]. When treated with 0.25 equivalents of [Rh$_2$Cl$_2$(C$_2$H$_4$)$_4$] a

Table 3. ^{31}P spectral data for the dcpp-^{15}N complexes[a]

Complex	Signal	$\delta^{31}P$[b]	$J(^{103}Rh—^{31}P)$[c]	$J(^{31}P—^{31}P)$
[*cis*-RhCl(PPh$_3$)$_2$(dcpp-^{15}N)][d]	dd	55.6	195.4	47.2
	ddd[f]	49.6	166.3	47.2
[*cis*-Rh(SC$_6$F$_5$)(PPh$_3$)$_2$(dcpp-^{15}N)]	ddd[f]	49.5	168.3	44.9
	dd	46.8	175.8	44.9
[RhCl(PPh$_3$)(C$_2$H$_4$)(dcpp-^{15}N)][d]	dd	52.7	165.6	
[RhCl(PPh$_3$)(CO)(dcpp-^{15}N)][d]	dd	44.4	158.6	
[Rh(H)$_2$Cl(PPh$_3$)$_2$(dcpp-^{15}N)]	d	47.6	117.7	
[Rh(H)$_2$(SC$_6$F$_5$)(PPh$_3$)$_2$(dcpp-^{15}N)][e]	d	49	117.6	
[Rh(H)(C$_2$Ph)Cl(PPh$_3$)$_2$(dcpp-^{15}N)][d]	d	40.2	104.3	
[Rh(H)(C$_2$Ph)(OCN)(PPh$_3$)$_2$(dcpp-^{15}N)]	d	39.6	102.7	
[Rh(H)(C$_2$Ph)(N$_3$)(PPh$_3$)$_2$(dcpp-^{15}N)]	d	38.8	104.2	
[Rh(H)(C$_2$Ph)$_2$(PPh$_3$)$_2$(dcpp-^{15}N)]	d	43.5	103.8	

[a] Solution in toluene at 22°C unless otherwise specified.
[b] In ppm from PPh$_3$ at δ −4.70 ≡ H_3PO_4, zero at 22°C.
[c] Coupling constants (absolute magnitude) in Hz.
[d] −25°C.
[e] −50°C.
[f] See Table 2 for values of $J(^{31}P—^{15}N)$.

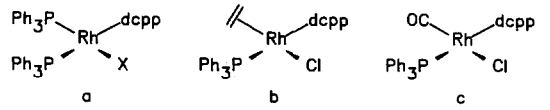

Fig. 3. Coordination geometries of the rhodium(I)-dcpp complexes; X = Cl, SC_6F_5.

mixture of $[RhCl(PPh_3)_3]$ (0.05 M) and dcpp (0.15 M) in toluene at 22°C is converted almost entirely to [*cis*-$RhCl(PPh_3)_2$(dcpp)] and some $[RhCl(PPh_3)(C_2H_4)$dcpp)]. By increasing the amount of $[Rh_2Cl_2(C_2H_4)_4]$ used in the reaction $[RhCl(PPh_3)(C_2H_4)$(dcpp)] can be obtained as the major product: of three possible isomers only one [Fig. 3(b)] is formed. On bubbling carbon monoxide through the solution the ethylene is readily replaced by CO to give the carbonyl derivative [Fig. 3(c)].

The complexes $[Rh(H)(C_2Ph)(X)(PPh_3)_2$(dcpp)] (X = Cl, OCN, N_3) (Fig. 4) are formed from $[RhX(PPh_3)_3]$ and PhC_2H in the presence of dcpp as the major products, even where the concentration of [*cis*-$RhX(PPh_3)_2$(dcpp)] is very low, thus removing the need for a phosphine scavenger. It would appear that one or both $[RhX(PPh_3)_3]$ and [*cis*-$RhX(PPh_3)_2$(dcpp)] combine with phenylacetylene to give a product which readily binds dcpp, but is reluctant to bind a third phosphine. The complex $[Rh(H)(C_2Ph)(X)(PPh_3)_2$(dcpp)] (X = N_3) undergoes further reaction with PhC_2H to give $[Rh(H)(C_2Ph)_2(PPh_3)_2$(dcpp)]; with X = Cl or OCN this tendency is greatly reduced.

Figure 2 shows the hydride signal in the ^1H spectrum of $[Rh(H)(C_2Ph)(N_3)(PPh_3)_2$(dcpp)] in both unenriched and 99% ^{15}N-enriched forms (with decoupling of the pyridine 2- and 6-hydrogens in order to improve the line shape). In Fig. 2(a) (unenriched) it is a doublet of triplets (coupling to rhodium—100% ^{103}Rh, nuclear spin 1/2—and two equivalent phosphines), while in Fig. 2(b) it is a doublet of doublets of triplets [the multiplet in Fig. 2(a) is further split by coupling to ^{15}N]. In Fig. 5 the $^{15}N\{^1H\}$ spectra of three complexes are shown: Figs 5(a) and (b) were obtained using INEPT delay times corresponding to $J(^{15}N—^1H) = 10.6$ Hz (polarization transfer from the pyridine 2- and 6-

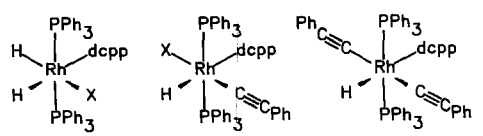

Fig. 4. Coordination geometries of the rhodium(III)-dcpp complexes. (a): X = Cl, SC_6F_5; (b): X = Cl, OCN, N_3.

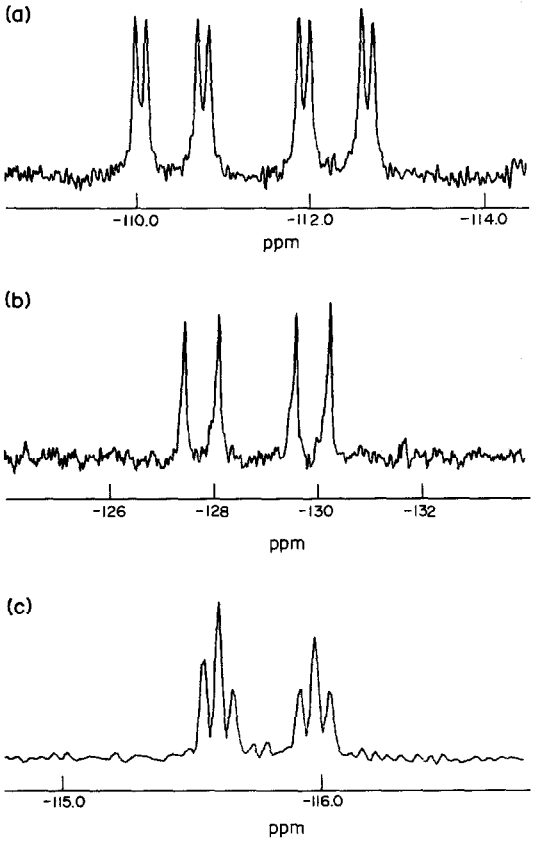

Fig. 5. $^{15}N\{^1H\}$ spectra of: (a) [*cis*-$Rh(SC_6F_5)(PPh_3)_2$(dcpp-^{15}N)] (0.07 M, 0.5 cm^3, 22°C, 25,000 scans); (b) $[RhCl(PPh_3)(CO)$(dcpp-^{15}N)] (0.015 M, 3.0 cm^3, −25°C, 1000 scans); (c) $[Rh(H)(C_2Ph)(OCN)(PPh_3)_2$(dcpp-$^{15}N$)] (0.05 M, 0.5 cm^3, 22°C, 14,000 scans). Solutions in toluene, $\delta^{15}N$ relative to CH_3NO_2 (ext. standard).

hydrogens), while Fig. 5(c) was obtained using a delay time corresponding to 22.8 Hz (polarization transfer from the hydride positioned *trans* to nitrogen).

In [*cis*-$Rh(SC_6F_5)(PPh_3)_2$(dcpp-^{15}N)] the nitrogen resonates as a doublet of doublets of doublets [Fig. 5(a)], coupling to rhodium and to phosphorus (two non-equivalent nuclei); the magnitude of the $^{31}P—^{15}N$ *trans* coupling (38.2 Hz) being approximately 15 times larger than that of $^{31}P—^{15}N$ *cis* (Table 2). The $^{15}N\{^1H\}$ signal from $[RhCl(PPh_3)(CO)$(dcpp-^{15}N)] [Fig. 5(b)] is a doublet of doublets with $J(^{31}P—^{15}N) = 43.5$ Hz, indicating a *trans*-phosphorus–nitrogen geometry [Fig. 2(c)]. The geometry of the complex $[Rh(H)(C_2Ph)(OCN)(PPh_3)_2$(dcpp-$^{15}N$)] [Figs 4(b) and 5(c)] is established unambiguously by a combination of ^1H (the magnitude of the $^{15}N—^1H$ coupling in the hydride signal indicates a *trans* configuration), ^{15}N

(the nitrogen resonates as a doublet of triplets, with coupling to rhodium and two equivalent phosphines) and ^{31}P (the phosphines give a single doublet confirming that they are equivalent, i.e. positioned mutually *trans*) NMR data.

Ligand exchange effects in the complexes [*cis*-$RhX(PPh_3)_2L$] (X = Cl, SC_6F_5; L = py, dcpp) are observed only at higher concentrations of N-donor ligand than were used in the present study, and become evident in the $^{31}P\{^1H\}$ spectrum as a broadening of the signals. Such effects are likely to be responsible for the broadening of the lines in the $^{15}N\{^1H\}$ spectra of $[Rh(H)_2X(PPh_3)_2(dcpp\text{-}^{15}N)]$ {X = Cl, SC_6F_5; formed from [*cis*-$RhX(PPh_3)_2$ (dcpp-^{15}N)] by treatment with hydrogen under ambient conditions} to the point where ^{31}P—^{15}N *cis* coupling cannot be observed. The spectrum of [*cis*-$RhCl(PPh_3)_2$(dcpp-^{15}N)] was recorded at −25°C in order to reduce the rate of conversion of the complex to $[Rh_2Cl_2(PPh_3)_4]$, a process that is accelerated by the removal from solution of free PPh_3. The complexes $[RhCl(PPh_3)(L)$(dcpp-^{15}N)] are also unstable in solution under the conditions required to generate them, their lifetime being prolonged at reduced temperature.

^{15}N NMR studies of complexes of rhodium have been reported for the ligands N_2,[11–13] NO,[14] ArN_2,[15,16] ArNSO,[17] NH_3,[18] 5-hydro-3,8-*R*,*R*-1,6-dioxa-4,9-diaza-5-phosphaspiro[4,4]nonane[19] (all with ^{15}N enrichment), pyridine, ethylenediamine, 1,2- and 1,3-diaminopropane, bipyridyl, 1,10-phenanthrolinc[20] and pyridine-2-carboxylate and related compounds[1] (natural abundance). ^{15}N studies of complexes of other metals have been comprehensively reviewed.[21–24] The change in chemical shift of nitrogen on complexation to a metal is considered to arise principally from three factors:[22] circulation of non-bonding and π-electrons (deshielding), asymmetry of the valence electrons (deshielding) and the energy separation (ΔE) between the ground and lowest excited states (the smaller the separation the greater the deshielding). The upfield shift (or, more correctly in the case of pulsed FT NMR, the shift to low frequency) of the ^{15}N resonance of pyridine on protonation is attributed largely to a change in ΔE when the lone pair electrons form a bond to hydrogen. Similar shifts have been observed on bonding of pyridine and derivatives to rhodium[1,20] and in the present study upfield shifts of *ca* 50 ppm were found in the dcpp-^{15}N signal. The values of δ^{15}N for the dcpp-^{15}N complexes show no obvious correlation with the properties of the other ligands: this may be a result of the fact that the ligand positioned *trans* to nitrogen is in all cases either PPh_3 or hydride and an investigation of the effects of a wide range of *trans* ligands is required before further comment can be made. Work in this direction is in progress.

Although the value of $J(^{103}Rh—^{15}N)$ (Table 2) appears to be related to the oxidation state of the metal these differences cannot be generalized and disappear when a wider range of complexes is considered: $[Rh(H)_2(O_2CArN)(PPh_3)_2]$ (O_2CArN = isoquinoline-1-carboxylate),[1] $J(^{103}Rh—^{15}N)$ = 10.1 Hz; $[RhCl(N_2Ph)(PMePh_2)_3][PF_6]$,[16] $J(^{103}Rh—^{15}N)$ = 15.9 Hz; [*trans*-$Rh(py)_4Cl_2$]Cl,[20] $J(^{103}Rh—^{15}N)$ = 17.1 Hz.

Acknowledgements—We thank the University of the Witwatersrand and the FRD for financial support.

REFERENCES

1. L. Carlton and M.-P. Belciug, *J. Organomet. Chem.* 1989, **378**, 469.
2. G. A. Morris and R. Freeman, *J. Am. Chem. Soc.* 1979, **101**, 760.
3. L. Carlton, M.-P. Belciug and G. Pattrick, *Polyhedron* 1992, **11**, 1501.
4. T. Chennat and U. Eisner, *J. Chem. Soc., Perkin I* 1975, 926.
5. L. Carlton and R. Weber, to be published.
6. J. A. Osborn, F. H. Jardine, J. F. Young and G. Wilkinson, *J. Chem. Soc. A* 1966, 1711.
7. L. Carlton, *J. Organomet. Chem.* 1992, **431**, 103.
8. D. F. Steele and T. A. Stephenson, *J. Chem. Soc., Dalton Trans.* 1972, 2161.
9. A. Maisonnat and R. Poilblanc, *Inorg. Chim. Acta* 1978, **29**, 203.
10. C. A. Tolman, P. Z. Meakin, D. L. Lindner and J. P. Jesson, *J. Am. Chem. Soc.* 1974, **96**, 2762.
11. D. L. Thorn, T. H. Tulip and J. A. Ibers, *J. Chem. Soc., Dalton Trans.* 1979, 2022.
12. J. R. Dilworth, S. Donovan-Mtunzi, C.-T. Kan, R. L. Richards and J. Mason, *Inorg. Chim. Acta* 1981, **53**, L161.
13. S. Donovan-Mtunzi, R. L. Richards and J. Mason, *J. Chem. Soc., Dalton Trans.* 1984, 469.
14. L. K. Bell, D. M. P. Mingos, D. G. Tew, L. F. Larkworthy, B. Sandell, D. C. Povey and J. Mason, *J. Chem. Soc., Chem. Commun.* 1983, 125.
15. J. R. Dilworth, C.-T. Kan, R. L. Richards, J. Mason and I. A. Stenhouse, *J. Organomet. Chem.* 1980, **201**, C24.
16. B. L. Haymore, M. Hughes, J. Mason and R. L. Richards, *J. Chem. Soc., Dalton Trans.* 1988, 2935.
17. R. Meij, D. J. Stufkens, K. Vrieze, W. van Gerresheim and C. H. Stam, *J. Organomet. Chem.* 1979, **164**, 353.
18. T. G. Appleton, J. R. Hall and S. F. Ralph, *Inorg. Chem.* 1988, **27**, 4435.
19. E. E. Nifantyev, K. N. Gavrilov, G. I. Timofeeva, A. T. Teleshev, S. N. Krasnokutsky, E. Y. Zhorov,

V. A. Pavlov and E. I. Klabunovsky, *J. Organomet. Chem.* 1990, **397**, 245.
20. K. S. Bose and E. H. Abbott, *Inorg. Chem.* 1977, **16**, 3190.
21. M. Witanowski, L. Stefaniak and G. A. Webb, *Ann. Rep. NMR Spectrosc.* 1981, **11B**, 1.
22. J. Mason, *Chem. Rev.* 1981, **81**, 205.
23. W. von Philipsborn and R. Müller, *Angew. Chem., Int. Edn Engl.* 1986, **25**, 383.
24. M. Witanowski, L. Stefaniak and G. A. Webb, *Ann. Rep. NMR Spectrosc.* 1986, **18**, 1.

Polyhedron Vol. 12, No. 11, pp. 1383–1390, 1993
Printed in Great Britain

0277–5387/93 $6.00+.00
© 1993 Pergamon Press Ltd

TRIPHOSPHA-FERROCENES AS LIGANDS: CRYSTAL AND MOLECULAR STRUCTURES OF $[Fe(\eta^5\text{-}C_5Me_5)(\eta^5\text{-}C_2Bu^t{}_2P_3)Cr(CO)_5]$ AND OF THE NOVEL NICKEL COMPLEX $[Fe(\eta^5\text{-}C_5Me_5)(\eta^5\text{-}C_2Bu^t{}_2P_3)Ni(CO)_2]_2$ CONTAINING TWO INTERLINKED $[Fe(\eta^5\text{-}C_5Me_5)(\eta^5\text{-}C_2Bu^t{}_2P_3)]$ SYSTEMS

CHRISTIAN MÜLLER, RAINER BARTSCH,* AXEL FISCHER and PETER G. JONES

Institut für Anorganische und Analytische Chemie der Technischen Universität, Hagenring 30, W-3300 Braunschweig, Germany

(*Received* 18 *December* 1992; *accepted* 27 *January* 1993)

Abstract—The lone pair electrons of the two adjacent phosphorus atoms of the $C_2Bu^t{}_2P_3$ ring in the triphospha-ferrocene complex $[Fe(\eta^5\text{-}C_5Me_5)(\eta^5\text{-}C_2Bu^t{}_2P_3)]$ can ligate to other metal centres to afford novel bi- and tetrametallic complexes, whose structures have been elucidated by NMR and single-crystal X-ray studies. In the reaction of $[Fe(\eta^5\text{-}C_5Me_5)(\eta^5\text{-}C_2Bu^t{}_2P_3)]$ with $Ni(CO)_4$ the tetrametallic complex $[Fe(\eta^5\text{-}C_5Me_5)(C_2Bu^t{}_2P_3)Ni(CO)_2]_2$ is formed. This complex is of particular interest because it represents the first example of the intermolecular interlinkage of two phospha-ferrocene units by two metal centres. A six-membered ring consisting of four phosphorus and two nickel atoms forms the core of the molecule and exhibits a boat configuration. The starting material $[Fe(\eta^5\text{-}C_5Me_5)(\eta^5\text{-}C_2Bu^t{}_2P_3)]$ reacts with $Cr(CO)_5(thf)$, $W(CO)_5(thf)$ and $Fe_2(CO)_9$ to yield the η^1-complexes $[Fe(\eta^5\text{-}C_5Me_5)(\eta^5\text{-}C_2Bu^t{}_2P_3)M(CO)_n]$ (M = Cr, W, $n = 5$; M = Fe, $n = 4$). Variable-temperature $^{31}P\{^1H\}$ NMR studies reveal that these complexes are fluxional in solution.

Syntheses and structures of di-, tri-, penta- and hexaphosphorus analogues of ferrocenes, hexaphosphorus analogues of chromocene and η^3-transition metal complexes of the $C_2Bu^t{}_2P_3$ ring system have been described.[1–7] Unlike their simple metallocene analogues, however, these complexes have further ligating potential towards other transition metal centres by virtue of the availability of the ring phosphorus lone-pair electrons not already utilized in their η^3- or η^5-metal ligation. In a previous paper[8] we have described the synthesis and structural characterization of four such compounds: $[Fe(\eta^5\text{-}C_2Bu^t{}_2P_3)_2Fe(CO)_4]$, $[Fe(\eta^5\text{-}C_2Bu^t{}_2P_3)_2W(CO)_5]$, $[Fe(\eta^5\text{-}C_3Bu^t{}_3P_2)(\eta^5\text{-}C_2Bu^t{}_2P_3)W(CO)_5]$ and $[Fe(\eta^5\text{-}C_2Bu^t{}_2P_3)_2Ru_3(CO)_{10}]$ (**1**). The latter is of special interest since it represents the first example of (1) attachment of a transition metal carbonyl cluster to another $(\eta^5\text{-}C_2Bu^t{}_2P_3)$ metal complex and (2) interlinkage of both $(\eta^5\text{-}C_2Bu^t{}_2P_3)$ ligated ring systems in hexaphospha-ferrocene complexes.

Very recently[9] we described the synthesis and structural characterization of the ruthenium compound $[Fe(\eta^5\text{-}C_5Me_5)(\eta^5\text{-}C_2Bu^t{}_2P_3)Ru_3(CO)_9]$ (**2**) as a first example of a triphospha-ferrocene in which adjacent phosphorus atoms act as η^1-donors (see Fig. 1).

In this paper we report the synthesis of the tetrametallic complex $[Fe(\eta^5\text{-}C_5Me_5)(\eta^5\text{-}C_2Bu^t{}_2P_3)Ni(CO)_2]_2$ (**4**), by treatment of $[Fe(\eta^5\text{-}C_5Me_5)(\eta^5\text{-}C_2Bu^t{}_2P_3)]$ (**3**) with $Ni(CO)_4$. The nickel complex **4** represents the first example of intermolecular interlinkage of two phospha-ferrocene systems by two metal centres. Furthermore, we describe the syntheses of the complexes $[Fe(\eta^5\text{-}C_5Me_5)(\eta^5\text{-}C_2Bu^t{}_2P_3)Cr(CO)_5]$ (**5**). $[Fe(\eta^5\text{-}C_5Me_5)(\eta^5\text{-}C_2Bu^t{}_2P_3)W(CO)_5]$ (**6**) and $[Fe(\eta^5\text{-}C_5Me_5)(\eta^5\text{-}C_2Bu^t{}_2P_3)Fe(CO)_4]$ (**7**) by treatment of **3** with $Cr(CO)_5(thf)$, $W(CO)_5(thf)$ and $Fe_2(CO)_9$, respectively. X-ray crystal structures of the complexes **4** and **5** have been determined in order to elucidate

* Author to whom correspondence should be addressed.

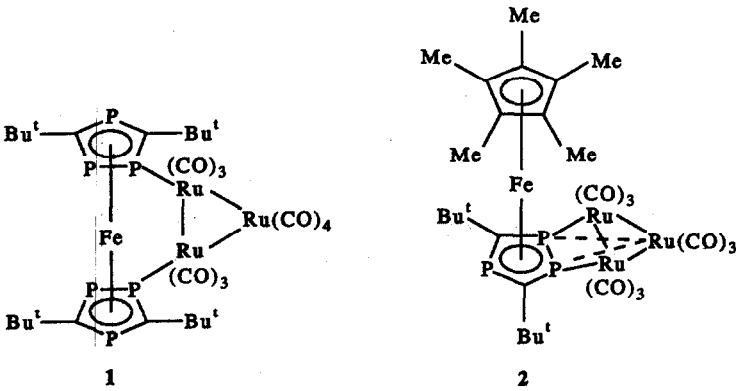

Fig. 1.

structural relationships within a series of related phospha-ferrocenes (see Table 1).

EXPERIMENTAL

All experiments were performed under oxygen-free nitrogen using conventional Schlenk techniques. Solvents were dried over sodium wire and distilled prior to use. The complexes $Cr(CO)_5(thf)$,[10] $W(CO)_5(thf)$[10] and $[Fe(\eta^5\text{-}C_5Me_5)(\eta^5\text{-}C_2Bu^t{}_2P_3)]$ (**3**)[9] were prepared according to literature procedures; all other starting materials were commercially available. IR spectra were obtained using a Nicolet 320 FT-IR spectrometer. NMR

Table 1. Crystal data and details of X-ray analyses for compounds **4** and **5**

	4	**5**
Formula	$C_{44}H_{66}Fe_2Ni_2O_4P_6$	$C_{25}H_{33}CrFeO_5P_3$
M_r	1073.9	614.3
Crystal habit	Red prism	Red–brown prism
Crystal size (mm)	$0.5\times0.4\times0.2$	$0.55\times0.3\times0.15$
Space group	$P2_1/c$	$P2_1/n$
Cell constants:		
a (Å)	20.347(6)	9.521(2)
b (Å)	16.138(5)	15.058(3)
c (Å)	15.738(5)	19.744(4)
β (°)	106.96(3)	90.81(3)
V (nm^3)	4.943	2.8305
Z	4	4
D_x (Mg m^{-3})	1.443	1.441
$F(000)$	2240	1272
μ (mm^{-1})	1.56	1.10
$2\theta_{max}$ (°)	50	50
Transmissions	0.64–1.00	0.76–0.83
No. of reflections		
Measured	12,259	7309
Independent	8740	4998
R_{int}	0.038	0.024
Significant [$>4\sigma(F)$]	5586	4100
R	0.038	0.033
wR	0.041	0.037
g	0.0006	0.0003
Number of parameters	589	349
S	1.0	1.6
Max. Δ/σ	0.003	0.002
Max. $\Delta\rho$ (e Å^{-3})	0.56	0.31

spectra were recorded on a Bruker spectrometer AC 200 (200.1 MHz). Positive shifts are to lower field. Mass spectra were obtained using a Finnigan spectrometer MAT 8430.

$[Fe(\eta^5\text{-}C_5Me_5)(\eta^5\text{-}C_2Bu^t{}_2P_3)Ni(CO)_2]_2$ (**4**)

A solution of nickel tetracarbonyl (2.64 g, 15.46 mmol) in DME (3 cm^3) was added to a solution containing $[Fe(\eta^5\text{-}C_5Me_5)(\eta^5\text{-}C_2Bu^t{}_2P_3)]$ (**3**) in DME (10 cm^3) with stirring at 0°C. Carbon monoxide was released immediately and stirring was continued for 16 h at room temperature. After removal of the volatile material *in vacuo* the orange residue was extracted with n-hexane and fractionated by column chromatography (kieselgel/n-hexane). Some starting material and impurities were eluted with n-hexane, then the nickel complex **4** was isolated by elution with toluene. Some orange coloured crystals of **4** suitable for X-ray analysis were obtained by recrystallization from n-hexane. However, the compound could not be isolated without traces of impurities and, therefore, the yield was not determined and a microanalysis was not performed. FAB-MS: $C_{44}H_{66}Fe_2Ni_2O_4P_6$ (1074), *m/z* (%): 1018 (0.7) $[M-2\ CO]^+$, 959 (1.6) $[M-Ni(CO)_2]^+$, 422 (100) $[\mathbf{3}]^+$, 284 (18) $[\mathbf{3}-C_2Bu^t{}_2]^+$, 253 (7) $[\mathbf{3}-C_2Bu^t{}_2-P]^+$. IR (n-hexane): ν(CO) = 2013 (vs), 1969 (s) cm^{-1}.

$[Fe(\eta^5\text{-}C_5Me_5)(\eta^5\text{-}C_2Bu^t{}_2P_3)Cr(CO)_5]$ (**5**)

A THF solution of $Cr(CO)_5$(thf) prepared from $Cr(CO)_6$ (280 mg, 1.27 mmol) in THF[10] was added to a solution of **3** (385 mg, 0.91 mmol) in THF (3 cm^3) and the reaction mixture was stirred for 4 h at room temperature. The volatile material was removed *in vacuo* and the orange–brown residue was extracted with n-hexane and fractionated by column chromatography (kieselgel/n-hexane). After the removal of the solvent and recrystallization from n-hexane deep brown crystals of **5** were obtained, which were suitable for X-ray analysis. Yield: 510 mg (91%); m.p. 162°C (dec.). Found: C, 48.8; H, 5.6; P, 15.1. Calc. for $C_{25}H_{33}CrFeO_5P_3$ (614.30): C, 48.9; H, 5.4; P, 15.1%. IR (n-hexane): ν (CO) = 2063 (vs), 1987 (s), 1944 (vs) cm^{-1}.

$[Fe(\eta^5\text{-}C_5Me_5)(\eta^5\text{-}C_2Bu^t{}_2P_3)W(CO)_5]$ (**6**)

Complex **6** was prepared using $W(CO)_5$(thf), prepared from $W(CO)_6$ (380 mg, 1.08 mmol)[10] and **3** (325 mg, 0.77 mmol) as starting materials. Deep brown crystals of **6** were obtained from n-hexane. Yield: 521 mg (91%); m.p. 159°C (dec.). Found: C, 40.4; H, 4.5; P, 12.5. Calc. for $C_{25}H_{33}FeO_5P_3W$ (746.15): C, 40.2; H, 4.5; P, 12.4%. IR (n-hexane): ν (CO) = 2071 (vs), 1984 (s), 1944 (vs) cm^{-1}.

$[Fe(\eta^5\text{-}C_5Me_5)(\eta^5\text{-}C_2Bu^t{}_2P_3)Fe(CO)_4]$ (**7**)

Compound **7** was prepared from **3** (423 mg, 1.00 mmol) and $Fe_2(CO)_9$ (510 mg, 1.40 mmol). Brown crystals of **7** were obtained from n-hexane. Yield: 515 mg (87%); m.p. 134°C (dec.). Found: C, 49.0; H, 5.6; P, 19.0. Calc. for $C_{24}H_{33}Fe_2O_4P_3$ (590.14): C, 48.8; H, 5.6; P, 18.9%. IR (n-hexane): ν (CO) = 2058 (vs), 2048 (vs), 1976 (vs), 1949 (vs) cm^{-1}.

Crystal structure determination for complexes **4** *and* **5**

Crystals were mounted in inert oil on glass fibres and transferred to the cold gas stream of the diffractometer (**4**: Siemens R3, $T = -95$°C; **5**: Stoe STADI-4, $T = -115$°C). Data were collected using monochromated Mo-K_α radiation. Absorption corrections based on ψ-scans were applied. Cell constants were refined from setting angles (**4**) or $\pm\omega$ angles (**5**) of *ca* 50 reflections in the 2θ range 20–23°. The structures were solved by direct methods and refined anisotropically. Hydrogen atoms were included using a riding model: weighting schemes of the form $w^{-1} = \sigma^2(F)+gF^2$ were employed. The program system was "Siemens SHELXTL PLUS". Full details of the structure determinations have been deposited at the Fachinformationszentrum Karlsruhe, Gesellschaft für Wissenschaftlich-technische Information mbH, D-7514 Eggenstein-Leopoldshafen 2, Germany. Any request for this material should quote a full literature citation and the reference number CSD 56974.

RESULTS AND DISCUSSION

Synthesis and spectroscopy

We recently[9] described the preparation of $[Fe(\eta^5\text{-}C_5Me_5)(\eta^5\text{-}C_2Bu^t{}_2P_3)]$ (**3**). Treatment of this complex with nickel carbonyl results in the formation of the tetrametallic complex **4**, in which two phosphaferrocenes (**3**) are linked by two $Ni(CO)_2$ centres. The ^{31}P NMR spectrum of **4** represents an AB_2 spin system with $\delta(P^A)$ 36.14 and $\delta(P^B)$ 35.00 ppm (Table 2). No molecular ion could be detected in the EI mass spectrum of **4**. Only the mass peak of complex **3** and its fragments could be established. Complex **4** cannot be transferred into the gas phase without decomposition because of its high mass. The molecular ion of **4** could also not be detected in the FAB

Table 2. $^{31}P\{^1H\}$ NMR data[a]

Complex	δ_P	$^1J(PP)$ (Hz)	$^2J(PP)$ (Hz)
4	36.14 (A)		46.9
	35.00 (B)		
5[b]	39.10 (A)	404.3	35.6 (AB)
	16.41 (B)		49.4 (AX)
	79.11 (X)		
6[b]	35.93 (A)	544.7	35.5 (AB)
	19.73 (B)		48.2 (AX)
	25.45 (X)		
7	37.19 (A)	435.0	37.0 (AB)
	−4.34 (B)		49.3 (AX)
	94.08 (X)		

[a] In $CDCl_3$; chemical shifts in ppm downfield from 85% H_3PO_4 as an external standard.
[b] −35°C.

mass spectrum, but fragments of lower intensity could be observed that resulted from the loss of carbonyl groups and a $Ni(CO)_2$ fragment. Again, the molecular ion of **3** represents the strongest peak, corresponding to the typical fragmentation pattern[9] (see Experimental). Treatment of **3** with $Cr(CO)_5$(thf), $W(CO)_5$(thf) and $Fe_2(CO)_9$ afforded the η^1-complexes **5**, **6** and **7** as deep brown crystals. The new complexes were characterized by microanalysis, IR spectroscopy (see Experimental) and ^1H, ^{31}P and ^{13}C NMR spectroscopy (see Scheme 1, Tables 2 and 3). The molecular structure of **5** was confirmed by a single-crystal X-ray diffraction study, indicating that the $C_2Bu^t_2P_3$ ring is bonded in an η^5-η^1-fashion to the iron and chromium atom, respectively, with the iron atom sandwiched between the two five-membered rings (Fig. 2). The $^{31}P\{^1H\}$NMR spectra of **5**, **6** and **7** represent ABX spin systems with values of chemical shifts and coupling constants lying in the same region as described for $[Fe(\eta^5\text{-}C_5H_5)(\eta^5\text{-}C_2Bu^t_2P_3)W(CO)_5]$[7] (see Table 2). For all complexes $^2J(P^AP^B)$ is smaller than $^2J(P^AP^X)$. In contrast to the corresponding cyclopentadienyl compound,[7] no ^{183}W satellites could be observed for the pentamethylcyclopentadienyl compound **6**. Variable-temperature $^{31}P\{^1H\}$ NMR studies reveal that complexes **5**, **6** and **7** are fluxional in solution. At −35°C the spectra of **5** and **6** exhibit the characteristic ABX pattern expected for the rigid structure. As the temperature is raised resonances P^B and P^X broaden and become featureless at room temperature (see Fig. 3 for the

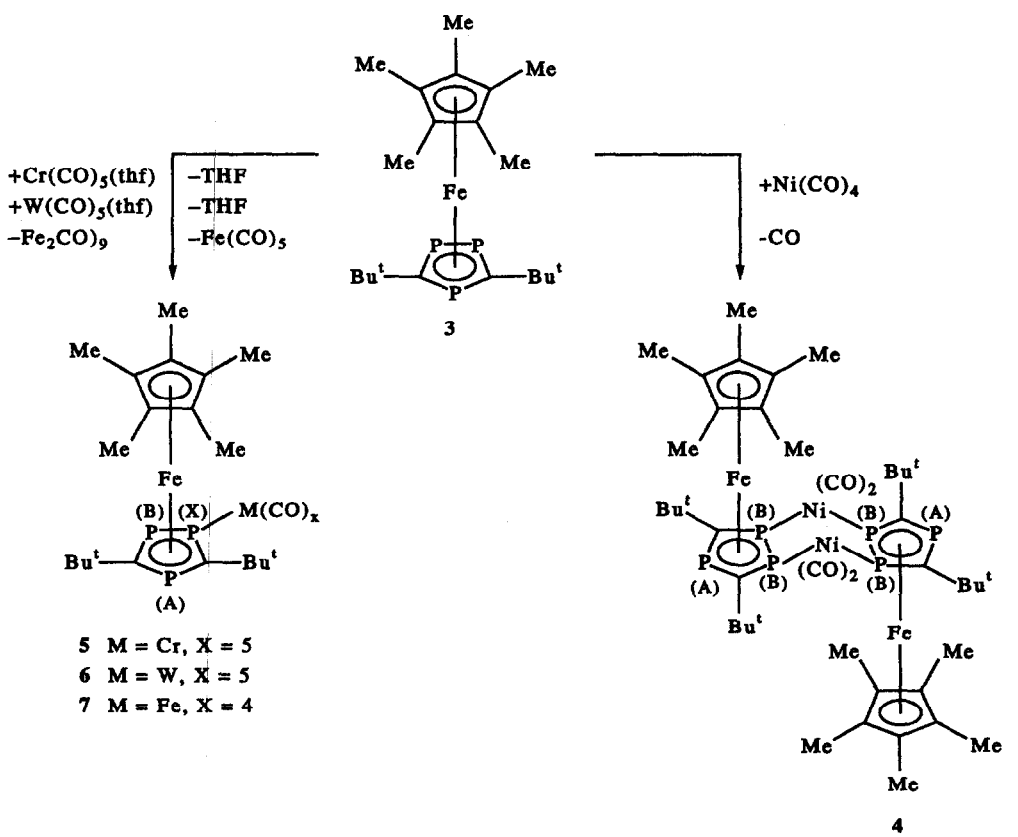

Scheme 1.

Table 3. ^1H and ^{13}C NMR data[a]

Complex	δ_H	δ_C
5	1.43 (s, 18H, CMe_3)	12.67 (s, C_5Me_5)
	1.90 (s, 15H, C_5Me_5)	36.06 (m, CMe_3)
		38.68 (m, CMe_3)
		88.41 (s, C_5Me_5)
		216.14 (s, *CO, cis*)
		222.03 (s, *CO, trans*)
6	1.43 (s, 18H, CMe_3)	12.68 (s, C_5Me_5)
	1.88 (s, 15H, C_5Me_5)	36.13 (m, CMe_3)
		38.76 (m, CMe_3)
		88.48 (s, C_5Me_5)
		196.59 (s, *CO, cis*)
7	1.41 (s, 18H, CMe_3)	12.37 (s, C_5Me_5)
	1.90 (s, 15H, C_5Me_5)	35.95 (m, CMe_3)
		38.99 (m, CMe_3)
		88.81 (s, C_5Me_5)
		214.02 (eq)
		[^2J(PC) = 12.3 Hz]

[a] In $CDCl_3$; chemical shifts in ppm downfield from $SiMe_4$; s = singlet, m = multiplet.

chromium complex **5**). This fluxional process is best visualized as an intramolecular 1,2-shift of chromium, tungsten or iron between P^B and P^X, as shown in Scheme 2 for chromium. In contrast to the chromium and tungsten compounds **5** and **6** the intramolecular 1,2-shift is slow for the $Fe(CO)_4$ adduct **7**. Although the signals in the $^{31}P\{^1H\}$ NMR spectrum of **7** are broadened at room temperature, the coupling constants $^2J(P^AP^B)$ and $^2J(P^AP^X)$ can still be observed.

This type of mechanism has been postulated for the complex *trans*-[$MCl(C_2R_2P_3)(PEt_3)_2$] (R = Bu^t, 1-adamantyl; M = Pd, Pt),[4] in which the 1,2,4-triphosphacyclopentadienyl system is η^1-ligated, and for related systems involving nitrogen, sulphur and selenium heterocycles.[11,12] The ^1H NMR spectra of the complexes **5**, **6** and **7** show only one resonance for the protons of the Bu^t groups. The intramolecular 1,2-shift of the metal fragment $M(CO)_x$ is obviously so fast, relative to the ^1H NMR time-scale, that even at −35°C no splitting of the signal could be observed. The ^{13}C NMR spectrum of **5** exhibits two signals for the carbonyl groups in *cis*/*trans* positions, whereas **6** shows only one resonance for the carbonyl groups in a *cis* position. Furthermore, only one resonance appears in the ^{13}C NMR spectrum of **7** for the carbonyl groups in equatorial positions. The value of the phosphorus–carbon coupling in **7** is 12.3 Hz (slow 1,2-shift), whereas no phosphorus–carbon couplings could be observed in the ^{13}C NMR spectra of **5** and **6** at room temperature because of the intramolecular 1,2-shift of the metal fragment $M(CO)_x$, which is fast relative to the ^{13}C NMR time-scale.

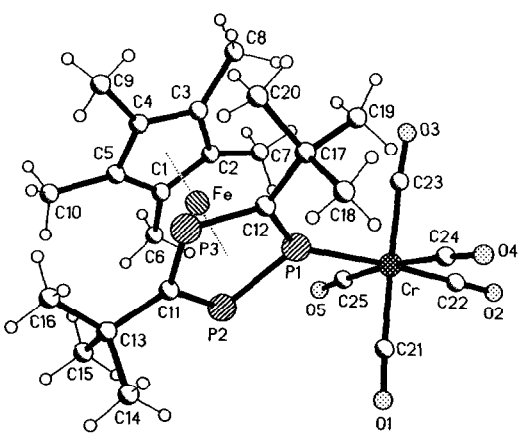

Fig. 2. Molecular structure of **5**.

X-ray investigations

The molecular structures of compounds **4** and **5** with analogous atomic numbering schemes are shown in Figs 2 and 4. Selected bond lengths and angles are given in Table 4. The molecule of **4** consists of two triphospha-ferrocene groups (**3**), doubly bridged by two $Ni(CO)_2$ fragments via the two adjacent phosphorus atoms of the $C_2Bu^t{}_2P_3$ ring

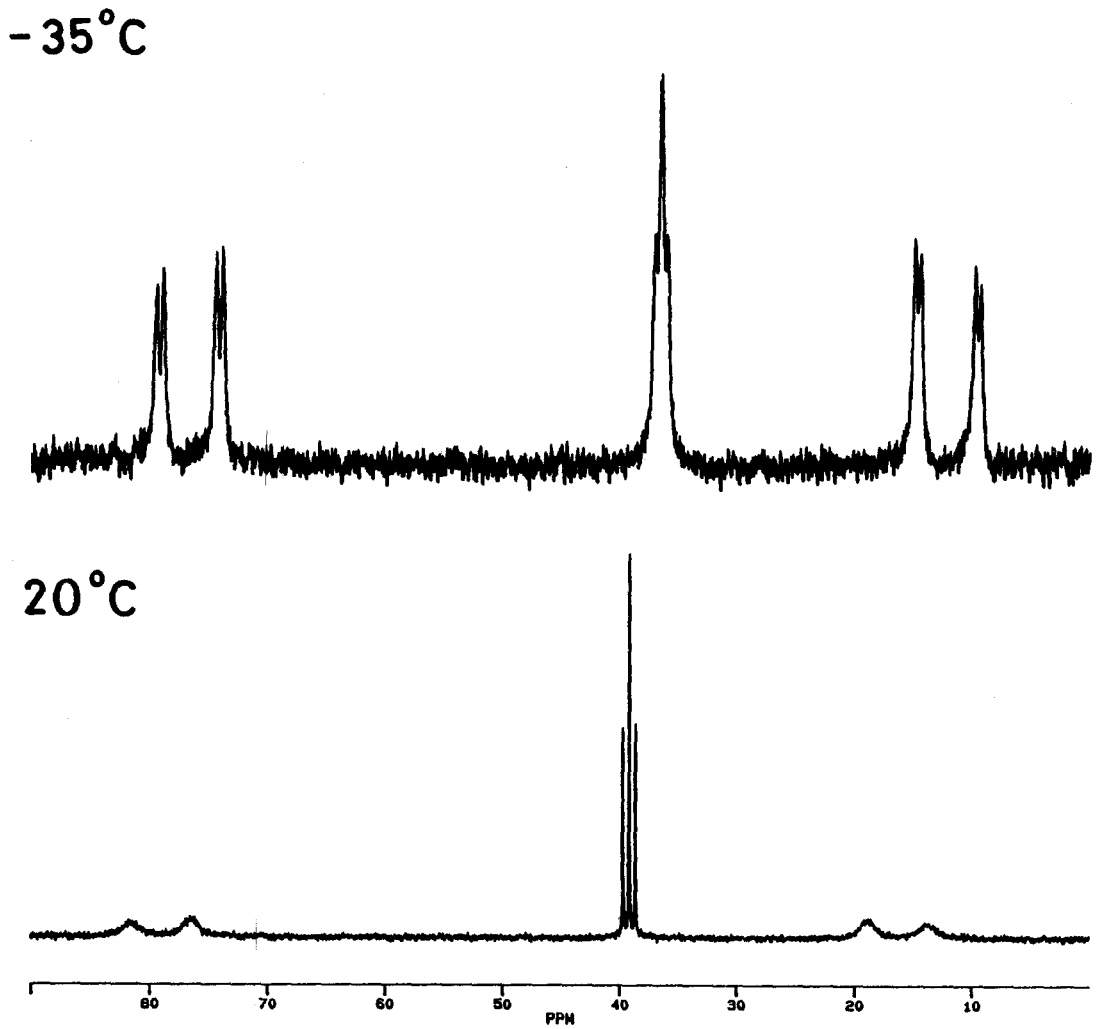

Fig. 3. Temperature-dependent $^{31}P\{^{1}H\}$ NMR spectra of the chromium complex **5**.

systems. Bond lengths and angles in the [Fe(η^5-C_5Me_5)(η^5-$C_2Bu^t{}_2P_3$)] moieties agree well with those of closely related sandwich compounds.[1-9] The triphosphacyclopentadienyl systems reveal only negligible deviation from planarity (av. 0.003 Å). The C_5Me_5 and $C_2Bu^t{}_2P_3$ ring systems are essentially parallel (dihedral angle 3.1°) and almost eclipsed. The observed iron-cyclopentadienyl ring centre distance of 1.711 Å and the iron-triphosphacyclopentadienyl ring distance of 1.656 Å are very similar to those of the ruthenium complex **2**.[9] The nickel atoms in the phosphorus–nickel six-membered ring in **4** occupy the centres of distorted tetrahedrons, in which the P—Ni—P,

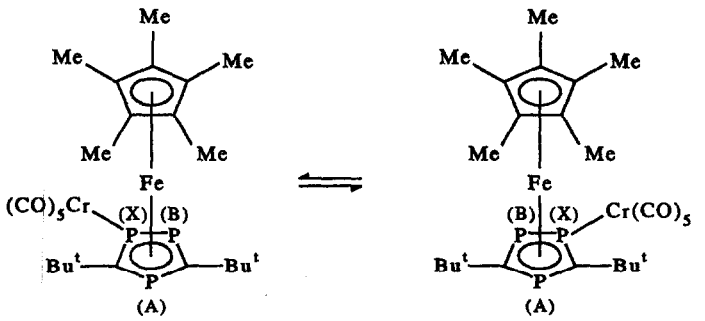

Scheme 2.

Table 4. Relevant bond lengths (Å) and angles (°) in compounds **4** and **5**

4		**5**	
Ni—P(1)	2.217(2)	Fe—P(1)	2.330(1)
Ni—P(1′)	2.221(2)	Fe—P(2)	2.346(1)
Ni′—P(2)	2.216(2)	Fe—P(3)	2.315(1)
Ni′—P(2′)	2.213(2)	P(1)—P(2)	2.110(1)
P(1)—P(2)	2.111(2)	P(1)—C(12)	1.759(3)
P(2)—C(11)	1.764(5)	P(3)—C(11)	1.758(3)
P(3)—C(11)	1.759(4)	P(2)—C(11)	1.760(3)
P(3)—C(12)	1.759(5)	P(3)—C(12)	1.762(3)
P(1)—C(12)	1.759(5)	P(1)—Cr	2.402(1)
Ni—C(22)	1.781(5)	Cr—C(21)	1.896(3)
Ni—P(1)—P(2)	124.5(1)	P(2)—C(11)—P(3)	122.4(2)
P(1)—Ni—P(1′)	106.0(1)	P(1)—C(12)—P(3)	118.9(1)
Ni—P(1′)—P(2′)	125.9(1)	P(2)—P(1)—C(12)	101.7(1)
P(2)—Ni′—P(2′)	105.4(1)	P(1)—P(2)—C(11)	97.2(1)
P(1)—P(2)—Ni′	126.3(1)	C(11)—P(3)—C(12)	99.7(1)
Ni′—P(2′)—P(1′)	124.9(1)	Cr—P(1)—C(12)	140.0(1)
P(2)—C(11)—P(3)	120.2(2)	P(2)—P(1)—Cr	116.7(1)
P(2)—P(1)—C(12)	99.3(2)	P(1)—Cr—C(21)	87.2(1)
P(1)—C(12)—P(3)	120.7(2)	P(1)—Cr—C(22)	175.1(1)
P(1)—P(2)—C(11)	99.7(1)	P(1)—Cr—C(23)	93.3(1)
C(11)—P(3)—C(12)	100.0(2)	P(1)—Cr—C(24)	94.1(1)
Ni—P(1)—C(12)	135.8(1)	P(1)—Cr—C(25)	88.8(1)
C(11)—P(2)—Ni′	133.8(1)		
Ni—C(21)—O(1)	175.9(5)		
Ni—C(22)—O(2)	175.9(6)		

P—Ni—C and C—Ni—C bond angles deviate by up to 5° from ideal angles. The six-membered ring that forms the core of the molecule exhibits a boat configuration. The values of the Ni—P bond lengths in **4** lie in the range 2.213–2.221 Å and agree well with those of known $Ni(CO)_2$-bridged structures.[13,14] The Ni—C—O angles show only minor deviations from linearity (Fig. 4).

The molecular structure of the chromium complex **5** illustrated in Fig. 2 agrees well with that of the closely related tungsten complex $[Fe(\eta^5\text{-}C_5H_5)(\eta^5\text{-}C_2Bu^t{}_2P_3)W(CO)_5]$.[7] The observed P—P and P—C distances in the $C_2Bu^t{}_2P_3$ ring system are very similar in both complexes. The triphosphacyclopentadienyl ring in **5** shows a slight deviation of 0.015 Å (av.) from planarity. The distances between the iron atom and the centres of the cyclopentadienyl and triphosphacyclopentadienyl ring systems (1.716 and 1.663 Å) resemble those in the nickel complex (**4**). The ring systems are almost parallel (dihedral angle 1.8°) and show an eclipsed configuration. The chromium pentacarbonyl fragment possesses the structure of a slightly distorted tetrahedron. Due to the steric demand of the tert-butyl groups, the neighbouring carbonyl groups display wider bond angles. The Cr—P(1) bond distance of 2.402 Å in **5** is in good agreement with the corresponding distance in $(Ph_3P)Cr(CO)_5$ (2.422 Å).[15,16] The Cr—C—O bond angles show only minor deviations from linearity. Bond lengths and angles of the chromium pentacarbonyl fragment in **5** are very similar to those in chromium pentacarbonyl adducts of comparable phosphaferrocenes.[17,18]

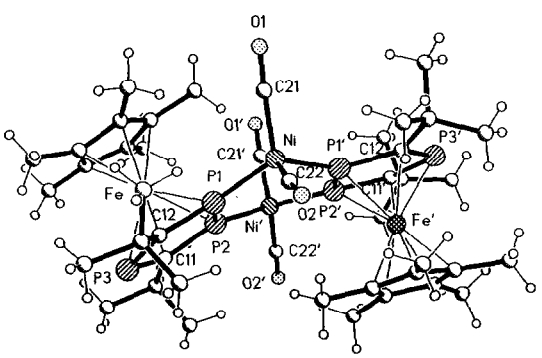

Fig. 4. Molecular structure of **4**.

We conclude that the geometry of the 2,5-di-

t-butyl-1,3,4-triphosphacyclopentadienyl ring in **4** and **5** is hardly changed on complexation from that in the parent complex $[Fe(\eta^5\text{-}C_2Bu^t{}_2P_3)_2]$.[1]

Acknowledgements—We thank Professor R. Schmutzler for his generous support, Mr A. Weinkauf for technical assistance and the Fonds der Chemischen Industrie for financial support.

REFERENCES

1. R. Bartsch, P. B. Hitchcock and J. F. Nixon, *J. Chem. Soc., Chem. Commun.* 1987, 1146.
2. R. Bartsch, P. B. Hitchcock and J. F. Nixon, *J. Chem. Soc., Chem. Commun.* 1988, 819.
3. R. Bartsch, P. B. Hitchcock and J. F. Nixon, *J. Organomet. Chem.* 1988, **356**, C1.
4. R. Bartsch, D. Carmichael, P. B. Hitchcock, M. F. Meidine, J. F. Nixon and G. J. D. Sillett, *J. Chem. Soc., Chem. Commun.* 1988, 1615.
5. R. Bartsch, P. B. Hitchcock and J. F. Nixon, *J. Organomet. Chem.* 1989, **373**, C17.
6. R. Bartsch, P. B. Hitchcock and J. F. Nixon, *J. Chem. Soc., Chem. Commun.* 1990, 472.
7. R. Bartsch, P. B. Hitchcock and J. F. Nixon, *J. Organomet. Chem.* 1988, **340**, C37.
8. R. Bartsch, A. Gelessus, P. B. Hitchcock and J. F. Nixon, *J. Organomet. Chem.* 1992, **430**, C10.
9. C. Müller, R. Bartsch, A. Fischer and P. G. Jones, *J. Organomet. Chem.* 1993, in press.
10. W. Strohmeier and F.-J. Müller, *Chem. Ber.* 1969, **102**, 3608.
11. M. Kooti and J. F. Nixon, *J. Organomet. Chem.* 1976, **105**, 217.
12. E. W. Abel, P. K. Mittal, K. G. Orrell and V. Sik, *J. Chem. Soc., Dalton Trans.* 1985, 1569 and refs therein.
13. C. Krüger and Y. H. Tsay, *Cryst. Struct. Commun.* 1974, **3**, 455.
14. J. A. J. Jarvis, R. H. B. Mais, P. G. Owston and D. T. Thompson, *J. Chem. Soc. (A)* 1970, 1867.
15. H. J. Plastas, J. M. Stewart and S. O. Grim, *J. Am. Chem. Soc.* 1969, **91**, 4326.
16. H. J. Plastas, J. M. Stewart and S. O. Grim, *Inorg. Chem.* 1973, **12**, 265.
17. L. Weber, R. Kirchhoff, R. Boese and H.-G. Stammler, *J. Chem. Soc., Chem. Commun.* 1991, 1293.
18. O. J. Scherer, T. Brück and G. Wolmershäuser, *Chem. Ber.* 1989, **122**, 2049.

Polyhedron Vol. 12, No. 11, pp. 1391–1397, 1993
Printed in Great Britain

0277–5387/93 $6.00+.00
© 1993 Pergamon Press Ltd

ELECTROCHEMICAL SYNTHESIS OF METAL(II) COMPLEXES OF SCHIFF BASES: THE CRYSTAL STRUCTURE OF ACETONITRILE-BIS{2-[(2-PYRROLE)METHYLIMINO]-4,6-DIMETHYLPHENOLATO}ZINC(II)

J. A. CASTRO, J. ROMERO, J. A. GARCIA-VAZQUEZ, A. MACIAS and A. SOUSA*

Departamento de Química Inorgánica, Universidad de Santiago, Santiago de Compostela, Galicia, Spain

and

U. ENGLERT

Institut für Anorganische Chemie de Technischen Hochschule Aachen, Aachen, Germany

(*Received* 23 *November* 1992; *accepted* 27 *January* 1993)

Abstract—The electrochemical oxidation of anodic metals (Co, Ni, Cu, Zn and Cd) in acetonitrile solution containing a Schiff base (H_2L) derived from H-pyrrole-2-carbaldehyde and a substituted *o*-aminophenol yielded the complexes $M(HL)_2$ and acetonitrile-bis{2-[(2-pyrrole)methylimino]-4,6-dimethylphenolato}zinc(II). X-ray data show the latter to have a distorted bipyramidal coordination polyhedron that does not include the pyrrole nitrogen atoms.

In previous papers we have reported the electrochemical synthesis of complexes of various metals with Schiff bases derived from H-pyrrole-2-carbaldehyde and anilines,[1,2] cysteamine or (2-aminophenyl)disulphide.[3] The electrochemical oxidation of a metal in a cell containing a solution of a ligand is simple, affords high yields and allows the one-step preparation of mixed complexes by inclusion of a second ligand in the cell solution [recently published examples include mixed complexes containing 2-pyrrole-N-(*o*-hydroxyphenyl)-aldimines and either 1,10-phenanthroline or 2,2′-bipyridine].[4] In continuation of our work in this field we have now synthesized complexes of metals with 2-[(2-pyrrole-)-methylimino]phenols (H_2L):

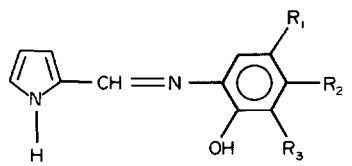

where $R_1 = R_2 = R_3 = H$ (HL^a); $R_1 = Cl$, $R_2 = R_3 = H$ (HL^b); $R_1 = CH_3$, $R_2 = R_3 = H$ (HL^c); $R_2 = CH_3$, $R_1 = R_3 = H$ (HL^d); $R_1 = R_3 = CH_3$, $R_2 = H$ (HL^e).

The crystal structure of acetonitrile-bis{2-[(2-pyrrole)methylimino]-4,6-dimethylphenolato}zinc(II) is also reported.

EXPERIMENTAL

Cobalt, nickel, copper, zinc and cadmium (Ega Chemie) were used as plates (*ca* 2 × 2 cm). All other reagents, including acetonitrile, H-pyrrole-2-carbaldehyde and amines were commercial products and were used without further purification.

Schiff base formation

Equimolecular amounts of the H-pyrrole-2-carbaldehyde and amine in chloroform solution were refluxed until the theoretical amount of water had been collected in a Dean–Stark trap. The solids isolated were crystallized from n-hexane and their purity was confirmed by elemental microanalysis and their IR and ^1H NMR spectra.

* Author to whom correspondence should be addressed.

Preparation of complexes

These compounds were obtained using an electrochemical procedure similar to that described by Tuck *et al.*[5] The cell consisted of a 100 cm^3 tall-form beaker containing an acetonitrile solution of the Schiff base (with a small amount of tetraethylammonium perchlorate as a current carrier), a platinum wire cathode and a sacrifical metal anode. Direct current was obtained from a purpose-built d.c. power supply. Applied voltages of 15–30 V allowed sufficient current flow for smooth dissolution of the metal. The cells can be summarized as $Pt_{(-)}/CH_3CN + H_2L/M_{(+)}$.

The solution compositions and experimental conditions are given in Table 1. In some cases the product formed during electrolysis was recrystallized from hot acetonitrile. The analytical data of the compounds are given in Table 2.

X-ray crystal structure analysis

$[Zn(C_{13}H_{13}N_2O)_2 \cdot CH_3CN]$, *Crystal data.* $C_{28}H_{29}N_5O_2Zn$, $M = 532.95$, orthorhombic, space group *Pbcn*, $a = 14.398(4)$, $b = 8.190(2)$, $c = 22.298(4)$ Å, $V = 2629(2)$ Å^3, $Z = 4$, $D_c = 1.346$ g cm^{-3}, $F(000) = 1112$, $\lambda(\text{Cu-}K_\alpha) = 1.5418$ Å, $\mu = 15.79$ cm^{-1}.

Data collection and processing. Structure determination was performed at room temperature with an Enraf–Nonius CAD4 diffractometer using a crystal of approximate dimensions $0.3 \times 0.2 \times 0.1$ mm. Lattice constants were obtained from the setting angles of 25 reflections. In the $+h+k+l$ quadrant of the reflection sphere 4509 reflections in the range $5 < \theta < 65°$ were recorded with Cu-K_α radiation (graphite monochromator) by the ω/θ scan technique. After averaging 2322 unique reflections remained ($R_{int} = 0.023$). Lorentz, polarization and

Table 1. Experimental conditions for the electrochemical syntheses

M	Ligand H_2L	Amount of $LH_2(g)$[a]	Initial voltage (V)[b]	Time (h)	Metal dissolved (mg)	E_f (mol F^{-1})
Co	H_2L^a	0.42	26	2.0	44.6	0.51
Co	H_2L^b	0.44	30	1.75	38.5	0.50
Co	H_2L^c	0.45	28	2.0	43.5	0.49
Co	H_2L^d	0.47	28	2.0	44.1	0.50
Co	H_2L^e	0.49	25	2.0	44.0	0.50
Ni	H_2L^a	0.14	15	1.0	19.1	0.44
Ni	H_2L^b	0.33	20	1.0	21.9	0.50
Ni	H_2L^c	0.32	22	2.0	42.1	0.48
Ni	H_2L^d	0.35	30	2.0	42.9	0.51
Ni	H_2L^e	0.23	23	1.5	32.0	0.49
Cu	H_2L^a	0.25	20	0.5	20.0	0.95
Cu	H_2L^b	0.20	18	0.5	22.6	0.95
Cu	H_2L^c	0.20	20	1.0	44.3	0.93
Cu	H_2L^d	0.30	20	0.5	26.1	1.10
Cu	H_2L^e	0.32	15	1.0	47.9	1.01
Zn	H_2L^a	0.20	20	1.0	26.5	0.54
Zn	H_2L^b	0.20	15	1.0	21.9	0.45
Zn	H_2L^c	0.20	18	1.0	23.7	0.49
Zn	H_2L^d	0.20	15	1.0	22.4	0.46
Zn	H_2L^e	0.18	27	1.0	33.8	0.55
Cd	H_2L^a	0.20	20	1.0	42.8	0.51
Cd	H_2L^b	0.25	18	1.0	44.0	0.52
Cd	H_2L^c	0.20	20	1.0	42.6	0.51
Cd	H_2L^d	0.20	10	1.0	45.4	0.54
Cd	H_2L^e	0.35	20	2.0	84.5	0.50

[a] Plus $[NMe_4]ClO_4$ (*ca* 10 mg).
[b] Voltage to produce a current of 20 mA.

Table 2. Analytical data for the complexes

Compound **1**	% Found (Calc.) N	C	H
$Co(HL^a)_2$	13.3(13.1)	61.6(61.6)	4.2(4.2)
$Co(HL^b)_2 \cdot H_2O$	11.0(11.8)	50.8(51.2)	3.5(3.5)
$Co(HL^c)_2$	11.8(12.2)	63.2(63.0)	4.6(4.8)
$Co(HL^d)_2 \cdot H_2O$	11.8(11.8)	60.3(60.6)	4.7(5.1)
$Co(HL^e)_2 \cdot 0.5H_2O$	11.6(11.3)	63.0(63.1)	5.0(5.6)
$Ni(HL^a)_2$	13.9(13.1)	61.6(61.6)	4.6(4.2)
$Ni(HL^b)_2$	11.2(11.9)	52.2(53.0)	3.3(3.2)
$Ni(HL^c)_2 \cdot H_2O$	11.6(11.7)	60.0(60.7)	5.6(5.5)
$Ni(HL^d)_2 \cdot H_2O$	11.7(11.7)	61.4(60.7)	5.6(5.5)
$Ni(HL^e)_2 \cdot 3H_2O$	10.0(10.4)	57.7(58.0)	4.8(5.9)
$Cu(HL^a)_2$	12.4(12.9)	60.6(60.9)	4.6(4.1)
$Cu(HL^b)_2$	11.1(11.1)	52.0(52.5)	5.2(3.2)
$Cu(HL^c)_2$	11.2(12.1)	61.9(62.4)	6.4(4.8)
$Cu(HL^d)_2$	12.4(12.1)	62.5(62.4)	5.0(4.8)
$Cu(HL^e)_2 \cdot H_2O$	10.7(11.0)	62.3(61.5)	6.2(5.5)
$Zn(HL^a)_2$	12.9(12.9)	59.3(60.1)	4.2(4.1)
$Zn(HL^b)_2$	11.3(11.1)	51.7(52.3)	4.5(3.2)
$Zn(HL^c)_2$	11.6(12.1)	61.3(62.2)	4.9(4.7)
$Zn(HL^d)_2$	12.1(12.1)	61.3(62.2)	5.0(4.7)
$Zn(HL^e)_2 \cdot CH_3CN$	12.9(13.1)	62.9(63.1)	4.8(5.4)
$Cd(HL^a)_2$	11.2(11.6)	54.2(54.7)	4.0(3.7)
$Cd(HL^b)_2$	9.7(10.1)	48.3(47.9)	3.6(2.9)
$Cd(HL^c)_2$	10.6(10.9)	55.9(56.4)	4.6(4.3)
$Cd(HL^d)_2 \cdot H_2O$	10.8(10.6)	55.2(54.5)	4.9(4.5)
$Cd(HL^e)_2 \cdot 3H_2O$	9.0(9.5)	52.8(52.8)	5.0(5.4)

empirical absorption corrections[6] were applied (max. and min. transmission factors 100 and 97%, respectively). Three standard reflections showed no significant variation in intensity during the course of data collection. The structure was solved by Patterson and difference-Fourier methods. Refinement was performed using 1627 independent observations with $I > 1.0\ \sigma(I)$ by minimizing the function $\Sigma w(|F_o| - |F_c|)^2$ with $w^{-1} = \sigma^2(F_o)$. Hydrogen atom positions were calculated (C—H = 0.98 Å; $B_{iso} = 1.3 \times B_{eq}$ of the atom bonded to it) and were not refined, but included isotropically in structure-factor calculations. In the final least-squares cycles all non-hydrogen atoms were refined with anisotropic displacement parameters and a correction for secondary extinction was applied. Refinement converged at $R = 0.039$, $R_w = 0.048$ for a total of 174 variables. A final difference-Fourier map showed a local electron density maximum of 0.54 e $Å^{-3}$ close to the metal atom. Calculations were performed on a VAXstation 3100 computer with the SDP system[7] and the program ORTEP.[8] Further details of the crystal structure investigation are available on request from the Fachinformationszentrum Karlsruhe, Gesellschaft für wissen-schaftlich-technischs Information mbH, D-7514 Eggenstein-Leopoldshafen 2, on quoting the depository number CSD-56729. Atomic coordinates have also been deposited at the Cambridge Crystallographic Data Centre.

Physical measurements

Carbon, hydrogen and nitrogen microanalyses were performed using a Carlo–Erba EA 1108 elemental analyser. IR spectra were recorded in KBr mulls on a Perkin–Elmer 180 spectrophotometer. Solid spectra were recorded on a Perkin–Elmer Lambda 9 spectrophotometer. Magnetic moment data were obtained with a SQUID susceptometer. Proton NMR spectra were recorded in $CDCl_3$ or DMSO solutions using a Bruker WM250 MHz spectrometer; chemical shifts were determined with respect to TMS as an internal standard.

RESULTS AND DISCUSSION

The elemental analyses (Table 2) indicate that the above electrochemical method can be satisfactorily used for the synthesis of compounds of the general formula $M(HL)_2$, where HL is the monoanionic form of the Schiff base ligands and M is cobalt(II), nickel(II), copper(II), zinc(II) or cadmium(II).

The electrochemical efficiency, E_F, defined as the amount of metal dissolved per Faraday of charge, was found to be close to 1.0 mol F^{-1} for the copper complexes. This and the release of hydrogen at the cathode are compatible with the formation of copper(I) at the anode in accordance with the process:

$$\text{Cathode:}\quad H_2L + e^- \longrightarrow 1/2H_{2(g)} + HL^-$$

$$\text{Anode:}\quad Cu + HL^- \longrightarrow [Cu(HL)] + e^-$$

followed by oxidation to copper(II) in the solution

$$[Cu(HL)] + H_2L \longrightarrow [Cu(HL)_2] + 1/2H_{2(g)}.$$

For the other complexes the E_F values are close to 0.5 mol F^{-1} and the reaction mechanism may accordingly be written:

$$\text{Cathode:}\quad H_2L + e^- \longrightarrow 1/2H_{2(g)} + HL^-$$

$$\text{Anode:}\quad M + 2HL^- \longrightarrow [M(HL)_2] + 2e^-.$$

Structure of $[Zn(C_{13}H_{13}N_2O)_2 \cdot CH_3CN]$

As illustrated in Fig. 1 the structure consists of monomeric $[Zn(C_{13}H_{13}N_2O)_2 \cdot CH_3CN]$ units situated on a two-fold crystallographic axis with the central zinc atom penta-coordinated to the imino nitrogen and phenolato oxygen atoms of two bidentate HL^- ligands and an acetonitrile nitrogen atom. The solvent molecule is disordered around the two-fold axis and shows large displacement parameters perpendicular to the axis. The pyrrole nitrogen atoms of each Schiff base ligand are not coordinated to the zinc. The environment of the zinc atom must be described as a distorted trigonal bipyramid, with the oxygen atoms of the Schiff bases and the acetonitrile nitrogen atom occupying equatorial sites and the imino nitrogen atoms axial sites. The zinc and the equatorial donors are co-planar to within the limits of experimental error.

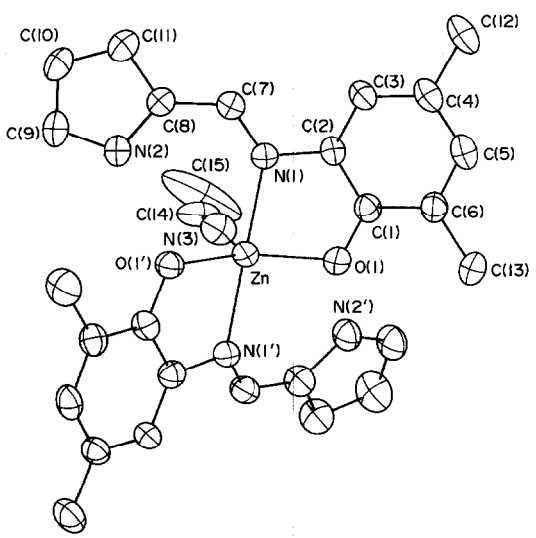

Fig. 1. Molecular structure of acetonitrile-bis{2-[(2-pyrrole)methylimino]-4,6-dimethylphenolato}zinc(II).

Angular distortions are observed both in the equatorial plane (Table 3), with the two O(1)—Zn—N(3) angles close to 112.99(6)° and an O(1)—Zn—O(1) angle of 134.0(1)°, and along the axial direction of the trigonal bipyramid, with an N(1)—Zn—N(1) angle of 176.2(1)°.

The deviation from strictly trigonal bipyramidal geometry also emerges in the difference between the Zn—O and Zn—N bond lengths. The average Zn—O(1) (phenolato) bond length, 1.938(2) Å, is in good agreement with those found in the perchlorate of {1,5,9-triazacyclododecane[2-(2-phenolate)aquo]}zinc(II)[9] [1.930(4) Å], [N,N'-ethylene-bis(salicylideneiminato)aquo zinc(II)][10] (1.94 Å) and other salicylaldiminates complexes of zinc(II), in which the metal is, as here, five-coordinated (1.944–1.965 Å).[11] The average Zn—N(1) (imino) bond length, 2.169(2) Å, is longer than those found in five-coordinated salicylaldiminates of zinc (II) (2.051–2.097 Å),[10,11] but is similar to those reported for several five-coordinated complexes of zinc(II) with non-salicylaldimine Schiff bases [e.g. 2.175(5) Å in {2,6-bis[1-(2-imidazol-4-ylethylimino)ethyl]pyridine}zinc(II) perchlorate[12] and 2.191(7) Å in bis[(2-thiobenzaldimino)-2,6-diacetylpyridine]zinc(II)].[13]

The distance between zinc and the acetonitrile nitrogen atom, 2.114(4) Å, is significantly longer than that reported in the tetrahedrally coordinated $[ZnCl_2 \cdot (CH_3CN)_2]$, 2.046(3) Å,[14] and even a little longer than those found in the six-coordinated zinc (II) complex $[Zn(15\text{-crown-}5) \cdot CH_3CN]$, 2.093(13) and 2.069(12) Å.[14]

The mean N—C and C—C distances in the pyrrole ring [1.355(4) and 1.378(5) Å respectively], the mean C—C distance in the phenyl ring [1.392(4) Å] and the mean C(sp^2)—C(methyl) distance [1.504(4) Å] are essentially identical to those found in other complexes and are unremarkable. The C(7)—N(1) distance [1.288(3) Å] is as expected for azomethine C=N bonds.[15] C(1)—O(1) [1.339(3) Å] is shorter than for a C—O single bond, but not as long as for C=O double bonds.[16] In the acetonitrile molecule

the C(14)—N(3) distance [1.075(6) Å] does not differ from the normal C≡N triple bond length.[17]

The phenyl and pyrrole rings are essentially planar, the maximum deviation of any atom being 0.01 Å. However, the ligand as a whole deviates considerably from planarity (the largest deviation of any atom from the best least-squares plane is 0.4 Å), since the phenyl and pyrrole rings are twisted with respect to each other so that the phenolato oxygen atom of each Schiff base is involved in a strong hydrogen bond with the pyrrole N—H ring group of the other Schiff base (O···N = 2.74 Å).[18]

Vibrational spectra

The IR spectrum of the free Schiff base shows bands attributable to ν(N—H) and ν(O—H) at 3340–3440 cm^{-1} and 3290–3300 cm^{-1}, respectively. One of these bands is absent from the complexes, suggesting that one of the two hydrogen atoms is lost during synthesis. The other is replaced by bands over 2700–2900 cm^{-1}, characteristic of NH groups involved in hydrogen bonds. The hypothesis that it is the phenolic group which is deprotonated and that the ligand is, therefore, coordinated in monoanionic form via the phenolate oxygen is corroborated by the observed shift to higher frequencies of the band attributable to ν(C—O). At the same time coordination via the azomethine nitrogen is indicated by the shift to lower frequencies of bands assignable to azomethine ν(C=N). These conclusions are in accordance with the structure found for $[Zn(C_{13}H_{13}N_2O)_2 \cdot CH_3CN]$ by X-ray diffraction. On this basis we proposed that the ligands are bidentate in the $[M(HL)_2]$ complexes, in which the coordination number of the metal is, therefore, four. In the spectrum of $[Zn(C_{13}H_{13}N_2O)_2 \cdot CH_3CN]$ the coordination of the acetonitrile nitrogen to the zinc is reflected by the two ν(C≡N) bands at 2305 and 2280 cm^{-1} being located at higher frequencies than those observed for free CH_3CN.

Table 3. Selected bond distances and angles for $[Zn(C_{13}H_{13}N_2O)_2 \cdot CH_3CN]$

Bond lengths (Å)			
Zn—O(1)	1.938(2)	Zn—O(1′)	1.938(2)
Zn—N(1)	2.169(2)	Zn—N(1′)	2.170(2)
Zn—N(3)	2.114(4)	O(1)—C(1)	1.336(3)
N(3)—C(14)	1.075(6)	N(1)—C(2)	1.421(3)
N(1)—C(7)	1.287(3)	N(2)—C(8)	1.365(3)
C(1)—C(2)	1.407(3)	N(2)—C(9)	1.349(3)
C(1)—C(6)	1.406(3)	C(2)—C(3)	1.393(3)
C(3)—C(4)	1.383(3)	C(4)—C(5)	1.388(4)
C(4)—C(12)	1.523(3)	C(5)—C(6)	1.380(4)
C(6)—C(13)	1.511(4)	C(7)—C(8)	1.417(3)
C(8)—C(11)	1.398(3)	C(9)—C(10)	1.375(4)
C(10)—C(11)	1.386(4)	C(14)—C(15)	1.55(2)
Bond angles (°)			
O(1)—Zn—O(1′)	134.0(1)	O(1)—Zn—N(3)	112.99(6)
O(1)—Zn—N(1)	81.84(7)	O(1′)—Zn—N(1′)	96.65(7)
O(1)—Zn—N(2)	112.99(6)	O(1)—Zn—N(1′)	96.70(7)
O(1′)—Zn—N(1)	81.82(7)	N(2)—Zn—(N1)	91.91(5)
N(2)—Zn—N(1′)	91.88(5)	N(1)—Zn—(N1′)	176.2(1)
C(2)—N(1)—C(7)	120.4(2)	C(8)—N(2)—C(9)	109.2(2)
O(1)—C(1)—C(2)	120.6(2)	O(1)—C(1)—C(6)	120.6(2)
C(2)—C(1)—C(6)	118.9(2)	N(1)—C(2)—C(1)	115.3(2)
N(1)—C(2)—C(3)	124.7(2)	C(1)—C(2)—C(3)	120.0(2)
C(2)—C(3)—C(4)	121.1(2)	C(3)—C(4)—C(5)	118.4(2)
C(3)—C(4)—C(12)	120.9(3)	C(5)—C(4)—C(12)	120.7(2)
C(4)—C(5)—C(6)	122.2(2)	C(1)—C(6)—C(5)	119.4(3)
C(1)—C(6)—C(13)	119.0(2)	C(5)—C(6)—C(13)	121.6(2)
N(1)—C(7)—C(8)	126.6(3)	N(2)—C(8)—C(7)	126.1(2)
N(2)—C(8)—C(11)	107.2(2)	C(7)—C(8)—C(11)	126.7(3)
N(2)—C(9)—C(10)	108.9(3)	C(9)—C(10)—C(11)	107.3(3)
C(8)—C(11)—C(10)	107.4(3)	N(3)—C(14)—C(15)	156.0(2)

Table 4. ^{1}H NMR data for the complexes

Compound	H^a	H^b	H^c	H^d	H^e	H^f	H^g
H_2L^a	6.6	6.2	6.9	8.5	11.8	8.8	
H_2L^b	6.7	6.2	6.9	8.5	11.8	9.0	
H_2L^c	6.6	6.2	6.7	8.5	11.8	8.6	2.2
H_2L^d	6.6	6.2	6.7	8.5	11.8	8.7	2.2
H_2L^e	6.6	6.2	6.7	8.4	11.8	8.6	2.2; 2.1
$Zn(HL^a)_2$	6.6	6.3	6.9	8.7	13.1	—	—
$Zn(HL^b)_2$	6.8	6.3	7.0	8.8	13.3	—	—
$Zn(HL^c)_2$	6.7	6.3	6.8	8.7	13.0	—	2.2
$Zn(HL^d)_2$	6.7	6.3	6.9	8.7	13.2	—	2.2
$Zn(HL^e)_2$	6.7	6.3	6.9	8.7	14.1	—	2.2; 2.2
$Zn(HL^e)_2CH_3CN$	6.8	6.3	6.9	8.7	14.4	—	2.2; 2.2
$Cd(HL^a)_2$	6.7	6.3	6.8	8.4	13.0	—	—
$Cd(HL^b)_2$	6.7	6.3	6.9	8.4	13.2	—	—
$Cd(HL^c)_2$	6.6	6.2	6.8	8.5	12.9	—	2.2
$Cd(HL^d)_2$	6.6	6.2	6.8	8.5	13.0	—	2.2
$Cd(HL^e)_2$	6.7	6.2	6.8	8.4	13.2	—	2.1; 2.1

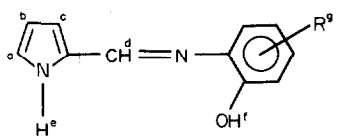

NMR spectra

For the zinc and cadmium complexes the ^{1}H NMR data (Table 4) are in keeping with the above conclusions. The single signal between 13 and 14.5 ppm in the spectra of the complexes is attributable to a hydrogen of the N—H group involved in a hydrogen bond.[4] This signal lies at 11.8 ppm in the free ligand and in pyrrole complexes, in which the N—H group is not involved in hydrogen bonds.[2] The azomethine signal shifts downfield, and the peak attributable to the phenolic hydrogen is absent from the spectra of the complexes.

Electronic studies

The solid state electronic spectra of the cobalt(II) complexes in the near-IR–vis region show two *d–d* transition bands in the 8300–9200 and 12,500–15,000 cm^{-1} ranges, both of the type expected for distorted tetrahedral cobalt(II) compounds.[19] The band in the visible region has been assigned to a $^4A_2 \rightarrow {}^4T_1(P)(\nu_3)$ transition and the multicomponent band in the near IR region to a $^4A_2 \rightarrow {}^4T_1(F)(\nu_2)$ transition. No $^4A_2 \rightarrow {}^4T_2(\nu_1)$ transition was observed and the band at *ca* 20,000 cm^{-1} may be attributed to a charge-transfer transition.

The magnetic moments of the nickel complexes lie in the 3.01–3.60 B.M. range at room temperature. These values are as expected for octahedral and tetrahedral complexes. The diffuse reflectance spectra of these complexes show bands in the 7300–8000 and 14,900–15,600 cm^{-1} regions, which can be assigned to $^3T_1(F) \rightarrow {}^3A_2(\nu_2)$ and $^3T_1(F) \rightarrow {}^3T_1(P)(\nu_3)$ transitions and are consistent with tetrahedral coordination geometry. The weak band observed in some complexes at *ca* 11,000 cm^{-1} is attributed to a spin-forbidden transition.

The magnetic moments of the copper complexes at room temperature lie in the 1.8–1.9 B.M. range, corresponding to one unpaired electron. The solid state electronic spectra show a very broad band at 15,000–18,000 cm^{-1}, compatible with square-planar geometry. The high intensity band observed at 20,500–23,000 cm^{-1} may be attributed to a charge-transfer transition.

REFERENCES

1. J. Castro, J. Romero, J. A. García-Vázquez, M. L. Durán, A. Sousa, E. E. Castellano and J. Zukerman-Schpector, *Polyhedron* 1992, **11**, 235; J. Castro, J. Romero, J. A. García-Vázquez, A. Castiñeiras, M. L. Durán and A. Sousa, *Z. Anorg. Allg. Chem.* 1992, **615**, 155.
2. J. Castro, J. Romero, J. A. García-Vázquez, A. Sousa, E. E. Castellano and J. Zukerman-Schpector, *Polyhedron* 1993, **12**, 31; J. Castro, J. Romero, J.

A. García-Vázquez, M. L. Durán, A. Sousa, E. E. Castellano and J. Zukerman-Schpector, *Z. Anorg. Allg. Chem.* 1992, **612**, 83.
3. J. Castro, J. Romero, J. A. Carcía-Vázquez, M. L. Durán, A. Castiñeiras, A. Sousa and D. E. Fenton, *J. Chem. Soc., Dalton Trans.* 1990, 3255.
4. J. A. Castro, J. Romero, J. A. Garcia-Vazquez, A. Castiñeiras and A. Sousa, *Z. Anorg. Allg. Chem.* 1993, **619**, 601.
5. D. G. Tuck, *Pure Appl. Chem.* 1979, **51**, 2005.
6. N. Walker and D. Stuart, *Acta Cryst.* 1983, **A39**, 159.
7. B. A. Frentz, The Enraf–Nonius CAD-4 SPD, A Realtime System for Concurrent X-Ray Data Collection and Crystal Structure Determination in Computing in Crystallography, pp. 64–71. VAXSPD Version 2.2. Delft University Press, The Netherlands (1985).
8. C. K. Johnson, ORTEP, Report ORNL-3794. Oak Ridge National Laboratory, Tennessee (1965).
9. E. Kimura, T. Koike and K. Toriuni, *Inorg. Chem.* 1988, **27**, 3687.
10. D. Hall and F. H. Moore, *Proc. Chem. Soc.* 1960, 256.
11. P. L. Orioli, M. Di Vaira and L. Sacconni, *Inorg. Chem.* 1968, **5**, 400; E. Labisbal, J. A. García-Vázquez, C. Gómez, A. Macías, J. Romero, A. Sousa, U. Englert and D. E. Fenton, *Inorg. Chim. Acta*, 1993, **203**, 67.
12. J. A. Korp, I. Bernal, C. L. Merril and L. J. Wilson, *J. Chem. Soc., Dalton Trans.* 1981, 1951.
13. V. L. Goedken and G. G. Crystoph, *Inorg. Chem.* 1973, **12**, 2316.
14. V. K. Bel'sky, N. R. Streltsova, B. M. Bulychev, P. A. Storozhenko, L. V. Ivankina and A. I. Gorbunov, *Inorg. Chim. Acta* 1989, **164**, 211.
15. J. N. Brown, R. L. Towns and L. M. Trefonas, *J. Am. Chem. Soc.* 1972, **92**, 7436.
16. G. Berthier and J. Serre, in *The Chemistry of the Carbonyl Group* (Edited by S. Patai), Ch. 1. Interscience, New York (1966).
17. V. Chebolu, R. R. Whittle and A. Sen, *Inorg. Chem.* 1985, **24**, 3082 and refs therein.
18. S. N. Vinogrador and R. A. Linnel, *Hydrogen Bonding*. Von Nostrand Reinhold Company, New York (1971).
19. A. B. P. Lever, *Inorganic Electronic Spectroscopy*, 2nd edn. Elsevier, Amsterdam (1984).

Polyhedron Vol. 12, No. 11, pp. 1399–1402, 1993
Printed in Great Britain

0277–5387/93 $6.00+.00
© 1993 Pergamon Press Ltd

SYNTHESIS AND CHARACTERIZATION OF NOVEL HOMO- AND HETEROLEPTIC NONAISOPROPOXODIZIRCONATOSAMARIUM(III) COMPLEXES

G. GARG, A. SINGH* and R. C. MEHROTRA†

Department of Chemistry, University of Rajasthan, Jaipur 302 004, India

(*Received* 13 *July* 1992; *accepted* 26 *January* 1993)

Abstract—Heterobimetallic isopropoxide derivatives of samarium(III) of the types $[Cl_{3-n}Sm\{Zr_2(OPr^i)_9\}_n]$ ($n = 1$, 2 or 3) have been prepared by the interaction of $SmCl_3 \cdot 3Pr^iOH$ with $K\{Zr_2(OPr^i)_9\}$ in the desired molar (1:1, 1:2 or 1:3) ratios in benzene. Chloride-isopropoxo (or tetraisopropoxoaluminato) exchange reactions have led to the formation of interesting hetero-(bi- or tri-) metal isopropoxides of samarium(III), $L_{3-n}Sm\{Zr_2(OPr^i)_9\}_n$ [$L = OPr^i$, $n = 1$ or 2; $L = Al(OPr^i)_4$, $n = 1$]. All these products have been characterized by elemental analyses and spectroscopic (IR, NMR) studies.

During the last few years there has been an unprecedented spurt of interest in the alkoxide chemistry of yttrium and lanthanum, due to various reasons such as (1) the formation of alkoxide derivatives of unusual compositions and structural patterns,[1–7] (2) the presence of yttrium and lanthanum in high temperature oxide superconductors,[8] (3) heterometal alkoxide derivatives proving to be useful precursors for ceramic materials via the sol–gel process,[9–12] (4) the possibility of utilization of volatile heterometal alkoxides as convenient precursors for oxide films by MOCVD techniques,[13,14] and (5) the high technological applications of samarium based magnets such as Sm_5Co.

Although samarium diiodide has recently proved to be a versatile stoichiometric reagent in various organic transformations,[15,16] the chemistry of metal-organic derivatives of samarium is mainly restricted to organometallics[15,16] except for derivatives like $[Sm\{N(SiMe_3)_2\}_3]$,[17] $[Sm\{Al(OPr^i)_4\}_3]$,[18] and $Li_5Sm(OBu^t)_8$[19] and $Sm[TeC_6Me_3\text{-}2,3,6]_2(THF)_2$.[20]

Further, although organometallic[15,16] derivatives of samarium are now well known in both tri- and bivalent states, the alkoxide and amide chemistry of samarium is so far limited to the trivalent state.[17,21,22]

In view of the above we report herein the synthesis and characterization of homo- and heteroleptic alkoxo-zirconates of samarium(III), with the intuition that derivatives of the types $[ClSm\{Zr_2(OPr^i)_9\}_2]$ and $[Cl_2Sm\{Zr_2(OPr^i)_9\}]$ may prove useful as precursors for the synthesis of heterometallic alkoxide systems, and that these chloro-precursors would make accessible the hetero-bimetallic alkoxides of samarium(II).

EXPERIMENTAL

In view of the highly moisture-sensitive nature of the heterometal isopropoxide systems, stringent precautions were taken to exclude moisture during all of the experimentation.

All solvents were dried by refluxing and distilling over the appropriate agent (in parentheses): benzene, toluene and n-hexane (Na/benzophenone), isopropanol [Na; $Al(OPr^i)_3$] prior to use. Finally, traces of moisture from benzene and isopropanol were removed by azeotropic distillation after adding 1–2 cm^3 of dry isopropanol or benzene, respectively.

Anhydrous samarium trichloride was prepared by heating a mixture of hydrated samarium trichloride and ammonium chloride (in excess) in a current of dry chlorine and hydrogen chloride

* Author to whom correspondence should be addressed.
† Present address: Vice-Chancellor, University of Allahabad, Allahabad 211002, U.P., India.

gases; the heating temperature was carefully regulated to avoid the formation of fusible oxychloride [SmOCl]. The anhydrous chloride was finaly converted into $SmCl_3 \cdot 3Pr^iOH$, by dissolving and crystallizing using isopropyl alcohol as a solvent. Zirconium isopropoxide isopropanolate was prepared by the literature procedure.[23]

Zirconium was estimated as ZrO_2 after precipitation as mandelate and ignition to the oxide. After removal of zirconium as mandelate the samarium content in the filtrate was precipitated as oxalate and estimated as Sm_2O_3.

Isopropoxy contents in the new derivatives were estimated by the oxidimetric method[24] using N—$K_2Cr_2O_7$ solution in 12.5% H_2SO_4. Chlorine was estimated by Volhard's method.[25]

IR spectra [4000–200 cm^{-1}] were recorded on Nujol mulls on Perkin–Elmer 557 and Carl–Zeiss M80 spectrophotometers using CsI optics. ^1H (89.55 MHz) and ^{13}C (22.49 MHz) NMR were recorded on a JEOL FX 90Q FT NMR spectrometer in $CDCl_3$ or C_6H_6, respectively. Chemical shifts were referenced internally to protio solvent impurities (δ 7.25/$CDCl_3$) and solvent ^{13}C references (δ 128.5, C_6H_6) and have been reported in ppm downfield of tetramethylsilane (TMS).

Synthesis of $Cl_2Sm\{Zr_2(OPr^i)_9\}$

A benzene (*ca* 25 cm^3) solution of $K\{Zr_2(OPr^i)_9\}$ [freshly prepared by the interaction of potassium (0.114 g, 2.91 mmol) in isopropyl alcohol (*ca* 5 cm^3) and refluxing with $Zr(OPr^i)_4 \cdot Pr^iOH$ (2.25 g, 5.80 mmol) in (*ca* 20 cm^3) benzene, followed by removal of volatiles under reduced pressure] was added dropwise to a benzene suspension (*ca* 20 cm^3) of $SmCl_3 \cdot 3Pr^iOH$. The reaction mixture was stirred for *ca* 12 h, during which time the colour of the reaction mixture was changed from light yellow to dirty white. Precipitated KCl (0.21 g, 2.82 mmol) was separated by filtration and the excess solvent from the filtrate was removed under reduced pressure to afford a crystalline solid product of the composition $Cl_2Sm\{Zr_2(OPr^i)_9\}$ (2.71 g, 99%), which was recrystallized from n-hexane in 60% yield. Found: Sm, 15.9; Zr, 20.5; Cl, 7.5; OPr^i, 56.7. Calc. for $Cl_2Sm\{Zr_2(OPr^i)_9\}$: Sm, 16.1; Zr, 19.5; Cl, 7.5; OPr^i, 56.9%.

Preparation of $[ClSm\{Zr_2(OPr^i)_9\}_2]$

A benzene (*ca* 20 cm^3) solution of $K\{Zr_2(OPr^i)_9\}$ [freshly prepared by dissolving potassium (0.4 g, 6.13 mmol) in isopropyl alcohol (*ca* 5 cm^3) and benzene (*ca* 10 cm^3) and then interacting under refluxing conditions with $Zr(OPr^i)_4 \cdot Pr^iOH$ (4.85 g, 12.50 mmol), followed by stripping off the volatiles under reduced pressure] was slowly added to a continuously stirred suspension of $SmCl_3 \cdot 3Pr^iOH$ (1.36 g, 3.11 mmol) in benzene (*ca* 20 cm^3). After stirring the reaction mixture at room temperature for 12 h the precipitated KCl (0.53 g, 7.11 mmol) was separated by filtration. Volatiles were removed from the filtrate under reduced pressure to afford a dirty white solid product of the composition $[ClSm\{Zr_2(OPr^i)_9\}_2]$ (4.69 g, 93%). The compound was purified by distillation at (145°C/0.5 mm) in 60% yield. Found: Sm, 9.1; Zr, 22.8; Cl, 2.2; OPr^i, 65.3. Calc. for $[ClSm\{Zr_2(OPr^i)_9\}_2]$: Sm, 9.3; Zr, 22.6; Cl, 2.2; OPr^i, 65.9%.

Preparation of $[Sm\{Zr_2(OPr^i)_9\}_3]$

A solution of $K\{Zr_2(OPr^i)_9\}$ [freshly prepared by dissolving potassium (0.31 g, 7.92 mmol) in the presence of dry isopropyl alcohol (*ca* 5 cm^3) and benzene (*ca* 20 cm^3) followed by refluxing and removal of volatiles under reduced pressure] in benzene (*ca* 20 cm^3) was added slowly to a suspension of $SmCl_3 \cdot 3Pr^iOH$ (1.15 g, 2.63 mmol) in benzene (*ca* 15 cm^3). The reaction mixture was refluxed for 3 h. The precipitated KCl (0.59 g, 7.92 mmol) was filtered off. After the removal of volatiles from the filtrate under reduced pressure an off-white sticky solid product of the composition $[Sm\{Zr_2(OPr^i)_9\}_3]$ (5.72, 95%) was obtained. The compound was purified by sublimation at 182°/0.5 mm in 80% yield. Found: Sm, 6.4; Zr, 24.2; OPr^i, 69.3. Calc. for $[Sm\{Zr_2(OPr^i)_9\}_3]$: Sm, 6.5; Zr, 23.8; OPr^i, 69.5%.

Reaction of $[ClSm\{Zr_2(OPr^i)_9\}_2]$ *with* $K(OPr^i)$

A benzene (*ca* 20 cm^3) suspension of $KOPr^i$ [prepared by the interaction of potassium with isopropyl alcohol (*ca* 20 cm^3), followed by the removal of volatiles] was added dropwise to a solution of $[ClSm\{Zr_2(OPr^i)_9\}_2]$ (3.05 g, 1.88 mol) in benzene (*ca* 15 cm^3). The reaction mixture was stirred at room temperature for *ca* 8 h. The precipitated KCl (0.18 g, 2.14 mmol) was removed by filtration. After removal of the volatiles from the filtrate under reduced pressure a dirty white sticky solid of the composition $[(OPr^i)Sm\{Zr_2(OPr^i)_9\}_2]$ (3.03 g, 97%) was obtained, which was distilled at 174°C/0.5 mm in 50% yield. Found: Sm, 9.4; Zr, 22.5; OPr^i, 68.5. Calc. for $[(OPr^i)Sm\{Zr_2(OPr^i)_9\}_2]$: Sm, 9.2; Zr, 22.3; OPr^i, 68.5%.

A similar procedure was adopted to prepare the off-white solid product of the composition $[(OPr^i)_2Sm\{Zr_2(OPr^i)_9\}]$ (1.29 g, 99%) by the interaction of $KOPr^i$ and $Cl_2Sm\{Zr_2(OPr^i)_9\}$ in a 2:1 molar ratio. The compound was recrystallized from

an n-hexane and toluene mixture. Found: Sm, 15.2; Zr, 19.6; OPr^i, 66.0. Calc. for $[(OPr^i)_2Sm\{Zr_2(OPr^i)_9\}]$: Sm, 15.2; Zr, 18.5; OPr^i, 66.1%.

Reaction of $[Cl_2Sm\{Zr_2(OPr^i)_9]$ *with* $K\{Al(OPr^i)_4\}$ *in a* 1:2 *molar ratio*

A benzene (*ca* 20 cm^3) suspension of $K\{Al(OPr^i)_4\}$ [freshly prepared from potassium (0.24 g, 6.13 mmol) and $Al(OPr^i)_3$ (1.25 g, 6.11 mmol) in isopropyl alcohol (*ca* 15 cm^3) and benzene (*ca* 15 cm^3) followed by the removal of the volatiles] was slowly added to a benzene solution (*ca* 20 cm^3) of $[Cl_2Sm\{Zr_2(OPr^i)_9\}]$ (2.87 g, 3.06 mmol). The reaction mixture was stirred at room temperature for 12 h and the precipitated KCl (0.50 g, 6.71 mmol) was separated by filtration. Removal of volatiles from the filtrate under reduced pressure afforded a pale white sticky mass of the composition $\{Al(OPr^i)_4\}_2Sm\{Zr_2(OPr^i)_9\}$ (3.54 g, 83%), which was distilled at 235°C/0.05 mm in 50% yield. Found: Sm, 10.2; Zr, 14.4; OPr^i, 72.0. Calc. for $\{Al(OPr^i)_4\}_2Sm\{Zr_2(OPr^i)_9\}$: Sm, 10.8; Zr, 13.1; OPr^i, 72.2%.

RESULTS AND DISCUSSION

Interaction of $SmCl_3 \cdot 3Pr^iOH$ and $K\{Zr_2(OPr^i)_9\}$ in different molar ratios (1:1, 1:2 and 1:3) in benzene results in the formation of hetero- and homoleptic nonaisopropoxodizirconatosamarium(III) complexes, according to the following reactions:

$$SmCl_3 \cdot 3Pr^iOH + nK\{Zr_2(OPr^i)_9\} \longrightarrow [Cl_{3-n}Sm\{Zr_2(OPr^i)_9\}_n] + nKCl\downarrow + 3Pr^iOH$$

Ia: $n = 1$; **Ib**: $n = 2$; **Ic**: $n = 3$.

Replacement of chloride in the derivatives **Ia** and **Ib** with alkoxo and/or alkoxometallato groups produced derivatives according to the reaction shown below:

$$[Cl_{3-n}Sm\{Zr_2(OPr^i)_9\}_n] + (3-n)KL \xrightarrow{(3-n)KCl} [(L)_{3-n}Sm\{Zr_2(OPr^i)_9\}_n]$$

IIa: $L = OPr^i, n = 1$;
IIb: $L = OPr^i, n = 2$;
IIc: $L = Al(OPr^i)_4, n = 2$.

All of these new hetero-(bi- or tri-)metallic isopropoxo derivatives are off-white coloured solids (in some cases sticky in nature), highly moisture-sensitive, soluble in common organic solvents and generally volatile.

IR spectral studies

The IR spectra of hetero-(bi- or tri-)metallic isopropoxides[26–29] of samarium(III) exhibit characteristic absorptions in the region (cm^{-1}): 1160–1190 (Me_2C skeleton vibrations), 950–1070, ν(C—O terminal), 920–950, ν(C—O bridging); 670–699, ν(Al—O); 540–570, ν(Zr—O); and 400–470, ν(Sm—O). Samarium–chlorine stretching absorptions[30,31] have been observed in **Ia** and **Ib** in the range 210–380 cm^{-1}.

NMR (^1H *and* ^{13}C) *spectral studies*

The ^1H NMR spectra of the new derivatives (in $CDCl_3$ at room temperature) exhibit doublets ($J = 6$ Hz) for gem-dimethyl protons at δ 1.24 (**IB**), 1.36 (**IIa**), 1.21 (**IIb**) and 1.26 (**IIc**), while methine protons of these complexes are observed as averaged septets ($J = 6$ Hz) at δ 4.39, 4.48, 4.04 and 4.31 ppm, respectively. However, the derivative **Ic** exhibits two doublets ($J = 6$ Hz) of gem-dimethyl protons at δ 1.24 and 1.35, but the methine protons appear as a broad peak centred at δ 4.28 ppm. Similarly, ^{13}C NMR spectra of the two typical derivatives **Ib** and **IIc** display only two types of resonances (**Ib**, 69.67, 26.49; **IIc**, 66.30, 26.50 ppm), characteristic of α- and β-carbons of the isopropoxy groups, respectively. The ^1H NMR signals of the above derivatives could not be resolved further, even at −65°C, to throw any light on their structural features.

Interestingly, the spectrum of **Ia** exhibits the following chemical shifts for gem-dimethyl protons, which could be grouped in the intensity ratio 5:2:2, respectively: (a) two overlapping doublets ($J = 6$ Hz) at δ 1.55 and 1.63 (terminal OPr^i); (b) a doublet ($J = 6$ Hz) at δ 2.35 (μ_2-OPr^i); and (c) a doublet ($J = 6$ Hz) at δ 9.22 (μ_3-OPr^i) ppm. A broad peak centred at δ 4.89 ppm may be ascribed to the methine protons of the terminal and μ_2-OPr^i groups, whereas the methine proton resonances of μ_3-OPr^i could not be distinguished in the range −50 to +55 ppm. Although any conjectures may be rather speculative in the absence of a single-crystal X-ray structure so far, these data appear to conform essentially to three types of isopropoxy groups, as observed in the ^1H NMR spectrum of $[\{Cd\{Zr_2(OPr^i)_9\}(\mu\text{-}Cl)\}_2]$,[32] the X-ray structure[33] of which showed a tetradentate ligation mode of $\{Zr_2(OPr^i)_9\}^-$ units.

The above results, coupled with (1) the tendency of samarium(III) (ionic radii = 1.10 Å) to achieve higher coordination states,[34,35] (2) the ability of $\{Zr_2(OPr^i)_9\}^-$ to function in a bi-,[36] tri-[36] or tetradentate[32,37] fashion, and (3) the observed

molecular complexities in benzene tend to favour tetradentate ligation of $\{Zr_2(OPr^i)_9\}^-$ in **Ia** and **IIa**, tridentate bonding in **Ib** and **IIb** and bidentate ligation in **Ic** and **IIc**. Furthermore, in derivatives **Ib**, **IIb**, **Ic** and **IIc** the possibility of ligation of a more suitably situated isopropoxy group(s) to increase the coordination state of the samarium(III) ion cannot be ruled out.

Acknowledgement—The authors are thankful to the Department of Science and Technology, New Delhi, India, for financial support.

REFERENCES

1. R. A. Anderson, D. H. Templeton and A. Zalkin, *Inorg. Chem.* 1978, **17**, 1962.
2. W. J. Evans and M. S. Sollberger, *Inorg. Chem.* 1988, **27**, 4417.
3. W. J. Evans, M. S. Sollberger and T. P. Hanusa, *J. Am. Chem. Soc.* 1988, **110**, 1841.
4. O. Poncelet, W. J. Sartain, L. G. Hubert-Pfalzgraf and K. Folting, *Inorg. Chem.* 1989, **28**, 263.
5. W. J. Evans, J. M. Olofson and J. W. Ziller, *J. Am. Chem. Soc.* 1990, **112**, 2308.
6. W. J. Evans, R. E. Golden and J. W. Ziller, *Inorg. Chem.* 1991, **30**, 4963.
7. D. C. Bradley, H. Chudzynska, M. B. Hursthouse and M. Motevalli, *Polyhedron* 1991, **10**, 1049.
8. A. Muller and J. G. Bednorz, *Science* 1987, **217**, 1133.
9. R. C. Mehrotra, *Chemtracts* 1990, **2**, 389 and refs therein.
10. L. G. Hubert-Pfalzgraf, *New J. Chem.* 1987, **1**, 663.
11. C. Sanchez and J. Livage, *New J. Chem.* 1990, **14**, 513.
12. R. C. Mehrotra, *J. Non-Cryst. Solids* 1990, **121**, 1.
13. D. C. Bradley, *Chem. Rev.* 1989, **89**, 1317.
14. D. C. Bradley, *Phil. Trans. Roy. Soc. A* 1990, **330**, 167.
15. H. B. Kagan, *New J. Chem.* 1990, **14**, 453 and refs therein.
16. W. J. Evans, *Adv. Organomet. Chem.* 1985, **24**, 131.
17. D. C. Bradley, J. S. Ghotra and F. A. Hart, *J. Chem. Soc., Dalton Trans.* 1973, 1021.
18. R. C. Mehrotra, M. M. Agrawal and A. Mehrotra, *Synth. React. Inorg. Met.-Org. Chem.* 1973, **3**, 181.
19. H. Schumann, G. Kociok-koehn, A. Dietrich and F. H. Goerlitz, *Z. Naturforsh. B: Chem. Sci.* 1991, **46**, 896.
20. A. R. Strzelecki, P. A. Timinski, B. A. Helsel and P. A. Bianconi, *J. Am. Chem. Soc.* 1992, **114**, 3159.
21. M. H. Chisholm and I. P. Rothwell, in *Comprehensive Coordination Chemistry* (Edited by G. Wilkinson, R. D. Gillard and J. M. Cleverty), Vol. 2, p. 335. Pergamon Press, Oxford (1988).
22. D. C. Bradley, R. C. Mehrotra and D. P. Gaur, *Metal Alkoxides*. Academic Press, London (1978).
23. D. C. Bradley, R. C. Mehrotra and W. Wardlaw, *J. Chem. Soc.* 1952, 2027.
24. R. C. Mehrotra, *J. Ind. Chem. Soc.* 1953, **30**, 585.
25. A. I. Vogel, *A Text Book of Quantitative Inorganic Analysis*. Longman Group Limited, London (1978).
26. C. N. R. Rao, *Chemical Applications of Infrared Spectroscopy*. Academic Press, New York (1963).
27. C. G. Barraclough, D. C. Bradley, J. Lewis and I. M. Thomas, *J. Chem. Soc.* 1961, 2601.
28. L. J. Bellamy, *The Infrared Spectra of Complex Molecules*. Methuen, London (1958).
29. L. J. Bellamy, *Advances in Infrared Group Frequencies*. Methuen, London (1968).
30. J. Murphy, H. H. Caspers and R. A. Buchanan, *J. Chem. Phys.* 1964, **40**, 743.
31. M. D. Taylor, T. T. Cheung and M. A. Hussein, *J. Inorg. Nucl. Chem.* 1972, **34**, 3073.
32. S. Sogani, A. Singh and R. C. Mehrotra, *Main Group Met. Chem.* 1990, **13**, 375.
33. S. Sogani, A. Singh, R. Bohra, R. C. Mehrotra and M. Nottemeyer, *J. Chem. Soc., Chem. Commun.* 1991, 738.
34. F. A. Cotton and G. Wilkinson, *Advanced Inorganic Chemistry*, 5th edn. John Wiley, New York (1988).
35. G. J. Palenik, in *Systematics and the Properties of the Lanthanides* (Edited by S. P. Sainha), p. 153. D. Reidel Publishing Company, Dordrecht/Boston (1983).
36. A. Shah, A. Singh and R. C. Mehrotra, *Inorg. Chim. Acta* 1988, **141**, 289.
37. B. A. Vaartstra, J. C. Huffman, W. E. Streib and K. G. Caulton, *J. Chem. Soc., Chem. Commun.* 1990, 1750; *Inorg. Chem.* 1991, **30**, 3068.

Polyhedron Vol. 12, No. 11, pp. 1403–1407, 1993
Printed in Great Britain

0277–5387/93 $6.00+.00
© 1993 Pergamon Press Ltd

IONIZATION OF THE Fe—X BOND IN POLAR SOLVENTS: A SPECTROSCOPIC STUDY OF CpFe(dppe)X COMPLEXES

C. DÍAZ,† N. YUTRONIC and B. WEISS

Departamento de Química, Facultad de Ciencias, Universidad de Chile, Las Palmeras 3425, Santiago, Chile

(*Received* 23 *November* 1992; *accepted* 26 *January* 1993)

Abstract—Electronic absorption spectra for complexes CpFe(dppe)X [with X = Cl, I and CN; dppe = $(Ph)_2PCH_2CH_2P(Ph)_2$; Cp = η^5-C_5H_5] and the cationic derivative $[CpFe(dppe)NCCH_3]PF_6$ in different solvents have been measured. The lower energy bands were assigned to iron *d–d* orbital transitions on the basis of intensities, solvent effects and extended Hückel MO calculations. The complexes CpFe(dppe)X (with X = Cl and I) undergo ionization in polar solvents to give the cationic solvated species [CpFe(dppe)(solvent)]$^+$. This behaviour can be explained on the basis of the theoretical calculations.

Compounds containing CpMLL′ moieties (with M = Fe, Ru; L, L′ = CO, phosphines and phosphites) are among the most versatile systems in organo-transition metal chemistry.[1–5] Although the carbonyl derivatives have been extensively studied, the phosphine and phosphite counterparts have not been so well investigated.[4,5]

Interest in compounds containing the fragment CpMLL′ (with L, L′ = phosphine and diphosphine) arises mainly because they show interesting catalytic properties in some C—C bond deformation[6] and C—H bond activation reactions.[7] The CpM(diphosphine) moiety activates coordinated π-bonds towards nucleophilic attack[8] and stabilizes alkylidene[9] and vinylidene groups.[10] Therefore, these structures are of considerable interest in organic synthesis.

A theoretical study on Cp-iron diphosphine derivatives has been recently made,[11] but only a few spectroscopic studies have been reported.[7] In this paper we present a UV–vis absorption study of the complexes CpFe(dppe)X (with X = Cl, I and CN) and $[CpFe(dppe)NCCH_3]PF_6$. Recently it has been shown that these cyclopentadienylphosphinoethane iron(II) halide compounds are also useful precursors of both mononuclear[12] and binuclear complexes[13] containing the above-mentioned moiety. To support the experimental results an extended Hückel calculation was performed on CpFe(dppe)Cl and some properties discussed.

RESULTS AND DISCUSSION

Figure 1 shows the absorption spectrum of CpFe(dppe)I and CpFe(dppe)CN in $CHCl_3$. The

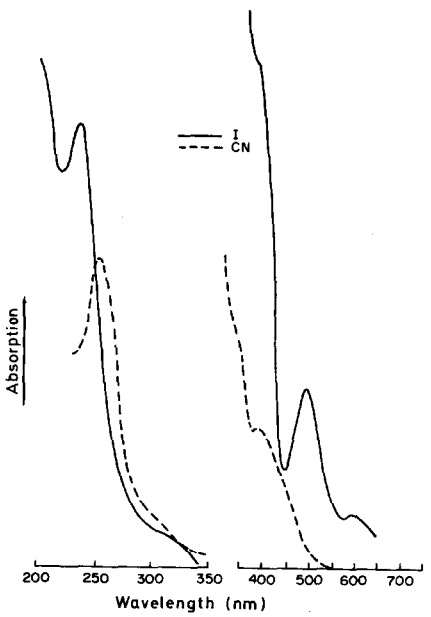

Fig. 1. UV–vis absorption spectra of the complexes CpFedppeX [X = I(– – – –), CN(· · · ·)] in $CHCl_3$ solution at room temperature.

† Author to whom correspondence should be addressed.

iodide complex (solid line) shows absorptions at 600, 490 and 390 nm with low intensities. The spectrum of the chloride is very similar to that of the iodide, as can be seen from Table 1, but is not shown in Fig. 1. The band at 600 nm is responsible for the red colour of the halide complexes. This band, as well as the more intense one located at 490 nm and the shoulder at *ca* 390 nm, is only slightly influenced by the polarity of the solvent, as shown in Table 2. This behaviour is typical of *d–d* bands and has been reported before in other complexes.[14] The low intensities of these bands also support the *d–d* character of these transitions. These assignments are in agreement with those reported for the Cp^*ML_2X complexes.[7] Additional information on the nature of these transitions has been obtained from an extended Hückel MO calculation, performed on CpFe(dppe)Cl. The geometry of the heavy atom skeleton was obtained from an X-ray diffraction study on the iodide derivative[15] and the hydrogen atoms were located at standard positions. Some results of this calculation are shown in Table 3. The HOMO and the next three internal orbitals are mainly localized on the metal and their composition is largely accountable to the contribution of the iron *d*-orbitals. The next inner orbitals contain important contributions from the π-orbitals of the cyclopentadienyl ligand. These results are in agreement with previously reported MO calculations in similar systems.[16] The LUMO is also predominantly iron *d*-orbitals, with a small contribution from Cp π-orbitals. The character of the next unfilled orbitals, as well as the LUMO, contains some iron *d*-orbital contribution, but the participation of phosphorus and Cp π-orbitals is also important. The higher energy orbitals are mainly localized around the chlorine and phosphorus atoms. It is interesting to note that because of the low contribution of phosphorus and chlorine orbitals to the nature of the MO near the frontier orbital zone, they have similar character to those obtained for the related complexes $CpM(CO_2)X$[16] and $CpM(PH_3)_2X$.[11] Participation from the phenyl groups to the calculated molecular orbitals is observed at higher and lower energies than the orbitals discussed before. The X substituents with π-donor–acceptor capabilities have a strong influence on the character of the frontier orbitals. For instance, the π- and π^*-orbitals of acetylide and vinylidene ligands are known to make a significant contribution to the character of the frontier orbitals.[11]

The calculated atomic charges on the chloride complex are shown in Fig. 2. The high negative charge on the chlorine atom is strong evidence in support of the ionic character of the iron–chlorine bond. On the other hand, the Cp ligand shows a total charge of -0.45, possibly due to a charge-transfer of $(Fe)d \rightarrow Cp\pi^*$, and is consistent with the anionic formulation commonly used for this group in transition metal chemistry.[17]

As expected the coordination of dppe to iron induces a positive charge on the phosphorus atoms, also in agreement with the calculation. Atomic overlap population values indicate that the order of degree covalency is Fe—Cp $\approx$ Fe—P $\gg$ Fe—Cl and this trend correlates with the corresponding bond distances.[15,18]

According to this MO scheme the first three predicted electronic transitions involve *d*-orbitals from the iron atom, in agreement with the characteristics of the observed spectra. Besides, the band centred at 250 nm, present in the CpFe(dppe)X complexes, can be assigned mainly to an internal charge-transfer in the Cp ligand, in agreement with previously reported assignments in similar compounds.[19] Consistent with this interpretation, the MOs with significant contribution from the Cp π-orbitals appear above and below the frontier orbitals. The shoulder at *ca* 295 nm could be ascribed to transitions that belong to the phenyl groups in dppe.

The spectrum of the halide complexes could not be measured in polar solvents because the formation of the cationic species $[CpFe(dppe)(solvent)]^+$ occurs. This is due to the high ionic character of the Fe—X bond, in agreement with the calculation. The formation of these cationic complexes (in propane-1,2-diolcarbonate as the solvent)

Table 1. Energy maxima absorption[a] (nm) and extinction coefficients (in parenthesis) (M^{-1} cm^{-1}) for $(\eta^5\text{-}C_5H_5)Fe(dppe)X$ and $[(\eta^5\text{-}C_5H_5)Fe(dppe)NCCH_3]PF_6$ complexes in $CHCl_3$

$(\eta^5\text{-}C_5H_5)Fe(dppe)Cl$	265(11,000)	300(4700)[b]	394(720)[b]	505(460)	600(360)
$(\eta^5\text{-}C_5H_5)Fe(dppe)I$	255(3700)	295(1200)[b]	388(1900)[b]	493(450)	593(80)
$(\eta^5\text{-}C_5H_5)Fe(dppe)CN$	255(6100)	290(1900)[b]	400(400)		
$[(\eta^5\text{-}C_5H_5)Fe(dppe)NCCH_3]PF_6$	270(21,000)[b]	379(950)[b]	453(720)		

[a] At room temperature.
[b] Shoulder.

Table 2. Solvent dependence of electronic absorption bands of $(C_5H_5)Fe(dppe)X$ and their cationic $[(C_5H_5)Fe(dppe)(NCCH_3)]PF_6$ complexes

Solvent	ε^a	$(C_5H_5)Fe(dppe)Cl$			$(C_5H_5)Fe(dppe)I$			$(C_5H_5)Fe(dppe)CN^b$	$[(C_5H_5)Fe(dppe)NCCH$
Chloroform	4.8	394	505	600	388	493	593	397	458
Dichloromethane	8.9	385	500	605	390	505	600	395	450
Acetone	20.7	380	500	590	390	505	605	400	457
Nitromethane	35.9	395	495	605	—	450	—	395	
Acetonitrile	37.5	390	496	595	—	450	—	397	450
Ethylene sulphite	41	—	443	—	—	[c]	—		
Sulpholane	42	—	445	—	—	450[d]	—		
Propane-1,2-diolcarbonate	69	378	497	600[d]	400	497	600[d]	400	456

[a] Dielectric constant value from ref. 21.
[b] Solvent effect performed only on the *d–d* band.
[c] Decomposed with this solvent.
[d] Slow ionization, see text.

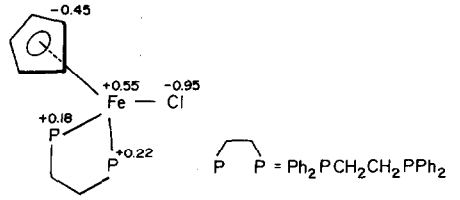

Fig. 2. Extended Hückel atomic charges of the CpFedppeCl complex.

is slow (minutes) for the iodide derivative and very slow (hours) for the chloride derivative. After this time absorptions at 465 and 450 nm, characteristic of the cationic complexes, are observed. The iodide complex undergoes ionization in solvents with $\varepsilon > 35$, whereas the chloride complex requires higher dielectric constants, $\varepsilon > 38$. This observation is consistent with an easy halide abstraction from CpFe(dppe)X complexes by $TlPF_6$ and NH_4PF_6 salts in the synthesis of cationic mononuclear[12] and binuclear complexes.[13]

The spectrum of the CpFe(dppe)CN complex (see Fig. 1) shows an absorption band at *ca* 400 nm, which is not sensitive to the nature of the solvent (see Tables 1 and 2). Similar to the halide derivatives, these absorptions can be assigned principally to *d–d* iron orbital transitions. The low energy band of the halide derivatives suffers a shift to higher energy in the cyanide complex. This observation can be rationalized in terms of the extra stabilization of the HOMO due to the participation of π^*-unfilled orbitals from the CN group. The stabilization of the HOMO by ligand π-acceptors has been reported in related systems.[20] This observation can also be explained in terms of the ligand field strength of the CN moiety.[21] The high frequency region of the spectrum shows similar characteristics to those observed for the halide complexes.

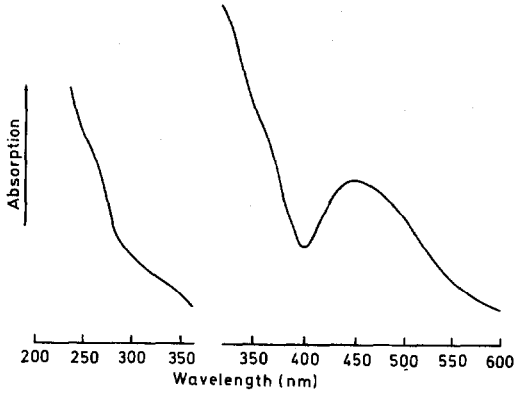

Fig. 3. UV–vis absorption spectrum of $[CpFe(dppe)NCCH_3]PF_6$ in $CHCl_3$ solution at room temperature.

Table 3. Energies and per cent compositions of important MOs in (η^5-C_5H_5)Fe(dppe)Cl

Orbital	E (eV)	Fe 3*d*	Fe 3*s*	Cl 3*p*	P 3*d*	P 3*s*	P 3*p*	π-C_5H_5	π-C_6H_6
97	−9.11				49	17			34
98	−9.26	5			47		5		
99	−10.46	50				6	16	22	
100	−10.90(LUMO)	89	4					6	
101	−11.43(HOMO)	94	5						
102	−11.51	96		3					
103	−11.60	94		3					
104	−11.83	61					3	34	
105	−11.98	14						86	
106	−12.42						10	27	63

The spectrum of the cationic methylcyanide complex exhibits a broad and asymmetric band around 450 nm, as shown in Fig. 3. This may suggest the existence of more than one absorption near 450 nm. Similar to the complexes mentioned before, intensities and solvent effects were used as criteria for the assignment, showing that this transition has strong *d–d* iron orbital character. Finally, the shift to high energy of the maxima of the absorptions on going from neutral to cationic species can be explained by the increase of the HOMO–LUMO gap, as found in calculations of $CpFe(PH_3)_2X$ and $[CpFe(PH_3)_2NCH]^+$.[11]

EXPERIMENTAL

The complexes CpFe(dppe)X, with X = Cl, I, CN, and $[CpFe(dppe)NCCH_3]PF_6$ were prepared using previously reported synthetic routes.[12,13] UV–vis absorption spectra were recorded using Cary-17 and Varian DMS-90 spectrophotometers, with 1 cm optical path cuvettes. The concentration of the complex was 10^{-3}–10^{-4} M. The solvents were all previously purified by standard methods.

The extended Hückel calculation[22] was performed using the program FORTICON8 (QCPE catalogue 344). The parametrizations employed were those reported in previous work.[23]

Acknowledgements—This work was funded by DTI, University of Chile (Q3280/9214 and Q3075/9222) and Fondecyt (084791).

REFERENCES

1. F. G. A. Stone, G. Wilkinson and E. W. Abel (Editors), *Comprehensive Organometallic Chemistry*, Vol. 4. Pergamon Press, Oxford (1982).
2. A. R. Cutler, P. K. Hanna and A. C. Vites, *Chem. Rev.* 1988, **88**, 1363.
3. H. Schumann, A. M. Arif, A. L. Rheingold, Ch. Janiak, R. Hoffmann and N. Kuhn, *Inorg. Chem.* 1991, **30**, 1618.
4. H. Schumann, L. Eguran and J. W. Ziller, *J. Organomet. Chem.* 1991, **408**, 361.
5. H. Schumann and J. W. Ziller, *J. Organomet. Chem.* 1991, **410**, 365.
6. H. Felkin and B. Meunier, *J. Organomet. Chem.* 1978, **146**, 169.
7. R. G. Gray, J. E. Bercaw, H. B. Gray, M. D. Hopkins and R. A. Paciello, *Organometallics* 1987, **6**, 922.
8. M. I. Bruce and F. Wong, *J. Organomet. Chem.* 1981, **C5**, 210.
9. M. P. Gamasa, J. Gimeno, E. Lastra, M. Lanfranchi and A. Tiripicchio, *Organomet. Chem.* 1991, **405**, 333.
10. M. P. Gamasa, J. Gimeno, E. Lastra, B. M. Martín, A. Anillo and A. Tiripicchio, *Organometallics* 1992, **11**, 1373.
11. N. M. Kostic and R. F. Fenske, *Organometallics* 1982, **1**, 947.
12. C. Díaz and R. Latorre, *Bol. Soc. Chil. Quim.* 1992, **37**, 211.
13. G. Barrado, G. A. Carriedo, C. Díaz and V. Riera, *Inorg. Chem.* 1991, **30**, 4416.
14. C. Díaz and N. Yutronic, *Polyhedron* 1987, **6**, 503.
15. D. H. Hill, M. Parvez and A. Sen, *Acta Cryst.* 1990, **C46**, 133.
16. D. L. Lichtenberger and R. F. Fenske, *J. Am. Chem. Soc.* 1976, **98**, 50.
17. Ch. Elschenbroich and A. Salzer, *Organometallics*. Springer-Verlag, Berlin (1989).
18. A. G. Orpen, L. Brammer, F. H. Allen, O. Kennard, D. G. Watson and R. Taylor, *J. Chem. Soc., Dalton Trans.* 1989, S1.
19. R. Jimenez, M. C. Barral, V. Moreno and A. Santos, *J. Organomet. Chem.* 1979, **174**, 281.
20. D. L. Lichtenberger and A. R. Chaudhuri, *J. Am. Chem. Soc.* 1991, **113**, 2923.

21. C. J. Ballhausen, *Ligand Field Theory*. McGraw Hill, New York (1962).
22. R. Hoffmann, *J. Chem. Phys.* 1963, **39**, 1397; R. Hoffmann and W. N. Lipscomb, *J. Chem. Phys.* 1962, **36**, 3179; 1962, **36**, 3489; 1962, **37**, 2872.
23. T. A. Albright, R. Hoffmann, J. C. Thibeault and D. L. Thorn, *J. Am. Chem. Soc.* 1979, **101**, 3801.
24. I. R. Griffiths and D. C. Pugh, *Coord. Chem. Rev.* 1979, **29**, 129.

Polyhedron Vol. 12, No. 11, pp. 1409–1410, 1993
Printed in Great Britain

0277–5387/93 $6.00+.00
© 1993 Pergamon Press Ltd

COMMUNICATION

CHROMIUM(V) SPECIES CAN BE GENERATED DURING THE REACTION OF SOLID WELDING FUME WITH SOLUTIONS OF GLUTATHIONE

PAUL O'BRIEN* and GUOFANG WANG

Department of Chemistry, Queen Mary and Westfield College, University of London, Mile End Road, London E1 4NS, U.K.

(*Received* 5 *January* 1993; *accepted* 5 *March* 1993)

Abstract—Welding fume, when suspended in neutral solutions of glutathione (40 mM), leads to the generation of chromium(V) species, as detected by ESR spectroscopy ($g = 1.986$ and 1.996). Such complexes have been implicated in the formation of DNA lesions in *in vitro* assays.

Chromium, in oxidation state six, in many different compounds is a well-established carcinogen,[1–5] although the exact effect appears to depend to some extent on the nature of the chromium(VI) containing material.[6] One major potential source of occupational exposure to high oxidation state chromium species is from "welding fume" (the complex particulate material generated during welding, especially of high chrome steels such as stainless steel).[1] The reduction of chromate is essential for the formation of DNA lesions *in vitro* and the peptide glutathione (γ-glutamyl cysteinyl glycine, GSH) is a likely intracellular reductant.[3–5] Consequently, we were interested to see if a sample of welding fume, in combination with GSH, could generate the kind of reactive intermediates known to be of significance in the generation of DNA lesions, such as strand breaks.[7–16] In the present communication we report on the interaction of solid welding fume with neutral solutions of GSH and show that similar chromium(V) species are formed to those well established during the reduction of chromate by GSH.[14–17]

Samples of welding fume were obtained from fume extractor dust from a system carrying two types of electrodes: (a) 20% chromium, 32% nickel and 1.3% niobium and (b) 25% chromium and 9% nickel. The brown material was fairly insoluble in water and the supernatant gave little or no ESR signal [Fig. 1(a)]. However, when a sample was shaken with a 40 mM solution of GSH (5 mg welding fume, 1 cm^3 solution, pH 7) strong ESR signals were generated at $g = 1.986$ and 1.996 [Fig. 1(b)], typical of the chromium(V) species known to be generated in the reaction of chromate with glutathione.[13–16] Furthermore, in the presence of the spin trap 5,5-dimethyl-1-pyrroline-N-oxide (DMPO), the species characteristic[4,9,12] of $RS^{\bullet}$ is generated [Fig. 1(c)]. The behaviour of the system is further confirmed to be similar to that of chromate, in that when the above experiment is performed in the presence of H_2O_2 (10 mM) and EtOH (10% solution) the ethanolate radical is trapped, typical of the generation of $OH^{\bullet}$.

Chromium(V) species and the combination of chromate and GSH are known to be able to cause the generation of single strand breaks in DNA *in vitro* assays.[7,8,10,13] Furthermore, intermediates of the kind detected in the present paper are believed to be important in mediating such lesions. One possible mechanism by which welding fume could cause lung/nasal toxicity could involve particles of welding fume being taken up by pinocytosis. The subsequently slow-release hypervalent chromium species could, after activation by reductive processes, lead to DNA lesions.

* Author to whom correspondence should be addressed.

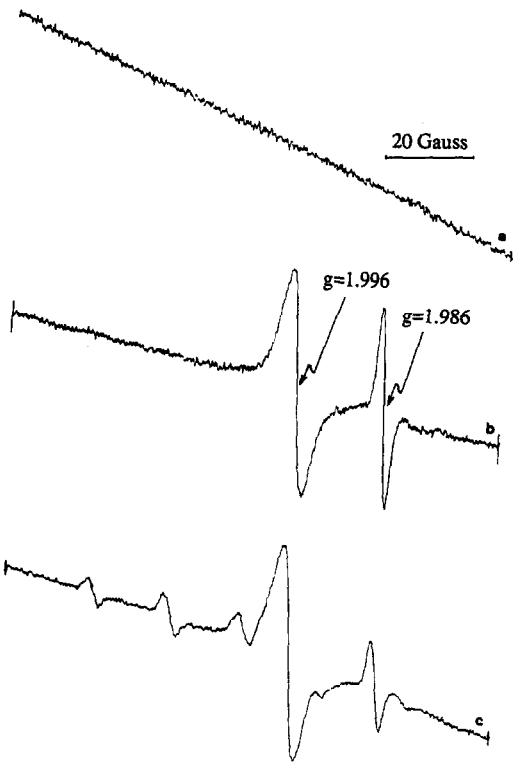

Fig. 1. ESR spectra obtained on the reaction of welding fume with glutathione (40 mM) at neutral pH (7.0) and room temperature (close to 20°C). (a) 5 mg welding fume in 1 cm^3 distilled water, (b) 5 mg welding fume and 40 mM glutathione and (c) 5 mg welding fume, 40 mM glutathione and 100 mM DMPO. ESR spectra were recorded 5 min after mixing with a gain 2.5×10^5, scan range 100 G and scan time 100 s using a Bruker ER/200/d.

Acknowledgements—We thank: the Cancer Research Campaign for their generous support of our work at Q.M.W.; Dr L. Levy (Occupational Health, University of Birmingham) for the "welding fume"; Dr A. Kortenkamp (School of Pharmacy, University of London) and Prof. D. Beyersmann (Universitat Bremen) for innumerable stimulating discussions concerning the problem of chromate toxicity.

REFERENCES

1. IARC (1990), Monographs on the Evaluation of the Carcinogenic Risk of Chemicals to Humans, Vol. 49, Chromium, Nickel and Welding. International Agency for the Research on Cancer, Lyon.
2. V. Bianchi and A. G. Levis, *Toxicol. Environ. Chem.* 1987, **15**, 1.
3. S. De Flora and K. E. Wetterhahn, *Life Chem. Rep.* 1989, **7**, 169.
4. P. O'Brien and G. Wang, *Environ. Geochem.* 1989, **11**, 75.
5. M. Sugiyama, *Free Rad. Biol. Med.* 1992, **12**, 397.
6. L. S. Levy and S. Venitt, *Carcinogenesis* 1986, **7**, 831.
7. A. Kortenkamp, Z. Ozolins, D. Beyersmann and P. O'Brien, *Mutat. Res.* 1989, **216**, 19.
8. A. Kortenkamp, G. Oetken and D. Beyersmann, *Mutat. Res.* 1990, **232**, 155.
9. J. Aiyar, K. M. Borges, R. A. Floyd and K. E. Wetterhahn, *Toxicol. Environ. Chem.* 1989, **22**, 135.
10. R. P. Farrell, R. J. Judd, P. A. Lay, N. E. Dixon, R. S. U. Baker and A. M. Bonin, *Chem. Res. Toxicol.* 1989, **2**, 227.
11. X. Shi and N. S. Dalal, *Biochem. Biophys. Res. Comm.* 1989, **163**, 627.
12. J. Aiyar, H. J. Berkovits, R. A. Floyd and K. E. Wetterhahn, *Environ. Health Perspect.* 1991, **92**, 53.
13. K. M. Borges and K. E. Wetterhahn, *Chem. Res. Toxicol.* 1991, **4**, 638.
14. A. M. Standeven and K. E. Wetterhahn, *Chem. Res. Toxicol.* 1991, **4**, 616.
15. P. O'Brien, J. Barrett and F. Swanson, *Inorg. Chim. Acta* 1985, **108**, L19.
16. D. M. L. Goodgame and A. M. Joy, *J. Inorg. Biochem.* 1986, **26**, 219.
17. P. O'Brien, J. Pratt, F. Swanson, P. Thornton and G. Wang, *Inorg. Chim. Acta* 1990, **169**, 265.

Polyhedron Vol. 12, No. 11, pp. 1411–1413, 1993
Printed in Great Britain

0277–5387/93 $6.00+.00
Pergamon Press Ltd

COMMUNICATION

SYNTHESIS AND X-RAY CRYSTAL STRUCTURE OF $TaBr_2(PPhMe_2)_4$

LILIANE G. HUBERT-PFALZGRAF* and ABDENASSER ZAKI

Laboratoire de Chimie Moléculaire, URA-CNRS, Université de Nice-Sophia Antipolis, 06108 Nice Cedex 2, France

and

LOIC TOUPET

Laboratoire de Cristallochimie, URA-CNRS, Campus de Beaulieu, 35042 Rennes Cedex, France

(*Received* 22 *February* 1993; *accepted* 4 *March* 1993)

Abstract—The reduction of $TaBr_5$ by $LiBEt_3H$ in toluene in the presence of dimethylphenylphosphine offers a tantalum(II) complex, $TaBr_2(PhPMe_2)_4$, which has been characterized by X-ray crystallography. The coordination polyhedron, in which the bromide ligands are in *cis* positions [∠ BrTaBr 84.23(4)°], is severely distorted towards a bicapped tetrahedron.

Low-valent early transition metal halide adducts have generally been obtained by the reduction of halide derivatives using various metals or sodium amalgam. In the case of niobium and tantalum[1] the issue of the system metal halide–tertiary phosphine, MX_n–PR_3 (M = Nb or Ta), has been found to be highly dependent on the nature of the reductant, of the phosphine and of the solvent. Mononuclear,[2] dinuclear[3] or trinuclear[4] units have been reported for the trivalent halide adducts, while the divalent ones are limited to the monomeric chloride complexes *t*-$MCl_2(PMe_3)_4$ and *t*-$TaCl_2(dmpe)_2$ (dmpe = dimethylphosphinoethane).[5] The use of bromide derivatives as precursors to group 15 low-valent derivatives has been less explored. $NbBr_n(PPhMe_2)_3$ complexes ($n = 4$ and 3) have been obtained by reduction of $NbBr_5$ by the phosphine and sodium amalgam (1 equivalent), respectively.[6] The reduction of $TaBr_5$ by Na/Hg over 1 h and in the presence of dimethylphenylphosphine leads to the *cis*-$TaBr_4(PhPMe_2)_2$ polymorphs, independently of the stoichiometry—one or two—of the reductant used.[7] When the latter reaction (1 : 2 stoichiometry) was achieved with longer reaction times (24 h) or when greater amounts of reductant were used, no compound suitable for X-ray structural determination could be isolated. We were thus interested in finding alternative reductive routes. Hydrides have been less investigated as reductants for access to non-cyclopentadienyl low-valent niobium and tantalum derivatives, although R_3SnH has, for instance, been used for the large scale preparation of $NbCl_3(DME)$ (DME = dimethoxyethane), which might be used in organic synthesis.[8] The use of vitride offered one of the few tantalum(I) derivatives as a mixed-metal $TaH_2Al(OC_2H_4OMe)(dmpe)_2$ species.[1]

Superhydride $LiBEt_3H$ is a versatile reactant, acting as a reductant[9] and a source of either hydride or alkyl ligands.[10] Its use offered access to a monomeric tantalum(II) adduct, $TaBr_2(PhPMe_2)_4$, whose synthesis and molecular structure are reported here.

Reaction between $TaBr_5$ in toluene in the presence of $PhPMe_2$ (3.5 equivalents) with an excess of $LiBEt_3H$ (3.5 equivalents) in THF led to an immediate gaseous evolution (probably hydrogen), while

* Author to whom correspondence should be addressed.

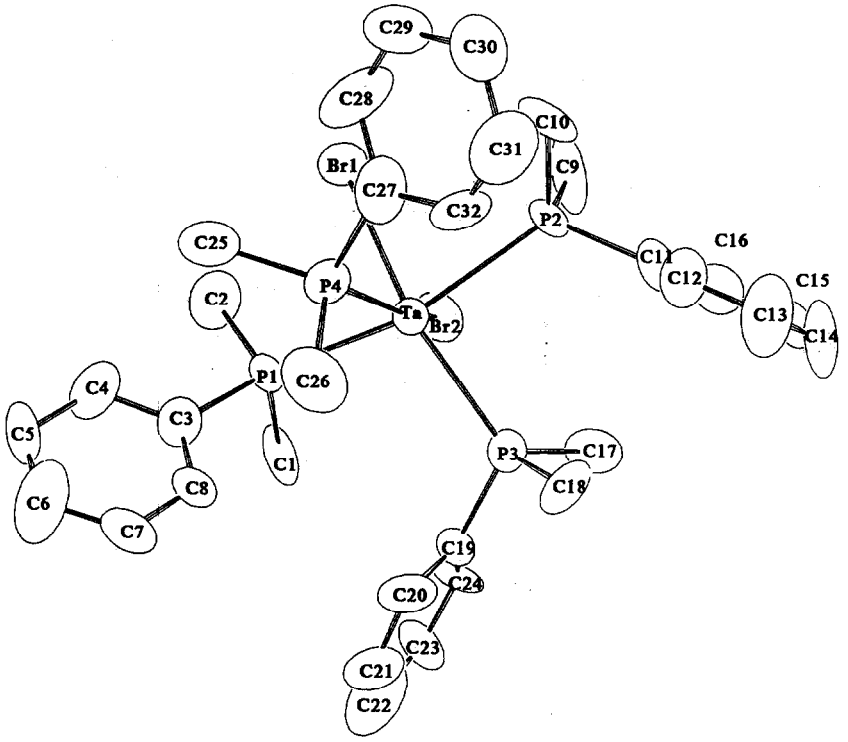

Fig. 1. Molecular structure of $TaBr_2(PPhMe_2)_4$ showing the atom labelling scheme. Selected bond lengths (Å): Ta—Br(1) 2.680(1), Ta—Br(2) 2.702(1), Ta—P(1) 2.675(4), Ta—P(2) 2.650(5), Ta—P(3) 2.587(4), Ta—P(4) 2.574(2); selected angles (°): Br(1)—Ta—Br(2) 84.23(4), Br(1)—Ta—P(1) 76.77(6), Br(1)—Ta—P(2) 83.11(7), Br(1)—Ta—P(3) 80.34(7), Br(1)—Ta—P(4) 158.34(7), Br(2)—Ta—P(1) 85.01(9), Br(2)—Ta—P(2) 77.41(9), Br(2)—Ta—P(3) 161.95(8), Br(2)—Ta—P(4) 77.62(8), P(1)—Ta—P(2) 154.46(9), P(1)—Ta—P(3) 100.4(1), P(1)—Ta—P(4) 89.8(1), P(2)—Ta—P(3) 91.4(1), P(2)—Ta—P(4) 104.1(1), P(3)—Ta—P(4) 119.3(1).

the colour of the reaction medium turned from yellow to brown–green and finally red. After elimination of the colloidal metal particles by filtration, a paramagnetic, extremely air-sensitive compound (**1**) was isolated as red crystals* by concentration and cooling of the filtrate.

Since this red compound is only slightly soluble in toluene and displays a poor stability in polar solvents, its identity was established by X-ray diffraction.† It corresponds to a tantalum(II) monomer, $TaBr_2(PhPMe_2)_4$, whose molecular structure is shown in Fig. 1. The bromide ligands occupy *cis* positions [∠ BrTaBr 84.23(4)°] in a distorted six-coordinated tantalum surrounding. Compound **1** is thus not isostructural with $TaCl_2(PMe_3)_4$[5] or with other MX_2L_4 species (M = Nb, X = OAr, L = 1/2 dmpe;[11] M = Mo, L = PMe_3, X = Cl, Br, M = W, X = I[12]). In fact, the geometry around the metal centre is severely distorted with respect to an octahedron and the various angles of the coordination polyhedron range from 76.77(6) to 161.95(8)° and the stereochemistry around tantalum tends towards a bicapped tetrahedron.[13] Since trimethylphosphine and dimethylphenylphosphine have almost the same cone angles, the change in the metal geometry with respect to $TaCl_2(PMe_3)_4$ is probably induced by the relative orientation of the phenyl rings. X-ray data on tantalum bromide adducts remain scarce and limited to the *cis*-$TaBr_4(PMe_2Ph)_2$ poly-

* Spectroscopic data: IR (cm^{-1}): 1576 [ν(C=C)]; 1180, 1097, 1020, 939, 918, 744, 729sh, 703, 580, 492, 401. ESR (toluene, room temperature): ⟨g⟩: 1.96, ⟨A⟩ = 133 G. Found: C, 42.5; H, 4.7; Br, 19.6. Calc. for $C_{32}H_{44}Br_2P_4Ta$: C, 43.0; H, 5.0; Br, 17.9%.

† Crystal data: $C_{32}H_{44}Br_2P_4Ta$, M = 893.4, a = 9.737(3), b = 9.950(9), c = 19.384(8) Å, α = 86.52(3), β = 75.73(6), γ = 77.14(4)°, V = 1774 Å^3, Z = 2, triclinic P-1, μ = 54.92. The structure was solved using conventional heavy-atom methods, R = 0.046, Rw = 0.052 from 1812 unique observed reflections with $2\theta < 50°$, measured with Mo-K_α radiation (λ = 0.71073 Å) and corrected for absorption. Atomic coordinates, bond lengths and angles and thermal parameters have been deposited as supplementary data with the Editor, from whom copies are available on request. Atomic coordinates have also been deposited with the Cambridge Crystallographic Data Centre.

morphs[7] and to $(\eta^5\text{-}C_5Me_4Et)_2Ta_2(\mu\text{-}Br)_2Br_4$[14] and for niobium to the $NbBr_n(PPhMe_2)_3$ adducts, $n = 3$, 4.[6] The tantalum(II)–bromide distances observed for $TaBr_2(PhPMe_2)_4$ are significantly longer (2.691 Å av.) than those previously reported for the tantalum(IV) adducts [Ta—Br (*trans*-P) 2.53 Å];[7] this may originate from decreases in the metal's oxidation state, as well as from a *trans* effect due to the phosphine ligands. Indeed, the Ta—P bond distances vary from 2.580 Å av. for those *trans* to the bromides to 2.667 Å av. when another phosphine is in the *trans* position. The Ta···Me distances are slightly shorter than the Ta···Ph ones (3.76 vs 3.83 Å), but their values exclude agostic CH interactions.[15]

The novel 15-electron tantalum(II) complex isolated in a 43% yield[16] is highly reactive. It is unstable in the polar solvents required for its solubilization. In acetonitrile, for instance, its evolution leads to ionic derivatives, as evidenced by the appearance in the ^{31}P NMR spectrum of a doublet ($J = 520$ Hz) at -2 ppm characteristic of the $HPPhMe_2^+$ cation. Another salient feature is the presence of a broad signal at *ca* 3.7 ppm in the proton NMR spectrum, which has been tentatively attributed to a Ta—Me resonance.[17] Ionic low-valent complexes stabilized by phosphonium cations have been identified for niobium and tantalum[18] as well as for the molybdenum[19] derivatives, but no indication has been given regarding the source of the proton. The formation of ionic, diamagnetic species, the presence of resonances due to Ta—C bonds and thus of P—C bond cleavage reactions suggest complex modification of the metal coordination sphere and the behaviour has not been further investigated.

REFERENCES

1. L. G. Hubert-Pfalzgraf, M. Postel and J. G. Riess, *Comprehensive Coordination Chemistry*, Ch. 34. Pergamon Press, Oxford (1987).
2. H. W. Turner, R. R. Schrock, J. D. Fellman and S. J. Holmes, *J. Am. Chem. Soc.* 1983, **105**, 4942.
3. A. P. Sattelberger, R. B. Wilson and J. C. Huffman, *Inorg. Chem.* 1982, **22**, 2392; 4179.
4. F. A. Cotton, M. P. Diebold, X. Feng and W. J. Roth, *Inorg. Chem.* 1988, **27**, 3413.
5. M. L. Luetkens, J. C. Huffman and A. P. Sattelberger, *J. Am. Chem. Soc.* 1983, **105**, 4474.
6. F. A. Cotton, M. P. Diebold and W. J. Roth, *Inorg. Chim. Acta* 1985, **105**, 41.
7. N. Hovnanian, L. G. Hubert-Pfalzgraf and G. Le Borgne, *Acta Cryst. C* 1990, **46**, 1207.
8. E. J. Roskamp and S. F. Pedersen, *J. Am. Chem. Soc.* 1987, **109**, 655.
9. H. Bonnemann, W. Brijoux and T. Joussen, *Angew. Chem., Int. Edn* 1990, **29**, 273.
10. E. Thaler, K. Folting, J. C. Huffman and K. G. Caulton, *Inorg. Chem.* 1987, **26**, 374; T. Cuenca, W. A. Herrmann and T. V. Ashworth, *Organometallics* 1986, **5**, 2514.
11. T. W. Coffindafer, I. P. Rothwell, K. Folting, J. C. Huffman and W. E. Streib, *J. Chem. Soc., Chem. Commun.* 1985, 1519.
12. P. R. Sharp and K. G. Frank, *Inorg. Chem.* 1985, **24**, 1808; P. R. Sharp, *Organometallics* 1984, **3**, 1217; R. A. Jones, F. M. Real, G. Wilkinson, A. M. R. Girdas, M. B. Hursthouse and K. M. A. Malik, *J. Chem. Soc., Dalton Trans.* 1980, 511; D. Rabinovitch and G. Parkin, *J. Am. Chem. Soc.* 1993, **115**, 353.
13. R. Hoffmann, J. M. Howell and A. R. Rossi, *J. Am. Chem. Soc.* 1976, **98**, 2484.
14. C. Ting and L. Messerle, *Inorg. Chem.* 1989, **29**, 173.
15. M. Brookhardt and M. L. H. Green, *J. Organomet. Chem.* 1983, **250**, 295.
16. Crystallization requires an extremely pure reaction medium, if not only brown oily products are obtained.
17. N. Hovnanian and L. G. Hubert-Pfalzgraf, *J. Organomet. Chem.* 1986, **299**, C29; V. C. Gibson, T. P. Kee, S. T. Carter, R. D. Sanner and W. Clegg, *J. Organomet. Chem.* 1991, **418**, 197.
18. F. A. Cotton and R. C. Najjar, *Inorg. Chem.* 1981, **20**, 1866; F. A. Cotton, P. A. Kibala and W. J. Roth, *J. Am. Chem. Soc.* 1988, **110**, 298.
19. F. A. Cotton and R. Poli, *Inorg. Chem.* 1987, **26**, 3310.

Polyhedron Vol. 12, No. 11, pp. 1415–1417, 1993
Printed in Great Britain

0277–5387/93 $6.00+.00
© 1993 Pergamon Press Ltd

COMMUNICATION

SYNTHESIS AND CHARACTERIZATION OF RUTHENIUM DIIMINODIPHOSPHINE COMPLEXES. X-RAY STRUCTURE OF *TRANS*-$Ru(P_2N_2)Cl_2 \cdot 2H_2O$ (P_2N_2 = N,N′-BIS [*o*-(DIPHENYLPHOSPHINO)BENZYLIDENE]ETHYLENEDIAMINE)

WAI-KWOK WONG*

Department of Chemistry, Hong Kong Baptist College, Kowloon, Hong Kong

and

JING-XING GAO

Department of Chemistry, Xiamen University, Xiamen 361005, Fujian, P.R.C.

and

ZHONG-YUAN ZHOU and THOMAS C. W. MAK*

Department of Chemistry, The Chinese University of Hong Kong, Shatin, N.T., Hong Kong

(*Received* 22 *February* 1993; *accepted* 4 *March* 1993)

Abstract—The interaction of $Ru(OAc)_2(Ph_3P)_2$ with 1 equivalent of N,N′-bis[*o*-(diphenylphosphino)benzylidene]ethylenediamine (P_2N_2) in refluxing dichloromethane gives *trans*-$Ru(OAc)_2(P_2N_2)$ (**I**) in moderate yield (63%); in refluxing toluene the reaction gives a red product, which upon recrystallization in $CHCl_3$/hexane gives *trans*-$Ru(OAc)_2Cl_2 \cdot 2H_2O$ (**III**) in good yield (92%). Compounds **I** and **III** have been fully characterized by analytical and spectroscopic methods. The structure of **III** has been determined by an X-ray diffraction study.

$Ru(OAc)_2(Ph_3P)_2$ is a very versatile reagent. It provides a very good entry to ruthenium(II) complexes. Since its preparation a large number of ruthenium carboxylate complexes have been synthesized, and most of the known mononuclear acetates are Ph_3P complexes. Recently, ruthenium diphosphine and triphosphine complexes have been synthesized.[1,2] Ruthenium acetate complexes have been shown to display various catalytic properties,[3] particularly those with chiral chelating diphosphine ligands.[4] Chelating multidentate phosphine ligands offer several advantages over monodentate phosphines containing similar phosphino groups. They can provide better control over the coordination number and stereochemistry of the resulting complexes, increase basicity at the metal centres and slow down intra- and intermolecular exchange processes.[5] N,N′ - bis[*o* - (diphenylphosphino)benzylidene]ethylenediamine (P_2N_2), a polydentate ligand, can serve as a bi-, tri- and tetradentate ligand depending on the reaction conditions.[6–8] It is likely that a ruthenium acetate complex containing the P_2N_2 ligand may display some interesting structural, chemical and catalytic properties that are not observed in other chelating phosphine complexes. In this communication the interaction of $Ru(OAc)_2(Ph_3P)_2$ with the polydentate diiminodiphosphine ligand P_2N_2 is reported.

When $Ru(OAc)_2(Ph_3P)_2$ was treated with 1 equi-

* Authors to whom correspondence should be addressed.

valent of P_2N_2 in refluxing dichloromethane for 16 h, work-up gave red crystals of the stoichiometry $[Ru(P_2N_2)(CH_3COO)_2]\cdot 2H_2O$ (**I**)* in moderate yield (63%) after recrystallization from an acetone/Et_2O mixture. Compound **I** exhibits absorptions at 1562vs and 1380s cm^{-1} in the IR spectrum and a singlet at δ 1.06 ppm in the ^1H NMR spectrum for the acetate groups. The $^{31}P\{^1H\}$ NMR spectrum of **I** exhibits a singlet at δ 48.6 ppm, indicating that the two phosphino groups of the P_2N_2 ligand are coordinated and equivalent. The IR and ^1H NMR data indicate that the two acetate groups are monodentate and equivalent. This rules out the salt formulation $[Ru(O_2CCH_3)(P_2N_2)][CH_3CO_2]$. There are two possible isomers for **I**. These are the *cis*- and *trans*-isomers, as shown below.

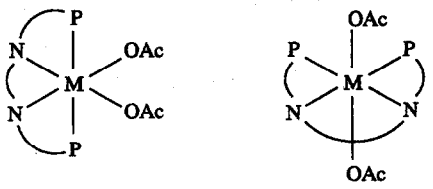

Cis *Trans*

The available spectroscopic data cannot distinguish between the two isomers. However, since the corresponding chloro complex, $Ru(P_2N_2)Cl_2$, adopts a *trans*-configuration (*via infra*), a *trans*-configuration is assigned to **I**.

When the above reaction was performed in refluxing toluene for 16 h, work-up gave a red solid (**II**), whose IR and ^1H NMR spectra showed the absence of the acetate groups. Compound **II** has a very complex ^1H NMR spectrum; however, its $^{31}P\{^1H\}$ NMR spectrum exhibits only a singlet at δ 3.8 ppm. Attempts to obtain an analytically pure sample of **II** for analysis were unsuccessful. When **II** was recrystallized from a $CHCl_3$/hexane mixture, dark red crystals of stoichiometry $Ru(P_2N_2)Cl_2\cdot 2H_2O$ (**III**)† were obtained in high yield (92%). This showed that **II** reacted with chloroform to give **III** and the chloro ligands of **III** originated from chloroform. The IR and ^1H NMR spectra of **III** do not exhibit any absorption due to acetate groups. The ^1H NMR spectrum of **III** exhibits resonances due to the P_2N_2 alone, whereas a resonance due to the methyl protons of acetate is not observed. $^{31}P\{^1H\}$ NMR of **III** exhibits a singlet at δ 46.1 ppm, indicating that the two phosphino groups of the P_2N_2 ligand are coordinated and equivalent. Since the available spectroscopic data again cannot be used to distinguish between the cis- and *trans*-isomers of **III**, an X-ray diffraction study‡ was performed to establish the structure unequivocally. A perspective drawing and selected bond lengths and angles of **III** are shown in Fig. 1 and its caption. All bond lengths and angles are normal.

The solid state structure of **III** reveals a *trans*-configuration for the complex. The structure shows that the two chloro ligands are mutually *trans* to each other and the P_2N_2 ligand acts as a tetradentate ligand with the two phosphino groups *cis* to each other.

---

* $Ru(CH_3COO)_2(C_{40}H_{34}N_2P_2)\cdot 2H_2O$: red crystals, m.p. 216–219°C (dec.). Found: C, 61.3; H, 4.8; N, 3.1. Calc.: C, 61.5; H, 5.1; N, 3.3%. IR (cm^{-1}, in KBr): 3400s, 3048w, 1608s, 1582vs, 1562vs, 1478w, 1430s, 1380s, 1326w, 1264w, 1182w, 1138w, 1090m, 1020w, 740m, 684m, 508m, 458m. $^{31}P\{^1H\}$ NMR ($CDCl_3$): δ 48.6(s) ppm. ^1H NMR ($CDCl_3$): olefinic protons, δ 8.97 (2H, m); phenyl protons, δ 6.80–7.53 (28H, m); NCH_2CH_2N protons, δ 4.59 (4H, s); water protons, δ 1.69 (4H, s); acetate methyl protons, δ 1.07 (6H, s) ppm.

† $RuCl_2(C_{40}H_{34}N_2P_2)\cdot 2H_2O$: dark red crystals, m.p. 168–171°C (dec). Found: C, 59.3; H, 4.5; N, 3.3; Cl, 9.0. Calc.: C, 59.1; H, 4.7; N, 3.4; Cl, 8.7%. IR (cm^{-1}, in KBr): 3476br, 3044m, 2916w, 1628m, 1478m, 1428s, 1344w, 1298m, 1264m, 1216w, 1186w, 1156w, 1134w, 1088m, 740s, 686vs, 476m. $^{31}P\{^1H\}$ NMR ($CDCl_3$): δ 46.1 ppm. ^1H NMR ($CDCl_3$): olefinic protons, δ 8.99 (2H, m); phenyl protons, δ 6.80–7.60 (28H, m); NCH_2CH_2N protons, δ 4.35 (4H, s); water protons, δ 1.53 (4H, s) ppm.

‡ Crystal data for $(C_{40}H_{34}N_2P_2)RuCl_2\cdot 2H_2O$: mol. wt 812.71, monoclinic, space group $C2/c$ (No. 15), $a = 38.751(15)$, $b = 10.299(4)$, $c = 25.377(9)$ Å, $\beta = 123.13(13)°$, $U = 8479.9(6)$ Å^3, $Z = 8$, $D_{calc} = 1.27$ g cm^{-3}, $F(000) = 3328$, Mo-K_α radiation ($\lambda = 0.71073$ Å), $\mu = 6.02$ cm^{-1}. Data were collected to $2\theta_{max} = 59°$ using a crystal (0.24 × 0.36 × 0.35 mm) on a Siemens P4 diffractometer in the variable ω-scan mode and corrected for absorption ($\mu r = 0.20$, transmission factors 0.834–0.975); 7991 unique reflections, of which 4493 with $|F_o| \geq 6\delta(|F_o|)$ were employed in structure analysis using the SHELXTL-PC program system. Other than the four independent water oxygen atoms which exhibit half site occupancy, all non-hydrogen atoms were subjected to anisotropic refinement. All hydrogen atoms, except those of the disordered water molecules, were placed in their idealized positions with assigned isotropic thermal parameters and included in structure-factor calculations. The weighting scheme used was $w = [\sigma^2(|F_o|) + 0.0003|F_o|^2]^{-1}$ and the final residuals were $R = 0.062$ and $R' = 0.074$. Atomic coordinates are available from the Director of the Cambridge Crystallographic Data Centre, University Chemical Laboratory, Lensfield Road, Cambridge CB2 1EW, U.K. Any request should be accompanied by a full literature citation for this communication.

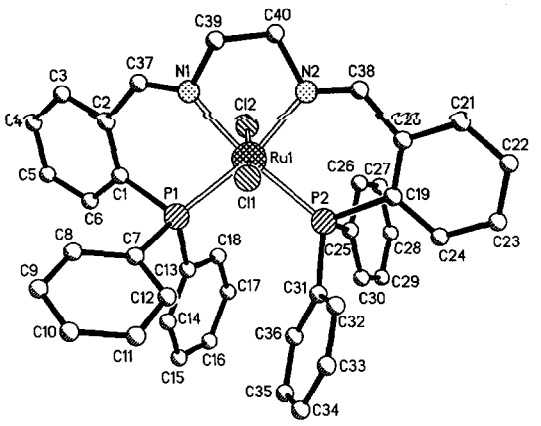

Fig. 1. A perspective view of the structure of *trans*-$RuCl_2(C_{40}H_{34}N_2P_2)$. Selected bond lengths (Å) and angles: Ru(1)—Cl(1), 2.419(3); Ru(1)—Cl(2), 2.427(3); Ru(1)—P(1), 2.292(2); Ru(1)—P(2), 2.298(3); Ru(1)—N(1), 2.094(9); Ru(1)—N(2), 2.097(6); N(1)—C(37), 1.297(9); N(1)—C(39), 1.47(1); N(2)—C(38), 1.285(9); N(2)—C(40), 1.48(1); Cl(1)—Ru(1)—Cl(2), 170.0(1); P(1)—Ru(1)—N(2), 169.5(2); P(2)—Ru(1)—N(1), 170.6(2); P(1)—Ru(1)—P(2), 100.3(1); N(1)—Ru(1)—N(2), 80.8(3); P(1)—Ru(1)—N(1), 88.7(2); P(2)—Ru(1)—N(2), 90.2(2); Cl(1)—Ru(1)—P(1), 95.6(1).

Acknowledgements—Financial support from the Hong Kong Baptist College and the UPGC (Hong Kong) is gratefully acknowledged.

REFERENCES

1. E. B. Boyar, P. A. Harding and S. D. Robinson, *J. Chem. Soc., Dalton Trans.* 1986, 1771.
2. G. Jia, A. L. Rheingold, B. S. Haggerty and D. W. Meek, *Inorg. Chem.* 1992, **31**, 900.
3. R. Noyori, *Chem. Soc. Rev.* 1989, **18**, 187 and refs therein.
4. R. Noyori and H. Takaya, *Accts Chem. Res.* 1990, **23**, 345 and refs therein.
5. D. W. Meek, *Homogeneous Catalysis with Metal Phosphine Complexes* (Edited by L. Pignolet), Ch. 8. Plenum Press, New York (1983).
6. W. K. Wong, J.-X. Gao, Z.-Y. Zhou and T. C. W. Mak, *Polyhedron* 1992, **11**, 2965.
7. W. K. Wong, J.-X. Gao and W. T. Wong, *Polyhedron*, submitted.
8. J. C. Jeffrey, T. B. Rauchfuss and P. A. Tucker, *Inorg. Chem.* 1980, **19**, 3306.

Polyhedron Vol. 12, No. 11, pp. 1419–1421, 1993
Printed in Great Britain

0277–5387/93 $6.00+.00
© 1993 Pergamon Press Ltd

COMMUNICATION

OXIDATION REACTIONS BY THE COORDINATED NITROSYL GROUP

ALOK K. DEB and SREEBRATA GOSWAMI*

Department of Chemistry, North-Eastern Hill University, Shillong 793 003, India

(*Received* 17 *November* 1992; *accepted* 4 *March* 1993)

Abstract—The oxidation reaction by the coordinated nitrosyl group in $[Ru(NO)(NO_2)(m\text{-tap})_2](ClO_4)_2$ (**1**) (*m*-tap = *m*-tolylazopyridine) is described. Complex **1** brings about the oxidative coupling of N,N-dimethylaniline (DMA) to tetramethylbenzidine (TMB) and the oxidation of $RuCl_2(bpy)_2$ (bpy = 2,2′-bipyridine) to $[RuCl_2(bpy)_2]^+$. These redox reactions have been studied voltametrically and the results have been analysed in terms of the electrophilicity of the coordinated NO^+ in **1**.

Examples of the electrophilic coordinated nitrosonium ion (NO^+) acting as an oxidant in a net chemical reaction are uncommon.[1–5] In the present communication we report two examples illustrating (1) oxidative coupling of N,N dimethylaniline (DMA) and (2) oxidation of $RuCl_2(bpy)_2$ by a highly electrophilic mononitrosyl complex, $[Ru(NO)(NO_2)(m\text{-tap})_2](ClO_4)_2$ (**1**) (*m*-tap = *m*-tolylazopyridine, L). Recently, the electrochemical properties of **1** have been described.[6] It undergoes electrochemically reversible one-electron reduction in acetonitrile at 0.76 V and a second irreversible one-electron reduction at 0.17 V vs S.C.E. at a platinum working electrode. Complex **1** is an example where electron transfer occurs to and from a coordinated ligand and it is a moderately strong oxidant.

Oxidative coupling

The cationic nitrosyl complex **1** is converted to the corresponding cationic $[Ru(CH_3CN)(NO_2)(m\text{-tap})_2]^+$ (**2**) complex by DMA in acetonitrile. In an electrochemical experiment a solution of **1** (1 mmol) in acetonitrile was mixed with DMA (1 mmol) and the resultant solution was examined cyclic voltametrically. It shows the characteristic reversible response[7] at $E^0_{298} = 0.4$ V ($\Delta E_p = 60$ mV) of N,N,N′,N′-tetramethylbenzidine (TMB), evidently formed by the oxidative coupling reaction shown in eq. (1). The voltamograms are displayed in Fig. 1.

$$2DMA + 2\,\mathbf{1} \xrightarrow{CH_3CN} TMB + 2\,\mathbf{2} + 2NO + 2H^+ \quad (1)$$

The cyclic voltametric current height of the TMB response corresponds to 35–40% utilization of the

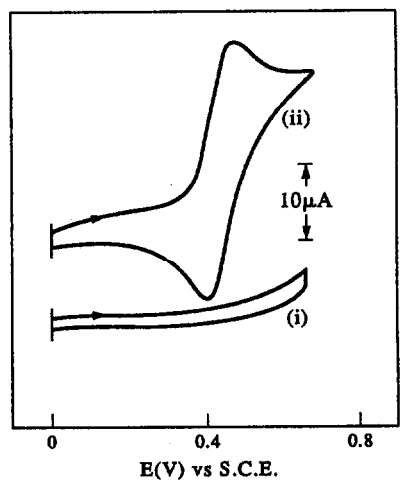

Fig. 1. Segmented cyclic voltamograms of: (i) free DMA and (ii) DMA mixed with an equimolar quantity of **1** in CH_3CN.

* Author to whom correspondence should be addressed.

oxidation equivalent for the coupling reaction. The rest of the amine is evidently lost in the side reactions.[8] In the preparative scale reaction (1) was performed in acetonitrile and on column chromatographic purification TMB and **2** were isolated. Complex **2** was crystallized as the perchlorate salt and was characterized[9] by molar conductance and spectral data. The electrochemical behaviour of compound **2**, thus isolated, was examined cyclic voltametrically at a platinum working electrode using tetraethylammoniumperchlorate (TEAP) as a supporting electrolyte. This showed[10] the reversible oxidative response at $E^0_{298} = 1.64$ V ($\Delta E_p = 120$ mV). It may be noted here that in the case of primary amines the present nitrosyl complex has been successfully used[9] as a nitrosating agent, whereas in the case of tertiary amines the same nitrosyl complex behaves as an oxidant. The difference in the oxidation potentials[11] of primary and tertiary amines is no doubt the controlling factor in driving the two reactions. The first reduction potential of **1** [E^0(**1**)] is just enough for the oxidation of DMA, whereas it is a weaker oxidant with respect to the primary amines.

Formation of trivalent ruthenium

Cis-dichlorobis(2,2′-bipyridyl)ruthenium(II), *cis*-$RuCl_2(bpy)_2$, is quantitatively oxidized to the corresponding ruthenium(III) chelate, $[RuCl_2(bpy)_2]^+$, by **1** [eq. (2)].

$$\mathbf{1} + RuCl_2(bpy)_2 \xrightarrow{CH_3CN} \mathbf{2} + [RuCl_2(bpy)_2]^+ \qquad (2)$$

This reaction was followed cyclic voltametrically. The cyclic voltamogram of a mixture of **1** and $RuCl_2(bpy)_2$ is shown in Fig. 2. A solution prepared by mixing $RuCl_2(bpy)_2$ (*ca* 10^{-3} mol) with **1** (*ca* 10^{-3} mol) shows the characteristic cyclic voltamogram[12] of $[RuCl_2(bpy)_2]^+$ and an additional reversible response at $E^0_{298} = 1.63$ V ($\Delta E_p = 120$ mV) was also observable due to the formation[10] of **2** (Fig. 2).

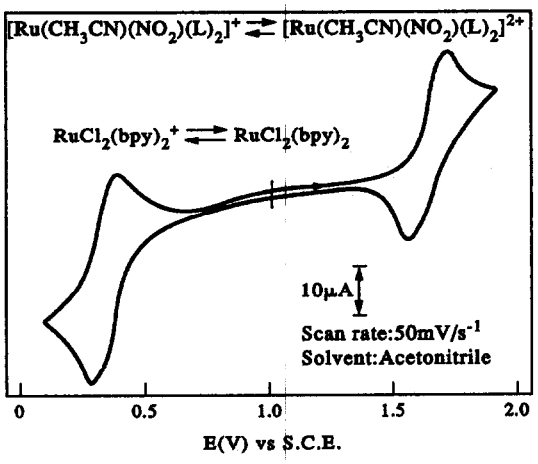

Fig. 2. Cyclic voltamogram of a mixture of **1** and $RuCl_2(bpy)_2$ in CH_3CN.

The origin of the solvento complex **2** from reactions (1) and (2) is perhaps one-electron reduction of Ru^{II}–NO^+ to give Ru^{II}–NO^0, followed by a rapid solvolysis reaction to form **2**. The mechanism and more general applicability of the oxidation reactions are under study.

EXPERIMENTAL

Complex **1** was prepared as described previously.[6]

Electrochemical reactions

(1) *Oxidative coupling.* A sample of **1** (0.006 g, 0.008 mmol) and TEAP (0.200 g, 0.87 mmol) was dissolved in deaerated acetonitrile (8 cm^3) in an electrochemical cell. To it a solution of DMA (0.001 g, 0.008 mmol) in acetonitrile (2 cm^3) was added. The resulting solution was then studied cyclic voltametrically at a platinum working electrode. A reversible oxidative couple at $E^0_{298} = 0.4$ V ($\Delta E_p = 60$ mV), indicating the formation of TMB, was observable. A similar experiment, without the addition of **1**, showed no response in the range 0.0–0.60 V. The yield of TMB formed in the experiment as stated above was assessed from the current height data of the reversible couple at 0.4 V.

(2) *Formation of trivalent ruthenium.* A sample of **1** (0.011 g, 0.014 mmol) and TEAP (0.200 g, 0.87 mmol) was dissolved in deaerated acetonitrile (10 cm^3) in an electrochemical cell. To it was added *cis*-$RuCl_2(bpy)_2$ (0.007 g, 0.014 mmol) and the mixture was stirred under nitrogen for 5 min. The resulting solution showed a reversible reductive response at $E^0_{298} = 0.33$ V ($\Delta E_p = 80$ mV), indicating the formation of $[RuCl_2(bpy)_2]^+$. Another oxidative response due to the oxidation of **2** was also recorded at $E^0_{298} = 1.63$ V ($\Delta E_p = 120$ mV). In the absence of **1** $RuCl_2(bpy)_2$ showed an oxidative response at 0.32 V.

Chemical reactions

Reaction of **1** *with* DMA. The salt of **1** (0.125 g, 0.16 mmol) was dissolved in acetonitrile (10 cm^3) and DMA (0.02 g, 0.16 mmol) was added. The mixture was stirred for 30 min at room temperature (298 K) and then evaporated to dryness. The crude

product was then dissolved in dichloromethane (10 cm^3) and subjected to column chromatography on a silica gel column. The first yellow fraction was eluted with benzene. The second brownish-red fraction was eluted with a 1:9 acetonitrile–dichloromethane mixture.

The yellow solution was concentrated in benzene and a yellow crystalline compound was obtained. This was filtered and dried *in vacuo* over P_4O_{10}; yield 40%; m.p. 139°C. Found: C, 80.1; H, 8.4; N, 11.7. Calc. for $C_{16}H_{20}N_2$: C, 80.0; H, 8.3; N, 11.7%.

The second brownish-red fraction was evaporated to dryness and recrystallized from a 1:1 dichloromethane–hexane mixture. A dark crystalline compound was obtained, yield 50%. Found: C, 44.7; H, 3.9; N, 16.1. Calc. for $C_{26}H_{27}N_8O_7ClRu$: C, 44.6; H, 3.9; N, 16.0%. Λ_M (298 K, CH_3CN): 145 Ω^{-1} cm^2 mol^{-1}. ν_{max} (KBr): 1370(NO_2), 2300(C≡N) and 1365 cm^{-1} (N=N). λ_{max} (CH_3CN): 518, 350 and 305 (sh)nm (ε, 6600, 12,200 and 12,000 dm^3 mol^{-1} cm^{-1}).

Acknowledgement—Financial support received from the Council of Scientific and Industrial Research, New Delhi, is gratefully acknowledged.

REFERENCES

1. B. L. Haymore and J. A. Ivers, *J. Am. Chem. Soc.* 1974, **96**, 3325.
2. R. W. Callahan, G. M. Brown and T. J. Meyer, *J. Am. Chem. Soc.* 1975, **97**, 894.
3. R. W. Callahan and T. J. Meyer, *Inorg. Chem.* 1977, **16**, 574.
4. J. A. McCleverty, *Chem. Rev.* 1979, **79**, 53.
5. B. F. G. Johnson and S. Bhaduri, *J. Chem. Soc., Chem. Commun.* 1973, 650.
6. A. K. Deb, P. C. Paul and S. Goswami, *J. Chem. Soc., Dalton Trans.* 1988, 2051.
7. T. Mizoguchi and R. N. Adams, *J. Am. Chem. Soc.* 1962, **84**, 2058.
8. (a) Z. Galus and R. N. Adams, *J. Am. Chem. Soc.* 1962, **84**, 2061; (b) Z. Galus, R. M. White, F. S. Rowland and R. N. Adams, *J. Am. Chem. Soc.* 1962, **84**, 2065.
9. A. K. Deb and S. Goswami, *Polyhedron* 1991, **10**, 1799.
10. A. K. Deb, PhD Thesis, North-Eastern Hill University, Shillong, India (1992).
11. (a) R. L. Hand and R. F. Nelson, *J. Am. Chem. Soc.* 1974, **96**, 850; (b) J. Bacon and R. N. Adams, *J. Am. Chem. Soc. (L)* 1968, **90**, 6596.
12. E. C. Johnson, B. P. Sullivan, D. J. Salmon, S. A. Adeyemi and T. J. Meyer, *Inorg. Chem.* 1978, **17**, 2211.

Polyhedron Vol. 12, No. 11, pp. 1423–1425, 1993
Printed in Great Britain

0277–5387/93 $6.00+.00
© 1993 Pergamon Press Ltd

COMMUNICATION

THE PREPARATION AND X-RAY CRYSTAL STRUCTURE OF THE FIRST HOMOBIMETALLIC $\mu(\eta^2\text{-O,O}':\eta^1\text{-C})$ CARBON DIOXIDE COMPLEX: (dppp)$(CO)_2ReO_2CRe(CO)_3$(dppp)

SANTOSH K. MANDAL, JEANETTE A. KRAUSE and MILTON ORCHIN†

Department of Chemistry, University of Cincinnati, OH 45221 0172, U.S.A.

(*Received* 8 *December* 1992; *accepted* 4 *March* 1993)

Abstract—The molecular structure of the title compound involves a carboxylate group acting as a bidentate ligand to one rhenium atom, while acting as a monodentate ligand to the other rhenium atom. It was prepared in a one-step reaction by treating a THF solution of *fac*-(dppp)$(CO)_3ReCO_2H$ with solid KOH.

Bimetallic bridging carboxylates or μ-CO_2 complexes may have either structure **1** or **2**:

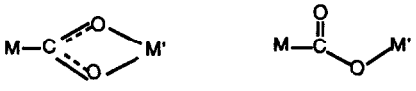

1 **2**

As is evident, the two structures differ with respect to whether or not there is symmetrical bonding between M′ and the two oxygen atoms. Both structures may be regarded as metal salts of carboxylic acids and both, perhaps responding to current interest in carbon dioxide fixation,[1] have been called μ-CO_2 bridging complexes. There are no reports on the interconversion of the two structures.

Complexes having structure **1**, where M and M′ are both transition metals, have been prepared by several groups of workers.[2] Also such complexes where M is a transition metal and M′ is a group IV element (Si, Ge, Sn, Pb) have been prepared.[3] Examples of complexes having structure **2**, where both transition metals are the same[4] or different,[5a] have been reported as well as an example where M′ is a group IV element.[5b] Also μ_3-CO_2 bridging complexes involving three or more metal centres are known.[6] We wish to report here the first example of a fully characterized complex having structure **1**, where M = M′, namely the complex (dppp)$(CO)_2$ $ReO_2CRe(CO)_3$(dppp), where dppp is 1,3-bis(diphenylphosphino)propane. The synthesis of this complex was achieved by treating a THF solution of *fac*-(dppp)$(CO)_3ReCO_2H$ with solid KOH. Although we have not investigated all the details of this reaction we believe the use of solid KOH is critical.

EXPERIMENTAL

Preparation of (dppp)$(CO)_2ReO_2CRe(CO)_3$(dppp)

To *fac*-(dppp)$(CO)_3ReCO_2H$[7] (1 g, 1.3 mmol) in THF (200 cm^3) was added solid KOH (5 g). After stirring for 24 h the mixture, which became red during this time, was filtered through a bed of celite and the THF was removed from the filtrate on a rotary evaporator. The residue was triturated with benzene (100 cm^3) and the benzene then evaporated. The residue was recrystallized from CH_2Cl_2/benzene/hexane to give 0.54 g (0.39 mmol) of the desired product; light brown crystals, m.p. 183–185°C. Data: IR (cm^{-1}, C_6H_6): ν(C≡O) 2022vs, 1946s, 1921vs, 1908s, 1835s. ^{1}H NMR (δ, CD_2Cl_2): 7.32 (m, 40H, C_6H_5), 2.78 (m, CH_2 12H). ^{13}C NMR (δ, CD_2Cl_2): 229.5 (t, J = 11 Hz, CO_2), 203.9 (t, J = 8 Hz, C≡O), 200.6 (dd, J = 71 Hz, 8 Hz, 2C≡O), 196.7 (t, J = 8 Hz, C≡O), 191.7 (t, J = 45 Hz, C≡O), 142.5–128.1 (m, C_6H_5), 31.9–19.5 (m, CH_2). ^{31}P NMR (δ, CD_2Cl_2, reference: 85%

† Author to whom correspondence should be addressed.

H_3PO_4): 11.85 (d, $J = 18$ Hz), 0.39 (d, $J = 18$ Hz), −9.55 (d, $J = 31$ Hz), −10.26 (d, $J = 31$ Hz). Found: C, 52.0; H, 3.7. Calc. for $C_{60}H_{52}O_7P_4Re_2$: C, 52.1; H, 3.8%.

X-ray structure determination

$(dppp)(CO)_2ReO_2CRe(CO)_3(dppp)\cdot C_6H_6$, mol. wt 1459.4, triclinic, space group $P\bar{1}$, $a = 10.902(2)$, $b = 13.657(3)$, $c = 21.591(4)$ Å, $\alpha = 98.90(2)$, $\beta = 99.900(10)$, $\gamma = 93.639(10)°$, $V = 3115.4(10)$ Å^3, $Z = 2$, $D_{calc} = 1.556$ g cm^{-3}, $F(000) = 1440$, Mo-K_α radiation ($\lambda = 0.71073$ Å), $\mu = 4.085$ mm^{-1}.

Diffraction intensities (crystal size $0.25 \times 0.40 \times 0.30$ mm, $2\theta = 3.5$–$45°$, 8201 unique data) were collected at 20°C on a Siemens R3m/V diffractometer using the 2θ–θ scan mode (1.5–14.65° min^{-1} in ω) in the range $3.5 \leqslant 2\theta \leqslant 45°$. Data processing, absorption corrections, structure solution and full-matrix least-squares refinement were performed with the SHELXTL-PLUS program package.[8] The non-hydrogen atoms were refined anisotropically. All the hydrogen atoms were generated geometrically (C—H = 1.00 Å), assigned isotropic temperature factors and included in the structure-factor calculations. The final residuals were $R = 4.60\%$ and $wR = 6.47\%$ for 6017 observed data with $F > 4.0\sigma(F)$.

RESULTS AND DISCUSSION

The IR spectrum of the complex exhibits five ν(C≡O)s. The ^{13}C NMR spectrum shows a resonance at δ 229.5 (t) for the CO_2 group and four resonances due to five terminal C≡Os. The ^{31}P NMR spectrum shows four doublets for the four non-equivalent phosphorus atoms.

The molecular structure of the complex was confirmed by X-ray determination. A distorted octahedral environment is observed for each rhenium atom (Fig. 1). The bridging carboxylate occupies two *cis* positions on Re(1) acting as a bidentate ligand, whereas the same ligand is monodentate on Re(2). This homobimetallic compound represents the first example reported of a carboxylate group acting as a bidentate ligand to one transition metal atom, while acting as a monodentate ligand to another identical atom. Other structural features involve one terminal CO and one phosphorus atom *trans* to the carboxylate ligand on Re(1) and the remaining terminal CO group and the phosphorus atom *cis* to the carboxylate. One terminal CO is *trans* to the carboxylate ligand on Re(2). The remaining two phosphorus atoms and COs occupy positions *cis* to the carboxylate.

The two oxygen atoms of the carboxylate group

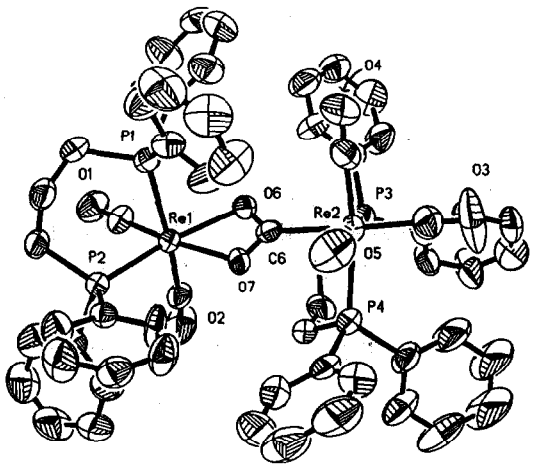

Fig. 1. Perspective drawing of the molecule $(dppp)(CO_2)ReO_2CRe(CO)_3(dppp)$. Selected bond distances (Å) and angles (°): Re(1)—P(1) = 2.474(3), Re(1)—P(2) = 2.343(3), Re(1)—O(6) = 2.208(8), Re(1)—O(7) = 2.198(8), Re(1)—C(1) = 1.867(13), Re(1)—C(2) = 1.916(11), Re(1)—C(6) = 2.633(13), Re(2)—P(3) = 2.483(3), Re(2)—P(4) = 2.467(4), Re(2)—C(3) = 1.937(17), Re(2)—C(4) = 1.919(15), Re(2)—C(5) = 1.939(14), Re(2)—C(6) = 2.191(13); P(1)—Re(1)—P(2) = 89.5(1), P(2)—Re(1)—O(6) = 163.0(2), P(2)—Re(1)—O(7) = 106.0(2), P(1)—Re(1)—C(7) = 85.9(4), P(1)—Re(1)—C(2) = 171.5(4), O(6)—Re(1)—C(2) = 94.6(4), C(1)—Re(1)—C(2) = 85.7(5), P(3)—Re(2)—C(3) = 97.6(4), P(3)—Re(2)—C(4) = 94.9(4), C(3)—Re(2)—C(4) = 89.0(7), P(4)—Re(2)—C(5) = 90.2(4), C(4)—Re(2)—C(5) = 88.5(6), P(4)—Re(2)—C(6) = 83.3(3), C(4)—Re(2)—C(6) = 87.7(6), P(3)—Re(2)—C(5) = 174.8(4), P(4)—Re(2)—C(4) = 171.0(5), C(3)—Re(2)—C(6) = 173.0(5), O(6)—C(6)—O(7) = 112.9(11).

are bonded to Re(1) in a symmetrical fashion with the Re—O distances being essentially equal [Re(1)—O(6) = 2.208(6) and Re(1)—O(7) = 2.198(8) Å]. The Re(2)—C(6) distance of 2.191(13) Å is slightly longer than the corresponding distance of 2.058(9) Å in $Cp^*(PPh_3)(NO)ReCO_2SnPh_3$[3a] and 2.04(4) Å in $[Cp^*(CO)(NO)ReCO_2WCp_2][BF_4]$.[2c] The C(6)—O(6) distance of 1.260(15) Å is slightly shorter than the C(6)—O(7) distance of 1.289(14) Å. The O(6)—C(6)—O(7) angle of 112.9(11)° is almost equal to the corresponding angle of 112.2(8)° in $Cp^*(PPh_3)(NO)ReCO_2SnPh_3$.[3a] However, this angle is significantly smaller than the corresponding angle of 115.8° in $(PMe_3)_2(CO)_2Mn(O_2CCH_3)$[9] and 118(1)° in $(PPh_3)_2(CO)_2Re(O_2CCH_3)$[10] and larger than the angle of 106(3)° in $[Cp^*(CO)(NO)ReCO_2WCp_2][BF_4]$.[2c]

Supplementary materials. Tables of positional and isotropic thermal parameters, anisotropic thermal parameters and bond distances and angles (7

pages); tables of structure factors (30 pages). Directions for ordering are given on any current masthead page.

REFERENCES

1. (a) A. Behr, *Angew. Chem., Int. Edn Engl.* 1988, **27**, 661; *Carbon Dioxide Activation by Metal Complexes.* VCH Publishers, Weinheim, Germany (1988); (b) P. Braunstein, D. Matt and D. Nobel, *Chem. Rev.* 1988, **88**, 747; (c) *Catalytic Activation of Carbon Dioxide* (Edited by W. M. Ayers), ACS Symposium Series 363. American Chemical Society, Washington, DC (1988); (d) D. Walther, *Coord. Chem. Rev.* 1987, **79**, 135; (e) D. J. Darensbourg and R. A. Kudaroski, *Adv. Organomet. Chem.* 1983, **22**, 129; (f) D. A. Palmer and R. van Eldik, *Chem. Rev.* 1983, **83**, 651; (g) R. P. A. Sneden, in *Comprehensive Organometallic Chemistry* (Edited by G. Wilkinson, F. G. A. Stone and F. W. Abel), Vol. 8, Ch. 50.4. Pergamon Press, New York (1982).
2. (a) C. T. Tso and A. R. Cutler, *J. Am. Chem. Soc.* 1986, **108**, 6069; (b) J. C. Vites, B. D. Steffey, M. E. Giuseppetti-Derry and A. R. Cutler, *Organometallics* 1991, **10**, 2827; (c) R. S. Pilato, C. Housmekerides, P. Kernakoff, D. Rubin and G. L. Geoffroy, *Organometallics* 1990, **9**, 2333.
3. (a) D. R. Senn, J. A. Gladysz, K. Emerson and R. D. Larsen, *Inorg. Chem.* 1987, **26**, 2739; (b) M. E. Giuseppettil and A. R. Cutler, *Organometallics* 1987, **6**, 970; (c) D. H. Gibson, T.-S. Ong and M. Ye, *Organometallics* 1991, **10**, 1811.
4. (a) M. A. Bennett, G. B. Robertson, A. Rokicki and W. Wickramasinghe, *J. Am. Chem. Soc.* 1988, **110**, 7098; (b) E. Fujita, D. J. Szalda, C. Creutz and N. Sutin, *J. Am. Chem. Soc.* 1988, **110**, 4870; (c) A. Doehring, P. W. Jolly, C. Krueger and M. J. Romao, *Z. Naturforsch. B: Anorg. Chem., Org. Chem.* 1985, **40B**, 484; (d) G. Fachinetti, C. Floriani, A. Chiesi-Villa and C. Guastini, *J. Am. Chem. Soc.* 1979, **101**, 1767.
5. (a) J. D. Audett, T. J. Collins, B. D. Santarsiero and G. H. Spies, *J. Am. Chem. Soc.* 1982, **104**, 1352; (b) see also ref. 2(a).
6. (a) E. G. Lundquist, J. C. Huffman, K. Folting, B. E. Mann and K. G. Caulton, *Inorg. Chem.* 1990, **29**, 128; (b) W. Beck, K. Raab, V. Nagel and M. Steinmann, *Angew. Chem., Int. Edn Engl.* 1982, **21**, 526; (c) G. R. Jahn, B. F. G. Johnson, J. Lewis and K. C. Wong, *J. Organomet. Chem.* 1979, **169**, C23; (d) C. R. Eady, J. J. Guy, B. F. Johnson, J. Lewis, M. C. Malatesta and G. M. Sheldrick, *J. Chem. Soc., Chem. Commun.* 1976, 602.
7. S. K. Mandal, D. M. Ho and M. Orchin, *J. Organomet. Chem.* 1992, **439**, 53.
8. SHELXTL PLUS, version 3.43 for R3/V and R3m/V crystallographic systems: G. M. Sheldrick, University of Göttingen, Germany, and Siemans/Nicolet Analytical X-Ray Instruments, Inc. Madison, WI, U.S.A. (1988).
9. W. K. Dean, G. L. Simon, P. M. Treichel and L. F. Dahl, *J. Organomet. Chem.* 1973, **50**, 193.
10. G. La Monica, S. Cenini, E. Forni, M. Manassero and V. G. Albano, *J. Organomet. Chem.* 1976, **112**, 197.

Polyhedron Vol. 12, No. 11, pp. 1427–1429, 1993
Printed in Great Britain

0277–5387/93 $6.00+.00
© 1993 Pergamon Press Ltd

COMMUNICATION

EPR STUDIES ON COPPER(II) IN FOUR DIVALENT DIAMAGNETIC METALLIC COMPLEXES OF 3-AMINO,5-METHYLISOXAZOLE

S. ZAMEERUDDIN and B. A. SASTRY*

Solid State and Molecular Physics Laboratory, Department of Physics, Osmania University, Hyderabad 500 007, India

and

G. PONTICELLI and M. MASSACESI

Dipartimento di Chimica E Technologie Inorganiche E Metallorganiche, Universita Degli Studi di Cagliari Via Ospedale 72, 09124 Cagliari, Italy

(*Received* 27 *November* 1992; *accepted* 25 *February* 1993)

Abstract—From EPR studies on copper(II)-doped $Cd(3\text{-AMI})_2(SCN)_2$, $Zn(3\text{-AMI})_2(SCN)_2$, $Cd(3\text{-AMI})Cl_2$ and $Ca(3\text{-AMI})_2Cl_2\cdot H_2O$ (3-AMI = 3-amino,5-methylisoxazole) it was found that 3-AMI bonds via the N_{ring} and the coordination polyhedra of the former three complexes are distorted more towards compressed tetrahedral symmetry than the latter one, which is at variance with earlier conclusions.

The IR and electronic spectral studies on metal complexes of 3-amino, 5-methylisoxazole

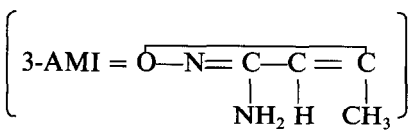

tentatively indicated that this ligand acts either as a monodentate (N_{ring} or O_{ring} bonded), bidentate or bridging bidentate (N_{ring} and O_{ring} bonded) ligand in metal complexes.[1,2] From the above studies it was also tentatively concluded that $Cd(3\text{-AMI})_2(SCN)_2$, $Zn(3\text{-AMI})_2(SCN)_2$[1] and $Ca(3\text{-AMI})_2Cl_2\cdot H_2O$[2] complexes are monomeric and tetrahedrally distorted complexes having CdN_2O_2, ZnN_2O_2 and CaN_2Cl_2 atomic sets in coordination polyhedra, respectively, unlike the polymeric bridging chloride octahedral complex $Cd(3\text{-AMI})Cl_2$,[1] which was tentatively interpreted as having the $CdCl_4NO$ moiety. Since the metal–ligand stretching frequencies of Cu—O and Cu—N fall in the same range, it will be difficult to conclude from IR spectra the actual coordinating atom among the above two if the ligands like 3-AMI contain both these donor atoms. Hence, the authors felt that EPR spectroscopy, with copper(II) as the paramagnetic probe, is the right method to unambiguously determine the type of coordinating atoms and the type of distortion in the coordination geometry of the above four complexes. EPR results obtained from polycrystalline samples are presented here.

EXPERIMENTAL

The complexes under investigation were synthesized as described earlier.[1,2] Small single crystals of 1% copper-doped complexes under consideration were grown following the usual procedure from solutions. The EPR spectra of these complexes after crushing to a fine powder form were recorded as described earlier.[3] TCNE (tetracyanoethylene), which gives a very sharp EPR signal, is used as a g (= 2.00277) marker. The errors in g and A are *ca* ± 0.001 and ± 2 G, respectively.

* Author to whom correspondence should be addressed.

RESULTS AND DISCUSSION

The EPR spectra of these complexes are shown in Fig. 1. The spin-Hamiltonian constants, metal–ligand σ-bond parameter α_σ^2 and the value of R (cm) ($|g_\parallel/A_\parallel|$) for these complexes are given in Table 1. The values of α_σ^2 in the case of $Cd(Cu)(3\text{-AMI})_2(SCN)_2$, where the ligand hyperfine structure on the parallel features is obtained, can be calculated using the procedure of Maki and McGarvey.[4] For the remaining complexes this is calculated using the expression[5] given below.

$$\alpha_\sigma^2 = \frac{|A_\parallel|}{P} + [g_\parallel - 2.0023] + 3/7[g_\perp - 2.0023] + 0.04 \quad (1)$$

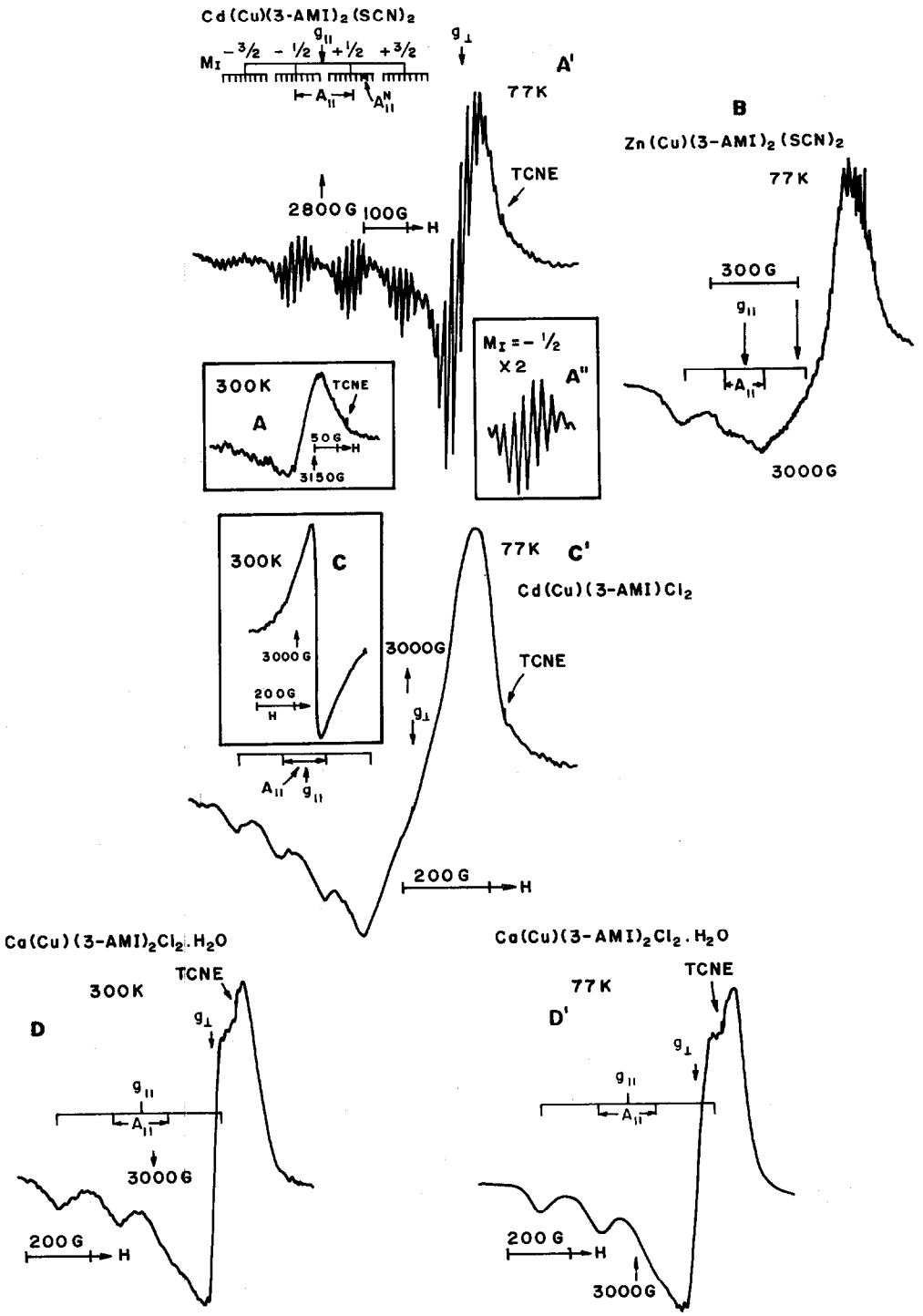

Fig. 1. ESR spectra of copper(II) in diamagnetic metal complexes of 3-AMI in polycrystalline form.

Table 1. Spin-Hamiltonian constants, α_σ^2 and R (cm) values of copper(II) in diamagnetic complexes

Sample	Temperature (K)	$g_\parallel$	$g_\perp$	$A_\parallel$ ($\times 10^4$ cm^{-1})	$A_\parallel^N$	R (cm)	α_σ^2
Cd(Cu)(3-AMI)$_2$(SCN)$_2$	77	2.305	2.069	117.9	13.75	196	0.68
Cd(Cu)(3-AMI)Cl$_2$	77	2.348	2.059	109.2	—	215	0.73
Zn(Cu)(3-AMI)$_2$(SCN)$_2$	77 and 300	2.208	2.104	143.7	—	153	0.69
Ca(Cu)(3-AMI)$_2$Cl$_2$·H$_2$O	300	2.200	2.049	179.0	—	123	0.76
	77	2.198	2.058	184.1	—	119	0.77

The following structural information for these complexes has been extracted from the above data.

(1) The greater resolution of the EPR spectra observed at low temperatures in the case of copper (II)-doped cadmium complexes (Fig. 1A, A′, A″, C and C′) indicates the presence of strong spin-lattice interactions. In addition larger $g_\parallel$ and smaller $A_\parallel$ values (Table 1) are obtained in these complexes. These two facts strongly support the presence of tetrahedral distortion in the coordination geometries of the above two complexes. The R (cm) values in both complexes indicate a dihedral angle[6] of *ca* 70°. Even though IR studies indicated this tetrahedral distortion in Cd(3-AMI)$_2$(SCN)$_2$, it failed to identify the above distortion in Cd(3-AMI)Cl$_2$.[1]

(2) The nine ligand hyperfine lines (LHL) on each copper(II) hyperfine line of the parallel features of the EPR spectrum of Cd(Cu)(3-AMI)$_2$(SCN)$_2$ (Fig. 1A′ and A″) clearly indicate a CuN_4 moiety, which differs from the conclusions drawn on the basis of IR studies. Even though LHL are not observed on the parallel features, LHL on the perpendicular features (Fig. 1B) and the $g_\parallel$ and $A_\parallel$ values of Zn(Cu)(3-AMI)$_2$(SCN)$_2$ are similar to those of Cu(TC-55) (TC = tropocoronand),[7] where the dihedral angle of CuN_4 coordination tetrahedral geometry is 61°. In this case also the IR spectral predictions about the coordinating atoms failed. In both the above two complexes the metal–ligand σ-bond is stronger than in the other two complexes.

(3) High $A_\parallel$ and low $g_\parallel$ and R (cm)(119) values observed in Ca(Cu)(3-AMI)$_2$Cl$_2$·H$_2$O rule out the possibility of considerable tetrahedral distortion, as predicted by IR studies, since the dihedral angle from the value of R (cm) is only 40°.[6]

(4) From the above observation it is evident that 3-AMI acts as a monodentate N_{ring}-bonded ligand in all the complexes.

REFERENCES

1. G. Devoto, M. Massacesi, G. Ponticelli and R. Ruggiri, *J. Inorg. Nucl. Chem.* 1977, **39**, 355.
2. M. Massacesi, R. Pinna, G. Ponticelli and A. Mangia, *Spectrochim. Acta* 1981, **37**, 251.
3. B. A. Sastry, S. Md. Asadullah, G. Ponticelli and M. Massacesi, *J. Chem. Phys.* 1979, **70**, 2834.
4. A. H. Maki and B. R. McGarvey, *J. Chem. Phys.* 1958, **29**, 31, 35.
5. D. Kivelson and R. Neimann, *J. Chem. Phys.* 1961, **35**, 149.
6. J. Gouteron, S. Jeannin, Y. Jeannin, J. Livage and C. Sanchez, *Inorg. Chem.* 1984, **23**, 3387.
7. W. M. Davis, A. Zask, K. Nakanishi and S. J. Lippard, *Inorg. Chem.* 1985, **24**, 3737.

Polyhedron Vol. 12, No. 11, pp. 1431–1432, 1993
Pergamon Press Ltd. Printed in Great Britain.

ANNOUNCEMENTS

LATIN-AMERICAN INORGANIC CHEMISTRY MEETING

13–17 SEPTEMBER 1993

Santiago de Compostela, Spain

Please address correspondence to:

Prof. Dr A. Castiñeiras
Departamento de Química Inorganíca
Facultad de Farmacia
Universidade de Santiago de Compostela
15706 Santiago de Compostela
Spain
Tel.: 34(9)81 594636
Fax: 34(9)81 594912

2ND ANAIC INTERNATIONAL CONFERENCE ON MATERIALS SCIENCE AND ENVIRONMENTAL CHEMISTRY ON MAIN GROUP ELEMENTS

8–11 NOVEMBER 1993

Kuala Lumpar, Malaysia

Please address correspondence to:

Prof. V. G. Kumar Das
Dean's Office, Faculty of Science
University of Malaya
59100 Kuala Lumpar
Malaysia
Tel.: (603) 756 7819
Fax: (603) 756 6343

ANNUAL POLYHEDRON PUBLICATION AWARD

Pergamon Press Ltd is pleased to announce the award annually of a cash prize of US$1000 for the best paper published in *Polyhedron*.

The award will be made to the authors of the original research paper (not including *Polyhedron* Reports) judged to be the best on the basis of scientific originality, significance, clarity and style of presentation. Members of the Editorial Board will each be invited to nominate two papers for the award and the final selection will be made by an anonymous committee appointed by the Editors who themselves will not be eligible for the award.

The award for 1992 will be announced this year.

The recipients of the yearly award:

1987 A. J. SCIOLY, M. L. LUETKENS JR. R. B. WILSON JR, J. C. HUFFMAN and A. P. SATTELBERGER, "Synthesis and characterization of binuclear tantalum hydride complexes", *Polyhedron* Vol. 6. No. 4, pp. 741–757 (1987).

1988 G. PARKIN and J. E. BERCAW, "Halide, hydride, alkyl, oxo and related derivatives of bis(pentamethylcyclopentadienyl)tungsten(IV)", *Polyhedron* Vol. 7, No. 19/20, pp. 2053–2082 (1988)

1989 FU-MIN SU, J. C. BRYAN, SOONHEE JANG and J. M. MAYER, "Tungsten complexes with strong π-donor and π-acceptor ligands: $W(E)Cl_2(L)(PR_3)_2$ (E = O, NR, S, and L = CO, CNR, CH_2=CHR and O=CHMe)", *Polyhedron* Vol. 8, No. 10, pp. 1261–1277 (1989).

1990 P. W. JOLLY and co-workers, "η^3-Allyl complexes of tungsten—I. Preparation and reactions of $[(\eta^3\text{-}C_3H_5)_3WCl]_2$" and "$\eta^3$-Allyl complexes of tungsten—II. Reaction of $[(\eta^3\text{-}C_3H_5)_3WCl]_2$ with organomagnesium compounds", *Polyhedron* Vol. 9, No. 1, pp. 11–22 and 23–34 (1990).

1991 D. H. BERRY, J. CHEY, H. S. ZIPIN and P. J. CARROLL, "Reactivity of molybdenum and tungsten disilene complexes", *Polyhedron* Vol. 10, No. 11, pp. 1189–1201 (1991).

Polyhedron Vol. 12, No. 12, pp. 1433–1435, 1993
Printed in Great Britain

0277–5387/93 $6.00+.00
© 1993 Pergamon Press Ltd

PREPARATION AND CRYSTAL STRUCTURE OF $MoO_2Cl_2(H_2O)_2 \cdot H_2O \cdot Et_4NCl$ IN RELATION TO THE NATURE OF THE MOLYBDENUM(VI) SPECIES IN HYDROCHLORIC ACID SOLUTIONS

MICHAEL J. TAYLOR,* WANG JIRONG and CLIFTON E. F. RICKARD

Department of Chemistry, University of Auckland, Auckland, New Zealand

(*Received* 5 *January* 1993; *accepted* 5 *March* 1993)

Abstract—Crystallization of a solution of Mo^{VI} in HCl containing Et_4NCl yields the molecular complex dioxodichlorodiaquamolybdenum(VI) in association with Et_4N^+ and Cl^- ions. Structure determination of the title compound by X-ray crystallography reveals $MoO_2Cl_2(H_2O)_2$ units with *cis,trans,cis* arrangement of ligands, which are linked by forming hydrogen bonds to the H_2O molecule of crystallization. Vibrational spectroscopic data confirm this complex as the predominant Mo^{VI} species in hydrochloric acid solutions.

The coordination chemistry of molybdenum (VI) oxo complexes holds continuing interest.[1,2] Recently, the molecular structures of MoO_2Cl_2 and MoO_2Br_2 have been redetermined by electron diffraction in the gas phase and shown to have C_{2v} symmetry, the bond angle O=Mo=O measuring 106.3° (Cl) or 107.8° (Br).[3] Derivatives of the type $MoO_2Cl_2L_2$ (L = neutral donor) are numerous;[4] the general structure is one in which the oxo-atoms are *cis*, the anionic ligands are *trans* and the neutral ligands are *trans* to oxo and thus *cis* to each other. Exceptions may arise if the neutral donors are in the form of a bidentate ligand such as tetramethylethylenediamine; an example is MoO_2Cl_2 (tmen), which is thought to have one N-donor *trans* to oxygen but the other *trans* to chlorine.[5]

In previous work we have gained structural evidence relating to the species $MoO_2X_2(H_2O)_2$ (X = Cl or Br) in solution using ^{95}Mo NMR and vibrational spectroscopy[6] and have also identified $[MoO_2Cl_4]^{2-}$ as the Cs^+ salt which can be prepared from a solution of Mo^{VI} in hydrochloric acid. Seeking to obtain oxohalogenomolybdenum(VI) species in crystalline form suitable for X-ray investigation, we have prepared the compound $(Et_4N)MoO_2Cl_3 \cdot 3H_2O$. This could possibly have contained an Mo^{VI} anion such as $[MoO_2Cl_3]^-$, $[Mo_2O_4Cl_6]^{2-}$ or $[MoO_2Cl_3(H_2O)]^-$, but instead reveals the molecular complex $[MoO_2Cl_2(H_2O)_2]$ whose structure and dimensions we have determined by means of crystallography.

EXPERIMENTAL

Preparation of $[(C_2H_5)_4N]MoO_2Cl_3 \cdot 3H_2O$

Tetraethylammonium chloride (1.00 g, 6.0 mmol) dissolved in concentrated hydrochloric acid (4 cm^3) was added slowly with stirring to a solution of $Na_2MoO_4 \cdot 2H_2O$ (0.97 g, 4.0 mmol) in a warm mixture of concentrated HCl (3 cm^3) and water (1 cm^3). The white precipitate (NaCl) was removed by filtration. The filtrate was allowed to stand; crystallization began after 1 h and was completed overnight. The colourless crystals were collected and dried on filter paper. The product is air-stable although the crystals become cloudy on long exposure, probably through partial loss of water of crystallization. A freshly prepared sample was analysed after drying over silica gel at room temperature. Found: C, 23.4; H, 6.2; N, 3.3; Cl, 26.7. Calc. for $C_8H_{26}Cl_3MoO_5N$: C, 23.0; H, 6.2; N, 3.3; Cl, 25.4%.

Attempted preparation of other complexes

Attempts to prepare analogous compounds using Pr^n_4NCl, Bu^n_2NCl or Et_4NBr and $Na_2MoO_4 \cdot 2H_2O$

* Author to whom correspondence should be addressed.

using similar methods did not give well-defined products.

Crystallography

A colourless crystal of the title compound was mounted on a silica fibre on an Enraf–Nonius CAD-4 diffractometer. Unit cell parameters were obtained from a least-squares fit to the four circle coordinates of 25 reflections using monochromatic Mo-K_α radiation ($\lambda = 0.71069$ Å). Intensity data were collected using ω–2θ scans with scan width $0.8 + 0.35 \tan\theta$, giving 3804 unique reflections in the range $2° < 2\theta < 55°$. The data were corrected for Lorentz and polarization effects and an absorption correction applied using empirical phi scans.

Crystal data. $C_8H_{26}Cl_3MoO_5N$, $M = 418.29$, triclinic, space group $P\bar{1}$, $a = 11.141(4)$, $b = 7.242(1)$, $c = 11.810(4)$ Å, $\alpha = 96.46(2)$, $\beta = 114.45(3)$, $\gamma = 77.87(2)°$, $U = 847.7$ Å^3, $Z = 2$, $D_o = 1.65$, $D_c = 1.638$ g cm^{-3}, $F(000) = 428$, μ(Mo-K_α) = 11.7 cm^{-1}.

The structure was solved by conventional Patterson and difference-Fourier techniques and refined by full-matrix least-squares. Non-hydrogen atoms were assigned anisotropic thermal parameters. Hydrogen atoms of the tetraethylammonium group were included in calculated positions and allowed to ride on the atom to which they were attached. Hydrogen atoms of the water molecule were located from difference Fourier maps and allowed to refine with restrained O—H distances and a common thermal parameter. The final R and R' values were 0.041 and 0.042, respectively, for the 3626 observed data ($I > 3\sigma\{I\}$) and weights $1.0/[\sigma(F^2) + 0.016F^2]$. Final atomic coordinates, thermal parameters and tables of observed and calculated structure factors have been deposited with the Editor.

Spectroscopy

IR spectra were measured using a Digilab FTS-60 spectrometer and Raman spectra using a Jobin–Yvon U1000 system with the green line of a Spectra Physics argon-ion lazer as the excitation source.

RESULTS AND DISCUSSION

The X-ray structure determination shows that the solid which forms from a solution of Mo^{VI} in hydrochloric acid, containing tetraethylammonium chloride, consists of Et_4N^+ and Cl^- ions co-crystallized with $MoO_2Cl_2(H_2O)_2$ molecules. The arrangement of these species in the unit cell is displayed in Fig. 1. The third H_2O molecule [oxygen O(5)] exists in the solid as water of crystallization; its position shows it to be involved in hydrogen bonding between the ligand H_2O groups of different molecules of the molybdenum complex, such that these are linked throughout the structure. The distances, O(1)—O(5) of 2.75 and O(5)—O(2′) of 2.75 Å, are normal for hydrogen bonds between oxygen atoms. The Et_4N^+ cation has the expected values of bond lengths and angles; these dimensions are not cited here but form part of the supplementary material.

A view of the $MoO_2Cl_2(H_2O)_2$ molecule is given in Fig. 2 and the bond distances and angles are listed in Table 1. The structure is distorted octahedral with *cis*-oxo groups, *cis*-H_2O ligands and *trans*-chlorine atoms, which is the expected pattern for a complex of this type.[4] The Mo=O distances of 1.685(2) and 1.690(2) Å are slightly less than the average value of 1.704 Å derived from a large number of dioxomolybdenum structures,[7] whilst the O=Mo=O angle of 103.5° is at the low end of the established range (102–114°).[1] The Cl—Mo—Cl angle of 157.9° is far removed from the nominal

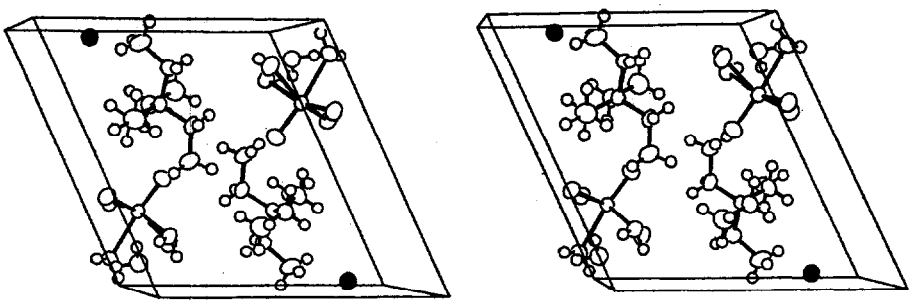

Fig. 1. The contents of the unit cell of $MoO_2Cl_2(H_2O)_2 \cdot H_2O \cdot Et_4NCl$. The chloride ions are shown in black.

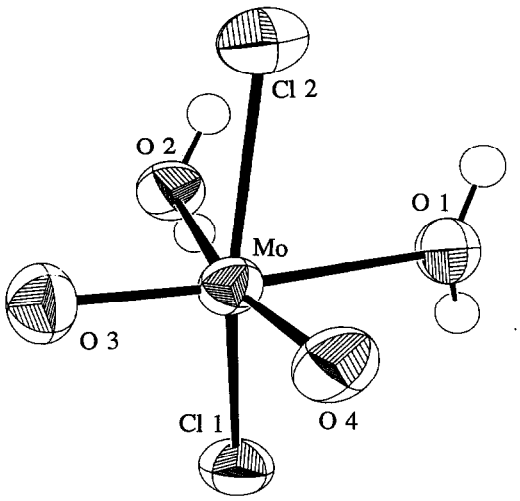

Fig. 2. A perspective view of the $MoO_2Cl_2(H_2O)_2$ molecule.

180° owing to repulsion between the Mo=O and Mo—Cl groups. The Mo—Cl bond lengths are practically equal at 2.346(1) Å. However, the distances to the H_2O ligands differ significantly, being 2.261(2) and 2.283(2) Å, perhaps in consequence of their involvement in hydrogen bonding to the third water molecule. The structure is akin to that of $MoO_2Cl_2(H_2O)_2 \cdot 2C_5H_5NHCl$, which is built up from the neutral molybdenum complex, pyridinium and chloride ions,[8] but lacks the water of crystallization which occurs in the present compound.

It is worthwhile to compare the structure of $MoO_2Cl_2(H_2O)_2$ with that of the uncomplexed MoO_2Cl_2 molecule in which r(Mo=O) = 1.686(4) and r(Mo—Cl) = 2.258(3) Å, ∠O=Mo=O = 106.3 and ∠Cl—Mo—Cl = 113.9°.[3] The introduction of the water molecules as ligands *trans* to the oxo groups appears to cause no change in the Mo=O bond lengths, whereas the Mo—Cl bonds are increased in length by almost 0.1 Å. The unsaturation of the MoO_2Cl_2 molecule is evident from the fact that anhydrous MoO_2Cl_2 has a layer structure in the solid state, in which both oxygen atoms participate in an Mo—O—Mo bridging system.[9] In the monohydrate, $MoO_2Cl_2 \cdot H_2O$, the entry of a water molecule into the coordination sphere of molybdenum atoms breaks down the layers into chains of octahedra, in which one oxo oxygen atom is bridging and one is terminal.[10]

The IR and Raman spectra of the solid $MoO_2Cl_2(H_2O)_2 \cdot H_2O \cdot Et_4NCl$ were investigated in the range 100–1200 cm^{-1}. After making allowances for bands due to the Et_4N^+ ion the remaining features are in good agreement with the spectra assigned to $MoO_2Cl_2(H_2O)_2$ in our earlier work.[6] Assignments for the solid (with the solution-state values in parentheses) are ν_{sym}(Mo—Cl) 318 (310), ν_{asym}(Mo—Cl) 353 (346), ν_{asym}(Mo=O) 910 (922) and ν_{sym}(Mo=O) 950 (960) cm^{-1}. Our previous study of molybdenum(VI) complexes[6] gave evidence that $MoO_2Cl_2(H_2O)_2$ is the predominant species in aqueous solution at high HCl concentration, and is the form in which molybdenum(VI) enters the organic phase during solvent extraction by ether or a ketone. The co-crystallization of $MoO_2Cl_2(H_2O)_2$ with Et_4NCl supports its presence in HCl solutions (notwithstanding the fact that the addition of CsCl leads to the separation of $Cs_2MoO_2Cl_4$ crystals). Ease of replacement of ligands *trans* to the oxo groups is a characteristic property of oxomolybdates, which has been widely used in the synthesis of such complexes.[4] The observation that either $MoO_2Cl_2(H_2O)_2$ or $MoO_2Cl_4^{2-}$ can be obtained from the Mo^{VI}/HCl solution simply by choice of the added halide salt is in harmony with this fact.

Table 1. Selected bond distances (Å) and angles (°) for $MoO_2Cl_2(H_2O)_2$

Mo—O(1)	2.283(2)	Mo—Cl(1)	2.347(1)
Mo—O(2)	2.261(2)	Mo—Cl(2)	2.346(1)
Mo—O(3)	1.685(2)		
Mo—O(4)	1.690(2)		
O(1)—Mo—O(2)	78.5(1)		
O(3)—Mo—O(4)	103.5(1)		
Cl(1)—Mo—Cl(2)	157.9(0)		

REFERENCES

1. E. I. Stiefel, *Prog. Inorg. Chem.* 1977, **22**, 1.
2. P. Román, A. Luque, J. M. Gutiérrez-Zorrilla and S. García-Granda, *Polyhedron* 1991, **10**, 2057.
3. H. Thomassen and K. Hedberg, *J. Molec. Struct.* 1992, **273**, 197.
4. E. J. Steifel, *Comprehensive Coordination Chemsitry* (Edited by G. Wilkinson, R. D. Gillard and J. A. McCleverty), Vol. 3, Ch. 36, p. 1375. Pergamon Press, Oxford (1987).
5. K. Dreisch, C. Andersson and C. Stålhandske, *Polyhedron* 1992, **11**, 2143.
6. J. M. Coddington and M. J. Taylor, *J. Chem. Soc., Dalton Trans.* 1990, 41.
7. J. M. Mayer, *Inorg. Chem.* 1988, **27**, 3899.
8. B. Kamenar and M. Penavić, *Acta Cryst.* 1976, **B32**, 3323.
9. L. O. Atovmyan, Z. G. Aliev and B. M. Tarakanov, *Zh. Strukt. Khim.* 1968, **9**, 1097.
10. F. A. Schröder and H. Schulz, *Acta Cryst.* 1973, **A29**, 333.

Polyhedron Vol. 12, No. 12, pp. 1437–1441, 1993
Printed in Great Britain

0277–5387/93 $6.00+.00
© 1993 Pergamon Press Ltd

A DIRUTHENIUM(III)-μ-OXO COMPLEX WITH AMINO ACID BRIDGES AND ITS OXIDATIVE DEAMINATION IN THE PRESENCE OF OXYGEN

M. M. TAQUI KHAN,* AMJAD HUSSAIN,* M. A. MOIZ, DEBABRATA CHATTERJEE and R. B. THORAT

Discipline of Coordination Chemistry and Homogeneous Catalysis, Central Salt and Marine Chemicals Research Institute, Bhavnagar 364 002, India

(*Received* 31 *July* 1992; *accepted* 5 *March* 1993)

Abstract—A stable diamagnetic complex of the type $[(Ru^{III}edta)_2\text{-}\mu\text{-}(amino\text{-}acidato)_2\text{-}\mu\text{-}oxo]^{6-}$ is reported. The amino acid bridge in the presence of oxygen undergoes oxidative deamination, as shown by the formation of an α-keto acid and the liberation of NH_3. The reaction is catalytic.

μ-Oxo-μ-diacetato diiron(II) cores in non-haeme proteins are known to be active centres.[1,2] Depending on the nature of the bridging groups these proteins act as oxygen carriers,[1,2] oxygen activating systems[3,4] and in the hydrolysis of phosphoric acid esters.[5,6] This led to extensive research in the chemistry of μ-oxo-μ-diacetato diiron(III) complexes with reference to their optical and magnetic properties and structures.[7] There has been a growing interest in developing the parallel chemistry of μ-oxo-ruthenium(III) complexes.[8,9] The iron and ruthenium complexes studied so far incorporate simple carboxylates as bridges[10] rather than amino acids, as in the natural systems.[1–6] In this paper we report diruthenium(III)-μ-oxo complexes with bridged amino acids, viz. alanine, phenylalanine and valine complexes, which have been characterized in solution as well as in the solid state. The complexes are stable under inert atmosphere and undergo oxidative deaminations under oxygen. The reactions were found to be catalytic.

EXPERIMENTAL

Materials

$RuCl_3$ was purchased from Johnson Matthey. All other chemicals used were of A.R. grade. All organic solvents were purified using known procedures.[11,12]

$K[Ru(edtaH)Cl]\cdot 2H_2O$ (**1**) was prepared by a known procedure.[13]

Syntheses of $Na_6[(edtaRu)_2\text{-}\mu_2\text{-amino acid-}\mu\text{-oxo}]$

Compound **1** *(0.2 mmol) and the appropriate* amino acid were dissolved in H_2O (10 cm^3) and the solution degassed with nitrogen. The pH was raised to 10.5 and the solution left overnight when it turned maroon. The solution was transferred to a flask containing degassed acetone (100 cm^3) and left under nitrogen for a week at 0°C. A dark purple solid separated, which was washed with ethanol, acetone and dried *in vacuo*. All operations were performed using the Schlenk technique. The yields ranged from 22 to 25%. Physicochemical data for the complexes are presented in Table 1.

Physical measurements

Absorption spectra were recorded on a Shimadzu UV–vis 160 spectrophotometer equippd with a TCC-240A temperature controller. Electrochemical studies were performed on PAR (model 174A) electrochemical equipment. The cyclic voltammogram (CV) at pH 10.5 was recorded using a mercury electrode as the working electrode and S.C.E. as the reference electrode. Raman spectra were recorded on a Spex Ramalog spectrometer

* Authors to whom correspondence should be addressed.

Table 1. Physicochemical data for $Na_6[(EDTARu)_2$-μ^2-amino acid-μ-O] complexes

Amino acid	Elemental analysis[a] C	H	N	λ_{max} (ε)[b]
Phenylalanine (**2**)	35.8(36.2)	3.2(3.5)	6.4(6.7)	548(14,500)
α-Alanine (**3**)	27.9(28.1)	2.4(2.3)	7.2(7.6)	552(12,600)
Valine (**4**)	31.0(30.9)	3.7(3.8)	7.1(7.2)	554(10,800)

[a] Values in parentheses are calculated.
[b] In degassed H_2O.

using 514.5 nm line of an Ar ion laser (Spectra-physics) for excitation.

Kinetics

The complex was dissolved in degassed NaOH (0.001 M) and the pH was adjusted to 10.5 with HCl and oxygen was then bubbled through. The kinetics of the deamination of amino acid bridged complexes were followed spectrophotometrically by monitoring the disappearance of the characteristic peak λ_{max} of the bridged dimer complexes. The concentration of dissolved oxygen was varied by passing through an oxygen and nitrogen mixture of varying composition. The rate constant data are reproducible to within $\pm 4\%$.

Detection of NH_3 *and α-keto acids*

The complex was dissolved in degassed NaOH, the pH adjusted to 10.5 and then oxygen was slowly bubbled through. The outlet of the reaction vessel was connected to another vessel containing HCl (0.1 M). Bubbling was continued for 24 h, after which time the HCl was back-titrated with standard NaOH. Meanwhile, bubbling of oxygen was continued and NH_3 collected as described above. This procedure was continued for 72 h until there was no appreciable change in the titre value of NaOH. From the difference in titre values before and after back-titration the amount of NH_3 was determined. From another experiment the presence of NH_3 was confirmed using Nesslers reagent.

After completion of the reaction with oxygen (72 h) the solution was acidified and the complex precipitated with ethanol and filtered. The filtrate was reduced to 4 cm^3, again acidified and the volume reduced *in vacuo*. A white solid separated, which gave a positive test for the keto group with 2,4-dinitrophenylhydrazine, and the presence of the —COOH group was confirmed by the effervescence of CO_2 on addition of $NaHCO_3$.

RESULTS AND DISCUSSION

Characterization of complexes **2–4**

Complexes **2–4** are formulated as $Na_6[Ru_2(edta)_2$-μ-(amino acid)$_2$-μ-O] on the basis of elemental analysis, UV–vis and proton NMR spectra. The absorption spectra of the complexes exhibit a strong band around 550 nm, which is assigned to M ← O charge-transfer in the Ru^{III}—O—Ru^{III} group. The assignment is based on comparison of the absorption spectra of the μ-oxo-diacetato diruthenium(III) complexes reported so far.[8–11] A similar complex of ethylenediamine exhibits a band at 565 nm. The shift in the reported complexes may be due to stronger binding of edta. These complexes, as also reported, are essentially diamagnetic (Evan's method). For the sake of clarity the details for complex **2** will be given. Similar results were obtained with complexes **3** and **4**. λ_{max} and $E_{1/2}$ were of course different.

The proton NMR spectrum exhibits peaks at 2.328 (CH_2 of ethylenediamine), 2.775 (CH_2 of —CH_2COO in edta), 3.050 (CH of amino acid), 3.375 (CH_2 of amino acid) and 7.550 ppm (phenyl protons of amino acid).

The laser Raman spectrum exhibits bands due to symmetric and asymmetric stretching of Ru^{III}—O—Ru^{III} at 636 and 729 cm^{-1} (Fig. 4), respectively. These values are *ca* 80 cm^{-1} towards a higher frequency compared with Fe^{III} complexes[14] and may be due to more diffused 4*d* orbitals in ruthenium(III).

The DPP and CV of the complex exhibit peaks at −0.28 and −0.44 V, due to stepwise reduction of Ru^{3+} to Ru^{2+}.

Complex **2** was dissolved in degassed NaOH (0.001 M) solution and the pH was adjusted to 10.5 by adding HCl (0.1 M). The absorption spectrum of complex **2** at pH 10.5 exhibited a band at 539 nm [Fig. 1(b)], whose intensity was low compared with those of μ-oxo-μ-carboxylato complexes pre-

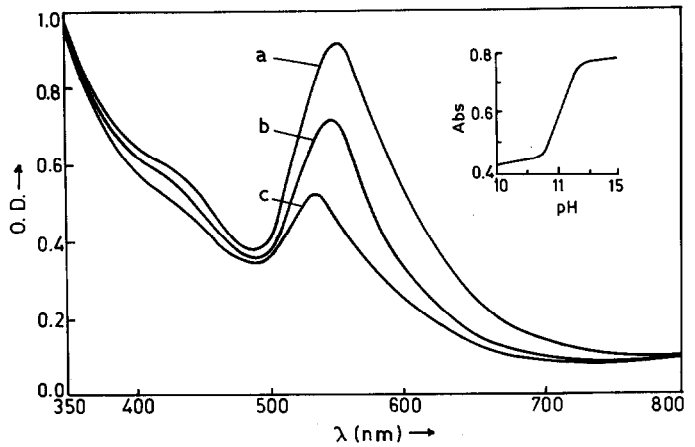

Fig. 1. Absorption spectra of complex **2**: (a) under nitrogen at pH 11.2, (b) under nitrogen at pH 10.5 and (c) after passing oxygen through (15 min) at pH 10.5. (Inset shows plot of absorbance at 548 nm as a function of pH under nitrogen.)

viously reported.[8-11] One of the reasons could be the dissociation of the complex to a monomeric species.

$$\mathrm{LMOML} \underset{-H_2O}{\overset{+H_2O}{\rightleftharpoons}} 2\mathrm{LMOH} \underset{-H^+}{\overset{+H^+}{\rightleftharpoons}} 2\mathrm{ML(H_2O)}$$

If this is so then an increase in pH would favour the formation of the dimer and the spectrum at higher pH would have shown an increase in absorbance. However, the spectrum of **2** at pH 11 showed a shift in λ_{max} to 548 nm with ε_{max} comparable to those of reported complexes.[8-11] Such behaviour is reminiscent of the protonation/deprotonation of the μ-oxo group.[11]

$$\mathrm{LMOML} \overset{+H^+}{\rightleftharpoons} \mathrm{L\overset{H}{M}OML} \qquad (1)$$

Decreasing the pH of the solution from 11.0 to 10.5 resulted in the reappearance of the peak at 539 nm. When the pH of the complex solution was again adjusted to 11.0 (addition of NaOH) the peak at 548 nm reappeared. Thus, increases and decreases of pH back and forth reproduced the spectrum at the corresponding pH value, demonstrating the existence of an equilibrium [eq. (1)]. From the plot of absorbance vs pH (Fig. 1 inset) the dissociation constant (pK_a) for reaction (1) was found to be 10.9 ± 0.1 ($T = 35°C$, $\mu = 0.1$). Thus, the species at pH 10.5 under nitrogen is a μ-hydroxo rather than a μ-oxo species.

On passing oxygen through the above solution the peak shifts further to 533 nm [Fig. 1(c)]. This may be due to the coordination and concomitant reduction of oxygen by transfer of electrons from Ru^{3+}. DPP (Fig. 2) and CV of this solution exhibit a peak at +0.04 V, assigned to an Ru^{4+}/Ru^{3+} couple. Due to oxidation of Ru^{3+} to Ru^{4+} the acidity of μ-OH increases and, therefore, it becomes deprotonated to form a μ-oxo species. Thus, the

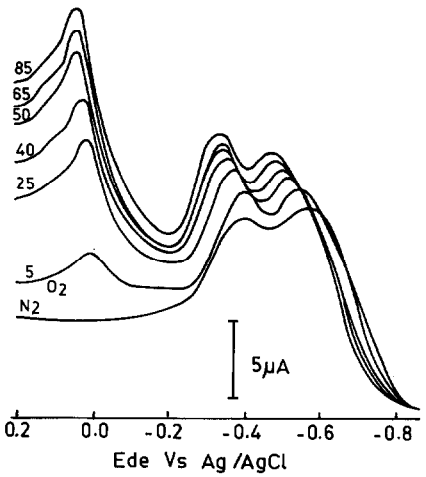

Fig. 2. DPP of **2** under nitrogen and under oxygen at different time intervals (indicated on DPP in minutes); $T = 35°C$, $\mu = 0.10$ M (KCl).

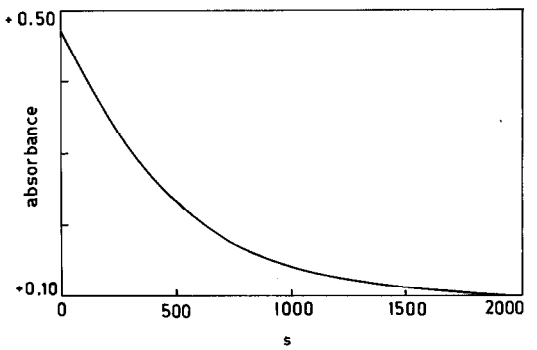

Fig. 3. Trace showing the decrease in intensity of the peak at 533 nm after passing oxygen through a solution of complex **2**; $T = 35°C$, $\mu = 0.10$ M (KCl).

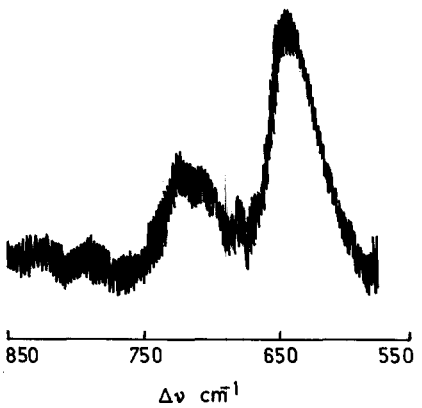

Fig. 4. Raman spectrum of complex **2**, excitation line: 514.5 nm, Ar ion 50 mW. Average of two scans.

species at pH 10.5 under oxygen is a μ-oxo peroxo diruthenium(IV) complex (**2a**).

$$\overset{H}{LMOML} \xrightarrow{O_2} LMOML(O_2)+H^+ \qquad (2)$$

Complex **2a** could not be isolated due to its instability under oxygen.

Oxidation of amino acid

On passing oxygen through a solution of the complex the peak at 533 nm starts decreasing (Fig. 3) until the spectrum resembles that of **1** in the absence of the amino acid. The reaction mixture gives a positive test for the α-keto acid and NH_3 as produced. The amount of NH_3 varied between 70–75% of the theoretical value. To account for these observations a possible mechanism is given below in Scheme 1.

In Scheme 1 hydride is abstracted from the α-carbon atom of the coordinated amino acid, which ultimately transfers its $2e^-$ to two ruthenium(IV) centres resulting in an Ru^{III}–Ru^{III} hydroperoxo species (**2d**). The cleavage of the C—H bond is facilitated by the presence of the R groups on C(2) atoms. An OH^- is then transferred to the α-carbonium ion thus produced to give **2c**.[15] The prototropic changes result in the formation of the keto acid and elimination of NH_3 to give complex **2d**. Species **2d** once again undergoes the same sequence of reactions and a second molecule of coordinated amino acid is oxidized (reaction requires **2c** and **2d** in Scheme 1). If at this stage the solution is degassed with argon and fresh amino acid added then the 539 nm peak again builds up. On passing oxygen through once again it disappears, repeating the cycle. Several such cycles could be run, indicating the catalytic nature of the reaction. If hydride abstraction takes place as proposed above then k_{obs} should follow the order valine > α-alanine > phenylalanine, since the R group with better electron donating properties will facilitate the hydride abstraction. The k_{obs} calculated are 1.31×10^{-3}, 0.85×10^{-3} and 0.68×10^{-3}

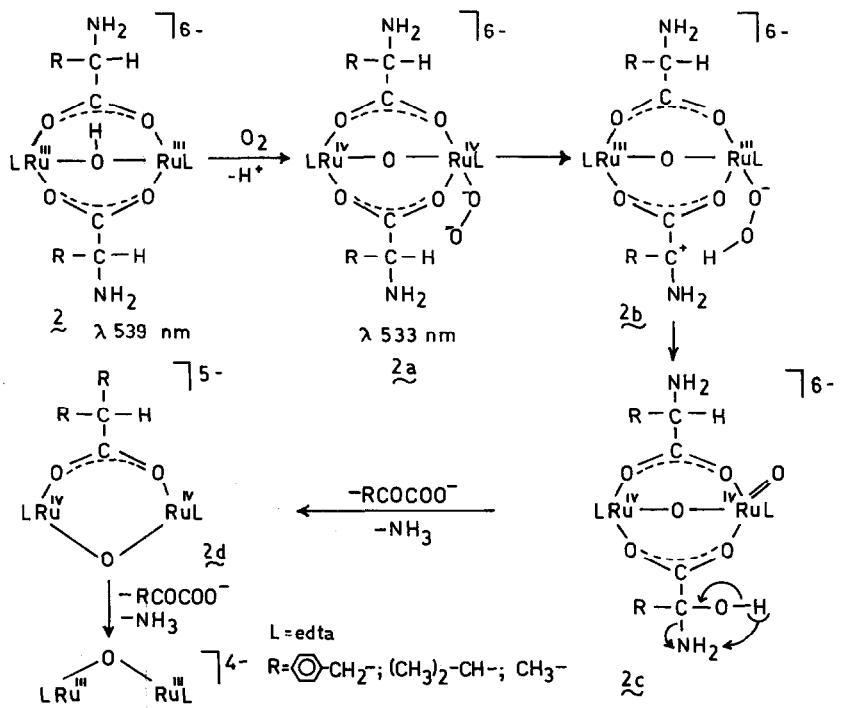

Scheme 1.

s^{-1} for valine, alanine and phenylalanine, respectively, thus supporting the assumption.

REFERENCES

1. R. E. Stenkamp, L. A. Sieker, L. H. Jensen and J. Sanders-Loehr, *Nature (London)* 1981, **291**, 263.
2. R. E. Stenkamp, L. A. Sieker and L. J. Jensen, *J. Am. Chem. Soc.* 1984, **106**, 618.
3. I. J. Higgins, D. J. Best and R. C. Hammond, *Nature (London)* 1980, **286**, 581.
4. H. Dalton, *Adv. Appl. Microbiol.* 1980, **26**, 71.
5. B. C. Antanaitis and P. J. Aisen, *Biol. Chem.* 1982, **257**, 1855.
6. B. C. Antanaitis and P. J. Aisen, *Adv. Inorg. Biochem.* 1985, **5**, 11.
7. D. M. Kurtz, *Chem. Rev.* 1990, **90**, 585.
8. Y. Sasaki, M. Suzuki, A. Tokiwa, M. Ebihara, T. Yamaguchi, C. Kabuto and T. Ito, *J. Am. Chem. Soc.* 1988, **110**, 625.
9. A. Syamala and A. R. Chakravarty, *Inorg. Chem.* 1991, **30**, 4699.
10. B. K. Das and A. R. Chakravarty, *Inorg. Chem.* 1990, **29**, 2078.
11. P. Neubold, K. Wieghardt, B. Nuber and J. Weiss, *Inorg. Chem.* 1989, **28**, 459.
12. A. I. Vogel, *A Text Book of Practical Organic Chemistry*. Orient-Longman, London (1950).
13. A. A. Diamantis and J. V. Dubrawski, *Inorg. Chem.* 1982, **21**, 1142.
14. J. S. Loehr, W. D. Wheeler, A. K. Shiemke, B. A. Averill and T. M. Loehr, *J. Am. Chem. Soc.* 1989, **111**, 8084.
15. Due to the μ-oxo-μ-carboxylato core an electron can be transferred to the other metal ion via bridges. Thus, Ru^{III}–Ru^{V} species, which may have formed initially, results in Ru^{IV}–Ru^{IV} species ultimately.

Polyhedron Vol. 12, No. 12, pp. 1443–1451, 1993
Printed in Great Britain

0277–5387/93 $6.00+.00
© 1993 Pergamon Press Ltd

OXIDATION OF TERTIARY PHOSPHINES BY MOLECULAR OXYGEN CATALYSED BY Ru^{III}-EDTA COMPLEX. ELECTRONIC EFFECT OF PHOSPHINE SUBSTITUENT ON THE OXYGEN ATOM TRANSFER REACTION; X-RAY CRYSTAL STRUCTURE OF THE COMPLEX $[Ru^{III}(EDTA\text{-}H)PPh_3]$

M. M. TAQUI KHAN,†‡ DEBABRATA CHATTERJEE, M. R. H. SIDDIQUI, S. D. BHATT, H. C. BAJAJ, K. VENKATASUBRAMANIAN and M. A. MOIZ

Discipline of Coordination Chemistry and Homogeneous Catalysis, Central Salt and Marine Chemical Research Institute, Bhavnagar 364002, India

(*Received* 30 *September* 1992; *accepted* 10 *February* 1993)

Abstract—The catalytic oxidation of tertiary phosphines, PR_3 (R = *p*-fluorophenyl, phenyl and cyclohexyl), by molecular oxygen to the corresponding phosphine oxide, (PR_3O), catalysed by $Ru^{III}(EDTA\text{-}H)(H_2O)$ is reported as a function of catalyst, substrate (PR_3) and molecular oxygen concentration at a constant pH 3.0 in water–dioxan (50% v/v) medium. The reactivity of PR_3 towards catalytic oxidation by molecular oxygen decreases in the order tris(*p*-fluorophenyl)phosphine > triphenylphosphine > tris-(cyclohexyl)-phosphine. A reverse reactivity order was observed in the case of stoichiometric oxidation of PR_3 by $[O{=}Ru^{V}(EDTA)]^-$. The proposed mixed-ligand complex Ru^{III}-EDTA-PR_3 intermediate in the catalytic oxidation of PR_3 with molecular oxygen has been isolated and its structure solved by single-crystal X-ray diffraction. The experimental results are discussed in terms of the σ-basic and π-acidic character of the phosphine substrates in the homolytic bond cleavage of O—O bonds of the μ-peroxo intermediate and oxygen atom transfer to the substrate. The bond dissociation energy for O—O bond cleavage is computed by the kinetic data obtained for oxygen atom transfer from the oxo complex $[O{=}Ru^{V}(EDTA)]^-$.

The oxidation of phosphines by transition-metal oxo complexes has been the subject of much current interest.[1–5] In our laboratory we have been engaged in developing non-porphyrinic ruthenium(III) complex catalysts for the oxidation of a variety of organic substrates.[6–10] These non-porphyrinic ligands involve aminopolycarboxylic acids such as ethylenediaminetetraacetic acid (EDTA), propylenediaminetetraacetic acid (PDTA), N-hydroxyethylethylenediaminetriacetic acid (HEDTA), Schiff bases and dimethylglyoxime, which do not undergo self-oxidation during the catalytic processes. In our earlier contribution[11] we reported the oxidation of PPh_3 to PPh_3O with molecular oxygen catalysed by the Ru^{III}-EDTA complex where we proposed the formation of a mixed-ligand Ru-EDTA-PPh_3 intermediate in the catalytic cycle. We have now successfully isolated the complex $Ru^{III}(EDTA\text{-}H)PPh_3$ and determined its structure.

In order to gain an insight into the mechanistic details of the reaction, such as coordination of the phosphine ligand to the metal ion and the nature of the oxygen atom transfer, we have studied the oxidation of various phosphines (PR_3; R = *p*-fluorophenyl, phenyl and cyclohexyl) by molecular oxygen catalysed by complex **1**. We have also studied the stoichiometric oxygen atom transfer reaction in the oxidation of PR_3 by the $Ru^{V}(EDTA)(O)^-$ complex. The experimental results are discussed in terms of σ-basicity and π-acidity of PR_3 substrates, which governs the reactivity of Ru^{III} and Ru^{V} complexes.

EXPERIMENTAL

The complex $K[Ru^{III}(EDTA\text{-}H)Cl]$ (**1**) was prepared following the published procedure.[12] Dis-

† Author to whom correspondence should be addressed.
‡ Present address: 17-3-479 Yakutpura, Hyderabad 500023, A.P., India.

tilled dioxane (HPLC grade) and doubly distilled water were used to prepare all solutions. All other chemicals used were of A.R. grade.

Synthesis of $K[Ru^{V}{=}O(EDTA)]\cdot 2H_2O$

The complex $K[Ru^{V}{=}O(EDTA)]$ was prepared by interacting $K[Ru^{III}(EDTA\text{-}H)Cl]$ with iodosylbenzene.[13] To a stirred solution of K[Ru(EDTA-H)Cl] [1 mmol in 10 cm^3 water–dioxane (1 : 1)] was added iodosylbenzene (1.1 mmol) and the solution was stirred for 1 h in the dark. The greenish-brown product, $[Ru^{V}{=}O(EDTA)]^-$, thus formed was precipitated by adding acetone, immediately filtered and washed with a cold acetone–water mixture (9 : 1) and dried. Found: C, 24.9; H, 3.3; N, 5.8. Calc.: C, 25.0; H, 3.3; N, 5.8%. UV–vis spectra, λ_{max} (nm) [ε_{max} (mol^{-1} dm^3 cm^{-1})] = 390(1860). IR spectra: ν(Ru=O), 870 cm^{-1}. $E_{1/2}$ (determined by cyclic voltammetric studies) for Ru^{5+}/Ru^{4+}, Ru^{4+}/Ru^{3+} and Ru^{3+}/Ru^{2+} redox couples are 0.91, 0.14 and −0.21 V (vs S.C.E.), respectively.

Synthesis of [Ru(EDTA-H)(PR_3)] *complexes*

[Ru(EDTA-H)(PPh_3)] (**2**). To a refluxing solution of $K[Ru^{III}(EDTA\text{-}H)Cl]$ (500 mg, 1 mmol) was slowly added triphenylphosphine (260 mg, 1 mmol) dissolved in a minimum volume of dioxane. The mixture was refluxed (under nitrogen) for a period of 2 h until the colour of the solution changed from yellow to orange–yellow. The solution was then allowed to cool down and an orange–yellow product precipitated. The product was filtered, washed with cold water several times and finally with ether and dried *in vacuo* (yield: 89%). Found: C, 51.0; H, 4.8. Calc.: C, 51.5; H, 4.3%. UV–vis in H_2O, λ_{max} (nm) [ε_{max} (mol^{-1} dm^3cm^{-1})]: 485 (3.8×10^2), 375 (1.6×10^3), 260 (6.7×10^3). IR: ν(Ru—P) = 532 cm^{-1}, μ_{eff} (Evans' method): 1.78 B.M. at 300 K.

Complexes $[Ru^{III}(EDTA\text{-}H)(P(C_6H_4{-}F)_3)]$ (**3**) and $[Ru^{III}(EDTA\text{-}H)(C_6H_{11})_3]$ (**4**) were prepared following a similar procedure as described for the preparation of **2**. Found: C, 49.4; H, 5.8; N, 3.9. Calc. for $[Ru^{III}(EDTA\text{-}H)P(C_6H_4{-}F)_3]$: C, 50.1; H, 6.9; N, 4.3%. UV–vis, λ_{max} (nm) [ε_{max} (mol^{-1} dm^3 cm^{-1})] = 481 (3.67×10^2).

$[Ru^{III}(EDTA\text{-}H)P(C_6H_{11})_3]$. Found: C, 47.5; H, 3.4; N, 3.9. Calc.: C, 47.6; H, 3.5; N, 4.0%. UV–vis, λ_{max} (nm) [ε_{max} (mol^{-1} dm^3 cm^{-1})] = 487 (4.1×10^2).

The redox potentials for the Ru^{3+}/Ru^{2+} couple of complexes **2**, **3** and **4** determined by cyclic voltammetric studies (vs S.C.E.) are −0.11, −0.14 and −0.27 V, respectively. The ^{31}P NMR spectra of complexes **2**, **3** and **4** give a singlet at δ (ppm) = 25.79, 23.51 and 52.3, respectively. The shifts are in accordance with the decreasing shielding on the phosphorus atom in the phosphines in the order **4**, **2**, **3**.

Instrumentation and techniques

Microanalyses were performed using a Carlo–Erba elemental analyser. The electronic spectra of the complexes were recorded with a Shimadzu-160 UV–vis spectrophotometer. The IR and far-IR spectra were recorded on Beckman Aculab-10 (4000–600 cm^{-1}) and Perkin–Elmer-621 (600–200 cm^{-1}) spectrometers, respectively. pH measurements were performed using a Digisun pH meter with an accuracy of ±0.01 unit. Electrochemical studies were performed with PAR 174A electrochemical apparatus. Cyclic voltammetric studies were performed in 0.1 M $HClO_4$ medium using a glassy carbon working electrode.

Kinetic studies

Kinetics of the catalytic oxidations of PR_3 with molecular oxygen were followed by measuring the absorption of oxygen with time as described earlier.[11] Stoichiometric oxygen atom transfer from $Ru^{V}(EDTA)O^-$ to PR_3 was studied spectrophotometrically by following the decrease in the peak at 393 nm of the complex$Ru^{V}(EDTA)O^-$ with time. For this purpose equal volumes (1 cm^3) of solutions (pre-equilibrated at the desired temperature) of the oxo complex (5×10^{-4} M) and PR_3 (2.5×10^{-3}–2.5×10^{-2} M) were mixed in a spectrophotometric cell and the corresponding pseudo-first-order rate constant (k_{obs}) values were obtained from the absorbance vs time trace by the usual procedure. The rate constant data are reproducible to within ±4%.

Product analysis

The oxidation products PR_3O were analysed by ^{31}P and ^{19}F [(*p*-fluorophenyl)$_3$P] NMR spectra recorded on a JEOL FX-100 NMR spectrometer using phosphoric acid and trifluoroacetic acid, respectively, as standards. The formation of tertiary phosphine oxide with time is shown in Fig. 1.

X-ray crystallographic studies

Large yellowish-orange crystals of the complex could be obtained by recrystallization from an aqueous solution. A crystal of the dimensions $0.19\times0.28\times0.31$ mm was used for data collection. Crystal data are summarized in Table 1. Density

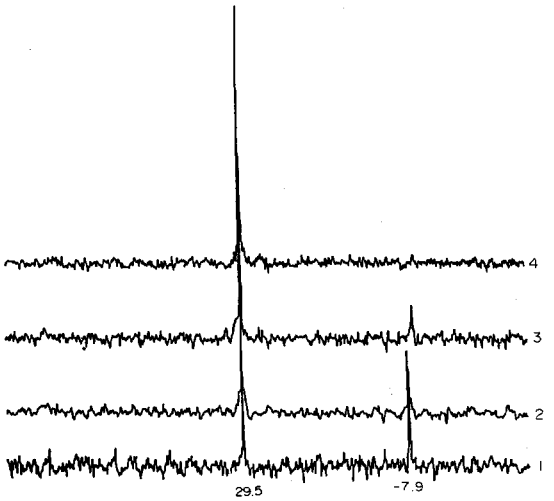

Fig. 1. ^{31}P NMR spectra for the formation of $(C_6H_4—F)_3PO$ with time at 35°C: (a) $t = 30$, (b) 60, (c) 90 and (d) 120 min.

considerations (Table 1) indicated the presence of two independent [Ru(EDTA-H)PPh_3] moieties with some solvent of crystallization. Two sets of reflection controls were used to monitor orientation and decay. Absorption corrections were applied using three intense reflections near Chi = 90°, employing the empirical absorption correction method.[14]

Table 1. Crystal data for $[Ru(EDTA\text{-}H)PPh_3]_2 \cdot 3H_2O$

Formula	$Ru_2P_2O_{19}N_4C_{55}H_{62}$
Molecular weight	1359.22
a (Å)	18.572(2)
b (Å)	14.786(2)
c (Å)	22.000(2)
β (°)	110.33(2)
Space group	$P2_1/a$
V (Å^3)	5665.0(9)
Z	4
Density (g cm^{-3})	1.593
(Cu-K_α)	1.54184
$F(000)$	2784
μ(Cu-k_α) (cm^{-1})	56.230
2θ range (°)	4–130
No. of reflections measured	7103
No. of reflections observed	3207
Data collected	$+h, +k, \pm l$
Temperature (K)	293
Transmission factors	Min. 51.67%
	Max. 99.25%
	Av. 75.08
R	0.031
R_w	0.039
(Δ/δ)	0.03

The structure was solved by the heavy atom method and was developed by alternating cycles of isotropic least-squares followed by difference-Fourier syntheses. Three water molecules in addition to two [Ru(EDTA-H)PPh_3] moieties could be located. Hydrogens could be either generated using stereochemical constraints or obtained from difference maps. A mixed mode refinement was adopted in which ruthenium, phosphorus and oxygen were refined anisotropically and carbon and nitrogen isotropically. The hydrogens were fixed employing a weighting scheme with a Dunitz–Seiler factor.[15] This resulted in convergence at an R of 0.031 ($Rw = 0.039$). Because of the large number of atoms refinement was performed in blocks. At the end of the refinement the largest shift-to-error ratio of refined parameters was 0.03; the difference map had ripples of 0.9 e Å^{-1} around the ruthenium atoms. The scattering factors for ruthenium, phosphorus, carbon, nitrogen and oxygen were from Vol. IV of the International Tables for Crystallography,[16] while those of hydrogens were from Stewart *et al.*[17] All the crystallographic computations were obtained using the SDP set of programs available on the PDP-11/73 system.[18]

RESULTS AND DISCUSSION

Figure 2 shows a PLUTO view of molecule **1**; the structure of molecule **2** is similar. The selected bond lengths and angles along with e.s.d.s are shown in Table 2. The PPh_3 moiety is *trans* with respect to one of the nitrogens of the bound EDTA ligand in both the molecules and the resulting ruthenium(III) octahedra are distorted; the dis-

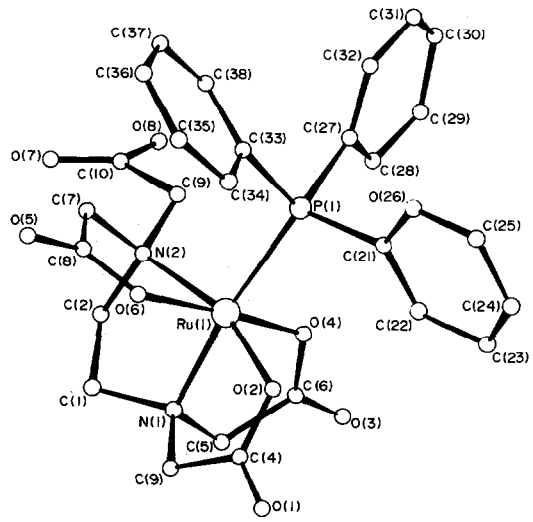

Fig. 2. PLUTO of Ru^{III}(EDTA-H)(PPh_3) (molecule **1**).

Table 2. Some important bond distances (Å) and angles (°) in structures **1** and **2**

Atoms	1	2	Atoms	1	2
Ru—P	2.351(2)	2.376(2)	P—Ru—O(2)	92.6(2)	92.9(2)
Ru—N(1)	2.061(5)	2.079(7)	P—Ru—O(4)	92.9(1)	95.7(2)
Ru—N(2)	2.116(8)	2.136(6)	P—Ru—O(6)	91.4(1)	88.9(2)
Ru—O(2)	1.998(6)	1.995(6)	P—Ru—N(1)	173.2(2)	172.9(2)
Ru—O(4)	1.981(5)	1.984(6)	P—Ru—N(2)	102.2(2)	101.4(2)
Ru—O(6)	2.060(5)	2.041(6)	O(2)—Ru—O(4)	94.1(3)	93.8(2)
C(4)—O(1)	1.20(2)	1.24(2)	O(2)—Ru—O(6)	88.3(3)	90.9(2)
C(6)—O(2)	1.313(8)	1.26(1)	O(2)—Ru—N(1)	82.1(3)	80.2(2)
C(6)—O(3)	1.18(2)	1.24(2)	O(2)—Ru—N(2)	160.6(2)	162.5(3)
C(6)—O(4)	1.332(8)	1.28(1)	O(4)—Ru—O(6)	175.0(2)	173.2(2)
C(8)—O(5)	1.24(2)	1.17(2)	O(4)—Ru—N(1)	83.5(2)	83.3(2)
C(8)—O(6)	1.27(2)	1.32(2)	O(4)—Ru—N(2)	97.7(3)	94.8(2)
C(10)—O(7)	1.21(1)	1.18(2)	O(6)—Ru—N(1)	92.5(2)	92.8(3)
C(10)—O(8)	1.33(1)	1.32(1)	O(6)—Ru—N(2)	78.8(2)	79.4(2)
C(1)—N(1)	1.5(1)	1.500(5)	N(1)—Ru—N(2)	84.1(3)	85.7(3)
C(2)—N(2)	1.518(9)	1.54(2)	O(1)—C(4)—O(2)	127.7(8)	123.3(7)
C(1)—C(2)	1.52(1)	1.53(1)	O(3)—C(6)—O(4)	123.2(7)	124.8(8)
			O(5)—C(8)—O(6)	123.3(8)	124.8(9)
			O(7)—C(10)—O(8)	125.2(9)	127.0(2)

tortion being reflected in the *cis* angles which span from 78.8(2)° to 102.2(2)° in molecule **1** and from 79.4(2)° to 101.4(2)° in molecule **2**. The range from *trans* angles in molecule **1** is 160.6(2)–175.0(20)° and for **2** 162.5(2)–173.2(2)°. The EDTA-aquo complex has a span of 17° in *cis* angles. Part of the increase in the span of *cis* angles in our complex is due to the steric effects produced by the bulky PPh_3 group and part of it comes from the elongated Ru(1)—N(1) distance produced by the *trans* influence of the PPh_3 ligand. The distances involving oxygen atoms coordinating as a pair are smaller [1.998(6), 1.981(5), av. 1.990(6) Å in molecule **1**; 1.999(5), 1.984(6), av. 1.992(6) Å in molecule **2**] than those which coordinate singly [2.060(8) and 2.041(6) Å in molecules **1** and **2**]; a phenomenon found in other metal–EDTA structures[6,19,20] and may have resulted due to the greater coordinating ability of the carboxylate group when both the oxygens are pulled into the coordination sphere of the metal ion. The difference in Ru—O and Ru—N distances involving the coordinated acetato groups and the connecting amino moiety are 0.071(6) and 0.056(6) Å for molecule **1** and 0.087(6) Å for molecule **2**. While part of the difference arises from the difference in the ionic radii of oxygen and nitrogen, the remainder can be attributed to steric factors. Other metal–aminopolycarboxylate derivatives also exhibit the same trend.

The Ru^{III}—O and Ru^{III}—N distances in the structure are within the range reported for [Ru(EDTA-H)(H_2O)],[19] as well as in K[Ru(EDTA-H)Cl]·$2H_2O$.[20] The Ru^{III}—P distances of 2.351(2) Å in the structure compare well with those found for $Ru_2O[O_2(Ph)_2MeCN(PPh_3)_2](ClO_4)\cdot H_2O$,[21] $Ru_2O(O_2C—C_6H_4—P—OMe_4(PPh_3)_2$[22] and $Ru_2Cl_6(DPPM)_2$.[23]

The coordinated C—O lengths (Table 2) in molecule **1** [av. 1.305(1) Å] and molecule **2** [av. 1.287(15) Å] are longer than the uncoordinated C—O bonds (Table 2) [av. 1.21(2) Å] in molecules **1** [av. 1.23(2) Å] and **2**; a situation encountered in other metal complexes of aminopolycarboxylic acids. A difference of 0.07–0.09 Å exists between the C—O lengths, of which the larger value is associated with the oxygen involved in coordination resulting in a stronger metal–oxygen binding. By this complexation the single bond is shortened by 0.03 Å, while the double bond becomes elongated by 0.04 Å.

The O—C—O angle is widened from the value of 120° by 3.3° in **1** and 4° in **2**, which is compensated for by a contraction in the —CCO angles in the coordinated carboxylate groups. In the protonated non-coordinating carboxyl group the difference in C—O lengths is more pronounced; 0.12(1) Å in **1** and 0.14(1) Å in **2**. One of the —CCO angles is widened and the other compressed in molecule **1**, whereas in molecule **2** both the —CCO angles are compressed. The compression of the —CCO angles is due to its involvement in hydrogen bond formation.

The bond lengths and angles in the EDTA moiety lie in the range reported for other structures.[19,20] The torsion angles [N(1)—C(1)—C(2)—N(2)] in **1** and **2** have values of $-56.6(8)°$ and lie in the range (53–63°) reported for similar structures. The ethylenediamine ring adopts an unusual envelope conformation, with the atom C(1) displaced by 0.668(6) Å from the plane of Ru(1)N(1)N(2)C(2) [maximum deviation 0.086(6) Å]. This conformation has been found in other mono-substituted pentadentate EDTA complexes of ruthenium.[19,20] Rings R_1 in **1** and **2** are planar within 0.015(6) and 0.035(6) Å, while rings R_2 and G are more strained and exist as envelopes with N(2) out of the Ru(1)C(7) C(8)O(6) plane by 0.413(6) Å. In ring G N(1) is displaced by $-0.508(6)$ Å from Ru(1)C(3) C(4)O(6) in **1**. The acetate groups are planar within experimental error.

Equilibrium studies for the formation of mixed-ligand $[Ru^{III}(EDTA)(PR_3)]^-$ *complexes*

The formation constants (K_1) of Ru^{III}-EDTA-PR_3 mixed-ligand complexes determined spectrophotometrically[11] at $\lambda_{max} = 481$ nm under nitrogen are summarized in Table 3. The values of the formation constants decrease with a decrease in π-acidity of the PR_3 ligands (Table 3). The stability of the mixed-ligand complex $[Ru^{III}(EDTA)(PR_3)]^-$ decreases in the following order:

$$[Ru^{III}(EDTA)P(C_6H_4—F)_3]^- > [Ru^{III}(EDTA)P(C_6H_5)_3]^- > [Ru^{III}(EDTA)P(C_6H_{11})_3]^-.$$

Catalytic oxidation of PR_3 *with oxygen*

Catalytic oxidations of PR_3 to PR_3O with molecular oxygen were studied in 50% water–dioxane medium. The rate of reaction was found to be first-order with respect to catalyst concentration for each substrate studied. The rate of reaction increases with an increase in PR_3 concentration. At high PR_3 concentration ($[PR_3]/[Cat] > 10^2$) a limit in rate[11] was observed for all the phosphine substrates studied. At constant catalyst (5×10^{-4} M) and PR_3 (5×10^{-3} M) concentrations the rate of reaction was found to be half-order with respect to dissolved oxygen concentration. The kinetic details are similar to those published earlier[11] at 35°C. Based on the above kinetic results a mechanism is proposed, as outlined in Scheme 1, which is similar to that reported earlier.[11]

The catalyst $K[Ru^{III}(EDTA\text{-}H)Cl]$ (**1**) is rapidly aquated when dissolved in water to the corresponding aquo complex (**1a**) at low pH ($\simeq 3$).[23] Complex **1a** reacts with PR_3 to give a mixed-ligand complex (**2**) in a pre-equilibrium step (1) (Scheme 1). The formation of this complex is supported by the successful isolation of (Ru^{III}-EDTA-PR_3) complexes in the present studies. Complex **2** subsequently reacts with dissolved molecular oxygen to form a transient μ-peroxo intermediate (**3**), which undergoes a homolytic cleavage of the O—O bond with one oxygen atom transfer to the substrate in a concerted rate-determining step to give the catalyst (Ru^{III}-EDTA complex) along with the oxidation product (PR_3O). The equilibrium constant (K_2) (determined kinetically)[11] and the rate constant (k) values are summarized in Tables 3 and 4, respec-

Table 3. Values of equilibrium constants (K_1 and K_2) for the oxidation of PR_3 with oxygen catalysed by the Ru^{III}-EDTA complex

System	Temperature (°C)	K^a (M^{-1})	K_2^b (M^{-2})
$LRu^{III}/P(C_6H_4F)_3/O_2$	25	87	3.3×10^3
	35	136	3.9×10^3
	45	228	4.3×10^3
$LRu^{III}/P(C_6H_5)_3/O_2$	25	78	3.9×10^3
	35	115	4.7×10^3
	45	172	4.9×10^3
$LRu^{III}/P\text{-}(C_6H_{11})_3/O_2$	25	55	4.3×10^3
	35	68	4.9×10^3
	45	87	5.3×10^3

[a] Determined spectrophotometrically.[11]
[b] Determined kinetically.[11]

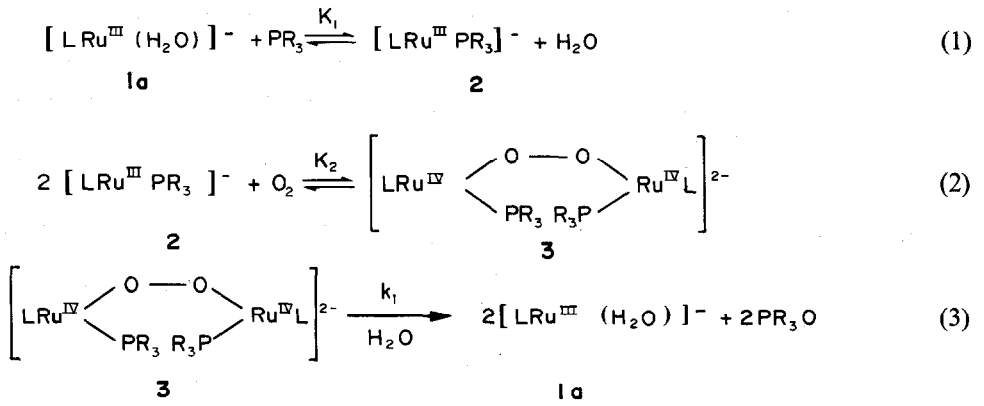

Scheme 1.

tively. The reactivity of the phosphines towards oxidation by molecular oxygen decreases in the order $P(C_6H_4F—P)_3 > P(C_6H_5)_3 > P(C_6H_{11})_3$, which can be explained in terms of the stability of the Ru^{III}-EDTA phosphine and Ru—μ-peroxo bond strengths in the intermediate **3** (Table 3). The fluoro-substituted substrate $P(C_6H_4—F)_3$ has maximum reactivity since it is more π-acidic in nature than $P(C_6H_5)_3$. The electron density at the ruthenium centre is depleted by increasing π-acidity of the PR_3 ligands in the $[Ru^{III}(EDTA)(PR_3)]^-$ mixed-ligand complexes. This is further supported by the positive shift of the redox potentials for Ru^{3+}/Ru^{2+} couples, increasing in the order **3** > **2** > **4**. The stability (K_2) of the μ-peroxo ternary $[Ru^{IV}(EDTA)PR_3]_2O_2$ complexes also increases in the same order.

It is of interest to note that Taqueshi has synthesized Ru^{IV}=O complexes with phosphine coordinated *cis* to the oxo ligand in the complex $[O=Ru^{IV}(bipy)(PPh_3)]$.[24] The coordinated phosphine in this complex is not oxidized to $OPPh_3$. The complex nevertheless oxidizes PPh_3 in solution by an outer sphere mechanism, without the "spectator" phosphine coordinating to the metal ion. In our case, however, the presence of the σ-basic EDTA ligand makes the oxo oxygen of the Ru=O intermediate (after cleavage of the O—O bond in **3**) sufficiently labile for oxygen atom transfer to coordinated phosphine. Thus, the oxygen atom transfer in our case occurs through a coordinated phosphine, as supported by the kinetic evidence (first-order dependence on phosphine concentration). The reaction is slowest in the case of the most basic $P(C_6H_{11})_3$, in which the σ-donation of electrons from phosphine to the metal centre strengthens the O—O bond towards homolytic cleavage. Triphenylphosphine falls between the fluoro and the tricyclohexylphosphine in terms of σ-basicity and π-acidity and thus has a reactivity intermediate of the two extremes.

The catalytic oxidation of PR_3 with molecular

Table 4. Rate and activation parameters for the catalytic oxidations of different aryl-phosphines (PR_3) with molecular oxygen; [Cat] = 5×10^{-4} M, O_2 pressure = 1 atm., pH = 3.0

System	Temperature (°C)	k_1 (s^{-1})	$\Delta H^{\ddagger}$ (kcal mol^{-1})	$\Delta S^{\ddagger}$ (cal ° mol^{-1})	$\Delta G^{\ddagger}$ (kcal mol^{-1})
$Ru^{III}(EDTA)(H_2O)^-/P(C_6H_4F)_3/O_2$	25	1.8×10^{-4}			
	35	3.0×10^{-4}	8±1	−48±2	22.5
	45	4.6×10^{-4}			
$Ru^{III}(EDTA)(H_2O)^-/P(C_6H_5)_3/O_2$	25	1.4×10^{-4}			
	35	2.2×10^{-4}	9±1	−46±2	22.6
		3.9×10^{-4}			
$Ru^{III}(EDTA)(H_2O)^-/P(C_6H_{11})_3/O_2$	25	0.5×10^{-4}			
	35	1.0×10^{-4}	13±2	−36±3	23.3
	45	1.9×10^{-4}			

oxygen was studied at three different temperatures and the activation parameters calculated from the temperature dependence of the rate constant are summarized in Table 4. The low value of $\Delta H^{\ddagger}$ and negative value of $\Delta S^{\ddagger}$ are consistent with the concerted oxygen atom transfer process, as shown in Scheme 1.

Stoichiometric oxygen atom transfer from $Ru^{V}(EDTA)(O)^{-}$ *to* PR_3

In order to probe into the nature of the oxygen atom transfer step in the catalytic oxidation of PR_3 with oxygen we have studied the stoichiometric oxygen atom transfer reaction from the oxo complex $Ru^{V}(EDTA)(O)^{-}$ to the phosphine PR_3 under the pseudo-first-order condition of excess phosphine, where the rate of reaction was found to be first-order with respect to the oxo complex concentration. The rate of reaction increases with an increase in PR_3 concentration (Fig. 3). The above kinetic data suggest the following mechanism [eq. (4)] for the oxo transfer reaction:

$$[Ru^{V}(EDTA)(O)]^{-} + PR_3 \xrightarrow[\mathbf{4}]{k_2} [Ru^{III}(EDTA)(OPR_3)]^{-} \xrightarrow[H_2O]{\text{Fast}} \underset{\mathbf{5}}{} [Ru^{III}(EDTA)(H_2O)]^{-} + OPR_3. \quad (4)$$

In the above mechanism the substrate PR_3 attacks the oxo oxygen in a rate determining redox step to give an $[Ru^{III}(EDTA)(OPR_3)]^{-}$ intermediate, which undergoes rapid hydrolysis to give the $Ru^{III}(EDTA)(H_2O)^{-}$ complex and PR_3O as an oxidation product.

The reactivity order for the oxygen atom transfer reaction in the oxidation of PR_3 by $Ru^{V}(EDTA)(O)^{-}$ decreases in the order $P(C_6H_{11})_3 > P(C_6H_5)_3 > P(C_6H_4—F)_3$, in accordance with the decrease in nucleophilicity of the phosphines. The rate and the activation parameters are reported in Table 5. The small positive value of $\Delta H^{\ddagger}$ and negative $\Delta S^{\ddagger}$ values are in good agreement to the proposed mechanism [eq. (4)].

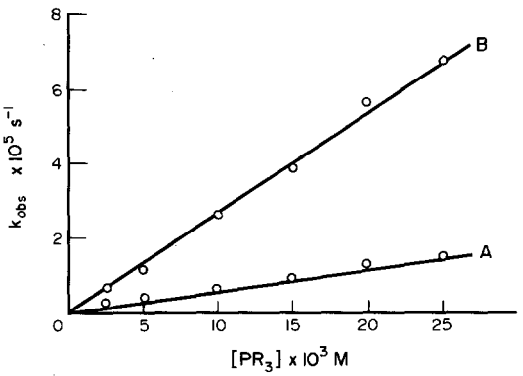

Fig. 3. Effect of $[PR_3]$ on rate constant (k_{obs}) at 30°C: (a) $P(C_6H_5)_3$, (b) $P(C_6H_4—F)_3$; $[Ru^{V}]_T = 5 \times 10^{-4}$ M, pH = 3.0 and μ = 0.2 M (KCl).

It is of interest to compare the free energy of activation, $\Delta G^{\ddagger}$, for the catalytic oxidation of phosphine by molecular oxygen to those observed for the stoichiometric reaction with the oxo complex **4**. $\Delta G^{\ddagger}$ is more positive (2–3 kcal mol^{-1}) for the molecular oxygen reaction compared with $\Delta G^{\ddagger}_2$ for the stoichiometric reaction with complex **4**. The small difference ($\Delta G^{\ddagger} - \Delta G^{\ddagger}_2$), which is significant, reflects on the lowering of the O—O bond dissociation energy in the intermediate μ-peroxo complex **3**.

The interaction of one π^* orbital of the oxygen

Table 5. Rate and activation parameters for the reaction $(EDTA)Ru^{V}{=}O^{-} + PR_3 \rightarrow (EDTA)Ru^{III}(H_2O)^{-} + PR_3O$; $[Ru^{V}] = 5 \times 10^{-4}$ M, pH = 3.0

System	Temperature (°C)	k_2 (M^{-1} s^{-1})	$\Delta H^{\ddagger}_2$ (kcal mol^{-1})	$\Delta S^{\ddagger}_2$ (cal ° mol^{-1})	$\Delta G^{\ddagger}_2$ (kcal mol^{-1})
$Ru^{V}(EDTA)(O)^{-}P(C_6H_4F)_3$	30	0.7×10^{-3}			
	40	1.5×10^{-3}	14±1	−26±1	21.9
	50	3.1×10^{-3}			
$Ru^{V}(EDTA)(O)^{-}/P(C_6H_5)$	30	2.7×10^{-3}			
	40	5.0×10^{-3}	12±1	−31±2	21.2
	50	9.8 ± 10^{-3}			
$Ru^{V}(EDTA)(O)^{-}/P(C_6H_{11})_3$	30	3.8×10^{-2}			
	40	6.7×10^{-2}	10±1	−34±2	20.5
	50	12.1×10^{-2}			

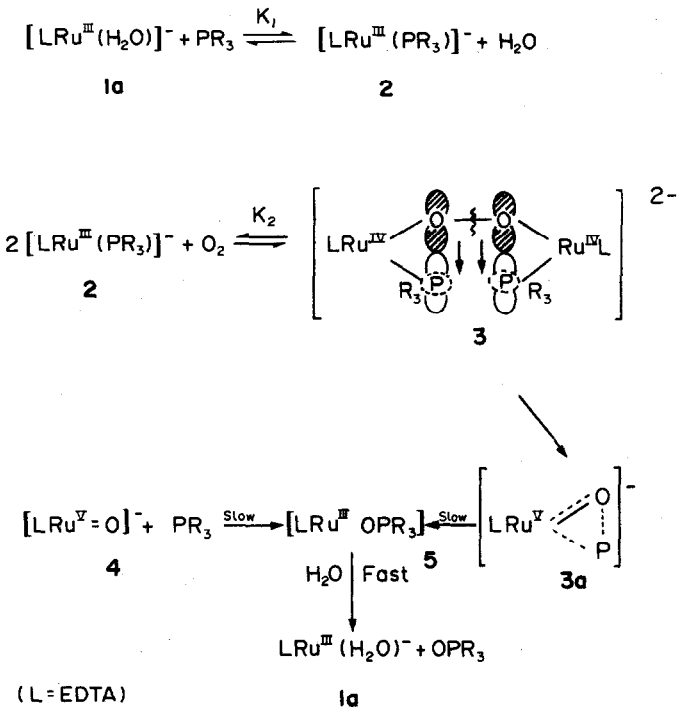

Scheme 2.

atom of the μ-peroxo group with the substrate has been suggested by Solomon *et al.*[25] as the crucial step in the oxygen atom transfer reaction in tyrosinases. The oxygen atom transfer to phosphine in the molecular oxygen oxidation occurs through a concentrated homolytic cleavage of the μ-peroxo bond, assisted by electron withdrawal by the substrate and transfer of oxo oxygen to phosphine to form Ru^{III}-OPR_3 (**5**) species. This interaction may be triangular **3a** with the association of phosphine either with the metal ion or/and the oxo oxygen. The rate-determination step in this case is the transfer of oxo oxygen to the phosphine to form Ru^{III}-OPR_3 species (Scheme 2).

REFERENCES

1. R. P. Hanzlik and D. Williamson, *J. Am. Chem. Soc.* 1976, **98**, 6570.
2. R. Durant, C. D. Garner, M. R. Hyde and F. E. Mabbs, *J. Chem. Soc., Dalton Trans.* 1977, 955.
3. G. J. J. Chen, J. W. McDonald and W. E. Newton, *Inorg. Chem.* 1976, **15**, 2612.
4. C. D. Garner, R. Ourant and F. E. Mabbs, *Inorg. Chim. Acta* 1977, **24**, 29.
5. B. A. Moyer, B. K. Sipe and T. J. Meyer, *Inorg. Chem.* 1981, **20**, 1475.
6. M. M. Taqui Khan, D. Chatterjee, R. R. Merchant, P. Paul, S. H. R. Abdi, D. Srinivas, M. A. Moiz, K. Venkatasubramanian and M. M. Bhadbhade, *Inorg. Chem.* 1992, **31**, 2711.
7. M. M. Taqui Khan, S. A. Mirza, A. Prakash Rao and Ch. Sreelatha, *J. Molec. Catal.* 1988, **44**, 107.
8. M. M. Taqui Khan, D. Chatterjee, N. H. Khan, R. I. Kureshy and K. N. Bhatt, *J. Molec. Catal.* 1992, **77**, 153.
9. M. M. Taqui Khan, R. R. Merchant and D. Chetterjee, *J. Molec. Catal.* 1991, **66**, 23.
10. M. M. Taqui Khan, M. A. Moiz, R. R. Merchant, S. D. Bhatt and D. Chatterjee, *J. Molec. Catal.* 1991, **67**, 1.
11. M. M. Taqui Khan, M. R. H. Siddiqui, A. Hussain and M. A. Moiz, *Inorg. Chem.* 1986, **25**, 2765.
12. A. A. Diamentis and J. V. Dubrawski, *Inorg. Chem.* 1981, **20**, 1142.
13. M. M. Taqui Khan, D. Chatterjee, S. A. Samad and R. R. Merchant, *J. Molec. Catal.* 1990, **61**, 55.
14. A. C. T. North, D. C. Phillips and F. S. Mathews, *Acta Cryst.* 1968, **A24**, 351.
15. J. D. Duniez and P. Sciller, *Acta Cryst.* 1973, **A29**, 589.
16. *International Tables for Crystallography*, Vol. IV. D. Reidel Publishing Company, Dordrecht (1985).
17. R. F. Stewart, E. R. Davidson and W. T. Simpson, *J. Chem. Phys.* 1965, **42**, 3175.
18. B. A. Frentz and Associatcs, Collcge Station, Texas and Enraf–Nonius (1985).
19. M. M. Taqui Khan, H. C. Bajaj, K. Venkatasubramanian and Z. Shirin, *Ind. J. Chem.* 1992, **31A**, 303.
20. M. M. Taqui Khan, K. Venkatasubramanian, M. M.

Bhadbhade, M. R. H. Siddiqui, H. C. Bajaj and Z. Shirin, *Acta Cryst.* 1990, **A46**, C-227.
21. B. K. Das and A. R. Chakrabarti, *Inorg. Chem.* 1990, **29**, 2078.
22. A. R. Chakrabarti, F. A. Cotton, M. P. Diebold, D. B. Lewis and W. J. Ruth, *J. Am. Chem. Soc.* 1986, **108**, 97.
23. T. Matsubara and C. Creuz, *Inorg. Chem.* 1979, **18**, 1956.
24. J. G. Muller and K. Takeuchi, *Inorg. Chem.* 1987, **26**, 3634.
25. P. K. Ross and F. I. Solomon, *J. Am. Chem. Soc.* 1991, **113**, 3246.

Polyhedron Vol. 12, No. 12, pp. 1453–1458, 1993
Printed in Great Britain

0277-5387/93 $6.00+.00
© 1993 Pergamon Press Ltd

THE SYNTHESIS AND CHARACTERIZATION OF $Pb(O_2CCH_3)_2$(18-CROWN-6)·$3H_2O$, A MONOMERIC LEAD(II) CARBOXYLATE COMPOUND

YEUNG-GYO SHIN,* MARK J. HAMPDEN-SMITH,† TOIVO T. KODAS†‡ and EILEEN N. DUESLER*

Departments of Chemistry* and Chemical Engineering‡ and Center for Micro-Engineered Ceramics, University of New Mexico, Albuquerque, NM 87131, U.S.A.

(*Received* 16 *December* 1992; *accepted* 4 *March* 1993)

Abstract—The compound $Pb(O_2CCH_3)_2$(18-crown-6)·$3H_2O$ was synthesized via the reaction of either an aqueous solution of lead(II) acetate with 18-crown-6 or by reaction of lead(II) carbonate with acetic acid and 18-crown-6 in water. The product was shown to be monomeric in the solid state, as determined by single-crystal X-ray diffraction. The molecule is markedly asymmetric with both acetate ligands chelating to the same side of the 10-coordinate lead(II) centre. Solid-state FTIR of a crystalline sample revealed a difference, Δ, in ν_{asym}(C—O) and ν_{sym}(C—O) of 612 cm^{-1}. Solution ^{207}Pb NMR spectroscopy was consistent with coordination of the 18-crown-6 ligand to the lead centre in aqueous solution. Thermogravimetric analysis studies showed that $Pb(O_2CCH_3)_2$(18-crown-6)·$3H_2O$ thermally decomposed in air to form crystalline PbO at 380°C.

There has been considerable interest in the formation of perovskite phase mixed-metal oxide materials because they exhibit a variety of interesting physical and chemical properties including dielectric, pyroelectric, ferroelectric and piezoelectric phenomena,[1–3] superconductivity,[4] catalytic activity[5] and oxygen transport.[6] For many applications it is desirable that crystalline thin films of these materials be formed at low temperatures. The deposition of thin, crystalline films of these materials is being attempted by gas phase routes such as chemical vapour deposition (CVD) and liquid phase routes[7] commonly involving sol–gel reaction chemistry.[8] Both these routes suffer from the common problem that metal–organic complexes of a number of the necessary components, most notably the metal-organic complexes of the divalent metals Pb, Ca, Sr and Ba, have a strong tendency to oligomerize. These cations are large,[9–11] exhibit high coordination numbers and their oligomerization reduces both the volatility and solubility of their complexes.[12–15] However, these problems are being circumvented by either reducing the cation coordination number through introduction of sterically demanding ligands, or introducing polydentate ligands into the coordination sphere of the metal. For example, the monomeric barium(II) compound $Ba[N(SiMe_3)_2]_2(THF)_2$[16] with sterically demanding amido ligands, and the monomeric polyether complexes M(18-crown-6)$(hfac)_2$ (18-crown-6 = 1,4,7,10,13,16-hexaoxacyclooctadecane), where M = Sr, Ca and Ba,[17] Ba(2,5,8,11,14-pentaoxapentadecane)$(hfac)_2$[18,19] and $Ba[O(CH_2CH_2O)_nCH_3]_2$ (n = 2, 3)[20] were recently prepared. However, much less work has been devoted to developing soluble or volatile lead compounds suitable for the synthesis of lead-based metal oxide ceramics.

Here we report the synthesis, characterization and solid-state single-crystal X-ray diffraction study of a monomeric lead(II) carboxylate compound, $Pb(O_2CCH_3)_2$(18-crown-6)·$3H_2O$. This species was prepared to investigate the ester elimination reaction between lead(II) carboxylates and titanium alkoxides that has been proposed to result in the formation of crystalline $PbTiO_3$.[21–26]

† Authors to whom correspondence should be addressed.

EXPERIMENTAL

General procedures

All reactions were performed under ambient conditions with no attempt to exclude atmospheric oxygen or moisture. All hydrocarbon and ethereal solvents were dried and distilled from sodium benzophenone ketyl and stored over 4 Å molecular sieves. Acetic acid, lead(II) carbonate, lead(II) acetate and 18-crown-6 starting materials were purchased from Aldrich Chemical Co. and used without further purification. Elemental analyses were performed by Ms R. Ju at the University of New Mexico, Department of Chemistry. NMR data were recorded on a Bruker AC-250P NMR spectrometer using the protio impurities of the deuterated solvents as references for the ^{1}H NMR and the ^{13}C resonance of the solvents as a reference for ^{13}C NMR spectroscopy. Temperatures were calibrated with either ethylene glycol or methanol. ^{207}Pb NMR data were recorded on a Bruker AC-250P NMR spectrometer at 52.3 MHz using the $Pb(NO_3)_2$ resonance (−2900 ppm) as an external reference. IR data were recorded on a Perkin–Elmer model 7000 series instrument under an air atmosphere.

Syntheses

Preparation of $Pb(O_2CCH_3)_2(18\text{-crown-6})\cdot 3H_2O$. $PbCO_3$ (0.58 g, 2.17 mmol) and 18-crown-6 (1.25 g, 4.72 mmol) were suspended in water (20 cm^3) and acetic acid (0.28 g, 4.67 mmol) was added. Alternatively, $Pb(O_2CCH_3)_2$ (1.75 g, 4.61 mmol) and 18-crown-6 (2.58 g, 9.76 mmol) can be dissolved in water (30 cm^3). The resulting clear solutions were stirred for at least 3 h and the volatile portion of the mixture was removed to leave a sticky white solid. Excess 18-crown-6 was removed by washing with dried pentane and the resulting white powder was air-dried; yield 93%. Characterization data: $Pb(O_2CCH_3)_2(18\text{-crown-6})\cdot H_2O$: ^{1}H NMR ($D_2O$, 300 K, 250 MHz): 3.43 (s, O_2CCH_3), 1.98 ppm [s, $(CH_2CH_2O)_6$]. IR (KBr pellets): 3456 (s), 2889 (s), 1567(vs), 1406 (s), 1100 (vs). Found: C, 30.9; H, 5.9. Calc. for $C_{16}H_{36}O_{13}Pb$: C, 29.9; H, 5.6%. Calc. for $Pb(O_2CCH_3)_2(18\text{-crown-6})\cdot 2H_2O$, $C_{16}H_{34}O_{12}Pb$: C, 30.7; H, 5.9% TGA (air, 1 atm.): 96.4% at 120°C [$Pb(O_2CCH_3)_2(18\text{-crown-6})\cdot 2H_2O$, calc. 97.2%], 46.5% at 270°C [$Pb(CH_3COO)_2$, calc. 50.5%], 33% at 380°C (PbO, calc. 34.9%). The final decomposition product was confirmed to be a mixture of α-PbO and Massicot phases by powder X-ray diffraction.

X-ray crystallographic studies

Crystals suitable for single-crystal X-ray diffraction study of $Pb(O_2CCH_3)_2(18\text{-crown-6})\cdot 3H_2O$ were grown by slow evaporation of water and were sealed in a glass capillary. The crystal data collection and refinement parameters are collected in Table 1. The determination of the space group $P2_1$ in the monoclinic crystal system was unambiguous. A semi-empirical correction for absorption was applied to the data. Of the 4580 data collected (max. $2\theta = 50°$), 3664 were both observed ($3\sigma F_o$) and independent. All non-hydrogen atoms were refined with anisotropic thermal parameters and hydrogen atoms were treated as idealized contributions. At convergence, $R(F) = 3.45\%$, $R(wF) = 2.81\%$, GOF = 1.07, highest unassigned peak in the final difference map = 1.50 Å^3. All computations used SHELXTL-PLUS software systems (G. Sheldrick, Siemens Corp., Madison, WI, U.S.A.). Selected bond lengths and angles are given in Tables 2 and 3. The atom numbering scheme of the molecule is shown in Figs 1 and 2 and a ball-and-stick drawing showing the positions of the water molecules is given in Fig. 3. Figure 4 is a schematic representation of the coordination environment about lead(II). Supplementary material is available from the Cambridge Crystallographic Database.

RESULTS AND DISCUSSION

The compound $Pb(O_2CCH_3)_2(18\text{-crown-6})\cdot 3H_2O$ was synthesized either by reacting $PbCO_3$, 18-crown-6 and acetic acid in a 1:2:2 molar ratio or the direct reaction of $[Pb(O_2CCH_3)_2]$ and 18-

Table 1. Summary of crystallograpahic data for $Pb(OAc)_2(18\text{-crown-6})\cdot 3H_2O$

Chemical formula	$C_{16}H_{36}O_{13}Pb$
Formula weight	643.6
Colour, habit	Clear, transparent prism
Unit cell dimensions	
a (Å)	9.1660(10)
b (Å)	8.351(2)
c (Å)	16.198(4)
Volume (Å^3)	1218.6(3)
Z	2
Space group	$P2_1$
Density (calc.) (g cm^{-3})	1.754
$R(F)$ (%)	2.93
$R_w(F)$ (%)	2.81

Parameters in common include temperature, 293 K; diffractometer, Siemens $R3_m/V$; radiation, Mo-K_α ($\lambda = 0.71073$ Å). Other data are available as supplementary material.

Table 2. Selected bond lengths for $Pb(OAc)_2$(18-crown-6)·$3H_2O$

Pb—O(1)	2.929(7)	Pb—O(2)	3.008(7)
Pb—O(3)	3.066(7)	Pb—O(4)	2.867(7)
Pb—O(5)	2.990(7)	Pb—O(6)	3.148(7)
Pb—O(7)	2.497(7)	Pb—O(8)	2.457(6)
Pb—O(9)	2.375(7)	Pb—O(10)	2.745(6)
C(2)—O(2)	1.413(11)	O(1)—C(12)	1.418(11)
C(3)—C(4)	1.480(13)	O(2)—C(3)	1.416(10)
C(3)—C(5)	1.429(12)	C(4)—O(3)	1.416(11)
C(6)—O(4)	1.420(11)	C(5)—C(6)	1.485(14)
C(7)—C(8)	1.508(13)	O(4)—C(7)	1.426(11)
O(5)—C(9)	1.436(11)	C(8)—O(5)	1.400(12)
C(10)—O(6)	1.414(11)	C(9)—C(10)	1.492(14)
C(11)—C(12)	1.480(13)	O(6)—C(11)	1.430(11)
O(8)—C(13)	1.285(11)	O(7)—C(13)	1.236(11)
O(10)—C(15)	1.229(12)	C(13)—C(14)	1.472(12)
O(1)—C(1)	1.433(11)	O(9)—C(15)	1.264(11)
C(1)—C(2)	1.507(11)	C(15)—C(16)	1.503(13)

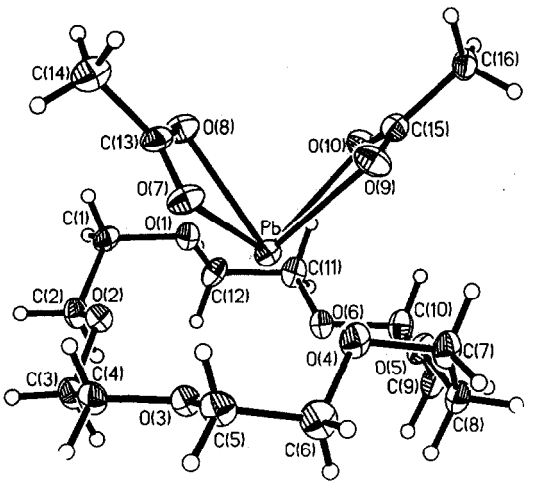

Fig. 1. ORTEP plot of the molecular structure of $Pb(O_2CCH_3)_2$(18-crown-6)·$3H_2O$, emphasizing the asymmetric nature of the coordination environment about lead(II).

crown-6 in a 1:2 molar ratio in aqueous solution. The reaction mixtures were stirred for 3 h after they became clear. A sticky white solid was collected upon removal of the volatile components *in vacuo*, which was washed with hexane until all free 18-crown-6 was removed. The resulting white solid *completely* dissolved in water and the ^1H NMR spectrum in D_2O showed two resonances at 3.43 (CH_2) and 1.98 ppm (CH_3) in the integrated ratio 24:6, respectively, corresponding to the empirical formula $Pb(O_2CCH_3)_2$(18-crown-6). The presence of water in the crystalline material could not be distinguished unambiguously from these NMR data obtained in D_2O. Elemental analysis was consistent with the empirical formula $Pb(O_2CCH_3)_2$(18-crown-6)·$2H_2O$ and the presence of the hydroxyl functionality was confirmed by IR spectroscopy through observation of a band at 3456

Table 3. Selected bond angles for $Pb(OAc)_2$(18-crown-6)·$3H_2O$

O(7)—Pb—O(8)	52.6(2)	O(7)—Pb—C(13)	25.8(2)
O(8)—Pb—C(13)	26.9(2)	O(7)—Pb—O(9)	81.0(2)
O(8)—Pb—O(9)	82.5(2)	C(13)—Pb—O(9)	81.9(3)
O(7)—Pb—O(10)	116.3(2)	O(8)—Pb—O(10)	79.8(2)
C(13)—Pb—O(10)	99.8(2)	O(9)—Pb—O(10)	49.8(2)
O(1)—C(1)—C(2)	112.8(7)	C(2)—O(2)—C(3)	111.5(6)
C(1)—C(2)—O(2)	107.9(7)	O(2)—C(3)—C(4)	109.9(7)
C(4)—O(3)—C(5)	112.3(7)	C(3)—C(4)—O(3)	109.2(7)
O(3)—C(5)—C(6)	108.2(7)	C(6)—O(4)—C(7)	112.8(7)
C(5)—C(6)—O(4)	110.1(8)	O(4)—C(7)—C(8)	112.2(8)
C(8)—O(5)—C(9)	113.5(7)	C(7)—C(8)—O(5)	108.0(7)
O(5)—C(9)—C(10)	109.0(8)	C(10)—O(6)—C(11)	111.6(6)
C(9)—C(10)—O(6)	110.1(7)	O(6)—C(11)—C(12)	109.2(7)
O(1)—C(12)—C(11)	108.2(7)	Pb—O(8)—C(13)	93.3(5)
Pb—O(7)—C(13)	92.8(5)	Pb—C(13)—O(8)	59.8(4)
Pb—C(13)—O(7)	61.4(4)	Pb—C(13)—C(14)	177.0(8)
O(7)—C(13)—O(8)	121.1(8)	O(8)—C(13)—C(14)	118.0(8)
O(7)—C(13)—C(14)	120.9(8)	Pb—O(10)—C(15)	85.8(5)
Pb—O(9)—C(15)	102.6(6)	O(9)—C(15)—C(16)	116.2(9)
O(9)—C(15)—O(10)	121.9(9)		
O(10)—C(15)—C(16)	121.9(8)		

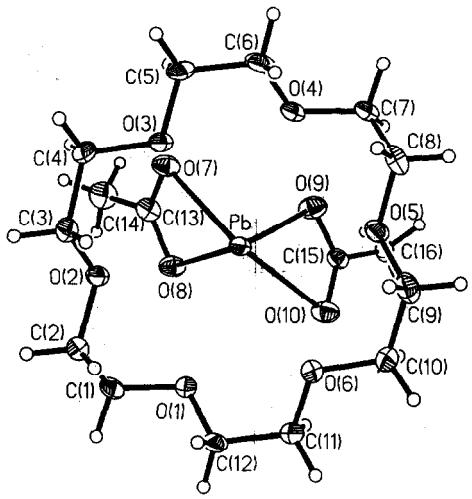

Fig. 2. ORTEP plot of the molecular structure of $Pb(O_2CCH_3)_2(18\text{-crown-6})\cdot 3H_2O$, emphasizing the coordination environment about lead(II).

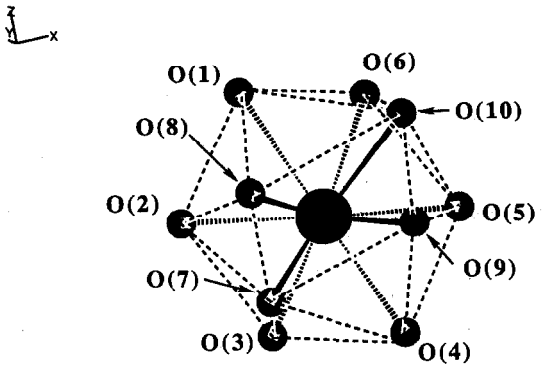

Fig. 4. Schematic diagram showing the geometry of the 10-fold coordination environment about lead(II) in $Pb(O_2CCH_3)_2(18\text{-crown-6})\cdot 3H_2O$.

cm^{-1}. This solid did not completely dissolve in benzene-d_6, the integration ratio of the soluble material changed to 48 (3.46 ppm): 6 (1.98 ppm) with the precipitation of $Pb(O_2CCH_3)_2$. Attempts to sublime this material at *ca* 10^{-2} torr and 120°C resulted in the sublimation of 18-crown-6 only. This observation indicated that the strength of interaction between the lead centre and the polyether ligand was weak.

For further investigation of the nature of the interaction between the lead centre and the 18-crown-6 ligand a saturated aqueous solution of $Pb(O_2CCH_3)_2$ was titrated with aliquots of 18-crown-6 and monitored by ^{207}Pb NMR spectroscopy.[27-29] The ^{207}Pb resonance of saturated $Pb(O_2CCH_3)_2$ aqueous solution was observed at −1338.2 ppm, consistent with the literature data.[28] The addition of the 0.5 equivalent amount of 18-

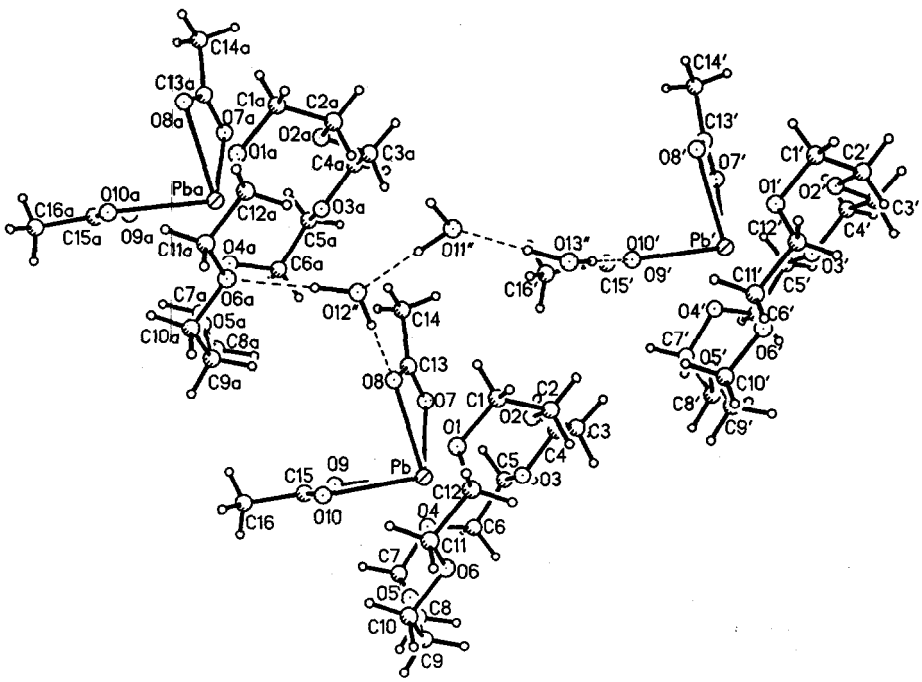

Fig. 3. Ball-and-stick drawing of the crystal structure of $Pb(O_2CCH_3)_2(18\text{-crown-6})\cdot 3H_2O$, emphasizing the intermolecular hydrogen bonding interactions.

crown-6 lead to complete disappearance of the intense ^{207}Pb resonance, probably as the result of an exchange process on the NMR time-scale. The ^{207}Pb resonance reappeared at −2492.5 ppm, and was sharp only after 2 equivalents of 18-crown-6 were added. Further addition of 18-crown-6 did not affect either the peak position or intensity. These data show that the presence of the 18-crown-6 ligand has a marked effect on the chemical environment of the lead.

To provide further information on the interaction between $Pb(O_2CCH_3)_2$ and 18-crown-6 a solid-state single-crystal X-ray diffraction study was performed. This revealed the presence of three water molecules of crystallization with the empirical formula $Pb(O_2CCH_3)_2$(18-crown-6)·$3H_2O$. ORTEP plots of two views of the molecular structure are shown in Figs 1 and 2 and relevant bonds lengths and angles are given in Tables 2 and 3, respectively. The lead atom is bonded to two chelating acetate groups at distances consistent with the sums of the covalent radii for lead oxygen (2.52 Å), with Pb—O(10) slightly longer (2.745 Å).[11] The 18-crown-6 ligand is asymmetrically coordinated to the lead with Pb—O distances that range from 2.867 to 3.184 Å. These distances are significantly longer than Pb—O bonding interactions and are consistent with the observed lability of this ligand. Some of the asymmetry in the coordination of the 18-crown-6 and acetate ligands maybe due to hydrogen bonding between the water molecules and these ligands. The water molecules are hydrogen bonded between O(6) of the 18-crown-6 ligand of one molecule and either O(8) or O(10) of an acetato ligand of an adjacent molecule, as shown in Fig. 3. It is interesting that the Pb—O(8) distance is normal, while Pb—O(10) is significantly lengthened.

Other lead(II) carboxylate compounds that have been characterized to date exhibit oligomeric or polymeric structures in the solid state and typically possess bridging carboxylate ligands as a general structural feature.[30–34] The complete abstinence of the acetate ligands in bridging interactions in the case of $Pb(O_2CCH_3)_2$(18-crown-6)·$3H_2O$ is highly unusual and is probably a result of the steric protection and coordinative saturation afforded by the 18-crown-6 ligand. The lead(II) centre is approximately 10-coordinate with no obvious free coordination site apparent for a stereochemically active lone pair. The coordination geometry is shown in Fig. 4. This geometry is quite different to that recently observed for $Pb(NO_3)_2$(18-crown-6),[35] which exhibits a more symmetrical structure where the lead ion lies in the centre of the 18-crown-6 ring and the bidentate nitrate ligands are coordinated above and below this plane.

The monomeric nature of this complex, which results in the presence of *chelating* acetate ligands that do not participate in bridging to another metal centre, provides a point of comparison with the literature correlation between the carbonyl stretching frequencies and carboxylate ligand coordination mode. It has been proposed that unidentate, chelating and bridging carboxylate ligands can be distinguished by the difference (Δ) between the asymmetric and symmetric carbonyl stretching frequencies.[36,37] Complexes that contain unidentate carboxylate ligands exhibit Δ values that are greater than that of the free carboxylate ion (164 cm^{-1} for acetate), while those that are chelating exhibit values that are significantly lower. Bridging carboxylate ligands exhibit Δ values that are similar to those of the free ion. In this case crystalline $Pb(O_2CCH_3)_2$(18-crown-6)·$3H_2O$ exhibited ν_{asym}(C—O) of 1567 cm^{-1} and ν_{sym}(C—O) of 1406 cm^{-1}, giving a Δ value of 161 cm^{-1}. Thus, based on this correlation, it might have been predicted that the acetate ligand was bidentate and bridging. However, these predictions are somewhat complicated by the presence of water which is hydrogen bonded to the acetate ligands in this compound.

Thermogravimetric analysis of this compound showed three distinct transformations as a function of increasing temperature. On heating to 120°C a weight loss corresponding to the loss of one water molecule was observed, consistent with the formation of $Pb(O_2CCH_3)_2$(18-crown-6)·$2H_2O$. This observation is also consistent with the elemental analysis data. Further heating to 270°C resulted in a weight loss consistent with the loss of the remaining water molecules and 18-crown-6 to form lead acetate. This species then lost weight, consistent with the formation of PbO at 380°C. X-ray powder diffraction analysis showed that crystalline PbO had been formed, which existed as a mixture of two phases, α-PbO and Massicot.

CONCLUSIONS

The synthesis and characterization of a monomeric lead(II) carboxylate compound have been achieved through steric and electronic saturation of the lead coordination environment with the polyether 18-crown-6 ligand. The resultant molecule is surprisingly asymmetric in the solid state and the 18-crown-6 ligand appears to be weakly coordinated to the lead centre. IR spectra reveal ν(C—O) stretching mode differences which are inconsistent with literature trends, although this may be complicated by the water molecules of crystallization present. Thermal decomposition of the title compound resulted in the formation of

crystalline lead(II) oxide at 380°C. Further studies are in progress to examine the reactivity of this species towards metal alkoxide compounds and to utilize this lead compound for the formation of perovskite phase mixed-metal oxide materials.

Acknowledgements—We thank the New Mexico Research Development Initiative Program for funding this work. We thank the NSF Chemical Instrumentation Program for the purchase of a low-field NMR spectrometer and ONR for analytical facilities.

REFERENCES

1. A. R. West, in *Solid State Chemistry and Its Applications*. John Wiley and Sons, New York (1989).
2. E. R. Meyers and A. I. Kingon (Editors), *Ferroelectric Thin Films*, Vol. 200. Materials Research Society, Pittsburgh, PA (1990).
3. A. S. Bhalla and K. M. Nair (Editors), *Ceramic Transactions: Ferroelectric Films*, Vol. 25. American Ceramic Society, Westerville, OH (1992).
4. H. Muller-Buschbaum, *Angew. Chem., Int. Edn Engl.* 1989, **28**, 1472: *Phys. Today* 1991, **44**, 22; J. G. Bednorz and K. A. Muller, *Z. Pys B: Condensed Matter* 1986, **64**, 189.
5. See e.g. L. G. Tejuca, L. G. Fierro and J. M. D. Tascon, in *Advances in Catalysis* (Edited by D. D. Eley, H. Pines and P. B. Weisz), Vol. 36, p. 237. Academic Press, London (1989).
6. See e.g. W. F. Libby, *Science* 1971, **171**, 449.
7. See e.g. *Better Ceramics Through Chemistry V* (Edited by M. J. Hampden-Smith, C. J. Brinker and W. Klemperer), Vol. 271. Materials Research Society Symposium Proceedings. Pittsburgh, PA (1992).
8. C. J. Brinker and G. W. Scherer, *Sol–Gel Science, The Physics and Chemistry of Sol–Gel Processing*. Academic Press, New York (1990).
9. F. A. Cotton and G. Wilkinson, in *Advanced Inorganic Chemistry*, 5th edn. John Wiley and Sons, New York (1988).
10. N. N. Greenwood and A. Earnshaw, in *Chemistry of the Elements*, 1st edn. Pergamon Press, Oxford (1984).
11. J. E. Huheey, *Inorganic Chemistry, Principles of Structure and Reactivity*, 3rd edn. Harper and Row, San Francisco (1983).
12. S. R. Drake, W. E. Strieb, M. H. Chisholm and K. G. Caulton, *Inorg. Chem.* 1990, **29**, 2707.
13. S. C. Goel, M. Y. Chiang and W. E. Buhro, *Inorg. Chem.* 1990, **29**, 4640.
14. S. C. Goel, M. A. Matchett, M. Y. Chiang and W. E. Buhro, *J. Am. Chem. Soc.* 1991, **113**, 1845.
15. A. Gleizes, D. Medes and S. Sans-Lenain, in *Better Ceramics Through Chemistry V* (Edited by M. J. Hampden-Smith, W. G. Klemperer and C. J. Brinker), Vol. 271, p. 919, Materials Research Society Symposium Proceedings. Materials Research Society, Pittsburgh, PA (1992).
16. B. A. Vaarstra, J. C. Huffman, W. E. Strieb and K. G. Caulton, *Inorg. Chem.* 1991, **30**, 121.
17. J. A. T. Norman and G. P. Pez, *J. Chem. Soc., Chem. Commun.* 1991, 971.
18. P. van der Sluis, A. L. Spek, K. Timmer and D. A. Meinema, *Acta Cryst., Sect. C* 1990, **46**, 1741.
19. K. Timmer, C. I. M. Spee, A. Mackor and H. A. Meinema, European Patent 0 405 634 A2 (1991).
20. W. S. Rees and D. A. Moreno, *J. Chem. Soc., Chem. Commun.* 1991, 1759.
21. D. C. Bradley and I. M. Thomas, *J. Chem. Soc. A* 1959, 3404.
22. H. K. Sharma and P. N. Kapoor, *Polyhedron* 1988, **7**, 1389.
23. K. D. Budd, S. K. Dey and D. A. Payne, *Mat. Res. Soc., Symp. Proc.* 1986, **73**, 711.
24. S. R. Gurkovich and J. B. Blum, *Ultrastructure Processing of Ceramics Glasses and Composites* (Edited by L. L. Hench and D. R. Ulrich), Ch. 12. Wiley-Interscience, New York (1984).
25. S. R. Gurkovich and J. B. Blum, *Ferroelectrics* 1985, **62**, 189.
26. S. R. Gurkovich and J. B. Blum, *J. Mat. Sci.* 1985, **20**, 4479.
27. See e.g. R. K. Harris and B. E. Mann, *NMR and the Periodic Table C*. Academic Press, New York (1978).
28. C. Brevard and P. Granger, *Handbook of High Resolution Multinuclear NMR*. Wiley and Sons, New York (1981).
29. B. Wrackmeyer and K. Horchler, *Ann. Rep. NMR Spectrosc.* (Edited by G. A. Webb) 1990, **22**, 249.
30. P. G. Harrison and A. T. Steel, *J. Organomet. Chem.* 1982, **239**, 105.
31. W. Clegg, I. R. Little and B. P. Straughan, *Acta Cryst.* 1986, **C42**, 1319.
32. K. A. Beveridge and G. W. Buchnell, *Can. J. Chem.* 1979, **57**, 2498.
33. G. M. Sheldrick and R. Taylor, *Acta Cryst.* 1975, **B31**, 2740.
34. C. D. Chandler, M. J. Hampden-Smith and E. N. Duesler, *Inorg. Chem.* 1992, **31**, 4891.
35. R. D. Rogers and A. H. Bond, *Inorg. Chem. Acta* 1992, **192**, 163.
36. G. B. Deacon and R. J. Phillips, *Coord. Chem. Rev.* 1980, **33**, 227.
37. K. Nakamoto, *Infrared and Raman Spectra of Inorganic and Coordination Compounds*, 4th edn. Wiley and Sons, New York (1986).

Polyhedron Vol. 12, No. 12, pp. 1459–1463, 1993
Printed in Great Britain

0277–5387/93 $6.00+.00
© 1993 Pergamon Press Ltd

A ^{197}Au MÖSSBAUER STUDY OF SOME CHLOROGOLD DERIVATIVES OF NITROGEN-CONTAINING HETEROCYCLES

S. CALOGERO*

Dipartimento di Chimica Fisica, Università, I-30123 Venezia, Italy

and

F. E. WAGNER

Physik Department, Technische Universität München, D-8046 Garching, F.R.G.

and

G. PONTICELLI

Dipartimento Chimica e Tecnologie Inorganiche e Metallorganiche, Università, I-09124 Cagliari, Italy

(*Received* 27 *January* 1993; *accepted* 3 *March* 1993)

Abstract—The ^{197}Au Mössbauer spectra of some chloro-gold(III) and -gold(I) compounds with N-alkylimidazole- or -benzoaxole-type ligands are reported and discussed. Two sites of types $AuNCl_3$ and $[AuCl_4^-][HNR^+]$, or AuNCl and $[AuCl_2^-][HNR^+]$ (where N indicates the 3-nitrogen atom of the imidazole- or benzoxazole-type ligands, R), are evidenced. Their ratio depends on a delicate balance between electronic and steric effects.

Gold compounds are interesting, *inter alia*, for their biological and medical applications: some gold(III) complexes seem to have antitumoral activity[1,2] and the presence of N-donor ligands has been considered suitable for modern chrysotherapy.[3,4] Understanding the mechanism of the biological activity of such compounds requires an understanding of their chemistry, i.e. knowledge of their structure and bonding. X-ray crystal data are not always available because of the lack of suitable crystals and such an occurrence is not rare in the field of gold chemistry.

In spite of the disadvantages of ^{197}Au Mössbauer spectroscopy,[5,6] in comparison with that of ^{57}Fe or ^{119m}Sn, such as the short half-life of the ^{197}Pt parent isotope and the low recoil-free fraction which requires the use of low temperatures, the technique provides a useful method for elucidating the structure and bonding of gold compounds in the solid state.[7–9] Progress in the interpretation of the ^{197}Au spectra has resulted, in particular, from the availability of the increasingly reliable correlations of isomeric shift and quadrupole splitting with chemical properties such as the oxidation state and the gold coordination number, as well as with the electronic influence of the ligands.[6]

Since the presence of azoles, purines and pyrimidines as constitutive parts of nucleic acids, vitamins, coenzymes and antibiotics is well known, it seemed useful to investigate the coordinating behaviour of azole-type ligands toward gold(III) and gold(I) to detect the influence of different substituents on the electronic structure and hence on their possible biological activity.[10] For this purpose Mössbauer spectroscopy has been employed in the study of some chloro-gold(III) and -gold(I) compound with N-alkylimidazole- or -benzoaxole-type ligands, in order to extract structural and electronic information.

* Author to whom correspondence should be addressed.

RESULTS AND DISCUSSION

The spectra exhibit two superimposed Mössbauer quadrupole doublets, except for those of samples **4** and **6** (Fig. 1). The parameters such as isomer shift, IS, quadrupole splitting, QS, and linewidth, LW, are listed in Table 1. As shown in Fig. 2, where the observed IS and QS parameters are reported, together with the literature linear relationships for gold(III) and gold(I) complexes[11] samples **1–6** are considered containing gold(III) and samples **7** and **8** gold(I) sites. The unsplit line, with shift of *ca* -1.25 mm s^{-1}, in the spectrum of **3** or **4** (Fig. 1) indicates the presence of metallic gold[5] formed because of partial decomposition of the sample.

The spectrum of **6** (Fig. 1) exhibits, within the limits of detection of the ^{197}Au resonance,[5] one electric quadrupole interaction. Its spectral parameters compare well with those reported[12] for $C_5H_5NAuCl_3$ (IS 1.45 mm s^{-1}) and $(C_5H_5)_2N_2AuCl_3$ (QS 2.22 mm s^{-1}) suggesting a similar stereochemistry, i.e. a more-or-less distorted square-planar site $AuNCl_3$. The larger doublet exhibited from samples **1–3** and **5**, with QS and IS in the range 1.87–2.20 and 1.34–1.40 mm s^{-1}, respectively, is analogously indicative of the site $AuNCl_3$, in agreement with their IR, UV and ^1H NMR data.[10]

The spectrum of **4** (Fig. 1) consists of a quadrupole-split doublet together with a more intense unsplit line, assigned to metallic gold. The doublet with larger splitting, before attributed to the site $AuNCl_3$, is not evidenced in the fit indicating the complete reduction of its site to metallic gold. The parameters of the quadrupole interaction detected in sample **4** (and for the similar interaction exhibited from the second site in **1–3** and **5**), requiring a donor more electronegative than the heterocyclic nitrogen, are more consistent with a site of type $AuCl_4$ than $AuNCl_3$.

Such a spectral component is not attributable to the starting material $HAuCl_4 \cdot 4H_2O$ (IS 0.71 and QS 0.98 mm s^{-1}),[13] since its presence is not consistent with conductivity data[10] or the fitting procedure. The alternative possibility of an increase in the gold coordination number in the site $AuNCl_3$ is ruled out since the expected splitting should be too small in comparison with the observed ones. The last possiblity demands the attribution of such a spectral component to the $AuCl_4$ hydrogen bonded

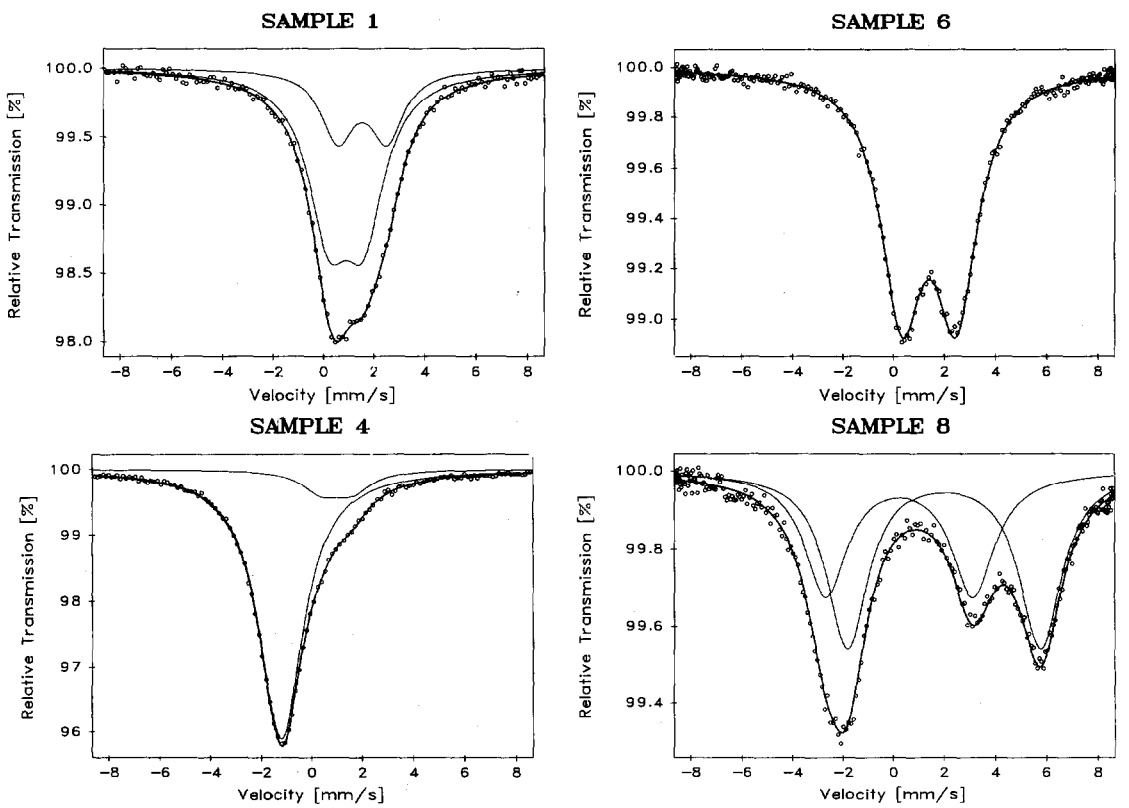

Fig. 1. Mössbauer spectra at 4.2 K of gold(III)-containing samples **1**, **4** and **6** and gold(I)-containing sample **8**.

Table 1. ^{197}Au Mössbauer parameters at 4.2 K

Sample[a]	Site	IS[b,c]	QS[c]	LW[c]	A[d]	
1	$Au(N\text{-}MeIm)Cl_3$	1.35	1.87	1.90	46	
	$[AuCl_4^-][H\text{-}(N\text{-}MeIm)^+]$	0.84	1.27	1.92	54	
2	$Au(N\text{-}EtIm)Cl_3$	1.37	1.91	1.95	86	
	$[AuCl_4^-][H\text{-}(N\text{-}EtIm)^+]$	0.85	1.30	2.05	14	
3	$Au(N\text{-}PrIm)Cl_3$	1.40	2.20	2.13	75	85[e]
	$[AuCl_4^-][H\text{-}(N\text{-}PrIm)^+]$	0.85	1.20	2.11	8	9[e]
	Metallic gold	−1.25	0.00	2.10	17	6[e]
4	$Au(BO)Cl_3$	—	—	—	—	
	$[AuCl_4^-][H\text{-}(BO)^+]$	0.93	1.20	1.90	12	31[e]
	Metallic gold	−1.25	0.00	2.12	88	69[e]
5	$Au(2\text{-}MBO)Cl_3$	1.34	2.07	1.92	77	
	$[AuCl_4^-][H\text{-}(2\text{-}MeBO)^+]$	1.10	1.30	2.00	23	
6	$Au(2,5\text{-}diMeBO)Cl_3$	1.39	2.14	1.99	100	
7	Au(N-EtIm)Cl	1.77	7.42	1.98	60	
	$[AuCl_2^-][H\text{-}(N\text{-}EtIm)^+]$	0.01	5.64	2.10	40	
8	Au(N-PrIm)Cl	1.97	7.58	1.96	58	
	$[AuCl_2^-][H\text{-}(N\text{-}PrIm)^+]$	0.22	5.79	2.05	42	

[a] N-MeIm, N-methylimidazole; N-EtIm, N-ethylimidazole; N-PrIm, N-propylimidazole; BO, benzoxazole; 2-MeBO, 2-methylbenzoxazole; 2,5-diMeBO, 2,5-dimethylbenzoxazole.

[b] The shifts are relative to Au(Pt). In order to refer these shifts to metallic gold 1.25 mm s^{-1} have to be added.

[c] In mm s^{-1}.

[d] Percentage of the gold site estimated assuming equal *f*-factors.

[e] Percentage of the gold site estimated using the experimetnal ratio fAu^{III}: $fAu = 3:10$.

to the heterocyclic nitrogen in the site of type $[AuCl_4^-][HNR^+]$ (where N indicates the 3-nitrogen atom of the imidazole- or benzoxazole-type ligands, R).

Compared with $HAuCl_4 \cdot 4H_2O$ the larger splitting for the sites $[AuCl_4^-][HNR^+]$ in **1**–**5** implies a larger anisotropy among the σ-bonding orbitals and then a larger principal component of the electric field gradient tensor along the symmetry axis. The imbalance in electron charge would arise from differences in the gold *p*- and *d*-electron involvement in the Au—Cl bonds. As a consequence a large difference in the Au—Cl bond lengths is predicted for the sites of type $[AuCl_4^-][HNR^+]$ in comparison with those reported for $HAuCl_4 \cdot 4H_2O$: Au—Cl 2.283 (×2) and 2.286 Å (×2).[14]

As shown in Fig. 2 the two quadrupole-split doublets of samples **7** or **8** have parameters typical of linearly coordinated gold(I), in agreement with their IR and ^{1}H NMR measurements.[10] Additional evidence for linearly coordinated gold(I) is provided, in the framework of the point-charge model, by the agreement between the experimental splitting and that predicted using the partial quadrupole splitting values of −1.57 for Cl[6] and −2.09 mm s^{-1} (the value for 2-isopropylimidazole[8] as a working approximation) for N-EtIm or N-PrIm. Since the predicted splittings for the sites AuNCl and $AuCl_2^-$ are −7.32 and −6.28 mm s^{-1}, respectively, the observed larger splittings in **7** and **8** can be attributed to AuNCl and the smaller ones tentatively to the site of type $AuCl_2$.

In comparison with $AuCl_2^-$ (IS 0.59 and QS 6.28 mm s^{-1}),[12] the second site of samples **7** or **8** presents less *s*-electron density, not delocalized in the *sp* hybridization, and less population in the p_z-orbital. These effects cannot be explained with the possible presence of distortions in the $AuCl_2$ site since the plot of Fig. 3 shows that the quadrupole splitting calculated by the point-charge[15] does not reproduce the observed splittings of **7** and **8** within a realistic Cl—Au—Cl angular distortion. Instead a possible cause is the involvement of one chloride in hydrogen bonding of type $[AuCl_2^-][HNR^+]$ (N is the 3-nitro-

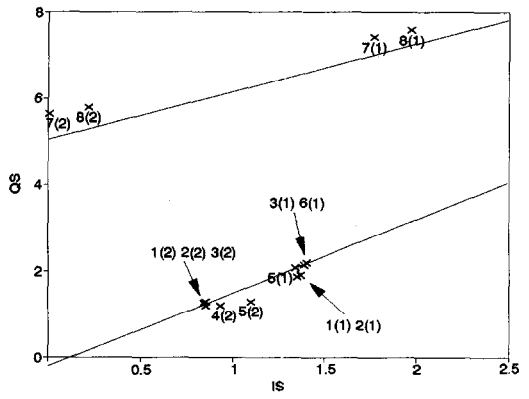

Fig. 2. Plot of QS vs IS values. The first number is that of Table 1. The second number indicates the gold site: 1 for $AuNCl_3$ or AuNCl, 2 for $[AuCl_4^-][HNR^+]$ or $[AuCl_2^-][HNR^+]$. The linear relationships for gold(III) and gold(I) compounds are QS = $-0.22+1.74$ IS and QS = $5.05+1.06$ IS, respectively.

gen atom of N-EtIm or N-PrIm) in cases connected to an increase in the gold coordination number.

On going from the sample **1** to **6** is generally observed an increase in the *s*-electron density, not involved in the dsp^2 hybridization, together with an increase in *p*-asymmetry or *d*-symmetry around the gold centre. Both effects are due to the small increase of the σ-donor strength produced by alkyl substitution at the N-atom in the imidazole-type ligands or by methyl insertion in benzoxazole. Therefore, the ligands may be roughly ordered following their increasing donor ability: Cl < N-MeIm < N-EtIm < N-PrIm and 2-MeBO < 2,5-diMeBO. The trend is also confirmed by the spectral parameters of the two gold(I) samples **7** and **8**.

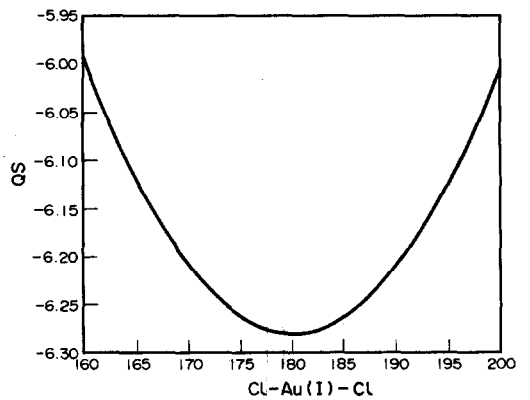

Fig. 3. Plot of the quadrupole splitting (in mm s^{-1}) calculated by the point-charge model[15] vs the angular distortion Cl—Au—Cl in (°).

The presence in the samples of two gold sites, one without hydrogen bonding and the other hydrogen bonded, in a variable ratio seems to be the result of steric and electronic effects. In fact the growing steric hindrance of the alkyl in the imidazole-type ligands (samples **1–3**, **7** and **8**), or that of one or two methyls in benzoxazole (**4–6**), may hamper the formation of the weaker hydrogen-bonded gold site among close molecular units. The accommodation of ligands with growing steric hindrance may introduce substantial deviations in the gold coordination geometry up to steric inhibition in the formation of weaker bonding. This effect is generally observed in Table 1, where the per cent of the hydrogen bonded site is larger in the presence of the less hindered ligand (sample **1**), decreases for more hindered ligands (samples **2**, **3**, **7** and **8**) and is negligible in the presence of the ligand 2,5-diMeBO (sample **6**).

The introduction of an additional hydrogen-bonded gold site might improve the comprehension of the Mössbauer spectra reported, *inter alia*, for some chlorogold nucleosides. In particular it might give a better comprehension of the Mössbauer spectra of $Au(trino)Cl_3$ and $Au(trguo)Cl_3$ (trino, triacetylinosine; trguo, triacetylguanosine) interpreted in the past on the basis of the presence of the sole gold site $AuNCl_3$.[16] Since the observed quadrupole doublet for such nucleosides (as reported in Fig. 2 and Table 1 or ref. 14) is asymmetric, the fit has been performed using a couple of different lines. On the contrary the introduction of an additional gold site might improve the fit by using couples of lines with equal width and equal intensity. In conclusion two sites of the types $AuNCl_3$ and $[AuCl_4^-][HNR^+]$ or AuNCl and $[AuCl_2^-][HNR^+]$ (where N indicates the 3-nitrogen atom of the imidazole- or benzoxazole-type ligands, R) are generally present in the reported chlorogold derivatives. Their ratio depends on the delicate balance between electronic and steric effects.

EXPERIMENTAL

The compounds have been prepared using solvents with gold and monodentate ligands in the required stoichiometric ratio. The compounds are microcrystalline, generally soluble in DMSO, DMF and $CHCl_3$ and non-conductors in DMSO. The compounds have been characterized by elemental analysis, conductivity measurements, UV, IR and ^1H NMR data.[10] The IR spectra were recorded again after the Mössbauer measurements and no change was observed.

The ^{197} Pt activity feeding the 77.3 keV Mössbauer transition was produced by neutron irradiation of enriched ^{196}Pt metal. Both source and

absorber were kept at 4.2 K. A sinusoidal velocity wave-form and an intrinsic Ge detector were used. The spectra have been fitted by the program MOS 90 with sets of equal Lorentzian lines. The calculated errors were *ca* 0.02 mm s^{-1} or 1 for per cent data.

For high-energy Mössbauer transitions the approximation of equal Lamb–Mössbauer factors is not correct[7] and in particular when metallic gold and gold(III) are present, as in samples **3** or **4**, the contributions to the resonance area are not proportional to their masses. In order to estimate the ratio of the Lamb–Mössbauer *f*-factors for gold (III) and metallic gold sample **6** was selected as a probe, since it contains merely one gold(III) site. The Mössbauer spectrum of the specimen containing sample **6** (74.92 mg Au cm^{-2}) together with the reference metallic gold (8.84 mg Au cm^{-2}) was collected at 4.2 K and the ratio $fAu^{III} : fAu = 3:10$ used to calculate the per cent data for samples **3** and **4** in Table 1.

Acknowledgements—Financial support from the Consiglio Nazionale delle Ricerche (Rome), MURST and NATO (CRG 920179 to S.C. and F.E.W.) is gratefully acknowledged. The authors thank Mr L. Stievano, University of Venice, for technical assistance.

REFERENCES

1. I. Haiduc and C. Silvestri, *Coord. Chem. Rev.* 1990, **99**, 253.
2. B. M. Sutton, in *Platinum, Gold and Other Metal Chemotherapeutic Agents* (Edited by S. J. Lippard), p. 355. A.C.S. Symposium Series 209, Washington, DC (1983).
3. P. J. Sadler, *Struct. Bonding (Berlin)* 1976, **28**, 171.
4. A. Lorber and T. M. Simon, *Gold Bull.* 1979, **12**, 149.
5. H. D. Bartunik and G. Kaindl, in *Mössbauer Isomer Shift* (Edited by G. Shenoy and F. E. Wagner), p. 515. North Holland, Amsterdam (1978).
6. R. V. Parish, in *Mössbauer Spectroscopy Applied to Inorganic Chemistry* (Edited by G. J. Long), Vol. 1, p. 577. Plenum Pres, New York (1984).
7. F. Bonati, A. Burini, B. R. Pietroni, S. Calogero and F. E. Wagner, *J. Organomet. Chem.* 1986, **309**, 363.
8. F. Bonati, A. Cingolani, S. Calogero and F. E. Wagner, *Inorg. Chim. Acta* 1987, **127**, 87.
9. F. Bonati, A. Burini, B. R. Pietroni, S. Calogero and F. E. Wagner, *J. Organomet. Chem.* 1991, **408**, 125.
10. Z. Matovic, G. Ponticelli, P. Scano, I. A. Efimenko and A. P. Kurbakova, *Inorg. Chem. Acta*, submitted.
11. P. Guetlich, R. Link and A. Trautwein, in *Mössbauer Spectroscopy and Transition Metal Chemistry*, p. 211. Springer-Verlag, Berlin (1978).
12. P. G. Jones, A. G. Maddock, M. J. Mays, M. M. Muir and F. A. Williams, *J. Chem. Soc., Dalton Trans.* 1977, 1434.
13. J. Friedl, F. E. Wagner, B. Nkosi, M. Towert, N. J. Coville, M. D. Adams and G. J. Hutchings, *Hyp. Inter.* 1991, **69**, 767.
14. J. M. Williams and S. W. Peterson, *J. Am. Chem. Soc.* 1969, **91**, 776.
15. S. Calogero and C. D'Arrigo, Quantum Chemistry Program Exchange Newsletters, 1978, 63, 47, n.367.
16. G. H. M. Calis and N. Hadjiliadis, *Inorg. Chim. Acta* 1984, **91**, 203.
17. H. Schmidbaur, C. Hartmann and F. E. Wagner, *Angew. Chem., Int. Edn Engl.* 1987, **26**, 1148.

Polyhedron Vol. 12, No. 12, pp. 1465–1469, 1993
Printed in Great Britain

0277–5387/93 $6.00+.00
© 1993 Pergamon Press Ltd

STRUCTURE AND MAGNETIC EXCHANGE OF AN IMIDAZOLATE-BRIDGED COPPER DIMER: [(dtma)Cu(im)Cu(dtma)]$ClO_4 \cdot 2.5H_2O$

MAO ZONGWAN, FU DEGANG, HANG QINWEI and TANG WENXIA*

Coordination Chemistry State Key Laboratory, Department of Chemistry, Nanjing University, Nanjing 210008, P.R.C.

and

YU KAIBEI

Analysis Center, Chengdu Branch of Chinese Academy of Science, Chengdu 610041, P.R.C.

(*Received* 27 *November* 1992; *accepted* 3 *March* 1993)

Abstract—The compound of the formula [(dtma)Cu(im)Cu(dtma)]$ClO_4 \cdot 2.5H_2O$ (where dtmaH is 4-diethylenetriamineacetic acid and im is the imidazolate anion) was synthesized and its crystal structure determined by X-ray diffraction methods. The structure consists of a dimeric complex bridged by the deprotonated imidazole. The geometries of the coordination polyhedron around the copper(II) ions are very near to tetragonal pyramid. The *X*-band ESR powder spectrum shows broad $\Delta M = 1$ and weak $\Delta M = 2$ absorptions. Variable-temperature (4.2–300 K) magnetic susceptibility data gave the antiferromagnetic interaction parameters $J = -37$ cm^{-1}. This behaviour is best accounted for by a superexchange mechanism involving σ- and π-exchange pathways.

Binding of imidazole-type molecules to metal complexes is a subject of considerable interest because of the frequency occurrence of imidazole derivatives in biologically important metal complexes. One of the most extensively studied members of this group is the Cu—Zn superoxide dismutase,[1] which has been shown by X-ray crystallography to have an imidazole bridge between the two metals. Temperature-dependent ESR measurements on the modified enzyme, in which zinc(II) has been substituted by copper(II), show that the two copper(II) ions are antiferromagnetically coupled with a singlet–triplet separation ($2J$) of -52 cm^{-1}.[2]

Consequently a number of imidazolate bridged polynuclear copper(II) units have been prepared.[3–7] In most of them the non-bridging ligands are polydentate amine ligands. These studies have shown that the magnitude of the antiferromagnetic exchange is strongly dependent upon the geometry and energy of the singly occupied metal orbitals and the highest occupied orbitals of the bridging group.

Most recently, an interesting new compound, [(dtma)Cu(im)Zn(dtma)]$ClO_4 \cdot 2.5H_2O$, containing an imidazolate-bridged copper(II)–zinc(II) binuclear unit, was reported as a possible model for the Cu, Zn-SOD,[8] in which the non-bridging ligand contains a carboxylate. In this paper the synthesis and structure of the compound [(dtma)Cu(im)Cu(dtma)]$ClO_4 \cdot 2.5H_2O$ is reported and the magnetic susceptibility data are discussed in detail.

EXPERIMENTAL

Preparation of [(dtma)Cu(im)Cu(dtma)]$ClO_4 \cdot 2.5H_2O$

The ligand dtmaH (4-diethylenetriamineacetic acid, $C_6H_{15}N_3O_2$) and the complex [Cu(dtma)]ClO_4 were prepared as described in the literature.[8,9] The title complex was prepared as follows:

[Cu(dtma)]ClO_4 (0.646 g, 2 mmol) and imH

* Author to whom correspondence should be addressed.

(0.068 g, 1 mmol) were mixed in water (15 cm^3) and then NaOH solution (1.0 cm^3, 1.0 N) was added with stirring. By slow evaporation of the solution, blue prismatic crystals were obtained. After being filtered, washed with water and ethanol and dried the title compound was obtained, 0.433 g (yield 65.6%). Found: C, 27.3; H, 5.2; N, 16.7; Cu, 19.1. Calc. for $C_{15}H_{36}ClN_8O_{10.5}Cu_2$: C, 27.3; H, 5.5; N, 17.0; Cu, 19.2%.

Crystal structure determination of [(dtma)Cu(im)Cu(dtma)]$ClO_4 \cdot 2.5H_2O$

Crystal data. $C_{15}H_{36}ClN_8O_{10.5}Cu_2$, $M = 659.02$, monoclinic, space group $P2_1/a$, $a = 13.133(2)$, $b = 14.224(3)$, $c = 15.788(3)$ Å, $\beta = 114.22(2)°$, $V = 2690(1)$, $Z = 4$, $D_c = 1.63$ g cm^{-3}, (Mo-K_α) = 0.71073 Å, (Mo-K_α) = 17.46 cm^{-1}, $F(000) = 1364$.

Data collection. A blue single crystal ($0.20 \times 0.40 \times 0.40$) was mounted on an R3M/E four-circle X-ray diffractometer. Data were collected at room temperature, in the ω–2θ scan mode with 8° min^{-1} scan speed and graphite-monochromated Mo-K_α radiation. Of the 4498 reflections measured (h: 0–15, k: 0–16, l: −18–18, $2° \leqslant 2\theta \leqslant 47°$), 4408 were unique and 3088, having $I > 3\sigma(I)$, were used for the fine refinement. The intensities of three standard reflections measured revealed no significant variation (<3%). Data for intensities were corrected for Lorentz–polarization effects and no absorption corrections have been made.

Structure solution and refinement. The structure was solved by heavy-atom techniques. The atomic coordinates of metal atoms were first obtained by analysing Patterson functions. The other non-hydrogen atom coordinates were gradually obtained by Fourier synthesis. After all the coordinates and isotropic and anisotropic thermal parameters of the non-hydrogen atoms were refined the hydrogen atom coordinates were obtained from difference-Fourier synthesis and analysis of geometry. Finally, the coordinates, the anisotropic thermal parameters of non-hydrogen atoms and the isotropic thermal parameters of hydrogen atoms were refined by block diagonal-matrix least-squares. All calculations were performed on an Eclipse/S140 computer with the SHELXTL program system (SHELXTL, 1985). The final R was 0.0669, $R_w = 0.0581$, where $w = [1 - \exp(-5 \sin\theta/\lambda)^2]/[\sigma^2(F) + 0.0001(F)^2]$, for all observed reflections. Further details are presented as supplementary data, together with thermal parameters, bond lengths and angles, mean average planes and structure factors.

Physical measurements

The ESR spectra at X-band frequency were recorded with a Bruker ER 200D-SRC spectrometer at 110 K. Magnetic susceptibility measurements in the temperature range 4.2–300 K were obtained on a model CF-1 vibrating-sample magnetometer using the Faraday method.

RESULTS AND DISCUSSION

Description of structure

Selected bond lengths and angles are given in Table 1. The structure of the title compound is shown in Fig. 1, together with the atomic numbering system.

The structure consists of one complex cation, $[(dtma)Cu(im)Cu(dtma)]^+$, one ClO_4^- anion and two and a half water molecules. In the cation two copper atoms are bridged by a deprotonated imidazole to form a binuclear complex. The coordination polyhedron around the copper(II) ions is better described as a distorted tetragonal pyramid. Each copper atom is penta-coordinate, surrounded by an approximate basal plane of four nitrogen atoms from the dtma and imidazolate ligands and by one oxygen atom of the dtma ligand situated on the axis of a distorted tetragonal pyramid. The best planes are calculated through N(1), N(2), N(3) and N(4) and N(5), N(6), N(7) and N(8) atoms, the dihedral angle of which is 46.3° and the separations of Cu(1) and Cu(2) from which are 0.235 and 0.236 Å, respectively. The average values of the angles $\angle O_{axial}—Cu—O_{basal}$ are 96° for both Cu(1) and Cu(2), while those of the angles $\angle N—Cu—N$ (neighbouring) in the basal plane are 89°. Likewise, the distortion (Δ) of the coordination polyhedron, from trigonal bipyramid ($\Delta = 0$) towards a regular tetragonal pyramid ($\Delta = 1$), has been calculated according to Mutterties and Galy.[10,11] The values obtained, $\Delta = 0.82$ and $\Delta = 0.64$ for Cu(1) and Cu(2), respectively, indicate that the geometry of coordination around the copper atoms is close to TP in a different degree.[13,14]

The average bond lengths of Cu—N (at the apex of the dtma ligand) and Cu—O are 2.076 and 2.184 Å, respectively. The distance between two copper atoms in the Cu—im—Cu moiety is 5.984 Å. The bond distances of N—C and C—C in the imidazolate anion group range from 1.330 to 1.371 Å and the bond angles from 103.9 to 113.5°, which are very close to the corresponding values in other imidazolate-bridged compounds.[8,12] While the constituent atoms of the imidazolate anion all lie within ±0.004 Å of the best mean plane through the ring

Table 1. Selected bond lengths (Å) and angles (°) for the title complex

Cu(1)—N(1)	2.087(5)	Cu(1)—N(2)	2.034(6)
Cu(1)—N(3)	2.032(6)	Cu(1)—N(4)	1.969(5)
Cu(1)—O(2)	2.180(6)	Cu(2)—N(5)	1.962(5)
Cu(2)—N(6)	2.065(5)	Cu(2)—N(7)	2.052(7)
Cu(2)—N(8)	2.024(6)	Cu(2)—O(3)	2.188(6)
N(1)—C(1)	1.469(12)	N(1)—C(3)	1.500(10)
N(1)—C(5)	1.490(11)	N(2)—C(4)	1.486(9)
N(3)—C(6)	1.475(9)	N(4)—C(7)	1.371(9)
N(4)—C(9)	1.342(8)	N(5)—C(8)	1.366(9)
N(5)—C(9)	1.330(8)	N(6)—C(11)	1.494(12)
N(7)—C(12)	1.475(9)	N(8)—C(14)	1.482(9)
N(6)—C(13)	1.495(11)	N(6)—C(15)	1.483(10)
O(1)—C(2)	1.252(10)	O(2)—C(2)	1.264(7)
O(3)—C(10)	1.255(8)	O(4)—C(10)	1.256(11)
C(1)—C(2)	1.508(13)	C(3)—C(4)	1.491(12)
C(5)—C(6)	1.498(12)	C(7)—C(8)	1.350(10)
C(10)—C(11)	1.485(12)	C(12)—C(13)	1.496(12)
C(14)—C(15)	1.506(11)		

N(1)—Cu(1)—N(2)	84.5(2)	N(1)—Cu(1)—N(3)	84.0(2)
N(2)—Cu(1)—N(3)	158.1(3)	N(1)—Cu(1)—N(4)	172.7(3)
N(2)—Cu(1)—N(4)	93.8(2)	N(3)—Cu(1)—N(4)	95.2(2)
N(1)—Cu(1)—O(2)	81.1(2)	N(2)—Cu(1)—O(2)	100.8(2)
N(3)—Cu(1)—O(2)	95.9(2)	N(4)—Cu(1)—O(2)	106.2(2)
N(5)—Cu(2)—N(6)	177.8(3)	N(5)—Cu(2)—N(7)	94.5(2)
N(6)—Cu(2)—N(7)	84.2(2)	N(5)—Cu(2)—N(8)	96.1(2)
N(6)—Cu(2)—N(8)	84.3(2)	N(7)—Cu(2)—N(8)	153.1(3)
N(5)—Cu(2)—O(3)	100.6(2)	N(6)—Cu(2)—O(3)	81.3(2)
N(7)—Cu(2)—O(3)	95.2(3)	N(8)—Cu(2)—O(3)	107.0(3)
Cu(1)—N(4)—C(7)	126.6(4)	Cu(1)—N(4)—C(9)	129.5(4)
C(7)—N(4)—C(9)	103.9(5)	Cu(2)—N(5)—C(8)	126.1(4)
Cu(2)—N(5)—C(9)	129.0(4)	C(8)—N(5)—C(9)	104.8(5)
N(4)—C(7)—C(8)	109.1(6)	N(5)—C(8)—C(7)	108.6(6)
N(4)—C(9)—N(5)	113.5(5)		

Cu(1) and Cu(2) are 0.016 and 0.041 Å, respectively, out of the plane. The two ions are attached on the same side of this plane.

Magnetic properties

The X-band ESR spectra of the title complex measured in undiluted polycrystalline powder and DMSO frozen solution at 110 K are shown in Fig. 2. In both cases a $\Delta M = 1$ signal appears as a single broad absorption at $g = 2.075$ or $g = 2.079$. A much weaker signal is observed at $g = 4.611$ and is recognized as a $\Delta M = 2$ transition. The broadening of the $\Delta M = 1$ transition and the absence of hyperfine structure suggest that the interaction would be mainly dipolar in character. The appearance of the $\Delta M = 2$ signal indicates a magnetic interaction between the copper(II) ions of the binuclear complex bridged by imidazolate.

Variable-temperature (4.2–300 K) magnetic susceptibility data for the title compound show antiferromagnetic interactions with a maximum in their susceptibility against temperature curve at *ca* 47 K. The magnetism of this compound is analysed on the basis of the revised Bleaney–Bowers equation[15]:

$$\chi_M = \frac{2Ng^2\beta^2}{kT}[3+\exp(-2J/kT)]^{-1}(1-\rho) + \rho\frac{2Ng^2\beta^2S(S+1)}{3kT} + N_\alpha. \quad (1)$$

Here ρ is the mole fraction of paramagnetic impurity.[16]

The temperature-independent paramagnetism N_α was taken as 60×10^{-6} e.m.u. mol^{-1} for copper.[17] The other symbols have their usual meaning. The best-fit parameters are $g = 2.177$, $J = -37.3$ cm^{-1} and $\rho = 0.00025$. The generalized R factor, $R = [\Sigma\chi_M(\text{obs.}) - \chi_M(\text{calc.})]^2/\Sigma\chi_M(\text{obs.})^2$, a convenient statistical indicator of the quality of fit, was

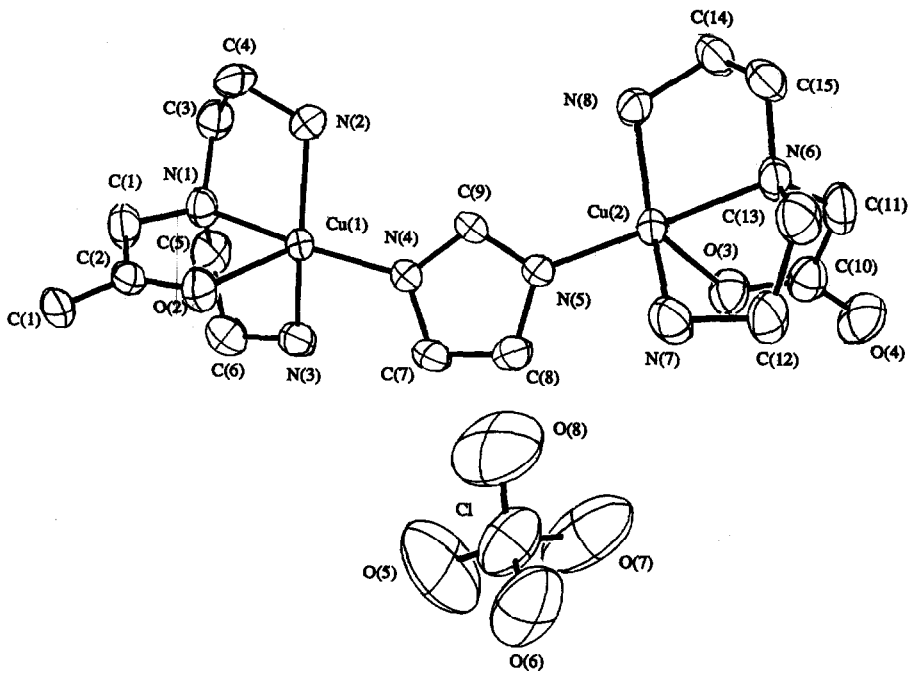

Fig. 1. Molecular structure of $[(dtma)Cu(im)Cu(dtma)]ClO_4$.

0.0008. The susceptibility against temperature data obtained are given in Fig. 3, together with a theoretical curve calculated from eq. (1), which is represented by a solid line, and obviously the fit to the experimental data is good for the whole range of temperatures.

Exchange mechanism

All the imidazolate-bridged copper(II) complexes having been reported exhibit antiferromagnetic exchange interactions with J varying from 0 to -88 cm^{-1}. The value of J of the title complex is just in this range and is almost equal to that of the compound $[(tren)Cu(im)Cu(tren)](ClO_4)_3$ [$J = -38$ cm^{-1}, trend = tri(2-ethylamine)amine], which has the same bridging ligand and a similar terminal ligand. The structural study of the title complex shows that the copper–copper distance in the Cu—im—Cu moiety is 5.984 Å. The observed coupling is too large to result from direct, through-space copper–copper interactions; the exchange is, there-

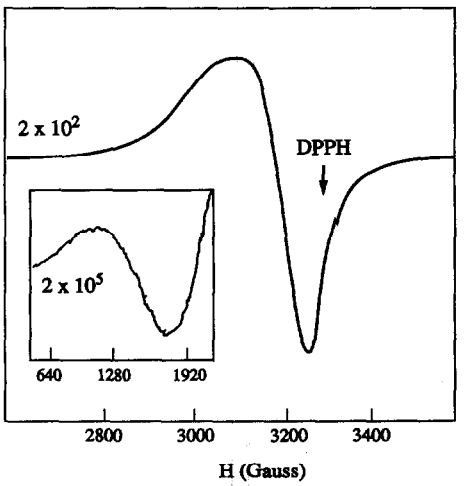

Fig. 2. Polycrystalline powder ESR spectrum of the title complex at 110 K.

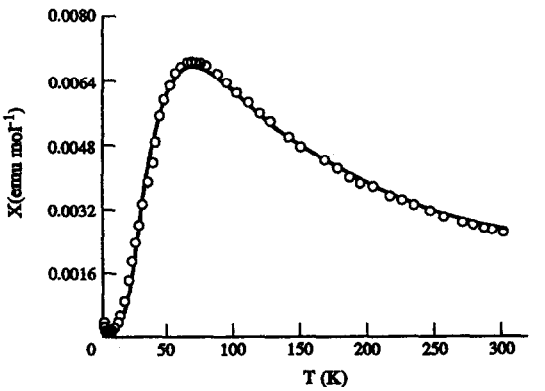

Fig. 3. The temperature dependence of the magnetic susceptibility (χ_M/e.m.u. mol^{-1}) of $[(dtma)Cu(im)Cu(dtma)]ClO_4 \cdot 2.5H_2O$. The experimental data are represented as circles and the line results from a least-squares fit to eq. (1).

fore, mediated by the bridging imidazolate ligand.

For square-planar or square-pyramidal copper(II) complexes the unpaired electron is in the $d_{x^2-y^2}$ orbital. In terms of Hoffmann's model[18] linear combinations of the two $d_{x^2-y^2}$ orbitals are given by eqs (2) and (3), where a and b refer to the two copper atoms.

$$\varphi_S \simeq d^a_{x^2-y^2} + d^b_{x^2-y^2} \quad (2)$$

$$\varphi_A \simeq d^a_{x^2-y^2} - d^b_{x^2-y^2} \quad (3)$$

In the absence of a bridging ligand φ_A and φ_S are degenerate in energy. On combining with bridging ligand orbitals of appropriate symmetry the antibonding orbitals of the resulting species are separated by an energy difference of $E_1 - E_2$. $-2J$ is related to $E_1 - E_2$ by eq. (4), where K_1 and K_2 are nearly constant quantities for small perturbations of the system. Equation (4) indicates that the larger the energy difference $E_1 - E_2$ the stronger the antiferromagnetic exchange interaction.

$$-2J = E_T - E_S = -2K_1 + (E_1 - E_2)^2/K_2 \quad (4)$$

It has been suggested that both the σ- and π-orbitals of the imidazole ligand are capable of acting as the superexchange pathways between copper atoms.[3,19] In a σ-pathway two linear combinations of the nitrogen lone pair orbitals interact with the metal linear combination φ_S and φ_A, respectively. The magnitude of J perhaps correlates the ϕ angle of $\angle$Cu—N—$C(2)_{im}$.[3] The ϕ angles are generally

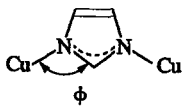

in the range 120–130° and the J values vary from -17 to -38 cm^{-1}. In a π-pathway the $d_{x^2-y^2}$ orbitals of copper atoms may interact with the π-orbitals of the imidazolate ion. The π-exchange pathway should be appreciable only when θ, which is defined as the dihedral angle between the imidazolate ring and copper coordination square plane, differs considerably from 0 to 90°. Spatial overlap of the copper $d_{x^2-y^2}$ and imidazolate π-orbitals is expected to be quite poor compared with the overlap with imazolate σ-orbitals (nitrogen lone pair) due to the long ($\geqslant 3$ Å) copper–carbon distance.[19]

The values of ϕ_1, ϕ_2, θ_1 and θ_2 of the title complex have been calculated and are 129.5, 129.0, 27.9 and 22.6°, respectively. The φ angles are in range 120–130° and θ angles are considerably different from 0°. These facts indicate that the exchange interactions involve two pathways. However, the average copper–carbon distance of imidazolate is 2.991 Å, approximately 3 Å, which indicates that the π-exchange interaction is very weak. The above results show that the σ-orbitals of the bridging imidazolate group provide the main, not the only, superexchange pathway in the compound reported here.

REFERENCES

1. J. S. Richardson, K. A. Thomas, B. H. Rubin and D. C. Richardson, *Proc. Natl. Acad. Sci. U.S.A.* 1975, **72**, 1349.
2. J. A. Fee and R. G. Briggs, *Biochem. Biophys. Acta* 1975, **400**, 439.
3. M. S. Hadded and D. N. Hendrickson, *Inorg. Chem.* 1978, **17**, 2622.
4. A. Bencini, D. Gatteschi, C. Zanchini, J. G. Haasnoot, R. Prins and J. Reedisk, *Inorg. Chem.* 1985, **24**, 2812.
5. H. M. J. Hendriks, P. J. M. W. L. Birker, G. C. Verschoor and J. Reedijk, *J. Chem. Soc., Dalton Trans.* 1982, 623.
6. J. P. Costes, J. F. Scrra, F. Dahan and J. P. Laurent, *Inorg. Chem.* 1986, **25**, 2790.
7. R. Quinn, M. Nappa and J. S. Valentin, *J. Am. Chem. Soc.* 1982, **104**, 2588.
8. Z. W. Mao, D. Chen, W. X. Tang, K. B. Yu and L. Liu, *Polyhedron* 1992, **11**, 191.
9. P. W. Schneder and J. P. Collman, *Inorg. Chem.* 1968, **7**, 2010.
10. E. L. Muetterties and L. J. Guggenberger, *J. Am. Chem. Soc.* 1974, **96**, 1748.
11. J. Galy, J. I. Bonnet and S. Anderson, *Acta Chem. Scand.* 1979, **33**, 383.
12. Z. W. Mao, K. B. Yu, D. Chen, S. Y. Han, Y. X. Sui and W. X. Tang, *Inorg. Chem.*, in press.
13. B. J. Hathaway and D. E. Billing, *Coord. Chem. Rev.* 1970, **5**, 143.
14. B. J. Hathaway, *Struct. Bond.* 1984, **57**, 55.
15. R. L. Carlin, *J. Chem. Educ.* 1966, **43**, 521.
16. A. P. Ginsberg, *Inorg. Chim. Acta* 1971, **5**, 45.
17. E. P. Maarschall, A. C. Botterman, S. Vegu and A. R. Miedema, *Physica* 1969, **41**, 473.
18. P. J. Hay, J. C. Thibeault and R. Hoffmann, *J. Am. Chem. Soc.* 1975, **97**, 4884.
19. G. Kolks, S. J. Lippard, J. V. Waszczak and R. Lilienthal, *J. Am. Chem. Soc.* 1982, **104**, 717.

Polyhedron Vol. 12, No. 12, pp. 1471–1475, 1993
Printed in Great Britain

0277–5387/93 $6.00+.00
© 1993 Pergamon Press Ltd

SYNTHESIS AND CHARACTERIZATION OF A SERIES OF $[Mo_3O_4(CN)_{9-x}(H_2O)_x]^{(5-x)-}$ ($x = 0$–3) IONS

J. SZKLARZEWICZ and A. SAMOTUS*

Faculty of Chemistry, Jagiellonian University, Ingardena 3, 30-060 Kraków, Poland

(*Received* 27 *January* 1993; *accepted* 26 *February* 1993)

Abstract—Thermal or photochemical decomposition of $(bpyH)_3(H_3O)[Mo(CN)_8]\cdot H_2O$ in aqueous solutions gives amorphous salts with anions formulated as $[Mo_3O_4(CN)_{9-x}(H_2O)_x]^{(5-x)-}$ ($x = 0$–3). The series of mixed-ligand complexes was characterized by chemical analyses, UV–vis, IR and ESR spectrometry, as well as cyclic voltammetry, thermogravimetry and electrophoresis measurements. Chemical reactions, typical of molybdenum(IV) trimers, support the formulation of salts as containing the (Mo_3O_4) core.

The composition and structure of molybdenum(IV) complexes in acidic aqueous solutions has been the subject of several investigations.[1–15] X-ray crystallographic studies of $Cs_2[Mo_3O_4(C_2O_4)_3(H_2O)_3]\cdot 4H_2O\cdot 0.5H_2C_2O_4$,[2] $Cs_2[Mo_3O_4(C_2O_4)_3(H_2O)_3]\cdot CF_3SO_3\cdot 3H_2O$,[8] $Na_2[Mo_3O_4((O_2CCH_2)_2NCH_3)_3]\cdot 7H_2O$,[6] $Na_4[(Mo_3O_4)_2(edta)_3]\cdot 14H_2O$,[3] $[(CH_3)_4N]_4[Mo_3O_4(NCS)_8(H_2O)]\cdot 3H_2O$,[5] $[Pt(en)_2][Mo_3O_4(C_2O_4)_3(H_2O)_3]\cdot 3H_2O$[9] and $[Mo_3O_4(H_2O)_9](CH_3C_6H_4SO_3)_4\cdot 13H_2O$[13] have demonstrated that all possess the incomplete cuboidal (metal depleted) trinuclear core $Mo_3O_4^{4+}$ (Fig. 1), with near C_{3v} symmetry, Mo—Mo distance of *ca* 2.5 Å, Mo—μ_3-O, 2.0–2.1 Å, Mo—μ_2-O, 1.90–1.95 Å and Mo—O_3—Mo angle of *ca* 76°. It was established that in this type of cluster the oxygen atoms of the core are extremely inert,[4,9,10,13] whereas other ligands (e.g. H_2O, SCN^- and $C_2O_4^{2-}$) are much more labile and susceptible to substitution.[1,4,9,12,13]

Considerable effort has been devoted to the synthesis of the trimeric Mo^{IV}_{aq} and related complexes. These are obtained in acidic solutions (HCl, CH_3SO_3H, Hpts = *p*-toluenesulphonic acid) by the comproportionation reaction of molybdenum(II) or molybdenum(III) and molybdenum(V) or molybdenum(VI).[4,7,13] To obtain pure solutions of Mo^{IV}_3 cation-exchange chromatography is generally used, but this lowers the yield of the reaction.

In recent years we have studied the chemistry and photochemistry of the reaction of $[M(CN)_8]^{4-}$ with bpy (M = Mo, W; bpy = 2,2′-bipyridine).[16–20] In this work we have found that $(bpyH)_3(H_3O)[Mo(CN)_8]\cdot H_2O$ can be converted with relatively good yield into a compound whose properties are analogous to those of the molybdenum(IV) trimers. To date there have been no such studies on trimeric molybdenum(IV) ions with cyano ligands. The latter cannot be prepared by standard methods due to the evolution of HCN in acidic solution required for synthesis.

EXPERIMENTAL

Reagents and physical measurements

The synthesis of initial $(bpyH)_3(H_3O)[Mo(CN)_8]\cdot H_2O$, analytical methods and physical measurements (IR, UV–vis, ESR and thermogravimetry) were as described earlier.[16,17] Reflectance spectra (in $BaSO_4$) were recorded on a VSU 2P (Carl Zeiss, Jena) spectrophotometer.

Electrophoresis was performed using an OE210 apparatus (Hungary) with silica gel plates and aqueous 0.5 M $NaClO_4$ as an electrolyte. Cyclic

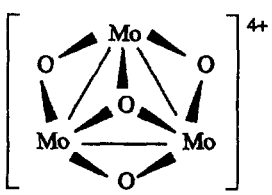

Fig. 1. Structure of the $Mo_3O_4^{4+}$ core.

* Author to whom correspondence should be addressed.

Table 1. Syntheses and analytical data for the complexes of $[Mo_3O_4(CN)_{9-x}(H_2O)_x]^{(5-x)-}$ ($x = 0$–3)

Complex	Colour	Yield (%)	Conditions	Analysis (%)[a] C	N	H	Mo	H_2O[b]
$(bpyH)_2[Mo_3O_4(CN)_6(H_2O)_3]\cdot 1.5H_2O$ (1)	Red–brown	10	$c = 2.5\times10^{-3}$, $t = 4$ h	34.5 (34.5)	15.4 (15.5)	3.5 (3.0)	31.6 (31.9)	2.8 (3.0)
$(bpyH)_3[Mo_3O_4(CN)_7(H_2O)_2]$ (2)	Red–brown	30	$c = 2.5\times10^{-2}$, $t = 4$ h	42.7 (42.6)	17.3 (17.5)	3.1 (3.0)	27.3 (27.6)	— —
$(bpyH)_3[Mo_3O_4(CN)_7(H_2O)_2]$ (2)	Red–brown	30	$c = 2.5\times10^{-2}$, hν, $t = 8$ h	43.4 (42.6)	17.5 (17.5)	3.4 (3.0)	27.9 (27.6)	— —
$(bpyH)_3(H_3O)[Mo_3O_4(CN)_8(H_2O)]\cdot 4H_2O$ (3)	Brown	40	$c = 0.1$[c], $t = 2$ h	40.7 (40.0)	17.0 (17.2)	4.1 (3.5)	25.4 (25.2)	8.1 (7.9)
$(bpyH)_3(H_3O)_2[Mo_3O_4(CN)_9]\cdot 8H_2O$ (4)	Dark brown	40	$c = 0.3$[c], $t = 1$ h	37.6 (37.8)	17.0 (16.9)	3.2 (4.0)	23.0 (23.2)	14.2 (14.5)

[a] Calculated values in parentheses.
[b] Isothermal dehydration *in vacuo* over P_4O_{10}.
[c] Solutions were prepared in hot water.

voltammetry measurements* were obtained as described earlier[21] (the potentials are reported vs NHE). Ion exchange measurements were performed using a Dovex IR120 ion exchange resin (in H^+ form).

Steady-state photolysis was performed using a medium-pressure mercury quartz lamp with open output in a glass flask under argon. Irradiation of an aqueous solution of 0.1 M $(bpyH)_3(H_3O)[Mo(CN)_8]$ was performed for periods of up to 6 h.

Syntheses

The trimeric complexes were prepared from $(bpyH)_3(H_3O)[Mo(CN)_8]\cdot H_2O$ using two simple methods and only one example of each procedure is given.

Tris-2,2′-bipyridinium diaquaheptacyanotetraoxotrimolybdate(IV), $(bpyH)_3[Mo_3O_4(CN)_7(H_2O)_2]$. Method (a): A solution (2.5×10^{-2} M) of $(bpyH)_3(H_3O)[Mo(CN)_8]\cdot H_2O$ (natural pH = 2.8) was heated at 80°C for 2 h. The resulting reddish-brown amorphous product was filtered, washed with water and ethanol and then dried in air.

Method (b): The same solution (2.5×10^{-2} M) of $(bpyH)_3(H_3O)[Mo(CN)_8]\cdot H_2O$ was irradiated with a medium-pressure mercury quartz lamp (main line 365 nm) under argon for 6 h to obtain a solid product, which was treated as above.

Details of the synthesis, yields and analytical data for the complexes are given in Table 1.

*The measurements were performed at the Department of Chemistry of the University of Ferrara, Ferrara, Italy.

The conversion of **1–4** *into* $Mo_3O_4^{4+}{}_{aq}$ *and* $[Mo_3O_4(NCS)_{9-x}(H_2O)_x]^{(5-x)-}$

The following methods were used to convert the $[Mo_3O_4(CN)_{9-x}(H_2O)_x]^{(5-x)-}$ complexes into trimers described in the literature:

(a) The solid complex was treated with $AgNO_3$ (0.5 M) in HNO_3 (0.2 M) and the mixture was heated up to 40°C and allowed to stand for 4 h. After filtration excess Ag^+ ions in the supernatant were removed by the addition of KCl and the resulting AgCl was filtered to yield a red solution of $Mo_3O_4^{4+}{}_{aq}$ ions. The identity of these ions was confirmed by electrophoresis, ion exchange experiments and UV–vis spectrophotometry.

(b) A similar procedure was used to obtain a solution of $Mo_3O_4^{4+}{}_{aq}$, except $HgCl_2$ was used as the precipitating agent for cyano ligands.

(c) The solid complex was treated with an aqueous solution (1.3 M) of NH_4SCN in Hpts (0.2 M). After 3 days standing the mixture was filtered to leave a red solution. Ion exchange experiments and electrophoresis show the negative charge of the ion (as expected for $x \leqslant 4$). Electronic absorption spectra match those previously reported for this type of complex.

RESULTS AND DISCUSSION

Syntheses

Thermal decomposition of $(bpyH)_3(H_3O)[Mo(CN)_8]\cdot H_2O$ in aqueous solutions of natural pH (pH $\leqslant$ 3) yields a brown amorphous salt. The same result can be obtained upon irradiation of an aqueous solution of this salt with polychromatic light. The composition of the product

depends on the concentration of $(bpyH)_3(H_3O)[Mo(CN)_8]\cdot H_2O$ (Mo:CN ratio changes from 1:2 in diluted solutions to 1:3 in saturated ones), but the analytical data always fit the trimeric compound (Table 1). In the conditions described repeated syntheses and analyses always produced the same results; the analytical data at concentrations between those reported in Table 1 indicate a mixture of compounds. It is noteworthy that the maximum number of cyano ligands per $Mo_3O_4^{4+}$ core was nine and no more ligands could be incorporated into the coordination sphere of the trimer. Thus, compound **4** should be the last complex of the series and not a mixture of higher and lower cyano analogues. In more dilute solutions ($c < 10^{-3}$ M) no precipitation of salt was observed. The change in colour suggests, however, the presence of lower cyano trimers, which are probably more soluble. Ion exchange experiments and electrophoresis of such solutions indicate the positive charge of the red ions.

The characteristic feature is that the complex with nine cyano ligands is formed only in more concentrated ($c > 0.3$ M) solutions where a large concentration of CN^- is present. The other compounds are formed by reversible aquation of the cyano complex in more dilute solutions. Similarly, a single-crystal X-ray study[5] showed that the typical complex formed with SCN^- as the ligand is $[Mo_3O_4(NCS)_8(H_2O)]^{4-}$, while the nine thiocyanato analogue requires very rigorous concentration conditions.

The reaction of **1–4** with $AgNO_3$ or $HgCl_2$:

$$[Mo_3O_4(CN)_{9-x}(H_2O)_x]^{(5-x)-} + (9-x)Ag^+ \longrightarrow [Mo_3O_4(H_2O)_9]^{4+} + (9-x)AgCN + xH_2O \quad (1)$$

resulted in the formation of $Mo_3O_4^{4+}{}_{aq}$, with $\lambda_{max} = 505$ nm and $\varepsilon = ca\ 60\ M^{-1}\ dm^3\ cm^{-1}$ per molybdenum (lit. data: $\lambda_{max} = 505$ nm, $\varepsilon = 63\ M^{-1}\ dm^3\ cm^{-1}$[7,12]). The red salt thus obtained is positively charged (as discovered by electrophoresis and ion exchange chromatography) and its electrochemical behaviour is identical to that described for $Mo_3O_4^{4+}{}_{aq}$ (quasi-reversible reduction at -0.154 V in 0.5 M $HClO_4$; the potential increases with increasing acid concentration).[22–25]

The reaction with a concentrated solution of thiocyanate:

$$[Mo_3O_4(CN)_{9-x}(H_2O)_x]^{(5-x)-} + 9SCN^- \longrightarrow [Mo_3O_4(NCS)_9]^{5-} + (9-x)CN^- + xH_2O \quad (2)$$

is expected to give the $[Mo_3O_4(NCS)_9]^{5-}$ ion,[9,26]

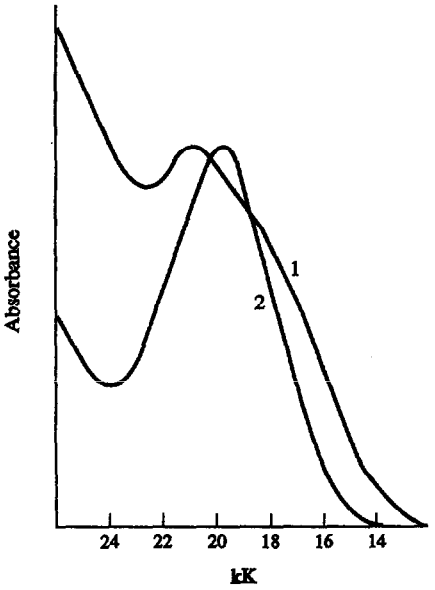

Fig. 2. Visible electronic spectra of **1** after treatment with concentrated KSCN solution in Hpts (curve 1) and after dilution with 1 M Hpts (curve 2).

which shows the appropriate ion-exchange and electrophoresis properties (negative charge) and electronic spectra (Fig. 2). The spectrum of the solution diluted by 1 M Hpts correlates very well to the spectrum of $[Mo_3O_4(H_2O)_9]^{4+}$. All these data suggest that the parent compounds also contain the Mo_3O_4 entity.

Characterization of the complexes

The products are stable towards air oxidation. They are insoluble in polar and non-polar solvents, but they dissolve in alkaline aqueous solution or basic solvents (such as pyridine) with decomposition and oxidation to molybdates.

The ESR spectra indicate that complexes **1–4** are diamagnetic, whereas the redox titration with $KMnO_4$ (under argon) indicates the two-electron oxidation per molybdenum, showing the presence of molybdenum(IV) but the absence of $Mo(CN)_8^{4-}$ ions which are oxidized to molybdenum(V). In the reflectance spectra the band at *ca* 520 nm is attributed to the transition within the quasi-aromatic cluster $Mo_3O_4^{4+}$ [27] and bands typical of the $bpyH^+$ cation and Mo^{IV}-CN anions (at 240 and 310 nm) also appear. No peaks can be seen for the complexes in the near-IR region (mixed-valence band).

As expected the complexes show strong IR bands at 2105–2115 cm^{-1}, typical for C≡N stretching vibrations (Table 2). When the charge of the anion decreases from -2 to -5 (from **1** to **4**), the strength

Table 2. Selected IR frequencies (in cm^{-1}) for salts **1–4**

Complex	Band (intensity) ν(M—O)		ν(CN)	ν(OH)	Intensity ratio[a] ν(OH)/ν(CN)	Molar ratio H_2O/CN^-
1	743(10)	960(10)	2115(10)	3400(5.4)	0.39	0.50
2	747(5.8)	956(7)	2115(10)	3400(4.2)	0.27	0.29
3	747(8.0)	955(10)	2110(10)	3400(2.7)	0.12	0.13
4	748(10)	961(10)	2105(10)	3400(1.5)	—	—

[a] The intensity of OH stretching vibrations was corrected assuming as a background the intensity of the band for salt **4**, which contains only the lattice water.

of the C≡N bonds also decreases. The lack of any shift compared with monomeric cyano complexes of molybdenum(IV) indicates that no CN^- bridging of the two molybdenum centres occurs. In the region typical of OH stretching vibrations (3100–3400 cm^{-1}) we observed a band at 3400 cm^{-1}, assigned to coordinated water molecules. The relative intensity of this band can be roughly correlated (after subtraction of the background) with the molar ratio of H_2O to CN^- in the complex anions (Table 2). All four complexes show bands at 956 and 747 cm^{-1}, assigned to the molybdenum–oxygen–molybdenum bridging system.

CONCLUSIONS

It is now well established that the reddish coloured $[Mo_3O_4(H_2O)_9]^{4+}$ ion is present in acidic solution containing only weakly complexing acids such as HCl, CH_3SO_3H or Hpts. In the presence of complexing agents the substituted ions are formed. We have found simple synthetic procedures based on the thermal or photochemical decomposition of $(bpyH)_3(H_3O)[Mo(CN)_8]\cdot H_2O$ leading to cyano-substituted compounds, $[Mo_3O_4(CN)_{9-x}(H_2O)_x]^{(5-x)-}$ ($x = 0$–3). It was established that the $Mo_3O_4^{4+}$ core can be transferred from one to the other compound, whereas CN^- ligands are labile and susceptible to substitution.

Acknowledgement—This work was supported in part by the Polish Research Grants Committee (KBN No. 1335/P3/91/02).

REFERENCES

1. M. Ardon, A. Bino and G. Yahav, *J. Am. Chem. Soc.* 1976, **98**, 2338.
2. A. Bino, F. A. Cotton and Z. Dori, *J. Am. Chem. Soc.* 1978, **100**, 5252.
3. A. Bino, F. A. Cotton and Z. Dori, *J. Am. Chem. Soc.* 1979, **101**, 3842.
4. R. K. Murmann and M. E. Shelton, *J. Am. Chem. Soc.* 1980, **102**, 3984.
5. E. O. Schlemper, M. Sakahawat and R. K. Murmann, *Cryst. Struct. Commun.* 1982, **11**, 89.
6. S. F. Cheller, T. W. Hambler, R. T. C. Brownlee, M. J. O'Connor, M. R. Snow and A. G. Wedd, *J. Am. Chem. Soc.* 1983, **105**, 1527.
7. F. A. Cotton, D. O. Marler and W. Schwotzer, *Inorg. Chem.* 1984, **23**, 3671.
8. E. Benory, A. Bino, D. Gibson, A. F. Cotton and Z. Dori, *Inorg. Chim. Acta* 1985, **99**, 137 and refs therein.
9. K. R. Rodgers, R. K. Murmann, E. O. Schlemper and M. E. Shelton, *Inorg. Chem.* 1985, **24**, 1313.
10. G. D. Hinch, D. E. Wycoff and R. K. Murmann, *Polyhedron* 1986, **5**, 487.
11. G. Wilkinson, R. D. Gillard and J. A. McCleverty, in *Comprehensive Coordination Chemistry* (Edited by G. Wilkinson), Vol. 3, p. 1243. Pergamon Press, Oxford (1987).
12. B. L. Ooi and A. G. Sykes, *Inorg. Chem.* 1988, **27**, 310.
13. D. T. Richens, L. Helm, P. A. Pittet, A. E. Merbach, F. Nicolo and G. Chapuis, *Inorg. Chem.* 1989, **28**, 1394.
14. D. T. Richens and Ch. Guille-Photin, *J. Chem. Soc., Dalton Trans.* 1990, 407.
15. T. Shibahara, *Adv. Inorg. Chem.* 1991, **37**, 143.
16. J. Szklarzewicz, A. Samotus and A. Kanas, *Polyhedron* 1986, **11**, 1733.
17. J. Szklarzewicz and A. Samotus, *Trans. Met. Chem.* 1988, **13**, 69.
18. A. Samotus, J. Szklarzewicz and N. W. Alcock, *Inorg. Chim. Acta* 1990, **172**, 129.
19. J. Szklarzewicz, A. Samotus, N. W. Alcock and M. Moll, *J. Chem. Soc., Dalton Trans.* 1990, 2959.
20. A. Al-Alousy, J. Burgess, A. Samotus and J. Szklarzewicz, *Spectrochim. Acta* 1991, **47A**, 985.
21. J. Szklarzewicz, *Inorg. Chim. Acta* 1993, **205**, 85.

22. D. T. Richens and A. G. Sykes, *Inorg. Chem.* 1982, **21**, 418.
23. M. T. Paffett and F. C. Anson, *Inorg. Chem.* 1983, **22**, 1347.
24. M. H. Chisholm, K. Folting, J. C. Huffman and E. M. Kober, *Inorg. Chem.* 1985, **24**, 241.
25. E. F. Hills and A. G Sykes, *J. Chem. Soc., Dalton Trans.* 1987, 1397.
26. M. Sagawa and Y. Sasaki, *J. Am. Chem. Soc.* 1985, **107**, 5565.
27. Z. Chen, J. Lu, Ch. Liu and Q. Zhang, *Polyhedron* 1991, **10**, 2779.

Polyhedron Vol. 12, No. 12, pp. 1477–1481, 1993
Printed in Great Britain

0277-5387/93 $6.00+.00
© 1993 Pergamon Press Ltd

HIGHEST Co^{III}–Co^{II} REDOX POTENTIAL IN $Co^{II}N_6$ ($S = 3/2$) COMPLEXES OF TRIDENTATE LIGANDS. PREDOMINANCE OF STERIC OVER ELECTRONIC EFFECT

S. MAHAPATRA, T. K. LAL and R. N. MUKHERJEE*

Department of Chemistry, Indian Institute of Technology, Kanpur 208 016, India

(*Received* 7 *January* 1993; *accepted* 26 *February* 1993)

Abstract—Using the tridentate ligand 2,6-bis(pyrazol-1-ylmethyl)pyridine and its methyl-substituted derivatives a new group of high-spin grossly octahedral cobalt(II) complexes has been synthesized and characterized. The field strength of these ligands with high-spin cobalt(II) progressively decreases with an increase in the number of methyl substituents near the donor site, as revealed from their crystal-field spectral analysis. The trends in the anodic peak potentials (Co^{III}–Co^{II} couple with $E_{1/2}/E_{pa}$ values of 0.78–1.06 V vs S.C.E.) are rationalized on the basis of predominance of the steric effect over the electronic effect of the methyl groups present near the donor site.

We have recently reported the synthesis of a group of three tridentate pyridylpyrazole ligands (L^1—L^3) and demonstrated the novel redox behaviour of their high-spin manganese(II), high-spin iron(II) and low-spin ruthenium(II) bis chelates.[1–3] It has been found that a systematic fine tuning of the M^{III}/M^{II} redox potentials from steric[1,2] over electronic to effectively an electronic[3] effect can be achieved. Additionally, we have discovered that the ligand L^1 induces temperature-dependent spin-transitions toward Fe^{2+}.[4]

The present work originates from our search for unusually stable cobalt(II) states toward oxidation in $Co^{II}N_6$ ($S = 3/2$) coordination, exploiting the steric effects of L^1–L^3 ligands. Here we report the outcome of this endeavour.

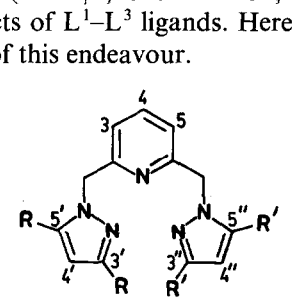

H_4bpp : R = R′ = H (L^1)

H_2Me_2bpp : R = H; R′ = Me (L^2)

Me_4bpp : R = R′ = Me (L^3)

* Author to whom correspondence should be addressed.

EXPERIMENTAL

Materials

Solvents were purified as before.[5] Tetrabutylammonium perchlorate was prepared/purified as reported previously.[6]

Synthesis of complexes

$[Co(L^1)_2](ClO_4)_2 \cdot 2H_2O$. To an ethanolic solution (5 cm^3) of L^1 (100 mg, 0.42 mmol) was added an aqueous solution (5 cm^3) of $CoCl_2 \cdot 6H_2O$ (50 mg, 0.21 mmol). The mixture was stirred at room temperature for 30 min, after which time a saturated aqueous solution (1 cm^3) of sodium perchlorate was added. The pale yellow microcrystalline solid was collected, washed with C_2H_5OH–H_2O (1:1 v/v) and dried *in vacuo* (yield *ca* 68%). Found: C, 40.4; H, 3.7; N, 18.2. Calc. for $C_{26}H_{30}N_{10}O_{10}Cl_2Co$: C, 40.4; H, 3.9; N, 18.1%. Λ_M (298 K, MeCN) = 270 Ω^{-1} cm^2 mol^{-1}. ^1H NMR (CD_3CN, δ downfield of $SiMe_4$): −10.2 (H^4), −8.0 (CH_2), −6.6 ($H^{3'}$). 17.2 ($H^{4'}$), 55.2 ($H^{5'}$), 60.4 (CH_2), 62.2 ($H^{3,5}$).

$[Co(L^2)_2](ClO_4)_2 \cdot 2H_2O$. To a stirred solution of L^2 (150 mg, 0.56 mmol) in ethanol (10 cm^3) was added an aqueous solution (5 cm^3) of $Co(ClO_4)_2 \cdot 6H_2O$ (100 mg, 0.27 mmol). The mixture was stirred for 1 h and kept at room temperature for slow evaporation. Orange crystals were

collected after 48 h, washed with C_2H_5OH/H_2O (1 : 1 v/v) and dried *in vacuo* (yield *ca* 62%). Found: C, 43.3; H, 4.6; N, 16.7. Calc. for $C_{30}H_{38}N_{10}O_{10}Cl_2Co$: C, 43.5; H, 4.6; N, 16.9%. Λ_M (298 K, MeCN) = 260 Ω^{-1} cm^2 mol^{-1}.

$[Co(L^3)_2](ClO_4)_2 \cdot 2H_2O$. This complex was synthesized following a similar method as described above for the ligand L^2 (yield *ca* 75%). Found: C, 46.0; H, 5.3; N, 15.9. Calc. for $C_{34}H_{46}N_{10}O_{10}Cl_2Co$: C, 46.2; H, 5.2; N, 15.8%. Λ_M (298 K, MeCN) = 263 Ω^{-1} cm^2 mol^{-1}. ^{1}H NMR (CD_3CN, δ downfield of $SiMe_4$): −28.8 ($Me^{3'}$), −9.6 (H^4), −3.2 (CH_2), 16.8 ($H^{4'}$), 22.8 ($Me^{5'}$), 63.8 ($H^{3,5}$), 82.0 (CH_2).

CAUTION! Although no problem was experienced in handling these complexes, perchlorate salts of complexes with organic groups should be regarded as potentially explosive.

Measurements

Conductivity and spectroscopic data were obtained as described previously.[5,6] Solution-state magnetic susceptibility was obtained by the NMR technique of Evans[7] in MeCN with a PMX-60 Jeol (60 MHz) NMR spectrometer.

The magnetic susceptibility of a powdered sample of $[Co(L^1)_2](ClO_4)_2 \cdot 2H_2O$ was measured by using the Faraday method between 8 and 300 K. Diamagnetic contributions (-306×10^{-6} cm^3 mol^{-1}) were applied with the use of Pascal's constants.[8] The details of the measurements are as described previously.[9] The system was calibrated using $Hg[Co(SCN)_4]$ and $[Fe(acac)_3]$ (acac = acetylacetonate anion). Variable-temperature magnetic moment data for $[Co(L^1)_2](ClO_4)_2 \cdot 2H_2O$ (T/K, μ_{eff}/μ_B): 300, 5.12; 280, 5.18; 260, 5.24; 240, 5.30; 220, 5.32; 200, 5.39; 180, 5.38; 160, 5.44; 140, 5.51; 120, 5.53; 100, 5.53; 80, 5.51; 60, 5.47; 40, 5.35; 20, 5.12; 11.8, 5.07; 8.8, 5.07.

All electrochemical experiments were performed under a dinitrogen atmosphere using a Princeton Applied Research (PAR) Model 370-4 electrochemistry system, as described previously.[5,6] The data were collected at 298 K, referenced to an aqueous S.C.E. and are uncorrected for junction potentials. The cyclic voltammetric measurements utilized a planar Beckman Model 39273 platinum inlay as a working electrode. The solutions were *ca* 1.0 mM in the complex and 0.2 M in the supporting electrolyte. The $E_{1/2}$ values were calculated as the average of the cathodic (E_{pc}) and anodic (E_{pa}) peak potentials.

RESULTS AND DISCUSSION

Synthesis, magnetism and ligand field spectra

The synthetic method reported herein for the preparation of cobalt(II) bis-chelates is relatively straightforward. The reaction of $CoCl_2 \cdot 4H_2O$ or $Co(ClO_4)_2 \cdot 6H_2O$ with the appropriate tridentate ligand in aqueous methanol affords complexes with a 1 : 2 metal-to-ligand ratio, having the general formula $[CoL_2](ClO_4)_2 \cdot 2H_2O$ (when $CoCl_2 \cdot 4H_2O$ was used a saturated aqueous solution of $NaClO_4 \cdot H_2O$ was added to isolate the desired product). The orange to pale yellow complexes are indefinitely stable in air. The complexes are 1 : 2 electrolytes[10] in MeCN solution.

Solution-state magnetic susceptibility measurements reveal that these cobalt(II) complexes are high-spin octahedral with a ground term of $^4T_{1g}$ origin.[11–13] The temperature-dependent solid-state magnetic behaviour of $[Co(L^1)_2](ClO_4)_2 \cdot 2H_2O$ has been examined (see Experimental) and is prototypical of the magnetically dilute high-spin cobalt(II) ion in a grossly octahedral field.[13]

The absorption spectral properties of these complexes were examined (Table 1) in MeCN solutions and the behaviour of a representative complex is displayed in Fig. 1. The spectra of these complexes are similar to those observed for grossly octahedral high-spin cobalt(II) complexes.[11] In the present complexes the number of *d–d* transitions are more due to low symmetry (*vide infra*) in the ligand field component. Following Figgis,[14] Dq and B were calculated (as it was not possible to obtain an unambiguous choice of parameters[13] to fit the solid-state magnetic data we have ignored the spin-orbit coupling term) as 1200 and 750 cm^{-1}, respectively. Similarly, for $[Co(L^2)_2]^{2+}$ and $[Co(L^3)_2]^{2+}$ the Dq values were calculated as 1120 and 1080 cm^{-1}, respectively, and the corresponding B values are 770 and 830 cm^{-1}, respectively. From the above three com-

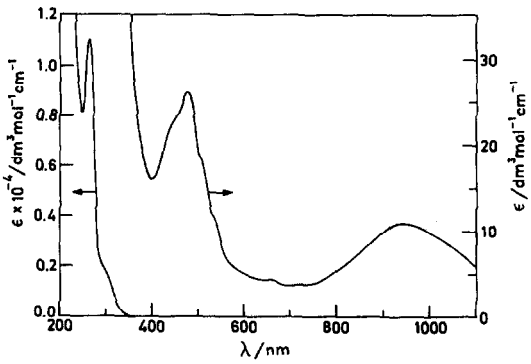

Fig. 1. Absorption spectrum of $[Co(L^1)_2](ClO_4)_2 \cdot 2H_2O$ in MeCN.

Table 1. Magnetic moment,[a] electronic spectra and cyclic voltammetric[b] data of the complexes at 298 K in acetonitrile

Complex	μ_{eff}/μ_B	λ (nm) (ε/dm^3 mol^{-1} cm^{-1})	Co^{III}–Co^{II} couple E_{pa} (V)	E_{pc} (V)
$[Co(L^1)_2](ClO_4)_2 \cdot 2H_2O$	4.78 (5.07)	934 (11), 539 (sh) (11), 510 (sh) (18), 479 (26), 435 (sh) (21), 302 (sh) (1670), 265 (11,100)	0.78	0.70
$[Co(L^2)_2](ClO_4)_2 \cdot 2H_2O$	4.86	992 (14), 655 (sh) (12), 545 (sh) (31), 485 (sh) (70), 308 (sh) (2330), 265 (10,900)	0.88	0.78
$[Co(L^3)_2](ClO_4)_2 \cdot 2H_2O$	4.80 (5.20)	1050 (11), 537 (sh) (16), 486 (31), 310 (sh) (2400), 267 (11,600)	1.06	0.88

[a] Using Evans' method; room temperature solid-state values in parentheses.

[b] Supporting electrolyte (n-Bu_4N)ClO_4; all potentials are referenced to S.C.E.; $E_f = (E_{pa} + E_{pc})/2$; scan rate 50 mV s^{-1} at a platinum working electrode.

plexes B_{av} was calculated as 786 cm^{-1}, which is approximately 70% of the free-ion value (1120 cm^{-1}).[14] This indicates *ca* 30% covalent character in the metal–ligand bonds. A most interesting result that is emerging is the gradual reduction in $10Dq$ values toward cobalt(II) in going from L^1 to L^2 to L^3. It is the increased steric crowding near the donor sites (3-methyl substituents) that progressively decreases the value of $10Dq$ due to interligand steric interactions. Similar effects were also observed in the iron(II)[1] and nickel(II)[15] complexes of these ligands.

^{1}H *NMR spectra*

To extract structural information in these six-coordinate cobalt(II) ($S = 3/2$) complexes in CD_3CN we have investigated the ^{1}H NMR spectral

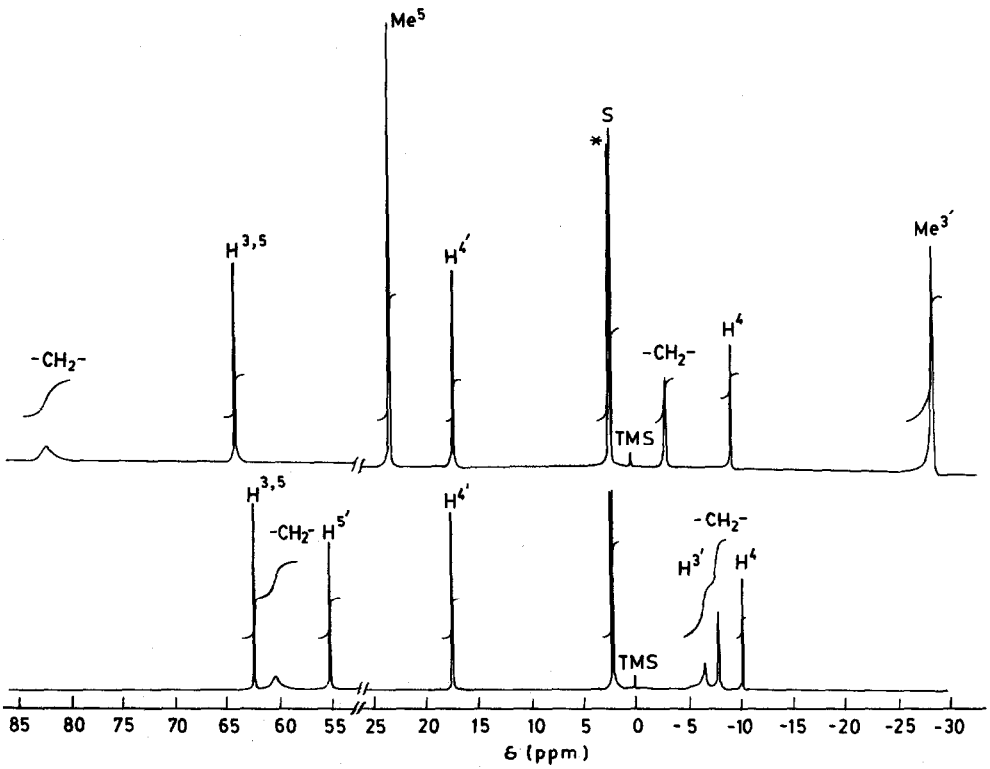

Fig. 2. 400 MHz ^{1}H NMR spectra of $[Co(L^1)_2](ClO_4)_2 \cdot 2H_2O$ and $[Co(L^3)_2](ClO_4)_2 \cdot 2H_2O$ in CD_3CN (solvent and water peaks marked by S and *, respectively).

properties of two representative complexes, $[Co(L^1)_2]^{2+}$ and $[Co(L^3)_2]^{2+}$ (Fig. 2). These two complexes are sufficient to establish the assignments given (see Experimental). The ligand proton assignments have been made on the basis of intensity, the effects of substitution of the methyl group for hydrogen, relative line widths and comparison with the spectra of related iron(II)[1] and nickel(II)[15] complexes. The singlet nature of all the pyridine and pyrazole ring proton resonances is consistent with two equivalent chelate rings, reflecting the grossly octahedral symmetry of these high-spin cobalt(II) complexes in CD_3CN solution. However, the occurrence of two methylene proton resonances is indicative of a non-planar chelate ring conformation, as observed in the solid-state structures of $[Fe(L^2)_2](ClO_4)_2$[16] and $[Ni(L^1)_2](ClO_4)_2$.[17] The ^1H NMR spectra, as shown in Fig. 2, have been reported very recently[18] utilizing cobalt(II) complexes of pyrazole-rich tridentate ligands.

Redox properties

(a) *The* Co^{III}/Co^{II} *couple.* Cyclic voltammetric studies using a platinum electrode gave an oxidative response with $i_{pc}/i_{pa} \approx 1.0$. The one-electron nature of this redox response has been identified by comparison of current height with the redox response[1] of a sample of $[Fe(L^1)_2]^{2+}$ under the same experimental conditions. The peak differences were 80 ($[Co(L^1)_2]^{2+}$), 100 ($[Co(L^2)_2]^{2+}$) and 180 mV ($[Co(L^3)_2]^{2+}$) at a scan rate of 50 mV s^{-1}. Thus, the Co^{III}–Co^{II} couple is electrochemically reversible[5,19] for the unsubstituted complex; however, the reversibility progressively decreases for $[Co(L^2)_2]^{2+}$ and $[Co(L^3)_2]^{2+}$. This is understandable, given an incremental steric crowding at the $Co^{II}N_6$ coordination unit on passing from $[Co(L^1)_2]^{2+}$ to $[Co(L^3)_2]^{2+}$, which in turn causes a substantial structural change between the redox states Co^{II} and Co^{III} and hence a decrease in the reversibility. The $E_{1/2}$ values of the Co^{III}–Co^{II} couple are 0.74 and 0.83 V vs S.C.E. for $[Co(L^1)_2]^{2+}$ and $[Co(L^2)_2]^{2+}$, respectively. For $[Co(L^3)_2]^{2+}$ the E_{pa} value is 1.06 V vs S.C.E. To the best of our knowledge the $E_{1/2}$ (E_{pa}) values[2] observed for the present complexes are the highest[20] (the $[Co(bpym)_3]^{3+}/[Co(bpym)_3]^{2+}$ couple[20f] is 0.80 V vs S.C.E.; bpym = 2,2′-bipyrimidine) known so far for high-spin cobalt(II) bis- or tris-chelates having CoN_6 coordination.

(b) *Effect of methyl substituents.* Since the observed oxidative responses are not reversible for all the three complexes, for the purpose of comparison the emphasis is given to the anodic peak potentials[2] which are the potentials measured when the anodic peak current is at its maximum. The

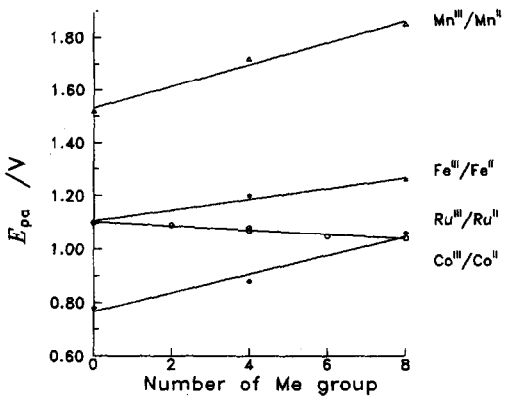

Fig. 3. Plot of anodic peak potentials (E_{pa} V vs S.C.E.) for the M^{III}–M^{II} couple against the total number of methyl groups in the complex with ligands L^1, L^2 and L^3.

observed unusual trend in the E_{pa} values (Table 1) can be rationalized[1,2] by considering the predominance of steric factors caused by substitution at the 3-position(s) over the electronic contribution prevailing at the 5-position(s) in the ligands L^2 and L^3. In the bis complexes of ruthenium(II)[3] we observed the predominance of electronic over steric effects. Figure 3 neatly summarizes our experimental findings for the M^{III}/M^{II} couple (M = Mn, Fe, Co and Ru; a positive slope signifies steric predominance and a negative slope indicates electronic predominance) in the bis complexes of the present ligands.

Acknowledgements—Financial assistance from the Department of Science and Technology, Government of India, and the Council of Scientific and Industrial Research, New Delhi, India, is gratefully acknowledged. We thank Professor S. Mitra and Mr B. T. Kansara of the Tata Institute of Fundamental Research (TIFR), Bombay, India, for solid-state magnetic susceptibility measurements. One of us (RNM) acknowledges the financial assistance from TIFR during his stay.

REFERENCES

1. S. Mahapatra, N. Gupta and R. N. Mukherjee, *J. Chem. Soc., Dalton Trans.* 1991, 2911.
2. S. Mahapatra, D. Bhuniya and R. N. Mukherjee, *Polyhedron* 1992, **11**, 2045.
3. S. Mahapatra and R. N. Mukherjee, *J. Chem. Soc., Dalton Trans.* 1992, 2337.
4. S. Mahapatra and R. N. Mukherjee, *Polyhedron*, submitted.
5. N Gupta, S. Mukerjee, S. Mahapatra, M. Ray and R. N. Mukherjee, *Inorg. Chem.* 1992, **31**, 139.
6. M. Ray, S. Mukerjee and R. N. Mukherjee, *J. Chem. Soc., Dalton Trans.* 1990, 3635.
7. D. F. Evans, *J. Chem. Soc.* 1959, 2003.

8. C. J. O'Connor, *Prog. Inorg. Chem.* 1982, **29**, 203.
9. S. Mahapatra, N. Gupta and R. N. Mukherjee, *J. Chem. Soc., Dalton Trans* 1992, 3041.
10. W. J. Geary, *Coord. Chem. Rev.* 1971, **7**, 81.
11. F. A. Cotton and G. Wilkinson, *Advanced Inorganic Chemistry*, 5th edn, pp. 729–731. John Wiley, New York (1986).
12. L. Banci, A. Bencini, C. Benelli, D. Gatteschi and C. Zanchini, *Struct. Bonding (Berlin)* 1982, **52**, 37.
13. L. L. Martin, R. L. Martin, K. S. Murray and A. M. Sargeson, *Inorg. Chem.* 1990, **29**, 1387.
14. B. N. Figgis, *Introduction to Ligand Fields*, pp. 168, 223–225. Wiley Eastern Limited, New Delhi (1976).
15. S. Mahapatra and R. N. Mukherjee, *Ind. J. Chem.* 1993, **32A**, 64.
16. S. Mahapatra, R. J. Butcher and R. N. Mukherjee, submitted.
17. A. A. Watson, D. A. House and P. J. Steel, *Inorg. Chim. Acta* 1987, **130**, 167.
18. J. C. Calabrese, P. J. Domaille, S. Trofimenko and G. J. Long, *Inorg. Chem.* 1991, **30**, 2795.
19. R. S. Nicholson and I. Shain, *Analyt. Chem.* 1964, **36**, 706.
20. (a) T. Saji and S. Aoyagui, *J. Electroanal. Chem.* 1975, **60**, 1; (b) J. M. Rao, M. C. Hughes and D. J. Macero, *Inorg. Chim. Acta* 1976, **16**, 231; (c) J. M. Rao, D. J. Macero and M. C. Hughes, *Inorg. Chim. Acta* 1980, **41**, 221; (d) K. Wieghardt, W. Schmidt, W. Herrmann and H.-J. Kuppers, *Inorg. Chem.* 1983, **22**, 2953; (e) C. A. Koval, R. L. A. Pravata and C. M. Reidsema, *Inorg. Chem.* 1984, **23**, 545; (f) R. R. Ruminski and J. D. Petersen, *Inorg. Chim. Acta* 1985, **97**, 129; (g) D. Ventur, K. Wieghardt, B. Nuber and J. Weiss, *Z. Anorg. Allg. Chem.* 1987, **551**, 33.

Polyhedron Vol. 12, No. 12, pp. 1483–1485, 1993
Printed in Great Britain

0277–5387/93 $6.00+.00
© 1993 Pergamon Press Ltd

SYNTHESIS AND CRYSTAL STRUCTURE OF THE HETEROPOLYVANADATE ANION $[AsV_{12}O_{40}(VO)_2]^{9-}$

GUI-QING HUANG, SHI-WEI ZHANG,* YONG-GE WEI and MEI-CHENG SHAO

Institute of Physical Chemistry, Peking University, Beijing 100871, P.R.C.

(*Received* 27 *October* 1992; *accepted* 26 *February* 1993)

Abstract—The structure of $(Et_4N)_3H_6[AsV_{12}O_{40}(VO)_2]\cdot 20H_2O$ has been determined by single-crystal X-ray diffraction analysis. In the anion the central AsO_4 tetrahedron and $12VO_6$ octahedra form the usual Keggin structure (α-isomer) and the remaining two VO^{3+} groups occupy the cavities in the Keggin structure, where a two-fold axis passes to form *trans*-located tetragonal pyramidal caps.

A number of heterotungstates and -molybdates adopt either the Keggin structure or a structure derived from fragments of it.[1] In these polyanions some of the molybdenum or tungsten atoms are replaced by vanadium atoms.[2,3] However, our knowledge on heteropolyvanadates containing a tetrahedrally-coordinated heteroatom is still limited. The mineral structure $[AlV_{14}O_{40}]^{9-}$ [4] and its isostructural anion $[AsV_{14}O_{40}]^{7-}$ [5] contain octahedrally coordinated heteroatoms. A series based on capping by VO or As_2O the sets of O_4-square faces of the rhombicuboctahedron of the Keggin anions has been synthesized and reported.[6,7] For a normal Keggin anion of vanadium, $XV_{12}O_{40}$, a high negative charge might prevent its formation, but it could be stabilized by capping two VO^{3+} or AsO^{3+} groups to form a bicapped Keggin structure.[8,9] We report here a bicapped Keggin structure in which arsenic is the tetrahedrally coordinated heteroatom.

EXPERIMENTAL

Synthesis and elemental analysis

The title compound was prepared by mixing NH_4VO_3 (0.83 g), Na_2HAsO_4 (0.49 g) and NH_2OH HCl (0.88 g) in water (50 cm^3) and 1 N HCl solution (2 cm^3). The mixture was heated at reflux temperature for *ca* $1\frac{1}{2}$ h followed by adding Et_4NBr (0.35 g) after the reaction solution had cooled to room temperature. Dark blue crystals were obtained from the above solution and dark red crystals were recrystallized from water at room temperature.

Found: C, 13.7; N, 1.9; V, 32.3; As, 3.6. Calc. for $C_{24}N_3H_{106}O_{82}V_{14}As$: C, 13.0; N, 1.9; V, 32.2; As, 3.40%.

Crystal structure determination

A single crystal of the dimensions $0.3\times0.4\times0.5$ mm^3 was used for the data collection on a Siemens R3m/V diffractometer equipped with graphite monochromatized Mo-K_α radiation ($\lambda = 0.7073$ Å). $\omega/2\theta$ scans with variable speeds, 4.88–29.3° min^{-1}, were used. The cell parameters were refined by a least-squares method on the basis of 25 reflections with $17 \leqslant 2\theta \leqslant 25$; two standard reflections were monitored every 100 reflections and showed no significant change; 2901 reflections were collected ($2\theta_{max} = 45°$, $0 \leqslant h \leqslant 16$, $0 \leqslant k \leqslant 26$, $0 \leqslant l \leqslant 45$) and merged to give 2603 independent reflections, of which 2034 reflections with $F > 5\sigma(F)$ were used in the calculations.

Crystal data. $C_{24}N_3H_{106}O_{62}V_{14}As$, orthorhombic, space group *Fddd*, $M = 2217$, $a = 14.938(4)$, $b = 24.712(7)$, $c = 42.619(12)$ Å, $V = 15.732(7)$ Å^3, $Z = 8$, $D_m = 1.867$ g cm^{-1}, $D_x = 1.87$ g cm^{-1}, $F(000) = 8976$, μ(Mo-K_α) = 2.049 mm^{-1}.

The positions of the arsenic and vanadium atoms were obtained by direct methods, subsequent Fourier syntheses yielded the coordinates of the remaining oxygen, nitrogen and carbon atoms by standard least-squares techniques (SHELXTL PLUS program system). No hydrogen atoms were included. The final R value was 0.0595.

* Author to whom correspondence should be addressed.

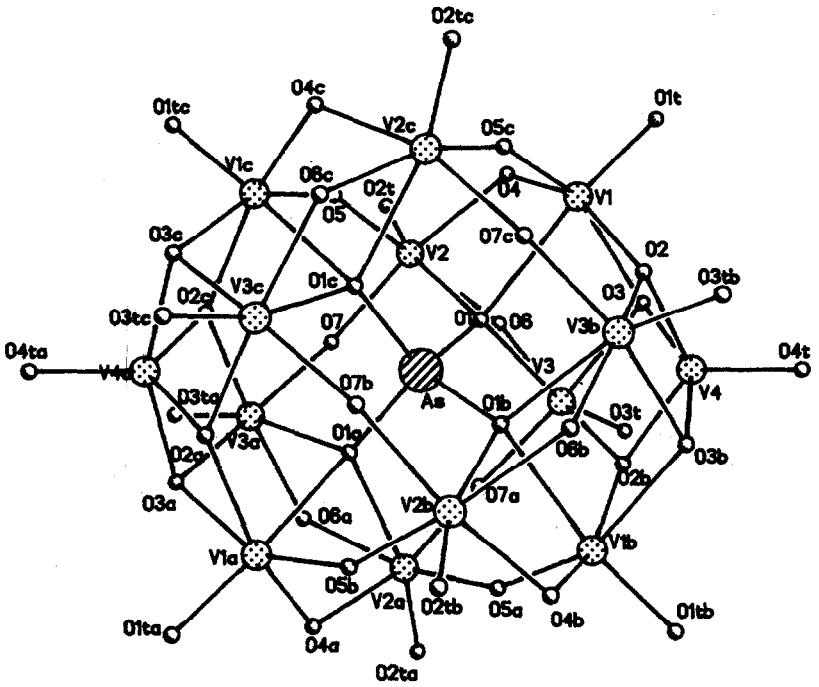

Fig. 1. A view of the $[AsV_{12}O_{40}(VO)_2]^{9-}$ anion.

Atomic positional coordinates, displacement factor coefficients, full lists of bond lengths and angles and a list of F_o/F_c values have been deposited as supplementary data with the Editor, from whom copies are available on request. Atomic coordinates have also been deposited with the Cambridge Crystallographic Data Centre.

RESULTS AND DISCUSSION

The anion structures are shown in Figs 1 and 2. Selected bond distances and bond angles are listed in Tables 1 and 2, respectively.

In the anion the central tetrahedral AsO_4 shares its oxygen atoms with four V_3O_{13} groups, each of which is made up of $V(1)O_6$, $V(2)O_6$ and $V(3)O_6$ edge-sharing octahedra. These four V_3O_{13} groups are connected to each other by a shared corner. This part is the well-known α-Keggin structure. The AsO_4 tetrahedron is almost perfectly regular. The As—O distances are all 1.686 Å and the O—As—O angles are 108.9–110.1°, the average being 109.5°. The AsO_4 tetrahedron thus has *Td* symmetry and the four V_3O_{13} units are linked in *Td* symmetry with a central AsO_4 group. Two other VO units, through which a crystallographic two-fold axis passes,

Table 1. Selected bond distances (Å) of the $[AsV_{12}O_{40}(VO)_2]^{9-}$ anion

As—O(1)	1.685(5)	V(1)—O(1)	2.299(5)
V(1)—O(1t)	1.619(7)	V(1)—O(2)	1.998(6)
V(1)—O(3)	2.129(6)	V(1)—O(4)	1.892(6)
V(1)—O(5)	1.724(6)	V(2)—O(1)	2.326(6)
V(2)—O(2t)	1.595(6)	V(2)—O(4)	1.977(6)
V(2)—O(5)	1.919(6)	V(2)—O(6)	1.928(6)
V(2)—O(7)	1.834(6)	V(3)—O(1)	2.319(6)
V(3)—O(3t)	1.588(6)	V(3)—O(2)	2.031(6)
V(3)—O(3)	2.075(6)	V(3)—O(6)	1.834(6)
V(3)—O(7)	1.794(6)	V(4)—O(4t)	1.586(9)
V(4)—O(2)	1.819(6)	V(4)—O(3)	1.938(6)

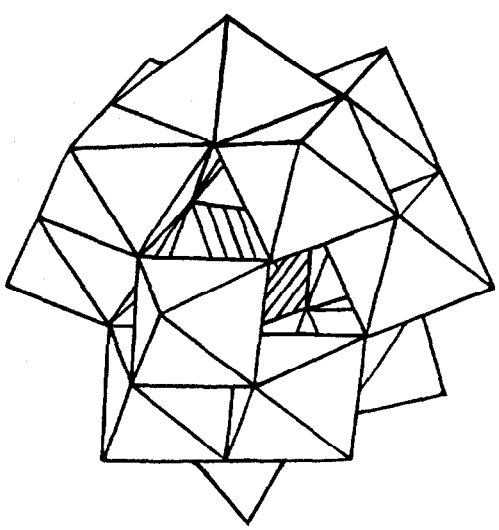

Fig. 2. Polyhedral model of the $[AsV_{12}O_{40}(VO)_2]^{9-}$ anion (idealized for clarity).

Table 2. Selected bond angles (°) of the $[AsV_{12}O_{40}(VO)_2]^{9-}$ anion

O(1)—As—O(1b)	109.5(4)	O(1t)—V(1)—O(1)	163.4(3)
O(1t)—V(1)—O(2)	99.5(3)	O(1t)—V(1)—O(3)	96.6(3)
O(1t)—V(1)—O(4)	97.5(3)	O(1t)—V(1)—O(5a)	104.9(3)
O(1)—V(1)—O(2)	85.8(2)	O(1)—V(1)—O(3)	69.3(2)
O(1)—V(1)—O(4)	74.3(2)	O(1)—V(1)—O(5a)	90.9(2)
O(2)—V(1)—O(3)	74.7(2)	O(2)—V(1)—O(4)	158.5(2)
O(2)—V(1)—O(5a)	88.8(3)	O(3)—V(1)—O(4)	89.9(2)
O(3)—V(1)—O(5a)	155.2(3)	O(4)—V(1)—O(5a)	99.3(3)
O(2t)—V(2)—O(1)	167.3(3)	O(2t)—V(1)—O(4)	97.5(3)
O(2t)—V(2)—O(5)	102.4(3)	O(2t)—V(1)—O(6)	98.2(3)
O(2t)—V(2)—O(7)	103.3(3)	O(1)—V(2)—O(4)	72.2(2)
O(1)—V(2)—O(5)	85.0(2)	O(1)—V(2)—O(6)	74.0(2)
O(1)—V(2)—O(7)	87.3(2)	O(4)—V(2)—O(5)	87.6(3)
O(4)—V(2)—O(6)	85.6(3)	O(4)—V(2)—O(7)	159.1(2)
O(5)—V(2)—O(6)	159.0(3)	O(5)—V(2)—O(7)	86.7(3)
O(6)—V(2)—O(7)	92.7(3)	O(3t)—V(3)—O(1)	164.8(3)
O(3t)—V(3)—O(2a)	98.9(3)	O(3t)—V(3)—O(3)	96.7(3)
O(3t)—V(3)—O(6)	98.4(3)	O(3t)—V(3)—O(7a)	105.5(3)
O(1)—V(3)—O(2a)	84.9(2)	O(1)—V(3)—O(3)	69.8(2)
O(1)—V(3)—O(6)	75.8(2)	O(1)—V(3)—O(7a)	89.3(2)
O(2a)—V(3)—O(3)	75.9(2)	O(2a)—V(3)—O(6)	159.9(2)
O(2a)—V(3)—O(7a)	87.1(2)	O(3)—V(3)—O(6)	92.1(2)
O(3)—V(3)—O(7a)	153.9(2)	O(6)—V(3)—O(7a)	97.9(3)
O(2)—V(4)—O(2a)	124.8(4)	O(3)—V(4)—O(3a)	155.6(4)
O(4t)—V(4)—O(2)	117.6(2)	O(4t)—V(4)—O(3)	102.2(2)
O(2)—V(4)—O(3)	84.4(2)		

occupy *trans*-located sites forming two tetragonal pyramidal caps.

All of the oxygen atoms in the polyanion are classified into four groups—Oa, Ob, Oc and Od. Oa is the oxygen atom bound to one central arsenic atom and to three vanadium atoms of the same V_3O_{13} unit, and Ob is shared by two vanadium atoms. Oc is a three-coordinate oxygen atom, which is bound to one capping and two other vanadium atoms of V_3O_{13} units; Od is a terminal oxygen atom combined with only one vanadium atom.

The metal–oxygen bonds in VO_6 and VO_5 are not equivalent. V—Od bond lengths are the shortest; range 1.586–1.620 Å with an average of 1.597 Å; the distances for the V—Oa bond, which is opposite to the V—Od bond, are the longest; range 2.298–2.326 Å with an average of 2.314 Å, and an average Od—V—Oa angle of 165.1°. The V—Ob distances are between 1.724 and 1.977 Å with an average of 1.863 Å, while the values for V—Oc are between 1.819 and 2.129 Å with an average of 1.982 Å. For VO_5 tetragonal pyramidal caps the V—Od bond length is 1.585 Å, three-coordinated V—Oc distances are 1.819 and 1.938 Å, respectively, and the average is 1.879 Å.

There are five kinds of crystallographically different water molecules in the crystals, each one having significant hydrogen bonds to the anion and other water molecules. A total of 20 water molecules, together with three Et_4N^+ cations, play an important role in stabilizing the crystals.

Acknowledgement—This work is supported by the National Natural Science Foundation of China.

REFERENCES

1. M. T. Pope, *Heteropoly and Isopoly Oxometalates*. Springer, New York (1983).
2. K. Nishikawa, A. Kobayashi and Y. Sasaki, *Bull. Chem. Soc. Japan* 1975, **48**, 3152.
3. A. Bjornberg and B. Hedman, *Acta Cryst.* 1980, **B36**, 1018.
4. H. T. Evans Jr and J. A. Konnert, *Am. Min.* 1978, **63**, 836.
5. A. Müller, J. Döring, M. I. Khan and V. Wittneben, *Angew. Chem., Int. Edn Engl.* 1990, **30**, 210.
6. A. Müller, J. Döring and H. Bögge, *J. Chem. Soc., Chem. Commun.* 1991, **30**, 273.
7. M. T. Pope and A. Müller, *Angew. Chem., Int. Edn Engl.* 1991, **30**, 34.
8. R. Kato, A. Kobayashi and Y. Sasaki, *Inorg. Chem.* 1982, **21**, 240.
9. G. Huang, S. Zhang and M. Shao, *Inorg. Chem.*, submitted.

Polyhedron Vol. 12, No. 12, pp. 1487–1490, 1993
Printed in Great Britain

0277–5387/93 $6.00+.00
© 1993 Pergamon Press Ltd

IRON–MOLYBDENUM–SULPHUR AND IRON–TUNGSTEN–SULPHUR COMPLEXES OF DIIMINES

VASANTHI LAKSHMANAN, K. S. NAGARAJA* and M. R. UDUPA†

Department of Chemistry, Indian Institute of Technology, Madras 600 036, India

(*Received* 23 *November* 1992; *accepted* 25 *February* 1993)

Abstract—The complexes $FeLMS_4$ (L = bipy or phen; M = Mo or W) were prepared and characterized. The linearity of the χ_M^{-1} vs T plot and Mössbauer spectral parameters (δ: 0.28 mm s^{-1}; E_Q: 0.37 mm s^{-1}) of $[Fe(bipy)_2MoS_4]$ suggested that iron(II) assumes a distorted octahedral geometry with an intermediate spin state. The thiometallate acts as a bidentate chelating ligand towards iron(III), as evidenced by IR spectral results. An irreversible anodic wave observed at +1.04 V vs S.C.E. in the cyclic voltammogram of $[Fe(bipy)_2MoS_4]$ in DMSO suggested the oxidation of iron(II) to iron(III) and the reduction of the bipyridyl ligand occurs at −1.40 V.

Although several iron–molybdenum–sulphur complexes have been reported,[1,2] the mechanism of redox reaction and the coordination environment around molybdenum in the nitrogenase enzyme have not been understood in detail. Thus, more studies on iron–molybdenum–sulphur complexes are demanded. We reported in this paper the preparation and characterization of iron–molybdenum–sulphur and iron–tungsten–sulphur complexes of 2,2′-bipyridine (bipy) and 1,10-phenanthroline (phen).

EXPERIMENTAL

Ammonium tetrathiometallates, $(NH_4)_2MoS_4$ and $(NH_4)_2WS_4$, and $[Fe(bipy)_2MoO_4]$ were prepared by the reported procedures.[3]

Preparation of $[Fe(bipy)_2MoS_4]$

Ammonium tetrathiomolybdate (0.26 g, 0.001 mol) solution was added to the deep red solution resulting from mixing an aqueous solution of iron(II) sulphate heptahydrate (0.28 g, 0.001 mol) and 2,2′-bipyridine (0.45 g, 0.003 mol). The mixture was stirred for 1 h. The red complex formed was filtered, washed with water, ethanol and acetone and dried over anhydrous calcium chloride. Yield: 55%. Complexes $[Fe(phen)_2MoS_4]$, $[Fe(bipy)WS_4]$ and $[Fe(phen)_2WS_4]$ were prepared by a similar procedure. Yield: 50–55%.

Carbon, hydrogen and nitrogen analyses were performed on a Hewlett–Packard CHN 185 analyser. The magnetic susceptibility studies were measured on a VSM sample magnetometer. UV–vis, IR and FIR spectra were recorded on Perkin–Elmer Cary 2300, Perkin–Elmer 983 and Polytech IR 12 spectrophotometers, respectively. Mössbauer spectra were recorded using an ECI MBS 35 spectrometer, operating at constant acceleration mode with a ^{57}Co source diffused in a rhodium matrix mounted on a transducer. The chemical isomer shifts (δ) were measured relative to the mid-point of the spectrum of an absorber of natural iron. The cyclic voltammetric measurements were performed in DMSO using tetraethylammonium perchlorate as the supporting electrolyte. The thermal decomposition studies were performed on a Stanton–Redcroft STA-780 thermobalance with a heating rate of 10°C min^{-1}.

RESULTS AND DISCUSSION

The analytical data of the complexes are given in Table 1. The complexes are insoluble in water and common organic solvents and undergo thermal decomposition (Table 2) in two stages. The chemical analysis and X-ray diffraction patterns of the products obtained on heating the complexes confirmed the intermediate phases to be a mixture of FeS and

* Department of Chemistry, Loyola College (autonomous), Madras, India.

† Author to whom correspondence should be addressed.

Table 1. Analytical and magnetic data of Fe–Mo–S complexes

Complex	Found (Calc.) (%) C	H	N	S	Mo/W	Fe	μ_{eff} (B.M.)
$[Fe(bipy)_2MoS_4]$	40.1 (20.6)	2.7 (2.7)	9.4 (9.5)	21.5 (21.6)	16.3 (16.3)	9.3 (9.4)	2.70
$[Fe(bipy)_2WS_4]$	35.8 (35.3)	2.5 (2.4)	8.1 (8.2)	18.9 (18.9)	26.7 (27.0)	8.4 (8.2)	2.72
$[Fe(phen)_2MoS_4]$	45.0 (45.0)	2.6 (2.5)	8.7 (8.7)	20.1 (20.1)	15.4 (15.0)	8.6 (8.7)	2.69
$[Fe(bipy)_2WS_4$	39.8 (39.6)	2.2 (2.2)	7.7 (7.7)	17.7 (17.6)	25.1 (25.2)	7.7 (7.7)	2.71

Table 2. TG and DTA data of Fe–Mo–S complexes

Complex	Temperature range (°C)	Weight loss (%)		Phases formed	DTA peaks[a] (°C)
$[Fe(bipy)_2MoS_4]$	180–250	52.0	52.7	$FeS+MoS_3$	250(+), 350(+)
	380–535	64.7	63.6	$Fe_2O_3+MoO_3$	475(+)
$[Fe(bipy)_2WS_4]$	230–290	45.9	45.7	$FeS+WS_3$	259(+), 280(+)
	425–510	64.2	64.9	$Fe_2O_3+WO_3$	460(+)
$[Fe(phen)_2MoS_4]$	300–400	56.3	56.0	$FeS+MoS_3$	350(+)
	470–500	66.3	66.9	$Fe_2O_3+MoO_3$	460(+)
$[Fe(phen)_2WS_4]$	330–400	49.5	49.3	$FeS+WS_3$	400(+)
	450–530	58.7	57.3	$Fe_2O_3+WO_3$	485(+)

[a] (+) = exotherm.

MoS_3, from thiomolybdates, and FeS and WS_3, from thiotungstates. The sulphides undergo further decomposition to the oxides as shown by IR[4] from the X-ray powder patterns of the end residues. The magnetic susceptibility measurements of $[Fe(bipy)_2MoS_4]$ indicated that the plot of χ_M^{-1} vs T (Fig. 1) is linear. The absence of Neel's temperature ruled out the presence of antiferromagnetic exchange interactions. The octahedral iron(II) complexes exhibited unusual magnetic behaviour[5] due to a spin cross-over mechanism ($^5T_2 - {}^1A_1$). However, complexes $[Fe(bipy)(CH_2CO_2CO_2)]$ and $[Fe(bipy)_2C_2O_4]$, with μ_{eff} at room temperature around 3.1 B.M., exhibited[6] linearity in the χ_M^{-1} vs T plot, which is attributed to the presence of an inherent half-quenched spin-state ($^3T_1$) of iron(II). The intermediate spin-state arises when the ligand field strength lies between strong and weak fields and thus the linear behaviour of the χ_M^{-1} vs T plot is attributed to the presence of an intermediate spin-state of iron(II) in $[Fe(bipy)MoS_4]$ and not due to antiferromagnetic coupling. The Mössbauer spectra of $Fe(bipy)MoS_4$ is given in Fig. 2 and the room-

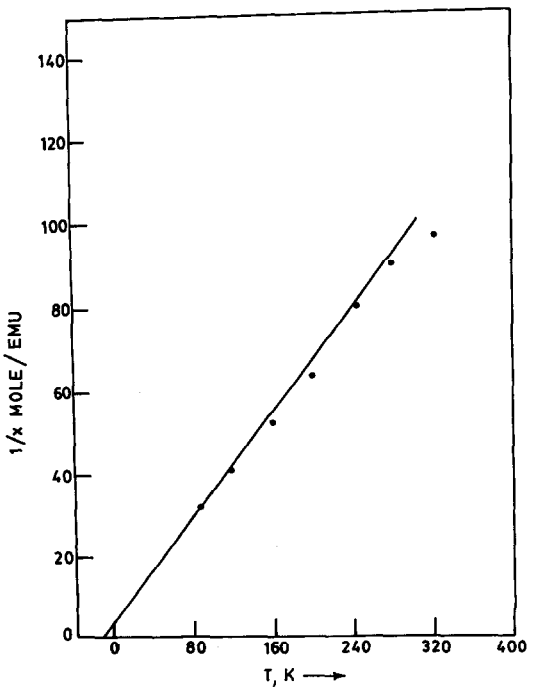

Fig. 1. $1/x$ vs T plot for $[Fe(bipy)_2MoS_4]$.

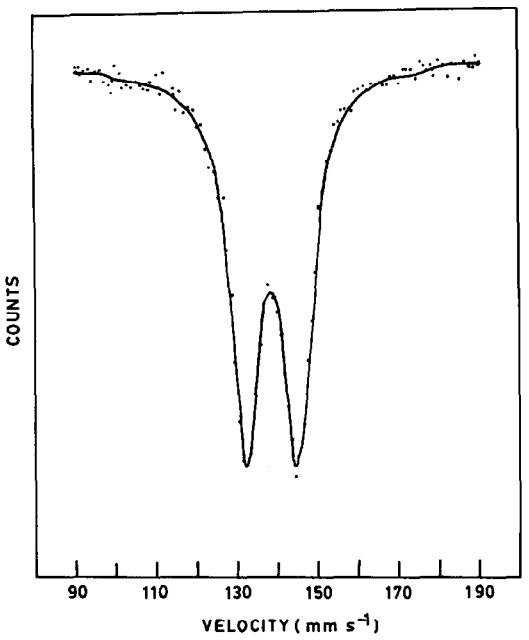

Fig. 2. Mössbauer spectrum of the complex $[Fe(bipy)_2MoS_4]$ at room temperature.

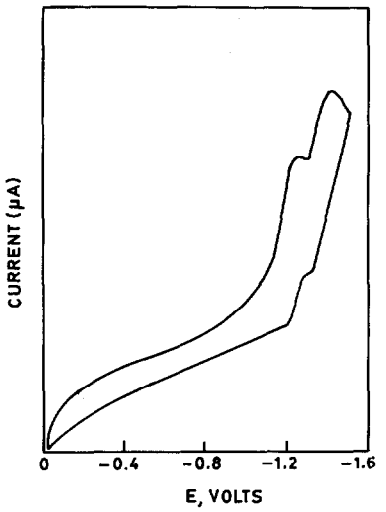

Fig. 3. CVM of $[Fe(bipy)_2MoS_4]$ in DMSO at a sweep rate of 100 mV s^{-1}.

temperature spectral parameters δ and ΔE_Q are 0.28 and 0.37 mm s^{-1}, respectively. These values are found[6] to be of the same order as observed for the intermediate spin-state complex $[Fe(bipy)C_2O_4]$. If iron(II) was in a high-spin state the reported[6] δ value would be in the range 1.65–1.45 mm s^{-1}. The low value of ΔE_Q may be due to a small electric field gradient[7] arising from the almost spherical electron distribution around the iron nucleus. Thus, magnetic data with a room-temperature effective magnetic moment of 2.7 B.M. and the Mössbauer data confirm that iron(II) in $[Fe(bipy)_2MoS_4]$ is in a distorted octahedral geometry with intermediate spin-state.

The electronic spectral transitions observed for the complexes at 520, 500 and 390 nm are attributed[8,9] to d (Fe) $\rightarrow \pi_1$ (diimine) and d (Fe) $\rightarrow \pi_2$ (diimine) charge-transfer transitions of the $[Fe(diimine)_2]^{2+}$ moiety. Additional bands due to π(S) $\rightarrow$ d(W) charge-transfer transitions occur around 410 and 330 nm. The charge transfer bands π(S) $\rightarrow$ dM^{VI} of $(MS_4)^{2+}$ suffer bathochromic shifts in the complexes.[10,11] The transition observed around 310 nm in all the complexes is characteristic[12] of the $\pi_1 \rightarrow \pi_2$ transition of the diimine ligand.

The IR frequencies ν(CN) and ν(CC) of bipyridine and phenanthroline undergo positive shifts of 10–30 cm^{-1} in the complexes, suggesting coordination through the diimine nitrogen atoms. The IR bands observed around 240 cm^{-1} for $[Fe(bipy)_2MS_4]$ complexes and 290 cm^{-1} for $[Fe(phen)_2MS_4]$ complexes are assigned[13] to M—S stretching frequencies. The splitting of these frequencies suggested that the MS_4 group probably acts as a bridging ligand towards iron(II). Thus, iron(II) is bonded through 4s atoms of the thiometallate and the coordination is completed by the bidentate diimine ligands.

The cyclic voltammogram of $[Fe(bipy)_2MoS_4]$ is given in Fig. 3. The CVM displays an irreversible anodic wave at +1.04 V and two quasi-reversible cathodic waves at −1.40 and −1.25 V. The anodic wave at +1.04 V is attributed[14] to the oxidation of iron(II) to iron(III). The quasi-reversible cathodic waves observed at −1.40 and −1.25 V in the cyclic voltammogram of $[Fe(bipy)_2MoS_4]$ are due to the reduction[15,16] of the bipyridyl ligand bonded to iron(II). In order to compare the electrochemical behaviour with that of $[Fe(bipy)_2MoO_4]$ the cyclic voltammogram of the latter was taken. It exhibited two quasi-reversible cathodic waves at −1.40 and −1.25 V, which are attributed[15,16] to the reduction of the bipyridine ligand bonded to iron(II). However, no anodic wave was observed to indicate the oxidation of iron(II) to iron(III). An irreversible wave did however appear at −0.20 V, which disappeared when the scan was reversed prior to the reduction of $[Fe(bipy)_2]^{2+}$. Thus suggests that the oxidation of iron(II) to iron(III) is difficult when the oxo ligand is coordinated to iron(II).

The geometries of Fe^{II} and M^{VI} are tetrahedral in $FeLMO_4$. However, in FeL_2MS_4 complexes Fe^{II} is six-coordinate and M^{VI} is four-coordinate. Oxo coordination probably saturates the hard acid character of iron(II) and thus only one diimine ligand can be accommodated, giving rise to a tetrahedral geometry around iron(II). In the case of oxometallates, both oxygen and nitrogen of the

diimine ligand compete for similar molecular orbitals, σ and p_π, and, therefore, only one diimine ligand coordinates to iron(II). In sulphido complexes the sulphur atoms compete for *d*-orbitals, whereas the nitrogen of diimine competes for σ- and p_π-orbitals. Thus, two diimine ligands could be accommodated around iron(II). This may be the reason for obtaining a tetrahedral iron(II) complex when oxo metallate is used and an octahedral iron(II) complex when thiometallate is used.

Acknowledgement—We are grateful to the Council of Scientific and Industrial Research (India) for the financial support.

REFERENCES

1. D. Coucouvanis, *Accts Chem. Res.* 1981, **14**, 201.
2. E. I. Stiefel, *Proceedings of the International Conference on the Chemistry and Uses of Molybdenum* (Edited by H. F. Barry and P. C. H. Mitchell), p. 56. Climax Molybdenum Co., Ann Arbor, Michigan (1982).
3. J. W. McDonald, G. D. Priesen, L. D. Rosenhein and W. E. Newton, *Inorg. Chim. Acta* 1983, **72**, 205.
4. *Inorganic Index to Power Diffraction File*, Sets 6–10 (Edited by L. G. Berry), Vol. 40, pp. 6–289; Vol. 42, pp. 11–151. JCPDS, Pennsylvania (1971 and 1972).
5. R. F. Gould (Editor), *Adv. Chem. Ser.* 1967, **7**, 1848.
6. E. Koning and K. Madeja, *Inorg. Chem.* 1968, **7**, 1848.
7. A. Muller, M. Dartmann, C. Romer, W. Clegg and G. M. Scheldrick, *Angew. Chem., Int. Edn Engl.* 1981, **20**, 1060.
8. A. A. Schiett, *J. Am. Chem. Soc.* 1960, **82**, 300.
9. R. J. P. Williams, *J. Chem. Soc.* 1955, 137.
10. S. R. Acott, C. D. Garner, J. R. Nicholson and W. Clegg, *J. Chem. Soc., Dalton Trans.* 1983, 713.
11. A. Muller, N. Weinstock and H. Schulze, *Spectrochim. Acta* 1972, **28A**, 1075.
12. G. M. Bryant, J. E. Fergusson and H. K. J. Powell, *Aust. J. Chem.* 1971, **24**, 257.
13. J. R. Ferraro, L. J. Basile and D. L. Kovacic, *Inorg. Chem.* 1966, **5**, 391.
14. K. Tanaka, M. Morimoto and T. Tanaka, *Inorg. Chim. Acta* 1981, **56**, L61.
15. T. Saje and S. Avyagre, *J. Electroanal. Chem. Int. Electrochem.* 1975, **60**, 1.
16. D. E. Pratt, S. H. Lawrie and R. H. Dahm, *Inorg. Chim. Acta* 1987, **135**, L21.

Polyhedron Vol. 12, No. 12, pp. 1491–1497, 1993
Printed in Great Britain

0277–5387/93 $6.00+.00
© 1993 Pergamon Press Ltd

GROUP 15 COMPLEXES WITH CARBOXYLIC ACIDS—VI.* PREPARATION AND CRYSTAL STRUCTURES OF POTASSIUM ANTIMONY(III) CITRATE, $\{[K_2Sb_4(citrate)_8(H_2O)_2]\}$ AND LITHIUM ANTIMONY(III) CITRATE, $\{[LiSb(citrate)_2(H_2O)]\cdot 2H_2O\}$

GRAHAM SMITH,† DALIUS S. SAGATYS, RAYMOND C. BOTT and DANIEL E. LYNCH

School of Chemistry, Queensland University of Technology, P.O. Box 2434, Brisbane 4001, Australia

and

COLIN H. L. KENNARD

Department of Chemistry, The University of Queensland, Brisbane 4072, Australia

(*Received* 29 *October* 1992; *accepted* 25 *February* 1993)

Abstract—Potassium antimony(III) citrate, $\{[K_2Sb_4(citrate)_8(H_2O)_2]\}$ (**1**), and lithium antimony(III) citrate, $\{[LiSb(citrate)_2(H_2O)]\cdot 2H_2O\}$ (**2**), have been prepared and their structures determined by X-ray diffraction. With **1** each of the two independent centrosymmetric tetramers in the repeating unit of the complex comprises four independent antimony ions and eight citrate residues interlinked by two potassium centres [K—O range 2.62–3.06(1) Å]. The difference between the two tetramers is that potassium is seven-coordinate in one and eight-coordinate in the other. The water molecules are coordinated to the potassium ions. Each antimony forms the usual distorted pseudo-trigonal bipyramidal four-coordinate complex through the α-hydroxy carboxylate oxygens of two citrate residues. A feature of the structure is the presence of three differently charged citrate species (1-, 2-, 3-), giving the formula $\{K_2[Sb(C_6H_6O_7)_2]_2[Sb(C_6H_7O_7)(C_6H_5O_7)]_2(H_2O)_2\}$. The coordination about antimony in **2** is similar, but the lithium links the two citrate residues together via a carboxyl and a hydroxyl oxygen from one ligand and a carboxyl oxygen from the second. A water completes the tetrahedral coordination sphere [mean Li—O, 1.942(5) Å]. Except for the four-coordination about lithium, the complex is similar to the analogous sodium complex $\{[NaSb(citrate)_2(H_2O)_2]\cdot H_2O\}$.

Antimony(III) complexes with citrate have shown only one coordination type, irrespective of the charge carried by the ligand species. This involves the α-hydroxycarboxyl moieties of two citrate residues in a bis-chelate mode, giving a very distorted pseudo-trigonal bipyramidal four-coordination about antimony. Known example types are $\{[NaSb(citrate)_2]_2(H_2O)_2]\cdot H_2O\}$,[2] $\{[AgSb(citrate)_2]_2$[2] [both (2−)]}, $\{[Co(NH_3)_6][Sb(citrate)_2]\cdot 5H_2O\}$[3] and $\{K_3[Sb(citrate)_2]\cdot 2H_2O\}$[3] [both (3−)]. The only previously described example in which mixed-valence citrate species are found is $[CuSb(citrate^{2-})(citrate^{3-})(H_2O)_2]\cdot 2.5H_2O$,[4] in which a terminal carboxyl proton is lost from one citrate residue, providing a cross-link between chains formed through five-coordinate copper(II) centres.

In all structures the observation is that deprotonation of the α-hydroxy group occurs at quite low pH (*ca* 1.5), due to lowering of its effective pK_a after initial coordination of the adjacent carboxyl group. As part of a program of investigation in our laboratories into the phenomenon of univalent and divalent metal ion stabilization of group 15 complexes with hydroxy acids the title compounds were prepared using similar pH conditions to those for

* Part V ref. 1.

† Author to whom correspondence should be addressed.

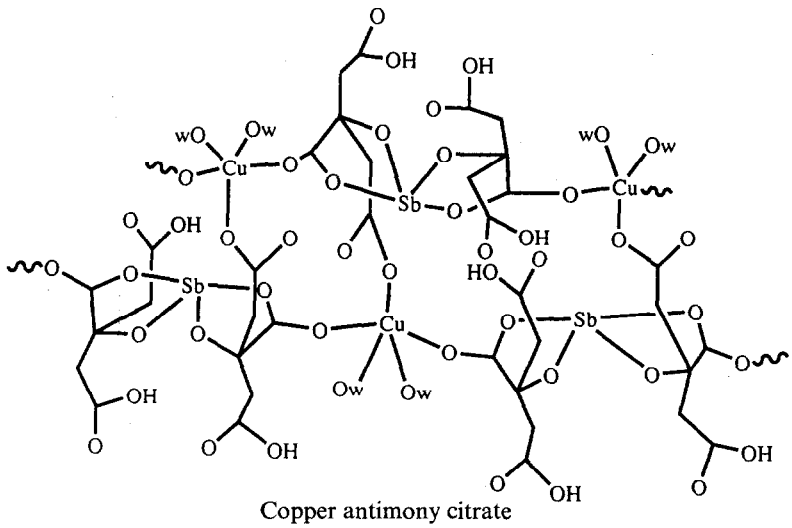

Copper antimony citrate

the silver, sodium and copper analogues.[2,4] For the potassium analogue (**1**) reported here the stoichiometry determined from elemental analysis, preliminary X-ray examination and density determination, $[KSb_2(citrate)_4(H_2O)]$, suggested probable mixed-valence citrate species. This has been confirmed by the X-ray structure determination. For the lithium complex (**2**) the stoichiometry, $[LiSb(citrate)_2(H_2O)_3]$, was the same as that of the sodium analogue,[2] although the structure determination has shown that the two are not isostructural.

EXPERIMENTAL

Preparation

Compounds were prepared using a previously described procedure[2] by the digestion of antimony(III) oxide in aqueous citric acid solution with subsequent addition of potassium or lithium nitrate to the syrupy concentrate. Large, hard colourless prismatic crystals grew from the digests after several weeks at room temperature.

Crystal data

1: $C_{48}H_{54}K_2O_{38}Sb_4$, $Mr = 1803.6$, $a = 12.239(9)$, $b = 16.085(10)$, $c = 18.458(9)$ Å, $\alpha = 79.12(5)$, $\beta = 76.84(5)$, $\gamma = 79.83(5)°$, $V = 3440(4)$ Å^3, space group $P\bar{1}$, $Z = 2$, $D_c = 1.748$, $D_m = 1.77$ g cm^{-3}, $\mu = 17.9$ cm^{-1}, Mo-K_α radiation ($\lambda = 0.71073$ Å), $F(000) = 1776$, $T = 297$ K.

2: $C_{12}H_{18}LiO_{17}Sb$, $Mr = 562.9$, $a = 7.712(6)$, $b = 10.763(7)$, $c = 12.756(9)$ Å, $\alpha = 75.600(9)$, $\beta = 77.29(6)$, $\gamma = 74.85(6)°$, $V = 976(1)$ Å^3, space group $P\bar{1}$, $Z = 2$, $D_c = 1.914$, $D_m = 1.93$ g cm^{-3}, $\mu = 15.0$ cm^{-1}, Mo-K_α radiation ($\lambda = 0.71073$ Å), $F(000) = 560$, $T = 297$ K.

Data collection, structure solution and refinement

X-ray diffraction data were collected from crystals of dimensions $0.25 \times 0.20 \times 0.20$ mm (**1**) and $0.20 \times 0.20 \times 0.15$ mm (**2**), mounted on an Enraf–Nonius CAD-4 diffractometer using graphite crystal monochromatized Mo-K_α X-radiation. Although the unit cell volume for **1** suggested the possibility of a non-reduced cell, standard cell reduction procedures failed to show any higher symmetry involving a smaller molecular asymmetric unit. Of 9972 (**1**) and 3715 (**2**) reflections collected up to $2\theta_{max} = 50°$, 8593 ($R_{int} = 0.021$) and 3433 ($R_{int} = 0.009$), respectively, were unique, while 6105 and 3232 with $I > 2.5\sigma(I)$ were considered observed and used in structure refinement. Collection ranges were h, -14 to 14; k, -19 to 19, l, 0 to 21 (**1**) and h, 0 to 9, k, -12 to 12 and l, -15 to 15 (**2**). The data were corrected for Lorentz and polarization effects and for absorption [empirical corrections: maximum and minimum transmission factors: 0.98, 0.85 (**1**) and 0.99, 0.96 (**2**)]. The structures were solved using the automatic Patterson procedure of SHELXS 86[5] and refined to residuals $R = 0.041$ and $R_w = 0.045$ ($S = 0.97$) (**1**) and 0.017 and 0.019 ($S = 1.5$) (**2**) using blocked-matrix least-squares (SHELX 76[6]), with anisotropic thermal parameters for all non-hydrogen atoms. Weighting schemes with $w = [\sigma^2(F_o) + 1.9 \times 10^{-3}(F_o)^2]^{-1}$ (**1**) and $[\sigma^2(F_o) + 1.8 \times 10^{-4}(F_o)^2]^{-1}$ (**2**) were used. Hydrogens were located by difference methods and were included in the respective refinements with coordinates and temperature factors refined (**2**), but with isotropic U values set invariant at 0.05 Å^2 for **1**. For **1** two atoms [O(111) and O(121)] gave non-positive definite temperature factor conditions and so were restored to isotropic refinement.

Atomic coordinates, anisotropic thermal parameters, observed and calculated structure factors

and intraligand bond distances and angles have been deposited with the Editor as supplementary material; copies are available on request. Atomic coordinates have also been deposited with the Cambridge Crystallographic Data Centre. Bond distances and angles about the metal coordination polyhedra are given in Table 1. The atom numbering scheme follows the convention adopted for previous structures of this series.[1,2,4]

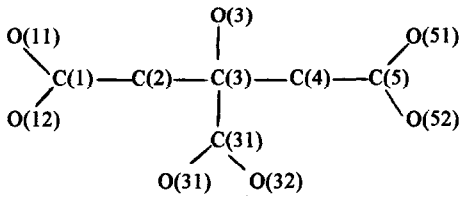

DISCUSSION

$[K_2Sb_4(citrate)_8(H_2O)_2]$

The two centrosymmetric tetramers in the repeating unit of compound **1** comprise four independent antimony(III) centres and eight citrate residues bound together by two potassium ions (Fig. 1). However, in one tetramer the potassiums are eight-coordinate, the other seven. The two waters in each are also bonded to the potassium ions. The units are related by a pseudo-A-face centring in a triclinic cell, although this symmetry could not be invoked crystallographically. The reason for this lies in asymmetry due to the conformational variations in the citrate residues, particularly at the terminal carboxylate groups, and in the difference in the coordination polyhedra about the two potassium centres. Figure 2 shows the stereochemistry about one of the antimony centres [Sb(1)], which is typical of all centres and involves four oxygens from two bidentate chelate α-hydroxycarboxyl groups of two citrate residues. The four-coordination is similar to that found for all known antimony(III) citrates,[1-4] with very distorted pseudo-trigonal bipyramidal stereochemistry, although this is less easily recognized due to some bond elongation and angle distortion. However, the axial sites are occupied typically by the carboxylate oxygens [O(31)], while in the equatorial sites are found the shorter bonds to hydroxyl oxygens [O(3)]. With the silver(I),[2] sodium[2] and copper(II)[4] antimony citrates the Sb—O(carboxyl) distances are 2.096 and 2.218(2), 2.153 and 2.164(1) and 2.177 and 2.230(6) Å, respectively, compared with Sb—O(hydroxyl): 2.007 and 2.008(2), 1.988 and 1.998(1) and 1.974 and 2.009(5) Å, respectively. In the present complex the comparative Sb—O bond distances are used to identify the protonated functional groups on the citrate residues, to enable the justification of the unusual stoichiometry in the overall complex, arising from a requirement to balance the net (14+) charge of the two potassium and four antimony(III) ions. It would normally be expected that a basic (2−) charge would arise on each citrate residue from deprotonation of both functional groups of the subterminal α-hydroxycarboxy moiety. This occurs even at the pH levels which are employed using the

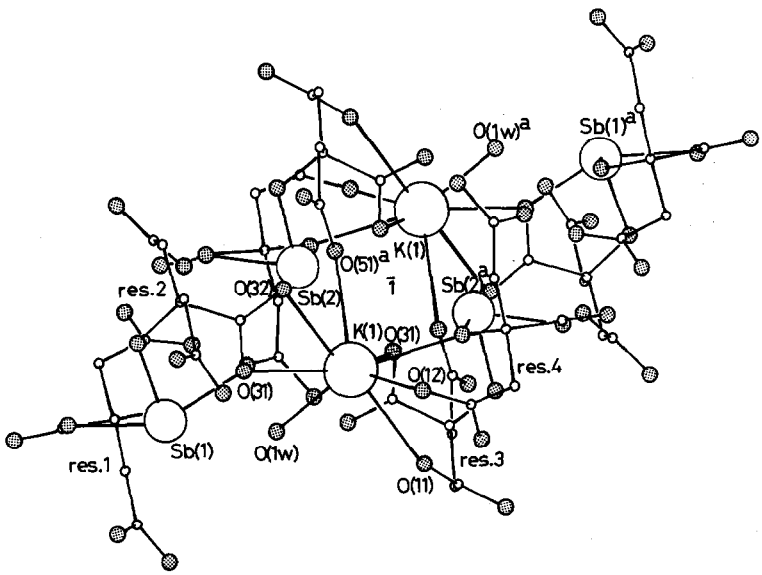

Fig. 1. A view of the centrosymmetric molecular repeating unit in the complex tetramer. Only one unit [involving K(1), Sb(1)–Sb(4) and citrate residues 1–4] is shown. The second unit [involving K(2), Sb(5)–Sb(8) and citrate residues 5–8] is configurationally similar.

Table 1. Bond distances (Å) and angles (°) about the coordination polyhedra for complexes **1** and **2**

(a) Distances

1

Sb(1)—O(31)	2.00(1)	Sb(3)—O(35)	2.00(1)
Sb(1)—O(32)	1.98(1)	Sb(3)—O(36)	2.01(1)
Sb(1)—O(311)	2.34(1)	Sb(3)—O(315)	2.11(1)
Sb(1)—O(312)	2.11(1)	Sb(3)—O(316)	2.26(1)
Sb(2)—O(33)	2.01(1)	Sb(4)—O(37)	2.02(1)
Sb(2)—O(34)	2.00(1)	Sb(4)—O(38)	2.00(1)
Sb(2)—O(313)	2.07(1)	Sb(4)—O(317)	2.11(1)
Sb(2)—O(314)	2.30(1)	Sb(4)—O(318)	2.30(1)
K(1)—O(1w)	2.76(1)	K(2)—O(2w)	2.74(1)
K(1)—O(34)	2.82(1)	K(2)—O(36)	2.87(1)
K(1)—O(113)	2.90(1)	K(2)—O(116)	2.62(1)
K(1)—O(124)	2.72(1)	K(2)—O(317)	3.01(1)
K(1)—O(312)	2.86(1)	K(2)—O(327)	3.03(1)
K(1)—O(313)	2.94(1)	K(2)—O(515)	2.76(1)
K(1)—O(513)	3.06(1)	K(2)—O(115)	2.97(1)
		K(2)—O(315)	2.88(1)

2

Sb(1)—O(31)	1.998(2)	Li—O(1w)	1.919(4)
Sb(1)—O(321)	2.117(2)	Li—O(121)	1.930(5)
Sb(1)—O(32)	2.009(2)	Li—O(32)	1.940(5)
Sb(1)—O(322)	2.195(2)	Li—O(512)	1.979(5)

(b) Angles

1

O(31)—Sb(1)—O(32)	100.5(2)	O(33)—Sb(2)—O(34)	100.3(2)
O(31)—Sb(1)—O(311)	74.4(2)	O(33)—Sb(2)—O(313)	79.8(2)
O(31)—Sb(1)—O(312)	82.3(2)	O(33)—Sb(2)—O(314)	79.2(2)
O(32)—Sb(1)—O(311)	78.5(2)	O(34)—Sb(2)—O(313)	81.2(2)
O(32)—Sb(1)—O(312)	79.7(2)	O(34)—Sb(2)—O(314)	74.5(2)
O(311)—Sb(1)—O(312)	144.4(2)	O(313)—Sb(2)—O(314)	144.2(2)
O(35)—Sb(3)—O(36)	102.9(2)	O(37)—Sb(4)—O(38)	99.9(2)
O(35)—Sb(3)—O(316)	81.3(2)	O(37)—Sb(4)—O(317)	77.9(2)
O(35)—Sb(3)—O(315)	78.9(2)	O(37)—Sb(4)—O(318)	77.1(2)
O(36)—Sb(3)—O(316)	75.2(2)	O(38)—Sb(4)—O(317)	80.2(2)
O(36)—Sb(3)—O(315)	79.6(2)	O(38)—Sb(4)—O(318)	74.7(2)
O(316)—Sb(3)—O(315)	143.3(2)	O(317)—Sb(4)—O(318)	140.6(2)
O(1w)—K(1)—O(34)	127.1(2)	O(2w)—K(2)—O(36)	131.1(2)
O(1w)—K(1)—O(113)	77.6(2)	O(2w)—K(2)—O(116)	135.6(2)
O(1w)—K(1)—O(124)	138.5(2)	O(2w)—K(2)—O(317)	69.3(2)
O(1w)—K(a)—O(312)	74.8(2)	O(2w)—K(2)—O(327)	110.9(2)
O(1w)—K(1)—O(313)	75.8(2)	O(2w)—K(2)—O(515)	110.9(2)
O(1w)—K(1)—O(513)	98.5(2)	O(2w)—K(2)—O(115)	71.0(2)
O(34)—K(1)—O(113)	66.0(2)	O(2w)—K(2)—O(315)	82.0(2)
O(34)—K(1)—O(124)	69.7(2)	O(36)—K(2)—O(116)	68.4(2)
O(34)—K(1)—O(312)	157.2(2)	O(36)—K(2)—O(317)	159.6(2)
O(34)—K(1)—O(313)	54.8(2)	O(36)—K(2)—O(327)	117.1(2)
O(34)—K(1)—O(513)	75.7(2)	O(36)—K(2)—O(515)	80.8(2)
O(113)—K(1)—O(124)	77.7(2)	O(36)—K(2)—O(115)	71.0(2)
O(113)—K(1)—O(312)	132.4(2)	O(36)—K(2)—O(315)	54.7(2)
O(113)—K(1)—O(313)	65.2(2)	O(116)—K(2)—O(317)	98.4(2)
O(113)—K(1)—O(513)	125.8(2)	O(116)—K(1)—O(327)	75.9(2)
O(124)—K(1)—O(312)	98.7(2)	O(116)—K(2)—O(515)	111.8(2)
O(124)—K(1)—O(313)	121.6(2)	O(116)—K(2)—O(315)	121.1(2)
O(124)—K(1)—O(513)	123.0(2)	O(116)—K(2)—O(115)	84.5(2)
O(312)—K(1)—O(313)	139.6(2)	O(115)—K(2)—O(317)	124.7(2)
O(312)—K(1)—O(513)	96.3(2)	O(115)—K(2)—O(327)	152.8(2)

Table 1—*continued*

O(313)—K(1)—O(513)	61.6(2)	O(115)—K(2)—O(515)	139.5(2)
		O(115)—K(2)—O(315)	65.5(2)
		O(317)—K(2)—O(327)	42.8(2)
		O(317)—K(2)—O(515)	90.6(2)
		O(317)—K(2)—O(315)	140.5(2)
		O(327)—K(2)—O(515)	66.6(2)
		O(327)—K(2)—O(315)	141.3(2)
		O(515)—K(2)—O(315)	74.7(2)
2			
O(31)—Sb(1)—O(32)	98.42(8)	O(1w)—Li—O(32)	117.5(2)
O(31)—Sb(1)—O(321)	78.93(8)	O(1w)—Li—O(121)	121.7(2)
O(31)—Sb(1)—O(322)	80.75(8)	O(1w)—Li—O(512)	109.4(2)
O(32)—Sb(1)—O(321)	80.98(8)	O(32)—Li—O(121)	104.9(2)
O(32)—Sb(1)—O(322)	76.21(8)	O(32)—Li—O(512)	97.0(2)
O(321)—Sb(1)—O(322)	146.70(8)	O(121)—Li—O(512)	102.6(2)

usual method of preparation. However, in the case of **1** variable negative charges arise on the citrate residues, (1−) from loss of the hydroxyl proton (all residues), (2−) from loss of both α-hydroxyl and carboxyl protons and (3−) from loss of an additional terminal carboxyl proton. The Sb—O(31) and Sb—O(3) distances involving residue 1 [to Sb(1)], residue 4 [to Sb(2)], residue 6 [to Sb(3)] and residue 8 [to Sb(4)] are 2.34(1) and 2.00(1), 2.30(1) and 2.00(1), 2.26(1) and 2.01(1) and 2.30(1) and 2.00(1) Å, respectively, indicating that the carboxyl groups remain protonated with a (1−) charge carried by each residue. The corresponding distances in residue 2 [to Sb(1)], residue 3 [to Sb(2)], residue 5 [to Sb(3)] and residue 7 [to Sb(4)] are 2.11(1) and 1.98(1), 2.07(1) and 2.01(1), 2.11(1) and 2.00(1) and 2.11(1) and 2.02(1) Å, indicating that both hydroxyl and carboxyl groups are deprotonated. The additional two charges arise from deprotonation of terminal carboxyl groups on residues 2 and 3. The total formula is, therefore, made up as follows:

[Sb(1)(residue 1)$^-$(residue 2)$^{3-}$]

[Sb(2)(residue 4)$^-$(residue 3)$^{3-}$] (tetramer **1**)

and

[Sb(3)(residue 6)$^-$(residue 5)$^{2-}$]

[Sb(4)(residue 8)$^-$(residue 7)$^{2-}$] (tetramer **2**),

with their inversion-related halves. Identification of the terminal carboxyl group which carries the (1−) charge is on the basis of located hydrogen atoms and on C—O bond distances, which become more equidimensional with deprotonation compared with their free acid values [typically, C=O 1.20 Å, C—OH 1.32 Å[7]].

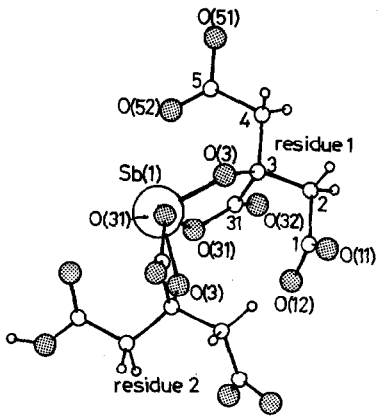

Fig. 2. Molecular configuration and atom naming scheme for the Sb(citrate)$_2$ complex centres. Only that for Sb(1) is shown. The centres about Sb(2), Sb(3) and Sb(4) are similar. Unless otherwise indicated, atoms are carbon.

The irregular coordination centres about each potassium ion [K(1) and K(2)] are similar (Fig. 3), involving oxygens from a single water molecule and from both carboxyl and hydroxyl groups of the α-hydroxycarboxyl moieties. However, K(1) is seven-coordinate while K(2) is eight-coordinate, with the K—O distances significantly longer about K(1) [2.72–3.06(1) cf. 2.62–3.01(1) Å for K(2)]. Bonds to K(1) are from a water [O(1w)], from carboxyl oxygens [O(11) (terminal) and O(31) (central) of citrate 3; O(12) (terminal carboxyl) and O(3) (hydroxyl) from citrate 4], a carboxylate link to O(31) (central carboxyl) from citrate 2 and one bridging link to an inversion-related carboxyl oxygen [O(513) $(-x, -y, 1-z)$]. The mean K—O distance is 2.87(1) Å. An almost identical stereochemistry is found about K(2), with bonds to O(2w), O(115) and O(315), O(116) and O(36), O(317) and O(327) [symmetric bidentate] and O(515) (also across an inversion centre). The eighth

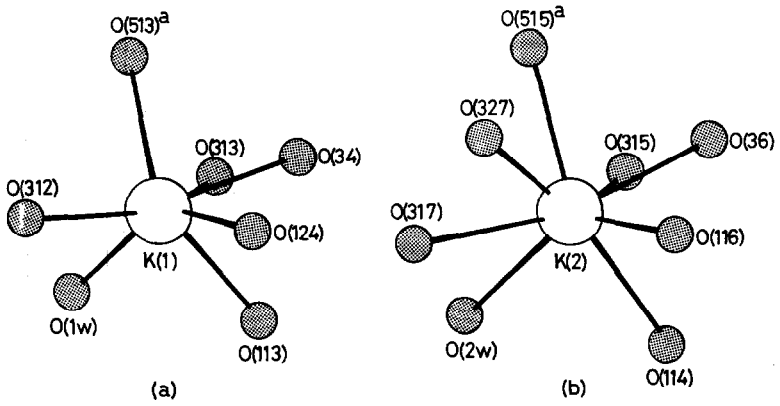

Fig. 3. The coordination polyhedra about the two potassium centres.

bond to K(2) corresponds to the second in the symmetric bidentate carboxylate association [K—O 3.01, 3.03(1) Å]. With K(1) this group becomes asymmetric, with significant elongation of the second bond [K(1)—O(312), 2.85(1); K(1)—O(322), 3.20(1) Å]. The mean K—O distance about K(2) is 2.86(1) Å. The stability of this basic tetramer unit in **1** is reflected in the isomorphous and isostructural rubidium complex $[Rb_4Sb_4(citrate)_8(H_2O)_2]$, which has now been prepared and its structure determined.[8]

$[LiSb(citrate)_2(H_2O)]\cdot 2H_2O$

The lithium antimony citrate complex (**2**) is monomeric (Fig. 4) and structurally similar to the sodium analogue $[NaSb(citrate)_2(H_2O)_2]\cdot H_2O$,[2] both of which involve only citrate(2−) species. However, lithium adopts its most usual tetrahedral coordination, with two oxygens from one citrate residue {one carboxyl [O(512)], one hydroxyl [O(32)], the latter also bridging to antimony}, one carboxyl oxygen from the second citrate residue [O(121)] and a single water. The mean Li—O distance is 1.942(5) Å. Also, in contrast to the sodium analogue, the third carboxyl oxygen (from the second citrate residue) is from the terminal rather than the central acid group. Furthermore, the five-coordinate sodium complex has an additional water in the distorted trigonal bipyramidal coordination sphere. With complex **2**, having the same stoichiometry, the additional water moves into the lattice as a molecule of solvation. Despite these variations in the peripheral coordination the stereochemistry about antimony is comparable to both the sodium analogue[2] and to other antimony citrates.[3,4] This involves hydroxyl oxygens in the axial sites of a very distorted pseudo-trigonal bipyramid [Sb—O 1.998 and 2.009(2) Å, cf. 1.988 and 1.998(1) Å for the sodium analogue] and oxygens of the central carboxyl groups in the equatorial sites [Sb—O 2.117 and 2.195(2) Å, cf. 2.153 and 2.164(1) Å].

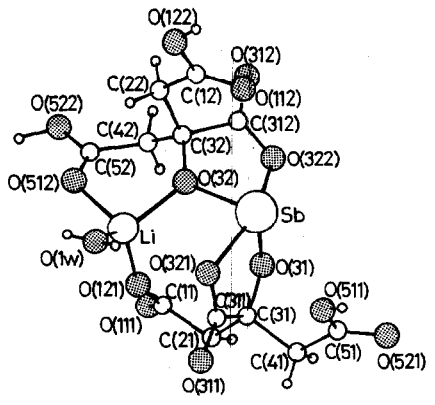

Fig. 4. Atom numbering scheme and molecular configuration for **2**.

Acknowledgements—The authors thank the Australian Research Council, Queensland University of Technology and The University of Queensland for financial support.

REFERENCES

1. R. C. Bott, G. Smith, D. S. Sagatys, T. C. W. Mak, D. E. Lynch and C. H. L. Kennard, *Aust. J. Chem.*, in press.
2. D. W. Hartley, G. Smith, D. S. Sagatys and C. H. L. Kennard, *J. Chem. Soc., Dalton Trans.* 1991, 2735.
3. I. F. Burshstein, G. A. Kiosse, A. B. Ablov, T. I. Malinovskii, B. M. Shehedrin and N. V. Rainier, *Dokl. Akad. SSSR* 1978, **238**, 90.

4. G. Smith, D. S. Sagatys, R. C. Bott, D. E. Lynch and C. H. L. Kennard, *Polyhedron* 1992, **11**, 631.
5. G. M. Sheldrick, SHELXS 86, Structure Solution Package. University of Göttingen, F.R.G. (1986).
6. G. M. Sheldrick, SHELX 76, Program for Crystal Structure Determination. University of Cambridge, U.K. (1976).
7. L. Lieserowitz, *Acta Cryst.* 1972, **B32**, 775.
8. R. C. Bott, D. S. Sagatys, G. Smith, D. E. Lynch and C. H. L. Kennard, unpublished data.

Polyhedron Vol. 12, No. 12, pp. 1499–1504, 1993
Printed in Great Britain

0277–5387/93 $6.00+.00
© 1993 Pergamon Press Ltd

STRUCTURE AND BONDING IN CHAIN-LIKE POLYHALONIUM CATIONS AND POLYHALIDE ANIONS

ZHENYANG LIN and MICHAEL B. HALL*

Department of Chemistry, Texas A&M University, College Station, TX 77843, U.S.A.

(*Received* 7 *December* 1992; *accepted* 25 *February* 1993)

Abstract—*Ab initio* calculations with both all-electron basis sets and effective core potentials (ECP) were employed to study the bonding in chain-like polyhalogen cations and anions. An electron density analysis based on Bader's theory of atoms in molecules shows that these polyhalogen cations and anions can be described in terms of the VSEPR model. On the basis of this analysis one can also distinguish covalent and dative bonds in these polyhalogen cations and anions. Covalent bonds exist only between atoms where both are four-coordinate (including the number of lone pairs), because higher coordinate halogens must form a three-centre four-electron bond with its adjacent atoms. The arrangement of iodine–fluorine contacts in the crystal structure of $(I_5^+)(AsF_6^-)$ can be explained by the distributions of lone pairs associated with the relevant iodines.

Heavy halogens (X) exhibit a strong tendency to form chain-like polyhalonium cations and polyhalide anions.[1] For example, I_3^+, $I_5^+(Br_5^+)$, $I_3^+(Br_3^-)$ and I_5^- molecules have been well characterized.[2–7] It is striking that the X_3^+ cation has a V-shaped structure while its corresponding X_3 anion adopts a linear one, and that X_5^+ has a Z-shaped structure but X_5^- is V-shaped. The geometrical features of these polyhalogen cations and anions can be rationalized in terms of the VSEPR model.[8] Based on the available structural parameters of these polyhalogen cations and anions we deduced the valence structures shown in Fig. 1. Based on the X—X bond lengths we make a distinction between dative and covalent bonds, which is also shown in Fig. 1. For the X_5^+ molecule the valence structure predicts that the central halogen carries the most positive charge. The fact that the crystal structure of I_5^+ in its AsF_6^- salt[2] shows the presence of iodine–fluorine contacts for the four non-central iodines, however, seems to imply little positive charge in the central halogen atom. This contradiction led to a bonding description that involves the resonance structures **I** and **II**.[2] Recent density functional calculations also gave support for these resonance structures.[9] In this paper *ab initio* calculations were used to reinvestigate the electronic structures of these polyhalogen ions. These results provide the connection between the VSEPR model and accurate measures of the electron density and resolve several controversies.

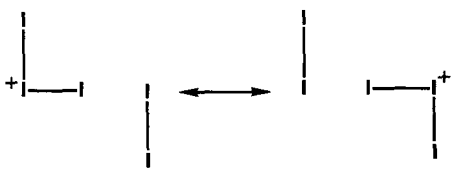

(I) (II)

Theoretical details

Both all-electron basis sets and effective core potentials (ECP)[10] were employed in these calculations. Geometries were optimized with the restricted Hartree–Fock calculations; HF/all electron and HF/ECP calculations, and with the second-order Moller–Plesset method (MP2/ECP).

In the all-electron calculations the 3-21G split-valence basis sets, augmented with polarization functions [$\zeta_d(I) = 0.266$, $\zeta_d(Br) = 0.389$, $\zeta_d(Cl) = 0.514$], were used.[11] In the ECP calculations double-ζ basis sets and the same polarization functions were used. All calculations were performed with the GAMESS package[12] at the Super-

* Author to whom correspondence should be addressed.

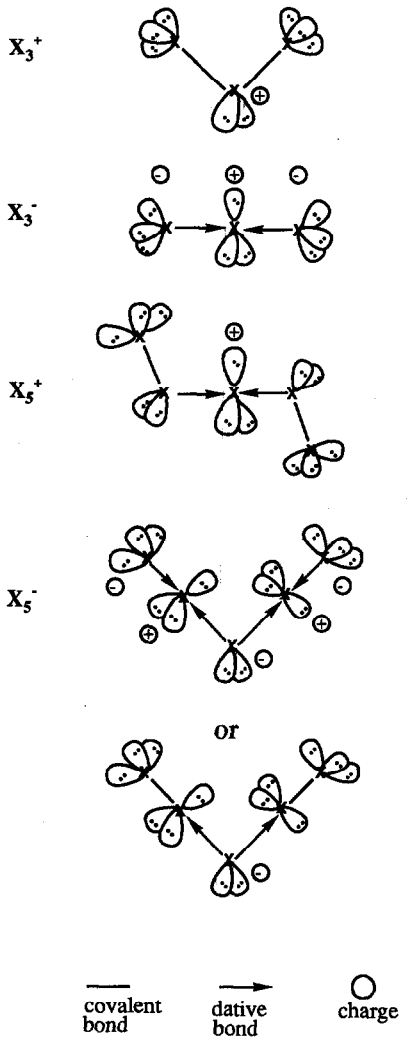

Fig. 1. The VSEPR structures for tri-atomic and penta-atomic halogen molecules.

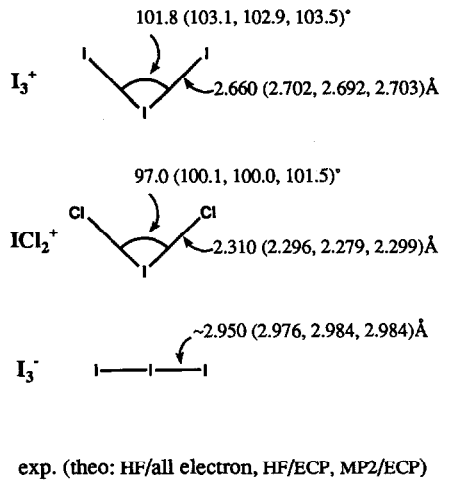

Fig. 2. Optimized geometries for some selected tri-atomic halogen molecules.

computer Center of Texas A&M University on a Cray Y-MP2/116 and on our Silicon Graphic Iris Indigo workstation. The net atomic charges were based on Bader's theory of atoms in molecules and calculated with the OMEGA program.[13] The Laplacian of valence electron density was plotted with the use of the program MOPLOT.[14]

RESULTS AND DISCUSSION

Geometry optimizations have been completed on tri-atomic and penta-atomic halogen cations and anions. The calculated structural parameters together with experimental results are shown in Figs 2 and 3. Overall, the theoretical predictions at both HF and MP2 levels agree quite well with the experimental results (see Figs 2 and 3). The predictions of bond angles are not as good as those of bond lengths. The results of all-electron calculations (HF/all electron) show a slightly better agreement than those of HF/ECP calculations. The MP2/ECP results show that the electron correlation is not very important in predicting the structural parameters for these polyhalogen systems, particularly in predicting the geometrical trends.

The density functional calculations[9] showed that the lowest energy geometry for the free Br_5^+ is a skew structure with the three central bromine atoms forming an angle of 168.6° and the two terminal bromine atoms exhibiting a dihedral angle of 82°, a result which is in contrast to the planar *trans* geometry found in the solid state.[4] Our all-electron calculations yield a slightly different skew structure with a linear unit for the three central atoms and a dihedral angle of 90° between the two terminal atoms. For the all-electron calculations the energy of this skew structure is only 0.16 kcal mol^{-1} lower in energy than that of the planar *trans* structure. Therefore, we expect an essentially free rotation of the two terminal Br_2 (or I_2) units about the central atom for the Br_5^+ (or I_5^+) molecule.

To investigate the charge distribution in these polyhalogen cations and anions we calculated the net atomic charges from the all-electron HF results using Bader's theory of atoms in molecules.[15] The results are listed in Table 1. As can be seen in Table 1 the central atom for I_3^+, I_3^- and I_5^+ carries the most positive charge, while the central atom for I_5^- carries the most negative charge. These results support the valence structures in Fig. 1, although these structures oversimplify the true electronic structures. The charge analyses can also explain the site preference for mixed polyhalogen cations and

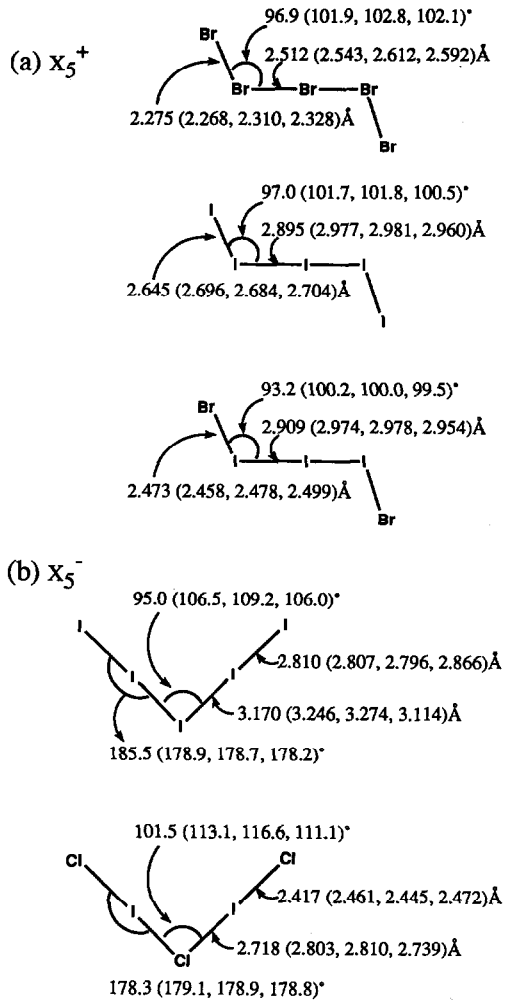

Fig. 3. Optimized geometries for some selected pentaatomic halogen molecules.

anions, in which the less electronegative atom prefers to occupy the site with the most positive charge (see examples of mixed molecules in Figs 2 and 3).

To further examine the bonding in these polyhalogen cations and anions we calculated the Laplacian of the valence electron density, $-\nabla^2\rho$,[15] from the HF/ECP wavefunctions. Plots in the molecular plane for the I_3^+, I_3^-, I_5^+ and I_5^- molecules are shown in Figs 4 and 5. In the contour plot solid lines denote $-\nabla^2\rho > 0$, where the electron density

Table 1. The Bader atomic charges in selected polyiodine molecules

Molecule	Central atom	Terminal atom	Adjoining atom[a]
I_3^+	+0.36	+0.32	
I_3^-	+0.14	−0.57	
I_5^+	+0.30	+0.21	+0.14
I_5^-	−0.58	−0.35	+0.14

[a] The atom connecting central and terminal atoms.

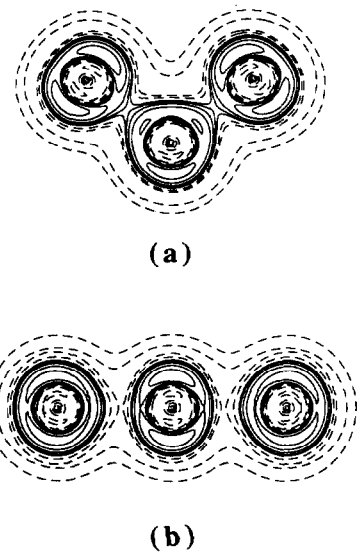

Fig. 4. The plots of $-\nabla^2\rho$ based on HF/ECP results for (a) I_3^+ and (b) I_3^-.

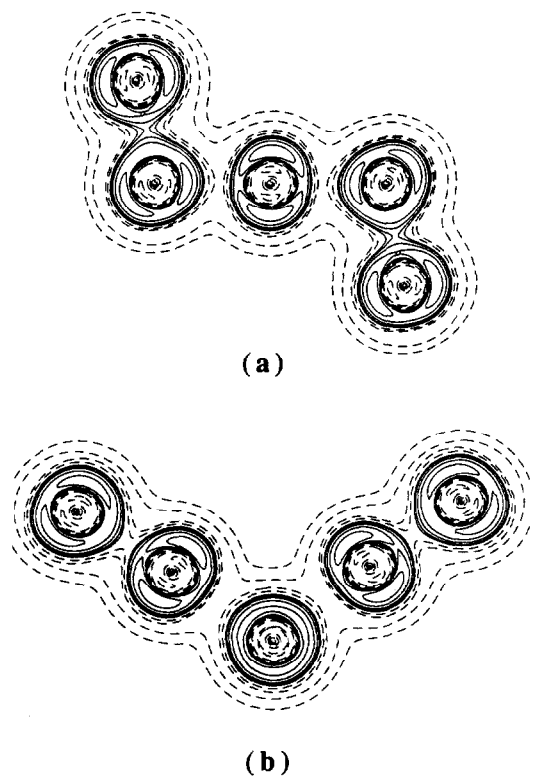

Fig. 5. The plots of $-\nabla^2\rho$ based on HF/ECP results for (a) I_5^+ and (b) I_5^-.

is locally concentrated, and dashed lines denote $-\nabla^2\rho < 0$, where the electron density is locally depleted.

Figure 4 shows significant electron density accumulations between iodine atoms in I_3^+, but much less in I_3^-. This is expected from the valence model (see Fig. 1), because in I_3^+ the bonds are covalent but in I_3^- they are dative. For I_5^+ Fig. 5(a) indicates covalent bonds between the terminal and adjoining atoms (an adjoining atom is an atom which connects both terminal and central atoms), but dative bonds from the adjoining atom to the central atom. In Fig. 5(b) the central atom of I_5^- exhibits a spherical-like electron density with slightly larger charge concentrations in the directions of I—I bonds. This result implies weak dative bonds, with electron pairs donated from the central atom, whose formal charge is -1, to the adjoining atoms. In the second valence structure for X_5^- molecules (see Fig. 1) covalent bonds were drawn between the adjoining and terminal atoms. However, the dative bonds from the central atom to the adjoining atoms significantly destabilize the bonds between the adjoining and terminal atoms. This destabilizing effect is consistent with the observed very long I—I bond length (2.810 Å, compared to the covalent bond length, 2.645 Å, in the I_5^+ molecule) and with the electron density map of Fig. 5(b), in which, unlike Fig. 5(a), there is no significant electron accumulation in the centre of the corresponding I—I bond. Thus, bonds between the adjoining and terminal atoms in the I_5^- molecule are almost dative in nature, i.e. more contributions from the first of the two X_5^- valence structures in Fig. 1.

In summary, all analyses above strongly support the valence structures in Fig. 1. The question now is how can we explain the experimentally observed iodine–fluorine contacts in the structure of $(I_5^+)(AsF_6^-)$. The crystal structure of this salt indicates that each adjoining atom has two iodine–fluorine contacts (less than the sum of van der Waals radii), while each terminal atom has only one such contact.[2] The central atom has no iodine–fluorine contact, although it carries the most positive charge according to our calculations.

The valence structure for the I_5^+ molecule (see Fig. 1) indicates that the central atom has three lone pairs plus two dative bonds, each adjoining atom has two lone pairs plus one dative and one covalent bond, and each terminal atom has three lone pairs plus one covalent bond. The $-\nabla^2\rho$ plots suggest that the adjoining atom has the most capacity to attract electron pairs from fluorine atoms of the AsF_6^- anion. Since it has the fewest lone pairs (large charge concentrations), it has larger holes in the valence shell. Two fluorines can weakly cap the holes around each of these adjoining atoms. Thus, the two capping fluorines are co-planar with the molecular plane, which is indeed observed in the solid state.[2a] For each terminal atom in I_5^+ a hole is seen in the *trans* direction of the I—I bond, which can be capped by a fluorine to make the third observed close contact. The iodine–fluorine contacts are also found in the AsF_6^- salt of I_3^+.[2b] The contact pattern in I_3^+, where the central atom has two contacts and each terminal atom has one, is analogous to that found in I_5^+. For solid $[ICl_2^+][SbF_6^-]$[16] the central iodine atom has two iodine–fluorine contacts and the terminal chlorine atoms have none. Since the more electronegative chlorine atom has lower polarizability and smaller holes, it has less tendency to form large chain-like polyhalogen molecules of any type.

For polyhalogen anions, the negative charge on the molecule decreases the ability of each halogen atom to attract electron pairs from its cationic counterpart in the solid state. In addition, the cationic counterpart usually does not contain electronegative fluorine ligands. Therefore, few reports on the corresponding cation–anion contacts have been found.

At this stage we have satisfactorily explained the relationship between structure and bonding in these polyhalogen cations and anions. One may raise questions on the distinction between dative and covalent bonds in Fig. 1. For example, the V-shape X_3^+ molecule has two covalent bonds around the central atom, while the X_5^- molecular has two dative bonds around the central atom. Examining the number of lone pairs in the relevant molecules we see that each atom in the X_3^+ molecule is four-coordinate (including the lone pairs). In X_5^- both adjoining atoms are five-coordinate (three lone pairs and two bonds). Each adjoining atom forms a three-centre four-electron bond with the central and terminal atoms by using a *p*-orbital with maximum amplitudes along the bonding axis. The three-centre four-electron bond around a five-coordinate halogen is, therefore, responsible for long X—X bonds. The first four valence structures in Fig. 1 summarize our conclusion that covalent bonds only exist between atoms having a coordination number of four (taking into account the number of lone pairs).

Other chain-like polyhalogen cations and anions

Other chain-like polyhalogen cations and anions have been reported.[17] They can be taken as aggregations of the triatomic and pentaatomic units discussed in this paper. For example, the largest poly-

iodine cation,[2c] I_{15}^{3+}, consists of three I_5^+ units linked by weak iodine–iodine interactions. In these weak interactions a lone pair of a terminal atom in one I_5^+ aligns itself with the hole of a terminal atom in another I_5^+ unit (see Fig. 1).

Two forms of I_8^{2-} have been reported (see **III**).[17a] The difference in I—I···I angles between the two forms indicates weak I···I bonding. Qualitatively, both forms can be viewed as two linear I_3^- units being weakly connected by an I_2 molecule. For the I_2 molecule theory predicts a single covalent bond between iodine atoms and three lone pairs on each iodine arranged as the lone pairs of terminal atoms in Fig. 1. Therefore, each iodine atom in the I_2 molecule has a hole *trans* to the covalent bond. This hole can weakly attract electron pairs from other polyhalogen units. The two holes in both iodine atoms of the I_2 molecule attract the lone pairs of the terminal atom of I_3^- to form the I_8^{2-} unit. The largest polyiodine anion,[17b] I_{16}^{4-}, can be viewed as an aggregation of two I_8^{2-} units (see **IV**), although we do not have an explanation of how the two are linked together. Each I_8^{2-} unit in I_{16}^{4-} is in an eclipsed form, while those shown in **III** are in the staggered form.

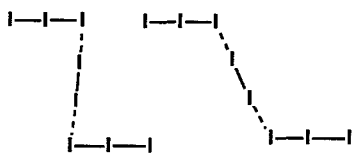

I_8^{2-}

(III)

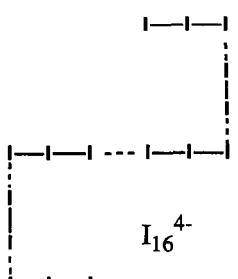

I_{16}^{4-}

(IV)

Linear I_4^{2-} deserves comment here. Two structural forms have been identified.[17a] One has three almost equal I—I bond distances (*ca* 3.14–3.18 Å), while the other one has two long terminal bonds (3.34 Å) and one short central bond (2.80 Å). The MP2/ECP geometry optimization only gave the latter structure. One can view this structural form as two terminal I^- units bonded to an I_2 molecule (see **V**).

I_4^{2-}

(V)

CONCLUSIONS

The electron density analyses from *ab initio* calculations indicate that the structure in the chain-like polyhalogen cations and anions can be satisfactorily rationalized in terms of the VSEPR model. A covalent bond exists only between atoms with a coordination number, including the number of lone pairs, of four. Since they are less electronegative and more polarizable, heavy atoms in the polyatomic cations can attract additional electron pairs from atoms such as fluorine in the anion. This attraction depends only on the number of lone pairs and on the size of holes associated with the relevant atom and not on its formal charge.

In the discussion of heteroconjugated organic molecules[18] it was argued that those atoms which are more electronegative prefer to occupy sites which bear a larger negative charge in the parent polyenes. Based on the formal charge assignment in Fig. 1 one can predict the site preference for other heterohalogen chain-like clusters. For example, fluorine atoms in ClF_2^+ and BrF_2^+ occupy terminal sites in a V-shaped structure. In the linear $[Y—X—Y]^-$ molecules the central X atom is always the least electronegative, e.g. ClF_2^-, BrF_2^-, $BrCl_2^-$, IF_2^- and ICl_2^-.[2] Again, the site preference in $I_3Cl_2^+$, $I_3Br_2^+$, $I_2Cl_3^-$ and $I_2Br_3^-$[3,7] can be understood through the formal charge assignment in Fig. 1.

Acknowledgements—We thank the National Science Foundation (Grant No. CHE 91-13634) and the Robert A. Welch Foundation (Grant No. A-648) for financial support.

REFERENCES

1. (a) F. A. Cotton and G. Wilkinson, *Advanced Inorganic Chemistry*, 5th edn, pp. 570–580. John Wiley, New York (1988); (b) N. N. Greenwood and A. Earnshaw, *Chemistry of the Elements*, pp. 978–988. Pergamon Press, Oxford (1984).
2. (a) A. Apblett, F. Grein, J. P. Johnson, J. Passmore and P. S. White, *Inorg. Chem.* 1986, **25**, 422; (b) J. Passmore, G. Sutherland and P. S. White, *Inorg. Chem.* 1981, **20**, 2169; (c) J. Passmore, P. Taylor, T. Whidden and P. S. White, *Can. J. Chem.* 1979, **57**, 968.

3. S. Pohl and W. Saak, *Z. Naturforsch.* 1981, **B36**, 283.
4. H. Hartl, J. Nowicki and R. Minkwitz, *Angew. Chem., Int. Edn Engl.* 1991, **30**, 328.
5. N. N. Greenwood and A. Earnshaw, *Chemistry of the Elements*, p. 979. Pergamon Press, Oxford (1984).
6. I. Broekema, E. E. Havinga and E. H. Wiebenga, *Acta Cryst.* 1957, **10**, 596.
7. (a) A. Parlow and H. Hartl, *Acta Cryst.* 1979, **B35**, 1930; (b) A. Parlow and H. Hartl, *Z. Naturforsch.* 1985, **B40**, 45.
8. R. J. Gillespie and I. Hargittai, *The VSEPR Model of Molecular Geometry*. Allyl and Bacon, Massachusetts (1991).
9. K. O. Christe, D. A. Dixon and R. Minkwitz, *Z. Anorg. Allg. Chem.* 1992, **612**, 51.
10. P. J. Hay and W. R. Wadt, *J. Chem. Phys.* 1985, **82**, 270.
11. (a) M. S. Gordon, J. S. Binkley, J. A. Pople, W. J. Pietro and W. J. Hehre, *J. Am. Chem. Soc.* 1982, **104**, 2797; (b) K. D. Dobbs and W. J. Hehre, *J. Comput. Chem.* 1986, **6**, 359; (c) S. Huzinaga, *Gaussian Basis Sets for Molecular Calculations*. Elsevier, Amsterdam (1984).
12. M. F. Guest and P. Sherwood, Daresbury Laboratory, Warrington WA4 4AD, U.K.
13. F. W. Biegler-Konig, T. T. Nguyen-Dang, Y. Tal, R. F. Bader and A. J. Duke, *J. Phys. B: Atom. Molec. Phys.* 1981, **14**, 2739; current version of OMEGA modified by K. E. Laidig.
14. Interactive MOPLOT: a package for the interactive display and analysis of molecular wave-functions incorporating the program MOPLOT (D. Lichtenburger), PLOTDEN (R. F. W. Bader, D. J. Kenworthy, P. M. Beddal, G. R. Runtz and S. G. Anderson), SCHUSS (R. F. W. Bader, G. R. Runtz, S. G. Anderson and F. W. Biegler-Koenig) and EXTREM (R. F. W. Bader and F. W. Biegler-Koenig), P. Sherwood and P. J. MacDougall (1989).
15. (a) R. F. W. Bader, P. J. MacDougall and C. D. H. Lau, *J. Am. Chem. Soc.* 1984, **106**, 1594; (b) R. F. W. Bader, *Accts Chem. Res.* 1985, **18**, 9; (c) R. F. W. Bader, *Atoms in Molecules, a Quantum Theory*. Clarendon Press, Oxford (1990).
16. R. Birchall and R. D. Myers, *Inorg. Chem.* 1981, **20**, 2207.
17. (a) P. K. Hon, T. C. W. Mak and J. Trotter, *Inorg. Chem.* 1979, **18**, 2916 and refs therein; (b) F. H. Herbstein and M. Kapon, *J. Chem. Soc., Chem. Commun.* 1975, 67718.
18. A. Streitwieser Jr, *Molecular Orbital Theory for Organic Chemists*. John Wiley & Sons, Inc., New York (1961).

Polyhedron Vol. 12, No. 12, pp. 1505–1508, 1993
Printed in Great Britain

0277–5387/93 $6.00+.00
© 1993 Pergamon Press Ltd

THE MANGANESE(II) COMPLEX OF A HYDRAZONE LIGAND DERIVED FROM PYRUVIC ACID AND SEMICARBAZIDE—SYNTHESIS, PROPERTIES AND CRYSTAL STRUCTURE

WANG LIUFANG,* PENG ZHOUREN and WANG XIN

Department of Chemistry, Lanzhou University, Lanzhou 730000, P.R.C.

and

YU SHUYAN and LUO QINHUI

Coordination Chemistry Institute, Nanjing University, Nanjing 210008, P.R.C.

and

WANG QI

Lanzhou Institute of Chemical Physics, Chinese Academy of Sciences, Lanzhou, P.R.C.

(*Received* 13 *July* 1992; *accepted* 19 *February* 1993)

Abstract—Pyruvic acid semicarbazonato manganese(II) hydrate, $Mn(C_4H_6N_3O_3)_2 \cdot H_2O$, has been prepared and its IR spectra and thermal decomposition (TG) have been investigated. The crystal structure was determined by X-ray diffraction analysis. The crystal is triclinic, space group $P\bar{1}$ with unit cell dimension $a = 8.916(2)$, $b = 9.362(2)$, $c = 10.067(2)$ Å, $\alpha = 101.92(3)$, $\beta = 91.25(2)$, $\gamma = 117.08(3)^\circ$ and $V = 725.6(7)$ Å^3, $Z = 2$, $D_c = 1.644$ g cm^{-3}. The structure was solved by the heavy-atom technique from 3586 observed, independent reflections recorded at 293 K and refined to a final $R = 0.053$. The manganese atom has a distorted octahedral coordination with ONO donor sets from hydrazone ligands. The crystal structure contains one water molecule of crystallization. The tight hydrogen-bonding network in the crystal packing gives rise to high thermal stability of the complex.

Hydrazone ligands derived from pyruvic acid (a significant metabolism intermediate) and hydrazides are generally superior in medicinal activity to the unique hydrazides.[1,2] Besides, the metal complexes with particular configuration and reactivity can probably provide us with some information about the pharmaceutical metabolism catalysed by metal enzymes.[3] Therefore, we have studied the synthesis, structure, property and biological activity of a series of complexes with pyruvic acid hydrazones as ligands.[4] Here we report the metal complex of another hydrazone ligand—pyruvic acid semicarbazone. Owing to their remarkable antitumor, antiviral and antimalarial activities semicarbazones and their thio-analogues have received considerable attention and intensive investigation in coordination chemistry.[5] As for the pyruvic acid hydrazones their complexes were first studied by Ablov *et al.*[6–8] in 1970. To date, the ligands reported can be summarized with the general formula (**I**):

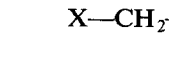

(**I**)

where R = H, CH_3, CH_3CH_2; X = H, C_6H_5, 4-$CH_3C_6H_4$; H_2Y = $H_2NNHCONH_2$,[6,9,10] $H_2NNHCSNH_2$,[6–13] $H_2NN{=}C(SCH_3)NH_2$,[14] $H_2NNHCOC_6H_5$,[15] H_2NNHCO— 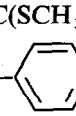 .[4]

However, only a few crystal structures of complexes are known, including $[Cr(Hthpu)(thpu)] \cdot H_2O$,[11] $\{[Cu(Hpt)Cl] \cdot 2H_2O\}_n$, $[Cu(ept)Cl]_2$[13] and $[Mn(H_2PAPH)(OH_2)_2] \cdot 2.5H_2O$.[4] Perhaps because of

* Author to whom correspondence should be addressed.

tautomerism the structure of the complexes varies with the synthetic conditions.

EXPERIMENTAL

Preparations

The hydrazone ligand, pyruvic acid semicarbazone, was obtained by a previous method.[3]

Freshly prepared solid $Mn_2(OH)_2CO_3$ (over 1 mmol) was added in portions to a stirred solution of the ligand (2 mmol) in distilled water (20 cm^3) at 80°C. At pH = 7 the solution was filtered and yellow crystals suitable for X-ray structural analysis were obtained after the filtrate was allowed to stand for *ca* 2 weeks at room temperature.

Measurements

IR spectra were measured with an American 5 DX-FTIR spectrometer and the TG spectra with a Du Pont 1090B-951 thermogravimeter.

Structure determination. A yellow crystal ($0.2 \times 0.2 \times 0.3$ mm) was mounted on an Enraf–Nonius CAD-4 diffractometer. The unit cell was measured by centring 25 reflections ($10 \leqslant \theta \leqslant 15°$) and refined by least-squares. Mo-K_α radiation was used. Intensities were measured with an ω–2θ scan technique, scan width : $0.52 \pm 0.34 \tan\theta$ ($h = -11$–11; $k = -12$–12; $l = 0$–13). 3686 independent reflections were collected, of which 3192 were considered observed [$I \geqslant 3\sigma(I)$]. Lorentz and polarization but no absorption corrections were made.

The manganese atom was located from a Patterson synthesis and the remaining non-hydrogen atoms from Fourier syntheses. The structure was refined isotropically and anisotropically by least-squares refinement. The function minimized was $\Sigma w(|F_o| - |F|)^2$, where w = 1. All hydrogen atoms were located from a difference synthesis and refined with an overall isotropic thermal parameter. Final $R = 0.048$ ($wR = 0.053$); $(\Delta/\sigma)_{max} = 0.59$ and the final difference-Fourier map showed peaks at 0.39 e $Å^{-3}$. Atomic scattering factors were taken from ref. 16. All calculations were performed on a PDP 11/44 computer using the SDP package.[17]

RESULTS AND DISCUSSION

Crystal structure of $Mn(C_4H_6N_3O_3)_2 \cdot H_2O$

Selected interatomic distances and bond angles are given in Table 1. Chemical analysis of the complex suggested the formula $Mn(C_4H_6N_3O_3)_2 \cdot H_2O$. Structural analysis indicates one complex unit $Mn(C_4H_6N_3O_3)_2$ and one lattice water molecule in the unit. The structure of the complex is shown in Fig. 1 and a diagram showing the unit cell contents is given in Fig. 2.

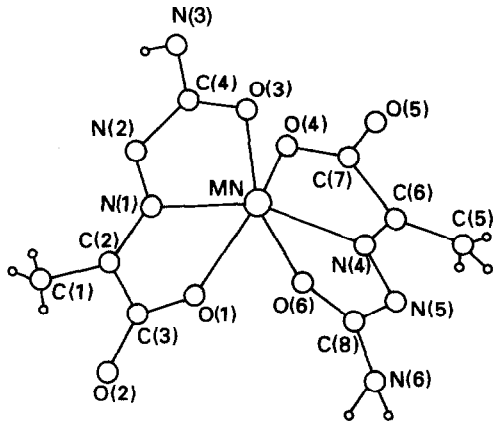

Fig. 1. Structure of the title compound showing the atomic numbering scheme.

It is notable that the unit cell consists of two $Mn(C_4H_6N_3O_3)_2 \cdot H_2O$ molecules bound with a tight hydrogen bond network, which is similar to that of $[Cr(Hthpu)(thpu)] \cdot H_2O$.[11] This network leads to a high thermal stability, which was confirmed by TG analysis. The crystal water is situated just in the hydrogen bond network.

As seen in Fig. 1 each ligand is a tridentate chelate with its ONO atoms bonded to the metal. The coordination sphere about manganese is a slightly distorted octahedron, the coordination atoms of the same ligand and the manganese atom are nearly co-planar.

From the torsion angles (Table 2) the relative spatial arrangement of the complex can be examined. Taking the first ligand (left part in Fig. 1) as an example, the torsion angles of Mn—N(1)—N(2)—C(4), 5.30°, and Mn—O(3)—C(4)—N(2), 3.01°, indicate that Mn metal is situated in the chelate plane of Mn—N(1)—N(2)—C(4)—O(3)—Mn. Similarly, the second chelate

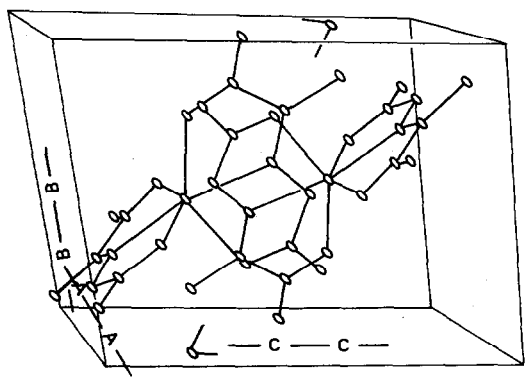

Fig. 2. Cell packing diagram.

Table 1. Selected distances (Å) and angles (°) of the complex $Mn(C_4H_6N_3O_3)_2 \cdot H_2O$

(a) Coordination sphere of manganese			
Mn—O(1)	2.171(1)	Mn—O(4)	2.136(1)
Mn—O(6)	2.271(2)	Mn—O(3)	2.166(1)
Mn—N(4)	2.208(1)	Mn—N(1)	2.229(1)
O(1)—Mn—O(6)	89.25(6)	O(4)—Mn—O(3)	93.98(5)
O(6)—Mn—N(4)	70.02(4)	O(3)—Mn—N(1)	71.06(4)
O(4)—Mn—N(4)	72.49(5)	O(1)—Mn—N(1)	71.07(5)
(b) Ligand			
O(1)—C(3)	1.267(2)	O(3)—C(4)	1.245(2)
O(4)—C(7)	1.271(2)	O(6)—C(8)	1.243(2)
O(2)—C(3)	1.235(2)	O(5)—C(7)	1.224(2)
N(1)—C(2)	1.270(2)	N(2)—C(4)	1.375(2)
N(3)—C(4)	1.327(2)	N(4)—C(6)	1.268(2)
N(5)—C(8)	1.365(2)	N(6)—C(8)	1.332(2)
N(1)—N(2)	1.359(2)	N(4)—N(5)	1.366(2)
C(1)—C(2)	1.491(2)	C(2)—C(3)	1.519(2)
C(5)—C(6)	1.492(2)	C(6)—C(7)	1.522(3)
O(1)—C(3)—O(2)	124.7(2)	O(1)—C(3)—C(2)	116.9(2)
O(4)—C(7)—O(5)	125.4(2)	O(4)—C(7)—C(6)	116.4(2)
O(2)—C(3)—C(2)	118.5(2)	O(5)—C(7)—C(6)	118.3(1)
C(1)—C(2)—C(3)	120.9(2)	C(5)—C(6)—C(7)	120.7(2)
C(1)—C(2)—N(1)	127.7(2)	C(5)—C(6)—N(4)	127.3(2)
C(3)—C(2)—N(1)	111.5(1)	C(7)—C(6)—N(4)	112.1(1)
N(1)—N(2)—C(4)	113.3(1)	N(4)—N(5)—C(8)	113.9(8)
N(2)—N(1)—C(2)	123.9(1)	N(5)—N(4)—C(6)	123.5(1)
N(2)—C(4)—O(3)	120.6(1)	N(5)—C(8)—O(6)	120.8(1)
N(2)—C(4)—N(3)	116.7(1)	N(5)—C(8)—N(6)	114.7(2)
N(3)—C(4)—O(3)	122.7(2)	N(6)—C(8)—O(6)	124.5(2)

Table 2. Selected torsion angles (°)

O(6)—Mn—O(1)—C(3)	76.8(0.3)	O(6)—Mn—N(4)—N(5)	11.9(0.3)
N(1)—Mn—O(1)—C(3)	−14.9(0.3)	O(6)—Mn—N(4)—C(6)	−174.6(0.4)
O(1)—Mn—O(3)—C(4)	11.6(0.3)	Mn—O(1)—C(3)—C(2)	16.0(0.4)
O(6)—Mn—O(3)—C(4)	−88.4(0.2)	Mn—O(3)—C(4)—N(2)	3.0(0.4)
N(1)—Mn—O(3)—C(4)	0.0(0.4)	Mn—O(4)—C(7)—C(6)	6.4(0.5)
O(1)—Mn—O(4)—C(7)	−95.7(0.3)	Mn—O(6)—C(8)—N(5)	21.5(0.5)
O(6)—Mn—O(4)—C(7)	9.7(0.5)	Mn—N(1)—N(2)—C(4)	5.3(0.3)
N(4)—Mn—O(4)—C(7)	−2.5(0.3)	C(2)—N(1)—N(2)—C(4)	177.1(0.3)
O(1)—Mn—O(6)—C(8)	80.2(0.3)	Mn—N(1)—C(2)—C(3)	−8.6(0.4)
O(1)—Mn—N(1)—N(2)	−175.4(0.2)	N(2)—N(1)—C(2)—C(3)	180.0(0.3)
O(3)—Mn—N(1)—N(2)	−3.0(0.2)	N(1)—N(2)—C(4)—O(3)	−5.6(0.5)
O(3)—Mn—N(1)—C(2)	−175.1(0.3)	Mn—N(4)—N(5)—C(8)	−6.3(0.5)
O(4)—Mn—N(1)—N(2)	−83.4(0.3)	C(6)—N(4)—N(5)—C(8)	−179.4(0.4)
O(6)—Mn—N(1)—N(2)	95.9(0.2)	Mn—N(4)—C(6)—C(7)	6.1(0.5)
O(1)—Mn—N(4)—C(6)	98.7(0.3)	N(5)—N(4)—C(6)—C(7)	179.1(0.4)
O(3)—Mn—N(4)—N(5)	100.1(0.3)	N(4)—N(5)—C(8)—O(6)	−10.6(0.6)
O(3)—Mn—N(4)—C(6)	−86.4(0.3)	N(1)—C(2)—C(3)—O(1)	−4.7(0.5)
O(4)—Mn—N(4)—N(5)	−176.0(0.3)	N(4)—C(6)—C(7)—O(4)	−8.2(0.6)

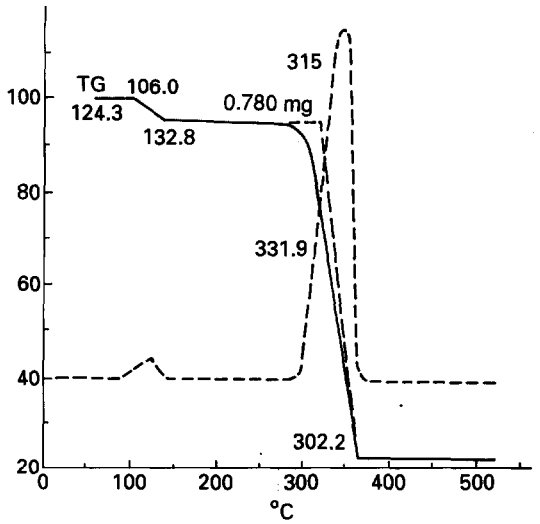

Fig. 3. TG of the complex.

ring of the same ligand, composed of Mn, N(1), N(2), C(4) and O(3), is also almost co-planar. Also from the torsion angles the two least-squares planes are staggered to each other at an angle somewhere between 60 and 100°, but not the ideal perpendicular.

In a normal octahedron all the angles between adjacent planes should be 90°. However, in this complex only the angles between the coordination atoms of different ligands and the metal are approximately 90°: O(3)—Mn—O(4) = 93.98(5) and O(1)—Mn—O(6) = 89.25(6). The angles between atoms of the same ligand and Mn are averaged to 71°. As for the bond lengths, among the four Mn—O bonds Mn—O(6) is the longest, which is due to hydrogen bond formation with non-coordinated NH_2. This fact also reveals that the effect of hydrogen bonds between molecules cannot be ignored in this crystal.

TG analysis and IR spectra

The TG curve of the complex is given in Fig. 3 and it can be seen that the temperature at which water is lost is rather high (106.0–132.8°C); this is probably due to the existence of a tight hydrogen bond network between different complex molecules, as stated above.

The IR spectra of the complex gives ν(Mn—O) = 540 cm^{-1} and the absorption bands which appear at 1750 [ν(C=O)(COOH)], 1679 [ν(C=O)(semicarbazide)] and 1620 cm^{-1} [ν(C=N)] in the ligand are shifted relatively far to the low wave number region at 1681, 1626 and 1607 cm^{-1}, respectively. This fact also indicates that the coordination between the ligand and Mn^{2+} is rather strong. The IR spectra also reflect the coordination characteristics that the ligand is coordinated to Mn^{2+} by its O—N—O atoms.

Acknowledgement—Project supported by NSFC of Gansu.

REFERENCES

1. Antibiotic Industrial Institute of Sichuan (P.R.C.), *Pharmaceuticals(2)*, Ch. 37B. Shanghai Science and Technology Publisher, Shanghai (1981).
2. R. Cao Vazquez and A. D. Garcia, *Rev. Cubana Farm.* 1989, **23**, 25.
3. M. Pankaskie and M. M. Abdol-Monem, *J. Pharm. Sci.* 1980, **69**, 1000.
4. W. Liu-fang, Z. Ying, Y. Zheng-yin, W. Ji-gui and W. Qi, *Polyhedron* 1991, **10**, 2477.
5. S. Padhye and G. B. Kauffman, *Coord. Chem. Rev.* 1985, **63**, 127.
6. A. V. Ablov, N. I. Belichuk and L. F. Chapurine, *Zhur. Neorg. Khim.* 1970, **15**, 112.
7. A. V. Ablov, and N. V. Berbeleu, *Zhur. Neorg. Khim.* 1970, **15**, 1854.
8. A. V. Ablov, N. V. Berbeleu, N. Ya. Negryatse and M. D. Revenko, *Zhur. Neorg. Khim.* 1970, **15**, 123.
9. B. L. Sauhney, J. S. Baijal, S. Chandra and K. B. Pandeya, *Acta Chim. Acad. Scient. Hung.* 1981, **108**, 325.
10. S. Chandra and K. K. Sharma, *Trans. Met. Chem.* 1984, **9**, 1.
11. M. D. Timken, S. R. Wilson and D. N. Hendrickson, *Inorg. Chem.* 1985, **24**, 3450.
12. N. V. Berbeleu, A. I. Shames, A. V. Verczhan, D. A. Bologa and B. S. Tsukerblat, *Zhur. Neorg. Khim.* 1987, **32**, 1396.
13. M. B. Ferrari, B. B. Fava, D. Tarasconi and C. Pelizzi, *J. Chem. Soc., Dalton Trans.* 1989, 361.
14. V. M. Leovac, V. I. Cesljevic, D. Z. Obadovic, D. M. Petrovic and S. Yu. Chundak, *Z. Anorg. Allg. Chem.* 1989, **570**, 177.
15. A. K. Bhagi, S. B. Tyagi, B. Singh and R. N. Kapoor, *Ind. J. Chem.* 1989, **28A**, 995.
16. *International Tables for X-ray Crystallography*, Vol. IV. Kynoch Press, Birmingham (1974).
17. B. A. Frenz, *Enraf–Nonius Structure Determination Package, SDP Users Guide*, Version of April (1983). Enraf–Nonius, Delft, The Netherlands (1983).

Polyhedron Vol. 12, No. 12, pp. 1509–1513, 1993
Printed in Great Britain

0277–5387/93 $6.00+.00
© 1993 Pergamon Press Ltd

REACTIONS OF 1,3-BUTANEDIOL WITH HEXACHLOROCYCLOTRIPHOSPHAZENE: UNUSUAL NON-EQUIVALENCE OF PHOSPHORUS NUCLEI IN THE SPIROCYCLIC PRODUCT $N_3P_3Cl_4[OCH(CH_3)CH_2CH_2O]$

M. G. MURALIDHARA, N. GROVER and V. CHANDRASEKHAR*

Department of Chemistry, Indian Institute of Technology, Kanpur 208016, India

(*Received* 21 *October* 1992; *accepted* 19 *February* 1993)

Abstract—The reaction of hexachlorocyclotriphosphazene, $N_3P_3Cl_6$ (**1**), with 1,3-butanediol affords the tetrachloro derivative $N_3P_3Cl_4[OCH(CH_3)(CH_2)_2O]$ (**2**). This product (**2**) and its derivative $N_3P_3(NMe_2)_4[OCH(CH_3)(CH_2)_2O]$ (**3**) possess spirocyclic structures. The phosphorus NMR spectrum of **2** is of the AMX type instead of the expected AB_2 or AX_2 types observed for other spirocyclic products. The synthesis of **2** and **3** and their characterization by proton and phosphorus NMR are discussed.

There are four main products possible in a reaction between hexachlorocyclotriphosphazene, $N_3P_3Cl_6$ (**1**), and any difunctional reagent such as a diamine or a diol. These are (a) spirocyclic, (b) ansa, (c) open-chain and (d) inter-molecular bridging.[1]

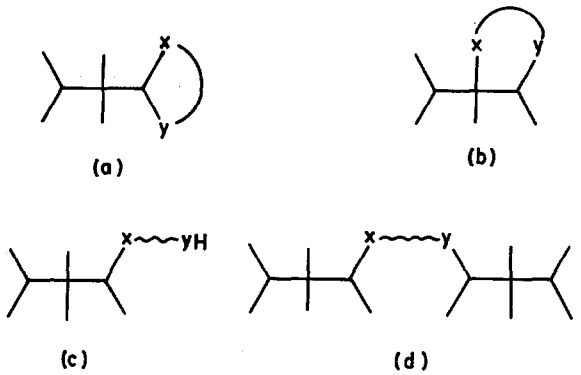

The type of product formed depends on the nature of the difunctional reagent. Thus, with a number of aliphatic difunctional reagents, $HY(CH_2)_nXH$ (X = Y = NH, n = 2, 3, 4, 5; X = Y = NCH_3, n = 2, 3; X = H, Y = NCH_3, n = 2; X = NH, Y = O, n = 2, 3; X = Y = O, n = 2, 3, 4), the reaction proceeds to afford predominantly the spirocyclic product.[2] Similarly reactions with aromatic difunctional reagents also give products containing five-, six- or seven-membered spirocyclic rings.[3] The first example where an "*ansa*" product is obtained in high yields consists of an indirect route:[4]

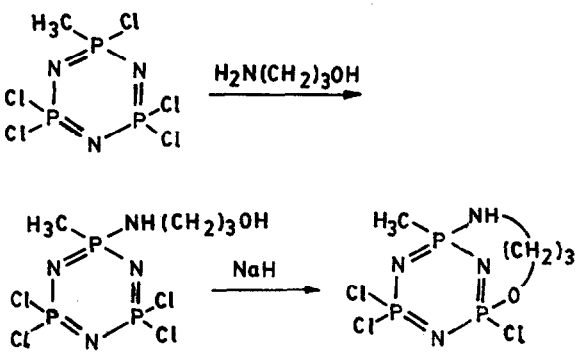

A French group has reported that the reaction of bis-2-amino ethyl ether with $N_3P_3Cl_6$ leads predominantly to the formation of an *ansa* product, $N_3P_3Cl_4[NH(CH_2)_2O(CH_2)_2NH]$.[5] More recently there have been reports that in reactions between aliphatic diols and $N_3P_3Cl_6$ small amounts of the *ansa* product could also be isolated, in addition to the major spirocyclic product.[6] In order to explore this possibility further we have studied the reactions of $N_3P_3Cl_6$ with an unsymmetrical difunctional reagent, 1,3-butanediol. It was reasoned that with such a reagent product characterization would be unambiguous. Thus, a spirocyclic product would show an AB_2 or AX_2 spin pattern, while an *ansa* product would be of the ABX, AMX or ABC spin type in the phosphorus NMR. The other two possibilities can be distinguished by analytical data

* Author to whom correspondence should be addressed.

alone. Surprisingly in our investigations of the above reaction we find that the spectroscopic behaviour of the product belies such simplistic reasoning. Thus, the product obtained in the above reaction, $N_3P_3Cl_4[OCH(CH_3)CH_2CH_2O]$ (**2**), shows a three-spin system (AMX) in the phosphorus NMR. However, more careful analysis of the NMR data reveals that the structure is spirocyclic as a result of the diastereotropic nature of the two $\equiv PCl_2$ groups. These results are discussed below.

EXPERIMENTAL

$N_3P_3Cl_6$ (Aldrich) was recrystallized from light petroleum ether (60–80°C); 1,3-butanediol (Fluka) was used as received. Anhydrous dimethyl amine was liberated from an aqueous solution (40% w/v) by treatment with KOH. The liberated amine was further dried by passing over KOH towers before collecting in a trap cooled at −78°C. The other solvents and reagents were purified by standard procedures.[7]

The proton and phosphorus NMR spectra were recorded on a Bruker 400 MHz instrument and chemical shifts are reported in ppm relative to Me_4Si in $CDCl_3$ and 85% H_3PO_4(ext.), respectively. Mass spectra were measured on a Kratos MS 80 RFA instrument (E.I./70 eV).

Preparation of $N_3P_3Cl_4[OCH(CH_3)(CH_2)_2O]$ (**2**)

$N_3P_3Cl_6$ (3.50 g, 10.1 mmol) was dissolved in dry benzene (150 cm^3). 1,3-Butanediol (0.91 g, 10.1 mmol) and triethyl amine (3.10 g, 30.6 mmol) were also dissolved in dry benzene (50 cm^3) and added over a period of 30 min to the solution of the trimeric chloride, with constant stirring. A calcium chloride guard tube was used to prevent moisture. After the addition was complete the reaction mixture was heated under reflux for 5 h. The reaction was monitored by TLC by the disappearance of $N_3P_3Cl_6$ (eluant: petroleum ether 60–80°C). The reaction mixture was allowed to cool and was then filtered to remove triethylamine hydrochloride. The filtrate was then washed with water (2×30 cm^3) and dried (Na_2SO_4). Benzene was stripped off *in vacuo*, affording a "semi" solid. This was pumped overnight and purified by crystallization from methylene chloride and petroleum ether (60–80°C) (1 : 1). The product isolated was identified as $N_3P_3Cl_4[OCH(CH_3)CH_2CH_2O]$ (**2**); m.p. 153–154°C. Yield 2.04 g, 55.60%. Mass spectra: parent ion at m/z 363 (^{35}Cl) showing the four chlorine isotope pattern. ^1H NMR: C(4)H_3: 1.44 (d of d), ^3J(H—H), 6.3 Hz, ^4J(P—H) 2.6 Hz; C(2)H_2: 1.80(m), 2.05(m); O—C(3)H_2: 4.39(m), 4.56(m); OC(1)H: 4.82(m).

A similar product was obtained in lesser yield when 2 equivalents of triethyl amine was used as a hydrogen chloride acceptor.

Preparation of $N_3P_3(NMe_2)_4[OCH(CH_3)(CH_2)_2O]$ (**3**)

Compound (**2**) (3.659 g, 10 mmol) was reacted with an excess of anhydrous dimethyl amine (25 g, 0.56 mol) in boiling chloroform (200 cm^3) for 4 h. The reaction mixture was allowed to reach room temperature and then washed with water (4×50 cm^3) to remove dimethyl amine hydrochloride and excess dimethyl amine. The organic layer was dried ($CaCl_2$) and the removal of solvent afforded an oil, which was identified as compound **3**. Mass spectra: parent ion at m/z 409. ^{31}P NMR: complex pattern, multiplets centred at 27.92 and 16.02 ppm. Spectrum recorded under proton coupled conditions affects both multiplets. ^1H NMR: CH—C(4)H_3: 1.32 (d of d), ^3J(H—H), 6.3 Hz; ^4J(P—H), 2.2 Hz. C(2)H_2: 1.56(m), 1.91(m); N—CH_3 2.61, ^3J(P—H) 11.2 Hz; 2.60, ^3J(P—H) 11.3 Hz; O—C(3)H_2: 4.16(m), 4.5(m), O—C(1)H, 4.73(m).

RESULTS AND DISCUSSION

The reaction of $N_3P_3Cl_6$ (**1**) with 1,3-butanediol proceeds smoothly with the replacement of two chlorines, in the presence of triethylamine:

$$N_3P_3Cl_6 + HO—CH(CH_3)(CH_2)_2OH \xrightarrow{2Et_3N}$$

$$N_3P_3Cl_4[OCH(CH_3)(CH_2)_2O]\,(\mathbf{2}) + 2Et_3N \cdot HCl.$$

The remaining four chlorines in **2** are easily replaced by $HNMe_2$ giving $N_3P_3(NMe_2)_4[OCH(CH_3)(CH_2)_2O]$ (**3**). The proton and phosphorus NMR of **2** are shown in Figs 1 and 2, respectively.

The proton NMR spectrum of **2**, even at 400 MHz, is quite complex. Homonuclear decoupling experiments have enabled the assignment of the peaks. The CH_3 group attached to C(1) appears as a doublet of doublets as a result of a three-bond coupling to OCH and a four-bond coupling to phosphorus. Such four-bond couplings are quite rare in phosphazenes. The OC(1)H is the most deshielded (4.82 δ). This is easily assigned since decoupling of the CH_3 resonance at 1.44 δ affects only the peak at 4.82 δ. The methylene protons of O—C(3)H_2 and C—C(2)H_2 are non-equivalent. The protons of C—C(2)H_2 appear as two multiplets centred at 1.80 and 2.05 δ. The complex multiplicity is as a result of coupling to the two non-equivalent protons of O—C(3)H_2 and O—C(1)H. Similarly, the O—C(3)H_2 protons appear as two sets of complex multiplets.

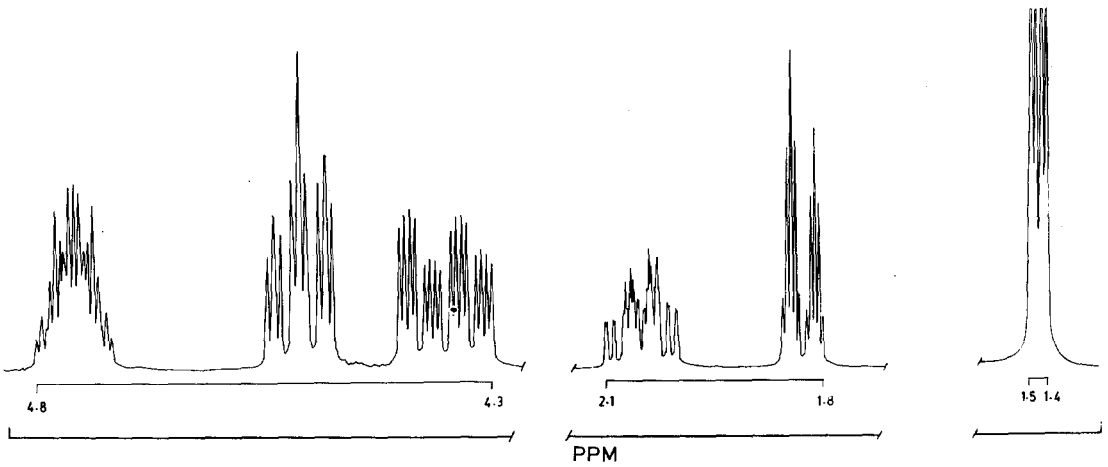

Fig. 1. ^1H NMR spectrum of $N_3P_3Cl_4[OCH(CH_3)(CH_2)_2O]$ (**2**).

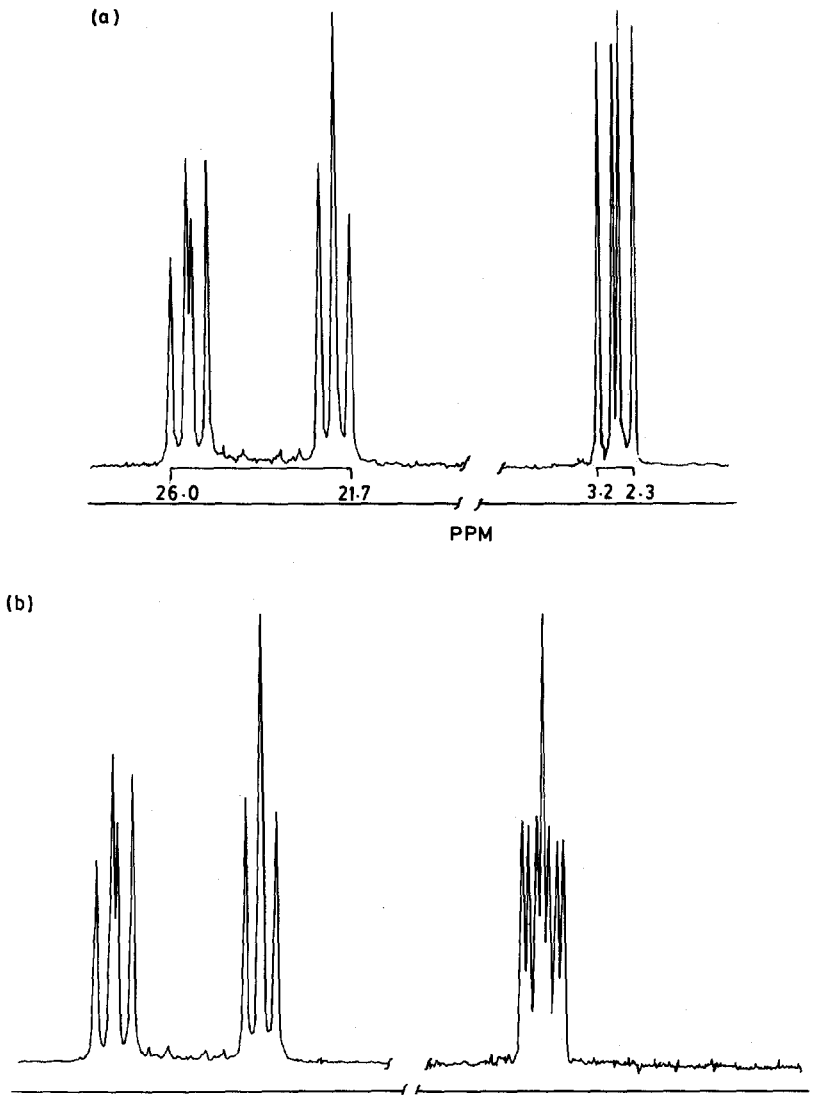

Fig. 2. (a) $^{31}P\{^1H\}$ NMR spectrum of **2** and (b) ^{31}P NMR spectrum of **2**.

Table 1. ^{31}P NMR data

Compound	Structure	δP_A	δP_B	δP_X	J(P—N—P) (Hz)	Ref.
$N_3P_3(CH_3)Cl_3[NH(CH_2)_3O]$	*Ansa*	31.2[a]	29.3	24.5	[b]	4
$N_3P_3Cl_4[O(CH_2)_2O(CH_2)_2O]$	*Ansa*	22.3[c]	27.6[d]	27.6[d]	70.8	6c
$N_3P_3Cl_4[O(CH_2)_2O(CH_2)_2O]$	Spiro	4.9[e]	23.2[c]	23.2[c]	70.8	6c
$N_3P_3Cl_4[HN(CH_2)_3O]$	Spiro	7.20[e]	22.40[c]	22.40[c]	53.9	2k
$N_3P_3Cl_4[N(CH_3)(CH_2)_2O]$	Spiro	22.40[e]	25.1[c]	25.1[c]	53.9	2i
$N_3P_3Cl_4[OCH(CH_3)(CH_2)_2O]$ (2)	Spiro	22.10[c]	25.59[e]	2.74[e]	[f]	This work

[a] $\delta P_A = P(CH_3)(NHR)$; $\delta P_B = P(Cl)(O)$; $\delta P_X = P(Cl_2)$.
[b] J(A—B) = 4.0; J(A—X) = 9.8; J(B—X) = 48.8 Hz.
[c] δPCl_2.
[d] $\delta PCl(OR)$
[e] δP(spiro).
[f] J(A—B) = 57.9; J(A—X) = 61.7; J(B—X) = 78.6 Hz.

The proton NMR spectrum of the dimethyl amino derivative $N_3P_3(NMe_2)_4[OCH(CH_3)(CH_2)_2O]$ (3) shows similar features to that of 2; in addition, two N—CH_3 signals are seen, both without virtual coupling.

The phosphorus NMR spectrum of 2 is of the AMX type (Fig. 2). The results are presented in Table 1. Spirocyclic products obtained with other unsymmetrical difunctional reagents, $N_3P_3Cl_4[N(CH_3)CH_2CH_2O]$,[2i] $N_3P_3Cl_4[HNCH_2CH_2O]$[2b] and $N_3P_3Cl_4[HN(CH_2)_3O]$,[2k] exhibit an AB_2 type of phosphorus NMR spectrum. The *ansa* product $N_3P_3Cl_3CH_3[HN(CH_2)_3O]$[4] shows an ABX spectrum. Therefore, an AMX type of pattern in the phosphorus NMR for 2 suggests an *ansa* structure. If this were so the phosphorus atom containing the chlorines would be of the X type and the phosphorus atoms having one chlorine and one oxygen each would belong to the AM type.

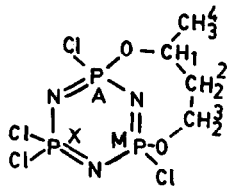

Ansa

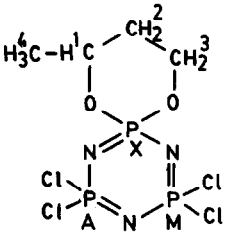

Spirocyclic

However, this would mean assigning the peak at 2.7 ppm to $\equiv PCl_2$. All known $\equiv PCl_2$ resonances in six-membered cyclophosphazenes are much more downfield than this value (+15.0 to +25.0 ppm).[1] Further, when the phosphorus NMR spectrum is recorded under proton coupled conditions, if the structure were *ansa* the A and M portions of the spectrum (downfield region) should be affected. However, as can be seen from Fig. 2 it is the X portion *alone* which is affected, leaving the A and M regions untouched. This is possible only if the structure is spirocyclic. Also, in a spirocyclic structure the A and M portions are assignable to $\equiv PCl_2$ (25.59 and 22.10 ppm), whose chemical shifts are now completely in agreement with the literature observations.

The non-equivalence of the methylene protons [C—C(2)H_2 and O—C(3)H_2], as well as the two phosphorus nuclei bearing chlorines, is presumably due to the influence of the —CH_3 substituent on C(1) of the spirocyclic ring. This would render the two $\equiv PCl_2$ groups diastereotropic. Such an influence of an asymmetric carbon substituent on the phosphorus chemical shifts has recently been demonstrated in *gem* alkyl (hydroxy alkyl) tetrachlorocyclotriphosphazenes, $N_3P_3Cl_4(CH_3)(CR^1R^2OH)$, where R^1 and R^2 are different.[8] Another reason for the observed non-equivalence of $\equiv PCl_2$ in 2 could be that the CH_3 substituent on C(1) would prefer an equatorial position of the energetically favourable chair conformation of the six-membered phosphate ring. This preference would substantially freeze the conformation leading to the observed pattern. In the absence of such effects the phosphorus NMR of spirocyclic products would be of the AB_2 type. We are investigating more examples of this nature to substantiate this point.

Acknowledgements—We are thankful to DST (India) for financial support. Thanks are due to Dr R. Yamadagni,

University of Calgary, Alberta, Canada, for help in recording some of the spectra.

REFERENCES

1. V. Chandrasekhar, M. G. Muralidhara and I. I. Selvaraj, *Heterocycles* 1990, **31**, 2231.
2. (a) V. Chandrasekhar, S. S. Krishnamurthy, A. R. Vasudeva Murthy, R. A. Shaw and M. Woods, *Inorg. Nucl. Chem. Lett.* 1981, **17**, 161; (b) S. S. Krishnamurthy, K. Ramachandran, A. R. Vasudeva Murthy, R. A. Shaw and M. Woods, *J. Chem. Soc., Dalton Trans.* 1980, 840; (c) T. Chivers and R. Hedgeland, *Can. J. Chem.* 1972, **50**, 1017; (d) B. D. Ruiter, G. Kuipers, J. H. Bijlart and J. C. Van de Grampel, *Z. Natursch.* 1982, **37b**, 1425; (e) W. F. Deutsch, M. Hursthouse, Z. Kilic, H. G. Parkes, L. S. Shaw and R. A. Shaw, *Phosphorus Sulfur* 1987, **32**, 81; (f) P. Castera, J. P. Faucher, J. F. Labarre and B. Perly, *J. Molec. Struct.* 1987, **160**, 365; (g) P. Castera, J. P. Faucher, G. Guerch, R. Laahana, A. Mahmoun, F. Sournies and J. F. Labarre, *Inorg. Chim. Acta* 1985, **108**, 29; (h) J. F. Labarre, *Top. Curr. Chem.* 1985, **129**, 173; (i) V. Chandrasekhar, S. S. Krishnamurthy, H. Manohar, A. R. Vasudeva Murthy, R. A. Shaw and M. Woods, *J. Chem. Soc., Dalton Trans.* 1984, 621; (j) V. Chandrasekhar and N. S. Reddy, *Heterocycles* 1989, **28**, 611; (k) K. C. Kumaraswamy and S. S. Krishnamurthy, *Ind. J. Chem.* 1984, **23A**, 717; (l) A. H. Alkubaisi, H. G. Parkes and R. A. Shaw, *Heterocycles* 1989, **28**, 347.
3. (a) H. R. Allcock and R. L. Kugel, *Inorg. Chem.* 1966, **5**, 1016; (b) K. Brandt and Z. Jedlinski, *J. Org. Chem.* 1980, **45**, 1672.
4. P. J. Harris and K. B. Williams, *Inorg. Chem.* 1984, **23**, 1496.
5. R. Enjalbert, J. Gah, P. Castera and J. F. Labarre, *Acta Cryst.* 1988, **C44**, 1813; (b) F. Sournies, A. E. Bakili, J. F. Labarre and B. Perly, *J. Molec. Struct.* 1989, **196**, 201; (c) R. Enjalbert, J. Galy, A. E. Bakili, P. Castera, J. P. Faucher, F. Sournies and J. F. Labarre, *J. Molec. Struct.* 1989, **195**, 207; (d) A. E. Bakili, P. Castera, J. P. Faucher, F. Sournies and J. F. Labarre, *J. Molec. Struct.* 1989, **195**, 21.
6. (a) A. H. Alkubaisi, H. G. Parkes and R. A. Shaw, *Heterocycles* 1989, **28**, 347; (b) H. A. Al-Madfa, R. A. Shaw and S. Ture, *Phosphorus, Sulfur, Silicon* 1990, **53**, 333; (c) R. A. Shaw and S. Ture, *Phosphorus, Sulfur, Silicon* 1991, **57**, 103.
7. A. I. Vogel, *Textbook of Practical Organic Chemistry*. English Language Book Society, Harlow, Essex, U.K. (1989).
8. P. L. Buwalda, A. Steenbergen, G. E. Oosting and J. C. Van de Grampel, *Inorg. Chem.* 1990, **29**, 2658.

Polyhedron Vol. 12, No. 12, pp. 1515–1522, 1993
Printed in Great Britain

0277–5387/93 $6.00+.00
© 1993 Pergamon Press Ltd

CHIRAL DISCRIMINATION IN DIASTEREOISOMERIC SYSTEMS OF CADMIUM WITH 1,10-PHENANTHROLINE AND *S*-AMINOACIDATES

A. DECINTI,† P. AGUIRRE and G. LARRAZÁBAL

Departamento de Química Inorgánica y Analítica,
Facultad de Ciencias Químicas y Farmacéuticas, Universidad de Chile,
Casilla 233, Santiago, Chile

(*Received* 2 *February* 1993; *accepted* 18 *February* 1993)

Abstract—Δ,Λ-[Cd(phen)$_2$(*S*-aa)]$^+$NO$_3^-$ diastereomeric systems (where phen = 1,10-phenanthroline and *S*-aa = *S*-alaninate, *S*-serinate, *S*-threoninate, *S*-prolinate, *S*-valinate, *S*-leucinate and *S*-phenylalaninate) have been prepared in the form of methanolic solutions and characterized by spectral (UV, CD, ORD) and conductance measurements. The CD spectra of these systems in the β' band region of the diimine ligand exhibit residuary exciton splittings, whose intensities and sign patterns suggest the following decreasing order of [Λ]/[Δ] diastereoisomeric equilibrium constants: *S*-prol > *S*-phenala > *S*-val > 1 > *S*-ala > *S*-leu > *S*-ser > *S*-threo. The same order is inferred from the ORD data over the range 400–600 nm. Comparison with the selectivities observed for some zinc analogues and the analysis of molecular models suggest that in the cadmium systems the chiral discriminations are governed mainly by a balancing between intramolecular steric repulsion, differential solvation and discriminating ion association. Solvent effects on the optical activity of some cadmium and zinc systems in methanol/n-propanol and methanol/benzene mixtures have also been studied. The corresponding results are discussed in terms of the contributions of the above discriminating forces.

The circular dichroism (CD) spectra in the aromatic region of Δ,Λ-[M(diimine)$_2$(aa)]$^{(z-q)+}$ systems, where M^{z+} is a transition or an $(n-1)d^{10}$ metal ion, diimine is 1,10-phenanthroline or 2,2′-bipyridine and aa^{q-} is an optically active α-aminoacidate, in aqueous or methanolic solution, exhibit residuary exciton bands whose intensities and sign patterns can be mainly connected with the particular positions of the respective diastereoisomeric equilibria:[1–4]

$$\Delta\text{-[M(diimine)}_2\text{(aa)]}^{(z-q)+} \rightleftharpoons \Lambda\text{-[M(diimine)}_2\text{(aa)]}^{(z-q)+}.$$

The equilibrium constants for the preceding reactions show, in turn, a clear dependence upon the nature of the side-chain of the chiral ligand. Usually, the chelation of an *S*-aminoacidate having an apolar side-chain induces an equilibrium shift towards an increase in concentration of the Λ-isomer. Here, the origin of chiral discrimination has been ascribed to a prevalence of intramolecular ligand–ligand steric repulsive interactions in the less preferred Δ-isomer.[2–6] On the other hand, the chelation of an *S*-aminoacidate having a polar side-chain may lead to the predominance of either the Δ- or the Λ-diastereoisomer, depending on the particular metal ion and diimine ligand involved. Thus, concerning the trend to Δ-isomer predominance, for systems containing *S*-serinate the order Ru^{II} > Co^{III} can be established from the data reported at present.[1,7] The order 2,2′-bipy > 1,10-phen is also observed for the above tendency in systems of ruthenium(II) with *S*-serinate, *S*-aspartate or *S*-glutamate.[1,8,9] This sequence has been ascribed to the greater flexibility of the bipyridine ligand,[8] which should cause a decrease in the intramolecular ligand–ligand steric repulsion, thus enhancing other types of non-covalent interactions that are referred to below. Indeed, for 1,10-phen systems in aqueous solution chiral induction involving Δ/Λ > 1 occurs only in Δ,Λ-[Ru(phen)$_2$(*S*-glu)]^0 and Δ,Λ-

† Author to whom correspondence should be addressed.

$[Ru(phen)_2(S\text{-threo})]^+$, whereas Δ,Λ-$[Ru(phen)_2(S\text{-asp})]^0$ and Δ,Λ-$[Ru(phen)_2(S\text{-ser})]^+$ show no stereoselectivity.[1,8–10] In general, chiral discrimination favouring the stability of one diastereoisomer would arise partly from a balancing between steric repulsive interactions and other intramolecular forces, such as hydrogen bonding and possible hydrophobic bonding interactions.[8,9] Further, some intermolecular factors have also been suggested as sources of stereoselectivity, namely differential solvation[11] and hydrogen bonding interactions with the surrounding chiral solvent sheaths,[12] which are concomitant with the dissymmetry of the complex ions. A structural feature of rather obvious interest for the study of the different kinds of interactions previously mentioned would be the metal ion size. An increase in the metal ion radius should diminish the intramolecular steric repulsion effects, which are usually predominant, thus allowing other discriminating forces to become apparent with relatively higher intensities. This report is concerned with the stereoselective effects of non-resolvable *S*-aminoacidatobis(1,10-phenanthroline)cadmium(II) complexes in methanolic solution. In these complexes the metal–ligand bond lengths should be nearly 0.2 Å larger than those of the corresponding complexes of zinc or ruthenium(II). Hence, a somewhat different balancing of intramolecular interactions should be expected here regarding the analogues of those metal ions. Similarly to zinc systems, cadmium systems exhibit very rapid diastereoisomeric equilibration rates. This prevents both the use of ordinary resolution procedures and the experimental estimation of the respective Δ/Λ equilibrium constants from optical activity measurements. Notwithstanding the above restraints, these complexes provide in return the certainty of dealing with truly equilibrated diastereoisomeric systems.

EXPERIMENTAL

Nitrate salts of the heterochelated ions Δ,Λ-$[Cd(phen)_2(S\text{-aa})]^+$ were prepared as 0.007 or 0.018 M solutions in methanol, by means of the following general reaction:

$$Cd(NO_3)_2\cdot 4H_2O + 2phen\cdot H_2O + S\text{-aaH} + (1/2)Ba(OH)_2\cdot 8H_2O \longrightarrow \Delta,\Lambda\text{-}[Cd(phen)_2(S\text{-aa})]NO_3 + (1/2)Ba(NO_3)_2 + 11H_2O;$$

where *S*-aaH = *S*-alanine, *S*-serine, *S*-threonine, *S*-valine, *S*-leucine, *S*-phenylalanine or *S*-proline. Stoichiometric amounts of the analytical reagent or CP-grade chemicals were mixed in methanol *pro analysi* as a solvent, and heated at 60°C in stoppered flasks until complete reaction of the amino acid. Once cooled the resulting mixtures were ultrasonically stirred and allowed to stand at room temperature for 2 days. Barium nitrate was discarded by filtration under suction. The resulting solutions were concentrated by boiling and standardized to 0.007 or 0.018 M at 25°C. For the sake of comparison chloride and sulphate salts of similar zinc complexes were also prepared as methanolic solutions (0.007 or 0.018 M in complex ions) by methods previously reported.[4] Electronic spectral measurements in the UV region were performed at room temperature on a Carl–Zeiss DMR-21 spectrophotometer using 5.6×10^{-5} M solutions in 0.1 cm cells. CD spectra were recorded on a Cary 60 spectropolarimeter, at room temperature, using 2.1×10^{-4} or 4.2×10^{-4} M solutions in closed 0.1 cm cells. Optical rotatory dispersion (ORD) spectra were measured at 25°C on a modified Perkin–Elmer 141 polarimeter, using 0.007 M solutions in thermostated closed 2 or 10 cm cells. Conductivity measurements were performed at 25°C with a YSI model 32 conductance bridge and an immersion cell ($1.022\ cm^{-1}$), using 0.007 M solutions. Molar ratio studies of optical rotation at 450 nm of the systems Cd^{II} : phen : *S*-aa = $1:x:1$ were performed at 25°C over the range $1 \leqslant x \leqslant 3$ for *S*-aa = *S*-threo and *S*-val. Moreover, solvent effects of increasing concentrations of n-propanol and benzene on the optical activity of some 0.0018 M cadmium systems were tested over the ranges 0–12 M and 0–10 M, respectively. Some zinc systems were also considered in these experiments. The effects of the relatively small water contents of the complex salt solutions on diastereoisomeric and formation equilibria were assumed to be neglible for comparative purposes.

RESULTS AND DISCUSSION

Spectral properties and diastereoisomeric equilibria

Results of the molar ratio studies on the systems Cd^{II} : phen : *S*-aa^- : NO_3^- = $1:x:1:1$ of *S*-valinate and *S*-threoninate are compared in Fig. 1, where the molecular rotations at 450 nm are plotted against $x = [phen]_{total} : [Cd^{II}]_{total}$. From these data it becomes apparent that the species responsible for the optical activity in the above system are $[Cd(phen)_2(S\text{-aa})]^+$ diastereoisomeric complexes. This inference agrees with the conductance data listed in Table 1. Although these values are not accurate, they strongly suggest that the cadmium systems prepared consist predominantly of uniu-

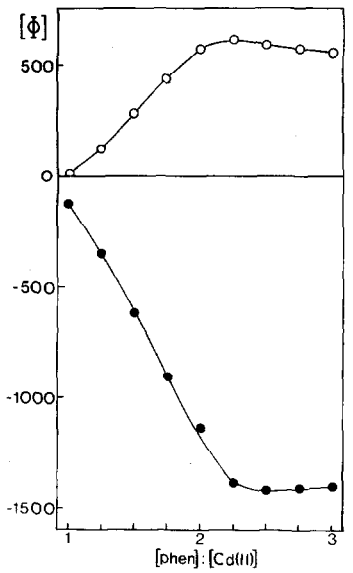

Fig. 1. Variation of molar rotation at 450 nm of systems Cd^{II} : phen : *S*-aa$^-$: NO_3^- = 1 : *x* : 1 : 1, in methanol, as a function of the $[phen]_{total}$: $[Cd^{II}]_{total}$ molar ratio. $[Cd^{II}]_{total}$ = 0.007 M; 25°C. *S*-aa$^-$ = *S*-val$^-$ (○) and *S*-threo$^-$ (●).

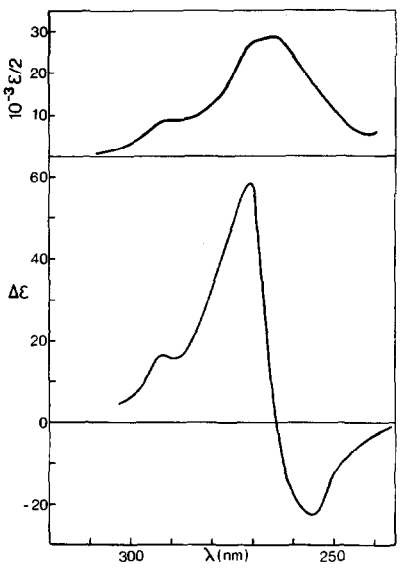

Fig. 2. Absorption and CD spectra in the UV region (*p*- and *β*′-bands) of the system Δ,Λ-[Cd(phen)$_2$(*S*-prol)]NO_3, in methanol, at room temperature.

nivalent electrolytes.[13,14] Moreover, the UV absorption spectra in the region of the long-axis-polarized π–π^* transitions of the diimine ligand, which are virtually identical for the different cadmium systems, show bathochromic shifts of the *β*′- and *p*-bands that are similar to those of Δ,Λ-[Ni(phen)$_2$(*S*-aa)]$^+$ and Δ,Λ-[Zn(phen)$_2$(*S*-aa)]$^+$ complexes[4] (Figs 2 and 3). Some features of the CD spectra in the *β*′-band region of the studied cadmium systems are given in Table 1 and CD spectra in the *β*′- and *p*-band region of some selected systems are shown in Figs 2, 3 and 4. According to these data residuary exciton bands are always present in the CD spectra, their intensities and sign patterns being clearly dependent upon the structure of the side-chain of the chiral ligand. In fact, the typical sign pattern indicating the predominance of the Λ-diastereoisomer is observed only in the systems of *S*-phenylalaninate, *S*-prolinate and *S*-valinate, i.e. in systems of *S*-aminoacidates having

Table 1. CD data at room temperature and molar conductances at 0.007 M and 25°C of Δ,Λ-[Cd(phen)$_2$(*S*-aa)]NO_3 systems in methanol

S-aa[a]	λ (nm) (Δε)	Λ^b (Ω^{-1} cm^2 mol^{-1})
S-prol	271 (+58.8); 256 (−22.0)	80
S-phenala	275 (+17.4); 253 (−8.7)	—
S-val	271 (+8.7); 253 (−4.6)	76
S-ala	275 (−6.5); 264 (+7.6)	78
S-leu	273 (−9.3); 259 (+2.9)	78
S-ser	273 (−9.9); 256 (+1.7)	81
S-threo	272 (−13.1); 256 (+2.9)	79

[a] Abbreviations: *S*-prol = *S*-prolinate, *S* = phenala = *S*-phenylalaninate, *S*-val = *S*-valinate, *S*-ala = *S*-alaninate, *S*-leu = *S*-leucinate, *S*-ser = *S*-serinate, *S*-threo = *S*-threoninate.

[b] Not corrected for the presence of small varying concentrations of barium nitrate.

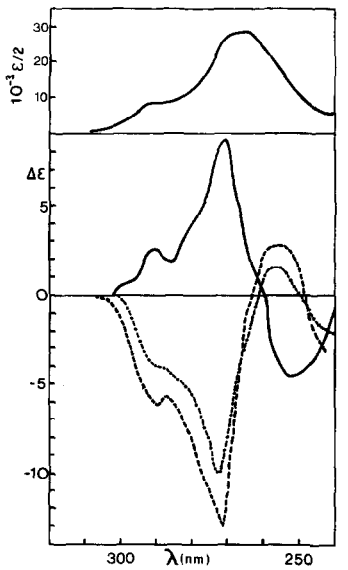

Fig. 3. Absorption and CD spectra in the UV region (*p*- and *β*′-bands) of systems Δ,Λ-[Cd(phen)$_2$(*S*-aa)]NO_3, in methanol, at room temperature. *S*-aa = *S*-val (——), *S*-ser (–·–·–) and *S*-threo (– – – –).

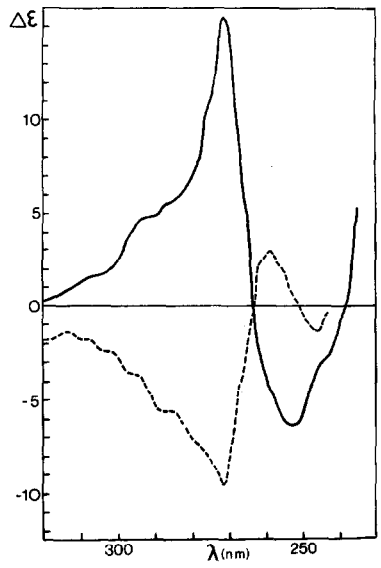

Fig. 4. CD spectra of Δ,Λ-[M(phen)$_2$(*S*-leu)]$^+$ systems (*p*- and *β*′-bands), in methanol, at room temperature. M = Zn (——) and Cd (– – – –).

bulky, exceedingly rigid or *β*-substituted side-chains, respectively. Chiral discrimination arising from intramolecular steric repulsive interations must be preponderant in the above systems.[2,5] On the other hand, the exciton CD spectra of the remaining cadmium systems exhibit sign patterns characteristic of Δ-diastereoisomer predominance. Here, discriminating forces other than steric effects would be determinant. Interestingly, two systems containing aminoacidate ligands with apolar side groups are found amongst those exhibiting chiral induction with a preference for the Δ-isomer, viz. the *S*-ala and *S*-leu systems. The exciton CD spectrum of the latter is compared with its zinc analogue in Fig. 4. From a general point of view the above dependences of the CD spectra upon the nature of the side groups of the aminoacidates indicate at least that these ligands are acting as chelating agents.

Molecular rotation values for the cadmium systems are listed in Table 2. As can be seen, these data are in good agreement with the respective CD spectra. This fact is reflected by the plot of the molecular rotation at 450 nm against the maximum of circular dichroism of the low-energy long-axis-polarized π–π^* transition, which gives a fairly good linear correlation ($r = 0.994$). Taking into account the relative intensities of the low-energy exciton CD bands (Table 1) and the molecular rotation values at 450 nm (Table 2), the following sequence of diastereoisomeric equilibrium constants can be proposed for the cadmium systems: K(*S*-prol) > K(*S*-phenala) > K(*S*-val) > 1 > K(*S*-ala) > K(*S*-leu) > K(*S*-ser) > K(*S*-threo), where K(*S*-aa) = [Λ]/[Δ]. The preceding sequence differs noticeably from that obtained for analogues of zinc,[3] where steric effects are always predominant and no cases are observed of chiral discrimination enhancing the equilibrium concentration of the Δ-isomer: K(*S*-val) > K(*S*-prol) > K(*S*-threo) > K(*S*-ser) > K(*S*-leu) > K(*S*-ala) > 1 (Table 2).

Exciton splitting and hydrophobic interactions

For the sake of comparison the ORD spectra of the cadmium and zinc systems under study were

Table 2. Molecular rotations at 450 nm and Drude equation parameters of Δ,Λ-[M(phen)$_2$(*S*-aa)]X$_{1/q}$ systems of cadmium[a] and zinc[b] in methanol, at 25°C

M	*S*-aa	$[\Phi]^{25°C}_{450\,nm}$	$\lvert\Sigma\rvert$ (cm^{-1})	C_1	C_2	10^3C_3
Cd	*S*-prol	+3693	82.4	+40.260	−39.861	15.3
Cd	*S*-phenala	+1086	108.0	+11.832	−11.765	4.8
Cd	*S*-val	+571	97.0	+6.236	−6.181	−2.3
Cd	*S*-ala	−500	51.0	−5.455	+5.366	1.7
Cd	*S*-leu	−557	98.5	−6.064	+6.024	−4.8
Cd	*S*-ser	−829	88.6	−9.044	+8.966	−4.6
Cd	*S*-threo	−1136	77.0	−12.361	+12.225	−3.8
Zn	*S*-val	+2179	105.5	+23.764	−23.637	17.2
Zn	*S*-prol	+2018	91.3	+22.023	−21.857	17.3
Zn	*S*-threo	+1271	86.4	+13.885	−13.759	5.3
Zn	*S*-ser	+763	116.0	+8.321	−8.297	9.4
Zn	*S*-leu	+756	115.0	+8.231	−8.192	2.2
Zn	*S*-ala	+729	85.0	+7.950	−7.871	0.2

[a] $X^{q-} = NO_3^-$.
[b] $X^{q-} = SO_4^{2-}$.

described over the range 400–600 nm through many-term Drude equations of the form:[4]

$$[\Phi]_\lambda = \frac{10^4}{1.4}\left[\frac{C_1\lambda_1^2}{\lambda^2-\lambda_1^2}+\frac{C_2\lambda_2^2}{\lambda^2-\lambda_2^2}+C_3\right];$$

where subscripts 1 and 2 are the β'-exciton bands, $\lambda_1 > \lambda_2$, and C_3 is a term comprising the weaker contributions. If the same excitation resonance splitting is assumed for both Δ and Λ isomers, the wavelengths of the absorption maxima of the exciton bands become $\lambda_1 = 10^7\lambda_0/(10^7-|\Sigma|\lambda_0)$ and $\lambda_2 = 10^7\lambda_0/(10^7+|\Sigma|\lambda_0)$, where λ_0 is the wavelength in nm of the baricenter of the β'-band and $|\Sigma|$ is the mean absolute value of the excitation resonance energy in cm^{-1}. The parameters C_1, C_2 and C_3 were calculated from the molecular rotation data at 400, 450 and 550 nm by iterating $|\Sigma|$ values until $C_1 \approx 0.1091\ [\Phi]_{450\,nm}$ was obtained. This condition arises from an assumed proportionality between C_1 and $[\Phi]_{450\,nm}$. The above proportionality constant was obtained from the previously studied system Δ,Λ-[Zn(phen)$_2$(*S*-ala)]Cl, for which $|\Sigma| = 100$ cm^{-1} was arbitrarily taken.[4] In other words this approximation implies that in these systems the intensity of the ORD spectrum depends much more upon the position of the Λ/Δ diastereoisomeric equilibrium than on the extent of the excitation resonance splitting. The $|\Sigma|$, C_1, C_2 and C_3 parameters thus obtained are shown in Table 2. The ORD curves calculated with these figures are in excellent agreement with the experimental ones. This fact becomes apparent on plotting the experimental against the calculated molecular rotation values over the range 400–600 nm. Straight lines almost passing through the origin are thus obtained, whose slopes are very close to unity, the corresponding correlation coefficients always being greater than 0.9996. Although the pairs of C_1 and C_2 values listed in Table 2 show the right sign patterns, they do not reflect the relative intensities of the residuary exciton bands (Table 1). However, some uncertainty could also be expected in the magnitudes of the residuary exciton bands since the diimine ligand exerts strong absorption in the aromatic spectral region, rendering the CD measurements difficult in most cases. On the other hand, for both cadmium and zinc systems the variation of $|\Sigma|$ through the aminoacidate series shows no correlation with the remaining Drude equation parameters. Nevertheless, for systems with *S*-aminoacidates having apolar side-chains amazingly good correlations are observed with a rather rough topological index consisting of the total number of atoms of the side-chain. Such correlations are shown in Fig. 5, where the systems of *S*-serinate and *S*-threoninate are also included, although they are not considered in the regression analysis. As can be seen these diagrams result in similar arrangements for the systems of both metal ions, even concerning the positions of the systems that contain *S*-aminoacidates with polar side-chains. Intramolecular non-covalent interactions could also be responsible for this behaviour. These forces should induce small geometrical changes that modify the effective distance between the transition dipoles located at the molecular centres of the adjacent diimine ligands. This assumption agrees with the fact that for each aminoacidate ligand the $|\Sigma|$ value of the zinc system is always greater than that of the cadmium system (Table 2), consistent with the dipole–dipole approximation.[15] Moreover, the $|\Sigma|$ values of systems containing *S*-aminoacidates with apolar side-chains follow the order *S*-phenala > *S*-leu > *S*-val > *S*-prol > *S*-ala, which parallels the hydrophobicity scale for side-chains of aminoacids.[16] Hence, the above defined topological index would also be reflecting the variation in this property through the aminoacidate series. Further, since the variation of the [Λ]/[Δ] equilibrium position of the cadmium and zinc systems through the aminoacidate series does not parallel the aforementioned hydrophobicity scale, it can be concluded that the contributions of intramolecular hydrophobic interactions are not determinant for the observed stereoselective effects. Indeed, intramolecular hydrophobic interactions would rather

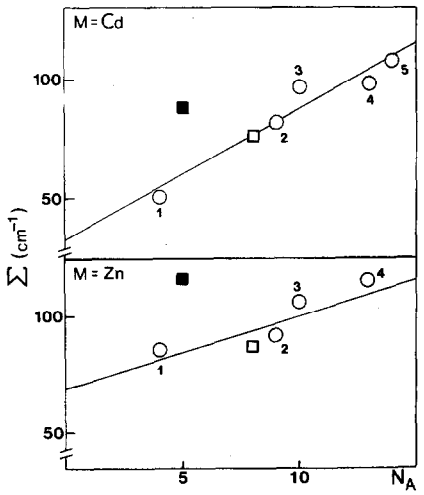

Fig. 5. Correlation of mean excitation resonance energies of Δ,Λ-[M(phen)$_2$(*S*-aa)]$^+$ systems vs side-chain sizes. N_A = total number of atoms of the side-chain. *S*-alaninate (1); *S*-prolinate (2); *S*-valinate (3); *S*-leucinate (4); *S*-phenylalaninate (5); *S*-serinate (■); *S*-threoninate (□). M = Cd (r = 0.97); Zn (r = 0.92).

enhance the stability of the Λ-isomer, as can be shown from the structure proposed by Sigel *et al.*[17] for the folded form of the species [Zn(phen)(*S*-leu)]$^+$.

Solvent effects

It seems reasonable to assume that both polar solvation and ion-pairing interactions of the diastereoisomeric species occur mainly through the amino group, because its hydrogen atoms would carry a substantial fraction of the positive charge of the metal chelates.[18] Thus, both differential polar solvation and discriminating ion association would take place on account of the different intramolecular environments that surround the coordinating amino group in each diastereoisomer. Analysis of molecular models suggests that although the Δ-diastereoisomer must be sterically less favoured than the Λ-form, it should be subjected in turn to better polar solvation on the amino group and stronger ion-pairing interactions, which would obviously contribute to increasing its thermodynamic stability. The above observations are illustrated in Fig. 6, where a comparison is attempted of the intramolecular environment of the assumed main polar solvation sites in the Δ- and Λ-isomers of the *S*-leucinate system. In these schematic representations the diastereoisomeric chelates are viewed along the $H_2N—Cd^{2+}$ bonds; consequently, the metal ions are eclipsed by the amino nitrogen donors. Moreover, both species are shown in folded form. As can be seen, in the Δ-isomer one of the hydrogen atoms of the NH_2 group remains freely exposed towards the bulk of the solvent, whatever the conformation adopted by the side-chain. Further, such a hydrogen atom would lie nearly 2.6 Å over the molecular plane of the phenanthroline ligand having both nitrogen donors in *cis* positions to the amino group. On the contrary, in the folded form of the Λ-isomer polar solvation should be somewhat hindered by the hydrophobic groups of the side-chain. As previously mentioned, in the case of the Λ-isomer the folded conformer would correspond to the "closed" form proposed by Sigel to account for the intramolecular hydrophobic interactions in the [Zn(phen)(*S*-leu)]$^+$ system.[17] Such interactions would be responsible for the slightly higher stability of the above 1 : 1 : 1 system in comparison with the *S*-alaninate analogue.[17] From the above considerations it could be proposed that, at least for the cadmium systems containing aminoacidates with apolar side-chains, the position of the [Λ]/[Δ] equilibrium is mainly determined by balancing between polar differential solvation, discriminating ion association and steric repulsive interactions. These factors in combination with hydrophobic solvation could also account for the observed effects that the increasing concentration of n-propanol has on chiral discrimination of cadmium and zinc systems in methanol/n-propanol mixtures (Figs 7 and 8). As can be seen, in systems containing aminoacidates with apolar side-chains the increasing concentration of n-propanol usually induces an equilibrium shift towards an increase in concentration of the Δ-isomer. This fact would be ascribed to the solvating properties of n-propanol. Apart from the ability to solvate the amino group, which is common for both solvents, n-propanol must be more

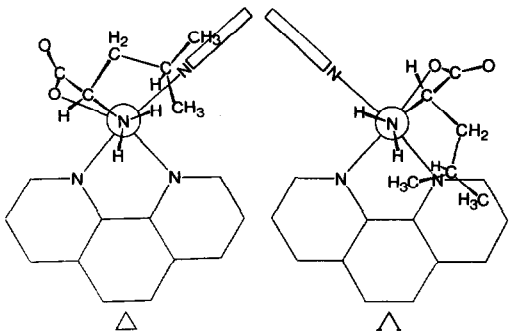

Fig. 6. Schematic representation of the assumed main solvation sites of the Δ- and Λ-diastereoisomers of [M(phen)$_2$(*S*-leu)]$^+$ complexes.

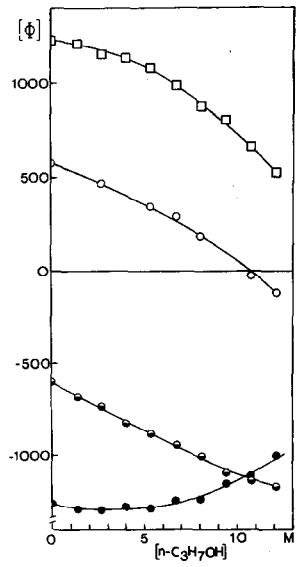

Fig. 7. Variation of molecular rotation at 450 nm of systems Δ,Λ-[M(phen)$_2$(*S*-aa)]X in methanol/n-propanol mixtures with varying n-propanol concentration, at room temperature. M^{II}, *S*-aa$^-$, X$^-$ = Zn^{II}, *S*-leu$^-$, Cl$^-$ (□); Cd^{II}, *S*-val$^-$, NO_3^- (○); Cd^{II}, *S*-leu$^-$, NO_3^- (◒); Cd^{II}, *S*-threo$^-$, NO_3^- (●).

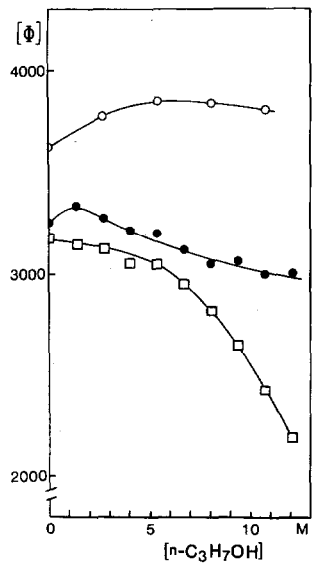

Fig. 8. Variation of molecular rotation at 450 nm of systems Δ,Λ-[M(phen)$_2$(*S*-aa)]X in methanol/n-propanol mixtures with varying n-propanol concentration, at room temperature. M^{II}, *S*-aa$^-$, X$^-$ = Cd^{II}, *S*-prol$^-$, NO$_3^-$ (○); Cd^{II}, *S*-prol$^-$, *S*-prol$^-$ (●); Zn^{II}, *S*-val$^-$, Cl$^-$ (□).

capable than methanol of interacting hydrophobically through its apolar end with the phenanthroline ligand lying almost perpendicular to the H_2N—Cd^{2+} bond (Fig. 6). The simultaneous occurrence of both types of interactions would be more favourable for the Δ-isomer, contributing to its stabilization. Moreover an increase in the discriminating ion-pair effects, favouring the Δ-form, would be expected from the decrease in dielectric constant of the solvent mixture. On the other hand, in the case of the system [Cd(phen)$_2$(*S*-prol)]NO$_3$ the optical rotation varies slightly, exhibiting a tendency to increase with increasing concentration of n-propanol (Fig. 8). This behaviour could be ascribed to the predominance of the unstabilizing effects of intramolecular steric repulsive forces in the Δ-isomer, owing to the extreme rigidity of the side-chain of the *S*-prolinate ligand. The small ascent in molecular rotation can be attributed to a shift of the formation equilibrium:

$$\Delta,\Lambda\text{-}[Cd(phen)_2(solv)_2]^{2+} + S\text{-prol}^- \rightleftharpoons \Delta,\Lambda\text{-}[Cd(phen)_2(S\text{-prol})]^+ + 2solv$$

towards the diastereoisomeric species, because of the decrease in dielectric constant of the solvent mixture. This assumption is supported by the fact that on counteracting the effects of such an equilibrium shift, i.e. in the system [Cd(phen)$_2$(*S*-prol)]*S*-prol (Fig. 8), the behaviour of molecular rotation as a function of n-propanol concentration is similar to those of the cadmium systems of *S*-leucinate or *S*-valinate (Fig. 7). The cadmium system containing *S*-threoninate, where the effects of polar differential solvation and discriminating ion association are predominant (Fig. 7), also exhibits a slight variation in optical rotation as a function of n-propanol concentration. Moreover, such a variation tends to be opposite to those observed for the remaining systems. This behaviour can be explained by assuming that the decrease in the dielectric constant of the solvent mixture causes the polar group of the side-chain to draw near the carboxylate or amine groups; thus, CO---HO or NH---OH hydrogen bonding would be promoted. The conformational changes involved here would be sterically more favourable in the Λ-isomer, as can be recognized from the analysis of molecular models. Hence, an increase in concentration of the Λ-isomer would be responsible for the slight rise in optical rotation observed on increasing the concentration of n-propanol above 6 M. The results obtained for the cadmium system with *S*-threoninate in methanol/benzene mixtures seem to be in support of the validity of the above assumptions (Fig. 9). In this case a conspicuous rise in optical rotation is observed with an increase in benzene concentration above 3.5 M; the greater intensity of this effect being in agreement with the more drastic decrease in dielectric constant involved here.

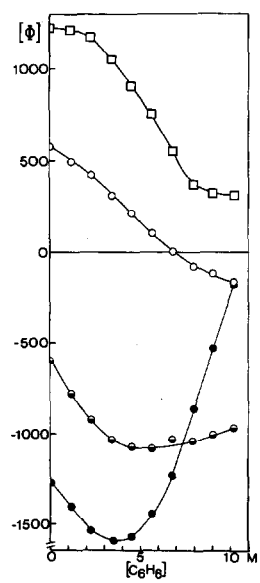

Fig. 9. Variation of molecular rotation at 450 nm of systems Δ,Λ-[M(phen)$_2$(*S*-aa)]X in methanol/benzene mixtures with varying benzene concentration, at room temperature. M^{II}, *S*-aa$^-$, X$^-$ = Zn^{II}, *S*-leu$^-$, Cl$^-$ (□); Cd^{II}, *S*-val$^-$, NO$_3^-$ (○); Cd^{II}, *S*-leu$^-$, NO$_3^-$ (◒); Cd^{II}, *S*-threo$^-$, NO$_3^-$ (●).

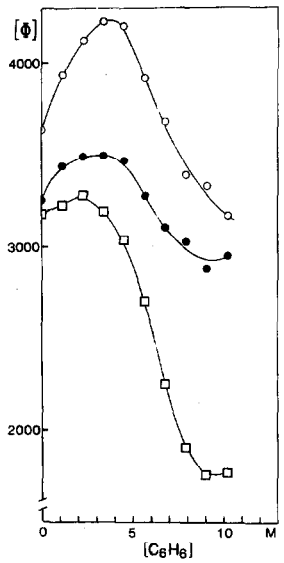

Fig. 10. Variation of molecular rotation at 450 nm of systems Δ,Λ-[M(phen)$_2$(*S*-aa)]X in methanol/benzene mixtures with varying benzene concentration, at room temperature. M^{II}, *S*-aa$^-$, $X^- = Cd^{II}$, *S*-prol$^-$, NO_3^- (○); Cd^{II}, *S*-prol$^-$, *S*-prol$^-$ (●); Zn^{II}, *S*-val$^-$, Cl^- (□).

From a general point of view, for the systems in methanol/benzene mixtures (Figs 9 and 10) the observed effects of the increasing concentration of benzene could be ascribed in part to the fact that the polar groups of the chiral ligand, mainly the amino group, tend to keep the polar ends of the methanol molecules clustered at the solvation sites of the metal chelates, making polar differential solvation prevail as the discriminating factor. Moreover, discrimination arising from differential ion pairing should become more operative on decreasing the dielectric constant. Thus, for the cadmium system containing *S*-threoninate the above effects would predominate at least up to 3.5 M benzene. However, in all of the systems under study, both in methanol/benzene and methanol/n-propanol mixtures, chiral discriminating effects are obviously superposed with the effects arising from equilibrium shifts towards the formation of 1 : 2 : 1 diastereoisomeric species. Such equilibrium shifts would account for the more negative slopes of variation in optical rotation observed in the concentration range 0–3.5 M of benzene for the cadmium systems of *S*-leucinate or *S*-threoninate, as compared with the cadmium system containing *S*-valinate or the zinc system containing *S*-leucinate (Fig. 9). Instead, for the systems of cadmium and zinc containing *S*-prolinate and *S*-valinate, respectively, the effects of the formation equilibrium shifts clearly predominate in the range 0–4 M (Fig. 10). For the systems containing *S*-aminoacidates with apolar side-chains, except that of cadmium with *S*-leucinate, the effects of the polar differential solvation and discriminating ion association on the [Λ]/[Δ] ratios seem to predominate in almost all the concentration range considered, or at least above 3.5 M. The different behaviour of the cadmium system containing *S*-leucinate (Fig. 9) would be ascribed to a predominance above 5 M of the effects of an apolar differential solvation, which would arise from a more favourable hydrophobic solvation of the folded form of the Λ-isomer.[19] These effects would also be responsible for the changes in curvature or slight rises in optical rotation observed above 8 M benzene for the remaining systems containing *S*-aminoacidates with apolar side-chains (Figs 9 and 10).

Acknowledgements—The authors thank Professors Sergio Bunel, Carmen Ibarra and Exequíel Moraga for help in the experimental, and Professors Fresia Pérez and Claudio Telha for technical assistance in writing this manuscript. This work was supported by FONDECYT (Project 93-1009).

REFERENCES

1. R. S. Vagg and P. A. Williams, *Inorg. Chim. Acta* 1981, **52**, 69.
2. R. S. Vagg and P. A. Williams, *Inorg. Chim. Acta* 1981, **51**, 65.
3. S. Bunel, G. Larrazábal and A. Decinti, *J. Inorg. Nucl. Chem.* 1981, **43**, 2781.
4. A. Decinti, M. Contreras, E. Moraga and G. Larrazábal, *Polyhedron* 1992, **11**, 1235.
5. A. Tatehata, *Inorg. Chem.* 1982, **21**, 2496.
6. F. S. Stephens, R. S. Vagg and P. A. Williams, *Inorg. Chim. Acta* 1983, **72**, 253.
7. A. Pasini, *Gazz. Chim. Ital.* 1983, **113**, 793.
8. T. J. Goodwin, P. A. Williams and R. S. Vagg, *Inorg. Chim. Acta* 1982, **63**, 133.
9. R. S. Vagg and P. A. Williams, *Inorg. Chim. Acta* 1982, **58**, 101.
10. T. J. Goodwin, P. A. Williams, F. S. Stephens and R. S. Vagg, *Inorg. Chim. Acta* 1984, **88**, 165.
11. D. A. Buckingham, L. G. Marzilli and A. M. Sargeson, *J. Am. Chem. Soc.* 1967, **89**, 5133.
12. D. P. Craig and D. P. Mellor, *Topics Curr. Chem.* 1976, **63**, 1.
13. W. J. Geary, *Coord. Chem. Rev.* 1971, **7**, 81.
14. J. Barthel, M. Krell, L. Iberl and F. Feuerlein, *Electroanalyt. Chem.* 1986, **214**, 485.
15. C. J. Hawkins, *Absolute Configuration of Metal Complexes*, pp. 230–233. John Wiley and Sons, New York (1971).
16. Y. Nozaki and C. Tandford, *J. Biol. Chem.* 1971, **246**, 2211.
17. B. E. Fischer and H. Sigel, *J. Am. Chem. Soc.* 1980, **102**, 2998.
18. K. Ito, *Inorg. Chem.* 1983, **22**, 2872.
19. H. Sigel, R. Malini-Balakrishnan and U. K. Häring, *J. Am. Chem. Soc.* 1985, **107**, 5137.

Polyhedron Vol. 12, No. 12, pp. 1523–1526, 1993
Printed in Great Britain

0277–5387/93 $6.00+.00
© 1993 Pergamon Press Ltd

SYNTHESIS AND MAGNETIC PROPERTIES OF BINUCLEAR Cu^{II}–Ni^{II} COMPLEXES WITH N,N′-BIS(2-AMINOETHYL)OXAMIDOCOPPER(II)

SHU-LIN MA,* DAI-ZHENG LIAO, ZONG-HUI JIANG, SHI-PING YAN and GENG-LIN WANG†

Department of Chemistry, Nankai University, Tianjin, P.R.C.

(*Received* 27 *January* 1993; *accepted* 18 *February* 1993)

Abstract—Four binuclear complexes have been synthesized, namely $[Cu(oxae)Ni(L)_2](ClO_4)_2 \cdot H_2O$, where oxae denotes the N,N′-bis(2-aminoethyl)oxamido dianion and L denotes 2,2′-bipyridyl (bpy), 4,4′-dimethyl-2,2′-bipyridyl (Me_2bpy), 1,10-phenanthroline (phen) or 5-nitro-1,10-phenanthroline ($NO_2 \cdot$phen). Based on IR, elemental analyses, conductivity measurements and electronic spectra these complexes are proposed to have extended oxamido-bridged structures and to consist of the copper(II) ion in a square environment and the nickel(II) ion in an octahedral environment. The temperature dependences of the magnetic susceptibilities of $[Cu(oxae)Ni(bpy)_2](ClO_4)_2 \cdot H_2O$ and $[Cu(oxae)Ni(Me_2bpy)_2](ClO_4)_2$ have been studied in the 4.2–300 K range, giving the exchange integral $J = -112.7$ cm^{-1} for bpy and $J = -123.8$ cm^{-1} for Me_2bpy. These results are commensurate with antiferromagnetic interactions between the adjacent metal ions.

Binuclear metal complexes with extended bridged structures are of current interest due to spin-exchange and charge-transfer between metal ions and homogeneous catalysis.[1] In view of the effective bridged ability of the oxamido group Ojima and Nonoyama[2] first utilized N,N′-bis(2-aminopropyl)oxamidocopper(II), [Cu(oxap)], and N,N′-bis(3-aminopropyl)oxamidocopper(II), [Cu(oxpn)], as a bidentate mononuclear fragment to prepare the binuclear complex, but its detailed physicochemical properties have not been reported. Recently, complexes of this kind with various terminal ligands and other metal ions, such as $[Cu(oxap)M(L)_2](ClO_4)_2$ (M = Zn, Ni, Co, Mn, L = bpy, phen and $NO_2 \cdot$phen)[3–6] and $[Cu(oxpn)M(L)_2](ClO_4)_2$ (M = Zn, Ni, Co, Mn, L = bpy, phen and $NO_2 \cdot$phen)[7–10] were synthesized in our laboratory and their magnetic properties and some crystal structures were studied. As an extension of that investigation in this paper we report the synthesis, characterization and magnetism of four new complexes, $[Cu(oxae)Ni(L)_2](ClO_4)_2$ [where L = 2,2′-bipyridyl (bpy), 4,4′-dimethyl-2,2′-bipyridyl (Me_2bpy), 1,10-phenanthroline (phen) and 5-nitro-1,10-phenanthroline ($NO_2 \cdot$phen)].

EXPERIMENTAL

Preparation of Cu(oxae)

The procedure for the synthesis of Cu(oxae) has been reported previously by Ojima *et al.*[11] We have used a modification of this procedure in our study.

To an absolute ethanol solution (75 cm^3) of ethylenediamine (24.6 g, 0.4 mol) was added dropwise an absolute ethanol solution (200 cm^3) of diethyl oxalate (29.2 g, 0.2 mol). The mixture was refluxed for 4 h and then cooled. A suspension of copper(II) hydroxide (15.6 g, 0.16 mol) in water (100 cm^3) was added, which led to a blue solution and a violet–red solid residue. By adding $Cu(OH)_2$ in less than a stoichiometric amount, the formation of the green binuclear complex is avoided. The mixture was filtered and the solid residue was washed with water in order to extract all the expected compound. Violet–red microcrystals of Cu(oxae) were obtained by the addition of ethanol; Cu(oxae) is very soluble in water and insoluble in methanol or ethanol.

* Tianjin College of Commerce.
†Author to whom correspondence should be addressed.

Preparation of $[Cu(oxae)Ni(bpy)_2](ClO_4)_2 \cdot H_2O$

To Cu(oxae) (94.2 mg, 0.4 mmol) stirred in methanol (5 cm^3) were successively added a solution of $Ni(ClO_4)_2 \cdot 6\,H_2O$ (146.3 mg, 0.4 mmol) in methanol (10 cm^3) and bpy (125.0 mg, 0.8 mmol) in methanol (10 cm^3). After stirring for 5 h the solution was filtered. Violet–red microcrystals were obtained, washed several times with absolute methanol and diethyl ether and dried *in vacuo*. Found: C, 37.5; H, 3.4; N, 13.6; Cu, 7.7; Ni, 7.0. Calc. for $C_{26}H_{28}N_8O_{10}Cl_2CuNi \cdot H_2O$: C, 37.9; H, 3.7; N, 13.6; Cu, 7.7; Ni, 7.1%.

Preparation of $[Cu(oxae)Ni(Me_2bpy)_2](ClO_4)_2$

This complex was obtained as violet–red microcrystals by the same procedure but using Me_2bpy instead of bpy. Found: C, 41.4; H, 4.2; N, 12.9; Cu, 7.1; Ni, 6.6. Calc. for $C_{30}H_{36}N_8O_{10}Cl_2CuNi$: C, 41.8; H, 4.2; N, 13.0; Cu, 7.4; Ni, 6.8%.

Preparation of $[Cu(oxae)Ni(phen)_2](ClO_4)_2 \cdot 0.5H_2O$

This complex was prepared in the same way but using phen instead of bpy. Light red microcrystals were obtained. Found: C, 41.7; H, 3.3; N, 12.7; Cu, 7.4; Ni, 6.7. Calc. for $C_{30}H_{28}N_8O_{10}Cl_2CuNi \cdot 0.5H_2O$: C, 41.8; H, 3.4; N, 13.0; Cu, 7.4; Ni, 6.8%.

Preparation of $[Cu(oxae)Ni(NO_2 \cdot phen)_2](ClO_4)_2$

This complex was obtained in the same way but replacing bpy with $NO_2 \cdot$phen. Apricot–red microcrystals were obtained. Found: C, 38.0; H, 2.6; N, 14.4; Cu, 6.6; Ni, 6.1. Calc. for $C_{30}H_{26}N_{10}O_{14}Cl_2CuNi$: C, 38.2; H, 2.8; N, 14.8; Cu, 6.7; Ni, 6.2%.

Measurements

Elemental analyses of carbon, hydrogen and nitrogen were performed using a Perkin–Elmer elemental analyser, Model 240. Metal contents were determined by EDTA titration, IR spectra were measured on a Shimadzu IR spectrophotometer, Model 408, using KBr pellets, and the electronic spectra (methanol solution) were measured on a Hitachi-240 spectrophotometer. The molar conductance was measured with a DDS-11A conductometer. Variable temperature magnetic susceptibilities were measured on a vibrating sample magnetometer, Model CF-1. Diamagnetic corrections were made with Pascal's constants for all the constituent atoms, and the magnetic moments were calculated using the equation $\mu = 2.828(\chi T)^{1/2}$. ESR spectra were measured with a JES-FEIXG ESR apparatus using the *X*-band.

RESULTS AND DISCUSSION

General characterization

Elemental analyses indicated that the reaction of Cu(oxae) with $Ni(ClO_4)_2 \cdot 6H_2O$ and bpy, Me_2bpy, phen or $NO_2 \cdot$phen yielded the binuclear complexes. For the four $[Cu(oxae)Ni(L)_2](ClO_4)_2$ complexes, the molar conductance values (see Table 1) fall in the expected range for 1:2 electrolytes,[12] indicating that the two perchlorate anions are situated outside the metal coordination sphere. The significant bands in the IR spectra of the complexes are given in Table 1. The $\rangle C{=}O$ (carbonyl) stretching vibration at 1615 cm^{-1} for Cu(oxae) and the $\rangle C{=}N-$ stretching vibration at 1450–1500 cm^{-1} for the terminal ligands (bpy, Me_2bpy, phen and $NO_2 \cdot$phen) were shifted to higher frequencies in their binuclear complexes. It is likely that the bond order of C=O in the binuclear complexes is higher than that in the mononuclear complexes. These shifts have often been used as definite proof for the existence of the oxamido bridge.[2] In addition, the $-NH_2$ vibration at 3250 cm^{-1} for Cu(oxae) was present for all complexes and a broad, intense band is observed at 1085 cm^{-1},

Table 1. Physical data for the complexes

Complexes	Colour	Λ_m (Ω^{-1} cm^2 mol^{-1})	IR (cm^{-1})				UV ($10^3 \times cm^{-1}$)		
			$-NH_2$	C=O	$-N{=}C$	ClO_4^-	*d–d*	CT	
1	Violet–red	171	3250	1635	1600	1080	18.4	33.9	41.7
2	Violet–red	169	3250	1632	1615	1080	18.5	33.8	40.8
3	Light red	163	3250	1639	1580	1080	18.3	37.3	44.4
4	Apricot–red	193	3250	1640	1580	1080	18.5	36.9	44.1

1 = $[Cu(oxae)Ni(bpy)_2](ClO_4)_2 \cdot H_2O$; **2** = $[Cu(oxae)Ni(Me_2bpy)_2](ClO_4)_2$; **3** = $[Cu(oxae)Ni(phen)_2](ClO_4)_2 \cdot 0.5H_2O$; **4** = $[Cu(oxae)Ni(NO_2 \cdot phen)_2](ClO_4)_2$.

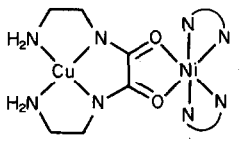

Fig. 1. Proposed chemical structure of $[Cu(oxae)Ni(L)_2]^{2+}$ (L = bpy, Me_2bpy, phen and $NO_2 \cdot$ phen).

which is typical for a non-coordination perchlorate ion.[13] Two strong absorptions in the UV range and only a weak absorption in the visible range can be observed. The former may be attributed to the charge-transfer absorption bands and the latter to the *d–d* transition.[8] Based on the discussion above these complexes are proposed to have an extended oxamido-bridged structure and to contain copper(II) in a planar environment and nickel(II) in an octahedral environment, as shown in Fig. 1.

Magnetic properties

The observed magnetic moment for the binuclear complexes at room temperature (2.74 B.M. for bpy and Me_2bpy) is considerably less than the spin-only value (3.32 B.M.). This suggests the operation of an antiferromagnetic spin-exchange interaction in these complexes. Variable-temperature susceptibility data were collected for bpy and Me_2bpy (Figs 2 and 3) and the magnetic analysis was performed using the susceptibility equation based on the Heisenberg spin operator ($\hat{H} = -2J\hat{S}_1\hat{S}_2$, $S_1 = 1/2$, $S_2 = 1$).[14]

$$\chi_M = \frac{N\beta^2}{4KT}\frac{g_{1/2} + 10g_{3/2}\exp(3J/KT)}{1 + 2\exp(3J/KT)}, \qquad (1)$$

where χ_M denotes the susceptibility per binuclear complex and $g_{1/2}$ and $g_{3/2}$ are g factors associated with the doublet and the quartet states, respectively. They are related to the local g factors g_{Ni} and g_{Cu}, assumed to be isotropic through $g_{1/2} = (4g_{Ni} - g_{Cu})/3$, $g_{3/2} = (2g_{Ni} + g_{Cu})/3$. The remaining symbols have their usual meanings. As shown in Figs 2 and 3 and good fits to the experimental data were obtained for $J = -112.7$ cm^{-1}, $g_{Ni} = 2.29$, $g_{Cu} = 2.10$, $\bar{g} = 2.20$ (bpy) and $J = -123.8$ cm^{-1}, $g_{Ni} = 2.29$, $g_{Cu} = 2.00$, $\bar{g} = 2.15$ (Me_2bpy). The agreement factor F defined here as $F = \Sigma[(\chi_M)_{obs} - (\chi_M)_{calc}]^2/\Sigma(\chi_M)_{obs}$ is then equal to 1×10^{-4}.

To describe the mechanism of exchange interaction several models have been proposed.[15–17]

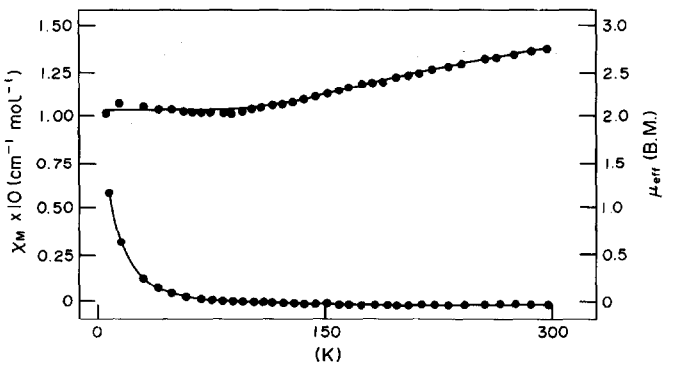

Fig. 2. Temperature variation of the magnetic susceptibility and magnetic moment for $[Cu(oxae)Ni(bpy)_2](ClO_4)_2 \cdot H_2O$. The curve is drawn based on eq. (1) using the magnetic parameters given in the text.

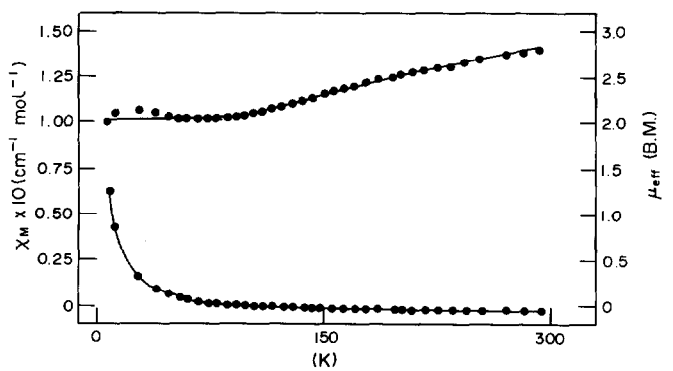

Fig. 3. Temperature variation of the magnetic susceptibility and magnetic moment of $[Cu(oxae)Ni(Me_2bpy)_2](ClO_4)_2$.

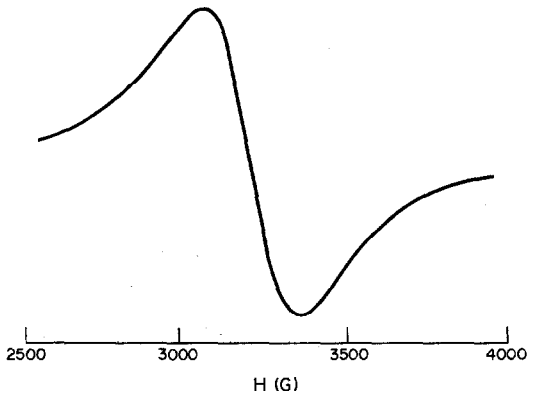

Fig. 4. *X*-band powder ESR spectra of [Cu(oxae)Ni $(Me_2bpy)_2](ClO_4)_2$ at room temperature.

According to these models strict orbital orthogonality results in ferromagnetism. For the present complexes if the overall molecular symmetry is considered to be C_{2v}, the 3*d* orbitals of the copper(II) and nickel(II) ions transform as a_1 (d_{z^2} and $d_{x^2-y^2}$), a_2 (d_{yz}), b_1 (d_{xy}) and b_2 (d_{xz}).[14] Since there is no orthogonality between the *b* magnetic orbitals centred on the copper(II) and nickel(II) ions, an antiferromagnetic interaction should be observed.

ESR spectra

As shown in Fig. 4 the *X*-band powder ESR spectrum at room temperature for complex **2** only exhibits a large, broad and intense band centred at $g = 2.20$, which corresponds to the allowed $|1/2, -1/2\rangle \rightarrow |1/2, 1/2\rangle$ transition in the $S = 1/2$ ground state.

REFERENCES

1. R. D. Willett, D. Gatteschi and Kahn (Editors), *Magneto-Structural Correlation in Exchange-Coupled Systems*, pp. 523–554. NATO ASI Series, Reidel, Dordrecht, Holland (1985).
2. H. Ojima and K. Nonoyama, *Coord. Chem. Rev.* 1988, **92**, 85.
3. L. C. Li, D. Z. Liao and G. L. Wang, *Jiegou Huaxue, J. Struct. Chem.* 1991, **10**, 89.
4. D. Z. Liao, L. C. Li, Z. H. Jiang, S. P. Yan, P. Cheng and G. L. Wang, *Trans. Met. Chem.* 1992, **17**, 356.
5. D. Z. Liao, L. C. Li and G. L. Wang, *Polyhedron* 1991, **10**, 1785.
6. D. Z. Liao, B. Lin and G. L. Wang, *Acta Chim. Sin.* 1992, **50**, 269.
7. Z. M. Liu, Z. H. Jiang, D. Z. Liao, G. L. Wang, X. K. Yao and H. G. Wang, *Acta Chim. Sin.* 1991, **49**, 981.
8. Z. Y. Zhang, D. Z. Laio, Z. H. Jiang, S. Q. Hao, X. K. Yao, H. G. Wang and G. L. Wang, *Inorg. Chim. Acta* 1990, **173**, 201.
9. D. Z. Liao, Z. Y. Zhang and Z. H. Jiang, *Chem. J. Chin. Univ. (B)* 1990, **6**, 226.
10. Z. M. Liu, D. Z. Liao, Z. H. Jiang and G. L. Wang, *Synth. React Inorg. Met.-Org. Chem.* 1991, **21**, 289.
11. H. Ojima and K. Yamada, *Nippon Kaishi* 1968, **89**, 490.
12. W. J. Geary, *Coord. Chem. Rev.* 1971, **7**, 81.
13. M. R. Rosenthal, *J. Chem. Educ.* 1973, **50**, 331.
14. M. Badarau, M. Rerat, O. Kahn, J. Jaud and J. Galy, *Inorg. Chem.* 1982, **21**, 3050.
15. I. G. Dance, *Inorg. Chim. Acta* 1974, **9**, 77.
16. P. J. Hay, J. C. Thibeault and R. Hoffman, *J. Am. Chem. Soc.* 1975, **97**, 4884.
17. O. Kahn and M. F. Charlot, *Nouv. J. Chem.* 1980, **4**, 567.

Polyhedron Vol. 12, No. 12, pp. 1527–1532, 1993
Printed in Great Britain

0277–5387/93 $6.00+.00
© 1993 Pergamon Press Ltd

SYNTHESIS AND STRUCTURE OF $[Co_3(CO)_6(\mu_3\text{-}S)(\overline{COCH_2CH_2NH})(\mu\text{-}\eta^2\text{-}S\overline{COCH_2CH_2N})]$ CONTAINING A CARBENE LIGAND AND A BRIDGING BIDENTATE LIGAND

LIU QIWING, HU XIANG,* LIU SHUTANG, YAN HONG, WU BINFANG and JIN ZHENXING

Department of Chemistry, Inner Mongolia University, Huhhot, Inner Mongolia 010021, P.R.C.

and

SHI JIANQIU

Fujian Institute of Research on the Structure of Matter, Chinese Academy of Sciences, Fuzhou, Fujian 350002, P.R.C.

(*Received* 21 *December* 1992; *accepted* 18 *February* 1993)

Abstract—The reaction of $Co_2(CO)_8$ with the heterocyclic thioamide $S\overline{COCH_2CH_2NH}$ provided the synthesis of the chiral cluster $[Co_3(CO)_6(\mu_3\text{-}S)(\overline{COCH_2CH_2NH})(\mu\text{-}\eta^2\text{-}S\overline{COCH_2CH_2N})]$ (**1**), where $S\overline{COCH_2CH_2N}$ is a three-electron bridging bidentate ligand linked by nitrogen and sulphur to two cobalt atoms and $\overline{COCH_2CH_2NH}$ is a two-electron terminal carbene ligand linked by carbon to the third cobalt atom, as shown by X-ray structure analysis. The molecule has an almost perfect regular triangular-pyramidal Co_3S skeleton.

Heterocyclic thioamides, $S{=}\overline{CX(CH_2)_2NH}$ (where X = S, O, NH, etc.), have been shown to be the versatile reactants in the reactions of transition metal carbonyls giving the metal carbonyl cluster derivatives with a variety of new structures and bonding modes. This is due to the different fragments cleaved from heterocyclic thioamides (SAH) which can be linked to the metal cores by different coordination atoms and various shapes.

The interaction of SAH with triosmium clusters provided the syntheses of three new clusters containing the μ_2-η^1-SA, μ_3-1,3-η^2(S,N)-SA and μ_2-1,2-η^2(C,N)-A ligands, respectively (types 1, 2 and 3),[1] but the interaction of SAH with triruthenium yielded only the cluster product containing the μ_3-1,3-η^2(S,N)-SA ligand (type 2).[2] The reaction of SAH with triiron dodecarbonyl provided the synthesis of the cluster with a terminal carbene AH ligand (type 4).[3] The reaction of a linear thioamide with dicobalt octacarbonyl yielded a chiral cluster, $[Co_3(CO)_7(S)(\mu\text{-}SC(CH_3)NH)]$ (**2**), containing the bridging μ_2-1,3-η^2(S,N)SA ligand belonging to type 5.[4] In this paper we report that the reaction of SAH with dicobalt octacarbonyl provided syntheses of the cluster containing the μ_2-1,3-η^2(S,N)-SA ligand (type 5) and the cluster containing both AH and μ_2-1,3-η^2(S,N)-SA ligands (type 6).

All the structures of the new clusters are shown in Fig. 1.

The crystal and molecular structural determinations showed that the new chiral tricobalt sulphur carbonyl cluster $[Co_3(CO)_6(\mu_3\text{-}S)(\overline{COCH_2CH_2NH})(\mu\text{-}1,3\text{-}\eta^2\text{-}S\overline{COCH_2CH_2N})]$ (**1**) (type 6) contains a three-electron bridging bidentate $S\overline{COCH_2CH_2N}$(SA) ligand linked to the Co(1) and Co(3) atoms of the cluster by a cobalt–nitrogen and a cobalt–sulphur bond, respectively, and a two-electron terminal carbene $\overline{COCH_2CH_2NH}$ (AH) ligand linked to the Co(2) atom of the cluster by a

* Author to whom correspondence should be addressed.

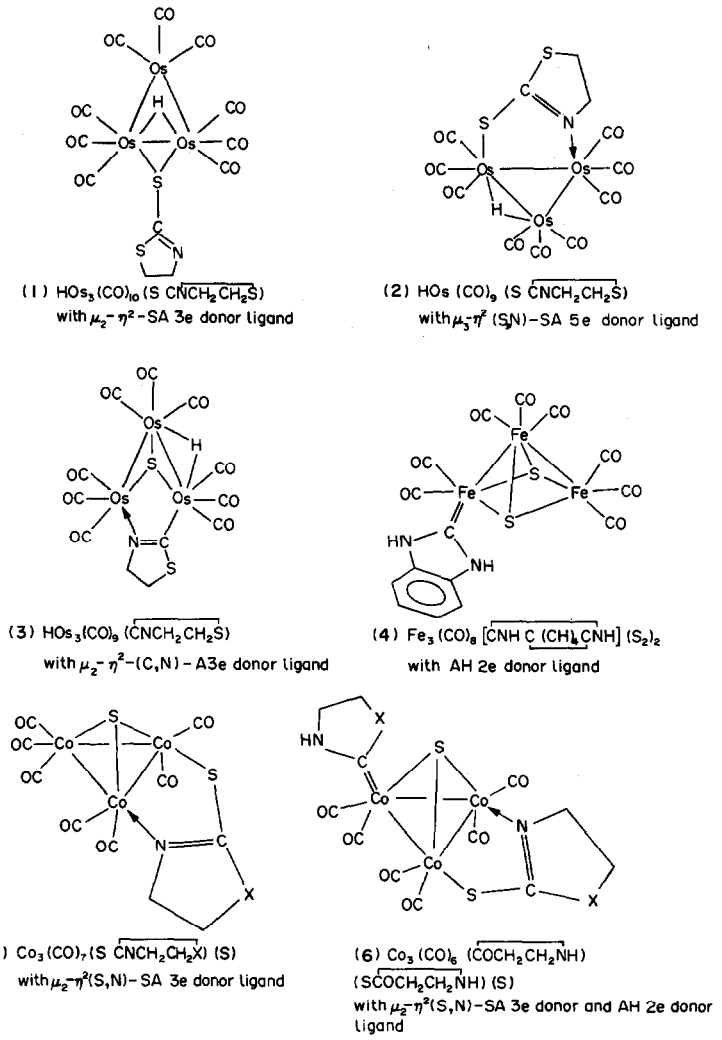

Fig. 1. The structures of trinuclear metal carbonyl clusters containing fragmental heterocyclic thioamides.

cobalt–carbon bond. We believe this is the first time that a trinuclear cobalt carbonyl cluster containing a terminal carbene ligand has been reported.

Herein we report the synthesis and structure of **1** and discuss the influence of the introduction of the bridging bidentate ligand and the terminal carbene ligand on the configuration change of the Co_3S cluster framework.

EXPERIMENTAL

Material and methods

Petroleum ether, THF and methylene chloride were dried by distillation with sodium-benzophenone and P_4O_{10}, respectively; $S\overline{COCH_2CH_2NH}$ was prepared by the literature method.[5] Dicobalt octacarbonyl was purchased and recrystallized from toluene as the solvent.

The synthetic reaction procedure was performed under a nitrogen atmosphere, using the Schlenk technique and degassed solvents. The IR spectrum was recorded on a Mattson Alpha–Centauri FTIR spectrophotometer in the range 1600–2200 cm^{-1} using CH_2Cl_2 as the solvent. ^1H NMR spectra were measured on a Varian FX-100 instrument using $CDCl_3$ as the solvent and TMS as the internal standard. Mass spectra were recorded on a Finigan MAT 711 instrument using the field dissociation method. Elemental analyses for carbon, hydrogen and nitrogen were conducted on an elemental analyser—Perkin–Elmer 240 C.

Table 1. Crystal and refinement data of **1**

Empirical formula	$C_{12}H_9N_2O_8S_2Co_3$
Formula weight	550.31
Crystal system	Orthorhombic
Lattice parameters	
a (Å)	19.256(4)
b (Å)	17.762(8)
c (Å)	10.996(3)
V (Å^3)	3761(4)
Space group	*Pbca*
Z	8
D_{calc} (g cm^{-3})	1.95
$F(000)$	2184
μ(Mo-K_α) (cm^{-1})	28.75
Diffractometer	Rigaku AFC5R
Radiation	Mo-K_α (λ = 0.71069 Å) Graphite-monochromated
Temperature (°C)	23
2θ (°)	50.0
Unique, $I \geqslant 3\sigma(I)$	1392
No. of variables	244
Residuals: R; Rw	0.057; 0.066
Goodness-of-fit indicator	1.31
Maximum shift in final cycle	0.004
Largest peak in final difference map (e Å^{-3})	0.76

Synthesis of $[Co_3(CO)_6(\mu_3\text{-}S)(\overline{COCH_2CH_2N})(\mu\text{-}S\overline{COCH_2CH_2N})]$ (**1**)

$Co_2(CO)_8$ (0.34 g, 1 mmol) and $S\overline{COCH_2CH_2NH}$ (0.20 g, 2 mmol) were dissolved in THF (10 cm^3). The solution was stirred for 24 h at 25°C and then evacuated to dryness. The resulting black residue was dissolved in CH_2Cl_2 and chromatographed on a silica gel column. The separation and crystallization yielded 0.04 g (yield 12%) of $[Co_3(CO)_7(\mu_3\text{-}S)(\mu\text{-}S\overline{COCH_2CH_2N})]$ from the first part of the eluant (petroleum ether: CH_2Cl_2 = 1 : 1) and 0.03 g (yield 8%) of $[Co_3(CO)_6(\mu_3\text{-}S)(\overline{COCH_2CH_2NH})(\mu\text{-}S\overline{COCH_2CH_2N})]$ (**1**) from the second part of the eluant (CH_2Cl_2). A dry sample of **1** was analysed. Found: C, 26.4; H, 1.9; N, 4.7. Calc. for $[C_{12}H_9N_2O_8S_2Co_3]$: C, 26.2; H, 1.6; N, 4.4%. IR data: ν(CO) (cm^{-1}): 2064(s), 2025(vs), 2003(s), 1972(w). ^{1}H NMR data, chemical shifts (ppm): 3.3 (t, 2H, NCH_2 of bridged ligand); 3.6 (t, 2H, NCH_2 of carbene ligand); 4.1 (t, 2H, OCH_2 of bridged ligand); 4.4 (t, 2H, OCH_2 of carbene ligand). Mass spectral data: m/z 550; calc. 550.31.

X-ray crystallography

The deep brownish block-shaped crystal (0.30 × 0.30 × 0.10 mm) was measured on a Rigaku AFC 5R diffractometer through graphite monochromated Mo-K_α radiation and diffraction data to $3° \leqslant 2\theta \leqslant 50°$ were collected in the θ–2θ scan mode. The 1392 unique reflections $[I \geqslant 3\sigma(I)]$ observed were obtained after correction of 3724 reflections for Lorentz, polarization and empirical absorption. The crystallographic data are given in Table 1.

Structure determination and refinement

All calculations were performed on a Micro VAX-II computer with the TEXSAN programs. At first the positions of a number of non-hydrogen atoms were obtained by direct methods from the electron density map. Then difference-Fourier syntheses were used to reveal the positions of all remaining non-hydrogen atoms. Final refinement was conducted through a full-matrix least-squares procedure with non-hydrogen atoms anisotropic and hydrogen atoms isotropic. Resulting R values were R = 0.057 and R_w = 0.066. The structure of **1** is shown in Fig. 2. The selected bond lengths and angles are listed in Table 2.

RESULTS AND DISCUSSION

Molecule **1** is formally derived from $Co_3(\mu_3\text{-}S)(CO)_9$ by replacing three terminal CO ligands with a three-electron donating bridging bidentate $S\overline{COCH_2CH_2N}$ ligand (nitrogen atom as a two-electron donor and sulphur as a one-electron

Table 2. Selected bond lengths (Å) and angles (°) for **1**

Co(1)—C(12)	1.81(2)	O(1)—C(1)	1.35(2)
Co(1)—C(11)	1.82(2)	O(1)—C(2)	1.46(2)
Co(1)—N(1)	1.98(1)	O(2)—C(4)	1.32(2)
Co(1)—S(1)	2.166(4)	O(2)—C(6)	1.46(2)
Co(1)—Co(3)	2.500(3)	O(11)—C(11)	1.13(2)
Co(1)—Co(2)	2.523(3)	O(12)—C(12)	1.13
Co(2)—C(13)	1.76(2)	O(13)—C(13)	1.18(2)
Co(2)—C(14)	1.82(2)	O(14)—C(14)	1.13(2)
Co(2)—C(4)	1.94(2)	O(15)—C(15)	1.11(2)
Co(2)—S(1)	2.173(5)	O(16)—C(16)	1.12(2)
Co(2)—Co(3)	2.499(3)	N(1)—C(1)	1.30(2)
Co(3)—C(16)	1.80(2)	N(1)—C(3)	1.45(2)
Co(3)—C(15)	1.82(2)	N(2)—C(4)	1.28(2)
Co(3)—S(1)	2.169(4)	N(2)—C(5)	1.46(2)
Co(3)—S(2)	2.299(4)	C(2)—C(3)	1.52(2)
S(2)—C(1)	1.71(2)	C(5)—C(6)	1.51(2)

C(12)—Co(1)—C(11)	101.0(7)	C(4)—Co(2)—Co(1)	101.0(5)
C(12)—Co(1)—N(1)	95.2(6)	S(1)—Co(2)—Co(3)	54.8(1)
C(12)—Co(1)—S(1)	149.4(5)	S(1)—Co(2)—Co(1)	54.3(1)
C(12)—Co(1)—Co(3)	99.3(5)	Co(3)—Co(2)—Co(1)	59.73(8)
C(12)—Co(1)—Co(2)	100.0(5)	C(16)—Co(3)—C(15)	101.4(8)
C(11)—Co(1)—N(1)	99.6(7)	C(16)—Co(3)—S(1)	101.5(6)
C(11)—Co(1)—S(1)	101.4(6)	C(16)—Co(3)—S(2)	100.1(6)
C(11)—Co(1)—Co(3)	155.4(5)	C(16)—Co(3)—Co(2)	101.8(6)
C(11)—Co(1)—Co(2)	103.0(6)	C(16)—Co(3)—Co(1)	155.3(6)
N(1)—Co(1)—S(1)	101.3(4)	C(15)—Co(3)—S(1)	146.5(5)
N(1)—Co(1)—Co(3)	92.2(3)	C(15)—Co(3)—S(2)	96.3(5)
N(1)—Co(1)—Co(2)	149.7(3)	C(15)—Co(3)—Co(2)	96.5(5)
S(1)—Co(1)—Co(3)	54.8(1)	C(15)—Co(3)—Co(1)	98.0(5)
S(1)—Co(1)—Co(2)	54.6(1)	S(1)—Co(3)—S(2)	103.4(2)
Co(3)—Co(1)—Co(2)	59.66(8)	S(1)—Co(3)—Co(2)	55.0(1)
C(13)—Co(2)—C(14)	101.9(9)	S(1)—Co(3)—Co(1)	54.7(1)
C(13)—Co(2)—C(4)	94.6(7)	S(2)—Co(3)—Co(2)	151.9(1)
C(13)—Co(2)—S(1)	145.5(5)	S(2)—Co(3)—Co(1)	92.9(1)
C(13)—Co(2)—Co(3)	96.2(5)	Co(2)—Co(3)—Co(1)	60.61(8)
C(13)—Co(2)—Co(1)	96.6(6)	Co(1)—S(1)—Co(3)	70.5(1)
C(14)—Co(2)—C(4)	96.1(7)	Co(1)—S(1)—Co(2)	71.1(1)
C(14)—Co(2)—S(1)	101.3(6)	Co(3)—S(1)—Co(2)	70.3(1)
C(14)—Co(2)—Co(3)	99.4(6)	C(1)—S(2)—Co(3)	102.4(6)
C(14)—Co(2)—Co(1)	153.7(6)	C(1)—O(1)—C(2)	108.0(1)
C(4)—Co(2)—S(1)	108.0(5)	C(4)—O(2)—C(6)	111.0(2)
C(14)—Co(2)—Co(3)	158.8(5)	C(1)—N(1)—C(3)	109.0(1)
C(1)—N(1)—Co(1)	124(1)	C(3)—N(1)—Co(1)	126(1)
C(4)—N(2)—C(5)	113(1)	N(1)—C(1)—O(1)	114(1)
N(1)—C(1)—S(2)	128(1)	O(1)—C(1)—S(2)	117(1)
O(1)—C(2)—C(3)	104(1)	N(1)—C(3)—C(2)	104(1)
N(2)—C(4)—O(2)	111(1)	N(2)—C(4)—Co(2)	123(1)
O(2)—C(4)—Co(2)	126(1)	N(2)—C(5)—C(6)	103(1)
O(2)—C(6)—C(5)	103(1)	O(11)—C(11)—Co(1)	179(2)
O(12)—C(12)—Co(1)	177(1)	O(13)—C(13)—Co(2)	178(2)
O(14)—C(14)—Co(2)	178(2)	O(15)—C(15)—Co(3)	179(2)
O(16)—C(16)—Co(3)	175(2)		

donor) and a two-electron donating carbene $\overline{COCH_2CH_2NH}$ ligand.

The three cobalt atoms form an almost equilateral triangle with Co—Co bond lengths = 2.499(3)–2.523(3) Å and average Co—Co—Co bond angles = 60°. The bond distances of diamagnetic species **1** are shorter than the paramagnetic parent cluster $Co_3S(CO)_9$ [mean value of the Co—Co bond length 2.637(3) Å],[6] which possesses an extra unpaired electron in delocalized anti-

Chart I Distance unit (Å)

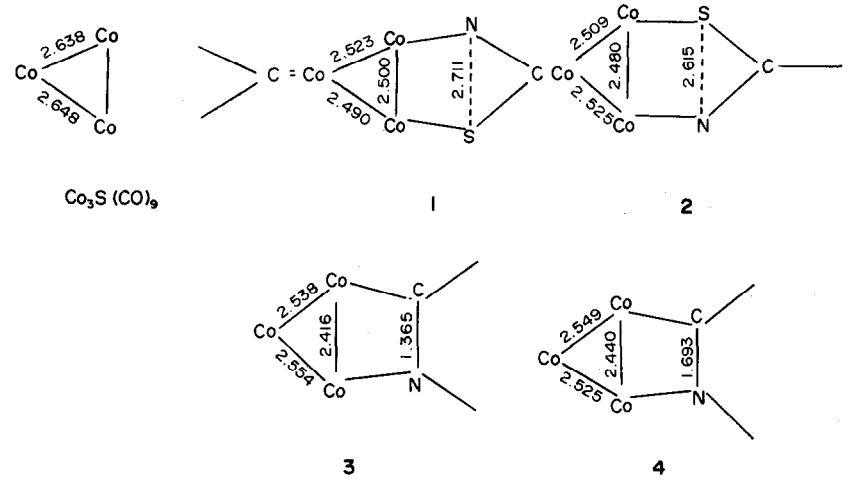

bonding orbitals. Benoit *et al.*[4] have discussed the compression effect in the bridging bidetate ligand-containing tricobalt sulphur carbonyl clusters and have shown that the bridged Co—Co edge is shorter than the other two Co—Co edges of the Co_3 triangle. Moreover, as shown below, modification of the geometrical constraint imposed by the bridge results in the progressive lengthening of the Co—Co bond as the "elongation effect" in $[Co_3(CO)_7(S)(\mu\text{-}CH_3C{=}NC_6H_{11})]$ (**3**) → $[Co_3(CO)_7(S)(\mu\text{-}CSNMe_2)]$ (**4**) → **2**. Comparison with the symmetrical cluster $Co_3S(CO)_9$ showed that significant modifications of the Co_3 core and Co_3S framework did appear in **3**, **4** and **2**.

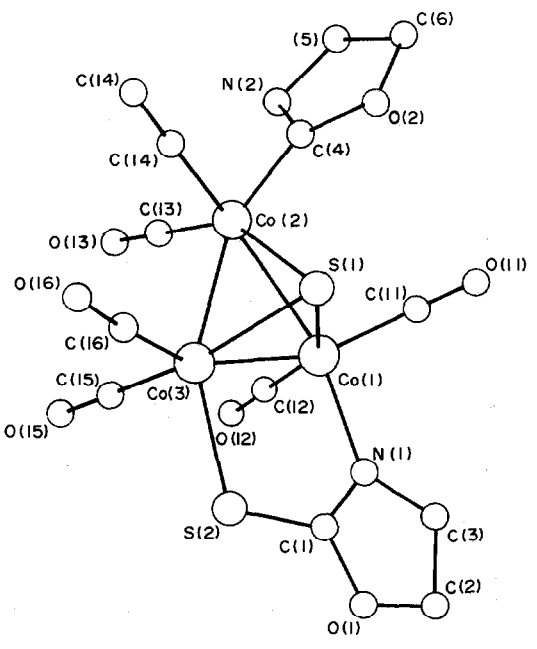

Fig. 2. Molecular structure of $[Co_3(CO)_6(\mu_3\text{-}S)(\overline{COCH_2CH_2NH})(\mu,\eta^2\text{-}S\overline{COCH_2CH_2N})]$.

The result on our tricobalt sulphur carbonyl cluster (**1**) is different. The compression effect of the bridged edge of the Co_3 triangle vanishes in **1** and the Co_3S framework of **1** is a regular triangular pyramid with the Co—S bond lengths = 2.166(4)–2.173(5) Å. This shows that the four electrons of the μ_3-S donor bond are almost equal to each of the Co_3 atoms. The big heterocyclic carbene ligand located in the vertex of the cobalt atom may play a counterpart role to the bridging bidentate ligand located in the opposite edge of two cobalt atoms to keep the Co_3 core remaining an equilateral triangle as a whole. The dihedral angle between the metallic triangle and the μ-$S\overline{COCH_2CH_2N}$ plane is 10.01°, C(1)—N(1) bond distance = 1.30(2) Å (in the range of carbon–nitrogen double bonds and the sp^2 hybridized C—N single bond length of 1.46 Å).[7] Bond angles around the C(1) and N(1) atoms (114–112°) and the total of the surrounding three bond angles (359°) clearly show the sp^2 character of the C(1) and N(1) atoms. The C(1)—S(2) bond length [1.71(2) Å] is closer to the value of a carbon–sulphur single bond than that of a carbon–sulphur double bond [1.741(2) vs 1.634(3) Å, respectively[8]]. All these characteristics of the ligand seem to favour the canonical formula **a** as a better representation of the electronic state of molecule **1** rather than the

alternative valence bond formulation such as **b**, suggested by Benoit *et al.*,[4] in which there is electron delocalization over the six atoms concerned because the S(1)—Co bond lengths (with the dashed lines) are significantly shorter than the S(1)—Co bond length (without the dashed line) of cluster **2**.

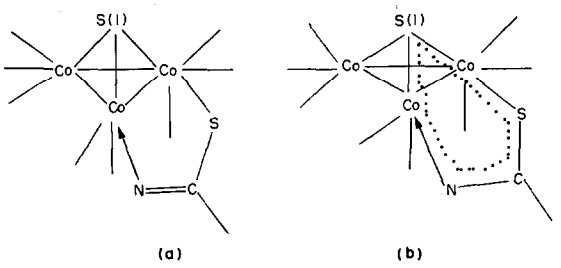

There is one two-electron donating heterocyclic carbene terminal $\overline{COCH_2CH_2NH}$ ligand in cluster **1**. The dihedral angle of the heterocyclic ring with the Co_3 plane is 76.16° and the heterocyclic ring acts as a carbene ligand to replace the axial carbonyl (according to the Co_3 plane) of the parent cluster $Co_3S(CO)_9$. The surrounding bond angles about C(4) [carbene] are 111(1)°, 123(1)° and 126(1)° and the total is 360°, which clearly shows the sp^2 character of the carbene. The Co(2)—C(4) distance [1.94(2) Å] corresponds to other cobalt stabilized bridging carbenes such as 1.953(3) Å in **3** and 1.958(5) Å in **4** are shorter than the Fe—C single bond average length of 2.151 Å[9] (the estimated single bond covalent radii of 1.165 and 1.162 Å for iron and cobalt, respectively, are virtually identical). Therefore, it has double bond character and stabilizes cluster **1**. However, we note that the Co(2)—C(4) distance observed must imply less double bond character than is present in the Co—CO bonds (average bond length 1.80 Å). The π-acceptor/σ-donor ratio is also significantly low for a carbene ligand where the neighbouring atoms are nitrogen and oxygen compared with CO. The shortest Co—CO bond of 1.76(2) Å, which is located in the *trans* position of the heterocyclic carbene ligand, once more clearly shows that the π-accepting ability is weak for this carbene ligand. The C(4)—N(2) and C(4)—O(2) bonds here have considerable double bond character, as indicated by their lengths of 1.28(2) and 1.32(2) Å, respectively (normal single bond lengths of sp^2 hybridized C—N and C—O are 1.46[7] and 1.43 Å,[10] respectively). The π-interaction between the carbene carbon and neighbouring nitrogen and oxygen atoms is another important factor in stabilizing cluster **1**.

The formulation and structure of **1** are consistent with experimental data obtained from elemental analysis, mass spectrometry, IR and ^1H NMR experiments. The IR spectrum in the carbonyl region has four bands with wave numbers of 1972–2064 cm^{-1}, which indicates the presence of only terminal COs. The wave numbers of ν(CO) of **1** were 25–61 cm^{-1} less than the values of $Co_3(S)(CO)_9$,[11] which provides further evidence that the π-accepting ability of the bridged $S\overline{COCH_2CH_2N}$ ligand and carbene $\overline{COCH_2CH_2NH}$ ligand of **1** is much weaker than the CO ligand.

Cluster **1** contains a Co_3 core and four kinds of ligands, namely μ_3-S, μ-$S\overline{COCH_2CH_2N}$, $\overline{COCH_2CH_2NH}$ and CO. The former three are fragments of the same reactant, heterocyclic thioamide SAH. This ligand precursor was cleaved to afford three kinds of fragments, namely S, SA and AH, during the reaction with $Co_2(CO)_8$ and all these fragments are linked to the same Co_3 core by the atoms carbon, nitrogen and sulphur (belonging to groups IVA, VA and VIA of the periodic table, respectively) and each coordinated atom locates in each Co of the Co_3 core. This is an interesting method of preparing a new type of metal carbonyl cluster derivative, by the cleavage of the reactant (ligand precursor) to obtain a variety of fragmental ligands in order to build the new cluster.

Supplementary material. The atomic coordinates and thermal parameters and a table of interatomic distances and angles have been deposited with the Editor, from whom copies are available on request. Atomic coordinates have also been deposited at the Cambridge Crystallographic Data Centre.

Acknowledgement—The project was supported by the Natural Science Foundation of China.

REFERENCES

1. A. M. Brodie, H. D. Holden, J. Lewis and M. J. Taylor, *J. Chem. Soc., Dalton Trans.* 1986, 633.
2. S. Jeannin, Y. Jeannin and G. Lavigne, *Inorg. Chem.* 1978, **17**, 2103.
3. Q. W. Liu, X. Hu, S. T. Liu, J. An and J. S. Huang, *Jiegou Huaxue* (*J. Struct. Chem.*) 1992, **11**, 104.
4. A. Benoit, A. Darchen, J. Y. Le Marouille, C. Mahé and H. Patin, *Organometallics* 1983, **2**, 555.
5. E. Tliger, *J. Am. Chem. Soc.* 1950, **72**, 4792.
6. C. H. Wei and L. F. Dahl, *Inorg. Chem.* 1967, **6**, 1229.
7. M. F. Lappert, P. L. Pye and G. M. McLaughlin, *J. Chem. Soc., Dalton Trans.* 1977, 1272.
8. H. Patin, G. Mignani, C. Mahé, J. Y. Le Marouille, A. Benoit and D. Grandjean, *J. Organomet. Chem.* 1980, **193**, 93.
9. F. A. Cotton and P. Lahuerta, *Inorg. Chem.* 1975, **14**, 116.
10. D. J. Cardin, B. Cetinkaya and M. F. Lappert, *Chem. Rev.* 1972, 545.
11. L. Marko and B. Marko, *Inorg. Chim. Acta* 1975, **14**, L39.

Polyhedron Vol. 12, No. 12, pp. 1533–1538, 1993
Printed in Great Britain

0277–5387/93 $6.00+.00
© 1993 Pergamon Press Ltd

THE SYNTHESIS AND CHARACTERIZATION OF CADMIUM AND ZINC COMPLEXES WITH DITHIOCARBAMATE DERIVATIVES OF DIAMINES

M. AZAD MALIK, TAHIR SAEED and PAUL O'BRIEN*

Department of Chemistry, Queen Mary and Westfield College, Mile End Road, London E1 4NS, U.K.

(*Received* 11 *December* 1992; *accepted* 8 *February* 1993)

Abstract—The synthesis and characterization of four new compounds, zinc or cadmium complexes with dithiocarbamates derived from N,N,N-trimethylethylenediamine or N,N,N-trimethylpropylinediamine as ligands are reported. Preliminary growth studies show that the cadmium complexes with N,N,N-trimethylpropylinediamine may be useful precursors for the deposition of the CdS, at temperatures as low as 350°C.

Thin films of cadmium sulphide have been used in solar cells,[1–6] light emitting diodes[7] and ultrasonic transducers.[8] A number of single-molecular precursors for the deposition of II/VI materials have been developed, including thiophosphinates,[9,10] thiocarbamates,[11,12] selenocarbamates,[13] thiolates,[14–16] bulky thiolates such as 2,4,6-tritertiarybutylphenylchalcogenides[15,16] and silicon-based systems [e.g. $M(ESi(SiCH_3)_3)_2$, M = Zn, Cd, Hg and E = Se, Te],[17] and alkyl-metal-thio/selenocarbamates.[18,19] We have recently reported the use of some mixed alkyl-dialkyldithiocarbamates of cadmium or zinc and the deposition of thin films of CdS or ZnS by metal organic chemical vapour deposition (MOCVD).[18] These compounds and the parent dithiocarbamates are in general dimers involving bridging sulphur atoms.[13,18]

In an attempt to improve the volatility of simple thiocarbamates we have developed thiocarbamates based on various diamines. These ligands have the potential to form additional coordinate linkages to the metal, via the nitrogen groups, which may influence both the degree and type of any aggregation and the strength of association between individual molecular units. In the present paper we report the synthesis and characterization of bistrimethylethylenediaminedithiocarbamatozinc(II) (**1**), bistrimethylethylenediaminedithiocarbamatocadmium(II) (**2**), bistrimethylpropylenediaminedithiocarbamatozinc(II) (**3**) and bistrimethylpropylenediaminedithiocarbamatocadmium(II) (**4**). Chalcogenide films have been deposited from **4** at temperatures as low as 350°C.

EXPERIMENTAL

All reagents were purchased from Aldrich Chemicals Ltd.

Physical measurements

IR spectra were recorded with a Mattson Polaris FT-IR spectrometer as Nujol mulls; ^{13}C and ^{1}H solution NMR were recorded with a Bruker AM 250 pulsed Fourier-transform NMR instruments; solid-state ^{13}C and ^{113}Cd NMR were recorded on a Bruker MSL-300 multinuclear instrument and mass spectra were recorded with a Kratos MS50 TC instrument. σ_1, σ_2 and σ_3 for ^{113}Cd NMR spectra were calculated using Herzselt and Berger's method.[20] Microanalyses were performed by the University College, London service, and EDAX was recorded with a JEOL 1200 EX II TEMSCAN electron microscope.

Synthesis of compounds **1** *and* **2**

A mixture of carbon disulphide (10 mmol) and N,N,N-trimethylethylenediamine (10 mmol) in water (20 cm^3) was stirred for 0.5 h at 5°C and then allowed to warm to room temperature. On addition of zinc nitrate (2.5 mmol) in water (10 cm^3) a white

* Author to whom correspondence should be addressed.

solid product was obtained. The product analysed as bistrimethylethylenediaminedithiocarbamatozinc (II) (**1**); yield 41%, m.p. 140°C. Found: C, 33.9; H, 6.1; N, 12.9; S, 33.0. Calc. for $C_{12}H_{26}N_4S_4Zn$: C, 34.4; H, 6.2; N, 13.4; S, 30.5%.

The cadmium complex (**2**) was prepared by the same method using cadmium nitrate; yield 46%, m.p. 143°C. Found: C, 29.6; H, 5.7; N, 11.2; S, 26.2. Calc. for $C_{12}H_{26}N_4S_4Cd$: C, 30.9; H, 5.6; N, 12.0; S, 27.5%.

Synthesis of compounds **3** *and* **4**

Carbon disulphide (10 mmol) was added to a stirred solution of N,N,N-trimethylpropylenediamine (TMPDA) (10 mmol) in water (20 cm^3) at 5°C for 30 min. The mixture was warmed to room temperature and a solution of zinc nitrate (2.5 mmol) in water (10 cm^3) was added. A white solid product analysed as bistrimethylpropylenediaminedithiocarbamatozinc(II) (**3**) was obtained; yield 60%, m.p. 102°C. Found: C, 36.4; H, 6.9; N, 11.8; S, 27.3. Calc. for $C_{14}H_{30}N_4S_4Zn$: C, 37.6; H, 6.7; N, 12.6; S, 28.2%.

The cadmium complex (**4**) was prepared by the same method using cadmium nitrate; yield 60%, m.p. 131°C. Found: C, 33.7; H, 5.9; N, 10.9; S, 25.7. Calc. for $C_{14}H_{30}N_4S_4Cd$: C, 34.0; H, 6.07; N, 11.3; S, 25.2%.

All four compounds have been characterized by NMR and IR spectroscopies. Compounds **3** and **4** were additionally characterized by mass spectrometry.

$Zn[S_2CNCH_3(CH_2)_3N(CH_3)_2]_2$ (**1**). ^{13}C NMR (solid state), δ (ppm): 205.97 (CS_2), 44.42 (NCH_3), 45.11 (NCH_3), 49.199 (NCH_3), 55.263 (CH_2N), 58.413 (NCH_2). IR (cm^{-1}), major bands and assignments are: 455 (M—S), 993 (C—S), 1462 (C=N).

$Cd[S_2CNCH_3(CH_2)_2N(CH_3)_2]_2$ (**2**). ^{13}C NMR (solid state), δ (ppm): 205.82 (CS_2), 45.21 (NCH_3), 45.82 (NCH_3), 49.35 (NCH_3), 54.15 (CH_2N), 58.53 (NCH_2). IR (cm^{-1}), major bands and assignments are: 433 (M—S), 1008 (C—S), 1465 (C=N).

$Zn[S_2CNCH_3(CH_2)_3N(CH_3)_2]_2$ (**3**). ^1H NMR solution ($[^2H_6]$ $CHCl_3$, 250 MHz), δ (ppm): 1.97 [(4H, t, ^3J(H—H) = 7.5 Hz), (CH_2—CH_2—CH_2)], 2.35 [12H, s, $N(CH_3)_2$], 2.41 [(4H, t, ^3J (H—H) = 7.5 Hz), (CH_2—CH_2N)], 3.44 (6H, s, NCH_3), 3.91 [(4H, t, ^3J(H—H) = 7.5 Hz), (NCH_2—CH_2)]. ^{13}C NMR ($[^2H_6]C_6H_6$, 250 MHz), δ (ppm): 204.38 (CS_2), 24.98 (—NCH_3), 42.83 (CH_2—CH_2—CH_2), 45.94 $N(CH_3)_2$, 55.50 (CH_2—CH_2N), 57.09 (NCH_2—CH_2). IR (cm^{-1}), major bands and assignments are: 424 (M—S), 989 (C—S), 1461 (C=N). Mass spectrum (m/z): base peak 58.1 (100%) $[CH_2N(CH_3)_2]$; other peaks at 44.1 (20.7%) $[N(CH_3)_2]$, 88 (28.8%) $[CH_2N(CH_3)_2]$, 111.1 (10.8%) $[CH_3(CH_2)_3N(CH_3)_2]$, 159.1 (30.1%) (CH_3ZnCS_2).

$Cd[S_2CNCH_3(CH_2)_3N(CH_3)_2]_2$ (**4**). ^1H NMR solution ($[^2H_6]$ $CHCl_3$, 250 MHz), δ (ppm): 2.10 [(4H, t, ^3J(H—H) = 7.3 Hz), (CH_2—CH_2—CH_2)], 2.41 [12H, s, $N(CH_3)_2$], 2.52 [(4H, t, ^3J (H—H) = 7.4 Hz), (CH_2—CH_2N)], 3.46 (6H, s, NCH_3), 3.95 [(4H, t, ^3J(H—H) = 7.5 Hz), (NCH_2—CH_2)]. ^{13}C NMR ($[^2H_6]C_6H_6$, 250 MHz), δ (ppm): 205.71 (CS_2), 25.22 (—NCH_3), 44.29 (CH_2—CH_2—CH_2), 46.24 $N(CH_3)_2$, 56.96 (CH_2—CH_2N), 57.47 (NCH_2—CH_2). ^{113}Cd NMR (solution state): singlet at δ 298 ppm. IR (cm^{-1}), major bands and assignments are: 420 (M—S), 917 (C—S), 1461 (C=N). Mass spectrum (m/z): base peak 58.1 (100%) $[CH_2N(CH_3)_2]$; other peaks at 44.1 (45.4%) $[N(CH_3)_2]$, 88 (45.1%) $[CH_2N(CH_3)_2]$, 111.1 (7.9%) $[CH_3(CH_2)_3N(CH_3)_2]$, 159 (54.8%) $[CS_2CH_3N(CH_2)_3N]$.

Deposition of thin films

Cadmium sulphide or zinc sulphide thin films were deposited onto glass microscope slides or GaAs by chemical vapour deposition using compounds **3** or **4**, respectively. Samples (50 mg) were placed at one end of a Schlenk tube placed in a horizontal tube furnace. Glass slides were placed at the centre of the furnace. The tube was continuously pumped and a pressure of *ca* 10^{-2} Torr was maintained in the reactor. Cadmium sulphide thin film depositions were performed in the furnace at 350°C, whereas for zinc sulphide thin films the furnace temperature was 450°C. The precursor itself was located slightly outside the furnace and, therefore, was at a somewhat lower temperature than that of the furnace; thin specular films were obtained relatively rapidly, in *ca* 20 min. The films were characterized by elemental detection by analytical X-rays (EDAX) using electron microscopy and reflection high energy electron diffraction (RHEED) for CdS on GaAs.

DISCUSSION

Compounds **1** and **2** are insoluble, presumably polymeric materials, and **3** and **4** are microcrystalline solids soluble in toluene and benzene. Repeated attempts to obtain suitable samples of any of these compounds for single crystal X-ray diffraction studies were unsuccessful. Compounds **1** and **2** are intractable solids; however, the IR spectra of these compounds contain bands at 455, 993 and 1462 cm^{-1}, typical of coordinated thiocarbamate functions.[21] Vibrations due to M—N

bonding probably occur at too low an energy to be measured other than with specialized equipment ($<200\ cm^{-1}$).[22] The solid-state ^{13}C NMR spectra of both **1** and **2** have clear six-line spectra (Fig. 1). The CS_2 carbon appears at the lowest field, while the other five signals appear close to each other at higher field. The $N(CH_3)_2$ carbons give two overlapping signals, probably indicating a non-equivalance in the solid state. The ^{113}Cd solid-state NMR spectrum of **2** indicates the presence of two discrete cadmium centres (δ 289 and δ 278 trace impurities); this may be a similar phenomenon to the two cadmium sites observed for the powder form of bis(2-mercaptobenzothiazolato)cadmium(II).[23] The chemical shift δ 289 ppm probably indicates that cadmium is in a similar environment to that in bis(5-mercapto-1-methyltetrazolato)cadmium(II), δ 274 ppm, or bis(pyrolidinedithiocarbamato)cadmium(II), δ 280 ppm.[23] All three different σ-values suggest low symmetry and analysis of the spinning side band for the principal cadmium resonance leads to an anisotropy parameter of 0.40 and may suggest S_4CdN coordination with distorted trigonal bipyramidal coordination (see Table 1 for data).

Compounds **3** and **4** show similar bands in the IR spectra, confirming coordination of the thiocarbamate functionality.[21] Unlike **1** and **2** these compounds could be further purified by recrystallization to give good elemental analyses. These compounds have been characterized by ^1H and ^{13}C NMR spectroscopies in solution (see the Experimental). Both compounds **3** and **4** give similar ^1H NMR spectra. The α- and γ-methylene protons give triplets due to coupling with β-methylene protons with similar coupling constants. The β-methylene protons appear as a quintet at higher field through coupling with four equivalent neighbouring methylene protons. The $N(CH_3)_2$ and $N(CH_3)$ protons give singlets for both **3** and **4**, with the expected 2 : 1 intensity ratio. The chemical shifts for the cadmium compound are at lower field, for all protons, as compared to the corresponding zinc compound. The ^{13}C NMR of both compounds show the expected six-line spectra. The ^{113}Cd solid-state NMR spectrum of **4** shows a single line at δ 291 ppm, with no evidence for quadrupolar coupling to nitrogen (Fig. 2). The greater purity of **4** is not surprising as it was relatively easy to recrystallize the compound. The chemical shift δ 291 ppm is similar to that for **2** and indicates a similar cadmium environment; an analysis of the spinning side bands leads to anisotropy parameters similar to **2** and suggests a similar coordination sphere. The ^{113}Cd solution state NMR spectrum gives a singlet at δ 298 ppm, which shows that the cadmium maintains

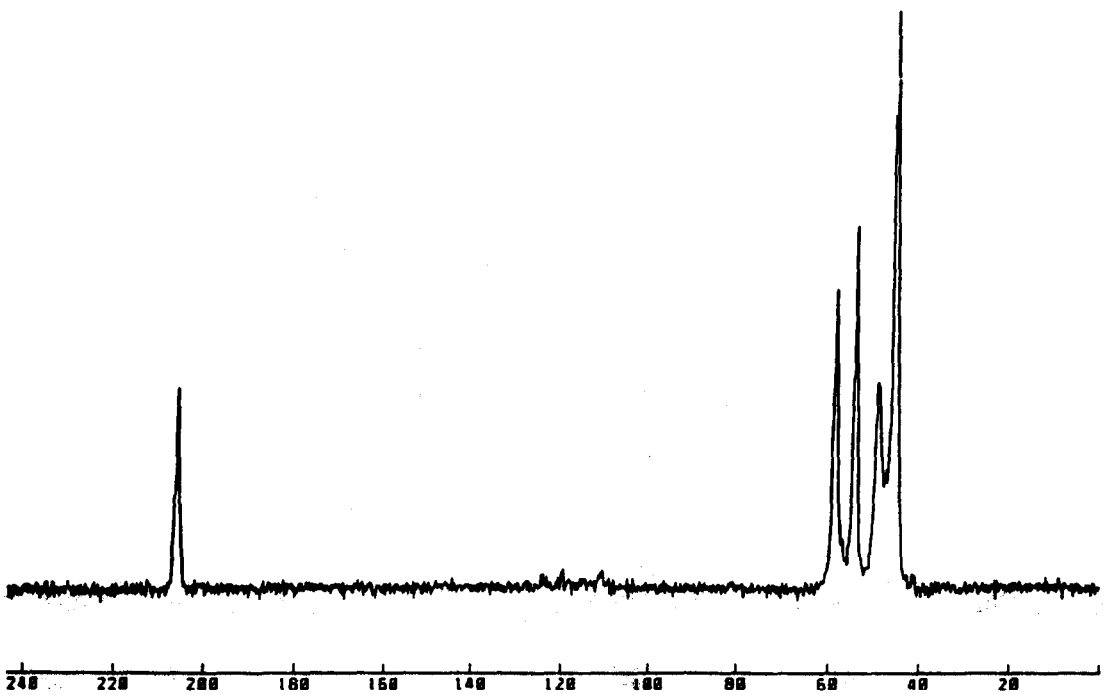

Fig. 1. ^{13}C NMR spectrum (solid state) of bis(trimethylethylenediaminedithiocarbamato)-cadmium(II) (**2**).

Table 1. Summary of solid-state ^{113}Cd NMR results

Compound coordination	δ(ppm)	σ_1	σ_2	σ_3
Bistrimethylethylene–CdS_4N (distorted diaminedithiocarbamato–trigonalbipyramid)-cadmium (**2**)	289	53	188	626
(impurity *ca* 5%)	276			
Bistrimethylpropylene–CdS_4N (distorted diaminedithiocarbamato–trigonalbipyramid)-cadmium (**4**)	291	40	203	631

a similar coordination environment in solution to that in the solid state.

The X-ray crystal structure of a related compound, $MeCdS_2CN(Me)(CH_2)_3N(Me)_2$, has been determined recently,[24] which may provide some idea of the bonding of the thiocarbamate group in **3** and **4**. In $MeCdS_2CN(Me)(CH_2)_3N(Me)_2$ the ligand bridges between adjacent cadmiums, giving a polymeric structure with CS_2N coordination at each cadmium centre. Given the similarity between the dimeric structures of metal bisthiocarbamates and mixed-alkyl complexes, such as $[MeMSCNEt_2]_2$ (MS_5 and MCS_3, respectively), it seems likely that compounds **3** and **4** have weakly bonded polymeric structures based on CdS_4N coordination.

Growth work

Compounds **3** and **4** have been successfully used to deposit thin films of metal sulphide on glass slides and GaAs by low-pressure metal organic chemical vapour deposition (MOCVD); some of the conditions and observations are summarized in Table 2. The 1 : 1 composition of CdS in the films have been confirmed by analytical X-ray (EDAX) measurements in the electron microscope. CdS films are polycrystalline with *ca* 10 micron crystallites.

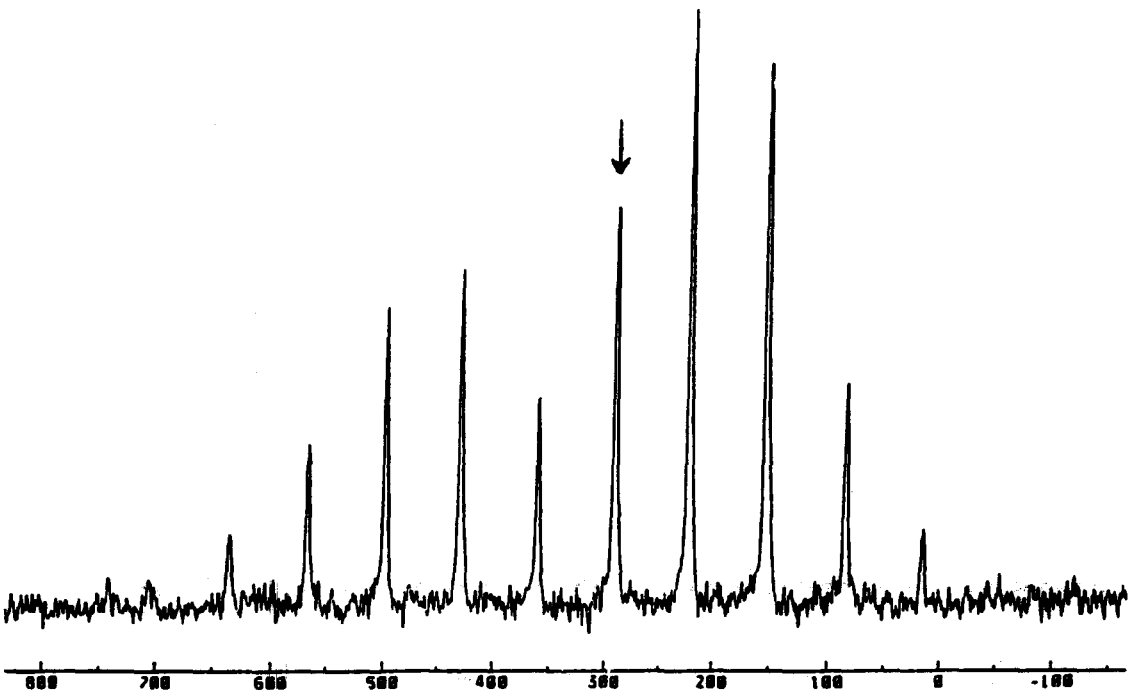

Fig. 2. ^{113}Cd NMR spectrum (solid state) of bis(trimethylpropylenediaminedithiocarbamato)-cadmium(II) (**4**).

Table 2. Summary of growth results using a hot wall LP-MOCVD apparatus

Compound	Film	Time (min)	Temperature (°C)	Substrate	Comments
3	ZnS	20	450	Glass	Poor morphology and uneven film thickness
	ZnS	20	425	Glass	Cloudy films
	ZnS	20	400	Glass GaAs	Very thin layers on GaAs substrate
4	CdS	20	400	Glass GaAs	Thick and even growth on both substrates
	CdS	20	375	Glass GaAs	Good even growth on glass and GaAs
	CdS	20	350	Glass GaAs	Thin even layers on both substrates
	CdS	20	325	Glass GaAs	Good specular layer on GaAs substrate

In the apparatus used in the present study deposition from the parent diethyldithiocarbamates was not observed at temperatures <400°C (20 min).

Both CdS and ZnS films were specular and adherent; their band gaps were 2.43 (lit. 2.425 eV)[25] and 3.57 eV (lit. 3.65 eV),[25] respectively. Compound **4** gave good even films on glass and GaAs substrates at temperatures as low as 325°C in 20 min. Using the present apparatus no deposition was observed from the parent diethydithiocarbamate in 20 min at temperatures less than 400°C,[12] indicating substantial advantages for the present compounds as a precursor. The film thickness appeared to decrease with temperatures (400–325°C) for a constant 20 min growth period.

The quality, as judged by reflectivity, of ZnS films grown from **3** (>400°C) was not better than that of equivalent films grown from zinc-diethyldithiocarbamate.[12] The films appeared cloudy with uneven thickness and lower growth rates.

CONCLUSIONS

Preliminary growth studies with these complexes indicate that better quality films of CdS can be obtained at a higher rate using bistrimethylpropylenediaminedithiocarbamatocadmium(II) as a precursor than those obtained with the parent diethyldithiocarbamate. The corresponding zinc derivative gave poorer quality films and only at higher temperatures; the overall performance of the zinc complex as a precursor is not substantially better than the parent bisdiethyldithiocarbamatozinc(II).

Acknowledgements—We thank the SERC for a grant to Paul O'Brien, Dr P Barrie of the ULIRS solid-state NMR service at University College, London, for recording the solid-state NMR spectra and assistance in their interpretation.

REFERENCES

1. H. Gerischer, *J. Electroanal. Interfac. Electrochem.* 1975, **58**, 263.
2. A. B. Ellis, S. W. Kaiser, J. M. Bolts and M. S. Wrighton, *J. Am. Chem. Soc.* 1977, **99**, 2839.
3. J. Masson, G. Hodes and D. Cahen, *J. Electrochem. Soc.* 1977, **124**, 532.
4. H. Minoura, T. Watanabe, T. Oki and M. Tsuiki, *J. Appl. Phys.* 1977, **16**, 865.
5. H. Minoura, M. Tsuiki and T. Oki, *Ber. Bunsenges. Physik. Chem.* 1977, **81**, 558.
6. M. Tsuiki, H. Minoura, T. Nakamura and Y. Ueno, *J. Appl. Electrochem.* 1978, **8**, 523.
7. H. Katayama, S. Oda and H. Kukimoto, *Appl. Phys. Lett.* 1975, **27**, 697.
8. H. J. Rohde, *Thin Solid Films* 1983, **100**, L125.
9. Y. Takahasi, R. Yuki, M. Motojima and K. Sugiyama, *J. Cryst. Growth* 1980, **50**, 491.
10. M. A. H. Evans and J. O. Williams, *Thin Solid Films* 1982, **87**, L1.
11. A. Saunders, A. Vecht and G. Tyrrell, Ternary Multinary Compound Proceedings, 7th International Conference 1986 (publ. 1987). (*Chem. Abstr.* 1988, **108**, 66226h).
12. D. M. Frigo, O. F. Z. Khan and P. O'Brien, *J. Cryst. Growth* 1989, **96**, 989.
13. M. B. Hursthouse, M. A. Malik, M. Motevalli and P. O'Brien, *Polyhedron* 1992, **11**, 45.
14. K. Osaka and T. Yamamoto, *Inorg. Chem.* 1991, **30**, 2328.
15. M. Bochman, K. Webb, M. Harman and M. B. Hursthouse, *Angew. Chem., Int. Edn Engl.* 1990, **29**, 638.

16. M. Bochman, K. Webb, M. B. Hursthouse and M. Mazid, *J. Chem. Soc., Dalton Trans.* 1991, 2317.
17. B. O. Dabbousi, P. J. Bonasia and J. Arnold, *J. Am. Chem. Soc.* 1991, **113**, 3186.
18. M. B. Hursthouse, M. A. Malik, M. Motevalli and P. O'Brien, *Organometallics* 1991, **10**, 730.
19. M. A. Malik and P. O'Brien, *Mater. Chem.* 1991, **3**, 999.
20. J. Herzselt and A. E. Berger, *J. Chem. Phys.* 1980, **73**, 6021.
21. D. Oktavec, E. Beinrour, B. Siles, J. Slefanec and J. Garaj, *Coll. Czech. Chem. Commun.* 1980, **45**, 1495.
22. K. Krishnan and R. A. Plane, *Inorg. Chem.* 1966, **5**, 852.
23. O. F. Z. Khan and P. O'Brien, *Polyhedron* 1991, **10**, 325.
24. M. A. Malik, T. Saeed and P. O'Brien, unpublished results, December 1991.
25. M. Kamiyama and E. Sugata, *Handbook for Thin Layer Engineering*. Ohm, Tokyo (1970).

Polyhedron Vol. 12, No. 12, pp. 1539–1543, 1993
Printed in Great Britain

0277–5387/93 $6.00+.00
© 1993 Pergamon Press Ltd

ELECTRON PARAMAGNETIC RESONANCE AND OPTICAL ABSORPTION SPECTRA OF MANGANESE(II) IONS IN LEAD ACETATE GLASSES

A. VENKATASUBBAIAH, J. LAKSHMANA RAO* and S. V. J. LAKSHMAN

Department of Physics, S.V. University, Tirupati 517 502, India

and

B. SREEDHAR

School of Physics, University of Hyderabad, Hyderabad 500 134, India

(*Received* 27 *August* 1992; *accepted* 8 *February* 1993)

Abstract—EPR and optical absorption studies have been made on lead acetate glasses containing 1–10 mol% $MnSO_4 \cdot H_2O$. The EPR spectra of Mn^{2+} ion-doped lead acetate glasses exhibit a sextet centred at $g = 2.02$. Remarkable changes have been observed in the EPR spectrum with changes in temperature, particularly at the glass transition temperature ($T_g = 317$ K). The optical absorption spectrum at room temperature shows five bands characteristic of Mn^{2+} ions in an octahedral symmetry. The crystal field parameter (Dq) and the Racah interelectronic repulsion parameters (B and C) have been evaluated. EPR and optical absorption studies reveal that the site symmetry around the transition metal ion is octahedral.

Interest in the research in common glasses and other less-common non-crystalline solids containing transition metal ions has grown in recent years, because of their potential use as optical fibres and efficient laser hosts. EPR and optical absorption spectra of transition metal ions in glasses have made it possible not only to interpret the energy levels involved in the observed transitions, but also to comment on the chemical and structural environment about the metal ion centre.

Glass-forming molten acetates have been studied extensively as these provide a bridge between essentially polymeric and ionic systems.[1] These glasses can be prepared over a wide range of glass compositions and these embrace cations of widely different chemistries.[2] This range includes (1) single component systems, e.g. LiOAc or $Pb(OAc)_2$; and (2) various mixtures, e.g. KOAc–$Ca(OAc)_2$ and KOAc–$Pb(OAc)_2$. Of particular interest to us is the lead acetate glass, because its glass transition temperature (T_g) lies within the range of the EPR measurements at different temperatures (123–423 K).

In the present investigation we describe the results of EPR and optical absorption spectra of Mn^{2+} ions in lead acetate glasses through the glass transition temperature (T_g).

EXPERIMENTAL

Glasses were prepared by melting appropriate amounts of Analar grade lead acetate with $MnSO_4 \cdot H_2O$ in an electric furnace at a temperature 50 K higher than that of the liquid. The melt was then quenched between two porcelain plates.

EPR spectra were recorded at 300 K at 9.205 GHz on a JEOL FE1X EPR spectrometer with a magnetic field modulation of 100 KHz. The magnetic field was scanned between 2250 and 4250 G. The EPR spectra were also recorded at different temperatures (123–423 K). The temperature was varied using a JES-VT-1A variable-temperature controller capable of regulating the temperature

* Author to whom correspondence should be addressed.

from 523 to 103 K. A temperature stability of ± 1 K was easily obtained by waiting for half an hour at the set temperature before recording the spectrum.

Optical absorption spectra were recorded using a Perkin–Elmer 551 spectrophotometer in the wavelength region 250–650 nm at 300 K. The wave number accuracy for sharp bands is ± 5 cm^{-1}.

RESULTS AND DISCUSSION

In undoped glasses no EPR signal is detected. When Mn^{2+} ions are introduced into the lead acetate glasses, all investigated samples exhibit absorption lines. Figure 1 shows the EPR spectrum of Mn^{2+} ions in lead actate glasses at 300 K. The spectrum shows the characteristic six-line hyperfine splitting spectrum centred at $g = 2.02 \pm 0.02$. There is also a relatively weak absorption centred at $g = 4.3 \pm 0.2$.

EPR spectra at different temperatures (123–423 K) were also recorded to study the temperature dependence of the intensity of the resonance line at $g = 2.02$. The intensity of the resonance line at $g = 2.02$ decreased gradually with increases in the temperature from 123 K, in proportion to the Boltzmann factor. A marked difference in the intensity of the resonance line at $g = 2.02$ was observed as the glass transition temperature was approached. The decrease in the intensity of the transition became more rapid at $T \sim T_g$ and the sextet almost disappeared leaving behind a single broad line. EPR spectra at different temperatures are shown in Fig. 2. From Fig. 2 it is clear that the intensity of the resonance line at $g = 2.02$ decreased with increases in temperature. The observed intensity of the resonance line at $g = 2.02$ at different temperatures is compared to the Boltzmann factor, i.e. $1/T$, and is shown in Fig. 3. For a derivative spectrum the measurement associated with the area under the absorption curve (i.e. intensity) is the peak-to-peak height $\times$ width^2.

The optical absorption spectrum measured at room temperature (300 K) for Mn^{2+} ions (10 mol %) in lead acetate glass is shown in Fig. 4. From the position and the number of observed bands the authors assumed Mn^{2+} ions in an octahedral symmetry. The optical absorption spectrum at 300 K consists of five bands centred at 17,235, 19,450, 24,445, 26,660 and 27,624 cm^{-1} and they are denoted as A, B, C, D and E, respectively. The bands C and E are sharp, whereas bands A and B are broad and band D is moderately sharp. Among the sharp bands band C is very sharp. When the number of t_{2g} electrons is the same in both the ground and excited states the energy expressions for the transitions are independent of Dq and the ligand field bands appear to be sharp.[3] The sharp band C is, therefore, assigned to the transition $^6A_{1g}(S) \rightarrow {}^4A_{1g}(G)$; $^4E_g(G)$ as the energy expression is independent of Dq. The broad bands A and B are assigned to the transitions $^6A_{1g}(S) \rightarrow {}^4T_{1g}(G)$ and $^6A_{1g}(S) \rightarrow {}^4T_{2g}(G)$, respectively. The bands at D and E are assigned to the transitions $^6A_{1g}(S) \rightarrow {}^4T_{2g}(D)$ and $^6A_{1g}(S) \rightarrow {}^4E_g(D)$, respectively.

The EPR spectrum of Mn^{2+} ions in glasses are characterized by an intense resonance at $g = 2.0$ with a hyperfine structure, an absorption at $g = 4.3$ and a distinct shoulder at $g = 3.3$[4].

The EPR spectra of manganese obtained for lead

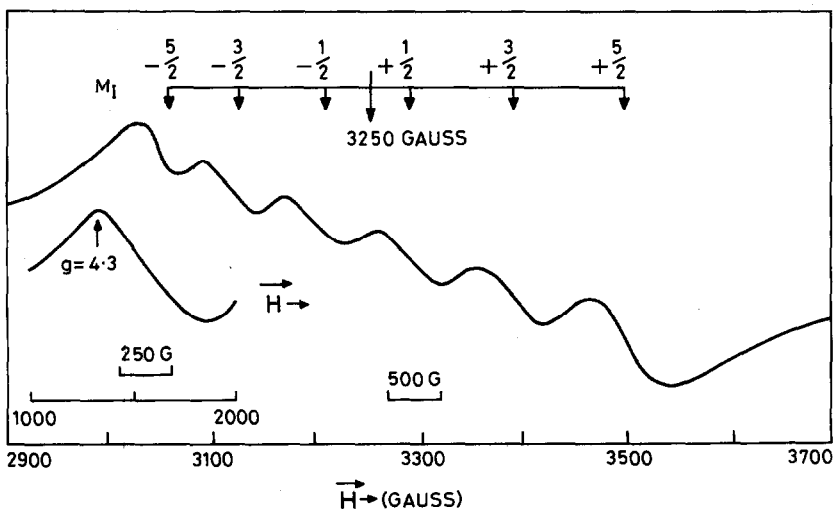

Fig. 1. EPR spectrum of Mn^{2+} ions in lead acetate glass at 300 K.

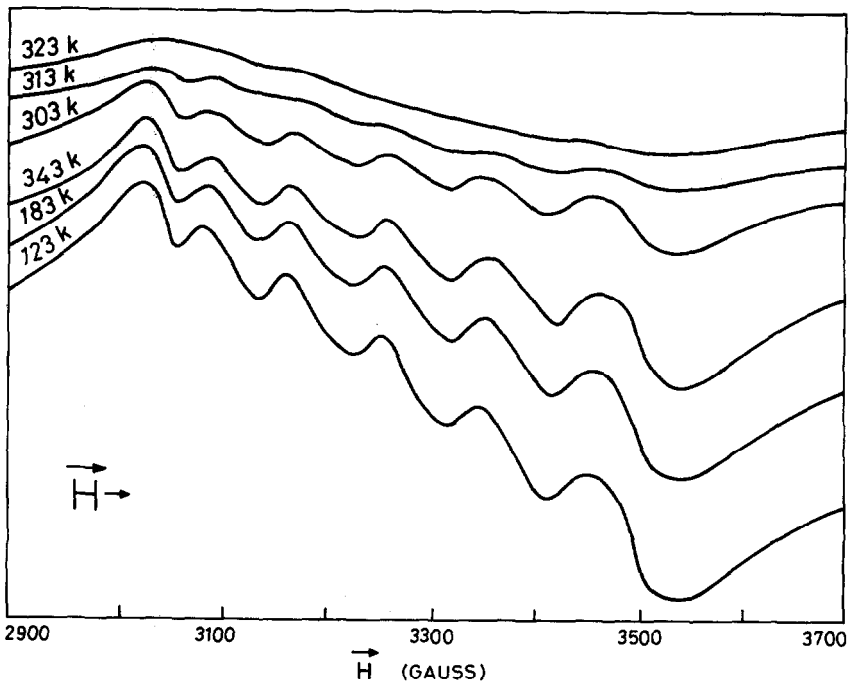

Fig. 2. EPR spectrum of Mn^{2+} ions in lead acetate glass at different temperatures.

acetate glasses are qualitatively very similar to those reported for Mn^{2+} ions in various glasses.[4-11] Due to this similarity one may conclude that Mn^{2+} ions are responsible for the EPR spectra.

The EPR spectrum comprising a sextet is analysed using the following expression for resonant fields:

$$H_m = H_0 - A_0 m - A_0^2(35-4m^2)/8H_0$$

where $H_0 = h\nu/g_0\beta$ and $m = -5/2, -3/2, \ldots +5/2$; g_0 is the isotropic g factor and A is the isotropic interaction parameter. The isotropic sig-

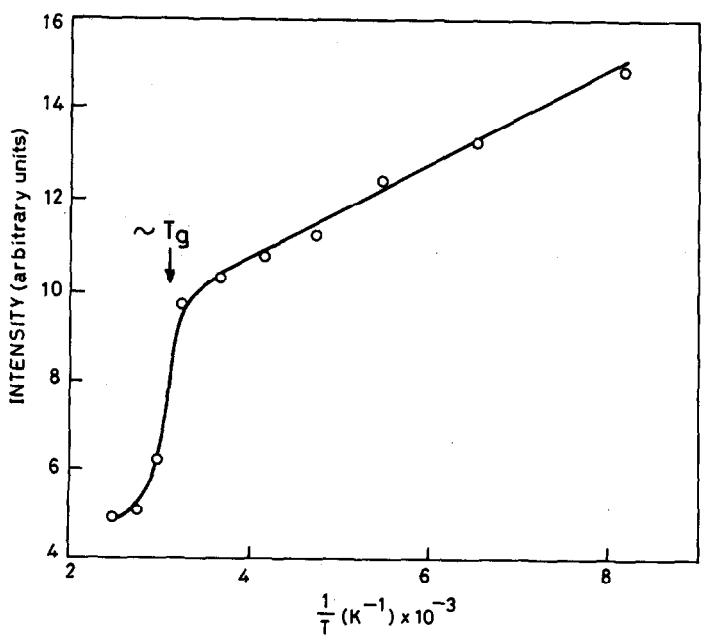

Fig. 3. Temperature dependence of the intensity of the resonance line at $g = 2.02$ at different temperatures is compared to the Boltzmann factor, i.e. $1/T$.

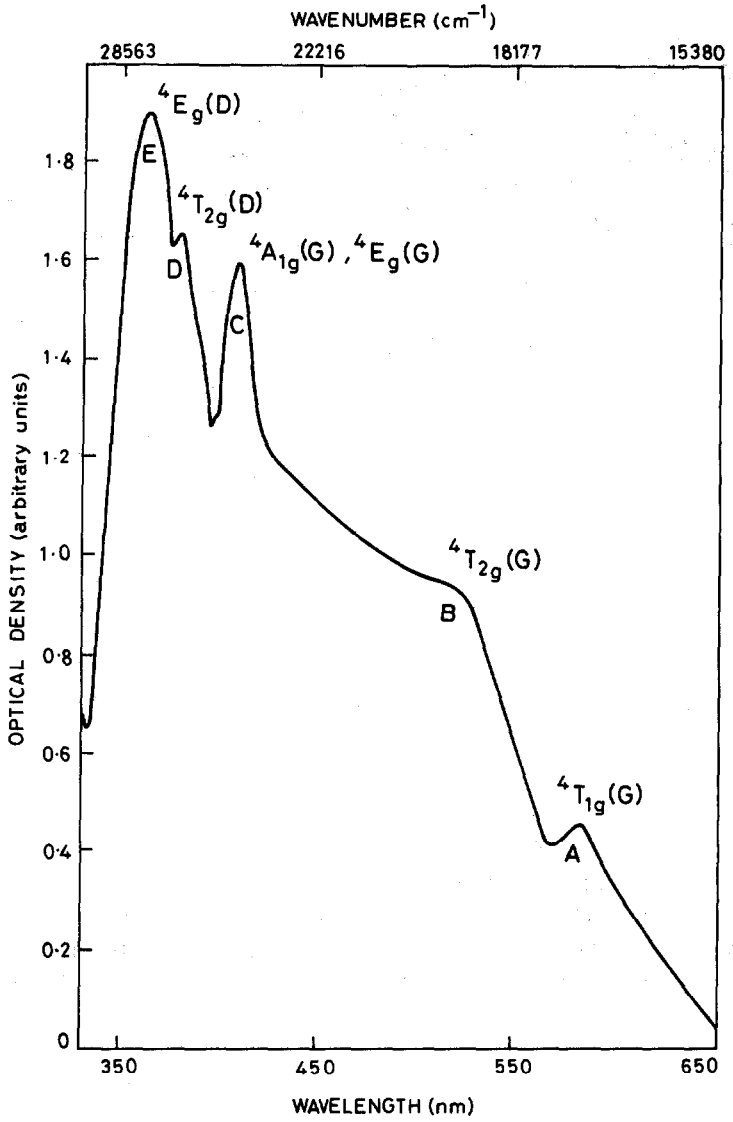

Fig. 4. Optical absorption spectrum of 10 mol % Mn^{2+} ions in lead acetate glass at room temperature (300 K).

nal at $g = 2.02$ is due to Mn^{2+} ions in an environment close to octahedral symmetry. The value of $A = 90$ G is consistent with Mn^{2+} ions in an octahedral coordination.[10,12–15]

The magnitude of the hyperfine splitting constant A provides a measure of covalency between the Mn^{2+} ion and its ligands. Van Wieringer[16] empirically determined a positive correlation between A and the ionicity of the manganese–ligand bond. On this basis it was found that Mn^{2+} ions in lead acetate glasses are quite ionic ($A = 90$ G), consistent with Mn^{2+} ions in alkali borate[5] and K_2SO_4–$ZnSO_4$[17] glasses ($A = 92$ G).

The decrease in the signal intensity of the resonance line at $g = 2.02$ with an increase in temperature from 123 K could be due to an efficient spin-lattice relaxation. A closer inspection reveals that the decrease in the intensity of the transitions becomes more rapid as the glass transition temperature, $T_g = 317$ K,[1] is approached. Similar observations were found for Mn^{2+} ions in the EPR studies of non-silicate inorganic glasses by Parthasarathy *et al.*[8] as the glass transition temperature (T_g) of sulphate (460 K), phosphate (469 K) and PbO—$PbCl_2$ (480 K) is approached. The glass transition temperature (T_g) for lead acetate glasses is 317 K,[1] at which temperature the authors observed a sudden decrease in the intensity of the resonance line at $g = 2.02$, as is shown in Fig. 3.

By diagonalizing the energy matrices[18] for the d^5 configuration the crystal-field parameter (Dq) and the Racah interelectronic repulsion parameters (B

Table 1. Experimental data and analysis of the absorption spectrum of Mn^{2+} ions in lead acetate glass at room temperature: $B = 600$, $C = 3395$, $Dq = 1000$, $\alpha = 76\ cm^{-1}$

Absorption peak	Transition $^6A_{1g}(S) \rightarrow$	Observed wavelength (nm)	Observed wave number (cm^{-1})	Calculated wave number (cm^{-1})
A	$^4T_{1g}(G)$	580	17,235	17,232
B	$^4T_{2g}(G)$	514	19,450	19,350
C	$^4A_{1g}(G)$; $^4E_g(G)$	409	24,445	24,445
D	$^4T_{2g}(D)$	375	26,660	26,360
E	$^4E_g(D)$	362	27,624	27,420

and C) have been evaluated. In the analysis of the optical absorption spectrum Tree's correction[19] parameter, α, has been incorporated, which is equal to 76 cm^{-1} in order to obtain a good fit to the observed and calculated values. The observed and calculated energies along with the assignments are given in Table 1.

In the present work the value of the inter-electronic repulsion parameter, $B = 600\ cm^{-1}$ (free ion value is 960 cm^{-1}),[20] was obtained, which indicates that the bonding is moderately ionic. This is also confirmed from the EPR spectra.

CONCLUSIONS

The EPR and optical absorption spectra of Mn^{2+} ions in lead acetate glasses have been investigated. EPR spectra at different temperatures reveal that there is a rapid fall in the intensity near the glass transition temperature T_g. The EPR and optical absorption studies of Mn^{2+} ions in lead acetate glasses show that the site symmetry around the transition metal ion is octahedral.

Acknowledgements—The authors thank the Department of Science and Technology, New Delhi, for the purchase of an ESR spectrometer. One of the authors (BS) thanks the Council for Scientific and Industrial Research, New Delhi, for the award of a Research Associateship.

REFERENCES

1. M. D. Ingram, G. G. Lewis and J. A. Duffy, *J. Phys. Chem.* 1972, **76**, 1035.
2. R. F. Bartholomew and S. S. Lewek, *J. Am. Ceram. Soc.* 1970, **53**, 445.
3. C. J. Ballhausen, *Introduction to Ligand Field Theory*. McGraw-Hill, New York (1962).
4. V. Cerny, B. Petrova and M. Frumar, *J. Non-Cryst. Solids* 1990, **125**, 17.
5. D. L. Griscom and R. E. Griscom, *J. Chem. Phys.* 1967, **47**, 2711.
6. R. C. Nicklin, H. A. Farach and C. P. Poole Jr, *J. Chem. Phys.* 1976, **65**, 2998.
7. I. Watanabe, Y. Inagaki and T. Shimizu, *J. Non-Cryst. Solids* 1976, **22**, 109.
8. R. Parthasarathy, K. J. Rao and C. N. R. Rao, *Chem. Phys.* 1982, **68**, 393.
9. L. D. Bogomolova, E. G. Grechko, N. A. Krasilnikova and V. V. Sakharov, *J. Non-Cryst. Solids* 1985, **69**, 299.
10. J. Lakshmana Rao, B. Sreedhar, Y. C. Ratnakar and S. V. J. Lakshman, *J. Non-Cryst. Solids* 1987, **92**, 175.
11. E. A. Harris, *Phys. Chem. Glasses* 1987, **28**, 196.
12. H. W. De Wijn and R. F. van Balderen, *J. Chem. Phys.* 1967, **46**, 1381.
13. S. Barnier, M. Guittard, M. Wintenberger and J. Flahaut, *J. Non-Cryst. Solids* 1983, **56**, 319.
14. J. M. Dance, J. J. Videan and J. Portier, *J. Non-Cryst. Solids* 1986, **86**, 88.
15. J. Lakshmana Rao, G. L. Narendra, B. Sreedhar and S. V. J. Lakshman, *Phys. Stat. Sol. (b)* 1989, **153**, 257.
16. J. S. Van Wieringer, *Disc. Faraday Soc.* 1955, **19**, 118.
17. H. G. K. Sundar and K. J. Rao, *J. Non-Cryst. Solids* 1982, **50**, 137.
18. Y. Tanabe and S. Sugano, *J. Phys. Soc. Japan* 1954, **9**, 753.
19. R. E. Trees, *Phys. Rev.* 1951, **83**, 756.
20. B. N. Figgis, *Introduction to Ligand Field*. Wiley, New Delhi (1976).

Polyhedron Vol. 12, No. 12, pp. 1545–1552, 1993
Printed in Great Britain

0277–5387/93 $6.00+.00
© 1993 Pergamon Press Ltd

SYNTHESIS, STRUCTURE AND ELECTROCHEMICAL PROPERTIES OF COMPLEXES WITH A (μ-OXO)BIS-(μ-CARBOXYLATO)DIRUTHENIUM(III) CORE

ARIYANCHIRA SYAMALA and AKHIL R. CHAKRAVARTY*

Department of Inorganic and Physical Chemistry, Indian Institute of Science, Bangalore 560 012, India

(*Received* 11 *December* 1992; *accepted* 1 *February* 1993)

Abstract—Reaction of $[Ru_2O(O_2CR)_2(MeCN)_4(PPh_3)_2](ClO_4)_2$ (**1**) with 1,2-diaminoethane (en) in MeOH–H_2O yielded a mixture of products, from which a purple diamagnetic and 1:2 electrolytic diruthenium(III) complex, $[Ru_2O(O_2CR)_2(en)_2(PPh_3)_2](ClO_4)_2$ (**2**), was isolated along with a trace by-product of $[Ru_2O(O_2CR)_2(en)_2(PPh_3)_2](ClO_4)(MeCONH)$ (**3**) (R = C_6H_4-*p*-X: X = H, **a**; OMe, **b**; Me, **c**). Complex **3b** has been characterized by X-ray diffraction analysis. The structure shows the presence of a $\{Ru_2(\mu\text{-}O)(\mu\text{-}O_2CR)_2^{2+}\}$ core, with the metal centre bonded to an unidentate PPh_3 and a bidentate chelating en terminal ligand. The Ru—Ru distance and the Ru—O—Ru angle in the core are 3.255(3) Å and 119.1(4)°. The amidate anion, formed presumably by nucleophilic attack of OH^- on the MeCN ligand in complex **1**, remains uncoordinated to the metal. In MeCN/0.1 M $[NBu^n_4]ClO_4$ complex **2** exhibits a nearly reversible $Ru_2^{III,III}$–$Ru_2^{III,IV}$ couple near 0.9 V and an irreversible $Ru_2^{III,III}$–$Ru_2^{III,II}$ process at −0.6 V (vs S.C.E.). The mechanistic aspects of the substitution and nucleophilic reactions in the formation of complexes **2** and **3** are discussed.

The chemistry of (μ-oxo)bis(μ-carboxylato)di-metal(III) complexes has gained considerable current interest[1] following the discovery of such a core in several non-haeme metalloproteins. Based on the chemical relevance of the low molecular weight transition-metal complexes as model systems, the major thrust was on the synthesis of di-iron complexes. However, in recent years several 3*d*- and 4*d*-metal complexes have also been reported.[2–8] Although the importance of the terminal sites of the core has earlier been recognized[9] in the biological activity of several μ-oxodi-iron proteins, the reaction chemistry at the facial positions in model systems is virtually unexplored[10] due to the presence of substitutionally inert terdentate or polydentate ligands in the majority of complexes. The easy accessibility of various oxidation states, the inert behaviour of ruthenium complexes and the ready availability of a precursor complex, $[Ru_2O(O_2CR)_2(MeCN)_4(PPh_3)_2](ClO_4)_2$ (**1**),[8] containing labile terminal ligands, have prompted us to investigate the effect of terminal ligands on the redox and spectral properties of the diruthenium(III) core.

In a previous report[8] we have shown that under mild reaction conditions the nitrile ligands in complex **1** undergo nucleophilic attack with 1,2-diaminoethane (en) to form amino-amidine moieties. In this paper we describe other reaction pathways leading to the formation of $[Ru_2O(O_2CR)_2(en)_2(PPh_3)_2](ClO_4)_2$ (**2**) and $[Ru_2O(O_2CR)_2(en)_2(PPh_3)_2](ClO_4)(MeCONH)$ (**3**) (R = C_6H_4-*p*-X: X = H, **a**; OMe, **b**; Me, **c**). Complex **3b** is structurally characterized by X-ray methods.

EXPERIMENTAL

The solvents and reagents were purchased from commercial sources. $Ru_2Cl(O_2CMe)_4$, $Ru_2Cl(O_2CR)_4$ and $[Ru_2O(O_2CR)_2(MeCN)_4(PPh_3)_2](ClO_4)_2$ (**1**) (R = C_6H_4-*p*-X: X = H, **a**; OMe, **b**; Me, **c**) were prepared by literature methods.[4a,6,11]

Preparation of the complexes

The complexes of formulations $[Ru_2O(O_2CR)_2(en)_2(PPh_3)_2](ClO_4)_2$ (**2a–2c**) and $[Ru_2O(O_2CR)_2$

* Author to whom correspondence should be addressed.

$(en)_2(PPh_3)_2](ClO_4)(MeCONH)$ (**3a**–**3c**) were prepared as a mixture, containing complex **2** as a major product along with a trace quantity of complex **3** (*ca* 5%), using a general procedure. A representative procedure is given below.

Complex **1b** (50 mg, 0.04 mmol) in a mixture of MeOH–H_2O (10 cm^3; 4:1 v/v) was reacted with 0.3 M en (0.3 cm^3, 0.09 mmol) in MeOH. The solution was heated under reflux for 2 h, followed by cooling to an ambient temperature. The resulting bluish-purple solution was added to an aqueous solution of $NaClO_4$ (10 cm^3). The purple precipitate thus formed was removed by filtration and washed with water. The crude product (yield: *ca* 60%), after drying *in vacuo* over P_4O_{10}, was subjected to chromatography on a silica gel column in petroleum ether (b.p. 60–80°C). A blue fraction was eluted first, followed by a purple band which was collected using a $CHCl_3$–MeOH mixture (9:1 v/v) as the eluant. A purple solid was obtained after removal of the solvent and crystallization from methanol by slow evaporation at 25°C. The product was found to be essentially complex **2b** with *ca* 5% complex **3b**, as observed from ^1H NMR studies. The yield after chromatographic separation was 10 mg (*ca* 20%). Found: C, 49.9; H, 5.1; N, 4.7. Calc. for $C_{56}H_{60}N_4O_{15}P_2Cl_2Ru_2$: C, 49.3; H, 4.4; N, 4.1%. Complex **2a**: Yield *ca* 20%. Found: C, 50.2; H, 4.5; N, 4.8. Calc. for $C_{54}H_{56}N_4O_{13}P_2Cl_2Ru_2$: C, 49.7; H, 4.3; N, 4.3%. Complex **2c**: yield *ca* 18%. Found: C, 50.9; H, 4.9; N, 4.7. Calc. for $C_{56}H_{60}N_4O_{13}P_2Cl_2Ru_2$: C, 50.5; H, 4.5; N, 4.2%.

Physical measurements

The elemental analyses were performed using a Heraeus CHN-O Rapid instrument. Electronic spectra were recorded on a Hitachi U-3400 spectrophotometer. The ^1H NMR spectra were obtained using Bruker WH-270 and AC(AF) 200-MHz spectrometers. Conductivity measurements were performed on a Century CC 603 digital conductivity meter. Cyclic voltammetric measurements were obtained using a three-electrode set-up on a PAR Model 174A polarographic analyser connected to a Houston Instruments Omnigraphic *X*–*Y* recorder. A platinum button, a platinum wire and a saturated calomel electrode (S.C.E.) were used as working, auxiliary and reference electrodes, respectively. The measurements were performed at 25°C in MeCN containing $[NBu^n_4]ClO_4$ (0.1 M). The data reported are uncorrected for junction potentials. Ferrocene, $(\eta^5\text{-Cp})_2Fe$, was used as a standard to verify the potentials observed against the S.C.E. and to obtain the electron-transfer stoichiometries of the redox couples by peak current measurements. The $Fe^{II/III}$ couple of ferrocene was observed at +0.42 V (vs S.C.E.) under similar experimental conditions.

Crystal structure determination of $[Ru_2O(O_2CC_6H_4\text{-}p\text{-}OMe)_2(en)_2(PPh_3)_2](ClO_4)(MeCONH)\cdot H_2O$ (**3b**)

The purple coloured rectangular crystals, obtained from slow evaporation of a methanolic solution of the purple mixture containing complex **2b** ≫ complex **3b**, were found to be unstable outside the mother liquor. A suitable crystal was sealed in a Lindemann capillary along with the mother liquor.

Crystal data. $C_{58}H_{66}N_5O_{13}P_2ClRu_2$, $M = 1340.7$, triclinic, $P\bar{1}$, $a = 13.066(6)$, $b = 13.531(3)$, $c = 19.132(2)$ Å, $\alpha = 95.53(1)$, $\beta = 94.62(2)$, $\gamma = 112.06(2)°$, $V = 3095(2)$ $Å^3$, $Z = 2$, $d_c = 1.44$ g cm^{-3}, $F(000) = 1376.0$, $\lambda = 0.7107$ Å, $\mu(\text{Mo-}K_\alpha) = 6.34$ cm^{-1}, $T = 293$ K.

Data collection, structure solution and refinement. CAD4 diffractometer, ω scan mode with scan width $= 0.90+0.35 \tan\theta$, prescan speed = 5.5° min^{-1} [the final scan with a speed calculated to satisfy the condition $\sigma(I)/I \leqslant 0.03$], graphite-monochromated Mo-K_α radiation; 9400 reflections measured ($4° \leqslant 2\theta \leqslant 46°$, h, $\pm k$, $\pm l$), 8589 unique giving 4829 with $I > 3\sigma(I)$. No decay was observed during data collection. Data were corrected for Lorentz and polarization effects. The data, collected in four stages using different orientation matrices due to the movement of the weakly diffracting crystal in the capillary, were not subjected to absorption correction (transmissions: 85–95%).

Direct methods (ruthenium and chlorine atoms) followed by normal heavy-atom procedures were used. Full-matrix least-squares refinement was performed (in three blocks for final, anisotropic cycles) with all non-hydrogen atoms anisotropic, except the positionally disordered perchlorate oxygens, the methoxy group atoms and the solvent water molecules with site-occupancy factors other than 1.0. The aryl group atoms of a bridging carboxylate, comprising atoms C(11)–C(16), were refined as a rigid group. Residuals: $R = 0.0767$ ($R_w = 0.0816$ for $w = 1/[\sigma^2(F_o) + 0.002853\ F_o^2]$), max. peak in final difference Fourier = 0.68 e $Å^{-3}$. The positional and thermal disorder of several atoms has contributed to the high values of the residuals. The ClO_4 anion is refined with two sets of four oxygens with site occupancy factors (s.o.f.) of 0.8 and 0.2. The disordered methoxy group is refined with a s.o.f. of 0.5. The probable source of water as the solvent of crystallization could be the methanol. All calculations were performed using a VAX88 computer and the SHELX system of programs[12]

at the Computer Centre of the Indian Institute of Science. Atomic scattering factors were taken from ref. 13. Positional and isotropic thermal parameters and bond lengths and angles have been forwarded to the Director, Cambridge Crystallographic Data Centre.

RESULTS AND DISCUSSION

Synthesis and spectral properties

The reaction of complex **1** with en under refluxing conditions in MeOH–H_2O leads to the formation of a mixture of products containing a blue, purple and yellow species. When the crude product is subjected to column chromatography a blue coloured minor product elutes first, followed by a purple band containing a (μ-oxo)diruthenium(III) complex, which is formulated as $[Ru_2O(O_2CR)_2(en)_2(PPh_3)_2](ClO_4)_2$ (**2**) from the analytical and conductivity data (Table 1). Preliminary studies[14] show that the yellow product is a monomeric ruthenium(III) complex. Earlier we have reported[8] the blue complex, which was isolated in a higher yield by conducting the reaction under mild thermal conditions. Complex **2** is stable in the solid state and in solution. It is soluble in polar organic solvents and exhibits a 1:2 electrolytic behaviour in MeCN. Subsequent studies on this purple species show the presence of a trace quantity (*ca* 5%) of $[Ru_2O(O_2CR)_2(en)_2(PPh_3)_2](ClO_4)(MeCONH)$ (**3**). The characterization of **3** has been unambiguously achieved by single-crystal X-ray diffraction studies.

Complex **2** is essentially diamagnetic. Relevant ^1H NMR data are presented in Table 1. Complexes **2b** and **2c** display a singlet for the methyl protons of two carboxylato bridging ligands, which are chemically equivalent in the solution phase. The chelating en ligands in complex **2** display four multiplets for the CH_2 protons in a static configuration. The amino protons appear in the aromatic region. While one is visible at δ 7.2, the other resonance is obscured by the phenyl proton signals of the PPh_3 ligands. The spectrum of the purple complex also shows the presence of a trace quantity (*ca* 5% from peak integrals) of the amidate anion of complex **3** (Fig. 1). A relatively weak signal, visible at δ 2.0, is tentatively assigned to the methyl protons of the amidate anion. The spectral features of the cationic species of complex **3** are identical with those of complex **2**.

Complex **2** displays a strong visible band at 559 nm (Table 1), which is assigned[4–8] to a charge-transfer transition involving the Ru^{III}-$d\pi$ and O(μ)-

Table 1. Physico-chemical data on $[Ru_2O(O_2CR)_2(en)_2(PPh_3)_2](ClO_4)_2$ (**2**)

	2a (R = C_6H_5)	**2b** (R = C_6H_4-*p*-OMe)	**2c** (R = C_6H_4-*p*-Me)
Conductivity (in MeCN)			
Λ_M (Ω^{-1} cm^2 mol^{-1})	205	195	197
Electronic spectra (in MeCN)			
λ_{max} (nm) (ε/M^{-1} cm^{-1})[a]	561(6300), 380(sh)	559(6500), 380(sh)	559(6400), 380(sh)
^1H NMR: δ(ppm) [nH, *J* (Hz)][b]			
$Me(O_2CR)$	—	3.76 s (6H)	2.34 s [6H]
CH_2(en)	2.42, 3.40, 3.82, 4.16 br [8H]	2.35, 3.44, 3.72, 3.94 br [8H]	2.40, 3.38, 3.83, 4.19 br [8H]
NH_2(en)[c]	7.15 br [4H]	7.03 br [4H]	
NH_2,[c] R,[d] PPh_3[e]	7.20–7.69 [44H][c,d,e]	6.79 d [4H, 9][d] 7.19–7.66 [38H][c,d,e]	6.63–8.07 [46H][c,d,e]
Electrochemistry: $E_{1/2}$(V) [ΔE_p (mV)][f]			
$Ru_2^{III,III} \rightleftharpoons Ru_2^{III,IV}$	0.94 (80)	0.93 (60)	0.93 (100)
$Ru_2^{III,III} \rightarrow Ru_2^{III,II}$	−0.60[g]	−0.63[g]	−0.63[g]

[a] Sh = shoulder.
[b] In $CDCl_3$ with Me_4Si as the standard; s, singlet; d, doublet; br, broad.
[c] NH_2 protons of en.
[d] Aryl carboxylato protons.
[e] PPh_3 protons.
[f] In MeCN/0.1 M $[NBu^n_4]ClO_4$; all potentials are referenced to S.C.E.; $E_{1/2} = 0.5\ (E_{pa} + E_{pc})$, where E_{pa} and E_{pc} are the anodic and cathodic peak potentials; scan rate 20 mV s^{-1} at a platinum working electrode; $\Delta E_p = E_{pa} - E_{pc}$.
[g] Cathodic peak (E_{pc}) of the irreversible reduction.

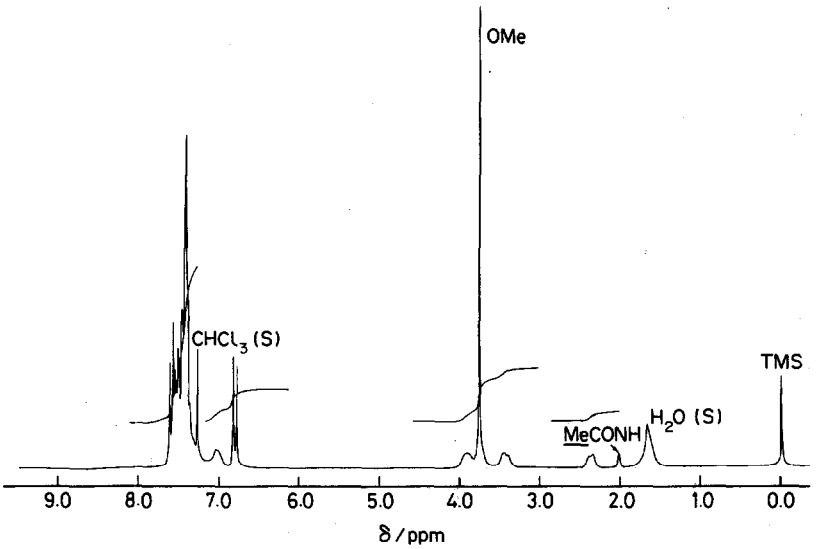

Fig. 1. ^{1}H NMR spectrum of $[Ru_2O(O_2CC_6H_4\text{-}p\text{-}OMe)_2(en)_2(PPh_3)_2](ClO_4)_2$ (**2b**) in $CDCl_3$. The peak at δ 2.0 is due to the amidate anion of **3b** (S, solvent peaks).

$p\pi$ orbitals. In complex **1** this band is observed[6] at 581 nm. The substitution of the π-acceptor MeCN ligands by σ-only donor en ligands caused a shift in the charge-transfer band to a higher energy.

Electrochemistry

The redox behaviour of **2** has been studied by cyclic voltammetry using a platinum button working electrode in MeCN containing 0.1 M $[NBu^n_4](ClO_4)$. Complex **2** undergoes a nearly reversible oxidation at *ca* 0.9 V and an irreversible reduction near *ca* −0.6 V *vs* S.C.E. (Fig. 2, Table 1). The one-electron stoichiometry of the redox processes is obtained from the peak current measurements using ferrocene as a standard. The ratio of cathodic and anodic peak currents for the oxidation couple is found to be *ca* 1.0 for scan rates 20–200 mV s^{-1}. The couples involved are given in eq. (1).

$$\{Ru_2^{III,IV}(\mu\text{-}O)(\mu\text{-}O_2CR)_2{}^{3+}\} \underset{-e}{\overset{+e}{\rightleftharpoons}} \{Ru_2^{III,III}(\mu\text{-}O)(\mu\text{-}O_2CR)_2{}^{2+}\} \xrightarrow{+e^-} \{Ru_2^{II,III}(\mu\text{-}O)(\mu\text{-}O_2CR)_2{}^{+}\} \quad (1)$$

Crystal structure

An ORTEP[15] view of the cationic complex of complex **3b** is shown in Fig. 3. It consists of a

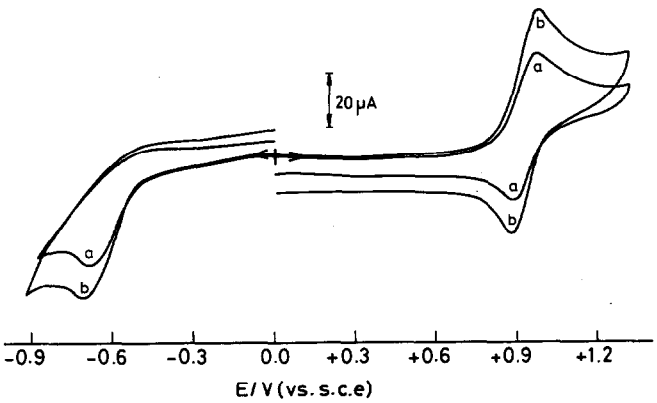

Fig. 2. Cyclic voltammograms of $[Ru_2O(O_2CC_6H_4\text{-}p\text{-}OMe)_2(en)_2(PPh_3)_2](ClO_4)_2$ (**2b**) in MeCN/0.1 M $[NBu^n_4]ClO_4$ at scan rates of (a) 20 and (b) 50 mV s^{-1}.

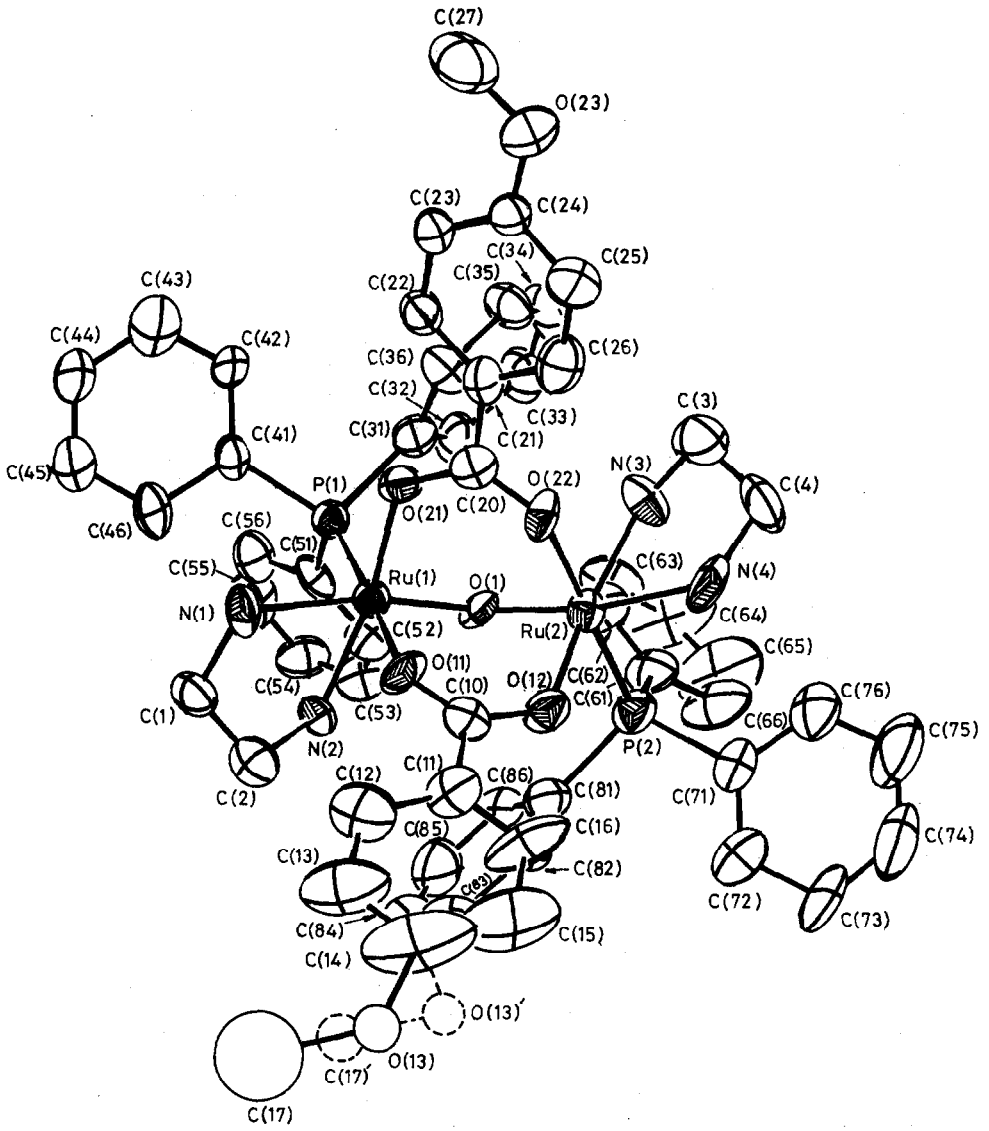

Fig. 3. An ORTEP view of $[Ru_2O(O_2CC_6H_4\text{-}p\text{-}OMe)_2(en)_2(PPh_3)_2]^{2+}$ in **3b**, showing 50% probability thermal ellipsoids, the atom numbering scheme and the positionally disordered methoxy group.

diruthenium(III) unit held by an oxo and two carboxylato bridges in a *cis* position to form a $\{Ru_2(\mu\text{-}O)(\mu\text{-}O_2CR)_2^{2+}\}$ core. The geometry around each metal centre is essentially octahedral, while the molecule has a staggered conformation. The facial sites of the core are occupied by chelating en and unidentate PPh_3 ligands. Selected bond distances and angles are listed in Table 2. The Ru(1)—Ru(2), av. Ru—O(1) distances and Ru(1)—O(1)—Ru(2) angle in the core are 3.255(3), and 1.888(9) Å and 119.1(4)°. In the chelate rings the Ru(1)—N(1) and Ru(2)—N(4) distances [av. 2.168(12) Å] are longer than the Ru(1)—N(2) and Ru(2)—N(3) bond lengths [av. 2.112(10) Å]. This is indicative of a significant *trans* influence of the μ-oxo ligand similar to that observed[4-8] in analogous μ-oxo complexes. A packing diagram showing the disposition of the complex cation and the anions in the unit cell is displayed in Fig. 4. The isolation of a single crystal of **3b** from the bulk of **2b** leads to the serendipitous discovery of nucleophilic attack by hydroxide in a triply-bridged dimeric system.

Mechanistic aspects

As shown in Scheme 1 the reactions pertaining to this work and in the formation of an amino-amidine complex[8] are believed to proceed through a common reactive intermediate (**I**), which involves a substitution of *trans*-MeCN to the μ-oxo ligand of complex **1** by η^1-en. In a recent study Sasaki *et al.* have shown[5] that $Ru_2O(O_2CMe)_2(py)_6^{2+}$ under-

Table 2. Selected bond distances (Å) and angles (°) for $[Ru_2O(O_2CC_6H_4\text{-}p\text{-}OMe)_2(en)_2(PPh_3)_2](ClO_4)(MeCONH)\cdot H_2O$ (**3b**)

Ru(1)—Ru(2)	3.255(3)	Ru(2)—O(1)	1.894(10)
Ru(1)—O(1)	1.882(8)	Ru(2)—P(2)	2.294(5)
Ru(1)—P(1)	2.281(5)	Ru(2)—O(12)	2.029(8)
Ru(1)—O(11)	2.149(10)	Ru(2)—O(22)	2.125(9)
Ru(1)—O(21)	2.034(9)	Ru(2)—N(3)	2.132(9)
Ru(1)—N(1)	2.183(10)	Ru(2)—N(4)	2.152(13)
Ru(1)—N(2)	2.092(11)	P(2)—C(61)	1.819(17)
P(1)—C(31)	1.831(12)	P(2)—C(71)	1.846(18)
P(1)—C(41)	1.841(14)	P(2)—C(81)	1.845(14)
P(1)—C(51)	1.839(16)	O(21)—C(20)	1.294(19)
O(11)—C(10)	1.259(17)	O(22)—C(20)	1.276(16)
O(12)—C(10)	1.296(15)	N(3)—C(3)	1.507(23)
N(1)—C(1)	1.476(18)	C(3)—C(4)	1.523(26)
C(1)—C(2)	1.532(22)	C(4)—N(4)	1.521(17)
C(2)—N(2)	1.499(17)	C(9)—O(6)	1.279(26)
C(9)—C(30)	1.151(30)		

Ru(1)—O(1)—Ru(2)	119.1(4)	N(3)—Ru(2)—N(4)	80.6(5)
N(1)—Ru(1)—N(2)	80.3(5)	O(22)—Ru(2)—N(4)	79.4(4)
O(21)—Ru(1)—N(2)	166.4(4)	O(22)—Ru(2)—N(3)	86.6(4)
O(21)—Ru(1)—N(1)	86.7(4)	O(12)—Ru(2)—N(4)	87.8(5)
O(11)—Ru(1)—N(2)	86.2(4)	O(12)—Ru(2)—N(3)	167.6(5)
O(11)—Ru(1)—N(1)	77.2(4)	O(12)—Ru(2)—O(22)	87.0(3)
O(11)—Ru(1)—O(21)	87.3(4)	P(2)—Ru(2)—N(4)	99.1(3)
P(1)—Ru(1)—N(2)	94.8(4)	P(2)—Ru(2)—N(3)	94.6(3)
P(1)—Ru(1)—N(1)	99.3(3)	P(2)—Ru(2)—O(22)	177.9(3)
P(1)—Ru(1)—O(21)	91.0(3)	P(2)—Ru(2)—O(12)	91.4(3)
P(1)—Ru(1)—O(11)	176.2(3)	O(1)—Ru(2)—N(4)	169.3(4)
O(1)—Ru(1)—N(2)	92.5(4)	O(1)—Ru(2)—N(3)	91.2(4)
O(1)—Ru(1)—N(1)	169.8(4)	O(1)—Ru(2)—O(22)	93.5(3)
O(1)—Ru(1)—O(21)	100.0(4)	O(1)—Ru(2)—O(12)	99.9(4)
O(1)—Ru(1)—O(11)	95.3(3)	O(1)—Ru(2)—P(2)	88.3(3)
O(1)—Ru(1)—P(1)	88.4(3)	Ru(2)—P(2)—C(81)	109.3(5)
Ru(1)—P(1)—C(51)	116.8(5)	Ru(2)—P(2)—C(71)	118.2(6)
Ru(1)—P(1)—C(41)	114.8(4)	Ru(2)—P(2)—C(61)	115.4(5)
Ru(1)—P(1)—C(31)	112.1(6)	C(71)—P(2)—C(81)	104.7(7)
C(41)—P(1)—C(51)	105.4(7)	C(61)—P(2)—C(81)	104.1(8)
C(31)—P(1)—C(51)	102.1(6)	C(61)—P(2)—C(71)	103.8(7)
C(31)—P(1)—C(41)	104.1(6)	Ru(2)—O(12)—C(10)	124.2(8)
Ru(1)—O(11)—C(10)	133.4(9)	Ru(2)—O(22)—C(20)	135.9(10)
Ru(1)—O(21)—C(20)	122.9(8)	Ru(2)—N(3)—C(3)	108.8(9)
Ru(1)—N(1)—C(1)	110.5(8)	N(3)—C(3)—C(4)	106.4(14)
N(1)—C(1)—C(2)	110.9(13)	C(3)—C(4)—N(4)	112.0(14)
C(1)—C(2)—N(2)	107.4(12)	Ru(2)—N(4)—C(4)	110.2(10)
Ru(1)—N(2)—C(2)	109.4(9)	O(21)—C(20)—O(22)	124.1(14)
O(11)—C(10)—O(12)	125.0(12)	N(5)—C(9)—C(30)	127.0(24)
O(6)—C(9)—C(30)	118.3(20)	O(6)—C(9)—N(5)	114.5(23)

goes an exclusive exchange of the *trans*-pyridine to the μ-oxo ligand with py-d_5 in CD_3CN. A similar regioselective process in complex **1** is expected to result in an exclusive *trans*-MeCN substitution as the first step. The X-ray structural data[6] for complex **1**, showing a longer *trans*-Ru—N bond compared with *cis*, also support this view.

The formation of complexes **2**, **3** and the reported[8] amino-amidine complex from the intermediate (**I**) can be rationalized by proposing three reaction pathways. (1) The intramolecular pathway, leading to the formation of a chelate ring by elimination of the *cis*-MeCN ligand, is expected to be a facile process. (2) The intramolecular pathway,

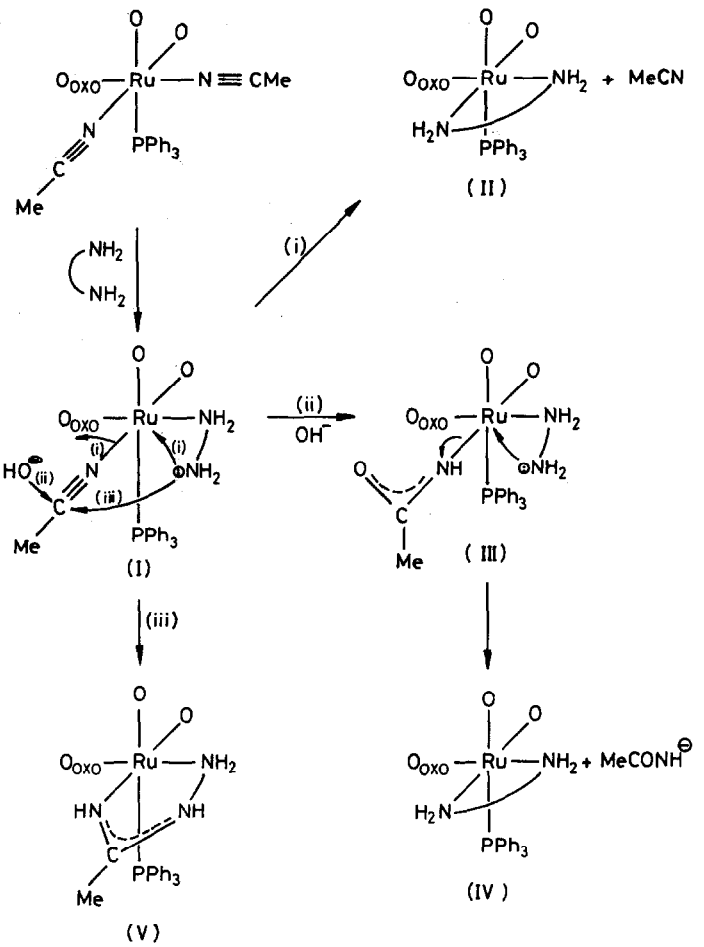

Scheme 1. A tentative mechanism for the nucleophilic reactions at the terminal nitrile ligands in $[Ru_2O(O_2CR)_2(MeCN)_4(PPh_3)_2]^{2+}$.

which involves nucleophilic attack of the free amino group of η^1-en on the carbon atom of the *cis*-nitrile ligand, forming a seven-membered amino-amidine chelate ring (**V**).[8] While the latter pathway is found to be more favourable under mild reaction conditions, the chelation process predominates at elevated reaction temperatures. The formation of **3** can be rationalized[16] by an intermolecular nucleophilic attack of hydroxide on the *cis*-nitrile carbon atom to form an η^1-bonded amidato intermediate (**III**), followed by an en-chelation (**IV**) by eliminating the amidato anion in a high dielectric medium such as an MeOH–H_2O mixture. The isolation of a trace quantity of complex **3** from the reaction indicates that the intramolecular processes are, as expected, more favourable than intermolecular.

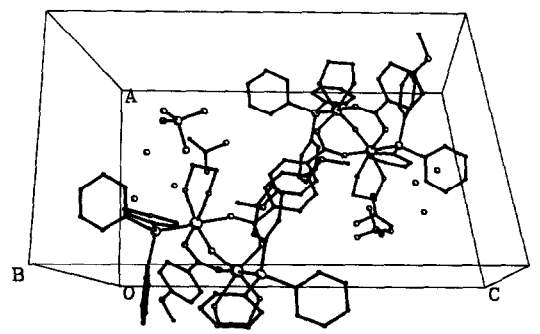

Fig. 4. A unit cell packing diagram of **3b**. The disorders in the ClO_4^- anion and the methoxy group are not shown for clarity.

Acknowledgement—We thank the Department of Science and Technology, Government of India, for financial support.

REFERENCES

1. (a) S. J. Lippard, *Angew. Chem., Int. Edn Engl.* 1988, **27**, 344; (b) D. M. Kurtz Jr, *Chem. Rev.* 1990, **90**, 585; (c) L. Que Jr and A. E. True, *Prog. Inorg. Chem.* 1990, **38**, 97; (d) J. B. Vincent, G. L. Olivier-Lilley and B. A. Averill, *Chem. Rev.* 1990, **90**, 1447.

2. P. Knopp and K. Wieghardt, *Inorg. Chem.* 1991, **30**, 4061 and refs therein.
3. (a) A. G. Blackman, J. C. Huffman, E. B. Lobkovsky and G. Christou, *J. Chem. Soc., Chem. Commun.* 1991, 989; (b) U. Bossek, K. Wieghardt, B. Nuber and J. Weiss, *Inorg. Chim. Acta* 1989, **165**, 123.
4. (a) R. W. Mitchell, A. Spencer and G. Wilkinson, *J. Chem. Soc., Dalton Trans.* 1973, 846; (b) P. Neubold, K. Wieghardt, B. Nuber and J. Weiss, *Inorg. Chem.* 1989, **28**, 459; (c) A. Llobet, M. E. Curry, H. T. Evans and T. J. Meyer, *Inorg. Chem.* 1989, **28**, 3131; (d) M. C. Barral, R. Jamenez-Aparicio, E. C. Royer, F. A. Urbanos, A. Monge and C. Ruiz-Valero, *Polyhedron* 1991, **10**, 113; (e) N. Gupta, S. Mukerjee, S. Mahapatra, M. Roy and R. N. Mukherjee, *Inorg. Chem.* 1992, **31**, 139.
5. Y. Sasaki, M. Suzuki, A. Nagasawa, A. Tokiwa, M. Ebihara, T. Yamaguchi, C. Kabuto, T. Ochi and T. Ito, *Inorg. Chem.* 1991, **30**, 4903.
6. B. K. Das and A. R. Chakravarty, *Inorg. Chem.* 1990, **29**, 2078.
7. A. Syamala, B. K. Das and A. R. Chakravarty, *Polyhedron* 1992, **11**, 335.
8. A. Syamala and A. R. Chakravarty, *Inorg. Chem.* 1991, **30**, 4699.
9. J. Sanders-Loehr, in *Iron Carriers and Iron Proteins* (Edited by T. M. Loehr), p. 373. VCH Publishers, New York (1989).
10. (a) R. H. Beer, W. B. Tolman, S. G. Bott and S. J. Lippard, *Inorg. Chem.* 1991, **30**, 2082; (b) S. Ménage and L. Que Jr, *New J. Chem.* 1991, **15**, 431.
11. B. K. Das and A. R. Chakravarty, *Polyhedron* 1988, **7**, 685.
12. (a) G. M. Sheldrick, SHELX-76, Program for Crystal Structure Determination. University of Cambridge (1976); (b) G. M. Sheldrick, SHELXS-86, Program for Crystal Structure Solution. Universität Göttingen, F.R.G. (1986).
13. *International Tables for X-ray Crystallography*, Vol. 4. Kynock Press, Birmingham (1974).
14. A. Syamala and A. R. Chakravarty, unpublished results.
15. C. K. Johnson, ORTEP-II. Oak Ridge National Laboratory, Oak Ridge, Tennessee (1976).
16. P. Paul and K. Nag, *Inorg. Chem.* 1987, **26**, 1586 and refs therein.

Polyhedron Vol. 12, No. 12, pp. 1553–1557, 1993
Printed in Great Britain

0277–5387/93 $6.00+.00
© 1993 Pergamon Press Ltd

SYNTHESIS AND CHARACTERIZATION OF A MONONUCLEAR IRON(III) COMPLEX WITH A TRIPODAL TRIAMIDE LIGAND

R. SHUKLA and P. K. BHARADWAJ*

Department of Chemistry, Indian Institute of Technology, Kanpur 208016, India

and

U. C. JOHRI

Department of Physics, Indian Institute of Technology, Kanpur 208016, India

(*Received* 8 *October* 1992; *accepted* 26 *January* 1993)

Abstract—A new potentially heptadentate tripodal ligand has been synthesized by the condensation reaction between tris(2-aminoethyl)amine and acetylsalicyclic acid in a 1:3 molar ratio. The *o*-acetyl linkage is cleaved by treating with KOH to form the desired ligand with the donors that include three amide nitrogens, three phenolate oxygens and one bridgehead nitrogen. $Fe(acac)_3$ readily forms a dark red 1:1 complex with the ligand. The complex behaves as a non-electrolyte in acetonitrile. The electronic absorption spectrum in the visible region is dominated by a strong absorption with λ_{max} at 425 nm, assignable to an LMCT transition from phenolate oxygen to iron(III) in an octahedral coordination geometry. The magnetic moment value at room temperature (5.5 μ_{eff}/μ_B) and the EPR spectra in the solid state and in solution ($g = 4.06$) are consistent with high-spin rhombically distorted octahedral iron(III). Room-temperature Mössbauer data provide the following values: isomer shift 0.37 mm s^{-1} and quadrupole splitting 0.82 mm s^{-1}. These data are consistent with a discrete, high-spin octahedral iron(III) complex.

Our interest in tripodal ligands stems from the fact that these ligands are capable of forming complexes with metal ions that can exhibit unusual coordination, high thermodynamic stability and kinetic inertness.[1,2] Besides, the tripodal ligands can serve as precursors to the synthesis of macrobicycles.[3–5] The present paper describes the synthesis of a new, potentially heptadentate tripodal ligand having an N_4O_3 donor set and its complexing ability towards iron(III). There has been continued interest in iron(III) chemistry with N,O-donor ligands. A large number of iron tyrosinate proteins are known where iron is bound mostly by nitrogen and oxygen atoms of the amino acid residues like histidine, tyrosine, aspartic acid, etc.[6–10] These proteins all contain high-spin iron(III), characterized by a $g = 4.3$ signal and an intense absorption in the visible region (400–600 nm) with an ε_{max} value in the range 2000–4000 M^{-1} cm^{-1}, due to a phenolate oxygen-to-iron(III) LMCT transition. Modelling these sites has been an active area of research.[11–15] The present work was undertaken for the dual purposes of modelling the iron tyrosinate active sites and probing the binding characteristics of the ligand towards a transition metal ion for the possible use of the complex as a precursor in the synthesis of various macrobicyclic compounds.[5]

* Author to whom correspondence should be addressed.

EXPERIMENTAL

Materials

Reagent grade tris(2-aminoethyl)amine, ethylchloroformate and acetylacetone (Merck), salicyclic acid, glacial acetic acid, acetic anhydride and ferric chloride (Glaxo, India) were used as received. All the solvents (Glaxo) were purified[16] prior to use.

Physical measurements were made as reported earlier.[17] The Mössbauer spectra were recorded with the help of a Wissel Mössbauer spectrometer (Wissel Electronik GmbH, Germany) operating in constant acceleration mode. The spectra were recorded at room temperature (300 K). Elemental analyses were performed at the Central Drug Research Institute, Lucknow, India.

Synthesis of the ligand L

The ligand was synthesized by the mixed anhydride method (Fig. 1).[18] Acetylsalicylic acid[19] (2 g, 11 mmol) was dissolved in THF (20 cm^3) under argon and cooled in an ice–salt bath. Freshly distilled triethylamine (1.12 g, 11 mmol) diluted with THF (20 cm^3) was added to the cold solution dropwise with constant stirring. After the addition was complete the solution was stirred for a further period of 20 min. Ethylchloroformate (1.2 g, 11 mmol) mixed with THF (20 cm^3) was then slowly added to the cold solution in 15 min. Finally, tris(2-aminoethyl)amine (0.54 g, 3.7 mmol) mixed with THF (20 cm^3) was added to the well-stirred solution over a period of 45 min. After all the additions were complete the reaction mixture was stirred at 0°C for 2 h and then left at room temperature overnight.

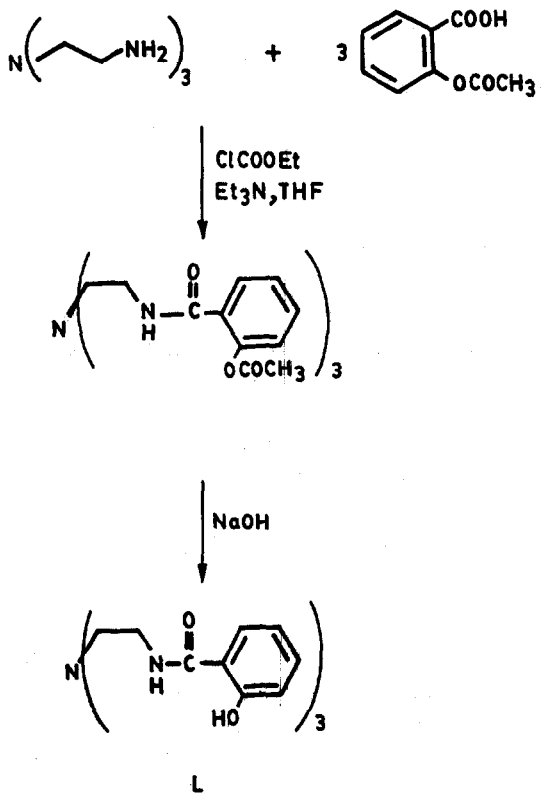

Fig. 1. Synthetic scheme for the tripodal ligand.

Solid triethylamine hydrochloride was removed by filtration and the almost colourless filtrate evaporated to dryness to obtain a pale yellow, thick, oily liquid. This was taken in $CHCl_3$ (25 cm^3) and washed four times with water. After drying the $CHCl_3$ layer the product was stripped of solvent to obtain the pure ligand (L) in 80% yield. ^1H NMR (80 MHz, $CDCl_3$, δ_{TMS} ppm): 7.5 (m, 12H), aromatic; 4.1 (m, 9H), $OCOCH_3$; 3.0 (t, 12H), CH_2.

Synthesis of the iron(III) *complex* (**1**)

A solution of $[Fe(acac)_3]$[20] (1 g, 2.8 mmol) in DMF (10 cm^3) was added dropwise with constant stirring at room temperature to a solution of the ligand, L (1.42 g, 2.8 mmol), in DMF (10 cm^3). The colour of the solution changed slowly to dark red. The dark red solution was allowed to reflux for 1/2 h and filtered after cooling to room temperature. All of the DMF was removed from the filtrate under low pressure and the residue was dissolved in methanol (25 cm^3). The red solution thus obtained was filtered and the filtrate was allowed to evaporate slowly at room temperature, affording a dark-red crystalline solid overnight; yield 47%. A small amount of the second crop of the product could be isolated on further evaporation. Found: C, 58.6; H, 4.8; N, 10.1; O, 17.5. Calc. for $C_{27}H_{27}N_4O_6Fe$: C, 58.0; H, 4.9; N, 10.0; O, 17.2%.

RESULTS AND DISCUSSION

The compound is stable at room temperature in the solid state or in solution in acetonitrile, alcohols, DMF, etc. The complex behaves as a non-electrolyte in these solvents. The IR spectrum in KBr shows a strong band at 1650 cm^{-1}, which is red-shifted by *ca* 35 cm^{-1} with respect to the free ligand, indicating that the three amide nitrogens are bonded to the metal ion.

The complex shows an intense band at 425 nm (λ_{max}), for which it has a dark red colour. The electronic spectra of a number of model iron(III) phenolate complexes have been studied.[12–15,21] Hexa-coordinated (distorted octahedral) iron(III) phenolates show an intense LMCT transition in the 420–470 nm region. This transition is assigned as due to the transition from a *p*-orbital on the phenolate oxygen to the half-filled *d*-orbital on iron(III).[22] In the present case the peak at 425 nm is similarly assigned. For di-iron(III) lactoferrin (Fe_2lf) this band appears at 465 nm (λ_{max}). The high molar absorptivity of the transition is due to a good Fe—O overlap. The IR and conductivity data show that the amides are not deprotonated in **1**. A protonated amide is a poor donor. In complex **1** the

poor donating abilities of the amide nitrogens are compensated by stronger bonds between iron(III) and phenolate oxygens—a fact corroborated by room-temperature Mössbauer data. This is reflected in the higher molar absorptivity for the LMCT band involving phenolate oxygens. The ligand field transitions are obscured due to the strong 42.5 nm band.

The room-temperature magnetic moment value after diamagnetic corrections is 5.5 μ_{eff}/μ_B, which is within the normal range found[15,21,23] for octahedral high-spin iron(III) complexes, corresponding to $S = 5/2$. The X-band EPR spectra of the complex in the solid state as well as in acetonitrile solution (*ca* 1×10^{-3} M) were examined at room temperature (300 K) and at liquid nitrogen temperature (77 K). In the solution phase the complex does not exhibit a well resolved spectrum either at room temperature or at 77 K. However, in the solid state it shows a well resolved signal at $g = 4.06$. The signal at $g = 4.06$ is due to a transition between the middle Kramers doublet. Iron tyrosinate proteins[6-8] and model iron(III) complexes[11-15] exhibit similar EPR spectra, which are typical of high-spin iron(III) complexes with rhombically distorted octahedral geometry.

Cyclic voltammograms for the complex were recorded at room temperature in acetonitrile (*ca* 1×10^{-3} M) at a glassy carbon electrode. When scanned in the positive direction first no well-defined peak could be observed either in the positive or in the negative side. However, when scanned in the negative direction first a broad cathodic peak appears at -1.02 V (vs S.C.E.) and on scan reversal the corresponding anodic peak appears at -0.5 V (vs S.C.E.). If the scan continues to *ca* $+0.6$ V then no peak appears anywhere. This signifies the breakdown of the ligand–metal ensemble on oxidation. The couple with $E_{1/2}$ at -0.76 V is attributable to the following redox process:

$$[FeL] + e^- = [FeL]^- \qquad (1)$$

The ligand-based nature of the couple is ruled out because nickel(II) and manganese(III) complexes of L do not show any couple at this $E_{1/2}$ value.[24] The large separation of the peaks can be attributed to extensive rearrangement of the product accompanying the redox process.

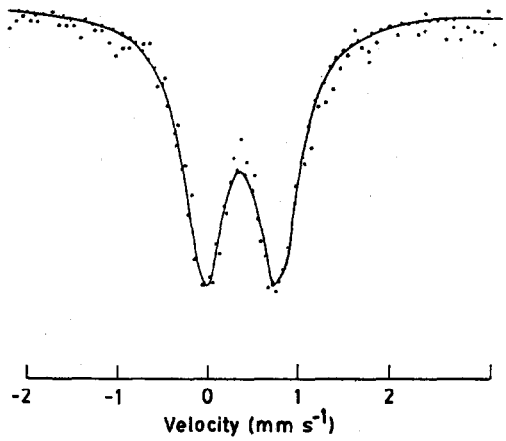

Fig. 2. Room-temperature Mössbauer spectrum for **1**.

The Mössbauer data for **1** and related systems are collected in Table 1. The complex shows (Fig. 2) an isomer shift of 0.37 mm s^{-1} with respect to iron metal, suggesting more covalency in the bonding between iron(III) and the ligands. This value lies close to that of lactoferrin[25] (0.39 mm s^{-1}) and transferrin[26] (0.38 mm s^{-1}), besides other octahedral high-spin iron(III) complexes. For octahedral complexes where the iron(III)–ligand bonding is more ionic an isomer shift of *ca* 0.5 mm s^{-1} with respect to the iron metal is observed.[12] Complex **1** shows quite a large value for the quadrupole splitting reflecting an unsymmetrical field around the ferric ion. Similar values are obtained in the case of structurally characterized, rhombically-distorted octahedral iron(III) complexes, as well as in cases of some iron tyrosinate proteins (Table 2).

CONCLUSION

A new tripodal ligand has been synthesized, which forms a rhombically-distorted octahedral complex with iron(III). The Mössbauer data for this complex closely resembles those of the iron tyrosinate proteins, lactoferrin and transferrin. The EPR and electronic spectral results are also very

Table 1. IR (selective) and electronic absorption spectral data

Compound	Selected IR bands (cm^{-1})	Electronic absorption bands λ_{max} (nm) (ε_{max}, $dm^3\ mol^{-1}\ cm^{-1}$)
L	3300s br; 1760s br; 1685s br	
1	3310s br; 1650s br	425(2620); 325(sh, 5400); 300(10,900)

Table 2. Mössbauer spectral data for **1** and related systems

Compound	Isomer shift (Fe, mm s^{-1})	Quadrupole splitting (E_q, mm s^{-1})	Ref.
1	0.37	0.82	This work
FeLf	0.39		25
FeTf	0.38	0.75	26
HCO^{3-} Free FeTf	0.47	0.72	27
$Fe(L_1)_3 \cdot 6H_2O$	0.41	0.92	28
$Fe(L_2)_3 \cdot 1.5H_2O$	0.38	0.72	12
Fe(EHGS)	0.54	1.60	11a

Lf = lactoferrin.
Tf = transferrin.
L_1 = nicotinylhydroxamic acid.
L_2 = 2-(5-methylpyrazol-3-yl)phenol.
EHGS = N-[2-((*o*-hydroxyphenyl)glycino)ethyl]salicylidenimine.

similar. These results suggest that effective electronic structural analogues of the iron tyrosinate proteins can be synthesized from ligands incorporating a number of phenolate groups in addition to nitrogen donors.

Acknowledgement—Financial help from the Department of Science and Technology, New Delhi, India, is gratefully acknowledged.

REFERENCES

1. R. M. Kirchner, C. Mealli, M. Bailey, M. Howe, L. P. Torre, L. J. Wilson, L. C. Andrews, N. J. Rose and R. C. Lingafelter, *Coord. Chem. Rev.* 1987, **77**, 89.
2. K. Ragunathan and P. K. Bharadwaj, *J. Chem. Soc., Dalton Trans.* 1992, 2417; C. Orvig, D. J. Berg and S. J. Rettig, *J. Am. Chem. Soc.* 1991, **113**, 2528; S. Liu, L. Gelmini, S. J. Rettig, R. C. Thompson and C. Orvig, *J. Am. Chem. Soc.* 1992, **114**, 6081.
3. K. Ragunathan and P. K. Bharadwaj, *J. Chem. Soc., Dalton Trans.* 1992, 1653; J. Hunter, J. Nelson, C. Harding, M. McCann and V. McKee, *J. Chem. Soc., Chem. Commun.* 1990, 1148.
4. J. de Mendoza, E. Meza, J. C. Rodriguez-Ubis, P. Vasquez, F. Vogtle, P. M. Windscheif, K. Rissanen, J. M. Lehn, D. Lilienbaum and R. Ziessel, *Angew. Chem., Int. Edn Engl.* 1991, **30**, 1331; T. J. McMurry, S. J. Rodgers and K. N. Raymond, *J. Am. Chem. Soc.* 1987, **109**, 3451.
5. K. Ragunathan and P. K. Bharadwaj, *Tetrahedron Lett.* 1992, 7581.
6. L. Que Jr, *Coord. Chem. Rev.* 1983, **50**, 73; L. Que Jr, *J. Chem. Ed.* 1985, **62**, 938.
7. B. F. Anderson, H. M. Baker, E. J. Dodson, G. E. Norris, S. V. Ramball, J. M. Watersand and E. N. Baker, *Proc. Natl. Acad. Sci. (USA)* 1987, **84**, 1769.
8. S. Bailey, R. W. Evans, R. C. Garratt, B. Gorinsky, S. Hasnain, C. Horsburg, H. Jhoti, P. F. Lindley, A. Mydin, R. Sarra and J. L. Watson, *Biochemistry* 1988, **27**, 5804.
9. J. W. Whittaker, J. D. Lipscomb, T. A. Kent and E. Munck, *J. Biol. Chem.* 1984, **259**, 4466.
10. D. H. Ohlendorf, J. D. Lipscomb and P. C. Weber, *Nature (London)* 1988, **336**, 403; F. C. Beadley, S. Lindstedt, J. D. Lipscomb, L. Que Jr, A. L. Roe and M. Rundgren, *Biochemistry* 1986, **261**, 11693.
11. C. J. Carrano, K. Spartalian, G. V. N. A. Rao, V. L. Pecoraro and M. Sundaralingam, *J. Am. Chem. Soc.* 1985, **107**, 1651; C. J. Carrano, M. W. Carrano, K. Sharma, G. Backes and J. S. Loehr, *Inorg. Chem.* 1990, **29**, 1865.
12. E. W. Ainscough, A. M. Brodie, J. E. Plowman, K. L. Brown, A. W. Addison and A. R. Gainsford, *Inorg. Chem.* 1980, **19**, 3655.
13. L. Casella, M. Gullotti, A. Pintar, L. Messori, A. Rochenbauer and M. Gyor, *Inorg. Chem.* 1987, **26**, 1031.
14. J. W. Pyrz, A. L. Roe, L. J. Stern and L. Que Jr, *J. Am. Chem. Soc.* 1985, **107**, 641.
15. M. R. McDevitt, A. W. Addison, E. Sinn and L. K. Thompson, *Inorg. Chem.* 1990, **29**, 3425.
16. D. D. Perrin, W. L. F. Armarego and D. R. Perrin, *Purification of Laboratory Chemicals*, 1st edn. Pergamon Press, Oxford (1966).
17. S. Mandal and P. K. Bharadwaj, *Polyhedron* 1992, **11**, 1037.
18. S. Mandal and P. K. Bharadwaj, *Polyhedron* 1993, **12**, 543.
19. B. R. Furniss, A. J. Hannaford, V. Rogers, P. W. G. Smith and A. R. Tatchell, *Vogel's Textbook of Practical Organic Chemistry*, 4th edn, pp. 832. Longman, U.K.
20. R. B. Roof Jr, *Acta Cryst.* 1956, **9**, 781.
21. K. Ramesh and R. N. Mukherjee, *J. Chem. Soc., Dalton Trans.* 1992, 83.

22. B. P. Gaber, V. Miskowski and T. G. Spiro, *J. Am. Chem. Soc.* 1974, **96**, 6868.
23. D. F. Cook, D. Cummins and E. D. McKenzie, *J. Chem. Soc. Dalton Trans.* 1976, 1369; R. C. Burrows and J. C. Bailer Jr, *J. Am. Chem. Soc.* 1966, **88**, 4150; J. C. Davis, W. J. Kung and B. A. Averill, *Inorg. Chem.* 1986, **25**, 394; R. W. Oehmbe and J. C. Bailar Jr, *J. Inorg. Nucl. Chem.* 1965, **27**, 2209.
24. R. Shukla and P. K. Bharadwaj, unpublished results.
25. J. Laidriere, R. Coussement and B. Theuwissen, *J. Phys. (Paris) Colloq.* 1974, 351.
26. K. Spartalian and W. T. Oosterhuis, *J. Chem. Phys.* 1973, **59**, 617.
27. C. P. Tsang, A. J. F. Boyle and E. H. Morgan, *Biochem. Biophys. Acta* 1975, **386**, 32.
28. L. M. Epstein and D. K. Straub, *Inorg. Chem.* 1969, **8**, 453.

Polyhedron Vol. 12, No. 12, pp. 1559–1568, 1993
Printed in Great Britain

0277–5387/93 $6.00+.00
Pergamon Press Ltd

PREPARATION, CHARACTERIZATION AND ELECTROCHEMICAL PROPERTIES OF TECHNETIUM(II) COMPLEXES WITH 1,2-BIS(DIETHYLPHOSPHINO)ETHANE (DEPE) AND DITHIOCARBAMATE LIGANDS. SINGLE-CRYSTAL STRUCTURAL ANALYSIS OF $[Tc((CH_3)_2NCS_2)(DEPE)_2](PF_6)$

KEN-ICHI OKAMOTO,† BAOHE CHEN, JON R. KIRCHHOFF,† DOUGLAS M. HO,† R. C. ELDER, WILLIAM R. HEINEMAN and EDWARD DEUTSCH†‡

Biomedical Chemistry Research Center, Department of Chemistry, University of Cincinnati, Cincinnati, OH 45221-0172, U.S.A.

and

MARY JANE HEEG‡

Department of Chemistry, Wayne State University, Detroit, MI 48202-3489, U.S.A.

(*Received* 9 *November* 1992; *accepted* 19 *January* 1993)

Abstract—Three technetium(II) complexes of the type $[Tc(dtc)(DEPE)_2]^+$ have been newly prepared and isolated, where DEPE denotes 1,2-bis(diethylphosphino)ethane and dtc represents dimethyldithiocarbamate (dmdc), diethyldithiocarbamate (dedc) or pentamethylenedithiocarbamate (pmdc). The complexes have been characterized by elemental analysis, UV–vis spectroscopy, FAB mass spectroscopy, electrochemistry and high performance liquid chromatography. Bidentate coordination of the dithiocarbamate ligand is confirmed by a single-crystal structural analysis of the prototypical complex $[Tc(dmdc)(DEPE)_2](PF_6)$. Bond lengths around the approximately octahedral technetium(II) centre are Tc—S = 2.449(6), Tc—P (*trans* to P) = 2.43(2) and Tc—P (*trans* to S) = 2.38(2) Å. The Tc—P length *trans* to the sulphur atom is significantly shorter than that which is *trans* to a phosphorus atom. Electrochemical measurements for the $[Tc(dtc)(DEPE)_2]^+$ complexes show a reversible technetium(II/I) couple between −0.517 and −0.544 V (vs Ag/AgCl) and another reversible technetium(III/II) couple ranging from +0.298 to +0.312 V (vs Ag/AgCl) in 0.5 M TEAP/DMF. The relevance of this chemistry to the design and development of new technetium radiopharmaceuticals is briefly discussed.

The interest in technetium complexes was initially, and still continues to be, derived largely from their utility in diagnostic medicine when prepared with the nuclide ^{99m}Tc.[1] Radiopharmaceutical design demands a careful control of many chemical factors, including reactivity, charge, lipophilicity and redox potential. Systematic studies through graduated classes of complexes, such as the technetium–diphosphine–thiolato series developed in our laboratory,[2–9] are necessary to understand and manipulate the complex factors responsible for *in vivo* metabolism.

As candidates for inclusion in our systematic investigations, dithiocarbamates provide an interesting group of sulphur donor ligands. These ligands possess a mixture of resonance forms and can bond in a variety of modes: unidentate, biden-

† Present addresses: Dr Ken-Ichi Okamoto, Department of Chemistry, The University of Tsukuba, Tsukuba, Ibaraki 305, Japan; Dr Jon R. Kirchhoff, Department of Chemistry, University of Toledo, Toledo, OH 43606, U.S.A.; Dr Douglas M. Ho, Department of Chemistry, Princeton University, Princeton, NJ 08544, U.S.A.; Dr Edward Deutsch, Mallinckrodt Medical, Inc., 675 McDonnell Blvd, P.O. Box. 5840, St Louis, MO 63134, U.S.A.

‡ Authors to whom correspondence should be addressed.

tate symmetric, bidentate asymmetric, S,S-bridging and μ-bridging. Unusual metal oxidation states are often stabilized by dithiocarbamate (dtc) ligands and their small chelate bite angle can accommodate high coordination numbers.[10]

In our continuing studies of low-valent, cationic technetium-bis(diphosphine) complexes[2-9] containing sulphur-donating ligands we were eager to incorporate the unusual properties of dithiocarbamate ligands and thus sought to synthesize $[Tc^{II}(dtc)(D)_2]^+$ (D = diphosphine ligand) complexes. When dtc functions as a chelating ligand the sulphur atoms are constrained to lie mutually *cis*, so the *cis*/*trans* interconversion reactions of $[Tc^{III/II}(SR)_2(D)_2]^{+/0}$ thiolato complexes are avoided. The charge on the dtc ligand is formally -1, as compared to a -2 contribution from two thiolato ligands, so that the overall charge of a dtc complex is relatively more positive than that of bis(thiolato) complexes. We were further interested in how the presence of the dtc ligand would affect the coordination geometry and redox potential of technetium-diphosphine complexes and especially what oxidation state of technetium would be favoured. This report contains the results of these investigations, highlighted by the syntheses and characterizations of three $[Tc(dtc)(DEPE)_2]^+$ complexes.

Acronyms and abbreviations

The following acronyms and abbreviations are used in this article: dedc = diethyldithiocarbamate; DEPE = 1,2-bis(diethylphosphino)ethane; dmdc = dimethyldithiocarbamate; DMF = N,N-dimethylformamide; DMPE = 1,2-bis(dimethylphosphino)ethane; DPPE = 1,2-bis(diphenylphosphino)ethane; dtc = dithiocarbamate; FAB = fast atom bombardment; HPLC = high performance liquid chromatography; LTMCT = ligand-to-metal charge transfer; Me = methyl; OTTLE = optically transparent thin-layer electrode; PDE = platinum disk electrode; Ph = phenyl; pmdc = pentamethylenedithiocarbamate; STE = structural *trans* effect; tdt = 3,4-toluenedithiolate; TEAP = tetraethylammonium perchlorate; TMT = tetramethylthiourea.

EXPERIMENTAL

CAUTION! Technetium-99 emits a low energy (0.292 MeV) β particle with a half-life of 2.12×10^5 years. When handled in milligram amounts ^{99}Tc does not present a serious health hazard since common laboratory materials provide adequate shielding. Bremsstrahlung is not a significant problem due to the low energy of the β particle emission, but normal radiation safety procedures must be used at all times, especially when dealing with solid samples, to prevent contamination and inadvertant inhalation. In this paper the symbol Tc refers only to technetium-99; the metastable isotope ^{99m}Tc was not used in these studies.

Reagents

Unless otherwise noted, all chemicals were of reagent grade. Technetium-99, in the form of solid ammonium pertechnetate, was obtained from Oak Ridge National Laboratory and purified.[11] The DEPE ligand was purchased from Strem Chemical Co. and used without further purification. The pmdc was prepared by a procedure similar to that published.[12] DMF was obtained from Burdick and Jackson Lab. Polarographic grade TEAP from G. F. Smith Chemicals was used in the electrochemical measurements. Prior to use the TEAP was dried at 60°C *in vacuo* over P_2O_5. No significant electroactive impurities were detected in either the solvent or supporting electrolyte. Na(dedc)·$3H_2O$ was purchased from Fisher Scientific and Na(dmdc)·$2H_2O$ from Aldrich Chemical.

Synthesis of $[Tc(dedc)(DEPE)_2](PF_6)$

The starting complex, *trans*-$[Tc(OH)(O)(DEPE)_2](PF_6)_2$, was prepared by the method similar to that described in a previous paper,[2] using NH_4TcO_4 (200 mg, 1.1×10^{-3} mol) and DEPE (1.5 cm^3, 4.8×10^{-3} mol). To a solution containing *trans*-$[Tc(OH)(O)(DEPE)_2](PF_6)_2$ (200 mg) in degassed 50/50 (v/v) ethanol–water (12 cm^3) was added a solution containing Na(dedc)·$3H_2O$ (350 mg) in degassed water (6 cm^3). The resultant mixture was stirred at *ca* 50°C for 5 min under argon. To this solution was gradually added a solution made up of formamidine sulphinic acid (110 mg) and NaOH (50 mg) in degassed water (12 cm^3). The mixture was continuously stirred at *ca* 50°C for 30 min under an argon atmosphere, during which time the colour of the precipitate gradually changed from yellow to red–brown. The precipitate was collected by filtration, washed with ethanol/water and water and dried in air; yield: 143 mg.

The complex was then recrystallized as follows. The crude product (above) (90 mg) was dissolved in ethanol (6 cm^3) in air. After 15 min an aqueous solution (7 cm^3) of NH_4PF_6 (700 mg) was added. After 1 h the red–brown precipitate was collected by filtration, washed with ethanol/water and water and dried in air; yield: 71 mg. Found: C, 37.3; H, 7.5; N, 1.7; P, 18.1; F, 13.4. Calc. for $[Tc(dedc)(DEPE)_2](PF_6)\cdot H_2O$, $C_{25}H_{60}NOS_2P_5F_6Tc$: C, 36.5; H, 7.4; N, 1.7; P, 18.8; F, 13.9%.

Synthesis of $[Tc(dmdc)(DEPE)_2](PF_6)$

This complex was prepared by a procedure similar to that above for $[Tc(dedc)(DEPE)_2](PF_6)$, using *trans*-$[Tc(OH)(O)(DEPE)_2](PF_6)_2$ (200 mg) and $Na(dmdc)\cdot 2H_2O$ (260 mg). A yellow impurity was insoluble in ethanol and acetonitrile, so the desired complex was extracted by ethanol. In the recrystallization procedure the resultant dmdc complex was dissolved in ethanol (5 cm^3) and acetonitrile (2 cm^3) and filtered. To the filtrate was added an aqueous solution (8 cm^3) containing NH_4PF_6 (800 mg). The precipitate was collected by filtration, washed with ethanol/water and water and dried in air; yield: 152 mg. Found: C, 35.6; H, 7.1; N, 1.8; P, 19.4; F, 14.3. Calc. for $[Tc(dmdc)(DEPE)_2](PF_6)$, $C_{23}H_{54}NS_2P_5F_6Tc$: C, 35.6; H, 7.0; N, 1.8; P, 19.9; F, 14.7%.

Single crystals suitable for X-ray analysis were obtained by dissolving the red–brown product in methanol at *ca* 50°C. The solution was filtered to remove insoluble materials. The filtrate was held at room temperature for 4 h under argon. The crystals which appeared were collected by filtration, washed with water and dried in air. These crystals were air stable throughout the duration of the X-ray diffraction experiment.

Synthesis of $[Tc(pmdc)(DEPE)_2](PF_6)$

This complex was prepared by a procedure similar to that above for $[Tc(dedc)(DEPE)_2](PF_6)$, using *trans*-$[Tc(OH)(O)(DEPE)_2](PF_6)_2$ (200 mg) and Na(pmdc) (315 mg). To recrystallize the pmdc complex the crude product was dissolved in ethanol (5 cm^3) and then filtered. (The colour of the undissolved material was yellow. This yellow complex was washed with ethanol/water and water and dried in air; yield: 55 mg.) To the filtrate was added an aqueous solution (8 cm^3) containing NH_4PF_6 (800 mg). The precipitate was collected by filtration, washed with ethanol/water and water and dried in air; yield: 126 mg. $[Tc(pmdc)(DEPE)_2](PF_6)$ is less soluble in both polar and non-polar solvents than the other dtc complexes reported here. Found: C, 37.0; H, 7.1; N, 1.7; P, 18.8; F, 13.3. Calc. for $[Tc(pmdc)(DEPE)_2](PF_6)\cdot 1/2H_2O$, $C_{26}H_{59}NO_{0.5}S_2P_5F_6Tc$: C, 37.8; H, 7.2; N, 1.7; P, 18.8; F, 13.8%.

HPLC analyses

HPLC experiments were conducted on an ISCO model 2350 liquid chromatograph with a gradient programmer model 2360, equipped with a guard column containing pellicular C-8 packing material and a reversed-phase C-8 analytical column (4.8 × 150 mm). The mobile phase was 97/3 ethanol/0.1 mol dm^{-3} NH_4CH_3COO (aqueous) and the flow rate 1 cm^3 min^{-1}. Spectrophotometric detection was performed with a Hewlett–Packard 1040A HPLC diode array detection system, which recorded the spectrum between 200 and 600 nm for selected points in each peak on the chromatogram.

Measurements

Elemental analyses were performed by Galbraith Laboratories, Knoxville, Tennessee. UV–vis spectra were recorded in acetonitrile on a Cary 210 spectrophotometer (Varian) at ambient temperature. FAB mass spectra were recorded using *m*-nitrobenzylalcohol as the matrix on a VG 30-250 spectrometer (VG Instruments). Xenon was used as the primary beam gas and the ion gun was operated at 8 KeV and 100 μA. The mass data were generally collected over the mass range 200–1000 Da at 0.7 s per scan.

Electrochemical measurements were obtained with a Bioanalytical Systems, Inc. (BAS) CV-1B voltammograph. Potentials were monitored with a Keithley 178 digital multimeter and voltammograms were recorded on a Hewlett–Packard 7015B *X–Y* recorder. Cyclic voltammograms were obtained in 0.5 M TEAP/DMF solutions under argon *vs* an Ag/AgCl (3 M NaCl) reference electrode,[13] using a platinum disk working electrode (BAS MF 2013) and a platinum wire auxiliary electrode. The reference electrode was isolated from the solution by a porous Vycor plug.

Crystallography

Single-crystal X-ray diffraction experiments were performed on a Nicolet R3m automated diffractometer with a graphite monochromator. Data are summarized in Table 1. All non-hydrogen atoms were refined anisotropically. Hydrogen atoms were allowed to ride on their respective carbon atoms with C—H = 0.96 Å and with isotropic thermal parameters fixed at 0.08 $Å^2$. The methyl groups of the dmdc ligand were treated as rigid groups with rotational freedom and all P—F bonds in the hexafluorophosphate anion were constrained to 1.56 Å. The inverse (enantiomeric) model was tested and found to converge at slightly higher residuals ($R = 0.041$ and $wR = 0.052$) and thus was rejected. Absorption corrections were empirically derived from psi scans. Structure solutions by Patterson methods and refinements used the programs of SHELXTL-PLUS,[14] including its stored values for neutral atom-scattering factors and corrections for anomalous dispersion.

Table 1. Crystallographic data for $[Tc(dmdc)(DEPE)_2]PF_6$

Formula	$Tc_1S_2P_5F_6N_1C_{23}H_{54}$
a (Å)	19.626(5)
b (Å)	10.854(1)
c (Å)	16.725(2)
V (Å^3)	3562.8(9)
Z	4
R^a	0.039
wR^a	0.050
Formula weight	776.59 amu
Space group	$Pca2_1$ (No. 29)
T (°C)	20
λ (Å)	0.71073
μ (cm^{-1})	7.74
ρ(calc) (g cm^{-3})	1.448
Transmission coefficients	1.000–0.850

$^a R = (\Sigma|\Delta F|)/\Sigma|F_o|$; w$R = [(\Sigma w|\Delta F|^2)/\Sigma wF_o^2]^{1/2}$.

RESULTS AND DISCUSSION

Synthesis and characterization

Three $[Tc^{II}(dtc)(DEPE)_2]^+$ complexes (dtc = dmdc, dedc and pmdc) were prepared by the reaction of *trans*-$[Tc(OH)(O)(DEPE)_2](PF_6)_2$ with dtc in the presence of the reducing agent formamidine sulphinic acid in alkaline solution. HPLC analysis shows that the crude initial product consists of two compounds. Recrystallization of the crude product from ethanol and aqueous NH_4PF_6 yields a solid product, the HPLC retention time of which corresponds to the latter eluted species in the HPLC of the crude product. This recrystallized solid is pure since the HPLC indicates only one band and identical 200–600 nm spectra were exhibited at multiple points within the HPLC band (thus confirming the homogeneity of the product). The absorption spectrum of the recrystallized precipitate in acetonitrile is identical to the corresponding spectra obtained from the HPLC measurements. The composition of one of the recrystallized products was determined by X-ray structural analysis to be $[Tc(dmdc)(DEPE)_2](PF_6)$. Therefore, we conclude that the latter eluted species in the crude product and the recrystallized materials are all members of the class of technetium(II) complexes $[Tc(dtc)(DEPE)_2]^+$.

The earlier eluted species observed in the dmdc and dedc preparations could not be obtained as a solid because they are unstable in solution. The colour of this species (for the dmdc preparation) is pale yellow; absorption maxima are observed at *ca* 364 and 290 nm using the HPLC detection system. Further, the positive ion-mode FAB mass spectrum for the earlier eluting, yellow component of the pmdc preparation suggests the same composite formulation as that of the latter eluting $[Tc^{II}(pmdc)(DEPE)_2]^+$ species: both exhibit a parent peak at $m/z = 671$. Therefore, since the two species of the crude product have the same atomic composition but different HPLC retention times, a difference in complex charge is implied. The assignment of a neutral technetium(I) species, i.e. $[Tc^{I}(pmdc)(DEPE)_2]^0$, is consistent with the more rapid HPLC elution under the given conditions. Therefore, the crude product of the pmdc synthetic reaction contains both $[Tc^{I}(pmdc)(DEPE)_2]^0$ and $[Tc^{II}(pmdc)(DEPE)_2]^+$. This assignment is supported by the facile technetium(II/I) redox chemistry discussed below.

Elemental analyses of the red–brown recrystallized materials are in acceptable agreement with the proposed formulations: $[Tc(dtc)(DEPE)_2](PF_6)\cdot nH_2O$ ($n = 0$ for dtc = dmdc; $n = 1$ for dtc = dedc; $n = 1/2$ for dtc = pmdc). These analyses are consistent with a +1 charged complex cation. Compositional assignments are also reliably made by positive ion-mode FAB mass spectrometry. A typical FAB mass spectrum is shown in Fig. 1; the interpretation of high molecular weight, positively charged, fragments is straightforward. Parent peaks occur at $m/z = 631$ for $[Tc(dmdc)(DEPE)_2]^+$, $m/z = 659$ for $[Tc(dedc)(DEPE)_2]^+$ and $m/z = 671$ for $[Tc(pmdc)(DEPE)_2]^+$, which are consistent with the calculated masses for those cations (631.17, 659.20 and 671.20 Da, respectively). Several fragment ions corresponding to the loss of C_2H_5 ($m/z = 29$), $CH_2CH_2P(C_2H_5)_2$ ($m/z = 117$) and/or DEPE ($m/z = 206$) are also observed as summarized in Table 2. Fragment ions resulting from loss of the dtc ligand and its components were not observed for the three complexes investigated.

Our previous attempt to prepare $[Tc(dtc)(DEPE)_2]^+$ complexes was conducted in acidic solution; this led to cleavage of the dtc moiety at the C—N bond and the formation of an unusual condensation product of the dtc fragment

Table 2. FAB mass spectral data for $[Tc(dtc)(DEPE)_2]PF_6$

dtc	Complex ion (M^+)	Fragment ion [M − ( )] C_2H_5	$CH_2CH_2P(C_2H_5)_2$	DEPE
dmdc	631[a]	602	—	—
dedc	659[a]	630	542	453
pmdc	671[a]	642	554	465

[a] Intense peak.

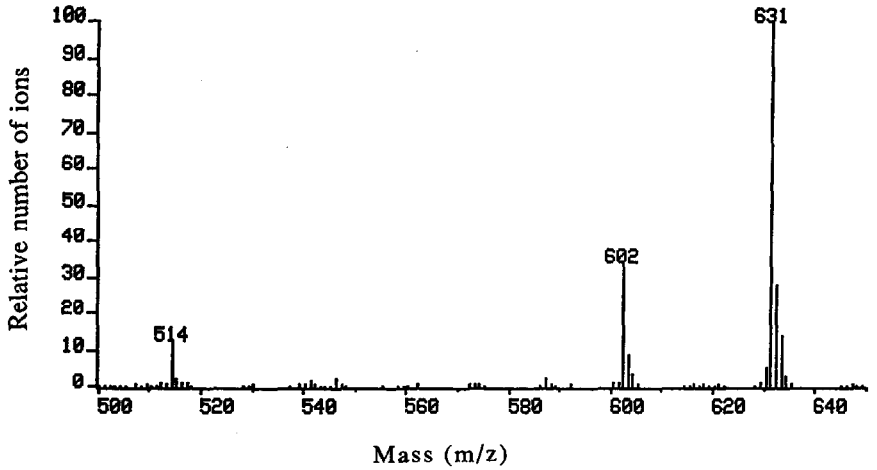

Fig. 1. The FAB mass spectrum of $[Tc(dmdc)(DEPE)_2]PF_6$ over the 500–650 *m/z* range.

and excess DMPE.[7] However, under alkaline conditions the dtc moiety remains intact and ligates to technetium. The reductant, formamidine sulphinic acid, used in these syntheses has been employed in other technetium-dtc preparations,[15] in which pertechnetate is the starting material. The present work demonstrates the utility of formamidine sulphinic acid as a reductant for the technetium(V) complex *trans*-$[Tc(OH)(O)(DEPE)_2]^{2+}$.

Although dtc ligands are capable of a large number of bonding modes, with technetium only the bidentate form of dtc bonding has been observed. A handful of technetium-dtc complexes have been structurally examined and include two five-coordinate technetium(V) complexes,[16,17] $[TcN(dedc)_2]$ and $[TcO(dmdc)(TMT)_2]$, a six-coordinate technetium(I) complex,[18] $[Tc(CO)_2(PPh_3)_2(dtc)]$, four seven-coordinate technetium(III) complexes,[15,19–21] $[Tc(dedc)_3(CO)]$, $[Tc(dedc)(PMe_2Ph)]$, $[Tc(dedc)_2Cl_2(NS)]$ and $[Tc(dedc)_2Br_2(NS)]$, and one other six-coordinate technetium(II) complex,[17] $[Tc(dmdc)(DPPE)_2]^+$. The latter complex was an accidental result of a synthesis intended to produce a mixed ligand complex containing a thiourea derivative. The presently reported $[Tc(dtc)(DEPE)_2]^+$ complexes are the first technetium(II)-dtc examples to be generated by a deliberate, rational synthesis and are more fully characterized than the others mentioned above. It is worth noting that those technetium complexes containing multiple dtc ligands are stable in higher oxidation states [technetium(III) and technetium(V)], which seems to attest to the effective σ-donor ability of dtc, while those dtc complexes in which technetium is in a lower formal oxidation state [technetium(I) and technetium(II)] contain π-accepting carbonyl and/or phosphine ligands.

All three $[Tc^{II}(dtc)(DEPE)_2]^+$ complexes exhibit

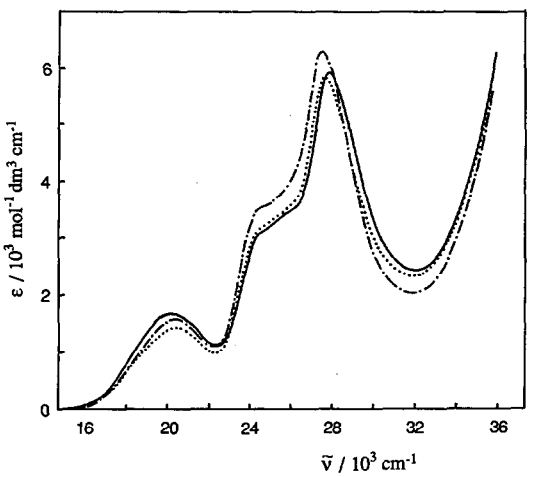

Fig. 2. The absorption spectra of $[Tc(dtc)(DEPE)_2]^+$ recorded in acetonitrile: dtc = dmdc (——), dedc (· · · ·) and pmdc (–·–·–).

similar UV–vis absorption spectral patterns, as shown in Fig. 2. The bands in this region consist of one peak at *ca* 20×10^3 cm^{-1}, an indistinct intermediate shoulder region and an intense absorption around 28×10^3 cm^{-1}. Extinction coefficients for these transitions are greater than 10^3 M^{-1} cm^{-1}. Absorption data are presented in Table 3. The X-ray analysis has definitively identified the $[Tc^{II}$

Table 3. UV–vis spectral data for $[Tc(dtc)(DEPE)_2]^+$ [a]

dtc	λ_{max} (10^3 cm^{-1}) ($\varepsilon/10^3$ M^{-1} cm^{-1})		
dmdc	20.20 (1.68)	25.00sh (3.22)	27.86 (5.93)
dedc	20.40 (1.43)	25.00sh (3.27)	27.66 (5.85)
pmdc	20.33 (1.58)	24.69sh (3.55)	27.55 (6.29)

[a] sh denotes a shoulder.

$(dmdc)(DEPE)_2]^+$ complex and the similarities in spectral characteristics of all three dtc complexes strongly suggest that they all contain technetium in the +2 oxidation state with similarly bound ligands.

LTMCT bands in the near UV–vis region typically occur at *ca* 540 and 440 nm for *trans*-$[Tc^{II}(S\text{-alkyl})(DMPE)_2]^0$ complexes (determined by OTTLE)[3] and around 520, 450 and 390 nm for *cis*-$[Tc^{II}(S\text{-aryl})_2(DMPE)_2]^0$ complexes (determined by OTTLE).[5] These bands are assigned to arise from $S(\pi) \rightarrow Tc(\pi^*)$ transitions; they mask the lower intensity *d–d* transitions observed in this region in the absorption spectra of $[Tc^{II}(DMPE)_3]^{2+}$ and $[Tc^{II}(DEPE)_3]^{2+}$.[22] In the three $[Tc^{II}(dtc)(DEPE)_2]^+$ complexes reported here, the intense LTMCT absorptions at 490 and 400 (sh) nm appear to be analogous to the 452 and 338 (sh) nm absorptions observed in $[Tc^{II}(tdt)(DMPE)_2]^0$ (determined by OTTLE)[7] with a similar pattern of intensities.

Crystallography, $[Tc(dmdc)(DEPE)_2](PF_6)$

A perspective view of the complex cation $[Tc(dmdc)(DEPE)_2]^+$ is illustrated in Fig. 3 along with the atomic labelling scheme. The independent portion of the structure consists of one discrete complex cation and one hexafluorophosphate anion. All atoms occupy general positions in the unit cell. The technetium ion is at the centre of a tris-chelate ligand arrangement, where the six donor atoms are as close to octahedral as possible within the constraints of the chelate bite angles. An evaluation of the *fac* twist angle[23] indicates that no trigonal distortion is exhibited by the ligands in $[Tc(dmdc)(DEPE)_2]^+$. Assigning the dmdc ligand a formal −1 charge leads to the conclusion that the technetium centre is in a formal +2 oxidation state.

Selected bond lengths and angles are reported in Table 4. The dmdc molecule acts as a symmetric bidentate (S,S) ligand. The two Tc—S bond distances are equivalent, implying a delocalization of the −1 charge in the dithiocarbamate. The entire dmdc ligand is planar (rmsd = 0.022 Å) and technetium is located 0.20 Å out of this plane. The dmdc bite angle is 71.5(1)°. The Tc—P distances average 2.43(2) Å when the *trans* ligand is a phosphine and 2.38(2) Å when the *trans* ligand is the dithiocarbamate. Therefore, in this complex the dmdc sulphur donor induces a *trans* shortening of 0.05 Å on the Tc—P bond distance. DEPE bite angles are normal at 81.8(1)° and 81.9(1)°.

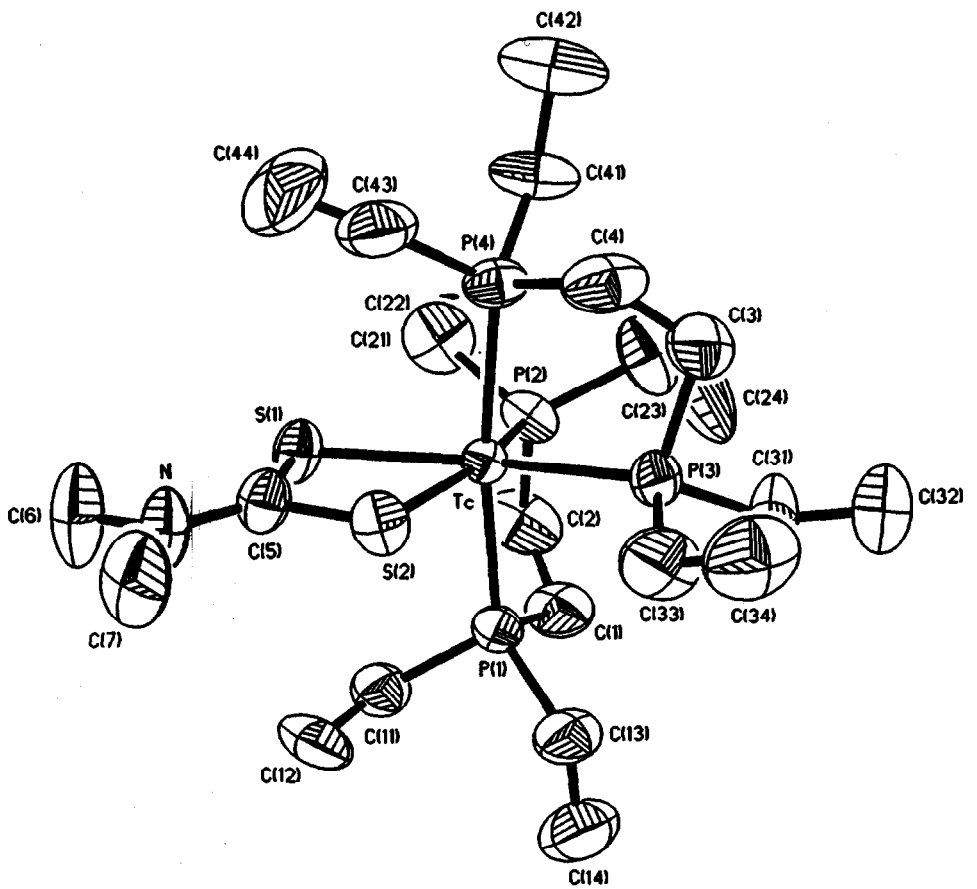

Fig. 3. Thermal ellipsoid drawing of the $[Tc(dmdc)(DEPE)_2]^+$ cation.

Table 4. Selected bond lengths (Å) and angles (°) in the cation $[Tc(dmdc)(DEPE)_2]^+$

Tc—S(1)	2.444(2)	P(1)—C(1)	1.86(1)
Tc—S(2)	2.453(2)	P(2)—C(2)	1.84(1)
Tc—P(1)	2.420(2)	P(3)—C(3)	1.83(1)
Tc—P(2)	2.364(2)	P(4)—C(4)	1.82(1)
Tc—P(3)	2.397(2)	N(1)—C(5)	1.31(1)
Tc—P(4)	2.442(2)	N(1)—C(6)	1.47(1)
S(1)—C(5)	1.710(8)	N(1)—C(7)	1.44(1)
S(2)—C(5)	1.737(8)	C(1)—C(2)	1.47(2)
		C(3)—C(4)	1.49(2)

S(1)—Tc—S(2)	71.5(1)	Tc—P(1)—C(1)	107.1(3)
S(1)—Tc—P(1)	92.4(1)	Tc—P(2)—C(2)	109.6(4)
S(2)—Tc—P(1)	93.8(1)	Tc—P(3)—C(3)	108.3(3)
S(1)—Tc—P(2)	92.9(1)	Tc—P(4)—C(4)	105.9(3)
S(2)—Tc—P(2)	163.6(1)	C(5)—N(1)—C(6)	118.7(8)
P(1)—Tc—P(2)	81.9(1)	C(5)—N(1)—C(7)	123.2(8)
S(1)—Tc—P(3)	164.5(1)	C(6)—N(1)—C(7)	118.1(8)
S(2)—Tc—P(3)	93.3(1)	P(1)—C(1)—C(2)	110.3(7)
P(1)—Tc—P(3)	91.7(1)	P(2)—C(2)—C(1)	110.4(7)
P(2)—Tc—P(3)	102.5(1)	P(3)—C(3)—C(4)	110.2(7)
S(1)—Tc—P(4)	94.6(1)	P(4)—C(4)—C(3)	110.4(7)
S(2)—Tc—P(4)	89.6(1)	S(1)—C(5)—S(2)	112.2(5)
P(1)—Tc—P(4)	172.8(1)	S(1)—C(5)—N(1)	125.7(6)
P(2)—Tc—P(4)	96.5(1)	S(2)—C(5)—N(1)	122.0(6)
P(3)—Tc—P(4)	81.8(1)		
Tc—S(1)—C(5)	88.6(3)		
Tc—S(2)—C(5)	87.7(3)		

The set of technetium–thiolato–diphosphine complexes characterized to date[2,4–8] show Tc—S(thiol) lengths to be dependent on technetium oxidation state; Tc^{III}—S averages 2.30(1) and Tc^{II}—S averages 2.42(1) Å. The Tc^{II}—S(dtc) lengths of 2.45(1) in $[Tc(dmdc)(DEPE)_2]^+$ and 2.44(1) Å in $[Tc(dmdc)(DPPE)_2]^+$[17] are close to the technetium(II)–thiolato length. Table 5 summarizes the structural parameters for technetium-dtc compounds. The first technetium(III) complexes of Table 5 all have expanded coordination numbers ($n = 7$) and this tends to lengthen bond distances.

Table 5. Structural comparison of technetium-dtc complexes[a]

Complex	n	Oxidation	Tc—S (Å)	S—C (Å)	C=N (Å)	N—C (Å)	S—Tc—S bite (°)	Ref.
$[TcN(dedc)_2]$	5	V	2.40	1.73	1.32	1.49	73	16
$[TcO(dmdc)(TMT)_2]$	5	V	2.35	1.75	1.28	1.48	74	17
$[Tc(NS)(dedc)_2Br_2]$	7	III	2.48	1.72	1.31	1.48	69	21
$[Tc(CO)(dedc)_3]$	7	III	2.47[b]	1.71	1.33	1.48	69	15
$[Tc(Cl)_2(NS)(dedc)_2]$	7	III	2.46	1.70	1.33	1.47	70	20
$[Tc(PMe_2Ph)(dedc)_3]$	7	III	2.48	1.71	1.33	1.46	69	19
$[Tc(dmdc)(DEPE)_2]^+$	6	II	2.45	1.72	1.31	1.46	72	[c]
$[Tc(dmdc)(DPPE)_2]^+$	6	II	2.44	1.67	1.36	1.46	71	17
$[Tc(CO)(PPh_3)_2(SC(NHPh)S)]$	6	I	2.51	1.70	1.34	1.42	71	18

[a] n is the coordination number, Oxidation is the oxidation state of technetium. E.s.d.s on lengths are of the order 0.01–0.03 Å. E.s.d.s on angles are of the order 1–2°. The bond lengths and angles quoted in the table are only those involved in the dtc ligands.

[b] One Tc—S length is 2.52 *trans* to CO and not included in this average.

[c] This work.

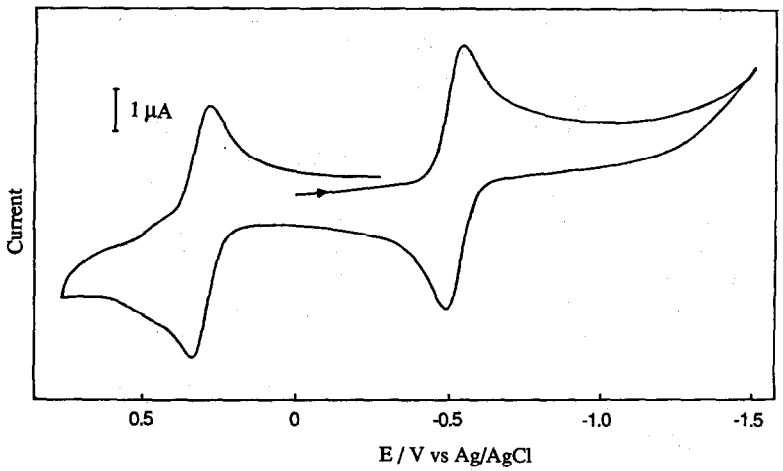

Fig. 4. A cyclic voltammogram of $[Tc(dmdc)(DEPE)_2]^+$ (6.2×10^{-4} g cm^{-3}) in 0.5 M TEAP/DMF at a PDE. Scan rate is 100 mV s^{-1}.

Taking this into account, Tc—S(dtc) lengths increase with decreasing technetium oxidation state, as we have observed with Tc—S(thiolato) lengths in the absence of other factors. The geometry of the dmdc ligand in $[Tc^{II}(dmdc)(DEPE)_2]^+$ is entirely in agreement with the other entries of Table 5.

The Tc^{II}—P length in $[Tc(dmdc)(DEPE)_2]^+$ averages 2.43(2) Å when *trans* to another phosphorus atom. The Tc^{II}—P(DMPE) length is *ca* 2.39 Å in similar complexes[4] and Tc—P(DMPE) lengths are slightly shorter than equivalent Tc—P(DEPE) lengths.[2] The Tc—P(DPPE) lengths (*trans* to phosphorus) in $[Tc^{II}(dmdc)(DPPE)_2]^+$ [17] are longer at 2.46(2) Å, due to the increasing bulk of the DPPE substituents; however, a *trans* shortening of the Tc—P length opposite the sulphur ligand is similarly observed. In contrast, technetium(III) and technetium(II) complexes containing thiols and DMPE exhibit Tc—P lengths which are longer when located *trans* to a thiolato ligand relative to those *trans* to another phosphine.[4,5] This indicates some fundamental bonding differences between thiolato and dtc ligands.

Electrochemistry

Cyclic voltammograms were obtained for solutions of the $[Tc(dtc)(DEPE)_2]^+$ (dtc = dmdc, dedc and pmdc) complexes in 0.5 M TEAP/DMF at a PDE. The voltammogram shown in Fig. 4 is that of $[Tc(dmdc)(DEPE)_2]^+$, but is typical of the other dtc complexes as well. For $[Tc(dmdc)(DEPE)_2]^+$ a negative potential scan initiated at 0.0 V exhibits a single reduction wave at −0.488 V. Upon reversing that scan at −1.5 V the corresponding reoxidation wave appears at −0.546 V. A positive potential scan to +0.75 V shows one other major redox couple centred at +0.312 V. These redox couples are assigned as diffusion-controlled, reversible, one-electron transfers on the basis of fulfilment of the accepted criteria for reversibility.[24] The formal reduction potentials, $E^{0\prime}$, are summarized in Table 6. With reference to the previously reported electrochemistry of technetium-diphosphine complexes,[2,3,5,7,11,22,25,26] these two redox processes are assigned as technetium(II/I) and technetium(III/II) reversible redox couples:

$$[Tc^{II}(dtc)(DEPE)_2]^+ + e^- \rightleftharpoons [Tc^{I}(dtc)(DEPE)_2]^0$$

$$E^{0\prime} = -0.52 \text{ to } -0.54 \text{ V}$$

$$[Tc^{III}(dtc)(DEPE)_2]^{2+} + e^- \rightleftharpoons [Tc^{II}(dtc)(DEPE)_2]^+$$

$$E^{0\prime} = +0.30 \text{ to } +0.31 \text{ V}.$$

Table 6 compares technetium(III/II) and technetium(II/I) redox potentials for similar complexes and shows that the reduction potentials characterizing $[Tc(dtc)(DEPE)_2]^+$ are unusual for technetium–sulphur/phosphine ligand complexes. In the dtc complexes the lower oxidation states are markedly stabilized relative to the dithiolato analogues. In general, the technetium(III) dithiocarbamate complexes are *ca* 500–900 mV easier to reduce to technetium(II) and the technetium(II) complexes are *ca* 600–1400 mV easier to reduce to technetium(I) than are the dithiolato analogues. From our studies of $[Re(SR)_2(DMPE)_2]^+$ complexes[27] it has been noted that rhenium(III/II) redox potentials vary only *ca* 50 mV between *cis* and *trans* geometries, the *cis*-$[Re(SR)_2(DMPE)_2]^+$ complexes being slightly easier to reduce than the *trans*. Therefore, the marked difference between the

Table 6. Comparison of redox potentials[a]

Complex ion	Technetium(III/II), $E^{0\prime}$ (V)	Technetium(II/I), $E^{0\prime}$ (V)	Ref.
$[Tc(dmdc)(DEPE)_2]^+$	+0.312	−0.517	This work
$[Tc(dedc)(DEPE)_2]^+$	+0.307	−0.544	This work
$[Tc(pmdc)(DEPE)_2]^+$	+0.298	−0.542	This work
$[Tc(DEPE)_3]^+$		+0.276	22
$[Tc(DMPE)_3]^+$		+0.422	22
Cis-$[Tc(SC_6H_4X)_2(DMPE)_2]^+$	−0.38 to −0.19	−1.2 to −1.1	5
Trans-$[Tc(SR)_2(DMPE)_2]^+$	−0.62 to −0.51	−1.9 to −1.7	3
$[Tc(tdt)(DMPE)_2]^+$	−0.60	−1.22	7
Trans-$[Tc(Cl)_2(DMPE)_2]^+$	−0.231	−1.41	22
Trans-$[Tc(Br)_2(DMPE)_2]^+$	−0.098	−1.27	22
Trans-$[Tc(SMe)_2(DEPE)_2]^+$	−0.554	−1.81	2
Trans-$[Tc(Cl)_2(DEPE)_2]^+$	−0.260	−1.44	22
Trans-$[Tc(Br)_2(DEPE)_2]^+$	−0.131	−1.29	22
Trans-$[Tc(NCS)_2(DPPE)_2]$	+0.390	−0.600	25
Trans-$[Tc(Cl)_2(DPPE)_2]^+$	−0.001		11
Trans-$[Tc(Br)_2(DPPE)_2]^+$	+0.103		11

[a] 25°C; PDE working electrode; scan rate 100 mV s^{-1}; 0.5 M TEAP/DMF; $E^{0\prime} = (E_{pc} + E_{pa})/2$ vs Ag/AgCl (3 M NaCl) from cyclic voltammetry.

reducibility of $[Tc^{III}(dtc)(DEPE)_2]^{2+}$ and the *cis*- and *trans*-$[Tc^{III}(SR)_2(D)_2]^+$ complexes of Table 6 signifies a profound effect on the energy levels of the complex engendered by the dtc ligand, not by the coordination geometry. The lowest unfilled orbital in $[Tc^{III}(dmdc)(DEPE)_2]^{2+}$ is at least 500 mV lower in energy than that of any other $[Tc^{III}(SR)_2(D)_2]^+$ complex examined. In fact, comparable redox potentials within this series occur only in *trans*-$[Tc^{III}(NCS)_2(DPPE)_2]^+$, where the NCS ligand binds to technetium through nitrogen and both NCS^- and DPPE are effective π-acceptors.[25] Both $[Tc^{II}(dtc)(DEPE)_2]^+$ and $[Tc^{II}(NCS)_2(DPPE)_2]$ are isolated as stable technetium(II) species. The comparable technetium(III/II) reduction potentials of $[Tc(dtc)(DEPE)_2]^{2+/+}$ and $[Tc(NCS)_2(DPPE)_2]^{+/0}$ are even more remarkable in light of the fact that DPPE ligands are better π-acceptors than DEPE ligands: otherwise equivalent $[Tc^{III}X_2(DPPE)_2]^+$ complexes are ~250 mV easier to reduce than $[Tc^{III}X_2(DEPE)_2]^+$ complexes (see Table 6). Therefore, the dtc ligand is very potent at lowering the technetium(III/II) reduction potential and this certainly implicates dtc as a significant π-acceptor ligand in technetium-diphosphine complexes. The effect of substituent exchanges within the ligands dmdc, dedc and pmdc leads to very little effect on the $E^{0\prime}$ values.

Animal experiments have shown that the technetium(III/II) couple of the prototypical bis(phosphine) complex $[TcCl_2(DMPE)_2]^{+/0}$ is biologically accessible and that the injected technetium(III) complex undergoes *in vivo* reduction to the technetium(II) form.[28] Replacement of the two chloride ligands by two thiolato ligands stabilizes the technetium(III) state, while replacement of the two chloride ligands by a dtc ligand stabilizes the technetium(II) state. Thus, careful control of the sulphur-donating ligands in bis(phosphine) technetium(III/II) complexes allows one to design and synthesize ^{99m}Tc radiopharmaceuticals with the properties (lipophilicity, charge, redox potential, etc.) required for specific imaging applications. For instance, it should be possible to design a neutral bis(phosphine) technetium(II) complex which can cross the blood–brain barrier and then undergo electron transfer within relatively oxidizing brain tissue[29] to a cationic technetium(III) species which will be trapped in the brain for a time long enough to allow imaging.[30] Some neutral bis(phosphine) technetium(II) complexes are already known to cross the blood–brain barrier.[30]

In addition to their readily tuneable redox properties, the $[Tc^{II}(dtc)(DIP)_2]^+$ complexes described in this work possess characteristics which are fundamental to the design of new ^{99m}Tc radiopharmaceuticals. These complexes are kinetically robust, do not undergo *cis*/*trans* isomerization reactions and have well-defined chemistry. It should

be noted that other classes of ^{99m}Tc-dtc complexes are also under active development as radiopharmaceuticals; Duatti and co-workers[31,32] are investigating [$^{99m}Tc^{V}N(dtc)_2$] as a myocardial perfusion imaging agent.

Acknowledgement—Financial support by the National Institute of Health grants nos HL-21276 (E.D. and R.C.E.) and CA-42179 (E.D.), by the Department of Energy grant DE-FG02-86ER60487 (W.R.H.) and by Mallinckrodt, Inc. (E.D.) is gratefully acknowledged.

REFERENCES

1. For reviews of technetium complexes as radiopharmaceuticals see E. Deutsch and K. Libson, *Comm. Inorg. Chem.* 1984, **3**, 83; M. J. Clarke and L. Podbielski, *Coord. Chem. Rev.* 1987, **78**, 253; C. L. Jones, in *Comprehensive Coordination Chemistry* (Edited by G. Wilkinson, R. D. Gillard and J. McCleverty), Vol. 6, pp. 881–1009. Pergamon Press, Oxford (1987); A. M. Verbruggen, *Eur. J. Nucl. Med.* 1990, **17**, 346.
2. T. Konno, M. J. Heeg and E. Deutsch, *Inorg. Chem.* 1988, **27**, 4113.
3. T. Konno, J. R. Kirchhoff, W. R. Heineman and E. Deutsch, *Inorg. Chem.* 1989, **28**, 1174.
4. T. Konno, M. J. Heeg and E. Deutsch, *Inorg. Chem.* 1989, **28**, 1694.
5. T. Konno, M. J. Heeg, R. Seeber, J. R. Kirchhoff, W. R. Heineman and E. Deutsch, *Trans. Met. Chem.* 1992, in press.
6. T. Konno, M. J. Heeg, J. A. Stuckey, J. R. Kirchhoff, W. R. Heineman and E. Deutsch, *Inorg. Chem.* 1992, **31**, 1173.
7. T. Konno, M. J. Heeg, J. R. Kirchhoff, W. R. Heineman and E. Deutsch, *J. Chem. Soc., Dalton Trans.* 1992, 3069.
8. K.-I. Okamoto, M. J. Heeg, J. R. Kirchhoff, W. R. Heineman and E. Deutsch, *Polyhedron*, submitted.
9. Other reports of similar complexes include: R. Münze, U. Abram, J. Stach and W. Hiller, *Inorg. Chim. Acta* 1991, **186**, 151; U. Abram, R. Beyer, P. Mading, I. Hoffman, R. Münze and J. Stach, *Z. Anorg. Allg. Chem.* 1989, **578**, 229; J. Stach, U. Abram and R. Münze, *Z. Chem.* 1989, **29**, 249.
10. For reviews of dithiocarbamates see D. Coucouvanis, *Prog. Inorg. Chem.* 1970, **11**, 233; D. Coucouvanis, *Prog. Inorg. Chem.* 1979, **26**, 301; R. Eisenberg, *Prog. Inorg. Chem.* 1970, **12**, 295; R. P. Burns, F. P. McCullough and C. A. McAuliffe, *Adv. Inorg. Chem. Radiochem.* 1980, **23**, 211.
11. K. Libson, B. L. Barnett and E. Deutsch, *Inorg. Chem.* 1983, **22**, 1695.
12. D. DeFilippo, P. Deplano, F. Devillanova, E. F. Trogu and G. Verani, *J. Org. Chem.* 1973, **38**, 560.
13. The potential of this electrode is 0.201 V to the NHE.
14. G. M. Sheldrick, SHELXTL. University of Göttingen, F.R.G. (1978).
15. J. Baldas, J. Bonnyman, P. M. Pojer, G. A. Williams and M. F. Mackay, *J. Chem. Soc., Dalton Trans.* 1982, 451.
16. J. Baldas, J. Bonnyman, P. M. Pojer, G. A. Williams and M. F. Mackay, *J. Chem. Soc., Dalton Trans.* 1981, 1798.
17. F. D. Rochon, R. Malanson and P.-C. Kong, *Inorg. Chim. Acta* 1992, **194**, 43.
18. R. Rossi, A. Marchi, L. Magon, U. Casellato and R. Graziani, *J. Chem. Res. (S)* 1990, 78.
19. A. S. Batsanov, Y. T. Struchkov, B. Lorenz and M. Wahren, *Z. Anorg. Allg. Chem.* 1984, **510**, 117.
20. J. Baldas, J. Bonnyman, M. F. Mackay and G. A. Williams, *Aust. J. Chem.* 1984, **37**, 751.
21. J. Baldas, S. F. Colmanet and G. A. Williams, *Aust. J. Chem.* 1991, **44**, 1125.
22. A. Ichimura, W. R. Heineman, J.-L. Vanderheyden and E. Deutsch, *Inorg. Chem.* 1984, **23**, 1272.
23. D. Kepert, *Inorganic Stereochemistry*. Springer-Verlag, New York (1982).
24. H. A. Strobel and W. R. Heineman, *Chemical Instrumentation: A Systematic Approach*, pp. 1112–1117. Wiley Interscience, New York (1989).
25. G. Bandoli, U. Mazzi, A. Ichimura, K. Libson, W. R. Heineman and E. Deutsch, *Inorg. Chem.* 1984, **23**, 2898.
26. R. W. Hurst, W. R. Heineman and E. Deutsch, *Inorg. Chem.* 1981, **20**, 3298.
27. L. Chang, M. J. Heeg and E. Deutsch, *Trans. Met. Chem.* 1992, in press.
28. J.-L. Vanderheyden, M. J. Heeg and E. Deutsch, *Inorg. Chem.* 1985, **24**, 1666.
29. N. Bodor, L. Prokai, W.-M. Wu, H. Farag, S. Jonalagadda, M. Kawamura and J. Simpkins, *Science* 1992, **257**, 1698.
30. M. Neves, K. Libson and E. Deutsch, *Nucl. Med. Biol.* 1987, **14**, 503.
31. L. Uccelli, C. Bolzati, V. Comazzi, A. Duatti, R. Pasqualini, M. Giganti and A. Piffanelli, *J. Nucl. Med.* 1992, **33**, 850.
32. R. Pasqualini, E. Bellande, V. Comazzi and A. Duatti, *J. Nucl. Med.* 1992, **33**, 989.

Polyhedron Vol. 12, No. 12, pp. 1569–1571, 1993
Printed in Great Britain

0277–5387/93 $6.00+.00
© 1993 Pergamon Press Ltd

COMMUNICATION

LOW TEMPERATURE ROUTES TO EUROPIUM AND YTTERBIUM CHALCOGENIDES

I. P. PARKIN* and J. C. FITZMAURICE

Department of Chemistry, The Open University, Walton Hall, Milton Keynes MK7 6AA, U.K.

(*Received* 18 *December* 1992; *accepted* 5 *April* 1993)

Abstract—Reaction of europium or ytterbium metal in liquid ammonia with sulphur, selenium or tellurium (at room temperature in a pressure tube) affords a convenient route to crystalline binary metal chalcogenides.

The solubility of alkali metals and alkaline metal earths in ammonia to generate blue or bronze solutions containing solvated electrons and metal cations is well known.[1] These solutions have been used to perform a range of reductions both in organic chemistry in, for instance, the Birch reduction[2] and in inorganic chemistry to afford metal polychalcogenide species, M_xE_y (M = group Ia, IIa; E = chalcogenide, $y \geqslant x$).[3] Europium and to a lesser extent ytterbium metal also dissolve in liquid ammonia to form deep blue or bronze solutions;[4] however, the synthetic utility of these solutions (to our knowledge) has not been reported.

Lanthanide sulphides, selenides and tellurides of varying stoichiometry LnE to Ln_3E_7 (E = S, Se, Te; Ln = lanthanide) have been synthesized by high temperature (> 1000°C) techniques, either by reduction of the metal oxide with H_2S and H_2Se or by direct combination of the elements.[5] Here we report the room temperature synthesis of crystalline europium and ytterbium chalcogenides.

RESULTS AND DISCUSSION

Reaction of europium metal in liquid ammonia at room temperature in a pressure tube with sulphur, selenium or tellurium affords the binary compounds EuE (E = S, Se, Te) (Table 1). The europium and chalcogenide were added under nitrogen to ammonia at −77°C to generate a deep blue or bronze solution, which was magnetically stirred and allowed to warm to room temperature (under pressure). The ammonia was maintained in the system by closing a Young's tap; after a couple of hours the blue or bronze colour was discharged and a green, yellow or purple homogeneous precipitate formed dependent on the ratio of europium to chalcogenide. After 12 h the solution was cooled and the ammonia allowed to evaporate under nitrogen. Removal of the final traces of ammonia *in vacuo* generally darkened the precipitate to black in the case of tellurium and dark red–brown for the selenium or sulphur derivatives. The reaction of excess europium with the chalcogenides leads to the formation of a pyrophoric material comprising of finely divided metal and metal chalcogenide. Reaction of excess chalcogenide with europium leads to the formation of the same metal species (Table 1) and unreacted chalcogenide, as detected both by X-ray powder diffraction and by extraction of the chalcogenide with CS_2.

The precipitates were characterized by microanalysis, S.E.M./EDAX, X-ray powder diffraction, magnetic moment measurement and IR spectroscopy. The IR spectra† showed only a broad band at 400 cm^{-1} for EuS with no evidence of any S—H or N—H stretches. The microanalysis of EuE showed no carbon, hydrogen or nitrogen present and chalcogenide analyses were satisfactory.

* Author to whom correspondence should be addressed.

† Measurements obtained by KBr pressed pellets on a Nicolet (CsI)205 spectrometer.

Table 1. Crystalline phases detected by X-ray powder pattern from evaporation of ammonia from reaction of europium or ytterbium with a chalcogen in liquid ammonia

	Chalcogenide			
Metal	O	S	Se	Te
Europium	Eu_2O_3[a]	EuS/Eu_3S_4	EuSe	EuTe
Ytterbium	Yb_2O_3[a]	YbS/Yb_3S_4	YbSe[b]	YbTe[b]

[a] Oxide formed by exposing the finely divided metal to air. **Caution:** extremely exothermic reaction.

[b] Material heated in the pressure tube to 250°C for 2 h after NH_3 evaporated.

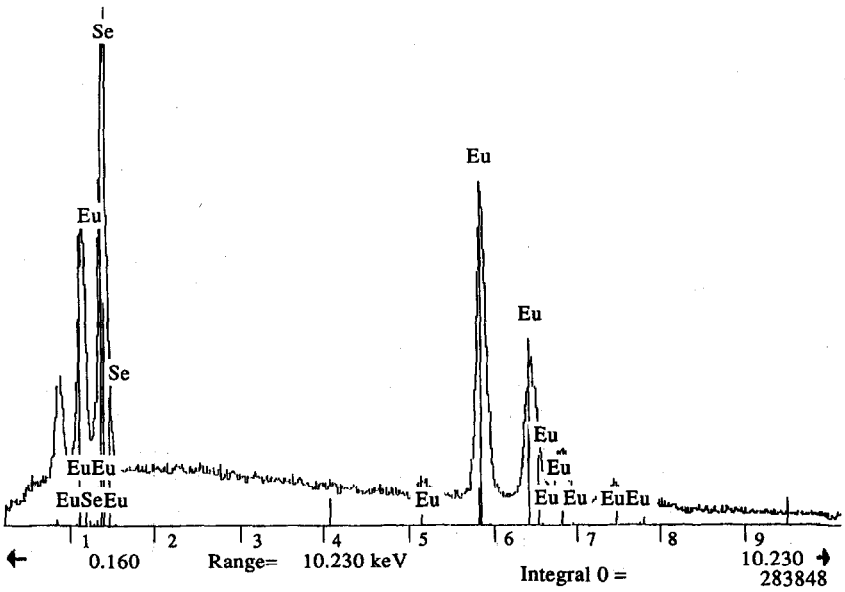

Fig. 1. S.E.M./EDAX elemental profile of europium selenide, EuSe.

The S.E.M./EDAX analysis* showed both a homogenous morphology and elemental profile standardized as EuE (Fig. 1). Samples of EuE decompose slowly in air, liberating H_2E and the formation of Eu_2O_3. Incorporation of oxygen was shown by a small peak in the EDAX analysis which increased in size with sample age.

The magnetic moments† and colours of the EuE compounds were identical to the literature.[5]

The X-ray powder diffraction data‡ showed that the product from the room temperature reaction was crystalline, with the predominant phase being EuE (Fig. 2). In the case of excess sulphur to europium a small amount of Eu_3S_4 and sulphur was also detected. When the reaction of selenium and tellurium with europium was performed with up to an eight-fold excess of the chalcogenide only EuSe and selenium metal or EuTe and tellurium metal were detected.

The analogous reactions with ytterbium were investigated. These showed that with selenium and tellurium even in excess only a small amount of YbSe and YbTe was formed after evaporation of the ammonia. The majority of material present was in the form of unreacted and finely divided metal. On exposure to air this powder ignited and pro-

*S.E.M. were obtained on a JEOL 820i with EDAX using a Kevex program.

†Magnetic moments were determined via the Evans method on a Johnson–Matthey balance.

‡X-ray powder diffraction data were obtained on a Siemens diffractometer D5000.

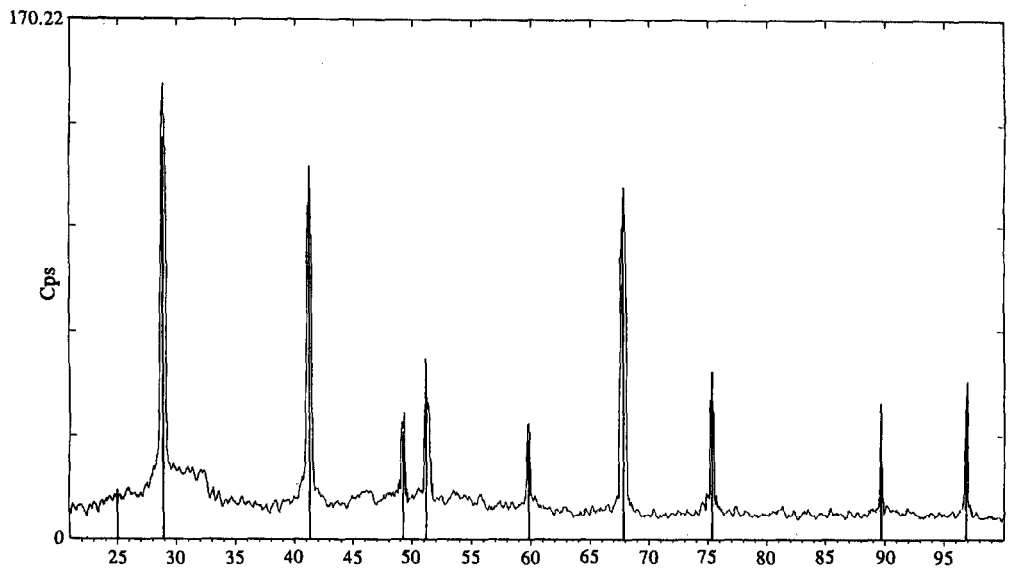

Fig. 2. X-ray powder diffraction pattern from reaction of europium with selenium in liquid ammonia at room temperature.

duced the metal oxide Yb_2O_3. However, YbSe and YbTe can be formed by gentle thermolysis of the ammonia precipitate (fully intermixed ytterbium and selenium or tellurium) at 250°C for 2 h under vacuum. Ytterbium sulphide formed at room temperature under the same conditions as the europium analogue.

Convenient preparation of both Eu_2O_3 and Yb_2O_3 can be achieved by generating finely divided metal by adding europium or ytterbium metal to liquid ammonia and allowing the ammonia to evaporate with vigorous stirring; careful pouring of the metal powder onto a ceramic dish (in air) causes spontaneous ignition and formation of the metal oxide.

The formation of europium and ytterbium chalcogenide by the ammonia route is significantly lower in energy than that of previous studies, where elevated temperatures were required.[5] However, it does seem limited to europium and ytterbium, as the other lanthanides are not soluble in ammonia. Indeed reaction of samarium and gadolinium under the same conditions failed to generate metal chalcogenides.

The chalcogenides are soluble in ammonia, forming a variety of different ions dependent on the concentration of the chalcogenide.[6] The reactions described here seem to proceed analogously to group IA and IIa chemistry where M_2E and ME compounds are known,[7] however, with excess chalcogenide no lanthanide polychalcogenide species are produced.

REFERENCES

1. W. L. Jolly and C. J. Mallada, in *Non-Aqueous Solvent Systems*, Ch. 1, pp. 1–45. Academic Press, London (1965).
2. A. Streitweiser and C. M. Heathcock, *Introduction to Organic Chemistry*, p. 672. Macmillan, New York (1981).
3. J. C. Bailar, H. J. Emeleus, R. Nyholm and A. F. Trotman-Dickenson, *Comprehensive Inorganic Chemistry*, Vol. 2, p. 837. Pergamon Press, Oxford (1973).
4. W. L. Jolly, *Prog. Inorg. Chem.* 1959, **1**, 235.
5. J. Flahaut and P. Laurelle, *Progress in the Science and Technology of the Rare Earths* (Edited by Le Roy Eyring), Vol. 3, pp. 149–155. Pergamon Press, Oxford (1968).
6. P. Dubais, J. P. Lelieur and G. Lepoutre, *Inorg. Chem.* 1989, **28**, 195.
7. Metal Ammonia Solution, Proceedings of the International Conference of the Nature of Metal-ammonia Solutions, Colloque Wey III, Ithaca, New York (1969). Butterworths, London (1970).

Polyhedron Vol. 12, No. 12, pp. 1573–1576, 1993
Printed in Great Britain

0277–5387/93 $6.00+.00
© 1993 Pergamon Press Ltd

COMMUNICATION

THE SYNTHESIS AND X-RAY CRYSTAL STRUCTURE OF MOLYBDENUM OXOMETHOXIDE $[MoO(OMe)_4]_2$

VADIM G. KESSLER,*† ANDREJ V. MIRONOV and NATALIYA YA. TUROVA

The Department of Chemistry, Lomonosov Moscow State University, Moscow, Leninskije Gory, 117234 Moscow, Russia

and

ALEXANDR I. YANOVSKY and YURI T. STRUCHKOV

The A.N.Nesmeyanov Institute of Organoelement Compounds, 28 Vavilov Street, 117813 Moscow, Russia

(*Received* 10 *September* 1992; *accepted* 27 *November* 1992)

Abstract—$MoO(OMe)_4$ has been prepared by anodic oxidation of molybdenum metal in anhydrous methanol containing LiCl as an electrolyte. The X-ray single crystal study showed the complex to consist of pseudo-centrosymmetric dimeric molecules, $[MoO(OMe)_3(\mu\text{-}OMe)]_2$. The general effect of the $M(\mu\text{-}OR)_2M$ ring upon the arrangement of bonds with increased multiplicity is discussed in this and related molecules.

The molybdenum(VI) oxoalkoxides, $MoO(OR)_4$, in spite of increasing interest as possible molecular precursors for MoO_3-based complex oxide materials, are scarcely studied. This seems to be a result of the low stability of these products, due to their significant tendency to ether elimination leading to the formation of $MoO_2(OR)_2$ species and high sensitivity to hydrolysis which is followed by the formation of "molybdenum blues".[1–3] $MoO(OMe)_4$—the only solid representative of the $MoO(OR)_4$ series—has been described in the literature as a brownish-yellow amorphous powder.‡ It was prepared by the alcohol interchange reaction of $MoO(OEt)_4$ with excess methanol. In the present work the synthesis and X-ray single-crystal investigation of $MoO(OMe)_4$ crystalline species (**I**) are described.

The anodic oxidation of metallic molybdenum in anhydrous MeOH was carried out in a cell without subdivision of the cathodic and anodic space, with water cooling. LiCl (0.025 M) was used as the electrolyte and the temperature in the cell did not exceed 50°C. Platelets of molybdenum with an area of *ca* 12–15 cm^2 were taken as anodes and cathodes (the average current density being 0.1 Å cm^{-2} as used earlier[4] for the anodic oxidation of tungsten). The duration of the synthesis in all the experiments was *ca* 36 h. Slow cooling of the solutions (the molybdenum concentrations reached *ca* 0.16–0.20 M) deposited $MoO(OMe)_4$ in the form of big, light yellow prismatic crystals.‡ The crystals of **I** are highly soluble in methanol, especially on heating, but poorly soluble in hexane. Their thermal decomposition, as well as for amorphous species, occurs at 110–140°C.

* Author to whom correspondence should be addressed.

† Present address: Laboratoire de Chimie Moléculaire, Université de Nice, Parc Valrose, 06108 Nice Cedex 2, France.

‡ The formation of **I** only as amorphous powder in the course of $MoO(OEt)_4$ alcohol interchange reactions is connected apparently with its insufficient purity. The easy formation of $MoO_2(OEt)_2$ due to ether elimination from the corresponding oxoethoxide gives rise to $MoO_2(OMe)_2$ which hinders the crystallization.

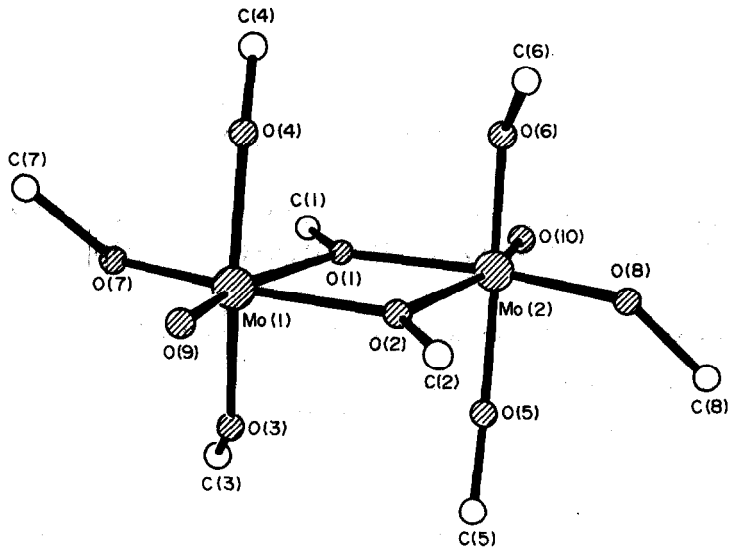

Fig. 1. The molecular structure of $MoO(OMe)_4$. Selected bond distances (Å) and angles (°): Mo(1a)—O(1a) 2.226(5), Mo(1a)—O(2a) 2.050(5), Mo(1a)—O(3a) 1.881(5), Mo(1a)—O(4a) 1.873(5), Mo(1a)—O(7a) 1.886(6), Mo(1a)—O(9a) 1.672(5); O(1a)—Mo(1a)—O(2a) 69.1(2), O(1a)—Mo(1a)—O(7a) 92.6(2), O(7a)—Mo(1a)—O(9a) 105.3(3), O(3a)—Mo(1a)—O(4a) 164.9(2).

The structure of **I** was determined by single-crystal X-ray investigation.*

The crystals of **I** are built up of $[MoO(OMe)_3(\mu\text{-}OMe)]_2$ pseudo-centrosymmetric dimeric molecules (Fig. 1) (two symmetrically independent molecules with practically identical geometric parameters in the unit cell). The molybdenum atoms possess distorted octahedral coordination: two longer Mo—O bonds are formed in the equatorial plane by the oxygen atoms of the bridging methoxo groups [Mo(1a)—O(1a) 2.226(5) and Mo(1a)—O(2a) 2.050(5) Å], the double-bonded oxo group being situated in the *trans* position to the longest of them, while other sites in the coordination sphere of the metal atom are occupied by terminal alkoxo groups. The latter are characterized by rather close values of bond lengths [1.886(6), 1.881(5) and 1.873(5) Å for one equatorial and two apical lengths, respectively]. It should be mentioned that in this case the coordination polyhedra of molybdenum atoms turn out to be seriously distorted in comparison with those usually determined for the various coordination compounds of molybdenum(VI).[6] While for the majority of molybdenum(VI) derivatives studied the sums of interatomic distances for atoms situated in *trans* positions to each other and to the molybdenum atom are nearly equal along all three dimensions of the octahedron. In the structure of **I** the distances are rather less for the apical substituents (3.754 Å) compared with the equatorial ones (3.898 and 3.936 Å). This fact, taking into consideration the considerably higher valent angles at the oxygen atoms of the apical alkoxo groups [Mo(1a)—O(3a)—C(3a) 134.5(5)°, Mo(1a)—O(4a)—C(4a) 137.2(6)°] compared with that of the equatorial angle [Mo(1a)—O(7a)—C(7a) 130.7(6)°], proves the absence of any significant "*trans* effect" in this structure. Such an unusual relationship between bond lengths and bond angles has already been mentioned in earlier descriptions of the molecular structures of $[Nb(OMe)_5]_2$,[7] $[W(NPh)(OMe)_3(\mu\text{-}OMe)]_2$[8] and the quite recently studied $[WO(OMe)_4]_2$,[9] which is apparently very similar to **I**. This can be

*Crystal data for $C_8H_{24}Mo_2O_{10}$ (**I**): $M = 472.2$, orthorhombic, space group $P2_12_12_1$, $a = 11.790(2)$, $b = 10.410(2)$, $c = 27.180(5)$ Å, $V = 3335.9(2)$ Å^3, $D_c = 1.880$ g cm^{-3} for $Z = 8$, $\lambda(\text{Mo-}K_\alpha) = 0.71073$ Å, 3946 reflections with $F^2 > 3\sigma(F^2)$ were collected at 20°C up to $2\theta_{max} = 45°$ with a CAD4 Enraf–Nonius diffractometer. The structure was solved by standard direct methods; the molybdenum atom coordinates were taken from the initial solution and the other non-hydrogen atoms were located in subsequent Fourier syntheses. The structure was refined by full-matrix least-squares in an isotropic and then in an anisotropic approximation. The positions of all the hydrogen atoms were calculated geometrically and included in the final cycles of refinement in an isotropic approximation. Final discrepancy factors are $R = 0.0397$ and $R_w = 0.0460$ (the absolute structure was determined by the Hamilton test, $R_{inv} = 0.0400$). All calculations were performed with an IBM PC using SHELXTL PC programs.[5] Atomic coordinates for this compound have been deposited at the Cambridge Crystallographic Data Center.

completely explained by the influence of the $M(\mu\text{-}OR)_2M$ cycle rigid geometry upon the ability of the M atom to π-bond. The formation of bridging σ-bonds (a significant input in which is made by the $d_{x^2-y^2}$ metal atom orbital) leads to a large deviation in the angle between the σ-bonding orbitals in the equatorial plane from 90°—in order to allow both metal and oxygen atoms of the bridging cycle to remain in the same plane [the endocyclic angle O(1a)—Mo(1a)—O(2a), 69.1(2)°; the exocyclic angle O(7a)—Mo(1a)—O(9a) 105.3(3)°]. However, this has practically no influence on the orbitals responsible for π-bonding—d_{xz}, d_{xy} and d_{yz}. Due to this distortion of the metal atom geometry, the effectiveness of π-bonding decreases for the oxygen atoms situated in the equatorial plane (Fig. 2), remaining unchanged for the apical oxygen atoms. This results apparently in the observed *trans* configuration of the M—OR bonds possessing increased multiplicity. The absence of this effect in the molecular structures of Ce, Zr and Hf solvated isopropoxides, $[M(OPr^i)_4Pr^iOH)]_2$,[10] which are also based on the $M(\mu\text{-}OR)_2M$ four-membered ring, can be explained by the fact that one of the apical positions of the metal-oxygen octahedron should be occupied by the solvating molecule of the alcohol, the active hydrogen atom, which is incorporated in the intramolecular hydrogen bonds. The arrangement of the latter is in this case responsible for the geometry of the molecule as a whole.

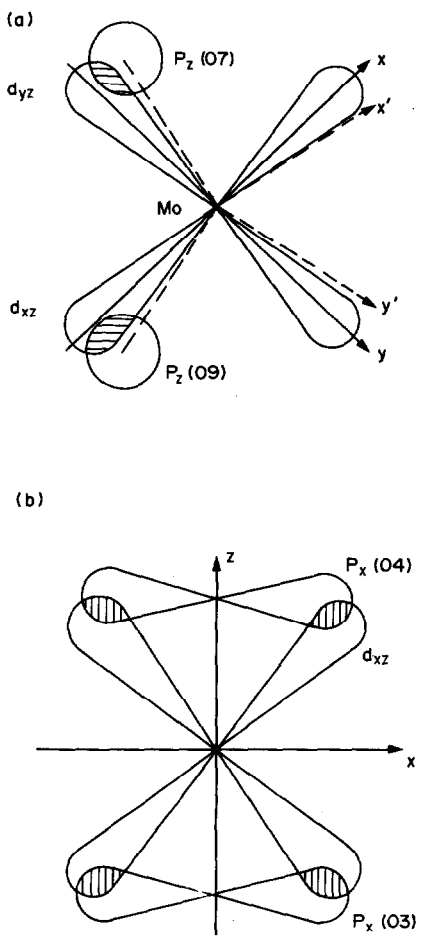

Fig. 2. Scheme of overlapping π-orbitals: (a) in the equatorial plane and (b) in the *xz* or *yz* plane.

The IR spectrum of the $MoO(OMe)_4$ crystalline species was found to be in accordance with the molecular structure described above: two bands at 950 and 920 cm^{-1}, respectively, correspond to the vibration of Mo=O terminal bonds (the appearance of the doublet in the spectrum is probably caused by superposition of stretching modes for two equivalent bonds in the structure), while the bands at 570 and 520 cm^{-1} correspond to the vibrations of terminal and bridging alkoxo groups, respectively. From the spectrum of the amorphous $MoO(OMe)_4$ species, that of **I** differs only by the higher intensity of the band at 520 cm^{-1} and better resolution of the Mo=O vibration bands. Such a difference might be caused by the presence of significant amounts of impurities [probably $MoO_2(OMe)_2$ or monomeric $MoO(OMe)_4$ in the species prepared by the alcohol interchange reaction of $MoO(OEt)_4$, which possesses a vigorous tendency to ether elimination and of which the molecular complexity is less than 2[1]].

Consequently, it is noteworthy that the investigated preparation, properties and structure of $MoO(OMe)_4$ provide one more illustration for the fundamental difference in the chemical nature of the analogous molybdenum(VI) and tungsten(VI) compounds. Thus, while the anodic oxidation of the molybdenum metal is a facile route to the oxotetraalkoxide, $WO(OMe)_4$ cannot be obtained in a pure form by this method; the samples prepared always contain a significant admixture of $W(OMe)_6$.[4] The reason for this fact probably lies in the rather higher stability of the initially formed *ortho* derivative $M(OMe)_6$ to both ether elimination and reduction–reoxidation processes for tungsten rather than for the molybdenum compound. It should also be mentioned that the dimeric alkoxo-bridged structure seems to be not only adaptable for $WO(OR)_4$, R = Me, Et. The IR and X-ray powder investigation of the latter compounds, prepared by exchange reaction of $WOCl_4$ with NaOR, showed them to be oxo-bridged polymeric species—analogues of $WOCl_4$.[11] The formation of a structure different from $MoO(OMe)_4$ for the tungsten compound is probably caused by the presence of traces of NaOR, irremovable by recrystallization which

is used for the purification of the products. It is interesting that for $MoO(OEt)_4$ and $MoO(OPr^i)_4$ [but not $MoO(OMe)_4$] polymerization in the presence of traces of NaOR also occurs, but only by the formation of alkoxo-bridges.[12] In the background of this difference in chemical and structural characteristics apparently lies the higher multiplicity and lower donor ability of Mo=O in comparison with W=O bonds.

Acknowledgements—The authors would like to express their gratitude to Dr A. A. Buchachenko for a fruitful discussion of electronic structure of the entitled and allied compounds.

REFERENCES

1. N. I. Kozlova, V. G. Kessler, N. Ya. Turova and A. I. Belokon, *Sov. J. Coord. Chem. (Engl.)* 1989, **15**, 867.
2. N. Ya. Turova and V. G. Kessler, *Zh. Obshch. Khim.* 1990, **60**, 113.
3. M. H. Chisholm, J. C. Huffman, K. Folting and C. C. Kirkpatric, *Inorg. Chem.* 1984, **23**, 1021.
4. S. I. Kucheiko, N. Ya. Turova and V. A. Shreider, *Zh. Obshch. Khim.* 1985, **55**, 2396.
5. R. M. Sheldrick, SHELXTL PC, Reference Manual (1990).
6. M. A. Porai-Koshits and L. O. Atovmyan, *Kristallokhimiya i stereokhimiya koordinatsionnykh soedinenii molibdena* (*Crystal Chemistry and Stereochemistry of Coordination Compounds of Molybdenum*). Nauka, Moscow (1974) (in Russian).
7. A. A. Pinkerton, D. Schwarzenbach, L. G. Hubert-Pfalzgraf and J. G. Riess, *Inorg. Chem.* 1976, **15**, 1196.
8. A. J. Nielson and J. M. Waters, *Polyhedron* 1982, **1**, 562.
9. W. Clegg, R. J. Errington, P. Kraxner and C. Redshaw, *J. Chem. Soc., Dalton Trans.* 1992, 1431.
10. B. A. Vaarstra, J. C. Huffman, P. S., Gradeff, L. G. Hubert-Pfalzgraf, J. C. Daran, S. Parraud, K. Yunlu and K. G. Caulton, *Inorg. Chem.* 1990, **29**, 3126.
11. S. I. Kucheiko, N. Ya. Turova, N. I. Kozlova and B. V. Zhadanov, *Sov. J. Coord. Chem. (Engl.)* 1985, **11**, 867.
12. N. Ya. Turova, V. G. Kessler and S. I. Kucheiko, *Polyhedron* 1991, **10**, 2617.

Polyhedron Vol. 12, No. 13, pp. 1577–1580, 1993
Printed in Great Britain

0277–5387/93 $6.00+.00
© 1993 Pergamon Press Ltd

THE COORDINATION CHEMISTRY OF MIXED PYRIDINE-PHENOL AND PHENANTHROLINE-PHENOL LIGANDS; SYNTHESIS AND CRYSTAL STRUCTURE OF $[PdL^1Cl]\cdot(CH_2Cl_2)$ [HL^1 = 6-(2-HYDROXYPHENYL)-2,2′-BIPYRIDINE]

DAVID BARDWELL, DANIEL BLACK, JOHN C. JEFFERY and MICHAEL D. WARD*

School of Chemistry, University of Bristol, Cantock's Close, Bristol BS8 1TS, U.K.

(*Received* 22 *February* 1993; *accepted* 30 *March* 1993)

Abstract—Reaction of the N,N,O-terdentate ligands 6-(2-hydroxyphenyl)-2,2′-bipyridine (HL^1) and 2-(2-hydroxyphenyl)-1,10-phenanthroline (HL^2) with $Na_2PdCl_4\cdot 3H_2O$ afforded the complexes $[PdL^1Cl]$ and $[PdL^2Cl]$; the crystal structure of $[PdL^1Cl]\cdot(CH_2Cl_2)$ shows it to be a square-planar monomer with extensive intramolecular π-stacking interactions involving the aromatic ligands.

We have recently been studying the structural properties of transition metal complexes containing polydentate aromatic ligands such as 6-(2-hydroxyphenyl)-2,2′-bipyridine (HL^1) and 2-(2-hydroxyphenyl)-1,10-phenanthroline (HL^2) and the competition between the various factors which influence their structures.[1–6] Complexes with metals which

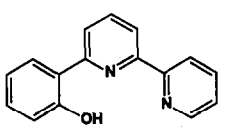

HL^1

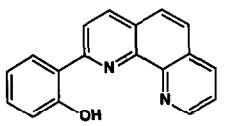

HL^2

have a strong electronic preference for octahedral geometries such as ruthenium(II), ruthenium(III), cobalt(III) and chromium(III) adopt the expected structures in which the metal adopts its most favoured geometry.[1,4,6] In complexes with copper(II) and nickel(II), however, which have weaker stereoelectronic preferences, some unexpected structures have arisen, in which other factors can be seen to be involved in contributing to the structures, in particular π-stacking between parallel fragments of aromatic rings.[1–3] Such π-stacking interactions occur frequently in coordination complexes containing aromatic ligands[7] and in purely organic systems[8] and as such have been the subject of extensive theoretical studies.[9] Although they are relatively weak and could not be said exclusively to control the structures of complexes in which they occur, we have shown that they may be sufficient to tip the balance between two different structural types; thus, the nickel(II) complexes of the two related ligands HL^1 and HL^2 have very different structures, because in the latter case the additional aromatic ring of HL^2 becomes involved in some very close inter-ring π-stacking interactions.[3]

To examine the π-stacking effects with these ligands systematically, we decided to prepare and structurally characterize their complexes of palladium(II) and platinum(II). These complexes would be expected to have planar structures in which any inter-ring stacking will be free to occur without any steric impedance from axial ligands. We report here the preparations of palladium(II) complexes with HL^1 and HL^2 and the crystal structure of $[PdL^1Cl]\cdot(CH_2Cl_2)$.

EXPERIMENTAL

^1H NMR spectra were recorded on a Jeol GX270 spectrometer. Fast-atom bombardment (FAB) mass spectra were recorded on a VG-Autospec at the SERC Mass Spectrometry Service Centre, Swansea, with 3-nitrobenzylalcohol as a matrix. All starting materials were purchased from Aldrich and used as received. HL^1 and HL^2 were prepared as

* Author to whom correspondence should be addressed.

described earlier.[1,3] The equipment used for the electrochemical measurements has been described previously.[1]

Preparation of [PdL^{1}Cl] *and* [PdL^{2}Cl]

A mixture of the appropriate ligand and 1 equivalent of $Na_2PdCl_4 \cdot 3H_2O$ in methanol was stirred for 4 h at room temperature. After this time the mixture was filtered and the yellow–orange solid washed with methanol and dried. Yields were typically 60%. Crystals of [PdL^{1}Cl]$\cdot(CH_2Cl_2)$ suitable for X-ray diffraction were grown by layering hexane on a concentrated solution of the complex in CH_2Cl_2 and allowing the layers to mix.

[PdL^{1}Cl]: FABMS, $m/z = 388$ (M^+), 353 ($M^+ - Cl$). ^{1}H NMR (270 MHz, CD_3SOCD_3): $\delta = 9.13$ (1H, d, $J = 5.3$), 8.57–8.65 (2H, m), 8.51 (1H, d, $J = 6.6$), 8.30–8.40 (2H, m), 8.04 (1H, dd, $J = 8.5, 1.5$), 7.78 (1H, td, $J = 6.7, 1.1$), 7.26 (1H, td, $J = 7.6, 7.1$), 6.99 (1H, dd, $J = 8.6, 1.3$), 6.74 (1H, td, $J = 7.5, 1.5$ Hz). Found: C, 48.7; H, 2.9; N, 7.0. Calc. for $C_{16}H_{11}N_2ClOPd$: C, 49.4; H, 2.8; N, 7.2%.

[PdL^{2}Cl]: FABMS, $m/z = 437$ ($M^+ + Na$), 412 (M^+), 377 ($M^+ - Cl$). ^{1}H NMR (270 MHz, CD_3SOCD_3): δ 9.40 (1H, dd, $J = 4.4, 1.5$), 8.99 (1H, d, $J = 8.2$), 8.93 (2H, s), 8.22–8.35 (3H, m), 8.13 (1H, dd, $J = 8.8, 5.2$), 7.34 (1H, t, $J = 8.0$), 7.08 (1H, d, $J = 8.8$), 6.81 (1H, td, $J = 8.4, 1.0$ Hz). Found: C, 51.5; H, 2.4; N, 6.5. Calc. for $C_{18}H_{11}N_2ClOPd$: C, 52.3; H, 2.7; N, 6.8%.

Crystal structure determination

Crystals of [PdL^{1}Cl]$\cdot(CH_2Cl_2)$ were grown from a CH_2Cl_2/hexane mixture as amber needles. The crystal used for data collection was sealed in a tube under an atmosphere of nitrogen saturated with CH_2Cl_2. Despite this precaution it is probable that some solvent loss occurred during data collection. Moreover, the intensity of three standard check reflections diminished by *ca* 18% during the course of the data collection. The latter observation together with the comparatively poor resolution of intensities along the *a*-axis mean that the overall accuracy of the structural determination should be treated with due caution. Data were collected using a Siemens R3m/V four-circle diffractometer (293 K, Mo-K_α *X*-radiation, graphite monochromator, $\bar{\lambda} = 0.71073$ Å). The data were corrected for Lorentz, polarization and X-ray absorption effects and an empirical absorption correction was applied using a method based upon azimuthal scan data.[10] Details of the crystal data and intensity collection are given in Table 1.

Table 1. Summary of crystal data and intensity collection for [PdL^{1}Cl]$\cdot(CH_2Cl_2)$

	[PdL^{1}Cl]$\cdot(CH_2Cl_2)$
Formula	$C_{17}H_{13}Cl_3N_2OPd$
M_r	474.0
Crystal system	Monoclinic
Space group	$C2/c$
a (Å)	30.02(2)
b (Å)	7.299(5)
c (Å)	18.276(13)
β (°)	119.35(5)
Cell volume	3491(4)
Molecules/unit cell	8
ρ(calc.) (g cm^{-3})	1.804
μ(Mo-K_α) (calc.) (cm^{-1})	15.28
F(000)	1872
Crystal dimensions (mm)	$0.7 \times 0.3 \times 0.2$
Unique reflections measured	4015
2θ range (°)	5.0–55.0
Reflections considered observed $\lvert F_o \rvert \geq 4\sigma(\lvert F_o \rvert)$	2219
R	0.051
R_w	0.046
Weight (G) ($w^{-1} = \sigma^2(F) + GF^2$)	0.0003
Absorption correction	Azimuthal scans
Min./max. transmission factors	0.686, 0.726
Largest and mean Δ/σ	0.005, 0.001
Largest difference peak and hole (e Å^{-3})	0.77, −0.64

The structure was solved by conventional heavy-atom methods and successive difference-Fourier syntheses were used to locate all non-hydrogen atoms. All non-hydrogen atoms were refined with anisotropic thermal parameters and hydrogen atoms were included in calculated positions (C—H 0.96 Å) with fixed isotropic thermal parameters ($U_{iso} = 0.08$). Final refinements by full-matrix least-squares procedures were performed on a μ-Vax computer with the SHELXTL system of programs.[10] Scattering factors with corrections for anomalous dispersion were taken from ref. 11.

RESULTS AND DISCUSSION

The complexes [PdL^{1}Cl] and [PdL^{2}Cl] were simply prepared by reaction of equimolar amounts of the appropriate ligand and $Na_2PdCl_4 \cdot 3H_2O$ in methanol at room temperature. The formulations of both were confirmed by elemental analysis and FAB mass spectrometry. In addition, proton NMR spectra in d^6-dimethylsulphoxide showed the

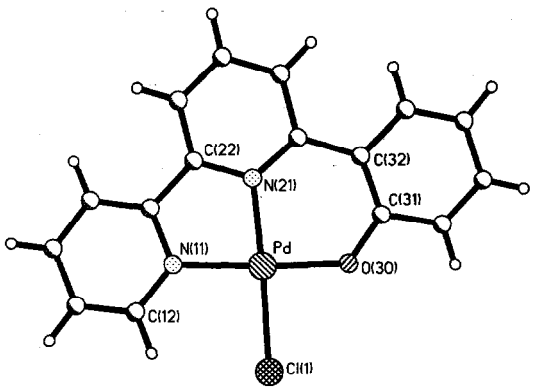

Fig. 1. The molecular structure of [PdL^{1}Cl].

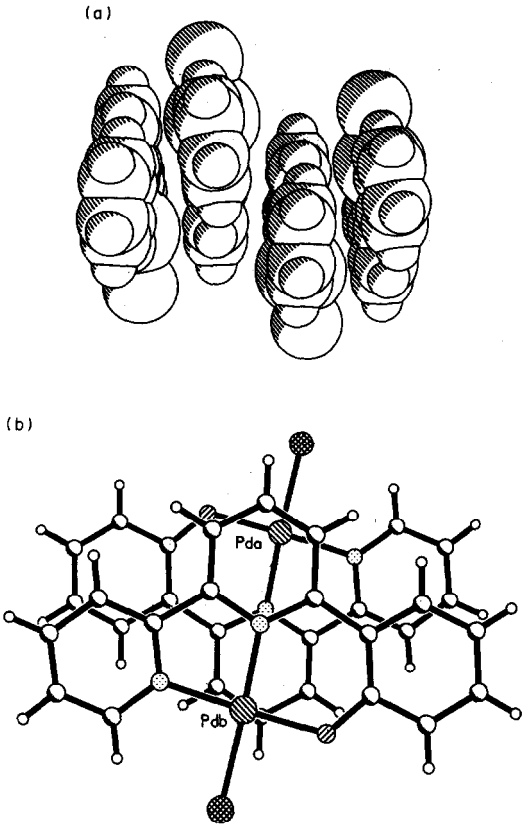

Fig. 2. Views showing π-stacking in the complex [PdL^{1}Cl].

expected number of resonances in the aromatic region in each case, although these have not been assigned. Electrochemical investigations showed only totally irreversible processes at high positive and negative potentials.

We were able to obtain X-ray quality crystals of [PdL^{1}Cl]·(CH_2Cl_2) by recrystallization from CH_2Cl_2/hexane; views of the structure are shown in Figs 1 and 2. Relevant bond lengths and angles are in Table 2. The basic square-planar structure of the complex is shown in Fig. 1; the distortions from idealized square geometry are small and arise principally because the 2,2′-bipyridyl fragment is not sufficiently flexible to attain a 90° bite angle in the five-membered chelate ring.[12] The ligand is very nearly flat, with dihedral twists of *ca* 1° between the pyridyl rings and *ca* 5° between the central pyridyl and terminal phenolate rings. This is in marked contrast to all other structures with this ligand, where inter-ring dihedral angles of up to 40° are observed, particularly between the central pyridyl and terminal phenolate rings. It also contrasts with the structure of [Pd(2-pp)$_2$][2-ppH = 2-(2-hydroxyphenyl)pyridine], where there is a 26° twist between the pyridyl and phenolate rings of each of the two ligands.[13] The stacking of the planar complex units is shown in Fig. 2(a). They are not all aligned in the same way, but alternate such that the two components of each pair are related by an inversion centre [Fig. 2(b)]; this is no doubt partly to avoid unfavourable steric and electronic interactions between chloride groups in adjacent complexes. The

Table 2. Selected internuclear distances (Å) and angles (°) for the complex [Pd^{1}Cl]·(CH_2Cl_2)

Pd—Cl(1)	2.312(3)	Pd—N(11)	1.995(7)	Pd—N(21)	1.982(6)	Pd—O(30)	1.939(6)
N(11)—C(12)	1.343(13)	N(11)—C(16)	1.360(8)	C(12)—C(13)	1.351(14)	C(13)—C(14)	1.367(11)
C(14)—C(15)	1.371(17)	C(15)—C(16)	1.371(13)	C(16)—C(22)	1.473(14)	N(21)—C(22)	1.364(11)
N(21)—C(26)	1.371(13)	C(22)—C(23)	1.374(9)	C(23)—C(24)	1.366(16)	C(24)—C(25)	1.348(14)
C(25)—C(26)	1.430(10)	C(26)—C(32)	1.470(12)	O(30)—C(31)	1.323(12)	C(31)—C(32)	1.401(10)
C(31)—C(36)	1.401(14)	C(32)—C(33)	1.421(16)	C(33)—C(34)	1.350(16)	C(34)—C(35)	1.394(14)
C(35)—C(36)	1.369(19)						

Cl(1)—Pd—N(11)	94.6(2)	Cl(1)—Pd—N(21)	176.1(2)	N(11)—Pd—N(21)	82.9(3)
Cl(1)—Pd—O(30)	88.2(2)	N(11)—Pd—O(30)	176.3(2)	N(21)—Pd—O(30)	94.4(3)
Pd—N(11)—C(12)	127.2(4)	Pd—N(11)—C(16)	113.6(6)	C(12)—N(11)—C(16)	119.2(7)
Pd—N(21)—C(22)	113.0(6)	Pd—N(21)—C(26)	126.0(5)	C(22)—N(21)—C(26)	120.9(6)
Pd—O(30)—C(31)	125.3(4)				

presence of π-stacking interactions between the complex units is evident. The separations of atoms in one ligand from the mean plane of the next vary from 3.30 [C(12)] to 3.59 Å [C(15)], with the average separation being 3.44 Å. Stacking appears to be maximized by overlap of all three aromatic rings of one complex unit with its neighbour. This precludes any axial interactions between the palladium atom of one complex and donor atoms from its neighbours, since the resulting substantial offset between the complexes would remove most of the stacking interaction.

REFERENCES

1. J. C. Jeffery, E. Schatz and M. D. Ward, *J. Chem. Soc., Dalton Trans.* 1992, 1921.
2. J. C. Jeffery and M. D. Ward, *J. Chem. Soc., Dalton Trans.* 1991, 2119.
3. B. M. Holligan, J. C. Jeffery and M. D. Ward, *J. Chem. Soc., Dalton Trans.* 1992, 3337.
4. B. M. Holligan, J. C. Jeffery, M. K. Norgett, E. Schatz and M. D. Ward, *J. Chem. Soc., Dalton Trans.* 1992, 3345.
5. J. P Maher, P. H. Rieger, P. Thornton and M. D. Ward, *J. Chem. Soc., Dalton Trans.* 1992, 3353.
6. D. Bardwell, D. Black, J. C. Jeffery, E. Schatz and M. D. Ward, *J. Chem. Soc., Dalton Trans.*, in press.
7. There are too many examples to list comprehensively, but some recent representative examples are given here: S. P. Perlepes, J. C. Huffman and G. Christou, *Polyhedron* 1992, **11**, 1471; A. Habiyakare, E. A. C. Lucken and G. Bernardinelli, *J. Chem. Soc., Dalton Trans.* 1992, 2591; A. Houlton, N. Jasim, R. M. G. Roberts, J. Silver, D.Cunningham, P. McArdle and T. Higgins, *J. Chem. Soc., Dalton Trans.* 1992, 2235; M.-T. Youinou, N. Rahmouni, J. Fischer and J. A. Osborn, *Angew. Chem., Int. Edn Engl.* 1992, **31**, 733; W. Jost, M. Adam, V. Enkelmann and K. Müllen, *Angew. Chem., Int. Edn Engl.* 1992, **31**, 878; N. Gupta, N. Grover, G. A. Neyhart, W. Liang, P. Singh and H. H. Thorp, *Angew. Chem., Int. Edn Engl.* 1992, **31**, 1048; E. C. Constable, S. M. Elder, J. V. Walker, P. D. Wood and D. A. Tocher, *J. Chem. Soc., Chem. Commun.* 1992, 229; E. C. Constable, M. D. Ward and D. A. Tocher, *J. Chem. Soc., Dalton Trans.* 1991, 1675 and refs therein; A. Yuchi, M. Shiro, H. Wada and G. Nakagawa, *Bull. Chem. Soc. Japan* 1991, **64**, 760; A. Furuhashi, I. Ono, A. Ouchi and A. Yamasaki, *Bull. Chem. Soc. Japan* 1991, **64**, 149; E. C. Constable, J. M. Holmes and P. R. Raithby, *Polyhedron* 1991, **10**, 127; L. A. Castonguay, A. K. Rappé and C. J. Casewit, *J. Am. Chem. Soc.* 1991, **113**, 7177; I. I. Mathews, P. A. Joy, S. Vasudevan and H. Manohar, *Inorg. Chem.* 1991, **30**, 2181; O. F. Schall, K. Robinson, J. L. Atwood and G. W. Gokel, *J. Am. Chem. Soc.* 1991, **113**, 7434.
8. S. C. Zimmerman and W. Wu, *J. Am. Chem. Soc.* 1989, **111**, 8054; A. V. Muehldorf, D. Van Engen, J. C. Warner and A. D. Hamilton, *J. Am. Chem. Soc.* 1988, **110**, 6561; B. Askew, P. Ballester, C. Buhr, K. S. Jeong, S. Jones, K. Parris, K. Williams and J. Rebek Jr, *J. Am. Chem. Soc.* 1989, **111**, 1082; J.-Y. Ortholand, A. M. Z. Slawin, N. Spencer, J. F. Stoddart and D. J. Williams, *Angew. Chem., Int. Edn Engl.* 1989, **28**, 1394 and refs therein; P. R. Ashton, C. L. Brown, E. J. T. Chrystal, T. T. Goodnow, A. E. Kaifer, K. P. Parry, D. Philp, A. M. Z. Salwin, N. Spencer, J. F. Stoddart and D. J. Williams, *J. Chem. Soc., Chem. Commun.* 1991, 634; F. Diederich, *Angew Chem., Int. Edn Engl.* 1988, **27**, 362.
9. C. A. Hunter and J. K. M. Sanders, *J. Am. Chem. Soc.* 1990, **112**, 5525; C. A. Hunter, *J. Chem. Soc., Chem. Commun.* 1991, 749; G: R. Desiraju and A. Gavezzotti, *J. Chem. Soc., Chem. Commun.* 1991, 621; G. Karlström, P. Linse, A. Wallqvist and B. Jönnson, *J. Am. Chem. Soc.* 1983, **105**, 3777; S. K. Burley and G. A. Petsko, *J. Am. Chem. Soc.* 1986, **108**, 7995.
10. G. M. Sheldrich, SHELXTL programs for use with a Siemens X-ray System.
11. *International Tables for X-ray Crystallography*, Vol. 4. Kynoch Press, Birmingham (1974).
12. E. C. Constable, *Adv. Inorg. Chem. Radiochem.* 1989, **34**, 1.
13. P. Ganis, A. Saporito, A. Vitagliano and G. Valle, *Inorg. Chim. Acta* 1988, **142**, 75.

Polyhedron Vol. 12, No. 13, pp. 1581–1586, 1993
Printed in Great Britain

0277–5387/93 $6.00+.00
© 1993 Pergamon Press Ltd

IRON CHROMIUM ANTIMONATES AND IRON GALLIUM ANTIMONATES: PREPARATION, STRUCTURAL AND MAGNETIC PROPERTIES

FRANK J. BERRY* and MEGAN I. SARSON

School of Chemistry, University of Birmingham, Edgbaston, Birmingham B15 2TT, U.K.

and

JAVIER TEJADA

Facultat de Fisica, Universitat de Barcelona, Diagonal 645, 080028 Barcelona, Spain

(*Received* 26 *February* 1993; *accepted* 23 *March* 1993)

Abstract—New mixed oxides of composition $Fe_{1-x}Cr_xSbO_4$ and $Fe_{1-x}Ga_xSbO_4$ have been prepared. New X-ray powder diffraction data for the compound $GaSbO_4$ are presented and the decrease in lattice parameters of $FeSbO_4$ when Fe^{3+} is substituted by smaller Cr^{3+} or Ga^{3+} ions is discussed. The temperature dependence of the inverse magnetic susceptibility of $Fe_{1-x}Cr_xSbO_4$ at temperatures exceeding *ca* 200 K follows a Curie–Weiss law. The Curie temperatures and effective magnetic moments decrease with decreasing iron content and are consistent with the substitution of Fe^{3+} by Cr^{3+} and a reduction in magnetic interaction between cations in the solid. Deviations from the Curie–Weiss law occur at lower temperatures with increasing chromium content and reflect the effect of chromium on the formation of clusters with short-range magnetic order amongst the Fe^{3+} species. A second Curie–Weiss law at even lower temperatures and a maximum in the magnetic susceptibility data recorded from $Fe_{0.85}Cr_{0.15}SbO_4$ and $Fe_{0.63}Cr_{0.37}SbO_4$ between 30 and 10 K is indicative of a spin glass-type transition in these materials. The trends in magnetic properties of materials of the type $Fe_{1-x}Ga_xSbO_4$ are similar, but more marked as a result of the substitution of paramagnetic Fe^{3+} by diamagnetic Ga^{3+}. The ^{57}Fe Mössbauer spectra recorded from $Fe_{1-x}Cr_xSbO_4$ and $Fe_{1-x}Ga_xSbO_4$ show an absence of magnetic splitting at 77 K, indicative of faster relaxation times than occur in $FeSbO_4$. The ^{121}Sb Mössbauer spectra recorded at low temperature show evidence for a super-transferred hyperfine magnetic field on the Sb^{5+} ion from iron via oxygen in the iron-rich mixed oxides.

In previous studies of rutile-related iron antimonate of composition $FeSbO_4$ we identified evidence for spin glass-type magnetic behaviour at low temperatures.[1,2] We report here on our subsequent studies of compounds of composition $Fe_{1-x}Cr_xSbO_4$ and $Fe_{1-x}Ga_xSbO_4$, where substitution of iron by chromium and diamagnetic gallium ions might induce weaker metal–metal magnetic interactions and thereby change the magnetic properties according to the degree of substitution.

* Author to whom correspondence should be addressed at the Department of Chemistry, The Open University, Milton Keynes, MK7 6AA, U.K.

EXPERIMENTAL

Materials of composition $Fe_{1-x}Cr_xSbO_4$ ($0 < x < 1$) and $Fe_{1-x}Ga_xSbO_4$ ($x = 0$–1) were prepared by co-precipitation techniques. Concentrated ammonia solution (Sp.Gr. 0.88) was added to stirred concentrated nitric acid (Sp.Gr. 1.42) solutions of the metal-nitrate hydrates or -chloride hydrates [$Fe(NO_3)_3 \cdot 9H_2O$, $Ga(NO_3)_3 \cdot xH_2O$, $CrCl_3 \cdot 6H_2O$] and antimony(V) chloride which had been prepared with molar ratios of total metal: antimony of 1 : 1. The resulting precipitates were removed by filtration, washed with water until the washings attained a pH between 6 and 7, dried at

110°C (18 h) in air, ground and calcined at 500°C (8 h) in air and subsequently at 1000°C (96 h) in air. The compound of composition $CrSbO_4$ was prepared by a similar method using concentrated hydrochloric acid (Sp.Gr. 1.18) solutions of chromium-chloride hydrate. The compound $GaSbO_4$ was also prepared by calcination of a ground mixture of gallium(III) oxide and antimony(V) oxide at 1200 °C in air.

X-ray powder diffraction data were recorded with a Philips PW 1050/70 diffractometer using Cu-K_α radiation. Energy dispersive X-ray microanalysis (e.d.x.) were performed with a Philips EM400T electron microscope interfaced with an EDAX energy dispersive X-ray analysis system. ^{57}Fe and ^{121}Sb Mössbauer spectra were recorded with a microprocessor-controlled Mössbauer spectrometer using $^{57}Co/Rh$ and $Ca^{121m}SnO_3$ sources. The drive velocities were calibrated with a $^{57}Co/Rh$ source and natural iron foil. All the spectra were computer fitted. The ^{57}Fe Mössbauer chemical isomer shifts were calculated relative to metallic iron and the ^{121}Sb Mössbauer chemical isomer shifts were calculated relative to indium antimonide. Magnetization measurements were performed with a Quantum Design SQUID magnetometer.

RESULTS AND DISCUSSION

Iron chromium antimonates

The X-ray powder diffraction patterns recorded from the materials of composition $Fe_{1-x}Cr_xSbO_4$ were all similar to those recorded from iron- and chromium-antimonate, which showed good agreement with data reported in the literature.[3] The variation of the lattice parameters with increasing chromium content, as determined by energy dispersive X-ray microanalysis, is contained in Table 1. The decrease in the *a* and *b* lattice parameters may be associated with the substitution of Fe^{3+} (0.645 Å in octahedral coordination)[4] by the smaller Cr^{3+} (0.615 Å in octahedral coordination),[4] which leads to a contraction of the unit cell.

Table 1. Lattice parameters of compounds of composition $Fe_{1-x}Cr_xSbO_4$

x	$a = b \pm 0.0005$ (Å)	$c \pm 0.0005$ (Å)
0.0	4.6180	3.0613
0.15	4.6170	3.0616
0.37	4.6150	3.0640
0.60	4.5848	3.0460
0.74	4.5789	3.0341
1.0	4.5743	3.0434

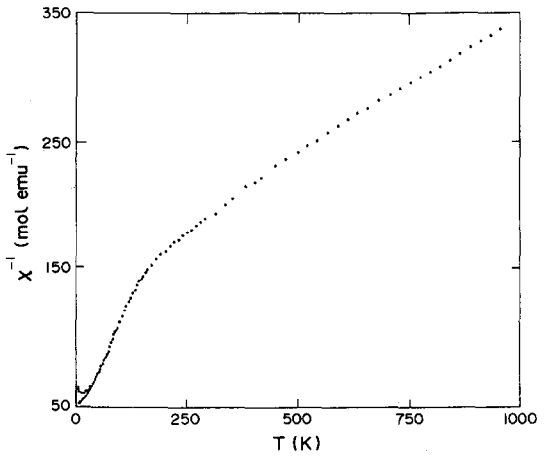

Fig. 1. The temperature dependence of the inverse zero field-cooled and field-cooled magnetic susceptibility recorded from iron antimonate in a magnetic field of 500 G.

The temperature dependence of the inverse zero field-cooled and the field-cooled magnetic susceptibility of iron antimonate recorded between 4 and 1000 K in a magnetic field of 500 G is shown in Fig. 1. The result shows that the susceptibility of the sample increases with decreasing temperature until the onset of irreversibility, which is attained at *ca* 70 K. At lower temperatures (*ca* 20 K) the zero field-cooled susceptibility begins to decrease, whereas the field-cooled susceptibility continues to increase. This low temperature behaviour is similar to that which characterizes a spin glass[5] and has been discussed in detail elsewhere.[1,2] However, in the high temperature region where the temperature exceeds *ca* 600 K a Curie–Weiss law is obeyed with the computer calculated effective magnetic moment of 6.0(1) B.M./ion, corresponding to high-spin paramagnetic Fe^{3+}, and the Curie temperature θ of +580 K being indicative of strong antiferromagnetic interactions.

The computer-calculated effective magnetic moments and Curie temperatures of compounds of composition $Fe_{1-x}Cr_xSbO_x$ were derived from magnetic susceptibility measurements and are collected in Table 2. The temperature dependence of the inverse magnetic susceptibility was influenced by the chromium content and was essentially of two types. The behaviour is illustrated by the data recorded from $Fe_{0.85}Cr_{0.15}SbO_4$ and $Fe_{0.26}Cr_{0.74}SbO_4$, which are shown in Figs 2 and 3. The magnetic susceptibility of the materials in the high temperature regions, i.e. > *ca* 200 K, obeyed the Curie–Weiss law. The temperature range over which the Curie–Weiss law is obeyed became

Table 2. Curie temperatures and effective magnetic moments of compounds of composition $Fe_{1-x}Cr_xSbO_4$

x	(θ) (K)	μ (B.M./ion)
0.0	580	6.0
0.15	446.5	5.73
0.37	355.8	5.29
0.60	249.9	4.86
0.74	189.4	4.62
1.0	107.8	4.01

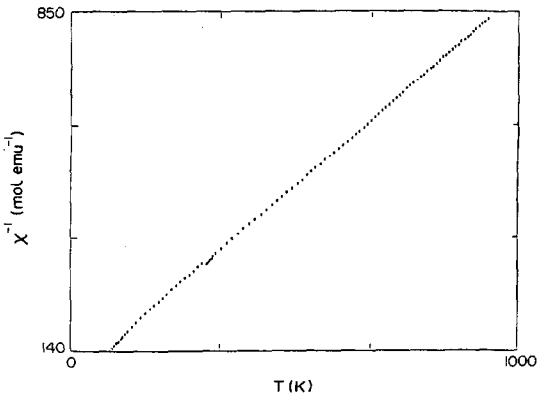

Fig. 3. The temperature dependence of the inverse zero field-cooled magnetic susceptibility recorded from the compound $Fe_{0.26}Cr_{0.74}SbO_4$.

greater as the iron content of the materials was reduced. The data contained in Table 2 show that the Curie temperatures and effective magnetic moments of compounds of composition $Fe_{1-x}Cr_xSbO_4$ decrease with decreasing iron content, indicating a reduction in the number of magnetic interactions between the cations in the solid. The results are consistent with the replacement of Fe^{3+} ions with five unpaired electrons by Cr^{3+} ions with three unpaired electrons and with the iron–chromium and chromium–chromium interactions in the iron chromium antimonates being much weaker than those between the iron species in iron antimonate. A deviation from the Curie–Weiss law was found to occur at temperatures which depended on the chromium content of the materials. The deviation for compounds of composition $Fe_{0.85}Cr_{0.15}SbO_4$, $Fe_{0.63}Cr_{0.37}SbO_4$, $Fe_{0.40}Cr_{0.60}SbO_4$ and $Fe_{0.26}Cr_{0.74}SbO_4$ occurred at *ca* 190, 160, 140, and 110 K, respectively. The deviations are similar to that recorded[1] in iron antimonate, which was associated with the development of clusters with short range magnetic order between the moments on the Fe^{3+} species. The progressively lower temperatures at which the deviation from the Curie–Weiss law begins is a reflection of the effect of smaller Fe^{3+} concentrations on the formation of clusters. Given that iron–chromium and chromium–chromium magnetic interactions are weaker than iron–iron interactions a decrease in Fe^{3+} concentration correlates with a decrease in magnetic interactions. The results reported here show that the antiferromagnetic ordering of the Fe^{3+} ions in a cluster in a sample dilute in iron can only be achieved at lower temperatures.

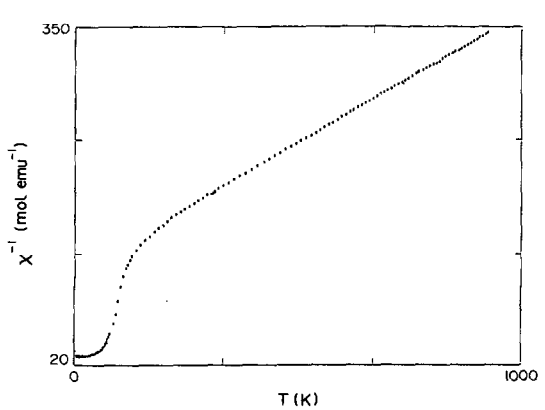

Fig. 2. The temperature dependence of the inverse zero field-cooled magnetic susceptibility recorded from the compound $Fe_{0.85}Cr_{0.15}SbO_4$.

An increase in magnetic susceptibility with further decreases in temperature was observed in $Fe_{0.85}Cr_{0.15}SbO_4$ and $Fe_{0.63}Cr_{0.37}SbO_4$ (as illustrated in Fig. 2), which indicated that a second Curie–Weiss law is obeyed at lower temperatures, which is analogous to that observed[1] in iron antimonate between 130 and 70 K. This new Curie–Weiss law may, as in the case of iron antimonate, be associated with the paramagnetic-like behaviour of small magnetically ordered clusters. At temperatures between 30 and 10 K a maximum was observed in the magnetic susceptibility data recorded from these two iron chromium antimonates (Fig. 2) which is similar to that associated with spin glass behaviour in iron antimonate. The absence of this low temperature behaviour in materials dilute in iron implies that the magnetic phenomena are inhibited by the reduction in the magnetic interactions or by the interference of substituted chromium with the cation order.

The ^{57}Fe Mössbauer spectra recorded at 298 K from materials of composition $Fe_{1-x}Cr_xSbO_4$ contained quadrupole split absorptions with ^{57}Fe Mössbauer parameters, δ *ca* 0.37 mm s^{-1}, Δ *ca* 0.71 mm s^{-1}, Γ *ca* 0.42 mm s^{-1}, characteristic of high-spin Fe^{3+}. Given that the magnetic susceptibility measurements indicate the existence of some short range magnetic order at this temperature the absence of magnetic splitting in the Mössbauer

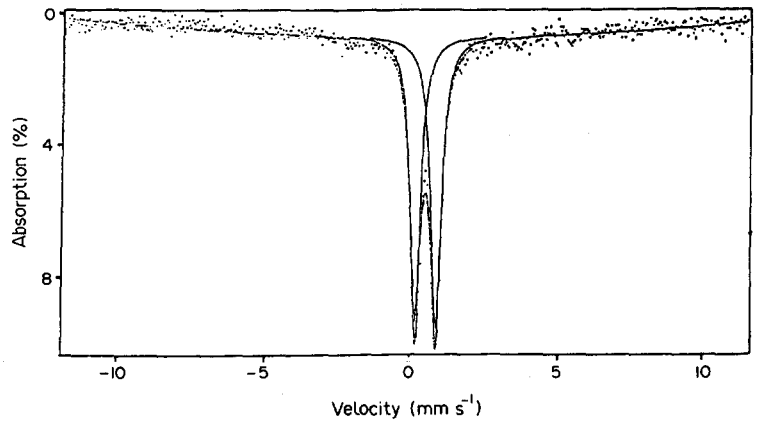

Fig. 4. ^{57}Fe Mössbauer spectrum recorded at 77 K from $Fe_{0.85}Cr_{0.15}SbO_4$.

spectrum indicates that the magnetic relaxation processes occurring in the clusters in the iron chromium antimonates have faster time scales than the Mössbauer time scale of 10^{-8} s. The ^{57}Fe Mössbauer spectra recorded at 77 K were similar (Fig. 4), δ *ca* 0.44 mm s^{-1}, Δ *ca* 0.71 mm s^{-1}, Γ *ca* 0.43 mm s^{-1}, and in contrast with the spectrum recorded[1] from iron antimonate at 77 K showed no evidence of magnetic splitting. The result is indicative of faster relaxation times between the magnetic interactions in iron chromium antimonates as a result of the smaller concentration of the Fe^{3+} species. The ^{121}Sb Mössbauer spectra recorded from the iron chromium antimonates at 298 and 77 K all gave single absorptions characteristic of Sb^{5+} (Fig. 5). The Mössbauer parameters are collected in Table 3. The samples with a high iron content, $x < 0.4$, showed a larger line width at 77 K than at 298 K. In the absence of a structural transformation the results are consistent with the presence of a super-transferred hyperfine magnetic field at antimony from iron via oxygen, as previously observed in iron antimonate at low temperature.[1] Presumably, the effect would be seen in the ^{57}Fe Mössbauer spectra recorded from iron-rich samples at very low temperature. It appears that the super-transferred hyperfine magnetic field is less significant as the iron content is decreased and, as shown by the magnetic susceptibility measurements, the magnetic interactions weaken.

Iron gallium antimonates

The X-ray powder diffraction data recorded from gallium antimonate prepared by both co-precipitation and solid state techniques were somewhat different from those reported in the literature.[6] The new data recorded here are contained in Table 4. The X-ray powder diffraction patterns recorded from materials of composition $Fe_{1-x}Ga_xSbO_4$ were all similar to each other and to those recorded from iron and gallium antimonate. The lattice parameters are collected in Table 5 and show a decrease as Fe^{3+} ions (ionic radii in six-fold coordination

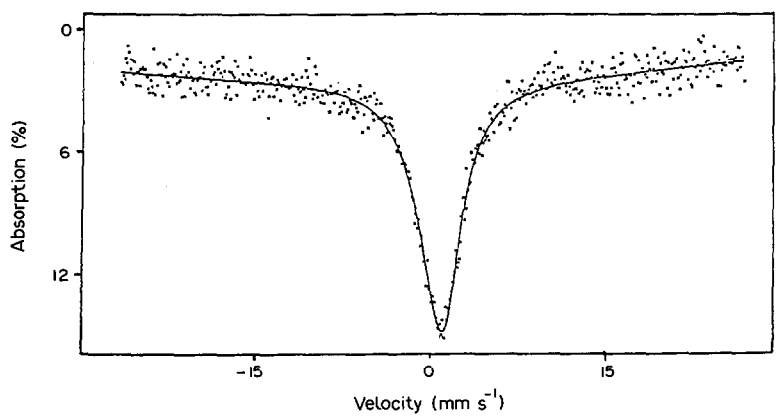

Fig. 5. ^{121}Sb Mössbauer spectrum recorded at 77 K from $Fe_{0.85}Cr_{0.15}SbO_4$.

Table 3. ^{121}Sb Mössbauer parameters recorded from compounds of composition $Fe_{1-x}Cr_xSbO_4$

x	Temperature (K)	$\delta \pm 0.05$ (mm s^{-1})	$\Gamma \pm 0.03$ (mm s^{-1})
0.0	298	8.28	3.73
	77	8.66	4.8
0.15	298	8.21	3.71
	77	8.31	4.29
0.37	298	8.27	3.64
	77	8.22	4.05
0.60	298	8.25	3.66
	77	8.18	3.85
0.74	298	8.22	3.59
	77	8.27	3.57
1.0	298	8.19	4.25
	77	8.10	4.19

0.645 Å)[4] are replaced by the smaller Ga^{3+} ions (ionic radii in six-fold coordination 0.62 Å).[4]

The temperature dependence of the inverse zero field-cooled magnetic susceptibility of the iron gallium antimonates is illustrated by the data recorded from $Fe_{0.90}Ga_{0.10}SbO_4$ and $Fe_{0.30}Ga_{0.70}SbO_4$, which are shown in Figs 6 and 7. The computer-calculated effective magnetic moments and Curie temperatures of the compounds of composition $Fe_{1-x}Ga_xSbO_4$ were derived from the magnetic susceptibility measurements and are collected in Table

Table 4. X-ray powder diffraction data for gallium antimonate

I_{obs}	hkl	d_{obs} (Å)	$d_{calc.}$ (Å)
100	110	3.2515	3.2520
81	101	2.5331	2.5330
20	200	2.2991	2.2995
9	111	2.2198	2.2187
70	211	1.7025	1.7026
14	220	1.6257	1.6260
11	002	1.5177	1.5174
13	310	1.4542	1.4543
19	112	1.3749	1.3750
19	301	1.3684	1.3683
8	202	1.2666	1.2665
9	321	1.1758	1.1759
4	400	1.1495	1.1497
8	222	1.1095	1.1093
4	330	1.0842	1.0840
10	312	1.0497	1.0499
4	420	1.0283	1.0284
5	103	0.9881	0.9880
4	213	0.9165	0.9164

Table 5. Lattice parameters of compounds of composition $Fe_{1-x}Ga_xSbO_4$

x	$a = b \pm 0.005$ (Å)	$c \pm 0.0005$ (Å)
0.10	4.6258	3.0655
0.32	4.6227	3.0612
0.52	4.6160	3.0553
0.70	4.6134	3.0491
1.00	4.5990	3.0347

Table 6. Curie temperatures and effective magnetic moments of compounds of composition $Fe_{1-x}Ga_xSbO_4$

x	θ (K)	μ (B.M./ion)
0.00	580	6.0
0.10	447.3	5.62
0.32	346.8	4.96
0.52	209.8	4.09
0.70	98.7	3.05

6. At temperatures exceeding *ca* 200 K the magnetic susceptibility data recorded from all the iron gallium antimonates followed the Curie–Weiss law. The trends of decreasing Curie temperatures and effective magnetic moments with decreasing Fe^{3+} content are more marked than those observed in the iron chromium antimonates because of the diamagnetic nature of Ga^{3+} which, by substitution for paramagnetic Fe^{3+} ions, dilutes the magnetic interactions between the Fe^{3+} species.

At temperatures below *ca* 200 K a deviation from the high temperature Curie–Weiss law was observed in the magnetic susceptibility data recorded from

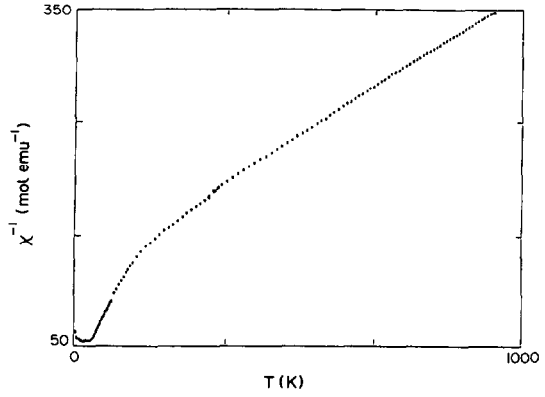

Fig. 6. The temperature dependence of the inverse zero field-cooled magnetic susceptibility recorded from the compound $Fe_{0.90}Ga_{0.10}SbO_4$.

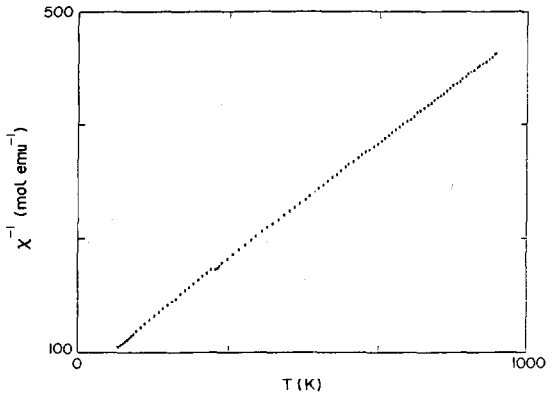

Fig. 7. The temperature dependence of the inverse zero field-cooled magnetic susceptibility recorded from the compound $Fe_{0.30}Ga_{0.70}SbO_4$.

the materials of composition $Fe_{1-x}Ga_xSbO_4$, ranging from 190 K when $x = 0.10$ to 100 K when $x = 0.70$. This deviation from the Curie–Weiss law may be associated with the formation of short-range magnetically ordered clusters, as observed in iron antimonate and the iron chromium antimonates, and the progressively lower temperatures at which these deviations begin may reflect the effect of larger Cr^{3+} concentrations on the formation of the clusters.

A second Curie–Weiss law was observed in the materials of composition $Fe_{0.90}Ga_{0.10}SbO_4$ and $Fe_{0.68}Ga_{0.32}SbO_4$ (see Fig. 6) at lower temperatures, which may be associated with the paramagnetic-like behaviour of the small magnetically ordered clusters as previously observed for iron antimonate and the iron chromium antimonates with high Fe^{3+} ion contents. At even lower temperatures between 10 and 30 K the magnetic susceptibility recorded from $Fe_{0.90}Ga_{0.10}SbO_4$ (Fig. 6) showed a maximum similar to that observed in the data obtained in high magnetic fields from iron antimonate, $Fe_{0.85}Cr_{0.15}SbO_4$ and $Fe_{0.63}Cr_{0.37}SbO_4$. The absence of a cusp in the magnetic susceptibility data recorded from iron gallium antimonates with lower iron concentrations may imply that the spin glass magnetic phenomena may be inhibited by the reduction in the magnitude and number of magnetic interactions or by interference of substituted gallium with the cationic anti-site ordered.

The ^{57}Fe and ^{121}Sb Mössbauer spectra recorded from the iron gallium antimonates at 298 K were similar to those recorded from the iron chromium antimonates (*vide supra*). The ^{57}Fe Mössbauer spectra recorded at 77 K from $Fe_{1-x}Ga_xSbO_4$ were also similar to those recorded from $Fe_{1-x}Cr_xSbO_4$ and failed to show any evidence for the magnetic interaction previously observed at 77 K in the spectrum recorded from iron antimonate.[1] The ^{121}Sb Mössbauer spectrum recorded at 77 K from $Fe_{0.90}Ga_{0.10}SbO_4$ showed a broader line as compared with that recorded at 298 K and may be associated with the onset of a super-transferred hyperfine magnetic interaction from iron to antimony via oxygen.

Acknowledgements—We thank the SERC, The British Council and the Ministerio de Education Y Ciencia for support.

REFERENCES

1. F. J. Berry, M. I. Sarson, A. Labarta, X. Obradors, R. Rodriguez and J. Tejada, *J. Solid State Chem.* 1987, **71**, 582.
2. F. J. Berry, M. I. Sarson, J. Tejada, A. Labarta, R. Rodriguez and X. Obradors, *J. Solid State Chem.* 1990, **87**, 237.
3. J. Amador and I. Rasines, *J. Appl. Cryst.* 1981, **14**, 348.
4. R. D. Shannon, *Acta Cryst.* 1976, **A32**, 751.
5. K. M. Fischer, *Phys. Stat. Sol.* 1985, **B130**, 13.
6. E. C. Shafer and R. Roy, *J. Am. Ceram. Soc.* 1956, **39**, 330.

Polyhedron Vol. 12, No. 13, pp. 1587–1591, 1993
Printed in Great Britain

0277–5387/93 $6.00+.00
© 1993 Pergamon Press Ltd

EXTRACTION BEHAVIOUR OF SILVER(I) WITH SOME CYCLIC TETRATHIOETHERS

KEIITSU SAITO,* SATOMI MURAKAMI and AKIHIKO MUROMATSU

Division of Natural Environment and Chemistry, Faculty of Human Development, Kobe University, Tsurukabuto, Nada, Kobe 657, Japan

and

EIICHI SEKIDO

Department of Chemistry, Faculty of Science, Kobe University, Rokkodai, Nada, Kobe 657, Japan

(*Received* 22 *February* 1993; *accepted* 23 *March* 1993)

Abstract—The extraction behaviour of silver(I) with 12-, 13-, 15- and 16-membered cyclic tetrathioethers (*n*-ane-S_4, where *n* represents the total number of carbon and sulphur atoms in the cyclic ligand ring) was examined stoichiometrically using the picrate ion (Pic^-) for the formation of the ion pair and chloroform and 1,2-dichloroethane as solvents. The composition of the extracted species and the extraction constant were determined. Silver(I) was extracted with these four ligands (L) into chloroform and 1,2-dichloroethane as the ion-pair compound $[AgL]^+Pic^-$. The extracted species with these four ligands is different from that previously reported for 14-ane-S_4, $[AgL_2]^+Pic^-$.

The complexing properties of macrocyclic polythioethers have been studied and metal complexes with macrocyclic polythioethers have been isolated and characterized.[1–8] Macrocyclic polythioethers have also been studied as an extraction reagent which is selective for soft metal ions.[9–15] Silver(I) belonging to soft Lewis acids[16] is extracted completely with macrocyclic polythioethers and an appropriate counter-anion under a large excess of the ligand and counter-anion. The extraction system has been applied to the spectrophotometric determination of silver using an appropriately coloured anion, such as picrate or Bromocresol Green.[10] Recently, the molecular structure of the dimeric silver(I)-13,14-benzo-1,4,8,11 - tetrathiocyclopentadec - 13 - ene picrate complex has been reported.[17] The structure of the dimeric silver(I) complex of 1,4,8,11-tetrathiacyclotetradecane has also been reported,[18] while studies concerning the extraction equilibria have shown that the extracted species is $[AgL_2]^+Pic^-$.[11] Therefore, it is of interest to determine whether the dimeric complex with a macrocyclic polythioether other than 1,4,8,11-tetrathiacyclotetradecane is formed or not in the organic solution in the presence of a large excess of the ligand. Moreover, it is of interest to study the composition of the extracted species of silver(I) with a continuous series of homologous macrocyclic polythioethers which have the same number of sulphur atoms. Thus, the extraction behaviour of silver(I) with 12-, 13-, 15- and 16-membered cyclic tetrathioethers (*n*-ane-S_4, where *n* represents the total number of carbon and sulphur atoms in the cyclic ligand ring) was examined using the picrate ion as the counter-anion. Chloroform and 1,2-dichloroethane were used as solvents. The results were compared with those previously reported for 14-ane-S_4.[11] The cyclic tetrathioethers considered in this work are shown in Fig. 1.

EXPERIMENTAL

Reagents

All cyclic tetrathioethers were synthesized according to the method of Ochrymowycz *et al.*[19]

* Author to whom correspondence should be addressed.

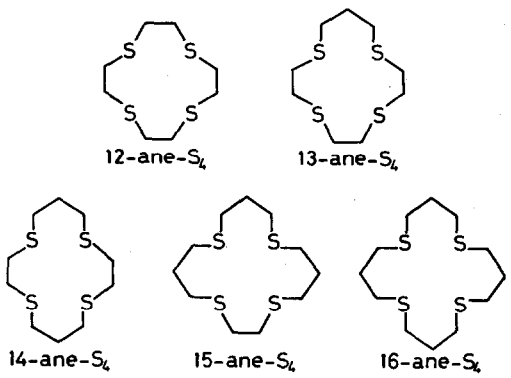

Fig. 1. Cyclic tetrathioethers investigated.

The products were purified by the method described previously.[15] Chloroform was shaken three times each with sulphuric acid (1 M), sodium hydroxide solution (2 M) and distilled water, dried over anhydrous sodium sulphate and distilled. 1,2-Dichloroethane was purified as described before.[15] Silver sulphate (analytical-reagent grade) was used to prepare a 2×10^{-2} M silver(I) stock solution. Other reagents were of analytical grade.

Apparatus

Extraction was performed in a Taiyo M-100 incubator at 25 ± 0.1°C. Seiko SAS-725 and Hitachi Z-8000 atomic absorption spectrometers were used to determine the concentration of the silver ion. The UV–vis absorption spectra were measured with a Hitachi U-3200 spectrophotometer. The pH of the aqueous phase was measured with a Toa HM-7E pH meter.

Liquid–liquid extraction of silver(I)

An aqueous solution (10 cm^3) containing silver(I), picrate ions and a buffer solution was taken in a 50 cm^3 glass cylindrical tube fitted with a glass stopper. The buffer solution was prepared with sulphuric acid (pH < 3) or acetic acid and sodium acetate (pH 3–6). The ionic strength was kept at 0.1 with sodium sulphate. After the addition of a cyclic tetrathioether solution (10 cm^3) of chloroform or 1,2-dichloroethane the mixture was shaken for 30 min at 200 inversions min^{-1} at 25 ± 0.1°C and then centrifuged for 5 min at 2000 rounds min^{-1}. After the two phases had separated the pH of the aqueous phase was measured and the concentration of the picrate ion in the aqueous phase was determined spectrophotometrically at 354 nm. The concentrations of silver ions in the aqueous and organic phases were determined by atomic absorption spectrometry. The silver ion concentration of the organic phase was determined as follows: a suitable volume of the organic phase was allowed to evaporate, the residue was treated with concentrated nitric acid (1 cm^3) and diluted with water (to 10 cm^3) and the concentration of silver ions was determined by atomic absorption spectrometry.

RESULTS AND DISCUSSION

Dependence on pH

The extraction of silver(I) with 12-ane-S_4 from an aqueous solution containing picrate ions (1×10^{-3} M) into 1,2-dichloroethane was examined in the pH range 2.5–5.5. A plot of the logarithmic distribution of silver(I), $\log D$, against the pH of the aqueous phase is shown in Fig. 2. The extractability of silver(I) is constant at > 99% ($\log D > 2$) in the pH range 2.5–5.5 under the present conditions.

Extraction of silver(I) *with cyclic tetrathioethers*

As crystallographic studies of silver(I) complexes with 14-ane-S_4[18] and 13,14-benzo-1,4,8,11-tetrathiacyclopentadec-13-ene[17] have shown that the 2:2 dimeric complex cation, $[Ag_2L_2]^{2+}$, is formed in the solid state, the formation of polynuclear complexes should be taken into account. If the species extracted into an organic phase is represented by $Ag_jL_m(Pic)_n$ the extraction equilibrium and the extraction constant, K_{ex}, are given by eqs (1) and (2), respectively:

$$jAg^+ + mL(o) + nPic^- \overset{K_{ex}}{\rightleftharpoons} Ag_jL_m(Pic)_n(o) \quad (1)$$

$$K_{ex} = [Ag_jL_m(Pic)_n]/[Ag^+]^j[L]_o^m[Pic^-]^n, \quad (2)$$

where (o) and subscript o indicate the species in the organic phase. When the complexation of silver(I) in the aqueous phase is neglected and the species present in the organic phase is only the ion-pair

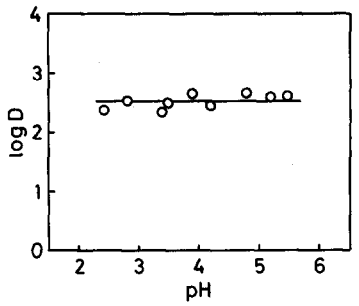

Fig. 2. Plot of $\log D$ vs pH. Initial concentrations: silver(I), 5×10^{-5} M; 12-ane-S_4, 5×10^{-3}M; picrate ion, 1×10^{-3} M.

$Ag_jL_m(Pic)_n$ the total concentration of silver(I) in the organic phase is presented by:

$$\log C_{Ag,o} = j\log[Ag^+] + m\log[L]_o + n\log[Pic^-] + \log j + \log K_{ex}. \quad (3)$$

Determination of the degree of polymerization of the extracted species

According to eq. (3) the plot of $\log C_{Ag,o}$ against $\log[Ag^+]$ at constant concentrations of the ligand and picrate ion should yield a straight line with a slope of j, the degree of polymerization. In order to determine the degree of polymerization of the extracted species the extraction of silver(I) at pH 4.8 was examined at various concentrations of silver(I) under constant concentrations of the ligand and picrate ion. Chloroform was used as the solvent because of the high extractibility of silver(I) into 1,2-dichloroethane in the presence of a large excess of the ligand and picrate ion. The results are shown in Fig. 3. Four straight lines with the slope of 1.0 were obtained, indicating that $j = 1$. This suggests that the monomer can be presented as the extracted species under these conditions.

Determination of the number of picrate ions involved in the extracted species

When the monomeric silver(I) species is extracted eqs (1) and (2) become:

$$Ag^+ + mL(o) + nPic^- \overset{K_{ex}}{\rightleftharpoons} AgL_m(Pic)_n(o) \quad (1')$$

$$K_{ex} = [AgL_m(Pic)_n]_o/[Ag^+][L]_o^m[Pic^-]^n. \quad (2')$$

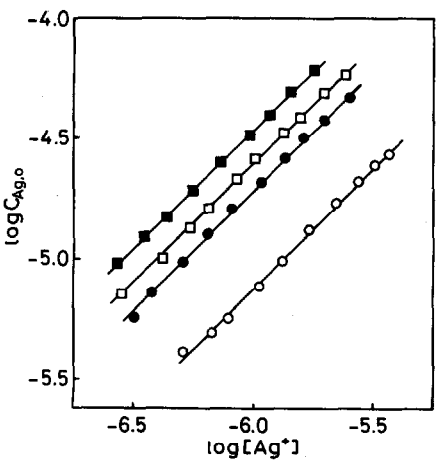

Fig. 3. Plots of $\log C_{Ag,o}$ vs $\log[Ag^+]$ at pH 4.8. Initial concentrations: n-ane-S_4, 1×10^{-3} M; picrate ion, 1×10^{-3} M. Ligands: (○) 12-ane-S_4; (●) 13-ane-S_4; (□) 15-ane-S_4; (■) 16-ane-S_4. Solid lines are straight with a slope of 1.0.

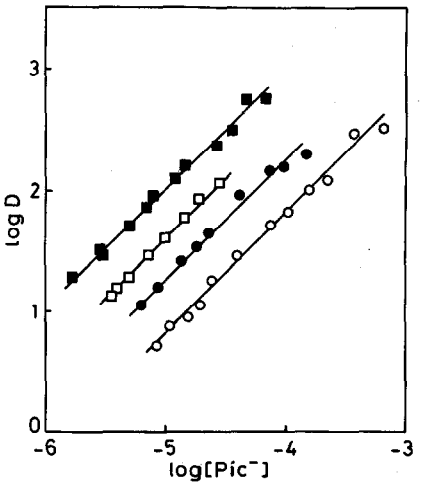

Fig. 4. Plots of $\log D$ vs $\log[Pic^-]$ at pH 4.9. Initial concentrations: silver(I), 5×10^{-5} M; n-ane-S_4, 5×10^{-3} M. Ligands: (○) 12-ane-S_4; (●) 13-ane-S_4; (□) 15-ane-S_4; (■) 16-ane-S_4. Solid lines are straight with a slope of 1.0.

The logarithmic distribution of silver(I) is presented by:

$$\log D = \log K_{ex} + m\log[L]_o + n\log[Pic^-]. \quad (4)$$

The extraction of silver(I) into 1,2-dichloroethane at pH 4.9 was examined at various concentrations of the picrate ion under constant concentration of the ligand. The results are shown in Fig. 4. Four straight lines with a slope of 1.0 were obtained, i.e. $n = 1$. This indicates that the molar ratio of the

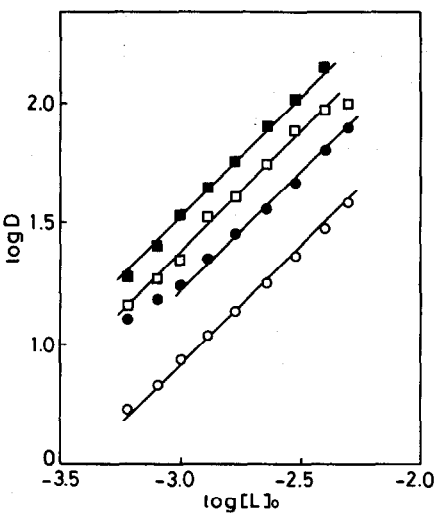

Fig. 5. Plots of $\log D$ vs $\log[L]_o$ at pH 4.8. Solvent: chloroform. Initial concentrations: silver(I), 5×10^{-5} M; picrate ion, 1×10^{-3} M. Ligands: (○) 12-ane-S_4; (●) 13-ane-S_4; (□) 15-ane-S_4; (■) 16-ane-S_4. Solid lines are straight with a slope of 1.0.

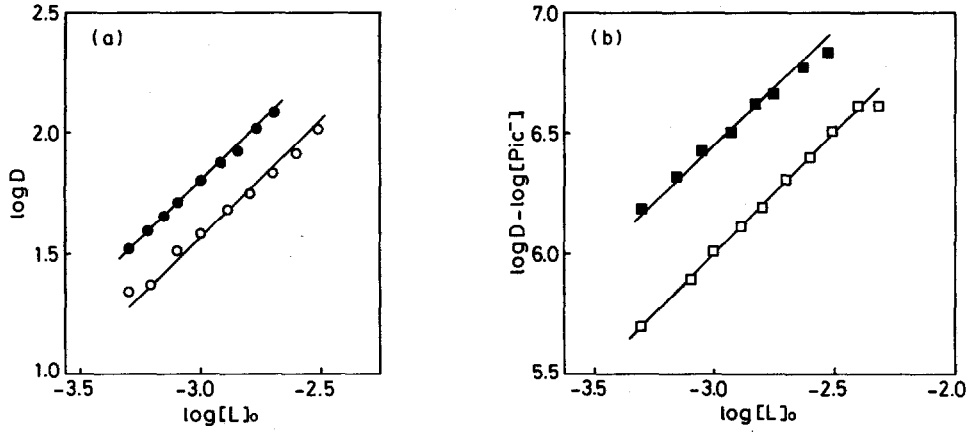

Fig. 6. Plots of (a) $\log D$ vs $\log[L]_o$ for (○) 12-ane-S_4 and (●) 13-ane-S_4 and (b) $\log D - \log[Pic^-]$ vs $\log[L]_o$ for (□) 15-ane-S_4 and (■) 16-ane-S_4; pH 4.8. Solvent: 1,2-dichloroethane. Initial concentrations: silver(I), 5×10^{-5} M for (a) and (b); picrate ion, 5×10^{-4} M for (a). Solid lines are straight with a slope of 1.0.

silver(I) and picrate ions is 1 : 1, as expected from the charges of the silver(I) and picrate ions.

Determination of the number of ligand molecules involved in the extracted species

The extraction of silver(I) into chloroform at pH 4.8 was examined at various concentrations of the ligand under constant concentration of the picrate ion. The relationships between $\log D$ and the logarithm of the ligand concentration in the organic phase are shown in Fig. 5. Four straight lines with the slope close to 1.0 were obtained, i.e. $m = 1$. This indicates that silver(I) is extracted with four cyclic tetrathioethers into chloroform as the complex $[AgL]^+$. The extraction of silver(I) into 1,2-dichloroethane was also examined at pH 4.8. The results obtained for 12-ane-S_4 and 13-ane-S_4 are shown in Fig. 6(a). Two straight lines with the slope close to 1.0 were obtained. The value of m for 15-ane-S_4 and 16-ane-S_4 could not be determined by the same method because of the high extractability of silver(I) into 1,2-dichloroethane in the presence of a large excess of the ligand and picrate ions to silver(I). Therefore, the extraction of silver(I) was performed at the total concentration of picrate ion, $[Pic^-]_t = 6.5 \times 10^{-5}$ and 6.0×10^{-5} M for 15-ane-S_4 and 16-ane-S_4, respectively, and $\log D - \log[Pic^-]$ was plotted against $\log[L]_o$. The results are shown in Fig. 6(b). Two straight lines with the slope close to 1.0 were obtained, i.e. $m = 1$. The molar ratio method for these two ligands has also shown that the extracted species is $[AgL]^+$. These results indicate that silver(I) is extracted with four ligands into 1,2-dichloroethane as the 1 : 1 complex $[AgL]^+$, as with chloroform.

Consequently, in the present extraction system the extraction equilibrium is expressed as follows:

$$Ag^+ + L(o) + Pic^- \rightleftharpoons AgL(Pic)(o).$$

Table 1. Compositions and extraction constants for silver(I)-cyclic tetrathioether complexes extracted into organic solvents

Ligand	$Ag^I : L : Pic^-$	Log K_{ex}[a] Chloroform	1,2-DCE[b]
12-ane-S_4	1 : 1 : 1	6.89 ± 0.03(4)	7.99 ± 0.12(2)
13-ane-S_4	1 : 1 : 1	7.23 ± 0.04(4)	8.33 ± 0.23(2)
14-ane-S_4[11]	1 : 2 : 1	10.9 ± 0.1	11.7 ± 0.2
15-ane-S_4	1 : 1 : 1	7.41 ± 0.04(3)	8.96 ± 0.05(2)
16-ane-S_4	1 : 1 : 1	7.56 ± 0.08(4)	9.37 ± 0.06(2)

[a] Mean value. The figures in parentheses are the number of measurements.

[b] 1,2-Dichloroethane.

Equation (4) becomes:

$$\log D = \log K_{ex} + \log [L]_o + \log [Pic^-]. \quad (4')$$

The logarithmic extraction constant was calculated according to eq. (4'). The results are shown in Table 1. As the studies concerning the extraction equilibria for the extraction of silver(I) picrate with 14-ane-S_4 have shown that the extracted species is $[AgL_2]^+Pic^-$,[11] the 1:2 molar ratio of silver(I)-to-ligand was expected for two smaller ligands, 12-ane-S_4 and 13-ane-S_4. However, the extracted species with 12-ane-S_4 and 13-ane-S_4 is $[AgL]^+Pic^-$.

REFERENCES

1. S. G. Murray and F. R. Hartley, *Chem. Rev.* 1981, **81**, 365.
2. V. B. Pett, L. L. Diaddario Jr, E. R. Dockal, P. W. R. Corfield, C. Ceccarelli, M. D. Glick, L. A. Ochrymowycz and D. B. Rorabacher, *Inorg. Chem.* 1983, **22**, 3661.
3. L. L. Diaddario Jr, E. R. Dockal, M. D. Glick, L. A. Ochrymowycz and D. B. Rorabacher, *Inorg. Chem.* 1985, **24**, 356.
4. J. A. Clarkson, R. Yagbasan, P. J. Blower, S. C. Rawle and S. R. Cooper, *J. Chem. Soc., Chem. Commun.* 1987, 950.
5. H. J. Küppers, K. Wieghardt, Y. H. Tsay, C. Krüger, B. Nuber and J. Weiss, *Angew. Chem.* 1987, **99**, 583.
6. D. Sevdić, M. Ćurić and Lj. Tušck-Božć, *Polyhedron* 1989, **8**, 505.
7. A. J. Blake, R. O. Gould, A. J. Holder, T. I. Hyde and M. Schröder, *Polyhedron* 1989, **8**, 513.
8. A. J. Blake and M. Schröder, *Adv. Inorg. Chem.* 1990, **35**, 1.
9. K. Saito, Y. Masuda and E. Sekido, *Anal. Chim. Acta* 1983, **151**, 447.
10. K. Saito, Y. Masuda and E. Sekido, *Bull. Chem. Soc. Japan* 1984, **57**, 189.
11. E. Sekido, K. Saito, Y. Naganuma and H. Kumazaki, *Anal. Sci.* 1985, **1**, 363.
12. E. Sekido, K. Chayama and M. Muroi, *Talanta* 1985, **32**, 797,
13. E. Sekido, H. Kawahara and K. Tsuji, *Bull. Chem. Soc. Japan* 1988, **61**, 1587.
14. M. Muroi, T. Tamiki and E. Sekido, *Bull. Chem. Soc. Japan* 1989, **62**, 1797.
15. K. Saito, S. Murakami, A. Muromatsu and E. Sekido, *Anal. Chim. Acta* 1990, **237**, 245.
16. R. G. Pearson, *J. Am. Chem. Soc.* 1963, **85**, 3533.
17. E. Sekido, K. Suzuki and K. Hamada, *Anal. Sci.* 1987, **3**, 505.
18. K. Chayama and E. Sekido, *Anal. Sci.* 1990, **6**, 883.
19. L. A. Ochrymowycz, C. P Mak and J. D. Michna, *J. Org. Chem.* 1974, **39**, 2079.

Polyhedron Vol. 12, No. 13, pp. 1593–1597, 1993
Printed in Great Britain

0277–5387/93 $6.00+.00
© 1993 Pergamon Press Ltd

SYNTHESIS AND X-RAY CRYSTAL STRUCTURE OF THE COBALT(III) COMPLEX OF 6-METHYL-6-(4-AMINO-2-AZABUTYL)-1-THIA-4-AZACYCLOHEPTANE (atac), *cis*-[Co(atac)Cl_2]$ClO_4 \cdot \frac{1}{2}H_2O$

THERESE M. DONLEVY and LAWRENCE R. GAHAN*

Department of Chemistry, The University of Queensland, Brisbane QLD 4072, Australia

and

TREVOR W. HAMBLEY

School of Chemistry, The University of Sydney, Sydney, NSW 2006, Australia

(*Received* 4 *January* 1993; *accepted* 23 *March* 1993)

Abstract—The crystal structure of *cis*-[Co(atac)Cl_2]$ClO_4 \cdot \frac{1}{2}H_2O$ [atac = 6-methyl-6-(4-amino-2-azabutyl)-1-thia-4-azacycloheptane] has been determined by X-ray diffraction methods. The tetradentate ligand atac contains the N_3S donor set and is coordinated to cobalt(III) through a secondary amine and a thioether in the cycloheptane ring, and through a pendant primary amine. The chloro ligands coordinated in a *cis* arrangement make up the octahedral environment of the metal ion.

Extensive use has been made of the reaction between 1,2-diaminoethane and suitably substituted neopentyl or pentaerythritol derivatives in order to prepare multidentate ligands containing the —$NHCH_2CH_2NH_2$ fragment.[1–8] The reaction permits large scale preparation of the desired ligands;[1] the propensity for the formation of a range of by-products, however, necessitates extensive purification procedures.[1,3] In a number of instances these by-products themselves represent interesting ligands and studies of their metal complexes have been pursued.[2,5] We have previously reported the characterization of the cobalt(III) complexes of two such by-products isolated from reactions in which sulphur-containing neopentyl moieties were reacted with 1,2-diaminoethane.[5] One of these complexes contained the seven-membered ring ligand 6-methyl-6-(4-amino-2-azabutyl)-1-thia-4-azacycloheptane (atac).[5] This paper now reports the isolation and characterization of the complex *cis*-[Co(atac)Cl_2]$ClO_4 \cdot \frac{1}{2}H_2O$.

RESULTS AND DISCUSSION

Reaction between 1,1,1-tris[{(benzenesulphonyl)oxy}methyl]ethane and the sodium salt of 2-aminoethanethiol, and subsequent reaction of the product with 1,2-diaminoethane, has been shown to result in a mixture of products. Depending on the reaction conditions and stoichiometry, the reaction has resulted in the isolation of the hexadentate ligands 5-methyl-5-(4-amino-2-azabutyl)-3,7-dithianonane-1,9-diamine[9] and 5-methyl-(4-amino-2-thiabutyl)-3,7-diazanonane-1,9-diamine.[10] The ligand 6-methyl-6-(4-amino-2-azabutyl)-1-thia-4-azacycloheptane (atac) has been shown to also be a major product from this type of reaction.[5] The formation of this product, which presumably arises from an intramolecular cyclization reaction,[2] is not unexpected and this type of product has been observed in similar systems. Indeed, for the reactions of 1,2-diaminoethane with pentaerythrityltetrabromide or 1,1,1-tris[{(toluenesulphonyl)oxy}methyl]ethane the products arising from the intramolecular pathway, 6,6-bis(4-amino-2-azabutyl)-1,4-diazacycloheptane[3] and 6-methyl-6-(4-amino-2-azabutyl)-1,4-diazacycloheptane,[2]

* Author to whom correspondence should be addressed.

respectively, were reported to constitute 30–50% of the products obtained.

The complex *cis*-$[Co(atac)Cl_2]^+$ was isolated as a major purple band from Dowex 50WX2 cation exchange chromatography and was isolated as the perchlorate salt from aqueous solution. The structure consists of two independent complex cations, two perchlorate anions, one of which is disordered, and a water molecule. The complex cations are not significantly different; each has a tetradentate ligand coordinated through three (N)amine and one (S)thioether donor groups to a cobalt(III) ion and two chloro ligands coordinated in a *cis* arrangement. The geometry about the cobalt is approximately octahedral although ligand constraints reduce some of the angles to *ca* 80°. The C(2)—C(4)—N(1) angle in the dichloro complex is 115.6(3)°, compared with 120.9(8)° in [Co(atac)en]$^{3+}$,[5] and is in fact comparable to the angle observed in the all-nitrogen complex $[Co(L)en]^{3+}$, where L = 6-methyl-6-(4-amino-2-azabutyl)-1,4-diazacycloheptane.[2] It appears then that the increased strain in this angle is not only a result of incorporation of the thioether into the cycloheptane ring, but may in addition be the result of strain induced by the coordination of the remainder of the ligand, e.g. some Co—N—C angles are opened to 122°. The Cl(1)—Co—Cl(2) bond angle 89.0(1)° is larger than the corresponding angle in [Co(atac)en]$^{3+}$ [83.8(3)°][5] and $[Co(L)en]^{3+}$ [84.3(1)°][2] and suggests the source of increased strain within the complex. The N(1)—C(7)—C(6)—S(1) torsion angle (~ 0.0°) indicates that this part of the chelate ring is essentially flat, with the hydrogen atoms eclipsed. The Co—N and Co—S bond lengths are longer than average, but not greatly so.[11,12] The Co—N(1) bond length in the dichloro complex is shorter than that observed in [Co(atac)en]$^{3+}$, 1.984(3) Å compared with 2.056(6) Å, respectively.[5] In contrast to the coordination observed in the [Co(atac)en]$^{3+}$ cation, where the primary amine of the ligand was *trans* to the thioether in the cycloheptane ring, in the present complex the primary amine of atac is *trans* to the secondary nitrogen in the cycloheptane ring. The Co—Cl bond lengths are slightly shorter (av. 2.268 Å) than those in $[Co(NH_3)_5Cl]Cl_2$ [2.286(2) Å][13] and those *trans* to sulphur are not significantly different to those *trans* to nitrogen.

EXPERIMENTAL

Fourier-transform $^{13}C[^1H]$ NMR spectra were recorded with a Bruker AC200F spectrometer. Chemical shifts for the spectra recorded in D_2O are reported in parts per million (δ) as positive downfield and negative upfield from the internal reference dioxane. Visible spectra were recorded with a Beckman DU7500 UV–vis spectrophotometer. Microanalyses were determined by the University of Queensland Microanalytical Service.

Ligand synthesis

1,1,1-Tris[{(benzenesulphonyl)oxy}methyl]ethane[14] (150 g, 0.28 mol) was reacted with the sodium salt of 2-aminoethanethiol (9.17 g, 0.092 mol) under reflux in ethanol (250 cm^3) and the yellow oil isolated upon removal of the solvent was refluxed with 1,2-diaminoethane, essentially as described previously.[1–5,9] The heavy oil obtained after removal of the solvent was employed without further purification in the preparation of the metal complex.

Synthesis of cis-$[Co(atac)Cl_2]ClO_4 \cdot \frac{1}{2}H_2O$

The oil obtained from the ligand synthesis was dissolved in methanol (250 cm^3) and whilst a slow stream of air was drawn through the solution a methanol solution (100 cm^3) of cobaltous chloride (22 g, 0.09 mol) was added dropwise over a period of 0.5 h. Air was continued to be drawn through the solution for 2 h after the completion of the addition, after which time the solution was filtered, diluted to a large volume with water and loaded on a column of Dowex 50WX2 cation exchange resin (H^+ form, 200–400 mesh). After washing with water and HCl (1 M) to remove minor bands, the intense purple band which eluted with HCl (2 M) was collected. Solvent was removed under reduced pressure and the purple residue obtained was dissolved in a large volume of water and loaded on a column of Sephadex C25 cation exchange resin (Na^+) form. After washing the column with water and NaCl (0.1 M) the purple band which eluted with NaCl (0.2 M) was collected on Dowex cation exchange resin, washed with water and HCl (0.5 M) and eluted with HCl (2 M). Removal of the solvent under reduced pressure and crystallization of the residue from an aqueous solution of $NaClO_4$ resulted in purple crystals. Found: C, 23.9; H, 4.8; N, 8.9. Calc. for $C_9H_{22}CoN_3SCl_3O_{4.5}$: C, 24.5; H, 5.0; N, 9.5%. ^{13}C NMR (D_2O): δ −5.37, −6.95, −9.36, −11.14, −24.00, −35.73, −27.75 (—CH_2); −26.21 (C_q); −44.04 (CH_3). Visible spectrum (0.1 HCl) [λ_{max} nm, ε (M^{-1} cm^{-1})]: 561 (218), 395 (175).

Single-crystal X-ray structure determination

Crystal data. *Cis*-$[Co(atac)Cl_2]ClO_4 \cdot \frac{1}{2}H_2O$: $C_9H_{22}Cl_3CoN_3O_{4.5}S$; $M = 441.65$, monoclinic,

Table 1. Bond lengths (Å) and angles (°) for *cis*-[Co(atac)Cl_2]$ClO_4 \cdot \frac{1}{2}H_2O$

S(1)—Co(1)	2.242(1)	Cl(1)—Co(1)	2.265(1)
Cl(2)—Co(1)	2.276(1)	N(1)—Co(1)	1.984(3)
N(2)—Co(1)	1.985(3)	N(3)—Co(1)	1.968(3)
C(3)—S(1)	1.813(5)	C(6)—S(1)	1.800(5)
C(4)—N(1)	1.497(5)	C(7)—N(1)	1.503(6)
C(5)—N(2)	1.495(5)	C(8)—N(2)	1.493(5)
C(9)—N(3)	1.478(6)	C(2)—C(1)	1.546(6)
C(3)—C(2)	1.520(7)	C(4)—C(2)	1.513(6)
C(5)—C(2)	1.519(7)	C(7)—C(6)	1.514(6)
C(9)—C(8)	1.483(7)	S(2)—Co(2)	2.225(1)
Cl(3)—Co(2)	2.264(1)	Cl(4)—Co(2)	2.268(1)
N(4)—Co(2)	1.978(3)	N(5)—Co(2)	1.995(3)
N(6)—Co(2)	1.965(3)	C(13)—S(2)	1.812(4)
C(17)—S(2)	1.818(5)	C(15)—N(4)	1.491(5)
C(18)—N(4)	1.482(5)	C(14)—N(5)	1.501(5)
C(16)—N(5)	1.483(6)	C(19)—N(6)	1.487(6)
C(12)—C(11)	1.549(6)	C(13)—C(12)	1.543(7)
C(14)—C(12)	4.522(6)	C(15)—C(12)	1.514(6)
C(17)—C(16)	1.512(8)	C(19)—C(18)	1.495(6)
O(1)—Cl(5)	1.422(4)	O(2)—Cl(5)	1.394(7)
O(3)—Cl(5)	1.357(7)	O(4)—Cl(5)	1.364(7)
O(5)—Cl(6)	1.403(6)	O(6)—Cl(6)	1.309(14)
O(7)—Cl(6)	1.404(14)	O(8)—Cl(6)	1.477(18)
O(5′)—Cl(6)	1.326(29)	O(6′)—Cl(6)	1.347(22)
O(7′)—Cl(6)	1.486(33)	O(8′)—Cl(6)	1.501(28)
O(5″)—Cl(6)	1.701(68)		

Cl(1)—Co(1)—S(1)	90.6(1)	Cl(2)—Co(1)—S(1)	170.5(1)
Cl(2)—Co(1)—Cl(1)	89.0(1)	N(1)—Co(1)—S(1)	80.8(1)
N(1)—Co(1)—Cl(1)	94.1(1)	N(1)—Co(1)—Cl(2)	89.7(1)
N(2)—Co(1)—S(1)	94.7(1)	N(2)—Co(1)—Cl(1)	169.2(1)
N(2)—Co(1)—Cl(2)	87.3(1)	N(2)—Co(1)—N(1)	96.1(1)
N(3)—Co(1)—S(1)	97.8(1)	N(3)—Co(1)—Cl(1)	85.1(1)
N(3)—Co(1)—Cl(2)	91.6(1)	N(3)—Co(1)—N(1)	178.5(1)
N(3)—Co(1)—N(2)	84.8(1)	C(3)—S(1)—Co(1)	104.2(2)
C(6)—S(1)—Co(1)	96.0(2)	C(6)—S(1)—C(3)	97.3(2)
C(4)—N(1)—Co(1)	114.8(2)	C(7)—N(1)—Co(1)	110.4(2)
C(7)—N(1)—C(4)	111.9(3)	C(5)—N(2)—Co(1)	121.7(3)
C(8)—N(2)—Co(1)	108.9(3)	C(8)—N(2)—C(5)	111.0(3)
C(9)—N(3)—Co(1)	109.7(3)	C(3)—C(2)—C(1)	107.1(4)
C(4)—C(2)—C(1)	107.9(4)	C(4)—C(2)—C(3)	114.1(4)
C(5)—C(2)—C(1)	107.3(4)	C(5)—C(2)—C(3)	109.4(4)
C(5)—C(2)—C(4)	110.8(4)	C(2)—C(3)—S(1)	116.5(3)
C(2)—C(4)—N(1)	115.6(3)	C(2)—C(5)—N(2)	113.3(4)
C(7)—C(6)—S(1)	110.8(3)	C(6)—C(7)—N(1)	112.6(3)
C(9)—C(8)—N(2)	108.5(4)	C(8)—C(9)—N(3)	106.4(4)
Cl(3)—Co(2)—S(2)	171.1(1)	Cl(4)—Co(2)—S(2)	90.0(1)
Cl(4)—Co(2)—Cl(3)	89.6(1)	N(4)—Co(2)—S(2)	93.9(1)
N(4)—Co(2)—Cl(3)	88.2(1)	N(4)—Co(2)—Cl(4)	168.5(1)
N(5)—Co(2)—S(2)	80.6(1)	N(5)—Co(2)—Cl(3)	90.6(1)
N(5)—Co(2)—Cl(4)	94.1(1)	N(5)—Co(2)—N(4)	97.2(1)
N(6)—Co(2)—S(2)	98.4(1)	N(6)—Co(2)—Cl(3)	90.5(1)
N(6)—Co(2)—Cl(4)	84.4(1)	N(6)—Co(2)—N(4)	84.3(1)
N(6)—Co(2)—N(5)	178.2(2)	C(13)—S(2)—Co(2)	103.6(2)
C(17)—S(2)—Co(2)	96.9(2)	C(17)—S(2)—C(13)	98.5(2)
C(15)—N(4)—Co(2)	122.2(3)	C(18)—N(4)—Co(2)	108.8(2)
C(18)—N(4)—C(15)	111.6(3)	C(14)—N(5)—Co(2)	115.8(2)
C(16)—N(5)—Co(2)	110.6(3)	C(16)—N(5)—C(14)	111.6(3)
C(19)—N(6)—Co(2)	110.7(3)	C(13)—C(12)—C(11)	108.3(4)

Table 1—*continued*

C(14)—C(12)—C(11)	107.5(4)	C(14)—C(12)—C(13)	114.5(4)
C(15)—C(12)—C(11)	106.9(4)	C(15)—C(12)—C(13)	109.3(4)
C(15)—C(12)—C(14)	110.0(4)	C(12)—C(13)—S(2)	116.8(3)
C(12)—C(14)—N(5)	115.4(4)	C(12)—C(15)—N(4)	113.3(3)
C(17)—C(16)—N(5)	111.5(4)	C(16)—C(17)—S(2)	111.1(4)
C(19)—C(18)—N(4)	106.7(3)	C(18)—C(19)—N(6)	106.2(4)
O(2)—Cl(5)—O(1)	109.9(3)	O(3)—Cl(5)—O(1)	110.9(4)
O(3)—Cl(5)—O(2)	107.2(5)	O(4)—Cl(5)—O(1)	107.7(3)
O(4)—Cl(5)—O(2)	111.2(4)	O(4)—Cl(5)—O(3)	110.0(5)

space group $C2/c$, $a = 30.291(3)$, $b = 9.282(1)$, $c = 24.883(3)$ Å, $\beta = 100.82(1)°$; $V = 6871.9$ Å^3 $Z = 16$, $D_c = 1.707$ g cm^{-3}, μ(Mo-K_α) 15.73 cm^{-1}. λ(Mo-K_α) 0.7107 Å, F(000) 3632 electrons.

Data collection and processing. For diffractometry a crystal of dimensions $0.25 \times 0.11 \times 0.10$ mm was mounted on a glass fibre with cyanoacrylate resin. Lattice parameters at 21°C were determined by least-squares fit to the setting parameters of 25 independent reflections, measured and refined on an Enraf–Nonius CAD4F four-circle diffractometer employing graphite monochromated Mo-K_α radiation.

Structure analysis and refinement. Intensity data were collected in the range $1 < \theta < 25°$ using an ω–1.33θ scan. The scan width and horizontal counter aperture employed were $(0.80 + 0.34 \tan\theta)°$ and $(2.70 + 1.05 \tan\theta)$ mm, respectively. Data reduction and application of Lorentz, polarization and absorption (max. trans. 0.865, min. trans. 0.714) corrections were performed using the Enraf–Nonius structure determination package.[15] Of the 5410 independent non-zero reflections collected 4407 with $I > 2.5\sigma(I)$ were considered observed and used in the calculations. The structure was solved by direct methods using SHELXS-86[16] and the solution was extended by difference-Fourier methods. Hydrogen atoms were included at calculated sites with group isotropic thermal parameters and all other atoms, with the exception of minor contributors to disordered species (one perchlorate anion), were refined anisotropically. Blocked-matrix least-squares refinement of an overall scale factor was performed and positional and thermal parameters converged (all shifts $< 0.10\sigma$) with $R = 0.039$, $R_w = 0.045$ and $w = 1.93/(\sigma^2(F_o) + 0.00026F_o^2)$ ($R = (||F_o| - |F_c||)/F_o$, $R_w = (w(|F_o| - |F_c|)^2/wF_o^2)^{1/2}$). Maximum excursions in a final difference map were +0.7 and −0.7 e Å^{-3}. Scattering factors and anomalous dispersion terms used for cobalt were taken from the International tables[17] and all others used were those supplied by SHELX-76.[18] All calculations were performed using SHELX-76[18] and plots were drawn using ORTEP.[19] The atom numbering scheme is given in Fig. 1. Bond lengths and angles are listed in Table 1. Positional parameters, listing of observed and calculated structure factors, hydrogen atom coordinates and thermal parameters (Tables S1–S4) are available from the Cambridge Crystallographic Data Centre.

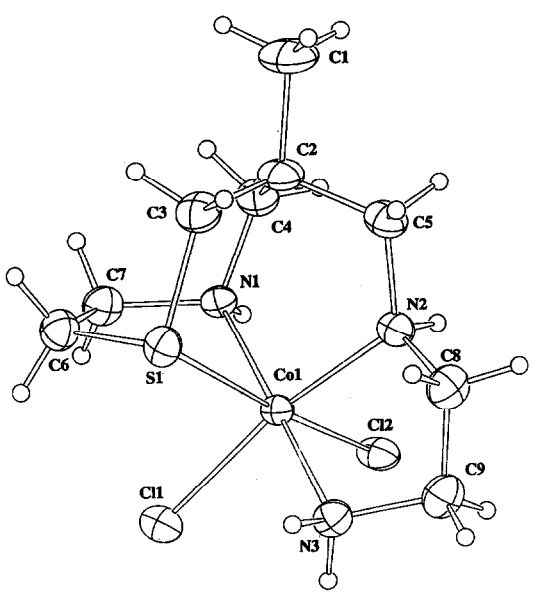

Fig. 1. ORTEP plot of the cation *cis*-[Co(atac)Cl$_2$]$^+$ (30% ellipsoids are shown).

REFERENCES

1. R. J. Geue and G. H. Searle, *Aust. J. Chem.* 1983, **36**, 927.
2. K. Tomioka, U. Sakaguchi and H. Yoneda, *Inorg. Chem.* 1984, **23**, 2863.
3. A. McAuley, K. Beveridge, S. Subramanian and T. Whitcombe, *Can. J. Chem.* 1989, **67**, 1657.
4. A. McAuley, S. Subramanian and T. Whitcombe, *Can. J. Chem.* 1989, **67**, 1650.

5. L. R. Gahan and T. W. Hambley, *Inorg. Chem.* 1987, **26** 2532.
6. A. McAuley, K. Beveridge, S. Subramanian and T. Whitcombe, *J. Chem. Soc., Dalton Trans.* 1991, 1821.
7. L. R. Gahan, K. E. Hart, C. H. L. Kennard, M. A. Kingston, G. Smith and T. C. W. Mak, *Inorg. Chim. Acta* 1986, **116**, 5.
8. A. A. Achilleos, L. R. Gahan, K. A. Nicholaidis and T. W. Hambley, *J. Chem. Soc., Chem. Commun.* 1988, 912.
9. T. M. Donlevy, L. R. Gahan, T. W. Hambley and R. Stranger, *Inorg. Chem.* 1992, **31**, 4376.
10. J. I. Bruce, L. R. Gahan, T. W. Hambley and R. Stranger, *Inorg. Chem.*, submitted.
11. T. W. Hambley, *Inorg. Chem.* 1988, **27**, 2496.
12. T. W. Hambley, *Acta Cryst., Sect. B; Cryst. Cryst. Chem.* 1988, **B44**, 601.
13. G. G. Messmer and E. L. Amma, *Acta Cryst., Sect. B; Cryst. Cryst. Chem.* 1968, **B24**, 417.
14. F. Heinz and R. Burkhardt, *Chem. Ber.* 1957, **90**, 921.
15. Enraf–Nonius Structure Determination Package, Enraf–Nonius, Delft, The Netherlands (1985).
16. G. M. Sheldrick, SHELXS-86, Program for the Solution of Crystal Structures. University of Göttingen, F.R.G. (1987).
17. *International Tables for X-ray Crystallography*, Vol. 4. Kynoch Press, Birmingham (1974).
18. G. M. Sheldrick, SHELX-76, A Program for X-ray Crystal Structure Determination. University of Cambridge (1976).
19. C. K. Johnson, ORTEP, A Thermal Ellipsoid Plotting Program. Oak Ridge National Laboratories, Oak Ridge (1965).

Polyhedron Vol. 12, No. 13, pp. 1599–1602, 1993
Printed in Great Britain

0277-5387/93 $6.00+.00
© 1993 Pergamon Press Ltd

ARENE RUTHENIUM COMPLEXES WITH PICOLINIC ACID, 1-AMINOETHYLPHOSPHONOUS ACID AND α-HYDROXYKETONES. X-RAY STRUCTURE OF [(η-1,3,5-$C_6Me_3H_3$)RuCl($NC_5H_4CO_2$)]

LEE CARTER, DAVID L. DAVIES,* JOHN FAWCETT and DAVID R. RUSSELL

Department of Chemistry, University of Leicester, Leicester LE1 7RH, U.K.

(*Received* 18 *December* 1992; *accepted* 23 *March* 1993)

Abstract—The ligands LH (LH = picolinic acid, 1-aminoethylphosphonous acid, ethyl maltol and N-methyl-3-hydroxy-2-ethyl-4-pyridinone) react with [(η-1,3,5-$C_6Me_3H_3$)$RuCl_2]_2$ and sodium methoxide to give the complexes [(η-1,3,5-$C_6Me_3H_3$)RuClL] (**1–3**), which are all soluble in water. The structure of [(η-1,3,5-$C_6Me_3H_3$)RuCl($NC_5H_4CO_2$)] (**1**) has been determined by X-ray diffraction.

It has been shown previously that [(arene)$RuCl_2]_2$ will react with biologically important ligands such as amino acids,[1–4] peptides[5] and also with substituted nucleobases such as 9-ethylguanine.[4] In addition their reactions with hydroxy pyridines have been studied.[6] We now report our results on the reactions of [(η-1,3,5-$C_6Me_3H_3$)$RuCl_2]_2$ with picolinic acid, 1-aminoethylphosphonous acid, the α-hydroxyketone ethyl maltol and a 3-hydroxy-4-pyridinone. Picolinic acid and aminoethylphosphonous acids are naturally occurring ligands related to α-amino acids, while hydroxypyrones and -pyridinones have found applications in medicinal chemistry.[7]

Refluxing the ligands LH and 1 equivalent of sodium methoxide with [(η-1,3,5-$C_6Me_3H_3$)$RuCl_2]_2$ gives moderate to good yields of the complexes [(η-1,3,5-$C_6Me_3H_3$)RuClL] (**1–3**), in which the ligands are bonded in a bidentate fashion. The sodium chloride by-product can be separated by dissolving the complexes in dichloromethane; however, in the case of **2** this does not work and the samples are always contaminated with some sodium chloride. Complexes **1** and **2** contain N, O chelates, while **3a** and **3b** have O, O donor atoms. The complexes are all soluble in water and also in dichloromethane. Water-soluble organometallic complexes are of interest because of the potential industrial benefits from aqueous soluble catalysts in terms of reduced costs of recovery and recycling of precious metal-based catalysts.[8]

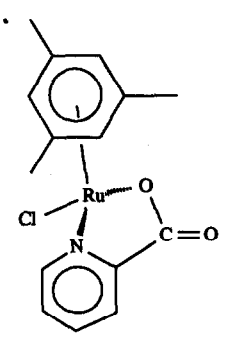

1

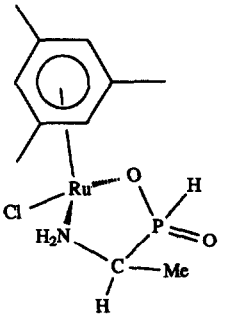

2

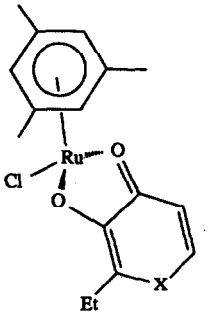

3a X=O
3b X=NMe

The complexes have all been characterized by microanalysis, ^1H NMR and mass spectroscopy, and $^{31}P\{^1H\}$ NMR spectroscopy for **2**. All the ^1H NMR spectra show signals due to coordinated mes-

* Author to whom correspondence should be addressed.

itylene and the relevant ligand. For complex **1** the ^1H NMR spectrum in D_2O shows the presence of two species. This is due to the substitution of the chloride ligand by D_2O, which has been observed previously for the amino acid complexes.[1] Addition of excess LiCl displaces the equilibrium in favour of chloride coordination. Complex **2** has three chiral centres, ruthenium, phosphorus and carbon, and exists as a mixture of diastereomers; as a result the ^1H NMR spectrum is very complicated. This is more clearly seen in the $^{31}P\{^1H\}$ NMR spectrum, where three signals are observed in CD_3OD. There are four possible diastereomeric pairs, of which only three are observed. In D_2O there are six signals which reduce to three in the presence of excess LiCl. Complexes **3a** and **3b** only show one species in the ^1H NMR spectrum in D_2O, which is believed to be that with D_2O coordinated in place of chloride. In this case the addition of LiCl does not cause an immediate coordination of chloride. The reason for this difference is not clear, but it could be that for **3a** and **3b** there is more hydrogen bonding with the coordinated water. Also, particularly for **3b**, it is possible to draw resonance structures in which the overall positive charge of $[(\eta\text{-}1,3,5\text{-}C_6Me_3H_3)RuL(D_2O)]^+$ can be delocalized onto the ligand. The extent of hydrogen bonding in these complexes can be important; it has previously been suggested that it plays a key role in determining the diastereomeric ratio in amino acid complexes.[4]

We have determined the structure of complex **1** as shown in Fig. 1 and selected bond lengths and angles are listed in Table 1. The Ru—N bond length of 2.102(4) Å is intermediate between that found for a related N,O-bound hydroxypyridine [2.084(7) Å][6] and that of a monodentate pyridine [2.127(7) Å].[9] However, the Ru—O bond length of 2.101(4) Å and the bite angle N—Ru—O of 77.9(2)° are comparable with those [2.085(8) and 2.093(9) Å and 76.4(4)° and 78.1(4)°] found for the five-membered chelate rings in the diastereomers of $[(\eta\text{-}1,3,5\text{-}C_6Me_3H_3)RuCl\{H_2NCH(Me)CO_2\}]$.[10] The complex crystallizes as the trihydrate. The hydrogen atoms of the water molecules were not located, but the O—O separations (2.78–2.85 Å) suggest hydrogen bonding between the water molecules. In addition, there are close contacts between a water molecule and the chlorine and also between the two carboxylate oxygens and the remaining two water molecules.

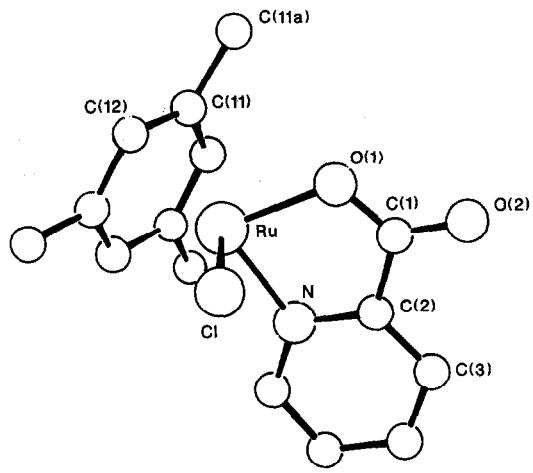

Fig. 1. Molecular structure of $[(\eta\text{-}1,3,5\text{-}Me_3C_6H_3)RuCl(NC_5H_4CO_2)]\cdot 3H_2O$ (**1**).

We are currently exploring the coordination of other biologically important molecules with organometallic complexes and also the use of some of these species as water-soluble catalysts.

EXPERIMENTAL

Petroleum ether and diethyl ether were dried by refluxing over purple sodium/benzophenone under

Table 1. Selected bond lengths (Å) and angles (°) for the complex $[(\eta\text{-}1,3,5\text{-}Me_3C_6H_3)RuCl(NC_5H_4CO_2)]\cdot 3H_2O$ (**1**)

Ru—Cl	2.420(1)	C(1)—O(1)	1.285(7)
Ru—N	2.102(4)	C(1)—O(2)	1.242(7)
Ru—O(1)	2.101(4)	C(1)—C(2)	1.502(8)
Ru—C(11)	2.185(5)	C(11)—C(12)	1.410(8)
Ru—C(12)	2.203(5)	C(12)—C(13)	1.436(10)
Ru—C(13)	2.220(6)	C(13)—C(14)	1.410(9)
Ru—C(14)	2.203(6)	C(14)—C(15)	1.438(8)
Ru—C(15)	2.206(5)	C(15)—C(16)	1.403(8)
Ru—C(16)	2.176(5)	C(16)—C(11)	1.419(8)
N—Ru—Cl	84.0(1)	O(2)—C(1)—O(1)	124.7(6)
O(1)—Ru—Cl	83.6(1)	C(2)—C(1)—O(1)	115.1(5)
O(1)—Ru—N	77.9(2)	C(2)—N—C(6)	119.3(5)

nitrogen, while dichloromethane was purified by refluxing over calcium hydride. The complex $[(1,3,5\text{-}Me_3C_6H_3)RuCl_2]_2$[11] and ligands 1-aminoethylphosphonous acid[12] were prepared using literature procedures, while N-methyl-3-hydroxy-2-ethyl-4-pyridinone was made by the same method as that used for the corresponding 2-methyl derivative.[13] The reactions described were performed in deoxygenated solvents under nitrogen; however, once isolated as pure solids the compounds are relatively air-stable and precautions for their storage are unnecessary.

^1H NMR spectra were recorded on Bruker AM300 or Varian EM390 spectrometers. Microanalyses were performed by Butterworth Laboratories Ltd, Middlesex. FAB mass spectra were performed at the SERC Mass Spectroscopy service centre at University College Swansea.

Preparation of $[(1,3,5\text{-}Me_3C_6H_3)RuCl(NC_5H_4CO_2)]$ (**1**)

Sodium methoxide (44 mg, 0.86 mmol) and picolinic acid (106 mg, 0.86 mmol) were added to a suspension of $[(1,3,5\text{-}Me_3C_6H_3)RuCl_2]_2$ (251 mg, 0.43 mmol) in methanol/water (1 : 1) (70 cm^3) and the mixture was refluxed for 3 h. The solvent was removed and the residue was dissolved in dichloromethane (100 cm^3) and filtered. Evaporation of the solvent gave $[(1,3,5\text{-}Me_3C_6H_3)RuCl(NC_5H_4CO_2)]$ (**1**) (267 mg, 82%) as a yellow solid. Found: C, 44.9; H, 4.5; N, 3.4. Calc. for $C_{15}H_{16}ClNO_2Ru \cdot H_2O$: C, 45.3; H, 4.6; N, 3.7%. ^1H NMR (D_2O+LiCl): δ 2.18 (s, 9H, Me), 5.37 (s, 3H, C_6H_3) [7.84 (t, 1H, $J = 6$), 7.92 (d, 1H, $J = 7$), 8.14 (t, 1H, $J = 7$), 9.20 (d, 1H, $J = 5$), all picolinic acid]. FAB-MS: m/z 379 $[M]^+$, 344 $[M-Cl]^+$.

Preparation of $[(1,3,5\text{-}Me_3C_6H_3)RuCl\{H_2NCH(Me)P(H)O_2\}]$ (**2**)

Sodium methoxide (34 mg, 0.74 mmol) and 1-aminoethylphosphonous acid (81 mg, 0.74 mmol) were added to a suspension of $[(1,3,5\text{-}Me_3C_6H_3)RuCl_2]_2$ (217 mg, 0.37 mmol) in methanol/water (1 : 1) (70 cm^3) and the mixture was refluxed for 3 h. The solvent was removed and the residue was dissolved in dichloromethane/methanol (15 cm^3 : 2 cm^3) and diethylether (3 cm^3) was added. A pale orange solid was removed by filtration and the remaining solution was evaporated to dryness to give $[(1,3,5\text{-}Me_3C_6H_3)RuCl\{H_2NCH(Me)P(H)O_2\}]$ (**2**) (100 mg, 37%) as a solid. Found: C, 30.9; H, 4.4; N, 3.1. Calc. for $C_{11}H_{19}ClNO_2PRu \cdot NaCl$: C, 31.2; H, 4.5; N, 3.3%. $^{31}P\{^1H\}$ NMR (CD_3OD): δ 40.52, 48.56, 48.72. FAB-MS: m/z 366 $[M]^+$.

Preparation of $[(1,3,5\text{-}Me_3C_6H_3)RuCl(EtMal)]$ (**3a**)

Sodium methoxide (68 mg, 1.32 mmol) and ethylmaltol (186 mg, 1.32 mmol) were added to a suspension of $[(1,3,5\text{-}Me_3C_6H_3)RuCl_2]_2$ (387 mg, 0.66 mmol) in methanol/water (1 : 1) (60 cm^3) and the mixture was refluxed for 2 h. The solvent was removed and the residue was dissolved in dichloromethane (80 cm^3) and filtered. The solvent was evaporated and the orange solid was recrystallized from dichloromethane/diethylether to give $[(1,3,5\text{-}Me_3C_6H_3)RuCl(EtMal)]$ (**3a**) (421 mg, 80%), as orange crystals. Found: C, 47.9; H, 4.8. Calc. for $C_{16}H_{19}ClO_3Ru$: C, 48.5; H, 4.8%. ^1H NMR ($CDCl_3$): δ 1.21 (t, 3H, CH_3, $J = 7.5$), 2.25 (s, 9H, Me_3), 2.80 (dq, 1H, CHH^1, $J = 15, 7.5$), 2.91 (dq, 1H, CHH^1, $J = 15, 7.5$), 4.91 (s, 3H, C_6H_3), 6.49 (d, 1H, CH, $J = 5$), 7.57 (d, 1H, CH, $J = 5$). FAB-MS: m/z 396 $[M]^+$, 361 $[M-Cl]^+$.

Preparation of $[(1,3,5\text{-}Me_3C_6H_3)RuCl(Pyr)]$ (**3b**)

Sodium methoxide (60 mg, 1.16 mmol) and N-methyl-3-hydroxy-2-ethyl-4-pyridinone (177 mg, 1.16 mmol) were added to a suspension of $[(1,3,5\text{-}Me_3C_6H_3)RuCl_2]_2$ (338 mg, 0.58 mmol) in methanol/water (1 : 1) (60 cm^3) and the mixture was refluxed for 2.5 h. The solvent was removed and the residue was dissolved in dichloromethane (80 cm^3) and filtered. The solvent was evaporated and the brown solid was recrystallized from methanol/diethylether to give $[(1,3,5\text{-}Me_3C_6H_3)RuCl(Pyr)]$ (**3b**) (320 mg, 68%) as a brown solid. Found: C, 50.1; H, 5.5; N, 3.5. Calc. for $C_{17}H_{22}ClNO_2Ru$: C, 49.9; H, 5.4; N, 3.4%. ^1H NMR (CD_3OD): δ 1.23 (t, 3H, CH_3, $J = 7.5$), 2.20 (s, 9H, Me_3), 2.95 (q, 2H, CH_2, $J = 7.5$), 3.77 (s, 3H, NMe), 5.05 (s, 3H, C_6H_3), 6.41 (d, 1H, CH, $J = 7.5$), 7.29 (d, 1H, CH, $J = 7.4$). FAB-MS: m/z 409 $[M]^+$, 374 $[M-Cl]^+$.

X-ray structure determination

Crystal data for $[(\eta\text{-}1,3,5\text{-}C_6Me_3H_3)RuCl(NC_5H_4CO_2)] \cdot 3H_2O$ (**1**). $M = 432.87$, monoclinic, space group $P2_1/a$, $a = 13.416(13)$, $b = 16.212(16)$, $c = 8.234(2)$ Å, $\beta = 99.63(1)°$, $U = 1766$ Å^3, $z = 4$, $\mu = 9.37$ cm^{-1}, $\lambda(Mo\text{-}K_\alpha) = 0.7107$ Å, $F(000) = 784$, $D_c = 1.47$ g cm^{-3}. Crystal dimensions $0.08 \times 0.36 \times 0.28$ mm.

The crystal used for data collection was mounted in air and the unit cell parameters were determined by least-squares refinement of ω measurements of

different layers.[14] Data were collected on a Stöe STADI-2 diffractometer with an ω scan technique in the range $7 < 2\theta < 54°$. Scattering factors were taken from ref. 15. The intensities of 3998 reflections were measured and these data were corrected for Lorentz and polarization effects to give 3600 unique reflections, of which 2660 had $I > 3\sigma(I)$. The structure was solved by conventional Patterson techniques and all subsequent calculations were performed with the computer programme SHELX-76.[16] All hydrogen atoms were included in calculated positions (C—H = 0.95 Å) with isotropic thermal parameters refined as groups. All non-hydrogen atoms were refined anisotropically. Final cycles of refinement employed a weighting factor w calculated from $w = (\sigma^2 F + 0.00027F^2)$ and gave final values of $R = 0.0462$ and $R_w = 0.0497$.

Acknowledgements—We thank the S.E.R.C. for a studentship (L.C.), the Hickinbotham Trust for financial support and Leicester University Computer Centre who provided support and facilities for X-ray single-crystal calculations. The FAB mass spectra were provided by the SERC mass spectrometry service at Swansea and by Dr G. Eaton at Leicester University.

REFERENCES

1. D. F. Dersnah and M. C. Baird, *J. Organomet. Chem.* 1977, **127**, C55.
2. R. Kramer, K. Polborn, H. Wanjek, I. Zahn and W. Beck, *Chem. Ber.* 1990, **123**, 767.
3. D. Carmona, A. Medoza, F. J. Lahoz, L. A. Oro, M. P. Lamata and E. San Jose, *J. Organomet. Chem.* 1990, **396**, C17.
4. W. S. Sheldrick and S. Heeb, *Inorg. Chim. Acta* 1990, **168**, 93.
5. W. S. Sheldrick and S. Heeb, *J. Organomet. Chem.* 1989, **377**, 357.
6. P. Lahuerta, J. Latorre, M. Sanau, F. A. Cotton and W. Schwotzer, *Polyhedron* 1988, **7**, 1311.
7. (a) W. O. Nelson, T. B. Karpishin, S. J. Rettig and C. Orvig, *Inorg. Chem.* 1988, **27**, 1045; (b) M. W. Finnegan, S. J. G. Lutz, W. O. Nelson and C. Orvig, *Inorg. Chem.* 1987, **26**, 2171.
8. M. Barton and J. D. Atwood, *J. Coord. Chem.* 1991, **24**, 43.
9. L. Carter, D. L. Davies, J. Fawcett and D. R. Russell, *Polyhedron* 1993, **12**, 1123.
10. L. Carter, D. L. Davies, J. Fawcett and D. R. Russell, unpublished results.
11. J. W. Hull Jr and W. L. Gladfelter, *Organometallics* 1984, **3**, 605.
12. J. G. Dingwall, C. D. Campbell and E. K. Baylis, *J. Chem. Soc., Perkin Trans. 1* 1984, 2845.
13. W. O. Nelson, T. B. Karpishin, S. J. Rettig and C. Orvig, *Can. J. Chem.* 1988, **66**, 123.
14. W. Clegg and G. M. Sheldrick, *Z. Krist.* 1984, **167**, 23.
15. *International Tables for X-ray Crystallography*, Vol. 4. Kynoch Press, Birmingham (1975).
16. G. M. Sheldrick, SHELX-76, Program for Crystal Structure Determination. University of Cambridge, U.K. (1976), updated Göttingen (1986).

Polyhedron Vol. 12, No. 13, pp. 1603–1606, 1993
Printed in Great Britain

0277–5387/93 $6.00+.00
© 1993 Pergamon Press Ltd

SINGLET⇌QUINTET TRANSITION IN A SIX-COORDINATE IRON(II) COMPLEX OF A TRIDENTATE BIS(PYRAZOLYL)PYRIDINE LIGAND

S. MAHAPATRA and R. N. MUKHERJEE*

Department of Chemistry, Indian Institute of Technology, Kanpur 208 016, India

(*Received* 27 *January* 1993; *accepted* 5 *March* 1993)

Abstract—The bis(ligand)iron(II) complex $[Fe(L^1)_2](ClO_4)_2 \cdot H_2O$ (**1**) [L^1 = 2,6-bis-(pyrazol-1-ylmethyl)pyridine] displays in the solid-state anomalous magnetic properties which are associated with a temperature-induced singlet ($^1A_1$)⇌quintet ($^5T_2$) transition. Mössbauer spectral data confirm this and reveal separate contributions from the singlet and quintet species with a strong temperature dependence of their relative intensities. Variable-temperature magnetic and Mössbauer studies establish that $[Fe(L^2)_2](ClO_4)_2 \cdot 2H_2O$ (**2**) [L^2 = 2-(3,5-dimethylpyrazol-1-ylmethyl)-6-(pyrazol-1-ylmethyl)pyridine] and $[Fe(L^3)_2](ClO_4)_2 \cdot 2H_2O$ (**3**) [L^3 = 2,6-bis(3,5-dimethylpyrazol-1-ylmethyl)pyridine] are purely high-spin species. For **1** three *d–d* transitions originating from the quintet and singlet state have been identified.

Recently we have been interested[1–5] in the identification of the steric effect of methyl substituent(s) adjacent to donor atoms in a group of bis-chelates, $M^{II}L_2^{2+}$ (M = Mn, Fe, Co, Ni or Ru), using a new family of tridentate heterocyclic ligands, L^1–L^3. We discovered that the ligand L^1 provides a field about iron(II) close to the critical value at the singlet/quintet cross-over from the absorption spectral data for the complex $[Fe(L^1)_2]^{2+}$ as well as from the data on the related nickel(II) complex.[1,4] To underscore a systematic spin-state behaviour of iron(II) bis-chelates we have undertaken the present study.

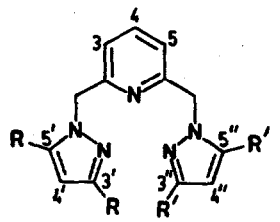

H_4bpp : R = R′ = H (L¹)

H_2Me_2bpp : R = H; R′ = Me (L²)

Me_4bpp : R = R′ = Me (L³)

We report here the characterization of a novel iron(II) system, $[Fe(L^1)_2]^{2+}$, exhibiting a spin transition in the solid-state from variable-temperature (8–300 K) magnetic susceptibility and ^{57}Fe Mössbauer spectral measurements. For the sake of completeness we also provide here the results on $[Fe(L^2)_2]^{2+}$ and $[Fe(L^3)_2]^{2+}$.

EXPERIMENTAL

Syntheses

$[Fe(L^1)_2](ClO_4)_2 \cdot H_2O$ (**1**), $[Fe(L^2)_2](ClO_4)_2 \cdot 2H_2O$ (**2**) and $[Fe(L^3)_2](ClO_4)_2 \cdot 2H_2O$ (**3**) were synthesized using literature methods.[1]

Measurements

Variable-temperature magnetic susceptibility measurements were obtained on powdered samples over the temperature range 8.0–300 K by the Faraday method using a locally built susceptometer at the Chemical Physics Group, Tata Institute of Fundamental Research (TIFR), Bombay, India. The details of the measurements are already described in the literature.[6] Effective magnetic moments were calculated from $\mu_{eff} = 2.828\,[\chi_M \cdot T]^{1/2}$, where χ_M is

* Author to whom correspondence should be addressed.

the corrected molar susceptibility. The diamagnetic contributions were calculated using values[7] of -239×10^{-6} cm^3 mol^{-1} for **1** and -400×10^{-6} cm^3 mol^{-1} for **3**. Mössbauer spectral measurements were performed at the Low-Temperature Physics Group, TIFR, India, using a standard, constant-acceleration spectrometer calibrated with metallic iron at room temperature. The observed spectra were computer-fitted to Lorentzian lines as described earlier.[6]

RESULTS AND DISCUSSION

Magnetism

First-row transition-metal complexes with electronic configurations d^4–d^7 have been found to exhibit thermally driven spin-state transitions between the high-spin state (HS) and the low-spin state (LS). This is because in these systems two electronic states of differing multiplicity become nearly equienergetic and a thermal population of the excited state is possible. Six-coordinate iron(II) complexes with heterocyclic nitrogen donor atoms and α-diimine ligands have been found to exhibit such a transition.[8]

From this background the variable-temperature (8–300 K) magnetic susceptibility studies on **1** were performed. Among the two other complexes we decided to study the fully methyl-substituted complex (**3**) to gain a better understanding. The magnetic properties are shown in Fig. 1 in the form of μ_{eff} vs T.

The magnetic properties of **1** are indicative of the occurrence of a temperature-induced singlet⇌quintet transition in the cation. The moments at high temperature are normal for iron(II) in the quintet $^5T_2$ state. At low temperatures **1** has very low magnetic moments, which are typical for the metal ion in the singlet $^1A_1$ state. As the temperature is increased the moment gradually increases and this is indicative of an increased population of quintet state species.

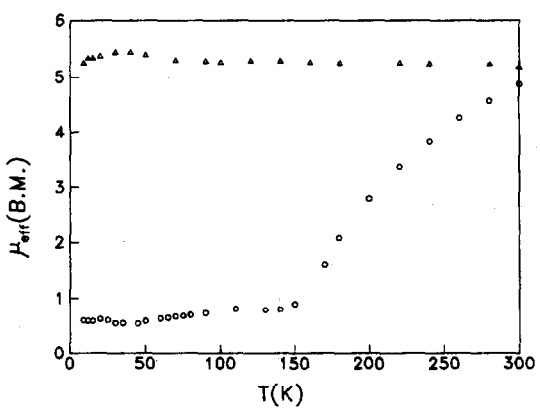

Fig. 1. Effective magnetic moment of **1** (○) and **3** (△) as a function of temperature.

Complex **3** follows the Curie–Weiss behaviour from room temprature down to 8 K. The Curie constant is in good agreement with that for an $S = 2$ ground state ($C = 3$ when $g = 2$) with a Curie–Weiss temperature of -1.45 K. Thus, no spin pairing was observed in **3** even at the lowest limit of the experimental temperature range. The methyl groups adjacent to the pyrazole nitrogen atoms apparently interfere with the close approach to the metal atom necessary for spin pairing.

An attempt to evaluate enthalpy and entropy changes for the spin transition of **1** [eq. (1)] was made using the standard equations.[9,10]

$$[Fe(L^1)_2]^{2+}(^1A_1, ls) \rightleftharpoons [Fe(L^1)_2]^{2+}(^5T_2, hs) \quad (1)$$

The pure high-spin data were evaluated from the data for **3** at the corresponding temperatures and the pure low-spin data were determined for **1** from the low-temperature data. Despite the limited range (170–300 K) over which a linear plot of ln K against $1/T$ was obtained it was possible to extract some information on the thermodynamic parameters. It is admitted that the data obtained from the present analysis (see below) are not that *accurate* compared with the more involved method of Zimmermann and König.[11] The derived ΔH and ΔS values are 13 kJ mol^{-1} and 56 J K^{-1} mol^{-1}, respectively. These thermodynamic parameters are similar to those found for other spin equilibria systems of iron(II).[9–13] The source of ΔH is the Fe—N bond length increase,[8] which accompanies the transition from low- to high-spin, i.e. reorganization of the inner coordination sphere. The entropy term for a simple spin equilibrium between singlet and quintet levels would be only 13.4 J K^{-1} mol^{-1}, due to the spin multiplicity change (R ln 5 = 13.4 J K^{-1} mol^{-1}).[12–14] The value of ΔS in excess of that predicted for a change in spin only is a feature of most of the examples of spin equilibria in six-coordinate iron(II) systems described so far. This could be accounted for in terms of a temperature dependence of the effective crystal field and on the different vibrational frequencies in the high-spin and low-spin states.

Mössbauer spectra

The origin of the temperature dependence of the magnetism of **1** is clearly revealed by Mössbauer spectral data. The Mössbauer spectral data (Table 1), like the magnetic data, show the temperature-induced change in the ground state for **1**. Figure 2

Table 1. Mössbauer data for iron(II) systems

Complex	Temperature (K)	Spin-state	δ (mm s^{-1})	ΔE_Q (mm s^{-1})
$[Fe(L^1)_2](ClO_4)_2 \cdot H_2O$	300	$^5T_2$	0.98	1.92
	200	$^5T_2$	0.71	2.42
		$^1A_1$	0.50	0.37
	80	$^1A_1$	0.53	0.39
$[Fe(L^2)_2](ClO_4)_2 \cdot 2H_2O$	300	$^5T_2$	1.06	2.45
	80	$^5T_2$	1.13	2.88
$[Fe(L^3)_2](ClO_4)_2 \cdot 2H_2O$	300	$^5T_2$	1.07	2.85

shows three typical spectra at 80, 200 and 300 K. With increasing temperature the $^5T_2$ state gains intensity, while the intensity of the $^1A_1$ state simultaneously decreases. At 300 K the contribution of the $^5T_2$ state is clearly predominant. At 80 K the contribution of the quintet state species has disappeared and the spectrum shows a doublet with small quadrupole splitting, characteristic of the $^1A_1$ state. The spectrum at 200 K reveals a superposition of separate spectra due to singlet and quintet state species.

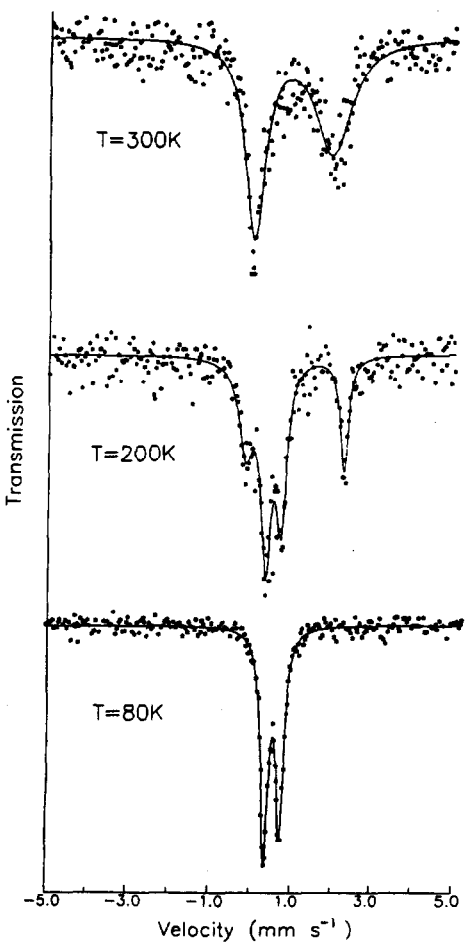

Fig. 2. ^{57}Fe Mössbauer spectra of **1** at 80, 200 and 300 K.

Complexes **2** and **3** display Mössbauer spectra (300 K) characteristic of purely high-spin states. The temperature dependence of **2** was also investigated. Interestingly, it remains high-spin even at 80 K (Table 1). The isomer shift and quadrupole splitting observed for the singlet and quintet state species in the spectra of **1**–**3** are comparable with those of the high-spin and low-spin complexes of related systems.[8]

d–d *transitions*

Even though the field strengths of L^1, L^2 and L^3 towards six-coordinate iron(II) were determined from their $^5T_2 \rightarrow {}^5E$ transitions, the present work adds to the previous assignments[1] of the bands for **1**. Among the three high-spin (at room temperature) iron(II) complexes, **1**–**3**, in acetonitrile solution **1** exhibits additional spectral features (an absorption at 543 nm of low intensity and a band at 415 nm with a shoulder at 368 nm);[1] the source of which was not appreciated earlier. Due to the high energy and the intensity of the band at 543 nm, we tentatively assign this band to the spin-allowed $^1A_1 \rightarrow {}^1T_1$ transition.[8] The band at 415 nm is probably due to[8] the transition $^1A_1 \rightarrow {}^1T_2$. The observed high intensity of this band could arise due to intensity stealing from the MLCT band at 368 nm. The feature observed at *ca* 400 nm is closely similar to a related spin equilibrium system.[13]

CONCLUSIONS

It follows from the temperature dependence of the magnetic susceptibility for **1** that the ligand field

arising from the two tridentate ligands (L^1) is such that the difference between the two spin states of the iron(II) ion is of the order kT and that the population of the states in question can be altered by changes in temperature. This has been substantiated by the Mössbauer results. The present investigation provides a clear indication of the existence of a spin-state transition for complex **1**. In contrast, methyl group substituents in the 3-position(s) of the pyrazole rings in L^2 and L^3 give rise to much weaker ligand fields to exhibit a high-spin configuration over the accessible temperature range. This arises from the steric crowding of the methyl group substituents near the donor site.

Acknowledgements—Financial assistance received from the Department of Science and Technology, Government of India and Council of Scientific and Industrial Research, New Delhi, India, is gratefully acknowledged. Our sincere thanks are due to Professor S. Mitra, TIFR, Bombay, for his hospitality in the use of his laboratory during the stay of one of us (RNM) as a visiting scientist. We thank Dr A. K. Nigam of TIFR for allowing us to use his Mössbauer set-up. We thank Mr B. T. Kansara, Mr R. S. Sannabhadti and Dr S. Veeturi for recording the solid-state magnetic data and Mössbauer data, respectively.

REFERENCES

1. S. Mahapatra, N. Gupta and R. N. Mukherjee, *J. Chem. Soc., Dalton Trans.* 1991, 2911.
2. S. Mahapatra and R. N. Mukherjee, *J. Chem. Soc., Dalton Trans.* 1992, 2337.
3. S. Mahapatra, D. Bhuniya and R. N. Mukherjee, *Polyhedron* 1992, **11**, 2045.
4. S. Mahapatra and R. N. Mukherjee, *Ind. J. Chem.* 1993, **32A**, 64.
5. (a) S. Mahapatra, T. K. Lal and R. N. Mukherjee, *Polyhedron* 1993, **12**, 1477; (b) S. Mahapatra, R. J. Butcher and R. N. Mukherjee, submitted.
6. S. Mahapatra, N. Gupta and R. N. Mukherjee, *J. Chem. Soc., Dalton Trans.* 1992, 3041.
7. C. J. O'Connor, *Prog. Inorg. Chem.* 1982, **29**, 203.
8. H. Toftlund, *Coord. Chem. Rev.* 1989, **94**, 67.
9. M. A. Hoselton, L. J. Wilson and R. S. Drago, *J. Am. Chem. Soc.* 1975, **97**, 1722.
10. H. Toftlund and S. Yde-Andersen, *Acta Chem. Scand.* 1981, **A35**, 575.
11. R. Zimmermann and E. König, *J. Chem. Phys. Solids* 1977, **38**, 779.
12. J. P. Jesson, S. Trofimenko and D. R. Eaton, *J. Am. Chem. Soc.* 1967, **89**, 3158.
13. H. L. Chum, J. A. Vanin and M. I. D. Holanda, *Inorg. Chem.* 1982, **21**, 1146.
14. M. J. Boylan, S. M. Nelson and F. A. Deeney, *J. Chem. Soc.* (*A*) 1971, 976.

Polyhedron Vol. 12, No. 13, pp. 1607–1611, 1993
Printed in Great Britain

0277–5387/93 $6.00+.00
© 1993 Pergamon Press Ltd

XPS STUDY OF METAL COMPLEXES WITH AN UNSYMMETRICAL TRIDENTATE SCHIFF BASE

ZHOU LIXIN

Department of Chemistry, Gansu Education College, Lanzhou 730000, P.R.C.

and

WANG BO, YANG SHIYAN* and JIN DAOSEN

Lanzhou Institute of Chemical Physics, Academia Sinica, Lanzhou 730000, P.R.C.

(*Received* 8 *January* 1993; *accepted* 5 *March* 1993)

Abstract—Complexes of 14 lanthanide metals with the new tridentate Schiff base derived from salicylaldehyde and furfuraldehyde with *o*-phenyldiamine (HL) have been prepared and studied using X-ray photoelectron spectroscopy (XPS). The nitrogen 1*s* peak for all the complexes is symmetrical relative to the two asymmetric peaks of the ligand. This behaviour suggests that a coordination conjugation of four equatorial nitrogens occurs, the complexes are in an octahedral structure and the nitrogen 1*s* electron BE increases from La to Lu in accordance with the "Four Subgroup Effect".

A large number of Schiff bases and their complexes have been studied for their interesting and important properties, e.g. their ability to reversibly bind oxygen,[1] catalytic activity in hydrogenations of olefins[2] and transfer of an amino group,[3] photochromic properties,[4] complexing ability towards some toxic metals,[5] and so on.

However, only a few compounds of this type have been studied by XPS, namely the symmetric tetradentate Schiff bases, such as H_2salen, H_2salphen and related metal complexes.[6] The main results have been obtained by comparing the spectra of different ligands of this type amongst themselves and with spectra of complexes containing the same cation. The variation of the nitrogen and nitrogen 1*s* electron BEs can be rationalized considering the reduction in electron density on the donor atoms after complexation. Protonation is accompanied by an even greater decrease in their electron density, therefore, the BEs increase follow the order: uncomplexed atom < complexed atom < protonated atom.

Most studies were restricted to a few metals, such as cobalt, nickel and copper, so that information on the role of the central atom is very limited. Our studies are aimed at bridging this gap. The present paper describes the XPS spectra of a set of complexes, $[LnL_2]ClO_4$, where HL denotes an asymmetrical Schiff base, but after complexing the four coordinated nitrogen atoms appear chemically identical.

EXPERIMENTAL

Methods and materials

All chemicals and solvents were analytical grade and were used without further purification. The preparation of the ligand has been described previously.[7] Lanthanide perchlorates were made from oxide and perchloric acid.

Preparation of the complexes

The same method of synthesis was adopted for all complexes. In a typical reaction an MeOH solution of $Ln(ClO_4)_3$ (1 mol) and the Schiff base (2 mol) was stirred and refluxed for 4 h, whereupon an ammonia solution was added dropwise. The solid product was filtered off, washed successively with MeOH and Et_2O and dried *in vacuo* (80 mm Hg) at 80° for 1 h. The complexes were thus prepared and their yields are given in Table 1.

* Author to whom correspondence should be addressed.

Table 1. Physical properties and analytical data of lanthanide complexes

Complex	Decomposition temperature (°C)	C	H	N	Ln	μ_{eff} (B.M.) (298 K)	Λ_M[a]
$[LaL_2]ClO_4$	212	52.8(52.9)	3.2(3.2)	6.9(6.9)	17.0(17.0)	dia.	40
$[CeL_2]ClO_4$	208	52.8(52.9)	3.1(3.2)	6.7(6.8)	17.0(17.1)	2.60	36
$[PrL_2]ClO_4$	203	52.7(52.8)	3.1(3.2)	6.7(6.8)	17.1(17.2)	3.70	38
$[NdL_2]ClO_4$	216	52.5(50.5)	3.2(3.2)	6.8(6.8)	17.5(17.5)	3.64	47
$[SmL_2]ClO_4$	212	52.1(52.2)	3.1(3.2)	6.7(6.8)	18.0(18.1)	1.68	41
$[EuL_2]ClO_4$	206	52.0(52.1)	3.1(3.2)	6.7(6.7)	18.0(18.3)	3.60	35
$[GdL_2]ClO_4$	224	51.5(51.6)	3.1(3.1)	6.6(6.7)	18.8(18.8)	7.91	35
$[TbL_2]ClO_4$	210	51.5(51.6)	3.1(3.1)	6.6(6.7)	18.9(19.0)	11.40	42
$[DyL_2]ClO_4$	205	51.5(51.4)	3.0(3.1)	6.6(6.7)	19.1(19.3)	10.26	41
$[HoL_2]ClO_4$	210	51.2(51.3)	3.0(3.1)	6.6(6.6)	19.6(19.5)	10.68	46
$[ErL_2]ClO_4$	215	51.1(51.1)	3.0(3.1)	6.4(6.6)	19.8(19.8)	8.94	40
$[TmL_2]ClO_4$	208	51.1(51.0)	3.1(3.1)	6.6(6.6)	19.8(19.9)	8.94	40
$[YbL_2]ClO_4$	204	50.6(50.7)	3.0(3.1)	6.5(6.6)	20.4(20.3)	4.60	38
$[LuL_2]ClO_4$	198	50.4(50.6)	3.0(3.1)	6.5(6.6)	20.5(20.5)	dia.	34

[a] S cm^2 mol^{-1} and *ca* 10^{-3} M DMSO.

Physical measurements

Molar conductances of the complexes in DMSO at 0.001 M concentration were measured with a DDS-IIA molar conductometer at 25°C. The IR spectra (CsI pellets) were obtained on a NIC-5DX spectrophotometer in the 200–4000 cm^{-1} region.

The X-ray photoelectron spectra were measured on a PHI-550 spectrometer. Non-monochromatic Mg-K_α (1253.6 eV) radiation was used from an X-ray gun operated at 15 kV and 20 mA. The base pressure was better than 7×10^{-11} mbra in the analyser. The samples were finely pulverized and spread on a gold holder as thin films. For all the samples the intense carbon 1*s* photopeak observed on the lowest energy side, whose FWHM was nearly 1.1 eV, was used as a standard for the binding energy. The peak mostly arises from carbon atoms of aromatic hydrocarbon character in the compounds to be studied, but not from possible impurities or surface contaminations, and the binding energy at the peak was assumed constant for all the compounds. The binding energy at the standard peak was determined to be 284.8 eV, such that it could reproduce the binding energies of N 1*s*, O 1*s* and Cl 1*s*. The observed spectra, subtracted from the background contribution, were reproduced by a superposition of Gaussians with an FWHM of *ca* 1.1 eV. The parameters to be determined were the line position and height for each composite peak. An optimum set of parameters was obtained in such a way that the root mean square deviations of the trial spectra were minimized by changing the parameters according to the simple method for function minimization.[6]

Room-temperature (298 K) magnetic susceptibility measurements were obtained by Gouy's method using solid samples with $Hg[Co(CNS)_4]$ as the calibrant. TG and DTA measurements were obtained in a nitrogen atmosphere between room temperature and 800°C using a Thermoflex TG–DTA meter.

RESULTS AND DISCUSSION

The complexes of HL are in a mononuclear form in which one metal ion is bonded to two ligands. This result has been confirmed by molecular weight determination (by Rast's method), which suggests that the complexes have the general formula $[LnL_2]ClO_4$. In the presence of metal ions HL is deprotonated, thus satisfying the charge on the metal. The complexes exhibit fairly high thermal stability and are moderately soluble in DMF and DMSO. The conductance values suggest that they are 1 : 1 electrolytes[7] (Table 1).

IR spectra

The IR spectra of the ligand and the complexes are complicated (see Table 2). However, attempts have been made to identify some important bands which furnish information regarding the mode of bonding. The absence of ν(OH) in the spectra of the complexes indicates deprotonation of the —OH group (structure **1**). The ν(C—O) frequency

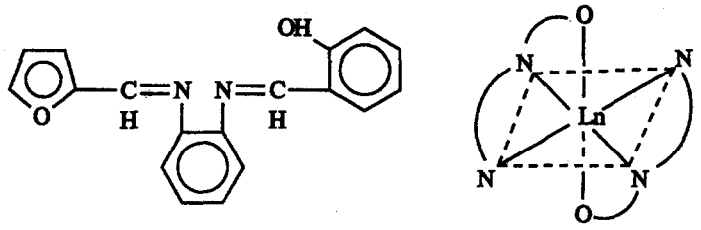

1

decreases by *ca* 10 cm^{-1} to 1555 cm^{-1} in the complexes, indicative of phenolic oxygen coordination. Similarly, ν(C=N) in the spectra of the complexes is at *ca* 1605 cm^{-1}, a lower frequency by *ca* 15–20 cm^{-1}, compared with two bands at 1624 and 1615 cm^{-1} which can be assigned to azomethine I and II, respectively. The absence of a ν(N—H) absorption in the spectra of the ligand and the complexes rules out the possibility of the C=N group in a protonated form. All complexes exhibit a ν(C—O—C) furfural ring frequency which is almost unshifted relative to the free ligand (1406 cm^{-1}), suggesting that the furfural ring oxygen[9] is not coordinated. Bands assignable to ν(Ln—O) and ν(Ln—N) are observed at *ca* 390 and 250 cm^{-1}, respectively.[10] The vibrational spectra indicate that perchlorate ions are not coordinated in the complexes studied.

XPS studies

The results of the XPS semi-quantitative analyses of the surface layers are in agreement with the sample compositions.

The 3*d* or 4*d* electron BEs of the metals and the values for the nitrogen 1*s* electron BEs are given in Table 3. Although the Ln 3*d* or 4*d* electron BE is closely related to the central atom charge and therefore to its valency, it is difficult to determine the valency only on the basis of this criterion since the intervals for various oxidation states may overlap. Nevertheless, we can obtain the same result as that reported previously.[11]

From the spectra we find only one symmetric nitrogen 1*s* peak for all the complexes relative to two 1*s* peaks of equal intensity for the ligand, as shown in Table 3. This behaviour suggests that the four nitrogen atoms in the complexes, $[LnL_2]ClO_4$, become chemically identical and a coordination conjugation of four equatorial nitrogens occurs, and as can be seen in structure **1**; the nitrogen 1*s* electron BEs in the complexes increase in the sequence: La > Ce < Pr < Nd < (Pm) > Sm < Eu < Gd > Tb < Dy < Ho < Er > Tm < Yb < Lu, which is exactly the same order as in the "Four Subgroup Effect" series of stability constants.[12] These energies reflect the amount of electron density transferred from the nitrogen

Table 2. Significant IR bands of HL and its complexes (cm^{-1})

Compound	ν(C—O) Phenolic	ν(C=N) I	II	ν(C—O—C)	ν(Ln—O)	ν(Ln—N)
HL	1565	1624, 1615		1406		
$[LaL_2]ClO_4$	1556	1606		1405	324	295
$[CeL_2]ClO_4$	1552	1604		1406	326	280
$[PrL_2]ClO_4$	1552	1604		1403	327	286
$[NdL_2]ClO_4$	1554	1606		1404	330	290
$[SmL_2]ClO_4$	1555	1602		1405	330	295
$[EuL_2]ClO_4$	1556	1605		1404	337	293
$[GdL_2]ClO_4$	1556	1606		1403	332	290
$[TbL_2]ClO_4$	1552	1602		1405	326	280
$[DyL_2]ClO_4$	1551	1601		1406	328	290
$[HoL_2]ClO_4$	1551	1604		1405	337	287
$[ErL_2]ClO_4$	1551	1603		1404	338	283
$[TmL_2]ClO_4$	1550	1602		1405	336	282
$[YbL_2]ClO_4$	1548	1601		1405	325	280
$[LuL_2]ClO_4$	1548	1600		1404	327	280

Table 3. The binding energy values of Ln 3*d* or 4*d*, Cl 2*p*, N 1*s* and O 1*s* electrons of the ligand and its complexes (eV)

Compound	N 1*s*	O 1*s*			Cl 2*p*	Ln	
HL	400.6, 398.8	532.6	532.0	531.7			
$[LaL_2]ClO_4$	399.2	533.0	532.1	531.7	209.1	$3d_{1/2}$	836.3
$[CeL_2]ClO_4$	399.1	533.1	532.0	531.8	209.2	$3d_{5/2}$	880.1
$[PrL_2]ClO_4$	399.2	532.8	532.0	531.6	209.1	$3d_{5/2}$	933.7
$[NdL_2]ClO_4$	399.3	532.8	532.1	531.8	209.2	$3d_{5/2}$	984.0
$[SmL_2]ClO_4$	399.3	532.9	532.1	531.8	209.2	$3d_{5/2}$	1084.0
$[EuL_2]ClO_4$	399.4	533.0	532.1	531.7	209.1	$3d_{5/2}$	1136.3
$[GdL_2]ClO_4$	399.5	533.0	532.1	531.7	209.1	$3d_{5/2}$	1191.1
$[TbL_2]ClO_4$	399.2	533.1	532.0	531.7	209.1	$3d_{5/2}$	1246.0
$[DyL_2]ClO_4$	399.4	533.0	532.1	531.7	209.1	$3d_{5/2}$	1217.9
$[HoL_2]ClO_4$	399.5	533.0	532.0	531.7	209.1	4*d*	162.4
$[ErL_2]ClO_4$	399.6	533.9	532.0	531.8	209.2	4*d*	170.6
$[TmL_2]ClO_4$	399.3	532.8	532.0	531.8	209.2	4*d*	178.8
$[YbL_2]ClO_4$	399.6	532.9	532.0	531.6	209.1	$4d_{5/2}$	185.9
$[LuL_2]ClO_4$	399.7	533.0	532.1	531.7	209.1	$4d_{5/2}$	192.3

atoms to a metal ion via coordination bonds and, as expected, correlate with the sum of the metal ionization potentials.[12]

Oxygen occurs in three different chemical environments in the complexes, i.e. in the perchlorate groups and in the furfural ring and the deprotonated phenolic oxygen. These three oxygen environments result in a broad O1*s* peak, which consists of two shoulder peaks and one sharp peak with relative intensities in the ratio 1 : 1 : 2. This is indicated by the FWHM values (full width at half height) of just above 5 eV for the complexes. Deconvolution indicates that the O 1*s* peaks are derived from the ClO_4^- group and the furfural ring remained almost unchanged for all the complexes compared with the values of the ligand and $La(ClO_4)_3$. However, the BE values of the O 1*s* peak from phenolic oxygen are slightly higher than that of the ligand.

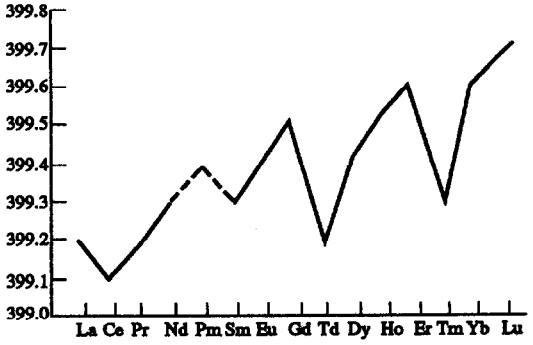

Fig. 1. The nitrogen 1*s* electron binding energies in $[LnL_2]ClO_4$ complexes.

Magnetic moments

The paramagnetic behaviour of the lanthanide(III) ions is consistent with the presence of unpaired electrons. The room-temperature magnetic moments of all the complexes show very little deviation from the Van Vleck values,[13] indicating little participation of the 4*f* electrons in bond formation.

TG and DTA

The thermolysis of all the compounds has similar patterns. In the first step the ClO_4^- group is split, with a strong exothermic effect. On increasing the temperature intermediate compounds decompose continuously and finally oxides formed.

On the basis of the above discussion a six-coordinated octahedral structure is suggested for the complexes and the "Four Subgroup Effects" can be confirmed by the XPS method.

REFERENCES

1. R. D. Jones, D. A. Summerville and F. Basolo, *Chem. Rev.* 1979, **79**, 133.
2. G. Henrici-Olie and S. Olive, *The Chemistry of the Catalyzed Hydrogenation of Carbon Monoxide*, p. 152. Springer, Berlin (1984).
3. H. Dugas and C. Penney, *Bioorganic Chemistry*, p. 435. Springer, New York (1981).
4. J. D. Margerrum and L. J. Miller, *Photochromism*, p. 569. Interscience, Wiley (1971).

5. W. J. Sawodny and M. Riederer, *Angew. Chem., Int. Edn Engl.* 1977, **16**, 859.
6. J. A. Nelder and R. Mead, *Computer J.* 1965, **7**, 308.
7. F. Dianzhong and W. Bo, *Trans. Met. Chem.* 1993, **18**, 101.
8. W. J. Geary, *Coord. Chem. Rev.* 1971, **7**, 81.
9. R. M. El-Shazly, M. M. Bekheit and F. I. Taha, *Trans. Met. Chem.* 1990, **15**, 337.
10. K. Nakamoto, *Infrared and Raman Spectra of Inorganic and Coordination Compounds*, 3rd edn. Wiley-Interscience, New York (1978).
11. L. Guo-Fa, *Acta Chem. Sin.* 1992, 473.
12. B. N. Figgs and J. Lewis, *Techniques of Inorganic Chemistry*, Vol. 24, p. 57. Interscience, New York (1978).
13. J. H. Burness, J. G. Dillard and L. T. Taylor, *J. Am. Chem. Soc.* 1975, **97**, 6080.

Polyhedron Vol. 12, No. 13, pp. 1613–1620, 1993
Printed in Great Britain

0277–5387/93 $6.00+.00
© 1993 Pergamon Press Ltd

PYRIDINE FUNCTIONALIZED ALKYLS OF TRANSITION METALS, SYNTHESIS OF BIS[C,N-2-PYRIDYLBIS(TRIMETHYLSILYL)METHYL]NICKEL

KEITH J. IZOD and PETER THORNTON*

Department of Chemistry, Queen Mary and Westfield College, Mile End Road, London E1 4NS, U.K.

(*Received* 26 *February* 1993; *accepted* 5 *March* 1993)

Abstract—Alternate lithiation and reaction with $ClSiMe_3$ of 2,6-dimethylpyridine gave the lithium derivatives of pyridine substituted at the 2- and 6-positions by mono- or bis(trimethylsilyl)methyl groups. The relative ease of formation of these compounds is discussed and compared to their reactivity with transition metal halides. The reaction of $NiCl_2$ with the lithium derivative of bis(trimethylsilyl)methylpyridine gives the remarkably air-stable nickel(II) alkyl bis[C,N-2-pyridylbis(trimethylsilyl)methyl]nickel(II).

Ligands of type **I**, the 2-functionalized pyridines, are of particular interest since they are often found to exhibit a wide variety of coordination patterns. A wide range of substituents X and Y have been employed to vary the properties of these ligands, usually combinations of X as H, alkyl or halogen and Y as O, S, NR, PR or CRR′.

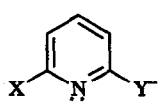

I

There are comparatively few studies of 2-pyridylalkyl compounds, Y = CRR′; of these over half are of the sterically hindered ligands with R = R′ = $SiMe_3$ or R = H, R′ = $SiMe_3$, here abbreviated as btsmp and tsmp, respectively. Both chelating and bridging modes of coordination have been established, but there is an intriguing variety of structures to be found among their homoleptic compounds. The isostructural cadmium, magnesium and zinc derivatives of btsmp have very distorted tetrahedral geometry, which in the cadmium compound leads to a C—Cd—C angle of 174.3°.[1] For these compounds the bite angle of 67° is comparable to those in pyridonate and pyridinethionates. In $[M(btsmp)_2]^+[MCl_4]^-$ (M = Al, Ga) the tetrahedral environment of the cation is more regular, but clashing of the two close $C(SiMe_3)_2$ groups is relieved by lengthening the M—N and M—C bonds to one of the ligands.[2] For tin(II) the stereochemically active lone pair appears to be responsible for compressing the bite angle to 59°.[3] In $Hg(btsmp)_2$] the characteristic two coordination of mercury is shown by the ligands bonding only through carbon, although there may be weaker links to nitrogen at a much longer distance.[1]

This varied coordination pattern of btsmp prompted us to study the coordination of btsmp and tsmp to first row transition metals. This paper describes the synthesis and properties of $[Ni(btsmp)_2]$ and points of interest on the ligand synthesis and reactivity.

Additional motivation for our work comes from the opportunity to study further the behaviour of lithiated alkylpyridines, which, despite having widespread use as intermediates in organic chemistry, for forty years,[4] were not used for transmetallations until much later.[5]

Alkylpyridines are much more acidic than toluene or xylene, which only undergo metallation by organolithium reagents when complexed by tertiary amines, as in Bu^nLi(tmeda), whereas alkylpyridines are deprotonated by uncomplexed organolithiums or by sodium amides in liquid ammonia. This may be attributed to the ring nitrogen's ability to accommodate much of the negative charge which is delocalized into the aromatic π-system away from the carbanion centre, as has been shown by ^1H and ^{13}C NMR spectroscopy correlated with electron

* Author to whom correspondence should be addressed.

densities calculated by the CNDO/2 method.[6] It has been known for a number of years that silyl groups adjacent to a carbon bearing a negative charge act to stabilize the carbanion, but this extra stabilization is thought to be lost on going from the free anion to a metallated derivative, although an intermediate situation may occur in solution.

The lithiation of 2-alkylpyridines is also facilitated by a complex-induced proximity effect.[7] In the first step of the deprotonation the ring nitrogen of the ligand coordinates the lithium atom of the metallating alkyllithium, e.g. Bu^nLi. This gives an increase in the nucleophilicity of the Bu^n group and a decrease in the molecular association of the organolithium. In such a pre-equilibrium complex the organolithium is held in a position where the alkyl group may be directed towards the active hydrogen of the free ligand. This allows the deprotonation step to proceed through a favoured six-membered ring intermediate, **II**.

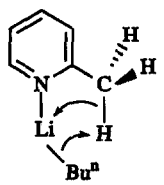

II

RESULTS AND DISCUSSION

Ligand formation

Despite the predicted order of carbanion stabilization $C(SiMe_3)_2 > CHSiMe_3 > CH_2$, discussed above, our initial metallation experiments suggested that the order of acidity of the 2-alkylpyridines was Htsmp > Hbtsmp > Hmp (Hmp = 2-methylpyridine). To study this anomaly further 2,6-dimethylpyridine was repeatedly lithiated and reacted with $ClSiMe_3$, with the results outlined in Scheme 1. The position of lithiation or silylation was identified by ^1H and ^{13}C NMR spectroscopy, allowing the relative acidities of unsubstituted mono- and bis-silylated alkyl groups in the ligand to be compared directly.

Reaction of 2,6-dimethylpyridine (**III**) with 2 equivalents of Bu^nLi in ether, followed by 2 equivalents of $ClSiMe_3$, leads to the disubstituted product **IV**, substitution occurring at one carbon only. Such a substitution pattern is expected since initial reaction of **III** would give a mono-subsituted product which was not isolated but which then reacts preferentially at the substituted carbon through a silyl-stabilized carbanion.

Further reaction of **IV** with Bu^nLi(tmeda) yielded a crystalline product whose ^1H NMR spectrum corresponded to **V**. Deprotonation occurs to give a carbanion stabilized by two Me_3Si groups rather than at the less sterically hindered methyl, clearly demonstrating the greater acidity of CH_2SiMe_3 and $CH(SiMe_3)_2$ substituents relative to CH_3.

Addition of $ClSiMe_3$ to a freshly prepared ether solution of **V** does not give the trisubstituted product **VI**, but yields **VII** through a tautomerization of the carbanion. This tautomerization may be compared to that observed in lithiated 2,4-dialkylpyridines and 2,4-dialkylquinolines. Reaction of Bu^nLi with 2,4-dimethylpyridine leads to the 2-lithiated product through a complex-induced proximity effect. However, this is seen to isomerize slowly to the thermodynamically more stable 4-lithio derivative in such coordinating solvents as THF.[8] The rate of isomerization is increased by the presence of tertiary amines such as tmeda and is dramatically increased by the presence of an extra equivalent of the parent heterocycle.[9,10] This has been interpreted as implying that the isomerization occurs through equilibration of small amounts of unreacted heterocycle with the carbanion. A marked dependence on solvent is also observed; in THF 2,4-dimethylquinoline undergoes lithiation at the 2-position with Bu^nLi. After 144 h this is found to have isomerized completely to the 4-lithio compound. In ether, however, the 2-lithio derivative does not isomerize even after prolonged periods in solution; indeed it is found that the 4-lithio derivatives isomerize to the 2-lithio derivatives in this solvent.

The isomerization observed in the present carbanion differs from those outlined above in three respects. First, for 2,4-dimethylpyridine isomerization favours the formation of a thermodynamically more stable product after initial kinetically controlled formation of the 2-lithio product, but in our compound the carbanion formed initially is both kinetically and thermodynamically favoured since it is stabilized by two $SiMe_3$ groups. The reaction occurs through an intermediate in which the negative charge is localized on the naked alkyl group, a situation relatively disfavoured thermodynamically. Second, the lithium derivative **V** is indefinitely stable in hexane, ether and THF solutions despite the presence of the tertiary amine tmeda. Third, isomerization is only observed when $ClSiMe_3$ is added.

From this it may be concluded that the tautomerization of **V** is neither a tautomerization from a carbanion formed under kinetic control to a more thermodynamically stable one, nor is it induced by solvent, the presence of tertiary amines or the unreacted parent heterocycle. The formation of **VII**

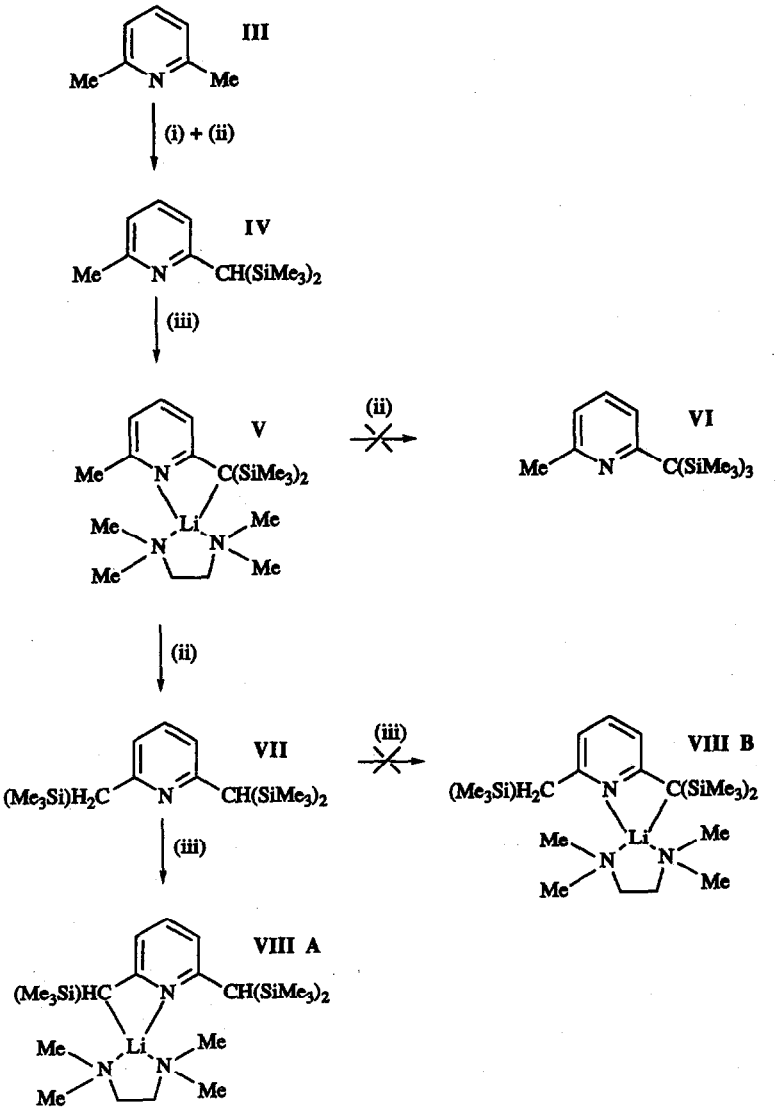

Scheme 1. (i) Bu^nLi in ether, 0°C; (ii) $ClSiMe_3$ in ether, 0°C; (iii) Bu^nLi(tmeda) in ether or pentane, 0°C.

may be rationalized as follows: In ether solution an equilibrium may exist between two carbanion tautomers **Va** and **Vb** (Scheme 2), with tautomerization occurring through a dianionic intermediate $[2\text{-}CH_2\text{-}6\text{-}C(SiMe_3)_2C_5H_3N]^{2-}$. Such a dianion has a precedent in the ready metallation of 2,6-bis(trimethylsilylmethyl)pyridine at both alkyl carbons with Bu^nLi(tmeda).[11]

The high polarizability of silicon suggests that nucleophilic attack of the carbanion on $ClSiMe_3$ would tend to favour an S_N2 mechanism, requiring the formation of a transition state in which the silicon atom is five-coordinate. It can be clearly seen that reaction through **Va** involves a transition state in which steric interactions between the silyl substitutents and the incoming group would be large, but in the transition state derived from **Vb** steric interactions between the alkyl protons and the silyl group would be minimal and so this route is favoured.

Metallation of **VII** provides a direct comparison of the acidities of mono- and disubstituted 2-alkyl groups. Reaction of **VII** with Bu^nLi(tmeda) in ether may give either **VIIIa** or **VIIIb**, but ^1H and ^{13}C NMR studies clearly indicate that deprotonation occurs at the mono-substituted alkyl, leading exclusively to the product **VIIIa**. Appreciable signal broadening in the ^1H resonance assigned to the $C(SiMe_3)_2$ protons suggests magnetic inequivalence of the methyl protons caused by restricted rotation about the C_{alkyl}—C_{ipso} bond in this very sterically crowded complex. The order of acidity of the alkyl groups of 2-alkylpyridines may now be confirmed as: $CH_2SiMe_3 > CH(SiMe_3)_3 > CH_3$, in agree-

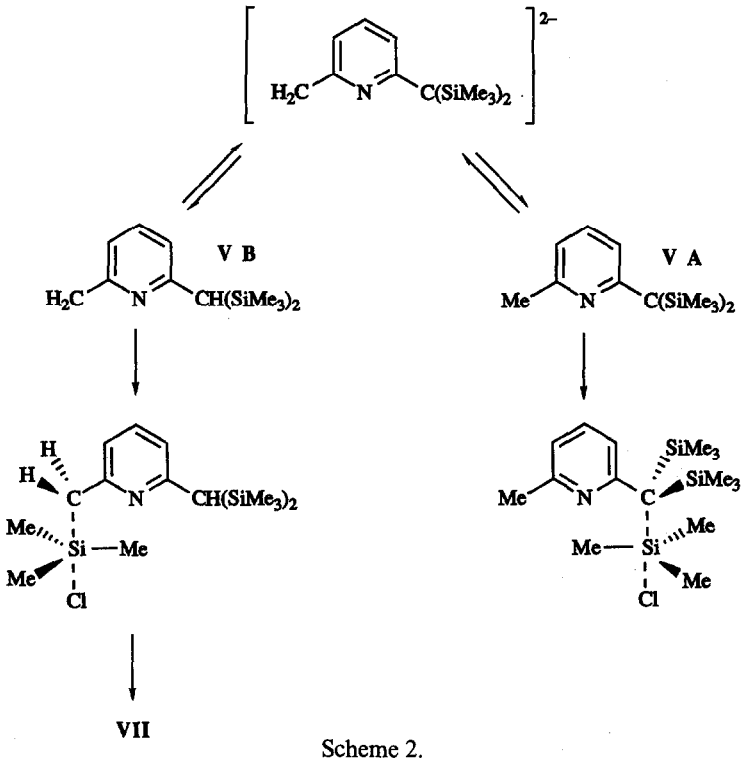

Scheme 2.

ment with competitive lithiation experiments[12] on a mixture of Hbtsmp and Htsmp.

Transmetallation reactions and ligand coupling

A convenient and frequently employed route to organometallic compounds is transmetallation:

$$n\mathrm{MR} + \mathrm{M'X}_n \longrightarrow n\mathrm{MX} + \mathrm{M'R}_n$$

where M is an electropositive metal such as lithium or sodium and X is a halogen. Since 2-alkylpyridines may readily be lithiated and many anhydrous transition metal halides are available, we adopted this route, which others have used to prepare $[M(btsmp)_2]$ (M = Zn, Cd, Hg)[1] and $[M_2(btsmp)_2]$ (M = Cu, Ag, Au).[13] However, our reactions turned out to be much more complex.

Reaction of lithiated alkylpyridines with transition metal halides in appropriate stoichiometric ratios rarely gave clean products and in several cases only intractable mixtures, particularly for the early heavy transition metals Nb, Mo and W, which have many easily accessible oxidation states. The unsubstituted 2-pyridylmethyl ligand, mp, was particularly intractable, giving a sticky brown oil with $ZrCl_4$ from which an ESR active zirconium(III) species was isolated.[14] It has previously been noticed that no tractable products are formed[15] on attempting to fully substitute $HfCl_4$ or $ThCl_4$ with Li(dmp) (Hdmp = 2,6-dimethylpyridine) and that reaction of $[Li_2(tsmp)_2(OEt_3)_2]$ with $AgBF_4$ or Au(CO)Cl gave a silver mirror and colloidal gold, respectively.[13] Only brief mention was made of these complications and in neither case was an explanation put forward. The complications seem to be caused by a redox process and we suggest that reduction of metals occurs through a ligand coupling reaction.

The reduction process was most effectively studied when $[Li_2(btsmp)_2]$ was used as a transmetallating agent. When an ether solution of this was added to a suspension of $NiCl_2$ in ether a large amount of grey solid, probably a mixture of LiCl and metallic nickel, was precipitated and a deep red solution was given. Attempts to isolate more than trace amounts of a pure product from the solution were unsuccessful.

When the reaction was repeated under the same conditions but with the additional presence of more than 4 mol of PEt_3 per mole of $NiCl_2$, much less grey solid was formed. Removal of this solid and crystallization of the red oil obtained from the filtrate from pentane gave crystals of $[Ni(PEt_3)_4]$.[16] The purely organic product could be isolated by removing solvent from the red filtrate, subliming away the excess PEt_3 *in vacuo* at 60°C and subliming the pale red residue at 150°C/10^{-2} Torr repeatedly. The sublimate could thus be divided into a little $[Ni(btsmp)_2]$ and some colourless crystals, although

these could not be completely separated. The ^1H NMR spectrum of this product (see Experimental) is consistent with the formation of 2-bis(trimethylsilyl)methyl-5-{2-pyridylbis(trimethylsilyl)-methyl}pyridine (**IX**), recently reported,[17] with crystal structure, from the reaction of $BiCl_3$ with $[Li_2(btsmp)_2]$.

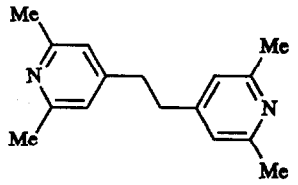

IX

The overall reaction consists of the formation of $[Ni(btsmp)_2]$ and a consequent competition between $NiCl_2$ and preformed $[Ni(btsmp)_2]$ for $[Li_2(btsmp)_2]$ with the subsequent formation of zero-valent nickel by a ligand coupling reaction:

$$NiCl_2 + [Li_2(btsmp)_2] \longrightarrow x[Ni(btsmp)_2] + yNi + z''(btsmp)_2''$$

A possible mechanism for the reduction process is shown in Scheme 3. The initial product is $[Ni(btsmp)_2]$. Addition of more lithium reagent results in nucleophilic attack of a btsmp carbanion at the 5-position of one of the pyridine rings of the preformed $[Ni(btsmp)_2]$ and transfer of electrons to nickel. Recovery of aromaticity by the loss of the 5-proton and its transfer to the remaining carbanion centre completes the reaction. Support for this mechanism is as follows: (1) Solutions of lithiated alkylpyridines are indefinitely stable, so the presence of a more readily reducible metal centre is essential to ligand coupling to take place. (2) $[Ni(btsmp)_2]$ is very stable to light, heat and hydrolysis, but is almost completely destroyed by addition to its solution in ether of $[Li_2(btsmp)_2]$. (3) Significantly lower yields are observed on reaction of $NiCl_2$ with the more nucleophilic carbanion formed upon lithiation of Htsmp.[16] This would be difficult to explain if the ligand coupling reaction proceeded by a reductive elimination mechanism. Isolation of the 5-coupled species only also argues against a radical based mechanism where a wider variety of products might be expected. (4) Electron transfer to a transition metal has been observed in nucleophilic additions to coordinated cyclopentadienyls, as in the reaction of $NaBH_4$ with $[Fe(C_5H_5)(CO)_2(PPh_3)]$ to give $[Fe(C_5H_6)(CO)_2(PPh_3)]$.[18]

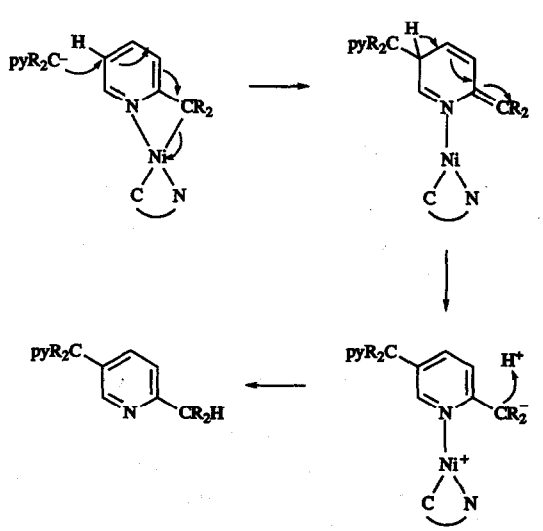

Scheme 3.

It has been suggested that lithiation of 2-alkylpyridines increases electron density at the 3- and 5-positions over the 2-, 4- and 6-positions[6,19] and consequently that nucleophilic attack at the former is disfavoured. Studies of uncharged pyridines coordinated to transition metals also suggest deactivation of the 3- and 5-positions towards nucleophilic attach may occur.[20] However, in the present case it appears that the presence of empty low-lying *d*-orbitals on the metal creates a situation whereby the 3- and 5-positions of the pyridine ring may readily undergo a form of reductive nucleophilic attack, whereas no such mechanism of electron transfer is available for the 2-, 4- or 6-positions.

The observed preference for substitution at the 5- over the 3-position may be attributed to efficient steric blocking of the latter by the two adjacent $SiMe_3$ groups, especially in conjunction with the large size of the incoming nucleophile.

$[Ni(btsmp)_2]$

Unlike the great majority of nickel alkyls $[Ni(btsmp)_2]$ is stable to air and dilute aqueous acids. The methyl groups of the $SiMe_3$ moieties probably lie above and below the nickel atoms and prevent attack by nucleophiles at the metal centre. The compound can be sublimed and its mass spectrum gives the molecular ion as a strong peak. It was not possible to obtain X-ray quality single crystals, but its diamagnetism and well-resolved ^1H and ^{13}C spectra indicate a square planar structure. The ^1H NMR spectrum shows significant upfield shifts of the ring protons compared with the free ligand, consistent with Ni—N $d\pi$–$p\pi$ back donation; the ^{13}C NMR spectrum is most remarkable for the small shift in the alkyl carbon resonance (3 ppm) when compared with the free ligand Hbtsmp, suggesting covalency in the Ni—C bond and in line with the spectra of $[M_2(btsmp)_2]$ (M = Au, Cu).[13]

EXPERIMENTAL

Materials

All compounds were assumed to be extremely air-sensitive until proven otherwise and were handled in a nitrogen atmosphere or under vacuum with standard Schlenk techniques. Solid materials were handled in a nitrogen-filled dry glove-box. Solvents were dried by standing over sodium wire, refluxing for 4 h over the sodium ketal of benzophenone, followed by distillation under dry nitrogen, and were stored in grease-free reservoirs over activated 3 Å molecular sieves. Deuterated solvents were dried over activated 3 Å molecular sieves and degassed by three freeze–pump–thaw cycles. Xylene, 2-methylpyridine, 2,6-dimethylpyridine and tmeda were dried and degassed by refluxing over CaH_2 and distillation under dry nitrogen. $ClSiMe_3$ (Aldrich) was distilled at reduced pressure onto 3 Å molecular sieves. Bu^nLi was used as a 2.5 M solution in hexanes (Aldrich) immediately after standardization.[21]

Instrumentation

^1H and ^{13}C NMR spectra were obtained on Bruker WP80 and WP250 spectrometers and mass spectra on AEI MS902 or Kratos M550 TC spectrometers.

2-*Trimethylsilylmethylpyridine*

The procedure is similar to that in the literature.[22] 2-Methylpyridine (10 cm^3, 0.102 mol) was added to an ice-cold solution of Bu^nLi (40 cm^3, 0.102 mol) in ether (100 cm^3). After stirring for 1 h the resulting orange solution was added dropwise to a solution of $ClSiMe_3$ (13 cm^3, 0.102 mol) in ether (100 cm^3). After stirring for 30 min the precipitated LiCl was removed by filtration, the solvent was removed by vacuum at 0°C and the product was distilled under reduced pressure (20°C/10^{-2} Torr). Yield: 12 g (71%). ^1H NMR (C_6D_6): δ 0.05 (s, 9H, Si*Me*$_3$), 2.20 (s, 2H, C*H*$_2$SiMe$_3$), 6.7 (m, 2H, 3,5-Ar*H*), 7.15 (m, 1H, 4-Ar*H*), 8.45 (m, 1H, 6Ar*H*).

Bis(trimethylsilyl)methylpyridine[22]

A solution of Bu^nLi (80 cm^3, 0.204 mol) and tmeda (30 cm^3, 0.2 mol) in ether (30 cm^3) was added to an ice-cold solution of 2-methylpyridine (10 cm^3, 0.102 mol) in ether (100 cm^3). After stirring for 1 h a solution of $ClSiMe_3$ (26 cm^3, 0.2 mol) in ether (60 cm^3) was added to the resulting orange solution. This mixture was stirred for 2 h, the precipitated LiCl removed by filtration, the solvent removed by vacuum at room temperature and the residue distilled under reduced pressure (65–70°C/10^{-2} Torr). Yield: 15 g (63%). ^1H NMR (C_6D_6): δ 0.15 [s, 18H, (Si*Me*$_3$)$_2$], 1.72 [s, 1H, C*H*(SiMe$_3$)$_2$], 6.60 (m, 2H, 3,5-Ar*H*), 7.10 (m, 1H, 4-Ar*H*), 8.45 (m, 1H, 6-Ar*H*).

2-*Methyl-6-bis(trimethylsilyl)methylpyridine* (IV)

$ClSiMe_3$ (22 cm^3, 0.17 mol) was added to the orange solution formed by the addition of Bu^nLi (63 cm^3, 0.17 mol) to an ice-cold solution of 2,6-dimethylpyridine (10 cm^3, 0.086 mol) and tmeda (26 cm^3, 0.17 mol) in ether (100 cm^3). The precipitated LiCl was removed by filtration and solvent removed by vacuum from the filtrate. The resulting colourless liquid was distilled under reduced pressure (85–90°C/10^{-2} Torr). ^1H NMR (C_6D_6): δ 0.12 [s, 18H, (Si*Me*$_3$)$_2$], 1.58 [s, 1H, C*H*(SiMe$_3$)$_2$], 2.32 (s, 3H, C*H*$_3$), 6.50 (m, 2H, 3,5-Ar*H*), 7.10 (m, 1H, 6-Ar*H*).

2-*Bis(trimethylsilyl)methyl-6-trimethylsilylmethylpyridine*(VII)

A solution of Bu^nLi (5.7 cm^3, 0.015 mol) and tmeda (1.8 cm^3, 0.015 mol) in ether (50 cm^3) was added to a solution of 2-methyl-6-bis(trimethysilyl)methylpyridine (5 cm^3, 0.015 mol) in ether (100 cm^3). $ClSiMe_3$ (1.9 cm^3, 0.015 mol) was added to the resulting solution, the precipitated LiCl removed by filtration, the solvent removed by vacuum and the product distilled under reduced pressure (100°C/10^{-2} Torr) as a colourless liquid. ^1H NMR (C_6D_6): δ 0.15 [s, 18H, (Si*Me*$_3$)$_2$], 0.30 (s, 9H, Si*Me*$_3$), 1.70 [s, 1H, C*H*(SiMe$_3$)$_2$], 2.27 (s, 2H, C*H*$_2$SiMe$_3$), 6.5 (m, 2H, 3,5-Ar*H*), 7.00 (m, 1H, 4-Ar*H*).

$Li(mp)(OEt_2)_n$, $Li_2(btsmp)_2$ *and* $Li_2(tsmp)_2(OEt_2)_2$

All these were prepared by the literature method[22] by the reaction of Bu^nLi with the respective ligands in ether. These lithium derivatives can be used in other reactions without further purification or isolation and appeared to form quantitatively.

[2-Me-6-C(SiMe$_3$)$_2$C$_5$H$_3$N]Li(tmeda) (V)

Bu^nLi (7 cm^3, 0.019 mol) was added to an ice-cold solution of 2-methyl-6-bis(trimethylsilyl)methylpyridine (8 cm^3, 0.019 mol) and tmeda (3 cm^3, 0.02 mol). After being stirred for 1 h the solvent was removed from the orange solution

by vacuum and the orange oil was recrystallized from pentane at −70°C to give the product as orange prisms. Yield: 4.4 g (61%). ^{1}H NMR (C_6D_6): δ 0.49 [s, 18H, (SiMe_3)$_2$], 1.70 (s, 4H, NCH_2), 1.85 (s, 12H, NMe_2), 2.15 (s, 3H, ArCH_3), 6.20 (m, 1H, 4-ArH), 6.90 (m, 2H, 3,5-ArH).

[2-CHSiMe$_3$-6-CH(SiMe$_3$)$_2$C$_5$H$_3$N]Li(tmeda) (**VIIIa**)

Bu^{n}Li (7.8 cm^3, 0.021 mol) was added to a solution of 2-bis(trimethylsilyl)methyl-6-trimethylsilylmethylpyridine (8 cm^3, 0.021 mol) and tmeda (3.2 cm^3, 0.02 mol) in pentane (30 cm^3). After being stirred for 1 h the solvent was removed by vacuum and the resulting orange oil was recrystallized from pentane at −70°C as orange prisms. ^{1}H NMR (C_6D_6): δ 0.37 (s, 9H, SiMe_3), 0.52 [s, br, 18H, (SiMe_3)$_2$], 1.85 [s, *ca* 8H, NCH_2+CH(SiMe$_3$)$_2$+CHSiMe$_3$], 2.05 (s, 12H, NMe_2), 5.85 (m, 2H, 3,5-ArH), 6.85 (m, 1H, 4-ArH). ^{13}C NMR (C_7D_8): δ 3.39 (q, SiMe_3), 7.64 [q, (SiMe_3)$_2$], 47.02 (q, NMe_2), 49.73 [d, CH(SiMe$_3$)$_2$], 57.99 (t, NCH$_2$), 100.89 (d, Ar), 105.69 (d, *Ar*), 136.09 (d, *Ar*), 169.5 (s, *Ar*).

Bis[*C,N*-2-*pyridylbis*(*trimethylsilyl*)*methyl*]*nickel*(II), [Ni(btsmp)$_2$]

Triethylphosphine (5 cm^3, 0.034 mol, > 4 equivalents) was added to a suspension of NiCl$_2$ (1.0 g, 7.71 mmol) in ether (50 cm^3) and stirred for 2 h. A solution of [Li$_2$(btsmp)$_2$] (7.75 mmol) in ether (40 cm^3) was then added over 2 h and stirring continued for 15 min. The dark precipitate produced was removed by filtration and the solvent removed from the filtrate by vacuum pumping to give a sticky red solid. This was redissolved in toluene (5 cm^3). This solution can now be handled in air. The solution in toluene was washed twice with water (10 cm^3) and chromatographed on Spence alumina, eluting with pentane. All the red fractions were combined, the solvent removed and the red solid recrystallized from pentane at −25°C to give twinned crystals of the product. Yield: 0.17 g (5%); m.p. 154–157°C. Found: C, 53.4; H, 8.7; N, 4.9. Calc. for $C_{24}H_{20}N_2NiSi_4$: C, 54.2; H, 8.4; N, 5.3%. IR: 2926s, 2855s, 1586s, 1558w, 1458s, 1425s, 1248s, 1212s, 1148m, 1103w, 1027w, 962w, 923s, 895s, 870m, 829s, 752m, 681w, 656s. MS: 530.1992 [20.6%, Ni(btsmp)$_2$ {calc. 530.1937}]; 294.1 [20%, Ni(btsmp)]; 222.1 (21.8%, btsmp—CH$_3$]; 73.04 [100%, SiMe$_3$]. ^{1}H NMR (C_6D_6): δ 0.52 (s, 18H, SiMe_3), 6.08 (m, 1H, 5-ArH), 6.62 (m, 1H, 3-ArH), 6.81 (m, 1H, 4-ArH), 7.62 (m, 1H, 6-ArH). ^{13}C NMR (C_7D_8): δ 4.096 (SiMe_3), 30.88 [C(SiMe$_3$)$_2$], 117.68, 125.57, 136.46, 149.10 (3,4,5,6-aromatics), 179.64 (2-Ar).

2-*Bis*(*trimethylsilyl*)*methyl*-5-[2-*pyridylbis*(*trimethylsilyl*)*methyl*]*pyridine* (**IX**)

The procedure of the synthesis of [Ni(btsmp)$_2$] was followed for the reaction of PEt$_3$, NiCl$_2$ and [Li$_2$(btsmp)$_2$]. After this mixture had been stirred for 15 h at room temperature the dark precipitate was removed by filtration and the solvent removed by vacuum. The sticky red solid was heated in vacuum to 60°C to remove excess PEt$_3$. The remaining solid was carefully sublimed (150°C/10^{-2} Torr), giving a colourless crystalline product which could be purified from the red impurity by repeated sublimation, but giving only small yields. ^{1}H NMR (C_6D_6): δ 0.21 [s, 18H, (SiMe_3)$_2$], 0.26 [s, 18H, (SiMe_3)$_2$], 1.78 [s, 1H, CH(SiMe$_3$)$_2$], 6.52 (m, 1H, ArH), 6.65 (m, 1H, ArH), 6.88–6.97 (m, 2H, ArH), 7.25 (m, 1H, ArH), 8.35 (m, 1H, ArH), 8.65 (m, 1H, ArH).

Acknowledgement—We thank Mr G. Coumbarides for NMR spectra and the Science and Engineering Research Council (U.K.) for a research studentship to K.J.I.

REFERENCES

1. M. J. Henderson, R. I. Paparsergio, C. L. Raston, A. H. White and M. F. Lappert, *J. Chem. Soc., Chem. Commun.* 1986, 672.
2. L. M. Engelhardt, U. Kynast, C. L. Raston and A. H. White, *Angew. Chem., Int. Edn Engl.* 1987, **26**, 681; U. Kynast, B. W. Skelton, A. H. White, M. J. Henderson and C. L. Raston, *J. Organomet. Chem.* 1990, **384**, C1.
3. L. M. Engelhardt, B. S. Jolly, M. F. Lappert, C. L. Raston and A. H. White, *J. Chem. Soc., Chem. Commun.* 1988, 336.
4. H. C. Brown and W. A. Murphey, *J. Am. Chem. Soc.* 1951, **73**, 3308.
5. R. I. Paparsergio, C. L. Raston and A. H. White, *J. Chem. Soc., Chem. Commun.* 1983, 1419.
6. K. Konishi and K. Takahashi, *Bull. Chem. Soc. Japan* 1977, **50**, 2512.
7. P. Beak and A. I. Meyers, *Accts Chem. Res.* 1986, **19**, 356.
8. E. M. Kaiser, *Tetrahedron* 1983, **39**, 2055.
9. E. M. Kaiser and W. R. Thomas, *J. Org. Chem.* 1974, **39**, 2659.
10. E. M. Kaiser, W. R. Thomas, T. E. Synos, J. R. McClure, T. S. Mansour, J. R. Garlich and J. E. Chastain, *J. Organomet. Chem.* 1981, **213**, 405.
11. R. Hacker, P. von R. Schleyer, G. Reber, G. Muller and L. Brandsma, *J. Organomet. Chem.* 1986, **316**, C4.
12. C. Jones, C. H. L. Kennard, C. L. Raston and G. Smith, *J. Organomet. Chem.* 1990, **396**, C39.

13. R. I. Papasergio, C. L. Raston and A. H. White, *J. Chem. Soc., Dalton Trans.* 1987, 3085,
14. M. B. Hursthouse, K. J. Izod, M. Motevalli and P. Thornton, *J. Chem. Soc., Dalton Trans.*, submitted.
15. S. M. Beshouri, P. E. Fanwick, I. P. Rothwell and J. C. Huffman, *Organometallics* 1987, **6**, 2498.
16. K. J. Izod, PhD Thesis, London (1991).
17. C. Jones, L. M. Engelhardt, P. C. Junk, D. S. Hutchings, W. C. Patalinghug, C. L. Raston and A. H. White, *J. Chem. Soc., Chem. Commun.* 1991, 1560.
18. C. M. Lukehart, *Fundamental Transition Metal Organometallic Chemistry*, p. 336. Brooks/Cole, Monterey (1985).
19. K. Takahashi, K. Konishi, M. Ushio, M. Takaki and R. A. Sami, *J. Organomet. Chem.* 1973, **50**, 1.
20. E. C. Constable, *Metals and Ligand Reactivity*. Ellis Horwood, Chichester (1990); E. C. Constable, *Inorg. Chim. Acta* 1988, **145**, 49.
21. H. Gilman and J. W. Morton, *Organic Reactions*, Vol. 8, p. 258. Wiley, New York (1954).
22. R. I. Papasergio, B. W. Skelton, P. Twiss, A. H. White and C. L. Raston, *J. Chem. Soc., Dalton Trans.* 1990, 1161.

Polyhedron Vol. 12, No. 13, pp. 1621–1634, 1993
Printed in Great Britain

0277–5387/93 $6.00+.00
Pergamon Press Ltd

MONOMERIC STRONTIUM AND BARIUM β-DIKETONATE ADDUCTS WITH POLYETHERS; THE X-RAY CRYSTAL STRUCTURES OF [Sr(Ph$_2$ACAC)$_2$(TETRAGLYME)] AND [Ba(THD)$_2$(TETRAGLYME)]

SIMON R. DRAKE* and STEWART A. S. MILLER

Department of Chemistry, Imperial College of Science, Technology and Medicine, South Kensington, London SW7 2AY, U.K.

and

MICHAEL B. HURSTHOUSE* and K. M. ABDUL MALIK

School of Chemistry and Applied Chemistry, University of Wales College of Cardiff, P.O. Box 912, Cardiff CF1 3TB, U.K.

(*Received* 10 *February* 1993; *accepted* 5 *March* 1993)

Abstract—The reaction of the ethanol solvated strontium ethoxide [Sr(OEt)$_2$(EtOH)$_4$]$_\infty$ with the β-diketonate thd-H in the presence of tetraglyme in hexane at ambient temperature yields [Sr(thd)$_2$(tetraglyme)] (**1**); while the analogous reaction of the *in situ* prepared [Sr(tfa)$_2$]$_\infty$ and triglyme produces [Sr(tfa)$_2$(triglyme)] (**2**). Reaction of [Sr(Ph$_2$acac)$_2$]$_\infty$ with tetraglyme yields [Sr(Ph$_2$acac)$_2$(tetraglyme)] (**3**). The corresponding barium complex [Ba(OEt)$_2$(EtOH)$_4$]$_\infty$ also reacts rapidly with thd-H and tetraglyme in hexane to yield the glyme-chelated monomeric complex [Ba(thd)$_2$(tetraglyme)] (**4**). These complexes are all monomeric and have been characterized by IR, ^{1}H and ^{13}C NMR spectroscopy, microanalysis, mass spectrometry, and in selected cases TGA and DSC. The X-ray structures of [Sr(Ph$_2$acac)$_2$(tetraglyme)] (**3**) and [Ba(thd)$_2$(tetraglyme)] (**4**) reveal that they are monomeric with similar nine-coordinate metal centres. The tetraglyme coordinates via all its available oxygen atoms which wrap in a meridional plane and the two β-diketonates are positioned on either side of this plane.

In the course of our research on alkaline earth metal chemistry directed towards volatile single source CVD precursors we have encountered a wide range of problems using the bulk metals as starting materials to a range of metal alkoxides or aryloxides.[1] Notable difficulties encountered include contamination of the metal surfaces by either hydroxide or oxide groups, which has frequently resulted in the incorporation of hydroxo or oxo groups into the end products. A further limitation has been passivation of the metal surface, which has often resulted in poor reproducibility of reactions. These problems have hindered the growth of the chemistry of the heavier metals of Group IIA, although seminal contributions have been made previously by Grignard, Beckman, Gilman, Bradley and Coates.[2] We have previously noted that cleavage of a range of organic ligands by alkaline non-aqueous solutions of these metals may occur, i.e. P—N cleavage of HMPA, C—O cleavage of THF and C—O scission of Bu^{t}OH.[1,3]

Given the above difficulties, a range of approaches has been used to overcome the inherent limitations of the bulk metal metallation route. Several strategies have recently been used; notable amongst these has been the use of metathesis, especially in the area of metal cyclopentadienyl complexes, which has only one drawback, i.e. the formation of "ate" complexes.[4] Other researchers active in

* Authors to whom correspondence should be addressed.

this area have used high-temperature metal vaporization techniques, pioneered by Green and Timms in the 1970s.[5] Less esoteric techniques have involved the use of metal trialkylsilylamido compounds [e.g. $Ba(N\{SiMe_3\}_2)_2(THF)_2$] prepared via transmetallation, using either mercury[6] or tin organometallic reagents.[7] This is an excellent route and the only small drawback is the additional cost/time in preparing the mercury or tin amide starting materials.

An alternative approach uses a mixed ammoniacal-organic solvent route, which has achieved a considerable degree of success. This is a remarkably low cost route, having one disadvantage, which is the tendency of bond cleavage reactions to occur as outlined above.[8]

Given the above state of the art we have sought to define the basic criteria that are essential for group IIA organometallic reagents.[9] Firstly, the materials should preferably be crystalline solids of known stoichiometry, which are hydrocarbon soluble (and not amorphous/insoluble polymeric solids). Secondly, they should have good thermal stability and be stable over extended periods (i.e. 3–6 months shelf-life) in a controlled atmosphere (e.g. a nitrogen or argon filled glove-box); and finally these reagents should be reactive enough that most reactions occur at or near ambient temperature. This last point effectively implies that they are low molecular weight species.

We have recently observed that the group IIA tetra-solvated metal ethoxides are suitable materials, which fulfil the fundamental criteria outlined above. These heavier alkaline earth (A.E.) ethoxides, $[M(OEt)_2(HOEt)_4]_\infty$ (M = Ca, Sr or Ba), are hydrocarbon-soluble crystalline sources of these metals.[10] These materials are proving to have an enormous versatility as organometallic A.E. precursors. Previously we have observed a facile reaction between these metal ethoxides and a range of β-diketonates in hexane at room temperature,[11] analogous to the work of Bradley *et al.*[12] on transition metal complexes.

The use of metal alkoxides or alternatively β-diketonates as organometallic chemical vapour deposition (OMCVD) precursors for metal oxides is a field of immense interest, due to their potential applications in the area of electroceramics. Prior researchers have extensively used either tetramethyl-heptane-2,4-dionato or hexafluoro-pentane-2,4-dionato-alkaline earth salts, but *such materials have been found to be not only highly dependent on their synthesis but also on their "later history".* Specific examples include $[Ba(thd)_2]_\infty$, which when prepared by an aqueous solvent route was found to actually be $[Ba_5(OH)(thd)_9(H_2O)_3]$,[13] while the more volatile hexafluoro-pentane 2,4-dionato salts available commercially have also been shown to be hydrated species, e.g. $[Ba(hfa)_2(H_2O)]_\infty$.[14]

A notable feature of complexes of the group IIA metals is their strong Lewis acidity, which ensures that in the absence of Lewis base solvents they *generally form polymeric insoluble materials.* However, on the addition of Lewis base solvents to group IIA organometallics the polymeric ensembles are cleaved to yield simpler molecular species.[1] A wide variety of molecular geometries are available, provided that judicious choice of hydrocarbyl ligands (or other organic substrates) and/or Lewis bases are used to achieve coordinative saturation of the large M^{2+} cations, to reduce potential polymerization processes. For such a strategy a precedent is available, with the prior use of macrocyclic ligands, e.g. crown ethers and cryptands.[15]

We now demonstrate that the oligomeric group IIA metal β-diketonate complexes prepared *in situ*[12] react readily at room temperature in hexane with multidentate Lewis bases (e.g. glymes) to yield monomeric air- and moisture-stable products.

EXPERIMENTAL

General procedures

All manipulations were carried out under dry (molecular sieves) nitrogen using standard dry-box and Schlenk techniques. All hydrocarbon solvents were rigorously pre-dried and then distilled first over calcium oxide and then over sodium metal by standard techniques. Elemental analyses were performed by the microanalytical department of the Department of Chemistry, Imperial College. The melting points were measured under argon in sealed capillaries and are uncorrected values.

Instrumentation

IR spectra were recorded on a Perkin–Elmer FTIR 1720 spectrometer as either Nujol or hexachlorobutadiene mulls between 25 × 4 mm KBr plates. The samples were protected from the atmosphere by an O-ring-sealed Presslok holder.

Mass spectra were run on a Kratos MS30 spectrometer using the instrument in electron impact positive mode at the Royal School of Pharmacy Mass Spec. Service, University of London.

NMR spectra were recorded on a Jeol GS 270 MHz NMR spectrometer, using the protio impurities of the deuterated solvent as a reference for ^1H spectra and the ^{13}C resonance of the solvent as a reference for ^{13}C spectra. Chemical shifts were also independently referenced to tetramethylsilane (*ca*

1%) added by volume. All chemical shifts are reported positive to high frequency of the standard.

Controlled thermal analysis of the complexes was investigated using a Polymer Laboratories 1500H simultaneous thermal analyser, controlled by an Omni Pro 486DX-33 PC connected to a Rioch 1200 Laser printer. The weight of the samples investigated was between 10 and 25 mg. The measurements were performed in alumina crucibles under an atmosphere of flowing dry nitrogen gas (25 cm^3 min^{-1}), using heating rates of 5°C min^{-1}.

Starting materials

Strontium and barium metal (as either granules or chunks) were purchased from Alfa–Ventron Chemicals and stored in an inert atmosphere glove-box. 2,2,6,6-Tetramethyl-3,5-heptanedione, trifluoroacetylacetone and tetraglyme were both obtained from Inorgtech of Mildenhall, Suffolk, U.K. Nujol and hexachlorobutadiene were obtained from Aldrich and dried over 4 A molecular sieves prior to use. The complexes $[Sr(OEt)_2(EtOH)_4]_\infty$ and $[Ba(OEt)_2(EtOH)_4]_\infty$ were prepared by literature routes.[11]

All of the complexes described here are air- and moisture-stable, but were routinely prepared under dry argon using thoroughly degassed and dry solvents.

CAUTION: Both strontium and barium metals and their respective solutions are toxic, with low LDA values, and must be handled with considerable care. For safest handling, fume cupboards with adequate ventilation rates are recommended.

Synthesis of $[Sr(thd)_2(tetraglyme)]$ (**1**)

$[Sr(OEt)_2(EtOH)_4]$ (2.72 g, 8.13 mmol) was weighed into a Schlenk tube and n-hexane (25 cm^3) added. To the resulting clear solution was added thd-H (3.46 cm^3, 16.25 mmol) and the reaction mixture left to stir for 5 min; tetraglyme (1.96 cm^3, 8.13 mmol) was then added and the reaction left for a further 10 min. The solvent and liberated ethanol were then removed *in vacuo* to yield a waxy solid, which was redissolved in hot n-hexane (20 cm^3) and stored at −25°C. Crystals were obtained over a period of 3 days. Yield 4.1 g, 66% based on strontium ethoxide; m.p. 56–60°C. Found: C, 56.6; H, 9.1. Calc. for $SrO_9C_{32}H_{60}$: C, 56.8; H, 9.2%. IR (Nujol, ν cm^{-1}): 1591(s), 1532(s), 1502(s) 1222(s), 1179(m), 1081(m), 1025(m), 952(s), 874(s), 855(m), 840(m), 788(m), 745(s), 729(s), 592(w), 469(w). IR (hexachlorobutadiene, ν cm^{-1}): 2969(s), 1505(s), 1452(s), 1425(s), 1356(s), 1272(m), 1224(s), 1104(s), 1068(m), 1012(m), 748(m), 731(m), 591(w). ^1H NMR (270 MHz, C_6D_6, 20°C): δ 1.24 (36H, s, Me), 3.10 (6H, s, OCH_3), 3.21 (4H, m, OCH_2 b), 3.24 (4H, m, OCH_2 a), 3.36 (4H, s, OCH_2 c), 3.39 (4H, s, OCH_2 d), 5.70 (2H, s, CH). $^{13}C\{^1H\}$ NMR (67.94 MHz, C_6D_6, 20°C): δ 28.81 (s, Me), 40.67 (s, CMe_3), 58.82 (s, OMe), 69.92 (s, OCH_2 b), 69.97 (s, OCH_2 a), 70.13 (s, OCH_2 c), 71.64 (s, OCH_2 d), 86.90 (s, H), 196.53 (s, CO). Mass spectrometry (electron impact positive ion): 725 $[Sr_2(thd)_3]$, 677 [Sr(thd)(tetraglyme)], 454 $[Sr(thd)_2]$, 397 [Sr(thd)(Bu^{t}COCHCOH)], 271 [Sr(thd)].

Synthesis of $[Sr(tfa)_2(triglyme)]$ (**2**)

Reacting $[Sr(OEt)_2(EtOH)_4]$ (2.15 g, 6.40 mmol) in n-hexane (20 cm^3) with tfa-H (1.55 cm^3, 12.78 mmol) and triglyme (1.21 cm^3, 6.40 mmol), in the same way as for **1**, yielded a pale orange solid, which was redissolved in hot toluene (20 cm^3) and left to crystallize at −20°C. Yield 2.2 g, 63.9% based on strontium ethoxide; m.p. 73–75°C. Found: C, 37.9; H, 4.7. Calc. for $SrO_8C_{18}F_6H_{26}$: C, 37.8; H, 4.5%. IR (Nujol, ν cm^{-1}): 1638(m), 1512(s), 1268(s), 1208(m), 1130(s), 948(s), 873(s), 852(m), 841(m), 764(m), 722(s). IR (hexachlorobutadiene, ν cm^{-1}): 2925(s), 1508(s), 1467(s), 1356(s), 1282(m), 1021(m), 765(m), 722(m), 549(w). ^1H NMR (270 MHz, C_6D_6, 20°C): δ 1.82 (36H, s, Me), 3.05 (6H, s, OCH_3), 2.96 (4H, m, OCH_2 b), 3.12 (4H, m, OCH_2 a), 3.21 (4H, s, OCH_2 c), 5.76 (2H, s, CH). $^{13}C\{^1H\}$ NMR (67.94 MHz, C_6D_6 20°C): δ 28.89 (s, Me), 58.83 (s, OMe), 68.98 (s, OCH_2 b), 69.31 (s, OCH_2 a), 70.73 (s, OCH_2 c), 93.26 (s, CH), 122.17 (q, CF_3, $^1J = 297$ Hz), 169.15 (q, CO, $^2J = 29$ Hz), 195.06 (s, CO). Mass spectrometry (electron impact positive ion): 572 $[Sr(tfa)_2(triglyme)]$, 397 [Sr(tfa)(triglyme)], 241 [Sr(tfa)].

Synthesis of $[Sr(Ph_2acac)_2(tetraglyme)]\cdot 0.5C_7H_8$ (**3**)

The complex was prepared by reacting [Sr(OEt)$_2$(EtOH)$_4$] (2.51 g, 6745 mmol) in $CHCl_3$ (20 cm^3) with Ph_2acac-H (3.34 cm^3, 14.92 mmol) and tetraglyme (1.64 cm^3, 7.46 mmol), in the same manner as for **1**. The yield is quantitative and the crystals were isolated in the atmosphere. M.p. 96–98°C. Found: C, 63.8; H, 6.1. Calc. for $SrO_9C_{43.5}H_{48}$: C, 63.5; H, 5.8%. IR (Nujol, ν cm^{-1}): 1620(s), 1582(s), 1512(s), 1324(s), 1222(s), 1108(m), 935(s), 870(s), 733(s), 580(w), 513(w). IR (hexachlorobutadiene, ν cm^{-1}): 2918(s), 1471(m), 1299(s), 1224(s), 1114(s), 1026(m), 748(m), 731(m), 691(w), 579(w). ^1H NMR (270 MHz, C_6D_6, 20°C): δ 2.09 (s, CH_3), 3.23 (6H,

s, OCH_3), 3.41 (4H, m, OCH_2 b), 3.42 (4H, m, OCH_2 a), 3.48 (4H, s, OCH_2 c), 3.51 (4H, s, OCH_2 d), 6.57 (2H, s, CH), 7.40 (m, Ph). $^{13}C\{^1H\}$ NMR (67.94 MHz, C_6H_6, 20°C): 58.72 (s, OMe), 70.28 (s, OCH_2 b), 70.48 (s, OCH_2 a), 71.97 (s, OCH_2 c), 72.12 (s, OCH_2 d), 92.36 (s, CH), 128.87 (m, Ph), 182.53 (s, CO).

Synthesis of [Ba(thd)$_2$(tetraglyme)] (**4**)

Reaction of [Ba(OEt)$_2$(EtOH)$_4$] (2.65 g, 6.45 mmol) in n-hexane (20 cm^3), with thd-H (2.70 cm^3, 12.9 mmol) and tetraglyme (1.43 cm^3, 6.45 mmol) in the same way as for **1**, yielded a white solid, which was redissolved in hot n-hexane (20 cm^3) and left to crystallize at −20°C. Yield is quantitative and the crystals were isolated in the atmosphere. M.p. 90–92°C. Found: C, 52.4; H, 6.0. Calc. for $BaO_9C_{32}H_{60}$: C, 52.9; H, 8.3%. IR (Nujol ν, cm^{-1}): 2373(w), 1971(w), 1602(s), 1532(s), 1504(s), 1354(s), 1287(m), 1224(s), 1179(s), 1099(s), 1026(s), 953(s), 858(s), 788(m), 744(s), 731(s), 590(w), 532(w). IR (hexachlorobutadiene, ν cm^{-1}): 2947(s), 1971(w), 1532(s), 1503(s), 1430(s), 1386(s), 1268(m), 1224(s), 1103(s), 1024(m), 746(m), 731(m), 590(w). ^1H NMR (270 MHz, C_6D_6, 20°C): δ 1.35 (36H, s, Me), 3.07 (6H, s, OCH_3), 3.26 (4H, m, OCH_2 b), 3.33 (4H, m, OCH_2 a), 3.36 (4H, s, OCH_2 c), 3.39 (4H, s, OCH_2 d), 5.83 (2H, s, CH). $^{13}C\{^1H\}$ NMR (67.94 MHz, C_6D_6, 20°C): δ 29.43 (s, Me), 41.16 (s, CMe_3), 59.04 (s, OMe), 69.89 (s, OCH_2 b), 69.32 (s, OCH_2 a), 70.08 (s, OCH_2 c), 70.87 (s, OCH_2 d), 87.11 (s, CH), 196.42 (s, CO). Mass spectrometry (electron impact positive ion): 629 [Ba(thd)(Bu^{t}COCHCOH)(tetraglyme)], 541 [Ba(thd)(tetraglyme)], 505 [Ba(thd)$_2$], 321 [Ba(thd)].

X-ray determinations of **3** *and* **4**

As the precise nature of the complexes could not be fully elucidated by spectroscopic investigations, X-ray single-crystal structural studies were undertaken for complexes **3** and **4** to unambiguously characterize these species and also to determine the disposition and coordination modes of the ligands.

The unit cell and intensity data were obtained at 150 K using a Delft-Instruments FAST TV area detector diffractometer and graphite monochromated Mo-K_α radiation at $\lambda = 0.71069$ Å, following previously described procedures.[16] The data were corrected for Lorentz and polarization effects and also for absorption.[17] The crystal data and details of data collection and structure refinement are presented in Table 1. The structures were solved via direct (compound **3**) and Patterson methods (compound **4**) and refined by full-matrix least-squares using the SHELX program system.[18] The non-hydrogen atoms were refined anisotropically.

For **3** the methyl hydrogens on the tetraglyme were located from the difference map and included in the calculation of F_c; the methylene hydrogens on the tetraglyme and those on the Ph_2acac groups were allowed to ride on their parents in calculated positions (C—H = 0.96 Å); a common U_{iso} was refined for all hydrogens; the hydrogens on the disordered toluene were ignored.

For **4** the CH and CH_2 hydrogens were included in the idealized positions with a common U_{iso} value, but the methyl hydrogens were ignored. The methyl carbon atoms of one tert-butyl group were refined in two orientationally disordered tetrahedra with occupancies of 0.6 and 0.4.

Selected bond lengths, angles and other geometry parameters for **3** and **4** are given in Tables 1, 2, 3 and 4, respectively. Atomic coordinates, displacement factor coefficients, full lists of bond lengths and angles and F_o/F_c values have been deposited as supplementary data with the Editor, from whom copies are available on request. Atomic coordinates have also been deposited with the Cambridge Crystallographic Data centre.

RESULTS

Synthesis

The reaction of the pre-formed metal ethoxides[10] $[M(OEt)_2(EtOH)_4]_\infty$ of the heavier alkaline earth metals, Sr and Ba, with tetramethylheptane-2,4-dione in hexane has been previously shown by us to yield the homoleptic aggregates, $[M(thd)_2]_\infty$, as shown in eq. (1).[11]

$$[M(OEt)_2(EtOH)_4]_\infty + 2\beta\text{-diket-H} \longrightarrow [M(\beta\text{-diket})_2]_\infty + 6EtOH \quad (1)$$

(M = Ca, Sr or Ba; β-diket = acac, Ph_2acac, tfa, hfa and thd).

These materials are highly sensitive to moisture, heat and the presence of external Lewis bases (e.g. H_2O or NH_3); given these shortcomings, we have sought to eliminate these handling problems.[19] We have investigated the reaction of the homoleptic group IIA β-diketonates with chelating O-donor Lewis base ligands, relying on the chelate effect to achieve our objective.

The *in situ* reaction of the "pre-formed" A.E. metal β-diketonates with O-donor glyme ligands (defined as L-L) has been found to yield monomeric air-stable products in *ca* 10 min at ambient temperature, as shown in eq. (2). These ligands are

Table 1. Crystallographic data for complexes **3** and **4**

	3	**4**
Formula	$C_{43.5}H_{48}SrO_9$	$C_{32}H_{60}BaO_9$
Molecular weight	802.474	726.15
Colour; habit	Clear blocks	Clear blocks
Crystal size (mm)	0.50 × 0.30 × 0.20	0.30 × 0.18 × 0.15
Crystal system	Monoclinic	Triclinic
a (Å)	12.950(2)	10.596(5)
b (Å)	27.008(4)	14.420(2)
c (Å)	12.373(7)	15.455(2)
α (°)	90	115.38(1)
β (°)	112.55(3)	97.82(1)
γ (°)	90	105.13(2)
V (Å^3)	3996.64	1974.59
Temperature (K)	150	298
Space group	$P2_1/c$	P-1
Z	4	2
D_{calc} (g cm^{-3})	1.334	1.221
λ(Mo-K_α) (Å)	0.71069	0.71069
μ(Mo-K_α) (cm^{-1})	13.6	10.4
F(000)	1676	760
θ range (°)	1.9–24.8	2.1–28.7
Total data measured	12,086	12,534
Absorption correction factors: min, max	0.945, 1.085	0.781, 1.277
No. of unique data	5877	5667
R_{int}	0.049	0.037
Observed data with $F > 3\sigma(F)$	4118	4105
No. of parameters	506	407
Final $\Delta\rho$ (e A^{-3})	0.49	0.61
Final Δ/σ	0.15	0.045
$R = \Sigma(\Delta F)/\Sigma(F_o)$	0.0378	0.0418
R_w	0.0477[a]	0.0493[a]

[a] $Rw = [\Sigma\{w(\Delta F)^2\}/\Sigma_w(F_o)^2\}]^{0.5}$ (w = 1).

exceptionally versatile, being non-toxic, cheap and easy to handle.

$$[M(\beta\text{-diketonate})_2]_\infty + \text{L-L} \longrightarrow [M(\beta\text{-diketonate})_2)\text{L-L})] \quad (2)$$

A wide variety of complexes may be made by this route and we have selected several examples to illustrate this strategy. The reaction of $[Sr(OEt)_2(EtOH)_4]_\infty$ with a range of β-diketonates in the presence of a glyme ligand yields $[Sr(thd)_2$(tetraglyme)] (**1**); with $[Sr(tfa)_2]_\infty$ this yields $[Sr(tfa)_2$(triglyme)] (**2**) and also $[Sr(Ph_2acac)_2$(tetraglyme)] (**3**). The related complex $[Ba(OEt)_2(EtOH)_4]_\infty$ reacts with thd-H and tetraglyme to yield the species $[Ba(thd)_2$(tetraglyme)] (**4**). All of the complexes are obtained as crystalline solids in greater than 65% yield on crystallization as air- and moisture-stable materials.

This synthetic strategy may be contrasted with other routes to alkaline earth metal β-diketonates. Purdy *et al.* have used the bulk metal as the starting source of the A.E. metal β-diketonates with the ligand suspended in thf and the reaction mixture refluxed for a period of several days, which results in poor to low yields of products being obtained.[20] Other researchers have recently used the well-known metal hydroxide route, e.g. $[Ba(OH)_2 \cdot 8(H_2O)]$ and thd-H, to yield the pentameric hydrated cluster $Ba_5(OH)(thd)_9(H_2O)_3$[13] and also separately with hfa-H the oligomeric complex $[Ba(hfa)_2(H_2O)]_\infty$ is obtained.[12] Since both of these barium complexes contain coordinated water, they consequently have poor mass transport properties and volatility. Finally, recent reports have mentioned the use of $BaCO_3$ as a barium source and its reaction with the highly acidic ligand hfa-H in EtOH to yield hydrated metal β-diketonates stabilized by crown ethers.[21] Commercial sources of these materials (e.g. Strem Chemicals) have

Table 2. Bond lengths (Å) for $[Sr(Ph_2acac)_2(tetraglyme)]\cdot 0.5(toluene)$

O(1)—Sr	2.563(6)	O(2)—Sr	2.500(6)
O(3)—Sr	2.534(6)	O(4)—Sr	2.564(6)
O(5)—Sr	2.708(6)	O(6)—Sr	2.770(6)
O(7)—Sr	2.755(6)	O(8)—Sr	2.718(6)
O(9)—Sr	2.791(7)	C(7)—O(1)	1.258(6)
C(9)—O(2)	1.261(6)	C(22)—O(3)	1.263(6)
C(24)—O(4)	1.270(7)	C(31)—O(5)	1.443(8)
C(32)—O(5)	1.423(7)	C(33)—O(6)	1.423(8)
C(34)—O(6)	1.443(7)	C(35)—O(7)	1.406(8)
C(36)—O(7)	1.455(8)	C(37)—O(8)	1.444(8)
C(38)—O(8)	1.433(8)	C(39)—O(9)	1.430(8)
C(40)—O(9)	1.424(8)	C(2)—C(1)	1.396(8)
C(6)—C(1)	1.388(8)	C(7)—C(1)	1.536(8)
C(3)—C(2)	1.395(8)	C(4)—C(3)	1.386(9)
C(5)—C(4)	1.376(9)	C(6)—C(5)	1.407(8)
C(8)—C(7)	1.408(7)	C(9)—C(8)	1.409(7)
C(10)—C(9)	1.526(8)	C(11)—C(10)	1.404(8)
C(15)—C(10)	1.401(8)	C(12)—C(11)	1.383(8)
C(13)—C(12)	1.394(9)	C(14)—C(13)	1.377(9)
C(15)—C(14)	1.404(8)	C(17)—C(16)	1.374(8)
C(21)—C(16)	1.408(8)	C(22)—C(16)	1.519(8)
C(18)—C(17)	1.403(8)	C(19)—C(18)	1.376(9)
C(20)—C(19)	1.368(9)	C(21)—C(20)	1.398(8)
C(23)—C(22)	1.415(8)	C(24)—C(23)	1.403(8)
C(25)—C(24)	1.514(9)	C(26)—C(25)	1.407(8)
C(30)—C(25)	1.396(8)	C(27)—C(26)	1.385(9)
C(28)—C(27)	1.394(10)	C(29)—C(28)	1.384(10)
C(30)—C(29)	1.388(9)	C(33)—C(32)	1.498(9)
C(35)—C(34)	1.502(11)	C(37)—C(36)	1.408(10)
C(39)—C(38)	1.466(9)		

also been shown to be hydrated materials, e.g. $[Ca(hfa)_2(H_2O)_2]_2$.[14]

When more stringent precautions are used the Lewis base solvated complexes $[Ba_2(thd)_4(L)_2]$ ($L = Et_2O$,[22] NH_3[23]) may be prepared. The materials reported here have an important advantage over the majority of the previous routes, that they yield *reproducible anhydrous products*, provided of course that anaerobic techniques are used. Most importantly reaction stoichiometry may be precisely controlled, which is not possible with the use of the commercial Group IIA metal hydrides, which are notoriously unreliable, since their metallation reactivity varies considerably from batch to batch.

If 2 equivalents or more of a glyme (e.g. triglyme or tetraglyme) are used in the preparations of complexes **1–4**, then generally an oily product results. This possibly implies that the complexes are highly soluble in an excess of the Lewis base, presumably forming more highly solvated species.

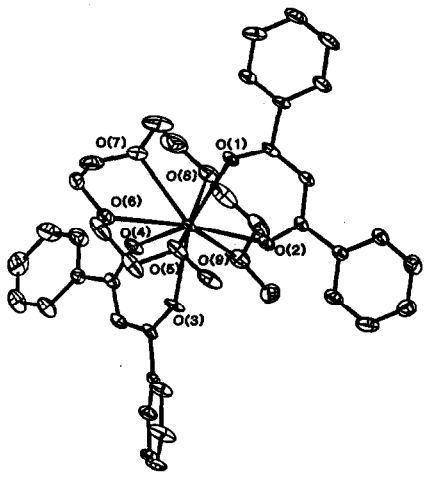

Fig. 1. Molecular structure of $[Sr(Ph_2acac)_2(tetraglyme)]$ (**3**) showing the atom numbering scheme. Hydrogen atoms have been omitted for clarity.

X-ray structures

The X-ray crystal structures of $[Sr(Ph_2acac)_2(tetraglyme)]\cdot 0.5(C_7H_8)$ (**3**) and $[Ba(thd)_2(tetraglyme)]$ (**4**) are shown in Figs 1 and 3, respectively. In both complexes the metal centres have a high coordination number, i.e. nine, although this is not excessive when compared with barium thiocyanate or β-diketonate complexes coordinated by crown or glyme ligands, e.g. $[Ba(hfa)_2(tetraglyme)]$.[24] In all of the above complexes the metals have very similar glyme ligand dispositions, with the O-donor ligand wrapped around the metal centre in a meridional plane and the two β-diketonates being positioned on either side of this plane.

The coordination geometry around the metal centres in complexes **3** and **4**, illustrated in Figs 2 and 4, is highly irregular and cannot be described in terms of any of the normal nine-coordinate polyhedra. However, it may be described as a distorted dodecahedron (eight-coordinate geometry)

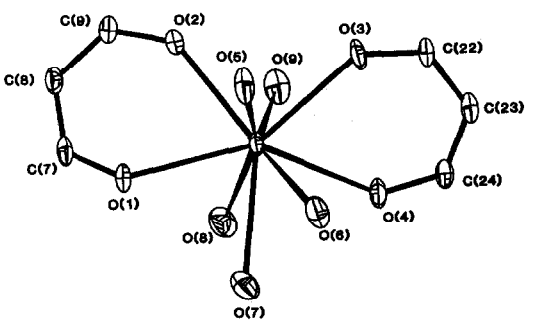

Fig. 2. The coordination polyhedron in $[Sr(Ph_2acac)_2(tetraglyme)]$ (**3**).

Table 3. Bond angles (°) for [Sr(Ph$_2$acac)$_2$(tetraglyme)] · 0.5(toluene) (**3**)

O(2)—Sr—O(1)	67.6(2)	O(3)—Sr—O(1)	150.6(1)
O(3)—Sr—O(2)	86.6(2)	O(4)—Sr—O(1)	139.8(1)
O(4)—Sr—O(2)	139.8(1)	O(4)—Sr—O(3)	69.4(2)
O(5)—Sr—O(1)	88.1(2)	O(5)—Sr—O(2)	76.8(2)
O(5)—Sr—O(3)	71.9(2)	O(5)—Sr—O(4)	121.8(2)
O(6)—Sr—O(1)	102.6(2)	O(6)—St—O(2)	136.8(1)
O(6)—Sr—O(3)	86.3(2)	O(6)—Sr—O(4)	75.2(2)
O(6)—Sr—O(5)	60.5(2)	O(7)—Sr—O(1)	70.3(2)
O(7)—Sr—O(2)	137.7(1)	O(7)—Sr—O(3)	135.2(1)
O(7)—Sr—O(4)	75.4(2)	O(7)—Sr—O(5)	106.3(2)
O(7)—Sr—O(6)	57.9(2)	O(8)—Sr—O(1)	71.6(2)
O(8)—Sr—O(2)	99.6(2)	O(8)—Sr—O(3)	129.0(2)
O(8)—Sr—O(4)	74.3(2)	O(8)—Sr—O(5)	158.9(1)
O(8)—Sr—O(6)	117.6(2)	O(8)—Sr—O(7)	62.3(2)
O(9)—Sr—O(1)	106.6(2)	O(9)—Sr—O(2)	69.1(2)
O(9)—Sr—O(3)	75.0(2)	O(9)—Sr—O(4)	73.6(2)
O(9)—Sr—O(5)	133.2(1)	O(9)—Sr—O(6)	147.7(1)
O(9)—Sr—O(7)	120.5(2)	O(9)—Sr—O(8)	61.0(2)
C(7)—O(1)—Sr	134.9(3)	C(9)—O(2)—Sr	139.2(3)
C(22)—O(3)—Sr	136.4(3)	C(24)—O(4)—Sr	136.2(3)
C(31)—O(5)—Sr	117.5(4)	C(32)—O(5)—Sr	112.2(4)
C(32)—O(5)—C(31)	110.9(5)	C(33)—O(6)—Sr	118.1(4)
C(34)—O(6)—Sr	120.3(4)	C(34)—O(6)—C(33)	112.6(5)
C(35)—O(7)—Sr	111.9(4)	C(36)—O(7)—Sr	111.1(4)
C(36)—O(7)—C(35)	119.5(6)	C(37)—O(8)—Sr	115.7(4)
C(38)—O(8)—Sr	116.1(4)	C(38)—O(8)—C(37)	109.0(6)
C(39)—O(9)—Sr	113.2(4)	C(40)—O(9)—Sr	119.6(4)
C(40)—O(9)—C(39)	111.9(5)	C(6)—C(1)—C(2)	119.5(5)
C(7)—C(1)—C(2)	117.8(5)	C(7)—C(1)—C(6)	122.7(5)
C(3)—C(2)—C(1)	120.0(6)	C(4)—C(3)—C(2)	120.4(6)
C(5)—C(4)—C(3)	119.7(6)	C(6)—C(5)—C(4)	120.5(6)
C(5)—C(6)—C(1)	119.8(6)	C(1)—C(7)—O(1)	116.5(5)
C(8)—C(7)—O(1)	126.4(5)	C(8)—C(7)—C(1)	117.0(5)
C(9)—C(8)—C(7)	123.3(5)	C(8)—C(9)—O(2)	125.0(5)
C(10)—C(9)—O(2)	115.9(5)	C(10)—C(9)—C(8)	119.0(5)
C(11)—C(10)—C(9)	123.9(5)	C(15)—C(10)—C(9)	117.8(5)
C(15)—C(10)—C(11)	118.2(5)	C(12)—C(11)—C(10)	121.6(6)
C(13)—C(12)—C(11)	119.2(6)	C(14)—C(13)—C(12)	120.6(6)
C(15)—C(14)—C(13)	120.1(6)	C(14)—C(15)—C(10)	120.2(6)
C(21)—C(16)—C(17)	118.5(5)	C(22)—C(16)—C(17)	119.6(5)
C(22)—C(16)—C(21)	121.9(5)	C(18)—C(17)—C(16)	120.7(6)
C(19)—C(18)—C(17)	120.0(6)	C(20)—C(19)—C(18)	120.5(6)
C(21)—C(20)—C(19)	119.8(6)	C(20)—C(21)—C(16)	120.5(6)
C(16)—C(22)—O(3)	116.5(5)	C(23)—C(22)—O(3)	126.2(5)
C(23)—C(22)—C(16)	117.2(5)	C(24)—C(23)—C(22)	126.4(5)
C(23)—C(24)—O(4)	124.9(5)	C(25)—C(24)—O(4)	116.5(5)
C(25)—C(24)—C(23)	118.6(5)	C(26)—C(25)—C(24)	123.4(6)
C(30)—C(25)—C(24)	118.8(5)	C(30)—C(25)—C(26)	117.8(6)
C(27)—C(26)—C(25)	120.8(6)	C(28)—C(27)—C(26)	120.3(6)
C(29)—C(28)—C(27)	119.5(6)	C(30)—C(29)—C(28)	120.1(7)
C(29)—C(30)—C(25)	121.4(6)	C(33)—C(32)—O(5)	108.9(5)
C(32)—C(33)—O(6)	108.8(5)	C(35)—C(34)—O(6)	109.0(6)
C(34)—C(35)—O(7)	105.9(6)	C(37)—C(36)—O(7)	114.4(7)
C(36)—C(37)—O(8)	108.6(7)	C(39)—C(38)—O(8)	109.1(6)
C(38)—C(39)—O(9)	108.9(6)		

Table 4. Bond lengths (Å) and angles (°) for $[Ba(C_{11}H_{19}O_2)_2(C_{10}H_{22}O_6)]$ (**4**)

O(1)—Ba	2.675(8)	O(2)—Ba	2.667(8)
O(3)—Ba	2.713(7)	O(4)—Ba	2.656(7)
O(5)—Ba	2.863(8)	O(6)—Ba	2.895(9)
O(7)—Ba	2.959(9)	O(8)—Ba	2.918(9)
O(9)—Ba	2.872(9)		

O(2)—Ba—O(1)	64.3(2)	O(3)—Ba—O(1)	139.8(1)
O(3)—Ba—O(2)	153.7(1)	O(4)—Ba—O(1)	141.9(2)
O(4)—Ba—O(2)	89.9(2)	O(4)—Ba—O(3)	64.3(2)
O(5)—Ba—O(1)	116.4(3)	O(5)—Ba—O(2)	70.3(3)
O(5)—Ba—O(3)	97.5(3)	O(5)—Ba—O(4)	75.7(3)
O(6)—Ba—O(1)	83.8(3)	O(6)—Ba—O(2)	93.4(3)
O(6)—Ba—O(3)	99.0(3)	O(6)—Ba—O(4)	127.5(3)
O(6)—Ba—O(5)	56.8(3)	O(7)—Ba—O(1)	72.3(3)
O(7)—Ba—O(2)	129.6(3)	O(7)—Ba—O(3)	76.1(3)
O(7)—Ba—O(4)	140.4(2)	O(7)—Ba—O(5)	110.6(3)
O(7)—Ba—O(6)	56.5(3)	O(8)—Ba—O(1)	73.4(3)
O(8)—Ba—O(2)	127.0(3)	O(8)—Ba—O(3)	68.6(3)
O(8)—Ba—O(4)	106.3(3)	O(8)—Ba—O(5)	162.1(2)
O(8)—Ba—O(6)	112.7(3)	O(8)—Ba—O(7)	56.3(3)
O(9)—Ba—O(1)	76.4(3)	O(9)—Ba—O(2)	81.2(3)
O(9)—Ba—O(3)	94.0(3)	O(9)—Ba—O(4)	72.1(3)
O(9)—Ba—O(5)	136.6(2)	O(9)—Ba—O(6)	159.9(2)
O(9)—Ba—O(7)	112.8(3)	O(9)—Ba—O(8)	58.3(3)
C(1)—O(1)—Ba	139.0(4)	C(3)—O(2)—Ba	139.7(4)
C(6)—O(3)—Ba	133.8(4)	C(8)—O(4)—Ba	134.5(4)
C(11)—O(5)—Ba	120.8(6)	C(12)—O(5)—Ba	116.9(6)
C(13)—O(6)—Ba	117.9(7)	C(14)—O(6)—Ba	118.5(7)
C(15)—O(7)—Ba	116.0(8)	C(16)—O(7)—Ba	116.8(8)
C(17)—O(8)—Ba	119.2(8)	C(18)—O(8)—Ba	115.3(7)
C(19)—O(9)—Ba	115.9(8)	C(20)—O(9)—Ba	119.8(7)

C(1)—O(1)	1.225(9)	C(3)—O(2)	1.229(8)
C(6)—O(3)	1.244(8)	C(8)—O(4)	1.243(8)
C(2)—C(1)	1.404(10)	C(4)—C(1)	1.548(12)
C(3)—C(2)	1.390(10)	C(5)—C(3)	1.546(11)
C(41)—C(4)	1.437(14)	C(42)—C(4)	1.477(14)
C(43)—C(4)	1.440(16)	C(51)—C(5)	1.528(14)
C(52)—C(5)	1.472(13)	C(53)—C(5)	1.527(14)
C(7)—C(6)	1.409(10)	C(9)—C(6)	1.548(10)
C(8)—C(7)	1.407(9)	C(10)—C(8)	1.559(11)
C(91)—C(9)	1.505(12)	C(92)—C(9)	1.509(12)
C(93)—C(9)	1.546(13)	C(101)—C(10)	1.533(17)
C(102)—C(10)	1.537(20)	C(103)—C(10)	1.547(20)
C(104)—C(10)	1.562(21)	C(105)—C(10)	1.504(20)
C(106)—C(10)	1.568(25)	C(11)—O(5)	1.420(10)
C(12)—O(5)	1.380(10)	C(13)—O(6)	1.340(13)
C(14)—O(6)	1.408(12)	C(15)—O(7)	1.274(14)
C(16)—O(7)	1.350(13)	C(17)—O(8)	1.332(12)
C(18)—O(8)	1.354(13)	C(19)—O(9)	1.377(13)
C(20)—O(9)	1.392(12)	C(13)—C(12)	1.357(15)
C(15)—C(14)	1.305(16)	C(17)—C(16)	1.299(17)
C(19)—C(18)	1.306(16)		

C(2)—C(1)—O(1)	126.0(8)	C(4)—C(1)—O(1)	116.4(7)
C(4)—C(1)—C(2)	117.6(8)	C(3)—C(2)—C(1)	125.3(8)
C(2)—C(3)—O(2)	125.6(7)	C(5)—C(3)—O(2)	114.5(7)
C(5)—C(3)—C(2)	119.9(7)	C(41)—C(4)—C(1)	116.4(8)
C(42)—C(4)—C(1)	110.2(8)	C(42)—C(4)—C(41)	108.2(12)
C(43)—C(4)—C(1)	107.3(10)	C(43)—C(4)—C(41)	110.2(11)

Table 4—*continued*

C(43)—C(4)—C(42)	103.9(11)	C(51)—C(5)—C(3)	109.2(8)
C(52)—C(5)—C(3)	108.3(8)	C(52)—C(5)—C(51)	109.1(10)
C(53)—C(5)—C(3)	113.9(8)	C(53)—C(5)—C(51)	105.6(9)
C(53)—C(5)—C(52)	110.6(11)	C(7)—C(6)—O(3)	125.5(7)
C(9)—C(6)—O(3)	116.7(7)	C(9)—C(6)—C(7)	117.8(7)
C(8)—C(7)—C(6)	125.5(7)	C(7)—C(8)—O(4)	125.2(7)
C(10)—C(8)—O(4)	116.1(7)	C(10)—C(8)—C(7)	118.7(7)
C(91)—C(9)—C(6)	113.6(7)	C(92)—C(9)—C(6)	110.2(7)
C(92)—C(9)—C(91)	109.5(9)	C(93)—C(9)—C(6)	105.2(7)
C(93)—C(9)—C(91)	109.4(8)	C(93)—C(9)—C(92)	108.9(9)
C(101)—C(10)—C(8)	108.4(9)	C(102)—C(10)—C(8)	111.1(9)
C(102)—C(10)—C(101)	110.7(12)	C(103)—C(10)—C(8)	104.9(9)
C(103)—C(10)—C(101)	107.1(13)	C(103)—C(10)—C(102)	114.3(12)
C(104)—C(10)—C(8)	106.2(10)	C(105)—C(10)—C(8)	116.1(10)
C(105)—C(10)—C(104)	114.1(15)	C(106)—C(10)—C(8)	107.9(11)
C(106)—C(10)—C(104)	96.9(14)	C(106)—C(10)—C(105)	113.9(15)
C(12)—O(5)—C(11)	115.4(8)	C(14)—O(6)—C(13)	123.4(9)
C(16)—O(7)—C(15)	126.2(10)	C(18)—O(8)—C(17)	124.5(10)
C(20)—O(9)—C(19)	113.3(11)	C(13)—C(12)—O(5)	117.1(9)
C(12)—C(13)—O(6)	122.1(11)	C(15)—C(14)—O(6)	118.6(11)
C(14)—C(15)—O(7)	127.7(13)	C(17)—C(16)—O(7)	122.6(12)
C(16)—C(17)—O(8)	122.8(11)	C(19)—C(18)—O(8)	124.5(11)
C(18)—C(19)—O(9)	121.6(12)		

with an additional atom [O(7)] intruding on the O(6)···O(8) edge.

The metal–oxygen bonds in both structures fall into two discrete categories. In **3** the Sr—$O_{(thd)}$ bonds range from 2.500(6) to 2.540(6) Å, average 2.540(6) Å, and the Sr—$O_{(glyme)}$ distances vary from 2.708(6) to 2.791(7) Å, average 2.748(5) Å. Similarly, in **4** the Ba—$O_{(thd)}$ values range from 2.656(7) to 2.713(7) Å, with an average of 2.678(7) Å, and the Ba—$O_{(glyme)}$ distances range from 2.863(8) to 2.959(9) Å, with an average of 2.901(9) Å. The fact that the M—O bonds in **4** are *ca* 0.20 Å longer than the corresponding values in **3** is consistent with the atomic radius difference of barium and strontium. The Ba—O distances in **4** are also comparable with the corresponding values in $[Ba(hfa)_2(tetraglyme)]$,[24] $[Ba(hfa)_2(18\text{-crown-6})]$[25] and the dimeric complexes $[Ba(thd)_2(L)_2]_2$ (where L = Et_2O[22] and NH_3[23]). It may be noted in this context that variations in the M—O distances involving the β-diketonate and tetraglyme ligands appear to be a common phenomenon in alkaline earth metal complexes.

An interesting observation may be made about the influence of the β-diketonate substituents (e.g. CMe_3 or CF_3) on the relative strengths of the Ba—O bonds. For example, in $[Ba(hfa)_2(tetraglyme)]$[24] the Ba—O(β-diketonate) and Ba—O(tetraglyme) distances are 2.683(2)–2.713(2) Å, average

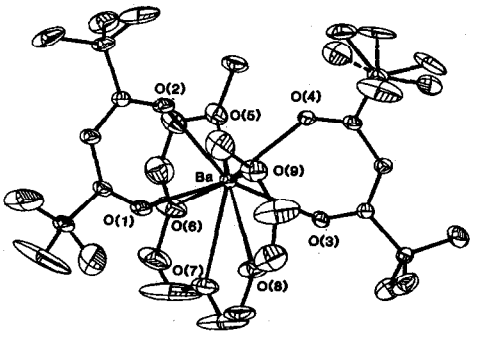

Fig. 3. Molecular structure of $[Ba(thd)_2(tetraglyme)]$ (**4**) showing the atom numbering scheme. Hydrogen atoms have been omitted for clarity. The t-butyl group [C(10)] is orientationally disordered between two tetrahedra, one indicated by solid lines (occupancy 0.6) and the other by dashed lines (occupancy 0.4).

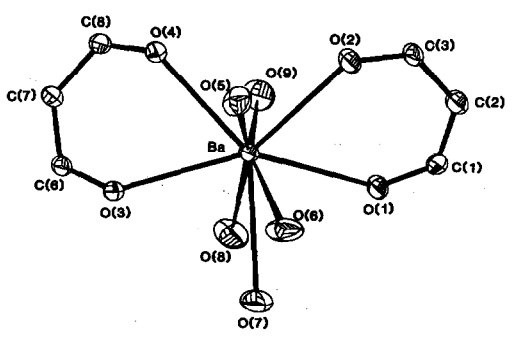

Fig. 4. The coordination polyhedron in $[Ba(thd)_2(tetraglyme)]$ (**4**).

2.703(2), and 2.809(2)–2.893(1), with an average of 2.857(2) Å, respectively. These values are respectively longer and shorter than the corresponding values in **4**. Although the differences are small (0.02–0.04 Å), the values seem to be real and may be correlated with the relative weakening of the Ba—$O_{(\beta\text{-diketonate})}$ bonds in the hfa derivatives due to the strong electron-withdrawing nature of the CF_3 substituents vs the strong electron-releasing nature of CMe_3 groups in **4** and the consequent relative strengthening of the Ba—$O_{(tetraglyme)}$ bonds in this compound.

The O—M—O chelate angles for the thd ligands of **4** are both 64.3(2) and those in the tetraglyme ligand fall within the narrow range 56.3(3)–58.3(3)°. These values are comparable with the corresponding values 63.9(2)°, 64.1(2)° and 56.8(2)–59.8(2)° in $[Ba(hfa)_2(tetraglyme)]$,[24] and seem to be mostly determined by the ligand geometry. The respective angles in the strontium complex (**3**) are similar and have values 76.6(2)°, 69.4(2)° and 57.9(2)–62.3(2)°.

The polyether ligands in these complexes bind to the metals via the chelate effect, to give a five pronged coordination mode. In both complexes the β-diketonates bind symmetrically to the metals; the metal centres lie very close to one OCCCO plane, while the other β-diketonate shows considerable fold about the O···O axis [12.0(2)° in **3** and 22.9(2)° in **4**]. These are probably caused by the steric requirements of the ligands around the metal centres. In **3** the phenyl rings are twisted relative to the OCCCO planes by 14.7(2)° and 31.2(2)° in one ligand and 14.1(2)° and 35.0(2)° in the other ligand. The polyether ligand adopts a conventional geometry with *gauche* and *anti* relationships around the C—C and C—O bonds, respectively.

Spectroscopic results

The formulation of these complexes as monomeric species is entirely consistent with the data acquired from IR, ^1H and ^{13}C NMR spectrocopy, mass spectrometer and microanalysis.

IR spectroscopic data

The IR spectra of complexes **1**–**4** show characteristic bands for the β-diketonates, with strong absorption bands in the region 1570–1635 cm^{-1} for C=O [in the parent thd-H ligand 1605 cm^{-1} C=O and 1500–1540 C=C]. These results may be contrasted with the IR spectra of the base-free complexes $[M(\beta\text{-diket})_2]_\infty$, where several bands are observed in the IR spectra, which is due to the differing coordination modes in their structures. Precise assignments of the different C=C and C=O modes is at present not possible since the bands are coupled.

The bands assigned as ν(C—O—C) in complexes **1**–**4** for the glyme ligands occur at slightly lower frequencies than the same peaks for the free ligands (either triglyme or tetraglyme), 1350–1360, 1270, 1220 and also at 1110±20 cm^{-1}. The shifts from the free ligand are *ca* 20 cm^{-1}, which is indicative of coordinated glyme ligands with relatively weak M—O ineractions.

NMR spectroscopic data

The most important features of both the ^1H and ^{13}C NMR spectra for complexes **1**–**4** are recorded in the Experimental. These spectroscopic data are in excellent accord with the reactions and structures described herein. There is no evidence of ethanol present in any of these complexes, from the starting complexes $[M(OEt)_2(EtOH)_4]_\infty$. The ^1H NMR spectra of all four complexes in d_6-benzene (see Experimental) show only a characteristic signal for one type of β-diketonate and glyme ligand environment at room temperature, which is also in accord with the solid state structures of complexes **3** and **4**. The integration ratio of β-diketonate to glyme ligand was observed to be 2 : 1. A shift downfield of the methylene signals in the glyme ligands is observed on coordination to the alkaline earth metal cations Ca, Sr and Ba. This effect has also been previously noted by other researchers using multidentate ligands.[15]

The ^{13}C NMR spectra have been assigned by direct comparison with both free ligands and the parent homoleptic complexes, $[M(\beta\text{-diketonate})_2]_\infty$. Signals due to the thd ligands in complexes **1** and **4** are observed at δ 28.8 (Me group), δ 40.6 (CMe_3 group) and a further singlet at δ 87.2±0.1 for the CH group. While the signals for the methyl and quarternary carbon have been shifted to lower field, those for the CH and CO are shifted to higher field with respect to the parent ligand thd-H. This effect has been observed previously and was ascribed to the formation of an electron-rich 1,3-diketonato chelating ring system. The electron density accumulates on the carbon atoms of the ring system (i.e. CH and CO), and this therefore results in electron withdrawal from the Bu^t groups and a resulting deshielding occurs.

The fluorinated β-diketonate complex $[Sr(tfa)_2$ (triglyme)] (**2**) shows additional features due to the CF_3 group, with both ^1J and ^2J coupling constants observed in the ^{13}C NMR spectrum of this

complex. The diphenylacac complex [Sr(Ph$_2$acac)$_2$(tetraglyme)] (**3**) has ^{1}H and ^{13}C NMR spectra in accord with its solid state structures.

Mass spectrometry

Mass spectroscopic data for complex **1** show not only the expected monomeric species. e.g. [Sr(thd)(tetraglyme)]$^+$ with *m/z* 677, but also *more intense peaks* due to [Sr$_2$(thd)$_3$] at 725. For this complex other intense peaks are observed at *m/z* 397 for [Sr(thd)(Bu^{t}COCHCO)]$^+$ and at *m/z* 271 for [Sr(thd)]$^+$. The related barium complex (**4**) also has a weak molecular ion, at *m/z* 629 for [Ba(thd)(Bu^{t}COCHCOH)(triglyme)]$^+$, and in a similar fashion to that of **1** shows more intense peaks due to oligomeric complexes, e.g. [Ba(thd)$_2$]$^+$ and [Ba(thd)]$^+$ with *m/z* 505 and 321, respectively. Cleavage of the thd ligand is also observed, with a peak at *m/z* of 127 corresponding to the fragment [Bu^{t}COCHCOH]$^+$.

Complex **2** reveals rather different behaviour to that of **1** and **2**, with a clear molecular ion being observed at 572 a.m.u. for [Sr(tfa)$_2$(triglyme)]$^+$, and then sequential loss of a tfa ligand to yield [Sr(tfa)(triglyme)]$^+$ at 397 a.m.u. and the lower clearly discernable molecular ion observed at 241 a.m.u. for [Sr(tfa)]$^+$. In contrast, complex **3** was not sufficiently volatile for a mass spectrum to be obtained.

The isotope patterns of the metal containing complexes are consistent with those which may be obtained from natural abundance patterns or by computer simulation. The *m/z* ratios which are given relate to the isotopes of greatest natural abundance, e.g. ^{88}Sr and ^{138}Ba.

These data imply that in the vapour state the two thd complexes readily dissociate to form the oligomeric donor-Lewis base free complexes, [M(thd)$_2$]$_\infty$. Such behaviour is important because as O-donor adducts we can now deliver these materials into the gas phase at *ca* 100°C lower than has previously been observed. While the corresponding strontium trifluoroacetylacetonate is far more stable in the vapour phase, the monomeric Lewis base-adducted complex evidently persists.

Physical properties

All of these complexes have extensive solubility in both aliphatic (except for **2** and **3**) and aromatic solvents and show appreciable solubility in coordinating solvents such as ethers (i.e. diethyl ether and thf) and DMSO. This pronounced solubility is undoubtedly due to the presence of both glyme and β-diketonate ligands chelating to the metal centre. These materials are all air- or moisture-stable and water coordination to these materials seems unlikely to occur.

The glyme stabilized complexes all have relatively low melting points (see Experimental) in the range 56–98°C at atmospheric pressure. This is a significant reduction in melting point when compared with their parent materials (e.g. [Sr(thd)$_2$]$_\infty$ 172–175, [Sr(tfa)$_2$]$_\infty$ dec. > 150 and [Ba(thd)$_2$]$_\infty$ 194–197°C). Sublimation studies are in accord with these results and also with our mass spectroscopic data; thus, complexes **1** and **3** decompose at *ca* 100°C and 10^{-3} torr to yield the unadducted thd complexes, while the strontium tfa complex (**2**) is stable and sublimes at 140–160°C and 10^{-3} torr. This difference in stability between thd and tfa complexes may possibly be ascribed to both steric and electronic effects due to the R-groups (i.e. Bu^t vs Me vs F$_3$C); thus, in the gas phase the binding of tetraglyme to the metal centre is considerably weakened when a thd ligand chelates. This is an important observation since we may thus use the adducted thd complexes of strontium and barium as low temperature sources of the parent thd complexes.

DSC/TGA data

Thermal gravimetric analysis has found extensive usage in both molecular and non-molecular chemistry, materials science and electronic engineering. This technique gives valuable information where a study of weight loss vs temperature may yield valuable information on thermal behaviour of materials over a wide temperature range. Differential scanning calorimetry allows the study of the entropy changes occurring during a controlled thermolysis and most importantly, whether a reaction is occurring (i.e. a phase change or melting point) or a chemical change (e.g. an irreversible decomposition). In our apparatus these two techniques are performed simultaneously.

Two complexes were selected as potentially suitable materials, these were [Sr(thd)$_2$(tetraglyme)] (**1**) and [Ba(thd)$_2$(tetraglyme)] (**4**).

The differential scanning calorimetry curve for complex **1** reveals a sharp reversible melting point endotherm at 75.38°C (−8.08 mcal mg^{-1}) and two other isotherms, the first at 215.48°C (−17.55 mcal mg^{-1}) and the second at 370.89°C (−6.85 mcal mg^{-1}). The first of these two isotherms is presumably due to loss of the glyme (see TGA discussion following) and the second is attributed to the end point of sublimation of the homoleptic [Sr(thd)$_2$]$_n$ material. The thermal gravimetric analysis curve of complex **1** has two steps (see Fig. 5), the

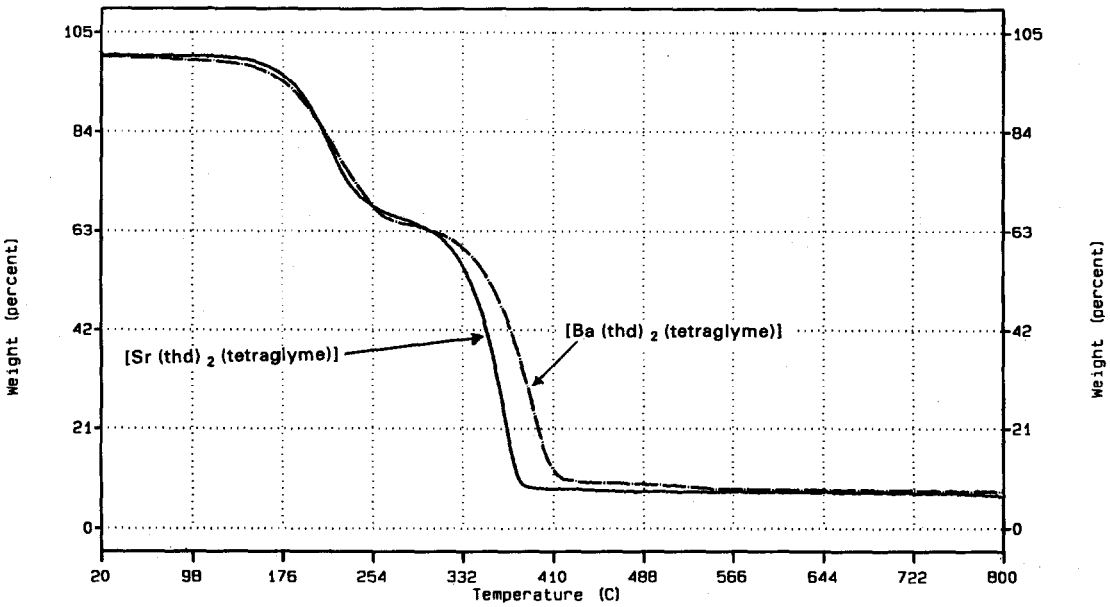

Fig. 5. Thermal gravimetric analysis of complexes **1** and **4**.

first starts at *ca* 150°C and is essentially complete by 260°C and represents the loss of the tetraglyme ligand (found 32.72%, expected 32.84%). This leaves the $[Sr(thd)_2]_n$ complex intact which sublimes intact between 250 and 382°C. A small amount of carbanceous solid remains (5.58%), which is probably due to some thermal decomposition of the thd ligand.

The barium complex (**4**) shows related behaviour in its DSC, with a sharp melting point at 103.8°C (-10.43 mcal mg^{-1}) and two further isotherms. The first of these is at 223.0°C (-20.12 mcal mg^{-1}) with the second at 396.6°C (-10.02 mcal mg^{-1}). The first of these two isotherms is attributed to the loss of the glyme and consequent structural change (see TGA discussion following), and the second at the end point of sublimation to the homoleptic $[Ba(thd)_2]_n$ compound. The TGA of complex **4** (see Fig. 5) is similar to that of **1** having two clearly defined steps (see Fig. 5), the first starts at *ca* 170°C and is essentially complete by 255°C and represents the loss of the tetraglyme ligand and also sublimation of the homoleptic compound $[Ba(thd)_2]_n$] (found 35.33%, expected 30.61%). This leaves $[Ba(thd)_2]_n$ remaining, which sublimes intact over the temperature range, *ca.* 250 to 410.7°C. A small amount of carbanaceous solid also remains (*ca* 6%).

The TGA data for these two complexes clearly reveal that these compounds do not sublime intact, which is in accord with our sublimation data. Yet they are important materials, since they are air- and moisture-stable precursors which will deliver the homoleptic thd complexes into the gas phase easily. Such materials are of importance if they can be obtained as liquids at or just above room temperature, and may then find application in bubblers for CVD work.

DISCUSSION

There have been considerable difficulties with the preparation of group IIA metal alkoxides and β-diketonates due to the continued unexpected appearance of either water, oxo or hydroxo ligands incorporated into the final products. Using a general synthetic strategy for complex **1**, we can switch not only β-diketonates, i.e. tfa to thd, but also donor chelating ligands, from triglyme to tetraglyme. We have thus explored the potential of using either strontium or barium β-diketonates as *in situ* prepared starting materials.[14] Such complexes have several pertinent properties; namely that they are readily obtainable as crystalline solids of known stoichiometry, soluble in hydrocarbons (both aliphatic or aromatic), stable in an inert atmosphere and are sufficiently reactive that most reactions occur at or slightly above room temperature.

The X-ray structural characterization of metal β-diketonates stabilized by a tetraglyme ligand has demonstrated that tailored synthetic strategies can and do work for the heavier metals of group IIA. It is our belief that this strategy has wide scope in developing the chemistry of the metallorganic complexes of this group, which have until recently

focused principally on the cyclopentadienyls and pentamethylcyclopentadienyls.[4]

There are several synthetic features that are important here: (i) this synthetic strategy of using a metal β-diketonate prepared *in situ* from a crystalline metal ethoxide is the first example for group IIA complexes and this leads to *anhydrous* complexes. (ii) The coordinative saturation of the hard acid metal centre by the multidentate Lewis base chelate and β-diketonate leads to *air- and moisture-stable* precursors of known stoichiometry and is thus highly flexible, since L-L may be varied. (iii) The designed synthesis of volatile discrete molecular alkaline earth metal organics is now possible without having to use large sterically hindered ligands, e.g. Ph_3CO^-, $OC_6H_2Bu^t_3$.

The use of such ligands will reduce the conventional problems of oligomerization and subsequent low volatility. We consider that an important requirement when designing A.E. molecule precursors is that sufficient coordinative saturation be incorporated into both ligand and Lewis base chelate, such that a low molecular mass volatile monomer will result. This approach of using a tailored synthetic rational for group IIA molecular precursors is currently being used for control of thin films by CVD, due to their high stability.

CONCLUSIONS

We postulate that for heavier alkaline earth complexes supported by O-chelates a coordination number of 7 appears to be the minimum required for such coordination complexes to be air- and moisture-stable. Data are rapidly accumulating to support this conjecture and a wide range of glyme/amine complexes of metal β-diketonates have been prepared, e.g. with L-L = diglyme, triglyme, tetraglyme, pentamethyldiethylenetriamine, hexamethyltriethylenetetramine, etc.

Careful design of such precursors should reap great benefit to not only the metal oxygen based chemistry, but one can envisage the use of these complexes as a template for further reactivity with either lithium organometallics, to yield stabilized alkaline earth organometallics, or other rare earth β-diketonates, to yield the as yet unexplored area of mixed metal β-diketonates.

Acknowledgements—This work was supported by the Nuffield Foundation (S.A.S.M.), the SERC (M.B.H., K.M.A.M., S.A.S.M.), the CASE sponsor Inorgtech (Dr T. Leedham) and the Royal Society. We would also like to acknowledge Dr H. E. Smith for invaluable advice. While this work was in progress, related work appeared: R. Gardiner, D. W. Brown, P. S. Kirlin and A. Rheingold, *Chem. Mat.* 1991, **3**, 1053.

REFERENCES

1. See for example: S. R. Drake, M. H. Chisholm, K. G. Caulton and W. E. Streib, *Angew. Chem., Int. Edn Engl.* 1990, **29**, 1483; S. R. Drake, M. H. Chisholm, K. G. Caulton and W. E. Streib, *Inorg. Chem.* 1990, **29**, 2707.
2. An excellent overview with many early references: T. P. Hanusa, *Polyhedron* 1990, **9**, 1345.
3. S. R. Drake, M. H. Chisholm, K. G. Caulton and K. Folting, *J. Chem. Soc., Chem. Commun.* 1990, 1345, 1498; S. R. Drake, M. H. Chisholm, K. G. Caulton and K. Folting, *Inorg. Chem.* 1991, **30**, 1500.
4. M. J. McCormick, R. A. Williams, C. J. Levine and T. P. Hanusa, *Polyhedron* 1988, **7**, 725.
5. P. B. Hitchcock, M. F. Lappert, G. A. Lawless and B. Royo, *J. Chem. Soc., Chem. Commun.* 1990, 1141, 1991, 724 and refs therein.
6. D. C. Bradley, M. B. Hursthouse, A. A. Ibrahim, K. M. A. Malik, M. Motevalli, R. Moseler, H. Powell, J. D. Runnacles and A. C. Sullivan, *Polyhedron* 1990, **9**, 2959.
7. H. Westerhausen, *Inorg. Chem.* 1991, **30**, 90.
8. S. R. Drake and D. J. Otway, *J. Chem. Soc., Chem. Commun.* 1991, 517; S. R. Drake and D. J. Otway, *Polyhedron* 1991, **10**, 745; S. R. Drake and D. J. Otway, *Polyhedron* 1992, **11**, 243; S. R. Drake, M. B. Hursthouse, K. M. A. Malik and D. J. Otway, *Polyhedron* 1992, **11**, 2006.
9. M. F. Lappert, M. J. Slade, A. Singh, J. L. Atwood, R. D. Rogers and R. Shakir, *J. Am. Chem. Soc.* 1983, **105**, 302.
10. V. C. Arunasalam, S. R. Drake, D. J. Otway and J. C. Huffman, *Inorg. Chem.* 1992, submitted.
11. V. C. Arunasalam, S. R. Drake, M. B. Hursthouse, K. M. A. Malik and D. J. Otway, *J. Chem. Soc., Chem. Commun.* 1993, 478.
12. D. C. Bradley, D. Gauer and R. Mehrotra, *Metal Alkoxides*. Academic Press, New York (1978); D. C. Bradley, *Chem. Rev.* 1989, **89**, 1317 and leading refs therein; K. G. Caulton and L. G. Hubert-Pfalzgraf, *Chem. Rev.* 1990, **90**, 969.
13. S. B. Turnipseed, R. M. Barkley and R. E. Sievers, *Inorg. Chem.* 1991, **30**, 1164.
14. D. C. Bradley, M. Hasan, M. B. Hursthouse, M. Motevalli, O. F. Z. Khan, R. G. Pritchard and J. O. Williams, *J. Chem. Soc., Chem. Commun.* 1992, 575.
15. Y. Y. Wei, B. Tinant, J.-P. Declerq, M. van Meerssche and J. Dale, *Acta Cryst.* 1987, **43C**, 1080.
16. A. A. Danopoulos, G. Wilkinson, B. Hussain-Bates and M. B. Hursthouse, *J. Chem. Soc., Dalton Trans.* 1991, 1855.
17. N. Walker and D. Stuart, *Acta Cryst.* 1983, **A39**, 158; adapted for FAST Geometry by A. Kazaulov, University of Wales College of Cardiff (1990).
18. G. M. Sheldrick, SHELX, Crystallographic Program System. University of Göttingen, F.R.G. (1980).

19. J. D. Mackenzie, *J. Non-Cryst. Solids* 1988, **110**, 162; M. Nemoto and M. Yanmanka, *J. Mat. Res.* 1990, **5**, 1; F. A. Kuznetsov, I. K. Igumenov and V. S. Danilovich, *Physica C* 1991, **185**, 1957.
20. A. P. Purdy, A. D. Berry, R. T. Holm, M. Fatemi and D. K. Gaskill, *Inorg. Chem.* 1989, **28**, 2799.
21. K. Timmer and H. A. Meinema, *Inorg. Chim. Acta* 1991, **187**, 99.
22. G. Rossetto, P. F. Benetollo, M. Porchia and P. Zanella, *Polyhedron* 1992, **11**, 979.
23. W. S. Rees Jr and M. W. Carris, *Inorg. Chem.* 1991, **30**, 4479.
24. C. I. M. A. Speck and A. Makor, in *Science and Technology of Thin Film Superconductors* (Edited by R. D. McConnell and S. A. Wolf), pp. 281–284. Plenum Press, New York (1989); P. van der Sluis, A. L. Spek, K. Timmer and D. A. Meinema, *Acta Cryst.* 1990, **C46**, 1741.
25. J. A. T. Norman and G. P. Pez, *J. Chem. Soc., Chem. Commun.* 1991, 971; J. A. T. Norman and G. P. Pez, Volatile Crown Ligand Beta-Diketonate Alkaline Earth Metal Complexes; Eur. Pat. Appl. EP. 460,627.

Polyhedron Vol. 12, No. 13, pp. 1635–1639, 1993
Printed in Great Britain

0277–5387/93 $6.00+.00
© 1993 Pergamon Press Ltd

OSMIUM(VI) COMPLEXES OF SULPHONYL AMIDO LIGAND. CRYSTAL STRUCTURES OF $[PPh_4]_2[Os_2O_4\{C_6H_4(C_7H_7SO_2N)_2\text{-}o\}_2(\mu\text{-}OH)_2]$ AND $Os_2N_2[C_6H_4(C_7H_7SO_2N)_2\text{-}o](\mu\text{-}OH)_2$

WA-HUNG LEUNG* and ERNEST KIN-FAI CHOW

Chemistry Department, Hong Kong University of Science and Technology, Clear Water Bay, Kowloon, Hong Kong

and

SHIE-MING PENG†

Department of Chemistry, National Taiwan University, Taipei 10764, Taiwan, R.O.C.

(*Received* 8 *February* 1993; *accepted* 5 *March* 1993)

Abstract—Interactions of $[PPh_4]_2[OsO_2Cl_4]$ and $[Bu^n{}_4N][OsNCl_4]$ with Li_2L [H_2L = 1,2-bis(*p*-toluenesulphonylamido)benzene] gave binuclear osmium(VI) compounds $(PPh_4)_2[Os_2O_4L_2(\mu\text{-}OH)_2]$ (**1**) and $Os_2N_2L_2(\mu\text{-}OH)_2$ (**2**), respectively. The structures of both compounds have been determined by X-ray crystallography. The crystal structure of the $[Os_2O_4L_2(\mu\text{-}OH)_2]^{2-}$ anion contains two *trans*-$OsO_2(L)$ units bridged by two OH groups; the Os—O(oxo) bond length is *ca* 1.74 Å. The crystal structure of **2** contains two OsN(L) units bridged by two OH groups; the Os—N(nitrido) bond length is *ca* 1.56 Å.

Multianionic chelating ligands are of current interest because they can stabilize metal ions in high oxidation states. High-valent metal complexes with deprotonated amido ligands, e.g. those of manganese(V),[1] iron(IV),[2] cobalt(IV),[3] nickel(III)[4] and copper(III),[5] are well documented. However, there are relatively few studies on complexes of sulphonyl amido groups. As the sulphonyl group is more electron-withdrawing than the carbonyl group one might expect that sulphonyl amido ligands can be deprotonated more readily and hence could display interesting coordination chemistry. To this end we set out to investigate the chemistry of complexes containing chelating sulphonyl amido ligands, e.g. bis-(toluenesulphonylamido)benzene (H_2L), as shown in Fig. 1. The unique features of the ligand H_2L are: (a) it is bidentate and dianionic; (b) it can stabilize highly oxidizing metal centres due to the strong σ-donating deprotonated sulphonyl amido groups; and (c) it is sterically bulky. Recently, the crystal structures of some copper complexes of H_2L have been described.[6] We herein report the synthesis and crystal structures of two osmium(VI) compounds of the ligand.

EXPERIMENTAL

The ligand H_2L,[6a] $[PPh_4]_2[OsO_2Cl_4]$[7] and $[Bu^n{}_4N][OsNCl_4]$[8] were prepared according to the literature procedures. Organic solvents were purified by standard methods and distilled before use. ^1H NMR spectra were recorded on a JEOL EX 400 spectrometer. Chemical shifts (δ) were reported referenced to $Si(CH_3)_4$. IR spectra (Nujol) were

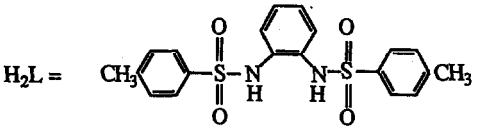

Fig. 1.

* Author to whom correspondence should be addressed.

† Author to whom inquiries concerning X-ray crystallography should be addressed.

obtained on a Perkin–Elmer 1600 FT-IR spectrophotometer. Elemental analyses were performed by MEDAC Ltd (Middlesex, U.K.).

Preparation of $[PPh_4]_2[Os_2O_4L_2(\mu\text{-}OH)_2]$ (**1**)

To a suspension of H_2L (0.4 g, 0.96 mmol) in THF (20 cm^3) at −40°C was added 2 equivalents of Bu^nLi (*ca* 1.25 cm^3 of a 1.6 M solution in hexanes). The resulting mixture was warmed to room temperature and stirred for 1 h. To this solution was added $[PPh_4]_2[OsO_2Cl_4]$ (0.51 g, 0.5 mmol) under nitrogen and the reaction mixture was stirred at room temperature overnight. After the removal of volatiles the dark red residue was extracted with acetonitrile/ether. Slow evaporation of the extract at room temperature afforded red crystals, which were collected and washed with ether (yield 0.25 g). ^1H NMR (CD_3CN): 2.34 (s, 12H, *p*-CH_3), 5.96 (br, s, 2H, OH) and aromatic protons. IR (Nujol)/cm^{-1}: ν(O—H) 3437; ν(S=O) 1152, 1108; $\nu(OsO_2)$ 859. Found: C, 53.2; H, 4.0; N, 3.3%. Calc. for $[Os_2C_{88}H_{78}N_4O_{14}P_2S_4]$: C, 53.2; H, 4.0; N, 2.8%.

Preparation of $Os_2N_2L_2(\mu\text{-}OH)_2$ (**2**)

The lithium salt of H_2L was prepared as for $[Os_2O_4(\mu\text{-}OH)_2]^{2-}$. To a THF solution of Li_2L (prepared from 0.41 g H_2L and 1.25 cm^3 Bu^nLi) was added $[Bu^n_4N][OsNCl_4]$ (0.29 g, 0.5 mmol). The reaction mixture was stirred overnight and evaporated to dryness. The dark yellow residue was extracted with THF. Careful addition of hexane to the extract afforded the crude product, which was recrystallized from THF/ether/hexane to give yellow crystals (yield 0.2 g). ^1H NMR (CD_3CN): 2.29 (s, 6H, *p*-CH_3); 6.28, 6.83, 7.06, 7.81 (all broad singlets, 12H, aroamtic protons). IR (cm^{-1}): ν(O—H) 3450; ν(S=O) 1150, 1126; ν(OsN) 986. Found: C, 61.5; H, 5.5; N, 11.0. Calc. for $[Os_2C_{40}H_{38}N_6O_{10}S_4]$: C, 62.3; H, 4.9; N, 10.9%.

X-ray crystallography

Diffraction measurements were performed on an Enraf–Nonius CAD-4 diffractometer. Lattice parameters of **1** were obtained from 25 reflections with 2θ angles in the range 17.00–21.00°, whereas cell dimensions of complex **2** were determined from 25 reflections with 2θ angles in the range 11.06–20.40°. All reflections were collected for Lorentz, polarization and adsorption effects. All data reduction and refinement were performed using the NRCC-SPD-VAX packages. The structures were solved by direct methods and refined by full-matrix least-squares; all non-hydrogen atoms were refined with anisotropic thermal parameters. Both complexes **1** and **2** crystallize in the triclinic system with the space group $P\bar{1}$. Hydrogen atoms on the organic ligands were calculated in idealized positions and were included in the structure factor calculation. The combined data collection and refinements are given in Table 1. Selected bond lengths and angles for complexes **1** and **2** are given in Tables 2 and 3, respectively.

Table 1. Experimental data for the X-ray diffraction studies[a]

Compound	**1**	**2**
Formula	$C_{90}H_{78}N_4O_{14}P_2Os_2\cdot(MeCN)_2$	$C_{40}H_{38}N_6O_{10}S_4Os_2\cdot(THF)\cdot2(H_2O)\cdot1/2(Et_2O)$
Crystal system	Triclinic	Triclinic
Spacc group	$P\bar{1}$ (No. 2)	$P\bar{1}$ (No. 2)
a (Å)	12.867(5)	11.363(8)
b (Å)	14.418(4)	14.289(9)
c (Å)	14.621(4)	18.580(7)
α (°)	66.69(3)	109.55(5)
β (°)	64.69(3)	102.62(3)
γ (°)	64.48(3)	90.23(5)
V (Å^3)	2137(1)	27,656(2)
Mol. wt	2008	1270
Z	1	2
D_c (g cm^{-3})	1.608	1.697
μ(Mo-K_α) (cm^{-1})	31.7	48.0
Transmission factors	0.696–1.00	0.745–1.00
R; R_w[b]	0.043; 0.055	0.062; 0.062

[a] Features common to all determinations: λ(Mo-K_α) = 0.7107 Å; temperature = 297 K.
[b] $R = \Sigma||F_o|-|F_c||/\Sigma|F_o|$, $R_w = [\Sigma w(F_o-F_c)^2/\Sigma wF_o^2]^{1/2}$.

Table 2. Selected bond lengths (Å) and angles (°) for the $[Os_2O_4L_2(\mu\text{-}OH)_2]^{2-}$ anion

Os—O(1)	1.740(6)	S(1)—O(4)	1.428(7)
Os—O(2)	1.747(7)	S(1)—N(1)	1.646(6)
Os—O(3)	2.051(6)	N(1)—C(1)	1.40(1)
Os—N(1)	2.022(6)		
O(1)—Os—O(2)	175.7(3)	Os—N(1)—C(1)	118.4(5)
O(1)—Os—O(3)	86.7(3)	O(1)—Os—N(1)	92.5(3)
O(3)—Os—O(3′)	71.3(2)	N(1)—Os—N(2)	78.3(3)
O(3)—Os—N(1)	175.7(2)	O(3)—Os—N(2)	105.9(2)
O(4)—S(1)—N(1)	110.8(4)	N(1)—S(1)—C(7)	106.6(3)
Os—O(3)—Osa	108.7(3)	O(4)—S(1)—N(1)	110.8(4)
Os—N(1)—S(1)	123.9(4)	O(4)—S(1)—C(7)	107.7(4)
N(1)—C(1)—C(2)	129.1(7)	N(1)—C(1)—C(6)	114.2(7)

RESULTS AND DISCUSSION

Interaction of $[PPh_4]_2[OsO_2Cl_4]$ with 2 equivalents of the lithium salt of H_2L [H_2L = 1,2-bis(*p*-toluenesulphonylamido)benzene] in THF gave the air-stable binuclear hydroxo-bridged osmium(VI)-dioxo compound (**1**), isolated as its $[PPh_4]^+$ salt. A monomeric compound could not be obtained even when excess ligand was used, presumably because the ligand is too bulky for formation of a planar bischelate complex. The IR spectrum of **1** does not show any sharp N—H band, indicating that the sulphonyl amido group is in the deprotonated form. The broad band near 3470 cm^{-1} can be assigned to the ν(O—H) stretch. The Os=O stretch at 845 cm^{-1} is within the range expected for *trans*-OsO_2 compounds.

The binuclear structure of **1** was confirmed by an X-ray diffraction study. A diagram of the $[Os_2O_4L_2(\mu\text{-}OH)_2]^{2-}$ anion is shown in Fig. 2; selected bond lengths and angles are given in Table 2. The geometry around each osmium is best described as octahedral with the two oxo groups as axial ligands and L and two hydroxo groups as equatorial ligands. The two *trans*-OsO_2L units are bridged by the two hydroxo ligands with the Os—O(H)—Os′ bond angle of *ca* 108.7°. A similar structure has been observed for the binuclear oxo-bridged $Os_2O_6py_4$.[9] The Os—O(oxo) bond lengths (*ca* 1.74 Å) are normal by comparison with *trans*-osmium(VI)-dioxo compounds. The Os—N(sulphonyl amido) bond length of *ca* 2.03 Å is similar to that for Os—N(amido) found in a related osmium(VI)-nitrido compound of a tetradentate amido ligand.[10] Of note, the four toluenesulphonyl groups of the ligands adopt a "two-up–two-down" geometry.

Treatment of $[Bu^n_4N][OsNCl_4]$ with 2 equivalents of Li_2L gave the neutral dimeric osmium(VI)-nitrido compound **2**. Again, the steric bulk of the ligand L precludes the formation of the monomeric bischelate complex. The presence of the bridging hydroxo group is indicated by the broad IR band at 3450 cm^{-1}. The Os—N stretch at 986 cm^{-1} is

Table 3. Selected bond lengths (Å) and angles (°) for $Os_2N_2L_2(\mu\text{-}OH)_2$ (**2**)

Os(1)—O(9)	1.99(2)	S(1)—N(1)	1.60(2)
Os(1)—N(1)	1.97(2)	S(1)—O(1)	1.46(2)
Os(1)—N(5)	1.52(2)	N(1)—C(1)	1.47(3)
Os(2)—N(6)	1.61(2)		
O(9)—Os(1)—O(10)	74.5(7)	O(1)—S(1)—N(1)	105(1)
O(9)—Os(1)—N(1)	92.4(7)	O(1)—S(1)—C(7)	108(1)
O(9)—Os(1)—N(2)	140.2(7)	N(1)—S(1)—C(7)	106(1)
O(9)—Os(1)—N(5)	110.0(9)	Os(1)—O(9)—Os(2)	104.2(7)
N(1)—Os(1)—N(2)	85.6(7)	Os(1)—N(1)—S(1)	124(1)
N(1)—Os(1)—N(5)	113.1(9)	Os(1)—N(1)—C(1)	116(2)
N(2)—Os(1)—N(5)	109.5(9)	N(1)—C(1)—C(2)	126(2)
N(1)—C(1)—C(6)	112(2)	S(1)—C(7)—C(8)	120.7(8)

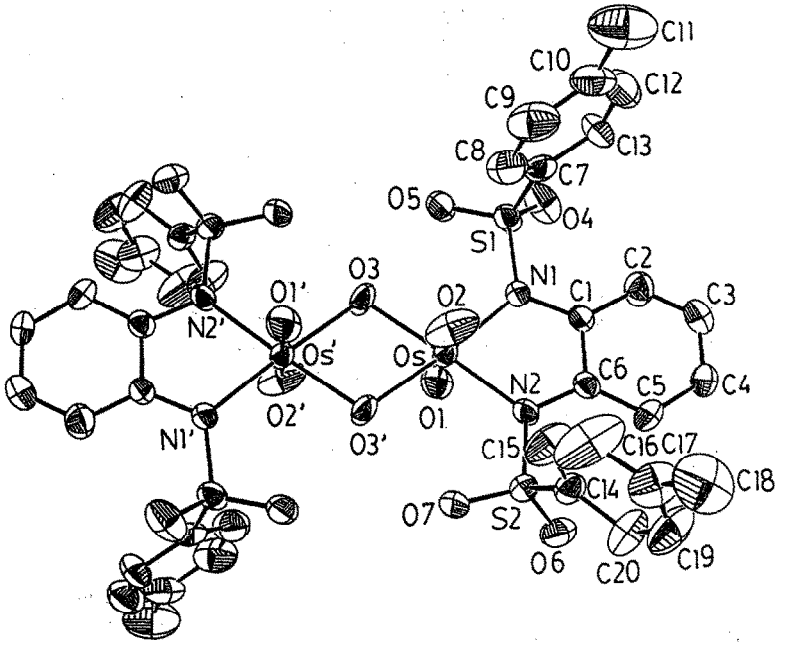

Fig. 2. A perspective view of the $[Os_2O_4L_2(\mu\text{-}OH)_2]^{2-}$ anion.

normal for nitrido compounds. The ^1H NMR spectrum of **2** is consistent with the solid-state structure.

The structure of **2** has been determined by X-ray crystallography. An ORTEP drawing of **2** is shown in Fig. 3 and selected bond lengths and angles are given in Table 3. The geometry around each osmium is square pyramidal with the nitrido group as an axial ligand. The two Os(N)L units are bridged by the two hydroxo ligands with the two nitrido ligands on the same side. The Os(1)—O(H)—Os(2) bond angle of 104.2° and Os—N(amido) bond length of 1.973 Å are similar to those for **1**. The Os—N(nitrido) bond length is normal for osmium(VI)-nitrido compounds.[11] It might be noted that this is the first structure of a binuclear osmium-nitrido compound.

The reactivity of these two osmium complexes is being studied.

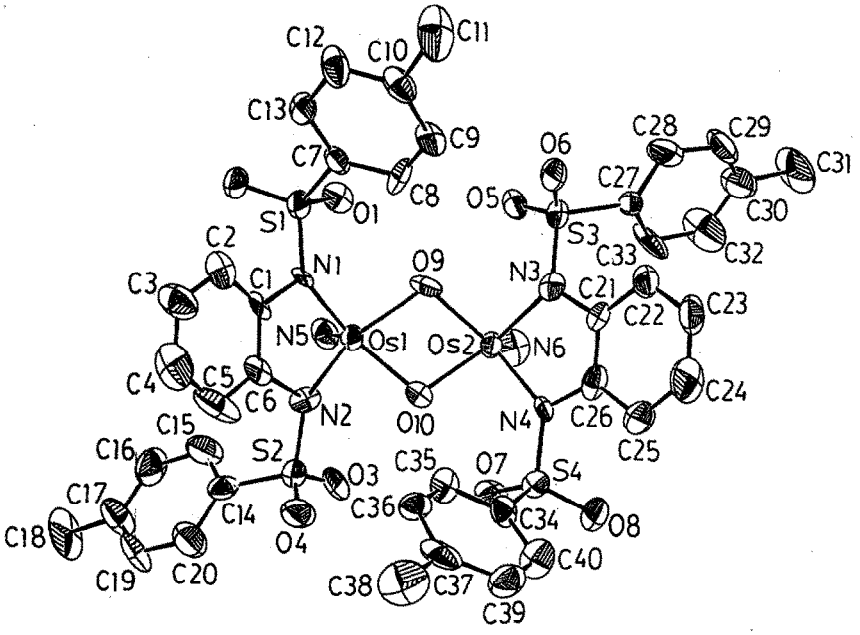

Fig. 3. A perspective view of **2**.

Acknowledgements—We thank the Hong Kong University of Science and Technology, Hong Kong Research Grants Council and the National Science Council of the Republic of China for support. W.-H.L. thanks Prof. Chi-Ming Che for helpful discussions.

REFERENCES

1. T. J. Collins, R. D. Powell, C. S. Slebodnich and E. S. Uffelman, *J. Am. Chem. Soc.* 1990, **112**, 899.
2. T. J. Collins, K. L. Kostka, E. Munich and E. S. Uffelman, *J. Am. Chem. Soc.* 1990, **112**, 5637.
3. F. C. Anson, T. J. Collins, R. J. Coots, S. L. Gibson and T. G. Richmond, *J. Am. Chem. Soc.* 1984, **106**, 5037.
4. L. Fabbrizzi, T. A. Kaden, A. Perotti, B. Seghi and L. Siegfried, *Inorg. Chem.* 1986, **25**, 321.
5. S. T. Kirsey Jr, J. A. Neubecker and D. W. Margerum, *J. Am. Chem. Soc.* 1979, **101**, 1631.
6. (a) H.-Y. Cheng, P.-H. Cheng, C.-F. Lee and S.-M. Peng, *Inorg. Chim. Acta* 1991, **181**, 145; (b) H.-Y. Cheng, G.-H. Lee and S.-M. Peng, *Inorg. Chim. Acta* 1992, **191**, 25.
7. P. A. Shapley, H. S. Kim and S. R. Wilson, *Organometallics* 1988, **7**, 928.
8. W. P. Griffith and D. Pawson, *J. Chem. Soc., Dalton Trans.* 1973, 1315.
9. A. M. R. Galas, M. B. Hursthouse, E. J. Behrman, W. R. Midden, G. Green and W. P. Griffith, *Trans. Met. Chem.* 1981, **6**, 194.
10. (a) C. J. Barner, T. J. Collins, B. E. Mapes and B. D. Santersiero, *Inorg. Chem.* 1986, **25**, 4322; (b) C. M. Che, H. W. Lam, W. T. Wong and T. F. Lai, unpublished work.
11. W. A. Nugent and J. M. Mayer, *Metal Ligand Multiple Bonds*, p. 186. Wiley-Interscience, New York (1988).

Polyhedron Vol. 12, No. 13, pp. 1641–1646, 1993
Printed in Great Britain

0277–5387/93 $6.00+.00
© 1993 Pergamon Press Ltd

STUDIES ON CROWN ETHER COMPLEXES—XXVIII. SYNTHESIS, CHARACTERIZATION AND STRUCTURE OF THE COMPLEXES OF HEAVIER LANTHANIDE NITRATES (Gd–Lu) WITH DIBENZO-24-CROWN-8

TONGBU LU, XINMIN GAN* and MINYU TAN

Department of Chemistry, Lanzhou University, Lanzhou 730000, P.R.C.

and

CHANGZHENG LI

Xinxiang Medicine College, Xinxiang, Henan 453003, P.R.C.

and

KAIBEI YU

Chengdu Centre of Analysis, Academia Sinica, Chengdu 610041, P.R.C.

(*Received* 8 *February* 1993; *accepted* 5 *March* 1993)

Abstract—The heavier lanthanide nitrate complexes with dibenzo-24-crown-8 (DB24C8) have been prepared in acetonitrile. These new complexes with the general formula $[Ln(NO_3)_3(OH_2)_3]\cdot(DB24C8)$ (Ln = Gd–Lu) have been characterized by means of elemental analysis, IR spectra, ^1H NMR spectra and conductivity measurements. The crystal and molecular structure of $[Gd(NO_3)_3(OH_2)_3]\cdot(DB24C8)$ has been determined by single-crystal X-ray diffraction. The gadolinium(III) ion is coordinated to the six oxygen atoms of three bidentate nitrate groups and three water molecules. The crown ether molecule is hydrogen bonded to these three water molecules. The average Gd—O(nitrate) and Gd—O(water) distances are 2.464(4) and 2.388(3) Å, respectively. The average O(water)···O(crown ether) separation is 2.787 Å. The coordination polyhedron is a distorted tricapped trigonal prism.

A large number of lanthanide-crown ether complexes have been investigated and some have been studied by single-crystal X-ray diffraction methods.[1,2] Among these studies the lanthanide complexes with large cavity crown ethers were little reported.[3,4] In order to investigate the coordination power of large cavity crown ethers with these ions we synthesized a series of lanthanide complexes with large cavity crown ethers.[5–8] We found that the lanthanide isothiocyanates reacted with DB24C8, dicyclohexyl-24-crown-8 (DCH24C8) and dibenzo-30-crown-10 (DB30C10) to yield $RE(NCS)_3\cdot DB24C8\cdot 2H_2O\cdot CH_3CN$ (RE = La–Lu, Y),[5,6] $RE(NCS)_3\cdot(DCH24C8)\cdot nH_2O$ (RE = La–Er, Yb, Lu, Y, n = 1–3)[7] and $Ln(NCS)_3\cdot(DB30C10)\cdot nH_2O$ (Ln = La–Lu, n = 1–3),[8] in which the ligands are all directly coordinated to the metal ions. In order to investigate the influence of different inorganic anions on the coordination properties of crown ethers in complexes we recently synthesized the complexes of lanthanide nitrates with DB24C8 and studied their composition, properties and structures.

EXPERIMENTAL

Reagents

Hydrated lanthanide nitrates were prepared by dissolving Ln_2O_3 (AnalaR) in 1 : 1 nitric acid. The

* Author to whom correspondence should be addressed.

ligand was obtained from Shanghai Reagent Company and purified by recrystallization from ethanol before use; m.p. = 101.5–102.0°C. All other chemicals were AnalaR grade.

Chemical and physical measurements

The metal ion contents were determined by EDTA titration using xylenol orange as an indicator. Carbon, nitrogen and hydrogen contents were determined using a Carlo–Erba 1106 elemental analyser. The IR spectra were recorded in the 4000–200 cm^{-1} region using KBr pellets and a 170 SX FTIR spectrometer. The ^1H NMR spectra were recorded on a FT-80A spectrophotometer using acetone-d_6 as a solvent and TMS as an internal standard. Conductivity measurements were carried out with a DDS-11A type conductivity bridge for freshly prepared solutions in acetone at 25°C. The crystal data were collected on a R3M/E diffractometer by the $\theta/2\theta$ scan technique.

Preparation of the complexes

A solution of $Ln(NO_3)_3 \cdot nH_2O$ (Ln = Gd–Lu) (0.63 mmol) in acetonitrile (2 cm^3) was added dropwise to a solution of DB24C8 (0.3 mmol) in acetonitrile (2 cm^3). The mixture was stirred at room temperature for 36 h. The precipitated solid complexes was filtered, washed with ethyl acetate and dried in a desiccator (0.1 mm Hg) over P_4O_{10} for 2 days. All the complexes were powdered solids with the characteristic colour of the corresponding lanthanide nitrates.

Single crystals of the gadolinium complex were obtained by dissolving the powdered solid complex in nitromethane and leaving the solution in a desiccator over $CaCl_2$ at room temperature. After *ca* 1 month colourless crystals suitable for X-ray analysis formed from the solution.

Under the same preparation conditions we could not obtain the solid complexes when DB24C8 was reacted with the lighter lanthanide nitrates (La–Eu).

X-ray structure determination

The structure was solved by the Patterson method and subsequent difference-Fourier techniques and refined by full-matrix least-squares methods with anisotropic thermal factors for all non-hydrogen atoms. The crown ether hydrogen atoms were placed in calculated positions. All calculations were performed using the SHELXTL system of computer programs. The final values $R = 0.053$ and $Rw = 0.044$ were obtained. The crystal data are listed in Table 1.

Table 1. Crystal data

Formula	$C_{24}H_{38}N_3O_{20}Gd$
Molecular weight	845.7
Crystal dimensions (mm)	$0.28 \times 0.32 \times 0.40$
System	Monoclinic
Space group	$P2_1/n$
Temperature (°C)	20
Lattice parameters	
a (Å)	10.552(2)
b (Å)	20.347(4)
c (Å)	15.709(3)
β (°)	98.77(1)
Cell volume (Å^3)	3333(1)
Molecules/unit cell (Z)	4
D_c (g cm^{-3})	1.69
D_o (g cm^{-3})	1.68
$\mu_{calc.}$ (cm^{-1})	20.81
Radiation, graphite monochromator	Mo-K_α ($\lambda = 0.71073$)
$F(000)$	1708
Scan type and rate (° min^{-1})	$\theta/2\theta$, 8
Standard reflection	2, 10, 0 and 5, 0, 3
2θ range (°)	$2 < 2\theta < 45$
Unique data measured	4826
Observable data with $I \geqslant 3.0\sigma(I)$	3466
No. of variables	546
GOF (or S)	1.009
R	0.0316
Rw	0.0277

RESULTS AND DISCUSSION

The composition of the complexes

The analytical data for these new complexes, listed in Table 2, indicate that they all conform to 1 : 1 stoichiometry of the metal ion to the crown ether.

IR spectra

The most important IR peaks of the ligand and the complexes are reported in Table 3.

Compared with those of the free ligand, the absorptions of ν(Ar—O—R) and ν(R—O—R) of the complexes showed small shifts towards lower wave numbers. This suggests that the ligand does not coordinate directly to the lanthanide(III) ion.[9]

In the IR spectra of the complexes the absorptions appearing in the 3239–3270, 1656–1664 and 569–578 cm^{-1} regions are clearly due to ν(OH), δ(HOH) and ρ_r(HOH), respectively, indicating that coordinated water molecules exist in the complexes.[10] Compared with normal ν(OH) (*ca* 3400 cm^{-1}) bands for water molecules the absorptions of ν(OH) of these complexes show a red-shift, which

Table 2. Elemental analysis and molar conductance data

Compound	C% Found (calc.)	N% Found (calc.)	H% Found (calc.)	Ln% Found (calc.)	Molar conductance (Ω^{-1} cm^2 mol^{-1})
$[Gd(NO_3)_3(OH_2)_3]\cdot$DB24C8	33.6 (34.1)	4.9 (5.0)	4.4 (4.5)	18.8 (18.6)	4.7
$[Tb(NO_3)_3(OH_2)_3]\cdot$DB24C8	34.3 (34.0)	4.9 (5.0)	4.4 (4.5)	18.3 (18.8)	3.5
$[Dy(NO_3)_3(OH_2)_3]\cdot$DB24C8	33.8 (33.9)	4.6 (4.9)	4.3 (4.5)	19.4 (19.1)	2.4
$[Ho(NO_3)_3(OH_2)_3]\cdot$DB24C8	33.5 (33.8)	4.8 (4.9)	4.4 (4.4)	19.5 (19.3)	2.3
$[Er(NO_3)_3(OH_2)_3]\cdot$DB24C8	33.4 (33.7)	5.0 (4.9)	4.2 (4.4)	19.6 (19.5)	1.6
$[Tm(NO_3)_3(OH_2)_3]\cdot$DB24C8	33.3 (33.6)	4.7 (4.9)	4.7 (4.4)	20.0 (19.7)	1.2
$[Yb(NO_3)_3(OH_2)_3]\cdot$DB24C8	33.2 (33.4)	4.7 (4.9)	4.3 (4.4)	19.7 (20.1)	2.0
$[Lu(NO_3)_3(OH_2)_3]\cdot$DB24C8	33.7 (33.4)	4.8 (4.9)	4.3 (4.4)	20.5 (20.3)	2.5

suggests that hydrogen bonding exists in the title complexes.[11,12]

The characteristic frequencies of coordinating nitrate groups appear in the IR spectra of the complexes (see Table 3), the difference between the two strongest absorptions (ν_1 and ν_4) of the nitrate groups being *ca* 200 cm^{-1}, indicating that the nitrate groups in the complexes coordinate to the metal ions as bidentate ligands.[10] The absence of absorptions around 1360 cm^{-1} indicates that all the nitrate groups in the complexes coordinate to the lanthanide ions.[10] This result is consistent with

Table 3. The most important IR bands (cm^{-1})

						$\nu(NO_3)$					
Compound	ν(Ar—O—R)	ν(R—O—R)	ν(OH)	δ(HOH)	$\rho_r(H_2O)$	$\nu_2+\nu_5$	$\nu_2+\nu_6$	ν_1	ν_4	ν_2	ν_3
DB24C8	1256s 1224s	1126s 1102s									
Gd	1250s 1192m	1102s 1078m	3254s	1662s	569w	1770w	1731w	1501s	1288s	1027s	849m 814s
Tb	1254s 1192s	1110s 1084m	3270s	1656m	570w	1771w	1729w	1506s	1287s	1026s	844m 814s
Dy	1251s 1192m	1103s 1080m	3243s	1662m	570w	1774w	1733w	1502s	1291s	1029s	849m 813s
Ho	1251s 1192m	1103s 1079m	3248s	1662m	571w	1775w	1733w	1502s	1293s	1030s	849m 813s
Er	1250s 1191m	1103s 1079m	3242s	1664m	571w	1777w	1735w	1503s	1294s	1031s	849m 814s
Tm	1251s 1192m	1104s 1080m	3239s	1661m	573w	1780w	1735w	1502s	1297s	1031s	850m 814s
Yb	1251s 1192m	1105s 1081m	3246s	1660m	576w	1781w	1735w	1504s	1299s	1033s	849m 814m
Lu	1251s 1192m	1104s 1080m	3246s	1661m	578w	1782w	1736w	1503s	1301s	1033s	850m 824s

Table 4. Selected bond lengths (Å)

Gd—O(9)	2.457(4)	Gd—O(10)	2.460(4)
Gd—O(12)	2.466(3)	Gd—O(13)	2.467(3)
Gd—O(15)	2.472(4)	Gd—O(16)	2.463(4)
Gd—O(18)	2.407(3)	Gd—O(19)	2.383(3)
Gd—O(20)	2.373(4)		

those of the molar conductance values (Table 2) and the crystal structure determination.

^{1}H *NMR spectra*

Comparing the proton chemical shifts of the free ligand [δ(Ar—H) = 6.92, δ(—CH_2—) = 3.75–4.19 ppm] with those of the lutetium complex [δ(Ar—H) = 6.91, δ(—CH_2—) = 3.75–4.19 ppm] it can be found that these values are almost the same, indicating that the ligand does not directly coordinate to the lutetium(III) ion. This conclusion is consistent with the IR spectrum and the crystal structure determination.

Solubility and molar conductance

All the complexes are sparingly soluble in benzene and tetrachloromethane, slightly soluble in ethyl acetate, ethyl ether and chloroform and soluble in acetonitrile, nitromethane and acetone. The molar conductances measured in acetone at 25°C lie in the range 1.2–4.7 Ω^{-1} cm^2 mol^{-1} (Table 2), indicating that all the complexes are non-electrolytes.[13] This indicates that all the nitrate groups in the complexes are coordinated to the metal ions.

Crystal and molecular structure of the gadolinium complex

Selected bond lengths and angles are given in Tables 4 and 5, respectively. Figure 1 shows the molecular structure of the gadolinium(III) complex whilst Fig. 2 illustrates the molecular packing arrangement in the unit cell.

The gadolinium(III) ion is nine-coordinated with three bidentate nitrates and three water molecules, forming a distorted tricapped trigonal prism (Fig. 3). Three oxygen atoms of three water molecules form one bottom plane of the trigonal prism and another bottom plane is formed by three oxygen atoms from three nitrate groups; the other three nitrate oxygen atoms cap each quadrilateral face of the trigonal prism. The average Gd—O(nitrate) and Gd—O(water) bond lengths are 2.464(4) and 2.388(3) Å, respectively.

Although the positions of the hydrogen atoms of the coordinated water molecules were not located, the presence of hydrogen bonding can be inferred from the close O···O non-bonded contacts.[14] It can be seen that five hydrogen atoms of three coordinated water molecules are bonded to five oxygen atoms in the crown ether (Table 6). The hydrogen bonding contacts range from 2.707 to 2.843 Å and average 2.787 Å. This value is close to those observed in $[Y(OH_2)_8]Cl_3 \cdot (15C5)$ [average 2.76(7) Å][14] and $[UO_2(NO_3)_2(OH_2)_2] \cdot (DB18C6)_2$ (average 2.860 Å).[15] The O(1)···O(19)···O(7) and

Table 5. Selected bond angles (°)

O(9)—Gd—O(10)	51.6(1)	O(9)—Gd—O(12)	115.8(1)
O(10)—Gd—O(12)	124.0(1)	O(9)—Gd—O(13)	74.2(1)
O(10)—Gd—O(13)	74.9(1)	O(12)—Gd—O(13)	51.4(1)
O(9)—Gd—O(15)	117.1(1)	O(10)—Gd—O(15)	73.0(1)
O(12)—Gd—O(15)	119.1(1)	O(13)—Gd—O(15)	121.4(1)
O(9)—Gd—O(16)	127.6(1)	O(10)—Gd—O(16)	79.8(1)
O(12)—Gd—O(16)	72.9(1)	O(13)—Gd—O(16)	75.3(1)
O(15)—Gd—O(16)	51.7(1)	O(9)—Gd—O(18)	79.8(1)
O(10)—Gd—O(18)	88.7(1)	O(12)—Gd—O(18)	147.0(1)
O(13)—Gd—O(18)	154.0(1)	O(15)—Gd—O(18)	70.7(1)
O(16)—Gd—O(18)	122.2(1)	O(9)—Gd—O(19)	71.3(1)
O(10)—Gd—O(19)	122.9(1)	O(12)—Gd—O(19)	78.7(1)
O(13)—Gd—O(19)	92.2(1)	O(15)—Gd—O(19)	146.4(1)
O(16)—Gd—O(19)	150.8(1)	O(18)—Gd—O(19)	79.8(1)
O(9)—Gd—O(20)	146.4(1)	O(10)—Gd—O(20)	152.3(1)
O(12)—Gd—O(20)	72.8(1)	O(13)—Gd—O(20)	124.0(1)
O(15)—Gd—O(20)	79.5(1)	O(16)—Gd—O(20)	85.9(1)
O(18)—Gd—O(20)	79.0(1)	O(19)—Gd—O(20)	79.4(1)

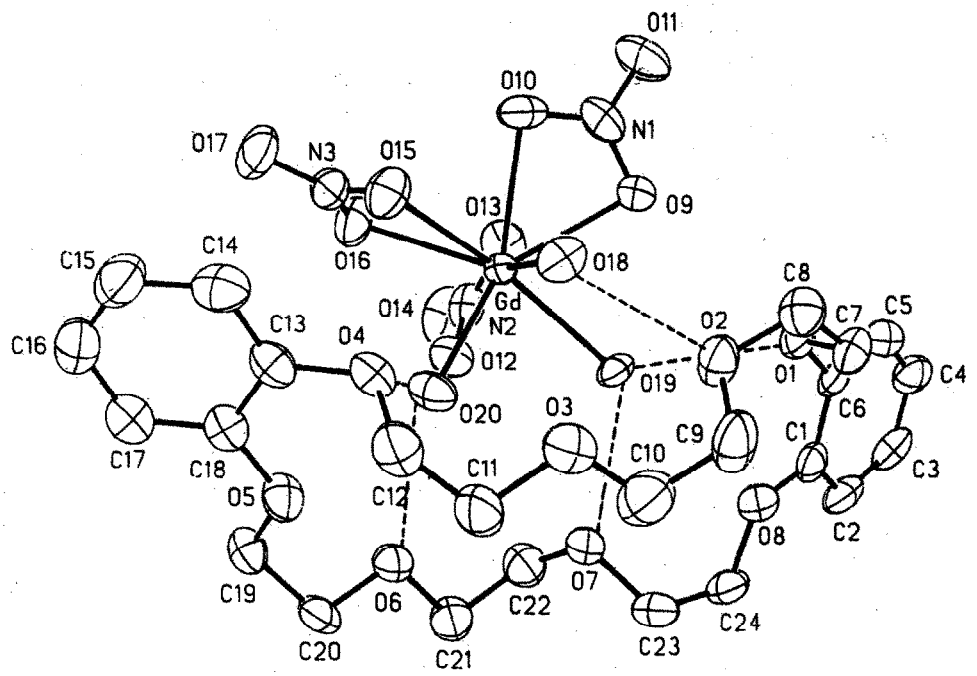

Fig. 1. The molecular structure of $[Gd(NO_3)_3(OH_2)_3]\cdot$(DB24C8).

O(4)···O(20)···O(6) angles are 109.1° and 107.4°, respectively, close to the H—O—H bond angle.

Owing to the unsuitable HO—H···O(crown) angle, a hydrogen atom in O(18) cannot form hydrogen bonds with the crown ether oxygen atom and this allows the other hydrogen atom in O(18) to form more efficient hydrogen bonds with O(2). This can be proved by the existence of the shortest O(18)···O(2) hydrogen bonding contact (see Table 6).

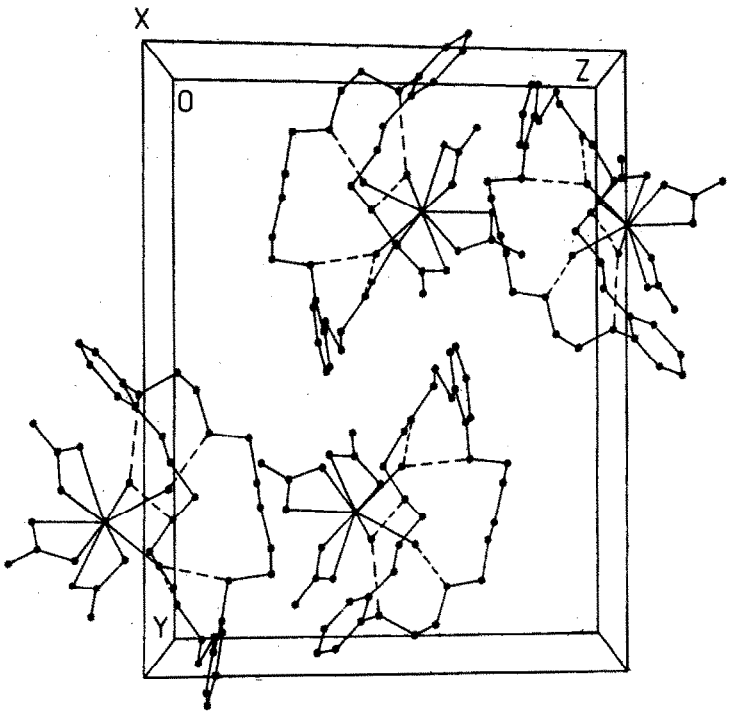

Fig. 2. The molecular packing arrangement in the unit cell.

Table 6. The hydrogen bonding contacts (Å) and angles (°)

O(18)···O(2)	2.707	O(19)···O(1)	2.843
O(19)···O(7)	2.771	O(20)···O(4)	2.797
O(20)···O(6)	2.815		
O(1)···O(19)···O(7)	109.1	O(4)···O(20)···O(6)	107.4

CONCLUSIONS

The Ln^{3+} ions can react with large cavity crown ethers to form two kinds of complexes with two different modes of coordination:

(1) In the presence of isothiocyanate groups the number of coordination atoms from the anions is only three, so the large cavity crown ethers (DB24C8, DCH24C8 and DB30C10) can directly coordinate to the Ln^{3+} ions to meet the need of the higher coordination numbers of the Ln^{3+} ions.[5–8]

(2) In the presence of the strong bidentate nitrates DB24C8 cannot directly coordinate to the Ln^{3+} ions due to its too large cavity and limited flexibility. The neutral $[Ln(NO_3)_3(OH_2)_3]$ unit and DB24C8 are linked together by hydrogen bonding through the intermediary water molecules.

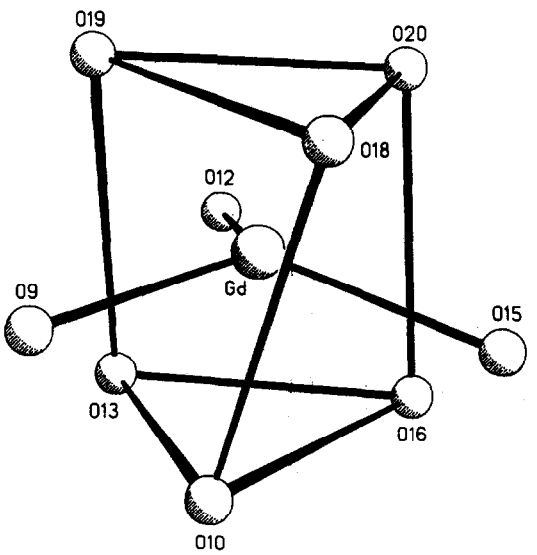

Fig. 3. The coordination polyhedron.

Acknowledgement—The authors are grateful to the China National Natural Science Foundation for financial support.

REFERENCES

1. J.-C. Bünzli, in *Handbook on the Physics and Chemistry of Rare Earths* (Edited by K. A. Gschneidner Jr and L. Eyring), Vol. 9, Ch. 60. North Holland Publ. Co., Amsterdam (1987).
2. Y. Inoue and G. W. Gokel, *Cation Binding by Macrocycles Complexation of Cationic Species by Crown Ethers*. Marcel Dekker, Inc., New York (1990).
3. M. Ciamplini and N. Nardi, *Inorg. Chim. Acta* 1979, **32**, L9.
4. W. Xin and T. Minyu, *Acta Chim. Sin.* 1984, **42**, 434.
5. L. Tongbu, G. Xinmin, T. Ning and T. Minyu, *Polyhedron* 1990, **9**, 2371.
6. L. Tongbu, G. Xinmin, T. Ning and T. Minyu, *J. Chin. Rare Earth Soc.* (Chinese Edition) 1992, **10**, 68.
7. G. Xinmin, L. Tongbu, Y. Wenfu, T. Ning, L. Weisheng and T. Minyu, *Syn. React. Inorg Metal-org. Chem.*, in press.
8. L. Tongbu, G. Xinmin, T. Ning and T. Minyu, *Chem. Res. Chin. Univ.* 1992, **8**, 319.
9. R. D. Rogers and L. K. Kurihara, *Inorg. Chim. Acta* 1987, **130**, 131.
10. K. Nakamoto, *Infrared and Raman Spectra of Inorganic and Coordination Compounds*, 3rd edn. John Wiley, New York (1978).
11. G. Xinmin, T. Ning, Z. Ying, Z. Yingli and T. Minyu, *J. Chin. Rare Earth Soc.* 1990, **8**, 10.
12. L. J. Bellamy, *The Infra-red Spectra of Complex Molecules*. Science Press, Beijing (1975).
13. W. J. Geary, *Coord. Chem. Rev.* 1971, **7**, 81.
14. R. D. Rogers and L. K. Kurihara, *Inorg. Chim. Acta* 1986, **116**, 171.
15. X. Gan, N. Tang, X. Wang, Y. Zhu and M. Tan, *J. Coord. Chem.* 1989, **20**, 21.

Polyhedron Vol. 12, No. 13, pp. 1647–1653, 1993
Printed in Great Britain

0277–5387/93 $6.00+.00
© 1993 Pergamon Press Ltd

SYNTHESIS AND STRUCTURAL CHARACTERIZATION OF TWO NOVEL HETERONUCLEAR CLUSTER COMPOUNDS, $[NEt_4]_4[WS_4Cu_5Br_7]$ AND $+WS_4Cu_6I_4(Py)_4+_n$

LANG JIANPING,* WEIYANG ZHOU and XIN XINQUAN

State Key Laboratory of Coordination Chemistry, Department of Chemistry, Nanjing University, Nanjing, Jiangsu 210008, P.R.C.

and

CAI JINHUA and KANG BEISHENG

Fuzhou Laboratory of Structural Chemistry and Fujian Institute of Research on the Structure of Matter, Chinese Academy of Sciences, Fuzhou, Fujian 350002, P.R.C.

and

YU KAIBEI

Chengdu Center of Analysis and Measurement, Chinese Academy of Sciences, Chengdu 610041, P.R.C.

(*Received* 11 *November* 1992; *accepted* 3 *March* 1993)

Abstract—The title compounds have been obtained by the reaction of $[NH_4]_2[WS_4]$, CuBr, $[NEt_4]_4Br$ and $[Bu^n_4N]Br$ in the solid state (**1**), or by the reaction of $[NH_4]_2[WS_4]$, CuI and $[Bu^n_4N]I$ in the solid state and the pyridine substitution of the solid-state product in acetonitrile (**2**). X-ray diffraction analysis confirms that in the structure of **1** five of the six edges of the $[WS_4]^{2-}$ tetrahedron are coordinated by CuBr units forming an open, double cubane-like structure, which possesses crystallographically imposed C_2 symmetry. The structure of **2**, which possesses a crystallographic $\bar{4}$ symmetry axis situated at the tungsten atom, consists of a tetrahedral WS_4 core enveloped by an octahedral array of six copper atoms, forming a WS_4Cu_6 aggregate. Linked by $—Cu_{eq}—I—Cu_{eq}—$ bridges, this aggregate connects with its nearest neighbours and develops a two-dimensional network. The substitution reactions of the solid-state product with pyridine are discussed.

The tetrathiometallate anions MS_4^{z-} (M = Mo, W, V, Re) have been shown to act as multidentate ligands to a wide variety of metal ions[1] and particularly with copper. The reaction of Cu^+ with MS_4^{z-} has led to a large number of heteronuclear compounds.[2–12] So far, almost all of these M—Cu—S cluster compounds reported in the literature have been prepared in solution. Recently, we have undertaken investigations on cluster compounds formed by reaction of $[NH_4]_2[MS_4]$ (M = Mo, W) with CuX (X = Cl, Br, I, CN, NCS) in the solid state and have prepared and structurally characterized a number of mixed-metal cluster compounds.[13–15] As a novel extension of this research, we herein report the synthesis and structural characterization of two new heteronuclear cluster compounds, $[NEt_4][WS_4Cu_5Br_7]$ (**1**) and $+WS_4Cu_6I_4(Py)_4+_n$ (**2**).

EXPERIMENTAL

All solid-state reactions were performed in an atmosphere of pure argon. IR spectra (KBr pellets) were recorded with a Fourier–Nicolet FT-170 SX spectrophotometer and electronic spectra on a

* Author to whom correspondence should be addressed.

Shimada UV-240 spectrophotometer (CH_3CN solution, 10^{-3} dm^3 mol^{-1} cm^{-1}). Cyclic voltammetry measurements of **1** were performed on a PAR Model 370 electrochemical apparatus equipped with an *X–Y* recorder at room temperature, under anaerobic conditions, using a three-electrode system with a platinum working electrode, a platinum wire auxiliary electrode and an S.C.E. references electrode. Potentials were also referenced to the ferrocene/ferrocinium system. The supporting electrolyte was Bu_4NBF_4 (0.1 M) and the sample was dissolved in DMF solution (5×10^{-3} M). The scan rate was 100 mV s^{-1}. $[NH_4]_2[WS_4]$ was prepared by the literature method.[16] Other reactants and solvents were used as purchased.

Synthesis of $[NEt_4]_4[WS_4Cu_5Br_7]$ **(1)**

A well-ground mixture of $[NH_4]_2[WS_4]$ (0.35 g, 1.0 mmol), CuBr (0.29 g, 2.0 mmol), $[NEt_4]Br$ (0.42 g, 2.0 mmol) and $[Bu^n_4N]Br$ (0.65 g, 2.0 mmol) was put into a reaction tube. A reddish-orange solid was obtained by heating the mixture in the solid state at 115°C for 14 h. After extracting the product with CH_2Cl_2 (40 cm^3) and filtering the reddish-orange coloured extract, the filtrate, on slow evaporation by standing in air, deposited 0.14 g (20.5%) of the reddish-orange crystals of the title compound. Found: C, 21.0; H, 4.6; N, 3.5; W, 9.9; Cu, 18.5. Calc. for $C_{32}H_{80}Br_7Cu_5N_4S_4W$: C, 21.1; H, 4.7; N, 3.3; W, 10.7; Cu, 18.6%.

Synthesis of $-[WS_4Cu_6I_4(Py)_4]-_n$ **(2)**

A well-ground mixture of $[NH_4]_2[WS_4]$ (0.35 g, 1.0 mmol), CuI (0.38 g, 2.0 mmol) and $[Bu^n_4N]I$ (1.48 g, 4.0 mmol) was placed in a reaction tube. A red solid was obtained by heating the mixture in the solid state at 120°C for 15 h. After extracting the product with CH_2Cl_2 (40 cm^3) and filtering the red coloured extract the filtrate, on slow evaporation by standing in air, deposited 0.16 g of the red crystals (as an intermediate). The product thus obtained was dissolved in CH_3CN (20 cm^3) in a tube, which was then placed in a closed beaker containing a small amount of pyridine. Slow diffusion of pyridine vapour into the tube at room temperature formed red octahedral crystals of the title compound a month later. Yield: 0.10 g (19.8%). Found: C, 15.6; H, 1.2; N, 3.9; W, 11.7; Cu, 24.8. Calc. for $C_{20}H_{20}Cu_6I_4N_4S_4W$: C, 15.8; H, 1.3; N, 3.7; W, 12.1; Cu, 25.1%.

Crystal data and structure determination

The crystals obtained directly from the preparations were suitable for single-crystal X-ray works. A single crystal was mounted in a random orientation of a glass fibre. Data were collected using a Nicolet R3m/E (**1**) or MSC/Rigaku (**2**) four-circle diffractometer with graphite-monochromated Mo-K_α [$\lambda = 0.71073$ (**1**) or 0.71069 Å (**2**)] radiation at room temperature. Cell constants were obtained by least-squares analysis on 23 (**1**) or 20 (**2**) diffraction maxima [the search limits of 2θ: 7.08–24.28° (**1**) or 10–25° (**2**)]. Details of the data collection together with structure refinement are summarized in Table 1.

Intensity data were corrected for Lorentz–polarization factors and for absorption empirically. For **1** there was no evidence of crystal decay from standard reflections monitored every 1.5 h of exposure. For **2**, as a check on crystal and electronic stability, three representative reflections were measured every 300 reflections and there was also no evidence of crystal and electronic decay.

The structure of **1** was solved by the heavy-atom method. Three-dimensional Patterson maps revealed the position of the tungsten atom. Successive least-squares refinements and difference-Fourier calculations revealed the positions of the remaining non-hydrogen atoms. Anisotropic temperature factors were introduced for all atoms of the anion and the cations. Hydrogen atoms were not included in the refinements. Neutral atom scattering factors with anomalous dispersion corrections were taken from ref. 17. Atomic parameters were refined by the full-matrix least-squares method using the SHELXTL program package (Nicolet corporation, 1986) on an Eclipse S/140 computer.

The structure of **2** was solved by direct methods. Six atoms were located from an E map; successive least-squares refinements and difference-Fourier calculations revealed the positions of the remaining atoms. The structure was refined by full-matrix least-squares with anisotropic thermal parameters for all non-hydrogen atoms and isotropic thermal parameters for all hydrogen atoms. Neutral atom scattering factors with anomalous dispersion corrections were taken from ref. 17. All calculations were performed on a VAX computer using the SDP/VAX program package.[18]

Important bond lengths and angles for **1** and **2** are given in Tables 2 and 3, respectively.

RESULTS AND DISCUSSION

The structure determination confirms that compound **1**, in which the anion has crystallographically imposed C_2 symmetry, is isostructural to $[NMe_4]_4[MS_4Cu_5Cl_7]$ (M = Mo,[5] W[4]) and $[PPh_4][NEt_4][ReS_4Cu_5X_7]$ (X = Cl, Br).[12] A perspective view of the cluster anion is shown in Fig.

Table 1. Crystallographic data

Compound	$[NEt_4]_4[WS_4Cu_5Br_7]$ (1)	$+WS_4Cu_6I_4(Py)_4+_n$ (2)
Chemical formula	$C_{32}H_{80}Br_7Cu_5N_4S_4W$	$C_{20}H_{20}Cu_6I_4N_4S_4W$
Formula weight	1710.3	1517.4 (for the monomer)
Crystal system	Monoclinic	Tetragonal
Space group	$C2/c$	$I\bar{4}2d$
a (Å)	23.054(4)	14.797(4)
b (Å)	10.809(2)	14.797(4)
c (Å)	22.118(4)	15.661(4)
β (°)	94.08(1)	90.00
V (Å^3)	5497(2)	3429.0
Z	4	4
μ (cm^{-1})	92.52	109.0
$F(000)$	3311	2768
D_{calc} (g cm^{-3})	2.07	2.94
Crystal dimensions (mm)	$0.36 \times 0.36 \times 0.42$	$0.40 \times 0.40 \times 0.30$
Radiation	Mo-K_α ($\lambda = 0.71073$ Å)	Mo-K_α ($\lambda = 0.71069$ Å)
Transmission factors	0.761–0.951	0.700–0.997
Scan mode	θ–2θ	ω–2θ
Scan width (°)	1.6	$0.40 + 0.35 \tan\theta$
Scan rate (° min^{-1})	8	16
2θ range (°)	2–54	1–54
Unique data measured	6541	1107
Unique data used	3919 [$I > 3.0\sigma(I)$]	765 [$I > 3.5\sigma(I)$]
No. of variables	242	110
Range of h, k, l	h, −29–28; k, 0–13; l, 0–28	h, 0–18; k, 0–12; l, 0–20
$(\Delta/\alpha)_{max}$	0.132	0.48
R(int)	0.019	0.020
R,[a] R_w[b]	0.0774, 0.062	0.055, 0.042
GOF (or S)	1.152	0.940
Largest/smallest peaks in final difference map (e Å^{-3})	1.60/−1.85	0.76/−0.76

[a] $R = \Sigma||F_o| - |F_c||/\Sigma|F_o|$.

[b] $R_w = [\Sigma w(|F_o| - |F_c|)^2/\Sigma w|F_o|^2]^{1/2}$. For **1**, $w = 1/[\sigma^2(|F_o| + 0.00015|F_o|^2)]$. For **2**, $w = F_o/114.0$ if $F_o < 114.0$; $w = 114.0/F_o$ if $F_o > 114.0$.

1. The geometry about the tungsten atom is nearly tetrahedral, see Table 2. Five CuBr units are bound to the WS_4 core [Cu—S 2.287(3)–2.371(4) Å] through double-bridged copper atoms, the sixth edge of the WS_4 tetrahedron remaining uncoordinated. The overall geometry can be viewed as a distorted double cube with two long Cu—Br distances [Cu(2)—Br(4) 2.685(2) and Cu(3a)—Br(4) 2.713(2) Å], as reported in other similar dicubane structures. The W—Cu distances [2.682(2)–2.705(2) Å] are comparable to the W—Cu distances observed in $[NEt_4]_4[WS_4Cu_5Cl_7]$ [2.656(2)–2.689(1) Å][4] or $\{Cu_3WS_3Br\}(PPh_3)_3S$ [2.715(2)–2.733(2) Å].[15]

A perspective view of the molecular structure and the cell packing of compound **2** are shown in Figs 2 and 3, respectively. The structure consists of an essentially tetrahedral WS_4 moiety encapsulated by a slightly distorted octahedron of six copper atoms, forming a WS_4Cu_6 aggregate with a crystallographic $\bar{4}$ symmetry axis situated at the tungsten atom. Linked by $—Cu_{eq}—I—Cu_{eq}—$ bridges, this aggregate connects with its nearest neighbours and develops a two-dimensional network. It is worth noting that the structure of the $[WCu_6]$ core in this cluster is very different from that of the $[MoCu_6]$ core in similar heptanuclear clusters, $[NMe_4]_5[MoS_4Cu_6Cl_9]$[6], or the $[VCu_6]$ core in $[VS_4Cu_6(PPh_3)_5Cl_3]\cdot CH_2Cl_2$.[10] The symmetry of the $[WCu_6]$ core in compound **2** is D_{4h}, while the symmetry of $[MoCu_6]$ in $[NMe_4]_5[MoS_4Cu_6Cl_9]$[6] is C_{3v} and the $[VCu_6]$ core in $[VS_4Cu_6(PPh_3)_5Cl_3]\cdot CH_2Cl_2$[10] possesses practically no symmetry element. The WS_4 core has retained the ideal geometry of free thiotungstate with the same W—S length [2.260(2) Å] and similar S—W—S angles [108.8(1)–109.8(3)°]. Each copper atom is bound across an edge of the WS_4 tetrahedron, giving each

Table 2. Selected bond lengths (Å) and angles (°) for $[NEt_4][WS_4Cu_5Br_7]$ (1)

W—Cu(1)	2.682(3)	W—Cu(2)	2.705(2)	W—Cu(3)	2.696(2)
W—S(1)	2.263(3)	W—S(2)	2.229(4)	W—Cu(2a)	2.705(2)
W—Cu(3a)	2.696(2)	W—S(1a)	2.263(3)	W—S(2a)	2.229(4)
Cu(1)—Br(1)	2.305(3)	Cu(1)—S(1)	2.287(3)	Cu(1)—S(1a)	2.287(3)
Cu(2)—Br(3)	2.339(2)	Cu(2)—Br(4)	2.685(2)	Cu(2)—S(1)	2.371(4)
Cu(2)—S(2)	2.325(4)	Cu(3)—Br(2)	2.327(2)	Cu(3)—S(1)	2.352(4)
Cu(3)—Br(4a)	2.713(2)	Cu(3)—S(2a)	2.311(4)	Br(4)—Cu(3a)	2.713(2)
S(2)—Cu(3a)	2.311(4)				
Cu(1)—W—Cu(2)	82.4(1)	Cu(1)—W—Cu(3)	83.0(1)	Cu(2)—W—Cu(3)	104.7(1)
Cu(1)—W—S(1)	54.3(1)	Cu(2)—W—S(1)	56.2(1)	Cu(3)—W—S(1)	55.8(1)
Cu(1)—W—S(2)	125.3(1)	Cu(2)—W—S(2)	55.2(1)	Cu(3)—W—S(2)	135.5(1)
S(1)—W—S(2)	109.9(1)	Cu(1)—W—Cu(2a)	82.4(1)	Cu(2)—W—Cu(2a)	164.7(1)
Cu(3)—W—Cu(2a)	73.4(1)	S(1)—W—Cu(2a)	113.7(1)	S(2)—W—Cu(2a)	136.4(1)
Cu(1)—W—Cu(3a)	83.0(1)	Cu(2)—W—Cu(3a)	73.4(1)	Cu(3)—W—Cu(3a)	166.1(1)
S(1)—W—Cu(3a)	114.9(1)	S(2)—W—Cu(3a)	55.0(1)	Cu(1)—W—S(1a)	54.3(1)
Cu(2)—W—S(1a)	113.7(1)	Cu(3)—W—S(1a)	114.9(1)	S(1)—W—S(1a)	108.6(2)
S(2)—W—S(1a)	109.6(1)	Cu(1)—W—S(2a)	125.3(1)	Cu(2a)—W—S(2a)	136.4(1)
Cu(3)—W—S(2a)	55.0(1)	S(1)—W—S(2a)	109.6(1)	S(2)—W—S(2a)	109.3(2)
W—Cu(1)—Br(1)	180.0(1)	W—Cu(1)—S(1)	53.5(1)	Br(1)—Cu(1)—S(1)	126.5(1)
W—Cu(1)—S(1a)	53.5(1)	Br(1)—Cu(1)—S(1a)	126.5(1)	S(1)—Cu(1)—S(1a)	107.0(2)
W—Cu(2)—Br(3)	159.0(1)	W—Cu(2)—Br(4)	93.6(1)	Br(3)—Cu(2)—Br(4)	107.4(1)
W—Cu(2)—S(1)	52.5(1)	Br(3)—Cu(2)—S(1)	121.9(1)	Br(4)—Cu(2)—S(1)	99.1(1)
W—Cu(2)—S(2)	51.9(1)	Br(3)—Cu(2)—S(2)	122.8(1)	Br(4)—Cu(2)—S(2)	97.3(1)
S(1)—Cu(2)—S(2)	103.1(1)	W—Cu(3)—Br(2)	156.8(1)	W—Cu(3)—S(1)	52.7(1)
Br(2)—Cu(3)—S(1)	121.3(1)	W—Cu(3)—Br(4a)	93.1(1)	Br(2)—Cu(3)—Br(4a)	110.0(1)
S(1)—Cu((3)—Br(4a)	98.0(1)	W—Cu(3)—S(2a)	52.2(1)	Br(2)—Cu(3)—S(2a)	121.7(1)
S(1)—Cu(3)—S(2a)	103.8(1)	Cu(2)—Br(4)—Cu(3a)	73.5(1)	W—S(1)—Cu(1)	72.2(1)
W—S(1)—Cu(2)	71.4(1)	Cu(1)—S(1)—Cu(2)	99.2(1)	W—S(1)—Cu(3)	71.5(1)
Cu(1)—S(1)—Cu(3)	100.5(1)	Cu(2)—S(1)—Cu(3)	129.7(2)	W—S(2)—Cu(2)	72.9(1)
W—S(2)—Cu(3a)	72.8(1)	Cu(2)—S(2)—Cu(3a)	88.3(1)		

sulphur atom a μ_4-S coordination. There are two types of copper atoms in the Cu_6 octahedron: two axial Cu(1) atoms and four equatorial Cu(2) atoms. Each axial Cu(1) atom has one terminal iodine atom and two μ_4-S atoms, forming a trigonal geometry. Each equatorial Cu(2) atom is four-coordinated by a pair of μ_4-S atoms, one μ_2-I atom and one nitrogen atom of a pyridine molecule with a distorted tetrahedral $ICu(\mu_4\text{-}S)_2N$ unit. It is of interest to note that the Cu_{eq}—I length [2.764(3) Å], which is comparable to the values observed in compounds containing tetrahedrally-coordinated copper (e.g. 2.700 Å in $[PEt_3CuI]_4$[19] or 2.629(1)–2.639(1) Å in $[MoS_4Cu_4I_2(Py)_6]$[20]), is 0.322 Å longer than that of

Table 3. Selected bond lengths (Å) and angles (°) for $[WS_4Su_6I_4(Py)_4]$ (2)

W—S	2.260(2)	W—Cu(1)	2.668(2)	W—Cu(2)	2.694(3)
S—Cu(1)	2.282(2)	S—Cu(2)	2.325(4)	Cu(1)—I(1)	2.442(4)
Cu(2)—I(2)	2.764(3)	Cu(2)—N	1.916(5)		
S—W—S(1)	109.8(3)	S(1)—W—S′	108.8(1)	S—W—S(1′)	109.8(3)
W—S—Cu(1)	72.0(1)	W—S—Cu(2)	71.9(2)	W—S(1)—Cu(2)	71.6(2)
Cu(1)—W—Cu(2)	95.93(6)	Cu(1)—W—Cu(1′)	180.01(2)	Cu(1′)—W—Cu(2)	84.08(6)
Cu(1)—S—Cu(2)	119.7(3)	Cu(1′)—S—Cu(2)	102.0(2)	Cu(2)—S—Cu(2′)	110.2(2)
W—Cu(1)—I(1)	180.1(2)	W—Cu(2)—I(2)	100.1(1)	W—Cu(2)—N	160.3(3)
S—Cu(2)—I(2)	95.1(2)	S—Cu(1)—I(1)	126.4(1)	S—Cu(1)—S′	107.6(2)
S—Cu(2)—S(1)	105.1(2)	S—Cu(2)—N	127.1(3)	I(2)—Cu(2)—N	99.5(3)
Cu(2)—N—C(1)	126.0(4)	Cu(2)—N—C(5)	118.4(5)		

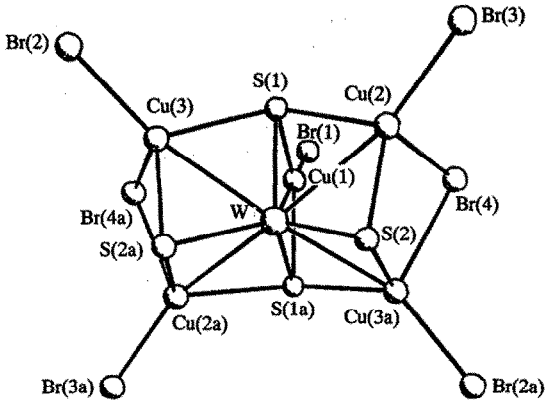

Fig. 1. Structure of the cluster anion $[WS_4Cu_5Br_7]^{4-}$.

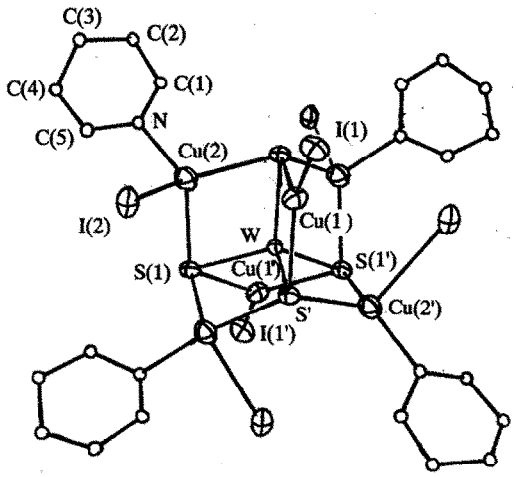

Fig. 2. Structure of the cluster compound $-[WS_4Cu_6I_4(Py)_4]-_n$.

the Cu_{ax}—I length [2.442(4) Å]. The Cu—S lengths also reflect the mode of coordination of the copper atoms: 2.282(2) Å for trigonal geometry, 2.325(4) Å for a tetragonal environment. These Cu—S lengths are very similar to those reported for $[NMe_4]_5[MoS_4Cu_6Cl_9]$[6] or $[VS_4Cu_6(PPh_3)_5Cl_3]\cdot CH_2Cl_2$.[10] Owing to the slight distortion of the Cu_6 octahedron, the W—Cu lengths are slightly different: 2.668(2) Å for the W—Cu_{ax} length and 2.694(3) Å for the W—Cu_{eq} length, respectively. These values are typical of corresponding lengths observed in other W—Cu—S clusters (e.g. 2.656(2)–2.689)(1) Å in $[NMe_4]_4[WS_4Cu_5Cl_7]$[4] or 2.6885(7)–2.6932(8) Å in $[NEt_4]_2[WS_4(CuNCS)_4]$[9]).

Since the W—Cu(1)—I(1) and Cu(1)—W—Cu(1′) angles are 180° and the tungsten atom remains situated on the 4-axis, the W, Cu(1), Cu(1′), I(1) and I(1′) atoms are co-linear. The Cu(1)—W—Cu(2) angle is 95.93(6)°, indicating that the tungsten atom is slightly above or below the mean plane composed of the four Cu_{eq} atoms.

In the IR spectrum of compound **1** bands at 447s and 421s cm^{-1} are assigned to the bridged WS_4 group. In the 350–250 cm^{-1} region bands at 310m, 290m, 260m and 253m are considered as the

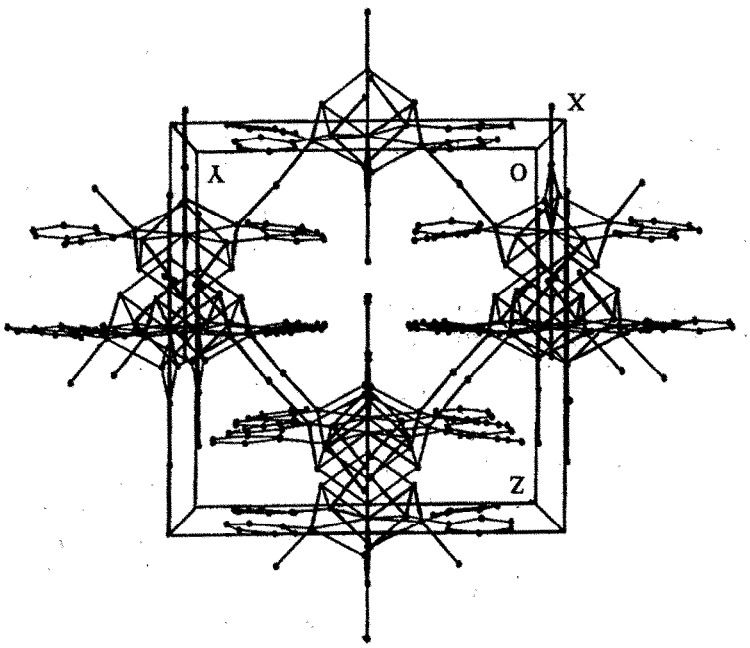

Fig. 3. Cell packing of $-[WS_4Cu_6I_4(Py)_4]-_n$.

ν(Cu—Br) vibrations. The electronic spectrum shows the expected $s \rightarrow w$ charge transfer at 438(3.7), 330(sh) and 310(12.2) nm.

In the IR spectrum of compound **2** the band at 430s cm^{-1} is assigned to the symmetric bridged WS_4 group. The electronic spectrum shows the expected $s \rightarrow w$ charge transfer at 443(5.3), 335(sh) and 263(26.2) nm.

Cyclic voltammetric measurements for $[WS_4Cu_5Br_7]^{4-}$ in DMF in the range -2.0 to -0.0 V display one pair of quasi-reversible oxidation–reduction waves ($E_{pa} = -0.275$, $E_{pc} = -0.55$, $\Delta E = 0.275$ V) and one irreversible reduction wave at -1.25 V.

The $[Bu^n_4N]Br$ compound is used to decrease the melting point of the solid mixture in the solid-state synthesis of compound **1**. It is noted that the title compound contains no $[Bu^n_4N]^+$ cation, only four $[NEt_4]^+$ cations are present. We cannot explain this priority at present.

In the synthesis of compound **2** the possible formula of the red solid-state intermediate product was concluded to be $[Bu^n_4N]_4[WS_4Cu_6I_8]$ using IR spectroscopy [ν(W—μ_4—S): 436.12s, 417.58 cm^{-1}] and elemental analysis. Found: C, 28.2; H, 5.2; N, 2.4; Cu, 14.0; W, 6.5. Calc. for $C_{64}H_{144}Cu_6I_8N_4W$: C, 28.7; H, 5.4; N, 2.1; Cu, 14.2; W, 6.9%. Attempts to obtain a single crystal of good quality failed. Interestingly, when the pyridine vapour slowly diffused into the acetonitrile solution of the intermediate product and partly substituted four of the eight iodine groups a beautiful octahedral crystal of the title compound formed. A possible substitution reaction is given as follows:

$$[Bu^n_4N]_4[WS_4Cu_6I_8] \xrightarrow[1\text{ month}]{\text{Pyridine vapour}} +[WS_4Cu_6I_4(Py)_4]+_n.$$

When the intermediate product was dissolved in excess pyridine one red brick-like crystal was formed in a couple of days and a reddish-orange needle crystal was deposited on standing in air a month later. Based on the elemental analysis and IR spectra of these two products the red brick-like crystal and the reddish-orange needle crystal were concluded to be the known compounds $[WS_4Cu_4I_2(Py)_6]$[21] and $[WS_4Cu_2(Py)_4]$,[22] respectively. The formation of these two cluster compounds was attributed to the collapse of the framework of the cluster core WS_4Cu_6. The two reactions are given as follows:

$$[Bu^n_4N]_4[WS_4Cu_6I_8] \xrightarrow[1\text{–}2\text{ days}]{\text{Pyridine}} [WS_4Cu_4I_2(Py)_6]$$

$$[Bu^n_4N]_4[WS_4Cu_6I_8] \xrightarrow[1\text{ month}]{\text{Pyridine}} [WS_4Cu_2(Py)_4].$$

It is expected that a series of new cluster compounds can be prepared from substitution of iodine groups in this intermediate product with other strong ligands, such as PPh_3, dppm and $S_2CNMe_2^-$[1]. Research on this aspect of the work is currently under way.

Acknowledgements—This research was supported by the National Natural Science Foundation of China and the State Education Commission Foundation of China.

REFERENCES

1. A. Müller, E. Diemann, R. Jostes and H. Bögge, *Angew. Chem., Int. Edn Engl.* 1981, **20**, 934.
2. A. Müller, H. Bögge, M. Penk, K. Nieradzik, M. Dartmann, E. Krickemeyer, J. Schimanski, C. Romer, M. Romer, H. Dornfeld, U. Weinboker, W. Hellmann and M. Zimmermann, *Monat. Chem.* 1989, **120**, 367.
3. F. Secheresse, S. Bernes, F. Robert and Y. Jeannin, *J. Chem. Soc., Dalton Trans.* 1991, 2875.
4. F. Secheresse, J. M. Manoli, C. Potvin and S. Marzak, *J. Chem. Soc., Dalton Trans.* 1988, 3055.
5. F. Secheresse, F. Robert, S. Marzak, J. M. Manoli and C. Potvin, *Inorg. Chim. Acta* 1991, **182**, 221.
6. S. Bernes, F. Secheresse and Y. Jeannin, *Inorg. Chim. Acta* 1992, **191**, 11.
7. J. R. Nicholson, A. C. Flood, C. D. Garner and W. Clegg, *J. Chem. Soc., Chem. Commun.* 1983, 1179.
8. S. F. Gheller, T. W. Hambley, J. R. Rodgers, R. T. C. Brownlee, M. J. O'Connors, M. R. Snow and A. Wedd, *Inorg. Chem.* 1984, **23**, 2519.
9. J. M. Manoli, C. Potvin, F. Secheresse and S. Marzak, *Inorg. Chim. Acta* 1988, **150**, 257.
10. C. D. Scattergood, P. G. Bonney, J. M. Slater, C. D. Garner and W. Clegg, *J. Chem. Soc., Chem. Commun.* 1987, 1749.
11. A. Müller, E. Krickemeyer, A. Hildebrand, H. Bögge, K. Schneider and M. Lemke, J. Chem. Soc., Chem. Commun. 1991, 1685.
12. A. Müller, E. Krickemeyer and H. Bögge, *Z. Anorg. Allg. Chem.* 1987, **554**, 61; *Angew. Chem.* 1986, **98**, 987; *Angew. Chem., Int. Edn Engl.* 1986, **25**, 990.
13. J. G. Li, X. Q. Xin, Z. Y. Zhou and K. B. Yu, *J. Chem. Soc., Chem. Commun.* 1991, 250.
14. X. Q. Xin, J. P. Lang, K. B. Yu, Z. Y. Zhou, J. H. Cai, B. S. Kang, M. Q. Chen and P. Q. Zheng, *J. Inorg. Chem.* 1992, **8**, 472.
15. J. P. Lang, H. Z. Zhu, X. Q. Xin, M. Q. Chen, K. Liu and P. J. Zheng, *Chin. J. Chem.* 1992, **10**, 521.
16. J. W. McDonald, G. D. Friesen, L. D. Rosenhein and W. E. Newton, *Inorg. Chim. Acta* 1983, **72**, 205.
17. *International Tables for X-ray Crystallography*, Vol. IV, pp. 72–98. Kynoch Press, Birmingham (1974).
18. B. A. Frenz, *The Enraf–Nonius CAD 4 SDP—A Real-time System for Concurrent X-ray Data Collection and Structure Determination in Computing in*

Crystallography, pp. 64–71. Delft University Press, The Netherlands (1978).
19. M. R. Churchill, B. G. Deboer and S. J. Mendak, *Inorg. Chem.* 1975, **14**, 2041.
20. J. G. Li, F. J. Gao, J. P. Lang, X. Q. Xin and M. Q. Chen, *J. Struct. Chem.* 1992, **11**, 351.
21. G. X. Jin, PhD Thesis, Nanjing University, China (1987).
22. F. J. Gao, H. Z. Zhu, X. Q. Xin, A. B. Dai, W. X. Liu, B. Y. Wang and P. J. Zheng, *Chem. J. Chin. Univ.* 1990, **11**, 1045.

Polyhedron Vol. 12, No. 13, pp. 1655–1660, 1993
Printed in Great Britain

0277–5387/93 $6.00+.00
© 1993 Pergamon Press Ltd

COMPLEXES OF 1,6-BIS(BENZIMIDAZOL-2-YL)-2,5-DITHIAHEXANE (BBDH) WITH ZINC(II), CADMIUM(II) AND MERCURY(II) HALIDES. CRYSTAL STRUCTURE OF $[Hg(BBDH)Cl_2] \cdot C_2H_5OH$

R. CARBALLO,* A. CASTIÑEIRAS† and M. C. G. CONDE

Departamento de Química Inorgánica, Universidad de Santiago de Compostela, E-15706 Santiago de Compostela, Spain

and

W. HILLER

Anorganisch-chemisches Institut der Technisches Universität München, Lichtenbergstr. 4, D-8046 Garching, F.R.G.

(*Received* 28 *January* 1993; *accepted* 5 *March* 1993)

Abstract—We describe the synthesis and characterization by elemental analysis, conductance measurements and ^1H NMR and IR spectrometry of compounds with the general formula $[M(BBDH)X_2]$ [M = Zn, Cd or Hg; X = Cl, Br or I; BBDH = 1,6-bis(benzimidazol-2-yl)-2,5-dithiahexane], which were prepared by reaction of zinc, cadmium or mercury dihalides with BBDH in ethyl alcohol. In addition, the structure of $Hg(BBDH)Cl_2 \cdot EtOH$ (**VI**) was determined by single-crystal structure analysis. The mercury atom is coordinated with slightly distorted tetrahedral geometry to the unprotonated nitrogen atoms of the BBDH benzimidazolyl groups [Hg—N = 225.8(5) and 223.6(6) pm] and to two chlorine atoms [Hg—Cl = 251.3(3) and 249.9(2) pm].

Acquisition of the fairly comprehensive knowledge we now have of the coordination chemistry of transition metals (especially cobalt, nickel and copper) with linear NSSN tetradentate ligands, in which the sulphur atoms belong to a thioether and the nitrogen atoms to heterocycles such as imidazole, benzimidazole, pydidine or quinoline,[1–5] has been prompted in part by the fact that the resulting complexes seem to be acceptable models of the active centres of metallobiomolecules;[6,7] all four donors of the *facultative* ligands being theoretically able to coordinate simultaneously to the metal atom. The versatility of these ligands as regards the number of donor atoms actually involved in coordination, and the relative ease with which they can adapt to a variety of coordination geometries, has been repeatedly demonstrated in complexes with the above-mentioned transition metals.[8–12]

By contrast, NSSN ligands have rarely been complexed with post-transition metals such as zinc, cadmium and mercury, in spite of zinc being a metal of considerable importance in many biological systems.[13]

In continuation of our studies on the coordination chemistry of the halides of divalent group 12 metals[14–19] in this work we report the synthesis and structures of the products of reaction between zinc, cadmium or mercury dihalides and 1,6-bis(benzimidazol-2-yl)-2,5-dithiahexane (BBDH), a linear NSSN tetradentate ligand whose capacity to coordinate with transition metals is well documented.[5,8,20–25]

* Present address: Departamento de Química Pura y Aplicada, Universidad de Vigo, Vigo, Spain.

† Author to whom correspondence should be addressed.

EXPERIMENTAL

Materials

BBDH was prepared using a published method.[26] Metal(II) halides and solvents were reagent-grade commercial products.

Metal complexes

All the complexes were prepared by the following general procedure. A solution of BBDH (1 mmol) in hot ethanol (15 cm^3) was added to a solution of metal(II) halide (1 mmol) in ethyl alcohol (25 cm^3) and the mixture kept stirring for several days. The solid products were filtered off, washed thoroughly with cold ethanol and dried over $CaCl_2$ (yield 70–95%). Crystals of **VI** were grown by dissolving the crude product in EtOH and slow evaporation of the solvent.

Physical measurements

Carbon, hydrogen and nitrogen analyses were performed on a Perkin–Elmer 240B microanalyser. Conductance measurements in methylcyanide at *ca* 10^{-3} M were obtained at 293 K on a WTW Type LF-3 conductivity bridge. ^1H NMR spectra were recorded in DMSO-d_6 on a Bruker WM250 spectrometer using TMS as an internal standard. IR spectra were recorded over the range 4000–400 cm^{-1} on a Perkin–Elmer 1330 spectrophotometer using KBr pellets and in the range 500–100 cm^{-1} on a Perkin–Elmer 180 spectrophotometer using Nujol mulls between polyethylene windows. Analytical data are listed in Table 1.

X-ray analysis

A colourless crystal of **VI** with the dimensions $0.20 \times 0.30 \times 0.10$ mm was mounted on an Enraf–Nonius CAD4 diffractometer and intensities were measured at room temperature using graphite-monochromated Mo-K_α radiation ($\lambda = 0.71073$ Å). The cell constants were determined from the setting angles of 25 reflections. Crystal data are summarized in Table 2. 4516 reflections were collected in the range $3 < \theta < 25°$ in the ω–θ scan mode. Of 3884 unique data measured ($R_{int} = 0.025$) 3221 with $I > 3\sigma(I)$ were used in the structure determination and refinement. Lp corrections and an empirical absorption correction[27] were applied to the data.

The structure was solved by direct methods[28] and refined on F by full-matrix least-squares procedures.[29] In the last refinement all non-hydrogen atoms were assigned anisotropic temperature parameters. the hydrogen atoms were located on a difference map and included in structure–factor calculations with B_{iso} fixed at 4.0 $Å^2$, but not refined. A secondary extinction correction was made[30] and the final coefficient refined in the least-squares cycle was 1.248×10^{-7}. The final R value was 0.035 with $Rw = 0.039$ [weighting scheme $w = 1/\sigma^2(F)$; 272 parameters; $S = 1.967$; maximum Δ/σ in final cycle < 0.001; maximum $\Delta\rho = 0.799$ e $Å^{-3}$]. Scattering factors were taken from the International Tables.[31]

Table 1. Analytical and other data for the complexes

Compound	Colour	M.p. (°C)	Analytical data[a] C	H	N	Λ_M[b]
$Zn(BBDH)Cl_2$ (I)	White	200	45.1 (44.1)	3.9 (3.7)	11.7 (11.4)	5.8
$Zn(BDDH)Br_2$ (II)	White	196	38.6 (37.3)	3.8 (3.1)	9.1 (9.7)	5.5
$Cd(BBDH)Cl_2$ (III)	White	290	40.3 (40.2)	3.7 (3.4)	10.8 (10.4)	10.6
$Cd(BBDH)Br_2 \cdot 2H_2O$ (IV)	White	275	32.1 (32.6)	3.2 (3.3)	8.4 (8.5)	11.2
$Cd(BBDH)I_2 \cdot EtOH$ (V)	Yellow	124	30.8 (31.3)	3.5 (3.2)	6.5 (7.3)	13.5
$Hg(BBDH)Cl_2 \cdot EtOH$ (VI)	White	141	35.5 (35.7)	3.5 (3.6)	8.1 (8.3)	23.8
$Hg(BBDH)Br_2$ (VII)	White	151	29.9 (30.2)	2.9 (2.5)	8.0 (7.8)	19.7
$Hg(BBDH)I_2$ (VIII)	Yellow	220	26.5 (26.7)	2.2 (2.2)	6.7 (6.9)	29.4

[a] Calculated values are given in parentheses.
[b] S cm^2 mol^{-1}, in methylcyanide at *ca* 10^{-3} M (20°C).

Table 2. Crystal data for **VI**

Formula	$C_{20}H_{24}Cl_2HgN_4OS_2$
Mr	672.06
Space group	$P\bar{1}$
a (pm)	1117.7(5)
b (pm)	1368.3(3)
c (pm)	833.1(5)
α (°)	104.99(4)
β (°)	95.63(4)
γ (°)	77.67(4)
$V \times 10^6$ (pm^3)	1198.4
D_c ($g\ cm^{-3}$)	1.862
μ(Mo-K_α) (cm^{-1})	68.321
Z	2
F(000)	652
Temperature (K)	293

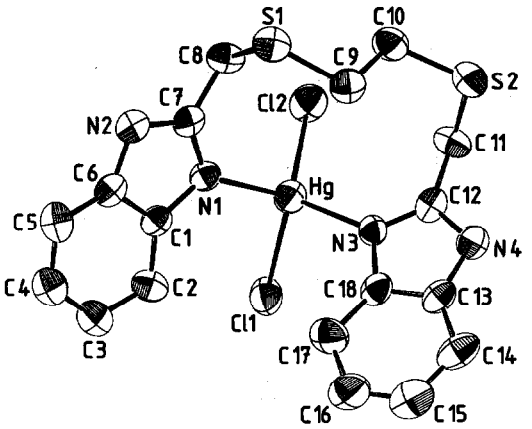

Fig. 1. View of the structure of $Hg(BBDH)Cl_2$ showing the numbering scheme.

Computations were performed on a DEC Micro VAXII computer.

RESULTS AND DISCUSSION

The metal complexes are quite stable at room temperature, having shown no signs of decomposition since their synthesis. The conductivities of *ca* 10^{-3} M solutions in methylcyanide at 20°C (5.0–30.0 S m^2 mol^{-1}; Table 1) class them as non-electrolytes[32] and hence show that their halogen atoms are coordinated to the metal.

Structure of VI

Compound **VI** is a 1:1 $HgCl_2$-BBDH complex with an ethyl alcohol molecule included in the crystal structure. The conformation of the complex is shown with the atom labelling used in Fig. 1. The bond lengths and angles involving the mercury atom are listed in Table 3.

The mercury atom has a slightly distorted tetrahedral coordination sphere involving two chlorine atoms and two unprotonated nitrogen atoms of the benzimidazolyl groups of the ligand. The Hg—Cl distances are within the range of divalent Hg—Cl bond lengths reported in other studies.[33,34]

In a comprehensive statistical analysis of interatomic distances in accurately determined structures of inorganic and organometallic complexes Allen *et al.*[34] observed that Hg—N distances fall into two fairly well-defined groups, with means of 214.0 and 240.0 pm, although no chemical distinction between long and short bonds was apparent. The Hg—N distances in **VI**, 225.8(5) and 223.6(6) pm, are intermediate. In this structure the Hg—N bond may involve weak back-donation from mercury due to the electron-withdrawing effect of the chlorine ligands.[18,19]

The extent of the tetrahedral distortion is shown by the angles about the mercury atom varying from 101.0(2)° in Cl(1)—Hg—N(3) to 117.0(2)° in Cl(2)—Hg—N(3).

IR spectra

The assignments of some of the IR bands of free BBDH and its complexes are listed in Table 4.

4000–500 cm^{-1} *Range.* The IR spectra of the compounds are very similar to one another and to that of BBDH itself. The most significant differences are in the NH stretching region, the frequency of ν(NH) increasing by 350–500 cm^{-1} on coordination, and in the 1450–1400 cm^{-1} region,

Table 3. Coordination distances (pm) and angles (°) in **VI**

Hg—Cl(1)	251.3(3)	Hg—N(1)	225.8(5)
Hg—Cl(2)	249.9(2)	Hg—N(3)	223.6(6)
Cl(1)—H—Cl(2)	111.44(9)	Cl(2)—Hg—N(1)	108.9(2)
Cl(1)—Hg—N(1)	109.1(2)	Cl(2)—Hg—N(3)	117.0(2)
Cl(1)—Hg—N(3)	101.0(2)	N(1)—Hg—N(3)	109.1(1)

Table 4. Selected IR bands of the complexes and BBDH (cm^{-1})

BBDH	I	II	III	IV	V	VI	VII	VIII	Assignments
—	—	—	—	—	3508 s	3450 s	—	—	ν(OH)
2800 s(b)	3240 m	3300 m	3170 m	3170 s	3317 s	3240 s	3320 s	3160 m	ν(NH)
1630 m	1625 m	1624 m	1628 m	1623 m	1628 m	1626 s	1623 m	1624 m	ν(CN)
1597 m	1598 m	1598 m	1598 m	1597 m	1602 m	1600 m	1597 m	1600 m	ν(CN)
1438 s	1394 w	1405 w	1410 m	1410 m	1412 m	1395 w	1404 w	1408 m(sh)	δ(NH)
700 w	700 w	695 w	700 vw	702 w	701 w	698 w	700 w	690 m	ν(CS)
—	352 m	—	340 m	333 w	328 w	338 m	339 m	—	ν(MN)
	307 m	300 w	292 w	—	285 w	297 m	301 m	310 w	
—	278 m	206 m	268 m	213 m	165 m	252 m	186 m	163 m	ν(MX)
	263 m	191 m	233 m	187 w	147 m	216 m	166 w	142 w	

where δ(NH) shifts from 1438 cm^{-1} in the free ligand to around 1400 cm^{-1} in the complexes. These changes indicate direct bonding between the unprotonated nitrogen atoms of the benzimidazolyl groups and the metal atom. A weak band observed at 700 cm^{-1} and assigned mainly to the ν(CS) stretching vibration[35] is unshifted upon coordination, suggesting that these complexes are not sulphur-bonded.

BBDH exhibits absorptions at 1630 and 1597 cm^{-1}, which are assumed to be due mainly to C—N stretching in the imidazole ring. The complexes all exhibit the same two bands, the lower energy band maintaining the same position while the higher energy band shifting to 1598–1602 cm^{-1}. These shifts in ν(CN) to lower frequencies indicate delocalization of the imidazole ring, in keeping with the C—N distances found in compound **VI**.

500–100 cm^{-1} *Range*. The IR spectra of all the complexes have two strong bands in the region 280–140 cm^{-1} and two weak-to-medium absorptions around 350–330 and 310–280 cm^{-1}. The strong bands are assigned to ν(MX), their observed frequencies being consistent with reported values for non-bridging halogen–metal bonds in a distorted tetrahedral MN_2X_2 skeleton with ideal C_{2v} symmetry.[19,36,37] For a given metal ν(MX) decreases in the order M—Cl > M—Br > M—I. In addition, the frequency ratios ν(MBr)/ν(MCl) = 0.73–0.80 and ν(MI)/ν(MCl) = 0.62–0.66 are consistent with those of tetrahedral structures which have appeared in the literature.[38,39] The bands in the 350–330 and 310–280 cm^{-1} regions may be attributed to the symmetric and assymmetric ν(MN) modes.[37,40]

^1H *NMR spectra*

The NMR spectral data obtained in this work are presented in Table 5, together with those of the free ligand.[9] The methylene and ethylene proton resonances occur as singlets, indicating equivalent protons. The methylene protons are shifted downfield and the ethylene protons upfield, but the magnitude of these shifts is insufficient to suggest

Table 5. ^1H NMR spectral data of BBDH and the complexes (δ ppm) relative to TMS[a]

Compound	HC(3), HC(4) HC(15), HC(16)	HC(2), HC(5) HC(14), HC(17)	$H_2C(8)$ $H_2C(11)$	$H_2C(9)$ $H_2C(10)$	HN(2) HN(4)
BBDH	7.50 m	7.14 m	3.97 s	2.79 s	12.55
I	7.65 m	7.22 m	4.10 s	2.68 s	13.07
II	7.63 m	7.20 m	4.08 s	2.71 s	nd
III	7.58 m	7.20 m	4.06 s	2.76 s	nd
IV	7.55 m	7.18 m	4.02 s	2.77 s	nd
V[b]	7.53 m	7.17 m	4.00 s	2.77 s	nd
VI[b]	7.72 m	7.23 m	4.20 s	2.70 s	nd
VII	7.76 m	7.29 m	4.23 s	2.69 s	nd
VIII	7.68 m	7.25 m	4.18 s	2.74 s	nd

[a] For proton nomenclature see the description of the structure of **VI**. The abbreviation nd indicates not detected.

[b] The ethanol resonances are found at 1.04 (t), 3.42 (q) and 1.05 (t) , 3.45 (q), respectively.

coordination via the thioether sulphur atoms. BBDH thus acts as a bidentate ligand, as was shown for **VI** by X-ray studies.

BBDH exhibits two groups of aromatic proton resonances approximately 0.36 ppm apart. These two groups also appear in the spectrum of all the complexes, but the high-field group is shifted downfield by up to 0.15 ppm and the low-field group by up to 0.26 ppm. It is assumed that the low-field group comprizes the benzene ring protons nearest to the imidazole ring and that coordination via an imidazole nitrogen atom deshields one of these protons much more than the other ring protons. Since only one set of benzimidazolyl proton resonances appears in the spectrum, it is further assumed that both benzimidazolyl groups coordinate to the same metal atom.

The presence of well-resolved, deshielded, imidazole-ring proton resonances in the NMR spectrum complex **I** also indicates M—N binding.

Regardless of which halogen was present, the aromatic proton signals are shifted most in mercury complexes and least in cadmium complexes. This difference may reflect the strength of the metal–ligand bond.*

REFERENCES

1. E. Bouwman, W. L. Driessen and J. Reedijk, *Coord. Chem. Rev.* 1990, **104**, 143.
2. A. Castiñeiras, W. Hiller, J. Strähle, M. V. Paredes and J. Sordo, *Acta Cryst.* 1985, **C41**, 41.
3. A. Castiñeiras, R. Carballo, W. Hiller and J. Strähle, *Z. Krystallogr.* 1990, **193**, 251.
4. E. Bermejo, R. Carballo, A. Castiñeiras, A. Lombao, W. Hiller and J. Strähle, *Polyhedron* 1991, **10**, 1579.
5. J. M. M. Smits, R. Janssen, P. T. Beurskens, J. Van Rijn and R. Reedijk, *Polyhedron* 1987, **6**, 1843.
6. A. E. Martell, *Metal Ions in Biological Systems*, Vol. 2. Marcel Dekker Inc., New York (1973).
7. K. D. Karlin and J. Zubieta, *Biological and Inorganic Copper Chemistry*. Adenine Press, New York (1986).
8. G. R. Brubaker, J. N. Brown, M. K. Yoo, R. A. Kinsey, M. T. Kutchan and E. A. Motell, *Inorg. Chem.* 1979, **18**, 299.
9. P. J. M. W. L. Birker, J. Helder, G. Henkel, B. Krebs and J. Reedijk, *Inorg. Chem.* 1982, **21**, 357.
10. M. J. Schilstra, P. J. M. W. L. Birker, G. C. Verschoor and J. Reedijk, *Inorg. Chem.* 1982, **21**, 2637.
11. A. Castiñeiras, W. Hiller, J. Strähle, R. Carballo, M. R. Bermejo and M. Gayoso, *Z. Naturforsch.* 1990, **45b**, 1267.
12. R. Carballo, A. Castiñeiras, W. Hiller and J. Strähle, *Acta Cryst.* 1991, **C47**, 1736.
13. M. J. Kendrick, M. T. May, M. J. Plishka and K. D. Robinson, *Metals in Biological Systems*. Ellis Horwood, New York (1992).
14. A. Arquero, J. R. Masaguer and A. Castiñeiras, *Z. Anorg. Allg. Chem.* 1985, **531**, 183.
15. W. Hiller, A. Castiñeiras, A. Arquero and J. R. Masaguer, *Acta Cryst.* 1986, **C42**, 151.
16. A. Castiñeiras, A. Arquero, J. R. Masaguer, S. Martinez-Carrera and S. García-Blanco, *Z. Anorg. Allg. Chem.* 1986, **539**, 219.
17. A. Castiñeiras, C. F. Vidal, R. Bastida, A. Macías and W. Hiller, *Polyhedron* 1988, **7**, 2503.
18. A. Castiñeiras, G. Díaz, F. Florencia, S. García-Blanco and S. Martinez-Carrera, *J. Cryst. Spectrosc. Res.* 1988, **18**, 395.
19. A. Castiñeiras, G. Díaz, F. Florencio, S. García-Blanco and S. Martinez-Carrera, *Z. Anorg. Allg. Chem.* 1988, **567**, 101.
20. M. F. Cabral, J. O. Cabral, J. Van Rijn and J. Reedijk, *Inorg. Chim. Acta* 1984, **87**, 87.
21. J. Ochocki, P. H. Chaudhuri, W. L. Driessen, R. A. G. De Graaf, F. B. Hulsbergen and J. Reedijk, *Inorg. Chim. Acta* 1990, **167**, 15.
22. L. A. Oro, D. Carmona and J. Reedijk, *Inorg. Chim. Acta* 1983, **71**, 115.
23. A. Castiñeiras, R. Carballo, W. Hiller and J. Strähle, *Acta Cryst.* 1990, **C46**, 1739.
24. W. Hiller, J. Strähle, A. Castiñeiras, R. Carballo, M. R. Bermejo and M. Gayoso, *An. Quím.* 1990, **86**, 506.
25. A. Castiñeiras, R. Carballo, W. Hiller and J. Strähle, *Acta Cryst.* 1991, **C47**, 1725.
26. A. W. Addison and P. J. Burke, *J. Heterocyc. Chem.* 1981, **18**, 803.
27. N. Walker and D. Stuart, *Acta Cryst.* 1983, **A39**, 159.
28. G. M. Sheldrick, SHELXS86, A Program for the Solution of Crystal Structures from X-ray Diffraction Data. University of Göttingen, F.R.G. (1986).
29. B. A. Frenz, The Enraf–Nonius CAD4-SDP. A real-time system for concurrent X-ray data collection and crystal structure solution. In *Computing in Crystallography* (Edited by H. Schenk, R. Olthof-Hazekamp, H. Van Koningsueld and G. G. Bassi). Delft University Press, Delft (1976).
30. W. H. Zachariasen, *Acta Cryst.* 1963, **16**, 1139.
31. W. C. Hamilton and J. A. Ibers (Editors), *International Tables for X-ray Crystallography*, Vol. IV. Kynoch Press, Birmingham (1974) (Present distributor, Kluwer Academic Publishers, Dordrecht).
32. W. J. Geary, *Coord. Chem. Rev.* 1971, **7**, 81.
33. D. P. Graddon, *Rev. Inorg. Chem.* 1982, **4**, 211.
34. A. G. Orpen, L. Brammer, F. H. Allen, D. G. Watson and R. Taylor, *J. Chem. Soc., Dalton Trans.* 1989, S1.
35. M. Ohsaku, *Bull. Chem. Soc. Japan* 1975, **48**, 707.

* Further details of the structure determination have been deposited as Supplementary Publication No. CSD-53222. Copies may be obtained through the Fachinformationszentrum Karlsruhe, D-7514 Eggenstein-Leopoldshafen 2, Germany.

36. G. E. Coates and D. Ridley, *J. Chem. Soc.* 1964, 166.
37. R. J. H. Clark and C. S. Williams, *Inorg. Chem.* 1965, **4**, 350.
38. I. M. Cheremisina, *J. Struct. Chem.* 1978, **19**, 286.
39. E. N. Yurchenko, E. B. Burgina, L. V. Konovalov, V. G. Pogareva and V. I. Bugaev, *J. Struct. Chem.* 1982, **22**, 708.
40. K. H. Tan and M. J. Taylor, *Aust. J. Chem.* 1980, **33**, 1753.

Polyhedron Vol. 12, No. 13, pp. 1661–1667, 1993
Printed in Great Britain

0277–5387/93 $6.00+.00
© 1993 Pergamon Press Ltd

CRYSTAL STRUCTURE AND SPECTROSCOPIC PROPERTIES OF $(NH_4)[UBr_2(CH_3CN)_2(H_2O)_5]Br_2$

E. ZYCH, P. STARYNOWICZ, T. LIS and J. DROŻDŻYŃSKI*

Institute of Chemistry, University of Wrocław, 50-383 Wrocław, Poland

(*Received* 27 *January* 1993; *accepted* 5 *March* 1993)

Abstract—The synthesis, crystal structure and spectroscopic properties of a uranium(III) compound of the formula $(NH_4)[UBr_2(CH_3CN)_2(H_2O)_5]Br_2$ is reported. The IR, Raman and electronic spectra of the compound have been recorded in the 30–4000 and 4000–26,000 cm^{-1} spectral ranges, respectively, and are discussed. The assignments of the IR and Raman frequencies are given.

In a previous paper[1] the synthesis and characterization of a compound with an incorrectly assumed formula, $NH_4UBr_4 \cdot 1.5CH_3CN \cdot 6H_2O$, was reported. The crystal structure determination presented in this paper reveals that the correct formula of the compound is $(NH_4)[UBr_2(CH_3CN)_2(H_2O)_5]Br_2$. For the first time uranium(III)–nitrogen bond lengths have been determined from single crystal data. The paper also reports an analysis of the IR and electronic spectra of the compound.

EXPERIMENTAL

Synthesis

In order to obtain single crystals of the compound uranium tetrabromide (5–6 g) together with an excess of ammonium bromide were added to acetonitrile (*ca* 100 cm^3). The mixture was shaken from time to time and left standing for 10–15 h. Subsequently, propionic acid (0.7 cm^3) and freshly distilled ethyl ether (15 cm^3) were added. After filtering, the solution, together with *ca* 1 cm^3 of liquid zinc amalgam, was transferred to a glass tube *ca* 15 cm long and 1.5 cm in diameter. The solution was added until its level reached a narrowing of 0.5 cm in the middle of the tube. Next, the tube was transferred to a flask and the solution was degassed by connecting the flask to a vacuum pump, reduced by gentle shaking and finally kept under nitrogen. A 100 : 15 : 0.7 : 0.9 solution of acetonitrile, ethyl ether, propionic acid and water, respectively, had been prepared separately. Approximately the same volume of solution as before was degassed and carefully transferred into the upper part of the tube. Afterwards the glass tube was sealed off and left standing for a couple of days. Several single crystals which grew around the constriction were separated in an inert gas glove-box and placed in Lindemann capillaries under paraffin oil.

Crystal structure determination

Crystal data for $(NH_4)[UBr_2(CH_3CN)_2(H_2O)_5]Br_2$: $C_4H_{20}Br_4N_3O_5U$, $M = 747.9$, orthorhombic, space group *Pnma* (D_{2h}^{16}), $a = 8.98(2)$, $b = 9.99(2)$, $c = 20.24(4)$ Å, $Z = 4$, $V = 1816(7)$ Å^3, $D_c = 2.74(1)$ g cm^{-3}, $D_m = 2.81$ g cm^{-3}, $F(000) = 1348$, $\lambda(\text{Mo-}K_\alpha) = 0.71069$ Å, $\mu = 96.5$ mm^{-1}.

A brown parallelepiped crystal of approximate dimensions $1.0 \times 0.6 \times 0.08$ mm^3 was sealed in a deoxygenated capillary and mounted on a KM4 Kuma diffractometer with κ geometry. The cell parameters were determined from angular settings of 25 reflections with 2θ between 16 and 25°. 3978 reflections were measured in the $4 \leqslant 2\theta \leqslant 42°$ range. Out of these 1359 had $I \geqslant 3\sigma(I)$. The data collection was performed at 298 K using Mo-K_α radiation and the $\omega/2\theta$ scan mode with variable scan speed. Three control reflections were monitored after 50 measured intensities. The mean relative variation was 3.1%. The data were corrected for the Lorentz and polarization factors, as well as for absorption calculated from the crystal shape. For the latter correction a grid composed of 4096

* Author to whom correspondence should be addressed.

points imposed on the crystal volume was used. Thus, calculated transmission factors were between 0.014 and 0.252. The position of the uranium atom was determined by the Patterson method and the other atoms were found from a difference-Fourier map. No attempt was made to locate the hydrogen atoms. Then, 245 weak reflections with the largest e.s.d.s were removed from the reflection file. The structure was refined using the full-matrix least-squares method. For the final refinement 932 unique reflections, yielded from merging 1114 data ($R_{int} = 0.076$), were used. The minimized function was $S = \Sigma w(|F_o| - |F_c|)^2$, with the weights $w = 1/\sigma^2(F)$. The scattering factors of neutral carbon, nitrogen and oxygen atoms, as well as those of U^{3+} and Br^-, were included[2] in the refinement. The C—N distances were constrained, with the common distance refined as an additional variable. The restraint of 1.45 Å was imposed on the C—C distances. As an additional variable the scaling length for absorption was applied. The uranium and bromine atoms had anisotropic thermal parameters, all other atoms were isotropic. The refinement of 59 parameters converged at $R = 0.0461$ and $R_w = 0.0391$; the maximum Δ/σ was less than 0.01 and the residual electron density was between -0.86 and 1.73. The highest peaks were around the uranium cation. The SHELXS86[3] program was used for solution and the locally modified SHELX76[4] for the refinement. The atomic parameters as well as the full list of bond lengths and angles have been deposited as supplementary material.

IR and Raman spectra

The IR transmission measurements were performed at room temperature on a Bruker JFS 88 FT-IR spectrometer in the 30–4000 cm^{-1} spectral range. The KBr disc and Nujol mull suspension techniques were applied.

The Raman spectra were observed in back-scattering geometry at 300 K. The 5145 Å line of an Ar^+ ion laser and the line of a solid Nd : YAG laser were the excitation sources. For measurements of the Raman spectra DFS 24 and Yvon Jobin monochromators were used. They were supplied with photon detection systems from Product for Research INC (Massachusetts, U.S.A.).

Electronic spectrum

The solid-state electronic spectrum of the compound was recorded on a Cary–Varian 2300 spectrophotometer in the 4000–26,000 cm^{-1} absorption range. In order to obtain the spectrum a well-ground mixture of the compound with a few drops of chlorinated naphthalene (index of refraction = 1.635) was placed between two quartz windows, approximately 1 cm in diameter, pressed to obtain a transparent layer and placed into the cell compartment of the spectrophotometer.

RESULTS AND DISCUSSION

Crystal structure

The crystal is composed of complex monomeric pentaaquabis(methyl cyanide)dibromouranium cations, ammonium cations and bromide anions. The uranium atom is placed on the *m* (C_s) plane and is surrounded by two bromide anions, two methyl cyanide nitrogen atoms and five oxygen atoms of the water molecules. The shortest U—U distance is 7.05(2) Å. Other selected bond lengths are presented in Table 1. The coordination figure of uranium is intermediate between a tricapped trigonal prism and a capped square antiprism. In the former case the best fitted figure had the upper and lower bases defined by Br(1), O(1), O(2′) and Br(1′), O(1′), O(2), respectively, and the caps by N(2), N(1), O(3). The parameter Δ, defined as $\Sigma d_i^2/9$ is equal to 0.066 $Å^2$, where d_i is the distance between the *i*th atom and the relevant vertex of the idealized least-squares fitted polyhedron.[5] In the latter case the non-capped base was spanned by O(3), O(2′), N(1), O(2), the capped base by Br(1), O(1), O(1′), Br(1′) with N(2) being the cap, $\Delta = 0.066$ $Å^2$. The structure is held together by N—H · · · Br and O—H · · · Br hydrogen bonds, the former probably disordered. An ORTEP[6] view of the complex cation is presented in Fig. 1. and that of the crystal cell in Fig. 2.

Symmetry-based vibrational data

The IR transmission spectra for $(NH_4)[UBr_2(CH_3CN)_2(H_2O)_5]Br_2$ are presented in Fig. 3 and those of the Raman spectra are shown in Fig. 4. The unit cell of the compound consists of four

Table 1. Lengths of bonds formed by the uranium cation

U—Br(1),Br(1′)[a]	3.074(4)
U—O(1),O(1′)	2.538(12)
U—O(2),O(2′)	2.549(14)
U—N(1)	2.517(30)
U—N(2)	2.688(26)
U—O(3)	2.652(20)

[a] Primed atoms are related to those unprimed through the mirror plane at *x*, 1/2 − *y*, *z*.

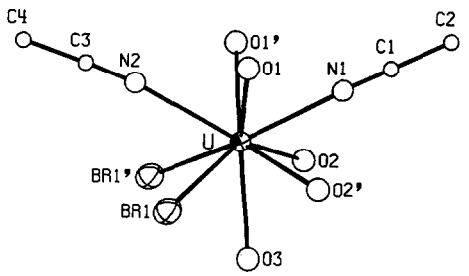

Fig. 1. View of the complex cation. Symmetry generated atoms are marked with primes, see Table 1.

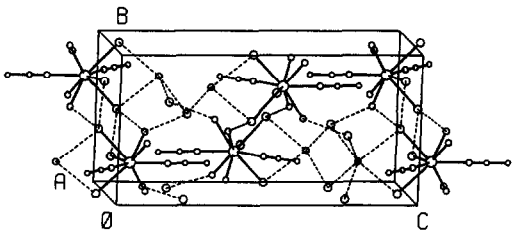

Fig. 2. View of the unit cell. The possible hydrogen bonds are marked with dashed lines.

formula units comprising 148 atoms. As mentioned before, the uranium ion lies inside the polyhedron with nine vertices. Since the uranium ion occupies the *c*-position of the unit cell, the structure of the coordination polyhedron is described by C_s symmetry. Hence, the 444 vibrational modes of the unit cell decompose according to the following representation:

$$T = 61A_g + 50B_{1g} + 61B_{2g} + 50B_{3g} + 50A_u + 61B_{1u} + 50B_{2u} + 61B_{3u},$$

where $B_{1u}+B_{2u}+B_{3u}$ are acoustic modes. Thus, there are 441 optical zone-centre modes, 45 of which are translational lattice modes, 24 librational lattice modes and 372 internal modes connected with the $[UBr_2(CH_3CN)_2(H_2O)_5]$ core. Table 2 lists these phonons with their symmetries and the polarizations necessary for their observations.

Since the $UBr_2N_2O_5$ coordination polyhedron has C_s symmetry, all the internal vibrations have IR and Raman components. 24 normal vibrations of this skeleton are described by the $13A'+11A''$ representation, which consists, amongst others, of two $A'+A''$ stretching $\nu(UBr_2)$, two $A'+A''$ stretching $\nu(UN_2)$ and five $3A'+2A''$ stretching $\nu(UO_5)$ modes. The interaction between the four molecules in the unit cell leads to the splitting of these modes as shown below.

Site symmetry C_s	Factor group symmetry D_{2h}
A'	A_g
	B_{2g}
	B_{1u}
	B_{3u}
A''	B_{1g}
	B_{3g}
	A_u
	B_{2u}

The remaining 19 fundamentals correspond to the bending vibrations of the $UBr_2N_2O_5$ skeleton. Based on the theoretical considerations, Table 3 lists the frequencies of the IR and RS bands along with the line assignments.

The IR and Raman studies reveal all characteristic lines expected for coordinated CH_3CN and H_2O ligands. Coordination through nitrogen is indicated by the bands at 202 (IR) and 282 (R) cm^{-1}, which correspond to the $\nu(UN_2)$ modes. The $\nu(CH_3)$, $\delta(CH_3)$, ν(C—C) and $\nu(C\equiv N)$ frequencies appear in energy ranges characteristic for the free ligand,[7,8] as well as for the cerium and uranium trichloride monoacetonitrile complexes.[9] The peaks near 2307 cm^{-1} have been assigned to a $\nu_3+\nu_4$ combination band of the symmetric $\delta_s(CH_3)$ and ν_s(C—C) modes. The pattern of lines typical for coordinated water molecules are observed both in the IR and RS spectra. This multiplet appears in the 400–770 cm^{-1} range with components at *ca* 600–670 and 700–770 cm^{-1} and is related to the wagging and rocking modes.

Very broad and poorly resolved bands observed in the 300–550 cm^{-1} region correspond to the $\nu(U—OH_2)$ and δ(OUO) vibrations of the UO_5 skeleton. The uranium–bromine vibrations appear in two regions: 110–190 cm^{-1} for the $\nu(UBr_2)$ stretching modes and 50–100 cm^{-1} for the δ(BrUBr) modes.

For a more detailed mode identification of some data on polarization properties of the modes observed in single crystals are required. One can note from Table 2 that all Raman modes have an IR counterpart and that the number of IR and R modes is less than expected from the theoretical FGA prediction. This is due to the use of polycrystalline samples in the measurements. Besides, due to the limited resolution and poor signal-to-noise the weaker oscillators can be dominated by the stronger ones, as well as by emission bands. The strong contour observed in the Raman spectra at *ca* 18,550 cm^{-1} has been assigned to emission connected with the Laporte allowed $5f^2 \rightarrow 5f^26d^1$ transitions.

Table 2. Factor group analysis for the $(NH_4)[UBr_2(CH_3CN)_2(H_2O)_5]Br_2$ complex; space group *Pnma* (D_{2h}^{16}), $Z = 4$

	E	$2_1(z)$	$2(y)$	$2_1(x)$	i	$a(xy)$	$m(xz)$	$n(yz)$	$n_i(N)$	$n_i(T)$	$n_i(T')$	$n_i(L)$	$n_i(n)$	Activity IR R
A_g	1	1	1	1	1	1	1	1	61	0	7	4	50	— xx, yy, zz
B_{1g}	1	1	−1	−1	1	1	−1	−1	50	0	5	2	43	— xy
B_{2g}	1	−1	1	−1	1	−1	1	−1	61	0	7	4	50	— xz
B_{3g}	1	−1	−1	1	1	−1	−1	1	50	0	5	2	43	— yz
A_u	1	1	1	1	−1	−1	−1	−1	50	0	5	2	43	— —
B_{1u}	1	1	−1	−1	−1	−1	1	1	61	1	6	4	50	T_z —
B_{2u}	1	−1	1	−1	−1	1	−1	1	50	1	4	2	43	T_y —
B_{3u}	1	−1	−1	1	−1	1	1	−1	61	1	6	4	50	T_x —
$\pm 1+2\cos\Phi_R$	3	−1	−1	−1	−3	1	1	1	444	3	45	24	372	
$1\pm 2\cos\Phi_R$	3	−1	−1	−1	3	−1	−1	−1						
$U_R(p)$	148	0	0	0	0	0	44	0						
$U_R(s)$	16	0	0	0	0	0	8	0						
$U_R(s-u)$	8	0	0	0	0	0	8	0						
$[X_\rho(R)]_N$	444	0	0	0	0	0	44	0						
$[X_\rho(R)]_T$	3	−1	−1	−1	−3	1	1	1						
$[X_\rho(R)]_{T'}$	45	1	1	1	3	−1	7	−1						
$[X_\rho(R)]_R$	24	0	0	0	0	0	8	0						

$n_i(N)$ = overall number of vibrational freedom; $n_i(T)$ = acoustic modes, $n_i(T')$ = translational lattice modes: $n_i(L)$ = librational lattice modes; $n_i(i)$ = internal vibrations.

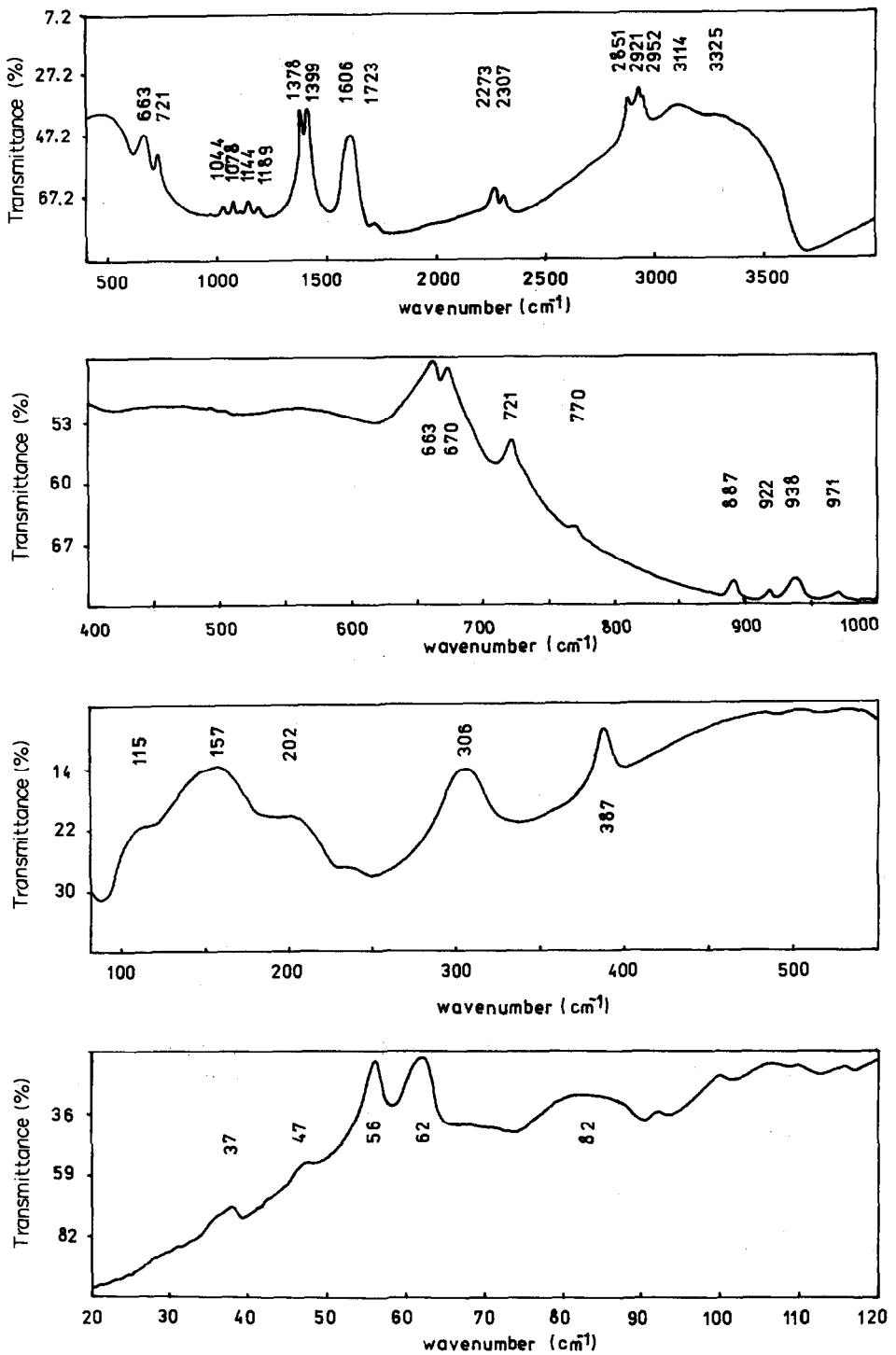

Fig. 3. IR transmission spectra.

Electronic spectrum

The solid-state electronic absorption spectrum of the compound is typical for all those uranium(III) compounds which possess some of the uranium–ligand bonds of more covalent character.[10]

In the 4000–15,000 cm^{-1} absorption range one observes the characteristic $5f^3 \rightarrow 5f^3$ transitions of

Table 3. IR and Raman frequencies and band assignment for the $(NH_4)[UBr_2(CH_3CN)_2(H_2O)_5]Br_2$ complex

IR	R	Assignment
3325s,b		$\nu(H_2O)$ with hydrogen bond character
3114s,b		
2952w		
2921w		$\nu(CH_3)$
2851w		
2307w		Combination band
2273w	2280m	$\nu_s(C{\equiv}N)$
1606m	1631m	$\delta(HOH)$
1399s	1415w	$\delta_{as}(CH_3)$
1378s	1356m	
1189w	1261w	$\delta_s(CH_3)$
1144w	1186w	
1078w	1123m	$\delta(U{-}OH_2)$
1044w	1063m	$\rho(CH_3)$
971w	952w	$\nu(C{-}C)$
938w		
922w	826w	
887w		
770w	729w	$\rho(U{-}OH_2)$
721w		
663vs,b	651w	$\omega(U{-}OH_2)$
670vs,b	611w	
400–590s,vb	536w	$\nu(U{-}OH_2)$
387m	455m,b	
306m	326w	
202m	282w	$\nu(UN_2)$
157m,b	195sh	$\nu(UBr_2)$
115sh	149	
82w	Broad band of	$\delta(UBr_2)$
62w	Rayleigh	
59w	scattering	
47w		
37w		

the U^{3+} ion with energies (in cm^{-1}) of the band maxima at 4325, 4490, 4595 ($^4I_{11/2}$),* 6920 ($^4F_{3/2}$),* 7999, 8200, 8457, 8650 ($^4I_{13/2}$),* 9092, 9302, 9393 ($^2H_{9/2}$),* 9633, 9850, 9940, 10,202 ($^4F_{5/2}$),* 11,112, 11,506, 11,795 ($^4S_{3/2}$, $^4G_{5/2}$, $^4I_{15/2}$, $^4F_{7/2}$),* 13,159, 13,690 ($^4G_{7/2}$)* and 14,797 ($^4F_{9/2}$).* One may note, however, that the bands are not well resolved and do not exhibit all crystal-field components.

Above this region the $5f^3 \rightarrow 5f^3$ transitions are obscured by strong and broad $5f^3 \rightarrow 5f^2 6d^1$ bands with centres at 16,705, 17,462, 18,870, 19,510, 21,650 and 25,000 cm^{-1}. A red shift of the first *f–d* bands from wavelengths higher than 20,000 cm^{-1} to the visible range has been attributed[10,11] to the formation of inner-sphere complexes, with some of the uranium–ligand bonds of a markedly more covalent character compared with those of the U^{3+} aquo ion.[10] The results of the hitherto investigated bromo complexes confirm the above:

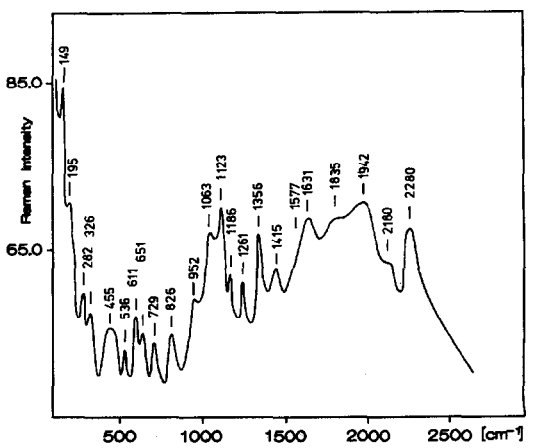

Fig. 4. Raman spectrum.

* Level assignment ≡ major component of eigenvector.[13]

Compound	UBr_3[10]	$NH_4UBr_4 \cdot 2CH_3CN \cdot 5H_2O$	Rb_2UBr_5[12]	K_2UBr_5[14]	Cs_2NaUBr_6[15]
d(U—Br) (pm)	306.2–315.0	307.4	297.6–307.6	294.8–303.2	254.2
$\nu(f \rightarrow d)$ (cm^{-1})	19,500	16,705–17,462	16,026	15,974	15,708–15,780

The U—Br distances in Rb_2UBr_5 and Cs_2NaUBr_5 have been calculated from X-ray powder diffraction data using the atomic coordinates of the isotypic compounds K_2PrCl_5[16] and β-K_2NaAlF_6,[17] respectively.

Acknowledgement—The authors thank Dr J. Hanuza from the Institute for Low Temperature and Structure Research of the Polish Academy of Science in Wrocław for his kind assistance in recording and interpretation of the Raman and IR spectra. This work was supported by Komitet Badań Naukowych within the project 0424/P3/92/03, which is gratefully acknowledged.

REFERENCES

1. E. Zych and J. Drożdżyński, *J. Less-Comm. Met.* 1990, **161**, 233.
2. *International Tables for X-Ray Crystallography*, Vol. 4. Kynoch Press, Birmingham (1974).
3. G. M. Sheldrick, SHELXS86, Program for the Solution of Crystal Structures from X-ray Diffraction Data. University of Göttingen, F.R.G. (1986).
4. G. M. Sheldrick, SHELX76, Program for Crystal Structure Determination. University of Cambridge, U.K. (1976).
5. M. G. B. Drew, *Coord. Chem. Rev.* 1977, **24**, 179.
6. C. K. Johnson, ORTEPII, Report ORNL-5138. Oak Ridge National Laboratory, Tennessee, U.S.A. (1976).
7. J. Wenkateswarlu, *J. Chem. Phys.* 1951, **19**, 293.
8. A. Walton, *Q. Rev.* 1965, **19**, 126.
9. J. Mac-Cordick and C. Brun, *C.R. Acad. Sci. C* 1970, **270**, 620.
10. J. Drożdżyński, in *Handbook on the Physics and Chemistry of the Actinides* (Edited by A. J. Freeman and C. Keller), Vol. 6, pp. 281–336. Elsevier, Amsterdam (1991).
11. M. Shiloh and Y. Marcus, *Isr. J. Chem.* 1965, **3**, 123.
12. K. Krämer, PhD Dissertation, Universität Giessen, F.R.G. (1991).
13. H. M. Crosswhite, H. Crosswhite, W. T. Carnall and A. P. Paszek, *J. Chem. Phys.* 1980, **72**, 5103.
14. K. Krämer, L. Keller, P. Fischer, B. Jung, N. Edelstein, H.-U. Güdel and G. Meyer, *J. Solid State Chem.* 1993, **103**, 152.
15. N. A. Aurov, V. A Volkov, and D. E. Chirkst, *Radiokhimiya* 1983, **25**, 366.
16. G. Meyer, J. Soose, A. Moritz, V. Vitt and Th. Holjes, *Z. Anorg. Allg. Chem.* 1985, **161**, 521.
17. R. W. G. Wyckoff, *Crystal Structures*, Vol. 3, 2nd edn. Interscience, New York (1965).

Polyhedron Vol. 12, No. 13, pp. 1669–1673, 1993
Printed in Great Britain

0277–5387/93 $6.00+.00
© 1993 Pergamon Press Ltd

CRYSTAL STRUCTURE OF CATIONIC SQUARE PLANAR PLATINUM(II) COMPLEXES CONTAINING THE TRIDENTATE CHELATE LIGAND 2,6-BIS(METHYLTHIOMETHYL)PYRIDINE

GIAMPAOLO MARANGONI* and BRUNO PITTERI

Dipartimento di Chimica, Universitá di Venezia, Calle Larga S. Marta 2137, 30123 Venezia, Italy

and

VALERIO BERTOLASI, VALERIA FERRETTI and PAOLA GILLI

Dipartimento di Chimica e Centro di Strutturistica Diffrattometrica, Università di Ferrara, Via Borsari 46, 44100 Ferrara, Italy

(*Received* 27 *January* 1993; *accepted* 5 *March* 1993)

Abstract—The crystal structures of four platinum(II) complex cations containing the organic ligand 2,6-bis(methylthiomethyl)pyridine (SNS), $[Pt(SNS)Cl]^+$ (**1**), $[Pt(SNS)(SCN)]^+$ (**2**), $[Pt(SNS)Br]^+$ (**3**) and $[Pt(SNS)(Py)]^{2+}$ (**4**) have been determined by X-ray diffraction. In all complexes SNS behaves as a tridentate neutral ligand with the two sulphur atoms in *trans* positions to each other. The fourth coordination position, *trans* to the nitrogen atom of SNS, is occupied either by a monodentate chloride, sulphur-bonded thiocyanate, bromide or nitrogen of a pyridine molecule, respectively, in a square planar arrangement. No Pt—Pt interactions in the linear chain are present. Pt—N(pyridine) bond distances are related to the charge of the complexes.

As part of our interest in the synthesis, structure and reactivity of coordination compounds of d^8 metal ions with chelating ligands containing the pyridine moiety,[1–9] we have recently studied the binding ability of the tridentate ligand 2,6-bis-(methylthiomethyl)pyridine (SNS) with protons, palladium(II) and copper(II) and determined the formation constants of the palladium(II) and copper(II) cationic complexes $[Pd(SNS)Tu]^{2+}$ (Tu = thiourea) and $[Cu(SNS)(H_2O)]^{2+}$ in aqueous solutions.[10] Due to the much higher formation constant of the palladium complex (log $K = 28.92 \pm 0.09$) with respect to its copper counterpart ($\log K = 4.6 \pm 0.1$), which certainly stresses the fact that the ligands being exchanged are different (Tu vs H_2O), it was thought the polymers functionalized with SNS groups would be selective for the extraction of palladium(II) from mixtures of palladium(II) and copper(II) in aqueous solutions. A chelating resin was thus prepared by reacting the derived ligand 2,6-bis(methylthiomethyl)-3-hydroxypyridine with a chloromethylated macroporous cross-linked polystyrene, which has been shown to be able to separate quantitatively and rapidly ($t_{1/2} = 11$ min) palladium(II) from copper(II), even when present in 150-fold excess, from acidic chloride (pH = 1) aqueous solutions.[11]

Successively, the complex cation of platinum(II), $[Pt(SNS)Cl]^+$, has been prepared and the kinetics of the associatively activated replacement of chloride by a wide variety of anionic and neutral nucleophiles has been studied in water.[12] Here we report the X-ray crystal structure of the chloro complex cation $[Pt(SNS)Cl]^+$ (**1**), as well as those of the substitution cationic products $[Pt(SNS)(SCN)]^+$ (**2**), $[Pt(SNS)Br]^+$ (**3**) and $[Pt(SNS)(Py)]^{2+}$ (**4**).

* Author to whom correspondence should be addressed.

EXPERIMENTAL

Preparation of the complexes

The complexes were prepared and crystallized as previously reported.[12]

Determination of the structures

Intensity data were collected on an Enraf–Nonius CAD4 diffractometer with monochromated Mo-K_α radiation using the $\omega/2\theta$ scan technique. Cell parameters were obtained from least squares refinement of 25 centred reflections in the range $7 < \theta < 14°$. Crystal data are reported in Table 1. Intensities were corrected for Lorentz, polarization and absorption (minimum transmission factors: 0.86, 0.43, 0.35 and 0.78 for compounds **1**, **2**, **3** and **4**, respectively). Scattering factors and anomalous dispersion parameters were taken from ref. 13; solution was by Patterson and Fourier methods. The structure of compound **2** was refined by full-matrix least-squares using anisotropic thermal parameters for all non-hydrogen atoms and isotropic ones for hydrogens. All the other structures were refined by full-matrix least-squares using anisotropic thermal parameters for all non-hydrogen atoms and hydrogen atoms in calculated fixed positions. Weights for the last cycle were applied according to the scheme given in Table 1. All calculations were performed by the MolEN[14] and PARST[15] programs. Final positional and thermal parameters, as well as supplementary material, have been deposited with the Editor.

RESULTS AND DISCUSSION

ORTEP[16] drawings of the four square-planar tetra-coordinate cation complexes of platinum (II) bis-2,6-(methylthiomethyl)pyridine derivatives, showing the atom number scheme, are given in Fig. 1. Bond distances and angles are reported in Tables 2 and 3, respectively. In all complexes the organic ligand behaves as a tridentate neutral ligand with

Table 1. Crystal data[a]

Compound	**1**[b]	**2**[b]	**3**[b]	**4**[b]
M	529.3	524.1	554.2	672.4
Crystal size (mm)	0.10 × 0.12 × 0.31	0.24 × 0.36 × 0.43	0.07 × 0.19 × 0.24	0.21 × 0.36 × 0.43
Space group	*Pbca*	*P*-1	*P*-1	*Fdd*2
Crystal system	Orthorombic	Triclinic	Triclinic	Orthorombic
a (Å)	12.705(1)	9.851(3)	7.234(1)	13.372(2)
b (Å)	10.618(3)	10.521(3)	7.696(1)	20.664(3)
c (Å)	22.283(3)	8.069(1)	12.440(1)	14.985(2)
α (°)	90	104.03(3)	97.46(1)	90
β (°)	90	105.55(2)	92.08(1)	90
γ (°)	90	85.98(2)	101.07(2)	90
V (Å^3)	3006(1)	781.6(4)	672.6(2)	4141(1)
F(000)	2000	484	508	2592
Z	8	2	2	8
D_c (g cm^{-3})	2.336	2.230	2.167	2.156
μ(Mo-K_α) (cm^{-1})	100.50	95.64	166.96	73.41
Independent reflections	3272	4768	3904	3773
Observed reflections	1505	4360	3007	1037
No. of variables (last cycle)	173	225	137	134
R[c]	0.035	0.022	0.040	0.017
R_w[c]	0.038	0.028	0.055	0.025
Max. shift/error	0.03	0.09	0.02	0.26
Largest ΔF peak (e Å^{-3})	0.84	0.80	0.75	0.63
p[d]	0.04	0.03	0.06	0.04
GOF	1.120	1.357	1.324	0.851

[a] Data common to the determinations: graphite-monochromated Mo-K_α radiation, $\lambda = 0.71069$ Å; $T = 22°C$, $\Theta_{mn} - \Theta_{max} = 2$–$27°$.

[b] **1**: $[PtCl(C_9H_{13}NS_2)]^+ \cdot ClO_4^-$; **2**: $[PtSCN(C_9H_{13}NS_2)]^+ \cdot SCN^-$; **3**: $[PtBr(C_9H_{13}NS_2)]^+ \cdot Br^-$; **4**: $[Pt(C_5H_5N)(C_9H_{13}NS_2)]^+ \cdot 2ClO_4^-$.

[c] $R = \Sigma|\Delta F_o|/\Sigma|F_o|$; $R_w = (\Sigma w|\Delta F_o|^2/\Sigma w|F_o|^2)^{1/2}$.

[d] $w = 4F_o^2/[\sigma^2(F_o^2) + (pF_o^2)^2]$.

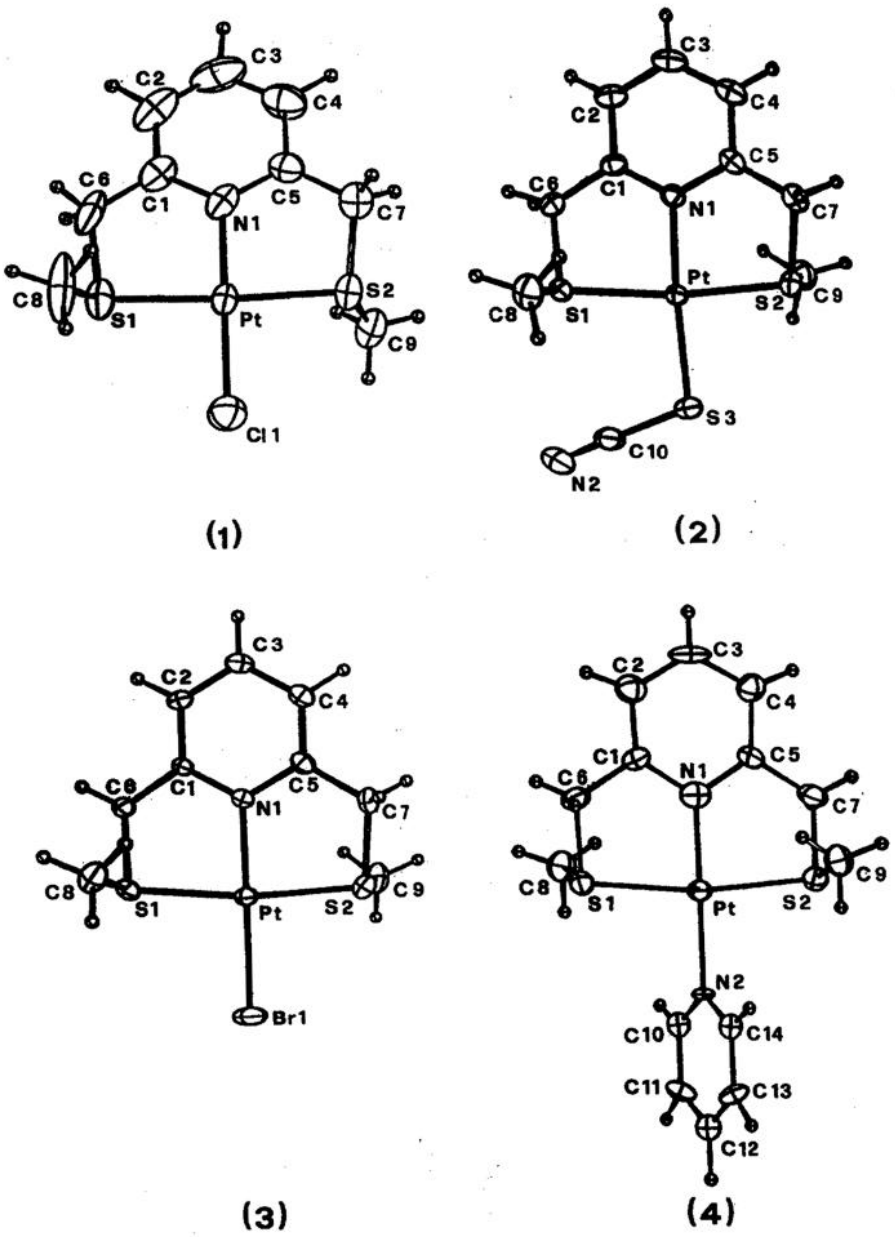

Fig. 1. ORTEP views of the complex cations $[Pt(SNS)Cl]^+$ (**1**), $[Pt(SNS)(SCN)]^+$ (**2**), $[Pt(SNS)Br]^+$ (**3**) and $[Pt(SNS)(Py)]^{2+}$ (**4**). Thermal ellipsoids are drawn at the 30% probability level.

the two sulphur atoms *trans* to each other. The cations of compounds **1**, **3** and **4** have a C_2 symmetry, but only the cation of compound **4** lies on a two-fold crystallographic axis passing through the Pt, N(1), N(2), C(3) and C(12) atoms. In general the tridentate ligands containing the pyridine moiety, as 2,2′,2″-terpyridine, 6-phenyl-2,2′-bipyridine and 2,6-pyridine dicarboxylate, usually give rise to strained square-planar platinum(II) complexes with exceptionally short Pt—N(pyridine) bond distances, observed in the range 1.88–1.97 Å, and N—Pt—X(*cis*) angles far from the ideal value of 90°, the average value being 81.0(8)° as calculated from a sample of 14 angles.[17–20]

In the compounds under examination, owing to the C(6) and C(7) sp^3 hybridized atoms and the Pt—S long distances, which are in the range 2.27–2.29 Å, the straining is less pronounced, with the N—Pt—S angles in the range 85.6–87.6° and Pt—N(pyridine) distances of 2.004(9), 2.014(13) and 2.004(7) Å in compounds **1**, **2** and **3**, respectively. In compound **4**, however, the Pt—N(1) distance remains very short, that is 1.937(9) Å, but it can be stressed in this case the *trans* position to N(1)

Table 2. Bond distances (Å) with e.s.d.s in parentheses

	1	2	3	4
Pt—Cl(1)	2.291(4)			
Pt—Br(1)			2.423(1)	
Pt—S(1)	2.272(3)	2.2777(9)	2.281(2)	2.291(1)
Pt—S(2)	2.270(3)	2.292(1)	2.280(2)	2.291(1)
Pt—S(3)		2.289(1)		
Pt—N(1)	2.004(9)	2.014(3)	2.004(7)	1.937(9)
Pt—N(2)				2.069(7)
S(1)—C(6)	1.780(14)	1.811(4)	1.820(9)	1.823(7)
S(1)—C(8)	1.753(16)	1.793(4)	1.804(11)	1.813(8)
S(2)—C(7)	1.810(15)	1.811(5)	1.812(11)	1.823(7)
S(2)—C(9)	1.749(17)	1.809(4)	1.810(12)	1.813(8)
S(3)—C(10)		1.686(4)		
N(1)—C(1)	1.361(15)	1.346(4)	1.366(9)	1.385(8)
N(1)—C(5)	1.348(14)	1.365(4)	1.352(11)	1.385(8)
N(2)—C(10)		1.140(5)		1.332(7)
C(1)—C(2)	1.372(19)	1.379(6)	1.375(12)	1.415(10)
C(1)—C(6)	1.501(17)	1.498(4)	1.477(12)	1.464(10)
C(2)—C(3)	1.380(23)	1.378(5)	1.385(14)	1.393(8)
C(3)—C(4)	1.351(22)	1.372(6)	1.382(12)	1.393(8)
C(4)—C(5)	1.352(19)	1.387(6)	1.379(14)	1.415(10)
C(5)—C(7)	1.476(18)	1.480(5)	1.484(11)	1.464(10)
C(10)—C(11)				1.358(9)
C(11)—C(12)				1.379(10)

Table 3. Bond angles (°) with e.s.d.s in parentheses

	1	2	3	4
Cl(1)—Pt—S(1)	93.3(1)			
Cl(1)—Pt—S(2)	92.4(1)			
Cl(1)—Pt—N(1)	179.6(3)			
Br(1)—Pt—S(1)			94.85(7)	
Br(1)—Pt—S(2)			93.70(7)	
Br(1)—Pt—N(1)			178.9(2)	
S(1)—Pt—S(2)	173.2(1)	171.47(4)	171.45(9)	170.04(4)
S(1)—Pt—S(3)		97.52(4)		
S(1)—Pt—N(1)	86.7(3)	86.05(8)	85.6(2)	85.02(4)
S(1)—Pt—N(2)				94.98(4)
S(2)—Pt—S(3)		90.92(4)		
S(2)—Pt—N(1)	87.6(2)	85.6(1)	85.8(2)	85.02(4)
S(3)—Pt—N(1)		175.66(8)		
N(1)—Pt—N(2)				180
Pt—S(1)—C(6)	98.8(4)	98.1(1)	96.7(3)	95.6(2)
Pt—S(1)—C(8)	103.6(4)	103.8(1)	105.6(4)	104.5(2)
C(6)—S(1)—C(8)	102.0(7)	102.5(2)	100.9(4)	99.7(4)
Pt—S(2)—C(7)	97.6(5)	96.4(1)	96.7(3)	95.6(2)
Pt—S(2)—C(9)	107.6(5)	104.5(2)	103.9(4)	104.5(2)
C(7)—S(2)—C(9)	101.3(7)	101.6(2)	101.1(5)	99.7(4)
Pt—S(3)—C(10)		106.9(1)		
Pt—N(1)—C(1)	119.0(7)	120.5(2)	119.8(5)	122.2(4)
Pt—N(1)—C(5)	119.5(8)	119.4(2)	119.8(5)	122.2(4)
C(1)—N(1)—C(5)	121(1)	120.1(3)	120.4(7)	115.5(7)
Pt—N(2)—C(10)				118.6(4)
C(10)—N(2)—C(14)				122.8(5)
N(1)—C(1)—C(2)	119(1)	121.0(3)	120.9(7)	124.1(6)
N(1)—C(1)—C(6)	119(1)	118.2(3)	117.7(7)	115.5(6)
C(2)—C(1)—C(6)	122(1)	120.7(3)	121.4(7)	120.4(6)
C(1)—C(2)—C(3)	119(1)	119.4(3)	119.5(8)	117.0(7)
C(2)—C(3)—C(4)	121(1)	119.7(4)	118.6(9)	122.1(8)
C(3)—C(4)—C(5)	119(1)	119.8(4)	121.0(9)	117.0(7)
N(1)—C(5)—C(4)	120(1)	120.0(3)	119.6(8)	124.1(6)
N(1)—C(5)—C(7)	119(1)	117.4(3)	117.9(7)	115.5(6)
C(4)—C(5)—C(7)	121(1)	122.5(3)	122.5(8)	120.4(6)
S(1)—C(6)—C(1)	114.0(9)	114.4(2)	113.4(6)	113.1(5)
S(2)—C(7)—C(5)	116.3(9)	113.1(3)	113.2(6)	113.1(5)
S(3)—C(10)—N(2)		177.4(4)		
N(2)—C(10)—C(11)				119.0(6)
C(10)—C(11)—C(12)				120.8(7)
C(11)—C(12)—C(13)				117.6(9)

is occupied by the N(2) nitrogen of a pyridine with a Pt—N(2) distance of 2.069(7) Å. This complex, unlike the other three, contains a neutral molecule *trans* to the N(1) atom and consequently the cation has two positive charges; the two different values of Pt—N(1) and Pt—N(2) could be related to a different positive charge redistribution on the cation. To support this hypothesis it can be noted that the average value of the two Pt—N bond lengths, 2.003 Å, corresponds very well to the Pt—N distances found in the other three complexes and to the Pt—N(pyridine) distances observed in other chelated platinum(II) square-planar derivatives, where the chelated ions or molecules are mono- or bidentate.[20–27] All the other distances are normal; the Pt—S distances can be compared with the Pt—S distances between platinum(II) and neutral sulphur in other square-planar complexes.[27–30] All the crystals contain ions with no short interatomic distances. No Pt—Pt distance less than 4.50 Å has been observed and consequently no metal–metal interactions in the linear chains are present, as in similar square-planar complexes where molecules or ions are stacked in columns with Pt—Pt distances in the range 3.24–3.73 Å.[17,18,20,23,24,28,31,32]

Acknowledgements—We thank M.U.R.S.T. and C.N.R. (Rome) for financial support and Miss Tatiana Bobbo for technical assistance.

REFERENCES

1. A. Baldo, G. Chessa, G. Marangoni and B. Pitteri, *Polyhedron* 1985, **4**, 1429.
2. G. Annibale, L. Cattalini, G. Chessa, G. Marangoni, B. Pitteri and M. L. Tobe, *Gazz. Chim. Ital.* 1985, **115**, 279.
3. G. Annibale, L. Canovese, L. Cattalini, G. Marangoni and M. L. Tobe, *J. Chem. Soc., Dalton Trans.* 1984, 1641.
4. L. Canovese, L. Cattalini, G. Marangoni, G. Michelon and M. L. Tobe, *J. Chem. Soc., Dalton Trans.* 1985, 731.
5. L. Cattalini, G. Marangoni, G. Paolucci, B. Pitteri and M. L. Tobe, *Inorg. Chem.* 1987, **26**, 2450.
6. G. Marangoni, B. Pitteri, V. Bertolasi, G. Gilli and V. Ferretti, *J. Chem. Soc., Dalton Trans.* 1987, 2235.
7. L. Cattalini, G. Chessa, G. Marangoni, B. Pitteri and E. Celon, *Inorg. Chem.* 1989, **28**, 1944.
8. B. Pitteri, L. Cattalini, G. Chessa, G. Marangoni, N. Stevanato and M. L. Tobe, *J. Chem. Soc., Dalton Trans.* 1991, 3049.
9. V. Ferretti, P. Gilli, V. Bertolasi, G. Marangoni and B. Pitteri, *Acta Cryst.* 1992, **C48**, 814.
10. L. Canovese, G. Chessa, G. Marangoni, B. Pitteri and P. Uguagliati, *Inorg. Chim. Acta* 1991, **186**, 79.
11. G. Chessa, G. Marangoni, B. Pitteri and F. Visentin, *React. Polym.* 1992, **18**, 7.
12. B. Pitteri, L. Canovese, G. Chessa, G. Marangoni and P. Uguagliati, *Polyhedron* 1992, **11**, 2363.
13. D. T. Cromer and J. T. Waber, *International Tables for X-ray Crystallography*, Vol. 4, Table 2.2A. Kynoch Press, Birmingham (1974).
14. MolEN, *An Interactive Structure Solution Procedure*. Enraf–Nonius, Delft, The Netherlands (1990).
15. M. Nardelli, *Comput. Chem.* 1983, **7**, 95.
16. C. K. Johnson, ORTEP II, A Fortran Thermal-Ellipsoids Plot Program for Crystal Structure Illustrations, Report ORLN-5138. Oak National Laboratory, Oak Ridge, TN (1976).
17. K. W. Jannette, J. T. Gill, J. A. Sadownick and S. J. Lippard, *J. Am. Chem. Soc.* 1976, **98**, 6159.
18. E. C. Constable, R. P. G. Nenney, T. A. Leese and D. A. Tocher, *J. Chem. Soc., Chem. Commun.* 1990, 513.
19. X.-Y. Zhou and N. M. Kostic, *Inorg. Chem.* 1988, **27**, 4402.
20. G. Chessa, G. Marangoni, B. Pitteri, V. Bertolasi, G. Gilli and V. Ferretti, *Inorg. Chim. Acta* 1991, **185**, 201.
21. P. Colamarino and P. L. Orioli, *J. Chem. Soc., Dalton Trans.* 1975, 1656.
22. M. R. Caira and L. R. Nassimbeni, *Acta Cryst., Sect. B* 1975, **31**, 581.
23. K. W. Nordquest, D. W. Phelps, W. F. Little and D. J. Hodgson, *J. Am. Chem. Soc.* 1976, **98**, 1104.
24. D. W. Phelps, W. F. Little and D. J. Hodgson, *Inorg. Chem.* 1976, **15**, 2263.
25. G. Annibale, L. Cattalini, L. Canovese, B. Pitteri, A. Tiripicchio, M. Tiripicchio Camellini and M. L. Tobe, *J. Chem. Soc., Dalton Trans.* 1986, 1101.
26. P. Bergamini, V. Bertolasi, V. Ferretti and S. Sostero, *Inorg. Chim. Acta* 1987, **126**, 151.
27. K. Umakoshi, I. Kinoshita, Y. Fukui-Yasuba, K. Matsumoto, S. Ooi, H. Nakai and M. Shiro, *J. Chem. Soc., Dalton Trans.* 1989, 815.
28. V. Theodorou, I. Photaki, N. Hadjiliadis, R. W. Gellert and R. Bau, *Inorg. Chim. Acta* 1982, **60**, 1.
29. B. T. Khan, K. Venkatasubramanian, K. Najmuddin, S. Shamsuddin and S. M. Zakeeruddin, *Inorg. Chim. Acta* 1991, **179**, 117.
30. A. J. Blake, G. Reid and M. Schroeder, *Acta Cryst. Sect. C.* 1991, **47**, 64.
31. G. Gliemann and H. Yersin, *Struct. Bonding Berlin* 1985, **62**, 87.
32. R. S. Osborne and D. Rogers, *J. Chem. Soc., Dalton Trans.* 1974, 1002.

Polyhedron Vol. 12, No. 13, pp. 1675–1680, 1993
Printed in Great Britain

0277–5387/93 $6.00+.00
© 1993 Pergamon Press Ltd

SPECTROELECTROCHEMISTRY OF IRON COMPLEXES OF THE C_2-CAPPED PORPHYRIN LIGAND

JAMES H. CAMERON* and STEVEN C. TURNER

Department of Chemistry, Heriot-Watt University, Riccarton, Edinburgh EH14 4AS, U.K.

(*Received* 27 *January* 1993; *accepted* 5 *March* 1993)

Abstract—The coordination chemistry of iron complexes of C_2-capped porphyrin ligand has been examined by spectroelectrochemistry. In solution, in dimethylsulphoxide (DMSO), the chloride ion of [$Fe^{III}(C_2cap)Cl$] remained bound to iron(III). In the presence of 1-methylimidazole (1-MeIm) the Cl^- ion is substituted by OH^-, generated by reaction of 1-MeIm with trace amounts of water in the system. Controlled potential reduction of [$Fe^{III}(C_2cap)(OH)$] in DMSO solution produced the six-coordinate iron(II) complex [$Fe^{II}(C_2cap)$(1-MeIm)(DMSO)], with the DMSO ligand bound within the capping group. Reduction of [$Fe^{III}(C_2cap)Cl$], in solution in CH_2Cl_2 containing 1-MeIm, produced the five coordinate iron(II) species, $Fe^{II}(C_2cap)$(1-MeIm).

The coordination chemistry of iron porphyrin complexes has been a topic of great interest, largely because of the widespread use of the haem group in bioinorganic chemistry and the desire to model the physical characteristics of the natural systems.[1] Early attempts to model the chemistry of the oxygen carrying proteins, haemoglobin and myoglobin, led to the conclusion that unhindered porphyrin complexes were not suitable because of the strong driving force for the iron(II) to achieve a six-coordinate, low spin state. This resulted in the formation of a number of families of substituted porphyrins with some form of steric protection for one, or more, of the axial binding sites of the iron(II) ion.[2] One of the earliest examples of this strategy, and one of the most successful, was the "capped porphyrin" molecule of Baldwin and co-workers, first reported in 1975.[3] [$Fe^{II}(C_2cap)$] (**1**) has a benzenoid "cap", attached to the porphyrin ring by four side-arm groups, forming a protected cavity, from which all but the smallest molecules are excluded. Thus, even in the presence of large quantities of ligands such as pyridine, the metal centre remains five-coordinate.[4] These systems may thus be regarded as exercizing a form of molecular recognition, where the physical dimensions of the cavity act to select or exclude potential binding groups for the metal centre.

A number of reports have appeared concerning the binding of dioxygen and carbon monoxide to both this complex and its analogues, producing six-coordinate complexes.[5] Relatively little work has been reported on the interaction of [$Fe^{II}(C_2cap)$] with other ligands. Basolo and co-workers reported the binding of ammonia to [$Fe^{II}(C_2cap)$(1-MeIm)] [1-MeIm = 1-methyl-imidazole], producing six-coordinate species with ammonia bonded inside the cap.[6] In an interesting paper Collman *et al.* used magnetic circular dichroism (MCD) spectra to characterize the coordination number and spin state of, amongst others, [$Fe^{II}(C_2cap)$] in the presence of ligands of varying steric bulk.[7] With the larger

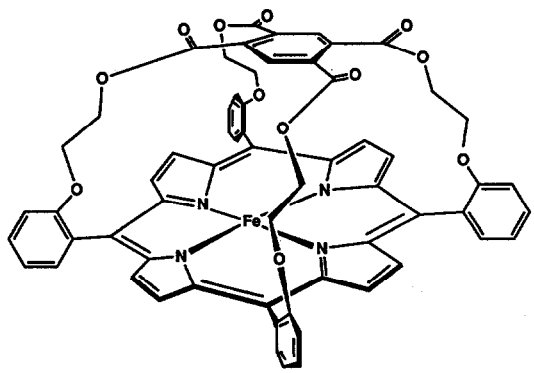

1

* Author to whom correspondence should be addressed.

ligands, such as 1-MeIm or pyridine, the five-coordinate, high spin ($S = 2$) nature of the resultant complex was confirmed, but a somewhat different situation was encountered using the smaller n-propylamine. In the presence of a dilute solution of Pr^nNH_2 (0.1 mol dm^{-3}) the complex was still predominantly five-coordinate, but there was evidence in the spectrum for some six-coordinate, low spin ($S = 0$) material. Increasing the concentration of Pr^nNH_2 (to 1.0 mol dm^{-3}) increased the relative concentration of six-coordinate material, but some five-coordinate complex was still evident. Related behaviour with i-butylamine was also reported, although formation of the six-coordinate species was very slow.

Recently Brewer and Brewer reported on the formation of binuclear complexes involving $[Fe^{III}(C_2cap)]^+$ species, formed by ligation of an imidazolate group of a copper(II) complex to the iron(III) centre, giving a five-coordinate iron(III) ion.[8]

Although the spectroelectrochemistry of $[Co^{III}(C_2cap)]$ has been reported,[9] the electrochemistry of the corresponding iron complex has not been discussed in the open literature. Some work concerning the electrochemistry of $[Fe^{II}(C_2cap)]$ and its oxygen adduct has appeared in the patent literature,[10] but the electrochemical behaviour of the complexes was not reported in detail. Saveant and co-workers have reported on the electrochemistry of some strapped and bridged iron(III) porphyrin complexes, which display unusual properties derived from the restricted solvation of the bulky porphyrin species.[11] In this work we report on the spectroelectrochemistry of $[Fe^{II}(C_2cap)]$ in different solvents and also report upon the formation of an unusual six-coordinate iron(II) complex in solution in DMSO.

RESULTS AND DISCUSSION

The cyclic voltammogram of $[Fe^{III}(C_2cap)Cl]$ dissolved in a DMSO solution, containing 10% by volume of 1-MeIm (1.25 mol dm^{-3}) is shown in Fig. 1. In the range 0 to -2 V (vs an S.C.E.) four reduction waves were observed, each having an associated oxidation wave on the reverse sweep (Table 1). This behaviour is similar to that observed for other iron(III) porphyrin complexes and, by analogy, the four one-electron reduction steps are assigned as two reductions of the metal ion, followed by two reductions of the porphyrin ring.[12]

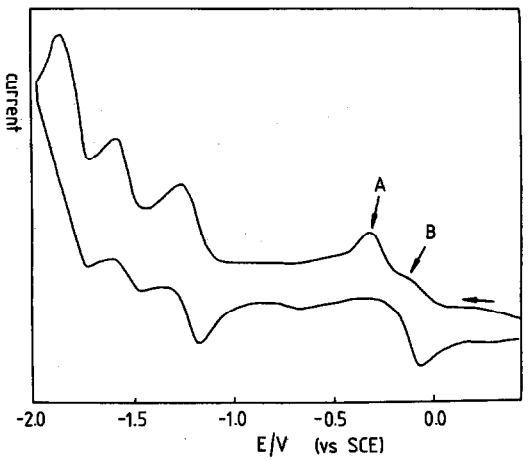

Fig. 1. Cyclic voltammogram of $Fe^{III}(C_2cap)Cl$ (5×10^{-3} mol dm^{-3}) dissolved in DMSO containing 10% by volume of 1-MeIm, with Bu_4NBF_4 (0.1 mol dm^{-3}) as an electrolyte.

Table 1. Electrochemical data for reduction of $Fe^{III}(C_2cap)Cl$

Couple	$E_{1/2}$ (V)	ΔE_p (mV)
$Fe^{III}(P)/Fe^{II}(P)$[a]	−0.20 (−0.10)	300 (100)
$Fe^{II}(P)/Fe^{I}(P)$	−1.22	110
$Fe^{I}(P)/Fe^{I}(P^{\cdot-})$	−1.52	130
$Fe^{I}(P^{\cdot-})/Fe^{I}(P^{2-})$	−1.80	140

[a] Two overlapping processes.

$$[Fe^{III}(Por)]^+ \xrightarrow{+e^-} [Fe^{II}(Por)] \xrightarrow{+e^-} [Fe^{I}(Por)]^- \xrightarrow{+e^-} [Fe^{I}(Por)^-]^{2-} \xrightarrow{+e^-} [Fe^{I}(Por)^{2-}]^{3-}$$

where Por represents a generalized porphyrin ligand. The ratio of current peak heights for each cathodic/anodic couple was approximately unity, indicating that the electron-transfer reactions were largely unaffected by any subsequent chemical reactions. The peak separation, ΔE_p, was in each case in excess of the theoretical value for a one-electron process of 59 mV and so each couple is best described as being quasi-reversible. This is in good agreement with the literature data for related systems.[12]

No oxidation reactions involving $[Fe^{III}(C_2cap)]^+$ were observed up to the anodic potential limit of the solvent (*ca* 0.8 V). This is in keeping with the results of a study of the oxidation reactions of $[Co^{II}(C_2cap)]$, in dichloromethane solution,[9] in which two oxidations of the porphyrin ring were observed, at 1.02 and 1.20 V vs S.C.E., and hence the corresponding oxidations of the iron(III) complex are beyond the solvent limit of the present system.

Closer examination of the wave assigned to the iron(III)/iron(II) couple suggests that two over-

lapping reduction steps are observed (A and B), indicating the presence of two distinct reducible species in solution. This behaviour is ascribed to the occurrence of an equilibrium between different species of the general formula $[Fe^{III}(C_2cap)X]$, where X is Cl^- or OH^- (*vide infra*).

$$[Fe^{III}(C_2cap)Cl]_{(solv)} + OH^-_{(solv)} \underset{}{\overset{DMSO}{\rightleftharpoons}} [Fe^{III}(C_2cap)(OH)]_{(solv)} + Cl^-_{(solv)}$$

Similar behaviour has been noted by Saveant and co-workers in the oxidation of the iron(II) complex of a strapped porphyrin ligand, where Cl^- competes successfully with dimethyl formamide as a ligand to iron(II), producing two oxidizable species.[11] In this work the electronic spectrum of the iron(III) species is sensitive to the nature of the axial ligand.[13] Since the electronic spectrum of $[Fe^{III}(C_2cap)Cl]$ in the non-coordinating solvent $CHCl_3$ (λ_{max} 514 nm) is identical to that in DMSO, then it is believed that DMSO does not displace chloride ions from the complex, nor does DMSO bind within the capping group in the sixth coordination site. DMSO is normally regarded as a good solvent for charged species, having a relatively high dielectric constant, but in this case dissociation of the neutral complex does not occur, instead strong ion pairing is favoured. Similar behaviour has been reported in the literature for other iron(III) porphyrin complexes, albeit in solvents of lower polarity than DMSO.[14] Thus, a species of the form $[Fe^{III}(C_2cap)(DMSO)]^+$ can be eliminated from discussion. This behaviour is in marked contrast to the situation found for the corresponding complex of the tetraphenylporphyrin ligand (TPP) $[Fe^{III}TPPCl]$. In DMSO solution the chloride ion is displaced by DMSO and a six-coordinate complex, $[Fe^{III}TPP(DMSO)_2]^+$, is formed.[15] This difference may arise because the bound Cl^- requires to be labilized by a *trans*-ligated DMSO molecule before substitution is favoured. This can occur readily with the TPP complex, but is disfavoured with the capped species. By analogy with other sulphoxide-ligated iron(III) porphyrin complexes, the DMSO would have to bind via the oxygen atom and it would appear that the capping group is unable to accommodate the DMSO in this coordination mode.[16]

In contrast the spectrum of $[Fe^{III}(C_2cap)Cl]$ in solution, in DMSO containing 10% by volume of 1-MeIm, has λ_{max} at 575 nm, indicating that the Cl^- ion is displaced, but not apparently by 1-MeIm since the spectrum is markedly different from a literature report of an imidazole ligand bonded to $[Fe^{III}(C_2cap)]^+$.[8] Brewer and Brewer have also observed the species with λ_{max} at 575 nm and have assigned it as the OH^- ligated complex $[Fe^{III}(C_2cap)OH]$.[8] In this work the spectrum retains a shoulder at *ca* 510 nm, ascribed to the presence of a small amount of the chloro complex. In solution in neat 1-MeIm this should be absent and only the peak assigned to $[Fe^{III}(C_2cap)OH]$, λ_{max} = 575 nm, is observed. The appearance of this OH^- ligated species presumably arises from the presence of trace amounts of water in the system. Deprotonation of this water by 1-MeIm produces the OH^- ion which is able to compete successfully for the iron(III) coordination site, even in neat 1-MeIm. The involvement of H_2O was confirmed by treating a $CHCl_3$ solution of $[Fe^{III}(C_2cap)Cl]$ with 1-MeIm, to which some water had been deliberately added. Whereas no reaction was observed in the absence of water, in the presence of water the characteristic spectrum of $[Fe^{III}(C_2cap)OH]$ was generated. Treating a DMSO solution of $[Fe^{III}(C_2cap)Cl]$ with aqueous NaOH also produced the spectrum of the hydroxo complex.

In the cyclic voltammogram the more negative, and larger, iron(III) reduction wave (A) is assigned, therefore, to reduction of the major species in solution, $[Fe^{III}(C_2cap)OH]$. The observed potential shift between waves A and B is ascribed to the stronger Lewis basicity of OH^-, relative to the chloride ion, making the iron(III) ion in $[Fe^{III}(C_2cap)OH]$ more difficult to reduce than that in $[Fe^{III}(C_2cap)Cl]$.

The corresponding oxidation reaction involves only a single peak and hence it is believed that the anionic ligand of $[Fe^{II}(C_2cap)X]^-$ (X = Cl^- or OH^-) is replaced by 1-MeIm, generating a single iron(II) species. The coordination environment of this iron(II) complex is discussed below.

Spectroelectrochemistry results

The above discussion has highlighted the utility of both electrochemistry and electronic spectroscopy in the characterization of the various iron-capped porphyrin species. An obvious extension is to combine the two techniques for simultaneous examination of the behaviour of the complexes and to this end the spectroelectrochemistry of $[Fe^{III}(C_2cap)X]$ (X = Cl^- or OH^-) was performed using an optically transparent thin layer electrode (OTTLE) cell. The spectroscopic changes accompanying the reduction of $[Fe^{III}(C_2cap)X]$ in DMSO/10% 1-MeIm solution are shown in Fig. 2. The initial spectrum, as described above, is assigned as belonging to a mixture of predominantly $[Fe^{III}(C_2cap)OH]$ with a small amount of $[Fe^{III}(C_2cap)Cl]$. During reduction of the system at −0.4 V a new spectrum, with λ_{max} 535 and 570 nm, grew in over a period of *ca* 5 min. This spectrum strongly

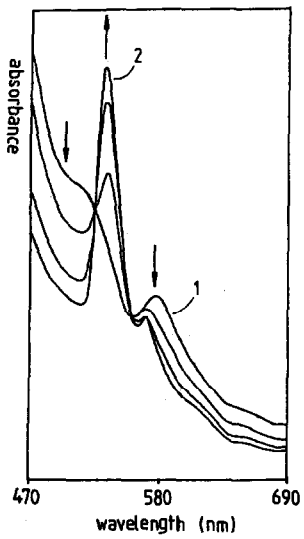

Fig. 2. Time resolved thin-layer electronic spectra during reduction of [$Fe^{III}(C_2cap)OH$] in solution in DMSO/10% 1-MeIm. Applied potential −0.4 V; 1, $t = 0$, 2, $t = 5$ min.

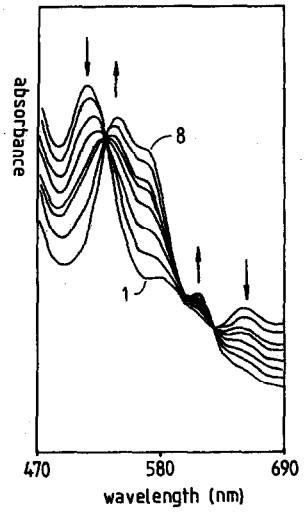

Fig. 3. Visible spectra during reduction of $Fe^{III}(C_2cap)Cl$ in solution in CH_2Cl_2/10% 1-MeIm. Applied potentials were: 1, +0.2; 2, −0.15; 3, −0.2; 4, −0.24; 5, −0.28; 6, −0.30; 7, −0.4; and 8, −0.55 V.

resembles literature results for six-coordinate, low spin iron(II) porphyrin complexes.[17]

The aim in designing the capped porphyrin was to produce a sterically protected binding site which only small molecules, such as O_2 or CO, could access. The crystal structure of [$Fe^{III}(C_2cap)Cl$] demonstrated that this had been achieved, with the capping group lying only 403 pm from the N_4 plane of the porphyrin.[18] This meant that the cavity must expand to accommodate even diatomic ligands. As described above Baldwin and co-workers showed that 1-MeIm was too large to enter the cavity of [$Fe^{II}(C_2cap)$],[4] but Basolo and co-workers[6] and Collman *et al.*[7] showed that smaller ligands, such as ammonia or n-propylamine or i-butylamine, respectively, could bind to the protected axial coordination site. In this work the only ligand present which is small enough to enter the cavity and bind to the iron(II) is DMSO, and so the six-coordinate iron(II) species generated in the electrolysis reaction is assigned as being [$Fe^{II}(C_2cap)$(1-MeIm)(DMSO)]. It is presumed that the DMSO ligand binds to iron(II) via its sulphur atom, although this remains to be confirmed. There is precedent for DMSO binding within the cavity of capped porphyrins. In an NMR study of zinc(II) species Williams and co-workers found evidence from NMR spectroscopy for DMSO entering the cavity of C_3-capped porphyrin and binding to the metal centre.[19]

The spectroscopic changes observed in the electrochemical experiment were reproduced when the [$Fe^{III}(C_2cap)Cl$] species was chemically reduced to [$Fe^{II}(C_2cap)$], isolated and then dissolved in DMSO/10% 1-MeIm solution. Moreover, the initial spectrum in Fig. 2 can be regenerated fully by applying an oxidizing potential of +0.2 V. This confirms that the redox reaction

$$Fe^{III} + e^- \rightleftharpoons Fe^{II}$$

is fully reversible under anaerobic conditions. The electron pathway that accounts for all of the observed results is shown in Scheme 1.

To confirm the involvement of DMSO in the coordination chemistry of the system, the spectroelectrochemistry of [$Fe^{III}(C_2cap)Cl$] in solution in dichloromethane containing 10% by volume of 1-MeIm was examined and the results are illustrated in Fig. 3. The initial spectrum (λ_{max} = 514, 588 and 650 nm) is typical of [Fe^{III}(tetraphenylporphyrin)Cl] species,[20] indicating that in CH_2Cl_2 solution the Cl^- ion is not replaced by 1-MeIm. This again represents a dramatic difference in behaviour

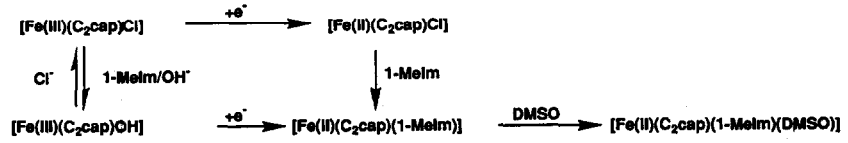

Scheme 1.

relative to that of [Fe^{III}TPPCl], which readily forms a bis(base) adduct in solvents of low polarity.[21] Since CH_2Cl_2 is more readily kept dry than DMSO, there is no involvement of OH^- in the coordination chemistry of [$Fe^{III}(C_2cap)]^+$ in this solvent. If water is deliberately added to the system, however, the hydroxo complex is again observed, underlining the necessity of working in anhydrous conditions with the capped complex. The inability of 1-MeIm to replace Cl^- ions in anhydrous conditions is in keeping with the strong binding of Cl^- to iron(III), reported by Walker *et al.* for [Fe^{III}TPPCl].[13] Although this species does undergo substitution, K_{diss} for Cl^- in $CHCl_3$ solution is very small ($< 10^{-6}$ mol dm^{-3}).

The electronic spectrum of the fully reduced material in CH_2Cl_2/10% 1-MeIm is very different from that of the fully reduced material in DMSO/10% 1-MeIm solution. It has λ_{max} at 540 nm with a shoulder at *ca* 564 nm, strongly resembling the spectrum of the five-coordinate $Fe^{II}(C_2cap)$(pyridine) species reported in the literature.[4] Therefore, the product of electrochemical reduction is assigned as the five-coordinate complex [$Fe^{II}(C_2cap)$(1-MeIm)]. The reaction pathway for reduction of $Fe^{III}(C_2cap)Cl$ in CH_2Cl_2/100% 1-MeIm is described by Scheme 2.

$$[Fe^{III}(C_2cap)Cl] \xrightarrow{+e^-} [Fe^{II}(C_2cap)Cl]^- \xrightarrow{-Cl^-}$$

$$[Fe^{II}(C_2cap)] \xrightarrow{1\text{-MeIm}} [Fe^{II}(C_2cap)(1\text{-MeIm})$$

Scheme 2.

The spectroelectrochemical results indicate that electron transfer is accompanied by isosbestic points in the electronic spectra. This implies that the intermediate species in the scheme are but transient, and Cl^- dissociation from [$Fe^{II}(C_1cap)Cl]^-$ and 1-MeIm binding to [$Fe^{II}(C_2cap)$] are both rapid processes. Notably the spectroscopic changes of Fig. 3 are completely reversible upon controlled potential oxidation of the system. This indicates that $Fe^{III}(C_2cap)Cl$ is reformed during the oxidation step and we ascribe this behaviour to the poor ability of CH_2Cl_2 to stabilize ions, which leads to rapid association of [$Fe^{III}(C_2cap)]^+$ and Cl^- to reform the starting material.

The electrochemical behaviour of the iron C_2-capped porphyrin complex in the presence of dioxygen will form the basis of a separate report.

CONCLUSIONS

The chloride ion of [$Fe^{III}(C_2cap)Cl$] is not displaced by DMSO when the complex is dissolved in that solvent. In contrast, when 1-MeIm is added to the solvent system the Cl^- ion is replaced by OH^-, formed from trace amounts of water, to produce a five-coordinate complex, [$Fe^{III}(C_2cap)OH$]. This species undergoes four quasi-reversible one-electron reduction steps in the region 0 to -2 V (vs S.C.E.). Controlled potential reduction at -0.4 V produces a six-coordinate iron(II) complex, [$Fe^{II}(C_2cap)$(1-MeIm)(DMSO)], where the DMSO ligand binds within the capping group. This redox reaction was shown to be reversible by spectroelectrochemistry.

Spectroelectrochemistry of [$Fe^{III}(C_2cap)Cl$] in CH_2Cl_2 containing 1-MeIm indicates that the Cl^- ion is not replaced by 1-MeIm until reduction has occurred. The iron(II) product of controlled potential reduction is the five-coordinate species $Fe^{II}(C_2cap)$(1-MeIm). Re-oxidation generates [$Fe^{III}(C_2cap)Cl$].

EXPERIMENTAL

All solvents and 1-MeIm were carefully dried using standard literature procedures. Tetrabutylammonium tetrafluoroborate was recrystallized from ethanol and dried *in vacuo* at 80°C. The C_2-capped porphyrin ligand was prepared by the method of Baldwin and co-workers.[3]

Preparation of [$Fe^{III}(C_2cap)Cl$]

This was prepared by a modification of the literature procedure.[22] A solution of the free-base ligand (0.100 g, 9.65×10^{-5} mol) and $Fe^{II}Cl_2 \cdot 4MeCN$ (0.360 g, 1.24 mmol) in THF was heated at reflux, under nitrogen, for 5 days. The flask was protected from light during this process. The THF was removed, the residue was dissolved in $CHCl_3$ and the organic layer was extracted with three portions of 1 M HCl (15 cm^3). The organic layer was dried, reduced in volume to *ca* 1 cm^3 and then chromatographed on neutral alumina using $CHCl_3$ as an eluant. The fast-moving coloured band was collected and HCl gas was bubbled through the solution, to react with the μ-oxo dimer by product. Removal of the solvent gave the product as a lustrous, dark blue solid (yield 0.080 g, 76%).

The electrochemical apparatus was that described in detail in a previous report.[23] The internal resistance of the solvent was compensated for by the PAR 273 potentiostat. Potentials were referenced externally to a sample of ferrocene, run immediately prior to each experiment. In addition an OTTLE cell based upon the design of Scherson *et al.*[24] was also used. This allowed incorporation of an S.C.E. reference electrode rather than the platinum wire pseudo-reference of the other system.

Qualitatively the results were identical in either cell. All potentials quoted in this work are with respect to the S.C.E. reference. Typically the electrochemical experiments were run on solutions *ca* 3.3×10^{-3} mol dm^{-3} in the porphyrin complex and 0.1 mol dm^{-3} in the supporting electrolyte $[Bu_4NBF_4]$. The electronic spectra were recorded using Shimadzu UV-240 or Philips Analytical SP1800 spectrophotometers.

Acknowledgements—We thank S.E.R.C. and British Aerospace plc for a CASE award (to S.C.T.) and Dr P. C. Morgan for useful discussion.

REFERENCES

1. *Iron Porphyrins* (Edited by A. B. P. Lever and H. B. Gray), Parts 1 and 2. Addison-Wesley, Reading, MA (1983).
2. J. P. Collman, *Accts Chem. Res.* 1977, **10**, 265.
3. J. Almog, J. E. Baldwin, R. L. Dyer and M. Peters, *J. Am. Chem. Soc.* 1975, **97**, 226.
4. J. Almog, J. E. Baldwin and J. Huff, *J. Am. Chem. Soc.* 1975, **97**, 227.
5. J. R. Budge, P. E. Ellis Jr, R. D. Jones, J. E. Linard, T. Szymanski, F. Basolo, J. E. Baldwin and R. L. Dyer, *J. Am. Chem. Soc.* 1979, **101**, 4762; J. E. Linard, P. E. Ellis Jr, J. R. Budge, R. D. Jones and F. Basolo, *J. Am. Chem. Soc.* 1980, **102**, 1896; J. E. Baldwin, J. H. Cameron, M. J. Crossley, I. J. Dagley, S. R. Hall and T. Klose, *J. Chem. Soc., Dalton Trans.* 1984, 1739.
6. T. Hashimoto, R. L. Dyer, M. J. Crossley, J. E. Baldwin and F. Basolo, *J. Am. Chem. Soc.* 1982, **104**, 2101.
7. J. P. Collman, F. Basolo, E. Bunnenburg, T. J. Collins, J. H. Dawson, P. E. Ellis Jr, M. L. Marrocco, A. Moscowitz, J. L. Sessler and T. Szymanski, *J. Am. Chem. Soc.* 1981, **103**, 5636.
8. C. T. Brewer and G. Brewer, *J. Chem. Soc., Dalton Trans.* 1990, 843.
9. L. A. Bottomley, J.-N. Gorce and W. M. Davis, *J. Electroanal. Interfac. Electrochem.* 1986, **202**, 111.
10. E. P. Appl. 176 446 (1986); U.S.P. Appl. 653 549 (1984).
11. D. Lexa, M. Momenteau, P. Rentien, G. Rytz, J.-M. Saveant and F. Xu, *J. Am. Chem. Soc.* 1984, **106**, 4755.
12. K. M. Kadish, *Iron Porphyrins* (Edited by A. B. P. Lever and H. B. Gray), Part 2, Ch. 4. Addison-Wesley, Reading, MA (1983).
13. F. A. Walker, M.-W. Lo and M. T. Ree, *J. Am. Chem. Soc.* 1976, **98**, 5552.
14. L. A. Constant and D. G. Davis, *Anal. Chem.* 1975, **47**, 2253.
15. K. M. Kadish, L. A. Bottomley and D. Beroiz, *Inorg. Chem.* 1978, **17**, 1124.
16. T. Mashiko, M. E. Kastner, K. Spartalian, W. R. Scheidt and C. A. Reed, *J. Am. Chem. Soc.* 1978, **100**, 6354.
17. D. Brault and M. Rougee, *Biochemistry* 1974, **13**, 4591.
18. M. Sabat and J. A. Ibers, *J. Am. Chem. Soc.* 1982, **104**, 3715.
19. N. J. Clayden, G. R. Moore, R. J. P. Williams, J. E. Baldwin and M. J. Crossley, *J. Chem. Soc., Perkin Trans. 2* 1982, 1693.
20. J. W. Buchler, *Porphyrins and Metalloporphyrins* (Edited by K. M. Smith), p. 189. Elsevier, Amsterdam (1975).
21. J. D. Satterlee, G. N. LaMar and J. S. Frye, *J. Am. Chem. Soc.* 1976, **98**, 7275.
22. J. Almog, J. E. Baldwin, M. J. Crossley, J. F. DeBernadis, R. L. Dyer, J. R. Huff and M. K. Peters, *Tetrahedron* 1981, **37**, 3589.
23. J. H. Cameron and S. C. Turner, *J. Chem. Soc., Dalton Trans.* 1992, 3285.
24. D. A. Scherson, S. Sarangapani and F. L. Urbach, *Anal. Chem.* 1985, **57**, 1501.

Polyhedron Vol. 12, No. 13, pp. 1681–1687, 1993
Printed in Great Britain

0277–5387/93 $6.00+.00
© 1993 Pergamon Press Ltd

NEW COMPLEXES OF NICKEL AND NICKEL/COBALT WITH TETRAHYDROFURAN-2,3,4,5-TETRACARBOXYLIC ACID, $THF(COOH)_4$. CRYSTAL STRUCTURES OF $Ni[THF(COOH)_2(COO)_2](H_2O)_3$ AND $Ni_{0.7}Co_{0.3}[THF(COOH)_2(COO)_2](H_2O)_3 \cdot H_2O$ AND THEIR THERMAL BEHAVIOUR

M. C. GUILLEM* and J. LATORRE

Departamento de Química Inorgánica, Universidad de Valencia, Dr.Moliner 50, Burjassot, 46100 Valencia, Spain

and

R. MARTÍNEZ-MÁÑEZ† and J. PAYÁ‡

†Departamento de Química and ‡Departamento de Ingeniería de la Construcción, Universidad Politécnica de Valencia, Camino de Vera s/n, 46071 Valencia, Spain

and

S. GARCÍA-GRANDA,* E. PÉREZ-CARREÑO and F. GÓMEZ-BELTRÁN

Departamento de Química Física y Analítica, Facultad de Química, Universidad de Oviedo, Julián Clavería s/n, 33006 Oviedo, Spain

(*Received* 5 *January* 1993; *accepted* 5 *March* 1993)

Abstract—The reaction of $NiCl_2 \cdot 6H_2O$ with tetrahydrofuran-2,3,4,5-tetracarboxylic acid, $THF(COOH)_4$, partially deprotonated by Na_2CO_3 (1 : 1 metal/ligand molar ratio), yielded $Ni[THF(COOH)_2(COO)_2](H_2O)_3$ (**1**). The molecular structure of **1** was determined by X-ray diffraction on the monocrystal. The structure consists of a mononuclear neutral unit with the nickel atom coordinated by a $[THF(COOH)_2(COO)_2]^{2-}$ ligand, which acts as a tridentate ligand, and three water molecules. Direct interaction of $NiCl_2 \cdot 6H_2O$ and $CoCl_2 \cdot 6H_2O$ (1 : 1 molar ratio) with $THF(COOH)_4$ previously deprotonated by Na_2CO_3 (1 : 1 metal/ligand molar ratio) gave, by slow evaporation of the solution obtained, green crystals of the non-stoichiometric complex $Ni_{0.7}Co_{0.3}[THF(COOH)_2(COO)_2](H_2O)_3 \cdot H_2O$ (**2**). Its crystal structure was solved by single-crystal X-ray diffraction methods. The structure is similar to that determined for compound **1**, but with 30% of the sites for the metal atom occupied by cobalt and including a water molecule of crystallization. The thermal decomposition of both compounds showed three effects: An endothermic effect, corresponding to the loss of water which occurred at about 150°C and second and third exothermic processes, which overlapped each other at *ca* 310 and 330°C, corresponding to the decomposition of the complex and subsequent formation of oxides at very low temperatures.

Ligands containing more than one functional group can be used efficiently to bond two or more metal centres, depending on the number of functional groups contained in the ligand. Dicarboxylic acids like oxalic acid have been used extensively in the synthesis of dinuclear homonuclear and heteronuclear complexes.[1,2] However, polycarboxylic

* Authors to whom correspondence should be addressed.

acids have not been used to the same extent. Tetrahydrofurantetracarboxylic acid, $THF(COOH)_4$, is commercially available as a mixture of diastereoisomers. It has been described that this ligand acts as a metal trapping agent in detergents,[3,4] although a small number of studies concerning the formation of complexes with this ligand have been performed. Thus, as far as we know, only three structures containing the $THF(COOH)_4$ ligand have been published: that of $[Co(en)_3][THF(COO)(COOH)_3][THF(COO)_2(COOH)_2] \cdot 2.5H_2O$,[5] where the dihydrogen and trihydrogen tetrahydrofurantetracarboxylates are present as anionic species, balancing the charge of the $[Co(en)_3]^{3+}$ cation, but are not acting as proper ligands; and those of polymeric $[Cs(THF(COO)(COOH)_3)]$ and $[Ca_2(THF(COO)_4(H_2O)_6)] \cdot 2H_2O$,[6] in which, in contrast, the ligand coordinates several metal atoms to give complicated three-dimensional structures.

The presence of four carboxylate groups in the ligand creates the possibility of acting with different coordination modes, for example, coordinating a unique atom as bidentate or tridentate, coordinating two metal atoms as bis-bidentate or acting as polydentate. In this sense we are interested in the coordination behaviour of this ligand with transition metal cations. We report here preliminary studies with nickel and cobalt.

EXPERIMENTAL

Preparation of the compounds

Preparation of $Ni[THF(COOH)_2(COO)_2](H_2O)_3$. Na_2CO_3 (106 mg, 1.0 mmol) was added to an aqueous solution (10 cm^3) of tetrahydrofuran-2,3,4,5-tetracarboxylic acid (248 mg, 1.0 mmol) and carbon dioxide evolved. The mixture was stirred for 5 min and an aqueous solution (10 cm^3) of $NiCl_2 \cdot 6H_2O$ (237 mg, 1.0 mmol) was added. Slow evaporation of the resulting green solution gave after several days suitable crystals for X-ray diffraction studies (yield 60%).

The IR spectrum of the compound obtained gave the following bands: 3480(m), 3380(m), 3220(m), 1730(s), 1670(m), 1590(s), 1410(s), 1335(w), 1295(w), 1235(w), 1220(w), 1190(m), 1100(w), 1055(m), 1020(w), 970(w), 955(w), 930(m), 870(w), 805(m), 760(m), 690(w) cm^{-1}.

Preparation of $Ni_{0.7}Co_{0.3}[THF(COOH)_2(COO)_2](H_2O)_3 \cdot H_2O$. Na_2CO_3 (106 mg, 1.0 mmol) was slowly added to an aqueous solution (10 cm^3) of tetrahydrofuran-2,3,4,5-tetracarboxylic acid (248 mg, 1.0 mmol) and the mixture was stirred for 5 min. A mixture of $NiCl_2 \cdot 6H_2O$ and $CoCl_2 \cdot 6H_2O$ (1 : 1 molar ratio) was then added in a metal/ligand molar ratio of 1 : 1. Slow evaporation of the solution thus obtained yielded after several days green crystals suitable for X-ray diffraction studies (yield 54%).

The IR spectrum of the compound obtained gave the following bands: 3420(m), 3376(m), 3243(m), 1739(s), 1670(m), 1599(s), 1415(s), 1343(w), 1305(w), 1251(w), 1232(w), 1189(m), 1108(w), 1067(m), 1020(w), 981(w), 965(w), 940(m), 876(w), 815(m), 766(m), 697(w) cm^{-1}.

The Ni/Co molar ratio was determined by flame atomic absorption and confirmed by microanalysis using scanning electron microscopy (SEM).

Materials and measurements

Tetrahydrofuran-2,3,4,5-tetracarboxylic acid $[THF(COOH)_4]$ was used as commercially available (Aldrich). Anhydrous sodium carbonate and hexahydrate nickel(II) and cobalt(II) chlorides were from Panreac.

IR spectra were recorded on KBr discs with a Perkin–Elmer 781 IR spectrophotometer between 600 and 4000 cm^{-1}. The two complexes were also studied in the solid state by UV–vis spectroscopy by the diffuse reflectance technique, with a UV–vis–NIR double beam spectrometer in the frequency range 4000–50,000 cm^{-1}. The thermal behaviour of both complexes was studied by TGA, DTG and DTA with Perkin–Elmer DTA1700 and TGA7 apparatus, between 20 and 600°C at a heating rate of 5 K min^{-1}, in a platinum crucible in air with a flow rate of 45.00 cm^3 min^{-1} and using alumina as a reference.

Analysis for metals was performed by flame atomic absorption spectroscopy using a Perkin–Elmer flame atomic absorption spectrometer. Microanalyses by scanning electron microscopy (SEM) (Hitachi S-2500) and energy dispersive X-ray analyses (EDX) (KEVEX, Delta IV quantum 8000) were performed on single crystals with 20 kV accelerating voltage; crystals being mounted on brass stubs with colloidal silver.

X-ray crystallographic procedures

Well-formed crystals of $Ni[THF(COOH)_2(COO)_2](H_2O)_3$ (**1**) and $Ni_{0.7}Co_{0.3}[THF(COOH)_2(COO)_2](H_2O)_3 \cdot H_2O$ (**2**) were grown by slow evaporation of aqueous solutions of the corresponding metal/ligand system and used for the structure determination. Crystallographic constants and experimental details for both structures are summarized in Table 1. X-ray diffraction data were collected on an Enraf–Nonius CAD4 single-crystal diffractometer using graphite-monochromated

Table 1. Crystallographic data for compounds **1** and **2**

	1	**2**
Crystal colour	Green	Green–brown
Crystal size	0.26 × 0.20 × 0.10	0.17 × 0.17 × 0.17
Molecular formula	$C_8H_{12}O_{12}Ni$	$C_8H_{12}O_{12}Ni_{0.7}Co_{0.3}\cdot H_2O$
fw	358.7	376.7
Space group	*P*-1	*P*-1
a (Å)	5.648(1)	5.655(1)
b (Å)	7.774(3)	7.795(3)
c (Å)	15.63(1)	15.64(1)
α (°)	103.92(4)	104.02(4)
β (°)	94.84(3)	94.81(3)
γ (°)	97.52(3)	97.54(2)
V (Å^3)	665.8	658.2(5)
Z	2	2
λ (Å)	0.71073	0.71073
D_{calc} (g cm^{-3})	1.82	1.90
μ(Mo-K_α) (cm^{-1})	14.58	14.58
F(000)	368	387
θ limits	0–25	0–25
hkl range	(−6, −9, −18) ↔ (6, 9, 18)	(−6, −9, −18) ↔ (6, 9, 18)
R_{int}[a]	0.022	0.022
Drift correction	0.95 ↔ 1.07	0.95 ↔ 1.07
Measured reflections	4580	4611
Unique reflections	2290	2302
Observed reflections ($I > 3\sigma(I)$)	2020	1790
Absorption correction		
Ψ-scans	0.78 ↔ 1.00	0.95 ↔ 1.00
DIFABS	1.42 ↔ 0.78	1.00 ↔ 0.98
R	0.116	0.054
Rw[b]	0.116	0.055
ρ, max. ↔ min. (e Å^{-3})	1.30 ↔ −2.00	1.56 ↔ −0.78
Number of variables	209	234

[a] $R_{int} = \Sigma(|I| - \langle I \rangle)/\Sigma I$.
[b] $\Sigma w(F_o - F_c)^2$, $w = 1/[\sigma^2(F_o) + g(F_o)^2]$.

Mo-K_α radiation. Unit cell parameters were determined from the angular settings of 25 reflections with $11° < \theta < 18°$. A triclinic cell was obtained and the space group *P*-1 was confirmed from structure determination in both complexes. Reflections were measured in each case using the ω–2θ scan technique and a variable scan rate with a maximum scan time of 60 s per reflection. The intensity was checked throughout data collection by monitoring three standard reflections every 60 min. A profile analysis was performed on all reflections.[7,8] An empirical absorption correction was applied using ψ-scans.[9] Some Friedel pairs were averaged, $R_{int} = \Sigma(|I| - \langle I \rangle)/\Sigma I$. Lorentz and polarization corrections were applied and data reduced to $|F_o|$ values.

The structures were solved by the Patterson interpretation using the program SHELX86[10] and completed by DIRDIF.[11] Isotropic least-squares refinement was performed using SHELX76.[12] An additional empirical absorption correction was applied.[13] Further anisotropic refinements followed by difference-Fourier syntheses allowed the location of most of the hydrogen atoms. Positional parameters and anisotropic thermal parameters of non-hydrogen atoms were refined in complex **1**, except O(41) and O(42) which were found strongly disordered with two alternative positions, named O(41′) and O(42′), with a refined occupation factor of 0.63(3) for O(41) and 0.61(2) for O(42), and they were isotropically refined. In complex **2** occupation factors for the heavy atom were fixed from the atomic absorption analysis data, i.e. 0.7 for nickel and 0.3 for cobalt, and they were isotropically refined. All hydrogen atoms were refined isotropically, riding on their parent atoms with a com-

mon thermal parameter. The final difference-Fourier map showed no peaks higher than 1.30 e $Å^{-3}$ and deeper than -2.00 e $Å^{-3}$ for complex **1**; most of the highest peaks were found near the disordered carboxylic group and some of the weakest around the central nickel atom. Atomic scattering factors were taken from the International Tables for X-ray Crystallography.[14] Geometrical calculations were performed with PARST[15] and the molecular illustration was drawn with PLUTO.[16] All calculations were made on a MicroVax-3400 at the Scientific Computer Center, University of Oviedo.*

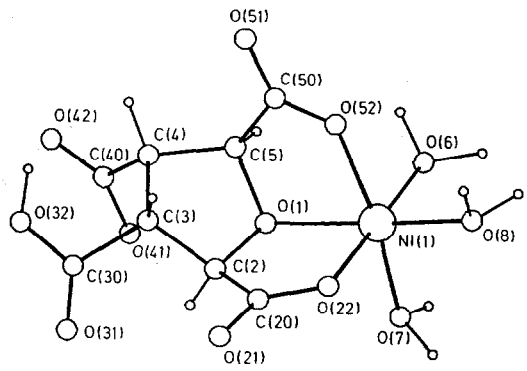

Fig. 1. Molecular structure of $Ni[THF(COOH)_2(COO)_2](H_2O)_3$.

RESULTS AND DISCUSSION

The reaction in aqueous medium of $THF(COOH)_4$ with $NiCl_2 \cdot 6H_2O$ in the presence of Na_2CO_3 (1 : 1 : 1 molar ratio) gave the compound $Ni[THF(COOH)_2(COO)_2](H_2O)_3$ (**1**) in good yield. Although the reaction was performed using the $THF(COOH)_4$ ligand as a commercially available mixture of diasteroisomers, complex **1** contains the coordinated ligand (partially deprotonated) in a *trans–cis–trans* conformation. The same behaviour is observed for other examples reported in the literature.[5,6] Inter- and intramolecular forces or packing forces may be related to the presence of only the *trans–cis–trans* isomer in the solid state, starting from a mixture of diastereoisomers in solution. This observation is supported by the fact that when crystals are separated the remaining solution refuses to crystallize, indicating that under these experimental conditions only the *trans–cis–trans* isomer is able to produce crystals.

Figure 1 shows a perspective view of the molecule for compound **1** with the atomic numbering scheme. Table 1 summarizes crystallographic data for compounds **1** and **2**. Selected bond distances and angles for compounds **1** and **2** are given in Tables 2 and 3, respectively.

The structure of compound **1** consists of a mononuclear neutral unit with the nickel atom coordinated by a $[THF(COOH)_2(COO)_2]^{2-}$ ligand acting as tridentate by coordinating two oxygen atoms from the carboxylate groups and one furanic oxygen from the ring. Three water molecules complete the coordination sphere. The crystallographic packing includes an extensive three-dimensional hydrogen-bond network involving carboxylic groups and water molecules. For compound **2** the crystal structure is very similar to that found for compound **1**, already shown in Fig. 1. However, for complex **2** nickel is substituted by cobalt in 30% of the sites of the heavy atom. We have confirmed the presence of cobalt in complex **2** quantitatively by flame atomic absorption spectroscopy and also semi-quantitatively by scanning electron microscopy, as well as by UV–vis spectroscopy, on the same crystals used for X-ray diffraction.

For both complexes the metal atom shows quite a regular octahedral environment with *cis* angles from 78.2(3) to 97.8(4)° for complex **1** and from 77.7(1) to 98.5(2)° for complex **2** and *trans* angles from 166.8(4) to 176.2(4)° (complex **1**) and from 166.1(2) to 175.8(2)° (complex **2**). The metal–oxygen bond distances fall in the ranges 2.103(8)–2.013(9) Å (compound **1**) and 2.143(4)–2.030(4) Å (compound **2**), averaging 2.050 and 2.086 Å, respectively. In the ligand the average C—C distance is 1.53 Å. The C(5)—O(1) and C(2)—O(1) bond distances are 1.45(1) and 1.46(1) Å for compound **1** and 1.457(6) and 1.453(6) Å for compound **2**; the average value given for the same distance in related structures being 1.43 Å. In the carboxylate groups the mean values for the bond length between carbon and oxygen atoms are C—OH 1.32 (complex **1**) and 1.27 Å (complex **2**), C—O 1.27 Å for both complexes and C=O 1.20 and 1.17 Å, respectively; average values reported for the same distances in the coordinated ligand are 1.31, 1.26 and 1.19 Å, respectively.

It has been suggested that the carboxylate groups on C(20) and C(50)[6] are more acidic than the remainder. Accordingly in compounds **1** and **2** these two carboxylate groups are deprotonated, which allows the ligand to act as a tridentate ligand (see

* Fractional positional and thermal parameters, full list of bond lengths and bond angles, anisotropic temperature factors for non-hydrogen atoms, fractional positional parameters for hydrogen atoms, bond lengths and bond angles involving hydrogen atoms, angles between least-squares planes, hydrogen contacts, principal torsion angles and observed and calculated structure factors have been deposited.

Table 2. Selected bond distances (Å) and angles (°) (with e.s.d.s) for compound **1**

N(1)—O(1)	2.103(8)	Ni(1)—O(6)	2.058(9)	Ni(1)—O(7)	2.028(9)
Ni(1)—O(8)	2.04(1)	Ni(1)—O(22)	2.013(9)	Ni(1)—O(52)	2.055(9)
O(1)—C(2)	1.46(1)	O(1)—C(5)	1.45(1)	C(2)—C(3)	1.52(2)
C(2)—C(20)	1.52(2)	C(3)—C(4)	1.57(2)	C(3)—C(30)	1.55(2)
C(4)—C(5)	1.53(2)	C(4)—C(40)	1.53(2)	C(5)—C(50)	1.54(2)
C(20)—O(21)	1.24(2)	C(20)—O(22)	1.27(2)	C(30)—O(31)	1.20(3)
C(30)—O(32)	1.33(2)	C(40)—O(41)	1.33(3)	C(40)—O(41′)	1.31(4)[a]
C(40)—O(42)	1.21(2)	C(40)—O(42′)	1.22(4)[a]	C(50)—O(51)	1.24(2)
C(50)—O(52)	1.26(2)	O(41)—O(41′)	0.71(4)[a]	O(42)—O(42′)	0.84(3)[a]

O(1)—Ni(1)—O(6)	97.0(3)	O(1)—Ni(1)—O(7)	90.3(4)
O(1)—Ni(1)—O(8)	166.8(4)	O(1)—Ni(1)—O(22)	80.8(3)
O(1)—Ni(1)—O(52)	78.2(3)	O(6)—Ni(1)—O(7)	87.6(4)
O(6)—Ni(1)—O(8)	93.8(4)	O(6)—Ni(1)—O(22)	176.2(4)
O(52)—Ni(1)—O(6)	89.7(4)	O(7)—Ni(1)—O(8)	97.8(4)
O(7)—Ni(1)—O(22)	89.3(4)	O(7)—Ni(1)—O(52)	167.8(4)
O(8)—Ni(1)—O(22)	88.8(4)	O(8)—Ni(1)—O(52)	94.3(4)
O(22)—Ni(1)—O(52)	92.9(4)	Ni(1)—O(1)—C(2)	111.1(7)
Ni(1)—O(1)—C(5)	110.4(7)	Ni(1)—O(22)—C(20)	118.0(8)
Ni(1)—O(52)—C(50)	117.7(8)		

[a] O(41) and O(42), which were found strongly disordered with two alternative positions, named O(41′) and O(42′), with a refined occupation factor of 0.63(3) for O(41) and 0.61(2) for O(42) were isotropically refined.

Fig. 1). In addition, compounds **1** and **2** are the only crystalline solids separated from solutions at different pH values (pH < 8 in order to avoid metal hydroxide formation).

The crystal structure of compound **2** contains one H_2O molecule of crystallization, whereas complex **1** is anhydrous. This molecule participates in an extensive three-dimensional hydrogen-bond network together with the carboxylic groups and the water coordination molecules.

The difference between the final conventional *R*-factor (0.116 for compound **1** and 0.054 for com-

Table 3. Selected bond distances (Å) and angles (°) (with e.s.d.s) for compound **2**

Ni(1)—O(1)	2.143(4)	Ni(1)—O(6)	2.078(4)	Ni(1)—O(7)	2.037(4)
Ni(1)—O(8)	2.034(4)	Ni(1)—O(22)	2.030(4)	Ni(1)—O(52)	2.061(4)
O(1)—C(2)	1.453(6)	O(1)—C(5)	1.457(6)	C(2)—C(3)	1.533(8)
C(2)—C(20)	1.528(8)	C(3)—C(4)	1.564(8)	C(3)—C(30)	1.55(1)
C(4)—C(5)	1.541(8)	C(4)—C(40)	1.511(8)	C(5)—C(50)	1.544(8)
C(20)—O(21)	1.250(7)	C(20)—O(22)	1.262(7)	C(30)—O(31)	1.18(1)
C(30)—O(32)	1.27(1)	C(40)—O(41)	1.143(8)	C(40)—O(42)	1.265(9)
C(50)—O(51)	1.226(2)	C(50)—O(52)	1.273(6)		

O(1)—Ni(1)—O(6)	97.0(1)	O(1)—Ni(1)—O(7)	89.9(2)
O(1)—Ni(1)—O(8)	166.1(2)	O(1)—Ni(1)—O(22)	80.0(1)
O(1)—Ni(1)—O(52)	77.7(1)	O(6)—Ni(1)—O(7)	87.5(2)
O(6)—Ni(1)—O(8)	94.4(2)	O(6)—Ni(1)—O(22)	175.8(2)
O(6)—Ni(1)—O(52)	89.6(2)	O(7)—Ni(1)—O(8)	98.5(2)
O(7)—Ni(1)—O(22)	89.6(2)	O(7)—Ni(1)—O(52)	166.9(2)
O(8)—Ni(1)—O(22)	89.0(2)	O(8)—Ni(1)—O(52)	94.5(2)
O(22)—Ni(1)—O(52)	92.6(2)	Ni(1)—O(1)—C(2)	111.0(3)
Ni(1)—O(1)—C(5)	109.7(3)	Ni(1)—O(22)—C(20)	118.6(3)
Ni(1)—O(52)—C(50)	118.5(3)		

Occupation factors for Ni(1): Ni(0.7), Co(0.30).

pound **2**) must be associated with disorder problems in the oxygen atoms of the non-coordinated carboxylate groups for complex **1**.

The UV–vis spectrum of complex **1** (Fig. 2) shows three absorption bands in agreement with the octahedral coordination of nickel(II): (a) a medium band at 9000 cm^{-1} corresponding to the $^3T_{2g}(F) \leftarrow {}^3A_{2g}(F)$ transition; (b) a strong band with a maximum at 15,300 cm^{-1} attributed to the $^3T_{1g}(F) \leftarrow {}^3A_{2g}(F)$ transition, and (c) a strong band at 25,700 cm^{-1} due to $^3T_{1g}(P) \leftarrow {}^3A_{2g}(F)$. The spectrum for complex **2** (Fig. 2) shows these bands of octahedral nickel(II) with a little lower intensity than for complex **1** and the first band displaced to 8800 cm^{-1}, and, in addition, two strong bands at 19,600 and 20,750 cm^{-1}. These two bands correspond, respectively, to $^4A_{2g}(F) \leftarrow {}^4T_{1g}(F)$ and $^4T_{1g}(P) \leftarrow {}^4T_{1g}(F)$ transitions for octahedral cobalt(II), while the displacement of the lower frequency band towards 8800 cm^{-1} can be explained as due to two overlapping transitions: the $^4T_{2g}(F) \leftarrow {}^4T_{1g}(F)$ transition of cobalt(II) and the $^3T_{2g}(F) \leftarrow {}^3A_{2g}(F)$ transition of nickel(II). Therefore, it is clear from these spectra that in compound **2** nickel(II) has been substituted to some extent by cobalt(II).

Complexes with metal atoms coordinated to ligands containing only carbon, oxygen and hydrogen are useful as precursors for producing the corresponding oxides at low temperatures. In this way we performed the thermal decomposition of the title compounds by TGA, DTG and DTA. The thermogravimetric study confirms the stoichiometry of complexes **1** and **2** found in the structural study. Figure 3 shows the thermal behaviour of compound **1**. Three thermal effects are clearly detected on the DTA curve. The first appears as a small endothermic peak between 110 and 185°C, with a maximum at 157°C. The other two appear as asymmetric overlapped exothermic peaks, one between 225 and 318°C with a maximum at 310°C and the other, much larger than the former, between 318 and 350°C with a maximum at 340°C. The endothermic effect corresponds to a weight loss which is observed in TGA and DTG curves between 125 and 175°C with a maximum at 154°C for compound **1** and 115 and 210°C with a maximum at 151°C for compound **2**, due to water evolution (three and four water molecules, respectively). The exothermic effects are accompanied by two overlapping larger weight losses corresponding to the decomposition of the complexes to the metal oxides, the second occurring at a much higher rate and developing a large amount of heat. The first loss takes place at 175–323°C with a maximum at 310°C for complex **1** and at 210–321°C with a maximum at 313°C for complex **2**, and the second loss occurs at 323–338°C with a maximum at 330°C and at

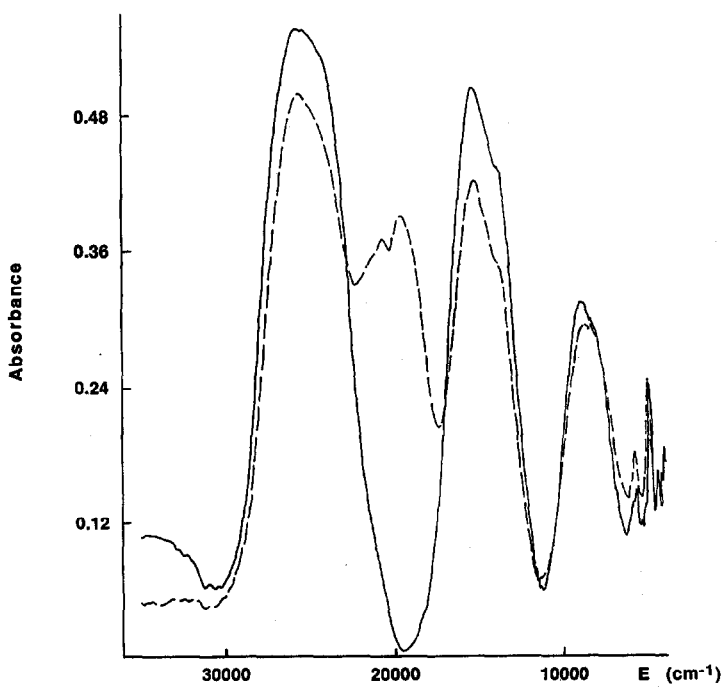

Fig. 2. UV–vis spectra of $Ni[THF(COOH)_2(COO)_2](H_2O)_3$ (**1**) (continuous line) and $Ni_{0.7}Co_{0.3}[THF(COOH)_2(COO)_2](H_2O)_3 \cdot H_2O$ (**2**) (broken line).

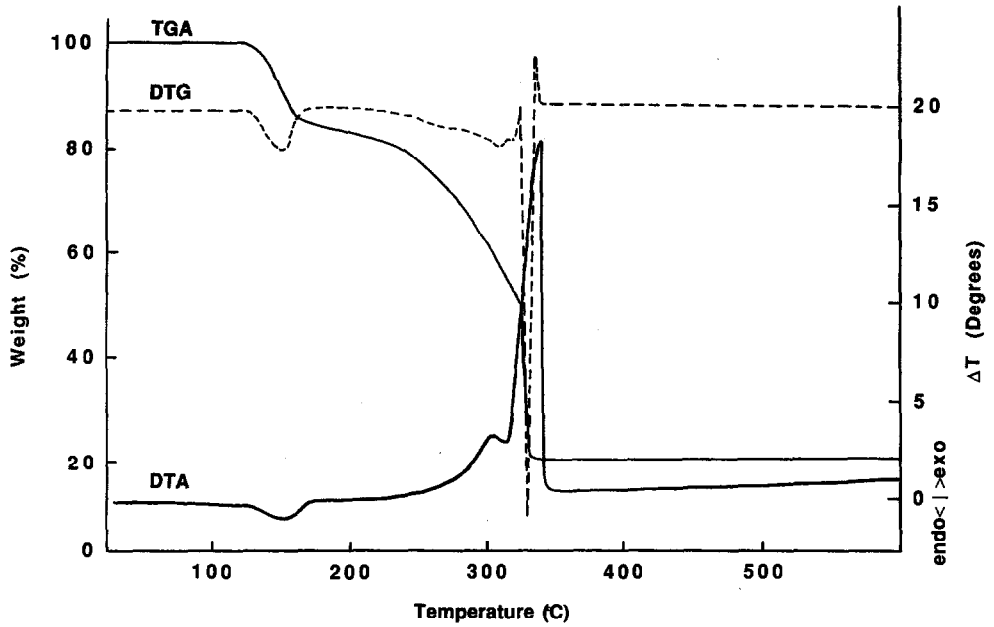

Fig. 3. TGA, DTG and DTA curves of $Ni[THF(COOH)_2(COO)_2](H_2O)_3$.

321–334°C with a maximum at 327°C, respectively.

As a conclusion this study reveals the ability of the $THF(COOH)_4$ ligand to give non-stoichiometric complexes; in fact, complex **2** should be considered as a non-stoichiometric compound. Studies oriented to the preparation of complexes with variable compositions of nickel and cobalt and the influence of the composition on structural parameters are now in progress. Furthermore, from this study the possibility of using this ligand to prepare precursors for the production of mixed oxides is opened.

Acknowledgement—We thank the Instituto de Tecnología Cerámica de Castellón for thermogravimetric measurements.

REFERENCES

1. K. V. Krishnamurty and G. M. Harris, *Chem. Rev.* 1961, **61**, 213.
2. O. Kahn, *Angew. Chem., Int. Edn Engl.* 1985, **24**, 834.
3. M. D. Konort, German Patent 2057259 (*Chem. Abstr.* 75, No. 111128r), 1971.
4. M. T. Yang, US Patent 3580852 (*Chem. Abstr.* 71, No. 50713d), 1971.
5. J. C. Barnes and J. D. Paton, *Acta Cryst.* 1982, **B38**, 1588.
6. J. C. Barnes and J. D. Paton, *Acta Cryst.* 1984, **C40**, 1809.
7. M. S. Lehman and F. K. Larsen, *Acta Cryst.* 1974, **A30**, 580.
8. D. F. Grant and E. J. Gabe, *J. Appl. Cryst.* 1978, **11**, 114.
9. A. C. T. North, D. C. Philips and F. S. Mathews, *Acta Cryst.* 1968, **A24**, 351.
10. G. M. Sheldrick, SHELX86, in *Crystallographic Computing 3* (Edited by G. M. Sheldrick, C. Kruger and R. Goddard), p. 175. Clarendon Press, Oxford (1985).
11. P. T. Beurskens, W. P. Bosman, R. O. Doesburg, J. M. M. Gould, Th. E. M. van den Hark, P. A. J. Prick, J. M. Noordik, G. Beurkens, V. Parthasarathi, H. J. Bruins-Slot, R. C. Haltiwanger, M. K. Strumpel, J. M. M. Smits, S. García Granda, C. Smykalla, H. Behm, H. Schäfer and G. Admiraal, ERICE90, Lecture Notes (1990).
12. G. M. Sheldrick, SHELX, A Program for Crystal Structure Determination. University Chemical Laboratory, Cambridge, U.K. (1976).
13. N. Walker and D. Stuart, *Acta Cryst.* 1983, **A39**, 158.
14. *International Tables for X-ray Crystallography*, Vol. IV. Kynoch Press, Birmingham (Present distributor Kluwer Academic Publishers, Dordrecht) (1974).
15. M. Nardelli, *Comput. Chem.* 1983, **7**, 95.
16. W. D. S. Motherwell and W. Clegg, PLUTO, A Program for Plotting Molecular and Crystal Structures. University Chemical Laboratory, Cambridge, U.K. (1978).

Polyhedron Vol. 12, No. 13, pp. 1689–1696, 1993
Printed in Great Britain

0277–5387/93 $6.00+.00
© 1993 Pergamon Press Ltd

ALLYL(CARBORANE) COMPLEXES OF THE GROUP 6 METALS: PROTONATION STUDIES WITH AQUEOUS HI*

SIHAI LI and F. GORDON A. STONE†

Department of Chemistry, Baylor University, Waco, TX 76798-7348, U.S.A.

(*Received* 22 *February* 1993; *accepted* 3 *March* 1993)

Abstract—Treatment of CH_2Cl_2 solutions of $[N(PPh_3)_2][closo\text{-}1,2\text{-}Me_2\text{-}3\text{-}(\eta^3\text{-}C_3H_5)\text{-}3,3\text{-}(CO)_2\text{-}3,1,2\text{-}WC_2B_9H_9]$ with aqueous HI in the presence of CO affords $[N(PPh_3)_2][closo\text{-}1,8\text{-}Me_2\text{-}2\text{-}I\text{-}2,2,2\text{-}(CO)_3\text{-}2,1,8\text{-}WC_2B_9H_9]$ in virtually quantitative yield. In contrast, the reaction between $[N(PPh_3)_2][closo\text{-}1,2\text{-}Me_2\text{-}3\text{-}(\eta^3\text{-}C_3H_5)\text{-}3,3\text{-}(CO)_2\text{-}3,1,2\text{-}MoC_2B_9H_9]$ and aqueous HI gives initially $[N(PPh_3)_2][closo\text{-}1,2\text{-}Me_2\text{-}3\text{-}I\text{-}3,3,3\text{-}(CO)_3\text{-}3,1,2\text{-}MoC_2B_9H_9]$, but the latter undergoes a cage framework rearrangement to afford $[N(PPh_3)_2][closo\text{-}1,8\text{-}Me_2\text{-}2\text{-}I\text{-}2,2,2\text{-}(CO)_3\text{-}2,1,8\text{-}MoC_2B_9H_9]$, which is slow at room temperature. Protonation of $[NEt_4][closo\text{-}1,2\text{-}Me_2\text{-}3\text{-}(\equiv CC_6H_4Me\text{-}4)\text{-}3,3\text{-}(CO)_2\text{-}3,1,2\text{-}MoC_2B_9H_9]$ with aqueous HI yields initially $[NEt_4][closo\text{-}1,2\text{-}Me_2\text{-}8\text{-}(CH_2C_6H_4Me\text{-}4)\text{-}3\text{-}I\text{-}3,3,3\text{-}(CO)_3\text{-}3,1,2\text{-}MoC_2B_9H_8]$, which isomerizes at room temperature to give $[NEt_4][closo\text{-}1,8\text{-}Me_2\text{-}11\text{-}(CH_2C_6H_4Me\text{-}4)\text{-}2\text{-}I\text{-}2,2,2\text{-}(CO)_3\text{-}2,1,8\text{-}MoC_2B_9H_8]$. The reaction between $[N(PPh_3)_2][closo\text{-}1,8\text{-}Me_2\text{-}2\text{-}I\text{-}2,2,2\text{-}(CO)_3\text{-}2,1,8\text{-}MoC_2B_9H_9]$ and $[W(\equiv CC_6H_4Me\text{-}4)(CO)_2(\eta\text{-}C_5H_5)]$ in CH_2Cl_2 in the presence of $TlPF_6$ affords mainly $[MoW(\mu\text{-}CC_6H_4Me\text{-}4)(CO)_3(\eta^5\text{-}nido\text{-}2,8\text{-}Me_2\text{-}2,8\text{-}C_2B_9H_9)(\eta\text{-}C_5H_5)]$ together with some of its polytopal isomer $[MoW(\mu\text{-}CC_6H_4Me\text{-}4)(CO)_3(\eta^5\text{-}nido\text{-}7,8\text{-}Me_2\text{-}7,8\text{-}C_2B_9H_9)(\eta\text{-}C_5H_5)]$.

We have recently reported the synthesis of the allyl(carborane)-molybdenum and -tungsten complexes $[N(PPh_3)_2][closo\text{-}1,2\text{-}Me_2\text{-}3\text{-}(\eta^3\text{-}C_3H_5)\text{-}3,3\text{-}(CO)_2\text{-}3,1,2\text{-}MC_2B_9H_9]$ (**1**, M = W or Mo) and have described some protonation ($HBF_4\cdot Et_2O$) reactions of these species in the presence of donor molecules.[1] The products isolated are of the formulation expected if it is assumed that the acid releases the allyl ligand as $MeCH{=}CH_2$ and the resultant coordinatively unsaturated carborane–metal fragment captures donor substrate molecules. The compounds $[closo\text{-}1,2\text{-}Me_2\text{-}3,3\text{-}(CO)_2\text{-}3,3\text{-}(L)_2\text{-}3,1,2\text{-}MC_2B_9H_9]$ (**2**, L = CO or PPh_3) and $[closo\text{-}1,2\text{-}Me_2\text{-}3\text{-}(CO)\text{-}3,3\text{-}(RC_2R)_2\text{-}3,1,2\text{-}MC_2B_9H_9]$ (**3**, M = W, R = Ph; M = Mo, R = Me) are examples of species obtained by this procedure.

Earlier we described reactions of salts of the anionic alkylidyne complexes $[closo\text{-}1,2\text{-}Me_2\text{-}3\text{-}(\equiv CR)\text{-}3,3\text{-}(CO)_2\text{-}3,1,2\text{-}MC_2B_9H_9]^-$ (M = W or Mo, R = alkyl or aryl) with $HBF_4\cdot Et_2O$ in the presence of donor molecules.[2] The compounds $[closo\text{-}1,2\text{-}Me_2\text{-}8\text{-}(CH_2C_6H_4Me\text{-}4)\text{-}3,3\text{-}(CO)_2\text{-}3,3\text{-}(L)_2\text{-}3,1,2\text{-}MC_2B_9H_8]$ (**4**, L = CO or PPh_3)[2a,b] and $[closo\text{-}1,2\text{-}Me_2\text{-}8\text{-}(CH_2C_6H_4Me\text{-}4)\text{-}3\text{-}(CO)\text{-}3,3\text{-}(PhC_2Ph)_2\text{-}3,1,2\text{-}WC_2B_9H_8]$ (**5**)[2a] are simple examples of the species obtained and are clearly structurally related to compounds **2** and **3**. However, the presence of the cage $CH_2C_6H_4Me$-4 substituents in **4** and **5** suggests that their formation proceeds via an intermediate alkylidene–metal complex, the alkylidene group subsequently inserting into a cage B—H vertex. This process is accompanied at some stage by ligation of CO, PPh_3 or PhC_2Ph molecules to the coordinatively and electronically unsaturated metal centres, as discussed elsewhere.[2a,3]

In a parallel study[2d,e] treatment of the complexes $[NEt_4][closo\text{-}1,2\text{-}Me_2\text{-}3\text{-}(\equiv CR)\text{-}3,3\text{-}(CO)_2\text{-}3,1,2\text{-}WC_2B_9H_9]$ [R = Me (**6a**), C_6H_4Me-4 (**6b**) or C_6H_4OMe-2 (**6c**)] with aqueous HI yielded the salts $[NEt_4][closo\text{-}1,8\text{-}Me_2\text{-}11\text{-}(CH_2R)\text{-}2\text{-}I\text{-}2,2,2\text{-}(CO)_3\text{-}2,1,8\text{-}WC_2B_9H_8]$ (**7a–c**). The reactions were rapid and occurred below ambient temperatures and it

* This paper is dedicated with best wishes to the distinguished chemist Professor Heinz Nöth on the occasion of his 65th birthday on 20 June 1993.

† Author to whom correspondence should be addressed.

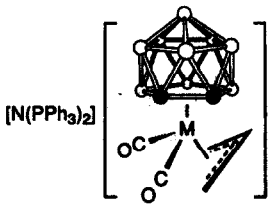

	M
1a	W
1b	Mo

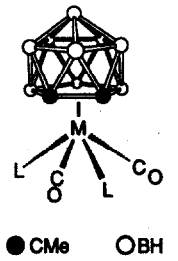

● CMe ○ BH

	M	L
2a	W	CO
2b	Mo	CO
2c	W	PPh_3
2d	Mo	PPh_3

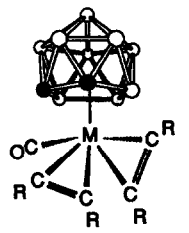

	M	R
3a	W	Ph
3b	Mo	Me

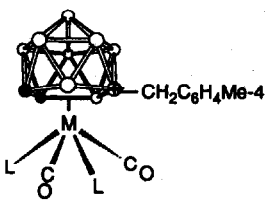

	M	L
4a	W	CO
4b	Mo	CO
4c	W	PPh_3

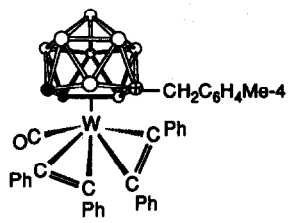

5

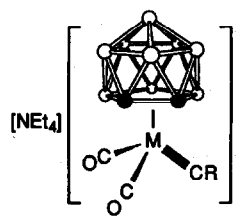

	M	R
6a	W	Me
6b	W	C_6H_4Me-4
6c	W	C_6H_4OMe-2
6d	Mo	C_6H_4Me-4

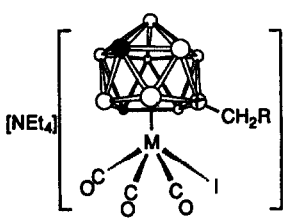

	M	R
7a	W	Me
7b	W	C_6H_4Me-4
7c	W	C_6H_4OMe-2
7d	Mo	C_6H_4Me-4

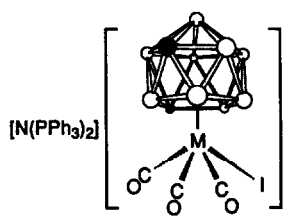

	M
8a	W
8b	Mo

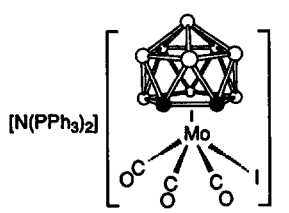

9

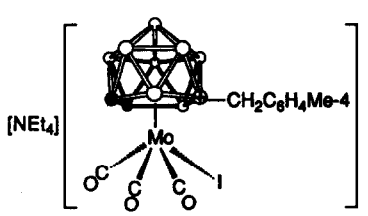

● CMe ○ BH ⊕ B

10

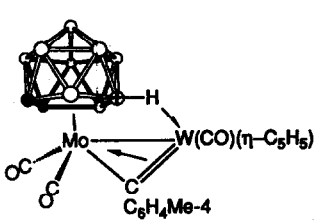

11a

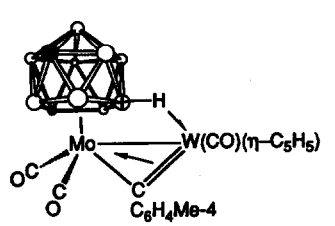

11b

was not possible to determine if the cage rearrangement took place prior or subsequent to insertion of the initially formed alkylidene group into the B—H vertex.

In this paper we describe further protonation studies, using aqueous HI as the proton source and the compounds **1** and $[NEt_4][closo\text{-}1,2\text{-}Me_2\text{-}3\text{-}(\equiv CC_6H_4Me\text{-}4)\text{-}3,3\text{-}(CO)_2\text{-}3,1,2\text{-}MoC_2B_9H_9]$ (**6d**) as the reagents. It was hoped that the results obtained would provide further information about the cage framework rearrangement process.

RESULTS AND DISCUSSION

Treatment of a CO saturated CH_2Cl_2 solution of **1a** at room temperature with aqueous HI, followed by column chromatography of the reaction mixture on silica at −20°C gave the complex $[N(PPh_3)_2][closo\text{-}1,8\text{-}Me_2\text{-}2\text{-}I\text{-}2,2,2\text{-}(CO)_3\text{-}2,1,8\text{-}WC_2B_9H_9]$ (**8a**) in essentially quantitative yield. The compound was fully characterized by the data given in Tables 1 and 2.

The ^1H and $^{13}C\{^1H\}$ NMR data (Table 2) are crucial in establishing that **8a** has the unsymmetrical 2,1,8-WC_2B_9 icosahedral core structure with no connectivity between the carbon vertices. This is reflected in the $^{13}C\{^1H\}$ NMR spectrum with the appearance of three CO resonances at δ 231.8, 221.6 and 221.2, and four signals for the cage CMe groups at δ 63.3 and 63.0 (*C*Me) and at δ 32.8 and 29.3 (C*Me*). The peak at δ 63.3 is appreciably broader than that at 63.0. This is diagnostic for a 2,1,8-WC_2B_9 cage framework in which the two non-adjacent CMe groups occupy vertices in different pentagonal rings of the cage.[2d,3] In such an arrangement one cage carbon nucleus (δ 63.3) is more strongly influenced by the quadrupolar effect of adjacent ^{11}B nuclei than the other (δ 63.0). This was initially observed for the compound $[NEt_4][closo\text{-}1,8\text{-}Me_2\text{-}11\text{-}(CH_2C_6H_4Me\text{-}4)\text{-}2\text{-}Cl\text{-}2,2,2\text{-}(CO)_3\text{-}2,1,8\text{-}WC_2B_9H_8]$, an analogue of **7**, for which an X-ray structure determination confirmed the cage topology.[2d] In contrast with **8a** the $^{13}C\{^1H\}$ spectrum of its precursor **1a** displays a single *C*Me resonance (δ 57.2),[1] as does that of **4a** (δ 70.3),[2a] where both cage carbon vertices lie in the pentagonal C_2B_3 ring ligating the tungsten atom. Consistently, the ^1H NMR spectrum of **8a** shows two C*Me* resonances at δ 1.62 and 1.94, whereas the spectra of **1a** and **4a** each display one signal at δ 2.29 and 2.44, respectively.

In contrast to the results obtained with **1a**, the reaction between CO-saturated CH_2Cl_2 solutions of **1b** and aqueous HI gave the compound $[N(PPh_3)_2][closo\text{-}1,2\text{-}Me_2\text{-}3\text{-}I\text{-}3,3,3\text{-}(CO)_3\text{-}3,1,2\text{-}MoC_2B_9H_9]$ (**9**), in which the 3,1,2-MoC_2B_9 core

Table 1. Analytical[a] and other data for the new compounds

Compound		Colour	Yield (%)	ν_{max} (CO)[b] (cm^{-1})	Analysis (%) C	H
7d	$[NEt_4][closo\text{-}1,8\text{-}Me_2\text{-}11\text{-}(CH_2C_6H_4Me\text{-}4)\text{-}2\text{-}I\text{-}2,2,2\text{-}(CO)_3\text{-}2,1,8\text{-}MoC_2B_9H_8]$[c]	Red-brown	62	2018s, 1938s,br		
8a	$[N(PPh_3)_2][closo\text{-}1,8\text{-}Me_2\text{-}2\text{-}I\text{-}2,2,2\text{-}(CO)_3\text{-}2,1,8\text{-}WC_2B_9H_9]$	Orange-red	99	2013vs, 1927vs, 1911sh	47.2 (47.2)[d]	3.9 (4.2)
8b	$[N(PPh_3)_2][closo\text{-}1,8\text{-}Me_2\text{-}2\text{-}I\text{-}2,2,2\text{-}(CO)_3\text{-}2,1,8\text{-}MoC_2B_9H_9]$	Brown	35	2016vs, 1934vs,br	51.1 (51.3)[e]	4.8 (4.5)
9	$[N(PPh_3)_2][closo\text{-}1,2\text{-}Me_2\text{-}3\text{-}I\text{-}3,3,3\text{-}(CO)_3\text{-}3,1,2\text{-}MoC_2B_9H_9]$	Red	100	2022vs, 1946vs, 1925sh	51.1 (51.3)[e]	4.8 (4.5)
11b	$[MoW(\mu\text{-}CC_6H_4Me\text{-}4)(CO)_3(\eta^5\text{-}nido\text{-}2,8\text{-}Me_2\text{-}2,8\text{-}C_2B_9H_9)(\eta\text{-}C_3H_5)]$[f]	Green	70	2009vs, 1958vs, 1942sh	34.2 (34.7)	4.1 (3.9)

[a] Calculated values are in parentheses.
[b] Measured in CH_2Cl_2. For all carborane compounds there is a broad B—H stretching absorption at 2550 cm^{-1}.
[c] Oil, formed as a mixture with **10**, see text.
[d] N, 1.3 (1.3).
[e] N, 1.4 (1.4).
[f] Formed as a mixture with **11a**, see text.

Table 2. ^{1}H, ^{13}C and ^{11}B NMR data[a] for the new compounds

Compound	$^{1}H(\delta)$[b]	$^{13}C(\delta)$[c]	$^{11}B(\delta)$[d]
7d	1.29 [t, br, 12H, CH_2Me, J(HH) 7], 1.58 (s, 3H, Me), 1.71 (s, 3H, Me), 2.23 (s, 3H, Me-4), 2.34 (s, br, 2H, BCH_2), 3.14 [q, 8H, NCH_2, J(HH) 7], 6.84, 6.91 [$(AB)_2$, 4H, C_6H_4, J(AB) 8]	[e]242.2, 230.0, 228.5 (CO), 145.7, 132.3, 129.2, 128.2 (C_6H_4), 53.5 (NCH_2), 32.4, 29.3 (CMe), 21.1 (vbr, BCH_2), 21.0 (Me-4), 8.2 (CH_2Me)	8.0 (1B, BCH_2), −3.0 to −13.6 (8B)
8a	1.62 (s, 3H, Me), 1.94 (s, 3H, Me), 7.46–7.69 (m, 30H, Ph)	231.8 [CO, J(WC) 125], 221.6 [CO, J(WC) 132], 221.2 [CO, J(WC) 135], 134.1–126.8 (Ph), 63.3 (vbr, CMe), 63.0 (br, CMe), 32.8, 29.3 (CMe)	−2.4 (1B), −3.3 (1B), −4.2 (1B), −7.2 (3B), −11.1 (2B), −12.2 (1B)
8b	1.61 (s, 3H, Me), 1.74 (s, 3H, Me), 7.45–7.67 (m, 30H, Ph)	243.3, 229.9, 229.3 (CO), 134.1–126.8 (Ph), 68.2 (vbr, CMe), 64.4 (br, CMe), 32.4, 29.0 (CMe)	−1.2, −2.4, −2.8, −4.7, −6.0, −6.6, −10.6, −11.2, −11.9 (9B)
9	2.40 (s, 6H, Me), 7.46–7.68 (m, 30H, Ph)	243.9 (CO), 230.8 (2 × CO), 134.1–126.8 (Ph), 71.0 (br, CMe), 33.4 (CMe)	−0.4 (1B), −4.6 (3B), −5.9 (1B), −6.7 (2B), −8.6 (2B)
11b[f]	−8.25 [q, br, 1H, BHW, J(BH) 55], 1.39 (s, 3H, Me), 1.76 (s, 3H, Me), 2.55 (s, 3H, Me-4), 5.42 (s, 5H, C_5H_5), 6.97, 7.40 [$(AB)_2$, 4H, C_6H_4, J(AB) 8]	[e]384.2 (μ-C), 232.5, 217.9, 214.6 (CO), 162.1–120.2 (C_6H_4), 92.6 (C_5H_5), 32.7, 28.1 (CMe), 21.2 (Me-4)	19.0 [1B, BHW, J(HB) 55], −0.6 (1B), −4.0 (1B), −6.8 (2B), −8.2 (1B), −9.6 (1B), −11.6 (1B), −15.3 (1B)

[a] Chemical shifts (δ) in ppm, coupling constants (J) in Hz. Measurements at ambient temperatures in CD_2Cl_2.
[b] Proton resonances for terminal B—H groups occur as broad unresolved peaks in the range δ *ca* −2 to +3.
[c] Hydrogen-1 decoupled, chemical shifts are positive to the high frequency of $SiMe_4$.
[d] Chemical shifts are positive to the high frequency of $BF_3 \cdot Et_2O$ (external). Signals ascribed to more than one boron nucleus may result from overlapping peaks and do not necessarily indicate symmetry equivalence.
[e] Resonances due to cage carbon atoms were too broad to be identified.
[f] Formed as a mixture with **11a**, therefore, some resonances are obscured by those of **11a**, see text.

structure of the precursor is retained. This is evident from the ^1H and $^{13}C\{^1H\}$ NMR data (Table 2). Thus, in the ^1H NMR spectrum there is only one resonance at δ 2.40 for the cage CMe groups. Correspondingly, in the $^{13}C\{^1H\}$ NMR spectrum the equivalent CMe vertices give rise to two signals at δ 71.0 (*C*Me) and 33.4 (C*Me*). As expected there are two peaks for the CO ligands and these occur at δ 243.9 and 230.8, with the latter resonance having twice the intensity of the former. This is the pattern expected for a symmetrical structure with a plane of symmetry through the molybdenum and iodine atoms, the mid-point of the cage C—C connectivity and the CO group transoid to the iodide ligand.

Interestingly, some changes were observed in the $^{13}C\{^1H\}$ NMR spectrum of **9** during the time of data acquisition. After recording the spectrum, fresh ^1H NMR measurements on the sample suggested that the complex had undergone a partial polytopal rearrangement in solution. Accordingly, a CH_2Cl_2 solution of **9** was heated under reflux for 8 h, after which time column chromatography afforded $[N(PPh_3)_2][closo\text{-}1,8\text{-}Me_2\text{-}2\text{-}I\text{-}2,2,2\text{-}(CO)_3\text{-}2,1,8\text{-}MoC_2B_9H_9]$ (**8b**), but in relatively low yield (*ca* 35%). The formation of another product was observed, but it could not be identified. It was also found that if CD_2Cl_2 solutions of **9** are left at ambient temperatures, ^1H NMR measurements revealed that after 10 days approximately 90% of the sample decomposed, with a small amount of **8b** being formed. Possibly the low yield of **8b** and the formation of the unidentified species is due to the instability of some intermediate along the slow pathway for isomerization of **9** into **8b**, since **8a** was prepared in high yield.

The spectroscopic data for **8b** are very similar to those of **8a**, as expected. In particular, the 2,1,8-MoC_2B_9 cage framework leads to the appearance in the $^{13}C\{^1H\}$ NMR spectrum of four resonances for the CMe groups [δ 68.2 and 64.4 (*C*Me), and 32.4 and 29.0 (C*Me*)]. Moreover, the more deshielded *C*Me signal was very broad. The three carbonyl ligands give rise to three peaks at δ 243.3, 229.9 and 229.3. These are more deshielded than those observed for **8a** as is usual for CO groups ligating molybdenum rather than tungsten. In accordance with the lack of symmetry the ^1H NMR spectrum revealed two signals for the CMe groups at δ 1.61 and 1.74. The $^{11}B\{^1H\}$ NMR spectrum displayed nine resonances for the non-equivalent boron nuclei.

As mentioned earlier treatment of the tungsten species **6a–c** with aqueous HI yielded the salts **7a–c**, respectively, in reactions that involved framework rearrangements of the cages from 3,1,2-WC_2B_9 to 2,1,8-WC_2B_9 core structures. These reactions also resulted in migration and hydroboration of the alkylidyne groups in the precursors and it was not apparent whether the migratory process preceded or followed the polytopal rearrangement of the cages. Since this work was restricted to tungsten complexes, it was hoped that a similar study with the molybdenum compound $[NEt_4][closo\text{-}1,2\text{-}Me_2\text{-}3\text{-}(\equiv CC_6H_4Me\text{-}4)\text{-}3,3\text{-}(CO)_2\text{-}3,1,2\text{-}MoC_2B_9H_9]$ (**6d**) might allow a resolution of this matter.

Addition of aqueous HI to a CH_2Cl_2 solution of **6d**, followed by column chromatography of the reaction mixture on silica at $-20°C$ gave a red–brown oil. The ^1H, $^{13}C\{^1H\}$ and $^{11}B\{^1H\}$ NMR measurements on this material revealed that it was a mixture of the two isomers $[NEt_4][closo\text{-}1,8\text{-}Me_2\text{-}11\text{-}(CH_2C_6H_4Me\text{-}4)\text{-}2\text{-}I\text{-}2,2,2\text{-}(CO)_3\text{-}2,1,8\text{-}MoC_2B_9H_8]$ (**7d**) and $[NEt_4][closo\text{-}1,2\text{-}Me_2\text{-}8\text{-}(CH_2C_6H_4Me\text{-}4)\text{-}3\text{-}I\text{-}3,3,3\text{-}(CO)_3\text{-}3,1,2\text{-}MoC_2B_9H_8]$ (**10**). Repeated experiments showed that depending on the time taken to work up the mixture, the isomer ratio varied because **10** slowly converts to **7d**, together with the formation of some unidentified carborane cage-containing material. Complete conversion of **10** into **7d** in solution requires about 10 h at ambient temperatures and is thus faster than the isomerization of **9** into **8b**. This must be due to the presence of the $CH_2C_6H_4Me$-4 substituent on the boron atom β to the two carbon atoms in the pentagonal CCB*B*B face of the cage ligating the molybdenum atom of **10**.

Assignment of resonances in the ^1H NMR spectrum of a mixture of **7d** and **10** was readily accomplished because the signals due to the latter species become weaker as the conversion to **7d** progressed. Indeed, in the $^{13}C\{^1H\}$ NMR spectrum only signals due to **7d** were observed. The ^1H NMR spectrum displayed two sets of $(AB)_2$ patterns due to the C_6H_4 groups of the two isomers. The signals at δ 6.81 and δ 6.89 [J(AB) 8 Hz] are assigned to **10** and the other peaks at δ 6.84 and 6.91 [J(AB) 8 Hz] to compound **7d**. Two resonances at δ 2.23 and 2.22 may be attributed to the Me-4 groups of **7d** and **10**, respectively. As expected the spectrum of **10** displays one peak at δ 2.39 for the two equivalent cage CMe groups, whereas **7d** has two signals for these groups at δ 1.58 and 1.71. A broad peak at δ 2.34 may be attributed to a BCH_2 group, very probably that of **7d**. The corresponding signal in the ^1H NMR spectrum of **7b** ($[N(PPh_3)_2]$ salt) is at δ 2.40.[2d] In the $^{11}B\{^1H\}$ NMR spectrum of the isomeric mixture there are diagnostic signals for the $BCH_2C_6H_4Me$-4 groups of the two isomers at δ 8.0 (**7d**) and 14.7 (**10**).[3] As mentioned above the $^{13}C\{^1H\}$ NMR spectrum of the mixture reveals resonances due only to **7d**. The non-equivalent CO ligands of the latter species display peaks at δ 242.2,

230.0 and 228.5. The signals due to the cage *C*Me nuclei were not observed, probably because broadening resulted in their being lost in the base-line. However, peaks due to the non-equivalent C*Me* groups were seen at δ 32.4 and 29.3, and there is a typical broad signal at δ 21.1 attributable to the $BCH_2C_6H_4Me$-4 nucleus.[3]

The dimetal complex $[MoW(\mu\text{-}CC_6H_4Me\text{-}4)(CO)_3(\eta^5\text{-}nido\text{-}7,8\text{-}Me_2\text{-}7,8\text{-}C_2B_9H_9)(\mu\text{-}C_5H_5)]$ (**11a**)* has been previously prepared by treating THF solutions of $Tl_2[closo\text{-}1,2\text{-}Me_2\text{-}3,3,3\text{-}(CO)_3\text{-}3,1,2\text{-}MoC_2B_9H_9]$ with 2 equivalents of $AgBF_4$ in the presence of $[W(\equiv CC_6H_4Me\text{-}4)(CO)_2(\eta\text{-}C_5H_5)]$.[1] In the present study an attempt to obtain **11a** by treating **1b** with $HBF_4 \cdot Et_2O$ in the presence of $[W(\equiv CC_6H_4Me\text{-}4)(CO)_2(\eta\text{-}C_5H_5)]$ was unsuccessful. However, compound **11a** was obtained when complex **9** in CH_2Cl_2 solution was treated with $TlPF_6$ in the presence of $[W(\equiv CC_6H_4Me\text{-}4)(CO)_2(\eta\text{-}C_5H_5)]$. The compound $[MoW(\mu\text{-}CC_6H_4Me\text{-}4)(CO)_3(\eta^5\text{-}nido\text{-}2,8\text{-}Me_2\text{-}2,8\text{-}C_2B_9H_9)(\eta\text{-}C_5H_5)]$ (**11b**), the isomer of **11a**, having the 2,1,8-MoC_2B_9 topology for the cage framework, was not formed in this reaction. However, treatment of a mixture of the compounds **8b** and $[W(\equiv CC_6H_4Me\text{-}4)(CO)_2(\eta\text{-}C_5H_5)]$ in CH_2Cl_2, with the addition of $TlPF_6$ to remove iodide as insoluble TlI, gave a mixture of the two isomeric dimetal compounds **11a** and **11b** in a *ca* 1:3 ratio, based on relative peak intensities in the NMR spectra. No interconversion between **11a** and **11b** was observed at room temperature and refluxing mixtures in CH_2Cl_2 or THF led only to decomposition.

In the $^{13}C\{^1H\}$ NMR spectrum of **11b** the resonance for the μ-C nucleus of the alkylidyne ligand occurs at δ 384.2, to be compared with that for **11a** at δ 380.1.[1] Both isomers are electronically unsaturated, with 32 cluster valence electrons, and the relatively deshielded chemical shifts observed for the μ-^{13}C nuclei in the two species are in accordance with this feature.[4] Isomer **11b** shows three CO peaks at δ 232.5, 217.9 and 214.6 in the $^{13}C\{^1H\}$ NMR spectrum, while those for **11a** occur at δ 226.1, 217.8 and 213.3.[1] The signals for the carbon vertices of the cage for **11b** were not observed probably due to the broadening discussed above. However, signals for the non-equivalent C*Me* groups were observed at δ 32.7 and 28.1, to be compared with those in the spectrum of **11a** at δ 31.6 and 31.3.[1] Generally, cages with the 3,1,2-MC_2B_9 topology, and with non-equivalent CMe groups, have ^{13}C NMR signals for these fragments which are less disparate than those for cages with 2,1,8-MC_2B_9 frameworks where the CMe groups are always non-equivalent.

The ^1H NMR spectrum of **11b** showed a diagnostic resonance for the B—H→W group at δ −8.25 [J(BH) 55 Hz].[3] The corresponding quartet signal in the ^1H NMR spectrum of **11a** is at δ −8.10.[1] The peaks in the spectrum of **11b** for the Me groups are seen at δ 1.39 and 1.76 for the cage CMe fragments and at δ 2.55 for the Me-4 substituent on the aryl ring.

The new reactions described in this paper give further information about the proton-induced icosahedral cage framework rearrangements from the 3,1,2- to the 2,1,8-MC_2B_9 topology. Thus, treatment of **1b** with aqueous HI yields initially compound **9**, which subsequently isomerizes to **8b**. This contrasts with the reaction of **1a** with the acid, in which no tungsten analogue of **9** was detected prior to the formation of **8a**. Correspondingly, whereas treatment of the tungsten compound **6b** with aqueous HI yields **7b** directly, the reaction of the molybdenum analogue **6d** with the acid proceeds in such a manner that complex **10** can be identified along the reaction profile before the final product **7d** is obtained. This observation is particularly important because it establishes that the polytopal rearrangement from a 3,1,2- to a 2,1,8-icosahedral framework occurs after protonation of the alkylidyne and insertion of the resulting alkylidene moiety into the cage B—H vertex. In the earlier studies with the tungsten species, because **7a–c** were formed so rapidly, it was not established that the two processes were independent with the framework rearrangement as the final step. However, some indication of the stepwise process came from an earlier observation[2d] that **4a** reacts slowly with NEt_4Cl in THF to give $[NEt_4][closo\text{-}1,8\text{-}Me_2\text{-}11\text{-}(CH_2C_6H_4Me\text{-}4)\text{-}2\text{-}Cl\text{-}2,2,2\text{-}(CO)_3\text{-}2,1,8\text{-}WC_2B_9H_8]$, the chloro-analogue of the iodo complex **7b**.

It is perhaps surprising that the skeletal rearrangements proceed more slowly with the molybdenum complexes than with their tungsten analogues. The mechanism of these cage isomerizations remains to be established, but as a consequence of proposals made elsewhere[5] we favour attack of I^- at the metal in species like **9** or **10** to yield a *nido*-12-vertex metallacarborane, with a formally 14-electron count for the polyhedral skeleton. This skeletal framework would be free to undergo rearrangement through diamond–square–diamond

* This compound has a 1,2-dicarba-3-tungsta-dodecacarborane structure. However, use of this numbering system for dimetal complexes leads to an impossibly complex nomenclature. For this reason we treat the cages in dimetal species as *nido*-11 vertex ligands with numbering as for an icosahedron from which the 12th vertex has been removed.

processes with rotation of a triangular face having a carbon and two boron atoms. Closure of the *nido*-intermediate would yield a 2,1,8-MC_2B_9 core structure as the final step.

EXPERIMENTAL

All solvents were freshly distilled over appropriate drying agents prior to use. Light petroleum refers to the fraction with b.p. 40–60°C. Chromatography columns were *ca* 15 cm long and 3 cm in diameter and unless otherwise stated were packed with silica (Aldrich, 70–230 mesh). All experiments were performed under nitrogen using Schlenk-tube techniques. The NMR measurements were obtained using a Bruker AMX 360 MHz spectrometer and IR spectra were recorded with a Bruker IFS 25 instrument. The reagents **1**,[1] **6d**[4c] and [W(≡CC_6H_4Me-4)$(CO)_2(\eta$-$C_5H_5)$][6] were obtained by methods described previously.

Protonation of the allyl(carborane)metal complexes [$N(PPh_3)_2$][closo-1,2-Me_2-3-(η^3-C_3H_5)-3,3-$(CO)_2$-3,1,2-$MC_2B_9H_9$] (M = W *or* Mo)

(i) A CH_2Cl_2 (50 cm^3) solution of **1a** (0.10 g, 0.10 mmol) was saturated with CO at room temperature and treated with HI (0.10 cm^3, 57% aqueous solution, 0.70 mmol). The mixture was stirred for 0.5 h, while maintaining the CO atmosphere. The solvent was removed *in vacuo* and the residue was extracted with CH_2Cl_2 (10 cm^3) and chromatographed at −20°C. Elution with CH_2Cl_2 removed an orange–yellow band. The solvent was removed *in vacuo* and the product was dried *in vacuo* giving orange–red microcrystals of [$N(PPh_3)_2$][*closo*-1,8-Me_2-2-I-2,2,2-$(CO)_3$-2,1,8-$WC_2B_9H_9$] (**8a**) (0.11 g).

(ii) In a similar experiment a CO-saturated CH_2Cl_2 (40 cm^3) solution of **1b** (0.10 g, 0.11 mmol) was treated with HI (0.10 cm^3, 57% aqueous solution, 0.70 mmol). After removal of the solvent the residue was extracted with CH_2Cl_2–light petroleum (10 cm^3, 1:1) and chromatographed at −20°C using neat CH_2Cl_2 as the eluant. The solvent was removed *in vacuo* from the red eluate to give red microcrystals of [$N(PPh_3)_2$][*closo*-1,2-Me_2-3-I-3,3,3-$(CO)_3$-3,1,2-$MoC_2B_9H_9$] (**9**) (0.11 g).

Framework rearrangement of the icosahedral cage

(i) A CH_2Cl_2 (20 cm^3) solution of **9** (0.10 g, 0.10 mmol) was refluxed for 8 h. The solvent was reduced in volume *in vacuo* to *ca* 10 cm^3 and the mixture chromatographed (2 × 5 cm column) at −20°C. Elution with CH_2Cl_2 gave a red–brown solution. The solvent was removed *in vacuo* to yield brown microcrystals of [$N(PPh_3)_2$][*closo*-1,8-Me_2-2-I-2,2,2-$(CO)_3$-2,1,8-$MoC_2B_9H_9$] (**8b**) (0.035 g).

(ii) The NMR spectra (^1H and $^{11}B\{^1H\}$) of a sample of **9** (0.30 g, 0.03 mmol) were recorded and the NMR tube kept for 10 days at room temperature. Remeasurement of the spectra revealed a more than 90% conversion to complex **8b**, together with some unidentified species.

Protonation of the complex [NEt_4][closo-1,2-Me_2-3-(≡CC_6H_4Me-4)-3,3-$(CO)_2$-3,1,2-$MoC_2B_9H_9$]

A CH_2Cl_2 (20 cm^3) solution of **6d** (0.10 g, 0.18 mmol) was treated with HI (0.20 cm^3, 57% aqueous solution, 1.40 mmol) at room temperature and the mixture was stirred for 0.5 h. The solvent was removed *in vacuo*, the residue extracted with CH_2Cl_2 (10 cm^3) and the extracts chromatographed at −20°C (2 × 5 cm column). Elution with CH_2Cl_2 removed a red–brown band, which after removal of solvent *in vacuo* afforded an oily mixture of [NEt_4][*closo*-1,8-Me_2-11-($CH_2C_6H_4$Me-4)-2-I-2,2,2-$(CO)_3$-2,1,8-$MoC_2B_9H_8$] (**7d**) and [NEt_4][*closo*-1,2-Me_2-8-($CH_2C_6H_4$Me-4)-3-I-3,3,3-$(CO)_3$-3,1,2-$MoC_2B_9H_8$] (**10**) (0.08 g).

Synthesis of the isomers [MoW(μ-CC_6H_4Me-4)$(CO)_3(\eta^5$-nido-$Me_2C_2B_9H_9)(\eta$-$C_5H_5)$] (**11**)

A CH_2Cl_2 (20 cm^3) solution of a mixture of **8b** (0.10 g, 0.11 mmol) and [W(≡CC_6H_4Me-4)$(CO)_2(\eta$-$C_5H_5)$] (0.04 g, 0.11 mmol) was treated with $TlPF_6$ (0.07 g, 0.20 mmol) and stirred at room temperature for 2 h. The solvent was removed *in vacuo*, the residue extracted with CH_2Cl_2–light petroleum (10 cm^3, 1:1) and chromatographed on alumina (Brockmann activity II). Elution with the same solvent mixture gave a green fraction. The solvent was removed *in vacuo* and the residue washed with light petroleum (2 × 2 cm^3) and dried *in vacuop* to give green microcrystals (0.05 g) of [MoW(μ-CC_6H_4Me-4)$(CO)_3(\eta^5$-7,8-*nido*-Me_2-7,8-$C_2B_9H_9)(\eta$-$C_5H_5)$] (**11a**) and [MoW(μ-CC_6H_4Me-4)$(CO)_3(\eta^5$-*nido*-2,8-Me_2-2,8-$C_2B_9H_9)(\eta$-$C_5H_5)$] (**11b**).

Acknowledgement—We thank the Robert A. Welch Foundation for support (Grant AA-1201).

REFERENCES

1. S. J. Dossett, S. Li and F. G. A. Stone, *J. Chem. Soc., Dalton Trans.* 1993, 1585.
2. (a) S. A. Brew, D. D. Devore, P. D. Jenkins, M. U. Pilotti and F. G. A. Stone, *J. Chem. Soc., Dalton Trans.* 1992, 393; (b) M. D. Mortimer, PhD thesis, Bristol University (1991); (c) S. A. Brew, P. D.

Jenkins, J. C. Jeffery and F. G. A. Stone, *J. Chem. Soc., Dalton Trans.* 1992, 401; (d) S. A. Brew, N. Carr, J. C. Jeffery, M. U. Pilotti and F. G. A. Stone, *J. Am. Chem. Soc.* 1992, **114**, 2203; (e) J. C. Jeffery, S. Li, D. W. I. Sams and F. G. A. Stone, *J. Chem. Soc., Dalton Trans.* 1992, 877.

3. S. A. Brew and F. G. A. Stone, *Adv. Organomet. Chem.* 1993, **35**, 135.
4. (a) S. J. Dossett, A. F. Hill, J. C. Jeffery, F. Marken, P. Sherwood and F. G. A. Stone, *J. Chem. Soc., Dalton Trans.* 1988, 2453; (b) S. J. Dossett, I. J. Hart and F. G. A. Stone, *J. Chem. Soc., Dalton Trans.* 1990, 3481; (c) S. A. Brew, N. Carr, M. D. Mortimer and F. G. A. Stone, *J. Chem. Soc., Dalton Trans.* 1991, 811.
5. G. M. Edvenson and D. F. Gaines, *Inorg. Chem.* 1990, **29**, 1210.
6. E. O. Fischer, T. L. Lindner, B. Huttner, P. Friedrich, F. R. Kreissl and J. O. Besenhard, *Chem. Ber.* 1977, **110**, 3397.

Polyhedron Vol. 12, No. 13, pp. 1697–1703, 1993
Printed in Great Britain

0277–5387/93 $6.00+.00
© 1993 Pergamon Press Ltd

CYANO-BRIDGED COPPER(I)–RUTHENIUM(II) COMPLEXES: SYNTHESES, CHARACTERIZATION AND SPECTROSCOPIC STUDIES

RAMSHARAN SINGH and S. K. DIKSHIT†

Department of Chemistry, Indian Institute of Technology Kanpur, Kanpur (U.P.) 208016, India

(*Received* 28 *January* 1993; *accepted* 26 *February* 1993)

Abstract—New complexes of the formulae [(N-N)Cu(PPh_3)CN] (N-N = 2,2′-bipyridine, 1,10-phenanthroline) have been isolated and used to synthesize the novel cyano-bridged copper(I)–ruthenium(II) complexes [(N-N)Cu(PPh_3)(μ-CN)Ru(bpy)$_2$Cl]PF_6 (bpy = 2,2′-bipyridine) and [(N-N)Cu(PPh_3)(μ-CN)Ru(η^5-Cp)(PPh_3)$_2$]PF_6 (Cp = cyclopentadienyl anion). In addition, the complexes [(PPh_3)$_2$Cu(μ-CN)Ru(bpy)$_2$Cl]PF_6 and [(PPh_3)$_2$Cu(μ-CN)Ru(η^5-Cp)(PPh_3)$_2$]PF_6 or BF_4 have been synthesized using [(PPh_3)$_2$CuCN]. All the complexes have been characterized on the basis of elemental analyses, spectroscopic data (IR, UV–vis, ^{1}H, ^{13}C and ^{31}P NMR), and magnetic and conductivity measurements. Spectroscopic data clearly indicate that in these complexes copper(I) and ruthenium(II) are bonded via a cyanide bridge.

The design of suitable chromophores to be used as sensitizers in the photochemical conversion of solar energy is one of the goals of coordination chemists.[1] In this context ruthenium(II)-polypyridine complexes have attracted the attention of many workers because of their excellent properties involving the role of light absorption and a light emission sensitizer.[2] In recent years much work has been performed on cyano-bridged homo- and heteropolynuclear complexes[3–7] to explore the various photophysical properties, including sensitization. The copper(I) centre, a d^{10} system, is very electron rich in nature and can be stabilized by ligands having π-acidic character, viz PPh_3, bpy, phen, CO, CN^-, etc. Extensive studies of copper(I) cyanide,[8] cyanide phosphine mixed-ligand complexes[9] and the phosphine polypyridine complexes[10,11] are reported in the literature. There are some reports[4,12,13] on heteronuclear bimetallic cyanide-bridged complexes containing ruthenium(II) and other metal centres, but, to the best of our knowledge, these are the first cyano-bridged heteronuclear bimetallic complexes containing copper(I) and ruthenium(II) metal centres. Since copper(I) complexes also show the photophysical and photochemical properties,[14] it stimulated us to study the various aspects of copper(I)–ruthenium(II) dinuclear complexes. Our interests are four-fold: (a) to study the nature of the stretching frequency of the cyano group when it is bonded to two electron-rich metal centres, copper(I)–ruthenium(II); (b) how this cyanide bridging affects the electronic and photophysical properties of the spectator ligands and the sub units; (c) to study the photo-induced intramolecular energy and electron transfer in the partially oxidized state; and (d) to study the electrochemical properties. In this paper we would like to report the syntheses, characterization and the study of IR stretching frequencies of the cyano group and the electronic (UV–vis) spectral properties of these complexes.

EXPERIMENTAL

The ^{1}H NMR spectra were recorded on a Jeol PMX-60 MHz spectrometer in the range 0–20 ppm(δ) using TMS as an internal calibrant. The ^{13}C and ^{31}P NMR spectra were recorded on a Bruker WM-400 NMR spectrometer. For ^{31}P NMR spectra 85% H_3PO_4 was used as an external calibrant, whereas ^{13}C NMR peaks were relative to TMS (0 ppm). IR spectra were recorded on Shimadzu IR-

† Author to whom correspondence should be addressed.

420 and Perkin–Elmer IR-841 double-beam spectrophotometers as KBr pellets in the ranges 4000–400 and 2500–2000 cm^{-1}, respectively. The electronic (UV–vis) spectra were recorded on a Shimadzu double-beam UV-160 spectrophotometer in acetonitrile solution. Conductivity measurements were performed on an Elico conductivity bridge type CM 82T in nitrobenzene or acetonitrile solutions. Magnetic measurements were performed using a parallel-field vibrating sample magnetometer (VSM), model-150A (Princeton Applied Research Corporation, Princeton, New Jersey). Melting points of the complexes were recorded on a Fisher–John melting point apparatus and are uncorrected. Microanalyses were performed at the RSIC, CDRI Lucknow, India.

All the chemicals used were either of Analar or chemically pure grade. Invariably manipulations were performed under dry oxygen-free nitrogen using standard Schlenk line and other techniques.[15] The solvents were dried by standard procedures[16] before use.

The complexes $[(\eta^5\text{-Cp})Ru(PPh_3)_2Cl]$[17] and $[(bpy)_2RuCl_2]\cdot 2H_2O$[18] were prepared according to the literature procedures. Cuprous cyanide[19] and the complex $[Cu(PPh_3)_2CN]$[20] were prepared by modifying the literature methods.

Syntheses

Cuprous cyanide. In a warm (60°C) water solution of $CuSO_4\cdot 5H_2O$ (2.5 g, 0.01 mol, 50 cm^3) with a constant bubbling of sulphur dioxide gas a solution of an equivalent amount of sodium cyanide (0.49 g, 0.01 mol, 25 cm^3) in water was added with vigorous stirring. A precipitate immediately appeared, which was filtered and washed thoroughly with water, ethanol and finally with ether and dried *in vacuo* over P_4O_{10} for several hours. The yield was almost quantitative.

Cyanobis(triphenylphosphine)copper(I) (**1**). To a suspension of CuCN (0.01 mol) in benzene (50 cm^3) was added a solution of triphenylphosphine (0.04 mol) in benzene (70 cm^3) and the mixture was refluxed for 2 h. The clear solution thus obtained was cooled and filtered to remove any insoluble materials and the solvent was removed under reduced pressure. The residue was washed many times with ether to ensure the complete removal of excess triphenylphosphine. It was recrystallized from benzene/petroleum ether and dried *in vacuo*.

Cyanobipyridinetriphenylphosphinecopper(I) (**2**). To a solution of $[Cu(PPh_3)_2CN]$ (1 mmol) in benzene (30 cm^3) was added a solution of bipyridine (1 mmol) in benzene (30 cm^3) with constant stirring. The resulting yellow solution was refluxed for 1 h. The clear solution thus obtained was cooled, the volume was reduced to half and excess petroleum ether (60–80°C) (100 cm^3) was added, which resulted in the precipitation of a pale yellow compound. It was washed several times with petroleum ether and dried *in vacuo*.

Cyano-1,10-phenanthrolinetriphenylphosphinecopper(I) (**3**). To solution of $[Cu(PPh_3)_2CN]$ (1 mmol) in benzene (30 cm^3) was added a solution of 1,10-phenanthroline (1 mmol) in benzene (30 cm^3) with constant stirring. Immediately an orange–red precipitate appeared. This mixture was refluxed for half an hour. After cooling excess petroleum ether (60–80°C) (100 cm^3) was added to ensure the complete precipitation of the complex. The complex was centrifuged and washed several times with petroleum ether and dried *in vacuo*.

Bis(triphenylphosphine)copper(I)(*μ-cyano*)*chlorobis*(2,2′-*bipyridine*)*ruthenium*(II)*hexafluorophosphate* (**4**). A mixture of $[Cu(PPh_3)_2CN]$ (1 mmol) and $[Ru(bpy)_2Cl_2]\cdot 2H_2O$ (1 mmol) was suspended in ethanol (30 cm^3) and the suspension was refluxed for 1 h. An equal volume of water was then added and the solution was further refluxed for 1 h. The solution was cooled and filtered to remove any insoluble material present. To the filtrate was added a highly concentrated solution of NH_4PF_6 in water (1 cm^3), which effected the immediate precipitation of the complex. The precipitate was centrifuged and washed thoroughly with water and finally with ether and dried *in vacuo*.

Bis(triphenylphosphine)copper(I)(*μ-cyano*)*cyclopentadienylbis(triphenylphosphine)ruthenium*(II)*hexafluorophosphate* (**5**). A mixture of $[Cu(PPh_3)_2CN]$ (1 mmol), $[(\eta^5\text{-Cp})Ru(PPh_3)_2Cl]$ (1 mmol) and NH_4PF_6 (1.2 mmol) was suspended in methanol (60 cm^3) and refluxed for 1 h. During reflux all the $[(\eta^5\text{-Cp})Ru(PPh_3)_2Cl]$ was dissolved and a pale yellow precipitate appeared. The solvent was evaporated to dryness *in vacuo* and the residue was extracted with a small amount of dichloromethane and filtered. To the filtrate was added excess petroleum ether (100 cm^3) and the complex was precipitated, which was centrifuged and washed several times with petroleum ether and dried *in vacuo*.

Bis(triphenylphosphine)copper(I)(*μ-cyano*)*cyclopentadienylbis(triphenylphosphine)ruthenium*(II)*tetrafluoroborate* (**6**). The procedure of the hexafluorophosphate was followed except $NaBF_4$ was used in place of NH_4PF_6.

2,2′-*Bipyridinetriphenylphosphinecopper*(I)(*μ-cyano*)(*chlorobis*(2,2′-*bipyridine*)*ruthenium*(II)*hexafluorophosphate* (**7**). A mixture of $[Cu(bpy)(PPh_3)CN]$ (0.2 mmol) and $[Ru(bpy)_2Cl_2]\cdot 2H_2O$ (0.2 mmol) in a 1:1 mixture of water and ethanol (50 cm^3) was suspended and refluxed for 3 h.

The resulting solution was cooled and filtered to remove any insoluble material. To the filtrate was added a concentrated aqueous solution of NH_4PF_6 (1 cm^3). A precipitate immediately appeared, which was centrifuged, washed several times with water and ether and dried over P_4O_{10} for several hours *in vacuo*.

1,10-*Phenanthrolinetriphenylphosphinecopper*(I)-(*μ-cyano*)*chlorobis*(2,2′-*bipyridine*)*ruthenium*(II)-*hexafluorophosphate* (**8**). The above procedure for the 2,2′-bipyridine analogue was followed, but in place of [Cu(bpy)(PPh_3)CN] its 1,10-phenanthroline analogue was used.

2,2′-*Bipyridinetriphenylphosphinecopper*(I)(*μ-cyano*)*cyclopentadienylbis*(*triphenylphosphine*)*ruthenium*(II)*hexafluorophosphate* (**9**). To a solution of [(η^5-Cp)Ru(PPh_3)$_2$Cl] (0.1 mmol) in methanol (30 cm^3) was added solid [(phen)Cu(PPh_3)CN] (0.1 mmol) and the mixture was refluxed for 2.5 h, whereby a clear solution was obtained. After cooling the reaction mixture was filtered to remove any insoluble material. To the filtrate was added a concentrated aqueous solution of NH_4PF_6 (2 cm^3) to precipitate the complex. The complex obtained was centrifuged and washed several times with water and ether and dried *in vacuo* over P_4O_{10} for several hours.

1,10-*Phenanthrolinetriphenylphosphinecopper*(I)-(*μ-cyano*)*cyclopentadienylbis*(*triphenylphosphine*)*ruthenium*(II)*hexafluorophosphate* (**10**). The above procedure for the 2,2′-bypiridine analogue was followed using the 1,10-phenanthroline analogue in place of [(bpy)Cu(PPh_3)CN].

RESULTS AND DISCUSSION

The analytical data for the complexes are given in Table 1, which are consistent with the stoichiometries proposed. Conductivity measurements were performed in nitrobenzene or acetonitrile solutions. The conductivity data of complexes **1**, **2** and **3** show their non-electrolytic nature, whereas the other cation complexes are 1:1 electrolytes.[21] All the complexes are diamagnetic at room temperature.

IR spectra

The ν(CN) stretching frequency data of the complexes are given in Table 2. The ν(CN) band of [Cu(PPh_3)$_2$CN] occurs at 2121 cm^{-1} (lit.,[22] 2105 cm^{-1}). In solid cuprous cyanide ν(CN) occurs[23–26] at 2172 cm^{-1}. A red shift of *ca* 51 cm^{-1} indicates that the CN group is terminal. In addition copper(I)

Table 1. Analytical and physical data of the complexes

Compound	Colour	Analysis Found (Calc.) (%) C	H	N	M.p.[a] (θ/°C)	Yield[b] (%)
1, [Cu(PPh_3)$_2$CN]	Dirty white	72.3 (72.4)	4.9 (5.0)	2.2 (2.3)	155	90
2, [Cu(bpy)(PPh_3)CN]	Yellow	68.5 (68.6)	4.6 (4.6)	8.0 (8.3)	138	80
3, [Cu(phen)(PPh_3)CN]	Orange	56.6 (56.7)	3.9 (3.8)	6.0 (5.8)	198	92
4, [(PPh_3)$_2$Cu(*μ*-CN)Ru(bpy)$_2$Cl]PF_6	Orange–red	64.5 (64.6)	4.7 (4.5)	1.1 (1.0)	218d	84
5, [(PPh_3)$_2$Cu(*μ*-CN)Ru(η^5-Cp)(PPh_3)$_2$]PF_6	Yellowish-white	64.5 (64.6)	4.7 (4.5)	1.1 (1.0)	222d	70
6, [(PPh_3)$_2$Cu(*μ*-CN)Ru(η^5-Cp)(PPh_3)$_2$]BF_4	Pale yellow	67.2 (67.3)	4.6 (4.7)	0.9 (0.9)	130	80
7, [(bpy)(PPh_3)Cu(*μ*-CN)Ru(bpy)$_2$Cl]PF_6	Maroon	43.6 (43.4)	3.4 (3.6)	9.0 (8.9)	173d	80
8, [(bpy)(PPh_3)Cu(*μ*-CN)Ru(η^5-Cp)(PPh_3)$_2$]PF_6	Yellowish-white	62.4 (62.6)	4.5 (4.4)	2.9 (3.1)	130d	40
9, [(phen)(PPh_3)Cu(*μ*-CN)Ru(bpy)$_2$Cl]PF_6	Orange–red	54.2 (54.4)	3.5 (3.7)	8.8 (8.7)	185d	85
10, [(phen)(PPh_3)Cu(*μ*-CN)Ru(η^5-Cp)(PPh_3)$_2$]PF_6	Yellow	63.0 (63.2)	4.5 (4.4)	3.4 (3.1)	128d	60

[a] d indicates the decomposition.

[b] Based on copper compounds **1**, **2**, **3** and on ruthenium for the other compounds.

Table 2. Spectral data of the complexes

Compound	UV–vis bands[a] λ_{max} (nm)	Assignment	ν(CN)[b] (cm^{-1})	^{1}H NMR signal[c] of Cp (δ/ppm)	^{13}C NMR signal[c,d] (δ/ppm)	^{31}P NMR signal (δ/ppm)
1	236.0	IL	2121		128–135 (m, —C_6H_5 groups); 151.9 (s[broad] CN)	−2.6 (s, Cu—P)
	259.5	CT				
2	261.0sh	CT	2108			
3	268.0	CT	2106			
4	244.0	$\pi^* \leftarrow \pi$(bpy) IL	2087			
	291.0	$\pi^* \leftarrow \pi$(bpy) IL				
	340.0	π_2^*(bpy) $\leftarrow d\pi$(Ru) CT				
	475.0	π^*(bpy) $\leftarrow d\pi$(Ru) CT				
5	228.0	IL	2075	4.23		
	268.0sh	CT				
6	229.0	IL	2084	4.33	85.6 (s, Cp); 128–138 (m, —C_6H_5 groups)	−3.4 (s, Cu—P) 48.9 (s, Ru—P)
	269.0sh	CT				
7	244.0	$\pi^* \leftarrow \pi$(bpy) IL	2091			
	287.0	$\pi^* \leftarrow \pi$(bpy) IL				
	345.0	π_2^*(bpy) $\leftarrow d\pi$(Ru) CT				
	471.0	π^*(bpy) $\leftarrow d\pi$(Ru) CT				
8	270.0	CT	2079	4.27		
9	244.0	$\pi^* \leftarrow \pi$(bpy) IL	2087			
	291.0	$\pi^* \leftarrow \pi$(bpy) IL				
	344.0	π_2^*(bpy) $\leftarrow d\pi$(Ru) CT				
	478.0	π^*(bpy) $\leftarrow d\pi$(Ru) CT				
10	267.0	CT	2085	4.37		

[a] In acetonitrile solution, sh denotes shoulder.
[b] In KBr discs.
[c] In $CDCl_3$.
[d] The ^{13}C NMR signal of the bridging cyano group was not observed.

is an electron-rich centre, which is also bonded to triphenylphosphine, a stronger σ-donor than π-acceptor, therefore, a strong back-donation from copper(I) to the cyanide group is expected, which may also be contributing to the red shift of ν(CN) in $[Cu(PPh_3)_2CN]$. There is a small red shift of ν(CN) in $[Cu(bpy)(PPh_3)CN]$ (*ca* $\Delta = 13\ cm^{-1}$) and $[Cu(phen)(PPh_3)CN]$ (*ca* $\Delta = 15\ cm^{-1}$) compared with ν(CN) of $[Cu(PPh_3)_2CN]$, which is in accordance with the analogy that as the coordination number increases the net positive charge on the metal centre decreases and in turn the σ-bonding from the cyanide group decreases, resulting in a decrease in ν(CN).[27]

In general the bridging cyano group gives the stretching band at a higher wave number[27] than the terminal cyano group. The shifting of the ν(CN) group to the higher region on bridging has been explained on the basis of force field arguments.[23] However, this is not always the case and the band position of the cyano group depends upon many other factors. The ^{13}C and ^{15}N NMR and IR studies[28] of cyano (ligand) cobaloximes have furnished evidence for cobalt(I)-to-cyanide π-bonding. The ν(CN) band tends to decrease with increasing basicity of the ligand *trans* to CN^-. Strong bases make cobalt(I) richer in electron density, resulting in increased back-bonding to π^* of CN^- which causes a decrease in ν(CN). The complexes reported here also show a red shift of ν(CN) on bridging. Both copper(I) and ruthenium(II) centres are electron rich and are also bonded to strong σ-donor and poor π-acid ligand triphenylphosphine and/or electron rich ligands. Lowering of the ν(CN) stretching frequency on bridging may be because of enhanced π-back donation from ruthenium and copper to the π^*-orbitals of the cyano group. All the characteristic bands due to the other ligands, namely triphenylphosphine, 2,2′-bipyridine and 1,10-phenanthroline, are found in their spectral region. The characteristic vibrational frequency due to Cp was completely masked by the strong, broad, characteristic peak of PF_6^- in the complexes having this group, but the presence

of the Cp group in the respective complexes is evident by the NMR signal of the Cp group.

^{1}H *NMR chemical shifts*

The ^{1}H NMR data are collected in Table 2. Complexes having the Cp group show a sharp singlet signal in the range 4.1–4.4 ppm(δ), which is diagnostic. The Cp peak of the complexes shifts slightly to higher δ (low field) in comparison to the parent complex [(η^5-Cp)Ru(PPh_3)$_2$Cl]. The shifting of the Cp proton signal to the higher δ (low field) on coordination through the nitrogen atom of the CN group is consistent with the literature reported observation.[5,29,30] The high δ value of the Cp protons in these complexes also suggest that the complexes must be cationic in nature.[5,6] The proton signals of the phenyl groups and the bpy and phen ligands appear in the region 7.0–8.0 ppm as broad multiplets.

^{13}C *and* ^{31}P *NMR chemical shifts*

The ^{13}C and ^{31}P NMR data of compounds **1** and **6** are collected in Table 2. All the peaks in the ^{13}C NMR spectra are found in the expected region of the phenyl group[31,32] for compound **1**. However, the ^{13}C NMR peaks due to the phenyl groups associated with copper and ruthenium metal centres for compound **6** become too complicated to be assigned properly (Fig. 1). The distinct ^{13}C NMR peak at 85.6 ppm(δ) is due to the cyclopentadienyl group, which is in the expected region.[33–36] Compound **1** shows only one ^{31}P NMR signal at -2.6 ppm, which is at a lower field relative to the free triphenylphosphine ^{31}P NMR signal[31] at -6.00 ppm(δ). This is expected as the formation of complex **1** causes deshielding of the phosphorus nuclei, because of the shifting of electron density from the phosphorus atom to the copper metal centre, which is in accordance with the greater σ-donating than the π-accepting properties of the triphenylphosphine ligand. The dinuclear complex **6** as expected shows two ^{31}P NMR signals at 48.9 and -3.4 ppm, which are assigned for the phosphorus atoms of the triphenylphosphine ligands associated with ruthenium[37] and copper metal centres, respectively. The ^{31}P NMR signal in compound **6**, at -3.4 ppm due to the copper sub-unit, is at higher field [less ppm(δ)] in comparison with compound **1** and at lower field (higher ppm) than the free triphenylphosphine. This shows that the back π-bonding from ruthenium to the cyanide group is predominant over the σ-donation of the cyano group to ruthenium. The electron density increases on the cyano group, which in turn affects the σ-donating and π-accepting behaviour of the cyano group, which results in the shielding of the phosphorus nuclei of triphenylphosphine of the copper sub-unit and, therefore, shifting of the ^{31}P NMR signal to high field [less ppm(δ)]. These types of trends indicate that shifting of electron density from a ruthenium centre to a cyano group may cause the deshielding of the phosphorus nuclei associated with the ruthenium sub-unit and hence shifting of the ^{31}P NMR signal to lower field [high ppm(δ)]. In fact the ^{31}P signal of the ruthenium sub-unit is observed at 48.9 ppm, which is much higher in comparison to the parent compound, [(η^5-Cp)Ru(PPh_3)$_2$Cl] (lit.,[29] 38.6 ppm), which supports the discussed trend of the shifting of ^{31}P NMR signals and ruthenium to the cyano group π-back-bonding.

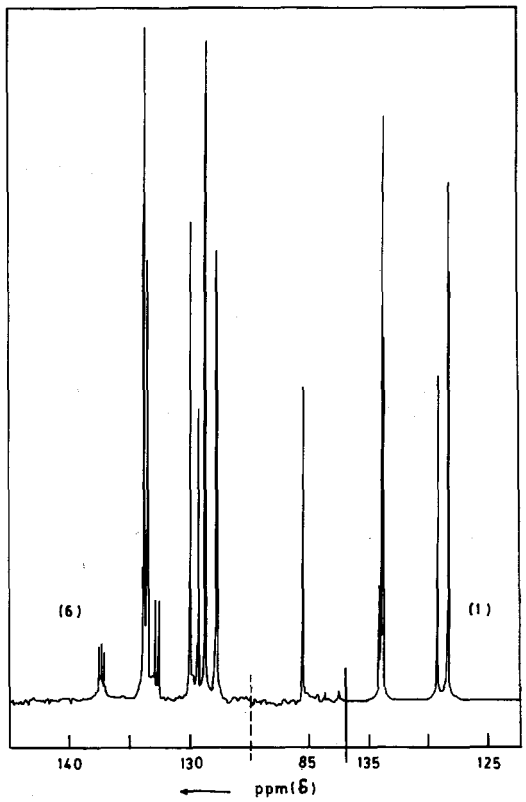

Fig. 1. The ^{13}C NMR spectra of complexes **1** and **6**.

Electronic (UV–vis) properties

Data for the electronic spectra are given in Table 2. In the electronic absorption spectra of complexes **4** and **9** four peaks and a shoulder at 244 nm are observed. These bands are denoted as I–V in order of increasing energy (Fig. 2). These are characteristic bands of the Ru(bpy)$_2^{2+}$ chromophore.[18,38,39] Assignments of these bands are given in Table 2. In all the complex having this chromophoric

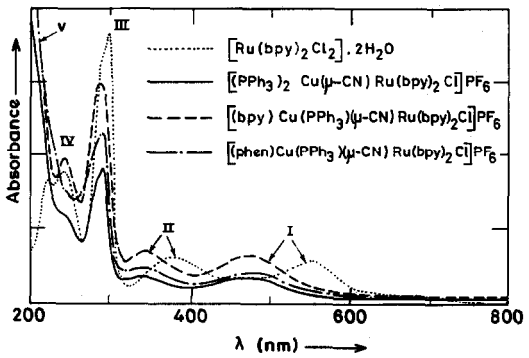

Fig. 2. The electronic (UV–vis) spectra of complexes **4**, **7**, **9** and $[Ru(bpy)_2Cl_2]\cdot 2H_2O$.

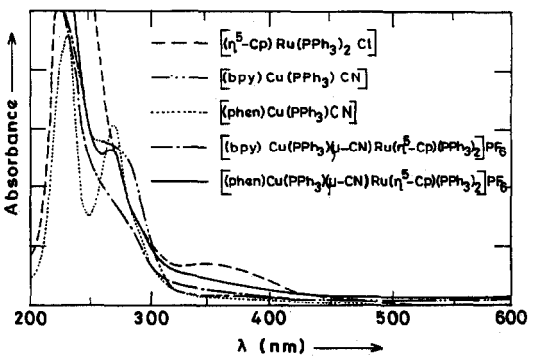

Fig. 3. The electronic (UV–vis) spectra of complexes **2**, **3**, **8**, **10** and $[(\eta^5\text{-Cp})Ru(PPh_3)_2Cl]$.

group, band III, which is assigned as the $\pi^* \leftarrow \pi$(bpy) intraligand transition, has very slightly shifted to the higher energy in comparison to the parent complex $[Ru(bpy)_2Cl_2]\cdot 2H_2O$. Assignments of bands I $[\pi^*_{bpy} \leftarrow d\pi(Ru)]$ and II $[\pi^*_{bpy} \leftarrow d\pi(Ru)]$ as charge-transfer transitions is based on literature reports.[18,38,39] In these complexes, due to the strong back bonding from ruthenium(II) to the cyano group, both bands I and II move to higher energies. This behaviour is expected if the *d*-orbitals are increasingly stabilized, because of increased back bonding from ruthenium(II) to the cyano group. In this context the π^*(bpy) $\leftarrow d\pi$(Ru) transitions act as spectator transitions for the CN–Ru interactions. This indicates the strong back bonding from ruthenium to the cyano group, which is also evident from the shifting of the ν(CN) stretching frequency to the lower energy region. Band IV appears as a shoulder on band V and can be assigned to the intraligand $\pi^* \leftarrow \pi$(bpy) transition[18,39] or, where aromatic phosphines are present, to a mixture of π(bpy)-π^*(bpy) and π(phenyl)-π^*(phenyl) transitions.[18] It is clearly seen in the absorption spectrum of complex **7**, as this complex has relatively less PPh_3 and more bpy groups, it shows a well-resolved peak of band IV at 244 nm (Fig. 2). Complexes **1**, **2** and **3** give absorption bands at 259.5, 268 and 261 nm (shoulder), respectively, which are assigned as MLCT transitions and the other bands in the higher energy region are assigned as $\pi^* \leftarrow \pi$ intraligand (IL) transitions. The band at 259.5 nm of complex **1** appears as a shoulder on band III of compound **4** at 280 nm. Similarly the band at 268 nm of complex **3** appears as a shoulder on band III of complex **9** at 270 nm. On the other hand in the case of complex **7**, because its band III occurs reasonably well in the higher energy (287 nm) region there is mixing of the band at 261 nm of compound **2** and no shoulder is observed. The higher energy IL bands of complexes **1**, **2** and **3** are mixed with $\pi^* \leftarrow \pi$(IL) bands at 222 nm of the bpy ligand and appear as band V in complexes **4**, **7** and **9**. The absorption spectra of compounds **2**, **3**, **8** and **10** are given in Fig. 3. The MLCT transition at 349 nm of the complex $[(\eta^5\text{-Cp})Ru(PPh_3)_2Cl]$ is shifted to the higher energy region on the formation of the bridged complexes **8** and **10** and becomes a very broad shoulder. This higher shifting of the band indicates the increasing stabilization of the ruthenium *d*-orbitals by back bonding from ruthenium to the cyanide group. Such shifting is also observed in the complexes having the $Ru(bpy)_2Cl^+$ sub-unit, as discussed earlier, and is in very good agreement with the shifting of ν(CN) to lower energy in the IR spectra. The shoulder at 261 nm in complex **2** and an absorption peak at 268 nm in complex **3**, which are assigned as the MLCT transitions for the copper sub-units, are almost unaffected in their corresponding complexes **8** and **10**, respectively, on bridge formation. The IL bands, in the higher energy regions, which are mainly localized on the phenyl group, in complexes **2** and **3** are mixed with the strong IL bands at 240 nm due to the complex $[(\eta^5\text{-Cp})Ru(PPh_3)_2Cl]$, in the bridged complexes (Fig. 3). On bridge formation the MLCT transition at 260 nm in complex **1** becomes broad and appears as a shoulder, whereas the MLCT transition band of the complex $[(\eta^5\text{-Cp})Ru(PPh_3)_2Cl]$ shifts towards the higher energy region and becomes broad due to the reasons discussed earlier.

Acknowledgement—We thank Mr N. Ahmed (Department of Chemistry, I.I.T. Kanpur, India) for recording ^1H NMR and UV–vis spectra and RSIC, CDRI Lucknow, India, for ^{13}C and ^{31}P NMR spectra and elemental analyses.

REFERENCES

1. V. Balzani, L. Moggi, M. F. Monfrin, F. Bolletta and M. Gleria, *Science* 1975, **189**, 852.
2. V. Balzani, F. Barigelletti and L. De Cola, *Top. Curr. Chem.* 1990, **158**, 31.

3. F. Scandola, C. A. Bignozzi, C. Chiorboli, M. T. Indelli and M. A. Rampi, *Coord. Chem. Rev.* 1990, **97**, 299 and refs therein.
4. C. A. Bignozzi and F. Scandola, *Inorg. Chem.* 1984, **23**, 1540.
5. K. M. Rao, R. Prasad and U. C. Agarwala, *Synth. React. Inorg. Met.-Org. Chem.* 1987, **17**, 469.
6. R. Prasad, L. Mishra and U. C. Agarwala, *Ind. J. Chem.* 1991, **30A**, 45, 162 and refs therein.
7. G. A. Carriedo, N. G. Connelly, M. C. Crespo, I. C. Duarmby, V. Riera and G. H. Worth, *J. Chem. Soc., Dalton Trans.* 1991, 315.
8. A. G. Sharpe, *The Chemistry of Cyano Complexes of the Transition Metals*. Academic Press, London (1976).
9. P. Rigo and A. Turco, *Coord. Chem. Rev.* 1974, **13**, 133.
10. A. A. D. Paggio and D. R. McMillin, *Inorg. Chem.* 1983, **22**, 691.
11. R. A. Rader, D. R. McMillin, M. T. Buckner, T. G. Matthews, D. J. Casadonte, R. K. Lingel, S. B. Whittaker, L. M. Darmon and F. G. Lytle, *J. Am. Chem. Soc.* 1981, **22**, 691.
12. G. J. Baird, S. G. Davies, S. D. Moon, S. J. Simpson and R. H. Jones, *J. Chem. Soc., Dalton Trans.* 1985, 1479.
13. A. Christofides, N. G. Connelly, N. J. Larson, A. C. Loyns, A. G. Orpen, M. O. Simmonds and G. H. Worth, *J. Chem. Soc., Dalton Trans.* 1991, 1595.
14. C. Kutal, *Coord. Chem. Rev.* 1990, **99**, 213 and refs therein.
15. R. Singh and S. K. Dikshit, *Chem. Educ.* 1992, **9**, 51.
16. B. S. Furniss, A. J. Hannaford, P. W. G. Smith and A. R. Tatchell, *Vogel's Textbook of Organic Chemistry*, 5th edn. English Language Book Society, Essex (1989).
17. M. I. Bruce, C. Hameister, A. G. Swincer and R. C. Wallis, *Inorg. Synth.* 1982, **21**, 78.
18. B. P. Sullivan, D. J. Salmon and T. J. Meyer, *Inorg. Chem.* 1978, **17**, 3334.
19. W. T. Reichle, *Inorg. Chim. Acta* 1971, **5**, 325.
20. W. J. Geary, *Coord. Chem. Rev.* 1971, **7**, 81.
21. H. J. Barber, *J. Chem. Soc.* 1924, 125.
22. D. Cooper and R. A. Plane, *Inorg. Chem.* 1966, **5**, 2209.
23. D. A. Dows, A. Haim and W. K. Wilmarth, *J. Inorg. Nucl. Chem.* 1961, **21**, 33.
24. J. H. Clark, C. V. A. Duke, J. M. Miller and S. J. Brown, *J. Chem. Soc., Chem. Commun.* 1986, 877.
25. R. A. Penneman and L. H. Jones, *J. Chem. Phys.* 1956, **24**, 292.
26. J. Han, N. J. Blackburn and T. M. Loehr, *Inorg. Chem.* 1992, **31**, 3223.
27. K. Nakamoto, *Infrared and Raman Spectra of Inorganic and Coordination Compounds*, p. 278. John Wiley, New York (1986).
28. K. L. Brown and S. Satyanarayana, *Inorg. Chem.* 1992, **31**, 1366.
29. T. Wilezewski, M. Bochenska and J. F. Niernat, *J. Organomet. Chem.* 1981, **215**, 87.
30. T. Blackmore, M. I. Bruce and F. G. A. Stone, *J. Chem. Soc.* (*A*) 1971, 2376.
31. R. Singh and S. K. Dikshit, *Polyhedron* 1992, **11**, 2099 and refs therein.
32. M. L. Ganadu, L. Naldini, G. Crisponi and V. Nurchi, *Spectrochim. Acta* 1991, **47A**, 615.
33. I. W. Robertson, T. A. Stephenson and D. A. Tocher, *J. Organomet. Chem.* 1982, **228**, 171.
34. M. I. Bruce, A. Catlow, M. G. Hamphery, G. A. Coutsantonis, M. R. Snow and E. R. T. Tiekink, *J. Organomet. Chem.* 1988, **338**, 59.
35. M. I. Bruce, P. A. Hamphery, M. R. Snow and E. R. T. Tiekink, *J. Organomet. Chem.* 1986, **303**, 417.
36. N. A. Ogorodnikova and D. N. Kravtsov, *Polyhedron* 1985, **4**, 311.
37. J. Amarasekera, T. B. Rauchfurs and S. R. Wilson, *Inorg. Chem.* 1987, **26**, 3328.
38. J. E. Fergusson and G. M. Harris, *J. Chem. Soc.* (*A*) 1966, 1293.
39. G. M. Bryant, J. E. Fergusson and H. K. J. Powell, *Aust. J. Chem.* 1971, **24**, 257.

Polyhedron Vol. 12, No. 13, pp. 1705–1710, 1993
Printed in Great Britain

0277–5387/93 $6.00+.00
© 1993 Pergamon Press Ltd

SYNTHESIS AND STRUCTURAL CHARACTERIZATION OF THE FIRST METAL COMPLEX WITH AN INDOLE NITROXIDE

ALEXEI B. BURDUKOV, VIKTOR I. OVCHARENKO,*
NATALIE V. PERVUKHINA and VLADIMIR N. IKORSKI

Institute of Inorganic Chemistry, Russian Academy of Sciences,
Siberian Branch, Lavrent'ev avenue 3, Novosibirsk 630090, Russia

and

LUCEDIO GRECI, PATRICIA CARLONI, ELISABETTA DAMIANI
and PIERLUIGI STIPA

Dipartimento di Scienze dei Materiali e Della Terra, Università di Ancano,
Via Brecce Bianche, 60131 Ancona, Italy

and

VLADIMIR A. REZNIKOV

Novosibirsk Institute of Organic Chemistry, Russian Academy of Sciences,
Siberian Branch, Lavrent'ev avenue 7, Novosibirsk 630090, Russia

(*Received* 18 *December* 1992; *accepted* 18 *February* 1993)

Abstract—Copper hexafluoroacetylacetonate reacts with an indole nitroxide (1,2-dihydro-3-oxo-2,2-diphenyl-3*H*-indole-1-oxyl) in hexane to yield a trinuclear complex with two bridging nitroxides, bis-[μ-(1,2-dihydro-3-oxo-2,2-diphenyl-3*H*-indole-1-oxyl)-O; O′]hexakis(hexafluoroacetylacetonato)tricopper(II), which has been structurally characterized by X-ray crystallography. The nitroxide functions of the paramagnetic ligands are coordinated to the terminal copper atoms. Magnetic measurements revealed strong antiferromagnetic coupling between the spins of the nitroxides and of the terminal copper atoms.

At present a good deal of information concerning the chemical, structural and magnetochemical properties of the complexes of the hexafluoroacetylacetonates of first row transition metals, [M(hfac)$_2$], with stable nitroxide radicals have been amassed, the results of these studies being summarized in a number of reviews.[1–3] Major efforts were devoted to the complexes of 3-imidazoline-1-oxyl and 2-imidazoline-1-oxyl 3-oxide derivatives, while the other types of nitroxides have been considerably less studied. For this reason we attempted to extend the range of nitroxides involved by studying the adducts formed by M(hfac)$_2$ with indole nitroxide derivatives. To the best of our knowledge nitroxides of this type have never been used as ligands. The choice of a strong acceptor—M(hfac)$_2$—as the metal salt was dictated by the well-known weakness of the nitroxide group as a donor. In this paper we report the results of the investigation of the Cu(hfac)$_2$ complex with 1,2-dihydro-3-oxo-2,2-diphenyl-3*H*-indole-1-oxyl (L^1).

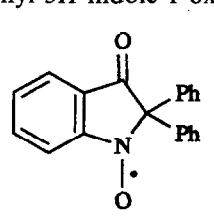

L^1

* Author to whom correspondence should be addressed.

EXPERIMENTAL

The nitroxides 1,2-dihydro-3-oxo-2,2-diphenyl-3*H*-indole-1-oxyl, 2,2,6,6-tetramethyl-4-oxo-piperidine-1-oxyl, 2,2,5,5-tetramethyl-3-oxo-pyrrolidine-1-oxyl and $Cu(hfac)_2$ were synthesized by literature methods.[4-6] Reagent-grade hexane was used as purchased.

Preparation of $[Cu(hfac)_2]_3L^1_2$

A mixture of L^1 (100 mg, 0.33 mmol) and anhydrous $Cu(hfac)_2$ (160 mg, 0.34 mmol) was dissolved in boiling hexane (approximately 40 cm^3) to form a brown coloured solution. After filtration the solution was kept at ambient temperature for 12 h. During this time greenish-brown table-shaped crystals deposited, which were filtered off and washed with cold hexane. Yield 100 mg (30%). The crystals appeared to be suitable for X-ray diffraction study; m.p. 138–140°C. Found: Cu, 9.4; C, 40.4; H, 1.5; N, 1.7. Calc. for $Cu_3C_{70}H_{34}F_{36}N_2O_{16}$: Cu, 9.4; C, 41.3; H, 1.7; N, 1.4%.

Crystal structure solution and refinement

The intensity data were obtained on a Syntex $P2_1$ diffractometer with Cu-K_α (graphite monochromator) radiation and corrected for Lorentz and polarization effects. The absorption correction was performed with the DIFABS package.[7] The structure was solved by the heavy atom method. Anisotropical full-matrix least-squares refinement was performed using the YANX package,[8] atomic scattering factors being taken from ref. 9. Hydrogen atoms were included in the last refinement cycle in idealized positions.

Crystal data for the compound are summarized in Table 1 and selected bond lengths and angles are reported in Table 2.

Magnetic measurements

The magnetic susceptibility of the complex was measured by Faraday's method over a 77–300 K temperature range. The data were corrected for diamagnetic contributions, estimated from Pascal's constants, and for copper(II) temperature-independent paramagnetism.

ESR spectra

The ESR spectrum of a finely ground solid $[Cu(hfac)_2]_3L^1_2$ was recorded on a P-1306 spectrometer (*X*-band) at 77 K (800 G scan, 200 G min^{-1} scan rate, −20 Db microwave power, 2.8 G modulation amplitude).

Table 1. Crystal data for $[Cu(hfac)_2]_3L^1_2$

Complex formula	$Cu_3C_{70}H_{34}F_{36}N_2O_{16}$
Fw	2033.68
Space group	$P\bar{1}$
a (Å)	12.412(3)
b (Å)	10.173(2)
c (Å)	17.204(4)
α (°)	92.43(2)
β (°)	114.32(2)
γ	95.33(2)
V (Å^3)	1963.1(7)
Z	1
λ (Å)	1.54178
T (K)	295
ρ_{calc} (g cm^{-3})	1.72
μ (cm^{-1})	23.1
F_{meas}	3878
$F_{obs} > 5\sigma$	2087
$R(F_o)$	0.067

RESULTS AND DISCUSSION

Copper hexafluoroacetylacetonate reacts with indole nitroxide L^1 in hexane forming the complex of composition $[Cu(hfac)_2]_3L^1_2$. No other adducts were obtained upon variation of the starting $Cu(hfac)_2 : L^1$ ratio from 1 : 1 to 3 : 2 or cooling of the reaction mixture to −15°C. The anhydrous $Cu(hfac)_2$ may be substituted by its hydrated forms, the same product being obtained. This indicates, taking into account the rather low solubility of $Cu(hfac)_2$ in hexane, that L^1 molecules effectively replace coordinated water.

The investigation of the $[Cu(hfac)_2]_3L^1_2$ structure has shown that this complex has a trinuclear structure (Fig. 1). In $[Cu(hfac)_3]_3L^1_2$ three $Cu(hfac)_2$ fragments are bridged by two O,O′-coordinated nitroxides. The central copper atom lies on the inversion centre (0,0,0) and has a tetragonally distorted octahedral coordination environment with four $hfac^-$ oxygen atoms in the equatorial plane (mean Cu—O = 1.93 Å) and two oxygen atoms of the paramagnetic ligands in the axial positions [Cu(1)—O(3) = 2.41(1) Å]. The terminal copper atoms have a distorted trigonal-bipyramidal coordination geometry similar to that found in the other trinuclear $Cu(hfac)_2$-nitroxide complexes reported so far.[10-12] The paramagnetic ligand is coordinated in the equatorial plane of the bipyramid, the Cu(2)—O(4) bond being equal to 2.00(1) Å. It is noteworthy that the equatorial Cu(2)—O(6) bond is elongated to 2.19(1) Å, while the other Cu—O_{hfac} bonds have the usual lengths of approximately 2.0 Å. Similar elongation of Cu—O bonds was observed in different $Cu(hfac)_2$-nitroxide complexes

Table 2. Selected bond lengths (Å) and angles (°) for $[Cu(hfac)_2]_3L^1_2$

Cu(1)—O(1)	1.91(1)	Cu(1)—O(2)	1.95(1)
Cu(1)—O(3)	2.41(1)	Cu(2)—O(4)	2.00(1)
Cu(2)—O(5)	1.88(1)	Cu(2)—O(6)	2.19(1)
Cu(2)—O(7)	1.97(1)	Cu(2)—O(8)	1.89(1)
C(6)—O(3)	1.24(1)	O(4)—N(1)	1.28(1)
O(1)—Cu(1)—O(2)	87.8(4)	O(5)—Cu(2)—O(6)	89.1(4)
O(1)—Cu(1)—O(3)	87.3(3)	O(5)—Cu(2)—O(7)	89.5(4)
O(2)—Cu(1)—O(3)	88.8(3)	O(5)—Cu(2)—O(8)	170.8(6)
O(4)—Cu(2)—O(5)	89.0(4)	O(6)—Cu(2)—O(7)	99.3(4)
O(4)—Cu(2)—O(6)	94.8(3)	O(6)—Cu(2)—O(8)	99.5(4)
O(4)—Cu(2)—O(7)	165.9(5)	O(7)—Cu(2)—O(8)	92.0(4)
O(4)—Cu(2)—O(8)	87.3(4)		

with the trigonal-bipyramidal environment of the copper atom.[10,11,13,14]

From the structural point of view the nitroxide L^1 manifests one interesting property: it contains chemically inequivalent but structurally similar nitroxide and carbonyl groups; therefore, the whole molecule has a C_2-pseudosymmetry axis.

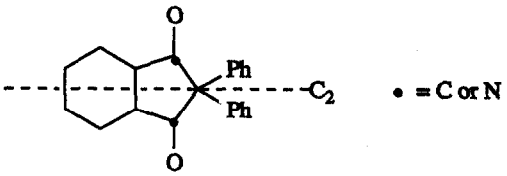

For this reason, on the examination of the $[Cu(hfac)_2]_3L^1_2$ structure the question arises whether L^1 is coordinated to the central copper atom by the nitroxide or the carbonyl group. Both variants were attempted in the course of the refinement. They appeared to be indistinguishable according to Hamilton's test[15] at the 99% level of probability. However, the variant of the terminal copper–nitroxide coordination was chosen for further refinement because the opposite one yielded a "non-positive" nitrogen atom and somewhat worse thermal parameters for adjacent atoms. The final values of the bond lengths for the carbonyl and nitroxide groups are in good accord with the refinement model. The bond length of 1.28(1) Å, found for the group coordinated to the terminal copper atom, is close to the value of 1.27 Å suggested as a "standard" for a nitroxide group.[16] The group coordinated to the central copper atom has the bond length equal to 1.24(1) Å, this value falling between the average bond lengths reported for free and coordinated carbonyl groups.[17,18] Thus, it is reasonable to suppose that the N→O group is coordinated to the terminal copper atom and the C=O group to the central copper atom.

Magnetic susceptibility measurements for $[Cu(hfac)_2]_3L^1_2$ showed that the room-temperature magnetic moment of the compound was equal to 1.82 B.M. and remained constant down to 77 K. This indicates the presence of strong antiferromagnetic coupling between the copper and nitroxide spins, resulting in the $S = 1/2$ ground state. According to the results of the ESR study of solid $[Cu(hfac)_2]_3L^1_2$ the odd electron is localized on a copper(II) ion: a typical spectrum of a copper(II) ion ($g_\parallel = 2.32$, $g_\perp = 2.06$, $A_\parallel = 147$ G) was observed (Fig. 2). The presence of well-resolved hyperfine splitting in parallel orientation shows that the magnetic sites are well-shielded, the exchange energy between copper(II) ions being negligible in comparison with the hyperfine splitting energy.

These results are easily understood if the N→O group is coordinated to the terminal copper atom. Such a coordination mode is known to result in effective pairing of the copper and nitroxide electron spins.[1,2] In the present case the remaining unpaired electron resides on the central copper atom, which is fully consistent with the observed magnetic moment and ESR spectrum of $[Cu(hfac)_2]_3L^1_2$.

It should be noted that very similar magnetic properties were reported for another trinuclear complex with nitroxide to terminal copper coordination—$[Cu(hfac)_2]_3(NITEt)_2$ (NITEt = 4,4,5,5-tetramethyl-2-ethyl-2-imidazolinyl-1-oxyl 3-oxide).[13]

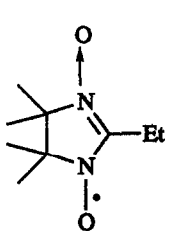

NITEt

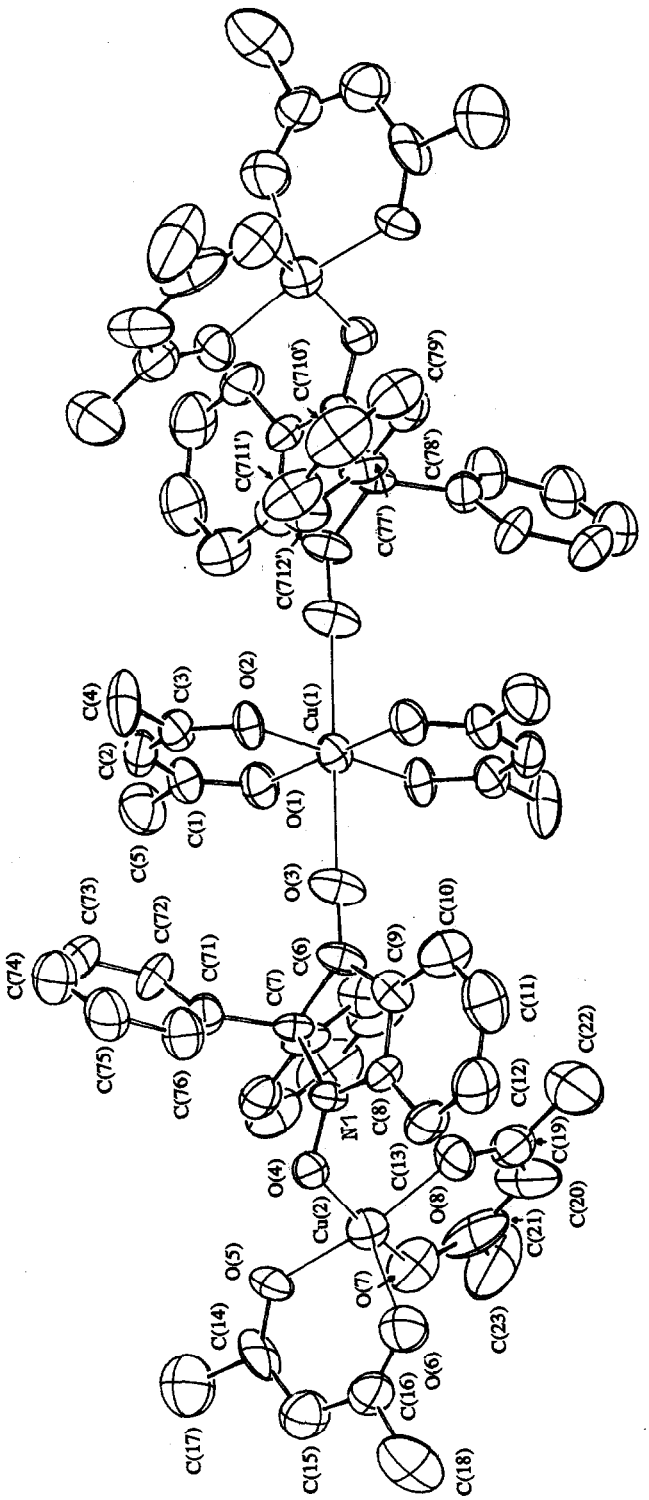

Fig. 1. ORTEP drawing of the $[Cu(hfac)_2]_3L^1_2$ molecule (ellipsoids are contoured at the 50% probability level, fluorine atoms are omitted for clarity). The labels with primes are given to the atoms related by the inversion centre.

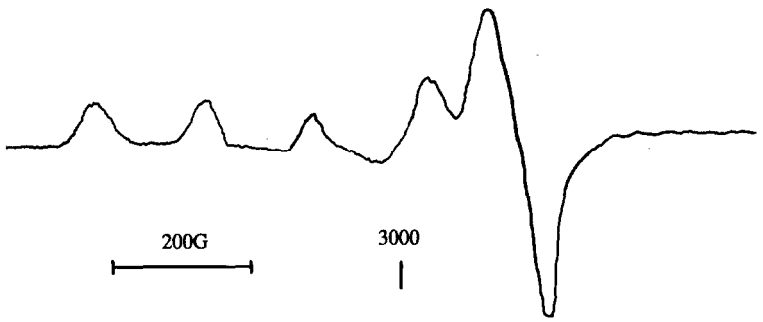

Fig. 2. *X*-band ESR spectrum of solid $[Cu(hfac)_2]_3L^1_2$ at 77 K.

Therefore, the results of the structural and magnetochemical investigation of the complex create a sound basis for the existence of N→O groups of L^1 molecules coordinated to the terminal copper ions.

The $[Cu(hfac)_2]_3L^1_2$ molecule manifests one specific feature when compared with other known complexes of the same stoichiometry: the N→O groups of both bridging paramagnetic ligands are always coordinated to the central copper atom, but not to the terminal one; the complex of symmetric NITEt being the only known exception.[13] It should be noted that the "terminal" bonds (approximately 2.0 Å) are always shorter than the "central" bonds (2.4–2.5 Å) and in the case of imidazoline derivatives, the shorter "terminal" bonds are formed by the stronger (imine) donor functions.[10,11]

account that both TEMPO and acetone are aliphatic bases and in L^1 both groups are conjugated with the aromatic π-system. However, the difference in ΔH seems to be large enough to assume that in the L^1 molecule the N→O group still remains the stronger donor. It is quite probable that this fact accounts for the "inversion" of the nitroxide radical.

These considerations have encouraged us to attempt to synthesize more trinuclear $Cu(hfac)_2$ complexes with "inverted" paramagnetic ligands, using nitroxides having structurally distinct N→O and C=O donor sites. For this purpose we engaged 2,2,6,6-tetramethyl-4-oxo-piperidine-1-oxyl (L^2) and 2,2,5,5-tetramethyl-3-oxo-pyrrolidine-1-oxyl (L^3). However, these nitroxides appeared to form

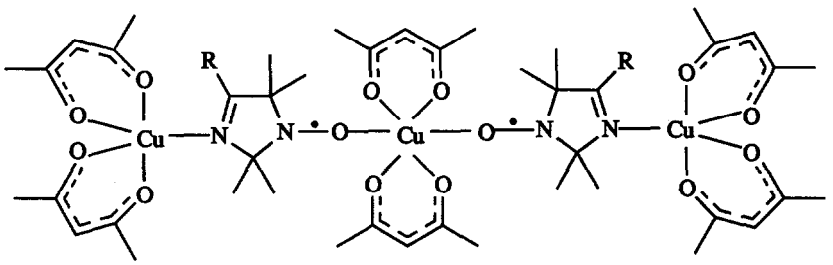

R = Et, Pr^i, Ph

Therefore, it is reasonable to suppose that in the case of L^1 the N→O group has stronger, or at least the same donor properties as the carbonyl group of the ligand. These considerations gain some support from the estimate of the donor ability of the N→O and C=O groups towards $Cu(hfac)_2$, on the basis of Drago's equation.[19] The calculations of the adduct formation enthalpy yield approximately -12 kcal mol^{-1} for the N→O group [2,2,6,6-tetramethylpiperidinyl-1-oxyl (TEMPO) as the base] and -7 kcal mol^{-1} for the C=O group (acetone as the base). Apparently, these figures should be considered as very rough estimates, taking into

only adducts of 1 : 1 stoichiometry under conditions that yielded $[Cu(hfac)_2]_3L^1_2$ in the case of the indole nitroxide. Therefore, the presence of peculiar donor groups is insufficient to result in the formation of a trinuclear complex.

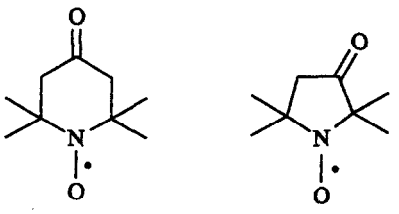

L^2 L^3

To conclude it is worth pointing out that the synthesized complex of the indole nitroxide is the first example of a trinuclear $Cu(hfac)_2$ nitroxide adduct with an "inverted" nitroxide. Further investigations of the complexes of indole nitroxide derivatives are in progress.

Acknowledgements—The authors are grateful to Dr E. Boguslavski (Institute of Inorganic Chemistry, Novosibirsk) for recording the ESR spectra and helpful discussions. The financial support of the International Tomographic Center (Novosibirsk) is gratefully acknowledged.

REFERENCES

1. A. Caneschi, D. Gatteschi and P. Rey, *Prog. Inorg. Chem.* 1991, **89**, 331.
2. V. I. Ovcharenko, A. B. Gel'man and V. N. Ikorski, *Zh. Strukt. Khim.* 1989, **30**, 142.
3. S. V. Larionov, *Zh. Strukt. Khim.* 1982, **23**, 127 and refs therein.
4. R. Benassi, F. Taddei, L. Greci, L. Marchetti, G. D. Andreetti, G. Bocelli and P. Sgarabotto, *J. Chem. Soc., Perkin Trans. II* 1980, 786.
5. E. G. Rozantzev, *Svobodnye iminoksil'nye radikaly*, pp. 185, 189. Khimiya, Moskva (1970).
6. J. A. Bertrand and R. I. Kaplan, *Inorg. Chem.* 1965, **5**, 489.
7. N. Walker and D. Stuart, *Acta Cryst.* 1983, **39A**, 158.
8. R. G. Gerr, L. I. Yanovski and Yu. T. Struchkov, *Kristallographiya* 1983, **28**, 1029.
9. *International Tables for X-ray Crystallography*, Vol. IV, pp. 99, 149. Kynoch Press, Birmingham (1974).
10. V. I. Ovcharenko, V. N. Ikorski, N. V. Pervukhina and N. V. Podberezskaya, *Zh. Neorg. Khim.* 1987, **32**, 1403.
11. A. B. Burdukov, V. I. Ovcharenko, N. V. Pervukhina, N. V. Podberezskaya and V. N. Ikorski, *Zh. Neorg. Khim.* 1991, **36**, 2058.
12. D. Luneau, P. Rey, J. Laugier, P. Fries, A. Caneschi, D. Gatteschi and R. Sessoli, *J. Am. Chem. Soc.* 1991, **113**, 1245.
13. A. Caneschi, D. Gatteschi, R. Sessoli, S. K. Hoffman, J. Laugier and P. Rey, *Inorg. Chem.* 1988, **27**, 2390.
14. N. V. Pervukhina, N. V. Podberezskaya and V. I. Ovcharenko, *Zh. Struct. Khim.* 1991, **32**, 92.
15. W. C. Hamilton, *Acta Cryst.* 1965, **18**, 502.
16. R. J. Doedens and M. H. Dickman, *Inorg. Chem.* 1982, **21**, 682.
17. F. H. Allen, O. Kennard, D. G. Watson, L. Brammer, A. G. Orpen and R. Taylor, *J. Chem. Soc., Perkin Trans. II* 1987, S1.
18. A. G. Orpen, L. Bramer, F. H. Allen, O. Kennard, D. G. Watson and R. Taylor, *J. Chem. Soc., Dalton Trans.* 1989, S1.
19. R. S. Drago, G. C. Vogel and T. E. Needham, *J. Am. Chem. Soc.* 1971, **93**, 6014.

Polyhedron Vol. 12, No. 13, pp. 1711–1714, 1993
Printed in Great Britain

0277-5387/93 $6.00+.00
© 1993 Pergamon Press Ltd

COMMUNICATION

TRISPYRAZOLYLBORATE DEGRADATION AND THE CRYSTAL STRUCTURE OF $[Mo(NO)(CO)_2\{HB(OPr^i)(3\text{-}Pr^i\text{-}5\text{-}MeC_3HN_2)_2\}]$

MERCEDES CANO, JOSE V. HERAS, ELENA SANTAMARIA and ELENA PINILLA*

Departamento de Quimica Inorganica, Facultad de Ciencias Quimicas, Universidad Complutense, Madrid 28040, Spain

and

ANGELES MONGE

Instituto de Ciencias de los Materiales sede D, C.S.I.C., Serrano 113, Laboratorio de Diffracion de Rayos-X, Facultad de Ciencias Quimicas, Universidad Complutense, Madrid 28040, Spain

and

CHRISTOPHER J. JONES†

School of Chemistry, The University of Birmingham, Edgbaston, Birmingham B15 2TT, U.K.

and

JON A. McCLEVERTY†

School of Chemistry, University of Bristol, Cantock's Close, Bristol BS8 1TS, U.K.

(*Received* 23 *March* 1993; *accepted* 22 *April* 1993)

Abstract—The complex $[Mo(NO)\{HB(OPr^i)(3\text{-}Pr^i\text{-}5\text{-}MeC_3HN_2)_2\}(CO)_2]$ has been isolated from one attempt to prepare $[Mo(NO)\{HB(3\text{-}Pr^i\text{-}5\text{-}MeC_3HN_2)_3\}(CO)_2]$; a crystal structure shows the presence of an isopropoxide group with the alkoxy oxygen bound to the boron and molybdenum atoms [Mo—O = 2.225(5) Å].

Following their initial development by Trofimenko[1] the trispyrazolylborate ligand and its derivatives have assumed an important role in modern coordination chemistry.[2] These ligands have found applications in a wide variety of contexts, including organometallic systems which exhibit photochemical reactivity,[3,4] models for bio-inorganic systems[5–8] and complexes used to study intramolecular electron transfer processes.[9,10] Although it is generally assumed that the trispyrazolylborate ligand system represents an inert group capable of occupying three facial coordination sites on a metal, several examples are known in which the ligand itself undergoes reactions. These reactions may

* Contribution also from Laboratorio de Diffracion de Rayos-X, Facultad de Ciencias Quimicas, Universidad Complutense, Madrid 28040, Spain.

† Authors to whom correspondence should be addressed.

involve varying degrees of ligand degradation. At one extreme asymmetrically substituted trispyrazolylborates carrying bulky substituents may undergo boratropic rearrangements which involve ligand reorganization without the loss of any pyrazolyl groups.[1,12] Presumably these rearrangements are driven by the energy benefit of achieving the most sterically efficient disposition of the bulky substituents within the complex when this substitution pattern differs from that initially present in the ligand. At the other extreme, complete degradation of the trispyrazolylborate ligand has been observed in the reaction[13] of K[HB(3,5-$Me_2C_3HN_2)_3$] with [{Ru(η^6-C_6H_6)Cl_2}$_2$] to give [Ru(η^6-C_6H_6){NH=CMe(Me_2pz)}Me_2Hpz)]$^{2+}$ and in deboronation of [Mo(NO){HB(3,5-$Me_2C_3HN_2)_3$}I_2] by catechol to give [Mo(NO)($O_2C_6H_4$)(Me_2pzH)$_2$(Me_2pz)].[14] Between these extremes there are examples in which one pyrazolyl group is displaced from a trispyrazolylborate ligand by another group. Evidence has been obtained that the reactions between [Mo(NO){HB(3,5-$Me_2C_3HN_2)_3$}I_2] and 2-aminobenzenethiol or 1,2-diaminobenzene result in the replacement of one of the dimethylpyrazolyl groups by the aminoaryl moiety, although the structures of the products could not be definitively assigned.[15] In this communication we report a further example of the partial degradation of a trispyrazolylborate ligand associated with the {Mo(NO)} moiety and describe the crystal structure of the product.

The synthesis of [Mo(NO){HB(MePr^i$C_3$$HN_2)_3$}(CO)$_2$] according to the previously reported method[12] has been successfully repeated on a number of occasions in our laboratory. However, on one occasion the product obtained was not the expected compound but a derivative having a different NMR spectrum. This contained doublets [J(HH) = 7 Hz] of relative areas 6:6:6 at 1.30, 1.18 and 1.03 ppm, attributable to three pairs of isopropyl methyl groups, a singlet of relative area 6 at 2.31 ppm, attributable to two equivalent pyrazolyl methyl substituents, two multiplets of relative areas 2:1 at 3.15 and 4.09 ppm, attributable to the isopropyl Me_2CH- groups, and a singlet of relative area 2 at 5.80 ppm, attributable to two equivalent pyrazolyl 4-CH protons. The spectrum was lacking in signals attributable to the methyl and 4-CH protons of a third pyrazolyl group. The IR spectrum contained bands at 2480, 2010, 1915 and 1660 cm^{-1} attributable to the BH, NO and CO groups. These spectroscopic data are in accord with the formulation [Mo(NO){HB(OPr^i)(3-Pr^i-5-$MeC_3HN_2)_2$}(CO)$_2$], in which one pyrazolyl group in the tripodal ligand has been replaced by an isopropoxide group. This formulation is also in accord with the structure established by X-ray methods and described below. The source of the isopropoxide remains unclear. Except for the sample of butyl nitrite, the reagents used in the preparation were taken from the same samples used in previous reactions and which afforded the expected product. It is possible that the butyl nitrite was impure but none of this sample remained for further investigation. We have found that heating [Mo(NO){HB(MePr^i$C_3HN_2)_3$}(CO)$_2$] under reflux in either Pr^{i}OH or Me_2CO, for longer than the reaction time used in its preparation, does not lead to the formation of [Mo(NO){HB(OPr^i)(3-Pr^i-5-$MeC_3HN_2)_2$}(CO)$_2$]. Thus, it appears that the degradation reaction must have occurred prior to, or during, the formation of [Mo(NO){HB(OPr^i)(3-Pr^i-5-$MeC_3HN_2)_2$}(CO)$_2$].

The crystal structure* of [Mo(NO){HB(OPr^i)(3-Pr^i-5-$MeC_3HN_2)_2$}(CO)$_2$] reveals a *fac* arrangement of the {(NO)(CO)$_2$} ligand set within a dis-

* *Crystal data.* Crystals of $MoBN_5O_4C_{19}H_{30}$ are orthorhombic, space group $P2_12_12_1$, a = 8.146(3), b = 16.886(3), c = 17.812(2) Å, U = 2450(1) Å^3, $F(000)$ = 1032, μ = 5.52 cm^{-1}, Z = 4, D_c = 1.35 g cm^{-3}. A crystal of dimensions 0.3 × 0.3 × 0.2 mm^3 was coated with epoxy resin and mounted in a kappa diffractometer. The cell dimensions were refined by least-squares fitting of the values of 25 reflections. The intensities of 4010 unique reflections within $2 < \theta < 30$ and indices from (0,0,0) to (11,23,25) were measured at 295 K with monochromatic Mo-K_α radiation (λ = 0.71069 Å) and an $\omega/2\theta$ scan technique. There was no appreciable drop in the intensity of standard reflections monitored every hour. The intensities were corrected for Lorentz and polarization effects and 2475 with $\{I < 2\sigma(I)\}$ were considered observed and used in the analysis. Scattering factors for neutral atoms and anomalous dispersion corrections for molybdenum were taken from ref. 16. The structure was solved by Patterson and Fourier methods. An empirical absorption correction[17] was applied at the end of the isotropic refinement. Final refinement with fixed isotropic thermal parameters and coordinates for hydrogen atoms and unit weights led to R = 0.44 and R_w = 0.051. No trend in F vs F_0 or $(\sin\theta)/\lambda$ was observed. Average shift-to-error ratios were < 0.03. A final difference synthesis showed no significant electron density.

The nitrogen atom of the nitrosyl ligand and the carbon atoms of the carbonyl ligands became indistinguishable. The positions of these three atoms were considered occupied by carbon and nitrogen atoms with population factors 0.66 and 0.34, respectively. The atom labelled as O(1) has been assigned as an oxygen atom on the basis of the spectroscopic data. Calculations were performed using the X-ray 80 system.[18] Additional material available from the Cambridge Crystallographic Data Centre comprises atom coordinates and thermal parameters.

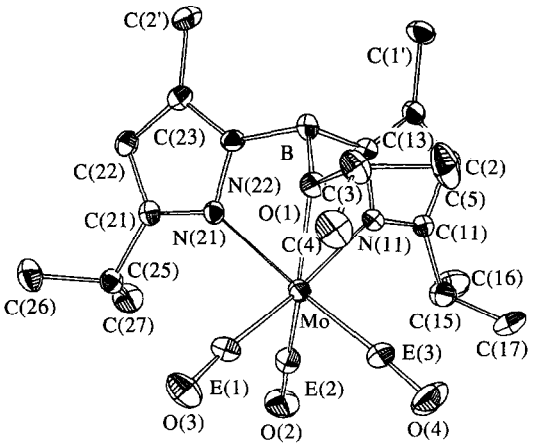

Fig. 1. A view of $[Mo(NO)\{HB(OPr^i)(3\text{-}Pr^i\text{-}5\text{-}MeC_3HN_2)_2\}(CO)_2]$ showing the atom numbering with 20% probability ellipsoids. Hydrogen atoms have been omitted for clarity. Selected bond lengths (Å) and angles (°): Mo—O(1), 2.225(5); Mo—N(11), 2.227(7); Mo—N(21), 2.204(7); Mo—E(1), 1.987(9); Mo—E(2), 1.955(10); Mo—E(3), 1.809(7); B—O(1), 1.501(11) Å; E(1)—Mo—E(2), 87.5(4); E(1)—Mo—E(3), 86.5(4); E(2)—Mo—E(3), 85.2(4); E(1)—Mo—O(1), 99.8(4); E(2)—Mo—O(1), 100.9(3); E(3)—Mo—O(1), 171.3(3); Mo—O(1)—B, 102.8(5); Mo—E(1)—O(3), 174.3(9); Mo—E(3)—O(4), 177.0(9); Mo—E(2)—O(2), 178.9(8); B—O(1)—C(3), 119.3(7)°.

torted octahedral coordination geometry around the formally 18-electron molybdenum centre (Fig. 1). The remaining three coordination sites are occupied by two pyrazolyl nitrogens and an oxygen atom derived from an isopropoxide moiety, which has replaced one of the pyrazolyl groups in the tripodal ligand. Within the first coordination sphere of the molybdenum atom the Mo—O(Pr^i) distance [2.225(5) Å] is comparable with the two Mo—N(pyrazolyl) distances [av. 2.216(7) Å], which in turn are similar to those found[19] in $[Mo(NO)\{HB(pz)_3\}(CO)_2]$ [av. 2.213(4) Å] but smaller than in $[Mo(NO)\{HB(C_3H_2N_2C_6H_4OMe\text{-}4)_3\}(CO)_2]$ [av. 2.253; range 2.23(1)–2.27(1) Å].[20] In contrast the E—Mo—E′ (E, E′ = N, C) angles in $[Mo(NO)\{HB(OPr^i)(3\text{-}Pr^i\text{-}5\text{-}MeC_3HN_2)_2\}(CO)_2]$ (av. 86.4°) are smaller than in $[Mo(NO)\{HB(pz)_3\}(CO)_2]$ [av. 90.45(30)°] and more comparable with the average value of 85.0° found in the more sterically constrained complex $[Mo(NO)\{HB(C_3H_2N_2C_6H_4OMe\text{-}4)_3\}(CO)_2]$. These findings indicate that, compared with $HB(pz)_3$, the $HB(OPr^i)(3\text{-}Pr^i\text{-}5\text{-}MeC_3HN_2)_2$ ligand produces some steric compression of the $\{Mo(NO)(CO)_2\}$ moiety, but that this is not reflected in the Mo—N pyrazolyl distances, unlike the situation in $[Mo(NO)\{HB(C_3H_2N_2C_6H_4OMe\text{-}4)_3\}(CO)_2]$. The average Mo—E(O) distance of 1.917 Å in $[Mo(NO)\{HB(OPr^i)(3\text{-}Pr^i\text{-}5\text{-}MeC_3HN_2)_2\}(CO)_2]$ lies between the average values of 1.907 and 1.930 Å found respectively in $[Mo(NO)\{HB(C_3H_2N_2C_6H_4OMe\text{-}4)_3\}(CO)_2]$ and $[Mo(NO)\{HB(pz)_3\}(CO)_2]$.

The findings described here provide a further example of the friability of the trispyrazolylborate ligand system and emphasize the need for those working with these ligands to be alert to the possibility of ligand degradation reactions.

Acknowledgement—We are grateful to MEC (Spain DGICVT) for the support of this work on project PB/890127.

REFERENCES

1. S. Trofimenko, *Chem. Rev.* 1972, **72**, 497.
2. S. Trofimenko, *Prog. Inorg. Chem.* 1986, **34**, 115.
3. C. K. Ghosh and W. A. G. Graham, *J. Am. Chem. Soc.* 1987, **109**, 4726; 1989, **111**, 375.
4. A. J. Rest, N. Wells, R. B. Hitam, M. Herberhold, W. Kremitz, C. J. Jones and J. A. Thomas, manuscript in preparation.
5. S. A. Roberts, C. G. Young, W. E. Cleland, R. B. Ortega and J. H. Enemark, *Inorg. Chem.* 1988, **27**, 3044.
6. S. A. Roberts, C. G. Young, C. A. Kipke, W. E. Cleland, K. Yamanouchi, M. D. Carducci and J. H. Enemark, *Inorg. Chem.* 1990, **29**, 3650.
7. W. H. Armstrong, A. Spool, G. C. Papaefthymiou, R. B. Frankel and S. J. Lippard, *J. Am. Chem. Soc.* 1984, **106**, 3653.
8. P. N. Turowski, W. H. Armstrong, M. E. Roth and S. J. Lippard, *J. Am. Chem. Soc.* 1991, **113**, 681.
9. A. Das, J. A. McCleverty, M. D. Ward, C. J. Jones and A. M. W. Cargill Thompson, *Polyhedron* 1992, **11**, 2119.
10. N. M. Rowley, S. S. Kurek, M. W. George, S. M. Hubig, J. M. Kelly, P. D. Beer, C. J. Jones and J. A. McCleverty, *J. Chem. Soc., Chem. Commun.* 1992, 497.
11. S. Trofimenko, J. C. Calabrese, P. J. Domaille and J. S. Thompson, *Inorg. Chem.* 1989, **26**, 1091.
12. M. Cano, J. V. Heras, S. Trofimenko, A. Monge, E. Gutierrez, C. J. Jones and J. A. McCleverty, *J. Chem. Soc., Dalton Trans.* 1990, 3577.
13. C. J. Jones, J. A. McCleverty and A. S. Rothin, *J. Chem. Soc., Dalton Trans.* 1986, 109.
14. H. Adams, N. A. Bailey, A. S. Drane and J. A. McCleverty, *Polyhedron* 1983, **2**, 465.
15. N. AlObaidi, C. J. Jones and J. A. McCleverty, *Polyhedron* 1989, **8**, 1033.
16. *International Tables for X-ray Crystallography*, Vol. 4, pp. 72–98. Kynoch Press, Birmingham (1974).
17. N. Walker and D. Stuart, *Acta Cryst., Sect. A* 1983, **39**, 158.

18. J. M. Stewart, The X-Ray 80 System, Computer Science Centre, University of Maryland, College Park (1985).
19. E. M. Holt, S. M. Holt, F. Cavalito and K. J. Watson, *Acta Chem. Scand., Ser. A* 1976, **30**, 225.
20. M. Cano, J. V. Heras, A. Monge, E. Gutierrez, S. L. W. McWhinnie, C. J. Jones and J. A. McCleverty, *J. Chem. Soc., Dalton Trans.* 1992, 2435.

Polyhedron Vol. 12, No. 13, pp. 1715–1717, 1993
Printed in Great Britain

0277–5387/93 $6.00+.00
© 1993 Pergamon Press Ltd

COMMUNICATION

ORTHOMETALLATION REACTION IN DIRHODIUM(II) COMPOUNDS. SELECTIVE FORMATION OF DOUBLY-METALLATED COMPOUNDS WITH HEAD-TO-HEAD STRUCTURE

M. V. BORRACHERO, F. ESTEVAN, P. LAHUERTA,* J. PAYÁ and E. PERIS

Departamento de Química Inorgánica, Universitat de Valencia, C/Dr. Moliner 50, E-46100 Burjassot-Valencia, Spain

(*Received* 10 *November* 1992; *accepted* 20 *April* 1993)

Abstract—The reaction of the mono-metallated compound $Rh_2(O_2CCH_3)_3[(C_6H_4)P(CH_3)(C_6H_5)]\cdot 2(HO_2CCH_3)$ with PPh_3 (1:1 molar ratio) has been studied by ^{31}P NMR spectroscopy. The reaction yields the doubly-metallated compound $Rh_2(O_2CCH_3)_2[(C_6H_4)P(CH_3)(C_6H_5)][(C_6H_4)P(C_6H_5)_2]\cdot 2(HO_2CCH_3)$ with a head-to-head (H-H) configuration. An intermediate reaction compound, not previously observed, has been spectroscopically detected in solution. Analogous intermediate compounds have been detected using $P(p\text{-}CH_3C_6H_4)_3$ and $P(p\text{-}ClC_6H_4)_3$ instead of triphenylphosphine.

It is known[1,2] that rhodium acetate reacts with triarylphosphines (PR_3) or alkylarylphosphines $\{P(CH_3)(C_6H_5)_2$ or $P(CH_3)_2(C_6H_5)\}$ to give mono- and doubly-metallated dirhodium(II) compounds. In the course of our investigation on the reactivity of dirhodium(II) tetracarboxylate and arylphosphines we have observed[1d,e] two general reaction pathways yielding doubly-metallated compounds with head-to-head (H-H) and head-to-tail (H-T) configurations. As a rule compounds with H-H configuration were only formed when excess phosphine was present in solution.

It has been reported that $Rh_2(O_2CCH_3)_4$ and $P(CH_3)(C_6H_5)_2$ (in a 1:2 molar ratio) react in refluxing acetic acid to yield the doubly-metallated compound $Rh_2(O_2CCH_3)_2[(C_6H_4)P(CH_3)(C_6H_5)]_2\cdot 2(HO_2CCH_3)$, which has been structurally characterized.[2a] We have found that the same reaction performed using an Rh_2:P molar ratio of 1:1 yields a mixture of the mono-metallated compound $Rh_2(O_2CCH_3)_3[(C_6H_4)P(CH_3)(C_6H_5)]\cdot 2(HO_2CCH_3)$ (**1**)† and the already reported doubly-metallated compound.[2a] When **1** reacts with $P(CH_3)(C_6H_5)_2$ (1:1 molar ratio) in chloroform at room temperature for 4 days only the titled compound with H-T configuration, $Rh_2(O_2CCH_3)_2[(C_6H_4)P(CH_3)(C_6H_5)]_2\cdot 2(HO_2CCH_3)$,[2a] is isolated (yield 70%). When **1** is reacted with triphenylphosphine in the same reaction conditions the doubly-metallated compound with H-H configuration, $Rh_2(O_2CCH_3)_2[(C_6H_4)P(CH_3)(C_6H_5)][(C_6H_4)P(C_6H_5)_2]\cdot$

* Author to whom correspondence should be addressed.

† Preparation of compound **1**: $Rh_2(O_2CCH_3)_4\cdot 2(CH_3OH)$ (300 mg, 0.59 mmol) was added to a solution of $PMePh_2$ (0.114 cm^3, 0.6 mmol) in CH_2Cl_2 (30 cm^3). The resulting brown suspension was stirred at room temperature for 10 min. The solvent was removed and a mixture of toluene: acetic acid (60 cm^3, 3:1) was added. The solution was refluxed for 45 min and the solvent was evaporated to dryness. The crude solid was dissolved in CH_2Cl_2 (5 cm^3) and transferred into a chromatography column. By elution with CH_2Cl_2: hexane: acetic acid (10:10:5) a purple band containing $Rh_2(O_2CCH_3)_2[(C_6H_4)P(CH_3)(C_6H_5)]_2\cdot 2(HO_2CCH_3)$ was separated. Further elution with CH_2Cl_2: hexane: acetic acid (10:10:10) separated a violet band of **1**, which was precipitated in a mixture (5 cm^3) of hexane: CH_2Cl_2 (yield 52%).

Characterization of **1**: Spectroscopic data: $^{31}P\{^1H\}$NMR: δ_P = 13.7 ppm, ^1J(Rh—P) = 147.7 Hz, ^2J(RhP) = 6.2 Hz. ^1H NMR (in ppm): 1.15 (3H, CH_3, s), 1.69 (3H, CH_3, s), 1.85 [3H, CH_3, d, ^1J(H—P) = 12 Hz], 2.28 (6H, CH_3, s), 2.32 (3H, CH_3, s), 6.9–7.7 (8H, aromatics, m), 8.43 (1H, aromatic, q). $^{13}C\{^1H\}$NMR (in ppm): 11.4 [CH_3, d, ^1J(P—C) = 32 Hz), 21.6 (CH_3, s), 23.4 (CH_3, s), 23.9 (CH_3, s), 122–145 (aromatics, m), 162.7 (metallated C, m), 179.2 (OCO, s), 182.3 (OCO, s) 189.5 (OCO, s), 189.9 (OCO, s). Found: C, 38.6; H, 4.2. Calc. for $Rh_2PO_{10}C_{23}H_{29}$: C, 39.3; H, 4.2%.

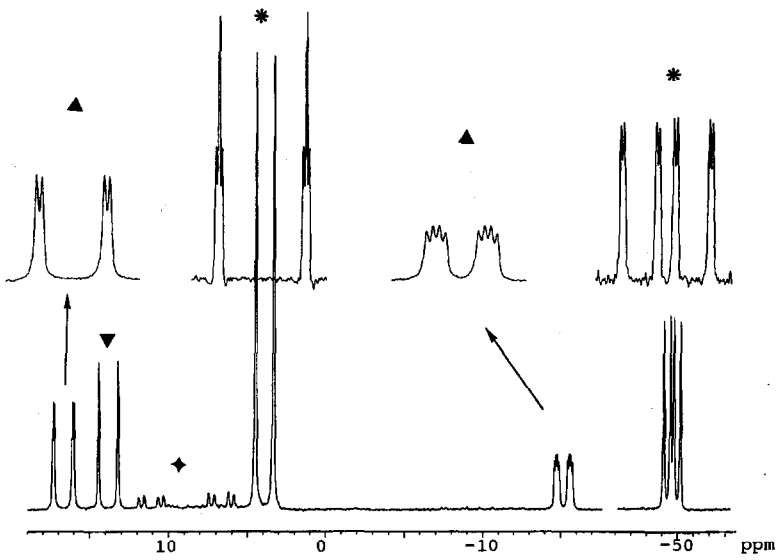

Fig. 1. ^{31}P NMR spectrum of a mixture of **1** and PPh_3 (molar ratio $P/Rh_2 = 0.8$) in $CDCl_3$ at $-50°C$: ▼ signals due to unreacted **1**, ▲ signals due to **1**·PPh_3, * signals due to **2** and ◆ signals due to impurities.

$2(HO_2CCH_3)$ (**3**),* is obtained in 6 h (yield 62%). The observation of a $^2J(P—P')$ coupling constant value of 42 Hz in the ^{31}P NMR spectrum of **3** is diagnostic of an H-H configuration of the two metallated ligands.[1e] Up until now we had only observed the formation of compounds with H-H structure when excess phosphine was present in solution. This is the first time that we observe the formation at room temperature of a compound with H-H structure under stoichiometric amounts of ligand (see Scheme I).

We have monitored the reaction **1** → **3** by ^{31}P NMR spectroscopy. The spectrum of the solution resulting from adding triphenylphosphine to a chloroform solution of **1** (molar ratio $P:Rh_2 = 1$) at $-40°C$ shows the presence of two main species: the phosphine mono-adduct $Rh_2(O_2CCH_3)_3[(C_6H_4)P(CH_3)(C_6H_5)]\cdot(PPh_3)(HO_2CCH_3)$ (**1**·PPh_3)[1e,3] and a new species **2**, which has two resonances

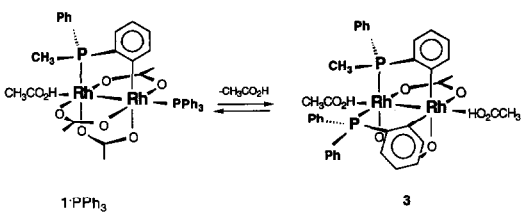

Scheme I.

at -49.23 and 3.90 ppm (Fig. 1). Different spectra recorded in the temperature range -40 to $+20°C$ show that the species **1**·PPh_3 and **2** are in equilibrium. The amount of species **2** in solution increases as the temperature decreases. Some line broadening is observed in the spectra recorded at 20°C.

At 30°C there is already a slow chemical evolution and signals due to the doubly-metallated compound **3** appear in the spectrum while those corresponding to **1**·PPh_3 and **2** disappear. The reaction is completed after 12 h and compound **3** can be isolated from the reaction mixture in moderate yield. Compound **3** could be obtained as a mixture of two isomers (with the methyl group attached to the phosphine in an *endo* or *exo* configuration relative to the dihedral angle formed by the two metallated ligands). The observation of very sharp resonances in the ^{31}P NMR spectra suggests that the reaction is regio-selective and only one of the two possible isomers, we propose the less sterically crowded, is formed.

In the two reported[1d,e] reaction pathways the observed intermediate species (**I** and **II**, Scheme II)

* Characterization of **3**: Spectroscopic data: $^{31}P\{^1H\}$NMR: $\delta_{P1} = 24.4$ ppm, $^1J(Rh(1)—P(1)) = 150$ Hz, $^2J(Rh(2)—P(1)) = 6.0$ Hz; $\delta_{P2} = 5.8$, $^1J(Rh(1)—P(2)) = 145$ Hz, $^2J(Rh(2)—P(2)) = 6.4$ Hz, $^2J(P(1)—P(2)) = 42$ Hz. ^1H NMR (in ppm): 0.85 (3H, CH_3, s), 1.27 [3H, CH_3, d, $^1J(H—P) = 15$ Hz], 1.63 (3H, CH_3, s), 2.11 (6H, CH_3, s), 6.2–8.1 (23H, aromatics, m). $^{13}C\{^1H\}$NMR (in ppm): 14.2 (CH_3, s), 22.8 (CH_3, s), 23.4 [CH_3, d, $^1J(P—C) = 32$ Hz], 29.9 (CH_3, s), 127–145 (aromatics, m), 161.8 (metallated C, m), 163.6 (metallated C, m), 181.7 (OCO, s), 182.6 (OCO, s) 182.8 (OCO, s). Found: C, 51.1; H, 4.7. Calc. for $Rh_2P_2O_8C_{39}H_{40}$: C, 51.8; H, 4.4%.

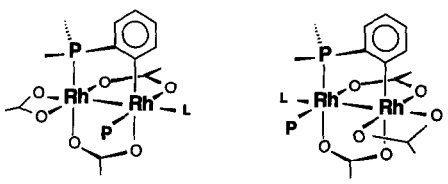

I II

L= H_2O, CH_3CO_2H

Scheme II.

contained one equatorial phosphine in a previous situation to the transfer of one proton to a partially displaced acetate group. The spectroscopic data observed for **2** indicate that this intermediate compound is structurally different to species **I** and **II**. The high-field resonance at −49.23 ppm cannot be assigned to one triphenylphosphine in the equatorial coordination position, which usually has chemical shift values in the range 30–50 ppm.[4] The ^{1}H NMR spectrum of the reaction mixture does not show any resonance indicative of agostic interactions or Rh—H bond formation.

Based on the spectroscopic data we are not able to make a definitive structural assignment for compound **2**. Even though the resonance at 3.90 ppm [^1J(Rh—P) = 140.1 Hz, ^2J(Rh—P) = 4.8 Hz and J(P(1)—P(2)) = 4.7 Hz] can be assigned to a metallated dimethylphenylphosphine the assignment of the signal at −49.23 ppm [^1J(Rh—P) = 76.5 Hz, ^2J(Rh—P) = 51.2 Hz and ^3J(P(1)—P(2)) = 4.7 Hz] is not completely clear to us. The ^{13}C NMR spectrum of this sample at −40°C did not give any additional information.

In a separate experiment we performed the same reaction using $P(C_6D_5)_3$.* The same equilibrium between species **1** and **2** was obtained. After adding CH_3CO_2H (0.1 cm^3) to the NMR tube the sample was warmed at 20°C for several minutes and was immediately cooled to −40°C. The process was repeated several times, after which only the two species **1** and **2** were still observed in solution. The ^{1}H NMR spectrum did not show any signal in the aromatic region indicative of the occurrence of exchange in the $P(C_6D_5)_3$ ligand. This experiment rules out the equilibrium **1**·$PPh_3 \leftrightarrow$ **2**, involving metallation and demetallation of the triphenylphosphine ligand. The same reaction performed with **1** and $P(p\text{-}CH_3C_6H_4)_3$ or $P(p\text{-}ClC_6H_4)_3$ behaved in a very similar way, yielding doubly-metallated compounds with H-H structure through reaction intermediates that show analogous ^{31}P NMR spectra.

The only possible structure for the intermediate **2** is the one involving axial coordination of the entering phosphine at the same rhodium atom that is bonded to the phosphorus of the metallated phosphine.

The spectroscopic data do not reject this assignment, which is fully consistent with the structure of the reaction product obtained. This particular adduct at room temperature might selectively undergo axial to equatorial rearrangement of the phosphine so explaining the H-H configuration of the reaction product.

Further experiments, aimed at a better elucidation of the mechanistic aspects of this particular metallation reaction, are in progress.

Acknowledgement—We thank the CICYT for the financial support of this work (MAT90-0656-C02-01).

REFERENCES

1. (a) A. R. Chakravarty, F. A. Cotton, D. A. Tocher and J. H. Tocher, *Organometallics* 1985, **4**, 8; (b) P. Lahuerta, J. Payá, E. Peris, M. A. Pellinghelli and A. Tiripicchio, *J. Organomet. Chem.* 1989, **373**, C5; (c) P. Lahuerta, J. Paya, E. Peris, A. Aguirre, S. García-Granda and F. Gómez-Beltrán, *Inorg. Chim. Acta* 1992, **192**, 43; (d) P. Lahuerta, J. Payá, X. Solans and M. A. Ubeda, *Inorg. Chem.* 1992, **31**, 385; (e) P. Lahuerta, J. Payá, M. A. Pellinghelli and A. Tiripicchio, *Inorg. Chem.* 1992, **31**, 1224.
2. (a) E. C. Morrison and D. A. Tocher, *Inorg. Chim. Acta* 1989, **157**, 139; (b) E. C. Morrison and D. A. Tocher, *J. Organomet. Chem.* 1991, **408**, 105.
3. E. Rotondo, B. E. Mann, P. Piraino and G. Tresoldi, *Inorg. Chem.* 1989, **28**, 3070.
4. (a) F. Barceló, F. A. Cotton, P. Lahuerta, R. LLúsar, M. Sanaú, W. Schwotzer and M. A. Ubeda, *Organometallics* 1986, **5**, 808; (b) P. Piraino, G. Bruno, G. Tresoldi, S. Lo Schiavo and F. Nicolo, *Inorg. Chem.* 1980, **28**, 139.

* We have performed the same reaction adding other substituted triarylphosphines. The same equilibrium was observed and type **2** compounds were spectroscopically detected.

Spectroscopic data for type **2** compounds: Adding $P(p\text{-}CH_3C_6H_4)_3$: δ_{P1} = 2.6 ppm [^1J(Rh—P(1)) = 141 Hz, ^2J(Rh—P(1)) = 4.6 Hz and ^3J(P(1)—P(2)) = 4.6 Hz], δ_{P2} = −52.5 ppm [^1J(Rh—P(2)) = 79 Hz and ^2J(Rh—P(2)) = 52 Hz]; adding $P(p\text{-}ClC_6H_4)_3$: δ_{P1} = 1.8 ppm [^1J(Rh—P(1)) = 139 Hz, ^2J(Rh—P(1)) = 4.4 Hz and ^3J(P(1)—P(2)) = 4.4 Hz], δ_{P2} = −52.9 ppm [^1J(Rh—P(2)) = 70 Hz and ^2J(Rh—P(2)) = 55 Hz].

Polyhedron Vol. 12, No. 14, pp. 1719–1724, 1993
Printed in Great Britain

0277–5387/93 $6.00+.00
Pergamon Press Ltd

OXIDATION OF INDOLES BY N-CHLORO-N-SODIO-*p*-TOLUENESULPHONAMIDE IN ALKALINE MEDIUM CATALYSED BY OSMIUM(VIII): A KINETIC STUDY

KANCHUGARAKOPPAL S. RANGAPPA*† and DANIEL T. ESTERLINE

Department of Chemistry, Miami University, Oxford, Ohio 45056, U.S.A.

and

CHIRCHINGI K. MYTHILY, DANDINASIVARA S. MAHADEVAPPA and SARVOTTAM Y. AMBEKAR

Department of Studies in Chemistry, University of Mysore Manasagangotri, Mysore 570006, India

(*Received* 24 *July* 1992; *accepted* 1 *April* 1993)

Abstract—The kinetics of oxidation of indoles (**1a–d**) to the corresponding oxindole by the title oxidant in alkaline medium catalysed by osmium(VIII) at 30°C has been studied. The reaction shows first-order each in [chloramine-T] (**2**), [Os^{VIII}] (**3**) and [indole] (**1a**). Effects of added anions and *p*-toluenesulphonamide (**5**) as well as varying ionic strength and dielectric constant of the medium have been investigated. Activation parameters have been computed. An isokinetic relationship was observed with $\beta = 325$, indicating enthalpy as the rate-controlling factor. With the available data, including the substituent effects ($\rho^+ = -1.0$) which were obtained from a Hammett plot, the proposed mechanism and the derived rate laws are in agreement with the observed kinetics.

Enzymatic oxidation of indole (**1a**) has attracted the attention of chemists for the past several decades. The metabolic oxidation of study of **1a** to indoxyl was attempted by Laroche and Desbordes.[1] Although the indole (**1a**) has been oxidized by sodium performate in the presence of acetone and methyl paraoxane as a promoter,[2] very few kinetic investigations of indole oxidations have been reported. The studies presented in this paper were undertaken to investigate the oxidation of various indoles by N-halogenated compounds. Specifically of interest is chloramine-T, a versatile oxidant.[3] Mechanistic studies of the oxidation of various organic substrates by organic haloamines have been earlier reported from this laboratory;[4–6] however, there seems to have been no report on the oxidation of indoles (**1a–d**) by chloramine-T (**2**). In this paper the kinetics and mechanism of base and osmium tetroxide (**3**) catalysed 5-substituted indole (**1a–d**) oxidations (30°C, 10% aqueous methanol) are reported.

EXPERIMENTAL

Chloramine-T, CAT (**2**, LobaChemie), was purified by the method of Morris *et al.*[7] An aqueous solution was prepared iodometrically standardized and stored in brown bottles to prevent photochemical deterioration. Indoles (**1a–d**, Aldrich Co.) were of accepted grades of purity and were used as such. Solutions of the compounds were prepared in 10% methanol (v/v). Osmium tetroxide (Johnson and Mathey, London) was prepared in 0.2 M NaOH. All other reagents used were analytical grades of purity. Doubly distilled water was employed in solution preparations. The ionic strength of the system was maintained at a constant

* Author to whom correspondence should be addressed.
† Present address: Department of Studies in Chemistry, University of Mysore, Manasagangotri, Mysore 570 006, India.

high value ($\mu = 0.5$ M) using a concentrated solution of sodium perchlorate.

Kinetics

The reaction was performed in stoppered Pyrex glass tubes with outer surfaces coated black to eliminate the possible photochemical effects. For each run, requisite amounts of solutions of NaOH, $NaClO_4$, OsO_4, water and methanol (to maintain the total volume constant and 10% methanol medium throughout) were added into a glass tube. Indoles (**1a–d**) and CAT solution pre-equilibrated separately at 30°C were added successively to the reaction mixture to initiate the reaction. The course of the reaction was followed by iodometric determination of unreacted CAT present in the measured aliquots of the reaction mixture withdrawn at different intervals of time. The reaction was studied for two half-lives. The pseudo-first-order rate constants calculated were reproducible within ±3%.

Product studies

Reaction products of the oxidation of indole with **2** in the presence of NaOH and OsO_4 (**3**) in 10% MeOH were isolated from varying amounts of known excess of CAT over indole at 30°C for 24 h. Determination of unreacted CAT in the reaction mixture showed that every mole of indole consumed 1 mol of CAT [eq. (1)].

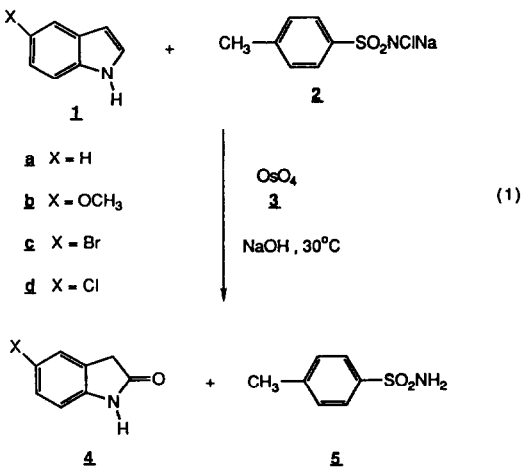

The residual brown solid obtained by the product studies was subjected to column chromatography on silica gel (60–200 mesh) using gradient elution (dichloromethane to acetone). After initial separation, reaction products were further purified by recrystallization. Reaction products were characterized by ^{1}H NMR, IR and GC/MS. Materials were identified by comparison to commercially available samples.

Oxindole (**4**). Recrystallized from dichloromethane/petroleum ether (m.p. = 118–120°C), known m.p. = 125–127°C (Beil. **21**, 282). The *Rf* value (0.13) was determined from TLC (CH_2Cl_2). IR (KBr): 3217 (N—H stretch), 3070 and 3032 (aromatic C—H stretch), 2925 (aliphatic C—H stretch), 1701 (C=O stretch), 1619 (C=C stretch), 1473, 1333, 1234, 749, 674 and 552 cm^{-1}. ^{1}H NMR ($CDCl_3$): δ = 7.22–6.83 (m, 4H, aromatic C—H), 3.54 (S, 2H, aliphatic C—H), and 1.71 (s, 1H, N—H). GC/MS, *m/z*: 133 (m^+), 104 ($m^+ - NH_2$), 78 ($m^+ - C_2HNO$), 77, 51 and 36 (15% yield).

p-*Toluenesulphonamide* (*PTS*) (**5**). Recrystallized from dichloromethane/petroleum ether (m.p. = 134–135.5°C), known m.p. = 137–140°C (Beil **11**, 104). The *Rf* value (0.84) was determined from TLC (CH_2Cl_2). IR (KBr): 3332 and 3244 (N—H stretch), 3125 (aromatic C—H stretch), 2925 (aliphatic C—H stretch), 1576 (C=C stretch), 1326 and 1172 (SO_2 stretch), 1094, 808, 665, 558 and 532 cm^{-1}. ^{1}H NMR ($CDCl_3$): δ = 7.87–7.26 (m, 4H aromatic C—H), 4.68 (s, 2H, N—H) and 2.43 (s, 3H, aliphatic C—H). GC/MS, *m/z*: 171 (m^+), 155 ($m^+ - NH_2$), 91 ($m^+ - SO_2NH_2$), 65 and 39 (65% yield).

RESULTS

The oxidation of **1a–d** with **2** in the presence of NaOH and OsO_4 in 10% MeOH proceeds in a pseudo-first-order fashion for at least two half-lives. At constant [OH^-] and [**3**] with substrate **1a** in excess plots of log [CAT] vs time were linear, indicating a first-order dependence of rate on [**2**]. Values of pseudo-first-order rate constants (k') are given in Table 1. The rate increases initially with increase in [**1a**], which levels off at higher [**1a**]. Plot of log k' vs

Table 1. Pseudo-first-order rate constants for the variation of [**2**] and [**1a**] at 30°C

[**1a**] = 2.5×10^{-3} M		[**2**] = 8.0×10^{-5} M	
[**2**] (10^{-5} M)	k' (10^{-5} s^{-1})	[**1a**] (10^{-3} M)	k' (10^{-5} s^{-1})
6.0	9.90	0.8	2.98
7.0	9.75	1.0	4.00
7.5	9.82	2.0	7.39
8.0	9.73	2.5	9.37
8.5	10.00	3.0	10.68
9.0	10.02	4.0	12.76
10.0	9.81	5.0	15.98
—	—	6.0	15.78
—	—	8.0	15.84

[**3**] = 15.7×10^{-6} M; [OH^-] = 0.002 M

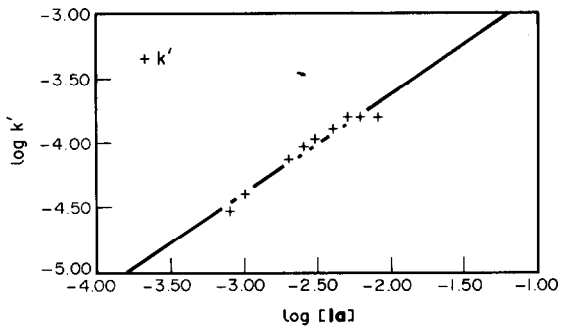

Fig. 1. Plot of log k' vs log [**1a**] at 30°C (k' are pseudo-first-order rate constants). [**2**] = 8.0×10^{-5} M; [OH^-] = 0.002 M; [**3**] = 15.7×10^{-6} M.

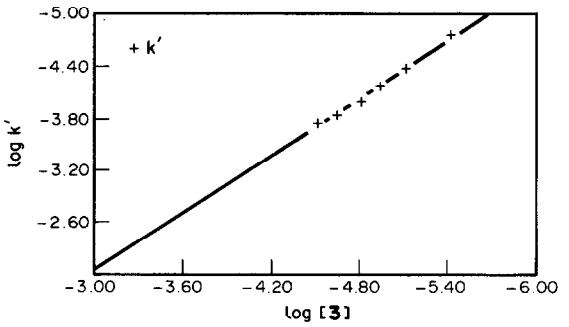

Fig. 2. Plot of log k' vs log [**3**] at 30°C. [**2**] = 8.0×10^{-5} M; [OH^-] = 0.002 M; [**1a**] = 2.5×10^{-3} M.

log [**1a**] was linear ($\gamma = 0.992$, Fig. 1) with unit slope (Table 1). At constant [**2**], [**1a**] and [**3**] the rate is independent of [OH^-] (Table 2). Dependence of rate on [**3**] was studied and found that the rate is accelerated by increasing [**3**] (Table 2). A plot of log k' vs log [**3**] was linear ($r = 0.997$, Fig. 2) with unit slope. Rate studies were made in water–methanol mixtures of varying composition. The rate decreases with an increase in methanol content of the reaction mixture. A plot of log k' vs $1/D$ (D is the dielectric constant of the medium) gave a straight line with negative slope supporting a rate limiting step with partial ionization.[8] Blank experiments with methanol, however, showed that there is slight decomposition of solvent under experimental conditions. This was allowed for in the calculation of the net reaction rate constant for the oxidation of indole. The effect of varying the ionic strength of the medium by adding a concentrated solution of $NaClO_4$ did not alter the rate of the reaction. Addition of the reduced product (**5**) had no effect on the rate. No effect of anions, such as Cl^- or Br^-, on the rate were observed.

From the Arrhenius plots of log k' vs $1/T$ kinetic and thermodynamic parameters were calculated (Table 3). A plot of log k'_2 (Table 3, second-order rate constants k'_2) vs the σp (σ^+) parameter for the ring substituents of **1a–d** is shown in Fig. 4. The Hammett correlations[9,10] were fitted with the $\sigma p = \sigma_I + \sigma_{R^-}$ scale.

DISCUSSION

N-Chloro-N-sodio-*p*-toluenesulphonamide (**2**) acts as an oxidizing agent in both acidic and alkaline

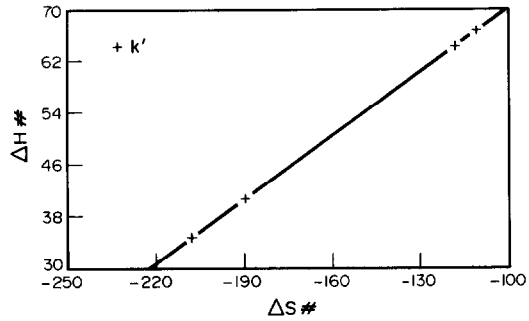

Fig. 3. Isokinetic plots of $\Delta H^{\ddagger}$ vs $\Delta S^{\ddagger}$ for the oxidation of **1a–d** by **2**.

Table 2. Pseudo-first-order rate constants for the variation [OH^-] and [**3**] at 30°C

[**3**] = 15.7×10^{-6} M		[OH^-] = 0.002 M	
[OH^-] (M)	k' (10^{-5} s^{-1})	[**3**] (10^{-6} M)	k' (10^{-5} s^{-1})
0.0008	9.98	3.93	1.74
0.0010	10.10	7.86	4.07
0.0020	9.73	11.78	6.46
0.0025	10.06	15.70	9.73
0.0030	10.07	23.60	13.75
0.0040	10.07	31.40	16.95

[**2**] = 8.0×10^{-5} M; [**1a**] = 2.5×10^{-3} M

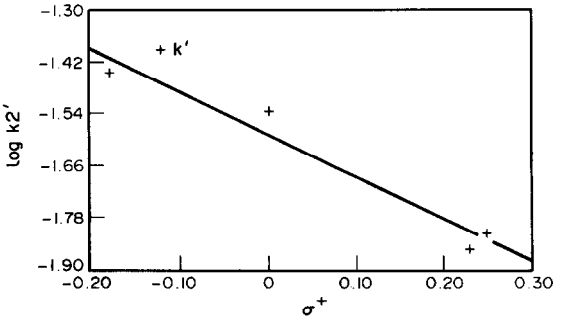

Fig. 4. Log k'_2 (second-order rate constants) vs σ^+ for **1a–d** at 29.4°C.

Table 3. Kinetic and thermodynamic parameters for the oxidation of **1a–d** by **2** in NaOH catalysed by **3**

1	*Ea* (kJ mol^{-1})	$\Delta H^{\ddagger}$ (kJ mol^{-1})	$\Delta G^{\ddagger}$ (kJ mol^{-1})	$\Delta S^{\ddagger}$ (J K^{-1} mol^{-1})	$k' \times 10^5$ s^{-1} at 29.4°C	$k'_2 = k'/$[**1a–d**] (m^{-1} s^{-1})
a	43.2	40.7	98.09	−189.7	7.30	2.92×10^{-2}
b	37.2	34.7	97.66	−208.1	9.02	3.61×10^{-2}
c	66.6	64.1	99.83	−118.1	3.80	1.52×10^{-2}
d	69.0	66.5	100.02	−110.8	3.50	1.40×10^{-2}

[**2**] = 8.0×10^{-6} M; [**1a–d**] = 2.5×10^{-3} M; [**3**] = 15.7×10^{-6} M and [OH^-] = 0.002 M

media. In general **2** undergoes a two-electron change in its reactions, the products being **5** and sodium chloride. The reduction potential of **2**/**5** is pH dependent and decreases with an increase in the pH of the medium, having values of 1.14 V at pH 0.65 and 0.5 V at pH 12. Depending on the pH of the medium, **2** furnishes different types of reactive species in solution, such as **7**, **8** [eqs (3) and (4)], HOCl and possibly H_2OCl^+ in acid solutions.[4,6,10]

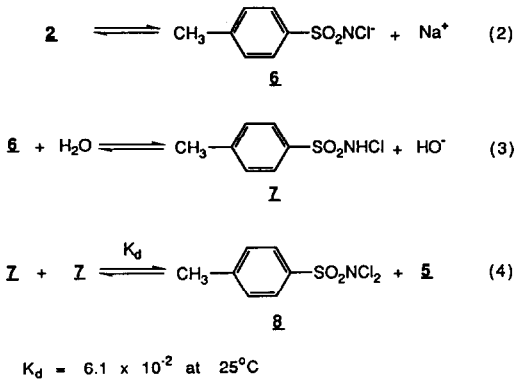

In alkaline solutions **8** does not exist and the predominant species are **6**, **7**, HOCl and the OCl^- ion. Hardy and Johnston[11] have calculated the concentrations of species present in alkaline **2** solutions. At pH *ca* 11 the concentration of the OCl^- ion is small and it does not make a significant contribution to the oxidation of **1a–d**. This potent oxidant (**2**) is of special interest for studying reaction mechanisms as it behaves both as a chlorinating and as an oxidizing agent. Compound **2** behaves as a strong electrolyte in aqueous solutions and dissociates as shown in eq. (2). It has been suggested[4,6] that the reactivity of **2** in weakly alkaline solutions is due to the formation of conjugate acid **7** from **6** in a base retarding step [eq. (3)]. Therefore, the possible oxidant species of **2** in alkaline solution is **6**.

The observed first-order dependence of rate on [**2**] and nearly first-order in [**1a**], which becomes gradual saturation at higher [**1a**], and the rate independence of [OH^-] can be explained by Scheme 1.

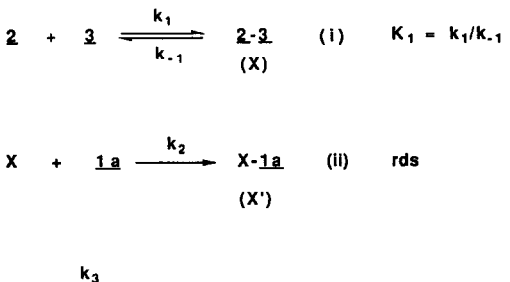

Scheme 1.

According to Scheme 1,

$$\text{rate} = k_2[\text{X}]\,[\mathbf{1a}]. \tag{5}$$

Assuming steady state for [X],

$$\text{rate} = \frac{k_1 k_2 [\mathbf{2}]\,[\mathbf{3}]_0\,[\mathbf{1a}]}{k_{-1} + k_1[\mathbf{2}] + k_2[\mathbf{1a}]} \tag{6}$$

because

$$[\mathbf{3}] = [\mathbf{3}]_0 - [\text{x}] = \frac{k_{-1} + k_2[\mathbf{1a}]}{k_{-1} + k_1[\mathbf{2}] + k_2[\mathbf{1a}]}\,[\mathbf{3}]_0. \tag{7}$$

The most probable structure of X is **10** and X^1 are **11** and **12** from Scheme 2. A proposed mechanism of the oxidation of **1a–d** by **2** catalysed by **3** in alkaline medium is shown in Scheme 2. Osmium(VIII) (**3**) exists[12] in alkaline medium as $[OsO_4(OH)]^-$ (**13**), which on further coordination with OH^- gives $[OsO_4(OH)_2]^{2-}$. Since the reactions were performed under comparable conditions of alkalinity and there is independence of [OH^-] in the oxidation of **1a–d**, it is unlikely that $[OsO_4(OH)_2]^{2-}$ reacts with the substrate. Compound **2** first coordinates with **3**, activating chloramine-T via stabilization of the nitrogen's anionic charge and polarizing the nitrogen–chlorine bond. Since **3** is known to bind with one or even two hydroxide anions, the hydroxide anion(s) can then be replaced by **2**. Then, the base-catalysed indole chlorination via activated chloramine-T (**10**) affords the 3-

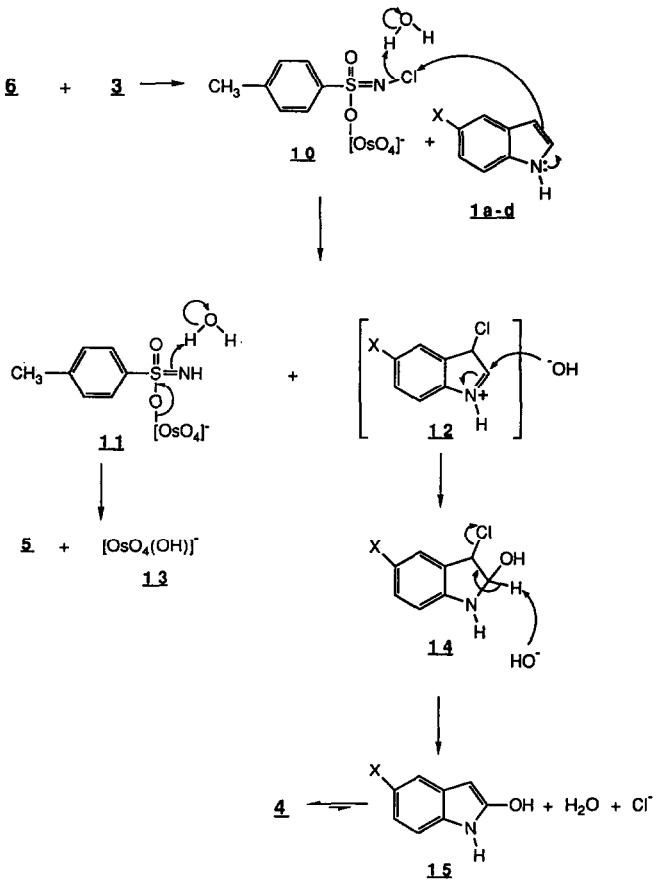

Scheme 2.

chloroindoleninium ion (**12**), a short-lived cationic intermediate and a *p*-toluenesulphonamide-osmium tetroxide complex (**11**). Hydration of complex **11** results in **5** and a hydroxide anion/osmium tetroxide complex (**13**). The formation of the 3-bromoindoleninium cation as an intermediate has been reported during the oxidation of indole to oxindole by NBS.[13] Hydroxylation of **12** to 2-hydroxy-3-chloroindoline (**14**) followed by base-catalysed removal of hydrogen chloride affords 2-hydroxyindole (**15**); **15** being in equilibrium with its more stable keto form (**4**). The low sensitivity of k'_2 to ring substituents ($\rho^+ = -1.0$, Fig. 4) indicates significant bond formation between the substrate and the oxidant in the rate limiting step.

The calculated activation enthalpies and entropies of oxidation of **1a–d** were linearly related by plotting $\Delta H^\ddagger$ vs $\Delta S^\ddagger$ (Fig. 3). From the slope the computed value of isokinetic temperature (β) is 325 K. Further verification of the isokinetic relation was completed by the Exner criterion[14] from which β is determined to be 325 K. The values of β from both the plots calculated are higher than the experimental temperature (303 K), indicating enthalpy as a controlling factor. The linear correlation and the consistency of $\Delta G^\ddagger$ values (Table 3) indicate that **1a–d** undergo oxidation via the same mechanism. Corbett *et al.*[15] have studied the enzymatic oxidation of **1a** to **4** by peroxide employing chloroperoxidase enzyme. They observed a first-order reaction with respect to [**1a**] up to 8 mM, which was the highest concentration of **1a** that could be investigated. On the other hand, 2-methylindole was not effected by peroxide and chloroperoxidase, but its presence largely inhibited **1a** oxidation. The isomer 2-methylindole was a poor substrate for chloroperoxidase oxidation and a weak inhibitor of **1a** oxidation. Their results suggest the possibility that chloroperoxidase oxidation of the carbon atom adjacent to nitrogen atom in part results from hydrogen bonding of the substrate N—H to the enzyme active site. Our studies show that the reaction rate becomes independent of [**1a**] from 5 mM to 15 mM at constant [OH^-] (5 mM). Hence, it is probable that the change in mechanism may be attributed to the fact that the oxidation of [**1a**] does not occur with either **3** or **2** alone. It can be assumed that a complex of these two serves as an oxidant.[16] The possible oxidizing species in this case would be **7**. Based on the oxidizing capacity observed, a cyclic

structure (**9**) can be proposed for the complex. The structure shows that the electron density around the nitrogen atom is lowered, resulting in a weakening of the N—Cl bond. The subsequent oxidizing capacity of N-chlorotoluene-*p*-sulphonamide is increased after complexation, which results in a fast interaction of complex **9** with the appropriate form of the substrate. The detailed study of this aspect as well as with strong electron withdrawing ($-NO_2$) and electron donating ($-CH_3$) groups as 5-position substituents on indole to critically examine substituent effects (ρ^+) is currently under investigation.

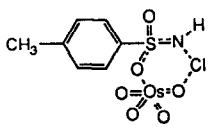

1

Acknowledgements—One of us (CKM) gratefully acknowledges the award of a Senior Research Fellowship by the UGC, New Delhi. We thank Professor Michael Novak, Department of Chemistry, Miami University, Oxford, OH, who extended the hospitality of his laboratory where this manuscript was prepared.

REFERENCES

1. G. Laroche and J. Desbordes, *Compt. Rend. Soc. Biol.* 1932, **109**, 271.
2. Z. Skuric and K. Weber, *Croat. Chem. Acta* 1966, **38**, 23.
3. M. M. Campbell and G. Johnson, *Chem. Rev.* 1978, **78**, 65.
4. D. S. Mahadevappa, K. S. Rangappa, N. M. M. Gowda and B. T. Gowda, *J. Phys. Chem.* 1981, **85**, 3651.
5. D. S. Mahadevappa, S. Ananda, A. S. A. Murthy and K. S. Rangappa, *Tetrahedron* 1984, **10**, 1673.
6. D. S. Mahadevappa, S. Ananda, N. M. M. Gowda and K. S. Rangappa, *J. Chem. Soc., Perkin Trans. II* 1985, 39.
7. J. C. Morris, J. A. Salazar and M. A. Wineman, *J. Am. Chem. Soc.* 1948, **70**, 12036.
8. J. A. Riddick and W. B. Burger, *Organic Solvents, Physical Properties and Methods of Purification*, 3rd edn. Wiley-Interscience, New York (1970).
9. M. S. Morales-Rios, R. E. del Rio and P. Joseph-Nathan, *Magnet. Reson. Chem.* 1989, **27**, 1038.
10. S. Ehrenson, R. T. C. Brownlee and R. W. Taft, *Prog. Phys.-Org. Chem.* 1973, **10**, 13.
11. F. F. Hardy and J. P. Johnson, *J. Chem. Soc., Perkin Trans.* 1973, **2**, 742.
12. R. D. Sanerbraun and E. B. Sandel, *J. Am. Chem. Soc.* 1953, **75**, 4171.
13. R. L. Hinman and C. P. Bauman, *J. Org. Chem.* 1964, **29**, 1206.
14. O. Exner, *Coll. Czech. Chem. Comm.* 1964, **29**, 1094.
15. M. D. Corbett and R. B. Chipko, *Biochem. J.* 1979, **183**, 269.
16. M. C. Agrawal and S. K. Upadhyay, *J. Sci. Ind. Res.* 1983, **42**, 508.

Polyhedron Vol. 12, No. 14, pp. 1725–1731, 1993
Printed in Great Britain

0277–5387/93 $6.00+.00
© 1993 Pergamon Press Ltd

SYNTHESIS AND PROPERTIES OF TETRA-μ-ACETATODIRUTHENIUM(II,III) PHENYLPHOSPHINATE AND PHENYLPHOSPHONATE COMPLEXES: X-RAY CRYSTAL STRUCTURES OF $[Ru_2(\mu\text{-}O_2CCH_3)_4(HPhPO_2)_2]H$ AND $[Ru_2(\mu\text{-}O_2CCH_3)_4(PhPO_3H)_2]H \cdot H_2O$

MALACHY McCANN* and EAMONN MURPHY

Chemistry Department, St Patrick's College, Maynooth, Co. Kildare, Ireland

and

CHRISTINE CARDIN and MAIRE CONVERY

Chemistry Department, Trinity College, Dublin, Ireland

(*Received* 8 *February* 1993; *accepted* 30 *March* 1993)

Abstract—Phenylphosphinic acid ($HPhPO_2H$) and phenylphosphonic acid ($PhPO_3H_2$) react with a methanolic solution of $[Ru_2(\mu\text{-}O_2CCH_3)_4(O_2CCH_3)_2]H \cdot 0.7H_2O$ at room temperature to give $[Ru_2(\mu\text{-}O_2CCH_3)_4(HPhPO_2)_2]H$ (**1**) and $[Ru_2(\mu\text{-}O_2CCH_3)_4(PhPO_3H)_2]H \cdot H_2O$ (**2**), respectively. The X-ray crystal structures of **1** and **2** each show the Ru—Ru core to be ligated by four bridging bidentate acetate ligands [Ru—Ru distances: **1** = 2.272(1) Å; **2** = 2.267(2) Å] and two axial phenylphosphinate and phenylphosphonate ligands, respectively. In each complex the individual bimetallic molecules are linked together by a hydrogen ion which bridges the oxygen atoms of neighbouring axial ligands. In **2** the water molecule is also hydrogen-bonded to one of the axial phenylphosphonate groups. Spectroscopic, magnetic and cyclic voltammetric data for the complexes are given.

Phenylphosphinic acid ($HPhPO_2H$) and phenylphosphonic acid ($PhPO_3H_2$) are each renowned for their ability to form polymeric layered complexes with the *d*-block metals.[1–3] Recently,[4] we have shown that by employing pyridine as the reaction solvent monomeric copper(II) phenylphosphonate complexes can be prepared and the complexes $[Cu(PhPO_3H)_2(C_5H_5N)_4] \cdot 2CH_3OH$ and $[Cu(PhPO_3H)_2(C_5H_5N)_4]$ were structurally characterized. Herein, we present details of the synthesis, structure and physical properties of the monomeric[5] tetra-μ-acetatodiruthenium(II,III) phenylphosphinate and phenylphosphonate complexes $[Ru_2(\mu\text{-}O_2CCH_3)_4(HPhPO_2)_2]H$ (**1**) and $[Ru_2(\mu\text{-}O_2CCH_3)_4(PhPO_3H)_2]H \cdot H_2O$ (**2**), respectively.

Excess phenylphosphinic acid and phenylphosphonic acid each react at room temperature with a methanolic solution of the diruthenium (II,III) complex $[Ru_2(\mu\text{-}O_2CCH_3)_4(O_2CCH_3)_2]H \cdot 0.7H_2O$[6–8] to give **1** and **2**, respectively. During both of these reactions the $[Ru_2(\mu\text{-}O_2CCH_3)_4]^+$ moiety remains intact and the axial $CH_3CO_2^-$ ligands are replaced by $HPhPO_2^-$ and $PhPO_3H^-$.[9] The reaction of phenylphosphinic acid with $[Ru_2(\mu\text{-}O_2CCH_3)_4(O_2CCH_3)_2]H \cdot 0.7H_2O$ contrasts with that found for the dicopper(II,II) complex $[Cu_2(\mu\text{-}O_2CCH_3)_4(H_2O)_2]$.[4] In the latter reaction the phenylphosphinic acid is oxidized to phenylphosphonic acid and is recovered as the monomeric copper(II) complex $[Cu(PhPO_3H)_2(C_5H_5N)_4] \cdot H_2O$. This conversion of phenylphosphinic acid to the copper(II) phenylphosphonate complex was accompanied by the loss of the ν(P—H) IR stretching band. In the IR spectrum of **2** this medium intensity ν(P—H) band was present at 2370 cm^{-1}.

The X-ray crystal structure of the phenylphos-

*Author to whom correspondence should be addressed.

phinate complex $[Ru_2(\mu\text{-}O_2CCH_3)_4(HPhPO_2)_2]H$ (**1**) (Fig. 1) shows that the Ru—Ru core is ligated by four equatorial bridging bidentate acetate groups and two axial monodentate phenylphosphinate ligands. Individual $[Ru_2(\mu\text{-}O_2CCH_3)_4(HPhPO_2)_2]^-$ units in **1** are linked together at neighbouring O(6) atoms by a proton to give an infinite hydrogen-bonded chain. Thus, the complex is best formulated as $[Ru_2(\mu\text{-}O_2CCH_3)_4(HPhPO_2)_2]H$. This formulation is similar to that proposed[7] for the structurally characterized[8] starting complex $[Ru_2(\mu\text{-}O_2CCH_3)_4(O_2CCH_3)_2]H \cdot 0.7H_2O$.

The structure of the phenylphosphonate complex $[Ru_2(\mu\text{-}O_2CCH_3)_4(PhPO_3H)_2]H \cdot H_2O$ (**2**) (Fig. 2) is similar to that of the phenylphosphinate complex **1**. Although the hydrogen-bonding hydrogen was not located directly in **2** the intermolecular distances between the oxygen atoms on neighbouring axial phenylphosphonate ligands [O(52)—O(62) = 2.431 Å] suggested that there was a proton bridging these two ligands. Hydrogen bonding was also present between the water molecule and one of the phenylphosphonate ligands. Thus, complex **2** is best formulated as $[Ru_2(\mu\text{-}O_2CCH_3)_4(PhPO_3H)_2]H \cdot H_2O$. It is interesting to note that in the structure of the phenylphosphinate complex **1** the phenyl groups are in the expected *trans* configuration with respect to each other, whereas in the phenylphosphonate complex **2** they are in the more sterically congested *cis* arrangement. It is thought that the latter stereochemistry may have been imposed, in part, by the more extensive hydrogen-bonding network that pervades **2**.

The more important bond distances and angles for structures **1** and **2** are listed in Tables 1 and 2, respectively. The Ru—Ru and Ru—O(carboxylate) distances in each complex are similar to those reported for other Ru_2^{5+} complexes.[7,8,10–12] In addition, the Ru—O(phenylphosphinate or phenyl-

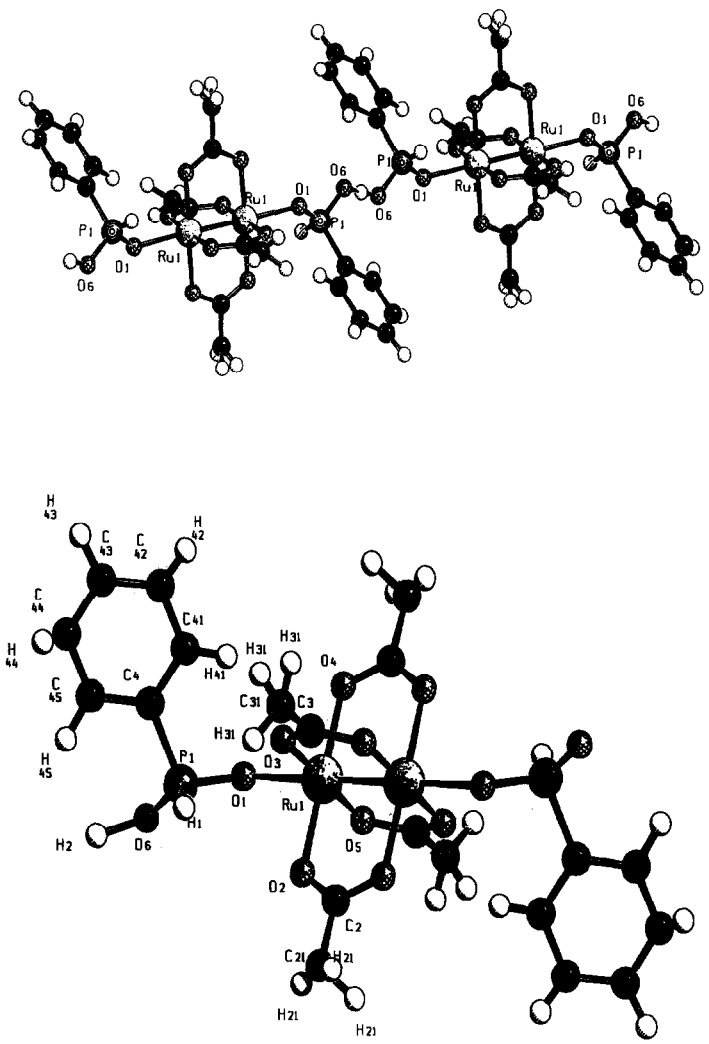

Fig. 1. X-ray crystal structure of $[Ru_2(\mu\text{-}O_2CCH_3)_4(HPhPO_2)_2]H$ (**1**).

Table 1. Selected bond lengths (Å) and angles (°) for **1**

Ru(1)—Ru(1)	2.272(1)	Ru(1)—O(1)	2.214(2)
Ru(1)—O(2)	2.026(2)	Ru(1)—O(3)	2.021(2)
Ru(1)—O(4)	2.026(2)	Ru(1)—O(5)	2.017(2)
P(1)—O(1)	1.495(2)	P(1)—O(6)	1.517(2)
P(1)—C(4)	1.791(3)	P(1)—H(1)	0.458(1)
O(6)—H(2)	1.202(2)		

O(2)—Ru(1)—O(1)	91.1(1)	O(3)—Ru(1)—O(1)	92.2(1)
O(3)—Ru(1)—O(2)	88.4(1)	O(4)—Ru(1)—O(1)	90.0(1)
O(4)—Ru(1)—O(2)	178.8(1)	O(4)—Ru(1)—O(3)	91.1(1)
O(5)—Ru(1)—O(1)	88.9(1)	O(5)—Ru(1)—O(2)	91.5(1)
O(5)—Ru(1)—O(3)	178.9(1)	O(5)—Ru(1)—O(4)	89.1(1)
O(6)—P(1)—O(1)	113.5(1)	P(1)—O(1)—Ru(1)	134.1(1)
H(2)—O(6)—P(1)	125.2(2)		

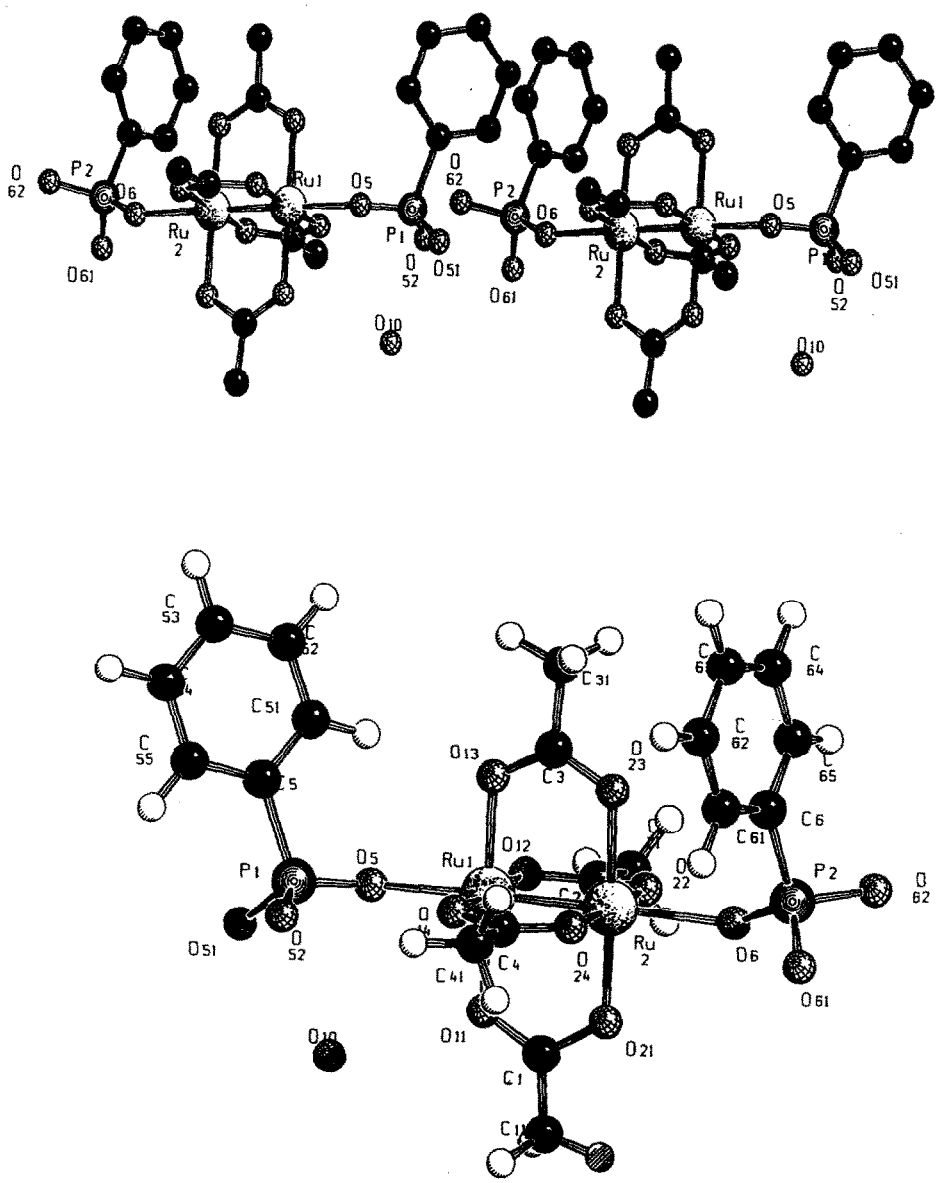

Fig. 2. X-ray crystal structure of $[Ru_2(\mu\text{-}O_2CCH_3)_4(PhPO_3H)_2]H \cdot H_2O$ (**2**).

Table 2. Selected bond lengths (Å) and angles (°) for **2**

Ru(1)—Ru(2)	2.267(2)	Ru(1)—O(11)	2.03(1)
Ru(1)—O(12)	2.03(1)	Ru(1)—O(13)	2.04(1)
Ru(1)—O(14)	1.99(1)	Ru(1)—O(5)	2.24(1)
Ru(2)—O(21)	1.99(1)	Ru(2)—O(22)	2.04(1)
Ru(2)—O(23)	2.02(1)	Ru(2)—O(24)	2.01(1)
Ru(2)—O(6)	2.22(1)	P(1)—O(5)	1.47(1)
P(1)—O(51)	1.54(1)	P(1)—O(52)	1.51(1)
P(2)—O(6)	1.48(2)	P(1)—C(5)	1.82(1)
P(2)—O(61)	1.57(1)	P(2)—O(62)	1.56(1)
P(2)—C(6)	1.80(1)	O(52)—O(62)	2.43(1)
O(5)—Ru(1)—Ru(2)	174.4(3)	O(5)—Ru(1)—O(12)	85.3(5)
O(5)—Ru(1)—O(14)	96.0(5)	O(6)—Ru(2)—Ru(1)	176.8(4)
O(6)—Ru(2)—O(22)	88.2(6)	O(6)—Ru(2)—O(24)	94.7(5)
P(1)—O(5)—Ru(1)	133.1(8)	P(2)—O(6)—Ru(2)	143.(1)

phosphonate) distances in **1** and **2** are also similar to those found in other Ru_2^{5+} carboxylates containing axial oxygen donor ligands.[7,8,12] The mean Ru—O(phenylphosphonate) distance in **2** (2.23 Å) is only slightly shorter than the mean Cu—O(phenylphosphonate) distances in $[Cu(PhPO_3H)_2(C_5H_5N)_4]\cdot 2CH_3OH$ (2.42 Å) and $[Cu(PhPO_3H)_2(C_5H_5N)_4]$ (2.32 Å).[4]

Complexes **1** and **2** behaved as 1 : 1 electrolytes in methanol and their electronic absorption spectra and magnetic moments were very similar to those normally found for Ru_2^{5+} carboxylates.[13–15]

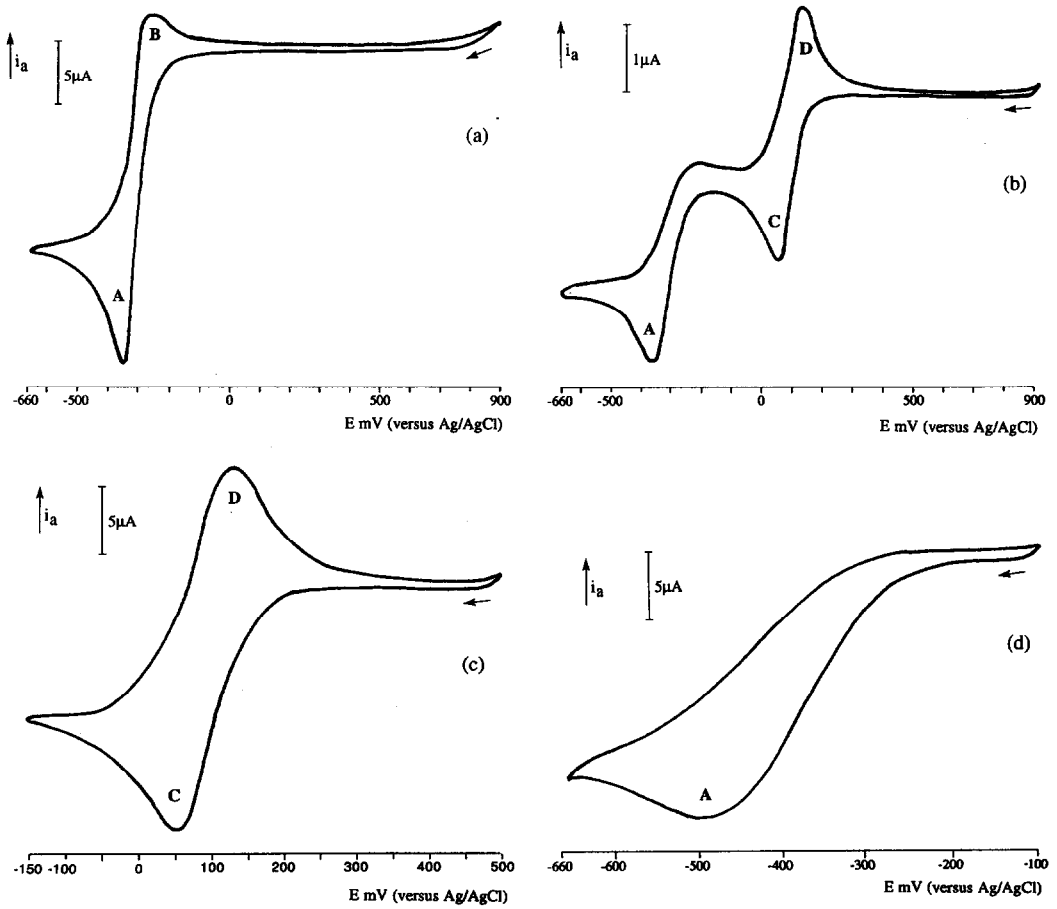

Fig. 3. Cyclic voltammograms of: (a) free phenylphosphinic acid; (b)–(d) $[Ru_2(\mu\text{-}O_2CCH_3)_4(HPhPO_2)_2]H$ (**1**) between different switching potentials. Potentials are quoted with respect to the Ag/AgCl reference electrode. Scan rate = 20 mV s^{-1}.

Cyclic voltammograms of free phenylphosphinic acid and $[Ru_2(\mu\text{-}O_2CCH_3)_4(HPhPO_2)_2]H$ (**1**) are displayed in Fig. 3. In the potential range +0.90 to −0.66 V (vs Ag/AgCl) the free acid [Fig. 3(a)] showed a single quasi-reversible wave AB with $E_{1/2} = -298$ mV. Within the same potential limits complex **1** [Fig. 3(b)] showed a reversible wave (CD; $E_{1/2} = +100$ mV) for the Ru_2^{5+}/Ru_2^{4+} couple[7,13] and an irreversible reduction wave (A; $E_c = -337$ mV), which is thought to be associated with the phenylphosphinate moieties. Figures 3(c) and 3(d) show the voltammograms of **1** recorded between the narrow potential ranges +0.50 to −0.15 V and −0.10 to −0.66 V, respectively, and these clearly demonstrate the reversibility of the Ru_2^{5+}/Ru_2^{4+} couple and the irreversibility of the phenylphosphinate reduction.

Voltammograms of free phenylphosphonic acid and $[Ru_2(\mu\text{-}O_2CCH_3)_4(PhPO_3H)_2]H \cdot H_2O$ (**2**) are shown in Fig. 4. In the range +0.90 to −0.66 V (vs Ag/AgCl) the phenylphosphonic acid [Fig. 4(a)] showed an essentially reversible redox couple (EF; $E_{1/2} = -369$ mV).[16] Across the same potential range complex **2** [Fig. 4(b)] exhibited an irreversible Ru_2^{5+}/Ru_2^{4+} reduction (G; $E_c = +21$ mV) as well as a pair of broad ill-defined peaks (EF), which are thought to arise from the redox activity of the liberated phenylphosphonic acid. Figure 4(c) shows the voltammogram of **2** between the constricted potential limits of +0.30 to −0.05 V and this clearly illustrates the somewhat unusual irreversibility of the Ru_2^{5+}/Ru_2^{4+} couple.

It is envisaged that **1** and **2** may be useful starting materials for the synthesis of polymeric phenylphosphinate and phenylphosphonate complexes containing strongly metal-to-metal bonded diruthenium centres.[9]

EXPERIMENTAL

$[Ru_2(\mu\text{-}O_2CCH_3)_4(O_2CCH_3)_2]H \cdot 0.7H_2O$ was prepared by the literature method.[8] IR spectra (KBr

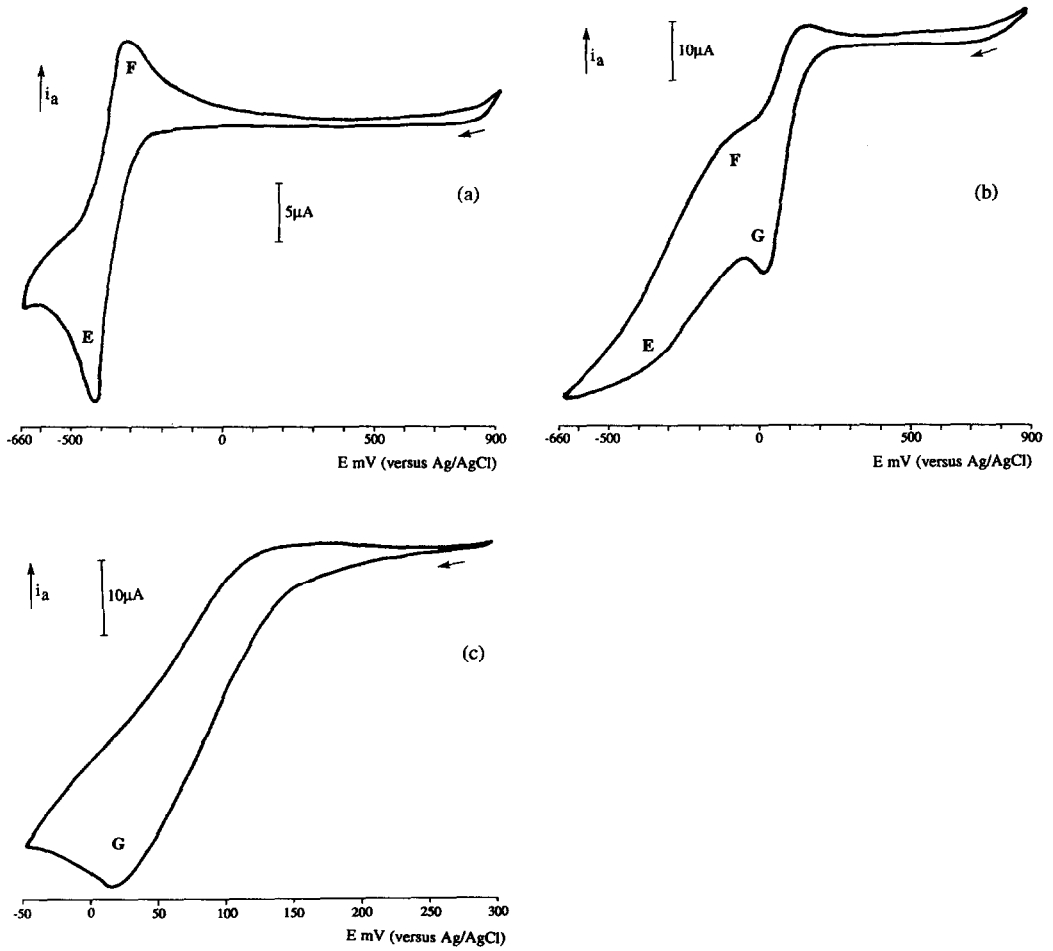

Fig. 4. Cyclic voltammograms of: (a) free phenylphosphonic acid; (b), (c) $[Ru_2(\mu\text{-}O_2CCH_3)_4(PhPO_3H)_2]H \cdot H_2O$ (**2**) between different switching potentials. Potentials are quoted with respect to the Ag/AgCl reference electrode. Scan rate = 20 mV s^{-1}.

discs) were recorded in the region 4000–200 cm^{-1} on a Perkin–Elmer 783 grating spectrometer and UV–vis spectra were obtained using a Milton Roy Spectronic 3000 Array. Room-temperature magnetic susceptibility measurements were made on a Johnson–Matthey Magnetic Susceptibility balance. An AGB Scientific Model 10 Conductivity meter was used for conductivity measurements. Cyclic voltammograms were recorded (*ca* 20°C and under nitrogen) using an EG&G Model 264A polarographic analyser and the data were analysed using the EG&G Condecon software package. A platinum bead and a platinum wire were used as the working and counter-electrodes, respectively. Tetra-n-butylammonium perchlorate in methanol (0.1 M) was used as the supporting electrolyte/solvent system. Sample concentration was 4.0×10^{-3} M and the scan rate was 20 mV s^{-1}. Potentials were recorded with respect to a silver–silver chloride reference electrode (3.5 M aqueous KCl), against which the ferrocene/ferrocenium(1+) couple had $E_{1/2} = +514$ mV. Elemental analyses were performed by the Microanalytical Laboratory, University College Cork, Ireland.

Crystallography

Complex **1**. A brown needle-shaped cystal was mounted on an Enraf–Nonius CAD4 diffractometer and the intensities of 2683 reflections were measured in the range $1° < \theta < 26°$ using graphite monochromated Mo-K_α radiation. The accurate cell dimensions were obtained by refining the setting angles of 25 reflections ($16° < \theta < 18°$). The data were reduced to give 2465 unique reflections, $R_{merg} = 0.0174$. Of these 2373 had $|F_{obs}| > 4\sigma|F_{obs}|$ and were used in the structure solution and refinement.

Crystal data for $C_{20}H_{25}O_{12}P_2Ru_2$ (**1**), $M_r = 721.496$. Triclinic, $P\bar{1}$ (No. 2), $a = 7.585(2)$, $b = 8.002(2)$, $c = 12.413(3)$ Å, $\alpha = 99.76(1)$, $\beta = 93.69(1)$, $\gamma = 117.29(1)°$, $U = 652.7(3)$ $Å^3$, $D_c = 1.835$ g cm^{-3}, $Z = 1$, $F(000) = 358$, $\lambda = 0.71069$ Å, μ(Mo-K_α) = 12.00 cm^{-1}.

The structure was solved using the Patterson method of SHELXS-86 with some operator intervention and was found to have half a molecule in the asymmetric unit. The rutheniums were found to have bridging acetate groups and the phenylphosphinate ligands in the axial positions. The structure was refined by full-matrix least-squares with all the non-hydrogen atoms anisotropic. The hydrogen atoms were located from difference-Fourier and allowed to refine with the exception of the bridging hydrogen, which is disordered and the hydrogen attached to the phosphorus. These hydrogens were located but were not allowed to refine. The refinement was weighted to give a flat analysis of variance and a final R of 0.0344 and R_w of 0.0373. The difference-Fourier had a highest peak of 1.2 e $Å^{-1}$ in the vicinity of the ruthenium atom.

Complex **2**. A small brown crystal was mounted on the above-mentioned diffractometer. The cell parameters were determined by refining the setting angles of 25 reflections with $14° < \theta < 16°$. The intensities of 3797 reflections ($\pm h$, $\pm k$, $+l$) in the range $1° < \theta < 22°$ were measured using graphite monochromated Mo-K_α radiation. The Laue symmetry of the diffraction pattern was not clear (although the lattice geometry was very close to orthorhombic) so the data were collected in triclinic symmetry. The structure was solved satisfactorily in the space group $P2_1$. The data were merged to give the unique non-centrosymmetric quadrant of data—1908 unique reflections (merging $R = 0.1144$), of which 1695 had $F_{obs} > 4\sigma F_{obs}$ and were used for structure solution and refinement.

Crystal data for $C_{20}H_{27}O_{15}P_2Ru_2$ (**2**), $M_r = 771.509$. Monoclinic, $P2_1$ (No. 4), $a = 11.361(4)$, $b = 11.040(5)$, $c = 11.679(6)$ Å, $\beta = 90.92(3)°$, $U = 1464(1)$ $Å^3$. $D_c = 1.750$ g cm^{-3}, $Z = 2$, $F(000) = 770$, $\lambda = 0.71069$ Å, μ(Mo-K_α) = 10.76 cm^{-1}.

The structure was solved by both the Patterson and direct methods of SHELXS-86 in space group $P2_1$. The structure was refined to a final R factor of 0.0564 using full-matrix least-squares analysis. The ruthenium, phosphorus and oxygen atoms of the "lantern" ligands were refined with anisotropic temperature factors. The phenyl rings were refined with fixed geometries. The hydrogen atoms on the phenyl ring were placed geometrically and their common temperature factor refined to 0.03(1) $Å^2$. The methyl hydrogens were placed using SHELX76, but not refined, and their common temperature factor refined to 0.18(6) $Å^2$. The hydrogen-bonding hydrogens could not be located from difference-Fourier, but hydrogen-bond distances were observed between the two molecules and between the molecule and the solvent. The weighting scheme was refined to give a flat analysis of variance and an R_w value of 0.0619. The final difference-Fourier had a highest peak of 1.06 e $Å^{-1}$.

The programs SHELXS and SHELX 76 were used with kind permission of Prof. G. M. Sheldrick (Universität Göttingen).

$[Ru_2(\mu\text{-}O_2CCH_3)_4(HPhPO_2)_2]H$ (**1**)

To a solution of $[Ru_2(\mu\text{-}O_2CCH_3)_4(O_2CCH_3)_2]H \cdot 0.7H_2O$ (0.30 g, 0.52 mmol) in methanol (60 cm^3) under nitrogen was added phenylphosphinic acid

(0.77 g, 5.42 mmol). The resulting red–brown solution was stirred at room temperature for 48 h. The solution was then concentrated under high vacuum (without heating) until the mustard–brown product precipitated. The solid was filtered off, washed with small amounts of methanol and with water and it was then dried *in vacuo*. Crystals suitable for X-ray diffraction studies were obtained by allowing the reaction filtrate to evaporate slowly in air. Yield: 0.26 g (69%). Found: C, 33.5; H, 3.3. Calc.: C, 33.3; H, 3.5%. IR: 3440, 3050, 2940, 2370, 1590, 1440, 1400, 1360, 1140, 1050, 1000, 970, 750, 690, 530, 400, 340 cm^{-1}; $\mu = 3.97$ B.M. per Ru_2 unit; λ_{max} (CH_3OH) = 429 nm ($\varepsilon = 712$ mol^{-1} dm^3 cm^{-1}); Λ_M (CH_3OH) = 49 S cm^2 mol^{-1} [for free phenylphosphinic acid Λ_M (CH_3OH) = 15 S cm^2 mol^{-1}].

$[Ru_2(\mu\text{-}O_2CCH_3)_4(PhPO_3H)_2]H \cdot H_2O$ (**2**)

To a solution of $[Ru_2(\mu\text{-}O_2CCH_3)_4(O_2CCH_3)_2]H \cdot 0.7H_2O$ (0.30 g, 0.52 mmol) in methanol (60 cm^3) under nitrogen was added phenylphosphonic acid (0.85 g, 5.38 mmol). The resulting red–orange solution was stirred at room temperature for 48 h. The solution was then concentrated under high vacuum (without heating) to *ca* 5 cm^3. Water (2 cm^3) was slowly added and on stirring in air the mustard–brown product precipitated. The solid was filtered off, washed with small amounts of methanol and with water and it was then dried *in vacuo*. Crystals suitable for X-ray diffraction studies were obtained by allowing the reaction filtrate to evaporate slowly in air. Yield: 0.24 g (60%). Found: C, 30.9; H, 4.3. Calc.: C, 31.1; H, 3.5%. IR: 3460, 3060, 2950, 1450, 1405, 1150, 1050, 960, 700, 570, 515, 405, 345 cm^{-1}; $\mu = 3.97$ B.M. per Ru_2 unit; λ_{max} (CH_3OH) = 428 nm ($\varepsilon = 765$ mol^{-1} dm^3 cm^{-1}); Λ_M (CH_3OH) = 53 S cm^2 mol^{-1} [for free phenylphosphonic acid Λ_M (CH_3OH) = 5 S cm^2 mol^{-1}].

Acknowledgement—We thank Johnson–Matthey plc for the loan of ruthenium trichloride.

REFERENCES

1. M. Shieh, K. J. Martin, P. J. Squattrito and A. Clearfield, *Inorg. Chem.* 1990, **29**, 958.
2. G. Cao, H. Lee, V. M. Lynch and T. E. Mallouk, *Inorg. Chem.* 1988, **27**, 2781.
3. K. J. Martin, P. J. Squattrito and A. Clearfield, *Inorg. Chim. Acta* 1989, **155**, 7.
4. M. McCann, E. Murphy, C. Cardin and M. Convery, *Polyhedron* 1992, **11**, 3101.
5. Although complexes **1** and **2** are essentially polymeric in the solid state by virtue of the intermolecular hydrogen bonding at the axial ligands we wish to distinguish them from those polymeric solids in which each phenylphosphinate and phenylphosphonate ligand uses two of their oxygen atoms to bridge adjacent metal centres (see refs 1–3).Thus, in terms of the monodentate coordination of the phenylphosphinate and phenylphosphonate ligands in **1** and **2** these complexes are best described as being monomeric.
6. $[Ru_2(\mu\text{-}O_2CCH_3)_4(O_2CCH_3)_2]H \cdot 0.7H_2O$ (see ref. 7) was originally incorrectly formulated as $[Ru_2(\mu\text{-}O_2CCH_3)_4(O_2CCH_3)_2] \cdot H_2O$ (see ref. 8).
7. F. A. Cotton, M. Matusz and B. Zhong, *Inorg. Chem.* 1988, **27**, 4368.
8. M. G. B. Drew, P. Higgins and M. McCann, *J. Chem. Soc., Chem. Commun.* 1987, 1385.
9. When excess phenylphosphinic acid and phenylphosphonic acid are each reacted with $[Ru_2(\mu\text{-}O_2CCH_3)_4(O_2CCH_3)_2]H \cdot 0.7H_2O$ in refluxing methanol paramagnetic brown solids are obtained. The IR spectra of these solids only show bands attributable to the phenylphosphinate and phenylphosphonate groups (no acetate bands are observed). Efforts are currently being made to try and further characterize these two solids.
10. M. J. Bennett, K. G. Caulton and F. A. Cotton, *Inorg. Chem.* 1969, **8**, 1.
11. A. Bino, F. A. Cotton and T. R. Felthouse, *Inorg. Chem.* 1979, **18**, 2599.
12. M. Spohn, J. Straehle and W. Hiller, *Z. Naturforsch.* (*B*) 1986, **41**, 541.
13. F. A. Cotton and E. Pedersen, *Inorg. Chem.* 1975, **14**, 388.
14. M. Mukaida, T. Nomura and T. Ishimori, *Bull. Chem. Soc. Japan* 2143, **45**, 1972.
15. J. G. Norman, G. E. Renzoini and D. A. Case, *J. Am. Chem. Soc.* 5256, **101**, 1979.
16. We have found (see ref. 4) that in the potential region +0.80 to −1.70 V (vs Ag/AgCl) free phenylphosphonic acid was electroinactive in a 1:4 pyridine:methanol solution. It is likely that in this solvent mixture the pyridinium salt $[C_5H_5NH]^+[PhPO_3H]^-$ is formed and that the $[PhPO_3H]^-$ ion is electroinactive. This suggests that in the voltammogram of **2** it is the free phenylphosphonic acid (and not the phenylphosphonate anion) that is liberated upon dissolving the complex in methanol that is giving rise to the broad waves EF in Fig. 4(b). In the same pyridine:methanol solvent mixture free phenylphosphinic acid has also been found to be electroinactive between +0.80 to −1.00 V. However, beyond −1.10 V a large irreversible reduction wave was observed for this acid.

Polyhedron Vol. 12, No. 14, pp. 1733–1738, 1993
Printed in Great Britain

0277–5387/93 $6.00+.00
© 1993 Pergamon Press Ltd

REDOX CHEMISTRY AND SPECTROSCOPY OF THE MANGANESE-QUINIZARINE-THIOSALICYLIC ACID MIXED-LIGAND COMPLEX IN APROTIC MEDIUM

MARIO E. BODINI,* M. ANGÉLICA DEL VALLE and VERÓNICA ARANCIBIA

Departamento de Química Analítica y Electroquímica Facultad de Química, Pontificia Universidad Católica de Chile, Casilla 306, Santiago de Chile, Chile

(*Received* 27 *January* 1993; *accepted* 30 *March* 1993)

Abstract—The addition of the monoanion of thiosalicylic acid to the insoluble compound formed between manganese(II) and the dianion of quinizarine forms a very intense blue soluble new complex. The stoichiometry of this complex is Mn : Qz : 2-MBA = 1 : 1 : 2, in the presence of 4 equivalents of base in order to neutralize the two hydroxylic protons of quinizarine and the carboxylic proton of each equivalent of 2-MBA. This mixed-ligand complex is oxidized in several steps and a total of 4 equivalents of charge per metal ion are transferred in this process. The complete oxidation at +0.90 V vs S.C.E. produces the destruction of this mixed-ligand complex. However, it is possible to oxidize sequentially at +0.35 and +0.65 V vs S.C.E. and the association between the metal ion and the ligands prevails. These two oxidations involve 1 equivalent of charge each and lead to the formation of a dark red complex. The stoichiometry of this complex is maintained with respect to the original blue compound and it is proposed that the metal ion is in the +3 oxidation state, the quinizarine has been oxidized to its semi-quinonic form and the monoanion of thiosalicylic acid has not changed. The final process at +0.90 V vs S.C.E. corresponds to the oxidation of the monoanion of the latter which leads to the decomposition of the complex. It is concluded that the mixed-ligand complex formed after the two-electron oxidation process can be considered as a very good model for biological systems in which it is known that manganese plays an important role as a catalyst for redox processes and ligands such as those studied here are present.

Interest in the chemistry of manganese catecholate and semi-quinonate complexes has greatly increased in recent years.[1–6] An important reason has been the recognition of the fundamental role of quinone and catechol-containing groups in biology.

Our group has studied for some time the complexes of manganese with this type of ligand.[7–9] On the other hand, it is known that higher oxidation states of manganese are involved in some biological systems[10,11] and that a mixed-ligand association is most likely to occur in these systems.[12–15] Therefore, based on our previous results concerning the stabilization of manganese(III) in the presence of thiosalicylic acid[16] and quinizarine,[17] which can be oxidized to the corresponding semi-quinone, we have now undertaken the study of mixed-ligand complexes of manganese with these two ligands in order to obtain an analogue of an amino acid (cysteine in the case of thiosalicylic acid) which tends to stabilize a higher oxidation state of the metal ion, and a second ligand such as quinizarine in the coordination sphere so that its dihydroxylic system can be oxidized to the corresponding semi-quinone at a potential positive enough to allow the stabilization of manganese(III) in this system. The characteristics of these compounds should be very important in understanding the role of manganese in different biological systems.

The monoanion of thiosalicylic acid forms a 1 : 2 complex with manganese(II), which can be oxidized reversibly to manganese(III) at −0.45 V vs S.C.E., yielding another 1 : 2 complex. The corresponding reduction to manganese(II) is observed at −0.50 V vs S.C.E.[16]

* Author to whom correspondence should be addressed.

In the case of quinizarine it is an important fact that manganese(II) forms a slightly soluble 1 : 1 compound with the semi-quinone produced by the oxidation of the dianion of this ligand. This compound presents two low intensity oxidation peaks at +0.50 and +0.75 V vs S.C.E. Therefore, these oxidation potentials are favourable to our purpose.

It is important to remark that the voltammetric and spectroscopic results obtained with the latter species are the same as those presented by a solution of manganese(III) and the dianion of quinizarine. Consequently, an internal charge-transfer is produced from the metal to the ligand (MLCT).[17]

EXPERIMENTAL

Equipment

A three-electrode potentiostat (Tacussel Model PRT 20-2X potentiostat–galvanostat with a Model GSTP wave generator) was used for the cyclic voltammetric and controlled-potential electrolysis experiments. A current integrator based on operational amplifiers was used as a coulometer in the controlled-potential electrolyses. Cyclic voltammograms were recorded on a Hewlett–Packard Model 7004 A *X–Y* recorder. The electrochemical cell was equipped with a Beckman platinum-inlay working electrode (area 0.23 cm^2), a platinum coil auxiliary electrode and an Ag/AgCl reference electrode filled with an aqueous tetramethylammonium chloride solution and adjusted to 0.00 V vs S.C.E. The latter was contained in a Pyrex tube with a soft-glass cracked tip; this electrode was placed inside a Luggin capillary. For controlled potential electrolysis a platinum-mesh working electrode was employed. A Beckman Model ACTA CV spectrophotometer was used for UV–vis spectrophotometric measurements. Air-sensitive compounds were handled in a glove-bag (Aldrich) under a nitrogen atmosphere and the oxygen content was monitored with a Beckman Model Monitor II Oxygen Analyser.

Reagents

The reagents for the investigation and syntheses included $Mn(ClO_4)_2 \cdot 6H_2O$ (G. Frederick Smith), tetraethylammonium hydroxide (TEAOH) (1.0 M in methanol, Eastman), tetramethylammonium chloride (Aldrich) and tetraethylammonium perchlorate (TEAP) (G. Frederick Smith). The ligands thiosalicylic acid and quinizarine were obtained from Aldrich and were purified by reduced pressure sublimation and recrystallization in acetic acid, respectively.

Aldrich "Gold Label" solvents were used without further purification for all the experiments. High purity argon was used to deaerate solutions.

Since the solvation water of $Mn(ClO_4)_2 \cdot 6H_2O$ interfered with the stoichiometric formation of the complexes under study, $[Mn^{II}(DMU)_6][ClO_4]_2$ (DMU = dimethylurea)[18] was used in all the experiments in which the manganese complexes were formed *in situ*. As a source of manganese(III) $[Mn^{III}(urea)_6][ClO_4]_3$[19] was used in all the experiments.

RESULTS AND DISCUSSION

Solutions of different combinations of manganese(II), quinizarine (Qz) and thiosalicylic acid (2-MBA) in dimethylsulphoxide were analysed electrochemically and spectroscopically in order to verify the possible formation of a mixed-ligand complex and to establish its redox chemistry. The amount of base present in these solutions was varied in order to generate the unprotonated species of the ligands. In most cases the electrochemical and spectroscopic behaviour of the solutions corresponds either to the free ligands or to the manganese complexes already reported, plus the excess of the second ligand. If the amount of base is enough to neutralize all the protons from Qz and 2-MBA the solution presents a behaviour indicating that a simple complex between manganese and 2-MBA has formed in the presence of excess Qz. Therefore, in this case there is no mixed-ligand complex formation and the more stable species $Mn(2\text{-}MBA)_2$ prevails in the presence of excess quinizarine.

A different behaviour was observed only when the mole ratio Mn^{II} : Qz : 2-MBA : base was 1 : 1 : 2 : 4. In this case the dark blue solution and the solid formed when manganese(II) and Qz are combined in a 1 : 1 mole ratio shows a dramatic change upon addition of the dianion of 2-MBA. The solid dissolves and the solution turns deep blue. The UV–vis spectrum of this solution is shown in Fig. 1(C). The absorption maxima in the visible region are different from those of either the simple complexes with the ligands under study or the combination of these ligands in the absence of the metal ion, as shown in Figs 1(A) and (B). Therefore, we conclude that a new species is being formed under these conditions.

The cyclic voltammograms of the solution with a Mn^{II} : Qz : 2-MBA : base = 1 : 1 : 2 : 4 mole ratio [Figs 2(A)–(D)] show that no reduction peak is observed for free manganese(II), indicating that this ion is present as a complex. On the other hand, the voltammetric peaks that have been assigned to the ligands are not observed in this case, which indicates that under these conditions the mole ratio in the

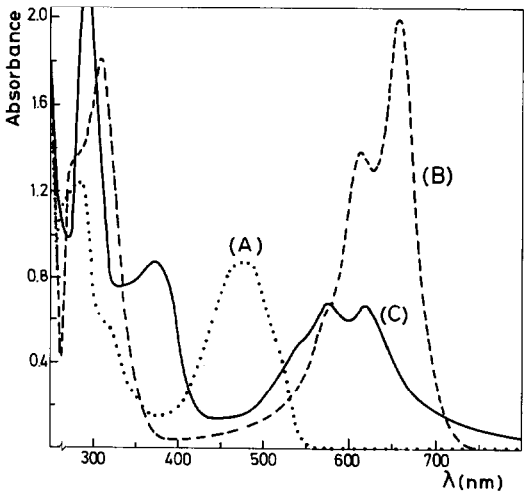

Fig. 1. UV–vis spectra of solutions in dimethylsulphoxide that are: (A) 1.0 mM Qz and 2.0 mM 2-MBA, (B) 1.0 mM Qz, 2.0 mM 2-MBA and 4.0 mM TEAOH and (C) same as (B) upon addition of 1.0 mM manganese(II).

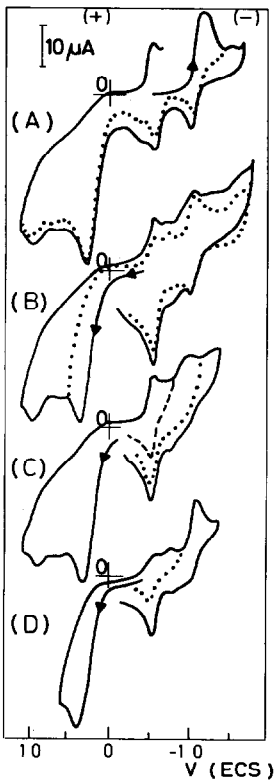

Fig. 2. Cyclic voltammograms of a solution of 1.0 mM Qz, 2.0 mM 2-MBA, 4.0 mM TEAOH and 1.0 mM manganese(II) in which: (A) illustrates the initial negative scan direction and (B), (C) and (D) illustrate initial positive scan directions with different reversal potentials. The solution is 0.1 M TEAP and the scan rate is 100 mV s^{-1}.

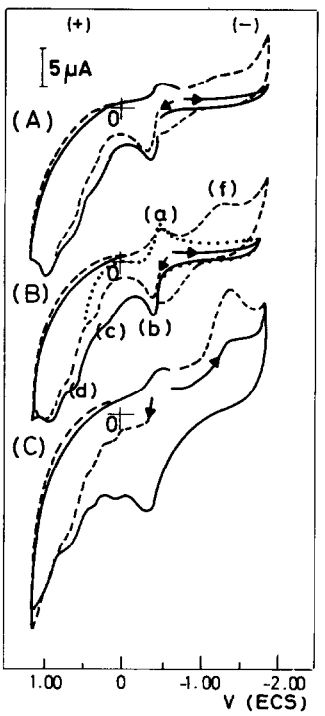

Fig. 3. Cyclic voltammograms of 1.0 mM 2-MBA, 2.0 mM TEAOH solutions and: (A) 0.33 mM manganese(II) (metal: ligand = 1:3), (B) 0.66 mM manganese(II) (metal: ligand = 1:2) and (C) 1.0 mM manganese(II) (metal: ligand = 1:1). The solutions are 0.1 M TEAP and the scan rate is 100 mV s^{-1}.

solution corresponds exactly to the stoichiometric relation and, therefore, we do not observe an excess either of the metal ion or of any of the ligands. The reduction peaks observed are different from those shown by the simple complexes with Qz or 2-MBA (Figs 3 and 4), therefore, we conclude that a new mixed-ligand species has formed.

Figures 2(B)–(D) indicate that when the mixed-ligand complex is oxidized this process occurs in steps which take place at +0.35, +0.65 and +0.90 V vs S.C.E. Controlled-potential electrolysis at +0.60 V vs S.C.E. indicates that 2 equivalents of charge are transferred per mole of manganese. It is impossible in this case to separate the two oxidation processes which might involve one electron each. The cyclic voltammogram of the final solution obtained shows no reduction peak corresponding to free manganese(II) [Fig. 5(B)], so that we can conclude that the metal ion is present as a complex in solution. This solution is dark red and the UV–vis spectra are illustrated in Fig. 6(C). The absorption maxima presented by the solution before the oxidation process [Fig. 6(B)] now show a bathochromic shift and can be observed at 675, 540 and a shoulder at 510 nm.

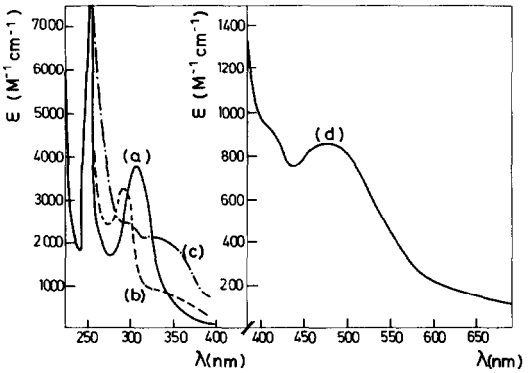

Fig. 4. UV spectra of solutions that are: (a) 1.0 mM 2-MBA and 2.0 mM TEAOH, (b) same as (a) plus 0.5 mM manganese(II), (c) same as (b) after controlled-potential oxidation at −0.25 V vs S.C.E. and (d) visible spectrum of solution (c).

The last 2 equivalents of charge transferred per mole of metal ion correspond to the oxidation of 1 of the 2 mol of 2-MBA present (the Mn^{II} : 2-MBA mole ratio is 1 : 2 in this solution). The oxidation of the —SH group would explain the destruction of the complex by formation of the corresponding dimer and the reprotonation of the dianion of quinizarine to regenerate the original ligand, as indicated by its UV–vis spectrum in Fig. 7.

Further oxidation of the dark red solution at +0.90 V vs S.C.E. again indicates that 2 equivalents of charge have been transferred per mole of metal ion before a residual current is obtained [Fig. 5(D)]. The solution becomes light orange, which is characc-

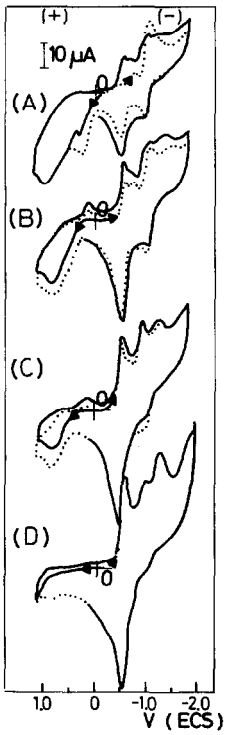

Fig. 5. Cyclic voltammograms of a solution of 1.0 mM Qz, 2.0 mM 2-MBA, 4.0 mM TEAOH and 1.0 mM manganese(II) after controlled-potential oxidation at: (A) 0.35 (1 equivalent of charge transferred), (B) 0.65 (2 equivalents of charge transferred), (C) 0.9 (3 equivalents of charge transferred) and (D) 0.9 V vs S.C.E. (4 equivalents of charge transferred). The solutions are 0.1 M TEAP and the scan rate is 100 mV s^{-1}.

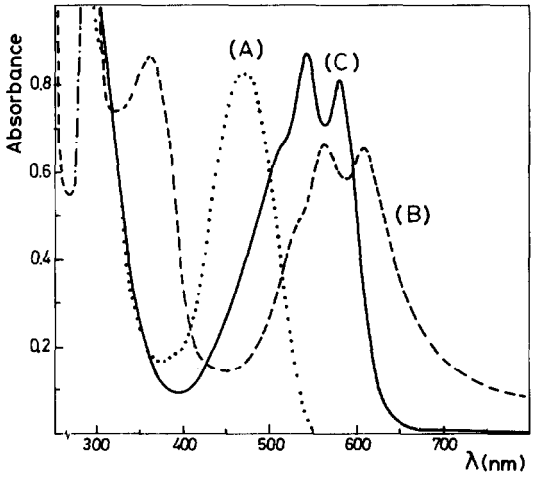

Fig. 6. UV–vis spectra of solutions that are: (A) 1.0 mM Qz, 2.0 mM 2-MBA and 1.0 mM manganese(II), (B) same as (A) plus 4.0 mM TEAOH and (C) same as (B) after controlled-potential oxidation at +0.65 V vs S.C.E. (2 equivalents of charge transferred).

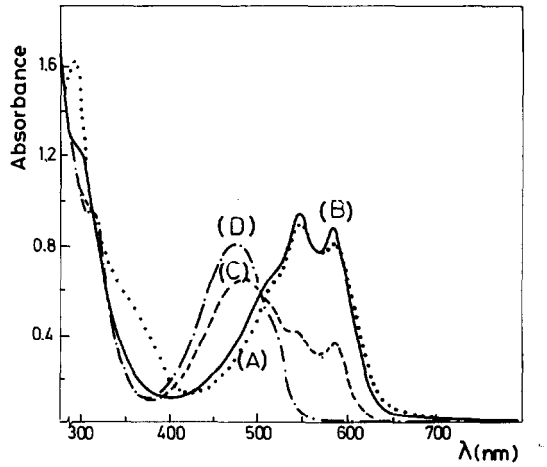

Fig. 7. UV–vis spectra of a solution of 1.0 mM Qz, 2.0 mM 2-MBA, 4.0 mM TEAOH and 1.0 mM manganese(II) after controlled-potential oxidation at: (A) 0.35 (1 equivalent of charge transferred), (B) 0.65 (2 equivalents of charge transferred), (C) 0.9 (3 equivalents of charge transferred) and (D) 0.9 V vs S.C.E. (4 equivalents of charge transferred).

teristic of quinizarine. The cyclic voltammograms, Figs 5(C) and (D), and the spectra shown in Fig. 7 indicate that in this case we have a mixture of the metal ion and the anions of the ligands with no complex formation, as the spectrum in Fig. 7(D) is identical to that in Fig. 1(A) which corresponds to a mixture of the ligands in the absence of manganese.

If we consider that the 4 equivalents of base added with respect to the metal ion correspond to the neutralization of the carboxylic protons of each mole of 2-MBA and of both hydroxylic protons of quinizarine the result is a species in which the 2-MBA residues would maintain their —SH groups. Therefore, it is conceivable to explain the behaviour of the system as follows: in the first oxidation process the 2 equivalents of charge that are transferred per mole of metal ion (at the end of which manganese appears to be forming a complex species) can be attributed either to the bound quinizarine or to the oxidation of the metal ion. In the first case the diquinone (DQ) species would be formed, which, as has been previously reported, does not form a complex species with manganese.[17] On the other hand, if the metal ion is oxidized its final oxidation state would be 4+ and the resulting complex would be neutral. Consequently, this species would be either insoluble or difficult to oxidize by electrolysis, which was not observed in our case.

Therefore, the following alternatives can explain the first oxidation process observed and both lead to the same oxidized species in solution. The only way to establish the correct alternative would be to isolate the intermediate species, which unfortunately was not possible. The first alternative would be to oxidize the dianion of quinizarine to the corresponding semiquinone and manganese(II) to manganese(III):

$$[Mn^{II}(Qz^{2-})(2\text{-MBA})_2]^{4-} \rightarrow [Mn^{III}(SQ^{-})(2\text{-MBA})_2]^{2-} + 2e^{-}. \quad (1)$$

The second alternative would be the oxidation of bound quinizarine to the corresponding semiquinone and then an internal charge transfer to produce manganese(III) and regenerate quinizarine. A second charge transfer process would oxidize quinizarine again and the final product would be the same as that illustrated in eq. (1).

Notice that upon the generation of the semi-quinone of quinizarine it is conceivable to consider its reprotonation, as described in the study of its simple manganese complex,[17] which would eliminate the possibility of forming a neutral species. If this reprotonation process occurs after the first oxidation step the oxidation of bound 2-MBA to the corresponding dimer with the consequent destruction of the complex would involve the $-S^{-}$ group instead of —SH. Therefore, the last oxidation step can be represented by:

$$[Mn^{III}(SQ)(2\text{-MBA})_2]^{0} \rightarrow Mn^{II} + DQ + (2\text{-MBA})_2 + 2e^{-}. \quad (2)$$

The reprotonation of the quinizarine semiquinone through an internal proton transfer from 2-MBA would give more stability to the manganese(III) complex as compared with manganese(II). Consequently, the oxidation of the mixed-ligand complex is totally irreversible as the manganese(III) species cannot be reduced. Furthermore, this oxidation process also involves the modification of the ligands which cannot be regenerated electrochemically.

In this work the manganese(II) and manganese(III) species have been stabilized with a coordination sphere that can be very relevant for some biological systems. It is important to notice that the oxidized species presents a sort of shoulder at 510 nm, which is coincident with the wavelength of absorption of the enzyme acid purple phosphatase[20] (the only protein that for certain has a sulphur atom in its first coordination sphere). Although the values of the wavelength for the absorption maxima can be affected by the solvent, the really interesting feature of the spectra is the shift of the maxima for one species or other, which would be indicative that, according to Christou,[21] the different nature of the atoms that are part of the coordination sphere of the metal ion determines its properties in every metalloprotein.

For these reasons we think it is convenient to study the mixed-ligand complexes in which we have a semi-quinone or catechol as one of the ligands and a second species in the coordination sphere that favours the Mn—N bond. That way the resulting complex would have an analogous structure to that proposed by O'Hara *et al.*[22] for the enzyme acid purple phosphatase. A species such as this would have a better redox reversibility and would be more useful to mimic its biological activity.

On the basis of Sekido *et al.*'s results[23] we can mention that the presence of 2-MBA (analogue of cysteine) is fundamental, because this amino acid is found at the active site of this enzyme. It is also feasible to find an Mn—O bond given by the presence of a quinonic or semi-quinonic ligand. This fact is inferred because the 8-mercaptoquinolinate complexes of both manganese(II) and manganese(III) (—N,S donor ligand) do not present either the spectroscopic or redox characteristics of the purple acid phosphatase or any other biological system.

Finally, it must be mentioned that we have been able to generate the semi-quinone of quinizarine in the presence of manganese at a very positive potential as compared with the oxidation observed in the absence of the metal ion.[17] Therefore, we have undertaken the study of analogous dihydroxy ligands such as 2,5-dihydroxybenzoic acid (2,5-DHBA), which presents a carboxylic group that deactivates the benzene ring leading to more positive oxidation potentials and which has been reported by the authors.[24] The metal ion presents in this complex a coordination sphere that is very common in biological systems, so that the system studied in this work is an important contribution to the basic knowledge in our field of interest.

Acknowledgement—This work was supported by CONICYT-Chile through the Fondecyt No. 309/88 Research Grant.

REFERENCES

1. J. Q. Chambers, *The Chemistry of Quinoid Compounds*. Wiley Interscience, New York (1973).
2. G. D. Lawrence and D. T. Sawyer, *Coord. Chem. Rev.* 1978, **27**, 173.
3. M. D. Stallings, M. M. Morrison and D. T. Sawyer, *Inorg. Chem.* 1981, **20**, 2655.
4. P. Mathur and G. Dismukes, *J. Am. Chem. Soc.* 1983, **105**, 7093.
5. M. W. Lynch, D. N. Hendrickson, B. J. Fitzgerald and G. C. Pierpont, *J. Am. Chem. Soc.* 1984, **106**, 2041.
6. S. C. Shoner and P. P. Power, *Inorg. Chem.* 1992, **31**, 1001.
7. V. Arancibia and M. Bodini, *An. Quím.* 1986, **82(B)**, 309.
8. V. Arancibia and M. Bodini, *An. Quím.* 1988, **84(C)**, 26.
9. M. Bodini and V. Arancibia, *Polyhedron* 1989, **8**, 1407.
10. A. N. Srinivasan and R. R. Sharp, *Biochim. Biophys. Acta.* 1986, **850**, 211.
11. S. Padhye, T. Kambara, D. N. Hendrickson and D. N. Govindjee, *Photosyn. Res.* 1986, **9**, 103.
12. W. M. Parker and C. S. F. Blake, *J. Molec. Biol.* 1988, **199**, 649.
13. K. Wieghardt, *Angew. Chem., Int. Edn Engl.* 1989, **101**, 1179.
14. J. B. Vincent and G. Christou, *Adv. Inorg. Chem.* 1989, **33**, 197.
15. G. Brudvig and R. H. Crabtree, *Prog. Inorg. Chem.* 1989, **37**, 99.
16. M. Bodini and M. A. del Valle, *Polyhedron* 1990, **9**, 1181.
17. M. Bodini and V. Arancibia, *Polyhedron* 1991, **10**, 1929.
17(a). S. Fujimoto, K. Murakami and A. O'Hara, *J. Biochem.* 1985, **97**, 1777.
17(b). J. S. Bashkin, J. C. Huffman and G. Christou, *J. Am. Chem. Soc.* 1986, **108**, 5038.
18. P. Van Leeuwen and W. Groeneveld, *Inorg. Chem.* 1967, **3**, 145.
19. H. Oghakozorg and J. Summers, *Inorg. Chem.* 1982, **21**, 3903.
20. S. Fujimoto, K. Murakami and A. O'Hara, *J. Biochem.* 1985, **97**, 1777.
21. J. S. Bashkin, J. C. Huffman and G. Christou, *J. Am. Chem. Soc.* 1986, **108**, 5038.
22. Y. Sugiura, H. Kawabe, H. Tanaka, S. Fujimoto and A. O'Hara, *J. Biol. Chem.* 1981, **256**, 10664.
23. Y. Nakabayashi, Y. Masuda and E. Sekido, *J. Electroanal. Chem.* 1984, **176**, 243.
24. M. Bodini and M. A. del Valle, *Bol. Soc. Chil. Quím.* 1990, **35**, 233.

Polyhedron Vol. 12, No. 14, pp. 1739–1744, 1993
Printed in Great Britain

0277–5387/93 $6.00+.00
© 1993 Pergamon Press Ltd

VOLTAMMETRIC AND SPECTROSCOPIC STUDIES OF THE BEHAVIOUR OF MANGANESE(II) AND MANGANESE(III) COMPLEXES WITH ISOQUINOLINECARBOXYLIC ACID IN APROTIC MEDIUM

MARIO E. BODINI,* ROBERTO LEIVA, MARÍA A. DEL VALLE and VERÓNICA ARANCIBIA

Departamento de Química, Analítica y Electroquímica, Facultad de Química, Pontificia Universidad Católica de Chile, Casilla 306, Santiago, Chile

(*Received* 8 *February* 1993; *accepted* 23 *March* 1993)

Abstract—The redox chemistry of the manganese(II) and manganese(III) complexes with 1-isoquinolinecarboxylate (1-IQC) in dimethylsulphoxide has been studied. Cyclic voltammetry, polarography, controlled-potential electrolysis, UV–vis spectroscopy and magnetic susceptibility measurements have been performed on the solutions. In the presence of the anion 1-isoquinolinecarboxylate the manganese(II) ion forms an $Mn^{II}(1\text{-IQC})_2$ complex, whose conditional formation constant has been evaluated polarographically and turns out to be $5 \times 10^7\ M^{-2}$ at 25°C. The polarograms of the solution of this complex show a cathodic wave with $E_{1/2} = -1.60$ V vs S.C.E., corresponding to the reduction of the metal ion with its subsequent destruction. On the other hand the voltammograms on a platinum electrode show the reduction of the bound ligand at −1.66 V vs S.C.E., probably to a bound radical species, and two oxidation processes at −1.37 and −1.49 V vs S.C.E. The manganese(II) complex does not decompose after this reduction, but the species produced was not obtained quantitatively as the reduction potential was too close to the solvent discharge. The manganese(II) complex is oxidized to the $Mn^{III}(1\text{-IQC})_3$ mononuclear complex, whose conditional formation constant was evaluated polarographically and turns out to be $4 \times 10^{14}\ M^{-3}$ at 25°C.

The coordination chemistry of manganese has been a rather neglected field until fairly recently, perhaps because high-spin manganese(II) has historically been the dominant oxidation state in well-characterized compounds. Not only does the high-spin d^5 manganese(II) ion have a zero crystal field stabilization energy (CFSE), but it gives no useful UV–vis spectral information from *d–d* bands. The majority of manganoproteins utilize only manganese(II). In these redox-inactive proteins other divalent metal ions frequently can functionally substitute for manganese and in many cases it is unclear whether manganese is even the physiologically relevant cation.[1–4]

The higher valence states of manganese have been increasingly studied and it has led to the discovery of a whole series of stable coordination complexes, mainly of d^4 manganese(III) and d^3 manganese(IV). A further difficulty is that in the absence of suitable ligands manganese(III) tends to disproportionate to manganese(II) and manganese(IV). The manganese(III) state can be stabilized by anionic strongly donating ligands. The *d–d* transitions have substantial intensity in manganese(III) complexes and most are green, red or brown; charge-transfer bands are probably also of importance in certain cases. Interest in binuclear and polynuclear complexes of manganese in relatively high oxidation states stems largely from the involvement of such species in a wide variety of biological oxidative processes; the most relevant example to the present work is the water oxidizing enzyme in photosystem II, disproportionation of hydrogen peroxide (catalase activity) in microorganisms and their potential use as redox catalysts.[5–9]

* Author to whom correspondence should be addressed.

Carboxylate groups show a tendency to bind to manganese in either a monodentate or bidentate manner; in the latter case with the formation of a symmetrical μ-carboxylato bridge.[10-14] Our group has studied the mononuclear complexes with manganese(II) and binuclear complexes with manganese(III) formed with the ligand 4-methoxy-2-quinolinecarboxylate[15] and we now report the study of complexes of this metal ion with 1-isoquinoline-carboxylate in order to compare their behaviour, considering that in this case the carboxylic group is in a different position and that this ligand has no substitution groups in their structure. Therefore, the redox chemistry and the stabilities of the complexes formed should be different from those reported in the past.

EXPERIMENTAL

Equipment

A three-electrode potentiostat (Bioanalytical Systems) Model CV-1A 230 and a Linear Model 8036 *X–Y* recorder were used for the cyclic voltammetric experiments. Controlled-potential coulometric electrolysis was accomplished with a Bioanalytical Systems Model SP-2 potentiostat and PUC coulometer.

The electrochemical cell was equipped with a Beckman platinum-inlay electrode for the voltammetric experiments. The auxiliary electrode was a platinum-coil electrode, which was isolated from the bulk solution by a glass tube with a fine-porosity glass frit at the end; it contained a concentrated solution of supporting electrolyte. The reference electrode was an Ag/AgCl (aqueous tetramethylammonium chloride) cracked glass-bead electrode, which was adjusted to 0.00 V vs S.C.E.[16] The reference electrode was located inside a Luggin capillary in the cell assembly. A platinum-mesh working electrode was used for the controlled-potential electrolysis experiments.

The UV–vis spectra were obtained with a Hewlett–Packard Model 8452 A spectrophotometer.

The magnetic susceptibility measurements were made by the Evans[17] method as modified by Rettig[18] using an NMR spectrometer Varian Model XL-100.

Reagents

The reagents for the investigation and syntheses included $Mn(ClO_4)_2 \cdot 6H_2O$ (G. Frederick Smith), tetrabutylammonium hydroxide (TBAOH) (1.0 M in methanol, Aldrich), tetramethylammonium chloride (Aldrich) and tetraethylammonium perchlorate (TEAP) (G. Frederick Smith). The ligand 1-isoquinolinecarboxylic acid was obtained from Aldrich.

Aldrich "Gold Label" solvents were used without further purification for all of the experiments. High purity argon was used to deaerate the solutions.

Since the solvation water of $Mn(ClO_4)_2 \cdot 6H_2O$ interfered with the stoichiometric formation of the complexes under study, $[Mn^{II}(DMU)_6][ClO_4]_2$ (DMU = dimethylurea)[19] was used in all the experiments in which the manganese complexes were formed *in situ*. As a source of manganese (III) $[Mn^{III}(urea)_6][ClO_4]_3$[20] was used in all the experiments.

RESULTS AND DISCUSSION

The cyclic voltammogram of a solution of 1-isoquinolinecarboxylic acid (1 mM) in dimethylsulphoxide (DMSO) is illustrated in Fig. 1. Two reduction processes are observed at -1.23 and -1.33 V vs S.C.E. (peaks a and b) and the corresponding anodic processes occur at -0.50 and $+0.08$ V vs S.C.E. (peaks c and d), which are due to the oxidation of the species generated on the surface of the electrode. A very reversible post-peak is also observed in Fig. 1, with $E_{p,c} = -1.66$ and $E_{p,a} = -1.64$ V vs S.C.E. The electrochemical behaviour of this ligand has been previously studied by our group.[21]

If 1 equivalent of base (TBAOH) is added to this solution the proton of the carboxylic group is neutralized and its cyclic voltammogram is shown in Fig. 1(B). Notice that the only electrochemical process shown by this compound is the irreversible oxidation of the carboxylate group[22] at $+0.95$ V vs S.C.E.

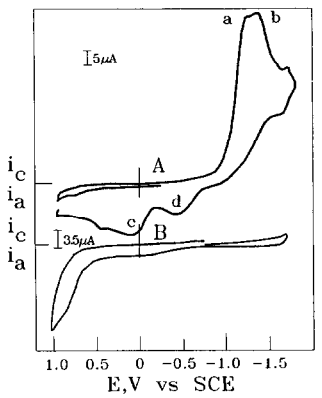

Fig. 1. Cyclic voltammograms in DMSO (TEAP 0.1 M, $V = 0.10$ V s^{-1}) of solutions that are: (A) 3.0 mM in 1-isoquinolinecarboxylic acid and (B) 3.0 mM in 1-isoquinolinecarboxylic acid + 3.0 mM in TBAOH.

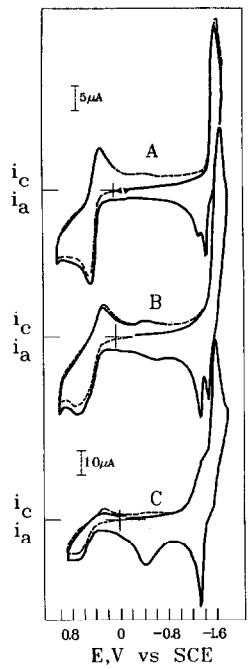

Fig. 2. Cyclic voltammograms in DMSO (TEAP 0.1 M, $V = 0.10$, V s^{-1}) of solutions 9.0 mM in 1-isoquinolinecarboxylic acid and 9.0 mM in TBAOH in the presence of: (A) $Mn(DMU)_6(ClO_4)_2$ (3.0 mM), (B) $Mn(DMU)_6(ClO_4)_2$ (4.5 mM) and (C) $Mn(DMU)_6(ClO_4)_2$ (9.0 mM).

Figure 2 illustrates the cyclic voltammograms of solutions of the anion of the ligand in the presence of increasing amounts of $Mn^{II}(DMU)_6(ClO_4)_2$ so that 1 : 3, 1 : 2 and 1 : 1 metal-to-ligand mole ratios are obtained [Figs 2(A), (B) and (C), respectively]. In this medium the manganese(II) ion reduces at -1.35 V vs S.C.E. and the oxidation of manganese metal depends on the negative potential limit at which the scan is reversed. In this case the corresponding anodic peak occurs at -0.40 V vs S.C.E. At the 1 : 3 and 1 : 2 metal-to-ligand mole ratios [Figs 2(A) and (B)] stable complexes are formed, which can be concluded from the fact that the reduction of free manganese(II) to manganese(0) is not observed. Only when the metal-to-ligand mole ratio is 1 : 1 does this process become evident.

Figure 3 shows the UV–vis spectra of these solutions, in which the monoanion of the ligand presents absorption maxima at 278 ($\varepsilon = 5451$ M^{-1} cm^{-1}), 314 ($\varepsilon = 4006$ M^{-1} cm^{-1}) and 326 nm ($\varepsilon = 4280$ M^{-1} cm^{-1}) [Fig. 3(A)]. In the presence of manganese(II) the absorption maximum is shifted from 278 to 282 nm and a lower absorbance is observed if the metal-to-ligand mole ratio is 1 : 3. The maximum at 314 nm disappears and a wide absorption band becomes evident between 322 and 338 nm, whose absorption is maximum for a metal-to-

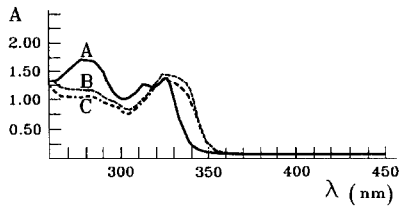

Fig. 3. UV absorption spectra in DMSO of: (A) 9.0 mM in 1-isoquinolinecarboxylic acid + 9.0 mM in TBAOH, (B) solution A in the presence of $Mn(DMU)_6(ClO_4)_2$ (3.0 mM) and (C) solution A in the presence of $Mn(DMU)_6(ClO_4)_2$ (4.5 mM).

ligand mole ratio of 1 : 2 [Fig. 3(C)]. For a 1 : 1 ratio the absorption spectrum does not change because the excess free manganese(II) is spectroscopically inactive in this wavelength region.

Therefore, according to voltammetric and spectroscopic results we can conclude that the 1-isoquinolinecarboxylate ligand forms a mononuclear complex with manganese(II) with a 1 : 2 metal-to-ligand stoichiometry.

If the potential is scanned initially in the negative direction (Fig. 2) a reduction process is observed at -1.66 V vs S.C.E. and two oxidations associated to this process appear at -1.37 and -1.49 V vs S.C.E. The electrochemical reduction must correspond to electron transfer to the bound ligand because the presence of free manganese(II) is not observed after this process. If free manganese(II) is released after the decomposition of the complex its reduction to manganese metal and the oxidation of the metallic deposit should become evident in the manganese(II) complex solution cyclic voltammograms.

When controlled-potential electrolysis at -1.80 V vs S.C.E. is performed on a solution of 1-isoquinolinecarboxylate and manganese(II) with a metal-to-ligand mole ratio of 1 : 2, in order to obtain quantitatively the reduced complex, the solution becomes a little darker, but unfortunately the applied potential was too close to the solvent discharge and the complete electrolytic process was not possible.

Based on our previous experience on the reduction of an analogous ligand[15] we can propose in this case that the bound ligand is reduced to a radical species, which is stabilized by the presence of the metal ion.

$$Mn^{II}(1\text{-IQC})_2 + e^- \longrightarrow Mn^{II}(1\text{-IQC})(1\text{-IQC}^{\cdot})^- \quad (1)$$

The presence of two oxidation peaks can be explained in terms of two different radicals, produced when this type of ligand is reduced.[15]

If a dropping mercury electrode (D.M.E.) is used the reduction of the manganese(II) complex to the corresponding amalgam is observed before the reduction of the ligand and it shifts to more negative potentials as the concentration of the ligand is increased in the solutions. This polarographic behaviour of our system was used to confirm the stoichiometry of the complex and to evaluate its conditional formation constant. The difference, $E_{3/4}-E_{1/4}$, of the polarographic wave was 78 mV, which was used to determine the value of the charge-transfer coefficient (α), which was 0.378. From the slope of the straight line obtained for the dependence of the half-wave potential with the concentration of the ligand in the solutions[23] (-0.168) it was confirmed that the manganese(II) complex had a 1 : 2 stoichiometry and from its intercept with the ordinate axis (-0.603) its conditional formation constant was estimated to be 5×10^7 M^{-2}.

Reference to Fig. 2 indicates that if the potential is scanned initially in the positive direction an oxidation process is observed at +0.46, +0.68 or +0.72 V vs S.C.E., depending on the manganese(II) concentration in the solutions. These potentials correspond to 1 : 3, 1 : 2 and 1 : 1 metal-to-ligand mole ratios, respectively. The corresponding reduction occurs at −0.22 V vs S.C.E. and it does not shift as the concentration of the metal ion is varied, indicating that the electrochemical process becomes more irreversible.

In order to quantitatively oxidize the species of manganese(II) in solution controlled-potential electrolysis was performed at +0.70 V vs S.C.E. of a solution with a metal-to-ligand mole ratio of 1 : 3 (oxidation peak potential = +0.46 V vs S.C.E.). The original pale yellow solution turned red–brown and a residual current was obtained after the transfer of 1 equivalent of charge. The magnetic susceptibility of the resulting solution was 4.91 B.M., which indicates that a manganese(III) species has been generated in solution. When solutions with 1 : 2 or 1 : 1 metal-to-ligand mole ratios were electrolysed at +0.75 V vs S.C.E. the same mononuclear manganese(III) complex was obtained, presenting a 1 : 3 stoichiometry. The cyclic voltammograms of these solutions are shown in Fig. 4.

In order to generate directly the oxidized species solutions of 1-isoquinolinecarboxylate and $[Mn^{III}(Urea)_6](ClO_4)_3$ with 1 : 3, 1 : 2 and 1 : 1 metal-to-ligand mole ratios were prepared. The cyclic voltammograms of these solutions are shown in Fig. 5 and the corresponding visible spectra are illustrated in Fig. 6. Figure 5(A) shows the cyclic voltammograms of a solution of $[Mn^{III}(Urea)_6](ClO_4)_3$ (5 mM). Although the crystal structure of this com-

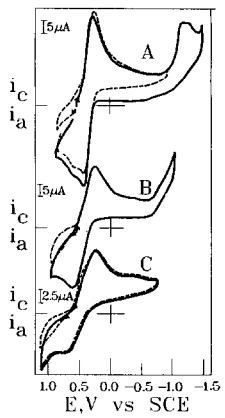

Fig. 4. Cyclic voltammograms in DMSO (TEAP 0.1 M, $V = 0.10$ V s^{-1}) of: (A) 9.0 mM in 1-isoquinolinecarboxylic acid + 9.0 mM in TBAOH + $Mn(DMU)_6(ClO_4)_2$ (3.0 mM) after electrolysis at +0.70 V vs S.C.E., (B) 9.0 mM in 1-isoquinolinecarboxylic acid + 9.0 mM in TBAOH + $Mn(DMU)_6(ClO_4)_2$ (4.5 mM) after electrolysis at +0.80 V vs S.C.E. and (C) 3.0 mM in 1-isoquinolinecarboxylic acid + 3.0 mM in TBAOH + $Mn(DMU)_6(ClO_4)_2$ (3.0 mM) after electrolysis at +0.85 V vs S.C.E.

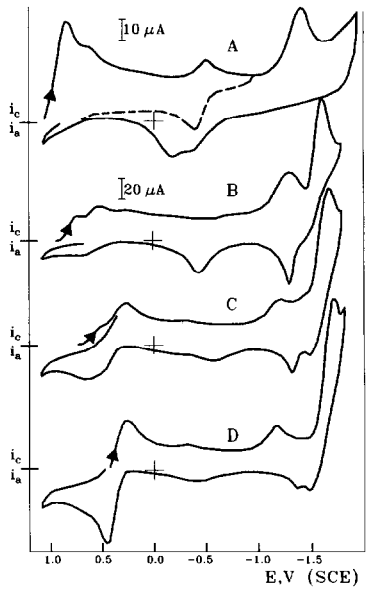

Fig. 5. Cyclic voltammograms in DMSO (TEAP 0.1 M, $V = 0.10$ V s^{-1}) of: (A) a solution of $Mn(Urea)_6(ClO_4)_3$ (5.0 mM), (B) the same as (A) and in the presence of 1-isoquinolinecarboxylate (5 mM), (C) the same as (A) and in the presence of 1-isoquinolinecarboxylate (10 mM) and (D) the same as (A) and in the presence of 1-isoquinolinecarboxylate (15 mM).

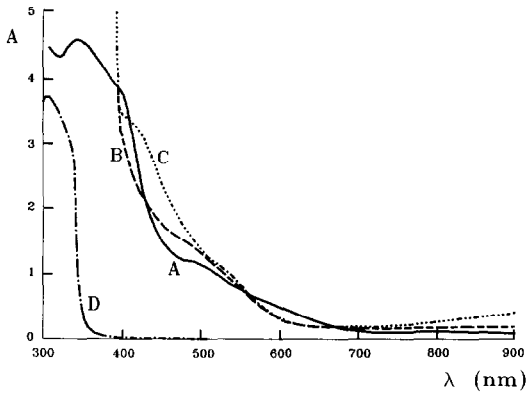

Fig. 6. UV–vis spectra in DMSO of solutions that are: (A) 5.0 mM in $Mn(Urea)_6(ClO_4)_3$, (B) 5.0 mM in $Mn(Urea)_6(ClO_4)_3$ and 10 mM in 1-isoquinolinecarboxylate, (C) 5.0 mM in $Mn(Urea)_6(ClO_4)_3$ and 15 mM in 1-isoquinolinecarboxylate and (D) 15 mM in 1-isoquinolinecarboxylic acid and 15 mM in TBAOH.

pound has been obtained[20] and it corresponds to a mononuclear complex, it is observed that in solution a polynuclear species is formed which presents reduction peaks at +0.87, +0.62 and −0.48 V vs S.C.E. Controlled-potential electrolysis after the third reduction process indicates that 1 equivalent of charge is being transferred, generating the manganese(II) complex. Upon addition of 1-isoquinolinecarboxylate to the solution of manganese(III) ions (5 mM) the intensity of these cathodic peaks decrease and a new reduction process is observed at +0.26 V vs S.C.E. This reduction peak presents its maximum intensity after the addition of three equivalents of the monoanionic ligand [Fig. 5(D)]. On the other hand the manganese(III)-urea complex is very unstable if it is electrochemically reduced [Fig. 5(A)] and the corresponding oxidation of the manganese(II) species is not observed. Only in the presence of 1-isoquinolinecarboxylate and in a 1:3 metal-to-ligand mole ratio is it possible to stabilize a mononuclear species. This solution presents the same cyclic voltammogram and spectrum as the solution obtained by electrolytic oxidation of the manganese(II) complex with this stoichiometric ratio. If the metal-to-ligand mole ratio is 1:1 or 1:2 the presence of free manganese(III) is observed and its reduction takes place at a higher potential due to the instability of this metal ion.

The UV–vis spectra of solutions of $[Mn^{III}(Urea)_6](ClO_4)_3$ are shown in Fig. 6. This compound has absorption maxima at 350 ($\varepsilon = 920\ M^{-1}\ cm^{-1}$), 400 ($\varepsilon = 760\ M^{-1}\ cm^{-1}$), 490 ($\varepsilon = 240\ M^{-1}\ cm^{-1}$) and a little shoulder at 600 nm ($\varepsilon = 100\ M^{-1}\ cm^{-1}$) [Fig. 6(A)]. The monoanionic ligand presents an absorption maximum at 309 nm ($\varepsilon = 253\ M^{-1}\ cm^{-1}$) and it contributes to the overall absorption spectrum up to approximately 380 nm [Fig. 6(D)]. The mononuclear tris complex $[Mn(IQC)_3]$ presents an absorption maximum at 410 ($\varepsilon = 650\ M^{-1}\ cm^{-1}$) and a little shoulder at 520 nm ($\varepsilon = 240\ M^{-1}\ cm^{-1}$) [Fig. 6(C)].

A polarographic analysis of solutions of the mononuclear species of manganese(III) indicates a wave with $E_{1/2} = 0.26$ V vs S.C.E., corresponding to the reduction of $Mn^{III}(IQC)_3$ to $Mn^{II}(IQC)_2$. From the shift in the half-wave potential with the concentration of the ligand we can obtain the ratio of the formation constants of the two complexes involved. As we had previously determined the constant for the manganese(II) complex the corresponding manganese(III) complex conditional formation constant is $4 \times 10^{14}\ M^{-3}$ at 25°C.

Therefore, we can conclude from this work that the 1-isoquinolinecarboxylate ligand forms mononuclear complexes both with manganese(II) and manganese(III). This is different from the behaviour presented by the previously reported ligand 4-methoxy-2-quinolinecarboxylate,[15] where a binuclear complex of manganese(III) formed in solution. This indicates that the position of the carboxylate group is very important in determining the structure of the oxidized species. Probably a steric effect precludes the formation of a bridge between the two metal centres in the case of the 1-isoquinolinecarboxylate ligand.

REFERENCES

1. G. W. Brudvig, H. H. Thorp and R. H. Crabtree, *Accts Chem. Res.* 1991, **24**, 311.
2. G. L. Lawrence and D. T. Sawyer, *Coord. Chem. Rev.* 1978, **27**, 173.
3. J. Livorness and T. D. Smith, *Struct. Bond.* 1982, **48**, 2.
4. F. A. Cotton and G. Wilkinson, *Advanced Inorganic Chemistry*, 3rd edn, p. 845. Wiley Interscience, New York (1972).
5. J. E. Sheats, R. S. Czernuszewicz, G. C. Dismukes, A. L. Rheingold, V. Petrouleas, J. Stubbe, W. H. Armstrong, R. H. Beer and S. J. Lippard, *J. Am. Chem. Soc.* 1987, **109**, 1435.
6. M. P. Heyward and C. F. Wells, *Inorg. Chim. Acta* 1989, **165**, 105.
7. M. Perré-Fauvet, A. Gaudemer, J. Bonvoisin, J. J. Girerd, C. Boucly-Goester and P. Boucly, *Inorg. Chem.* 1989, **28**, 3533.
8. K. Wieghardt, *Angew. Chem., Int. Edn Engl.* 1989, **28**, 1153.
9. G. C. Dismukes, J. E. Sheats and J. A. Smegal, *J. Am. Chem. Soc.* 1987, **109**, 7202.
10. T. Matsushita, L. Spencer and D. Sawyer, *Inorg. Chem.* 1988, **27**, 1167.

11. E. Libby, R. J. Webb, W. E. Streib, K. Folting, J. C. Huffman, D. N. Hendrickson and G. Christou, *Inorg. Chem.* 1989, **28**, 4037.
12. M. Suzuki, M. Mikuriya, S. Murata, A. Uehara, H. Oshio, S. Kida and K. Saito, *Bull. Chem. Soc. Japan* 1987, **60**, 4305.
13. K. Wieghardt, U. Bossek, J. Bobvoisin, P. Beauvillain, J. Girerd, B. Nuber, J. Weiss and J. Heinze, *Angew. Chem., Int. Edn Engl.* 1986, **25**, 1030.
14. A. Caneschi, F. Ferraro, D. Gatteschi, M. C. Melandri, P. Rey and R. Sessoli, *Angew. Chem., Int. Edn Engl.* 1989, **28**, 1365.
15. M. E. Bodini and V. Arancibia M., *Polyhedron* 1992, **17**, 2195.
16. D. Sawyer and J. L. Roberts Jr, *Experimental Electrochemistry for Chemists*, p. 53. John Wiley & Sons, New York (1974).
17. D. F. Evans, *J. Chem. Soc.* 1959, 2003.
18. M. F. Rettig, private communication. University of California, Riverside, California (1975).
19. P. W. van Loewen and W. L. Groenwald, *J. Inorg. Nucl. Chem. Lett.* 1967, **3**, 145.
20. H. Oghakozorg, G. J. Palenik, R. C. Stoufer and J. Summers, *Inorg. Chem.* 1982, **21**, 3903.
21. R. Leiva, H. Licenciate Thesis. Faculty of Chemistry, Catholic University of Chile (1992).
22. A. J. Bard and L. R. Faulkner, *Electrochemical Methods, Fundamentals and Applications*. John Wiley & Sons, New York (1980).

Polyhedron Vol. 12, No. 14, pp. 1745–1750, 1993
Printed in Great Britain

0277–5387/93 $6.00+.00
© 1993 Pergamon Press Ltd

ZINC(II) COMPLEXES WITH THE REDUCTION PRODUCTS OF 2,3-DIMETHOXY-1,4-NAPHTHOQUINONE IN DIMETHYL SULPHOXIDE REDOX CHEMISTRY AND SPECTROSCOPY

VERÓNICA ARANCIBIA and MARIO BODINI*

Departamento de Química Analítica Electroquímica, Facultad de Química, Pontificia Universidad Católica de Chile, Casilla 306, Santiago, Chile

(*Received* 23 *November* 1992; *accepted* 23 *March* 1993)

Abstract—In dimethylsulphoxide the 2,3-dimethoxy-1,4-naphthoquinone (Q) is reduced in two successive one-electron steps, which are electrochemically reversible at low scan rates. At −0.72 V vs S.C.E. the semiquinone anion radical is formed and at −1.42 V vs S.C.E. a second reduction to the corresponding dianion is observed. A mixture of zinc(II) and the dianion of 2,3-dimethoxy-1,4-naphthoquinone at a mole ratio of 1 : 1 in Me_2SO yields a stable complex. The zinc(II)-semiquinone complex is formed only on the surface of the electrode because under these conditions this radical ligand disproportionates producing the corresponding quinone and the dianion. The different forms of the ligand and the zinc(II)-dianion complex have been characterized by cyclic voltammetry, UV–vis spectroscopy and magnetic susceptibility measurements. The stability constants for the 1 : 1 zinc(II)-dianion and zinc(II)-semiquinone complexes are large, but it was not possible to determine their exact value as their voltammetric behaviour was irreversible. However the high stability of the dianion complex causes the disproportionation of the ligand in the semiquinone complex.

There is considerable interest in metal complexes containing quinone and quinone-derived ligands. These ligands can potentially bind to metal ions in three different forms, namely quinone, semiquinone or dianion. Quinones are present in a number of biological systems, and their role appears to be as electron transfer agents in redox reactions.[1–7] The interaction of quinones and their reduced species with metal ions such as manganese(II), manganese(III), iron(II), iron(III) and copper(II) has been used as a model for some biological systems, for example Photosystem II of green plant photosynthesis.[8–10]

Most of the work in this area has been performed with three ligands in their various electronic forms: 3,5-di-t-butylbenzoquinone, 9,10-phenanthrenequinone and tetrachloro-1,2-benzoquinone.[11–13]

The zinc(II) ion, which is redox inactive under the conditions where the bound dianion (DA^{2-}) and the semiquinone ($SQ^{\cdot -}$) are electroactive, is a hard acid and forms strong coordinate bonds with oxo ligands.[14] This characteristic should favour strong complexation of zinc(II) by DA^{2-}-$ySQ^{\cdot -}$ and the degree of interaction should be equal to or greater than that of these ligands with manganese(II) or iron(II).

The present paper summarizes the results of an electrochemical, spectroscopic and magnetic characterization of the complexes of zinc(II) with different forms of the ligand 2,3-dimethoxy-1,4-naphthoquinone in dimethyl sulphoxide (Me_2SO).

EXPERIMENTAL

Equipment

A three-electrode potentiostat (Bioanalytical Systems) Model CV-1A 230 and a Linear Model 8036 *X–Y* recorder were used for the cyclic voltammetric experiments. Controlled-potential electrolysis was accomplished with a Bioanalytical Systems Model SP-2 potentiostat and PUC coulometer.

* Author to whom correspondence should be addressed.

The electrochemical cell was equipped with a Beckman platinum-inlay electrode (area 0.23 cm^2) for the voltammetric experiments. The auxiliary electrode was a platinum-coil electrode, which was isolated from the bulk solution by a glass tube with a fine-porosity glass frit at the end; it contained a concentrated solution of supporting electrolyte. An Ag/AgCl reference electrode filled with an aqueous tetramethylammonium chloride solution and adjusted to 0.00 V vs S.C.E. was used in all the experiments.[15] This electrode was contained in a Pyrex tube with a soft-glass cracked tip and was located inside a Luggin capillary in the cell assembly. A platinum-mesh working electrode was used for the controlled-potential electrolysis experiments.

The UV–vis spectra were obtained with a Hewlett–Packard Model 8452 A diode-array spectrophotometer.

The magnetic susceptibility measurements were made by the Evans[16] method as modified by Rettig,[17] using an NMR Varian Model XL-100 spectrometer. Diamagnetic corrections were made.[18]

Air-sensitive compounds were handled in a glove-bag (Aldrich) under a nitrogen atmosphere and the oxygen content was monitored with a Beckman Model Monitor II Oxygen Analyser.

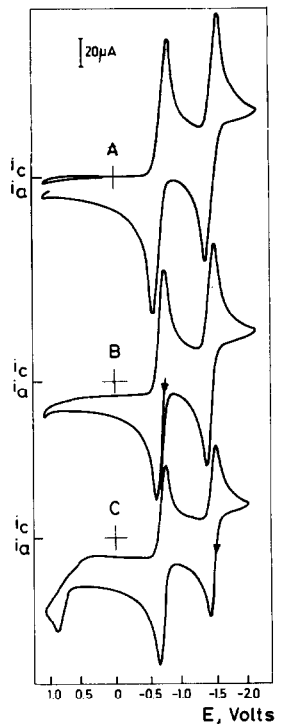

Fig. 1. Cyclic voltammograms in Me_2SO (0.1 M TEAP; $v = 0.1$ V s^{-1}) of solutions that are 3.0 mM in (A) 2,3-dimethoxy-1,4-naphthoquinone (Q), (B) 2,3-dimethoxy-1,4-naphthoquinone after electrolysis at −0.92 V vs S.C.E: ($n = 1$, $SQ^{\cdot -}$) and (C) 2,3-dimethoxy-1,4-naphthoquinone after electrolysis at −1.62 V vs S.C.E. ($n = 2$, DA^{2-}).

Reagents

2,3-Dimethoxy-1,4-naphthoquinone (Q) was obtained from Aldrich Chemical Co., $[Zn^{II}(DMU)_6](ClO_4)_2$[19] (DMU = dimethylurea) was used as the source of zinc(II) ions; tetramethylammonium chloride was obtained from INC Pharmaceuticals Inc.; tetraethylammonium perchlorate (TEAP) was obtained from reaction of a 25% aqueous solution of tetraethylammonium hydroxide (Aldrich) and concentrated perchloric acid (Merck) and recrystallized from anhydrous ethyl alcohol; dimethyl sulphoxide (Me_2SO) was obtained from Aldrich (water < 0.005%) and was used without further purification. High-purity argon was used to deaerate the solutions.

RESULTS AND DISCUSSION

Figure 1 shows the cyclic voltammograms of the ligand 2,3-dimethoxy-1,4-naphthoquinone (Q) in dimethylsulphoxide (Me_2SO). The quinone presents two reduction processes at −0.72 V vs S.C.E. and −1.42 V vs S.C.E. with the corresponding oxidations at −0.58 V vs S.C.E. and −1.29 V vs S.C.E. A 3 mM solution of this ligand is yellow and controlled-potential electrolysis at −0.92 V vs S.C.E. indicates that 1 equivalent of charge is being transferred in the process. A dark brown solution is obtained, which is extremely sensitive to the presence of oxygen. The magnetic susceptibility of this solution is 1.75 B.M., which indicates that a radical species is being formed in this electrolysis [Fig. 1(B)]. Controlled-potential electrolysis on this solution at −1.62 V vs S.C.E. yields a red–brown solution and again 1 equivalent of charge is transferred. The compound produced in this process is very sensitive to oxidation by oxygen as well. Its cyclic voltammogram is shown in Fig. 1(C), where it can be observed that a new oxidation peak occurs at +0.86 V vs S.C.E.

On the other hand, controlled-potential electrolyses at −1.09 V vs S.C.E. and −0.38 V vs S.C.E. to produce oxidations of the compound generated in the former elecrolytic processes indicated that 1 equivalent of charge is transferred in each case and the initial compound is regenerated.

We suggest that the following reactions are taking place in our system:

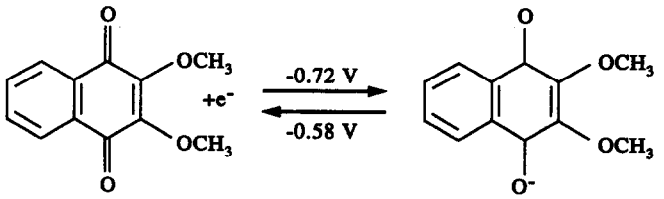

Quinone (Q) Semiquinone ($SQ^{\cdot-}$)

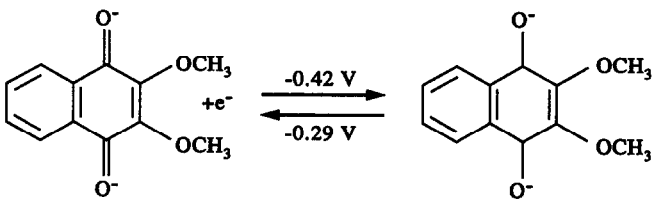

Semiquinone ($SQ^{\cdot-}$) Dianion (DA^{2-})

The semiquinone does not dimerize on the timescale of the electrolysis experiment and in the presence of oxygen it is oxidized to the original quinone. In the case of the dianion it is very reactive and gets oxidized on the surface of the electrode first to the semiquinone and then to the quinone. The latter presents a new oxidation peak at +0.86 V vs S.C.E.

The UV–vis spectra of the quinone, the semiquinone ($SQ^{\cdot-}$) and the dianion (DA^{2-}) are shown in Figs 2(A), (B) and (C). It can be observed that the quinone presents an absorption maximum at 330 nm ($\varepsilon = 3331\ M^{-1}\ cm^{-1}$), whereas the semiquinone shows its maxima at 300 ($\varepsilon = 8014\ M^{-1}\ cm^{-1}$), 406 ($\varepsilon = 6600\ M^{-1}\ cm^{-1}$) and 460 nm ($\varepsilon = 6491\ M^{-1}\ cm^{-1}$). On the other hand, the dianion presents its absorption maxima at 300 ($\varepsilon = 5899\ M^{-1}\ cm^{-1}$) and 410 nm ($\varepsilon = 6686\ M^{-1}\ cm^{-1}$).

Figure 3 shows the cyclic voltammograms of a solution of 2,3-dimethoxy-1,4-naphthoquinone in the presence of increasing amounts of zinc(II), so that 1:1, 1:2 and 1:3 metal-to-ligand stoichiometric ratios are obtained in solution. It can be observed that as the concentration of metal ion increases the peak current at −0.72 V vs S.C.E.

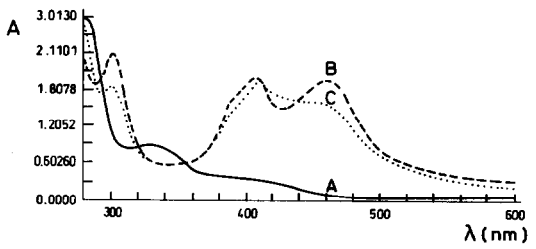

Fig. 2. Absorption spectra of solutions in Me_2SO containing: (A) 2,3-dimethoxy-1,4-naphthoquinone (3 mM) (Q), (B) 2,3-dimethoxy-1,4-naphthoquinone (3 mM) after electrolysis at −0.92 V vs S.C.E. ($n = 1$, $SQ^{\cdot-}$) and (C) 2,3-dimethoxy-1,4-naphthoquinone (3 mM) after electrolysis at −1.62 V vs S.C.E. ($n = 2$, DA^{2-}).

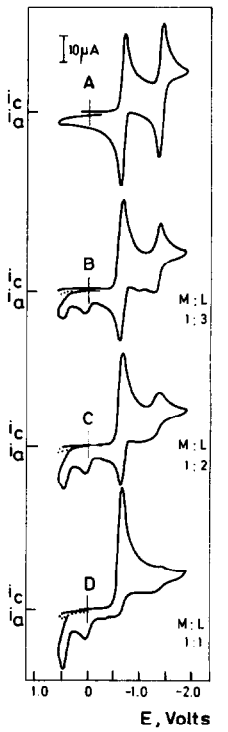

Fig. 3. Cyclic voltammograms in Me_2SO (0.1 M TEAP; $v = 0.1\ V\ s^{-1}$) of: (A) a solution (3 mM) of 2,3-dimethoxy-1,4-naphthoquinone, (B), (C) and (D) after the addition of 1, 1.5 and 3 mM $[Zn(DMU)_6](ClO_4)_2$, respectively.

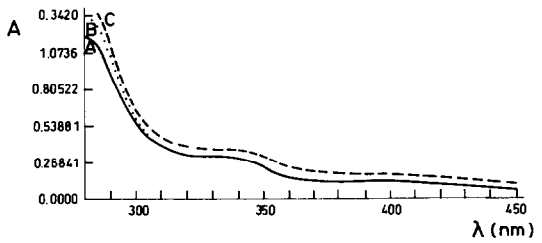

Fig. 4. Absorption spectra of solutions in Me_2SO containing: (A) 2,3-dimethoxy-1,4-naphthoquinone (3 mM); (B) and (C): solution (A) after the addition of 1.5 and 3 mM $[Zn(DMU)_6](ClO_4)_2$, respectively.

increases as well, whereas the current intensities associated with the processes at −1.42, −1.29 and −0.58 V vs S.C.E. decrease. On the other hand, new oxidations are observed at +0.05 and −0.50 V vs S.C.E. The most important effect is observed when the metal-to-ligand stoichiometric ratio is 1 : 1.

In order to prepare this compound a solution (3 mM) of both the quinone and zinc(II) was prepared and controlled-potential electrolysis at −0.92 V vs S.C.E. was attempted (peak potential = −0.72 V vs S.C.E.). As the electrolysis starts the current drops almost immediately to the residual value and the desired compound is not formed. Apparently, this compound precipitates and passivates the electrode.

The cyclic voltammograms of Fig. 3 show that the reduction of free quinone does not shift to more negative potentials in the presence of the metal ion, as would be the case if some interaction exists between these two species. Furthermore, the UV–vis spectra of the quinone ligand do not change in the presence of zinc(II), as is illustrated in Figs 4(B) and (C). Therefore, we can conclude that there is no interaction between the metal ion and the quinone.

As the peak current for the reduction of quinone to semiquinone almost doubles and the reduction of the free semiquinone to the corresponding dianion almost disappears, this would be indicative that a very stable complex forms between the metal ion and the dianion produced as a consequence of the reduction of the ligand.

The dianion was produced by controlled-potential electrolysis at −1.62 V vs S.C.E. of a solution (3.0 mM) of the quinone and then zinc(II) ions were added to the solution to produce 1 : 1 and 1 : 2 metal-to-ligand mole ratios. The cyclic voltammograms of the resulting solutions are shown in Fig. 5, whereas the corresponding UV–vis spectra are illustrated in Fig. 6. Notice that the cyclic voltammograms and the spectra indicate that when the metal-to-dianion stoichiometric mole ratio is 1 : 2

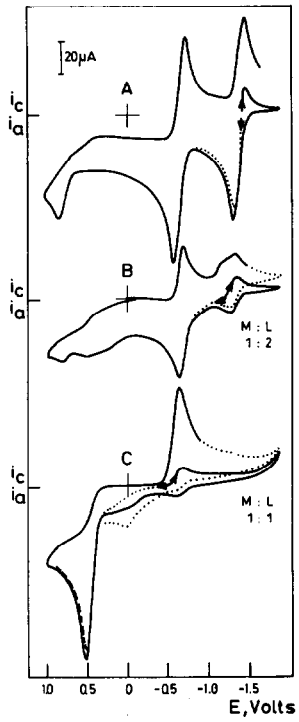

Fig. 5. Cyclic voltammograms (0.1 M TEAP; $v = 0.1$ V s^{-1}) of solutions in Me_2SO containing: (A) 2,3-dimethoxy-1,4-naphthoquinone (3 mM) after electrolysis at −1.62 V vs S.C.E. (DA^{2-}); (B) and (C): solution (A) after the addition of 1.5 and 3 mM $[Zn(DMU)_6](ClO_4)_2$, respectively.

the free dianion is absent, because its oxidation peak at −1.29 V vs S.C.E. is not observed and its characteristic absorption maxima at 300 and 410 nm do not occur. Therefore, we can conclude that a very stable 1 : 2 zinc(II)-dianion complex is formed, which is oxidized very easily at −0.66 and +0.50 V vs S.C.E.

$$Zn^{2+} + 2DA^{2-} \longrightarrow Zn(DA)_2^{2-}$$

$$Zn(DA)_2^{2-} \xrightarrow{-0.66\,V} ZnDA + Q + 2e^-$$

$$ZnDA \xrightarrow{+0.50\,V} Zn^{2+} + Q + 2e^-$$

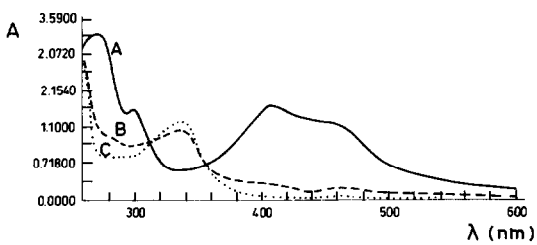

Fig. 6. Absorption spectra of solutions in Me_2SO containing: (A) 2,3-dimethoxy-1,4-naphthoquinone (3 mM) after electrolysis at −1.62 V vs S.C.E. (DA^{2-}); (B) and (C): solution (A) after the addition of 1.5 and 3 mM $[Zn(DMU)_6](ClO_4)_2$, respectively.

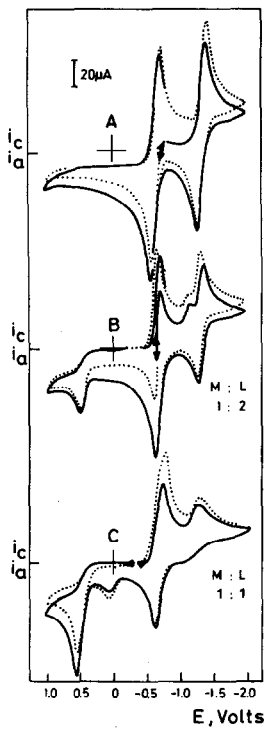

Fig. 7. Cyclic voltammograms (0.1 M TEAP; $v = 0.1$ V s^{-1}) of solutions in Me_2SO containing: (A) 2,3-dimethoxy-1,4-naphthoquinone (3 mM) after electrolysis at −0.92 V vs S.C.E. ($SQ^{\cdot -}$); (B) and (C): solution (A) after the addition of 1.5 and 3 mM $[Zn(DMU)_6](ClO_4)_2$, respectively.

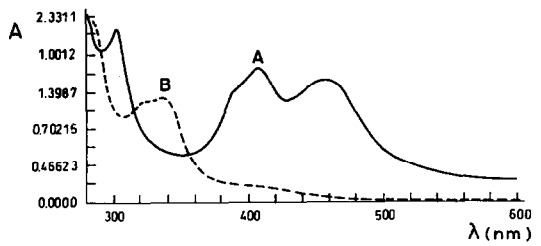

Fig. 8. Absorption spectra of solutions in Me_2SO containing: (A) 2,3-dimethoxy-1,4-naphthoquinone (3 mM) after electrolysis at −0.92 V vs S.C.E. ($SQ^{\cdot -}$); (B) solution (A) after the addition of 3 mM $[Zn(DMU)_6](ClO_4)_2$.

In the presence of excess zinc(II) the solution becomes colourless and another very stable complex with a 1 : 1 stoichiometric mole ratio is formed, which is oxidized in a single step at +0.50 V vs S.C.E. to the corresponding quinone and the free metal ion.

$$Zn^{2+} + DA^{2-} \longrightarrow ZnDA$$

$$ZnDA \underset{-0.65\,V}{\overset{+0.50\,V}{\rightleftharpoons}} Zn^{2+} + Q + 2e^-$$

This complex has an absorption maximum at 338 nm ($\varepsilon = 5113\ M^{-1}\ cm^{-1}$), which is very close to the absorption maximum of the quinone (330 nm, $\varepsilon = 3301\ M^{-1}\ cm^{-1}$) but with a larger extinction coefficient.

Upon the addition of zinc(II) the semiquinone completely disproportionates and as a consequence both the concentration of free quinone and the zinc-dianion complex increase.

$$Zn^{2+} + SQ^{\cdot -} \longrightarrow 1/2ZnDA + 1/2Q + 1/2Zn^{2+}$$

The UV–vis spectrum of this solution [Fig. 8(B)] shows an absorption band that ranges from 300 to 338 nm with an extinction coefficient of 4380 M^{-1} cm^{-1}, which confirms that half of the ligand is present as the quinone (330 nm; $\varepsilon = 3301\ M^{-1}\ cm^{-1}$) and half as the zinc-dianion complex (338 nm; $\varepsilon = 5113\ M^{-1}\ cm^{-1}$). Therefore, if we consider a contribution of 50% of the concentration as the quinone and 50% as the zinc-dianion complex the result is an absorbance such as that shown in Fig. 8(B).

Notice that if the complex is produced by direct combination of the metal ion and the dianion of the ligand it is oxidized in one step (+0.50 V) to the corresponding quinone and the free metal ion, whereas when the quinone is reduced in the presence of Zn^{2+} [Figs 3(B), 3(C), 3(D), 5(C) and 7(C)] the species being formed on the surface of the electrode is oxidized in two steps, which is probably due to the formation of a lower stability complex with the semiquinone. It was not possible to study the latter complex because in the presence of the metal ion the semiquinone disproportionates and the formation of the dianion complex is favoured.

Based on the behaviour of the zinc(II) complexes with 3,5-di-tert-butyl-catechol[11] we assume that the semiquinone complex formed on the surface of the electrode has 1 : 1 stoichiometry and from the shift in the oxidation potentials we could estimate their conditional formation constants.[11] Unfortunately, the voltammetric behaviour of these species is not reversible and it was not possible to determine their exact value. However, the oxidation of bound semiquinone to free quinone occurs 1.08 V more positive than the oxidation of free semiquinone, whereas the oxidation of bound dianion to bound semiquinone occurs 1.34 V more positive than the oxidation of the free dianion. This indicates that the corresponding conditional formation constants are large.

From our observations we can conclude that in this case the stability of the *para*-semiquinone complex is not enough to preclude the disproportionation of the ligand, considering that the dianion complex is much more stable. The complex

with the dianion is further stabilized due to the presence of methoxy groups in the *ortho* position with respect to the hydroxylic oxygens. This observation may be pertinent to the redox chemistry of related systems in biology.

REFERENCES

1. S. Patai, *The Chemistry of the Quinonoid Compounds*, Part 2. John Wiley and Sons, London (1974).
2. R. H. Thomson, *Naturally Occurring Quinones*. Butterworths Publications Ltd, London (1957).
3. R. A. Morton, *Biochemistry of Quinones*. Academic Press, New York (1965).
4. V. Arancibia and M. E. Bodini, *An. Quím.* 1986, **82B**, 309.
5. V. Arancibia and M. Bodini, *An. Quím.* 1988, **84C**, 26.
6. M. E. Bodini and V. Arancibia, *Polyhedron* 1989, **8**, 1407.
7. M. E. Bodini and V. Arancibia, *Polyhedron* 1991, **10**, 1929.
8. G. L. Lawrence and D. T. Sawyer, *Coord. Chem. Rev.* 1978, **27**, 173.
9. S. E. Jones, D. H. Chin and D. T. Sawyer, *Inorg. Chem.* 1981, **20**, 4257.
10. C. G. Pierpont and R. M. Buchanan, *Coord. Chem. Rev.* 1981, **38**, 45.
11. M. E. Bodini, G. Copia, R. Robinson and D. T. Sawyer, *Inorg. Chem.* 1983, **22**, 126.
12. P. J. Crowley and H. M. Haendler, *Inorg. Chem.* 1962, **1**, 905.
13. S. R. Sofen, D. C. Ware, S. R. Cooper and K. N. Raymond, *Inorg. Chem.* 1979, **18**, 234.
14. R. G. Pearson, *J. Chem. Ed.* 1968, **45**, 581.
15. D. T. Sawyer and J. Roberts, *Experimental Electrochemistry for Chemists*, p. 212. Wiley Interscience, New York (1974).
16. D. F. Evans, *J. Chem. Soc.* 1959, 2003.
17. M. F. Rettig, private communication, University of California, Riverside, California, U.S.A.
18. B. N. Figgis and J. Lewis, *Modern Coordination Chemistry* (Edited by J. Lewis and R. G. Wilkins). Interscience, New York (1960).
19. P. W. van Loenwen and W. L. Groenwald, *J. Inorg. Nucl. Chem. Lett.* 1967, **3**, 145.

Polyhedron Vol. 12, No. 14, pp. 1751–1756, 1993
Printed in Great Britain

0277–5387/93 $6.00+.00
© 1993 Pergamon Press Ltd

SYNTHESIS, SPECTRAL AND STRUCTURAL CHARACTERIZATION OF A BRIDGING CHLORO COMPLEX OF MANGANESE(II) WITH PICOLINIC ACID; $[Mn(C_5H_4NCO_2H)(C_5H_4NCO_2)Cl]_2$

MOHAMED A. S. GOHER

Department of Chemistry, Faculty of Science, Alexandria University, Alexandria 21321, Egypt

and

MORSY A. M. ABU-YOUSSEF* and FRANZ A. MAUTNER†

Institut für Physikalische und Theoretische Chemie, Technische Universität Graz, A-8010 Graz, Austria

and

ALOIS POPITSCH

Institut für Anorganische Chemie, Karl-Franzens-Universität Graz, A-8010 Graz, Austria

(*Received* 10 *February* 1993; *accepted* 30 *March* 1993)

Abstract—The title compound of manganese(II) with picolinic acid was synthesized and characterized by spectroscopic and X-ray crystallographic methods. In the structure of the complex $[Mn(C_5H_4NCO_2H)(C_5H_4NCO_2)Cl]_2$ each manganese(II) atom is coordinated by two nitrogen atoms at Mn—N distances of 2.268(6) Å and two carboxylic oxygen atoms O(1) at Mn—O bond lengths of 2.191(4) Å, belonging to two picolinato groups. The Cl^- anions act as bridging ligands to build edge-sharing dimeric Mn_2Cl_2 units [Mn—Cl = 2.500(2) Å] with the Mn···Mn separation of 3.608(2) Å and Cl···Cl separation of 3.462(1) Å. The four-membered dimeric Mn_2Cl_2 rings are planar and oriented along the *c*-axis of the unit cell. The O(2)···O(2) separation between non-coordinated carboxylate oxygen atoms of adjacent dimeric coordination polyhedra is 2.423(7) Å. The IR and Raman spectral results confirm the existence of neutral picolinic acid as well as the picolinate anion. The vibrational bands of diagnostic value are compared with the values of the carboxylic acid and the free anion.

There is continuing interest in the synthesis and characterization of manganese(II)-picolinic acid complexes.[1–4] This, on one hand, is due to the identification of several manganese biomolecules that appear to contain di- and tetranuclear manganese units, including the water oxidation/oxygen evolution centre within the photosynthesis apparatus of green plants and cyanobacteria,[5] the manganese catalases[6] and even the recently identified manganese ribonucleotide reductases.[7] A further reason comes from the fact that picolinic acid and its derivatives have a broad spectrum of physiological effects on the activity functions of both animal and plant organisms, which have been attributed to their ability to form complexes with transition metals.[8] In this regard many complexes of picolinic acid and its derivatives together with their crystal structures have been reported.[9–12]

* On leave from the Department of Chemistry, Faculty of Science, Alexandria University.

† Author to whom correspondence should be addressed.

Recently we described the preparation and characterization of gold(III) halide complexes of picolinic acid (hereafter abbreviated as: H-pic), together with the crystal structure of $[AuBr_4][K(H\text{-}pic)_2(H_2O)_2]\cdot(H\text{-}pic)_2$[13] as well as the structure of $Mn(pic)(N_3)(H_2O)$.[14] In the present work we employed picolinic acid in preparing the title manganese(II) chloride complex and determined its structure by spectroscopic and X-ray crystallographic methods, in order to elucidate the molecular and coordination geometry.

EXPERIMENTAL

Preparation of the $[Mn(C_5H_4NCO_2H)(C_5H_4NCO_2)Cl]_2$ *complex*

The complex compound was prepared by dissolving $MnCl_2\cdot 4H_2O$ (1.44 g, 10 mmol) in ethanol (20 cm^3) with stirring at 298 K. Picolinic acid (2.46 g, 20 mmol) was then dissolved in warmed ethanol (15 cm^3) and added dropwise. The turbidity was filtered off and the clear solution mixture allowed to stand in a dark, cold place for several days. Transparent yellow crystals of the complex were obtained, filtered, washed with a little amount of ethanol, air dried and kept in a desiccator. The complex is insoluble in many polar solvents, e.g. water, alcohols, acetone, $CHCl_3$, etc., as well as benzene and CCl_4. Found: C, 42.6; H, 2.1; N, 8.0; Cl, 10.8. Calc.: C, 42.9; H, 2.7; N, 8.3; Cl, 10.6%.

The experimental procedures and instruments used for spectral measurements have been given previously.[14]

X-ray analysis

The density of the crystals was determined by flotation in CCl_4/CH_2Br_2. A prism-shaped crystal was measured at 300(2) K on a modified STOE four-circle diffractometer. The cell dimensions were determined from setting angles of 50 reflections. Intensity data were collected with graphite monochromatized Mo-K_α radiation ($\lambda = 0.71069$ Å) and processed in the usual way (corrections: LP factor, but no absorption or extinction).

The structure was solved via the heavy-atom procedure and Fourier syntheses (following full-matrix least-squares, with scattering factors calculated using the data from ref. 15). All non-hydrogen atoms were refined with anisotropic displacement factors. Four hydrogen atoms were identified in difference maps and included in the refinements with isotropic U values, but with constraints applied to the positional parameters. The programs SHELX-76,[16] SHELXS-86,[17] PLATON[18] and THE XRAY SYSTEM[19] were used for computations. Crystallographic data and processing parameters are given in Table 1 and selected bond distances and bond angles in Table 2. Positional parameters, anisotropic thermal parameters, a full list of bond lengths and angles and observed and

Table 1. Crystallographic data of $[Mn(H\text{-}pic)(pic)Cl]_2$

Chemical formula	$C_{24}H_{18}Cl_2Mn_2N_4O_8$
Formular mass	671.2
Crystal system	Tetragonal
a (Å)	14.836(5)
c (Å)	24.346(9)
V (Å^3)	5359(3)
Space group	$I4_1/acd$ (No. 142; choice 2)
N	16
$F(000)$	2704
D_{calc}/D_{obs} (Mg m^{-3})	1.66(2)/1.664
Approx. crystal size (mm)	$0.50\times0.16\times0.15$
Data collection limits (°)	$2\theta < 50$
Scan mode	ω-scan, $\Delta\omega = 1.5°$
Number of observed reflections (criterion)	549 [$I > 4\sigma(I)$]
Least squares parameters	96
μ(Mo-K_α) (mm^{-1})	1.16
R	0.045
R_w	0.040
Weighting scheme	$2.660/\sigma^2(F_o)$
Residual extrema in final difference map (e Å^{-3})	0.33/−0.39

Table 2. Selected bond distances (Å) and angles (°)

Mn—Cl	2.500(2) 2x	Mn—O(1)	2.191(4) 2x
Mn—N	2.268(6) 2x	O(1)—C(6)	1.250(8)
O(2)—C(6)	1.266(8)	N—C(1)	1.330(9)
N—C(5)	1.334(10)	C(1)—C(6)	1.502(9)
C(1)—C(2)	1.377(9)	C(2)—C(3)	1.381(12)
C(3)—C(4)	1.368(12)	C(4)—C(5)	1.390(11)
Mn···Mn(b)	3.608(2)	Cl···Cl(a)	3.462(1)
O(2)···O(2d)	2.243(7)		

Mn—Cl—Mn(b)	92.38(4)	Cl—Mn—Cl(a)	87.63(5)
Cl—Mn—O(1)	106.9(1)	Cl—Mn—N	93.5(1)
O(1)—Mn—N	73.3(2)	O(1)—Mn—O(1a)	154.2(2)
O(1)—Mn—N(a)	88.3(2)	N—Mn—O(1a)	88.3(2)
N—Mn—N(a)	89.4(2)	Mn—O(1)—C(6)	118.1(4)
Mn—N—C(1)	114.8(4)	Mn—N—C(5)	127.4(5)
C(1)—N—C(5)	117.8(6)	N—C(1)—C(6)	114.6(6)
N—C(1)—C(2)	123.3(6)	C(6)—C(1)—C(2)	122.1(6)
C(1)—C(2)—C(3)	118.6(7)	C(2)—C(3)—C(4)	118.9(7)
C(3)—C(4)—C(5)	118.9(8)	N—C(5)—C(4)	122.5(7)
O(1)—C(6)—C(1)	118.8(6)	O(1)—C(6)—O(2)	123.6(6)
C(1)—C(6)—O(2)	117.6(6)		

Symmetry code: (a) $3/4-y, 3/4-x, 3/4-z$; (b) $-x, 1/2-y, z$; (c) $1/4+y, 3/4+x, 3/4-z$; (d) $1/2-x, y, -z$.

calculated structure factors have been deposited with the Editor as supplementary material.

RESULTS AND DISCUSSION

The reaction between picolinic acid and manganese(II) chloride afforded a complex of the formula $[Mn(H\text{-pic})(pic)Cl]_2$, which differs from the frequently produced complexes of the type $M(pic)_2 \cdot nH_2O$, $n = 0$, 2 or 4, which have been described previously.[3,9–12] The manganese complex is similar to those obtained for cobalt(II), nickel(II) and copper(II) of the type M(H-pic)(pic)X, reported earlier.[20–22]

The room-temperature magnetic moment value of 5.8 B.M. found for the manganese(II) complex falls very well within the range reported for octahedral manganese(II) complexes.[23] This result is consistent with the X-ray structure analysis of the complex given in Fig. 1, which illustrates its essential structural features. $[Mn(H\text{-pic})(pic)Cl]_2$ crystallizes in the tetragonal I-centred lattice with 16 formulae per unit cell. Both heavy atoms occupy special positions with site symmetry 2; the manganese(II) centre, the special position 16d (0, 1/4, z), the Cl^- anion, the special position 16f (x, $x+1/4$, 1/8). The 16 neutral H-pic and 16 picolinato anions are located on the general position 32g of space group $I4_1/acd$. Thus, in this crystal structure it is not possible by X-ray crystallography to distinguish between the H-pic and (pic^-) molecules.

As seen from Fig. 1, each manganese(II) atom is six-coordinated via the N and O(1) atoms of H-pic

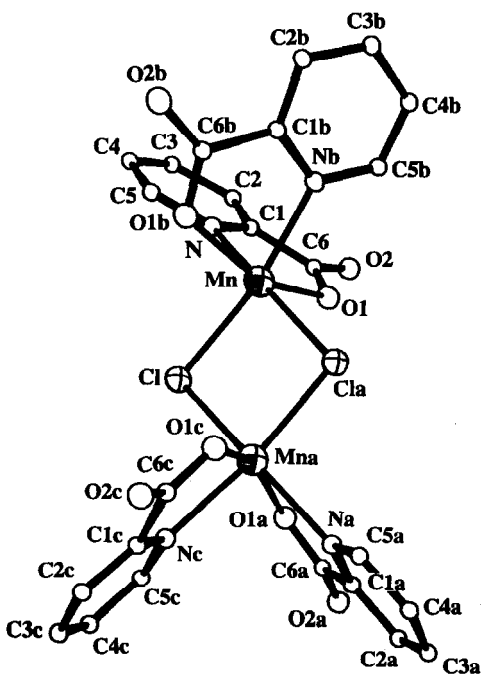

Fig. 1. The molecular structure of $[Mn(H\text{-pic})(pic)Cl]_2$ and the atom numbering scheme. Hydrogen atoms are omitted.

and (pic^-) molecules with Mn—N and Mn—O(1) bond lengths of 2.268(6) and 2.191(4) Å, respectively, and two Cl^- anions. The Cl^- anions act as bridging ligands to build edge-sharing dimeric units. The dimeric units are oriented along the *c*-axis of the unit cell. There is evidence that a hydrogen bond of the type O(2)—H(5)···O(2d) exists. The O(2)···O(2d) separation between adjacent coordination polyhedra is 2.423(7) Å. Attempts to locate the H(5) atom on the calculated position (with site occupation of 1/2; due to space group symmetry the vice versa hydrogen bond O(2d)—H(5d)···O(2) is also generated) failed. The O(2)···O(2d) separation is very close to that found in the structure of the silver(I) picolinate complex, $Ag(C_5H_4NCO_2H_{1/2})_2 \cdot H_2O$;[11] the hydrogen atoms are, therefore, equally shared by the $—COO^-$ groups and there is no distinct molecule of silver(I) picolinate. Within the dimeric units the Mn···Mn(b) separation is 3.608(2) Å and the Cl···Cl(a) separation equals 3.462(1) Å. The four-membered Mn_2Cl_2 ring is planar (restriction of the two two-fold rotation axes normal to each other). The Mn—Cl distances are equal [2.500(2) Å] and the Mn—Cl—Mn(b) angle is 92.38(4)°, whereas the Cl—Mn—Cl(a) angle equals 87.63(5)°. These manganese–chloride bonds and angles are comparable with those reported for other manganese(II) complexes, e.g. $[(CH_3)_3NH]_3Mn_2Cl_7$ [Mn—Cl from 2.369(3) to 2.559(3) Å, Mn···Mn = 3.208(3) Å, Mn—Cl—Mn = 77.46(8)° and Cl—Mn—Cl = 85.20(9) and 95.00(9)°].[24]

The coordination mode of the picolinato group in the title complex differs from that found in the $Mn(pic)(N_3)(H_2O)$ complex.[14] In the latter complex the picolinato anion chelates a metal atom via its ring nitrogen and a carboxylate oxygen to form a five-membered ring. The chelating carboxylate oxygen is further bridging another manganese(II) centre, giving rise to dimeric Mn_2O_2 units.[14] The type of bonding of the picolinate anion in the title complex, however, is similar to that observed in the structure of $[Mg(pic)_2(H_2O)_2]$.[9]

The room-temperature IR and Raman spectra of the crystalline picolinic acid, the sodium salt of the picolinic acid and the $[Mn(H\text{-}pic)(pic)Cl]_2$ complex are given together with tentative assignments of the bands in Table 3. The (N—Mn—N) bending, (Mn-pic) torsion and (Mn-pic) rocking vibrational modes are expected to be of lower energy and probably responsible for the complex group of bands between 30 and 180 cm^{-1}. Coupling of these modes with lattice vibrations and Mn_2Cl_2 deformations may also produce spectral features in this region.

In the high energy region hydrogen bonding involving the carboxylic acid group is considerable and causes very broad bands of the type (O—H···O) centred around 3400 cm^{-1}, which is observed in both the free acid as well as the solid complex, indicating the presence of the picolinic acid form (—COOH) in the complex. Hydrogen bonding of the type (O—H···N) is indicated in the free acid by the presence of broad, medium strong bands near 2565, 2150 and 2070 cm^{-1}.[25] These bands are completely absent in the spectra of the solid complex, as well as the corresponding salt, indicating that all nitrogen atoms are involved in the coordination with the central metal ion.[26]

The ν_{as}(—COOH) vibration frequencies of the free picolinic acid at 1719 s,br, 1655 m (IR)[27,28] and 1691 ms, 1655 vw (Raman) are shifted to lower frequencies at 1655 s, 1625 s (IR) for the sodium salt of picolinic acid. The solid complex shows a broad medium to strong band at 1713 cm^{-1}, a very strong band at 1636 cm^{-1} (IR) and a medium to strong band at 1638 cm^{-1} (Raman). This result suggests that the complex contains both coordinated picolinic acid and picolinate anion, since complexes containing only picolinate anions, and as shown in the sodium salt, do not show any absorption in the vicinity of 1700 cm^{-1}.[3,4] Compared with the sodium salt, the complex shows a slight increase of $\nu_{as}(—COO^-)$, 1636 vs (IR) and 1638 wm (Raman), and a decrease of $\nu_s(—COO^-)$, to 1355 s (IR) and 1388 m (Raman), which is indicative of bidentate coordination as was found for acetato complexes.[29,30]

It is noticeable that some bands of the free picolinic acid are broad, similar to those of the pyridine moiety, and not shifted. However, the bands related to the pyridine ring in the solid complex are shifted to higher frequencies, e.g. the ring breathing mode *ca* 1014 vs, 1018 vs (IR) and 1010 vs, 1020 vs (Raman), indicating also the presence of two different pyridine moieties. N,O-bidentate neutral picolinic acid exhibits the ν_{as}(—COOH) mode at a little higher wave number in the spectrum of the $[AuBr_4][K(H\text{-}pic)_2(H_2O)_2] \cdot (H\text{-}pic)_2$ complex[13] when compared with that of the free acid. Thus, while the above IR and Raman spectral results indicate the N,O-bidentate picolinato anion, it is not clear from ν_{as}(—COOH) that the H-pic molecule is linked via its carbonyl oxygen atom. However, as no bands in the range 1340–1310 cm^{-1} attributable to ν_s(—COOH) could be detected in the spectrum of the complex, one may suggest N,O-bidentate coordination for the neutral picolinic acid molecule in the title complex as well (cf. structural data).

In the far-IR region we tentatively assigned the medium strong bands at 376 (IR) and 335 cm^{-1} (Raman) as ν(Mn—O(pic)) and 230 vs (IR) and 240 w (Raman) to ν(Mn—N(pic)). According to the

Table 3. Vibrational frequencies (cm^{-1}) in the IR, far-IR and Raman spectra of [Mn(H-pic)(pic)Cl]$_2$, picolinic acid and Na-picolinate

Picolinic Acid IR	Picolinic Acid Raman	Na-Picolinate IR	[Mn(H-pic)(pic)Cl]$_2$ IR	[Mn(H-pic)(pic)Cl]$_2$ Raman	Assignments
				32 (200)	
	46 (25)			48 (80)	(pic)N—Mn—N(pic)
65 m	68 (250)	76 m	70 w	70 (300)	bends, Mn—pic
82 ms	86 (300)	84 m	99 m	95 (80)	rocks and torsions[a]
97 ms	100 (500)	102 s	105 m	118 (250)	and Mn_2Cl_2
113 ms	115 (25)		131 ms	130 (80)	deformation
148 s	153 (25)	161 vs	139 m		
177 vw	200 (50)	193 vs	151 m	160 (35)	
			185 sh	182 (20)	ν (Mn—Cl)
			205 vs	198 (110)	
			230 vs	240 (20)	ν (Mn—N(pic))
266 vs	268 (10)	265 sh	284 vs	275 (10)	
			376 m	335 (20)	ν (Mn—O(pic))
			416 s	410 (10)	2×205
405 vs	405 (5)	405 s	440 sh	432 (15)	Pyridine
420 vs	420 (20)	431 sh	455 sh	449 (10)	
500 s		520 m	500 s	505 (5)	
540 s					
618 ms	616 (25)	620 ms	625 sh	620 (10)	Pyridine
630 vs	631 (30)	625 ms	638 vs	631 (40)	Pyridine
680 vs	676 (5)				δ (COO)
688 vs					
698 m	696 (15)	708 s	695 vs	695 (15)	Pyridine
705 s					
752 vs	775 (5)	752 s	758 vs	767 (10)	Pyridine + 2×370
768 vs			770 vs		
802 s	800 (5)	800 sh	800 s,br		2×405
820 ms	823 (15)	836 ms	818 s,br		$405 + 420$
838 ms	833 (5)	848 ms	835 ms	832 (40)	Pyridine
	841 (50)		860 s,br		
966 s					δ(OH) out of plane
995 s	997 (20)	996 ms	1005 s	980 (10)	Pyridine
1010 s	1011 (100)	1010 ms	1014 s	1010 (100)	Pyridine
			1018 s	1018 (70)	
1048 s	1038 (25)	1049 s	1048 s	1038 (30)	Pyridine
	1051 (30)				
1088 s	1088 (10)	1091 wm	1096 s	1088 (30)	Pyridine
1159 s	1150 (20)	1154 m	1159 ms	1150 (30)	Pyridine
1170 s	1170 (20)	1175 wm	1180 m	1170 (30)	
1198 s	1236 (8)	1238 m	1242 m	1250 (15)	Pyridine
1220 s			1262 m		
1252 s	1258 (5)	1260 m	1278 sh	1258 (20)	2×630
1294 vs	1296 (2)	1291 m	1300 ms	1294 (20)	Pyridine
1307 vs	1302 (10)	1392 vs	1353 ms	1388 (25)	ν_s (—COO^-)
1343 vs	1355 (25)		1385 m	1410 (35)	Pyridine
1372 sh	1377 (25)	1412 vs	1423 wm		Pyridine
1410 wm	1410 (10)				δ (OH) in plane
1439 s	1440 (5)	1439 s	1447 m	1442 (25)	Pyridine
1455 vs	1487 (5)	1474 wm	1485 m	1472 (35)	Pyridine
1529 s	1573 (40)	1565 vs	1570 s	1562 (50)	Pyridine
1573 s					
1595 vs	1596 (60)	1584 vs	1593 vs	1582 (40)	Pyridine
1608 vs	1610 (10)	1607 vs			4×405
	1621 (20)				
1655 ms	1655 (5)	1625 s	1636 vs	1638 (20)	ν_{as}(—COO^-) and/or
		1655 s			
1719 s	1691 (20)		1713 s		ν_{as}(—COOH)

v = very, m = medium, s = strong, w = weak, br = broad, sh = shoulder, ν_{as} = asymmetric vibration, ν_s = symmetric vibration; relative intensities of the Raman bands are given in parentheses.

[a] The notation for the metal–ligand bends, rocks and torsions is that used in ref. 34.

bridging nature of the chloride ion, forming a four-membered ring (Mn_2Cl_2), ν(Mn—Cl) are shifted to lower frequencies at 205 vs, 185 (sh) (IR) and 198 vs, 182 sh (Raman). The assignments of both ν(Mn—N) and ν(Mn—Cl) are given in accordance with those reported earlier[31–33] for complexes of the type MnL_2Cl_2 (L = substituted pyridine ligand) containing bridging octahedral geometry.

Acknowledgements—F.A.M. thanks Doz. Dr Ch. Kratky for the use of his equipment. M.A.M.A.-Y. thanks Prof. H. P. Fritzer for very helpful correspondence and the Austrian Academic Exchange Service ÖAD for the award of a research studentship.

REFERENCES

1. B. N. Figgis, C. L. Raston, R. P. Sharma and A. H. White, *Aust. J. Chem.* 1978, **31**, 2545.
2. E. Libby, R. J. Webb, W. E. Streib, K. Folting, J. C. Hoffman, D. N. Hendrickson and G. Christou, *Inorg. Chem.* 1989, **28**, 4037.
3. A. Kleinstein and G. A. Webb, *J. Inorg. Nucl. Chem.* 1971, **33**, 405.
4. D. L. Hoof, D. G. Tisley and R. A. Walton, *Inorg. Nucl. Chem. Lett.* 1973, **9**, 571.
5. T. K. Goindjee and W. Coleman, *Photochem. Photobiol.* 1985, **42**, 187; J. Amesz, *Biochim. Biophys. Acta* 1983, **1**, 726.
6. W. F. Beyer Jr and I. Fridovich, *Biochemistry* 1985, **24**, 6460; R. M. Franko, J. E. Penner-Hahn and C. J. Bender, *J. Am. Chem. Soc.* 1988, **110**, 7554.
7. A. Willing, H. Follman and G. Auling, *Eur. J. Biochem.* 1988, **170**, 603.
8. B. A. Bovikin, A. M. Omel'Chenko, R. N. Sharonina and I. A. Zanina, Abstracts of Proceedings of the 15th All-Union Chugaevskii Conference on the Chemistry of Complex Compounds, Vol. 1, p. 229. Ukraine (1985).
9. P. J.-P. Deloume, H. Loiseleur and G. Thomas, *Acta Cryst.* 1973, **B29**, 668.
10. P. J.-P. Deloume and H. Loiseleur, *Acta Cryst.* 1974, **B30**, 607.
11. P. J.-P. Deloume, R. Faure and H. Loiseleur, *Acta Cryst.* 1977, **B33**, 2709.
12. Z. G. Aliev, L. O. Atovmyan, E. A. Saratovskikh, V. I. Krinichnii and V. G. Kartsev, *Izv. Akad. Nauk SSSR, Ser. Khim.* 1988, **11**, 2495.
13. M. A. S. Goher, A. E. H. Abdou, W.-H. Yijs and T. C. W. Mak, *Polyhedron*, accepted.
14. M. A. S. Goher, M. A. M. Abu-Youssef, F. A. Mautner and A. Popitsch, *Polyhedron* 1992, **11**, 2137.
15. *International Tables for X-ray Crystallography*, Vol. IV, pp. 99 and 149. Kynoch Press, Birmingham (1974).
16. G. M. Sheldrick, SHELX-76, A Program for Crystal Structure Determination. University Chemical Laboratory, Cambridge (1976).
17. G. M. Sheldrick, SHELXS-86. Universität Göttingen, F.R.G. (1986).
18. A. L. Spek, in *Computational Crystallography* (Edited by D. Sayre), p. 528. Clarendon Press, Oxford (1982).
19. J. M. Stewart, The X-RAY SYSTEM, version of 1976, Technical Report TR-466. University of Maryland, College Park (1976).
20. G. W. A. Fowles, R. W. Matthews and R. A. Walton, *J. Chem. Soc. (A)* 1968, 1108.
21. V. M. Ellis, R. S. Vagg and E. C. Watton, *J. Inorg. Nucl. Chem.* 1974, **36**, 1031.
22. V. M. Ellis, R. S. Vagg and E. C. Watton, *Aust. J. Chem.* 1974, **27**, 1191.
23. B. N. Figgis and J. Lewis, *Prog. Inorg. Chem.* 1964, **6**, 37.
24. R. E. Caputo, S. Roberts, R. D. Willet and B. C. Gerstein, *Inorg. Chem.* 1976, **15**, 820.
25. Y. Ichida, Y. Kuroda, D. Nakamura and M. Kubo, *Spectrochim. Acta* 1972, **28A**, 2433.
26. R. F. Evans and W. Kynaston, *J. Chem. Soc.* 1962, 1005.
27. S. Yoshida and M. Asai, *Chem. Pharm. Bull (Japan)* 1959, **7**, 162.
28. I. Nakagawa and T. Shimanouchi, *Spectrochim. Acta* 1964, **20**, 429.
29. A. B. P. Lever, J. Lewis and R. S. Nyholm, *J. Chem. Soc.* 1962, 5262.
30. K. Nakamoto, *Infrared and Raman Spectra of Inorganic and Coordination Compounds*. John Wiley, New York (1978).
31. M. Goldstein and W. D. Unsworth, *Inorg. Nucl. Chem. Lett.* 1970, **6**, 25.
32. M. Goldstein and W. D. Unsworth, *Spectrochim. Acta* 1972, **28A**, 1297.
33. A. B. P. Lever and B. S. Ramaswamy, *Can. J. Chem.* 1973. **51**, 1582.
34. C. D. Flint and A. B. Matthews, *Inorg. Chem.* 1975, **14**, 1008.

Polyhedron Vol. 12, No. 14, pp. 1757–1765, 1993
Printed in Great Britain

0277–5387/93 $6.00+.00
© 1993 Pergamon Press Ltd

STRUCTURES AND PROPERTIES OF ANTHRANILATO- AND N-PHENYLANTHRANILATO-RHODIUM(I) COMPLEXES CONTAINING TRIPHENYLPHOSPHINE LIGANDS

ANDRZEJ F. BOROWSKI*

Institute of Coal Chemistry, Polish Academy of Sciences, 5 Sowinskiego St, 44-100 Gliwice, Poland

and

DAVID J. COLE-HAMILTON*

Department of Chemistry, University of St Andrews, St Andrews, Fife KY16 9ST, U.K.

(*Received* 26 *February* 1993; *accepted* 30 *March* 1993)

Abstract—The structures of two triphenylphosphine rhodium(I) complexes with anthranilic and N-phenylanthranilic acid, which are active in hydrogenation of some alkenes, dienes, aromatic and heteroaromatic compounds, are described, together with some of their catalytic properties. A monomeric aminocarboxylate analogue of Wilkinson's catalyst is postulated for the anthranilate complex (**1**) and a dimeric structure with carboxylate bridges and two *cis*-triphenylphosphine molecules coordinated to each rhodium atom is proposed for N-phenylanthranilate (**2**). On treatment with hydrogen both complexes give *cis*-dihydrides, but variable temperature ^1H and ^{31}P NMR studies of the product derived from **1** reveal that a temperature-dependent equilibrium involving dissociation of PPh_3 occurs. Complexes **1** and **2** are stable under hydrogenation conditions and enable slow hydrogenation of 1-alkenes and cyclohexadienes. For cyclohexadienes some selectivity to cyclohexene formation is observed, especially in DMF. Although the activities of **1** and **2** towards the hydrogenation of arenes and heteroaromatics are generally very low, pyridine can be hydrogenated to piperidine to a substantial degree.

A rhodium complex of N-phenylanthranilic acid formulated as $[H\{Rh_2(PAA)_2Cl\}]$ (HPAA = N-phenylanthranilic acid) has been reported as one of a few homogeneous catalysts capable of arene hydrogenation.[1,2] Its structure as well as the structure of the other amino carboxylic acid complexes have not been fully elucidated. Khidekel[1] and co-workers suggest the existence of a rhodium to phenyl π-bond, apart from the bidentate O—C—O bond in the N-phenylanthranilato complex.[1,3]

Our previous studies revealed[4–6] that N-phenylanthranilate tends to form a bridging rather than a chelate linkage through the carboxylate anion, while the anthranilate (HAA = anthranilic acid) is liable to form monomeric structures with N—Rh—O bonds.[7–11]

The rhodium complexes with these two amino carboxylic acids and 1,5-COD (1,5-cyclooctadiene) described previously[7] turned out to be unstable under hydrogenation conditions. In this paper we report our structural and catalytic studies of the two anthranilato and N-phenylanthranilato complexes containing triphenylphosphines, i.e. ligands which are better than 1,5-COD at stabilizing the low oxidation state of the metal under a hydrogen atmosphere.

RESULTS AND DISCUSSION

Reaction of the green dirhodium cation Rh_2^{4+}, in a methanolic solution of triphenylphosphine,[12] with lithium or sodium anthranilate (NaAA) and

* Authors to whom correspondence should be addressed.

Table 1. Characteristic vibrational frequencies of the complexes **1**, **2** and sodium salts of the aminocarboxylic acids

Frequency (cm^{-1})[a]				
Sodium anthranilate	Sodium N-phenylanthranilate	**1**	**2**	Assignment
3440 w		3440 w		ν_{as}(N—H)
3330 w		3340 w		ν_{s}(N—H)
	3320 mbr		3270 mbr	ν(N—H)
		1635 vs		ν(C=O)
1530 vs	1610 m		1630 vs	$\nu_{as}(COO^{-})$
		1435 vs	1435 vs	ν(P—C_6H_5)
1395 vs	1380 vs		1395 vs	$\nu_{s}(COO^{-})$
		1360 vs		ν(C—O)
		1090 vs[b]	1090 vs[b]	δ(P—C_6H_5)

[a] In Voltalef 3S oil, if not stated otherwise.
[b] Nujol mulls.

the reaction of sodium N-phenylanthranilate (NaPAA) with $[\{RhCl(PPh_3)_2\}_2]$,[13] respectively, give products of stoichiometry $[Rh(AA)(PPh_3)_3]$ and $[Rh(PAA)(PPh_3)_2]$, which have been characterized by spectral methods.

IR spectra

Table 1 shows the characteristic vibrational frequencies of the two complexes, as well as of sodium salts of the amino carboxylic acids.

The N—H stretching vibrations of the anthranilic acid complex (**1**) appear almost at the same frequencies as those of sodium anthralinate, suggesting that the amine nitrogen remains uncoordinated in the complex.[7] Instead of ν_{as} and $\nu_{s}(COO^{-})$ bands present in the spectrum of sodium anthranilate there are two new bands in the spectrum of the complex at 1635 and 1360 cm^{-1}. The increase observed for ν_{as}(COO) is characteristic of carboxylic acids coordinated through only one of the oxygen atoms.[7,14]

The N—H stretching vibrations in **2** (Table 1) are only slightly shifted when compared with those of the sodium N-phenylanthranilate, suggesting that the nitrogen is uncoordinated in the complex. The positions of $\nu_{as}(COO^{-})$ and $\nu_{s}(COO^{-})$, differing marginally as compared with those found for sodium N-phenylanthranilate, and $\Delta\nu$ = 235 cm^{-1} favour a bridging O—C—O coordination[7,15] between two rhodium atoms.

Vibrational spectra of the solutions of the complexes under a hydrogen atmosphere reveal solvent independent bands in the region associated with ν(Rh—H) at *ca* 2000 cm^{-1} (Table 2). After solvent evaporation in a stream of hydrogen a bright yellow or a white precipitate for **1** and **2**, respectively, has been obtained. The solids darken when exposed to air, but are stable enough for their IR spectra to be taken. The IR spectrum of **2** shows two absorptions in the solid state and a single, broad signal in solution, whereas generally two bands are present for **1** both in the solid state and in solution. An additional absorption at 825 cm^{-1}, assignable to δ(Rh—H), has been observed for **2**. No further new bands could be found in the 800–600 cm^{-1} region for complex **1** in the solid state and for **1** and **2** in solution after treatment with hydrogen.

Table 2. IR [ν(Rh—H) region] bands for **1** and **2** after their treatment with hydrogen[a]

Complex	Solution ν(Rh—H)[b] (cm^{-1})	Solid ν(Rh—H)[b] (cm^{-1})
1+H_2	2125 brsh (CH_2Cl_2) 2120 br (C_6H_6)	2120 sh[c] 2060 m
2+H_2	2130 m, 2085 sh (DMF)	2160 m[d] 2120 m
	2115 m, 2070 m (C_6H_6)	2130 sh[e] 2070 m
	2130 brsh (CH_2Cl_2)	

[a] Ambient conditions.
[b] br = broad, m = medium, sh = shoulder.
[c] Solid obtained in CH_2Cl_2; Nujol mulls.
[d] Solid obtained in diethyl ether; silicone grease mull.
[e] Solid obtained in CH_2Cl_2; Voltalef 3S oil mull.

Solution studies followed via ^1H *and* ^{31}P *NMR spectroscopies*

Room-temperature ^1H NMR spectra of both complexes in CD_2Cl_2 show broad multiplet resonances from the phenyl protons of the amino carboxylic acids and PPh_3 with shifts of around δ 7 ppm (Table 3). There is no evidence for π-bonding of the phenyl ring in **2**. The amine proton resonances are broadened and appear centred at δ *ca* 5 (**1**) and δ *ca* 9 (**2**). The relative intensities of the amine to aromatic protons suggest the composition of one anthranilate per three PPh_3 in **1** and one N-phenylanthranilate group per two triphenylphosphine groups in complex **2**.

At room temperature in benzene only broad resonances are observed in the ^{31}P NMR spectrum of **1**. The low-temperature (223 K) spectrum in CH_2Cl_2 shows a doublet of doublets at δ −33.1 [$J(RhP_A)$ = 152 Hz], assignable to two equivalent ^{31}P nuclei and a doublet of triplets at δ 50.6 [$J(RhP_B)$ = 176.7, $J(P_AP_B)$ = 4 Hz] due to the unique phosphorus nucleus *trans* to oxygen, consistent with the structure shown in Scheme 1. Such a structure has been reported for many similar complexes containing other carboxylate anions.[16,17] However, some irreversible decomposition appears to occur after warming the solution to room temperature, as evidenced by a signal from free PPh_3 at δ *ca* −4 ppm and by the appearance of some weak sharp lines in the ^{31}P NMR spectrum.

On reaction of **1** with hydrogen (1 mol per 1 mol of rhodium is absorbed) at room temperature at least two hydrido compounds are formed. In the ^{31}P NMR (at 223 K where the resolution is better) one compound shows (Table 4) a doublet of doublets (δ 39.8) that has been assigned to two *trans* phosphorus atoms and a doublet of triplets (δ 24) originating from the unique phosphorus atom coupled to the mutually *trans* triphenylphosphines. Such a spectrum along with the hydride region of the ^1H NMR spectrum [δH_A −6.61, δH_B −17.1, $J(P_BH_A)$ = 165 Hz] allows unambiguous assignment of the compound as configuration **B** (Scheme 1).

The other resonance (a doublet at *ca* 43 ppm) arises from a different compound (**C**), since its relative intensity varies for different solvents and at different temperatures. The stereochemistry for **C** (Scheme 1) is assigned on the basis of the ^{31}P chemical shift of the phosphorus atoms, which is similar to that of the mutually *trans* phosphorus atoms in **1**. The important finding is that the two compounds (**B** and **C**) are interconvertible. At low temperatures (223 K, d_8-toluene) only **B** is observed, whilst at high temperatures (323 K) there are only signals attributable to **C**. At intermediate temperatures **B**

Table 3. Proton NMR data for rhodium complexes and for compounds formed in solution from **1** and **2** under hydrogen[a]

Complex	δ					Coupling (*J*/Hz)							
	N—H[b]	Ar[c]	H	H_A	H_B	H_AH_B	RhH	RhH_A	RhH_B	PH	P_AH_A	P_AH_B	P_BH_A	P_BH_B
$[Rh(AA)(PPh_3)_3]^d$ (**1**)	4.9(brs)[d]	7.9–5.9(m)[d]												
$[RhH_2^{A,B}(AA)(PPh_3)_3]^e$ (**B**)				−6.61(dm)[e]	−17.1(m)[e]	~9.5		5	16					
$[RhH_2(AA)(PPh_3)_2]^e$ (**C**)			−19.0(dt)[e]				22			17				
$[\{Rh(PAA)(PPh_3)_2\}_2]^d$ (**2**)	9.03(brs)[d]	8.0–6.3(m)[d]									10	16	165	8
$[RhH_2(PAA)(PPh_3)_2]^f$ (**D**)			−20.4(dt)[f]				24.5			17.1				

[a] Chemical shifts are in ppm relative to $SiMe_4$.
[b] Amine protons.
[c] Arene protons.
[d] In CD_2Cl_2, 298 K.
[e] In C_7D_8, 273 K.
[f] In C_6D_6, 183 K.

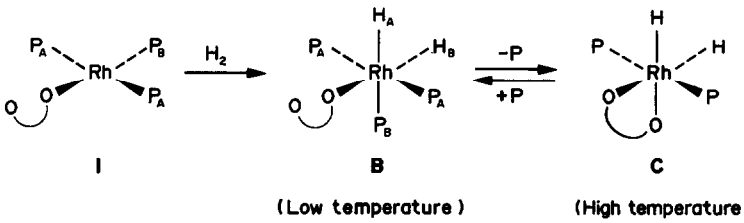

Scheme 1. Structure of **1** and the products of its reaction with hydrogen. P = PPh_3, O—O = anthranilato.

and **C** are observed in varying amounts (e.g. **B**/**C** ratio is *ca* 3.5 at 273 K in d_8-toluene), although some decomposition is observed after high temperature measurements.

The ^1H NMR spectrum of **C** consists of a doublet of triplets [δ −19.0 ppm, J(PH) = *ca* 17 Hz, J(RhH) = *ca* 22 Hz] and is changed into a doublet [J(RhH) = 21.8 Hz] on decoupling phosphorus.

These NMR spectral data indicate that under hydrogen at 243 K and above the new complex (**C**) is formed at the expense of **B**. Additionally, the existence of a coupling of rhodium to both dihydrides as well as to the two phosphorus atoms implies that a temperature dependent equilibrium between **B** and **C** occurs (Scheme 1).

Free triphenylphosphine is observed as a broad signal at δ −4 ppm at room temperature, but the breadth of the signal indicates that it is exchanging with compound **B** for which the signals are also broadened. Such an exchange is well established for the complex $[RhH_2Cl(PPh_3)_3]$, which has analogous stereochemistry.

It is very difficult to rationalize why no signal from free PPh_3 is observed at high temperature where compound **C** predominates, particularly as there does not appear to be exchange of the bound phosphines [J(RhP) is preserved], however, the stoichiometry of compounds **B** and **C** is certain since all the couplings have been confirmed by heteronuclear double resonance experiments. At 223 K the complex exists only in form **B**, hence no free phosphine is present in solution.

The ^{31}P NMR spectrum of **2** shows a doublet at δ 58.1 [J(RhP) = 200 Hz]. On the basis of this chemical shift, which is similar to that of the unique phosphorus atom in **1**, we assign this as arising from P *trans* to carboxylate and hence the compound must have two mutually *cis* phosphorus atoms.

We assumed the complex as a dimer (Scheme 2) on the basis of the known preference of N-phenylanthranilato anions for bridging rather than chelate binding to rhodium[4–6] and because monomeric *cis*-bis-triphenylphosphine complexes of rhodium(I) are unknown. On hydrogenation the phosphorus atoms remain equivalent (a doublet), but the resonance moves to higher fields (δ 42.1 ppm). The coupling constant also changes to a smaller value [J(RhP) = 119 Hz] that is consistent with a change of oxidation state from rhodium(I) to rhodium(III).[18,19] The proton NMR spectrum in C_6D_6 at 183 K shows a doublet of triplets [δ −20.4 ppm, J(PH) = 17.1 Hz, J(RhH) = 24.5 Hz].

Table 4. ^{31}P NMR data for rhodium complexes and for compounds formed in solution from **1** and **2** under a hydrogen atmosphere[a]

Complex	δ			Coupling (J/Hz)			
	P	P_A	P_B	RhP	RhP_A	RhP_B	P_AP_B
$[(Rh(AA)(PPh_3)_3]$[b] (**1**)		33.1(dd)[b]	50.6(dt)[b]		152[b]	176.7[b]	41[b]
$[RhH_2^{A,B}(AA)(PPh_3)_3]$[c] (**B**)		39.8(dd)[c]	24.0(dt)[c]		118.5[c]	83.3[c]	17[c]
$[RhH_2(AA)(PPh_3)_2]$[d] (**C**)	42.6(d)[d]			121.3[d]			
$[\{Rh(PAA)(PPh_3)_2\}_2]$[e] (**2**)	58.1(d)[e]			200[e]			
$[RhH_2(PAA)(PPh_3)_2]$[e] (**D**)	42.1(d)[e]			119[e]			

[a] Chemical shifts are in ppm to high-frequency of external 85% H_3PO_4. For assignment see Schemes 1 and 2.
[b] In CH_2Cl_2, 223 K.
[c] In C_7D_8, 223 K.
[d] In C_7D_8, 363 K.
[e] In C_6D_6, 297 K.

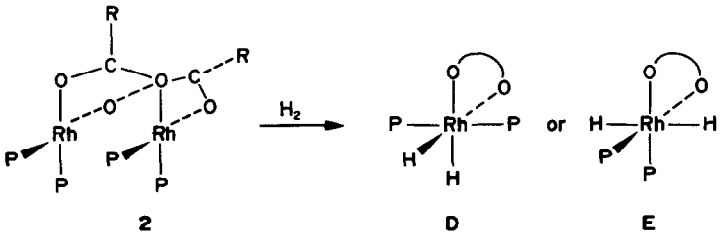

Scheme 2. Structure of **2** and the possible products of its reaction with hydrogen. P = PPh_3, O—O = N-phenylanthranilato.

Based on the findings suggesting that both phosphorus atoms as well as both hydrides are equivalent one can put forward two possible structures for the hydrido species formed (Scheme 2).

Structure **D** seems to be more likely since it can be formed directly from **2** by hydrogen activation, while **E** requires a rearrangement. Moreover, the upfield shift of the phosphorus resonance would be much smaller for **E** than that observed (Table 4) since in the starting complex (**2**) and in **E** the phosphorus atoms are *trans* to oxygen atoms. Additional support for structure **D** is provided by the IR studies of **2** under hydrogen, which show two ν(Rh—H) in the isolated solid. The dihydrido complex is formulated as a monomer since a dimeric formation with mutually *trans*-PPh_3 groups on the rhodium atoms would place two PPh_3 groups on different rhodium atoms unacceptably close together.

Catalytic studies

The catalytic activities of both complexes were evaluated for hydrogenation reactions of unsaturated compounds under ambient conditions or under pressure (Table 5). Reaction rates, expressed as the number of catalytic cycles per rhodium h^{-1}, are low and do not exceed *ca* 12 for 1-alkenes up to C_{10}.

The two isomers of cyclohexadiene are hydrogenated with slower rates than 1-alkenes and the hydrogen consumption remains constant throughout the course of the reaction. The hydrogenation of cyclohexa-1,3-diene in toluene catalysed by **2** produces 2 : 1 cyclohexene : cyclohexane after 10 h, suggesting that a two-stage hydrogenation process is in operation. The reaction stops after *ca* 10% total conversion as an uncharacterized yellow solid precipitates.

Generally, complexes **1** and **2** show similar activities in hydrogenation reactions of cycloalkadienes after comparable reaction times, but the 1,3-isomer is reduced a little faster than the 1,4-isomer. A similar phenomenon has been observed in the hydrogenation of cyclohexadiene isomers in the presence of cationic complexes of rhodium(I).[20] That process was, however, accompanied by a large degree of isomerization of 1,4-cyclohexadiene to the 1,3-isomer. Such an isomerization has not been observed in our studies.

By carrying out the hydrogenation of cyclohexadienes in DMF the catalyst lifetime can be enhanced and the conversion increased. The reaction still occurs in two stages and selectivities up to 7 : 1 in favour of cyclohexene can be obtained at low conversion. Since the substrate is not completely soluble in DMF, the reason for such a product composition may not be purely kinetic. It may depend on diffusion processes between DMF soluble and DMF insoluble layers.

Hydrogenation of mono- and bicyclic arenes and nitrogen containing heteroaromatics is generally ineffective with conversions below 3% being observed both at ambient conditions and under elevated pressure. However, pyridine, which normally inhibits hydrogenation by Wilkinson's catalyst, can be hydrogenated to piperidine in reasonable yield. This is a most unusual specificity and suggests that decomposition to rhodium metal is not responsible for the hydrogenation. In experiments performed under elevated pressure using neat benzene a pale yellow precipitate soluble in polar solvents was found when **1** was used. No such effects were observed for pyridine. Both bicyclic substrates naphthalene and quinoline are not susceptible to hydrogenation at ambient conditions, but naphthalene shows low conversion, at elevated pressure in acetone, to decalins in the presence of **1** or to a mixture of tetralin and decalins when **2** is used.

EXPERIMENTAL

Apparatus

Elemental analyses were performed by the Research Centre of Molecular and Macromolecular Studies, Polish Academy of Sciences, Lodz. Melting points were evaluated on an Electrothermal melting point apparatus in capilliary tubes sealed under

Table 5. Hydrogenation of selected alkenes, cyclohexadienes and aromatic compounds in the presence of **1** and **2** at 293 K[a]

Substrates	**1** Reaction time (h)	**1** Mol of prod. / mol of Rh (h)	**1** Products, wt (%)	**2** Reaction time (h)	**2** Mol of prod. / mol of Rh (h)	**2** Products, wt (%)
1-Hexene	10	11	n-Hexane, 100	10	11	n-Hexane, 100
1-Decene	10	11	n-Decane, 100	10	11	n-Decane, 100
Cyclohexene	16	7	Cyclohexane, 100	12	9	Cyclohexane, 100
1,3-Cyclohexadiene[b]	12		Cyclohexane, 6.5 Cyclohexene, 50	9		Cyclohexane, 8 Cyclohexene, 55
	30		Cyclohexane, 14 Cyclohexene, 75	24		Cyclohexane, 32 Cyclohexene, 68
1,3-Cyclohexadiene[c]	2[d]	1.1 6.2[e]	Cyclohexane, 2 Cyclohexene, 7	10	3.4 7 (10.3)[e]	Cyclohexane, 30 Cyclohexene, 62
				20	3.8 1.8 (5.6)[e]	Cyclohexane, 67 Cyclohexene, 33
1,4-Cyclohexadiene[c]	2[d]	2.8 6.7[e]	Cyclohexane, 5 Cyclohexene, 7	15	2.5 4.8 (7.3)[e]	Cyclohexane, 33 Cyclohexene, 65
Benzene	21		Cyclohexane, Traces	6	—	Cyclohexane, Traces
Benzene[f]				6	—	Cyclohexane, Traces
				20	1.1	Cyclohexane, 1

Benzene[f,g]	6	19	Cyclohexane, 1.9			
Benzene[f,h]				6	30	Cyclohexane, 2
Naphthalene[i]	10	—	No conversion	10	—	No conversion
Naphthalene[g,j]	6	0.2	*Cis*-decalin, 0,8	6	—	*Cis*-decalin, Traces
			Trans-decalin, 1,8		—	*Trans*-decalin, Traces
					0.5	Tetralin, 2.1
Pyridine[f,k]				6	1.1	Piperidine, 3.3
Pyridine	9	2.1	Piperidine, 17	7	1.4	Piperidine, 9
Quinoline	6	—	No conversion	6	—	No conversion

[a] Unless mentioned otherwise: 0.05 mmol of rhodium and 5.6 mmol of substrate in DMF (40 cm^3), pressure 0.1 MPA.
[b] Sparingly soluble in DMF; GC analysis performed for DMF soluble part of the reaction solution.
[c] Toluene.
[d] Reaction time for homogeneous solutions.
[e] Calculated based on the assumption that cyclohexane is formed in a two-stage reaction. It involves hydrogenation of the diene to cyclohexene (stage 1), followed by its hydrogenation to cyclohexane (stage 2).
[f] 112 mmol.
[g] 0.02 mmol of rhodium, 5 MPa.
[h] 0.012 mmol of rhodium, 5 MPa.
[i] In acetone (40 cm^3).
[j] 3 mmol of naphthalene in acetone (10 cm^3).
[k] 0.05 mmol of rhodium, 5 MPa.

vacuum and are uncorrected. IR absorption spectra in Nujol and Voltalef 3S oil were recorded on a Specord 71 IR spectrophotometer. ^1H and ^{31}P NMR spectra were acquired on a Bruker WM 250 spectrometer (University of Liverpool) operating in the Fourier-transform mode with proton noise decoupling (^{31}P). GC analyses of napthalene and the products of its hydrogenation were performed on a Chrom-4 apparatus using a steel column (3 m × 3 mm) packed with EGA (10%) on Chromosorb W (80–100 mesh). The other GC analyses were performed as described previously.[6]

Materials

Analytical grade reagents and solvents were used throughout. $RhCl_3 \cdot 3H_2O$ (40% rhodium) was purchased from Fluka AG, N-phenylanthranilic acid from Loba and anthranilic acid from POCH. DMF was freshly distilled and dried over molecular sieves. Toluene and benzene were dried over sodium and distilled under argon. Triphenylphosphine and naphthalene were recrystallized from ethyl alcohol. Solvents and reagents were degassed prior to use and reactions as well as other operations were performed under oxygen-free (BTS catalyst) argon or hydrogen using standard Schlenk-line and catheter-tubing techniques.

Preparation of the complexes

Preparation of the anthranilato complex was based on the techniques described by Mitchell *et al.*[21] for a range of carboxylate analogues of Wilkinson's catalyst.

Anthranilato-O-tris(triphenylphosphine)rhodium(I), $[Rh\{O_2C(C_6H_4)NH_2\}(PPh_3)_3]$ (**1**). To a solution of PPh_3 (0.5 g, 1.9 mmol) in methanol (50 cm^3) was added a green methanol solution of Rh_2^{4+}[12] (10 cm^3, *ca* 0.2 mmol of rhodium), followed by an excess of a methanolic solution (20 cm^3) of lithium anthranilate (0.86 g, 6 mmol). The resulting orange–red solution was boiled for *ca* 20 min and filtered hot. On cooling the orange–yellow crystals were collected, washed with methanol and vacuum dried (yield 0.16 g, 80%). Found: C, 70.8; H, 5.2; N, 1.3; P, 8.6; Rh, 10.1. Calc. for $RhC_{61}H_{51}NO_2P_3$: C, 71.3; H, 5.0; N, 1.4; P, 9.1; Rh, 10.0%. This compound always crystallizes in two forms; the major one gives orange needles, m.p. 135–138°C (decomposition), whilst the minor one forms yellow rhombs, m.p. 192–196°C (decomposition).

Di-μ-N-phenylanthranilato-O,O′-tetrakis(triphenylphosphine)dirhodium(I), $[Rh_2\{O_2C(C_6H_4)NH(C_6H_5)\}_2(PPh_3)_4]$ (**2**). A mixture of $[\{RhCl(PPh_3)_2\}_2]$[13] (0.33 g, 0.25 mmol) and sodium N-phenylanthranilate (0.18 g, 0.75 mmol) was heated under reflux in THF (20 cm^3) for 4 h. After cooling a red solution was decanted and the solvent evaporated under vacuum. The resulting red precipitate was washed thoroughly with water, vacuum dried at *ca* 40°C and dissolved in acetone (12 cm^3). The red solution was filtered promptly and left overnight at room temperature. The reddish-brown (terracotta) crystals were collected and washed with cold (0°C) acetone before drying *in vacuo* (yield 0.19 g, 45%); m.p. 180°C (darkens), 192–197°C (melts). Found: C, 69.5; H, 4.9; N, 1.7; P, 7.1; Rh, 11.9 ± 0.6. Calc. for $Rh_2C_{98}H_{80}N_2O_4P_4$: C, 70.0; H, 4.8; N, 1.7; P, 7.4; Rh, 12.2%.

Hydrogenation apparatus and procedure

Apparatus. Hydrogenations under atmospheric pressure were performed in a glass reactor (500 cm^3) fitted with a reflux condenser, a set of stopcocks to allow inlet and outlet of gases and introduction of reagents and a mercury burette for pressure equilibration. Intensive agitation was ensured by means of a magnetic stirrer. A catalyst was placed in a teflon bucket and suspended inside the reactor over the surface of a solvent and could be brought into contact with the solvent on turning the arm on which it was hanging.

Reactions under elevated pressure were performed in an apparatus consisting of a stainless reactor (250 cm^3) equipped with a glass vessel (*ca* 70 cm^3) closed with a stopper containing a capilliary orifice for pressure equilibration, a set of stopcocks to allow inlet and outlet of gases and a magnetic stirrer ensuring effective agitation.

Procedure. Hydrogenations under ambient conditions. To a reactor containing the solvent, degassed prior to its saturation with hydrogen, a catalyst was introduced and agitation ensured. After *ca* 15 min of exposure to hydrogen the degassed substrate was added. The amount of hydrogen consumed during the course of the reaction was estimated from the pressure drop in the closed reactor–burette system.

Hydrogenations under elevated pressure. To a glass vessel filled with hydrogen and containing a catalyst, a solvent saturated with hydrogen was introduced. After the catalyst was dissolved a degassed substrate was added. The vessel was closed with the stopper containing a capillary orifice and installed inside the reactor filled with hydrogen. The reactor was then flushed with hydrogen and after setting up a required pressure magnetic stirring was ensured. Conversions were measured using GC analysis of the product solution.

REFERENCES

1. O. N. Efimov, M. L. Khidekel', V. A. Avilov, P. S. Chekrii, O. N. Eremenko and A. G. Ovcharenko, *J. Gen. Chem., USSR* 1968, **38**, 2581.
2. O. N. Efimov, O. N. Eremenko, A. G. Ovcharenko, M. L. Khidekel' and P. S. Chekrii, *Bull. Acad. Sci., USSR Chem. Sect.* 1969, 778.
3. I. Rajca, *Pol. J. Chem.* 1981, **55**, 775.
4. V. A. Avilov, Yu. G. Borod'ko, V. B. Panov, M. L. Khidekel' and P. S. Chekrii, *Kinet. Catal. (USSR)* 1968, **9**, 582.
5. I. Rajca, A. Borowski and A. Marzec, *Erdöl u. Kohle* 1982, **35**, 36.
6. A. F. Borowski, *Trans. Met. Chem.* 1983, **8**, 266.
7. A. F. Borowski and I. Rajca, *Trans. Met. Chem.* 1984, **9**, 109.
8. A. G. Hill and C. Curran, *J. Phys. Chem.* 1960, **64**, 1519.
9. J. Decker and H. Frye, *Z. Naturforsch.* 1966, **21b**, 522.
10. G. S. Shephard and D. A. Thornton, *J. Molec. Struct.* 1973, **16**, 321.
11. E. Kwaskowska-Chec and J. J. Ziolkowski, *Trans. Met. Chem.* 1983, **8**, 103.
12. P. Legzdins, R. W. Mitchell, G. L. Rempel, J. D. Ruddick and G. Wilkinson, *J. Chem. Soc. A* 1970, 3322.
13. J. A. Osborn, F. H. Jardine, J. F. Young and G. Wilkinson, *J. Chem. Soc. (A)* 1966, 1711.
14. K. Nakamoto, *Infrared and Raman Spectra of Inorganic and Coordination Compounds*, 3rd edn, p. 232. Wiley-Interscience, New York (1978).
15. K. Nakamoto, *Infrared and Raman Spectra of Inorganic and Coordination Compounds*, 3rd edn, p. 304. Wiley-Interscience, New York (1978).
16. F. H. Jardine and P. S. Sheridan, in *Comprehensive Coordination Chemistry* (Edited by G. Wilkinson, R. D. Gillard and J. A. McCleverty). Pergamon Press, Oxford (1987).
17. L. Carlton, M.-P. Belciug and G. Pattrick, *Polyhedron* 1992, **11**, 1501.
18. P. Meakin, J. P. Jesson and C. A. Tolman, *J. Am. Chem. Soc.* 1972, **94**, 3240.
19. C. A. Tolman, P. Z. Meakin, D. L. Lindner and J. P. Jesson, *J. Am. Chem. Soc.* 1974, **96**, 2762.
20. R. R. Schrock and J. A. Osborn, *J. Am. Chem. Soc.* 1976, **98**, 4450.
21. R. W. Mitchell, J. D. Ruddick and G. Wilkinson, *J. Chem. Soc. (A)* 1971, 3224.

Polyhedron Vol. 12, No. 14, pp. 1767–1768, 1993
Printed in Great Britain

0277-5387/93 $6.00+.00
© 1993 Pergamon Press Ltd

^{31}P NMR STUDIES OF THE REACTIONS OF PHOSPHITES WITH SOME DICYANOPHOSPHINES

ROBERT M. K. DENG

Chemistry Department, University of Botswana, P/Bag 0022, Gaborone, Botswana

and

KEITH B. DILLON*

Chemistry Department, University of Durham, South Road, Durham DH1 3LE, U.K.

(*Received* 3 *March* 1993; *accepted* 30 *March* 1993)

Abstract—The reactions of some dicyanophosphines, $RP(CN)_2$ (R = Me, Et or Ph), with phosphites have been investigated in solution by means of ^{31}P NMR spectroscopy. In each instance a new P—P coupled compound was obtained, with no indication of organocyanophosphide ion, $RP(CN)^-$, formation, even when $NaPO(OEt)_2$ was used.

Although dicyanophosphines, $RP(CN)_2$, are well-established compounds, their reactions with phosphites have not been investigated. Schmidpeter and Zwaschka have shown that phosphorus tricyanide, $P(CN)_3$, reacts with $NaPO(OR)_2$ (R = Me or Et) and with $HPO(OR)_2$ in the presence of Et_3N to form salts of the dicyanophosphide ion,[1,2] eqs (1) and (2).

$$P(CN)_3 + NaPO(OR)_2 \longrightarrow Na^+P(CN)_2^- + NCPO(OR)_2 \quad (1)$$

$$P(CN)_3 + HPO(OR)_2 + Et_3N \longrightarrow Et_3NH^+P(CN)_2^- + NCPO(OR)_2 \quad (2)$$

(R = Me or Et)

The products were unstable in solution, but the anion could be stabilized as its [18]-crown-6 sodium derivative,[1] the crystal structure of which was subsequently determined.[2] In the absence of triethylamine, however, $P(CN)_3$ reacted with $HPO(OEt)_2$ to give a compound with a P—P bond, δ ^{31}P P_A-14, P_B-121 ppm, $^1J(PP)$ = 88 Hz [eq. (3)].

$$P(CN)_3 + HPO(OEt)_2 \longrightarrow HCN + (NC)_2P_BP_AO(OEt)_2 \quad (3)$$

The dicyanophosphide ion can also be prepared by reaction of $P(CN)_3$ with cyanide ions, when the initially formed phosphoranide $P(CN)_4^-$ loses cyanogen, eq. (4).[3,4]

$$P(CN)_3 + CN^- \longrightarrow [P(CN)_4]^- \longrightarrow P(CN)_2^- + (CN)_2 \quad (4)$$

We have shown that cyanide ions react with dicyanophosphides, $RP(CN)_2$ (R = Me, Et or Ph), leading to the formation of organocyanophosphide(I) ions by a similar pathway.[5] It was, therefore, of considerable interest to study the reactions of some dicyanophosphines with phosphites.

RESULTS AND DISCUSSION

In contrast with the behaviour of $P(CN)_3$ mentioned above, $MeP(CN)_2$ reacted in acetonitrile solution with $NaPO(OEt)_2$ yielding a P—P bonded compound **I**, to which the structure $Me(NC)P_BP_AO(OEt)_2$ may be attributed, eq. (5). (The ^{31}P NMR parameters for the new phosphorus compounds prepared in this work are given in Table 1.)

$$MeP(CN)_2 + NaPO(OEt)_2 \longrightarrow NaCN + Me(NC)P_BP_AO(OEt)_2 \quad (5)$$

I

*Author to whom correspondence should be addressed.

Table 1. δ ^{31}P (ppm) for the new P—P bonded compounds I–IV

Compound	δ ^{31}P (P_A)	δ ^{31}P (P_B)	^1J(PP) (Hz)	Solvent
I	26.6	−90.3	119	MeCN
II	30.9(±0.7)	−91.7(±0.6)	126(±10)	CH_2Cl_2
III	27.5	−77.5	158	CCl_4
IV	25.1	−76.6	117	CCl_4

All ^{31}P resonances are doublets.

This reaction parallels that reported for $P(CN)_3$ with $HPO(OEt)_2$ in the absence of base.[1]

A similar result was obtained for $MeP(CN)_2$ and $HPO(OMe)_2$ in CH_2Cl_2 solution. When a solution of the phosphite in this solvent was treated with $MeP(CN)_2$ two new doublets were seen in the ^{31}P spectrum (Table 1), as well as a doublet at 11.3 ppm, $^1J(PH) = 707$ Hz, from unreacted phosphite.[6] The phosphite doublet disappeared after the addition of more $MeP(CN)_2$, but the two new doublets were still present, together with a resonance at −81.5 ppm from excess $MeP(CN)_2$.[7] The reaction thus follows eq. (6), with the product **II** apparently stable in the presence of either excess phosphite or excess $MeP(CN)_2$.

$$MeP(CN)_2 + HPO(OMe)_2 \longrightarrow HCN + Me(NC)P_BP_AO(OMe)_2 \quad (6)$$

II

There was no evidence for formation of a cyanophosphide ion in either case.

Interestingly, $EtP(CN)_2$ did not react with $HPO(OMe)_2$ in CH_2Cl_2 solution, but yielded the analogous P—P bonded compound **III** in CCl_4 as the solvent.

$$EtP(CN)_2 + HPO(OMe)_2 \longrightarrow HCN + Et(NC)P_BP_AO(OMe)_2 \quad (7)$$

III

Similar behaviour was observed for $PhP(CN)_2$. No reaction was apparent with $HPO(OMe)_2$ in CH_2Cl_2, but the coupled compound **IV** was detected in CCl_4.

$$PhP(CN)_2 + HPO(OMe)_2 \longrightarrow HCN + Ph(NC)P_BP_AO(OMe)_2 \quad (8)$$

IV

We thus conclude that the dicyanophosphines react with either $NaPO(OEt)_2$ or $HPO(OMe)_2$ with the elimination of NaCN or HCN, respectively, and the formation of P—P coupled species, as clearly shown by ^{31}P NMR evidence. The main difference from the previously reported[1] reactions of $P(CN)_3$ with phosphites arises in the interaction of $MeP(CN)_2$ with $NaPO(OEt)_2$, where there was no indication of the presence of the $MeP(CN)^-$ ion[5] and the P—P derivative appeared to be stable in solution. The choice of solvent also seems to be critical for larger R groups in $RP(CN)_2$, with CCl_4 superior to CH_2Cl_2 in promoting reaction, although the reason for this behaviour was not readily apparent. The $P(CN)_2^-$ ion is likely to be appreciably more stable than $RP(CN)^-$, so the non-observation of the latter in these reactions is not surprising.

EXPERIMENTAL

All manipulations, including NMR sample preparation, were performed either *in vacuo* or under dry nitrogen. The dicyanophosphines were prepared as reported in a previous publication.[7] Sodium diethylphosphite, $NaPO(OEt)_2$, was synthesized by the method of Pudovik and Arbuzov.[8]

^{31}P NMR spectra were recorded at 307.2 K relative to external 85% H_3PO_4, as described previously,[7,9] with the higher frequency (lower field) direction taken as positive.

Acknowledgement—We thank the British Council for the award of a Postgraduate Technical Training grant (to R.M.K.D.).

REFERENCES

1. A. Schmidpeter and F. Zwaschka, *Angew. Chem., Int. Edn Engl.* 1977, **16**, 704.
2. W. S. Sheldrick, J. Kroner, F. Zwaschka and A. Schmidpeter, *Angew. Chem., Int. Edn Engl.* 1979, **18**, 934.
3. K. B. Dillon and A. W. G. Platt, unpublished work; A. W. G. Platt, PhD Thesis, Durham (1980).
4. A. Schmidpeter, personal communication.
5. R. M. K. Deng and K. B. Dillon, *J. Chem. Soc., Chem. Commun.* 1981, 1170.
6. V. Mark, C. H. Dungan, M. M. Crutchfield and J. R. Van Wazer, *Top. Phosphorus Chem.* 1967, **5**, 227.
7. R. M. K. Deng, K. B. Dillon and W. S. Sheldrick, *J. Chem. Soc., Dalton Trans.* 1990, 551.
8. A. N. Pudovik and B. A. Arbuzov, *Izvest. Akad. Nauk SSSR., Otdel Khim. Nauk* 1949, 522.
9. R. M. K. Deng and K. B. Dillon, *J. Chem. Soc., Dalton Trans.* 1984, 1911.

Polyhedron Vol. 12, No. 14, pp. 1769–1777, 1993
Printed in Great Britain

0277–5387/93 $6.00+.00
Pergamon Press Ltd

SYNTHESIS AND REACTIVITY OF TECHNETIUM(VII) IMIDO COMPLEXES

JEFFREY C. BRYAN,* ANTHONY K. BURRELL, MARY M. MILLER, WAYNE H. SMITH, CAROL J. BURNS and ALFRED P. SATTELBERGER

Los Alamos National Laboratory, Los Alamos, New Mexico 87545, U.S.A.

(*Received* 2 *January* 1993; *accepted* 30 *March* 1993)

Abstract—The synthesis, characterization and electrochemistry of a series of new technetium complexes, $Tc(NAr)_3X$ and $Tc(NAr')_3X$ ($X = OSiMe_3$, alkyl, I)†, is reported. These complexes are shown to be resistant to reduction and moderately air-sensitive. The siloxy complex $Tc(NAr)_3(OSiMe_3)$ (**1a**) reacts with fluoride ion to give the tris(imido)oxo anion $[TcO(NAr)_3]^-$. Less sterically hindered $M(NAr')_3(OSiMe_3)$ complexes react with Ar'NCO in a net [2+2] fashion to give the urylene complexes $M(NAr')_2(NAr'C(O)NAr')(OSiMe_3)$ (**2a**, M = Tc; **2b**, M = Re). The X-ray crystal structures of **1a**, **2b** and $Tc(NAr)_3I$ (**4a**) suggest that the imido ligands moderate their level of electron donation to reflect the electronic requirements of the metal and the ancillary ligands.

The coordination of multiple π-donors to a metal centre (π-loading) can result in increased stabilization of high-valent metal centres and/or in increased nucleophilicity of relatively inert ligands such as oxo (O^{2-}) or imido (RN^{2-}).[1,2] Technetium(VII) complexes are relatively rare, usually requiring stabilization by highly electronegative oxo, fluoride or chloride ligands, and are typically very sensitive to moist air and unstable towards reduction.[3] We set out to prepare new, stable technetium(VII) complexes using imido ligands. Rhenium complexes containing the imido (NR^{2-}) ligand are known for a variety of oxidation states and coordination numbers,[1,4–6] while technetium imido complexes have only recently been reported.[7] This paper describes the preparation of a series of new technetium(VII) imido complexes that are only slightly air-sensitive and remarkably stable towards reduction. Some of these complexes have been previously communicated.[8]

* Author to whom correspondence should be addressed.

† Abbreviations: Ar = 2,6-diisopropylphenyl; Ar' = 2,6-dimethylphenyl; PPN^+ = bis(triphenylphosphine) *iminium*.

RESULTS

Synthesis

When a hexamethyldisiloxane solution of $TcO_3(OSiMe_3)$[9] is treated with 3 equivalents of 2,6-diisopropylphenylisocyanate at 100°C for 18 h deep green $Tc(NAr)_3(OSiMe_3)$ (**1a**, Ar = 2,6-diisopropylphenyl) is formed (Scheme 1). Similar reactivity is observed for 2,6-dimethylphenylisocyanate and $TcO_3(OSiMe_3)$, forming $Tc(NAr')_3(OSiMe_3)$ (**1b**, Ar' = 2,6-dimethylphenyl),[10] although the reaction temperature must be lowered to 60°C and the reaction time shortened to 6 h. This prevents formation and subsequent thermal decomposition of the urylene complex $Tc(NAr')_2(NAr'C(O)NAr')(OSiMe_3)$ (**2a**, described below). Complex reactivity, involving the loss of $SiMe_3$, is observed when the less sterically hindered *p*-tolylisocyanate reacts with $TcO_3(OSiMe_3)$ under similar conditions. The latter result suggests that steric bulk about nitrogen is critical to the success of this reaction.

Preparations of **1b** can be complicated by the formation of the urylene complex $Tc(NAr')_2(NAr'C(O)NAr')(OSiMe_3)$ (**2a**). This complex most likely arises from the net [2+2] addition of the C=N bond of Ar'NCO with a Tc=N bond of **1b**. Similar [2+2] additions between imido ligands

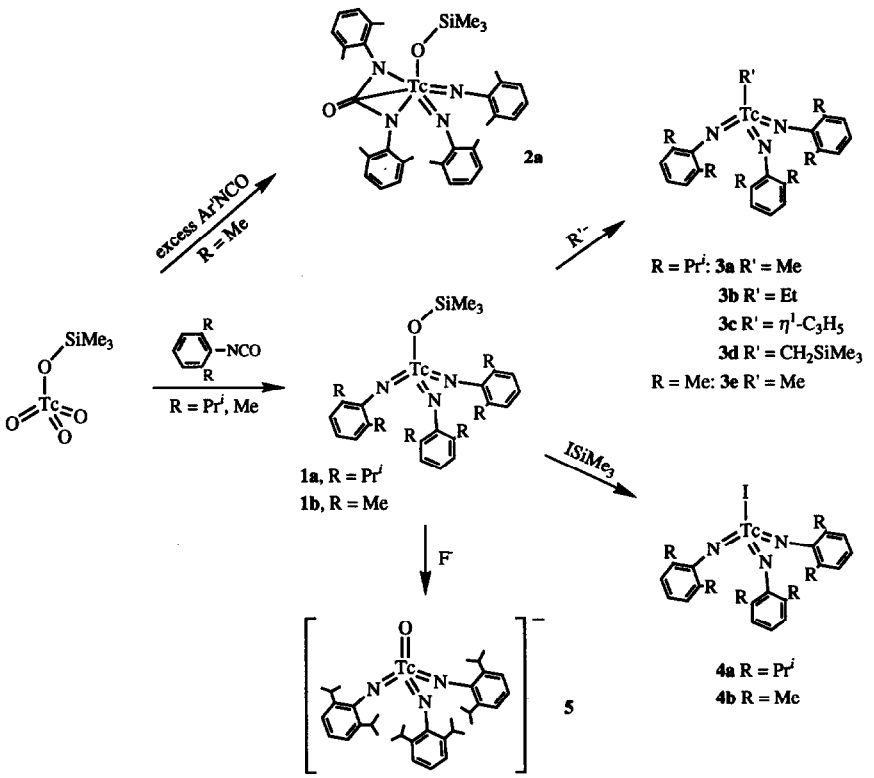

Scheme 1.

and isocyanates have recently been reported.[6,11] Formation of the urylene complex **2a** can be minimized by careful control of the relative amounts of reactants, temperature and time of reaction. Complex **2a** can be prepared in reasonable yield by heating an excess of Ar'NCO with $TcO_3(OSiMe_3)$ to 80°C in hexamethyldisiloxane solvent overnight. The rhenium analogue of **2a**, $Re(NAr')_2(NAr'C(O)NAr')(OSiMe_3)$ (**2b**), can be prepared by heating $Re(NAr')_3(OSiMe_3)$[5] and an excess of Ar'NCO in hexamethyldisiloxane solvent to 120°C for 15 h [eq. (1)].

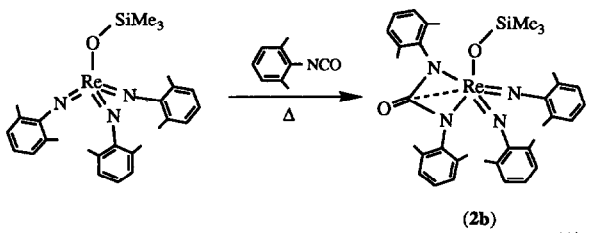

(1)

The bulkier tris(2,6-diisopropylphenylimido) complexes **1a** and $Re(NAr)_3(OSiMe_3)$[5] are not observed to react with excess ArNCO to form urylene complexes analogous to **2a** and **2b**.

The trimethylsiloxy ($^-OSiMe_3$) ligand in **1a, b** is readily substituted (Scheme 1). THF solutions of $Tc(NAr)_3(OSiMe_3)$ (**1a**) react quickly at room temperature with Grignard reagents to form deep blue–green $Tc(NAr)_3R$ (**3a–c**, R = Me, Et, η^1-allyl) and with $LiCH_2SiMe_3$ to form $Tc(NAr)_3(CH_2SiMe_3)$ (**3d**). Similarly, $Tc(NAr')_3(OSiMe_3)$ (**1b**) reacts with methyl Grignard in THF to form $Tc(NAr')_3Me$ (**3e**). Complexes **1a** and **1b** also react with trimethylsilyliodide in toluene forming $Tc(NAr)_3I$ (**4a**)[8c] and $Tc(NAr')_3I$ (**4b**), respectively. When this reaction is performed in a sealed NMR tube 1 equivalent of hexamethyldisiloxane is the only other observed product.

The trimethylsilyl group can be selectively removed from the trimethylsiloxy ligand in **1a** by fluoride ions (Scheme 1). A methylene chloride solution of **1a** reacts with [PPN]F [$PPN^+ = (Ph_3P)_2N^+$] to form the tris(imido)oxo anion $[TcO(NAr)_3]^-$ (**5**).[12] Complex **5** is a tris(imido) analogue of pertechnetate and is also formed, albeit in lower yields, when **1a** is treated with $^-OSiMe_3$.

Characterization

Complexes **1–5** have been characterized by NMR and combustion analysis. Additionally, complexes **1, 2b** and **3a–c** have been characterized by UV–vis and complexes **1b, 2** and **5** by IR. Generally, NMR spectra show a single set of resonances for the terminal imido ligands at room temperature, indi-

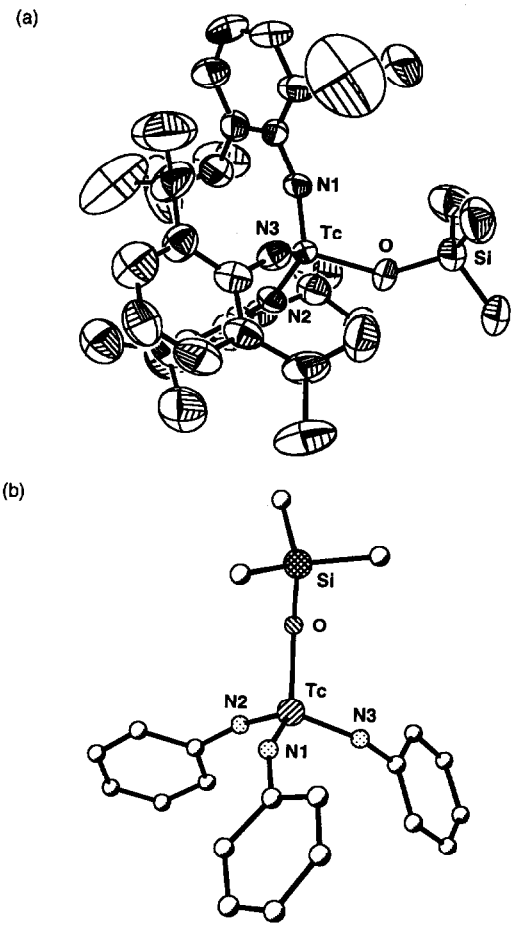

Fig. 1. Representations of $Tc(N\text{-}2,6\text{-}Pr^i_2C_6H_3)_3(OSiMe_3)$ (**1a**). (a) 40% thermal ellipsoids with hydrogen atoms omitted. (b) Ball and stick diagram with hydrogen atoms and isopropyl groups omitted. Selected bond angles (°) not already presented in Table 1. O—Tc—N(1) 111.3(3), O—Tc—N(2) 105.2(3), O—Tc—N(3) 109.9(3), N(1)—Tc—N(2) 111.3(3), N(1)—Tc—N(3) 109.9(3), N(2)—Tc—N(3) 109.1(3).

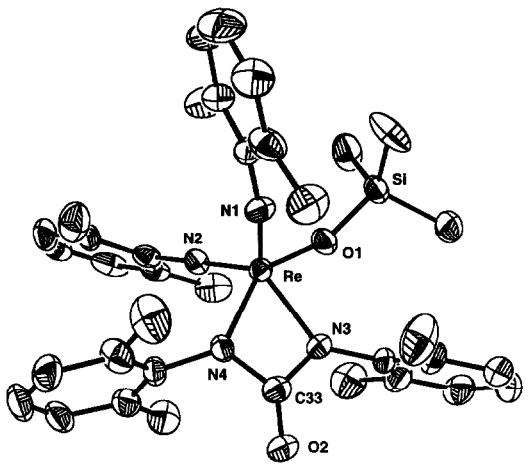

Fig. 2. ORTEP representation of $Re(NAr')_2(NAr'C(O)NAr')(OSiMe_3)$ (**2b**, Ar′ = 2,6-dimethylphenyl) with hydrogen atoms omitted. Selected bond distances (Å) and angles (°) not already presented in Table 1: Re—N(3) 2.035(7), Re—N(4) 2.052(7), Re···C(33), 2.627(9), O(1)—Re—N(1) 100.8(3), O(1)—Re—N(2) 100.2(3), O(1)—Re—N(3) 84.0(3), O(1)—Re—N(4) 146.0(3), N(1)—Re—N(2) 110.3(3), N(1)—Re—N(3) 119.6(3), N(1)—Re—N(4) 102.4(3), N(2)—Re—N(3) 128.1(3), N(2)—Re—N(4) 94.6(3), N(3)—Re—N(4) 63.0(3).

cating free rotation about the N—C bonds. The urylene complexes **2** exhibit three resonances in a 2:2:4 ratio attributable to CH_3 on the 2,6-dimethylphenyl groups. The largest of these three resonances can be assigned to the terminal imido ligands and the smaller two to the methyls on each of the Ar′ groups of the urylene ligand. This assumes free rotation about all N—C bonds, symmetry-related terminal imido groups and inequivalent environments for the 2,6-dimethylphenyl groups on the urylene ligand. This is consistent with the solid state structure (described below, see Fig. 2) determined for **2b**, where a mirror plane relates the two imido ligands and one urylene Ar′ is *cis* to the siloxy ligand and the other *trans*. The urylene carbonyl functionality is observed in the IR at 1676 and 1696 cm^{-1} and in the $^{13}C\{^1H\}$ NMR at δ 165.8 and 161.6 ppm for **2a** and **2b**, respectively. These values are comparable to known urylene complexes.[6,11] NMR spectra of $Tc(NAr)_3(C_3H_5)$ (**3c**) indicate that the allyl ligand is σ-bound to technetium in an η^1 fashion, as observed for a related rhenium complex, $Re(NBu^t)_3(C_3H_5)$,[6] and for the cyclopentadienyl ligand in $CpTc(NAr)_3$.[8b]

Complexes **1a**, **2b** and **4a** have been characterized by X-ray crystallography. The structures are shown in Figs 1–3, as are selected bond distances and angles specific to an individual structure. Additional bond distances and angles are presented in Table 1. The coordination geometry about the metal is approximately tetrahedral in all three complexes, assuming the urylene ligand in **2b** occupies one coordination site. Alternatively, the urylene complex **2b** could be described as a distorted square-based pyramid, where N(1) occupies the apex. All three structures exhibit short M—N bond lengths and large M—N—C angles for the terminal imido ligands, indicating considerable multiple bond character.[1] Similarly the M—O bond lengths and the M—O—Si angles in **1a** and **2b** suggest that there may be multiple bond character to the trimethylsiloxy ligand. In general, the bond distances and angles in **1a** and **4a** are similar to those observed for related $M(NR)_3X$ (X = monoanionic ligand) complexes.[2a,8b,13]

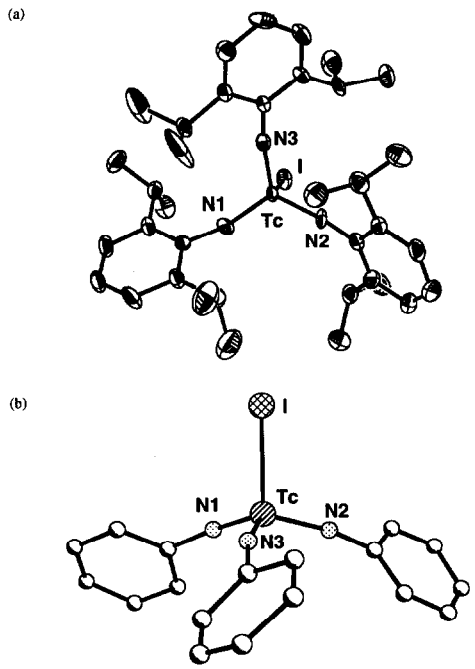

Fig. 3. Representations of $Tc(N\text{-}2,6\text{-}Pr^i_2C_6H_3)_3I$ (**4a**). (a) 40% thermal ellipsoids with hydrogen atoms omitted. (b) Ball and stick diagram with hydrogen atoms and isopropyl groups omitted. Selected bond distance (Å) and angles (°) not already presented in Table 1: Tc—I 2.654(1), I—Tc—N(1) 107.5(2), I—Tc—N(2) 105.7(2), I—Tc—N(3) 105.0(2), N(1)—Tc—N(2) 114.3(3), N(1)—Tc—N(3) 111.4(3), N(2)—Tc—N(3) 112.2(3).

The UV–vis spectra of these complexes exhibit very intense absorptions. Since these are d^0 complexes it is assumed that ligand-to-metal charge transfer is responsible for the observed transitions. The lowest energy absorption in the spectrum (200–800 nm) for $Tc(NAr)_3(OSiMe_3)$ (**1a**) is red shifted by 120 cm^{-1} relative to the same feature observed in the spectrum for $Re(NAr)_3(OSiMe_3)$. Such a shift

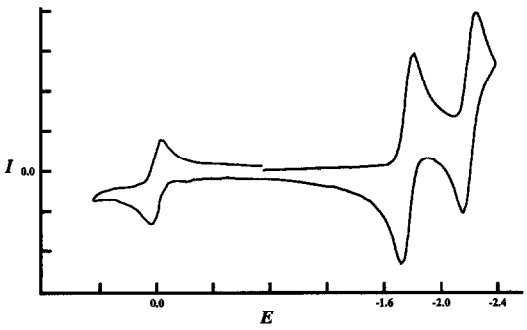

Fig. 4. Cyclic voltammogram showing reversible reductions of $Tc(NAr)_3(OSiMe_3)$ (**1a**, −1.77 V) and $Re(NAr)_3(OSiMe_3)$ (−2.21 V) and the Cp_2Fe/Cp_2Fe^+ couple as a reference (0.0 V).

is expected since the empty technetium-based 4*d* orbitals should be lower in energy, and therefore closer in energy to the filled ligand-based orbitals, than the analogous rhenium-based 5*d* orbitals.

Electrochemistry

Reductions of the d^0 complexes **1**, **3a**, **4a** and **5** were explored by cyclic voltammetry. Results are presented in Table 2. The tris(imido) complexes **1** and **3a** exhibit only a single reversible reduction up to −2.5 V. When scanned beyond this value additional features (irreversible reductions and oxidations) are observed in the voltammogram and the reversibility of the original reduction becomes questionable. As expected,[3a] the rhenium complex $Re(NAr)_3(OSiMe_3)$ is more difficult (440 mV) to reduce than its technetium analogue **1a** (Fig. 4). The tris(imido)iodide complex **4a** exhibits an irreversible reduction wave at −1.62 V when scanned at 0.20 V s^{-1}, which becomes reversible at higher scan rates (see Table 3). The chemical reduction of **4a** has been previously communicated.[8c] Additional details of

Table 1. Selected bond lengths (Å) and angles (°) in $Tc(NAr)_3(OSiMe_3)$ (**1a**), $\overline{Re(NAr')_2(NAr'C(O)NAr')}(OSiMe_3)$ (**2b**) and $Tc(NAr)_3I$ (**4a**)

	$Tc(NAr)_3(OSiMe_3)$	$\overline{Re(NAr')_2(NAr'C(O)NAr')}(OSiMe_3)$	$Tc(NAr)_3I$
M=N(1)	1.759(6)	1.746(7)	1.740(7)
M=N(2)	1.753(6)	1.749(7)	1.759(7)
M=N(3)	1.749(7)		1.763(6)
M—O	1.909(6)	1.889(6)	
Si—O	1.615(7)	1.654(7)	
M—N(1)—C	154.3(6)	165.8(6)	164.8(6)
M—N(2)—C	158.5(5)	175.5(6)	169.4(6)
M—N(3)—C	154.7(6)		165.6(6)
M—O—Si	145.7(4)	148.0(4)	

Table 2. Electrochemically measured *reduction* potentials for **1a**, **1b**, $Re(NAr)_3(OSiMe_3)$, **3a**, **4a** and **5**

Complex	No.	Ep_{red} (V)[a]	Ep_{ox} (V)[a]	ΔEp (V)
$Tc(NAr)_3(OSiMe_3)$	**1a**	−1.82	−1.72	0.10
$Tc(NAr')_3(OSiMe_3)$	**1b**	−1.76	−1.55	0.21
$Re(NAr)_3(OSiMe_3)$		−2.16	−2.26	0.10
$Tc(NAr)_3Me$	**3a**	−2.02	−1.80	0.22
$Tc(NAr)_3I$[b]	**4a**	−1.62	−1.39	0.23
$[PPN][Tc(NAr)_3O]$[c]	**5**	−2.51		

[a] Peak potentials relative to ferrocene/ferrocenium internal standard.
[b] Scan rate 0.5 V s^{-1}.
[c] CH_3CN was used as the solvent.

the chemical and electrochemical reductions of **4a** will be the subject of a future publication. The tris (imido)oxo anion **5** is the most difficult to reduce of all the complexes reported here, exhibiting an irreversible reduction wave at −2.51 V. Since complexes **1a**, **3a**, **4a** and **5** all contain the $[Tc(NAr)_3]^+$ fragment and differ only in the identity of the final ligand, an arrangement of these complexes by ease of reduction should reflect the relative donor ability of the unique ligand:

$$I^-, \mathbf{4a} > {}^-OSiMe_3, \mathbf{1a} > Me^-, \mathbf{3a} > O^{2-}, \mathbf{5}$$

$$\longleftarrow \text{ease of reduction}$$

Finally, it is more difficult to reduce **1a** than **1b**, which may indicate that 2,6-diisopropylphenylimido is a better donor than 2,6-dimethylphenylimido.

DISCUSSION

The complexes reported here contain several strong π-donor ligands, as such they are heavily "π-loaded". As a result of the competition between the strong π-donor ligands the imido ligands in these complexes are best represented by resonance structure **I**:

Table 3. Crystallographic data for $Tc(NAr)_3(OSiMe_3)$ (**1a**), $\overline{Re(NAr')_2(NAr'C(O)NAr')}(OSiMe_3)$ (**2b**) and $Tc(NAr)_3I$ (**4a**)

Complex	$Tc(NAr)_3(OSiMe_3)$	$\overline{Re(NAr')_2(NAr'C(O)NAr')}(OSiMe_3)$	$Tc(NAr)_3I\cdot(THF)_{0.5}$
Formula	$C_{39}H_{60}N_3OSiTc$	$C_{36}H_{45}N_4O_2SiRe$	$C_{38}H_{55}IN_3O_{0.5}Tc$
f_w	713.9	781.0	787.7
Crystal dimensions (mm)	0.20 × 0.24 × 0.40	0.49 × 0.40 × 0.08	0.39 × 0.36 × 0.37
Space group	*Cc*	$P2_1/n$	*Fdd*2
a (Å)	12.077(2)	10.541(4)	36.867(6)
b (Å)	19.477(4)	19.581(12)	39.261(10)
c (Å)	17.914(4)	17.388(4)	10.485(2)
β (°)	95.90(3)	94.71(2)	
V (Å^3)	4191.3(14)	3577(3)	15,177(5)
Z	4	4	16
ρ_{calc} (g cm^{-3})	1.13	1.45	1.38
μ (cm^{-1})	3.91	35.1	12.2
Temperature (K)	298	298	203
θ limits (°)	1–25	1–25	2–27.5
Transmission factors	0.888–0.829	0.514–0.812	0.223–0.324
Total number of reflections	8136	6734	9528
	$\pm h, k, \pm l$	$\pm h, k, l$	$h, k, \pm l$
Observed reflections	5341	4554	6552
	$F > 6\sigma_F$	$F > 2.5\sigma_F$	$F > 3\sigma_F$
Final number of variables	404	398	381
R	0.044	0.048	0.060
R_w	0.066	0.048	0.072

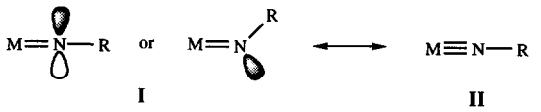

I II

where the metal–nitrogen bond order is lowered, bending at nitrogen *may* be observed and electron density is displaced from the metal–nitrogen bond to the nitrogen atom making the imido ligand more nucleophilic at nitrogen.[1,2]

The effects of π-loading can be observed in the structures of **1a** and **4a**. Terminal imido ligands can generally be expected to be linear at nitrogen when they are able to donate both pairs of p-π electrons. All the Tc—N—C angles in complexes **1a** ($\angle$Tc—N—C_{av} = 155.8°) and **4a** ($\angle$Tc—N—C_{av} = 166.6°) are bent significantly from 180°, falling within the range often observed for complexes with multiple π-donors.[1,2a,8b,13] The iodo complex (**4a**) is closer to being linear at nitrogen than the siloxy complex (**1a**), and while **1a** is very close to tetrahedral about technetium **4a** is distorted towards a trigonal-based pyramid where the iodide occupies the apex. These differences are probably due to the greater electronic dominance of the imido ligands in **4a**, where there is less competition from the more weakly donating I^-. Similar comparison of the structures for **1a** and **2b** ($\angle$Tc—N—C_{av} = 170.6°) suggests that replacement of an imido with a urylene ligand allows the remaining imido ligands to donate more strongly. These three structures suggest that the imido ligands moderate their donor ability depending on donor strength of the other ligands.

π-loading can also be used to rationalize some of the reactivity reported here. Extra electron density at the imido nitrogen is observed in the formation of the urylene complexes **2**, if the reaction is viewed as nucleophilic attack by an imido nitrogen on the isocyanate carbon.[11a,14] Subsequent reaction of the remaining imido ligands in **2** with isocyanate, forming additional urylene ligands, is probably inhibited because the imido ligands in **2** have less competition for π-electron density, are able to donate to technetium more strongly and are, therefore, less nucleophilic at nitrogen.[11a] Since the trimethylsiloxy ligand in complexes **1** is a good π-donor on a π-loaded complex, it may also exhibit nucleophilic character at oxygen. This is observed in the reactions of Me_3SiI with complexes **1**, which can be thought of as electrophilic attack of Me_3Si^+ at the siloxy oxygen.

The tris(imido) fragment "$[Tc(NAr)_3]^+$" imparts a high degree of stability to the normally oxidizing Tc^{VII} centre. For instance, electrochemical studies on the tris(imido) complexes demonstrate that they are difficult to reduce. Additionally, the tris(imido)siloxy (**1**) and tris(imido)alkyl (**3**) complexes are stable to air as solids for extended periods. Complex **1a** decomposes in solutions exposed to air over 2–3 days. $Tc(NAr)_3(CH_2SiMe_3)$ (**3d**) is stable to 1 equivalent of water in Et_2O solution at room temperature for 18 h! The tris(imido)technetium fragment is even capable of stabilizing iodide, a ligand that is quite susceptible to oxidation.[15] In fact, complexes **4** are the first examples of technetium(VII) iodide complexes.[16] $Tc(NAr)_3I$ (**4a**) is also stable to moist air in solution for short periods. All of this contrasts strongly with known oxotechnetium(VII) complexes, which are generally more sensitive to moist air and unstable towards reduction.[3]

EXPERIMENTAL

General considerations

CAUTION! ^{99}Tc is a weak β^--emitter (E = 0.3 MeV, $t_{1/2} = 2.12 \times 10^5$ years). All experiments are performed in designated laboratories approved for low-level radioactive materials following procedures and techniques described below and elsewhere.[17] All manipulations were performed in a helium atmosphere dry-box equipped with a freezer (−40°C) or in a well-ventilated fume hood with the appropriate secondary containment. Personnel are trained in the safe handling of radioactive materials, use beta–gamma counters to detect areas of contamination and wear protective lab. coats, approved safety glasses and disposable gloves at all times. Every reasonable effort was made to recover ^{99}Tc from reaction residues. Radioactive wastes were disposed of in appropriate containers.

Toluene, hexane, THF, diethyl ether, hexamethyldisiloxane and dimethoxyethane were distilled under nitrogen from sodium or sodium/potassium alloy and methylene chloride from phosphorous pentoxide. Ammonium pertechnetate was obtained from Oak Ridge National Laboratory and was purified as described previously.[18] $[(Ph_3P)_2N]F$,[19] $Tc(O)_3(OSiMe_3)$,[9] $Re(NAr')_3(OSiMe_3)$[5] and **4a**[8c] were prepared following published procedures. Arylisocyanates and $ISiMe_3$ (Aldrich) were distilled and stored in a dry-box prior to use. Alkylating reagents were used as supplied from Aldrich.

NMR spectra were recorded in C_6D_6 on an IBM AF-250 or a Bruker WM-300 spectrometer, referenced to solvent unless otherwise noted and reported below as chemical shift in δ (multiplicity, integral, coupling constant in Hz, assignment). IR spectra were obtained as Nujol mulls using a Per-

kin–Elmer 1500 or a Bio–Rad FTS-40 spectrometer and are reported in cm^{-1}. Elemental analyses were obtained on a Perkin–Elmer 2400 analyser. UV–vis spectra were recorded on a Hewlett–Packard 8450A spectrophotometer and are reported as λ_{max} (ε) unless otherwise noted. Cyclic voltammograms were measured with a Princeton Applied Research Model 273 electrochemistry system using a platinum disk working electrode (BAS Model MF2013), a platinum wire counter electrode and a silver wire quasi-reference electrode separated from the bulk solution via a fine porosity glass frit. Test solutions were approximately 2 mM of the measured compound with approximately 0.1 M of $[Bu^n_4N]BF_4$ (anhydrous and recrystallized) as the supporting electrolyte in THF. The scan rate was 0.2 V s^{-1} unless otherwise noted. Potentials are quoted relative to the ferrocene/ferrocenium redox couple used as an internal reference standard.

$Tc(NAr)_3(OSiMe_3)$ (**1a**)

A solution of $TcO_3(OSiMe_3)$ (0.50 g, 2.1 mmol) and ArNCO (1.28 g, 6.3 mmol) in hexamethyldisiloxane (12 cm^3) was stirred at 110°C under argon for 21 h. The reaction mixture was concentrated to 5 cm^3 and cooled to −40°C. The resulting solids were filtered, washed with cold hexamethyldisiloxane (3 × 2 cm^3) and dried *in vacuo*, yielding 0.88 g (60%) of deep green **1a**. ^1H NMR: 7.00 (m, 9, Ar), 3.50 (sept, 6, $J = 6.8$, $CHMe_2$), 1.10 (d, 36, $J = 6.8$, $CHCH_3$), 0.45 (s, 9, $SiCH_3$). $^{13}C\{^1H\}$ NMR: 139.5 (Ar), 126.9 (Ar), 122.7 (Ar), 29.1 ($CHMe_2$), 23.7 ($CHCH_3$), 2.6 ($SiCH_3$). Found: C, 65.8; H, 8.3; N, 5.9. Calc. for $C_{39}H_{60}N_3OSiTc$: C, 65.6; H, 8.4; N, 5.9%. UV–vis (nm): 277 (30,000), 319 (35,000), 588 (4500).

$Tc(NAr')_3(OSiMe_3)$ (**1b**)

A solution of $TcO_3(OSiMe_3)$ (0.24 g, 1.0 mmol) and Ar'NCO (0.45 g, 3.1 mmol) in hexamethyldisiloxane (15 cm^3) was stirred at 62°C under argon for 5 h. The reaction mixture was cooled to −40°C. The resulting solids were filtered, washed with hexamethyldisiloxane (2 × 5 cm^3) and dried *in vacuo*, yielding 0.33 g (61%) of **1b**. Preparations of **1b** often contain **2a**, which can be selectively crystallized from hexane or hexamethyldisiloxane. ^1H NMR: 6.75 (m, 9, Ar), 2.24 (s, 18, $ArCH_3$), 0.37 (s, 9, $SiCH_3$). $^{13}C\{^1H\}$ NMR (CD_2Cl_2): 130.2 (Ar), 127.9 (Ar), 126.5 (Ar), 18.9 ($ArCH_3$), 2.1 ($SiCH_3$). IR: 1274 vs, 1246 s, 1158 m, 1094 m, 951 vs br, 834 s, 772 vs, 762 m, 744 m, 726 m. Found: C, 59.5; H, 6.2; N, 8.1. Calc. for $C_{27}H_{36}N_3OSiTc$: C, 59.4; H, 6.6; N, 7.7%. UV–vis (nm): 237 (40,000), 310 (30,000), 584 (4500).

$\overline{Tc(NAr')_2(NAr'C(O)NAr')}(OSiMe_3)$ (**2a**)

A solution of $TcO_3(OSiMe_3)$ (0.22 g, 0.92 mmol) and Ar'NCO (1.02 g, 6.9 mmol) in hexamethyldisiloxane (40 cm^3) was stirred at 80°C under argon for 11 h. The reaction mixture was cooled to −40°C. The resulting solids were filtered, washed with cold hexamethyldisiloxane (3 × 4 cm^3) and dried *in vacuo*, yielding 0.32 g (50%) of red–brown **2a**. ^1H NMR: 6.69 (m br, 5, Ar), 6.57 (m, 7, Ar), 2.80 (s, 6, $ArCH_3$), 2.33 (s, 6, $ArCH_3$), 2.23 (s, 12, $ArCH_3$), −0.15 (s, 9, $SiCH_3$). $^{13}C\{^1H\}$ NMR (CD_2Cl_2): 165.8 (*C*O), 137.3 (Ar), 136.9 (Ar), 131.6 (Ar), 128.7 (Ar), 128.5 (Ar), 128.0 (Ar), 126.7 (Ar), 126.4 (Ar), 19.3 ($ArCH_3$), 18.8 ($ArCH_3$), 1.6 ($SiCH_3$). IR: 1676 vs [ν(CO)], 1312 w sh, 1284 m, 1247 m, 899 s, 890 m sh, 840 m, 774 m, 764 m. Found: C, 62.7; H, 6.5; N, 8.3. Calc. for $C_{36}H_{45}N_4O_2SiTc$: C, 62.5; H, 6.6; N, 8.1%.

$\overline{Re(NAr')_2(NAr'C(O)NAr')}(OSiMe_3)$ (**2b**)

A solution of $Re(NAr')_3(OSiMe_3)$ (0.10 g, 0.2 mmol) and Ar'NCO (0.26 g, 1.8 mmol) in hexamethyldisiloxane (5 cm^3) was stirred at 120°C for 15 h. Volatiles were pumped away and hexane (3 cm^3) was added. The suspension was cooled to −40°C and the resulting solids were filtered, washed with hexane (3 × 2 cm^3) and dried *in vacuo*, yielding 0.84 g (68%) of red **2b**. ^1H NMR: 7.02 (m, 2, Ar), 6.73 (m, 8, Ar), 6.56 (m, 2, Ar), 2.78 (s, 6, $ArCH_3$), 2.39 (s, 6, $ArCH_3$), 2.29 (s, 12, $ArCH_3$), −0.22 (s, 9, $SiCH_3$). $^{13}C\{^1H\}$ NMR (THF-d_8): 161.6 (*C*O), 153.6 (Ar), 147.5 (Ar), 145.7 (Ar), 141.0 (Ar), 140.6 (Ar), 139.8 (Ar), 133.3 (Ar), 131.7 (Ar), 131.2 (Ar), 130.1 (Ar), 129.7 (Ar), 19.9 ($ArCH_3$), 19.2 ($ArCH_3$), 18.4 ($ArCH_3$), 1.4 ($SiCH_3$). IR: 1696 vs [ν(CO)], 1315 w sh, 1294 s, 1249 m, 907 vs, 841 m, 772 m, 763 m. Found: C, 55.6; H, 5.7; N, 7.0. Calc. for $C_{36}H_{45}N_4O_2ReSi$: C, 55.4; H, 5.8; N, 7.2%. UV–vis (all λ_{sh}) (nm): 236 (40,000), 275 (25,000), 396 (9000), 486 (4500).

$Tc(NAr)_3Me$ (**3a**)

A solution (3 M) of MeMgCl (0.04 cm^3, 0.1 mmol) in THF was added dropwise to a THF (20 cm^3) solution of $Tc(NAr)_3(OSiMe_3)$ (0.082 g, 0.1 mmol). The reaction mixture was stirred for 90 min. Volatiles were pumped away and hexane (3 cm^3) was then added. The resulting suspension was filtered through Celite®, which was then washed with hexane (2 × 5 cm^3). The filtrates were pumped to

dryness, yielding 0.055 g (75%) of deep blue–green **3a**. ^{1}H NMR: 7.01 (m, 9, Ar), 3.72 (sept, 6, $J = 7.0$, C*H*Me$_2$), 2.61 (s, 3, TcC*H*$_3$), 1.13 (d, 36, $J = 7.0$, CHC*H*$_3$). ^{13}C{^{1}H} NMR (CD_2Cl_2): 140.2 (Ar), 132.2 (Ar), 126.4 (Ar), 122.6 (Ar), 30.1 (Tc*C*H$_3$), 29.0 (*C*HMe$_2$), 23.2 (CH*C*H$_3$). Found: C, 69.5; H, 8.1; N, 6.1. Calc. for $C_{37}H_{54}N_3Tc$: C, 69.6; H, 8.5; N, 6.6%. UV–vis (nm): 257 (30,000), 336 (30,000), 598 (5500).

Tc(NAr)$_3$Et (**3b**)

This was prepared from EtMgCl in 86% yield as a deep blue–green solid following the procedure for **3a**. ^{1}H NMR: 7.02 (m, 9, Ar), 3.75 (sept, 6, $J = 6.8$, C*H*Me$_2$), 3.74 (q, 2, $J = 7.3$, C*H*$_2$CH$_3$), 2.21 (t, 3, $J = 7.3$, CH$_2$C*H*$_3$), 1.14 (d, 36, $J = 6.8$, CHC*H*$_3$). ^{13}C{^{1}H} NMR (CD_2Cl_2): 155.4 (Ar), 140.5 (Ar), 126.3 (Ar), 122.6 (Ar), 34.7 (*C*H$_2$CH$_3$), 28.8 (*C*H), 23.4 (CH*C*H$_3$), 22.0 (CH$_2$*C*H$_3$). Found: C, 69.9; H, 8.6; N, 6.4. Calc. for $C_{38}H_{56}N_3Tc$: C, 69.8; H, 8.6; N, 6.4%. UV–vis (nm): 258 (35,000), 339 (30,000), 604 (6000).

Tc(NAr)$_3$(C$_3$H$_5$) (**3c**)

This was prepared from (C$_3$H$_5$)MgCl in 70% yield as a deep blue–green solid following the procedure for **3a**. ^{1}H NMR: 7.01 (m, 9, Ar), 6.66 (m, 1, C*H*=CH$_2$), 5.25 (d, 1, $J = 17$, *trans*-CH=C*H*H′), 4.99 (d, 1, $J = 10$, *cis*-CH=CH*H*′), 4.33 (d, 2, $J = 8$, TcC*H*$_2$), 3.71 (sept, 6, $J = 6.8$, C*H*Me$_2$), 1.12 (d, 36, $J = 6.8$, CHC*H*$_3$). ^{13}C{^{1}H} NMR (CD_2Cl_2): 143.3 (Ar), 140.9 (Ar), 126.7 (Ar), 122.7 (Ar), 113.4 (*C*H=CH$_2$), 66.2 (CH=*C*H$_2$), 34.8 (Tc*C*H$_2$), 28.8 (*C*HMe$_2$), 23.5 (CH*C*H$_3$). Found: C, 70.8; H, 9.1; N, 5.9. Calc. for $C_{39}H_{56}N_3Tc$: C, 70.3; H, 8.5; N, 6.3%. UV–vis (nm): 255 (45,000), 339 (30,000), 606 (6500).

Tc(NAr)$_3$(CH$_2$SiMe$_3$) (**3d**)

This was prepared from Li(CH$_2$SiMe$_3$) in 70% yield as a deep blue–green solid following the procedure for **3a**. ^{1}H NMR: 7.00 (m, 9, Ar), 3.84 (sept, 6, $J = 6.9$, C*H*Me$_2$), 2.69 (s, 2, TcC*H*$_2$), 1.18 (d, 36, $J = 6.9$, CHC*H*$_3$), 0.25 (s, 9, SiC*H*$_3$). ^{13}C{^{1}H} NMR (CD_2Cl_2): 155.3 (Ar), 141.7 (Ar), 126.9 (Ar), 122.9 (Ar), 34.3 (*C*H$_2$Si), 28.6 (*C*HMe$_2$), 23.7 (CH*C*H$_3$), 1.4 (Si*C*H$_3$). Found: C, 67.3; H, 8.9; N, 6.0. Calc. for $C_{40}H_{62}N_3SiTc$: C, 67.6; H, 8.8; N, 5.9%.

Tc(NAr′)$_3$Me (**3e**)

This was prepared from Tc(NAr′)$_3$(OSiMe$_3$) in 74% yield [together with < 10% yield of red Tc$_2$(NAr′)$_4$(μ-NAr′)$_2$[20]] as a deep green oil following the procedure for **3a**. ^{1}H NMR: 6.75 (m, 9, Ar), 2.48 (s, 3, TcC*H*$_3$), 2.27 (s, 18, ArC*H*$_3$). Found: C, 64.0; H, 6.6; N, 9.1. Calc. for $C_{25}H_{30}N_3Tc$: C, 63.8; H, 6.4; N, 8.9%.

Tc(NAr′)$_3$I (**4b**)

A solution of Tc(NAr′)$_3$(OSiMe$_3$) (0.10 g, 0.19 mmol) and Me$_3$SiI (0.027 cm^3, 0.19 mmol) in toluene (10 cm^3) was stirred at room temperature for 40 min. Volatiles were pumped away yielding 0.085 g (76%) of **4b** as a deep green solid. ^{1}H NMR: 6.70 (m, 9, Ar), 2.21 (s, 3, ArC*H*$_3$). Found: C, 49.5; H, 4.8; N, 7.0. Calc. for $C_{24}H_{27}N_3ITc$: C, 49.5; H, 4.7; N, 7.2%.

[(Ph$_3$P)$_2$N][TcO(NAr)$_3$] (**5**)

A solution of Tc(NAr)$_3$(OSiMe$_3$) (0.10 g, 0.14 mmol) and [(Ph$_3$P)$_2$N]F (0.10 g, 0.16 mmol) in CH_2Cl_2 (10 cm^3) was stirred at room temperature for 5 min. Volatiles were pumped away and dimethoxyethane/Et$_2$O (5:1, 12 cm^3) was then added. The resulting suspension was cooled to −40°C and filtered through Celite®, which was then washed with Et$_2$O (2 × 3 cm^3). The filtrates were pumped to dryness, yielding 0.12 g (73%) of red **5**. ^{1}H NMR: 7.45 (m, 30, P*Ph*$_3$), 6.97 (m, 9, Ar), 4.06 (sept, 6, $J = 6.8$, C*H*Me$_2$), 1.29 [d, 36, $J = 6.8$, CH(C*H*$_3$)$_2$]. IR: 1411 s, 1324 vs, 1264 vs br, 1183 w, 1111 s, 997 w, 960 m, br, 932 w sh, 834 m, 808 m, 744 s, 720 vs, 691 s, 545 s, 533 vs, 497 m. Found: C, 72.8; H, 6.5; N, 4.7. Calc. for $C_{72}H_{81}N_4OP_2Tc$: C, 73.3; H, 6.9; N, 4.7%.

X-ray structure determinations for Tc(NAr)$_3$(OSiMe$_3$) (**1a**), Re(NAr′)$_2$(NAr′C(O)NAr′)(OSiMe$_3$) (**2b**) *and* Tc(NAr)$_3$I (**4a**)

Data were collected on crystals mounted on glass fibres. Preliminary photographic examination and data collection were performed on a Siemans R3m/V diffractometer with graphite monochromated Mo-K_α radiation. Cell constants and an orientation matrix were obtained by least-squares refinement, using the setting angles of at least 25 reflections. Good crystal quality was also suggested by measuring omega scans of several intense reflections and by examining axial photographs. Intensity data were obtained using θ–2θ (**1a** and **2b**) or ω scans (**4a**). The data were scaled for linear decay and a semi-empirical absorption correction based on the average relative intensity curve of azimuthal scan data was applied. The structures were solved using standard heavy atom methods and refined

with full-matrix least-squares. All non-hydrogen atoms were refined anisotropically, hydrogen atom positions were calculated (C—H = 0.96 Å) and were added to the structure–factor calculations without refinement. All calculations were performed using SHELXTL PLUS programs provided by Siemans Analytical. Crystallographic data are given in Table 3. Positional and thermal parameters and complete tabulations of bond lengths and angles are available as supplementary material from the Cambridge Crystallographic Data Center.

Acknowledgements—This work was supported by Laboratory Directed Research and Development and performed under the auspices of the U.S. Department of Energy at Los Alamos National Laboratory. We also thank S. D. McKee and D. L. Clark for helpful discussions.

REFERENCES

1. W. A. Nugent and J. M. Mayer, *Metal–Ligand Multiple Bonds*. John Wiley, New York (1988).
2. (a) Y.-W. Chao, P. M. Rogers, D. E. Wigley, S. J. Alexander and A. L. Rheingold, *J. Am. Chem. Soc.* 1991, **113**, 6326 and refs therein; D. P. Smith, K. D. Allen, M. D. Carducci and D. E. Wigley, *Inorg. Chem.* 1992, **31**, 1319; B. L. Haymore, E. A. Matta and R. A. D. Wentworth, *J. Am. Chem. Soc.* 1979, **101**, 2063; (b) T. R. Cundari, *J. Am. Chem. Soc.* 1992, **114**, 7879; (c) W. A. Herrmann, P. Kiprof, K. Rypdal, J. Tremmel, R. Blom, R. Alberto, J. Behm, R. W. Albach, H. Bock, B. Solouki, J. Mink, D. Lichtenberger and N. E. Gruhn, *J. Am. Chem. Soc.* 1991, **113**, 6257 and refs therein; M. H. Schofield, T. P. Kee, J. T. Anhaus, R. R. Schrock, K. H. Johnson and W. M. Davis, *Organometallics* 1991, **30**, 3595.
3. (a) E. Deutsch, K. Libson, S. Jurisson and L. F. Lindoy, *Prog. Inorg. Chem.* 1983, **30**, 75; (b) W. A. Herrmann, R. Alberto, P. Kiprof and F. Baumgärtner, *Angew. Chem.* 1990, **102**, 208; R. M. Pearlstein and A. Davison, *Polyhedron* 1988, **7**, 1981.
4. See for example: R. Toreki, R. R. Schrock and W. M. Davis, *J. Am. Chem. Soc.* 1992, **114**, 3367; V. Saboonchian, A. A. Danopoulos, A. Gutierrez, G. Wilkinson and D. J. Williams, *Polyhedron* 1991, **10**, 2241; M. R. Cook, W. A. Herrmann, P. Kiprof and J. Takacs, *J. Chem. Soc.* 1991, 797; I. A. Weinstock, R. R. Schrock, D. S. Williams and W. E. Crowe, *Organometallics* 1991, **10**, 1; A. Gutierrez, G. Wilkinson, B. Hussain-Bates and M. B. Hursthouse, *Polyhedron* 1990, **9**, 2081; G. R. Clark, A. J. Nielson and C. E. F. Rickard, *Polyhedron* 1988, **7**, 117.
5. A. D. Horton and R. R. Schrock, *Polyhedron* 1988, **7**, 1841.
6. W. A. Herrmann, G. Weichselbaumer, R. A. Paciello, R. A. Fischer, E. Herdtweck, J. Okuda and D. W. Marz, *Organometallics* 1990, **9**, 489.
7. C. M. Archer, J. R. Dilworth, P. Jobanputra, R. M. Thompson, M. McPartlin, D. C. Povey, G. W. Smith and J. D. Kelly, *Polyhedron* 1990, **9**, 1497; T. Nicholson, A. Davison and A. G. Jones, *Inorg. Chim. Acta* 1991, **187**, 51; 1990, **168**, 227; T. Nicholson, S. L. Storm, W. M. Davis and A. Davison, *Inorg. Chim. Acta* 1992, **196**, 27.
8. (a) J. C. Bryan, C. J. Burns and A. P. Sattelberger, *Isotope and Nuclear Chemistry Division Annual Report FY* 1990, pp. 40–41. National Technical Information Service, US Department of Commerce, LA-12143-PR; (b) A. K. Burrell and J. C. Bryan, *Organometallics* 1992, **11**, 3501; (c) A. K. Burrell and J. C. Bryan, *Angew. Chem.* 1993, **105**, 85.
9. W. A. Nugent, *Inorg. Chem.* 1983, **22**, 965.
10. Similar synthetic methodologies are reported for $Re(NAr)_3(OSiMe_3)$ and $Re(NAr')_3(OSiMe_3)$.[5]
11. (a) P. Legzdins, E. C. Phillips, S. J. Rettig, J. Trotter, J. E. Veltheer and V. C. Yee, *Organometallics* 1992, **11**, 3104; (b) R. I. Michelman, R. A. Andersen and R. G. Bergman, *J. Am. Chem. Soc.* 1991, **113**, 5100; W.-H. Leung, G. Wilkinson, B. Hussain-Bates and M. B. Hursthouse, *J. Chem. Soc., Dalton Trans.* 1991, 2791.
12. The rhenium analogue $[ReO(NAr)_3]^-$ has been reported, from the reaction of $Re(NAr)_3^-$ and Me_3NO. D. S. Williams, J. T. Anhaus, M. H. Schofield, R. R. Schrock and W. M. Davis, *J. Am. Chem. Soc.* 1991, **113**, 5480.
13. A. A. Danopoulos, C. J. Longley, G. Wilkinson, B. Hussain and M. B. Hursthouse, *Polyhedron* 1989, **8**, 2657; A. Gutierrez, G. Wilkinson, B. Hussain-Bates and M. Hursthouse, *Polyhedron* 1990, **9**, 2081; V. Saboonchian, A. A. Danopoulos, A. Gutierrez, G. Wilkinson and D. J. Williams, *Polyhedron* 1991, **10**, 2241.
14. The dominant resonance structure for isocyanates locates a positive charge on the isocyanate carbon. R. G. Arnold, J. A. Nelson and J. J. Verbanc, *Chem. Rev.* 1957, **57**, 47.
15. F. A. Cotton and G. Wilkinson, *Advanced Inorganic Chemistry*, 5th edn. John Wiley, New York (1988).
16. To the best of our knowledge, $[Tc^V(O)I_4]^-$ is the highest valent technetium iodide complex previously reported: G. Peters and W. Preetz, *Z. Naturforsch., B: Anorg. Chem., Org. Chem.* 1981, **36B**, 138; R. W. Thomas, A. Davison, H. S. Trop and E. Deutsch, *Inorg. Chem.* 1980, **19**, 2840.
17. C. J. Burns, *Operations Involving Natural Thorium (Th-232) and Depleted Uranium (U-238). Addendum: Operations Involving Technetium-99*. Los Alamos National Laboratory, Standard Operating Procedure No. INO-88-02, copies may be obtained from the author; see also A. Davison, C. Orvig, H. S. Trop, M. Sohn, B. V. DePamphilis and A. G. Jones, *Inorg. Chem.* 1980, **19**, 1988; A. Roodt, J. G. Leipoldt, E. A. Deutsch and J. C. Sullivan, *Inorg. Chem.* 1992, **31**, 1080.
18. K. Libson, B. L. Barnett and E. Deutsch, *Inorg. Chem.* 1983, **22**, 1695.
19. W. Douglas and J. K. Ruff, *J. Organomet. Chem.* 1974, **65**, 65.
20. A. K. Burrell and J. C. Bryan, unpublished results.

Polyhedron Vol. 12, No. 14, pp. 1779–1783, 1993
Printed in Great Britain

0277-5387/93 $6.00+.00
© 1993 Pergamon Press Ltd

CRYSTAL AND MOLECULAR STRUCTURE OF PENTA(4-METHYLBENZYL)TANTALUM, [Ta($CH_2C_6H_4$-4Me)$_5$]

CHRISTOPHER J. PIERSOL, ROBERT D. PROFILET, PHILLIP E. FANWICK and IAN P. ROTHWELL†

Department of Chemistry, 1393 Brown Building, Purdue University, West Lafayette, IN 47907, U.S.A.

(*Received* 14 *December* 1992; *accepted* 29 *March* 1993)

Abstract—Reaction of the dichloride [$TaCl_2(CH_2$—C_6H_4-4Me)$_3$] (**1**) (CH_2—C_6H_4-4Me = 4-methylbenzyl) with the dialkylmagnesium compound [$Mg(CH_2$—C_6H_4-4-Me)$_2$] leads to the homoleptic 4-methylbenzyl compound [$Ta(CH_2$—C_6H_4-4Me)$_5$] (**2**). The solid state structure of **2** shows a distorted square-pyramidal geometry for the central TaC_5 core. Four of the 4-methylbenzyl ligands are σ-bound to the tantalum with Ta—CH_2—C angles of 108.4(5)–125.7(5)°, while the remaining ligand has an acute Ta—CH_2—C angle of 90.4(5)°. In solution all alkyl groups are equivalent by ^{1}H and ^{13}C NMR even at −60°C, indicating facile exchange of non-equivalent alkyl groups on the NMR time-scale.

The study of the simple alkyl derivatives of the group 5 metals niobium and tantalum has played an important role in organometallic chemistry. This importance stems from the discovery by Schrock of the α-hydrogen abstraction process that can lead to stable alkylidene and alkylidyne derivatives of these metals.[1] This early work has now resulted in the development of a whole new field of organometallic chemistry, much of which is focussed on the stoichiometric and catalytic reactivity of these functional groups.[2]

During our studies of the catalytic hydrogenation of arene rings by group 5 metal compounds[3] we required a mononuclear, homoleptic alkyl derivative of tantalum as a molecular precursor to oxide surface bound organometallic species of tantalum.[4] Our attention focussed upon the penta-benzyl compound [$Ta(CH_2C_6H_5)_5$] reported by Schrock to be an isolable,[5] although thermally unstable,[5,6] red crystalline material. We wish to report here our synthesis of the analogous 4-methylbenzyl derivative as well as upon the solid state and solution structure of the compound.

RESULTS AND DISCUSSION

The 4-methylbenzyl compound [$Ta(CH_2C_6H_4$-4-Me)$_5$] (**2**) was obtained via the intermediate [$TaCl_2(CH_2$—C_6H_4-4-Me)$_3$] (**1**) by using a procedure essentially identical to that reported by Schrock[5] (Scheme 1). The red–orange dichloride **1**, generated by treating $TaCl_5$ with [$Zn(CH_2$—C_6H_4-4-Me)$_2$] in hexane/toluene, was a crude, low melting solid that was used without further purification. The penta(4-methylbenzyl) compound (**2**) was obtained as deep red crystals from hexane solution after allowing **1** and [$Mg(CH_2$—C_6H_4-Me)$_2$] to react in toluene at room temperature. The rapid isolation of **2** from the reaction mixture is necessary due to its thermal instability (*vide infra*).

The homoleptic alkyl **2** was subjected to a single-crystal X-ray diffraction analysis. The data set was collected at −98°C due to the thermal instability of the compound. The diffraction study (Figs 1 and 2 and Table 1) confirmed the stoichiometry of the compound and shows some interesting features. The solid state structure of **2** can best be described as

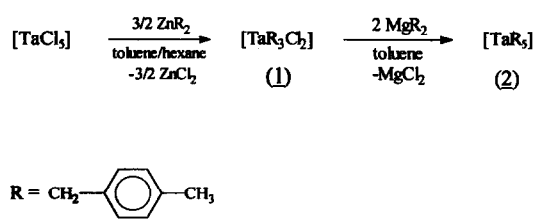

Scheme 1.

† Author to whom correspondence should be addressed.

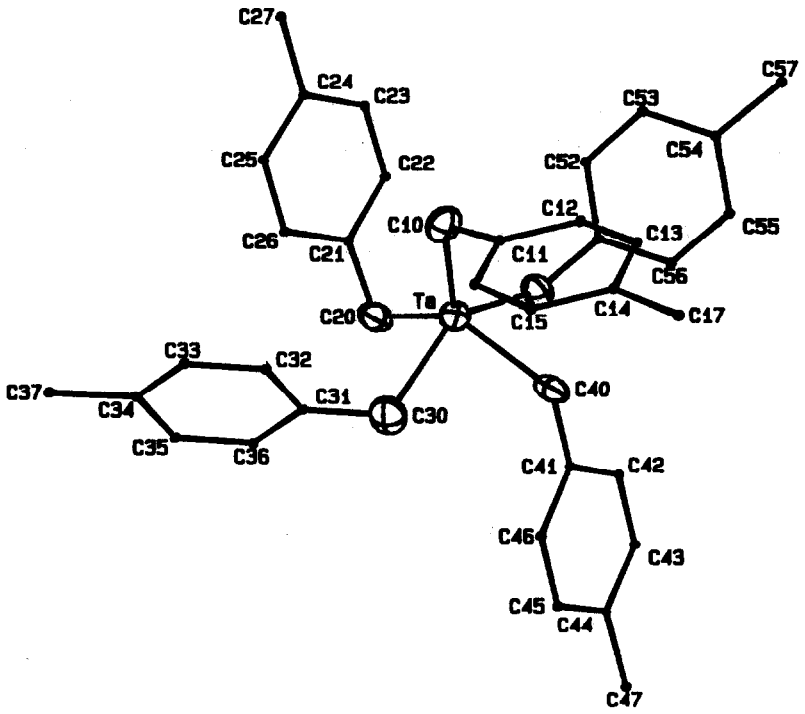

Fig. 1. ORTEP view of **2** with labelling scheme.

distorted square-pyramidal for the central TaC_5 core. The axial benzyl group Ta—C(10) makes an angle of 104.7(3)–118.2(3)° to the four basal benzyl ligands. The angles between each of these four basal groups lies in the narrow range 80.6(3)–84.6(3)°. The electronic aspects involved in determining which geometry is adopted in five-coordinate transition metal compounds have been thoroughly evaluated by Hoffman and Lauer.[7] There are now a significant number of five-coordinate compounds of the group 5 metals that have been structurally characterized.[8] The observed structures are normally rationalized using a combination of electronic arguments along with the steric influence of ligands containing non-trivial bulk. Of particular importance for high valent metal derivatives (typically d^0-metal configuration) has been the influence of π-donor ligation that tends in large part to dictate the structure that is observed.[9] In compound **2** the central coordination sphere contains donor atoms only capable of σ-bonding. On the basis of simple VSEPR rules one would, therefore, predict a trigonal bipyramidal structure, cf. heavier group 15 metal derivatives, $[MX_5]$ (M = P, As, Sb). However, the importance of crystal packing forces in determining observed solid state structures should not be overlooked. This is clearly demonstrated in the structures of the isoelectronic pentaalkyl compounds $[Sb(C_6H_5)_5]$[10] and $[Sb(C_6H_4\text{-}4\text{-}Me)_5]$,[11] where the former adopts an unexpected square-pyramidal geometry in contrast to a regular trigonal bipyramid for the latter. The influence of crystal packing forces was argued to influence which of the two structures were adopted in solution.[11] Another factor that may also influence the structure of **2** is the acute Ta—CH_2—C angle observed for one of the basal benzyl ligands (*vide infra*).

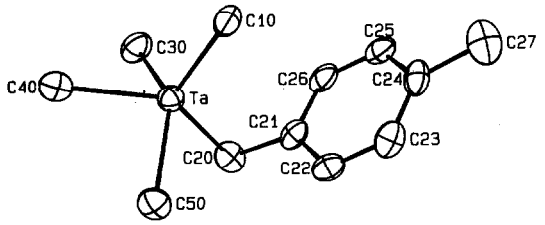

Fig. 2. ORTEP view of the central coordination sphere in **2** showing the orientation of the benzyl ligand bound through C(20).

The five Ta—CH_2 distances span the narrow range 2.151(8)–2.216(8) Å and are essentially identical to values found in the tantalum aryloxide compounds of the formula $[Ta(OAr)_2(CH_2Ph)_3]$ (Table 2). An important characteristic of benzyl ligands is their ability to interact in an η^n ($n > 1$) fashion to electron deficient metal centres. This type of bonding is typified by the η^3-benzyl compound $[CpMo(\eta^3\text{-}CH_2\text{—}C_6H_4\text{-}4Me)(CO)_2]$,[12] where the metal makes close contacts with the α, *ipso*- and

Table 1. Selected bond distances (Å) and angles (°) for [Ta(CH$_2$—C$_6$H$_4$-4Me)$_5$] (2)

Ta—C(10)	2.151(8)	Ta—C(40)	2.202(8)
Ta—C(20)	2.216(8)	Ta—C(50)	2.213(8)
Ta—C(30)	2.189(8)		
C(10)—Ta—C(20)	118.2(3)	C(20)—Ta—C(40)	137.0(3)
C(10)—Ta—C(30)	107.5(3)	C(20)—Ta—C(50)	82.8(3)
C(10)—Ta—C(40)	104.7(3)	C(30)—Ta—C(40)	80.6(3)
C(10)—Ta—C(50)	113.7(3)	C(30)—Ta—C(50)	138.1(3)
C(20)—Ta—C(30)	84.6(3)	C(40)—Ta—C(50)	81.9(3)
Ta—C(10)—C(11)	108.4(5)	Ta—C(40)—C(41)	125.7(5)
Ta—C(20)—C(21)	90.4(5)	Ta—C(50)—C(51)	113.2(5)
Ta—C(30)—C(31)	119.9(6)		

ortho-carbon atoms with distances of 2.269(7), 2.364(5) and 2.480(6) Å, respectively. In the case of high valent, early *d*-block metals multisite bonding of benzyl ligands to the electron deficient metal centre has been established in a number of cases. However, a broad spectrum of interactions appears to exist. This is exemplified by the homoleptic benzyl derivatives of the group 4 metals, [M(CH$_2$Ph)$_4$] (M = Ti, Zr, Hf).[13] In these compounds the M—CH$_2$—Ph angles at the α-carbon atom vary from 85° to 115°. The close contact of the aryl rings is often quoted as justification for the thermal stability of these compounds compared to simple alkyl derivatives. The stepwise substitution of benzyl ligands by aryloxide groups leads to an increase in the average M—CH$_2$—Ph angles, reflecting either decreasing electron deficiency of the metal centre or, more likely, steric congestion precluding close approach of the arene ring.[14]

In compound **2** one of the benzyl ligands has a small angle at the α-carbon, Ta—C(20)—C(21) = 90.4(5)°. The four remaining benzyl ligands have corresponding angles of 108.4(5)–125.7(5)°. A search of the Cambridge Crystallographic Database uncovered a limited number of benzyl compounds of tantalum that had been subjected to single-crystal X-ray diffraction analysis.[15–21] In Table 2 are listed the values of M—CH$_2$ and M—CH$_2$—Ar reported for the most relevant of these compounds. It can be seen that the M—C

Table 2. Structural parameters for selected tantalum benzyl compounds

Compound	M—CH$_2$ (Å)	M—CH$_2$—C (°)	Ref.
[Ta(CH$_2$—C$_6$H$_4$-4Me)$_5$]	2.216(8)	90.4(5)	This work
	2.151(8)	108.4(5)	
	2.189(8)	119.9(6)	
	2.202(8)	125.7(5)	
	2.213(8)	113.2(5)	
[Ta(OC$_6$H$_3$Me$_2$-2,6)$_2$(CH$_2$Ph)$_3$]	2.204(6)	114.9(5)	15
	2.204(7)	94.8(4)	
	2.163(7)	111.5(4)	
[Ta(OC$_6$H$_3$Ph$_2$-2,6)$_2$(CH$_2$—C$_6$H$_4$-4Me)$_3$]	2.154(7)	114.3(4)	16
	2.179(6)	110.8(4)	
	2.161(6)	116.2(4)	
[Cp$_2$Ta(=CHPh)(CH$_2$Ph)]	2.30(1)	123.1(10)	17
	2.07(1)	135.2(7)	
[Cp*Ta(=CHPh)(CH$_2$Ph)$_2$]	2.188(15)	126.1(8)	18
	2.233(14)	114.7(8)	
	1.883(14)	166.0(10)	

distances lie in a narrow range. The longest distances are found in benzyl compounds containing two cyclopentadienyl ancillary ligands. It is also apparent that the majority of benzyl ligands have "normal" M—C—Ph angles between 100° and 120°. However, the acute benzyl ligand in **2** and one of the ligands in the aryloxide compound $[Ta(OC_6H_3Me_2\text{-}2,6)_2(CH_2Ph)_3]$ have angles below 100°.

Despite the square-pyramidal geometry observed in the solid state structure of **2** only one set of resonances for the benzyl ligands are detected in the ^1H and ^{13}C NMR spectra. Cooling à toluene-d_8 solution of **2** to −60°C showed only one Ta—C*H*$_2$ and 4-*Me* resonance in the ^1H NMR, indicating that exchange of non-equivalent benzyl ligands is facile on the NMR time-scale at this temperature. In the ^{13}C NMR spectrum of **2** the benzylic carbon was found to resonate at δ 105.2 ppm and appears as a triplet of triplets. The observed $^1J(^{13}C—^1H)$ coupling of 123.3 Hz is identical to the value of 123 Hz reported by Schrock *et al.* for $[Ta(CH_2Ph)_5]$. The value of this coupling constant is very close to that expected for an undistorted sp^3-CH bond and correlates well with the average Ta—CH$_2$—C angle of 111.5° found in the solid state structure of **2**.

A fresh, deep-red benzene-d_6 solution of crystalline **2** was found to undergo decomposition at room temperature to produce a dark brown solution along with a dark precipitate. Analysis of this reaction by ^1H NMR showed that 2–3 equivalents of *p*-xylene per tantalum metal centre were generated in solution. This reactivity is identical to that reported for $[Ta(CH_2Ph)_5]$.[5,6]

EXPERIMENTAL

All operations were performed under a dry nitrogen atmosphere either in a Vacuum Atmospheres dri-lab or by standard Schlenk techniques. Hydrocarbon solvents were dried by distillation from sodium benzophenone under a nitrogen atmosphere. ^1H and ^{13}C NMR spectra were performed on a Gemini 200 MHz spectrometer.

Preparation of $[Zn(CH_2C_6H_4\text{-}4Me)_2]$

A sample of magnesium turnings (26.73 g, 1.09 mol, 50% excess) was dried in an oven overnight and placed in a 5 dm^3 flask. The metal was further dried with a heat gun under vacuum for 10 min. Diethylether (750 cm^3) was added to the flask followed by α-chloro-*p*-xylene (70 cm^3, 734 mmol) in diethylether (50 cm^3) dropwise over a period of 1 h. The resulting mixture was allowed to stir for an additional 3 h. Dry $ZnCl_2$ (50 g, 3.66 mol) was added over an hour and the reaction mixture was left to stir overnight. The solvent was removed under vacuum to leave a white–brown mixture and excess magnesium turnings. The mixture was extracted with toluene. The solvent was removed *in vacuo* from the yellow filtrate and the resulting residue washed with hexane yielding 68.62 g (68%) of white $[Zn(CH_2C_6H_4\text{-}4Me)_2]$.

Preparation of $[TaCl_2(CH_2C_6H_4\text{-}4Me)_3]$ **(1)**

Solid $TaCl_5$ (21.99 g, 61 mmol) was placed in a 500 cm^3 flask and a 1:1 mixture of toluene and hexane (200 cm^3) was added to the solid. $[Zn(CH_2C_6H_4\text{-}4Me)_2]$ (25.4 g, 0.092 mol) was added over 15 min. The reaction was allowed to stir for an additional 45 min. The solvent was removed *in vacuo* and the dried residue was extracted with hexane and filtered. The resulting deep red–orange filtrate was evaporated to a liquid containing the crude product.

Preparation of $[Ta(CH_2C_6H_4\text{-}4Me)_5]$ **(2)**

$[TaCl_2(CH_2C_6H_4\text{-}4Me)_3]$ (1.00 g, 1.763 mmol) was dissolved in toluene (10 cm^3) in a 50 cm^3 flask. A sample of $[Mg(CH_2C_6H_4\text{-}4Me)_2(EtO_2)_2]$ (0.675 g, 1.763 mmol) was dissolved in toluene (10 cm^3) and added dropwise to the flask over 30 min. The reaction was then allowed to stir for an additional 20 min. The mixture was filtered and the filtrate evaporated to dryness. Toluene (3 cm^3) was added and the red solution was layered with hexane. Cooling at −20°C yielded crystals of $[Ta(CH_2C_6H_4\text{-}4Me)_5]$. Yield = 0.20 g (18%).

^1H NMR (δ, C_6D_6, 25°C): 7.00 (d), 6.78 (d), 2.71 (s, C*H*$_2$), 2.25 (s, C*H*$_3$). Selected ^{13}C NMR data (δ, C_6D_6): 105.2 [t–t, *C*H$_2$, $^1J(^{13}C—^1H)$ = 123.3 Hz, $^3J(^{13}C—^1H)$ = 4.36 Hz]; 21.0 [q–t, *C*H$_3$, $^1J(^{13}C—^1H)$ = 126.0 Hz, $^3J(^{13}C—^1H)$ = 4.38 Hz].

Acknowledgement—We thank the National Science Foundation for support of this research.

REFERENCES

1. (a) R. R. Schrock, *J. Organomet. Chem.* 1986, **300**, 249; (b) R. R. Schrock, *Accts Chem. Res.* 1986, **19**, 342; (c) R. R. Schrock, *Accts Chem. Res.* 1979, **12**, 98.
2. (a) W. A. Nugent and J. A. Mayer, *Metal–Ligand Multiple Bonds*. Wiley, New York (1988); (b) J. Feldman and R. R. Schrock, *Prog. Inorg. Chem.* 1991, **39**, 1 and refs therein.
3. J. S. Yu, B. C. Ankianiec, M. T. Nguyen and I. P. Rothwell, *J. Am. Chem. Soc.* 1992, **114**, 1927.

4. R. D. Profilet and I. P. Rothwell, *J. Chem. Soc., Chem. Commun.* 1993, 42.
5. R. R. Schrock, *J. Organomet. Chem.* 1976, **122**, 209.
6. V. Malatesta, K. U. Ingold and R. R. Schrock, *J. Organomet. Chem.* 1978, **152**, C53.
7. A. R. Rossi and R. Hoffman, *Inorg. Chem.* 1975, **14**, 365.
8. C. H. Zambrano, R. D. Profilet, J. E. Hill, P. E. Fanwick and I. P. Rothwell, *Polyhedron* 1993, **12**, 689.
9. M. H. Chisholm, L. S. Tan and J. C. Huffman, *J. Am. Chem. Soc.* 1982, **104**, 4879.
10. P. J. Wheatley, *J. Chem. Soc.* 1964, 3718.
11. C. Brabart, J. Hubert and A. L. Beauchamp, *Can. J. Chem.* 1973, **51**, 2952.
12. (a) F. A. Cotton and M. D. LaPrade, *J. Am. Chem. Soc.* 1968, **90**, 5418; (b) F. A. Cotton and T. J. Marks, *J. Am. Chem. Soc.* 1969, **91**, 1339; (c) R. B. King and H. Fronzaglia, *J. Am. Chem. Soc.* 1966, **88**, 709.
13. (a) G. R. Davies, J. A. J. Jarvis, B. T. Kilbourn and A. J. P. Pioli, *J. Chem. Soc., Chem. Commun.* 1971, 677; (b) G. R. Davies, J. A. J. Jarvis and B. T. Kilbourn, *J. Chem. Soc., Chem. Commun.* 1971, 1511; (c) C. Pellechia, A. Grassi and A. Immirzi, *J. Am. Chem. Soc.* 1993, **115**, 1160; (d) R. F. Jordan, R. E. LaPointe, C. S. Bajgur, S. F. Echols and R. Willett, *J. Am. Chem. Soc.* 1987, **109**, 4111; (e) M. Bochmann, G. Karger and A. Jagger, *J. Chem. Soc., Chem. Commun.* 1990, 1038.
14. S. L. Latskey, A. K. McMullen, G. P. Niccolai and I. P. Rothwell, *Organometallics* 1985, **4**, 902.
15. L. R. Chamberlain, I. P. Rothwell, K. Folting and J. C. Huffman, *J. Chem. Soc., Dalton Trans.* 1987, 155.
16. R. W. Chesnut, G. G. Jacobs, J. S. Yu, P. E. Fanwick and I. P. Rothwell, *Organometallics* 1991, **10**, 321.
17. R. R. Schrock, L. W. Messerle, C. D. Wood and L. J. Guggenberger, *J. Am. Chem. Soc.* 1978, **100**, 3793.
18. L. W. Messerle, P. Jennische, R. R. Schrock and G. Stucky, *J. Am. Chem. Soc.* 1980, **102**, 6744.
19. A. van Asselt, M. S. Trimmer, L. M. Henling and J. E. Bercaw, *J. Am. Chem. Soc.* 1988, **110**, 8254.
20. H. C. L. Abbenhuis, D. M. Grove, G. P. M. van Mier, A. L. Spek and G. van Koten, *Recl. Trans. Chim. Pays-Bas* 1990, **109**, 361.
21. H. C. L. Abbenhuis, D. M. Grove, G. P. M. van Mier, A. L. Spek and G. van Koten, *J. Chem. Soc., Chem. Commun.* 1989, 1581.

Polyhedron Vol. 12, No. 14, pp. 1785–1792, 1993
Printed in Great Britain

0277-5387/93 $6.00+.00
© 1993 Pergamon Press Ltd

SYNTHESIS AND CHARACTERIZATION OF 1,1,1,5,5,5-HEXAFLUOROACETYLACETONATO-(1,5-CYCLOOCTADIENE)SILVER(I) DIMER. AN UNUSUAL β-DIKETONATE COORDINATION MODE

ALEC BAILEY,† TOM S. CORBITT,† MARK J. HAMPDEN-SMITH,†‡
E. N. DUESLER† and TOIVO T. KODAS§

Departments of †Chemistry and §Chemical Engineering and Center for Micro-Engineered Ceramics, University of New Mexico, Albuquerque, NM 87131, U.S.A.

(*Received* 20 *November* 1992; *accepted* 29 *March* 1993)

Abstract—The compound (hfac)Ag(1,5-cod) was synthesized by the reaction of 1,1,1,5,5,5-hexafluoroacetylacetone (hfacH) with Ag_2O and 1,5-cyclooctadiene (1,5-cod) and characterized in the solid state by single-crystal X-ray diffraction. In contrast to the corresponding copper(I) compound (hfac)Ag(1,5-cod) exhibited lower volatility and was found to be dimeric in the solid state, containing the two unusual β-diketonate coordination modes, namely, μ^4-η^2-hfac and μ^2-hfac. The deterioration of the crystal and extensive disorder precluded a detailed comparison of the metrical parameters of this compound with other literature data. However, the solid-state FTIR data showed substantial differences in the ν(C—O) and ν(C—C) stretching regions compared with the chelated hfac ligand in (hfac)Cu(1,5-cod). These data will be useful in assigning the coordination mode of β-diketonate ligands in metal-organic β-diketonate complexes by FTIR.

The rational design of metal-organic compounds as precursors for the chemical vapour deposition (CVD) of metals is a topic of intense research interest.[1] These precursors need to meet certain design criteria if they are to be used to deposit high-quality metal films that are likely to be integrated into semiconductor device technology as, for example, vertical interconnects. The design criteria for such compounds are that they exhibit high volatility (vapour pressure preferably greater than 100 mtorr at the evaporation temperature), are thermally stable at room temperature, deposit pure metal films at high rates and relatively low temperatures (< 400°C) and can deposit selectively on one material in the presence of another. Some of these criteria have been attained for the CVD of copper from a number of Lewis base adducts of copper(I) β-diketonate compounds, (β-diketonate)CuL.[2–13] It has been shown that these species undergo a thermally-induced disproportionation reaction on a variety of surfaces to deposit pure copper metal with near bulk resistivity, according to the reaction in eq. (1) below.

$$2(\beta\text{-diketonate})\text{CuL} \longrightarrow \text{Cu} + \text{Cu}(\beta\text{-diketonate})_2 + 2\text{L} \quad (1)$$

In this system the 1,1,1,5,5,5-hexafluoroacetylacetonato (hfac) derivatives are most useful because they exhibit higher volatility compared to the other β-diketonate derivatives investigated. The Lewis base ligands, L, have been chosen from triorganophosphines, olefins and alkynes.

In this work we set out to examine the possibility of extending this work to investigate the chemistry of analogous (β-diketonate)ML compounds of group 11 and to compare their propensity for the formation of metal via disproportionation from volatile silver(I) precursors. While disproportionation reactions of copper(I) [eq. (1)] and gold(I) [eq. (2)] are well known the disproportionation of silver(I) [eq. (3)] is poorly characterized.[14] However, complexes of both silver(II) and silver(III) are known with oxygen ligands.

$$3\text{Au}^{\text{I}} \longrightarrow 2\text{Au} + \text{Au}^{\text{III}} \quad (2)$$

‡Author to whom correspondence should be addressed.

$$2Ag^{I} \longrightarrow Ag + Ag^{II} \quad (3)$$

Here we describe the synthesis and characterization of the silver(I) compound (hfac)Ag(1,5-cod), where 1,5-cod = 1,5-cyclooctadiene, which exhibits an unexpected structure in the solid state.

EXPERIMENTAL

General procedures

All manipulations were performed under a dinitrogen atmosphere using standard Schlenk techniques or in a nitrogen atmosphere dry-box.[15] Hydrocarbon and ethereal solvents were predried over sodium wire, distilled from sodium benzophenone ketyl and stored over 4 Å molecular sieves under nitrogen. Combustion element analyses were performed by Ms R. Ju in the Department of Chemistry at the University of New Mexico. NMR data were recorded on a Bruker AC-250P NMR spectrometer using the protio impurities of the deuterated solvents as references for the ^{1}H NMR and the ^{13}C resonance of the solvents as reference for ^{13}C NMR specroscopy. Temperatures were calibrated with either ethylene glycol or methanol. IR data were recorded on a Perkin–Elmer Model 1620 FTIR spectrophotometer.

Synthesis of [(hfac)Ag(1,5-cod)]$_2$

A suspension of Ag_2O (2.122 g, 9.16 mmol) in THF (69 cm^3) was stirred in a 250 cm^3 Schlenk flask for 10 min under nitrogen. A slight excess of 1,5-cyclooctadiene (2.4 cm^3, 19.6 mmol, *ca* 2.1 equivalents) was added dropwise over a 5 min period and the entire solution was stirred under nitrogen for 10 min. A small excess of hexafluoroacetylacetone (2.7 cm^3, 19.3 mmol, *ca* 2.1 equivalents) was added dropwise over a 5 min period. The black Ag_2O solution gradually dissolved forming a cloudy solution. This solution was stirred under nitrogen for 3 h. Removal of the volatile components under vacuum gave a dirty brown/tan solid which was dissolved in toluene (100 cm^3) and filtered to remove any unreacted Ag_2O. The filtered solution was brown/yellow and translucent. Removal of toluene *in vacuo* gave colourless, crystalline (hfac)Ag(1,5-cod) (4.9946 g, 11.8 mmol, 65.5% yield). Crystals of (hfac)Ag(1,5-cod) were obtained by dissolving *ca* 50 mg of the product in toluene and room temperature and cooling to −10°C. Found: C, 36.7; H, 3.3. Calc. for $C_{13}H_{13}O_2F_6Ag$: C, 36.9; H, 3.1%. Spectroscopic data: NMR data: ^{1}H (C_6D_6, 20°C) (ppm): 1.70 (s, br, 8H, CH_2 in 1,5-COD), 5.30 (s, br, 4H, CH in 1,5-COD), 6.26 (s, 1H, CH in hfac). $^{13}C\{^{1}H\}$ (ppm): 27.65 (s, CH_2 in 1,5-COD), 87.18 (s, CH in hfac), 124.62 (s, CH in 1,5-COD), 177.5 ($CF_3C{=}O$ in hfac). ^{19}F (ppm): 132.08 (s, CF_3 in hfac).

Crystallographic data

Single crystals were isolated from a saturated solution in toluene, cooled to −10°C. The crystal data collection and refinement parameters are summarized in Table 1. The crystal showed signs of deterioration during the data collection. The crystal was originally clear and colourless, but was dark grey and translucent at the end of data collection. The peak profiles also broadened by *ca* 20% during the data collection. The space group assignment of $P2(1)/n$ is consistent with the observed extinctions. A semi-empirical absorption correction was applied to the data set. Direct methods were used to find initial silver coordinates and the rest of the non-hydrogen atoms were located by full-matrix refinements on the trial positions and subsequent interpretation of the difference-Fourier maps. The R factor converged to 18% for all non-hydrogen atoms isotropic. At this point large isotropic Us for the Fs and some of the 1,5-cod carbon atoms were evident. Also, there were large deviations from the expected bond lengths: C—F ranged from 1.22(5) to 1.43(4); C—C bond lengths ranged from 1.34(6) to 1.71(6). In spite of the large deviations these are still within 3.4 standard deviations of the expected values. Difference-Fourier primary F sites (occupation factors > 50%) and secondary F sites were based on residual difference Fourier peaks. The positions of the primary sites were allowed to vary and

Table 1. Crystallographic data for [(hfac)Ag(1,5-cod)]$_2$

Chemical formula	$C_{13}H_{13}F_6O_2Ag$
Formula weight	23.1
Space group	$P2_1/n$
a (Å)	10.700(1)
b (Å)	14.427(2)
c (Å)	120.684(4)
V (Å^3)	3093.4(1)
Z	8
T (°C)	20
λ (Å)	0.71073
ρ_{calc} (g cm^{-3})	1.817
μ (cm^{-1})	12.93
$R(F_o)^a$ (%)	10.10
$R_w(F_o)^b$ (%)	10.33

$^a R(F_o) = \Sigma(|F_o|-|F_c|)/\Sigma|F_o|$.

$^b R_w(F_o) = \Sigma(w^{1/2}(|F_o|-|F_c|))/(w^{1/2}|F_o|)$; $w^{-1} = \sigma^2(F_o)+0.0027F_o^2$.

the positions of the secondary sites were fixed. Each of these sets had common isotropic *U*s, which were also varied. The CF_3 group on C(5) did not have any difference-Fourier peaks which could be associated to a second set of Fs. These F positions were constrained to have the average C—F bond length of 1.310 Å in a tetrahedral arrangement about C(5). These Fs also shared a common variable isotropic *U*. Hydrogen atoms in idealized positions (riding model) with isotropic *U*s set to 1.25*U*(equiv.) of their parent atoms were included in the final refinements. The final *R* factor is 10.10%. All software and the source of scattering factors are contained in the SHELXTL program library (G. Sheldrick, Nicolet Corp., Madison, WI). Selected bond distances and angles are given in Tables 2 and 3, respectively.

There is one independent molecule in the asymmetric unit. The two hfac units are bonded differently to the silver atoms, but the two 1,5-cod units are similarly bonded, one to each silver atom. The bond lengths and angles show large standard deviations, a result of the marginal data set. However, this data is sufficient to show the general structure and dimeric nature of the molecule.

Table 2. Bond lengths (Å)

Ag(1)—Ag(2)	2.955(2)	Ag(1)—O(1)	2.468(9)
Ag(1)—O(3)	2.559(9)	Ag(1)—O(4)	2.541(9)
Ag(1)—C(11)	2.499(17)	Ag(1)—C(14)	2.606(21)
Ag(1)—C(15)	2.508(25)	Ag(1)—C(18)	2.579(21)
Ag(2)—O(2)	2.445(9)	Ag(2)—O(3)	2.579(10)
Ag(2)—O(4)	2.507(9)	Ag(2)—C(19)	2.583(21)
Ag(2)—C(22)	2.489(17)	Ag(2)—C(23)	2.501(26)
Ag(2)—C(26)	2.676(22)	O(1)—C(1)	1.239(18)
O(2)—C(3)	1.276(17)	O(3)—C(6)	1.254(17)
O(4)—C(8)	1.252(18)	C(1)—C(2)	1.406(22)
C(1)—C(4)	1.655(28)	C(2)—C(3)	1.370(19)
C(3)—C(5)	1.553(17)	C(4)—F(1)	1.281(18)
C(4)—F(2)	1.257(20)	C(4)—F(3)	1.334(22)
C(4)—F(1′)	1.251(16)	C(4)—F(2′)	1.328(22)
C(4)—F(3′)	1.289(23)	C(5)—F(4)	1.310(13)
C(5)—F(5)	1.311(12)	C(5)—F(6)	1.310(15)
C(6)—C(7)	1.401(20)	C(6)—C(9)	1.503(25)
C(7)—C(8)	1.378(21)	C(8)—C(10)	1.536(23)
C(9)—F(7)	1.345(26)	C(9)—F(8)	1.247(23)
C(9)—F(9)	1.372(27)	C(9)—F(7′)	1.326(16)
C(9)—F(8′)	1.286(22)	C(9)—F(9′)	1.277(17)
C(10)—F(10)	1.374(23)	C(10)—F(11)	1.318(26)
C(10)—F(12)	1.283(30)	C(10)—F(10′)	1.333(18)
C(10)—F(11′)	1.314(22)	C(10)—F(12′)	1.304(18)
C(11)—C(12)	1.525(32)	C(11)—C(18)	1.311(36)
C(12)—C(13)	1.458(34)	C(13)—C(14)	1.462(29)
C(14)—C(15)	1.240(37)	C(15)—C(16)	1.467(47)
C(16)—C(17)	1.415(44)	C(17)—C(18)	1.545(43)
C(19)—C(20)	1.551(44)	C(19)—C(26)	1.358(47)
C(20)—C(21)	1.361(37)	C(21)—C(22)	1.389(37)
C(22)—C(23)	1.291(39)	C(23)—C(24)	1.333(39)
C(24)—C(25)	1.358(54)	C(25)—C(26)	1.475(47)

RESULTS AND DISCUSSION

The species (hfac)Ag(1,5-cod) was prepared according to the literature method,[16,17] where silver(I) oxide was first mixed with 1,5-cod and then reacted with hfacH according to the stoichiometry of eq. (4).

$$Ag_2O + 2hfacH + 2\,1,5\text{-cod} \xrightarrow{(thf)} [(hfac)Ag(1,5\text{-cod})]_2 + H_2O \quad (4)$$

After removal of the volatile components *in vacuo* the product was recrystallized from toluene to give satisfactory analytical data. As in the case of (hfac)Cu(1,5-cod) ^1H and ^{13}C NMR data for (hfac)Ag(1,5-cod) revealed a solution structure in which all the aliphatic proton resonances were equivalent and where all four olefinic carbon and all four aliphatic carbon environments were identical. These data are consistent with the corresponding data for the copper(I) analogue, (hfac)Cu(1,5-cod), which has been structurally characterized in the solid state and shown to exhibit an unusual "3+1" coordination mode for the olefin ligand, as shown in Fig. 1, where one copper–olefin distance is considerably longer than the other.[18] For the copper analogue the NMR data have been interpreted in terms of the degenerate rearrangement according to eq. (5), although a dissociative mechanism could not be ruled out.

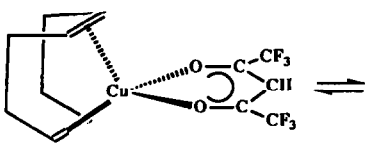

1

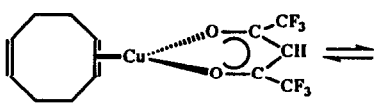

2

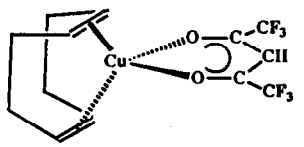

(5)

1

A similar situation is possible for the case of (hfac)Ag(1,5-cod), although a number of incon-

Table 3. Bond angles (°)

Ag(2)—Ag(1)—O(1)	61.2(2)	Ag(2)—Ag(1)—O(3)	55.2(2)
O(1)—Ag(1)—O(3)	77.7(3)	Ag(2)—Ag(1)—O(4)	53.6(2)
O(1)—Ag(1)—O(4)	114.8(3)	O(3)—Ag(1)—O(4)	67.1(3)
Ag(2)—Ag(1)—C(11)	144.0(5)	O(1)—Ag(1)—C(11)	92.0(5)
O(3)—Ag(1)—C(11)	98.2(6)	O(4)—Ag(1)—C(11)	144.0(6)
Ag(2)—Ag(1)—C(14)	137.1(4)	O(1)—Ag(1)—C(14)	112.4(5)
O(3)—Ag(1)—C(14)	166.5(5)	O(4)—Ag(1)—C(14)	113.7(5)
C(11)—Ag(1)—C(14)	73.2(7)	Ag(2)—Ag(1)—C(15)	135.3(5)
O(1)—Ag(1)—C(15)	140.1(8)	O(3)—Ag(1)—C(15)	142.1(8)
O(4)—Ag(1)—C(15)	91.6(6)	C(11)—Ag(1)—C(15)	80.7(7)
C(14)—Ag(1)—C(15)	28.0(9)	Ag(2)—Ag(1)—C(18)	144.1(5)
O(1)—Ag(1)—C(18)	117.8(7)	O(3)—Ag(1)—C(18)	88.9(6)
O(4)—Ag(1)—C(18)	114.5(6)	C(11)—Ag(1)—C(18)	29.9(8)
C(14)—Ag(1)—C(18)	78.4(7)	C(15)—Ag(1)—C(18)	71.3(9)
Ag(1)—Ag(2)—O(2)	57.7(2)	Ag(1)—Ag(2)—O(3)	54.6(2)
O(2)—Ag(2)—O(3)	112.3(3)	Ag(1)—Ag(2)—O(4)	54.7(2)
O(2)—Ag(2)—O(4)	75.2(3)	O(3)—Ag(2)—O(4)	67.3(3)
Ag(1)—Ag(2)—C(19)	143.1(7)	O(2)—Ag(2)—C(19)	88.1(7)
O(3)—Ag(2)—C(19)	155.3(7)	O(4)—Ag(2)—C(19)	107.0(7)
Ag(1)—Ag(2)—C(22)	134.0(4)	O(2)—Ag(2)—C(22)	121.9(6)
O(3)—Ag(2)—C(22)	104.5(6)	O(4)—Ag(2)—C(22)	162.7(6)
C(19)—Ag(2)—C(22)	73.7(8)	Ag(1)—Ag(2)—C(23)	136.5(6)
O(2)—Ag(2)—C(23)	151.8(7)	O(3)—Ag(2)—C(23)	86.8(7)
O(4)—Ag(2)—C(23)	132.7(7)	C(19)—Ag(2)—C(23)	80.2(9)
C(22)—Ag(2)—C(23)	30.0(9)	Ag(1)—Ag(2)—C(26)	146.3(4)
O(2)—Ag(2)—C(26)	110.0(7)	O(3)—Ag(2)—C(26)	125.6(8)
O(4)—Ag(2)—C(26)	92.8(5)	C(19)—Ag(2)—C(26)	29.9(10)
C(22)—Ag(2)—C(26)	79.6(6)	C(23)—Ag(2)—C(26)	70.4(8)
Ag(1)—O(1)—C(1)	120.1(8)	Ag(2)—O(2)—C(3)	123.6(8)
Ag(1)—O(3)—Ag(2)	70.2(3)	Ag(1)—O(3)—C(6)	121.0(8)
Ag(2)—O(3)—C(6)	119.8(8)	Ag(1)—O(4)—Ag(2)	71.7(2)
Ag(1)—O(4)—C(8)	121.4(9)	Ag(2)—O(4)—C(8)	120.5(8)
O(1)—C(1)—C(2)	129.3(12)	O(1)—C(1)—C(4)	111.3(13)
C(2)—C(1)—C(4)	119.3(13)	C(1)—C(2)—C(3)	123.8(14)
O(2)—C(3)—C(2)	127.4(14)	O(2)—C(3)—C(5)	111.9(11)
C(2)—C(3)—C(5)	120.6(12)	C(1)—C(4)—F(1)	106.9(16)
C(1)—C(4)—F(2)	108.2(17)	F(1)—C(4)—F(2)	114.9(12)
C(1)—C(4)—F(3)	105.4(11)	F(1)—C(4)—F(3)	109.7(17)
F(2)—C(4)—F(3)	111.2(17)	C(1)—C(4)—F(1′)	106.9(18)
C(1)—C(4)—F(2′)	103.3(13)	F(1′)—C(4)—F(2′)	109.5(14)
C(1)—C(4)—F(3′)	116.3(14)	F(1′)—C(4)—F(3′)	112.6(15)
F(2′)—C(4)—F(3′)	107.7(18)	C(3)—C(5)—F(4)	110.2(9)
C(3)—C(5)—F(5)	110.1(9)	F(4)—C(5)—F(5)	109.2(9)
C(3)—C(5)—F(6)	108.7(9)	F(4)—C(5)—F(6)	109.4(9)
F(5)—C(5)—F(6)	109.3(9)	O(3)—C(6)—C(7)	125.9(13)
O(3)—C(6)—C(9)	115.4(14)	C(7)—C(6)—C(9)	118.8(14)
C(6)—C(7)—C(8)	123.9(13)	O(4)—C(8)—C(7)	127.0(13)
O(4)—C(8)—C(10)	113.5(13)	C(7)—C(8)—C(10)	119.5(13)
C(6)—C(9)—F(7)	115.2(17)	C(6)—C(9)—F(8)	115.6(15)
F(7)—C(9)—F(8)	109.4(17)	C(6)—C(9)—F(9)	110.9(16)
F(7)—C(9)—F(9)	104.6(15)	F(8)—C(9)—F(9)	99.5(18)
C(6)—C(9)—F(7′)	105.2(13)	C(6)—C(9)—F(8′)	106.4(14)
F(7′)—C(9)—F(8′)	107.9(13)	C(6)—C(9)—F(9′)	110.2(14)
F(7′)—C(9)—F(9′)	111.9(15)	F(8′)—C(9)—F(9′)	114.7(14)
C(8)—C(10)—F(10)	106.7(13)	C(8)—C(10)—F(11)	111.6(17)
F(10)—C(10)—F(11)	105.5(18)	C(8)—C(10)—F(12)	112.8(17)
F(10)—C(10)—F(12)	104.7(17)	F(11)—C(10)—F(12)	114.7(16)
C(8)—C(10)—F(10′)	109.5(11)	C(8)—C(10)—F(11′)	110.9(16)
F(10′)—C(10)—F(11′)	106.8(13)	C(8)—C(10)—F(12′)	111.4(13)

Table 3—*continued*

F(10′)—C(10)—F(12′)	108.5(16)	F(11′)—C(10)—F(12′)	109.7(11)
Ag(1)—C(11)—C(12)	103.0(12)	Ag(1)—C(11)—C(18)	78.5(12)
C(12)—C(11)—C(18)	128.6(21)	C(11)—C(12)—C(13)	120.1(17)
C(12)—C(13)—C(14)	121.0(18)	Ag(1)—C(14)—C(13)	106.5(15)
Ag(1)—C(14)—C(15)	71.6(15)	C(13)—C(14)—C(15)	125.4(22)
Ag(1)—C(15)—C(14)	80.4(15)	Ag(1)—C(15)—C(16)	101.2(18)
C(14)—C(15)—C(16)	136.0(23)	C(15)—C(16)—C(17)	117.2(23)
C(16)—C(17)—C(18)	113.0(21)	Ag(1)—C(18)—C(11)	71.7(12)
Ag(1)—C(18)—C(17)	108.0(16)	C(11)—C(18)—C(17)	120.5(22)
Ag(2)—C(19)—C(20)	100.3(14)	Ag(2)—C(19)—C(26)	78.8(13)
C(20)—C(19)—C(26)	121.9(25)	C(19)—C(20)—C(21)	123.3(23)
C(20)—C(21)—C(22)	126.2(22)	Ag(2)—C(22)—C(21)	105.0(13)
Ag(2)—C(22)—C(23)	75.6(14)	C(21)—C(22)—C(23)	128.3(20)
Ag(2)—C(23)—C(22)	74.5(14)	Ag(2)—C(23)—C(24)	111.1(20)
C(22)—C(23)—C(24)	128.4(28)	C(23)—C(24)—C(25)	123.8(28)
C(24)—C(25)—C(26)	126.9(24)	Ag(2)—C(26)—C(19)	71.3(13)
Ag(2)—C(26)—C(25)	100.9(15)	C(19)—C(26)—C(25)	124.7(25)

sistencies were noted between the spectroscopic data and physical properties of the copper(I) and silver(I) analogues. The FTIR spectra of the two compounds exhibited some substantial differences. For chelating, bidentate β-diketonate monoanionic ligands a number of characteristic bands are typically observed in the region between 1700 and 1400 cm^{-1}. For monomeric (hfac)Cu(L) complexes[19–23] in the solid state, for example, (hfac)Cu(1,5-cod),[18] there are two strong bands at 1636 and 1482 cm^{-1}, two medium intensity bands at 1554 and 1527 cm^{-1}, a medium intensity shoulder at 1668 cm^{-1} and a weak band at 1593 cm^{-1}. For (hfac)Ag(1,5-cod) a quite different envelope was observed in this region. Five bands were observed at different positions, namely, 1672, 1643, 1542, 1527 and 1492 cm^{-1}. A comparison of these two IR spectra is shown in Fig. 2. These differences can be interpreted in terms of the different coordination modes of the β-diketonate ligand in these two complexes, where it was shown by a single-crystal X-ray diffraction study (see later) that for (hfac)Cu(1,5-cod) the β-diketonate ligand only chelates, whereas for [(hfac)Ag(1,5-cod)] the β-diketonate ligands bridge two metal centres in addition to chelating. An alternative explanation is that these differences could be attributed to solid-state effects, such as the different point group symmetries of the copper(I) and silver(I) imposed by the solid state. However, we and others[24–26] have shown that in copper(I) and copper(II) β-diketonate compounds the solid-state and gas-phase IR data are similar where no intermolecular interactions exist in the solid state and that the differences generally involve changes in intensity rather than the position of the IR bands. No intermolecular interactions were observed in the solid-state structure of [(hfac)Ag(1,5-cod)]. Therefore, we believe that the difference in the hfac coordination mode is likely to be the predominant effect.

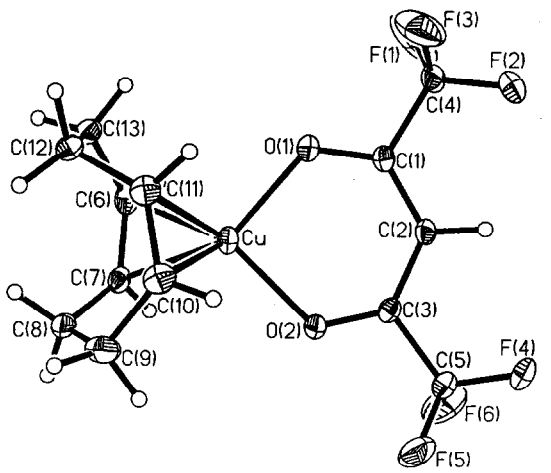

Fig. 1. ORTEP plot showing the solid-state structure of (hfac)Cu(1,5-cod).

In addition to these differences between the copper(I) and silver(I) compounds observed in the IR spectra a substantial difference was observed, qualitatively, in volatility. The silver compound was noticeably less volatile than the copper analogue, which was consistent with a higher degree of oligomerization for the silver(I) species. To investigate the nature of (hfac)Ag(1,5-cod) further a single-crystal X-ray diffraction study was performed which revealed the origin of the differences observed in the spectroscopic data and physical properties.

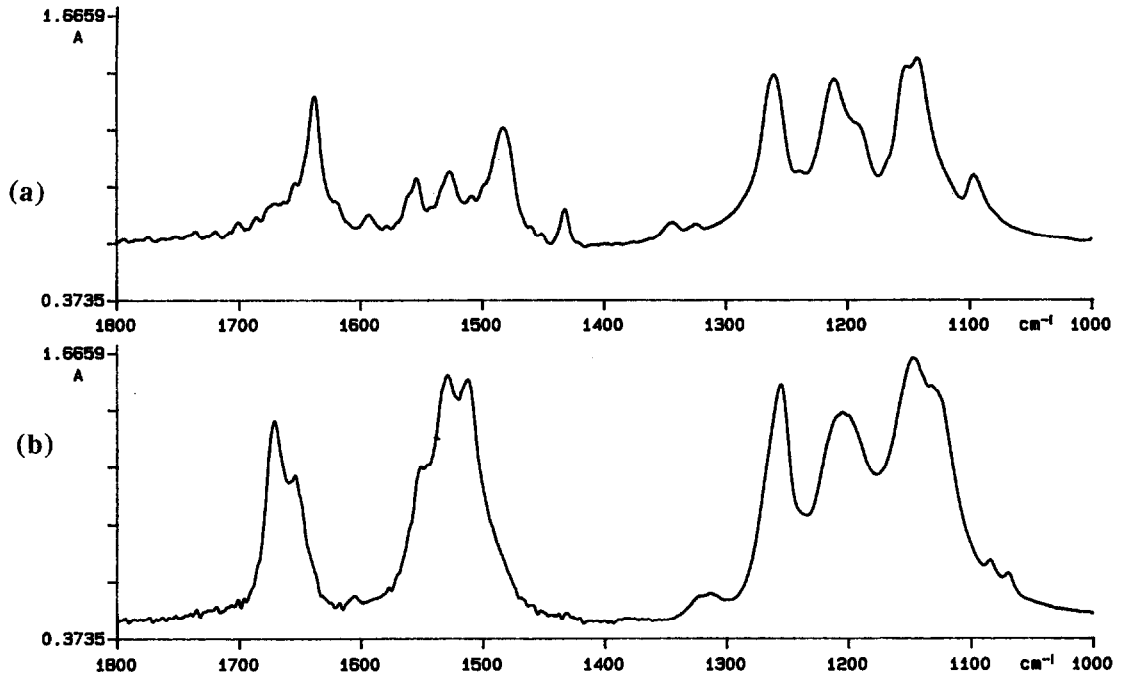

Fig. 2. Comparison of the FTIR data for (hfac)M(1,5-cod), M = (a) Cu and (b) Ag in the region 1800–1000 cm^{-1}.

An ORTEP plot is shown in Fig. 3, together with the atom labelling scheme. This species is dimeric in the solid state with one β-diketonate ligand, which both chelates and bridges two silver atoms in a μ^4,η^2-fashion, and a β-diketonate ligand, which bridges the two metal centres in an μ^2-fashion. The μ^4,η^2-β-diketonate binding mode is not common and has been observed only in three previous structures, namely, $[Ba_4(2,2,6,6,tetramethylheptandionato)_2]_4$,[27,28] Ca(1,3-diphenyl-1,3-propanedionate)$_2$ hemiethanolate[29] and Sr(1,3-diphenyl-1,3-propanedionate)$_2$ hemiethanolate.[30] The structure can be described as exhibiting an octahedral core with four β-diketonate oxygen atoms in an approximate square plane with silver atoms on opposite apices. Unfortunately, this compound is photosensitive and deteriorated significantly during the data collection. There is also significant disorder in the CF_3 groups. As a result it is unwise to interpret these data in great detail. However, it seems that the μ^4,η^2-hfac ligand bridges the silver(I) centres with similar Ag—O bond lengths (2.56 Å av.), while the other hfac ligand is markedly asymmetric with one short Ag—O bond length (2.46 Å av.) and one long distance (2.72 Å av.) that is longer than the sum of the covalent radii of silver and oxygen. Each silver atom is also coordinated to one 1,5-cod ligand through both double bonds. The marked asymmetry that was observed in the coordination of the copper(I) centre to the two double bonds of 1,5-cod in (hfac)Cu(1,5-cod) is not observed in the case of silver. The C=C distance in the 1,5-cod ligand of (hfac)Ag(1,5-cod) is close to the value of the double bond. These bonds lengths are similar to those observed for silver(I) complexes of 1,5-cod[31,32] and other olefins.[33–50]

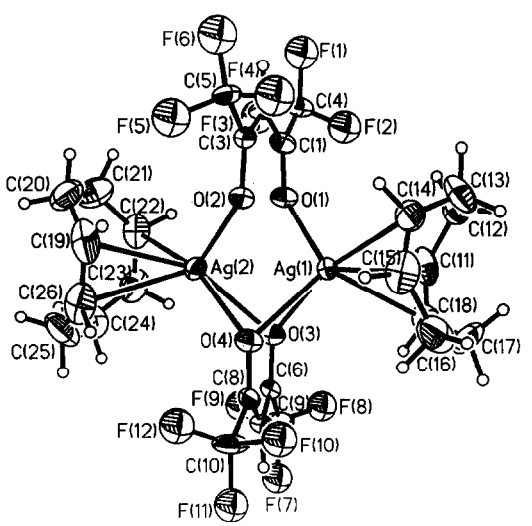

Fig. 3. ORTEP plot of the molecular structure of [(hfac)Ag(1,5-cod)]$_2$.

CONCLUSIONS

The compound (hfac)Ag(1,5-cod) was synthesized by the literature method and characterized

in the solid state by single-crystal X-ray diffraction. In contrast to the corresponding copper(I) compound it was found to be dimeric in the solid state and contained two unusual β-diketonate coordination modes, μ^4,η^2-hfac and μ^2-hfac. The deterioration of the crystal and extensive disorder precluded a detailed comparison of the metrical parameters of this compound with other literature data. However, the solid-state FTIR data showed substantial differences in the ν(C—O) and ν(C—C) stretching regions compared with the chelated hfac ligand in (hfac)Cu(1,5-cod). The data presented here will be useful in assigning the coordination mode of β-diketonate ligands in metal-organic complexes and on metal and metal oxide surfaces by FTIR.[24–26]

The dimeric nature of $[(hfac)Ag(1,5\text{-cod})]_2$ compared with the copper(I) analogue is probably the result of the larger size of silver(I) compared with copper(I), with the resulting desire for a higher coordination number for silver(I). It is interesting to note that analogous rhodium(I) complexes are monomeric even though rhodium(I) and silver(I) have a similar size and are from the same period.[51] However, for silver(I) there is no *d*-orbital-imposed geometrical preference as there is in the case of rhodium(I), which is probably a major influence in determining the coordination number and geometry of the rhodium(I) analogues.

Acknowledgements—M.H.-S. thanks the NSF REU program and ONR for partially funding this work. M.H.-S. thanks the NSF chemical instrumentation program for purchase of a low-field NMR spectrometer and Dr Todd Alam for assistance in obtaining NMR data.

REFERENCES

1. A. Zinn, B. Neimer and H. D. Kaesz, *Angew. Chem., Adv. Mat.* 1992, **4**, 375.
2. H. K. Shin, K.-M. Chi, M. J. Hampden-Smith, T. T. Kodas, M. F. Paffett and J. D. Farr, *Angew. Chem. Adv. Mat.* 1991, **3**, 246.
3. H. K. Shin, K.-M. Chi, M. J. Hampden-Smith, T. T. Kodas, N. F. Paffett and J. D. Farr, *Chem. Mat.* 1992, **4**, 788.
4. A. Jain, K.-M. Chi, M. J. Hampden-Smith, T. T. Kodas, M. F. Paffett and J. D. Farr, *J. Mat. Res.* 1992, **7**, 261.
5. S. K. Reynolds, C. J. Smart, E. F. Baran, T. H. Baum, C. E. Larson and P. J. Brock, *Appl. Phys. Lett.* 1991, **59**, 2332.
6. R. Kumar, A. W. Maverick, F. R. Fronczek, G. Lai and G. L. Griffin, 200th American Chemical Society Meeting, Atlanta, April 1991, Abstract INOR 256.
7. J. A. T. Norman, B. A. Muratore, P. N. Dyer, D. A. Roberts and A. K. Hochberg, *J. Phys.* 1992, **IV**, 1, C2-271.
8. A. Jain, K.-M. Chi, M. J. Hampden-Smith, T. T. Kodas, M. F. Paffett and J. D. Farr, *J. Electrochem. Soc.*, in press.
9. A. Jain, K.-M. Chi, H. K. Shin, M. J. Hampden-Smith, T. T. Kodas, M. F. Paffett and J. D. Farr, *SPIE Conference Proceedings*, Vol. 1596, p. 23. San Jose, CA (1991).
10. M. E. Gross and V. M. Donnelly, in *Advanced Metallization for ULSI Applications* (Edited by V. S. Rana and R. V. Joshi), p. 355. Materials Research Society, Pittsburgh (1991).
11. A. Jain, K.-M. Chi, M. J. Hampden-Smith, T. T. Kodas, M. F. Paffett and J. D. Farr, *Chem. Mat.* 1991, **3**, 995.
12. T. H. Baum and C. E. Larson, *Chem. Mat.* 1992, **4**, 365.
13. S. L. Cohen, M. Liehr and S. Kasi, *Appl. Phys. Lett.* 1992, **60**, 1585.
14. F. A. Cotton and G. Wilkinson, *Advanced Inorganic Chemistry*, 5th edn. Wiley, New York (1988).
15. D. F. Shriver and M. A. Drezden, *The Manipulation of Air-Sensitive Compounds*, 2nd edn, p. 78. Wiley-Interscience, New York (1986).
16. W. Partenheimer and E. H. Johnson, *Inorg. Chem.* 1972, **11**, 2840.
17. G. Doyle, K. A. Eriksen and D. Van Engen, *Organometallics* 1985, **4**, 830.
18. K.-M. Chi, H. K. Shin, M. J. Hampden-Smith, T. T. Kodas and E. N. Duesler, *Polyhedron* 1991, **10**, 2293.
19. H. K. Shin, M. J. Hampden-Smith, T. T. Kodas and E. N. Duesler, *Polyhedron* 1991, **6**, 645.
20. H. K. Shin, K.-M. Chi, J. Farkas, M. J. Hampden-Smith, T. T. Kodas and E. N. Duesler, *Inorg. Chem.* 1992, **31**, 424.
21. K.-M. Chi, H. K. Shin, M. J. Hampden-Smith, T. T. Kodas and E. N. Duesler, *Inorg. Chem.* 1991, **30**, 4293.
22. F. D. Hardcastle, J. Farkas, C. H. F. Peden, T. R. Omstead, R. S. Blewer, M. J. Hampden-Smith and T. T. Kodas, in *Advanced Metallization for ULSI Applications* (Edited by V. S. Rana and R. V. Joshi), p. 413. Materials Research Society, Pittsburgh (1991).
23. R. Rye, J. A. Knapp, K. M. Chi, M. J. Hampden-Smith, A. Jain and T. T. Kodas, *J. Appl. Phys. Lett.* 1992, **72**, 5941.
24. F. D. Hardcastle, J. Farkas, C. H. F. Peden, T. R. Omstead, R. S. Blewer, M. J. Hampden-Smith and T. T. Kodas, in *Advanced Metallization for ULSI Applications* (Edited by V. S. Rana and R. V. Joshi), p. 413. Materials Research Society, Pittsburgh (1991).
25. L. H. Dubois, *J. Electrochem. Soc.*, to be published.
26. A. Jain, J. Farkas, M. J. Hampden-Smith and T. T. Kodas, *Appl. Phys. Lett.* 1992, **62**, 2662.
27. A. Gleizes, S. Sans-Lenain and D. Medus, *Comp. Rendu*, Acad. Sci. Paris, Serie II, 1991, 761.
28. A. Gleizes, D. Medus and S. Sans-Lenain, in *Better Ceramics Through Chemistry V* (Edited by M. J. Hampden-Smith, W. G. Klemperer and C. J. Brinker), Vol. 271, p. 27. Materials Research Society, Pittsburgh (1992).

29. F. L. Hollander, D. H. Templeton and A. Zalkin, *Acta Cryst.* 1973, **B29**, 1295.
30. F. L. Hollander, D. H. Templeton and A. Zalkin, *Acta Cryst.* 1973, **B29**, 1303.
31. A. Albinati, S. V. Meille and G. Carturan, *J. Organomet. Chem.* 1979, **182**, 269.
32. F. S. Mathews and W. N. Lipscomb, *J. Am. Chem. Soc.* 1959, **63**, 845.
33. P. Ganis, V. Giuliano and U. Lepore, *Tetrahedron Lett.* 1971, **10**, 765.
34. C. S. Gibbons and J. Trotter, *J. Chem. Soc.* 1971, **A**, 2058.
35. O. Ermer, H. Eser and J. D. Dunitz, *Helv. Chim. Acta* 1971, **54**, 2469.
36. I. W. Bassi and G. Fagherazzi, *J. Organomet. Chem.* 1968, **13**, 535.
37. N. C. Baenziger, H. L. Haight, R. Alexander and J. R. Doyle, *Inorg. Chem.* 1966, **5**, 1399.
38. T. C. W. Mak, W. C. Ho and N. Z. Huang, *J. Organomet. Chem.* 1983, **251**, 413.
39. T. C. W. Mak, *J. Organomet. Chem.* 1983, **246**, 331.
40. S. C. Nyburg and J. Hilton, *Acta Cryst.* 1959, **12**, 116.
41. R. B. Jackson and W. E. Streib, *J. Am. Chem. Soc.* 1967, **89**, 2539.
42. J. E. McMurry, G. J. Haley, J. R. Matz, J. C. Clardy and J. Mitchell, *J. Am. Chem. Soc.* 1986, **108**, 515.
43. R. Faure, H. Loiseleur, G. Haute and H. Trauer, *Acta Cryst.* 1985, **C41**, 1593.
44. A. T. McPhail and G. A. Sim, *J. Chem. Soc.* 1966, **B**, 112.
45. K. Shelly, D. C. Finster, Y. J. Lee, W. R. Scheidt and C. A. Reed, *J. Am. Chem. Soc.* 1985, **107**, 5955.
46. E. A. H. Griffith and E. L. Amma, *J. Am. Chem. Soc.* 1974, **96**, 5407.
47. P. F. Rodesiler, E. A. H. Griffith and B. L. Amma, *J. Am. Chem. Soc.* 1972, **94**, 761.
48. E. A. H. Griffith and E. L. Amma, *J. Am. Chem. Soc.* 1971, **93**, 3167.
49. I. F. Taylor, E. A. Griffith and E. L. Amma, *J. Am. Chem. Soc.* 1969, **91**, 5745.
50. R. Usón, A. Laguna, M. Laguna and B. R. Manzano, *J. Chem. Soc., Dalton Trans.* 1984, 285.
51. Z. Duan, M. J. Hampden-Smith, A. L. Rheingold and E. N. Duesler, *Inorg. Chem.*, submitted.

Polyhedron Vol. 12, No. 14, pp. 1793–1795, 1993
Printed in Great Britain

0277–5387/93 $6.00+.00
© 1993 Pergamon Press Ltd

SYNTHESES, PROPERTIES AND STRUCTURE OF THE COMPLEXES OF N-HYDROXYETHYL-N-BENZIMIDAZOLYLMETHYLETHYLENEDIAMINEDIACETIC ACID WITH COPPER(II) AND NICKEL(II)

LUQIN YANG, GENGLIN WANG,* SHIPING YAN, DAIZHENG LIAO, ZONGHUI JIANG and PANWEN SHEN

Department of Chemistry, Nankai University, Tianjin 300071, P.R.C.

and

HONGGEN WANG, RUJI WANG and XINKAN YAO

Central Laboratory, Nankai University, Tianjin 300071, P.R.C.

(*Received* 27 *January* 1993; *accepted* 23 *March* 1993)

Abstract—Two new complexes, $NiL \cdot 3H_2O$ and $CuL \cdot H_2O$ (L = N-hydroxylethyl-N-benzimidazolylmethylethylenediaminediacetic actate), have been synthesized and characterized by elemental analysis, IR and ESR spectra. The crystal structure of $NiL \cdot 3H_2O$ has been determined by single-crystal X-ray diffraction. The nickel centre is six-coordinate with distorted octahedral symmetry. IR and ESR spectra show that the structure of the copper compound is different from that of the nickel compound. The former may be a dimer and with a $d_{x^2-y^2}$ ground state. The hyperfine structure splitting parameter in copper is $A_2^N = 37.2$ G.

The aminopolycarboxyl complexes have attracted great interest in recent years for their use as the contrast-enhancing agents in magnetic resonance imaging, as probes in biochemistry and medical science.[1–3] Metal complexes of polydentate ligands containing imidazole are of current interest due to their being potential models for metalloenzymes and metalloproteins.[4,5] When preparing the ligand N-hydroxylethyl-N,N′,N′-tribenzimidazolylmethylethylenediamine we obtained the title ligand, a new benzimidazole aminopolycarboxyl acid. This paper reports the complexes of copper and nickel with the title ligand L.

EXPERIMENTAL

Synthesis of $CuL \cdot 2H_2O$ **(1)**

A water solution containing $CuAc_2$ (2 mmol) was added to an L–water solution (1 mmol). The mixture was heated for 2 h and then kept at room temperature for 1 week. A blue precipitate was formed slowly. The product was collected and dried in air. Found: C, 42.4; H, 5.0; N, 12.6. Calc. for $C_{16}H_{24}N_4O_7Cu$: C, 42.8; H, 5.4; N, 12.6%.

Synthesis of $NiL \cdot 3H_2O$ **(2)**

The compound was obtained in a similar manner to **1**, except $Ni(ClO_4)_2$ was used instead of $CuAc_2$ and the reaction solution was left in air for 1 month. Found: C, 40.8; H, 4.9; N, 12.5. Calc. for $C_{16}H_{26}N_4O_8Ni$: C, 41.7; H, 5.6; N, 12.2%.

Compound **2** was dissolved in hot water and slowly evaporated at room temperature for several weeks until a single crystal suitable for X-ray structure analysis was obtained.

X-ray data collection, structure determination and refinement for **2**

A transparent blue crystal of complex **2** having approximate dimensions $0.05 \times 0.2 \times 0.3$ mm was

* Author to whom correspondence should be addressed.

mounted on a glass fibre in a random orientation. The determination of the unit cell and the data collection were performed with Mo-K_α radiation ($\lambda = 0.71073$ Å) on an Enraf-Nonius CAD4 diffractometer equipped with a graphite crystal monochromator. A total of 3458 independent reflections were collected in the range $2° \leqslant \theta \leqslant 24°$ by the ω–2θ scan technique at room temperature, in which 1136 reflections with $[I \geqslant 3\sigma(I)]$ were considered to be observed and used in the succeeding refinement. A correction for Lp effects was applied to the data.

Crystals are rhombic, space group *Pbca*, $a = 10.863(2)$, $b = 13.874(2)$, $c = 25.727(7)$ Å, $V = 3877(3)$ Å^3, $Mr = 461.12$, $Z = 8$, $D_x = 1.58$ g cm^{-3}, $\mu = 10.54$ cm^{-1}, $F(000) = 1936$.

The structure was solved by direct methods (MULTAN 82). The nickel was located on an *E*-map. All the other non-hydrogen atoms were determined from successive difference-Fourier syntheses. The final refinement by full-matrix least-squares with anisotropic thermal parameters for non-hydrogen atoms converged with agreement factors of $R = \Sigma|\Delta F|/\Sigma|F_o| = 0.049$ and $Rw = [\Sigma_w|F|^2/\Sigma_w|F_o|^2]^{1/2} = 0.055$ (unit weights for all observed reflections). The highest peak on the final difference-Fourier map had a height of 0.48 e Å^{-3}.

All calculations were performed on a PDP11/44 computer using the SDP-PLUS program system.

Tables of final atomic positional and thermal parameters, full lists of bond lengths and angles and equations of least-squares planes have been deposited as supplementary material with the Editor.

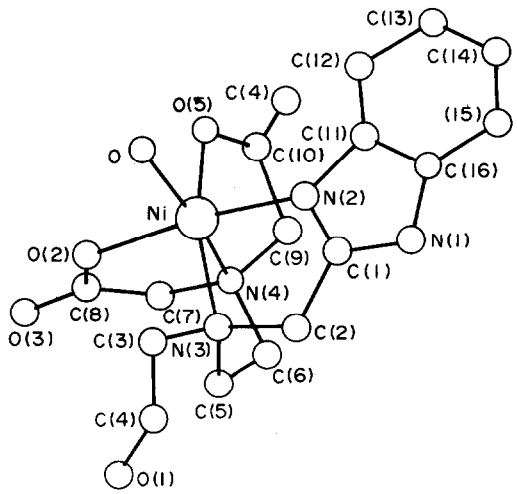

Fig. 1. Perspective view of NiL · $3H_2O$.

RESULTS AND DISCUSSION

The structure of compound **2**

The molecular structure of the complex NiL · $3H_2O$ is shown in Fig. 1. Selected bond lengths and angles are collected in Table 1.

Table 1. Bond distances (Å) and angles (°)

Ni—O	2.069(4)	N(3)—C(3)	1.521(6)
Ni—O(2)	2.063(4)	N(3)—C(5)	1.477(7)
Ni—O(5)	2.107(4)	N(4)—C(6)	1.504(7)
Ni—N(2)	2.051(4)	N(4)—C(7)	1.506(6)
Ni—N(3)	2.203(4)	N(4)—C(9)	1.485(6)
Ni—N(4)	2.072(4)	C(1)—C(2)	1.524(7)
O(1)—C(4)	1.420(7)	C(3)—C(4)	1.548(8)
O(2)—C(8)	1.268(7)	C(5)—C(6)	1.529(8)
O(3)—C(8)	1.268(7)	C(7)—C(8)	1.510(8)
O(4)—C(10)	1.232(6)	C(9)—C(10)	1.554(8)
O(5)—C(10)	1.289(7)	N(1)—C(1)	1.360(6)
N(1)—C(16)	1.407(6)	N(2)—C(1)	1.303(6)
N(2)—C(11)	1.412(6)	N(3)—C(2)	1.514(7)

O—Ni—O(2)	88.1(1)	O(2)—Ni—N(4)	82.3(2)
O—Ni—O(5)	95.5(1)	O(5)—Ni—N(2)	93.7(2)
O—Ni—N(2)	92.2(2)	O(5)—Ni—N(3)	159.8(2)
O—Ni—N(3)	104.0(2)	O(5)—Ni—N(4)	78.0(2)
O—Ni—N(4)	167.7(2)	N(2)—Ni—N(3)	80.4(2)
O(2)—Ni—O(5)	95.4(1)	N(2)—Ni—N(4)	98.5(2)
O(2)—Ni—N(2)	170.8(2)	N(3)—Ni—N(4)	83.8(2)
O(2)—Ni—N(3)	90.7(1)		

Numbers in parentheses are estimated standard deviations in the least significant digits.

In the molecule NiL·3H$_2$O, L is a pentadentate ligand. The five-coordinate atoms are N(2) (imidazole), N(3) (amine), N(4) (amine) and O(2), O(4) (two different acetic acids). The hydroxyl group is not coordinated to nickel in the molecule. The coordination number of nickel is six. The sixth coordinated atom is oxygen, which is from one water molecule. The six atoms around nickel make up a distorted coordination octahedron. The other two non-coordinated waters in the molecule are linked to L by hydrogen bonds.

The Ni—N distances in the molecule range from 2.051 to 2.203 Å (mean 2.109 Å) and Ni—O from 2.063 to 2.107 Å (mean 2.079 Å). The Ni—N(3) distance is longer than the others.

The O(2), O(5), N(2) and N(3) atoms lie approximately in a plane (plane 1). The maximum deviation from the plane is 0.1765 Å (nickel). The dihedral angle between plane 1 and the benzimidazole plane is 11.97°.

IR spectra

The IR spectra of these two complexes have the features of the spectrum L. No absorptions can be attributed to ClO_4^- and Ac^-. This result is in accordance with the constituents. In complex **1** the C=O stretching vibrations appear at 1625, 1575 and 1534 cm^{-1} [ν_{as}(CO)] and 1380 and 1400 cm^{-1} [ν_s(CO)], indicating different CO_2^- environments. From the values of $\Delta\nu = \nu_{as}(CO) - \nu_s(CO)$ we can deduce that both monodentate CO_2^- ($\Delta\nu > 220$ cm^{-1}) and bridging CO_2^- ($\Delta\nu$ 130–190 cm^{-1}) may be present in the complex.[6]

In the nickel complex the CO_2^- stretching vibrations appear at 1675, 1640, 1400 and 1365 cm^{-1}. Only monodentate CO_2^- is present. The result is also confirmed by the crystal structure. Two sets of CO_2^- absorptions imply two different CO_2^- types in the structure. For the free ligand H_2L the CO_2^- vibrations are at 1640, 1380 and 1365 cm^{-1} (sh).

The IR spectra indicate that the structure of the copper compound is different from that of nickel. The former may exist as a dimer.

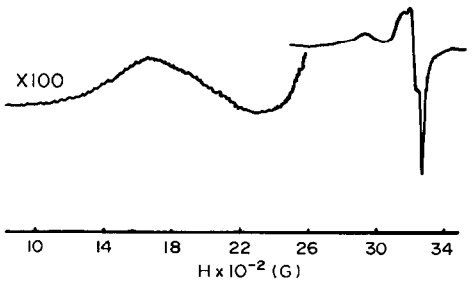

Fig. 2. *X*-band ESR powder spectrum of CuL·H$_2$O at 120 K.

ESR spectra

The powder ESR spectrum of the copper complex at −120 K is shown in Fig. 2. Three g values have been observed: $g_1 = 2.023$, $g_2 = 2.070$ and $g_3 = 2.247$. $R = (g_2 - g_1)/(g_3 - g_2) < 1$, which indicates that a predominant $d_{x^2-y^2}$ ground state is present. The coordinate structure of copper may be square pyramidal (coordinate number 5) or elongated tetragonal octahedron (coordinate number 6).[7]

The hyperfine structure was also found at g_2 for nuclear nitrogen (N, $I = 2$) at low temperature. The splitting parameter is *ca* $A_2^N = 37.2$ G.

The half-field line was also observed with a g-value centred at *ca* 4.0. The peak is weaker due to the forbidden transition $\Delta Ms = 2$. The appearance of the half-field line reveals that the complex is binuclear.

The intensity of the signals for $\Delta Ms = 1$ decreases upon cooling down towards 120 K. This confirms that the resonance occurs within the triplet excited state and a spin exchange interaction exists between copper ions.[8] Thus, the structure of the copper complex may be dimeric with the carboxyl acting as a bridging group.

The effective magnetic moments of the copper complex (**1**) are 1.3 B.M. at 4 K and 1.6 B.M. at 100 K. These values are lower than the spin-only magnetic moment 1.73 B.M. The effective magnetic moment decreases with decreasing temperature which implies the existence of an antiferromagnetic spin exchange interaction between the two copper ions in the dimer.

Acknowledgement—This project was supported by the National Natural Science Foundation of China.

REFERENCES

1. R. B. Lauffer, *Chem. Rev.* 1987, **87**, 901.
2. A. D. Sherry, C. A. Stark, J. R. Ascenso and C. F. G. C. Geraldes, *J. Chem. Soc., Dalton Trans.* 1981, 2078.
3. F. S. Richardson, *Chem. Rev.* 1982, **82**, 541.
4. P. Gomez-Romero, E. H. Witten, W. M. Reiff and G. B. Jameson, *Inorg. Chem.* 1990, **29**, 5211.
5. T. N. Sorrell, *Tetrahedron* 1989, **45**, 3.
6. K. Nakamoto, *Infrared and Raman Spectra of Inorganic and Coordination Compounds*, 3rd edn. John Wiley & Sons, New York (1978).
7. B. J. Hathaway and D. E. Billing, *Coord. Chem. Rev.* 1970, **5**, 143.
8. F. Tinti, M. Verdaguer, O. Kahn and J.-M. Savariault, *Inorg. Chem.* 1987, **26**, 2380.

Polyhedron Vol. 12, No. 14, pp. 1797–1804, 1993
Printed in Great Britain

0277–5387/93 $6.00+.00
© 1993 Pergamon Press Ltd

SYNTHESIS AND REACTIVITY OF BIMETALLIC ACETYLIDE-BRIDGED Pt—Pt COMPLEXES. CRYSTAL AND MOLECULAR STRUCTURE OF $[(PPh_3)(C_6F_5)Pt(\mu\text{-}C{\equiv}CPh)_2Pt(C_6F_5)(PPh_3)]$

J. R. BERENGUER, J. FORNIÉS,* F. MARTÍNEZ and J. C. CUBERO

Departamento de Química Inorgánica, Instituto de Ciencia de Materiales de Aragón, Universidad de Zaragoza-Consejo Superior de Investigaciones Científicas, 50009 Zaragoza, Spain

and

E. LALINDE* and M. T. MORENO

Universidad de La Rioja, 26001 Logroño, Spain

and

A. J. WELCH

Department of Chemistry, University of Edinburgh, Edinburgh EH9 3JJ, U.K.

(*Received* 27 *January* 1993; *accepted* 23 *March* 1993)

Abstract—The binuclear double-bridged acetylide complexes $[Pt(\mu\text{-}C{\equiv}CR)(C_6F_5)(PPh_3)]_2$ [R = Ph (**1**), Bu^t (**2**), $SiMe_3$ (**3**)] have been synthesized from [*trans*-$Pt(C{\equiv}CR)_2(PPh_3)_2$] and [*cis*-$Pt(C_6F_5)_2(THF)_2$] (THF = tetrahydrofuran). The crystal structure of $[Pt(\mu\text{-}C{\equiv}CPh)(C_6F_5)(PPh_3)]_2$ (**1**) has been established by X-ray diffraction methods. The structure shows that two identical $[(PPh_3)(C_6F_5)PtC{\equiv}CPh]$ units are joined together through η^2-bonding of M—C≡CPh units. This indicates that the complex is formed via a rearrangement of groups between the two metal centres. Treatment of $[Pt(\mu\text{-}C{\equiv}CR)(C_6F_5)(PPh_3)]_2$ with L (L = PPh_3, py = pyridine) produces simple bridge-cleavage reactions giving the mononuclear complexes [*trans*-$Pt(C_6F_5)(C{\equiv}CR)(PPh_3)L$] (**4–9**).

Over the past decade intense research activity has been expended on homo- and heterobinuclear complexes stabilized through bridging acetylide ligands.[1–3] This is due both to their structural interest and to the possibility of observing new useful transformations by means of the activation of the acetylenic fragment (—C≡CR) coordinated to two reactive metal centres.[4–6]

Following our recent studies on the chemical reactivity of platinum acetylide complexes we have shown that [*cis*-$M(C_6F_5)_2(THF)_2$] (M = Pt, Pd) are excellent precursors for the synthesis of complexes containing the moiety "$M(C_6F_5)_2$". Thus, the neutral bis-acetylide complexes [*cis*-$L_2Pt(C{\equiv}CR)_2$] react with [*cis*-$M(C_6F_5)_2(THF)_2$] to yield the neutral asymmetric binuclear complexes $[\{L_2Pt(C{\equiv}CR)_2\}M(C_6F_5)_2]$, in which the unit "*cis*-$L_2Pt(C{\equiv}CR)_2$" is acting as a chelating metallo ligand towards the "$M(C_6F_5)_2$" fragment. By contrast, treatment of [*cis*-$M(C_6F_5)_2(THF)_2$] with the anionic derivatives Q_2[*cis*-$Pt(C_6F_5)_2(C{\equiv}CR)_2$] gives, probably through intramolecular σ-alkynyl migration reactions, doubly acetylide-bridged complexes of the type $Q_2[(C_6F_5)_2Pt(\mu\text{-}C{\equiv}CR)_2M(C_6F_5)_2]$.[7] In this paper we describe the reactions between [*trans*-$Pt(C{\equiv}CR)_2(PPh_3)_2$] (R = Ph, Bu^t, $SiMe_3$) and [*cis*-$Pt(C_6F_5)_2(THF)_2$], which

* Authors to whom correspondence should be addressed.

Table 1. ^{19}F and ^{31}P NMR data of the complexes ($CDCl_3$, J in Hz)

Complex	^{19}F $F_{oo'}$	F_p	$F_{mm'}$	J(Pt—F_o)	$^{31}P\{^1H\}$ δ(P)	^1J(Pt—P)
1 $[Pt(\mu\text{-}C{\equiv}CPh)(C_6F_5)(PPh_3)]_2$	−118.2	−164.3	−165.4	261	14.04	3976
2 $[Pt(\mu\text{-}C{\equiv}CBu^t)(C_6F_5)(PPh_3)]_2$[a]	−109.7		−162.1	246	13.19	4006
		−162.6				
	−117.7		−164.6	256		
3 $[Pt(\mu\text{-}C{\equiv}CSiMe_3)(C_6F_5)(PPh_3)]_2$	−115.1	−163.5	−164.8	273	15.30	3991
4 [*trans*-$Pt(C_6F_5)(C{\equiv}CPh)(PPh_3)_2$]	−118.2	−165.3		280	20.26	2723
5 [*trans*-$Pt(C_6F_5)(C{\equiv}CBu^t)(PPh_3)_2$]	−118.1	−165.7		299	20.47	2761
6 [*trans*-$Pt(C_6F_5)(C{\equiv}CSiMe_3)(PPh_3)_2$]	−118.1	−165.4		286	20.03	2741
7 $[Pt(C_6F_5)(C{\equiv}CPh)(PPh_3)py]$	−119.5	−163.1	−163.4	212	9.10	3768
8 $[Pt(C_6F_5)(C{\equiv}CBu^t)py]$	−119.2	−163.5	−164.2	280	9.37	3829
9 $[Pt(C_6F_5)(C{\equiv}CSiMe_3)(PPh_3)py]$	−119.4	−163.1	−164.0	282	8.97	3786

[a] In CD_3COCD_3; data at −85°C; see text for data at different temperatures.

take place with redistribution of the ligands. The neutral binuclear doubly acetylide bridged complexes $[Pt(\mu\text{-}C{\equiv}CR)(C_6F_5)(PPh_3)]_2$ are obtained and the reactions of such binuclear complexes with neutral ligands are studied.

RESULTS AND DISCUSSION

The reactions between [*trans*-$Pt(C{\equiv}CR)_2(PPh_3)_2$] and [*cis*-$Pt(C_6F_5)_2(THF)_2$] in CH_2Cl_2, at room temperature and under nitrogen, render neutral double-bridged binuclear acetylide complexes **1–3** in good yield [eq. (1)]. These complexes have been characterized by elemental analysis and spectroscopic methods [mass spectrometry, IR, ^1H (Experimental), ^{31}P and ^{19}F NMR (Table 1)], together with the X-ray structure of complex **1**. Compound **2** crystallizes with CH_2Cl_2, which is supported by elemental analysis and ^1H NMR spectroscopy.

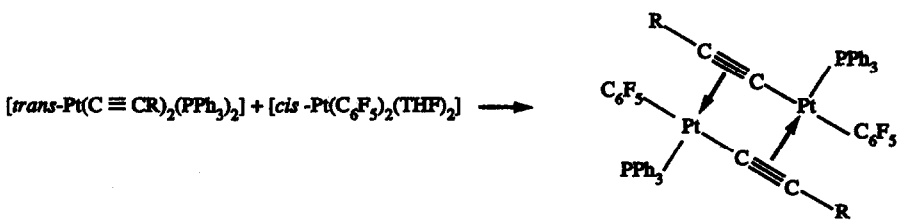

(1)

R = Ph (1)
R = Bu^t (2)
R = $SiMe_3$ (3)

As is well known acetylide bridging ligands can display a range of different bonding situations[1] and in order to ascertain the structural characteristics of the acetylide groups in these neutral complexes, an X-ray diffraction study of complex **1** has been performed. Suitable crystals for X-ray study have been obtained by slow diffusion of n-hexane into a dichloromethane solution of the compound at room temperature.

A drawing of the molecular structure of **1** is shown in Fig. 1. Selected bond distances and angles are listed in Table 2. Compound **1** is a centrosymmetric alkynyl-bridged dimer formed by the mutual interaction of two identical $(PPh_3)(C_6F_5)Pt(C{\equiv}CPh)$ units. In each unit the platinum atom is in an approximately square-planar environment formed by the phosphorus atom of the PPh_3 ligand, two carbon atoms mutually *trans* (the C-*ipso* atom of the C_6F_5 group and the C_α atom of the C≡CPh ligand) and the midpoint of the C≡C triple bond of the phenylacetylide ligand of the other unit. The central C_4Pt_2 core atoms are co-planar, although both planar[3,8] and non-planar[4,7] C_4M_2 cores have been found in double-bridged binuclear acetylide complexes. The Pt(1)—P(1) [2.250(2) Å], Pt(1)—C(1) [2.026(6) Å] and Pt(1)—C(9) [2.049(6) Å] distances are similar to those found in other platinum complexes with these types of ligands.[7,9–11]

The most significant feature is that the platinum

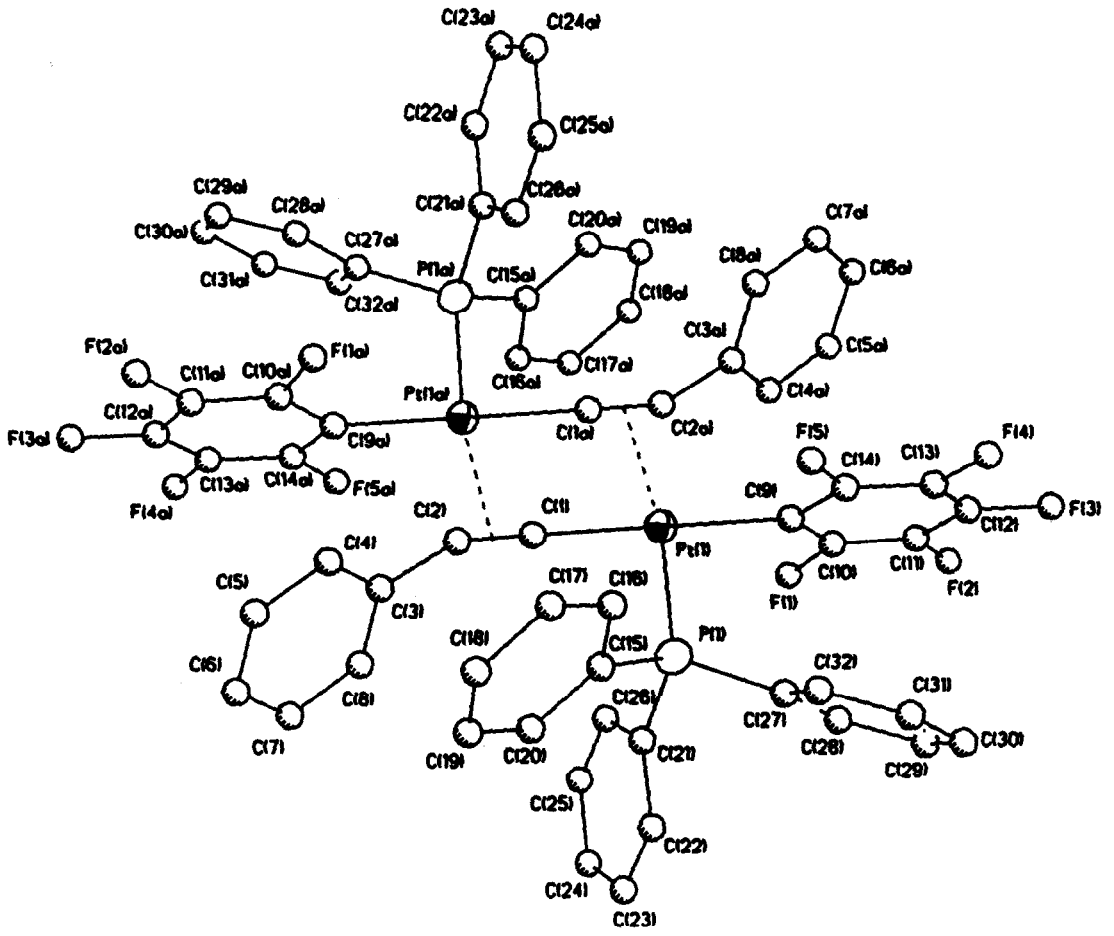

Fig. 1. View of the structure of the complex $[Pt(\mu\text{-}C{\equiv}CPh)(C_6F_5)(PPh_3)]_2$ (**1**) with the atomic numbering scheme.

acetylide π-linkages are asymmetric, as is reflected by the bond lengths from Pt(1A) to the two carbon atoms C(1) and C(2); the Pt(1A)—C(2) distance [2.261(6) Å] being substantially shorter than Pt(1A)—C(1) [2.362(6) Å]. Although this very characteristic structural feature contrasts with the symmetrical π-linkages found in the binuclear anion $[(C_6F_5)_2Pt(\mu\text{-}C{\equiv}CPh)_2Pt(C_6F_5)_2]^{2-}$ (**A**),[7] it has been previously observed in other σ–π acetylide-bridging binuclear complexes[4,8a,12,13] and is partly explained by the resonance structures shown in Scheme 1.

Table 2. Selected bond lengths (Å) and angles (°) for complex **1**

Pt(1)—Pt(1A)	3.653(1)	Pt(1)—P(1)	2.250(2)
Pt(1)—C(1)	2.026(6)	Pt(1)—C(9)	2.049(6)
C(1)—C(2)	1.199(8)	C(1)—Pt(1A)	2.362(6)
C(1)—C(1A)	2.454(1)	C(2)—C(3)	1.469(7)
C(2)—Pt(1A)	2.261(6)		
P(1)—Pt(1)—C(1)	88.1(2)	P(1)—Pt(1)—C(9)	90.4(2)
P(1)—Pt(1)—C(1A)	155.7(1)	P(1)—Pt(1)—C(2A)	174.1(1)
C(1)—Pt(1)—C(9)	177.3(2)	C(1)—Pt(1)—C(1A)	67.5(3)
C(9)—Pt(1)—C(1A)	113.9(2)	C(1)—Pt(1)—C(2A)	97.4(2)
C(9)—Pt(1)—C(2A)	84.1(2)	Pt(1)—C(1)—C(2)	175.1(5)
C(1)—C(2)—C(3)	151.2(6)		

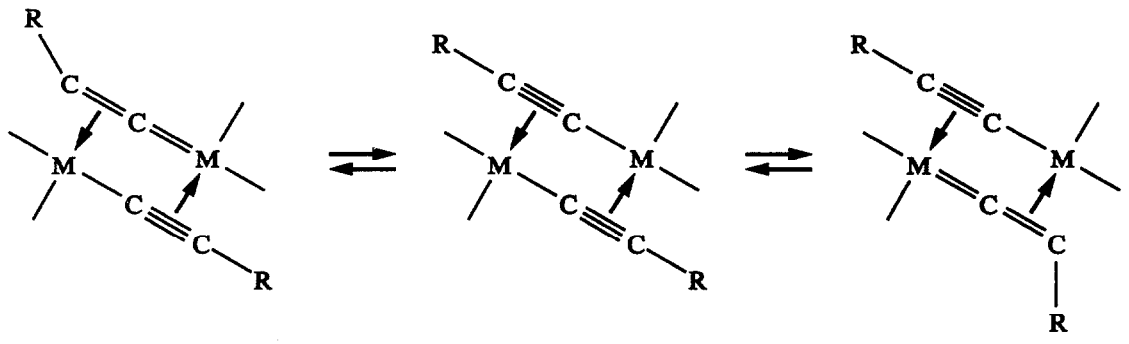

B C B'

On coordination the Pt(1)—C(1)—C(2) unit remains almost linear [175.1(5)°], but the phenyl group is slightly bent away [∠C(1)—C(2)—C(3) = 151.2(6)°] from the side-on coordinated metal centre Pt(1A). The acetylide groups adopt a *cis*-bent arrangement. The C(1)—C(2) distance [1.199(8) Å] is identical (within experimental error) to the corresponding distances found in the binuclear anion **A**.[7] In contrast, the distance between the platinum atoms is much longer in complex **1** [3.653(1) Å] than in the binuclear anion **A** (3.43 Å).[7]

The IR spectra of compounds **1–3** all show a medium intensity absorption in the 1915–1986 cm^{-1} region due to $\nu(C{\equiv}C)$. As expected these absorptions appear at lower frequencies than those in the starting materials [*trans*-$Pt(C{\equiv}CR)_2(PPh_3)_2$] [R = Ph,[14] Bu^t,[9] $SiMe_3$ (see Experimental)] (2110–2041 cm^{-1}). Complexes **2** and **3** show an absorption due to the *X*-sensitive mode of the C_6F_5[15] groups (B_u), in good agreement with that expected for a compound of C_{2h} symmetry. The assignment of this *X*-sensitive band in **1** is precluded because of the presence, in this region, of an internal absorption of —C≡CPh.

The ^{31}P NMR spectra of **1–3** exhibit the expected singlet flanked by two platinum satellites (Table 1). The magnitude of $^1J(^{195}Pt—^{31}P)$ (3976–4006 Hz) is larger than that of the corresponding asymmetric isomers [$\{(PPh_3)_2Pt(C{\equiv}CR)_2\}Pt(C_6F_5)_2$] (*ca* 2600 Hz) reported previously.[7] These values are also considerably larger than those reported for mononuclear acetylide complexes having a tertiary phosphine *trans* to a terminal acetylide group (*ca* 2100 Hz).[16] This suggests that acetylide groups bound in a π-fashion exert a lower *trans* influence than corresponding groups which are σ-bonded. In complexes **2** and **3** both acetylide ligands are equivalent, giving rise in their ^1H NMR spectra to the expected singlet for the Bu^t and $SiMe_3$ groups, respectively (see Experimental). The ^{19}F NMR spectra of complexes **1** and **3** exhibit the typical pattern of three signals in a 2:1:2 ratio (Table 1) due to two equivalent C_6F_5 groups, for which the plane of coordination is a plane of symmetry. By contrast the corresponding ^{19}F NMR spectrum of the t-butyl derivative **2** at room temperature shows five signals: one sharp resonance at −163.7 ppm (Fp), two broad *ortho*-fluorine resonances centred on −111.7 and −117.1 ppm, respectively, and two broad *meta*-fluorine signals (−164.2 and −165.9 ppm). By lowering the temperature (see Fig. 2 and Table 1 for data at −85°C) the five signals are clearly resolved. This spectral pattern indicates the lack of a symmetry plane in this molecule and can be explained by assuming a non-planar structure for complex **2** at low temperature. Similar non-planar structures have been previously found in doubly acetylide-bridged binuclear complexes.[4,7] At higher temperatures (40°C, 55°C) the two *ortho*-fluorine signals (as well as the two *meta*-fluorine signals) collapse to give broad unresolved signals (δF_{ortho} = −112.8; δF_{meta} = −164.9 ppm) at 55°C, suggesting the beginning of dynamic behaviour.

Finally, it is interesting to emphasize the different behaviour of both [*cis*-$M(C{\equiv}CR)_2L_2$] and [*trans*-$M(C{\equiv}CR)_2L_2$] towards [*cis*-$M(C_6F_5)_2(THF)_2$]. With the *cis*-derivatives binuclear asymmetric complexes [$\{L_2Pt(C{\equiv}CR)_2\}M(C_6F_5)_2$], with the bis-acetylide complex acting as a chelate ligand, are formed,[7] while the reactions with the *trans*-derivatives result in a redistribution of ligands and formation of the symmetric binuclear complexes **1–3**.

In order to explore the reactivity of these doubly acetylide-bridged diplatinum complexes (**1–3**) a few reactions with neutral donor ligands have been performed. Treatment of the bridged complexes **1–3** with PPh_3 or py brings about bridge splitting to give mononuclear complexes [*trans*-$Pt(C_6F_5)(C{\equiv}CR)(PPh_3)_2$] [R = Ph (**4**), R = Bu^t (**5**), R = $SiMe_3$ (**6**)] and [$Pt(C_6F_5)(C{\equiv}CR)(PPh_3)py$] [R = Ph (**7**), R = Bu^t (**8**), R = $SiMe_3$ (**9**)], respectively [eq. (2)].

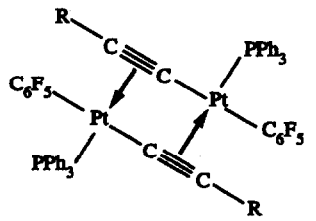

$$+2L \longrightarrow 2\ [Pt(C_6F_5)(C{\equiv}CR)(PPh_3)L] \quad (2)$$

R = Ph;	L = PPh_3(4)	R = Ph;	L = py(7)
R = Bu^t;	L = PPh_3(5)	R = Bu^t;	L = py(8)
R = $SiMe_3$;	L = PPh_3(6)	R = $SiMe_3$;	L = py(9)

We have observed that the fastest and easiest reactions occur with complex **1**. Thus, whereas **1** reacts readily with a stoichiometric amount of PPh_3 or py, the reaction between **2** and PPh_3 requires 6 h for completion and a large excess of py must be used to bring about complete reaction (see Experimental). On the other hand, although the acetylide bridges in complex **3** are easily cleaved by using a stoichiometric amount of PPh_3, the reaction with pyridine is more complex. Thus, treatment of **3** with a slight excess of pyridine (4 h under reflux and 12 h at room temperature) renders a colourless solution, from which a first fraction containing **9** and unreacted **3** (IR spectroscopy) and a second fraction of **9** (25% yield) can be isolated. However, with a shorter reaction time (3 h at room temperature) **3** did not react appreciably with py and longer reaction times or a large excess of py only produce mixtures which contain [*cis*-$Pt(C_6F_5)_2py_2$] (IR spectroscopy), **6**, **9** (^{31}P NMR spectroscopy) and an unidentified material with $\delta(P) = 14.8$ and $^1J(^{195}Pt—^{31}P) = 3674$ Hz. The formation of **6** indicates that the reaction occurs with ligand rearrangement. On the other hand, **1**, the most reactive, does not react in CH_2Cl_2 with CO at room temperature, and from the reactions between **1** or **3** with 2,2′-bipy (molar ratio 1 : 1) in CH_2Cl_2 (at room temperature or at reflux), only the starting materials are recovered.

Analysis, yields, relevant IR data and ^1H NMR data for complexes **4**–**9** are given in the Experimental. ^{19}F and ^{31}P NMR data are listed in Table

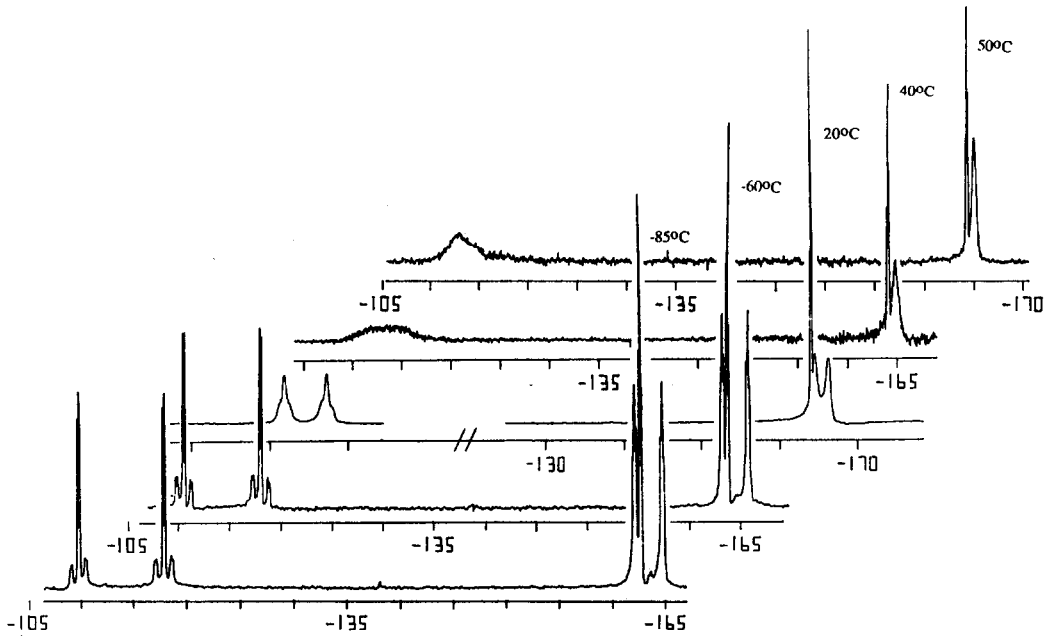

Fig. 2. ^{19}F NMR spectra of the complex [Pt(μ-C≡CBu^t)(C_6F_5)(PPh_3)]$_2$ (**2**) in CD_3COCD_3 at different temperatures.

1. The IR spectra of all the complexes show an absorption in the 2047–2119 cm^{-1} range, due to $\nu(C{\equiv}C)$, which indicates terminal coordination of the acetylide ligand.[17] The ^{31}P NMR spectra of complexes **4–6** show (Table 1) that both phosphorus nuclei are equivalent, indicating a *trans* structure for these complexes. Moreover, the absence of an absorption due to PPh_3 in the 540–560 cm^{-1} region (IR spectra) agrees with this assertion.[18] For the complexes $[Pt(C_6F_5)(C{\equiv}CR)(PPh_3)py]$ [R = Ph (**7**), R = Bu^t (**8**), R = $SiMe_3$ (**9**)] the structure with pyridine and PPh_3 ligands *trans* to one another is tentatively assigned on the basis of $^1J(^{195}Pt—^{31}P)$. Thus, the three compounds show one phosphorus resonance with this platinum–phosphorus coupling constant in the range (3768–3829 Hz), characteristic of $[trans\text{-}PtX_2(PR_3)py]$[19] and $[PtXY(PR_3)py]$[20] (phosphine *trans* to py) compounds.

EXPERIMENTAL

General considerations

Carbon, hydrogen and nitrogen analyses were performed on a Perkin–Elmer 240-B microanalyser. IR spectra were recorded (in the range 4000–200 cm^{-1}) on a Perkin–Elmer 883 spectrometer using Nujol mulls between polyethylene sheets. Proton, ^{19}F and ^{31}P NMR spectra were recorded on a Varian XL-200 or Unity-300 spectrometer. Chemical shifts are reported in ppm relative to external standards ($SiMe_4$, $CFCl_3$ and 85% H_3PO_4). Mass spectra were recorded on a VG Autospec. Literature methods were used to prepare: $[PtCl_2(tht)_2]$,[21] $[cis\text{-}PtCl_2(PPh_3)_2]$,[22] $[cis\text{-}Pt(C_6F_5)_2(THF)_2]$[23] and $[trans\text{-}Pt(C{\equiv}CPh)_2(PPh_3)_2]$.[14] $[Trans\text{-}Pt(C{\equiv}CR)_2(PPh_3)_2]$ (R = Bu^t, $SiMe_3$) were prepared as described below.

$[Trans\text{-}Pt(C{\equiv}CBu^t)_2(PPh_3)_2]$[24]

$[PtCl_2(tht)_2]$ (0.7 g, 1.583 mmol) was added, under nitrogen, to an ethereal solution of $LiC{\equiv}CBu^t$ at −10°C (8.706 mmol)[10] and the stirred mixture was allowed to warm to room temperature over 30 min. Moist ether (10 cm^3) was added to destroy the excess $LiC{\equiv}CBu^t$ and the solution was evaporated to dryness. The residue was treated with EtOH (40 cm^3) and acetone (20 cm^3), giving a colourless solution which was stirred with PPh_3 (1.24 g, 4.746 mmol) for 12 h. The resulting white solid, $[trans\text{-}Pt(C{\equiv}CBu^t)_2(PPh_3)_2]$, was filtered off, washed with acetone and air dried, yield 84%.

$[Trans\text{-}Pt(C{\equiv}CSiMe_3)_2(PPh_3)_2]$

A solution of $LiBu^n$ in hexane (1.8 mol dm^{-3}, 1.67 cm^3, 3.036 mmol) was added dropwise, under nitrogen, to an ethereal (20 cm^3) solution of $Me_3SiC{\equiv}CH$ (0.29 g, 2.0357 mmol) at −10°C. After 30 min stirring $[cis\text{-}PtCl_2(PPh_3)_2]$ (0.8 g, 1.0119 mmol) was added and the mixture stirred overnight at room temperature. The resulting white suspension was evaporated to dryness and the residue extracted with CH_2Cl_2 (50 cm^3) and filtered. The resulting solution was evaporated to dryness and the residue was treated with acetone (20 cm^3), giving $[trans\text{-}Pt(C{\equiv}CSiMe_3)_2(PPh_3)_2]$ as a white solid; yield 65%. Found: C, 60.4; H, 5.3. Calc.: C, 59.7; H, 5.6%. IR data (cm^{-1}): $\nu(C{\equiv}C)$ 2041 (s). ^1H NMR ($CDCl_3$, 200 MHz): δ −0.49 (s, $SiMe_3$), δ 7.35, 7.74 (m, Ph). $^{31}P\{^1H\}$ NMR ($CDCl_3$): δ 18.46 [$^1J(^{195}Pt—^{31}P)$ = 2690 Hz].

Preparation of the complexes

$[Pt(\mu\text{-}C{\equiv}CPh)(C_6F_5)(PPh_3)]_2$ (**1**). $[Cis\text{-}Pt(C_6F_5)_2(THF)_2]$ (0.0704 g, 0.1085 mmol) was added, under N_2, to a CH_2Cl_2 solution of $[trans\text{-}Pt(C{\equiv}CR)_2(PPh_3)_2]$ (0.1 g, 0.1085 mmol) and the mixture was stirred at room temperature for 4 days. The yellow solution was filtered, reduced in volume (*ca* 1 cm^3) and mixed with hexane (*ca* 10 cm^3). The resulting solid was recrystallized from dichloromethane–hexane giving white crystals of **1**. Yield 73%. Found: C, 52.8; H, 2.9. Calc.: C, 53.0; H, 2.8%. IR data (cm^{-1}): $\nu(C{\equiv}C)$ 1963 (m). EI–MS: m/z = 1450 [M^+].

$[Pt(\mu\text{-}C{\equiv}CR)(C_6F_5)(PPh_3)]_2$ [R = Bu^t (**2**), R = $SiMe_3$ (**3**)]. A mixture of $[cis\text{-}Pt(C_6F_5)_2(THF)_2]$ (0.07635 g, 0.1134 mmol) and $[trans\text{-}Pt(C{\equiv}CR)_2(PPh_3)_2]$ (0.1 g for R = Bu^t or 0.1037 g for R = $SiMe_3$; 0.1134 mmol) in CH_2Cl_2 (20 cm^3) was stirred at room temperature for 4 days under nitrogen. Concentration of the resulting yellow solution and addition of EtOH (*ca* 30 cm^3) afforded **2** or **3** as white crystals, which were washed with EtOH; yields: **2**, 60%; **3**, 63%.

$[Pt(\mu\text{-}C{\equiv}CBu^t)(C_6F_5)(PPh_3)]_2 \cdot CH_2Cl_2$ (**2**). Found: C, 48.9; H, 3.2. Calc.: C, 48.9; H, 3.4%. IR data (cm^{-1}): $\nu(C{\equiv}C)$ 1986 (m), νX-sens(C_6F_5) 786 (vs). ^1H NMR ($CDCl_3$, 300 MHz): δ 0.4 (s, Bu^t); δ 5.30 (CH_2Cl_2); δ 7.36, 7.66 (m, Ph). E.I.–MS: m/z = 1410 [M^+].

$[Pt(\mu\text{-}C{\equiv}CSiMe_3)(C_6F_5)(PPh_3)]_2$ (**3**). Found: C, 48.1; H, 3.2. Calc.: C, 48.3; H, 3.3%. IR data (cm^{-1}): $\nu(C{\equiv}C)$ 1915 (s); νX-sens(C_6F_5) 790. ^1H NMR ($CDCl_3$, 200 MHz): δ −0.7 (s, $SiMe_3$); δ 7.4, 7.66 (m, Ph). E.I.–MS: molecular peak not observed.

[*Trans*-Pt(C≡CR)(C_6F_5)(PPh_3)$_2$] [R = Ph (**4**), R = Bu^t (**5**), R = $SiMe_3$ (**6**)]. Compound **4**: Triphenylphosphine (0.036 g, 0.1314 mmol) was added to a CH_2Cl_2 (15 cm^3) solution of **1** (0.1 g, 0.0662 mmol) and the mixture stirred at room temperature for 30 min. The solvent was removed and EtOH (5 cm^3) was added to the residue affording a white solid (**4**) which was washed with EtOH; yield 85%. Complexes **5** (yield 60%) and **6** (yield 63%) were prepared similarly. For **5** the initial yellow mixture of **2** and PPh_3 in CH_2Cl_2 was stirred until a colourless solution was obtained (*ca* 6 h). **4**. Found: C, 61.3; H, 3.6. Calc.: C, 60.8; H, 3.6%. IR data (cm^{-1}): ν(C≡C) 2119 (s); νX-sens(C_6F_5) 800 (s). E.I.–MS: m/z = 987 [M$^+$]. **5**: Found: C, 59.5; H, 3.9. Calc.: C, 59.6; H, 4.3%. IR data (cm^{-1}): ν(C≡C) 2129 (w); νX-sens(C_6F_5) 787 (s). ^{1}H NMR ($CDCl_3$, 200 MHz): δ 0.4 (s, Bu^t); δ 7.7, 7.4 (m, Ph). E.I.–MS: m/z = 967 [M$^+$]. **6**: Found: C, 57.1; H, 4.0. Calc.: C, 57.4; H, 4.0%. IR data (cm^{-1}): ν(C≡C) 2052 (m); νX-sens(C_6F_5) 789 (m). ^{1}H NMR ($CDCl_3$, 200 MHz): δ −0.6 (s, $SiMe_3$); δ 7.6, 7.3 (m, Ph). E.I.–MS: molecular peak not observed, m/z = 886 [M−C≡C$SiMe_3$].

[Pt(C_6F_5)(C≡CPh)(PPh_3)py] (**7**). To a solution of **1** (0.1 g, 0.0689 mmol) in CH_2Cl_2 (10 cm^3) was added pyridine (0.11 cm^{-3}, 0.1378 mmol). Immediately the solution turned deep yellow. The mixture was stirred for 2 h and then evaporated to dryness. Addition of n-hexane (10 cm^3) to the residue rendered **7** as a yellow solid, which was washed with n-hexane and air dried; yield 78%. Found: N, 1.6; C, 55.0; H, 3.1. Calc.: N, 1.7; C, 55.2; H, 3.1%. IR data (cm^{-1}): ν(C≡C) 2118 (s); νX-sens(C_6F_5) 781 (m). ^{1}H NMR ($CDCl_3$, 200 MHz): δ 6.98, 7.24, 7.30, 7.72 (m, overlapping, aromatic, PPh_3, py); δ 8.95 (m,. py). E.I.–MS: m/z = 804 [M$^+$].

[Pt(C_6F_5)(C≡CBu^t)(PPh_3)py] (**8**). Excess pyridine (0.2 cm^{-3}, 2.5054 mmol) was added to a yellow solution of **2** (0.124 g, 0.0878 mmol) in CH_2Cl_2 and the mixture was stirred at room temperature for 12 h. The resulting colourless solution was evaporated to dryness and n-hexane (20 cm^3) was added to give **8** as a white solid; yield 90%. Found: N, 1.9; C, 53.6; H, 3.6. Calc.: N, 1.8; C, 53.6; H, 3.7%. IR data (cm^{-1}): ν(C≡C) 2110 (w); νX-sens(C_6F_5) 787 (s). ^{1}H NMR ($CDCl_3$, 200 MHz): δ 0.8 (s, Bu^t); δ 7.3 (m, aromatic, PPh_3); δ 7.7 (m, overlapping, aromatic PPh_3, py); δ 8.97 (m, py). E.I.–MS: m/z = 784 [M$^+$].

[Pt(C_6F_5)(C≡C$SiMe_3$)(PPh_3)py] (**9**). Py (0.021 cm^3, 0.258 mmol) was added to a dichloromethane solution of **3** (0.125 g, 0.086 mmol) and the mixture stirred under reflux for 4 h and finally at room temperature for 12 h. Evaporation of the resulting solution and addition of isopropanol (2 cm^3) and n-hexane (5 cm^3) caused the precipitation of a white solid, which was identified by IR spectroscopy as a mixture of **3** [ν(C≡C) 1915 cm^{-1}] and **9** [ν(C≡C) 2047 cm^{-1}]. The resulting filtrate was concentrated and cooled to −30°C, yielding white crystals of **9** (25% yield). Found: N, 1.6; C, 51.0; H, 3.6. Calc.: N, 1.7; C, 51.0; H, 3.6%. IR data (cm^{-1}): ν(C≡C) 2047 (w): νX-sens(C_6F_5) 788 (s). ^{1}H NMR ($CDCl_3$, 200 MHz): δ −0.3 (s, $SiMe_3$); δ 7.32 (m, aromatic, PPh_3); δ 7.7 (m, overlapping, aromatic Ph_3, py); δ 8.93 (m, py). E.I.–MS: m/z = 800 [M$^+$].

Crystal structure determination

The crystal data for compound **1** are summarized in Table 3, together with some experimental details. Data were collected on an Enraf–Nonius CAD4 diffractometer using Mo-K_α radiation (λ = 0.71069 Å) at room temperature. The lattice dimensions and Laue group of the crystal were based on 25 reflections ($12° < \theta < 13°$). The structure was solved by Patterson synthesis (SHELXTL PLUS).[25] Most non-hydrogen atoms were located in the succeeding difference Fourier synthesis. The structure was refined by full-matrix least-squares with anisotropic thermal parameters for all atoms.

Table 3. Crystallographic data for complex **1**

Empirical formula	$C_{64}H_{40}F_{10}P_2Pt_2$
Crystal system	Monoclinic
Space group	$P2_1/n$
Unit cell dimensions	
a (Å)	8.384(2)
b (Å)	14.120(3)
c (Å)	22.664(5)
β (°)	99.90(3)
Volume (Å^3)	2643.1(10)
Z	2
Formula weight	1451.1
Density (calc.) (Mg m^{-3})	1.82
Absorption coefficient (mm^{-1})	5.423
2θ range (°)	4.0–50.0
Index ranges	$0 \leqslant h \leqslant 9$, $0 \leqslant k \leqslant 16$, $-27 \leqslant l \leqslant 27$
Reflections collected	4971
Observed reflections	3945 [$F > 5.0\sigma(F)$]
Abs.min.,Max.	1.141, 1.523
Weighting scheme	$w^{-1} = \sigma^2(F)+0.0004F^2$
Final R indices (obs. data)	R = 0.0277, wR = 0.0457
Largest shift/e.s.d.	< 0.001
Largest difference peak (e Å^{-3})	0.71

An empirical absorption correction was applied[26] after isotropic convergence. Hydrogen atoms were not included and C_6H_5 rings were treated as rigid, planar hexagons (C—C = 1.395 Å). The computer programs SHELXTL PLUS,[25] CADABS[27] and DIFABS[26] were used. Geometrical calculations were performed with the program PARST.[28] In the final converging refinement 304 parameters were fitted using 3945 data for a data-to-parameter ratio of 12.97.

Supplementary materials. Tables of interatomic distances, bond angles, positional and anisotropic thermal parameters, and observed and calculated structure factors have been deposited at the Cambridge Crystallographic Data Centre.

Acknowledgement—We thank the DGICYT (Spain) (Proyect PB-89-0057) for financial support and for a grant to J.R.B. and the British Council and Spanish Ministry of Education and Science for an Acciones Integradas Grant.

REFERENCES

1. P. N. V. Pavan Kumar and E. D. Jemmis, *J. Am. Chem. Soc.* 1988, **110**, 125 and refs therein.
2. W. J. Evans, D. K. Drummond, T. P. Hanusa and J. M. Olofson, *J. Organomet. Chem.* 1989, **376**, 311.
3. G. L. Wood, C. B. Knobler and M. F. Hawthorne, *Inorg. Chem.* 1989, **28**, 382.
4. J. Muller, M. Tschampel and J. Pichardt, *J. Organomet. Chem.* 1988, **355**, 513.
5. T. Cuenca, R. Gómez, P. Goémez-Sal, G. M. Rodriguez and P. Royo, *Organometallics* 1992, **11**, 1229.
6. (a) J. H. Teuben and H. J. De LiefdeMeijer, *J. Organomet. Chem.* 1969, **17**, 87; (b) D. G. Sekutowski and G. D. Stucky, *J. Am. Chem. Soc.* 1976, **98**, 1376; (c) W. J. Evans, R. A. Keyer and J. W. Ziller, *Organometallics* 1990, **9**, 2628.
7. F. Forniés, M. A. Gómez-Saso, E. Lalinde, F. Martínez and M. T. Moreno, *Organometallics* 1992, **11**, 2873.
8. (a) G. Erker, W. Frömberg, R. Mynott, B. Gabor and C. Krüger, *Angew. Chem., Int. Edn Engl.* 1986, **25**, 463; (b) G. Erker, W. Frömberg, R. Benn, R. Mynott, K. Angermund and C. Krüger, *Organometallics* 1989, **8**, 911.
9. P. Espinet, J. Forniés, F. Martínez, M. Sotés, E. Lalinde, M. T. Merono, A. Ruiz and A. J. Welch, *J. Organomet. Chem.* 1991, **403**, 253.
10. P. Espinet, J. Forniés, F. Martínez, M. Tomás, E. Lalinde, M. T. Moreno, A. Ruiz and A. J. Welch, *J. Chem. Soc., Dalton Trans.* 1990, 791.
11. J. Forniés, M. A. Gómez Saso, F. Martínez, E. Lalinde, M. T. Moreno and A. J. Welch, *New J. Chem.* 1992, **16**, 483.
12. M. Akita, M. Terada, S. Oyama and Y. Moro-Oka, *Organometallics* 1990, **9**, 816.
13. K. G. Frank and J. P. Selegue, *J. Am. Chem. Soc.* 1990, **112**, 6414.
14. I. Collamati and A. Furlani, *J. Organomet. Chem.* 1969, **17**, 457.
15. F. Maslowsky Jr, *Vibrational Spectra of Organometallic Compounds*, p. 437. John Wiley, New York (1977) and refs therein.
16. R. J. Cross and J. Gemmill, *J. Chem. Soc., Dalton Trans.* 1984, 199.
17. R. Nast, *Coord. Chem. Rev.* 1982, **47**, 89.
18. S. H. Martin, *Inorg. Chem.* 1974, **13**, 1003.
19. (a) V. K. Jain and G. S. Rao, *Inorg. Chim. Acta* 1987, **127**, 161; (b) H. C. Clark, G. Ferguson, V. K. Jain and M. Parvez, *Inorg. Chem.* 1985, **24**, 1477; (c) A. Pidcock, R. E. Richards and L. M. Venanzi, *J. Chem. Soc. A* 1966, 1707.
20. (a) C. Eaborn, K. J. Odell and A. Pidcock, *J. Chem. Soc., Dalton Trans.* 1978, 1288; (b) V. K. Jain, R. P. Patel and K. Venkatasubramanian, *Polyhedron* 1991, **10**, 857.
21. R. Usón, J. Forniés, F. Martínez and M. Tomás, *J. Chem. Soc., Dalton Trans.* 1980, 888.
22. J. C. Bailar Jr and H. Itatani, *Inorg. Chem.* 1965, **4**, 1618.
23. R. Usón, J. Forniés, M. Tomás and B. Menjón, *Organometallics* 1985, **4**, 1912.
24. This compound has been prepared previously by reacting [*cis*-$PtI_2(PPh_3)_2$] and $[Ag(C{\equiv}CBu^t)]_n$, although in lower yield.[9]
25. SHELXTL-PLUS, Software Package for the Determination of Crystal Structures, Release 4.0. Siemens Analytical X-ray Instruments, Inc. Madison, WI (1990).
26. N. Walker and D. Stuart, *Acta Cryst., Sect. A* 1983, **39**, 158.
27. R. O. Gould and D. E. Smith, University of Edinburgh (1986).
28. M. Nadelli, *Comput. Chem.* 1983, **7**, 95.

Polyhedron Vol. 12, No. 14, pp. 1805–1809, 1993
Printed in Great Britain

0277–5387/93 $6.00+.00
© 1993 Pergamon Press Ltd

LANTHANIDE COMPLEXES OF A SULPHUR–NITROGEN–OXYGEN LIGAND DERIVED FROM THIOSEMICARBAZONES

WANG BO, YANG SHIYAN* and JIN DAOSEN

Lanzhou Institute of Chemical Physics, Academia Sinica, Lanzhou 730000, P.R.C.

and

ZHOU LIXIN

Department of Chemistry, Gansu Education College, Lanzhou 730000, P.R.C.

(*Received* 8 *January* 1993; *accepted* 23 *March* 1993)

Abstract—Fourteen lanthanide complexes of 1-phenyl-3-(2-hydroxylphenyl)-2-propenone with thiosemicarbazone (HL) of the composition $[LnL_2]ClO_4$ have been prepared and characterized on the basis of their chemical analyses, magnetic measurements, conductance, visible and IR spectra, TG–DTA and XPS data. It was found that HL acts as an SNO tridentate ligand; the electronic spectra of Pr^{3+}, Nd^{3+} and Sm^{3+} show characteristic *f–f* transitions and the nephelauxetic parameter ($\bar{\beta}$), the bonding parameter ($b^{1/2}$) and covalency parameter (δ) have been evaluated.

Studies relating the nature of metal complexes to an aspect of their biological activity are increasingly important. The reported antifungal properties of 2-acetyl-pyridine thiosemicarbazone[1] prompted a series of reports on the metal complexes of thiosemicarbazides and their thiosemicarbazones containing 3*d*, 4*d* and 5*d* electrons.[2–4] But lanthanide complexes of thiosemicarbazone with 1-phenyl-3-(2-hydroxyphenyl)-2-propenone have not been reported. It was therefore thought of interest to investigate the lanthanide complexes of thiosemicarbazones. The work described here is an attempt in this direction and deals with the synthesis of lanthanide metal complexes of ligand (HL) and the bonding model by the XPS method.

EXPERIMENTAL

Methods and materials

All chemicals and solvents were analytical grade and used without further purification. 1-Phenyl-3-(2-hydroxylphenyl)-2-propenone was prepared by a literature procedure.[5] Lanthanide metal perchlorates were made from their oxides and perchloric acid.

Physical measurements

Molar conductance of the complexes in DMSO at 0.001 mol l^{-1} concentration was measured with a DDS-IIA molar conductometer at 25°C. Electronic spectra of the solutions of the complexes in the 190–700 nm region were recorded on a Shimayu 240 spectrophotometer from Japan. The IR spectra (CsI pellets) were obtained on a NIC-5DX spectrophotometer in the 200–4000 cm^{-1} region. The magnetic measurement was made by the Guoy method using $Hg[Co(CNS)_4]$ as a calibrant. XPS were taken on a PHI-550 X-ray photoelectron spectrophotometer. Non-monochromatic Mg-K_α radiation was used from an X-ray gun operated at 15 kV and 20 mA. The base pressure was better than 7×10^{-9} mbar in the analyser. TG and DTA measurements were made in a nitrogen atmosphere between room temperature and 800°C using a thermoflex TG-DTA meter. The C, H, N, S and Cl contents were microanalysed on a Perkin–Elmer 240C Elemental Analyser. Metals were determined volumetrically by EDTA titrations[6] using xylenol orange as the indicator.

*Author to whom correspondence should be addressed.

Preparation of the ligand

1-Phenyl-3-(2-hydroxylphenyl)-2-propenone (1 mol), dissolved in the minimum quantity of MeOH (40 cm^3), and a solution of thiosemicarbazone (1 mol) in MeOH (20 cm^3) were mixed and refluxed for 2 h on a water-bath. The resulting solution was cooled and a crystalline product separated. The solid was filtered, washed with cold EtOH and Et_2O, dried *in vacuo*.

Preparation of the complexes

The same method of synthesis for the complexes was adopted as with the ligand. In a typical reaction, a dioxane solution of lanthanide (III) perchlorate and the ligand in a 1 : 2 molar ratio was refluxed for 3 h, then the product precipitated. It was filtered off, washed with dioxane followed by Et_2O and dried *in vacuo*.

RESULTS AND DISCUSSION

Elemental analyses, functional group tests, IR and XPS spectral data indicate the structure shown (structure **1**) for the ligand. The geometry of the ligand ruled out tetradentate coordination to a single metal ion and binuclear or multinuclear complex forms can also be excluded by molecular weight determinations (by Rast's method).

The complexes have the general formula $[LnL_2]ClO_4$, where Ln = lanthanide (excluding Pm). They are air-stable yellow solids, soluble in

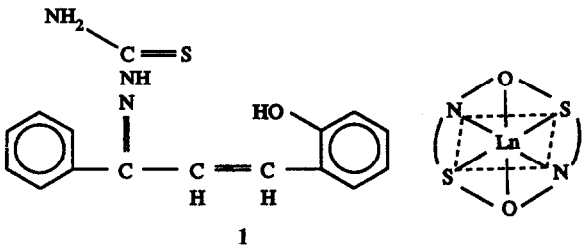

1

dimethylformamide, dimethylsulphoxide and methanol, but insoluble in benzene and ethylacetate. The molar conductances of the complexes fall in the range expected for 1 : 1 electrolytes[7] and show little solvolytic tendency in DMSO.

IR spectra

The important bands observed in the IR spectra of the ligand as well as in its metal complexes are given in Table 2 along with their assignments. These assignments are based on the corresponding assignments of thiosemicarbazone[8] and the metal complexes derived from it.

The strong band observed at 3540 cm^{-1} in the IR spectra of the ligand has been assigned to the —OH stretching vibration. The disappearance of this band in the IR spectra of all the complexes indicates that the OH group of the ligand is involved in bond formation.

The absorption bands in the region 3340–3045 cm^{-1} in the free ligand and its metal complexes are assigned to NH stretching frequencies.[3] The ν(C=N) band of the ligand at 1625 cm^{-1} was

Table 1. Physical properties and analytical data of lanthanide complexes

Complex	Decomposition temperature (°C)	Found (Calc.) % C	H	N	S	Ln	μ (B.M.) (298 K)	Λ_M[a]
$(LaL_2)ClO_4$	326	46.1(46.1)	3.8(3.9)	10.0(10.1)	7.6(7.7)	16.8(16.6)	dia	40
$(CeL_2)ClO_4$	319	45.9(45.9)	3.8(3.9)	10.0(10.1)	7.6(7.7)	16.7(16.8)	dia	36
$(PrL_2)ClO_4$	316	45.9(45.9)	3.8(3.9)	10.0(10.0)	7.5(7.7)	16.9(16.8)	3.72	37
$(NdL_2)ClO_4$	314	45.6(45.7)	3.8(3.8)	10.1(10.0)	7.5(7.6)	16.9(17.2)	3.56	43
$(SmL_2)ClO_4$	314	45.5(45.4)	3.8(3.8)	9.8(9.9)	7.5(7.6)	17.7(17.6)	1.64	39
$(EuL_2)ClO_4$	308	45.2(45.3)	3.7(3.8)	9.7(9.9)	7.4(7.6)	18.0(17.9)	3.52	38
$(GdL_2)ClO_4$	313	44.8(45.0)	3.5(3.8)	9.7(9.9)	7.4(7.5)	18.1(18.4)	7.85	46
$(TbL_2)ClO_4$	311	44.7(44.9)	3.6(3.8)	9.6(9.8)	7.4(7.5)	18.4(18.6)	6.81	32
$(DyL_2)ClO_4$	311	44.9(44.7)	3.6(3.8)	9.8(9.8)	7.5(7.5)	19.0(18.9)	10.18	48
$(HoL_2)ClO_4$	309	44.6(44.6)	3.7(3.8)	9.7(9.8)	7.2(7.4)	19.2(19.1)	10.63	42
$(ErL_2)ClO_4$	312	44.7(44.5)	3.9(3.7)	9.7(9.7)	7.3(7.4)	19.2(19.4)	8.91	40
$(TmL_2)ClO_4$	310	44.2(44.4)	3.6(3.7)	9.5(9.7)	7.4(7.4)	19.4(19.5)	3.68	34
$(YbL_2)ClO_4$	308	44.2(44.2)	3.7(3.7)	9.6(9.7)	7.3(7.4)	20.0(19.9)	4.46	35
$(LuL_2)ClO_4$	309	44.1(44.1)	3.6(3.7)	9.7(9.7)	7.2(7.4)	20.0(20.1)	dia	32

[a] S cm^2 mol^{-1} and *ca* 10^{-43} M DMSO.

Table 2. Significant IR bands of the ligand and its complexes (cm^{-1})

Compound	ν(HN)	ν(NN)	ν(CN)	ν(CS)	ν(Ln—O)	ν(Ln—N)	ν(Ln—S)
HL	3380br	1125	1625	865			
$(LaL_2)ClO_4$	3384br	1130	1610	814	390	260	224
$(CeL_2)ClO_4$	3384br	1138	1608	810	394	256	217
$(PrL_2)ClO_4$	3386br	1138	1608	810	385	257	220
$(NdL_2)ClO_4$	3389br	1140	1605	809	384	257	215
$(SmL_2)ClO_4$	3380br	1134	1600	809	390	262	222
$(EuL_2)ClO_4$	3380br	1128	1604	810	394	250	215
$(GdL_2)ClO_4$	3380br	1139	1600	805	387	262	217
$(TbL_2)ClO_4$	3378br	1141	1600	805	397	257	217
$(DyL_2)ClO_4$	3382br	1136	1658	803	385	264	214
$(HoL_2)ClO_4$	3382br	1136	1601	801	392	250	216
$(ErL_2)ClO_4$	3385br	1138	1601	802	380	252	220
$(TmL_2)ClO_4$	3378br	1140	1659	802	388	252	221
$(YbL_2)ClO_4$	3376br	1140	1658	801	387	248	216
$(LuL_2)ClO_4$	3376br	1140	1658	801	384	248	216

shifted down to *ca* 1600 cm^{-1} in the complexes, indicating participation of the azomethine nitrogen.[9] The decrease in ν(CS) from 865 cm^{-1} to *ca* 800 cm^{-1} shows the coordination of the thiol sulphur.[10] The characteristic bands around 1140 and 625 cm^{-1} arise from the ionic perchlorate which is uncoordinated. Of the several bands observed in the far-IR spectra, some may be tentatively assigned to ν(Ln—N), ν(Ln—S) and ν(Ln—O) vibrations. On the basis of the discussion referred to above, it is possible to conclude that the ligand is attached to the metal ion at three coordination sites involving one phenolic oxygen, one thioketosulphur and one nitrogen of the unsaturated CN group.

Magnetic moments and electronic spectra

The magnetic moments of the lanthanide complexed in Table 1 show little deviation from the Van Vleck values,[11] thereby indicating that 4*f*-electrons do not participate in bond formation in these complexes. Thus, the magnetic moments of these complexes are within the range predicted and observed in the compounds of the lanthanide ions.

The *f–f* transitions normally show weak perturbations on complexation. Increase in the intensity, shift of the centre and splitting of certain bands due to crystal field with respect to those of aquo ions are effects that can be observed on complex formation. The electronic spectra of Pr^{III} and Sm^{III} complexes were recorded in 2×10^{-3} M DMSO solutions. The spectra of the complexes show a shift of the spectral bands towards lower energy as compared with those of the aquo ions[12] due to the nephelauxetic effect (which is regarded as a measure of covalency). The bonding parameter ($b^{1/2}$), the covalency parameter (δ) and nephelauxetic ratio ($\bar{\beta}$) have been calculated[13] and compiled in Table 3. The lower nephelauxetic parameter ($\bar{\beta}$), positive bonding parameter ($b^{1/2}$) and Sinhas' parameter (δ) indicate some covalent character of the bond between the metal and ligand.

XPS spectra

The results of the XPS semi-quantitative analyses of the surface layers are in agreement with sample compositions. The only exception is the Cl:Ln ratio which decreases during irradiation of the sample. A new peak simultaneously appears with a Cl 2*p*-electron BE about 10 eV smaller, indicating decomposition of perchlorate anions. No other change either in positions or intensities of the other peaks was observed during the measurements.

The 3*d*- or 4*d*-electron BEs of the metals and the values for the N(C=N) 1*s* and the S 1*s* electron BEs are given in Table 4. The Ln 3*d*- or 4*d*-electron BE is closely related to the central atom charge and therefore to its valency.[14] The N 1*s*-electron spectra of the complexes are asymmetric and their deconvolution yields three binding energy components with an intensity ratio 1:1:1. The component with the highest BE value, belonging to the azomethine nitrogen, relative to that in the ligand indicates that the two coordinated nitrogens are in a symmetric form (structure).

The sulphur 1*s* peak of both the complexes and ligand is symmetric but with an intensity ratio 2:1.

Table 3. Electronic spectra of Pr^{III}, Nd^{III} and Sm^{III} of complexes HL[a]

Complex	λ_{max} (cm^{-1}) Solution	Solid	Assignments	Calculated spectral parameter β	$b^{1/2}$	(%)
$(PrL_2)ClO_4$	16,830	16,715	$^3H_4$—$^1D_2$			
	20,620	20,410	—$^3P_0$	0.986	0.084	0.42
	21,190	21,080	—$^3P_1$			
	22,330	22,145	—$^3P_2$			
$(NdL_2)ClO_4$	11,470	11,435	$^4I_{9/2}$—$^4F_{3/2}$			
	12,380	12,360	—$^4F_{5/2}$			
	13,320	13,410	—$^4F_{7/2}$			
	17,095	17,095	—$^4G_{5/2}$, $^2G_{7/2}$	0.990	0.050	0.40
	19,045	18,980				
	19,420	19,300				
$(SmL_2)ClO_4$	20,680	20,900	$^6H_{5/2}$—$^4L_{11/2}$			
	21,300	21,370	—$^4I_{9/2}$			
	23,785	23,820	—$^4P_{9/2}$	0.992	0.056	0.58
	2405	24,515	—$^4F_{9/2}$			

[a] Various spectral parameters were calculated from the solid-state spectra of the complexes only.

Table 4. The binding energies (eV) of the ligand and its complexes

Compound	N 1*s* (C=N)	S 1*s*	O 1*s* (phenolic)	Ln	
HL	399.16	161.4	533.2		
$(LaL_2)ClO_4$	400.90	161.9	533.2		
$(PrL_2)ClO_4$	401.01	162.1	533.6	$3d_{5/2}$	836.40
$(NdL_2)ClO_4$	401.00	162.2	533.8		984.01
$(SmL_2)ClO_4$	400.80	162.2	534.1		1084.05
$(EuL_2)ClO_4$	400.80	162.2	534.1		1136.22
$(TbL_2)ClO_4$	400.85	162.3	534.2		1245.80
$(DyL_2)ClO_4$	400.60	162.0	534.6		1297.90
$(HoL_2)ClO_4$	400.62	162.4	534.5	4*d*	162.40
$(TmL_2)ClO_4$	400.10	162.3	534.6		178.80
$(YbL_2)ClO_4$	400.08	162.5	534.7	$4d_{5/2}$	185.90

The higher BE value relative to the ligand suggests thiol sulphur participation in coordination with the lanthanide metal. The measured 1*s* peak of O and deconvolution also revealed the symmetric character of the complexes. Carbon occurs in different chemical environments in the studied complexes, i.e. in phenyl groups (C is at 284.60 eV), in keto carbon (C is at 286.4 eV), and in N=C—C=C— groups (C is at 285.2 eV).

TG and DTA

Thermogravimetric analyses show all the complexes in a similar decomposition and in an anhydrous state. It can be seen from the diagrams that the complexes, $[LnL_2]ClO_4$, begin decomposing at *ca* 310°C exothermically. Decomposition is completed at *ca* 690°C with the formation of the lanthanide oxide.

From the above discussion a possible octahedral structure of these complexes is proposed.

REFERENCES

1. H. K. Parwana and G. Singh, *Ind. J. Chem.* 1987, **26A**, 581.
2. M. C. Jain and P. C. Jain, *J. Inorg. Nucl. Chem.* 1977, **39**, 2183.

3. M. C. Jain, A. R. Srivastava and P. C. Jain, *Inorg. Chem. Acta* 1977, **23**, 199.
4. M. C. Jain and P. C. Jain, *Croat. Chim. Acta* 1977, **49**, 717.
5. H. H. Freedman, *J. Am. Chem. Soc.* 1961, **83**, 2900.
6. S. S. Lyle and M. M. Rahaman, *Talanta* 1963, **10**, 1177.
7. W. J. Geary, *Coord. Chem. Rev.* 1971, **7**, 81.
8. G. R. Burns, *Inorg. Chem.* 1968, **7**, 227.
9. R. Rita, C. S. Manik and R. S. Parag, *Trans. Met. Chem.* 1990, **15**, 51.
10. D. X. West, C. S. Carlson, C. P. Galloway, A. B. Liberta and C. R. Daniel, *Trans. Met. Chem.* 1990, **15**, 91.
11. F. A. Cotton and G. Wilkinson, *Advanced Inorganic Chemistry*, 3rd edn. John Wiley & Sons, New York (1972).
12. W. T. Carnall, P. R. Fields and K. Rajnak, *J. Chem. Phys.* 1961, **34**, 4424.
13. D. E. Henric and G. R. Choppin, *J. Chem. Phys.* 1968, **49**, 477.
14. C. D. Wagner, *J. Electron Spectrosc. Relat. Phenom.* 1983, **32**, 99.

Polyhedron Vol. 12, No. 14, pp. 1811–1816, 1993
Printed in Great Britain

0277–5387/93 $6.00+.00
© 1993 Pergamon Press Ltd

THE STRUCTURES OF CROWN-ETHER/OXONIUM/AsF_6^- SPECIES

H. FEINBERG, I. COLUMBUS, S. COHEN, M. RABINOVITZ, H. SELIG* and G. SHOHAM

Institute of Chemistry, The Hebrew University of Jerusalem, Jerusalem 91904, Israel

(*Received* 7 *January* 1993; *accepted* 23 *March* 1993)

Abstract—The reaction of $XeF^+AsF_6^-$ with a series of crown ethers (containing *ca* 0.1 weight % H_2O) resulted in three new oxonium complexes of crown ethers, two of whose structures have been determined in detail by X-ray crystallography. Complex **I**, 18-C-6/H_3O^+/AsF_6^-, m.p. 180°C, is orthorhombic. In this structure the oxonium occupies the centre of the crown cavity, coordinated to its six ether oxygens with hydrogen bonds of average distance 2.75 Å. The AsF_6^- counter-ion is perfectly octahedral at a distance of 7.1 Å from the oxonium oxygen, forming no direct contacts with the crown ether. 18-C-6 adopts the most common "D_{3d}-like" conformation. Complex **II**, 2(15-C-5)/H_3O^+/AsF_6^-, m.p. 285°C, is tetragonal. The crystal structure shows a sandwich complex where the oxonium is located between the crown ethers. The counter-anion, AsF_6^-, is 8.0 Å from the oxygen atom of the oxonium and has no direct contacts with the crown ethers. The crown ether molecules are disordered. Complex **III**, 2(12-C-4)/H_3O^+/AsF_6^-, m.p. 150°C, is monoclinic. This structure is also a sandwich complex, where the oxonium is located between two crown ethers. Only five of the eight crown ether oxygens are involved in hydrogen bonds to the oxonium ion. The distances O_C—O_W range from 2.53 to 2.84 Å. The other three oxygens are at distances exceeding 3 Å from the oxonium ion.

Although $H_3O^+AsF_6^-$ is one of the most stable oxonium salts its crystallographic structure has not yet been determined. The lack of structural analysis of this species results probably from the fact that it exists at room temperature in a plastic phase, where the ions, centred on the atomic positions of an NaCl structure, are in large oscillatory motions.[1] Crown ethers are known for their abilities of complexation and stabilization of various ions and some of their complexes with oxonium salts have been characterized. Most of the complexes reported, such as 18-C-6/H_3O^+/Cl_2H^-,[2] DCH-18-C-6/H_3O^+/ClO_4^-,[3] 18-C-6$(COOH)_4/H_3O^+/Cl^-$[4] and 18-C-6/H_3O^+/BF_4^-,[5] are those with the common 18-C-6 crown ether, probably because of its cavity diameter, 2.6–3.2 Å, which is commensurate with the size of the oxonium ion. This is not the case with the smaller crown ethers, 15-C-5 and 12-C-4, which have cavities of 2.0 and 1.2 Å, respectively.[6] Oxonium ions cannot enter these cavities without severe distortions and until now no crystal structures of oxonium complexes involving these crown ethers have been reported.

We present here a series of oxonium complexes with the crown ethers 18-C-6, 15-C-5 and 12-C-4 and we follow the mode of complexation of the oxonium ion from encapsulation in the first instance to sandwich formation in the others.

EXPERIMENTAL

Materials

The crown ethers were obtained from Aldrich Co. and were used as supplied. They contained *ca* 0.1 wt % of water, as obtained by a Karl Fischer titration. $XeF^+AsF_6^-$ was prepared by the reported photochemical synthesis.[7] This species was identified by its Raman spectrum.[8]

* Author to whom correspondence should be addressed.

Preparation

Our original intention had been to encapsulate the XeF^+ cation in crown ethers by reacting $XeF^+AsF_6^-$ with a solution of the crown ether in CH_2Cl_2 solution, for **I** and **II**, or in CH_3CN, in the case of 15-C-5. However, during the experimental analysis it was realized that the water impurity in the crown ethers hydrolyses XeF^+ according to the equation:

$$XeF^+AsF_6^- + 2H_2O \longrightarrow Xe + 1/2O_2 + H_3O^+AsF_6^- + HF$$

and the resulting oxonium ion is encapsulated instead. Attempts to remove the water by refluxing with thionyl chloride or by azeotropic distillation with benzene were only partially successful, but were not sufficient to remove the H_2O completely. The reactants were loaded into a three-necked flask in a glove-bag under dry nitrogen. One of the side-arms was fitted with a $CaCl_2$ drying tube. $XeF^+AsF_6^-$ was added to the solution under a dry nitrogen flow with constant magnetic stirring. This was done by inverting an L-shaped side-arm connected via a ground glass joint, which was fitted with a Teflon sleeve. Crystals were obtained from the resulting solution by slow evaporation of the solvent. Similar results were obtained by pre-synthesizing $H_3O^+AsF_6^-$ [9] and reacting it with the crown ether in solution. However, this salt is less soluble in CH_2Cl_2. Complete crystallographic analyses were obtained on complexes **I** and **III**. An incomplete crystallographic analysis was obtained for complex **II**, but its stoichiometry was ascertained by chemical analysis. 2(15-C-5)/H_3O^+/AsF_6^-. Found: As, 11.9; C, 37.8; H, 6.8. Calc.: As, 11.5; C, 37.0; H, 6.7%.

Crystal structure analyses

Crystal structure determination of **I**. Crystal data: 18-crown-6/H_3O^+/AsF_6^-, $C_{12}O_7H_{27}F_6As$, $Mr = 472.25$, orthorhombic, *Pbam* (No. 55), $a = 10.097(2)$, $b = 8.877(1)$, $c = 10.958(2)$ Å, $V = 982.2(5)$ Å^3, $Z = 2$, $D_c = 1.60$ g cm^{-3}, Cu-K_α radiation, $\lambda = 1.54178$ Å, $\mu = 31.6$ cm^{-1}, $F(000) = 484$, T = room temperature.

Data collection and processing: Crystallographic measurements for compound **I** were performed on an Enraf–Nonius CAD-4 automatic four-circle diffractometer with graphite monochromated Cu-K_α radiation. Cell constants and an orientation matrix for data collection were obtained from a least-squares refinement based on the setting angles of 25 carefully centred high-order reflections. The data were collected using an $\omega/2\theta$ scan procedure to a maximum 2θ angle of 140°. A total of 1030 unique reflections were collected. The intensity of three reflections measured every 60 min remained constant throughout data collection and hence no decay correction was applied. An azimuthal scan of several reflections indicated no need for absorption corrections.

Structure analysis and refinement: The structure of **I** was solved by direct methods.[10] All non-hydrogen atoms were found in the initial *E*-map. For convenience all hydrogen atoms of the crown ether were initially calculated at idealized positions relative to the corresponding carbon atoms and were refined as "riding" atoms on their carbon atoms, with ideal C—H bond lengths and ideal H—C—H bond angles. The final cycle of full-matrix least-squares refinement was based on 783 observed reflections [with $I > 3\sigma(I)$] and 68 variable parameters and converged smoothly (with maximum shift/e.s.d. of 0.01) to crystallographic agreement parameters of $R = 5.4\%$ and $R_W = 8.2\%$. The maximum and minimum peaks in the final difference electron density map corresponded to 0.60 and -0.38 e Å^{-3}, respectively. All calculations were performed using the TEXSAN crystallographic software package.[10]

Crystal structure determination of **II**. Crystal data: 2(15-crown-5)/H_3O^+/AsF_6^-, $C_{20}O_{11}H_{43}F_6As$, $Mr = 648.47$, tetragonal, $P4_2$ (No. 77), $a = b = 9.187(2)$, $c = 17.884(3)$ Å, $V = 1509.4(9)$ Å^3, $Z = 2$, $D_c = 1.43$ g cm^{-3}, Mo-K_α radiation, $\lambda = 0.71069$ Å, $\mu = 11.99$ cm^{-1}, $F(000) = 676$, T = room temperature.

Data collection and processing: Crystallographic measurements for compound **II** were performed on a Phillips 1100/20 automatic four-circle diffractometer with graphite monochromated Mo-K_α radiation. Cell constants and an orientation matrix for data collection were obtained from a least-squares refinement using the setting angles of 22 carefully centred high-order reflections. Intensity data were collected in the $\omega/2\theta$ scan mode in the range $4° < 2\theta < 46°$, using a constant scan speed. Due to the small absorption coefficient and insignificant radiation damage, it was unnecessary to make corrections for radiation decay or absorption. The integrated intensities of 1254 reflections were measured, of which 1102 are unique.

Structure analysis and refinement: The structure of **II** was partially solved by direct methods. Most of the non-hydrogen atoms could be located in the initial *E*-map, which indicated that the crown ether molecules in the crystal are disordered. Most of the electron density observed in the map could be interpreted with a set of molecules of partial statistical occupancy of *ca* 0.6–0.7. The positional par-

ameters of these molecules were partially refined, using only the non-hydrogen atoms and isotropic temperature factors. Refinement was performed with considerable difficulties because of the unaccounted residual electron density, probably due to the alternative positions of the crown ethers at lower occupancy. The model at this stage clearly indicated a "sandwich" complex with two 15-C-5 macrocycles encapsulating each oxonium ion and a separate, non-interacting, AsF_6^- counter-anion. Refinement was stopped, however, because of the poor electron density map and insufficient observed data for a full atomic refinement. At this point the crystallographic R factor was 13.8%. Due to the relatively low level of confidence in the resulting structure it was decided not to continue with the crystal structure analysis, and hence the final model is not presented here in detail. The general features of the structure, the complex stoichiometry (which is supported by chemical analysis) and the oxonium–macrocycle interaction scheme are used here, therefore, only for comparison purposes.

Crystal structure determination of **III**. Crystal data: 2(12-crown-4)/H_3O^+/AsF_6^-, $C_{16}O_9H_{35}F_6As$, $Mr = 560.36$, monoclinic, $P2_1/c$ (No. 14), $a = 9.524(2)$, $b = 11.901(3)$, $c = 21.214(5)$ Å, $\beta = 98.8(2)°$, $V = 2376.2(9)$ Å^3, $Z = 4$, $D_c = 1.57$ g cm^{-3}, Mo-K_α radiation, $\lambda = 0.71069$ Å, $\mu = 15.1$ cm^{-1}, $F(000) = 1160$, $T =$ room temperature.

Data collection and processing: All measurements were made on a Phillips 1100/20 automatic four-circle diffractometer, with graphite monochromated Mo-K_α radiation. The cell constants and orientation matrix for data collection were obtained from least-squares refinement of 25 carefully centred high-order reflections. Intensity data were collected in the $\omega/2\theta$ scan mode in the range $4° < 2\theta < 50°$, using a constant scan speed. Out of the 3820 measured reflections, only 3708 unique reflections ($R_{int} = 0.016$) were used for refinement. No corrections for radiation damage or absorption effects were needed.

Structure analysis and refinement: The structure of **III** was solved by direct methods.[10] As for the case of compound **I** all the non-hydrogen atoms were found in the initial electron density map and all hydrogens were subsequently placed at calculated ideal positions. Cycles of full-matrix least-squares refinement were based on 2910 observed reflections [for which $I > 3\sigma(I)$] and 289 variable atomic parameters. The refinement converged in the last cycle (max. shift/e.s.d. of 0.02) to crystallographic agreement factors of $R = 4.3\%$ and $R_W = 5.3\%$. The maximum and minimum peaks in the final electron density difference map were 0.51 and -0.54 e Å^{-3}, respectively. All the steps of refinement and density maps were calculated with the TEXSAN crystallographic software package.[10]

RESULTS AND DISCUSSION

Final intramolecular bond lengths in complexes **I** and **III** are listed in Tables 1(a) and 1(b), respectively. Final intramolecular bond angles in complexes **I** and **III** are listed in Tables 2(a) and 2(b), respectively. The final crystal structure and the numbering scheme of **I** are shown in Fig. 1, while a stereoview of the crystal packing is shown in Fig. 2. Similarly, the numbering scheme and the structure of complex **III** is shown in Fig. 3, while the crystal packing is shown in Fig. 4.

In complex **I** (Fig. 1) the crown adopts the common round configuration of symmetry, "D_{3d}-like", where the oxonium ion occupies the centre of the macrocycle.[11] The oxonium ion is located practically equidistant (2.71–2.79 Å) from the six ether oxygens. Of these, three alternating oxygens are pointing "down" and three are pointing "up". The

Table 1(a). Relevant intramolecular distances involving the non-hydrogen atoms for **I**

As—F(1)	1.702(5)	O(1)—C(2)	1.399(7)
As—F(2)	1.719(2)	C(2)—C(3)	1.518(9)
As—F(3)	1.762(4)	O(4)—C(3)	1.364(7)
Ow—O(4)	2.712(3)	O(4)—C(5)	1.410(7)
Ow—O(1)	2.788(6)		

Table 1(b). Relevant intramolecular distances involving the non-hydrogen atoms for **III**

As—F(1)	1.714(2)	O(5)—C(16)	1.415(5)
As—F(2)	1.711(2)	O(6)—C(10)	1.411(5)
As—F(3)	1.715(2)	O(6)—C(11)	1.427(5)
As—F(4)	1.709(2)	O(7)—C(12)	1.445(5)
As—F(5)	1.709(2)	O(7)—C(13)	1.430(6)
As—F(6)	1.716(2)	O(8)—C(14)	1.388(5)
O(1)—C(1)	1.433(4)	O(8)—C(15)	1.426(5)
O(1)—C(8)	1.423(5)	C(1)—C(2)	1.465(6)
O(2)—C(2)	1.411(5)	C(3)—C(4)	1.498(6)
O(2)—C(3)	1.426(4)	C(5)—C(6)	1.475(6)
O(3)—C(4)	1.415(5)	C(7)—C(8)	1.486(6)
O(3)—C(5)	1.423(4)	C(9)—C(10)	1.486(6)
O(4)—C(6)	1.423(5)	C(11)—C(12)	1.486(7)
O(4)—C(7)	1.418(5)	C(13)—C(14)	1.493(8)
O(5)—C(9)	1.442(4)	C(15)—C(16)	1.465(6)
Ow—O(1)	2.637(3)	Ow—O(5)	2.532(3)
Ow—O(8)	2.823(3)	Ow—O(2)	2.837(3)
Ow—O(7)	2.598(4)		

Distances are in Å. Estimated standard deviations in the least significant digit are given in parentheses.

Table 2(a). Relevant intramolecular bond angles involving the non-hydrogen atoms for **I**

F(1)—As—F(2)	90.00	O(1)—C(2)—C(3)	109.8(5)
F(1)—As—F(3)	90.00	O(4)—C(3)—C(2)	106.2(4)
F(2)—As—F(3)	91.0(2)	C(3)—O(4)—C(5)	110.3(4)
		O(4)—C(5)—C(5)	112.1(5)

Table 2(b). Relevant intramolecular bond angles involving the non-hydrogen atoms for **III**

F(1)—As—F(2)	90.0(1)	C(10)—O(6)—C(11)	116.2(4)
F(1)—As—F(3)	90.4(1)	C(12)—O(7)—C(13)	115.0(4)
F(1)—As—F(4)	89.6(1)	C(14)—O(8)—C(15)	114.8(3)
F(1)—As—F(5)	90.3(1)	O(1)—C(1)—C(2)	109.2(3)
F(1)—As—F(6)	179.8(1)	O(2)—C(2)—C(1)	113.9(3)
F(2)—As—F(3)	89.7(1)	O(2)—C(3)—C(4)	110.9(3)
F(2)—As—F(4)	90.3(1)	O(3)—C(4)—C(3)	108.3(4)
F(2)—As—F(5)	179.6(1)	O(3)—C(5)—C(6)	108.9(3)
F(2)—As—F(6)	90.0(1)	O(4)—C(6)—C(5)	111.2(3)
F(3)—As—F(4)	179.9(1)	O(4)—C(7)—C(8)	108.3(3)
F(3)—As—F(5)	90.1(1)	O(1)—C(8)—C(7)	114.1(3)
F(3)—As—F(6)	89.4(1)	O(5)—C(9)—C(10)	109.6(3)
F(4)—As—F(5)	89.9(1)	O(6)—C(10)—C(9)	107.2(4)
F(4)—As—F(6)	90.5(1)	O(6)—C(11)—C(12)	106.9(4)
F(5)—As—F(6)	89.7(1)	O(7)—C(12)—C(11)	109.2(4)
C(1)—O(1)—C(8)	113.7(3)	O(7)—C(13)—C(14)	112.8(4)
C(2)—O(2)—C(3)	115.7(3)	O(8)—C(14)—C(13)	108.1(4)
C(4)—O(3)—C(5)	113.6(3)	O(8)—C(15)—C(16)	108.6(3)
C(6)—O(4)—C(7)	113.9(3)	O(5)—C(16)—C(15)	112.8(3)
C(9)—O(5)—C(16)	115.8(3)		

Angles are in °. Estimated standard deviations in the least significant digit are given in parentheses.

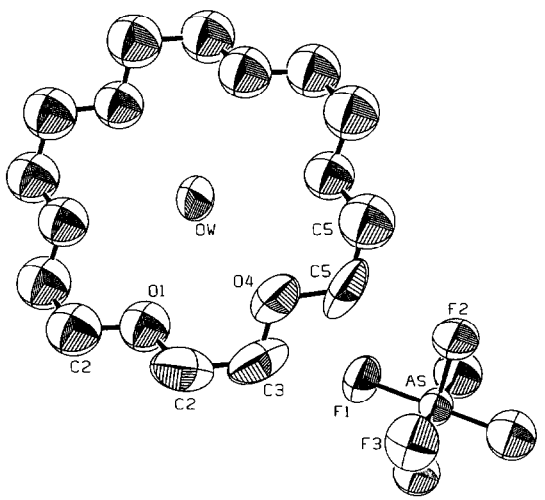

Fig. 1. The final crystal structure of the complex 18-crown-6/$H_3O^+AsF_6^-$ (compound **I**). Note the almost symmetrical interactions of the oxonium ion (Ow, centre) and the six macrocyclic etheral oxygens.

planes defined by these two sets of oxygens are nearly parallel to each other (interplanar angle of 173° and interplanar distance of 0.34 Å) and the oxonium ion is positioned midway between these

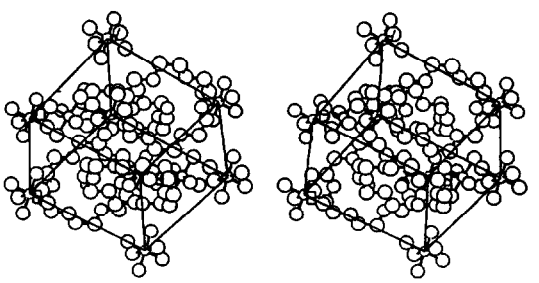

Fig. 2. A stereo view of the crystallographic unit cell packing of compound **I**. The packing scheme demonstrates that there are no intermolecular contacts between the counter-ion and either the oxonium ion or the crown ether.

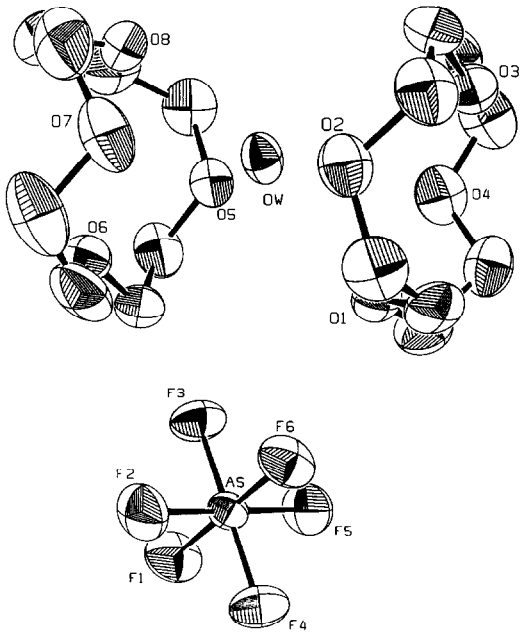

Fig. 3. The final crystal structure of the complex 2(12-crown-4)/$H_3O^+AsF_6^-$ (compound **III**). The oxonium ion (Ow, upper centre) is trapped nearly symmetrically between two 12-C-4 macrocycles, while the counter-ion (bottom) is outside of the interaction range.

planes. Since we are unable to locate the hydrogens of the oxonium ions in the electron density maps, we assume that the oxonium ion adopts two alternative orientations (each at 50% statistical occupancy) around the oxygen, such that two alternative sets of hydrogen positions are formed. One set involves the crown oxygens pointing "down" and the other set involves those pointing "up". The AsF_6^- anion, which is perfectly octahedral, is positioned 7.05 Å from the oxonium ion and is located 3.96 Å above the average plane of the six ether oxygens. The anion is not involved in any direct intermolecular contacts (Fig. 2). Complex **I** can also be considered a "sandwich structure" where the oxonium ion is sandwiched between the two alternative oxygen planes of the crown ether.

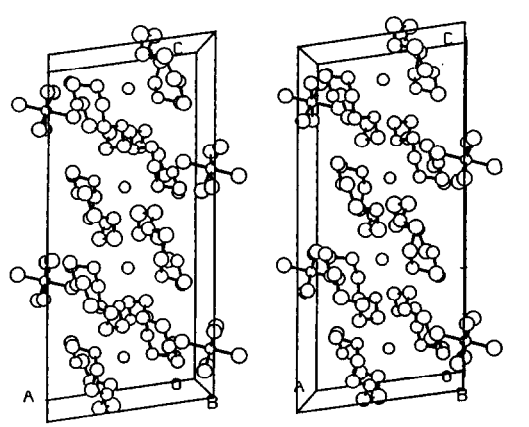

Fig. 4. A stereo view of the crystallographic unit cell packing of compound **III**, demonstrating no significant intermolecular interactions by the AsF_6^- counter-ion.

In complex **III**, 2(12-C-4)/H_3O^+/AsF_6^- (Fig. 3), the oxonium is sandwiched between two crown molecules, probably because of the size of the cavity, which is only 1.2 Å, not permitting encapsulation. In this complex the 12-C-4 molecules have practically no internal symmetry. In each molecule three of the ether oxygens [O(1), O(2) and O(4)] of one crown ether and three [O(5), O(7) and O(8)] of the other crown ether are pointing towards the oxonium, while one oxygen [O(3) and O(6)] of each crown ether is directed "outside". Since we are unable to locate the oxonium hydrogens in the electron density maps, we have to assume that they are located between the three macrocycle ether oxygens located at hydrogen bond distances from the oxonium ion. The "outside" pointing oxygens [O(3) and O(6)] are located at distances of 3.16 and 3.04 Å, respectively, from the oxonium oxygen and thus are not involved in hydrogen bonding. The other six oxygens are pointing "inside" towards the oxonium ion. Of these only five, O(1) and O(2) from one crown ether and O(5), O(7) and O(8) from the other crown ether, are at hydrogen bond distances of 2.64, 2.84 Å, and 2.53, 2.60 and 2.82 Å, respectively. The O(4) oxygen, despite its orientation, is located at a distance of 3.24 Å from the oxonium oxygen and hence cannot be involved in the hydrogen bonding scheme. This deviation is probably explained by crystal limitations or coordination sphere problems. It should also be pointed out that in one of the crown ethers four oxygens, O(1)–O(4), are in one plane (plane 1) within 0.22 Å, while in the other crown ether the four oxygens, O(5)–O(8), are in the plane (plane 2) within only 0.47 Å. The distance of plane 1 to O_W is 2.15 Å and that of plane 2 is 1.99 Å. The averages of the two planes are not exactly parallel, but at a dihedral angle of 16.4°. The counter-anion, AsF_6^-, is not involved in any direct intermolecular contacts (Fig. 4). The distance As—O_W is 6.80 Å and it is situated nearer plane 1 than plane 2.

As explained above no complete structure was obtained for complex **II** and only the oxygen of the oxonium ion and the atoms of AsF_6^- were located with certainty. The crown molecules were disordered. However, chemical analyses supported the 2 : 1 sandwich stoichiometry.

To our knowledge this is the first crystallographic report on a series of simple oxonium complexes with crown ethers and AsF_6^- counter-anions. The parameter of significance in this series appears to be the size of the "cavity", which determines whether

the oxonium ion is encapsulated or forms a sandwich with two crown ether molecules. In the case of 18-C-6 the size of the oxonium is exactly commensurate with the size of the "cavity", while with 15-C-5 and 12-C-4 the cavity is too small and hence sandwich compounds are formed. In all cases the AsF_6^- counter-anion is used to neutralize the overall charge of the system, but it is not in direct contact with the oxonium cation or the crown ether. The lack of such interactions could be explained, as least in part, by the softness and relative stability of the AsF_6^- species.

Supplementary material. Lists of the fractional coordinates of all atoms of 18-crown-6/H_3O^+/AsF_6^- (compound **I**) and 2(12-crown-4)/H_3O^+/AsF_6^- (compound **III**) [Tables S1(a), S1 (b)], anisotropic temperature factors for non-hydrogen atoms of **I** and **III** [Tables S2(a), S2(b)], all intramolecular distances in **I** and **III** (Tables S3(a), S3(b)], all intramolecular bond angles in **I** and **III** [Tables S4(a), S4(b)], all torsion angles for non-hydrogen atoms in **I** and **III** [Tables S5(a), S5(b)] and lists of observed and calculated structure factors for **I** and **III** [Tables S6(a), S6(b)] are provided as supplementary material (39 pages).

REFERENCES

1. K. O. Christie, P. Charpin, E. Soulie, R. Bougon, J. Fawcett and D. R. Russell, *Inorg. Chem.* 1984, **23**, 3756.
2. J. A. Atwood, S. G. Boot, A. W. Coleman, K. D. Robinson, S. V. B. Whetstone and C. M. Means, *J. Am. Chem. Soc.* 1987, **109**, 8100.
3. Y. A. Simonov, N. F. Krasnova, A. A. Dvorkin, V. V. Yashkin, V. M. Abashkin and B. N. Laskorin, *Dokl. Akad. Nauk. SSSR* 1983, **272**, 1120.
4. J. P. Behr, P. Dumas and D. Moras, *J. Am. Chem. Soc.* 1982, **104**, 4540.
5. H. Selig, H. Sheshinski, S. Cohen, I. Columbus and G. Shoham, *J. Fluor. Chem.* 1991, **54**, 359.
6. C. J. Pederson and H. K. Frensdorff, *Angew. Chem., Int. Edn Engl.* 1972, **11**, 16.
7. J. Binenboym, H. Selig and J. Shamir, *J. Inorg. Nucl. Chem.* 1968, **30**, 2863.
8. R. J. Gillespie and B. Landa, *Inorg. Chem.* 1973, **12**, 1383.
9. K. O. Christe, C. J. Schack and R. D. Wilson, *Inorg. Chem.* 1975, **14**, 2224.
10. TEXSAN: Single Crystal Structure Analysis Software, Version 5.0. Molecular Structure Corporation, The Woodlands, TX, 777381, U.S.A. (1989).
11. M. Dobler, *Chimia* 1984, **38**, 415.

Polyhedron Vol. 12, No. 14, pp. 1817–1820, 1993
Printed in Great Britain

0277–5387/93 $6.00+.00
© 1993 Pergamon Press Ltd

EXISTENCE AND DISTRIBUTION OF GEOMETRICAL ISOMERS OF BIS(*VIC*-DIOXIMATO)NICKEL(II) COMPLEXES IN SOLUTION

REIKO HIROTA,* YUMI YOSHIDA and YOSHIKI IIDA

Department of Chemistry, Faculty of Science, Rikkyo University, Nishi-ikebukuro, Toshima-ku, Tokyo 171, Japan

and

HIROKO SUEZAWA

Department of Synthetic Chemistry, Faculty of Engineering, Yokohama National University, Hodogaya-ku, Yokohama 240, Japan

and

TAMIZO KOGANE

Industrial Research Institute of Kanagawa Prefecture, Showamachi, Kanazawa-ku, Yokohama 236, Japan

(*Received* 11 *November* 1992; *accepted* 23 *March* 1993)

Abstract—The existence of geometrical isomers of several bis(*vic*-dioximato)nickel complexes with non-symmetrical ligands has been clarified by ^{1}H NMR. The general formula of the ligands is $CH_3C(=NOH)C(=NOH)R$, here R = Et, Pr^n, Bu^n, Ph, *p*-MeC_6H_4, *p*-$MeOC_6H_4$ and *p*-ClC_6H_4. The *trans* isomer of each complex is predominant in pyridine-d_5 solution. The *cis–trans* equilibrium constants of these complex in pyridine-d_5 have been estimated.

The structures of $Ni(Hdioxm)_2$ complexes (H_2dioxm = *vic*-dioxime) have been investigated and it has been established that, in the solid state or in chloroform solution, they take the square planar configuration.[1] On the other hand, they tend to be coordinated by one or two solvent molecules at the apical positions in pyridine or in other nucleophilic solvents, leading to square pyramidal or tetragonally distorted geometry.[2] Therefore, the existence of the *cis* and *trans* isomers of $Ni(Hdioxim)_2$ with non-symmetrical ligands was considered to be reasonable and several chemists have attempted to distinguish and separate the isomers.

In 1932 Sugden reported the separation of α- and β-forms of bis(1-phenyl-2,3-butanedione dioximato)nickel(II) by taking advantage of the difference in their solubilities in benzene. He assigned them to the *cis* and *trans* isomers, respectively.[3] Cavell and Sugden further reported that they also succeeded in separating geometrical isomers of bis(2,3-hexanedione dioximato)nickel(II).[4] However, Jensen *et al.* reinvestigated Sugden's

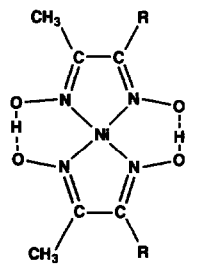

cis

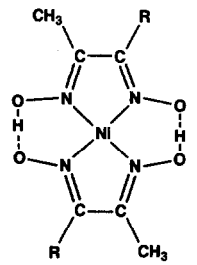

trans

*Author to whom correspondence should be addressed.

experiment on bis(1-phenyl-2,3-butanedione dioximato)nickel(II) and concluded that the separated compounds are not geometrical isomers but isomers with different crystal forms.[5] Later, Pedersen and Larsen also investigated the isomerism of bis(1-phenyl-1,2-propanedione dioximato)nickel(II) by ^{1}H NMR. They concluded that only the *trans* isomer is present in a chloroform-d solution of the complex.[6]

We now report the presence of *cis* and *trans* isomers of Ni(Hdioxm)$_2$ complexes in equilibrium in solutions of chloroform and pyridine.

EXPERIMENTAL

Preparation of the oximes

1-*Phenyl*-1,2-*propane dionedioxime* (H_2phg). This compound was prepared by an ordinary synthetic method used in organic chemistry.[7] 1-Phenyl-1,2-propanedione was heated with approximately twice the molar amount of hydroxylamine hydrochloride in a 1 : 1 ethanol–water mixture under reflux for *ca* 1 h. The white precipitate which formed was recrystallized from ethanol.

2,3-*Pentanedione dioxime* (H_2ethg), 2,3-*hexanedione dioxime* (H_2prg) *and* 2,3-*heptanedione dioxime* (H_2butg). These compounds were prepared from commercially obtained 2,3-pentanedione, 2,3-hexanedione and 2,3-heptanedione, respectively, in a similar manner to the synthesis of H_2phg.

1-(p-*Methylphenyl*)-1,2-*propanedione dioxime* (H_2mephg). The preparation of this compound was performed according to the method of Hartung.[8] As a first step 1-(*p*-methylphenyl)-1,2-propanedione 2-oxime was synthesized by introducing freshly prepared gaseous nitromethane to an ethereal solution of equimolar *p*-methylpropiophenone for 15 min. After standing overnight the product was extracted with aqueous 10% NaOH solution and the extract was neutralized with cold hydrochloric acid. The white crystals which separated were recrystallized from toluene. The 1-(*p*-methylphenyl)-1,2-propanedione 2-oxime thus obtained was dissolved in aqueous 20% NaOH solution and an equimolar amount of hydroxylamine hydrochloride was added to the solution. The mixture was heated for 1 h and on adding sodium acetate a white precipitate was formed, which was recrystallized from 80% aqueous acetic acid.

1-(p-*Methoxyphenyl*)-1,2-*propanedione dioxime* (H_2mophg) *and* 1-(p-*chlorophenyl*)-1,2-*propanedione dioxime* (H_2clphg). These compounds were prepared in a similar manner to that used in the synthesis of H_2mephg described above, the starting materials being *p*-methoxypropiophenone and *p*-chloropropiophenone, respectively.

Preparation of the nickel complexes

The preparation of the nickel complexes with dioximes, i.e. Ni(Hethg)$_2$,[9] Ni(Hprg)$_2$,[9] Ni(Hbutg)$_2$,[3] Ni(Hphg)$_2$,[10] Ni(Hmophg)$_2$,[11] Ni(Hmephg)$_2$[11] and Ni(Hclphg)$_2$[11], has been reported. Each complex was prepared by mixing an oxime (2 mmol) in ethanol (30 cm^3) with nickel acetate 4-hydrate (1 mmol) in water (10 cm^3). After the mixture was heated on a water bath for 30 min an orange to orange–red precipitate was formed, which was recrystallized from chloroform and dried *in vacuo*. The elemental analyses of the nickel complexes are summarized in Table 1.

NMR measurement

^{1}H NMR spectra of the complexes were measured by a JNM GSX 400 spectrometer equipped with a temperature control apparatus.

The deuterated solvents were purchased from Aldrich Chemical Co. The concentrations of the samples were in the range 2×10^{-2}–5×10^{-2} mol dm^{-3} for pyridine-d$_5$ solutions and 5×10^{-3}–1×10^{-2} mol dm^{-3} for chloroform-d solutions.

The molar ratio of the isomers of each complex was estimated from the ratio of the areas of the two methyl peaks derived from each isomer in the spectrum. As the two peaks were slightly overlapped in most cases the area of each peak was calculated graphically on a computer by assuming them to be Lorentz curves. A cutting and weighing method was used in cases where overlapping regions of the peaks were negligible.

RESULTS AND DISCUSSION

The ^{1}H chemical shifts of the CH_3 groups of the complexes in chloroform-d and pyridine-d$_5$ at room temperature are summarized in Table 1. As shown in Table 1, each complex gives a single methyl peak or two largely overlapped methyl peaks in chloroform-d solution. For example, the separation between the two peaks is 0.003 ppm for Ni(Hmephg)$_2$. However, at -30°C, as shown in Table 1, all the single methyl peaks split into two peaks except Ni(Hprg)$_2$. The intensity ratio of the two peaks is approximately unity in every case. It is suggested that the two peaks derive from each of the geometrical isomers and that rapid interchange between them may occur at room temperature.

A broad peak at *ca* 18 ppm was observed for every complex in chloroform-d, which was assigned

Table 1. Elemental analyses and ^1H chemical shifts for CH_3 groups of $Ni(Hdioxm)_2$ complexes

Complex	Analysis: Found (Calc.) (%) C	H	N	Solvent	Chemical shift (ppm) CH_3—C=N[a]	Other CH_3 group		
$Ni(Hethg)_2$	38.0	5.7	17.7	$CDCl_3$	2.05	CH_3CH_2	1.07	
	(37.9)	(5.7)	(17.7)		(2.110) (2.115)			
				C_5D_5N	1.989 2.005		0.961	0.975
$Ni(Hprg)_2$	41.6	6.4	16.1	$CDCl_3$	2.04	$CH_3(CH_2)_2$	0.964	
	(41.7)	(6.4)	(16.2)		(2.097)			
				C_5D_5N	2.010 2.021		0.784	0.801
$Ni(Hbutg)_2$	45.1	7.0	15.1	$CDCl_3$	2.06	$CH_3(CH_2)_3$	0.933	
	(45.1)	(7.0)	(15.0)		(2.106) (2.109)			
				C_5D_5N	2.026 2.039		0.779	0.794
$Ni(Hmophg)_2$	50.4	4.6	11.6	$CDCl_3$	2.06	$CH_3OC_6H_4$		
	(50.7)	(4.7)	(11.7)		(2.013) (2.019)			
				C_5D_5N	2.076[b] 2.110		3.679	3.698[b]
$Ni(Hmephg)_2$	52.5	4.9	12.1	$CDCl_3$	2.03	$CH_3C_6H_4$	2.39	
	(54.5)	(5.0)	(12.7)		(1.989) (1.996)			
				C_5D_5N	2.043[b] 2.007		2.218	2.240[b]
$Ni(Hphg)_2$	51.7	4.3	13.5	$CDCl_3$	2.010 2.020			
	(52.3)	(4.4)	(13.6)		(2.005) (2.043)			
				C_5D_5N	2.005[b] 2.043			
$Ni(Hclphg)_2$	44.7	3.3	11.6	$CDCl_3$	2.024 2.040			
	(44.9)	(3.4)	(11.6)					
				C_5D_5N	2.029[b] 2.059			

[a] Chemical shifts (in $CDCl_3$) at $-30°C$ are given in parentheses.
[b] More intense signal.

to the hydrogen-bonded O—H···O proton in bis(dioximato)nickel complexes coordinated by nitrogen atoms.[6] Marov *et al.* reported, however, three peaks in this region for $Ni(Hdioxm)_2$ with non-symmetrical ligands for some solvents at room temperature. They suggested that this proved the existence of the *cis* and *trans* isomers.[12] The absence of split peaks in the region of our experiment may be due to rapid exchange reactions of hydrogen-bonded hydrogen atoms or fast isomeric exchange reactions of these complexes in chloroform-d.

The ^1H NMR spectrum of each complex in pyridine-d_5 showed a single CH_3C=N methyl peak immediately after dissolution, followed by the gradual appearance of a second peak in the lower field. The second peak grew with time, while the intensity of the first peak decreased, until a finite intensity ratio of the two peaks was attained. It can be concluded from the above observation that in the solid state only one of the isomers exists and on dissolution in pyridine it slowly isomerizes to the other, until the equilibrium

$$\textit{trans}\text{-Ni(Hdioxm)}_2 \rightleftharpoons \textit{cis}\text{-Ni(Hdioxm)}_2$$

$$K = [\textit{cis}\text{-Ni(Hdioxm)}_2]/[\textit{trans}\text{-Ni(Hdioxm)}_2]$$

is reached. As the table shows CH_3 groups other than from the CH_3—C=N group also split in the ^1H spectra. X-ray analysis of $Ni(Hethg)_2$ has already revealed that it has *trans* geometry in the solid state.[13] It follows that in the case of $Ni(Hethg)_2$ the primary signal arises from the *trans* isomer and the second from the *cis* isomer. For other complexes similarly only *trans* isomers may probably be prepared in an ordinary recrystallization process. Therefore, the primary peak can be assigned to the *trans* isomer in each case. The isomerization reaction of these complexes reaches its equilibrium in several hours at room temperature.

It can, therefore, be concluded that these complexes isomerize much faster in chloroform than in pyridine. These square planar complexes in chloroform probably isomerize by rapid intramolecular ligand rotation through a tetrahedral intermediate. The evidence in support of this mechanism is the absence of ligand exchange reactions between two different kinds of $Ni(Hdioxm)_2$ complexes in chloroform-d solution.[6]

The substituent effects of the complexes on the equilibrium constants of the isomerization reactions were estimated for these complexes at several

temperatures ranging from 303 to 343 K in pyridine-d_5. For the series $Ni(Hethg)_2$, $Ni(Hprg)_2$ and $Ni(Hbutg)_2$ $K = 1$ was given.

In the series $Ni(Hmophg)_2$, $Ni(Hmephg)_2$, $Ni(Hphg)_2$ and $Ni(Hclphg)_2$ the K values at room temperature are 0.95, 0.80, 0.74 and 0.71, respectively. In this series the electronic effects of the substituents on the phenyl groups appear to contribute to the K values as it is shown that the order of increase in K values coincides with that of the decrease in σ-values of Hammett's constants of the substituent on the phenyl group.

Acknowledgement—The authors are grateful to Dr Minoru Hirota of Yokohama National University for helpful comments.

REFERENCES

1. A. Chakravorty, *Coord. Chem. Rev.* 1974, **13**, 1.
2. C. V. Banks and R. W. Vander Haar, *U.S. Atom. Energ. Comm.* 1952, ISC-250.
3. S. Sugden, *J. Chem. Soc.* 1932, 246.
4. J. Cavell and S. Sugden, *J. Chem. Soc.* 1935, 621.
5. K. A. Jensen, B. Nygaard and R. B. Jensen, *Acta Chem. Scand.* 1965, **19**, 770.
6. S. B. Pedersen and E. Larsen, *Acta Chem. Scand.* 1973, **27**, 3291.
7. H. Muller and H. von Beckmann, *Chem. Ber.* 1889, **22**, 2127.
8. W. H. Hartung, *Org. Syn. Coll.* 1943, **2**, 363.
9. C. L. Tschugaeff, *Z. Anorg. Allg. Chem.* 1905, **46**, 144.
10. G. Ponzio, *Gazz. Chim. Ital.* 1921, **51**, 213.
11. K. Takagi, M. Sugai, H. Matsuda, A. Mizuno and K. Tokami, *Memoirs Wakayama Tech. Coll.* 1981, **16**, 27.
12. I. N. Marov, A. T. Panilov, E. K. Ivanova and N. A. Plekhanov, *Koord. Khim.* 1975, **1**, 1516.
13. E. Frasson and C. Panattoni, *Acta Cryst.* 1960, **13**, 893.

Polyhedron Vol. 12, No. 14, pp. 1821–1824, 1993
Printed in Great Britain

0277–5387/93 $6.00+.00
© 1993 Pergamon Press Ltd

SYNTHESIS, THERMAL AND SPECTRAL INVESTIGATION OF A NEW BERYLLIUM PERIODATE HYDRATE

M. MANEVA* and M. GEORGIEV

Department of Inorganic Chemistry, Sofia Technology University, 1156 Sofia, Bulgaria

(*Received* 17 *June* 1992; *accepted* 23 *March* 1993

Abstract—A new beryllium periodate hydrate has been synthesized whose composition is $Be_2HIO_6 \cdot 6.5H_2O$. It has been identified by DTA, TG, DSC, IR spectra and X-ray powder diffraction. The compound is thermally stable up to 60°C, followed by three-step dehydration and decomposition to form BeO. The IR spectra prove the presence of the following structural groups: HIO_6^{4-}, BeO_4 and H_2O.

Published data about beryllium periodates are rather scanty. The first communications have been made by Atterberg[1–3] and are related to a meso-periodate of composition $Be_3(IO_5)_2 \cdot nH_2O$, where $n = 5, 11, 13$. Data have also been quoted in prominent literature about the formation of $Be_3(IO_5)_2 \cdot nH_2O$, where $n = 8, 12$.[4,5] More extensive studies have been reported for $Be(IO_4)_2 \cdot 8H_2O$[6–8] and, accordingly, $Be(H_4IO_6)_2 \cdot 4H_2O$. There is also information about the preparation and identification of $Be(H_4IO_6)_2 \cdot 2H_2O$.[7]

Interest in compounds of this group accounts for further studies in this direction. They resulted in the elaboration of a method of synthesizing a new beryllium periodate hydrate of composition $Be_2HIO_6 \cdot 6.5H_2O$, identified by DTA, TG, IR spectra and X-ray diffraction. This is the subject of the present publication.

EXPERIMENTAL

$Be_2HIO_6 \cdot 6.5H_2O$ was obtained using H_5IO_6 and $Be(NO_3)_2 \cdot 4H_2O$—p.a. Merck.

A solution of $Be(NO_3)_2 \cdot 4H_2O$ (20 g) in H_2O (20 cm^3) was added with continuous stirring using a magnetic agitator to a solution of H_5IO_6 (6 g) in H_2O (20 cm^3), the temperature being maintained at 60 ± 1°C. The homogeneous solution obtained was concentrated to a jelly-like mass, which was cooled and then treated several times with absolute C_2H_5OH under continuous trituration of the precipitate on the walls of the beaker. A white, fine crystalline substance was finally obtained and, after filtration, left in the air until a constant mass was obtained.

The compound was analysed by quantitative analysis: Be^{2+} was determined by weight as BeO upon heating to 950°C, while iodine was determined iodometrically.[9]

The thermal investigations of $Be_2HIO_6 \cdot 6.5H_2O$ were performed using a derivatograph MOM OD-102 Paulic–Paulic–Erdey system in the temperature range 25–1000°C, at a heating rate of 10° min^{-1} and 200 mg sensitivity. The DSC curves were obtained using an apparatus of the Mettler company—System TA 3000—at a heating rate of 10° min^{-1} in the 30–500°C temperature interval and 5 mg mass of the sample.

The IR spectra were taken in the 4000–2800 cm^{-1} range in Hostaflon and over 2800–400 cm^{-1} in KBr tablets on an IR "Shimatsu" spectrophotometer and on a UR-10 Zeiss spectrometer.

The diffractograms of the newly obtained compound and products of its decomposition were obtained using the apparatus HZG 4C-Zeiss with Cu-K_α radiation, $\lambda = 1.54178$ Å, and a nickel filter in the interval 4.03–78.18°.

RESULTS AND DISCUSSION

The data from the quantitative analysis, averaged from three different syntheses, are: Be = 5.07% and I = 35.33%. Those theoretically calculated for a compound with the formula $Be_2HIO_6 \cdot 6.5H_2O$ are, accordingly, Be = 5.02% and I = 35.36%.

* Author to whom correspondence should be addressed.

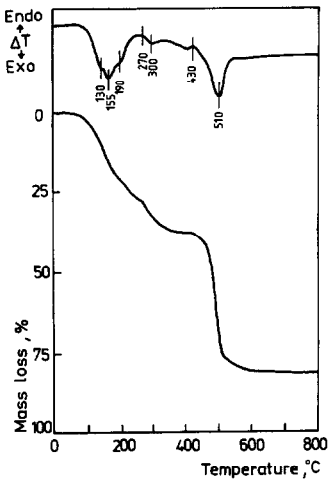

Fig. 1. DTA and TG curves of $Be_2HIO_6 \cdot 6.5H_2O$.

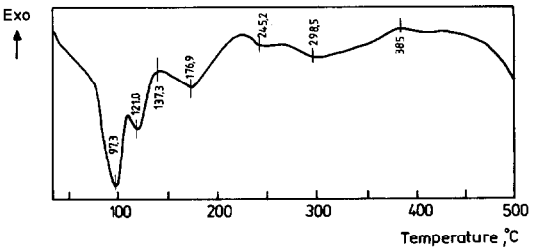

Fig. 2. DSC curve of $Be_2HIO_6 \cdot 6.5H_2O$.

The DTA and TG curves of $Be_2HIO_6 \cdot 6.5H_2O$ are shown in Fig. 1, while the DSC curve is shown in Fig. 2.

Table 1 shows the diagrams of thermal dehydration and decomposition, together with the values of the change in enthalpies of some phase transitions determined by the DSC curve. Figure 3 shows the IR spectrum of $Be_2HIO_6 \cdot 6.5H_2O$.

The curves shown in Figs 1 and 2 and the data from Table 1 indicate that the compound is stable up to 60°C. The process of dehydration takes place at three stages, the last also being associated with a process of decomposition of the compound.

The first endothermal effect observed in the DTA curve has a particularly marked width and makes it possible to record three temperatures—130°C, 155°C and 190°C. At the first two temperatures it is possible to record along the TG a change in the character of the curve, corresponding to $\Delta m_{exp} = 20.1\%$ theoretically and according to the proposed diagram of dehydration [Table 1, eq. (1)], $\Delta m_{calc} = 20.15\%$.

Corresponding to the examined effects in DSC there are two distinct and separate peaks with $T_{max} = 97.3°C$ and $T_{max} = 121.0°C$, with a total ΔH^0 of 60.3 kJ mol^{-1}. This ΔH^0 value is, however, relatively small for the release and evaporation of 4 mol H_2O under the conditions of DSC and leads to the formation of a three-phase systems: solid, liquid and vapours. This is corroborated by the small exothermal effect observed with $T_{max} =$ 137.3°C in DSC, which may be due to crystallization or dissolution of the newly obtained intermediate phase. The same exothermal effect is not seen in the DTA curve. The second dehydration stage, associated with the expansion of the endo effect observed in DTA, corresponds to $T_{max} = 190°C$. Corresponding to this in TG is $\Delta m_{exp} = 30.4\%$, as opposed to $\Delta m_{calc} = 30.08\%$ according to Table 1, eq. (2). This change in mass is recorded well due to the existence of distinct retention in TG. The examined degree of dehydration is registered along DSC by a separate endothermal effect with $T_{max} = 176.9°C$, characterized by $\Delta H^0 = 30.2$ kJ mol^{-1}.

The further course of the curves in DTA and DSC is analogous, with identical effects. There follows a

Table 1. DTA, TG and DSC data for $Be_2HIO_6 \cdot 6.5H_2O$

No.	Scheme of thermal decomposition	DTA and TG data			DSC data	
		T_{max} (°C)	Calc.	Exp.	T_{max} (°C)	ΔH^0 (kJ mol^{-1})
1	$Be_2HIO_6 \cdot 6.5H_2O \rightarrow$ $Be_2HIO_6 \cdot 2.5H_2O + 4H_2O$	130; 150	20.05	20.1	97.3; 121.0 137.3	60.3 −10.9
2	$Be_2HIO_6 \cdot 2.5H_2O \rightarrow$ $Be_2HIO_6 \cdot 0.5H_2O + 2H_2O$	190	30.08	30.4	176.9	30.2
3	$Be_2HIO_6 \cdot 0.5H_2O \rightarrow$ $3BeO + Be(IO_3)_2 + O_2 + 2H_2O$	270; 300	39.55	40.2	245.2; 2928.5	−2.14; 20.3
4	$Be(IO_3)_2 \rightarrow BeO + I_2 + 2.5O_2$	430; 510	86.07	86.9	385	
5	BeO residue	over 600	—	—		

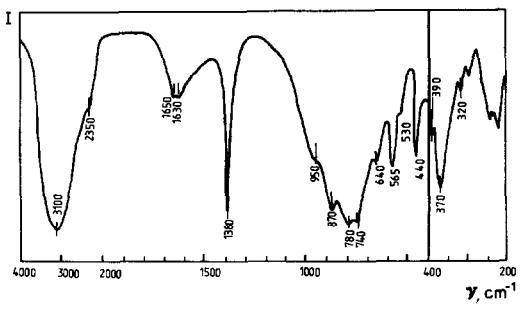

Fig. 3. IR spectra of $Be_2HIO_6 \cdot 6.5H_2O$.

small exo effect (T_{max} = 270°C at DTA and 245.2°C at DSC), which is probably due to crystallization of the compound obtained. The compound is unstable and a large endo effect (300°C DTA and 298.5° at DSC) corresponds to its decomposition. The products of the decomposition are BeO and $Be(IO_3)_2$, which are proved by X-ray phase analysis.

The amount of released oxygen and water leads to a decrease in the mass of 40.2% along the TG curve, with theoretically calculated Δm_{calc} = 39.55%. The change in enthalpy at the decomposition of the compound, recorded along DSC, is 20.3 kJ mol^{-1}. The horizontal section in the TG curve is proof of the stability of the intermediate mixture of BeO and $Be(IO_3)_2$. Corresponding to the decomposition of $Be(IO_3)_2$ is the exo effect at T_{max} = 430°C along DTA, which passes abruptly into an endo effect, in line with the decomposition of I_2O_5—fully analogous to those observed by us at the thermal investigations of other beryllium iodates and periodates.[7,18] The final product of the decomposition is BeO, which is identified using IR spectra and X-ray phase analysis. The thermal decomposition of $Be_2HIO_6 \cdot 6.5H_2O$ may be referred to one of the four diagrams for the decomposition of periodates, namely periodate–iodate–oxide, which is typical for the decomposition of the other beryllium periodates we examined.

Table 2. Crystallographic data for $Be_2HIO_6 \cdot 6.5H_2O$

No.	d (Å)	I/I_0 (%)	No.	d (Å)	I/I_0 (%)	No.	d (Å)	I/I_0 (%)
1	10.996	84.4	32	2.203	7.7	63	1.479	10.3
2	5.993	63.6	33	2.186	15.5	64	1.466	14.2
3	5.791	47.4	34	2.161	7.1	65	1.449	11.6
4	5.651	100	35	2.106	7.1	66	1.438	8.4
5	5.385	63.6	36	2.075	7.1	67	1.417	8.4
6	4.853	27.2	37	2.049	14.9	68	1.397	14.9
7	4.730	11.6	38	2.023	17.5	69	1.381	6.4
8	4.315	30.5	39	2.006	33.7	70	1.363	14.2
9	4.198	26.6	40	1.979	20.7	71	1.359	11.0
10	3.886	14.2	41	1.936	44.1	72	1.352	9.7
11	3.732	55.8	42	1.902	15.5	73	1.321	7.7
12	3.671	54.5	43	1.885	12.9	74	1.288	24.0
13	3.433	28.5	44	1.867	22.7	75	1.247	12.9
14	3.328	23.3	45	1.851	22.0	76	1.201	16.2
15	3.283	35.7	46	1.838	12.9	77	1.111	11.9
16	3.029	33.1	47	1.799	27.2	78	1.070	7.7
17	3.123	18.1	48	1.771	10.3	79	0.999	5.2
18	3.066	16.8	49	1.735	27.9	80	0.980	12.1
19	3.005	22.0	50	1.705	8.4	81	0.958	8.6
20	2.938	20.1	51	1.683	22.7	82	0.931	7.0
21	2.901	10.3	52	1.672	22.0	83	0.905	5.1
22	2.826	7.7	53	1.651	8.4	84	0.885	4.1
23	2.755	40.9	54	1.634	9.0	85	0.864	9.1
24	2.733	27.2	55	1.619	13.6	86	0.847	3.2
25	2.648	32.4	56	1.613	20.7	87	0.828	4.0
26	2.621	18.8	57	1.608	14.2	88	0.817	3.1
27	2.552	18.8	58	1.564	11.6	89	0.804	2.6
28	2.490	27.9	59	1.548	7.1	90	0.794	1.1
29	2.339	8.4	60	1.529	26.6	91	0.787	1.2
30	2.288	26.6	61	1.505	12.3			
31	2.228	10.3	62	1.495	11.6			

The interpretation of the IR spectra of $Be_2HIO_6 \cdot 6.5H_2O$ is of particular interest, because it is possible that a compound with the formula $Be_4I_2O_{11} \cdot 14H_2O$ may correspond to the same chemical composition. This is why it was of interest to firstly identify the character of the anion. The anion of the type HIO_6^{4-} is best proved by the presence of the two bending vibrations of the I—O—H group, namely δ(I—OH) and γ(I—OH), whose absorption bands are observed in the spectrum of the compound (Fig. 3) at 1380 and 780 cm^{-1}. Reference of these absorptions to the bending vibrations is on the basis of published data.[10,11] The presence of the IO_6^{5-} ion is also identified with the appearance in the spectrum of the absorption band at 640 cm^{-1}, which is attributed to the asymmetric stretching vibration (ν_3)[11,12] of I—O for this periodate ion. The analogous vibration for IO_4^- lies at 850 cm^{-1}.[11,12] The $\nu_3(F_2)$ vibration examined appears in immediate proximity to the strong and relatively broad absorption bands with maxima at 870, 780 and 740 cm^{-1}, on account of which it appears with reduced intensity. It is possible that some of the components of the triply degenerated ν_3 vibration, upon disturbed symmetry, could also lie in this region.

The absorptions (780, 740 cm^{-1}) may be differentiated by attributing the librational vibration (R) of the coordinated water molecules to the band at 740 cm^{-1} due to the weak absorption observed at 2630 cm^{-1}, which is in turn due to the composite vibration $\delta(H_2O)+R$.

According to data published in the prominent literature the absorption band observed at 440 cm^{-1} may be attributed to the bending vibration of the O—I—O group.[13]

The spectrum (Fig. 3) also shows an absorption band at 565 cm^{-1}, which we refer to as the $\nu_1(A_1)$ vibration of the BeO_4 group participating in the structure of the investigated compound,[14–17] while that at 370 cm^{-1} may be attributed to the stretching vibration ν(Be—O). The weak absorption band at 320 cm^{-1} (ν_4) is also due to the same group.

The data on hydrated water [$\nu(H_2O)$ and ν(OH)] show the presence of two crystallographically different water molecules [$\nu(H_2O)$ is split—1650 and 1630 cm^{-1}]. In this case four water molecules are coordinated around beryllium, while the remaining ones are involved in hydrogen bonds.

The information on $Be_2HIO_6 \cdot 6.5H_2O$ obtained from the IR spectra makes it possible to propose the following molecular formula:

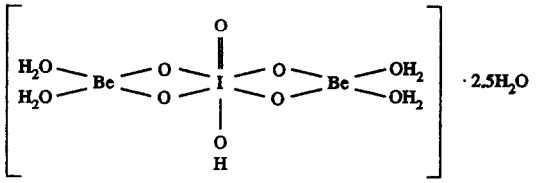

The newly synthesized compound has been characterized by X-ray powder diffraction and the data for *d*-spacings and intensity ratios are given in Table 2.

REFERENCES

1. A. Atterberg, *Bull. Soc. Chim.* 1875, **2**, 358.
2. A. Atterberg, *Ber.* 1874, **7**, 472.
3. A. Atterberg, *Svenska Acad. Hendl.* 1873, **12**, 20.
4. M. Dratovsky and V. Prejkova, *Collect. Czech. Chem. Commun.* 1963, **28**, 1280.
5. J. Julak, *Collect. Czech. Chem. Commun.* 1972, **37**, 1247.
6. V. Biber, I. Neiman and A. Bragina, *Zh. Obst. Khim.* 1941, **11**, 861.
7. M. Maneva, M. Georgiev and A. Pavlova, *J. Therm. Anal.* 1988, **33**, 589.
8. M. Maneva, M. Georgiev, N. Lange and H. Lutz, *Z. Naturforsch.* 1991, **46b**, 795.
9. G. Sharlo, *Methodi Analiticheskoi Khim.*, p. 1015. Khimiya, Moskwa (1969).
10. B. K. Chaudhuri and H. G. Mutherjee, *J. Ind. Chem. Soc.* 1979, **56**, 1098.
11. T. Balicheva and G. Petrova, *Coll. Problemi Sovremennoy Khim. Koord. Soed. L., Leningr. Gos. Univ.* 1978, **B6**, 62.
12. H. Siebert, *Z. Anorg. Allg. Chem.* 1962, **B303**, 162.
13. K. Petrov. V. Kravchenko, M. Verfolomeev, N. Shamray and V. Pluschev, *Zh. Neorg. Khim.* 1974, **19**, 903.
14. V. Sipachev and A. Grigoriev, *Zh. Strukt. Khim.* 1969, **10**, 820.
15. A. Grigoriev, V. Sipachev and A. Novoselova, *Dokl. Acad. Nauk. SSSR* 1965, **160**, 383.
16. A. Grigoriev, V. Sipachev and E. Pogofilova, *Zh. Strukt. Khim.* 1970, **11**, 485.
17. F. Bertin and J. Derouaut, *C. R. Acad. Sc. Paris* 1975, **280**, 973.
18. M. Maneva and M. Georgiev, *Thermochim. Acta* 1985, **92**, 627.

Polyhedron Vol. 12, No. 14, pp. 1825–1827, 1993
Printed in Great Britain

0277–5387/93 $6.00+.00
© 1993 Pergamon Press Ltd

COMMUNICATION

COVALENT ATTACHMENT OF TWO IMPORTANT DICOPPER(II) SYSTEMS IN A ONE-DIMENSIONAL POLYMERIC CHAIN: AN X-RAY STRUCTURE OF $[\{Cu_2(en)_2(OH)_2 \cdot Cu_2(O_2CMe)_4\}(PF_6)_2 \cdot 0.5EtOH]_\alpha$ SHOWING THE SHORTEST Cu···Cu DISTANCE IN THE TETRAACETATO CORE

SHANMUGAM MEENAKUMARI and AKHIL R. CHAKRAVARTY*

Department of Inorganic and Physical Chemistry, Indian Institute of Science, Bangalore 560 012, India

(*Received* 26 *February* 1993; *accepted* 2 *April* 1993)

Abstract—Reaction of $Cu_2(O_2CMe)_4(H_2O)_2$ with 1,2-diaminoethane(en) in ethanol, followed by the addition of NH_4PF_6, led to the formation of a covalently linked 1D polymeric copper(II) title complex showing alternating $\{Cu_2(en)_2(OH)_2^{2+}\}$ and $\{Cu_2(O_2CMe)_4\}$ units in the chain and the shortest Cu···Cu separation of 2.558(2) Å in the tetraacetato core.

Current interests in the chemistry of spin-coupled dimeric and polymeric copper(II) complexes lie towards understanding the magneto-structural relationships of such systems.[1–3] The discrete dimeric species that are subjected to extensive studies belong primarily to two important classes of copper(II) complexes, viz. $[Cu_2(O_2CMe)_4L_2]$ and $[Cu_2(OH)_2L'_2]^{2+}$, where L and L′ are neutral unidentate and bidentate ligands, respectively. While the copper(II) centres in the tetraacetato core are known[2] to be antiferromagnetically coupled, the magnetic interaction phenomena in the other core are dependant on the Cu—OH—Cu angle.[3a–c] In this communication we report a unique copper(II) complex, $[\{Cu_2(en)_2(OH)_2 \cdot Cu_2(O_2CMe)_4\}(PF_6)_2]_\alpha$ (**1**), in which two different dimeric units belonging to the above mentioned classes of complexes are covalently linked in a one-dimensional polymeric chain.

Complex **1** was prepared by reacting $Cu_2(O_2CMe)_4(H_2O)_2$ (1 mmol) with 1,2-diaminoethane (1 mmol) in ethanol (10 cm^3) with stirring at 50°C for 10 min. The solution after cooling to an ambient temperature was filtered and NH_4PF_6 (1 mmol) was added to the filtrate. The blue coloured precipitate thus obtained was isolated, washed with an ice-cold 1:1 (v/v) ethanol–water mixture and dried *in vacuo* over P_4O_{10} (yield 70%). Complex **1** has been structurally characterized†[4,5] by X-ray diffraction.

*Author to whom correspondence should be addressed.

† Analytical data for **1**: Found: C, 15.5; H, 3.5; N, 5.7. Calc. for $C_{12}H_{30}N_4O_{10}F_{12}P_2Cu_4$: C, 15.4; H, 3.2; N, 6.0%. Single crystals, suitable for X-ray studies, were obtained by slow evaporation of an ethanolic solution of **1**. Crystal data: $[C_{12}H_{30}N_4O_{10}F_{12}P_2Cu_4 \cdot 0.5EtOH]_\alpha$, mol. wt (polymer unit) = 957.54, monoclinic, a = 11.945(1), b = 21.044(3), c = 8.073(1) Å, β = 123.79(1)°, U = 1686.5(4) Å^3, Z = 2, space group $C2/m$, D_c = 1.89 g cm^{-3}, T = 290 K, μ = 27.02 cm^{-1}, $F(000)$ = 954, $R(R_w)$ = 0.0570 (0.0662) for 1148 reflections with $I > 2.5\sigma(I)$, weighting scheme $w = [\sigma^2|F_o| + 0.003767|F_o|^2]^{-1}$. Intensity data, collected on an Enraf-Nonius CAD4 diffractometer (Mo-K_α radiation, λ = 0.7107 Å) using a dark blue needle-shaped crystal of dimensions 0.3 × 0.1 × 0.1 mm, were corrected for Lorentz, polarization and absorption[4] effects (transmission coefficients: 0.89–1.00). The structure was solved and refined by Fourier syntheses and full-matrix least-squares using the SHELX 76 program.[5a] Atomic coordinates, full lists of bond lengths and angles and thermal parameters have been deposited at the Cambridge Crystallographic Data Centre. Magnetic susceptibility data at 288 K using a Faraday balance: $\chi_g = 3.185 \times 10^{-6}$ cm^3 g^{-1}, χ_M^{corr}/Cu = 0.85×10^{-3} cm^3 mol^{-1}, μ_{eff}/Cu = 1.40 B.M. at 2100 G and $\chi_g = 3.805 \times 10^{-6}$ cm^3 g^{-1}, χ_M^{corr}/Cu = 1.0×10^{-3} cm^3 mol^{-1}, μ_{eff}/Cu = 1.52 B.M. at 850 G (diamagnetic correction: $\chi^{dia} = -442 \times 10^{-6}$ cm^3 mol^{-1}; molecular weight of **1** = 934.5).

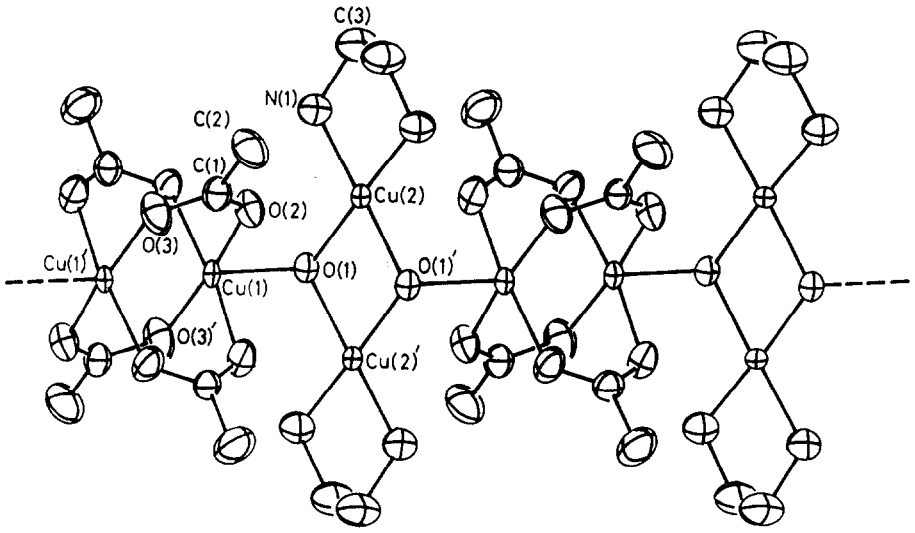

Fig. 1. An ORTEP view of the one-dimensional chain structure in **1** with atom numbering scheme.

The crystal structure of **1** consists of one-dimensional chains of the cationic polymers with PF_6 anions and the lattice ethanol molecules lying in between the isolated chains. An ORTEP[6] view of a portion of the polymeric chain is shown in Fig. 1. The chains are formed by covalent attachment of the $\{Cu_2(O_2CMe)_4\}$ and $\{Cu_2(en)_2(OH)_2^{2+}\}$ units by the μ_3-OH ligand. The geometries around the Cu(1) and Cu(2) atoms are essentially square-pyramidal and square-planar, respectively. The Cu(1)···Cu(1)′, Cu(2)···Cu(2)′ and Cu(1)···Cu(2) distances in **1** are 2.558(2), 3.005(3) and 3.231(1) Å, respectively. The Cu(1)···Cu(1)′ length is the shortest among known[2,7,8] tetra-μ-carboxylatodicopper(II) complexes. The Cu···Cu distance in $Cu_2(O_2Me)_4(H_2O)_2$[7] is 2.614(2) Å. The shortening of the Cu(1)···Cu(1)′ separation may be attributed to the Cu(1)′···Cu(1)—O(2), O(3) angles which are much lower than 90° (Table 1). The Cu(1)—O(1) distance is, however, similar to that observed[7] for the diaqua adduct. The inter-unit intrachain Cu(1)···Cu(2) distance in **1** is also found to be the shortest among related complexes having a covalent and/or hydrogen-bond linkage between discrete mono-, bi- or polynuclear units.[9-11] In the 1D chain the Cu(1)···Cu(1)′ and Cu(2)···Cu(2)′ axes are orthogonal to each other.

The *X*-band ESR spectrum of an aqueous solution of **1** at 77 K exhibits an isotropic signal with a g_{av} value of 2.12. Preliminary susceptibility measurements on **1** at 288 K show a field depen-

Table 1. Selected bond distances (Å) and angles (°) for $[\{Cu_2(en)_2(OH)_2 \cdot Cu_2(O_2CMe)_4\}(PF_6)_2 \cdot 0.5EtOH]_\alpha$

Cu(1)···Cu(1)′	2.558(2)	Cu(2)—O(1)	1.951(4)
Cu(2)···Cu(2)′	3.005(3)	Cu(2)—N(1)	1.981(6)
Cu(1)···Cu(2)	3.231(1)	Cu(2)···O(2)	2.695(7)
Cu(1)—O(1)	2.161(9)	O(2)—C(1)	1.261(11)
Cu(1)—O(2)	1.976(4)	O(3)—C(1)	1.258(11)
Cu(1)—O(3)′	1.975(4)	N(1)—C(3)	1.492(11)
C(1)—C(2)	1.486(10)		

Cu(1)′···Cu(1)—O(1)	176.2(2)	O(1)—Cu(2)—O(1)′	79.3(1)
Cu(1)—O(1)—Cu(2)	103.4(1)	O(1)—Cu(2)—N(1)	97.8(2)
Cu(2)—O(1)—Cu(2)′	100.7(1)	O(2)—Cu(1)—O(3)′	90.3(2)
O(1)—Cu(1)—O(2)	91.9(1)	O(2)—C(1)—O(3)	124.3(6)
O(1)—Cu(1)—O(3)′	97.7(2)	Cu(2)—N(1)—C(3)	108.9(5)
Cu(1)′···Cu(1)—O(2)	85.4(2)		
Cu(1)′···Cu(1)—O(3)′	85.0(2)		

dence. The average μ_{eff}/Cu value* indicates the presence of antiferromagnetically coupled copper(II) centres in **1**. Further studies aimed towards understanding the magnetic exchange behaviour of **1** are in progress.

Acknowledgements—We thank Dr S. Vasudevan and Mr S. K. Tiwari for the magnetic susceptibility measurements.

REFERENCES

1. B. J. Hathaway, in *Comprehensive Coordination Chemistry* (Edited by G. Wilkinson, R. D. Gillard and J. A. McCleverty), Vol. 5, p. 533. Pergamon Press, Oxford (1987) and refs therein.
2. (a) M. Kato and Y. Muto, *Coord. Chem. Rev.* 1988, **92**, 45; (b) M. Melnik, *Coord. Chem. Rev.* 1982, **42**, 259; 1981, **36**, 1; (c) R. J. Doedens, *Prog. Inorg. Chem.* 1976, **21**, 209; (d) P. deLoth, P. Cassoux, J. P. Daudey and J. P. Malrieux, *J. Am. Chem. Soc.* 1981, **103**, 407; (e) R. W. Jotham, S. F. A. Kettle and J. A. Marks, *J. Chem. Soc., Dalton Trans.* 1972, 429.
3. (a) W. E. Hatfield, *Comm. Inorg. Chem.* 1981, **1**, 105; (b) D. J. Hodgson, *Prog. Inorg. Chem.* 1975, **21**, 209; (c) Van H. Crawford, H. W. Richardson, J. R. Wasson, D. J. Hodgson and W. E. Hatfield, *Inorg. Chem.* 1976, **15**, 2107; (d) O. Kahn, *Angew. Chem., Int. Edn Engl.* 1985, **24**, 834; (e) W. E. Hatfield and L. W. ter Haar, in *Biological and Inorganic Copper Proteins* (Edited by K. D. Karlin and J. Zubieta), Vol. 1, p. 173. Adenine Press, New York (1985).
4. A. C. T. North, D. C. Phillips and F. S. Mathews, *Acta Cryst.* 1968, **A24**, 351.
5. (a) G. M. Sheldrick, SHELX 76, Program for Crystal Structure Determination. University of Cambridge, U.K. (1976); (b) International Tables for X-ray Crystallography, Vol. 4. Kynoch Press, Birmingham (1974).
6. C. K. Johnson, ORTEP II, Oak Ridge National Laboratory, Oak Ridge, Tennessee (1976).
7. (a) G. M. Brown and R. Chidambaram, *Acta Cryst.* 1973, **B29**, 2393; (b) P. de Meester, S. R. Fletcher and A. C. Skapski, *J. Chem. Soc., Dalton Trans.* 1973, 2575.
8. (a) M. M. Borel and A. Leclaire, *Acta Cryst.* 1976, **B32**, 3333; (b) V. Mohan Rao, D. N. Sathyanarayana and H. Manohar, *J. Chem. Soc., Dalton Trans.* 1983, 2167; (c) B. Morosin, R. C. Hughes and Z. G. Soos, *Acta Cryst.* 1975, **B31**, 762.
9. (a) B. Chiari, O. Piovesana, T. Tarantelli and P. F. Zanazzi, *Inorg. Chem.* 1988, **27**, 3246; (b) R. J. Butcher, J. W. Overman and E. Sinn, *J. Am. Chem. Soc.* 1980, **102**, 3276; (c) G. Christou, S. P. Perlepes, E. Libby, K. Folting, J. C. Huffman, R. J. Webb and D. N. Hendrickson, *Inorg. Chem.* 1990, **29**, 3657; (d) B. Chiari, W. E. Hatfield, O. Piovesana, T. Tarantelli, L. W. ter Haar and P. F. Zanazzi, *Inorg. Chem.* 1983, **22**, 1468; (e) B. Chiari, J. H. Helms, O. Piovesana, T. Tarantelli and P. F. Zanazzi, *Inorg. Chem.* 1986, **25**, 870, 2408; (f) D. B. W. Yawney, J. A. Moreland and R. J. Doedens, *J. Am. Chem. Soc.* 1973, **95**, 1164; (g) S. P. Perlepes, E. Libby, W. E. Streib, K. Folting and G. Christou, *Polyhedron* 1992, **11**, 923.
10. S. Meenakumari and A. R. Chakravarty, *J. Chem. Soc., Dalton Trans.* 1992, 2305, 2749.
11. (a) I. I. Mathews, P. A. Joy, S. Vasudevan and H. Manohar, *Inorg. Chem.* 1991, **30**, 2181; (b) M. Beneto', L. Soto, J. Garcia-Lozano, E. Escriva', J.-P. Legros and F. Dahan, *J. Chem. Soc., Dalton Trans.* 1991, 1057; (c) B. Morosin, *Acta Cryst.* 1975, **B31**, 632.

* See footnote to p. 1825.

Polyhedron Vol. 12, No. 15, pp. 1829–1848, 1993
Printed in Great Britain.

0277–5387/93 $6.00+.00
Pergamon Press Ltd

POLYHEDRON REPORT NUMBER 48

LEWIS BASE ADDUCTS OF ALANE AND GALLANE

CAMERON JONES, GEORGE A. KOUTSANTONIS and COLIN L. RASTON*

Faculty of Science and Technology, Griffith University, Nathan,
Brisbane 4111, Australia

CONTENTS

1. INTRODUCTION 1829

2. SYNTHESIS OF ADDUCTS OF ALANE AND GALLANE 1830
2.1. Tertiary and secondary amine adducts 1830
2.2. Tertiary phosphine adducts 1833
2.3. Mixed donor adducts and others 1834

3. STABILITY CONSIDERATIONS 1836

4. STRUCTURAL STUDIES 1839
4.1. Alane derivatives 1839
4.2. Gallane derivatives 1841

5. REACTIONS 1843
5.1. Metallation 1843
5.2. Hydrometallation/reduction 1843
5.3. Miscellaneous 1844

6. SURFACE CHEMISTRY 1845

7. CONCLUSIONS 1846

1. INTRODUCTION

Lewis base adducts of alane, AlH_3, have a wide range of applications in organic synthesis as selective reducing agents,[1] the preparation of transition metal aluminohydrides[2] and in materials science, with the latter evolving in recent years mainly in relation to the application of volatile Lewis base adducts in chemical vapour deposition (CVD) technology.[3–8] Adducts of gallane are starting to gain attention for application in CVD technology[9] and in synthesis.[10]

Advantages of the use of adducts of alane and gallane in CVD over conventional group 13 alkyl precursors include (i) facile M—H bond cleavage relative to M—C cleavage[8] and (ii) a reduction in the amount of carbonaceous contaminant in the deposited metal, in consequence of the lack of direct metal–carbon bonds in the precursors. The primary process in the decomposition of adducts of alane is thought to be ligand loss,[7,11,12] which is followed by aluminium catalysed hydrogen loss, forming AlH then metal.[6] Thus, varying the nature of the ligands, in particular base strength, is likely to effect the thermal stability of the adducts, as for gallane adducts. Other applications of adducts of alane include (i) the use of solutions of triethylamine-alane, H_3AlNEt_3, and $LiAlH_4$ to

* Author to whom correspondence should be addressed.

electroplate aluminium onto copper surfaces[13] and (ii) the generation of silane from SiF_4 and $AlH_3(NEt_3)$.[14]

The recent resurgence in the chemistry of the adducts of alane and gallane follows on the pioneering work of the 60s and 70s.[11,15–17] The characterization of uncoordinated gallane was detailed as recently as 1990.[18,19] It is a symmetrical dimer in the gas phase, $[H_2Ga(\mu\text{-}H)_2GaH_2]$, although it tends to associate into oligomers of *ca* four units in the condensed phase. In contrast, alane yields polymeric and involatile solids. One fully characterized phase shows octahedral aluminium with each hydride bridging two metal centres.[20] On structural considerations alone gallane is more like the ubiquitous diborane, $[H_2B(\mu\text{-}H)_2BH_2]$, which reflects the trend in group 13 electronegativities: boron, 2.0; aluminium, 1.5; gallium, 1.8 (Allred and Rochow). Thus, the more polarized Al—H bonds result in a greater tendency for MH_3 to associate and greater reactivity relative to Ga—H bonds.[21,22] Indane (InH_3) and thallane (TlH_3) are apparently too unstable to exist in the uncoordinated state, but may have a transitory existence in ethereal solutions at reduced temperatures.[23] For these heavier elements the only structurally authenticated compounds with M—H bonds are mixed potassium salts of bulkyalkylindane species.[24,25]

Prior to 1991 the structural elucidation of alane adducts was confined to a few poorly refined cases[26–29] and to a single, poorly defined structure of a gallane, H_3GaNMe_3.[30] Much conjecture has surrounded the solid state structure of tertiary amine adducts of the type H_3AlNR_3, with uncertainty as to whether they are monomeric or dimeric through hydride bridges. For $H_3AlN(Bu^n)_3$ the X-ray structural determination shows the compound to be monomeric,[26] but when the amine substituents are less sterically demanding dimerization may occur.[12] The structure of amine adducts in solution has also been a controversial issue with the degree of association being put at anywhere from 1 to 2, depending on the nature of the substituent, the solvent or the concentration of the adduct.[12,31,32] Lewis base adducts of gallane are seemingly simplified by almost exclusively forming four-coordinate species, exemplified by H_3GaNMe_3 being monomeric in both the vapour and solid phases.[22,30,33,34]

Our recent endeavours in this field include further elaborating the chemistry of Lewis base adducts of alane and gallane. Structure elucidation via X-ray crystallography, coupled with theoretical studies and the investigation of surface adsorption characteristics, has provided a firm base for the continuing study into applications of these adducts. Closely related work has led to the preparation of alane and gallane amido complexes. These are of interest for application in CVD technology, e.g. $(H_2GaNH_2)_3$ yields semi-conducting GaN.[35] Some of our publications on alane chemistry have been recently reviewed in Chemtracts (Inorganic Chemistry).[36]

2. SYNTHESIS OF ALANE AND GALLANE ADDUCTS

2.1. *Tertiary and secondary amine adducts*

Synthesis of tertiary amine adducts of alane and gallane mainly follows the methods developed by earlier workers.[11] For alane this involves treating $LiAlH_4$ with the hydrochloride of the amine (salt elimination)[37,38] and ligand displacement whereby etherates, e.g. H_3AlOEt_2, or amine adducts are treated with an amine. This takes advantage of the greater affinity of N-donors to alane,[39] amine base strength differences,[40] e.g. quinuclidine > trimethylamine, and the tendency for alane to form five-coordinate adducts with multidentate amines. Indeed, ligand displacement involving readily available H_3AlNMe_3 is the preferred method for the synthesis of multidentate tertiary amine adducts of alane, thus removing problems associated with the ability of these amines to solubilize the LiCl generated in the salt elimination method using $LiAlH_4$.[41] Less common methods of preparation include (i) the reduction of aluminium halide adducts using a hydride source, e.g. in the synthesis of H_3AlNMe_3 from Cl_3AlNMe_3 and LiH,[42] (ii) the direct synthesis from aluminium powder and amine under high pressure of hydrogen, as in the synthesis of polymeric $[H_3Al\{N(CH_2CH_2)_3N\}]_\infty$,[43] and (iii) the more recent treatment of $LiAlH_4$ with a tertiary amine, e.g. eq. (1), although it is seemingly of limited scope since NEt_3 fails to react and the loss of some aluminium hydride as the by-product.[1]

$$3LiAlH_4 + 2NMe_2Et \xrightarrow{\text{Toluene}} 2H_3AlNMe_2Et + Li_3AlH_6 \quad (1)$$

Bidentate tertiary amines afford five-coordinate species, (−)sparteine excepted which forms an alane rich compound possibly because of steric impediment at the N-centres.[40] Five-coordinate bis(monodentate amine) compounds are limited to the well-known trimethylamine adduct and the quinuclidine adduct.[40] Five-coordination is possible for monodentate amines via hydride bridging, at least in the solid state. Aspects of recent work in this area, including the synthesis of the (−)sparteine adduct, are shown in Schemes 1 and 2.[38,40,44,45] In many synthesis of H_3AlNMe_3, which is a key starting material for preparing a variety of amine adducts, as well as mixed donor species,[45] a significant amount of chloride is often present in the product and in some cases has resulted in the isolation of partially chlorinated species, e.g. $H_{2-x}Cl_xAl\{NMe(CH_2CH_2)_2O\}$, see Section 3.1.[40] This appears to arise from hydride/chloride exchange between preformed H_3AlNMe_3 and LiCl derived from $LiAlH_4$ and $NMe_3 \cdot HCl$, and work-up of reaction mixtures using this salt elimination route should follow immediately after evolution of hydrogen gas has ceased. Similarly, close attention to stoichiometry should be paid as excess hydrochloride salt can also result in partial chlorination.

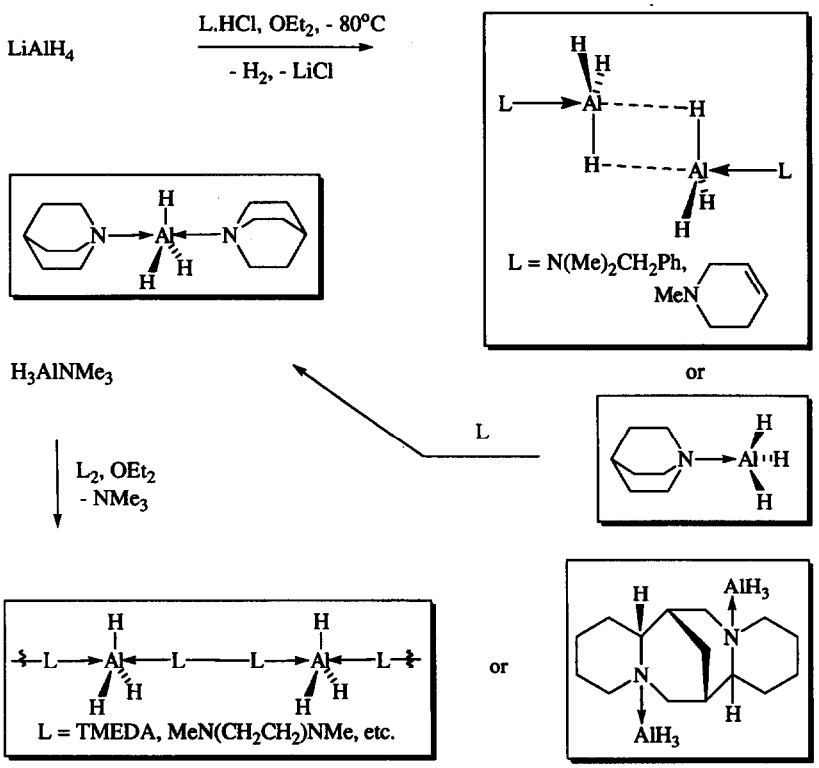

Scheme 1.

Treatment of H_3AlNMe_3 with the polydentate tertiary amines, Me_3TRIAZ (1,3,5-trimethylhexahydro-1,3,5-triazine), PMDETA (N,N,N′,N″,N″-pentamethyldiethylenetriamine) or $Me_4CYCLAM$ (N,N′,N″,N‴-tetramethylcyclam), yield either neutral, five-coordinate adducts or the first examples of cationic aluminium hydride species, Scheme 2.[44,46] For Me_3TRIAZ the formation of four-membered chelate rings, and thus ionic species, is favourable and additional uptake of alane by the polymeric $[H_3Al(Me_3TRIAZ)]_\infty$ is not observed.

Several methods have been reported for the synthesis of tertiary amine adducts of gallane. Some of these outlined below include the reaction of $LiGaH_4$ with a hydrochloride salt of the amine.[15] The ligand displacement method which is common for alane is limited to a few examples for gallane. These are shown in Scheme 3, along with examples of the salt elimination route. The 1 : 1 reaction of TMEDA (N,N,N′,N′-tetramethylethylenediamine) with H_3GaNMe_3 yields the unstable intermediate $H_3GaTMEDA$,[46] which may be five-coordinate like the TMEDA adduct of alane, but it readily loses half an equivalent of TMEDA *in vacuo* affording the "gallane rich" species.[9,46] A 2 : 1

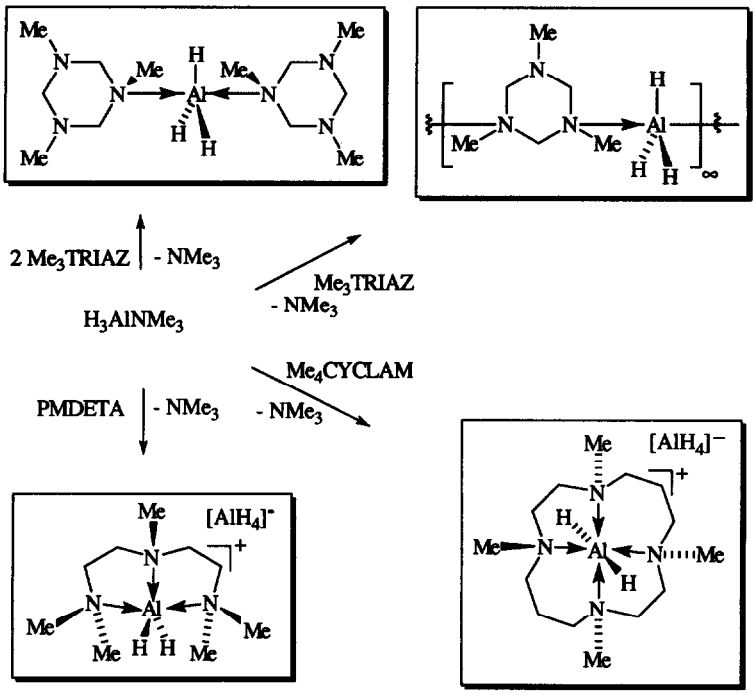

Scheme 2.

adduct of H_3GaNMe_3 and $Me_4CYCLAM$ has been prepared, but attempts to isolate higher adducts result in rapid decomposition to gallium metal, hydrogen and the free ligand. Indeed, attempts at preparing a range of other tertiary amine gallane adducts of PMDETA and of the mixed donor ligands N-methylmorpholine and N-methylthiomorpholine results in decomposition above *ca* $-20°C$.

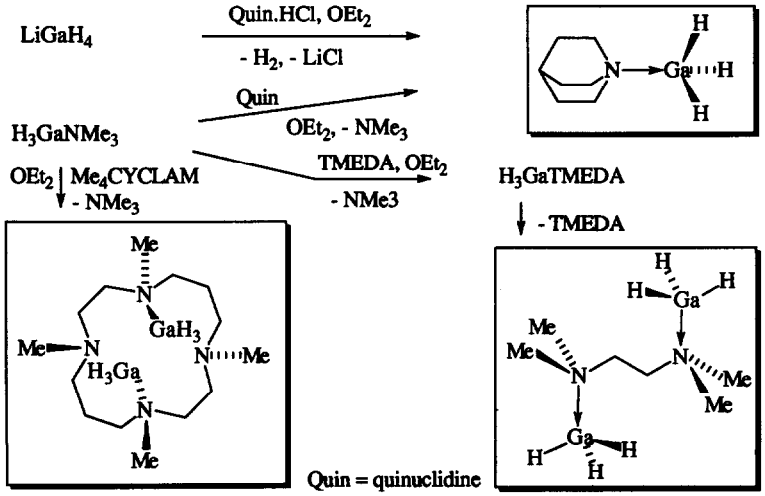

Scheme 3.

Significant differences in the synthesis of tertiary amine adducts of alane and gallane relate to the tendency for alane to form stable five-coordinate and ionic species and the tendency for polydentate amines to yield inherently unstable adducts of gallane. While the reaction of uncoordinated gallane with trimethylamine at low temperature results in symmetrical cleavage of Ga—H—Ga bridges, affording five-coordinate $H_3Ga(NMe_3)_2$, loss of amine takes place at $> -20°C$, eq. (2).[19] A novel route to H_3GaNMe_3 has recently been described by Downs *et al.*,[47]

eq. (3).

$$1/n[GaH_3]_n \xrightarrow[-95°C]{2NMe_3} H_3Ga(NMe_3)_2 \xrightarrow[-NMe_3]{> 20°C} H_3GaNMe_3 \quad (2)$$

$$H_2Ga(\mu\text{-}H)_2BH_2 \xrightarrow[-95°C]{NMe_3} H_2GaBH_4(NMe_3)_n \xrightarrow{23°C} H_3GaNMe_3 + H_3BNMe_3 \quad (3)$$

Secondary amine adducts are less common because of their tendency to eliminate hydrogen above *ca* −20°C and 20°C for alane and gallane, respectively, affording amido alane and gallane species with amido groups bridging the metal centres.[15] However, the bulky amine 2,2,6,6-tetramethylpiperidine provides an example of a stable alane-secondary amine adduct. Ethereal solutions of AlH_3 and 2,2,6,6-tetramethylpiperidine in diethyl ether afford the adduct (solid decomposes > 145°C), but ethereal solutions of H_3AlNMe_3 result in the formation of a novel monomeric amide at 0°C, Scheme 4.[48] The kinetic stability of the adduct arises from poor donor properties of diethyl ether towards alane, compared with NMe_3.

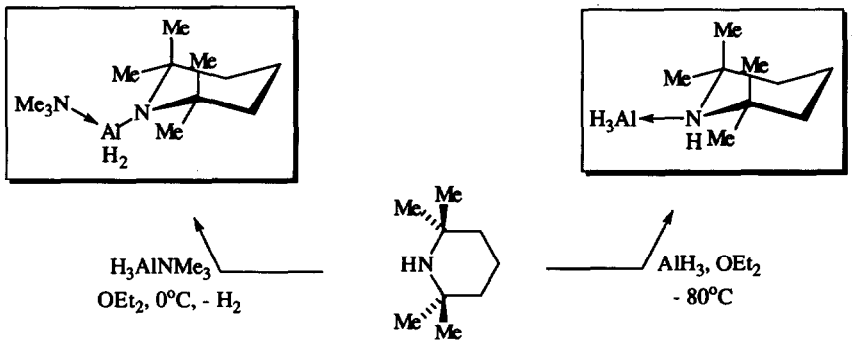

Scheme 4.

2.2. *Tertiary phosphine adducts*

Stable tertiary phosphine adducts require the use of bulky trialkyl phosphines to circumvent the formation of polymeric alane at low temperature, e.g. H_3AlPEt_3 decomposes at −20°C.[49] Synthetic procedures involve treating ethereal solutions of $LiAlH_4$ with dry HCl and phosphine; $(Pr^i_2PCH_2)_2$ gives the only example of a five-coordinate species, Scheme 5.[50] The ligand displacement method involving H_3AlNMe_3 either fails, notably for aryl substituted phosphines, or gives mixed donor adducts. These can decompose *in vacuo* to simple phosphine adducts, e.g. in the synthesis of $H_3AlPBu^t_3$ (Section 2.3).[45,51,52] Interestingly, the formation of "alane rich" adducts of bifunctional phosphines has only one parallel with tertiary amines, viz the adduct of (−)sparteine. In the case of amines polymeric material normally results with an alane-to-ligand ratio of 1 : 1, with the polymer formed in the presence of excess amine even when the ratio is 2 : 1.

The synthesis of phosphine adducts of gallane is simpler; the ligand displacement method is not complicated by the formation of five-coordinate bis(phosphine) or mixed donor adducts, in accordance with the tendency for gallane to only form stable four-coordinate species. Typically, the starting material is H_3GaNMe_3.[9,51,53] Addition of phosphines to $LiGaH_4$ can yield the adduct directly with the extrusion of LiH in some cases, although the yields are not as high.[53] There is no evidence for the formation of the intermediate 1 : 1 compound, $H_3Ga(PMe_2CH_2)_2$, of the type found in the analogous displacement reaction involving TMEDA, Scheme 3.[46]

Tertiary phosphine adducts of gallane have similar stabilities to tertiary amine adducts, in consequence of the comparable donor strength of the bases towards gallane, established for the equilibrium in eq. (4), $K = 2.94$ (benzene). This suggests that back-donation from filled gallium 3*d* orbitals to vacant phosphorus 3*d* orbitals may explain the anomalously high stability of the P—Ga bond.[54]

$$H_3GaPMe_3 + NMe_3 \rightleftharpoons H_3GaNMe_3 + PMe_3 \quad (4)$$

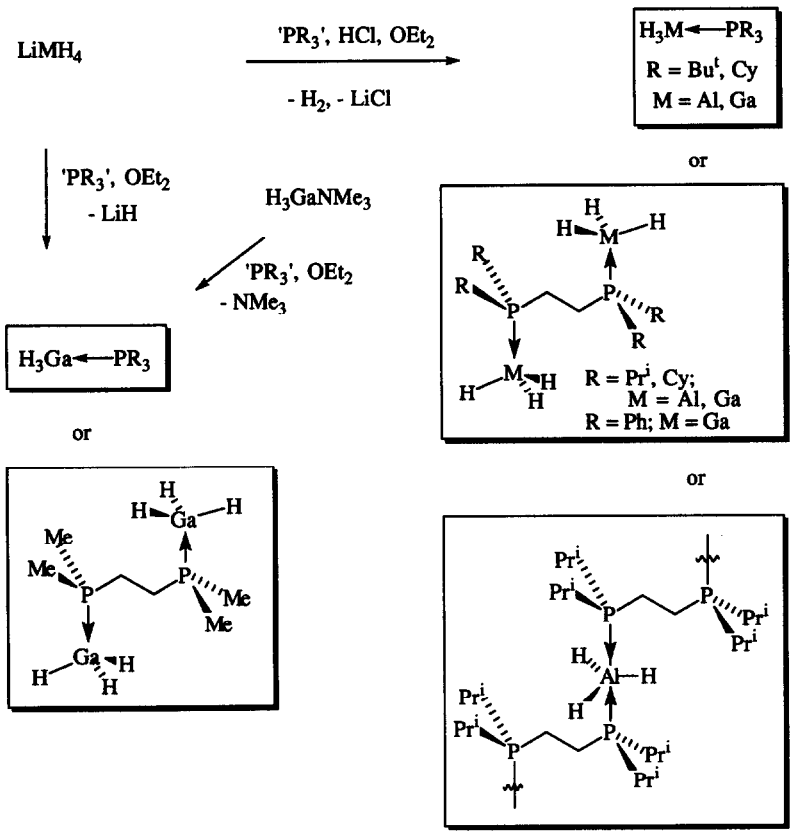

Scheme 5.

2.3. *Mixed donor adducts and others*

Mixed tertiary phosphine/amine adducts of alane have been briefly mentioned in Section 2.2. Treatment of H_3AlNMe_3 with a trialkyl phosphine can result in these novel species, Scheme 6.[45,51]

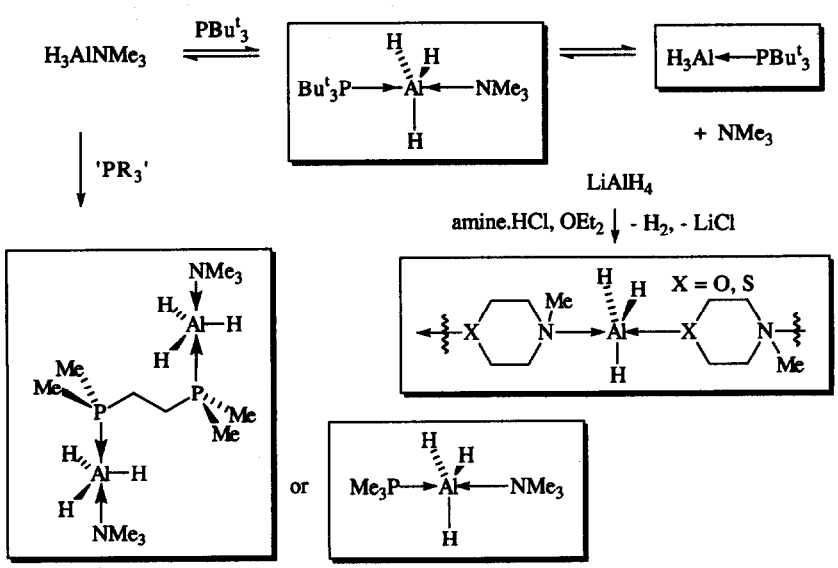

Scheme 6.

The loss of trimethylamine from the tri-t-butyl adduct *in vacuo* is unusual given the donor strengths of the ligands towards alane and theoretical considerations.[38,44,50] Presumably, the exceptionally

large steric demand of the phosphine coupled with the volatility of the amine shifts the equilibrium in favour of $H_3AlPBu^t_3$.[51] Mixed donor species have not been identified for gallane, although they are likely intermediates in ligand displacement reactions. In general ligand displacement reactions of alane or gallane are likely to proceed via complexation as the primary process, even for reactions with secondary and primary amines, phosphines, thiols, etc., where ultimately ligand displacement and hydrogen evolution is possible.[15]

Alane also forms mixed donor adducts with N-methylmorpholine[45] and N-methylthiomorpholine,[40] containing N and heteroatom interactions in the solid state, Scheme 6. The amide $[H_2Al\{N(CH_2CH_2)_2S\}]_2$ results from the reaction of thiomorpholine with trimethylamine alane and can be considered to be a mixed donor complex by virtue of the weak intermolecular Al···S interactions observed in the solid state structure of the amide, Fig. 1.

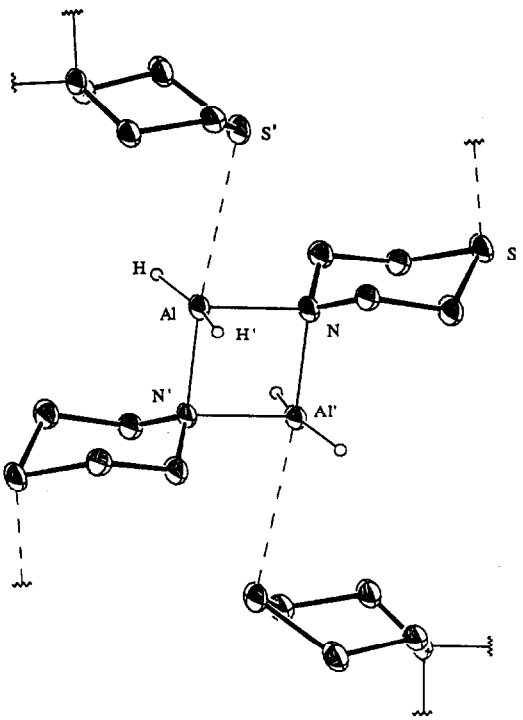

Fig. 1. Molecular structure of $[AlH_2(Thiomorph)]_2$; Al—S′ 3.26(1) Å.

The mixed donor adduct of N-methylmorpholine can be regarded as (i) a model compound for surface binding of H_3AlNMe_3 to oxidized silicon (see Section 6), (ii) as a model intermediate for the displacement of weakly bound etherates to alane[12] and (iii) as a model for Wiberg and Nöth's hydrolysis of amine adducts of alane, where complexation precedes hydrolysis of $H_2O(H)_3AlNR_3$.[55] In one report[56] the complex $Et_2O(H_3Al)NMe_3$ is postulated for the dissolution of H_3AlNMe_3 in diethyl ether. More recently, Smith *et al.* have structurally characterized tetrahydrofuran (THF) adducts of alane.[57] $[H_3Al(THF)]_2$ and $[H_3Al(THF)_2]$ are accessible either from the displacement of NMe_3 from $[H_3Al(NMe_3)]_2$ by THF or the action of concentrated sulphuric acid on lithium aluminium hydride[57] in THF solvent. The hydride-bridged dimer is in equilibrium with the bis-THF monomer and the position of the equilibrium can be disturbed by the addition of excess petrol in the crystallization process giving the monomer. The dimer is favoured by excess THF.[57] $[H_3Al(THF)]_2$ is unstable with respect to loss of THF, in the absence of excess THF, giving $[H_3Al(THF)]_2$ which itself loses the ether donor under dynamic vacuum at 60°C to give polymeric alane, Scheme 7.

Treatment of H_3GaNMe_3 with BF_3 in the presence of SMe_2 is an effective method for generating S-donor adducts of gallane, eq. (5);[58] claims that uncoordinated gallane is formed in the absence of SMe_2[59] have been disputed. It is now thought that some hydride–halide exchange takes place,

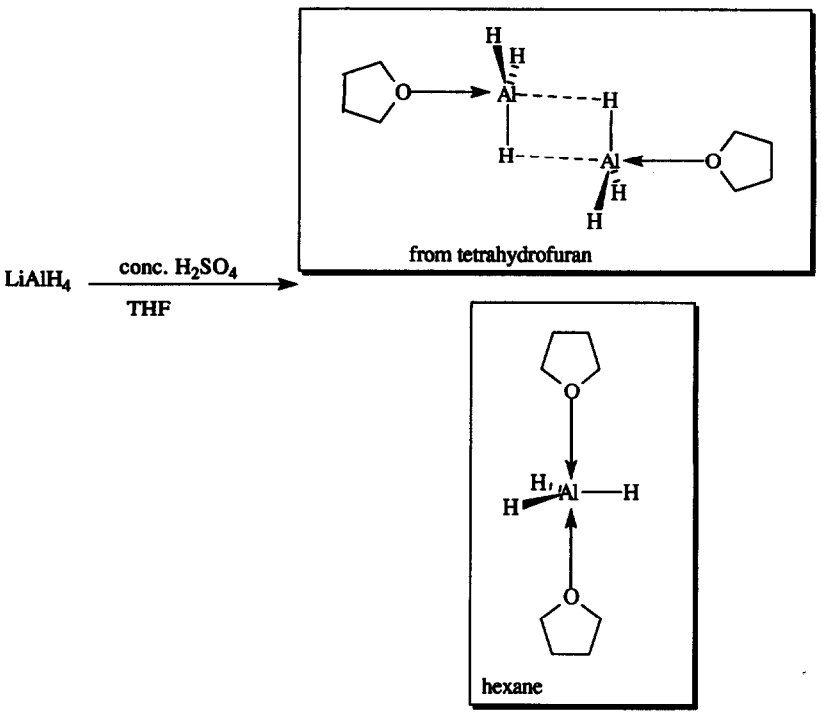

Scheme 7.

giving rise to compounds of the type $[GaH_xF_{3-x}]_n$ in the condensed phase[19] and GaH_2F in the gas phase.[60]

$$H_3GaNMe_3 + BF_3 \overset{SMe_2}{\rightleftharpoons} H_3GaSMe_2 + F_3BNMe_3 \qquad (5)$$

A remarkably stable adduct of alane results from the treatment of 1,3-bis(2,4,6-trimethylphenyl)imidazol-2-ylidene with $[H_3Al(NMe_3)]_2$, Scheme 8.[61] This carbene alane adduct has a melting point of 246–247°C and contains a tetrahedral aluminium centre.

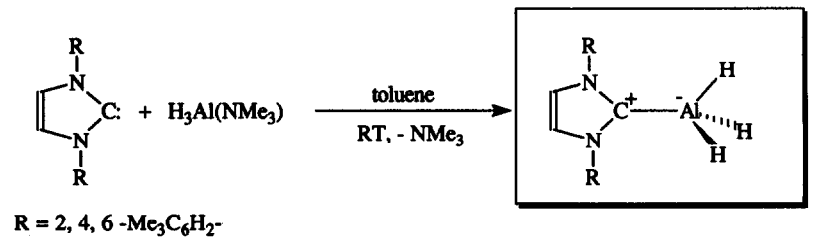

Scheme 8.

3. STABILITY CONSIDERATIONS

Thermal decomposition pathways for tertiary amine adducts of alane and gallane are poorly understood, despite their emerging importance as precursors in CVD technology. The primary process for the decomposition of $H_3Al(NMe_3)_2$ is the loss of one amine group at 100°C.[27] In contrast, the bis(quinuclidine) adduct $H_3Al\{N(CH_2CH_2)_3CH\}_2$ sublimes without decomposition at >120°C and the greater stability here relates to the greater donor strength of the amine. Only above 190°C does it decompose directly to the metal, hydrogen and amine, possibly with the loss of one amine as the limiting process. The five-coordinate mixed donor compound $\{Me_3N(H_3Al)(PMe_2CH_2)_2\}_2$ is also thermally robust and can be sublimed without the loss of either amine or phosphine at 50°C.[45] Theoretical studies (HF/DZP-ECP) on model systems show that $H_3Al(NH_3)_2$

is only 10.74 kcal mol^{-1} more stable relative to fragmentation to H_3AlNH_3 and NH_3[44] and *ab initio* studies of the dissociation energy of H_3AlNH_3 was predicted to be 26 kcal mol^{-1}, after zero point energy corrections.[62] For gallane (D95*+DZP) $H_3Ga(NH_3)_2$ is only 7.8 kcal mol^{-1} more stable relative to H_3GaNH_3 and NH_3,[63] in accordance with the preference for gallane to form four-coordinate species, $H_3Ga(NMe_3)_2$ excepted which is stable below -23.4°C.[59] Similarly, the stabilization energy (D95*//D95*) of $Me_3P(H_3Al)NH_3$ relative to H_3AlNH_3 and PMe_3 is low, at 2.72 kcal mol^{-1} and 9.02 kcal mol^{-1} relative to NH_3 and H_3AlPMe_3,[51] and thus the origin of the stability of $\{Me_3N(H_3Al)(PMe_2CH_2)_2\}_2$ is uncertain. As to the mixed N,O-donor complex based on N-methylmorpholine, the stabilization energy of the model compound $H_2O(H)_3AlNH_3$(D95P) relative to H_3AlNH_3 and OH_2 is only 4.71 kcal mol^{-1} and 13.16 kcal mol^{-1} relative to H_3AlOH_2 and free amine.[64] The compound $H_3Al(PR_3)_2$, modelling the only example of a bis(phosphine) adduct of alane, viz. polymeric $H_3Al\{(PPr^i_2CH_2)_2\}$, Scheme 5, has a low stabilization energy relative to H_3AlPR_3 and free phosphine, 1.82 or 2.26 kcal mol^{-1}, when R = H or Me, respectively (D95*).[64]

The mono-tertiary amine adducts of alane decompose with the formation of aluminium mirrors between 100 and 170°C,[38,40] whereas bidentate tertiary amines have higher temperatures for the same process, *ca* 170–215°C.[40,44] The enhanced stability of these compounds relates to their polymeric structures, with a reluctance to undergo Al—N cleavage and form monomeric species, as evidenced by their low vapour pressures. For higher amines, which form ionic species predominantly, there is also greater thermal stability relative to monodentate species; the PMDETA and Me_4CYCLAM complexes, Scheme 2, decompose at 182 and 243°C, respectively.[65]

Mono(amine) alane adducts are thought to decompose via an initial and irreversible amine dissociation yielding polymeric alane, which further decomposes to its constituents.[12,27] However, at reduced pressure thermal decomposition of H_3AlNMe_3 yields the highly reactive monomeric alane species AlH_3,[7] which spontaneously decomposes to aluminium and hydrogen before association to dialane and higher aggregates of alane. Thermodynamic studies show that decomposition of AlH_3 to aluminium and hydrogen is favoured by 11 kcal mol^{-1}.[66]

While polydentate tertiary amines enhance the stability of alane, there is no improvement for gallane; H_3GaNHe_3 slowly decomposes to its constituents at room temperature, whereas the "gallane rich" TMEDA compound, Scheme 3, Me_4CYCLAM and PMDETA derivatives decompose rapidly at the same temperature. Seemingly, there is no advantage in having additional donor sites, because of the preference for four-coordinate species. The higher stability of gallane adducts is imparted by the use of stronger Lewis bases such as quinuclidine. This yields an adduct of remarkably high thermal stability, decomposing to its constituents above *ca* 100°C.[67] Tertiary amine adducts of gallane decompose at lower temperatures than analogous alane species, due to weaker metal–nitrogen bonds in gallane adducts, in turn a consequence of the lower acidity of the GaH_3[22] and also because of the frailty of Ga—H bonds.[68]

In adducts containing ligands with methylene linkages between the N-donor groups there is cleavage of N—C bonds, as in tetramethylmethylenediamine (ambient temperature)[69] and alane Me_3TRIAZ adducts, Scheme 2.[44] The monomeric Me_3TRIAZ adduct decomposes at 123°C via the polymeric adduct, yielding on hydrolysis NMe_3, $CH_2(NMe_2)_2$ and some Me_3TRIAZ.[44]

Ammonia will also form a thermally unstable 1 : 1 adduct with alane.[70] This loses 1 equivalent of hydrogen at -40°C, with a further loss at room temperature and at 150°C cross-linked aluminium nitride results. Primary and secondary amine adducts of alane are thermally unstable, the tetramethylpiperidine adduct excepted, Scheme 4,[48] a consequence of the reactivity of hydride substituents towards acidic amine protons resulting in hydrogen elimination and the formation of N-bridging oligomeric amides.[12,71,72] The stability of the piperidine adduct, Scheme 4 (decomposition > 145°C), relates to the steric demand of the amine, disfavouring amido bridges. Steric demand is also important in the formation of the alane-rich amido species in eq. (6); the intermediate amido/amine complex is proposed on the basis of the isolation of the corresponding hydrido/chloro species.[73]

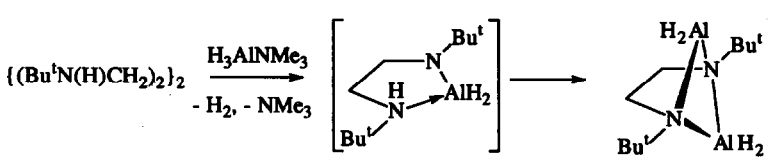

(6)

Free gallane and excess ammonia, at low temperature, afford an ionic ammonia-gallane adduct, eq. (7),[19] which remarkably is stable to hydrogen loss at room temperature. The proposed ionic structure of the product is directly comparable with $[AlH_2(PMDETA)]^+[AlH_4]^-$ and $[AlH_2(Me_4CYCLAM)]^+[AlH_4]^-$.[65]

$$2/n[GaH_3]_n + 2NH_3 \xrightarrow{-78°C} [H_2Ga(NH_3)_2]^+[GaH_4]^- \quad (7)$$

Ammonia condenses with the trimethylamine adduct of gallane yielding the hydrogen elimination product as a cyclic trimer, $[(H_2GaNH_2)]_3$, in the solid state,[35] although earlier reports claimed it was polymeric, eq. (8).[74] As for aluminium (above) heating the trimer above 150°C results in the formation of the metal nitride, as cubic GaN. Secondary amine adducts of gallane usually decompose via hydrogen elimination yielding gallane amides, cf. eq. (8),[75] and typically this takes place at *ca* 20°C, which compares with *ca* −20°C for secondary amine alane adducts, which is higher on account of the greater polarity of the Al—H bond.

$$H_3GaNMe_3 + NH_3 \xrightarrow[-H_2]{ca\ 20°C} \quad (8)$$

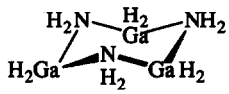

Tertiary aryl phosphine adducts of alane based on PPh_3, $(Ph_2PCH_2)_2$ and $(Ph_2PCH_2CH_2)_2PPh$ rapidly decompose to polymeric alane at room temperature or lower. Trialkyl phosphine adducts similarly decompose, unless the alkyl groups are bulky. Decomposition then occurs at *ca* 160°C for both four- and five-coordinate species, Scheme 5, yielding the metal, hydrogen and the ligand.[50,51] In accordance with theoretical considerations the association of alane and release of phosphine are favoured, but for bulky alkyl groups they are kinetically inhibited.[50]

Tertiary phosphine adducts of gallane are in general more stable than alane analogues. Aryl phosphine adducts slowly decompose at room temperature, yielding the metal, hydrogen and the ligand, e.g. $\{H_3Ga(PPh_2CH_2)_2\}_2$,[55] unlike alane analogues which yield polymeric alane and phosphine. Steric hindrance is not necessary to stabilize trialkylphosphine adducts of gallane; $[\{H_3Ga(PMe_2CH_2)_2\}_2]$ and the tricyclohexylphosphine adduct decompose to their constituents at 100 and 130°C.[51] Lower stabilities of aryl phosphine adducts of gallanes (and alanes) are consistent with the lower base strength of aryl-substituted ligands.

Computed stabilization energies (D95*) for various complexation reactions of model phosphine adducts of alane and gallane include:[51]

$$AlH_3 + PH_3 \longrightarrow H_3AlPH_3 \qquad -10.65\ kcal\ mol^{-1}$$

$$AlH_3 + PMe_3 \longrightarrow H_3AlPMe_3 \qquad -21.54\ kcal\ mol^{-1}$$

$$GaH_3 + PH_3 \longrightarrow H_3GaPH_3 \qquad -8.06\ kcal\ mol^{-1}$$

$$GaH_3 + PMe_3 \longrightarrow H_3GaPMe_3 \qquad -16.01\ kcal\ mol^{-1}$$

The trimethylphosphine adducts have greater stabilization energies relative to PH_3, in accordance with donor strength considerations. The potential energy hypersurface of $(H_3AlPH_3)_2$ (6-31G*+DZP) results in convergence on dialane $H_2Al(\mu\text{-}H)_2AlH_2$ and free PH_3, favoured by 5.84 kcal mol^{-1} relative to H_3AlPH_3,[50] Fig. 2. This is consistent with the instability of phosphine adducts of alane relative to polymeric alane, unless the phosphine is bulky enough to suppress association via hydride bridges. Similar calculations on H_3AlNH_3 give a dimer, $H_3N(H)_2Al(\mu\text{-}H)_2Al(H)_2NH_3$, favoured by just 0.4 kcal mol^{-1},[38] and thus the finding of both dimers and monomers for mono(tertiary) amine adducts of alane is not unreasonable.[38,45] No hydride-bridged dimers have detectable energy minima for H_3GaXH_3, X = N or P, with or without binding of the group 15 centres. Indeed, H_3GaPH_3 has been isolated as a colourless solid [m.p. *ca* −50°C (decomposition > −30°C)] by treatment of gallane with excess phosphine[19] and the absence of IR bands diagnostic of Ga—H—Ga bridging suggests it is monomeric in the condensed phase, in agreement with theory.[51,53] Theory also predicts that H_3GaAsH_3 should be a stable monomeric species.[76] Secondary phosphine adducts of gallane are poorly characterized oils of the type H_3GaPHR_2.[75] These are generally unstable to hydrogen elimination and phosphide formation in a similar fashion to that seen for secondary amine gallane adducts.

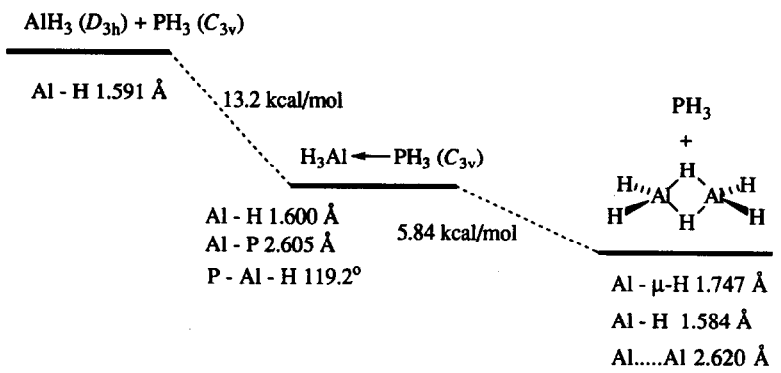

Fig. 2. Computed structures and energies (6–31 G*+DZP) for interaction of AlH_3 and PH_3.

The stability of Lewis base adducts in air varies considerably. In general, adducts of gallane are less reactive than alane due to the lower polarity of the Ga—H bond. Mono(amine) adducts of alane are very reactive and can spontaneously ignite in air, e.g. H_3AlNMe_3. In contrast, bis(amine) and mixed donor adducts decompose slowly due to steric protection of the metal centres/blocking of complexation by reactive species such as water and oxygen (see Section 2.3). Bulky alkylphosphines also impart higher stability in air, even though there is in principle a vacant coordination site available, polymeric $H_3Al\{(PPr^i_2CH_2)_2\}$ expected. Bulky alkylphosphine adducts of gallane also have improved stability in air, to the extent that the tricyclohexylphosphine adduct is air stable.[77]

4. STRUCTURAL STUDIES

4.1. *Alane derivatives*

Four structural types have been identified for adducts of alane: viz (i) monomeric four-coordinate species; (ii) dimeric mono-Lewis base adducts with unsymmetrical hydride bridges, at least for tertiary amines; (iii) five-coordinate bis-Lewis base adducts; and (iv) ionic compounds based on five- or six-coordinate cationic species, $H_2Al(ligand)^+$, and the ubiquitous AlH_4^- ion. X-ray diffraction and electron diffraction studies provide the most definitive structural assignments. However, ^1H NMR and to a lesser extent ^{27}Al NMR spectroscopy is informative, as is the position of ν(Al—H) IR bands, which for example are typically 1680 cm^{-1} for bis(amine) adducts and 1760 cm^{-1} for mono(tertiary amine) adducts.[40,78,79] While the ^1H NMR hydride resonances are broad they are usually *ca* 0.3 ppm upfield, at *ca* 3.8 ppm, for four five-coordinate bis(amine) adducts relative to mono(amine)adducts.[40]

The quinuclidine[45] and tri-n-butyl[26] adducts of alane are monomeric in the solid. The gas phase electron diffraction structure of H_3AlNMe_3[28] shows it to also be monomeric, although there is a discrepancy between the Al—N distance, 2.063(8) Å, in this structure with those in the solid, 1.991(4) and 1.98(2) Å, respectively. Typical Al—H distances are close to 1.60 Å, which are close to theoretical values for H_3AlNH_3.[38,62] The greater basicity of the amines, and thus greater metal centre electron saturation, in monomeric solid state structures relative to those amines found in the bridging hydride adducts, Scheme 1, may account for the existence of monomeric species. However, the difference in energy, monomer versus dimer, is comparable to crystal packing forces.[38] The structure of the alane rich (−)sparteine adduct has been modelled using Chem 3D, Fig. 3.

Solid state structures of H_3AlPR_3, R = Cy,[50] Bu^t,[51] $\{H_3Al(PR_2CH_2)\}_2$, R = Cy,[50] Pr^i,[51] all possess four-coordinate species, with the distances in the range Al—P 2.460(2)–2.467(1) Å. The computed structure at the MP2/D95* level of theory for H_3AlPMe_3, C_{3v} symmetry, is longer, 2.498 Å, which is a common result for phosphine adducts of alane and gallane.[51] The lack of dimeric structures with bridging hydrides is predetermined by the necessity to use hindered ligands to block formation of polymeric alane, Fig. 2.[50,51]

The X-ray crystal structures of the trimethylamine, dimethylbenzylamine, 4-methyltetrahydropyridine and tetrahydrofuran adducts of alane, Schemes 1 and 7, have the unsymmetrical hydride bridge structure, illustrated by the methyltetrahydropyridine adduct in Fig. 4.[38] In each

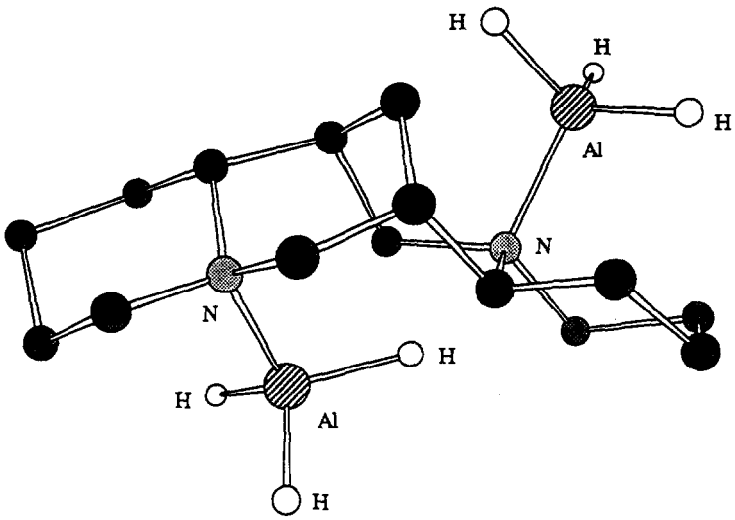

Fig. 3. Chem 3D structurally minimized molecular model of $(H_3Al)_2(-)$sparteine.

case the aluminium coordination environment can be considered as pseudo-trigonal bipyramidal. The Al—N distances are significantly longer than in the four coordinate species, 2.08 Å, with the Al—O distance 1.967(2) Å. The Al···H contact at *ca* 2.05 Å was long and no significant elongation occurred of the associated short distance, *ca* 1.59(4) Å—amine adducts; *ca* 1.39 Å—THF adducts, relative to terminal Al—H distances. The computed structure for the model compound $(H_3AlNH_3)_2$ agrees well with these structures, as does the computed structure of H_3AlNH_3 with the above monomers, DZP,[38] TZ2P+*f*basis.[62] Prior to the finding of a dimeric structure in the solid for H_3AlNMe_3, originally proposed by Ruff and Hawthorne,[12] the generally accepted view was that complexes of the type H_3AlNR_3 were monomeric in the solid state.

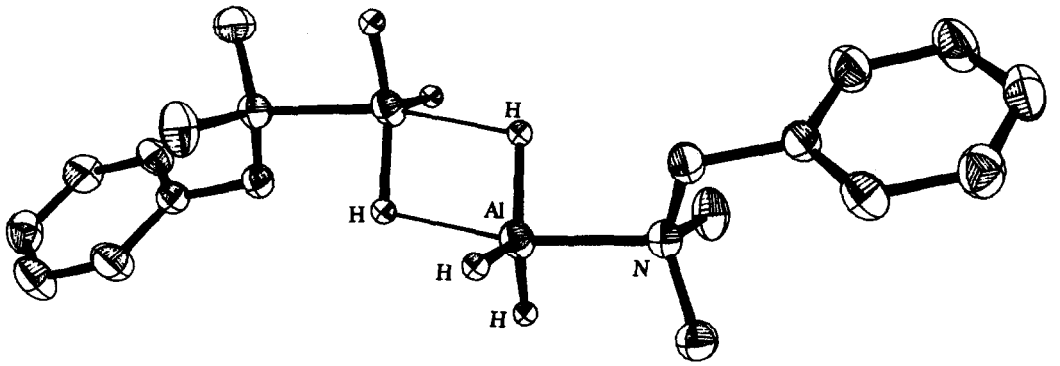

Fig. 4. Dimeric structure of $H_3Al(NMe_2CH_2Ph)$; Al—H 2.088(2) Å; Al—μ-H 1.56, 2.07 Å; Al—H 1.56 Å (mean); Al···Al 2.883 Å; H—Al—H 122(1)°; Al—μ-H—Al 104.7(5)°; μ-H—Al—μ-H 75(1)°.

The foregoing dimeric structures can be considered as tertiary amine stabilized adducts of the as yet unknown dialane $[H_2Al(\mu\text{-}H)]_2$. Theory predicts a binding energy comparable to that of the well-known diborane $[H_2B(\mu\text{-}H)]_2$.[80] Vaporization cleaves the hydride bridges, at least for H_3AlNMe_3 which is monomeric in the gas phase,[28] and the dimeric nature of this compound in the solid explains why it has a lower vapour pressure than the monomeric bis(amine) adduct.[32] The degree of association of the solid state dimers in benzene is close to 1.40,[27,40] cf. with 1.21 for the mono(quinuclidine) adduct which is monomeric in the solid.[16,45] The degree of association of the 3-chloroquinuclidine adduct of alane in benzene is higher, 1.64,[40] possibly in consequence of the chloro group acting as a weak donor rather than association via hydride bridging. This is also supported by IR and ^{27}Al NMR studies.[40]

Davidson and Wartik[37] had previously reported the TMEDA adduct having a high vapour

pressure and a dimeric structure was proposed for the gas phase in which the TMEDA was thought to adopt a bidentate coordination mode. Structurally characterized $[H_3Al\{Me_2N(CH_2)_nNMe_2\}]_\infty$ [$n = 2$ (TMEDA),[29] 3 (TMPDA),[41] 4 (TMBDA)[44]] are all polymeric in the solid state, the alane moiety defining a trigonal plane and N-centres in apical positions of a trigonal bipyramid, as shown by the structure of the TMEDA analogue in Fig. 4.[44,81] Thus, it seems unlikely that TMEDA would adopt a bidentate mode of bonding with octahedral aluminium as previously suggested.[37] More likely is a gas phase cyclic dimer in which the aluminium atoms are five-coordinate with nitrogen atoms in apical positions, as suggested for the solution state structure of $[H_3Al\{Me_2N(CH_2)_3NMe_2\}]_\infty$.[41] The structures of the Me_3TRIAZ derivatives, Scheme 2, have a similar coordination environment, as has the earlier structure of the TMEDA adduct, albeit for space group $P2_12_12_1$[29] cf. $P2_1/c$, and the structure of $H_3Al(NMe_3)_2$.[27] The range of Al—N distances for all five-coordinate species is 2.183(4)–2.24(2) Å, which encompasses the distance for the computed structure for $H_3Al(NH_3)_2$, 2.20 Å. This has D_{3h} symmetry and thus a linear N—Al—N arrangement, cf. experimental values for the foregoing structures $>174.9(2)°$.[44] Placing the nitrogen centres in apical positions is supported by theory (HF/DZP-ECP); starting with the C_{2v} and C_s trigonal bipyramidal isomers of $H_3Al(NH_3)_2$ resulted in fragmentation to H_3AlNH_3 and NH_3.[44]

Related structures include (i) those of the mixed donor species, the alane adduct of N-methylmorpholine and $\{Me_3N(H)_3Al(PMe_2CH_2\}_2$[45] and (ii) the structure of polymeric $H_3Al(PPr^i{}_2CH_2)_2$, Fig. 5.[50] All have the trigonal bipyramidal structure with the donor atoms in apical positions, as predicted by theory on model compounds (D95P),[50] D95*//D95*[51] and D95*,[51] respectively. The adduct of N-morpholine crystallizes in $P2_12_12_1$, but with *ca* 17% chloride content (see Section 2.0) it crystallizes in $P2_1/c$;[43] the chloride replaces hydride groups at only one site/metal centre for the two independent strands and thus without disruption to the polymeric structure. The Al—N distance is slightly shorter than for the above compounds, 2.15 Å, and Al—O is 2.19 Å. The mixed P—N— donor adduct has a similarly short Al—N distance, 2.155(9) Å, which is offset by an exceptionally long Al—P distance, 2.688(5) Å. In fact this distance is more akin to that in polymeric $H_3Al(PPr^i{}_2CH_2)_2$, mean 2.755(3) Å,[51] Fig. 6, some 0.3 Å longer than in monophosphine adducts of alane (see above) and some 0.5 Å longer than in bis(amine) adducts, which reflects very weak solvation of alane by P-donors and the tendency of unhindered phosphine adducts of alane to decompose to polymeric alane under mild conditions, via association.

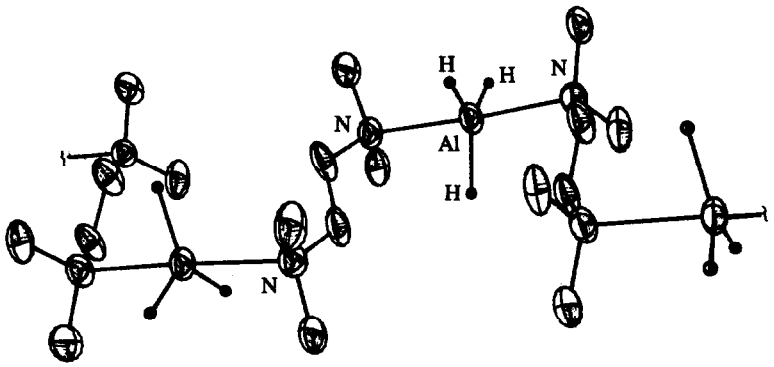

Fig. 5. Polymeric structure of H_3Al(TMEDA) [Al—N 2.24(2) and Al—H 1.55 Å (mean), N—Al—N 178.4(2)°].

Five- and six-coordination is achieved in the cationic species H_2AlL^+, L = PMDETA (trigonal bipyramidal with hydrogen atoms in the trigonal plane) and L = Me_4CYCLAM, *trans*-octahedral, Fig. 7.[65] ν(Al—H) reflect complex structures, both with a band at 1660 cm^{-1} for $[AlH_4]^-$ and another at 1822 cm^{-1}, L = PMDETA; 1740 cm^{-1}, L = Me_2CYCLAM.[65]

4.2. *Gallane derivatives*

Unlike alane, gallane has only one authenticated structural type, monomeric four-coordinate species. The ^{1}H NMR chemical shifts for the hydrides are typically 4.5–5.0 ppm and ν(Ga—H)

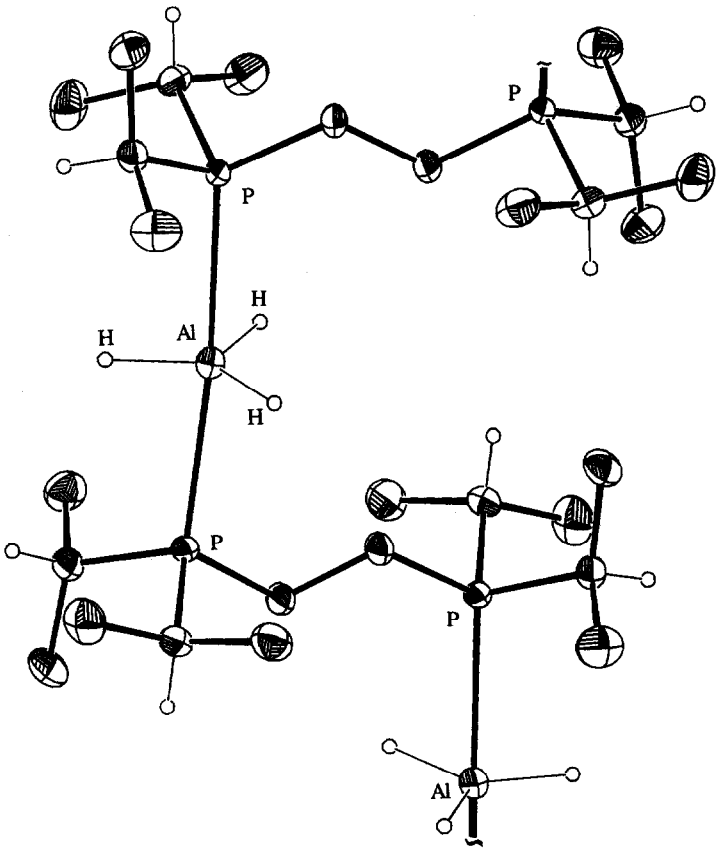

Fig. 6. Polymeric structure of $H_3Al(PPr^i_2CH_2)_2$ [Al—P 2.724 and Al—H 1.59 Å (mean), P—Al—P 175.0(3)°].

1800–1850 cm^{-1}, both significantly higher than for alane adducts. The 1 : 1 gallane adduct of TMEDA, Scheme 3, has a lower ν(Ga—H) band at 1790 cm^{-1}, which suggests it has a polymeric structure, as for the alane analogue,[81] and along with $H_3Ga(NMe_3)_2$ (< 23.4°C) are seemingly the only examples of five-coordinate species. Interestingly, theory predicts five-coordinate $H_2O(H)_3GaNH_3$ has a stabilization energy of 7.8 kcal mol^{-1} relative to H_3GaNH_3 and H_2O (D95* + DZP),[63] so that mixed N–O-donor five-coordinate species are possibly accessible.

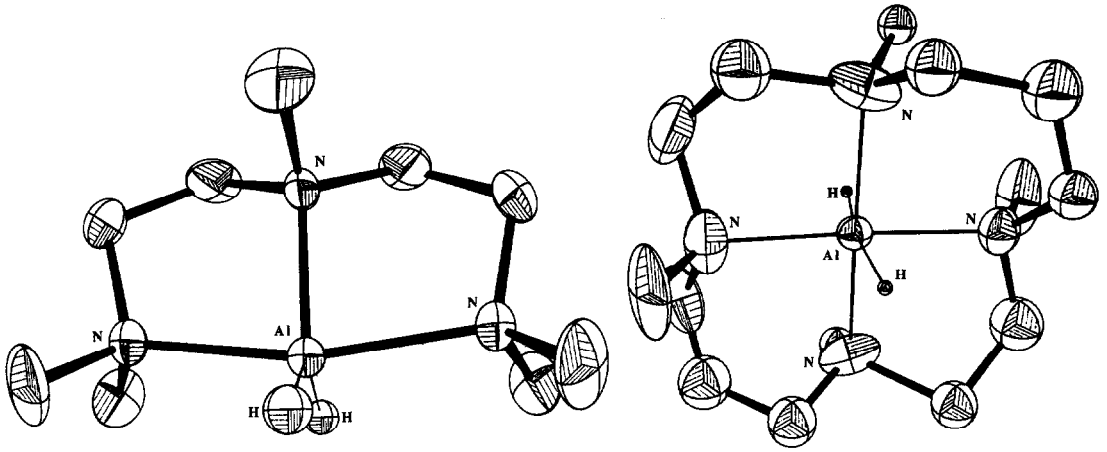

Fig. 7. Structures of the cationic alanes, $H_2Al(PMDETA)^+$ and $H_2Al(Me_4CYCLAM)^+$.

Tertiary amine adducts structurally characterized include $(H_3Ga)_2$TMEDA, Ga—N 2.094(4) Å,[9,67] and the quinuclidine adduct, Ga—N 2.063(4) Å,[46] with the difference in Ga—N reflecting the

high difference in stabilities of the two compounds (Section 3). The gas-phase structure of H_3GaNMe_3 has Ga—N of 2.124 Å.[22] [An inaccurate and incomplete X-ray structure determination of this compound gives Ga—N 1.97(9) Å.[82]] The STO-3G/ECP-DZ level of theory on H_3GaNH_3 yields a slightly flattened tetrahedron environment around the metal centre, N—Ga—H 99.57° with Ga—N 2.074 Å, Ga—H 1.57 Å,[53] which is close to the solid state structures.[67]

H_3GaPMe_3 is X-ray sensitive, but other compounds have been authenticated in the solid: H_3GaPR_3, R = Cy[53] or Bu^t,[51] and $\{H_3Ga(PMe_2CH_2)\}_2$,[9,53] Ga—P 2.460(2), 2.444(6) and 2.399(4) Å, respectively. The agreement with theory for both H_3GaPH_3 (MP2/DZP) and H_3GaPMe_3 (RHF/DZP) for the Ga—P distance is poor, 2.576 and 2.550 Å, respectively, but there is reasonable agreement for other geometries.

5. REACTIONS

5.1. *Metallation*

Metallation reactions have in part been discussed in Section 3, dealing with the stability of secondary and primary amine adducts of alane, for example, Scheme 4, eq. (6). N,N′-Dimethylethylenediamine and H_3GaNMe_3 afford a novel gallane-rich metal amide, $[H_5Ga_3\{(NMeCH_2)_2\}_2]$.[67] Alcohols and thiols react with H_3AlNMe_3, yielding alkoxy- or mercapto-alanes.[67,83,84] Reaction with *p*-tert-butylcalix[4]arene results in trimetallation and deprotonation by the tertiary amine, yielding a bis(calix[4]arene), eq. (9), which included methylene chloride "hydrogen-bonded" to the centroids of opposing arene rings.[77] Reaction of H_3MNMe_3, M = Al or Ga, with 1,3-diketones, $X_3CC(O)CH_2C(O)CX'_3$, X = X′ = H; X = H, X′ = F; X = X′ = Me, affords exclusively the metallation products, as tri(acetylacetonato)metal(III) species, but for X = X′ = F metallation and addition prevails (see below).[85]

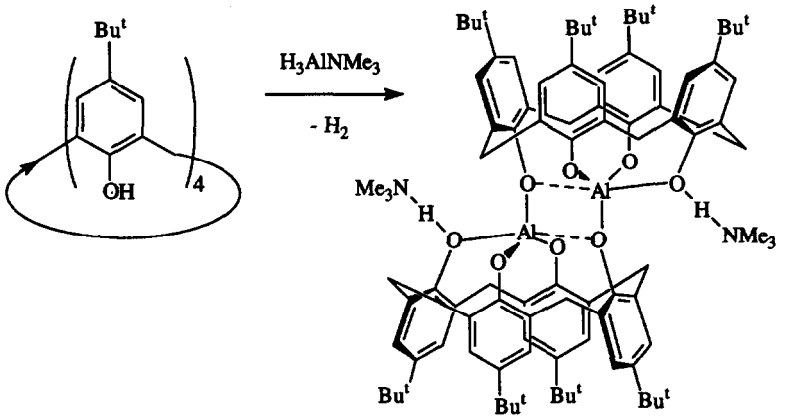

(9)

A monomeric mercaptoalane has been authenticated (X-ray structure) for an N-functionalized thiol, eq. (10).[48]

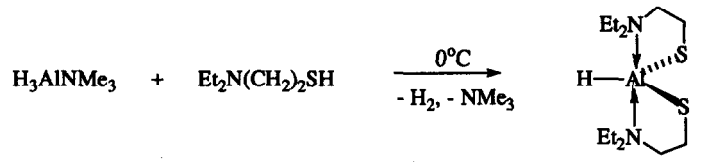

(10)

5.2. *Hydrometallation/reduction*

Tertiary amine adducts of alane reduce a variety of functional groups, often in high yield and with selectivity,[1] e.g. H_3AlNEt_2Me reduces carboxylic acids to alcohols and nitriles and amides to amines, but will not attack alkyl or halide groups. There is little work on synthetic applications of gallane, although recent work suggest some differences with alane analogues.[86] For example, H_3GaNMe_3 does not reduce ethylbenzoate, whereas H_3AlNMe_3 reduces the same compound to benzyl alcohol. Di-t-butylketone is reduced by both the trimethylamine adducts of alane and gallane,

although the isolated compounds have different solid state structures, further reflecting the tendency for gallane to achieve four fold coordination, e.g. (11).[48]

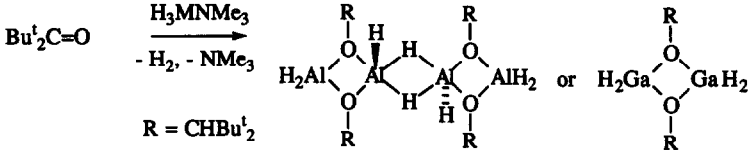

(11)

Metallation and addition prevails on treating H_3AlNMe_3 with $F_3CC(O)CH_2C(O)CF_3$, eq. (12), but metallation only for other 1,3-diketones (see below).[85]

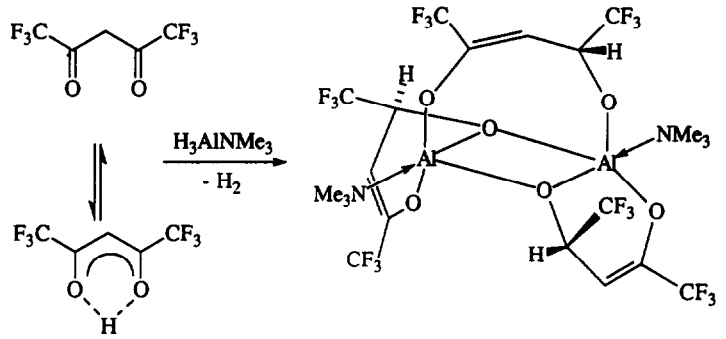

(12)

1,4-Di-t-butyldiazabutadiene reacts differently with the trimethyl amine adducts of alane and gallane; alane affords a paramagnetic species, whereas gallane results in complete hydrometallation, Scheme 9,[10,87] isolated as a "gallane-rich" species which is isolobal with the aluminium compound derived from metallation of N,N′-di-t-butylethylenediamine, eq. (6).[72] 1,4-Di-i-propylbutadiene also gives addition, but as a dimeric species, Scheme 9. Interestingly, the treatment of 1,4-di-t-butylbutadiene with a mixture of metal powder, M′, and $LiMH_4$ gives radical species, $[M\{(NBu^tCH)_2\}_2]^{\bullet}$, with one ligand reduced to a dianion, the other to a radical, M = M′ = Ga or Al, M′ = Al or Ga, M = Ga.[10,87,88]

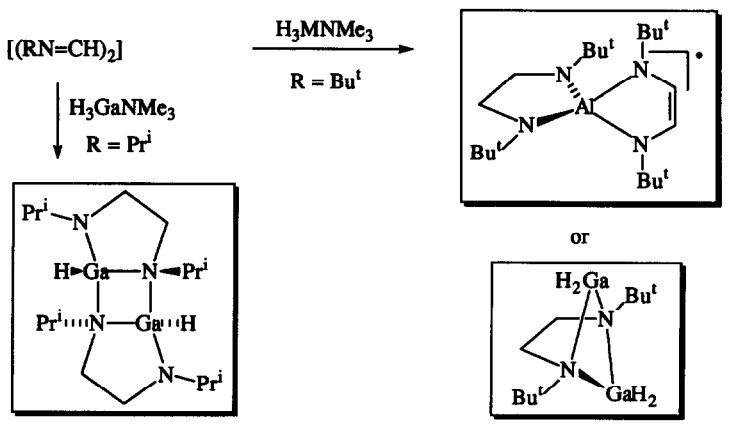

Scheme 9.

Addition to C=C bonds requires rather forcing conditions, even for intramolecular addition, e.g. hydrometallation of $H_3AlN(Me)_2CH_2CH{=}CH_2$, yielding a polymer—$\{(H)_2AlNMe_2(CH_2)_3\}^-$.[27]

5.3. *Miscellaneous*

Lithium hydride will displace the amine from H_3AlNMe_3 yielding $LiAlH_4$.[89] Similarly, mercury or lithium alkyls will displace hydrides in H_3AlNMe_3, affording amine adducts of alkylalanes,[31,90] and mercury(II) halides afford haloalane compounds.[31] Monoalkylgallane can also be prepared from mercury alkyl and H_3GaNMe_3.[91]

6. SURFACE CHEMISTRY

Tertiary amine adducts have found applications in materials science as precursors for delivering aluminium metal to surfaces. In addition to the useful vapour pressure of these adducts the absence of metal–carbon bonds in the precursors results in little deleterious carbonaceous material in the metal deposits.[7] Moreover, the compounds are less air-sensitive than trialkylaluminium compounds which have been used extensively in CVD technology.[6,8,92]

Both H_3AlNMe_3 and $H_3Al(NMe_3)_2$ have been successfully used to prepare thin films of aluminium using laser induced CVD,[7] low pressure CVD[6,8,92,93] and molecular beam epitaxy MBE.[94] They have also been used in electroless[95] and electrosolution aluminium plating.[13] More recently the mixed group 13 tertiary amine adduct $Me_3N(H)_2Al(\mu\text{-}H)_2BH_2$ has been used in depositing high purity aluminium under mild conditions, 100°C or 25°C with substrates pretreated with $TiCl_4$.[96].

Studies on the surface reactivity of H_3AlNMe_3 and $H_3Al(NMe_3)_2$ pecursors on Si, Al and GaAs substrates have yielded the following reactions, eqs (13)–(16), with the assumption that for $H_3Al(NMe_3)_2$ the primary process is the formation of NMe_3 and H_3AlNMe_3 prior to any surface adsorption.[38,92,93]

$$H_3AlNMe_3(g) \longrightarrow H_3AlNMe_3(ads) \qquad T = 150\,K$$

$$H_3AlNMe_3(ads) \longrightarrow AlH_3(ads) + NMe_3(g) \qquad T = 200\text{–}400\,K$$

$$AlH_3(ads) \longrightarrow Al(m) + H_2(g) + H(ads) \qquad T = 500\,K$$

$$2H(ads) \longrightarrow H_2(g) \qquad T = 600\,K$$

The adsorption of H_3AlNMe_3 on thermally grown oxidized silicon under UHV conditions has at least two pressure dependent processes, Scheme 10.[64] Molecular adsorption prevails at the dosing pressure *ca* 5.0×10^{-7} mbar with the aluminium centres becoming five-coordinate via binding to surface oxygen centres. High XPS X-ray flux (>240 W) results in migration of NMe_3 to silicon centres, ascertained by comparison of adsorption of NMe_3 gas. At dosing pressures of H_3AlNMe_3 *ca* $>10^{-7}$ mbar an aluminium rich species is formed, with the Al : N close to 2 : 1, possibly with hydride bridge formation, Scheme 10. Similar results are obtained for dosing of bis-trimethylamine alane, $H_3Al(NMe_3)_2$.

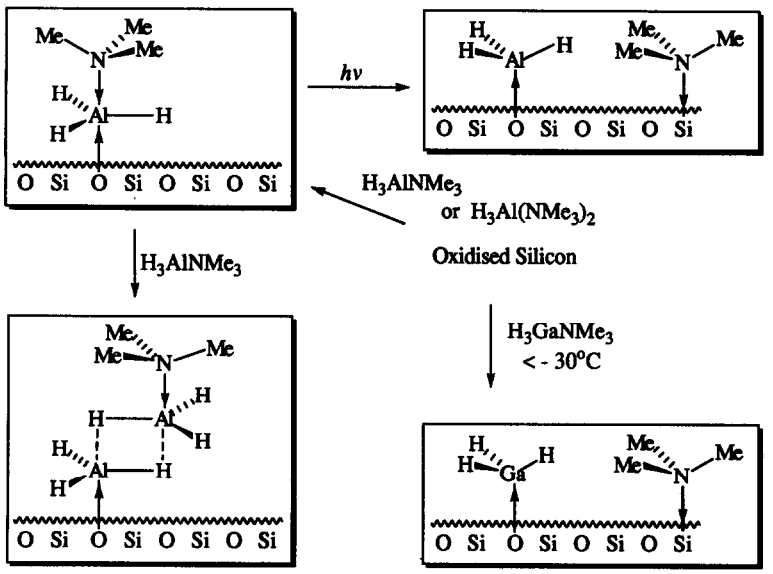

Scheme 10.

Calculations on H_3AlNH_3 and H_2O, and H_3AlOH_2(HF/D95*), as model systems for the interaction of H_3AlNMe_3 with surface oxygen centres have the formation of $H_3AlNH_3(OH_2)$ as energetically favoured by 4.53 kcal mol^{-1} and its fragmentation to H_3AlOH_2 and NH_3 requiring 13.16 kcal mol^{-1}; association of H_3AlOH_2 and H_3AlNH_3 to $H_2(H_3N)Al(\mu\text{-}H)_2Al(OH_2)H_2$, as a model

for the aluminium rich species, is also favoured, by 3.39 kcal mol^{-1}. At the higher dosing pressure where there is greater chance of molecular encounter of H_3AlNMe_3 with adsorbed H_3AlNMe_3, dissociation of $H_3Al(NMe_3)_2$ yielding surface bound "$H_3Al{\leftarrow}O{=}$" is possible, eq. (13). Association of such species with H_3AlNMe_3 via hydride bridges, of the type found in the solid for H_3AlNMe_3, is then possible, eq. (14).

$$H_3AlNMe_3(g) + Me_3N(H)_3Al{\leftarrow}O{=} \rightleftharpoons H_3Al(NMe_3)_2 + H_3Al{\leftarrow}O{=} \quad (13)$$

$$H_3AlNMe_3(g) + H_3Al{\leftarrow}O{=} \rightleftharpoons H_2(NMe_3)Al(\mu\text{-}H)_2Al{\leftarrow}O{=} \quad (14)$$

Adsorption characteristics for the trimethylamine adduct of gallane on oxidized silicon, also under UHV conditions, are different. For temperatures below *ca* −30°C dissociative adsorption occurs, with some of the trimethyl amines trapped on silicon sites. This is consistent with the preference for gallane to form four-coordinate species, although the primary process is likely to be the formation of a five-coordinate "mixed-donor" species. Calculations (D95* + DZP) show the five-coordinate species $H_2O(H)_3GaNH_3$ to be energetically favoured relative to (i) H_3GaNH_3 and H_2O by 0.67 kcal mol^{-1} and (ii) H_3GaOH_2 and NH_3 by 7.8 kcal mol^{-1}.[63]

7. CONCLUSIONS

Overall, the differences between Lewis base adducts of alane and gallane are: (i) a stronger tendency of aluminium to form "hyper"-valent structures compared to gallium; gallane forms four-coordinate species in the gas phase and the solid, even with potentially polydentate ligands such as TMEDA; (ii) the frailty of Ga—H bonds compared with Al—H bonds; and (iii) the polarizing influence/back-bonding participation of the d^{10} core for gallium. Recent rapid developments in the chemistry of Lewis base adducts of alane and gallane include applications in synthesis and materials science. Further developments in the former are likely because of differences in the reactivity of alanes and gallanes between various functional groups, viz differences in stereo-, chemo- and regioselectivity. Moreover, with a careful choice of optically active Lewis base there is scope for developing chiral reducing agents of gallane, possibly with different enantioselectivity than reagents based on alane. New applications in materials science are possible in developing volatile hetero-bimetallic compound for CVD generation of alloys, such as aluminium or gallium transition metal materials which have favourable lattice parameters relative to group 13–15 compound semiconductor materials, to circumvent breakdown of the interface and corruption of the device characteristics.[97] The incorporation of boron in aluminium is advantageous in high current density and deposition of such a material has recently been achieved using $Al(BH_4)_3$.[96] There is also scope for: (i) using alanes (and gallanes) as precursors for Ziegler Natta catalysts, along the lines developed for aluminium alkyls; (ii) developing arsine, and other heavier main group element adducts of alane and gallane; (iii) developing the chemistry of indane; and (iv) developing mixed group 13 hydride species, as well as gallane aggregates similar to the extensive types developed for borane, noting the nexus between borane and gallane and the distinctiveness of alane.

REFERENCES

1. E. M. Marlett and W. S. Park, *J. Org. Chem.* 1990, **55**, 2968.
2. B. M. Bulychev, *Polyhedron* 1990, **9**, 387.
3. L. H. Dubois, B. R. Zegarski, M. E. Gross and R. G. Nuzzo, *Surf. Sci.* 1991, **244**, 89.
4. P. Zanella, G. Rossetto, N. Brianese, F. Ossola and M. Porchia, *Chem. Mat.* 1991, **3**, 225.
5. A. A. Melas, Patent US No. 4740606 (1988).
6. W. L. Gladfelter, D. C. Boyd and K. F. Jensen, *Chem. Mat.* 1989, **1**, 339.
7. T. H. Baum, C. E. Larson and R. L. Jackson, *Appl. Phys. Lett.* 1989, **55**, 1264.
8. A. T. S. Wee, A. J. Murrell, N. K. Singh, D. O'Hare and J. S. Foord, *J. Chem. Soc., Chem. Commun.* 1990, 11.
9. D. O'Hare, J. S. Foord, T. C. Page and T. J. Whitaker, *J. Chem. Soc., Chem. Commun.* 1991, 1445.
10. M. J. Henderson, C. H. L. Kennard, C. L. Raston and G. Smith, *J. Chem. Soc., Chem. Commun.* 1990, 1203.
11. E. Wiberg and E. Amberger, in *Hydrides of the Elements of Main Groups I–IV*, Ch. 5. Elsevier, London (1971).

12. J. K. Ruff and M. F. Hawthorne, *J. Am. Chem. Soc.* 1960, **82**, 2141.
13. T. E. Daenen, Patent No. G. B. 2,021,646 (1979).
14. E. M. Marlett, Patent No. US 4 474 743 (1984).
15. E. Wiberg and E. Amberger, in *Hydrides of the Elements of Main Groups I–IV*, Ch. 6. Elsevier, London (1971).
16. N. N. Greenwood and B. S. Thomas, *J. Chem. Soc.* (*A*) 1971, 814.
17. S. Cucinella, A. Mazzei and W. Marconi, *Inorg. Chim. Acta Rev.* 1970, **4**, 51.
18. A. J. Downs, M. J. Goode and C. R. Pulham, *J. Am. Chem. Soc.* 1989, **111**, 1936.
19. C. R. Pulham, A. J. Downs, M. J. Goode, D. W. H. Rankin and H. E. Robertson, *J. Am. Chem. Soc.* 1991, **113**, 5149.
20. J. W. Turley and H. W. Rinn, *Inorg. Chem.* 1969, **8**, 18.
21. G. Trinquier and J.-P. Malrieu, *J. Am. Chem. Soc.* 1991, **113**, 8634.
22. P. L. Baxter, A. J. Downs and D. W. H. Rankin, *J. Chem. Soc., Dalton Trans.* 1984, 1755.
23. N. N. Greenwood and A. Earnshaw, in *Chemistry of the Elements*, 1st edn, Ch. 7. Pergamon Press, Oxford (1984).
24. O. T. Beachley, S.-H. L. Chao, M. R. Churchill and R. F. See, *Organometallics* 1992, **11**, 1486.
25. A. G. Avent, C. Eaborn, P. B. Hitchcock, J. D. Smith and A. C. Sullivan, *J. Chem. Soc., Chem. Commun.* 1986, 988.
26. E. B. Lobkovski and K. N. Semenenko, *Zh. Strukt. Khim.* 1975, **16**, 150.
27. C. W. Heitsch, C. E. Nordman and R. W. Parry, *Inorg. Chem.* 1963, **2**, 508.
28. A. Almenningen, G. Gundersen, T. Haugen and A. Haaland, *Acta Chem. Scand.* 1972, **26**, 3928.
29. G. J. Palenik, *Acta Cryst.* 1964, **17**, 1573.
30. D. F. Shriver and C. E. Nordman, *Inorg. Chem.* 1963, **2**, 1298.
31. J. K. Ruff, *J. Am. Chem. Soc.* 1961, **83**, 1798.
32. D. G. Hendricker and C. W. Heitsch, *J. Phys. Chem.* 1967, **71**, 2683.
33. N. N. Greenwood, A. Storr and M. G. H. Wallbridge, *Proc. Chem. Soc. London* 1962, 249.
34. J. R. Durig, K. K. Chatterjee, Y. S. Li, M. Jalilian, A. J. Zozulin and J. D. Odom, *J. Chem. Phys.* 1980, **73**, 21.
35. J. Hwang, S. A. Hanson, D. Britton, J. F. Evans, K. F. Jensen and W. L. Gladfelter, *Chem. Mat.* 1990, **2**, 342.
36. M. R. M. Mason and A. R. Barron, *Chemtracts* (*Inorg. Chem.*) 1992, 179.
37. J. M. Davidson and T. Wartik, *J. Am. Chem. Soc.* 1960, **82**, 5506.
38. J. L. Atwood, F. R. Bennett, F. M. Elms, C. Jones, C. L. Raston and K. D. Robinson, *J. Am. Chem. Soc.* 1991, **113**, 8183.
39. K. M. Mackay, in *Hydrogen Compounds of the Metallic Elements*, p. 110. Spon, London (1966).
40. C. Jones and C. L. Raston, unpublished results.
41. A. R. Young and R. Ehrlich, *Inorg. Chem.* 1965, **4**, 1358.
42. M. J. Taylor, in *Comprehensive Coordination Chemistry* (Edited by G. Wilkinson), Vol. 3. Pergamon Press, Oxford (1987).
43. E. C. Ashby, *J. Am. Chem. Soc.* 1964, **86**, 1883.
44. J. L. Atwood, F. R. Bennett, C. Jones, G. A. Koutsantonis, C. L. Raston and K. D. Robinson, *J. Chem. Soc., Chem. Commun.* 1992, 541.
45. J. L. Atwood, K. W. Butz, M. G. Gardiner, C. Jones, G. A. Koutsantonis, C. L. Raston and K. D. Robinson, *Inorg. Chem.*, in press.
46. J. L. Atwood, S. G. Bott, F. M. Elms, C. Jones and C. L. Raston, *Inorg. Chem.* 1991, **30**, 3792.
47. C. R. Pulham, P. T. Brain, A. J. Downs, D. W. H. Rankin and H. E. Robertson, *J. Chem. Soc., Chem. Commun.* 1990, 177.
48. G. A. Koutsantonis, F.-C. Lee and C. L. Raston, unpublished results.
49. A. E. Finholt, C. Helling, V. Imhof, L. Neilsen and E. Jacobsen, *Inorg. Chem.* 1963, **2**, 504.
50. J. L. Atwood, F. R. Bennett, F. M. Elms, G. A. Koutsantonis, C. L. Raston and D. J. Young, *Organometallics* 1992, **11**, 1475.
51. F. M. Elms, M. G. Gardiner, G. A. Koutsantonis, C. L. Raston, J. L. Atwood and K. D. Robinson, *J. Organomet. Chem.* 1993, in press.
52. F. M. Elms and C. L. Raston, unpublished results.
53. J. L. Atwood, K. D. Robinson, F. R. Bennett, F. M. Elms, G. A. Koutsantonis, C. L. Raston and D. J. Young, *Inorg. Chem.* 1992, **31**, 2674,
54. N. N. Greenwood, E. J. F. Ross and A. Storr, *J. Chem. Soc.* 1965, 1400.
55. E. Wiberg and H. Nöth, *Z. Naturforsch.* 1955, **10(B)**, 237.
56. E. Wiberg, H. Graf and R. Usón, *Z. Anorg. Allg. Chem.* 1953, **272**, 221.
57. I. B. Gorrell, P. B. Hitchcock and J. D. Smith, *J. Chem. Soc., Chem. Commun.* 1993, 189.
58. N. N. Greenwood, A. Storr and M. G. H. Wallbridge, *Inorg. Chem.* 1963, **2**, 1036.

59. N. N. Greenwood and M. G. H. Wallbridge, *J. Chem. Soc.* 1963, 3912.
60. A. E. Shirk and J. S. Shirk, *Inorg. Chem.* 1983, **22**, 72.
61. A. J. Arduengo III, H. V. R. Dias, J. C. Calabrese and F. Davidson, *J. Am. Chem. Soc.* 1992, **114**, 9724.
62. C. M. B. Marsh, T. P. Hamilton, Y. Xie and H. F. Schaefer, *J. Chem. Phys.* 1992, **96**, 5310.
63. K. W. Butz, F. M. Elms, C. L. Raston, R. N. Lamb and P. J. Pigram, *Inorg. Chem.*, in press.
64. F. M. Elms, R. N. Lamb, P. J. Pigram, M. G. Gardiner, B. J. Wood and C. L. Raston, *J. Chem. Soc., Chem. Commun.* 1992, 1423.
65. J. L. Atwood, K. D. Robinson, C. Jones and C. L. Raston, *J. Chem. Soc., Chem. Commun.* 1991, 1697.
66. G. G. Sinke, L. C. Walker, F. L. Qetting and D. R. Stull, *J. Chem. Phys.* 1967, **47**, 2759.
67. J. L. Atwood, S. G. Bott, F. M. Elms, C. Jones and C. L. Raston, *Inorg. Chem.* 1991, **30**, 4868.
68. C. R. Pulham, A. J. Downs, D. W. H. Rankin and H. E. Robertson, *J. Chem. Soc., Dalton Trans.* 1992, 1509.
69. N. R. Fetter, B. Bartocha, F. E. Brinkman and D. W. Moore, *Can. J. Chem.* 1963, **41**, 1359.
70. E. Wiberg and A. May, *Z. Naturforsch.* 1955, **10(B)**, 229.
71. K. Ouzounis, H. Riffel, H. Hess, U. Kohler and J. Weidlein, *Z. Anorg. Allg. Chem.* 1983, **504**, 67.
72. C. Cucinella, T. Salvatori, C. Busseto, G. Perego and A. Mazzei, *J. Organomet. Chem.* 1974, **78**, 185.
73. J. L. Atwood, S. Lawrence and C. L. Raston, unpublished results.
74. A. Storr, *J. Chem. Soc.* (*A*) 1968, 2605.
75. N. N. Greenwood, E. J. F. Ross and A. Storr, *J. Chem. Soc.* (*A*) 1966, 706.
76. K. D. Dobbs, M. Trachtman, C. W. Bock and A. H. Cowley, *J. Phys. Chem.* 1990, **94**, 5210.
77. J. L. Atwood, S. G. Bott, C. Jones and C. L. Raston, *J. Chem. Soc., Chem. Commun.* 1992, 1349,
78. H. Roszinski, R. Dautel and W. Zeil, *Z. Phys. Chem.* 1963, **36**, 26.
79. J. W. Lauher, D. Dougherty and P. J. Harley, *Acta Cryst.* (*B*) 1979, **35**, 1454.
80. B. J. Duke, C. Liang and H. F. Schaefer, *J. Am. Chem. Soc.* 1991, **113**, 2884.
81. J. L. Atwood, C. Jones, C. L. Raston and K. D. Robinson, unpublished results.
82. D. F. Shriver and C. E. Nordman, *Inorg. Chem.* 1963, **2**, 1299.
83. W. Marconi, A. Mazzei, S. Cucinella and M. de Maldé, *Makromol. Chem.* 1964, **71**, 134.
84. W. Marconi, A. Mazzei, F. Bonati and M. de Maldé, *Z. Naturforsch.* 1963, **18(B)**, 3.
85. J. L. Atwood, F.-C. Lee, C. L. Raston and K. D. Robinson, unpublished results.
86. C. Tranter, C. L. Raston and D. J. Young, unpublished results.
87. F. G. N. Cloke, C. I. Dalby, M. J. Henderson, P. B. Hitchcock, C. H. L. Kennard, R. N. Lamb and C. L. Raston, *J. Chem. Soc., Chem. Commun.* 1990, 1394.
88. M. G. Henderson and C. L. Raston, unpublished results.
89. J. K. Ruff and M. F. Hawthorne, *J. Am. Chem. Soc.* 1961, **83**, 535.
90. F. M. Peters and B. Bartocha and A. J. Bilbo, *Can. J. Chem.* 1963, **41**, 1051.
91. A. Storr and V. G. Wiebe, *Can. J. Chem.* 1968, **47**, 673.
92. B. E. Bent, R. G. Nuzzo and L. H. Dubois, *J. Am. Chem. Soc.* 1989, **111**, 1634.
93. L. H. Dubois, B. R. Zegarski, C. T. Kao and R. G. Nuzzo, *Surf. Sci.* 1990, **236**, 77.
94. J. S. Foord, A. J. Murrell, D. O'Hare, N. K. Singh, A. T. S. Wee and T. J. Whitaker, *Chemtronics* 1989, **4**, 262.
95. D. L. Schmidt and R. Hellmann, Patent No. US 3,462,288 (1969).
96. J. A. Glass, S. S. Kher and T. Spencer, *Chem. Mat.* 1992, **4**, 530.
97. H. D. Kaesz, R. S. Williams, R. F. Hicks, J. I. Zink, Y.-J. Chen, H.-J. Muller, Z. Xue, D. Xu, D. K. Shuh and Y. K. Kim, *New J. Chem.* 1990, **14**, 527.

Polyhedron Vol. 12, No. 15, pp. 1849–1853, 1993
Printed in Great Britain

0277–5387/93 $6.00+.00
© 1993 Pergamon Press Ltd

PROPOSED STRUCTURE OF THE FIRST *HYPHO* CARBABORANE, $C_3B_4H_{12}$

MARK A. FOX, ROBERT GREATREX,* NORMAN N. GREENWOOD and MARTIN KIRK

School of Chemistry, University of Leeds, Leeds LS2 9JT, U.K.

(*Received* 23 *March* 1993; *accepted* 20 *April* 1993)

Abstract—The reaction between *arachno*-B_4H_{10} and propyne under hot/cold conditions affords in low yield the first unsubstituted neutral *hypho* carbaborane, $C_3B_4H_{12}$, a colourless volatile liquid. The new tricarbaborane has been characterized by high-resolution mass spectrometry and ^1H, $^1H\{^{11}B\}$, $^1H\{^{11}B$ selective$\}$, 2D ^1H—$^1H\{^{11}B\}$ COSY, $^1H\{^{11}B\}$ n.O.e., ^{11}B, $^{11}B\{^1H\}$, 2D ^{11}B—$^{11}B\{^1H\}$ COSY and ^{13}C NMR spectroscopy. The data imply a mirror-plane symmetry and are consistent with an unprecedented open seven-vertex carbaborane framework.

A continuing and important theme in polyhedral borane chemistry is that of establishing relationships between cluster geometry and bonding.[1] Species belonging to the *closo*, *nido* and *arachno* classes have been well studied, but boranes having *hypho* electron counts (i.e. containing $n+4$ framework electron pairs, where n is the number of cluster atoms) are sparse and consequently their structural and bonding patterns are less well understood. Known examples, including a new series of eight- and nine-vertex dithiaborane clusters, have been summarized recently.[2]

Perhaps surprisingly, among the thousands of known carbaboranes the only authenticated example that falls into the *hypho* category is $Me_3N \cdot CB_5H_{11}$,[3] in which the 3,4-H-bridge of B_5H_{11} is replaced by the —$CHNMe_3$— linkage. The main route into carbaborane chemistry has been through the reactions of boranes with unsaturated hydrocarbons,[4] the type of product depending on the conditions employed. High-temperature "flash" reactions or electric discharges tend to form *closo*-carbaboranes, whereas less energetic conditions lead to *nido* clusters. It is tempting to speculate that *hypho*- and *arachno*-carbaboranes might occur as unstable intermediates in the formation of the more familiar *closo* and *nido* species, and that the hot/cold reaction technique might offer a viable method of isolating them. Interestingly, the classic compound $B_4H_8 \cdot C_2H_4$, obtained from the hot/cold reaction between B_4H_{10} and ethene,[5] has a *hypho* formula and electron count, but is generally regarded as being simply a dimethylene-substituted derivative of *arachno*-B_4H_{10}. No diffraction data have yet been published for this compound,[6] but IR[7] and NMR[8] data have been interpreted in terms of a symmetrical "basket-like" structure of C_{2v} symmetry and recent *ab initio*/IGLO/NMR calculations are in agreement with this.[9] The idea that an analogous molecule having a bridging unsaturated C=C function could be formed in the reaction between B_4H_{10} and alkynes has been suggested,[4e] but does not appear to have been followed up.

In view of the fact that the hot/cold technique has not previously been applied generally to reactions between boranes and acetylenes we decided to embark on a systematic study in this area in an attempt to generate new carbaborane intermediates and to shed further light on the mechanisms involved in these reactions. We have recently communicated preliminary results on the new *hypho*-carbaborane $C_3B_4H_{12}$;[10] in this fuller account we present additional NMR data on this interesting compound and discuss their structural implications.

* Author to whom correspondence should be addressed.

Dedicated to Professor Heinz Nöth on his 65th birthday.

EXPERIMENTAL

Reactions were performed in standard high-vacuum systems fitted with greaseless O-ring taps and spherical joints [J. Young (Scientific Glassware) Ltd]. MeC≡CH was obtained commercially (Cambrian Gases) and B_4H_{10} was produced by the action of BF_3 on $[NMe_4]B_3H_8$, as described in the literature.[11] The hot/cold reactor was of the concentric tube type,[12] constructed of Pyrex and having a reaction volume of approximately 650 dm^3.

In a typical reaction B_4H_{10} (5 mmol) and MeC≡CH (4 mmol) were measured manometrically, condensed into the vessel and then allowed to warm to the temperature of the acetone/CO_2 slush bath maintained at −35°C surrounding the reactor. Silicone fluid (Dow Corning 550) was added to the inner reservoir, heated rapidly with a 1000 W heater to 100°C and controlled at that temperature for the desired period. The hot oil was then removed, the vessel cooled to −196°C and the volatile products pumped into a U-trap held at −196°C as the vessel was allowed to warm to room temperature. The volatiles were subjected to fractionation on a low-temperature column[13] and the distillate monitored directly by low-resolution mass spectrometry on a Kratos MS30 instrument. A species with a mass cut-off at *m/z* 92, which left the column at −60°C, was isolated in low yield (*ca* 1%) and characterized by high-resolution mass spectrometry (on a VG AutoSpec operated by Mr D. Singh) and by NMR spectroscopy. Attempts to improve the yield of this species by altering the reaction conditions have so far proven unsuccessful. Samples for NMR spectroscopy were pumped under vacuum into 5 mm soda-glass traps, which were sealed off and used as NMR tubes. Low-field measurements were made at 2.35 Tesla (100 MHz ^1H; 32 MHz ^{11}B) on a Jeol FX100 instrument. High-field spectra were obtained at 9.4 Tesla (400 MHz ^1H; 128 MHz ^{11}B; 100 MHz ^{13}C) on a Bruker AM-400 instrument. The $^1H\{^{11}B$ selective$\}$ and 2D ^1H—$^1H\{^{11}B\}$ COSY experiments were performed as described in previous publications from this laboratory.[14]

RESULTS AND DISCUSSION

High-resolution mass-spectrometric measurements on the new product with a mass cut-off at *m/z* 92 confirmed the assignment of this fragment to the parent molecular ion $[^{12}C_3{}^{11}B_4{}^1H_{12}]^+$ (observed *m/z* 92.1306, calc. *m/z* 92.1311). The 128 MHz $^{11}B\{^1H\}$ NMR spectrum in $CDCl_3$ at 223 K of the purest sample consisted essentially of two signals of equal integrated intensity [Fig. 1(i) and Table 1]. Significantly there were no cross peaks between these two boron resonances in the 2D ^{11}B—$^{11}B\{^1H\}$ COSY NMR spectrum. In the line-narrowed, undecoupled spectrum [Fig. 1(ii)] the peak at δ −20.1 (relative to $BF_3 \cdot OEt_2$) comprised a doublet of doublets of doublets [J(BH) = 165, 63, 37 Hz] and the peak at δ 1.60 appeared as a broadened doublet [J(BH) = 145.0 Hz].

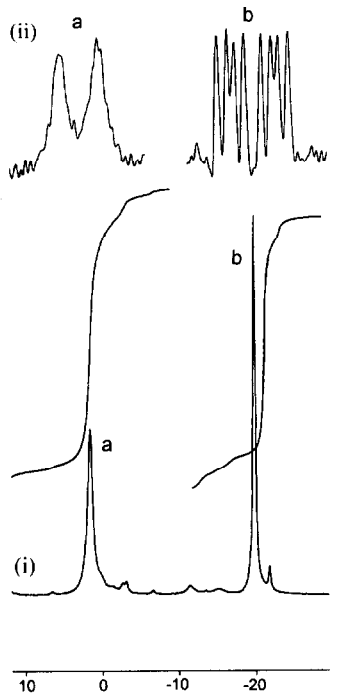

Fig. 1. Boron NMR spectra of *hypho*-$C_3B_4H_{12}$: (i) 128 MHz $^{11}B\{^1H\}$, (ii) 128 MHz line-narrowed ^{11}B. Chemical shifts referenced to $BF_3 \cdot Et_2O$ = 0.00 ppm.

The 400 MHz boron-decoupled ^1H NMR spectrum in $CDCl_3$ at 223 K consisted of seven signals of approximate relative intensity 2:2:2:2:1:1:2 at δ values (relative to Me_4Si) of 3.25, 2.23, 1.61, 0.68, −0.90, −1.40 and −2.16, respectively (labelled c–j in Fig. 2). Comparison of proton spectra with and without boron decoupling allowed peaks e, g and h at δ 1.61, −0.90 and −1.40 to be assigned to C—H protons. The $^1H\{^{11}B$ selective$\}$ experiments have revealed that the resonances from the two bridging hydrogen atoms are in fact coincident and comprise the peak at δ −2.16, despite the fact that the integrated intensity of this peak is nearer 1.6 than 2 (relative to peaks g and h which are both of intensity 1). The signal labelled with an asterisk at δ 0.24 was originally thought to be part of the main spectrum and was assigned to the hydrogen atom bridging the two boron atoms B_a.[10] However, this peak has since been shown to vary in intensity from sample to sample, and is now

Table 1. NMR data of *hypho*-$C_3B_4H_{12}$

Boron	δ (ppm)[a]	J(BH) (Hz)[b]
a	1.60	$J(BH_c) = 145$
b	−20.1	$J(BH_d) = 165$; $J(BH_f) = 63$; $J(BH_j) = 37$

Carbon	δ (ppm)[c]	Proton[d]
k	−24.5	
l	18.0	1

Proton	δ[e]	δ[f]	Boron[g]	J(HH)[h]	J(HH)[i]	H···H[j]
c		3.25	a			$H_f = 4$; $H_g = 2.5$
d		2.33	b		$J(H_dB_bH_f)$	$H_f = 2.5$; $H_{i,j} = 2$
e	1.61	1.61				
f		0.68	b		$J(H_fB_bH_j)$; $J(H_fB_bH_d)$	$H_d = 4.3$; $H_h = 2.5$; $H_{i,j} = 3.2$; $H_c = 2$
g	−0.91	−0.91		$J(H_gC_kH_h) = 15.7$; $J(H_h\cdots H)^k \sim 4.1$ doublet of quintets	$J(H_gC_kH_h)$	$H_h = 13$
h	−1.40	−1.40		$J(H_hC_kH_g) = 15.7$; $J(H_i\cdots H)^k = 5.7$ doublet of triplets	$J(H_hC_kH_g)$	$H_g = 12$
i		−2.16	a	$J(H_j\cdots H)^k = 7.5$		$H_d = 3$, $H_c = 1$
j			b	quintet	$J(H_jB_bH_f)$	$H_f = 8.7$

[a] In ppm ($BF_3\cdot Et_2O$ = 0.00 ppm); 128 MHz $^{11}B\{^1H\}$ spectrum; solvent $CDCl_3$, 230 K. There were no cross peaks relating these two boron resonances in the 2D ^{11}B—$^{11}B\{^1H\}$ NMR.

[b] In Hz; 128 MHz line-narrowed ^{11}B spectrum.

[c] In ppm (Me_4Si = 0.00 ppm); 100 MHz $^{13}C\{^1H\}$ spectrum; solvent $CDCl_3$, 230 K.

[d] Number of protons attached to each carbon; $^{13}C\{^1H\}$ A.P.T. (attached proton test) spectrum. The δ −24.5 peak is too broad for assignment.

[e] In ppm (Me_4Si = 0.00 ppm); 400 MHz ^1H spectrum.

[f] In ppm; 400 MHz $^1H\{^{11}B\}$ spectrum.

[g] Boron atom to which the proton is bonded; 400 MHz $^1H\{^{11}B$(selective)$\}$—^1H spectra.

[h] In Hz; 100 MHz line-narrowed ^1H spectrum; solvent CD_2Cl_2 233 K. The peak appearance is also described.

[i] By cross peaks; 2D ^1H—$^1H\{^{11}B\}$ COSY spectrum; solvent $CDCl_3$, 233 K.

[j] Peaks of other protons observed, with relative intensities; 400 MHz $^1H\{^{11}B\}$ n.O.e. (nuclear Overhauser effect) spectra.

[k] Protons unknown.

attributed to a minor impurity. In the ^1H—^1H COSY spectrum very strong cross-peaks were observed between H_f and H_j, H_f and H_d and H_g and H_h, but none between H_d and H_j or H_c and H_i.

These NMR data point to a structure of C_s mirror-plane symmetry with B_2H_5, B_2H_3, CH_2 and two equivalent CH groups. The favoured structure and a corresponding (2243) topological diagram are shown in Figs 3(i) and (ii). Each pair of symmetry-related boron atoms is associated with a bridging hydrogen atom and the CH_2 group has non-identical protons. The lack of connectivity between the two sets of boron atoms is indicated by the absence of cross-peaks in the ^{11}B—$^{11}B\{^1H\}$ COSY NMR spectrum.

The boron signal at δ 1.60 is attributed to the two boron atoms B_a, for which the coupling to the bridging hydrogen H_i is unresolved, even in the line-narrowed spectrum. The complex splitting of the boron signal at δ −20.1 is attributed to the coupling of boron atoms B_b to the three sets of protons H_f, H_d and H_j. The coupling constants of 165 and 37 Hz (revealed in the line-narrowed ^{11}B NMR spectrum [Fig. 1(ii)]) are typical of *exo*-terminal and bridg-

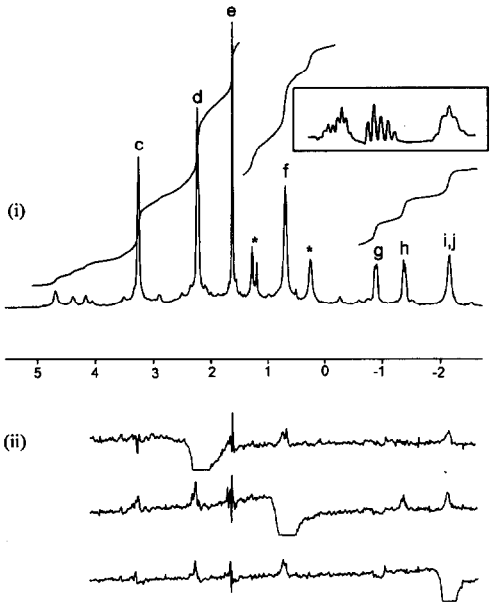

Fig. 2. Proton NMR spectra of *hypho*-$C_3B_4H_{12}$: (i) 400 MHz $^1H\{^{11}B\}$ (* = impurities); inset: 100 MHz line-narrowed $^1H\{^{11}B\}$ of peaks H_g, H_h and $H_{i,j}$; (ii) 400 MHz $^1H\{^{11}B\}$ n.O.e. spectra with irradiation at H_d, H_f and $H_{i,j}$ peak positions, respectively. Chemical shifts referenced to Me_4Si = 0.00 ppm.

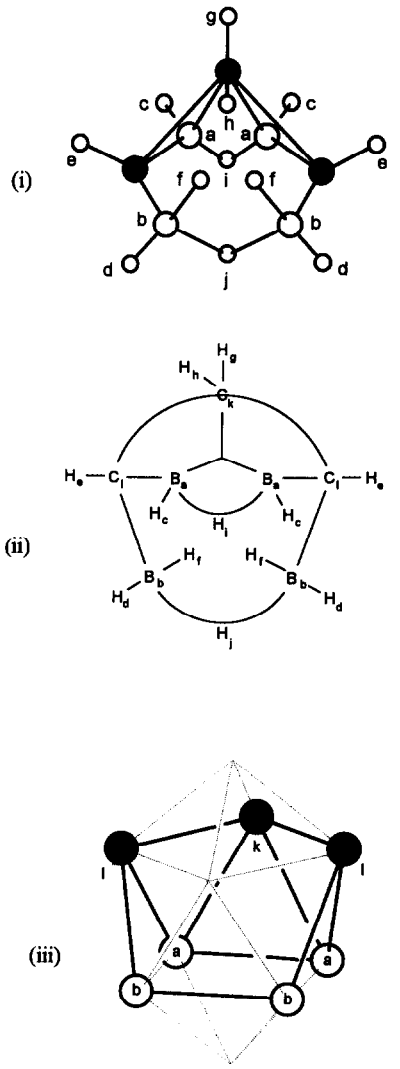

Fig. 3. (i) The proposed molecular structure of $C_3B_4H_{12}$, see text. (ii) A possible (2243) topological description of the bonding in *hypho*-$C_3B_4H_{12}$. An alternative (and effectively equivalent) bond network involves two closed three-centre CBC bonds in place of the closed three-centre BCB and open three-centre CCC bonds shown. (iii) Formal relationship between the cluster framework geometry of *hypho*-$C_3B_4H_{12}$ and *closo*-$B_{10}H_{10}^{2-}$. Large open circles B, shaded circles C, small open circles H.

ing hydrogen atoms, respectively, and these are assigned to H_d and H_j. The coupling constant of 63 Hz is unusual, but a similar value (J = 55–60 Hz[15]) has been obtained for the coupling constant associated with the unique *endo*/face-capping hydrogen atom in pentaborane(11)[16] and it therefore seems likely that the two H_f protons in $C_3B_4H_{12}$ are also *endo* in character. The possibility that they might be bridging between B_b and C_l is rejected because any such structure would feature too many three-centre bonds to enable a topological description to be formulated in which all 11 framework electron pairs were accommodated. Moreover, the observation that a ^1H n.O.e. enhancement was observed for protons H_h and H_c when proton H_f was irradiated, but not when H_d or $H_{i,j}$ are irradiated [Fig. 2(iii)], strongly suggests that the H_f protons are indeed disposed towards H_h, whereas the terminal H_d protons and the bridge protons $H_{i,j}$ point away from H_h. The 100 MHz $^{13}C\{^1H\}$ spectrum showed peaks at δ 18.0 and −24.5, assigned to C_l and C_k, respectively, by an attached proton test.

The cluster framework geometry, which conforms to 2243 *styx* topology, can be formally viewed as a seven-atom fragment of a closed triangular 10-vertex bicapped Archimedean antiprism [Fig. 3(iii)]. This description of the molecule is consistent with the Williams–Wade electron counting rules for *hypho*-$C_3B_4H_{12}$, which require a contribution of 11 electron pairs to the framework bonding. However, the absence of any direct bonding between the two sets of boron atoms, revealed in the COSY data, suggests considerable flexibility in the structure and an alternative description of the *molecular* geometry would be as a 1,2,5-tricarbapentaborane fragment in which the C(2) and C(5) atoms are bridged by a

B_2H_5 fragment, giving an overall *hypho* electron count. It is also noteworthy that the compound is isoelectronic with the non-classical norbornene carbocation $C_7H_9^+$. By contrast, the view that the framework geometry is that of a *hypho* six-vertex trigonal prismatic C_2B_4 cluster with a μ_2-bridging CH_2 group can be confidently rejected: proton peaks g and h in Fig. 2(i), each of which features geminal coupling, are at unusually high field for a normal methylene grouping, suggesting that the latter is not acting simply as a pendant moiety. Such a description would also be impossible to formulate topologically.

The reaction mechanism by which the *hypho*-tricarbaborane $C_3B_4H_{12}$ is formed from propyne and tetraborane is not obvious. It is noteworthy that the product has three contiguous carbon atoms —CH—CH_2—CH—, but there is no sign of the methyl group initially present in propyne, $CH_3C{\equiv}CH$.

Acknowledgements—We thank the SERC, the U.S. Army Research and Standardization Group (Europe) and Borax Research for financial support, Dr X. L. R. Fontaine for recording some of the high-field NMR data, Ellen Leuschner for help in preparing a sample of the compound for the ^{11}B—^{11}B COSY measurement and Professor P. Paetzold (Aachen) for useful comments on this work.

REFERENCES

1. K. Wade, *Adv. Inorg. Chem. Radiochem.* 1976, **18**, 1.
2. S. O. Kang and L. G. Sneddon, *J. Am. Chem. Soc.* 1989, **111**, 3281 and refs therein.
3. J. Duben, S. Hermánek and B. Štíbr, *J. Chem. Soc., Chem. Commun.* 1978, 287.
4. (a) R. N. Grimes, *Carboranes*. Academic Press, New York (1970); (b) C. L. Bramlett and R. N. Grimes, *J. Am. Chem. Soc.* 1966, **88**, 4269; (c) R. N. Grimes and C. L. Bramlett, *J. Am. Chem. Soc.* 1967, **89**, 2557; (d) R. N. Grimes, C. L. Bramlett and R. L. Vance, *Inorg. Chem.* 1968, **7**, 1066; (e) D. A. Franz and R. N. Grimes, *J. Am. Chem. Soc.* 1971, **93**, 387; (f) D. A. Franz, J. W. Howard and R. N. Grimes, *J. Am. Chem. Soc.* 1969, **91**, 4010; (g) D. A. Franz and R. N. Grimes, *J. Am. Chem. Soc.* 1970, **92**, 1438; (h) D. A. Franz, V. R. Miller and R. N. Grimes, *J. Am. Chem. Soc.* 1972, **94**, 412; (i) D. C. Finster and R. N. Grimes, *J. Am. Chem. Soc.* 1981, **103**, 2675.
5. B. C. Harrison, I. J. Solomon, R. D. Hites and M. J. Klein, *J. Inorg. Nucl. Chem.* 1960, **14**, 195.
6. We are collaborating with Professor D. W. H. Rankin to determine the structure of this molecule in the gas phase by electron diffraction and will report the results in due course.
7. I. Shapiro, R. E. Williams and S. G. Gibbins, *J. Phys. Chem.* 1961, **65**, 1061.
8. T. Onak, K. Gross, J. Tse and J. Howard, *J. Chem. Soc., Dalton Trans.* 1973, 2633.
9. M. Bühl and P. von R. Schleyer, Private communication (1991).
10. R. Greatrex, N. N. Greenwood and M. Kirk, *J. Chem. Soc., Chem. Commun.* 1991, 1510.
11. M. A. Toft, J. B. Leach, F. L. Himpsl and S. G. Shore, *Inorg. Chem.* 1982, **21**, 1952.
12. J. Klein, B. C. Harrison and I. J. Solomon, *J. Am. Chem. Soc.* 1958, **80**, 4149.
13. (a) J. Dobson and R. Schaeffer, *Inorg. Chem.* 1970, **9**, 2183; (b) D. F. Shriver and M. A. Drezdzon, *The Manipulation of Air-sensitive Compounds*, 2nd edn, p. 193. Wiley-Interscience, New York (1986).
14. (a) X. L. R. Fontaine and J. D. Kennedy, *J. Chem. Soc., Dalton Trans.* 1987, 1573; (b) X. L. R. Fontaine, J. D. Kennedy, M. McGrath and T. R. Spalding, *Magnet. Reson. Chem.* 1991, **29**, 711; (c) X. L. R. Fontaine and J. D. Kennedy, *J. Chem. Soc., Chem. Commun.* 1986, 779.
15. (a) T. Onak and J. B. Leach, *J. Am. Chem. Soc.* 1970, **92**, 3513; (b) R. R. Rietz, R. Schaeffer and L. G. Sneddon, *J. Am. Chem. Soc.* 1970, **92**, 3514; (c) J. B. Leach, T. Onak, J. Spielman, R. R. Rietz, R. Schaeffer and L. G. Sneddon, *Inorg. Chem.* 1970, **9**, 2170.
16. R. Greatrex, N. N. Greenwood, D. W. H. Rankin and H. E. Robertson, *Polyhedron* 1987, **6**, 1849.

Polyhedron Vol. 12, No. 15, pp. 1855–1862, 1993
Printed in Great Britain

0277–5387/93 $6.00+.00
© 1993 Pergamon Press Ltd

LOW-TEMPERATURE SOLID-STATE ROUTES TO TRANSITION METAL OXIDES VIA METATHESIS REACTIONS INVOLVING LITHIUM OXIDE

A. HECTOR and I. P. PARKIN*

Department of Chemistry, The Open University, Milton Keynes MK7 6AA, U.K.

(*Received* 18 *March* 1992; *accepted* 19 *April* 1993)

Abstract—Thermolysis of a mixture of lithium oxide and anhydrous transition metal halide, MX_n (M = Ti, Zr, Hf, V, Nb, Ta, Cr, Mo, W, Fe, Co, Ni, Cu, Zn, X = Cl; M = Mn, X = I), at oven temperatures of 450°C for 5 h produces crystalline transition metal oxide via a solid-state metathesis reaction. DSC studies show that the reaction is initiated at 300°C for M = Hf and Nb. When M = Ta or Nb the product is $LiMO_3$. The metal oxides and lithium-metal oxides were characterized by X-ray powder diffraction, S.E.M., EDAX, FT-IR and magnetic moment measurements.

Metal oxides of various formulations are known for all the transition elements.[1] They have widespread technological importance as powders for catalysts,[2] ceramics,[3] engineering materials[4] and as thin films for reflectance coatings. Recently the use of mixed metal oxides as high-temperature superconductors[5] has seen rapid growth and could lead to great improvements in power transmission.

Metal oxides have been made by heating the metal in air, often at high temperature. The refractory nature of some metal oxides means that annealing has often been required to produce a crystalline material. New developments in metal oxide and mixed metal oxide synthesis have involved the use of either molecular precursors or hydrothermal processes.[6] The thermal decomposition of metal nitrates or alkoxides has allowed lower temperature preparation of oxides either as bulk solids or as thin films via MOCVD. Occasionally competitive degradation pathways incorporate other elements in the oxide lattice in these lower temperature preparations.[7] Hydrothermal processes have allowed lower temperature mixed-metal oxide synthesis and have several advantages, including intimate mixing of the reagents and stoichiometric composition control.

Solid-state "self-propogating high-temperature synthesis" (SHS) routes to ceramic materials including nitrides, sulphides, phosphides and oxides have been developed by Russian workers.[8] Kaner[9–12] has elegantly developed this work for metathesis type reactions and has synthesized a range of main group and transition metal pnictides, mixed pnictides and mixed chalcogenides. Solid-state metathesis routes have some advantages when compared to traditional methods of metal oxide synthesis: firstly, no solvent is involved in the reaction; secondly, low synthesis temperatures are required often with the reaction exhibiting high exothermicity once initiated; thirdly, the by-products in the reactions are removeable from the oxide lattice allowing ready separation of products. Additionally, stoichiometric control of the reagents allows the possibility of making a range of mixed metal oxides.

An early example of a metathesis route to metal oxides was developed in 1932 by Hilpert and Wille,[13] who reported the preparation of mixed-metal ferrates at moderate temperature (400–500°C) by reaction of metal dichlorides with lithium ferrate. Recently, reaction[10,14] of sodium peroxide with CuF was found to produce Cu_2O.

We report here the reaction of lithium oxide with anhydrous transition metal halides, to produce crystalline transition metal oxides.

* Author to whom correspondence should be addressed.

EXPERIMENTAL

All reactions and preparations were conducted under vacuum or in a dinitrogen filled dry-box. Glass ampoules were made out of either pyrex, borosilicates or quartz glass and were either flame dried under vacuum or heated to 400°C for 6 h prior to reaction. All solvents were degassed; THF was distilled from sodium/benzophenone and stored over 4 Å molecular sieves prior to use. Metal halides and lithium oxide were purchased from Aldrich Chemical Company. The metal halides were dried over thionyl chloride prior to use. X-ray powder diffraction patterns were obtained using a Siemens D5000 diffractometer using nickel filtered Cu-K_α radiation (1.5406 Å); SEM and EDAX analyses were obtained on a Jeol JSM 820 instrument equipped with the Kevex program;[15] FT-IR spectra were obtained as pressed KBr pellets on a Nicolet 205(CsI); GC were obtained on a Pye–Unicam 204 with 5 Å molecular sieves using a thermal conductivity detector with helium carrier gas; magnetic moment measurements were determined by a Johnson–Matthey balance. DSC analyses were performed in open aluminum pans under argon flow on a Polymer Laboratories DSC using a ramp rate of 5°C min^{-1} from 200 to 620°C. Thermal initiation of the reactions was performed in a Lenton Thermal Design tube furnace. Microanalyses were performed by Medac LTD, Brunel University.

Transition metal oxide preparation (M = Ti, Zr, Hf, V, Cr, Mo, W, Mn, Fe, Co, Ni, Cu, Zn, Hg)

Lithium oxide (50–100 mg) and anhydrous metal halide, MX_y (equimolar quantities of lithium and halide), were ground together using an agate pestle and mortar in a nitrogen filled dry-box. The powder was added to a thick-walled glass ampoule, sealed under vacuum and sonicated with ultrasound for 10 min. The ampoule was then wrapped in glass wool and placed in a conventional oven at 450°C for 2–10 h, during which time the solids invariably fused into a large lump and changed colour. The ampoule was removed from the oven, allowed to cool to room temperature and broken open in a dinitrogen filled glove-box. Trituration of the fused solid with THF (3×20 cm^3) for 10 h produced a coloured precipitate and a cloudy THF layer. Evaporation of the THF filtrate produces lithium chloride. The coloured powders were identified as transition metal oxides by X-ray powder diffraction (Table 1), EDAX analysis, FT-IR and magnetic moment measurements. Ceramic yields, based on the metal after THF trituration varied from 60 to 90% dependent on the sample.

Table 1. Crystalline phases observed from reaction of MX_n and Li_2O

Initial metal halide	Crystalline phase detected	Colour	Yield (%)	Reaction time (h)	Observed lattice *a* spacing[20]	Literature lattice *a* spacings
$TiCl_4$	TiO_2 (Li_2TiO_3)	White	60	2	4.585 (5.06)	4.593 (5.072)
$TiCl_3$	TiO_2	White/grey	60	2	5.069	5.067
$ZrCl_4$	ZrO_2	Grey	65	2	5.32	5.313
$HfCl_4$	HfO_2	Grey	65	2	5.12	5.12
VCl_4	VO_2 (Li_3VO_4)	Black	55	2	9.083 (5.499)	9.083 (5.447)
VCl_3	V_2O_3 ($LiVO_2$)	Black	60	2	5.42	5.43
$NbCl_5$	$LiNbO_3$	Light grey	90	2	5.149	5.149
$TaCl_5$	$LiTaO_3$	Grey	90	2	5.167	5.153
$CrCl_3$	Cr_2O_3	Grey	60	10	4.955	4.958
$MoCl_5$	MoO_2	Brown	65	10	5.609	5.607
$MoCl_3$	MoO_2	Black	70	10	5.610	5.607
WCl_4	WO_2	Black	70	2	5.575	5.575
MnI_2	MnO (Mn_3O_4)	Brown	85	2	4.440	4.445
$FeCl_3$	Fe_3O_4 (Fe_2O_3)	Dark brown	80	2	8.396	8.396
$CoCl_2$	CoO	Brown	85	10	5.040	5.036
$NiCl_2$	NiO	Light green	75	10	4.277	4.260
CuI	Cu_2O	Yellow	40	2	4.177	4.176
$ZnCl_2$	ZnO	Light grey	90	2	4.271	4.270
$HgCl_2$	HgO	Yellow	45	10	3.257	3.350

Note: not all lattices are cubic; only the *a* value is reported. Minor phases detected are shown in parentheses.

Alternative procedure

(1) An identical procedure to that outlined above can be carried out by initiating the reaction using a 750 W industrial microwave oven with a variable heating period dependent on the sample. The work-up and properties of the materials obtained were identical to those initiated in the conventional oven.

(2) The metal oxides could also be washed free of lithium chloride by-products by washing with degassed water for 10 min.

(3) Attempts at making mixed metal oxides were investigated under the same reaction and work-up conditions as above, except equimolar quantities of the starting metal halide powders were ground together before mixing in the ground lithium oxide powder.

CAUTION! Reaction of hydrated metal halides with lithium oxide can lead to an explosion of the ampoules on thermolysis. Care must be taken in the reactions of Li_2O with metal halides because a vigorous exothermic reaction can result. All preparations should be routinely performed behind a toughened glass safety screen.

RESULTS AND DISCUSSION

Reaction of ground powders of Li_2O and anhydrous transition metal halides at an oven temperature of 450°C in sealed ampoules produce crystalline transition metal oxides and lithium halides via a solid state metathesis reaction, eqs (1), (2), (3) and (4).

$$MCl_4 + 2Li_2O \longrightarrow MO_2 + 4LiCl \quad (M = Hf, Zr, W) \quad (1)$$

$$MX_2 + Li_2O \longrightarrow MO + 2LiX \quad (M = Zn, Hg, Cd, Co, Ni, X = Cl; M = Mn, X = I) \quad (2)$$

$$FeCl_3 + Li_2O \longrightarrow Fe_2O_3 + Fe_3O_4 + 3LiCl \quad (3)$$

$$2CuI + Li_2O \longrightarrow Cu_2O + 2LiCl \quad (4)$$

The product of the reactions [eqs (1), (2), (3) and (4)] was often contained as a fused grey lump and a small amount of a white solid was sublimed onto the walls of the ampoule. The white sublimed solid was analysed as lithium halide (either LiCl or LiI dependent on the initial reagents) by X-ray powder diffraction (XRPD), lithium flame test and EDAX analysis. The grey fused material showed a smooth morphology by S.E.M., Fig. 1(a); metal, oxygen and a small amount of halide (15 mol%) by EDAX analysis, both of which are consistent with the formation of a metal oxide that is coated with sublimed lithium halide. The metal oxide was purified by either washing with THF or water; this removed the co-product lithium halide. The metal oxides after trituration were characterized by X-ray powder diffraction (Table 1), FT-IR, magnetic moment measurements, S.E.M., EDAX analysis and microanalysis.

The S.E.M. profile of the triturated metal oxides showed micron sized particles with sharp angles and faces as illustrated in Fig. 1(b), whilst the EDAX analysis revealed only metal and oxygen with no halides present (2–3% detection limit). The samples of ZnO and Cr_2O_3 made in this study showed less than 0.5% lithium by microanalysis, indicating that the metal oxide lattices do not contain appreciable amounts of LiX after trituration. The FT-IR spectra of the metal oxides showed a broad band at *ca* 450 cm^{-1} due to M—O stretches. The magnetic moment measurements were typical for each of the metal oxides and showed no deviation from literature values.[16]

The X-ray powder diffraction data for the transition metal oxides formed from reaction of Li_2O and metal halide are summarized in Table 1. In general, after a reaction time of 5 h at 450°C a crystalline transition metal oxide was formed, however, the degree of crystallinity as judged by the Scherrer equation[17] varied from crystallite sizes of 800 Å (ZnO) to 150 Å (HfO_2). The metal oxides after trituration showed no lithium halide present and only one phase of metal oxide (by XRD), with the exception of iron and manganese where two phases, Fe_2O_3, Fe_3O_4 and MnO, Mn_3O_4, were detected. Representative XRD patterns for ZnO and MnO, Mn_3O_4 made in this study, are shown in Figs 2(a) and 2(b).

The phase of metal oxide detected by XRD invariably showed the metal in the same oxidation state as in the initial metal halide. In general no reduction or oxidation of the metal occurred and no gases (O_2) were detected from the reaction by GC, however, for reactions involving $TiCl_3$ and $MoCl_3$, TiO_2 and MoO_2 were detected indicating an oxidation at the metal. For reactions involving VCl_3 and VCl_4 the metal oxides formed were V_2O_3 and VO_2, respectively. A small amount of the phases associated with $LiVO_2$ and Li_3VO_4 were also detected in these reactions by XRD. Analogous solid-state reactions of Li_3N and metal halides do lead to reduction at the metal and formation of dinitrogen,[18] with the tendency increasing across the periodic table such that when starting with $HfCl_4$ partial reduction occurs at the metal and HfN and N_2 are formed. To the right of the *d*-block reduction becomes increasingly more important

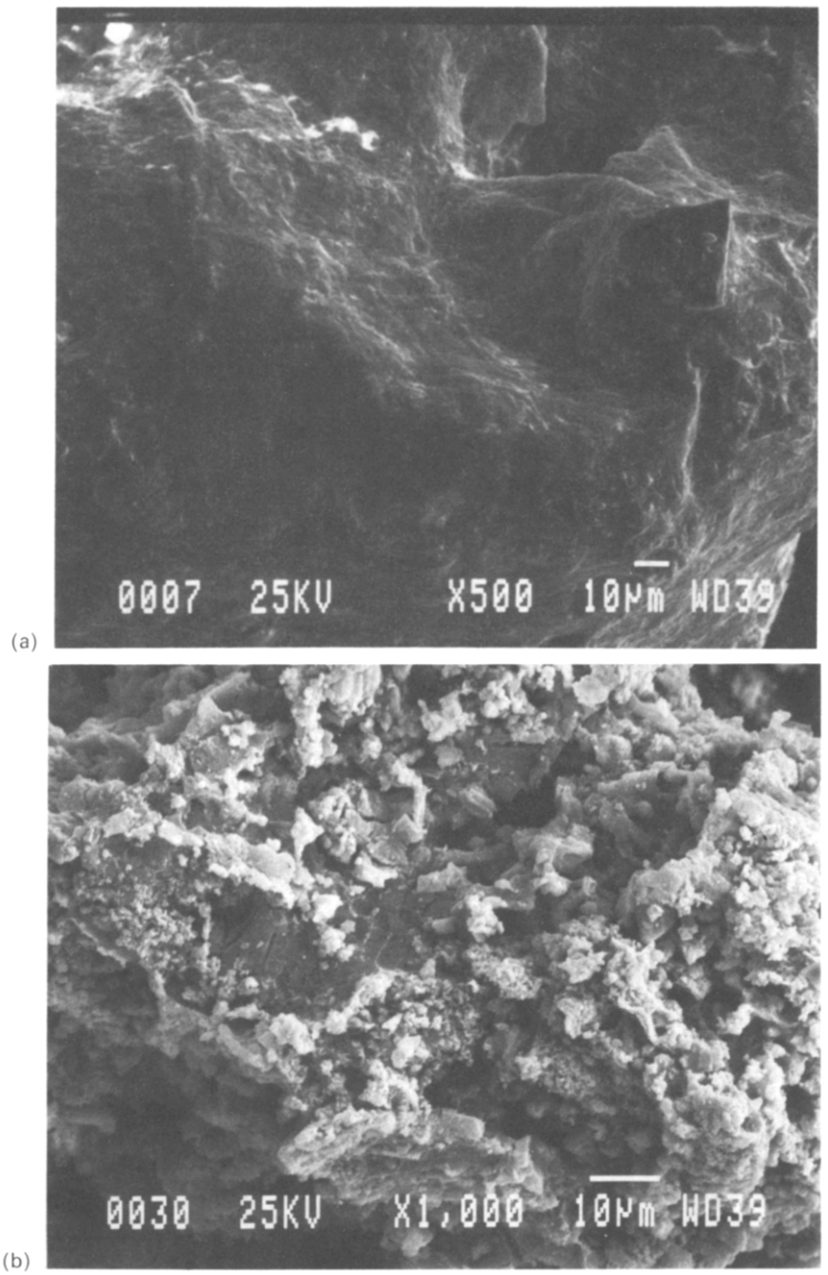

Fig. 1. S.E.M. profiles of the solid produced by reaction of MnI_2 and Li_2O (a) without and (b) after trituration with water.

and the reaction between $ZnCl_2$ and Li_3N yields only zinc metal and dinitrogen. This trend is not seen for the reactions of Li_2O and transition metal halides where metal oxides (or lithium metallates) are formed for all the metal halides studied independent of the position of the metal in the periodic table. The reason for the difference in reactivity for similar solid-state reactions involving Li_2O and Li_3N and metal halides may be due to the fact that many of the late transition metal nitrides are thermally unstable and undergo facile reduction to metal and dinitrogen, whereas metal oxides are comparatively more thermally stable.

The reaction of $HfCl_4$ with Li_2O was studied by DSC, which revealed a large exotherm at 310–325°C (Fig. 3). Similar results were also obtained for reaction of $NbCl_5$ and Li_2O. The energy released (120–300 kJ mol^{-1}) corresponds to the expected heat of reaction on forming metal oxide and LiCl. Interestingly the exotherm takes place over a time scale of a few minutes, indicating that the reaction is not as violently exothermic as reactions of $MoCl_5$–

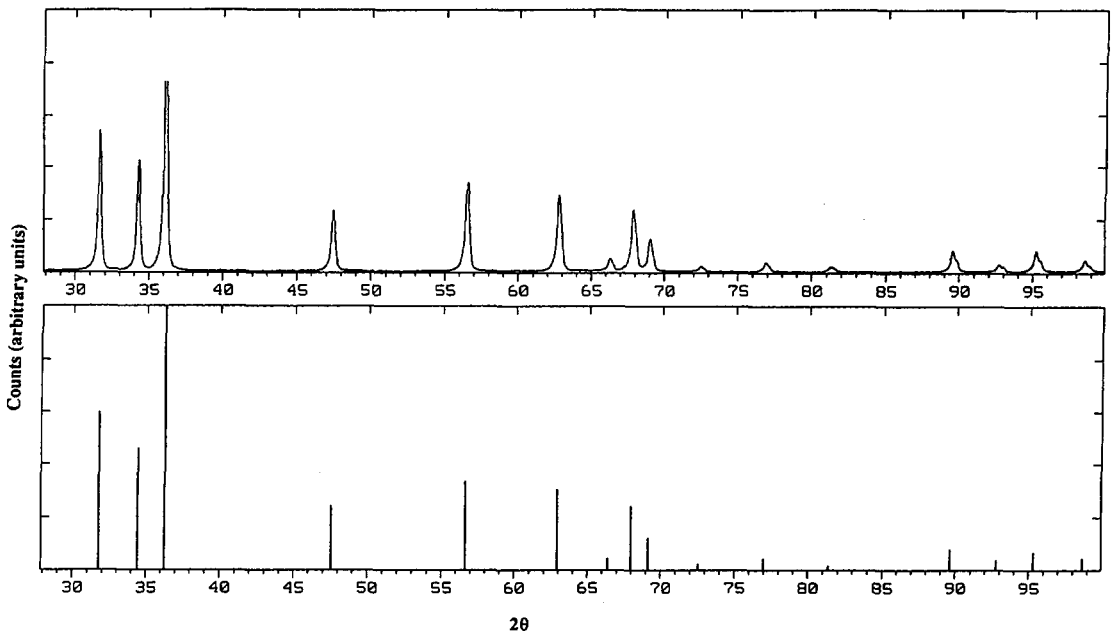

Fig. 2(a). Upper trace X-ray powder diffraction pattern for the solid produced from reaction of $ZnCl_2$ and Li_2O; lower trace standard X-ray powder diffraction line pattern for ZnO.

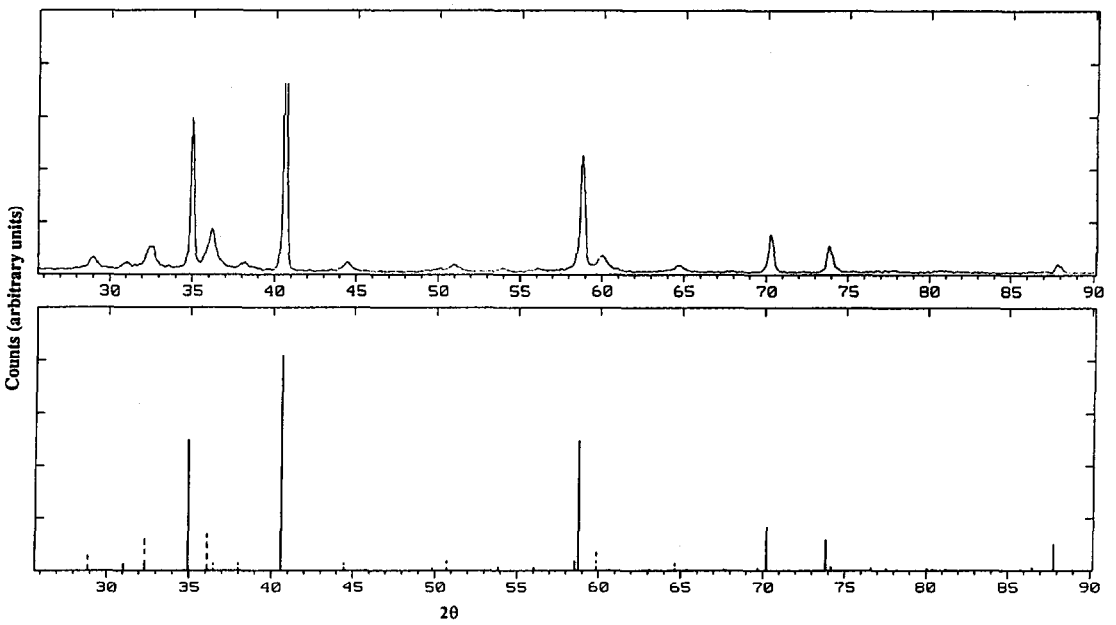

Fig. 2(b). Upper trace X-ray powder diffraction pattern for the solid produced from reaction of MnI_2 and Li_2O; lower trace standard X-ray powder diffraction line pattern form MnO (——) and Mn_3O_4 (– – – –).

Na_2S and Li_3N–$HfCl_4$ which are over in a few seconds.[9,18] However, the reaction of $ZnCl_2$ and Li_2O is extremely exothermic with the products spraying the inside of the DSC cell; initiation temperature in this case proved to be around 250°C. It is probable that heat transfer in the DSC cell is easier than in the glass ampoule reactions and that the observed tube furnace initiation temperatures of 400–450°C actually correspond to 310–325°C at the sample surface after the effects of thermal gradient through the glass and the bulk sample are taken into account. Blank runs of Li_2O and $HfCl_4$

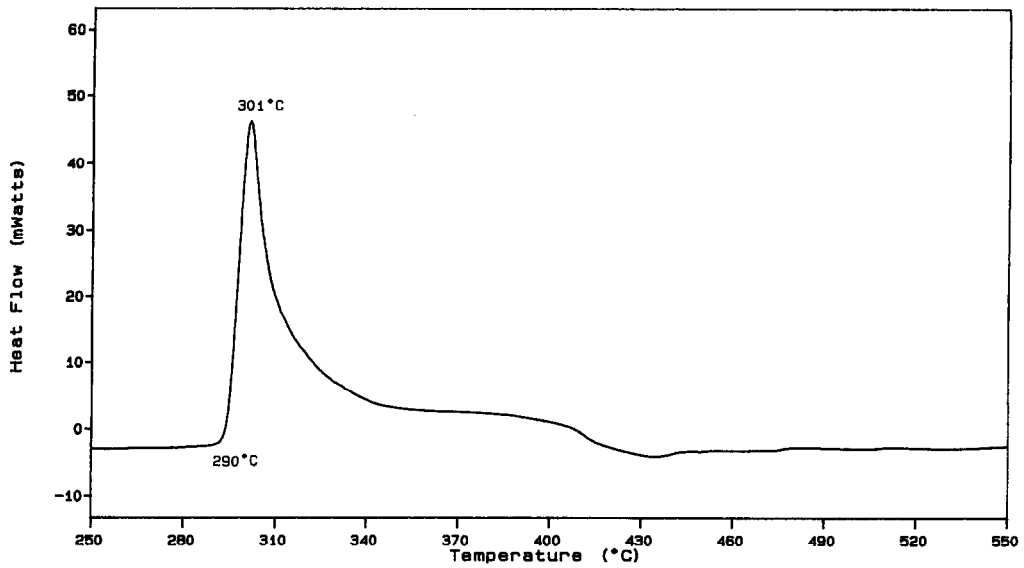

Fig. 3. Differential scanning calorimetry trace for reaction of $HfCl_4$ and Li_2O.

in the same apparatus showed no features of the same magnitude from 200 to 650°C. A sample of $HfCl_4$ and Li_2O held at 295°C showed heat evolved over a 15 min period, corresponding approximately to the calculated heat of reaction. The heat evolved from the reaction suggests high temperatures are generated; this is confirmed by the crystallinity of the product. Analogous reactions of lithium nitride or lithium sulphide with transition metal halides are very exothermic, inducing temperatures[9,18] in excess of 1000°C.

Hess' Law calculations[19] of the reaction of Li_2O with metal halides indicate that the reaction is exothermic with ΔH_f varying from -100 to -600 kJ mol^{-1} dependent on the metal. Initiation of the reaction in a small region of the solid may occur, but propagation throughout the bulk material may not be as facile in these uncompressed mixed Li_2O/MX_n powders than with analogous Li_3N reactions. Thus, a number of independent propagations throughout the solid could account for the observed fused crystalline product and partially sublimed metal halide.

The major exceptions to the formation of metal oxides in the reactions of Li_2O with transition metal halides were those involving niobium and tantalum pentachlorides, where $LiNbO_3$ and $LiTaO_3$ were the only phases detected [eq. (5)]. However, in reactions involving titanium and vanadium halides with Li_2O a small amount of crystalline lithium metallate was observed in addition to the main metal oxide phase by XRPD. The X-ray powder diffraction patterns of $LiTaO_3$ and $LiNbO_3$

$$MCl_5 + 3Li_2O' LiMO_3 + LiCl \quad (M = Ta, Nb) \qquad (5)$$

were phase pure (Fig. 4) after THF trituration and the EDAX analysis showed only metal and oxygen with no chlorine present (lithium could not be determined by EDAX analysis on the instrument used). The samples of $LiMO_3$ were diamagnetic as expected, indicating that the metals had not been reduced.

Attempts at making mixed-metal oxides, $M_xM_yO_z$, by reaction of preground metal halides and lithium oxide did not prove successful at oven temperatures of 450°C. This is illustrated in Fig. 5 for the reaction of equimolar amounts of $ZnCl_2$ and MnI_2 with Li_2O, which produced both ZnO and MnO rather than a mixed metal oxide, Zn_xMn_yO.

The oxygen incorporated in the transition metal oxides formed from metathesis reactions involving Li_2O comes predominantly from the lithium oxide, because blank experiments under exactly the same conditions produced only unreacted metal halide (as demonstrated by XRPD and EDAX analysis). However, for the reactions involving $TiCl_3$ and $MoCl_3$, where oxidized products TiO_2 and MoO_2 are produced, some oxygen is probably incorporated in the product either due to work-up or from the glassware. One specialist utility of this reaction could be in incorporating isotropically labelled oxygen into a metal oxide lattice by starting with initially labelled lithium oxide.

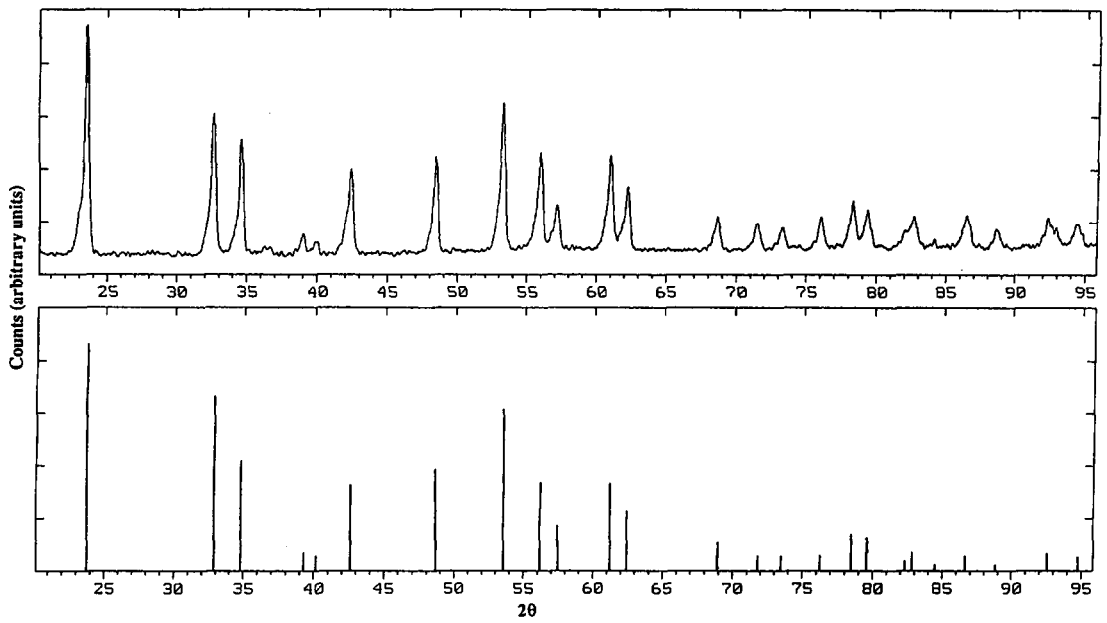

Fig. 4. Upper trace X-ray powder diffraction pattern for the solid produce from reaction of $TaCl_3$ and Li_2O; lower trace standard X-ray powder diffraction line pattern for $LiTaO_3$.

CONCLUSIONS

Current routes to metal oxides either by direct combination of the elements or by hydrothermal molecular precursor routes often involve high-temperature pyrolysis of the materials or prolonged annealing to produce a crystalline material. The solid-state metathesis routes described here to form metal oxides are at a reasonably low initiation temperature (300°C) and comparatively short reaction times (5 h for ampoule reactions, 6–10 min in a DSC cell). Unfortunately mixed-metal oxides seem

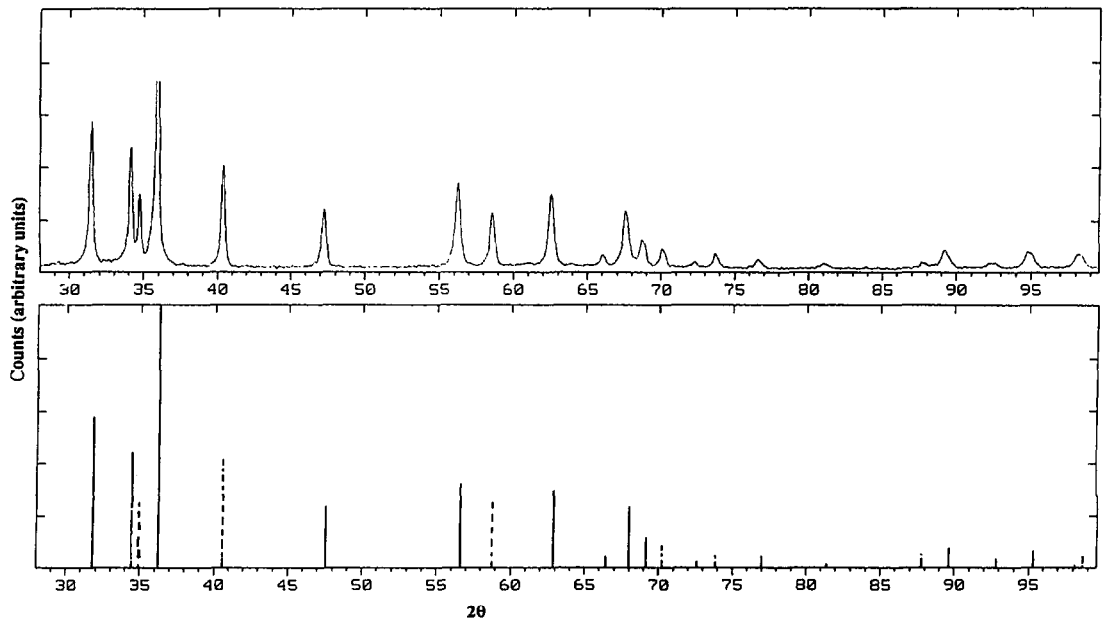

Fig. 5. Upper trace X-ray powder diffraction pattern for the solid produce from reaction of equimolar amounts of $ZnCl_2$ and MnI_2 with Li_2O; lower trace standard X-ray powder diffraction line pattern for ZnO (——) and MnO (– – – –).

difficult to form by this low external energy route, probably because of a lack of intimate mixing of the reagents. All the transition metal halides studied react with Li_2O to form metal oxide with little redox chemistry at the metal, however, for Ta and Nb the only phase produced is $LiMO_3$ and for V and Ti a small amount of $LiMO_x$ phases are also seen. The solid-state metathesis reaction of Li_2O and MX_n offers a convenient, rapid, low external energy route to industrially useful metal oxides such as TiO_2 and ZnO.

Acknowledgement—Open University Research Award (AH), Leverhulme Trust, The Royal Society, Nuffield Trust.

REFERENCES

1. C. S. G. Phillips and R. J. P. Williams, *Inorganic Chemistry*. Oxford University Press, Oxford (1965).
2. P. W. Lednor, *Catalysis Today* 1992, **15**, 243.
3. N. Ichinose, *Introduction to Fine Ceramics*. Wiley, Chichester (1987).
4. N. N. Greenwood and A. Earnshaw, *Chemistry of the Elements*, p. 1118. Pergamon Press, Oxford (1990).
5. L. Smart and E. Moore, *Solid State Chemistry*, Ch. 8. Chapman and Hall, London (1992).
6. P. P. Phule and S. H. Risbud, *J. Mat. Sci.* 1990, **25**, 1169; L. G. Hubert-Pfalzgraf, *Appl. Organomet. Chem.* 1992, **6**, 627.
7. A. Ayral, T. Assin, M. A. Benoza, J. Pholippou, A. Lecomte and A. Douder, *J. Mat. Sci.* 1990, **25**, 1268.
8. Z. A. Munir, *J. Mat. Sci.* 1990, **25**, 1159.
9. R. B. Kaner, P. R. Bonneau and R. F. Jarvis, *Inorg. Chem.* 1992, **32**, 2127.
10. R. B. Kaner, P. R. Bonneau and R. F. Jarvis, *Nature* 1991, **349**, 519.
11. P. R. Bonneau, R. F. Jarvis and R. B. Kaner, *Inorg. Chem.* 1992, **31**, 2127.
12. R. E. Treece, G. S. Macala and R. B. Kaner, *Chem. Mat.* 1992, **4**, 9.
13. S. Hilpert and A. Wille, *Z. Phys. Chem.* 1932, **18B**, 291.
14. J. B. Wiley and R. B. Kaner, *Science* 1992, **255**, 1093.
15. Quantex 6.2, with quantum detector Kevex delta 4.
16. *Handbook of Chemistry and Physics*, 55th edn, p. E121. CRC Press, Cleveland (1974).
17. H. P. Klug and L. E. Alexander, *X-ray Diffraction Procedure for Polycrystalline and Amorphous Materials*, 2nd edn. John Wiley, New York (1974).
18. J. C. Fitzmaurice, A. H. Hector and I. P. Parkin, *Polyhedron* 1993, **12**, 1295.
19. D. D. Wayman, W. H. Evans, V. B. Parker, R. H. Schumm, J. Halow, S. M. Bailey, K. C. Chumey and R. L. Nuttal, *The NBS Tables of Chemical Thermodynamics Properties*. American Chemical Society, Washington DC (1982).
20. PDF-2 Data Base, International Centre for Diffraction Data, Swarthmore, PA 19081 (1990).

Polyhedron Vol. 12, No. 15, pp. 1863–1870, 1993
Printed in Great Britain

0277-5387/93 $6.00+.00
© 1993 Pergamon Press Ltd

PREPARATION, CRYSTAL STRUCTURE AND SPECTROSCOPIC STUDY OF AZIDO(N,O-QUINALDATO)TRIAQUAMANGANESE(II) MONOHYDRATE AND THIOCYANATO(N,O-QUINALDATO)-(O-QUINALDIC ACID)DIAQUAMANGANESE(II), $[Mn(NC_9H_6COO)(N_3)(H_2O)_3]\cdot H_2O$ AND $[Mn(NC_9H_6COO)(NC_9H_6COOH)(NCS)(H_2O)_2]$

MOHAMED A. S. GOHER

Department of Chemistry, Faculty of Science, Alexandria University, Alexandria 21321, Egypt

and

FRANZ A. MAUTNER*

Institut für Physikalische und Theoretische Chemie, Technische Universität Graz, A-8010 Graz, Austria

(*Received* 2 *February* 1993; *accepted* 19 *April* 1993)

Abstract—Two mixed ligand complexes of quinaldic acid and manganese(II) azide or thiocyanate, namely azido(N,O-quinaldato)triaquamanganese(II) monohydrate (**1**) and thiocyanato(N,O-quinaldato)(O-quinaldic acid)diaquamanganese(II) (**2**), have been prepared and characterized by single-crystal X-ray methods. The coordination environment of the manganese(II) atom in complex **1** is a distorted octahedron. Each metal atom is chelated by a quinaldate anion [via its nitrogen atom, Mn—N = 2.292(3) Å, and a carboxylate oxygen atom, Mn—O = 2.147(3) Å] and links three aqua molecules [Mn—O distances from 2.189(3) to 2.217(3) Å] and a terminal azido ligand [Mn—N = 2.181(3) Å]. The structure of complex **2** features distorted octahedral manganese(II) coordination geometry, chelated quinaldate anion [Mn—N = 2.271(7) Å and Mn—O = 2.158(5) Å], O-bonded neutral quinaldic acid molecule [Mn—O = 2.228(5) Å], two aqua molecules [Mn—O = 2.180(5) and 2.203(6) Å] and a terminal N-thiocyanato group at an Mn—N distance of 2.119(7) Å. The IR spectra of these two complexes are presented and discussed in relation to their structures.

Quinaldic acid (hereafter abbreviated as H-quin) has long been accepted as a chelating ligand for many di- and trivalent metal ions forming five-membered rings through the ligation of the quinaldate anion.[1–17] Quinaldic acid, however, was found to function as a neutral monodentate ligand in its gold(III) complex, $[(H_3O)(H\text{-quin})_2][AuBr_4]$, coordinating via its carbonyl oxygen with long Au—O bonds (av. = 3.414 Å).[18] Elman *et al.*[19,20] and Csöregh *et al.*[21] studied the effects of various substituents on the coordinating properties of pyridine- and quinoline-carboxylic acids and the stereochemistry of the resulting complexes.

It is well known that the azide group may function as a terminal monodentate or bridging bi-, tri- or tetradentate ligand with a variable manner of binding.[22,23] Recently we described the synthesis and X-ray structural characterization of a polymeric complex of manganese(II) azide with picolinic acid, otherwise called 2-pyridinecarboxylic acid, which crystallizes with an additional water molecule.[24] We now report our investigation of the corresponding complex of quinaldic acid (**1**), along with the manganese(II) thiocyanato complex of quinaldic acid (**2**). We anticipated that a comparative

* Author to whom correspondence should be addressed.

study of these mixed ligand complexes might yield interesting results. The present work constitutes part of our continuing study of metal pseudohalides containing substituted pyridine and quinoline ligands;[25,26] further impetus is derived from the recent surge of interest in the structural features of azide binding to biological metals.[27]

EXPERIMENTAL

Quinaldic acid was obtained from Aldrich. The other chemicals were of analytical grade quality.

Preparation of [Mn(quinaldato)$(N_3)(H_2O)_3]\cdot H_2O$

This complex was prepared by dissolving $MnCl_2\cdot 4H_2O$ (0.52 g, 5 mmol) in ethanol (10 cm^3). Quinaldic acid (1.73 g, 10 mmol) dissolved in warmed ethanol was then added dropwise. This mixture was filtered off. To the clear solution NaN_3 (0.65 g, 10 mmol) in distilled water (5 cm^3) was also added dropwise with stirring and the mixture became a yellow solution. Yellow crystals were obtained by slow evaporation in a desiccator charged with anhydrous $CaCl_2$, kept in the dark for several days. The same yellow crystals were obtained by the same procedure using an aqueous medium instead of ethanol. Found: C, 35.3; H, 4.2; N, 16.2; Mn, 16.3. Calc.: C, 35.2; H, 4.1; N, 16.4; Mn, 16.1%.

Preparation of [Mn(quinaldato)(quinaldic acid) $(NCS)(H_2O)_2$]

This complex was prepared by dissolving $MnCl_2\cdot 4H_2O$ (0.52 g, 5 mmol) in ethanol (10 cm^3). Upon addition of quinaldic acid (1.73 g, 10 mmol) dissolved in warmed ethanol (10 cm^3) the solution became turbid. Drops of distilled water were added until the solution became clear. To this solution KSCN (0.97 g, 10 mmol) in distilled water (3 cm^3) was added and the mixture became very faint yellow. Upon allowing this final solution mixture to stand in an open conical flask over several days red crystals were obtained. These crystals were filtered off and the filtrate allowed to stand over several days more to produce the title complex as yellow crystals or needles. Found: C, 51.2; H, 3.4; N, 8.3; Mn, 11.3. Calc.: C, 51.0; H, 3.5; N, 8.5; Mn, 11.1%.

X-ray crystallography

Lattice parameters of both compounds have been determined by least-squares refinement of X-ray powder patterns at 298(1) K (Philips APD 1700

Table 1. Crystallographic data and processing parameters of Mn[(quin)$(N_3)(H_2O)_3]H_2O$ (**1**) and Mn(H-quin)(quin)$(NCS)(H_2O)_2$ (**2**)

Compound	**1**	**2**
Chemical formula	$C_{10}H_{14}N_4O_6Mn$	$C_{21}H_{17}N_3O_6SMn$
Molecular weight	341.18	494.38
Crystal system	Triclinic	Triclinic
a (Å)	7.505(3)	8.479(4)
b (Å)	7.770(5)	10.853(5)
c (Å)	12.150(5)	11.949(5)
α (°)	91.65(3)	95.68(4)
β (°)	92.01(4)	94.99(3)
γ (°)	92.18(3)	95.00(4)
V (Å^3)	707.2(6)	1084.9(9)
Space group	P-1 (No. 2)	P-1 (No. 2)
Z	2	2
$F(000)$	350	506
D_{calc} (Mg m^{-3})	1.602	1.513
Approx. crystal size (mm)	$0.45\times0.17\times0.15$	$0.30\times0.10\times0.05$
Data collection limits (°)	$\pm h, \pm k, l; 2\theta < 50$	$\pm h, \pm k, l; 2\theta < 45$
Scan mode	ω-scan, $\Delta\omega = 1.5°$	ω-scan, $\Delta\omega = 1.5°$
Least squares parameters	228	321
$F_o > 3\sigma(F_o)$	2008	1191
μ(Mo-K_α) (mm^{-1})	0.93	0.72
R	0.044	0.041
R_w	0.044	0.039
Weighting scheme	$1.890\sigma^{-2}(F_o)$	$1.238\sigma^{-2}(F_o)$
Residual electron density (e Å^{-3})	+0.40/−0.61	+0.27/−0.24

powder diffractometer) with silicon (NIST 640b) as an internal standard. Single-crystal intensity data were collected on a modified STOE four-circle diffractometer at 300(2) K with graphite monochromated Mo-K_α radiation ($\lambda = 0.71069$ Å) and processed in the usual way (corrections: LP factor, absorption,[28] no extinction). Crystallographic data are given in Table 1.

Table 2. Selected bond distances (Å) and angles (°)

(a) Mn[(quin)(N$_3$)(H$_2$O)$_3$]H$_2$O (**1**)

Mn—O(1)	2.147(3)	Mn—O(3)	2.189(3)
Mn—O(4)	2.217(3)	Mn—O(5)	2.200(3)
Mn—N(1)	2.292(3)	Mn—N(11)	2.181(3)
O(1)—C(1)	1.245(4)	O(2)—C(1)	1.243(4)
N(1)—C(2)	1.333(4)	N(1)—C(6)	1.373(4)
N(11)—N(12)	1.167(4)	N(12)—N(13)	1.157(4)
O(1)—Mn—O(3)	89.2(1)	O(1)—Mn—O(4)	91.7(1)
O(1)—Mn—O(5)	88.3(1)	O(1)—Mn—N(1)	74.0(1)
O(3)—Mn—O(4)	91.8(1)	O(3)—Mn—O(5)	90.5(1)
O(3)—Mn—N(1)	163.1(1)	O(3)—Mn—N(11)	88.6(1)
O(4)—Mn—O(5)	177.7(2)	O(4)—Mn—N(1)	90.7(1)
O(4)—Mn—N(11)	92.4(1)	O(5)—Mn—N(1)	87.1(1)
O(5)—Mn—N(11)	87.7(1)	N(1)—Mn—N(11)	108.1(1)
Mn—O(1)—C(1)	119.5(2)	O(1)—Mn—N(11)	175.4(1)
Mn—N(1)—C(2)	112.1(2)	Mn—N(1)—C(6)	128.8(2)
Mn—N(11)—N(12)	127.9(3)	N(11)—N(12)—N(13)	179.4(5)
O(1)—C(1)—C(2)	117.4(3)	O(1)—C(1)—O(2)	124.6(3)
C(2)—C(1)—O(2)	118.0(3)	N(1)—C(2)—C(1)	115.6(3)
N(1)—C(2)—C(3)	123.2(3)	N(1)—C(6)—C(5)	121.5(3)
N(1)—C(6)—C(10)	119.0(3)	C(2)—N(1)—C(6)	118.6(3)

(b) Mn(H-quin)(quin)(NCS)(H$_2$O)$_2$ (**2**)

Mn—O(1)	2.158(5)	Mn—O(4)	2.228(5)
Mn—O(5)	2.180(5)	Mn—O(6)	2.203(6)
Mn—N	2.119(7)	Mn—N(1)	2.271(7)
S—C	1.626(9)	O(1)—C(10)	1.257(10)
O(2)—C(10)	1.273(10)	O(3)—C(20)	1.231(9)
O(4)—C(20)	1.266(9)	N—C	1.140(11)
N(1)—C(1)	1.354(10)	N(1)—C(5)	1.366(10)
N(2)—C(11)	1.331(10)	N(2)—C(15)	1.387(9)
O(1)—Mn—O(5)	171.4(2)	O(6)—Mn—N	172.5(3)
O(1)—Mn—O(4)	80.1(2)	O(1)—Mn—O(6)	89.9(2)
O(1)—Mn—N	97.5(2)	O(1)—Mn—N(1)	73.4(2)
O(4)—Mn—O(5)	96.6(2)	O(4)—Mn—O(6)	92.7(2)
O(4)—Mn—N	88.1(2)	O(4)—Mn—N(1)	153.4(2)
O(5)—Mn—O(6)	82.2(2)	O(5)—Mn—N	90.3(2)
O(5)—Mn—N(1)	109.9(2)	N—Mn—N(1)	93.7(3)
O(6)—Mn—N(1)	89.0(2)	Mn—N(1)—C(1)	114.4(5)
Mn—O(1)—C(10)	119.8(5)	Mn—O(4)—C(20)	131.5(5)
Mn—N—C	154.9(7)	N—C—S	178.7(7)
Mn—N(1)—C(5)	128.9(5)	C(1)—N(1)—C(5)	116.6(7)
C(11)—N(2)—C(15)	124.1(6)	N(1)—C(5)—C(6)	118.1(7)
N(1)—C(1)—C(10)	114.0(7)	N(1)—C(1)—C(2)	123.6(7)
N(1)—C(5)—C(4)	123.2(8)	O(1)—C(10)—C(1)	117.7(7)
O(1)—C(10)—O(2)	124.3(7)	C(1)—C(10)—O(2)	118.0(7)
C(20)—C(11)—N(2)	118.9(6)	N(2)—C(11)—C(12)	119.0(6)
N(2)—C(15)—C(14)	118.8(6)	N(2)—C(15)—C(16)	120.3(6)
O(4)—C(20)—O(3)	126.9(7)	O(3)—C(20)—C(11)	117.0(6)
O(4)—C(20)—C(11)	116.0(6)		

The structures were solved by direct methods. Anisotropic displacement parameters were only applied to the non-hydrogen atoms in blocked-matrix least-squares refinements. Hydrogen atoms with bonds to carbon atoms were geometrically generated; the positions of the remaining hydrogen atoms were located from difference fourier maps and included in the final refinement cycles with isotropic displacement values. The programs DIFABS,[28] SHELX-76,[29] SHELXS-86,[30] PLATON[31] and THE XRAY SYSTEM[32] were used for computations. Analytical expressions of neutral-atom scattering factors were employed and anomalous dispersion corrections were incorporated.[33] Selected bond distances and bond angles are given in Table 2, hydrogen bonding systems are collected in Table 3. Positional parameters, anisotropic thermal parameters, a full list of bond lengths and angles and observed and calculated structure factors have been deposited with the Editor as supplementary material.

Physical measurements

The IR absorption spectral bands of free and coordinated ligands are collected in Table 4. The experimental procedures and instruments used for spectral and other measurements have been given previously.[34]

DISCUSSION

The reaction between manganese(II) ion and quinaldic acid in the presence of azide ions in aqueous or aqueous ethanolic medium afforded only the title complex (**1**), whereas the same reaction in the presence of thiocyanate anion afforded two complexes, a yellow complex (**2**) and red crystals of a complex that has not yet been investigated. Trials to prepare crystals suitable for X-ray structure determination of the red complex are in progress. Complexes **1** and **2** are insoluble in cold or hot water, ethanol and acetone, but soluble in boiled DMF and DMSO giving rise to non-conducting solutions in these solvents.

The principal structural features of [Mn(quin)$(N_3)(H_2O)_3]\cdot H_2O$ (**1**) are illustrated in Figs 1 and 2. The coordination environment of each manganese(II) atom is distorted octahedron. The quinaldate anion chelates a metal atom via its ring nitrogen atom [Mn–N(1) = 2.292(3) Å] and a carboxylate oxygen atom [Mn—O(1) = 2.147(3) Å] to form a five-membered ring. The chelate ring deviates only 0.075(5) Å from planarity. Each manganese atom is further bonded to three aqua molecules at Mn—O distances from 2.189(3) to 2.217(3) Å. The coordination number six of the manganese atom is completed through its binding to a terminal azido group at an Mn—N(11) bond length of

Table 3. Hydrogen bond systems [bond lengths (Å) and angles (°)]

(a) Mn[(quin)$(N_3)(H_2O)_3]H_2O$ (**1**)

D—H···A	D···A	D—H	H···A	D—H···A
O(3)—H(1)···O(2)	2.737(4)	0.93(3)	1.85(3)	160(3)
O(3)—H(2)···N(13)	2.892(5)	0.88(3)	2.03(3)	166(4)
O(4)—H(3)···O(2)	2.708(4)	0.93(3)	1.78(3)	172(4)
O(4)—H(4)···O(6)	2.767(4)	0.91(3)	1.87(3)	169(3)
O(5)—H(5)···N(13)	2.913(4)	0.88(3)	2.04(2)	173(4)
O(5)—H(6)···O(6)	2.756(4)	0.89(3)	1.87(4)	172(4)
O(6)—H(7)···O(1)	3.018(4)	0.90(5)	2.42(5)	124(4)
O(6)—H(7)···O(1)	2.980(4)	0.90(5)	2.24(5)	140(4)
O(6)—H(8)···N(13)	2.935(5)	0.92(4)	2.08(5)	153(4)

(b) Mn(H-quin)(quin)$(NCS)(H_2O)_2$ (**2**)

D—H···A	D···A	D—H	H···A	D—H···A
O(5)—H(13)···O(2)	2.681(8)	0.96(5)	1.77(5)	159(6)
O(5)—H(14)···O(4)	2.747(7)	0.93(5)	1.83(5)	172(5)
O(6)—H(15)···O(3)	2.752(7)	0.96(7)	1.81(7)	166(7)
O(6)—H(16)···O(2)	2.815(8)	0.94(6)	1.91(5)	161(6)
N(2)—H(17)···O(1)	2.779(7)	0.99(5)	1.84(6)	159(6)
N(2)—H(17)···O(4)	2.724(7)	0.99(5)	2.27(6)	107(4)

D = donor atom, A = acceptor atom.

Table 4. IR spectral data (frequencies, cm^{-1})

Quinaldic acid	Complex **1**	Complex **2**	Assignments
3450 m	3450 vs, br	3500–3200 vs	Free or hydrogen-bonded H_2O
3100–2800 s	3200 vs		+hydrogen-bonded COOH+NH
2500 m, 1900 m			
	2060 vs, sp	2040 vs, sp	$\nu_{as}(N_3)$ or ν(CN)
1690 wm		1690	ν(CO)
	1650	1645	$\delta(H_2O)$
1640 ms	1625 vs	1615 vs	$\nu(COO^-)$
1380 vs[a]	1390 vs	1390 vs	ν(C—O)
1320 vs	1365 vs	1370 vs	
		1350 vs	
1615 vs	1625 vs	1615 vs	Quinoline ring
1580 vs	1610 vs	1585 vs	vibrations
1555 s	1555 s	1555 s	
1145 s	1170 m	1180 m	
1110 m	1150 m	1160 m	
		1140 wm	
		1120 w	
	1335 m		$\nu_s(N_3)$
	640 wm	480	$\delta(N_3)$ or δ(NCS)
	380 m	365 m	ν(Mn—O(H$_2$O))
	360 ms	340 m	ν(Mn—N$_3$) or ν(Mn—NCS)
	260 s	270 s	ν(Mn—O(quin))
	235 s	225 s	ν(Mn—N(quin))

v = very, s = strong, m = medium, w = weak, sp = sharp, br = broad.
[a] Split band.

2.181(3) Å, which is shorter than Mn—N(quin) but comparable with the corresponding distances [2.161(23) Å] found in the complex [Mn(3-pic)$_2$(N$_3$)$_2$(H$_2$O)$_2$][35] (**3**) also containing terminal azido groups. The terminal azido ligand in the title complex is linear [angle N—N—N = 179.4(5)°] and slightly asymmetric [N(11)—N(12) = 1.167(4) and N(12)—N(13) = 1.157(4) Å]. The maximum deviation [0.088(5) Å] from planarity within the quinaldato ligand anion shows the non-coordinated oxygen atom O(2). The isolated manganese(II) polyhedra are linked via hydrogen bonds of the types O—H···N and O—H···O to form a two-dimensional layer structure extended along the *ab*-plane of the unit cell. In this hydrogen bond system the oxygen atoms O(3)–O(6) of the water molecules act as donor atoms forming hydrogen bonds to the N(13) atom of the azide group, to both oxygen atoms of the quinaldate ligand and also to O(6) of the lattice water molecule (Table 3).

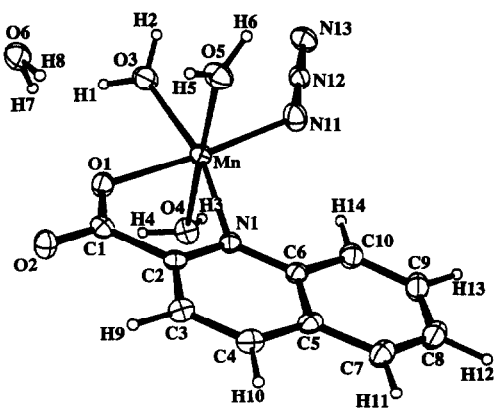

Fig. 1. Molecular structure and atom numbering scheme of Mn[(quin)(N$_3$)(H$_2$O)$_3$]H$_2$O (**1**).

The title complex (**1**) differs from the polymeric [Mn(picolinato)(N$_3$)(H$_2$O)] complex **4**, although both have octahedral manganese atoms. While the quinaldate anion acts as an N,O-bidentate ligand in complex **1**, the picolinato anion behaves as a tridentate ligand in complex **4**; it chelates a manganese atom via its nitrogen and carboxylate oxygen atom. This coordinated carboxylate oxygen atom further bridges another manganese atom giving rise to cyclic Mn$_2$O$_2$ units. These centrosymmetric dimeric units are connected by bridging μ(1,3) azido groups to form a two-dimensional layer structure along the *ab*-plane (Fig. 2, see ref. 24).

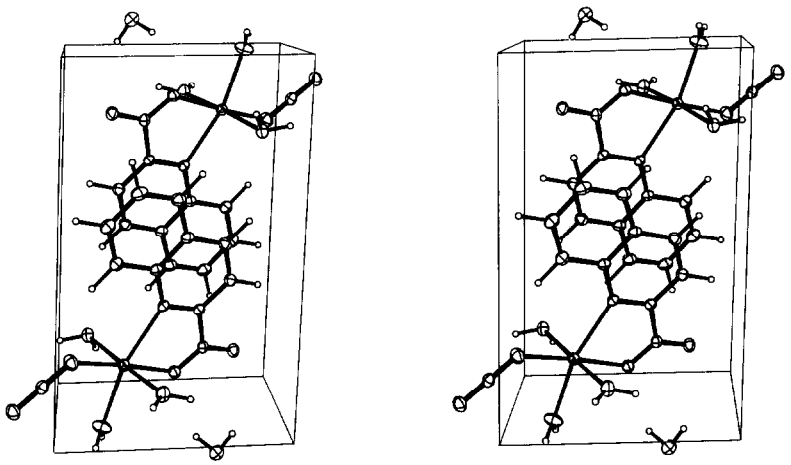

Fig. 2. Packing plot of $Mn[(quin)(N_3)(H_2O)_3]H_2O$ (**1**), viewed down the *b*-axis of the unit cell.

A plot with the atom numbering scheme of the $[Mn(quin)(H\text{-}quin)(NCS)(H_2O)_2]$ complex (**2**) is given in Fig. 3. The coordination geometry of the manganese(II) atom is also distorted octahedral. The quinaldate anion chelates a manganese atom, as in complex **1**, through its heterocyclic nitrogen atom [Mn—N(1) = 2.271(7) Å] and a carboxylate oxygen atom [Mn—O(1) = 2.158(5) Å]. These bond lengths are similar to the corresponding values in complex **1**. The manganese atom further links an O-monodentate neutral quinaldic acid molecule via its carboxylic oxygen at an Mn—O(4) distance of 2.228(5) Å, which is longer than the corresponding Mn—O distance with the quinaldate anion and two aqua molecules at Mn—O bond lengths of 2.180(5) and 2.203(6) Å, which are very close to those found in complex **1**. The octahedral geometry of the manganese atom is completed through its binding to a terminal N-thiocyanato group [Mn—N = 2.119(7) Å]. The thiocyanate group is linear [angle N—C—S = 178.7(7)°]. The manganese(II) atom is almost co-planar [0.039(4) Å] to the quinaldato anion molecule. The heteroatomic ring system of the quinaldate ligand is planar within experimental error, but its carboxylate group has a distortion of approximately 9(1)° from the ring plane. The maximum deviation from planar geometry within the neutral quinaldic acid molecule has the oxygen atom O(4) [0.09(1) Å]. Intermolecular hydrogen bonds of the type O—H···O between the water molecules and the oxygen atoms of the carboxylic groups of both heteroatomic ring ligands link manganese(II) polyhedra to form one-dimensional chains along the *a*-axis of the unit cell. In addition, possible intramolecular hydrogen bonds of the type N—H···O occur (Table 3).

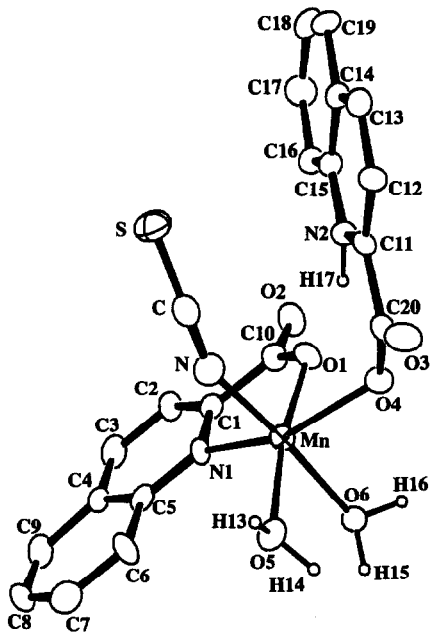

Fig. 3. Molecular structure and atom numbering scheme of $Mn(H\text{-}quin)(quin)(NCS)(H_2O)_2$ (**2**). H(1)–H(12) are omitted for clarity.

It is of interest to compare the mixed-ligand complexes **1**–**4** and $Mn(pyridine)_2(N_3)_2$ (**5**).[36] A common structural feature of this series is a six-coordination about the manganese atoms. In complexes **3** and **5** with monodentate picoline and pyridine, respectively, the azido groups function as $\mu(1,3)$ bridging in **5**, whereas in **3** the presence of two aqua molecules hinders the bridging mode of the azido ligands enforcing them to act as terminal groups. In complex **4** the picolinato anion acts as a chelating

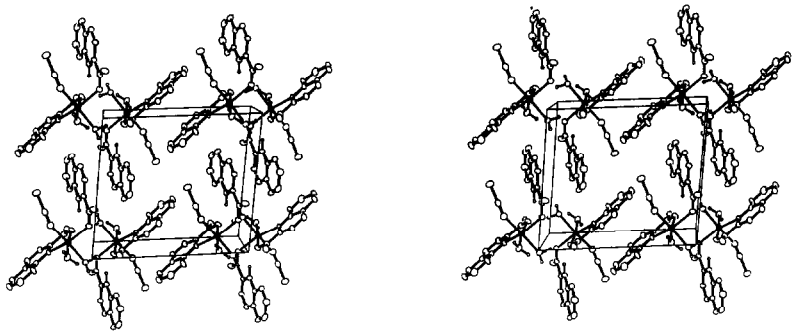

Fig. 4. Packing plot of Mn(H-quin)(quin)(NCS)(H$_2$O)$_2$ (**2**), viewed down the *a*-axis of the unit cell. H(1)–H(12) are omitted for clarity.

bridging tridentate ligand and the fourth coordination site is occupied by an aqua molecule, therefore, the other two sites are satisfied by bridging the azido ligand in the fashion $\mu(1,3)$ between two metal centres. In complexes **1** and **2** a quinaldate anion acts as a bidentate chelating ligand. The remaining four sites are occupied by three aqua molecules and a terminal azido group in complex **1**, whereas two aqua molecules and a terminal N-thiocyanato ligand occupies three sites in complex **2** which makes the neutral quinaldic acid molecule act as a monodentate ligand. It is noticeable that in all manganese(II) azido complexes known up until now the azido ligands act either as terminal or as $\mu(1,3)$ bridging ligands. Bridging azido ligands of the type $\mu(1,1)$ were observed only once before in the structure of [(CO)$_3$Mn(N$_3$)$_3$Mn(CO)$_3$].[37]

Previous studies have shown that no bands due to the C=O stretching vibration could be observed in the vicinity of 1700 cm^{-1} in the IR spectrum of free quinaldic acid as a result of hydrogen-bond formation between carboxylic hydrogen and the nitrogen atoms.[38] In accordance with this a weak-to-medium intensity band is observed at 1690 cm^{-1} in the IR spectrum of our sample. The hydrogen-bond formation is indicated by the appearance of the N—H stretching vibrations[39] around 3200–2400 and 1950–1900 cm^{-1}. Examination of Table 4 shows that a medium band at 1690 cm^{-1} due to ν(C=O) appears only in the spectrum of complex **1**. In the IR spectra of both complexes, however, a very strong band is observed around 1620 cm^{-1} due to the COO$^-$ stretching vibration. The C—O stretching vibration which appears at 1320 cm^{-1} in the IR spectrum of free acid is shifted to higher frequencies and appears at 1365 cm^{-1} in complex **1**. The appearance of two very strong bands at 1370 and 1350 cm^{-1} associated with ν_s(C—O) in the spectrum of complex **2** indicates the existence of a coordinated quinaldate anion as well as a neutral quinaldic acid molecule. The vibration frequencies related to the quinoline ring are shifted to higher frequencies in the spectrum of complex **1** as compared with the corresponding frequencies in the spectrum of free quinaldic acid. These results suggest that the quinaldate anion acts as an N,O-bidentate ligand in complex **1**. The IR spectrum of complex **2**, on the other hand, shows quinoline ring vibrations at higher frequencies as well as vibrations at more or less the same frequencies for free H-quin. This result suggests that complex **2** contains N,O-bidentate as well as O-monodentate ligand molecules. Free and coordinated water molecules as well as hydrogen-bonded carboxylic groups are indicated by the appearance of strong and broad bands in the range 3500–2500 cm^{-1}.[40] The above results are consistent with the X-ray structures given above for both complexes (Figs 2 and 4).

The ν_{as}(N$_3$) mode which appears as a very strong and sharp band at 2060 cm^{-1} in the spectrum of the manganese(II) azide complex is consistent with a structure containing only terminal azide ligands. The medium band at 1335 cm^{-1} associated with the ν_s(N$_3$) mode supports the asymmetric nature of the azide group.[41] In the IR spectrum of complex **2** ν(CN) which appears as a very intense band at 2040 cm^{-1} is consistent with the terminal N-bonded thiocyanato group.[42] This conclusion is supported by the appearance of δ(NCS) at 480 cm^{-1}.

In the far-IR region we tentatively assigned to the metal–ligand vibrations the following frequencies;[42] bands around 370 cm^{-1} to ν[Mn—O(H$_2$O)], those around 350 cm^{-1} due to ν[Mn—N(N$_3$ or NCS)], bands around 270–250 cm^{-1} to ν[Mn—O(quin)] and 240–220 cm^{-1} to ν[Mn—N(quin)].

Acknowledgement—The authors thank Prof. Ch. Kratky for use of his experimental equipment.

REFERENCES

1. A. Vogel, *A Textbook of Quantitative Inorganic Analysis*, 3rd edn. Longman, London (1962).
2. R. A. K. Majumdar and J. O. Gupta, *Z. Anal. Chem.* 1958, **161**, 100.
3. R. A. K. Majumdar and J. O. Gupta, *Z. Anal. Chem.* 1958, **161**, 181.
4. R. A. K. Majumdar and J. P. Bag, *Anal. Chim. Acta* 1960, **22**, 549.
5. B. W. Banerjee and J. P. Ray, *Ind. Chem. Soc.* 1958, **35**, 299.
6. K. Shinra and K. Y. Kawa, *J. Chem. Soc. Japan* 1954, **75**, 44.
7. F. Holms and W. R. C. Crimmen, *J. Chem. Soc.* 1955, 1175.
8. F. Holms and W. R. C. Crimmen, *J. Chem. Soc.* 1955, 3467.
9. J. Ray and D. Nathser, *J. Ind. Chem. Soc.* 1948, **25**, 479.
10. G. Thomas and R. A. Paris, *Anal. Chim. Acta* 1961, **25**, 159.
11. P. O. Lumme, *Suom. Kemi.* 1959, **B32**, 203.
12. M. B. Koromantzou and G. A. Pneimeticakis, *Chem. Ind.* 1967, **25**, 1089.
13. A. Kumar and J. Buddhodwesen, *J. Ind. Chem. Soc.* 1950, **27**, 245.
14. R. L. Dutta and L. Subratta, *Sci. Cult.* 1962, **26**, 139.
15. P. O. Lumme, *Suom. Kemi.* 1962, **B35**, 294.
16. G. Condorelli and A. Siminara, *Bull. Acad. Gioenia (Catania)* 1966, **48**, 799.
17. A. Siminara and A. Musumesi, *J. Inorg. Nucl. Chem.* 1977, **39**, 599.
18. M. A. S. Goher, R.-J. Wang and T. C. W. Mak, *Inorg. Chim. Acta* 1990, **20**, 245.
19. B. Elman, A. G. S. Högberg, M. Weber and M. Muhammed, *Polyhedron* 1985, **4**, 1197.
20. B. Elman, A. G. S. Högberg, C. Moberg and M. Muhammed, *Polyhedron* 1986, **5**, 1917.
21. I. Csöregh, B. Elman, A. G. S. Högberg, C. Moberg and M. Nygren, *Inorg. Chem.* 1988, **27**, 235.
22. M. A. S. Goher and T. C. W. Mak, *Inorg. Chim. Acta* 1985, **99**, 223.
23. Z. Dori and R. F. Ziolo, *Chem. Rev.* 1973, **73**, 247.
24. M. A. S. Goher, M. A. M. Abu-Youssef, F. A. Mautner and A. Popitsch, *Polyhedron* 1992, **11**, 2137.
25. F. A. Mautner and M. A. S. Goher, *Polyhedron* 1992, **11**, 2537.
26. M. A. S. Goher and F. A. Mautner, *Z. Naturforsch.* 1991, **46B**, 687.
27. K. D. Karlin and J. Zubieta (Editors), *Copper Coordination Chemistry; Biochemical and Inorganic Perspectives*. Adenine Press, New York (1983).
28. N. Walker and D. Stuart, *Acta Cryst.* 1983, **A39**, 158.
29. G. M. Sheldrick, SHELX-76, A Program for Crystal Structure Determination. University Chemical Laboratory, Cambridge (1976).
30. G. M. Sheldrick, SHELXS-86. Universität Göttingen, F.R.G. (1986).
31. A. L. Spek, in *Computational Crystallography* (Edited by D. Sayre), p. 528. Clarendon Press, Oxford (1982).
32. J. M. Stuart, The X-RAY SYSTEM, Version of 1976, Technical Report TR-466. University of Maryland, College Park (1976).
33. *International Tables for X-ray Crystallography*, Vol. IV, pp. 99 and 149. Kynoch Press, Birmingham (1974).
34. M. A. S. Goher, R.-J. Wang and T. C. W. Mak, *Polyhedron* 1992, **11**, 829.
35. F. A. Mautner and M. A. S. Goher, *Cryst. Res. Technol.* 1990, **25**, 1271.
36. M. A. S. Goher and F. A. Mautner, *Croat. Chim. Acta* 1990, **63**, 559.
37. R. Mason, G. A. Rasholme, W. Beck, H. Engelmann, K. Joos, B. Lindenberg and H. S. Smedal, *J. Chem. Soc., Chem. Commun.* 1971, 496.
38. G. Thomas, *Bull. Soc. Chim. Fr.* 1960, 796.
39. N. N. Greenwood and K. Wade, *J. Chem. Soc.* 1960, 1130.
40. L. C. Nathan, D. C. Zapien, A. M. Mooring, C. A. Doyle and J. A. Brown, *Polyhedron* 1989, **8**, 745.
41. M. A. S. Goher, *Acta Chim. Hung.* 1990, **127**, 227 and refs therein.
42. K. Nakamoto, *Infrared and Raman Spectra of Inorganic and Coordination Compounds*. John Wiley, New York (1978).

Polyhedron Vol. 12, No. 15, pp. 1871–1878, 1993
Printed in Great Britain

0277–5387/93 $6.00+.00
© 1993 Pergamon Press Ltd

SYNTHESIS AND CHARACTERIZATION OF SOME METAL(II) COMPLEXES OF QUINOLINIC ACID (H_2-Quin) AND X-RAY CRYSTAL STRUCTURES OF $[Ni(H\text{-}Quin)_2(H_2O)_2]$ AND $[Mn(H_2O)_6][Mn(H\text{-}Quin)_3]_2$

MOHAMED A. S. GOHER* and ADEL A. YOUSSEF

Department of Chemistry, Faculty of Science, Alexandria University, P.O. Box 426 Ibrahimia, Alexandria 21321, Egypt

and

ZHONG-YUAN ZHOU and THOMAS C. W. MAK

Department of Chemistry, The Chinese University of Hong Kong, Shatin, New Territories, Hong Kong

(*Received* 22 *February* 1993; *accepted* 2 *April* 1993)

Abstract—Complexes of the types $M(H\text{-}Quin)_2 \cdot 2H_2O$ (M = Mn, Co, Ni and Zn) and $M(H_2\text{-}Quin)(Quin) \cdot 2H_2O$ (M = Fe and Co), where H_2-Quin = quinolinic acid, have been prepared and characterized. The spectral results suggest that all these complexes contain distorted octahedral metal atoms. The crystal structures of the nickel(II) and manganese(II) complexes were determined by single-crystal X-ray diffraction methods. The nickel atom in centrosymmetric $Ni(H\text{-}Quin)_2 \cdot 2H_2O$ is octahedrally coordinated by two nitrogen atoms [Ni—N = 2.030(2) Å] and two oxygen atoms [Ni—O = 2.027(2) Å] belonging to the two $H\text{-}Quin^-$ anions and two *trans*-aqua molecules at Ni—O distances of 2.117(2) Å. The structure is consolidated by intra- and intermolecular O—H···O hydrogen bonds. X-ray analysis of the $Mn(H\text{-}Quin)_2 \cdot 2H_2O$ complex revealed that it should be formulated as $[Mn(H_2O)_6][Mn(H\text{-}Quin)_3]_2$. The octahedral $[Mn(H\text{-}Quin)_3]^-$ and $[Mn(H_2O)_6]^{2+}$ units lie on different three-fold axes and are connected together by O—H···O hydrogen bonds between the aqua ligands and the non-coordinated oxygen of a carboxylato group or oxygen atoms of the carboxy group in position 3 in the pyridine ring.

The reaction of some metal(II) salts with quinolinic acid, otherwise called pyridine-2,3-dicarboxylic acid, have been reported to produce complexes of the type $M(quinolinato) \cdot nH_2O$, where M = Mn, Fe, Co, Ni, Cu and Zn and n = 0–2, and the thermal properties of these solid complexes were studied.[1] Other metal(II) complexes of this ligand, either anhydrous or hydrated, have also been mentioned in the literature,[2–7] but definitive crystallographic data are lacking for these materials. X-ray structure determination has been performed only for the dihydrated silver(II) complex of quinolinic acid.[7] Recently we have been interested in the study of metal complexes of pyridine dicarboxylic acids[8] and described the structure of $[AuBr_4][K(dinicotinic\ acid)_6]$.[9] In this paper we report the synthesis and characterization of Mn^{II}, Fe^{II}, Co^{II}, Ni^{II} and Zn^{II} complexes of quinolinic acid (hereafter abbreviated as H_2-Quin) and X-ray structures of the nickel and manganese complexes.

EXPERIMENTAL

Quinolinic acid was obtained from Aldrich and the other chemicals were of analytical grade.

Preparation of the complexes

Complexes of the type $M(H\text{-}Quin)_2 \cdot 2H_2O$ were generally prepared by mixing metal(II) nitrate or

* Author to whom correspondence should be addressed.

Table 1. Analytical data

Complex	Colour	Analysis: Found (Calc.) C	H	N	M
$Mn(H\text{-}Quin)_2 \cdot 2H_2O$	Yellow	39.6 (39.7)	3.0 (2.9)	6.5 (6.6)	13.3 (13.0)
$Co(H\text{-}Quin)_2 \cdot 2H_2O$	Orange	39.5 (39.4)	2.7 (2.8)	6.8 (6.6)	14.0 (13.8)
$Ni(H\text{-}Quin)_2 \cdot 2H_2O$	Sky blue	39.2 (39.4)	2.9 (2.8)	6.7 (6.6)	13.7 (13.8)
$Zn(H\text{-}Quin)_2 \cdot 2H_2O$	Colourless	39.0 (38.8)	3.0 (2.8)	6.3 (6.5)	15.3 (15.1)
$Co(H_2\text{-}Quin)(Quin) \cdot 2H_2O$	Pink	39.4 (39.4)	2.6 (2.8)	6.6 (6.6)	13.6 (13.8)
$Fe(H_2\text{-}Quin)(Quin)_2 \cdot 2H_2O$	Red–brown	39.7 (39.7)	2.9 (2.8)	6.7 (6.6)	13.5 (13.2)

sulphate (5 mmol) and the ligand (12 mmol) in water (30 cm^3) and boiling the mixture for several minutes until a clear solution was obtained. The mixture was then allowed to stand over several days until a crystalline product of the complex separated. In the case of the manganese complex $MnCl_2 \cdot 3H_2O$ was used and the final mixture allowed to stand in the dark.

Complexes of the type $M(H_2\text{-}Quin)(Quin) \cdot 2H_2O$ (M = Fe or Co) were prepared in the same manner except that ethanol was used as a solvent instead of water. The products were filtered off, washed with hot water or ethanol and dried *in vacuo*.

Elemental analyses of the complexes isolated are given in Table 1.

Physical measurements

Magnetic susceptibility measurements were performed on the modified Faraday balance SUS 10 (A. Paar KG, Graz, Austria). The accuracy and reproducibility of the data is about 2%. Corrections were made using Pascal's constants. IR and electronic spectra and other measurements were performed as described previously.[10]

Table 2 contains the magnetic moments as well as spectral data of the isolated complexes.

X-ray structure analysis

The nickel(II) and manganese(II) complexes are handled in the same manner. Diffraction measurements were made on a Nicolet R3m/V four-circle diffractometer (graphite-monochromatized Mo-K_α radiation, $\lambda = 0.71069$ Å) and determination of the crystal class, orientation matrix and accurate unit cell parameters were performed according to established procedures.[11] Intensities were recorded at 18°C and data collection and processing parameters are summarized in Table 3. The raw inten-

Table 2. Magnetic and spectra data

Compound	Magnetic moment, μ_B[a]	Electronic spectra (λ, cm^{-1})	ν(C=O)+ν_{as}(COO)	ν_s(COO)
$Mn(H\text{-}Quin)_2 \cdot 2H_2O$	5.73		1695s, 1640 m	1360 s
$Co(H\text{-}Quin)_2 \cdot 2H_2O$	5.12	21,505 sh, 20,000, 18,690 sh	1680 m, 1535 sh	1370 s
$Ni(H\text{-}Quin)_2 \cdot 2H_2O$	3.27	26,300 sh, 19,200, 16,400	1675 ms, 1530 sh	1365 m
$Zn(H\text{-}Quin)_2 \cdot 2H_2O$	Diamagnetic		1685 s, 1640 m	1370 s
$Co(H_2\text{-}Quin)(Quin) \cdot 2H_2O$	5.18	26,600, 19,200	1740, 1725 s 1640 s	1375 s, 13490 s 1310 s
$Fe(H_2\text{-}Quin)(Quin) \cdot 2H_2O$	5.35	19,000, 11,000	1740 vs, 1720 s 1610 s	1380 s, 1330 s 1310 ms
H_2-Quin			1710 m, 1665 m	1305 m

[a] At 296 K, m = medium, s = strong, sh = shoulder, v = very.

Table 3. Data collection and processing parameters

Molecular formula	$Ni(C_7H_4NO_4)_2(H_2O)_2$	$2[Mn(C_7H_4NO_4)]\cdot[Mn(H_2O)_6]$
Molecular weight	426.99	1269.66
Colour and habit	Colourless prism	Yellow plate
Unit cell parameters		
a (Å)	9.228(5)	14.633(3)
b (Å)	7.946(3)	14.633(3)
c (Å)	10.400(6)	6.349(2)
α (°)	90	90
β (°)	95.02(5)	90
γ (°)	90	120(2)
V (Å^3)	759.7(0.7)	1177.3(0.6)
Z	2	1
$F(000)$	436	645
Density (calc.) (g cm^{-3})	1.87	1.79
Space group	$P2_1/n$ (No. 14)	$P\bar{3}$ (No. 143).
Radiation	Graphite monochromatized Mo-K_α, $\lambda = 0.71073$ Å	
Standard reflections	(0, 5, −1), (3, 2, 3)	(6, 3, 0); (6, −2, 1)
Intensity variation	±1.4%	±1.1%
R_{int} (from merging of equivalent reflections)	±0.0162	0.042
Absorption coefficient (cm^{-1})	13.44	8.67
Crystal size (mm^3)	0.40 × 0.32 × 0.04	0.16 × 0.68 × 0.42
Mean μr	0.24	0.24
Transmission factors	0.510–0.599	0.693–0.945
Scan type and rate (° min^{-1})	ω-scan: 3.00–15.62	
Scan range	0.8° below $K\alpha_1$ to 0.8° above $K\alpha_2$	
Background counting	Stationary counts for one-fifth of scan time at each end of scan range	
Collection range	$h, k, \pm 1$; $2\theta_{max} = 65°$	$h, k, \pm 1$; $2\theta_{max} = 60°$
Unique data measured	2940	3394
Observed data with $\|F_o\| \geq 6\sigma(\|F_o\|)$, n	2069	2789
No. of variables, p	124	244
$R_F = \Sigma\|\|F_o\|-\|F_c\|\|/\Sigma\|F_o\|$	0.039	0.038
Weighting scheme, w	$[\sigma^2(F_o)+0.0003\|F_o\|^2]^{-1}$	
$R_G = [\Sigma w(\|F_o\|-\|F_c\|)^2/\Sigma w\|F_o\|^2]^{1/2}$	0.053	0.047
$S = [\Sigma w(\|F_o\|-\|F_c\|)^2/(n-p)]^{1/2}$	2.05	1.89
Residual extrema in final difference map (e Å^3)	+0.30 to −0.50	+0.61 to −0.32

sities were processed with a learnt-profile procedure[12] and absorption corrections were applied using a pseudo-ellipsoidal fit to azimuthal scans of selected strong reflections.[13,14]

The structure was solved by Patterson superposition and Fourier methods. All non-hydrogen atoms in the asymmetric unit were subjected to anisotropic refinement. The aromatic hydrogen atoms were generated geometrically (C—H fixed at 0.96 Å), allowed to ride on their respective parent carbon atoms and included in structure factor calculations with assigned isotropic thermal parameters. The carboxyl and aqua hydrogen atoms were located from difference maps. All computations were performed using a DEC MicroVAX-II computer with the SHELXTL-PLUS system.[15,16] Analytical expressions of neutral atom scattering factors incorporating the real and imaginary components of anomalous dispersion were employed.[17] Least-squares refinement converged to the R indices and other parameters listed in Table 3. Selected bond distances and bond angles are given in Table 4. Anisotropic thermal parameters and structure factors are available from the last author upon request and have also been deposited with the Editor and the Cambridge Crystallographic Data Centre.

RESULTS AND DISCUSSION

The reactions between Mn^{II}, Co^{II}, Ni^{II} and Zn^{II} salts and H_2-Quin in aqueous solution afforded complexes of the type $M(H\text{-}Quin)_2\cdot 2H_2O$. On the other hand, reactions in ethanolic media led to the

Table 4. Bond lengths (Å) and angles (°)

$Ni(H\text{-}Quin)_2 \cdot 2H_2O$, complex **1**

Ni(1)—N(1)	2.030(2)	Ni(1)—O(1)	2.027(2)
Ni(1)—O(5)	2.117(2)		
N(1)—C(1)	1.351(3)	N(1)—C(5)	1.333(3)
O(2)—C(6)	1.251(2)	O(2)—C(6)	1.261(3)
O(3)—C(7)	1.291(3)	O(4)—C(7)	1.231(3)
C(1)—C(2)	1.410(3)	C(1)—C(6)	1.536(3)
C(2)—C(3)	1.402(3)	C(2)—C(7)	1.522(3)
C(3)—C(4)	1.372(3)	C(4)—C(5)	1.388(3)
N(1)—Ni(1)—O(1)	79.3(1)	N(1)—Ni(1)—O(5)	89.0(1)
O(1)—Ni(1)—O(5)	90.1(1)		
Ni(1)—N(1)—C(1)	116.2(1)	Ni(1)—N(1)—C(5)	122.7(1)
C(1)—N(1)—C(5)	121.1(2)		
Ni(1)—O(1)—C(6)	116.5(1)	N(1)—C(1)—C(2)	120.7(2)
N(1)—C(1)—C(6)	110.8(2)	N(1)—C(5)—C(4)	121.5(2)
C(2)—C(1)—C(6)	128.5(2)	C(1)—C(2)—C(3)	117.0(2)
C(1)—C(2)—C(7)	128.2(2)	C(3)—C(2)—C(7)	114.8(2)
C(2)—C(3)—C(4)	121.3(2)	C(3)—C(4)—C(5)	118.4(2)
O(1)—C(6)—O(2)	122.4(2)	O(1)—C(6)—C(1)	117.1(2)
O(2)—C(6)—C(1)	120.5(2)	O(3)—C(7)—O(4)	120.1(2)
O(3)—C(7)—C(2)	120.9(2)	O(4)—C(7)—C(2)	118.9(2)

$2[Mn(H\text{-}Quin)_3] \cdot [Mn(H_2O)_6]$, complex **2**

Mn(1)—O(1)	2.142(3)	Mn(1)—N(1)	2.286(3)
Mn(2)—O(5)	2.131(3)	Mn(2)—N(2)	2.257(4)
Mn(3)—O(9)	2.168(3)	Mn(3)—O(10)	2.173(4)
O(1)—C(6)	1.248(4)	O(2)—C(6)	1.257(5)
O(3)—C(7)	1.335(5)	O(4)—C(7)	1.210(6)
O(5)—C(13)	1.265(6)	O(6)—C(13)	1.237(4)
O(7)—C(14)	1.272(5)	O(8)—C(14)	1.211(4)
N(1)—C(1)	1.331(4)	N(1)—C(5)	1.312(5)
N(2)—C(8)	1.363(5)	N(2)—C(12)	1.355(4)
C(1)—C(2)	1.392(4)	C(1)—C(6)	1.506(5)
C(2)—C(3)	1.337(4)	C(2)—C(7)	1.486(4)
C(3)—C(4)	1.435(4)	C(4)—C(5)	1.387(4)
C(8)—C(9)	1.398(6)	C(8)—C(13)	1.523(5)
C(9)—C(10)	1.428(4)	C(9)—C(14)	1.507(5)
C(10)—C(11)	1.324(6)	C(11)—C(12)	1.380(7)
O(1)—Mn(1)—N(1)	74.3(1)	O(1)—Mn(1)—O(1a)	97.5(1)
N(1)—Mn(1)—O(1a)	100.2(1)	O(5)—Mn(2)—N(2)	74.6(1)
N(1)—Mn(1)—N(1b)	92.7(1)	N(2)—Mn(2)—O(5a)	101.1(2)
O(5)—Mn(2)—O(5a)	94.3(1)	N(2)—Mn(2)—N(2a)	92.8(1)
O(9)—Mn(3)—O(10)	85.0(1)	O(9)—Mn(3)—O(9a)	93.3(1)
O(10)—Mn(3)—O(10a)	94.1(1)	O(10)—Mn(3)—O(9b)	87.6(1)
Mn(1)—O(1)—C(6)	119.8(3)	Mn(2)—O(5)—C(13)	119.5(2)
Mn(1)—N(1)—C(1)	111.2(2)	Mn(1)—N(1)—C(5)	127.0(2)
C(1)—N(1)—C(5)	121.3(3)	Mn(2)—N(2)—C(8)	113.3(2)
Mn(2)—N(2)—C(12)	129.2(3)	C(8)—N(2)—C(12)	117.0(4)
N(1)—C(1)—C(2)	120.6(3)	N(1)—C(1)—C(6)	116.8(3)
C(2)—C(1)—C(6)	122.6(3)	C(1)—C(2)—C(3)	119.4(3)
C(1)—C(2)—C(7)	124.4(3)	C(3)—C(2)—C(7)	116.2(3)
C(2)—C(3)—C(4)	119.8(3)	C(3)—C(4)—C(5)	116.7(3)
N(1)—C(5)—C(4)	121.8(3)	O(1)—C(6)—O(2)	124.7(4)

Table 4—*continued.*

O(1)—C(6)—C(1)	116.7(3)	O(2)—C(6)—C(1)	118.3(3)
O(3)—C(7)—O(4)	120.9(3)	O(3)—C(7)—C(2)	112.8(3)
O(4)—C(7)—C(2)	126.1(3)	N(2)—C(8)—C(9)	123.0(3)
N(2)—C(8)—C(13)	113.0(4)	C(9)—C(8)—C(13)	123.6(3)
C(8)—C(9)—C(10)	116.7(3)	C(8)—C(9)—C(14)	122.5(3)
C(10)—C(9)—C(14)	120.6(4)	C(9)—C(10)—C(11)	119.9(4)
C(10)—C(11)—C(12)	120.6(3)	N(2)—C(12)—C(11)	122.6(4)
O(5)—C(13)—O(6)	126.1(3)	O(5)—C(13)—C(8)	117.3(3)
O(6)—C(13)—C(8)	116.6(4)	O(7)—C(14)—O(8)	129.9(4)
O(7)—C(14)—C(9)	111.1(3)	O(8)—C(14)—C(9)	118.6(3)

Symmetry transformation: a $(-y, x-y, z)$, b $(y-x, -x, z)$.

isolation of $M(H_2\text{-Quin})(Quin)\cdot 2H_2O$ only in the case of M = Fe and Co. Complexes of the first type are insoluble in cold water, alcohol, acetone and chloroform, but slightly soluble in hot water and DMF and reprecipitated upon cooling. Those of the other type are soluble in water and ethanol.

IR spectral data (Table 2) of the solid complex differentiate between the two types of compounds. Complexes of the type $M(H\text{-Quin})_2\cdot 2H_2O$ (M = Mn, Co, Ni and Zn) exhibit spectra which are consistent with $H\text{-Quin}^-$ coordination. In this case ν(C=O) of the carboxyl group in position 3 appears as a medium to strong band just below 1700 cm^{-1} and $\nu_{as}(COO^-)$ of the α-carboxylate group as a shoulder or medium band around 1635 cm^{-1}. On the other hand, ν_s(COO) which appeared at 1305 cm^{-1} in the free acid is shifted to higher frequencies in the spectra of these complexes and appears around 1360–1380 cm^{-1}. Complexes of the other type exhibit at least two IR bands above 1700 cm^{-1}, similar to those observed for coordinated neutral dipicolinic acid,[18] in addition to a band around 1630 cm^{-1}. In the region 1300–1280 cm^{-1} where ν_s(COO) appears, several bands corresponding to H_2-Quin and $Quin^{2-}$ are observed. Crystal structure determination has shown that bis(pyridine-2,6-dicarboxylate)silver(II) monohydrate contains two different ligand molecules, namely anionic dipicolinate and neutral dipicolinic acid.[19] Both ligands, however, have the same tridentate coordination modes. One may assume a similar composition for the pyridine-2,3-dicarboxylic acid molecules in complexes of the type $M(H_2\text{-Quin})(Quin)\cdot 2H_2O$. The typical upward shift of the major pyridine ring bands is indicative of coordination of the ring nitrogen in all complexes of both types. A strong broad band centred at *ca* 3450 cm^{-1} appears in the spectra of all complexes due to the presence of aqua molecules.[20,21] The extremely broad band in the 3100–2400 cm^{-1} range due to hydrogen bonded COOH groups in H_2-Quin or $H\text{-Quin}^-$ appears in the spectra of the above complexes.

The electronic spectra of the complexes are summarized in Table 2. Spectra of nickel(II) and cobalt (II) complexes are typical of six-coordinate species, most of the absorption bands having clearly defined shoulders that suggest distortions from octahedral symmetry. The iron(II) complex shows the broad spin-allowed $^5T_{2g}$–$^5F_{2g}$ transition band in O_h symmetry,[22] which is similar to other iron(II) complexes.[23]

Room-temperature magnetic data (Table 2) are consistent with high-spin six-coordinate $M(H\text{-Quin})_2\cdot 2H_2O$ and $M(H_2\text{-Quin})(Quin)\cdot 2H_2O$ com-

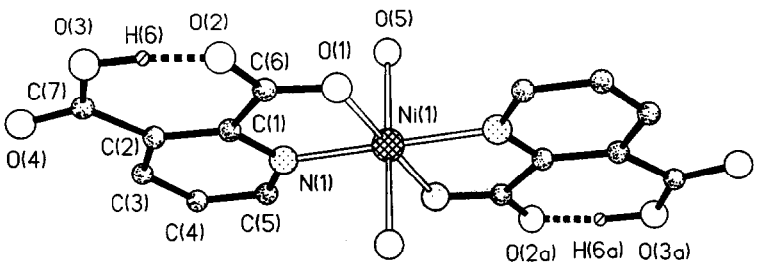

Fig. 1. The coordination environment of the nickel(II) atom in the complex $Ni(H\text{-Quin})_2\cdot 2H_2O$ (1), along with the atom numbering scheme.

plexes. The observed magnetic moments are similar to those of $M(H\text{-dipic})_2 \cdot 3H_2O$, $M(dipic) \cdot nH_2O$ and $M_2(dipic)(H\text{-dipic})_2 \cdot nH_2O$.[24,25] The magnetic susceptibility of the $Ni(H\text{-Quin})_2 \cdot 2H_2O$ complex was measured over the range 78–296 K. The χ_M data obey very well the Curie–Weiss law and $1/\chi_M$ vs T gives a straight line. The small θ value (-1.1 K) is indicative of the absence of magnetic interaction between nickel centres. These results are consistent with the results of crystal structure determination of the nickel(II) complex.

Figure 1 illustrates the structural features of the centrosymmetric $Ni(H\text{-Quin})_2 \cdot 2H_2O$ complex **1**. The (2 + 2 + 2) coordination about the nickel atom can be described as an elongated octahedron with aqua ligands occupying the axial positions. The Ni—N bond length of 2.030(2) Å is a little longer, whereas Ni—O(L) distances of 2.027(2) Å a little shorter than the corresponding distances reported for $Ni(H\text{-dipic})_2 \cdot 2H_2O$ [1.974(14) Å for Ni—N and 2.105(15)–2.207(6) Å for Ni—O].[26,27] Structurally the present complex is very similar to *trans*-diaquabis(pyridine-2-carboxylato)nickel(II) tetrahydrate, which has a comparable axial Ni—O(aqua) bond of 2.100(11) Å and longer equatorial Ni—L bonds [Ni—O = 2.053(7), Ni—N = 2.068(10) Å].[28]

The structure of complex **1** differs from that of $Ag(H\text{-Quin})_2 \cdot 2H_2O$ (**3**).[7] The latter complex consists of $Ag(H\text{-Quin})_2$, where each ligand molecule is strongly bonded to the silver(II) atom through the nitrogen atom and an oxygen atom of the carboxy group in the 2-position. The ketonic oxygen atoms of the twisted 3-carboxy groups form weak interactions [2.98 Å] with the silver atom in adjacent molecules, giving rise to a tetragonally distorted octahedron. The lattice water molecules are in positions to form hydrogen bonds with the oxygen atoms of the carboxy groups in the 2- and 3-positions.

A perspective view of the crystal structure of **1** along the *b*-axis is shown in Fig. 2. There are two kinds of hydrogen bonding interactions: an intramolecular O(3)—H···O(2) hydrogen bond similar to that in the crystal structure of free quinolinic acid [O···O = 2.398(3) Å][29] and an intermolecular O(5)—H···O(4) hydrogen bond linking the aqua ligand of one complex with the carboxy group of an adjacent complex. The structure is consolidated by intermolecular hydrogen bonds that are arranged in spirals along the two axes in the unit cell.

The X-ray structural analysis revealed that the complex $Mn(H\text{-Quin})_2 \cdot 2H_2O$ (**2**) should be reformulated as $[Mn(H_2O)_6][Mn(H\text{-Quin})_3]_2$, as seen from Fig. 3 which illustrates the essential structure components. The structure consists of a packing of octahedral $[Mn(H\text{-Quin})_3]^-$ and $[Mn(H_2O)_6]^{2+}$ ions that lie on different three-fold axes in the unit cell. The two independent anionic units exhibit different Mn—N bond lengths [2.286(3) and 2.257(4) Å], but nearly equal Mn—O bond lengths [2.142(3) and 2.131(3) Å]. The Mn—O distances in the hexaaqua cation [2.168(3) and 2.173(4) Å] are longer than the Mn—O(Quin) distances in the anions. The non-coordinated oxygen of the carboxy group in position 2 in the pyridine ring forms two hydrogen bonds of the type O···H—O, the first with the OH group of the non-coordinated carboxy

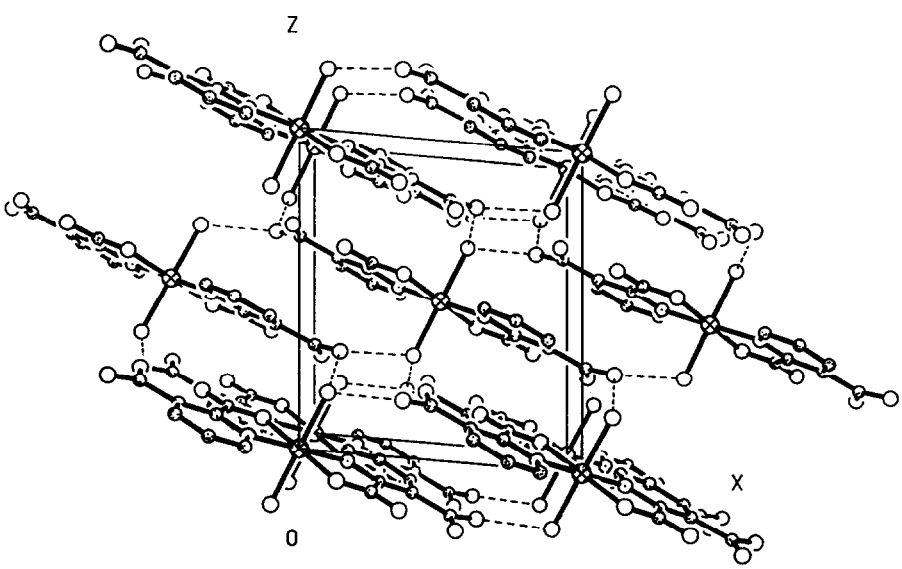

Fig. 2. Perspective view of the crystal structure of complex **1** along the *b*-axis.

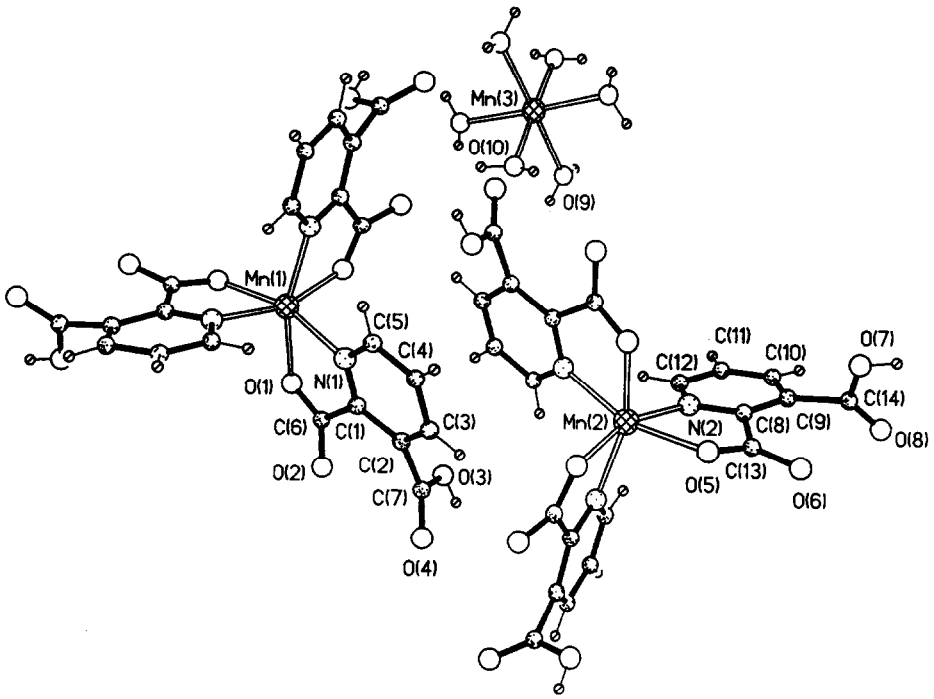

Fig. 3. The coordination environments of the manganese(II) atoms in the cation and anions in the complex $2[Mn(H\text{-}Quin)_3]\cdot[Mn(H_2O)_6]$ (**2**), along with the atom numbering scheme.

group (position 3) of another anionic unit and the second with an aqua molecule from the cationic unit. A third hydrogen bond of the same type exists between the cationic oxygen of the non-coordinated carboxy group from an anionic unit and the oxygen atom of a water molecule of the cation. These hydrogen bonds, therefore, connect the anions and the cation together into a three-dimensional network structure (Fig. 4).

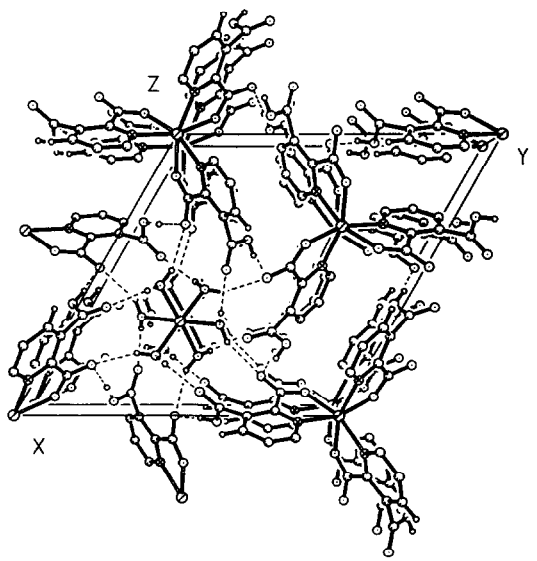

Fig. 4. Packing in the unit cell of complex **2** viewed down the *c*-axis.

The structure of the anionic unit $[Mn(H\text{-}Quin)_3]^-$ in complex **2** may be compared with that of Mn(picolinato)$_3\cdot H_2O$,[30] in which the picolinato anions function as N,O-bidentate ligands and are arranged in a very similar way in both compounds. The Mn^{III}—N distances in the picolinate complex vary from 2.059(5) to 2.254(5) Å, which are shorter than the Mn^{II}—N bond lengths found for the quinolinato anions (Table 4). The Mn^{II}—N distances, however, are very close to that observed [2.278(3) Å] in Mn(picolinato)$(N_3)(H_2O)$.[31] The above Mn—N distances are all longer than the Mn^{IV}—N bond lengths of 2.006(4) Å found in the Mn_2O_2(picolinato)$_4\cdot$MeCN complex.[32] This comparison demonstrates a progressive decrease in the Mn—N bond length as the oxidation state of the manganese atom increases.

REFERENCES

1. G. D'Ascsnzo, U. B. Ceipidor, A. Marino and A. Magri, *Anal. Chim. Acta* 1973, **65**, 105.
2. A. Anagnostopoulos, *J. Coord. Chem.* 1975, **4**, 231.
3. B. Chaterjee, *J. Inorg. Nucl. Chem.* 1981, **43**, 2553.
4. B. F. Gomez and L. T. Alfaro, *Rev. Acad. Cienc.*

Exactas, Fis-Quim., Net. Zeragoza 1973, **29**, 229 (*Chem. Abstr.* 83 : 90076v.).
5. A. Anagnostopoulos, *Inorg. Nucl. Chem. Lett.* 1974, **10**, 525.
6. G. W. A. Fowles, R. W. Matthews and R. A. Walton, *J. Chem. Soc.* (*A*) 1968, 1108.
7. M. G. B. Drew, R. W. Matthews and R. A. Walton, *J. Chem. Soc. A* 1971, 2959.
8. M. A. S. Goher and A. A. Youssef, *Syn. React. Inorg. Met.-Org. Chem.* 1992, **22**, 615.
9. M. A. S. Goher, R.-J. Wang and T. C. W. Mak, *J. Cryst., Spectrosc. Res.* 1990, **20**, 265.
10. M. A. S. Goher, R.-J. Wang and T. C. W. Mak, *Polyhedron* 1992, **11**, 829.
11. R. A. Sparks, in *Crystallographic Computing Techniques* (Edited by F. R. Ahmed), pp. 442–467. Munksgraad, Copenhagen (1976).
12. R. Diamond, *Acta Cryst.* 1969, **A25**, 43.
13. G. Kopfmann and R. Huber, *Acta Cryst.* 1968, **A24**, 348.
14. A. C. T. North, D. C. Phillips and F. S. Mathews, *Acta Cryst.* 1968, **A24**, 351.
15. G. M. Sheldrick, in *Computational Crystallography* (Edited by D. Sayre), pp. 506–514. Oxford University Press, New York (1982).
16. G. M. Sheldrick, in *Crystallographic Computing 3: Data Collection, Structure Determination, Proteins, and Databases* (Edited by G. M. Sheldrick, C. Kruger and R. Goddard), pp. 175–183, Oxford University Press, Oxford (1985).
17. *International Tables for X-ray Crystallography*, Vol. IV, pp. 55, 99, 149. Kynock Press, Birmingham (1974) (New distributed by Kluwer Acad. Academic Publishers, Dordrecht).
18. D. L. Hoof and R. A. Walton, *Inorg. Chem. Acta* 1975, **71**, 12.
19. M. G. B. Drew, R. W. Matthews and R. A. Walton, *J. Chem. Soc.* (*A*) 1970, 1405.
20. S. Yoshida and M. Asai, *Chem. Pharm. Bull.* (*Japan*) 1959, **5**, 162; I. Nakagawa and T. Shimanouchi, *Spectrochim. Acta* 1964, **20**, 429.
21. L. S. Gelfand, L. L. Pytlewski, A. N. Speca, C. M. Mikulski and N. M. Karayannis, *J. Inorg. Nucl. Chem.* 1980, **42**, 209.
22. F. A. Cotton and M. D. Myers, *J. Am. Chem. Soc.* 1960, **82**, 5023.
23. D. M. L. Goodgame, M. Goodgame, M. Hitchman and M. Eecks, *Inorg. Chem.* 1966, **5**, 635.
24. R. W. Matthews, A. D. Hamer, D. L. Hoof, D. G. Tisley and R. A. Walton, *J. Chem. Soc., Dalton Trans.* 1973, 1035.
25. M. Biagini, A. Chiesi-Villa, C. Guestini and M. Nardelli, *Gazz. Chim. Ital.* 1971, **101**, 825.
26. A. Chiesi-Villa, C. Gaustini, A. Musatti and M. Nardelli, *Gazz. Chim. Ital.* 1972, **102**, 226.
27. P. P. Quaglieri, H. Loiseleur and G. Thomas, *Acta Cryst.* 1972, **B28**, 2593.
28. H. Loiseleur, *Acta Cryst.* 1972, **B28**, 816.
29. F. Takusagawa, K. Hirotsu and A. Shimada, *Bull. Chem. Soc.* (*Japan*) 1973, **46**, 2372; F. Takusagawa and T. F. Koetzle, *Acta Cryst.* 1978, **B34**, 1149.
30. B. N. Figgis, C. L. Raston, R. P. Sharma and A. H. White, *Aust. J. Chem.* 1978, **31**, 2545.
31. M. A. S. Goher, M. A. M. Abu-Youssef, F. A. Mautner and A. Popitsch, *Polyhedron* 1992, **11**, 2137.
32. E. Libby, R. J. Webb, W. E. Streib, K. Folting, J. C. Hoffman, D. N. Hendrickson and G. Christou, *Inorg. Chem.* 1989, **28**, 4037.

Polyhedron Vol. 12, No. 15, pp. 1879–1885, 1993
Printed in Great Britain

0277–5387/93 $6.00+.00
© 1993 Pergamon Press Ltd

PREPARATION AND CHARACTERIZATION OF GOLD(III) HALIDE COMPLEXES OF PICOLINIC ACID (pic-H) AND X-RAY CRYSTAL STRUCTURE OF $[K(pic\text{-}H)_2(H_2O)_2][AuBr_4]\cdot(pic\text{-}H)_2$

MOHAMED A. S. GOHER† and AZZA E. H. ABDOU

Department of Chemistry, Faculty of Science, Alexandria University, P.O. Box 426, Ibrahimia, Alexandria 21321, Egypt

and

WAI-HING YIP and THOMAS C. W. MAK†

Department of Chemistry, The Chinese University of Hong Kong, Shatin, New Territories, Hong Kong

(*Received* 22 *February* 1993; *accepted* 30 *March* 1993)

Abstract—Complexes of the types $MAuX_4\cdot 4(pic\text{-}H)\cdot 2H_2O$ (M = Na for X = Cl and M = K for X = Br), $NaAu(pic)_2X_2\cdot 2H_2O$ (where X = Cl or I) and $NaAuCl_4\cdot Na(pic\text{-}H)\cdot(pic)\cdot 2H_2O$ (where pic-H = picolinic acid) have been prepared and characterized. Picolinic acid functions as a neutral N,O-bidentate ligand in the first type and as an O-monodentate picolinate anion in the second type. The IR results suggest that the last complex contains both neutral and anionic organic moieties. The conductivities of these complexes were measured and are discussed. X-ray single-crystal analysis of the $KAuBr_4\cdot 4(pic\text{-}H)\cdot 2H_2O$ complex revealed that it should be formulated as $[K(pic\text{-}H)_2(H_2O)_2]\cdot[AuBr_4]\cdot(pic\text{-}H)_2$. The potassium atom in the centrosymmetric cation is octahedrally coordinated by two *trans*-N,O-bidentate neutral picolinic acid molecules [K—N = 2.790(6) Å and K—O = 2.888(5) Å] and two aqua ligands at K—O distances of 2.769(4) Å. The other two picolinic acid molecules are involved in hydrogen bonding with the oxygen atoms of the coordinated pic-H and aqua molecules.

The broad spectrum of physiological effects of picolinic acid, also known as 2-pyridinecarboxylic acid, and its derivatives on activity functions of both animal and plant organisms has been attributed to their ability to form complexes with transition metals.[1] In this regard many complexes of picolinic acid together with their crystal structures have been reported.[2–10]

Alkali metal complexes, on the other hand, play vital roles in biological systems, many of which are not fully understood as yet. Speakman[11] has reviewed the structures of "acid salts" formed by alkali metals and carboxylic acids, such as MHX_2, where M = K, Rb, NH_4 and HX = salicylic acid, and drawn attention to the very short hydrogen bonds which generally occur in these compounds. Although some of the "acid salts" of potassium formed by inorganic[12] or organic acids[13,14] have been structurally characterized, to our knowledge potassium compounds containing both organic acids and inorganic anions have been reported only once in hexa(3,5-dicarboxypyridine)potassium tetrabromoaurate(III).[15] In the present study, we prepared some gold(III) halide complexes of picolinic acid (hereafter abreviated as pic-H) and determined the crystal structure of $KAuBr_4\cdot 4(pic\text{-}H)\cdot 2H_2O$ by X-ray diffraction.

EXPERIMENTAL

Picolinic acid was obtained from Aldrich and the other chemicals were of analytical grade quality.

† Authors to whom correspondence should be addressed.

Preparation of the complexes

(1) $NaAu(pic)_2Cl_2 \cdot 2H_2O$. A mixture of sodium tetrachloroaurate(III) dihydrate (0.40 g, 1 mmol) and picolinic acid (0.248 g, 2 mmol) in acetone (30 cm^3) was boiled for *ca* 10 min. The mixture was allowed to stand overnight to produce the complex.

(2) $NaAu(pic)_2I_2 \cdot 2H_2O$. A mixture of sodium tetrachloroaurate(III) dihydrate (0.42 g, *ca* 1 mmol) and picolinic acid (0.27 g, 2.2 mmol) in ethanol (*ca* 40 cm^3) was boiled and reduced to half its original volume. After cooling NaI (0.9 g, 6 mmol) dissolved in the least amount of distilled water was added and the final mixture allowed to stand for *ca* 2 weeks.

(3) $NaAuCl_4 \cdot 4(pic\text{-}H) \cdot 2H_2O$. $NaAuCl_4 \cdot 2H_2O$ (4.3 g, *ca* 1 mmol) in ethanol (10 cm^3) and picolinic acid (0.62 g, 5 mmol) in warmed ethanol (20 cm^3) were mixed together and the mixture reduced to *ca* half of its original volume by boiling, and allowed to stand in an open beaker for several days.

(4) $KAuBr_4 \cdot 4(pic\text{-}H) \cdot 2H_2O$. This complex was prepared by mixing $NaAuCl_4 \cdot 2H_2O$ (0.41 g, 1 mmol) and picolinic acid (0.55 g, 4.5 mmol) in ethanol (30 cm^3). The mixture was boiled for *ca* 15 min and after cooling an aqueous solution of KBr (0.72 g, 6 mmol) was added. The final mixture was allowed to stand for *ca* 2 weeks to produce the complex. Alternatively, $NaAuCl_4 \cdot 2H_2O$, picolinic acid and KBr were mixed together in the above molar ratio, using acetone instead of ethanol. The mixture was boiled for *ca* 10 min and then allowed to stand over several days, after which the brown colour of the solution disappeared. Several days later the complex was separated as dark brown crystals.

(5) $NaAuCl_4 \cdot Na(pic\text{-}H)(pic) \cdot 2H_2O$. This complex was prepared according to procedure (3), except that water was used as a medium instead of ethanol.

Elemental analysis results of the isolated complexes together with some of their physical properties are given in Table 1.

Physical measurements

The IR absorption bands of free and coordinated ligands and the gold–halogen stretching vibrations are given in Table 2. Conductivity measurements were performed using 10^{-3} mol of each complex in acetone solution. The experimental procedures and instruments used for various physical measurements are as described previously.[16,17]

X-ray structure analysis of $[AuBr_4][K(pic\text{-}H)_2(H_2O)_2] \cdot (pic\text{-}H)_2$

Details of the crystal parameters, data collection and structure determination are given in Table 3. The raw intensities collected on a Nicolet R3m/V four-circle diffractometer at room temperature (294 K) were processed with the profile-fitting procedure of Diamond[18] and corrected for absorption using ψ-scan data.[19] The gold and bromine atoms were located by the Patterson method and the coordinates of the other non-hydrogen atoms were determined from successive difference-Fourier syntheses. All non-hydrogen atoms were subjected to anisotropic refinement and the hydrogen atoms of the pyridyl groups were generated geometrically (C—H bonds fixed at 0.96 Å) and assigned the same isotropic temperature factor of $U = 0.08$ Å^2. Computations were performed using the SHELTXL-PLUS program package[20] on a DEC MicroVAX-II computer. Analytic expressions of atomic scattering factors were employed and anomalous dispersion corrections were incorporated.[21] The residual maxima in the last difference map all lie

Table 1. Analytical data for some gold(III) halide complexes of picolinic acid (pic-H)

No.	Complex	Colour	M.p. (°C)	Ω^{-1} cm^2 mol^{-1}	Analysis: Found (Calc.) (%) C	H	N	X
1	$NaAu(pic)_2Cl_2 \cdot 2H_2O$	Light yellow crystalline powder	130	132	25.8 (25.2)	2.3 (2.1)	5.1 (4.9)	12.0 (12.4)
2	$NaAu(pic)_2I_2 \cdot 2H_2O$	Red needles	350	112	18.8 (19.1)	1.9 (1.6)	3.7 (3.7)	34.0 (33.7)
3	$NaAuCl_4 \cdot 4(pic\text{-}H) \cdot 2H_2O$	Bright yellow crystals	207	118	32.4 (32.0)	2.7 (2.5)	6.3 (6.1)	15.9 (16.2)
4	$KAuBr_4 \cdot 4(pic\text{-}H) \cdot 2H_2O$	Red–brown needles	195[a]	125	26.6 (26.2)	2.2 (2.3)	5.2 (5.4)	29.5 (30.0)
5	$NaAuCl_4 \cdot Na(pic)(pic\text{-}H) \cdot 2H_2O$	Pale yellow fine crystals	215	115	22.2 (21.6)	2.6 (2.0)	4.1 (4.2)	21.7 (21.3)

[a] At 130°C the colour fades.

Table 2. IR spectral data for picolinic acid and its gold(III) halide complexes

pic-H	Complex **1**	Complex **4**	Complex **5**	Assignments
2600 s,br	3450 s,br	3450 m,br	3550–3300 m	ν(O···H—O)+ν(N···H—O)
	2500 s,br	3100 s,br		
2100–1900 m	2100–1900 wm			
1715 s,br		1740 s,br	1700 vs	ν(C=O)
1650 ms	1645 vs,br		1640 s,br	$\nu(COO^-)_{asym}$
1600 vs	1590 vs	1610	1610 s, 1590 s	Pyridine ring vibrations
1565 ms	1560 sh	1580 sh	1560 ms	
1520 ms	1520 s	1530 m	1520 w	
1445 s	1440 ms	1460 m	1470 s, 1450 ms	
1340 vs	1385 vs	1380 s,br	1385 m, 1370 ms	ν(C—O)+$\nu(COO)_{sym}$
1300 vs,br	1345 vs	1350 s,br, 1300 m	1310 vs	
1000 ms	995 m	1020 m,br	1020 wm	Ring breathing
985 m	975 m	1005 m, 990 m	980 wm	
670 vs	685 vs	570 ms	695 m, 675 wm	δC(=O)O
530 ms	515 m	600 m, 505 m	555 wm	Ring vibrations
405 s	400 ms	430 m, 405 wm	420 wm, 405 wm	

s = strong, m = medium, w = weak, v = very, sh = shoulder, br = broad.

in the neighborhood of the $[AuBr_4]^-$ anion. Selected bond lengths and angles are given in Table 4. Anisotropic thermal parameters and structure factors are available from the last author and along with atomic coordinates have been deposited with the Editor and the Cambridge Crystallographic Data Centre.

DISCUSSION

The reaction between picolinic acid and gold(III) halides in different media afforded complexes of the types $MAuX_4 \cdot 4(pic\text{-}H) \cdot 2H_2O$, NaAu $(pic)_2X_2 \cdot 2H_2O$ and $NaAuCl_4 \cdot Na(pic)(pic\text{-}H) \cdot 2H_2O$. These complexes differ from nicotinic acid and isonicotinic acid complexes formulated as AuL_nX_3, where $n = 1$, 2 or 3,[16,17] as well as from those of quinaldic acid for the formula $[(H_3O)(quin\text{-}H)_2][AuBr_4]$.[22]

Pertinent IR data for the products of interaction of pic-H with gold(III) halides are given in Table 2. Complexes of the type $MAuBr_4 \cdot 4(pic\text{-}H) \cdot 2H_2O$ exhibit the ν(C=O) band around 1745 cm^{-1} and no absorption due to ν(COO), whereas those of the type $NaAu(pic)_2X_2 \cdot 2H_2O$ show only very strong bands around 1645 cm^{-1} [ν(COO)]. The result for these latter complexes is indicative of O-picolinate anions, since the vibrations of the pyridine ring are not influenced by coordination. However, the IR spectrum of 3,5-pyridinedicarboxylic acid coordinated to potassium atom *via* its carbonyl oxygen exhibits a shift of ν(C=O) to higher frequencies.[15,23] Accordingly picolinic acid in its complexes of the former type is coordinated via its carbonyl oxygen to an alkali metal atom. The strong shoulder at 1710 cm^{-1} indicates the existence of picolinic acid molecules that are similar to free pic-H. This conclusion is supported by the appearance of pyridine ring vibrations at higher frequencies, in addition to bands at more or less the same frequencies as in free pic-H. These results suggest that $MAuX_4 \cdot 4(pic\text{-}H) \cdot 2H_2O$ complexes possess N,O-bidentate pic-H molecules as well as uncoordinated pic-H, as found in $[Mg(H_2O)_6]$ (nicotinate)$_2 \cdot (H_2O)_4$.[24] The existence of hydrogen bonds of the types O—H···O and N···H—O between aqua molecules and/or carboxylic groups and nitrogen atoms of the pyridine moiety are indicated by broad bands in the region 3500–2000 cm^{-1} (Table 2).[25–27] The spectra of $MAuX_4 \cdot 4(pic\text{-}H) \cdot 2H_2O$ exhibit ν(Au—X) bands at 360, 345 and 265 cm^{-1} for X = Cl and Br, respectively, which are very similar to those found for other complexes containing $[AuX_4]^-$ anions.[23,28,29] Complexes of this type may, therefore, be formulated as $[M(pic\text{-}H)_2(H_2O)_2][AuX_4] \cdot (pic\text{-}H)_2$. This formulation is consistent with the molar conductivities of these complexes in acetone (Table 1), which are indicative of 1 : 1 electrolytes.[30] In the case of the NaAu $(pic)_2Cl_2 \cdot 2H_2O$ complex no bands are attributable to ν(Au—Cl), so that ionic or bridging halogen atoms may be present. As these complexes behave as 1 : 1 electrolytes in acetone (Table 1) one

Table 3. Data collection and processing parameters

Molecular formula	$KAuBr_4 \cdot 4C_5H_4NCOOH \cdot 2H_2O$
Molecular weight	1084.2
Colour and habit	Dark brown needles
Crystal size (mm^3)	$0.14 \times 0.18 \times 0.20$
Crystal system	Triclinic
Space group	$P\bar{1}$ (No. 2)
Unit cell parameters	
a (Å)	7.114(1)
b (Å)	7.199(1)
c (Å)	17.247(3)
α (°)	94.06(1)
β (°)	101.75(1)
γ (°)	109.57(1)
V ($Å^3$)	805.5(3)
Z	1
$F(000)$	514
Density (calc.) ($g\ cm^{-3}$)	2.235
Radiation	Graphite-monochromatized Mo-K_α $\lambda = 0.71073$ Å
Standard reflections	(3, 3, 3); 1, 2, −6)
Intensity variation	±1.0%
Absorption coefficient (cm^{-1})	97.14
Mean μr	0.65
Transmission factors	0.153–0.571
Scan type and rate (° min^{-1})	ω-scan; 3.08–14.65
Scan range	0.80° below $K\alpha_1$ to 0.80° above $K\alpha_2$
Background counting	Stationary counts for one-fifth of scan time at each end of scan range
Collection range	$0 \leqslant h \leqslant 9$, $-8 \leqslant k \leqslant 9$, $-21 \leqslant l \leqslant 22$; $2\theta_{max} = 55°$
Unique data measured	3678
Observed data with $\|F_o\| \geqslant 3\sigma(\|F_o\|)$, n	2743
No. of variables, p	222
Weighting scheme	$w = [\sigma^2\|F_o\| + 0.0015\|F_o\|^2]^{-1}$
Extinction correction	$\chi = 0.00017(1)$, where $F^* = F[1 + 0.002\chi F^2/\sin(2\theta)]^{-1/4}$
$R_F = \Sigma\|\|F_o\| - \|F_o\|\|/\Sigma\|F_o\|$	0.044
$wR = [\Sigma w^2(\|F_o\| - \|F_c\|)^2/\Sigma w^2\|F_o\|^2]^{1/2}$	0.052
$S = [\Sigma w(\|F_o\| - \|F_c\|)^2/(n-p)]^{1/2}$	0.89
Residual extrema in final difference map ($e\ Å^{-3}$)	+2.11 to −1.60

may suggest the $Na[Au(pic)_2X_2] \cdot 2H_2O$ formulation, in which the gold atom is in a square planar arrangement of four bridging halogen atoms and further ligated at long Au—O distances by a pair of *trans*-O-monodentate picolinate groups. Six-coordinate gold atoms are found in the structure of $[(H_3O)(quin\text{-}H)_2][AuBr_4]$.[22] The IR data of the $NaAuCl_4 \cdot Na(pic)(pic\text{-}H) \cdot 2H_2O$ complex (Table 2) suggest that it contains O,N-bidentate pic^- and uncoordinated pic-H and may, therefore, be formulated as $Na[AuCl_4] \cdot [Na(pic)(H_2O)_2] \cdot (pic\text{-}H)$. This formula is consistent with the conductivity measurement (Table 1) and the far-IR results, which exhibit ν(Au—Cl) bands at 378 and 333 cm^{-1}. The IR spectral results given above for $MAuX_4 \cdot 4(pic\text{-}H) \cdot 2H_2O$ are confirmed by the X-ray structure analysis of the bromide complex.

The X-ray structure analysis of $KAuBr_4 \cdot 4(pic\text{-}H) \cdot 2H_2O$ revealed that it should be formulated as $[K(pic\text{-}H)_2(H_2O)_2][AuBr_4] \cdot (pic\text{-}H)_2$. Figure 1 illustrates the principal structural features of the complex, which consists of $AuBr_4^-$ anions, $[K(pic\text{-}H)_2(H_2O)_2]^+$ cations and pic-H molecules. The potassium atom is located at an inversion centre and six-coordinated by pairs of *trans*-N,O-bidentate chelating picolinic acid molecules [K—N = 2.790(6) and K—O = 2.888(5) Å] and aqua ligands at K—O distances of 2.769(4) Å. The remaining independent picolinic acid molecules form acceptor hydrogen bonds with the coor-

Table 4. Bond lengths (Å) and angles (°)

K(1)—O(1W)	2.769(4)	K(1)—O(1)	2.888(5)
K(1)—N(1)	2.790(6)	Au(1)—Br(1)	2.409(1)
Au(1)—Br(2)	2.406(2)	Au(1)—Br(3)	2.413(8)
Au(1)—Br(4)	2.482(7)	O(1)—C(1)	1.313(9)
O(2)—C(1)	1.200(8)	C(1)—C(2)	1.515(7)
C(2)—C(3)	1.391(10)	C(2)—N(1)	1.331(8)
C(3)—C(4)	1.382(8)	C(4)—C(5)	1.382(10)
C(5)—C(6)	1.369(11)	C(6)—N(1)	1.339(7)
O(3)—C(7)	1.268(8)	O(4)—C(7)	1.217(8)
C(7)—C(8)	1.525(7)	C(8)—C(9)	1.384(9)
C(8)—N(2)	1.357(8)	C(9)—C(10)	1.377(7)
C(10)—C(11)	1.404(10)	C(11)—C(12)	1.366(10)
C(12)—N(2)	1.355(6)	O(1)···O(3)	2.603(6)
O(1W)···O(4a)	2.717(7)	O(1W)···N(2b)	2.741(7)
O(3c)···O(1W)	2.905(7)		

O(1W)—K(1)—O(1)	110.2(1)	O(1W)—K(1)—N(1)	80.9(1)
O(1)—K(1)—N(1)	55.3(1)	Br(1)—Au(1)—Br(2)	90.1(1)
Br(3)—Au(1)—Br(4)	89.9(3)	K(1)—O(1)—C(1)	121.7(3)
O(1)—C(1)—O(2)	125.0(5)	O(1)—C(1)—C(2)	113.0(5)
O(2)—C(1)—C(2)	122.0(6)	C(1)—C(2)—C(3)	118.6(5)
C(1)—C(2)—N(1)	117.2(6)	C(3)—C(2)—N(1)	124.1(5)
C(2)—C(3)—C(4)	117.3(6)	C(3)—C(4)—C(5)	119.6(7)
C(4)—C(5)—C(6)	118.2(5)	C(5)—C(6)—N(1)	124.1(6)
K(1)—N(1)—C(2)	123.1(4)	K(1)—N(1)—C(6)	116.4(4)
C(2)—N(1)—C(6)	116.6(6)	O(3)—C(7)—O(4)	129.0(5)
O(3)—C(7)—C(8)	114.5(5)	O(4)—C(7)—C(8)	116.5(6)
C(7)—C(8)—C(9)	123.6(5)	C(7)—C(8)—N(2)	116.1(5)
C(9)—C(8)—N(2)	120.3(5)	C(8)—C(9)—C(10)	119.2(6)
C(9)—C(10)—C(11)	119.7(7)	C(10)—C(11)—C(12)	119.2(5)
C(11)—C(12)—N(2)	120.6(6)	C(8)—N(2)—C(12)	120.9(6)

Symmetry transformations: a $(-x, -y, 1-z)$; b $(1-x, -y, 1-z)$; c $(-1+x, -1+y, z)$.

dinated oxygen atom O(1) of the picolinic acid ligand and an oxygen atom of an aqua molecule (Fig. 1). A similar situation exists in the structure of $[Mg(H_2O)_6]\cdot(\text{nicotinate})_2(H_2O)_2$, in which the nicotinate molecules are hydrogen-bonded to the water molecules and not coordinated directly to magnesium.[24] Other hydrogen bonds of the types O(3c)—H···O(1W) and O(1W)—H···N(2b) between the aqua ligand and the uncoordinated picolinic acid link the latter with the cations to form a thick layer concentrated about the plane $z = 1/2$ (Fig. 2). The C=O and C—OH bonds of the carboxy group in either the coordinated or uncoordinated picolinic acid molecule are clearly distinguishable, so that the donor and acceptor atoms in all hydrogen bonds can be assigned, although the carboxy and aqua hydrogen atoms could not be located from the final difference map.

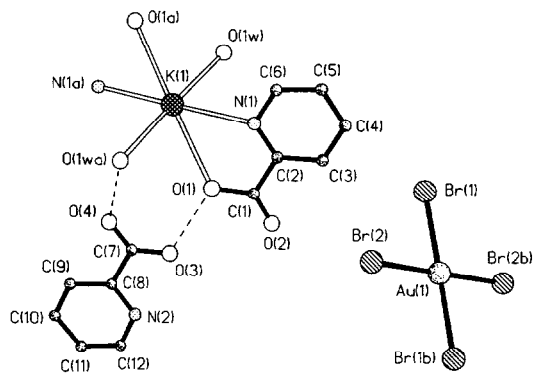

Fig. 1. The coordination environments of the potassium and gold(III) atoms in the complex $[K(\text{pic-H})_2(H_2O)_2][AuBr_4]\cdot(\text{pic-H})_2$ along with the atom numbering scheme.

The mode of bonding of picolinic acid in the present complex is similar to that found in the structure of Mn(pic-H)(pic)Cl.[31] The K—O distances are much longer than those [2.56(1) Å] in $[K(3,5\text{-dicarboxypyridine})_6][AuBr_4]$,[15] but agree very well with those (2.71–2.86 Å) in other KO_6 octahedra.[13] Likewise, the K—N distances of 2.790(6) Å are close to those in other KN_6 coordination

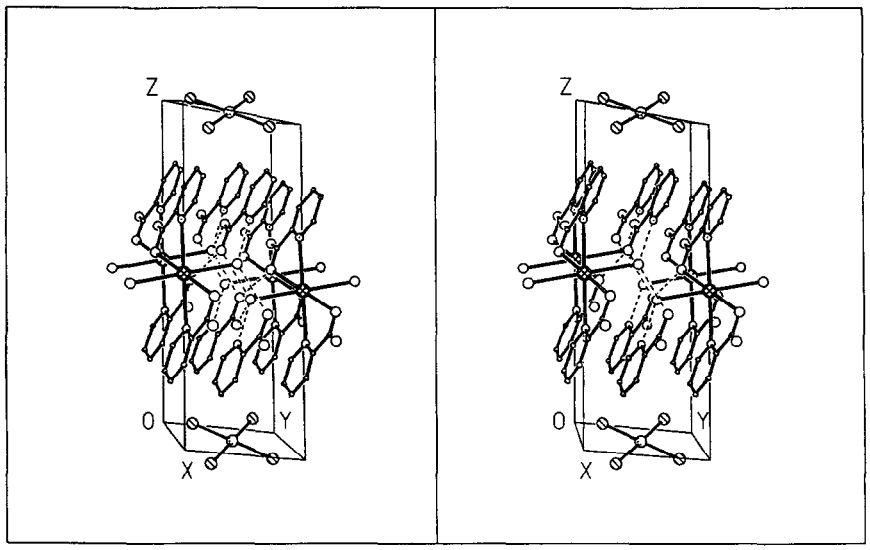

Fig. 2. A stereoview of the crystal structure. Hydrogen bonds are represented by broken lines.

octahedra,[14,32,33] but longer than those (2.556–2.603 Å) found in the structure of $KCr(pyridine)_4(N_3)_4$.[34]

REFERENCES

1. B. A. Bovikin, M. M. Omel'chenko, R. N. Sharonina and I. A. Zanina, Abstracts of Proceedings of the 15th All-Union Chungaevskii Conference on the Chemistry of Complex Compounds, Vol. 1, p. 229. Ukraine (1985).
2. P. J.-P. Deloume, H. Loiseleur and G. Thomas, *Acta Cryst.* 1973, **B29**, 668.
3. S. C. Chang, J. K. H. Ma, J. S. Wang and N. C. Li, *J. Coord. Chem.* 1972, **2**, 31.
4. P. J.-P. Deloume and H. Loiseleur, *Acta Cryst.* 1974, **B30**, 607.
5. A. Takenaka, N. Utsumi, T. Yamamoto and I. Nitta, *Nippon Kagaku Zsashi* 1970, **91**, 928.
6. B. N. Figgis, C. L. Raston, R. P. Sharma and A. H. White, *Aust. J. Chem.* 1977, **31**, 2545.
7. P. J.-P. Deloume, R. Faure and H. Loiseleur, *Acta Cryst.* 1977, **B33**, 2709.
8. E. Libby, R. J. Webb, W. E. Streib, K. Folting, J. C. Hoffmann, D. N. Hendrickson and G. Christou, *Inorg. Chem.* 1989, **28**, 4037.
9. H. Loiseleur, G. Thomas, B. Chevrier and D. Grandjean, *J. Chem. Soc., Chem. Commun.* 1967, 182.
10. M. A. S. Goher, M. A. M. Abu-Youssef, F. A. Mautner and A. Popitsch, *Polyhedron* 1992, **11**, 2137.
11. J. C. Speakman, *Struct. Bonding (Berlin)* 1972, **12**, 141.
12. L. Y. Y. Chan and F. W. B. Einstein, *Can. J. Chem.* 1971, **49**, 468.
13. L. Manojlovic and J. C. Speakman, *Acta Cryst.* 1968, **B24**, 323, 326.
14. M. A. Bush and M. R. Truter, *J. Chem. Soc. (A)* 1971, 745.
15. M. A. S. Goher, R.-J. Wang and T. C. W. Mak, *J. Cryst. Spect. Res.* 1990, **20**, 245.
16. M. A. S. Goher, *Bull. Soc. Chim. Fr.* 1982, I-262.
17. M. A. S. Goher, *Bull. Soc. Chim. Fr.* 1985, I-159.
18. R. Diamond, *Acta Cryst.* 1969, **A25**, 43.
19. G. Kopfmann and R. Huber, *Acta Cryst.* 1968, **A24**, 348.
20. G. M. Sheldrick, in *Crystallographic Computing 3: Data Collection, Structure Determination, Proteins, and Databases* (Edited by G. M. Sheldrick, C. Kruger and R. Goddard), p. 175. Oxford University Press, New York (1985).
21. *International Tables for X-ray Crystallography*, Vol. IV, pp. 55, 99, 149. Kynoch Press, Birmingham (1974) (now distributed by Kluwer Academic Publishers, Dordrecht).
22. M. A. S. Goher, A. K. Hafez, R.-J. Wang and T. C. W. Mak, unpublished work.
23. M. A. S. Goher and A. A. Youssef, *Synth. React. Inorg. Met.-Org. Chem.* 1992, **22**, 615.
24. L. B. Cole and E. M. Holt, *Inorg. Chim. Acta* 1985, **108**, 159.
25. S. Yoshida and M. Assai, *Chem. Pharm. Bull. (Japan)* 1959, **7**, 163.
26. I. Nakagawa and T. Shimanouchi, *Spectrochim. Acta* 1964, **20**, 429.
27. L. S. Gelfand, L. L. Pytlewski, A. N. Speca, C. M. Mikulski and N. M. Karayannis, *J. Inorg. Nucl. Chem.* 1980, **42**, 209.
28. H. Stammreich and K. Forneris, *Spectrochim. Acta* 1960, **16**, 363.
29. A. Sabatini, L. Sacconi and V. Schettino, *Inorg. Chem.* 1964, **3**, 1775.

30. E. W. Einscough and R. A. Plowman, *Aust. J. Chem.* 1970, **23**, 1269.
31. M. A. S. Goher, M. A. M. Abu-Youssef and F. A. Mautner, result to be published.
32. P. L. Johnson, R. L. Musselman and J. M. Williams, *Acta Cryst.* 1977, **B33**, 3155.
33. R. K. Brown, P. L. Johnson, T. J. Lynch and J. M. Williams, *Acta Cryst.* 1978, **B34**, 1955.
34. M. A. S. Goher, M. A. M. Abu-Youssef, F. A. Mautner and H. P. Fritzer, *Z. Naturforsch.* 1992, in press.

Polyhedron Vol. 12, No. 15, pp. 1887–1893, 1993
Printed in Great Britain

0277–5387/93 $6.00+.00
© 1993 Pergamon Press Ltd

MOLECULAR STRUCTURE AND SPECTRAL STUDIES OF BIS(ACETYLPYRAZINE ^{4}N-DIMETHYLTHIOSEMICARBAZONATO)NICKEL(II), $[Ni(Pz4DM)_2] \cdot CH_2Cl_2$

DOUGLAS X. WEST,† MARK A. LOCKWOOD and HAILESELASSIE GEBREMEDHIN

Department of Chemistry, Illinois State University, Normal, IL 61761, U.S.A.

and

A. CASTINEIRAS

Departamento de Química Inorganica, Universidad de Santiago de Compostela, E-15706 Santiago de Compostela, Spain

and

ANTHONY E. LIBERTA

Department of Biological Sciences, Illinois State University, Normal, IL 61761, U.S.A.

(*Received* 14 *January* 1993; *accepted* 7 *April* 1993)

Abstract—A nickel(II) complex of acetylpyrazine ^{4}N-dimethylthiosemicarbazone, $[Ni(Pz4DM)_2]$, has been synthesized and characterized by its spectral properties. Its crystal structure shows the two ligands coordinated in a *mer*-configuration and bond lengths and angles are compared with other thiosemicarbazone complexes. The complex, in contrast to the uncoordinated thiosemicarbazone, shows no growth inhibition against two human pathogenic fungi, *Aspergillus niger* and *Paecilomyces variotii*.

Heterocyclic thiosemicarbazones, as well as their metal complexes, are important because of potentially beneficial biological activity.[1] Although there have been numerous studies involving the isolation of complexes and their spectral and magnetic characterization,[2,3] comparatively few crystal structures of these complexes have been determined. Results of studies of bis(ligand)chromium(III) and -iron(III) complexes that are relevant are: The thione $\{=^1N-^2NH-C(=S)^4NH_2\}$ and thiol $\{=N-N=C(-S^-)NH_2\}$ forms of pyruvic acid thiosemicarbazone are coordinated to chromium(III) as tridentate ligands in a meridional conformation with the expected bond length differences for the metal–ligand and thiosemicarbazone moiety.[4] Bis(salicylaldehyde thiosemicarbazonato)-chromium(III) perchlorate has two equivalent tridentate ONS ligands arranged in a meridional conformation,[5] as does an iron(III) complex with two anionic 2-acetylpyridine 3-azabicyclo-[3.2.2]nonylselenosemicarbazones (i.e. loss of ^{2}NH).[6] However, the structure of bis(isoquinoline-1-carboxaldehyde thiosemicarbazonato)nickel(II) monohydrate was reported[7] with small differences in the bond lengths of the two coordinated ligands.

Most crystal studies have been reported for four-coordinate nickel(II) and copper(II) thiosemicarbazone complexes, that demonstrated the most biological activity.[8] A tetrahedral nickel(II) complex, NiS_2Cl_2, with two acetophenone thiosemicarbazone ligands, does not have the imine nitrogens coordinated.[9] *Cis*-bis(acetonethiosemicarbazonato)nickel(II) has been found to have con-

† Author to whom correspondence should be addressed.

siderable tetrahedral distortion from planar stereochemistry.[10] Planar nickel(II) complexes have been reported for complexes of 2-acetylpyridine azabicyclo[3.2.2]nonylthiosemicarbazone,[11] salicylaldehyde ^{4}N-phenylthiosemicarbazone[12] and two acetylpyrazine ^{4}N-substituted thiosemicarbazones.[13] Representative copper(II) complexes of heterocyclic thiosemicarbazones are the following: [Cu(HPictsc)H_2O]Cl·H_2O, where H_2Pictsc is 3-hydroxy-5-hydroxymethyl-4-formyl-2-picoline thiosemicarbazone,[14] the dinuclear complex of 2-formylpyridine thiosemicarbazone,[15,16] the mononuclear complex formed from the aforementioned dinuclear copper(II) complex and saccharin,[17] as well as additional complexes of 2-formylpyridine thiosemicarbazone.[18] The structure of a 2-acetylpyridine-3-hexamethyleneiminylthiosemicarbazone nickel(II) complex has also been reported.[19] Here we report the structure and spectral properties of bis(acetylpyrazine ^{4}N-dimethylthiosemicarbazonato)nickel(II) dichloromethane, [Ni(Pz4DM)$_2$]·CH_2Cl_2.

EXPERIMENTAL

Syntheses and materials

The yellow thiosemicarbazone was prepared by adding ^{4}N-methyl-^{4}N-phenyl thiosemicarbazide to an ethanolic-aqueous mixture of acetylpyrazine and dimethylamine followed by gentle refluxing for 2 h as described previously.[20] The bis complex [Ni(Pz4DM)$_2$] was prepared by refluxing for 2 h an anhydrous ethanol 1:2 mixture of nickel(II) acetate (Alfa) and acetylpyrazine ^{4}N-dimethylthiosemicarbazone. The brown product (*ca* 70% yield), which formed on cooling, was filtered after about half of the solvent was evaporated, washed with cold isopropanol and dried on a warm plate (35°C). The crystal was grown from dimethyl sulphoxide by slow diffusion of methylene chloride into the solution.

Physical measurements

The spectral, physical and biological measurements of the powder sample were made as previously reported.[2]

Determination of the crystal structure of [Ni($C_9H_{12}N_5S$)$_2$]·CH_2Cl_2([Ni(Pz4DM)$_2$]·CH_2Cl_2)

A brown prismatic crystal of approximate dimensions 0.25 × 0.20 × 0.50 mm was mounted on a glass fibre and used for data collection on a CAD4 Enraf–Nonius four-circle automatic diffractometer. Cell constants and an orientation matrix for data collection were obtained by least-squares refinement of the diffraction data from 25 reflections in the range 18–29°. The systematic absences observed suggested the space group to be $P2_1/n$. Data were collected at 293 K using Cu-K_α radiation (λ = 1.54056 Å) and the $\omega/2\theta$ scan technique. The intensities were corrected for Lorentz and polarization effects, and for absorption by an empirical method.[21] The structure was solved by direct methods,[22] which revealed the position of all non-hydrogen atoms. The positional and individual displacement (initially isotropic then anisotropic) parameters were refined by full-matrix least-squares.[23] The positions of the pyrazine hydrogen atoms were found from a difference map and those of methyl groups and of the dichloromethane were calculated from geometry. All hydrogen atoms were included in the structure factor calculations with B_{iso} = 4.0 Å^2, but not refined. A secondary extinction correction was applied[24] and the final coefficient, refined in the last cycle, was 8.248(1) × 10^{-7}. The final R value was 0.062, with R_w = 0.069 (weighting scheme $w^{-1} = \sigma^2(F)$; 326 parameters; S = 2.260; maximum Δ/σ in final cycle 0.001; maximum $\Delta\rho$ = 1.009 e Å^{-3}). Computations were performed on a DEC MicroVAX 3500 computer. For a summary of crystal data, see Table 1.

Table 1. Crystallographic data for [Ni(Pz4DM)$_2$]·CH_2Cl_2

Chemical formula	$C_{19}H_{26}C_{12}N_{10}NiS_2$
Formula weight	588.21
Crystal class	Monoclinic
Space group	$P2_1/n$
a (Å)	9.185(1)
b (Å)	19.929(1)
c (Å)	14.313(2)
β (°)	91.476(6)
V (Å^3)	2619.1(5)
Z	4
λ(Cu-K_α) (Å)	1.54056
ρ_{calc} (g cm^{-3})	1.502
μ (cm^{-1})	46.963
F(000)	1216
Min./max. abs. correction	0.928/1.506
Max. (sin θ)/λ	0.605
Total no. of reflections measured (θ range)	5350 (4–69°)
No. of unique reflections (R_{int})	4702 (0.016)
No. of observed reflections (criterion)	4476 [$I > 3\sigma(I)$]
R	0.062
Rw	0.069

Table 2. Selected bond lengths (Å) for $[Ni(Pz4DM)_2]$

Ni—S(11)	2.380(1)	Ni—S(21)	2.409(1)
Ni—N(11)	2.110(6)	Ni—N(21)	2.096(4)
Ni—N(12)	2.014(3)	Ni—N(22)	2.017(4)
S(11)—C(16)	1.714(4)	S(21)—C(26)	1.729(5)
N(11)—C(11)	1.346(6)	N(21)—C(21)	1.343(6)
N(11)—C(14)	1.343(9)	N(21)—C(24)	1.337(6)
N(12)—N(13)	1.371(6)	N(22)—N(23)	1.366(6)
N(12)—C(15)	1.297(6)	N(22)—C(25)	1.300(6)
N(13)—C(16)	1.347(6)	N(23)—C(26)	1.335(7)
N(14)—C(16)	1.350(6)	N(24)—C(26)	1.353(7)
N(14)—C(141)	1.462(7)	N(24)—C(241)	1.457(8)
N(14)—C(142)	1.456(7)	N(24)—C(242)	1.445(8)
N(15)—C(12)	1.329(7)	N(25)—C(22)	1.342(8)
N(15)—C(13)	1.345(9)	N(25)—C(23)	1.321(8)
C(11)—C(12)	1.402(7)	C(21)—C(22)	1.396(7)
C(11)—C(15)	1.445(7)	C(21)—C(25)	1.463(7)
C(13)—C(14)	1.366(9)	C(23)—C(24)	1.390(8)
C(15)—C(151)	1.498(7)	C(25)—C(251)	1.497(8)

Numbers in parentheses are estimated standard deviations in the least significant digits.

RESULTS AND DISCUSSION

Structure of $[Ni(Pz4DM)_2]$

The most important bond lengths and angles are included in Tables 2 and 3, respectively. Both tables are arranged in order to allow for a convenient comparison of the two ligands. A complete list of bond distances and angles, as well as final atomic coordinates, equivalent isotropic temperature factors and lists of F_o/F_c values are included in the supplementary material deposited with the Editor. A view of the structure of the molecule is shown in Fig. 1.[25]

The nickel(II) ion is octahedrally coordinated by the two approximately planar tridentate ligands arranged in a *mer*-configuration and a single isomer of this chiral molecule is present. Coordination for both ligands is via a pyrazinyl nitrogen, the azomethine nitrogen and the thiolato sulphur atoms. The greatest difference between the two ligand's metal donor atom bond lengths, 0.029 Å, occurs for the Ni—S bonds. This is larger than the 0.013 Å found for bis(isoquinoline-1-carboxaldehyde thiosemicarbazonato)nickel(II), $[Ni(Iq4DH)_2]$, which had a difference in the Ni—N(12) and Ni—N(22), azomethine nitrogen, bond lengths of the same magnitude.[7] The Ni—N(12) and Ni—N(22) bonds in $[Ni(Pz4DM)_2]$ are quite similar, but Ni—N(11) and Ni—N(21), pyrazinyl nitrogens, differ by 0.014 Å, while the analogous isoquinonyl Ni—N bonds differed by only 0.004 Å. The two complexes have similar distances for the S(11)—C(16) and S(21)—C(26) bonds; for $[Ni(Iq4DH)_2]$ 1.719 and 1.735 Å and for $[Ni(Pz4DM)_2]$ 1.714 and 1.729 Å. There is similar agreement between the bond distances for the remaining thiosemicarbazonato moieties of the two complexes.

Table 4 is a more complete compilation of some

Table 3. Selected bond angles (°) for $[Ni(Pz4DM)_2]$

S(11)—Ni—S(21)	97.54(5)		
S(11)—Ni—N(11)	159.0(1)	S(21)—Ni—N(21)	158.2(1)
S(11)—Ni—N(12)	81.7(2)	S(21)—Ni—N(22)	81.3(2)
S(11)—Ni—N(21)	91.9(2)	S(21)—Ni—N(11)	91.0(1)
S(11)—Ni—N(22)	97.6(2)	S(21)—Ni—N(12)	103.6(2)
N(11)—Ni—N(12)	77.8(1)	N(11)—Ni—N(21)	87.0(1)
N(11)—Ni—N(22)	102.6(1)	N(12)—Ni—N(21)	97.2(1)
N(12)—Ni—N(22)	175.1(1)	N(21)—Ni—N(22)	78.0(1)
C(11)—N(11)—C(14)	118.1(4)	C(21)—N(21)—C(24)	117.6(4)
N(13)—N(12)—C(15)	116.7(4)	N(23)—N(22)—C(25)	117.1(4)
N(12)—N(13)—C(16)	112.2(3)	N(22)—N(23)—C(26)	112.9(4)
C(16)—N(14)—C(141)	121.4(5)	C(26)—N(24)—C(241)	120.2(4)
C(16)—N(14)—C(142)	121.3(5)	C(26)—N(24)—C(242)	123.9(5)
C(141)—N(14)—C(142)	117.4(5)	C(241)—N(24)—C(242)	115.7(5)
N(11)—C(11)—C(15)	116.5(4)	N(21)—C(21)—C(25)	116.1(4)
N(12)—C(15)—C(11)	114.7(4)	N(22)—C(25)—C(21)	114.2(4)
N(12)—C(15)—C(151)	122.6(4)	N(22)—C(25)—C(251)	124.3(4)
S(11)—C(16)—N(13)	126.5(3)	S(21)—C(26)—N(23)	126.3(3)
S(11)—C(16)—N(14)	119.4(3)	S(21)—C(26)—N(24)	119.6(3)
N(13)—C(16)—N(14)	114.1(4)	N(23)—C(26)—N(24)	114.2(4)

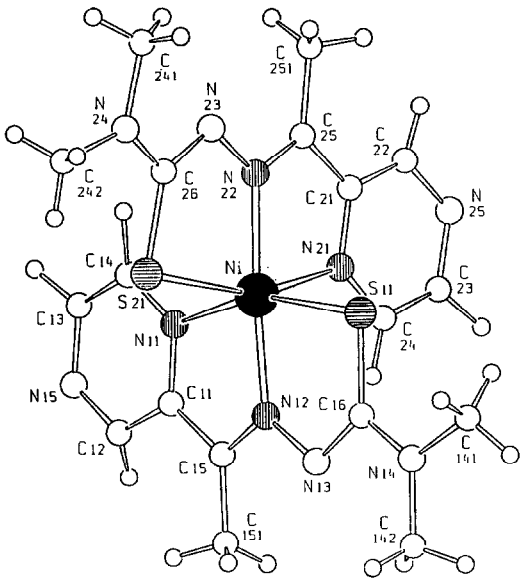

Fig. 1. Schakal diagram of $[Ni(Pz4DM)_2]$.

of the relevant bond lengths of the thiosemicarbazone moiety in the various nickel(II) complexes, as well as examples of copper(II) and chromium(III) complexes. The copper(II) complex has a coordinated heterocyclic thiosemicarbazonato ligand and displays considerable growth inhibition against a range of fungi.[19,26] The thiosemicarbazone bond lengths that would be expected to be most affected by coordination would be the imine C=N and thiolato C—S bonds and, therefore, the largest differences in these bonds would also be expected in the complexes listed in Table 4. There is small variation in C=N with $[Ni(Pz4DM)_2]$ having somewhat shorter bonds and, therefore, weaker bonding to the nickel(II) centre in the six-coordinate complex than for the four-coordinate nickel(II) complexes, except for *cis*-$[NiAc4DH)_2]$. $[Ni(Pz4DM_2]$ has longer C=N bonds than $[Ni(Iq4DH)_2]$, which has the bulkier isoquinoline rings which would presumably weaken imine nitrogen coordination. The bonds are of comparable length to those of $[Cr(HSal4DH)_2]^+$, but considerably longer than found for the four-coordinate copper(II) complex. Similar trends are found for the C—S bond length, except that $[Cr(HSal4DH)_2]^+$ has shorter bonds indicating that the soft sulphur donor atom does not bond as strongly to the hard chromium(III) ion as the nitrogen donor. Also, in contrast to the C=N bond, the C—S bond is considerably longer in the four-coordinate copper(II) complex, indicating stronger bonding of the sulphur donor; most of the four-coordinate nickel(II) complexes also have long C—S bonds. The remaining complexes listed in Table 4 show less differences in the thiosemicarbazone moiety's bond lengths, since they change to a lesser degree on complexation.

Table 4. Comparison of the thiosemicarbazone moiety and metal–donor atom bond lengths (Å) for metal complexes (e.s.d.s range from 0.003 to 0.009 Å)

Compound	C=N	N—N	N—C(S)	C—S	C(S)—N	M—S	M—N	M—N(rg)	Ref.
$[Ni(Pz4DM)_2]$	1.297	1.371	1.347	1.714	1.350	2.380	2.014	2.110	This
	1.300	1.366	1.335	1.729	1.353	2.409	2.017	2.096	work
$[Ni(Iq4DH)_2]^a$	1.279	1.357	1.331	1.719	1.345	2.412	2.026	2.114	7
	1.295	1.356	1.326	1.735	1.350	2.425	2.013	2.110	
$[Ni(Ac4DH)_2]^b$	1.281	1.433	1.309	1.734	1.373	2.162	1.934		10
	1.290	1.417	1.277	1.760	1.369	2.166	1.921		
$[Ni(Lbcn)NCS]^c$	1.300	1.373	1.317	1.764	1.346	2.138	1.846	1.912	11
$[Ni(Pz4M)Cl]^d$	1.312	1.376	1.317	1.756	1.327	2.169	1.852	1.923	13
[Ni(Pz4DM)Cl]	1.304	1.370	1.320	1.756	1.342	2.141	1.855	1.918	13
$[Ni(Sal4Ph)NH_3]^e$	1.316	1.393	1.333	1.717	1.357	2.166	1.844		12
$[Cu(Lhexim)Br]^f$	1.275	1.373	1.301	1.759	1.377	2.236	1.963	2.016	19
$[Cr(HSal4DH)_2]^{+g}$	1.307	1.393	1.336	1.702	1.311	2.407	2.034		5
	1.288	1.388	1.344	1.707	1.307	2.425	2.041		

[a] Iq4DH = anion (loss of ^{2}N proton) of isoquinoline thiosemicarbazones.
[b] Ac4DH = anion (loss of ^{2}N proton) of acetone thiosemicarbazone.
[c] Lbcn = anion (loss of ^{2}N proton) of 2-acetylpyridine 3-azabicyclo[3.2.2]nonylthiosemicarbazone.
[d] Pz4M = anion (loss of ^{2}H proton) of acetylpyrazine ^{4}N-methyl-thiosemicarbazone.
[e] Sal4Ph = dianion (loss of hydroxy and ^{2}N proton) of salicylaldehyde ^{4}N-phenylthiosemicarbazone.
[f] Lhexim = anion (loss of ^{2}N proton) of 2-acetylpyridine 3-hexamethyleneiminylthiosemicarbazone.
[g] HSal4DH = monoanion (loss of hydroxy proton) and salicylaldehyde thiosemicarbazone.

As expected and consistent with the discussion of the bond lengths of the thiosemicarbazone moiety, the six-coordinate complexes all have significantly longer M—S and M—N bonds (Table 4) than the four-coordinate complexes. Somewhat surprising is that the metal–thiosemicarbazone ligand bonds for $[Cr(HSal4DH)_2]ClO_4$ are longer than the metal–sulphur and metal–nitrogen bonds for [Ni(Pz4DM)$_2$]. Additional studies of complexes having different ^4N {i.e. $=^1N—^2NH—C(=S)^4NR_2$} substituents are needed to establish this function's effect on the M—S and C=S bond lengths. Note that there is considerable difference in the M—S bond lengths between [Ni(Pz4M)Cl] and [Ni(Pz4DM)Cl] with a change from ^4NHMe to $^4NMe_2$ (Table 4), but the two compounds have identical C—S bond lengths.

The metal–thiosemicarbazone ligand bond angles (Table 5) also show a difference with a change in coordination number; the six-coordinate complexes have similar bond angles and the angles are smaller for the six-coordinate complexes than for the four-coordinate complexes. A comparison of the angles between [Ni(Pz4DM)$_2$] and [Ni(Pz4DM)Cl] shows a large difference in the S—Ni—N(ring) bond angle, *ca* 159.0° and 158.2° vs 170.6°, respectively. The much smaller angles found for [Ni(Pz4DM)$_2$] must be due to an inter-ligand steric effect, as are the *ca* 5° differences in the other metal–ligand bond angles.

Spectroscopic studies of HPz4DM *and* [Ni(Pz4DM)$_2$]

A decrease in the energy of ν(C=N) from 1605 cm^{-1} in the spectrum of HPz4DM to 1565 cm^{-1} in the spectrum of [Ni(Pz4DM)$_2$] is consistent with coordination of the azomethine nitrogens, as is the presence of a band at 430 cm^{-1} which is assignable to ν(Ni—N).[27] A second band at 1600 cm^{-1} assignable to ν(C=N) is expected in this complex's spectrum since the anionic ligands formally have a double bond between ^2N and ^3C {i.e. $=^1N—^2NH—C(=S)^4NR_2$}. Coordination of the thiol sulphurs is indicated by a decrease in energy of the thioamide IV band at 857 to 749 cm^{-1}, as well as a band at 335 cm^{-1} assignable to ν(NiS).[28] We recorded the spectrum of acetylpyrazine to aid us in assigning the ring deformation band in the 600 cm^{-1} region of the spectrum of the uncomplexed ligands; this band increases by 30 cm^{-1} in the spectrum of [Ni(Pz4DM)$_2$] on coordination of one of the ring nitrogens. The ν(NiN) band for a pyrazinyl nitrogen is expected below 250 cm^{-1} and we are unable to assign it with our spectrometer. Pyrazine derivatives have bands assignable to the ring's $\pi \rightarrow \pi^*$ and $n \rightarrow \pi^*$ transitions at *ca* 38,500 and 30,500 cm^{-1}, respectively.[29] A DMSO solution of acetylpyrazine shows its ring's $\pi \rightarrow \pi^*$ and $n \rightarrow \pi^*$ transitions at 36,900 and 32,890 cm^{-1}, respectively, with $\log \varepsilon = 2.911$ for the latter band. A third band in the spectrum at 29,410 cm^{-1} is assignable to the $n \rightarrow \pi^*$ band involving the acetyl oxygen's lone electron pair(s). In the solution spectrum of HPz4DM the ring's $n \rightarrow \pi^*$ band must merge with the $n \rightarrow \pi^*$ band of the azomethine group to give a $\log \varepsilon$ value of 4.33 for a band at 31,350 cm^{-1}. Lower energy $n \rightarrow \pi^*$ bands at 23,040 and 18,520 cm^{-1}, which involve the thiosemicarbazone moiety, are present in the solid-state spectra of HPz4DM, as well as [Ni(Pz4DM)$_2$] (24,510 and 20,620 cm^{-1}).

In DMSO solution, other than the intense $n \rightarrow \pi^*$

Table 5. Comparison of the thiosemicarbazone moiety and coordination site bond angles (°) for metal complexes

Compound[a]	S—M—N(rg)	S—M—N	N(rg)—M—N	M—S—C	M—N—N	Ref.
[Ni(Pz4DM)$_2$]	159.0	81.7	77.8			This
	158.2	81.3	78.0			work
[Ni(Iq4DH)$_2$]	158.9	81.1	78.2	93.2	125.1	7
	159.0	81.3	77.7	93.7	124.3	
[Ni(Ac4DH)$_2$]		85.4		93.5	118.1	10
		86.0		94.6	116.6	
[Ni(Lbcn)NCS]	171.0	87.0	84.0	95.5	124.4	11
[Ni(Pz4M)Cl]	170.0	86.7	83.3	95.2	124.1	13
[Ni(Pz4DM)Cl]	170.6	87.3	83.4	95.3	123.8	13
[Ni(Sal4Ph)NH$_3$]		87.7		95.9	121.5	12
[Cu(Lhexim)Br]	165.3	85.1	80.5	94.5	122.7	19
$[Cr(Sal4DH)_2]ClO_4$		82.0		97.5	118.7	5
		81.5		97.0	119.0	

[a] Identification of the ligands is under Table 4.

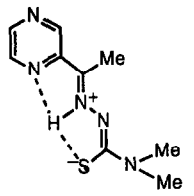

Fig. 2. Bifurcated isomer of HPz4DM with extended conjugation.

band at *ca* 30,000 cm^{-1}, only a single band at *ca* 23,000 cm^{-1} is present for HPz4DM. This coupled with ^1H NMR results[13] indicate that HPz4DM possesses a significant percentage of the bifurcated isomer (Fig. 2) with its conjugated thiosemicarbazone moiety. The DMSO spectrum of $[Ni(Pz4DM)_2]$ has bands at 28,990, 25,640 and 21,740 cm^{-1} with $\log \varepsilon$ values of 4.47, 4.28 and 4.34, respectively. The highest energy band is due to an intraligand $n \rightarrow \pi^*$ transition, while the next band includes the thiosemicarbazone moiety's $n \rightarrow \pi^*$ and $Ni^{II} \rightarrow$ ring charge transfer transitions. The lowest energy band is likely due to an $S \rightarrow Ni^{II}$ charge transfer transition, since it is too intense for a *d–d* band. Weak bands are found in the mull transmission spectrum at 6760 and 13,160 cm^{-1}, which can be assigned as $^3A_{2g} \rightarrow {}^3T_{2g}$ and $^3A_{2g} \rightarrow {}^3T_{1g}(F)$, respectively. However, their ratio falls outside the values normally associated with octahedral symmetry[30] and do not yield meaningful ligand field parameters.

Antifungal activity of HPz4DM *and* $[Ni(Pz4DM)_2]$

Although HPz4DM strongly inhibits the growth of *Paecilomyces variotii* (i.e. a 22 mm diameter of growth inhibition is achieved by a 1000 $\mu g\ cm^{-3}$ solution), and to a slightly lesser extent *Aspergillus niger* (i.e. 19.5 mm at 1000 $\mu g\ cm^{-3}$), $[Ni(Pz4DM)_2]$ shows no activity against either fungus. The four-coordinate nickel(II) complexes of this ligand, [Ni(Pz4DM)Cl] and [Ni(Pz4DM)Br] also showed no activity.[13] Copper complexes of NPz4DM show significant activity against both fungi,[20] indicating that ease of reduction of the metal centre and the thiosemicarbazone ligand may be important for antifungal activity.[31]

Acknowledgement—The Donors of the Petroleum Research Fund, administered by the American Chemical Society, are acknowledged for the partial support of this research.

REFERENCES

1. J. P. Scovill, D. L. Klayman and C. F. Franchino, *J. Med. Chem.* 1982, **25**, 1261.
2. D. X. West, C. S. Carlson, A. E. Liberta, J. N. Albert and C. R. Daniel, *Trans. Met. Chem.* 1990, **15**, 341 and refs therein.
3. B. S. Garg, M. R. P. Kurup, S. K. Jain and Y. K. Bhoon, *Trans. Met. Chem.* 1988, **13**, 247 and refs therein.
4. M. D. Timken, S. R. Wilson and D. N. Hendrickson, *Inorg. Chem.* 1985, **24**, 3450.
5. M. Soriano-Garcia, J. Valdes-Martinez, R. A. Toscano and J. Gomez-Lara, *Acta Cryst.* 1985, **C41**, 500.
6. D. X. West, P. M. Ahrweiler, G. Ertem, J. P. Scovill, D. K. Klayman, J. L. Flippen-Anderson, R. Gilardi, C. George and L. K. Pannell, *Trans. Met. Chem.* 1985, **10**, 264.
7. M. Mathew and G. J. Palenik, *J. Am. Chem. Soc.* 1969, **91**, 6310.
8. A. E. Liberta and D. X. West, *BioMetals* 1992, **5**, 121.
9. P. Dapporto, G. De Munno and A. A. G. Tomlinson, *J. Chem. Res.* 1984, 40.
10. J. Valdes-Martinez, R. A. Toscano, M. Soriano-Garcia, M. Rubio, J. Gomez-Lara, M. A. Vazquez-M. and S. Carranza, *Polyhedron* 1989, **8**, 727.
11. D. X. West, J. P. Scovill, J. V. Silverton and A. Bavoso, *Trans. Met. Chem.* 1986, **11**, 123.
12. M. Soriano-Garcia, R. A. Toscano, J. Valdes-Martinez and J. M. Fernandez-G., *Acta Cryst.* 1985, **C41**, 498.
13. D. X. West, M. A. Lockwood, A. E. Liberta, X. Chen and R. D. Willett, *Trans. Met. Chem.*, in press.
14. M. B. Ferrari, G. G. Fava, C. P. Pelizzi, P. Tarasconi and G. Tosi, *J. Chem. Soc., Dalton Trans.* 1987, 227.
15. C. F. Bell and C. R. Theocharis, *Acta Cryst.* 1987, **C43**, 26.
16. A. G. Bingham, H. Bogge, A. Muller, E. W. Ainscough and A. M. Brodie, *J. Chem. Soc., Dalton Trans.* 1987, 493.
17. E. W. Ainscough, E. N. Baker, A. M. Brodie, R. J. Cresswell, J. D. Ranford and J. M. Waters, *Inorg. Chim. Acta* 1990, **172**, 185.
18. E. W. Ainscough, A. M. Brodie, J. D. Ranford and J. M. Waters, *J. Chem. Soc., Dalton Trans.* 1991, 2195.
19. R. J. Butcher and D. X. West, *Trans. Met. Chem.*, in press.
20. D. X. West, C. S. Carlson, A. E. Liberta and J. P. Scovill, *Trans. Met. Chem.* 1990, **15**, 383.
21. N. Walker and D. Stuart, *Acta Cryst.* 1983, **A39**, 158.
22. C. M. Sheldrick, SHELXS86, A Program for the Solution of Crystal Structures from X-ray Diffraction Data. University of Göttingen, F.R.G. (1986).
23. B. A. Frenz & Associates Inc., Structure Determination Package SDP/VAX, V. 2.2. College Station, TX, U.S.A. and Enraf–Nonius, Delft, The Netherlands (1985).
24. W. H. Zachariasen, *Acta Cryst.* 1963, **16**, 1139.
25. E. Keller, SCHAKAL, A Program for Plotting

Molecular and Crystal Structures. University of Freiburg, F.R.G. (1988).
26. D. X. West, C. S. Carlson, K. J. Bouck and A. E. Liberta, *Trans. Met. Chem.* 1991, **16**, 271.
27. P. Souza, J. A. Garcia-Vazquez and J. R. Masaguer, *Trans. Met. Chem.* 1984, **9**, 318; *Synth. React. Inorg. Met-Org. Chem.* 1985, **15**, 247; T. R. Rao, M. Sahay and R. C. Aggarwal, *Synth. React. Inorg. Met-Org. Chem.* 1985, **15**, 175.
28. S. K. Senkupta, S. K. Sahni and R. N. Kapoor, *Acta Chim. Acad. Sci. Hungary* 1980, **104**, 89.
29. S. F. Mason, in *Physical Methods in Heterocyclic Chemistry* (Edited by A. R. Katritzky), Vol. II, Ch. 7. Academic Press, New York (1963).
30. A. P. B. Lever, *J. Chem. Educ.* 1968, **45**, 711.
31. A. S. Kumbhar, S. B. Padhye, D. X. West and A. E. Liberta, *Trans. Met. Chem.* 1991, **16**, 276; 1992, **17**, 247.

Polyhedron Vol. 12, No. 15, pp. 1895–1900, 1993
Printed in Great Britain

0277–5387/93 $6.00+.00
© 1993 Pergamon Press Ltd

NINE-COORDINATE ADDUCTS OF TETRAKIS(THENOYLTRIFLUOROACETONATO)URANIUM(IV): EQUILIBRIUM CONSTANTS FROM ^{1}H NMR AND ELECTRONIC SPECTROSCOPY

J. I. BULLOCK* and M. OULABI

Chemistry Department, University of Surrey, Guildford, Surrey GU2 5XH, U.K.

(*Received* 23 *March* 1993; *accepted* 6 *April* 1993)

Abstract—Time-averaged chemical shifts in the ^{1}H NMR spectra of aniline, pyridine and some derivatives, induced by coordination in 1:1 complexes to the paramagnetic $5f^2$ uranium(IV) as its complex with the thenoyltrifluoroacetonato anion [U(TTA)$_4$], have been used to find equilibrium constants in benzene and acetone solution. The bound chemical shifts are shown to be solvent independent. In acetone the equilibrium constant for the formation of U(TTA)$_4$·H$_2$O was found to be 4.0±0.2 dm^3 mol^{-1} from ^{1}H NMR spectroscopy. Equilibrium constants have also been determined by electronic spectroscopy in benzene solution, in which U(TTA)$_4$ itself is eight-coordinate. The results were correlated with the basicity of the substrate and the effects of steric hindrance were evaluated. U(TTA)$_4$ is nine-coordinate in acetone through solvent coordination and the addition of substrate caused no or small changes to the electronic spectrum.

The addition of a neutral donor ligand, S, to a benzene solution of U(TTA)$_4$ containing excess HTTA caused[1] changes in the shape and intensity of an *f–f* absorption near 670 nm, which were interpreted in terms of a change in coordination number at uranium(IV) from eight to nine. There is no published evidence that U(TTA)$_4$ forms 10-coordinate adducts.

$$U(TTA)_4 + S \rightleftharpoons U(TTA)_4S \quad (1)$$

with

$$\beta_1 = [U(TTA)_4S]/[U(TTA)_4][S] \quad (2)$$

and

$$L_0 = U_{total} = [U(TTA)_4] + [U(TTA)_4S] \quad (3)$$

$$S_0 = S_{total} = [S] + [U(TTA)_4S] \quad (4)$$

With triphenylphosphine oxide (TPPO), for example,[1] successive additions produced a set of spectra with two isosbestic points from which the equilibrium constant β_1 [eqs (1) and (2)] was calculated with the mass balance equations (3) and (4). The extinction coefficients of U(TTA)$_4$, ε_1, and the adduct U(TTA)$_4$S, ε_2, were found when the TPPO concentration was zero (ε_1) and when further addition of TPPO caused no change to the spectrum (ε_2), i.e. when the nine-coordinate U(TTA)$_4$·TPPO was fully formed. Between 450 and 500 nm $\varepsilon_2 > \varepsilon_1$ and the nine-coordinate adduct has a characteristic absorption maximum near 670 nm. Oxidation of uranium(IV) to uranium(VI) was said to be prevented by the addition of a 10-fold excess of HTTA. The Th(TTA)$_4$ adduct with trioctylphosphine oxide is nine-coordinate in the solid state.[2]

The computer program SQUAD[3–5] used in the present work for the calculation of β_1 from electronic spectroscopy requires no predetermined values of ε_1 and ε_2, which are calculated at each analytical wavelength. This provides a useful internal validation of the results since ε_1 is readily found from solutions where the concentration of S is zero.

In addition to electronic spectroscopy it is also possible to find β_1 from an analysis[6,7] of the ^{1}H NMR spectra of S, which are shifted but little broadened by the presence of the paramagnetic $5f^2$ uranium(IV). This method should be applicable in solvents which bind to U(TTA)$_4$, e.g. acetone, where changes in the electronic spectrum might be too small for the determination of β_1 because no

* Author to whom correspondence should be addressed.

change in coordination number occurs on the addition of S.

Here, we extend the electronic spectroscopic method to organic nitrogen bases and further demonstrate the usefulness of ^{1}H NMR techniques for β_1 and the bound chemical shifts of S, Δ_B.

EXPERIMENTAL

Materials

4-Picoline (BDH) was purified by distillation and 4-toluidene (Aldrich) by recrystallization (petroleum ether). Pyridine (BDH, 99.5%, AnalaR), 3,5-lutidene (Aldrich, 98%), 3,4-lutidene (Aldrich, 98%), 2,4,6-collidine (Aldrich, 99%), aniline (BDH, 99.5%, AnalaR), 3-chloroaniline (Aldrich, 99%), 4-nitroaniline (BDH), $UO_2SO_4 \cdot 3.5H_2O$ (BDH), HTTA (Aldrich, 99%), benzene (BDH, AnalaR, water content 0.04% Karl Fischer), acetone (BDH, AnalaR, water content 0.2%, chromatography), benzene-d_6 (Merck, 99.6 atom %D) and acetone-d_6 (CEN, 99.8 atom %D) were used as supplied.

Tetrakis(thenoyltrifluoroacetonato)uranium(IV), U(TTA)$_4$

Uranyl sulphate in dilute hydrochloric acid was reduced with zinc amalgam. Caesium chloride and concentrated hydrochloric acid were added to the reduced solution, which was then saturated with gaseous hydrogen chloride. On cooling green crystals of Cs_2UCl_6 precipitated. HTTA in ethanol was added to a suspension of Cs_2UCl_6 in ethanol. The dark brown precipitate of U(TTA)$_4$ which eventually formed was recrystallized from toluene. Found: C, 34.6; H, 1.6. Calc. for $C_{32}H_{16}F_{12}O_8S_4U$: C, 34.3; H, 1.4%. ^{1}NMR (C_6D_6), 293 K: σ 5.25, 5.20, 5.16 (1H, m), δ 7.02, 6.96 (1H, m), δ 7.43, 7.39 (1H, m), 13.71 (1H, singlet), m = multiplet.

Use of nitrogen box

Solutions of U(TTA)$_4$ and the adducts were prepared by conventional degassing procedures in an atmosphere of purified nitrogen using a Faircrest glove-box. These solutions were transferred under nitrogen to sealed cells for use in the spectrophotometer.

Spectrometric measurements

Electronic spectra were recorded with a Pye–Unican SP8-100 between 445 and 500 nm (determination of $\log_{10}\beta_1$) and 620–700 nm (to monitor oxidation) in matched quartz cells at 20 ± 1°C using pure solvent as the reference. The nitrogen bases did not absorb at these wavelengths. Equilibrium constants were determined with SQUAD. The conditions are summarized in the footnote to Table 1.

In a system $A + nB \rightleftharpoons AB_n$, if $n = 1$ then a plot of $A_T B_T/\Delta A_s$ against $A_T + B_T$ will be linear,[9] where A_T = total concentration of A, B_T = total concentration of B, ΔA_s = absorbance at a given wavelength (at which B does not absorb) minus $\varepsilon_A A_T$ (ε_A = extinction coefficient of A at the same wavelength). This behaviour was found at 450 nm for U(TTA)$_4$ adducts and helps confirm the stoichiometry of the reaction.

^{1}H NMR spectra were recorded in d_6-benzene and d_6-acetone using a Bruker WH90 FT spectrometer operating at 90.0229 MHz. Chemical shifts (ppm) relative to the internal standard TMS for the coordinated and free ligand were subtracted to give values of $\sigma\Delta$. The experimental conditions are summarized in the footnotes to Table 2.

The upfield, experimental chemical shifts, $\sigma\Delta$, observed when various amounts of S were added to solutions containing a fixed concentration of U(TTA)$_4$ were used to find β_1 and ΔB, the bound chemical shift of any proton on S.

Table 1. Complexation (1 : 1) of the nitrogen bases with U(TTA)$_4$ in benzene—results from electronic spectroscopy[a]

Ligand	$\log_{10}\beta_1$	pK_a	% Oxidation (min^{-1})
2,4,6-Collidene	0.94 (0.01)	7.43	0.15
3,4-Lutidene	2.31 (0.02)	6.46	0.08
3,5-Lutidene	2.37 (0.01)	6.17	0.03
4-Picoline	2.44 (0.01)	6.03	0.03
2-Picoline	0.83 (0.01)	5.95	0.10
Pyridine	1.98 (0.01)	5.23	0.09
4-Toluidene	1.09 (0.01)	5.08	0.03
Aniline	0.74 (0.02)	4.63	0.04
3-Chloroaniline	0.76 (0.07)	3.46	0.03
4-Nitroaniline	see text	1.00	—

[a] Figures in parentheses give one standard deviation; $\log_{10}\beta_1$ from SQUAD; no. of solutions 5–7; wavelength range 445–500 nm, interval 5 nm; U concentration 2.05–2.48×10^{-4} mol dm^{-3}; ligand concentration 1×10^{-4}–2 mol dm^{-3} dependent on magnitude of β_1; $T = 20 \pm 1$°C; % oxidation measured with U concentration 5×10^{-3} mol dm^{-3} and ligand concentration 3×10^{-2} mol dm^{-3}; mean experimental value of ε (dm^3 mol^{-1} cm^{-1}) for U(TTA)$_4$ at 445 nm, 1603 ± 45 and at 500 nm, 703 ± 34, mean values calculated from SQUAD at 445 nm, 1605 ± 48 and at 500 nm, 698 ± 38; degree of complex formation 10–90%.

Table 2. ^{1}H bound chemical shifts (ΔB, ppm) and $\log_{10}\beta_1$ for nitrogen bases complexed 1:1 with U(TTA)$_4$ in benzene and acetone[a]

		ΔB[c]				$\log_{10}\beta_1$			
		Benzene		Acetone		Benzene[d]		Acetone	
Ligand[b]	Proton	Eq. (5)	Eq. (6)	Eq. (5)	Eq. (6)	Eq. (5)	Eq. (6)	Eq. (5)	Eq. (6)
3,5-lut	—CH$_3$	6.4 (0.6)	5.8 (0.2)	6.1 (0.3)	5.7 (0.5)	2.13 (0.14)	2.41 (0.08)	1.76 (0.07)	1.83 (0.09)
	4-H	8.0 (0.8)	7.1 (0.3)	7.0 (0.8)	7.4 (0.7)	2.13 (0.14)	2.42 (0.09)	1.79 (0.16)	1.63 (0.10)
	2-H	31.3 (3.1)	28.3 (0.8)	31.4 (2.5)	31.6 (2.2)	2.18 (0.12)	2.48 (0.09)	1.64 (0.11)	1.61 (0.08)
4-pic	—CH$_3$			7.6 (0.2)	7.4 (0.1)			1.56 (0.02)	1.58 (0.02)
	3-H			12.9 (0.3)	12.1 (0.4)			1.45 (0.03)	1.52 (0.02)
	2-H			35.1 (0.7)	33.1 (0.7)			1.45 (0.03)	1.54 (0.03)
4-tol	—CH$_3$	[e]	2.5 (0.1)			[e]	1.04 (0.08)		
	3-H	11.3 (1.2)	11.6 (1.0)			0.78 (0.06)	1.10 (0.08)		
	2-H	12.6 (0.9)	12.6 (1.9)			1.00 (0.04)	1.00 (0.08)		
	—NH$_2$	[e]	96.0 (9.6)			[e]	0.90 (0.05)		

[a] Figures in parentheses give one standard deviation; % oxidation see Table 1; $T = 20 \pm 1$°C; U concentration 1.78×10^{-2}–4.83×10^{-3} mol dm^{-3}; ligand concentration range 1.01×10^{-1}–8.90×10^{-3} mol dm^{-3}; no. of solution 5–7.

[b] 3,5-lut = 3,5-lutidene; 4-pic = 4-picoline; 4-tol = 4-toluidene.

[c] Degree of complex formation 5–25%.

[d] Table 1, 3,5-lutidene 2.37 ± 0.01, 4-toluidene 1.09 ± 0.01.

[e] No convergence.

(1) A graphical method was used which employed the relationship:[6]

$$S_0(1-\sigma\Delta/\Delta B) = L_0\Delta B/\sigma\Delta - (\beta_1^{-1} + L_0), \quad (5)$$

where L_0 = constant concentration of U(TTA)$_4$ and S_0 = variable concentration of S.

A value of ΔB was guessed to calculate $S_0(1-\delta\Delta/\Delta B)$, which was plotted against $1/\sigma\Delta$. The slope ($L_0\Delta B$) of the plot was found using linear least-squares analysis and the new value of ΔB was used to recalculate S_0 $(1-\delta\Delta/\Delta B)$, which in turn was replotted against $1/\sigma\Delta$. This process was repeated until the difference in successive values of ΔB was insignificant (less than 1 part in 1000 for both slope and intercept). The final value of the intercept was used to find β_1.

(2) The general relationship[6–8]

$$\sigma\Delta = [\mathrm{U(TTA)_4S}]\Delta B/S_0 \quad (6)$$

was analysed with eqs (2)–(4) using the Newton-Raphson method with a locally-written program which gave values of β_1 and ΔB with their standard deviations and the degree of formation of the complex.

The results from SQUAD and the two NMR methods, eqs (5) and (6), are given in Tables 1 and 2 with one standard deviation given in parentheses. Allowing for systematic and other experimental errors the true uncertainty is likely to be at least two to three times greater than these values.

Equilibrium constant and bound chemical shift for water

The ^{1}H NMR spectrum of a sample (1 cm^3) of d_6-acetone was recorded and the H_2O resonance recognized. Known amounts of H_2O were added to samples (1 cm^3) of d_6-acetone and the spectra recorded. By measuring the peak areas it was then possible to find the amount of H_2O initially present in the d_6-acetone. D_2O at various concentrations was then added to solutions of U(TTA)$_4$ at fixed concentration in d_6-acetone. The ^{1}H NMR spectra of these solutions were recorded and the shifts analysed using eqs (5) and (6) as before. Results are given in Table 3. Similar experiments could not be conduced in d_6-benzene because of the low solubility of water in the solvent. There was no evidence from the electronic spectra in benzene to suggest that water coordination was significant in this solvent.

RESULTS AND DISCUSSION

Oxidation of uranium(IV)

Uranium(IV) is oxidized to uranium(VI) by atmospheric dioxygen in non-aqueous solvents.[10–12] There is no consistent kinetic pattern, but the rate of oxidation may depend[10–12] on (1) the initial concentration of uranium(IV), (2) the partial pressure

Table 3. Complexation of water with $U(TTA)_4$ in acetone[a]

Range of H_2O/D_2O concentration (mol dm^{-3})	Number of solutions	Degree of formation	ΔB (ppm) Eq. (5)	Eq. (6)	β_1 (dm^3 mol^{-1}) Eq. (5)	Eq. (6)
5.590×10^{-1}–6.450×10^{-2}	7	2–6% based on H_2O	46.8(1.4)	48.1(1.0)	4.0(0.2)	4.0(0.2)

[a] $\log_{10}\beta_1 = 0.60$; $[U(TTA)_4] = 1.890 \times 10^{-2}$ mol dm^{-3}.

of O_2, (3) the solvent and its water content, (4) the nature of the coordinated ligands and (5) exposure to light. In solution the oxidation of $U(TTA)_4$ and its adducts can be readily followed between 610 and 720 nm, since uranium(VI) does not absorb appreciably above 500 nm.

We made preliminary experiments in which uranium(IV) absorbances near 660 nm were measured using benzene and acetone solutions of $U(TTA)_4$ and its adducts. Solutions were prepared in air and a nitrogen box, but with no excess HTTA. In general, the rate of oxidation was acceptably slow in air (Table 1). The percentage oxidation of $U(TTA)_4$ in unit time increased with a decrease in the initial $U(TTA)_4$ concentration and with an increase in the total concentration of S. We found that $U(TTA)_4$ alone was less susceptible to oxidation in benzene where it is eight-coordinate than in acetone where nine-coordination is achieved with a solvent molecule as ligand; on the addition to acetone and benzene solutions of a ligand S at a concentration which would result in the complete formation of a nine-coordinate adduct in benzene, the oxidation was more rapid but became much less solvent dependent.

Although the rate of oxidation decreased for solutions prepared in a nitrogen box it could not be totally prevented in our hands. All of the results presented here refer to solutions made up in the air.

Our purpose was to find conditions under which oxidation was minimized in subsequent studies to find equilibrium constants and NMR parameters. Measurements were made rapidly and were always complete within 30 min of solution preparation. Initial rates of oxidation are recorded in Table 1. The good agreement found between calculated and experimental values of extinction coefficients of $U(TTA)_4$ and the small standard deviations in $\log_{10}\beta_1$ (Tables 1 and 2) suggested that oxidation was relatively unimportant. Experiments with results showing marked variation in extinction coefficients or with high standard deviations in $\log_{10}\beta_1$ or with absorption spectra with weak shoulders below 500 nm typical of uranium(VI), or with new, weak resonances indicative of uranium(VI) complexes in the ^1H NMR spectra, were repeated. No excess HTTA was used in our experiments since this produced many additional resonances in the ^1H NMR spectra, which made it difficult to monitor shifts in the resonances of S protons and, in addition, results from NMR and electronic spectroscopy could be compared under very similar experimental conditions.

Electronic spectroscopy in benzene solution

The analysis (Table 1) gave values of $\log_{10}\beta_1$ with small standard deviations, indicating a good fit to the experimental data. There was also good agreement between the calculated and experimental values for the extinction coefficients of $U(TTA)_4$.

In general, $\log_{10}\beta_1$ increases with an increase in the pK_a of the nitrogen bases, except when steric hindrance is present (Table 1). Thus, 2,4,6-collidene and 2-picoline have $\log_{10}\beta_1$ at least an order of magnitude smaller than might be expected from the pK_a values.

The method becomes less satisfactory as $\log_{10}\beta_1$ decreases since large excesses of the base are required to give a wide range in the degree of formation of the complex (see footnote to Table 1 and Experimental). For 4-nitroaniline no changes in the spectrum of $U(TTA)_4$ were observed.

There is good evidence that the uranium(IV) absorption maximum near 670 nm is sensitive to a change in coordination number,[1] which was confirmed in the present work through comparison between benzene and acetone solutions. The peak at 656 nm in benzene shifts to that found in acetone at 662 nm and the pronounced shoulder near 685 nm declines as base is added. These are accompanied by changes in the overall shape of the band envelope. Adding the base to an acetone solution caused small or no change in λ_{max} and the

shape of the envelope, although we do know from ^{1}H NMR measurements that complex formation takes place. Our conclusion is that U(TTA)$_4$ is eight-coordinate in benzene and nine-coordinate in acetone.

Experiments for a given base with variation in the initial uranium(IV) concentration gave consistent values of $\log_{10}\beta_1$, indicating that no polymeric species were present.

The use of carefully-dried benzene had little effect on the values of $\log_{10}\beta_1$. For example, a value of 2.44 ± 0.03 was found for 4-picoline in dry benzene, which is the same as that given in Table 1 for which the water content was 0.04%.

The bound chemical shift (ΔB) *and* β_1 *from* ^{1}H *NMR studies*

For 3,5-lutidene the bound chemical shifts of equivalent protons are solvent independent (Table 2) within experimental error, as might be expected for complexes of similar structure. ΔB (ppm) decreased as the number of bonds separating a proton from the metal centre increased; two bonds, NH_2 in 4-tol 96, H in H_2O 47; three bonds, 2-H in 4-pic 34, 2-H in 3,5-lut 31; four bonds, 2-H in 4-tol 13, 3-H in 4-pic 12.5; five bonds, 3-H in 4-tol 11, CH_3 in 3,5-lut 6, 4-H in 3,5-lut 7; six bonds, CH_3 in 4-pic 7; seven bonds, CH_3 in 4-tol 2. These results do not provide evidence for a predominant contact shift mechanism. There are through-space relationships (r^{-3}, θ) with ΔB decreasing with an increase in r as expected for a pseudo-contact mechanism. A simple analysis using r^{-3} only found from known bond lengths reproduced the correct order of ΔB, but overestimated the relative values in most cases. Nothing is known of the true symmetry of these complexes in solution. We are currently undertaking a full analysis in selected cases using ^{13}C in addition to ^{1}H NMR spectroscopy.

The values for ΔB obtained by the two methods of data analysis agree within the likely experimental errors in all cases.

There is also reasonable agreement between values of $\log_{10}\beta_1$ obtained from benzene solutions using both the electronic and NMR spectroscopic methods (Tables 1 and 2, for 3,5-lutidene 2.37 and 2.30, for 4-toluidene 1.09 and 0.97, respectively). The values of $\log_{10}\beta_1$ found in acetone are rather less than an order of magnitude smaller than those found in benzene and could reflect the nine-coordination of U(TTA)$_4$ itself in acetone.

^{1}H NMR spectroscopy is thus established as a satisfactory method for the determination of an equilibrium constant for uranium(IV) complexes, particularly in cases where changes in the electronic spectrum are too small for use in the determination. The method is limited in terms of the range in the degree of formation of complex across the experiments because of the decrease in intensity of the resonances of the base as the concentration is reduced (see Experimental). For example, ΔB for the amine protons of 4-toluidene was found to be 96 ppm, which is very much larger than the observed shifts $\delta\Delta$. Nonetheless, relatively small (10%) standard deviations were observed.

Comparison with values of $\log_{10}\beta_1$ *found previously*

Previously values of $\log_{10}\beta_1$, with U(TTA)$_4$ in benzene solution,[13] were found to be 2.55 for N,N-diethylacetamide and 3.02 for triethylphosphate and for U(acac)$_4$ in benzene β_1 (kg mol^{-1}) was found[14] to be 63.8 for dimethyl sulphoxide at 40°C from a ^{1}H NMR kinetic study ($\log_{10}\beta_1 \cong 1.80$). With oxygen donor ligands and U(TTA)$_4$ in benzene the values shown below for $\log_{10}\beta_1$ are reported,[1,15,16] determined by electronic spectroscopy.

tri-n-octylphosphine oxide	6.23
tri-phenylphosphine oxide	4.72
di-n-butyl n-butylphosphinate	4.04
dioctyl sulphoxide	3.64
dihexyl sulphoxide	3.62
dimethyl sulphoxide	3.23
dibenzyl sulphoxide	3.10
tri-n-butyl phosphate	3.04
tri-iso-octylthiophosphate	1.04
methyl-iso-butylketone	0.1

The values for triethyl phosphate[13,15] are in good agreement.

Using SQUAD[3-5] we found $\log_{10}\beta_1$ in benzene to be 3.14 ± 0.01 for tri-n-butyl phosphate and 4.00 ± 0.01 for di-n-butyl n-butylphosphonate from electronic spectroscopy. The very different values for dimethyl sulphoxide[14,16] may be attributed[17] to the apparent poorer acceptor properties of U(acac)$_4$ compared with U(TTA)$_4$. As far as we know there are no comparable values for the nitrogen bases with uranium(IV).

Complexation between U(TTA)$_4$ *and water in acetone solution*

Nine-coordinate adducts of thorium(IV) with one molecule of water are well-established in the solid state. The structures[18,19] of aquatetrakis(1,1,1-trifluoropentan-2,4-dionato)thorium(IV) and the corresponding tropolonato complex are based on the nine-coordinate monocapped square antiprism.

The ^1H NMR method was modified (see Experimental) to allow estimations of β_1 and ΔB for water (Table 3). The value of β_1 is at the lower limit of the useful range for the method, as indicated by the degree of formation of the complex. The concentration of water in the experimental solutions cannot be conveniently lowered whilst the concentration of $U(TTA)_4$ is limited by solubility. Nonetheless, satisfactory standard deviations were obtained for β_1 and ΔB with very similar values from the two methods of data analysis. The value of ΔB was large, as expected (see results for the $-NH_2$ group in 4-toluidene, Table 2). As far as we know this is the first determination of β_1 for complexation of water with a uranium(IV) complex.

Acknowledgement—We thank the Syrian Atomic Energy Commission for granting study leave to M.O.

REFERENCES

1. V. V. Ramakrishna, S. K. Patil and A. Ramanujam, *J. Inorg. Nucl. Chem.* 1980, **42**, 1009.
2. J. G. Leipoldt, G. F. S. Wessels and L. D. C. Bok, *J. Inorg. Nucl. Chem.* 1975, **37**, 2487.
3. D. J. Leggett and W. A. E. McBryde, *Talanta* 1975, **22**, 781.
4. D. J. Leggett and W. A. E. McBryde, *Analyt. Chem.* 1975, **47**, 1065.
5. D. J. Leggett, *Analyt. Chem.* 1977, **49**, 276.
6. B. C. Mayo, *Chem. Soc. Rev.* 1973, **2**, 49.
7. B. L. Shapiro and M. D. Johnston Jr, *J. Am. Chem. Soc.* 1972, **94**, 8185.
8. M. D. Johnston Jr, B. L. Shapiro, M. J. Shapiro, T. W. Proulx, A. D. Godwin and H. L. Pearce, *J. Am. Chem. Soc.* 1975, **97**, 542.
9. F. J. C. Rossotti and H. Rossotti, *The Determination of Stability Constants*, p. 476. McGraw-Hill, New York (1961).
10. K. Juznic and M. Senegacnik, *Inorg. Nucl. Chem. Lett.* 1975, **11**, 349.
11. B. J. M. A. Busch, J. G. H. Du Preez, G. J. Gerber, H. E. Rohwer and C. P. J. Van Vuuren, *Inorg. Chim. Acta* 1977, **24**, L87.
12. S. Sosero, O. Traverso, L. Magon, P. Zanella and G. Scibona, *J. Chem. Soc., Dalton Trans.* 1980, 1324.
13. J. I. Bullock and A. J. Sweatman, *Inorg. Chim. Acta* 1982, **64**, L1.
14. H. Fukutomi, H. Ohno and H. Tomiyasu, *Bull. Chem. Soc. Japan* 1986, **59**, 2303.
15. S. K. Patil, V. V. Ramakrishna and A. Ramanujam, *Proc. Ind. Acad. Sci.* 1979, **88**, 303.
16. A. Ramanujam, N. M. Gudi, M. N. Nadkarni, S. K. Patil and V. V. Ramakrishna, *Proc. Ind. Acad. Sci.* 1982, **91**, 347.
17. L. D. C. Bok, G. F. S. Wessels and J. G. Leipoldt, *Z. Anorg. Allg. Chem.* 1974, **404**, 76.
18. T. W. Hambley, D. L. Kepert, C. L. Raston and A. H. White, *Aust. J. Chem.* 1978, **31**, 2635.
19. R. J. Hill and C. E. F. Rickard, *J. Inorg. Nucl. Chem.* 1975, **37**, 2481.

Polyhedron Vol. 12, No. 15, pp. 1901–1905, 1993
Printed in Great Britain

0277–5387/93 $6.00+.00
© 1993 Pergamon Press Ltd

MULTIDENTATE FERROCENYLPHOSPHINES—I. TRIS-(DIPHENYLPHOSPHINO)FERROCENES

IAN R. BUTLER,* LOIS J. HOBSON, STEPHAN M. E. MACAN and DENIS J. WILLIAMS

Department of Chemistry, The University of Wales, Bangor, Gwynedd LL57 2UW, U.K.

(*Received* 23 *March* 1993; *accepted* 6 *April* 1993)

Abstract—New potentially tridentate ferrocenylphosphines have been prepared by the lithiation of diphenylphosphinoferrocene (dppf) followed by reaction of the dilithiated products with chlorodiphenylphosphine. The reaction of the new ligands with $Pd(COD)Cl_2$ has been studied using ^{31}P NMR to determine the preferential bidentate coordination modes.

The tertiary alkyl- and aryl-phosphines are probably the most widely used class of ligands in organometallic chemistry. One of the ligands in this class, dppe, diphenylphosphinoethane (diphos), is the prototype for the bidentate series of ligands and is probably the most commonly used bidentate ligand for complexation of *soft* transition metal centres. The ferrocenylphosphine ligands constitute a subgroup of the aforementioned general ligand class and in their own right are among the most widely used in active homogeneous catalysis. The prototype ligand of this group, bis-diphenylphosphinoferrocene,† bdppf[1–5] (**2**), the ferrocenyl analogue of dppe, was first described by Davison in 1972.[1]

The advantage of ferrocene-based ligands over more conventional linear alkyl based ligands is that they are amenable to chemical modification by incorporation of different functionalities into the ferrocenyl side-chain with consequent changes in the overall steric, electronic and solubility properties.

There are very surprisingly few tridentate trisphosphine ligands available for use in inorganic chemistry. Of these triphos, bis-(2-phenylphosphinoethyl)phenylphosphine, is probably the most well known. There is a significant literature database covering the chemistry of triphos complexes and in many cases the chemical reactivity of such complexes is very different from that of closely-related complexes containing bidentate phosphine ligands. It would be useful to prepare an equivalent series of ferrocene based ligands with the prototype **3** as shown in Fig. 1, with the inherent advantages allowing the possibility of further facile chemical modification. With this in mind several years ago

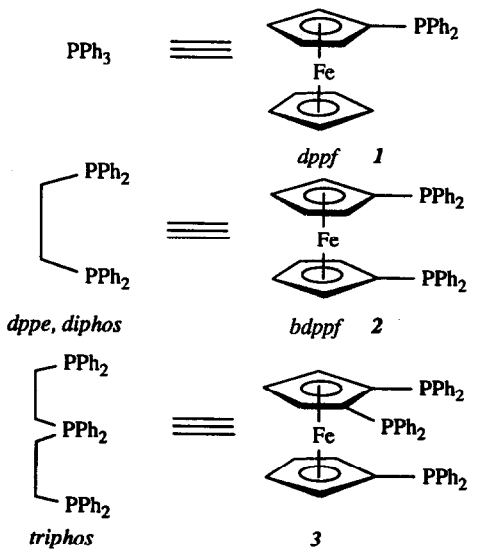

Fig. 1. Common tertiary phosphines and their ferrocenyl analogues.

* Author to whom correspondence should be addressed.

† The acronyms dppf and bdppf are used to represent diphenylphosphinoferrocene and 1,1′-bis-diphenylphosphinoferrocene, respectively, in this paper, although in the literature currently dppf is commonly used to represent the latter compound, which can cause confusion.

we investigated the lithiation of diphenylphosphinoferrocene, but we were unable to effectively isolate individual isomers of the derived substituted products from crude reaction mixtures. In view of the differences observed between the chemistries of dppe and triphos complexes which have developed since that time we felt this area of work should be further explored. This paper describes initial results in this area.

EXPERIMENTAL

All reactions were performed under an inert atmosphere of dry nitrogen or argon. Chromatographic separations were performed in a glovebox, although minimal oxidation occurs under normal aerobic chromatography. ^{1}H NMR spectra were obtained using Bruker WH-400 or WM-250 instruments. ^{31}P NMR spectra were recorded at 101.26 MHz. Mass spectra were recorded using the solid probe on a Finnegan 1020 instrument.

Preparation of tris-diphenylphosphinoferrocenes

A solution of diphenylphosphinoferrocene (dppf) in diethylether was treated with 2 molar equivalents of an n-butyllithium solution (2.5 M) and 1 molar equivalent of tetramethylethylenediamine, TMED. After stirring for 16 h the solution was treated with 2 mol equivalents of chlorodiphenylphosphine. After refluxing for 1 h the reaction mixture was hydrolysed with a dilute solution of sodium carbonate. The mixture was extracted with dichloromethane (until no more yellow product was extracted) and the combined extracts concentrated to a small volume, dried over anhydrous $MgSO_4$ and filtered. Following solvent removal a yellow oil was obtained. This was then chromatographed carefully on a neutral alumina column: a series of fractions were collected eluting with n-hexane and diethyl ether (increasing polarity), the solvent was removed from each fraction and the ^{31}P{H} NMR spectrum of each was recorded. Following identification of the product containing fractions which were still mixtures at this stage, fractions containing identical products were combined and these were rechromatographed on a silica gel column to give the following products in order of elution: 1,1′-bis-diphenylphosphinoferrocene (bdppf), 1,3,1′-tris-diphenylphosphinoferrocene (tdppf-**3**) and finally 1,2,1′-tris-diphenylphosphinoferrocene (tdppf-**2**). The solvents used for elution were increasingly polar mixtures of hexane and diethyl ether. The yields tend to vary with the scale of the reaction; however, as an example the reaction when carried out on a 10 mmol scale of dppf gave the following approximate product composition based on integration of ^{31}P resonances: unreacted dppf 22%, bdppf 15%, tdppf-**3** 51% and tdppf-**2** 6%. A similar reaction performed using neat TMED as a solvent gave slightly higher product yields of tdppf-**3** (54%) and tdppf-**2** (6%). The isolated yields are somewhat lower especially for tdppf-**2**, which is typically only about 4%.

tdppf-**2**. ^{1}H NMR ($CDCl_3$): 3.73 (q, 2H, Hc), 4.06 (1:2:2:2:1 ddd, 2H, Ha), 4.18 (t, 1H, Hb), 4.40 (t, 2H, Hd). ^{31}P{H} ($CDCl_3$): −18.36 δ (mono-substituted ring), −25.35 δ (di-substituted ring). Mass spectrum *m/z*: 738 (mass ion, 2), 662 (3), 586 (4), 570 (3), 569 (2), 553 (15), 476 (8), 381 (12), 370 (20), 355 (19), 321 (30), 183 (100). Found: C, 74.7; H, 5.1. Calc. for $C_{46}H_{37}FeP_3$: C, 74.8; H, 5.0%.

tdppf-**3**. ^{1}H NMR ($CDCl_3$): 3.89 (q, 2H, Hc), 4.04 (bq, 2H, Ha), 4.07 (bm, 1H, Hb), 4.10 (t, 2H, Hd), 7.20–7.40 (ms, 30H). ^{31}P{H} ($CDCl_3$): −18.86 (s). Mass spectrum *m/z*: 740 (2), 738 (4), 678 (5), 662 (9), 630 (2), 553 (13), 476 (8), 370 (18), 226 (23), 215 (28), 185 (100). Elemental analysis: Found: C, 75.11; H, 5.15. Calc. for $C_{46}H_{37}FeP_3$: C, 74.81; H, 5.05.

Reaction of tdppf-**2** *and* -**3** *with* $Pd(COD)Cl_2$

In 3 mm NMR tubes containing either tdppf-**2** or tdppf-**3** was added a filtered solution of $Pd(COD)Cl_2$ (0.5 molar equivalents) in $CDCl_3$. After a few minutes the ^{31}P{H} NMR spectrum was recorded, then again after 2 h and again after 1 week. The new resonances located are as listed in Table 1.

The resultant solutions were then further treated with a deutero-chloroform solution of $Pd(COD)Cl_2$ to give a slight molar excess of the palladium complex and the reaction mixtures were crystallized by slow diffusion of a hexane top layer to give nodules

Table 1. ^{31}P NMR data of tdppf-**2**·$PdCl_2$ and tdppf-**3**·$PdCl_2$

Ligand	Original resonances	New resonances on addition of $Pd(COD)Cl_2$
tdppf-**2**	−18.36, −25.35	−18.49, 41.85
tdppf-**3**	−18.86	32.57 (2 resonances), 27.65, −18.91, −19.94

in the case of tdppf-**3**·$PdCl_2$ or microcrystals in the case of tdppf-**2**·$PdCl_x$. ^{1}H NMR: 7.90–8.10 (bm, 4H), 7.20–7.70 (bm, 26H), 4.48–4.56 (bm, 2H), 3.50–3.70 (bm, 2H), three other broadened resonances present of low intensity. ^{31}P NMR: 41.75(bs), 25.64(bs). tdppf-**3**·$PdCl_2$ ^{1}H NMR: 4.03 (bs, [m], 2H), 4.12 (bs, 2H), 4.23 (bs, 1H), 4.29 (bs, 1H), 4.45 (bs, 1H), 7.10–7.60 (ms, 22H), 7.70–8.00 (ms, 8H). ^{31}P NMR: −19.76 (s), 32.45 (s).

RESULTS AND DISCUSSION

The ferrocene based ligands dppf and bdppf are prepared either by Friedel–Crafts procedures or by reaction of lithioferrocenes with chlorodiphenylphosphine.[6–8] The dilithiation of dppf is known to give mixtures of 2,1′- and 3,1′-dilithiodiphenylphosphinoferrocene, albeit in rather poor yields as observed by trapping experiments with sulphur.[9] By a simple modification of the experimental conditions the yield of these dilithiated intermediates can be increased and, therefore, subsequent reaction with chlorodiphenylphosphine results in the formation of the tris-diphenylphosphinoferrocenes. The separation of the isomers **3a** and **3b** from each other and from reaction by-products on a large scale posed the greatest experimental problem, since on TLC they have almost identical R_f values in a range of solvent mixtures. This was overcome by repeated careful chromatography using both neutral alumina and silica gel supports. The products **3a** and **3b** were identified by ^{1}H NMR spectroscopy, since their spectra are diagnostic of the substitution pattern on the cyclopentadienyl rings, Fig. 2. Compound **3b** which elutes first from the column shows only minor shifts in its ^{1}H NMR spectrum in comparison to bdppf (**2**). The mono-phosphorus substituted ring

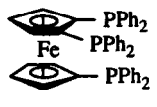

3a, tdppf-2

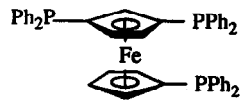

3b, tdppf-3

protons of **3b** are observed at 3.89 and 4.10 δ and the di-substituted ring protons at 4.04 and 4.07 δ, respectively, the latter being the unique proton. The ferrocenyl proton region in the spectrum of **3a** exhibits a greater chemical shift spread: 3.73 and 4.40 δ for the mono-substituted ring protons and 4.06 and 4.18 δ for the di-substituted ring protons, the

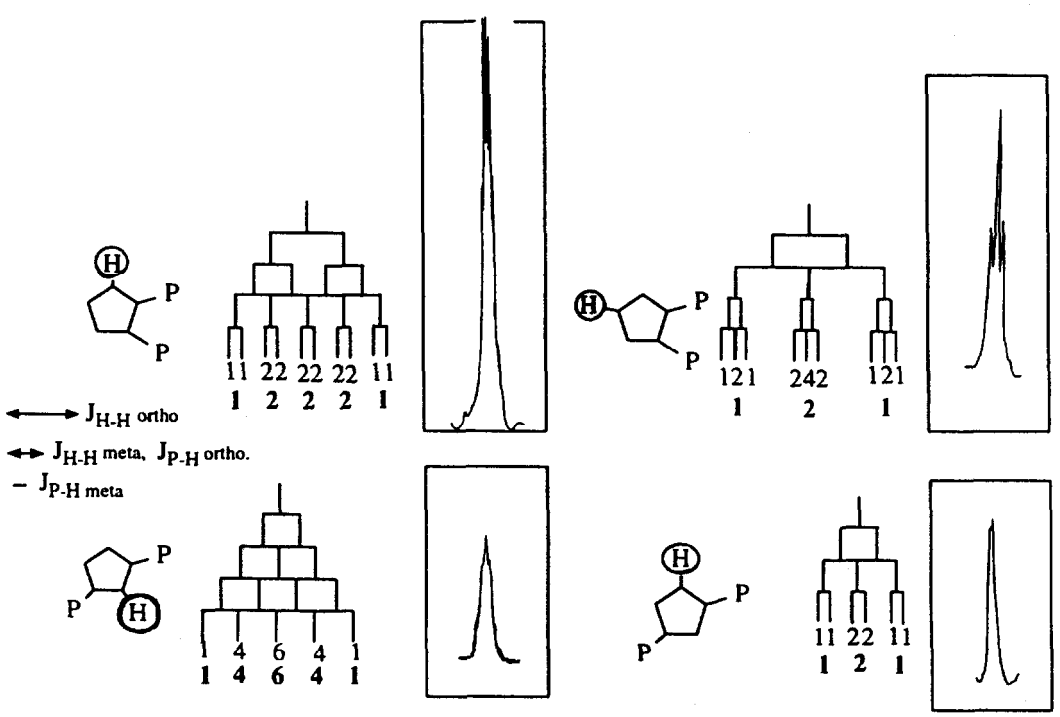

Fig. 2. The predicted resonance line shapes for individual proton resonances of the di-substituted cyclopentadienyl rings, assuming that J(H—H)(*ortho*) values are approximately double those of J(H—H)(*meta*) and J(H—P)(*ortho*) with J(H—P)(*meta*) not resolved. In the boxes are the experimentally observed resonances.

latter shift value being that of the unique proton. The $^{31}P\{H\}$ NMR of **3b** is interesting in that only one singlet is observed at -18.86 δ at MHz, with only a minor shift when compared to bdppf (-17.75 δ) or dppf (-16.82 δ). This result infers that there is very little steric or electronic effect on 1,3 di-substitution of the ferrocenyl ring. The similar $^{31}P\{H\}$ NMR spectrum of **3a** is as expected with two resonances observed at -18.36 and -25.35, the latter of which is due to the di-substituted ring. The significant chemical shift difference in this case is presumably due to the proximity of the two phosphorus atoms and the phenyl rings. This is also mirrored to some extent in the ^1H NMR resonance of the phenyl protons, which also show a wider chemical shift range in comparison to both bdppf and compound **3b**. There is also evidence both in the crude reaction mixture and in the fractions collected following column chromatography for the presence of 1,2- and 1,3-diphenylphosphinoferrocenes. This is corroberated by the proton ^1H NMR data: these are two additional singlets in the ferrocenyl region of early fractions collected following column chromatography indicative of unsubstituted cyclopentadienyl rings and in the ^{31}P NMR there are three unassigned peaks at -24.99, -17.94 and -17.82 δ.

The reaction of tdppf-**3** with $Pd(COD)Cl_2$ gave a mixture of products. The initial $\{H\}^{31}P$ singlet resonance at -18.86 δ was slowly replaced by new resonances at 32.57 (2s) and -19.94 δ, respectively, with low intensity resonances observed at 27.65 and -18.91. The complex **4c** would be expected to show three different ^{31}P NMR resonances, two of which would be of very similar chemical shift and intensity. This is, therefore, indeed what is observed with the two closely spaced resonances at $+32.57$ δ, being assigned to the palladium-bound phosphorus atoms. This chemical shift value compares well with that of the ^{31}P resonance of $(bdppf)PdCl_2$, which,

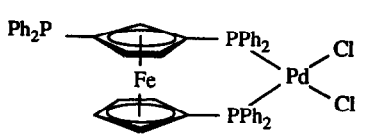

4c

under the same conditions, appears at $+33.36$ δ. It is not, however, altogether clear if the other low-field, low-intensity resonance is due to a palladium-bound species or not, since it is unlikely that complexes of the type $(tdpff\text{-}3)_2(PdCl_2)_3$ (**4d**) would be formed under these reaction conditions. On standing spherical nodules of $(tdpff\text{-}3)PdCl_2$ can be isolated, which show one broad ^{31}P resonance at 32.45 δ and a second sharper resonance at -19.75 δ, the latter being due to the uncoordinated phosphorus

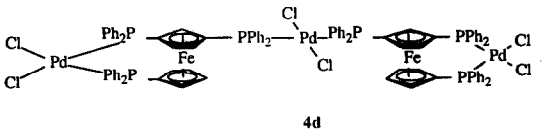

4d

atom. The ^1H NMR spectrum of the latter indicates the expected non-equivalence of all three di-substituted ring protons. This is also evidence for an oligomeric product since a brown insoluble powder is also deposited. In the case of the reaction of tdpff-**2** with $Pd(COD)Cl_2$ there should be two distinct possibilities for coordination modes as shown below:

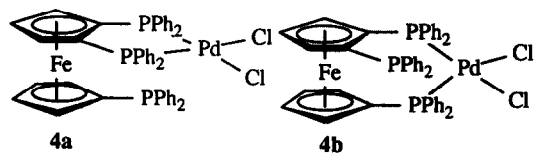

4a **4b**

In the case of **4b** there should be three phosphorus resonances, two of which again should be similarly shifted of roughly equal intensity, while in the case of **4a** only two resonances should be observed, one of which should be shifted downfield. The observation is that both complexes **4a** and **4b** are obtained, however, **4a** predominates initially since a high intensity singlet is rapidly observed at 41.85 δ following addition of $Pd(COD)Cl_2$, with the expected two low-field singlets due to **4b** at 32.57 δ present in only minor concentration. Associated with this resonance is the weaker resonance at -18.49, which is due to the uncoordinated phosphorus atom. However, on addition of a stoichiometric amount of the palladium complex and prolonged standing leads to the formation and isolation of a small quantity of a solid sample, which exhibits two low-field singlets in approximately a 1:2 ratio at 25.64 and 41.75 δ, respectively. The resonance at 41.75 δ is clearly due to coordinated phosphorus atoms as was observed in the reaction mixture; however, it is not clear whether the uncoordinated phosphorus atom is bound to a second palladium atom or simply oxidized (the phosphine oxides of dppf and bdppf are observed at similar chemical shift values, *ca* 28.47and 27.57 δ, respectively). The ^1H NMR spectrum is extremely broad and, therefore, another possibility is that all three phosphorus atoms are bound to one palladium centre with chloride dissociation, although this will obviously produce a different coordination mode compared with the normal square planar coordination geometry.

Our studies on the coordination chemistry of these new ligands and the related series of tetradentate tetra-diphenylphosphinoferrocenes is con-

tinuing and will be the subject of following publications in this series.

Acknowledgements—The aid of the SERC mass spectroscopy service at Swansea is greatly acknowledged and Eric Lewis of the University of Wales, Bangor, for recording the large number of NMR spectra used in these investigations.

REFERENCES

1. J. J. Bishop, A. Davison, M. L. Katcher, D. W. Merrill and J. C. Smart, *J. Organomet. Chem.* 1971, **27**, 241.
2. I. R. Butler, W. R. Cullen, T.-J. Kim, S. J. Rettig and J. Trotter, *Organometallics* 1985, **4**, 972.
3. D. A. Clemente, G. Pilloni, B. Corrain, B. Longato and M. Tiripicchio-Camellini, *Inorg. Chim. Acta* 1986, **115**, L9.
4. H. S. O. Chan, A. T. S. Hor, L. T. Phang and K. L. Kuang, *J. Organomet. Chem.* 1991, **407**, 353.
5. S. T. Chacon, W. R. Cullen, M. I. Bruce, O. B. Shawkataly, F. W. B. Einstein, R. H. Jones and A. C. Willis, *Can. J. Chem.* 1990, **68**, 2001.
6. C. E. Sulliven and W. E. McEwen, *Org. Prep. Proc.* 1970, **2**, 157.
7. J. C Kotz and C. L. Nivert, *J. Organomet. Chem.* 1973, **52**, 387.
8. A. W. Smalley, *Org. Prep. Proc.* 1978, **10**, 195.
9. I. R. Butler and W. R. Cullen, *Organometallics* 1986, **5**, 2537.

Polyhedron Vol. 12, No. 15, pp. 1907–1918, 1993
Printed in Great Britain

0277–5387/93 $6.00+.00
© 1993 Pergamon Press Ltd

THE SYNTHESIS AND CHARACTERIZATION OF VOLATILE COMPLEXES OF FLUORINATED ALKOXIDES OF YTTRIUM. X-RAY STRUCTURES OF $[Y\{OCMe(CF_3)_2\}_3(thf)_3]$ AND $[Y\{OCMe(CF_3)_2\}_3(DIGLYME)]$

DONALD C. BRADLEY,* HALINA CHUDZYNSKA, MICHAEL B. HURSTHOUSE† and MAJID MOTEVALLI

Department of Chemistry, Queen Mary and Westfield College, Mile End Road, London E1 4NS, U.K.

(*Received* 26 *February* 1993; *accepted* 2 *April* 1993)

Abstract—From the reactions of $(CF_3)_2CHOH$ (hfip.H), $(CF_3)Me_2COH$ (tftb.H) and $(CF_3)_2MeCOH$ (hftb.H) with $Y\{N(SiMe_3)_2\}_3$ in benzene, thf or diethyl ether as solvents the following compounds have been isolated and characterized by elemental analysis, IR, NMR and mass spectroscopy: $[Y\{OCMe_2(CF_3)\}_3]_n$ (**1**), $[Y\{OCMe_2(CF_3)\}_3(thf)_{2.5}]$ (**2**), $[Y\{OCMe(CF_3)_2\}_3]_n$ (**3**), $[Y\{OCMe(CF_3)_2\}_3(NH_3)_{0.5}]$ (**4**), $[Y\{OCMe(CF_3)_2\}_3(NH_3)_3]$ (**5**), $[Y\{OCMe(CF_3)_2\}_3(thf)_3]$ (**6**), $[Y\{OCMe(CF_3)_2\}_3(Et_2O)_{0.33}]$ (**7**), $[Y\{OCMe(CF_3)_2\}_3$ (diglyme)] (**8**), $[Y\{OCMe(CF_3)_2\}_3(Bu^tOH)_3]$ (**9**), $[Y\{OCH(CF_3)_2\}_3(NH_3)_{0.5}]$ (**10**) and $[Y\{OCH(CF_3)_2\}_3(thf)_3]$ (**11**). Sublimation *in vacuo* is usually accompanied by loss of some of the neutral ligand, but **8** sublimes intact. Single-crystal X-ray structures of **6** and **8** showed that these mononuclear octahedral complexes have the facial configuration. ^{89}Y NMR chemical shifts were obtained for **2**, δ 93.66; **6**, 66.44; **8**, 78.63; and **11**, 82.78.

Recently we reported the synthesis and characterization of a number of tris-tertiary alkoxides of yttrium and lanthanum as part of a programme aimed at developing suitable precursors for depositing metal oxides by the MOCVD technique.[1]

Volatility in metal alkoxides, $[M(OR)_3]_x$, is usually limited because of their oligomeric nature ($x > 2$), which is caused by μ_2-OR of μ_3-OR bridges.[2] With tetravalent or pentavalent metals volatile mononuclear alkoxides, $M(OR)_4$ or $M(OR)_5$, are readily obtained by using tertiary butoxide ligands to prevent oligomerization by steric hindrance,[2] but with trivalent metals much bulkier (higher tertiary alkoxide) ligands are required. Thus, yttrium tert-butoxide was obtained as the trinuclear species $[Y_3(\mu_3\text{-}OBu^t)_2(\mu\text{-}OBu^t)_3(OBu^t)_4(Bu^tOH)_2]$, which could be sublimed (with loss of Bu^tOH) at 235°C/10^{-2} Torr and even with the very bulky OCMeEtPr^i ligand a dimer, $[Y_2(OCMeEtPr^i)_6]$, subliming at 170°C/10^{-3} Torr resulted.[1] In terms of enhancing volatility by increasing the bulk of the ligand, there is a trade-off between lowering the degree of oligomerization (x) and increasing the total number of atoms in the molecule. Thus, Lappert *et al.*[3] obtained mononuclear species, $M(OC_6H_2Bu^t_2\text{-}2,6\text{-}Me\text{-}4)_3$, by using the very bulky aryloxo ligand, but due to the large number of atoms in the molecule (one metal, three oxygens, 45 carbons and 69 hydrogens) the volatility was comparatively low (sublimes 250–260°C/10^{-3} Torr). In a further effort to enhance volatility we have explored the use of fluorinated alkoxide ligands. Thus, by replacing CH_3 groups by CF_3 groups we anticipated that three factors would be operating. Firstly there would be a small increase in bulkiness because the CF_3 group is slightly larger than CH_3; secondly the inductive effect of the electron attracting fluoro derivative will make the oxygen a weaker electron donor (e.g. pK_a values: Bu^tOH, 19.2; $C_4F_9{}^tOH$, 5.4) and thus a weaker bridging ligand; and thirdly the abnormally weak intermolecular forces between CF_3 groups would lower the enthalpy of vaporization.

* Author to whom correspondence should be addressed.

† Present address: Department of Chemistry and Applied Chemistry, University of Wales—Cardiff, PO Box 912, Cardiff CF1 3TB, U.K.

Unfortunately, perfluoro-tert-butanol ($C_4F_9{}^tOH$) is not commercially available, so we were restricted to the use of three partially fluorinated alcohols; one secondary alcohol, $(CF_3)_2CHOH$ (hexafluoroisopropyl, hfip), and two tertiary alcohols, $(CF_3)(Me)_2COH$ (trifluoro-tert-butyl, tftb) and $(CF_3)_2MeCOH$ (hexafluoro-tert-butyl, htfb). Encouraged by our previous success in preparing yttrium tris-tert-alkoxides by the reaction of the tert-alcohol with the chloride-free three-coordinated silylamido-derivative $Y\{N(SiMe_3)_2\}_3$ [eq. (1)]

$$Y\{N(SiMe_3)_2\}_3 + 3R^tOH \longrightarrow Y(OR^t)_3 + 3(Me_3Si)_2NH \quad \textbf{(1)} \quad (1)$$

we adopted the same approach for the synthesis of the fluoroalkoxides. Some preliminary results on these and other metal fluoroalkoxides have already been published[4] and we now report full details.

RESULTS AND DISCUSSION

When the fluorinated alcohols R^tOH were added to $Y\{N(SiMe_3)_2\}_3$ the silylamide groups were completely replaced by fluoroalkoxides but the products obtained were sensitive to experimental details such as solvent and temperature and also depended on the acidity of the fluorinated alcohol. Besides the tris-fluoroalkoxides $[Y(OR^t)_3]_n$ a number of adducts, $\{Y(OR^t)_3\}_xLy$ (where L = NH_3, thf or Et_2O), were also obtained.

Trifluoro-tert-butoxides (tftb)

From the reaction of excess tftb.H with $Y\{N(SiMe_3)_2\}_3$ in benzene the tris-fluoroalkoxide $[Y(tftb)_3]_n$ (**1**) was obtained as a white solid (m.p. 118–120°C), which could not be sublimed *in vacuo* due to thermal decomposition. The ^1H NMR spectrum in C_7D_8 gave a single peak at 333 K (δ 1.49), which broadened and split at lower temperatures. At 253 K a five-line spectrum (δ 1.66, 1.58, 1.48, 1.37 and 1.24) with integral ratios 2 : 2 : 2 : 1 : 2 was obtained. At 233 K the ^{19}F spectrum also gave five lines in the ratios 1 : 2 : 2 : 2 : 2. These NMR spectra were consistent with a trinuclear species, $[Y_3(\mu_3\text{-}tftb)_2(\mu\text{-}tftb)_3(tftb)_4]$, having the same structure as that revealed by single-crystal X-ray analysis for $[Pr_3(tftb)_9]$.[4] This structure consists of a triangle of metal atoms capped by two μ_3-ligands and three bridging ligands distinguishable by symmetry into two types (ratio 2 : 1). One metal has two terminal ligands giving it a distorted octahedral configuration, whilst the other two, which are equivalent, each have one terminal ligand giving a five-coordinate configuration. In the praseodymium compound the X-ray structure showed that the five-coordinated metals were interacting intramolecularly at the vacant octahedral sites with fluorine from CF_3 groups and it is possible that this occurs in **1**.

When the reaction of tftb.H and the silylamide was performed in thf as the solvent, the product **2** obtained after crystallization from toluene had the composition $[Y(tftb)_3(thf)_{2.5}]$ and its ^1H NMR spectrum suggested that more than one species was present. When **2** was redissolved in thf and the excess solvent pumped off *in vacuo* the ^1H NMR spectrum of the residual solid corresponded to $[Y(tftb)_3(thf)_3]$. The NMR data can be interpreted on the basis that the tris-thf complex dissociates reversibly in toluene solution with the formation of a dimeric species, $[Y_2(\mu\text{-}tftb)_2(tftb)_4(thf)_4]$, as depicted in eq. (2).

$$2Y(tftb)_3(thf)_3 \Leftrightarrow Y_2(tftb)_6(thf)_4 + 2thf \quad (2)$$

The product **2** obtained by crystallization from toluene is thus a mixture of the two compounds shown in eq. (2).

Hexafluoro-tert-butoxides (hftb)

When hftb.H (3 mol) was added to $Y\{N(SiMe_3)_2\}_3$ (1 mol) in benzene a white precipitate formed, which redissolved on heating under reflux. The tris-fluoroalkoxide $[Y(hftb)_3]_n$ (**3**) crystallized out on cooling (m.p. 175–177°C) and in contrast to **1** it readily sublimed at 110–120°C/10^{-2} Torr. Unfortunately the low solubility of **3** precluded the collection of reliable NMR spectra, which might have provided structural information. If compound **3** is a dimer or trimer the alkoxide bridges must be very weak to allow such a high volatility compared with $[Y_3(OBu^t)_9(Bu^tOH)_2]$ (sublimed at 235°C/10^{-2} Torr) and $[Y_3(tftb)_9]$ (thermally unstable).

Refluxing yttrium silylamide (1 mol) with excess hftb.H (*ca* 4.5 mol) in benzene gave on cooling a crystalline product (**4**), which had the analysis for $[Y_2(hftb)_6(NH_3)]$. The presence of coordinated ammonia was confirmed by IR [ν(NH), 3396 and 1607 cm^{-1}) and ^1H NMR (δ 0.87) spectra, although the ratio of hftb : NH_3 in the ^1H NMR spectrum was closer to 3 : 1. Compound **4** sublimed at 105–110°C/10^{-2} Torr giving a sublimate with a hftb : NH_3 ratio of 3 : 1. Its mass spectrum gave a series of dinuclear fragmentations, $Y_2F_x(hftb)^+_{5-x}$ (x = 1–5).

Concerning the origin of the ammonia in **4** we presume it is formed in a side reaction involving

$(Me_3Si)_2NH$ liberated in the primary reaction [eq. (1)] and the excess of hftb.H which is acidic (pK_a 9.6), according to eq. (3).

$$2(CF_3)_2MeCOH + (Me_3Si)_2NH \longrightarrow NH_3 + 2Me_3SiOCMe(CF_3)_2 \quad (3)$$

Support for this hypothesis was given by an experiment in which $Y(hftb)_3$ was suspended in benzene to which hftb.H and $(Me_3Si)_2NH$ were than added. The $Y(hftb)_3$ slowly dissolved and after standing overnight the solution was stripped of volatiles *in vacuo* and the residue crystallized from toluene. Analysis of the product (**5**) showed it to be the tris-ammine $[Y(hftb)_3(NH_3)_3]$ [m.p. 130–135°C; ν(NH), 3408 and 1605 cm^{-1}; δ_H 0.63 (9H, NH_3), 1.39 (9H, $O(CH_3)(CF_3)_2$]. Compound **5** sublimed at 80–110°C/10^{-2} Torr with loss of ammonia giving a sublimate similar in properties to that obtained from **4**. The variable-temperature ^1H NMR spectra of **4** and **5** both suggested the presence of more than one species due to dissociation of weakly coordinated ammonia molecules. In view of the formation of the dimer $[Pr_2(hftb)_6(NH_3)_4]$, whose structure was established by single-crystal X-ray diffraction,[4] it is reasonable to suppose that yttrium forms an analogous compound which could be in equilibrium with **5** in solution [eq. (4)].

$$2Y(hftb)_3(NH_3)_3 \Leftrightarrow [Y_2(hftb)_6(NH_3)_4] + 2NH_3 \quad (4)$$

The sublimates obtained from **4** and **5** both gave complex ^1H and ^{19}F NMR spectra at low temperatures, which could be interpreted in terms of trinuclear complexes such as $[Y_3(hftb)_9(NH_3)_2]$ analogous to the known species $[Y_3(OBu^t)_9(Bu^tOH)_2]$ and $[Y_3(OBu^t)_9(thf)_2]$.[1]

When the reaction of $Y\{N(SiMe_3)_2\}_3$ with excess hftb.H was performed in thf solution instead of benzene the product was the tris-thf adduct $[Y(hftb)_3(thf)_3]$ (**6**), which could be crystallized from toluene. It is noteworthy that no ammine was formed under these conditions and it may be that reaction (3) only occurs if $Y(hftb)_3$ is available to complex the ammonia thus produced. When thf is present the stable complex (**6**) is formed because thf is a better ligand than ammonia. Compound **6** was established by elemental analysis, ^1H NMR spectroscopy and a single-crystal X-ray structure determination, which showed that the mononuclear octahedral complex existed as the facial isomer (Fig. 1).

Compound **6** readily sublimed at 110–120°C/10^{-2} Torr with loss of thf and the sublimate had a composition close to that of $[Y_2(hftb)_6(thf)]$ and was sparingly soluble in benzene. It readily dissolved in thf to reform $[Y(hftb)_3(thf)_3]$. The ^1H NMR spectrum of **6** in C_7D_8 at room temperature gave a single resonance for hftb (δ 1.56) and the two multiplets for thf (δ 1.43 and 3.69), but at low temperature (233 K) all three peaks were split (δ 1.13, 1.26, 1.63, 1.73, 3.48, 3.79) suggesting that more than one species was present. An obvious possibility is dissociation of thf giving either a five-coordinated complex, $[Y(hftb)_3(thf)_2]$, or the six-coordinated dimer $[Y_2(hftb)_6(thf)_4]$. The mass spectrum of **6** gave a series of fragment ions, $Y_2F_x(hftb)^+_{(5-x)}$ (x = 1–5), due to abstraction of fluoride by the yttrium, suggesting that loss of thf in the vapour leads to the formation of dinuclear $Y_2(hftb)_6$.

Treatment of $Y\{N(SiMe_3)_2\}_3$ with excess hftb.H in diethyl ether gave an etherate, which was crystallized from toluene as $[Y(hftb)_3(Et_2O)_x]$ (**7**). According to elemental analysis x = 1/3, but from the ^1H NMR spectrum x was closer to 1/2. Compound **7** readily sublimed at 75–100°C/10^{-2} Torr to form the unsolvated $[Y(hftb)_3]_n$ (**3**). Interestingly the mass spectrum of **7** was identical with those of **4** and **6**, which gave the dinuclear species $Y_2F_x(hftb)^+_{(5-x)}$ (x = 1–5).

Since diethyl ether is a weaker ligand than thf, it is not surprising that a tris-etherate was not obtained. Nevertheless, compound **7** proved to be the most volatile complex of $Y(hftb)_3$. Since the tris-thf complex readily lost thf when heated *in vacuo*, it was decided to try the potentially chelating tridentate ether ligand diglyme ($CH_3OCH_2CH_2OCH_2CH_2OCH_3$) in an attempt to prepare an adduct which was thermally stable. Excess diglyme was added to a suspension of $[Y(hftb)_3]_n$ (**3**) in toluene. Compound **3** rapidly dissolved and after concentrating the solution the 1 : 1 adduct $[Y(hftb)_3(diglyme)]$ (**8**) crystallized out. At 140–150°C/10^{-2} Torr compound **8** sublimed completely without loss of diglyme. Its mass spectrum gave the fragment ion $[Y(hftb)_2(diglyme)]^+$ and the species $[YF(hftb)(diglyme)]^+$, in both of which the diglyme remains coordinated to a mononuclear yttrium species. A single-crystal X-ray structure confirmed that **8** is an octahedral complex with facial configuration (Fig. 2).

In another experiment excess htfb.H was added to a solution of $[Y_3(OBu^t)_9(Bu^tOH)_2]$ in benzene. After removal of solvent and tertiary alcohols *in vacuo* the residue was crystallized from toluene giving compound **9**, which was characterized by elemental analysis and ^1H NMR as the tris-alcoholate $[Y(hftb)_3(Bu^tOH)_3]$ [ν(OH) 3572 cm^{-1}]. Compound **9** readily sublimed at 70–120°C/10^{-2} Torr with loss of tertiary alcohols (mainly Bu^tOH). Heating **9** *in vacuo* at 60°C until no more alcohol

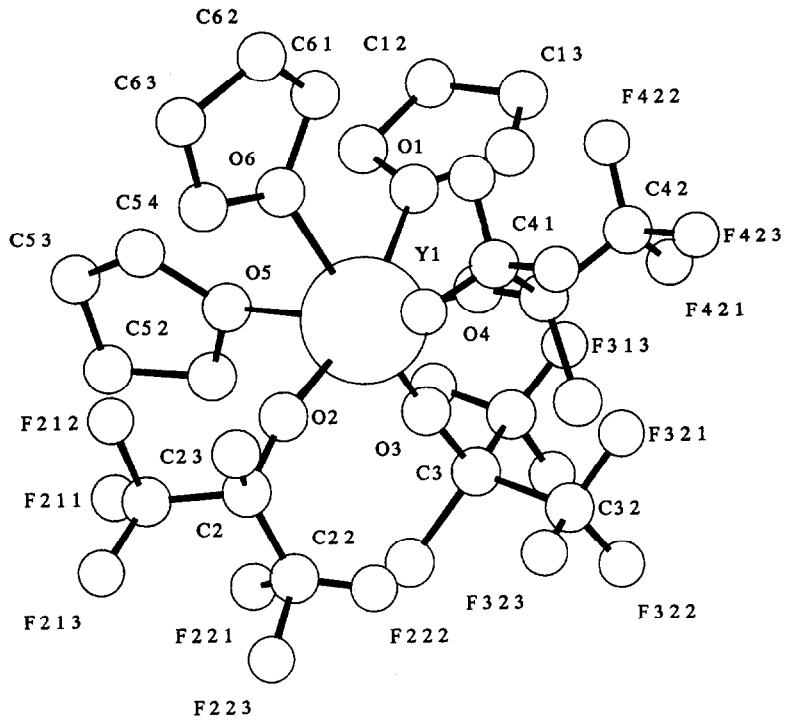

Fig. 1.

was released and then subliming the residue (110°C/10^{-2} Torr) gave a sublimate which had an analysis corresponding to $[Y_2(hftb)_5(OBu^t)]$.

Although the room-temperature ^1H NMR of **9** gave single peaks for OH (δ 3.13), hftb (δ 1.45) and Bu^tO (1.17) in the correct ratio for $[Y(hftb)_3(Bu^tOH)_3]$, low-temperature (213 K) spectra showed the presence of four OH resonances, three hftb and four Bu^tO resonances indicating a mixture of species. Similarly the ^{19}F NMR spectrum gave a single peak for hftb at room temperature, but split into four peaks (4:2:3:2 ratios) at 193 K.

In formulating compound **9** as $[Y(hftb)_3(Bu^tOH)_3]$ it is assumed that the more electronegative ligand $hftb^-$ is present as the covalently bonded anion in preference to Bu^tO^-. This complex could exist as facial or meridional isomers. In the latter the three hftb ligands have two which are equivalent and *trans* to each other and the third which is *cis* to the other two. Similarly the three Bu^tOH ligands will be distinguishable in a 2:1 ratio. Thus, at low temperatures a mixture of *fac* and *mer* isomers in the absence of fluxional interconversion might be expected to show six different hftb and Bu^tO peaks in the ^1H NMR spectrum and three hftb peaks in the ^{19}F NMR spectrum. Since the ^1H NMR gave seven and the ^{19}F NMR gave four it appears that other species must also be present. It is possible that some $[Y(hftb)_2(OBu^t)(hftb.H)(Bu^tOH)_2]$ is also present, which would give rise to even more isomeric species. One of the OH peaks (δ 6.27) at 213 K could well be due to coordinated hftb.H. Careful removal of coordinated alcohol (60°C/10^{-2} Torr) left a residual compound, whose analysis was close to that required for $[Y_2(hftb)_5(OBu^t)]$. However, it must be remembered that hftb.H (b.p. 60°C) is more readily evaporated *in vacuo* than Bu^tOH (b.p. 82°C) and the action of removing alcohol from **9** may promote the exchange of ligands [eq. (5)].

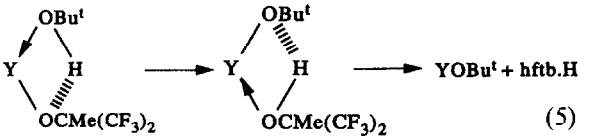

(5)

Treatment of **9** with thf caused the complete removal of coordinated Bu^tOH, leaving the previously established compound $[Y(hftb)_3(thf)_3]$ (**6**).

Hexafluoro-isopropoxides (hfip)

Although hexafluoro-isopropanol (hfip.H) is not a tertiary alcohol, it was of special interest in view of the fact that yttrium tris-isopropoxide was found to be unstable because of its facile breakdown to give the pentanuclear oxo-species $[Y_5(\mu_5\text{-}O)(\mu_3\text{-}OPr^i)_4(\mu\text{-}OPr^i)_4(OPr^i)_5]$.[6,7] It is very acidic (pK_a 9.3) compared with isopropanol (pK_a 17.1) and more volatile (b.p.: hfip.H, 59°C; Pr^iOH, 82°C).

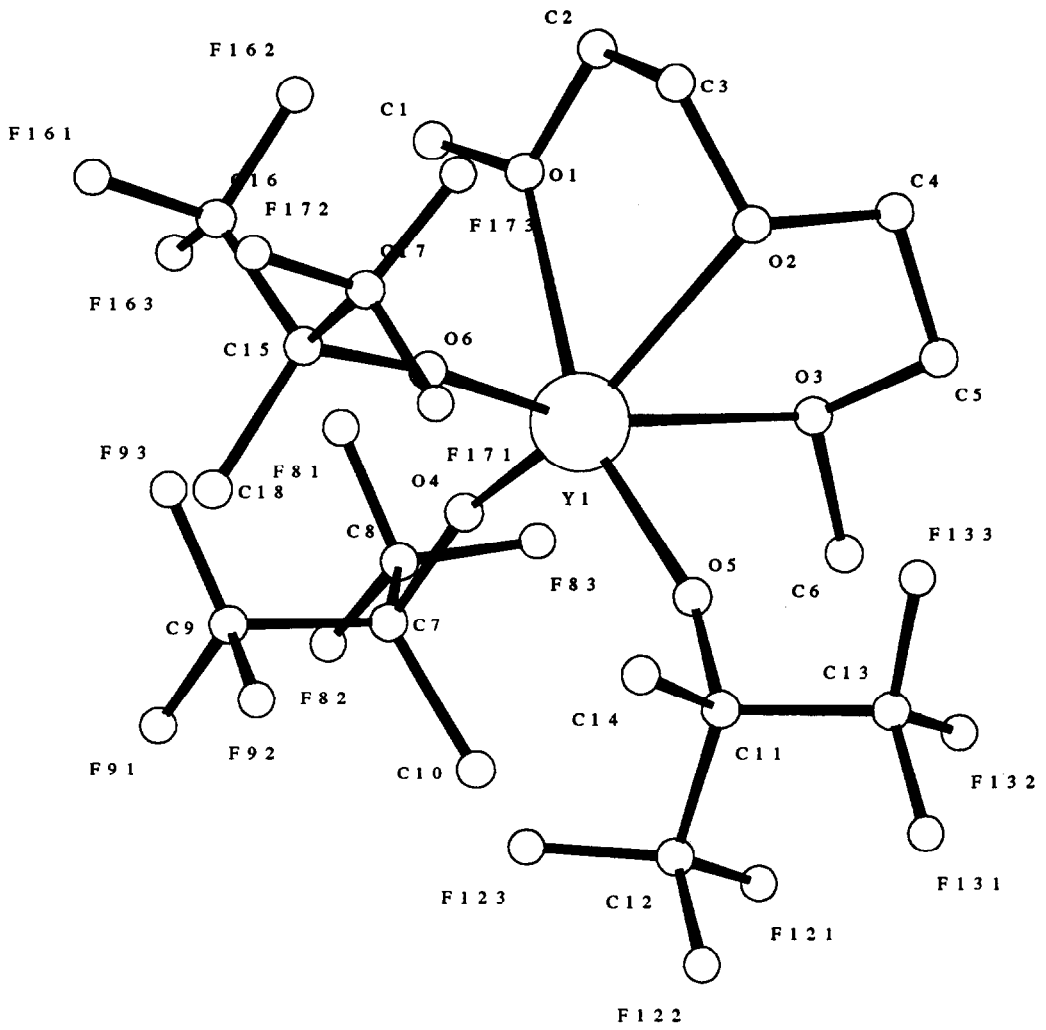

Fig. 2.

From the reaction involving excess hfip.H with $Y\{N(SiMe_3)_2\}_3$ in boiling benzene a product (**10**) crystallized out, which analysed as $[Y_2(hfip)_6(NH_3)]$. The presence of coordinated ammonia was confirmed by IR [ν(NH), 3652, 3394, 1618 cm^{-1}] and ^1H NMR (C_6D_6, δ 0.90, NH_3; 4.65 hfip) spectroscopy. In the mass spectrum peaks were observed corresponding to $[Y_2F_x(hfip)_{(5-x)}]^+$ ($x = 1$, 2 and 4), suggesting that dinuclear species were present in the vapour phase. The compound sublimed with decomposition at *ca* 140°C/10^{-2} Torr. The ammonia was doubtless formed by the side reaction of excess hfip.H with $(Me_3Si)_2NH$ liberated in the primary reaction. The composition of **10** was probably determined by the amount of excess hfip.H present, since according to eqs (1) and (3) an excess of 200% would be needed to convert all the $(Me_3Si)_2NH$ to ammonia, but only 40% excess was used in the experiment.

Mazdiyasni and Schaper[8] obtained the compound $[Y(hfip)_3(NH_3)_2]$ from the reaction of YCl_3 and hfip.H in the presence of excess ammonia, but we assume that it has the dinuclear structure $[Y_2(hfip)_6(NH_3)_4]$ by analogy with the corresponding scandium and praseodymium complexes, whose structures were determined by single-crystal X-ray diffraction analysis.[4]

The formation of ammine was completely suppressed when the reaction was performed in thf and the crystalline adduct $[Y(hfip)_3(thf)_3]$ (**11**) (m.p. 164–169°C) was obtained by crystallizing from toluene. The formula of **11** was confirmed by elemental analysis and ^1H NMR (C_7D_8; δ 4.68 sept. 3H, hfip; 3.74 m. 12H, thf; 1.44 m. 12H, thf) spectroscopy. Sublimation (90–130°C/10^{-2} Torr) occurred with loss of thf and the sublimate, which was sparingly soluble in benzene, had an analysis corresponding to $[Y(hfip)_3(thf)_{0.33}]$. The mass spectrum of **11** con-

tained peaks corresponding to the fragment ions $[Y_2(hfip)_6CF_3]^+$ and $[Y_2(hfip)_5]^+$. Although **11** behaved as a single species in the ^1H and ^{19}F NMR spectra at room temperature, at low temperature both ligands showed evidence of fluxional behaviour (e.g. broadening and splitting into two peaks). At 215 K the ^1H spectrum gave a ratio of 4:7 for the two species of hfip and at 189 K the ^{19}F spectrum gave a ratio of 2:3. Therefore, it appears that in solution either *fac/mer* isomerization or some dissociation of thf is occurring. Formation of a five-coordinate complex, $[Y(hfip)_3(thf)_2]$, or a six-coordinate dimer, $[Y_2(hfip)_6(thf)_4]$, are obvious possibilities as was suggested in the case of the hftb complex (**6**).

The structure of $[Y(hftb)_3(thf)_3]$ (**6**)

The single-crystal X-ray diffraction analysis of **6*** showed that this mononuclear complex has a distorted octahedral structure with the two sets of ligands disposed in the facial configuration (Fig. 1). Some bond lengths and angles relating to the core of the structure are given in Tables 1 and 2. The Y—O(hftb) bond distances (av. 2.10 Å) are notably shorter than those for Y—O(thf) (av. = 2.43 Å). This is as expected because the Y—O(hftb) bond involving the anionic ligand should be a stronger covalent bond than the Y—O(thf) coordinate bond. The very bulky hftb ligands would be expected on steric grounds to adopt the meridional arrangement and the actual adoption of the facial arrangement implies the operation of strong electronic interactions opposing the *mer* configuration. An obvious explanation would be the presence of considerable oxygen-to-metal π-donation from the oxygen lone pairs to the vacant *d*-orbitals (t_{2g}) of the d^0Y^{3+} ion. Both ligands could in principle be π-donors, but so long as one ligand type is a stronger π-donor than the other then the facial configuration will be favoured. If the hftb ligand is strongly π-donating its oxygen lone pairs then the $\widehat{YOC}$ should widen towards the limiting angle of 180°. Inspection of Table 2 shows that the angles are 167.7, 159.2 and 173.5°, which does suggest that π-donation is present. Although the inductive electronic effect of the electronegative CF_3 groups will reduce the donor capability of the oxygen (hftb.H is acidic) the short Y—O σ-bond will assist π-overlap. Turning to the coordinated thf ligands, it is noteworthy that the $\widehat{YOC}$s are all close to 120° (av. 123, 122 and 123° for each thf) and the $\widehat{COC}$s are around 111° so that the sum of the angles at each oxygen is close to 360° (358, 357 and 358°). Thus, the oxygens are in the trigonal planar configuration, which is required for π-donation to the yttrium. Although the structural evidence lends support to π-donation by both hftb and thf ligands it must be remembered that the bulky nature of the hftb ligands may cause distortions in the structure. Caulton *et al.*[5] have reported the structure of the complex $[Y(OSiPh_3)_3(thf)_3]$, which also adopts the facial configuration. The core structure of this complex is strikingly close in detail to that of **6** showing that replacement of hftb by $OSiPh_3$ makes little difference to bond lengths or angles.

Table 1. Some bond lengths (Å) for $[Y(hftb)_3(thf)_3]$ (**6**)

O(1)—Y(1)	2.428(11)	O(2)—Y(1)	2.123(11)
O(3)—Y(1)	2.079(12)	O(4)—Y(1)	2.094(10)
O(5)—Y(1)	2.453(10)	O(6)—Y(1)	2.413(12)
C(11)—O(1)	1.452(18)	C(14)—O(1)	1.463(18)
C(2)—O(2)	1.372(17)	C(3)—O(3)	1.374(18)
C(4)—O(4)	1.370(16)	C(51)—O(5)	1.472(20)
C(54)—O(5)	1.469(20)	C(61)—O(6)	1.489(19)
C(64)—O(6)	1.508(20)		

The structure of $[Y(hftb)_3(diglyme)]$ (**8**)

The single-crystal X-ray diffraction analysis of **8** showed it to be a distorted octahedral complex exhibiting the facial configuration (Fig. 2). The bond distances [Y—O(hftb) av. 2.06; Y—O(diglyme) av. 2.47 Å, Table 3] are very close to those found in **6**, as are also the angles $\widehat{YOC}$(hftb) of 160.3, 159.1 and 171.0° (Table 4). The replacement of three thf ligands by the tridentate diglyme has, therefore, had little effect on the structure and bonding of the hftb ligands. In the coordinated diglyme it is noteworthy that whilst O(1) is trigonal planar, the sum of the angles around O(2) and O(3) are 343°, suggesting that diglyme is less effective as a π-donor than thf.

Judging by the Y—O bond lengths [Y—O(thf) 2.43; Y—O(diglyme) 2.47 Å] it appears that diglyme is slightly less strongly bonded to yttrium than thf and, therefore, the greater stability of **8** to dissociation must be due to the chelate effect of diglyme coupled with its lower volatility than thf.

^{89}Y *NMR spectra*

In our previous work on the tertiary alkoxides of yttrium some ^{89}Y NMR data were obtained.[1] It

*The structure of **6** was reported in a preliminary communication[4] and all data have been deposited therein.

Table 2. Some bond angles (°) for $[Y(hftb)_3(thf)_3]$ (6)

O(2)—Y(1)—O(1)	163.6(3)	O(3)—Y(1)—O(1)	87.9(5)
O(3)—Y(1)—O(2)	101.8(4)	O(4)—Y(1)—O(1)	88.1(4)
O(4)—Y(1)—O(2)	102.4(5)	O(4)—Y(1)—O(3)	102.5(5)
O(5)—Y(1)—O(1)	79.7(4)	O(5)—Y(1)—O(2)	87.3(5)
O(5)—Y(1)—O(3)	88.3(5)	O(5)—Y(1)—O(4)	163.4(3)
O(6)—Y(1)—O(1)	79.9(4)	O(6)—Y(1)—O(2)	88.2(4)
O(6)—Y(1)—O(3)	164.8(4)	O(6)—Y(1)—O(4)	86.2(4)
O(6)—Y(1)—O(5)	80.7(4)	C(11)—O(1)—Y(1)	126.7(10)
C(14)—O(1)—Y(1)	120.0(10)	C(14)—O(1)—C(11)	111.5(13)
C(2)—O(2)—Y(1)	167.7(10)	C(3)—O(3)—Y(1)	173.5(10)
C(4)—O(4)—Y(1)	159.2(10)	C(51)—O(5)—Y(1)	120.7(10)
C(54)—O(5)—Y(1)	123.9(10)	C(54)—O(5)—C(51)	113.0(13)
C(61)—O(6)—Y(1)	123.5(10)	C(64)—O(6)—Y(1)	123.5(10)
C(64)—O(6)—C(61)	109.6(13)		

was noted that the chemical shifts for the octahedral trinuclear complexes $[Y_3(OBu^t)_9(Bu^tOH)_2]$ (δY 166.8) and $[Y_3(OAm^t)_9(Am^tOH)_2]$ (δY 199.1) were considerably downfield compared with the tetrahedral complexes, which appeared to be in the range δY 36.8–45.6. However, it was recently reported by Coan *et al.*[10] that the tetrahedral complex $[Y_2(OSiPh_3)_6]$ gave a chemical shift of 263.2 ppm, i.e. further downfield than the values for our octahedral complexes. We have now re-determined the spectra of the tetrahedral complexes and found that the values had been incorrectly identified due to "fold-over" of the spectra. The correct values (all in C_7D_8) are: $[Y_2(OCMe_2Pr^i)_6]$ (δ 249.04), $[Y_2(OCMeEtPr^i)_6]$ (δ 237.48) and $[Y_2(OCEt_3)_6]$ (δ 245.42). These values are clearly in the same region as found for $[Y_2(OSiPh_3)_6]$. It is noteworthy that the earlier chemical shifts for $[Y_5O(OPr^i)_{13}]$ reported by Poncelet *et al.*[7] were also shown by Coan *et al.*[10] to be in error due to fold-over. We have now determined the ^{89}Y chemical shifts of the new octahedral complexes of the fluorinated tertiary alkoxides. The following values were obtained: $[Y(tftb)_3(thf)_3]$ (δY 93.66), $[Y(hftb)_3(thf)_3]$ (δY 66.44), $[Y(hftb)_3(diglyme)]$ (δY 78.63) and $[Y(hfip)_3(thf)_3]$ (δY 82.78). These chemical shifts are considerably upfield compared with the octahedral complexes containing unfluorinated tertiary alkoxides. These data are collected together with some of Coan *et al.*'s[10] results in Table 5. The shift to higher fields caused by replacement of CH_3 groups by CF_3 in the tertiary butoxide complexes is evident.

Table 3. Some bond lengths (Å) for $[Y(hftb)_3(diglyme)]$ (8)

O(1)—Y(1)	2.486(15)	O(2)—Y(1)	2.429(15)
O(3)—Y(1)	2.430(15)	O(4)—Y(1)	2.059(16)
O(5)—Y(1)	2.084(16)	O(6)—Y(1)	2.074(15)
C(1)—O(1)	1.362(24)	C(2)—O(1)	1.386(25)
C(3)—O(2)	1.411(28)	C(4)—O(2)	1.488(25)
C(5)—O(3)	1.477(24)	C(6)—O(3)	1.478(27)
C(7)—O(4)	1.413(26)	C(11)—O(5)	1.384(28)
C(15)—O(6)	1.348(24)		

CONCLUSIONS

This work has shown that volatile mononuclear octahedral complexes of yttrium can be synthesized using highly-fluorinated alkoxide ligands. In addition to the steric effect of tertiary alkoxides the electronegative effect of CF_3 groups destabilizes the alkoxide bridges and promotes the formation of stable adducts of the type $[Y(OR^1)_3L_3]$. However, the mass spectra of some of these compounds show evidence of fluorine abstraction by the yttrium under the conditions within the mass spectrometer.

EXPERIMENTAL

All manipulations were performed under dry nitrogen using vacuum-line, glove-box and Schlenk-style apparatus. Solvents were dried using the sodium ketyl of benzophenone and freshly distilled. The fluorinated alcohols (Fluorochem Ltd) were dried over molecular sieves and diglyme (Aldrich) was treated first with sodium then refluxed over CaH_2 (2 h) and finally distilled under reduced pressure. $Y\{N(SiMe_3)_2\}_3$ was prepared as previously described.[9]

NMR spectra were obtained using Bruker WM 250 FT and WH 400 FT spectrometers, using solvent signals from incomplete deuteration for ^1H

Table 4. Some bond angles (°) for [Y(hftb)$_3$(diglyme)] (**8**)

O(2)—Y(1)—O(1)	65.5(6)	O(3)—Y(1)—O(1)	86.9(6)
O(3)—Y(1)—O(2)	66.4(6)	O(4)—Y(1)—O(1)	87.3(6)
O(4)—Y(1)—O(2)	145.1(5)	O(4)—Y(1)—O(3)	91.9(6)
O(5)—Y(1)—O(1)	162.2(5)	O(5)—Y(1)—O(2)	97.4(6)
O(5)—Y(1)—O(3)	81.2(7)	O(5)—Y(1)—O(4)	106.2(7)
O(6)—Y(1)—O(1)	87.1(7)	O(6)—Y(1)—O(2)	92.6(6)
O(6)—Y(1)—O(3)	158.8(5)	O(6)—Y(1)—O(4)	108.2(6)
O(6)—Y(1)—O(5)	99.2(7)	C(1)—O(1)—Y(1)	128.9(14)
C(2)—O(1)—Y(1)	116.5(13)	C(2)—O(1)—C(1)	114.3(18)
C(3)—O(2)—Y(1)	113.8(13)	C(4)—O(2)—Y(1)	116.3(12)
C(4)—O(2)—C(3)	110.1(18)	C(5)—O(3)—Y(1)	113.2(13)
C(6)—O(3)—Y(1)	115.5(13)	C(6)—O(3)—C(5)	114.7(17)
C(7)—O(4)—Y(1)	160.3(15)	C(11)—O(5)—Y(1)	159.1(16)
C(15)—O(6)—Y(1)	171.0(13)		

and ^{13}C chemical shifts which are quoted relative to TMS. Fluorine chemical shifts are relative to $CFCl_3$ and ^{89}Y chemical shifts are relative to YCl_3.

Mass spectra were obtained using a Kratos MS 50 TC mass spectrometer operating at 70 eV. IR spectra were obtained as Nujol mulls in the range 4000–200 cm^{-1} using a Perkin–Elmer FT 1720 spectrophotometer. Carbon, hydrogen and nitrogen analyses were obtained from the Microanalytical service, University College, London, or from B.M.A.C. Yttrium was determined gravimetrically as Y_2O_3.

Preparation of $[Y\{OCMe_2(CF_3)\}_3]_n$ (**1**)

To a suspension of $Y\{N(SiMe_3)_2\}_3$ (6.5 g) in benzene (180 cm^3) was added $Me_2(CF_3)COH$ (5.8 g) in benzene (40 cm^3), causing the solid to dissolve immediately. After standing overnight the solution was refluxed for a minute and the volatiles removed *in vacuo*. The residue was crystallized from toluene giving **1** (2.5 g, 46% yield, m.p. 118–120°C dec.). Found: Y, 19.0; C, 30.7; H, 3.9. Calc. for $Y\{OCMe_2(CF_3)\}_3$: Y, 18.9; C, 30.6; H, 3.9%. ^1H NMR ($C_6D_5CD_3$): at 333 K (δ 1.49); at 290 K (δ 1.59 br, 1.47, 1.31 br); at 253 K (δ 1.66, 2H; 1.58, 2H; 1.48, 2H; 1.37, 1H; 1.24, 2H). ^{13}C NMR (C_6D_6): δ 26.54. ^{19}F NMR ($C_6D_5CD_3$): ambient temperature (δ −74.70 br, −76.11 br, −78.28 br, −79.80, −80.08 br); at 233 K (δ −75.45, 1F; −74.76, 2F; −75.70, 2F; −80.91, 2F; −82.34, 2F). IR: 1710 vw, 1397 m, 1320 m, 1212 s, 1148 s, 1020 m, 989 m, 876 m, 799 w, 755 m, 616 m, 587 m, 516 m, 497 m, 482 m, 432 w, 404 w, 378 w, 289 w, 228 w cm^{-1}.

Table 5. Some ^{89}Y NMR chemical shifts for yttrium complexes with oxygen-donor ligands

Compound	Coordination number	Chemical shift	Ref.
$[Y(O\text{-}2,6\text{-}^tBu_2\text{-}4\text{-}MeC_6H_2)_3]$	3	170.8	10
$[Y(O\text{-}2,6\text{-}^tBu_2\text{-}4\text{-}MeC_6H_2)_3(OPMe_2Ph)]$	4	148.1	10
$[Y_2(OSiPh_3)_6]$	4	263.2	10
$[Y_2(OCMe_2Pr^i)_6]$	4	249.0	This work
$[Y_2(OCMeEtPr^i)_6]$	4	237.5	This work
$[Y_2(OCEt_3)_6]$	4	245.4	This work
$[Y(OSiPh_3)_3(OPBu^n_3)_2]$	5	221.6	10
$[Y_3(OAm^t)_9(Am^tOH)_2]$	6	199.1	1
$[Y_3(OBu^t)_9(Bu^tOH)_2]$	6	166.8	1
$[Y(OSiPh_3)_3(thf)_3]$	6	157.1	10
$[Y(tftb)_3(thf)_3]$	6	93.7	This work
$[Y(hftb)_3(thf)_3]$	6	66.4	This work
[Y(hftb)$_3$(diglyme)]	6	78.6	This work
$[Y(hfip)_3(thf)_3]$	6	82.8	This work

Preparation of $[Y\{OCMe_2(CF_3)\}_3(thf)_x]$ (**2**)

$(CF)_3Me_2COH$ (2.18 g) in thf (10 cm^3) was added to a solution of $Y\{N(SiMe_3)_2\}_3$ (2.80 g) in thf (100 cm^3) and left overnight. After removal of the volatiles *in vacuo* the residue was crystallized from toluene giving **2** (2.31 g, m.p. 115–121°C). Found: Y, 13.7; C, 40.1; H, 5.9. Calc. for $Y\{OCMe_2(CF_3)\}_3(thf)_{2.5}$: Y, 13.7; C, 40.6; H, 5.9%. ^1H NMR ($C_6D_5CD_3$): at 297 K [δ 3.72 m, 10H, (thf); 1.49 m, 10H (thf); 1.46, 18H (tftb)]; at 213 K [δ 3.59, 3.53 (thf); 1.68, 1.53 (tftb); 1.33, 1.32 (thf)]. ^{19}F NMR ($C_6D_5CD_3$): ambient temperature (δ −78.51, −81.29, −81.64, −82.04, −82.28 br, −82.58, −83.52); at 268 K (δ −78.58, −81.21, −81.58, −82.09, −82.20, −82.55, −83.20, −83.71). ^{89}Y NMR (thf-d_8): δ 93.66. IR: 1317 s, 1218 s, 1137 vs, 1029 s, 989 m, 921 m, 879 s, 755 m, 672 w, 611 s, 598 m, 482 m, 441 w, 373 m, 345 w, 286 s, 232 m, 222 s, 217 m cm^{-1}.

Compound **2** was redissolved in thf and the solvent pumped off *in vacuo*, leaving a solid residue of $[Y(thb)_3(thf)_3]$. ^1H NMR (C_6D_6): at 297 K (δ 3.73 m, 12H (thf); 1.49, 18H (tftb); 1.46 m, 12H (thf)]; at 213 K ($C_6D_5CD_3$) [δ 3.59 (thf); 1.62, 1.49, 1.48, (tftb); 1.38 (thf)]. Mass spectrum: *m/z*. Found: 871.0413. Calc. for $[Y_2(tftb)_6CF_3]$: 871.0390. Found: 812.9878. Calc. for $[Y_2(tftb)_5]$: 812.9971. Compound **2** was sublimed in small yield (*ca* 20%) at 105–110°C/10^{-2} Torr.

Preparation of $[Y\{OCMe(CF_3)_2\}_3]_n$ (**3**)

Addition of $(CF_3)_2MeCOH$ (2.98 g) in benzene (10 cm^3) to a solution of $Y\{N(SiMe_3)_2\}_3$ (3.11 g) in benzene (190 cm^3) caused immediate precipitation of a white solid which redissolved under reflux. On cooling the product **3** crystallized (2.94, 85% yield, m.p. 175–177°C). Found: Y, 14.3; C, 21.7; H, 1.3. Calc. for $Y\{OCMe(CF_3)_2\}_3$: Y, 14.1; C, 22.8; H, 1.4%. The compound was sparingly soluble in hydrocarbon solvents making NMR measurements unreliable. ^1H NMR (C_6D_6): at 323 K (δ 1.80, 1.54, 1.50, 1.39). IR: 1315 s, 1256 s, 1206 s, 1186 s, 1100 s, 1080 s, 1020 m, 995 m, 980 m, 965 m, 954 m, 866 m, 760 m, 701 s, 681 w, 658 w, 624 m, 534 m, 502 w, 455 w, 430 w, 305 w, 283 w, 227 m, 217 w.

Compound **3** sublimed at 110–120°C/10^{-2} Torr (m.p. 176–178°; Found: Y, 13.4; C, 22.3; H, 1.3%).

Preparation of $[Y\{OCMe(CF_3)_2\}_3(NH_3)_x]$ (**4**)

Addition of $(CF_3)_2MeCOH$ (7.0 g) in benzene (40 cm^3) to a solution of $Y\{N(SiMe_3)_2\}_3$ (5 g) in benzene (180 cm^3) caused a white precipitate which dissolved on warming. After refluxing for 2 h the solution was allowed to cool and deposited needle crystals of **4** (4.7 g; m.p. 108–130°C). Found: Y, 14.2; C, 21.9; H, 1.7; N, 1.2. Calc. for $[Y\{OCMe(CF_3)_2\}_3(NH_3)_{0.5}]$: Y, 13.9; C, 22.5; H, 1.6; N, 1.1%. ^1H NMR (C_6D_6): at 297 K [δ 1.37 (9H, hftb), 0.87 br (3H, NH_3)]. ^{19}F NMR ($C_6D_5CD_3$): at 333 K [δ −77.45 (1F), −78.55 br (3F), −79.37 (1F), −79.48 (6F)]. IR: 3396 w, 1607 w, 1309 s, 1260 s, 1171 s, 1077 s, 993 m, 979 m, 967 m, 865 m, 801 w, 759 m, 701 s, 688 m, 679 m, 656 w, 624 m, 535 m, 503 m, 458 m, 433 w, 384 w, 336 w, 295 w, 280 w, 230 w, 220 w, 215 w, 209 w cm^{-1}. Mass spectra: *m/z*. Found: 758.8275. Calc. for $Y_2F_2\{OCMe(CF_3)_2\}_3$: 758.8350. Found: 596.8282. Calc. for $Y_2F_3\{OCMe(CF_3)_2\}_2$: 596.8246. Found: 434.8177. Calc. for $Y_2F_4\{OCMe(CF_3)_2\}$: 434.8142. Found: 272.8045. Calc. for $[Y_2F_5]$: 272.8116. Found: 250.7975. Calc. for $[Y_2F_3O]$: 250.8019.

Compound **4** sublimed at 105–110°C/10^{-2} Torr (m.p. 125–130°C). Found: Y, 13.6; C, 21.7; H, 1.9; N, 1.7. Calc. for $[Y\{OCMe(CF_3)_2\}_3(NH_3)]$: Y, 13.7; C, 22.2; H, 1.9; N, 2.2%. ^1H NMR ($C_6D_5CD_3$): at 298 K [δ 1.47 (1H), 1.40 (3H), 1.38 (1H), 1.15 (4H)]: at 220 K (δ 1.54, 1.38 br, 0.85): at 333 K (δ 1.50, 1.38, 1.22 br, 0.92 br). ^{19}F NMR ($C_6D_5CD_3$): at 296 K [−77.45 (2F), −78.55 br (6F), −79.37 (2F), −79.62 (9F)]. IR: 3399 w, 1613 w, 1311 s, 1258 s, 1186 s, 1110 s, 1077 s, 977 m, 895 m, 865 m, 802 w, 760 m, 702 s, 629 m, 656 w, 618 m, 534 m, 503 m, 458 w, 384 m, 295 w, 280 m, 231 w cm^{-1}. Compound **4** was refluxed in thf and the volatiles removed *in vacuo*, leaving a residue of $[Y\{OCMe(CF_3)_2\}_3(thf)_3]$ (**6**).

Preparation of $[Y\{OCMe(CF_3)_2\}_3(NH_3)_3]$ (**5**)

To $[Y\{OCMe(CF_3)_2\}_3]_n$ (0.90 g) suspended in benzene was added $(Me_3Si)_2NH$ (1 cm^3) and $(CF_3)_2MeCOH$ (1.3 cm^3). The solid slowly dissolved and was left overnight before evaporating off the volatiles *in vacuo*, leaving a residue which was crystallized from toluene (**5**, 0.73 g, m.p. 130–135°C). Found: Y, 12.1; C, 20.5; H, 2.4; N, 5.4. Calc. for $[Y\{OCMe(CF_3)_2\}_3(NH_3)_3]$: Y, 13.0; C, 21.1; H, 2.6; N, 6.1%. ^1H NMR ($C_6D_5CD_3$): at 297 K [δ 1.39 (9H, hftb), 0.63 br (9H, NH_3)]: at 228 K (major peaks, δ 1.49, 0.28 br; minor peaks, 1.42, 1.16, 0.46). ^{19}F NMR ($C_6D_5CD_3$): δ −79.96. IR: 3408 m, 1605 w, 1306 s, 1202 s, 1110 s, 1072 s, 978 m, 857 m, 762 w, 700 s, 672 m, 614 w, 535 m, 458 w, 379 w, 328 w, 294 w, 284 w, 259 w, 250 w, 240 w, 228 w, 216 w cm^{-1}.

Compound **5** sublimed with loss of NH_3 at 80–110°C/10^{-2} Torr (m.p. 128–136°C). ^1H NMR ($C_6D_5CD_3$): at 297 K [δ 1.45 (1H), 1.39 (3H), 1.36

(1H), 1.28 (4H) (hftb); 0.89 br (3H) (NH_3)]; at 233 K (δ 1.58, 1.50, 1.40, 1.25, 1.17, 0.93, 0.77, 0.49). IR: 3669 w, 3405 w, 1614 w, 1310 s, 1260 s, 1186 s, 1109 s, 1077 s, 978 m, 864 m, 864 m, 800 m, 761 m, 701 s, 674 m, 616 m, 535 m, 502 m, 456 w, 384 m, 295 w, 280 m, 253 w, 228 m.

Preparation of $[Y\{OCMe(CF_3)_2\}_3(thf)_3]$ (**6**)

To a solution of $Y\{N(SiMe_3)_2\}_3$ (3.91 g) in thf (100 cm^3) was added $(CF_3)_2MeCOH$ (4.5 g) and the solution left overnight. After removal of volatiles *in vacuo* the residue was crystallized from toluene **6** (5.67 g, 98% yield, m.p. 164–182°C). Found: Y, 10.6; C, 33.7; H, 4.0. Calc. for $[Y\{OCMe(CF_3)_2\}_3(thf)_3]$: Y, 10.5; C, 34.0; H, 3.9%. ^1H NMR ($C_6D_5CD_3$): at 297 K [δ 3.69 m (12H, thf); 1.56 (9H, hftb); 1.43 m (12H, thf)]; at 233 K [major peaks: 3.48 m (thf), 1.73 (hftb), 1.26 m (thf); minor peaks: 3.79 m, 1.63, 1.13]. ^{19}F NMR ($C_6D_5CD_3$): at 297 K (δ −74.65); at 203 K (−74.32 plus a small peak at −74.09). ^{89}Y NMR (thf): δ 66.44. IR: 1306 s, 1223 s, 1186 s, 1111 s, 1078 s, 1024 s, 977 s, 925 m, 871 s, 800 w, 761 w, 701 s, 671 m, 614 m, 533 m, 497 m, 380 m, 368 m, 332 w, 291 m, 280 m, 265 m, 227 m, 217 m cm^{-1}. Mass spectra: *m/z*. Found: 920.8556. Calc. for $[Y_2F\{OCMe(CF_3)_2\}_4]$: 920.8454. Found: 758.8436. Calc. for $[Y_2F_2\{OCMe(CF_3)_2\}_3]$: 758.8350. Found: 596.8285. Calc. for $[Y_2F_3\{OCMe(CF_3)_2\}_2]$: 596.8246. Found: 434.8157. Calc. for $[Y_2F_4\{OCMe(CF_3)_2\}]$: 434.8142. Found: 272.8045. Calc. for $[Y_2F_5]$: 272.8116. Found: 250.7997. Calc. for $[Y_2F_3O]$: 250.8019.

Compound **6** sublimed with loss of thf at 110–120°C/10^{-2} Torr (m.p. 170–175°C). Found: Y, 13.2; C, 24.9; H, 2.0. Calc. for $[Y_2(hftb)_6(thf)]$: Y, 13.3; C; 25.2; H, 2.0%. The sublimate was sparingly soluble in benzene giving a poor ^1H NMR spectrum (C_6D_6) (δ 3.81 m and 1.39 m, thf; 1.74 br, 1.44, 1.24, 0.97 br, hftb). The sublimate dissolved in thf and reformed complex **6**.

Preparation of $[Y\{OCMe(CF_3)_2\}_3(Et_2O)_x]$ (**7**)

$(CF_3)_2MeCOH$ (3.75 g) was added to a solution of $Y\{N(SiMe_3)_2\}_3$ (2.83 g) in diethyl ether (150 cm^3) and the solution left overnight. After removing the volatiles *in vacuo* the residue was crystallized from toluene (**7**, 2.97 g, m.p. 126–132°C). Found: Y, 13.7; C, 23.7; H, 1.9. Calc. for $[Y\{OCMe(CF_3)_2\}_3(Et_2O_{0.33}]$: Y, 13.5; C, 24.4; H, 1.9%. ^1H NMR (C_6D_6): at 297 K [δ 3.51 q (4H, Et_2O—CH_2); 1.40 (18H, hftb); 0.98 t (6H, Et_2O—CH_3)]; in ($C_6D_5CD_3$) at 297 K [δ 3.45 q (4H, Et_2O—CH_2); three overlapping broad peaks at 1.41, 1.35 and 1.27 (18H, hftb); 0.99 t (6H, Et_2O—CH_3)]; at 253 K (3.24 q, 1.37, 1.11 t, 0.94). ^{19}F NMR ($C_6D_5CD_3$): at 320 K [−73.14, −74.23, −74.80 br (major peak), −75.41]; at 283 K [−73.13, −74.22 br, −75.07, −75.28]; at 203 K [−72.25 (1F), −72.51 (3F), −73.02 (9F), −73.67 (4F), −73.90 (4F), −74.49 (14F), −74.86 (3F), −75.62 (4F)]. IR: 1314 s, 1259 s, 1175 s, 1079 s, 1042 m, 994 m, 976 m, 954 m, 889 w, 865 m, 799 m, 784 m, 761 m, 702 s, 676 w, 656 w, 619 m, 536 m, 499 m, 454 w, 434 w, 381 m, 281 m, 227 m, 213 m cm^{-1}. Mass spectra: *m/z*. Found: 920.8581. Calc. for $[Y_2F\{OCMe(CF_3)_2\}_4]$: 920.8454. Found: 758.8373. Calc. for $[Y_2F_2\{OCMe(CF_3)_2\}_3]$: 758.8350. Found: 596.8242. Calc. for $[Y_2F_3\{OCMe(CF_3)_2\}_2]$: 596.8246. Found: 434.8131. Calc. for $[Y_2F_4\{OCMe(CF_3)_2\}]$: 434.8142. Found: 272.8030. Calc. for $[Y_2F_5]$: 272.8116. Found: 250.8004. Calc. for $[Y_2F_3O]$: 250.8019.

Compound **7** sublimed at 75–100°C/10^{-2} Torr (m.p. 120–150°C). Found: Y, 13.8; C, 22.1; H, 1.5. Calc. for $Y\{OCMe(CF_3)_2\}_3$: Y, 14.1; C, 22.8; H, 1.4%. ^1H NMR (C_6D_6): at 297 K (δ 1.72, 1.48, 1.42 br, 1.38, 1.26, 0.98 br). IR: 1314 s, 1191 s, 1117 s, 1088 s, 1037, 990 m, 962 m, 869 m, 802 m, 768 m, 761 m, 703 s, 692 m, 653 w, 617 m, 536 m, 501 m, 454 w, 438 w, 381 m, 337 w, 322 w, 296 m, 278 m, 226 m, 219 m, 213 m cm^{-1}. The sublimate was sparingly soluble in hydrocarbon solvents.

Preparation of $[Y\{OCMe(CF_3)_2\}_3(diglyme)]$ (**8**)

Diglyme (3 cm^3) was added to a suspension of $[Y\{OCMe(CF_3)_2\}_3]_n$ (3.41 g) in toluene (100 cm^3) and the solid rapidly dissolved. The solution was concentrated to approximately 50 cm^3 and the product crystallized out (3.42 g, m.p. 201–204°C). Found: Y, 11.7; C, 27.7; H, 2.9. Calc. for $[Y\{OCMe(CF_3)_2\}_3(diglyme)]$: Y, 11.6; C, 28.2; H, 3.0%. ^1H NMR ($C_6D_5CD_3$): at 297 K [δ 3.27 s (6H, CH_3-diglyme); 3.08 m (4H, CH_2-diglyme); 2.90 m (4H, CH_2-diglyme); 1.60 s (9H, hftb)]; at 203 K [3.23 (CH_3-diglyme), 3.28 sh, 2.97 (CH_2-diglyme), 2.32, 2.25 (CH_2-diglyme); 1.69 (hftb)]; at 183 K [3.26, (CH_3-diglyme); {3.12, 3.00, 2.92, 2.88 (CH_2-diglyme)}; {2.26, 2.19 (CH_2-diglyme)}; 1.71, 1.69 (hftb)]. ^{19}F NMR ($C_6D_5CD_3$): at 297 K (δ −79.42); at 194 K (δ −78.14, −78.94, −79.20). ^{89}Y NMR (C_7D_8/diglyme, 2:3 v/v): δ 78.63. IR: 1305 s, 1176 s, 1110 s, 1077 s, 1045 s, 1008 s, 978 s, 931 m, 864 s, 834 m, 809 w, 762 m, 701 s, 675 m, 615 m, 533 m, 499 m, 382 m, 368 m, 332 w, 282 s, 261 m, 222 s, 217 m cm^{-1}. Mass spectra: *m/z*. Found: 585.0175. Calc. for $[Y\{OCMe(CF_3)_2\}_2$

(diglyme)]: 585.0175. Found: 423.0090. Calc. for [YF{OCMe$(CF_3)_2$}(diglyme)]: 423.0074.

Compound **8** completely sublimed at 140–150°C/10^{-2} Torr (m.p. 199–203°C). ^{1}H NMR (C_6D_6): at 297 K [δ 3.29 s (6H, CH_3-diglyme); 3.00 t (4H, CH_2-diglyme); 2.84 t (4H, CH_2-diglyme); 1.67 s (9H, hftb)]. IR spectrum identical with **8**.

Preparation of [Y{OCMe$(CF_3)_2$}$_3$($Bu^tOH)_3$] (**9**)

$(CF_3)_2$MeCOH (3.75 g) was added to a solution of [$Y_3(OBu^t)_9(Bu^tOH)_2$] (1.42 g) in benzene (80 cm^3) and the solution kept at room temperature overnight. After refluxing for 0.5 h the volatiles were removed *in vacuo*, leaving a residue which was crystallized from toluene (**9**, 2.97 g, m.p. 174–184°C). Found: Y, 10.7; C, 32.4; H, 4.1. Calc. for [Y{OCMe$(CF_3)_2$}$_3$($Bu^tOH)_3$]: Y, 10.4; C, 33.7; H, 4.6%. ^{1}H NMR ($C_6D_5CD_3$): at 298 K [δ 3.13 (3H, OH); 1.45 (9H, hftb); 1.17 (27H, Bu^tO)]; at 213 K [6.27 (1H), 4.46 (1H), 4.04 (1H), 3.70 (2H) OH; 1.60 (12H), 1.52 (6H), 1.27 (6H) (hftb); 1.12 sh, 1.11 (45H), 1.04 (18H), 0.94 (18H)]. ^{19}F NMR ($C_6D_5CD_3$): at 293 K (δ −78.59); at 233 K [−78.03 (11F); −78.54 (4F); −78.74 br (3F)]; at 203 K [−77.78 (2F): −78.19 br (1F); −78.44 br (3F)]; at 193 K [−77.71 (4F); −78.11 (2F); −78.33 (3F); −78.39 (2F)]. IR: 3572 m, 1307 s, 1191 s, 1110 s, 1077 s, 1025 m, 975 m, 882 m, 860 m, 803 w, 762 w, 749 m, 702 s, 674 m, 615 w, 533 w, 498 m, 441 w, 382 m, 279 w, 233 w, 223 w, 214 w cm^{-1}.

Compound **9** sublimed with loss of alcohol at 70–120°C/10^{-2} Torr. When **9** was heated at 60°C *in vacuo* until all the coordinated alcohol had been removed the residue sublimed at 110°C/10^{-2} Torr. Found: Y, 15.2; C, 25.1; H, 2.4. Calc. for [Y_2{OCMe$(CF_3)_2$}$_5$(OBu^t)]: Y, 15.4; C, 24.9; H, 2.1%. The sublimate was sparingly soluble in hydrocarbon solvents rendering the NMR measurements unreliable. ^{1}H NMR (C_6D_6): at 298 K [δ 1.49, 1.40 (hftb); 1.12 (OBu^t) approximate ratio hftb: OBu^t, 4:3]. The mixture of alcohols [δ 5.80 (OH), 1.32 sept (hftb); 1.47 (OH), 1.04 (Bu^tO)] pumped off (**9**) appeared to be in the ratio Bu^tOH: hftb.H = 2:1. Found: C, 45.5; H, 7.8. Calc.: C, 43.6; H, 7.9%.

Preparation of [Y{OCH$(CF_3)_2$}$_3$($NH_3)_x$] (**10**)

Addition of $(CF_3)_2$CHOH (6.8 g) in benzene (40 cm^3) to a solution of Y{$N(SiMe_3)_2$}$_3$ (5.5 g) in benzene (180 cm^3) caused immediate precipitation. The precipitate dissolved under reflux (2 h) and on cooling gave a crystalline product (**10**, 4.5 g, m.p. 108–109°C). Found: Y, 15.1; C, 17.3; H, 0.8; N, 1.1. Calc. for [Y_2{OCH$(CF_3)_2$}$_6$(NH_3)]: Y, 14.8; C, 18.1; H, 0.7; N, 1.2%. Compound **10** was sparingly soluble in hydrocarbon solvents, which caused problems in obtaining reliable NMR measurements. ^{1}H NMR (C_6D_6): at 298 K [(δ 4.65 m (hfip); 0.90 (NH_3)]. ^{19}F NMR ($C_6D_5CD_3$): at 296 K [δ −75.91 d (J = 4.2 Hz)]; at 213 K [δ −75.42 d (J = 5.7 Hz)]. IR: 3652 w, 3394 w, 3312 w, 1667 w, 1618 w, 1293 s, 1218 s, 1105 s, 1054 m, 978 w, 890 s, 850 s, 746 s, 690 s, 673 w, 642 w, 536 m, 520 m, 494 w, 455 m, 375 m, 311 m, 292 m, 250 w, 240 w cm^{-1}. Mass spectra: *m/z*. Found: 864.8803. Calc. for [Y_2F{OCH$(CF_3)_2$}$_4$]: 864.7829. Found: 716.7297. Calc. for [Y_2F_2{OCH$(CF_3)_2$}$_3$]: 716.7881. Found: 420.7029. Calc. for [Y_2F_4{OCH(CF_3)}$_2$]: 420.7986.

Compound **10** sublimed with decomposition at 140°C/10^{-2} Torr. It dissolved in thf to form the tris-thf complex (**11**) [^{1}H NMR (thf-d_8) at 298 K, δ 4.72 sept (hfip)].

Preparation of [Y{OCH$(CF_3)_2$}$_3$(thf)$_3$] (**11**)

$(CF_3)_2$CHOH (3.78 g) in thf (10 cm^3) was added to a solution of Y{$N(SiMe_3)_2$}$_3$ (3.8 g) in thf (90 cm^3) and left overnight before removing the volatiles *in vacuo*. The residue was crystallized from toluene (**11**, 4.23 g, 80% yield, m.p. 164–169°C). Found: Y, 11.0; C, 31.2; H, 3.3. Calc. for [Y{OCH$(CF_3)_2$}$_3$(thf)$_3$]: Y, 11.0; C, 31.3; H, 3.4%. ^{1}H NMR ($C_6D_5CD_3$): at 297 K [δ 4.68 sept (3H, hfip); 3.74 m (12H, thf); 1.44 m (12H, thf)]; at 215 K [4.90 (4H) 4.72 (7H) (hfip); 3.67 (32H) 3.46 (15H) (thf); 1.38 (15H) 1.31 (33H) (thf)]. ^{19}F NMR ($C_6D_5CD_3$): at 298 K (δ −77.6 d; J = 7.1 Hz); at 235 K (δ −76.99 br); at 216 K [(−76.86 br (5F); −77.20 br (2F)]; at 189 K [−76.56 br (2F); −77.14 d (J = 4.7 Hz) (3F)]. ^{89}Y NMR (thf): δ 82.78. IR: 1291 s, 1211 s, 1178 s, 1092 s, 1025 s, 928 m, 885 s, 843 s, 742 s, 686 s, 655 m, 528 m, 369 m, 333 w, 281 m, 212 m cm^{-1}. Mass spectra: *m/z*. Found: 871.0413. Calc. for [Y_2{OCH$(CF_3)_2$}$_6$$CF_3$]: 871.0390. Found: 812.9878. Calc. for [Y_2{OCH$(CF_3)_2$}$_5$]: 812.9971.

Compound **11** sublimed with loss of thf at 90–130°C/10^{-2} Torr (m.p. 148–160°C). Found: Y, 14.2; C, 20.4; H, 0.8. Calc. for [Y{OCH$(CF_3)_2$}$_3$(thf)$_{0.33}$]: Y, 14.5; C, 20.2; H, 0.9%. Due to the sparing solubility of the sublimate it was difficult to obtain a reliable NMR spectrum. ^{1}H NMR (C_6D_6): at 297 K [δ 4.91 br (1H, hfip); 3.79 m (2H, thf); 1.23 m (2H, thf)]. IR: 1295 s, 1228 s, 1180 s, 1095 s, 1008 m, 890 s, 848 s, 745 s, 688 s, 521 m, 446 m, 374 m, 354 w, 289 m, 224 w, 218 w cm^{-1}.

X-ray crystallography

The crystal structure of $[Y\{OCMe(CF_3)_2\}_3(thf)_3]$ (**6**) has already been reported[4] and all supplementary data have been deposited with the Cambridge Crystallographic Data Centre.

$[Y\{OCMe(CF_3)_2\}_3(diglyme)]$ (**8**). A single crystal was grown from toluene solution and X-ray measurements were made using a CAD 4 diffractometer operating in the $\omega/2\theta$ mode with graphite-monochromated Mo-K_α radiation.

Details of the crystal data, intensity measurements and structure refinement are given in Table 6.

Table 6. Crystal data, intensity measurements and structure refinement

Formula	$C_{18}H_{23}O_6F_{18}Y$
M	766.254
Crystal system	Orthorhombic
Space group	$P2_12_12_1$
a (Å)	9.863(2)
b (Å)	18.322(3)
c (Å)	16.399(3)
α (°)	90
β (°)	90
γ (°)	90
U (Å^3)	2963.46(9.44)
Z	4
D_c (g cm^{-1})	1.717
$F(000)$	1520
Radiation	Mo-K_α
λ (Å)	0.71069
μ (cm^{-1})	21.177
$\theta_{min/max}$ (°)	1.5, 25
Total no. of reflections	3292
No. of unique reflections	2947
No. of observed reflections $[F_o > 3\sigma(F_o)]$	1614
No. of refined parameters	412
Weighting scheme parameter g in $w = 1/[\sigma^2(F)+gF^2]$	Unit
Final R	0.0744
Final R_w	0.0744

Acknowledgements—With thanks to SERC for financial support. We are very grateful to Mr Peter Cook for obtaining the mass spectra; Mr Greg Coumbarides for the 250 MHz NMR spectra; Mr P. Haycock for the 400 MHz NMR spectra, using the University of London Intercollegiate Research Service (ULIRS) and Mrs Jane Hawkes and Mr J Cobb for the ^{19}F NMR spectra using the Bruker WM 250 machine (ULIRS) at King's College, London.

REFERENCES

1. D. C. Bradley, H. Chudzynska, M. B. Hursthouse and M. Motevalli, *Polyhedron* 1991, **10**, 1049.
2. D. C. Bradley, R. C. Mehrotra and D. P. Gaur, *Metal Alkoxides*. Academic Press, London (1978).
3. P. B. Hitchcock, M. F. Lappert and A. Singh, *J. Chem. Soc., Chem. Commun.* 1983, 1499; P. B. Hitchcock, M. F. Lappert and R. G. Smith, *Inorg. Chim. Acta* 1987, **139**, 183; P. B. Hitchcock, M. F. Lappert and A. MacKinnon, *J. Chem. Soc., Chem. Commun.* 1988, 1557.
4. D. C. Bradley, H. Chudzynska, M. E. Hammond, M. B. Hursthouse, M. Motevalli and W. Ruowen, *Polyhedron* 1992, **11**, 375.
5. M. J. McGeary, P. S. Coan, K. Folting, W. E. Streib and K. G. Caulton, *Inorg. Chem.* 1991, **30**, 3570.
6. D. C. Bradley, H. Chudzynska, D. M. Frigo, M. B. Hursthouse and M. A. Mazid, *J. Chem. Soc., Chem. Commun.* 1988, 1258; D. C. Bradley, H. Chudzynska, D. M. Frigo, M. E. Hammond, M. B. Hursthouse and M. A. Mazid, *Polyhedron* 1990, **9**, 719.
7. O. Poncelet, W. J. Sartain, L. G. Hubert-Pfalzgraf, K. Folting and K. G. Caulton, *Inorg. Chem.* 1989, **28**, 263.
8. K. S. Mazdiyasni and B. J. Schaper, *J. Less-Comm. Metals* 1973, **30**, 105.
9. D. C. Bradley, J. S. Ghotra and F. A. Hart, *J. Chem. Soc., Dalton Trans.* 1973, 1021.
10. P. S. Coan, L. G. Hubert-Pfalzgraf and K. G. Caulton, *Inorg. Chem.* 1992, **31**, 1262.

Polyhedron Vol. 12, No. 15, pp. 1919–1925, 1993
Printed in Great Britain

0277–5387/93 $6.00+.00
© 1993 Pergamon Press Ltd

CHROMIUM TRICARBONYL η^6-COMPLEXES OF (η^5-CYCLOPENTADIENYL)(η^4-TETRAPHENYLCYCLOBUTADIENE)COBALT

FUNG-E HONG* and YUAN-TERNG CHANG

Department of Chemistry, National Chung-Hsing University, Taichung 40227, Taiwan, R.O.C.

and

MING-CHU CHENG and YU WANG

Department of Chemistry, National Taiwan University, Taipei 10764, Taiwan, R.O.C.

(*Received* 22 *February* 1993; *accepted* 2 *April* 1993)

Abstract—The reaction of (η^5-cyclopentadienyl)(η^4-tetraphenylcyclobutadiene)cobalt (**1**) with excess $Cr(CO)_6$ leads to four identified heterometallic compounds. They are compounds **2**, **3** (**3′** and **3″**) and **4** with one, two, and three phenyl ring(s) being complexed with $Cr(CO)_3$ fragment(s), respectively. Compounds **3′** and **3″** are two structural isomers with two arene $Cr(CO)_3$ groups in the *trans* and *cis* positions, respectively. These compounds were characterized by mass, IR, E.A. and ^1H and ^{13}C NMR spectra. The X-ray crystal structure of **3′** has been determined and can be regarded as three metals linked by three connected π-rings. It shows that two $Cr(CO)_3$ complexed phenyl rings are about parallel to the cyclobutadiene ring which causes the downfield shift of the Cp signal of **3′** in the ^1H NMR spectrum. Steric effects are more important than electronic effects in **3′** in the interpretation of the geometry of the two arene$Cr(CO)_3$ fragments.

The applications of arene$Cr(CO)_3$ in organic synthesis are well known and numerous derivatives of arene$Cr(CO)_3$ compounds have been made.[1] However, examples of the synthesis of mixed-metal compounds through bridging π-rings are rare.[2] We know that the heteronuclear metal complexes offer the chance to observe cooperative effects of the different metal centres when the metals are held in close proximity by bridging ligands.[3] The cooperative effect should be enhanced through directly joined π-rings. Therefore, it was of interest to prepare this type of compound and examine their physical and chemical properties.

(η^5-Cyclopentadienyl)(η^4-tetraphenylcyclobutadiene)cobalt (**1**) is a sandwich-like compound with four phenyl rings attached to four carbons of the cyclobutadiene ring. It has four active sites, four phenyl groups, for metal π-complexation. The dihedral angle between each phenyl and the cyclobutadiene ring is around 50–60°.[4] It seems that the space between the phenyl rings is too small to accommodate any $Cr(CO)_3$ fragment without significant structural change of **1**. It was therefore of interest to study the possibility of incorporating metal fragment(s) into phenyl rings and to monitor the structural change and effects caused. We now report the preparation of **2**, **3** (**3′** and **3″**) and **4** and the crystal structure of **3′**, which contains mixed metals through the directly joined π-rings.

RESULTS AND DISCUSSION

The reaction of **1** with $Cr(CO)_6$ in dibutyl ether in the presence of a small amount of THF resulted in attachment of $Cr(CO)_3$ fragments to the phenyl groups (Scheme 1).

The yields of **2**, **3′**, **3″** and **4** are 44.2%, 14.0%, 7.3% and 10.8%, respectively. Compounds **3′** and **3″** are structural isomers (Fig. 1). They are both orange and very close in R_f values (0.21 for **3″**, 0.19

* Author to whom correspondence should be addressed.

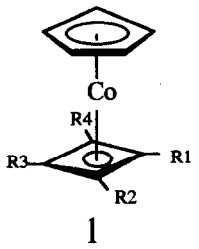

1

+ Cr(CO)6 → (Dibutyl ether, THF) 2 + 3' + 3" + 4

1: R1=Ph, R2=Ph, R3=Ph, R4=Ph
2: R1=areneCr(CO)3, R2=Ph, R3=Ph, R4=Ph
3': R1=areneCr(CO)3, R2=Ph, R3=areneCr(CO)3, R4=Ph
3": R1=areneCr(CO)3, R2=areneCr(CO)3, R3=Ph, R4=Ph
4: R1=areneCr(CO)3, R2=areneCr(CO)3, R3=areneCr(CO)3, R4=Ph

Scheme 1.

for **3'** in CH_2Cl_2/hexanes = 1 : 1). A slight difference in solubilities makes the separation of these two isomers by CTLC possible; **3"** was eluted first before **3'**. The fact that the yield of **3'** is higher than **3"** is reasonable from the viewpoint of steric effects.

Compound **3'** was crystallized by diffusing CH_2Cl_2 from the solution to the toluene and dark red crystals were obtained. The crystal data of **3'** shows that the dihedral angles between the $Cr(CO)_3$ complexed phenyl rings and cyclobutadiene ring are around 10° (Fig. 2 and Table 3). This is a significant structural change compared with that of **1**. The change in structure might help in releasing the tension between areneCr(CO)$_3$ and non-complexed phenyl rings. Also, the downfield shift of the Cp in ^{1}H NMR from 4.63 in **1** to 4.89 in **3'** can be attributed to this structural change. It can be explained by a better overlap between the cyclobutadiene ring and the two $Cr(CO)_3$ complexed phenyl rings through π-interaction (Fig. 3). By that process the two $Cr(CO)_3$ complexed phenyl rings may donate more electron density to the electron-withdrawing cyclobutadiene ring and then to the Cp ring that causes the downfield shift. It is also supported by the fact that a sequential downfield shift from **2** to **3** to **4** with more $Cr(CO)_3$ complexed **1** (**2**: 4.76, **3'**: 4.89, **3"**: 4.93, **4**: 5.05). ^{1}H NMR also shows an obvious upfield shift for the phenyl ring(s) of arene-$Cr(CO)_3$ and the almost unaffected phenyl group(s) in the same molecule, which is consistent with the well-known observations.[5]

The two $Cr(CO)_3$ fragments are pointed in different directions from the CoCp fragment in **3'**, which might avoid the repulsion between $Cr(CO)_3$ and CoCp. The dihedral angle between cyclobutadiene and one of the non-complexed phenyls, 75.9°, is larger than that in **1**. This might also help to relieve the tension between the phenyl and the $Cr(CO)_3$ fragment. The bond lengths of four cyclobutadiene carbon–carbon bonds in the planar cyclobutadiene ring is about the same, which is around 1.46 Å. The Cp and C_4 rings are almost coplanar [dihedral angle 1.9°]. Compound **3'** can be regarded as three metal fragments that are linked

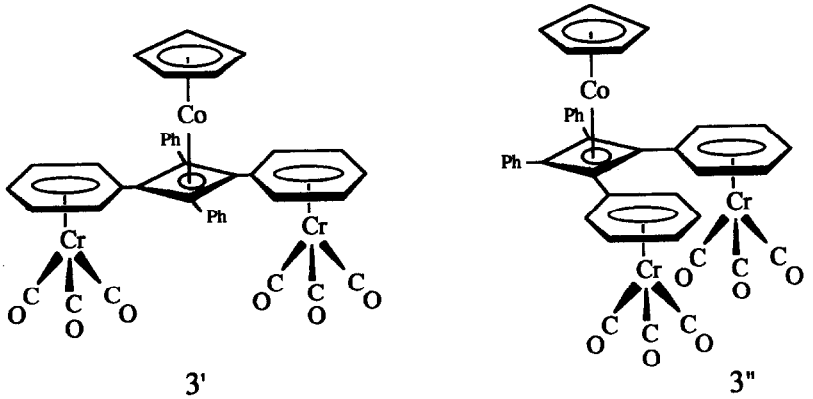

3' 3"

Fig. 1. The isomeric structures of **3'** and **3"**.

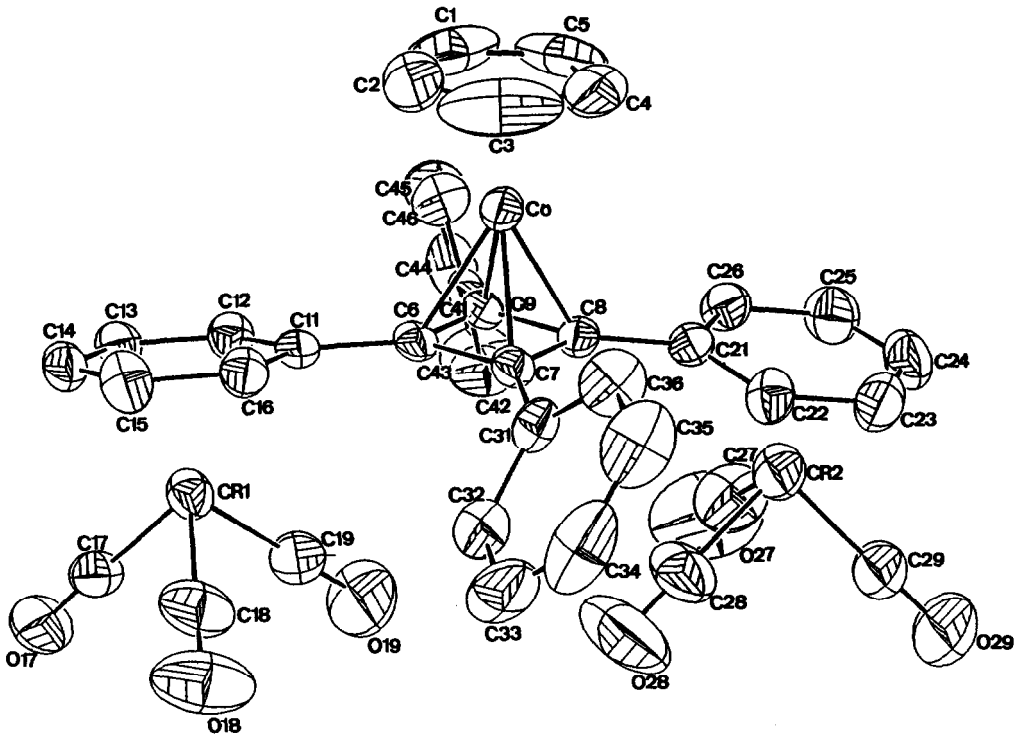

Fig. 2. ORTEP drawing with the numbering scheme for the non-hydrogen atoms of 3′.

by a 6–4–6 conjugated π–π ring system, which is rare according to the literature.

Hunter pointed out that the planarity of the arene ring can be distorted by a substituent.[6] An inward distortion, $\delta d < 0$, will take place when the substituent is an electron-withdrawing group. On the other hand, an outward distortion, $\delta d > 0$, is expected for an electron-donating substituent.[7] The above rule is obeyed unless a very bulky substituent is present. The cyclobutadiene ring is an electron-withdrawing group due to its tendency of aromaticity with six π-electrons. It is also supported by the fact that the positive values of $\Delta\pi$ in the ^{13}C NMR spectrum of the η^6-complexed phenyl group (2.04 ppm for **2**, 1.72 ppm for **3′**, 1.66 and 1.36 ppm for **3″**, 2.946, 0.285 and 0.294 ppm for **4**) were observed. According to Hunter, a positive $\Delta\pi$ in ^{13}C NMR indicates that the substituent, a C_4 ring, is an electron-withdrawing group.[8] However, in our case a slightly outward distortion is observed, even though an electron-withdrawing group (C_4 ring) is attached to the arene$Cr(CO)_3$ ring (Table 2). This opposite result to the above rule strongly suggests that the steric effect is more important than the electronic effect in this case. An inward distortion will not be favoured for the strong steric interaction between $Cr(CO)_3$ and the rest of the molecular fragment.

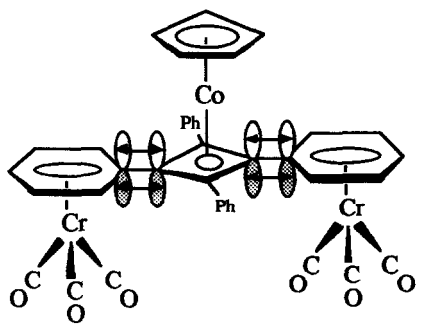

Fig. 3. The enhancement of interaction through the overlap of *p*-orbitals in the π-rings.

The orientation of $Cr(CO)_3$ in arene$Cr(CO)_3$ has been the subject of extensive studies. An *anti*-eclipsed form is observed for arene$Cr(CO)_3$ with an electron-withdrawing substituent. On the other hand, a *syn*-eclipsed form is observed for arene-$Cr(CO)_3$ with an electron-donating substituent.[9] However, it will be distorted to a nearly staggered structure when the substituent is very bulky. In the structure of (1′-t-butyl-2′,2′-dimethylpropyl)-π-(tricarbonylchromium)benzene the chromium carbonyl group was found to eclipse 44° away from its expected *syn*-eclipsed form due to its bulky substituent.[10] It is about 30° in **3′** for both arene-

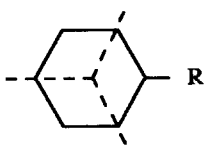

anti-eclipse

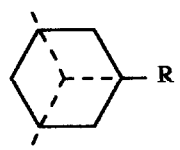

syn-eclipse

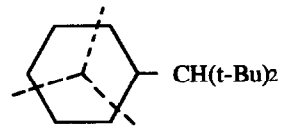

1'-t-butyl-2',2'-dimethylpropyl)-π-(tricarbonylchromium)benzene

$Cr(CO)_3$ fragments. This result also supports the observation that arene$Cr(CO)_3$ is attached by a very bulky, even though electron-withdrawing, group in **3'**.

Compound **4** was obtained in a reasonable amount. It is interesting to find that three $Cr(CO)_3$ fragments are able to insert into the already crowded area. In a related case Grimes was only able to place two $Cr(CO)_3$ fragments into a carborane, nido-2,3-$(PhCH_2)_2C_2B_4H_6$, even though four phenyl groups and more room are available in that compound.[11]

EXPERIMENTAL

Preparation of (η^5-C_5H_5)(PPh_3)Co(C_4Ph_4)

The synthesis of the title compound was patterned on the procedure in the literature.[12]

Preparation of **1**, (η^5-C_5H_5)Co(C_4Ph_4)

By refluxing (η^5-C_5H_5)(PPh_3)Co(C_4Ph_4) in toluene for 12 h one may obtain a quantitative yield of the title compound.

Apparatus and materials

All operations were performed in a nitrogen-flushed glove-box or in a vacuum system. Freshly distilled solvents were used. All processes of separation of the products were performed by Centrifugal Thin Layer Chromtography (CTLC), Chromatotron, Harrison model 8924. ^1H and ^{13}C NMR spectra were recorded on a Varian-300 spectrometer at 300 and 75.46 MHz, respectively. Chemical shifts are reported in ppm downfield from internal TMS. IR spectra were recorded in CH_2Cl_2 on a Hitachi 270-30. Mass spectra were recorded on a Joel JMS-SX/SX 102A GC/MS/MS. Elementary analyses were recorded on a Heraeus CHN-O-S-Rapid. X-ray diffraction data were collected on an Enraf–Nonius CAD4 diffractometer; the essential crystal data of **3'** are given in Table 1. Structure analyses are processed on a microvax computer using NRC VAX software.[13]

Reaction of (η^5-C_5H_5)Co(C_4Ph_4) *with* $Cr(CO)_6$

Into a 250 cm^3 round-bottom flask equipped with a condenser and a magnetic stirrer were placed (η^5-C_5H_5)Co(C_4Ph_4) (0.6 g, 1.24 mmol) and chromium hexacarbonyl (2.74 g, 12.42 mmol). Anhydrous dibutyl ether (120 cm^3) and anhydrous tetrahydrofuran (THF) (12 cm^3) were added and the reaction mixture was refluxed under dry nitrogen for 36 h. The reactor was cooled to room temperature and filtered and the solvent removed *in vacuo*.

The residue was dissolved in a small amount of CH_2Cl_2 and then was loaded onto CTLC for separation. Four bands were collected through the elution of a mixture of solvents. The ratio of solvent mixture (CH_2Cl_2/hexanes) changed from 4:1 to

Table 1. Crystal data for **3'**

Formula	$C_{39}H_{25}O_6Co_1Cr_2$
Formula weight	752.5481
Diffractometer used	CAD4
a (Å)	13.765(6)
b (Å)	16.765(14)
c (Å)	28.841(7)
V (Å^3)	6656(6)
Z	8
D_c (g cm^{-3})	1.502
Space group	Orthorhombic, *Pbca*
$F(000)$	3056
μ (cm^{-1})	11.64
Transmission	0.97–1.0
R^a	0.042
$R_w{}^b$	0.034
G.O.F.	2.36
Crystal size (mm)	0.2 × 0.3 × 0.25
$2\theta_{max}$ (°)	45
Temperature (K)	298
No. of reflections measured	4321
No. of observed reflections	3013
$(\Delta/\sigma)_{max}$	0.071
$(\Delta\rho)_{max,min}$ (e Å^{-3})	0.5, −0.5
Second extinction coeff.	2.2(2) × 10^{-4}

^{a} $R = [\Sigma\|\|F_o|-|F_c\|\|/|F_o|]$.
^{b} $R_w = [\Sigma w(\|F_o|-|F_c\|)^2/\Sigma w(|F_o|^2)^{1/2}]$; $w = 1/\sigma^2 F_o$.

Table 2. Selected bond distances (Å) and angles (°)

Co—C(1)	2.044(6)	Cr—C(17)	1.845(6)
Co—C(2)	2.037(6)	Cr—C(18)	1.834(6)
Co—C(3)	2.027(6)	Cr—C(19)	1.814(6)
Co—C(4)	2.012(6)	Cr(2)—C(21)	2.258(5)
Co—C(5)	2.038(6)	Cr(2)—C(22)	2.178(5)
Co—C(6)	1.979(5)	Cr(2)—C(23)	2.180(6)
Co—C(7)	1.971(5)	Cr(2)—C(24)	2.202(6)
Co—C(8)	1.974(5)	Cr(2)—C(25)	2.210(7)
Co—C(9)	1.969(5)	Cr(2)—C(26)	2.237(5)
Cr—C(11)	2.251(5)	Cr(2)—C(27)	1.897(7)
Cr—C(12)	2.222(6)	Cr(2)—C(28)	1.859(7)
Cr—C(13)	2.215(5)	Cr(2)—C(29)	1.821(6)
Cr—C(14)	2.217(5)	C(6)—C(7)	1.461(7)
Cr—C(15)	2.211(5)	C(6)—C(9)	1.454(7)
Cr—C(16)	2.215(5)	C(7)—C(8)	1.456(7)

C(6)—Co—C(7)	43.39(21)	C(6)—Co—C(8)	62.26(21)
C(6)—Co—C(9)	43.23(21)	C(7)—Co—C(8)	43.32(21)
C(7)—Co—C(9)	63.44(22)	C(8)—Co—C(9)	43.14(21)
C(17)—Cr—C(18)	89.4(3)	C(17)—Cr—C(19)	86.9(3)
C(18)—Cr—C(19)	89.4(3)	C(27)—Cr(2)—C(28)	87.6(3)
C(27)—Cr(2)—C(29)	87.8(3)	C(28)—Cr(2)—C(29)	92.3(3)
C(7)—C(6)—C(9)	90.6(4)	C(7)—C(6)—C(11)	136.2(5)
C(9)—C(6)—C(11)	133.2(5)	C(6)—C(7)—C(8)	89.0(4)
C(6)—C(7)—C(31)	135.0(5)	C(8)—C(7)—C(31)	134.8(5)
C(7)—C(8)—C(9)	91.0(4)	C(7)—C(8)—C(21)	135.2(5)
C(9)—C(8)—C(21)	133.4(5)	C(6)—C(9)—C(8)	89.5(4)
C(6)—C(9)—C(41)	135.8(5)	C(8)—C(9)—C(41)	132.2(5)
Cr—C(17)—O(17)	178.0(5)	Cr—C(18)—O(18)	178.6(5)
Cr—C(19)—O(19)	178.1(6)	Cr(2)—C(27)—O(27)	177.8(7)
Cr(2)—C(28)—O(28)	176.5(7)	Cr(2)—C(29)—O(29)	177.9(7)

1 : 1 as the separation proceeded. The first yellow band, R_f (0.66) in 1 : 1 of CH_2Cl_2–hexanes, was identified as a small amount of unreacted **1**. Compound **2**, orange ($R_f = 0.42$), was collected as the second band. The third band contains **3′** and **3″**. Both are orange and are very close in R_fs; 0.21 for **3″** and 0.19 for **3′**. This mixture was separated further by CTLC with a slow solvent injection speed. Compound **3″** was eluted out before **3′**. Compound **4**, orange ($R_f = 0.08$), was collected as the last band. The separation in CTLC was under nitrogen.

2. ^{1}H NMR ($CDCl_3$): δ 4.76 (s, 5H, Cp), 5.16 (m, 1H, *p*-C_6H_5), 5.22 (m, 2H, *o*-C_6H_5), 5.28 (m, 2H, *m*-C_6H_5), 7.13 (m, 5H, phenyl), 7.39 (m, 6H, phenyl), 7.81 (m, 4H, phenyl). ^{13}C NMR ($CDCl_3$):[14] δ 83.022 (5C, Cp), 90.023 (1C, C11), 90.751 (2C : C13, C15), 92.790 (3C : C12, C14, C16), 110.783 (1C, C6), 126.388 (1C, C21), 128.107 (3C : C22, C24, C26), 127.398 (2C : C23, C25), 127.505 (2C : C31, C41), 128.320 (4C : C33, C35, C43, C45), 130.709 (6C : C32, C34, C36, C42, C44, C46), 134.486 (2C : C7, C9), 135.758 (1C, C8), 233.571 (3C, CO). IR (CH_2Cl_2): ν(CO) 1966, 1888 cm^{-1}. Mass spectrum : *m/z* 616 (P^+).

3′. ^{1}H NMR ($CDCl_3$): δ 4.89 (s, 5H, Cp), 5.11 (m, 10H, phenyl), 7.51 (m, 6H, phenyl), 7.97 (m, 4H, phenyl). ^{13}C NMR ($CDCl_3$) : δ 82.866 (5C, Cp), 90.138 (2C : C11, C21), 90.325 (4C, C13, C15, C23, C25), 92.052 (6C : C12, C14, C16, C22, C24, C26), 107.887 (2C : C6, C8), 128.324 (2C : C31, C41), 128.715 (4C : C33, C35, C43, C45), 131.430 (6C : C32, C34, C36, C42, C44, C46), 132.908 (2C : C7, C9), 233.117 (6C, CO). IR(CH_2Cl_2): ν(CO) 1974, 1890 cm^{-1}. Mass spectrum : *m/z* 752 (P^+). Found : C, 62.1 ; H, 3.6. Calc. : C, 62.24 ; H, 3.3%.

3″. ^{1}H NMR ($CDCl_3$): δ 4.93 (s, 5H, Cp), 5.40 (m, 6H), 5.69 (m, 2H), 5.93 (m, 2H), 7.27 (m, 6H), 7.45 (m, 4H). ^{13}C NMR ($CDCl_3$): δ 83.313 (5C, Cp), 90.754 (1C, C31), 91.368 (2C : C33, C35), 92.178 (1C, C11), 92.285 (2C : C13, C15), 93.024 (3C : C32, C34, C36), 93.647 (3C : C12, C14, C16), 108.361 (2C : C6, C7), 127.427 (2C : C21, C41), 128.353 (4C : C23, C25, C43, C45), 129.688 (6C :

Table 3. Dihedral angle between planes A and B

A	B	Angle (°)
1	2	1.9(3)
1	3	10.46(25)
1	4	9.3(3)
1	5	53.3(3)
1	6	104.1(3)
2	3	12.2(3)
2	4	8.1(3)
2	5	52.9(3)
2	6	104.0(3)
3	4	19.47(20)
3	5	51.57(21)
3	6	99.95(20)
4	5	58.77(22)
4	6	110.30(21)
5	6	51.56(22)

Plane 1 : C(1)–C(5) ; plane 2 : C(6)–C(9) ; plane 3 : C(11)–C(16) ; plane 4 : C(21)–C(26) ; plane 5 : C(31)–C(36) ; plane 6 : C(41)–C(46).

C22, C24, C26, C42, C44, C46), 130.738 (2C: C8, C9), 233.057 (6C, CO). IR (CH_2Cl_2): ν(CO) 1970, 1892 cm^{-1}. Mass spectrum: m/z 752 (P^+).

4. ^1H NMR ($CDCl_3$): δ 5.05 (s, 5H, Cp), 5.19 (m, 5H), 5.26 (m, 3H), 5.50 (m, 3H), 5.73 (m, 2H), 5.99 (m, 2H), 7.45 (m, 3H), 7.80 (m, 2H). ^{13}C NMR ($CDCl_3$): δ 83.266 (5C, Cp), 91.312 (2C: C11, C21), 91.624 (2C: C13, C15), 91.722 (2C: C23, C25), 91.918 (3C: C12, C14, C16), 92.007 (3C: C22, C24, C26), 92.113 (1C, C31), 92.585 (2C: C33, C35), 95.531 (3C: C32, C34, C36), 105.803 (2C: C6, C8), 106.142 (1C, C7), 128.581 (1C, C41), 128.786 (2C: C43, C45), 131.305 (3C: C42, C44, C46), 131.519 (1C, C9), 232.502 (3C, CO), 232.867 (6C, CO). IR (CH_2Cl_2): ν(CO) 1974, 1894 cm^{-1}. Mass spectrum: m/z 888 (P^+).

Supplementary material available. Tables of atomic coordinates and thermal parameters, bond lengths and angles, anisotropic thermal parameters and hydrogen atom coordinates for **3'**.

Acknowledgement—Financial support of the National Research Councils of the R.O.C. under Grant NSC-82-0208-M-005-022 is gratefully acknowledged.

REFERENCES

1. (a) J. P. Collman, L. S. Hegedus, J. R. Norton and R. G. Finke, *Principles and Applications of Organotransition Metal Chemistry*. University Science Books, Mill Valley, CA (1987); (b) R. Davis and L. A. P. Kane-Maguire, *Comprehensive Organometallic Chemistry* (Edited by G. Wilkinson, F. G. A. Stone and E. W. Abel), Vol. 3, p. 953. Pergamon Press, Oxford (1982) and refs therein; (c) W. E. Watts, *Comprehensive Organometallic Chemistry* (Edited by G. Wilkinson, F. G. A. Stone and E. W. Abel), Vol. 8, p. 1013. Pergamon Press, Oxford (1982); (d) H. M. Colquhoun, J. Holton, D. J. Thompson and M. V. Twigg, *New Pathways for Organic Synthesis: Practical Applications of Transition Metals*. Plenum Press, New York (1984); (e) E. P. Kundig, N. P. Do Thi, P. Paglia, D. P. Simmons, S. Spichiger and E. Wenger, *Organometallics in Organic Synthesis* (Edited by A. de Meijere and T. Dieck), Vol. 1. Springer-Verlag, Berlin, Heidelberg (1988); (f) K. Schlogl, *Organometallics in Organic Synthesis* (Edited by A. de Meijere and T. Dieck), Vol. 2. Springer-Verlag, Berlin, Heidelberg (1988).
2. Ferrocenylphenyl chromium tricarbonyl, Cp_2Fe-$areneCr(CO)_3$, has two π-rings (Cp and arene) which are joined directly. (a) S. P. Gubin and V. S. Khandkarova, *J. Organomet. Chem.* 1970, **22**, 449. Examples of the synthesis of homonuclear compounds through bridging π-rings are few. (b) L. D. Schulte and R. D. Rieke, *J. Org. Chem.* 1987, **52**, 4829; (c) E. W. Neuse, *J. Organomet. Chem.* 1972, **40**, 387.
3. (a) D. A. Roberts and G. L. Geoffroy, *Comprehensive Organometallic Chemistry* (Edited by G. Wilkinson, F. G. A. Stone and E. W. Abel), Ch. 40. Pergamon Press, Oxford (1982); (b) R. M. Bullock and C. P. Casey, *Accts Chem. Res.* 1987, **20**, 167.
4. The crystal structure of **1** is not available; however, the structure of a closely related compound, $CpCo(C_4Ph_4BH)$, is known. (a) F.-E. Hong, C. W. Eigenbrot and T. P. Fehlner, *J. Am. Chem. Soc.* 1989, **111**, 949. The dihedral angle of another closely related compound, $Fe(CO)_3(C_4Ph_4)$, is relatively smaller. (b) R. P. Dodge and V. Schomaker, *Acta Cryst.* 1965, **18**, 614.
5. (a) R. V. Emanuel and E. W. Randall, *J. Chem. Soc. A* 1969, 3002; (b) M. J. McGlinchey and T. S. Tan, *Can. J. Chem.* 1974, **52**, 2439; (c) M. J. McGlinchey and J. L. Fletcher, *Can. J. Chem.* 1975, **53**, 1525; (d) C. S. Keller, *Tetrahedron Lett.* 1978, 2361.
6. (a) A. D. Hunter, L. Shilliday, W. S. Furey and M. J. Zaworotko, *Organometallics* 1992, **11**, 1550; (b) J. Li, A. D. Hunter, R. McDonald, B. D. Santarsiero, S. G. Bott and J. L. Atwood, *Organometallics* 1992, **11**, 3050.
7. The parameter δd is defined as the difference between the Cr—C_{ipso} bond length and the average of the other Cr—C(H) bond lengths. $\delta d = d$Cr—$C_{ipso} - d$Cr—$C(H)_{av}$.
8. The $\Delta\pi$ is defined as the difference (in ppm) between the measured chemical shifts of the *para*- and *meta*-substituted carbon atoms in the mono-substituted complexes. $\Delta\pi = \delta_{para} - \delta_{meta}$. A. D. Hunter, L. Shilliday, W. S. Furey and M. J. Zaworotko, *Organometallics* 1992, **11**, 1550.
9. (a) T. A. Albright and B. K. Carpenter, *Inorg. Chem.* 1980, **19**, 3092; (b) T. A. Albright, P. Hofmann and R. Hoffmann, *J. Am. Chem. Soc.* 1977, **99**, 7546.
10. (a) F. van Meurs and H. van Konigsveld, *J. Organomet. Chem.* 1974, **78**, 229; (b) F. van Meurs and H.

van Konigsveld, *J. Organomet. Chem.* 1976, **118**, 295.

11. (a) T. Whelan, J. T. Spencer, M. R. Pourian and R. N. Grimes, *Inorg. Chem.* 1987, **26**, 3116; (b) J. T. Spencer, M. R. Pourian, R. J. Butcher, E. Sinn and R. N. Grimes, *Organometallics* 1987, **6**, 335.
12. H. Yamazaki and Y. Wakatsui, *J. Organomet. Chem.* 1977, **139**, 157.
13. E. J. Gabe, Y. LePage, J.-P. Charland and F. L. Lee, *J. Appl. Cryst.* 1989, **22**, 384.
14. All the ^{13}C NMR labelling of carbon atoms are referred to the labelling on crystal structure **3'**.

Polyhedron Vol. 12, No. 15, pp. 1927–1931, 1993
Printed in Great Britain

0277–5387/93 $6.00+.00
© 1993 Pergamon Press Ltd

STUDIES ON LANTHANIDE COMPLEXES WITH OPEN CHAIN MULTIDENTATE LIGANDS—IX. SYNTHESIS, CHARACTERIZATION AND STRUCTURE OF THE COMPLEXES OF LANTHANIDE NITRATES WITH N,N′-BIS(4-METHOXYPHENYL)TETRAGLYCOLLIC DIAMIDE

XINMIN GAN, ZHIJIAN LIANG, NING TANG and MINYU TAN*

Department of Chemistry, Lanzhou University, Lanzhou 730000, P.R.C.

and

KAIBEI YU

Chengdu Centre of Analysis, Academia Sinica, Chengdu 610016, P.R.C.

and

GANZU TAN

Lanzhou Institute of Chemical Physics, Academia Sinica, P.R.C.

(*Received* 7 *January* 1993; *accepted* 1 *April* 1993)

Abstract—Lanthanide nitrate complexes with N,N′-bis(4-methoxyphenyl)tetraglycollic diamide (L) have been prepared in non-aqueous medium. These new complexes with the general formula $[Ln(L)(NO_3)_3]$ (Ln = La, Ce, Pr, Nd and Sm) have been characterized by elemental analysis, conductivity measurements and IR spectra. An X-ray crystallographic structural determination of the praseodymium complex shows that the pentadentate organic ligand wraps around the lanthanide ion which is also bonded to three bidentate nitrate groups, achieving the uncommon undeca-coordination.

Macrocyclic ligands, such as crown ethers, show a high complexation selectivity, which makes them suitable reagents for investigations of separation of lanthanide ions.[1] On the other hand, non-cyclic polydentate ligands, the open-chain analogues of crown ethers,[2] can also be used in the separation and analysis of the rare earths.[3–5] Some polyethylene glycols and their derivatives exhibit a "crown-like" behaviour in the lanthanide complexes[6] and some of them have been studied as lanthanide extractants.[3,4] As part of a systematic investigation on the lanthanide complexes with open chain multidentate ligands[7] this paper reports the preparation and structure of the complexes of lanthanide nitrates with N,N′-bis(4-methoxyphenyl)tetraglycollic diamide.

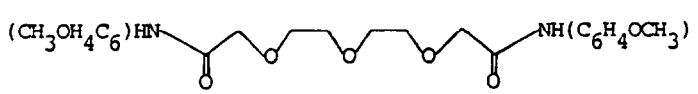

N,N'-Bis(4-methoxyphenyl)tetraglycollic diamide (L)

* Author to whom correspondence should be addressed.

EXPERIMENTAL

Reagents

Lanthanide nitrates were prepared by dissolving the corresponding oxides (AR) in 1 : 1 nitric acid. The ligand was obtained from the Lanzhou Institute of Chemical Physics. All other chemicals were AR grade and used without further purification.

Chemical and physical measurements

The metal ions were determined by EDTA titration using xylenol as an indicator. Carbon, nitrogen and hydrogen were determined using a Carlo–Erba 1106 elemental analyser. Conductivity measurements were performed with a DDS-11A type conductivity bridge using 10^{-3} mol dm^{-3} solutions in acetone at 25°C. The IR spectra were recorded on a Nicolet 170 SX FT-IR instrument using KBr discs in the 4000–400 cm^{-1} region. The crystal structure was determined on an R3M/E four-circle X-ray diffractometer.

Preparation of the complexes

A solution of lanthanide nitrate (1 mmol) in ethyl acetate (25 cm^3) was added dropwise to a solution of the ligand (0.432 g, 1 mmol) in ethyl acetate (25 cm^3) under stirring. The complex was precipitated gradually. After being stirred for 10 h the complex was isolated by filtration, washed with ethyl acetate and dried *in vacuo* over P_4O_{10} for 72 h; yield 60–65%. Single crystals of the praseodymium complex suitable for X-ray diffraction were obtained by recrystallizing the powdery complex from a solution of acetonitrile by slow evaporation.

X-ray structure determination

Crystal data. $C_{26}H_{34}N_7O_{16}Pr$, $M = 841.51$, monoclinic, space group Cc, $a = 21.324(8)$, $b = 11.456(4)$, $c = 14.495(4)$ Å, $\beta = 97.37(2)°$, $V = 3512(2)$ Å^3, $Z = 4$, $D_c = 1.59$ g cm^{-3}, λ(Mo-K_α) = 0.71073 Å, $\mu = 14.6$ cm^{-1}, $F(000) = 1704$.

A single crystal of dimensions $0.2 \times 0.4 \times 0.6$ mm was selected for the data collection on an R3M/E diffractometer with graphite-monochromated Mo-K_α radiation, $\theta/2\theta$ scan. 25 reflections were used for measuring lattice parameters and 2232 independent reflections were collected in the range $1° < 2\theta < 42°$. Of these 1777 reflections with $I \geqslant 1.5\sigma(I)$ were used in the structure determination and refinement. Lorentz–polarization corrections were applied. The structure was solved by Patterson methods and Fourier techniques and refined by full-matrix least-squares, with anisotropic thermal factors for all non-hydrogen atoms and isotropic thermal parameters for hydrogen atoms. Final $R = 0.049$, $R_w = 0.045$. Atomic coordinates, thermal parameters and a full set of bond lengths and angles have been deposited with the Editor as supplementary material.

RESULTS AND DISCUSSION

Analytical results are summarized in Table 1. The analytical data show that all of the complexes conform to a 1 : 1 metal-to-ligand stoichiometry.

All complexes are hygroscopic. They are soluble in methanol, ethanol, acetone and acetonitrile, slightly soluble in chloroform, ethyl acetate and nitromethane, and sparingly soluble in benzene, ether and cyclohexane. The molar conductance values of the complexes in acetone (Table 1) indicate that all the

Table 1. Elemental analysis, IR spectrum and molar conductance data

Compound	C% Found (Calc.)	H% Found (Calc.)	N% Found (Calc.)	Ln% Found (Calc.)	IR (cm^{-1}) ν(C—O—C)	ν(C=O)	Λ_m (s cm^3 mol^{-1})
L	61.3 (61.1)	6.5 (6.5)	6.8 (6.5)		1130s	1670s	
[La(L)(NO$_3$)$_3$]	35.3 (34.9)	3.7 (3.7)	9.0 (9.3)	18.2 (18.3)	1104s	1633s	31.6
[Ce(L)(NO$_3$)$_3$]	34.8 (34.8)	3.6 (3.7)	8.7 (9.2)	18.2 (18.5)	1103s	1632s	29.8
[Pr(L)(NO$_3$)$_3$]	35.1 (34.8)	3.7 (3.7)	9.1 (9.2)	18.7 (18.6)	1100s	1631s	28.5
[Nd(L)(NO$_3$)$_3$]	35.0 (34.6)	3.7 (3.7)	8.9 (9.2)	18.8 (18.9)	1100s	1629s	27.8
[Sm(L)(NO$_3$)$_3$]	33.9 (34.4)	3.8 (3.7)	8.9 (9.1)	19.5 (19.6)	1098s	1628s	28.4

Table 2. Selected bond lengths (Å)

Pr—O(1)	2.565(8)	Pr—O(7)	2.616(11)
Pr—O(2)	2.744(14)	Pr—O(9)	2.562(9)
Pr—O(3)	2.636(7)	Pr—O(10)	2.476(14)
Pr—O(4)	2.764(10)	Pr—O(12)	2.686(11)
Pr—O(5)	2.493(9)	Pr—O(13)	2.518(8)
Pr—O(6)	2.573(10)		

complexes act as non-electrolytes,[8] implying that all the nitrate groups are in the coordination sphere.

IR spectra

The most important IR bands of the ligand and the complexes are reported in Table 1. The ligand has a ν(C—O—C) band at 1130 cm^{-1} in its spectrum. This band appears at 1098–1104 cm^{-1} in the spectra of the complexes with a shift of 26–32 cm^{-1} to the lower frequency region, indicating that the ether oxygen atoms are coordinated to the metal ions. A very strong band assigned to ν(C=O) is observed at 1670 cm^{-1} in the spectrum of the free ligand. This band appears at 1628–1633 cm^{-1} in the spectra of the complexes with a shift of 37–42 cm^{-1}, showing that the C=O groups also take part in coordination to the metal ions. The IR spectral evidence above suggests the ligand is pentadentate, forming a ring-like structure, which is confirmed by the result of crystal structure determination.

Crystal structure of $[Pr(L)(NO_3)_3]\cdot 2CH_3CN$

Selected bond lengths and angles are given in Tables 2 and 3. Figure 1 shows the structure and the numbering scheme for the complex molecules. Figure 2 shows the packing arrangement in the unit cell.

The unit cell consists of the complex molecules and separate uncoordinated acetonitrile molecules. The ligand wraps around the metal ion with its oxygen atoms and assumes a ring-like structure similar to those of the crown ethers.[1] The praseodymium ion in the complex is 11-coordinated by three bidentate nitrate groups and one pentadentate ligand. Six Pr—O(nitrate) distances have values between 2.476 and 2.686 Å (mean 2.572 Å). The Pr—O(L)

Table 3. Selected bond angles (°)

O(1)—Pr—O(2)	56.9(3)	O(4)—Pr—O(6)	65.8(3)
O(1)—Pr—O(3)	114.7(3)	O(4)—Pr—O(7)	107.5(3)
O(1)—Pr—O(4)	172.9(3)	O(4)—Pr—O(9)	65.0(3)
O(1)—Pr—O(5)	126.2(3)	O(4)—Pr—O(10)	102.7(4)
O(1)—Pr—O(6)	110.2(3)	O(4)—Pr—O(12)	117.3(3)
O(1)—Pr—O(7)	66.5(3)	O(4)—Pr—O(13)	120.2(3)
O(1)—Pr—O(9)	120.3(3)	O(5)—Pr—O(6)	70.2(3)
O(1)—Pr—O(10)	79.6(4)	O(5)—Pr—O(7)	111.6(3)
O(1)—Pr—O(12)	65.5(3)	O(5)—Pr—O(9)	71.8(3)
O(1)—Pr—O(13)	66.7(3)	O(5)—Pr—O(10)	116.9(4)
O(2)—Pr—O(3)	58.3(4)	O(5)—Pr—O(12)	63.5(3)
O(2)—Pr—O(4)	117.8(3)	O(5)—Pr—O(13)	67.6(3)
O(2)—Pr—O(5)	176.1(4)	O(6)—Pr—O(7)	48.0(3)
O(2)—Pr—O(6)	106.9(4)	O(6)—Pr—O(9)	128.3(3)
O(2)—Pr—O(7)	67.0(4)	O(6)—Pr—O(10)	162.0(4)
O(2)—Pr—O(9)	108.9(4)	O(6)—Pr—O(12)	73.6(3)
O(2)—Pr—O(10)	65.1(4)	O(6)—Pr—O(13)	118.8(3)
O(2)—Pr—O(12)	118.6(4)	O(7)—Pr—O(9)	169.4(4)
O(2)—Pr—O(13)	116.3(4)	O(7)—Pr—O(10)	131.1(4)
O(3)—Pr—O(4)	59.6(3)	O(7)—Pr—O(12)	72.4(3)
O(3)—Pr—O(5)	118.2(3)	O(7)—Pr—O(13)	115.4(3)
O(3)—Pr—O(6)	81.2(4)	O(9)—Pr—O(10)	48.3(4)
O(3)—Pr—O(7)	82.4(4)	O(9)—Pr—O(12)	117.4(3)
O(3)—Pr—O(9)	87.2(4)	O(9)—Pr—O(13)	75.3(3)
O(3)—Pr—O(10)	81.0(4)	O(10)—Pr—O(12)	124.3(4)
O(3)—Pr—O(12)	152.3(4)	O(10)—Pr—O(13)	78.7(4)
O(3)—Pr—O(13)	158.9(4)	O(12)—Pr—O(13)	48.6(3)
O(4)—Pr—O(5)	58.9(3)		

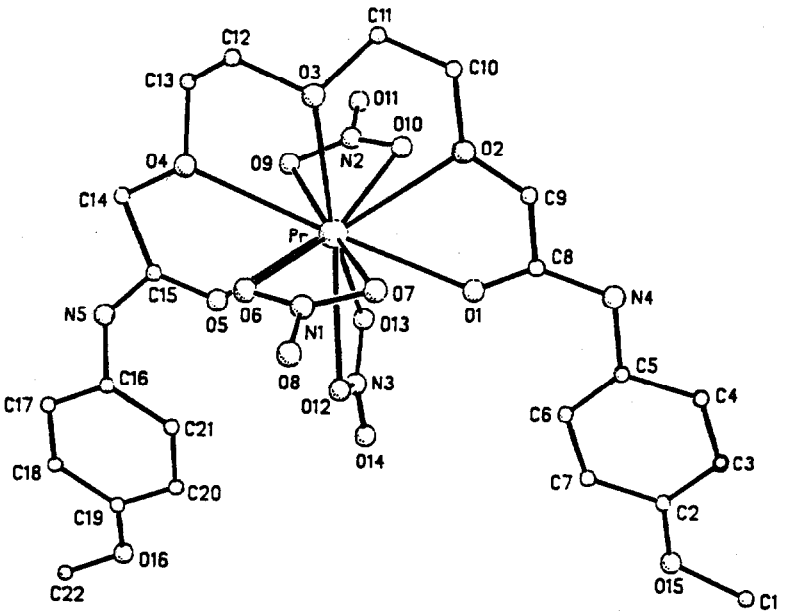

Fig. 1. Molecular structure of the praseodymium complex.

distances are of two types: as expected, the two terminal Pr—O(carbonyl) distances (mean 2.529 Å) are significantly shorter than the three Pr—O (etheric) distances (mean 2.715 Å). This is probably due to the higher electron density on the carbonyl oxygen.

A noteworthy feature of the molecular structure is the 11-coordinate polyhedron around the metal ion. Undeca-coordination is not common in inorganic chemistry.[9,10] The other reported undeca-coordinated lanthanide complexes with organic-type ligands are $[La(15\text{-crown-}5)(NO_3)_3]$,[11] $[La(monoaza\text{-}15\text{-crown-}5)(NO_3)_3]$,[12] $[La(naphtho\text{-}16\text{-crown-}5)(NO_3)_3]$,[13] $[La(TEG)(NO_3)_3]$ (where TEG = tetraethylenglycol),[14] $[La(DAPBAH)(NO_3)_3]$ [where DAPBAH = 2,6-diacetylpyridine-

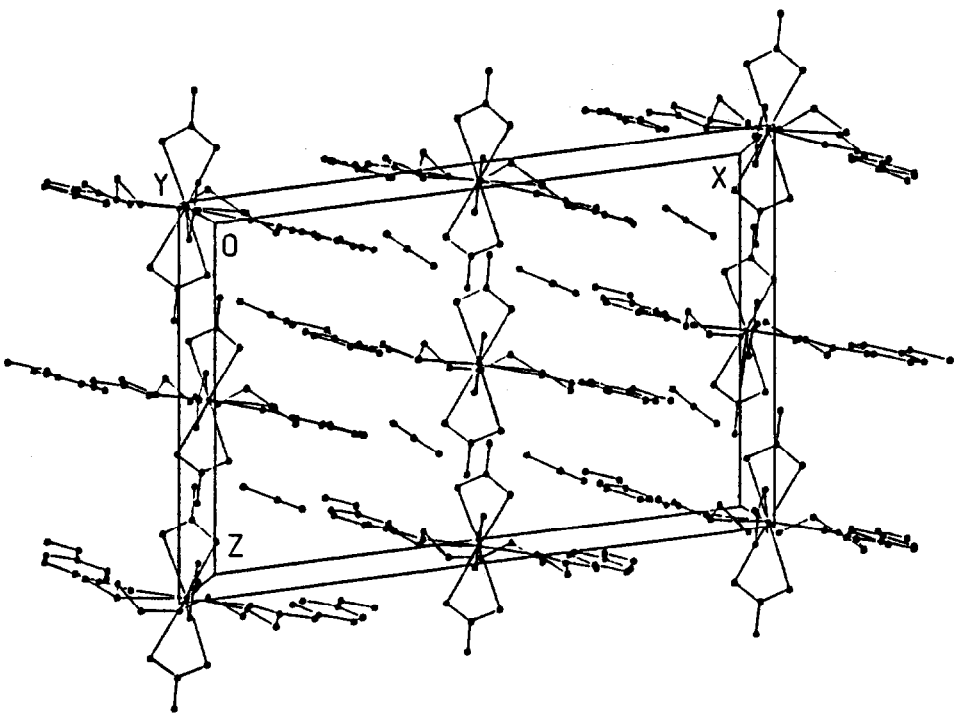

Fig. 2. Molecular packing in the unit cell.

bis(benzoic acid hydrazone)],[15] [Ce(15-crown-5)$(NO_3)_3$],[16] [Ce(4,4′-bipy)$(NO_3)_4(H_2O)_2]^-$ anion[17] and [Eu(15-crown-5)$(NO_3)_3$].[10] In general, the coordination polyhedra in these complexes are not easily definable or comparable and seem to be more determined by the shapes and characteristics of the bonded ligands than by the common coordination number.[9,14]

In conclusion, the open-chain multidentate ligand N,N′-bis(4-methoxyphenyl)tetraglycollic diamide can react with lanthanide nitrates in non-aqueous medium to form 1:1 (metal-to-ligand) stable solid complexes. The ligand acts as a pentadentate ligand forming a ring-like structure. Similar structures were also found for lanthanide complexes with other non-cyclic polyethers.[6]

Acknowledgements—The authors thank the Chinese National Natural Science Foundation for financial support.

REFERENCES

1. J.-C. G. Bünzli, in *Handbook on the Physics and Chemistry of Rare Earths* (Edited by K. A. Gschneidner Jr and L. Eyring), Ch. 60. Elsevier, Amsterdam (1987).
2. Y. Hirashima, K. Kanetsuki, I. Yonezu, K. Kamakura and J. Shiokawa, *Bull. Chem. Soc. Japan* 1983, **56**, 738.
3. Y. Yang, Y. Ding, G. Tan, J. Xu, Z. Yao and F. Zhang, *He Huaxue Yu Fangshe Huaxue* 1984, **6**, 196.
4. Y. Ding, J. Lu, Y. Yang, G. Tan and J. Xu, *Huaxue Shiji* 1986, **8**, 201.
5. Y. Yang and S. Cai, *Huaxue Shiji* 1984, **6**, 133.
6. Y. Hirashima, K. Kanetsuki, J. Shiokawa and N. Tanaka, *Bull. Chem. Soc. Japan* 1981, **54**, 1567.
7. X. Gan, T. Jiao, X. Guo, M. Tan and G. Tan, *J. Chin. Rare Earth Soc.* 1989, **7**, 71.
8. W. J. Geary, *Coord. Chem. Rev.* 1971, **7**, 81.
9. M. G. B. Drew, *Coord. Chem. Rev.* 1977, **24**, 179.
10. J.-C. G. Bünzli, B. Klein, G. Chapuis and K. J. Schenk, *Inorg. Chem.* 1982, **21**, 808.
11. R. D. Rogers and A. N. Rollins, *J. Cryst. Spectrosc. Res.* 1990, **20**, 389.
12. P. J. Cragg, S. G. Bott and J. L. Atwood, *Lanth. Act. Res.* 1988, **2**, 265.
13. G. Wang, S. Yan, X. Li, X. Yao, Z. Wan, Z. Rao and D. Liang, *Sci. Sin.* 1982, **B25**, 916.
14. U. Casellato, G. Tomat, P. Dibernardo and R. Graziani, *Inorg. Chim. Acta* 1982, **61**, 181.
15. J. E. Thomas, R. C. Palenik and G. J. Palenik, *Inorg. Chim. Acta* 1979, **37**, L459.
16. Y. Lin and Y. Xing, *Huaxue Xuebao* 1983, **41**, 97.
17. M. Bukowska-Stryzewska and A. Tosik, *Inorg. Chim. Acta* 1978, **30**, 189.

Polyhedron Vol. 12, No. 15, pp. 1933–1938, 1993
Printed in Great Britain

0277–5387/93 $6.00+.00
© 1993 Pergamon Press Ltd

CONFIGURATIONAL TREND IN THE COORDINATION ARRANGEMENT OF SOME LANTHANIDE(III) COMPLEXES. THE CRYSTAL AND MOLECULAR STRUCTURE OF $Yb(NCS)_3(THF)_4$—II*

GIOVANNI DEPAOLI,† PAOLO GANIS‡ and PIER LUIGI ZANONATO

Dipartimento di Chimica Inorganica Metallorganica ed Analitica, Università di Padova, Via L. Loredan 4, 35100 Padova, Italy

and

GIOVANNI VALLE

Centro Studi sui Biopolimeri del CNR, Via Marzolo 1, 35141 Padova, Italy

(*Received* 10 *February* 1993; *accepted* 30 *March* 1993)

Abstract—The series of lanthanide(III) complexes $Ln(NCS)_3(THF)_4$ [Ln = lanthanide(III) ion, THF = tetrahydrofuran] has been synthesized and examined by X-ray diffractometric methods. The study has shown that four oxygen atoms (THF) and three nitrogen atoms (NCS) are arranged around the Ln^{3+} ions according to well-defined coordination geometries: the square antiprism (SQA) for eight-coordination and the pentagonal bipyramid (PB) for seven-coordination. The dimeric square antiprismatic structures (Ln = Nd, Gd, Eu, Dy and Er) have been previously described. Here we report the crystal structure of $Yb(NCS)_3(THF)_4$. The coordination geometry of the metal ion consists of a slightly distorted pentagonal bipyramid, in which two nitrogen atoms (NCS) are in the apical positions and four oxygens atoms (4THF) and one nitrogen (NCS) lie in the equatorial plane. A correlation between the two coordination arrangements (SQA) and (PB) is discussed.

A preliminary X-ray analysis of the lanthanide series of the complexes $Ln(NCS)_3(THF)_4$ has recently revealed two isomorphous groups of crystal structures.[1a] The former includes the elements from La to Er; to the second belongs Yb and very likely the elements Tm and Lu, with completely different crystallographic features. (It was impossible to obtain crystals of Tm and Lu complexes suitable for an X-ray crystal analysis.)

The first group of complexes has already been described;[1b] it is characterized by a square antiprismatic octa-coordination about the metal ions; their geometrical features change regularly with the atomic number of the element according to the lanthanide contraction.[2]

The crystallographic data observed for the Yb complex are completely different; they are related to the smaller ionic size of the element and are attributable to a change into a seven-coordination. It is well known that such change is determined by the steric requirements of the ligands. For instance, the interconversion from octa- to seven-coordination occurs with Er in the case of $Ln(2,6\text{-dimethyl-4-pyrone})_7(ClO_4)_3$[3] and with Sm in the case of $Ln[(S_2P(OEt)_2]_2(\text{triphenylphosphine oxide})_3[S_2P(OEt)_2]$.[4] In the present case it takes place with Yb (or very likely with Tm). However, this behaviour has never been described on the basis of a systematic analysis of the full series of the lanthanide elements.

The seven coordination seems not to be favoured in all the periodic system[5] and is mostly char-

* For Part I see ref. 1(b).

† Author to whom correspondence should be addressed.

‡ On sabbatical leave from Dipartimento di Chimica, Università di Napoli, 80134 Napoli, Italy.

acterized by a capped octahedral or trigonal geometry,[6] specifically in complexes with non-equivalent ligands of the type (unidentateA)$_4$Me(unidentateB)$_3$.[7] As for the lanthanide metals only a few complexes are known with different unidentate ligands and all have three-fold symmetry or capped octahedral stereochemistry.[8]

Here we report the crystal and molecular structure of the complex Yb(NCS)$_3$(THF)$_4$, which shows a seven-coordination in the less common bipyramidal pentagonal configuration.[6]

A comparison will also be attempted with the molecular geometry found for the octa-coordinated homologous complexes already reported.[1]

The failure to obtain single crystals of the Tm complex is very likely attributable to the simultaneous presence of both the octa- and seven-coordination species in the product. Actually Tm is at the border line between the two series of these lanthanide complexes. For Lu the problem is related to its small ionic dimensions with respect to the donor ligands employed and its particular electronic configuration.

EXPERIMENTAL

The procedures for the preparation and manipulation of the ytterbium complex are exactly the same as adopted for the preparation of the dimeric square antiprismatic complexes (L = Nd, Eu and Er).[1] Moisture and oxygen were rigorously excluded using the glove-box technique. Anhydrous $YbCl_3$ was prepared according to reported methods.[9] Potassium thiocyanate was purified according to ref. 10. The solvents (THF and pentane) were purified by distillation from $LiAlH_4$ and K-benzophenone under nitrogen. The analysis of the metal was performed according to ref. 11. The Nujol IR spectrum was obtained with a Nicolet FTIR instrument.

Synthesis of Yb(NCS)$_3$(THF)$_4$

$YbCl_3$ and KSCN (molar ratio 1:3) were suspended in THF. The mixture was stirred for 1 day at room temperature and refluxed for 3 h under nitrogen. The resulting solution was centrifuged, the solid removed and the crude product isolated by evaporation of the solvent under reduced pressure. Crystals suitable for X-ray data collection were obtained by adding pentane to a THF solution of the compound. Found: Yb, 27.7. Calc. for $YbS_3O_4N_3C_{19}H_{32}$: Yb, 27.2%.

The Nujol IR spectrum of the title complex shows the frequencies characteristic of the N-monodentate group: ν(CN) 2037, ν(CS) 834, δ(NCS) 485 cm^{-1}.

Collection of X-ray data and structure solution

To prevent decomposition single crystals of Yb(NCS)$_3$(THF)$_4$ were sealed in Lindemann capillaries under nitrogen. Suitable crystals for an X-ray analysis were mounted on a Philips PW100 computer-controlled four-circle diffractometer with a graphite monochromator. Standard centring and auto-indexing procedures indicated the primitive monoclinic lattices $P2_1/a$. The orientation matrix and accurate unit cell dimensions were determined from a least-square fit of 25 symmetry-related reflections.

Intensity data were collected at 25°C using the θ–2θ scan method; two standard reflections, monitored every 150 reflection measurements, indicated a sensible decay of the crystals under X-ray radiation. Three crystals were used for data collection. The intensities were corrected for Lorentz and polarization effects, but not for absorption owing to the relatively low value of μ. Crystal data and details of intensity collection are reported in Table 1.

The positions of the lanthanide atoms were determined from three-dimensional Patterson syntheses. The light atoms were located from subsequent Fourier maps. The positions of the hydrogen atoms were geometrically calculated, assigned isotropic thermal parameters [with $U(H) = 1.2U_{eq}(C)$] and allowed to ride on their parent carbon atom. They were included in the final calculations, but not refined. Except for the carbon atoms of the THF groups anisotropic thermal parameters were used

Table 1. Summary of the crystal data and intensity collection for Yb(NCS)$_3$(THF)$_4$

Formula	$YbS_3O_4N_3C_{19}H_{32}$
M	635.90
a (Å)	25.583(11)
b (Å)	17.614(8)
c (Å)	12.075(6)
β (°)	90.5(1)
V (Å^3)	5441.0
Z	8
D_c (g cm^{-3})	1.55
Space group	$P2_1/a$
Crystal dimensions (mm)	0.25 × 0.25 × 0.35
T (K)	298
μ (cm^{-1})	40.5
Take off angle (°)	3
Scan speed (° min^{-1})	2.0 in the 2θ mode
2θ range (°)	$3.0 \leqslant 2\theta \leqslant 45$
Unique data	3694
$[F_o^2 \geqslant 2\sigma(F_o^2)]$	1701
R (on F_o)	0.059

for the non-hydrogen atoms. Blocked-cascade least-squares refinements were used; they converged to the conventional R index of 0.059. A unitary weighting scheme was used. Scattering factors for the atoms were taken from Cromer and Waber;[12] the scattering factors for Yb were corrected for the real and imaginary parts of anomalous dispersion using Cromer's values.[13] All computations were performed on a Cyber 76 computer using the SHELX-76 program.[14] Additional material available from the Cambridge Crystallographic Data Center comprises the final positional parameters of the non-hydrogen atoms, hydrogen atom coordinates and a full list of the bond lengths and angles.

DISCUSSION

The relevant molecular parameters are reported in Table 2 with reference to Fig. 1. The structural unit consists of two independent molecules of $Yb(NCS)_3(THF)_4$: **A** and **B**. They exhibit a slightly distorted bipyramidal pentagonal seven-coordination. The largest deviations from a symmetrical polyhedron concern the apical positions of the axial ligands in molecule **B**, for which some angles, L_{eq}—Yb′—L_{ax}, are *ca* 107–110°, as against the theoretical value of 90° and L_{ax}—Yb′—L_{ax}, is 166°. For both **A** and **B** the four THF ligands are disposed in the equatorial girdle with bond distances Yb—O of *ca* 2.36–2.40 Å, for THF groups inserted between two THF groups, and of *ca* 2.22–2.25 Å, for THF groups inserted between one THF and the equatorial NCS group, which indicates the dependence of these parameters upon sterical influences. The apical positions are occupied by NCS groups, giving rise to an idealized molecular C_2 symmetry with the pseudo-two-fold axis passing through the equatorial bond; Yb—N(1) and Yb′—N(1)′ for **A** and **B**, respectively (Fig. 1). The values of the Yb—ligand bonds are much more influenced by the coordination mode rather than the ionic radium of the metal; therefore, no simple correlation with the

Table 2. Selected bond distances (Å) and angles (°) with the estimated standard deviations for $Yb(NCS)_3(THF)_4$

Molecule **A**		Molecule **B**(′)	
Yb—O(1)	2.247(5)	Yb′—O(1)′	2.242(6)
Yb—O(2)	2.367(6)	Yb′—O(2)′	2.417(6)
Yb—O(3)	2.411(5)	Yb′—O(3)′	2.358(5)
Yb—O(4)	2.282(7)	Yb′—O(4)′	2.222(7)
Yb—N(1)	2.299(6)	Yb′—N(1)′	2.255(6)
Yb—N(2)	2.282(6)	Yb′—N(2)′	2.222(7)
Yb—N(3)	2.270(5)	Yb′—N(3)′	2.314(5)
N(1)—C(1)	1.12(2)	N(1)′—C(1)′	1.15(2)
N(2)—C(2)	1.10(2)	N(2)′—C(2)′	1.17(2)
N(3)—C(3)	1.14(2)	N(3)′—C(3)′	1.12(2)
C(1)—S(1)	1.56(1)	C(1)′—S(1)′	1.61(1)
C(2)—S(2)	1.62(1)	C(2)′—S(2)′	1.63(1)
C(3)—S(3)	1.59(1)	C(3)′—S(3)′	1.57(1)
O(1)—Yb—N(3)	92.9(5)	O(1)′—Yb′—N(3)′	85.9(7)
O(2)—Yb—N(3)	88.6(7)	O(2)′—Yb′—N(3)′	87.1(6)
O(3)—Yb—N(3)	82.2(6)	O(3)′—Yb′—N(3)′	87.2(6)
O(4)—Yb—N(3)	95.1(5)	O(4)′—Yb′—N(3)′	77.7(5)
N(2)—Yb—N(3)	87.8(7)	N(2)′—Yb′—N(3)′	108.6(7)
O(1)—Yb—N(1)	89.9(6)	O(1)′—Yb′—N(1)′	98.3(6)
O(2)—Yb—N(1)	86.4(5)	O(2)′—Yb′—N(1)′	82.1(6)
O(3)—Yb—N(1)	91.8(5)	O(3)′—Yb′—N(1)′	82.0(6)
O(4)—Yb—N(1)	85.8(7)	O(4)′—Yb′—N(1)′	106.5(7)
N(2)—Yb—N(1)	99.1(6)	N(2)′—Yb′—N(1)′	84.8(6)
O(1)—Yb—O(2)	71.6(4)	O(1)′—Yb′—O(2)′	72.3(7)
O(2)—Yb—O(3)	73.0(5)	O(2)′—Yb′—O(3)′	72.1(6)
O(3)—Yb—O(4)	69.1(6)	O(3)′—Yb′—O(4)′	73.9(7)
O(4)—Yb—N(2)	72.6(5)	O(4)′—Yb′—N(2)′	72.9(7)
N(2)—Yb—O(1)	75.4(6)	N(2)′—Yb′—O(1)′	76.4(6)
N(1)—Yb—N(3)	173.1(7)	N(1)′—Yb′—N(3)′	166.6(7)

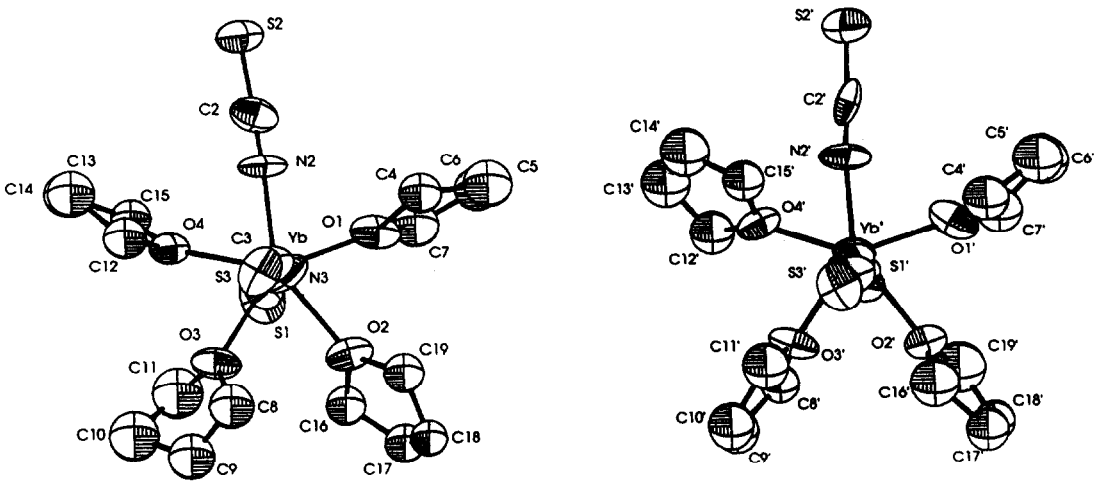

Fig. 1. Two molecules of $Yb(NCS)_3(THF)_4$ forming an independent structural unit, as viewed orthogonally to the equatorial YbL_5 girdle.

corresponding values observed in the octa-coordinated homologous series from Nd to Er is possible. The five atoms bonded to Yb in the equatorial girdle lie within ± 0.04 Å in a plane, the metal ion being way above this plane (*ca* 0.10 Å); in the case of molecule **B** the $Yb'L_5$ girdle is more distorted and only the oxygen atoms lie in a plane within ± 0.06 Å; N(2) and Yb′ are far above this plane (up to *ca* 0.20 Å). These facts and the sensible difference in the axial bond lengths Yb′—N(1)′ and Yb′—N(3)′ (2.25 and 2.31 Å, respectively) in unit **B** cannot be evidence of some *trans* effect[15] since the axial ligands here are identical; they can be ascribed only to intra- and/or intermolecular stereochemical influences.

In Table 3 some coordination parameters about

Table 3. Comparison between theoretical and experimental angular parameters for SQA and PB coordinations (°)

Atoms	Theoretical values for SQA configuration	Experimental values for $Er(NCS)_3(THF)_4$	Experimental values for $Yb(NCS)_3(THF)_4$	Theoretical values for BPP configuration
N(1)—Yb—O(1)	75	83	94	90
N(1)—Yb—O(2)	75	89	84	90
N(1)—Yb—O(3)	75	76	87	90
N(1)—Yb—O(4)	75	76	96	90
N(1)—Yb—N(2)	118	108	92	90
N(3)—Yb—O(1)	75	84	90	90
N(3)—Yb—O(2)	75	97	88	90
N(3)—Yb—O(3)	75	81	85	90
N(3)—Yb—O(4)	75	77	86	90
N(3)—Yb—N(2)	142	135	99	90
O(3)—Yb—O(2)	75	72	72	72
O(2)—Yb—O(1)	75	72	72	72
O(4)—Yb—O(3)	75	72	72	72
O(4)—Yb—N(2)	75	76	73	72
N(2)—Yb—O(1)	75	79	75	72
N(1)—Yb—N(3)	142	148	170	180

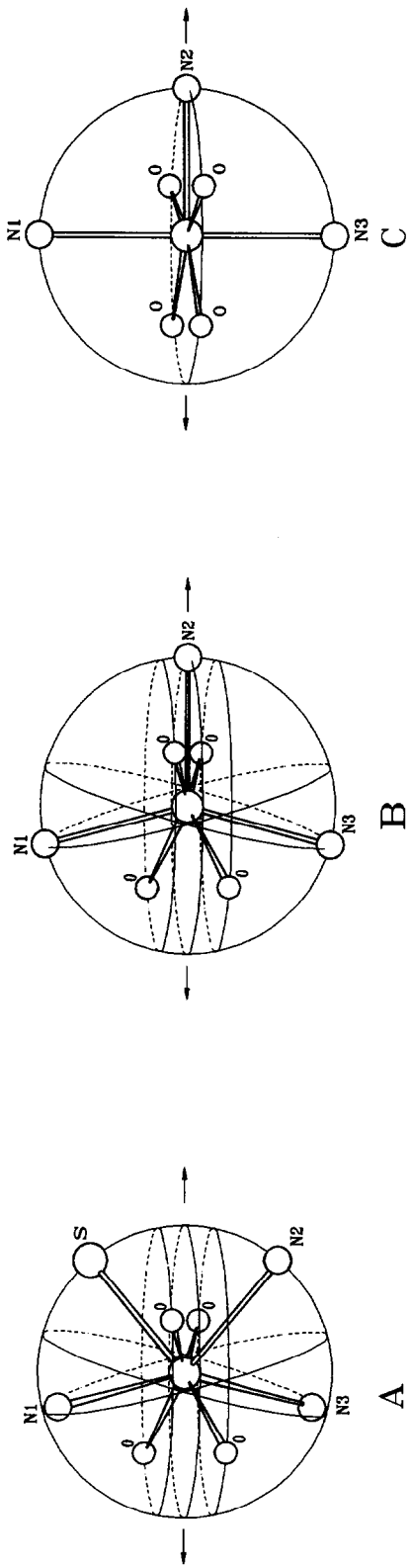

Fig. 2. Schematic interconversion path from square antiprism to pentagonal bipyramid with the retention of a two-fold symmetry axis. (A) Idealized symmetrical SQA coordination sphere; (B) the sites of S and N(2) coalesce in a single position on the equatorial plane, producing a distorted PB coordination; and (C) the oxygen atoms move towards the equatorial plane and N(2) and N(3) towards the meridional plane of the coordination sphere. A regular PB geometry is obtained.

the central ion, averaged between the values found for **A** and **B**, are compared with the corresponding values of a square antiprismatic, octa-coordinated homologous complex. As an example we have selected the complex $Er(NCS)_3(THF)_4$,[1] which is the closest to the Yb complex in this lanthanide series. It is noteworthy that the transformation from octa- to seven-coordination requires little geometrical rearrangement of the coordination sites, mainly involving the three positions occupied by the NCS groups; thus, we estimate that the bipyramidal pentagonal geometry is the seven-coordination mode closest to a square antiprismatic arrangement.

All these facts, together with the presence of two molecules in the structural unit, seem in some way to indicate a reminiscence in this structure of the dimeric nature of the complexes of the preceding lanthanide elements and their octa-coordination in the SQA configuration.[1]

A possible interconversion path from SQA to PB geometry for idealized symmetrical polyhedra is schematically shown in Fig. 2, assuming the retention of a two-fold symmetry axis [a pseudo-C_2 symmetry is present also in the molecular unit of $Er(NCS)_3(THF)_4$[1]].

Likely, such an interconversion does not require an appreciable change in energy,[16] which enhances the suggestion that in the case of the Tm complex both these geometries are present, so preventing or making difficult its crystallization from the mother solution.

The seven-coordination assumed by the Yb complex is the consequence of further contraction of the ionic radium from Er to Yb (*ca* 0.023 Å).[17]

Assuming an octa-coordination, with a sulphur atom of an adjacent molecular unit in the eighth site, we would expect a bond length of Yb—S (see ref. 1) larger than 3.28 Å, as found for the Er complex, that is too weak, and shorter bond lengths of Yb—O and Yb—N, giving rise to a much overcrowded coordination sphere around the central ion.

Acknowledgements—We thank Mr M. Griggio for the computer elaboration of the figures and for the technical assistance.

REFERENCES

1. (a) G. Depaoli, P. L. Zanonato and G. Valle, Proc. of the Conference on Rare Earth '92, Kioto (Japan) (1992); (b) G. Depaoli, P. Ganis, G. Valle and P. L. Zanonato, *Polyhedron* 1993, **12**, 676,
2. J. G. Palenic, in *Systematics and Properties of Lanthanides* (Edited by S. P. Sinha), pp. 153–210. D. Reidel Publishing Co., Dordrecht (1981).

3. C. Castellani Bisi, A. Coda and V. Tazzoli, *Cryst. Struct. Comm.* 1981, **10**, 703.
4. A. A. Pinkerton and D. Schwarzenbach, *J. Chem. Soc., Dalton Trans.* 1976, 2466.
5. J. L. Palenik, in *Systematics and Properties of Lanthanides* (Edited by S. P. Sinha), p. 173. D. Reidel Publishing Co., Dordrecht (1981).
6. D. L. Kepert, *Prog. Inorg. Chem.* 1979, **25**, 41.
7. M. G. B. Drew, J. D. Wilkins and A. P. Wolters, *J. Chem. Soc., Chem. Commun.* 1972, 1278; M. G. B. Drew and A. P. Wolters, *J. Chem. Soc., Chem. Commun.* 1972, 457; Lj. Manojlovic-Muir, *J. Chem. Soc., Dalton Trans.* 1976, 192.
8. M. G. B. Drew, *Prog. Inorg. Chem.* 1977, **23**, 67.
9. M. D. Taylor and C. P. Carter, *J. Inorg. Nucl. Chem.* 1962, **24**, 378.
10. D. D. Perrin, W. L. Armarego and D. R. Perrin, *Purification of Laboratory Chemicals*, p. 517. Pergamon Press, Oxford (1985).
11. S. L. Lyle and Md. M. Rahman, *Talanta* 1963, 1177.
12. D. T. Cromer and J. T. Waber, *Acta Cryst.* 1965, **18**, 184.
13. D. T. Cromer, *Acta Cryst.* 1965, **18**, 17.
14. G. M. Sheldricks, SHELX-76. Program for Crystal Structure Determination, Cambridge University, U.K. (1976).
15. E. M. Shustorovich, M. A. Porei-Koshits and Yu. A. Buslaev, *Coord. Chem. Rev.* 1975, **17**, 1.
16. H. B. Thompson and L. S. Bartell, *Inorg. Chem.* 1968, 7, 488.
17. R. D. Shannon, *Acta Cryst.* 1976, **A32**, 751.

Polyhedron Vol. 12, No. 15, pp. 1939–1945, 1993
Printed in Great Britain

0277-5387/93 $6.00+.00
© 1993 Pergamon Press Ltd

SYNTHESIS, CHARACTERIZATION AND LUMINESCENCE PROPERTIES OF LANTHANIDE(III) COMPLEXES WITH 2,6-BIS(BENZIMIDAZOL-2′-YL)PYRIDINE

SHUANGXI WANG and QINHUI LUO†

Coordination Chemistry Institute, Nanjing University, Nanjing 210008, P.R.C.

and

XIAOXIAN ZHOU and ZHENGZHI ZENG

Department of Chemistry, Lanzhou University, Lanzhou 730000, P.R.C.

(*Received* 8 *October* 1992; *accepted* 30 *March* 1993)

Abstract—New complexes of hydrated lanthanide(III) nitrates with 2,6-bis(benzimidazol-2′-yl)pyridine (BBP) having the formulae $[Ln(BBP)_2(NO_3)_2]NO_3 \cdot nH_2O$ (where Ln = La–Nd, Sm–Tb, n = 1, 2), $[Ln(BBP)(BBP—H)(NO_3)(OH_2)]NO_3 \cdot nH_2O$ (where Ln = Dy, Er, n = 3, 4) and $[Ln(BBP—H)(NO_3)_2(OH_2)] \cdot 2H_2O$ (where Ln = Lu) have been prepared and characterized by elemental analyses, IR and electronic spectra, molar conductance, thermal analyses and X-ray powder diffraction patterns. The emission spectra of all the complexes have also been examined. It has been found that all the complexes show the luminescence of the ligand. The Sm, Eu and Tb complexes also show the corresponding metal ion luminescence.

Luminescent lanthanide complexes are a subject of increasing interest, mainly due to their possible applications in bioinorganic chemistry.[1–5] To obtain luminescent lanthanide complexes it is necessary to bind lanthanide cations with chromophonic ligands, which are able to absorb energy and then transfer it effectively to the cation or shield the lanthanide ion from interaction with solvent (water) molecules which deactivate the luminiscent excited state. The tridentate ligand 2,6-bis-(benzimidazole-2′-yl)pyridine (BBP) (see Fig. 1), in which two benzimidazole and one pyridine rings can form an extensive conjugated system by coordination to a metal ion, may fulfil these requirements.[6] Although its complexes with some transition metals have been reported,[6–12] no paper concerning the study of lanthanide(III) complexes with BBP has been reported. Therefore, to investigate whether the BBP ligand would be effective in yielding ionic luminescence we have synthesized several lanthanide(III) complexes with BBP and discuss their luminescence properties.

EXPERIMENTAL

Reagents

The hydrated lanthanide(III) nitrates were prepared by dissolving the respective oxides (99.95%) in 50% nitric acid. The ligand 2,6-bis(benzimidazol-2′-yl)pyridine was prepared according to the literature method.[13] The other chemicals were analytical reagent grade.

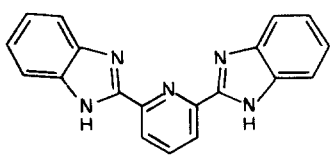

Fig. 1.

† Author to whom correspondence should be addressed.

Table 1. Analytical and physical data of the complexes

Complex[a]	Colour	Yield (%)	Elemental analysis: Found (Calc. %)[b] C	H	N	M	Decomposition interval (°C)	TGA analysis Weight loss (%)	Temperature range (°C)	Assignment
$[La(L)_2(NO_3)_2]NO_3 \cdot H_2O$	White	81	47.2 (47.3)	2.8 (2.9)	18.5 (18.9)	14.1 (14.4)	367–560	2.1 (1.9)	49–56	H_2O
$[Ce(L)_2(NO_3)_2]NO_3 \cdot H_2O$	Yellow	87	47.2 (47.2)	2.7 (2.9)	18.4 (18.8)	14.1 (14.5)	362–415	2.2 (1.9)	51–62	H_2O
$[Pr(L)_2(NO_3)_2]NO_3 \cdot H_2O$	Light green	82	47.5 (47.2)	3.0 (2.9)	18.5 (18.8)	14.2 (14.6)	358–432	1.9 (1.9)	62–77	H_2O
$[Nd(L)_2(NO_3)_2]NO_3 \cdot H_2O$	Light violet	78	46.7 (47.0)	3.1 (2.9)	18.3 (18.8)	14.4 (14.6)	354–441	2.3 (1.9)	71–96	H_2O
$[Sm(L)_2(NO_3)_2]NO_3 \cdot 2H_2O$	Cream	79	45.4 (45.9)	3.1 (3.0)	18.1 (18.3)	14.9 (15.1)	357–514	3.3 (3.6)	46–54	$2H_2O$
$[Eu(L)_2(NO_3)_2]NO_3 \cdot H_2O$	Light yellow	84	47.1 (46.6)	2.9 (2.9)	18.4 (18.6)	15.2 (15.5)	379–483	1.8 (1.8)	47–63	H_2O
$[Gd(L)_2(NO_3)_2]NO_3 \cdot H_2O$	White	81	46.4 (46.4)	2.6 (2.9)	18.5 (18.5)	15.6 (15.9)	307–505	2.1 (1.8)	52–58	H_2O
$[Tb(L)_2(NO_3)_2]NO_3 \cdot H_2O$	White	68	45.9 (46.3)	2.9 (2.8)	18.1 (18.5)	15.9 (16.1)	330–564	2.3 (1.8)	92–118	H_2O
$[Dy(L)(L—H)(NO_3)(OH_2)]NO_3 \cdot 4H_2O$	White	65	45.4 (45.7)	3.3 (3.5)	16.7 (16.8)	16.2 (16.3)	341–527	6.7 (7.2)	59–73	$4H_2O$
$[Er(L)(L—H)(NO_3)(OH_2)]NO_3 \cdot 3H_2O$	Cream	61	46.1 (46.3)	3.1 (3.4)	16.8 (17.1)	16.5 (16.9)	301–600	4.9 (5.5)	85–112	$3H_2O$
$[Lu(L—H)(NO_3)_2(OH_2)] \cdot 2H_2O$	White	57	34.4 (34.4)	2.8 (2.7)	14.4 (14.8)	25.9 (26.4)	298–580	5.9 (5.4)	80–107	$2H_2O$

[a] L = BBP.

[b] Required values are given in parentheses.

Preparation of the complexes

To a solution of BBP (20 mmol) in Me_2CO (40 cm^3) was added dropwise a solution of hydrated lanthanide(III) nitrates (10 mmol) in Me_2CO (10 cm^3) with stirring at room temperature. A precipitate was formed in a few minutes. After stirring for several hours the product was collected by filtration, washed several times with Me_2CO and Et_2O and dried in a vacuum desiccator over P_4O_{10}. The elemental analyses of these complexes are listed in Table 1.

Measurements

Carbon, nitrogen and hydrogen analyses were determined using a Carlo–Erba 1106 elemental analyser. The IR spectra were recorded on a Nicolet-170SX FT-IR spectrophotometer in CsI discs in the range 4000–200 cm^{-1}. Electronic spectra were recorded on a UV-240 spectrophotometer in the 190–900 nm region using a solution in methanol. Thermal characterization studies were performed with a Du Pont 1090 thermal analyser. Metal analyses were determined by titration with EDTA. Conductivity measurements were obtained using a 10^{-4} M solution in methanol on a DDS-II A conductometer at 25°C. The powder spectra were recorded on a Phillips PW 1700 automated powder diffractometer using Cu-K_α radiation ($\lambda = 1.54051$) with a diffracted-beam curved graphite monochromator. The experimental conditions were: focusing geometry with a θ–2θ scanning mode, stationary flat specimen, divergence slit (1°C), peak angle range 1–60°C, range in d spacing 2.34–14.33 Å, generator settings 40 KV, 100 mA. Electronic emission and excitation spectra were recorded with an 850 spectrophotofluorometer.

RESULTS AND DISCUSSION

The stoichiometries of the solid products obtained from the reaction of Me_2CO solutions of BBP and lanthanide(III) nitrates depend upon the lanthanide ion employed. Use of the lighter lanthanide ions (La–Tb except for Pm) gave the compounds $[Ln(BBP)_2(NO_3)_3 \cdot nH_2O]$ ($n = 1, 2$); the heavier lanthanide ions (Dy and Er) gave complexes of stoichiometry $[Ln(BBP)(BBP—H)(NO_3)_2(OH_2) \cdot H_2O]$ ($n = 3, 4$); whereas the Lu ion yields the 1:1 (metal:ligand) complex $[Lu(BBP—H)(NO_3)_2(OH_2)2H_2O]$. In the Dy, Er and Lu complexes an N proton on the benzimidazole ring of a ligand is lost, as indicated in the literature[12] and in the $Cd(BBP—H)_2$ complex, whose crystal structure has been determined by X-ray diffraction techniques.[14] These results indicate that the size of the metal ions affects the stoichiometry of the complexes. Besides, this change in stoichiometry most probably also results from the steric requirements of the nitrate ligands, which become increasingly forbidding from larger metal ions to smaller metal ions. The complexes are air-stable at room temperature, solution in CH_3OH, DMF and DMSO, slightly soluble in Me_2CO and insoluble in water and non-polar organic solvents. The molar conductances of the complexes (Table 2) indicate that the complexes, except for the Lu

Table 2. Important IR data (cm^{-1}) and molar conductances for the ligand and is complexes

Compound	ν(OH)	ν(NH)	$\nu(NO_3^-)$ (ionic)	$\nu(NO_3^-)$ (coordinate)				ν(M—N)	Λ_m[a]
BBP	—	3184brm	—	—	—	—	—	—	8
La	3421sh	3060brm	1386vs	1495s	1285s	1039m	824m	357vw	98
Ce	3428sh	3058brm	1391vs	1504s	1300s	1041m	828m	357vw	101
Pr	3386sh	3062brm	1389vs	1496s	1286s	1039m	824m	360vw	97
Nd	3480sh	3059brm	1384vs	1496s	1290s	1038m	826m	359vw	94
Sm	3460sh	3090brm	1382vs	1495s	1288s	1041m	825m	352vw	92
Eu	3420wb	3064brm	1382vs	1496s	1288s	1041m	825m	364vw	86
Gd	3430wb	3064brm	1382vs	1496s	1288s	1042m	825m	362vw	95
Tb	3361bm	3061brm	1384vs	1495s	1285s	1032m	824m	356vw	87
Dy	3584sp 3462bm	3062brm	1395vs	1496s	1293s	1020m	826m	362vw	106
Er	3561sp 3362bm	3060brm	1389vs	1496s	1293s	1036m	824m	366vw	88
Lu	3560sp 3401sh	3058brm	—	1510s	1294s	1024m	820m	374vw	49

[a] Ω^{-1} cm^2 mol^{-1}, in methanol.

v: very; s: strong; m: medium; w: weak; br: broad; sh: shoulder; sp: sharp.

complex, behave as 1 : 1 electrolytes in methanol, whereas the Lu complex is a non-electrolyte.

Thermal analysis

The TG curves of the complexes show a weight loss between 46 and 118°C. The weight loss corresponds to one water molecule for La–Nd and Eu–Tb complexes, two water molecules for Sm and Lu complexes, three water molecules for the Er complex and four water molecules for the Dy complex. These results are in accordance with the compositions of the complexes determined by elemental analyses and also show that the water molecules in these complexes are present as crystal water. The other water molecule (corresponding dehydrated temperature in the range 118–196°C) in the Dy, Er and Lu complexes is present as coordinated water. The complexes undergo decomposition within the temperature range 298–600°C, which shows that the complexes are more thermally stable than the parent ligand (decomposition temperature 250°C). The final products are metal oxides in all cases.

IR spectra

The important IR data of the complexes are listed in Table 2. The appearance of new bands at 3361–3480 cm^{-1} in the spectra of Ln complexes (Ln = La–Nd, Sm–Tb) indicates the antisymmetric and symmetric $OH(H_2O)$ stretching and N—OH bending modes. In the spectra of Dy, Er and Lu complexes the bands assigned to $\nu(H_2O)$ modes in the region 3401–3584 cm^{-1} are split or broadened, which indicates that the complexes contain both coordinated and cystal water, in agreement with the results of thermal studies. A broad band at 3184 cm^{-1} in the free ligand, assigned to the N—H group of the benzimidazole ring, is shifted to lower frequencies by *ca* 120 cm^{-1} in all complexes. This shift may be indicative of stronger hydrogen bonding between the ligand and the anions in the complexes than the intermolecular hydrogen bonding in the ligand in the solid state.[15,16] A new band at *ca* 361 cm^{-1} in the spectra of these complexes may be assigned to the metal–nitrogen stretching vibrations.

The bands characteristic of the ligand vibrations (C=C, C=N stretching) in the 1625–1500 cm^{-1} range are shifted towards high energy (*ca* 5–20 cm^{-1}) by complexation to the lanthanide(III) ions. The in-plane deformation mode of the pyridine ring appears at *ca* 635 cm^{-1}.[18,19] These indicate that the pyridine nitrogen and the nitrogens of the benzimidazole rings coordinate to lanthanide(III) ions. Presumably BBP acts as a tridentate ligand to lanthanide(III) ions.

Table 2 summarizes the IR spectral data of the nitrate groups. It can be seen that the IR spectra of the nitrate complexes exhibit four bands at *ca* 1496, 1288, 1038 and 825 cm^{-1}, which can be assigned to the vibrational modes of the coordinated (C_{2v}) nitrate groups. The magnitude of the splitting of the two bands at higher energies is *ca* 208 cm^{-1}, suggesting that the nitrate groups are present as bidentate ligands.[20] Meanwhile, the band at *ca* 1389 cm^{-1} due to ionic nitrate groups in the IR spectra of the complexes was also observed except for the Lu complex. This shows that these complexes have both ionic and coordinated nitrate groups. However, no band indicative of the ionic nitrate group at *ca* 1389 cm^{-1} in the Lu complex was observed, which shows that the Lu complex has only coordinated nitrate groups.

On the basis of the above discussion these complexes are formulated as: $[Ln(BBP)_2(NO_3)_2]NO_3 \cdot nH_2O$ (where Ln = La–Nd, Sm–Tb, n = 1, 2), $[Ln(BBP)(BBP—H)(NO_3)(OH_2)]NO_3 \cdot nH_2O$ (where Ln = Dy, Er, n = 3,4) and $[Ln(BBP—H)(NO_3)_2(OH_2)] \cdot 2H_2O$ (where Ln = Lu). The metal ion seems to be 10-coordinate for La–Nd and Sm–Tb, nine-coordinate for Dy and Er and eight-coordinate for Lu. The coordination number of central ions is variable (from 10 to 8) from the larger to the smaller lanthanide(III) ions, i.e. the coordination number of the central ion decreases due to lanthanide contraction.

Powder spectra

The X-ray powder patterns were recorded for selected Ce, Eu, Er and Lu complexes for comparison and are shown in Fig. 2. Comparison of the powder spectra of the complexes shows that Eu and Ce complexes are isomorphous, while as expected those of the Er and Lu complexes are different. Also, the powder spectra of the Er complex are different from those of the Lu complex. These results further support the above conclusion.

Electronic spectra

The electronic absorption spectra of all the complexes recorded in methanol (10^{-4} M) show similar features, containing an intense band at 324–328 nm with two shoulders at 306–309 and 331–334 nm attributable to an intraligand $\pi \rightarrow \pi^*$ transition. No absorption bands due to interconfiguration f–f transitions were observed due to their very low molar absorptivities ($\varepsilon < 3$).[21]

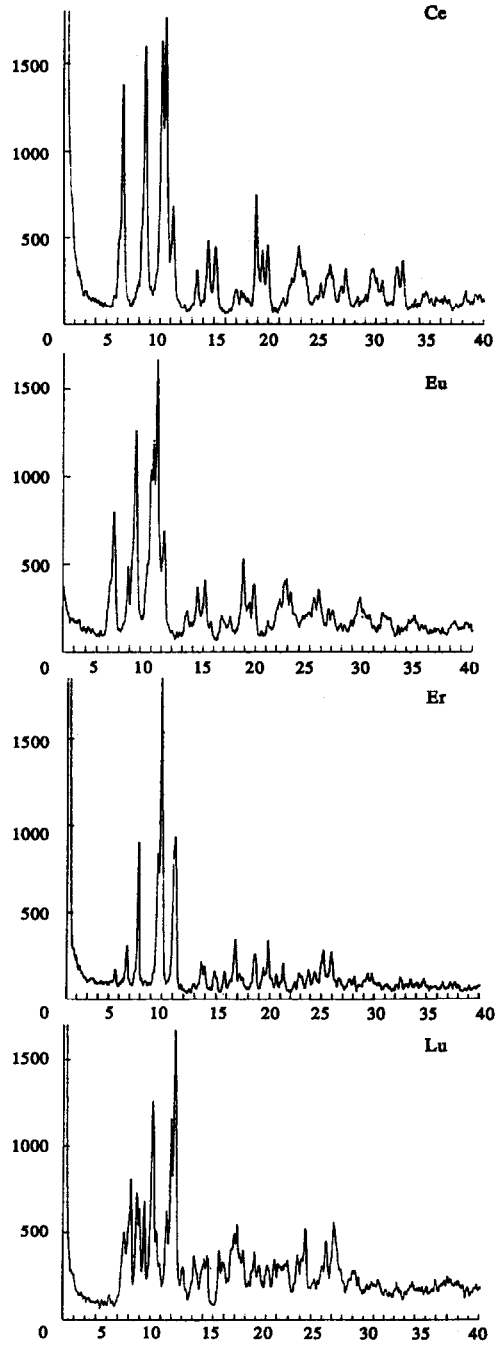

Fig. 2. X-ray diffraction powder patterns for Ce, Eu, Er and Lu complexes.

Table 3. Emission data and their assignments

Complex	λ_{ex} (nm)	λ_{em} (nm)[a]	Assignment
BBP	355	390	
La	355	389	Ligand
Ce	353	384	Ligand
Pr	350	387	Ligand
Nd	355	390	Ligand
Sm	355	390	Ligand
		560 (0.014)	$^4G_{5/2} \rightarrow {}^6H_{5/2}$
		597 (0.033)	$^4G_{5/2} \rightarrow {}^6H_{7/2}$
		645 (0.034)	$^4G_{5/2} \rightarrow {}^6H_{9/2}$
Eu	355	390	Ligand
		593 (0.460)	$^5D_0 \rightarrow {}^7F_1$
		618 (2.420)	$^5D_0 \rightarrow {}^7F_2$
		651 (0.040)	$^5D_0 \rightarrow {}^7F_3$
		695 (0.387)	$^5D_0 \rightarrow {}^7F_4$
Gd	355	389	Ligand
Tb	365	395	Ligand
		490 (0.101)	$^5D_4 \rightarrow {}^7F_6$
		545 (0.262)	$^5D_4 \rightarrow {}^7F_5$
		585 (0.058)	$^5D_4 \rightarrow {}^7F_4$
		620 (0.040)	$^5D_4 \rightarrow {}^7F_3$
		650 (0.006)	$^5D_4 \rightarrow {}^7F_2$
Dy	355	387	Ligand
Er	355	390	Ligand
Lu	354	385	Ligand

[a] Relative intensity given in parentheses.

Emission spectra

The emission spectra of all the complexes and the ligand were recorded using a compound concentration of 1.0×10^{-4} M in methanol at room temperature. The emission data and their assignments are summarized in Table 3. The results indicate that the only Sm^{III}, Eu^{III} and Tb^{III} complexes show corresponding metal luminescence, whereas

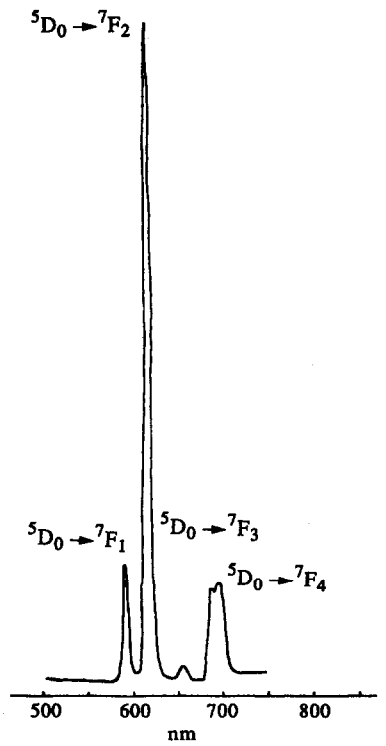

Fig. 3. Emission spectrum of $[EuL_2(NO_3)_2]NO_3 \cdot H_2O$ in methanol (10^{-4} M) at room temperature (λ_{ex} = 355 nm).

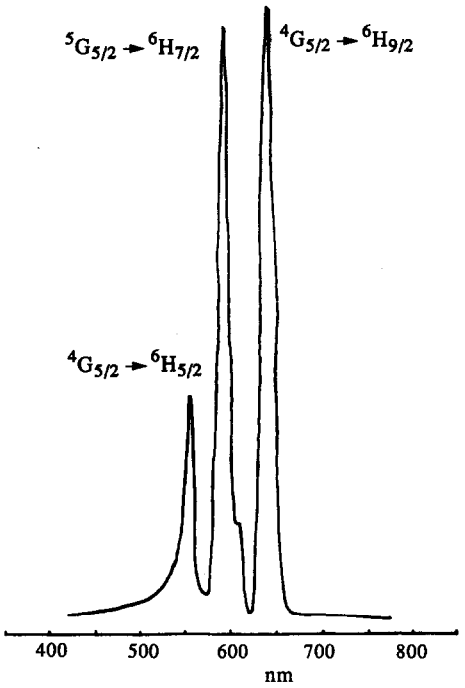

Fig. 4. Emission spectrum of $[SmL_2(NO_3)_2]NO_3 \cdot 2H_2O$ in methanol (10^{-4} M) at room temperature (λ_{ex} = 355 nm).

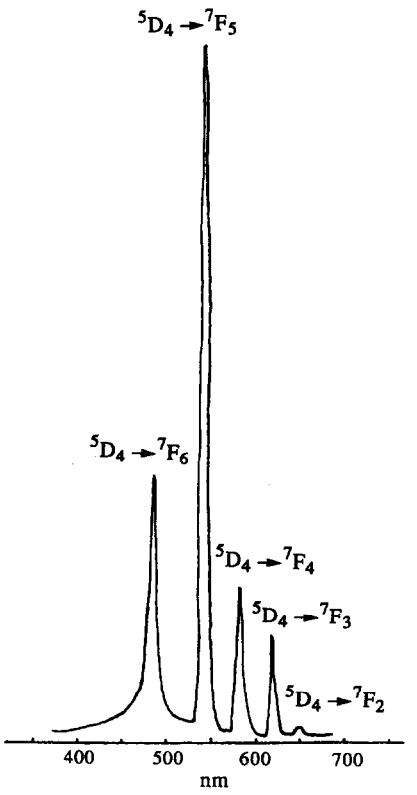

Fig. 5. Emission spectrum of $[TbL_2(NO_3)_2]NO_3 \cdot H_2O$ in methanol (10^{-4} M) at room temperature (λ_{ex} = 365 nm).

the other lanthanide(III) complexes do not. However, all the complexes exhibit luminescence of the ligand by excitation at *ca* 355 nm radiation. Figure 3 shows the emission spectrum of the Eu complex. It can be seen that the emisson arises mainly from a transition originating at the $^5D_0$ level and terminating in the $^7F_1$, $^7F_2$, $^7F_3$ and $^7F_4$ levels. The most intense band at 618 nm is due to the $^5D_0 \rightarrow {}^7F_2$ transition. The transition $^7D_0 \rightarrow {}^7F_3$ at 651 nm is of low intensity and can be reasonably taken as forbidden. The $^5D_0 \rightarrow {}^7F_4$ transition at 695 nm is slightly split into two almost equal intensity lines. The Sm complex shows weak metal ion luminescence and its emission spectrum (Fig. 4) exhibits three bands. Two stronger bands at 597 and 645 nm are assigned to $^4G_{5/2} \rightarrow {}^6H_{7/2}$ and $^4G_{5/2} \rightarrow {}^6H_{9/2}$, respectively. The intensity of the $^4G_{5/2} \rightarrow {}^6H_{5/2}$ transition at 560 nm is so low that this transition can be taken as forbidden. The emission spectrum of the Tb^{III} complex is depicted in Fig. 5. The most intense band at 545 nm is assigned to a $^5D_4 \rightarrow {}^7F_5$ transition. The three relatively weak bands at 490, 585 and 620 nm, assigned to $^5D_4 \rightarrow {}^7F_6$, $^5D_4 \rightarrow {}^7F_4$ and $^5D_4 \rightarrow {}^7F_3$ transitions, respectively, appear in the spectrum of this complex. A very weak band at 650 nm due to the $^5D_4 \rightarrow {}^7F_2$ transition can be taken as forbidden. Further developments about the luminescence properties of the lanthanide(III) complexes with BBP are in progress.

Acknowledgements—We thank Ms X. Lu for drawing the diagrams and helpful assistance.

REFERENCES

1. F. S. Richardson, *Chem. Rev.* 1982, **82**, 541.
2. W. D. Horrocks Jr and D. R. Sudnick, *Accts Chem. Res.* 1981, **14**, 384.
3. W. D. Horrocks Jr and M. Albin, *Prog. Inorg. Chem.* 1984, **31**, 1.
4. W. D. Horrocks Jr and D. R. Sudnick, *Science* (Washington D.C.) 1978, **1**, 1194.
5. V. Balzani, N. Sabbatini and F. Scandola, *Chem. Rev.* 1986, **86**, 319.
6. W. Shuangxi, Z. Ying, Z. Fangjie, W. Qiuying and W. Liufang, *Polyhedron* 1992, **11**, 1909.
7. S. M. Nelson, F. S. Fsho and M. G. B. Drew, *J. Chem. Soc., Dalton Trans.* 1982, 407.
8. S. B. Sanni, H. J. Behm, P. T. Beurskens, G. A. van Albada, J. Reedijk, A. T. H. Lenstra, A. W. Addision and M. J. Palaniandavar, *J. Chem. Soc., Dalton Trans.* 1989, 1429.
9. C. Piguet, B. Bocquet, E. Muler and A. F. Williams, *Helv. Chim. Acta* 1989, **72**, 323.

10. N. Shashikala, V. Gayathri, N. M. N. Gowda and G. K. N. Reddy, *J. Ind. Chem. Soc.* 1989, **66**, 537.
11. A. W. Addison, S. Burman, C. B. Wahlgren, O. A. Rajan, T. M. Rowe and E. Sinn, *J. Chem. Soc., Dalton Trans.* 1987, 2621.
12. S. Ruttimann, C. M. Moreau, A. F. Williams, G. Bernardinelli and A. W. Addition, *Polyhedron* 1992, **11**, 635.
13. A. W. Addison and P. J. Burke, *J. Heterocyc. Chem.* 1981, **18**, 803.
14. S. Wang, *Transition Met. Chem.* to be published.
15. F. Mani and G. Scapacci, *Inorg. Chim. Acta* 1976, **16**, 163.
16. J. B. Hodgson, G. C. Percy and D. A. Thornton, *J. Molec. Struct.* 1980, **66**, 75.
17. W. Radenka-Paryzek and E. Jankowska, *Inorg. Chim. Acta* 1987, **134**, 179.
18. W. Radecka-Paryzek, *Inorg. Chim. Acta* 1980, **45**, L147.
19. W. Radecka-Paryzek, *Inorg. Chim. Acta* 1981, **52**, 261.
20. K. Nakamoto, *Infrared and Raman Spectra of Inorganic and Coordination Compounds*, 3rd edn. John Wiley & Sons, New York (1978).
21. V. Banks and D. W. Klingman, *Anal. Chim. Acta* 1956, **15**, 356.

Polyhedron Vol. 12, No. 15, pp. 1947–1952, 1993
Printed in Great Britain

0277–5387/93 $6.00+.00
© 1993 Pergamon Press Ltd

PREPARATION AND CHARACTERIZATION OF HETEROLEPTIC TETRAISOPROPOXOALUMINATO-YTTRIUM(III) COMPLEXES

UPENDRA M. TRIPATHI, ANIRUDH SINGH* and RAM C. MEHROTRA†

Department of Chemistry, University of Rajasthan, Jaipur 302004, India

(*Received* 28 *January* 1993; *accepted* 1 *March* 1993)

Abstract—Novel heteroleptic tetraisopropoxoaluminato-yttrium(III) complexes $[\{Cl_2Y\{Al(OPr^i)_4\}\cdot 1.5Pr^iOH\}_2]$ **(I)** and $[\{Y\{Al(OPr^i)_4\}_2(\mu\text{-}Cl)(Pr^iOH)\}_2]$ **(II)**, synthesized by the reaction of $YCl_3\cdot 3Pr^iOH$ with $KAl(OPr^i)_4$ in 1 : 1 and 1 : 2 molar ratios, gave on prolonged evacuation the unsolvated complexes $[\{Y\{Al(OPr^i)_4\}(\mu\text{-}Cl)Cl\}_2]$ **(Ia)** and $[\{Y\{Al(OPr^i)_4\}_2(\mu\text{-}Cl)\}_2]$ **(IIa)**, respectively. Derivatives **Ia** and **IIa** have been used as precursors for the synthesis of interesting hetero-(bi- and tri-)metallic isopropoxides of yttrium of the type $[L_{3-x}Y\{Al(OPr^i)_4\}_x]$ [x = 1 and 2; L = OPr^i and $Zr_2(OPr^i)_9$]. All the new derivatives have been characterized by elemental analyses, IR, multinuclear (^1H, ^{13}C, ^{27}Al and ^{89}Y) NMR spectral studies and ebullioscopic molecular weight measurements.

In continuation of our investigations on the chemistry of alkoxides of the lanthanides,[1–4] we report here some interesting results on heteroleptic tetraisopropoxoaluminates of yttrium(III), particularly in view of the applications of alkoxides of yttrium, barium and copper as soluble molecular precursors in the sol–gel process[5–14] for the synthesis of high-temperature superconductors such as $YBa_2Cu_3O_{7-\delta}$.

For a comparative study of lanthanide chemistry, yttrium provides a convenient diamagnetic probe for ^1H, ^{13}C and even ^{89}Y NMR spectroscopy, which assumes significance particularly in view of the difficulties in obtaining single-crystals suitable for X-ray structural studies.

Heterometallic alkoxide chemistry of yttrium remains unexplored,[3,4,15] except for the synthesis of $[Y\{Al(OPr^i)_4\}_3]$,[16] and doubts have been cast recently even on the identity of the simple tris-isopropoxide $Y(OPr^i)_3$.[17,18] The product obtained by the dissolution of metallic yttrium in refluxing isopropyl alcohol has been recently characterized as $Y_5O(OPr^i)_{13}$. The authors have further reported that $Y_5O(OPr^i)_{13}$ does not interact with $Al(OPr^i)_3$ to give $[Y\{Al(OPr^i)_4\}_3]$, whereas the same can be obtained in a high yield by the addition of the required amount of $Al(OPr^i)_3$ to the initially obtained mother liquor, followed by distillation of the bimetallic isopropoxide. Mehrotra[19] has commented that the above observations indicate: (1) the presence of mainly tris-isopropoxide, $Y(OPr^i)_3$, in the mother liquor and (2) high stability of $[Y\{Al(OPr^i)_4\}_3]$. Hubert-Pfalzgraf *et al.*[20] have recently reported that the reaction of neodymium chips with isopropyl alcohol affords the major product $Nd(OPr^i)_3(Pr^iOH)$ in *ca* 76% yield as a first crop, while the second crop in *ca* 15% yield was established by X-ray diffraction to correspond to an oxoisopropoxide solvate, $Nd_5O(OPr^i)_{13}(Pr^iOH)_2$.

In view of the above the synthesis of a number of stoichiometric heteroleptic tetraisopropoxoaluminates of yttrium, $L_xY\{Al(OPr^i)_4\}_{3-x}$ [where L = Cl, OPr^i and $Zr_2(OPr^i)_9$; x = 1 and 2], are reported herein.

EXPERIMENTAL

Stringent precautions were taken to exclude moisture from the solvents, reactants as well as glassware employed throughout the investigations.

* Author to whom correspondence should be addressed.
† Present address: Vice-Chancellor, University of Allahabad, Allahabad 211002, U.P., India.

$YCl_3 \cdot 3Pr^iOH$,[21] $Zr(OPr^i)_4 \cdot Pr^iOH$[22] and $Al(OPr^i)_3$[23] were prepared by literature methods.

Zirconium in the reactant, $Zr(OPr^i)_4 \cdot Pr^iOH$, as well as in the derivatives was estimated as ZrO_2 after precipitation as mandelate and ignition to oxide. Similarly aluminium was estimated by the oxinate method. Yttrium was estimated by complexometric titration with EDTA using xylenol orange as an indicator. The isopropoxy content was estimated by oxidimetric methods.[24] Chloride was estimated by Volhard's method.[25] IR spectra (4000–200 cm^{-1}) were recorded as Nujol mulls using CsI plates on a Perkin–Elmer 557 spectrophotometer. ^1H (89.55 MHz), ^{27}Al (29.5 MHz) and ^{13}C (22.49 MHz) NMR were recorded at probe temperature on a Jeol FX 90Q FT NMR spectrometer in $CDCl_3$ or C_6H_6. ^1H and ^{13}C NMR spectra were referenced to tetramethylsilane. ^{27}Al NMR spectra were referenced to $Al(NO_3)_3 \cdot xH_2O$ (external). ^{89}Y NMR spectra were obtained using long pulse delay times (4 s) at a frequency of 4.37 MHz and were referenced to $\{Y(H_2O)_6\}Cl_3$. Better response signals were observed with 1 M solutions of yttrium(III) complexes containing *ca* 1% (by mole ratio) of analogous gadolinium complex. The paramagnetic gadolinium derivatives act as a relaxation reagent without appreciable alteration of the chemical shifts at these mole ratios; the number of scans generally required was *ca* 40.

Synthesis of the complexes

$[\{Cl_2Y\{Al(OPr^i)_4\} \cdot 1.5Pr^iOH\}_2]$ (**I**). A solution of $KAl(OPr^i)_4$ [freshly prepared by the reaction of potassium (0.33 g, 8.40 mmol) with isopropanol (*ca* 5 cm^3) containing benzene (*ca* 10 cm^3), followed by the addition of $Al(OPr^i)_3$ (1.70 g, 8.35 mmol) and refluxing the reaction mixture for 2 h] was added slowly to a suspension of $YCl_3 \cdot 3Pr^iOH$ (3.13 g, 8.35 mmol) in benzene (*ca* 20 cm^3) and stirred at 60°C for 12 h. Separation of precipitated KCl (0.61 g, 8.18 mmol) by filtration, followed by removal of the volatiles under reduced pressure (30°C/1 Torr) affords the title compound (**I**) (3.97 g, 99.2%). Found: Y, 17.3; Al, 5.4; Cl, 13.9; OPr^i, 63.2. Calc. for $C_{33}H_{80}Al_2Cl_4O_{11}Y_2$: Y, 17.3; Al, 5.3; Cl, 13.8; OPr^i, 63.6%.

The unsolvated compound, $[\{Cl_2Y\{Al(OPr^i)_4\}\}_2]$ (**Ia**), could be isolated by heating **I** at 60°C under reduced pressure for 4 h. Found: Y, 21.1; Al, 6.4; Cl, 16.7; OPr^i, 55.7. Calc. for $C_{24}H_{56}Al_2Cl_4O_8Y_2$: Y, 21.0; Al, 6.4; Cl, 16.7; OPr^i, 55.8%.

$[\{ClY\{Al(OPr^i)_4\}_2 \cdot Pr^iOH\}_2]$ (**II**). To a benzene (*ca* 15 cm^3) suspension of $YCl_3 \cdot 3Pr^iOH$ (2.54 g, 6.77 mmol) a solution of $KAl(OPr^i)_4$ [prepared by the interaction of potassium (0.53 g, 13.60 mmol) with isopropanol (*ca* 4 cm^3), followed by addition of a benzene (*ca* 20 cm^3) solution of $Al(OPr^i)_3$ (2.77 g, 13.57 mmol) and refluxing for 2 h] was added with continuous stirring. After stirring the reaction mixture at 60°C for 5 h, it was allowed to stir overnight at room temperature (*ca* 30°C). The precipitated KCl (1.00 g, 13.60 mmol) was separated by filtration. Volatiles were removed from the filtrate under reduced pressure (30°C/1 Torr) to yield the product (**II**) (4.74, 98%), which was recrystallized in *ca* 60% yield from an n-hexane–dichloromethane (2:1) mixture. Found: Y, 12.6; Al, 7.7; Cl, 5.0; OPr^i, 74.2. Calc. for $C_{54}H_{128}Al_4Cl_2O_{18}Y_2$: Y, 12.5; Al, 7.6; Cl, 5.0; OPr^i, 74.7%.

However, recrystallization of **II** from n-hexane–dichromethane (2:1) in the presence of isopropanol (1 cm^3) gave a product of composition $[\{ClY\{Al(OPr^i)_4\}_2(HOPr^i)_2\}]$ (**III**) in 55% yield. Found: OPr^i, 76.4; Cl, 4.7; Y, 11.5; Al, 7.0. Calc. for $C_{30}H_{72}Al_2ClO_{10}Y$: OPr^i, 76.6; Cl, 4.6; Y, 11.5; Al, 7.0%. ^1H NMR spectrum of **III** exhibits peaks (with the expected integration ratios) due to α- and β-protons as a septet and a doublet ($J = 6$ Hz) centred at δ 4.27 and 1.25 ppm, respectively, and a broad peak due to the hydroxyl proton of the coordinated isopropanol at δ 2.52 ppm.

Distillation of **II** at 203°C/0.1 Torr affords the unsolvated complex $[\{ClY\{Al(OPr^i)_4\}_2\}_2]$ (**IIa**) in 65% yield. Found: Y, 13.7; Al, 8.2; Cl, 5.5; OPr^i, 72.3. Calc. for $C_{48}H_{112}Al_4Cl_2O_{16}Y_2$: Y, 13.7; Al, 8.3; Cl, 5.4; OPr^i, 72.6%.

$[\{ClY\{Al(OPr^i)_4\}_2 \cdot THF\}_2]$ (**IVa**). To a benzene (*ca* 20 cm^3) solution of $[\{ClY\{Al(OPr^i)_4\}_2 \cdot Pr^iOH\}_2]$ (2.61 g, 3.67 mmol) was added THF (*ca* 3 cm^3) and the reaction mixture was stirred for *ca* 7 h at room temperature. Removal of the volatiles under reduced pressure, followed by recrystallization from an n-hexane–dichloromethane (2:1) mixture results in the product of composition $[\{ClY\{Al(OPr^i)_4\}_2 \cdot THF\}_2]$ in 60% yield. Found: Y, 12.4; Al, 7.5; Cl, 4.9; OPr^i, 65.1. Calc. for $C_{56}H_{120}Al_4Cl_2O_{18}Y_2$: Y, 12.3; Al, 7.4; Cl, 5.0; OPr^i, 65.3%.

$[\{ClY\{Al(OPr^i)_4\}_2 \cdot Py\}_2]$ (**IVb**). Adopting a similar procedure, interaction of $[\{ClY\{Al(OPr^i)_4\}_2 \cdot Pr^iOH\}_2]$ (1.95 g, 2.68 mmol) with pyridine (*ca* 1 cm^3) affords **IVb** in 98.3% yield. It was crystallized by n-hexane at −20°C in 60% yield. Found: Y, 12.3; Al, 7.4; Cl, 4.9; OPr^i, 64.3. Calc. for $C_{58}H_{122}Al_4Cl_2N_2O_{16}Y_2$: Y, 12.2; Al, 7.4; Cl, 4.8; OPr^i, 64.7%.

$[\{(OPr^i)Y\{Al(OPr^i)_4\}_2\}_2]$ (**Va**). A solution of $KAl(OPr^i)_4$ [freshly prepared by reacting potassium (0.61 g, 15.57 mmol) with isopropanol (*ca* 5 cm^3) containing benzene (*ca* 10 cm^3) followed by reflux-

ing after adding $Al(OPr^i)_3$ (3.18 g, 15.58 mmol)] was added slowly to a suspension of $YCl_3\cdot 3Pr^iOH$ (2.93 g, 7.79 mmol) in benzene (*ca* 15 cm^3). After stirring the reaction mixture for 6 h at 60°C a solution of $KOPr^i$ [prepared by reacting potassium (0.30 g, 7.67 mmol) with isopropanol (*ca* 2 cm^3) in benzene (*ca* 10 cm^3)] was added and the resulting reaction mixture was allowed to stir for 6 h. Separation of the precipitated KCl (1.72 g, 22.8 mmol) followed by removal of volatiles affords (**Va**) as a colourless solid (5.22 g, 99.0%), which was distilled unchanged in *ca* 70% yield at 163°C/0.05 Torr. Found: Y, 13.3; Al, 7.9; OPr^i, 78.2. Calc. for $C_{54}H_{126}Al_2O_{18}Y_2$: Y, 13.2; Al, 8.0; OPr^i, 78.8%.

Following a similar procedure interaction of $YCl_3\cdot 3Pr^iOH$, $KAl(OPr^i)_4$ and $KOPr^i$ in a 1:1:2 molar ratio affords $[\{(OPr^i)_2Y\{Al(OPr^i)_4\}\}_x]$ (**Vb**) in 99% yield as a white solid, which could be recrystallized from n-hexane in 60% yield.

$[\{Zr_2(OPr^i)_9\}Y\{Al(OPr^i)_4\}_2]$ (**Vd**). A solution of $KAl(OPr^i)_4$ [prepared by the interaction of potassium (0.27 g, 6.88 mmol) with isopropanol (*ca* 3 cm^3) and $Al(OPr^i)_3$ (1.40 g, 6.88 mmol) in benzene (*ca* 15 cm^3) followed by refluxing for 2 h and removal of volatiles in benzene (*ca* 20 cm^3)] was added slowly to a suspension of $YCl_3\cdot 3Pr^iOH$ (1.29 g, 3.45 mmol) in benzene (*ca* 15 cm^3). After stirring the resulting reaction mixture at 60°C for 10 h a benzene (*ca* 15 cm^3) solution of $KZr_2(OPr^i)_9$ [freshly prepared from potassium (0.13 g, 3.43 mmol) and $Zr(OPr^i)_4\cdot Pr^iOH$ (2.66 g, 6.86 mmol) in isopropanol (*ca* 2 cm^3) and benzene (*ca* 20 cm^3) mixture, followed by stripping off the volatiles] was added in a small proportion and then allowed to stir at 55°C for *ca* 12 h. Removal of precipitated KCl (0.77 g, 10.38 mmol) by filtration and volatiles from the filtrate under reduced pressure (0.9 Torr) affords the title compound (**Vd**) (4.56 g, 99.6%) as a colourless viscous mass. The product (**Vd**) was distilled in 80% yield unchanged at 193°C/0.5 Torr. Found: Y, 6.6; Al, 4.1; Zr, 14.8; OPr^i, 75.1. Calc. for $C_{51}H_{119}Al_2O_{17}YZr_2$: Y, 6.7; Al, 4.0; Zr, 14.7; OPr^i, 75.5%.

Adopting a similar procedure, interaction of $YCl_3\cdot 3Pr^iOH$, $KAl(OPr^i)_4$ and $KZr_2(OPr^i)_9$ in 1:1:2 molar ratios, affords the product of composition $[\{Zr_2(OPr^i)_9\}_2Y\{Al(OPr^i)_4\}]$ (**Vc**) in 99% yield, which could be distilled at 195°C/0.5 Torr in *ca* 90% yield. Found: Y, 4.9; Al, 1.6; Zr, 20.7; OPr^i, 72.6. Calc. for $C_{66}H_{154}AlO_{22}YZr_4$: Y, 5.0; Al, 1.5; Zr, 20.5; OPr^i, 73.0%.

RESULTS AND DISCUSSION

Reactions of $YCl_3\cdot 3Pr^iOH$ with $KAl(OPr^i)_4$ in 1:1 and 1:2 molar ratios yield products **I** and **II**, respectively:

$$YCl_3\cdot 3Pr^iOH + n KAl(OPr^i)_4 \longrightarrow 1/2[\{Cl_{3-n}Y\{Al(OPr^i)_4\}_n(Pr^iOH)_x\}_2] + (3-x)Pr^iOH + nKCl\downarrow$$

I: $n = 1, x = 1.5$

II: $n = 2, x = 1.$

Recrystallization of **II** from n-hexane–dichloromethane in the presence of isopropanol gave $[ClY\{Al(OPr^i)_4\}_2(Pr^iOH)_2]$.

The coordinated isopropanol in **I** and **II** could be removed on prolonged evacuation (1 Torr) at 60°C, yielding the unsolvated products **Ia** and **IIa**, respectively. Alternatively **IIa** can be obtained by distillation (at 203°C/0.1 Torr) of the derivatives (**II**) under reduced pressure.

The coordinated isopropanol in **II** can easily be displaced with comparatively stronger donor ligands, such as THF or pyridine (Py):

$$II + 2L \longrightarrow [\{ClY\{Al(OPr^i)_4\}_2\cdot L\}_2] + 2Pr^iOH$$

IVa: L = THF

IVb: L = Py.

Interestingly, yttrium(III) complexes of the type $[\{YCl(N(SiMe_3)_2)_2(THF)\}_2]$[26] could not be isolated in view of a facile tendency to disproportionate into symmetrical YCl_3 and $Y\{N(SiMe_3)_2\}_3$. Thus, the stability of complexes **II**, **IIa**, **IVa** and **IVb** may be due to the combined effects of steric crowding, coordinative saturation and the chelating effect of the bidentate tetraisopropoxoaluminate ligand.

In situ reactions of $YCl_3\cdot 3Pr^iOH$, $KAl(OPr^i)_4$ and $KOPr^i$ or $KZr_2(OPr^i)_9$ in appropriate molar ratios yield novel hetero-(bi- or tri-)metallic isopropoxides of yttrium(III) according to the following reaction:

$$YCl_3\cdot 3Pr^iOH + (3-x)KL \longrightarrow [L_{(3-x)}Y\{Al(OPr^i)_4\}_x] + 3KCl\downarrow$$

Va: $x = 2$, L = OPr^i

Vb: $x = 1$, L = OPr^i

Vc: $x = 1$, L = $Zr_2(OPr^i)_9$

Vd: $x = 2$, L = $Zr_2(OPr^i)_9$.

These new heterometallic isopropoxides are highly moisture sensitive, colourless solids or viscous liquids, soluble in common organic solvents, generally volatile under reduced pressure, and depict dimeric behaviour (ebullioscopically) in benzene, except the heterotrimetallic isopropoxides **Vc** and **Vd** which tend to be monomeric.

Spectroscopic studies

The characteristic IR frequencies of these new heteroleptic isopropoxometallates of yttrium(III) have been assigned on the basis of published data on metal alkoxides.[1,4,27] The $(CH_3)_2C<$ skeletal vibrations have been observed in the range 1170–1105 cm^{-1}. The ν(C—O) have been found to exhibit absorptions in the range 1085–935 cm^{-1}. Medium to strong broad absorptions displayed in the range 710–410 cm^{-1} may be related to ν(Al—O) (710–640 cm^{-1}), ν(Zr—O) (570–535 cm^{-1}) and ν(Y—O) (460–410 cm^{-1}). The chloro derivatives exhibited additional absorptions in the range 290–205 cm^{-1}, which may be tentatively assigned to Y—Cl stretching frequencies.

Despite the possibility of the inequivalent nature of the isopropoxy groups in plausible structures for the new derivatives, the room-temperature ^{1}H NMR spectra (in $CDCl_3$) of **I**, **Ia**, **II**, **IIa**, **III**, **IVa**, **IVb**, **Va** and **Vb** exhibit a doublet (J = 6 Hz) at δ 1.27, 1.21, 1.25, 1.27, 1.25, 1.24, 1.26, 1.26, 1.24 and a septet (J = 6 Hz) at δ 4.22, 4.03, 4.24, 4.24, 4.27, 4.23, 4.18, 4.31, 4.26 ppm, respectively, due to *gem*-dimethyl (β-H) and methine (α-H) protons. Derivatives **I**, **II** and **III** showed additional broad signals at δ 3.06, 3.40 and 2.52 ppm, respectively, due to OH of the coordinated isopropyl alcohol. The presence of coordinated THF in the derivative **IVa** is indicated by the signals at δ 1.83 (β-CH_2) and 3.69 (α-CH_2), while the appearance of three ^{1}H NMR signals at δ 7.22, 7.58 and 8.66 ppm in the case of the derivative **IVb** is characteristic of coordinated pyridine. The presence of pyridine in the complex **IVb** is further corroborated by the peaks at δ 124.5, 139.6 and 148.4 ppm in its ^{13}C NMR spectrum.

Interestingly, the ^{1}H NMR spectrum of **Vc** exhibits three doublets (J = 6 Hz) centred at δ 1.24, 1.39 and 1.62 ppm, respectively, due to terminal-, μ_2- and μ_3-OPr^i groups, which is consistent with a structure involving bidentate ligation modes of both the groups $Zr_2(OPr^i)_9^-$ and $Al(OPr^i)_4^-$ with a further possibility for a $Zr_2(OPr^i)_9$ unit to coordinate through an appropriately situated isopropoxy group. By contrast, the methine protons appear as an average septet (J = 6 Hz) at δ 4.39 ppm. The above structural possibility is further supported by its ^{13}C NMR spectrum with the appearance of the peaks at δ 25.74, 26.66, 27.31 (β-carbons) and 65.83, 69.03, 72.06 (α-carbons).

By contrast, the spectrum of **Vd** exhibits only two doublets (J = 6 Hz) centred at δ 1.22 and 1.23 ppm due to gem-dimethyl protons, while methine protons appear as an average septet (J = 6 Hz) at δ 4.27 ppm.

The ^{13}C NMR spectrum of the product **I** exhibits two signals at δ 24.9 and 26.5 ppm due to β-carbons and two signals at δ 65.65 and 66.12 ppm ascribable to α-carbons of the isopropoxy groups. The formulation of the product **I** as $[(Pr^iO)_2Al(\mu\text{-}OPr^i)_2Y(Cl)(Pr^iOH)(\mu\text{-}Cl)_2(\mu\text{-}Pr^iOH)Y(Cl)(Pr^iOH)(\mu\text{-}OPr^i)_2Al(OPr^i)_2]$ involving a hepta-coordinated environment around yttrium is supported by the elemental analyses, molecular weight measurements, integrated intensity ratio of the ^{1}H NMR signals at δ 1.27, 3.07 and 4.22 ppm and appearance of a single ^{89}Y NMR peak at δ 313.3 ppm.

The ^{13}C NMR spectrum of **Vb** shows a single peak at δ 26.97 (β-carbons) and two peaks at δ 64.51 and 66.14 (α-carbons) ppm of the isopropoxy groups.

The ^{89}Y NMR spectra of **I**, **Ia**, **II**, **IIa** and **Va** exhibit single peaks at δ 313.3, 361.9, 214.6, 256.9 and 195.1 ppm, respectively. The ^{89}Y NMR spectrum of the product **Vb** exhibits four sharp peaks at δ 219.26, 195.79, 157.20 and 155.01 ppm, probably due to the presence of yttrium(III) in different coordination (five, six or higher) geometries.[28]

In view of the available spectroscopic data and the observed molecular weight (molecular complexity 2.4), 1128 against 470 (calculated value for monomeric derivative), it appears that there might be an equilibrium of the type indicated below:

$$\underset{^{89}\text{Y NMR}:\,\delta\,157.2,\,155.01\text{ ppm}}{[\{Y\{Al(OPr^i)_4\}(OPr^i)(\mu\text{-}OPr^i)\}_2]\,(\mathbf{Vb})} \rightleftharpoons$$

$$\underset{^{89}\text{Y NMR}:\,\delta\,195.79}{(Pr^iO)Y\{Al(OPr^i)_4\}_2} + 1/n\underset{^{89}\text{Y NMR}:\,\delta\,219.26\text{ ppm}}{[Y(OPr^i)_3]_n}^{29}$$

(n = 4 or 5)

These data in conjunction with the recent X-ray crystallographic authentication of a praseodymium analogue,[2] $[\{Pr\{Al(OPr^i)_4\}_2(\mu\text{-}Cl)(Pr^iOH)\}_2]$, tend to support a dimeric type structure (Fig. 1) for the products **II**, **IVa**, **IVb**, **IIa** and **Va**.

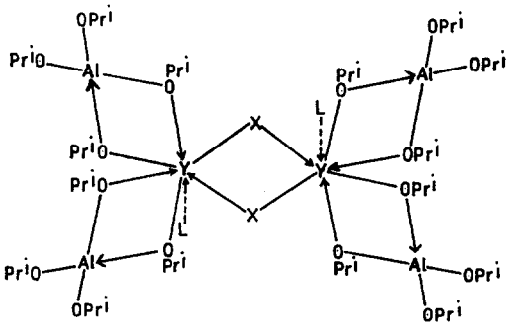

Fig. 1. Proposed structures of the derivatives $[\{XY\{Al(OPr^i)_4\}_2 \cdot L\}_2]$ [when X = Cl and L = Pr^iOH (**II**), THF (**IVa**), Py (**IVb**), absent (**IIa**); when L is absent and X = OPr^i (**Va**)].

The facile removal of coordinated isopropyl alcohol from **II** *in vacuo* is understandable in terms of steric congestion around the smaller Y^{3+} (0.881 Å) compared with that of the larger Pr^{3+} (1.013 Å). This is also reflected in the observed molecular weight (1319), which tends to suggest dissociation of the coordinated isopropyl alcohol in refluxing benzene.

The structural formulation of **IIa** and **Va** as dimeric species (Fig. 1) is mainly based on (1) their molecular weight measurements and (2) ^{89}Y NMR chemical shifts[30] (δ 191.8 ppm) for the derivative **Va**, in which each yttrium atom is surrounded by six oxygens. Interestingly, the ^{80}Y NMR spectrum of $[Y\{Al(OPr^i)_4\}_3]$, for which an octahedral geometry has been suggested on the basis of molecular weight measurements and ^1H NMR studies, exhibits a single sharp peak at δ 192.18 ppm.

The appearance of a single peak at δ 256.87 ppm in the ^{89}Y NMR spectrum of **IIa** is interpretable in terms of the lower electronegativity of Cl (3.0) compared with that (3.5) of O, causing a deshielding effect.

Further, it is interesting to note that (1) the ^1H NMR spectral studies of almost all the products indicate fast exchange (on the NMR time-scale) between bridging and terminal isopropoxy groups; (2) in agreement with the structural formulation depicted in the preceding account, the products **I**, **II**, **IIa**, **IVa**, **IVb**, **Va**, **Vb**, **Vc** and **Vd** exhibit rather broad ^{27}Al NMR signals centred respectively at δ 70.18, 75.15, 66.70, 75.00, 75.50, 80.86, 66.10, 56.05 and 58.58 ppm, characteristic of four-coordinated aluminium(III) species,[31–33] which is the form generally adopted by the $\{Al(OPr^i)_4\}^-$ ligand, as shown in the structures of $Al\{Al(OPr^i)_4\}_3$,[34,35] $\{C_6H_{11}NH_3\}^+\{Al(OPr^i)_4\}^-$[36] and $[\{Pr\{Al(OPr^i)_4\}_2(\mu\text{-}Cl)(Pr^iOH)\}_2]^2$; and (3) the labile nature of solvated products is in agreement with the tendency of yttrium(III) to attain an octahedral environment of the monodentate oxygen ligand.[37–40].

Attention may be finally drawn towards rather a novel dimension depicted in the extraordinary stability of volatile bi- and trimetallic alkoxide derivatives, which appear to involve chlorine/alkoxy bridges (without any metal–metal bonds, often characteristic of polymetal systems).

Acknowledgements—We (RCM & AS) thank the DST, New Delhi, for support of this work. We are grateful to Prof. C. L. Khetrapal, Indian Institute of Science, Bangalore, for his valuable assistance in connection with ^{89}Y NMR studies. We would also like to acknowledge the technical assistance of Mr Suman Gupta in recording ^{89}Y NMR spectra. UMT acknowledges the UGC, New Delhi, and the Rajasthan Government for providing JRF under the Special Assistance Programme.

REFERENCES

1. U. M. Tripathi, A. Singh and R. C. Mehrotra, *Polyhedron* 1991, **10**, 949.
2. U. M. Tripathi, A. Singh, R. C. Mehrotra, S. C. Goel, M. Chiang and W. E. Buhro, *J. Chem. Soc., Chem. Commun.* 1992, 152.
3. R. C. Mehrotra, A. Singh and U. M. Tripathi, *Chem. Rev.* 1991, **92**, 1287.
4. R. C. Mehrotra, P. N. Kapoor and J. M. Batwara, *Coord. Chem. Rev.* 1980, **31**, 67.
5. G. Kordas, *J. Non-Cryst. Solids* 1990, **21**, 436.
6. P. Catania, N. Novnanian, L. Cot, M. Pham Thi, R. Kormann and J. P. Ganne, *Mater. Res. Bull.* 1990, **25**, 631.
7. E. A. Hayri, M. Greenblatt, K. V. Ramanujachary, M. Nagano, J. Oliver, M. J. Miceli and R. Gerhart, *J. Mater. Res.* 1989, **4**, 1099.
8. H. S. Horowitz, S. J. McLain, A. W. Sleight, J. D. Drulinger, P. L. Gai, M. J. Van Kavelaar, J. L. Wangner, B. D. Biggs and S. J. Poon, *Science* 1989, **243**, 66.
9. S. Hirano, T. Hayashi, M. Miura and H. Tomonaga, *Bull. Chem. Soc. Japan* 1989, **62**, 688.
10. H. Zheng and J. D. Mackenzie, *Mater. Lett.* 1988, **7**, 182.
11. S. Shibata, T. Kitagawa, H. Okazake and T. Kimura, *Japan J. Appl. Phys.* 1988, **27**, L646.
12. M. R. Scozzafava, W. E. Rhine and M. J. Cima, *Better Ceramics Through Chemistry* 4, *Mater. Res. Soc. Symp. Proc.* 1990, **180**, 677.
13. K. Kani, M. Awano, Y. Kodama and H. Takagi, *Ceram. Trans.* 1991, **22**, 561.
14. S. C. Goel, K. S. Kramer, P. C. Gibbons and W. E. Buhro, *Inorg. Chem.* 1989, **28**, 3619.
15. R. C. Mehrotra, *Chemtracts* 1990, **2**, 389.
16. R. C. Mehrotra, M. M. Agrawal and A. Mehrotra, *Synth. React. Inorg. Met.-Org. Chem.* 1973, **3**, 181.
17. O. Poncelet, W. J. Sartain, L. G. Hubert-Pfalzgraf, K. Folting and K. G. Caulton, *Inorg. Chem.* 1989, **28**, 263; D. C. Bradley, H. Chudzynska, D. M. Frigo, M. E. Hammond, M. B. Hursthouse and M. A. Mazid, *Polyhedron* 1990, **9**, 719.
18. For comments on oxide–alkoxide formation, see W. J. Evans, M. S. Sollberger, J. L. Shreeve, J. M. Olofson, J. H. Hain Jr and J. W. Ziller, *Inorg. Chem.* 1992, **31**, 2492 and refs therein.
19. R. C. Mehrotra, *Chemtracts* 1990, **2**, 143.
20. G. Helgesson, S. Jagner, O. Poncelet and L. G. Hubert-Pfalzgraf, *Polyhedron* 1991, **10**, 1559.
21. A. Mehrotra, PhD Thesis, University of Rajasthan, Jaipur (1971).
22. D. C. Bradley, R. C. Mehrotra and W. Wardlaw, *J. Chem. Soc.* 1952, 2027.
23. L. M. Brown and K. S. Mazdiyasni, *Inorg. Chem.* 1970, **9**, 2783.
24. R. C. Mehrotra, *J. Ind. Chem. Soc.* 1953, **30**, 585.
25. A. I. Vogel, *Text Book of Quantitative Inorganic Analysis*. Longman, London (1978).
26. H. C. Aspinall, D. C. Bradley, M. B. Hursthouse, K.

D. Sales, N. P. C. Walker and B. Hussain, *J. Chem. Soc., Dalton Trans.* 1989, 623.
27. C. G. Barraclough, D. C. Bradley, J. Lewis and I. M. Thomas, *J. Chem. Soc.* 1961, 2601.
28. P. S. Coan, L. G. Hubert-Pfalzgraf and K. G. Caulton, *Inorg. Chem.* 1972, **31**, 1262.
29. U. D. Tripathi, PhD Thesis, University of Rajasthan, Jaipur, India (1971).
30. P. S. Coan, L. G. Hubert-Pfalzgraf and K. G. Caulton, *Inorg. Chem.* 1992, **31**, 1262.
31. J. W. Akitt and A. Farthing, *J. Chem. Soc., Dalton Trans.* 1981, 1615.
32. J. W. Akitt and A. Farthing, *J. Chem. Soc., Dalton Trans.* 1981, 1624.
33. J. W. Akitt and G. Gessnev, *J. Chem. Soc., Dalton Trans.* 1984, 147.
34. N. Ya. Turova, V. A. Kozunov, A. I. Yanovskii, N. G. Bokil, Yu. T. Struchkov and B. L. Tarnopolskii, *J. Inorg. Nucl. Chem.* 1978, **41**, 5.
35. K. Folting, W. E. Streib, K. G. Caulton, O. Poncelet and L. G. Hubert-Pfalzgraf, *Polyhedron* 1991, **10**, 1639.
36. B. Beagley, K. Jones, P. Parkes and R. S. Pritchard, *Synth. React. Inorg. Met.-Org. Chem.* 1988, **18**, 465.
37. W. J. Evans, J. M. Olofson and J. W. Ziller, *Inorg. Chem.* 1989, **28**, 4308.
38. M. J. McGeary, P. S. Coam, K. Folting, W. E. Streib and K. G. Caulton, *Inorg. Chem.* 1989, **28**, 3283.
39. W. J. Evans, M. S. Sollberger and T. P. Hanusa, *J. Am. Chem. Soc.* 1988, **110**, 1841.
40. W. J. Evans, J. M. Olofson and J. W. Ziller, *J. Am. Chem. Soc.* 1990, **112**, 2308.

Polyhedron Vol. 12, No. 15, pp. 1953–1955, 1993
Printed in Great Britain

0277–5387/93 $6.00+.00
© 1993 Pergamon Press Ltd

COMMUNICATION

POLYPYRAZOLYLBORATE DERIVATIVES OF THE LANTHANIDES. THE SYNTHESES OF OXIDATION STATE(II) COMPLEXES

MICHAEL A. J. MOSS, ROMAN A. KRESINSKI* and CHRISTOPHER J. JONES†

School of Chemistry, The University of Birmingham, Edgbaston, Birmingham B15 2TT, U.K.

and

WILLIAM J. EVANS

Department of Chemistry, University of California, Irvine, CA 92717, U.S.A.

(*Received* 20 *April* 1993; *accepted* 27 *April* 1993)

Abstract—Air-sensitive bivalent europium, samarium and ytterbium complexes have been prepared with the hydrotrispyrazolylborate and hydrotris(3,5-dimethyl-pyrazolyl)borate ligands and some reactions with CO, propene and $(Me_2NCS_2)_2$ investigated.

Since the first homoleptic polypyrazolylborate complexes $[Ln\{HBpz_3\}_3]$ [Ln = Y, La, Ce, Pr, Sm, Gd, Er, Yb, Lu; $HBpz_3$ = hydrotris(pyrazol-1-yl)borate] were reported by Bagnall and Takats,[1] a variety of compounds of the general formula $[Ln\{HBpz_3\}_2X]$ (X = a bidentate monoanionic chelating ligand) have been reported.[2–11] All of these compounds contain lanthanide ions in the tervalent state and some provide analogues of corresponding complexes containing cyclopentadienyl or pentamethylcyclopentadienyl ligands in place of $HBpz_3$.[12–16] However, the sterically demanding nature of $HBpz_3$ tends to produce monomeric species rather than the dimers or oligomers often obtained with the cyclopentadienyl ligands. A consideration of steric angle factors indicates that tridentate $HBpz_3$ is more sterically demanding than C_5Me_5.[8] This suggests that $HBpz_3$ would be a suitable ligand for the bivalent state lanthanide ions since it should be more effective than C_5Me_5 in achieving steric saturation in complexes of 2:1 ligand:metal stoichiometry. Thus, analogues of $[Sm(\eta^5\text{-}C_5Me_5)_2(THF)_2]$[17,18] and $[YB(\eta^5\text{-}C_5Me_5)_2(THF)]$[19] might be obtained using $HBpz_3^-$ or $HB(Me_2pz)_3^-$ in place of $C_5Me_5^-$. Three of the lanthanide elements have accessible bivalent states, samarium, europium and ytterbium.[20] Bivalent lanthanide complexes are generally highly air-sensitive; the most stable being the europium complexes, which are water stable in some cases. The diiodides LnI_2 (Ln = Sm, Yb) offer a convenient starting material for the synthesis of bivalent complexes.[21] They are soluble in THF and are readily formed by the reaction of the metallic element (Sm or Yb) with 1,2-diiodoethane.

The reaction between LnX_2 (Ln = Sm, Yb, X = I; Ln = Eu, X = Cl) and $K\{HBpz_3\}$ in a 2:1 molar ratio in THF leads to the formation of soluble brown, red and yellow complexes containing samarium, ytterbium and europium, respectively. The yellow europium complex was also prepared in aqueous media by the reaction of Eu^{2+} ions, gen-

*Present address: School of Science, Staffordshire University, College Road, Stoke on Trent, Staffordshire ST4 2DE, U.K.

† Author to whom correspondence should be addressed.

erated *in situ* from Eu^{3+} with amalgamated zinc, with $K\{HBpz_3\}$. However, the reaction product was unstable in acidic water and could not be isolated using this approach. As with their pentamethylcyclopentadienyl-containing counterparts, these complexes are all extremely air-sensitive.

The ^1H NMR spectrum of the samarium(II) complex contains signals attributable to coordinated THF. In addition, there are three singlets of area ratio 1:1:1 at δ_{TMS} 11.71, 4.10 and 0.09 ppm, attributable to the $HBpz_3$ ligands which are undergoing rapid exchange. The mass spectrum of this compound contains a molecular ion for $[Sm\{HBpz_3\}_2]^+$ as the most intense peak; other fragment ions observed correspond to $[Sm\{HBpz_3\}pz]^+$ (80%), $[Sm\{HBpz_3\}]^+$ (9%) and $[Smpz_2]^+$ (45%). The ^1H NMR spectrum of the red complex containing the diamagnetic ($4f^{14}$) ytterbium(II) ion exhibits three pyrazolyl resonances of equal area at δ_{TMS} 7.75(d), 7.40(d) and 6.09(t) ppm. The mass spectrum contains the molecular ion for $[Yb\{HBpz_3\}_2]^+$ at 28% of the intensity of the most intense ion, $(pzH)^+$. Other fragments observed correspond to $[Yb\{HBpz_3\}pz]^+$ (37%), $[Yb\{HBpz_3\}]^+$ (8%), $[Ybpz_2]^+$ (10%) and $[Ybpz]^+$ (7%). This compound could also be prepared from the direct reaction of the known complex $Yb\{HB(pz)_3\}_3$ with ytterbium metal in THF. The orange europium(II) complex could not be studied by ^1H NMR because of the highly paramagnetic nature of the $4f^7$ Eu^{2+} ion.

The IR spectra for the samarium(II) and europium(II) complexes are virtually identical suggesting that, like the samarium compound, the europium complex contains coordinated THF. The IR spectrum of the ytterbium compound is similar to those of the samarium and europium compounds, but shows slight differences which may be attributed to the absence of coordinated THF. All of the compounds exhibit ν(BH) at 2440 cm^{-1} and ν(CN) at 1500 cm^{-1}.

The reaction of LnX_2 (Ln = Sm, Yb, X = I; Ln = Eu, X = Cl) with $K\{HB(Me_2pz)_3\}$ [potassium hydrotris(3,5-dimethylpyrazolyl)borate] in a 1:2 molar ratio in THF affords air-sensitive, insoluble purple complexes for samarium and ytterbium and an insoluble orange complex for europium. The IR spectrum of all three solids contains a B—H stretching band at 2530 cm^{-1} and other characteristic ligand bands. These insoluble complexes are intimately mixed with alkali metal halide, but can be purified by sublimation at 200°C under dynamic high vacuum (10^{-6} Torr = 1.3×10^{-4} Nm^{-2}). However, attempts to prepare crystals of $[Sm\{HB(Me_2pz)_3\}_2]$ by heating at 200°C in a sealed evacuated (5×10^{-7} Torr = 7×10^{-5} Nm^{-2}) tube led to the formation of a green melt after 6 h. The orange europium complex can also be prepared from the reaction between $HB(Me_2pz)_3^-$ and Eu^{2+} in water, the orange precipitate being obtained free from alkali metal halide impurities.

In view of the novel reactivity observed[22–26] for the bispentamethylcyclopentadienyl samarium(II) complexes we were interested in determining whether a similar reactivity might be associated with the polypyrazolylborate lanthanide(II) complexes. However, we have not so far succeeded in establishing this. Unlike $[(\eta^5\text{-}C_5Me_5)_2Sm(THF)_2]$[22] a suspension of the samarium(II) trispyrazolylborate complex in toluene does not react with carbon monoxide at 6 atm. In an attempt to prepare a heteroleptic allyl complex, again following the precedent of $[(\eta^5\text{-}C_5Me_5)_2Sm(THF)_2]$,[27] it was found that both the samarium(II) and ytterbium(II) trispyrazolylborate complexes react with propene at 2.7 atm. and 20°C to give the insoluble $[Sm\{HBpz_3\}_3]$ and the soluble $[Yb\{HBpz_3\}_3]$, respectively, as the only characterizable products. In a similar reaction, performed in an attempt to demonstrate their reducing power, these bivalent complexes were reacted with $(Me_2NCS)_2S_2$ in THF. However, again $[Ln\{HBpz_3\}_3]$ (Ln = Sm, Yb) were isolated as the only characterizable products. This failure to establish a parallel to the chemistry of the pentamethylcyclopentadienyl complexes may reflect the relative thermodynamic stability of $[Ln\{HBpz_3\}_3]$ (Ln = Sm, Yb), which can be formed by ligand exchange reactions following oxidation of the oxidation state(II) complex.

Acknowledgements—We are grateful to the SERC and BP Chemicals for support (to M.A.J.M.) and to NATO for the provision of travel grant No. 175/84.

REFERENCES

1. K. W. Bagnall, A. C. Tempest, J. Takats and A. P. Masino, *Inorg. Nucl. Chem. Lett.* 1976, **12**, 555.
2. M. V. R. Stainer and J. Takats, *Inorg. Chem.* 1982, **21**, 4050.
3. M. A. J. Moss and C. J. Jones, Abstracts of the XXIV International Conference on Coordination Chemistry, Chimika Chronika, Association of Greek Chemists, A7-488 (1986).
4. D. L. Reger, J. A. Lindeman and L. Lebioda, *Inorg. Chim. Acta* 1987, **139**, 71.
5. M. A. J. Moss, C. J. Jones and A. J. Edwards, *Polyhedron* 1988, **7**, 79.
6. M. A. J. Moss and C. J. Jones, *Polyhedron* 1989, **8**, 117.

7. M. A. J. Moss and C. J. Jones, *Polyhedron* 1989, **8**, 555.
8. M. A. J. Moss, C. J. Jones and A. J. Edwards, *J. Chem. Soc., Dalton Trans.* 1989, 1393.
9. M. A. J. Moss and C. J. Jones, *J. Chem. Soc., Dalton Trans.* 1990, 581.
10. M. A. J. Moss and C. J. Jones, *Polyhedron* 1989, **8**, 2367.
11. M. A. J. Moss and C. J. Jones, *Polyhedron* 1990, **9**, 697.
12. R. S. Coutts and P. C. Wailes, *J. Organomet. Chem.* 1970, **25**, 117.
13. G. B. Deacon, G. D. Fallon, P. I. MacKinnon, R. H. Newnham, G. N. Pain, T. D. Tuong and D. L. Wilkinson, *J. Organomet. Chem.* 1984, **277**, C2.
14. T. D. Tilley, R. A. Andersen, A. Zalkin and D. H. Templeton, *Inorg. Chem.* 1982, **21**, 2644.
15. Z. Ye, Z. Zhou, S. Yuan and Z. Luo, *Youji Huaxue* 1984, 119; *Chem. Abstr.* 1984, **101**, 130815.
16. E. C. Baker, PhD Thesis, University of California, Berkeley (1977).
17. W. J. Evans, I. Bloom, W. E. Hunter and J. L. Atwood, *J. Am. Chem. Soc.* 1981, **103**, 6507.
18. W. J. Evans, L. A. Hughes and T. P. Hanusa, *J. Am. Chem. Soc.* 1984, **106**, 4270.
19. T. D. Tilley, R. A. Andersen, B. Spencer, F. L. Ruben, A. Zalkin and D. H. Templeton, *Inorg. Chem.* 1980, **19**, 2999.
20. L. R. Morse, *Chem. Rev.* 1976, **76**, 827.
21. J. L. Namy, P. Girard and H. B. Kagan, *Nouv. J. Chim.* 1981, **5**, 479.
22. M. J. Evans, J. W. Grate, L. A. Hughes, H. Zhang and J. L. Atwood, *J. Am. Chem. Soc.* 1985, **107**, 3728.
23. W. J. Evans, I. Bloom, W. E. Hunter and J. L. Atwood, *J. Am. Chem. Soc.* 1983, **105**, 1401.
24. W. J. Evans, L. A. Hughes, D. K. Drummond, H. Zhang and J. L. Atwood, *J. Am. Chem. Soc.* 1986, **108**, 1722.
25. W. J. Evans, D. K. Drummond, S. G. Bott and J. L. Atwood, *Organometallics* 1986, **5**, 2389.
26. W. J. Evans and D. K. Drummond, *J. Am. Chem. Soc.* 1986, **108**, 7440.
27. W. J. Evans, T. A. Ulibarri and J. W. Ziller, *J. Am. Chem. Soc.* 1990, **112**, 2314.

Polyhedron Vol. 12, No. 15, p. 1957, 1993
Pergamon Press Ltd. Printed in Great Britain

BOOK REVIEW

Electron Paramagnetic Resonance of *d* Transition Metal Complexes. By F. E. Mabbs and D. Collison. (Studies in Inorganic Chemistry, Vol. 16). Elsevier, Amsterdam, 1992 (obtainable in U.S.A./Canada from Elsevier, PO Box 882, Madison Square Station, NY 10159). ISBN 0-444-89852-2, xx + 1326 pp., $622/Dfl995.

EPR can be a very powerful technique for the study of paramagnetic transition metal compounds but, as the authors remark in their introduction, existing texts on EPR fall between the two stools of concentrating on free radicals (the majority) or treating the subject at an advanced level (e.g. Griffith, Abragam and Bleaney). This book is an attempt to produce a text that bridges that gap.

The early chapters are devoted to introducing the reader to basic EPR concepts; thus, the first nine (of 18) chapters only deal with $S = 1/2$ systems. Chapters 1 and 2, indeed, are concerned with the basics of the EPR experiment together with logistical problems, such as observing signals, sample handling, effect of spectrometer frequency and showing the reader ways of obtaining g values from powder and frozen solution spectra. The "hard bits" begin with Chapter 3, introducing the concept of the spin-Hamiltonian and the use of perturbation theory, subsequently discussing some simple single-crystal spectra; the ensuing chapters bring in the concept of nuclear hyperfine interaction, treated qualitatively then quantitatively, followed by quadrupole and Zeeman effects. Throughout the book lavish use is made of illustrative spectra, both "real" and simulations; this is a real strength of the book and their use will be a real help in the interpretation of spectra to any non-specialist. Chapter 7 goes into considerable detail in discussing simulation methods, including a worked example showing how matches between real and simulated spectra can be achieved (demonstrating the importance, even for an $S = 1/2$ system, of working at more than one frequency). Several groups' simulation techniques are discussed.

The second part of the book begins with a brief résumé of crystal field theory and then goes on to relate electronic structure to the spin-Hamiltonian parameters for $S = 1/2$ systems, including cases such as low-spin iron(III) and cobalt(II) as well as the more usual examples of copper(II) and titanium(III).

From Chapter 10 onwards the book discusses the less familiar systems with $S > 1/2$. Individual chapters are devoted to $S = 1$, $S = 3/2$, $S = 2$ and $S = 5/2$ cases, with plenty of simulated spectra shown at the end of each chapter showing how spectra vary with changes to the Hamiltonian parameters D and λ, as well as temperature, and the very useful frequency independent resonance (FIR) diagrams where resonance positions are shown as graphs of D against magnetic field; these enable approximate choices of D and λ to be made as preliminaries to accurate fitting.

Chapter 15 examines polynuclear complexes (including a limited number of simulated spectra for $S > 5/2$), whilst Chapter 16 goes through how to simulate spectra for the cases where $S > 1/2$. These are most valuable, for example, for $S = 5/2$ systems in those cases where the zero-field splitting is comparable to $h\nu$, as the observed spectrum is very sensitive to factors like the spin-Hamiltonian parameters. (Here the caveat is that at present computation times, even on a mainframe computer, can apparently run to hours in these "difficult" cases, in contrast to the situations where $D \gg h\nu$, often computable on a PC.) The book does not neglect factors like off-axis turning points, "forbidden" transitions, D- and A-strain. Chapter 17 looks at the effect of extended electron exchange on spectra, whilst Chapter 18 considers the factors responsible for line broadening in solids and solutions. The book is completed by useful appendices listing properties of solvents, physical constants and conversion factors, isotopic spins and abundances, mathematical relationships and expanded FIR diagrams. There are very thorough subject and chemical indexes.

Transition-metal EPR represents one of the "hard bits" of inorganic chemistry. The book is not intended as a guide to the literature of transition metal EPR, although plenty of references to the primary literature are given with, very commendably, a number of 1992 references. Misprints seem very few [e.g. J. S. Griffiths on p. 337, oxovanadium(V) on p. 438]. The immense number of simulated spectra make the book tremendously valuable for this alone (particularly with the cost of computing some of these). This book should go to a second edition, so here are some suggestions for inclusion! Although the concept of determining the sign of D is set out, it would have been nice to see the mathematical principles elucidated, with a real example. Likewise, I missed seeing an example of the application of EPR to spin-equilibrium situations. There are some of the conventional scatter plots of g vs A for ions like vanadyl and copper(II) indicating the dependence of g and A on ligand donor atoms, as well as a table of g values for low-spin d^5, but I think that a rather greater amount of tabulated data, for example, spin-Hamiltonian parameters for high-spin chromium(III) and iron(III), would have been valuable (although it may seem unfair to cavil with a book of over 1300 pages, collecting some data in a further appendix would have been very useful).

This work should be a *sine qua non* for inorganic chemistry departments, although the price will give librarians some sleepless nights.

Felixstowe College **SIMON COTTON**
Maybush Lane
Felixstowe
Suffolk IP11 7NQ, U.K.

Polyhedron Vol. 12, No. 16, pp. 1959–1966, 1993
Printed in Great Britain

0277–5387/93 $6.00+.00
© 1993 Pergamon Press Ltd

SYNTHESIS AND REACTIVITY OF BIS-4-PYRONE AND BIS-4-PYRIDINONE DICHLOROTIN(IV) COMPOUNDS

J. BURGESS* and S. A. PARSONS

Department of Chemistry, University of Leicester, Leicester LE1 7RH, U.K.

(*Received* 20 *April* 1993; *accepted* 30 *April* 1993)

Abstract—A number of tin(IV) complexes, $Sn(LL)_2X_2$, have been prepared in which LL is a 4-pyronate or 4-pyridinonate ligand and X is chloride or alkoxide. UV–vis, IR and NMR (^1H, ^{13}C, ^{119}Sn) spectra are reported for these complexes. Reactivities have been established through kinetic studies of nucleophilic substitution in acetonitrile solution. Ligand effects on spectra and reactivity are discussed and compared with those for similar metal(IV) complexes, especially of titanium.

The pyrones kojic acid (**1**) and maltol (**2**) are naturally occurring ligands. Maltol was first isolated from larch bark; kojic acid is derived from bacterial fermentation of carbohydrates, for instance of starch by *Aspergillus oryzae*.[1] Maltol (**2**) and ethylmaltol (**3**) are permitted food additives (E636 and E637) used in the baking industry. They are thus attractive ligands for use either in controlling metal ion concentrations in the human body, or for the introduction of appropriate isotopes for diagnosis or therapy.[2] In practice the closely related 4-pyridinones (e.g. **4**–**6**) are proving more suitable,[3] both since they form significantly more stable complexes and also since, with two variable groups R and R′, they can be tailored more readily than the pyrones.[4] Almost all present and potential applications involve the tris-ligand complexes of metal(III) cations, as for example in the administration of iron(III) complexes for the treatment of anaemia, the use of the ligand L1 (**4**) in clinical trials for dealing with iron overload in thalassaemia[3] and the proposal to use such ligands in the control of aluminium levels in the hope that the progress of senile dementias might at least be slowed.[5] Ligands of these types may also prove of value for the introduction of, for instance, complexes containing gadolinium(III) to act as contrast-enhancing agents in magnetic resonance imaging (MRI)[6] or $^{90}Y^{3+}$ for tumour targetting and destructive irradiation.[7] The most recent application of promise involves vanadium(IV), with the bis-maltolato complex $VO(malt)_2$ claimed to be of value in the treatment of diabetes.[8] In all these applications one of the biggest attractions is the possibility of oral administration.

Several β-diketone complexes of metal(IV) ions of the $M(\beta\text{-dik})_2X_2$ type have shown promise as anti-tumour agents.[9] In particular the benzoylacetonate (bzac) (**7**) compound $Ti(bzac)_2(OEt)_2$, budotitane, is showing considerable promise in the treatment of colon cancers.[10] A number of tin(IV) compounds,[11,12] including the dibenzoylmethanato complex $Sn(bzbz)_2Cl_2$,[13] have also shown some promise in this respect. We therefore felt that synthesis and study of a series of tin(IV) compounds, $Sn(LL)_2X_2$, with LL = a pyronate or pyridinonate ligand [known to form stable complexes, $Si(LL)_3^+$, with silicon[14]] and X = halide or alkoxide, would be interesting and possibly provide one or more compounds of pharmacological value. A further matter of interest to us was the kinetic behaviour of this type of complex, for which rather little information appears to be available. There is rate constant, activation parameter ($\Delta H^\ddagger$, $\Delta S^\ddagger$, $\Delta V^\ddagger$) and solvent effect information on racemization of $Ge(acac)_3^+$ (acacH = acetylacetone = pentane-2,4-dione, **8**)[15] and some kinetic information on intramolecular rearrangements within $Sn(\beta\text{-diketonate})_2Cl_2$ complexes,[16–18] but very little on kinetics of ligand replacement. For tin the only such data appear to be a few results on the relatively slow chloride exchange at $Sn(acac)_2Cl_2$ in chloroform[19] and kinetic parameters for hydrolysis of six dihalogenotin(IV) β-diketonates.[20]

* Author to whom correspondence should be addressed.

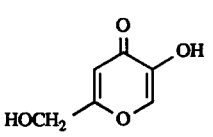

1 kojH

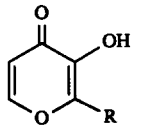

2 R=Me, memaltH
3 R=Et, etmaltH

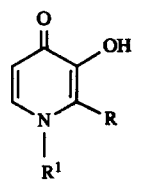

4 R=R¹=Me, dmppH
5 R=Et, R¹=Me, emppH
6 R=R¹=Et, deppH

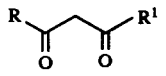

7 R=Me, R¹=Ph, bzacH
8 R=R¹=Me, acacH

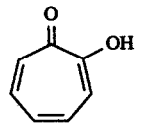

9 tropH

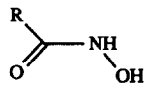

10 R=Me, ahaH
11 R=4MeC$_6$H$_4$, mbzH

We have, therefore, prepared a number of complexes of the $Sn(LL)_2Cl_2$ type, with LL = 4-pyronate or 4-pyridinonate, and characterized them, particularly by NMR and IR spectroscopy. We have also measured rates of ligand replacement in a range of conditions. We report our results here and discuss them in relation to other complexes, particularly of similar bidentate ligands such as β-diketonates (e.g. **7** and **8**), tropolonate (**9**) and hydroxamates (**10** and **11**).

EXPERIMENTAL

Preparation of complexes

The ethylmaltolate complex $Sn(etmalt)_2Cl_2$ was prepared from tin tetrachloride. Ethylmaltol (2.8 g, 0.02 mol) was dissolved in anhydrous acetone at room temperature. $SnCl_4$ (2.6 g, 0.01 mol) was added dropwise with stirring. The solution was refluxed for 30 min during which time a white precipitate formed. This was filtered and washed with diethyl ether. The crude product was recrystallized from dichloromethane/40–60 petroleum ether, to give 3.4 g of white crystals (85% yield). All the other complexes were prepared in an analogous manner. Their melting points, CHN analyses and UV–vis absorption maxima are given in Table 1, IR frequencies in Tables 2 and 3 and NMR data in Table 4.

Apparatus and techniques

IR spectra were obtained using Nujol mulls on a Perkin–Elmer FTIR instrument, NMR spectra on a Bruker AM300 and UV-vis spectra on a Pye–

Table 1. Melting points, wavelengths of maximum absorption and CHN microanalyses for compounds $Sn(LL)_2Cl_2$

Compound	λ_{max} (nm)	M.p. (°C)	(Calc.) Found (%) C	H	N
$Sn(etmalt)_2Cl_2$	337	142	(36.1) 37.0	(3.0) 3.1	
$Sn(memalt)_2Cl_2$	341	138	(27.0) 27.5	(2.3) 2.3	
$Sn(aha)_2Cl_2$	337	liq			
$Sn(mbz)_2Cl_2$	311	180[a]	(39.1) 38.7	(3.3) 3.3	(5.7) 5.4
$Sn(trop)_2Cl_2$	348	201	(36.1) 36.7	(3.7) 2.4	
$Sn(depp)_2Cl_2$	319	249[a]	(36.6) 36.0	(4.0) 4.0	(3.8) 3.4
$Sn(empp)_2Cl_2$	351	238	(36.5) 36.8	(3.8) 4.0	(5.3) 5.2
$Sn(dmpp)_2Cl_2$	360	258	(37.8) 37.3	(3.7) 4.0	(5.8) 5.8

[a] Decomposed.

Table 2. IR data for compounds $Sn(LL)_2Cl_2$

Compound	ν(C—O) ν(C—R)	σ(C—H)	σ(ring)	ν(C—R)	π(C—H)	ν(C—R)	ν(M—O)	ν(M—X)
$Sn(etmalt)_2Cl_2$	1604	1331	1261	1044	844	722	540	390
	1548			942	824		480	338
	1504							
$Sn(memalt)_2Cl_2$	1558	1322	1263	1027	842	720	538	385
	1540		1185				459	330
	1506							
$Sn(aha)_2Cl_2$	1616	1339		1093	810	722	540	370
	1520						458	
	1456							
$Sn(mbz)_2Cl_2$	1611	1401	1197	1085	830	721	542	
	1570						450	
$Sn(trop)_2Cl_2$	1558	1338	1261	1016	801	722	540	340
	1540						427	328
	1506							
$Sn(depp)_2Cl_2$	1607	1327	1237	1034	846	722	539	340
	1564			942			481	295
	1511							
$Sn(empp)_2Cl_2$	1609	1332	1253	1030	845	722	539	360
	1549				820		480	345
	1511							
$Sn(dmpp)_2Cl_2$	1575	1351	1260	1020			541	330
	1558						495	285
	1506							

Unicam SP1800. This last instrument, which was equipped with a thermostatted cell holder and PC for data analysis, was also used for the kinetic measurements.

RESULTS AND DISCUSSION

In all cases the product obtained was *cis*-bis-pyronato- or bis-pyridinato-dichlorotin(IV), as was clear from analysis (see above) and from IR and NMR spectroscopy (see below). In the case of the ethylmaltol (**3**) derivative a crystal of product of suitable quality for X-ray structural determination[21] was obtained. This was confirmed to be the expected *cis*-dichloro isomer, with its unsymmetrical bidentate ligands disposed as shown in **12**.

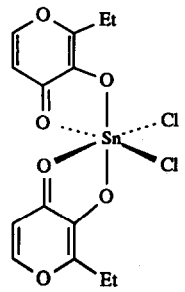

12

IR spectroscopy

IR frequencies and their assignments are given in Table 2, while tin–chloride stretching frequencies for these and a number of related complexes are

Table 3. Tin(IV)–chloride stretching frequencies

	ν(Sn—Cl) (cm^{-1})		ν(Sn—Cl) (cm^{-1})	Ref.
$Sn(etmalt)_2Cl_2$	390, 338	$Sn(koj)_2Cl_2$	336, 331(sh)	22
$Sn(memalt)_2Cl_2$	385, 330	$Sn(acac)_2Cl_2$	334, 264	16, 18, 23
$Sn(aha)_2Cl_2$	370	$Sn(bzac)_2Cl_2$	336, 314	13
$Sn(trop)_2Cl_2$	339, 328	$Sn(bzbz)_2Cl_2$	347, 334	13
$Sn(depp)_2Cl_2$	345, 295	$Sn(cp)_2Cl_2$	358, 336	24
$Sn(empp)_2Cl_2$	340, 295	$SnCl_6^{2-}$	300	25
$Sn(dmpp)_2Cl_2$	330, 285			

Table 4. NMR data for compounds $Sn(LL)_2Cl_2$

Compound	^1H NMR (ppm)	^{13}C NMR (ppm)	^{119}Sn NMR (ppm)	$J(^{119}Sn—^{13}C)$ (Hz)
$Sn(etmalt)_2Cl_2$	H_a 8.1, 7.9, H_b 6.9, 6.7, H_c 2.9, H_d 1.4 $CDCl_3$	C^1 10.6, C^2 22.7, C^3 146.1, C^4 160.9, C^5 172.3, C^6 110.0, C^7 155.9	−467.71 (3) −473.33 (1)	$^2J(Sn—C^5)$ 23.0 $^3J(Sn—C^6)$ 71.4
$Sn(memalt)_2Cl_2$	H_a 8.1, H_b 6.9, H_c 2.6 d^6 acetone		−465.51 (3) −471.62 (1)	
$Sn(aha)_2Cl_2$	H_a 4.1, H_b 6.0 d^6 acetone	C^1 17.8, C^2 165.8	−518.01 (2) −534.25 (2) −549.30 (1)	$^2J(Sn—C^1)$ 23.9 $^3J(Sn—C^2)$ 28.5
$Sn(mbz)_2Cl_2$	H_a 8.0, 7.9, H_b 7.3, H_c 2.4, H_d 5.2 d^6 acetone	C^1 21.5, C^2 128.9, C^3 128.1, C^4 130.0, C^5 130.2, C^6 130.7, C^7 143.4, C^8 168.3	−467.63 (3) −473.53 (1)	$^3J(Sn—C^7)$ 48.44
$Sn(trop)_2Cl_2$	H_a 7.4, H_b 6.8 d^6 acetone		−466.64 (3) −472.43 (1)	
$Sn(depp)_2Cl_2$	H_a 8.0, 7.9, 7.8, H_b 6.85, 6.7, H_c 3.1, H_d 1.33, He 4.4, H_f 1.55 d^6 acetone	C^1 11.1, C^2 20.6, C^3 135.8, C^4 149.5, C^5 164.7, C^6 109.2, C^7 158.1, C^8 51.5, C^9 17.5	−531.32	$^2J(Sn—C^4)$ 42.7 $^2J(Sn—C^5)$ 44.5 $^3J(Sn—C^6)$ 70.7 $^3J(Sn—C^3)$ 48.9
$Sn(empp)_2Cl_2$	H_a 7.7, H_b 6.65, H_c 2.9, H_d 1.3, He 3.7 d^6 acetone	C^1 11.8, C^2 20.7, C^3 136.5, C^4 149.5, C^5 164.3, C^6 109.2, C^7 140.9, C^8 43.6	−531.43	$^3J(Sn—C^6)$ 87.64 $\{^4J(Sn—H_b)$ 15$\}$
$Sn(dmpp)_2Cl_2$	H_a 7.8, H_b 6.9, H_c 3.0, H_d 1.2, He 4.0 d^6 acetone		−520.22	

collected together in Table 3.[22–25] In all cases, except for the broad band observed for the acethydroxamate complex and the single Sn—Cl stretch for $SnCl_6^{2-}$, two distinct bands assignable to ν(Sn—Cl) in *cis* geometry are found. The ν(Sn—Cl) for our complexes are similar to those for Sn(β-diketonate)$_2Cl_2$ and indeed for $Sn(cp)_2Cl_2$ and $SnCl_6^{2-}$, as is clear from the following order of mean ν(Sn—Cl) values (pyrone and pyridinone complexes in bold type) for complexes $Sn(LL)_2Cl_2$:

aha > **etmalt** > **memalt** > cp > bzbz > **koj** =

trop > bzac > **depp** > **empp** > acac > **dmpp**.

The more weakly bonding pyronate ligands produce higher ν(Sn—Cl) than pyridinonates; the most strongly bonding pyridinonate, dmpp, is associated with the lowest ν(Sn—Cl). The values for the β-diketonate complexes are consistent with this sequence. These IR results are correlated with kinetic results in the appropriate section later.

Discussion of ν(Sn—O) is potentially more complicated, since the bonds in question are incorporated in chelate rings. In practice ν(Sn—O) values are identical within experimental uncertainty for all the pyrone and pyridinone complexes (Table 2; values for the kojate complex are available already[22]). There are, however, significant differences between this very short range of values for the pyrone and pyridinone complexes and the ranges characteristic of tropolonates,[26] β-diketonates[27] and 8-hydroxyquinolinates[28] in complexes $Sn(LL)_2XY$.

NMR spectroscopy

The ^1H, ^{13}C and ^{119}Sn chemical shifts are listed in Table 4, which also includes $^{119}Sn—^{13}C$ coupling constants. Very few direct comparisons with published data appear to be possible.[29] ^1H, ^{13}C and ^{119}Sn chemical shifts and coupling constants are available for one $Sn(koj)_2X_2$ compound,[22,30] but here X = methyl rather than chloride. There is only limited proton NMR information on β-diketonate complexes, Sn(β-dik)$_2X_2$.[16,18]

Kinetics and mechanism

The complexes are indefinitely stable in solution in dry acetonitrile, but addition of water, thio-

Table 5. Observed first-order rate constants for the second stage of reactions of $Sn(LL)_2Cl_2$ with nucleophiles, in acetonitrile solution at 298.2 K

Compound	Nucleophile conc:	$10^3 k_{obs}$ ($dm^3 mol^{-1} s^{-1}$) 0.0005	0.001	0.002	0.005	0.01	0.015
$Sn(etmalt)_2Cl_2$	H_2O		3.0		7.4	12.3	
$Sn(etmalt)_2Cl_2$	Pyrazine				2.8	4.4	6.3
$Sn(etmalt)_2Cl_2$	NCS^-	7.35	15.1				
$Sn(memalt)_2Cl_2$	NCS^-	6.2	12.6				
$Sn(aha)_2Cl_2$	NCS^-	3.6	5.1	9.8			
$Sn(mbz)_2Cl_2$	NCS^-		3.1	4.0	8.1	14.3	
$Sn(trop)_2Cl_2$	NCS^-		2.6		5.11	10.1	15.0
$Sn(depp)_2Cl_2$	NCS^-		2.5	2.9	5.1	9.0	14.2
$Sn(empp)_2Cl_2$	NCS^-		2.3	2.6	4.9	7.7	12.5
$Sn(dmpp)_2Cl_2$	NCS^-		1.3	1.6	2.2	3.8	4.9

cyanate, pyrazine or other potential nucleophiles results in instant reaction. Such reactions are complete within the time needed to mix solutions and run their UV–vis spectra on a conventional spectrophotometer. Thereafter, there is a much slower second reaction, occurring on a time scale appropriate for kinetic monitoring. The products of the second stage are the bis-nucleophile complexes $Sn(LL)_2(nucl)_2$; we are able to obtain rate constants for the reactions:

$$Sn(LL)_2Cl(nucl)^+ + nucl \rightarrow Sn(LL)_2(nucl)_2^{2+} + Cl^-.$$

As both reactants on the left-hand side of this equation vary with the nature of the nucleophile it is not possible to establish relative reactivities for various incoming groups in the way that we were able to do with titanium(IV) analogues.[31] We have, therefore, carried out only a few runs comparing reactivities of water, thiocyanate and pyrazine as nucleophiles and have concentrated our kinetic investigations on the effects of the nature of the non-leaving ligands LL on reactivities with one nucleophile, viz. thiocyanate.

All kinetic runs were conducted in acetonitrile solution, at 298.2 K, with the incoming nucleophile present in considerable excess over the tin compound. First-order kinetics were followed in every run; observed first-order rate constants, computed from absorbance data collected over the first 2.5 half-lives, are reported as a function of nucleophile concentration in Table 5. In each series of runs over a range of nucleophile concentrations a plot of observed rate constant against nucleophile concentration was linear, but with a positive intercept

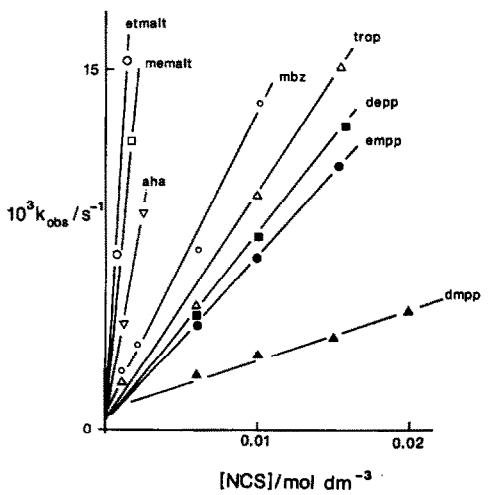

Fig. 1. Dependence of first-order rate constants on thiocyanate concentration for reactions of $Sn(LL)_2(NCS)Cl$ plus thiocyanate, in acetonitrile solution at 298.2 K.

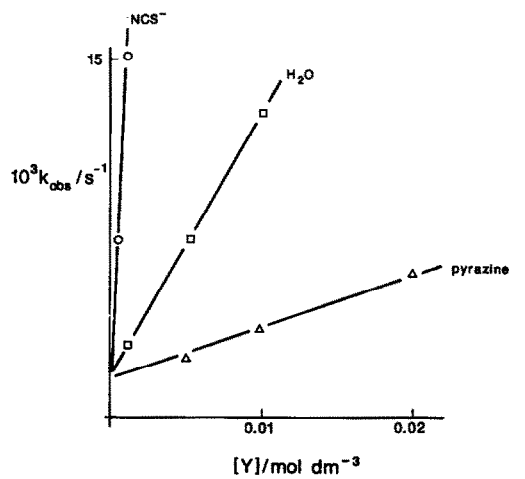

Fig. 2. Dependence of first-order rate constants on incoming nucleophile concentration for the second stage of the reactions of $Sn(etmalt)_2Cl_2$ with thiocyanate, water and pyrazine, in acetonitrile solution at 298.2 K.

Table 6. Derived first-order and second-order rate constants, with their attendant uncertainties, for the second stage of reactions of $Sn(LL)_2Cl_2$ with nucleophiles, in acetonitrile solution at 298.2 K

Compound	Nucleophile	$10^3 k_1$ (s^{-1})	σ	k_2 ($M^{-1}s^{-1}$)	σ
$Sn(etmalt)_2Cl_2$	H_2O	1.5	±0.11	1.08	±0.07
$Sn(etmalt)_2Cl_2$	Pyrazine	1.5	±0.13	0.24	±0.03
$Sn(etmalt)_2Cl_2$	NCS^-	1.6		13.3	
$Sn(memalt)_2Cl_2$	NCS^-	1.5		10.9	
$Sn(aha)_2Cl_2$	NCS^-	1.6	±0.01	4.23	±0.1
$Sn(mbz)_2Cl_2$	NCS^-	1.6	±0.08	1.25	±0.06
$Sn(trop)_2Cl_2$	NCS^-	1.4	±0.04	0.91	±0.06
$Sn(depp)_2Cl_2$	NCS^-	1.3	±0.1	0.84	±0.1
$Sn(empp)_2Cl_2$	NCS^-	1.2	±0.05	0.71	±0.02
$Sn(dmpp)_2Cl_2$	NCS^-	1.3	±0.1	0.24	±0.02

on the y (rate constant) axis:

$$k_{obs} = k_1 + k_2[\text{nucleophile}].$$

This is illustrated for the series of reactions with thiocyanate in Fig. 1 and for reaction of the ethylmaltol complex with thiocyanate, pyrazine and water in Fig. 2. Values of k_1 and k_2 are collected together, with their uncertainties, in Table 6.

All the values of k_1 (Table 6) are remarkably similar. For the series of thiocyanate reactions these rate constants correspond to solvolytic dissociation of the second chloride:

$$Sn(LL)_2(NCS)Cl + NCS^- \rightarrow Sn(LL)_2(NCS)_2 + Cl^-.$$

As the ligands LL are all two-oxygen chelators of rather similar properties, it is not unreasonable that non-leaving ligand effects on chloride loss should be small. It is rather more surprising that k_1 values for chloride loss from the three complexes Sn(etmalt)$_2$Cl(NCS), Sn(etmalt)$_2$Cl$(OH_2)^+$ and Sn(etmalt)$_2$Cl(pz)$^+$ are also so similar in value. However, a similarly small range of rate constants has recently been found for analogous titanium(IV) complexes.[31]

The relative reactivities of the series of complexes $Sn(LL)_2(NCS)Cl$ towards nucleophilic attack by thiocyanate (Fig. 1), i.e. the order of k_2 values (Table 6), is the same as that in analogous reactions of titanium(IV) complexes.[31] Indeed rate constants for nucleophilic attack at the tin and titanium complexes correlate well, as shown in Fig. 3. The slope of the correlation line in Fig. 3 is 30, indicating that

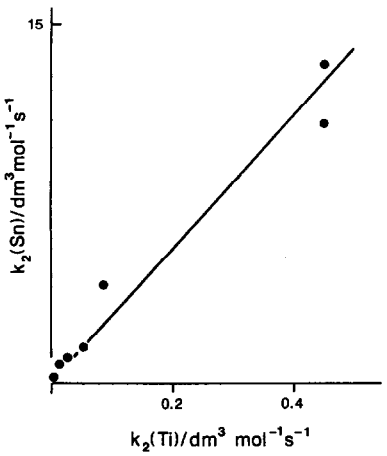

Fig. 3. Correlation of second-order rate constants for thiocyanate attack at tin(IV) and titanium(IV) complexes, $M(LL)_2(NCS)Cl$, under comparable conditions.

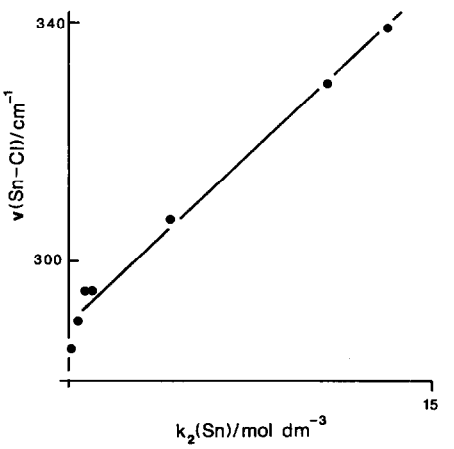

Fig. 4. Correlation of second-order rate constants for thiocyanate attack at complexes of $Sn(LL)_2(NCS)Cl$ with tin–chloride stretching frequencies for the respective complexes $Sn(LL)_2Cl_2$.

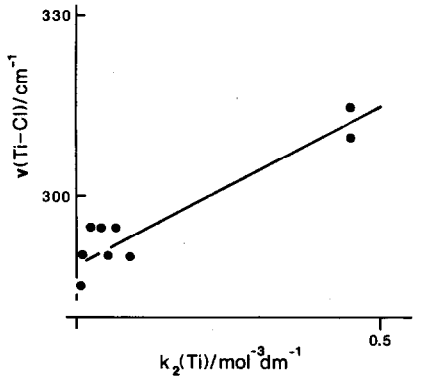

Fig. 5. Correlation of second-order rate constants for thiocyanate attack at complexes of $Ti(LL)_2(NCS)Cl$ with titanium–chloride stretching frequencies for the respective complexes $Ti(LL)_2Cl_2$.

the tin(IV) centre is considerably more reactive than titanium(IV) in this type of complex. This reactivity difference can be ascribed to the different sizes of the tin and the titanium, whose notional ionic radii in six-coordination differ by 8.5 pm, according both to the original Shannon estimates[32] (Sn 69, Ti 60.5 pm) and to the later Shannon and Prewitt values[33] (Sn 83, Ti 74.5 pm). Frazer and Haines found that second-order rate constants were very similar for the three β-diketonate complexes, $Sn(\beta\text{-dik})_2Cl_2$ ($k_2 = 8.8$ for β-dik = acac, 10.3 for bzac and 7.5 $dm^3\ mol^{-1}\ s^{-1}$ for bzbz, in chloroform at 30°C).[20] These values are remarkably close to ours for the ethylmaltol analogue, especially when allowance is made for the differences in solvent (chloroform vs acetonitrile) and in temperature. Frazer and Haines reported activation entropies of around $-50\ J\ K^{-1}\ mol^{-1}$ for the reactions of their three β-diketone complexes, which is consistent with bimolecular water attack at the tin.

Figure 4 shows that there is a strong correlation between IR stretching frequencies, ν(Sn—Cl), and second-order rate constants for thiocyanate attack. Stronger tin–chloride bonding makes attainment of the transition state harder since the bond to the leaving group has to be extended considerably to form the S_N2 transition state. There is a similar correlation for the analogous titanium complexes and reactions.[31]

Anti-tumour activity

The complex $Sn(empp)_2Cl_2$ was tested against a number of cell lines. It was found to have significant but rather modest activity against K562 leukemia and MAC13 murine tumour cells, and rather small activity against two other murine lines and HCT18 and HRT18, human colon and rectal carcinoma lines, respectively. It is interesting that the tin complex shows most activity against the leukemia cells, whereas analogous titanium complexes only appear to show significant activity against colon tumours. Earlier reports[11,34] also suggested greatest activity of complexes of the R_3SnOH, R_2SnO and $R_2SnOSnR_2$ type against P388 leukemia.

Acknowledgements—We are grateful to British Technology Group Plc and the Clinical Oncology Unit of the University of Bradford for the *in vitro* testing of the ethylmaltol complex.

REFERENCES

1. C. R. Noller, *Chemistry of Organic Compounds*, 2nd edn. W. B. Saunders, Philadelphia (1957); L. F. Fieser and M. Fieser, *Organic Chemistry*, 3rd edn. Reinhold, New York (1956).
2. J. Burgess, *Trans. Met. Chem.* 1993, **18**, in press.
3. G. J. Kontoghiorges, M. Aldouri, L. Sheppard and A. V. Hoffbrand, *Lancet* 1987, **1**, 1294; G. J. Kontoghiorges, M. A. Aldouri, A. V. Hoffbrand, J. Barr, B. Wonk, T. Kourouclaris and L. Sheppard, *Br. Med. J.* 1987, **295**, 1509; N. F. Olivieri, D. M. Templeton, G. Koren, D. Chung, C. Herman, M. H. Freedman and R. A. McClelland, *Ann. N. Y. Acad. Sci.* 1990, **612**, 369.
4. J. B. Porter, M. Gyparacki, L. C. Burke, E. R. Huehns, P. Sarpong, V. Saez and R. C. Hider, *Blood* 1988, **72**, 1497; J. B. Porter, E. R. Huehns and R. C. Hider, *Baillière's Clin. Haematol.* 1989, **2**, 257; P. S. Dobbin and R. C. Hider, *Chem. Br.* 1990, 565.
5. G. J. Kontoghiorges and J. Barr, First International Symposium on Chelation, p. (1989).
6. R. B. Lauffer, *Chem. Rev.* 1987, **87**, 901; S. Ahmed, J. Burgess and S. A. Parsons, *Polyhedron* submitted.
7. J. L. Humm, *J. Nucl. Med.* 1986, **27**, 1490; J. P. L. Cox, K. J. Jankowski, R. Kataky, D. Parker, N. R. A. Beeley, B. A. Boyce, M. A. W. Eaton, K. Millar, A. T. Millica, A. Harrison and C. Walker, *J. Chem. Soc., Chem. Commun.* 1989, 797; C. J. Broan, J. P. L. Cox, A. S. Craig, R. Kataky, D. Parker, A. Harrison, A. M. Randall and G. Ferguson, *J. Chem. Soc., Perkin Trans.* II 1991, 87.
8. C. Orvig, J. McNeill, V. Yuen and H. Hoveyda, *J. Med. Chem.* 1992, **35**, 1489.
9. B. K. Keppler, C. Friesen, H. G. Moritz, H. Vongerichten and E. Vogel, *Struct. Bonding* 1991, **78**, 97; B. K. Keppler and K. Michels, *Arzneim-Forsch.* 1985, **35 (II)**, 1837; B. K. Keppler and D. Schmähl, *Arzneim-Forsch.* 1986, **36 (II)**, 1822.
10. M. E. Heim, H. Flechtner and B. K. Keppler, *Prog. Clin. Biochem. Med.* 1989, **10**, 217.
11. A. J. Crowe and P. J. Smith, *Chem. Ind.* 1980, 200.
12. For example, A. J. Crowe, P. J. Smith and G. Atassi, *Inorg. Chim. Acta* 1984, **93**, 179; M. Gielen, R. Willem, T. Mancilla, J. Ramharter and E. Joosen, *Silicon, Germanium, Tin Lead Cpds* 1986, **9**, 349; A.

J. Crowe, *Drugs Future* 1987, **12**, 255; A. H. Penninks, M. Bol-Schoenmakers, M. Gielen and W. Seinen, *Main Group Met. Chem.* 1989, **12**, 1; M. Gielen, R. Willem, A. Delmotte, E. Joosen, A. Meriem, M. Mélotte, C. Vanbellinghen, B. Mahieu, P. Lelieveld, D. de Vos and G. Atassi, *Main Group Met. Chem.* 1989, **12**, 55.

13. D. Searle, P. J. Smith, N. A. Bell, L. A. March, I. W. Nowell and J. D. Donaldson, *Inorg. Chim. Acta* 1989, **162**, 143 and refs therein.
14. D. F. Evans and C. Y. Wong, *Polyhedron* 1991, **10**, 1131.
15. A. Nagasawa and K. Saito, *Bull. Chem. Soc. Japan* 1974, **47**, 131; F. B. Ueno, A. Nagasawa and K. Saito, *Inorg. Chem.* 1981, **20**, 3504.
16. R. W. Jones and R. C. Fay, *Inorg. Chem.* 1973, **12**, 2599.
17. Y. Kawasaki and T. Tanaka, *Inorg. Nucl. Chem. Lett.* 1967, **3**, 13.
18. J. W. Faller and A. Davison, *Inorg. Chem.* 1967, **6**, 182.
19. J. M. Bull, M. J. Frazer, L. I. B. Haines and J. Measures, *Abstr., Chem. Soc. Autumn Mtg.*, Southampton, A14 (1969).
20. M. J. Frazer and L. I. B. Haines, *J. Chem. Soc., Dalton Trans.* 1975, 1471.
21. J. Burgess, J. Fawcett, S. A. Parsons and D. R. Russell, to be submitted.
22. J. Otera, Y. Kawasaki and T. Tanaka, *Inorg. Chim. Acta* 1967, **1**, 294.
23. I. Douek, M. J. Frazer, Z. Goffer, M. Goldstein, B. Rimmer and H. A. Willis, *Spectrochim. Acta* 1967, **23A**, 373.
24. D. L. Tomaja and J. J. Zuckermann, *Synth. React. Inorg. Met.-Org. Chem.* 1976, **6**, 323.
25. I. R. Beattie, T. Gilson, K. Livingston, V. Fawcett and G. A. Ozin, *J. Chem. Soc. A* 1967, 712.
26. M. Komura, T. Tanaka and R. Okawara, *Inorg. Chim. Acta* 1968, **2**, 321.
27. Y. Kawasaki, T. Tanaka and R. Okawara, *Spectrochim. Acta* 1966, **22**, 1571.
28. T. Tanaka, M. Komura, Y. Kawasaki and R. Okawara, *J. Organomet. Chem.* 1964, **1**, 484.
29. R. Okawara and M. Ohara, in *Organotin Compounds* (Edited by A. K. Sawyer), Vol. 2. Marcel Dekker, New York (1971).
30. J. Otera, T. Hinoishi, Y. Kawabe and R. Okawara, *Chem. Lett.* 1981, 273.
31. J. Burgess and S. A. Parsons, *Appl. Organomet. Chem.*, 1993, 7, in press.
32. R. D. Shannon and C. T. Prewitt, *Acta Cryst.* 1969, **B25**, 925.
33. R. D. Shannon, *Acta Cryst.* 1976, **A32**, 751.
34. E. J. Bulten and H. A. Budding, *UK Patent Appl.* GB 2 077 266 A (1981).

Polyhedron Vol. 12, No. 16, pp. 1967–1971, 1993
Printed in Great Britain

0277-5387/93 $6.00+.00
© 1993 Pergamon Press Ltd

A ROUTE LEADING TO A STABLE M—H—B UNIT (M = Si, Ge, Sn). THE BIDENTATE AND TRIDENTATE BEHAVIOUR OF TETRAHYDROBORATE

K. S. SIDDIQI,* FATHI M. A. M. AQRA, S. A. SHAH and S. A. A. ZAIDI

Department of Chemistry, Aligarh Muslim University, Aligarh 202 002, India

(*Received* 27 *January* 1993; *accepted* 30 *April* 1993)

Abstract—The complex $[MLCl_2]$ [M = Si, Ge and Sn, L = NN′-ethylene bis-(salicylideneiminate)] reacts with KBH_4 in THF to give $[ML(BH_4)_2]$. The results indicate that the BH_4^- ion behaves as a bidentate ligand and the central metal atom possesses eight-coordination. The conductivity measurements reveal their covalent nature. Another series of compounds of the types $[R_2Sn(BH_4)_2]$ (R = Me, Bu and Ph) and $[R_3Sn(BH_4)]$ (R = Bu and Ph) have been synthesized by the direct interaction of R_2SnCl_2 and R_3SnCl with excess KBH_4 in THF, respectively. In this case it is found that the tetrahydroborate group acts as a tridentate ligand implying eight- and six-coordination of the tin atom, respectively. The molar conductance value ascertains their non-electrolytic character.

It is a conspicuous feature that a polydentate ligand provides unusual stabilization of different oxidation states as well as rigid coordination spheres for the metal.[1,2] Redox reactions carried out on transition metal chelate complexes lead either to a change in the oxidation state of the metal or to the generation of electrophilic and nucleophilic sites on the ligand.[3–8] Since a group(IV) metal in a low oxidation state is able to promote the coordination and the activation of small molecules,[9–11] our interest was focussed on some precursors of low-valent group(IV) metal complexes, containing ligands such as NN′-ethylene bis-(salicylideneiminate) (Fig. 1), which stabilize various oxidation states of these metals.[12]

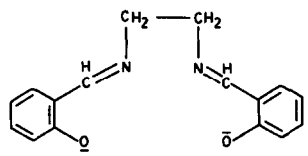

NN′-ethylene bis (Salicylideneiminate)

Fig. 1.

Transition metal tetrahydroborates are important as precursors to solid metal borides,[13] to metal hydrides[14] as well as alkyls.[15] From the structural point of view they are intriguing for the versatility displayed by the BH_4 group in the mode of its ligation to the metal centre, which may entail triple,[16] double[16] or single[17] hydrogen bridges.

The present paper reports two types of compounds: (1) $[ML(BH_4)_2]$ [M = Si, Ge, and Sn; L = NN′-ethylene bis-(salicylideneiminate)] and (2) $[R_2Sn(BH_4)_2]$ (R = Me, Bu, Ph) and $[R_3Sn(BH_4)]$ (R = Bu, Ph) with a view to exploring the nature and mode of bonding of the BH_4^- ion and to establish a group(IV) metal hydrido complex.

EXPERIMENTAL

Ethylenediamine (Koch Light), salicylaldehyde (E. Merck), $SiCl_4$, $GeCl_4$, $SnCl_4$ and KBH_4 (BDH), R_2SnCl_2 (R = Me, Bu, Ph) and R_3SnCl (R = Bu, Ph) (Fluka) were used as supplied. All the solvents were distilled and dried before use. Microanalyses were made on a Carlo–Erba analyser model 1106. Molar conductances were measured at room temperature on a Digisun electronic conductivity bridge. The IR spectra (200–4000 cm^{-1}) were recorded on a Carl Ziess Specord M-80 spectrophotometer as Nujol mulls. Chlorine and tin were estimated gravimetrically.

* Author to whom correspondence should be addressed.

Synthesis of the Schiff base

A methanolic solution (15 cm^3) of ethylene diamine (0.01 mol) was added dropwise to a methanolic solution (15 cm^3) of salicylaldehyde (0.02 mol). An immediate yellow precipitate was obtained which was filtered, washed, recrystallized from methanol and dried *in vacuo*.

Synthesis of the complexes $[MLCl_2]$ **(1)**

The Schiff base (0.01 mol) was taken in THF and added to MCl_4 (0.01 mol) (M = Si, Ge, Sn) in toluene. The mixture was refluxed along with stirring for 2 h and the yellow product obtained was filtered and washed with toluene and dried *in vacuo*.

Synthesis of the complexes $[ML(BH_4)_2]$

To a THF solution of excess KBH_4 (0.02 mol) was added a chloroform solution (0.01 mol) of **1**. The solution was refluxed for 4 h and after cooling for some time a coloured precipitate settled, which was washed with THF and dried *in vacuo*.

Synthesis of the complexes $[R_2Sn(BH_4)_2]$ *and* $[R_3Sn(BH_4)]$

R_2SnCl_2 (0.01 mol) or R_3SnCl (0.01 mol) was added to a THF solution of excess KBH_4 (0.02 mol or 0.01 mol), respectively. The mixture refluxed for 6 h yields a powdery compound after cooling, which was washed with THF and dried *in vacuo*.

RESULTS AND DISCUSSION

The analytical data (Table 1) agree well with the composition of the complexes. The molar conductance values of 10^{-3} M solutions of the complexes at room temperature in DMF (10–15 Ω^{-1}) fall well below those quoted for uni-univalent electrolytes, indicating their non-ionic nature.[18]

$[ML(BH_4)_2]$ *type*

The complex $[MLCl_2]$ reacts with a THF solution of KBH_4 according to eq. (1) yielding brown, green and yellow powders for tin, silicon and germanium complexes, respectively.

Table 1. Analytical data, melting points, % yield and colour of the complexes

Compound	% Yield	M.p. (°C)	Colour	C(%) Found (Calc.)	H(%) Found (Calc.)	N(%) Found (Calc.)	Sn(%) Found (Calc.)	Cl(%) Found (Calc.)
$C_{14}H_{22}N_2O_2B_2Si$	60	202	Green	58.5 (58.3)	7.7 (7.6)	9.6 (9.7)	—	—
$C_{14}H_{22}N_2O_2B_2Ge$	63	210	Light yellow	50.8 (50.6)	6.1 (6.6)	8.5 (8.4)	—	—
$C_{14}H_{22}N_2O_2B_2Sn$	72	242	Brown	44.6 (44.4)	5.9 (5.8)	7.3 (7.4)	31.0 (31.2)	—
$C_2H_{14}B_2Sn$	55	189	Grey	13.7 (13.6)	8.0 (7.9)	—	67.2 (67.0)	—
$C_8H_{26}B_2Sn$	55	192	White	37.0 (36.9)	10.0 (10.0)	—	45.1 (45.3)	—
$C_{12}H_{18}B_2Sn$	60	220	Light yellow	48.1 (48.0)	6.2 (6.0)	—	39.2 (39.3)	—
$C_{12}H_{31}BSn$	52	232	White	47.6 (47.5)	10.2 (10.2)	—	38.8 (38.9)	—
$C_{18}H_{19}BSn$	55	187	White	59.6 (59.5)	5.3 (5.2)	—	32.4 (32.5)	—
$C_{14}H_{14}N_2Cl_2Si$	70	132	Yellow	54.5 (54.3)	4.6 (4.5)	9.0 (9.0)	—	22.8 (22.9)
$C_{14}H_{14}N_2Cl_2Ge$	62	161	Yellow	47.7 (47.5)	4.0 (3.9)	8.0 (7.9)	—	20.0 (20.1)
$C_{14}H_{14}N_2Cl_2Sn$	81	150	Yellow	42.3 (42.1)	3.6 (3.5)	7.1 (7.0)	29.4 (29.5)	17.7 (17.8)

$$[MLCl_2]+2KBH_4 \xrightarrow{THF} [ML(BH_4)_2] + 2KCl \quad (1)$$

This reaction must be performed with excess KBH_4 since a KBH_4:M ratio lower than 2:1 results in the reduction of the metal atom.

The most significant spectroscopic information on these complexes comes from the IR spectrum. Strong bands occur at 2560, 2510, 2269 and 2220 cm^{-1}. These are attributed to B—H stretching modes, the higher two being due to the terminal hydrogens, while the lower two belong to the bridging hydrogens (the presence of the B—H_t stretching frequency rules out the possibility of polymerization). The stretching bands at 1990 and 1825 cm^{-1} must be considered as asymmetric and symmetric vibrations due to the MH_2 unit. The absence of the ν(M—Cl) band in the far-IR region suggests the replacement of Cl^- by the BH_4^- ion. Sharp absorption bands are observed in the 490–500 cm^{-1} range, assignable to ν(M—O). Since the ν(C=C) and ν(C=N) absorption bands generally appear in the same region, it is difficult to distinguish them. A strong band at 1520 cm^{-1} has been assigned to ν(C=N), but it may be due to ν(C=C) also. On this basis we suggest that the reaction of $[MLCl_2]$ with KBH_4 involves the substitution of Cl^- by BH_4^- and then the ligation of BH_4^- to the group(IV) metal in a bidentate manner (Fig. 2), as is the case with $Al(BH_4)_3$.[19] The characteristic IR bands are listed in Table 2. Since these compounds are not soluble in hydrocarbons (benzene, hexane and chloroform) and they are decomposed by coordinating solvents (when the compounds are dissolved in dry DMSO, DMF, THF and CH_3CN the evolution of hydrogen gas was not observed, but the colour of the solution changed probably indicating the chemical deformation of the compounds), any dynamic inspection of them by NMR spectroscopy is prevented.

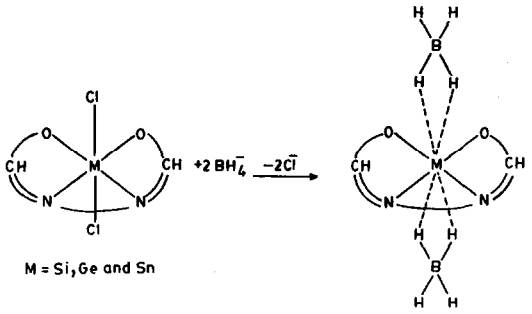

Fig. 2.

Table 2. The important characteristic IR bands of the complexes

Complex	Peak position (cm^{-1})						
	ν(B—H_t)	ν(B—H_b)	ν(M—H_b)	ν(M—C)	ν(M—O)	ν(M—N)	ν(Sn(μ—H)$_3$B)
$C_{14}H_{22}N_2O_2B_2Si$	2560 2510	2269 2220	1200	—	490	310	—
$C_{14}H_{22}N_2O_2B_2Ge$	2561 2510	2270 2222	1199	—	490	291	—
$C_{14}H_{22}N_2O_2B_2Sn$	2560 2510	2269 2222	1200	—	500	304	—
$C_2H_{14}B_2Sn$	2587	2200 2221 2241	1160	500	—	—	450
$C_8H_{26}B_2Sn$	2580	2211 2261 2205	1162	505	—	—	450
$C_{12}H_{18}B_2Sn$	2582	2200 2219 2225	1160	505	—	—	446
$C_{12}H_{31}BSn$	2587	2201 2252 2261	1171	500	—	—	421
$C_{18}H_{19}BSn$	2587	2215 2226 2242	1162	522	—	—	462

$[R_2Sn(BH_4)_2]$ and $[R_3Sn(BH_4)]$ type

The reaction of R_2SnCl_2 and R_3SnCl with excess KBH_4 in THF can be represented in accordance with eqs (2) and (3). All the synthesized compounds are air stable.

$$R_2SnCl_2 + \text{excess } KBH_4 \xrightarrow{THF} R_2Sn(BH_4)_2 + 2KCl \quad (2)$$

$$R_3SnCl + \text{excess } KBH_4 \xrightarrow{THF} R_3Sn(BH_4) + KCl \quad (3)$$

The relevant bands of the IR spectra are given in Table 2. The first salient point is the observation of a single intense absorption at 2587 cm^{-1}, taken in conjunction with the absence of any doublet near 2500 cm^{-1}, assigned to $\nu(B—H_t)$, which suggests the presence of only one terminal hydrogen. This is characteristic of tridentate tetrahydroborate groups.[16,19] Other features diagnostic of tridentate binding of the tetrahydroborate group include the appearance of a doublet near 2200 cm^{-1} and an intense band near 1200 cm^{-1}.[16,20] Such tridentate behaviour of BH_4^- was found in the cases of $Zr(BH_4)_4$,[21] $Hf(BH_4)_4$[22] and the actinide derivatives $M(BH_4)_3$[23] (M = Np and Pu). There is no sign of the features characteristic of bidentate binding, as exhibited by $Al(BH_4)_3$,[19] which gives us good grounds for believing that the tetrahydroborate groups are bound to tin exclusively via triple hydrogen bridges (Fig. 3).

The absorptions in the range 1000–1400 cm^{-1} are almost certainly due to fundamentals in which $H_b—B—H_t$ bending is the predominant motion.[21] Another band located near 450 cm^{-1} is assigned to the deformation of the $\nu(Sn(\mu\text{-}H)_3B)$ bridges.[21] The bands observed around 2585–2400 cm^{-1} are assigned to $\nu(B—H_t)$ and those at 2230–2155 cm^{-1} are assigned to $\nu(B—H_b)$. Two distinct bands appeared at 1160 and 500 cm^{-1}, definitively attributed to $\nu(Sn—H_b)$ and $\nu(Sn—C)$. It is noteworthy that the BH_4^- ligand can have a bidentate coordination mode in which only two orbitals are effective in donating electron density to the metal (C_{2v} symmetry), whereas in the tridentate coordination mode three orbitals are effective in this way (C_{3v} symmetry). Very recently the tridentate behaviour of the BH_4^- ion has been explored in the case of $Ti(BH_4)_3$.[24] It has been shown that the tetrahedral BH_4^- anion is characterized by four filled B—H bonding MOs and four vacant B—H antibonding MOs. When coordinated to a metal the local symmetry about the boron atom is reduced, to C_{3v} in the case of the tridentate mode and C_{2v} in the case of the bidentate mode of binding.

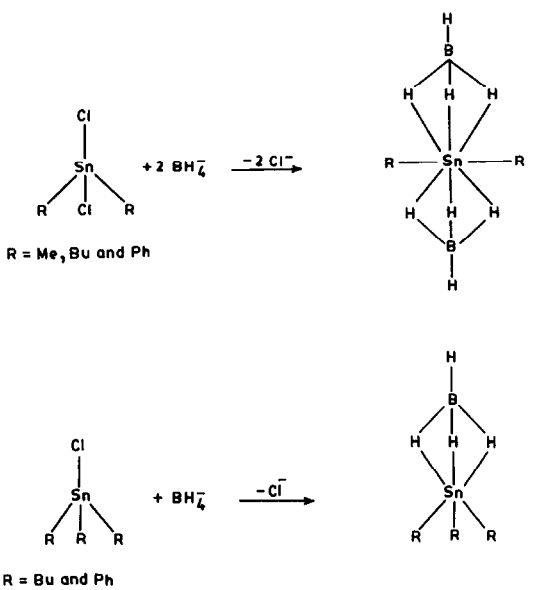

Fig. 3.

REFERENCES

1. D. P. Rillema, J. F. Endicott and E. Papaconstantinou, *Inorg. Chem.* 1971, **10**, 1739.
2. J. A. Stecky, D. G. Pillsbury and D. H. Busch, *Inorg. Chem.* 1980, **19**, 3148.
3. J. A. Switzer and J. F. Endicott, *J. Am. Chem. Soc.* 1980, **102**, 1181.
4. M. Millar and R. H. Holm, *J. Am., Chem. Soc.* 1975, **97**, 6052.
5. F. V. Lovecchio, E. S. Gore and D. H. Busch, *J. Am. Chem. Soc.* 1974, **96**, 3109.
6. R. R. Gange and D. M. Ingle, *Inorg. Chem.* 1981, **20**, 420.
7. J. K. Burdett and D. P. Williams, *Inorg. Chem.* 1980, **19**, 2779.
8. D. C. Olson and J. Vasilevskis, *Inorg. Chem.* 1969, **8**, 1611.
9. E. E. Van Tamelen, *Accts Chem. Res.* 1970, **3**, 361.
10. J. E. Bercaw, R. H. Marvich, L. G. Bell and H. H. Brintzinger, *J. Am. Chem. Soc.* 1972, **94**, 1219.
11. J. E. Bercaw, *J. Am. Chem. Soc.* 1974, **96**, 5087.
12. G. Fachinetti, C. Floriani, P. F. Zanazzi and A. R. Zangari, *Inorg. Chem.* 1979, **18**, 3469.
13. J. A. Jensen, J. E. Gozum, D. M. Pollina and G. S. Girolami, *J. Am. Chem. Soc.* 1988, **110**, 1643.
14. G. G. Hlatky and R. H,. Crabtree, *Coord. Chem. Rev.* 1985, **65**, 1.
15. J. A. Jensen, S. R. Wilson, A. J. Schultz and G. S. Girolami, *J. Am. Chem. Soc.* 1987, **109**, 8094.
16. T. J. Marks and J. R. Kolb, *Chem. Rev.* 1977, **77**, 263.
17. J. A. Gensen and G. S. Girolami, *Inorg. Chem.* 1989, **28**, 2107.

18. W. J. Geary, *Coord. Chem. Rev.* 1971, **7**, 81.
19. D. A. Coe and J. W. Nibler, *Spectrochim. Acta, Part A* 1973, **29**, 1789.
20. T. J. Marks, W. J. Kennelly, J. R. Kolb and L. A. Shimp, *Inorg. Chem.* 1972, **11**, 2540.
21. B. E. Smith, H. F. Shurvell and B. D. James, *J. Chem. Soc., Dalton Trans.* 1978, 710.
22. T. A. Keiderling, W. T. Wozniak, R. S. Gay, D. Jurkowitz, E. R. Bernstein, S. J. Lippard and T. G. Spiro, *Inorg. Chem.* 1975, **14**, 576.
23. R. H. Banks, N. M. Edelstein, R. R. Rietz, D. H. Templeton and A. Zalkin, *J. Am. Chem. Soc.* 1978, **100**, 1957.
24. C. J. Dain, A. J. Downs, M. J. Goode, D. G. Evans, K. T. Nicholls, D. W. H. Rankin and H. E. Robertson, *J. Chem. Soc., Dalton Trans.* 1991, 967.

Polyhedron Vol. 12, No. 16, pp. 1973–1976, 1993
Printed in Great Britain

0277–5387/93 $6.00+.00
© 1993 Pergamon Press Ltd

THE CRYSTAL AND MOLECULAR STRUCTURE OF TETRAKIS(μ-OCTANOATO-O,O')-BIS(PYRIDINE)DICOPPER(II)

M. PETRIČ*

Department of Wood Science and Technology, University of Ljubljana, Rožna dolina, C. VIII/34, 61000 Ljubljana, Slovenia

and

I. LEBAN and P. ŠEGEDIN

Department of Chemistry and Chemical Technology, University of Ljubljana, Aškerčeva 5, 61001 Ljubljana, POB 537, Slovenia

(*Received* 27 *January* 1993; *accepted* 27 *April* 1993)

Abstract—The crystal structure of the adduct of copper(II) octanoate with pyridine, $(Cu_2(C_7H_{15}COO)_4)(C_5H_5N)_2$, has been determined by X-ray diffraction. The complex forms discrete centrosymmetric tetracarboxylate-bridged dimers with pyridine moieties in the apical positions.

Copper(II) carboxylate adducts with a large variety of ligands have been extensively investigated and results have been summarized in several publications.[1–5] Investigations on copper(II) complexes with higher carboxylic acids apart from acetates, propionates and butyrates are rare. In spite of increased interest in copper(II) alkanoates containing linear chains and related adducts exhibiting a thermotropic columnar mesophase,[6,7,8] only two crystal structures of copper(II) complexes with higher carboxylic acids have been hitherto determined: anhydrous copper(II) octanoate[9] ($R = 0.159$) and anhydrous copper(II) decanoate[10] ($R = 0.134$).

It was the intention of this work to obtain crystallographic data on the copper(II) octanoate adduct with pyridine.

EXPERIMENTAL

Preparation

The complex was prepared by dissolving $Cu_2(C_7H_{15}COO)_4$ (0.7 g) in pyridine (5 cm^3). The addition of water (300 cm^3) resulted in the precipitation of small blue crystals, presumably monomeric species of copper(II) octanoate adduct with pyridine. The crystals were filtered off. Dark green crystals grew from the filtrate after standing in air for a period of 1 month at room temperature. Found: C, 58.6; H, 8.2; Cu, 15.0; N, 3.3. Calc. for $C_{42}H_{70}Cu_2N_2O_8$: C, 58.8; H, 8.2; Cu, 14.8; N, 3.3%.

Crystal data

$C_{42}H_{70}Cu_2N_2O_8$, $M_r = 858.1$, triclinic, $a = 8.379(3)$, $b = 10.921(6)$, $c = 13.286(6)$ Å, $\alpha = 108.42(4)$, $\beta = 96.21(4)$, $\gamma = 92.06(4)°$, $V = 1143.5$ Å^3, $D_m = 1.23$, $D_c = 1.246$ g cm^{-3}, $Z = 1$, Mo-K_α radiation, $\lambda = 0.7107$ Å, μ(Mo-K_α) $= 9.78$ cm^{-1}, space group $P\bar{1}$, $F(000) = 458$, $T = 293$ K.

Data collection, structure solution and refinement

Data were collected on an Enraf–Nonius CAD-4 diffractometer (crystal monochromatized Mo-K_α radiation, $\lambda = 0.7107$ Å) from a prismatic crystal of dimensions $0.14 \times 0.24 \times 0.32$ mm. Of 6651 reflections collected up to $2\theta_{max} = 60°$, 3036 with

* Author to whom correspondence should be addressed.

$I > 2.5\sigma(I)$ were used in structure refinement. Intensity variation of not greater than 2.5% in three standards monitored during the data collection period indicated negligible crystal decay. The structure was solved by a routine Patterson method followed by subsequent electron-density map calculations. Full-matrix least-squares refinement with anisotropic thermal parameters on all non-hydrogen atoms gave $R[=\Sigma\|F_o|-|F_c\|/\Sigma|F_o|]$ and $R_w[=\Sigma w(\|F_o|-|F_c\|^2/\Sigma w|F_o|^2)^{1/2}]$ of 0.049 and 0.061, respectively, with a value of $w = 1.85\ [\sigma^2(F_o)+0.0014(F_o)^2]^{-1}$. Hydrogen atom positions were generated and their positional and common isotropic thermal parameters were refined. Neutral

Table 1. Important bond lengths (Å) and angles (°) with standard deviations in parentheses

Cu coordination			
Cu—Cu^i	2.651(1)	Cu^i—Cu—N	178.4(1)
Cu—N	2.194(4)	Cu^i—Cu—O(1)	84.3(1)
Cu—O(1)	1.987(3)	Cu^i—Cu—O(2)^i	83.6(1)
Cu—O(2)^i	1.976(3)	Cu^i—Cu—O(3)	83.4(1)
Cu—O(3)	2.038(3)	Cu^i—Cu—O(4)^i	84.8(1)
Cu—O(4)^i	2.026(3)	N—Cu—O(1)	97.2(2)
		N—Cu—O(2)^i	94.9(2)
		N—Cu—O(3)	97.2(2)
		N—Cu—O(4)^i	94.6(2)
		O(1)—Cu—O(2)^i	167.9(1)
		O(1)—Cu—O(3)	87.9(2)
		O(1)—Cu—O(4)^i	90.5(2)
		O(2)^i—Cu—O(3)	90.7(2)
		O(2)^i—Cu—O(4)^i	88.4(2)
		O(3)—Cu—O(4)^i	168.2(1)
Pyridine moiety			
N—C(1)	1.349(6)	C(1)—N—C(5)	117.7(4)
N—C(5)	1.343(6)	N—C(1)—C(2)	124.0(4)
C(1)—C(2)	1.380(7)	C(1)—C(2)—C(3)	118.2(5)
C(2)—C(3)	1.371(7)	C(2)—C(3)—C(4)	118.8(4)
C(3)—C(4)	1.382(8)	C(3)—C(4)—C(5)	120.4(4)
C(4)—C(5)	1.392(7)	N—C(5)—C(4)	121.0(4)
Octanoate moieties			
O(1)—C(11)	1.262(6)	O(1)—C(11)—O(2)	125.0(3)
O(2)—C(11)	1.257(6)	O(1)—C(11)—C(12)	119.7(4)
C(11)—C(12)	1.511(6)	O(2)—C(11)—C(12)	115.3(4)
C(12)—C(13)	1.519(7)	C(11)—C(12)—C(13)	116.1(4)
C(13)—C(14)	1.548(8)	C(12)—C(13)—C(14)	110.0(4)
C(14)—C(15)	1.514(7)	C(13)—C(14)—C(15)	113.2(4)
C(15)—C(16)	1.551(8)	C(14)—C(15)—C(16)	112.4(5)
C(16)—C(17)	1.508(8)	C(15)—C(16)—C(17)	112.6(5)
C(17)—C(18)	1.517(8)	C(16)—C(17)—C(18)	112.3(5)
O(3)—C(21)	1.274(6)	O(3)—C(21)—O(4)	123.5(4)
O(4)—C(21)	1.260(6)	O(3)—C(21)—C(22)	120.0(4)
C(21)—C(22)	1.567(7)	O(4)—C(21)—C(22)	116.5(4)
C(22)—C(23)	1.419(10)	C(21)—C(22)—C(23)	113.2(5)
C(23)—C(24)	1.371(14)	C(22)—C(23)—C(24)	128.1(8)
C(24)—C(25)	1.356(15)	C(23)—C(24)—C(25)	130.0(9)
C(25)—C(26)	1.394(18)	C(24)—C(25)—C(26)	125.5(10)
C(26)—C(27)	1.32(2)	C(25)—C(26)—C(27)	129.9(11)
C(27)—C(28)	1.400(18)	C(26)—C(27)—C(28)	127.0(11)

Symmetry code: $^i 2-x, -y, -z$.

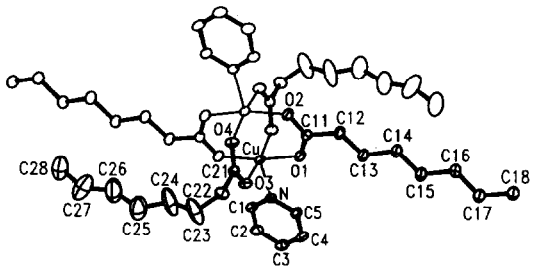

Fig. 1. ORTEP view of the dimeric complex with the atomic-numbering scheme. Thermal ellipsoids are drawn at 30% probability level.

atom scattering factors were used.[11] The system of computer programs NRCVAX,[12] adapted for the PC 386 computer, was used throughout the data reduction, determination, refinement and interpretation. The SHELX-76[13] program was used for the final refinement cycles.

Atomic fractional coordinates, hydrogen atom coordinates, anisotropic thermal parameters, intraligand bond distances and angles, and observed and calculated structure factors tables are deposited with the Editor as supplementary material, from whom copies are available on request. Atomic coordinates have also been deposited with the Cambridge Crystallographic Data Centre.

DISCUSSION

The structure of the title compound is shown in Fig. 1. The important bond lengths and angles are presented in Table 1. Pairs of copper ions are bridged by four n-octanoate ligands, forming a dimeric structure of the acetate hydrate type with pyridine rings instead of water molecules in the apical positions. The Cu—Cu separation of 2.651(1) Å and Cu—N distance of 2.194(4) Å compare well with 2.641(1) and 2.191(2) Å, respectively,

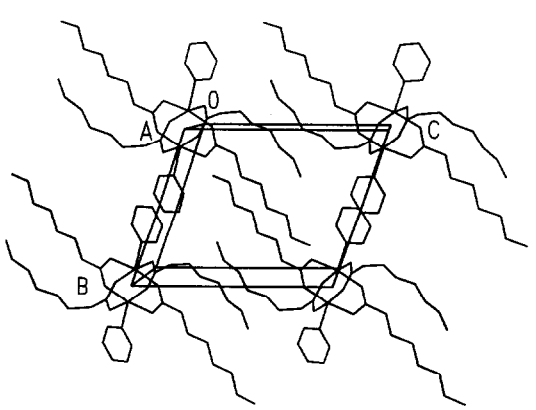

Fig. 2. View of the molecular packing along [1 0 0].

Table 2. Selected torsion angles (°)[a] with standard deviations in parentheses

O(1)—C(11)—C(12)—C(13)	4.7(4)
O(2)—C(11)—C(12)—C(13)	−176.0(6)
C(11)—C(12)—C(13)—C(14)	−178.3(6)
C(12)—C(13)—C(14)—C(15)	175.2(6)
C(13)—C(14)—C(15)—C(16)	−176.8(7)
C(14)—C(15)—C(16)—C(17)	176.7(7)
C(15)—C(16)—C(17)—C(18)	−177.3(7)
O(4)—C(21)—C(22)—C(23)	114.3(7)
O(3)—C(21)—C(22)—C(23)	−66.7(6)
C(21)—C(22)—C(23)—C(24)	−39.5(10)
C(22)—C(23)—C(24)—C(25)	−140.1(19)
C(23)—C(24)—C(25)—C(26)	159.3(22)
C(24)—C(25)—C(26)—C(27)	−154.3(24)
C(25)—C(26)—C(27)—C(28)	175.6(26)

[a] Sign convention taken from ref. 15.

in the orthorhombic copper(II) acetate-pyridine adduct.[14] Cu—O(equatorial) distances range from 1.976(3) to 2.038(3) Å and are considered to be normal for this type of system. The distance of copper from the plane consisting of four equatorial oxygen atoms has a value of 0.209(3) Å and is comparable with the value of 0.19 Å for copper acetate dihydrate.[5] As similarly found in anhydrous copper(II) octanoate[9] and decanoate[10] one pair of hydrocarbon chains in each dimer has the common plane zigzag conformation and the other pair of chains is distorted by rotations about the bonds C(21)—C(22) and C(22)—C(23) (Table 2), presumably because the long hydrocarbon chains if extended in directions at right angles to each other could not pack efficiently together. The structural parameters of the carboxylate groups are usual. C(23)–C(28) hydrocarbon chains are affected by high thermal motion and their bond distances and angles are less reliable. Angles and bond distances in pyridine are normal. The dihedral angle between best planes through C(11)–C(18) carbon atoms ("normal" chain) and C(23)–C(28) carbon atoms (part of the "distorted" chain) is 72.5(19)°.

The packing of the dimers in the unit cell involves no significant inter-dimer associations (Fig. 2). The distance of 3.435(12) Å between the C(3) atom from the pyridine moiety and the C(5) atom from the pyridine ring of a neighbouring molecule represents the closest interaction between discrete dimeric units.

REFERENCES

1. R. C. Mehrotra and R. Bohra, *Metal Carboxylates*. Academic Press, London (1983).

2. M. Kato, H. B. Jonassen and J. C. Fanning, *Chem. Rev.* 1964, **64**, 99.
3. C. Oldham, *Prog. Inorg. Chem.* 1968, **10**, 223.
4. J. Catterick and P. Thornton, *Adv. Inorg. Chem. Radiochem.* 1977, **20**, 291.
5. M. Melnik, *Coord. Chem. Rev.* 1981, **36**, 1.
6. A. M. Godquin-Giroud, J. C. Marchon, D. Guillon and A. Skoulios, *J. Phys. Lett.* 1984, **45**, L-681.
7. H. Abied, D. Guillon, A. Skoulios, P. Weber, A. M. Giroud-Godquin and J. C. Marchon, *Liq. Cryst.* 1987, **2**, 269.
8. P. Maldivi, A. M. Giroud-Godquin, J. C. Marchon, D. Guillon and A. Skoulios, *Physica B* 1989, **158**, 234.
9. T. R. Lomer and K. Perera, *Acta Cryst.* 1974, **B30**, 2913.
10. T. R. Lomer and K. Perera, *Acta Cryst.* 1974, **B30**, 2912.
11. *International Tables for X-ray Crystallography*, Vol. 4. Kynoch Press, Birmingham (1974).
12. E. J. Gabe, Y. Le Page, J. P. Charland, F. L. Lee and P. S. White, *J. Appl. Cryst.* 1989, **22**, 384.
13. G. M. Sheldrick SHELX-76, Program for Crystal Structure Determination. University of Cambridge, U.K. (1976).
14. H. Uekusa, S. Ohba, Y. Saito, M. Kato, T. Tokii and Y. Muto, *Acta Cryst.* 1989, **C45**, 377.
15. W. Klyne and V. Prelog, *Experientia* 1960, **16**, 521.

Polyhedron Vol. 12, No. 16, pp. 1977–1981, 1993
Printed in Great Britain

0277–5387/93 $6.00+.00
© 1993 Pergamon Press Ltd

THE STRUCTURE AND BONDING OF *nido*-7,9-$X_2B_9H_9$ (X = S OR Se)

O. NI DHUBHGHAILL

Institut de Chimie Minérale et Analytique, Université de Lausanne, 3 Place du Château, CH-1005 Lausanne, Switzerland

and

D. REED

Department of Chemistry, University of Edinburgh, King's Buildings, West Mains Road, Edinburgh EG9 3JJ, U.K.

and

T. R. SPALDING*

Chemistry Department, University College, Cork, Ireland

(*Received* 6 *April* 1993; *accepted* 22 *April* 1993)

Abstract—The structure of *nido*-$Se_2B_9H_9$ has been determined unambiguously to be the 7,9-isomer by ultra high-field (192.48 MHz) ^{11}B NMR spectroscopy. The He(I) PE spectrum of 7,9-$Se_2B_9H_9$ is compared with the results of an MNDO MO calculation of the dithiaborane analogue 7,9-$S_2B_9H_9$.

The two possible structures of *nido*-$Se_2B_9H_9$ shown in diagrams **I** and **II** are the 7,8- and 7,9-isomers, respectively. The former structure has been suggested for $Se_2B_9H_9$,[1,2] whilst the latter was

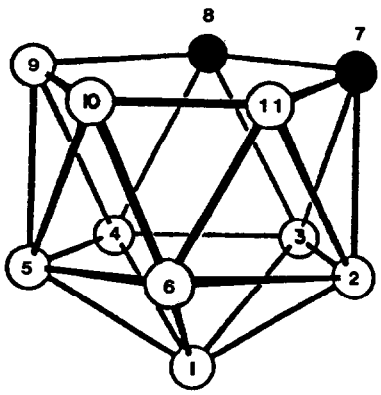

(I)

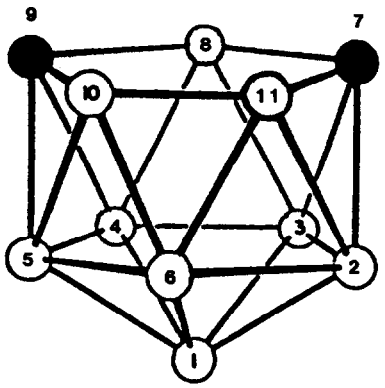

(II)

suggested for $SSeB_9H_9$.[3] All previous attempts to identify the correct structure of $Se_2B_9H_9$ have been unsuccessful. In the present work we have used ultra high-field two-dimensional NMR to resolve this problem and to completely assign the ^{11}B and ^{1}H spectra. The compound is the 7,9-isomer, diagram **II**. In order to better understand the cluster bonding

* Author to whom correspondence should be addressed.

in this type of compound we have investigated the electronic structure of the analogous thiaborane 7,9-$S_2B_9H_9$ using the MNDO programme[4] and compared the results with the published PE spectrum of $Se_2B_9H_9$.[5]

RESULTS AND DISCUSSION

NMR spectroscopy

The present study used a combination of ^{11}B, $^{11}B\{^1H\}$, homonuclear ^{11}B COSY[6] and ^{11}B—^1H HETCOR[7] to establish the structure of $Se_2B_9H_9$ as the 7,9-isomer and assign the resonances in the ^1H and ^{11}B spectra. The 192.48 MHz ^{11}B and $^{11}B\{^1H\}$ NMR spectra show six different boron signals at δ values of +2.1, +1.6, −0.6, −1.0, −8.6 and −34.6 ppm with relative intensities 1:2:2:2:1:1, as shown in Fig. 1. These signals are consistent with either of the structures shown in diagrams **I** and **II**, as each has a plane of symmetry passing through the B—H units in positions (1), (3) and (10) or (1), (6) and (8), respectively. To distinguish between these possibilities a 192.48 MHz ^{11}B COSY experiment was performed, Fig. 2. Of the three resonances with unit relative intensity the two at $\delta = +2.1$ and −34.6 ppm have three cross-peaks, whilst that at $\delta = -8.6$ ppm exhibits only one. In structure **I** B(1) would be expected to have three cross-peaks and B(3) and B(10) two each. For structure **II** B(1) and B(6) would be expected to show three correlations and B(8) only one. Thus, **II** is the correct structure. The signal at δ −8.6 is, therefore, assigned to B(8) and using this information the ^{11}B assignments can be extracted from the COSY data, Table 1. The boron and proton chemicals shifts were correlated from a ^{11}B—^1H HETCOR experiment. The results are summarized in Table 1.

Electronic structure of $X_2B_9H_9$ (X = S *or* Se)

Both the 7,9- and 7,8-isomers of $S_2B_9H_9$ were calculated with the MNDO programme.[4] In both molecules the contributions of the sulphur atoms to the molecular orbitals were notably diffuse, much more so than the contributions from the boron atoms. In general, this diffuseness makes specific comments about particular orbitals difficult. However, in both the isomers the four most stable orbitals were clearly seen to be cluster bonding in nature, even though the other nine cluster bonding orbitals which were expected were not so easily located. The heat of formation of the 7,9-isomer was calculated to be −28.2 kcal mol^{-1}, which was 48.2 kcal mol^{-1} more stable than the 7,8-isomer. The energies of the 14 highest occupied orbitals

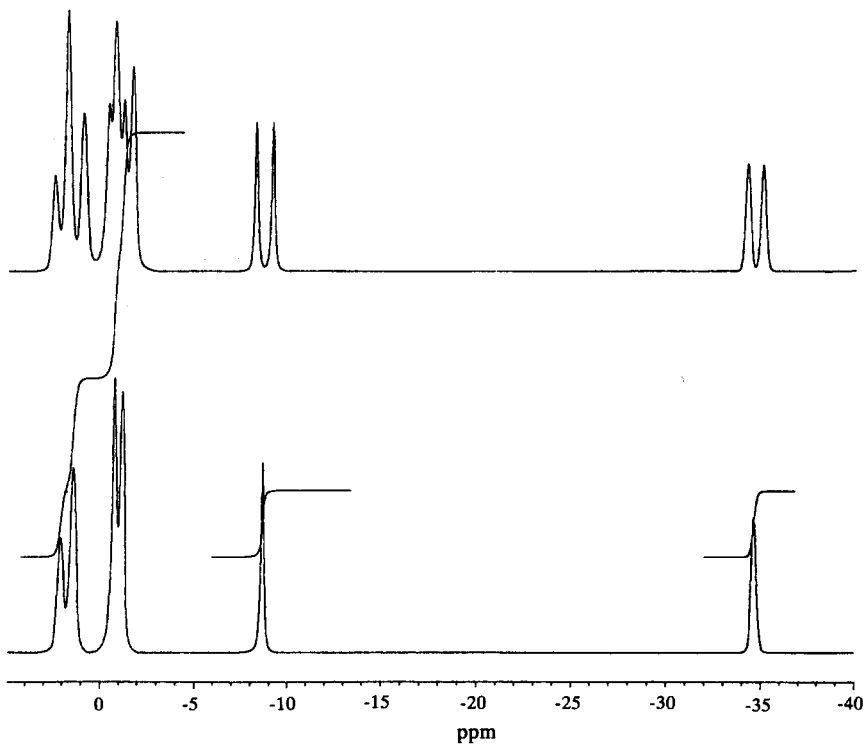

Fig. 1. 192.48 MHz ^{11}B and $^{11}B\{^1H\}$ NMR spectra of 7,9-$Se_2B_9H_9$.

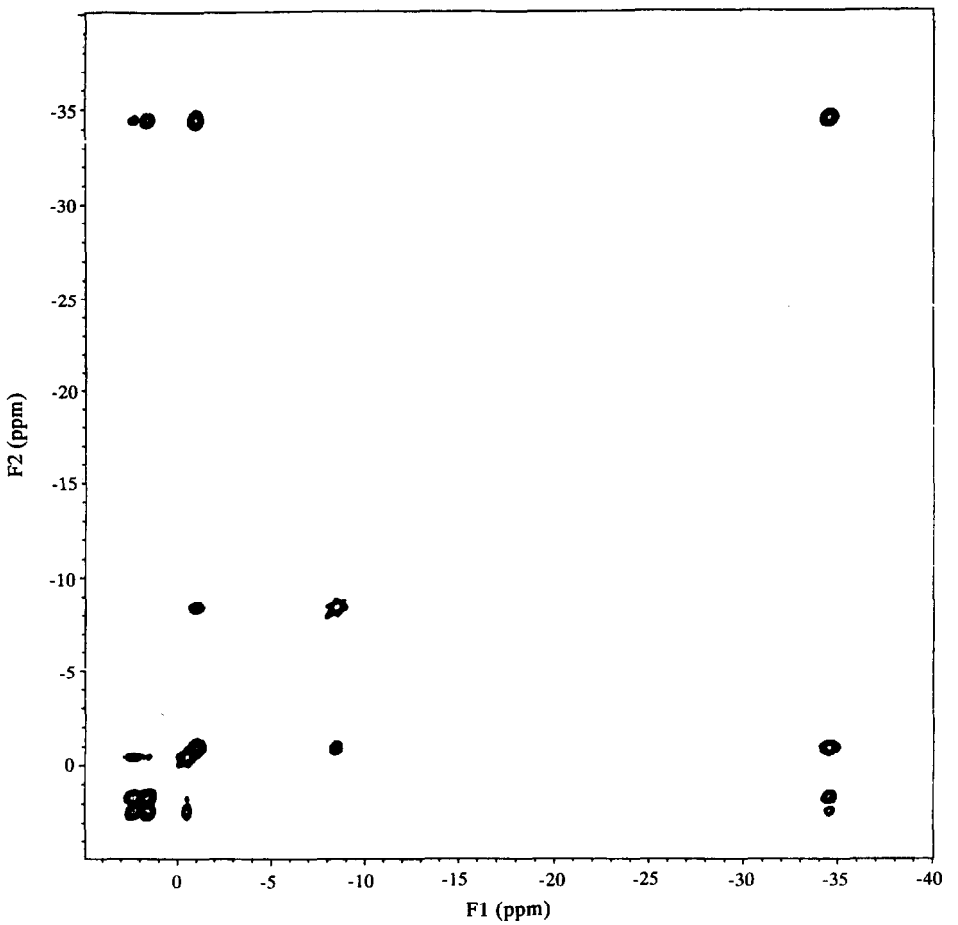

Fig. 2. 192.48 MHz $^{11}B\{^1H\}$ COSY plot for 7,9-$Se_2B_9H_9$. During the experiment 512 increments, each of 384 transients, were collected. Recycle delay 0.3 s; spectrum width 10,500 Hz in both dimensions; final data matrix 2048 × 2048 points. Pseudo-echo window functions were used in both dimensions.

in 7,9-$S_2B_9H_9$ are compared with data from the published PE spectrum[5] of 7,9-$Se_2B_9H_9$ in Table 2. The difference of *ca* 2 eV between the MNDO calculated and observed PE energies in Table 2 is typical of calculations which contain third row atoms.[8] In a previous study of 12-atom heteroborane clusters, 1-$XB_{11}H_{11}$ (X = S or Se), it was concluded that the contribution to cluster bonding from selenium was remarkably similar to that from sulphur.[5] The PE spectra of both 12-atom clusters were essentially the same and showed three broad bands, although there was a slight shift of the band maxima of 1-$SeB_{11}H_{11}$ to lower energies (by 0.5 to 0.7 eV) compared with 1-$SB_{11}H_{11}$. In the present study there is reasonably good agreement between the calculated and experimental data for the first three bands in terms of (a) the differences in energy between successive bands and (b) the number of energy levels or ionization processes. However, the energies of the subsequent ionization processes giving rise to the fourth band are not separated sufficiently well for a detailed analysis to be made. It appears from the calculation that there may be up to eight energy levels in the fourth band. The fifth band is separated by 1.5 eV from the previous one and appears to contain two ionization processes. This feature is reproduced in the calculation, Table 2.

Table 1. ^{11}B and ^1H NMR data for 7,9-$Se_2B_9H_9$

$\delta(^{11}B)$ (ppm)	$\delta(^1H)$ (ppm)	Assignment
+2.1	+3.65	6
+1.6	+3.42	2,5
−0.6	+3.02	10,11
−1.0	+3.24	3,4
−8.6	+2.64	8
−34.6	+2.33	1

Table 2. Calculated (MNDO) energy levels in 7,9-$S_2B_9H_9$ and observed ionizations in the PE spectrum of 7,9-$Se_2B_9H_9$[5]

MNDO Energy (eV)	Band	PE spectrum I.p. (eV)[a]	No. of ionization assigned
11.07	1	9.0	1
12.06	2	10.1	1
12.21	3	10.4(sh)	2
12.41		10.6	
12.85	4	11.0(sh)	[b]
13.04		11.4	
13.53		11.8(sh)	
14.01			
14.39			
14.55			
14.80			
14.99			
16.63	5	12.6(sh)	[c]
16.82		12.8	

[a] Values refer to band centres, except (sh) which indicates a shoulder feature.
[b] Estimated to be $\geqslant 6$.
[c] Estimated to be $\geqslant 2$.

A scheme of localized cluster bonding in 7,9-$S_2B_9H_9$ calculated with the MNDO programmme is shown in diagram **III**. Of the expected 13 cluster

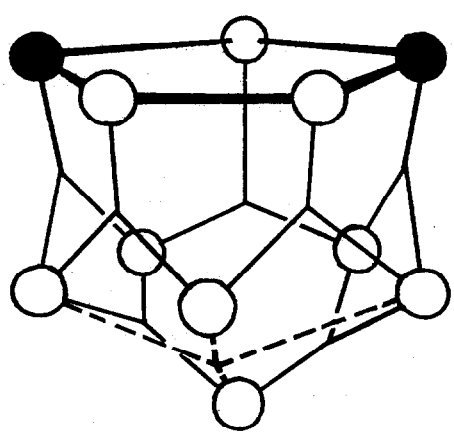

(III)

orbitals four are two-centre S—B localized, one is two-centre B—B, two are three-centre B—S—B, five are three-centre B—B—B and one is a four-centre B—B—B—B orbital. All the two-centre orbitals are located around the open B_3S_2-face. The remaining 12 localized orbitals comprise nine two-centre B—H and two lone-pair sulphur orbitals. The last mentioned correspond to filled 3*s* orbitals at very low energy. Hence, the sulphur atoms can be expected to show no donor properties. On the contrary, the positive charge calculated for the sulphur atoms (+0.34) suggests that these atoms are electrophilic. Some experimental evidence for their electrophilic nature comes from the observation of a compound postulated to be $[Se_2B_9H_{10}O]^-$, which was obtained by Friesen *et al.* from the reaction between $Se_2B_9H_9$ and $[OH]^-$.[3]

Finally, it is noteworthy that while there are many examples of heteroboranes with two or more hetero-atoms from groups IV/14 or V/15 in adjacent positions, apparently there are no heteroboranes with two adjacent atoms from group VI/16 nor any metal-heteroborane derivatives with two adjacent group VI/16 atoms.

EXPERIMENTAL

A sample of 7,9-$Se_2B_9H_9$ was prepared and purified according to a literature method.[3]

NMR spectroscopy

Experiments were performed using a Varian VXR600S spectrometer operating at 14.1 T and a Bruker WH360 spectrometer operating at 8.46 T. The solvent was toluene-d_8 and the spectrometer temperature was 50°C. All ^{11}B chemical shifts are quoted relative to external $BF_3 \cdot OEt_2$ and ^1H chemical shifts relative to internal TMS. The ^{11}B homonuclear correlation experiment (COSY) was performed on the VXR600S instrument, for which the ^{11}B resonance frequency is 192.48 MHz. Details are given in the caption to Fig. 1. The ^{11}B—^1H heteronuclear correlation experiments were performed with the WH360 instrument (for which the ^{11}B frequency is 115.55 MHz and the ^1H frequency is 360.13 MHz) using the sequence XHCORRD.AU provided by Bruker Spectrospin Ltd.

Acknowledgement—We wish to thank the SERC for provision of the ultra high-field NMR facility at the University of Edinburgh.

REFERENCES

1. K. Báse and B. Štíbr, *Chem. Ind.* 1977, 919.
2. J. L. Little, G. D. Friesen and L. J. Todd, *Inorg. Chem.* 1977, **16**, 869.
3. G. D. Friesen, A. Barriola, P. Daluga, P. Ragatz,

J. C. Huffman and L. J. Todd, *Inorg. Chem.* 1980, **19**, 458.
4. M. J. S. Dewar and M. L. McKee, *Inorg. Chem.* 1978, **17**, 1569.
5. O. Ni Dhubhghaill, J. MacCurtain, M. Myers, T. R. Spalding, P. Brint, T. McCabe, G. Ferguson and D. Reed, *Proc. Roy. Ir. Acad.* 1989, **89B**, 461.
6. T. L. Venable, W. C. Hutton and R. N. Grimes, *J. Am. Chem. Soc.* 1982, **104**, 4716; 1984, **106**, 29; D. Reed, *J. Chem. Res. (S)* 1984, 198.
7. D. C. Finster, W. C. Hutton and R. N. Grimes, *J. Am. Chem. Soc.* 1980, **102**, 400; I. Colquhoun and W. McFarlane, *J. Chem. Soc., Dalton Trans.* 1981, 2014.
8. J. MacCurtain, P. Brint and T. R. Spalding, *J. Chem. Soc., Dalton Trans.* 1985, 2591.

Polyhedron Vol. 12, No. 16, pp. 1983–1987, 1993
Printed in Great Britain

0277–5387/93 $6.00+.00
© 1993 Pergamon Press Ltd

A CONVENIENT ROUTE TO IRON(III)-THIOLATES: SYNTHESIS AND CHARACTERIZATION OF LOW-SPIN ($S = 1/2$) IRON(III) COMPLEXES HAVING THE CHROMOPHORE $FeN_2S_2^*S_2$ (S* = THIOETHER)

RAMESHWER SHUKLA and PARIMAL K. BHARADWAJ†

Department of Chemistry, Indian Institute of Technology, Kanpur, Kanpur 208016, India

(*Received* 5 *April* 1993; *accepted* 22 *April* 1993)

Abstract—Three air-stable iron(III) complexes with homoleptic hexadentate ligands with the donor set $N_2S_2^*S_2$ (S* = thioether, S = thiolate) have been isolated. The two thiol groups present in each ligand are initially protected as their t-butyl derivatives. When iron(III) chloride is allowed to reflux with any of these thiol-protected ligands the S—Bu^t linkages are cleaved forming the corresponding iron(III)-thiolates in high yields. The complexes are characterized by electronic absorption, EPR and room-temperature Mössbauer spectroscopic as well as room-temperature magnetic susceptibility studies. As the spectral data indicate each complex has a pseudo-octahedral coordination geometry around the metal ion. The effective magnetic moment values at 300 K lie in the range 2.24–2.30, corresponding to low-spin iron(III) ($S = 1/2$) complexes with significant orbital contribution. One of the complexes exhibits a quasi-reversible Fe^{III}/Fe^{II} couple at $E_f = -1.66$ V (vs S.C.E.), while another complex shows a quasi-reversible Fe^{IV}/Fe^{III} couple at $E_f = 0.86$ V (vs S.C.E.).

A number of proteins contain[1–3] iron in different oxidation states with donations mainly from sulphur. Besides these, a bacterial enzyme nitrile hydratase from *Brevibacterium* R312[4] and *Pseudomonas chlororaphis* B23[5] contains iron coordinated to sulphur and nitrogen/oxygen in an octahedral fashion. Detailed spectroscopic studies[6] on this enzyme indicate that iron is present in the +3 oxidation state with low spin ($S = 1/2$). In order to model these sites low molecular weight complexes of iron with sulphur ligation are necessary. A number of polynuclear Fe—S complexes are known,[7,8] where iron exists in different formal oxidation states. In contrast, studies on mononuclear iron complexes in the +3 oxidation state with sulphur ligation are somewhat sparse.[9,10] This is because of the facile redox decomposition of such systems. As a matter of fact, no general synthetic method for iron(III)-thiolates is available. In our quest to find a synthetic strategy to circumvent such redox instability, we present here a synthetic route to iron(III)-thiolates. The method involves cleavage of the S—Bu^t linkage(s) present in a multidonor ligand (as shown in Fig. 1) utilizing the Lewis acidity of the metal ion.[11] Previously, we had reported[12] the synthesis of stable copper(II)-thiolates from these ligands. We, therefore, started with the idea that the iron(III) ion, being a better Lewis acid compared with the copper(II) ion, should be able to cleave the S—Bu^t linkage. Once the free thiolate is formed it should be able to occupy the vacant coordination site on the iron(III). Herein, we describe this method of synthesis of iron(III)-thiolates and their characterization by different spectroscopic and electrochemical techniques.

EXPERIMENTAL

Materials

2-Nitrobenzaldehyde, 2-mercaptoaniline, 1,2-dibromoethane, mercaptoacetic acid, thiosalicyclic acid, t-butylthiol (Aldrich), ethyl chloroformate and iron(III) chloride (Merck) were used as received. All solvents were from Glaxo laboratories

† Author to whom correspondence should be addressed.

and were purified prior to use following standard methods.[13]

The electronic absorption, IR, proton NMR, EPR spectroscopic and room-temperature magnetic susceptibility studies were made as reported earlier.[12] The electrical conductivity of the complexes in acetonitrile solutions were measured using an Elico model CM-82T conductivity bridge. Cyclic voltammograms of the complexes were obtained on a PAR model 370-4 electrochemistry system using freshly purified DMF. The working electrode was glassy carbon and the standard electrode was a saturated calomel electrode. Under our experimental conditions the reversible[14] ferrocenium/ferrocene couple had $\Delta E_p = 80$ mV at $E_f = 0.360$ (mV vs S.C.E.) $[E_f = 0.5\ (E_{pa} + E_{pc})]$. Transmission Mössbauer spectra at 295 K were recorded with a Wiessel Mössbauer spectrometer (Wissel Electronik GmbH, Germany) operating in constant acceleration mode and a ^{57}Co/Rh source. The elemental analyses were performed at the Central Drug Research Institute, Lucknow, India.

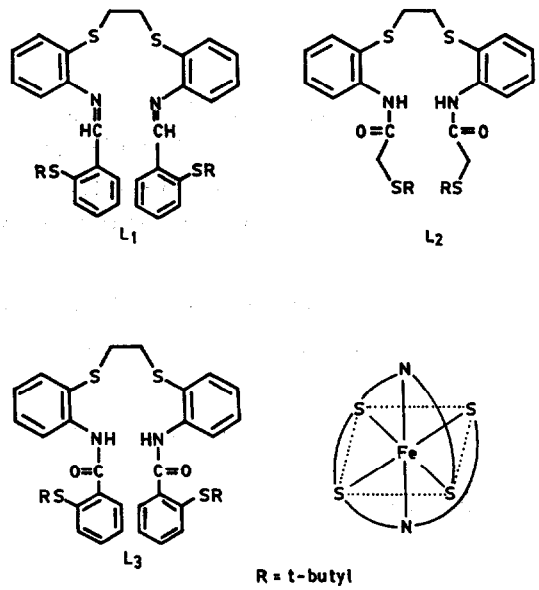

Fig. 1. Ligands used in the present study.

Synthesis of the ligands and complexes

The ligands shown in Fig. 1 were synthesized as described earlier.[12b,c]

Synthesis of complex **1**. To the ligand L_1 (1.25 g, 2 mmol) taken in ethanol (50 cm^3) was added an ethanolic solution (10 cm^3) of iron(III) chloride (0.33 g, 2 mmol) under dinitrogen. The colour of the solution changed to dark red in 5 min upon heating the mixture. After refluxing for 30 min the dark red solution was filtered in air, reduced in volume to *ca* 25 cm^3 in a rotary evaporator and finally allowed to evaporate at room temperature. A dark-red polycrystalline solid appeared overnight, which was collected and air-dried; yield 41%.

Synthesis of complex **2**. This complex was synthesized with L_2 following the method as described above; yield 46%.

Synthesis of complex **3**. Synthesis of this complex was achieved with L_3 as above in 43% yield.

Analytical data for the complexes are collected in Table 1.

RESULTS AND DISCUSSION

The complexes are readily formed as mononuclear cationic species by refluxing an iron(III) salt with the ligand in ethanol under a dinitrogen atmosphere. The reaction cleanly forms the desired products in high yields. They are air-stable both in the solid state as well as in solution (acetone, acetonitrile). In DMF the complexes are stable at least up to 2 h. This stability arises due to the hexadentate chelating ligand occupying all the six coordination sites on the iron(III) ion. The corresponding PF_6^-

Table 1. Cyclic voltammetric[a] and analytical[b] data of the complexes

Complex	Redox couple E_f (V)	ΔE_p (mV)	Analysis (%) C	H	N	S
1	−1.66	120	54.2(55.5)	3.7(3.6)	4.4(4.6)	21.0(21.2)
2	0.87	170	41.8(42.1)	3.5(3.5)	5.1(5.4)	24.8(25.0)
3	—	—	52.4(52.7)	3.3(3.5)	4.2(4.4)	19.9(20.0)

[a] Calculated values are given in parentheses.

[b] All results reported were obtained at 298 K at a scan rate of 100 mV s^{-1} and referenced to S.C.E.; $E_f = 0.5\ (E_{pa} + E_{pc})$; E_{pa} and E_{pc} are the anodic and cathodic peak potentials, respectively.

Table 2. Room-temperature magnetic, EPR and electronic spectral data of the complexes

Complex	μ_{eff}/μ_B	g_{av} values	λ_{max} (nm) (ε_{max}, $dm^3\ mol^{-1}\ cm^{-1}$)
1	2.29	2.01 (solid, 298 K) 2.03 (solid, 77 K) 2.12 (soln, 298 K) 2.01 (soln, 77 K)	770(410), 625(950), 305(6065)
2	2.24	2.01 (solid, 298 K) 2.01 (solid, 77 K) 2.03 (soln, 298 K) 2.01 (soln, 77 K)	810(280), 640(1450), 310(6135)
3	2.30	2.01 (solid, 298 K) 2.02 (solid, 77 K) 2.06 (soln, 298 K) 2.01 soln, 77 K)	750(180), 625(495), 380(3010)

salts are less soluble in solvents such as acetonitrile as they are precipitated when the chloride salts are treated with $NaPF_6$. The IR spectra of the PF_6^- salts are, however, not diagnostic of the presence of this anion as the ligand itself absorbs strongly in the same region. These complexes, having either PF_6^- or chloride counterions, afford only polycrystalline products. Isolation in single-crystal forms suitable for X-ray crystallography remained unachievable.

The solution electronic spectra for all the hexadentate complexes are quite similar (Table 2) and confirm the presence of iron(III)-thiolate bonds. Each exhibits a strong band in the UV region around 300 nm and one broad band centred near 620 nm with a low energy shoulder. Only a few authentic mononuclear iron(III)-thiolate complexes are known. The electronic spectra of the X-ray crystallographically characterized $[Fe^{III}S_4]$ cores exhibit[9] two charge-transfer bands at 280 and 350 nm, while the pseudo-octahedral FeN_3S_3 complex[10] shows two strong bands near 300 nm. Hence, the two bands around 300 nm are assigned as ligand-to-metal charge-transfer transitions involv-

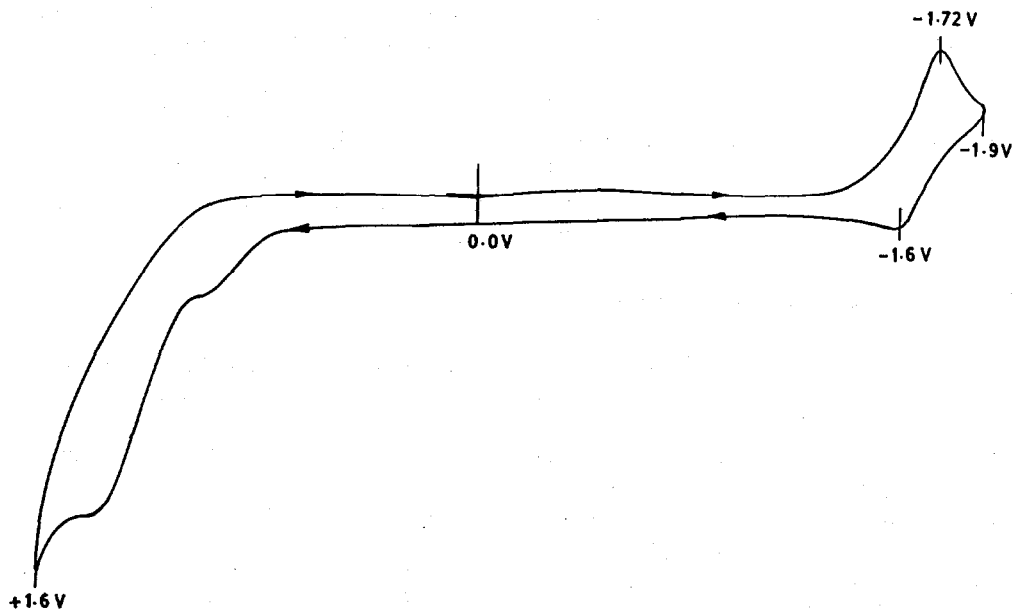

Fig. 2. Cyclic voltammogram (100 mV s^{-1}) of **1** in DMF at a glassy carbon electrode.

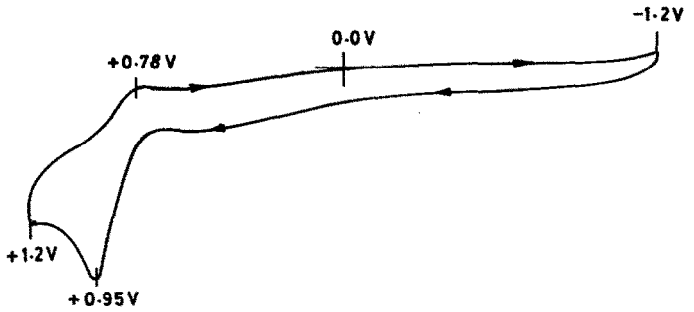

Fig. 3. Cyclic voltammogram (100 mV s^{-1}) of **2** in DMF at a glassy carbon electrode.

ing thiolate and iron(III). Unlike the $[Fe^{III}S_4]$ chromophores, which show a strong and broad band centred around 500 nm, each of the three complexes **1–3** shows one strong band centred near 620 nm with a low energy shoulder attributable to the ligand field transitions. The higher intensity of the ligand field transitions should be due[15] to increased metal–ligand covalency.

The electron-transfer properties of the complexes in DMF were probed by room-temperature cyclic voltammetry. Cyclic voltammograms are shown in Figs 2 and 3, while the redox data are given in Table 1. Complexes **1** and **2** show cyclic responses which are quasi-reversible. The copper(II) complexes of these ligands[12b,c] also exhibit cyclic responses, although at very different potentials. Therefore, the cyclic responses are concluded to be metal-centred. The response in **1** is due to the Fe^{III}/Fe^{II} couple, as eq. (1) below suggests:

$$[Fe(L_1)]^+ + e = [Fe(L_1)] \quad (1)$$

On the other hand, in **2** the response is due to the Fe^{IV}/Fe^{III} couple [eq. (2)]:

$$[Fe(L_2)]^{2+} + e = [Fe(L_2)]^+ \quad (2)$$

It is of relevance to note here that the copper(II) complex of the ligand L_2 shows[12c] a reversible Cu^{III}/Cu^{II} couple at $E_f = 0.55$ V (vs S.C.E.), suggesting the ability of this ligand to stabilize high oxidation states.

The effective magnetic-moment values (μ_{eff}/μ_B) for the complexes range between 2.24 and 2.30 (Table 1) at 300 K. Recently an $Fe^{III}N_3S_3$ complex has been reported[10] that has a pseudo-octahedral geometry around iron(III), consisting of three amino nitrogens of the 1,4,7-triazacyclononane backbone and three thiophenolato sulphurs. This complex shows temperature-dependent magnetic moments with predominantly low-spin (2.4 μ_B at 77 K and 2.9 μ_B at 300 K) at ambient temperatures. The magnetic data for **1–3** are consistent[16,17] with low-spin ($S = 1/2$) iron(III) complexes with significant orbital contributions. The *X*-band EPR spectra of the complexes also corroborate the low-spin nature of the complexes. All the complexes exhibit broad EPR signals near $g = 2$ at 298 or 77 K and no signal is seen near $g = 4$ under any circumstances. Resolved EPR spectra could not be observed either in the solid state or in dilute acetonitrile solutions. Lack of hyperfine splittings and the g value deviating from the free electron g value are indicative[18,19] of delocalization of the odd electron into the four bound sulphurs of the ligand moiety. Studies of molecular models indicate that the binding mode, as illustrated in Fig. 1, leads to the least strained conformation of the ligands as found earlier in the case of copper(II) complexes with these ligands.[12b,c] Thus, the singly occupied metal orbital of the t_{2g} set overlaps with the four equatorially-bound sulphur atoms in the complex leading to increased covalency of the metal–ligand bond.

In order to further confirm the presence of the low-spin iron(III) centres in **1–3** Mössbauer spectra were recorded at 295 K. Table 3 lists the relevant data; characteristic spectra are shown in Fig. 4. The zero-field spectra of the complexes display symmetrical quadrupole doublets. Both the isomer shifts and quadrupole splittings of the complexes are quite comparable with each other. This is attributed to the similar coordination environments

Table 3. Room-temperature Mössbauer spectral data of the complexes

Compound	Isomer shift (Fe, mm s^{-1})	Quadrupole splitting ΔE_q (mm s^{-1})
1	0.49	0.84
2	0.42	0.72
3	0.42	0.86

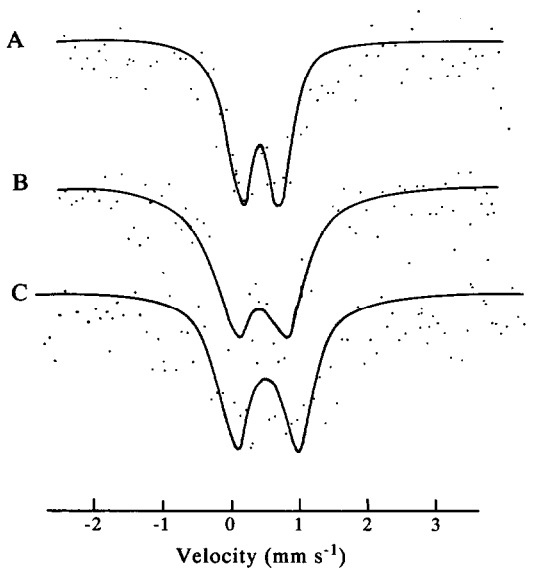

Fig. 4. Room-temperature Mössbauer spectra for (A) **1**, (B) **2** and (C) **3**.

around the iron(III) ion. Also, the magnitude of these parameters is consistent[10,20,21] with low-spin ($S = 1/2$) octahedral iron(III) complexes.

CONCLUSIONS

The present study shows that it is possible to have a general synthetic route to stable octahedral iron-(III)-thiolates. Both the thiolate sulphurs and the amines, being strong donors, form low-spin iron-(III) complexes. Interestingly, the ligand donor set for iron(III) is quite similar to the one present in the enzyme nitrile hydratase and in both the cases iron(III) is in the low-spin ($S = 1/2$) state. Mimicking the active sites of nitrile hydratase with different types of ligands having thiolate donors is in progress.

Acknowledgement—We thank the Department of Science and Technology, New Delhi, India, for financial support.

REFERENCES

1. T. R. Hawkes, P. A. McLean and B. E. Smith, *Biochem. J.* 1984, **217**, 217.
2. *Iron–Sulfur Proteins, Metal Ions in Biology* (Edited by T. G. Spiro), Vol. 4. John Wiley and Sons, New York (1982).
3. *Iron–Sulfur Proteins* (Edited by W. Lovenberg), Vol. 1. Academic Press, New York (1973).
4. T. Nagasawa, K. Ryuno and H. Yamada, *Biochem. Biophys. Res. Commun.* 1986, **139**, 1305.
5. T. Nagasawa, H. Nanba, K. Ryouno, K. Takeuchi and H. Yamada, *Eur. J. Biochem.* 1987, **162**, 691.
6. M. J. Nelson, H. Jin, I. M. Turner Jr, G. Grove, R. C. Scarrow, B. A. Brennan and L. Que Jr, *J. Am. Chem. Soc.* 1991, **113**, 7072.
7. B. R. Krebs and G. Henkel, *Angew. Chem., Int. Edn Engl.* 1991, **30**, 769 and refs therein.
8. S. Ciurli, M. Carrie, J. A. Weigel, M. J. Carney, T. D. P. Stack, G. C. Papaefthymiou and R. H. Holm, *J. Am. Chem. Soc.* 1990, **112**, 2654 and refs therein.
9. H. Sanghwa, S. C. Roman and T. G. Spiro, *Inorg. Chem.* 1986, **25**, 2276.
10. T. Beissel, K. S. Burger, G. Voigt, K. Wieghardt, C. Butzlaff and A. X. Trautwein, *Inorg. Chem.* 1993, **32**, 124.
11. H. Toftlund, J. Becher, P. H. Olesen and J. H. Pedersen, *Isr. J. Chem.* 1985, **25**, 56.
12. (a) S. Mandal and P. K. Bharadwaj, *Ind. J. Chem.* 1991, **30A**, 948; (b) S. Mandal and P. K. Bharadwaj, *Polyhedron* 1992, **11**, 1037; (c) S. Mandal, R. Shukla and P. K. Bharadwaj, *Polyhedron* 1992, **11**, 1855.
13. D. D. Perrin, W. L. F. Armarego and D. R. Perrin, *Purification of Laboratory Chemicals*, 1st edn. Pergamon Press, Oxford (1966).
14. M. A. Weiner and A. Basu, *Inorg. Chem.* 1980, **19**, 2797.
15. A. B. P. Lever, *Inorganic Electronic Spectroscopy*, 2nd edn, p. 452. Elsevier, New York (1984).
16. K. Weighardt, W. Schmidt, W. Hermann and H. J. Kuppers, *Inorg. Chem.* 1983, **22**, 2953.
17. L. L. Martin, R. L. Martin, K. S. Murray and A. M. Sargeson, *Inorg. Chem.* 1990, **29**, 1387.
18. D. Sellmann, M. Geck, F. Knoch, G. Ritter and J. Dengler, *J. Am. Chem. Soc.* 1991, **113**, 3819.
19. Y. Sugiura, J. Kuwahara, T. Nagasawa and H. Yamada, *J. Am. Chem. Soc.* 1987, **109**, 5848.
20. R. Richards, C. E. Johnson and H. A. O. Hill, *J. Chem. Soc. (A)* 1971, 797.
21. H. Oshio, K. Toriumi, Y. Maeda and Y. Takashima, *Inorg. Chem.* 1991, **30**, 4252.

Polyhedron Vol. 12, No. 16, pp. 1989–2000, 1993
Printed in Great Britain

0277–5387/93 $6.00+.00
© 1993 Pergamon Press Ltd

THE MOLECULAR STRUCTURES AND MAGNETIC PROPERTIES OF μ_3-TETRANUCLEAR β-DIKETONATE COPPER COMPLEXES $[Cu(bzac)(\mu_3\text{-}OC_2H_4OCH_3)]_4$ AND $[Cu(\mu\text{-}dbm)(\mu_3\text{-}OC_2H_4OCH_3)]_4$

G. D. FALLON, B. MOUBARAKI, K. S. MURRAY, A. M. VAN DEN BERGEN and B. O. WEST*

Centre for Chemical Synthesis and Department of Chemistry, Monash University, Clayton, Victoria 3168, Australia

(*Received* 23 *March* 1993; *accepted* 22 *April* 1993)

Abstract—$[Cu(bzac)(OC_2H_4OCH_3)]_4$† (**I**) and $[Cu(dbm)(OC_2H_4OCH_3]_4$† (**II**) have been shown to be tetrameric in the solid state. Compound **I** has a pseudo-cubane type structure with μ_3-alkoxide oxygens occupying four bridging positions. Two methoxy oxygens are also within bonding distance of copper(II) ions. Compound **II** has a stepped configuration with a chelate ring and alkoxide oxygens as bridging centres. None of the methoxy oxygens is clearly chelating. Magnetic susceptibility data versus temperature data to 4 K for the complexes show antiferromagnetic coupling which can be treated by "pairs of equal dimers" procedures. The complexes decompose in stages at temperatures below 350°C at atmospheric pressure to give CuO.

The search for suitable precursors for the preparation of layers of CuO or lanthanoid-Ba—Cu superconducting oxides by hydrolytic or MOCVD processes[1,2] has turned attention to the synthesis of soluble or volatile copper(II) complexes[3,4] involving alkoxides Cu(L)(OR'), particularly alkoxy-alkoxides.

Studies of their structural and other properties[5] are, therefore, important in the search for correlations which can predict combinations of ligand and alkoxide which give appropriate solubility, volatility, thermal stability and hydrolytic behaviour.

A substantial number of copper(II) complexes containing a β-diketonate[3,4,6,7] or related ligand, such as a hydroxy benzaldehyde[8] and an alkoxide group [Cu(lig)(OR)], have been reported since the initial study of the $[Cu(acac)(OCH_3)]$ complex by Bertrand and Kaplan.[9] However, only seven structural studies have been reported for such compounds,[7,10] five appearing in 1992.[4,11] The results have identified three types of structure with some variation within each type. Type 1 structures are dimers with alkoxide groups defining essentially square-planar arrays of Cu_2O_6 atoms (**i**). The copper ions can achieve square-pyramidal coordination by coordinating with other Lewis bases as in the sole example of this type so far reported, $[Cu(tfac)(OC_6F_5)(THF)]_2$.[4] Related alkoxy-bridged complexes have also been characterized, of the form $[M(acac)_2(OR)]_2$, R = CH_3, M = Fe^{III},[12] Cr^{III},[13,14] where each M ion is six-coordinate. Type 2 structures are formed by association of pairs of dimers to form tetramers of Cu_4O_4 core units and two subclasses have been reported. In type 2(a) (**ii**) association occurs between dimeric units with inter-dimer bonding between oxygens of chelate rings on one dimer and copper(II) ions on the other, together with additional inter-dimer bonding between bridging alkoxide oxygens (now μ_3-O) and copper(II)

* Author to whom correspondence should be addressed.

† Ligand abbreviations used for β-diketonate anions are as follows: bzac = benzoylacetonato(1-phenyl-1,3-butanedionato); tfac = 1,1,1-trifluoroacetylacetonato (1,1,1-trifluoro-2,4-pentanedionato); hfac = 1,1,1-5,5,5-hexafluoroacetylacetonato(1,1,1 - 5,5,5 - hexafluoro - 2,4-pentanedionato); acac = acetylacetonato(2,4-pentanedionato); pvac = dipivaloylacetonato(2,2,6,6-tetramethyl-3,5-heptanedionato); and dbm = dibenzoylmethanato (1,4-diphenyl-1,3-propanedionato).

ions as in the first characterized species, $[Cu(acac)(OCH_2Ph)]_4$[10] and $[Cu(tfac)(OCH_2CH_2OCH_3)]_4$.[4] Type 2(b) structures (**iii**) only involve inter-dimer bridging through alkoxide oxygens, as in the dipivaloylmethane-methoxide derivative $[Cu(dpm)(OCH_3)]_4$.[7] There are no chelate—O—Cu distances reported or commented on in this latter work and it is possible that further weak interactions do occur involving these ligands, making the structure similar to type 2(a). However, the bulky tert-butyl groups of the β-diketone ligands may prevent easy coordination. Such structures have been termed "stepwise"[10] or "ladder-like".[7]

The third type of structure (**iv**) also contains a tetrameric Cu_4O_4 core formed by the association of dimer units, but is of the pseudo-cubane type with axes of the pairs of copper ion in each "dimer" subunit arranged at approximately 90° to each other. The alkoxy oxygens act as μ_3-bridging groups. Three complexes having this type of structure have now been structurally characterized, $[Cu(hfac)(OCH_3)(THF)]_4$,[4] $[Cu(hfac)(OC_2H_4OCH_3)]_4$[4] and $[Cu(acac)(OC_2H_4OCH(CH_3)_2)]_4$.[11] The copper ions may be further coordinated to other Lewis bases, as in the first of the three examples, of the methoxy oxygen of $(OCH_2CH_2OCH_3)^-$.

A study[15] of the related cobalt(II) and nickel(II) derivatives, $[M(acac)(OCH_3)(CH_3OH)]$, shows them to have similar cubane-like structures with a molecule of methanol coordinated to each metal centre. Magnetic susceptibility vs temperature studies[6,16] on a number of such copper compounds have shown that the copper(II) ions are coupled antiferromagnetically, leading to values for room-temperature moments per copper ion less than the spin only value for one unpaired electron. However, the paucity of structural data on these types of complexes has not permitted any comparisons of the extent of coupling and structure. The recently[4] demonstrated structural variety of this class of copper(II) complexes strongly suggests that steric factors arising from ligand or alkoxide group substituents can determine the final molecular structure observed and hence the degree of magnetic coupling.

We wish to report further structural, magnetic and thermal studies of copper complexes containing the methoxyethoxide group and the non-symmetrically substituted ligand 1-phenyl-1,3-butanedione (benzoylacetone, bzac) and the symmetrical, bulkier variant 1,3-diphenyl-1,3-propanedione (bidenzoylmethane, dbm) to test the influence of ligand structure on complex structure type and hence on the degree of magnetic coupling. In addition ligand influence on whether the methoxyethoxide group can chelate to copper was sought

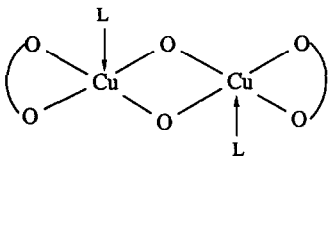

Type 1

(i)

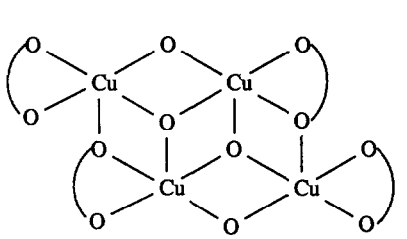

Type 2 (a)

(ii)

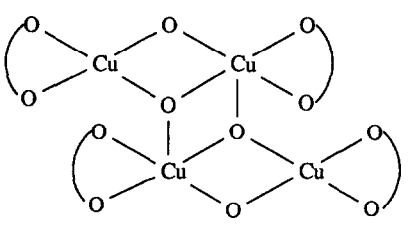

Type 2(b)

(iii)

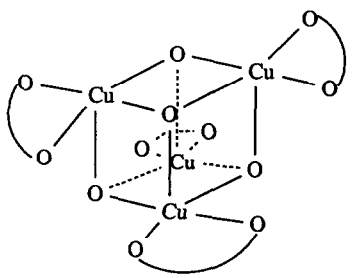

Type 3

(iv)

in the light of the differing situations in [Cu(acac)($OC_2H_4OCH(CH_3)_2$)]$_4$[11] (no chelation) and [Cu(hfac)($OC_2H_5OCH_3$)]$_4$[4] (chelation).

EXPERIMENTAL

The copper complexes are susceptible to hydrolysis in air in the solid state as well as in solution and all operations were performed using standard Schlenk manipulations under an atmosphere of dry nitrogen. IR spectral measurements were obtained with either Perkin–Elmer FT1600 or JASCO A100 spectrometers. Molecular weights were obtained at 60° in benzene using a Knauer Type II vapour phase osmometer (VPO). Microanalyses were by the National Analytical Laboratories. Thermogravimetric measurements were obtained on a Stanton Redcroft Model STA 1500 thermal analyser at heating rates of 10° min^{-1} and a nitrogen flow rate of 15 cm^3 min^{-1}.

Measurements of magnetic susceptibility

Powdered specimens were used and measurements of susceptiblity obtained at a field strength of 10,000 G between 300 K and 4.2 K using a Quantum Design M.P.M.S. Squid magnetometer. The calibration of the instrument was checked regularly against pure palladium and AR $CuSO_4 \cdot 5H_2O$. Samples were enclosed in gelatine capsules which were suspended at the middle of a plastic drinking straw, which was rigidly fixed to the end of the sample rod.

Syntheses

[Cu(bzac)($OC_2H_4OCH_3$)]$_4$ **(I)** *and* [Cu(acac)($OC_2H_4OCH_3$)]$_4$. Initial attempts to prepare the complexes by refluxing Cu(bzac)$_2$ or Cu(acac)$_2$ with KOH in 2-methoxyethanol yielded red Cu_2O. An alternate successful procedure was subsequently developed involving exchange of the methoxide group in [Cu(bzac)(OCH_3)] or [Cu(acac)(OCH_3)] for the 2-methoxyethoxide ion. The methoxide complexes were readily prepared by refluxing Cu(bzac)$_2$ or Cu(acac)$_2$ in methanol in the presence of 1 molar equivalent of KOH. A general procedure is described for the bzac derivative.

A solution of Cu(bzac)(OCH_3) (1.28 g, 5 mmol) in 2-methoxyethanol (10 cm^3) was refluxed for 5 min, during which time the solution colour changed from green to bright blue. The hot solution was filtered through a Celite pad and then allowed to cool. Blue–green dichroic crystals were formed (1.0 g, 60% yield). Further recrystallization of this material from 2-methoxyethanol gave crystals suitable for X-ray studies. Found: C, 52.1; H, 5.2. Calc. for $C_{13}H_{16}O_4Cu$: C, 52.1; H, 5.4%. IR (Nujol, cm^{-1}): 1020 m [ν(Cu—OR)], 505 s [ν(Cu—OR)], 460 [ν(Cu—O)]. Mol. wt (benzene, 60°): 0.0255 M, 1176±80; 0.058 M, 1076±80. Calc. for [Cu(bzac)($OC_2H_4OCH_3$)]$_4$, 1198. μ_{eff} = 1.48 B.M. (300 K).

[Cu(acac)($OC_2H_4OCH_3$)]. Found: C, 40.4; H, 5.9. Calc. for $C_8H_{14}O_4Cu$: C, 40.5; H, 6.1%. IR (Nujol, cm^{-1}): 1020 m [ν(Cu—OR)], 519 s (ν(Cu—OR)), 445 [ν(Cu—O)]. μ_{eff} = 1.39 B.M. (300 K).

[Cu(dbm)($OC_2H_4OCH_3$)]$_4$ **(II)**. Cu(dbm)$_2$ is insoluble in methanol, preventing direct formation of [Cu(dbm)(OCH_3)]$_4$ and hence negating the exchange route. However, 2-methoxyethanol, at reflux temperature, reacts with Cu(dbm)$_2$ in the presence of KOH and after filtration of the brown solid formed initially [Cu(dbm)$_2$ contaminated by traces of Cu_2O] the desired blue–green compound crystallized from the filtrate on cooling. Reycrystallization from 2-methoxyethanol gave material suitable for X-ray study. Found: C, 59.6; H, 5.0. Calc. for $C_{18}H_{18}O_4Cu$: C, 59.7; H, 5.0%. IR (Nujol, cm^{-1}): 1020 m [ν(Cu—OR)], 517 [ν(Cu—OR)], 457 [νCu—O]. μ_{eff} = 1.52 B.M. (300 K). The complex was also prepared by reaction of Cu(dbm)$_2$ with an equimolar quantity of preformed Na($OC_2H_4OCH_3$) in 2-methoxyethanol. The mixture was refluxed for 1–2 h under nitrogen and the complex crystallized out on cooling.

Crystallographic studies of [Cu(bzac)($OC_2H_4OCH_3$)]$_4$ **(I)** *and* [Cu(dbm)($OC_2H_4OCH_3$]$_4$ **(II)**

Crystals of approximate dimensions 0.17×0.20×0.11 mm **(I)** and 0.24×0.16×0.22 mm **(II)** were used for data collection. Intensity measurements were obtained on a Philips PW1100 diffractometer using graphite monochromated Cu-K_α radiation. Crystallographic data are collected in Table 1. Three standard reflections monitored every 4 h for each complex showed no significant variation over the data collection periods. Intensity data were processed as previously described.[17] Face-indexed numerical absorption corrections were applied, the maximum and minimum transmission factors, respectively, being **(I)** −0.804 and 0.540 and **(II)** −0.765 and 0.632. The atomic scattering factors for neutral atoms were taken from literature values[18] and corrected for anomalous dispersion. Calculations were performed on VAX 11/780 **(I)** and VAX 6250 **(II)** computers, the program for least-squares refinement being that due to Sheldrick.[19] The structures were solved by direct

Table 1. Crystallographic data for $[Cu(bzac)(OCH_2CH_2OCH_3)]_4$ (I) and $[Cu(dbm)(OC_2H_4OCH_3)]_4$ (II)

	$[Cu(bzac)(OC_2H_4OCH_3)]_4$ (I)	$[Cu(dbm)(OC_2H_4OCH_3)]_4$ (II)
Compound	$C_{52}H_{64}Cu_4O_{16}$	$C_{72}H_{72}Cu_4O_{16}$
Colour	Green–blue	Green
Molecular weight	1199.3	1447.6
Crystal system	Triclinic	Triclinic
Space group	$P\bar{1}$	$P\bar{1}$
a (Å)	20.062(2)	13.823(1)
b (Å)	14.970(1)	12.473(2)
c (Å)	10.658(2)	12.978(1)
α (°)	69.156(8)	91.699(5)
β (°)	74.597(9)	123.216(5)
γ (°)	65.637(8)	110.723(5)
U (Å^3)	2698.3(7)	1653.3(4)
Density calc. (g cm^{-3})	1.48	1.45
Density meas. (g cm^{-3})	1.47(1)	1.45(1)
Z	2	1
T (°C)	20(1)	20(1)
λ(Cu-K_α) (Å)	1.5418	1.5418
μ(Cu-K_α) (mm^{-1})	22.9	19.69
Scan mode	$\theta/2\theta$	$\theta/2\theta$
2θ range (°)	6–120	6–120
Symmetric scan range (°)	$\pm(0.80+0.10\tan\theta)$	$\pm(0.75+0.20\tan\theta)$
Scan rate (s^{-1})	0.05	0.03
Data collected	7991	4914
Data used [$I \geqslant 3\sigma(I)$]	5254	3953
$R(R')$	0.053 (0.057)	0.035 (0.037)

methods. Full-matrix least-squares refinements employed anisotropic thermal parameters for copper and oxygen and isotropic thermal parameters for all other atoms, including single isotropic thermal parameters for hydrogen [which refined to 0.094(3) Å^2 for **I** and 0.08 Å^2 for **II** positioned in geometrically idealized positions: C—H (**I**) = 0.97 Å, C—H (**II**) = 0.96 Å. $R' = \Sigma w^{1/2}(||F_o|-|F_c||)/\Sigma w^{1/2}|F_o|$ and $\omega = [\sigma^2(F_o)]^{-1}$. The goodness-of-fit values $([\Sigma w(|F_o|-|F_c|)^2/(N_{obs}-N_{para})]^{1/2})$ were 2.10 (**I**) and 1.81 (**II**), respectively. The highest peaks in the difference-Fourier syntheses were 0.58 (**I**) and 0.30 e Å^{-3}.

RESULTS AND DISCUSSION

Syntheses

A general method for the synthesis of copper β-diketone–alkoxide complexes involves reaction of alkoxide anions formed by reaction of KOH[9,20] or alkali metals alone[4,11] with an alcohol and the bis copper complex $Cu(lig)_2$. Reaction between 3,5-substituted salicylaldehydato-copper complexes and alcohols alone have been reported[8] to form OCH_3 and OC_2H_5 derivatives, but the salicylaldehyde complex requires a base to be present for reaction to occur. Although the copper-dbm-methoxyethoxide compound was prepared for the present study by the KOH method, reactions with $Cu(bzac)_2$ and, for comparison, $Cu(acac)_2$ produced red Cu_2O as the main product. Indeed the yield of $[Cu(dbm)(OC_2H_4OCH_3)]_4$ was low and the recovered $Cu(dbm)_2$ appeared to be contaminated with traces of the copper(I) oxide. This complex was however readily prepared by reaction of the preformed sodium alkoxide. A more general reaction involves exchange of one alkoxide group for another by reacting a preformed [Cu(lig)(OR)] complex with another alcohol, preferably of higher boiling point than ROH to facilitate its removal. The Cu-bzac-OCH_3 and analogous acac complex were readily prepared by reaction of $Cu(bzac)_2$ or $Cu(acac)_2$ with methanol and both compounds underwent ready replacement of the methoxide group by methoxyethoxide when refluxed in that alcohol. This synthetic route was introduced by Mehrotra[21] for the preparation of nickel β-diketone–alkoxide compounds and clearly obviates complications due to the reducing properties of

alcohols in strongly basic solution. Each complex showed a comparable IR absorption at 1020 cm^{-1}, which was associated with the presence of the alkoxide group.

The structures of the complexes

[Cu(bzac)($OC_2H_4OCH_3$)]$_4$ (**I**). A diagram of the structure determined by a single-crystal X-ray study is shown in Fig. 1 with selected bond lengths and angles in Table 2 and angles of intersection of the various planes of interest in Table 3. The molecule may be considered to consist of two dimeric units, [Cu(bzac)($OC_2H_4OCH_3$)]$_2$, in which the copper(II) ions are bridged by alkoxy groups, associated into a tetrameric pseudo-cubane (type 3) structure by further, longer bonds between the alkoxide oxygens of each dimer with copper(II) ions in the other. The Cu···Cu axes in each dimeric unit lie at 96.4° to each other. The "intra-dimer" Cu—alkoxy O bonds average 1.954 Å compared with the larger, "inter-dimer" Cu—O linkages averaging 2.436 Å. This indicates weaker coordination between "dimers" than between the monomer units [Cu(bzac)(OR)]. These distances are comparable with those found for the other tetrameric examples described previously (Table 4). The distances between two of the methoxyl-oxygen atoms and two copper(II) ions are short enough to indicate weak bonding [Cu(2)—O(10), 2.865(5) Å; Cu(4)—O(14), 2.867(5) Å] giving six-coordinate copper at these sites. The remaining Cu–methoxyl O distances are much longer (4.76 Å) and no significant bonding interaction would seem possible leaving these copper(II) ions five-coordinate. This situation can be compared with that in [Cu(hfac)($OC_2H_4OCH_3$)]$_4$,[4] where a bonding interaction is indicated between methoxyl oxygens and each copper(II) ion. The Cu—methoxyl O distances (2.67 and 2.56 Å) are shorter than those in the present case. In the third example known having this type 3 structure, [Cu(acac)($OC_2H_4OCH(CH_3)_2$)]$_4$,[7] the isopropoxy oxygen atoms are not within bonding distances of the copper(II) ions. In the bzac compound the planes defined by the Cu_2O_2 dimer units Cu(I)—O(II)—O(9)—Cu(2) and Cu(3)—O(13)—O(15)—Cu(4) are not parallel, but inclined at an angle of 5.5°. Similarly the various benzoylacetonate chelate rings are inclined at angles to these planes. For each "dimer unit" one chelate plane (C_3O_2Cu) intersects at *ca* 23° and the other at *ca* 10° (Table 4), i.e. each is deflected away from the Cu_2O_2 plane and the Cu_4O_4 core. The phenyl rings in each dimer have a *trans* relationship to each other. In the tetramer, however, the arrangement of the two dimers brings pairs of phenyl groups in each dimer towards one another, causing the phenyl rings to incline at angles of *ca* 18° or 30° to their respective chelate rings (Table 3). A view of the molecule through the Cu(1)—O(9)—O(13)—Cu(3) face (Fig. 2) displays this arrangement and shows how the methoxy oxygens of the two alkoxy-methoxide groups are turned away from Cu(1) and Cu(3), while the remaining two are able to interact with Cu(2) and Cu(4).

[Cu(dbm)($OC_2H_4OCH_3$)]$_4$ (**II**). An ORTEP dia-

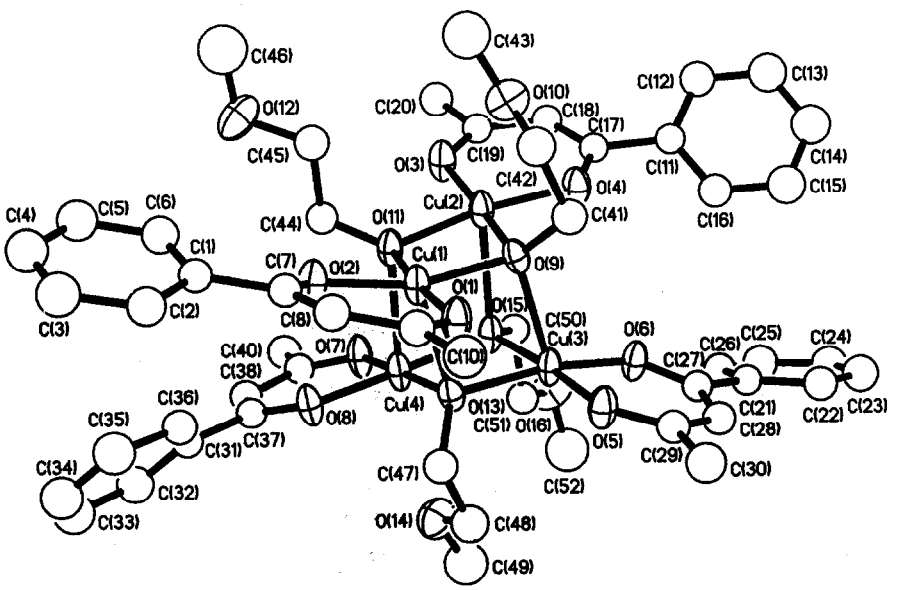

Fig. 1. ORTEP diagram of the molecular structure of [Cu(bzac)($OC_2H_4OCH_3$)]$_4$ (**I**) showing the atom-labelling scheme. Thermal ellipsoids at 50% probability.

Table 2. Selected bond lengths (Å) and angles (°)

[Cu(bzac)($OC_2H_4OCH_3$)]$_4$ (I)

Cu(1)—O(1)	1.925(5)	Cu(3)—O(9)	2.345(5)
Cu(1)—O(2)	1.916(5)	Cu(3)—O(13)	1.968(5)
Cu(1)—O(9)	1.977(4)	Cu(3)—O(15)	1.953(5)
Cu(1)—O(10)	2.868(5)	Cu(2)—O(11)	1.938(4)
Cu(1)—O(11)	1.955(5)	Cu(2)—O(15)	2.519(5)
Cu(1)—O(13)	2.347(5)	Cu(4)—O(11)	2.533(5)
Cu(2)—O(3)	1.928(6)	Cu(4)—O(13)	1.959(5)
Cu(2)—O(4)	1.912(5)	Cu(4)—O(14)	2.867(5)
Cu(2)—O(9)	1.953(5)	Cu(4)—O(15)	1.933(4)
Cu(2)—O(10)	2.865(3)		

O(1)—Cu(1)—O(2)	92.8(2)	Cu(1)—O(9)—Cu(3)	100.4(2)
O(1)—Cu(1)—O(9)	94.7(2)	Cu(1)—O(11)—Cu(2)	100.3(2)
O(1)—Cu(1)—O(13)	93.9(2)	Cu(1)—O(11)—Cu(4)	91.2(2)
O(2)—Cu(1)—O(11)	92.6(2)	Cu(1)—O(9)—C(41)	118.4(3)
O(2)—Cu(1)—O(13)	115.1(2)	Cu(1)—O(11)—C(44)	125.5(3)
O(9)—Cu(1)—O(11)	79.4(2)	Cu(2)—O(9)—Cu(3)	97.1(2)
O(9)—Cu(1)—O(13)	79.3(2)	Cu(2)—O(11)—Cu(4)	99.6(2)
O(11)—Cu(1)—O(13)	86.6(2)	Cu(1)—O(13)—Cu(3)	100.6(2)
O(9)—Cu(2)—O(11)	80.4(2)	Cu(2)—O(15)—Cu(3)	91.7(2)
O(9)—Cu(2)—O(15)	81.4(2)	O(9)—C(41)—C(42)	112.1(8)
O(11)—Cu(2)—O(15)	80.2(2)	C(41)—C(42)—O(10)	109.4(6)
Cu(1)—O(9)—Cu(2)	99.0(2)		

[Cu(dbm)($OC_2H_4OCH_3$)]$_4$ (II)

Cu(1)—O(1)	1.903(2)	Cu(2)—O(3)	1.928(2)
Cu(1)—O(2)	1.903(2)	Cu(2)—O(4)	1.927(3)
Cu(1)—O(5)	1.954(2)	Cu(2)—O(5)	1.985(2)
Cu(1)—O(6)	1.926(2)	Cu(2)—O(6)	1.925(2)
Cu(1)—O(3a)	2.697(3)	Cu(2)—O(5a)	2.312(3)

O(1)—Cu(1)—O(2)	93.55(9)	O(2)—Cu(1)—O(5)	173.83(10)
O(5)—Cu(1)—O(6)	81.04(8)	O(2)—Cu(1)—O(6)	92.80(9)
O(5)—Cu(1)—O(3a)	78.26(10)	O(2)—Cu(1)—O(3a)	102.04(11)
O(1)—Cu(1)—O(3a)	88.15(11)	O(6)—Cu(1)—O(3a)	89.16(10)
Cu(1)—O(5)—Cu(2)	97.7(1)	O(6)—Cu(2)—O(5a)	98.46(11)
Cu(1)—O(6)—Cu(2)	100.8(1)	O(3)—Cu(2)—O(5a)	89.26(11)
O(5)—Cu(2)—O(6)	80.27(8)	O(4)—Cu(2)—O(5a)	105.21(11)
O(5)—Cu(2)—O(5a)	82.65(9)		

gram of one dimer segment of the dibenzoylmethane complex is given in Fig. 3 and bond length and angle data in Tables 2 and 3. The complex in contrast to the monophenyl substituted β-diketone has a step structure of type 2(a), as shown in Fig. 4, with chelate ring oxygens being involved in coordinating the two dimer units as well as two bridging alkoxy oxygens. The inter-dimer Cu—O_{chel} bonds are longer than the inter-dimer Cu—O_{alkox} bonds by *ca* 0.4 Å. There is a centre of symmetry in the molecule. The methoxy oxygens of two of the alkoxide groups are certainly beyond even weak bonding interactions with the nearest copper ions with Cu—O > 4.6 Å. The remaining methoxy oxygens are 3.020(2) Å from the nearest copper ions, almost 0.2 Å further away than in compound **I**. [Cu(tfac)($OC_2H_4OCH_3$)]$_4$, where all four methoxyethoxide groups are considered to be in bonding distance with copper ions, has these Cu—O distances at 2.766 Å. Any bonding interaction must therefore be very weak if it may be considered at all.

Given the structural variety now disclosed for [Cu(lig)(OR)] compounds it is logical to expect that the type of structure adopted depends on the steric properties of both β-diketone and bridging alkoxide involved in a given compound. The possibility of alkoxyalkoxide groups chelating to copper ions as

Table 3. Relative orientations of planes of atoms and phenyl ring–chelate ring torsion angles

	Angles between planes	
[Cu(bzac)($OC_2H_4OCH_3$)]$_4$		
Cu(1)—O(11)—Cu(2)—O(9)	and Cu(3)—O(13)—Cu(4)—O(15)	5.5
	and Cu(1)—O(1)—O(2)—C(7)—C(8)—C(9)	22
	and Cu(2)—O(3)—O(4)—C(17)—C(18)—C(19)	9.5
Cu(3)—O(13)—Cu(4)—O(15)	and Cu(3)—O(5)—O(6)—C(27)—C(28)—C(29)	23.0
	and Cu(4)—O(7)—O(8)—C(37)—C(38)—C(39)	9.9
[Cu(dbm)($OC_2H_4OCH_3$)]$_4$		
Cu(1)—O(5)—Cu(2)—O(6)	and Cu(1)—O(1)—O(2)—C(1)—C(2)—C(3)	2.7
	and Cu(2)—O(3)—O(4)—C(16)—C(17)—C(18)	25.9

Torsion angles between phenyl rings and chelate rings (°)			
[Cu(bzac)($OC_2H_4OCH_3$)]$_4$		[Cu(dbm)($OC_2H_4OCH_3$)]$_4$	
C(6)—C(1)—C(7)—O(2)	−18.4	C(2)—C(1)—C(10)—C(11)	−17.9
C(36)—C(31)—C(37)—O(8)	30.2	C(2)—C(3)—C(4)—C(5)	16.7
O(6)—C(27)—C(21)—C(26)	−18.5	C(17)—C(18)—C(19)—C(20)	8.2
O(4)—C(17)—C(11)—C(16)	29.5	C(17)—C(16)—C(25)—C(26)	18.9

well as acting as bridging ligands may also further influence the final structure adopted. Although alkoxyalkoxide groups are known to chelate readily in molecules such as [$Y(OC_2H_4OCH_3)_3]_{10}$[22] and [$Mo(O)_2(OC_2H_4OCH_3)_2$],[23] steric features of individual molecules no doubt can prevent such bonding occurring in specific instances. Thus, with only one bulky CF_3 group on the diketone a type 3 pseudo-cubane structure results and chelation occurs at each copper via the methoxy oxygen in [Cu(tfac)($OC_2H_4OCH_3$)]$_4$.[4] Replacing this CF_3 group by a phenyl as in compound **I** allows the

Table 4. Comparison of average bond distances in [Cu(lig)(OR)]$_n$ complexes

Complex and structure type	Cu—alkoxide oxygen distances (Å) Intra-dimer	Inter-dimer	Cu—O (Å) External ligand
Type 1			
[Cu(tfac)(OC_6F_5)(THF)]$_2$[4]	1.952	—	2.279
Type 2			
[Cu(dbm)($OC_2H_4OCH_3$)]$_4$[a]	1.965 (av.)	2.312 (OR)	Two at 3.0, two > 4.0
	1.926	2.697 (chelate O)	
[Cu(tfac)(OC_2H_4OMe)]$_4$[4]	1.942	2.326 (OR)	2.766
		2.605 (chelate O)	
[Cu(acac)(OCH_2Ph)]$_4$[10]	1.875	2.42 (OR)	No bond
	1.945	2.71 (chelate O)	
[Cu(pvac)(OMe)]$_4$[7]	1.880	2.379 (OR)	No bond
	1.935		
Type 3			
[Cu(bzac)($OC_2H_4OCH_3$)]$_4$[a]	1.954	2.436	Two at 2.868
[Cu(acac)($OC_2H_4O^iPr$)]$_4$[11]	1.948	2.462	No bond
[Cu(hfac)(OC_2H_4OMe)]$_4$[4]	1.949	2.423	2.672
			2.560
[Cu(hfac)(OMe)(THF)]$_4$[4]	1.945	2.441	2.547

[a] This work.

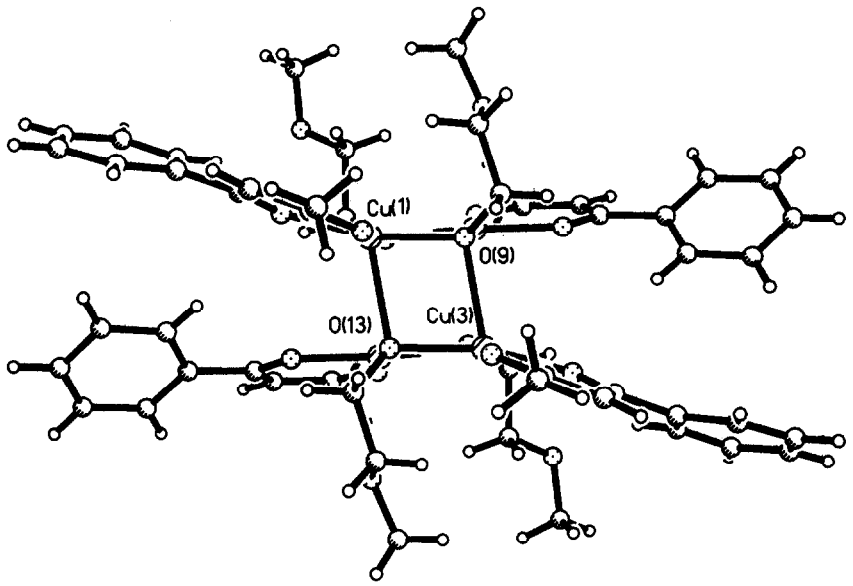

Fig. 2. ORTEP diagram of $[Cu(bzac)(OC_2H_4OCH_3)]_4$ (I) viewed through the Cu(1)—O(9)—Cu(3)—O(13) plane.

type 3 structure to be retained, but chelation by the alkoxyalkoxide group is restricted to two of the four copper ion sites. With two phenyl substituents, as in compound **II**, a type 2(a) structure results and chelation is prevented at each copper site although two alkoxy oxygens can approach two copper sites more closely than the others. The phenyl rings in this compound are set at angles to the chelate ring planes (Table 3). In each dimer unit three rings are rotated in the same direction as each other, while the fourth is turned in the opposite direction. The phenyl ring diametrically opposite to this latter is rotated through only half the angle of the other two. The overall effect is to prevent easy access of the methoxy groups to any copper ion site.

Dimer–tetramer equilibrium in solution

It is of interest to know whether the tetrameric forms of these types of complexes are retained in

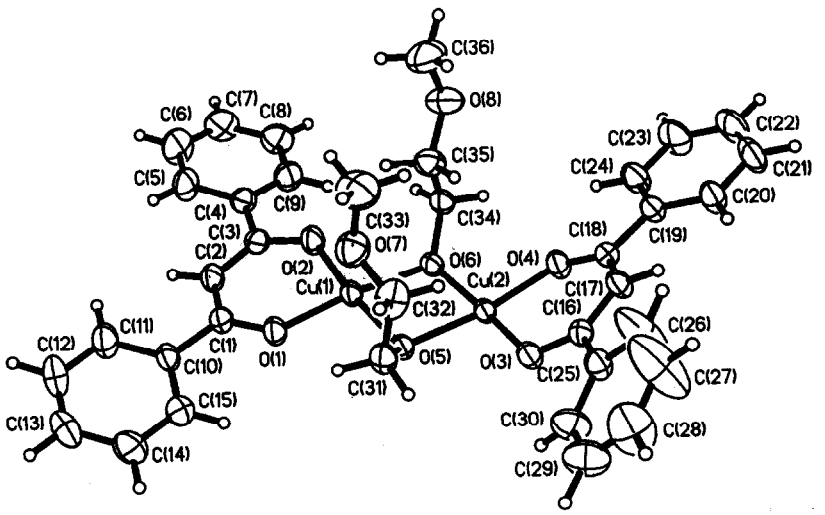

Fig. 3. ORTEP diagram of one dimer segment of the molecular structure of $[Cu(dbm)(OC_2H_4OCH_3)]_4$ (II) showing the atom-labelling scheme. Thermal ellipsoids at 50% probability.

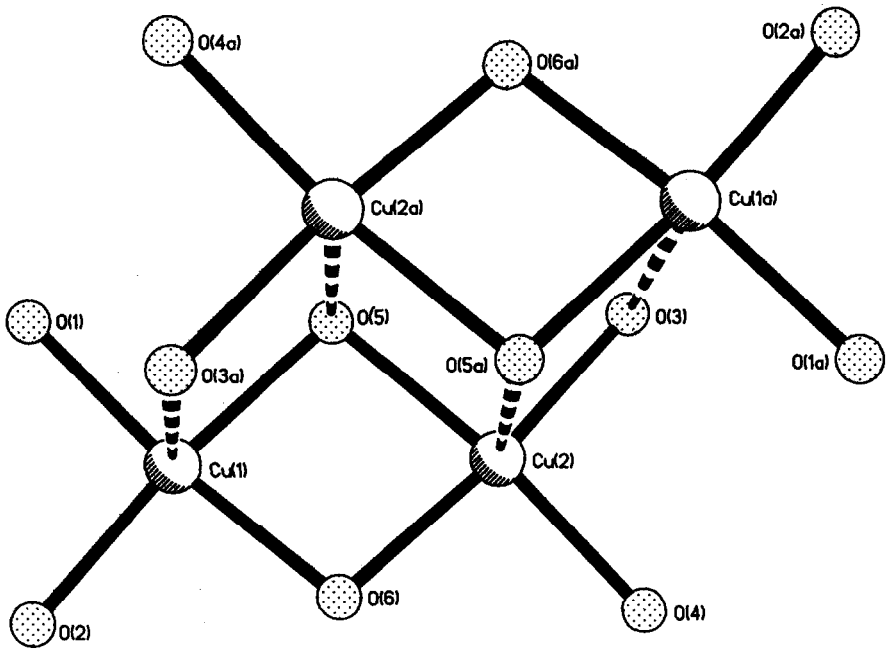

Fig. 4. Diagram of coordination core of [Cu(dbm)($OC_2H_4OCH_3$)]$_4$.

solution. Previous measurements of molecular weights of other copper β-diketonate-alkoxide complexes[4,9] have generally found values much closer to the dimer composition even for complexes shown to be tetrameric in the solid state, indicating that dissociation must be relatively easy. This could be correlated with the long Cu—O inter-dimer bonds. Interestingly the only dimer to be characterized so far by an X-ray diffraction study, [Cu(tfac)(OC_6F_5)THF]$_2$,[24] has a molecular weight in $CHCl_3$ indicating some degree of higher (presumably tetrameric) molecular weight species has formed. Berke *et al.*[4] also report molecular weight data showing that [Cu(hfac)($OC_2H_4OCH_3$)]$_4$ retains the tetrameric form in solution. The low solubility of the dibenzoylmethane complex (II) prevented measurement of its molecular weight by VPO, but the molecular weight of [Cu(bzac)($OC_2H_4OCH_3$)]$_4$ at 60°C in benzene indicates a substantial portion of that complex is still in the tetrameric form. Since the inter-dimer Cu—O distances are of similar dimensions in all the tetramer units so far examined, it is not clear what other factors determine the extent of the tetramer–dimer equilibrium in addition to the long inter-dimer Cu—O distances. Molecular weight studies on [Ni(lig)(OR)ROH] analogues[21] show them to be tetrameric in solution with little tendency to dissociate into constituent dimers. The limited X-ray data on such compounds indicate that the inter-dimer distances are much closer to the intra-dimer distances than is the case in the copper compounds.

Magnetic susceptibility measurements

The copper benzoylacetone and dibenzoylmethane-methoxyethoxide complexes show reduced magnetic moments at 300 K of 1.48 and 1.55 B.M., respectively, as do other such copper(II) complexes.[6,16] This indicates Cu···Cu magnetic coupling and a plot of susceptibility vs temperature from 300 to 4.2 K (Fig. 5) for [Cu(bzac)(OC_2H_4

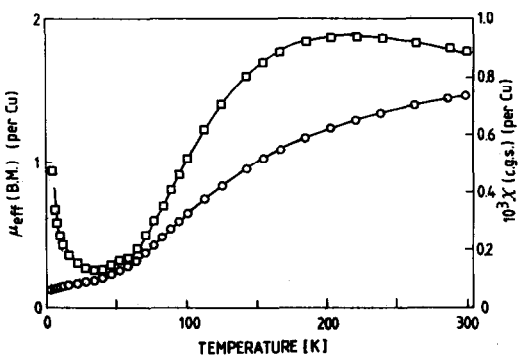

Fig. 5. Plots of magnetic susceptibility (□) and moments (○) vs temperature for [Cu(bzac)($OC_2H_4OCH_3$)]$_4$ (I). Solid lines are the calculated values using a "pair of equal dimers" model with $g = 2.01$, $J_{12} = -120.4$ cm^{-1}, TIP = 60×10^6 cm^3 mol%, copper(II) monomer = 0.5.

$OCH_3)]_4$ shows the typical curve expected for an antiferromagnetically coupled system with a χ_{max} value at *ca* 210 K. The corresponding μ_{eff} value falls to 0.1 B.M. at 4.2 K.

The observed data can be fitted very well by using an isolated "pair of equal dimers" model[24] (i.e. $J_{12} = J_{34}$; $J_{14} = 0$, etc.) with parameters $g = 2.01$, TIP $= 60 \times 10^{-6}$ cm^3 mol and $J_{12} = -120.4$ cm^{-1}. The small increase in χ observed at very low temperatures in the χ/T plot can be accounted for by assuming the presence of a trace amount ($\leqslant 0.5\%$) of a monomer copper(II) "impurity". Previous magnetic studies[6,16] on a range of other copper(β-diketone)(OR) complexes have used a similar model to treat the χ/T data down to 80 K and comparable g and J values have been obtained. The use of a "pair of equal dimers" model appears reasonable in view of the large inter-dimer Cu—alkoxide axial distances (Table 2), which should render any out-of-plane interactions very weak. Indeed, we found that fitting the data to models appropriate to the pseudo-cubane symmetry (type 3), in a manner similar to that previously used by Haase[24,25] and Hatfield[26] for chelating alkoxo species of the type $[Cu(X)(OCH_2CH_2NEt_2)]_4$ (X = NCO, NCS, halide), yielded the same value of J_{12} and a zero value for the cross-coupling parameters J_{14}. In these other studies[24–26] it was found necessary to incorporate non-zero values of the cross J terms, often ferromagnetic in sign, in order to get good fits and sensible values for g. However, the inter-dimer Cu—alkoxide distances were generally much shorter (*ca* 2.1 Å) than those observed here for **I** and the deduced intra-dimer J_{12} parameters were also of a much smaller negative value. The variable-temperature magnetic data for the dbm analogue (**II**) are broadly similar to those of **I**, although the room-temperature μ_{eff} value per copper, of 1.55 B.M., is slightly larger. The corresponding J value, again deduced from an excellent fit using a "pair of equal dimers" model, is a little less than in **I**, viz. $J = -104.3$ cm^{-1} ($g = 2.06$, TIP $= 60 \times 10^{-6}$ cm^3 mol^{-1}, % monomer = 0.5%). The use of a tetranuclear model,[27] appropriate to the symmetry of a stepped structure [type 2(a)] once more yielded the same values of g and J_{12} as found in the dimer model as well as a zero value for J_{14}, etc. Blake *et al.*[6] also found that cross-coupling terms were not required to fit the susceptibility data in a related type 2(b) complex, $[Cu(acac)(OCH_2Ph)]_4$, the J_{12} value being much larger (-313 cm^{-1}) in that case.[16] In other related type 2(a) systems we,[28] and others,[27,29] have found that non-zero inter-dimer interactions do occur and are sometimes ferromagnetic in nature, but this is not the case in complex **II**. Hubert-Pfalzgraf *et al.*[11] commented that preliminary measurements on $[Cu(acac)(OC_2H_4OCH(CH_3)_2)]_4$ might indicate a ferromagnetic contribution, but no further details have been published. In striving to sort out the many factors which might influence the size and sign of J_{12} values in di-μ-alkoxo copper(II) fragments complexes **II** and $[Cu(acac)(OCH_2Ph)]_4$ provide two structurally characterized type 2(a) analogues.[10] The geometrics of the $Cu_2(OR)_2$ bridging moieties are shown in Fig. 6. The main difference is the shorter Cu···Cu distance in **II** with correspondingly smaller Cu—O—Cu angles. This broadly correlates with the r (Cu···Cu) and average Cu—O—Cu angle (ϕ) dependencies noted some years ago by Melnik.[30] Use of Melnik's relation, $2J_{calc} = -101.5(\phi) + 9830$ cm^{-1}, yields J_{calc} values of -110 (**I**), -131 (**II**) and -287 cm^{-1} ($[Cu(acac)(OCH_2Ph)]_4$), in quite good agreement with the fitted values. Magnetic data for the other structurally characterized analogues now known (Table 4) would further test this structural relationship.

Also, di-μ-alkoxo systems displaying very large negative J values[6,31] (i.e. close to diamagnetism) require further structure/magnetism studies to be made in order to confirm an anticipated (ϕ) angle of *ca* 105°, predicted by the linear relationship given above.

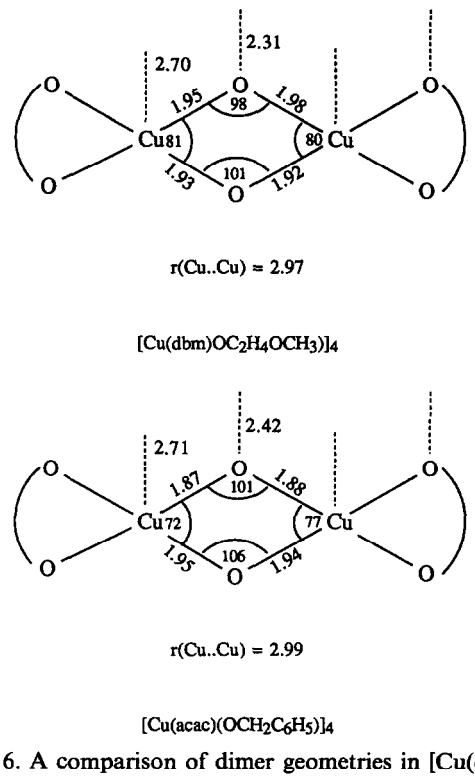

Fig. 6. A comparison of dimer geometries in $[Cu(dbm)(OC_2H_4OCH_3)]_4$ (**II**) and $[Cu(acac)(OCH_2C_6H_5)]$.

Thermal stability

A comparison of the thermal decomposition of compounds **I** and **II** with [Cu(acac)($OC_2H_4OCH_3$)]$_4$ has been made at atmospheric pressure under a dynamic nitrogen atmosphere. The TG and DTG curves for **I** (Fig. 7) show the first decomposition occurs near 100°C (where the weight loss is close to that of one $OC_2H_4OCH_3$ group per tetrameric unit (obs. 6.8%, theor. 6.25%). Further decomposition occurs around 200°C and the additional weight loss is just less than for two further OR groups (obs. 16.6%, theor. for a total of 3 OR groups, 18.7%). Further thermal decomposition has occurred by 280–290°C when a total 62.1% weight loss has taken place. Continuing heating to 500°C finally produces pure CuO (confirmed by XRD) as a film which firmly adheres to the surface of the rhodium sample container. Compound **II** shows somewhat more clearly two decomposition stages (Fig. 7). The first weight loss, *ca* 200°C, corresponds to removal of virtually the entire methoxyethoxide group (obs. 20.1%, calc. 20.7%). The second stage (*ca* 350°C) corresponds to the loss of the remaining organic material and formation of metal oxide is completed by *ca* 480°C. The final material (by XRD examination) was found to be a mixture of CuO and Cu_2O in almost equal proportions, together with a small amount (< 5%) of metallic copper. [Cu(acac)($OC_2H_4OCH_3$)] shows a broadly similar TG curve to those of the benzoyl compounds, without the clearer definition of the stages of decomposition shown by them. However, pure CuO was eventually produced by heating to 400°C a temperature lower than for either of the other complexes. CuO in this case was formed as a powder, which did not adhere to the floor of the sample container. Attempts to sublime [Cu(acac)($OC_2H_4OCH_3$)]$_4$ and [Cu(bzac)($OC_2H_4OCH_3$)]$_4$

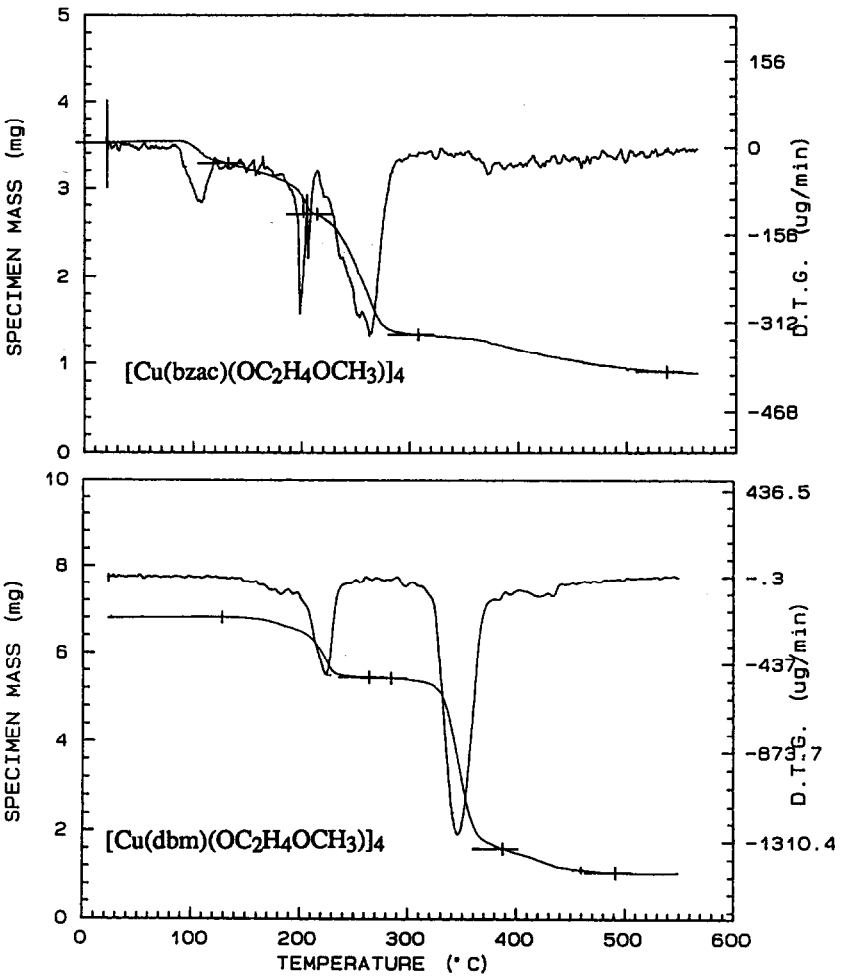

Fig. 7. TG and DTG curves for [Cu(bzac)($OC_2H_4OCH_3$)]$_4$ (**I**) and [Cu(dbm)($OC_2H_4OCH_3$)]$_4$ (**II**). Heating rate 10° min^{-1}, dinitrogen flow 15 cm^3 min^{-1}.

at 10^{-3} mm of Hg resulted in deposits of the bis $Cu(lig)_2$ complexes being obtained at 110°C [$Cu(acac)_2$] and 190°C [$Cu(bzac)_2$]. These latter complexes were identified by their IR spectra, which showed only bands for the $Cu(lig)_2$ compounds. There was no evidence for a band at 1020 cm^{-1} which is characteristic of the copper diketone-alkoxyalkoxides. Other solid decomposition products remained in the sublimation vessel. The [Cu(acac)$(OC_2H_4OCH(CH_3)_2)]_4$ complex is reported to sublime readily at 10^{-3} mm Hg/80°C, but the authors did not specifically refer to examination of the sublimate observed.

Acknowledgements—This work was supported by grants from the Australian Research Council (K.S.M. and B.O.W.) and by an Australian Postdoctoral Research Fellowship (B.M.).

REFERENCES

1. M. W. Rupich, B. Lagos and J. P. Hachey, *Appl. Phys. Lett.* 1989, **55**, 2447.
2. N. N. Sauer, E. Garcia, K. V. Salazar, R. R. Ryan and J. A. Martin, *J. Am. Chem. Soc.* 1990, **112**, 1524.
3. O. Poncelet, L. G. Hubert-Pfalzgraf and J. C. Daran, *Inorg. Chem.* 1990, **29**, 2883.
4. W. Bidell, V. Shklover and H. Berke, *Inorg. Chem.* 1992, **31**, 5561.
5. L. G. Hubert-Pfalzgraf, *Appl. Organomet. Chem.* 1992, **6**, 627.
6. J. E. Andrew and A. B. Blake, *J. Chem. Soc., Dalton Trans.* 1976, 477.
7. W. H. Watson and W. H. Holley, *Croat. Chem. Acta* 1984, **57**, 467.
8. T. Inazu, H. Okawa, I. Inazu and T. Yoshino, *Bull. Chem. Soc. Japan* 1969, **42**, 2291.
9. J. A. Bertrand and R. I. Kaplan, *Inorg. Chem.* 1965, **4**, 1657.
10. J. E. Andrew and A. B. Blake, *J. Chem. Soc., Dalton Trans.* 1973, 1102.
11. C. Sirio, O. Poncelet, L. G. Hubert-Pfalzgraf, J. C. Daran and J. Waissermann, *Polyhedron* 1992, **11**, 177.
12. C. S. Wu, G. R. Rossman, H. B. Gray, G. S. Hammond and H. J. Schugar, *Inorg. Chem.* 1972, **11**, 990.
13. E. D. Estes, R. P. Scaringe, W. E. Hatfield and D. J. Hodgson, *Inorg. Chem.* 1976, **15**, 1179.
14. K. Kasuga, T. Itou and Y. Yamamoto, *Bull. Soc. Chem. Japan* 1974, **47**, 1026.
15. J. A. Bertrand, A. P. Ginsberg, R. I. Kaplan, C. E. Kirkwood, R. L. Martin and R. C. Sherwood, *Inorg. Chem.* 1971, **10**, 240.
16. C. G. Barraclough, R. W. Brookes and R. L. Martin, *Aust. J. Chem.* 19174, **27**, 1843.
17. G. D. Fallon and B. M. G. Gatehouse, *J. Solid State Chem.* 1980, **34**, 193.
18. J. A. Ibers and W. C. Hamilton (Editors), *International Tables for X-ray Crystallography*, Vol. IV. Kynoch Press, Birmingham (1974).
19. G. M. Sheldrick, SHELX-76, Program for Crystal Structure Determination. Cambridge, U.K. (1975).
20. J. Bertrand and D. Caine, *J. Am. Chem. Soc.* 1964, **86**, 2298.
21. B. P. Baranwal and R. C. Mehrotra, *Trans. Met. Chem.* 1978, **3**, 220.
22. O. Poncelet, L. G. Hubert-Pfalzgraf, J. C. Daran and R. Astier, *J. Chem. Soc., Chem. Commun.* 1989, 1846.
23. V. G. Kessler, N. Ya. Turova, A. V. Korolev, A. I. Yanovskii and Y. T. Struchkov, *Mendeleev. Commun.* 1991, 89.
24. L. Merz and W. Haase, *J. Chem. Soc., Dalton Trans.* 1978, 1594.
25. L. Schwake and W. Haase, *J. Chem. Soc., Dalton Trans.* 1985, 1909.
26. J. W. Hall, W. E. Ester, E. D. Ester, R. D. Scaringe and W. E. Hatfield, *Inorg. Chem.* 1977, **16**, 1572.
27. W. E. Hatfield and W. G. Caman, *Inorg. Chem.* 1969, **8**, 1376.
28. W. Mazurek, K. J. Berry, K. S. Murray, M. J. O'Connor, M. R. Snow and A. R. Wedd, *Inorg. Chem.* 1982, **21**, 3071.
29. P. D. W. Boyd and R. L. Martin, *J. Chem. Soc., Dalton Trans.* 1977, 105.
30. M. Melnik, *Coord. Chem. Rev.* 1982, **42**, 259.
31. J. H. Timmons, J. W. L. Martin, A. E. Martell, P. Randolf, A. Clearfield, J. T. Loeb and C. J. Willis, *Inorg. Chem.* 1981, **20**, 181.

Polyhedron Vol. 12, No. 16, pp. 2001—2004, 1993
Printed in Great Britain

0277-5387/93 $6.00+.00
© 1993 Pergamon Press Ltd

SYNTHESIS AND MOLECULAR STRUCTURE OF $[Zn_2(CH_3COO)_3(OCH_3)]$

C. D. CHANDLER, G. D. FALLON and B. O. WEST*

Centre for Chemical Synthesis and Department of Chemistry, Monash University, Clayton, Victoria 3168, Australia

(*Received* 23 *March* 1993; *accepted* 22 *April* 1993)

Abstract—The compound $Zn_2(CH_3COO)_3(OCH_3)$ has been prepared by an exchange reaction between $Zn(CH_3COO)_2$ and $Sn(Bu^n)_2(OCH_3)_2$ in methanol and structurally characterized as a three-dimensional polymer.

There is considerable interest in the identification of heteronuclear complexes that can be formed by the interaction between alkanoate and alkoxide derivatives of metallic elements since they may have utility in the preparation of mixed metal oxides by hydrolysis, the so-called "sol–gel process".[1] When main group elements form the metals involved their compounds are usually labile and given the variety of coordinations possible with carboxyl and alkoxide groups (bridging, terminal coordination, chelation), the particular heteronuclear complex isolated will depend to a large degree on the relative solubilities of the various possible complexes that could form in solution. This in turn could lead to a different molar ratio of the RCOO and R'O groups in the product eventually isolated to that in the reaction mixture. Thus, the compound $[Cd_4Sn_4(\mu\text{-}O)_2(CH_3COO)_{10}(OCH_2Bu^t)_{10}]$ has resulted[2] from reaction between equimolar amounts of $Cd(CH_3COO)_2$ and $Sn(OCH_2Bu^t)_4$ which makes the isolated product "shorter" on alkoxide and "richer" in acetate than the initial mixture. The complex $Pb_2Ti_4(\mu_4\text{-}O)_2(CH_3COO)_2(OC_2H_5)_{14}$ is a more extreme example having been isolated[3] from an equimolar mixture of $Pb(CH_3COO)_2$ and $Ti(OC_2H_5)_4$. Such results raise the question as to whether homonuclear intermediates can form by exchange of alkanoate and alkoxide groups between the reactants before a more complex heteronuclear species is created. We present structural evidence for such a zinc compound of the empirical formula $Zn_2(CH_3COO)_3(OCH_3)_2$, formed by the reaction between $Zn(CH_3COO)_2$ and the alkoxide of restricted bridging ability, $Sn(Bu^n)_2(OCH_3)_2$.

EXPERIMENTAL

All manipulations were conducted using standard Schlenk procedures under an atmosphere of dry nitrogen. Spectral measurements: IR—Perkin–Elmer, FTIR 1600; NMR—Bruker AM-300; mass—VG Micromass 7070F; electron microprobe measurements—Cambridge S410 SEM, with NEC X-ray detector and Packard multichannel analyser. $Sn(Bu^n)_2(OPr^i)_2$ was prepared[4] by reaction of $Sn(Bu^n)_2Cl_2$ with $NaOPr^i$ in *iso*-propanol. The compound was finally distilled at 80°C 1 mm^{-1} Hg (lit.[5] 87°C/1.5 mm Hg). M.S.: *m/z* 293 $Sn(Bu)2(OPr)^+$, 235 $Sn(Bu)(OPr)^+$. ^1H NMR ($CDCl_3$): δ, 4.26 (CH); 1.7–0.8 mult. (CH_3, CH_2). Anhydrous $Zn(CH_3COO)_2$ was obtained by drying the dihydrate (BDH LR grade) at 100°C and 10^{-3} mm Hg for 2 h. IR examination of such material showed no evidence for OH absorptions and its spectrum agreed with that of another reported preparation.[6]

Reaction of $Sn(Bu^n)_2(OCH_3)_2$ *with* $Zn(CH_3COO)_2$

$Sn(Bu^n)_2(OPr^i)_2$ (0.75 g, 2 mmol) was dissolved in methanol (20 cm^3), stirred for 20 min and then evaporated rapidly under reduced pressure, yielding an oil. This was redissolved in methanol (40 cm^3) and anhydrous $Zn(CH_3COO)_2$ (0.4 g, 2 mmol) was added. The solid rapidly dissolved but within several minutes a white precipitate reappeared. The

* Author to whom correspondence should be addressed.

mixture was heated to redissolve the precipitate and then allowed to cool slowly. The clear, colourless crystals which formed were filtered, washed with cold methanol and dried in a stream of nitrogen. Crystals suitable for X-ray studies were obtained by a further recrystallization from methanol. The compound is reasonably soluble in methanol, but very sparingly soluble in chloroform or toluene. Found: C, 24.7; H, 3.5. Calc. for $C_7H_{12}O_7Zn_2$: C. 24.7; H, 3.5%. Electron microprobe showed no evidence for tin in the product. IR (Nujol): 1604(s) 1551(s), 1542(s), 1445(s), 1417(m), 1405(s), 1377(vs), 1364(sh), 1350(sh), 1053(m), 1028(m), 1014(m), 958(m), 702(s), 672(w), 663(w), 609(m) cm^{-1}. ^1H NMR ($CDCl_3$): δ, 3.88 (OCH_3), 3H; 2.12 (CH_3COO), 9H.

Crystallographic studies of $Zn_2(CH_3COO)_3(OCH_3)$

A representative fragment of a large clear crystal sealed in a Lindemann glass capillary was used for data collection. Intensity measurements were made on a Nicolet R3m/V diffractometer using graphite monochromated Mo-K_α radiation. Crystallographic data are collected in Table 1. Cell parameters were derived by least-squares calculations from angular settings of 29 reflections measured in the range $8° < 2\theta < 27°$. Three standard reflections monitored every 197 reflections showed no significant variation in intensity over the data collection period. Intensity data were corrected for Lorentz and polarization effects. Due to difficulty indexing the irregular crystal no absorption correction was applied. The atomic scattering factors for neutral atoms were taken from literature values.[7] All calculations were performed on a VAX11/780 computer, the program for least-squares refinement being that due to Sheldrick.[8] The structure was solved by Patterson methods and refined by full-matrix least-squares employing anisotropic thermal parameters for zinc and isotropic thermal parameters for all other atoms, including a single isotropic thermal parameter for hydrogen (which refined to 0.16(3) $Å^2$), positioned in geometrically idealized positions: C—H 0.96 Å. This treatment reduced R to 0.034 and R' to 0.045, respectively, at convergence where $R' = (\Sigma w(\|F_o\| - |F_c\|)^2/\Sigma w|F_o|^2)^{1/2}$ and $w = [\sigma^2(F_o) + 0.000267F_o^2]^{-1}$. The goodness-of-fit value $([\Sigma w(|F_o| - |F_c|^2/(N_{obs} - N_{para})]^{1/2})$ was 1.85. Refinement with the sense of the polar axis reversed resulted in $R = 0.036$ and $R' = 0.053$. The highest peak in the difference-Fourier synthesis was 0.48 $eÅ^{-3}$.

Table 1. Crystallographic data for $[Zn_2(CH_3COO)_3(OCH_3)]$

Compound	$C_7H_{12}O_7Zn_2$
Formula weight	338.9
Crystal system	Orthorhombic
Space group	$Pmn2_1$
a (Å)	12.468(4)
b (Å)	7.801(2)
c (Å)	6.105(1)
U ($Å^3$)	593.8(3)
Density calc. (g cm^{-3})	1.90
Z	2
T (°C)	20(1)
λ (Mo-K_α) (Å)	0.71073
μ (Mo-K_α) (mm^{-1})	4.15
F(000)	340
Scan mode	$\omega/2\theta$
2θ range (°)	3.5–55
Scan rate (° min^{-1})	1.5–15
Data collected	771
Data used [$F \geqslant 6\sigma(F)$]	636
$R(R')$	0.034 (0.045)

RESULTS AND DISCUSSION

Crystal structure of $Zn_2(CH_3COO)_3(OCH_3)$

The X-ray structural study has shown the compound to be a three-dimensional polymer in the solid state (Fig. 1). Each zinc atom is four-coordinate, surrounded by a distorted tetrahedron of oxygen atoms derived from three acetate groups and one alkoxide. The zinc atoms are linked in pairs by a bridging OCH_3 and a bridging acetate forming six-membered rings while each zinc atom is in turn linked to a zinc atom on a neighbouring "ring" by further bridging acetates. A list of relevant bond distances and angles is given in Table 2. The compound has a mirror plane through the middle of the six-membered ring, bisecting the bridging methoxide and acetate groups. Anhydrous $Zn(CH_3COO)_2$ is also polymeric in the solid state[9] with zinc atoms in distorted tetrahedral environments, although the departure from 109.5° angles is much less than in the present complex. Each zinc in $Zn(CH_3COO)_2$ is coordinated to four acetates, which in turn bridge to other zinc atoms. Thus, the structure of $Zn_2(CH_3COO)_3(OCH_3)$ can be regarded as derived from that of $Zn(CH_3COO)_2$ with the replacement of one acetate in four by the OCH_3 group. The more limited ability of the latter group to bridge through only one oxygen instead of the two available to the acetate then causes the change in structure. The Zn—O methoxide distances, 1.932 Å, are shorter than the acetate Zn—O distances, which range from 1.948 to 1.974 Å, and the acetate Zn—O

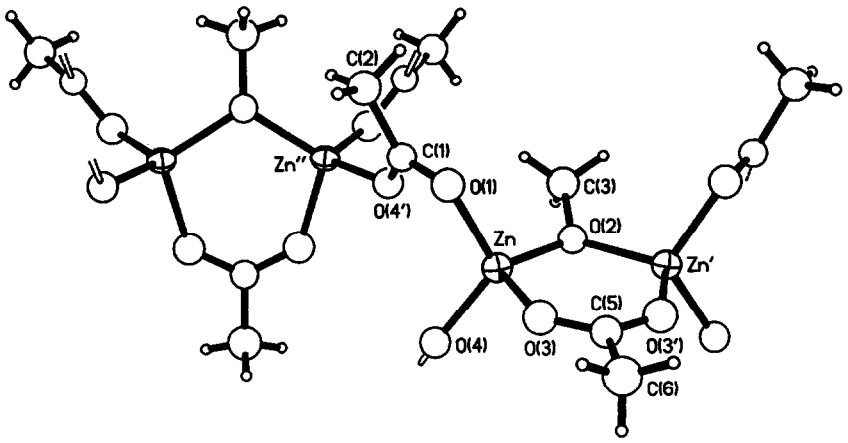

Fig. 1. Molecular structure diagram of $[Zn_2(CH_3COO)_3(OCH_3)]$, showing the atom labelling scheme. Thermal ellipsoids at 50% probability.

distances are longer than the average such bond in $Zn(CH_3COO)_2$. The bond distances are closer to those in basic zinc acetate,[10] $Zn_4(\mu_4\text{-O})(CH_3COO)_6$, where Zn—($\mu_4$-O) is 1.936(1) Å, and the Zn—O (bridging acetate) bonds average 1.946(4). The alkoxide $(CH_3ZnOCH_3)_4$ displays notably longer Zn—O distances (2.039–2.114 Å)[11] than in the present compound (1.932 Å), which can be ascribed to the μ_3 nature of each oxygen in the former. There are two types of acetate group in the alkoxy-acetate compound. One forms six-membered rings with OCH_3 groups and two zinc atoms, while the other bridges between such rings. The difference shows in the O—C—O angles, the former averaging 125° and bridging in a *syn–syn* mode while "ring bridging" acetate groups have O—C—O angles of 120.4° and are coordinated in a *syn–anti* mode. This latter mode of coordination is apparently necessary in order to bridge the long distances between the six-membered rings. The O—C—O angles in $Zn_4(\mu_4\text{-O})(CH_3COO)_6$ are also 125° and there is a striking geometric similarity between the six-membered rings in this compound involving the μ_4-O atom and in $Zn_2(CH_3COO)_3(OCH_3)$ involving the μ_2-OCH_3 group.

Spectroscopic properties

The bridging acetate carboxylate group in basic zinc acetate, $Zn_4(\mu_4\text{-O})(CH_3COO)_6$, gives rise to asymmetric and symmetric vibration frequencies of the CO_2 unit variously reported as $\nu_{asym} = 1600$[6] and 1639 cm^{-1}[12] and $\nu_{sym} = 1441$[6] and 1489 cm^{-1}.[12] The differences, Δ(asym–sym) = 159 or 150 cm^{-1}, are of the right order of magnitude suggested as a correlation for bridging acetate group frequencies.[13] The present complex shows absorptions of similar value which may be assigned to the bridging acetate in the six-membered $Zn_2(CH_3COO)(OCH_3)$ rings at $\nu_{asym} = 1604$ and $\nu_{sym} = 1445$ cm^{-1} ($\Delta = 159$ cm^{-1}). Since a second type of bridging acetate exists in the structure of the complex one further pair of frequencies in the asymmetric and symmetric regions is expected to

Table 2. Selected bond lengths (Å) and angles (°) for $[Zn_2(CH_3COO)_3(OCH_3)]$

Zn—O(1)	1.949(6)	O(3)—C(5)	1.244(8)
Zn—O(2)	1.932(5)	C(1)—C(2)	1.518(13)
Zn—O(3)	1.974(7)	O(2)—C(3)	1.443(16)
Zn—O(4)	1.948(5)	O(4)—C(1')	1.290(7)
O(1)—C(1)	1.236(10)	C(5)—C(6)	1.506(19)

O(1)—Zn—O(2)	112.4(3)	O(1)—Zn—O(3)	100.9(2)
O(2)—Zn—O(3)	108.0(3)	O(1)—Zn—O(4)	114.8(2)
O(2)—Zn—O(4)	118.4(2)	O(3)—Zn—O(4)	99.4(3)
Zn—O(1)—C(1)	116.7(4)	Zn—O(2)—C(3)	120.8(3)
Zn—O(2)—Zn'	113.7(4)	Zn—O(3)—C(5)	132.6(6)
O(1)—C(1)—O(4')	120.4(7)	O(3)—C(5)—O(3')	125.0(11)

be observed. There are indeed other strong absorptions at 1557 and 1542 cm^{-1} (ν_{asym} region) and 1417 and 1405 cm^{-1} (ν_{sym} region), the latter pair being distinguished from the Nujol peak by a structure subtraction procedure. The crystallographic evidence indicates that the acetates in this bridging mode are identical and a clear assignment of an appropriate pair of frequencies, therefore, cannot be made. Frequencies due to the methoxide group are also difficult to assign with confidence amongst the acetate bands. The clearest indication appears to be a band at 1014 cm^{-1} in the alkoxide stretching region beside the probable CH_3 rocking frequency of the acetate group (1053 cm^{-1}).

The ^1H NMR spectrum of $Zn_2(CH_3COO)_3(OCH_3)$ shows only one acetate and one methoxide resonance. If the ring formulation was retained in solution two acetate resonances could be expected in the ratio 2 : 1. The resultant spectrum indicates that rapid exchange is taking place between acetate groups whatever molecular species finally forms.

CONCLUSION

This study confirms that group exchange can take place between labile zinc and tin species to form the type of homo-binuclear ring system detected in larger heteronuclear species and suggests that such entities can form initially and act as building blocks in the formation of such large heteronuclear entities.

Acknowledgement—This work was supported by an Australian Research Council grant (to B.O.W.).

REFERENCES

1. L. G. Hubert-Pfalzgraf, *Appl. Organomet. Chem.* 1992, **6**, 627.
2. C. Chandler, G. D. Fallon and B. O. West, *J. Chem. Soc., Chem. Commun.* 1990, 1063.
3. J. Bates, Z. Qi, G. D. Fallon and B. O. West, to be published.
4. P. J. Smith, R. F. M. White and L. Smith, *J. Organomet. Chem.* 1972, **40**, 341.
5. R. C. Mehrotra and B. P. Bachlas, *J. Organomet. Chem.* 1970, **22**, 121.
6. A. I. Grigor'ev, *Russ. J. Inorg. Chem.* 1963, **8**, 409.
7. J. A. Ibers and W. C. Hamilton (Editors), *International Tables for X-ray Crystallography*, Vol. IV. Kynoch Press, Birmingham (1974).
8. SHELXTL PLUS, Revision 3.4, Siemens Analytical X-Ray Instruments Inc., Madison, Wisconsin, U.S.A. (1988).
9. V. Capilla and A. Aranda, *Cryst. Struct. Commun.* 1979, **8**, 795.
10. L. Hiltunen, M. Leskela, M. Makela and L. Niinisto, *Acta Chem. Scand.* 1987, **A41**, 548.
11. H. M. M. Shearer and C. B. Spencer, *Acta Cryst.* 1980, **B36**, 2046.
12. K. Nakamoto, Y. Morimoto and A. E. Martell, *J. Am. Chem. Soc.* 1961, **83**, 4528.
13. G. B. Deacon and R. J. Phillips, *Coord. Chem. Rev.* 1980, **33**, 227.

Polyhedron Vol. 12, No. 16, pp. 2005–2008, 1993
Printed in Great Britain

0277–5387/93 $6.00+.00
© 1993 Pergamon Press Ltd

A STUDY ON THE SCHIFF BASE Cu_2Zn_2SOD MODEL COMPLEXES—THE RELATIONSHIP BETWEEN STRUCTURE AND ACTIVITY

QIN LU, CHENG-YU SHEN and QIN-HUI LUO*

Coordination State Key Laboratory, Nanjing University, Nanjing 210008, P.R.C.

(*Received* 5 *April* 1993; *accepted* 22 *April* 1993)

Abstract—2-Acetylpyridine was condensed with $NH_2(CH_2)_nNH_2$ (n = 2,3,4). The di-Schiff base complexes of copper(II) were obtained for simulating superoxide dismutase. Studies on the relationship between dismutase O_2^- ability and coordination configuration were made. Linear relationships were obtained between $E_{1/2}$ of $Cu^{II}L/Cu^{I}L$, $g_\parallel/A_\parallel$ and catalytic activities of these complexes, respectively.

Superoxide dismutase (SOD) is a scavenger of the superoxide anion (O_2^-) and it plays an important role in protecting cells from the toxic effects of the superoxide ion, or some products derived from it.[1–3] The active site of Cu_2Zn_2SOD is similar to the imidazolate-bridged copper(II), zinc(II) binuclear complex. In Cu_2Zn_2SOD copper(II) is centred in a distorted square plane coordinated to four nitrogen atoms of four imidazolate radicals (His-44, His-46, His-118 and His-61), in which His-61 is bridged to the zinc(II) atom. His-69 and His-78 provide two more imidazolate nitrogens and the oxygen of the carboxylate group of Asp-81 acts as the fourth ligand to zinc(II), forming a distorted tetrahedral structure[4] (Fig. 1). The main function of the zinc(II) atom is to make the structure stable and has little effect on enzyme activity. Studies on the structure and function of SOD model compounds can lead to a profound understanding of the enzyme as well as to the coordination chemistry and biological medicine chemistry.[5] Up until now some copper (II) complexes have been synthesized with salicylate,[6] amino acids,[7] polypeptides[8] and other[9,10] ligands, but the relationship between structure and function has rarely been discussed.[9,11] In this work 2-acetylpyridine was condensed with ethanediamine, propane diamine-1,2 and butanediamine-1,2 to form three new Schiff base ligands (apen, appn and aptn). After their reaction with $Cu(ClO_4)_2$, we obtained three copper(II) complexes: [N,N′-ethylene bis-(2-acetylpyridine iminato)copper(II)] diperchlorate ([Cu(apen)]$(ClO_4)_2$ (**1**); [N,N′-propylene bis-(2-acetylpyridine iminato)copper(II)] diperchlorate ([Cu(appn)]$(ClO_4)_2$) (**2**); and [N,N′-butylene bis-(2-acetylpyridine iminato)copper(II)] diperchlorate ([Cu(aptn)]$(ClO_4)_2$) (**3**) (formula shown in Fig. 2). Among these three [Cu(aptn)]$(ClO_4)_2$ has been found in our early paper to have a high SOD activity.[12] In this work, the relationship between the structure and SOD activity was determined by the riboflavin illumination method, UV, EPR, electrochemistry and other techniques.

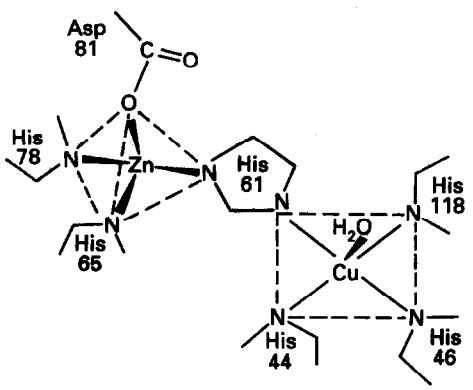

Fig. 1. The active site of Cu_2Zn_2 superoxide dismutase.

EXPERIMENTAL

Materials

2-Acetylpyridine and the diamines were C.P. grade. Cu_2Zn_2SOD was the product of Gansu

* Author to whom correspondence should be addressed.

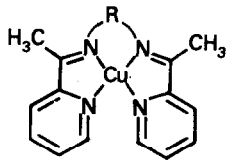

Fig. 2. Formula of model complexes.

Xiahe Pharmaceutical Factory, specific activity 3000 units mg^{-1} protein. KH_2PO_4 and K_2HPO_4 (A.R) were recrystallized twice in deionized water. Nitrotetrazolium blue (NBT), L-methionine and B.R. riboflavin were analysed by literature methods.[13]

Preparation of complexes

[Cu(apen)]$(ClO_4)_2$. To a methanol solution (30 cm^3) of 2-acetylpyridine (0.5 g, 4.13 mmol) ethanediamine was added dropwise (0.125 g) (distilled before use) with stirring. After refluxing for 20 min a methanol solution (20 cm^3) of $Cu(ClO_4)_2 \cdot 6H_2O$ (0.76 g, 2.07 mmol) was added and refluxing continued for another 30 min. On cooling blue–black microcrystals precipitated in 44% yield (0.52 g). Found: C, 35.1; H, 3.2; N, 10.1; Cu, 11.3. Calc. for $C_{16}H_{18}CuCl_2N_4O_8 \cdot H_2O$: C, 35.1; H, 3.7; N, 10.2; Cu, 11.6%. Λ_M (DMF, 298 K): 138 Ω^{-1} cm^2 mol^{-1}.

[Cu(appn)]$(ClO_4)_2$. The complex was obtained as heavy blue needle crystals in a similar manner using 2-acetylpyridine (0.5 g, 4.13 mmol) propanediamine-1,2 (0.153 g, 2.07 mmol) and $Cu(ClO_4)_2 \cdot H_2O$ (0.76 g, 2.07 mmol); yield 43% (0.48 g). Found: C, 37.2; H, 3.4; N, 9.9; Cu, 11.2. Calc. for $C_{17}H_{20}CuCl_2N_4O_8$: C, 37.6; H, 3.7; N, 10.3; Cu, 11.7%. Λ_M (DMF, 298 K): 144 Ω^{-1} cm^2 mol^{-1}.

[Cu(aptn)]$(ClO_4)_2$. The complex was obtained as heavy blue microcrystals in a similar manner; yield 50%. Found: C, 38.7; H, 4.2; N, 10.2; Cu, 11.2. Calc. for $C_{18}H_{22}CuCl_2N_4O_8$: C, 38.8; H, 3.9; N, 10.1; Cu, 11.4%. Λ_M (DMF, 298 K): 140 Ω^{-1} cm^2 mol^{-1}.

Measurements

Cyclic voltammetry was performed with a 79-1 electrochemical apparatus, connected to an *X–Y* recorder. A three-electrode system was used. The working electrode was glass carbon and platinum coil was used as the counter electrode. The reference electrode was a saturated calomel electrode (S.C.E.). Solutions were prepared using twice distilled water and the concentration of complexes was *ca* 1×10^{-3} mol dm^{-3}. In KCl (0.08 mol dm^{-3}) (A.R., recrystallized before use) a flow of high purity nitrogen was bubbled through the solution for 15 min before measurement. The procedure was performed at room temperature. The half-wave potential, $E_{1/2}$ of $Cu^{II}L/Cu^{I}L$ was obtained from an average of E_{pc} and E_{pa}.

X-band EPR spectra were recorded on a 200D-SRC spectrometer at 110 K with a frequency modulation of 100 kHz. The frequency was calibrated with Mn^{2+} ions in MgO powder.

Electronic spectra were recorded on a Shimadu UV-200 spectrophotometer in methanol solution.

Activity was assayed by illumination[14] of a solution containing 3.40×10^{-6} mol dm^{-3} riboflavin, 4.66×10^{-5} mol dm^{-3} NBT, 0.01 mol dm^{-3} methionine and various concentrations of complexes and SOD, prepared with pH = 7.8 phosphate buffer. The solution was illuminated by a fluorescent lamp with constant light strength at 25°C. The optical density of the solution with and without the complexes (Δ and Δ_0, respectively) was measured at 560 nm to determine their variations with time. The percentage of inhibiting NBT reduction was determined as $f\% = [(\Delta_0 - \Delta)/\Delta_0] \times 100\%$.

RESULTS AND DISCUSSION

Conductivity and electronic spectrum

In DMF the conductivity of all three complexes was *ca* 140 Ω^{-1} cm^2 mol^{-1}, behaving as a 1:2 electrolyte, which is consistent with the chemical formula predicted by elemental analysis (Fig. 2).

Table 1. Spectral parameters and activity data for copper(II) complexes and SOD

Complexes[a]	$\lambda_{max}(\varepsilon)$ (nm)	$g_\parallel$	$g_\perp$	$A_\parallel$ ($10^{-4} \times cm^{-1}$)	$g_\parallel/A_\parallel$	α^2	α'^2	Activity (μM)	Relative activity (%)
1	620(93)	2.227	2.040	187	119	0.804	0.286	11.04	0.5
2	623(88)	2.211	2.036	181	122	0.769	0.325	2.33	2.6
3	705(105)	2.226	2.082	142	157	0.696	0.403	0.56	10.7
Cu_2Zn_2SOD	680(155)	2.268	2.087	142	160	0.740	0.348	0.06	100

[a] **1**: [Cu(apen)]$(ClO_4)_2$; **2**: [Cu(appn)]$(ClO_4)_2$; **3**: [Cu(aptn)]$(ClO_4)_2$.

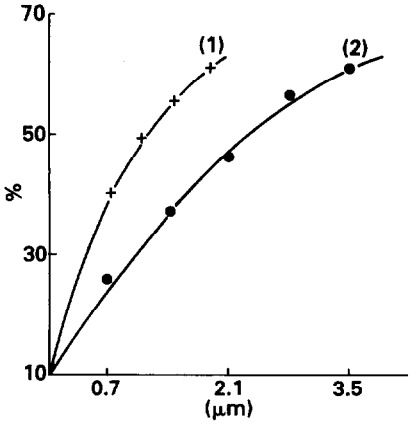

Fig. 3. Plots of percentage of inhibiting NBT reduction vs concentration of the complexes.

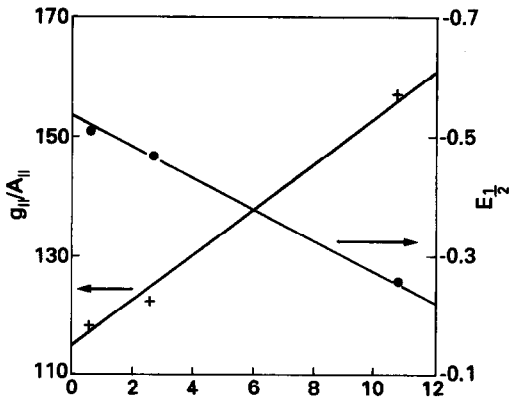

Fig. 4. Plots of $E_{1/2}$ and $g_{\parallel}/A_{\parallel}$ vs relative activity.

The electronic spectra data in Table 1 show that the maximum *d–d* absorption shifted from 620 nm to 705 nm as the carbon chain of the ligand increased. Their absorption intensity increased as well. $[Cu(aptn)](ClO_4)_2$ had a maximum *d–d* wavelength, which is between Cu_2Zn_2SOD and Cu_2ESOD [740(140)].[15] The red shift of absorption implies a distortion from square-planar to tetrahedron for copper(II) configuration.

EPR spectrum

We recorded the EPR spectra of the three compounds and their parameters are listed in Table 1. As previous scholars have reported[16] $g_{\parallel}/A_{\parallel}$ can be used as an empirical rule of configuration distortion. When $g_{\parallel}/A_{\parallel}$ falls between 105 and 135 cm CuN_4 forms a square planar configuration, whereas if $135 < g_{\parallel}/A_{\parallel} < 258$ a distorted tetrahedral configuration results. The $g_{\parallel}/A_{\parallel}$ values of complexes **1** and **2** in Table 1 indicates a square-planar structure. Whilst complex **3** is a distorted tetrahedron, its EPR parameter is very close to that of Cu_2Zn_2SOD.[17] The covalence parameters α^2 and α'^2 were obtained by the literature method[18] and we can see that the covalence of the complexes increases as the structure distortion increases.

Table 2. Electrochemistry data of $Cu^{II}L/Cu^{I}L$ compounds (S.C.E. is standard)

Complexes[a]	E_{pc}(V)	E_{pa}(V)	ΔE_p(V)	$E_{1/2}$(V)
1	−0.564	−0.443	−0.121	−0.504
2	−0.529	−0.414	−0.115	−0.472
3	−0.321	−0.207	−0.114	−0.264

[a] See footnote to Table 1.

Activity

The activity data in Table 1 were obtained by plotting the percentage of inhibiting NBT reduction against concentration of the complex (Fig. 3). The activity for dismuting superoxide ion (O_2^-) increased as the carbon chain of the diamine increased. Among them complex **3** was the highest, its spectral data were the closest to Cu_2Zn_2SOD, implying a close coordination environment of copper(II) to Cu_2Zn_2SOD.

Electrochemistry

Listed in Table 2 are the redox half-wave potentials of the three complexes obtained by cyclic voltammetry. The redox of $Cu^{II}L/Cu^{I}L$ was a quasi-reversible process. When the distortion of CuN_4 increased ($g_{\parallel}/A_{\parallel}$ increased) its reduction potential shifted positively and its activity also increased. Two straight lines were obtained when plotting half wave potential and $g_{\parallel}/A_{\parallel}$ against relative activity (Fig. 4). Former researchers have indicated[19] that the distortion of copper(II) from square planar toward tetrahedral was in favour of the reduction of copper(II) to form a $Cu^{I}L$ complex. In the dismutase reaction of O_2^- the easier $Cu^{I}L$ complex forms, the value of $E_{1/2}$ for $Cu^{II}L/Cu^{I}L$ is more positive and the catalytic activity will be higher. From this point of view, it is easy to understand why $[Cu(aptn)](ClO_4)_2$ gave the best result in simulating superoxide dismutase.

Acknowledgement—The project was supported by the National Natural Science Foundation of China.

REFERENCES

1. L. W. Oberley and G. R. Buettner, *Cancer Res.* 1979, **39**, 1141.
2. B. Halliwell and J. M. C. Gutteride, *Biochem. J.* 1984, **219**, 1.
3. B. Halliwell and J. M. C. Gutteride, *Arch. Biochem. Biophys.* 1986, **246**, 501.
4. T. A. Tainer, D. E. Getzoff, J. S. Richardson and D. C. Richardson, *Nature* 1983, **306**, 284.
5. J. A. Ibers and R. H. Holm, *Science* 1980, **209**, 4453.
6. R. G. Bhirud and T. S. Srivastava, *Inorg. Chim. Acta* 1990, **173**, 121.
7. M. Younes and U. Weser, *FEBS Lett.* 1976, **61**, 209.
8. E. Kimoto, H. Tanka, J. Gyotoka, F. Morishige and L. Pauling, *Cancer Res.* 1982, **43**, 824.
9. C. M. Perkins, N. J. Rose and R. E. Stenkamp, *Inorg. Chim. Acta* 1990, **172**, 119.
10. Q. Lu, Q. H. Luo, A. B. Dai, Z. Y. Zhou and G. Z. Hu, *J. Chem. Soc., Chem. Commun.* 1990, 1429.
11. B. M. Katz and V. I. Stenberg, *Polyhedron* 1985, **4**, 2031.
12. Q.-H. Luo, Q. Lu and A.-B. Dai, *J. Inorg. Biochem.*, in press.
13. *British Pharmacopoeia*, Vol. 1, p. 390. HMSO, London (1980).
14. C. Beauchamp and J. Fridovich, *Anal. Biochem.* 1971, **44**, 276.
15. M. W. Pantoliano, J. S. Valentine and L. A. Nafie, *J. Am. Chem. Soc.* 1982, **104**, 6310.
16. V. Sakaguchi and A. W. Addison, *J. Chem. Soc., Dalton Trans.* 1979, 600.
17. G. Rotilio, A. Finazzi-Agro, L. Calabrese, F. Borsa, P. Guerrieri and B. Mondovi, *Biochemistry* 1971, **10**, 616.
18. D. Kivelson and R. Neiman, *J. Chem. Phys.* 1961, **35**, 149.
19. H. Yokoi and A. W. Addison, *Inorg. Chem.* 1977, **16**, 1341.

Polyhedron Vol. 12, No. 16, pp. 2009–2012, 1993
Printed in Great Britain

0277–5387/93 $6.00+.00
© 1993 Pergamon Press Ltd

SYNTHESIS AND X-RAY CRYSTAL STRUCTURE OF OXOTRIMESITYLIRIDIUM(V)

ROBYN S. HAY-MOTHERWELL and GEOFFREY WILKINSON*

Johnson Matthey Laboratory, Chemistry Department, Imperial College, London SW7 2AY, U.K.

and

BILQUIS HUSSAIN-BATES and MICHAEL B. HURSTHOUSE*

Department of Chemistry and Applied Chemistry, University of Wales Cardiff, P.O. Box 912, Cardiff CF1 3TB, U.K.

(*Received* 23 *March* 1993; *accepted* 22 *April* 1993)

Abstract—The interaction of trimesityliridium(III) with trimethylamine oxide gives quantitative yields of the green iridium(V) complex $Ir(O)(mes)_3$, whose X-ray crystal structure has been determined. The oxo compound is also obtained by interaction of dioxygen with $Ir(mes)_3$ and $Ir(mes)_4$. A similar oxo species has also been obtained from $Ir(2,6\text{-}Me_2C_6H_3)_4$. The molecular structure of $Ir(O)(mes)_3$ is distorted tetrahedral with Ir=O and Ir—C bond lengths of 1.725(9) and 1.989–2.034(13) Å, respectively.

We have described[1] the syntheses and X-ray crystal structures of $Ir(mes)_3$, mes = mesityl, 2,4,6-trimethylphenyl, $Ir(mes)_4$ and $[Ir(mes)_4]^+$, the latter two being the first examples of tetrahedral Ir^{IV} and Ir^V, respectively.

It was noted[1] that brown solutions of $Ir(mes)_3$, which unlike its rhodium analogue is exceedingly air-sensitive, and also of $Ir(mes)_4$ react with dioxygen, the latter only on heating, becoming green. Since the formation of an oxo species was evident, a better procedure for the product, $Ir(O)(mes)_3$, was the interaction of $Ir(mes)_3$ with Me_3NO.

Neutral iridium(V) compounds are relatively rare,[2] being limited to tertiary phosphine and η^5-cyclopentadienyl polyhydrides and related compounds [2a,b] and to (triso)$Ir(H)_2SiR_2R'$ species,[2c] triso = tris(diphenyloxophosphoronyl methanide), R = Ph, R′ = Me and R,R′ = Et. Some aqua cationic dimeric species of Ir^V have been proposed in solution, but they have not been isolated.[2d]

No compounds with Ir=O groups have been previously characterized.

RESULTS AND DISCUSSION

From the reaction of $Ir(mes)_3$ and Me_3NO in diethylether, a quantitative reaction, small greenish-black air-stable crystals of $Ir(O)(mes)_3$ (**1**) can be obtained with some difficulty. The structure as determined by X-ray diffraction is shown in Fig. 1; selected bond lengths and angles are given in Table 1.

The molecular geometry is distorted tetrahedral. The O—Ir—C and C—Ir—C angles each show a considerable spread of *ca* 15° and this feature is probably due to steric interactions linked to the fitting of the bulky aryl groups into the coordination sphere. In addition, for each of the rings the aryl ring coordination is tilted, with Ir—C—C_α angles of 128 and 113; 127 and 117; 122 and 120(1)° for rings 1, 2 and 3, respectively. This feature is commonly found in the *o*-tolyl, 2,6-xylyl and mesityl derivatives previously studied.[1,3] The orientations of the rings relative to the Ir=O bond also vary, with angles between the lines of this bond and the perpendiculars to the ring planes of 40.7, 25.6 and 80.8° for rings 1, 2 and 3, respectively.

The Ir—C distances of 1.99–2.03(1) Å are to be compared with those found in the neutral tetra-

* Authors to whom correspondence should be addressed.

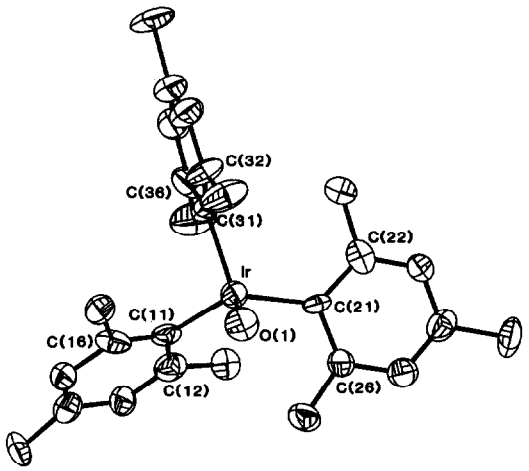

Fig. 1. The structure of oxotrimesityliridium(V).

hedral $Ir(mes)_4$ molecule, 1.99–2.04(1) Å, and the cation $[Ir^V(mes)_4]^+$, 2.00–2.04(1) Å. The Ir=O distance of 1.725(9) Å is significantly longer than Re=O distances[4] in the Re^{VI} complexes $(mes)_2ReO_2$ [Re=O = 1.688(5) Å] and $(mes)_4Re{=}O$ [1.646, 1.679(8) Å], where the Re—C distances [2.062(6) and 2.089(8)–2.194(8) Å] are somewhat longer than the Ir—C distances here, indicating a relative weakening of the Ir=O double bond. This weakening is reflected in the loss of the oxygen atom in the FAB mass spectrum, where only $Ir(mes)_3$ was observed.

The spectroscopic data for **1** are consistent with the solid-state structure. The ^1H NMR spectrum shows only mesityl group resonances, while the IR spectrum has a band at 802 cm^{-1} that can be assigned to Ir=O in addition to mesityl bands.

The compound is soluble in common solvents giving green solutions. Treatment of an Et_2O solution of **1** with aqueous sodium dithionite, $Na_2S_2O_4$, gives a clean reduction to $Ir(mes)_3$, which can be isolated from the ether layer and characterized by ^1H NMR. The compound does not react with CO_2 and from reactions with CO and with HCl in Et_2O no clean products could be isolated. Attempts to convert the Ir=O group to Ir=NR using isocyanates, RNCO, R = Ph, Bu^t, c-C_6H_{11} or $(Me_3Si)N_3$, gave only $Ir(mes)_3$ and decomposition products.

The rapid reaction of $Ir(mes)_3$ in d_6-benzene with dioxygen diluted with dinitrogen on injection via a syringe can be followed by ^1H NMR. The initial spectrum for $Ir(mes)_3$[1] changes (to br s at 2.27, 9H, Me; s, 6.51, 2 aromatic H) and there is clearly an intermediate, labile species which we have been unable to isolate or characterize; it is possibly an η^2-oxygen adduct. The final product has the spectrum of $Ir(O)(mes)_3$. The reaction is presumably of the type

$$Ir(mes)_3 \overset{O_2}{\rightleftharpoons} Ir^V(mes)_3(\eta^2\text{-}O_2) \xrightarrow{Ir(mes)_3} Ir^V(O)(mes)_3$$

involving cleavage of the O—O bond in the intermediate.

The reaction of $Ir(mes)_4$, which is air-stable both in the solid state and in solutions, and oxygen occurs only on heating to *ca* 60°C in toluene or hexane, and the green solution contains $Ir(O)(mes)_3$. When $Ir(mes)_4$ is heated at 60°C in d_8-toluene for 14 h in the absence of air $Ir(mes)_3$ and mesitylene-d_1 only are formed, the latter being detected in the solvent by GC/MS spectra: presumably this reaction involves a radical abstraction of deuterium from the solvent. The tetramesityl does not react with Me_3NO under similar conditions.

Although earlier attempts to obtain homoleptic species with other aryl groups were unsuccessful,[1] we have found that interaction of Li-2,6-dimethylphenyl in Et_2O with a partially dehydrated iridium chloride prepared by the action of $SOCl_2$ on "chloroiridic acid", $(H_3O)_2IrCl_6 \cdot 2H_2O$, using the work-up as for $Ir(mes)_4$,[1] gave $Ir(2,6\text{-xylyl})_4$ (**2**) as a brown solid in low yield (*ca* 6%). It is much less stable than $Ir(mes)_4$ decomposing even in the reaction mixture to give $Ir(2,6\text{-xylyl})_3$, which was characterized only by ^1H NMR; the latter was exceptionally sensitive to air giving $Ir(O)(2,6\text{-xylyl})_3$ identified by IR and NMR spectra. The *X*-band

Table 1. Selected bond lengths (Å) and angles (°)

Ir—O(1)	1.725(9)	Ir—C(11)	2.022(13)
Ir—C(21)	1.989(13)	Ir—C(31)	2.034(13)
C(11)—Ir—O(1)	111.0(5)	C(21)—Ir—O(1)	103.0(5)
C(21)—Ir—C(11)	15.7(6)	C(31)—Ir—O(1)	116.6(5)
C(31)—Ir—C(11)	100.6(6)	C(31)—Ir—C(21)	110.5(5)
C(12)—C(11)—Ir	128.4(10)	C(16)—C(11)—Ir	113.0(10)
C(22)—C(21)—Ir	126.5(9)	C(26)—C(21)—Ir	117.0(9)
C(32)—C(31)—Ir	121.8(10)	C(36)—C(31)—Ir	120.2(10)

EPR spectra of **2** in frozen toluene at 77 K is identical with that of Ir(mes)$_4$;[1] $g_{\parallel} = 2.489$ and $g_{\perp} = 2.009$.

EXPERIMENTAL

Analysis by Medac, Brunel University and Imperial College Laboratories. General methods and instrumentation are as previously described.[1] All reactions were performed under argon and solvents degassed and dried.

Oxo(trimesityl)iridium(V)

To a solution of Ir(mes)$_3$[1] (0.4 g, 0.07 mmol) in Et_2O (10 cm^3) was added dried Me_3NO (0.009 g, 0.12 mmol). The solution immediately turned bright green but stirring was continued for 12 h at room temperature. After filtration and removal of volatiles in vacuum the residue was extracted with petroleum (2×20 cm^3, 40–60°C) and the extracts reduced to *ca* 10 cm^3. After cooling at −20°C the yield of solid Ir(O)(mes)$_3$, m.p. 130–131°C, was essentially quantitative. Very small X-ray quality crystals were grown from petroleum. Found: C, 57.1; H, 6.0. Calc. for $C_{27}H_{33}IrO$: C, 57.3; H, 5.9%. ^{1}H NMR (C_6D_6, 270 MHz): δ 2.35 (s, 3H, *p*-Me); 2.52 (s, 6H, *o*-Me); 6.79 (s, 2H, aromatic-H).

2,6-*Dimethylphenyliridium compounds*

To Johnson Matthey "chloroiridic acid" (*ca* 1 g) was added thionyl chloride (20 cm^3) and the mixture refluxed under nitrogen (2 h) when the $SOCl_2$ was removed. The black residue (0.3 g) was stirred in Et_2O (15 cm^3) and a solution of 2,6-dimethylphenyl lithium (0.75 g in 15 cm^3 of Et_2O) added. After stirring (20 min) the Et_2O was removed and the residue extracted with petroleum (40–60°C, 2×15 cm^3). Reduction in volume (to *ca* 3 cm^3) and cooling (−20°C) yielded a brown crystalline solid (**2**) (0.04 g, 6.5% yield). We have been unable to obtain satisfactory analyses due to decomposition. In the presence of air the brown solutions become green over 2 h, but the oxo species is much less stable than **1**.

On attempting to prepare **2** from partially dehydrated $IrCl_3 \cdot nH_2O$ as for Ir(mes)$_4$[1] the brown solution was exceedingly sensitive to traces of air and on cooling gave a black powder that was unstable. The ^{1}H NMR spectrum (C_6D_6) taken rapidly corresponded to that of the intermediate found in the Ir(mes)$_3$ + O_2 reaction (δ 6.6, br.s, 3H, aromatic H; 2.2, s, 6H, *o*-Me), while the NMR of the final green solution corresponded to that of **1**. The final product isolated as a solid had an IR (Nujol mull) band at 803 cm^{-1} due to Ir=O, while the ^{1}H NMR spectrum was similar to that for **1**; in C_6D_6: δ 6.9 (d, $J = 7.3$ Hz, 1H aromatic *p*-H); 6.5 (t, $J = 7.3$ Hz, 2H aromatic, *m*-H); 2.4 (s, 6H *o*-Me).

X-ray crystallography

X-ray data were recorded on a FAST TV area detector diffractometer with Mo-K_α radiation ($\lambda = 0.71069$ Å) as previously described,[5] using a crystal of dimensions $0.2 \times 0.15 \times 0.1$ mm^3. The structure was solved via the heavy atom method and refined by full-matrix least-squares. The data were corrected for absorption using the DIFABS[6] method at the isotropic refinement stage. All non-hydrogen atoms were refined in the anisotropic approximation, whilst hydrogens were included in idealized positions and assigned group U_{iso} values. Crystal data and experimental details are as follows.

Formula: $C_{27}H_{33}OIr$, $M_r = 565.78$. Monoclinic, $a = 8.299(1)$, $b = 15.828(3)$, $c = 18.235(7)$ Å, $\beta = 101.21(3)°$, $V = 2349.6$ Å^3, space group $P2_1/a$, $Z = 4$, $D_c = 1.599$ g cm^{-3}, $F(000) = 1120$, μ(Mo-K_α) = 56.7 cm^{-1}. From the ranges scanned 11,805 data were recorded and merged to give 5747 unique ($R_{int} = 0.038$), 2531 observed [$F_o > 3(F_o)$]. $R = 0.039$, $Rw = 0.042$, 304 parameters. Tables of atomic coordinates, displacement factor coefficients, full lists of bond lengths and angles and F_o/F_c values have been deposited as supplementary material with the Editor. Atomic coordinates have also been deposited with the Cambridge Crystallographic Data Centre.

Acknowledgements—We thank Johnson Matthey plc for the loan of iridium halides, the SERC for provision of X-ray facilities (M.B.H.) and Mr R. Tye, ULIRS Mass Spectrometry Service, Kings College, London.

REFERENCES

1. (a) R. S. Hay-Motherwell, G. Wilkinson, B. Hussain-Bates and M. B. Hursthouse, *Polyhedron* 1991, **10**, 1457; (b) R. S. Hay-Motherwell, G. Wilkinson, B. Hussain-Bates and M. B. Hursthouse, *J. Chem. Soc., Dalton Trans.* 1992, 3477.
2. (a) F. A. Cotton and G. Wilkinson, *Advanced Inorganic Chemistry*, 5th edn, p. 916. Wiley, New York (1988); (b) X.-L. Luo and R. H. Crabtree, *J. Am. Chem. Soc.* 1989, **111**, 2527; (c) R. S. Tanke and R. H. Crabtree, *Organometallics* 1991, **10**, 615; (d) S. E. Castillo-Blum, D. T. Richens and A. G. Sykes, *Inorg. Chem.* 1989, **28**, 954.
3. P. Stavropoulos, P. D. Savage, R. P. Tooze, G.

Wilkinson, B. Hussain, M. Motevalli and M. B. Hursthouse, *J. Chem. Soc., Dalton Trans.* 1978, 557.
4. P. Stavropoulos, P. G. Edwards, T. Behling, G. Wilkinson, M. Motevalli and M. B. Hursthouse, *J. Chem. Soc., Dalton Trans.* 1987, 169.
5. A. A. Danopoulos, G. Wilkinson, B. Hussain-Bates and M. B. Hursthouse, *J. Chem. Soc., Dalton Trans.* 1991, 1855.
6. N. P. C. Walker and D. Stuart, *Acta Cryst., Sect. A* 1983, **39**, 158.

Polyhedron Vol. 12, No. 16, pp. 2013–2019, 1993
Printed in Great Britain

0277–5387/93 $6.00+.00
© 1993 Pergamon Press Ltd

COMPLEXES OF TUNGSTEN(IV,VI) AND MOLYBDENUM(V) DERIVED FROM 1,2-DIAMINOBENZENE. X-RAY CRYSTAL STRUCTURES OF *CIS,MER*-W(*o*-$NC_6H_4NH_2$)$Cl_2(PMe_3)_3$, {WCl[*o*-$(HN)_2C_6H_4]_2(PMe_3)_2$}(BPh_4) AND *MER,TRANS*-Mo(*o*-$NC_6H_4NH_2$)$Cl_3(PMePh_2)_2$

CARL REDSHAW and GEOFFREY WILKINSON†

Johnson Matthey Laboratory, Chemistry Department, Imperial College, London SW7 2AY, U.K.

and

TRACY K. N. SWEET and MICHAEL B. HURSTHOUSE†

School of Chemistry and Applied Chemistry, University of Wales Cardiff, P.O. Box 912, Cardiff CF1 3TB, U.K.

(*Received* 23 *March* 1993; *accepted* 22 *April* 1993)

Abstract—The compound $WCl_2(PMe_3)_4$ undergoes an oxidative-addition reaction with excess *o*-phenylenediamine (1,2-diaminobenzene) in refluxing toluene to give the tungsten(IV) imido complex *cis,mer*-W(*o*-$NC_6H_4NH_2$)$Cl_2(PMe_3)_3$ (**1**). A chloride substitution reaction of **1** with $NaBPh_4$ leads to the seven-coordinate tungsten(VI) complex {WCl[*o*-$(HN)_2C_6H_4]_2(PMe_3)_2$}(BPh_4) (**2**). Interaction of $MoOCl_2(PMePh_2)_3$ with excess *o*-phenylenediamine in the presence of base (Et_3N) gives the imido complex *mer,trans*-Mo(*o*-$NC_6H_4NH_2$)$Cl_3(PMePh_2)_2$ (**3**). X-ray structures of the compounds listed in the title have been determined. In **1** and **3** the pseudo-octahedral complexes contain unidentate near-linear imido groups, derived from the *o*-phenylenediamine ligand, whereas in complex **2** the geometry is distorted capped octahedral with chelating $(HN)_2C_6H_4$ groups.

In previous studies on *o*-phenylenediamine or its deprotonated compounds of Cr, Mo and W we have described the synthesis and X-ray crystal structures of a number of *o*-phenylenediamine compounds of chromium(II), (III) and (IV),[1] such as the tetra-triflate complex $Cr(O_3SCF_3)_4[(H_2N)_2C_6H_4]$, as well as the *o*-phenylenediamide complex $CrCl_2[(HN)_2C_6H_4](PMe_2Ph)_2$[2] and the binuclear tungsten complex $\{WCl_3[(HN)(H_2N)C_6H_4]\}_2[\mu$-1,2-$(N)_2C_6H_4]$,[3] in which the bridging ligand acts as a bis imido function.

We now describe the synthesis and characterization of the mono-imido complexes *cis,mer*-W(*o*-$NC_6H_4NH_2$)$Cl_2(PMe_3)_3$ and *mer,trans*-Mo(*o*-$NC_6H_4NH_2$)$Cl_3(PMePh_2)_2$. The only previous example[4] of a complex involving an imido group and "free" amino group derived from an *o*-phenylenediamine ligand is Mo(*o*-$NC_6H_4NH_2$)$Cl_2(S_2CNEt_2)_2$. The interesting seven-coordinate bis chelate {WCl[*o*-$(HN)_2C_6H_4]_2(PMe_3)_2$}(BPh_4) is also described.

RESULTS AND DISCUSSION

Tungsten complexes

Interaction of $WCl_2(PMe_3)_4$[5] with *o*-phenylenediamine in refluxing toluene yields large dark needles of *cis,mer*-W(*o*-$NC_6H_4NH_2$)$Cl_2(PMe_3)_3$ (**1**) in good yields (50–55%). Similar oxidative-addition reactions have been reported for the complexes $WCl_2(PR_3)_4$, PR_3 = $PMePh_2$, PMe_3, with hetero-cumulenes such as R′NCO, R′ = Bu^t, Ph,[6] and

† Authors to whom correspondence should be addressed.

the main group azides[7] (mesityl)$_2$B(N)$_3$ and (*o*-tolyl)$_3$Si(N$_3$). The IR spectrum of **1** has a strong ν(N—H) stretch at *ca* 3420 cm^{-1}, indicative of an uncoordinated NH$_2$ group,[8] together with a strong ν(C—N) stretch at *ca* 1279 cm^{-1}. In addition, the strong band at 1263 cm^{-1} can be attributed to the C—N stretch of a coordinated group. Confirmation of the unidentate nature of the ligand is provided by X-ray (see below) and NMR data. In the ^{1}H NMR spectrum the unsymmetrical nature of the bonding results in four distinct multiplets for the aromatic ring protons (see Experimental); a broad band at *ca* 4.9 ppm can be assigned to the NH$_2$ group, whilst the methyl signals of the PMe$_3$ ligands appear as a doublet [δ = 1.9, J(P—H) = 7.9 Hz, 9H] and a triplet [δ = 1.6, J(P—H) = 37 Hz, 18H]. In the ^{13}C NMR spectrum all six imido ligand carbon atoms appear at different chemical shifts (115.1–145.8 ppm). The ^{31}P NMR spectrum consists of two singlets, however, there is no phosphorus–phosphorus coupling between the two inequivalent phosphorus atoms; ^{183}W satellites are present.

Figure 1 depicts the *cis*-chlorine, *mer*-phosphine pseudo-octahedral geometry of one of the three crystallographically independent molecules of **1**. Selected bond lengths and angles for all three molecules are given in Table 1. An "inverse" *trans* influence is exerted by the near-linear (W$\widehat{\text{N}}$C = 177.2 Å) NC$_6$H$_4$NH$_2$ ligand in this complex. The *trans*-W—Cl bond distances are actually shorter than the W—Cl bond *cis* to the NC$_6$H$_4$NH$_2$ group in all three molecules. This effect, or at least the absence of a *trans* lengthening influence, seems to be common for tungsten(IV) species. Similarly no *trans* lengthening influence was reported for the phenylimido group in the related tungsten(IV) complex, W(NPh)Cl$_2$(PMe$_3$)$_3$.[9] There is also evidence of a *trans*-phosphine influence in **1**: the mutually *trans* phosphine distances (2.494 and 2.509 Å) are *ca* 0.04 Å longer than the remaining (*trans* to Cl) W—P distance (2.455 Å). Similar phosphine effects have been reported for the complex Mo(N-*p*-tol)Cl$_2$(PMe$_3$)$_3$[10] and may be ascribed to competitive π-back-bonding.

On the basis of the above X-ray data the compound previously reported[3] as WCl$_2$[1,2-(HN)$_2$C$_6$H$_4$](PMe$_3$)$_3$ is now best regarded as being compound **1** also.

Interaction of **1** with NaBPh$_4$ (2 equivalents) in refluxing MeCN (12 h) yields, after work-up, deep red prisms of {W[*o*(HN)$_2$C$_6$H$_4$]$_2$Cl(PMe$_3$)$_2$}BPh$_4$ (**2**). The IR spectra of **2** contains a sharp band at 3308 cm^{-1}, characteristic of the monoarylamide group.[11] There are no strong bands above 3300 cm^{-1} (uncoordinated NH$_2$). In the ^{1}H NMR spectrum a broad band at *ca* 11.7 ppm can be assigned to the NH protons;[12] the wide range of shifts observed for amido proton resonances, *ca* 2.2–16.8 ppm, has been noted.[12] The aromatic region is complex, whilst a triplet at *ca* 1.0 ppm can be assigned to PMe$_3$ resonances. The ^{31}P NMR spectrum contains

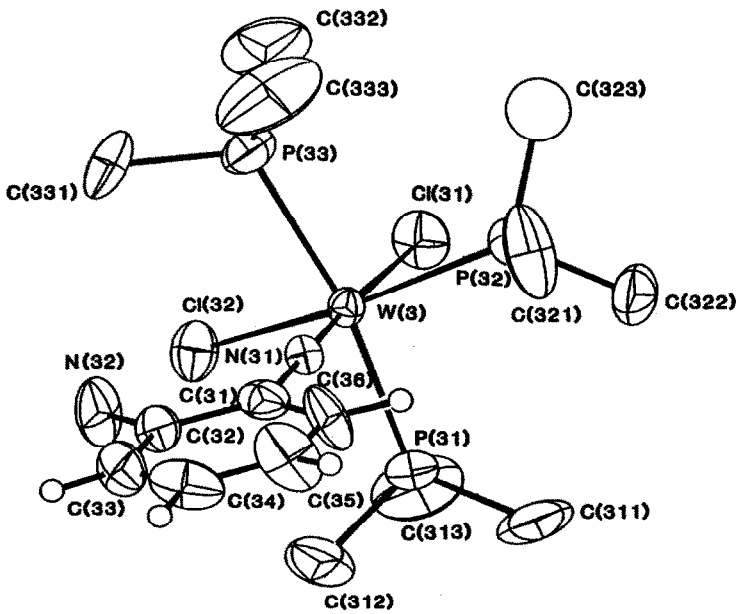

Fig. 1. The structure of one of the three crystallographically independent molecules of *cis*-Cl, *mer*-PMe$_3$-[W^{IV}(*o*-NC$_6$H$_4$NH$_2$)Cl$_2$(PMe$_3$)$_3$] (**1**).

Table 1. Selected bond lengths (Å) and angles (°) for compound **1**

	$n = 1$	$n = 2$	$n = 3$
Cl(*n*2)—W(*n*)	2.515(7)	2.540(6)	2.524(6)
Cl(*n*1)—W(*n*)	2.483(6)	2.483(8)	2.489(7)
P(*n*2)—W(*n*)	2.482(7)	2.500(8)	2.492(7)
P(*n*2)—W(*n*)	2.445(6)	2.443(8)	2.454(6)
P(*n*3)—W(*n*)	2.514(8)	2.491(8)	2.507(7)
N(*n*1)—W(*n*)	1.724(11)	1.716(11)	1.725(11)
	$n = 1$	$n = 2$	$n = 3$
Cl(*n*1)—W(*n*)—Cl(*n*2)	84.4(2)	84.5(2)	84.6(2)
P(*n*1)—W(*n*)—Cl(*n*2)	86.1(3)	86.3(3)	85.8(3)
P(*n*1)—W(*n*)—Cl(*n*1)	89.5(2)	85.4(3)	91.6(2)
P(*n*2)—W(*n*)—Cl(*n*2)	164.3(1)	171.8(2)	163.8(1)
P(*n*2)—W(*n*)—Cl(*n*1)	80.0(2)	87.4(3)	79.2(2)
P(*n*2)—W(*n*)—P(*n*1)	92.9(3)	93.1(3)	93.0(2)
P(*n*3)—W(*n*)—Cl(*n*2)	82.7(3)	86.5(3)	82.5(2)
P(*n*3)—W(*n*)—Cl(*n*1)	88.1(2)	86.4(3)	87.8(2)
P(*n*3)—W(*n*)—P(*n*1)	168.8(2)	169.6(2)	168.3(2)
P(*n*3)—W(*n*)—P(*n*2)	97.5(3)	93.0(3)	98.4(2)
N(*n*1)—W(*n*)—Cl(*n*2)	99.3(5)	96.8(5)	99.2(4)
N(*n*1)—W(*n*)—Cl(*n*1)	176.2(4)	178.7(4)	175.5(4)
N(*n*1)—W(*n*)—P(*n*1)	91.5(5)	94.7(5)	91.0(5)
N(*n*1)—W(*n*)—P(*n*2)	96.3(5)	91.3(5)	96.9(4)
N(*n*1)—W(*n*)—P(*n*3)	91.6(5)	93.6(5)	90.4(5)

two major peaks [$\delta = -1.1$ and $+8.6$ ppm singlet with satellites J(P—W) = 109 Hz]. The crystal structure of **2** is shown in Fig. 2, with bond lengths and angles given in Table 2. Most interestingly, the unidentate $NC_6H_4NH_2$ imido ligand in **1** has been converted to the chelating diamido of **2**.

Hydrogen atoms were experimentally located, one on each of the *o*-pda nitrogens and so the complex is clearly identified as a tungsten(VI) species. The W—N distances of 2.008(7) to 2.068(7) Å are slightly longer than might be expected for a tungsten(VI)–amido link where N → W $p\pi$–$d\pi$ donation might be expected. However, only limited π-bonding will occur since the metal electron count via sigma interactions is already 14e and a total of only two π-interactions are required. The *ca* 0.05 Å spread in W—N distances may reflect this and the different environments of the nitrogens in the

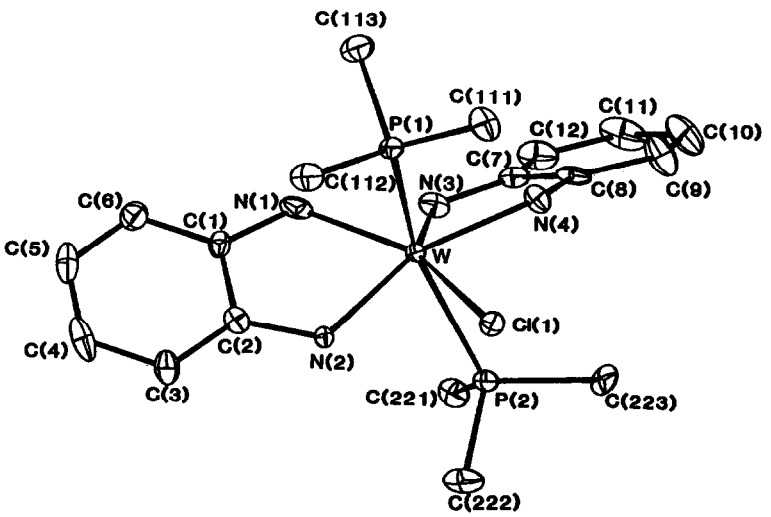

Fig. 2. The structure of $\{W^{VI}[o\text{-}(NH)_2C_6H_4]_2Cl(PMe_3)_2\}BPh_4$ (**2**).

Table 2. Selected bond lengths (Å) and angles (°) for compound **2**

P(1)—W	2.527(4)	P(2)—W	2.550(4)
N(1)—W	2.010(8)	N(2)—W	2.053(6)
N(3)—W	2.008(7)	N(4)—W	2.068(6)
Cl(1)—W	2.511(4)	C(1)—N(1)	1.371(8)
C(2)—N(2)	1.360(8)	C(7)—N(3)	1.385(8)
C(8)—N(4)	1.360(7)	C(51)—N(5)	1.128(9)
H(101)—N(1)	0.616(49)	H(201)—N(2)	0.917(58)
H(301)—N(3)	0.802(51)	H(401)—N(4)	0.904(55)
P(2)—W—P(1)	154.9(1)	N(1)—W—P(1)	79.8(2)
N(1)—W—P(2)	123.3(2)	N(2)—W—P(1)	97.9(2)
N(2)—W—P(2)	82.5(2)	N(2)—W—N(1)	71.4(3)
N(3)—W—P(1)	116.1(2)	N(3)—W—P(2)	81.6(2)
N(3)—W—N(1)	76.8(3)	N(3)—W—N(2)	127.8(3)
Cl(1)—W—N(1)	139.8(2)	Cl(1)—W—N(2)	78.5(2)
Cl(1)—W—N(3)	143.3(1)	Cl(1)—W—N(4)	77.8(2)
C(1)—N(1)—W	124.1(5)	C(2)—N(2)—W	122.1(5)
C(7)—N(3)—W	123.0(5)	C(8)—N(4)—W	120.9(5)
H(101)—N(1)—W	118.5(56)	H(201)—N(2)—W	120.5(36)
H(301)—N(3)—W	125.5(34)	H(401)—N(4)—W	121.0(35)
N(4)—W—P(1)	82.3(2)	H(4)—W—P(2)	87.3(2)
N(4)—W—N(1)	131.8(2)	N(4)—W—N(2)	155.8(2)
N(4)—W—N(3)	71.8(3)	Cl(1)—W—P(1)	78.6(1)
Cl(1)—W—P(2)	76.9(1)		

unsymmetrical coordination sphere. There is, however, some evidence of delocalization of the nitrogen lone pairs into the aromatic ring system. In fact the geometry is difficult to define, partly as a result of the bite restrictions of the *o*-pda ligands, but might reasonably be described as a distorted capped octahedron with N(3) as the capping atom. An alternative description would identify P(1) and P(2) as axial ligands in a distorted pentagonal bipyramidal geometry with considerable equatorial puckering.

Molybdenum. Addition of excess *o*-phenylenediamine to $MoOCl_2(PMePh_2)_3$ gives the paramagnetic complex *mer,trans*-$Mo(o\text{-}NC_6H_4NH_2)Cl_3(PMePh_2)_2$ (**3**), which can be isolated as red–brown crystals in low yield.

The IR spectrum of **3** again contains a ν(N—H) stretch at *ca* 3407 cm^{-1}, indicative of an uncoordinated NH_2 group, together with bands in the ν(C—N) region consistent with the presence of a coordinated group.

The *X*-band EPR spectrum (toluene, 298 K) is sharp with $g_{iso} = 1.978$; super-hyperfine coupling is observed to two equivalent ^{31}P nuclei (*ca* 27 G) comparable to those observed for the complexes $M(N\text{-}p\text{-tol})Cl_3(PR_3)_2$, R = $EtPh_2$, Me and Ph.[13] However, the hyperfine coupling to $^{95,97}Mo$ for **3** (*ca* 44 G) is double that observed by Maatta *et al.*[13] (21.4–22.4 G), but is comparable with that observed for the reduction product of $Mo(NC_6H_4S)Cl(S_2CNEt_2)_2$ (40 G)[14] and the value of 38 G reported for $Mo(S_2CNEt_2)(NHC_6H_4S)_2$.[15] This may be a reflection of the greater contribution of the bent compared with linear bonding in the MNR group in **3**. There is no observable hyperfine isotropic splitting to nitrogen for **3**.

The molecular structure of **3** is shown in Fig. 3, and important bond lengths and angles are given in Table 3. The molecule possesses a *mer* arrangement of chlorines with the phosphine ligands occupying *trans* positions, presumably to minimize steric constraints ($PMePh_2$, cone angle = 136°); whereas in the complex $Mo(N\text{-}p\text{-tol})Cl_2(PMe_3)_3$[10] containing the less sterically demanding PMe_3 ligand (cone angle = 118°) a *cis, mer* geometry is adopted. The molecule lies on a two-fold rotation axis passing through Cl(2), Mo(1), N(1) and the attached $C_6H_4NH_2$ group is disordered. The near-linear imido ligand [Mo—N(1)—C(121) = 169.9(2)°] in **3** shows a *trans* influence with Mo—Cl(2), *ca* 0.1 Å, longer than Mo—Cl(1). This is similar to the situation in the related molybdenum(V) complex $Mo(N\text{-}p\text{-tol})Cl_3(EtPh_2P)_2$.[10]

EXPERIMENTAL

Microanalyses were performed by the University College, London, and Medac Ltd, Brunel University.

The spectrometers and general techniques have

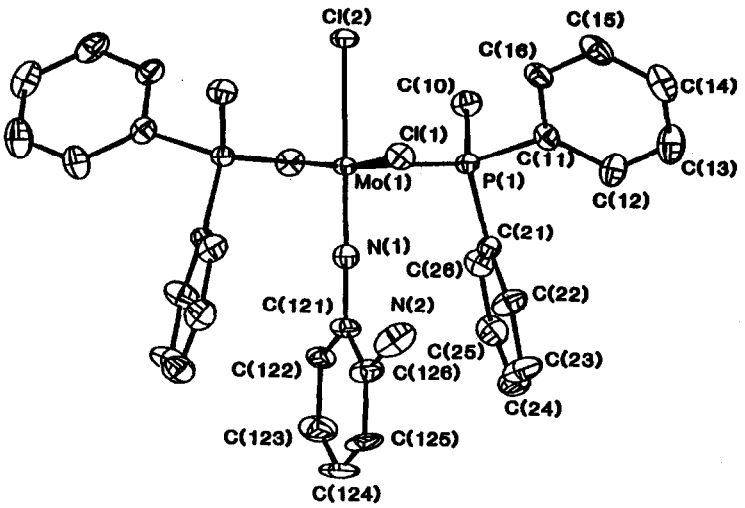

Fig. 3. The structure of *mer*-Cl, *trans*-$PMePh_2[Mo^{V}(o\text{-}NC_6H_4NH_2)Cl_3(PMePh_2)_2]$ (3).

been previously described.[16] The precursors $WCl_2(PMe_3)_4$[5] and $MoOCl_2(PPh_2Me)_3$[17] were prepared as described. Trimethylphosphine was prepared by the method of Wolfsberger and Schmidbaur.[18] Commercial chemicals are from Aldrich; $C_6H_4(NH_2)_2$-1,2 was recrystallized from toluene prior to use. All operations were performed under oxygen-free nitrogen or argon. NMR spectra: Bruker WM 250 Hz (^1H, ^{13}C and ^{31}P), δ in ppm referenced to Me_4Si, solvent and 85% H_3PO_4 (external), respectively. IR spectra as Nujol mulls (in cm^{-1}) and mass spectra by fast atom bombardment.

[(2 - *Aminophenyl*)*imido*]*dichlorotris*(*trimethylphosphine*)*tungsten*(IV) (1)

To $WCl_2(PMe_3)_4$ (1.0 g, 1.79 mmol) in toluene (*ca* 40 cm^3) was added 1,2-$C_6H_4(NH_2)_2$ (0.39 g, 3.6 mmol). The solution was refluxed for 12 h then filtered (hot) and allowed to stand at room temperature when large black needles formed. Yield: 50–55%; m.p. 254–258°C. Found: C, 30.9; H, 5.3; N, 4.8; Cl, 13.6. Calc. for $WC_{15}H_{33}Cl_2N_2P_3$: C, 30.6; H, 5.6; N, 4.8; Cl, 12.0%. Mass spectrum: *m/z* 589(M), 553(M − Cl), 513(M − PMe_3), 437(M − 2PMe_3). IR: 3420s, 3312s, 3205w, 2727w,

Table 3. Selected bond lengths (Å) and angles (°) for compound 3

Cl(1)—Mo(1)	2.400(3)	Cl(2)—Mo(1)	2.499(3)
P(1)—Mo(1)	2.562(4)	N(1)—Mo(1)	1.735(6)
C(10)—P(1)	1.820(5)	C(11)—P(1)	1.824(5)
C(21)—P(1)	1.808(5)	C(121)—N(1)	1.375(6)
N(2)—C(126)	1.400(11)		
Cl(2)—Mo(1)—Cl(1)	86.7(1)	P(1)—Mo(1)—Cl(1)	93.5(1)
P(1)—Mo(1)—Cl(2)	87.1(1)	N(1)—Mo(1)—Cl(1)	93.3(1)
N(1)—Mo(1)—Cl(2)	180.0(1)	N(1)—Mo(1)—P(1)	92.9(1)
Cl(1)—Mo(1)—Cl(1a)	173.4(1)	P(1)—Mo(1)—P(1a)	174.2(1)
Cl(1)—Mo(1)—P(1a)	86.1(1)	C(10)—P(1)—Mo(1)	113.1(2)
C(11)—P(1)—Mo(1)	117.5(2)	C(11)—P(1)—C(10)	102.3(2)
C(21)—P(1)—Mo(1)	109.8(2)	C(21)—P(1)—C(10)	106.3(2)
C(21)—P(1)—C(11)	107.1(2)	C(121)—N(1)—Mo(1)	169.9(2)
C(12)—C(11)—P(1)	124.6(3)	C(16)—C(11)—P(1)	116.7(3)
C(22)—C(21)—P(1)	119.4(3)	C(26)—C(21)—P(1)	121.7(3)
C(122)—C(121)—N(1)	122.0(3)	C(126)—C(121)—N(1)	117.9(3)
C(121)—N(1)—C(121)	20.1(4)	N(2)—C(126)—C(121)	118.5(5)

1716w, 1605s, 1558w, 1339s, 1322s, 1300s, 1279s, 1263s, 1159s, 1080w, 1033w, 990w, 945s, 847m, 824w, 751s, 733s, 668m, 591w, 577w, 532w, 495m, 448w, 420m, 395w, 375w, 342w, 280m. NMR ($CDCl_3$, 298 K): ^1H: δ 1.6 [t, 18H, *trans*-PMe_3, J(P—H) = 3.7 Hz]; 1.91d, 9H, *cis*-PMe_3, J(P—H) = 7.9 Hz; 4.9 (br s, 2H, NH_2); aromatic region δ = 6.37 (t*, 1H, J = 7.37 Hz, J' = 1.18 Hz), 6.48 (dd, 1H, J = 7.96 Hz, J' = 0.99 Hz), 6.78 (dd, 1H, J = 7.37 Hz, J' = 1.12 Hz), 6.95 (t*, 1H, J = 8.3 Hz, J' not seen—t* signifies singlet between two doublets). ^{13}C: δ 17.7 [t, J(C—P) = 13.3 Hz], 26.9 (d, J = 28.7 Hz) PMe_3; aromatics δ 115.1, 116.0, 123.3, 125.1, 143.0 and 145.8. $^{31}P\{^1H\}$: δ −23.9 [s with satellites, J(P—W) = 403 Hz, *cis*-PMe_3]; −25.5 [s with satellites, J(P—W) = 300 Hz, *trans*-PMe_3]; no P—P coupling observed.

Chlorobis(1,2-*phenylenediamido*)*bis*(*trimethylphosphine*)*tungsten*(VI)*tetraphenylborate* (**2**)

To **1** (0.3 g 0.51 mmol) in MeCN (*ca* 40 cm^3) was added $NaBPh_4$ (0.35 g, 1.02 mmol). The solution was refluxed for 12 h, cooled, filtered and concentrated (*ca* 5 cm^3), warmed to dissolve all solid and allowed to stand (24 h) at room temperature. The large, dark red prisms were collected: further crops may be obtained by concentration of the supernatant. Overall yield: *ca* 40%, m.p. *ca* 210°C. Found: C, 56.2; H, 5.7; N, 7.3. Calc. for $WC_{42}H_{50}BClN_4P_2$: C, 55.9; H, 5.6; N, 6.2%. IR: 3308s, 1580w, 1413m, 1360s, 1305m, 1286s, 1261s, 1230m, 1185w, 1150s, 1100s, 1032s, 951s, 846w, 802s, 790s, 737s, 727s, 707s, 612w, 577w, 557w, 453w. NMR (CD_3CN): ^1H: δ 11.7 (br.s, 4H, NH); 6.3–7.4 [m, 28H, B*Ph*$_4$ and 1,2-$C_6H_4(NH)_2$]; 1.0 (t, 18H, PMe_3). $^{31}P\{^1H\}$: −1.1 (br, s), +8.6; [s; satellites, J(P—W) = 109 Hz]. There was a weak impurity peak at +30.6 ppm with satellites J(P—W 109 Hz).

[(2-*Aminophenyl*)*imido*]*trichlorobis*(*methyldiphenylphosphine*)*molybdenum*(V) (**3**)

To $MoOCl_2(PMePh_2)_3$ (0.9 g, 1.15 mmol) in toluene (*ca* 40 cm^3) was added 1,2-$C_6H_4(NH_2)_2$ (0.25 g, 2.31 mol); after refluxing (12 h) and filtering hot, a hexane layer (*ca* 40 cm^3) was carefully added. After standing at room temperature (72 h) the large red prisms were collected and dried *in vacuo*. Yield: *ca* 20%, m.p. 232–234°C. Found: C, 54.2; H, 4.6; N, 4.8. Calc. for $MoC_{32}H_{32}Cl_3N_2P_2$: C, 54.2; H, 4.6; N, 4.0%. IR: 3407w, 3333w, 2609w, 1713w, 1622m,

Table 4. Crystal data, details of intensity measurements and structure refinements

Structure number	**1**	**2**	**3**
Formula	$WCl_2N_2C_{15}H_{31}P_3$	$WClN_4C_{42}H_{50}P_2B$	$MoCl_3N_2C_{32}H_{32}P_2$
Mr	587.101	902.95	708.867
Crystal system	Monoclinic	Monoclinic	Monoclinic
Space group	$P2_1/c$	$P2_1/n$	$C2/c$
a (Å)	9.344(4)	16.348(4)	11.423(4)
b (Å)	43.035(10)	9.808(3)	19.363(4)
c (Å)	18.159(7)	27.290(3)	15.117(2)
α (°)	90.0	90.0	90.0
β (°)	100.61(1)	106.75(2)	107.08(2)
γ (°)	90.0	90.0	90.0
V (Å^3)	7177.24	4189.77	3196.16
Z	12	4	4
D_c (g cm^{-3})	1.63	1.43	1.47
F(000)	3456	1824	1444
μ(Mo-K_α) (cm^{-1})	53.571	29.912	7.76
Total no. of reflections	23,169	12,640	10,167
No. of unique reflections	7803	6195	3913
No. of observed reflections ($F_o > 3\sigma(F_o)$)	6345	5129	2709
No. of refined parameters	603	485	258
Weighting scheme	$1/[\sigma^2(F)]$	$1/[\sigma^2(F)]$	Unit
Final R $R = \Sigma(\Delta F)/\Sigma(F_o)$	0.0516	0.0304	0.0277
Final Rw $wR = [\Sigma\{w(\Delta F)^2\}/\Sigma\{w(F_o)^2\}]^{1/2}$	0.0706	0.0389	0.0307

1595w, 1574w, 1552w, 1499w, 1292m, 1261s, 1153s, 1097s, 530w, 504m, 446m.

Crystallographic studies

X-ray diffraction data were recorded for the three compounds using a FAST TV area detector diffractometer and graphite monochromated Mo-K_α radiation following previously described procedures.[19] Crystals for compounds **2** and **3**, coated with silicone oil, were mounted on the end of glass fibres and the data collected at 150 K, using a CRYOSTREAM cooling device. Data for compound **1** were recorded at room temperature using a capillary mounted crystal. The structures were solved and developed via the heavy atom method and refined by full-matrix least-squares. During the refinement process the data for each structure were corrected for absorption using the DIFFAST program.[20] Crystal data and details of the data collection and structure refinement are given in Table 4.

REFERENCES

1. C. Redshaw, G. Wilkinson, B. Hussain-Bates and M. B. Hursthouse, *J. Chem. Soc., Dalton Trans.* 1992, 1803.
2. W.-H. Leung, A. A. Danopoulos, G. Wilkinson, B. Hussain-Bates and M. B. Hursthouse, *J. Chem. Soc., Dalton Trans.* 1991, 2501.
3. C. Redshaw, G. Wilkinson, B. Hussain-Bates and M. B. Hursthouse, *J. Chem. Soc., Dalton Trans.* 1992, 555.
4. M. Minelli, M. R. Carson, D. W. Whisenhurst Jr and J. L. Hubbard, *Inorg. Chem.* 1990, **29**, 442.
5. R. R. Sharp, J. C. Bryan and J. M. Mayer, *Inorg. Chem.* 1990, **28**, 329.
6. F. M. Su, J. C. Bryan, S. Jong and J. M. Mayer, *Polyhedron* 1989, **10**, 1261.
7. A. A. Danopoulos, C. Redshaw, A. Vaniche, G. Wilkinson, B. Hussain-Bates and M. B. Hursthouse, *Polyhedron* 1993, **12**, 1061.
8. J. Julde, L. F. Larkworthy, L. F. Oliver, D. L. Povey and G. W. Smith, *J. Chem. Soc., Dalton Trans.* 1991, 2045.
9. D. C. Bradley, M. B. Hursthouse, K. M. Abdul Malik, A. J. Nielson and R. L. Short, *J. Chem. Soc., Dalton Trans.* 1983, 2651.
10. C. Y. Chan, D. D. Devore, S. C. Huckett, E. A. Maatta, J. C. Huffman and F. Takusagawa, *Polyhedron* 1986, **5**, 301.
11. K. W. Chiu, W. W. Wong, G. Wilkinson, A. M. Galas and M. B. Hursthouse, *Polyhedron* 1982, **1**, 37.
12. C. Redshaw, W. Clegg and G. Wilkinson, *J. Chem. Soc., Dalton Trans.* 1992, 2059.
13. C. Y. Chou, J. C. Huffman and E. A. Maatta, *Inorg. Chem.* 1986, **25**, 822.
14. M. Minelli, M. R. Carson, D. W. Whisenhunt Jr, W. Imhof and G. Huttner, *Inorg. Chem.* 1990, **29**, 4801.
15. N. Pariyadath, W. E. Newton and E. I. Stiefel, *J. Am. Chem. Soc.* 1976, **98**, 5388.
16. A. A. Danopoulos, A. C. C. Wong, G. Wilkinson, M. B. Hursthouse and B. Hussain-Bates, *J. Chem. Soc., Dalton Trans.* 1990, 315.
17. A. V. Butcher and J. Chatt, *J. Chem. Soc. A* 1970, 2652.
18. W. Wolfsberger and H. Schmidbaur, *Synth. React. Inorg. Met.-Org. Chem.* 1974, **4**, 149.
19. A. A. Danopoulos, G. Wilkinson, B. Hussain-Bates and M. B. Hursthouse, *J. Chem. Soc., Dalton Trans.* 1991, 1855.
20. A. Karaulov, DIFFAST: Fast specific version of DIFABS. University Wales, Cardiff (1992).

Polyhedron Vol. 12, No. 16, pp. 2021–2025, 1993
Printed in Great Britain

0277–5387/93 $6.00+.00
© 1993 Pergamon Press Ltd

CHELATE COMPLEXES OF 1,3-BIS-(1′-PHENYL-3′-METHYL-5′-PYRAZOLONE-4′)-1,3-PROPANEDIONE AND 1,10-PHENANTHROLINE WITH LANTHANIDE

XIAOJING LI, LAN YAN,* HUI WANYAN and RUDONG YANG

Department of Chemistry, Lanzhou University, Lanzhou 730000, P.R.C.

(*Received* 30 *September* 1992; *accepted* 22 *April* 1993)

Abstract—A new ligand, 1,3-bis-(1′-phenyl-3′-methyl-5′-pyrazolone-4′)-1,3-propanedione (H_2L), and its chelated complexes, $Ln_2L_3(Phen)_2 \cdot nH_2O$ (where Phen = 1,10-phenanthroline, Ln = lanthanide and Y, n = 3–6), have been prepared by the reaction of H_2L and Phen with the relative metal nitrate in an aqueous alcoholic solution. The binuclear structure of the complexes is proposed according to the discussions of the elemental analyses, molar conductance, IR and ^1H NMR spectra. Fluorescence spectra prove Pr, Sm, Eu, Tb, Dy and Tm complexes have line emissions of metal ions.

4-Acyl-pyrazolones are thought of as ideal chelating agents and their complexes are also of interest to investigate the interaction between metal ions and complexing agents, catalytic activity and NMR shift reagents.[1–3] However, 4-acyl-bis-pyrazolones with four oxygen donors are also potential chelating agents for metal ions and are superior in extraction than monopyrazolone.[4] They are also able to form mononuclear, polynuclear or heteronuclear complexes with ions under differing conditions. These complexes, especially with some of the lanthanides, exhibit excellent fluorescence, which provides an opportunity to study their application in analysis of optical materials. Recently some 4-acyl-bis-pyrazolines and their complexes with lanthanide ions have been investigated,[5–9] but much less work has been performed with the new 4-acyl-bis-pyrazolone-1,3-bis-(1′-phenyl-3′-methyl-5′-pyrazolone-4′)-1,3-propanedione (noted H_2L) and its complexes. In this paper the preparation and various interesting properties of novel mixed-ligand complexes of lanthanide ions with H_2L and 1,10-phenanthroline (noted Phen) are reported.

EXPERIMENTAL

Physical measurements and analyses

The metal content of the reported complexes was obtained by the literature method.[9] Microanalyses for carbon, hydrogen and nitrogen contents were determined using a 1106 elemental analyser. The analytical data for the complexes are given in Table 1. Electrolytic conductance measurements were obtained with a DDS-11A molar conductometer. IR spectra were recorded on an FT-170SX IR spectrophotometer as KBr discs in the 4000–200 cm^{-1} region. ^1H NMR spectra in dimethyl sulphoxide-d_6 were measured with an FT-80A 80 MHz spectrometer; the chemical shifts are reported in ppm downfield from TMS. The UV and fluorescence spectra were obtained using a UV-730 spectrophotometer and a Hitachi-850 fluorescence spectrophotometer, respectively. Thermogravimetric and differential thermal analyses were performed in air at a heating rate of 10°C min^{-1}, using a PCT-2 precision thermobalance analyser.

Materials

Lanthanide nitrate solutions were obtained from the respective metal oxides and HNO_3. Propanedionyl chloride was the chemical reagent. 1-Phenyl-3-methyl-5-pyrazolone, Phen and other chemicals were analytical reagents.

Synthesis of 1,3-*bis*-(1′-*phenyl*-3′-*methyl*-5′-*pyrazolone*-4′)-1,3-*propanedione*

1-Phenyl-3-methyl-5-pyrazolone (21 g) was dissolved in dioxane (40 cm^3) at 75–80°C and calcium hydroxide (10 g) and propanedionyl chloride (5.5

* Author to whom correspondence should be addressed.

Table 1. Analytical results and conductivity data for the complexes

Compounds[a]	Analysis (%)[b] C	H	N	Metal	Λ_M (Ω^{-1} cm^2 mol^{-1})
$Y_2L_3(Phen)_2 \cdot 6H_2O$	59.0	4.7	11.7	9.3	8.6
	(59.1)	(4.4)	(11.9)	(9.4)	
$La_2L_3(Phen)_2 \cdot 3H_2O$	57.8	3.8	11.7	14.2	9.1
	(57.7)	(4.0)	(11.6)	(14.0)	
$Pr_2L_3(Phen)_2 \cdot 4H_2O$	57.3	3.8	11.5	14.3	8.6
	(57.1)	(4.0)	(11.5)	(14.4)	
$Nd_2L_3(Phen)_2 \cdot 4H_2O$	57.0	3.9	11.2	14.9	10.5
	(56.9)	(4.0)	(11.4)	(14.7)	
$Sm_2L_3(Phen)_2 \cdot 4H_2O$	56.4	3.7	11.6	15.0	14.8
	(56.5)	(4.0)	(11.3)	(15.2)	
$Eu_2L_3(Phen)_2 \cdot 4H_2O$	56.2	3.7	11.3	15.4	12.1
	(56.4)	(4.0)	(11.3)	(15.4)	
$Gd_2L_3(Phen)_2 \cdot 4H_2O$	56.0	3.9	11.3	16.1	13.7
	(56.1)	(4.0)	(11.3)	(15.8)	
$Tb_2L_3(Phen)_2 \cdot 4H_2O$	56.2	3.8	11.4	16.2	10.2
	(56.0)	(3.9)	(11.2)	(15.9)	
$Dy_2L_3(Phen)_2 \cdot 4H_2O$	55.8	3.7	11.1	16.3	11.0
	(55.8)	(3.9)	(11.2)	(16.2)	
$Ho_2L_3(Phen)_2 \cdot 4H_2O$	55.7	3.6	11.0	16.8	13.3
	(55.7)	(3.9)	(11.2)	(16.5)	
$Er_2L_3(Phen)_2 \cdot 4H_2O$	55.6	3.9	11.1	16.6	12.9
	(55.6)	(3.9)	(11.1)	(16.6)	
$Tm_2L_3(Phen)_2 \cdot 4H_2O$	55.7	3.8	11.1	16.7	9.9
	(55.5)	(3.9)	(11.1)	(16.8)	
$Yb_2L_3(Phen)_2 \cdot 4H_2O$	55.2	3.8	11.3	17.1	10.7
	(55.3)	(3.9)	(11.1)	(17.2)	

[a] L = BPMPTD ($C_{23}H_{18}N_4O_4$), Phen = ($C_{10}H_8N_2$).
[b] Calculated values in parentheses.

g) were added dropwise within 1 min with rapid stirring. The reaction mixture became a thick paste. After stirring for 5 min the mixture was heated to reflux for 1 h and was decomposed by pouring into dilute hydrochloric acid (200 cm^3, 2 N), which caused brown–yellow coloured crystals to separate. The crystals were collected on a Buchner funnel, washed with distilled water until the washing was neutral, recrystallized from chloroform–petroleum ether (3:2) and dried *in vacuo*. Yield: 4.2 g (35.5%); m.p. 200–201°C. Found: C, 66.1; H, 4.8; N, 13.5. Calc. for $C_{23}H_{20}N_4O_4$: C, 66.3; H, 4.8; N, 13.5%.

Preparation of complex compounds

A solution of H_2L (0.25 g, 0.6 mmol), which was dissolved in 95% alcohol (35 cm^3) by adding NaOH solution (1.2 mmol), was mixed together with Phen · H_2O · ethanol (0.06 g, 0.3 mmol) solution and stirring for a few minutes. Lanthanide nitrate (0.35 mmol) aqueous solution was added dropwise to the above solution and a precipitate appeared gradually. After stirring and refluxing the mixture for 3 h the precipitate was centrifugally separated, washed thoroughly with dilute aqueous HNO_3 solution (pH = 3–4), distilled water and warm chloroform until the washing did not contain Ln^{3+} or NO_3^- and was neutral, and dried *in vacuo*. All the compounds were obtained in high yield: 75–85%.

RESULTS AND DISCUSSION

According to the elemental analyses of the complexes their composition agrees with the general formula $Ln_2L_3(Phen)_2 \cdot nH_2O$ (Ln = Y, $n = 6$; Ln–La, $n = 3$; Ln = Pr, Nd, Sm, Eu, Gd, Tb, Dy, Ho, Er, Tm and Yb, $n = 4$). All the complexes are yellowish–brown. They are soluble in dimethylsulphoxide and chloroform, slightly soluble in ethanol and methanol and insoluble in water and petroleum ether.

The molar conductance values of the complexes (see Table 1) in dimethylsulphoxide lie in the range 8–15 Ω^{-1} cm^2 mol^{-1}. This indicates that in the DMSO solvent complexes are non-ionic in nature.[10]

IR spectra

The ligand H_2L contains a large number of bands in the region 3400–200 cm^{-1}, which rendered frequency assignment somewhat difficult. It is possible, however, to obtain some useful information regarding the metal–ligand bonding. For example, the IR spectra of the enolic form of H_2L shows a broad band at 2600 cm^{-1}, which is evidently due to hydrogen bonded OH, and this band disappears after chelation. The reason is that the intramolecular hydrogen bond is broken after chelating with lanthanide ions. The H_2L band at 1612 cm^{-1} is shifted to lower frequency, 1064 cm^{-1}, in the metal chelates and thus can be related to the C=O stretching. On the other hand, the bands at 2954–2915 and 1597 cm^{-1} in H_2L remain unaltered in the chelates and are, therefore, due to methyl-methylene and phenyl ring stretching. Similarly, another unaffected band at 1574 cm^{-1} appears to be due to C=C/C=N stretching. The H_2L band at 1551 cm^{-1}, which is displaced to 1535 cm^{-1}, and the strength of the vibration which decreases in the chelates provide major contributions to C=O stretching. The 1642 cm^{-1} band due to the stretching vibration of C=N of free Phen is absent in these chelates, whereas a new band is observed at 1623 cm^{-1}. The out-of-plane band frequencies [δ(C—H)] range from 855 and 737 cm^{-1} in Phen to 845 and 731 cm^{-1} in the complexes. All these facts can be taken as evidence of Phen being bonded to the lanthanide ions. The broad band in the chelates observed at 3400–3380 cm^{-1} is due to the water molecules. Low-frequency IR spectroscopy has been used to examine metal–ligand bonds. In the far-IR region new bands appear at 410–420 and 270–285 cm^{-1}, which we infer are due to metal–ligand vibrations. As the metal–nitrogen bond is expected to be weaker than the metal–oxygen bond the 270–285 cm^{-1} bands are assigned to γ(Ln—N) and the bands at 410–420 cm^{-1} to γ(Ln—O). Indeed, the literature[11,12] also refers to Ln—N and Ln—O stretching vibrations appearing at 270–316 and 400–420 cm^{-1}, respectively.

UV spectra

The UV data of the compound dissolved in chloroform are listed in Table 2. It can be seen that the UV spectra of all the complexes are similar, but they are different from those of the ligands. The intense absorption bands of the complexes at 236–243 and 269–272 nm are ascribed to the *B* band ($\pi \rightarrow \pi^*$ transition) of the benzene and phenanthrene ring.[13] These absorption maxima remain either unchanged or suffer slight shifts compared with the ligands. However, the molar extinction coefficients measured at identical wavelengths show significant differences. The band at 375 nm in H_2L is also attributed to the *K* band ($\pi \rightarrow \pi^*$ transition), but in the complexes a bathochromic shift of *ca* 45 nm is observed. It is possible that the *f*-orbital of

Table 2. UV spectral data of ligands and complexes

Compounds	λ_1 max (nm)	$\varepsilon_1 \times 10^{-3}$ (dm^{3}cm^{-1}mol^{-1})	λ_2 max (nm)	$\varepsilon_2 \times 10^{-4}$ (dm^{3}cm^{-1}mol^{-1})	λ_3 max (nm)	$\varepsilon_3 \times 10^{-3}$ (dm^{3}cm^{-1}mol^{-1})
Phen	238	13.5	265	3.3		
H_2L	241	1.8	277	0.2	377	1.2
$Y_2L_3(Phen)_2 \cdot 6H_2O$	239	6.8	271	1.1	422	4.0
$La_2L_3(Phen)_2 \cdot 3H_2O$	239	11.8	269	1.8	424	1.8
$Pr_2L_3(Phen)_2 \cdot 4H_2O$	241	10.1	270	1.4	423	4.7
$Nd_2L_3(Phen)_2 \cdot 4H_2O$	240	14.6	270	1.6	425	4.3
$Sm_2L_3(Phen)_2 \cdot 4H_2O$	240	8.2	272	1.3	423	4.5
$Eu_2L_3(Phen)_2 \cdot 4H_2O$	240	7.8	274	1.1	422	3.8
$Gd_2L_3(Phen)_2 \cdot 4H_2O$	240	13.0	271	1.4	423	4.6
$Tb_2L_3(Phen)_2 \cdot 4H_2O$	238	8.6	271	1.5	423	5.1
$Dy_2L_3(Phen)_2 \cdot 4H_2O$	240	8.6	270	2.0	422	9.2
$Ho_2L_3(Phen)_2 \cdot 4H_2O$	239	17.0	271	1.7	420	9.3
$Er_2L_3(Phen)_2 \cdot 4H_2O$	239	8.7	270	1.4	426	4.8
$Tm_2L_3(Phen)_2 \cdot 4H_2O$	239	8.8	272	1.1	421	4.0
$Yb_2L_3(Phen)_2 \cdot 4H_2O$	242	7.8	271	1.2	420	4.9

Table 3. ^{1}H NMR spectral data of ligands and complexes (chemical shifts in ppm relative to TMS)

Compounds	Methyl protons	Methylidyne protons	Benzene protons	Phen protons	Hydroxyl protons
H_2L	2.56 (sh, s 6H)	4.05 (sh, s 4H)	7.27–7.81 (br, m 10H)	—	—
Phen	—	—	—	7.98–9.12 (m 8H)	—
$Y_2L_3(Phen)_2 \cdot 6H_2O$	2.23 (s 6H) 1.95 (m 12H)	3.75 (m 6H)	7.25–7.80 (br, m 30H)	7.82–9.15 (m 16H)	3.41 (s 12H)
$La_2L_3(Phen)_2 \cdot 3H_2O$	2.24 (s 6H) 2.08 (m 12H)	3.84 ((m 6H)	7.18–7.72 (br, m 30H)	7.86–9.18 (m 16H)	3.45 (s 6H)
$Pr_2L_3(Phen)_2 \cdot 4H_2O$	—	—	6.20–9.20 (vbr, m)		—

sh: sharp; br: broad; s: singlet; m: multiplet; int: integrated intensity.

the metal atom and the *p*-orbital of H_2L overlap each other to form a greater conjugated system after enolizing and complexing.

^{1}H *NMR spectra*

The ^{1}H NMR spectra of the ligands and some complexes have been investigated using $(CD_3)_2SO$ as a solvent (see Table 3). The proton signals of the free ligand Phen are observed as multiplets at *ca* 7.98–9.12 ppm (8H). The benzene ring proton signals of the ligand H_2L are found as multiplets at *ca* 7.40–7.88 ppm (10H) and methyl and methylene proton signals as singlets at 2.54 (6H) and 4.05 ppm (2H), respectively. The enol proton signal is not observed. The ^{1}H NMR spectra of diamagnetic Y^{3+} and La^{3+} complexes undergo large shifts and changes in comparison with the spectra of the ligands. Almost all the protons show upfield shifts. The proton signals of Phen in the chelate which has also shifted upfield appears at 7.82–9.15 ppm (16H). This indicates that the deshielding effect of electron density in the phenanthrene ring decreases after complexation of the nitrogen atoms in Phen with the Ln^{3+} ion. The complex shows more signals in the region of 7.18–7.80 ppm (30H), which can be assigned to the phenyl protons. Water proton signals are present at 3.41 ppm (12H), which may be exchanged by D_2O. The methylene proton signals have shifted from 4.05 to 3.80 ppm (6H). In addition there are two distinctly different sets of methyl resonances, one set at *ca* 2.23 ppm (6H) and another at *ca* 2.08–1.95 ppm (12H), with a ratio of *ca* 1:2 which indicates that the structures of the complexes have non-equivalent ligands.

In the paramagnetic complexes the proton signals of the Pr^{3+} complex become much weaker and broader. The methyl and methylidyne signals have disappeared and the proton signals of the benzene and phenanthrene ring become a broad multiplet appearing at 6.20–9.20 ppm. The broadening may be ascribed to spin–spin relaxation processes.[14,15] With the Gd^{3+} complex no signal is observed due to extensive broadening of the signals, since Gd^{3+} has the maximum number of unpaired electrons and is, therefore, strongly paramagnetic.

Fluorescenes

Although many lanthanide chelates of β-diketonates fluoresce, the phenomenon of emission line fluorescence, that many lanthanide ions in the same chelate series exhibit, can be seen only in the lanthanide chelates of 4-acyl-bispyrazolone. In our ligands and complexes the fluorescence and assignments are as follows: —Phen, 361,179 nm (line emission ex. = 320 nm); H_2L, Nd, Gd, Ho and Er, 480 nm (band emission ex. = 360 nm). Pr, 604 $^3P_0 \rightarrow {}^3H_6$ (ex. = 359 nm); Sm, 566 $^4G_{5/2} \rightarrow {}^6H_{5/2}$; 646 $^4G_{5/2} \rightarrow {}^6H_{9/2}$; 714 $^4G_{5/2} \rightarrow {}^6H_{11/2}$ (ex. = 370 nm). Eu, 590 $^5D_0 \rightarrow {}^7F_1$; 612 $^5D_0 \rightarrow {}^7F_2$ (ex. = 363 nm). Tb, 490 $^5D_4 \rightarrow {}^7F_6$; 545 $^5D_4 \rightarrow {}^7F_5$; 586 $^5D_4 \rightarrow {}^7F_4$; 622 $^5D_4 \rightarrow {}^7F_3$ (ex. = 354 nm). Dy, 481 $^4F_{9/2} \rightarrow {}^6H_{15/2}$; 575 $^4F_{9/2} \rightarrow {}^6H_{13/2}$ (ex. = 365 nm). Tm, 478 $^1D_2 \rightarrow {}^3H_4$ (ex. = 360 nm). These luminescence phenomena of the lanthanide complexes have been discussed in the literature.[16] In addition terbium and samarium complexes in the solid state have no fluorescence when they are irradiated with UV light (λ = 254 nm), but in DMSO exhibited excellent green and red fluorescence, respectively.

Thermal analysis

In order to investigate the behaviour of the heated compounds we measured the TG–DTA

Table 4. The values of thermal peaks and total weight loss of the complexes

Compounds	T_{endo} (°C)	T_{exo} (°C) (1)	(2)	(3)	(4)	Total weight loss (%)[a]
$Y_2L_3(Phen)_2 \cdot 6H_2O$	147	359	413	497	577	88.4 (88.1)
$La_2L_3(Phen)_2 \cdot 3H_2O$	110	305	399	508	535	83.1 (83.5)
$Pr_2L_3(Phen)_2 \cdot 4H_2O$	124	331	406	490	540	83.0 (82.6)[b]
$Nd_2L_3(Phen)_2 \cdot 4H_2O$	121	332	392	490	534	82.8 (82.9)
$Sm_2L_3(Phen)_2 \cdot 4H_2O$	116	330	397	505	529	81.9 (82.4)
$Eu_2L_3(Phen)_2 \cdot 4H_2O$	119	337	411	492	531	81.9 (82.2)
$Gd_2L_3(Phen)_2 \cdot 4H_2O$	115	318	367	464	523	81.4 (81.8)
$Tb_2L_3(Phen)_2 \cdot 4H_2O$	105	355	427	500	566	80.9 (81.2)[b]
$Dy_2L_3(Phen)_2 \cdot 4H_2O$	96	336	404	501	545	81.3 (81.4)
$Ho_2L_3(Phen)_2 \cdot 4H_2O$	108	349	381	443	548	80.9 (81.2)
$Er_2L_3(Phen)_2 \cdot 4H_2O$	89	350	429	469	538	80.5 (81.0)
$Tm_2L_3(Phen)_2 \cdot 4H_2O$	115	366	403	473	548	80.4 (80.8)
$Yb_2L_3(Phen)_2 \cdot 4H_2O$	101	354	389	509	569	80.6 (80.5)

[a] Calculated values in parentheses.
[b] The products of decomposition for Pr and Tb complexes are Pr_3O_{11} and Tb_4O_7, respectively.

curves of the ligands and the complexes and found: H_2L begins to melt and decompose at 200°C and continuously decomposes at 245, 342, 430 and 597°C; Phen·H_2O loses water at 104°C and then melts at 123°C, until finally it decomposes in the temperature range 217–318°C.

The TG and DTA measurements of the complexes show that all of the complexes exhibit similar thermal analysis diagrams. They have a small endothermal peak on the DTA curve and on the TG curve have a weight-loss equal to the weight of the water molecules in the complexes. These types of complexes have no melting point, and thus after losing water molecules the compounds begin to decompose. There are mainly four exothermal peaks which appear successively on the DTA curve and obvious weight loss occurs on the TG curve between 300 and 750°C. The endothermal and exothermal peak temperatures of the complexes are summarized in Table 4.

It can be seen from Table 4 that the total weight loss of the complexes is nearly equal to that calculated and the complexes are more thermostable than the ligands.

CONCLUSIONS

Summarizing the above analysis we propose a binuclear structure for these complexes in which each of two Ln^{3+} ions combines with two complexing nitrogen atoms in each Phen and three H_2L as tetradentate ligands in the enolic form chelating two Ln^{3+} ions.

Acknowledgement—We wish to thank the National Natural Science Foundation of China for financial assistance with this work.

REFERENCES

1. B. S. Jensen, *Acta Chem. Scand.* 1959, **13**, 1347; 1668.
2. R. Yany, *Rare Earths* 1986, **5**, 1.
3. Y. Sasaki, *Inorg. Chem.* 1983, **22**, 2289.
4. A. Tayeb, G. J. Goetz-Grandmont, J. P. Brunette and M. J. F. Leroy, *Solv. Ext. Ion Exch.* 1990, **8**, 1.
5. X. C. Dong, F. C. Liu and Y. L. Zhao, *Acta Chim. Sin.* 1983, **41**, 848.
6. L. Q. Yang and R. D. Yang, *J. Lanzhou Univ.* 1988, **24**, 134.
7. L. Q. Yang and R. D. Yang, *Chem. J. Chin. Univ.* 1985, **10**, 225.
8. H. WanYan, W. J. Dong, X. J. Li, C. Z. Feng and R. D. Yang, *Rare Earths* 1989, **2**, 1.
9. X. J. Li, H. Wanyan, W. J. Dong and R. D. Yang, *Polyhedron* 1990, **9**, 2285.
10. W. J. Geary, *Coord. Chem. Rev.* 1971, **7**, 81.
11. C. Y. Liang, E. J. Schmitsehek and T. A. Trias, *J. Inorg. Nucl. Chem.* 1970, **32**, 811.
12. K. Iftikahr, M. Sayeed and N. Ahmad, *Bull. Chem. Soc. Japan* 1982, **55**, 2258.
13. Y. Z. Chem, *Organic Analysis*, p. 544. Advance Education Publishing House, Beijing (1983).
14. E. C. Okafor, *J. Inorg. Nucl. Chem.* 1979, **42**, 1455.
15. Y. L. Qi, C. C. Peng, X. J. Li, Y. S. Wu and R. D. Yany, *Chem. J. Chin. Univ.* 1988, **9**, 844.
16. R. H. Zhang, *Rare Earth Elemental Chemistry*, Vol. 70. Science and Technology Publishing House of Tianjin, Tianjin (1987).

Polyhedron Vol. 12, No. 16, pp. 2027–2037, 1993
Printed in Great Britain

0277–5387/93 $6.00+.00
© 1993 Pergamon Press Ltd

A STUDY ON THE COMPLEX FORMATION BETWEEN COPPER(II) AND SOME EPHEDRINES

RAFIE H. ABU-EITTAH* and A. ABDEL RAZIK

Department of Chemistry, Faculty of Science, Cairo University, Giza, Egypt

and

ZEIN MOBARAK and LAILA T. KAMEL

National Center for Social and Criminological Research, Cairo, Egypt

(*Received* 18 *December* 1992; *accepted* 20 *April* 1993)

Abstract—Complex formation between the copper(II) ion and ephedrine and norephedrine has been studied potentiometrically and spectrophotometrically. A spectral–structural correlation has been investigated for the complexes. Copper ephedrine and norephedrine complexes possessed a geometry which varied from octahedral to tetragonal to square planer depending on the experimental conditions. Semi-empirical MO calculations were performed on a model "copper–ephedrine complex" with different geometries, with satisfactory results.

Ephedrine and norephedrine are sympathomimetic agents with direct and indirect effects on adrenergic receptors.[1] They possess adrenergic activity and pronounced stimulating effects on the central nervous system.

Transition metal complexes of ephedrine are used as antiallergic drugs. The free energy of formation of such complexes has been related to their medical activity. Copper(II) ephedrine complexes are important, interesting and have drawn much attention. These complexes have some peculiar properties: they are readily soluble in non-polar solvents and react at room temperature with halogenated hydrocarbons.

Different complexes of copper(II) and some ephedrines were prepared and their crystal structure has been studied. Deep violet crystals were obtained from benzene with the structure $(C_{10}H_{14}ON)_2Cu \cdot \frac{2}{3}C_6H_6$,[2] whereas crystallization from cyclohexane led to crystals which have the composition $(C_{10}H_{14}ON)_2Cu \cdot \frac{1}{3}C_6H_{12}$.[3] The crystals from hexane have the composition $(C_{10}H_{14}ON)_2Cu \cdot \frac{1}{6}C_6H_{14}$.

The structure of the copper(II) norephedrine complex, $(C_9H_{12}NO)_2Cu \cdot 3H_2O$, was determined by X-ray diffraction.[4] The crystals were monoclinic where the two norephedrine groups were *trans* and coordinated through their nitrogen and oxygen atoms. The coordination was square pyramidal.

Ephedrine hydrochloride was obtained from the copper complex in alkaline medium[5] and by forming metal diaralkyldithiocarbamate with carbon disulphide and ammoniacal copper(II) and nickel (II) solutions.

Ephedrine and amine complexes of copper(II) combine reversibly with carbon dioxide and yield singly- and multiply-charged copper carbamate complexes.[6] The formation of unstable carbamate complexes was confirmed by EPR studies.[7]

The acid dissociation constant as well as the thermodynamic functions of dissociation were determined for ephedrinium ions by thermometric titration[8] and potentiometry.[9] A value of 9.014 was obtained for the pK_a of norephedrine in aqueous media at 25°C.

In this work the process of complex formation between copper(II) ephedrine and norephedrine was studied potentiometrically and spectrophotometrically and spectral/structural correlations were investigated. The variation of the spectrum with the proposed geometry is discussed. Molecular orbital

* Author to whom correspondence should be addressed.

calculations have been performed on octahedral, tetragonal and square-planar copper(II) ephedrine complexes. The results showed the variation of *d*-orbital splitting as a function of the geometry of the complex.

EXPERIMENTAL

All materials used were of BDH analar grade. L-ephedrine and D-norephedrine hydrochloride were supplied by Alderich Gillingham, Dorset, U.K. The free base of D-norephedrine was obtained by extracting from alkaline solution (5% ammonium hydroxide).

Preparation of complexes

Copper(II) ephedrine and norephedrine complexes were prepared by adding an aqueous solution of copper sulphate to an aqueous solution of ephedrine or norephedrine hydrochloride, respectively, followed by the dropwise addition of dilute sodium hydroxide solution until a blue violet colouration or precipitate was obtained. The copper(II) ephedrine complex was extracted by benzene, hexane or cyclohexane. Elemental analysis gave the following results: Found: C, 63.3; H, 7.1; N, 6.7; Cu, 13.5. Calc. for $(C_{10}H_{14}ON)_2Cu \cdot \frac{2}{3}C_6H_6$: C, 64.9; H, 7.2; N, 6.3; Cu, 14.3%. Crystals from hexane accounted for the formula $(C_{10}H_{14}ON)_2Cu \cdot \frac{1}{6}C_6H_{14}$. The deep blue–violet precipitate of the copper norephedrine complex was crystallized from methanol. Elemental analysis gave: Found: C, 52.5; N, 6.8; H, 6.9; Cu, 16.5. Calc. for $(C_6H_{12}ON)_2Cu \cdot 3H_2O$: C, 52.2; N, 6.7; H, 7.2; Cu, 15.3%.

Apparatus

pH titration and pH measurements were performed using an Orion 920 digital pH meter and the spectra were scanned on a Perkin–Elmer Lambda 4B spectrophotometer.

RESULTS AND DISCUSSION

1. *Complex formation*

1.1. *Formation constant.* The process of complex formation between copper(II) and ephedrine and norephedrine was studied using pH titration procedures.[10] The pK_a values for the protonated ligand, for the equilibrium:

$$HL^+ \rightleftharpoons H^+ + L,$$

were 8.74 ± 0.21 for norephedrine and 9.18 ± 0.14 for ephedrine. These results compare satisfactorily with values reported in the literature. At 37°C the

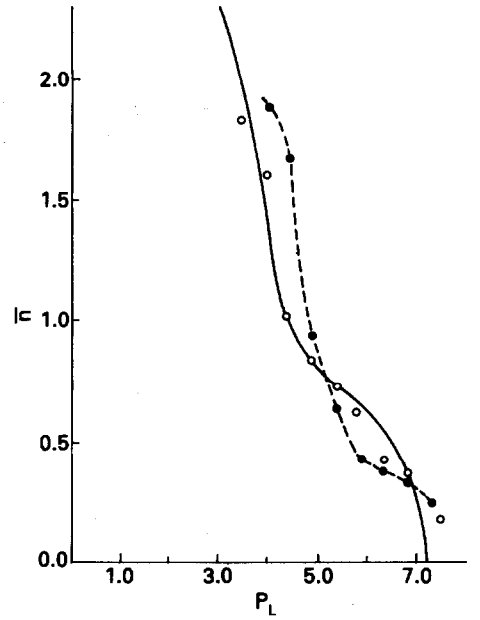

Fig. 1. The formation curves of copper(II) ephedrine (---) and copper(II) norephedrine (O--O) systems.

pK_a value for the ephedrinium ion is *ca* 9.2,[11] whereas that for the norephedrenium ion in aqueous solution is *ca* 9.014[9] at zero ionic strength.

Figure 1 shows the formation curves of copper complexes with ephedrine and norephedrine. Preliminary values of log K_1 and log K_2 for the formation of 1:1 and 1:2 copper complexes were obtained from Fig. 1. Accurate values were obtained from the relations

$$\log K_1 = \log \frac{n}{(1-n)[L]_n} \quad (1)$$

$$\log K_2 = \log \frac{(n-1)}{(2-n)[L]_n}, \quad (2)$$

where $1 > n > 0$ in eq. (1) and $2 > n > 1$ in eq. (2). For copper norephedrine complexes log K_1 and log K_2 were 6.39 ± 0.10 and 3.88 ± 0.90, respectively. For copper ephedrine complexes log K_1 and log K_2 were 5.64 ± 0.15 and 4.59 ± 0.05, respectively.

1.2. *Spectral–structural correlation.*

1.2.1. Copper(II) ephedrine system. The optically active alkaloids, ephedrines, occur naturally in the form of different isomers, namely, (−)-ephedrine(I), (−)-norephedrine(II), (+)-pseudo-ephedrine(III) and (+)-pseudo-nonrephedrine(IV) whose absolute configurations are:

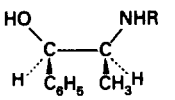

I. R = CH_3; (—) -ephedrine
II. R = H; (—) -norephedrine

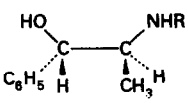

III. R = CH_3; (+) -ψ-ephedrine
IV. R = H; (+) -ψ-norephedrine

For an isolated molecule ephedrine has three possible conformations:

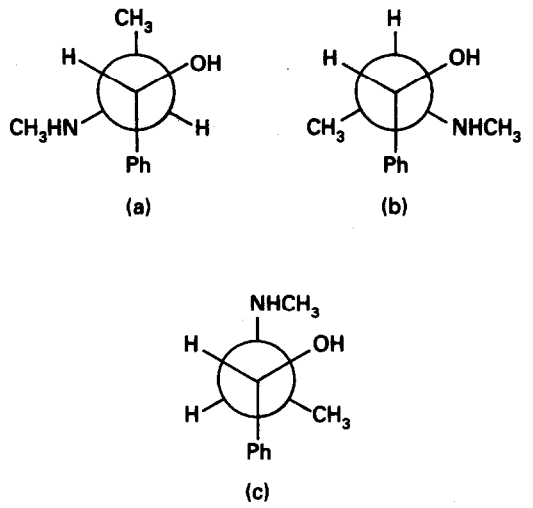

Conformation (a) has been proposed for free ephedrine,[12] whereas conformation (c) is found in the crystal structure of copper(II) ephedrine complex.[2]

The reaction between copper(II) and ephedrine is sensitive to the reaction medium. It was easier to prepare the neutral bis-copper(II) complexes of (+)-Hψ ephedrine than the corresponding complexes of (+)-H ephedrine.[13] Amano *et al.*[2] could identify three different copper(II) ephedrine complexes: pale violet–blue crystals, bis((−)-eph)diaquocopper(II), reddish–violet plates, bis((−)-eph)copper(II), and the violet hexagons which were shown by crystal structure to consist of trimeric units of the bis complex by intermolecular hydrogen bonding. The absorption spectra of a crystal of the latter complex and its solution in hexane were identical, which suggests that the trimer nature is retained in solution.

Gillard and Wootton[14] prepared copper(II) ephedrine which was extracted from aqueous medium by petroleum ether. The absorption spectra of the solution of the complex were solvent dependent and did not obey Beer's law. The spectra show two bands around 500–600 nm, the first band was assigned to the *d–d* transition in non-polar solvents. The monomer is considered to dominate in polar solvents, particularly water and the band around 500 nm became weaker. An equilibrium was assumed to exist between the monomer and the trimer.

The diastereoisomeric complex of ephedrine with copper(II) was precipitated in two forms, bis[(+)-ψ-eph]Cu^{II} and the tris form Cu[(+)-ψ-eph]$_2$(+)-Hψ-eph·$2H_2O$, which had identical reflectance spectra,[14] indicating that the third ψ-ephedrine molecule is not involved in coordination. Crystal structure determination establishes this formulation.[15]

Figure 2 shows the absorption spectra of copper(II) ephedrine solutions at a total constant concentration of 2.5×10^{-2} M, with pH ranging from

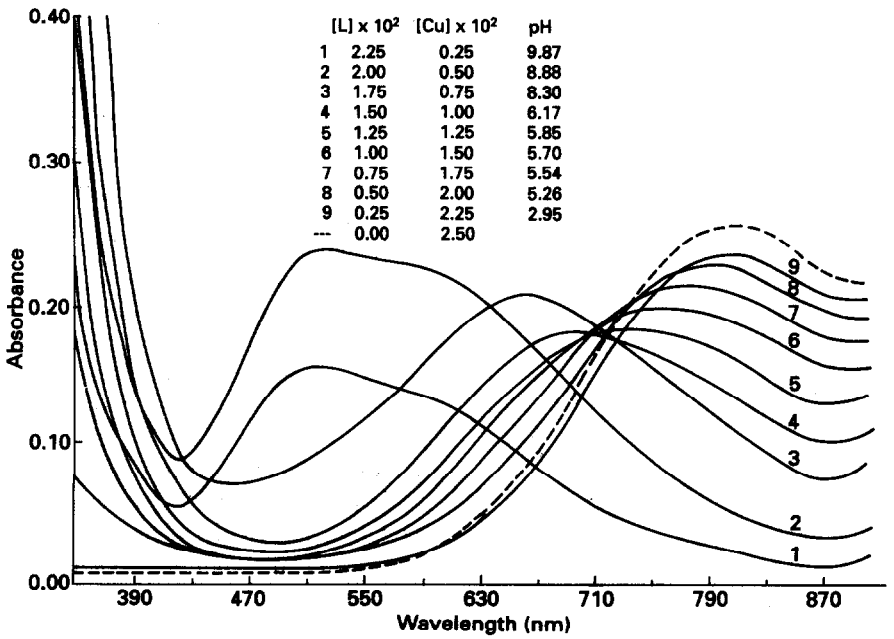

Fig. 2. Absorption spectra of copper(II) ephedrine solutions with a constant total concentration of 2.5×10^2 M.

2.95 to 9.87. The distribution curves for the formation of the different complexes are given in Fig. 3. The 1 : 1 copper(II) ephedrine complex starts to be formed at pH = 5.0 and is predominant in the pH range 5.3–7.5. The 1:2 complex biaquobisephedrinocopper(II) starts to be formed at pH = 7.5 and predominates at pH higher than 8.0. In the pH range 2.95–5.54 there is no indication of complex formation, Fig. 2, whereas in the pH range 5.7–8.30 the spectra of copper(II) ephedrine solutions show a broad band characteristic of tetragonal copper(II) complexes. The broad band has a maximum which ranges from 750–720 to 690–660 nm, depending on the pH of the solution. As the pH increases to 8.88 and 9.78 the spectra differ basically from those at lower pH. It is suggested that only the 1 : 1 Cu : ephedrine complex is formed in the pH range 5.7–8.30 as predicted by the distribution curve, Fig. 2, whereas the 1:2 copper: ephedrine complex is formed at higher pH. Both complexes are tetragonal. In the former complex four water molecules are in the inner coordination sphere, whereas in the latter two, water molecules are in the inner coordination sphere and are along the *z*-axis.

The variation of band maximum with the increase in the pH of the solution, which is attained by the increase in [eph], is due to the distortion of the geometry of the formed complex. Distortion is of the "*z*-out" type and in the limit when the two water molecules along the *z*-axis are removed a square-planar bisephedrinocopper(II) complex is formed. When one applied Job's[16] method to the results of Fig. 2 using the absorbance at $\lambda = 520$, 660 and 740 nm the existence of 1:1 and 1:2 copper(II) ephedrine complexes was evident.

The results of X-ray crystal analysis confirmed

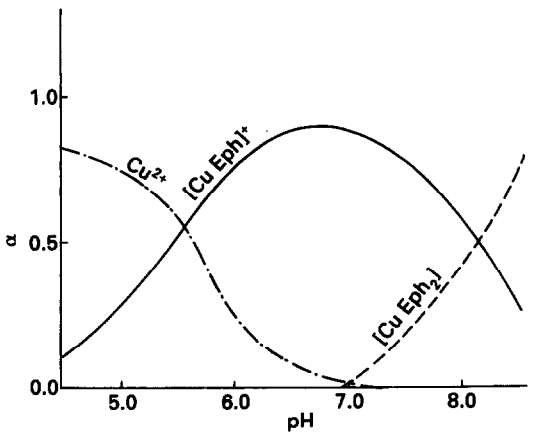

Fig. 3. Distribution curves for the copper(II) ephedrine complex.

that the hydrogen atom of the alcoholic hydroxyl group of the ephedrine molecule was replaced by the copper ion in chelate formation and that the chelate ring was built up by a four-coordinated square planar configuration.[2] No atoms were detected between the copper atoms in the adjacent unit cells in the direction perpendicular to the plane of the square. Based on the Jahn–Teller effect, most of the copper complexes have distorted octahedral configuration. The configuration of ephedrine copper chelate is considered as a limiting case of the usual distorted octahedral configuration with two ligands completely removed.

Figure 4 shows the absorption spectra of copper (II) ephedrine solutions where the ratio of $[Cu^{2+}]$:[eph] varies from 1 : 1 to 1 : 10 and the pH ranges from 6.27 to 10.08. It is clear that each solution has its own spectrum. Up to pH 8.70 the ratio $[LH^+]/[L]$ is of the order of 10, which means that the predominant complex is monoephedrinotetraaquocopper(II). The difference in the spectra for different solutions, Fig. 4, is attributed to different degrees of distortion from octahedral to tetragonal geometry. In a tetragonal field both ^2E_g and $^2T_{2g}$ states split and the single transition in the octahedral geometry splits into three transitions, ν_1 ($^2A_{1g} \leftarrow {}^2B_{1g}$), ν_2 [$^2B_{2g}(T) \leftarrow {}^2B_{1g}(E)$] and ν_3 ($^2E_g \leftarrow {}^2B_{1g}$). This splitting is quite evident on investigating the spectra in Fig. 4. The broad band, for example, in solution 3, is easily resolved to three overlapping bands which are assigned to $^3A_{1g} \leftarrow {}^2B_{1g}$ at 12,820 cm^{-1} (ν_3), $^2B_{2g} \leftarrow {}^2B_{2g}$ at 15,625 cm^{-1} (ν_2) and $^2E_{1g} \leftarrow {}^2B_{1g}$ at 18,518 cm^{-1} (ν_1). The calculation of the physical parameters Δ_0, δ and ρ gives 11,145, 1930 and 6410 cm^{-1}, respectively. The splitting of the ground state (2ρ = 12,820 cm^{-1}) is much larger than that of the excited $^2T_{2g}$ state ($\frac{3}{2}\delta$ = 2893 cm^{-1}). The appearance of three electronic transitions in the 400–800 nm region is quite apparent and there is a gradual blue shift of band maximum and ν_2 overlaps ν_1, which is an indication of the transformation from octahedral to square planar geometry. The spectrum of the aqueous solution of the prepared copper ephedrine complex is very much similar to that of aqueous solution prepared by mixing Cu^{2+} and ephedrine in the ratio 1 : 5 or 1 : 10. The prepared complex proved (elemental analysis) to be the bisephedrinocopper(II) complex.

Conformational effects on the stability of the chelate ring have been reviewed. The chelate ring in the bisephedrine copper(II) complex is subjected to different conformational effects which determine its stability.[17,18] The chelate ring is puckered to minimize the steric repulsions. A number of confomers have been suggested for bisephedrinocopper(II),

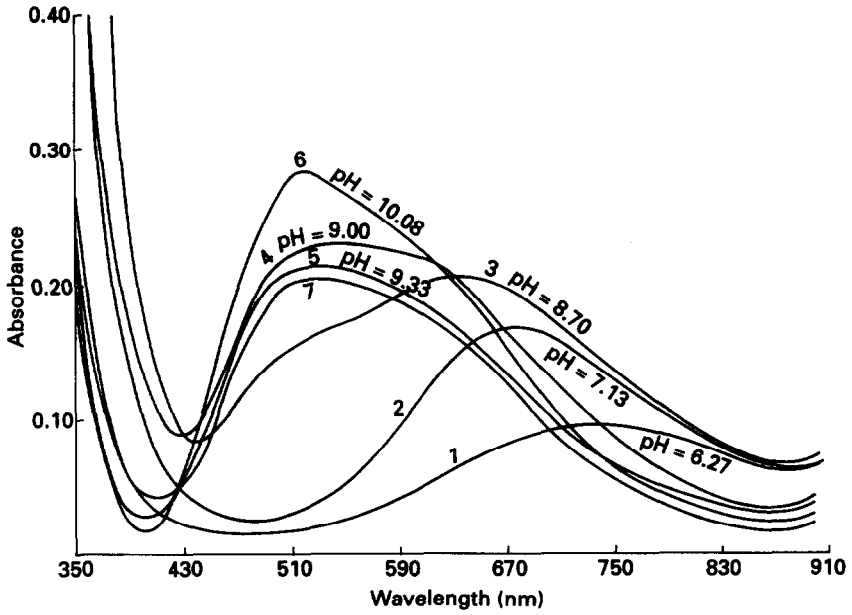

Fig. 4. Absorption spectra of copper(II) ephedrine solutions of varying [Cu^{II}]:[eph] ratios, 1 (1:1), 2 (1:2), 3 (1:3), 4 (1:4), 5 (1:5), 6 (1:10), 7 (free copper).

the most stable of which are:

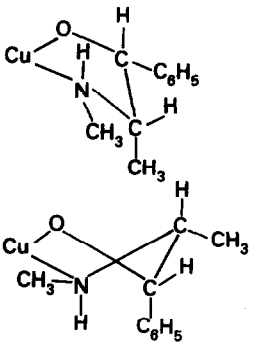

Each of the above conformers has an isomer whereby the substituents, H and $-CH_3$, on the totally asymmetric nitrogen atom exchange positions. Copper(II) complexes with ephedrine and ψ-ephedrine are optically active.[19,20] In a square copper(II) complex the copper atom is not asymmetric and the optical activity in the band of the *d–d* transitions[21] of the metal has been interpreted to result from the vicinal effect of an asymmetric atom in the ligand. The vicinal interaction on the visible optical rotatory dispersion, as measured by the Cotton effect amplitudes, was found to be very sensitive to the substituent in a number of amino acid copper (II) complexes. A large mixing of *d–d* transitions with charge transfer transition from ligand-to-metal or metal-to-ligand has been suggested to lead to the optical activity of these complexes.[21]

The CD spectra of copper(II) complexes with ephedrine and pseudoephedrine, in benzene solution, were almost enantiomeric.[14] The most stable conformations of the ligand describe opposite helicities about the copper atom. The (+)-Hψ-eph complex retains the same signs of Cotton effects in going from non-polar to polar solvents, whereas the Cotton effects of the (−)-H eph complex apparently change sign under the same circumstances; in water the two complexes have almost the same CD spectrum. This was attributed to the ligand having a different conformation when the complex is dissolved in different solvents compared to that adopted in aqueous solution.

Figure 5 shows the absorption spectra of the pre-

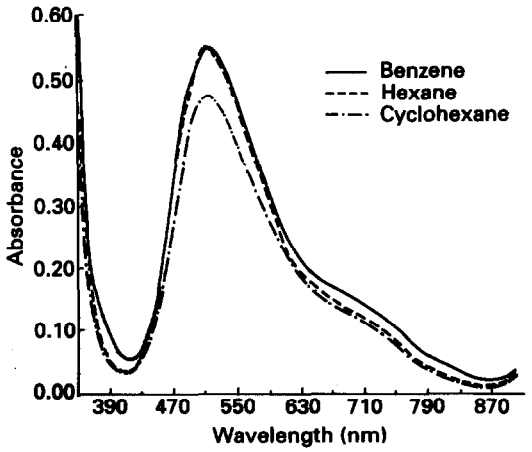

Fig. 5. Absorption spectra of the bisephedrinecopper(II) complex in different solvents.

pared bisephedrine copper(II) complex dissolved in benzene, hexane and cyclohexane. The spectra are for the square bisephedrinocopper(II) complex. The similarity of the spectra when benzene and cyclohexane are the solvents indicates the absence of any π-bonding between benzene and the metal ion in the formed chelate. The broad contour of the absorption band is resolved (Gaussian analysis) into three bands with λ_{max} at 520, 630 and 700 nm. The copper ephedrine complex crystallized from benzene had a 1 : 2 square planar geometry.

1.2.2. Copper(II) norephedrine system. On adding an aqueous solution of Cu^{2+} ion to an aqueous solution of norephedrine the copper complex precipitates immediately. However, when methanol was the solvent precipitation did not occur.

Figure 6 shows the absorption spectra of mixtures of copper perchlorate and norephedrine solutions with a constant total concentration of 1.25×10^{-2} M and using methanol as a solvent. The pH of the solutions (after correction) varied from 4.54 to 11.39. The process of complexation becomes clearer at higher concentrations of norephedrine and a gradual blue shift of band maxima is observed with increasing ligand concentration. One starts with a tetragonal tetraaquomononorephedrinocopper(II) complex and finishes up with the square bisnorephedrinocopper(II) complex. The gradual blue shift of band maxima (corresponding to a gradual change from tetragonal to square geometry of the complex) is evident on investigating Fig. 7, where the spectra of solutions containing constant $[Cu^{2+}]$ and varying [norephedrine] are given. For comparison the spectrum of a prepared bisnorephedrinocopper(II) complex, dissolved in methanol, is given.

The gradual change in the geometry of the complex is nicely reflected in the spectra. For the square bisnorephedrinocopper(II) complex one has the following assignment: ν_1 ($d_{xz}, d_{yz} \rightarrow d_{x^2-y^2}$) is observed at 19,610 cm^{-1}, ν_2 ($d_{z^2} \rightarrow d_{x^2-y^2}$) at 16,650 cm^{-1} and ν_3 ($d_{xy} \rightarrow d_{x^2-y^2}$) at 13,330 cm^{-1}.

The square bisnorephedrine copper(II) complex can exist only in two conformers:

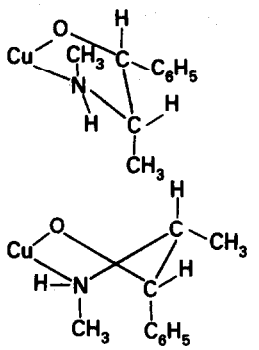

Both do not contain an asymmetric atom and the complex would be optically inactive.

2. *Molecular orbital calculation*

It is interesting to investigate theoretically the energy level splitting as the distortion from a pure octahedral geometry increases, via "z-out" dis-

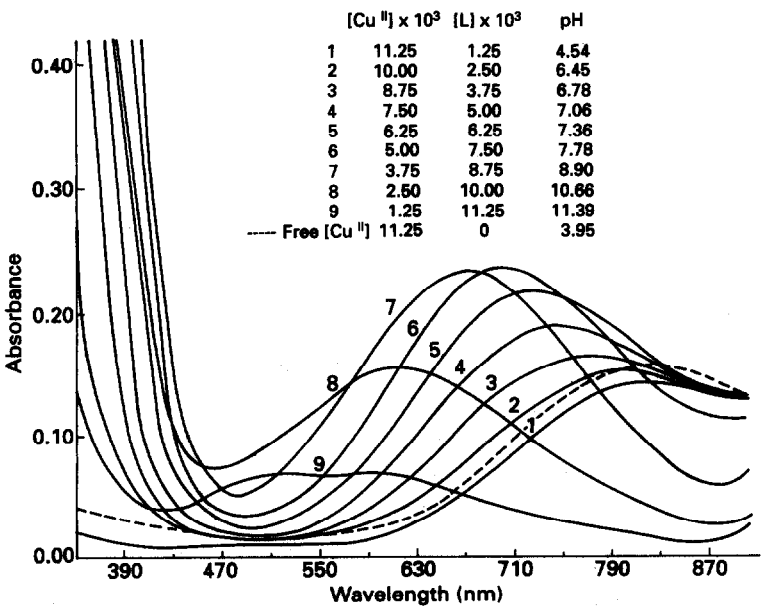

Fig. 6. Absorption spectra of copper(II) norephedrine complexation using methanol as a solvent, with a constant total concentration of 1.25×10^{-2} M.

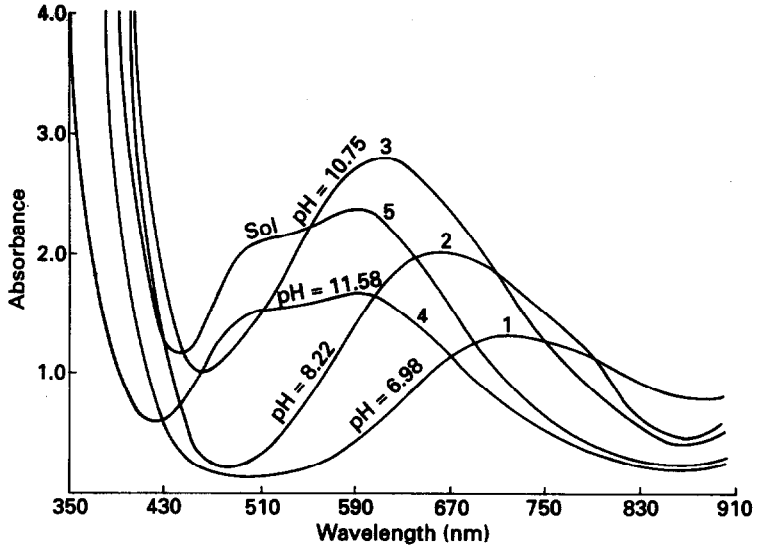

Fig. 7. Absorption spectra of copper(II) norephedrine solutions of varying [Cu^{II}]:[noreph] ratios, 1 (1:1), 2 (1:2), 3 (1:3), 4 (1:4), 5 (methanol solution of solid complex).

tortion until it arrives at a square planar geometry. The O_h complex of biaquobisephedrinocopper(II) is assumed to have the geometry shown. Assuming a D_{2h} local symmetry for the complex, the symmetry orbitals are given in Table 1.

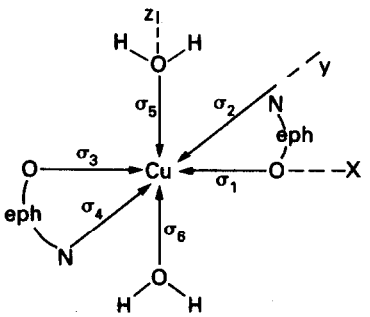

The general form of the molecular orbital is

$$\psi_i = \sum_j C_{ij} M(\phi_{ij}) + \sum_l C_{il} L(\phi_{il})$$

where CM is the coefficient of the metal ion orbital, ϕ_j, CL is the coefficient of the ligand atomic orbital, ϕ_l.

A symmetry secular determinant is set up and solved for each symmetry species. The diagonal and off-diagonal elements were calculated as

$$H_{ii} = \int \psi_i \hat{H} \psi_i \, d\tau$$

$$H_{ij} = \int \psi_i \hat{H} \psi_j \, dj$$

$$= 0.875[H_{ii} - H_{jj}]\delta_{ij}$$

$$S_{ij} = \int \psi_i \psi_j \, d\tau.$$

The value of H_{ii} is taken as the valence state ionization energy of orbital i and S_{ij} is the group overlap integral between orbital i and j. The values of H_{ij} are calculated using the Wolfsberg–Helmholz relation.[22]

Valence state ionization energies, VSIE, for the ligand orbital, were taken from charge transfer data.[23] The value of H_{ii} for the nitrogen atom of ephedrine was taken as -7.60 eV and that of the hydroxyl oxygen atom of ephedrine as -11.18 eV. A value of -12.16 eV was taken for the ionization energy of the n-electron of the water molecule.[23] The VSIE for the different atomic orbitals on Cu^{2+} ions are charge dependent. Assuming a $+0.25$ charge on the copper ion and a starting configuration of $3d^{9.25}\ 4s^{1.0}\ 4p^{0.5}$ the calculated VSIE were:[24]

$3d = 64{,}000\,cm^{-1}$,

$4s = 54{,}500\,cm^{-1}$ and $4p = 29{,}000\,cm^{-1}$.

Solving the different symmetry determinants one obtains the different eigenvalues and eigenfunctions for the O_h biaquobisephedrinocopper(II) complex. A complete MO energy level diagram is shown in Fig. 8.

Molecular orbital calculations were repeated where the bond length between copper ion and oxygen atom of water molecule was elongated from 1.93 to 2.3 Å. This elongation has its effect on the values of S_{ij} and H_{ij} and on the splitting of energy levels as shown in Fig. 9.

Finally, MO calculations were performed on the square $[Cu(eph)_2]^0$. Results are given in Fig. 10.

In spite of the approximation of the method of

Table 1. Orbital scheme for the biaquobis(ephedrine)copper(II) complex

Symmetry species	Copper(II) orbital	Ligand orbital	S_{ij}
a	$3d_{z^2}$	$\frac{1}{\sqrt{2}}(\sigma_5+\sigma_6)$	0.466
	$3d_{x^2-y^2}$	$\frac{1}{\sqrt{2}}(\sigma_1+\sigma_3-\sigma_2-\sigma_4)$	0.365
		$\frac{1}{\sqrt{2}}(\sigma_1+\sigma_2+\sigma_3+\sigma_4)$	−0.173
	$4s$	$\frac{1}{\sqrt{2}}(\sigma_1+\sigma_3)$	0.048
		$\frac{1}{\sqrt{2}}(\sigma_2+\sigma_4)$	0.107
		$\frac{1}{\sqrt{2}}(\sigma_5+\sigma_6)$	0.137
b_3	$3d_{yz}$	—	—
	$4p_x$	$\frac{1}{\sqrt{2}}(\sigma_3-\sigma_1)$	0.149
b_2	$3d_{xz}$	—	—
	$4p_y$	$\frac{1}{\sqrt{2}}(\sigma_2-\sigma_4)$	0.279
b_1	$3d_{xy}$	—	—
	$4p_z$	$\frac{1}{\sqrt{2}}(\sigma_5-\sigma_6)$	0.197

MO calculations used, some interesting and informative results were obtained. The molecular orbital energy diagram, Fig. 8, for biaquobisephedrinocopper(II) shows a tetragonal splitting of the *d*-orbital. It also shows an extensive mixing between the ligand and both the d_{x^2} and $d_{x^2-y^2}$ metal ion orbitals. The observed transition possesses a partial charge-transfer character, which explains the relatively high intensity of the observed transitions.

As the two water molecules are pulled "out" the MO energy-level diagram turns to that characteristic of a distorted tetragonal complex. A pronounced lowering in the energy of the d_{z^2} orbital is observed as compared with that of $d_{x^2-y^2}$, Fig. 9. Removal of the two water molecules along the *z*-axis leaves a square bisephedrinocopper(II) complex. In this case the MO energy-level diagram, Fig. 10, is characterized by the lowering of the d_{z^2} orbital, even lower than the d_{xy}, d_{xz} and d_{yz} orbitals. The $d_{x^2-y^2}$ orbital is extensively mixed with the ligand orbital. Three low-lying electronic transitions are predicted for the square complex compared with four transitions for the tetragonal complex.

CONCLUSIONS

Spectral–structural correlations have been investigated for the copper(II) ephedrine and norephedrine systems. In the case of the copper(II) ephedrine system both the 1:1 and 1:2 metal:ligand complexes showed spectra characteristic of distorted tetragonal geometry. As the ligand concentration increases the observed spectrum varied significantly and this was interpreted to be due to the increase in the extent of distortion via pulling out the two water molecules along the *z*-axis. The calculation of the crystal field parameters Δ_0 and δ showed an increase in the splitting of the ground

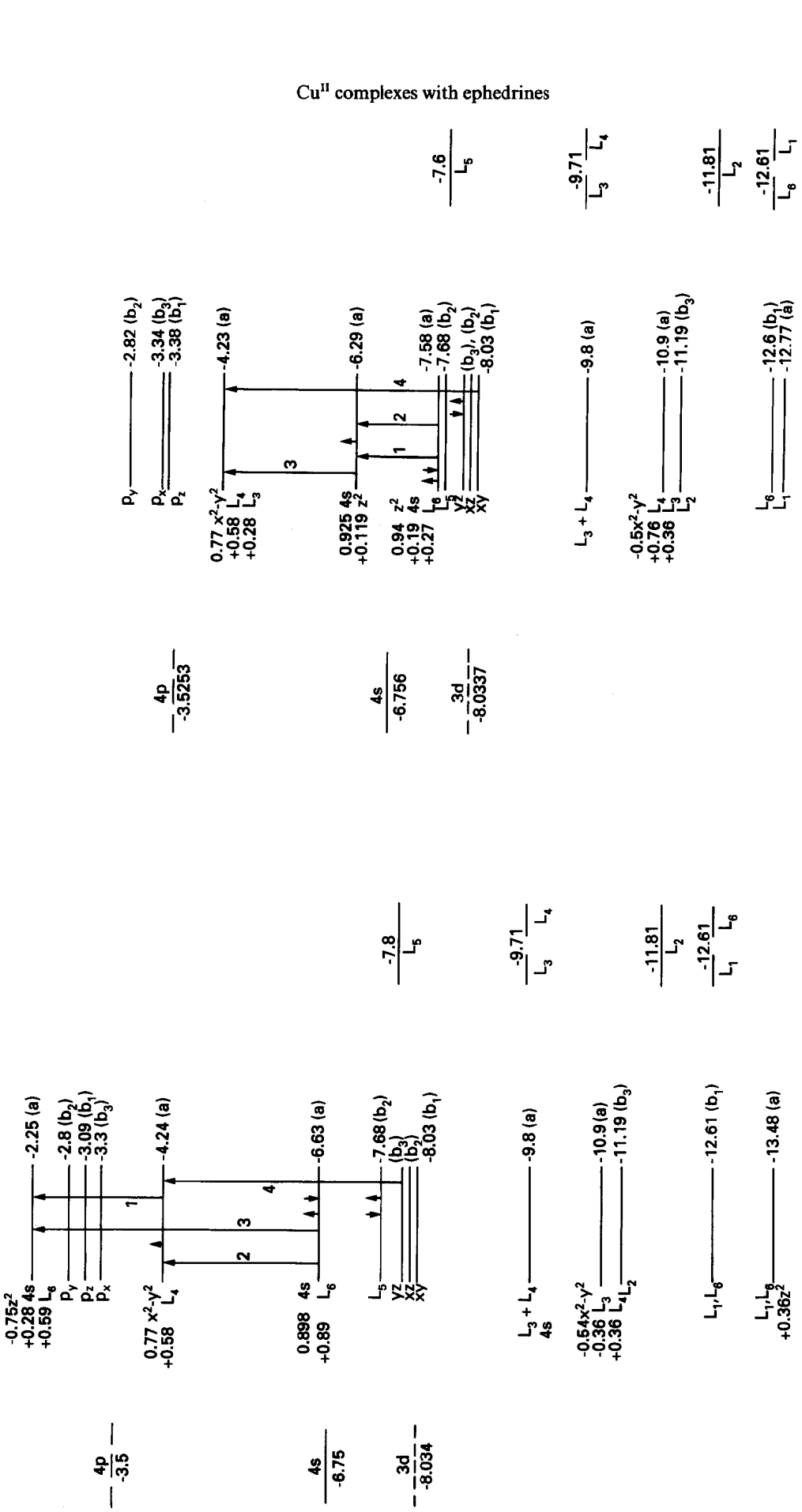

Fig. 8. A non-scale molecular orbital energy level diagram for the octahedral biaquobis(ephedrine)copper(II) complex.

Fig. 9. A non-scale molecular orbital energy level diagram for the distorted octahedral "z-out" biaquobis(ephedrine)copper(II) complex.

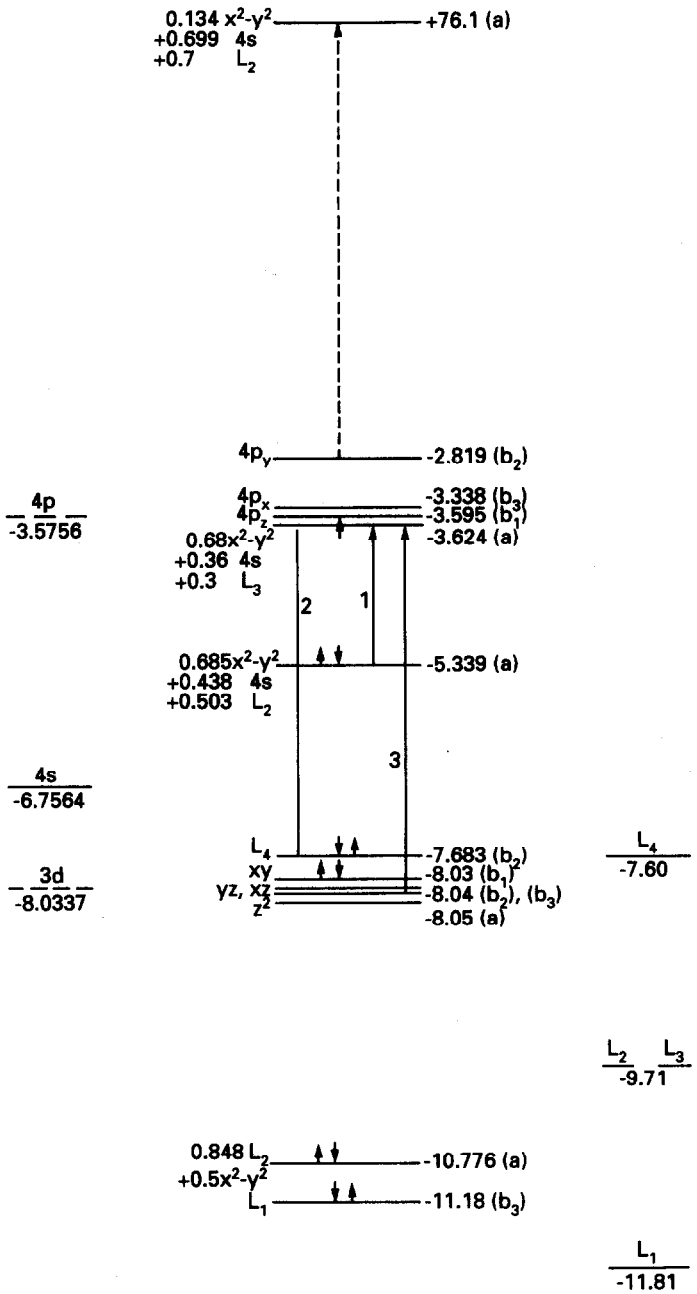

Fig. 10. A non-scale molecular orbital energy level diagram for the square bis(ephedrine)copper(II) complex.

state, a decrease in the splitting of the ground state and a decrease in the splitting of the excited state as the concentration of ephedrine increased with respect to that of Cu^{2+} ions. A further increase in the ligand concentration led to the formation of the bisephedrinocopper(II) complex, which gave an absorption spectrum characteristics of a square complex. The same spectral behaviour, a blue shift of λ_{max} with ligand concentration, was observed for the copper(II) norephedrine system using methanol as a solvent.

REFERENCES

1. J. E. F. Reynolds and A. B. Prasad (Editors), *Martindale The Extra Pharmacopia*, 28th edn, pp. 11 and 25. The Pharmaceutical Press, London (1982).
2. Y. Amano, K. Osaki and T. Watanabe, *Bull. Chem. Soc. Japan* 1964, **37**, 1363.
3. Y. Amano, K. Osaki and T. Uno, *Nippon Kagaku Zasshi* 1965, **86**, 1109.
4. J. F. Malone, M. Miskelly and M. Parvez, *Proc. H. Ir. Acad. Sect. B* 1977, **77B**, 19, 499.
5. A. A. Medvedovskii and T. V. Kovalchuk, *Otkrytiya*

Izobert, Prom. Obraztsy, Tovarnye Znaki 1979, **32**, 157; *Chem. Abstr.* 1989, **92**, 2.
6. E. G. Bogusavskii, A. A. Shklysev, N. G. Maksumov, Z. M. Alaudinova, I. S. Kolomnikov and V. F. Anufrienko, *Izv. Akad. Nauk. U.S.S.R. Ser Khim.* 1980, **6**, 1231; *Chem. Abstr.* 1980, **93**, 6.
7. E. O. Boguslavsku, I. S. Kolomnikov, A. A. Shklyaev, N. G. Maximov, G. K. Boreskov and V. F. Anufrienko, *Dok Akad. Nauk. U.S.S.R.* 1980, **251**, 904; *Chem. Abstr.* 1980, **93**, 22.
8. R. J. Raffa, M. J. Stern and L. Malspeis, *Anal. Chem.* 1968, **40**, 70.
9. S. Lukkari, *Farm. Alkerk* 1970, **79**, 95; *Chem. Abstr.* 1972, **77**, 4.
10. H. M. Irving and H. S. Rosotti, *J. Chem. Soc.* 1954, 2904.
11. C. Lagercrantz, *Acta Chem. Scand., Sect. B* 1987, **B41**, 526.
12. W. J. Close, *J. Org. Chem.* 1950, **15**, 1131.
13. Z. Foldi, T. Foldi and A. Foldi, *Chem. Ind.* 1955, 1297.
14. R. D. Gillard and R. Wootton, *J. Inorg. Nucl. Chem.* 1971, **33**, 2185.
15. N. A. Bailey, Pamela M. Harrison and R. Mason, *J. Chem. Soc., Chem. Commun.* 1968, 559.
16. P. Jop, *Ann. Chim. Phys.* 1928, **9**, 113.
17. R. D. Gillard and H. M. Irving, *Chem. Rev.* 1965, **65**, 603.
18. E. J. Corey and J. C. Bailer, *J. Am. Chem. Soc.* 1959, **81**, 2620.
19. J. H. Dunlop, R. D. Gillard and N. C. Payne, *J. Chem. Soc. (A)* 1967, 1469.
20. R. D. Gillard and R. Wootton, *J. Chem. Soc. (B)* 1967, 921.
21. S. F. Mason and B. J. Norman, *J. Chem. Soc. Chem. Commun.* 1965, 48.
22. M. Wofsberg and L. Helmholz, *J. Chem. Phys.* 1952, **20**, 837.
23. S. P. McGynn, L. G. Vanquickenborne, M. Kinoshika and D. G. Garroll, *Introduction to Applied Quantum Chemistry*. Holt, Rinehard and Winston Inc., New York (1972).
24. R. Abu-Eittah, Z. Mobarak and M. Abdou, *Gazz. Chim. Ital.* 1988, **118**, 275.

Polyhedron Vol. 12, No. 16, pp. 2039–2044, 1993
Printed in Great Britain

0277–5387/93 $6.00+.00
© 1993 Pergamon Press Ltd

VANADYL COMPLEXES IN AMBIENT-TEMPERATURE IONIC LIQUIDS. THE FIRST X-RAY CRYSTAL STRUCTURE OF A TETRACHLOROOXOVANADATE(IV) SALT

PETER B. HITCHCOCK

School of Chemistry and Molecular Sciences, University of Sussex, Falmer, Brighton BN1 9QJ, U.K.

and

RICHARD J. LEWIS and THOMAS WELTON†

Department of Chemistry, University of Exeter, Exeter EX4 4QD, U.K.

(*Received* 22 *February* 1993; *accepted* 1 *April* 1993)

Abstract—The novel salt $[emim]_2[VOCl_4]$ ($[emim]^+$ = 1-ethyl-3-methylimidazolium cation) has been prepared and characterized, both spectroscopically and crystallographically. The $[VOCl_4]^{2-}$ anion has an approximately square pyramidal structure in the solid state. This structure is maintained when the salt is dissolved in the [emim]Cl—$AlCl_3$ ambient-temperature ionic liquid.

Ambient-temperature chloroaluminate(III) ionic liquids have been used as solvents to study the spectroscopy and electrochemistry of a wide range of transition metal chloro complexes.[1] During these investigations a number of oxochloro complexes have been observed.[1–3] They have, generally, been treated as impurities rather than as interesting species in their own right. However, the ambient-temperature chloroaluminate(III) ionic liquids provide an ideal opportunity to observe these species, free from the distortions caused by solvation and solvolysis phenomena.[1]

The chemistry of vanadium(IV) is dominated by the vanadyl group (VO^{2+}). Hence, its roles in redox catalysis and oxo transfer reactions are of some interest.[4,5] As part of a wider investigation of oxygen atom transfer chemistry in ambient-temperature chloroaluminate(III) ionic liquids, we have prepared the salt 1-ethyl-3-methylimidazolium tetrachlorooxovanadate(IV) {$[emim]_2[VOCl_4]$}. We present here the X-ray crystal structure of the salt, together with a spectroscopic investigation of its structure in a basic (excess [emim]Cl) [emim]Cl—$AlCl_3$ ionic liquid.

EXPERIMENTAL

Solvents and starting materials

Dichloromethane (ex. B.D.H.) and ethanenitrile (ex. Aldrich) were distilled from phosphorus(V) oxide, under dinitrogen, immediately before use; thionyl chloride (ex. Aldrich) was distilled *in vacuo* prior to use. Anhydrous $VOCl_2$ was prepared from the dihydrate (ex. B.D.H.), using $SOCl_2$.[6] The non-stoichiometric $VOCl_2(CH_3CN)_x$ ($x \approx 2.5$) was prepared from the reaction of $VOCl_2$ with ethanenitrile.[6] [emim]Cl was prepared by the reaction of 1-methylimidazole with chloroethane.[7]

Preparation of $[emim]_2[VOCl_4]$

1-Ethyl-3-methylimidazolium chloride (2.6 g) and $VOCl_2(CH_3CN)_x$ (2.0 g) were added to dry dichloromethane (75 cm^3). The mixture was heated under reflux, under dry dinitrogen, for 48 h. The resulting mixture was allowed to cool to room temp-

† Author to whom correspondence should be addressed.

Supplementary data are deposited at the Cambridge Crystallographic Data Centre.

erature. After standing overnight green needle crystals were formed, from a green oil. The crystals were isolated by filtration, under dry dinitrogen, and washed with aliquots (10×10 cm^3) of dry dichloromethane. Finally the green crystals were dried *in vacuo*. Yield: 2.54 g (65%), m.p. 99°C. Found: C, 33.76; H, 5.22; N, 12.05%. Calc. for $C_{12}H_{22}Cl_4N_4OV$: C, 33.43; H, 5.14; N, 13.00%.

Spectra

IR spectra were recorded on a Nicolet Magna 550 IR spectrometer. Electronic absorption spectra were recorded on a Perkin–Elmer Lambda 2 spectrophotometer, using 1 cm path length cells.

Crystallographic data collection

A crystal of $[emim]_2[VOCl_4]$ ($0.5 \times 0.3 \times 0.2$ mm) was isolated and mounted in a Lindemann capillary tube. Data were collected on an Enraf–Nonius CAD4 diffractometer. There was no crystal decay. Non-hydrogen atoms were located by direct methods and refinement was by full-matrix least-squares, using an Enraf–Nonius SDP program, with anisotropic temperature factors. Hydrogen atoms were located on a difference map and refined isotropically. Other details of the methods are summarized in Table 1.

RESULTS AND DISCUSSION

IR spectra

The tetrachlorooxovanadate(IV) anion has six atoms and, therefore, 18 Cartesian vectors ($3n$) and 12 molecular vibrations ($3n-6$). Group theory can be used to find the symmetries of these vibrations. The ion has C_{4v} symmetry (*vide infra*); a reducible representation can be obtained by applying the symmetry operations of the group on the Cartesian vectors of the ion.

C_{4v}	E	$2C_4$	C_2	$2\sigma_v$	$2\sigma_d$
χ	18	2	−2	4	2

Table 1. Summary of the experimental conditions, data collection and refinements

Chemical formula	$C_{12}H_{22}Cl_4N_4OV$
Formula weight (g)	431.1
Crystal system	Monoclinic
Space group	$P2_1/c$ (No. 14)
Cell dimensions	
a (nm)	0.9035(1)
b (nm)	1.3257(2)
c (nm)	0.9280(2)
β (°)	113.80(1)
Unit cell volume (nm^3)	1.0170
No. of molecules per unit cell, Z	2
Total number of electrons in a unit cell, $F(000)$	442
Calculated density, D_c (g cm^{-3})	1.41
Monochromated Mo-K_α radiation	
λ (Å)	0.71069
μ (cm^{-1})	10.1
Scan mode	θ–2θ
θ limits (°)	2–28
Data reflection ranges	h, $0 \rightarrow 11$; k, $0 \rightarrow 17$; l, $-12 \rightarrow 12$
Total collected reflections	2694
Max. absorption correction	1.21
Min. absorption correction	0.56
No. of reflections $I > \sigma(I)$ in the least-squares refinement	1543
Final R	0.048
Final R'	0.061

This representation may then be reduced, using the C_{4v} character table, to give the irreducible representation.

$$\Gamma = 4A_1 + A_2 + 2B_1 + B_2 + 5E \quad (1)$$

From this, the translations (A_1+E) and the rotations (A_2+E) are subtracted to reveal the normal vibrations.

$$\Gamma_{vib} = 3A_1 + 2B_1 + B_2 + 3E \quad (2)$$

It can be shown that the V=O stretch has A_1 symmetry, whilst there are three V—Cl stretches with A_1, B_1 and E symmetries. Of these only A_1 and E are IR active.

The IR spectrum (2000–225 cm^{-1}) of the solid $[emim]_2[VOCl_4]$ as a Nujol mull is shown in Fig. 1. It can be seen that ν(V=O) is observed as a single strong sharp peak at *ca* 1001 cm^{-1} (cf. 1000 cm^{-1} for $[Et_4N]_2[VOCl_4]$[8]). In the far-IR spectrum a strong band is observed that can be attributed to ν(V—Cl). In the spectrum shown (Fig. 1) this band has resolved into two peaks at 361 and 340 cm^{-1}, in spectra where these peaks are not resolved the band is found at *ca* 350–355 cm^{-1} (cf. 350 cm^{-1} for $[Et_4N]_2[VOCl_4]$[8]). Group theory shows that, for C_{4v} symmetry, the ion $[VOCl_4]^{2-}$ should have both symmetric and asymmetric V—Cl stretches. The two peaks observed at 340 and 361 cm^{-1} can be assigned to the symmetric (A_1) and the asymmetric (E) stretches, respectively. The other peaks in the spectrum are due to the $[emim]^+$ cation and have been discussed elsewhere.[9]

A spectrum of a solution of $[emim]_2[VOCl_4]$ in a basic [emim]Cl—$AlCl_3$ ionic liquid shows a peak due to ν(V=O) at 993 cm^{-1}; ν(V—Cl) is obscured by the spectrum of the ionic liquid itself.

Electronic absorption spectra

The $[VOCl_4]^{2-}$ ion is a d^1 system and hence might be expected to have a simple electronic absorption spectrum. In fact, the spectra of oxovanadium(IV) compounds have been a source of some controversy. However, low-temperature polarized single-crystal measurements[8] of a number of oxovanadium(IV) compounds have led to definitive assignments of electronic absorption spectra. For $[Et_4N]_2[VOCl_4]$[8] three bands were observed at wave numbers below 30,000 cm^{-1}, all of which were assigned to *d–d* transitions, the energies increasing in the order I < II < III. The transitions occur due to an electron being excited from a singly occupied b_2 orbital, which arises from an interaction between the metal d_{xy} orbital and a ligand (Cl) π-orbital, and is weakly antibonding.[8,10]

Band I $b_2 \longrightarrow b_1$

Band II $b_2 \longrightarrow e$

Band III $b_2 \longrightarrow a_1$

Using the single-crystal spectra as a guide the electronic absorption spectrum of a solution of $[emim]_2[VOCl_4]$ (Fig. 2, Table 2) in basic ionic liquid can be analysed. It can be seen that the spectrum is dominated by a broad absorption in the visible region (λ_{max} = 739 nm, 13,530 cm^{-1}), its overall

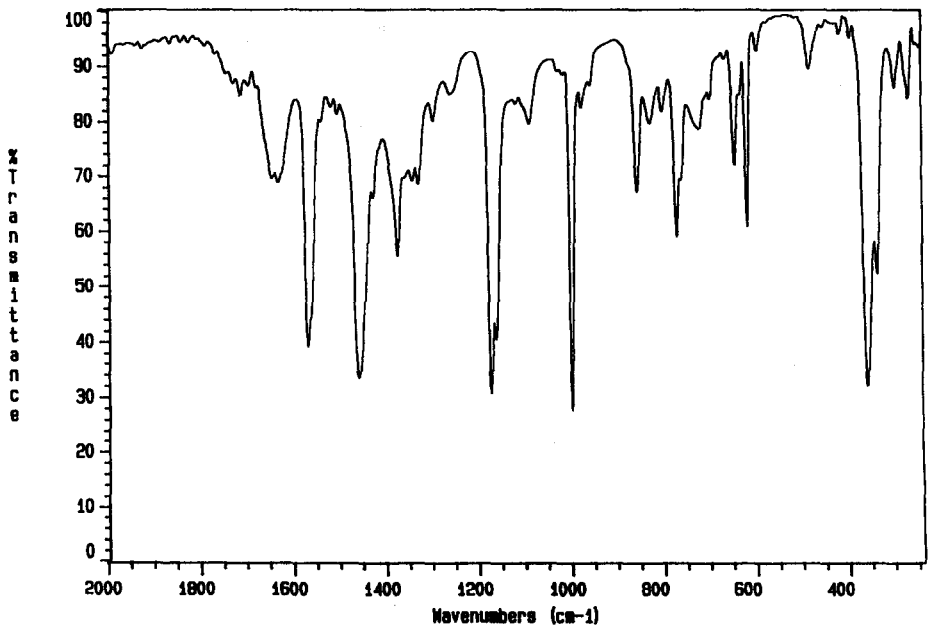

Fig. 1. The IR spectrum (2000–225 cm^{-1}) of $[emim]_2[VOCl_4]$.

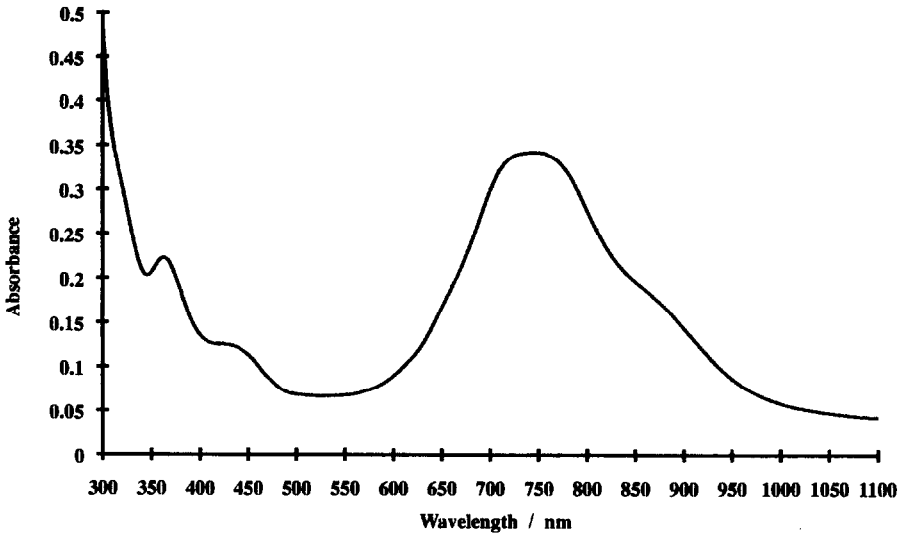

Fig. 2. The electronic absorption spectrum of $[emim]_2[VOCl_4]$ in a basic [emim]Cl—$AlCl_3$ ionic liquid.

appearance being similar to that of the room-temperature single-crystal spectrum of $[Et_4N]_2[VOCl_4]$.[8] The shoulder at 859 nm (11,640 cm^{-1}) can be attributed to the $b_2 \longrightarrow b_1$ transition (band I). The rest of this complicated absorption can be assigned to the $b_2 \longrightarrow e$ transition (band II). The remaining absorptions at 430 and 364 nm (23,280 and 27,470 cm^{-1}) are the beginning of the progression due to the $b_2 \longrightarrow a_1$ transition (band III). Most of this band is obscured by the solvent cut-off, which arises from a π–π^* transition of the imidazolium ring. The spectrum is entirely consistent with the ion maintaining C_{4v} symmetry in the basic ionic liquid.

The crystal structure

The crystal structure of $[emim]_2[VOCl_4]$ is presented in Figs 3 and 4. In this structure the $[VOCl_4]^{2-}$ ion is approximately square pyramidal (C_{4v} symmetry). In the anion there are two longer and two shorter V—Cl bonds (Table 3). However, it can be seen from the bond angles (Table 3) that the ion is not distorted toward trigonal bipyramidal symmetry. The anions lie on crystallographic inversion centres, with the vanadium atoms displaced off the inversion centre such that they, and the oxygen atoms, are disordered equally between both sides of the Cl_4 plane (Fig. 4). Disorder of this nature has been observed for other square pyramidal oxovanadium(IV) compounds.[11]

Although no other crystal structures of the $[VOCl_4]^{2-}$ ion have been recorded, the structures of a number of square-pyramidal complexes of the type $[VOCl_2L_2]$ are known.[11–13] The mean V—Cl bond length in these structures of 0.2326(14) nm is in good agreement with that found for the $[VOCl_4]^{2-}$ ion. However, the mean V=O bond length of 0.1600(12) nm is somewhat longer in these neutral molecules than that in the $[VOCl_4]^{2-}$ ion.

Table 2. The electronic absorption spectrum of $[emim]_2[VOCl_4]$

Transition	λ_{max} (nm)	ν_{max} (cm^{-1})	ε (dm^3 mol^{-1} cm^{-1})
$b_2 \longrightarrow b_1$	859	11,640	shoulder
$b_2 \longrightarrow e$	739	13,530	34.87
$b_2 \longrightarrow a_1$	430	23,280	7.33
	364	27,470	12.87

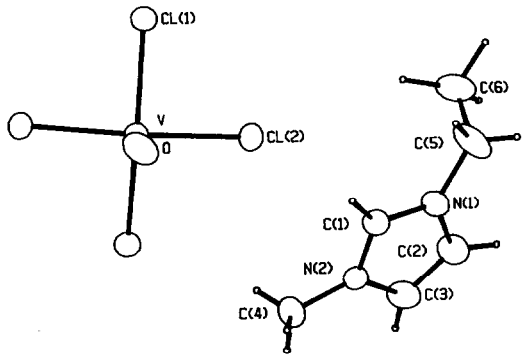

Fig. 3. A single cation and anion of the $[emim]_2[VOCl_4]$ unit, showing the numbering scheme employed.

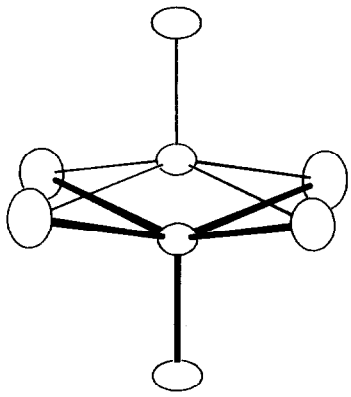

Fig. 4. The site disorder found in $[emim]_2[VOCl_4]$.

The structure of the hexachlorodioxodivanadate(IV) anion ($[V_2O_2Cl_6]^{2-}$) has been recorded[14] and the ion has been shown to consist of two distorted square-pyramidal VCl_4O units sharing a basal edge. As might be expected the V=O bond length of 0.1564(13) nm is in excellent agreement with that found here of 0.1560(5) nm. In $[V_2O_2Cl_6]^{2-}$ the square pyramids are distorted by the presence of both bridging [0.2403(4) nm] and terminal [0.2293(5) nm] V—Cl bonds.

Finally, it is useful to compare the structure of $[emim]_2[VOCl_4]$ with those of known tetrachlorooxovanadate(V) salts. Like the $[VOCl_4]^{2-}$ ion the $[VOCl_4]^-$ ion has a square-pyramidal, C_{4v}, structure. Of the three published structures[15–17] one $\{[P_2NCl_6][VOCl_4]\}$ is the result of diffraction by twinned crystals[17] and is not used for the comparison here. The remaining two structures are in good agreement, showing mean V=O and V—Cl distances of 0.1550 and 0.2252 nm, respectively. The molecular orbital description for $[VOCl_4]^{2-}$ shows that the ground state is $^2B_2$ with a b_2 antibonding HOMO. Oxidation of $[VOCl_4]^{2-}$ to $[VOCl_4]^-$ involves the removal of the electron from the antibonding orbital. Since this orbital has no oxygen character, little difference in the V=O bond lengths is expected. The HOMO does, however, have V—Cl antibonding character, hence the V—Cl bond length in $[VOCl_4]^{2-}$ (0.2330 nm) is expected to be longer than in $[VOCl_4]^-$ (0.2252 nm). This is indeed the case.

A survey of closest interionic contacts reveals that it is unlikely that any of the protons of the cation are involved in hydrogen bonding with the anion. This is consistent with conclusions previously drawn, on the hydrogen-bond acceptor properties of chlorometallate complexes.[18]

The internal dimensions of the $[emim]^+$ ion are unremarkable and in good agreement with those of other salts of this cation.[18,19]

CONCLUSIONS

In the salt $[emim]_2[VOCl_4]$ the anion has C_{4v} symmetry (square pyramidal), at room temperature. This symmetry is maintained when the salt is dissolved in basic compositions of the [emim]

Table 3. Intramolecular distances (Å) and angles (°) with estimated standard deviations in parentheses

V—Cl(1)	2.302(1)	V—Cl(1)′	2.355(1)
V—Cl(2)	2.348(1)	V—Cl(2)′	2.314(1)
V—O	1.560(5)	N(1)—C(1)	1.313(4)
N(1)—C(2)	1.357(5)	N(1)—C(5)	1.468(4)
N(2)—C(1)	1.311(4)	N(2)—C(3)	1.360(5)
N(2)—C(4)	1.452(4)	C(2)—C(3)	1.334(4)
C(5)—C(6)	1.500(9)		

Cl(1)—V—Cl(1)′	157.59(6)	Cl(1)—V—Cl(2)	87.48(4)
Cl(1)—V—Cl(2)′	89.46(5)	Cl(1)—V—O	100.2(2)
C(1)′—V—Cl(2)	87.39(5)	Cl(1)′—V—Cl(2)′	87.02(4)
Cl(1)′—V—O	102.2(2)	Cl(2)—V—Cl(2)′	157.59(6)
Cl(2)—V—O	102.0(2)	Cl(2)′—V—O	100.4(2)
C(1)—N(1)—C(2)	108.0(3)	C(1)—N(1)—C(5)	126.5(3)
C(2)—N(1)—C(5)	125.2(3)	C(1)—N(2)—C(3)	107.6(2)
C(1)—N(2)—C(4)	125.9(3)	C(3)—N(2)—C(4)	126.4(3)
N(1)—C(1)—N(2)	109.6(3)	N(1)—C(2)—C(3)	107.1(3)
N(2)—C(3)—C(2)	107.6(4)	N(1)—C(5)—C(6)	110.6(4)

Symmetry element ′ is $-x, -y, -z$

Cl—$AlCl_3$ ionic liquid. The electronic absorption spectrum of the salt dissolved in the ionic liquids was markedly better resolved than spectra recorded in conventional non-aqueous solvents (cf. ref. 10) and is of a quality comparable to that of single-crystal spectra.[8] This confirms the usefulness of [emim]Cl—$AlCl_3$ for the investigation of these interesting oxochloride systems.

REFERENCES

1. C. L. Hussey, *Pure Appl. Chem.* 1988, **60**, 1763.
2. I.-W. Sun and C. L. Hussey, *Inorg. Chem.* 1989, **28**, 2731.
3. H. Linga, Z. Stojek and R. A. Osteryoung, *J. Am. Chem. Soc.* 1981, **103**, 3754.
4. M. Otto and G. Werner, *Anal. Chim. Acta* 1981, **126**, 65.
5. Y. Zhang and R. H. Holm, *Inorg. Chem.* 1990, **29**, 911.
6. J. G. H. du Preez and F. G. Sadie, *Inorg. Chim. Acta* 1967, **1**, 202.
7. G. P. Smith, A. S. Dworkin, R. M. Pagni and S. P. Zingg, *J. Am. Chem. Soc.* 1989, **111**, 525.
8. D. Collison, B. Gahan, C. D. Garner and F. E. Mabbs, *J. Chem. Soc., Dalton Trans.* 1980, 667.
9. S. Tait and R. A. Osteryoung, *Inorg. Chem.* 1984, **23**, 4352.
10. J. E. Drake, J. E. Vekris and J. S. Wood, *J. Chem. Soc. (A)* 1969, 345.
11. S. Bristow, S. C. M. McAvilley, W. Clegg and D. Collison, *Polyhedron* 1989, **8**, 87.
12. J. Coetzer, *Acta Cryst.* 1970, **B26**, 872.
13. M. R. Caira and B. J. Gellatly, *Acta Cryst.* 1980, **B36**, 1198.
14. F. A. Cotton, M. W. Extine, L. R. Falvello, D. B. Lewis, G. E. Lewis, C. A. Murillo, W. Schwotzer, M. Thomas and J. M. Troup, *Inorg. Chem.* 1986, **25**, 3505.
15. G. Frenzen, W. Massa, T. Ernst and K. Dehnicke, *Z. Naturforsch.* 1990, **45b**, 1393.
16. G. Beindorf, J. Strahle, W. Liebelt and K. Dehnicke, *Z. Naturforsch.* 1980, **35b**, 522.
17. A. Zinn, U. Patt-Siebel, U. Muller and K. Dehnicke, *Z. Anorg. Allg. Chem.* 1990, **591**, 137.
18. P. B. Hitchcock, K. R. Seddon and T. Welton, *J. Chem. Soc., Dalton Trans.*, in press.
19. A. K. Abdul-Sada, A. M. Greenway, P. B. Hitchcock, T. J. Mohammed, K. R. Seddon and J. A. Zora, *J. Chem. Soc., Chem. Commun.* 1986, 1753.

Polyhedron Vol. 12, No. 16, pp. 2045–2050, 1993
Printed in Great Britain

0277–5387/93 $6.00+.00
© 1993 Pergamon Press Ltd

SYNTHESIS AND CHARACTERIZATION OF *CIS*-DIOXOMOLYBDENUM(VI) SCHIFF BASE COMPLEXES DERIVED FROM 1-PHENYL-3-METHYL-4-BENZOYL-5-PYRAZOLONE

N. SUMITA RAO, M. N. JAISWAL, D. D. MISHRA and R. C. MAURYA*

Department of Post-Graduate Studies and Research in Chemistry, R.D. Vishwavidyalaya, Jabalpur 482001, India

and

N. NAGESWARA RAO

Coordination Chemistry Discipline, Central Salt and Marine Chemicals Research Institute, Bhavnagar 364002, India

(*Received* 5 *January* 1993; *accepted* 1 *April* 1993)

Abstract—The synthesis and characterization of some *cis*-dioxomolybdenum(VI) complexes with bidentate and tetradentate Schiff base ligands derived from reactions of 1-phenyl-3-methyl-4-benzoyl-5-pyrazolone with amines, such as *p*-anisidine, *m*-phenitidine, *m*-toluidine, *o*-, *m*- and *p*-phenylenediamine, and benzidine are reported. Reaction of the bi- and tetradentate Schiff bases with $MoO_2(acac)_2$ in 2:1 and 1:1 ratios, respectively, gave diamagnetic molybdenum(VI) mononuclear complexes with the general formulae *cis*-$MoO_2(L)_2$ (L = bidentate Schiff base), *cis*-$MoO_2(L^1)$ (L^1 = tetradentate Schiff base with *o*- and *m*-phenylenediamine) and the ligand-bridged dinuclear complexes $Mo_2O_4(L^2)(S)_x$ (L^2 = tetradentate Schiff base with *p*-phenylenediamine and benzidene, $S = C_2H_5O^-$ and $x = 2$ or 4). These complexes were characterized by elemental analysis, molar conductance, IR, UV–vis, ^1H NMR and cyclic voltammetry.

The coordination complexes of molybdenum have gained considerable research interest due to their activity in biochemical redox reactions associated with several enzymes.[1–4] The valence of molybdenum varies depending on the nature of the enzyme and the function of some redox enzymes is dependent on variable-valence molybdenum cofactors. The coordination chemistry of the molybdenum(VI) state is based on oxo complexes to a large extent, which are important in oxidations catalysed by metals.[5,6] Most molybdenum(VI) coordination complexes contain *cis*-dioxo MoO_2^{2+} and an octahedral structure. Although many precursors are available, $MoO_2(acac)_2$ is a convenient source of MoO_2^{2+}.[7–9] In this paper we report the synthesis and characterization of some *cis*-dioxomolybdenum(VI) complexes with bi- and tetradentate Schiff bases. The bidentate Schiff bases form mononuclear molybdenum(VI) complexes having the general formula $MoO_2(L)_2$, where L = a bidentate Schiff base, namely, 1-phenyl-3-methyl-4-benzoyl-*p*-anisidine-5-pyrazolone (PMBP-A), 1-phenyl-3-methyl-4-benzoyl-*m*-phenitidine-5-pyrazolone (PMBP-P) and 1-phenyl-3-methyl-4-benzoyl-*m*-toluidine-5-pyrazolone (PMBP-T). The Schiff base ligand of *o*-phenylenediamine forms a mononuclear complex, *cis*-$MoO_2(L^1)$ [L^1 = 1-phenyl-3-methyl-4-benzoyl-*o*-phenylenediamine-5-pyrazolone (PMBP-*o*-phd)]. The Schiff base ligand of *m*-phenylenediamine behaves as a tridentate ligand and forms the mononuclear five-coordinate *cis*-$MoO_2(L^1)$ [L^1 = 1-phenyl-3-4-benzoyl-*m*-phenylenediamine-5-pyrazolone (PMBP-*m*-phd)]. The molyb-

* Author to whom correspondence should be addressed.

denum(VI) complexes of *p*-phenylenediamine and benzidine Schiff bases are five- and six-coordinate dinuclear complexes, respectively, bridging through azomethine nitrogens, represented as $(Mo_2O_4)(L^2)(S)_x$, where L^2 = 1-phenyl-3-methyl-4-benzoyl-*p*-phenylenediamine-5-pyrazolone (PMBP-*p*-phd) and 1-phenyl-3-methyl-4-benzoyl-benzidine-5-pyrazolone (PMBP-bz), $S = C_2H_5O^-$ and $x = 2$ or 4. Elemental analysis, molar conductance, spectroscopic (IR, UV–vis and ^{1}H NMR) and cyclic voltammetry data are given for all the complexes.

EXPERIMENTAL

Materials

All reagents required for compound preparation were of analytical grade. 1-Phenyl-3-methyl-5-pyrazolone was procured from Johnsons Chemical Company, Bombay, India. Ammonium molybdate, acetylacetone and the amines used in this study were procured from B.D.H., U.K.

Synthesis of the ligands

1-Phenyl-3-methyl-4-benzoyl-5-pyrazolone (PMBP) was prepared according to the reported method.[10] The synthesis of bidentate Schiff base ligands, namely 1-phenyl-3-methyl-4-benzoyl-*p*-anisidine-5-pyrazolone (PMBP-A) (**1a**), 1-phenyl-3-methyl-4-benzoyl-*m*-phenitidine-5-pyrazolone (PMBP-P) (**2a**) and 1-phenyl-3-methyl-4-benzoyl-*m*-toluidine-5-pyrazolone (PMBP-T) (**3a**), has been reported earlier.[11] The tetradentate Schiff bases were prepared by a general method wherein 2:1 ethanolic solutions of PMBP and *o*-, *m*- and *p*-phenylenediamine and benzidine were taken and refluxed with stirring for 4–5 h. The volume of the solution was reduced (*ca* 10 cm^3) by concentrating on a water bath. On cooling the solutions to room temperature crystals of yellow 1-phenyl-3-methyl-4-benzoyl-*o*-phenylenediamine-5-pyrazolone (PMBP-*o*-phd) (**4a**), greenish-yellow 1-phenyl-3-methyl-4-benzoyl-*m*-phenylenediamine-5-pyrazolone (PMBP-*m*-phd) (**5a**), yellow 1-phenyl-3-methyl-4-benzoyl-*p*-phenylenediamine-5-pyrazolone (PMBP-*p*-phd) (**6a**) and 1-phenyl-3-methyl-4-benzoyl-benzidine-5-pyrazolone (PMBP-bz) (**7a**) separated out from their respective solutions. The crystals thus obtained were filtered and recrystallized from ethanol (yield 70–75%).

Synthesis of the complexes

$MoO_2(acac)_2$ was prepared according to the reported method.[12] The *cis*-dioxomolybdenum bidentate Schiff base complexes $\{MoO_2(PMBP\text{-}A)_2\}$ (**1b**), $\{MoO_2(PMBP\text{-}P)_2\}$ (**2b**) and $\{MoO_2(PMBP\text{-}T)_2\}$ (**3b**) and tetradentate Schiff base complexes $\{MoO_2(PMBP\text{-}o\text{-}phd)\}$ (**4b**), $\{MoO_2(PMBP\text{-}m\text{-}phd)\}$ (**5b**), $\{Mo_2O_4(PMBP\text{-}p\text{-}phd)(C_2H_5O^-)_2\}$ (**6b**) and $\{Mo_2O_4(PMBP\text{-}bz)(C_2H_5O^-)_4\}$ (**7b**) were prepared by adding a hot ethanolic solution of the ligand to a hot ethanolic solution of $MoO_2(acac)_2$ in 2:1 and 1:1 ratios, respectively. The resulting solution was refluxed for 6–7 h when the colour of the solution changed to dark green. The volume of the solution was reduced (*ca* 10 cm^3) by concentrating on a water bath. Green complexes were obtained on cooling which were filtered, washed with small aliquots of ethanol to remove unreacted ligand and $MoO_2(acac)_2$ and then dried *in vacuo* (yield 60–65%).

Physical measurements

Microanalyses (C, H, N) of the ligands and the complexes were performed on a Carlo–Erba 1106 elemental analyser. Solution electrical conductivity was measured at 298 K using a Digisun Electronics Conductivity bridge. IR spectra were recorded at 298 K on an FT-IR (Bio-Rad) spectrometer as Nujol mulls/KBr pellets. Electronic spectra were recorded on a Shimadzu model UV-160 spectrophotometer. The ^{1}H NMR spectra were recorded at 298 K on a Jeol FX-100 FT-NMR spectrometer. Cyclic voltammetry traces of the complexes were recorded on a Princeton Applied Research Model 384 Polarographic Analyser.

RESULTS AND DISCUSSION

The elemental analyses, UV–vis, ^{1}H NMR and IR data of the bidentate Schiff base ligands (**1a–3a**) have been reported earlier,[11] whereas the data for the tetradentate Schiff base ligands (**4a–7a**) is presented in Table 1. The ^{1}H NMR spectra of all the Schiff base ligands (**1a–7a**) except **5a** and **7a**, show a peak at δ 12.4–12.8 ppm, which is due to the —OH proton, suggesting their existence in the enolic form. In the case of **5a** and **7a** the absence of the —OH proton and the presence of the —CH proton (δ 2.17 ppm) suggest their existence in the keto form. This is further supported by the IR spectra, wherein a band at 3476 cm^{-1} characteristic of ν(OH) is present in all the ligands except **5a** and **7a**. Further, the spectral data suggest that condensation to form tetradentate Schiff bases occurred at both the amino groups present in the diamines. The IR spectra of the ligands show ν(C=N) in the region 1592–1647 cm^{-1}, ν(C—O) at 1137–1165 cm^{-1} and in the case of **5a** and **7a** ν(C=O) appears at 1657 and 1642

Table 1. Melting point, elemental analysis, IR, UV–vis, ^{1}H NMR and cyclic voltammetric data for the ligands **4a**–**7a** and *cis*-MoO_2^{VI} Schiff base complexes **1b**–**7b**

Ligand/ complex No.	M.p. (°C)	Elemental analysis (%)[a] C	H	N	IR (cm^{-1})[b] ν (Mo=O)	Electronic[c] spectral data λ_{max} (nm) (ε, $M^{-1}\,cm^{-1}$)	^{1}H NMR[d] δ (ppm)		E_{pc}	$E_{1/2}$	E_{pa}[e] [Mo^{VI}/Mo^{V} (in V)]
1b	—	64.0 (64.5)	4.3 (4.5)	9.0 (9.4)	852, 906	428 (700) 410 (600) 327	6.72–8.2 3.72 1.49	(M, 28H) (S, 6H) (S, 6H)	−1.01	—	+0.20
2b	—	65.0 (65.1)	4.6 (4.8)	9.0 (9.1)	854, 904	424 (700) 410 (600) 332	6.7–8.2 3.84–4.1 1.49 1.23–1.37	(M, 2SH) (q, 4H) (S, 6H) (t, 6H)	0.97	—	+0.20
3b	—	66.8 (66.9)	4.6 (4.6)	9.7 (9.5)	861, 907	424 (600), 410 (500), 332	6.65–8.2 2.18 1.5	(M, 28H) (S, 6H) (S, 6H)	−0.96	—	+0.20
4a	200	76.2 (76.4)	5.0 (5.1)	13.2 (13.3)	—	330, 410	12.4 6.46–8.21 1.58	(S, 2H) (M, 24H) (S, 6H)	—	—	—
4b	—	63.2 (63.4)	4.2 (4.2)	11.0 (11.1)	908, 959	731 (120), 431 (800), 410 (900)	6.34–8.2 1.51	(M, 24H) (S, 6H)	—	−0.550	—
5a	170	76.0 (76.4)	5.0 (5.1)	13.0 (13.3)	—	330, 410	6.77–8.16 2.82	(M, 24) (S, 2H)	—	—	—
5b	—	63.0 (63.4)	4.0 (4.2)	10.9 (11.1)	910, 958	428 (1200), 410 (700)	6.34–8.2 1.51	(M, 24H) (S, 6H)	−0.88	—	—
6a	155	76.2 (76.4)	5.0 (5.1)	13.0 (13.3)	—	327, 410	12.8 6.45–8.21 1.49	(S, 2H) (M, 24H) (S, 6H)	—	—	—
6b	—	54.0 (54.3)	3.9 (4.1)	8.4 (8.6)	891 901 and 939, 955	689 (180), 443 (900), 410 (1000)	6.59–8.19 2.7–2.82 1.48 1.15–1.26	(M, 24H) (q, 4H) (S, 6H) (t, 6H)	—	0.57	—
7a	300	78.3 (78.4)	4.9 (5.1)	11.8 (11.9)	—	327, 410	6.76–8.1 2.17 1.5	(M, 28H) (S, 2H) (S, 6H)	—	—	—
7b	—	57.0 (56.8)	5.0 (4.9)	7.6 (7.4)	904, 946	682 (240), 449 (1000) 410 (500)	6.82[f]–8.2 2.91[f] (2H) 2.72 (2H) 2.13 (S, 2H) 1.53[g] (S, 6H) 1.05[g] (3H) 1.29 (3H)	(M, 28H)	—	−0.530	—

[a] Found (calc.).
[b] In KBr pellets at 298 K.
[c] The solvent is acetone for ligands **1a**–**7a** and complexes **1b**–**3b** and DMF for **4b**–**7b**.
[d] The solvent is acetone-d_6 for **1a**–**7a** and **1b**–**3b** and DMF-d_7 for **4b**–**7b**.
[e] A glassy-carbon electrode is the working electrode; the solvent is deaerated in acetone for **1b**–**3b** and DMF for **4b**–**7b**, the supporting electrolyte is tetra-butylammoniumhexafluorophosphate; the standard electrode is Ag/AgCl.
[f] Mid-positions of quartets.
[g] Mid-positions of triplets.

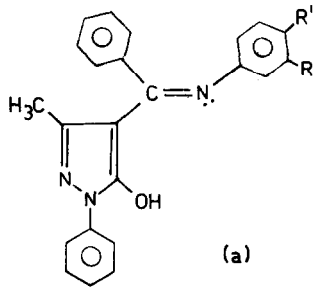

(a)

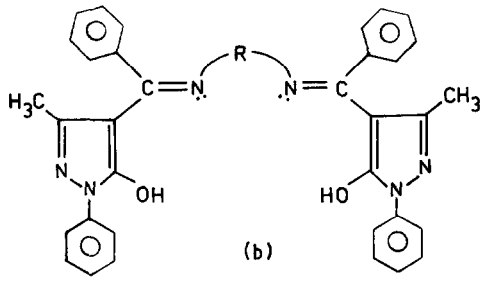

(b)

LIGAND	R	R'
1a	$-OCH_3$	-H
2a	-H	$-OC_2H_5$
3a	-H	$-CH_3$

LIGAND	R
4a	
5a	
6a	
7a	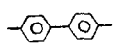

Structure I

cm^{-1}, respectively. On the basis of the data in Table 1 the structure of the bi- and tetradentate Schiff base ligands in general can be written as shown in structure **I**(a and b), respectively.

$MoO_2(acac)_2$ reacts with these bi- and tetradentate Schiff base ligands in ethanol to form stable molybdenum(VI) mononuclear (**1b–5b**) and ligand-bridged dinuclear complexes (**6b–7b**). That both the "acac" ligands in $MoO_2(acac)_2$ were displaced by these ligands was supported by the absence of characteristic peaks of "acac" groups in the IR and NMR spectra for these complexes.

The analytical data for the mononuclear and dinuclear *cis*-dioxomolybdenum(VI) Schiff base complexes (**1b–7b**) is presented in Table 1. The conductivities of freshly prepared solutions of **1b–3b** in acetone and **4b–7b** in DMF are in the range 2–7 $\Omega\ cm^{-1}\ mol^{-1}$, indicating that they are non-electrolytes.

The IR spectra of the complexes (**1b–7b**) (Table 1) exhibit bands in the regions 860–910 and 906–960 cm^{-1} due to ν_{as}(O=Mo=O) and ν_s(O=Mo=O), respectively.[13,14] This indicates the O=Mo=O species to be in the *cis* form as the *trans*-O=Mo=O species would exhibit only a single band in this region.[15,16] In the case of complex **6b** the peaks at 891 and 955 cm^{-1} due to the O=Mo=O species show a split, indicating the presence of two O=Mo=O moieties, one of which is probably present in a slightly different coordination environment. However, only two strong peaks attributable to *cis*-MoO_2^{2+} were seen in complex **7b**. The observed carbon, hydrogen and nitrogen analysis data for complexes **6b** and **7b** fit the ligand-bridged dinuclear complexes only. From the absence of new peaks in the regions 750–770 and 460–490 cm^{-1} in their IR spectra, the possibility of the formation of $\{O_2Mo—O—MoO_2\}^{4+}$ type[14] complexes could be excluded. Further, in the IR spectra of complexes **6b** and **7b** one new peak appeared at 844 and 854 cm^{-1}, respectively. This may be attributed to the M—OC_2H_5 vibration.[13]

The formation of a dinuclear complex may be due to the *para* position of the azomethine nitrogens in **6a** (PMBP-*p*-phd) and **7a** (PMBP-bz), wherein coordination of both azomethine nitrogens to the same metal atom is difficult. In complexes **1b–7b** the bands in the region 1592–1647 cm^{-1} due to the azomethine group of the ligand undergo a shift to lower frequency[17] (1574–1616 cm^{-1}) after complexation, indicating the coordination of azomethine nitrogen to molybdenum. In complex **5b** the ligand **5a** behaves as a tridentate ligand, one of the azomethine nitrogens being unable to coordinate to the metal due to its *meta* position. This is shown by the presence of ν(C=N) at 1647 cm^{-1} (as in the ligand) and the appearance of a new band at 1629 cm^{-1} due to coordinated ν(C=N). The coordination of both the azomethine nitrogens in **5b** to the same metal centre requires the bending of bonds of the phenylenediamine ring. In complex **5b** the band due to ν(C=O) at 1657 cm^{-1} is absent, indicating the enolization of the C=O group.[18] Instead, a new band appears at 1173 cm^{-1} due to coordinated ν(C—O)(enolic). The coordination of enolic oxygen to the metal centre in complexes **1b–6b** is indicated by the increase in ν(C—O) (1166–1180 cm^{-1}) compared with that of the free ligand (1137–1165 cm^{-1}).[11] The cyclic carbonyl coordination to the metal centres in **7b** is indicated by the decrease[19] in ν(C=O) (1635 cm^{-1}) compared with that of the free ligand (1642 cm^{-1}).[18]

The electronic spectra of complexes **1b–7b** (Table 1) were studied in the concentration range 1×10^{-4}–

1×10^{-3} M in acetone (**1b–3b**) and DMF (**4b–7b**). For the bidentate Schiff base complexes (**1b–3b**) a blue shift (327–332 nm) was observed for the ligand band at 347 nm. All the complexes (**1b–7b**) show an additional intense band in the region 424–443 nm, which may be due to ligand-to-metal charge transfer transitions. In the cases of the tetradentate Schiff base complexes **4b–7b**, except **5b**, an additional broad band of low intensity was also observed in the region 680–730 nm. The band appearing at such a low energy is unexpected for $4d^0$ molybdenum(VI) complexes. However, this has also been observed in the case of the tetradentate Schiff base complex *cis*-MoO_2(3-OCH_3-Saltrien).[20]

The mononuclear and dinuclear *cis*-MoO_2(VI) Schiff base complexes were found to be diamagnetic by ^{1}H NMR spectroscopy. The chemical shifts of various protons of the ligands in the molybdenum(VI) complexes **1b–7b** are shown in Table 1. The absence of —OH protons in complexes **1b–6b** suggests coordination through the enolic oxygen to the metal centre. The presence of —CH protons (δ 2.13 ppm) in complex **7b** suggests coordination through the cyclic carbonyl to the metal centre. In the case of complexes **6b** and **7b** the signals due to $-CH_3$ and $-CH_2$ protons (of OC_2H_5) appear as a quartet and a triplet in the regions 2.73–3.09 and 1.23–1.37 ppm, respectively, indicating coordination of the ethoxo group to the metal centre. Further, in the spectrum of complex **7b** two quartets and two triplets are seen in this region, indicating the variation in coordination environment of the two ethoxo groups per metal atom.

The cyclic voltammograms (scan range +1.3 to −1.5 V) vs Ag/AgCl for the bidentate Schiff base complexes **1b–3b** in acetone consist of an irreversible reduction wave at −1.01 V (±0.02 V) vs Ag/AgCl (Fig. 1). When cyclic voltammetry for these complexes was performed in DMF the irreversible reduction wave was found to shift to positive potentials (*ca* 0.05–0.1 V). This irreversible process is attributed to Mo^{VI}/Mo^{V} reduction.[21,22] The reoxidation of Mo^{V} to Mo^{VI} was not observed in **1b–3b**, instead dimerization of Mo^{V} species was seen, forming Mo^{V}—O—Mo^{V}, for which an oxidation wave was observed at +0.2 V (±0.02 V). However, on increasing the scan rate (0.1–2.5 V s^{-1}) it was seen that the anodic peak current at +0.2 V diminished and simultaneously the reoxidation wave of Mo^{V} to Mo^{VI} at −0.95 V tended to appear, especially at the highest scan rate used in this study. Such dimerization of molybdenum(V) species is well known.[22] However, when the scan was reversed at a potential relatively positive to the reduction wave at −1.01 V the oxidation peak at +0.2 V was not seen, indicating that the peak at +0.2 V is a consequence of the reduction peak at −1.01. The cyclic voltammetry of complexes **4b–7b**, except **5b**, showed a reversible redox couple at $E_{1/2} = 0.55$ V[22] (±0.02 V, $0.07 < \Delta E < 0.1$ V) (Fig. 1). In complex **5b** an irreversible reduction ($Mo^{VI} \rightarrow Mo^{V}$) wave was seen at −0.88 V. The reversible redox couple is attributed to $Mo^{VI} \rightarrow Mo^{V}$ reduction and reoxidation to Mo^{VI} in **4b**, **6b** and **7b**. Comparison of the cyclic voltammetry data of the bi- and tetradentate Schiff base complexes **1b–7b** reveals that the $Mo^{VI} \rightarrow Mo^{V}$ reduction is not only facile, but also reversible in the case of tetradentate Schiff base complexes. This may be due to the change in ligand structure,[23,24] wherein the phenylenediamine ring in the ligands **4a–7a** appears to delocalize the electron density effectively from the metal centre causing its easier reduction. In the bidentate Schiff base complexes it appears that the added electron during $Mo^{VI} \rightarrow Mo^{V}$ reduction is located on one of the Mo=O bonds (due to poor delocalization by the bidentate Schiff base ligand) and thus the reduced species may participate in the proton equilibrium leading to dimerization.

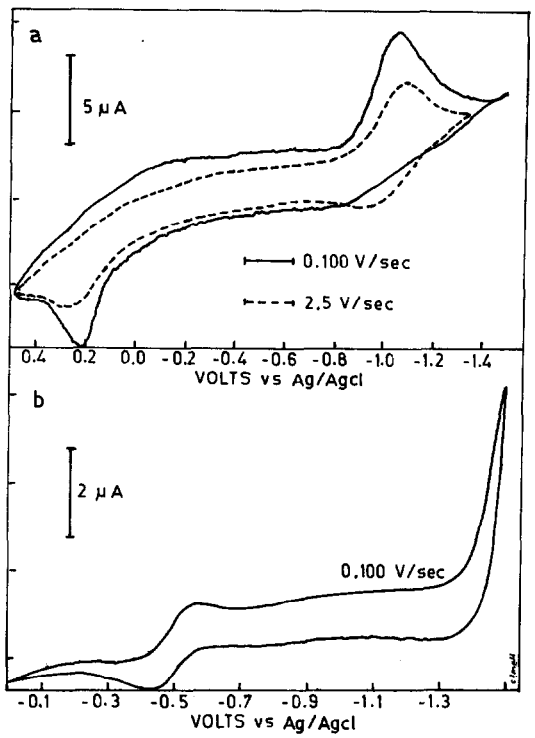

Fig. 1. Cyclic voltammograms of (a) MoO_2(PMBP-P)$_2$, representing bidentate Schiff base complexes, and (b) Mo_2O_4(PMBP-bz)$(C_2H_5O^-)_4$ (**7b**), representing tetradentate Schiff base complexes.

Thus, on the basis of the above data it is evident that the ligands coordinate through the azomethine nitrogen and enolic oxygen to the central metal

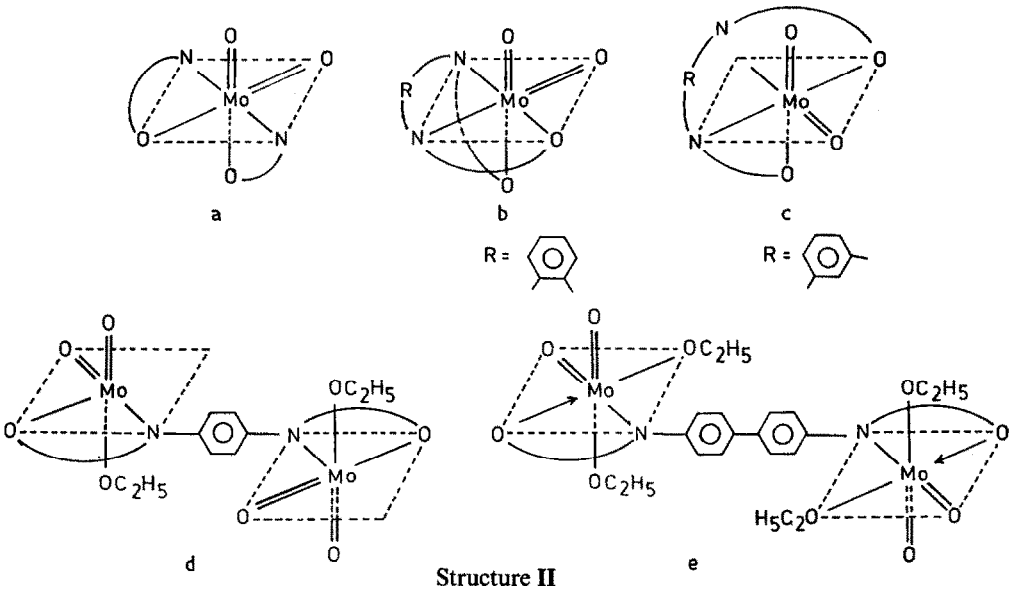

Structure II

atom in complexes **1b–6b** and through the cyclic carbonyl in **7b**. Complexes **6b** and **7b** are dinuclear complexes bridging through the azomethine nitrogen. In general, the structure of the bidentate Schiff base complexes *cis*-MoO_2^{VI} (**1b–3b**) can be represented as shown in structure **IIa**. The six- and five-coordinate complexes **4b** and **5b** can be written as shown in structures **IIb** and **IIc**, respectively. The binuclear five- and six-coordinate bridging complexes **6b** and **7b** can be represented as shown in structures **IId** and **IIe**, respectively. For complexes **6b** and **7b** the structures **IId** and **IIe** are preferred, wherein the two MoO_2 moieties are *trans* with respect to phenylenediamine and benzidine rings, in which the steric hindrance of the *p*-hydrogens of the phenyl rings attached to azomethine carbons is avoided. Efforts were made to obtain the crystals of these molybdenum(VI) complexes to study their X-ray crystallography, but due to their poor solubility in most of the organic solvents the desired results could not be attained. However, the work is still being continued in the same direction to obtain positive results.

Acknowledgements—NSR is grateful to CSIR for awarding a Research Associateship. The authors thank Prof. Natrajan, Director, CSMCRI, Bhavnagar, for providing analytical facilities.

REFERENCES

1. J. Topich and J. O. Bachert, *Inorg. Chem.* 1992, **31**, 511.
2. J. Topich and J. T. Lyon, *Polyhedron* 1984, **3**, 55.
3. A. Clearfield, A. Moini and P. R. Rudolf, *Inorg. Chem.* 1985, **24**, 4606.
4. A. Syamal and M. R. Maurya, *Ind. J. Chem.* 1986, **25A**, 1152.
5. J. K. Kochi, *Organometallic Mechanism and Catalysis*, Ch. II. Academic Press, New York (1978).
6. M. S. Reynolds, J. M. Berg and R. H. Holm, *Inorg. Chem.* 1984, **23**, 3057.
7. R. N. Mohanty and K. C. Dash, *Polyhedron* 1990, **9**, 1011.
8. O. A. Rajan and A. Chakravorty, *Inorg. Chem.* 1981, **20**, 660.
9. W. C. Fernelius, K. Terada and B. E. Bryant, *Inorg. Synth.* 1960, **6**, 147.
10. H. C. Arora and G. N. Rao, *Ind. J. Chem.* 1981, **20A**, 1539.
11. R. C. Maurya, D. D. Mishra, N. Sumita Rao and N. Nageswara Rao, *Polyhedron* 1992, **2**, 2837.
12. G. J. J. Chen, J. W. McDonald and W. E. Newton, *Inorg. Chem.* 1976, **15**, 2612.
13. A. Syamal and M. R. Maurya, *Coord. Chem. Rev.* 1989, **95**, 183.
14. C. Pickett, S. Kumar, P. A. Vella and J. Zubieta, *Inorg. Chem.* 1982, **21**, 908.
15. M. L. Larsen and F. W. Moore, *Inorg. Chem.* 1986, **5**, 80.
16. J. Goffart, J. P. Mevnier and G. Duyckaerto, *Inorg. Nucl. Chem. Lett.* 1980, **14**, 233.
17. S. Yamada, *Coord. Chem. Rev.* 1966, **1**, 415.
18. A. Syamal and K. S. Kale, *Ind. J. Chem.* 1978, **16A**, 46.
19. N. Sumita Rao, D. D. Mishra, R. C. Maurya and N. Nageswara Rao, *Trans. Met. Chem.* 1993, submitted.
20. M. Gulloti, A. Pasini and G. M. Sanderight, *J. Chem. Soc., Dalton Trans.* 1981, 902.
21. J. Topich, *Inorg. Chem.* 1981, **20**, 3704.
22. R. D. Taylor, J. P. Street, M. Minelli and J. T. Spence, *Inorg. Chem.* 1978, **17**, 3207.
23. D. A. Smith and F. A. Schultz, *Inorg. Chem.* 1982, **21**, 3035.
24. G. S. Patterson and R. H. Holm, *Inorg. Chem.* 1972, **11**, 2285.

Polyhedron Vol. 12, No. 16, pp. 2051–2056, 1993
Printed in Great Britain

0277–5387/93 $6.00+.00
© 1993 Pergamon Press Ltd

THE CRYSTAL AND MOLECULAR STRUCTURE OF (η^5-PENTAPHENYLCYCLOPENTADIENYL) (η^5-CYCLOPENTADIENYL)IRON(II), 1,2,3,4,5-PENTAPHENYLFERROCENE, [Fe(C_5Ph_5)(C_5H_5)]

M. J. ARONEY, I. E. BUYS, G. D. DENNIS, L. D. FIELD,* T. W. HAMBLEY, P. A. LAY and A. F. MASTERS*

Departments of Inorganic and Organic Chemistry, University of Sydney, NSW 2006, Australia

(*Received* 10 *February* 1993; *accepted* 30 *March* 1993)

Abstract—The preparation and characterization of [Fe(C_5Ph_5)(C_5H_5)] by single-crystal X-ray diffraction are reported. The compound crystallizes from chlorobenzene as a chlorobenzene solvate. The (C_5H_5) ring is planar to within 0.002 Å, whilst the C_5 ring of the (C_5Ph_5) ligand is planar to within 0.004 Å. The Fe—(ring centroid) distances are both 1.652 Å. The phenyl substituents of the (C_5Ph_5) ring are canted relative to the cyclopentadienyl frame at angles between 44.3° and 61.8°. The structure of [Fe(C_5Ph_5)(C_5H_5)] is compared with the structures of ferrocene, 1,2,3,4,5-pentamethylferrocene and 1,2,3,4,5-penta(*p*-tolyl) ferrocene. The synthesis and characterization of [Fe(C_5Ph_5)$(CO)_2]_2$ is also reported. [Fe(C_5Ph_5)$(CO)_2]_2$ is assigned a *trans* configuration on the basis of its IR spectrum.

Complexes of the pentaphenylcyclopentadienyl ligand are of considerable current interest, particularly in the context of the emerging field of supracyclopentadienyl chemistry.[1,2] The ligand is capable of conferring novel steric and electronic properties on metal centres. Thus, for example, the two parallel C_5 planes of [Sn(C_5Ph_5)$_2$] contrast with the bent structures of [Sn(C_5H_5)$_2$] and [Sn(C_5Me_5)$_2$].[3–5] [(C_5Ph_5)PdNO] is a purple solid, indefinitely stable at room temperature under dinitrogen, whereas the red oil [(C_5H_5)PdNO] is reported to be unstable at room temperature under an argon atmosphere.[6–8] Diamagnetic decaphenylnickelocene contrasts with paramagnetic nickelocene;[9–11] the dimer [{Ni(μ-Br)(C_5R_5)}$_2$] is unknown for R = H, must be stored below +10°C for R = Me and melts with decomposition above 200°C when R = Ph,[12] and the pentaphenylcyclopentadienyl anion stabilizes 17-, 19- and 20-electron species.[13–15] To date, the crystal structures of pentaphenylcyclopentadiene,[16] pentaphenylcyclopentadien-1-ol[17] and 14 complexes of the pentaphenylcyclopentadienyl anion have been reported.[3,12,18–28] Of these complexes only [Sn(C_5Ph_5)$_2$] has more than one pentaphenylcyclopentadienyl anion coordinated to a single metal atom and only [Ti(C_5Ph_5)(C_5H_5)Cl_2] and [Sn(C_5Ph_5)(C_5H_5)] have an additional cyclopentadienyl ligand. The crystal structure of the closely related [Fe(C_5(*p*-tol)$_5$)(C_5H_5)] has been reported recently.[29] However, there have been few opportunities to study the comparative structural chemistry of the ligands $(C_5R_5)^-$ (R = H, Me, *p*-tol, Ph) in analogous compounds.

We report here the structure and additional properties of pentaphenylferrocene, [Fe(C_5Ph_5)(C_5H_5)], and a comparison with the structures of the complexes [Fe(C_5R_5)(C_5H_5)] (R = H, Me, *p*-tol) and [Fe(C_5Ph_5)$(CO)_2$)Br].[20,29–31] In the course of synthesizing [Fe(C_5Ph_5)(C_5H_5)] we have unexpectedly prepared a pure sample of the elusive [Fe(C_5Ph_5)$(CO)_2]_2$, which is also reported here.

RESULTS AND DISCUSSION

[Fe(C_5Ph_5)(C_5H_5)] was prepared by thermolysis of the product of the reaction between [Fe(C_5Ph_5)$(CO)_2$Br] and cyclopentadienylsodium, as reported

* Authors to whom correspondence should be addressed.

previously.[32] We have recently reported that $[Fe(C_5(p\text{-tolyl})_5)(\eta^1\text{-}C_5H_5)(CO)_2]$ can be isolated as a deep red, air-stable solid from the reaction between $[Fe(C_5(p\text{-tolyl})_5)(CO)_2Br]$ and cyclopentadienyl sodium and is thermally converted to $[Fe(C_5(p\text{-tolyl})_5)(\eta^5\text{-}C_5H_5)]$.[29] The preparation of $[Fe(C_5Ph_5)(C_5H_5)]$ presumably follows an analogous route, as postulated previously by Pauson.[32] At a scan rate of 100 mV s^{-1} $[Fe(C_5Ph_5)(C_5H_5)]$ undergoes a reversible oxidation at $E_{1/2} = +0.240$ V ($\Delta E_p = 65$ mV) and a quasi-reversible reduction at $E_{1/2} = -1.491$ V ($\Delta E_p = 132$ mV). The stabilization of $[Fe(C_5Ph_5)(C_5H_5)]^-$ is unusual for ferrocene and its substituted derivatives and the reduction is almost certainly due to a small equilibrium concentration of the linkage isomer $[Fe(\eta^6\text{-}C_6H_5(C_5Ph_4))(C_5H_5)]$. The analogous compound, $[Fe(\eta^6\text{-}C_6H_5(C_5Ph_4))(\eta^5\text{-}C_5Ph_5)]$, is known[33] and the reduction potential of -1.49 V is typical of those observed for $[Fe(\eta^6\text{-arene})(\eta^5\text{-}C_5Ph_5)]^+$ complexes.[28] Since the reduction of $[Fecp_2]$ complexes typically occurs at *ca* -3 V,[34] it is most likely that the linkage isomer is responsible for the observed reduction behaviour. This can be explained by the processes of Scheme 1, in which the linkage isomerization occurs as a rapid pre-equilibrium and favours the parent complex, $[Fe(C_5Ph_5)(C_5H_5)]$, in the iron(II) oxidation state and the linkage isomer, $[Fe(\eta^6\text{-}C_6H_5(C_5Ph_4))(C_5H_5)]^-$ in the iron(I) oxidation state.

$[Fe(C_5Ph_5)(C_5H_5)]$ has a small (1.3 D) but significant dipole moment. It is not possible to differentiate between the dipole moments of $[Fe(C_5R_5)(C_5H_5)]$ (R = Me,[35] Ph) on the basis of the precision of the present measurements. 1,2,3,4,5-Pentamethylferrocene was shown by microwave absorption measurements to have a small (0.90 D) dipole moment directed along the molecular symmetry axis from the pentamethylcyclopentadienyl ligand towards the cyclopentadienyl ligand (at the negative end of the dipole), in accord with the electron donating properties of methyl groups.[35] The finite dipole moment of pentaphenylferrocene suggests that a small amount of electron charge transmission occurs between the substituent phenyl groups and the ferrocene system. The electrochemical results suggest that the phenyl groups are electron withdrawing and hence that the pentaphenylcyclopentadienyl ligand is at the negative end of the dipole.

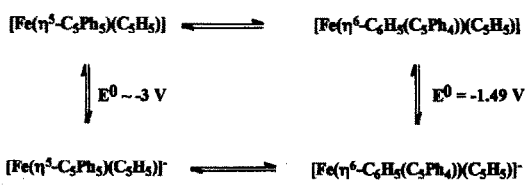

Scheme 1.

During an attempted preparation of $[Fe(C_5Ph_5)(CO)_2Br]$ a green crystalline solid which analysed as $[Fe(C_5Ph_5)(CO)_2]_2$ was isolated. The compound is assigned as *trans*-$[Fe(C_5Ph_5)(CO)_2]_2$ on the basis of its IR spectrum.[36] Although observed as a transitory species in the past,[32,37] pure *trans*-$[Fe(C_5Ph_5)(CO)_2]_2$ has not hitherto been isolated. The preparation of *trans*-$[Fe(C_5Ph_5)(CO)_2]_2$ by this route is not reproducible and the mechanism of its formation during the synthesis of $[Fe(C_5Ph_5)(CO)_2Br]$ is unclear. The most obvious difference in the preparations of the two materials is that $[Fe(C_5Ph_5)(CO)_2Br]$ is produced after 2 h reflux, whereas *trans*-$[Fe(C_5Ph_5)(CO)_2]_2$ was isolated after a similar solution had been refluxed for 18 h.

$[Fe(C_5Ph_5)(C_5H_5)]$ crystallizes as discrete molecules in which the iron atom is sandwiched between two near parallel five-membered rings. Final atomic positional coordinates, with estimated standard deviations, bond lengths and angles and anisotropic thermal parameters are deposited.* Selected interatomic bond distances and angles, with standard deviations derived from the refinement, are given in Tables 1 and 2. The atomic nomenclature is defined in Fig. 1. Figures 1 and 2 illustrate the molecular geometry viewed along, and perpendicular to, the normal to the C_5 planes of the ligands, respectively.

No intermolecular contacts of significance were observed in the solid; the closest intermolecular non-bonding approach between molecules being 3.494 Å.

$[Fe(C_5Ph_5)(C_5H_5)]$ crystallizes as a chlorobenzene solvate. There are no significant contacts between the chlorobenzene and the $[Fe(C_5Ph_5)(C_5H_5)]$ molecules in the solid. Disorder of the

Table 1. Selected bond lengths (Å) for $[Fe(C_5Ph_5)(C_5H_5)]$

Atoms	*d* (Å)	Atoms	*d* (Å)
C(1)—Fe(1)	2.051(4)	C(2)—Fe(1)	2.060(3)
C(3)—Fe(1)	2.055(3)	C(4)—Fe(1)	2.057(3)
C(5)—Fe(1)	2.056(3)	C(6)—Fe(1)	2.054(4)
C(7)—Fe(1)	2.069(4)	C(8)—Fe(1)	2.042(5)
C(9)—Fe(1)	2.023(5)	C(2)—C(3)	1.434(5)

* The atomic coordinates and thermal parameters have been submitted as supplementary material for deposition at the Cambridge Crystallography Data Centre (see deposition of crystallographic data).

Table 2. Selected bond angles (°) for $[Fe(C_5Ph_5)(C_5H_5)]$

Atoms	Angle (°)	Atoms	Angle (°)
C(2)—Fe(1)—C(1)	41.1(1)	C(3)—Fe(1)—C(1)	69.0(1)
C(3)—Fe(1)—C(2)	40.8(1)	C(4)—Fe(1)—C(1)	69.0(1)
C(4)—Fe(1)—C(2)	68.8(1)	C(4)—Fe(1)—C(3)	40.9(1)
C(5)—Fe(1)—C(1)	41.1(1)	C(5)—Fe(1)—C(2)	69.0(1)
C(5)—Fe(1)—C(3)	68.9(1)	C(5)—Fe(1)—C(4)	40.9(1)
C(6)—Fe(1)—C(1)	116.2(2)	C(6)—Fe(1)—C(2)	109.5(2)
C(6)—Fe(1)—C(3)	131.9(2)	C(6)—Fe(1)—C(4)	170.5(2)
C(6)—Fe(1)—C(5)	148.1(2)	C(7)—Fe(1)—C(1)	149.2(2)
C(7)—Fe(1)—C(2)	117.7(2)	C(7)—Fe(1)—C(3)	110.2(2)
C(7)—Fe(1)—C(4)	131.7(2)	C(7)—Fe(1)—C(5)	169.4(2)
C(7)—Fe(1)—C(6)	40.1(2)	C(8)—Fe(1)—C(1)	168.3(2)
C(8)—Fe(1)—C(2)	149.9(2)	C(8)—Fe(1)—C(3)	117.5(2)
C(8)—Fe(1)—C(4)	108.9(2)	C(8)—Fe(1)—C(5)	130.0(2)
C(8)—Fe(1)—C(6)	67.6(2)	C(8)—Fe(1)—C(7)	40.3(2)
C(9)—Fe(1)—C(1)	128.6(2)	C(9)—Fe(1)—C(2)	168.3(2)
C(9)—Fe(1)—C(3)	149.0(2)	C(9)—Fe(1)—C(4)	115.5(2)
C(9)—Fe(1)—C(5)	106.5(2)	C(9)—Fe(1)—C(6)	68.2(2)
C(9)—Fe(1)—C(7)	68.5(2)	C(9)—Fe(1)—C(8)	41.0(2)

chlorobenzene was obvious from the temperature factors. However, the type of disorder could not be deduced from the data refinement.

The $[Fe(C_5Ph_5)(C_5H_5)]$ *molecule*

The C_5 rings of $[Fe(C_5Ph_5)(C_5H_5)]$ are not significantly distorted from planarity (maximum deviation of the C_5C atoms from the C_5R_5 rings, 0.004 Å, R = C_6H_5; 0.002 Å, R = H). The two rings are almost parallel (angle between the normals to the rings 2.8°) and are nearly eclipsed in the solid state. All C—C bond distances are normal within statistical significance [av. 1.438 Å, (C_5Ph_5), 1.418 Å, (C_5H_5)], but may be slightly long by comparison with other iron cyclopentadienyl derivatives. Those of the $(C_5Ph_5)^-$ ligand are similar to those in $[Fe(C_5Ph_5)(CO)_2Br]$.[20] The bond angles within the C_5 rings are normal for the C_5 rings of cyclopentadienyl and substituted cyclopentadienyl derivatives. The Fe—(ring centroid) distances are 1.652 Å (C_5H_5) and 1.652 Å (C_5Ph_5), with the average Fe—C distances being 2.046 Å (C_5H_5) and 2.056 Å (C_5Ph_5). Thus, the separation between the ligand planes is 3.304 Å. These are within the ranges observed for substantially undistorted $[Fe(C_5R_5)$

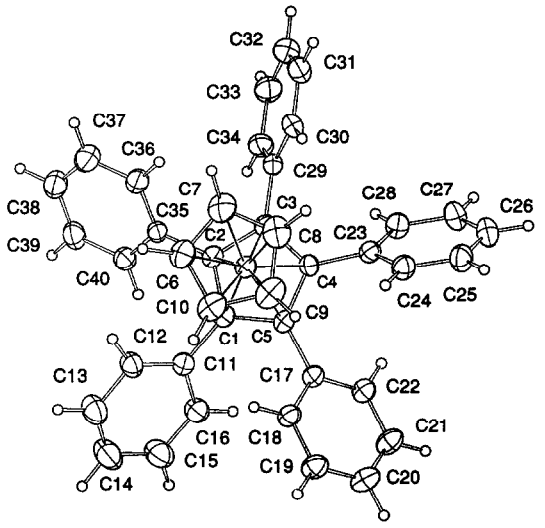

Fig. 1. ORTEP (50% probability) illustration of the molecular structure of $[Fe(C_5Ph_5)(C_5H_5)]$, showing the atom numbering. Viewed along the normal to the C_5Ph_5 plane.

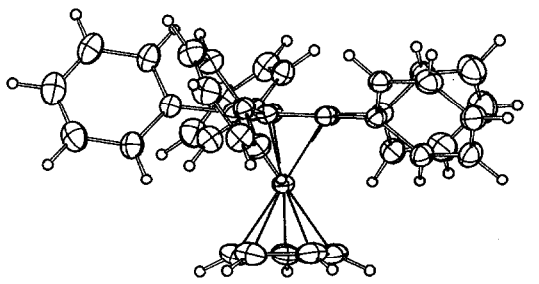

Fig. 2. ORTEP (50% probability) illustration of the molecular structure of $[Fe(C_5Ph_5)(C_5H_5)]$, showing the atom numbering. Viewed perpendicular to the normal to the C_5Ph_5 plane.

Table 3. Comparisons between $[Fe(C_5R_5)(C_5H_5)]$ (R = H, Me, *p*-tolyl, Ph)

Bond	Distance (Å) H[44]	Me[45]	*p*-tolyl[29]	Ph[a]
Fe—C_5H_5	1.654	1.663	1.660	1.651_8
Fe—C_5R_5	1.654	1.641	1.645	1.652_2
C_5H_5—C_5R_5	3.308	3.304(9)	3.305 Eclipsed	3.304 Eclipsed
C—C (C_5H_5)	1.389	1.399(6)	1.400	1.418
C—C (C_5R_5)	1.389	1.408(6)		1.438

[a] Ref: this work.

($C_5R'_5$)] derivatives [Fe—C *ca* 2.04 Å, Fe—(ring centroid) *ca* 1.645–1.66 Å] and outside the range observed for $[Fe(C_5H_5)L_1L_2L_3]$ derivatives [Fe—C *ca* 2.10 Å, Fe—(ring centroid) *ca* 1.74 Å]. The *ipso*-carbon atoms of each of the phenyl rings are displaced slightly from the C_5 plane by between 0.01 and 0.1 Å, with the average distance being 0.09 Å. These *ipso*-carbon atoms and the iron atom are on the opposite sides of the C_5 plane, similar to the configuration in $[Fe(C_5Ph_5)(CO)_2Br]$.[20] The phenyl rings are all also planar with normal dimensions and are oriented at between 44.3° and 61.8° to the C_5 ring of the $(C_5Ph_5)^-$ ligand. The average deviation of the phenyl rings from coplanarity with the C_5 ring of the $(C_5Ph_5)^-$ ligand is 52.0°. Selected bond distances of $[Fe(C_5R_5)(C_5H_5)]$ (R = H, Me, *p*-tolyl, Ph) are compared in Table 3.

EXPERIMENTAL

All synthetic manipulations were performed under an atmosphere of dinitrogen using standard inert-atmosphere techniques. All solvents used were analytical grade. Benzene (Merck) and THF (Merck) were pre-dried over sodium wire, distilled from sodium benzophenone ketyl under an atmosphere of dinitrogen and degassed for at least 30 min prior to use. Chlorobenzene (Fluka) was dried, distilled and stored over calcium hydride. Iron pentacarbonyl (Aldrich) was used as received. 1-Bromo-1,2,3,4,5-pentaphenylcyclopenta-2,4-diene was prepared as described previously.[38] Bromodicarbonylpentaphenylcyclopentadienyliron, $[Fe(C_5Ph_5)(CO)_2Br]$, was prepared by literature methods and was characterized spectroscopically.[20,32]

NMR spectra were recorded on a Bruker AC200F spectrometer. Spectra were referenced internally against the residual solvent resonances [CD_2Cl_2 ^1H NMR δ 5.30 ppm; ^{13}C NMR δ 54.20 ppm; $(CD_3)_2CO$ ^1H NMR δ 2.05 ppm]. IR spectra were recorded using a Digilab FTS-80 Fourier transform spectrometer with 20/80 FTS optics. Electrochemical experiments were performed using a BAS-100 electrochemical analyser. Data were transferred to an Osborne-PC Executive Microcomputer using BAS File Transfer software. A three-electrode configuration was used. The working electrode was a BAS glassy carbon disc (3 mm diameter), which was polished with an alumina (0.25 μm grade) suspension before each cyclic voltammogram was recorded. The auxiliary electrode was a platinum wire (0.5 mm diameter, 4 cm length) and the reference electrode was a BAS Ag/AgCl/KCl(sat.) electrode. All samples were thoroughly degassed with high purity argon (CIG), which was prebubbled through a Cr^{2+} scrubber (0.2 M Cr^{2+}/0.5 M $HClO_4$) and a sulphuric acid (18 M) bubbler tower to remove any traces of oxygen and water, respectively. All potentials are quoted relative to the ferrocinium/ferrocene redox couple, which was observed at +627 mV against the reference electrode. Samples were examined as *ca* 1 mM solutions in THF with tetra(1-butyl) ammonium tetrafluoroborate (*ca* 0.1 M) as the supporting electrolyte. The tetra(1-butyl) ammonium tetrafluoroborate was prepared from tetrafluoroboric acid (35% (v/v) Merck) and aqueous tetra(1-butyl)ammonium hydroxide (40% (w/w) Aldrich).

Solution densities were determined using a Paar precision density meter, model DMA-602 at 25.00 ± 0.01°. Refractive indices of solutions at the sodium D-line were determined using an Abbe 60 refractometer at 25.00 ± 0.05°. Solution dielectric constants were determined by measuring the capacitance at 100 kHz of a condenser filled alternatively with sample solution, solvent and air. A heterodyne beat method was used with a Sullivan precision variable condenser and a glass and nickel cell at 25.00 ± 0.05°.

X-ray diffraction data were recorded using an Enraf–Nonius CAD4-F diffractometer with Mo-K_α radiation, λ = 0.71069 Å.

Melting points were recorded on a Reichert hot platform in air and are uncorrected.

Synthesis of 1,2,3,4,5-*pentaphenylferrocene*

1,2,3,4,5-Pentaphenylferrocene was prepared following a variation on the procedure of McVey and Pauson.[32] A THF solution of cyclopentadienylsodium (2 cm^3, 0.15 g, 6.5 mmol sodium, 0.44 g, 6.8 mmol cyclopentadiene) was added to a stirred solution of $[Fe(C_5Ph_5)(CO)_2Br]$ (4.0 g, 6.3 mmol) in THF (75 cm^3) at room tem-

perature. After 3 h the solution was filtered and the solvent stripped from the filtrate. The combined dried solids were heated at 200°C under vacuum for 5 h and the cooled residue extracted with hot benzene (250 cm^3). The extract was filtered and the solvent evaporated to produce an orange–brown residue with weak IR absorptions at 2007 and 1955 cm^{-1}, consistent with the presence of a small amount of [Fe(η^5-C_5Ph_5)(η^1-C_5Ph_5)$(CO)_2$].[32] The products were separated by chromatography on flash silica (60–400 mesh) using a 1 : 1 (v/v) mixture of petroleum ether (40/60) and benzene as an eluent. The orange fraction, pentaphenylferrocene, was separated from colourless pentaphenylcyclopentadiene by fractional crystallization from chlorobenzene. After several recrystallizations from chlorobenzene, pentaphenylferrocene was obtained as orange tubular crystals, which were suitable for X-ray crystal structure analysis. Yield 2.04 g, 57%; m.p. >300°C (lit.[32] 356–358°C). ^{1}H NMR (CD_2Cl_2, 200.13 MHz): δ 7.1–7.0 (m, 25H, Ar—*H*), 4.3 (s, 5H, C_5H_5) ppm. ^{13}C NMR (CD_2Cl_2, 50.33 MHz): δ 136.6 (quaternary Ar—*C*) 132.7, 127.5, 126.5 (Ar—*C*H). 88.2 (quaternary Cp—*C*), 75.4 (C_5H_5) ppm. IR (KBr) ν_{max}: 1599(m), 1502(s), 1478(w), 1443(m), 1402(s), 1108(w), 1073(w), 1027(w), 1005(w), 814(m), 801(w), 742(s), 709(s), 699(s), 688(m) cm^{-1}.

Synthesis of trans-*bis(pentaphenylcyclopentadienyl)di(μ-carbonyl)dicarbonyldiiron*

A solution of pentaphenylcyclopentadienyl bromide (5.00 g, 9.55 mmol) was prepared by stirring the solid in freshly distilled benzene (100 cm^3) under an atmosphere of nitrogen for 4 h. Iron pentacarbonyl (2.4 g, 12 mmol) was added via a syringe to the orange solution. The deep purple colour characteristic of the pentaphenylcyclopentadienyl radical rapidly developed. The reaction mixture was refluxed for 18 h and cooled to room temperature to give an extremely deep green solution and a fine precipitate, which was separated by filtration. The solvent was stripped from the green filtrate leaving a brown solid, which was identified as [Fe(η^5-C_5Ph_5)$(CO)_2$Br] on the basis of its IR spectrum.[20] The residue in the reaction flask was a layered mixture of an orange–brown solid and a deep green microcrystalline solid. A sample of the green solid was mechanically separated, thoroughly dried under high vacuum and analysed by elemental analysis, IR and ^{1}H NMR spectroscopy. This sample was not sufficiently stable in solution to permit the acquisition of a ^{13}C NMR spectrum. The green material was formulated as the iron dimer, *trans*-[Fe(η^5-C_5Ph_5)$(CO)_2$]$_2$. Yield *ca* 0.4 g, 8%; m.p. 215–20°C (dec.). Found: C, 79.5; H, 4.7. Calc. for $C_{74}H_{50}Fe_2O_4$: C, 79.7; H, 4.5%. ^{1}H NMR [$(CD_3)_2CO$, 200.13 MHz]: δ 7.2–7.0 (m, Ar—*H*), 2.8 (s, broad) ppm. IR (KBr) ν_{max}: 2033(w), 1951(vs), 1913(m), 1787(vs), 1754(m), 1601(w), 1503(m), 1475(w), 1444(m), 1402(m), 1182(w), 1076(w), 1023(w), 802(w), 741(s), 703(s), 679(s), 597(s) cm^{-1}.

Structure determination

Cell constants were determined by a least squares fit to the θ values of 25 independent reflections, measured and refined on an Enraf–Nonius CAD-4 diffractometer with a graphite monochromator. Data were reduced and Lorentz, polarization and decomposition corrections were applied using the Enraf–Nonius Structure Determination Package.[39] The structure was solved by direct methods within the SHELXS-86 program.[40] Non-hydrogen atoms were refined anisotropically and hydrogen atoms were included at calculated sites (C—H 0.97 Å) with group isotropic thermal parameters. Blocked-matrix least-squares refinement was performed using the program SHELX-76.[41] Scattering factors and anomalous dispersion corrections for iron were taken from the International Tables,[42] and for all others the values supplied in SHELX-76 were used. Full tables of bond lengths and angles and listing of atom coordinates, thermal parameters, details of least-squares planes calculations and observed and calculated structure factor amplitudes have been deposited.* Figures were drawn using the program ORTEP.[43]

Crystal data

$C_{40}H_{30}Fe$, M = 566.5, monoclinic, space group, $C_{2/c}$, a = 42.646(8), b = 10.314(3), c = 14.655(4) Å, β = 96.16(2), U = 6408 $Å^3$, D_c (Z = 8) = 1.178 g cm^{-3}, $F(000)$ = 2368, μ(Mo-K_α) = 4.93 cm^{-1}. Specimen: orange tubes, 0.073 × 0.138 × 0.47 mm. N = 6315, N_0 = 3602, range of *hkl* $-50 \rightarrow 50$, $0 \rightarrow 12$, $0 \rightarrow 17$, merging R = 0.04, R = 0.048, R_w = 0.050, residual extrema +0.5011 and −0.3441 e $Å^3$.

Acknowledgements—We thank the Australian Research Council for financial support and Mr C. M. Lindall and Mr M. S. Davies for experimental assistance and helpful discussion.

* See footnote to p. 2052.

REFERENCES

1. C. Janiak and H. Schumann, *Adv. Organomet. Chem.* 1991, **33**, 291.
2. H. Schumann, *Pure Appl. Chem.* 1991, **63**, 813.
3. M. J. Heeg, C. Janiak and J. J. Zuckerman, *J. Am. Chem. Soc.* 1984, **106**, 4259.
4. J. L. Atwood, W. E. Hunter, A. H. Cowley, R. A. Jones and C. A. Stewart, *J. Chem. Soc., Chem. Commun.* 1981, 925.
5. P. Jutzi, F. Kohl, P. Hofmann, C. Kruger and Y. H. Tsay, *Chem. Ber.* 1980, **113**, 757.
6. E. O. Fischer and A. Volger, *Z. Naturforsch. B* 1963, **18**, 771.
7. E. O. Fischer and H. Schuster-Woldan, *Z. Naturforsch. B* 1964, **19**, 766.
8. T. R. Jack, C. J. May and J. Powell, *J. Am. Chem. Soc.* 1977, **99**, 4707.
9. G. Wilkinson, P. L. Pauson and F. A. Cotton, *J. Am. Chem. Soc.* 1954, **76**, 1970.
10. K. W. Barnett, *J. Organomet. Chem.* 1974, **78**, 139.
11. A. Schott, H. Schott, G. Wilke, J. Brandt, H. Hoberg and E. G. Hoffmann, *Liebigs Ann. Chem.* 1973, 508.
12. W. Klaui and L. Ramacher, *Angew. Chem., Int. Edn Engl.* 1986, **25**, 97.
13. F. Mao, C. E. Phibin, T. J. R. Weakley and D. R. Tyler, *Organometallics* 1990, **9**, 1510.
14. W. Klaui, M. Huhn and R. Herbst-Irmer, *J. Organomet. Chem.* 1991, **415**, 133.
15. R. J. Hoobler, M. A. Hutton, M. M. Dillard, M. P. Castellani, A. L. Rheingold, A. L. Rieger, P. H. Rieger, T. C. Richards and W. E. Geiger, *Organometallics* 1993, **12**, 116.
16. L. D. Field, T. W. Hambley, C. M. Lindall and A. F. Masters, *Inorg. Chem.* 1992, **31**, 2366.
17. C. M. Lindall, PhD Thesis, University of Sydney (1992).
18. U. Thewalt and G. Schmidt, *J. Organomet. Chem.* 1991, **412**, 343.
19. C. Janiak, M. Schwichtenberg and F. E. Hahn, *J. Organomet. Chem.* 1989, **365**, 37.
20. L. D. Field, T. W. Hambley, C. M. Lindall and A. F. Masters, *Polyhedron* 1989, **8**, 2425.
21. J. W. Chambers, A. J. Baskar, S. G. Bott, J. L. Atwood and M. D. Rausch, *Organometallics* 1986, **5**, 1635.
22. J. Powell and N. I. Dowling, *Organometallics* 1983, **2**, 1742.
23. D. W. Slocum, M. Matusz, A. Clearfield, R. Peascoe and S. Duraj, *J. Macromol. Sci., Chem.* 1990, **27A**, 1405.
24. H. Adams, N. A. Bailey, A. F. Browning, J. A. Ramsden and C. White, *J. Organomet. Chem.* 1990, **387**, 305.
25. E. Ban, P.-T. Cheng, T. Jack, S. C. Nyburg and J. Powell, *J. Chem. Soc., Chem. Commun.* 1973, 368.
26. U. Behrens and F. Edelmann, *Z. Naturforsch. B* 1986, **41**, 1426.
27. H. Hoberg, R. Krause-Going, C. Kruger and J. C. Sekutowski, *Angew. Chem., Int. Edn Engl.* 1977, **16**, 183.
28. L. D. Field, T. W. Hambley, P. A. Lay, C. M. Lindall and A. F. Masters, *J. Chem. Soc., Dalton Trans.* 1991, 1499.
29. L. D. Field, A. F. Masters, M. Gibson, D. R. Latimer, T. W. Hambley and I. E. Buys, *Inorg. Chem.* 1993, **32**, 211.
30. P. Seiler and J. D. Dunitz, *Acta Cryst., Sect. B* 1979, **35**, 1068.
31. D. P. Freyberg, J. L. Robbins, K. N. Raymond and J. C. Smart, *J. Am. Chem. Soc.* 1979, **101**, 892.
32. S. McVey and P. L. Pauson, *J. Chem. Soc.* 1965, 4312.
33. K. N. Brown, L. D. Field, P. A. Lay, C. M. Lindall and A. F. Masters, *J. Chem. Soc., Chem. Commun.* 1990, 408.
34. V. V. Strelets, *Coord. Chem. Rev.* 1992, **114**, 1.
35. L. Phillips and S. W. Filipczuk, *J. Molec. Liq.* 1991, **47**, 261.
36. J. G. Bullitt, F. A. Cotton and T. J. Marks, *Inorg. Chem.* 1972, **11**, 671.
37. N. G. Connelly and I. Manners, *J. Chem. Soc., Dalton Trans.* 1989, 283.
38. L. D. Field, K. M. Ho, C. M. Lindall, A. F. Masters and A. G. Webb, *Aust. J. Chem.* 1990, **43**, 281.
39. Enraf–Nonius Structure Determination Package, Enraf–Nonius, Delft (1985).
40. G. M. Sheldrick, SHELXS-86. Oxford University Press, Oxford (1985).
41. G. M. Sheldrick, SHELX-76, A Program for X-Ray Structure Determination. University of Cambridge, Cambridge, U.K. (1976).
42. *International Tables for X-ray Crystallography*, Vol. IV. Kynoch Press, Birmingham (1974).
43. C. K. Johnson, ORTEP, a Thermal Elipsoid Plotting Program. Oak Ridge National Laboratories, Oak Ridge, Tennessee (1965).
44. P. Seiler and J. D. Dunitz, *Acta Cryst., Sect. B* 1979, **35**, 1068.
45. D. P. Freyberg, J. L. Robbins, K. N. Raymond and J. C. Smart, *J. Am. Chem. Soc.* 1979, **101**, 892.

Polyhedron Vol. 12, No. 16, pp. 2057–2062, 1993
Printed in Great Britain

0277–5387/93 $6.00+.00
© 1993 Pergamon Press Ltd

DINUCLEAR RUTHENIUM(III) COMPLEXES AND THEIR REACTIONS WITH CO AND NOCl: SYNTHESIS, CHARACTERIZATION AND ELECTROCHEMICAL STUDIES

PARIMAL PAUL

Discipline of Coordination Chemistry and Homogeneous Catalysis, Central Salt and Marine Chemicals Research Institute, Bhavnagar 364002, India

(*Received* 5 *January* 1993; *accepted* 30 *March* 1993)

Abstract—A series of dinuclear ruthenium(III) complexes was synthesized by the reaction of $RuCl_3(AsPh_3)_2MeOH$ with the hexadentate ligands BDPE, BDAE and BDPX, with N_2P_4/N_2As_4 donor sites [BDPE = α,α′-bis(bis(2-(diphenylphosphino)ethyl)amino)ethane, BDAE = α,α′-bis(bis(2-(diphenylarsino)ethyl)amino)ethane and BDPX = α,α′-bis(bis(2-(diphenylphosphino)ethyl)amino)-*m*-xylene). In some cases the mixture of products was separated by column chromatography and characterized. By passing CO through the dichloromethane solution of the above complexes for 20 h the CO adducts were formed with the reduction of ruthenium(III) to ruthenium(II). The reactions of NOCl with ruthenium(III) complexes resulted in the displacement of one Cl or $AsPh_3$ per metal by NO and the ruthenium(III) was reduced to ruthenium(II). The geometry of the complexes was established by $^{31}P\{^1H\}$ NMR spectral data. The cyclic voltammetric behaviour of these complexes was also reported.

The chemistry of transition metal complexes with chelated tertiary phosphine or arsine ligands has gained considerable interest in recent years. Among many reports the chemistry of ruthenium with the ligands having donor sets P_3, NP_2 and NAs_2 are of special interest due to their interesting structural features and reactivities.[1–11] A number of such complexes were also reported from this laboratory with ruthenium and with other transition metal ions.[3–6,12–14] For extensive studies in this area three hexadentate ligands having σ-donor and π-acidic mixed donor sites (N_2P_4 and N_2As_4) have been synthesized and their chemistry with copper(I),[15–19] ruthenium(II),[20] nickel(II) and cobalt(II)[21] have been reported recently. This paper reports the synthesis and characterization of a number of dinuclear ruthenium(III) complexes with the ligands BDPE, BDAE and BDPX and their reactions with CO at normal pressure and ambient temperature and with NOCl [where BDPE = α,α′-bis(bis(2-(diphenylphosphino)ethyl)amino)ethane, BDAE = arsenic analogue of BDPE and BDPX = α,α′-bis(bis(2-(diphenylphosphino)ethyl)amino-*m*-xylene]. The cyclic voltammetric behaviour of these complexes is also reported.

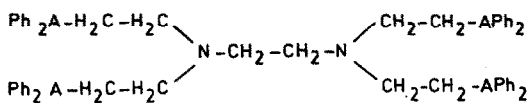

A=P (BDPE)
A=As (BDAE)

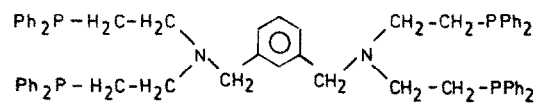

(BDPX)

EXPERIMENTAL

Materials

The ligands BDPE, BDAE and BDPX were synthesized by the procedure recently developed in this laboratory.[15] $RuCl_3(AsPh_3)_2MeOH$ was prepared by the published procedure.[22] CO gas was obtained by the dropwise addition of concentrated H_2SO_4 into sodium formate. NOCl was generated *in situ*

by the reaction of sodium nitrite with hydrochloric acid. All solvents used were of reagent grade and were purified and dried before use. All preparations, except reactions with CO, were performed under nitrogen.

Physical measurements

Elemental analyses were performed on a Carlo–Erba elemental analyser model 1106. A digisum Electronics digital conductivity meter model D1-909 was used for conductivity measurement. Magnetic measurements were performed with a PAR model 155 vibrating sample magnetometer. IR spectra were recorded on a Carl–Zeiss Specord M80 spectrometer, as KBr pellets. $^{31}P\{^{1}H\}$ NMR spectra were recorded on a Jeol FX-100 FT NMR using a 10 mm spinning tube with a capillary of deuterium oxide for the internal lock. The UV–Vis spectra were recorded on a Shimadzu UV-160 spectrometer. Electrochemical measurements were performed with a PAR electrochemical instrument; for cyclic voltammograms a PAR 175 Universal programmer coupled with the PAR 174A analyser was used with a glassy carbon working electrode. All potentials were measured against S.C.E. at 25°C and tetrabutylammoniumperchlorate was used as a supporting electrolyte.

Synthesis of metal complexes

$[Ru_2(BDPE)(AsPh_3)_2Cl_6]$ (**1**) *and* $[Ru_2(BDPE)Cl_6]$ (**2**). To a boiling solution of $RuCl_3(AsPh_3)_2MeOH$ (0.426 g, 0.5 mmol) in dichloromethane (50 cm^3) was added dropwise BDPE (0.227 g, 0.25 mmol) dissolved in dichloromethane (10 cm^3) and after complete addition refluxing was continued for 3 h. The solvent from the reaction mixture was removed by a rotary evaporator and the solid mass washed with benzene. The residue was passed through a silica gel column using a dichloromethane–methanol (9 : 1) solvent mixture; the first fraction of the eluant gave complex **1** (yield 0.24 g) and the second fraction yielded **2** (yield 0.1 g).

Complex **2** was also obtained as a single product in good yield when the above reaction was conducted in benzene. The reaction mixture was refluxed for 6 h and during this period complex **2** was separated by filtration and washed with benzene; yield 80%.

$[Ru_2(BDAE)Cl_6]$ (**3**) *and* $[Ru_2(BDPX)Cl_6]$ (**4**). These compounds were synthesized following the same procedure as described for **2** in benzene. Complexes **3** and **4** were recrystallized from a dichloromethane–n-hexane solvent mixture; yield 70–80%.

$[Ru_2(BDPE)(CO)_2Cl_4]$ (**5**, **5a**) $[Ru_2(BDAE)(CO)_2Cl_4]$ (**6**) *and* $[Ru_2(BDPX)(CO)_2Cl_4]$ (**7**). To a dichloromethane solution of complexes **1–4** (0.2 mmol) CO gas was passed through for 20 h at ambient temperature with stirring. During this period the colour of the solution changed from green to brown. The solution was then concentrated to *ca* 5 cm^3 and n-hexane was added dropwise with stirring. The brown microcrystalline compounds that deposited were collected by filtration and recrystallized from a dichloromethane–n-hexane solvent mixture; yield 85–90%.

$[Ru_2(BDPE)(NO)_2Cl_6]$ (**8**), $[Ru_2(BDPE)(NO)_2Cl_4]Cl_2$ (**8a**), $[Ru_2(BDAE)(NO)_2Cl_4]Cl_2$ (**9**) *and* $[Ru_2(BDPX)(NO)_2Cl_4]Cl_2$ (**10**). Complexes **1–4** (0.2 mmol) were taken in a suspension of methanol (50 cm^3) and to this mixture $NaNO_2$ (0.03 g) and concentrated HCl (0.2 cm^3) were added. The reaction mixture became clear after refluxing for 5 h. The solution was concentrated to *ca* 30 cm^3 and kept at room temperature overnight. The brown compounds which separated were collected by filtration, washed with water and ethanol and dried *in vacuo*; yield 65–70%.

RESULTS AND DISCUSSION

The reaction of $RuCl_3(AsPh_3)_2MeOH$ with BDPE in a 2 : 1 molar ratio in CH_2Cl_2 resulted in the formation of a mixture of two complexes of compositions $[Ru_2(BDPE)(AsPh_3)_2Cl_6$ (**1**) and $[Ru_2(BDPE)Cl_6]$ (**2**), separated by column chromatography. The same reaction when conducted in benzene gave complex **2**, which precipitated during the reaction. The ^{31}P NMR spectra of the filtrate indicated the formation of **1**, but the yield was so poor that the pure compound could not be isolated. Similar reactions with the ligands BDAE and BDPX in benzene gave dinuclear complexes $[Ru_2(BDAE)Cl_6]$ (**3**) and $[Ru_2(BDPX)Cl_6]$ (**4**), respectively. To a dichloromethane solution of complexes **1–4** CO gas was passed through for 20 h at ambient temperature. During this period the colour of the solution changed from green to brown and the isolated products were diamagnetic [low-spin ruthenium(II)] with the composition $[Ru_2L(CO)_2Cl_4]$, where L = BDPE (**5** and **5a**), BDAE (**6**) and BDPX (**7**), obtained from **1**, **2**, **3** and **4**, respectively. The reactions of complexes **1–4** with NOCl in methanol resulted in the formation of dinuclear diamagnetic complexes of the compositions $[Ru_2(BDPE)(NO)_2Cl_6$ (**8**) and $[Ru_2L(NO)_2Cl_4]Cl_2$, where L = BDPE (**8a**), BDAE (**9**) and BDPX (**10**), obtained from **1**, **2**, **3** and **4**, respectively. The compositions of all the complexes were confirmed by elemental analysis, presented in Table 1.

Table 1. Analytical data for the complexes[a]

Complex	Analysis (%) C	H	N
$[Ru_2(BDPE)(AsPh_3)_2Cl_6]$ (**1**)	58.5 (58.3)	4.8 (4.7)	1.4 (1.5)
$[Ru_2(BDPE)Cl_6]$ (**2**)	52.3 (52.6)	4.4 (4.5)	2.0 (2.1)
$[Ru_2(BDAE)Cl_6]$ (**3**)	46.1 (46.4)	3.9 (4.0)	1.8 (1.9)
$[Ru_2(BDPX)Cl_6]$ (**4**)	55.2 (54.9)	4.4 (4.6)	1.9 (2.0)
$[Ru_2(BDPE)(CO)_2Cl_4]$ (**5**)	54.9 (55.1)	4.7 (4.6)	2.0 (2.1)
$[Ru_2(BDPE)(CO)_2Cl_4]$ (**5a**)	55.0 (55.1)	4.5 (4.6)	2.0 (2.1)
$[Ru_2(BDAE)(CO)_2Cl_4]$	48.3 (48.5)	4.1 (4.0)	1.8 (1.9)
$[Ru_2(BDPX)(CO)_2Cl_4]$ (**7**)	57.4 (57.2)	4.7 (4.6)	1.9 (2.0)
$[Ru_2(BDPE)(NO)_2Cl_6]$ (**8**)	49.8 (50.3)	4.1 (4.3)	3.9 (4.1)
$[Ru_2(BDPE)(NO)_2Cl_4]Cl_2$ (**8a**)	50.0 (50.3)	4.2 (4.3)	4.0 (4.1)
$[Ru_2(BDAE)(NO)_2Cl_4]Cl_2$ (**9**)	44.9 (44.6)	3.8 (3.9)	3.4 (3.6)
$[Ru_2(BDPX)(NO)_2Cl_4]Cl_2$ (**10**)	52.2 (52.6)	4.3 (4.4)	3.7 (3.8)

[a] Calculated values are given in parentheses.

Conductivity measurements in DMF show that complexes **1–8** are non-electrolytes and **8a–10** correspond to 1 : 2 electrolytes (Table 2). These results indicate that in complexes **1–8** all of the chloride ions are coordinated to the metal ion and in **8a–10** two chlorides in each complex are not involved in coordination.

Magnetic susceptibility measurements showed that complexes **1–4** are paramagnetic (μ_{eff} in the range 1.8–1.96 B.M. per metal) and the moments correspond to one unpaired electron, as expected for low-spin octahedral ruthenium(III)-d^5 complexes. Complexes **5–10** are diamagnetic, as expected for spin-paired ruthenium(II)-d^6 octahedral complexes. These results indicate that the reaction of CO and NOCl with complexes **1–4** resulted in a reduction of ruthenium(III) to ruthenium(II) with the coordination of CO and NO^+ to the metal ion. A similar reductive addition of CO has also been reported for a number of ruthenium(III) complexes with π-acidic ligands such as PPh_3 and $AsPh_3$.[23]

Some selected IR bands of the complexes are shown in Table 2. The IR spectra of all the complexes having BDPE or BDPX as the ligand exhibit a band of medium intensity in the range 510–518 cm^{-1}, which is assigned to ν(Ru—P).[3,4,6,20] For the complexes of BDAE the band in the range 478–482

Table 2. Selected IR bands[a] and conductivity data[b] for the complexes

Complex	IR data (cm^{-1})[a] ν (Ru—P/As)	ν (Ru—Cl)	ν (CO)	ν (NO)	Conductivity[b] Λ_M ($\Omega^{-1}cm^2mol^{-1}$)	Comment
1	510 m, 480 m	320 w, 310 w			8	Non-electrolyte
2	515 m	318 w, 305 w			12	Non-electrolyte
3	482 m	320 w, 305 w			6	Non-electrolyte
4	515 m	330 w, 316 w			7	Non-electrolyte
5	515 m	322 w	1960 s		10	Non-electrolyte
5a	512 m	330 w, 318 w	1960 s		10	Non-electrolyte
6	480 m	328 w, 315 w	1982 s		12	Non-electrolyte
7	518 m	325 w, 300 w	1955 s		8	Non-electrolyte
8	510 m	330 w, 315 w		1850 s	12	Non-electrolyte
8a	508 m	330 w, 312 w		1850 s	136	1 : 2 electrolyte
9	478 m	332 w, 320 w		1875 s	145	1 : 2 electrolyte
10	515 m	332 w, 320 w		1865 s	130	1 : 2 electrolyte

[a] As KBr pellets.
[b] In DMF.
s = strong, m = medium, w = weak.

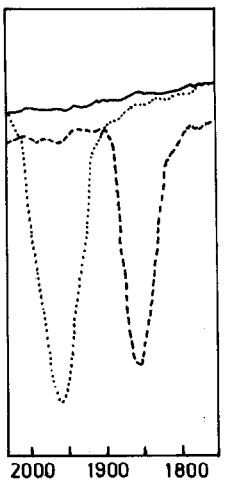

Fig. 1. IR spectra of the complexes **2**, **5a** and **8a** in the range 1750–2050 cm^{-1}, recorded as KBr pellets. (——) $[Ru_2(BDPE)Cl_6]$ (**2**), (·····) $[Ru_2(BDPE(CO)_2Cl_4]$ (**5a**) and (- - - -) $[Ru_2(BDPE)(NO)_2Cl_4]Cl_2$ (**8a**).

cm^{-1} is due to ν(Ru—As).[3,4,20] In all complexes two weak bands appeared in the range 305–332 cm^{-1}, which may be assigned to ν(Ru—Cl).[3–6,20] The bonding of CO or NO^+ in complexes **5–10** is confirmed by IR spectral data. Complexes **5–7** show a strong band in the range 1955–1982 cm^{-1} and **8–10** show a strong band in the range 1850–1875 cm^{-1}, which may be assigned to ν(CO)[7,10,23] and $\nu(NO^+)$,[24–26] respectively. The IR spectra of complex **2** and its CO (**5a**) and NO (**8a**) adducts in the range 1750–2050 cm^{-1} are shown in Fig. 1.

The electronic spectral data of complexes **1–10** in the range 700–300 nm in DMF are presented in Table 3. In this range all complexes exhibit four absorption bands. Similar observations were also reported for a number of ruthenium(III) and ruthenium(II) complexes with tertiary phosphine and arsine ligands.[3,6,20,27] The first two bands may be due to *d–d* transitions,[3,20] whereas the other higher energy bands can be assigned to LMCT; the charge-transfer involving phosphorus or arsenic lone pairs.

Geometry

The $^{31}P\{^1H\}$ NMR spectral data (Table 3) are extremely useful for geometrical assignment. All the complexes except **8** showed a singlet in the range δ 27.37–45.11, suggesting that all the phosphorus atoms in each complex are magnetically equivalent. Complex **1** shows a singlet at δ 45.11, whereas **2** and **4** exhibit singlets at δ 32.33 and 31.52, respectively. The δ value at 45 ± 2 is usually found for the phosphorus atoms of PPh_2 *trans* to chloride in ruthenium complexes with NP_2 donor sets.[3,4,6,20] With a similar donor set the δ value of 30 ± 2 was reported for a number of complexes where the phosphorus atoms of PPh_2 are *trans* to each other.[3,4,6,20] The data, therefore, suggest that in complex **1** two PPh_2 groups bonded to each metal ion are *trans* to chloride and in complexes **2** and **4** *trans* to each other. With this information and other data a dinuclear octahedral geometry for **1** with $AsPh_3$ and Cl in axial positions, as shown in structure **I**, is suggested. For complexes **2** and **4** an octahedral

Table 3. $^{31}P\{^1H\}$ NMR data, magnetic susceptibility and electronic spectral data for the complexes

Complex	$^{31}P\{^1H\}$ NMR data: Solvent	$^{31}P\{^1H\}$ NMR data: Chemical shift (δ)	Magnetic susceptibility (μ_{eff} B.M.)	Electronic spectral data in DMF λ_{max} (nm) [ε (M^{-1} cm^{-1})]
1	CH_2Cl_2	45.11	1.92	585(330), 465(600), 406(1600), 358(2250)
2	CH_2Cl_2	32.33	1.86	575(380), 462(720), 400(1800), 351(2650)
3	—	—	1.96	519(520), 440(700), 395(1950), 298(8000)
4	CH_2Cl_2	31.52	1.90	463(840), 460(950), 402(2250), 359(3600)
5	CH_2Cl_2	32.64	d	573(350), 442(1850), 405 (2450), 352(3100)
5a	CH_2Cl_2	28.37	d	563(250), 458(1050), 399(2400), 339(3125)
6	—	—	d	570(100), 470(521), 390(1750), 333(5800)
7	CH_2Cl_2	29.00	d	560(90), 442(700), 400(2200), 330(6200)
8	DMF	34.27, 5.33	d	575(325), 465(650), 400(1500), 324(2650)
8a	DMF	30.03	d	562(400), 455(860), 406(1850), 340(2900)
9	—	—	d	525(620), 458(620), 400(1600), 306(6200)
10	DMF	29.25	d	550(125), 454(725), 400(2000), 338(5100)

d = diamagnetic.

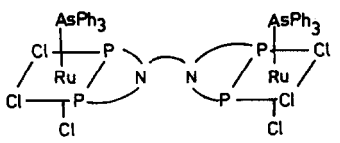

I

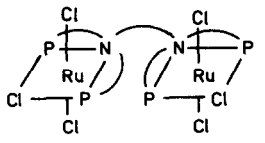

II

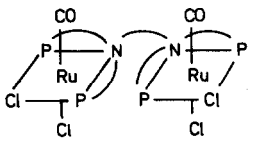

III

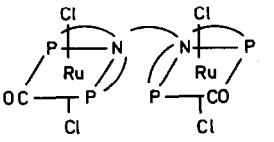

IV

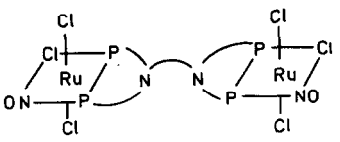

V

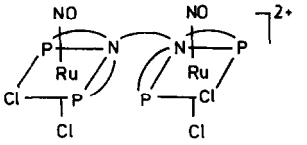

VI

geometry with a *trans* disposition of phosphorus atoms of PPh_2 in the square plane of the octahedron and two Cl in axial positions, as shown in structure **II**, are suggested. For complex **3** a similar geometry is expected. The CO adducts **5**, **5a** and **7** show singlets at 32.64, 28.37 and 29.00, respectively. For complexes **5a** and **7** there is no remarkable change in chemical shift of the phosphorus atom compared with the parent compounds, therefore, a similar geometry as found for **2** and **3** with the displacement of one Cl by CO in the axial position, as shown in structure **III**, is suggested. The displacement of Cl by CO in the axial position is also supported by the IR data, which exhibit two bonds of ν(Ru—Cl) indicating a *cis* disposition of Cl. In the case of complex **5** there is a considerable upfield shift of the ^{31}P signal compared with the parent compound (**1**). This result indicates that the replacement of $AsPh_3$ by CO with the reduction of ruthenium(III) to ruthenium(II) changes the geometry of the metal ion. The δ value (32.64) indicates that the position of the phosphorus atoms *trans* to chloride is unlikely and again the geometry is not the same as shown in structure **III** since the other physicochemical data of **5** and **5a** are not identical. This possibility is shown in structure **IV**. For complex **6** a similar geometry as shown in structure **III** is proposed. The NO complex (**8**) shows two broad signals at 5.33 and 34.27 with equal intensity, indicating the presence of two types of non-equivalent phosphorus atoms. The signal at 5.33 is assigned to the phosphorus atom *trans* to NO and a notable upfield shift of this signal may be due to the strong *trans* effect of NO^+. The splitting of the signals into a doublet, as expected from two non-equivalent phosphorus atoms, could not be observed at room temperature. The proposed geometry is shown in structure **V**. Complexes **8a** and **10** show singlets at δ 30.03 and 29.25, respectively, indicating the equivalence of all phosphorus atoms in each complex. This observation is similar to that of the CO adduct and, therefore, an octahedral geometry with NO in the axial position, as shown in structure **VI**, is suggested. For complex **9** one can expect a similar geometry as found for **8a**.

Electrochemical study

The cyclic voltammetric behaviour of complexes **1–10** was studied in the potential range 0 to +1.5 V (vs S.C.E.) in DMF at 25 ± 1°C, with scan rates of 100–500 mV s^{-1}. In this range all complexes show two quasi-reversible one-electron redox potentials (Table 4). The differences in potential for the anodic and cathodic peaks (ΔE_p) were in the range 80–110 mV, consistent with a quasi-reversible one-electron process. The two waves can be attributed to the sequential one-electron transfer process for the Ru^{III}/Ru^{II} couple, as found for other dinuclear complexes of different transition metal ions with the same ligands.[18–21] Similar observations were also reported for a number of dinuclear ruthenium complexes and are often used to calculate the stability of the mixed-valence species,[28] expressed in terms of the comproportionation constant K_{com}:

$$K_{com} = \mathrm{Exp}\,(nF(\Delta E/RT));$$

where ΔE is the difference between the two potentials in V. The K_{com} values thus calculated are presented in Table 4. The K_{com} values indicate that the mixed-valence species are moderately stable and

Table 4. Cyclic voltammetry data of the complexes in DMF

Complex	$E^1_{1/2}$	$E^2_{1/2}$	K_{com}
$Ru_2(BDPE)(AsPh_3)_2Cl_6]$ (1)	0.56	1.12	2.99×10^9
$[Ru_2(BDPE)Cl_6]$ (2)	0.48	0.92	2.79×10^7
$[Ru_2(BDAE)Cl_6]$ (3)	0.38	0.80	1.28×10^7
$[Ru_2(BDPX)Cl_6]$ (4)	0.40	0.86	6.07×10^7
$[Ru_2(BDPE)(CO)_2Cl_4]$ (5)	0.60	1.08	1.32×10^8
$[Ru_2(BDPE)(CO)_2Cl_4]$ (5a)	0.60	1.06	6.07×10^7
$[Ru_2(BDAE)(CO)_2Cl_4]$ (6)	0.52	1.02	2.88×10^8
$[Ru_2(BDPX)(CO)_2Cl_4]$ (7)	0.56	1.00	2.79×10^7
$[Ru_2(BDPE)(NO)_2Cl_6]$ (8)	0.76	1.18	1.31×10^7
$[Ru_2(BDPE)(NO)_2Cl_4]Cl_2$ (8a)	0.73	1.16	1.94×10^7
$[Ru_2(BDAE)(NO)_2Cl_4]Cl_2$ (9)	0.65	1.10	4.24×10^7
$[Ru_2(BDPX)(NO)_2Cl_4]Cl_2$ (10)	0.70	1.14	2.87×10^7

this is probably due to the presence of σ-donor and π-acceptor coordinating atoms in the principal ligands.

REFERENCES

1. M. M. Taqui Khan and A. E. Martell, *Inorg. Chem.* 1975, **14**, 676.
2. M. M. Taqui Khan and A. E. Martell, *Inorg. Chem.* 1974, **13**, 2961.
3. M. M. Taqui Khan and V. V. S. Reddy, *Inorg. Chem.* 1986, **25**, 208.
4. M. M. Taqui Khan and B. Swamy, *Inorg. Chem.* 1987, **26**, 178.
5. M. M. Taqui Khan and A. P. Reddy, *Polyhedron* 1987, **6**, 2009.
6. M. M. Taqui Khan and E. Rama Rao, *Polyhedron* 1988, **7**, 29.
7. A. Mezzetti, A. D. Zotto, P. Rigo and N. B. Pahor, *J. Chem. Soc., Dalton Trans.* 1989, 1045.
8. G. Jia, D. W. Meck and J. C. Ga'lucci, *Organometallics* 1990, **9**, 2549.
9. C. Bianchini, P. J. Perez, M. Peruzzini, F. Zanobini and A. Vacca, *Inorg. Chem.* 1991, **30**, 279.
10. P. W. Blosser, J. C. Gallucci and A. Wojcicki, *Inorg. Chem.* 1992, **31**, 2376.
11. A. M. Joshi, I. S. Thorburn, S. J. Rettig and B. R. James, *Inorg. Chim. Acta* 1992, **198**, 283.
12. M. M. Taqui Khan, H. C. Bajaj, R. H. Siddiqui, B. T. Khan, M. S: Reddy and K. V. Reddy, *J. Chem. Soc., Dalton Trans.* 1985, 2603.
13. M. M. Taqui Khan, V. V. S. Reddy and H. C. Bajaj, *Polyhedron* 1987, **6**, 921.
14. M. M. Taqui Khan and E. Rama Rao, *Polyhedron* 1987, **6**, 1727.
15. M. M. Taqui Khan, P. Paul, K. Venkatasubramanian and S. Purohit, *J. Chem. Soc., Dalton Trans.* 1991, 3405.
16. M. M. Taqui Khan, P. Paul, K. Venkatasubramanian and S. Purohit, *Inorg. Chim. Acta* 1991, **183**, 229.
17. M. M. Taqui Khan, P. Paul and K. Venkatasubramanian, *Polyhedron* 1991, **10**, 1827.
18. M. M. Taqui Khan and P. Paul, *Polyhedron* 1992, **11**, 805.
19. P. Paul and K. Venkatasubramanian, *Polyhedron*, submitted.
20. M. M. Taqui Khan, P. Paul and S. Purohit, *Inorg. Chim. Acta* 1991, **189**, 165.
21. P. Paul, K. Venkatasubramanian and S. Purohit, *J. Coord. Chem. Sec. A*, in press.
22. T. A. Stephenson and G. Wilkinson, *J. Inorg. Nucl. Chem.* 1966, **28**, 945.
23. L. Ruiz-Ramirez, T. A. Stephenson and E. S. Switkes, *J. Chem. Soc., Dalton Trans.* 1973, 1770.
24. B. L. Haymore and J. A. Ibers, *Inorg. Chem.* 1975, **14**, 3060.
25. R. E. Townsend and K. J. Coskran, *Inorg. Chem.* 1971, **10**, 1661.
26. L. F. Szczepura, J. G. Muller, C. A. Bessel, R. F. See, T. S. Janik, M. R. Churchill and K. J. Takeuchi, *Inorg. Chem.* 1992, **31**, 859.
27. M. Bressan and P. Rigo, *Inorg. Chem.* 1975, **14**, 2286.
28. D. V. Richardson and H. Taube, *Coord. Chem. Rev.* 1984, **60**, 107.

Polyhedron Vol. 12, No. 16, pp. 2063–2066, 1993
Printed in Great Britain

0277–5387/93 $6.00+.00
© 1993 Pergamon Press Ltd

COMMUNICATION

PREPARATION OF COPPER(I) BINAP-P_2N_2 COMPLEXES; CRYSTAL AND MOLECULAR STRUCTURE OF [Cu(Binap-P_2N_2)Br]

WAI-KWOK WONG*

Department of Chemistry, Hong Kong Baptist College, Kowloon, Hong Kong

and

JING-XING GAO

Department of Chemistry, Xiamen University, Xiamen 361005, Fujian, People's Republic of China

and

WING-TAK WONG* and CHI-MING CHE

Department of Chemistry, The University of Hong Kong, Pokfulam Road, Hong Kong

(*Received* 23 *March* 1993; *accepted* 25 *June* 1993)

Abstract—The interaction of a racemic mixture of N,N′-bis[*o*-(diphenylphosphino)benzylidene-2,2′-diimino-1,1′-binaphthyl (Binap-P_2N_2) (**I**) with 1 equivalent of $Cu(Ph_3P)_2Br$ and $[Cu(CH_3CN)_4]PF_6$ in CH_2Cl_2 gave Cu(Binap-P_2N_2)Br (**II**) and [Cu(Binap-P_2N_2)]PF_6 (**III**) in 60 and 74% yield, respectively. The structure of **II** was established by X-ray diffraction and can be described as distorted tetrahedral with the bromide ion and the two phosphino groups and one of the two imino groups of **I** coordinated to the copper. Variable temperature $^{31}P\{^1H\}$ NMR study of **II** shows that the coordinated and the uncoordinated imino groups of the tridentate Binap-P_2N_2 ligand undergo a facile intramolecular exchange even at −55°C.

The potential of polydentate ligands having both soft and hard centres being good bridging ligands for the preparation of heterobimetallic complexes containing an oxophilic metal and late transition metal has led to extensive study on the synthesis and reactivities of polydentate ligands containing both phosphine and nitrogen base groups.[1–3] Recently, we have examined the reactivity of N,N′-bis[*o* - (diphenylphosphino)benzylidene]ethylenediamine, (P_2N_2), toward transition metal complexes and have shown that the P_2N_2 ligand can act as bridging, bi-, tri-, or tetra-dentate ligand depending on the reaction conditions.[4–6] In this communication, we report the reactivity of the analogous diiminodiphosphine ligands, N,N′-bis[*o*-(diphenylphosphino)benzylidene]-2,2′-diimino-1,1′-binaphthyl (Binap-P_2N_2) (**I**) toward copper(I) complexes.

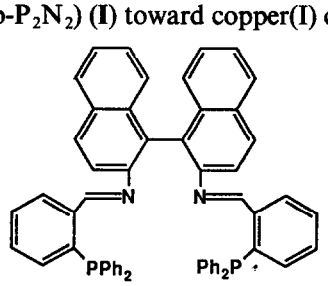

* Authors to whom correspondence should be addressed.

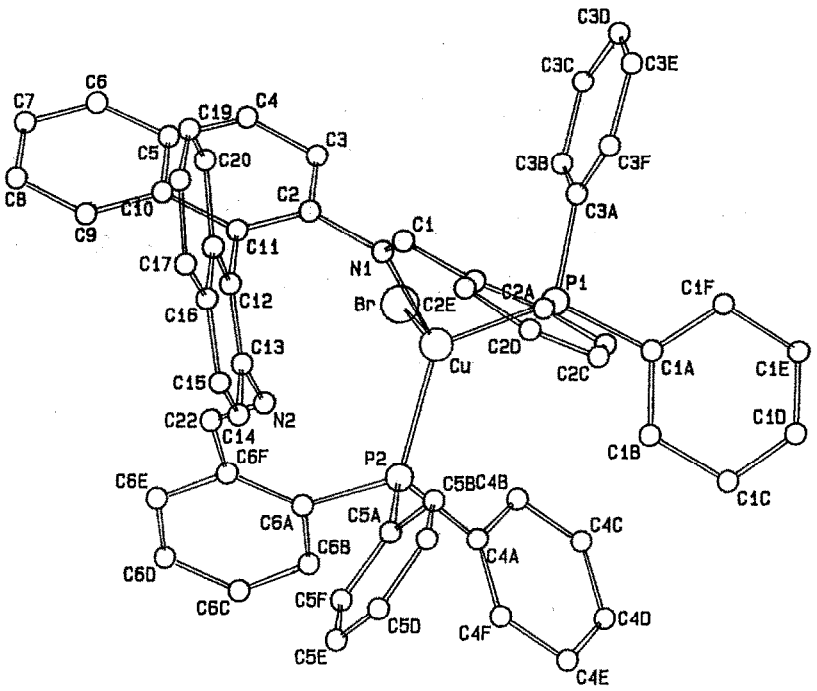

Fig. 1. A perspective view of the molecular structure of $Cu(C_{58}H_{42}N_2P_2)Br$. Selected bond lengths (Å) and bond angles (°): Cu—Br, 2.446(2); Cu—P(1), 2.261(4); Cu—P(2), 2.270(4); Cu—N(1), 2.28(1); C(1)—N(1) 1.27(2); C(22)—N(2), 1.24(2); Br—Cu—P(1), 118.3(1); Br—Cu—P(2), 104.1(1); Br—Cu—N(1), 108.5(3); P(1)—Cu—P(2), 122.0(2); P(1)—Cu—N(1), 82.6(4); P(2)—Cu—N(1), 120.5(3).

When a racemic mixture of Binap-P_2N_2 was treated with 1 equivalent of $Cu(Ph_3P)_2Br$ in refluxing dichloromethane for 12 h, work up gave orange crystals of stoichiometry $Cu(Binap\text{-}P_2N_2)Br \cdot CH_2Cl_2$ (**II**), in moderate yield (60%) after recrystallization from a CH_2Cl_2/Et_2O mixture.[7] The structure of **II** was established by an X-ray diffraction study. Crystals of stoichiometry $[Cu(Binap\text{-}P_2N_2)Br]2.5CHCl_3$ suitable for X-ray diffraction study were grown from a mixture of $CHCl_3$/hexane.* A perspective drawing and selected bond lengths and bond angles of **II** are shown in Fig. 1 and its caption. All bond lengths and bond angles are normal. The structure can be described as a distorted tetrahedral with the bromide ligand and the two phosphino groups and one of the two imino groups of the Binap-P_2N_2 ligand coordinated to the copper. The dihedral angle between the two least planes of the naphthene units in the binaphthenene moiety is 74.8°. The non-bonding distance between Cu and N(2) is 3.35(1) Å. ^1H NMR spectrum of **II** exhibits a singlet at δ 8.21 ppm for the imino protons and a complex multiplet at δ 6.80–7.75 ppm for the phenyl and binaphthyl protons. The ambient temperature $^{31}P\{^1H\}$ NMR spectrum of **II** exhibits a broad singlet (width at half-height is 150 Hz) which broadens slightly on cooling to −55°C (width at half-height is 160 Hz) at δ −12.4 ppm. This suggests that the coordinated imino group and the uncoordinated imino group of **II** undergo a facile intramolecular exchange as shown in Scheme 1. Similar dynamic behaviour has been reported for $[Cu(P_2N_2)(t\text{-}BuNC)]ClO_4$.[8]

When a racemic mixture of Binap-P_2N_2 was treated with 1 equivalent of $[Cu(CH_3CN)_4]PF_6$ in refluxing dichloromethane for 12 h, work up gave

* Crystal data for $C_{58}H_{42}N_2P_2CuBr \cdot 2.5CHCl_3$: F_w = 1270.82, monoclinic, $P2_{1/c}$ (No. 14), a = 14.114(3), b = 15.633(8), c = 27.429(9) Å, β = 99.56(4)°, V = 5968.1(4) Å^3, Z = 4, $F(000)$ = 2572, D_c = 1.414 g cm^{-3}, μ = 14.6 cm^{-1}. Crystal dimensions: 0.20 × 0.20 × 0.41 mm. Intensity data were collected on an Enraf–Nonius CAD-4 diffractometer with graphite monochromated Mo-K_α radiation (λ = 0.71073 Å) using ω–2θ scans ($2\theta_{max}$ = 45°). The structure was solved by a combination of Patterson and direct methods (DIRDIF) after an absorption correction (transmission factors 0.935–0.998) was applied and refined by full-matrix least-squares to give R = 0.089, R_w = 0.112 for 4069 independent observed reflections [$I \geqslant 3\sigma(I)$].

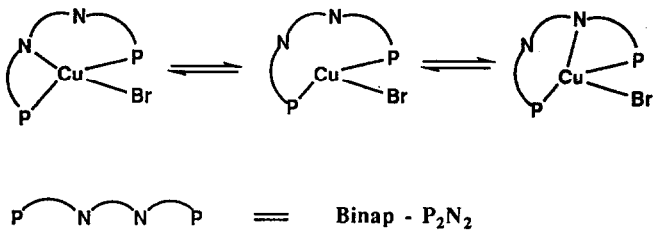

Scheme 1. Proposed mechanism for the dynamic behaviour of **II**.

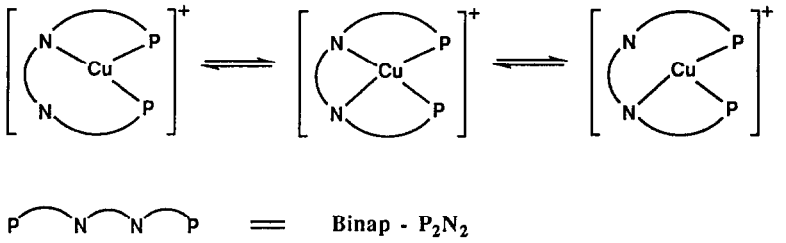

Scheme 2. Possible intramolecular exchange process for **III**.

orange crystals of stoichiometry [Cu(Binap-P_2N_2)]PF_6 (**III**) in good yield (74%) after recrystallization from a CH_2Cl_2/Et_2O mixture.[9] ^1H NMR spectrum of **III** exhibits a singlet at δ 8.28 ppm for the imino protons and a complex multiplet at δ 6.50–7.80 ppm for the phenyl and binaphthyl protons. The ambient temperature $^{31}P\{^1H\}$ NMR spectrum of **III** exhibits a broad singlet (width at half-height is 75 Hz) and a heptet [J(P—F) = 712.3 Hz] which remain unchanged on cooling to $-55°C$ at δ -11.6 and -145.1 ppm for the phosphorus of the Binap-P_2N_2 ligand and the PF_6^- anion, respectively. The spectroscopic data suggest that **III** is a tetrahedral complex with the Binap-P_2N_2 ligand acting as a tetradentate ligand. However, a recent X-ray diffraction study on the analogous silver complex, [Ag(Binap-P_2N_2)]BF_4, reveals that the silver is tri-coordinated with the two phosphino groups and one of the two imino groups of the Binap-P_2N_2 ligand coordinated to the silver.[10] Thus, one cannot rule out the possibility that **III** is a tri-coordinated complex having the coordinated and the uncoordinated imino groups of the tridentate ligand Binap-P_2N_2 undergoing a facile intramolecular exchange as shown in Scheme 2. We are in the process of growing crystals suitable for an X-ray diffraction study to confirm the solid state structure of **III**. Preliminary studies also show that **III** is an effective catalyst for aziridination of styrene by PhINTs (Ts = tosylate) at room temperature.

Acknowledgements—W.K.W. thanks the Hong Kong Baptist College, the UPGC (Hong Kong), and the Croucher Foundation for financial support, W-T.W. thanks the Hong Kong Research Grant Council and the University of Hong Kong for financial support.

REFERENCES

1. J. Powell, A. Kuksis, C. J. May, P. E. Meindl and S. J. Smith, *Organometallics* 1989, **8**, 2933.
2. L. Wei, A. Bell, K-H. Ahn, M. M. Holl, S. Warner, I. D. Williams and S. L. Lippard, *Inorg. Chem.* 1990, **29**, 825.
3. A. Balch, F. Neve and M. M. Olmstead, *J. Am. Chem. Soc.* 1991, **113**, 2995.
4. W. K. Wong, J-X. Gao, Z-Y. Zhou and T. C. W. Mak, *Polyhedron* 1992, **11**, 2965.
5. W. K. Wong, J-X. Gao and W. T. Wong, *Polyhedron* 1993, **12**, 1047.
6. W. K. Wong, J-X. Gao, Z-Y. Zhou and T. C. W. Mak, *Polyhedron* in press.
7. $Cu(C_{58}H_{42}N_2P_2)Br \cdot CH_2Cl_2$: Orange crystals, m.p. 278–281°C dec. Found: C, 66.5; H, 4.3; N, 2.1. Calc. for $C_{59}H_{44}N_2BrCl_2P_2Cu$: C, 66.9; H, 4.2; N, 2.6%. IR (cm^{-1}, in KBr): 3060m, 1612s, 1586w, 1470s, 1430vs, 1184w, 1092m, 814w, 738s, 690s, 498w. $^{31}P\{^1H\}$ NMR ($CDCl_3$): δ -12.4 (br, s) ppm. ^1H NMR ($CDCl_3$): imino protons, δ 8.12 (2H, s) ppm; phenyl protons, δ 6.80–7.75 (40H, m) ppm; CH_2Cl_2 protons, δ 5.30 (2H, s) ppm.
8. J. C. Jeffrey, T. B. Rauchfuss and P. A. Tucker, *Inorg. Chem.* 1980, **19**, 3306.

9. $[Cu(C_{58}H_{42}N_2P_2)][PF_6]$: Orange crystals, m.p. 206–209°C dec. Found: C, 67.6; H, 4.1; N, 2.5. Calc. for $C_{58}H_{42}N_2F_6P_3Cu$: C, 67.2; H, 4.1; N, 2.7%. IR (cm^{-1}, in KBr): 3050w, 1608s, 1586s, 1424w, 1030vs, 816w, 684w. $^{31}P\{^1H\}$ NMR ($CDCl_3$): δ −11.6 (br, s), δ −145.1 {heptet, [J(P—F) = 712.3 Hz} ppm. ^1H NMR ($CDCl_3$): imino protons, δ 8.28 (2H, s) ppm; phenyl protons, δ 6.50–7.80 (40H, m) ppm.
10. W. K. Wong, J-X. Gao, W. T. Wong, W. C. Cheng and C. M. Che, manuscripts in preparation.

Polyhedron Vol. 12, No. 16, pp. 2067–2068, 1993
Printed in Great Britain

0277–5387/93 $6.00+.00
© 1993 Pergamon Press Ltd

COMMUNICATION

THE REMARKABLE POLYMETALLATE CLUSTER: CRYSTAL STRUCTURE OF $Na_6[H_6Mo_{57}Fe_6O_{183}(NO)_6(H_2O)_{18}]\cdot 91H_2O$

GUI-QING HUANG, SHI-WEI ZHANG* and MEI-CHENG SHAO

Institute of Physical Chemistry, Peking University, Beijing, 100871, P.R.C.

(*Received* 2 *June* 1993; *accepted* 15 *June* 1993)

Abstract—The crystal structure of $Na_6[H_6Mo_{57}Fe_6O_{189}(NO)_6(H_2O)_{18}]\cdot 91H_2O$ has been determined and shown to consist of three 17-molybdate subunits connected by six FeO_6 octahedra and three $\{Mo_2O_9\}$ groups.

Understanding the driving force for the formation of high-nuclearity clusters is still a formidable challenge.[1] We recently reported the structure with the largest polymetallate cluster involving mixed-valence molybdenum and vanadium(IV).[2] In this communication, we report another remarkable polymetallate also involving mixed valence molybdenum with iron(III) instead of vanadium(IV).

The compound was prepared according to the method described by Zhang *et al.*[2,3] a mixture of $Na_2MoO_4\cdot 2H_2O$ (1.92 g), FeS (0.33 g) and NH_2OH–HCl (2.56 g) in water (40 cm^3) and 1 mol dm^{-3} HCl (2 cm^3) was heated under nitrogen at reflux temperature with stirring for 2 h. The resultant dark solution was opened to the air after it was cooled to room temperature. The dark orange hexagonal and yellow needle crystals were obtained from the filtered solution after a few days and the former was characterized by elemental analysis, IR† and single-crystal X-ray structure analysis.‡

The title compound consists of three 17-molybdate subunits connected by six FeO_6 octahedra and three $\{Mo_2O_9\}$ groups, each of which are linked by one bridging oxygen atom and two bridging water molecules, and the subunits related to each other by a three-fold rotation axis; the cluster centre sits on a special position with $\bar{6}m2$ crystallographic symmetry and each individual subunit has internal C_{2v} symmetry (see Figs 1 and 2). In the centre cavity there are 12 water molecules, which are situated around a $\bar{6}$ axis and are coordinated to six molybdate and six iron groups, respectively. Moreover, these 12 water molecules are linked to each other by hydrogen bonding to form two six-membered rings.

The 17-molybdate subunit consists of one compact group of five predominantly edge-sharing MoO_6 octahedra and two $MoO_6(NO)$ pentagonal bipyramids viewed as an $\{Mo_7O_{24}(NO)_2\}$ unit of C_{2v} symmetry, characteristic of the heptamolybdate structure; the $\{Mo_7O_{24}(NO)_2\}$ unit is circled by a ring of 10 corner-sharing distorted MoO_6 octahedra to form a 17-molybdate unit. Such linking may give an indication about the possible mechanism of formation for the 17-molybdate subunit and polymolybdate clusters, which may involve an intact compact unit link $\{Mo_7O_{24}(NO)_2\}$ as a starting nucleus.

The most remarkable feature of the structure, however, is the manner of linking of the 17-mo-

* Author to whom correspondence should be addressed.

† Found: Fe, 3.1; Mo, 50.0; Na, 0.9. Calc. for $Fe_6H_{250}Mo_{57}N_6Na_6O_{590}$: Fe, 3.0; Mo, 49.6; Na, 1.2%. IR (cm^{-1} in KBr): 3139s, 1618s, 1400vs, 944m, 880vs, 773s, 535m, 469m.

‡ Crystal data: single crystals of $Na_6[Mo_{57}Fe_6O_{183}H_6(NO)_6(H_2O)_{18}]\cdot 91H_2O$ at 293 K are hexagonal, space group $P6_3/mmc$, $a = 23.843(4)$, $c = 27.797(9)$ Å, $V = 13{,}685(7)$ Å^3 and $Z = 2$, $D_c = 2.69$, $D_x = 2.70$ g cm^{-3}. A total of 2602 independent reflections ($1 < 2\theta < 41$) were collected using $\omega/2\theta$ scans with graphite-monochromated Mo-K_α radiation. The structural parameters have been refined to convergence R (based on F^2) = 0.049 for 2076 observed reflections [$F > 4\sigma(F)$].

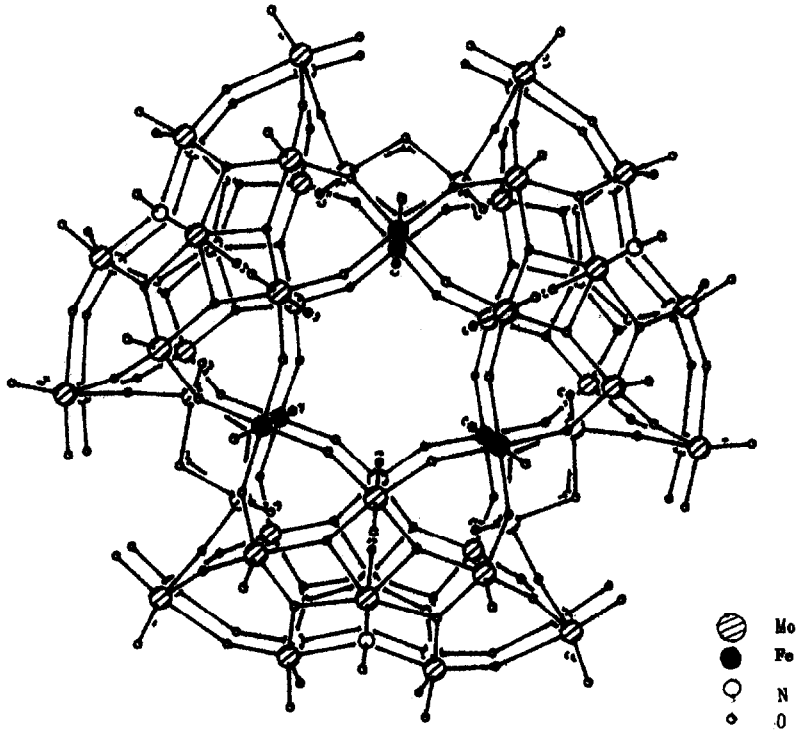

Fig. 1. Perspective drawing of the $[H_6Mo_{57}Fe_6O_{183}(NO)_6(H_2O)_{18}]^{6-}$ anion, viewed along the three-fold rotation axis.

lybdate subunits. In the Mo_{36} isopoly,[4] two 17-molybdate subunits are linked by two $Mo^{VI}O_6$ octahedra with four Mo—O bonds in $\bar{1}$ symmetry, but in the title high-nuclearity anions three 17-molybdate subunits are linked to each other by six $Fe^{III}O_6$ octahedra with four equatorial Fe—O bonds in C_{2v} symmetry, and three $\{Mo_2O_9\}$ groups occupy the three cavities of the anion.

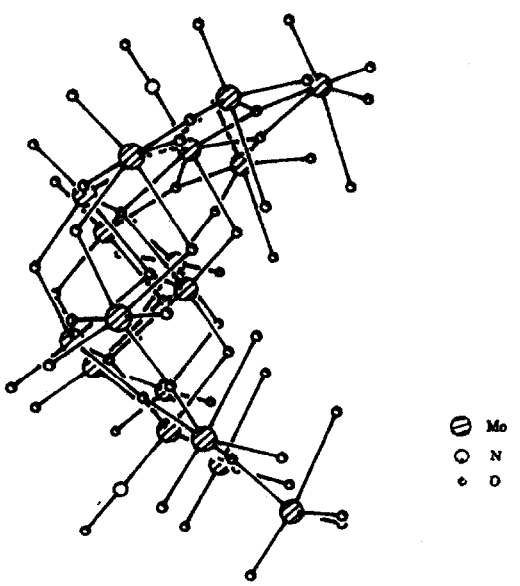

Fig. 2. The 17-molybdate subunit of the $[H_6Mo_{57}Fe_6O_{183}(NO)_6(H_2O)_{18}]^{6-}$ anion, viewed along the $2/m$ axis of the anion.

The same 17-molybdate unit exists in two polyanions also reported,[4] so we supposed that such a 17-molybdate unit is a relatively stable entity.[2] The title compound supports our idea. Moreover, we have synthesized the third high-nuclearity anion $[H_8MO_{57}Fe^{II}{}_6O_{185}(NO)_6(H_2O)_{16}(MoO)_2]^{6-}$, where the 17-molybdate subunit is linked by $Fe^{II}O_6$ instead of $Fe^{III}O_6$ or VO_6 octahedra by controlling the degree of oxidation.

Acknowledgement—We thank the National Natural Science Foundation of China for financial support.

REFERENCES

1. A. Müller and M. T. Pope, *Angew. Chem., Int. Edn Engl.* 1991, **30**, 34.
2. S. W. Zhang, G. Q. Huang, M. S. Shao and Y. Q. Tang, *J. Chem. Soc., Chem. Commun.* 1993, **1**, 37.
3. G. Q. Huang, S. W. Zhang and M. C. Shao, *Chin. Chem. Lett.*, accepted.
4. (a) S. W. Zhang, D. Q. Liao, M. C. Shao and Y. Q. Tang, *J. Chem. Soc., Chem. Commun.* 1986, 835; (b) B. Krebs and I. Paulat-Boschen, *Acta Cryst., Sect. B* 1982, **38**, 1710.

Polyhedron Vol. 12, No. 16, pp. 2069–2072, 1993
Printed in Great Britain

0277–5387/93 $6.00+.00
© 1993 Pergamon Press Ltd

COMMUNICATION

PREPARATION AND CHARACTERIZATION OF $[Cu_2Cl_4L_2]$: THE FIRST STRUCTURAL DETERMINATION OF A COMPLEX CONTAINING THE NOVEL LIGAND 2-(2′-PYRIDYL)QUINOXALINE (L)

JOHN C. PLAKATOURAS and NICK HADJILIADIS*

Department of Chemistry, University of Ioannina, 45110 Ioannina, Greece

and

SPYROS P. PERLEPES

Department of Chemistry, University of Patras, 26110 Patras, Greece

and

ALBERTO ALBINATI

Instituto di Chimica Farmaceutica e Tossicologica della Universita, Viale Abruzzi 42, 20131 Milano, Italy

and

GEORGE KALKANIS

Department of Chemistry, Physics and Material Technology, Technological Institution of Athens, Egaleo, Athens, Greece

(*Received* 7 *May* 1993; *accepted* 4 *June* 1993)

Abstract—The reaction of the unexpectedly formed ligand 2-(2′-pyridyl)quinoxaline (L) with $CuCl_2$ in ethanol, followed by recrystallization from methanol, yields the dinuclear copper (II) complex $[Cu_2Cl_4L_2]$. The crystal structure of this compound shows a bidentate chelating behaviour of L and different (terminal, asymmetric bridging) chloride coordination modes. Some properties of the dimer are also described.

We wish to report the first X-ray crystal structure of a complex containing the ligand 2-(2′-pyridyl)quinoxaline (L). We believe this molecule has great potential as a generally-useful new polyfunctional ligand in metal chemistry and that it will thus prove attractive to a variety of inorganic chemists. Compound L, which may combine the chelating properties of 2,2′-bipyridine[1] with the bridging properties of quinoxaline,[2] belongs to a class of aromatic nitrogen heterocycles whose coordination chemistry is currently a subject of intense research.[3–5] The study of complexes of such ligands is important in developing our understanding of the theory of electron transfer processes, of mixed-valence compounds, of excited-state acid–base properties of inorganic compounds and of magnetic coupling interactions. Such compounds are also used to model important bioinorganic systems and are finding applications as photosensitizers,

* Author to whom correspondence should be addressed.

catalysts and in low-dimensional coordination polymers.

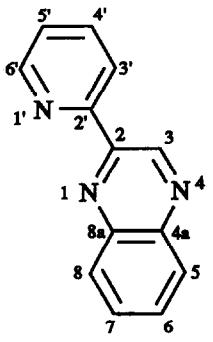

L

2-(2′-Pyridyl)quinoxaline was derived unexpectedly from an unusual cyclization reaction of 1,2-diaminobenzene and 2-acetylpyridine;[6] its identity was confirmed by microanalyses and spectroscopic techniques, including various types of mass spectroscopy and two-dimensional COSY NMR. A few 1 : 1 coordination compounds of L with transitional metal chlorides were also isolated and characterized by powder physical and spectroscopic methods.[6] In spite of many efforts neither the crystal structure of L nor that of any complex were known when we submitted our findings concerning the unexpected formation of this ligand.[6] During this period we did not stop seeking the crystal structure of a complex containing L, and we recently succeeded in growing single crystals of $[Cu_2Cl_4L_2]$ (**1**).

For the preparation of the complex, to a solution containing $CuCl_2$ (2.0 mmol) in ethanol (8 cm^3) was added dropwise a warm ethanol solution (10 cm^3) of L (1.9 mmol). Upon addition of the ligand a yellow precipitate was formed. Stirring was continued for 30 min. The solid was collected by filtration, washed with ethanol and diethyl ether and dried in air. The yield was 70–80%. The analytical data corresponded to the formula $CuCl_2L$. Brown crystals of **1** were obtained by recrystallization of the yellow material from hot methanol.*

The structure† of a molecule of **1** is shown in Fig. 1. The structure consists of two Cu^{II} centres bridged by two chloro ligands; a terminal chloro ligand and a bidentate chelating L molecule complete five-coordination at each metal. The molecules of **1** are well separated from each other. The bridging Cu_2Cl_2 is constrained to be planar by the presence of the crystallographic inversion centre in the middle of the dimer. Analysis of the shape-determining angles using the approach of Reedijk *et al.*[7] yields a value for trigonality index, τ, of 0.42 for Cu^{II} ($\tau = 0$ and 1 for perfect *sp* and *tbp* geometries, respectively). Thus, the geometry at each copper can be described as either a distorted square-pyramidal or a distorted trigonal-bipyramidal arrangement. With use of the *tbp* description the apical sites are occupied by Cl(2″) and N(1) with atoms Cl(1), Cl(2), N(1′) and Cu making up the equatorial plane with deviations from the best least-squares plane being −0.027(2), −0.023(2), 0.067(1) and −0.017(5) Å, respectively. The apical atoms, Cl(2″) and N(1), are located 2.310(2) and −1.931(5) Å, respectively, on either side of this plane. For the *sp* description the base plane would consist of the atoms Cl(1), Cl(2), Cl(2″) and N(1) with N(1′) occupying the apical site. The four basal atoms are not co-planar; N(1) and Cl(2″) lie 0.392(5) and 0.348(2) Å, respectively, above the best least-squares plane through the four atoms while Cl(1) and Cl(2) lie 0.356(2) and 0.384(2) Å,respectively, below it. The copper atom is 0.358(1) Å above the plane, i.e. toward the apical atom N(1′). These distortions from the ideal square-pyramidal geometry appear greater than in the trigonal-bipyramidal model. Using the distorted *tbp* description the axial Cu—N(1) distance was found to be shorter than the equatorial Cu—N(1′) distance; this variation of Cu—N as a function of axial *vs* equatorial location at copper is typical of trigonal-bipyramidal Cu^{II}/2,2′-bipyridine complexes.[8] Within the ligand L the angle between the plane of the pyridine ring and the plane of the quinoxaline ring is 7.1°.

Complex **1** joins only a handful of structurally characterized complexes of the type $[Cu_2X_2(\mu\text{-}X)_2(\text{bidentate ligand})_2]$ (X = Cl, Br), in which the geometry at copper is trigonal bipyramidal with the bridging ligands occupying apical and equatorial

* Far-IR, UV-vis and ESR data indicate that the yellow material is structurally different from the brown dinuclear complex. The yellow complex is believed to be a six-coordinate polymer with a mixed bidentate chelating N(1), N(1′)-monodentate N(4) coordination mode of L.[6]

† Crystal data: $C_{26}H_{18}N_6Cl_4Cu_2$, $M_r = 683.4$, monoclinic, space group $P2_1/n$, $a = 8.385(6)$, $b = 14.708(7)$, $c = 10.44(6)$ Å, $\beta = 92.59(5)°$, $V = 1283(1)$ Å^3, $Z = 2$, $D_c = 1.763$ g cm^{-3}, μ(Mo-K_α) = 21.075 cm^{-1}, $T = 25°C$, $2.5° < \theta < 25.0°$, $R(R_w) = 0.038(0.048)$ for 1175 unique reflections with $F > 2.5\sigma$ (F_o). The structure was solved by Patterson and Fourier techniques and refined by full-matrix least-squares analysis. All non-hydrogen atoms were readily located and refined with anisotropic thermal parameters. The contribution of the hydrogen atoms in their calculated positions was taken into account but not refined. All calculations were performed using the Enraf–Nonius crystallographic package MOLEN. Atomic coordinates, thermal parameters and bond lengths and angles have been deposited as supplementary data with the Editor.

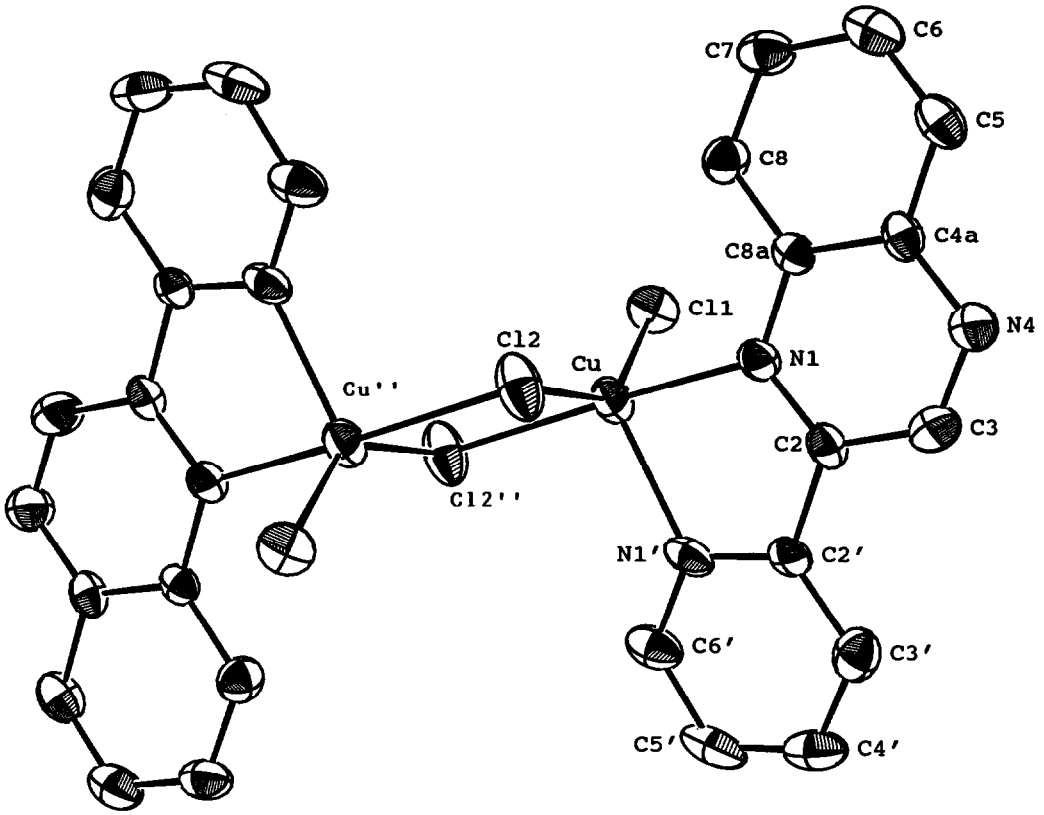

Fig. 1. The molecular structure of $Cu_2Cl_4L_2$ and atom numbering scheme. Double primed atoms are related to those unprimed by the symmetry operation $-x, -y, -z$. Selected bond distances (Å) and angles (°) are: Cu···Cu″ 3.522(1), Cu—N(1) 2.021(5), Cu—N(1′), 2.106(5), Cu—Cl(1), 2.272(2), Cu—Cl(2) 2.473(2), Cu—Cl(2″) 2.274(2); Cl(1)—Cu—Cl(2) 144.2(1), Cl(1)—Cu—Cl(2″) 96.0(1), Cl(1)—Cu—N(1) 94.0(2), Cl(1)—Cu—N(1′) 114.1(1), Cl(2)—Cu—Cl(2″) 84.3(1), Cl(2)—Cu—N(1) 86.1(1), Cl(2)—Cu—N(1′) 101.2(2), C(2″)—Cu—N(1) 169.7(2), Cl(2″)—Cu—N(1′) 98.5(1), N(1)—Cu—N(1′) 79.7(2), Cu—Cl(2)—Cu″ 95.7(1).

sites of each copper ion.[9–11] This structural type is relatively uncommon for halogen-bridged copper(II) dimers, which evidently prefer to form apical–basal bridges with square pyramidal geometry at copper.[9,10] Adopting the above described *sp* viewpoint complex **1** is the only known example, to our knowledge, of a dihalogen-C bridged square-pyramidal $[Cu_2X_4(\text{bidentate ligand})_2]$ complex in which the bridging halogens occupy two basal coordination sites of each copper(II).

The room-temperature effective magnetic moment of **1** is 1.87 B.M. per copper atom. The ESR spectrum obtained at 77 K from a powdered sample shows two poorly resolved lined at $g = 2.09$ and $g = 2.27$; in addition, a $\Delta M_S = 2$ transition is seen at $g = 4.20$. The latter transition is diagnostic of copper(II) dimers.[12] Detailed variable-temperature ESR and magnetic susceptibility studies on complex **1** are currently in progress. The appearance of a very sharp single band at 935 cm^{-1} in the IR spectrum of **1** characterizes a monodentate coordination of the quinoxaline system.[13]

In summary, the chelating N(1) and N(1′) behaviour of L has been confirmed in **1**. The mixed bidentate N(1), N(1′)-monodentate N(4) ligation mode is clearly possible. It is clear that the nature of L makes it a versatile new ligand for use with a variety of metals and for a variety of objectives/advantages, including variable metal oxidation states, bridging vs terminal modes, possible high-nuclearity aggregate formation and/or the linking of aggregates into polymeric arrays, and interesting types of magnetic exchange interactions. Such matters are currently under further investigation. Finally, it is worth noting that the coordination chemistry of the parent pyrazine ligand 2-(2′-pyridyl)pyrazine is also completely unexplored.[3]

REFERENCES

1. E. C. Constable, *Adv. Inorg. Chem.* 1989, **34**, 1.
2. W. Kaim, *Angew. Chem., Int. Edn. Engl.* 1983, **22**, 171.
3. E. C. Constable and P. J. Steel, *Coord, Chem. Rev.* 1989, **93**, 205.
4. P. J. Steel, *Coord. Chem. Rev.* 1990, **106**, 227.
5. J. G. Vos, *Polyhedron* 1992, **11**, 2285.
6. A. Garoufis, S. Kasselouri, A. Katehanakis, G. Kalkanis, S. P. Perlepes and N. Hadjiliadis, *Inorg. Chim. Acta*, 1993, **207**, 255.
7. A. W. Addison, T.N. Rao, J. Reedijk, J. V. Rijn and G. C. Verschoor, *J. Chem. Soc., Dalton Trans.* 1984, 1349.
8. G. Christou, S. P. Perlepes, E. Libby, K. Folting, J. C. Huffman, R. J. Webb and D. N. Hendrickson, *Inorg. Chem.* 1990, **29**, 3657 and refs therein.
9. W. E. Marsh, K. C. Patel, W. E. Hatfield and D. J. Hodgson, *Inorg. Chem.* 1983, **22**, 511 and refs therein.
10. For a recent tabulation see: A. Tosik, W. Maniukiewicz, M. Bukowska-Strzyzewska, J. Mrozinski, M. P. Sigalas and C. A. Tsipis, *Inorg. Chim. Acta* 1991, **190**, 193.
11. B. J. Hathaway, in *Comprehensive Coordination Chemistry* (Edited by G. Wilkinson, R. D. Gillard and J. A. McCleverty), Ch. 53, pp. 533–774. Pergamon Press, Oxford (1987).
12. S. G. N. Roundhill, D. M. Roundhill, D. R. Bloomquist, C. Landee, R. D. Willet, D. M. Dooley and H. B. Gray, *Inorg. Chem.* 1979, **18**, 831.
13. P. Lumme, S. Lindroos and E. Lindell, *Inorg. Chim. Acta* 1988, **144**, 75.

Polyhedron Vol. 12, No. 16, pp. 2073–2074, 1993
Printed in Great Britain

0277–5387/93 $6.00+.00
Pergamon Press Ltd

COMMUNICATION

OXIDATIVE ADDITION REACTIONS AND REVERSE YLIDE FORMATION INVOLVING MACROCYCLIC (TMTAA, $C_{22}H_{22}N_4$) COMPLEXES OF GERMANIUM(II) AND TIN(II)

DAVID A. ATWOOD, VICKI O. ATWOOD, ALAN H. COWLEY* and HALA R. GOBRAN

Department of Chemistry and Biochemistry, The University of Texas at Austin, Austin, TX 78712, U.S.A.

(*Received* 12 *April* 1993; *accepted* 25 *May* 1993)

Abstract—The germanium(II) and tin(II) macrocyclic complexes Ge(tmtaa) (**1**) and Sn(tmtaa) (**2**) (tmtaa = dibenzotetramethyltetraaza[14]annulene) undergo facile oxidative addition reactions and reverse ylide formation with MeI and C_6Fe_5I, respectively.

In comparison with main-group porphyrin and phthalocyanine complexes very little is known about other tetraaza macrocycles, such as the dibenzotetramethyltetraaza[14]annulene (tmtaa) ligand.[1] Use of the tmtaa ligand in the context of main-group chemistry is, in fact, limited to the elements Al,[2] Ga,[3,4] In,[3] Si,[5] Ge,[3] Sn[3,5] and Zn.[6] One of our objectives in using this ligand is to create unprecedented coordination environments and hence unusual reactivity patterns for main-group element fragments. In a previous communication[3] we have described the synthesis of Ge(tmtaa) (**1**) and Sn(tmtaa) (**2**). The structures of both molecules involve a unique square pyramidal geometry in which the $M^{(II)}$ centre lies 0.91 Å (Ge) and 1.15 Å (Sn) above the N_4 plane of the saddle-shaped tmtaa ligand. The purpose of the present communication is to report that the availability of an axially situated $M^{(II)}$ lone pair in **1** and **2** permits facile oxidative addition and reverse ylid formation to take place.

An excess of MeI was added to a stirred THF solution of either **1** or **2** at −78°C, following which the reaction mixture was allowed to warm slowly (8–12 h) to 25°C. Removal of the excess MeI and solvent under reduced pressure afforded virtually quantitative yields of the oxidative addition products Ge(tmtaa)(Me)(I) (**3**) and Sn(tmtaa)(Me)(I) (**4**). The foregoing formulations for **3** and **4** are in accord with the elemental analyses and mass spectroscopic data.† As noted by Cotton and Czuchajowska,[1] the coordination sphere of M(tmtaa)XY complexes can be regarded as a distorted trigonal prism in which the X and Y ligands adopt a mutually *cis* arrangement. Such a view is consistent with the ^{1}H NMR data for the tin com-

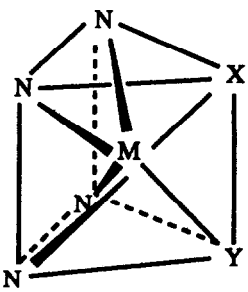

Structure 1.

* Author to whom correspondence should be addressed.

† Analytical data. Found: C, 50.6; H, 5.3. Calc. for **3**: C, 49.6; H, 4.5%. Found: C, 45.3; H, 4.9. Calc. for **4**: C, 45.8; H, 4.2%. Found: C, 46.5; H, 3.0. Calc. for **6**: C, 47.4; H, 3.1%. Found: C, 45.6; H, 3.3. Calc. for **7**: C, 44.5; H, 2.9%. MS data (Cl, CH_4), **3**: *m/z* 558 (M^+), 416 (M^+-MeI), 142 (MeI); **4**, 462 (M^+-MeI), 142 (MeI); **6**, 690 (M^+-F), 652 (M^+-3F), 294 (C_6F_5I); **7**, 462 ($M^+-C_6F_5I$), 294 (C_6F_5I). ^{1}H NMR data (300 MHz, 25°C, C_6D_6 for **3** and **4**, d^8-THF for **6** and **7**): **3**, δ 6.87 (m, 8H, C_6H_4), 4.69 (s, 2H, CH), 1.87 (s, 12H, CH_3), 0.69 (s, 3H, $GeCH_3$); **4**, 6.94 (m, 8H, C_6H_4), 5.40 (s, 1H, CH), 4.83 (s, 1H, CH), 2.43 (s, 6H, CH_3), 2.09 (s, 6H, CH_3), 0.02 (s, 3H, $SnCH_3$); **6**, 6.98 (m, 8H, C_6H_4), 4.84 (s, 2H, CH), 2.10 (s, 12H, CH_3); **7**, 6.95 (m, 8H, C_6H_4), 4.84 (s, 2H, CH), 2.08 (s, 12H, CH_3).

plex **4**. Thus, the methyl and methine protons are inequivalent while the aryl protons, being at the periphery of the complex, remain equivalent. Interestingly, in the case of the germanium analogue **3** the methyl and methine resonances remain equivalent down to −78°C. We attribute this observation to the existence of a rapid ionic-covalent equilibrium in solution.

$$Ge(tmtaa)(Me)(I) \rightleftharpoons [Ge(tmtaa)Me]^{+}I^{-}.$$

A recent report by Arduengo *et al.*[7] indicates that nucleophilic carbenes are capable of forming "reverse ylides" (**5**) with C_6F_5I in the sense that the formal charges at carbon and the halogen are inverted. It was, therefore, of interest to determine whether **1** and **2**, which are heavier carbene analogues, would undergo oxidative addition or reverse ylide formation.

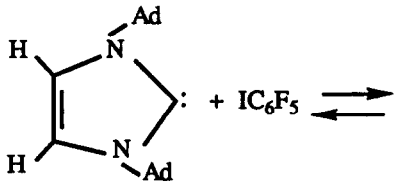

Ad = Adamantyl

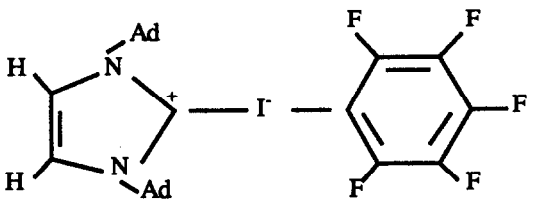

5

Compounds **1** and **2** react readily with C_6F_5I upon warming THF solutions of the reagents from −78°C to ambient temperature. Removal of the solvent and excess C_6F_5I affords virtually quantitative yields of products of composition

Table 1. ^{19}F NMR chemical shift data for C_6F_5I and compounds **5–7**

Compound	*Ortho*-F	*Para*-F	*Meta*-F
C_6F_5I	−119.4	−152.4	−159.6
5[a]	−123.75	−159.44	−163.63
6	−121.61	−155.83	−162.16
7	−121.62	−162.91	−163.75

[a] Data from ref. 7.

$Ge(tmtaa)(IC_6F_5)$ (**6**) and $Sn(tmtaa)(IC_6F_5)$ (**7**). Unfortunately, it has not been possible to obtain crystals of **6** and **7** that are suitable for X-ray analysis. However, based on the similarity of the *ortho*, *meta* and *para* ^{19}F chemical shifts of **5**, **6** and **7** (Table 1), we propose that reverse ylide formation has taken place.

Acknowledgements—We are grateful to the National Science Foundation (Grant CHE 9108228) and the Robert A. Welch Foundation for generous financial support.

REFERENCES

1. For an excellent review of tmtaa chemistry, see F. A. Cotton and J. Czuchajowska, *Polyhedron* 1990, **9**, 2553.
2. V. L. Goedken, H. Ito and T. Ito, *J. Chem. Soc., Chem. Commun.* 1984, 1453.
3. D. A. Atwood, V. O. Atwood, A. H. Cowley, J. L. Atwood and E. Román, *Inorg. Chem.* 1992, **31**, 3872.
4. N. W. Alcock, N. C. Blacker and M. G. H. Wallbridge, *J. Organomet. Chem.* 1991, **419**, C23.
5. G. R. Willey and M. D. Rudd, *Polyhedron* 1992, **11**, 2805.
6. D. R. Neves and J. C. Dabrawiak, *Inorg. Chem.* 1976, **15**, 129.
7. A. J. Arduengo, III, M. Kline, J. C. Calabrese and F. Davidson, *J. Am. Chem. Soc.* 1991, **113**, 9704.

Polyhedron Vol. 12, No. 16, pp. 2075–2077, 1993
Printed in Great Britain

0277-5387/93 $6.00+.00
© 1993 Pergamon Press Ltd

COMMUNICATION

$BaCo_2Si_2O_7$: A NEW ONE-DIMENSIONAL ANTIFERROMAGNET BASED ON CHAINS OF OXIDE BRIDGED CoO_4 TETRAHEDRA

RICHARD D. ADAMS* and RALPH LAYLAND

Department of Chemistry and Biochemistry, University of South Carolina, Columbia, SC 29208, U.S.A.

and

TIMIR DATTA

Department of Physics, University of South Carolina, Columbia, SC 29208, U.S.A.

and

CHRISTOPHE PAYEN*

Institut des Matériaux de Nantes, 2 rue de la Houssinière, 44072, Nantes Cedex 03, France

(*Received* 20 *May* 1993; *accepted* 14 *May* 1993)

Abstract—The new compound $BaCo_2Si_2O_7$ was obtained by heating the mixture $BaCO_3$, $CoCO_3$ and SiO_2 to 1300°C for 48 h. The material was characterized by single-crystal X-ray diffraction and magnetic susceptibility measurements. Each cobalt ion is surrounded by four oxygen atoms arranged in a distorted tetrahedral shape. These tetrahedra are linked into chains through the sharing of one of the oxygen atoms. The CoO_4 chains are cross-linked by bridging Si_2O_7 groups. The barium ions occupy channels that run parallel to the crystallographic *c*-axis. The effective magnetic moment, $\mu_{eff} = 4.70$ B.M., at 25°C is consistent with Co^{2+} in a tetrahedral environment having three unpaired electrons. Antiferromagnetic coupling of the electrons occurs between the nearest neighbour cobalt ions, as indicated by the sign of the Weiss constant, $\theta_p = -46$ K, and by the presence of a broad maximum in the susceptibility curve. At 26 K it undergoes a three-dimensional magnetic transition into a field-induced weak ferromagnet that is characteristic of a one-dimensional metamagnet.

Low-dimensional materials having anisotropic transport and magnetic properties have been the source of great interest.[1] Efforts to synthesize these materials have recently attracted considerable attention.[2] We now report the preparation, structural characterization and magnetic properties of the new material, $BaCo_2Si_2O_7$. Pure $BaCo_2Si_2O_7$ was obtained from the solid-state reaction of $BaCO_3$, $CoCO_3$, and SiO_2 by heating to 1300°C for 48 h.† Its three-dimensional structure was estab-

* Authors to whom correspondence should be addressed.

† A mixture of $BaCO_3$ (0.789 g, 4 mmol), $CoCO_3$ (0.9515 g, 8 mmol) and SiO_2 (0.4816 g, 8.01 mmol) was ground thoroughly in a mortar and then transferred to a platinum crucible. The crucible was placed in the oven (Lindberg Model 51333) and heated in air to 1300°C for 48 h. After this period the oven was cooled slowly (approx. 1°C min^{-1}) to 1000°C, and then allowed to cool quickly to 500°C. At this temperature the sample was removed from the oven.

lished by a single-crystal X-ray diffraction analysis. A projection of the crystallographic unit cell perpendicular to the *bc*-plane is shown in Fig. 1. Each cobalt ion is surrounded by four oxygen atoms arranged in the form of a distorted tetrahedron. These are represented by the tetrahedral shapes in the figure. The tetrahedra are linked into chains through the sharing of one of the oxygen atoms. Tetrahedral CoO_4 ions are exceedingly rare and there are no previous examples of such groupings that are linked to form chains.[3] The CoO_4 chains are cross-linked by Si_2O bridges that form Si_2O_7 groups by using the oxygen atoms surrounding the cobalt ions. The barium ions occupy channels that run parallel to the *c* crystallographic axis.*

Magnetic susceptibility measurements of $BaCo_2Si_2O_7$ show that it is paramagnetic with an effective magnetic moment, μ_{eff}, of 4.70 B.M. at 25°C.† This value is typical of a cobalt(II) ion in a tetrahedral environment with three unpaired electrons.[4] Antiferromagnetic coupling was indicated by a negative Weiss constant, $\theta_p = -46$ K, derived from the linear dependence of the inverse susceptibility, χ^{-1} vs *T*, and by the presence of a broad maximum in the susceptibility curve, near 35 K, which is typical of a low-dimensional antiferromagnet, see Fig. 2. At low temperatures the magnetic properties are very unusual. At 27 K the magnetic response increases rapidly and reaches a broad maximum at approximately 10 K, see Fig. 2. Isothermal magnetization measurements, shown in Fig. 3, have established that the transition is due to a weak *field-induced* ferromagnetic response. Above the transition temperature at 40 K only the anticipated linear paramagnetic response is observed, but at 12 K and 18 K the magnetization increases rapidly to a maximum of approximately 0.4 B.M./Co atom as soon as the magnetic field is applied. At 2.5 K and 5 K the magnetization initially increases slowly to

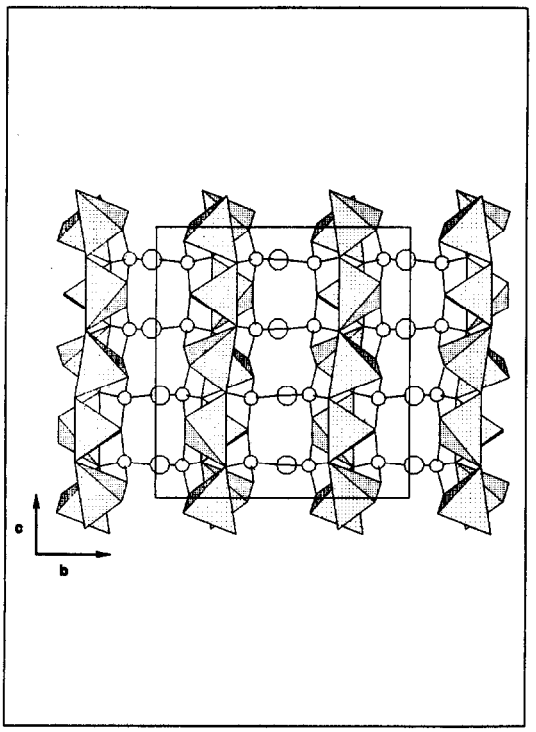

Fig. 1. A projection of the *bc*-plane of the solid-state structure of $BaCo_2Si_2O_7$ showing the chains of CoO_4 tetrahedra running parallel to the *c*-axis. CoO_4 tetrahedra are represented by the shaded polyhedra. Bonds between the silicon (small circles) and oxygen atoms are shown but the oxygen atoms are not drawn. The connectivities of the barium atoms (large circles) are not shown.

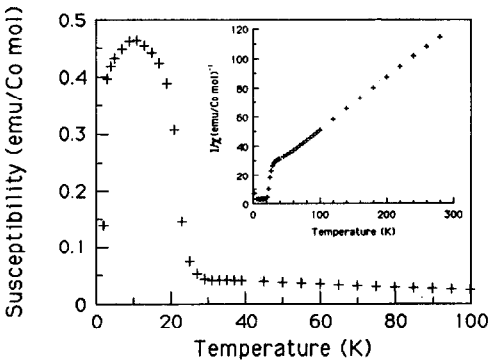

Fig. 2. A plot of the magnetic susceptibility of $BaCo_2Si_2O_7$ measured a 5 kOe in the range 2–100 K shows the broad 1D maximum at *ca* 35 K and the weak ferromagnetic response below 27 K. The insert shows a plot of the inverse susceptibility over the temperature range 2–280 K.

* A deep royal blue crystal was cleaved from the bulk and analysed by single-crystal diffractometry. Space group = *C*2/*c*, $a = 7.2131(6)$, $b = 12.781(1)$, $c = 13.762(1)$ Å, $\beta = 90.299(8)°$, $Z = 8$, 1370 reflections [$I > 3.0\sigma(I)$], $R = 0.042$. Diffraction measurements at 20°C were made on a Rigaku AFC6S four-circle diffractometer using Mo-K_α radiation. The structure solution and refinement was made by using the TEXSAN structure solving program library (v5.0) of the Molecular Structure Corp., The Woodlands, TX. An empirical absorption correction was applied to the data. An X-ray powder analysis showed the bulk sample to be pure $BaCo_2Si_2O_7$.

† Magnetic measurements were performed on a Quantum Design SQUID magnetometer using $BaCo_2Si_2O_7$ (41.9 mg), randomly-oriented small single crystals. The measurements were corrected for diamagnetism and effects of the sample holder. The sample was first cooled in the absence of an applied field. The susceptibility was then measured upon warming in a static field of 5 kOe. The Curie–Weiss law is obeyed in the region 120–220 K. The Curie constant $C = 2.8$ emu K^{-1} mol^{-1} and corresponds to $\mu_{eff} = 4.70$ B.M.

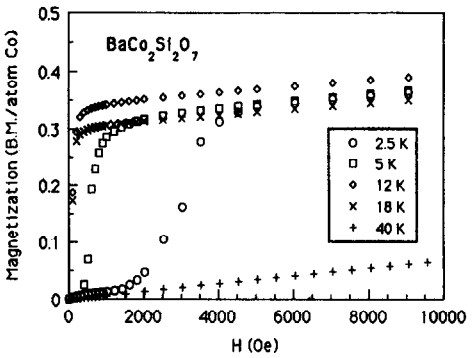

Fig. 3. Isothermal magnetization plots of $BaCo_2Si_2O_7$, μ (B.M./Co atom) vs H (Oersteds), at five different temperatures.

threshold values of 2000 Oe and 500 Oe, respectively, and then rapidly to approximately the same maximum value observed at 12 K and 18 K. Field-induced ferromagnetic phase transitions are characteristic of low-dimensional metamagnets and can be explained by a canting of the electron spins away from the principal magnetic axis.[5] The observation of the threshold fields cannot be attributed to spin-flop behaviour since neither saturation effects nor a weak ferromagnetic response of χ would have been observed for a spin-flop co-linear antiferromagnet.[6]

Supplementary materials available. Tables of crystal data, positional parameters, interatomic distances and angles, anisotropic thermal parameters and tables of structure factors (16 pages) for the structural analyses are available from the author RDA.

REFERENCES

1. (a) C. Schlenker and J. Dumas, *Crystal Chemistry and Properties of Materials with Quasi-One-Dimensional Structures. A Chemical and Physical Synthetic Approach* (Edited by J. Rouxel), p. 135. D. Reidel Publishing Co, Dordrecht/Boston/Lancaster/Tokyo (1986); (b) R. M. Metzger, P. Day and G. C. Papavassiliou (Editors), *Lower-Dimensional Systems and Molecular Electronics*. Plenum, New York (1990); (c) R. J. Cava, *Science* 1990, **247**, 656; (d) C. P. Poole Jr, T. Datta and H. A. Farach, *J. Superconduct.* 1989, **2**, 369; (e) M. Greenblatt, *Chem. Rev.* 1988, **88**, 31; (f) J. S. Miller and A. J. Epstein, *Prog. Inorg. Chem.* 1976, **20**, 1; (g) S. Wang and S.-J. Hwu, *J. Am. Chem. Soc.* 1992, **114**, 6920.
2. (a) A. Simon, *Angew. Chem., Int Edn Engl.* 1988, **27**, 159; (b) J. D. Corbett, in *Perspectives in Coordination Chemistry* (Edited by A. F. Williams, C. F. Floriani and A. E. Merbach), p. 219. VCH Publishers, Weinheim (1992); (c) R. P. Ziebarth, J. D. Corbett, *Accts Chem. Res.* 1989, **22**, 256; (d) J. D. Corbett, *Pure. Appl. Chem.* 1984, **56**, 1527; (e) G. Meyer, *Chem. Rev.* 1988, **88**, 93.
3. (a) M. Kimata, *Naturwis.* 1982, **69**, 40; (b) A. Riou and A. Lecerf, *Acta Cryst.* 1975, **B31**, 2487; (c) H. Yamaguchi, K. Akatsuka, M. Setoguchi and Y. Takaki, *Acta Cryst.* 1979, **B35**, 2680.
4. L. Banci, A. Bencini, C. Benelli, D. Gatteschi and C. Zanchini, *Struct. Bonding* 1982, **52**, 37.
5. E. Stryjewski and N. Giordano, *Adv. Phys.* 1977, **26**, 487.
6. A. Tressaud and J.-M. Dance, *Struct. Bonding* 1982, **52**, 87.

Polyhedron Vol. 12, No. 16, pp. 2079–2080, 1993
Printed in Great Britain

0277–5387/93 $6.00+.00
© 1993 Pergamon Press Ltd

COMMUNICATION

FIRST *ORTHO*-PALLADATION OF UNSUBSTITUTED BENZYLAMINE BY PALLADIUM(II) ACETATE

YOSHIO FUCHITA* and HAJIME TSUCHIYA

Laboratory of Chemistry, College of General Education, Kyushu University, Ropponmatsu, Chuo-ku, Fukuoka 810, Japan

(*Received* 27 *April* 1993; *accepted* 11 *May* 1993)

Abstract—The first *ortho*-palladation of unsubstituted benzylamine, achieved by the reaction of palladium(II) acetate with benzylamine in benzene at 60°C, is reported.

In 1968 Cope and Friedrich discovered that N,N-dimethylbenzylamine undergoes *ortho*-metallation on reaction with $PdCl_4^{2-}$, but that benzylamine itself did not.[1] Later Lewis and co-workers showed that disubstitution at the benzylic carbon also promotes *ortho*-palladation.[2] Shaw suggested that the reason for the different behaviour is that the disubstituted compounds lose less internal entropy on cyclization compared with the parent compounds, namely *gem*-disubstituted effect.[3] Furthermore, 10 years before Avshu and co-workers succeeded in preparing the *ortho*-palladated complex of benzylamine, $[\{PdI(C_6H_4CH_2NH_2)\}_2]$, by treating the adduct $[PdI_2(PhCH_2NH_2)_2]$ with a silver(I) salt. This finding is of value in a sense that *ortho*-palladation proceeds via a three-coordinate intermediate which was formed by abstraction of iodide by silver(I),[4] but did not change the general fundamental rule that direct activation of C—H bonds by palladium(II) to afford corresponding palladacycles is the most feasible in the case of tertiary amines, whereas primary and secondary amines are usually inert toward such activation.

Recently, we have found that N-methylbenzylamine can *ortho*-palladate on reaction with palladium(II) acetate, showing the higher ability for C—H bond activation of palladium(II) acetate compared with $PdCl_2$ or $PdCl_4^{2-}$.[5] This experience prompted us to investigate the reaction with benzylamine and we have found that even unsubstituted benzylamine can be *ortho*-palladated by palladium(II) acetate.

Palladium(II) acetate reacted with benzylamine in benzene at 60°C for 1 day to give yellow crystals $[\{Pd(C_6H_4CH_2NH_2)(\mu\text{-}O_2CMe)\}_2]$ (**1**). Its IR spectrum showed characteristic bridging acetato bands at 1570 and 1410 cm^{-1}. The ^1H NMR spectrum of **1** exhibited only one acetato-methyl signal at δ 2.09, indicating that **1** has the *anti* structure **A** and excluding the presence of the *syn* isomer **B** (Fig. 1). If complex **1** has the *syn* structure the two non-equivalent acetato-methyl groups are expected to have different chemical shifts. Reflecting the characteristic folded structure of the acetato-bridged dimer, two protons of the methylene group and those of the amino group were observed non-equivalently at δ 3.2 (complex) and 3.9 (complex) and at δ 2.95 (br) and 3.6 (br), respectively. As for the aromatic protons they appeared at δ 6.7–7.0 (8H) as multiplets. On the basis of these results and elemental analysis **1** was assigned to the dinuclear cyclopalladated complex of benzylamine having the *anti* configuration **A**.

The acetato bridged complex **1** reacted with NaCl to give the chloro-bridged analogue $[\{Pd(C_6H_4CH_2NH_2)(\mu\text{-}Cl)\}_2]$ (**2**), which was almost insoluble in common organic solvents. However, soluble mononuclear complexes $[PdCl(C_6H_4CH_2NH_2)$(3,5-lutidine)] (**3**) and $[PdCl(C_6H_4CH_2NH_2)$(2-picoline)] (**4**) were obtained on treatment of **2** with 3,5-lutidine and 2-picoline, respectively. The ^1H NMR spectrum ($CDCl_3$) of **3** exhibited aromatic protons in the *o*-phenylene moiety at

* Author to whom correspondence should be addressed.

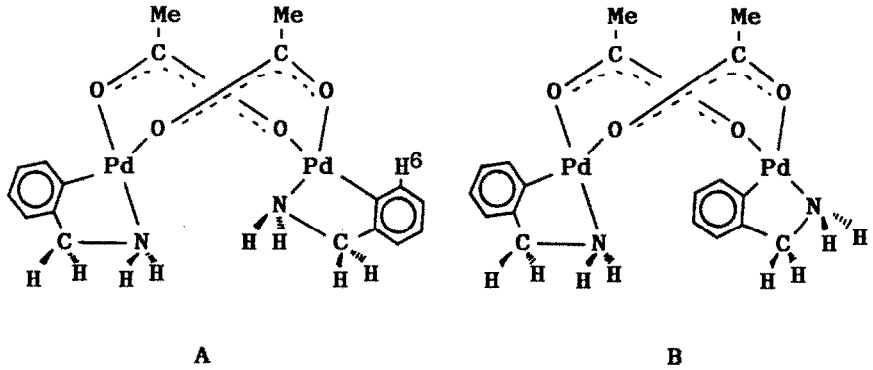

A B

Fig. 1. Structure of $[\{Pd(C_6H_4CH_2NH_2)(\mu\text{-}O_2CMe)_2\}]$ (1).

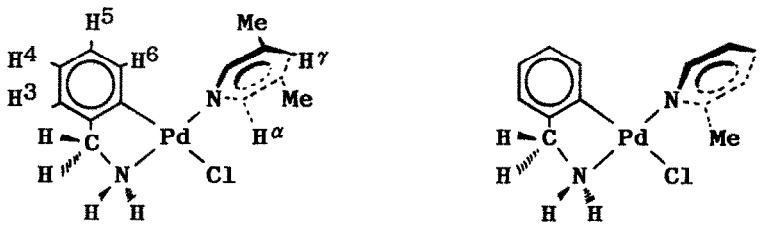

3 4

Fig. 2. Structures of $[PdCl(C_6H_4CH_2NH_2)(3,5\text{-lutidine})]$ (3) and $[PdCl(C_6H_4CH_2NH_2)(2\text{-picoline})]$ (4).

δ 6.41 [d, ^3J(HH) = 8.3 Hz, 1H], 6.6 (m, 1H) and 7.0 (m, 2H), together with two singlets due to H^α (δ 8.53) and H^γ (δ 7.42) of the 3,5-lutidine ligand. The doublet was assigned to H^6 of the *o*-phenylene moiety, in consideration of the magnetic anisotropy of the pyridine ring (Fig. 2). The benzylic protons were observed as a triplet owing to the coupling with NH_2 at δ 4.24 [^3J(HH) = 5.9 Hz], whereas NH_2 appeared as a broad signal at δ 3.8. As for the ^{1}H NMR spectrum ($CDCl_3$) of **4**, reflecting the unsymmetrical structure of the 2-picoline ligand which coordinates to the palladium atom perpendicular to the palladium square planar plane (Fig. 2), two protons of the amino group resonated separately at δ 3.8 and 4.3 as broad signals, while the benzyl-methyl protons were observed as a triplet at δ 4.25 [^3J(HH) = 5.4 Hz]. The above NMR data of **3** and **4** confirmed unambiguously the *ortho*-palladated structure of benzylamine and the formation of the 2-aminomethylphenyl-C^1, N chelate ring.

In conclusion our results show that palladium(II) acetate is a much better palladium(II) species for direct C—H bond activation than $PdCl_4^{2-}$. This difference might come from the enhanced electrophilicity of palladium(II) acetate itself and/or easier generation of coordinatively unsaturated species by losing one benzylamine from the initially formed bis-adduct $[Pd(O_2CMe)_2(PhCH_2NH_2)_2]$ compared with the adduct $[PdCl_2(PhCH_2NH_2)_2]$, owing to a relatively bulkier acetato ligand compared with the chloro ligand. Details are currently being investigated.

REFERENCES

1. A. C. Cope and E. C. Friedrich, *J. Am. Chem. Soc.* 1968, **90**, 909.
2. B. N. Cockburn, D. V. Howe, T. Keating, B. F. G. Johnson and J. Lewis, *J. Chem. Soc., Dalton Trans.* 1973, 404.
3. B. L. Shaw, *J. Am. Chem. Soc.* 1975, **97**, 3856.
4. A. D. Ryabov, *Chem. Rev.* 1990, **90**, 403.
5. Y. Fuchita and H. Tsuchiya, *Inorg. Chim. Acta*, 1993, **209**, 229.

Polyhedron Vol. 12, No. 17, pp. 2081–2090, 1993
Printed in Great Britain

0277–5387/93 $6.00+.00
© 1993 Pergamon Press Ltd

THE SYNTHESES AND STRUCTURES OF TWO LARGE IODOANTIMONATE ANIONS

CLAIRE J. CARMALT and NICHOLAS C. NORMAN*

Department of Chemistry, The University of Newcastle upon Tyne, Newcastle upon Tyne NE1 7RU, U.K.

and

LOUIS J. FARRUGIA

Department of Chemistry, The University of Glasgow, Glasgow G12 8QQ, U.K.

(*Received* 6 *April* 1993; *accepted* 10 *May* 1993)

Abstract—The structures of two iodoantimonate anions are reported, viz. $[Sb_8I_{28}]^{4-}$ and $[Sb_5I_{18}]^{3-}$ both of which resulted from hydrolysis in reactions between SbI_3, $AgBF_4$ and two equivalents of either DMPU or HMPA, respectively. The cations in the former case are $[H(DMPU)_2]^+$ and in the latter case are $[H(HMPA)_2]^+$, both of which contain O···H···O hydrogen bonds. The structure of a similar cation $[H(OPPh_3)_2]^+$, as its $[ICl_4]^-$ salt, is also described.

Antimony and bismuth trihalides readily form adducts with extra halide ions to give halogenoanions, for which a large number of structural types are known.[1] Most of the discrete anions which have been characterized (as opposed to polymeric forms) contain between two and four antimony or bismuth atoms, but in recent years a number of ionic complexes have been isolated in which anions containing up to eight antimony or bismuth atoms are present. Notable in this regard is the work of Pohl, to which we will refer later in more detail. Herein we describe the structures of two iodoantimonate anions, $[Sb_8I_{28}]^{4-}$ and $[Sb_5I_{18}]^{3-}$, the latter having an unprecedented structure, obtained as a result of adventitious hydrolysis in reactions involving antimony tri-iodide and two-electron, oxygen-donor ligands.

RESULTS AND DISCUSSION

The reaction between antimony tri-iodide, SbI_3, 1 equivalent of $AgBF_4$ and 2 equivalents of N,N′-dimethylpropylene urea (DMPU) in THF solution afforded, after work-up, an orange crystalline product. Spectroscopic and analytical data indicated, however, that no BF_4^- was present and, therefore, that a product of, or similar to, the anticipated formula $[SbI_2(DMPU)_2][BF_4]$ had not been formed. The nature of the crystalline material was established by X-ray crystallography (on crystals obtained by recrystallization of the orange powder from chlorobenzene/Et_2O mixtures) and found to be ionic with the formula $[H(DMPU)_2]^+_4[Sb_8I_{28}]^{4-}\cdot xC_6H_5Cl$ (**1**), the origin of which is clearly due to hydrolysis, most probably from traces of moisture associated with $AgBF_4$ which is hygroscopic.

The unit cell of **1** contains a crystallographically centrosymmetric $[Sb_8I_{28}]^{4-}$ anion, four $[H(DMPU)_2]^+$ cations (two per asymmetric unit) and two disordered C_6H_5Cl molecules (one per asymmetric unit) with no significantly short intermolecular or interionic contacts; selected bond lengths and angles for the anion are given in Table 1. A view of one of the two crystallographically independent cations ($\mathbf{1}^+$) is shown in Fig. 1 and in the diagram (the second is similar in all respects). Each cation consists of two DMPU molecules and a proton which, although not directly located, is assumed to lie between the two oxygen atoms in the form of an O···H···O hydrogen bond, in view

*Author to whom correspondence should be addressed.

Table 1. Selected bond lengths (Å) and angles (°) for **1**

Sb(1)—I(1)	2.798(2)	Sb(1)—I(2)	2.822(2)
Sb(1)—I(3)	2.771(2)	Sb(1)—I(4)	3.348(2)
Sb(1)—I(5)	3.350(2)	Sb(1)—I(11)	3.477(1)
Sb(2)—I(4)	2.933(2)	Sb(2)—I(5)	3.000(2)
Sb(2)—I(6)	2.761(1)	Sb(2)—I(7)	3.094(2)
Sb(2)—I(8)	3.159(2)	Sb(2)—I(8)	3.477(1)
Sb(3)—I(5)	3.494(1)	Sb(3)—I(7)	3.085(2)
Sb(3)—I(8)	3.188(2)	Sb(3)—I(9)	2.753(1)
Sb(3)—I(10)	2.914(2)	Sb(3)—I(11)	3.016(2)
Sb(4)—I(2)	3.580(2)	Sb(4)—I(10)	3.454(2)
Sb(4)—I(11)	3.398(2)	Sb(4)—I(12)	2.754(2)
Sb(4)—I(13)	2.788(2)	Sb(4)—I(14)	2.783(2)
I(1)—Sb(1)—I(2)	96.7(1)	I(1)—Sb(1)—I(3)	95.5(1)
I(1)—Sb(1)—I(4)	90.9(1)	I(1)—Sb(1)—I(5)	170.5(1)
I(1)—Sb(1)—I(11)	91.4(1)	I(2)—Sb(1)—I(3)	94.3(1)
I(2)—Sb(1)—I(4)	171.5(1)	I(2)—Sb(1)—I(5)	91.9(1)
I(2)—Sb(1)—I(11)	89.6(1)	I(3)—Sb(1)—I(4)	88.7(1)
I(3)—Sb(1)—I(5)	87.7(1)	I(3)—Sb(1)—I(11)	171.5(1)
I(4)—Sb(1)—I(5)	80.3(1)	I(4)—Sb(1)—I(11)	86.4(1)
I(5)—Sb(1)—I(11)	84.7(1)	I(4)—Sb(2)—I(5)	93.4(1)
I(4)—Sb(2)—I(6)	93.8(1)	I(4)—Sb(2)—I(7)	89.5(1)
I(4)—Sb(2)—I(8)	174.0(1)	I(4)—Sb(2)—I(8)	86.6(1)
I(5)—Sb(2)—I(6)	94.2(1)	I(5)—Sb(2)—I(7)	173.0(1)
I(5)—Sb(2)—I(8)	89.0(1)	I(5)—Sb(2)—I(8)	87.6(1)
I(6)—Sb(2)—I(7)	92.0(1)	I(6)—Sb(2)—I(8)	91.6(1)
I(6)—Sb(2)—I(8)	178.2(1)	I(7)—Sb(2)—I(8)	87.6(1)
I(7)—Sb(2)—I(8)	86.2(1)	I(8)—Sb(2)—I(8)	87.9(1)
I(5)—Sb(3)—I(7)	84.3(1)	I(5)—Sb(3)—I(8)	84.4(1)
I(5)—Sb(3)—I(9)	176.8(1)	I(5)—Sb(3)—I(10)	87.4(1)
I(5)—Sb(3)—I(11)	89.6(1)	I(7)—Sb(3)—I(8)	87.2(1)
I(7)—Sb(3)—I(9)	93.6(1)	I(7)—Sb(3)—I(10)	88.4(1)
I(7)—Sb(3)—I(11)	173.3(1)	I(8)—Sb(3)—I(9)	93.2(1)
I(8)—Sb(3)—I(10)	171.1(1)	I(8)—Sb(3)—I(11)	89.5(1)
I(9)—Sb(3)—I(10)	94.8(1)	I(9)—Sb(3)—I(11)	92.5(1)
I(10)—Sb(3)—I(11)	94.0(1)	I(2)—Sb(4)—I(10)	82.3(1)
I(2)—Sb(4)—I(11)	79.5(1)	I(2)—Sb(4)—I(12)	171.6(1)
I(2)—Sb(4)—I(13)	90.0(1)	I(2)—Sb(4)—I(14)	89.5(1)
I(10)—Sb(4)—I(11)	78.5(1)	I(10)—Sb(4)—I(12)	92.0(1)
I(10)—Sb(4)—I(13)	90.4(1)	I(10)—Sb(4)—I(14)	169.5(1)
I(11)—Sb(4)—I(12)	93.4(1)	I(11)—Sb(4)—I(13)	165.6(1)
I(11)—Sb(4)—I(14)	93.7(1)	I(12)—Sb(4)—I(13)	96.2(1)
I(12)—Sb(4)—I(14)	95.5(1)	I(13)—Sb(4)—I(14)	96.1(1)
Sb(1)—I(2)—Sb(4)	99.4(1)	Sb(1)—I(4)—Sb(2)	93.6(1)
Sb(1)—I(5)—Sb(2)	92.4(1)	Sb(1)—I(5)—Sb(3)	89.6(1)
Sb(2)—I(5)—Sb(3)	95.5(1)	Sb(2)—I(7)—Sb(3)	93.8(1)
Sb(2)—I(8)—Sb(2)	92.1(1)	Sb(2)—I(8)—Sb(3)	90.6(1)
Sb(2)—I(8)—Sb(3)	92.5(1)	Sb(3)—I(10)—Sb(4)	93.6(1)
Sb(1)—I(11)—Sb(3)	95.8(1)	Sb(1)—I(11)—Sb(4)	91.0(1)
Sb(3)—I(11)—Sb(4)	92.9(1)		

of the short O···O distances observed [2.37(2) and 2.39(2) Å] which are typical of such hydrogen bonded systems.

The structure of the $[Sb_8I_{28}]^{4-}$ anion ($\mathbf{1}^{4-}$) is shown in Fig. 2 and diagramatically. The simplest description of the structure is in terms of three layers

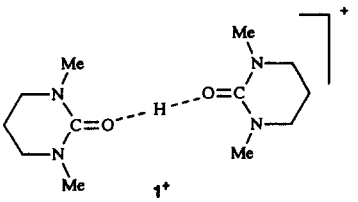

$\mathbf{1}^{+}$

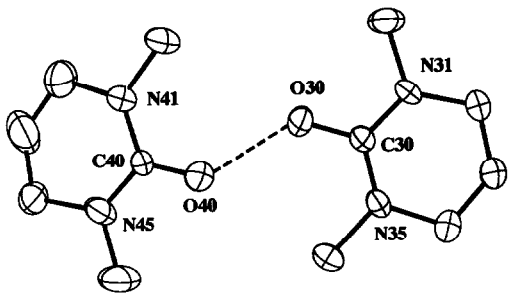

Fig. 1. A view of one of the $[H(DMPU)_2]^+$ cations in **1** ($\mathbf{1}^+$) showing the atom numbering scheme. Hydrogen atoms are omitted and the O···H···O interaction is indicated as a dotted line. Ellipsoids are drawn at the 20% probability level.

of closely packed iodine atoms with the antimony atoms occupying all of the octahedral holes. The iodines are present in terminal positions as well as in μ_2- and μ_3-bridging sites with Sb—I bond lengths in the ranges 2.753(1)–2.798(1), 2.822(1)–3.580(1) and 3.000(1)–3.494(1) Å, respectively; all of which are usual and deserve no special comment. The structure of $\mathbf{1}^{4-}$ is the same as that found in the salt $[Ph_4P]_4[Sb_8I_{28}]$ (**2**) reported by Pohl *et al.*,[2] although a different isomeric form is found in the structures of $[Me_4N]_4[Sb_8I_{28}]$ (**3**) and $[Me_3S]_4[Sb_8I_{28}]$ (**4**).[3] In **3** and **4** the $[Sb_8I_{28}]^{4-}$ anions have a more three-dimensional structure which is based on an approximately planar $[Sb_6I_{22}]^{4-}$ unit with additional SbI_3 groups coordinated on either site.

We will not comment in detail here on the structural complexity of iodoantimonate anions or related species (see ref. 1 for a general discussion and also refs. 2 and 3), but we draw attention to the fact that the structure of the $[Sb_8I_{28}]^{4-}$ anion found in **1** and **2** can be considered as the fourth member of a series with the general formula $[E_{2n}X_{6n+4}]^{4-}$. Examples of anions for $n = 1$ include $K_4[Bi_2Br_{10}]\cdot 4H_2O$,[4] $[C_2H_{10}N_4S]_2[Bi_2Cl_{10}]\cdot 4H_2O$,[5] $[C_2H_5N_4S]_4[Bi_2Br_{10}]$[6] and $[Sr(H_2O)_8]_2[Bi_2Br_{10}]$[7] and for $n = 2$ include $[Fe(\eta\text{-}C_5H_5)_2]_4[Bi_4Br_{16}]$,[8] $[C_2H_4N_3S]_4[Bi_4Br_{16}]$[9] and $[Mg(MeCN)_6]_2[Bi_4Cl_{16}]$.[10] For $n = 3$ the only examples so far characterized are $[Et_4P]_4[Bi_6I_{22}]$[11] and $[Fe(\eta\text{-}C_5H_5)_2]_4[Sb_6I_{22}]$,[12] although an isomeric form is found in the structure of $[Fe(phen)_3]_2[Sb_6I_{22}]\cdot 2MeCN$.[13]

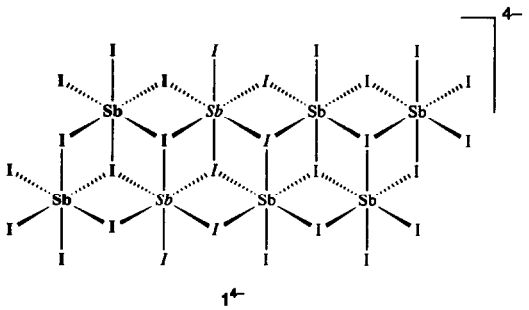

The structural relationship within this series is illustrated in the diagram of $\mathbf{1}^{4-}$. Complexes of the general formula $[E_2X_{10}]^{4-}$ (i.e. for $n = 1$) have an edge-shared bi-octahedral structure, as shown for the atoms on the left-hand side in bold face. Addition of an E_2X_6 unit, shown in italic face, affords the next member of the series $[E_4X_{16}]^{4-}$, where $n = 2$, and the third and fourth members of the series are constructed accordingly. Judicious choice of the cation(s) will no doubt allow structures with $n > 4$ to be synthesized. The isomeric structures of the form $[E_6X_{22}]^{4-}$ and $[E_8X_{28}]^{4-}$ result from a less symmetrical addition of successive E_2X_6 units; in fact these structures are based on the preceding $[E_{2n}X_{6n+4}]^{4-}$ structure, i.e. for $n-1$, where

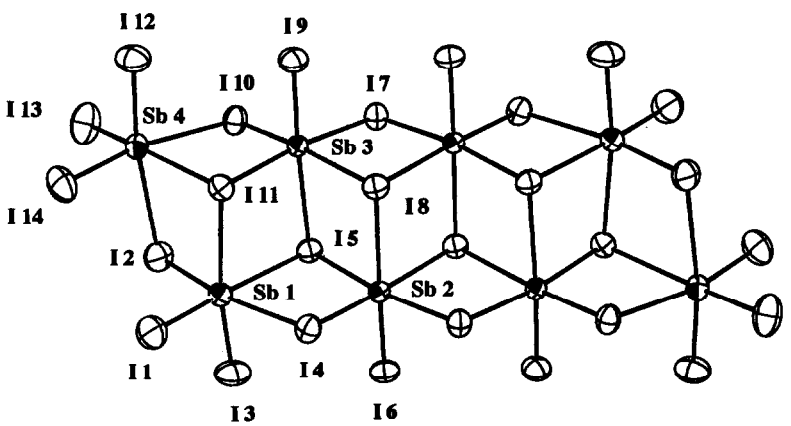

Fig. 2. A view of the centrosymmetric $[Sb_8I_{28}]^{4-}$ anion ($\mathbf{1}^{4-}$) showing the atom numbering scheme. Non-labelled atoms are related to the labelled atoms by a centre of symmetry at 0, 0, 0. Ellipsoids are drawn at the 50% level.

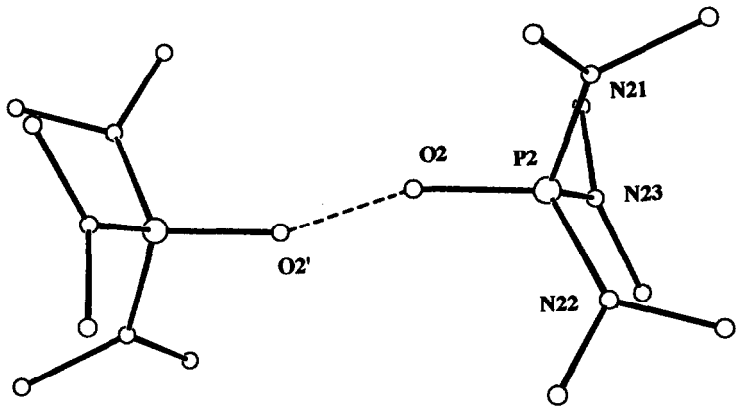

Fig. 3. A view of one of the $[H(HMPA)_2]^+$ cations in **5** (5^+) showing the atom numbering scheme. Hydrogen atoms are omitted and the O···H···O interaction is indicated as a dotted line. Atoms are drawn as circles of arbitrary size due to the large thermal motion associated with the NMe_2 groups.

the final E_2X_6 unit is added as separate EX_3 groups above and below the $[E_{2n}X_{6n+4}]^{4-}$ plane.

The analogous reaction between SbI_3, $AgBF_4$ and 2 equivalents of HMPA [hexamethylphosphoramide, $OP(NMe_2)_3$] also afforded an orange crystalline product, the nature of which was established by X-ray crystallography. The results of this analysis revealed an ionic compound having a similar constitution to **1** with the formula $[H(HMPA)_2]_3[Sb_5I_{18}]$ (**5**) and undoubtedly resulting from a similar hydrolysis reaction. The unit cell is centrosymmetric and contains one formula unit of **5** with each of the two asymmetric units containing one and a half cations $[H(HMPA)_2]^+$ (5^+) and half of the anion $[Sb_5I_{18}]^{3-}$ (5^{3-}). A picture of the cation lying on the centre of symmetry is shown in Fig. 3 and in the diagram. In neither of the cations were the protonic hydrogen atoms directly located, although, as in the case of the cations in **1**, their presence between the oxygen atoms is implied by the short O···O distances [O(1)—O(3) 2.41(2), O(2)—O(2′) 2.17(3) Å];* the P—O distances are P(1)—O(1) 1.552(13), P(2)—O(2) 1.515(19) and P(3)—O(3) 1.464(15) Å, and the P—O···O—P torsion angles are P(1)—O(1)—O(3)—P(3) 115(2) and P(2)—O(2)—O(2′)—P(2′) 180°.

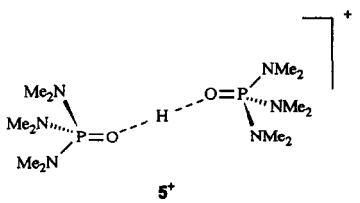

5^+

The structure of the anion 5^{3-} (shown in Fig. 4) has crystallographic C_i symmetry, although the molecular symmetry is close to D_{2h}. An illuminating description of the structure, particularly in terms of its electronic structure, is as an octahedral SbI_6^{3-} core in which four faces of the octahedron are capped by SbI_3 groups. This is reflected in the Sb—I bond lengths which are presented in Table 2. The shortest bonds are between the six terminal iodines, I(4)–I(9), and the antimony atoms to which they are bonded, Sb(2) and Sb(3), which range from 2.756(2) to 2.787(2) Å. The next longest bonds are to the central antimony, Sb(1), which range from 3.015(1) to 3.046(1) Å, with the longest interactions being between the face capping antimony atoms, Sb(2) and Sb(3), and the iodines I(1)–I(3), 3.393(1)–3.646(2) Å. The constraints of the structure are such that the iodines I(1)–I(3) are all triply bridging, although I(3) and the symmetry related I(3′) have a rather unusual T-shaped coordination geometry.† There is also a fairly close contact between I(5) and I(9), 3.866(1) Å.

We are not aware of any structures analogous to 5^{3-}, but an isomeric form is found in the structure

* The O(2)—O(2′) distance of 2.17(3) Å is very short, significantly more so than the other O···H···O bonds in **1**, **5** and **7** and O···H···O bonds in general. However, in view of the high thermal motion of the HMPA ligands and possible disorder (see Experimental) we cannot be confident of the accuracy of this value.

† A similar T-shaped geometry for a triply-bridging bromine and iodine is found in the structures of the halogenoarsenic anions in $[Et_3NH]_3[As_3Br_{12}]$ and $[Me_3NH]_3[As_3I_{12}]$, respectively.[26] Both of these anions are isostructural and, by analogy with the description given for 5^{3-}, can be viewed as a central, octahedral AsX_6^{3-} unit capped on two adjacent faces by AsX_3 molecules (X = Br, I).

Table 2. Selected bond lengths (Å) and angles (°) for **5**

Sb(1)—I(1)	3.046(1)	Sb(1)—I(2)	3.040(1)
Sb(1)—I(3)	3.015(1)	Sb(2)—I(1)	3.646(2)
Sb(2)—I(2)	3.605(2)	Sb(2)—I(3)	3.415(1)
Sb(2)—I(4)	2.765(2)	Sb(2)—I(5)	2.760(2)
Sb(2)—I(6)	2.756(2)	Sb(3)—I(1)	3.451(2)
Sb(3)—I(2)	3.568(2)	Sb(3)—I(3)	3.393(1)
Sb(3)—I(7)	2.767(2)	Sb(3)—I(8)	2.787(2)
Sb(3)—I(9)	2.773(2)		
I(1)—Sb(1)—I(1′)	180.0	I(1)—Sb(1)—I(2)	94.4(1)
I(1)—Sb(1)—I(2′)	85.6(1)	I(1)—Sb(1)—I(3)	89.8(1)
I(1)—Sb(1)—I(3′)	90.2(1)	I(2)—Sb(1)—I(2′)	180.0
I(2)—Sb(1)—I(3)	90.4(1)	I(2)—Sb(1)—I(3′)	89.6(1)
I(3)—Sb(1)—I(3′)	180.0	I(1)—Sb(2)—I(2)	69.5(1)
I(1)—Sb(2)—I(3)	74.5(1)	I(1)—Sb(2)—I(4)	161.1(1)
I(1)—Sb(2)—I(5)	101.2(1)	I(1)—Sb(2)—I(6)	92.3(1)
I(2)—Sb(2)—I(3)	74.8(1)	I(2)—Sb(2)—I(4)	97.4(1)
I(2)—Sb(2)—I(5)	99.1(1)	I(2)—Sb(2)—I(6)	158.3(1)
I(3)—Sb(2)—I(4)	89.1(1)	I(3)—Sb(2)—I(5)	173.4(1)
I(3)—Sb(2)—I(6)	89.4(1)	I(4)—Sb(2)—I(5)	94.2(1)
I(4)—Sb(2)—I(6)	97.1(1)	I(5)—Sb(2)—I(6)	95.9(1)
I(1)—Sb(3)—I(2)	72.1(1)	I(1)—Sb(3)—I(3)	77.7(1)
I(1)—Sb(3)—I(7)	96.2(1)	I(1)—Sb(3)—I(8)	163.9(1)
I(1)—Sb(3)—I(9)	93.6(1)	I(2)—Sb(3)—I(3)	76.2(1)
I(2)—Sb(3)—I(7)	159.7(1)	I(2)—Sb(3)—I(8)	92.7(1)
I(2)—Sb(3)—I(9)	102.8(1)	I(3)—Sb(3)—I(7)	85.3(1)
I(3)—Sb(3)—I(8)	93.8(1)	I(3)—Sb(3)—I(9)	171.1(1)
I(7)—Sb(3)—I(8)	96.6(1)	I(7)—Sb(3)—I(9)	94.3(1)
I(8)—Sb(3)—I(9)	95.1(1)	Sb(1)—I(1)—Sb(2)	81.2(1)
Sb(1)—I(1)—Sb(3)	81.3(1)	Sb(1)—I(1)—Sb(2)	81.2(1)
Sb(1)—I(1)—Sb(3)	81.3(1)	Sb(2)—I(1)—Sb(3)	97.6(1)
Sb(1)—I(2)—Sb(1)	0.0	Sb(1)—I(2)—Sb(2)	82.0(1)
Sb(1)—I(2)—Sb(3)	79.5(1)	Sb(1)—I(2)—Sb(2)	82.0(1)
Sb(1)—I(2)—Sb(3)	79.5(1)	Sb(2)—I(2)—Sb(3)	96.2(1)
Sb(1)—I(3)—Sb(2)	85.6(1)	Sb(1)—I(3)—Sb(3)	82.7(1)
Sb(1)—I(3)—Sb(2)	85.6(1)	Sb(1)—I(3)—Sb(3)	82.7(1)
Sb(2)—I(3)—Sb(3)	168.2(1)	Sb(3)—I(7)—I(7)	169.7(1)

of $[Me_4N]_3[Sb_5I_{18}]$ (**6**) reported by Pohl *et al.*[12] The structure of the $[Sb_5I_{18}]^{3-}$ anion in **6** ($\mathbf{6}^{3-}$) is shown in the diagram and has approximate C_{4v} symmetry with a μ_5-iodine in the basal plane. In terms of the structural description given above for $\mathbf{5}^{3-}$, we can look upon the structure of $\mathbf{6}^{3-}$ in terms of an SbI_6^{3-} octahedron with four edge-bridging SbI_3 groups, in which the four edges share a common vertex. The requirements of octahedral coordination around the bridging antimony atoms mean that each has two terminal iodines and two shared, μ_2-bridging iodines.

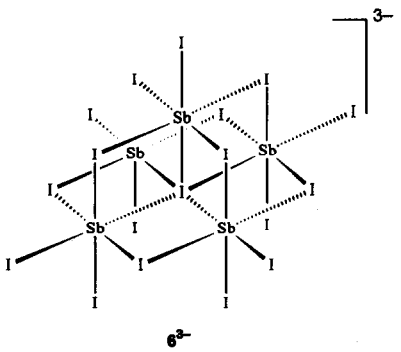

$\mathbf{6}^{3-}$

The structure of $\mathbf{5}^{3-}$, together with those of other iodoantimonate anions found in previous studies, illustrates the structural diversity in this field and this is almost certainly controlled by the nature of the cation and, probably to a lesser extent, by the solvent. In this regard we note the parallel with the structural chemistry of copper(I) halogenoanions,[14] wherein there is evidence that the species present in solution are relatively simple, the complex solid-state structures being a mani-

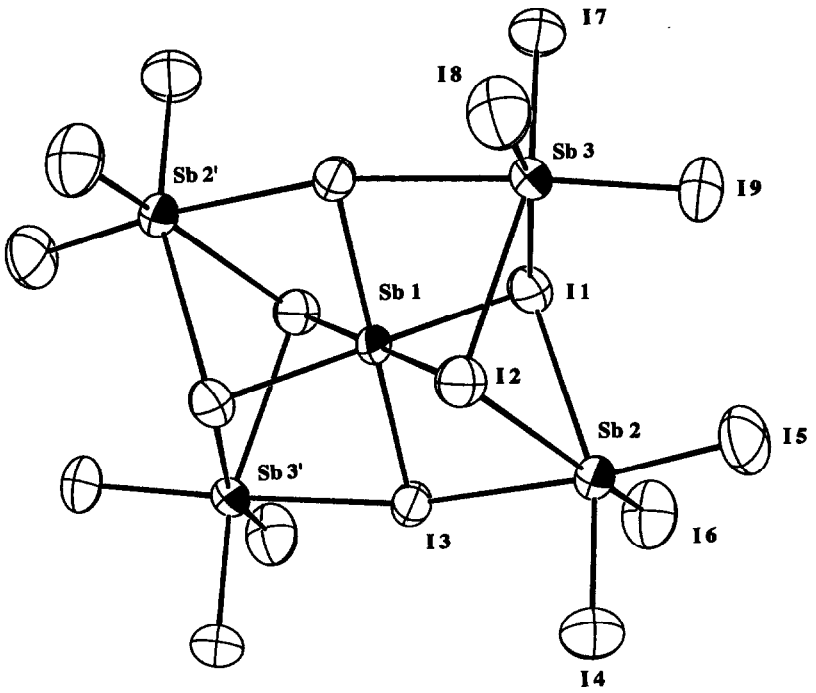

Fig. 4. A view of the centrosymmetric $[Sb_5I_{18}]^{3-}$ anion (5^{3-}) showing the atom numbering scheme. Non-labelled atoms are related to the labelled atoms by a centre of symmetry at 0, 0, 0, i.e. Sb(1). Ellipsoids are drawn at the 20% level.

festation of the crystallization process in which the nature of the cation (size and shape, etc.) is crucial.

The cation in **5** (5^+) is an example of a protonated phosphine oxide, which is hydrogen bonded to another phosphine oxide to give a complex cation of the form $R_3P{=}O\cdots H\cdots O{=}PR_3$. We obtained another example of this type of cation, viz. $[H(OPPh_3)_2]^+[ICl_4]^-$ (**7**), from the reaction between ICl_3 and two equivalents of Ph_3PO in CH_2Cl_2 resulting, as in the case of **5**, from partial hydrolysis, the structure of which is reported for comparison. The iodine of the $[ICl_4]^-$ anion in **7** resides on a crystallographic two-fold axis (0.0, *y*, 0.25), giving crystallographic C_{2v} symmetry although the actual molecular structure is very close to the expected D_{4h}, square-planar geometry. The only significant deviation from the idealized structure is in the I—Cl bond lengths, which differ by 0.037 Å (*ca* 18σ); I—Cl(1), 2.471(2), I—Cl(2) 2.508(2) Å. The cation $[H(OPPh_3)_2]^+$ (shown in Fig. 5) lies about a crystallographic inversion centre at 0.5, 0.0, 0.5. The presence of a hydrogen bonding interaction between the two phosphine oxides was indicated by the short O···O separation [O(1)—O(1′) 2.387(6) Å], which is comparable to the distances found in 5^+. However, in this case the hydrogen atom was located and the thermal parameter successfully refined, the O—H distance being 1.194(3) Å (the positional parameters are fixed at 0.5, 0, 0.5). Structurally characterized protonated phosphine oxides are not particularly common, but we note the structures of $Ph_3PO\cdots HF$,[15] $Ph_3PO\cdots HCl$[16] and $Ph_3PO\cdots HBr$.[17] The HBr complex with Ph_3PO has also been characterized as a hydrate (**8**), in which two Ph_3PO groups are hydrogen-bonded to an H_2O molecule which is, in turn, hydrogen bonded to HBr as shown below.[18] The P=O···O distances are 2.470(7) and 2.398(8) Å, although the protonic hydrogens were not detected.

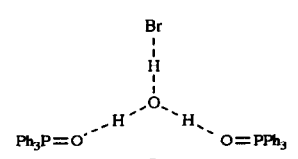

8

Other examples of O···H···O hydrogen bonds where one of the oxygen atoms is from a phosphine oxide are $Ph_3PO\cdots HOC(O)CH_2OC_6Cl_5$ [O···O 2.541(4) Å],[19] tri-*p*-tolylphosphine oxide hemihydrate [O···O 2.810(4) Å][20] and triphenylphosphine oxide hemihydrate [O···O 2.856(3) Å];[21] the O···O distances are understandably shorter in the cationic complexes.

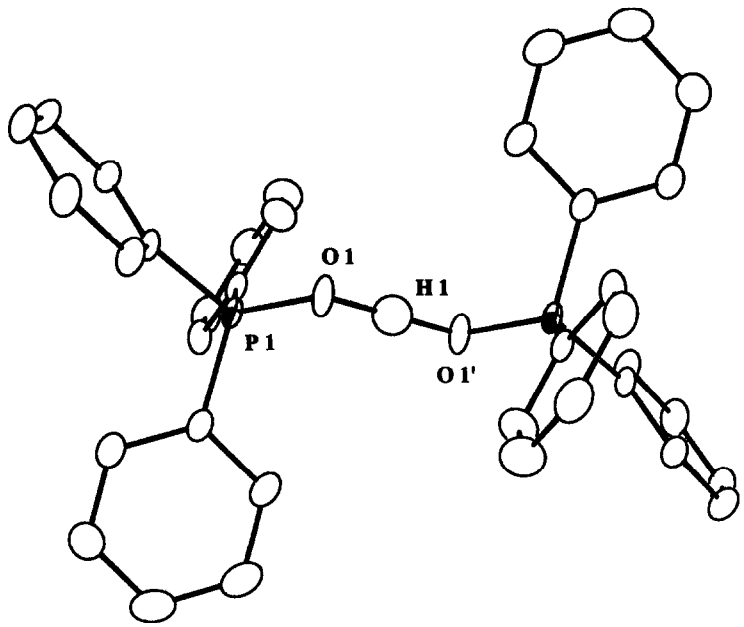

Fig. 5. A view of the $[H(OPPh_3)_2]^+$ cation in **7** showing the atom numbering scheme. Primed atoms refer to the symmetry operation $1-x, -y, 1-z$. Ellipsoids are drawn at the 20% level.

EXPERIMENTAL

General procedures

All reactions were performed using standard Schlenk techniques under an atmosphere of dry, oxygen-free dinitrogen. All solvents were distilled from appropriate drying agents immediately prior to use (sodium-benzophenone for THF, Et_2O and hexanes; CaH_2 for CH_2Cl_2; 4 Å molecular sieves for pyridine, nitromethane, chlorobenzene and 1,2-dichloroethane). SbI_3 (99%+), ICl_3, HMPA, DMPU, Ph_3PO and $AgBF_4$ were procured commercially and used without further purification. Microanalytical data were obtained at The University of Newcastle.

Preparations

$[H(DMPU)_2]_4[Sb_8I_{28}]$ **1**. DMPU (0.097 cm^3, 0.802 mmol) was added to a solution of of SbI_3 (0.201 g, 0.400 mmol) in THF (10 cm^3) resulting in a colour change from yellow to orange. $AgBF_4$ (0.078 g, 0.401 mmol) dissolved in THF (6 cm^3) was then added, which resulted in the formation of a pale yellow precipitate. The solution was stirred for 1 h and then filtered through Celite. The volume of the orange filtrate was reduced to *ca* 10 cm^3 by vacuum and hexane (25 cm^3) was added as an overlayer. Solvent diffusion over a period of days at $-30°C$ resulted in an orange oil. Crystallizations were attempted from CH_2Cl_2/hexane, pyridine-hexane and nitromethane/Et_2O, but X-ray quality crystals of **1** are finally obtained by solvent diffusion of Et_2O over a period of days into a chlorobenzene solution of the orange oil at room temperature (0.092 g, 32% based on antimony). Found: C, 12.1; H, 1.7; N, 3.5. Calc. for $C_{48}H_{100}I_{28}N_{16}O_8Sb_8 \cdot (C_6H_5Cl)_2$: C, 12.4; H, 1.9; N, 3.9%.

$[H(HMPA)_2]_3[Sb_5I_{18}]$ (**5**). HMPA (0.12 cm^3, 0.690 mmol) was added to a solution of SbI_3 (0.173 g, 0.344 mmol) in THF (10 cm^3), resulting in a colour change from yellow to orange. $AgBF_4$ (0.067 g, 0.344 mmol) dissolved in THF (6 cm^3) was then added, which resulted in the formation of a pale yellow precipitate. The solution was stirred for 1 h and then filtered through Celite. The volume of the orange filtrate was reduced to *ca* 10 cm^3 by vacuum and hexane (25 cm^3) was added as an overlayer. Solvent diffusion over a period of days at $-30°C$ resulted in an orange solid. Crystallizations were attempted from CH_2Cl_2/hexane, CH_2Cl_2/Et_2O and 1,2-dichloroethane/hexane, but X-ray quality crystals of **5** were finally obtained by solvent diffusion of Et_2O over a period of days into a CH_2Cl_2 solution of the orange solid at toom temperature (0.083 g, 30% based on antimony). Found; C, 11.3; H, 2.5; N; 5.8. Calc. for $C_{36}H_{111}I_{18}N_{18}O_6P_6Sb_5$: C, 11.1; H, 2.9; N, 6.5%.

$[H(OPPh_3)_2][ICl_4]$ (**7**). Ph_3PO (0.120 g, 0.431 mmol) was dissolved in CH_2Cl_2 (5 cm^3) and cooled to 0°C with an ice-bath. A solution of ICl_3 (0.050

Table 3. Crystallographic and structure solution data for compounds **1**, **5** and **7**

	1	**5**	**7**
Compound formula	$C_{48}H_{100}I_{28}N_{16}O_8Sb_8 \cdot (C_6H_5Cl)_x$	$C_{36}H_{111}I_{18}N_{18}O_6P_6Sb_5$	$C_{36}H_{31}Cl_4IO_2P_2$
M_r	2778.39 (not including C_6H_5Cl)	3971.28	684.5
Space group	$P\bar{1}$	$P\bar{1}$	$C2/c$
Crystal system	Triclinic	Triclinic	Monoclinic
a (Å)	13.484(1)	14.323(1)	19.726(3)
b (Å)	14.778(1)	15.323(1)	9.192(2)
c (Å)	20.515(1)	16.013(1)	20.700(5)
α (°)	70.167(4)	62.167(7)	
β (°)	84.696(5)	63.045(5)	105.42(2)
γ (°)	63.797(4)	79.798(7)	
V (Å^3)	3442.2(3)	2767.5(5)	3618(1)
Z	1	1	4
D_{calc} (g cm^{-3})	2.68 (not including C_6H_5Cl)	2.38	1.256
$F(000)$	2456 (not including C_6H_5Cl)	1800	1384
μ(Mo-K_α) (cm^{-1})	78.1 (not including C_6H_5Cl)	63.07	12.9
T (K)	298	298	298
Scan mode	$\theta/2\theta$	$\theta/2\theta$	$\theta/2\theta$
θ range (°)	$2 < \theta < 27.4$	$2 < \theta < 25.0$	$2 < \theta < 25.0$
Crystal size (mm)	$0.3 \times 0.2 \times 0.13$	$0.33 \times 0.33 \times 0.2$	$0.6 \times 0.3 \times 0.5$
Range of transmission coefficients	0.67–1.20	0.71–1.27	0.63–1.29
No. of data collected	18,032	10,079	6859
No. of unique data	15,597	9684	3179
hkl range	$0 \rightarrow 17, -19 \rightarrow 19, -26 \rightarrow 26$	$-17 \rightarrow 17, 0 \rightarrow 18, -19 \rightarrow 19$	$0 \rightarrow 23, 0 \rightarrow 10, -24 \rightarrow 24$
R_{merge}	0.038	0.032	0.041
Standard reflections	2 9 1, 2 0 $\bar{1}\bar{1}$, $\bar{7}$ $\bar{5}$ $\bar{5}$	$\bar{5}$ $\bar{3}$ 2, 0 $\bar{9}$ 5, $\bar{7}$ $\bar{1}$ $\bar{7}$	9 3 4, 10 $\bar{2}$ 4
Observability criterion	$I > 3\sigma(I)$	$I > 3\sigma(I)$	$I > 2\sigma(I)$
No. of data in refinement	7493	6176	2216
No. of refined parameters	533	442	170
Final R	0.042	0.049	0.043
Final R_w	0.052	0.060	0.060
Goodness of fit, S	1.82	2.30	2.54
Largest remaining feature in electron density map (e Å^{-3})	+1.12 (max), −1.49 (min)	+0.94 (max), −1.19 (min)	+0.58 (max), −0.81 (min)
Shift/e.s.d. in last cycle	0.42 (max), 0.10 (av)	2.6 (max), 0.11 (av)	0.077 (max), 0.004 (av)

g, 0.214 mmol) in CH_2Cl_2 (3 cm^3) was then added, which resulted in the formation of a bright yellow solution (ICl_3 is orange in CH_2Cl_2). Hexane (15 cm^3) was then layered over this solution and solvent diffusion over a period of days at −30°C afforded yellow crystals of **7** (0.087 g, 49% based on iodine). Some of these crystals were suitable for X-ray diffraction. Found: C, 51.7; H, 3.5. Calc. for $C_{36}H_{31}Cl_4IO_2P_2$: C, 52.3; H, 3.8%.

KBr disc IR spectra for all complexes showed absorptions due to the DMPU or phosphine oxide groups, but absorptions due to the O···H···O fragments were not detected.

X-ray crystallography

Crystallographic data and details of the data collection procedures and structure refinement for all structures are presented in Table 3. The following section deals with the structure of **1**; data for **5** where different are given in square brackets and data for **7** curly brackets. Data were collected on an Enraf–Nonius Turbo-CAD4 diffractometer, running under CAD4-Express software {Enraf–Nonius CAD4 diffractometer}, and with graphite monochromated *X*-radiation ($\lambda = 0.71069$ Å). Accurate unit cell parameters were determined by refinement of setting angles ($20.7° < \theta < 23.7°$) [$17.5° < \theta < 20.7°$] {$\theta \sim 12°$} of 25 reflections. Standard reflections were measured every 2 h during data collection and no significant variation in intensities was noted {a 6% decay was noted and corrected for}. Corrections were applied for Lorentz–polarization and absorption (DIFABS[22]) effects. {The systematic absences indicated either the centrosymmetric space group $C2/c$ or the non-centrosymmetric Cc. The former was chosen on the basis of E statistics and this choice was subsequently confirmed by successful solution and refinement.} The structure was solved for all antimony and iodine atoms by direct methods (SHELX86[23]) {the structure was solved by heavy atom methods for the iodine atom}. Subsequent difference syntheses gave all other atomic positions. All atoms were allowed anisotropic thermal motion. Hydrogen atoms were included at calculated positions (C—H 0.96 Å) and assigned thermal parameters 1.2 times that of the attached carbon atom [due to the extremely high thermal motion of the HMPA ligands, possibly disorder although this could not be modelled, no hydrogen atoms were included in the structure factor calculations]. {Phenyl hydrogens were included at calculated positions with C—H = 1.0 Å and were refined as rigid groups with idealized geometry (C—C = 1.395 Å), and allowed to ride on their attached carbon atoms during refinement. One common isotropic thermal parameter for all phenyl H atoms was refined.} The protonic hydrogens were not detected {the protonic hydrogen H(1) at the centre of inversion (0.5, 0, 0.5) was suspected from the short O···O contact and was observed in a difference map as a peak at 0.36 e $Å^{-3}$; a separate thermal parameter was refined for this hydrogen atom}. There was a severely disordered solvent molecule in the unit cell (presumably C_6H_5Cl), but it was not possible to model this satisfactorily. The electron density was finally modelled using a set of carbon atoms of full and half occupancy; atoms C(100)–C(110) [no solvent was present in crystals of **5** and **7**]. Refinement was by full matrix least-squares, with the function $\Sigma w(|F_o| - |F_c|)^2$ minimized, and with the weighting scheme $w = [\sigma^2(F_o)]^{-1}$ used and judged satisfactory. $\sigma(F_o)$ was estimated from counting statistics. Neutral atom scattering factors were taken from ref. 24 with corrections for anomalous dispersion. All calculations were carried out on a MicroVAX 3600 computer using the Glasgow GX suite of programs.[25]

Supplementary material available from the Cambridge Crystallographic Data Centre comprises complete tables of bond lengths and angles, atomic positional parameters, thermal parameters and hydrogen atom coordinates.

Acknowledgements—We thank the SERC for financial support and for a studentship (C.J.C.). N.C.N. also thanks the Royal Society for additional supporting funds.

REFERENCES

1. G. A. Fisher and N. C. Norman, *Adv. Inorg. Chem.*, in preparation.
2. S. Pohl, W. Saak and D. Haase, *Z. Naturforsch., Teil. B* 1987, **42**, 1493.
3. S. Pohl, R. Lotz, D. Haase and W. Saak, *Z. Naturforsch., Teil. B* 1988, **43**, 1144. A further isomeric form is found in the structure of $[Et_3NH]_4[As_8I_{28}]$, W. S. Sheldrick, H.-J. Häusler and J. Kaub, *Z. Naturforsch., Teil B* 1988, **43**, 789.
4. F. Lazarini, *Acta Cryst., Sect. B* 1977, **33**, 1954.
5. F. Bigoli, M. Lanfranchi and M. A. Pellinghelli, *Inorg. Chim. Acta* 1984, **90**, 215.
6. A. Benedetti, A. C. Fabretti and W. Malavasi, *J. Cryst. Spectrosc. Res.* 1992, **22**, 145.
7. F. Lazarini and I. Leban, *Acta Cryst., Sect. B* 1980, **36**, 2745.
8. A. L. Rheingold, A. D. Uhler and A. G. Landers, *Inorg. Chem.* 1983, **22**, 3255.
9. L. Antolini, A. Benedetti, A. C. Fabretti and A. Giusti, *J. Chem. Soc., Dalton Trans.* 1988, 2501.
10. G. R. Willey, H. Collins and M. G. B. Drew, *J. Chem. Soc., Dalton Trans.* 1991, 961.

11. W. Clegg, R. J. Errington, G. A. Fisher, M. E. Green, D. C. R. Hockless and N. C. Norman, *Chem. Ber.* 1991, **124**, 2457.
12. S. Pohl, R. Lotz, W. Saak and D. Haase, *Angew. Chem., Int. Edn Engl.* 1989, **28**, 344.
13. S. Pohl, D. Haase, R. Lotz and W. Saak, *Z. Naturforsch., Teil. B* 1988, **43**, 1033.
14. S. Jagner and G. Helgesson, *Adv. Inorg. Chem.* 1991, **37**, 1. See also L. Subramanian and R. Hoffmann, *Inorg. Chem.* 1992, **31**, 1021.
15. D. Thierbach and F. Huber, *Z. Anorg. Allg. Chem.* 1979, **451**, 137.
16. H. J. Haupt, F. Huber, C. Krüger, H. Preut and D. Thierbach, *Z. Anorg. Allg. Chem.* 1977, **436**, 229.
17. H. P. Lane, C. A. McAuliffe and R. G. Pritchard, *Acta Cryst., Sect. C* 1992, **48**, 2002.
18. D. Thierbach and F. Huber, *Z. Anorg. Allg. Chem.* 1979, **457**, 189.
19. D. E. Lynch, G. Smith, K. A. Byriel and C. H. L. Kennard, *Acta Cryst., Sect. C* 1993, **49**, 285 and refs therein.
20. M. R. Churchill, R. F. See, S. L. Randall and J. D. Atwood, *Acta Cryst., Sect. C* 1993, **49**, 345.
21. P. W. Baures and J. V. Silverton, *Acta Cryst., Sect. C* 1990, **46**, 715.
22. N. Walker and D. Stuart, *Acta Cryst., Sect. A* 1983, **39**, 158.
23. G. M. Sheldrick, University of Göttingen, F.R.G. (1986).
24. *International Tables for X-ray Crystallography*, Vol. 4. Kynoch Press, Birmingham (1974).
25. P. Mallinson and K. W. Muir, *J. Appl. Cryst.* 1985, **18**, 51.
26. W. S. Sheldrick and J. Kiefer, *Z. Naturforsch., Teil B* 1992, **47**, 1079.

Polyhedron Vol. 12, No. 17, pp. 2091–2096, 1993
Printed in Great Britain

0277–5387/93 $6.00+.00
© 1993 Pergamon Press Ltd

ACTIVATION OF LANTHANIDE ACETATES VIA HETEROMETALLIC ALKOXIDES: SYNTHESIS AND MOLECULAR STRUCTURE OF $Gd_2Zr_6(\mu_4\text{-}O)_2(\mu\text{-}OAc)_6(\mu\text{-}OPr^i)_{10}(OPr^i)_{10}$

STEPHANE DANIÈLE and LILIANE G. HUBERT-PFALZGRAF†

Laboratoire de Chimie Moléculaire, URA-CNRS, Université de Nice-Sophia-Antipolis, BP 71, 06108 Nice Cédex 2, France

and

JEAN-CLAUDE DARAN and RUBEN A. TOSCANO‡

Laboratoire de Chimie des Métaux de Transition, URA-CNRS, 4 Place Jussieu, 75230 Paris Cédex 05, France

(*Received* 5 *April* 1993; *accepted* 10 *May* 1993)

Abstract—The mixed-metal species $[Gd_2Zr_6(\mu_4\text{-}O)_2(\mu\text{-}OAc)_6(\mu\text{-}OPr^i)_{10}(OPr^i)_{10}]$ (**1**) was obtained by reacting anhydrous gadolinium acetate with $[Zr(OPr^i)_4(Pr^iOH)]_2$. Its X-ray structure analysis reveals two $Zr_3Gd(\mu_4\text{-}O)(\mu\text{-}OAc)_2(OPr^i)_{10}$ tetrahedral clusters associated via Gdμ-OAc linkages. The zirconium and gadolinium centres are hexa- and hepta-coordinated, respectively. The analogous yttrium derivative (**2**) was obtained by a similar route and characterized by microanalysis, IR, ^1H and ^{13}C NMR spectroscopies. Control of the stoichiometry between the metals can be achieved by varying the nature of the alkoxo group. Hydrolysis–polycondensation reactions proceed via differential hydrolysis and offered cubic zirconia containing various amounts of lanthanide oxides depending on the stoichiometry between the metals.

Ternary or complex metal oxides represent an important part of advanced materials due to their wide range of technical applications. Lanthanide oxides are involved in various advanced complex oxide materials such as electro-optical ceramics and high-temperature protonic or super conductors. Chemical routes such as the sol–gel process are versatile methods for obtained ceramics in a variety of shapes and are based on hydrolytic condensation reactions.[1] Molecular precursors of oxides mostly remain limited to alkoxides, which are oligomeric and difficult to handle especially for oxophilic metals and materials science purposes. The use of metal alkoxides in conjunction with less reactive and more easily accessible metal oxide precursors (β-diketonates, acetates) is a common alternative in the approach of mixed-metal oxide materials by chemical routes.[2] However, the molecular constitution of such solutions is not well known and a better understanding is required as a means to a better control of the passage from molecules to materials and a better selection of the homo- and heterometallic precursors for a given material.[3] Lanthanides are associated with zirconium in electro-optical ceramics, high-temperature protonic conductors, electrodes, etc. The most commonly used lanthanide alkoxides, isopropoxides, are generally pentanuclear $Ln_5(\mu_5\text{-}O)(OPr^i)_{13}$ clusters (Ln = Y, La, Yb, Pr)[4] and although they are reported to form mixed-metal alkoxides, for instance with $[Zr(OPr^i)_4(Pr^iOH)]_2$, their structural characterization turned out to be difficult.[5]

This paper relates the synthesis and char-

† Author to whom correspondence should be addressed.
‡ On leave from Instituto de Quimica, Univ. Nac. Autonoma de Mexico, cd. Universitaria, A. Obregon, 04510 Mexico D.F., Mexico.

acterization of mixed-metal lanthanide–zirconium acetatoalkoxides and the molecular structure of $Gd_2Zr_6(\mu_4\text{-}O)_2(\mu\text{-}OAc)_6(\mu\text{-}OPr^i)_{10}(OPr^i)_{10}$, the first heterometallic Ln—Zr species structurally characterized.

EXPERIMENTAL

All manipulations were routinely performed under argon using Schlenk tubes and vacuum-line techniques with solvents purified by standard methods. $[Zr(OPr^i)_4(Pr^iOH)]_2$[6] and anhydrous $Ln(OAc)_3$ (Ln = Y, Gd)[7] were obtained according to the literature. ^1H and ^{13}C NMR and IR spectra were obtained using Bruker WH-90, AC-200 and IR-FTS 45 spectrometers, respectively. IR spectra were obtained as Nujol mulls. Analytical data were obtained from the Centre de Microanalyses du CNRS.

Synthesis of $Ln_2Zr_6O_2(OAc)_6(OPr^i)_{20}$ [Ln = Gd (**1**), Y (**2**)]

$Gd(OAc)_3$ (0.6 g, 1.77 mmol) added to a solution of $[Zr(O^iPr)_4(Pr^iOH)]_2$ (2 g, 2.64 mmol) in toluene (40 cm^3). The reaction medium was then heated at reflux for 20 h leading to the progressive dissolution of the acetate. After evaporation to dryness the crude product was recrystallized at 5°C in a toluene–hexane mixture (10:1); yield: 2 g (90%) of **I**. The product is soluble in aliphatic and aromatic hydrocarbons and THF. Its solubilization in isopropanol is slow (1 h). Found: C, 34.9; H, 6.1; Gd, 12.9; Zr, 22.5. Calc. for $C_{36}H_{79}O_{17}GdZr_3$: C, 35.6; H, 6.5; Gd, 14.5; Zr, 22.6%. IR (cm^{-1}): 1637sh, 1610vs [$\nu_{as}(CO_2)$]; 1544sh, 1454, 1436 [$\nu_s(CO_2)$]; 553sh, 526vs, 487s, 437m, 519m [ν(M—OR)]. ESR (room temperature, toluene): $\langle g \rangle = 2.016$, $\mu = 11.8\ \mu_B$.

A similar procedure applies to the synthesis of the yttrium analogue **2** obtained in a 75% yield, but no crystals suitable for X-ray analysis could be grown. Found: C, 36.5; H, 6.4; Y, 8.1; Zr, 24.0. Calc. for $C_{36}H_{79}O_{17}YZr_3$: C, 37.8; H, 6.9; Y, 7.8; Zr, 23.9%. IR (cm^{-1}): 1645sh, 1616m, 1574vs [ν_{as}(CO)]; 542s, 499m, 465s [μ(M—OR)] ^1H (C_6D_6, ppm): 4.88 (m, 2H, CH), 4.45 (sep, $J = 6$ Hz, 8H, CH); 1.99s (6H, OAc), 1.94s (3H, OAc); 1.65d 1.59d, 1.51d, 1.45d ($J = 6$ Hz, 60H, CH_3). $^{13}C\{^1H\}$ ($CDCl_3$, ppm): 73, 71.8, 70.9, 70.1, 69, 64.7 (CH); 29.8, 26.6, 26, 25.6, 25, 23.8, 19.9, 19 (CH_3).

Synthesis of $Y_2Zr_2O(OAc)6(OC_2H_4OMe)_6$ (**3**)

$Y(OAc)_3$ (0.8 g, 3 mmol) was dissolved at room temperature in a solution of zirconium 2-methoxyethoxide (obtained by refluxing $[Zr(OPr^i)_4(Pr^iOH)]_2$ (1.04 g, 2.68 mmol) with $MeOC_2H_4OH$) in toluene (20 cm^3) over a period of 20 h. After elimination of the excess $Y(OAc)_3$ the filtrate was concentrated and crystallization of **3** was achieved by adding hexane (1.4 g, 89%). The product is soluble in toluene, THF, 2-methoxyethanol, but insoluble in aliphatic hydrocarbons. Found: Y, 15.0; Zr, 15.4. Calc. for $C_{30}H_{60}O_{25}Y_2Zr_2$: Y, 15.1; Zr, 15.5%. IR (cm^{-1}): 1616sh, 1560vs [ν(C—O)]; 588s, 514vs, 467s [ν(M—OR)]. ^1H (C_6D_6, ppm): 3.44 m (2H, $MOCH_2$), 3.1t ($J = 6.2$ Hz, 2H, CH_2); 3.01s (3H, OMe), 2.13s (3H, OAc). $^{13}C\{^1H\}$ ($CDCl_3$, ppm): 129.0, 128.2, 125.3 (CO_2); 73.7, 61.8, 58.9 (CH_2, OMe); 29.7, 24.5, 21.5 (OAc).

If the same reaction was achieved at refluxing toluene a different oxo compound was obtained. IR (cm^{-1}): 1583 [$\nu_{as}(CO_2)$], 1448 [$\nu_s(CO_2)$]; 585, 511, 464 [ν(M—OR)].

X-ray diffraction study of $Gd_2Zr_6(\mu_4\text{-}O)_2(\mu\text{-}OAc)_6(\mu\text{-}OPr^i)_{10}(OPr^i)_{10}$ (**1**)

A crystal grown from toluene–hexane solutions at 5°C was introduced into a Lindeman capillary and mounted onto an Enraf–Nonius CAD-4 automatic diffractometer. Systematic absences indicate monoclinic symmetry and space group $C2/c$. The lattice parameters were determined from 25 computer-centred reflections. The unit cell parameters and basic information about data collection are as follows.

Crystal data for $C_{66}H_{158}O_{34}Gd_2Zr_6,C_6H_{14}$. $M = 2357.8$, monoclinic, space group $C2/c$, $a = 39.55(2)$, $b = 12.274(7)$, $c = 22.91(1)$ Å, $\beta = 103.20(4)$, $U = 10827$ Å^3, $D_c = 1.415$ g cm^{-3} for $Z = 4$, μ(Mo-K_α) = 18.22 cm^{-1}. 3458 data were collected at low temperature (−100°C) using graphite-monochromated Mo-K_α radiation ($\lambda = 0.71073$ Å). Metal atoms were found by direct methods using SHELXS.[8] All remaining non-hydrogen atoms were located on successive difference electron density maps. The structure was refined by least-squares with an approximation (in three blocks) to the normal matrix using CRYSTALS.[9] 2760 reflections with $I > 3\sigma(I)$ were used to solve and refine the structure: $R = 0.0529$, $R_w = 0.0617$, 357 variables. The weighting scheme w was defined as $w = w'*[1-(\Delta F/6\sigma(F))^2]^2$, with $w' = 1.0/\Sigma_{r=1,n}\mathrm{ArTr}(x)$, where $x = F_c/F_c(\max)$ and three coefficients of Ar (7.32, −0.218, 4.42) for the Chebyshev polynomial Tr(x).[10] In view of the low ratio of variables/data only metals and oxygen atoms were refined anisotropically. Some of the carbon atoms of the alkoxide ligands have high

isotropic thermal parameters. For three of them a disordered distribution of the carbon atoms could be found, but other attempts to define possible disordered sites failed. Anomalous dispersion terms were applied. Empirical absorption corrections using DIFABS[11] were made. Positional parameters and equivalent isotropic thermal parameters are given as supplementary material.

RESULTS AND DISCUSSION

By contrast with lanthanide alkoxides, acetates of the compounds studied are easily accessible but poorly soluble. However, they can be activated by metal alkoxides, although they appear less reactive towards $M(OR)_n$ species than metal acetates of other elements such as lead(II) or magnesium.[3a] The reaction between anhydrous $Ln(OAc)_3$ (Ln = Y, Gd) and $[Zr(OPr^i)_4(Pr^iOH)]_2$ requires refluxing in toluene for 20 h and is evidenced by the dissolution of the acetate. In both cases compounds analysing as $Ln(OAc)_3 \cdot Zr_3O(OPr^i)_{10}$ [Ln = Gd (**1**), Ln = Y (**2**)] have been obtained in high yield (80%). These compounds are air-sensitive, soluble in non-polar media (hexane, toluene) and non-volatile. Their IR spectra show three stretching frequencies for the acetate ligands, shifted to higher frequencies with respect to $Gd(OAc)_3$ (1546 cm^{-1}) or to $Y(OAc)_3$ (1536 cm^{-1}). ^1H and ^{13}C NMR spectra of the yttrium derivative **2** display two types of acetate ligands in a 1 : 2 surface area and are quite complex for the isopropoxo region, while the paramagnetism of **1** results in poorly resolved NMR spectra. Suitable crystals could be obtained for **1** and its structure was thus elucidated by X-ray studies, which established its mixed-metal character as well as the presence of the oxo ligands.

Compound **1** appears to be an octanuclear heterometallic oxoacetatoalkoxide of the formula $Gd_2Zr_6(\mu_4\text{-}O)_2(\mu\text{-}OAc)_6(\mu\text{-}OPr^i)_{10}(OPr^i)_{10}$. Its molecular structure results from two $GdZr_3(\mu_4\text{-}O)(OAc)_2(OR)_{10}$ aggregates assembled by the two gadolinium atoms via bridging acetato ligands into the discrete centrosymmetric molecule shown in Fig. 1. Selected bond distances and angles are summarized in Table 1. The gadolinium atoms are hepta-coordinated, while all zirconium centres are hexa-coordinated. The tetranuclear $GdZr_3(\mu_4\text{-}O)(OAc)_2(OR)_{10}$ unit can be viewed either as a distorted flattened tetrahedron or as two cubane units (in which one metal apex is missing) sharing a face [Zr(1), Gd and the oxo ligand O(15)]. The gadolinium atom occupies the "apical" position of the distorted tetrahedron, while the zirconium atoms form an isosceles triangular unit: the distances Zr(1)···Zr(2) and Zr(1)···Zr(3) are comparable (3.42 Å av.), but Zr(2)···Zr(3) opens up to 4.074(2) Å. The oxo ligand O(15) is located at 0.46 Å from the plane of the three zirconium atoms and is the only ligand connecting the Zr(2) and Zr(3) atoms. The salient feature is the coordination of the μ_4-oxo O(15) ligand; this ligand is "concave" [Zr(2)—O(15)—Zr(3) 137.3(4)°] and thus drawn towards Gd and Zr(1). Such a stereochemistry contrasts with most $M_4(\mu_4\text{-}X)$ (X = C, N, O)[12] units, but is analogous with that of $Ce_4(\mu_4\text{-}O)(OPr^i)_{13}(Pr^iOH)$[13] or $Al_4(\mu_4\text{-}O)(OPr^i)_5Cl_4(Pr^iOH)$[14] species; in the latter the stereochemistry around the

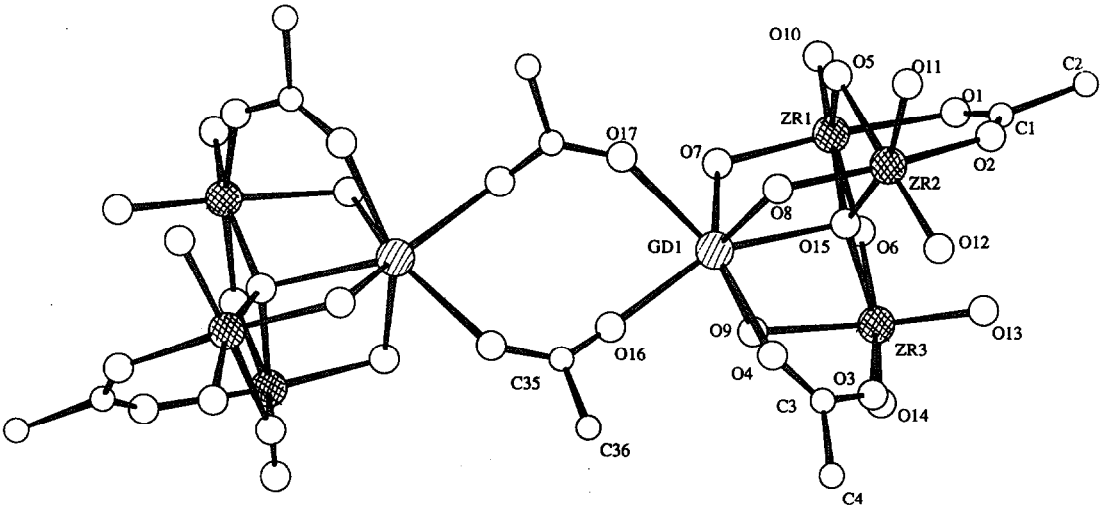

Fig. 1. Ball and stick view of the molecular structure of $Gd_2Zr_6(\mu_4\text{-}O)_2(\mu\text{-}OAc)_6(\mu\text{-}OPr^i)_{10}(OPr^i)_{10}$ showing the atom labelling.

Table 1. Selected bond distances (Å) and angles (°) for $Gd_2Zr_6O_2(OAc)_6(OPr^i)_{20}$

Gd(1)—Zr(1)	3.558(1)	Zr(1)—Zr(2)	3.437(2)
Gd(1)—Zr(2)	3.583(1)	Zr(1)—Zr(3)	3.413(2)
Gd(1)—Zr(3)	3.594(1)	Zr(1)—O(1)	2.21(1)
Gd(1)—O(4)	2.406(8)	Zr(1)—O(5)	2.094(8)
Gd(1)—O(7)	2.393(8)	Zr(1)—O(6)	2.100(9)
Gd(1)—O(8)	2.335(8)	Zr(1)—O(7)	2.066(8)
Gd(1)—O(9)	2.303(7)	Zr(1)—O(10)	1.912(8)
Gd(1)—O(15)	2.421(8)	Zr(1)—O(15)	2.151(8)
Gd(1)—O(16)	2.277(8)	Zr(3)—O(3)	2.146(9)
Gd(1)—O(17′)[a]	2.368(8)	Zr(3)—O(6)	2.179(9)
Zr(2)—O(2)	2.19(1)	Zr(3)—O(9)	2.168(8)
Zr(2)—O(5)	2.274(9)	Zr(3)—O(13)	1.899(9)
Zr(2)—O(8)	2.069(8)	Zr(3)—O(14)	1.906(9)
Zr(2)—O(11)	1.915(9)	Zr(3)—O(15)	2.195(8)
Zr(2)—O(12)	1.904(9)		
Zr(2)—O(15)	2.180(8)		

O(7)—Gd(1)—O(4)	148.4(3)	O(16)—Gd(1)—O(8)	126.1(3)
O(8)—Gd(1)—O(4)	77.7(3)	O(17′)[a]—Gd(1)—O(4)	133.2(3)
O(8)—Gd(1)—O(7)	106.1(3)	O(17′)[a]—Gd(1)—O(7)	77.4(3)
O(9)—Gd(1)—O(4)	76.6(3)	O(17′)[a]—Gd(1)—O(8)	79.4(3)
O(9)—Gd(1)—O(7)	79.2(3)	O(15)—Gd(1)—O(9)	70.2(3)
O(9)—Gd(1)—O(8)	134.2(3)	O(16)—Gd(1)—O(9)	85.9(3)
O(15)—Gd(1)—O(4)	83.0(3)	O(16)—Gd(1)—O(15)	153.7(3)
O(15)—Gd(1)—O(7)	69.8(3)	O(17′)[a]—Gd(1)—O(9)	143.6(3)
O(15)—Gd(1)—O(8)	69.6(3)	O(17′)[a]—Gd(1)—O(15)	125.3(3)
O(16)—Gd(1)—O(4)	80.9(3)	O(17′)[a]—Gd(1)—O(16)	80.6(3)
O(16)—Gd(1)—O(7)	117.4(3)	O(5)—Zr(2)—O(2)	80.5(3)
O(5)—Zr(1)—O(1)	82.5(3)	O(8)—Zr(2)—O(2)	164.7(4)
O(6)—Zr(1)—O(1)	84.4(3)	O(8)—Zr(2)—O(5)	87.2(3)
O(6)—Zr(1)—O(5)	148.5(3)	O(11)—Zr(2)—O(2)	91.5(4)
O(7)—Zr(1)—O(1)	172.3(3)	O(11)—Zr(2)—O(5)	88.4(4)
O(7)—Zr(1)—O(5)	94.0(3)	O(11)—Zr(2)—O(8)	97.2(4)
O(7)—Zr(1)—O(6)	95.3(3)	O(12)—Zr(2)—O(2)	92.4(4)
O(10)—Zr(1)—O(1)	89.3(4)	O(12)—Zr(2)—O(5)	168.7(4)
O(10)—Zr(1)—O(5)	106.1(4)	O(12)—Zr(2)—O(8)	98.3(4)
O(10)—Zr(1)—O(6)	102.1(4)	O(12)—Zr(2)—O(11)	100.6(4)
O(15)—Zr(1)—O(1)	91.0(3)	O(15)—Zr(2)—O(2)	88.0(3)
O(15)—Zr(1)—O(5)	75.2(3)	O(15)—Zr(2)—O(5)	71.1(3)
O(15)—Zr(1)—O(6)	76.6(3)	O(15)—Zr(2)—O(8)	79.4(3)
O(10)—Zr(1)—O(7)	98.3(4)	O(15)—Zr(2)—O(11)	159.3(4)
O(15)—Zr(1)—O(7)	81.5(3)	O(15)—Zr(2)—O(12)	100.1(4)
O(15)—Zr(1)—O(10)	178.7(4)	Zr(1)—O(7)—Gd(1)	105.6(3)
O(6)—Zr(3)—O(3)	163.4(3)	Zr(1)—O(15)—Gd(1)	102.0(3)
O(9)—Zr(3)—O(3)	83.4(3)	Zr(2)—O(15)—Gd(1)	102.2(3)
O(9)—Zr(3)—O(6)	87.4(3)	Zr(2)—O(15)—Zr(1)	105.0(3)
O(13)—Zr(3)—O(3)	90.6(4)	Zr(2)—O(5)—Zr(1)	103.7(3)
O(13)—Zr(3)—O(6)	96.1(4)	Zr(2)—O(8)—Gd(1)	108.8(3)
O(13)—Zr(3)—O(9)	169.2(4)	Zr(3)—O(6)—Zr(1)	105.8(3)
O(14)—Zr(3)—O(3)	99.1(4)	Zr(3)—O(9)—Gd(1)	107.0(3)
O(14)—Zr(3)—O(6)	94.9(4)	Zr(3)—O(15)—Gd(1)	102.2(3)
O(14)—Zr(3)—O(9)	91.6(4)	Zr(3)—O(15)—Zr(1)	103.5(3)
O(14)—Zr(3)—O(13)	98.2(4)	Zr(3)—O(15)—Zr(2)	137.3(4)
O(15)—Zr(3)—O(3)	90.3(3)	C(26)—O(12)—Zr(2)	177.5(10)
O(15)—Zr(3)—O(6)	74.1(3)	C(29)—O(13)—Zr(3)	171.0(17)
O(15)—Zr(3)—O(9)	77.0(3)	C(32)—O(14)—Zr(3)	168.6(9)
O(15)—Zr(3)—O(13)	94.1(4)	C(23)—O(11)—Zr(2)	156.3(12)
O(15)—Zr(3)—O(14)	164.3(4)	C(20)—O(10)—Zr(1)	165.2(9)

[a] Prime-related by an inversion centre.

oxo ligand is supported by a bridging $H(OPr^i)_2^-$ ligand resulting from hydrogen bonding. With the exception of the long Zr(2)···Zr(3) distance the tetranuclear unit is quite regular, with Gd···Zr distances of 3.57 Å av., and thus close to the Zr···Zr distances. A similar tetranuclear framework has also been observed for a mixed-metal lead–zirconium derivative, $PbZr_3(\mu\text{-}OAc)_2(\mu\text{-}OPr^i)_5(OPr^i)_5$.[3,15] The tetranuclear aggregates of **1** are connected by acetate ligands, thus resulting in hepta-coordination of the gadolinium centres and quite long Gd···Gd distances (5.58 Å). The M—O bond distances follow the pattern Zr—OR < Zr—μ-OR Zr—μ_4-O Zr—OAc and Gd—μ-OR < Gd—μ-OAc < Gd—μ-4O and range from 1.904(9) to 2.274(9) Å for zirconium and from 2.277(8) to 2.421(8) Å for gadolinium. The gadolinium–oxygen bond lengths are longer than the Zr—O ones, as expected on the basis of the larger gadolinium covalent radius. Quite large variations are observed for the Zr—μ-OR (2.10–2.27 Å) as well as for the Gd—OAc linkages (2.27–2.41 Å). Angles Zr—O—C to terminal alkoxide ligands are large (167.7° av.) and account for the short Zr—O bond lengths (av. 1.91 Å) with respect to the sum of the covalent radii (2.18 Å). The various metal–oxygen distances are in the range of the values reported for zirconium isopropoxide derivatives[16] or the gadolinium alkoxides structurally characterized so far, $Cp_5Gd(\mu_5\text{-}O)(OMe)_8$ and $Na_2Gd_4(\mu_6\text{-}O)(OBu^t)_{12}$.[17] Although both types of zirconium centres—depending on the number of terminal and bridging alkoxides—are hexa-coordinated, they depart from octahedral geometry. Gadolinium, like other lanthanides, can commonly accommodate high coordination numbers such as eight; however, only hexa-coordination has been observed so far in its alkoxide derivatives,[17] while the metal is six- or seven-coordinate in Gd_2O_3. The stereochemistry of the hepta-coordinated gadolinium centres of **1** correspond to a triangular prism capped by an acetate oxygen, O(4). The increase in the gadolinium coordination number in the acetatoalkoxide illustrates a common tendency of acetate ligands.

The NMR spectra of the yttrium derivative **2** account for a structure similar to that of compound **1** in solution. In view of the large yield of **1** and **2** and of the absence of formation of isopropylacetate (as shown by IR monitoring and by NMR), the origin of the oxo ligand most probably results from the alkoxide groups giving an oxo $Zr_3O(OR)_{10}$ unit. Such an oxo fragment has also been detected by mass spectrometry studies.[5] Reactions between metal alkoxides and acetates do not necesssarily proceed by elimination of an ester, since derivatives resulting from simple addition reactions such as $MNb_2(\mu\text{-}OAc)_2(\mu\text{-}OPr^i)_4(OPr^i)_6$ (M = Cd, Mg) have been obtained and structurally characterized.[3a,18]

Hydrolysis of **1** gives a powder still containing acetate ligands [$\nu_{as}(CO_2)$ 1541, $\nu_s(CO_2)$ 1404 cm^{-1}] and hydroxyl residues [ν(OH) 3375 cm^{-1}], as a result of the lower hydrolytic susceptibility of the carboxylate ligands as compared with alkoxides,[1] which are further eliminated by thermal treatment at 300°C as shown by thermogravimetric analysis. Temperatures as high as 700°C are usually required for the conversion of gadolinium acetate into the oxide.[19] After crystallization (starting at 600°C), cubic ZrO_2 containing 25% of Gd_2O_3 is obtained as a result of the existence of ZrO_2–Gd_2O_3 solid solutions over a large range of compositions.[20] Comparable results are obtained in the case of the yttrium derivative **1** {IR after hydrolysis 3382 [ν(OH)], 1558 [$\nu_{as}(CO_2)$], 1412 [$\nu_s(CO_2)$] cm^{-1}}.

The Ln—Zr stoichiometry of the mixed-metal species can be modified by varying the nature of the OR ligand. Heterometallic species in which the two metals, Ln and Zr, display a 1 : 1 stoichiometry[21] are obtained if zirconium 2-methoxyethoxide is used instead of the isopropoxide. The zirconium 2-methoxyethoxide is also more reactive and dissolution of the anhydrous $Ln(OAc)_3$ proceeds readily at room temperature. By contrast with the reactions with zirconium isopropoxide, refluxing leads in this case to the elimination of an ester, $MeOC_2H_4OAc$, detected by IR [$\nu(CO_2)$: 1726 cm^{-1}]. These condensation reactions result in species having a higher proportion of oxo ligands and which are also less soluble than **1** or **2**.

The overall data establish that the poor reactivity and insolubility of acetates can be overcome in the presence of a metal alkoxide, giving a soluble mixed-metal species. The reaction proceeds with redistribution of the acetate ligands, which act as assembling ligands between the different metals. The use of soluble—but less favourable in terms of ceramic yields—carboxylates such as 2-ethylhexanoates is thus not a prerequisite. The metal introduced via classical alkoxides such as isopropoxides or ethoxides is always predominant.[3a] Another interesting feature lies in the assistance of the organic residues, which allow thermal elimination of the acetate ligands (which remain after hydrolysis) in quite mild conditions as compared with the parent acetates.

Acknowledgements—We thank the CNRS (GRECO 93) for financial support and Dr A. Mari (Toulouse) for the magnetic measurements.

REFERENCES

1. L. G. Hubert-Pfalzgraf, *New J. Chem.* 1987, **11**, 663.
2. K. G. Caulton and L. G. Hubert-Pfalzgraf, *Chem. Rev.* 1990, **90**, 969.
3. (a) L. G. Hubert-Pfalzgraf, *Better Ceramics Through Chemistry V*, MRS Proceedings 1992, **271**, 15; (b) C. Chandler, G. D. Fallon and B. O. West, *J. Chem. Soc., Chem. Commun.* 1990, 1063.
4. O. Poncelet, W. J. Sartain, L. G. Hubert-Pfalzgraf, K. Folting and K. G. Caulton, *Inorg. Chem.* 1989, **28**, 263; W. J. Evans, M. S. Sollberger, J. L. Shreeve, J. M. Olofson, J. H. Hain and J. W. Ziller, *Inorg. Chem.* 1992, **31**, 2492.
5. N. Ya Turova, N. I. Kozlova and A. V. Novoselova, *Russ. J. Inorg. Chem.* 1980, **25**, 1788.
6. B. A. Vaarstra, J. C. Hufman, P. S. Gradeff, L. G. Hubert-Pfalzgraf, J. C. Daran, S. Parraud, K. Yunlu and K. G. Caulton, *Inorg. Chem.* 1990, **29**, 3126.
7. T. Moeller, V. Gralasyn and J. Xavier, *J. Inorg. Nucl. Chem.* 1963, **15**, 259.
8. G. M. Sheldrick, SHELXS 86, *Program for Crystal Structure Solution.* University of Göttingen, F.R.G. (1986).
9. D. J. Watkin, J. R. Carruthers and P. W. Betteridge, CRYSTALS User guide. Chemical Crystallography Laboratory, University of Oxford (1986).
10. E. Prince, *Mathematical Techniques in Crystallography.* Springer Verlag, Berlin (1992).
11. N. Walker and D. Stuart, *Acta Cryst.* 1983, **A39**, 158.
12. A. J. Blake, P. E. Y. Milne, P. Thornton and R. E. P. Winpenny, *Angew. Chem., Int. Edn Engl.* 1991, **30**, 1139; I. A. Kahwa, S. Folkes, D. J. Williams, S. V. Ley, C. A. O'Mahoney and G. L. McPherson, *J. Chem. Soc., Chem. Commun.* 1989, 1531.
13. K. Yunlu, P. S. Gradeff, N. Edelstein, W. Kot, G. Shalimoff, W. E. Streib, B. A. Vaarstra and K. G. Caulton, *Inorg. Chem.* 1991, **30**, 2317.
14. N. Ya, Turova, A. I. Yanovskaya, V. G. Kessler and N. I. Kozlova, *Russ. J. Inorg. Chem.* 1991, **36**, 2497.
15. S. Daniele, R. Papiernik, L. G. Hubert-Pfalzgraf, M. C. Massiani and J. Vaissermann, to be published.
16. B. Vaarstra, J. C. Huffman, W. E. Streib and K. G. Caulton, *Inorg. Chem.* 1991, **30**, 3068.
17. H. Schumann, G. Kociok-Köhn and J. Loebel, *Z. Anorg. Allg. Chem.* 1990, **581**, 69.
18. S. Boulmaaz, R. Papiernik, L. G. Hubert-Pfalzgraf and J. C. Daran, *Chem. Mat.* 1991, **3**, 779.
19. K. C. Patil, G. V. Chandrashekhar, M. V. George and C. N. Rao, *Can. J. Chem.* 1968, **46**, 258.
20. R. Collonges, *La Nouvelle Stoechiométrie*, Ed. Masson, Paris (1971).
21. The stoichiometry between the two metals has been established by microanalysis in the precursor and confirmed in the powder resulting from their hydrolysis.

Polyhedron Vol. 12, No. 17, pp. 2097–2104, 1993
Printed in Great Britain

0277–5387/93 $6.00+.00
© 1993 Pergamon Press Ltd

THE SYNTHESIS AND CHARACTERIZATION OF NOVEL DIOXIMES AND THEIR HETERONUCLEAR COMPLEXES CONTAINING CROWN ETHER MOIETIES

YASAR GOK,* HALIT KANTEKIN and ISMAIL DEGIRMENCIOGLU

Department of Chemistry, Karadeniz Technical University, 6180 Trabzon, Turkey

(*Received* 27 *April* 1993; *accepted* 7 *May* 1993)

Abstract—A novel vic-dioxime S,S′-bis[2-(4′-benzylidenamino-benzo-15-crown-5)]dithioglyoxime (**6**), with crown ether groups has been synthesized from the reaction of 4′-formylbenzo(15-crown-5) and S,S′-bis(2-aminophenyl)dithioglyoxime (**4**), which has been synthesized from the potassium salt of 2-aminothiophenol and dichloroglyoxime. Mononuclear complexes with a metal : ligand ratio of 1 : 2 have been isolated for nickel(II) and cobalt(III). The reaction of mononuclear complexes with copper(I) and cadmium(II) gives heterotrinuclear complexes. The structure of dioximes and their complexes are proposed according to elemental analyses, ^{1}H and ^{13}C NMR, IR, UV–vis and mass spectra.

Crown ether compounds which were first synthesized by Pedersen, who described their ion-binding properties,[1] have been the focus of a great deal of interest for the past 35 years. This is because of the possible chemical and biological applications of their unusual ion-binding capability, solvation and transport effect.[2] A number of investigations of these processes have been carried out,[3] as well as studies of the molecular structures of the complexes using IR, ^{1}H and ^{13}C NMR spectroscopy[4] and X-ray crystallography.[5] Recently, crown ether groups have also been extensively employed to construct new compounds with extraordinary properties; ion channels formed by the superposition of crown ether macrocycles in tetrakis(crown ether) substituted phthalocyanines.[6] Bis(crown ether) Schiff base[7] and quinoxaline,[8] and imidazoline[9] ligands containing recognition sites for alkali and transition metal guest cations have been reported.[10] The design and synthesis of macropolycyclic molecules containing more than one recognition site for binding several guest species is of considerable current interest in the chemical literature.[7b,11] These multisite receptors may exhibit allosteric properties[12] by binding sequentially two or more guest metal cations in close proximity to one another.

vic-Dioximes have received considerable attention as model compounds to mimic biofunctions such as reduction of vitamin B_{12}.[13] Their complexes have been the continuous source, through the decades, of many interesting reports. The reaction of thiols with (*E,E*)-dichloroglyoxime or cyanogen di-N-oxide yielded various symmetrically substituted dithioglyoxime derivatives.[14] The (*E,E*)- and (*E,Z*)-stereoisomers of *vic*-dioximes are capable of coordinating through N,N or N,O sites of the oxime groups, and only in a few cases is it possible to realize the interconversion of (*E,E*) and (*E,Z*) complexes.[9,15] The transition metal complexes of these vicinal dioximes are essentially N,N-coordinated square-planar structures.[16]

Especially the chemistry and molecular structure of bis(dioximato)cobalt(III) complexes have been extensively explored in the last few years[17] due to interest in them as models for important biochemical complexes, as well as to their usefulness as catalysts in many chemical processes[18] or as templates in many organic syntheses.[19]

Furthermore, the relevance of bimetallic compounds to bioinorganic systems has been one of the reasons for the increase in the amount of research on polynuclear compounds. In addition to these resulting polynuclear complexes may facilitate electron-transfer studies and serve as models of relevance to biological redox processes.

In the present paper we describe symmetrically substituted dithioglyoxime and its derivative carrying symmetrical benzylidenamino benzo(15-crown-5) units. The preparation of a bis-benzo

* Author to whom correspondence should be addressed.

crown ether ligand(6) containing a Schiff base diothioglyoxime linkage and its heteronuclear complexes has been achieved.

RESULTS AND DISCUSSION

The ligand used for this study, namely S,S′-bis(2-aminophenyl)dithioglyoxime (**4**), contains an amine and two sulphur donors and a *vic*-dioxime group. Its synthesis was accomplished in 62.8% yield by the reaction of dichloroglyoxime and the potassium salt of 2-aminothiophenol as shown in Scheme 1. The condensation reaction of **4** with 4′-formylbenzo(-15-crown-5) (**5**)[20] (2 mol) gave the Schiff base bis-crown ether (**6**), which is named S,S′-bis[2-(4′-benzylidenamino - benzo - 15 - crown - 5)]dithioglyoxime, as a white crystalline solid in good yield (24.94%) (Scheme 1). Both structures were verified by elemental analyses, mass spectrometry, ^{1}H and ^{13}C NMR, IR and UV–vis spectroscopy. The two novel *vic*-dioxime ligands **4** and **6** contain three recognition site for transition metals, whereas **6** contains two crown ether sites for alkali metal cations.

In the ^{1}H NMR spectrum of **4** a singlet which belongs to the thiol group disappears; a new resonance at $\delta = 11.77$ ppm is formed after the addition of (*E,E*)-dichloroglyoxime (Scheme 1). This resonance indicates that the OH protons are present in this compound (**4**). The =N—OH protons are also identified easily by D_2O exchange. The presence of only one singlet for the OH protons is consistent with the assumption that **4** has an *S-trans*-configuration, as do all known symmetrically substituted *vic*-dioximes.[21] A singlet at $\delta = 5.06$ and multiplets at $\delta = 6.54$–7.26 ppm corresponding to NH_2 and aromatic protons are not shifted considerably compared with the starting material (**1**). More detailed information about the structure of **4** is provided by the ^{13}C NMR spectrum. The signal

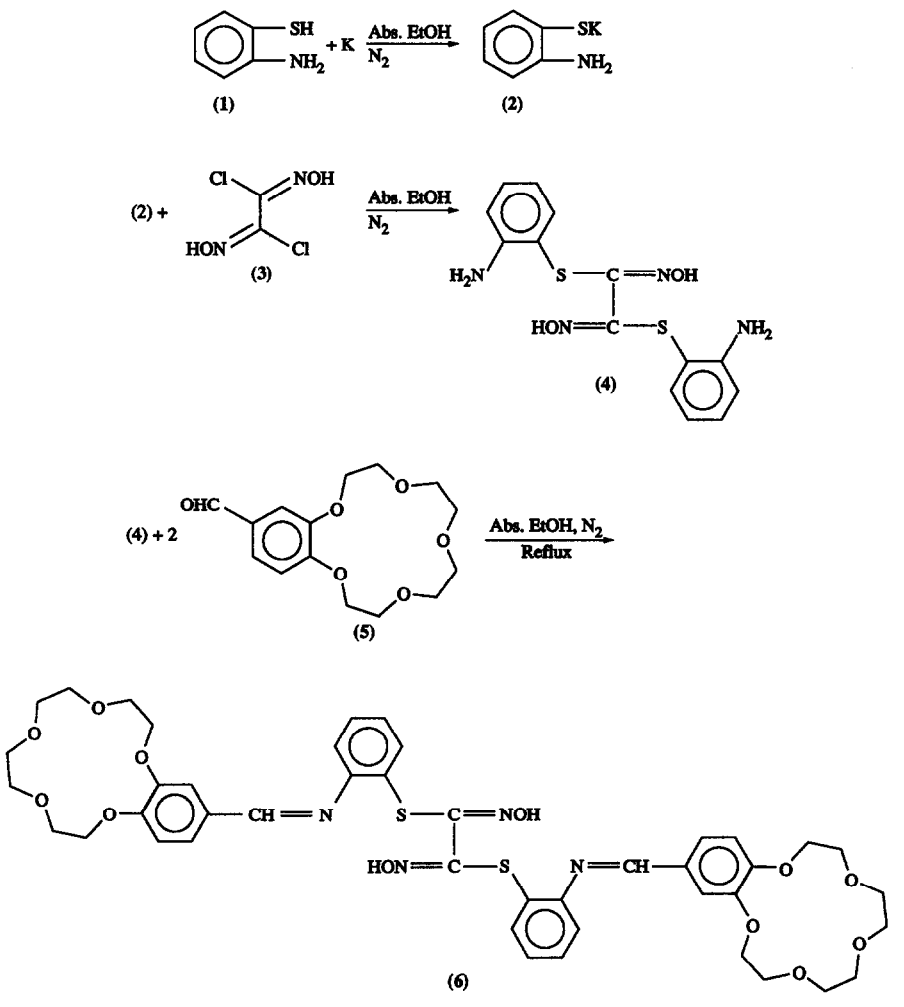

Scheme 1.

for the benzene carbon, C(1) with *ortho*-C—S substituents, is observed at $\delta = 143.97$ ppm,[22] while the other carbon [C(2)] having a proton with *ortho*-C—N and *meta*-C—S substituents is seen at $\delta = 109.51$ ppm. The other signals which belong to benzene carbons C(3), C(4), C(5) and C(6) are observed at $\delta = 128.36$, 114.57, 126.58 and 116.22 ppm, respectively. In addition to the chemical shifts of the carbon atoms (4) oxime groups exhibit a new signal belonging to C(7) (Table 1). The presence of only one resonance for oxime carbons in the ^{13}C NMR spectrum of **4** can be interpreted for the formation of an *S-trans*-configuration of **4**.[15] The carbon resonances of oximes in this compound are found at higher fields than values given for aldo- and keto-oximes.[22] The mass spectrum of **4**, which shows a molecular ion at *m/z* 334, confirms the proposed structure and rules out any polymeric form. In the IR spectrum of **4** the disappearance of the S—H stretching vibration along with the appearance of new vibrations at 3210 [(OH)], 1650 [(C=N)] and 980 cm^{-1} [(N—O)] are in agreement with the structure in Table 1. The aromatic and amine stretching and bending vibrations of **4** are very close to those of both **4** and **1**. In the ^1H NMR spectra of **6** OH protons appear as a singlet at $\delta = 12.21$ ppm, which disappears upon D_2O exchange. This result indicates that the structure of **6** is of the *S-trans* form[23] (Table 2). The singlets at $\delta = 5.06$ ppm, which belong to NH_2 protons of **4**, disappear after the condensation reaction with **5**. The chemical shifts which belong to aromatic and etheral protons were observed at $\delta = 8.05$, 7.62–7.38, 7.10 and 3.65–4.19 ppm, respectively. The carbonyl protons were shifted upfield[12a] as expected and appeared at $\delta = 9.84$ ppm. In the ^{13}C NMR spectrum of **6** all the carbon atoms of the aliphatic ether groups show absorptions between $\delta = 68.27$ and 70.46 ppm, as previously reported.[9b] The protonated benzene carbons with the *ortho*-carbonyl and O—CH_2 substituents appear at $\delta = 114.20$ ppm. The aromatic carbon atom attached to the carboxy group appears at $\delta = 128.22$ ppm. The chemical shifts for the azomethine carbons and carbohydroxyamide carbon atom are found at $\delta = 167.07$ and 151.28 ppm, respectively. These equivalent carbon atoms also confirm the *S-trans* configuration[24] and are also found at lower fields than values given for aldo- and keto-oximes. The mass spectrum of **6** did not exhibit a molecular ion;[8] however, peaks at *m/z* 841 (30), 804 (48), 708 (14), 589 (85), 440(8) and 402 (68) were observed. The observed chemical shifts either in ^1H or ^{13}C NMR for **6** reveal that upon condensation the HC=N, C=N—O, aromatic and O—CH_2 carbon bonds shift by a small degree. Little change in the positions of the above-mentioned absorptions were evidence suggesting Schiff base formation of **4**.

In the IR spectrum of **6** the stretching and bending vibrations at 3350 and 1630 cm^{-1}, respectively, disappear after the formation of the Schiff base and the new resonances, which belong to C=N group, appear at 1670 cm^{-1} as a broad band. The O—H, N—O and C=N vibrations which belongs to the oxime group were observed at 3220, 965 and 1640 cm^{-1}, respectively. In addition the stretching vibration (C=O) for **5** disappears after the condensation reaction of **4** with **5**. This result indicates that the formation of the Schiff base is completed.

The reaction of **4** with a salt of nickel(II) gives a product with a metal–ligand ratio of 1:2. This mononuclear complex was obtained even when the metal ion was used in an equivalent amount. Since a distinct lowering in the pH of the solution was observed during the complex formation, in the case of nickel(II) complex (**7**), deprotonation of (**4**) with subsequent N,N′-chelation with the *vic*-dioxime groups probably occurs (Fig. 1).

In the ^1H NMR spectrum of the diamagnetic nickel(II) complex (**7**) the resonances of intramolecular binding OH···O protons shifted to $\delta = 17.15$ ppm, which disappear by D_2O exchange. The usual hydrogen bridges of the square-planar vic-dioxime complexes were also characterized by the weak deformation bands[25] around 1730 cm^{-1}. Weak bands at *ca* 1730 cm^{-1} indicate OH···O bridges,[16a] while the C=N vibrations are at lower wave numbers, as expected for N,N-chelated vicinal dioxime complexes. This mononuclear complex **7** is diamagnetic, as expected for a square-planar d^8 metal ion.[26]

Table 1. ^{13}C NMR spectra of dioxime [D_6] [DMSO] (**4**)

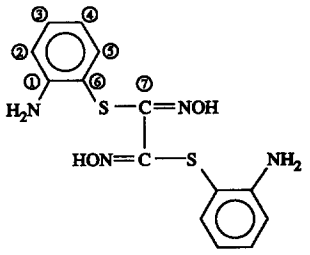

Assignment	δ (ppm) of **4**
C(1)	143.97
C(2)	109.51
C(3)	128.36
C(4)	114.57
C(5)	126.58
C(6)	116.22
C(7)	150.15

Table 2. ^{13}C NMR spectra of **6**, **9** and **10**

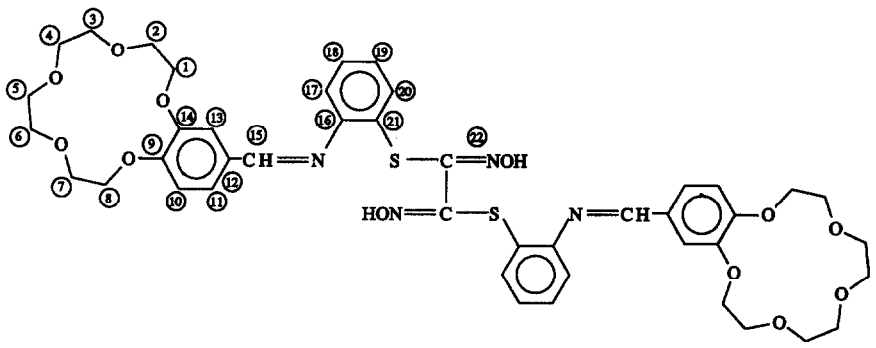

Assignment	δ (ppm) of **6**	δ (ppm) of **9**	δ (ppm) of **10**
	70.46	70.45	70.25
Crown-OCH_2	69.55	69.56	69.16
[C(1)—C(8)]	68.50	68.55	68.21
	68.27	68.33	68.08
C(15)	167.07	167.06	172.73
C(10)	113.17	113.27	113.61
C(13)	114.20	114.05	113.96
C(11)	122.07	121.04	121.18
C(12)	128.22	125.63	124.16
C(9)	144.19	143.87	143.63
C(14)	153.48	153.49	153.56
C(16)	148.67	148.71	150.58
C(17)	111.05	111.24	110.87
C(18)	134.04	134.20	134.51
C(19)	118.24	117.92	117.69
C(20)	130.43	126.40	126.17
C(21)	112.20	111.03	113.47
C(22)	151.28	151.32	151.53

To prepare the cadmium(II) complex of **7** a suspension of **7** in ethanol was refluxed for 17 h. Thus, the cadmium(II) complex (**8**) was obtained. This trinuclear complex is diamagnetic. The stability of the dithiadiamino complex of two cadmium(II) metal ions in solvents such as water and ethanol is the most important reason for the formation of this tri-nuclear complex. The difference in the ^1H NMR spectrum of **8** is the presence of small shifts for the NH_2 protons, which can be interpreted as the formation of the new complex. A close look at the IR spectrum of **8**, taken as KBr pellets, shows a high degree of similarity which suggests that it has the same geometrical configuration. The [(NH_2)] mode of **7** occurs at 3300 cm^{-1} and a band at 1605 cm^{-1} is attributed to [$\delta(NH_2)$]. This band is lowered to 3200–3265 cm^{-1} in the complex, suggesting Cd—N through the amine nitrogen atom. The [(S—C)] vibrations in the free ligand (**4**) appear as a split band at 690 and 585 cm^{-1}, a mode which is shifted in the spectra of the trinuclear complex of **4** and which appears at 663 and 572 cm^{-1} suggesting the bonding of the metal ion to the ligand sulphur atom. This is further supported by the presence of bands in the lower frequency region which can be attributed to Cd—S bonding. With regard to the nature of the perchlorate ion in **8**, the complex shows a strong band centred at 1095 cm^{-1}, a weak one at 960

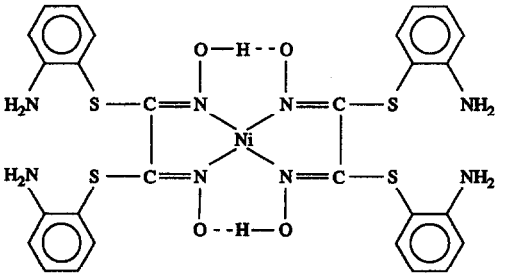

(7)

Fig. 1.

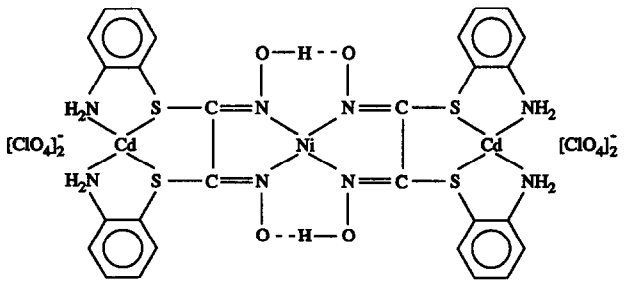

(8)

Fig. 2.

and a sharp one at 620 cm^{-1}, features typical of ionic perchlorates.[27a,b] The lack of appreciable splitting of the strong perchlorate bands supports a structure in which the perchlorate ions are not coordinated to the metal ions.[27c] A structural feature of this complex system is the presence of fused benzo groups, which serve to reduce the flexibility of the system.[28] The X-ray analysis indicates that in $[Cd(gly)_2]\cdot H_2O$[29] two glycino anions coordinate to the metal by forming a square-planar structure. The IR spectrum of the d^{10} complex of L-cysteine[30] shows that the structure of the complexes is square-planar, as shown in Fig. 2.

The cobalt(III) complex of **6** was prepared as previously reported[9a]. In the ^1H NMR spectrum of this complex the deuterium is exchangeable; intramolecular bridging, O—H · · · O protons appear as a singlet at $\delta = 14.35$ ppm for the pyridine derivative. ^{13}C NMR spectra of this compounds are very similar to those of the free ligand (**6**). The small shifts that take place in these spectra are due to complexation. The complex exhibits [(C=N)] absorptions at 1630 and 1660 cm^{-1}. In addition, after the complexation reaction of **6** the [(O—H)] vibrations at 3220 cm^{-1} disappear. These facts suggest that ligand **6** is N,N′-coordinated to cobalt(III) to look like the proposed structure (**9**) shown in Fig. 3.

The reaction of $[Cu(I)(CH_3CN)_4][PF_6]$[31] with **6** gave the corresponding diamagnetic copper(I) complex as a dark-yellow microcrystalline solid. This complex is especially suited for non-aqueous media syntheses of copper(I) compounds and the complex is moderately soluble in polar solvents and remarkably stable to air oxidation in CH_3CN solution. In this complex with **9** tetradentate coordination is achieved by the use of the two imino nitrogen and two sulphur atoms. Comparing the respective solutions, the ^{13}C NMR spectra of **9** and its copper(I) complex (Table 2) reveal that upon complexation shifts of the HC=N, SC and NC carbons by up to 5–7 pm result. Little change (0.7–1.0 ppm) in the position of the crown ether absorptions were evident, supporting the structure of the copper(I) cation in complex **10**. Subsequent complexation of the copper(I) complex with potassium hexafluorophosphate gave the respective heteropolymetallic complexes **10**, with the copper(I) cation in a square-planar coordination environment

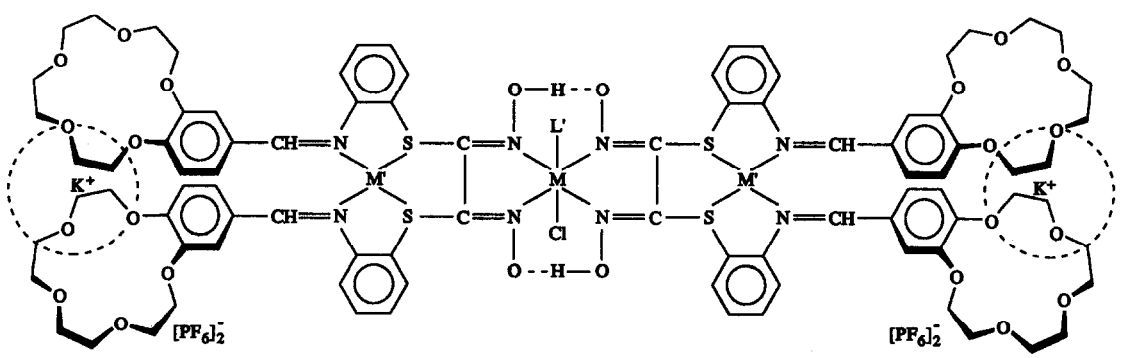

9:M = Co^{III},L′ = pyridine
10:M = Co^{III},L′ = pyridine
M′ = Cu^{I}

Fig. 3.

and (Fig. 3) the potassium cations bound by crown ether moieties. The structures of these sandwich complexes are proposed in Fig. 3. In the IR spectrum **10** shows small shifts for the stretching vibrations of the imine groups. The [(C=N)] vibrations of **10** appear at 1638 cm^{-1}. This azomethine stretch occurs at slightly lower energy in complex **9**, which indicates coordination of the imine nitrogen atom. As expected, shifts of the imine stretching vibrations to lower wave numbers are observed by complexation of copper(I) and potassium hexafluoro phosphate. In addition to these shifts of [(C=N)] suggest the bound alkali metal cations are influencing the electron density at the respective cobalt-bound copper(I) metal centres. The bands (850 and 557 cm^{-1}) which belong to [PF_6] support the structure in which the hexafluorophosphate ions are not coordinated to the centred copper(I) atom.[31]

EXPERIMENTAL

The ^1H and ^{13}C NMR spectra were recorded with a Bruker 200-AC instrument in DMSO-d_6 and the chemical shifts are reported in δ values relative to Me_4Si as an internal standard. IR spectra were recorded with a Perkin–Elmer 1600 FT-IR instrument. Mass spectra were measured on a Concept H Series Mass spectrometer. The metal contents of the complexes were determined by a Hitachi 180-80 atomic absorption spectrophotometer in solutions prepared by decomposing the compounds in the aqua regia and then subsequently digesting in concentrated HCl. 4′-Formylbenzo(15-crown-5)[32] (**5**) and dichloroglyoxime[33] were prepared as in the reference cited.

S,S′-Bis(2-aminophenyl)dithioglyoxime (**4**)

A solution of the potassium salt of 2-aminothiophenol was prepared by portionwise addition of the latter (2.5 g, 20 mmol) to KOEt solution, obtained by dissolving potassium metal (0.78 g, 20 mmol) in absolute ethanol (40 cm^3). This solution, together with a solution of (*E,E*)-dichloroglyoxime (1.57 g, 10 mmol) in absolute ethanol (40 cm^3), was simultaneously added dropwise over 6 h to absolute ethanol (180 cm^3) stirred at room temperature under nitrogen; stirring was continued overnight. The pale yellow reaction mixture was then filtered off and the filtrate volume was reduced to 30 cm^3 to precipitate the rest of the crude product. The crude product was filtered off, washed with water, cold ethanol and diethylether, respectively, and dried *in vacuo* over P_4O_{10}. After recrystallization from ethanol, yield; 2.10 g (62.8%) of needle crystals; m.p. 199°C (dec.). IR (KBr) = 3550, 3295, 3210, 3070, 2950, 1650, 1610, 1600, 1590, 1570, 1480, 1435, 1320, 1295, 1240, 1160, 980, 690, 585 cm^{-1}. ^1H NMR [D_6] DMSO: δ = 11.77 (s, 2H), 5.06 (s, 4H), 7.26–6.24 (m, 8H). ^{13}C NMR [D_6] DMSO: δ = 150.15, 143.97, 128.36, 126.58, 116.22, 114.57, 109.51. MS (E.I.), *m/z* (%): 334 (12) (M^+), 316 (16), 302 (10), 283 (100). UV–vis (DMF), λ_{max} (log ε): 276 (4.87), 306 (4.55), 323 (4.48), 348 (4.36), 364 (4.30). Found: C, 50.0; H, 4.1; N, 16.6. Calc. for $C_{14}H_{14}N_4O_2S_2$: C, 50.3; H, 4.2; N, 16.8%.

S,S-Bis[2-(4′-benzylidenamino-benzo-15-crown-5)] dithioglyoxime (**6**)

A solution of 4′-formylbenzo(15-crown-5) (2.96 g, 10 mmol) in absolute ethanol (35 cm^3) was added dropwise to a solution of compound **4** (1.67 g, 5 mmol) in absolute ethanol for a 30 min period at room temperature under nitrogen. The reaction mixture was refluxed and stirred for 22 h. The reaction was monitored by thin layer chromatography [*Rf* = 0.79, $CHCl_3$: CH_3—OH : H_2O (73 : 25 : 3)]. The mixture was cooled and the solvent was removed *in vacuo*. After crystallization of the product from ethanol, yield 1.11 g (24.9%) of white product; m.p. 117°C (dec.). IR (KBr): 3200, 3065, 2920, 2850, 1670, 1640, 1600, 1580, 1510, 1435, 1280, 1160, 1130, 1050, 965, 686, 582 cm^{-1}. ^1H NMR [D_6] DMSO: δ = 12.21 (s, 2H), 9.84 (s, 2H), 8.05 (s, 4H), 7.62–7.38 (m, 8H), 7.10 (s, 2H), 4.19–3.65 (m, 32H). ^{13}C NMR [D_6] DMSO: δ = 167.07, 153.48, 151.28, 148.67, 144.19, 134.04, 130.43, 128.22, 122.07, 118.24, 114.20, 113.17, 112.20, 111.05, 70.46, 69.55, 68.50, 68.27. MS (FAB.), *m/z* (%): 842 ($M^+ - NOH - OH$), 804 (45), 664 (18), 708 (12), 589 (85), 537 (90), 154 (100). UV–vis (DMF) (nm): λ_{max} (log ε) 270 nm (4.58), 305 nm (4.83), 361 nm (4.97), 391 nm (4.85). Found: C, 59.2; H, 5.5; N, 6.2. Calc. for $C_{44}H_{50}N_4O_{12}S_2$: C, 59.3; H, 5.6; N, 6.3%.

{*Bis[S,S′-bis(2-aminophenyl)dithioglyoximato]*} *nickel*(II) *complex* (**7**)

A solution of $NiCl_2 \cdot 6H_2O$ (0.474 g, 2 mmol) in ethanol (30 cm^3) was added to a solution of **4** (1.336 g, 4 mmol) in ethanol (60 cm^3) at room temperature, a distinct change in colour from colourless to red and a decrease in the "pH" of the solution was observed. While heating the mixture to 70°C $(C_2H_5)_3N$ (0.505 g, 5 mmol) in ethanol (5 cm^3) was added and an orange precipitate formed (**7**). After heating the mixture for 2 h the precipitate was filtered off, washed with water, ethanol and diethyl ether and then dried *in vacuo* over P_4O_{10}. Yield:

1.425 (98.3%); m.p. 297°C (dec.). IR (KBr): = 3305, 3030, 1730, 1635, 1605, 1595, 1565, 1480, 1440, 1310, 1235, 1190, 1160, 1130, 1060, 960, 910, 681, 583 cm^{-1}. ^1H NMR [D_6]DMSO: δ 5.13 (s, 8H), 7.35–6.68 (m, 16H), 17.35 (s, 2H). UV–vis (DMF), λ_{max} (nm) ($\log\varepsilon$): 275 (4.69), 304 (4.58), 322 (4.85), 342 (4.88), 395 (4.30), 516 (4.12). Found: C, 46.2; H, 3.4; N, 15.3; Ni, 7.9. Calc. for $C_{28}H_{26}N_8O_4S_4Ni$: C, 46.4; H, 3.6; N, 15.4; Ni, 8.1%.

Trinuclear complex of **4**

A solution of $Cd(ClO_4)_2 \cdot 6H_2O$ (0.836 g, 2 mmol) in ethanol (20 cm^3) was added to a suspension of **7** (0.724 g, 1 mmol) in ethanol (100 cm^3) and the mixture was refluxed for 17 h with vigorous stirring. The end of the reaction was determined by thin layer chromatograhy [$Rf = 0.65$, n-BuOH : CH_3COOH : H_2O (4 : 1 : 5)]. The precipitate was filtered off, washed with cold ethanol and diethyl ether and then dried *in vacuo* over P_4O_{10}. Yield (**8**): 1.112 g (82.5%); m.p. 319°C (dec.). IR (KBr): 3305, 3020, 1710, 1630, 1600, 1590, 1560, 1475, 1450, 1310, 1240, 1195, 1160, 1130, 1095, 960, 915, 663, 625, 572 cm^{-1}. ^1H NMR [D_6] DMSO: δ = 5.22 (br, 8H), 7.38–6.71 (m, 16H), 17.28 (s, 2H). UV–vis (DMF) (nm) λ_{max} ($\log\varepsilon$): 276 (4.82), 305 (4.50), 332 (4.81), 345 (4.76), 393 (4.15), 426 (3.94), 450 (3.63). Found: C, 24.6; H, 1.7; N, 8.2; Ni, 4.1; Cd, 16.4. Calc. for $[C_{28}H_{26}N_8O_4S_4NiCd_2][ClO_4]_4$: C, 24.9; H, 1.9; N, 8.3; Ni, 4.3; Cd, 16.7%.

The cobalt(III) *complex of* **6**

A solution of $CoCl_2 \cdot 6H_2O$ (0.1185 g, 0.5 mmol) in absolute ethanol (20 cm^3) was added to a solution of **6** (0.890 g, 1 mmol) in absolute ethanol (60 cm^3). While heating pyridine (0.395 g, 5 mmol) in ethanol (5 cm^3) was added to the above solution and dioxygen was bubbled through the mixture for 2 h at 70°C. The pale brown precipitate was filtered off, washed with water, ethanol and diethyl ether and then dried *in vacuo* over P_4O_{10}. Yield: 0.928 g, (95.1%); m.p. 326°C (dec.). IR (KBr): 3050, 2920–2845, 1660, 1630, 1600, 1580, 1470, 1440, 1310, 1300, 1245, 1160, 1140, 1030, 975, 940, 684, 584 cm^{-1}. ^1H NMR [D_6] DMSO: δ = 9.95 (s, 4H), 8.18–8.01 (m, 8H), 7.71 (s, 2H), 7.68–7.35 (m, 16H), 7.07 (s, 2H), 7.13 (s, 4H), 14.35 (s, 4H). ^{13}C NMR [D_6] DMSO: δ 167.06, 153.49, 151.32, 148.71, 143.87, 134.20, 126.40, 126.15, 125.82, 125.63, 124.79, 121.04, 117.92, 114.05, 113.27, 111.24, 111.03, 70.45, 69.59, 68.55, 68.33. UV–vis (DMF) (nm), λ_{max} ($\log\varepsilon$) = 272 (4.09), 303 (4.52), 322 (4.86), 365 (4.67), 420 (4.27), 525 (3.84). Found: C, 7.0; H, 5.2; N, 6.3; Co, 2.9. Calc. for $C_{93}H_{103}N_9O_{24}S_4ClCo$: C, 57.2; H, 5.3; N, 6.4; Co, 3.0%.

Trinuclear complex of **6**

A suspension of the mononuclear cobalt(III) complex of **6** (0.4878 g, 0.25 mmol) in dry acetonitrile (100 cm^3) was treated with excess $Cu(CH_3CN)_4PF_6$ (0.1829 g, 0.5 mmol) in dry acetonitrile (50 cm^3) under nitrogen and the mixture was refluxed for 18 h with stirring. The end of the reaction was determined by thin layer chromatography ($Rf = 0.68$, BAW 4 : 1 : 5). After the addition of KPF_6 (0.1104 g, 0.6 mmol) dissolved in dry acetonitrile (40 cm^3) under nitrogen the mixture was stirred at room temperature for 4 h and the solvent volume was reduced (30 cm^3) *in vacuo*. The precipitate was filtered off, washed with cold water, cold ethanol and diethyl ether and then dried *in vacuo* over P_4O_{10}. Yield (**10**): 0.627 g (87.87%), m.p. 380°C. IR (KBr): 3035, 2190–2840, 1720, 1638, 1625, 1600, 1580, 1560, 1530, 1450, 1430, 1380–1350, 1340, 1290, 1260, 1240–1210, 1175, 1030, 975, 895, 850, 667, 575, 557 cm^{-1}. ^1H NMR [D_6] DMSO: δ 9.91 (s, 4H), 8.25–8.03 (m, 8H), 7.78 (s, 2H), 7.68–7.43 (m, 16H), 7.22 (s, 4H), 7.12 (s, 2H), 15.64 (s, 4H). ^{13}C NMR [D_6] DMSO: δ 172.73, 153.56, 151.53, 150.58, 143.63, 134.51, 127.22, 126.17, 125.45, 124.68, 124.16, 121.18, 117.69, 113.96, 113.61, 113.47, 110.87, 70.25, 69.16, 68.21, 68.08. UV–vis (DMF) (nm), λ_{max} ($\log\varepsilon$): 278 (4.17), 302 (4.49), 331 (4.81), 348 (4.74), 366 (4.48), 444 (4.08) 536 (3.97). Found: C, 40.6; H, 3.6; N, 4.4; Co, 2.0; Cu, 4.4; K, 2.5. Calc. for $[C_{93}H_{103}N_9O_{24}S_4ClCoCu_2K_2][PF_6]_4$: C, 40.8; H, 3.8; N, 4.6; Co, 2.1; Cu, 4.6; K, 2.8%.

Acknowledgements—This work was supported by The Research Fund for Karadeniz Technical University (Trabzon, Turkey). We are indebted to Dr R. D. W. Kemmitt (Leicester, England) for mass spectra.

REFERENCES

1. C. J. Pedersen, *J. Am. Chem. Soc.* 1967, **89**, 7017.
2. A. V. Bajaj and N. S. Poonia, *Coord. Chem. Rev.* 1988, **87**, 55.
3. H. K. Frendsdorff, *J. Am. Chem. Soc.* 1971, **93**, 600.
4. D. Live and S. I. Chan, *J. Am. Chem. Soc.* 1976, **98**, 3769.
5. N. K. Dalley, D. E. Smith, R. M. Izatt and J. J. Christensen, *J. Chem. Soc., Chem. Commun.* 1972, 90.
6. C. Sirlin, L. Bosio, J. Simon, V. Ahsen, E. Yilmazer and Ö. Bekâroğlu, *Chem. Phys. Lett.* 1978, **139**, 362.
7. (a) A. Gül, A. I. Okur, A. Cihan, N. Tan and Ö. Bekâroğlu, *Synth. React. Inorg. Met.-Org. Chem.*

1986, **16**, 871; (b) P. D. Beer and C. G. Crane, *Polyhedron* 1988, **27**, 2649.
8. A. Gül, A. I. Okur, N. Tan and Ö. Bekâroğlu, *J. Chem. Res. (S)* 1986, 90.
9. (a) Y. Gök and H. Kantekin, *Chem. Ber.* 1990, **123**, 1479; (b) Y. Gök and H. Kantekin, *Synth. React. Inorg. Met.-Org. Chem.* 1990, **20**, 1085.
10. (a) Y. Gök and H. B. Şentürk, *Dyes Pigments* 1991, **15**, 279; (b) Y. Gök, *Org. Prep. Proc. Int.* 1990, **22**, 641.
11. (a) J. C. Chambron and J. P. Savage, *Tetrahedron Lett.* 1986, **27**, 865; (b) B. A. Boyce, A. Carroy, J. M. Lehn and D. Panker, *J. Chem. Soc., Chem. Commun.* 1984, 1546; (c) J. Rebeck Jr, J. R. Trend. R. V. Wattley and S. Chakravorti, *J. Am. Chem. Soc.* 1979, **101**, 4333; (d) J. P. Dix and F. Vögtle, *Chem. Ber.* 1980, **113**, 457.
12. (a) P. D. Beer and C. G. Crone, *Polyhedron* 1988, **27**, 2649; (b) J. Rebek Jr, *Accts Chem. Res.* 1984, **17**, 258; (c) P. D. Beer and H. Sikanyika, *Polyhedron* 1990, **9**, 1091; (d) P. D. Beer, H. Sikanyika, C. Blackburn, J. F. McAleer and M. G. B. Drew, *J. Chem. Soc., Dalton Trans.* 1990, 3295.
13. (a) G. N. Schrauzer, R. J. Windgassen and J. Kohnle, *Chem. Ber.* 1965, **98**, 3324; (b) A. Chakrovorty, *Coord. Chem. Rev.* 1974, **1**, 13.
14. (a) Y. Gök and Ö. Bekâroğlu, *Synth. React. Inorg. Met.-Org. Chem.* 1981, **11**, 621; (b) V: Ahsen, F. Gökceli and Ö. Bekâroğlu, *J. Chem. Soc., Dalton Trans.* 1987, 1818.
15. (a) Y. Gök and S. Serin, *Synth. React. Inorg. Met.-Org. Chem.* 1988, **18**, 975; (b) Y. Gök, H. Ertepınar and S. Z. Yıldız, *Spect. Lett.* 1990, **23**, 713.
16. (a) V. Ahsen, E. Musluoğlu, A. Gürek, A. Gül, Ö. Bekâroğlu and M. Zehnder, *Helv. Chim. Acta* 1990, **73**, 174; (b) Y. Gök and E. Özcan, *Trans. Met. Chem.* 1991, **16**, 393.
17. (a) N. M. Samus and A. V. Ablou, *Coord. Chem. Rev.* 1979, **28**, 177; (b) P. J. Toscano and L. G. Marzilli, *Prog. Inorg. Chem.* 1984, **31**, 105.
18. (a) A. Rockenbaver, M. Eyor, M. Kwiecinski and S. Tyrlik, *Inorg. Chim. Acta* 1982, **58**, 237; (b) S. Nemeth and L. Simondi, *J. Molec. Catal.* 1982, **14**, 87; (c) C. Lopez, S. Alvarez, X. Solons and M. Font-Altaba, *Inorg. Chem.* 1986, **25**, 2952.
19. (a) G. S. White and D. W. Stephan, *Inorg. Chem.* 1986, **25**, 1499; (b) Y. Gök and H. B. Şentürk, *Inorg. Chim. Acta* 1991, **180**, 53; (c) Y. Gök, M. Tüfekçi and E. Özcan, *Synth. React. Inorg. Met.-Org. Chem.* 1993, **23**, 861
20. (a) E. M. Hyde, B. L. Shaw and I. Shephard, *J. Chem. Soc., Dalton Trans.* 1978, 1696; (b) R. Ungaro, B. ElHaj and J. Smid, *J. Am. Chem. Soc.* 1976, **98**, 5198.
21. M. Erbaş, V. Ahsen, A. Gül and Ö. Bekâroğlu, *J. Organomet. Chem.* 1987, **333**, 383.
22. F. W. Wehri, A. P. Marchand and S. Wehrli, *Interperation of Carbon-13 NMR Spectra*, 2nd edn. John Wiley, New York (1988).
23. A. Gül and Ö. Bekâroğlu, *J. Chem. Soc., Dalton Trans.* 1983, 2537.
24. R. L. Lichter, D. E. Dorman and R. Wasyluhar, *J. Am. Chem. Soc.* 1974, **96**, 930.
25. (a) Y. Gök and S. Z. Yıldız, *Synth. React. Inorg. Met.-Org. Chem.* 1993, **22**, 1327; (b) Y. Gök, S. Z. Yıldız and M. Tüfekci, *J. Coord. Chem.* 1993, in press.
26. V. Ahsen, A. Gürek, A. Gül and Ö. Bekâroğlu, *J. Chem. Soc., Dalton Trans.* 1990, 5.
27. (a) R. M. Rosenthall, *J. Chem. Educ.* 1973, **50**, 331; (b) G. Mukherjee, S. N. Poddor, K. Choudhury and K. Dey, *Trans. Met. Chem.* 1988, **13**, 58; (c) P. A. Tasker and E. B. Fleischer, *J. Am. Chem. Soc.* 1970, **92**, 7072.
28. K. R. Adam, B. J. McCool, A. J. Leong, I. F. Lindoy, C. W. G. Ansell, P. J. Ballie and K. P. Doncoy, *J. Chem. Soc., Dalton Trans* 1990, 3435.
29. B. M. Low, F. L. Hirshfeld and F. M. Richards, *J. Am. Chem. Soc.* 1989, **81**, 4412.
30. K. Nakamoto, *Infrared Spectra of Inorganic and Coordination Compounds*. Wiley-Interscience, New York (1970).
31. G. J. Kubas, B. Monzya and A. L. Crubles, *Inorg. Synth.* 1971, **19**, 90.
32. (a) R. Ungaro, B. El Haj and J. Smid, *J. Am. Chem. Soc.* 1976, **98**, 5198; (b) E. M. Hyde, B. L. Shaw and I. Shephard, *J. Chem. Soc., Dalton Trans.* 1978, 1696.
33. K. A. Lance, K. A. Goldsby and D. H. Busch, *Inorg. Chem.* 1990, **29**, 4537.

Polyhedron Vol. 12, No. 17, pp. 2105–2109, 1993
Printed in Great Britain

0277–5387/93 $6.00+.00
© 1993 Pergamon Press Ltd

THE REACTIONS OF THE BIS(BUT-2-YNE) COMPLEX $[WI_2(CO)(NCMe)(\eta^2\text{-}MeC_2Me)_2]$ WITH BENZALDEHYDESEMICARBAZONE AND THIOSEMICARBAZONES

PAUL K. BAKER* and STEPHEN D. RIDYARD

Department of Chemistry, University of Wales, Bangor, Gwynedd LL57 2UW, U.K.

(*Received* 27 *April* 1993; *accepted* 7 *May* 1993)

Abstract—Reaction of equimolar quantities of $[WI_2(CO)(NCMe)(\eta^2\text{-}MeC_2Me)_2]$ and $Ph(H)CNNHCONH_2$ or $R(R^1)CNNHCSNH_2$ ($R = R^1 = Me$, Et; $R = H$, $R^1 = Ph$; $R = Me$, $R^1 = Et$, Pr^n, Bu^t, Ph) in CH_2Cl_2 at room temperature gave the cationic bis(but-2-yne) complexes $[WI(CO)\{Ph(H)CNNHCONH_2\}(\eta^2\text{-}MeC_2Me)_2]I$ or $[WI(CO)\{R(R^1)CNNHCSNH_2\}(\eta^2\text{-}MeC_2Me)_2]I$ in good yield. The cationic nature of these complexes was confirmed by reaction of $[WI(CO)\{Me(Ph)CNNHCSNH_2\}(\eta^2\text{-}MeC_2Me)_2]I$ with $Na[BPh_4]$ in acetonitrile to afford the tetraphenylborate exchanged product $[WI(CO)\{Me(Ph)CNNHCSNH_2\}(\eta^2\text{-}MeC_2Me)_2][BPh_4]$. Refluxing a $CHCl_3$ solution of $[WI(CO)\{Et_2CNNHCSNH_2\}(\eta^2\text{-}MeC_2Me)_2]I$ for 14 h gave the mono(but-2-yne) complex $[WI_2(CO)\{Et_2CNNHCSNH_2\}(\eta^2\text{-}MeC_2Me)]$.

Although a wide range of "classical" transition metal complexes containing semicarbazones and thiosemicarbazones have been described,[1–3] very few examples of organotransition metal complexes containing these attached ligands have been reported. The π-allyl molybdenum thiosemicarbazone complexes $[MoX(CO)_2\{R^1(R^{11})CNNHCSNH_2\}(\eta^3\text{-}C_3H_4R)]$ ($X = Cl$ or Br; $R = H$ or Me; $R^1 = H$ or Me; $R^{11} = Me$, Et, Pr^n or Ph)[4,5] and the closely related semicarbazone complexes $[MoX(CO)_2\{R^1(R^{11})CNNHCONH_2\}(\eta^3\text{-}C_3H_4R)]$ ($X = Cl$, Br or I; $R = H$ or Me; R′, R″ = H or Me and Me, Et, Pr^n or Ph)[6,7] have been prepared and characterized. Tripathi and coworkers[8] have described the synthesis of some zirconium cyclopentadienyl thiosemicarbazone complexes. The iron complexes $[Fe(CO)_2L(\eta^5\text{-}C_5H_5)][PF_6]$ [$L = R^1(R^{11})CNNHCSNH_2$, where $R^1 = R^{11} = Me$; $R^1 = H$, $R^{11} = Ph$; $R^1 = H$, $R^{11} = p\text{-}NO_2Ph$; $R^1 = Me$, $R^{11} = p\text{-}MePh$; $R^1R^{11} = C_5H_{10}$] have been prepared[9,10] and crystallographically characterized[10] for $R^1 = H$, $R^{11} = Ph$. The seven-coordinate thiosemicarbazone complexes $[WI_2(CO)_3\{R(R^1)CNNHCSNH_2\}]$ ($R = R^1 = Me$ or Et; $R = Me$, $R^1 = Pr^i$; $R = Ph$, $R^1 = H$) and $[Mo(\mu\text{-}I)I(CO)_2\{R(R^1)CNNHCSNH_2\}]_2$ have also been reported.[11]

In recent years we have been investigating the chemistry of the bis(alkyne) tungsten complexes $[WI_2(CO)(NCMe)(\eta^2\text{-}RC_2R)_2]$ ($R = Me$ or Ph),[12] which are prepared by reacting the bis(acetonitrile) complex $[WI_2(CO)_3(NCMe)_2]$ with an excess of RC_2R in CH_2Cl_2 at 0°C. In this paper we describe the reactions of the bis(but-2-yne) complex $[WI_2(CO)(NCMe)(\eta^2\text{-}MeC_2Me)_2]$ with benzaldehydesemicarbazone and thiosemicarbazones.

EXPERIMENTAL

The reactions were performed under dry nitrogen using standard Schlenk-line techniques. The compound $[WI_2(CO)(NCMe)(\eta^2\text{-}MeC_2Me)_2]$ was prepared by the published method.[12] The ligands benzaldehydesemicarbazone and the thiosemicarbazones $R(R^1)CNNHCSNH_2$ ($R = R^1 = Me$, Et; $R = H$, $R^1 = Ph$; $R = Me$, $R^1 = Et$, Pr^n, Bu^t, Ph) were synthesized by the method of Sah and Daniels.[13] All other chemicals used were purchased from commercial sources. IR spectra were recorded as $CHCl_3$ films between NaCl plates on a 1430 ratio recording IR spectrophotometer. Elemental analyses (carbon, hydrogen and nitrogen) were determined using a Carlo–Erba elemental analyser MOD 1106 (using helium as a carrier gas). ^1H and ^{13}C NMR spectra were recorded either on a Bruker AC 250 or a Bruker WH 400 MHz NMR spec-

*Author to whom correspondence should be addressed.

trometer (all spectra were calibrated against tetramethylsilane).

Preparation of [WI(CO){H(Ph)CNNHCONH$_2$}(η^2-MeC$_2$Me)$_2$]I (**1**)

To a stirred solution of [WI$_2$(CO)(NCMe)(η^2-MeC$_2$Me)$_2$] (0.5 g, 0.813 mmol) in CH_2Cl_2 (20 cm^3) was added H(Ph)CNNHCONH$_2$(0.13 g, 0.813 mmol). After stirring for 18 h the solution was filtered and the solvent removed *in vacuo* to give brown crystals of [WI(CO){H(Ph)CNNHCONH$_2$}(η^2-MeC$_2$Me)$_2$]I (**1**), which were recrystallized from CH_2Cl_2/Et_2O. Yield of pure complex = 0.24 g, 40% (see Table 1 for physical and analytical data).

Preparation of [WI$_2$(CO){Me(Ph)CNNHCSNH$_2$}(η^2-MeC$_2$Me)$_2$]I (**8**)

To a stirred solution of [WI$_2$(CO)(NCMe)(η^2-MeC$_2$Me)$_2$] (0.5 g, 0.813 mmol) in CH_2Cl_2 (20 cm^3) was added Me(Ph)CNNHCSNH$_2$ (0.16 g, 0.813 mmol). After stirring for 18 h the solution was filtered and the solvent removed *in vacuo* to give brown crystals of [WI(CO){Me(Ph)CNNHCSNH$_2$}(η^2-MeC$_2$Me)$_2$]I (**8**), which were recrystallized from CH_2Cl_2/Et_2O. Yield of pure complex = 0.32 g, 52%.

Similar reactions of [WI$_2$(CO)(NCMe)(η^2-MeC$_2$Me)$_2$] with an equimolar quantity of R(R^1)CNNHCSNH$_2$ [R = R^1 = Me (**2**), Et (**3**); R = H, R^1 = Ph (**4**); R = Me, R^1 = Et (**5**); Pr^n (**6**); Bu^t (**7**)] in CH_2Cl_2 at room temperature gave [WI(CO){R(R^1)CNNHCSNH$_2$}(η^2-MeC$_2$Me)$_2$]I (**2–7**). For physical and analytical data see Table 1.

Preparation of [WI(CO){Me(Ph)CNNHCSNH$_2$}(η^2-MeC$_2$Me)$_2$][BPh$_4$] (**9**)

To a stirred suspension of [WI$_2$(CO)(NCMe)(η^2-MeC$_2$Me)$_2$] (0.5 g, 0.813 mmol) in acetonitrile (25 cm^3) was added Me(Ph)CNNHCSNH$_2$ (0.16 g, 0.829 mmol) and Na[BPh$_4$] (0.28 g, 0.819 mmol). After stirring for 18 h removal of the solvent *in vacuo* afforded a yellow/white slurry, which was redissoved in CH_2Cl_2 (20 cm^3) and the solution was filtered twice to remove NaI. Finally, removal of the solvent *in vacuo* gave red/brown crystals of [WI(CO){Me(Ph)CNNHCSNH$_2$}(η^2-MeC$_2$Me)$_2$][BPh$_4$] (**9**), which were recrystallized from CH_2Cl_2/Et_2O. Yield of pure product = 0.37 g, 47%.

Preparation of [WI$_2$(CO){Et$_2$CNNHCSNH$_2$}(η^2-MeC$_2$Me)] (**10**)

To a stirred solution of [WI$_2$(CO)(NCMe)(η^2-MeC$_2$Me)$_2$] (0.5 g, 0.813 mmol) in $CHCl_3$ (40 cm^3)

Table 1. Physical and analytical data[a] for the benzaldehydesemicarbazone and thiosemicarbazone but-2-yne complexes of tungsten(II)

Complex	Colour	Yield (%)	C (%)	H (%)	N (%)
(**1**) [WI(CO){Ph(H)CNNHCONH$_2$}(η^2-MeC$_2$Me)$_2$]I	Brown	40	27.8 (27.7)	3.4 (2.9)	6.2 (5.7)
(**2**) [WI(CO){Me$_2$CNNHCSNH$_2$}(η^2-MeC$_2$Me)$_2$]I	Yellow	53	22.6 (22.2)	3.3 (3.0)	5.7 (6.0)
(**3**) [WI(CO){Et$_2$CNNHCSNH$_2$}(η^2-MeC$_2$Me)$_2$]I	Sandy yellow	63	24.5 (24.6)	3.7 (3.4)	5.3 (5.7)
(**4**) [WI(CO){H(Ph)CNNHCSNH$_2$}(η^2-MeC$_2$Me)$_2$]I	Brown	54	27.4 (27.1)	3.2 (2.8)	5.5 (5.5)
(**5**) [WI(CO){Me(Et)CNNHCSNH$_2$}(η^2-MeC$_2$Me)$_2$]I	Yellow	59	23.4 (23.4)	3.4 (3.2)	5.8 (5.8)
(**6**) [WI(CO){Me(Pr^n)CNNHCSNH$_2$}(η^2-MeC$_2$Me)$_2$]I	Yellow/ brown	67	24.6 (24.6)	3.6 (3.4)	5.3 (5.7)
(**7**) [WI(CO){Me(Bu^t)CNNHCSNH$_2$}(η^2-MeC$_2$Me)$_2$]I	Yellow/ brown	46	26.0 (25.7)	4.0 (3.6)	5.9 (5.6)
(**8**) [WI(CO){Me(Ph)CNNHCSNH$_2$}(η^2-MeC$_2$Me)$_2$]I	Brown	52	27.8 (28.2)	3.0 (3.0)	5.4 (5.5)
(**9**) [WI(CO){Me(Ph)CNNHCSNH$_2$}(η^2-MeC$_2$Me)$_2$][BPh$_4$]	Red/ brown	47	53.2 (53.8)	3.8 (4.0)	5.1 (4.9)
(**10**) [WI$_2$(CO){Et$_2$CNNHCSNH$_2$}(η^2-MeC$_2$Me)]	Brown	53	19.4 (19.5)	2.8 (2.8)	6.3 (6.2)

[a] Calculated values in parentheses.

was added $Et_2CNNHCSNH_2$ (0.13 g, 0.813 mmol). After refluxing for 14 h at 69°C cooling the solution, filtration and removal of the solvent *in vacuo* gave brown crystals of $[WI_2(CO)\{Et_2CNNHCSNH_2\}(\eta^2\text{-}MeC_2Me)]$ (**10**), which were recrystallized from CH_2Cl_2/Et_2O. Yield of pure product = 0.29 g, 53%.

RESULTS AND DISCUSSION

Equimolar quantities of $[WI_2(CO)(NCMe)(\eta^2\text{-}MeC_2Me)_2]$ and $Ph(H)CNNHCONH_2$ or $R(R^1)CNNHCSNH_2$ (R = R^1 = Me, Et; R = H, R^1 = Ph; R = Me, R^1 = Et, Pr^n, Bu^t, Ph) in CH_2Cl_2 at room temperature eventually gave the cationic complexes $[WI(CO)\{Ph(H)CNNHCONH_2\}(\eta^2\text{-}MeC_2Me)_2]I$ (**1**) and $[WI(CO)\{R(R^1)CNNHCSNH_2\}(\eta^2\text{-}MeC_2Me)_2]I$ (**2–8**) *via* displacement of an acetonitrile ligand and an iodide. Confirmation of the cationic nature of **1–8** was obtained by reacting equimolar amounts of $[WI(CO)\{Me(Ph)CNNHCSNH_2\}(\eta^2\text{-}MeC_2Me)_2]I$ and $Na[BPh_4]$ in acetonitrile to give the anion exchanged product $[WI(CO)\{Me(Ph)CNNHCSNH_2\}(\eta^2\text{-}MeC_2Me)_2][BPh_4]$ (**9**). Refluxing $[WI(CO)\{Et_2CNNHCSNH_2\}(\eta^2\text{-}MeC_2Me)_2]I$ (**3**) in chloroform (69°C) for 14 h eventually gave the neutral diiodo complex $[WI_2(CO)\{Et_2CNNHCSNH_2\}(\eta^2\text{-}MeC_2Me)]$ (**10**). All the new complexes **1–10** were characterized by elemental analysis (carbon, hydrogen and nitrogen) (Table 1), IR and ^1H NMR spectroscopy (Tables 2 and 3). Complexes **1–10** are moderately soluble in chlorinated solvents such as CH_2Cl_2 and $CHCl_3$, however, they are more soluble in acetone and dimethylsulphoxide. Complexes **1–10** are air-sensitive both in the solid state and in solution, however, they can be stored under nitrogen for several days. The reactions described in this paper are shown in Scheme 1.

The IR spectra of complexes **1–9** showed a strong single carbonyl band between 2020 and 2050 cm^{-1}, which was expected since the previously reported[14] bidentate nitrogen donor complexes $[WI(CO)(\widehat{N\,N})(\eta^2\text{-}RC_2R)_2]I$ (R = Me or Ph; $\widehat{N\,N}$ = 2,2′-bipy, 1,10-phen or *o*-phenylenediamine) have similar CO stretching bands in their IR spectra. The molecular structure of the tetraphenylborate complex $[WI(CO)(2,2'\text{-bipy})(\eta^2\text{-}MeC_2Me)_2][BPh_4]$ was crystallographically determined[14] and the structure of the related complexes described in this paper are likely to be similar, as shown in Fig. 1. The ^1H NMR spectra for **1–9** generally also show four but-2-yne methyl resonances, expected for the structure shown in Fig. 1. In the cases where there are three but-2-yne resonances the intensity ratio is 2:1:1, which indicates two of the resonances are overlapping. For the complexes $[WI(CO)(\widehat{O\,S}$ or $\widehat{N\,S})(\eta^2\text{-}MeC_2Me)_2]I$ (**1–8**) to obey the effective atomic number rule the two but-2-yne ligands in **1–8** must donate a total of six electrons to the metal, i.e. one four-electron and one two-electron donor to the tungsten centre. This was confirmed by the ^{13}C NMR spectrum obtained for $[WI(CO)\{Et_2CNNHCSNH_2\}(\eta^2\text{-}MeC_2Me)_2]I$ (**3**), which showed alkyne contact carbon resonances at $\delta(CDCl_3, +25°C)$ = 148.3, 156.3, 163.8 and 176.3 ppm, which from Templeton and Wards'[15] correlation suggest that the but-2-yne ligands are donating an average of "three" electrons each to the tungsten. However, it is likely that four- and two-electron alkynes are rapidly equilibrating on the NMR time-scale. Attempts to obtain the ^{13}C NMR spectra of all complexes **1–10** was unsuc-

Table 2. IR data[a] for the benzaldehydesemicarbazone and thiosemicarbazone but-2-yne complexes of tungsten(II)

Complex	ν(NH) (cm^{-1})	ν(C≡O) (cm^{-1})	$\nu(NH_2)$ (cm^{-1})	ν(C≡S) (cm^{-1})
(**1**)	3450 (br, m)	2020 (s)[b]	1570 (m), 1625 (m)	690 (m)
(**2**)	3420 (br, m)	2040 (s)	1640 (m), 1580 (m)	700 (m)
(**3**)	3430 (br, m)	2030 (s)	1640 (w), 1590 (w)	690 (s)
(**4**)	3370 (br, w), 3430 (br, w)	2050 (s)	1605 (m), 1590 (m)	695 (s)
(**5**)	3425 (br, m)	2030 (s)	1550 (m), 1510 (m)	695 (m)
(**6**)	3420 (br, m)	2020 (s)	1610 (m), 1580 (w)	695 (m)
(**7**)	3300 (m), 3450 (m)	2030 (s)	1610 (s), 1550 (m)	690 (m)
(**8**)	3350 (br, w), 3440 (br, w)	2050 (s)	1605 (m), 1520 (m)	665 (s)
(**9**)	3283 (m), 3415 (m)	2050 (s)	1690 (m), 1610 (w)	738 (s)
(**10**)	3375 (br, m)	1960 (s)	1630 (m), 1590 (m)	690 (m)

br = broad, w = weak, m = medium, s = strong.

[a] All spectra were recorded as thin films in $CHCl_3$ between NaCl plates.

[b] ν(C≡O) band at 1640s cm^{-1} for benzaldehydesemicarbazone.

Table 3. ^{1}H NMR data[a,b] for the benzaldehydesemicarbazone and thiosemicarbazone but-2-yne complexes of tungsten(II)

Complex	^{1}H (δ)
1[a]	2.90. 2.95, 3.02, 3.07 (4s, 12H, ≡C*Me*), 3.40 (s, 1H, =C*H*), 7.40 (brm, 5H, *Ph*), 9.06 (brs, 2H, NH_2), 10.12 (brs, 1H, N*H*)
2[b]	1.4, 1.7 (2s, 6H, CMe_2), 2.79, 2.92, 3.1 (3s, 12H, ≡C*Me*), 9.78 (brs, 2H, NH_2), 10.02 (brs, 1H, N*H*)
3[b]	1.6 (brt, 6H, CH_2CH_3), 2.1 (brq, 4H, CH_2CH_3), 2.72, 2.92, 3.0, 3.1 (4s, 12H, ≡C*Me*), 10.2 (brd, 2H, NH_2), 11.1 (brs, 1H, N*H*)
4[b]	2.91, 2.94, 3.03, 3.07 (4s, 12H, ≡C*Me*), 5.62 (s, 1H, =C*H*), 7.8 (m, 5H, *Ph*), 9.04 (brs, 2H, NH_2), 9.50 (brs, 1H, N*H*)
5[b]	1.6 (t, 3H, CH_2CH_3), 1.7 (s, 3H, =C*Me*), 2.0 (m, 2H, CH_2CH_3), 2.88, 2.92, 3.4 (3s, 12H, ≡C*Me*); 9.30 (brs, 2H, NH_2); 10.8 (brs, 1H, N*H*)
6[b]	1.18 (t, 3H, $CH_2CH_2CH_3$), 1.6 (m, 2H, $CH_2CH_2CH_3$), 2.0 (t, 2H, $CH_2CH_2CH_3$), 2.1 (s, 3H, C*Me*), 2.87, 2.92, 2.98 (3s, 12H, ≡C*Me*), 9.74 (brd, 2H, NH_2), 10.7 (brs, 1H, N*H*)
7[b]	1.18 (s, 9H, CMe_3), 1.7 (s, 3H, C*Me*), 2.89, 2.94, 3.02, 3.06 (4s, 12H, ≡C*Me*), 8.88 (brs, 2H, NH_2), 9.01 (brs, 1H, N*H*)
8[a]	1.8 (s, 3H, C*Me*), 2.68, 2.72, 2.9, 3.04 (4s, 12H, ≡C*Me*), 7.62 (m, 5H, *Ph*), 9.7 (brs, 2H, NH_2), 10.65 (brs, 1H, N*H*)
9[a]	1.8 (s, 3H, C*Me*), 2.67, 2.72, 2.91, 3.06 (4s, 12H, ≡C*Me*), 7.4–7.7 (brm, 25H, *Ph*), 9.4 (d, 2H, NH_2), 10.6 (brs, 1H, N*H*)
10[b]	1.4 (brt, 6H, CH_2CH_3), 1.8 (brq, 4H, CH_2CH_3), 2.9, 3.00 (2s, 6H, ≡C*Me*), 9.8 (d, 2H, NH_2), 11.6 (brs, 1H, N*H*)

[a] Spectra recorded in $CDCl_3$ or $(CD_3)_2CO$ at +25°C on a Bruker AC 250 NMR spectrometer.
[b] Spectra recorded in $CDCl_3$ or $(CD_3)_2CO$ at +25°C on a Bruker WH 400 NMR spectrometer.

cessful due to moderate solubility and instability in solution. It should be noted that we attempted the reactions of the more sterically crowded benzophenonethiosemicarbazone with [WI_2(CO)(NCMe)(η^2-MeC_2Me)$_2$] without success.

We have previously described[16] the reaction of the bidentate phosphines, $Ph_2P(CH_2)_nPPh_2$ (n = 1–6) with [WI_2(CO)(NCMe)(η^2-RC_2R)$_2$] (R = Me or Ph) to give the mono(alkyne) complexes [WI_2(CO){$Ph_2P(CH_2)_nPPh_2$}(η^2-RC_2R)]. Hence, we attempted to prepare the analogous mono(but-2-yne) complexes [WI_2(CO){Ph(H)CNNHCONH$_2$}(η^2-MeC_2Me)] and [WI_2(CO){R(R^1)CNNHCSNH$_2$}(η^2-MeC_2Me)] by refluxing **1–8** in CH_2Cl_2 or $CHCl_3$. In the case of R = R^1 = Et the neutral mono(but-2-yne) complex [WI_2(CO){Et_2CNNHCSNH$_2$}(η^2-MeC_2Me)] (**10**) was obtained in 53% yield, after refluxing [WI(CO){Et_2CNNHCSNH$_2$}(η^2-MeC_2Me)$_2$]I in $CHCl_3$ for 14 h. The carbonyl stretching band for **10** at 1960 cm^{-1} is at a considerably lower wave number than the bis(but-2-yne) complexes **1–9** and in a similar position to the bidentate phosphine complexes [WI_2(CO){$Ph_2P(CH_2)_nPPh_2$}(η^2-MeC_2Me)].[16] The differing behaviour of the $\widehat{N\,S}$ donor ligands and the $\widehat{P\,P}$ type ligands is likely to be due to the more electron-rich donor ability of $\widehat{N\,S}$, which helps to stabilize the bis(but-2-yne) complexes [WI(CO)($\widehat{N\,S}$)(η^2-MeC_2Me)$_2$]I. It should be noted that several unsuccessful attempts were made to prepare

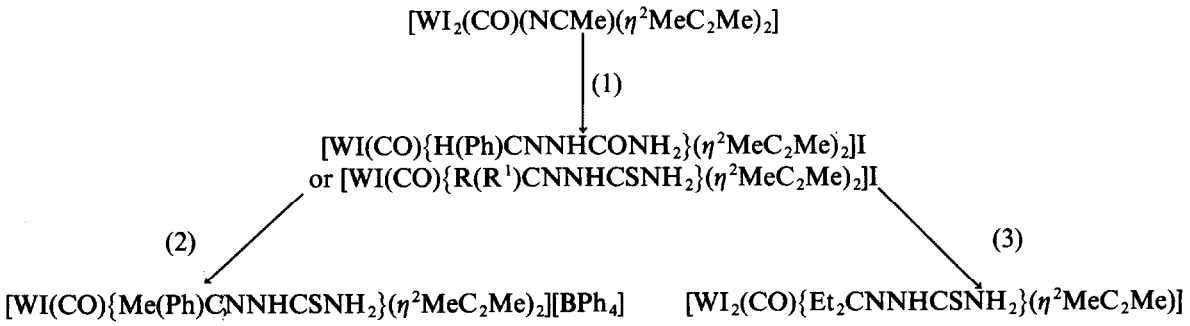

Scheme 1. Reagents: (1) H(Ph)CNNHCONH$_2$ or R(R^1)CNNHCSNH$_2$ (R = R^1 = Me, Et; R = H, R^1 = Ph; R = Me, R^1 = Et, Pr^n, Bu^t, Ph) in CH_2Cl_2 at room temperature. (2) For R = Me, R^1 = Ph, Na[BPh_4] in acetonitrile. (3) For R = R^1 = Et, reflux at 69°C in $CHCl_3$ for 14 h.

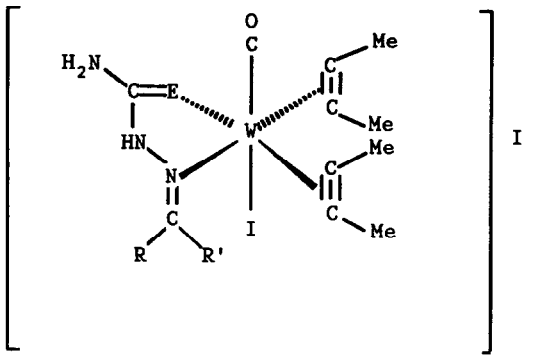

I

Fig. 1. Proposed structure for the cationic bis(but-2-yne) complexes $[WI(CO)\{R(R^1)CNNHCENH_2\}(\eta^2\text{-}MeC_2Me)_2]I$ (**1–8**) (E = O or S).

the diphenylacetylene complexes $[WI(CO)\{R(R^1)CNNHCSNH_2\}(\eta^2\text{-}PhC_2Ph)_2]I$ in a pure state by reacting $[WI_2(CO)(NCMe)(\eta^2\text{-}PhC_2Ph)_2]$ with $R(R^1)CNNHCSNH_2$. The IR spectra of these reactions showed mixtures of two complexes, probably $[WI(CO)\{R(R^1)CNNHCSNH_2\}(\eta^2\text{-}PhC_2Ph)_2]I$ and $[WI_2(CO)\{R(R^1)CNNHCSNH_2\}(\eta^2\text{-}PhC_2Ph)]$, which were difficult to separate in each case. The semicarbazone and thiosemicarbazone complexes **1–10** described in this paper are considerably less stable than the cationic bidentate nitrogen $[WI(CO)(\widehat{N}\widehat{N})(\eta^2\text{-}RC_2R)_2]I$[14] ($\widehat{N}\widehat{N}$ = 2,2′-bipy, 1,10-phen or *o*-phenylenediamine) and bidentate phosphine $[WI_2(CO)\{Ph_2P(CH_2)_nPPh_2\}(\eta^2\text{-}RC_2R)]$[16] donor ligand complexes.

Acknowledgements—We thank the European Social Fund for support for S.D.R. and we thank Dr O. W. Howarth for obtaining several ^1H and ^{13}C NMR spectra for us at the University of Warwick on the SERC NMR service.

REFERENCES

1. M. J. M. Campbell, *Coord. Chem. Rev.* 1975, **15**, 279.
2. S. Padhye and G. B. Kauffman, *Coord. Chem. Rev.* 1985, **63**, 127.
3. R. B. Singh, B. S. Garg and R. P. Singh, *Talanta* 1978, **25**, 619.
4. P. K. Baker, M. J. M. Campbell and M. V. White, *Inorg. Chim. Acta* 1985, **98**, L27.
5. M. J. M. Campbell, E. Morrison, V. Rogers and P. K. Baker, *Trans. Met. Chem.* 1986, **11**, 381.
6. M. J. M. Campbell, E. Morrison, V. Rogers and P. K. Baker, *Inorg. Chim. Acta* 1987, **127**, L17.
7. M. J. M. Campbell, E. C. Morrison, V. Rogers and P. K. Baker, *Polyhedron* 1988, **7**, 1719.
8. V. Srivastava, S. Sengupta and S. C. Tripathi, *Synth. React. Inorg. Met.-Org. Chem.* 1985, **15**, 163.
9. M. J. M. Campbell, E. Morrison, V. Rogers and P. K. Baker, *Polyhedron* 1987, **6**, 1703.
10. M. J. M. Campbell, E. Morrison, V. Rogers, P. K. Baker, D. C. Povey and G. W. Smith, *Polyhedron* 1989, **8**, 2371.
11. P. K. Baker and S. G. Fraser, *J. Coord. Chem.* 1989, **20**, 267.
12. E. M. Armstrong, P. K. Baker and M. G. B. Drew, *Organometallics* 1988, **7**, 319.
13. P. P. T. Sah and T. C. Daniels, *Recueil* 1950, **69**, 1545.
14. P. K. Baker, E. M. Armstrong and M. G. B. Drew, *Inorg. Chem.* 1988, **27**, 2287.
15. J. L. Templeton and B. C. Ward, *J. Am. Chem. Soc.* 1980, **102**, 3288.
16. E. M. Armstrong, P. K. Baker, M. E. Harman and M. B. Hursthouse, *J. Chem. Soc., Dalton Trans.* 1989, 295.

Polyhedron Vol. 12, No. 17, pp. 2111–2119, 1993
Printed in Great Britain

0277–5387/93 $6.00+.00
© 1993 Pergamon Press Ltd

ELECTROCHEMICAL AND EPR SPECTRAL STUDIES OF MONO- AND BIMETALLIC (TRISPYRAZOLYLBORATO)MOLYBDENUM AND TUNGSTEN COMPLEXES WITH EXTENDED DI-PHENOL BRIDGING LIGANDS; EVIDENCE FOR ELECTRON EXCHANGE BELOW THE FAST LIMIT

RICHARD COOK, JOHN P. MAHER, JON A. McCLEVERTY† and MICHAEL D. WARD†

School of Chemistry, University of Bristol, Cantock's Close, Bristol BS8 1TS, U.K.

and

ANDRZEJ WLODARCZYK†

Institute of Chemical Engineering and Physical Chemistry, Technical University of Krakow, 31-155 Krakow, Poland

(*Received* 23 *March* 1993; *accepted* 7 *May* 1993)

Abstract—Mononuclear diphenolato complexes [M(NO)L*X(OQOH)] and binuclear complexes [{M(NO)L*X}$_2$(μ-OQO)] {M = Mo, W; L* = [HB(3,5-$Me_2C_3HN_2$)$_3$]$^-$; X = Cl, I; Q = C_6H_4, 4,4′-$C_6H_4C(O)C_6H_4$, 4,4′-$C_6H_4S(O)_2C_6H_4$ or $C_6H_4C(O)(C_6H_4)_2C(O)C_6H_4$} were prepared. Some have been reported before; the new complexes were thoroughly characterized. Electrochemical interactions between the metal centres in the binuclear complexes with the three longer bridging ligands are small. The binuclear molybdenum complexes (which contain two 16-electron metal centres) with 4,4′-$OC_6H_4C(O)C_6H_4O$ or 4,4′-$OC_6H_4S(O)_2C_6H_4O$ as bridging ligands were reduced to dianionic species (two 17-electron centres), whose EPR spectra indicate pairwise electron exchange at or near the fast limit; with the longer bridging ligand $OC_6H_4C(O)(C_6H_4)_2C(O)C_6H_4O$ the more complex EPR spectrum of the reduced dianionic complex indicates that electron exchange is no longer "fast", but occurs at an intermediate rate. With the shortest bridging ligand OC_6H_4O the electrochemical interaction is sufficiently large to allow selective preparation of the mixed-valence 16-electron/17-electron species, whose EPR spectrum indicates that it is valence trapped; fast exchange is only initiated when *both* metal centres have a 17-electron configuration. The EPR spectra of the corresponding bimetallic tungsten dianions cannot be used to examine electron exchange processes since they show no resolved hyperfine signals.

In earlier papers[1,2] we reported that the bimetallic molybdenum complexes [{Mo(NO)L*X}$_2$E] [L* = tris(3,5-dimethylpyrazolyl)borate, HB(3,5-$Me_2C_3HN_2$)$_3$; E = *para*- or *meta*-OC_6H_4O; X = Cl or I] and [{Mo(NO)L*X}$_2$($OC_6H_4YC_6H_4O$)] (X = Cl or I; Y = nothing, O, S, SO_2, CO, $COC_6H_4C_6H_4CO$) underwent two one-electron reductions, affording a mono- and a di-anion. The $E_{1/2}$ data indicated that in those systems containing relatively short bridges, e.g. *para*-OC_6H_4O, the electrochemical interaction between the two redox centres was very strong (as measured by $\Delta E_{1/2}$, the difference between first and second reduction potentials), whereas in the complexes containing more extended bridges such as $OC_6H_4YC_6H_4O$ (above)

† Authors to whom correspondence should be addressed.

the interaction was weak or negligible. In the case of $[\{Mo(NO)L^*Cl\}_2(p\text{-}OC_6H_4O)]$ the two one-electron reductions are sufficiently well separated to permit selective one-electron reduction with a reducing agent of the appropriate potential;[1] with longer bridging ligands this is not possible. Whereas the neutral bimetallic complexes formally contain two 16-electron metal centres, the mixed-valence mono-anions have one 16- and one 17-electron centre and the dianions contain two 17-electron centres. The mixed-valence 16-electron/17-electron species could be either valence-trapped, if the asymmetry due to solvation differences at the two ends is sufficiently large, or delocalized with the electron "hopping" between the ends. The doubly-reduced 17-electron/17-electron species could have either singlet (coupled 17-electron centres) or triplet (uncoupled centres) states. The EPR properties of these paramagnetic species have not hitherto been studied in detail.

More recently we have found that analogous complexes containing bridging ligands such as 4,4′-bipyridines[3] and the "extended" α,ω-di(4-pyridyl)-polyenes[3,4] of the type $[\{Mo(NO)L^*Cl\}(pyr\text{–}E\text{–}pyr)]$ [E = $(CH_2)_n$, n = 0–3; $(CH{=}CH)_n$, n = 1–5; C_6H_4, N=N, etc.] contain two 17-electron molybdenum centres. The electrochemical interactions between those centres are substantial, being in fact an order of magnitude larger than the interactions found between $\{Ru(NH_3)_5\}^{2+}$ centres with the same bridging ligands.[5] EPR spectroscopy has shown that the two unpaired electrons in these species are apparently in fast exchange across the bridging ligand. This interaction can even occur across a saturated bridge,[3] its facility being explained partly by the fact that, unlike one-electron charge-transfer processes, there is no solvent reorganization required since both metals have the same number of electrons before and after any exchange.

Use of asymmetric bridging ligands, with one phenol terminus and one pyridyl terminus, has enabled the preparation of binuclear complexes with one 17-electron and one 16-electron terminus, e.g. $[\{Mo(NO)L^*Cl\}_2(OC_6H_4C_5H_4N)]$.[6,7] Due to the difference of 800 mV in redox potential between the two ends the single unpaired electron is "valence trapped", but one-electron reduction of the 16-electron terminus to give the *asymmetric* (17 + 17)-electron complex initiates apparent fast exchange of electrons between the two ends despite the asymmetry.

A re-examination of the doubly-reduced bimetallic complexes containing extended phenolic bridges, viz. $[\{Mo(NO)L^*X\}_2(OQO)]^{2-}$, has shown

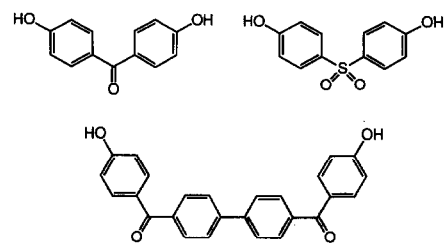

Fig. 1. Structures of the bridging ligands used in this paper.

that these species have EPR spectral characteristics analogous to their neutral bipyridyl analogues $[\{Mo(NO)L^*Cl\}(pyr\text{–}E\text{–}pyr)]$ and to $[\{Mo(NO)L^*Cl\}_2(OC_6H_4C_5H_4N)]^-$; all three types of system contain two 17-electron metal centres. In this paper we describe the full characterization of some neutral bi-molybdenum species and some tungsten analogues with the extended di-phenol bridging ligands shown in Fig. 1; some related mono-metallic compounds, $[Mo(NO)L^*X(OQOH)]$, are also described. In addition we describe a solution EPR spectroscopic study of the singly-reduced (16-electron/17-electron) and doubly-reduced (17-electron/17-electron) forms of $[\{Mo(NO)L^*Cl\}_2)p\text{-}OC_6H_4O)]^{n-}$ (n = 1, 2) and of the doubly-reduced (17-electron/17-electron) dianionic species $[\{Mo(NO)L^*X\}_2(OQO)]^{2-}$ with the longer bridging ligands. These new species now allow us to examine apparent fast exchange of electrons between phenolate-substituted molybdenum centres with bridging ligands from short to very long, i.e. we can compare dianionic [(17 + 17)-electron] species containing OC_6H_4O, $OC_6H_4COC_6H_4O$, $OC_6H_4S(O)_2C_6H_4O$ and $OC_6H_4CO(C_6H_4)_2COC_6H_4O$ as bridging ligands. We have previously established a lower limit of *ca* 100 MHz for the exchange interaction J between the electrons with relatively short bridging ligands;[1,6] the real rate is probably much faster. With sufficiently long bridging ligands, however, and provided intermolecular electron exchange does not occur, there must come a point at which the intramolecular exchange becomes slow and spectra characteristic of electrons localized at one metal centre may be observed.

EXPERIMENTAL

^1H NMR spectra were recorded on Jeol GX90 or GX270 spectrometers. Electron-impact (E.I.) mass spectra were measured on a Kratos MS9 instrument and fast-atom bombardment (FAB) mass spectra on a VG-Autospec at the SERC Mass Spectrometry Service Centre, Swansea, with 3-nitrobenzylalcohol

as a matrix. EPR spectra were recorded at room temperature on a Bruker ESP-300E spectrometer. Electrochemical experiments were performed using an EG&G PAR model 273A potentiostat. A standard three-electrode configuration was used, with platinum-bead working and auxiliary electrodes and a saturated calomel electrode (S.C.E.) reference. Ferrocene was added at the end of each experiment as an internal standard; all potentials are quoted vs the ferrocene/ferrocenium couple (Fc/Fc^+). The solvent was CH_2Cl_2, purified by distillation from CaH_2, containing $[NBu_4][PF_6]$ (0.1 mol dm^{-3}) as a base electrolyte.

Controlled-potential reductions *in situ* in the EPR cavity were performed using a platinum gauze working electrode in an EPR flat cell. The platinum wire working electrode and S.C.E. reference were positioned in a reservoir of solvent (CH_2Cl_2 containing 0.1 mol dm^{-3} $[NBu_4][PF_6]$) attached to the top of the EPR flat cell. The potential at the working electrode was applied using an EG&G PAR model 264A polarographic analyser. Alternatively, the reduced (17-electron/17-electron) forms of some complexes could be prepared by addition of cobaltocene to a solution of the neutral (16-electron/16-electron) species in distilled MeCN under nitrogen. After immersion of the mixture in a sonic cleaning bath for a few minutes a sudden and obvious colour change, from deep red/brown to a much paler brown, occurred. A few drops of the solution were then added by syringe to a nitrogen-flushed EPR tube; the reduced solutions were stable for several hours.

4,4′-Dihydroxybenzophenone ($HOC_6H_4COC_6H_4OH$), bis(4-hydroxyphenyl)sulphone ($HOC_6H_4S(O)_2C_6H_4OH$) and hexamethylenetetramine were obtained from Aldrich and used as received; $HOC_6H_4CO(C_6H_4)_2COC_6H_4OH$ was kindly donated by Dr H. Colquhoun of ICI Mond division. [{Mo(NO)L*Cl}$_2$(p-OC_6H_4O)] was prepared according to the published method.[1]

General procedure for syntheses of complexes

A mixture of [ML*(NO)X$_2$] (M = Mo, X = Cl, I; M = W, X = Cl), the appropriate ligand (5 equivalents) and hexamine (5 equivalents, except for [{Mo(NO)L*Cl}$_2$($OC_6H_4COC_6H_4C_6H_4CO$ C_6H_4OH)] where an excess of Et_3N was used) in dry toluene was heated to reflux under nitrogen. The reactions were monitored by thin-layer chromatography, the reaction times required for complete consumption of the starting metal complex being given in Table 1. After cooling the reaction mixture hexane was added (half the volume of the toluene solution) and the solution was refrigerated overnight to precipitate the unreacted ligand and the excess of hexamethylenetetramine and its salts. After filtration the residual solution was evaporated to dryness *in vacuo* and purified by column chromatography on silica. Initial elution with CH_2Cl_2 removed traces of unreacted [ML*(NO)X$_2$] and the green μ-oxo dimer, which always appeared as a by-product. The major two fractions were then collected, the first being the bimetallic complex [{ML*(NO)X}$_2$(μ-L)] and the second the monometallic complex [ML*(NO)X(HL)]. Addition of up to 2% THF to the CH_2Cl_2 was sometimes necessary to elute the more polar mononuclear complexes. The fractions from the columns were evaporated to dryness *in vacuo*, recrystallized from CH_2Cl_2/hexane (M = W) or CCl_4/hexane (M = Mo), collected by filtration and dried *in vacuo*. If necessary, fractions collected in this way could be purified further on a second short silica column.

Analytical and mass spectroscopic data are given in Table 1.

RESULTS AND DISCUSSION

Synthesis and characterization of complexes

All of the complexes with the "extended" ligands (Fig. 1) were prepared by reaction of [ML*(NO)X$_2$] (M = Mo, X = Cl, I; M = W, X = Cl) with $HOC_6H_4EC_6H_4OH$ (E = CO or SO_2) and $\{HOC_6H_4COC_6H_4\}_2$ in toluene at reflux with hexamethylenetetramine or Et_3N present as base. Due to the very low solubility of these ligands in hot toluene a large excess was always used. On chromatographic purification the relatively non-polar binuclear complexes eluted ahead of the much more polar mononuclear complexes, which have free pendant phenol groups and so could be separated easily. With $HOC_6H_4S(O)_2C_6H_4OH$ no mononuclear complexes were formed; only a binuclear complex was isolated in each case (Table 1). The three binuclear complexes [{Mo(NO)L*Cl}$_2$($OC_6H_4EC_6H_4O$)] [E = CO, SO_2, $CO(C_6H_4)_2CO$] have been mentioned earlier and their electrochemistry was described in some detail.[2] However, complete details of their characterization were not given, so they are included here for the sake of completeness. All of the complexes were characterized by elemental analysis and FAB mass spectrometry, strong molecular ions being seen in every case. Owing to the presence of a large number of possible isotope combinations of the elements Mo, W, Cl and B the molecular ion clusters span a wide mass range and the most intense peak of the cluster does not always cor-

Table 1. Synthetic, analytical, spectroscopic and electrochemical data for the new complexes

M_n[a]	X	(Bridging) Ligand	Colour	%Y[b]	RT[c]	ν(NO)[d]	FAB MS[e]	Elemental analysis[f] %C	%H	%N	$E_{1/2}$ (V)[g] (ΔE_p, mV)
Mo	I	$OC_6H_4C(O)C_6H_4OH$	Brown	12	1.5	1686	766 (765)	45.0 (44.1)	4.3 (4.1)	12.5 (12.8)	−0.75 (90)
Mo_2	I	$OC_6H_4C(O)C_6H_4O$	Brown	23	1.5	1683	1318 (1316)	40.0 (39.4)	4.4 (4.0)	14.0 (14.9)	−0.75 (200)
Mo	Cl	$OC_6H_4C(O)C_6H_4OH$	Brown	14	4.5	1686	673 (673)	49.3 (50.1)	4.7 (4.7)	14.3 (14.6)	−0.79 (90)
Mo_2	Cl	$OC_6H_4C(O)C_6H_4O$	Brown	32	4.5	1683	1133 (1132)	44.7 (45.7)	4.7 (4.6)	16.4 (17.4)	[h]
W	Cl	$OC_6H_4C(O)C_6H_4OH$	Green	10	6	1652	760 (759)	44.3 (44.3)	4.2 (4.1)	12.4 (12.9)	−1.35 (140)
W_2	Cl	$OC_6H_4C(O)C_6H_4O$	Green	59	6	1651	1299 (1304)	39.4 (39.6)	4.0 (4.0)	14.4 (15.0)	−1.33 (190)
Mo_2	I	$OC_6H_4S(O)_2C_6H_4O$	Brown	42	1	1681	1350 (1352)	37.2 (37.4)	3.8 (3.9)	13.9 (14.5)	−1.16 (120)
Mo_2	Cl	$OC_6H_4S(O)_2C_6H_4O$	Brown	23	5	1682	1169 (1168)	42.4 (43.3)	4.8 (4.5)	16.0 (16.8)	[h]
W_2	Cl	$OC_6H_4S(O)_2C_6H_4O$	Green	39	7	1650	1335 (1340)	37.4 (37.6)	3.9 (3.9)	14.4 (14.6)	−1.28 (160)
Mo	Cl	$OC_6H_4COC_6H_4—C_6H_4COC_6H_4OH$	Brown	22	1	1687	851 (853)	57.0 (57.8)	4.8 (4.6)	11.2 (11.5)	−0.78 (200)
Mo_2	Cl	$\{OC_6H_4COC_6H_4\}_2$	Brown	20	4	1688	1311 (1312)	49.7 (51.4)	4.6 (4.6)	14.8 (15.0)	[h]
Mo_2	I	$\{OC_6H_4COC_6H_4\}_2$	Brown	22	1.5	1684	1497 (1496)	45.6 (45.1)	4.2 (4.1)	13.1 (13.1)	−0.71 (100)
W_2	Cl	$\{OC_6H_4COC_6H_4\}_2$	Green	35	10	1651	1485 (1484)	45.4 (45.3)	3.9 (4.1)	12.9 (13.2)	−1.31 (120)

[a] M_n = monomer (n = 1) or bimetallic (n = 2).
[b] Percentage yield based on metal-containing starting materials.
[c] Reaction time (h).
[d] KBr discs.
[e] Calculated values in parentheses (based on most abundant isotopes).
[f] Calculated values in parentheses.
[g] Electrochemical measurements made at a platinum bead working electrode in CH_2Cl_2, at scan rate of 0.2 V s^{-1}; potentials vs the ferrocene/ferrocenium couple (Fc/Fc^+).
[h] Detailed electrochemical details in ref. 2.

Table 2. Proton NMR spectral data for the new complexes

M[a]	X[b]	(Bridging) Ligand	Methyl protons[c]	Pyrazolyl protons[c]	Ligand protons[c]
Mo	I[d]	$OC_6H_4C(O)C_6H_4OH$	2.00(3), 2.27(3), 2.40(3), 2.42(3), 2.48(3), 2.51(3)	5.91(1), 5.93(1), 5.97(1)	6.94 (2, d), 7.48 (2 d), 7.8–7.9 (4, m)
Mo_2	I[e]	$OC_6H_4C(O)C_6H_4O$	2.02(6), 2.31(6), 2.37(6), 2.40(6), 2.45(6), 2.53(6)	5.87(4), 5.91 (2)	7.50 (4, d), 7.90 (4 d)
Mo	Cl[e]	$OC_6H_4C(O)C_6H_4OH$	2.08(3), 2.20(3), 2.39(3), 2.42(6), 2.55(3)	5.77(1), 5.93(2)	6.90 (2, d), 7.38 (2, d), 7.7–7.9 (4, m)
Mo_2	Cl[e]	$OC_6H_4C(O)C_6H_4O$	2.10(6), 2.21(6), 2.40(6), 2.42(12), 2.56(6)	5.78(2), 5.94(4)	7.40 (4, d), 7.97 (4, d)
W	Cl[e]	$OC_6H_4C(O)C_6H_4OH$	2.20(3), 2.27(3), 2.39(9), 2.64(3)	5.84(1), 5.94(2)	6.88 (2, d), 7.31 (2, d), 7.7–7.9 (4, m)
W_2	Cl[d]	$OC_6H_4C(O)C_6H_4O$	2.21(6), 2.29(6), 2.42(12), 2.43(12), 2.62(6)	5.90(2), 6.00(4)	7.29 (4, d), 7.91 (4, d)
Mo_2	I[e]	$OC_6H_4S(O)_2C_6H_4OH$	1.95(6), 2.23(6), 2.36(6), 2.39(6), 2.44(6), 2.50(6)	5.82(2), 5.86(2), 5.89(2)	7.50 (4, d), 7.97 (4, d)
Mo_2	Cl[e]	$OC_6H_4S(O)_2C_6H_4O$	2.03(6), 2.13(6), 2.38(6), 2.41(6), 2.42(6), 2.53(6)	5.74(2), 5.93(4)	7.38 (4, d), 8.00 (4, d)
W_2	Cl[d]	$OC_6H_4S(O)_2C_6H_4O$	2.14(6), 2.17(6), 2.40(6), 2.41(6), 2.42(6), 2.59(6)	5.86(2), 5.98(2), 5.99(2)	7.30 (4, d), 7.97 (4, d)
Mo	Cl[d]	$OC_6H_4C(O)C_6H_4—C_6H_4C(O)C_6H_4O$	2.10(3), 2.18(3), 2.42(3), 2.44(6), 2.53(3)	5.83(1), 6.00(2)	6.95 (2, d), 7.0–7.2 (2, m), 7.39 (2, d), 7.7–8.1 (10, m)
Mo_2	Cl[e]	$\{OC_6H_4C(O)C_6H_4\}_2$	2.10(6), 2.20(6), 2.42(18), 2.56(6)	5.79(2), 5.94(4)	7.40 (4, d), 7.7–8.1 (12, m)
Mo_2	I[d]	$\{OC_6H_4C(O)C_6H_4\}_2$	2.03(6), 2.29(6), 2.40(6), 2.43(6), 2.48(6), 2.52(6)	5.92(2), 5.94(2), 5.98(2)	7.52 (4, d), 7.84 (4, d), 7.9–8.0 (8, m)
W_2	Cl[d]	$\{OC_6H_4C(O)C_6H_4\}_2$	2.22(6), 2.26(6), 2.42(12), 2.43(6), 2.61(6)	5.90(2), 6.01(4)	7.32 (4, d), 7.83 (4, d), 7.95 (8, d)

[a] M = monomer (n = 1) or bimetallic (n = 2).
[b] Solvent as indicated.
[c] Number of protons for which each signal integrates is given in parentheses.
[d] Recorded at 270 MHz in CD_2Cl_2.
[e] Recorded at 90 MHz in $CDCl_3$.

respond exactly to the value calculated from the most abundant isotopes.

In addition all complexes were characterized by ^{1}H NMR spectroscopy (Table 2). The pyrazolyl methyl protons occur as singlets between 2 and 2.7 ppm. In many cases all six signals were resolved, which is consistent with the low symmetry of the [ML*(NO)X(phenoxide)] centre; each pyrazolyl ring is *trans* to a different group (nitrosyl, halide, phenoxide) and are, therefore, all inequivalent. The fact that only six signals were ever observed for the binuclear complexes confirms that they have two-fold symmetry in solution, with each metal centre equivalent. The pyrazolyl protons, between 5.7 and 6.0 ppm, behave similarly. The protons of the aromatic ligands in the bridging ligands occur between 6.9 and 8.1 ppm in each case. In the mononuclear complexes [M(NO)L*X($OC_6H_4COC_6H_4OH$)] (M = Mo, X = Cl, I; M = W, X = Cl) the inequivalence of the coordinated and pendant aromatic rings is clear; in the binuclear complexes the signals due to the bridging ligand protons simplify consistent with the two-fold symmetry.

All of the tungsten complexes have ν(NO) at *ca* 1650 cm^{-1} in the IR spectrum; for the molybdenum complexes the nitrosyl stretch is at just above 1680 cm^{-1}. These values are to be expected by comparison with other phenoxide-substituted molybdenum and tungsten complexes and further confirm the identities of the complexes.

Electrochemistry

The complexes were examined by cyclic voltammetry and the results are summarized in Table 1. The results show that the metal–metal interactions across these long bridges in the binuclear complexes are fairly weak. In no cases are two waves resolved by cyclic voltammetry. Accordingly, the positions of the centres of the (rather broad) voltammetric waves are given in each case. No attempt has been made to deconvolute the electrochemical response to give separate $E_{1/2}$ values for the two closely-spaced reductions in the new binuclear complexes. For [{Mo(NO)L*Cl}$_2$(O$C_6H_4EC_6H_4O$)] [E = CO, SO_2 and $CO(C_6H_4)_2CO$] the electrochemical properties were reported earlier in some detail and the separate $E_{1/2}$ values estimated by analysis of the shapes of differential-pulse polarograms.[2] They showed separations of 85, 75 and 56 mV, respectively, between the two reductions. This is in marked contrast to complexes with bis(4-pyridyl) bridging ligands of similar lengths, where the electrochemical interactions were typically several hundred millivolts.[3,4]

EPR spectroscopy of molybdenum complexes

First, we examined the EPR properties of the reduced forms of [{Mo(NO)L*Cl}$_2$(p-OC_6H_4O)], in which the two metal-centred reductions are sufficiently far apart to allow selective one-electron or two-electron reductions by controlled-potential electrolysis. A controlled-potential reduction at -0.9 V vs Fc/Fc$^+$ generated the 16-electron/17-electron mixed-valence mono-anion. The EPR spectrum of the resultant solution is shown in Fig. 2(a). This spectrum clearly shows that the unpaired electron is localized on one molybdenum centre; since about 25% of molybdenum atoms have nuclear spin $I = 5/2$, there is a sextet ($A_{Mo} = 50 \pm 1$ Gauss) superimposed on a central singlet at $g = 1.97$. This spectrum is identical to those of several *mono-nuclear*, 17-electron molybdenum complexes.[1,3,4,8] The mixed-valence state is, therefore, valence-trapped on the EPR time-scale, i.e. it exhibits Class I behaviour according to the Robin and Day classification.[9]

Reduction at a potential more negative than the

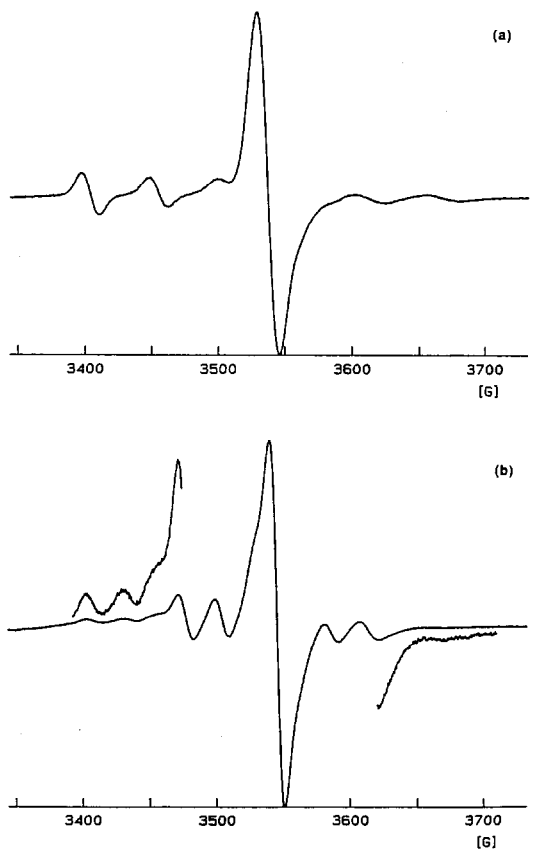

Fig. 2. EPR spectra of [{Mo(NO)L*Cl}$_2${OC_6H_4O}] after (a) one-electron reduction and (b) two-electron reduction, in MeCN at room temperature.

second reduction process—either electrochemically or by addition of cobaltocene—afforded a solution of the 17-electron/17-electron dianion, whose EPR spectrum is in Fig. 2(b). This spectrum clearly shows that the exchange interaction between the two unpaired electrons has been initiated. The apparent hyperfine splitting of the sextet (arising from the isotopomer containing one $I = 0$ and one $I = 5/2$ nucleus) has halved to 26 ± 1 Gauss, which is consistent with each electron coupling to two equivalent metal centres,[10] and additional outlying lines consistent with the presence of a 1:2:3:4:5:6:5:4:3:2:1 11-fold multiplet (arising from the isotopomer containing two nuclei which both have $I = 5/2$) are evident. The limit of "fast" electron exchange is the situation where the electron exchange interaction $|J|$ is much greater than the hyperfine coupling frequency;[10] with $A_{Mo} = 51 \pm 1$ Gauss, the signal centre at 3537 Gauss and a microwave frequency of 9.77 GHz, this means that $|J|$ must be *much greater* than $(51/3537) \times 9.77 \times 10^9$ Hz, i.e. 140 MHz, to give a first-order spectrum consistent with both electrons coupling equally to both molybdenum nuclei. This behaviour is identical to that observed with the asymmetric 16-electron/17-electron complex [{Mo(NO)L*Cl}$_2$($OC_6H_4C_5H_4N$)] where the single unpaired electron is also valence-trapped, but on reduction to the 17-electron/17-electron monoanion fast exchange is initiated.[6,7]

We next examined the EPR properties of the reduced mononuclear complexes [Mo(NO)L*Cl($OC_6H_4COC_6H_4OH$)]$^-$ and [Mo(NO)L*Cl{O$C_6H_4CO(C_6H_4)_2COC_6H_4OH$}]$^-$, and of the reduced binuclear complexes [{Mo(NO)L*Cl}$_2$(O$C_6H_4EC_6H_4O$)]$^{2-}$ [E = CO, SO_2 and $CO(C_6H_4)_2$CO], all of which contain 17-electron {MoL*(NO)Cl(OAr)} cores, in order to see whether or not the exchange interaction could be sustained over relatively long distances. Although we have shown that the exchange interaction is maintained (i.e. $|J| \gg A_{Mo}$, where $|J|$ is the electron–electron interaction and A_{Mo} the hyperfine coupling) over a long distance using α,ω-di(4-pyridyl)-polyenes and related ligands as bridges,[3,4] with diphenols as bridging ligands the mesomeric linkage between the metal centres is removed by the presence of formally sp^3-hybridized oxygen atoms in the bridge. The effect of this is illustrated by the observation that the inter-metal electrochemical interactions with diphenol bridges are substantially weaker than those in binuclear complexes with 4,4′-bipyridyl-type bridges of comparable lengths.

The reduction potentials of the molybdenum complexes are sufficiently anodic that complete two-electron reduction to the 17-electron species may be effected simply by addition of cobaltocene to the sample in acetonitrile solution. We have previously used this technique with CH_2Cl_2 as the solvent,[6,7] but with these rather large complexes the dianions slowly precipitated from solution (presumably as the cobalticenium salts) resulting in very poorly resolved EPR spectra. Accordingly we used MeCN, in which the reduced dianions are fully soluble.

The 17-electron mononuclear complexes [Mo(NO)L*Cl($OC_6H_4COC_6H_4OH$)]$^-$ and [{Mo(NO)L*Cl}$_2$($OC_6H_4CO(C_6H_4)_2COC_6H_4OH$)]$^-$ gave spectra which are essentially identical to the spectra of valence-localized 16-electron/17-electron complexes, such as in Fig. 2(a); these spectra indicate the presence of an unpaired electron localized at one molybdenum atom. Anisotropic broadening, due to the slow tumbling rate of the long molecules in solution, means that the high-field components of the sextet are poorly resolved. These spectra are identical to several other mononuclear, 17-electron molybdenum complexes.[1,3,4,8]

The reduced binuclear complexes [{Mo(NO)L*Cl}$_2$($OC_6H_4EC_6H_4O$)]$^{2-}$ (E = CO or SO_2) give spectra which are very similar to those we have observed for other 17-electron/17-electron biradicals such as in Fig. 2(b); halving of the apparent hyperfine splitting and the appearance of outlying components from the expected 11-fold multiplet are again evident. Although these spectra are slightly perturbed from ideality in that the intensities of the outlying components are not exactly as predicted (e.g. the first three weak components are predicted to have intensity ratios of 1:2:3), the positions and

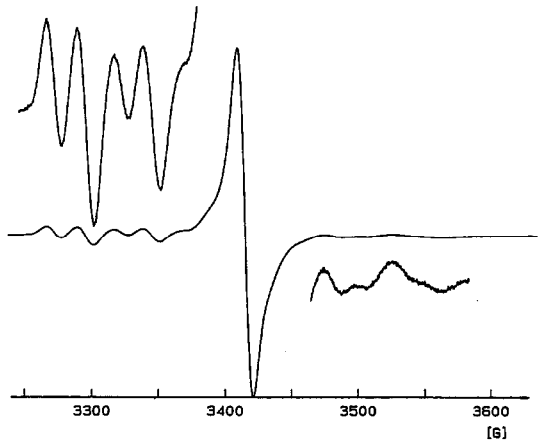

Fig. 3. EPR spectrum of [{MoL*(NO)Cl}$_2${OC_6H_4C(O)$(C_6H_4)_2$(CO)C_6H_4O}]$^{2-}$ (with two 17-electron centres) in MeCN at room temperature.

multiplicities of the signals confirm that the value of $|J|$ is still very large relative to A_{Mo}.

The EPR spectrum of $[\{Mo(NO)L^*Cl\}_2\{OC_6H_4CO(C_6H_4)_2COC_6H_4O\}]^{2-}$, which contains a much longer bridging ligand, is shown in Fig. 3. It is quite different from both of the previous two, showing five resolved peaks to the left of the central peak with separations of 18–20 Gauss between them. It appears that in this complex the exchange interaction between the unpaired electrons is sufficiently decreased by the greater length of the bridging ligand to give an intermediate situation where $|J|$ is now of the same order as A_{Mo}. This is expected to lead to a more complicated, second-order spectrum with several additional lines appearing (depending on the nuclear spin) and apparent line separations of less than either of the two simple extremes,[10] which is what we observe. In addition, the separation between the most outlying hyperfine component and the signal centre is larger than we observed for either extreme, which is another indication of second-order behaviour. We are currently attempting to simulate these EPR spectra and the preliminary results clearly show that a spectrum very similar to that of $[\{Mo(NO)L^*Cl\}_2\{OC_6H_4CO(C_6H_4)_2COC_6H_4O\}]^{2-}$ may be obtained with a value of $|J|$ of approximately 50 MHz (c.f. $A_{Mo} \approx 140$ MHz); a detailed report of the spectral simulation studies will be made in due course.[11]

In order to rule out intermolecular electron exchange processes contributing to the appearance of the spectrum we also performed a variable-temperature EPR study of $[\{Mo(NO)L^*Cl\}_2\{OC_6H_4CO(C_6H_4)_2COC_6H_4O\}]^{2-}$ in MeCN, from 240 to 340 K. No significant variation in the appearance of the spectrum was observed apart from a slight broadening of all of the lines at low temperatures as the solvent viscosity increased. This proves that inter-molecular electron exchange is not occurring, and that therefore the appearance of the spectrum is solely due to the intramolecular electron exchange interaction across $\{OC_6H_4COC_6H_4C_6H_4COC_6H_4O\}$.

EPR spectroscopy of tungsten complexes

The molybdenum complexes are particularly suitable for these studies since changes in the appearance of the hyperfine satellites is an excellent diagnostic tool for examining electron exchange interactions in the biradicals. In order to see if we could observe similar behaviour with tungsten complexes we examined the EPR spectra of the reduced 17-electron and 34-electron mono- and binuclear complexes. Electrochemical reduction of the mononuclear complex $[W(NO)L^*Cl(OC_6H_4COC_6H_4OH)]$ *in situ* in the EPR cavity yielded a paramagnetic species whose spectrum just consisted of a broad, single line at $g = 1.89$. Similar behaviour was observed with the corresponding binuclear complex $[\{W(NO)L^*Cl\}_2(OC_6H_4COC_6H_4O)]^{2-}$; the signal did not become much stronger with time, and after about an hour a small signal appeared at the free-spin value with a hyperfine coupling of 2.5 Gauss, i.e. an organic free radical with resolved hydrogen coupling, probably resulting from decomposition of $[\{W(NO)L^*Cl\}_2(OC_6H_4COC_6H_4O)]^{2-}$ and partial reduction of the free bridging ligand. Neither $[W(NO)L^*Cl(OC_6H_4COC_6H_4OH)]^-$ nor $[\{W(NO)L^*Cl\}_2(OC_6H_4COC_6H_4O)]^{2-}$ showed any evidence of clearly resolved hyperfine coupling to ^{183}W ($I = 1/2$, 14.4% natural abundance), which means unfortunately that electron-exchange between tungsten centres in the biradicals such as $[\{W(NO)L^*Cl\}_2(OC_6H_4COC_6H_4O)]^{2-}$ cannot be easily examined.

CONCLUSIONS

We have demonstrated that on addition of one electron to binuclear complexes of the type $[\{Mo(NO)L^*Cl\}_2(\mu\text{-}L)]$ (where H_2L is a *p*-diphenol-type bridging ligand) the odd electron is localized at one molybdenum terminus; addition of a second electron initiates delocalization. This delocalization (pairwise electron exchange) can also occur in biradicals containing $\{OC_6H_4COC_6H_4O\}$ and $\{OC_6H_4S(O)_2C_6H_4O\}$ as bridging ligands between $\{Mo(NO)ClL^*\}$ centres. With $\{OC_6H_4COC_6H_4C_6H_4COC_6H_4O\}$ as a bridging ligand, however, the EPR spectrum is second-order, consistent with a weaker exchange interaction between the two electrons; we are, therefore, seeing the first indications of control of the magnitude of $|J|$ with the length of the bridging ligand. The EPR spectra of the analogous tungsten complexes show no clearly-defined hyperfine satellites and are, therefore, unsuitable for examination of pairwise electron exchange.

Acknowledgements—We are grateful to the SERC for support of this work through a fellowship (AW) and via funds to purchase the EPR spectrometer, and to the Politechnika Krakowska, Poland, for leave of absence for AW while part of this work was completed. We thank Mr Dariusz Rams for technical assistance.

REFERENCES

1. S. M. Charsley, C. J. Jones, J. A. McCleverty, B. D. Neaves, S. J. Reynolds and G. Denti, *J. Chem. Soc., Dalton Trans.* 1988, 293.

2. S. M. Charsley, C. J. Jones, J. A. McCleverty, B. D. Neaves and S. J. Reynolds, *J. Chem. Soc., Dalton Trans.* 1988, 293.
3. S. L. McWhinnie, C. J. Jones, J. A. McCleverty, D. Collison and F. E. Mabbs, *J. Chem. Soc., Chem. Commun.* 1990, 940.
4. J. A. Thomas, C. J. Jones, J. A. McCleverty, D. Collison, F. E. Mabbs, C. J. Harding and M. G. Hutchings, *J. Chem. Soc., Dalton Trans.* 1992, 1796; A. Das, J. P. Maher, J. A. McCleverty, J. A. Navas Badiola and M. D. Ward, *J. Chem. Soc., Dalton Trans.* 1993, 681.
5. C. Creutz, *Prog. Inorg. Chem.* 1983, **30**, 1.
6. A. Das, J. C. Jeffery, J. P. Maher, J. A. McCleverty, E. Schatz, M. D. Ward and G. Wollermann, *Angew. Chem., Int. Edn. Engl.* 1992, **31**, 1515.
7. A. Das, J. C. Jeffery, J. P. Maher, J. A. McCleverty, E. Schatz, M. D. Ward and G. Wollermann, *Inorg. Chem.* 1993, **32**, 2145.
8. A. Abdul-Rahman, A. Das, C. J. Jones, J. A. McCleverty and M. D. Ward, to be published.
9. M. P. Robin and P. Day, *Adv. Inorg. Chem. Radiochem.* 1967, **10**, 247.
10. D. C. Reitz and S. Weissmann, *J. Chem. Phys.* 1960, **33**, 700.
11. J. P. Maher, J. A. McCleverty, M. D. Ward, C. Western and A. Wlodarczyk, unpublished results.

Polyhedron Vol. 12, No. 17, pp. 2121–2124, 1993
Printed in Great Britain

0277–5387/93 $6.00+.00
© 1993 Pergamon Press Ltd

METAL COMPLEXES OF FUNCTIONALIZED PHOSPHINES—II.* SYNTHESIS OF HYDROXYMETHYL- AND AMINOMETHYLDIPHENYLPHOSPHINE COMPLEXES OF PLATINUM. CRYSTAL STRUCTURE OF *cis*-[$PtCl_2(Ph_2PCH_2OH)_2$]

DAVID L. DAVIES,† JULIE NEILD, LESLEY J. S. PROUSE and DAVID R. RUSSELL

Department of Chemistry, University of Leicester, Leicester LE1 7RH, U.K.

(*Received* 22 *April* 1993; *accepted* 5 *May* 1993)

Abstract—The phosphine Ph_2PCH_2OH reacts with (COD)$PtCl_2$ to form *cis*-[$PtCl_2(Ph_2PCH_2OH)_2$], the structure of which has been determined by X-ray crystallography. Similarly, the phosphines Ph_2PCH_2NHR (R = Bu^t, C_6H_4Me-4) react with (COD)$PtCl_2$ to form *cis*-[$PtCl_2(Ph_2PCH_2NHR)_2$], although for R = C_6H_4Me-4 this complex is unstable and [$PtCl_2\{(Ph_2PCH_2)_2NR\}$] (R = C_6H_4Me-4) is isolated. The complexes [$PtCl_2\{(Ph_2PCH_2)_2NR\}$] can be prepared directly from (COD)$PtCl_2$ and $(Ph_2PCH_2)_2NR$.

In recent years functionalized phosphines containing one or more functional groups of various types have been synthesized and their properties investigated.[2] The ligands Ph_2PCH_2XH (X = O, NR) are formally analogous to the diphosphine $Ph_2PCH_2PPh_2$, which is most commonly found as a bridging ligand rather than as a chelate.[3] To our knowledge there are no examples of Ph_2PCH_2XH (X = O, NR) acting as chelates. This is presumably due to the strain involved in forming a four-membered ring since the related ligands $Ph_2PCH_2CH_2XH$ (X = O, NR) will form chelate complexes when bound to platinum.[1,4] Hydroxymethyldiphenylphosphine has been used as a bridging ligand to form early–late heterobimetallic complexes,[5] whilst aminomethyldiphenylphosphine ligands have also been used to form bimetallic platinum complexes.[6]

In this paper we report the synthesis of some hydroxymethyl- and aminomethyldiphenylphosphine complexes of platinum. Reaction of (COD)$PtCl_2$ with Ph_2PCH_2OH resulted in the formation of *cis*-[$PtCl_2(Ph_2PCH_2OH)_2$] (**1**). This complex has been made previously by hydrolysis of [$PtCl_2\{Ph_2PCH_2OCOMe\}_2$] with HCl.[7] The ^1H NMR spectrum exhibits a multiplet due to the phenyl protons at δ 7.6–7.0 and a broad, unresolved multiplet at δ 4.5, which also has broad platinum satellites and is assigned to the methylene protons. A broad signal at δ 3.9 is assigned to the hydroxyl protons. As pointed out previously the absence of P—CH_2 coupling makes determination of the stereochemistry of these complexes in solution difficult from ^1H NMR data. However, we now report the $^{31}P\{^1H\}$ NMR data which allows unequivocal assignment of stereochemistry. The $^{31}P\{^1H\}$ NMR spectrum displays a singlet at δ +7.3, with platinum satellites [J(Pt—P) = 3687 Hz]. The magnitude of the coupling constant indicates that the phosphine ligands are *trans* to chloride, in a mutually *cis* configuration.[8]

A single-crystal X-ray diffraction study of **1** was performed to establish the molecular geometry and whether there was any interaction of the hydroxyl groups with platinum or hydrogen bonding with the chlorides. In $Ni(CN)_2$ complexes of this phosphine there were found to be intermolecular hydrogen bonds between the hydroxyl protons and the nitrogens of cyanides in adjacent molecules.[9] The molecular structure of **1** is illustrated in Fig. 1, together with the crystallographic numbering system. A summary of important bond lengths and angles is

* For part I see ref. 1.

† Author to whom correspondence should be addressed.

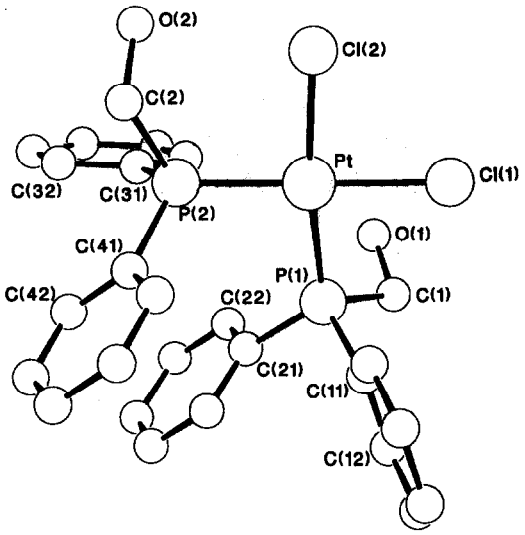

Fig. 1. Molecular structure of *cis*-$[PtCl_2(Ph_2PCH_2OH)_2]$ (**1**).

given in Table 1. The geometry around the platinum is effectively square planar. The molecule exists as the *cis* isomer with the phosphine ligands *trans* to the chloride ligands. The Pt—Cl and Pt—P bond lengths are of a similar magnitude to those reported for *cis*-$[PtCl_2(PPh_3)_2]$,[10] which has average Pt—Cl and Pt—P bond lengths of 2.345(16) and 2.258(10 Å, respectively. The Cl—Pt—Cl and P—Pt—P bond angles are slightly smaller than those recorded for *cis*-$[PtCl_2(PPh_3)_2]$ of 87.1(1)° and 97.8(1)°, respectively. The O(1)—Pt separation of 3.484 Å is too large for any bonding interaction. The hydroxyl hydrogens were located in the difference-Fourier map. The O—H bond lengths are 0.78 [O(1)—H(5)] and 1.39 Å [O(2)—H(6)], respectively. Both these hydrogen atoms have short separations from a chlorine atom. Thus, H(5) is 2.46 Å from a chlorine in an adjacent molecule with an O(1)—H(5)—Cl angle of 164°, both of which are consistent with an intermolecular hydrogen bond. For H(6) the intramolecular distance to Cl(2) is 2.05 Å, which is very short, and the O(2)—H(6)—Cl(2) angle is 123°, suggesting a bent hydrogen bond. This may also explain the rather long O(2)—H(6) bond length mentioned above. Thus, the structure of **1** shows evidence of inter- and intramolecular hydrogen bonding between chlorine atoms and hydroxyl hydrogens.

The reaction of $Ph_2PCH_2NHBu^t$ with (COD)$PtCl_2$ in a 2:1 ratio gave *cis*-$[PtCl_2(Ph_2PCH_2NHBu^t)_2]$ (**2a**). The $^{31}P\{^1H\}$ NMR spectrum of **2a** exhibits a signal at δ +4.0 ppm with platinum satellites [J(Pt—P) = 3710 Hz], consistent with phosphorus coordinated *trans* to chloride; hence, the two phosphorus ligands are in a mutually *cis* configuration. The ^1H NMR spectrum displays a multiplet in the region δ 8.0–7.1 due to the phenyl protons, a multiplet at δ 3.5 due to the methylene protons, as well as signals due to the tert-butyl and N—H protons.

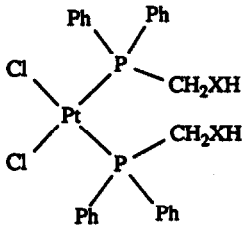

1 X=O
2a X=NBu^t
2b X=NC$_6$H$_4$Me-4

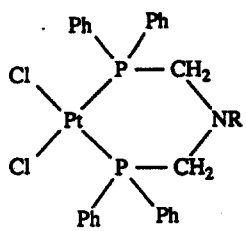

3a R=Bu^t
3b R=C$_6$H$_4$Me-4

Reaction of $Ph_2PCH_2NHC_6H_4Me$-4 with (COD)$PtCl_2$ gave a mixture of two products, as determined by $^{31}P\{^1H\}$ NMR spectroscopy. It is probable that a signal observed at δ +5.9 [J (Pt—P) = 3693 Hz] is due to *cis*-$[PtCl_2(Ph_2PCH_2$

Table 1. Selected bond lengths (Å) and angles (°) for *cis*-$[PtCl_2(Ph_2PCH_2OH)_2]$

Bond length	(Å)	Bond angle	(°)
Pt—P(1)	2.253(2)	P(2)—Pt—P(1)	96.8(1)
Pt—P(2)	2.249(2)	Cl(2)—Pt—Cl(1)	86.4(1)
Pt—Cl(1)	2.373(2)	Cl(2)—Pt—P(2)	91.1(1)
Pt—Cl(2)	2.358(2)	Cl(2)—Pt—P(1)	172.0(1)
P(1)—C(1)	1.872(10)	Cl(1)—Pt—P(1)	85.8(1)
P(2)—C(2)	1.856(9)	Cl(1)—Pt—P(2)	174.9(1)
C(1)—O(1)	1.385(14)	C(1)—P(1)—Pt	109.7(3)
C(2)—O(2)	1.445(16)	C(2)—P(2)—Pt	115.3(4)
O(1)—H(5)	0.78(11)	P(1)—C(1)—O(1)	108.0(7)
O(2)—H(6)	1.39(11)	P(2)—C(2)—O(2)	113.0(8)

Estimated standard deviations are given in parentheses.

$NHC_6H_4Me\text{-}4)_2$] (**2b**), since the chemical shift and size of J(Pt—P) are similar to those found in **2a**. The second signal of δ −6.1 [J(Pt—P) = 3417 Hz] is due to the chelate complex [$PtCl_2\{(Ph_2PCH_2)_2NR\}$] (**3b**), which was identified by comparison of its $^{31}P\{^1H\}$ NMR spectrum with that of an independently prepared sample, see below.

Reaction of $(COD)PtCl_2$ with $(Ph_2PCH_2)_2NR$ (R = Bu^t, C_6H_4Me-4) gave the complexes [$PtCl_2\{(Ph_2PCH_2)_2NR\}$] (**3a,b**). The $^{31}P\{^1H\}$ NMR spectra of **3a** and **3b** each display one signal at δ −5.9 and −6.1, respectively, with J(Pt—P) values of *ca* 3420 Hz. The coupling constant indicates that the phosphine ligands are *trans* to chloride, i.e. in a mutually *cis* configuration. The reduction in magnitude of J(Pt—P) going from complexes **2** to complexes **3** containing a six-membered chelate ring, is consistent with related platinum complexes containing diphenylphosphinoalkyl ligands.[11] The ^1H NMR spectra of **3a** and **3b** display broad multiplets at δ 3.4 and 3.9, respectively, due to the methylene protons, and signals due to the phenyl groups, Bu^t and C_6H_4Me-4, respectively.

The conversion of *cis*-[$PtCl_2(Ph_2PCH_2NHC_6H_4Me\text{-}4)_2$] (**2b**) to *cis*-[$PtCl_2\{(Ph_2PCH_2)_2NC_6H_4Me\text{-}4\}$] (**3b**) is in contrast to the previous reaction of $Ph_2PCH_2NHBu^t$ when only the non-chelate complex *cis*-[$PtCl_2(Ph_2PCH_2NHBu^t)_2$] (**2a**) is formed. The difference in reactivity of the two ligands is unlikely to be due to their nucleophilicity since Bu^t is the more nucleophilic, but it may be that the electron-withdrawing C_6H_4Me-4 group activates the α-C towards nucleophilic attack. It is interesting that complex **3a** can also be formed by refluxing **2a** in toluene with aqueous formaldehyde for 24 h. A similar transformation has been reported for the analogous *cis*-[$Mo(CO)_4(Ph_2PCH_2NHR)_2$] complexes.[12]

Further studies are in progress to investigate the effect of substituents on the reactivity of the phosphines and also the use of complexes **1** and **2a** as precursors to bimetallic species.

EXPERIMENTAL

Petroleum ether and toluene were all dried by refluxing over purple sodium/benzophenone in a nitrogen atmosphere. Dichloromethane was purified by refluxing over calcium hydride. The phosphines[12] and $(COD)PtCl_2$[13] were prepared by the literature methods. The syntheses of phosphorus-containing compounds were performed in deoxygenated solvents under a nitrogen atmosphere. Once isolated as pure solids, all new phosphine compounds are relatively air-stable and precautions for their storage are unnecessary.

^1H NMR spectra were recorded on a Bruker AM300 or Varian EM390 spectrometer as $CDCl_3$ solutions with internal $SiMe_4$ as a reference. $^{31}P\{^1H\}$ NMR spectra were recorded on a Jeol FX60 instrument at 24.15 MHz in CH_2Cl_2 solution and were referenced to external 85% H_3PO_4 with shifts to high frequency being positive. Microanalyses were performed by Butterworth Laboratories Ltd, Middlesex.

Reaction of $(COD)PtCl_2$ *with* Ph_2PCH_2OH

A mixture of Ph_2PCH_2OH (819 mg, 3.79 mmol) and $(COD)PtCl_2$ (650 mg, 1.79 mmol) in dichloromethane (50 cm^3) was stirred for 0.5 h at room temperature, after which time the solvent was removed under vacuum giving a white solid. The solid was crystallized from dichloromethane and petroleum ether to give white crystals of *cis*-[$PtCl_2(Ph_2PCH_2OH)_2$] (**1**) (1.6 g, 85%). Found: C, 44.5; H, 3.7. Calc. for $C_{26}H_{26}Cl_2O_2P_2Pt$: C, 44.7; H, 3.7%. ^1H NMR ($CDCl_3$): δ3.9 (s, br, 2H, OH), 4.5 (m, 4H, CH_2), 7.3 (m, 20H, Ph). $^{31}P\{^1H\}$ NMR: +7.3 [J(Pt—P) 3687 Hz].

Reaction of $(COD)PtCl_2$ *with* $Ph_2PCH_2NHBu^t$

A solution of $(COD)PtCl_2$ (750 mg, 2.0 mmol) in dichloromethane (40 cm^3) was added to a solution of $Ph_2PCH_2NHBu^t$ (0.99 mg, 4.05 mmol) in toluene (4 cm^3). The mixture was stirred for 0.5 h at room temperature, after which time the solvent was removed under vacuum to give a pale yellow solid. Crystallization of the solid from dichloromethane and petroleum ether afforded pale yellow crystals of *cis*-[$PtCl_2(Ph_2PCH_2NHBu^t)_2$] (**2a**) (1.11 g, 69%). Found: C, 50.6; H, 5.6; N, 3.2. Calc. for $C_{34}H_{44}Cl_2N_2P_2Pt$: C, 50.5; H, 5.5; N, 3.5%. ^1H NMR ($CDCl_3$): δ1.00 (s, 18H, Bu^t), 2.00 (s, br, 2H, NH), 3.50 (m, 4H, CH_2), 7.5 (m, 20H, Ph). $^{31}P\{^1H\}$ NMR: +4.0 [J(Pt—P) 3711 Hz].

Reaction of $(COD)PtCl_2$ *with* $Ph_2PCH_2NHC_6H_4Me$-4

A mixture of $Ph_2PCH_2NHC_6H_4Me$-4 (461 mg, 1.51 mmol) and $(COD)PtCl_2$ (221 mg, 0.59 mmol) in dichloromethane (50 cm^3) was stirred for 1 h at room temperature, after which time the solvent was removed under vacuum affording a white solid. The solid consisted of a mixture of two complexes, as determined by $^{31}P\{^1H\}$ NMR spectroscopy, *cis*-[$PtCl_2(Ph_2PCH_2NHC_6H_4Me\text{-}4)_2$] (**2b**), $^{31}P\{^1H\}$ NMR +5.9 [J(Pt—P) 3693 Hz], and [$PtCl_2\{(Ph_2PCH_2)_2NC_6H_4Me\text{-}4\}$] (**3b**) (see below).

Reaction of $(COD)PtCl_2$ *with* $(Ph_2PCH_2)_2NR$ (R = Bu^t, C_6H_4Me-4)

A mixture of $(COD)PtCl_2$ (200 mg, 0.54 mmol) and $(Ph_2PCH_2)_2NBu^t$ (251 mg, 0.54 mmol) in dichloromethane (50 cm^3) was stirred for 1 h, after which time the solvent was removed under vacuum giving a white solid. The solid was crystallized from dichloromethane and petroleum ether affording white crystals of $[PtCl_2\{(Ph_2PCH_2)_2NBu^t\}]$ (**3a**) (313 mg, 79%). Found: C, 45.9; H, 4.3; N, 1.8. Calc. for $C_{30}H_{33}Cl_2NP_2Pt\cdot(CH_2Cl_2)$: C, 45.3; H, 4.3; N, 1.7%. ^1H NMR ($CDCl_3$): δ0.8 (s, 9H, Bu^t), 3.4 (m, 4H, CH_2), 7.6 (m, 20H, Ph). $^{31}P\{^1H\}$ NMR: −5.9 [J(Pt—P) 3428 Hz].

Using a similar procedure starting from $(COD)PtCl_2$ (100 mg, 0.27 mmol) and $(Ph_2PCH_2)_2NC_6H_4Me$-4 (140 mg, 0.28 mmol) gave, after crystallization from dichloromethane and petroleum ether, $[PtCl_2\{(Ph_2PCH_2)_2NC_6H_4Me\text{-}4\}]$ (**3b**) as white crystals (153 mg, 74%). Found: C, 45.2; H, 3.4; N, 1.5. Calc. for $C_{33}H_{31}Cl_2NP_2Pt\cdot(2CH_2Cl_2)$: C, 44.8; H, 3.8; N, 1.5%. ^1H NMR ($CDCl_3$): δ2.2 (s, 3H, Me), 3.9 (m, 4H, CH_2), 7.5 (m, 24H, Ph). $^{31}P\{^1H\}$ NMR: −6.1 [J(Pt—P) 3418 Hz].

Crystal structure determination

Crystal data for *cis*-$[PtCl_2(Ph_2PCH_2OH)_2]$ (**1**). M = 698.4. Monoclinic, space group $P2_1/n$, a = 17.452(5), b = 15.878(5), c = 9.379(6) Å, β = 100.1(1)°, U = 2559 $Å^3$, z = 4, μ = 55.89 cm^{-1}, λ(Mo-K_α) = 0.7107 Å, $F(000)$ = 1360, D_c = 1.81 g cm^{-3}. Crystal dimensions 0.08 × 0.1 × 0.2 mm.

The crystal used for data collection was mounted in air and the unit cell parameters were determined by least-squares refinement of ω-measurements of different layers.[14] Data were collected on a Stöe STADI-2 diffractometer with an ω-scan technique in the range $7° < 2\theta < 60°$. The intensities of 4935 unique reflections were measured and these data were corrected for Lorentz and polarization effects to give 4706 unique reflections with $I > 3\sigma(I)$. The structure was solved by conventional Patterson techniques using SHELXS-86 and all subsequent calculations were performed with the computer programme SHELX-76.[15] Scattering factors were taken from ref. 16. An absorption correction was applied to the data, the maximum and minimum transmission factors being 0.7484 and 0.6443, respectively. The phenyl rings were included as rigid groups with D_{6h} symmetry and C—C distances of 1.395 Å. All hydrogen atoms were included in calculated positions (C—H = 0.95 Å) and refined with group isotropic thermal parameters, with the exception of the two hydroxyl hydrogen atoms which were located in a difference-Fourier map and their positional coordinates and isotropic parameters were refined. All non-hydrogen atoms were refined anisotropically. Final cycles of refinement employed a weighting factor w calculated from $w = k/(\sigma^2F + gF^2)$, where k = 0.95 and g = 0.0047, and gave final values of R = 0.0580 and R_w = 0.0627.

Acknowledgements—We thank the S.E.R.C. for a studentship (JN), the Nuffield Foundation for an award to newly appointed science lecturers (DLD), Johnson Matthey for a loan of platinum salts and Leicester University Computer Centre who provided support and facilities for X-ray single-crystal calculations.

REFERENCES

1. Part I. M. Bassett, D. L. Davies, J. Neild, L. J. S. Prouse and D. R. Russell, *Polyhedron* 1991, **10**, 501.
2. T. B. Rauchfuss, in *Homogeneous Catalysis with Metal Phosphine Complexes* (Edited by L. H. Pignolet), Ch. 7. Plenum Press, New York (1983).
3. R. J. Puddephatt, *Chem. Soc. Rev.* 1983, **12**, 99.
4. N. W. Alcock, A. W. G. Platt and P. G. Pringle, *J. Chem. Soc., Dalton Trans.* 1987, 2273.
5. S. M. Baxter, G. S. Ferguson and P. T. Wolczanski, *J. Am. Chem. Soc.* 1988, **110**, 4231.
6. (a) P. Dagnac, R. Turpin and R. Poilblanc, *J. Organomet. Chem.* 1980, **253**, 123. (b) R. Turpin, J. Casteran-Baumassy and P. Dagnac, *J. Chem. Res.* 1980, **(S) 138**, (M) 2073.
7. J. Chatt, G. J. Leigh and R. M. Slade, *J. Chem. Soc., Dalton Trans.* 1973, 2021.
8. A. Pidcock, R. E. Richards and L. M. Venanzi, *J. Chem. Soc. (A)* 1966, 1707.
9. H. Hope, M. M. Olmstead, P. P. Power and M. Viggiano, *Inorg. Chem.* 1984, **23**, 326.
10. G. Ferguson, G. K. Anderson, H. C. Clark, J. A. Davies and M. Parvez, *J. Cryst. Spectrosc. Res.* 1982, **12**, 449.
11. T. G. Appleton, M. A. Bennett and I. B. Tomkins, *J. Chem. Soc., Dalton Trans.* 1976, 439.
12. D. L. Davies, F. I. Healey, J. Howarth, D. R. Russell and L. J. S. Sherry, *J. Organomet. Chem.* 1989, **376**, C31.
13. J. X. McDermott, J. F. White and G. M. Whitesides, *J. Am. Chem. Soc.* 1976, **98**, 6521.
14. W. Clegg and G. M. Sheldrick, *Z. Krist.* 1984, **167**, 23.
15. G. M. Sheldrick, *Programs for Crystal Structure Determination*, SHELX-76. University of Cambridge, U.K. (1976); SHELXS-86, Göttingen, F.R.G. (1986).
16. *International Tables for X-ray Crystallography*, Vol. 4. Kynoch Press, Birmingham (1975).

Polyhedron Vol. 12, No. 17, pp. 2125–2131, 1993
Printed in Great Britain

0277–5387/93 $6.00+.00
© 1993 Pergamon Press Ltd

SYNTHESES AND MOLECULAR STRUCTURES OF MULTINUCLEAR ALUMINIUM COMPLEXES $R_{n+2}Al_nL_2$ ($n = 3,4$; L = DIAMINE, TRIAMINE) CONTAINING PENTA-COORDINATE ALUMINIUM ATOMS

C. C. CHANG,* C. C. HUANG, J. O. TSAI and M. D. LI

Department of Chemistry, National Sun Yat-Sen University, Kaohsiung, Taiwan, R.O.C.

and

L. K. LIU

Institute of Chemistry, Academia Sinica, Taipei, Taiwan, R.O.C.

(*Received* 17 *November* 1992; *accepted* 5 *May* 1993)

Abstract—Reactions of $Al_2R'_4[N(C_2H_5)_2]_2$ ($R' = CH_3$, C_2H_5) with ethylenediamine or N,N′-dimethylethylenediamine yield air-sensitive trialuminium products $[AlR'_2]_2[RNCH_2CH_2NR]_2[AlR']$ (**1a**: $R' = CH_3$, $R = H$; **1b**: $R' = CH_3$, $R = CH_3$; **2a**: $R' = C_2H_5$, $R = H$; **2b**: $R' = C_2H_5$, $R = CH_3$). Reactions of $Al_2R'_4[N(C_2H_5)_2]_2$ with diethylenetriamine, $[(NH_2CH_2CH_2)_2NH]$, yield air-sensitive tetraaluminium products, $(AlR'_2)_2[(HNCH_2CH_2)_2N]_2(AlR')_2$ (**3**: $R' = CH_3$; **4**: $R' = C_2H_5$). The polyaluminium complexes are well characterized. Some structures have been determined by X-ray crystallography. For both **1a** and **1b** the penta-coordination sphere around the central aluminium conforms to a square-pyramidal configuration and the tetra-coordination for the outer two aluminium atoms is a tetrahedral configuration. Complex **4** has two central aluminium atoms with a penta-coordinate square-pyramidal configuration and the outer aluminium atoms in a tetrahedral configuration.

The utilization of organo main group compounds as precursors to ceramic materials is currently a very popular area of study. Noteworthy are the organo aluminium–nitrogen compounds, which are precursors for aluminium nitride.[1–10] Smith *et al.* have reported a considerable amount of organoaluminium with primary and secondary monodentate amines.[1–5] We have been studying the selective synthesis of $R_4Al_2(NR'_2)_2$ in high yields, the Al_2N_2 framework being similar to cyclobutane.[11] As the chemistry of Al_2N_2 towards donor ligands has not been explored we have attempted reactions of the Al_2N_2 frame with multidentate nitrogen donor ligands to see to what extent a maximization of aluminium coordinate number occurs by association to different aggregations. The interaction of aluminium multidentate containing N—H ligands involving Al—C, Al—N and N—H bond cleavages via intermolecular condensation has been documented in the literature.[12–18]

EXPERIMENTAL

Apparatus and materials

All operations were performed in a nitrogen-flushed glove-bag, dry-box or in a vacuum system. All solvents were distilled prior to use. IR, mass, nuclear magnetic resonance and X-ray single diffraction data were obtained using a Hitachi 26030 IR spectrometer, VG-7025S spectrometer, Varian VXR-300 MHz FT-NMR spectrometer and Enraf–Nonius CAD4 spectrometer. Elemental analyses were performed at Galbraith Laboratory, U.S.A.

* Author to whom correspondence should be addressed.

Reactions of bis(di-μ-diethylamino-dialkylaluminium) with ethylenediamine

Ethylenediamine (0.24 cm^3, 12 mmol) was added slowly to a solution containing an ether solution (100 cm^3) of bis(di-μ-diethylamino-dialkylaluminium) (6 mmol) (R′ = CH_3, C_2H_5) under nitrogen. The reaction took place immediately and released heat and gases. The colourless solution became turbid, but cleared at later stages. After 4 h the residue $Al(alkyl)_3(NHCH_2CH_2NH)_2$ (R′ = CH_3, **1a**, and C_2H_5, **2a**) was obtained after removal of ether.

The complex (**1a**) (solid) was purified by sublimation at 80°C, 10^{-3} Torr; m.p.: 84.5–86°C. IR (Nujol mull): 3330(w), 3280(w), 2980(s), 2960(s), 2910(s), 2860(s), 2810(m), 1460(m), 1370(m), 1185(br), 1055(br), 690(br). Found: C, 39.8; H, 10.5; N, 19.1. Calc.: C, 39.7; H, 10.0; N, 20.6%. Characteristic fragment ions occur at *m/z* (E.I.: 70 eV, assignment in parentheses): 257 $(Al_3Me_4HC_4H_{12}N_4)^+$, 241 $(Al_3Me_3HC_4H_{11}N_4)^+$, 228 $(Al_3Me_2C_4H_{12}N_4)^+$, 199 $(Al_3Me_4C_2H_6N_2)^+$, 170 $(Al_2Me_2C_7H_{14}N_2)^+$, 141 $(Al_2Me_2C_2H_7N_2)^+$, 99 $(AlMeC_2H_5N_2)^+$, 84 $(AlC_2H_5N_2)^+$, 69 $(Al_2Me)^+$, 57 $(AlMe_2)^+$. The complex (**2a**) (liquid) was purified by distillation at 170°C; 10^{-3} Torr. IR(in KBr pellets): 3330(m), 3290(m), 1370(m), 1330(m), 1290(m), 1230(m), 1190(m), 1165(s), 1160(m), 1120(w), 1065(m), 800(br), 640(br) cm^{-1}. Their NMR chemical shifts are listed in Tables 1 (^1H) and 2 (^{13}C and ^{27}Al).

Reactions of bis(di-μ-diethylamino-dialkylaluminium) with N,N′-dimethylethylenediamine

A diethyl ether solution of N,N′-dimethylethylenediamine (68.2 mmol) was added slowly to an ether (50 cm^3) solution of bis(di-μ-diethylamino-dialkylaluminium) (34.1 mmol) (R′ = CH_3, C_2H_5) under nitrogen with stirring for 6 h and its colour turned to deep yellow. The residue $Al(alkyl)_3(MeNCH_2CH_2NMe)_2$ (alkyl = CH_3, **1b**, and C_2H_5, **2b**) was obtained after removal of ether.

The complex (**1b**) (solid) was purified by sublimation at 90°C, 10^{-3} Torr; m.p.: 200°C sublimated. IR (Nujol mull): 2950(m), 2880(m),

Table 1. ^1H NMR spectra

Compound	δ (ppm)	(C_6D_6)
1a	2.842, 2.700	(m, 8H, NCH_2CH_2N)
	0.55	(m, 4H, NH)
	−0.698	(s, 6H, $AlCH_3$)
	−0.743, −0.815	[s, 12H, $Al(CH_3)_2$]
2a	2.424, 1.982	(m, 8H, NCH_2CH_2N)
	1.300	[m, 12H, CH_3 of $Al(C_2H_5)_2$]
	1.068	(t, 3H, CH_3 of AlC_2H_5)
	0.187	(m, 4H, NH)
	0.700	[m, 8H, CH_2 of $Al(C_2H_5)_2$]
	−0.126	(q, 4H, CH_2 of AlC_2H_5)
1b	2.013	(s, 12H, NCH_3)
	2.814, 2.206	(m, 8H, NCH_2CH_2N)
	−0.501, −0.532	[s, 12H, $Al(CH_3)_2$]
	−0.645	(s, 3H, $AlCH_3$)
2b	2.17	(s, 12H, NCH_3)
	2.081, 2.016	(m, 8H, NCH_2CH_2N)
	1.254, 1.317, 1.356	[t, 15H, CH_3 of $Al(C_2H_5)_2$]
	0.186, 0.138, 0.001	(q, 10H, CH_2 of AlC_2H_5)
3	2.617	[m, 16H, $(NCH_2CH_2)_2N$]
	−0.487	[m, 12H, $Al(CH_3)_2$]
	−0.748	(s, 6H, $AlCH_3$)
	−0.12	(t, 4H, NH)
4	2.558, 2.260, 1.668	[m, 16H, $(NCH_2CH_2)_2N$]
	1.401	[q, 12H, CH_3 of $(Al(C_2H_5)_2$]
	1.140	(t, 6H, CH_3 of AlC_2H_5)
	0.445	(t, 4H, NH)
	1.16	(sept, 8H, CH_2 of $Al(C_2H_5)_2$]
	−0.72	(q, 4H, CH_2 of AlC_2H_5)

Table 2. ^{13}C and ^{27}Al NMR spectra

Compound	^{13}C NMR δ (ppm)	^{27}AL NMR δ (ppm)
1a	45.902 (NCH_2CH_2N)	162 (br, C.N. = 4)
	−8.821 [m, $Al(CH_3)_2$]	106 (br, C.N. = 5)
	−12.492 (m, $AlCH_3$)	
2a	43.838 (s, CH_2 of NCH_2CH_2N)	150 (br, C.N. = 4)
	10.482 (s, CH_3 of AlC_2H_5)	100 (br, C.N. = 5)
	9.695, 9.346 [s, CH_3 of $Al(C_2H_5)_2$]	
	−6.312 [m, CH_2 of $Al(C_2H_5)_2$]	
	−2.424 (m, CH_2 of AlC_2H_5)	
1b	51.194 (s, NCH_2CH_2N)	162 (br, C.N. = 4)
	40.153 (s, NCH_3)	106 (br, C.N. = 5)
	−11.323 (m, $AlCH_3$)	
2b	51.327, 39.155 (NCH_2CH_2N)	154 (br, C.N. = 4)
	11.629 (NCH_3)	98 (br, C.N. = 5)
	9.53, 9.599 (CH_2 of AlC_2H_5)	
	−1.152 (CH_2 of AlC_2H_5)	
4	52.327, 39.155 (NCH_2CH_2N)	149.5 (br, C.N. = 4)
	9.713, 9.896, 11.155 (s, CH_3 of AlC_2H_5)	98.8 (br, C.N. = 5)
	0, −2 (m, CH_2) of AlC_2H_5)	

2850(m), 1456(m), 1455(m), 1370(w), 1080(m), 1035(m), 990(br), 960(m) cm^{-1}. Found: C, 39.8; H, 10.5; N, 19.1. Calc: C, 47.5; H, 10.7; N, 17.1%. Characteristic fragment ions occur at *m/z* (E.I.: 20 eV, assignment in parentheses): 314 $(Al_3Me_4HC_8H_{20}N_4)^+$, 313 $(Al_3Me_4C_8H_{20}N_4)^+$, 270 $(Al_2Me_3C_8H_{19}N_2)^+$, 225 $(Al_2Me_2C_8H_{19}N_4)^+$, 127 $(AlMe_2C_4H_9N_2)^+$, 112 $(AlC_4H_9N_2)^+$, 98 $(AlC_3H_7N_2)^+$, 84 $(Al_2Me_2)^+$, 70 $(Al_2MeH)^+$, 57$(AlMe_2)^+$, 43 $(AlMeH)^+$. The complex (**2b**) (solid) was purified by distillation at 182°C; 10^{-3} torr; m.p.: 38–40°C. IR (in KBr pellet): 2960(s), 2930(s), 2840(s), 2790(s), 1470(s), 1450(s), 1405(m), 1365(m), 1338(s), 1270(s), 1238(m), 1190(m), 1155(m), 1125(w), 1100(m), 1075(m), 1025(w), 960(m), 840(m), 778(m), 660(br) cm^{-1}. Found: C, 53.9; H, 11.6; N, 131. Calc.: C, 54.3; H, 11.4; N, 14.1%. Characteristic fragment ions occur at *m/z* (E.I.: 70 eV, assignment in parentheses): 398 $(M)^+$, 370 $(Al_3Et_4HC_8H_{20}N_4)^+$, 369 $(Al_3Et_4C_8H_{20}N_4)^+$, 355 $(Al_3Et_4C_7H_{18}N_4)^+$, 283 $(Al_3EtHC_8H_{20}N_4)^+$, 255 $(Al_3H_2C_8H_{20}N_4)^+$, 195 $(Al_3C_4H_{10}N_4)^+$, 167 $(HAl_2C_4H_8N_4)^+$, 141 $(HAlC_4H_8N_4)^+$. Their NMR chemical shifts are listed in Tables 1 (^1H) and 2 (^{13}C and ^{27}Al).

Reactions of bis(di-μ-diethylamino-dialkylaluminium) with diethylethylenediamine

Diethylethylenediamine (0.69 cm^3, 6 mmol) was added to an ether solution (50 cm^3) of bis(di-μ-diethylamino-dialkylaluminium) (6 mmol) (R′ = CH_3, C_2H_5) under nitrogen, causing immediate reaction with the release of heat and gases. After stirring for 4 h the solution was decanted by centrifugation and the solid $Al_4R_6(HNCH_2CH_2NCH_2CH_2NH)$ (R = CH_3, **3**, C_2H_5, **4**) was obtained.

The complex (**3**) (solid) was purified by sublimation at 140°C, 10^{-3} Torr; m.p.: dec > 315°C, IR (Nujol mull): 3340(w), 3290(w), 2950(m), 2920(s), 2850(w), 1460(m), 1370(w), 1295(w), 1190(s), 1105(w), 1065(m), 1050(m), 1010(w), 925(m), 840(m), 760(br), 690(br), 650(w) cm^{-1}. Characteristic fragment ions occur at *m/z* (E.I.: 70 eV, assignment in parentheses): 398$(M)^+$, 384 $(Al_4Me_5HC_8H_{20}N_6)^+$, 383 $(Al_4Me_5C_8H_{20}N_6)^+$, 367 $(Al_4Me_4C_8H_{19}N_6)^+$, 354 $(Al_4Me_3HC_8H_{20}N_6)^+$, 311 $(Al_3Me_2C_8H_{20}N_6)^+$, 282 $(Al_4Me_5C_4H_9N_3)^+$, 183 $(Al_2Me_2C_4H_{10}N_3)^+$, 73 $(HAlMe_3)^+$, 57 $(AlMe_2)^+$. The complex (**4**) (solid) was purified by recrystallization (ether) m.p.: 139.5–140°C. Found: C, 49.2; H. 9.2. Calc.: C, 49.8; H, 9.5%. Characteristic fragment ions occur at *m/z* (E.I.: 20 eV, assignment in parentheses): 453 [bass peak, $(Al_4Et_5CH_2C_8H_{17}N_6)^+$], 339 [bass peak, $(Al_4Et_5C_8H_{20}N_6)^+$], 57 $(HAlEt)^+$, 393 $(Al_4Et_3C_8H_{18}N_6)^+$, 85 $(AlEt_2)^+$, 455 $(Al_4Et_3C_8H_{22}N_6)^+$, 212 $(Al_4Et_2C_4H_{10}N_3)^+$, 423 $(Al_4Et_4C_8H_{20}N_6)^+$, 154 $(Al_2C_4H_{10}N_3)^+$, 125 $(AlC_4H_{10}N_3)^+$. Their NMR chemical shifts are listed in Table 1 (^1H) and Table 2 (^{13}C and ^{27}Al).

X-ray structure analysis

Single crystals suitable for X-ray diffraction were obtained by thermal gradient vacuum sublimation

(**1a** and **1b**) or slow recrystallization from a suitable solvent (**4**, from ether). Data crystals were sealed in lithium glass capillaries to avoid decomposition by oxygen or moisture. Reflections were collected on a Enraf–Nonius CAD-4 automated diffractometer using graphite-monochromated Mo-K_α radiation for data up to $2\theta \leqslant 45°$. Structures were solved with MULTAN[19] and refined with a weighted full-matrix least-squares routine, NRCVAX,[20] on a Micro VAX 3600. Atomic scattering curves were derived from data taken from the International Tables, Vol. IV.[21] Crystal data and refinement details are listed in Table 3. The initially non-disordered models of **1a** and **1b** finished with very unreasonable C—C bond lengths (1.25–1.33 Å) for N—CH_2—CH_2—N, in addition to large thermal motions. Hence, 1 : 1 disordered structures were constructed later, resulting in much more reasonable thermal parameters for carbon atoms and C—C single bond distances. The R values were significantly decreased. For **4** no disorder has been found in the structure. We have obtained the crystal structure of **1a**, which is very similar to the structure reported earlier.[22] However, we believe that we obtained a different form of the crystal. Since it does not convey any more chemical information than what has already been published, we decided not to present the crystallographic data of **1a** here. Selected bond distances and angles of **1b** and **4** are listed in Tables 4 and 5, respectively.

RESULTS AND DISCUSSION

The bidentate ligands ethylenediamine or N,N′-dimethylethylene diamine were allowed to react with $Al_2R'_4(NEt_2)_2$ (R′ = Me, Et) to produce $[AlR'_2]_2[(HNCH_2CH_2)_2N]_2[AlR']$. Compounds **1a** and **1b** were the only aluminium containing products isolated besides the gaseous product and volatile amine. The overall reaction is given in eq. (1). Crystal data and refinement details of **1a** and **1b** are listed in Table 3, with bond lengths and angles in Tables 4 and 5, respectively.

$$3Al_2(NEt_2)R'_4 + 4RHNCH_2CH_2HNR \rightarrow 2[AlR'_2]_2(NHCH_2CH_2NR)_2 [AlR'] + 6Et_2NH + 2R'H \quad (R' = Me, Et;\ R = H, Me) \qquad (1)$$

The complexes (**1b**, **2a**, **2b**) display two different environments for the aluminium atoms and the ethylenediamines are bridged to three organoaluminium groups, such that two Al_2N_2 cores are linked by the central aluminium atom, as shown in Fig. 1. The coordination environment of the two

Table 3. Crystallographic data refinement details for compounds **1b** and **4**

Compound	**1b**	**4**
Formula	$C_{13}H_{35}Al_3N_4$	$C_{20}H_{50}Al_4N_6$
fw	328.39	482.58
a (Å)	14.668(7)	8.429(3)
b (Å)	16.682(2)	9.207(2)
c (Å)	8.160(3)	9.804(1)
α (°)	—	102.39(2)
β (°)	—	86.92(2)
γ(°)	—	109.68(2)
Crystal system	Orthorhombic	Triclinic
Space group	*Pnma*	$P\bar{1}$
2θ range (°)	14.84–32.16	11.49–29.46
Crystal size (mm)	0.75 × 0.50 × 0.31	0.46 × 0.28 × 0.36
V (Å^3)	1996.8(11)	699.6(13)
D_{calc} (mg m^{-3})	1.092	1.145
μ (mm^{-1})	0.18	0.18
λ (Å)	0.7093	0.7093
No. of reflections measured	1348	1974
No. of unique reflections	1348	1821
No. of reflections $I_0 > 2.0\sigma(I_0)$	945	1311
transmission factors (min; max)	—	0.966; 0.998
RF	0.056	0.033
*R*w	0.070	0.035
GOF	3.54	1.68
max Δ/δ	0.079	0.628

Table 4. Selected bond lengths (Å) for compounds **1b** and **4**

Compound **1b**		Compound **4**	
Al(1)—N(1)	1.926(4)	Al(1)—N(1)	2.083(3)
Al(1)—C(7)	1.948(6)	Al(1)—N(3)	2.034(2)
Al(2)—N(1)	2.029(4)	Al(1)—C(8)	1.976(4)
Al(2)—N(2)	2.043(4)	Al(2)—N(1)	1.904(3)
Al(2)—C(5)	1.959(8)	Al(2)—C(10)	1.960(4)
N(1)—C(1)	1.59(1)	N(1)—C(4)	1.481(4)
N(2)—C(4)	1.53(2)	N(3)—N(5)	1.475(4)
C(2)—C(2)	1.50(2)	N(3)—C(7)	1.467(4)
		C(4)—C(5)	1.512(5)
		C(6)—C(7)	1.509(5)
		C(8)—C(9)	1.490(6)

outer aluminium atoms is in the usual tetrahedral coordination. The central aluminium atom is bonded to four nitrogen atoms from two bidentate ligands and a methyl carbon atom. The penta-coordination of the central aluminium atom is obviously in a square-pyramidal configuration. The distances of central Al(2)—N(1), 2.029(4), and Al(2)—N(2), 2.043(4) Å bonds in **1b** are consistent with the mean Al—N distance of 2.022(3) Å in the published data,[15] and are slightly longer than the distances of the outer Al—N, Al(1)—N(1), 1.926(4), and Al(1)—N(2), 1.923(4) Å, in **1b**. The Al—N lengths of a penta-coordinate aluminium, therefore, are longer than those of a tetra-coordinate aluminium. The Al—C distances are similar in **1b**. The Al(1)···Al(2) contacts of 2.911(2) Å in **1b** are not indicative of any metal–metal interaction. The distance of C(1)—C(1′) = 1.526(20) Å in **1b** as extracted from the disordered five-membered ring AlN_2C_2 are consistent with a single bond distance of 1.55 Å. The tridentate diethylenetriamine was allowed to react with $Al_2R'_4(NEt_2)_2$(R′ = Me, Et) and $[AlR'_2]_2[(HNCH_2CH_2)_2N]_2[AlR']$ was isolated as the aluminium-containing products. The crystal data and structural parameters are listed in Tables 3, 4 and 5. The overall reaction is given in eq. (2)

$$2Al_2(NEt_2)_2R'_4 + 2(H_2NCH_2CH_2)_2NH \rightarrow Al_4R'_6[(HNCH_2CH_2)_2N]_2 + 4Et_2NH + 2R'H \quad (R' = Me, Et) \qquad (2)$$

The spectral data of **3** were consistent with the

Table 5. Selected bond angles (°) for compounds **1b** and **4**

Compound **1b**		Compound **4**	
N(1)—Al(1)—N(2)	88.2(2)	N(1)—Al(1)—N(2)	81.0(1)
N(1)—Al(1)—C(6)	114.4(3)	N(1)—Al(1)—N(3)	149.6(1)
N(1)—Al(1)—C(7)	112.9(2)	N(1)—Al(1)—N(3′)	84.0(1)
C(6)—Al(1)—C(7)	113.9(3)	N(1)—Al(1)—C(8)	105.3(2)
N(1)—Al(2)—N(1)a	84.1(2)	N(2)—Al(1)—N(3)	84.5(1)
N(1)—Al(2)—N(2)	82.1(2)	N(2)—Al(a)—N(3′)	124.4(2)
N(1)—Al(2)—N(2)a	139.0(2)	N(2)—Al(1)—C(8)	115.6(2)
N(1)—Al(2)—C(5)	110.9(2)	N(3)—Al(1)—N(3′)	82.4(1)
Al(1)—N(1)—Al(2)	94.9(2)	N(3)—Al(1)—C(8)	105.1(1)
Al(1)—N(1)—C(1)	107.1(6)	N(3′)—Al(1)—C(8)	119.9(2)
Al(1)—N(1)—C(3)	113.3(3)	N(1)—Al(2)—N(2)	87.6(1)
Al(2)—N(1)—C(1)	101.6(5)	N(1)—Al(2)—C(10)	114.7(2)
Al(2)—N(1)—C(3)	113.8(4)	N(1)—Al(2)—C(12)	109.2(2)
C(1)—N(1)—C(3)	122.2(6)	C(10)—Al(2)—C(12)	118.9(2)
Al(1)—N(2)—Al(2)	94.4(2)	Al(1)—N(1)—Al(2)	94.0(1)
Al(1)—N(2)—C(2)	108.5(5)	Al(1)—N(1)—C(4)	109.2(2)
Al(1)—N(2)—C(4)	114.4(4)	Al(2)—N(1)—C(4)	120.7(2)
Al(2)—N(2)—C(2)	115.5(7)	Al(1)—N(3)—C(7)	111.0(2)
Al(2)—N(2)—C(4)	113.6(4)	N(3)—C(7)—C(6)	109.4(3)

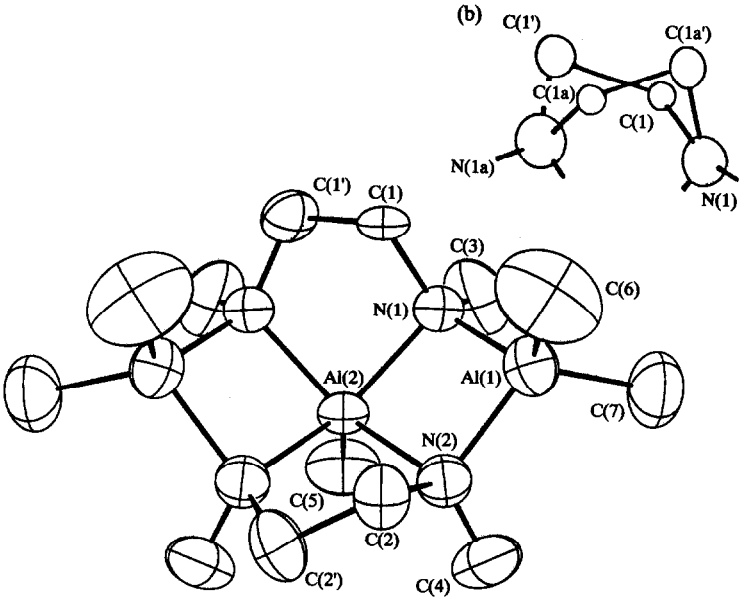

Fig. 1. Molecular structure of $[AlR'_2]_2[RNCH_2CH_2NR]_2[AlR']$ (**1b**, R′ = CH_3, R = CH_3).

published results.[5] Herein, we also report the X-ray crystal structure of **4**, which is similar to the work published by Robinson *et al.* Complex **4** consists of two different environments for the aluminium atoms and the diethylenetriamines bridge four organoaluminium groups, revealing three Al_2N_2 cores connected consecutively by two central aluminium atoms as shown in Fig. 2. The two outermost aluminium atoms are in the usual tetrahedral coordination and the two inner aluminium atoms are bonded to four nitrogen atoms and to a methyl carbon atom in a square-pyramidal configuration. The distances of Al(1)—N(1) = 2.083(3), Al(1)—N(2) = 1.980(3), Al(1)—N(3) = 2.034(2) and Al(1)—N(3)′ = 1.987(2) Å for square-pyramidal configuration are slightly longer than the distances of Al(2)—N(1) = 1.904(3) and Al(2)—N(2) = 1.912(3) Å for tetrahedral aluminium. The distances of Al(1)—C(8) = 1.976(4), Al(2)—C(10) = 1.960(4) and Al(2)—C(12) = 1.971(4) Å are essentially the same, despite the bonding geometry variations. The contacts of Al(1)···Al(2) = 2.919(1) and Al(2)···Al(1A) = 3.025(1) Å exclude any significant metal–metal interactions.

Alkanes and secondary amines were released due to cleavage of N—H, Al—R and Al—N bonds via an intermolecular condensation reaction, giving products possessing Al_2N_2 fragments. The for-

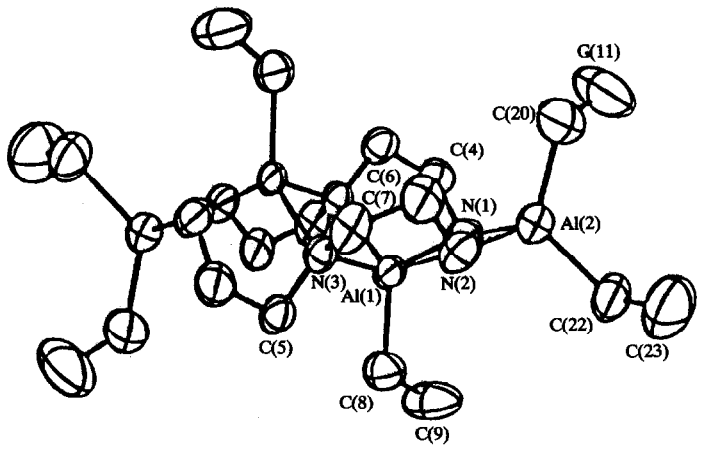

Fig. 2. Molecular structure of $[AlEt]_2[C_6H_{20}N_6]_2[AlEt_2]_2$.

mation of trialuminium or tetraaluminium organocomplexes depends on the number of nitrogen atoms present in the polydentate amines. Each nitrogen atom is able to donate two electron pairs to two different aluminium atoms after the cleavage of one N—H bond. The outer aluminium accepts two electron pairs from nitrogen atoms, keeping a tetrahedral configuration, and the central aluminium accepts four electron-pairs from four nitrogen atoms, forming a square-pyramidal configuration. Hence, substitutions of ethylenediamine and diethylenetriamine reactants on the Al_2N_2 skeleton result in the formation of trinuclear and tetranuclear aluminium complexes, respectively.

REFERENCES

1. A. W. Laubengayer, J. D. Smith and G. C. Ehrlich, *J. Am. Chem. Soc.* 1961, **83**, 542.
2. K. Gosling, J. D. Smith and D. H. W. Wharmby, *J. Chem. Soc. (A)* 1969, 1738.
3. K. J. Alfold, K. Gosling and J. D. Smith, *J. Chem. Soc., Dalton Trans.* 1972, 2203.
4. P. B. Hitchcock, J. D. Smith and K.M. Thomas, *J. Chem. Soc., Dalton Trans.* 1976, 1433.
5. S. Amirkhalili, P. B. Hitchcock and J. D. Smith, *J. Chem. Soc., Dalton Trans.* 1979, 1206.
6. S. Amirkhalili, P. B. Hitchcock, A. D. Jenkins, J. Z. Nyath and J. D. Smith, *J. Chem. Soc., Dalton Trans.* 1981, 377.
7. J. L. Atwood and G. D. Stucky, *J. Am. Chem. Soc.* 1970, **92**, 285.
8. G.M. McLaughlin, G. M. Sim and J. D. Smith, *J. Chem. Soc., Dalton Trans.* 1972, 2197.
9. G. Dozzi, S. Cucinella and A. Mazzei, *J. Organomet. Chem.* 1979, **164**, 1.
10. G. D. Piero, M. Cesari, G. Dozzi, S. Cucinella and A. Mazzei, *J.Organomet. Chem.* 1977, **129**, 281.
11. (a) T. Y. Her, C. C. Chang, J. O. Tsai, Y. Y. Lai, L. K. Liu, H. C. Chang and J. H. Chen, personal communication; (b) C. C. Chang, S. C. Lin and J.O. Tsai, *J. Chin. Chem. Soc.* 1992, **39**, 55.
12. Y. Y. Lai, MSc Thesis, National Sun Yat-sen University (1991).
13. G. H. Robinson, S. A. Sangokoya and R. D. Roger, *Polyhedron* 1988, **7**, 2727.
14. G. H. Robinson, S. A. Sangokoya, F. Moise and W. T. Pennington, *Organometallics* 1988, **7**, 1887.
15. G. H. Robinson and S. A. Sangokoya, *J. Am. Chem. Soc.* 1987, **109**, 6852.
16. G. H. Robinson, A. D. Rae, C. F. Campana and S. K. Byram, *Organometallics* 1987, **6**, 1227.
17. G. H. Robinson and S. A. Sangokoya, *Organometallics* 1988, **7**, 1453.
18. G. H. Robinson, B. Lee, W. T. Pennington and S. Sangokoya, *J. Am. Chem. Soc.* 1988, **110**, 6260.
19. G. Germain, P. Main and M. M. Woolfson, *Acta Cryst.* 1971, **A27**, 368.
20. E. J. Gabe, Y. Le Page, P. S. White and F. L. Lee, *Acta Cryst.* 1987, **A43**, S294.
21. *International Tables for X-ray Crystallography*, Vol. IV, Tables 2.2B and 2.3.1. Kynoch Press, Birmingham (1974).
22. Z. Jiang, L. V. Interrante, D. Kwon, F. S. Tham and R. Kullnig, *Inorg. Chem.* 1991, **30**, 995.

Polyhedron Vol. 12, No. 17, pp. 2133–2136, 1993
Printed in Great Britain

0277–5387/93 $6.00+.00
© 1993 Pergamon Press Ltd

CRYSTAL AND MOLECULAR STRUCTURE OF BIS(DIMETHYLPHENYLPHOSPHINE)(3,4-DIACETYL-4-HEXENE-2-ONE-5-OLATO-C^3,O)PLATINUM(II)

TOORU SAKAI

Faculty of Sciences, Kobe University, Kobe 657, Japan

and

ZENEI TAIRA*

Faculty of Pharmaceutical Sciences, Tokushima Bunri University, 180 Yamashiro-Cho, Tokushima 770, Japan

and

SHINSAKU YAMAZAKI*

Chemistry Laboratory, Kochi Gakuen College, 292 Asahi Tenjin-Cho, Kochi 780, Japan

(*Received* 27 *October* 1992; *accepted* 5 *May* 1993)

Abstract—The crystal and molecular structure of the first cyclometallated platinum(II) complex of 1,1,2,2-tetraacetylethane {bis(2,4-pentanediones)-3,4-diacetyl-2,4-hexadiene-2,5-diol (H_2-dahd)}, [Pt(dahd-C^3,O)(PMe_2Ph)$_2$], was determined by X-ray analysis.

The β-dicarbonyl and β-ketoesters, which have active methylene groups, have been widely known to function as versatile ligands to transition metal ions and a number of their bonding modes in a variety of metal complexes have been reported.[1,2] While the L-ascorbate platinum(II) complex with the Pt—C bond has been prepared, which is of interest as an antitumor reagent,[3] its structure interestingly resembles in its skeleton the central carbon-bonded platinum(II) complex of β-dicarbonyl. In contrast to these previous findings any function of γ,γ′-bis(β-dicarbonyls)[4] with the second- or third-row transition metals has strangely been elusive. 1,1,2,2 - Tetraacetylethane{3,4 - diacetyl - 2,4 - hexadiene-2,5-diol(H_2-dahd)} and the bis(β-diketones) with connecting links of L_2 (L = S, Se: 2,3 - disubstituted 1,1,4,4 - tetraacetylbutane) between the two β-diketones are always in the dienol form with six-membered hydrogens chelated intramolecularly, and their central carbons of the β-dicarbonyl groups are stabilized as quarternary carbons.[5,6] Nevertheless, we have recently found that the central carbons of the bis(β-dicarbonyls) are relatively readily activated under basic conditions to form a metallacycle to platinum(II) with a (C,O)-linkage (1,1,2,2-tetraacetylethane),[7–9] while the 2,3-disubstituted 1,1,4,4-tetraacetylbutane undergoes S—S, S—C and Se—C bond cleavage producing 3 - substituted 2,4 - pentanedionate dianions which relatively readily form unusual platinum(II) complexes with five-membered (S,O)-[10] and four-membered (η^2-L_2)-linkages (L = S, Se),[11] respectively. An analogous platinum(II) complex with an (Se, O) bond has been prepared by an oxidation reaction of $Pt(PPh_3)_4$ with 2,2,4,4-tetraacetyl-1,3-diselenetane.[12] Here, [Pt(dahd-C^3,O′)(SEt_2)$_2$] is interesting since inversion of one sulphur atom has been found to proceed via an unusual bond breakage (an intermolecular path-

* Authors to whom correspondence should be addressed.

way) from ^{1}H NMR, which may be accounted for as a relatively large *trans* influence of the metallated carbon (C^3).[9] In addition, the cyclometallated platinum(II) complex of 1,1,2,2-tetraacetylethane unusually activates the C—H bond of the monosubstituted acetylene to afford the dialkynyl complexes, as described previously.[13] The crystal and molecular structure of [Pt(dahd-C^3,O)(PMe_2Ph)$_2$] has thus been determined by X-ray analysis in this paper and it reveals that the five-membered metallacycle of 1,1,2,2-tetraacetylethane is approximately planar. The structure retains an almost square-planar configuration with a slight distortion towards tetrahedral, while large steric repulsions between PMe_2Ph and the C-bonded 2,4-pentanedione group from 1,1,2,2-tetraacetylethane has been observed. This is the first report of a structure of a cyclometallated platinum(II) complex of 1,1,2,2-tetraacetylethane crystallographically determined.

EXPERIMENTAL

[Pt(dahd-C^3,O′)(PMe_2Ph)$_2$]

The preparation of this compound has been described previously.[8]

X-ray crystal structural analysis of [Pt(dahd-C^3,O′)(PMe_2Ph)$_2$]

Pale yellow crystals were grown from an acetone–ethanol mixed solution under isothermal vaporization. A crystal of dimensions *ca* 0.1 × 0.13 × 0.20 mm was used during the measurements. Throughout the experiment Mo K_α radiation ($\lambda = 0.71069$ Å) was used with a graphite crystal monochromator on a Rigaku AFC four-circle diffractometer.

Crystal data of [Pt(dahd-C^3,O′)(PMe_2Ph)$_2$], $C_{26}H_{34}O_4P_2Pt$

$Mr = 667.59$, monoclinic, $a = 13.897(2)$, $b = 18.987(4)$, $c = 11.164(1)$ Å, $\beta = 112.471(9)$; $U = 2722.2(8)$ Å^3, space group $P2_1/n$, $Z = 4$, $D_x = 1.629$ g cm^{-3}, $F(000) = 1320$, μ(Mo K_α) = 5.62 mm^{-1}. The cell parameters were refined by least-squares for 25 reflections in the range $33° < 2\theta < 38°$. The space group was determined from the systematic absences ($0k0$; k odd, $h0l$; $h+l$ odd). The intensity data were measured using the ω–2θ scan technique, with a scan speed of 2° s^{-1}. The intensity of the incident beam was monitored throughout the data collection by measuring three reference reflections, (1,1,1), (1,0,1) and (0,−1,1), which showed no significant change in intensities ($0.97 < I_0 < 1.06$). A total of 5373 reflections were measured, ($0 \leqslant h \leqslant 16$, $0 \leqslant k \leqslant 22$, $-13 \leqslant l \leqslant 13$). Among these zero intensities were 417 and 681 were weak [$|F_0| < 3\sigma(F_0)$]. Non-zero unique reflections from 4275 planes were corrected for Lorentz and polarization, but not absorption effects. The position of the platinum atom was obtained by a Patterson synthesis. All other atoms were located by Fourier and difference syntheses. The structure was refined by the full-matrix least-square method with anisotropic thermal parameters for non-hydrogen atoms and isotropic factors for hydrogen atoms. The function minimized was $\Sigma w(|F_0| - |F_c|)^2$ with $w = 1/[\sigma^2(F_0)]$. The R values of the final refinement were $R = 0.045$ with $Rw = 0.049$. Goodness-of-fit, S, was 2.5. The maximum and minimum heights in the final difference-Fourier map were ±0.2 e Å^{-3}. A FACOM-M782 computer at the Data Processing Center, Kyoto University, and the UNICSII computation program system[14] were used for all calculations in the data reduction and the structure analysis. The atom scattering factors were taken from the International Tables for X-ray Crystallography.[15]

RESULTS AND DISCUSSION

A perspective view of [Pt(dahd-C^3,O′)(PMe_2Ph)$_2$] [dahd^{2-}-3,4-diacetyl-2,4-hexadiene-2,5-diolate dianion {bis(2,4-pentanediones)-1,1,2,2-tetraacetylethane}] with the numbering scheme is shown in Fig. 1. The bis(2,4-pentanedione) ligand forms a five-membered metallacycle, in which the 3-carbon atom and the carbonyl oxygen atom at the 5-position from the dahd^{2-} bond to platinum(II). The bond lengths and bond angles are shown in Fig. 2. Bond angles P(1)—Pt—C(3) and P(2)—Pt—O(1) are 165.8° and 177.2°, respectively, and P(1) and C(3), and P(2) and O(1) are displaced up to 0.1 Å out of the best plane in opposite directions. These show that the complex still retains an approximate square planar geometry, but with a slight tetrahedral distortion.[2] The Pt—C(3) bond distance 2.143 Å may be normal and comparable with the corresponding bond distance observed in the Pt—C bonded complex of a β-ketoester, *trans*-bis{methyl(α-methoxycarbonyl)[pyridine]-2-propanoate-C,N} platinum(II).[3] In the present case the bond distance C(3)—C(4), 1.549 Å, is slightly elongated from the corresponding bond length of the free ligand 1,1,2,2-tetraacetylethane (1.496 Å),[5,6] while C(4)—C(5), 1.368 Å, is so shortened that it is sufficiently close to a C=C bond length, 1.360 Å, found in the cyclometallated compound of the 2,4-pentanedionate dianion, [Pt(tfa-C,O)(Me_2-py)(PPh_3)] (tfa =

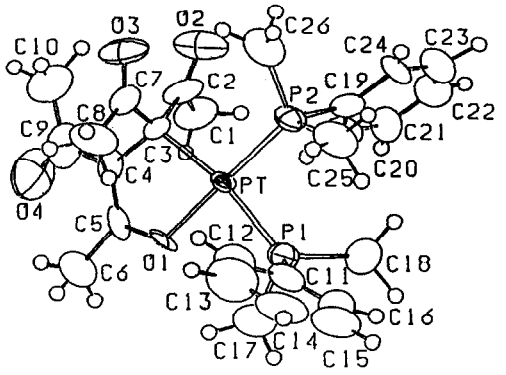

Fig. 1. A perspective view of the molecular structure of [Pt(dahd-C³,O)(PMe₂Ph)₂].

1,1,1-trifluoro-2,4-pentanedione) with a six-membered chelate ring.[16] The five-membered chelate ring Pt, O(1), C(5), C(4) and C(3) in the present case is in the envelope conformation, where the torsion angle C(3)—C(4)—C(5)—O(1) is −1.8°, C(4)—C(3)—Pt—O(1) −8.03° and C(5)—O(1)—Pt—C(3) 8.39°, respectively. Bond angles in the five-membered chelate ring, Pt—C(3)—C(4) 104.3° and C(3)—C(4)—C(5) 117.0°, are alternatively 5° and 3° less than the ideal bond angles 109° and 120° and these are probably the distortions due to the ring strain. The two carbonyls of the carbon-bonded 2,4-pentanedione group of 1,1,2,2-tetraacetylethane are in the same direction, opposite to the chelate ring with torsion

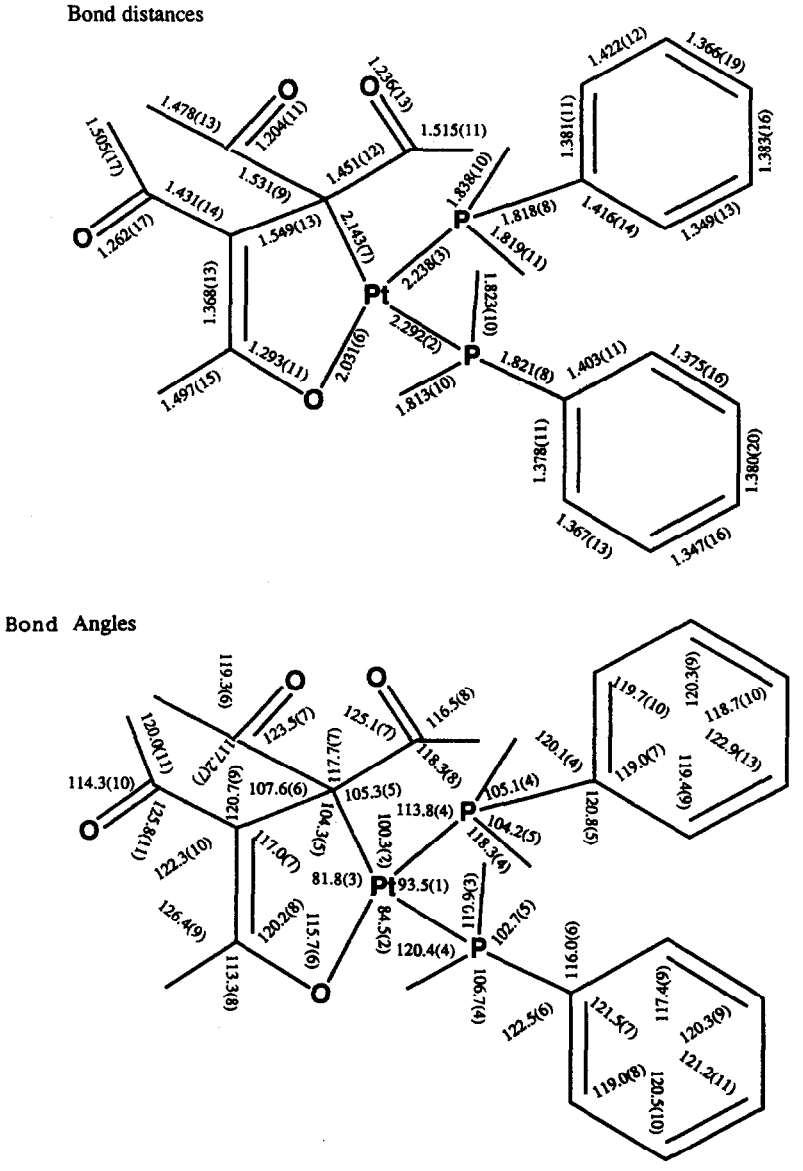

Fig. 2. Bond distances (Å) and angles (°) in [Pt(dahd-C³,O)(PMe₂Ph)₂].

angles C(2)—C(3)—C(7)—O(3) 1.7° and O(2)—C(2)—C(3)—C(7) 20.8°.

The steric size of PMe_2Ph and 1,1,2,2-tetraacetylethane is significant and an unusual short interatomic contact has been observed for O(2)···C(26), 2.99 Å, which is much shorter than the sum of the van der Waals radii of the methyl group (2.0 Å) and oxygen atom (1.5 Å). The bond angle C(3)—Pt—P(1), 100.3°, is also extraordinary being expanded from the ideal bond angle 90°, which may cause repulsion of C(3) in a direction towards O(1). As a result the interatomic contact O(2)···C(26), 2.82 Å, is considerably short and the bond angle O(1)—Pt—P(1) is 5.5° less than the ideal bond angle 90°.

The two phenyl rings of PMe_2Ph ligands orient in mutually opposite directions to the coordination plane and the dihedral angles between each phenyl ring and the coordination plane are 59.9° and 99.6°, respectively.

Although the lengths of the four carbonyl bonds from 1,1,2,2-tetraacetylethane were unfortunately accompanied with relatively large deviations and any significant differences were not clearly distinct, the bond length C(9)—O(4), 1.262 Å, seems to be slightly longer than the others in the keto form, C(7)—O(3) 1.204 and C(2)—O(2) 1.2364 Å, and it rather approaches that of the enol C(5)—O(1), 1.293 Å. Any elongation of bond distance C(9)—O(4) may not, however, be significant since its oxygen atom is apart by more than 7.8 Å from the adjacent platinum atom and an intermolecular interaction can be excluded. On the other hand, the IR carbonyl stretching vibrations in $[Pt(dahd\text{-}C^3,O')(PMe_2Ph)_2]$[8] have been observed as three distinct bands at 1515(s), 1627(s) and 1673(vs) cm^{-1} and these absorptions could be assigned as due to the O-bonding carbonyl in the enol form [$\nu(C^5—O^1)$], the acetyl group [$\nu(C^9=O^4)$] attached to the five-membered chelate ring and the C-bonded 2,4-pentanedione group [$\nu(C^7=O^3)$ and $\nu(C^2=O^2)$]. In the latter two bands the frequency at 1627 cm^{-1} is in the lower frequency region relative to the keto carbonyl, which may not, however, be unusual and is comparable with 1613–1621 cm^{-1} already found in $[Rh(acac\text{-}O)(CO)(PPr^i_3)_2]$[17] possessing an O-unidentate 2,4-pentanedione and $[Pt(M\text{-}ac\text{-}M,O)(PR_2Ph)_2]$ (M = S, R = Me;[9] M = Se, R = Ph;[11] M-ac = 3-mono-substituted-2,4-pentanedione).

In the present case a large *trans* influence related with a metallated carbon (3) could not be observed and the difference in bond lengths between Pt—P(2), 2.238 Å, and Pt—P(1), 2.292 Å, is not as pronounced as 2.24 and 2.34 Å found in $[PtCl(PMe_3)_3)]Cl$.[18]

REFERENCES

1. S. Kawaguchi, *Coord. Chem. Rev.* 1986, **70**, 51.
2. G. R. Newkome, K. J. Theriot, F. R. Fronczek and B. Villar, *Organometallics* 1989, **8**, 2513.
3. L. S. Hollis, A. R. Amundsen and E. W. Stern, *J. Am. Chem. Soc.* 1985, **107**, 274.
4. R. G. Charles, *J. Phys. Chem.* 1960, **64**, 1747.
5. J. P. Schaefer and P. J. Wheatley, *J. Chem. Soc. (A)* 1966, 528.
6. L. F. Power, K. E. Turner and F. H. Moore, *Inorg. Nucl. Chem. Lett.* 1972, **8**, 313.
7. S. Yamazaki, *Polyhedron* 1986, **5**, 1183.
8. S. Yamazaki, T. Ama and Z. Taira, *Polyhedron* 1988, **7**, 353.
9. S. Yamazaki and T. Ama, *Bull. Chem. Soc. Japan* 1989, **62**, 931.
10. S. Yamazaki, T. Ama, M. Hojo and T. Ueno, *Bull. Chem. Soc. Japan* 1989, **62**, 4036.
11. S. Yamazaki, T. Ueno and M. Hojo, *Bull. Chem. Soc. Japan* 1991, **64**, 1404.
12. S. Yamazaki, *Chem. Lett.* 1991, 1299.
13. S. Yamazaki, *Polyhedron* 1992, **11**, 1983.
14. UNICS II. Universal Crystallographic Computation Program System (Edited by T. Sakurai). The Crystallographic Society of Japan, Tokyo (1967).
15. *International Tables for X-ray Crystallography*, Vol. IV. Kynoch Press, Birmingham (1974).
16. S. Okeya, Y. Kawakita, S. Matsumoto, Y. Nakamura, S. Kawaguchi, N. Kanehisa, K. Miki and N. Kasai, *Bull. Chem. Soc. Japan* 1974, **55**, 2134.
17. S. Yoshida, Y. Ohgomori, Y. Watanabe, K. Honda, M. Goto and M. Kurahashi, *J. Chem. Soc., Dalton Trans.* 1988, 895.
18. R. Favez, R. Roulet, A. A. Pinkerton and D. Schwarzenbach, *Inorg. Chem.* 1980, **19**, 1356.

Polyhedron Vol. 12, No. 17, pp. 2137–2142, 1993
Printed in Great Britain

0277–5387/93 $6.00+.00
© 1993 Pergamon Press Ltd

THERMODYNAMICS OF SEVERAL BORON ACID COMPLEXATION REACTIONS STUDIED BY VARIABLE-TEMPERATURE ^{1}H AND ^{11}B NMR SPECTROSCOPY

R. D. PIZER,* P. J. RICATTO and C. A. TIHAL

Department of Chemistry, City University of New York, Brooklyn College, Brooklyn, NY 11210, U.S.A.

(*Received* 28 *January* 1993; *accepted* 4 *May* 1993)

Abstract—Borate ions, $RB(OH)_3^-$, react with polyols to form anionic complexes via the reaction $RB(OH)_3^- + H_2L \rightleftharpoons Cx^- + 2H_2O$. In the present study thermodynamic parameters of several such reactions were determined by variable-temperature ^{1}H and ^{11}B NMR spectroscopy. The systems studied were: $B(OH)_4^-$/1,2-ethanediol; $B(OH)_4^-$/1,2-propanediol; $C_6H_5B(OH)_3^-$/1,2-ethanediol; $CH_3B(OH)_3^-$/1,2-propanediol; and $CH_3B(OH)_3^-$/1,2-dihydroxybenzene. The first four systems have very similar stability constants and thermodynamic parameters. The reactions are all exothermic ($\Delta H° \sim -20$ kJ mol^{-1}) and values of $\Delta S°$ are quite negative ($\Delta S° \sim -60$ J mol^{-1} K^{-1}). The negative entropy is attributed primarily to a loss of configurational entropy in the ligand on complexation. This assertion was further investigated by studying the complexation of $CH_3B(OH)_3^-$ with the rigid ligand 1,2-dihydroxybenzene. The $CH_3B(OH)_3^-$/1,2-dihydroxybenzene reaction is characterized by a stability constant which is greater by four orders of magnitude than those of the other systems and this increase is shown to be entirely due to a much more positive value of $\Delta S°$.

Molecular recognition of carbohydrates and other polyhydroxy compounds by boron acids has been a subject of long and continuing interest.[1] The basis of this recognition is the formation of covalent bonds between the boron acid and appropriately oriented hydroxyl groups on the ligand. The overall reaction in basic media is a condensation reaction between borate ion and the ligand [eq. (1)]. In our continuing study of the mechanism of boron acid complexation reactions we have recently shown that polyols react only with borate ions,[2] while more acidic ligands such as dihydroxybenzenes[3] can react with trigonal boron acids, $RB(OH)_2$, as well.

We report here our first determination of thermodynamic parameters for these reactions. Although there have already been several reports[4–11] of thermodynamic parameters for borate/polyol complexation reactions in the literature, significant disagreement among the various studies is common and, as a result, the thermodynamic parameters remain somewhat uncertain. The two techniques used in these studies have been the measurement by pH techniques of stability constants as a function of temperature[4–8] and calorimetry.[9–11] One reason for the lack of agreement is that both techniques used in the determination of the thermodynamic

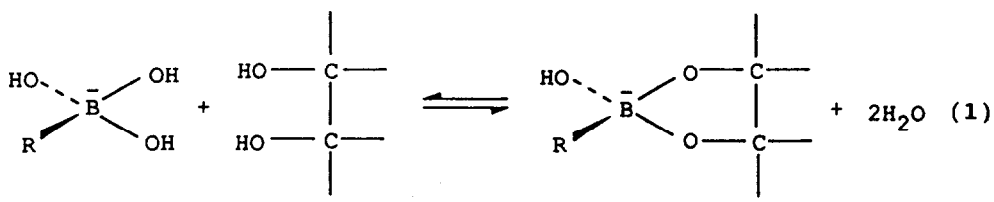

* Author to whom correspondence should be addressed.

parameters are dependent on accurate values of the reaction stability constants and here, too, differences exist in the literature.

The present paper demonstrates the efficacy of variable-temperature ^1H and ^{11}B NMR spectroscopy for the accurate determination of stability constants and thermodynamic parameters for boron acid complexation reactions. Although ^{11}B NMR spectroscopy has been used in the determination of stability constants for the reactions,[12-14] its use has not previously been extended to include a thermodynamic study.

EXPERIMENTAL

Boric acid, methylboronic acid, phenylboronic acid, 1,2-ethanediol, 1,2-propanediol, 1,2-dihydroxybenzene and D_2O (Aldrich) were all used as received. Stability constants for the various reactions were determined as a function of temperature by pH titration (NaOH titration), ^1H NMR spectroscopy and ^{11}B NMR spectroscopy. pH titrations were performed on a Fisher Accumet 950 pH meter and pH measurements were made in a thermostated cell under a nitrogen atmosphere. The activity coefficient of the hyrdogen ion was calculated using the Davies equation[15] as appropriate for each temperature and ionic strength. The pH meter was restandardized at each temperature. ^1H and ^{11}B NMR spectra were obtained using a Bruker IBM 250 MHz FT NMR spectrometer equipped with a Bruker BVT-1000 variable-temperature unit; 10 mm quartz NMR tubes were used in all ^{11}B experiments. The Bruker BB VSP 250 broad-band probe was modified to contain only quartz glassware. Therefore, there was no background boron signal. The accuracy of the ^{11}B NMR integration was checked by preparing a solution containing known (gravimetric) concentrations of $CH_3B(OH)_2$, $B(OH)_3$ and $C_6H_5B(OH)_2$ and comparing the NMR integrated areas with the gravimetric molar ratio. No measurable difference was observed. All solutions were prepared using D_2O/H_2O as the solvent mixture and the pH was adjusted by addition of deuterated NaOH or deuterated HCl. ^1H NMR spectra were recorded in 100% D_2O and ^{11}B NMR spectra were usually recorded in 30% D_2O. Solution pH was measured before and after recording each spectrum using a Fisher Ag/AgCl Microprobe combination pH electrode. In the case of ^{11}B NMR spectra these measurements were made directly in the NMR sample tube. pH measurements and NMR spectra were recorded over a temperature range from 276 to 318 K. Boron acid concentrations in various experiments ranged from 0.05 to 0.20 M and ligand concentrations ranged from 0.07 to 0.35 M. Ionic strength was adjusted by addition of the requisite amount of KNO_3 and it was typically maintained at 0.10 M.

RESULTS

Stability constants for the reactions at 25°C were variously determined by pH titration, ^{11}B NMR spectroscopy and ^1H NMR spectroscopy and agreement between the first two techniques has been previously demonstrated.[2,16] ^1H NMR spectroscopy also yields identical results.

Variable-temperature ^1H and ^{11}B NMR spectroscopy were used to determine the stability constants as a function of temperature. Since the ^{11}B NMR signals of $RB(OH)_3^-$ are relatively broad and often overlap with the resonances of the borate complex ions, ^1H NMR spectroscopy is frequently the method of choice for these systems. ^{11}B NMR spectroscopy is particularly useful for $B(OH)_4^-$ systems because the borate resonance is quite sharp and adequate separation of the resonances makes integration much more accurate. Both techniques were used in the $B(OH)_4^-$/1,2-propanediol study and representative spectra are shown in Figs 1 and 2.

The ^{11}B NMR spectrum of the system is presented in Fig. 1. The peak at -18 ppm is due to $B(OH)_4^-$ and the downfield peak (-14 ppm) is assigned to the 1 : 1 complex. Although $B(OH)_4^-$ is

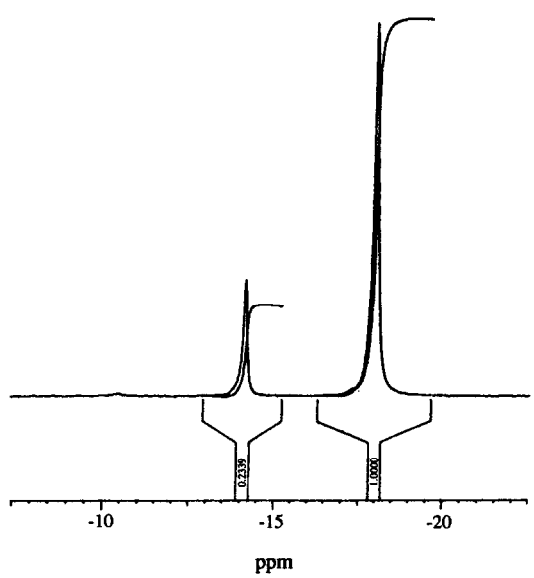

Fig. 1. ^{11}B NMR spectrum: $[B(OH)_4^-] = 0.10$ M; [1,2-propanediol] = 0.10 M; pH(D) = 12.0 in 30% D_2O/H_2O; $T = 25$°C. Chemical shifts are relative to external 0.15 M $B(OH)_3$ in 30% D_2O/H_2O at pH(D) = 2.0. The bracketed numbers are the relative integrations.

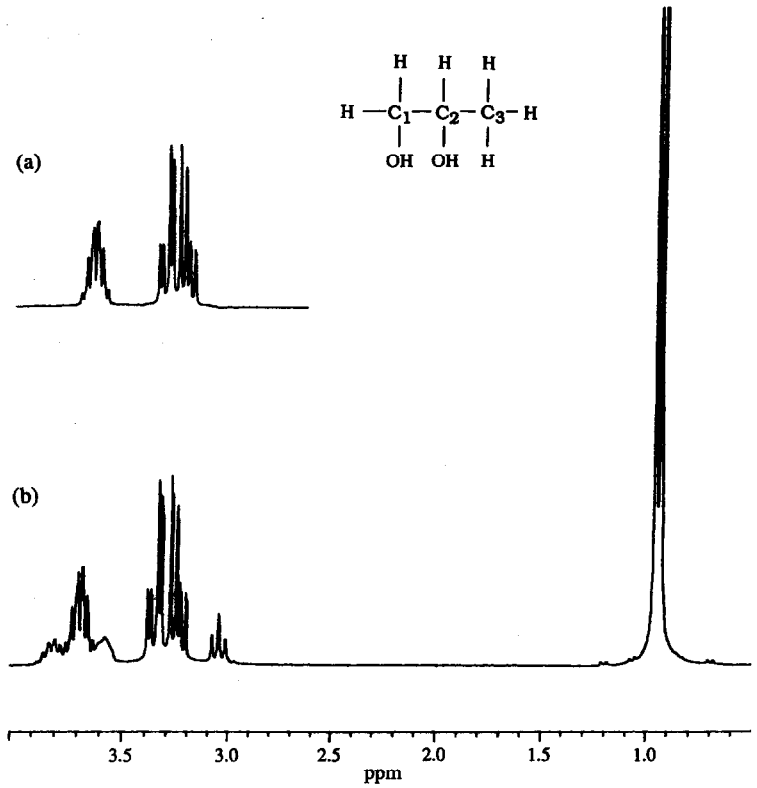

Fig. 2. ^{1}H NMR spectra: (a) The methylene/methyne [C(1)/C(2)] region of [1,2-propanediol] = 0.13 M in D_2O; pD = 12.0; T = 25°C. (b) $[B(OH)_4^-]$ = 0.10 M; [1,2-propanediol] = 0.13 M in D_2O; pD = 12.0; T = 25°C. The solvent H_2O/D_2O peak at 4.63 ppm is not shown. All ^{1}H NMR chemical shifts are relative to external 3-(trimethylsilyl)propionic acid in D_2O; pD = 12.0; T = 25°C.

also capable of forming bis complexes with diols,[17] reactant concentrations in our experiments were kept sufficiently low that only 1 : 1 complexes are formed in measurable concentration. An NMR signal due to the bis complex (−11 ppm) can be easily seen at higher reactant concentrations. Direct integration of the peaks in Fig. 1 allows a calculation of the reaction stability constant [eq. (1)].

The ^{1}H NMR spectrum of the same system is shown in Fig. 2. The spectrum of free 1,2-propanediol is presented in Fig. 2(a). The multiplet at 3.3 ppm is assigned to the two protons on C(1) and the multiplet at 3.7 ppm is due to the one proton on C(2). The spectrum with added $B(OH)_3$ is presented in Fig. 2(b). The methyl protons (1 ppm) are unaffected by complexation. The three non-methyl protons in the complex are non-equivalent and they give rise to three new multiplets in the spectrum. The new triplet at 3.1 ppm is well separated from the free ligand multiplet at 3.3 ppm and the stability constant can be calculated from the integration of these two multiplets.

Since ^{1}H and ^{11}B NMR experiments are performed in solvents which differ in D_2O concentration, this variable was also studied. ^{11}B NMR experiments were performed in 20%, 50% and 100% D_2O and results were obtained which agreed within experimental error. Similarly, although the ionic strength was maintained at 0.10 M by addition of the requisite amount of KNO_3, in a few experiments reactant concentrations alone provided an ionic strength in excess of 0.10 M. Therefore, the effect of ionic strength was evaluated. Ionic strength was increased up to 0.60 M by addition of KNO_3 and no measurable effect on either stability constants or thermodynamic parameters was observed. Our complete results on the $B(OH)_4^-$/1,2-propanediol system are presented in Fig. 3.

All of the NMR experiments except 1,2-dihydroxybenzene were performed at pH 12. At pH 12 the boron acids are all present predominantly as $RB(OH)_3^-$ and the various diols are unionized. Integration of the appropriate NMR signals provides a direct determination of the reaction stability constant [eq. (1)]. The $CH_3B(OH)_2$/1,2-dihydroxybenzene system, however, was studied at pH 6. This lower pH was selected to avoid problems associated with ligand oxidation in basic media.[3]

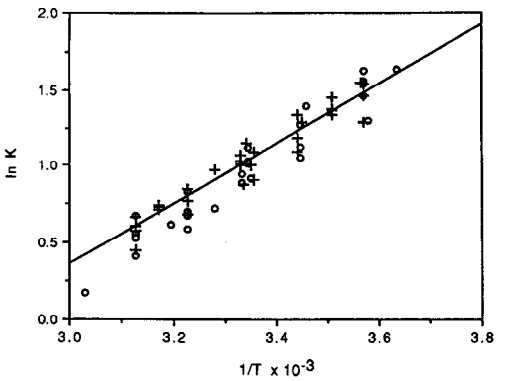

Fig. 3. van't Hoff plot of the $B(OH)_4^-$/1,2-propanediol system; ○ = ^1H NMR (experimental points); + = ^{11}B NMR (experimental points).

At this pH both $CH_3B(OH)_2$ and 1,2-dihydroxybenzene are unionized. Integration of the ^{11}B NMR spectrum at the measured pH allows the direct calculation of the stability constant for the reaction of trigonal $CH_3B(OH)_2$. The stability constant and thermodynamic parameters for the analogous reaction of $CH_3B(OH)_3^-$ with 1,2-dihydroxybenzene can be calculated from the $CH_3B(OH)_2$ values and the acid dissociation constant and thermodynamic parameters of $CH_3B(OH)_2$ ionization. The latter parameters were determined by pH titration of $CH_3B(OH)_2$ at several temperatures.

Stability constants and thermodynamic parameters for the various reactions are presented in Table 1. The error associated with the stability constants and the $CH_3B(OH)_2$ acid dissociation constant is ±10%. The values of ΔG° were calculated from the reported values of the equilibrium constants at 25°C and have an error of ±0.25 kJ mol^{-1}, which corresponds to the ±10% error in each of these constants. Errors associated with the other thermodynamic parameters were determined from the variances[18] of the slope and intercept of the appropriate van't Hoff plots (Fig. 3) and are specifically included in Table 1.

DISCUSSION

Although there have been several determinations of thermodynamic parameters of borate/polyol reactions in the literature,[4-11] significant disagreement among the various studies is not uncommon. For example, the reaction of $B(OH)_4^-$ with 1,2-dihydroxybenzene has been the subject of three investigations[5-7] and reported values of ΔH° vary from −0.24[5] to −23 kJ mol^{-1},[6] while determinations of ΔS° vary from +77[5] to −1.7 J mol^{-1} K^{-1}.[6] There have also been three different studies[7-9] of both the $B(OH)_4^-$/1,2-ethanediol and $B(OH)_4^-$/1,2-propanediol systems. The last of these[9] is a calorimetric investigation. Again, reported values of ΔH° vary widely (from −5.8[9] to −15.1 kJ mol^{-1}[8] for 1,2-ethanediol and from −9.3[9] to −21.4 kJ mol^{-1}[8] for 1,2-propanediol), as do values of ΔS° (−15[9] to −45.6 J mol^{-1} K^{-1}[8] for 1,2-ethanediol and −22[9] to −62 J mol^{-1} K^{-1}[8] for 1,2-propanediol). Several thermodynamic studies of more complex polyols[5,8-11] produce similar or greater differences.

Perhaps the most important reason for these large differences in reported thermodynamic parameters is the lack of accurate values of the reaction stability constants. Accurate stability constants are needed even if a calorimetric method is used,[9-11] because these reactions do not go to completion at any pH. The most common method which has been used in the determination of the stability constants is one in which the pH change on addition of diol to a borax buffer is measured.[17] It has been pointed out[7,17,19] that the equations which relate the pH change to the reaction stability constants can be solved exactly only for cases in which just one com-

Table 1. Thermodynamic parameters for several $RB(OH)_3^-$/1,2-diol reactions

Reaction	K^a	$\Delta G^{\circ a}$ (kJ mol^{-1})	ΔH° (kJ mol^{-1})	ΔS° (J mol^{-1} K^{-1})	NMR method
$B(OH)_4^-$ + 1,2-ethanediol	1.4	−0.83	−18(±2)	−58(±8)	^1H, ^{11}B
$B(OH)_4^-$ + 1,2-propanediol	2.8	−2.6	−17(±1)	−50(±2)	^1H, ^{11}B
$C_6H_5B(OH)_3^-$ + 1,2-ethanediol	2.4	−2.2	−20(±3)	−60(±9)	^1H
$CH_3B(OH)_3^-$ + 1,2-propanediol	6.0	−4.4	−26(±4)	−74(±10)	^1H
$CH_3B(OH)_3^-$ + 1,2-dihydroxybenzene[b]	4.0×10^4	−26	−28(±2)	−11(±10)	^1H

[a] Values of K and ΔG° are given at 25°C. The errors in K and ΔG° are ±10% and ±0.25 kJ mol^{-1}, respectively.

[b] Calculated from the values for the reaction of $CH_3B(OH)_2$ with 1,2-dihydroxybenzene and the thermodynamic parameters for the ionization of $CH_3B(OH)_2$. For $CH_3B(OH)_2$: $K_a = 4.0 \times 10^{-11}$; $\Delta G^\circ = -59$ kJ mol^{-1}; $\Delta H^\circ = 28 \pm 2$ kJ mol^{-1}; $\Delta S^\circ = -105 \pm 8$ J mol^{-1} K^{-1}.

plex is formed. An approximation must be made when bis complexes are also formed.[7,17] The determination of stability constants by ^{11}B NMR spectroscopy[12–14] involves no similar approximation. A tabulation[12] of pH change and ^{11}B NMR results shows that ^{11}B NMR spectroscopy leads to smaller values of stability constants in most cases. Given the uncertainty in the literature values of the stability constants, it is to be expected that the thermodynamic parameters determined using them would also be uncertain.

Reactions of $RB(OH)_3^-$

The study of simple 1,2-diols was chosen as a first test of the use of variable-temperature ^{11}B and ^1H NMR spectroscopy for the determination of thermodynamic parameters for borate complexation reaetions. The two $B(OH)_4^-$ systems involve a redetermination of previously reported[7–9] values of $\Delta H°$ and $\Delta S°$. The $CH_3B(OH)_3^-$ reactions complement some of our earlier kinetic studies.[2,3] The principal result (Table 1) is that the thermodynamic parameters for the reactions of aliphatic diols with the various borate ions are quite similar. The reactions are all exothermic with an average value of $\Delta H° \sim -20$ kJ mol^{-1}. All of the entropy changes are quite negative ($\Delta S° \sim -60$ J mol^{-1} K^{-1}) and this can be attributed to a loss of ligand configurational entropy on complexation. This assertion is supported by a comparison of the reactions of $CH_3B(OH)_3^-$ with 1,2-propanediol and 1,2-dihydroxybenzene, a rigid ligand. 1,2-Dihydroxybenzene is much more acidic than 1,2-propanediol and the reaction stability constant for this system exceeds that for the 1,2-propanediol system by four orders of magnitude. Surprisingly, this difference in stability constant turns out to be entirely related to a much more positive value of $\Delta S°$ and not at all to any real difference in $\Delta H°$. It is interesting to note that our previous kinetic study[3,20] concluded that the complexation reactions of 1,2-dihydroxybenzenes are likely to be characterized by a much more positive entropy of activation in the forward direction as compared with less rigid ligands. The present thermodynamic result is entirely in accord with the consequences of that idea. It should also be noted that a recent thermodynamic analysis[21] estimates the "entropic cost of restricting a rotor, within a hydrocarbon chain, as -1.6 to -3.6 kJ mol^{-1} ($T\Delta S°$ at 300 K)". Our results on the $CH_3B(OH)_3^-$/1,2-propanediol and $CH_3B(OH)_3^-$/1,2-dihydroxybenzene systems yield a comparable value of -1.9 kJ mol^{-1} if the difference in $\Delta S°$ between the two systems is attributed solely to the loss of configurational entropy in 1,2-propanediol. Although the comparison is certainly not exact (the —$CHOHCH_2OH$ moiety of 1,2-propanediol is not simply a hydrocarbon chain), it is significant to acknowledge the quantitative similarity between the two results.

The wide variation in previously reported thermodynamic parameters for borate/aliphatic 1,2-diol reactions has obscured the fact that these reactions are all very similar thermodynamically. Now that variable-temperature ^{11}B and ^1H NMR spectroscopy has been shown to be an accurate and reliable method for the determination of these parameters, we will extend its use to more complex polyols and also to the thermodynamic study of bis borate complexes.[22]

Acknowledgement—The support of the PSC/CUNY Faculty Research Award Program is gratefully acknowledged. The helpful suggestions of Professor Gary Mennitt regarding the ^{11}B NMR experiments are most appreciated.

REFERENCES

1. (a) M. Biot, *Compt. Rend.* 1842, **14**, 49; (b) J. Böeseken, *Adv. Carbohydr. Chem.* 1949, **4**, 189; (c) S. Shinkai, K. Tsukagoshi, Y. Ishikawa and T. Kunitake, *J. Chem. Soc., Chem. Commun.* 1991, 1039.
2. R. Pizer and C. Tihal, *Inorg. Chem.* 1992, **31**, 3243.
3. L. Babcock and R. Pizer, *Inorg. Chem.* 1977, **16**, 1677.
4. P. J. Antikainen, *Suomen Kemistilehti B* 1957, **30**, 185.
5. P. J. Antikainen and A. Kauppila, *Suomen Kemistilehti B* 1959, **32**, 141.
6. P. J. Antikainen and I. P. Pitkanen, *Suomen Kemistilehti B* 1968, **41**, 65.
7. J. M. Conner and V. C. Bulgrin, *J. Inorg. Nucl. Chem.* 1967, **29**, 1953.
8. T. Paal, *Acta Chim. Acad. Sci. Hung.* 1976, **91**, 393.
9. R. Aruga, *Talanta* 1985, **32**, 517.
10. R. Aruga, *J. Chem. Soc., Dalton Trans.* 1988, 2971.
11. W. J. Evans, V. L. Frampton and A. D. French, *J. Phys. Chem.* 1977, **81**, 1810.
12. W. G. Henderson, M. J. How, G. R. Kennedy and E. F. Mooney, *Carbohydr. Res.* 1973, **28**, 1.
13. M. van Duin, J. A. Peters, A. P. G. Kieboom and H. van Bekkum, *Tetrahedron* 1985, **41**, 3411.
14. M. Makkee, A. P. G. Keiboom and H. van Bekkum, *Recl. Trav. Chim. Pays-Bas* 1985, **104**, 230.
15. C. W. Davies, *J. Chem. Soc.* 1938, 2093.
16. R. Pizer and C. Tihal, *Inorg. Chem.* 1987, **26**, 3639.
17. G. L. Roy, A. L. Laferriere and J. O. Edwards, *J. Inorg. Nucl. Chem.* 1957, **4**, 106.
18. H. D. Young, *Statistical Treatment of Experimental Data*, p. 146. McGraw-Hill, New York (1962).
19. We have used a method similar to the pH change method in previous studies.[3,16] In some cases where

bis complexes are formed it is possible to avoid the necessity of making approximations in the data analysis. In these particular studies the pH change technique was complemented by additional methods of stability constant determination.

20. L. Babcock and R. Pizer, *Inorg. Chem.* 1980, **19**, 56.
21. M. S. Searle and D. H. Williams, *J. Am. Chem. Soc.* 1992, **114**, 10690.
22. L. Babcock and R. Pizer, *Inorg. Chem.* 1983, **22**, 174.

Polyhedron Vol. 12, No. 17, pp. 2143–2151, 1993
Printed in Great Britain

0277–5387/93 $6.00+.00
© 1993 Pergamon Press Ltd

PREPARATION AND THE UNIQUE ACIDIC PROPERTY OF A HEXAFLUORO-2,4-PENTANEDIONATOCOBALT(III) COMPLEX WITH ADDITIONAL ANIONIC LIGANDS

Y. KITAMURA† and A. SHIBATA

Department of Chemistry, Faculty of Science, Ehime University, Matsuyama 790, Japan

(*Received* 5 *April* 1993; *accepted* 30 *April* 1993)

Abstract—15 title complexes were newly prepared. Omitting the water of crystallization, these are: $[Co(hfac)L]ClO_4$, with L = *fac*(N)-(β-ala)(bpy), *fac*(N)-(L-ala)(bpy), *fac*(N)-(gly)(bpy), *mer*(N)-(gly)(en), *mer*-(NO_2)(dien), *mer*(N)-(pico)(en), *mer*(N)-(pico)(tn); [Co(hfac)L], with L = *cis*(O)-aeida, *trans*(O)-aeida, *cis*(O)-apida, β-eddp, C_2-*cis*(O)-$(gly)_2$, *cis*-$(ox)(NH_3)_2$, (ox)(en); and K[Co(hfac)(nta)], where the hfac acts as a bidentate and L is a mix of ligands occupying the residual four coordination sites. The abbreviations for the ligand are: Hhfac = hexafluoro-2,4-pentanedione, H(β-ala) = β-alanine, bpy = 2,2′-bipyridine, H(L-ala) = L-alanine, Hgly = glycine, en = ethylenediamine, dien = diethylenetriamine, Hpico = picolinic acid, tn = 1,3-propanediamine, H_2aeida = aminoethyliminodiacetic acid, H_2apida = aminopropyliminodiacetic acid, H_2eddp = ethylenediamine-N,N′-dipropionic acid, H_2ox = oxalic acid and H_3nta = nitrilotriacetic acid. The geometric structures of these complexes were assigned on the basis of UV–vis, proton NMR and fluorine NMR spectra. All these complexes show a pH-dependent rapid and reversible colour change in water and in methanol, which is ascribed to covalent bond formation and fission between a lyate anion and one of the carbonyl carbon atoms of the coordinating hfac ligand. The thermodynamic constants for this equilibrium in water, K_{OH}, and in methanol, K_{OMe}, were estimated spectrophotometrically. The pK_{OH} ranged from −7.4 to −4.8 and the pK_{OMe} from −8.4 to −4.2. Possible explanations are given for the following observations: K_{OH} and K_{OMe} are large when L involves a coordinating oxygen atom on the hfac plane in $[Co(hfac)L]^{n+}$, when L involves a pico or bpy ligand or when L is a tripod-type ligand. K_{OMe} is large when L is quadridentate. For a monopositive complex $K_{OH} < K_{OMe}$, whereas for a zero-valent complex $K_{OH} > K_{OMe}$.

In 1979 Kuroda found a pH-dependent rapid and reversible colour change of an aqueous solution of $[Co(hfac)(en)_2](ClO_4)_2$; orange in acid and violet in base.[1] He proposed a deprotonation of the methylidyne group of the coordinating hfac ligand as an origin for this phenomenon. Later, NMR spectra of this complex in D_2O were studied.[2] The methine proton signal shifted on addition of NaOD, but it returned to the original position without losing intensity on the subsequent reacidification by DCl. The ^{13}C signals in basic D_2O revealed that the two CF_3 and the two C—O groups are not equivalent. On these bases a reversible addition of an OH^- to one of the carbonyl carbon atoms of the coordinating hfac ligand was proposed [L = $(en)_2$, R = H and $n = 2$ in eq. (1)].[2]

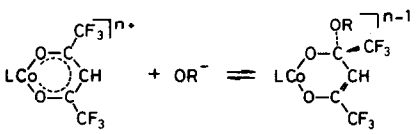

(1)

Subsequently, an analogous colour change was also observed for several related complexes, $[Co(hfac)L]^{n+}$, with L = $(NH_3)_4$, trien, i-dtma and edda (trien = 1,8-diamino-3,6-diazaoctane, Hi-dtma = 4-diethylenetriaminemonoacetic acid, H_2edda = ethylenediamine-N,N′-diacetic acid).[3] The fluorine NMR spectra of these complexes in basic D_2O indicated that two or four dia-

† Author to whom correspondence should be addressed.

stereoisomers are formed, except for the case of the highly symmetrical L = $(NH_3)_4$. This was consistent with eq. (1) (R = H) and eliminated the alternative possibility of the formation of $[Co(hfac)(OH)L]^{n-1}$ or $[Co(hfacOH)L(H_2O)]^{n-1}$, in which hfac or hfacOH coordinates to cobalt(III) as a monodentate ligand.[3] A single crystal of $[Co(hfacOH)(cn)_2]Br \cdot H_2O$ was obtained on addition of NaOH to an aqueous solution of $[Co(hfac)(en)_2]Br_2$.[4] It was studied by X-ray diffraction and the structure of the complex ion as given on the right of eq. (1) [L = $(en)_2$, R = H, $n = 2$] was confirmed.[4] The proton NMR spectrum of $[Co(hfac OH)(en)_2]Br \cdot H_2O$ in CH_3OD indicated that substitution of OH^- by OCH_3^- occurs and $[Co(hfac OCH_3)(en)_2]^+$ is formed.[4] The X-ray crystallographic study of crystals of β-$[Co(hfacOCH_3)(trien)]ClO_4$ and $[Co(hfacOCH_3)(en)_2]ClO_4$ confirmed the structure of these complexes, as given on the right of eq. (1) [R = CH_3, L = $(en)_2$ or β-trien, $n = 2$].[5,6] The thermodynamic equilibrium constants of eq. (1), K_{OH} in water (R = H) or K_{OMe} in methanol (R = CH_3), were determined by titration or from the UV–vis absorption intensity of the complex in appropriate buffers.[3,5,7,8] It was pointed out that in the case of 25 $[Co(hfac)L]^{2+}$ with tetraamine L ligands their values critically depend on the involvement as L ligands of a bpy or a phen ligand (phen = 1,10-phenanthroline).[8] $pK_{OH} \fallingdotseq -6.6$ and $pK_{OMe} \fallingdotseq -8.7$ when L does not involve bpy or phen ligands. $pK_{OH} \fallingdotseq -8.7$ and $pK_{OMe} \fallingdotseq -11.0$ when L involves either a bpy or a phen ligand. $pK_{OH} \fallingdotseq -11.5$ and $pK_{OMe} \fallingdotseq -14.6$ when L involves two bpy or phen ligands.

In the present report we are further interested in the effect of anionic L ligands on the magnitudes of K_{OH} and K_{OMe}. We have recently prepared 15 new complexes and estimated their K_{OH} and K_{OMe} values by UV spectrophotometry. Their geometric structures are assigned on the bases of UV–vis, proton NMR and fluorine NMR spectra.

EXPERIMENTAL

A Unisoku RS-450 stopped-flow apparatus, JEOL-GSX-270-FT-NMR instrument and a Shimadzu UV-2200 UV–vis spectrophotometer were used. The experimental procedures were similar to those described in a previous report.[5] In the proton and fluorine NMR measurements 2-methyl-2-propanol ($\delta = 0$ ppm) and trifluoroacetic acid ($\delta = -76.5$ ppm) were used as internal standard, respectively.

CAUTION! Although we have experienced no difficulty with the perchlorate salts described here, these should be regarded as potentially explosive and handled accordingly.

Cis(O)-Na[Co(aeida)$(NO_2)_2$]·$2H_2O$ (1)

This substance was prepared by a slight modification of a published method.[9] During the air-oxidation of the solution containing $CoCl_2$ and H_2aeida the pH value was controlled at *ca* 7 by the occasional addition of acetic acid. This prevented the decomposition of the complex and improved the yield by a magnitude of 1.5.

Cis(O)-M^1[Co(aeida)$(NO_2)_2$]·nH_2O ($M^1 = NH_4^+$, K^+, Rb^+, Cs^+; $n = 0$ or 1). A hot aqueous solution of **1** (38 g) was mixed with a saturated aqueous solution of CH_3COOM^1 (0.2 mol). Brilliant orange–brown crystals separated on cooling the solution and washed with methanol; yield 90%. *Cis*(O)-K[Co(aeida)$(NO_2)_2$]·H_2O was identified. Found: C, 18.9; H, 3.2; N, 14.7. Calc.: C, 19.1; H, 3.2; N, 14.9%. UV–vis absorption maxima: λ_{max} (nm) (ε) = 470 (252), 334 (6290).

Trans(O)-[Co(aeida)$(H_2O)_2$]NO_3 (2)

A mixture of *cis*(O)-NH_4[Co(aeida)$(NO_2)_2$] (10 g), acetic acid (60 cm^3) and H_2O (20 cm^3) was contained in an evaporating dish covered with a watch glass and was warmed on a water bath until the solid dissolved and the evolution of the gas stopped. The resultant solution was treated with 2 M HNO_3 (20 cm^3) and evaporated on a water bath by air blow (M = mol dm^{-3}). The tarry product was diluted by water (100 cm^3) and evaporated again. These dilution and evaporation procedures were repeated three times, while acetic acid escaped in the vapour. The final tarry product was dissolved in water (50 cm^3) and treated by 2 M HNO_3 (10 cm^3). It was evaporated at 70°C until crystal separation and left at room temperature overnight. The resultant red–violet crystals (5 g) were collected and washed with methanol. Found: C, 21.8; H, 4.2; N, 12.2. Calc.: C, 21.8; H, 4.3; N, 12.7%. λ_{max} (nm) (ε) = 538 (185), 382 (178).

Na[Co(apida)$(NO_2)_2$] (3)

This yellow–brown crystal was prepared analogously to **1** using tn; yield 30%.

H[$CoCl_2$(eddp)] (4)

An aqueous suspension (40 cm^3) of H_2eddp·2HCl (2.7 g) and $CoCO_3$ (1.3 g) was stirred at 50°C. The resultant red–brown solution was treated with NaOH (0.8 g) and oxidized by the addition

of 30% H_2O_2 (20 cm^3). The deep red solution was treated with HCl (20 cm^3) and evaporated on a water bath. Red–brown crystals (2 g) were obtained and washed with ethanol and ether.

[Co(β-ala)(CO_3)(bpy)] (**5**)

This substance (1.5 g) was prepared analogously to **6** using β-alanine (0.9 g). The crystal was washed with ethanol and ether (1 : 1).

[Co(L-ala)(CO_3)(bpy)] (**6**)

An aqueous solution of K[Co(CO_3)$_2$(bpy)] (3.8 g) and L-alanine (0.9 g) was stirred at 40°C for 2 h and evaporated to near dryness.[8] The residue was extracted with methanol and insoluble salts were removed. These evaporation and extraction procedures were repeated three times. Crystals separated on the final evaporation of the methanolic solution and were washed with ethanol and ether; yield 1.5 g.

[Co(CO_3)(gly)(bpy)] (**7**)

Glycine (0.8 g) was added to an aqueous solution (20 cm^3) of K[Co(CO_3)$_2$(bpy)] (4 g).[8] This solution was stirred at 50°C for 1 h. Red–violet precipitates were obtained and washed with ethanol and ether.

[Co(CO_3)(NO_2)(dien)] (**8**)

An aqueous solution (20 cm^3) of *mer*-[$CoCl_3$(dien)] (2.7 g) and Li_2CO_3 (1 g) was stirred at 60°C for 1 h.[10] After filtration the filtrate was treated with $NaNO_2$ (1 g), stirred at 60°C for 30 min and evaporated in the air to 10 cm^3. Inorganic salts were removed. An orange–yellow precipitate (2 g) separated on treatment of this filtrate by ethanol (10 cm^3), which was collected and washed with ethanol and ether. This complex is soluble in water and slightly soluble in methanol.

[Co(CO_3)(pico)(tn)] (**9**)

An aqueous solution of K[Co(CO_3)$_2$(tn)] (2.9 g) was slowly treated with an aqueous solution of Hpico (1.2 g).[8] This mixture was stirred at 50°C for 30 min and evaporated by air blow to near dryness. The resultant solid was separated by filtration and dissolved in methanol. This was evaporated giving violet crystals which were washed with methanol and ether (1 : 1).

K[Co(CO_3)(gly)$_2$] (**10**)

Glycine (7.5 g) was neutralized by KOH. This solution was added to a tricarbonatocobaltate solution prepared from $CoCl_2 \cdot 6H_2O$ (12 g).[11] The mixture was stirred at 50°C for 2 h and cooled. Salts were removed and the filtrate was treated with an equal volume of ethanol. The resultant violet crystals were recrystallized from water by the addition of ethanol and washed with ethanol and ether; yield 5 g.

Fac(N)-[Co(β-ala)(hfac)(bpy)]ClO_4

This substance (1 g) was prepared analogously to **11** using **5** (1.2 g). Found: C, 35.3; H, 2.5; N, 6.7. Calc.: C, 35.5; H, 2.5; N, 6.9%.

Fac(N)-[Co(L-ala)(hfac)(bpy)]ClO_4 (**11**)

Compound **6** (1.2 g) in water was decarbonized by 2 M $HClO_4$ (3 cm^3) and treated with drops of Hhfac (0.7 g) and 2 M NaOH (1.6 cm^3). The mixture was stirred at 50°C for 1 h and cooled. The resultant precipitates were recrystallized from acetone and washed with ethanol and ether (2 : 8) and ether; yield 1 g. Found: C, 35.5; H, 2.5; N, 7.2. Calc.: C, 35.5; H, 2.5; N, 6.9%.

Fac(N)-[Co(gly)(hfac)(bpy)]ClO_4

Compound **7** (3.5 g) was decarbonized in 2 M $HClO_4$ (10 cm^3) and combined with Hhfac (2.1 g) and 1 M NaOH (10 cm^3). The mixture was then stirred at 50°C for 1 h. The resultant orange–red crystals were recrystallized from methanol and water (9 : 1); yield 2 g. Found: C, 34.2; H, 2.2; N, 7.3. Calc.: C, 34.3; H, 2.2; N, 7.1%.

Mer(N)-[Co(gly)(hfac)(en)](ClO_4)$\cdot 2H_2O$

Mer(N)-[Co(CO_3)(gly)(en)]$\cdot H_2O$ (2.7 g) was decarbonized with 2 M $HClO_4$ (10 cm^3).[12] The resultant solution was treated with Hhfac (2.1 g) and NaOH (0.4 g) and stirred at 50°C for 1 h. Deep orange crystals separated on the addition of $HClO_4$, which were recrystallized from methanol containing drops of $HClO_4$ and washed with ethanol and ether (2 : 8); yield 3.7 g. Found: C, 19.9; H, 3.0; N, 7.9. Calc.: C; 20.2; H, 3.2; N, 7.9%.

Mer-[Co(hfac)(NO_2)(dien)]ClO_4

Compound **8** (1.4 g) was decarbonized by 1 M $HClO_4$ (10 cm^3). The solution was treated at 45°C with an aqueous solution of Hhfac (1 g) and NaOH

(0.2 g). The resultant yellow–orange precipitates were collected by filtration and extracted with acetone (30 cm^3) containing drops of $HClO_4$. The final product (1.6 g) was obtained by evaporation of the extract and washed with ethanol and ether (2:8). Found: C; 20.8; H, 2.8; N, 10.7. Calc.: C, 21.0; H, 2.7; N, 10.9%.

Mer(N)-[Co(hfac)(pico)(en)]ClO_4

This substance was prepared analogously to **12** using $K[Co(CO_3)_2(en)]$.[8] Found: C; 28.3; H, 2.6; N, 7.7. Calc.: C, 28.5; H, 2.4; N, 7.7%.

Mer(N)-[Co(hfac)(pico)(tn)]ClO_4 (**12**)

Compound **9** (3.3 g) was decarbonized with 2 M $HClO_4$ (10 cm^3). The solution was treated with Hhfac (2.1 g) and NaOH (0.4 g) and stirred at 50°C until the colour changed from violet to red–violet. The solution was evaporated to near dryness and the residue was extracted with acetone. The extracts were treated with drops of $HClO_4$ and evaporated and the resultant precipitates were extracted by methanol and water (9:1) with drops of $HClO_4$. The extracts were evaporated. These extraction and evaporation procedures were repeated three times and the product was obtained. Found: C, 25.8; H, 2.6; N, 7.4. Calc.: C, 25.8; H, 2.7; N, 7.5%.

Trans(O)-[Co(aeida)(hfac)]·$0.5H_2O$

An aqueous solution (40 cm^3) of **2** (6.7 g) was treated with an aqueous solution (5 cm^3) of Hhfac (4.2 g) and NaOH (0.9 g) and was stirred at 40°C for 2 h. Crystals appeared in the solution, which was then treated with 2 M HNO_3 (1 cm^3), concentrated at 40°C to half volume and left overnight. The resultant crystals were collected and washed with ether. This mixture of *trans*(O) and *cis*(O) products was then extracted with ethanol (25 $cm^3 \times 5$). The extracts were treated with water (10 cm^3) containing a few drops of 2 M HNO_3 and were evaporated at 50°C to near dryness. The resultant precipitates were extracted with ethanol and the extracts treated with water (quarter volume of the extracts) containing a drop of 2 M HNO_3 and evaporated to near dryness. These extraction, dilution and evaporation procedures were repeated three times. The resultant brown–violet crystals (1.8 g) were collected, washed with ethanol:ether (1:9), then ether and finally air-dried. Found: C, 29.4; H, 2.5; N, 6.1. Calc.: C, 29.4; H, 2.7; N, 6.2%.

Cis(O)-[Co(aeida)(hfac)]·$0.5H_2O$

The ethanol extraction residues in the above procedure for the *trans*(O) isomer were collected and dissolved in hot methanol and water (1:1). This solution was filtered and the filtrate was treated with a few drops of 2 M HNO_3. The mixture was evaporated at 60°C until the solution colour turned from red to violet and was left at room temperature. The resultant deep red crystals were collected by filtration. The filtrate containing the *trans*(O) product can be utilized through evaporation and ethanol extraction. It was recrystallized twice from methanol, washed with ethanol, acetone and air-dried; yield 4.5 g. Found: C, 29.4; H, 2.5; N, 6.4. Calc.: C, 29.4; H, 2.7; N, 6.2%.

Cis(O)-[Co(apida)(hfac)]·$1.5H_2O$

Compound **3** (8 g) was dissolved in warm 80% acetic acid (70 cm^3). The violet solution obtained was treated with 2 M $HClO_4$ (20 cm^3) and evaporated. The oily product was treated with ethanol and the resultant precipitates were collected by filtration and washed with ethanol. This product (4.5 g), which we presumed to be crude $[Co(apida)(H_2O)_2]ClO_4$, was dissolved in water (10 cm^3) and treated with a mixture of Hhfac (2.1 g) and 1 M NaOH (10 cm^3) and stirred at 60°C for 1 h. The resultant red–violet crystals were recrystallized from methanol and water (9:1); yield 1.5 g. This substance is sparingly soluble in water. Found: C, 30.3; H, 3.4; N, 5.8. Calc.: C, 30.0; H, 3.4; N, 5.8%.

β-[Co(eddp)(hfac)]·$2H_2O$

An aqueous solution (10 cm^3) of **4** (1.7 g) was neutralized with 2 M NaOH (2.5 cm^3) to pH = 4–5. The solution was then combined with Hhfac (1.0 g) and 1 M NaOH (5 cm^3) and stirred at 50°C for 1 h. The resultant red oily product was extracted with acetone. After filtration, the extracts were evaporated and the resultant oily substance was dissolved in ethanol. Red–violet crystals separated on evaporation of this ethanolic solution, which were washed with ethanol:ether (1:9) and ether; yield 0.5 g. Found: C, 30.9; H, 3.6; N, 5.6. Calc.: C, 31.0; H, 3.8; N, 5.6%.

C_2-cis(O)-[Co(hfac)$(gly)_2$]·$0.5H_2O$

This red–orange substance (2 g) was prepared analogously to **13** using **10** (3.4 g). Found: C, 25.5; H, 2.3; N, 6.4. Calc.: C; 25.6; H; 2.4; N, 6.6%.

Cis-$[Co(hfac)(ox)(NH_3)_2]\cdot 0.5H_2O$

An aqueous solution (10 cm^3) of *cis–cis*-$[Co(ox)(NH_3)_2(H_2O)_2]NO_3$ (2.8 g) was treated at 50°C with Hhfac (2.1 g) and 2 M NaOH (5 cm^3).[13] The resultant violet crystals were recrystallized from methanol containing drops of $HClO_4$ and washed with ethanol : ether (2 : 8); yield 2 g. This substance is light sensitive and should be kept in a refrigerator in the dark. Found: C; 20.9; H, 1.8; N, 7.1. Calc.: C, 21.2; H, 1.8; N, 7.1%.

$[Co(hfac)(ox)(en)]\cdot 1.5H_2O$ (13)

$K[Co(CO_3)(ox)(en)]\cdot H_2O$ (3.2 g) was decarbonized at 40°C by 1 M H_2SO_4 (10 cm^3).[11] The solution was treated by an aqueous solution (10 cm^3) of Hhfac (2.1 g) and NaOH (0.5 g) and stirred at 45°C for 1 h. The mixture was then acidified using drops of 3 M H_2SO_4 and evaporated. The resultant red–violet crystals were recrystallized twice from methanol and washed with ethanol : ether (2 : 8) and ether; yield 1.5 g. Found: C, 24.4; H, 2.2; N, 6.5. Calc.: C, 24.5; H, 2.7; N, 6.4%.

$K[Co(hfac)(nta)]\cdot 2H_2O$

An aqueous suspension (10 cm^3) of K[Co(OH)(nta)(H_2O)] (3.2 g) was treated with a methanolic solution (10 cm^3) of Hhfac (2.1 g).[14] The mixture was stirred at 30°C for 10 h and evaporated slowly at 30°C to dryness. The residue was washed with ether and extracted with ethanol. The extracts were evaporated at 30°C to dryness and the residue was extracted with ethanol and left at room temperature. The resultant red–violet crystals (1 g) were washed with ethanol : ether (2 : 8) and ether. Found: C, 24.9; H, 1.9; N, 2.4. Calc.: C, 25.0; H, 2.1; N, 2.7%.

RESULTS AND DISCUSSION

Preparations

The general preparative course for $[Co(hfac)L]^{n+}$ is that Nahfac reacts with the corresponding diaqua complex, which is derived from the carbonato, dichloro or dinitro precursor. $[Co(hfac)(nta)]^-$ is prepared by the reaction between Hhfac and the corresponding hydroxoaqua precursor.

Proton NMR spectra

The isomerism of the cobalt(III)-aeida complex can be assigned by the glycinate ring proton resonance spectra (Table 1). One pair of doublets with 4H intensity corresponds to the *trans*-(O) isomer, where the two glycinate rings are equivalent. Two pairs of doublets, each of which is of 2H intensity, corresponds to the *cis*(O) isomer, where the two glycinate rings are inequivalent.

UV–vis spectra

All the $[Co(hfac)L]^{n+}$ complexes obtained in this work show a distinct, rapid and reversible colour change with variation of the pH in water and methanol. Typical spectra are shown in Fig. 1 and the absorption maxima are summarized in Table 2. In acidic medium the first band and the charge transfer band around 350 nm are observed. In basic medium the first band shifts by 30–60 nm to lower energy and the charge-transfer band disappears. This disappearance is consistent with eq. (1), where a localization of the π-electron system occurs on the right. When L coordinates through three nitrogen and one oxygen atoms [L = (β-ala)(bpy), (L-ala)(bpy), (gly)(bpy), (gly)(en), (pico)(en) and (pico)(tn)] the *mer*(N) or *fac*(N) coordination mode of L can

Table 1. Glycinate ring proton resonance spectra for the cobalt(III)-aeida complex

Complex	δ (ppm)	J (Hz)	No. of Hs
Cis(O)-$[Co(aeida)(NO_2)_2]^-$	2.77, 2.71, 2.64, 2.58	16.5	2H
	2.81, 2.74, 2.72, 2.65	18.6	2H
Trans(O)-$[Co(aeida)(H_2O)_2]^+$	3.18, 3.12, 2.47, 2.41	16.6	4H
Cis(O)-[Co(aeida)(hfac)]	3.14, 3.08, 2.49, 2.43	16.2	2H
	2.91, 2.84, 2.83, 2.76	19.1	2H
Trans(O)-[Co(aeida)(hfac)]	3.47, 3.41, 2.65, 2.59	16.9	4H

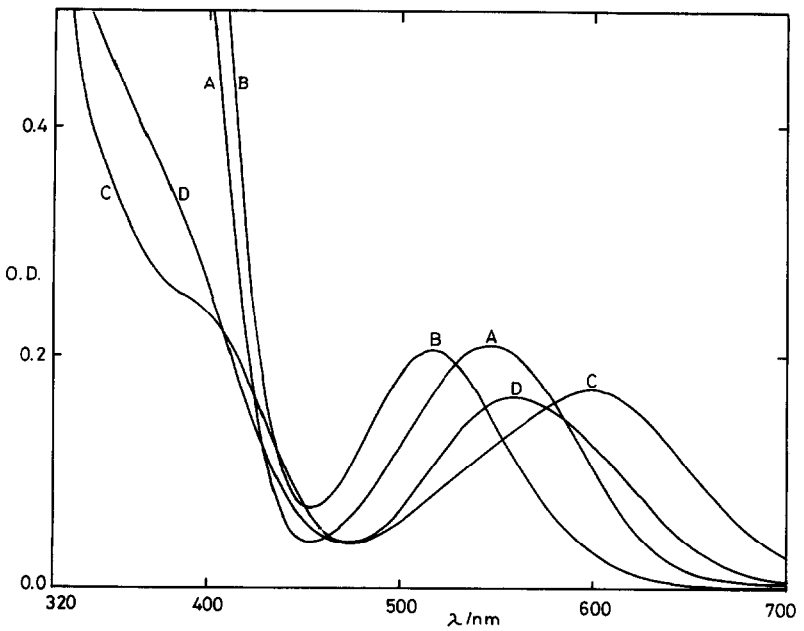

Fig. 1. Visible absorption spectra of [Co(aeida)(hfac)] in water. [Co^{III}] = 1 mM, path length = 1 cm. (A) *Trans*(O) isomer with 1mM $HClO_4$; (B) *cis*(O) isomer with 1 mM $HClO_4$; (C) *trans*(O) isomer with 10 mM NaOH; and (D) *cis*(O) isomer with 10 mM NaOH.

be assigned, comparing the first band position in water with those of [Co(hfac)(i-dtma)]$^+$: λ_{max} (nm) (ε) = 513 (182) for the *fac*(N) isomer and 493 (151) for the *mer*(N) isomer.[3] Similarly, when L coordinates through two nitrogen and two oxygen atoms [L = $(gly)_2$] the *cis*(O) or *trans*(O) coordination mode can be assigned comparing its first band position in water with those of *cis*(O)-[Co(aeida)(hfac)] (516 nm), β-[Co(edda)(hfac)] (507 nm), *trans*(O)-[Co(aeida)(hfac)] (547 nmm) and α-[Co(edda)(hfac)] (550 nm) (Fig. 2).[3] It can also be noticed in Table 2 that among [Co(hfac)L]$^{n+}$ of a similar L ligand that with the longer chelate ring shows the first absorption at the longer wave-

Table 2. UV–vis absorption maxima of [Co(hfac)L]$^{n+}$

L	λ (nm) (ε) in water		λ (nm) (ε) in methanol	
	1 mM $HClO_4$	10 mM Na_2CO_3	1 mM H_2SO_4	10 mM $NaOCH_3$
Fac(N)-(β-ala)(bpy)	517(209), 345(2790)sh[a]	552(178)	513(203), 345(2620)sh	560(161)
Fac(N)-(L-ala)(bpy)	510(183), 345(3040)sh	544(168)	506(189), 345(2910)sh	548(173)
Fac(N)-(gly)(bpy)	511(168), 345(2790)sh	552(168)	511(182), 345(2970)sh	551(172)
Mer(N)-(gly)(en)	492(114), 352(2520)	537(117)	494(120), 353(2240)	540(122)
Mer-(NO_2)(dien)	479(224), 335(4490)	505(186)	481(236), 338(5270)	508(186)
Mer(N)-(pico)(en)	486(152), 351(2450)	529(135)	485(140), 351(2120)	535(127)
Mer(N)-(pico)(tn)	495(95), 350(2240)	538(97)	501(84), 334(2010)	540(93)
Cis(O)-aeida	516(216), 353(2560)	559(178)	518(219), 350(2270)	567(177)
Trans(O)-aeida	547(202), 347(2370)	600(143)	546(207), 340(2230)	616(169)
Cis(O)-apida	529(128), 352(2070)	559(122)	522(132), 350(1800)sh	548(117)
β-eddp	508(240), 338(2020)	[b]	513(256), 350(1780)sh	[b]
C_2-*cis*(O)-$(gly)_2$	514(123), 354(1900)	559(112)	514(142), 338(2170)	564(126)
Cis-(ox)$(NH_3)_2$	546(98), 351(2500)	570(95)	546(108), 340(2270)	575(101)
(ox)(en)	531(125), 350(2200)	559(120)	534(132), 338(2050)	566(134)
nta	542(270), 348(2360)	590(173)	545(264), 336(2070)sh	612(166)

[a] sh = shoulder.
[b] Decomposition.

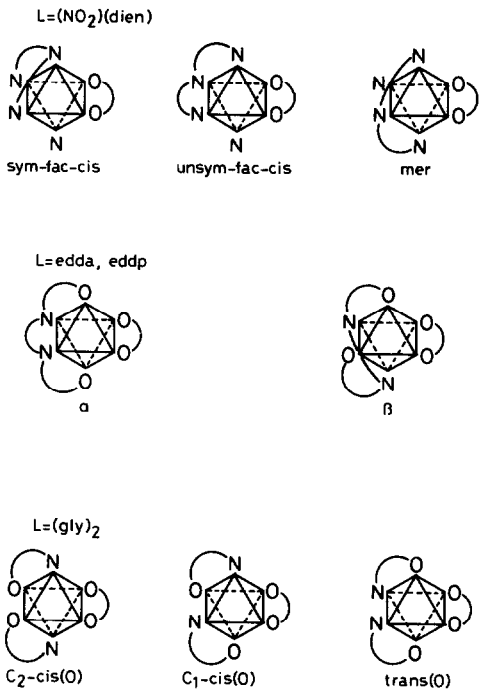

Fig. 2. Possible isomers of $[Co(hfac)L]^{n+}$.

length. The examples are: among L = *fac*(N)-(β-ala)(bpy), *fac*(N)-(L-ala)(bpy) and *fac*(N)-(gly)(bpy); between L = *mer*(N)-(pico)(en) and *mer*(N)-(pico)(tn); between L = *cis*(O)-aeida and *cis*(O)-apida.

Fluorine NMR spectra

The fluorine NMR spectra in D_2O are summarized in Table 3. One can interpret these results by considering the symmetry aspect of $[Co(hfac)L]^{n+}$.[3,8] The two CF_3 groups are equivalent in $[Co(hfac)L]^{n+}$ with C_{2v}, C_2 or $C_s(\perp)$ symmetry. They are inequivalent in $[Co(hfac)L]^{n+}$ with other symmetry or in $[Co(hfacOH)L]^{n-1}$. When $[Co(hfac)L]^{n+}$ is of C_2, $C_s(\perp)$ or $C_s(\parallel)$ symmetry two diastereoisomeric $[Co(hfacOH)L]^{n-1}$ are possible. When $[Co(hfac)L]^{n+}$ is of C_1 symmetry four diastereoisomeric $[Co(hfacOH)L]^{n-1}$ are possible. Thus, the point group of $[Co(hfac)L]^{n+}$ and, therefore, the coordination mode of the L ligand are assigned from the observed spectra and are given in Table 3. Symmetry types of alternative isomers are: $C_s(\perp)$ with L = *sym–fac–cis*-(NO_2)(dien), C_1 with L = *unsym–fac–cis*-(NO_2)(dien), C_2 with L = α-eddp, $C_s(\parallel)$ with L = *trans*(O)-(apida), C_1 with L = C_1-*cis*(O)-$(gly)_2$ and C_{2v} with L = *trans*-$(ox)(NH_3)_2$ (Fig. 2). The spectra with L = β-eddp indicate that two isomers co-exist with a mole ratio of 12:88 in acidic D_2O 20 min after dissolution, where the meridional secondary NH proton is either adjacent to or remote from the coordinated hfac oxygen.[15] On the other hand, the spectra with L = *mer*-(NO_2)(dien) indicate that only one of the two possible isomers with respect to the disposition of the meridional secondary NH proton exists in the solution.

Equilibrium constant

Values of K_{OH} and K_{OMe} were estimated from the absorption intensity at 350 nm of the complex in appropriate buffers as described elsewhere.[8] A typical example is shown in Fig. 3. In water tris was used as a buffering agent. In methanol tris (pK_b = 6.53) was used with $[Co(hfac)L]^+$ and 5,5-diethyl-

Table 3. Fluorine NMR spectra of $[Co(hfac)L]^{n+}$ in D_2O

L	Point group of $[Co(hfac)L]^{n+}$	$-\delta$ (ppm) (intensity) 1 mM CF_3CO_2H	5 mM Na_2CO_3
Mer-(NO_2)(dien)	$C_s(\parallel)$	76.12, 76.13	73.47(22), 74.05(78), 84.94(76), 86.02(24)
Cis(O)-aeida	C_1	75.78, 76.16	72.92(11), 73.04(17), 73.90(51), 74.00(21) 84.55(11), 84.84(21), 85.64(51), 86.10(17)
Trans(O)-aeida	$C_s(\parallel)$	75.74, 76.34	72.85(9), 74.00(91), 83.88(91), 85.69(9)
Cis(O)-apida	C_1	75.86, 76.29	72.71(28), 72.80(20), 73.68(23), 73.72(29) 84.56(27), 84.79(23), 85.47(30), 86.12(20)
β-eddp	C_1	76.06(12), 76.14(88)[a] 76.17(12), 76.22(88)	
C_2-*cis*(O)-$(gly)_2$	C_2	76.01	73.36(68), 76.01(32), 85.37(34), 85.42(66)
Cis-$(ox)(NH_3)_2$	C_1	75.76, 76.29	73.16(15), 73.23(9), 73.74(28), 73.97(48) 84.66(48), 85.06(13), 85.20(29), 85.40(10)
nta	$C_s(\parallel)$	75.65, 76.23	72.60(22), 73.79(78), 83.87(78), 85.69(22)

[a] After 20 min from dissolution.

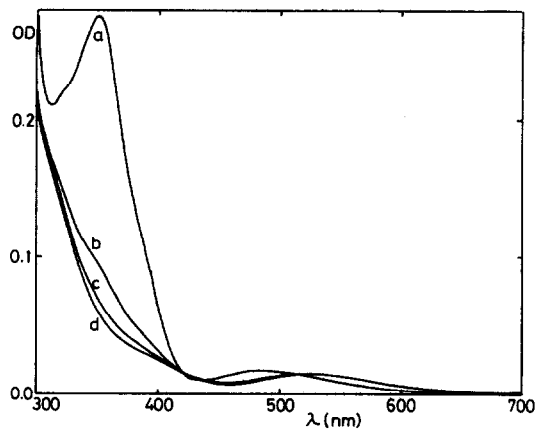

Fig. 3. pH-dependent absorption spectra of *mer*(N)-[Co(hfac)(pico)(en)]ClO_4 in water. $[Co^{III}] = 0.11$ mM, path length = 1 cm, 25°C. (a) 1 mM $HClO_4$; (b) tris-HCl buffer, pH = 7.40, ionic strength = 0.01; (c) tris-HCl buffer, pH = 8.10, ionic strength = 0.006; and (d) 5 mM NaOH.

Table 4. Lyate anion addition equilibrium [eq. (1)] constants for $[Co(hfac)L]^{n+}$ at 25°C

L	$-pK_{OH}$	$-pK_{OMe}$
Fac(N)-(β-ala)(bpy)	6.52	7.39
Fac(N)-(L-ala)(bpy)	7.11	8.00
Fac(N)-(gly)(bpy)	7.36	8.36
Mer(N)-(gly)(en)	6.49	6.73
Fac(N)-(i-dtma)[a]	6.15	6.95
Mer(N)-(i-dtma)	6.93	7.51
Mer-(NO_2)(dien)	5.82	6.48
Mer(N)-(pico)(en)	7.34	7.94
Mer(N)-(pico)(tn)	7.26	8.08
Cis(O)-aeida	6.26	5.52
Trans(O)-aeida	5.58	4.23
Cis(O)-apida[b]	5.51	5.3
α-edda[a]	4.95	3.95[c]
β-edda[a]	5.92	5.26
β-eddp[b]	4.76	5.2
C_2-*cis*(O)-$(gly)_2$[b]	6.91	5.5
Cis-(ox)$(NH_3)_2$	6.00	4.69
(ox)(en)	5.53	4.41
nta[b]	5.48	4.3

[a] Ref. 5.
[b] By the stopped-flow method.
[c] Previous value (5.0) was incorrect.

barbituric acid ($pK_b = 4.26$) with [Co(hfac)L] or $[Co(hfac)(nta)]^-$. In certain cases where the lyate anion combined species was labile the absorption intensity was measured immediately after mixing the complex with the base using a stopped-flow apparatus. The results are summarized in Table 4. The following deductions can be inferred, where we denote the K_{OH} and K_{OMe} values of $[Co(hfac)L]^{n+}$ as $K_{OH}(L)$ and $K_{OMe}(L)$, respectively.

(1) K_{OH} and K_{OMe} are large when a coordinating oxygen atom of the L ligand exists on the hfac plane in $[Co(hfac)L]^{n+}$. Examples are: K_{OH}(*fac*(N)-i-dtma) < K_{OH}(*mer*(N)-i-dtma); K_{OH}(α-edda) < K_{OH}(β-edda); K_{OH}(*trans*(O)-aeida) < K_{OH}(*cis*(O)-aeida); K_{OH}(*trans*(O)-aeida) or K_{OH}(α-edda) < K_{OH}(C_2-*cis*(O)-$(gly)_2$). One possible explanation for this may be that the back-donation of the *d* electrons of the cobalt(III) centre to the carbonyl π*-orbital co-planar with the hfac plane makes the carbonyl carbon atoms of the hfac ligand electron-deficient. This electron deficiency could be the driving force for the bond formation between one of the carbonyl carbon atoms and the lyate anion.

(2) K_{OH} and K_{OMe} are large when L involves a coordinating pyridine ring. Examples are: K_{OH}(*fac*(N)-i-dtma) < K_{OH}(*fac*(N)-(gly)(bpy)), K_{OH}(*fac*(N)-(β-ala)(bpy)) or K_{OH}(*fac*(N)-(L-ala)(bpy)); K_{OH}(*mer*(N)-i-dtma) < K_{OH}(*mer*(N)-(pico)(en)) or K_{OH}(*mer*(N)-(pico)(tn)). This may be explained analogously to the above by back-donation to the pyridine ring π*-orbital, which is, however, not co-planar with the hfac plane. The effect of a bpy ligand on the magnitude of K_{OH} or K_{OMe} is not so remarkable, as with L = tetraamine (see the introduction).[8] It may be that K_{OH} or K_{OMe}(*fac*(N)-i-dtma) is comparatively large owing to the tripod structure of the i-dtma ligand, as described below.

(3) K_{OH} and K_{OMe} are large when L is a tripod-type ligand. Examples are: K_{OH}(β-edda) < K_{OH}(*cis*(O)-aeida); K_{OH}(α-edda) < K_{OH}(*trans*(O)-aeida); K_{OH}(α-trien) or K_{OH}(β-trien) < K_{OH}(tren), where tren = tris-(2-aminoethyl)amine.[8]

(4) K_{OMe} is large when L is quadridentate. Examples are: K_{OMe}((ox)(en)) < K_{OMe}(*cis*(O)-aeida) or K_{OMe}(β-edda); K_{OMe}(*mer*(N)-(gly)(en)) < K_{OMe}(*mer*(N)-i-dtma); K_{OMe}(*cis*-(ox)$(NH_3)_2$) < K_{OMe}(*cis*(O)-aeida) or K_{OMe}(β-edda).

(5) The relatively small values of K_{OH} and K_{OMe} with $[Co(hfac)(nta)]^-$ are explained by the electronic repulsion between the anionic complex and lyate anion. The tripod structure of the nta ligand and the oxygen atom of nta existing on the hfac plane may overcome this repulsion.

(6) For a mono-positive complex $K_{OH} < K_{OMe}$, whereas for a zero-valent complex $K_{OH} > K_{OMe}$. The only exception is β-[Co(hfac)(eddp)]. This tendency can be explained by the change, ΔG_{el}, in the electrostrictive solvation free energy of the complex in eq. (1), as already indicated in a previous report.[5] According to the Drude–Nernst aproximation ΔG_{el}

in methanol is smaller than that in water for a mono-positive complex, whereas the former is larger than the latter for a zero-valent complex.

REFERENCES

1. K. Kuroda, *Chem. Lett.* 1979, 93.
2. Y. Fukuda, M. Ishige, T. Ito, K. Kuroda, K. Sone, Y. Suzuki, S. Yano and S. Yoshikawa, *Chem. Lett.* 1981, 1699.
3. S. Aygen, Y. Kitamura, K. Kuroda, R. Kume, H. Kelm and R. van Eldik, *Inorg. Chem.* 1985, **24**, 423.
4. S. Aygen, E. F. Paulus, Y. Kitamura and R. van Eldik, *Inorg. Chem.* 1987, **26**, 769.
5. Y. Kitamura, J. G. Leipoldt and A. Roodt, *Inorg. Chim. Acta* 1988, **149**, 125.
6. W. Purcell, J. G. Leipoldt and Y. Kitamura, *Inorg. Chim. Acta* 1990, **177**, 151.
7. Y. Kitamura, T. Katou and K. Watanabe, *Inorg. Chim. Acta* 1990, **178**, 41.
8. Y. Kitamura and A. Shibata, *Inorg. Chim. Acta* 1993, **203**, 37.
9. K. Kuroda, S. Ohtsuka and N. Matsumoto, *Bull. Chem. Soc. Japan* 1975, **48**, 1055.
10. P. H. Crayton, *Inorg. Synth.* 1963, **7**, 211.
11. M. Shibata, *Nippon Kagaku Zasshi* 1966, **87**, 771.
12. N. Matsuoka, J. Hidaka and Y. Shimura, *Bull. Chem. Soc. Japan* 1966, **39**, 1257.
13. Y. Enomoto, T. Ito and M. Shibata, *Chem. Lett.* 1974, 423.
14. T. P. Dasgupta and G. M. Harris, *Inorg. Chem.* 1974, **13**, 1275.
15. Y. Kitamura and A. Shibata, *Polyhedron* 1992, **19**, 2441.

Polyhedron Vol. 12, No. 17, pp. 2153–2156, 1993
Printed in Great Britain

0277–5387/93 $6.00+.00
© 1993 Pergamon Press Ltd

SYNTHESIS AND ELECTROCHEMICAL STUDY OF A NEW DOUBLY-METALLATED COMPOUND WITH THE FERROCENE-LABELLED PHOSPHINE $PPh_2(C_5H_4)Fe(C_5H_5)$

F. ESTEVAN,* J. LATORRE and E. PERIS

Departamento de Química Inorgánica, Universitat de Valencia, Dr. Moliner 50, E-46100 Burjassot-Valencia, Spain

(*Received* 5 *April* 1993; *accepted* 30 *April* 1993)

Abstract—Direct reaction of the metallated compound $Rh_2(\mu^2\text{-}O_2CCH_3)_3[\mu^2\text{-}(C_6H_4)PPh_2]\cdot(H_2O)_2$ with PPh_2Fc [$Fc = (C_5H_4)Fe(C_5H_5)$] in chloroform solution yields the corresponding mono-adduct $Rh_2(O_2CCH_3)_3[(C_6H_4)PPh_2]\cdot(PPh_2Fc)$ (**1**), which has been characterized by ^{31}P NMR spectroscopy. Photochemical irradiation of **1** in chloroform gives the compound $Rh_2(\mu\text{-}O_2CCH_3)_2(\eta^2\text{-}O_2CCH_3)[\mu^2\text{-}(C_6H_4)PPh_2][PPh_2Fc]\cdot(H_2O)$ (**2**) in practically quantitative yield. Compound **2**, by thermal treatment in chloroform solution, yields cleanly the doubly-metallated compound $Rh_2(\mu^2\text{-}O_2CCH_3)_2[\mu^2\text{-}(C_6H_4)PPhFc][\mu^2\text{-}(C_6H_4)PPh_2]\cdot(H_2O)_2$ (**3**). Complex **3** acts as a multiple electron-transfer system, showing by cyclic voltammetry in CH_2Cl_2 two well-defined one-electron oxidation processes: the first at 0.52 V, assigned to the redox couple Fe^{II}/Fe^{III}, and the second at 1.00 V, due to the redox couple Rh_2^{+4}/Rh_2^{+5}.

Orthometallation reactions of P-donor ligands in dirhodium(II) compounds have been extensively studied.[1] Reaction intermediates have been isolated and in some cases kinetic studies of single steps of the metallation process have been performed.[2] One intermediate step of the metallation reaction consists of the rearrangement of one phosphine from axial to equatorial coordination (step I → II in Scheme 1). This rearrangement can be selectively promoted by photochemical irradiation of the mono-adduct species **I**.[2]

We have recently studied the metallation of redox active phosphines such as PPh_2Fc ($Fc = \{(C_5H_4)Fe(C_5H_5)\}$) and $Fe\{(C_5H_4)PPh_2\}_2$ on $Rh_2(\mu^2\text{-}O_2CCH_3)_4$ as a new route to obtain complexes with two or more redox centres.[3] Crystal structures of the doubly-metallated complexes $Rh_2(\mu^2\text{-}O_2CCH_3)_2[\mu^2\text{-}(C_6H_4)PPhFc]_2(HO_2CCH_3)_2$ and $Rh_2(\mu^2\text{-}O_2CCH_3)_2\{[(C_6H_4)PPh(C_5H_4)]_2Fe\}(HO_2CCH_3)(CH_2Cl_2)$ have been determined by X-ray diffraction methods.[3]

The crystal structure of the acetic acid bis-adduct of complex **3**, $Rh_2(\mu^2\text{-}O_2CCH_3)_2[\mu^2\text{-}(C_6H_4)PPhFc][\mu^2\text{-}(C_6H_4)PPh_2]\cdot(HO_2CCH_3)_2$, has been recently reported.[4]

We describe in this paper the details of the synthesis of the mixed doubly-metallated complex $Rh_2(\mu^2\text{-}O_2CCH_3)_2[\mu^2\text{-}(C_6H_4)PPhFc][\mu^2\text{-}(C_6H_4)PPh_2]\cdot(H_2O)_2$ (**3**) from the intermediate product $Rh_2(\mu^2\text{-}O_2CCH_3)_2(\eta^2\text{-}O_2CCH_3)[\mu^2\text{-}(C_6H_4)PPh_2][PPh_2Fc]\cdot(H_2O)$ (**2**). The electrochemical behaviour of complex **3** as a new ferrocene-labelled dinuclear rhodium(II) complex is also discussed.

EXPERIMENTAL

All solvents were of analytical grade and were degassed prior to use by standard procedures. All the reactions were performed under argon using the Schlenk technique, although the isolated compounds were air-stable solids.

Preparation of the compounds

$Rh_2(\mu^2\text{-}O_2CCH_3)_4(MeOH)_2$,[5] $Rh_2(\mu^2\text{-}O_2CCH_3)_3[\mu^2\text{-}(C_6H_4)PPh_2](H_2O)_2$[1e] and $Rh_2(\mu^2\text{-}O_2CCH_3)_3[\mu^2\text{-}(C_6H_4)PPhFc]\cdot(HO_2CCH_3)_2$[3] were prepared according to literature methods.

*Author to whom correspondence should be addressed.

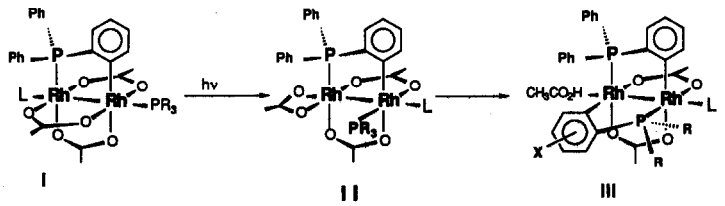

R= (XC_6H_4); X= H, pCH_3, mCH_3, pCl, mCl

L= H_2O, CH_3CO_2H

Scheme 1.

(a) $Rh_2(\mu^2\text{-}O_2CCH_3)_3[\mu^2\text{-}(C_6H_4)PPh_2]\cdot(PPh_2Fc)$ (**1**). This adduct was obtained in solution by adding the phosphine ligand PPh_2Fc to $Rh_2(\mu^2\text{-}O_2CCH_3)_3[\mu^2\text{-}(C_6H_4)PPh_2]\cdot(H_2O)_2$ ($[Rh_2]/[PPh_2Fc] = 1:1$) in $CHCl_3$. The ^{31}P NMR spectra were recorded from the resulting solution. $^{31}P\{^1H\}$ NMR ($CDCl_3$): δ P1 = 21.2 ppm, [^1J(Rh—P) = 156.1 Hz]; δ P2 = −8.5 ppm [^1J(Rh—P) = 109.4, ^2J(Rh—P) = 27.9, ^3J(P—P′) = 7.4 Hz).

(b) $Rh_2(\mu^2\text{-}O_2CCH_3)_2(\eta^2\text{-}O_2CCH_3)[\mu^2\text{-}(C_6H_4)PPh_2][PPh_2Fc]\cdot(H_2O)$ (**2**). $Rh_2(\mu^2\text{-}O_2CCH_3)_3[\mu^2\text{-}(C_6H_4)PPh_2]\cdot(H_2O)_2$ (100 mg, 0.13 mmol) and PPh_2Fc (48.1 mg, 0.13 mmol) were introduced in a photochemical reactor with a mercury vapour lamp (OSRAM-125). The solid mixture was dissolved in $CHCl_3$ (100 cm^3) yielding a brown–orange solution. After 45 min of irradiation the reaction was stopped and the solvent was removed under reduced pressure. The resulting crude solid was dissolved in a mixture of CH_2Cl_2: hexane (5 cm^3: 5 cm^3); slow evaporation of the solvent gave a brown crystalline product; yield 86%. Spectroscopic data: ^1H NMR ($CDCl_3$), δ (ppm): 1.05 (3H, s, Me), 1.21 (3H, s, Me), 1.41 (3H, s, Me) 3.6–4.9 (9H, m, C_5H_5; C_5H_4), 6.4–8.7 (24H, m, aromatics). $^{31}P\{^1H\}$ NMR ($CDCl_3$): δ P1 = 17.32 ppm [^1J(Rh—P) = 138.14, ^2J(Rh—P) = 8.7 Hz], δ P2 = 38.42 ppm [^1J(Rh—P) = 172.34 Hz]. Found: C, 52.8; H, 4.5. Calc. for $C_{46}H_{44}FeO_7P_2Rh_2$: C, 53.5; H, 4.3%.

(c) $Rh_2(\mu^2\text{-}O_2CCH_3)_2[\mu^2\text{-}(C_6H_4)PPhFc][\mu^2\text{-}(C_6H_4)PPh_2]\cdot(H_2O)_2$ (**3**). Compound **2** (100 mg, 0.091 mmol) was dissolved in chloroform (40 cm^3) and the solution was refluxed for 1 h when the colour changed to red–brown. The solvent was evaporated to dryness under vacuum and the resulting red–solution solid was dissolved in CH_2Cl_2. This solution was transferred to a chromatography column (30 × 2 cm) packed with silica gel in hexane. Elution with hexane: CH_2Cl_2: acetone (10:5:1) separated a yellow band, which was discarded. Further elution with hexane: CH_2Cl_2: acetone (2:1:2) separated a brown–red band, which was collected. This solution was evaporated to dryness and the solid was dissolved in a CH_2Cl_2: hexane (1:1) (5 cm^3) mixture. Red–brown crystals were obtained by slow evaporation of the solvent; yield 85%. Spectroscopic data: ^1H NMR ($CDCl_3$) δ (ppm): 1.18 (3H, s, Me), 1.23 (3H, s, Me), 2.41 (4H, b, H_2O), 3.47 (1H, s, C_5H_4), 3.77 (5H, s, C_5H_5), 4.07 (1H, s, C_5H_4), 4.43 (1H, s, C_5H_4), 4.55 (1H, s, C_5H_4), 6.19–7.92 (24H, m, aromatics). $^{31}P\{^1H\}$ NMR ($CDCl_3$): δ P1 = 17.24 ppm [^1J(Rh—P) = 167.5, ^2J(Rh—P) = 7.1 Hz], δ P2 = 14.92 ppm [^1J(Rh—P) = 160.5, ^2J(Rh—P) = 7.5 Hz]. Found: C, 53.5; H, 4.3. Calc. for $C_{44}H_{42}FeO_6P_2Rh_2$: C, 53.4; H, 4.3%.

Compound **3** can be recrystallized from a mixture of CH_2Cl_2: hexane: acetic acid (5:5:1) yielding quantitatively the acetic acid adduct $Rh_2(\mu^2\text{-}O_2CCH_3)_2[\mu^2\text{-}(C_6H_4)PPhFc][\mu^2\text{-}(C_6H_4)PPh_2](CH_3CO_2H)_2$.[4]

Instrumental

NMR measurements were recorded on Varian Unity-300 and Unity-400 spectrometers.

The electrochemical experiments were performed in a three-electrode cell; the working and auxiliary electrodes were platinum, the reference electrode was a saturated calomel electrode electrically connected to the solution by a "salt bridge" containing a saturated solution of the supporting electrolyte and the solvent. Cyclic voltammograms were obtained with a programming function generator 305 HQ instrument connected to a AMEL potentiostat and were recorded on a Riken–Denshi F-35 *X–Y* recorder. The solvent was CH_2Cl_2, which had been freshly distilled from P_2O_5. The supporting electrolyte, Bu_4NPF_6, was recrystallized from ethanol and dried at 80°C *in vacuo* for 48 h. Potential-controlled electrolysis was performed in a three-compartment cell separated by fritted glass. Working and auxiliary electrodes were a platinum mesh. The charge transferred was calculated by recording intensity vs the time and carrying out

a further integration. The system was calibrated against ferrocene.

RESULTS AND DISCUSSION

Rhodium(II) complexes containing a metallated arylphosphine react with additional amounts of phosphine yielding rhodium(II) doubly-metallated compounds. This thermal reaction generally yields a complex mixture of doubly-metallated compounds.[1d,3]

In the present case the first attempts to obtain the doubly-metallated compound $Rh_2(\mu^2\text{-}O_2CCH_3)_2[\mu^2\text{-}(C_6H_4)PPhFc][\mu^2\text{-}(C_6H_4)PPh_2](H_2O)_2$ (**3**) from the singly-metallated compounds $Rh_2(\mu^2\text{-}O_2CCH_3)_3[\mu^2\text{-}(C_6H_4)PPh_2](H_2O)_2$ or $Rh_2(\mu^2\text{-}O_2CCH_3)_3[\mu^2\text{-}(C_6H_4)PPhFc]\cdot(H_2O)_2$ with PPh_2Fc and PPh_3, respectively, by the thermal method, failed because a very complicated mixture of metallated compounds was obtained.

The photochemical irradiation of the phosphine mono-adduct $Rh_2(\mu^2\text{-}O_2CCH_3)_3[\mu^2\text{-}(C_6H_4)PPh_2](PPh_2Fc)$ (**1**) in chloroform promotes the rearrangement of the axial PPh_2Fc to an equatorial coordination yielding $Rh_2(\mu^2\text{-}O_2CCH_3)_2(\eta^2\text{-}O_2CCH_3)[\mu^2\text{-}(C_6H_4)PPh_2][PPh_2Fc](H_2O)$ (**2**). This reaction can be easily monitored by ^{31}P NMR spectroscopy, showing no other intermediates between the starting and the final compounds. The ^{31}P NMR spectrum of **2** shows a low-field resonance (38.42 ppm) characteristic of an equatorial phosphine[2,6] and another in the region of the metallated bridging phosphines (17.32 ppm). However, by irradiating the mono-metallated compound $Rh_2(\mu^2\text{-}O_2CCH_3)_3[\mu^2\text{-}(C_6H_4)PPhFc]\cdot(H_2O)_2$ with an equimolecular amount of PPh_3 in similar conditions a mixture of different metallated compounds is formed, together with small amounts of the intermediate compound containing the equatorial non-metallated phosphine, which, in this case, could not be isolated. The metallation of the intermediate compound $Rh_2(\mu^2\text{-}O_2CCH_3)_2(\eta^2\text{-}O_2CCH_3)[\mu^2\text{-}(C_6H_4)PPh_2][PPh_2Fc]\cdot(H_2O)$ (**2**) to give the doubly-metallated compound **3** occurs cleanly and selectively. This reaction can be easily followed by ^{31}P NMR spectroscopy. These results are summarized in Scheme 2.

Electrochemical results

Compound **3** shows by cyclic voltammetry [in CH_2Cl_2 $(NBu_4)PF_6$, 0.2 M, as a supporting electrolyte] two well-defined one-electron reversible oxidation peaks at 0.58 and 1.04 V (Fig. 1). The first peak must be associated to the redox couple Fe^{II}/Fe^{III} of the ferrocenyl ligand, whereas the second oxidation process must be due to the Rh_2^{4+}/Rh_2^{5+} couple. Both processes are electrochemically reversible at the sweep rate of 0.1 V s^{-1}. The voltammogram of **3** as the acetic acid bis-adduct $Rh_2(\mu^2\text{-}O_2CCH_3)_2[\mu^2\text{-}(C_6H_4)PPhFc][\mu^2\text{-}(C_6H_4)PPh_2](CH_3CO_2H)_2$ shows no important differences (E_p $[Fe^{II}/Fe^{III}] = 0.52$ V; E_p $[Rh_2^{4+}/Rh_2^{5+}] = 1.00$ V).

For compound **3** the oxidation value for the couple Rh_2^{4+}/Rh_2^{5+} is intermediate between those of the doubly-metallated complexes $Rh_2(\mu^2\text{-}O_2CCH_3)_2[\mu^2\text{-}(C_6H_4)PPhFc]_2\cdot(CH_3CO_2H)_2$ and $Rh_2(\mu^2\text{-}O_2CCH_3)_2[\mu^2\text{-}(C_6H_4)PPh_2]\cdot(CH_3CO_2H)_2$ previously reported.[3] The oxidation value for the couple Rh_2^{4+}/Rh_2^{5+} is lower in **3** than in the related ferrocene-labelled monometallated compound $Rh_2(\mu^2\text{-}O_2CCH_3)_3[\mu^2\text{-}(C_6H_4)PPhFc]\cdot(CH_3CO_2H)_2$, in good agreement with the trend that doubly-metallated compounds oxidize more easily than mono-metallated compounds.[3]

These differences show the influence that the more easily oxidizable couple produces on the

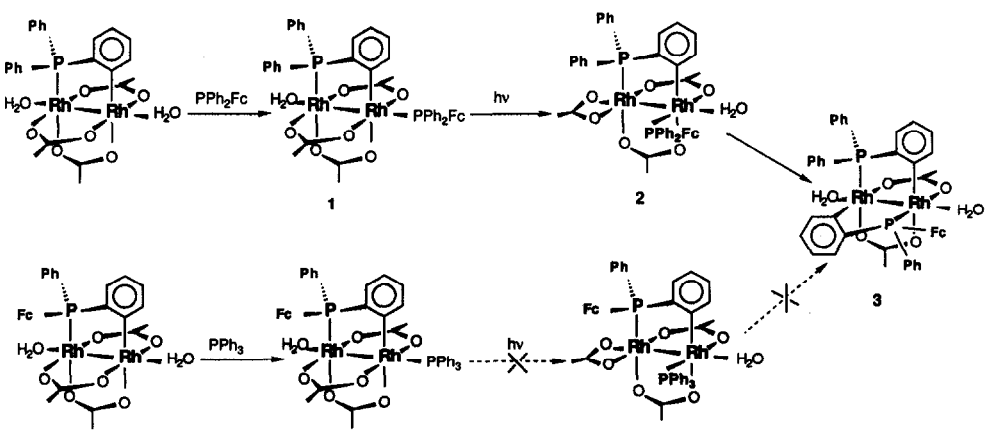

Scheme 2.

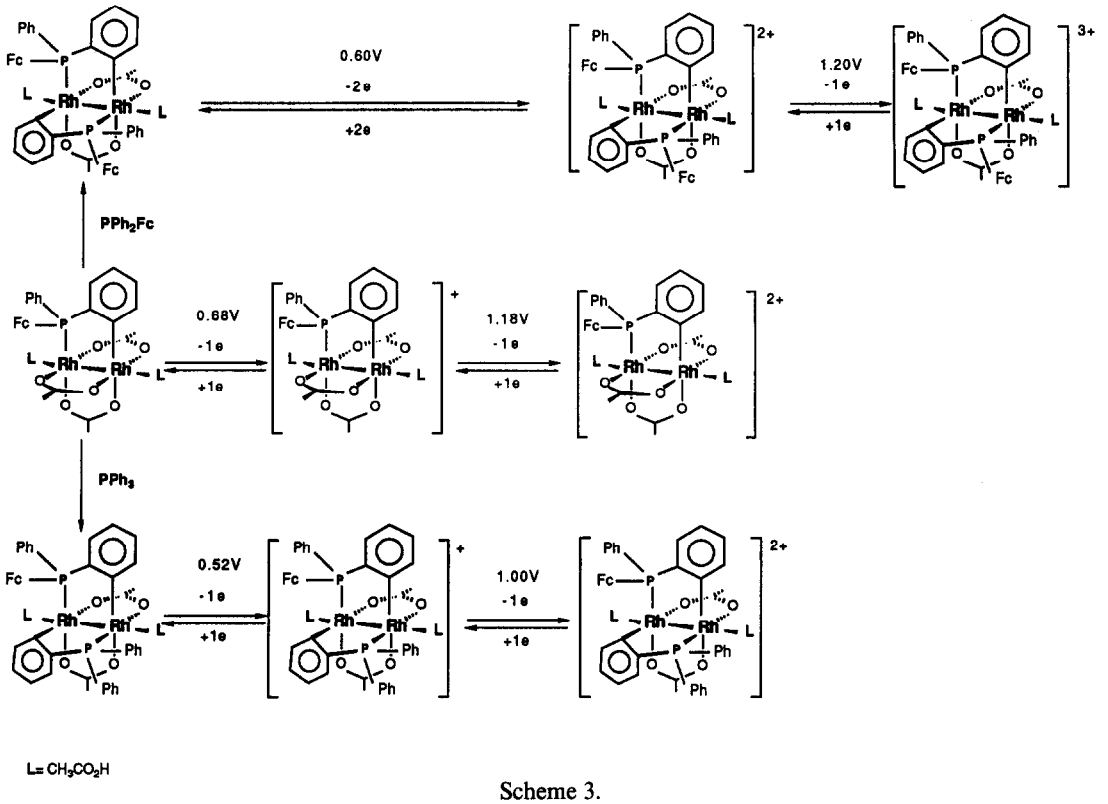

Scheme 3.

potential value of the second redox centre and with complex **3** a series of complexes which undergoes multiple electron-transfer processes is completed, as is summarized in Scheme 3.

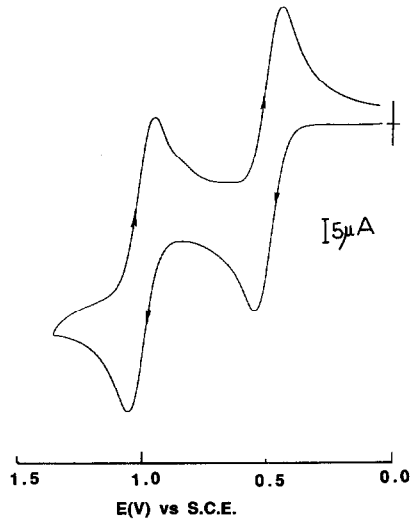

Fig. 1. Cyclic voltammogram of **3**, in CH_2Cl_2 (NBu_4PF_6 supporting electrolyte, sweep rate 0.1 V s^{-1}).

Acknowledgements—We thank the CICYT for the financial support of this work (MAT90-0656-C02-01).

REFERENCES

1. (a) P. Lahuerta, J. Payá, X. Solans and M. A. Ubeda, *Inorg. Chem.* 1992, **31**, 385; (b) P. Lahuerta, J. Payá, E. Peris, M. A. Pellinghelli and A. Tiripicchio, *J. Organomet. Chem.* 1989, **373**, C5; (c) P. Lahuerta, R. Martínez-Mañez, J. Payá, E. Peris and W. Díaz, *Inorg. Chim. Acta* 1990, **173**, 99; (d) P. Lahuerta, J. Payá, E. Peris, A. Aguirre, S. García-Granda and F. Gómez-Beltrán, *Inorg. Chem. Acta* 1992, **192**, 43; (e) P. Lahuerta, J. Payá, M. A. Pellinghelli and A. Tiripicchio, *Inorg. Chem.* 1992, **31**, 1224.
2. P. Lahuerta, E. Peris, M. Sanaú, G. González and M. Martínez, unpublished results.
3. F. Estevan, P. Lahuerta, J. Latorre, E. Peris, S. García-Granda, A. Aguirre and M. A. Salvadó, *J. Chem. Soc., Dalton Trans.* 1993, 1681.
4. S. García-Granda, *et al.*, *Acta Cryst.*, submitted.
5. G. A. Rempel, P. Ledgdins, H. Smith and G. Wilkinson, *Inorg. Synth.* 1972, **13**, 9.
6. F. Barceló, F. A. Cotton, P. Lahuerta, R. LLúsar, M. Sanaú, W. Schwotzer and M. A. Ubeda, *Organometallics* 1986, **5**, 808.

Polyhedron Vol. 12, No. 17, pp. 2157–2168, 1993
Printed in Great Britain

0277–5387/93 $6.00+.00
© 1993 Pergamon Press Ltd

NEW METALLABORANES OF THE EARLY TRANSITION METALS: REACTIONS OF DECABORANE(14) WITH $(\eta^5\text{-}C_5H_5)_2ZrX_2$ AND $(\eta^5\text{-}C_5H_5)_2ZrXY$, WHERE X, Y = H^-, CH_3^- OR BH_4^-. THE $(\eta^5\text{-}C_5H_5)_2Zr$ GROUP AS A CLUSTER VERTEX

R. A. BERTHON, R. J. ROUNSLEY and R. C. BURNS*

Department of Chemistry, The University of Newcastle, Callaghan 2308, N.S.W., Australia

(*Received* 6 *April* 1993; *accepted* 22 *April* 1993)

Abstract—Reaction of decaborane(14) with compounds of the type $(\eta^5\text{-}C_5H_5)_2ZrX_2$ and $(\eta^5\text{-}C_5H_5)_2ZrXY$, where X and Y are H^-, CH_3^- or BH_4^-, leads to a range of compounds, which include $[(\eta^5\text{-}C_5H_5)_2Zr(\mu\text{-}H)]B_{10}H_{13}$, $(\eta^5\text{-}C_5H_5)_2ZrB_{10}H_{10}$, $[(\eta^5\text{-}C_5H_5)_2Zr(\mu\text{-}H)]_2B_{10}H_{10}$ and probably $[(\eta^5\text{-}C_5H_5)_2Zr(BH_4)]B_{10}H_{13}$. All of these compounds exhibit three-centre/two-electron Zr—H—B interactions between $(\eta^5\text{-}C_5H_5)_2Zr^{2+}$ and the terminal hydrogen atoms on their (formal) anionic borane moieties. The formation of $B_{10}H_{10}^{2-}$ in the reactions when X and Y are both CH_3^- was found to be attributable to a previously unknown disproportionation/rearrangement reaction of $B_{10}H_{12}^{2-}$, which occurs above *ca* 60°C, i.e. $2B_{10}H_{12}^{2-} \rightarrow B_{10}H_{10}^{2-} + B_{10}H_{14}^{2-}$. When X and/or Y is BH_4^-, then at higher temperatures borane cluster anion enlargement occurs to give a mixture of species which contain the borane anions $B_{12}H_{12}^{2-}$, $B_{11}H_{11}^{2-}$ and $B_{10}H_{10}^{2-}$, again exhibiting Zr—H—B interactions from $(\eta^5\text{-}C_5H_5)_2Zr^{2+}$ to these anions through their terminal hydrogen atoms. It is suggested that these products arise through the agency of a metal-mediated disproportionation reaction(s), probably with the involvement of Zr—H—B interactions. The extent of Zr—B interaction in the Zr—H—B linkages was investigated using extended-Hückel LCAO–MO calculations in the case of $(\eta^5\text{-}C_5H_5)_2ZrB_{10}H_{10}$ and indicate a significant contribution from Zr—B overlap in the bonding. Finally, the ability of an $(\eta^5\text{-}C_5H_5)_2Zr$ fragment to act as a cluster vertex in a metallaborane is discussed in light of the types of metal to borane anion interactions observed for the species synthesized in this study.

An examination of the literature shows that, with the exception of tetrahydroborates, very few metallaboranes of the early transition metals have been reported.[1–4] Known examples include $(\eta^5\text{-}C_5H_5)_2TiB_3H_8$ and $(\eta^5\text{-}C_5Me_5)_2Ta_2(\mu\text{-}Br)_2(B_2H_6)$.[5,6] In the former the (formal) $B_3H_8^-$ ion is regarded as being linked to titanium by two Ti—H—B three-centre/two-electron bonds, while in the latter the bridging diborane unit is asymmetrically bound, with three Ta—H—B bridges, one direct Ta—B bond and a single B—H—B bridge. By way of comparison several metallacarbaborane species have been synthesized. These include compounds of the type $(\eta^8\text{-}C_8H_8)_2M(Et_2C_2B_4H_4)$, where M = Ti and V, which are cyclooctatetraene metal-carbaborane sandwich compounds,[7] and the species $(Et_4N)_2[M(C_2B_{10}H_{12})_2]$, M = Zr or Hf, and their related dimethyl analogues[8,9] (M also includes Ti[10]), which involve two metal-linked 13-vertex metallacarbaboranes. However, no large early transition metal species derived from decaborane(14), $B_{10}H_{14}$, are currently known.

The acidic nature of the bridging protons in $B_{10}H_{14}$ is well established. Indeed, $B_{10}H_{14}$ acts as a strong monoprotic acid in aqueous ethanol[11] (and in other organic solvents, e.g. CH_3CN). Of synthetic relevance to this study is the fact that $B_{10}H_{14}$ reacts with 1 equivalent of NaH in ether to give $B_{10}H_{13}^-$ and H_2.[12] With 2 equivalents of NaH a second mole

* Author to whom correspondence should be addressed.

of H_2 is evolved and $B_{10}H_{12}^{2-}$ is reported to form.[13] Similar reactions occur with $LiBH_4$ and $NaBH_4$ to give $B_{10}H_{13}^-$, H_2 and B_2H_6.[12,14] However, at higher temperatures (80–90°C in dioxane) cluster enlargement occurs with the formation of $B_{11}H_{14}^-$ and H_2,[14] while at even higher temperatures (160°C in diglyme) $B_{12}H_{12}^{2-}$ and H_2 are produced.[15] All of these reactions rely wholly or, in part, on the combination of protic and hydridic hydrogens to eliminate H_2. This approach should, in turn, be applicable to transition metal systems containing (hydridic) hydrogen and their reactions with decaborane. Condensation of the transition metal and borane fragments should, after elimination of H_2, lead to metallaboranes.

A related approach is to combine a borane with a metal alkyl or aryl (R), followed by elimination of RH and metallaborane formation as above. Such an approach has, however, been used infrequently. Some examples do exist; for example, $B_{10}H_{14}$ reacts with the dialkyls and diaryls of zinc and cadmium (where R = Me, Et, Ph) in ethereal solvents to yield RH and solvates of the formula $MB_{10}H_{12}\cdot nS$, where M = Zn, Cd and S = Et_2O, THF.[16,17] A more recent example involves the reaction of $B_{10}H_{14}$ and $(Et_3P)AuMe$ [and also $(Ph_3P)AuMe$] to give methane, H_2 and, ultimately, the triple gold and boron cluster $[(H_{12}B_{10}Au)(\mu\text{-}AuPEt_3)_4(AuB_{10}H_{12})]$.[18]

For the early transition metals a range of accessible hydride, methyl and tetrahydroborate ligand species is provided by the $(\eta^5\text{-}C_5H_5)_2MX_n$ compounds, where X is H^-, CH_3^- or BH_4^- and n may be 1, 2 or 3 depending on the metal and its formal oxidation state (III → V). Not all compounds are known, but many mixed-ligand species can also be synthesized, e.g. $(\eta^5\text{-}C_5H_5)_2Zr(H)CH_3$. Reaction of these organo-transition metal hydride-, methyl- and tetrahydroborate-containing species with $B_{10}H_{14}$ should, therefore, give rise to new metallaboranes of the early transition metals. Varing the transition metal, for the same oxidation state, will allow exploration of the effect of electron configuration (in conjunction with frontier orbital considerations) on metallaborane formation, although the reducing nature of the boranes may make some oxidation states unattainable. Moreover, in the case of (formally at least) H^- as a ligand the $(\eta^5\text{-}C_5H_5)_2MH_n$ compounds of groups IV and V exhibit hydridic character, whereas organo-transition metal hydrides of the latter transition metals are generally neutral or acidic in nature.[19] At the outset of these studies it was expected that these features would play some role in metallaborane formation and in this study only the results of our investigations into the zirconium system are reported.

EXPERIMENTAL

All operations and manipulations were performed under nitrogen or in a vacuum so as to exclude oxygen and water, using Schlenk apparatus or an inert atmosphere glove-box. All reagents were used as received, while $B_{10}H_{14}$ (Strem Chemical Co.) was sublimed under vacuum before use. Solvents were dried using standard methods and distilled either under nitrogen or in a vacuum immediately prior to use, and were transferred using gastight syringes or under a vacuum.

The compounds $(\eta^5\text{-}C_5H_5)_2ZrH_2$, $(\eta^5\text{-}C_5H_5)_2Zr(CH_3)_2$, $(\eta^5\text{-}C_5H_5)_2Zr(BH_4)_2$ and $(\eta^5\text{-}C_5H_5)_2Zr(H)BH_4$ were prepared as described in the literature,[20–22] while $(\eta^5\text{-}C_5H_5)_2Zr(H)CH_3$ was prepared from $(\eta^5\text{-}C_5H_5)_2Zr(Cl)CH_3$, which was prepared in turn from $[(\eta^5\text{-}C_5H_5)_2ZrCl]_2O$.[23,24] The compound $(\eta^5\text{-}C_5H_5)_2Zr(BH_4)CH_3$, previously characterized in solution by ^1H and ^{11}B NMR,[25] was obtained by reaction of $(\eta^5\text{-}C_5H_5)_2Zr(Cl)CH_3$ with $LiBH_4$ (in a 1 : 2 mole ratio, respectively) in toluene for 4 h, followed by filtration and removal of the solvent. Examination by ^1H NMR indicated no evidence of any starting material, while IR examination (Nujol mull) gave ν(B—H) at 2436, 2395 and 2102 cm^{-1} and $\delta(BH_2)$ at 1124 cm^{-1}.

IR spectra were recorded on a Bio-Rad FTS-7 spectrophotometer as either Nujol mulls between NaCl plates or as (dried) KBr discs. Gas-phase spectra were recorded using a 10 cm gas cell fitted with NaCl windows. All NMR spectra were recorded on a JEOL FX-90Q instrument operating at 28.75 and 89.60 MHz for ^{11}B and ^1H, respectively, and were referenced to $BF_3\cdot Et_2O$ and TMS. Acetonitrile (AR grade) for conductivity work was refluxed over CaH_2 for 3 days, then doubly distilled in an all-glass still under nitrogen. This resulted in CH_3CN of specific conductivity better than 8×10^{-8} S cm^{-1} at 25°C. Conductivities were measured using a Philips PR 9500/01 conductivity-measuring bridge with a PW 9512 cell. Microanalyses were performed by the Analytical Unit, Research School of Chemistry, at the Australian National University.

Reactions and preparations

$(\eta^5\text{-}C_5H_5)_2ZrH_2$ and $B_{10}H_{14}$; preparation of $[(\eta^5\text{-}C_5H_5)_2Zr(\mu\text{-}H)]B_{10}H_{13}$. In a typical reaction a solution of $B_{10}H_{14}$ (0.144 g, 1.18 mmol, 5% excess) in benzene (20 cm^3) was added to a well-stirred slurry containing $(\eta^5\text{-}C_5H_5)_2ZrH_2$ (0.25 g, 1.12 mmol) in benzene (30 cm^3) under nitrogen. A gas (presumably hydrogen) formed immediately and the slurry changed from white to yellow. The mix-

ture was stirred for a further 3 h, but to ensure completion of the reaction heating to 40–50°C for a period of *ca* 30 min was found to be necessary. The resulting solid was collected by filtration, washed with benzene and dried *in vacuo* (typical yield >90%). Found: C, 36.4; H, 7.5. Calc. for $[(\eta^5\text{-}C_5H_5)_2ZrH]B_{10}H_{13}$: C, 34.9; H, 7.0%. In a separate reaction, using similar quantities of reactants, $B_{10}H_{14}$ was added to $(\eta^5\text{-}C_5H_5)_2ZrH_2$ in benzene in an evacuated glass reaction vessel. After completion of the reaction the gas generated was transferred to a calibrated volume using a Toepler pump, giving 0.98 mol of hydrogen formed per mole of $(\eta^5\text{-}C_5H_5)_2ZrH_2$ consumed.

$(\eta^5\text{-}C_5H_5)_2Zr(CH_3)_2$ and $B_{10}H_{14}$; preparation of $(\eta^5\text{-}C_5H_5)_2ZrB_{10}H_{10}$ and $[(\eta^5\text{-}C_5H_5)_2Zr(\mu\text{-}H)]_2B_{10}H_{10}$.

(a) $(\eta^5\text{-}C_5H_5)_2Zr(CH_3)_2$ to $B_{10}H_{14}$, mole ratio 1:1 and 1:2. To a stirred solution of $B_{10}H_{14}$ (0.241 g, 1.97 mmol) in toluene (20 cm^3) was added a toluene solution (20 cm^3) of $(\eta^5\text{-}C_5H_5)_2Zr(CH_3)_2$ (0.500 g, 1.97 mmol). No reaction was observed and the solution temperature was raised slowly to *ca* 105°C, at which point the solution turned yellow, quickly followed by the formation of a bright yellow precipitate. Evidence of gas evolution was also noted. Using a gas-tight syringe a gas sample was taken from the reaction vessel at this point for IR examination, which indicated the presence of CH_4. After refluxing (*ca* 110°C) for 30 min the products were allowed to cool and the yellow product filtered, washed with toluene and dried *in vacuo* (yield 0.366 g, 78%). An identical product was also obtained with a mole ratio for $(\eta^5\text{-}C_5H_5)_2Zr(CH_3)_2$ to $B_{10}H_{14}$ of 1:2. Found: C, 36.1; H, 6.3. Calc. for $(\eta^5\text{-}C_5H_5)_2ZrB_{10}H_{10}$: C, 35.4; H, 5.9%. In two independent reactions measurement of the volume of non-condensable gas (CH_4+H_2) generated in this reaction indicated that 2.43 and 2.56 mol per mole of $(\eta^5\text{-}C_5H_5)_2Zr(CH_3)_2$ were formed.

(b) $(\eta^5\text{-}C_5H_5)_2Zr(CH_3)_2$ to $B_{10}H_{14}$, ratio 2:1. A solution of $(\eta^5\text{-}C_5H_5)_2Zr(CH_3)_2$ (0.570 g, 2.27 mmol) and $B_{10}H_{14}$ (0.140 g, 1.15 mmol) in toluene (45 cm^3) was heated to *ca* 105°C, at which point the solution turned yellow, gas evolution was observed and an orange solid formed. A sample taken for IR analysis indicated the presence of CH_4 but not, definitely, evidence of C_2H_6. After refluxing for *ca* 1 h the bright orange solid product was filtered, washed with toluene and dried in a vacuum (yield 0.375 g, 59%). Found: C, 42.5; H, 5.7. Calc. for $[(\eta^5\text{-}C_5H_5)_2ZrH]_2B_{10}H_{10}$: C, 42.7; H, 5.7%.

$(\eta^5\text{-}C_5H_5)_2Zr(BH_4)_2$ and $B_{10}H_{14}$. In a typical reaction a solution of $B_{10}H_{14}$ (0.122 g, 1.00 mmol) in benzene (20 cm^3) was added to a solution of $(\eta^5\text{-}C_5H_5)_2Zr(BH_4)_2$ (0.251 g, 1.00 mmol) in benzene (30 cm^3). No reaction was observed. The solution was then heated to *ca* 80°C, at which the first signs of reaction occurred. The mixture was subsequently refluxed for 3 h, yielding an orange precipitate. After cooling the product was filtered, washed with benzene (30 cm^3) and dried in a vacuum (yield 0.299 g). The reaction was repeated several times using different stoichiometries [both 1:1 and 1:2 $(\eta^5\text{-}C_5H_5)_2Zr(BH_4)_2$ to $B_{10}H_{14}$], variable reaction times (1–5 h) and also at a different temperature using refluxing toluene as the solvent. A reaction was also conducted in a closed, evacuated system, which demonstrated the formation of large quantities of a permanent gas (presumably hydrogen) and also the formation of B_2H_6 (by IR spectroscopy).

$(\eta^5\text{-}C_5H_5)_2Zr(H)CH_3$ and $B_{10}H_{14}$. A solution of $B_{10}H_{14}$ (0.149 g, 1.22 mmol) in benzene (25 cm^3) was added to a slurry of $(\eta^5\text{-}C_5H_5)_2Zr(H)CH_3$ (0.276 g, 1.16 mmol) in benzene (20 cm^3) in an evacuated glass vessel. No reaction was observed initially, but the solid turned yellow within 15 min with evidence for the formation of a yellow solution. After 24 h the mixture was heated to 50°C for 1 h to ensure complete reaction. IR examination of the gas generated in the reaction indicated the presence of CH_4. The yellow solution was decanted and the insoluble yellow product washed with benzene and dried in a vacuum (yield 0.269 g, 66%). IR and ^{11}B NMR examination established that the insoluble product was $[(\eta^5\text{-}C_5H_5)_2ZrH]B_{10}H_{13}$.

$(\eta^5\text{-}C_5H_5)_2Zr(H)BH_4$ and $B_{10}H_{14}$.

(a) Reaction at room temperature. A solution of $B_{10}H_{14}$ (0.155 g, 1.27 mmol) in benzene (20 cm^3) was added to $(\eta^5\text{-}C_5H_5)_2Zr(H)BH_4$ (0.301 g, 1.27 mmol) in benzene (30 cm^3). No reaction was observed initially, but the solution slowly turned yellow with time and a pale yellow precipitate also formed. At various stages the atmosphere above the solution was sampled and subject to IR examination, which indicated the generation of B_2H_6. After 4 days the solid was collected by filtration, washed with benzene (30 cm^3) and dried *in vacuo* (yield 0.233 g).

(b) Reaction at *ca* 80°C. A solution containing $(\eta^5\text{-}C_5H_5)_2Zr(H)BH_4$ (0.255 g, 1.07 mmol) and $B_{10}H_{14}$ (0.131 g, 1.07 mmol) in benzene (50 cm^3) was refluxed (*ca* 80°C) for 4 h, resulting in the formation of an orange solid. This material was isolated by filtration, washed with benzene (25 cm^3) and dried *in vacuo* (yield 0.310 g).

$(\eta^5\text{-}C_5H_5)_2Zr(BH_4)CH_3$ and $B_{10}H_{14}$. A solution of $(\eta^5\text{-}C_5H_5)_2Zr(BH_4)CH_3$ (0.203 g, 0.808 mmol) in toluene (30 cm^3) was added to one containing $B_{10}H_{14}$ (0.100 g, 0.818 mmol) in toluene (20 cm^3). No reaction was observed at room temperature. On heating reaction occurred at *ca* 90°C with evidence

of gas generation and the formation of a yellow orange solid. The reaction vessel and contents were subsequently refluxed for 2 h. On cooling the yellow–orange insoluble product was isolated, washed with toluene and dried in a vacuum (yield 0.193 g). IR and ^{11}B NMR spectroscopy indicated that the major component of this solid was $(\eta^5\text{-}C_5H_5)_2ZrB_{10}H_{10}$.

Extended-Hückel molecular orbital calculations

Molecular orbital calculations were made using the extended-Hückel approach, as described by Hoffmann.[26,27] The basis set used for zirconium consisted of single Slater orbitals for both the 5*s* and 5*p* functions, while the 4*d* function was taken as a linear combination of two Slater type functions. The Slater exponents (ζ) and valence-state ionization potentials (H_{ii}) for zirconium, as well as those of H, C and B, were as reported in the literature.[27,28] Off-diagonal elements of the Hamiltonian, H_{ij}, were calculated using a modified Wolfsberg–Helmholtz formula with K equal to 1.75.[29] Calculations were made on an isolated $(\eta^5\text{-}C_5H_5)_2Zr^{2+}$ group and on $(\eta^5\text{-}C_5H_5)_2ZrB_{10}H_{10}$ (see below).

RESULTS AND DISCUSSION

Reactions of $B_{10}H_{14}$ *with* $(\eta^5\text{-}C_5H_5)_2ZrX_2$ *and* $(\eta^5\text{-}C_5H_5)_2ZrXY$, *where* X, Y = H^-, CH_3^-, BH_4^-

In many ways the zirconium system represents an ideal case. Every compound (six in all) arising from all possible combinations of the ligands H^-, CH_3^- and BH_4^- has been synthesized for $(\eta^5\text{-}C_5H_5)_2ZrX_2$ and $(\eta^5\text{-}C_5H_5)_2ZrXY$ species. Moreover, reduction of zirconium from oxidation state IV to III is relatively difficult compared with titanium and most other group V and VI elements, while hafnium does not show the range of compounds exhibited by zirconium. This also pertains to the group V and VI $(\eta^5\text{-}C_5H_5)_2MX_n$ species.

The reactions of the six $(\eta^5\text{-}C_5H_5)_2ZrX_2$ and $(\eta^5\text{-}C_5H_5)_2ZrXY$ compounds produce a diverse array of products depending on the temperature of reaction and the ratio of reactants. In general, H^- was found to react at room temperature or just above, BH_4^- at 80–90°C and CH_3^- at 100–110°C, although some variation was observed with the mixed-ligand species. For each reaction product the boron-containing fragment(s) could be related to one of the known decaborane anions (e.g. $B_{10}H_{10}^{2-}$, $B_{10}H_{13}^-$) or, in the case of BH_4^- as a ligand, to borane cluster enlargement under the appropriate high-temperature reaction conditions. The reactions and their products can be conveniently arranged in three groups, which depend on the temperature at which reaction occurred, the borane anion to which the resulting boron-containing fragment of the product species is related and whether or not borane cluster enlargement occurred.

$(\eta^5\text{-}C_5H_5)_2ZrH_2$, $(\eta^5\text{-}C_5H_5)_2Zr(H)CH_3$ *and* $(\eta^5\text{-}C_5H_5)_2Zr(H)BH_4$: *reactions at* ca *room temperature; products related to the* $B_{10}H_{13}^-$ *ion*

The reaction between $(\eta^5\text{-}C_5H_5)_2ZrH_2$ and $B_{10}H_{14}$ occurs at room temperature in a 1 : 1 mole ratio to produce 1 mol of H_2 (hence implying $B_{10}H_{13}^-$ formation) and a compound of composition $[(\eta^5\text{-}C_5H_5)_2ZrH]B_{10}H_{13}$. The product does not have the "ionic" formulation suggested by this representation but is, rather, polymeric with Zr—H—Zr and Zr—H—B linkages. It is insoluble in non-polar solvents like benzene and toluene and is only slightly soluble in more polar solvents such as CH_3CN and DMF, which attests to its polymeric nature.

The IR spectrum of $[(\eta^5\text{-}C_5H_5)_2ZrH]B_{10}H_{13}$ in the range 2600–1900 cm^{-1} is shown in Fig. 1(a) and indicates a B—H_{ter} stretch (*ca* 2515 cm^{-1}) showing some structure, along with two bands at 2172 and 2135 cm^{-1}, which may be assigned as Zr—H—B stretches based on assignments for $(\eta^5\text{-}C_5H_5)_2Zr(BH_4)_2$, $(\eta^5\text{-}C_5H_5)_2Zr(H)BH_4$ and $(\eta^5\text{-}C_5H_4Me)_2Hf(BH_4)_2$ (see also the next section below).[22,30,31] Another weaker band occurred at *ca* 2298 cm^{-1} and this is also likely to be a Zr—H—B stretch. No evidence of a terminal Zr—H stretch was observed, as found in $[(\eta^5\text{-}C_5H_5)_2ZrH_2]_n$ (1520 cm^{-1}), $[(\eta^5\text{-}C_5H_4Me)_2Zr(\mu\text{-}H)H]_2$, (1565 cm^{-1}) and in monomeric $(\eta^5\text{-}C_5Me_5)_2ZrH_2$ (1555 cm^{-1}).[20,32,33] However, a strong band was observed at 1314 cm^{-1}, which can be assigned as a Zr—H—Zr stretch, based on assignments for this feature in the spectra of $[(\eta^5\text{-}C_5H_5)_2ZrH_2]_n$ (1300 cm^{-1}) and in $[(\eta^5\text{-}C_5H_4Me)_2Zr(\mu\text{-}H)H]_2$ (1330 cm^{-1}), the latter also subject to a structural study.[32] Two possible structures for this compound can be envisaged. The first is based on the hydrogen-bridged $Zr(\mu\text{-}H)_2Zr$ unit found in $[(\eta^5\text{-}C_5H_4Me)_2Zr(\mu\text{-}H)H]_2$ and is shown in **A** below. In this case the two terminal hydrogens bound to zirconium in the dimeric unit of $[(\eta^5\text{-}C_5H_4Me)_2Zr(\mu\text{-}H)H]_2$ have been replaced by two $B_{10}H_{13}^-$ groups, with zirconium bound to what would be in an isolated $B_{10}H_{13}^-$ ion terminal hydrogen atoms on boron. The second structure **B** also has $B_{10}H_{13}^-$ groups attached to zirconium, but is built around a non-linear $\cdots Cp_2Zr\text{—}H\text{—}Cp_2Zr\text{—}H\cdots$ backbone. However, this is considered less likely based on the known presence of the $Zr(\mu\text{-}$

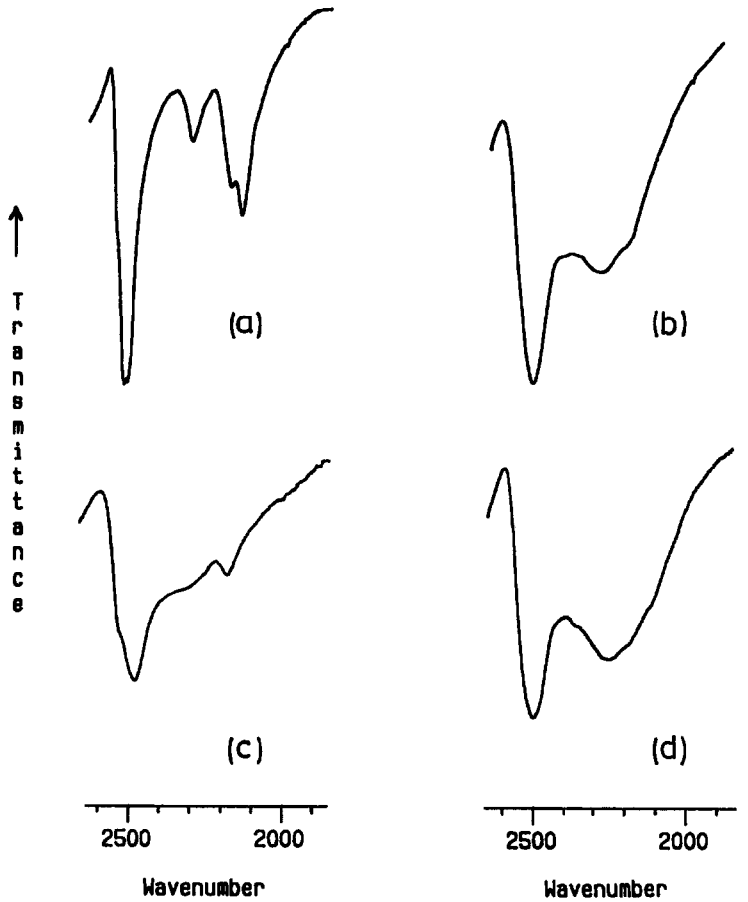

Fig. 1. IR spectra in the ν(B—H) and ν(Zr—H—B) stretching regions (2600–1900 cm^{-1}) of (a) $[(\eta^5\text{-}C_5H_5)_2Zr(\mu\text{-}H)]B_{10}H_{13}$, (b) $(\eta^5\text{-}C_5H_5)_2ZrB_{10}H_{10}$, (c) $[(\eta^5\text{-}C_5H_5)_2Zr(\mu\text{-}H)]_2B_{10}H_{10}$ and (d) the reaction product of $(\eta^5\text{-}C_5H_5)_2Zr(BH_4)_2$ and $B_{10}H_{14}$ (1 : 1 mole ratio) after refluxing in toluene for 2 h.

H)$_2$Zr unit in $[(\eta^5\text{-}C_5H_4Me)_2Zr(\mu\text{-}H)H]_2$ and, as established by ^{1}H NMR studies, in the precursor $[(\eta^5\text{-}C_5H_5)_2Zr(\mu\text{-}H)H]_2$.[34]

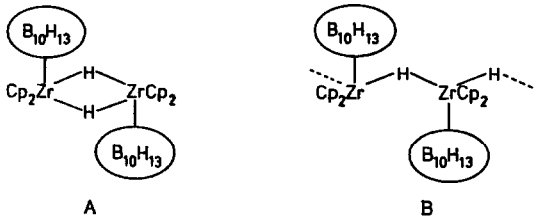

In both **A** and **B** due consideration has been given to the three frontier orbitals of an $(\eta^5\text{-}C_5H_5)_2Zr$ group (i.e. $1a_1$, b_2, $2a_1$; local C_{2v} symmetry) as discussed by Lauher and Hoffmann,[35] resulting in coordinatively saturated zirconium(IV) in either structural proposal, as is found in $[(\eta^5\text{-}C_5H_4Me)_2Zr(\mu\text{-}H)H]_2$. Without a structural study, however, it is not possible to tell which hydrogen atoms are involved in Zr—H—B bonding. While no calculations have been made on $B_{10}H_{13}^-$, *ab initio* SCF–MO calculations on isolated $B_{10}H_{12}^{2-}$ and on $B_{10}H_{14}$ have shown that the charge on the terminal hydrogens varies by only a small amount in each case (+0.04 to +0.08 e^- and +0.17 to +0.18 e^-, respectively[36]) so that, assuming an even charge distribution also pertains to $B_{10}H_{13}^-$, it is likely that more than one type of terminal hydrogen is involved in Zr—H—B bonding. This is the probable source of the many Zr—H—B bands found in the IR spectrum and use of different hydrogens in Zr—H—B bonding is probably related to at least two geometric packing arrangements for $B_{10}H_{13}^-$ within the structure. The possibility of bonding through a bridging hydrogen on $B_{10}H_{13}^-$ would seem unlikely as these would be the most positively charged hydrogen atoms in this species, while breakdown of a B—H—B unit to give a single Zr—H—B bond would leave the remaining boron electron deficient.

Although the compound was not highly soluble, ^{11}B NMR studies in acetonitrile and N,N-dimethylformamide showed the presence of free $B_{10}H_{13}^-$,[37] indicating breakdown of the polymeric structure in solution. Moreover, the ^1H NMR spectrum in d_3-CH_3CN exhibited a resonance at 6.33 ppm, which corresponds to the η^5-C_5H_5 protons, as well as a resonance at 3.29 ppm which can only be assigned as a terminal hydrogen on zirconium. The latter value may be compared with values of 3.85 and 3.75 ppm for the terminal hydrogen atoms in $[(\eta^5\text{-}C_5H_5)_2Zr(\mu\text{-}H)H]_2$ and $[(\eta^5\text{-}C_5H_4Me)_2Zr(\mu\text{-}H)H]_2$, respectively (the bridging hydrogens occur at -3.45 and at -2.98 ppm).[32,34] Presumably, the $[Cp_2Zr(\mu\text{-}H)_2ZrCp_2]^{2+}$ unit has also broken down to give solvated $(\eta^5\text{-}C_5H_5)_2ZrH^+$ ions, which have terminal hydrogen atoms. In agreement with this the molar conductivity of a 1.0×10^{-3} M solution of $[(\eta^5\text{-}C_5H_5)_2Zr(\mu\text{-}H)]B_{10}H_{13}$ in CH_3CN at 25°C was 108 S cm^2 mol^{-1}, slightly lower than the range expected for a 1:1 electrolyte (120–160 S cm^2 mol^{-1})[38] in this solvent. The low value may perhaps be associated with the fairly large sizes of the ions, leading to reduced ionic mobilities, or perhaps to some residual cation–anion (or even cation–cation) interactions in solution.

Reaction of $(\eta^5\text{-}C_5H_5)_2Zr(H)CH_3$ and $B_{10}H_{14}$ occurred between room temperature and 50°C to produce the same product, $[(\eta^5\text{-}C_5H_5)_2Zr(\mu\text{-}H)]B_{10}H_{13}$, as described above, as well as CH_4. The formation of the hydrogen-bridged zirconium species in this reaction is not surprising as the precursor $(\eta^5\text{-}C_5H_5)_2Zr(H)CH_3$ is also known to be polymeric with Zr—H—Zr bridging, with a ν(Zr—H—Zr) stretch (1310 cm^{-1}) evident in the IR spectrum.[24]

The reaction between $(\eta^5\text{-}C_5H_5)_2Zr(H)BH_4$ and $B_{10}H_{14}$ at room temperature was similar to that between $NaBH_4$ (or $LiBH_4$) and $B_{10}H_{14}$, in that the ultimate boron-containing products were compounds containing the $B_{10}H_{13}^-$ ion as well as B_2H_6.[12,14] The initial compound that formed appeared to be $[(\eta^5\text{-}C_5H_5)_2Zr(BH_4)]B_{10}H_{13}$ based on the formulation of the species $[(\eta^5\text{-}C_5H_5)_2Zr(\mu\text{-}H)]B_{10}H_{13}$ described above, in conjunction with IR data. The IR data showed a strong B—H_{ter} stretch at 2523 cm^{-1} and evidence of a doubly-bridged BH_4^- group,[22,30,31] with bands at 2429, 2384, 2156(sh) and 2124 cm^{-1}. Also, there was a strong peak at 1119 cm^{-1}, which is assignable as the $\delta(BH_2)$ mode. However, B_2H_6 was observed as a product in the reaction after several days and the IR spectrum of the solid product always indicated the presence of a strong, broad band at 1317 cm^{-1}, characteristic of the Zr—H—Zr stretch found in $[(\eta^5\text{-}C_5H_5)_2Zr(\mu\text{-}H)]B_{10}H_{13}$. It would thus appear that the initial product, that is $[(\eta^5\text{-}C_5H_5)_2Zr(BH_4)]B_{10}H_{13}$, decomposes slowly to $[(\eta^5\text{-}C_5H_5)_2Zr(\mu\text{-}H)]B_{10}H_{13}$ and B_2H_6. As the actual reaction between $(\eta^5\text{-}C_5H_5)_2Zr(H)BH_4$ and $B_{10}H_{14}$ is itself quite slow, taking several days, pure $[(\eta^5\text{-}C_5H_5)_2Zr(BH_4)]B_{10}H_{13}$ can never be obtained without the presence of some $[(\eta^5\text{-}C_5H_5)_2Zr(\mu\text{-}H)]B_{10}H_{13}$. The $^{11}B\{^1H\}$ NMR spectrum in CH_3CN of a typical product of this reaction after 3 days indicated the presence of free $B_{10}H_{13}^-$ and a resonance at -26.0 ppm, which is assignable to BH_4^- bound to zirconium based on a comparison with the BH_4^- resonance (-14.4 ppm) found in $(\eta^5\text{-}C_5H_5)_2Zr(BH_4)_2$.[20]

$(\eta^5\text{-}C_5H_5)_2Zr(CH_3)_2$: *reactions at* ca 105°C; *products related to the* $B_{10}H_{10}^{2-}$ *ion*

Reaction between $(\eta^5\text{-}C_5H_5)_2Zr(CH_3)_2$ and $B_{10}H_{14}$ produced two different products depending on the reaction stoichiometry. With a mole ratio for $(\eta^5\text{-}C_5H_5)_2Zr(CH_3)_2$ to $B_{10}H_{14}$ of 1:1 or 1:2 only $(\eta^5\text{-}C_5H_5)_2ZrB_{10}H_{10}$ was formed, while with a mole ratio of 2:1 $[(\eta^5\text{-}C_5H_5)_2Zr(\mu\text{-}H)]_2B_{10}H_{10}$ was isolated. The formation of $B_{10}H_{10}^{2-}$ in all of these reactions was initially surprising and will be addressed below, but its presence was established by ^{11}B NMR studies in N,N-dimethylformamide and dimethyl sulphoxide, in which both compounds are quite soluble, each compound exhibiting (see Fig. 2) signals at *ca* +1 and -28 ppm (with integrated intensities of 1:4) in agreement with the data reported for the $B_{10}H_{10}^{2-}$ ion.[39]

The IR spectra of both compounds, Figs 1(b) and (c), indicated considerable interaction between the $(\eta^5\text{-}C_5H_5)_2Zr^{2+}$ or $[(\eta^5\text{-}C_5H_5)_2Zr(\mu\text{-}H)]_n^{n+}$ cations and $B_{10}H_{10}^{2-}$ anions. In $(\eta^5\text{-}C_5H_5)_2ZrB_{10}H_{10}$, for example, there was a strong B—H_{ter} stretch at 2502 cm^{-1} with a very broad (*ca* 300 cm^{-1}) medium intensity band to lower frequencies, centred at 2300 cm^{-1}. The presence of broad, weak bands in the region 2400–2100 cm^{-1}, which are absent in alkali metal salts of $B_{10}H_{10}^{2-}$, are indicative of M—H—B bonding. This has been established on the basis of IR studies[40–42] on $\{[(C_6H_5)_3P]_2Cu\}_2B_{10}H_{10}$ and $Cu_2B_{10}H_{10}$, both of which exhibit Cu—H—B interactions in their solid-state structures.[42,43] In each case the Cu—H—B bridges involve both axial and equatorial BH interactions of the *closo*-$B_{10}H_{10}^{2-}$ ion with Cu(I). Evidence for similar interactions are also found for $[(\eta^5\text{-}C_5H_5)_2Zr(\mu\text{-}H)]_2B_{10}H_{10}$. In this case there is a broad, medium intensity band centred at 2280 cm^{-1} and a second, well-developed peak at 2177 cm^{-1}. One further feature in the IR spectrum of the latter compound is a strong band at 1194 cm^{-1}, which is

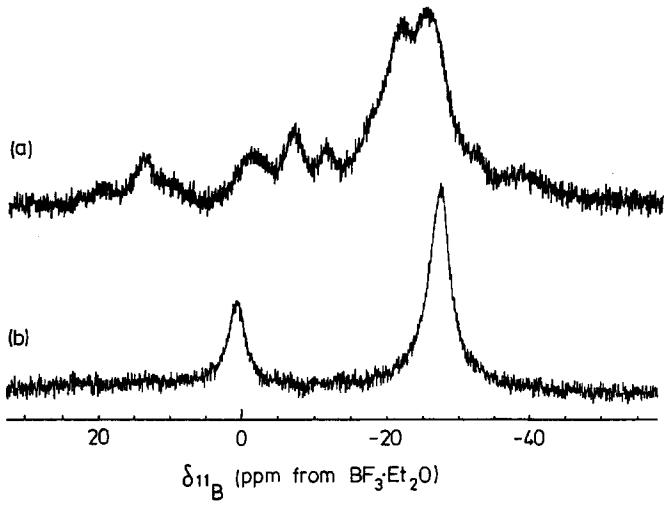

Fig. 2. $^{11}B\{^1H\}$ NMR spectra (at 27°C) of $(\eta^5\text{-}C_5H_5)_2ZrB_{10}H_{10}$ in (a) acetonitrile and (b) dimethyl sulphoxide.

assigned as a Zr—H—Zr stretch (see the previous section), leading to a polymeric structure.

Further evidence for strong Zr—H—B interactions in both compounds came from ^{11}B and ^1H NMR studies. Although both compounds dissociate on dissolution in DMF and DMSO to give free $B_{10}H_{10}^{2-}$, in CH_3CN their $^{11}B\{^1H\}$ spectra are considerably more complicated, exhibiting multiple boron environments. The interaction of one $(\eta^5\text{-}C_5H_5)_2Zr^{2+}$ group with a bidentate, "chelating" $B_{10}H_{10}^{2-}$ ion (a bicapped Archimedian antiprismatic structure) can occur in three ways, involving one axial–equatorial and two types of equatorial–equatorial linkages to the anion. These would lead, in turn, to a maximum of seven, seven and five boron environments, respectively, assuming no coincidences of chemical shifts. If some $B_{10}H_{10}^{2-}$ is also bound through only one of its terminal hydrogen atoms then the resulting spectra would be even more complex. The $^{11}B\{^1H\}$ NMR spectra of these compounds (see, for example, Fig. 2) are more complicated than might be expected, based on the presence of a single species in solution containing one bidentate $B_{10}H_{10}^{2-}$ ion, and suggest that more than one type of linkage is present and, by inference, also in the solid state. Indeed, it is likely that one $(\eta^5\text{-}C_5H_5)_2Zr^{2+}$ group could even link two $B_{10}H_{10}^{2-}$ ions in solution and in the solid state, as found in the structure of $Cu_2B_{10}H_{10}$.[43] It should be noted that different Pt—H—B linkages have been invoked to explain two (geometric) isomers of *cis*-$[(PPh_3)_2Pt(B_{10}H_{10})]$.[44] However, in *cis*-$[(PPh_3)_2Pt(B_{10}H_{10})]$ and also in $[(PPh_3)_2Cu]_2B_{10}H_{10}$ the $^{11}B\{^1H\}$ spectra are recognizably that of $B_{10}H_{10}^{2-}$, except for the increased width of the signals (with $w_{1/2} = 330$ Hz in the platinum compound) compared with free $B_{10}H_{10}^{2-}$ ($w_{1/2} = 51$ Hz).[41,44] This is not the case for the two zirconium-containing species obtained in this study, where multiple boron environments were observed.

The ^1H NMR spectra of $(\eta^5\text{-}C_5H_5)_2ZrB_{10}H_{10}$, $[(\eta^5\text{-}C_5H_5)_2Zr(\mu\text{-}H)]_2B_{10}H_{10}$, $[(PPh_3)_2Cu]_2B_{10}H_{10}$ and *cis*-$[(PPh_3)_2Pt(B_{10}H_{10})]$ also provide an interesting comparison, as well as strong evidence for Zr—H—B interactions. For $[(PPh_3)_2Cu]_2B_{10}H_{10}$ the ^1H NMR spectrum has been reported to show just *single*, broadened axial and equatorial resonances, consistent with a fluctional system, with chemical shifts (axial at 3.65 and equatorial at 0.85 ppm[41]) not too different from $B_{10}H_{10}^{2-}$ itself (4.3 and 0.9 ppm, respectively). For *cis*-$[(PPh_3)_2Pt(B_{10}H_{10})]$, on the other hand, the $^1H\{^1B\}$ NMR spectrum shows multiple axial and equatorial signals, consistent with a rigid species in solution.[44] In the case of $(\eta^5\text{-}C_5H_5)_2ZrB_{10}H_{10}$ the ^1H NMR spectrum shows two $\eta^5\text{-}C_5H_5$ resonances (6.45 and 6.38 ppm) and a broad ($w_{1/2} = 20$ Hz) resonance at 2.19 ppm. The two $\eta^5\text{-}C_5H_5$ resonances are of unequal integrated intensities, ruling out the possibility of two magnetically inequivalent $\eta^5\text{-}C_5H_5$ groups on a single $(\eta^5\text{-}C_5H_5)_2Zr$ group, and is consistent with at least two species in solution. The resonance at 2.19 ppm is tentatively assigned to axial hydrogens involved in Zr—H—B bonding, which are now observable in a non-^{11}B decoupled spectrum because of changed electric field gradient conditions operative in the Zr—H—B three-centre/two-electron bonds. For $[(\eta^5\text{-}C_5H_5)_2Zr(\mu\text{-}H)]_2B_{10}H_{10}$, there is only a single $\eta^5\text{-}C_5H_5$ resonance (6.38 ppm) and the axial hydrogens now

involved in Zr—H—B bonding appear at 2.16 ppm. There is also a sharp resonance at 2.35 ppm, which is assignable as a terminal hydrogen on zirconium formed by breakdown of the Zr—H—Zr link on dissolution in CH_3CN.

The presence of strong Zr—H—B linkages for $(\eta^5\text{-}C_5H_5)_2ZrB_{10}H_{10}$ was also supported by conductivity measurements in CH_3CN, which showed a Λ_M of only 27 S cm^2 mol^{-1} for a 1.0×10^{-3} M solution at 25°C, indicative of substantial cation–anion interactions even in this dilute solution (relative to the concentrations used in the NMR studies in CH_3CN, which were saturated solutions).

The formation of $B_{10}H_{10}^{2-}$ in the above reactions was surprising given that it is a *closo* species, while the precursor $B_{10}H_{14}$ is a *nido* species. Thus, conversion of $B_{10}H_{14}$ (i.e. "$B_{10}H_{10}^{4-}$") to $B_{10}H_{10}^{2-}$ is an oxidation process, but no change in metal oxidation state was observed. In the reaction between $(\eta^5\text{-}C_5H_5)_2Zr(CH_3)_2$ and $B_{10}H_{14}$ in a 1 : 1 mole ratio, after initial formation of CH_4 (i.e. "$CH_3^- + H^+$") to give $B_{10}H_{12}^{2-}$ as a likely intermediate based on the initial reaction stoichiometry, this suggests that one or more of the following reactions may operate:

$$2B_{10}H_{12}^{2-} \rightarrow B_{10}H_{10}^{2-} + B_{10}H_{14}^{2-} \quad (1)$$

$$B_{10}H_{12}^{2-} \rightarrow B_{10}H_{10}^{2-} + H_2 \quad (2)$$

$$B_{10}H_{14}^{2-} \rightarrow B_{10}H_{10}^{2-} + 2H_2. \quad (3)$$

Previously, it has been shown that pyrolysis of solid $Na_2B_{10}H_{12}$ or $Rb_2B_{10}H_{14}\cdot nH_2O$ at *ca* 240°C produces a mixture of $B_{10}H_{10}^{2-}$ and $B_9H_9^{2-}$.[45] However, no information on the thermal stabilities of $B_{10}H_{12}^{2-}$ and $B_{10}H_{14}^{2-}$ in solution is currently available.

A solution of $Na_2B_{10}H_{12}$ in THF was, therefore, prepared in a sealed, evacuated NMR tube and the thermal stability of $B_{10}H_{12}^{2-}$ investigated using ^{11}B NMR. Reaction began at *ca* 60°C and was subsequently monitored at 65°C, giving $B_{10}H_{10}^{2-}$ and $B_{10}H_{14}^{2-}$ in approximately equal amounts over several (*ca* 6) hours. Likewise, when $B_{10}H_{14}$ and excess NaH were vigorously refluxed in THF under nitrogen only $B_{10}H_{10}^{2-}$ and $B_{10}H_{14}^{2-}$ in approximately equal amounts (together with a small amount of BH_4^- <1%) were observed after 3 h by ^{11}B NMR. This suggests that the reaction between $(\eta^5\text{-}C_5H_5)_2Zr(CH_3)_2$ and $B_{10}H_{14}$ in a 1 : 1 mole ratio occurs according to the steps:

$$Cp_2Zr(CH_3)_2 + B_{10}H_{14} \rightarrow [Cp_2ZrB_{10}H_{12}] + 2CH_4 \quad (4)$$

$$2[Cp_2ZrB_{10}H_{12}] \rightarrow Cp_2ZrB_{10}H_{10} + Cp_2ZrB_{10}H_{14}. \quad (5)$$

The presence of $B_{10}H_{14}^{2-}$ as a product in this reaction was established (amongst other species) in the toluene-soluble fraction of the products by ^{11}B NMR in DMSO. However, the yield of toluene-insoluble $(\eta^5\text{-}C_5H_5)_2ZrB_{10}H_{10}$ was always 70–80%, while reaction (5) above would imply a maximum yield of 50%. A subsequent ^{11}B NMR investigation into the thermal stability of $B_{10}H_{14}^{2-}$ (a solution of $Cs_2B_{10}H_{14}\cdot CsCl$[46] in DMSO showed no decomposition up to 150°C, well above the reaction temperature of $(\eta^5\text{-}C_5H_5)_2Zr(CH_3)_2$ with $B_{10}H_{14}$. The reaction between $(\eta^5\text{-}C_5H_5)_2Zr(CH_3)_2$ and $B_{10}H_{14}$ (in a 1 : 1 mole ratio) was, therefore, studied under conditions whereby the total amount of gaseous product could be measured using a Toepler system. The amount of evolved gas was 24% greater (average of two determinations; see Experimental) than that based on the amount of CH_4 generated according to reaction (4) above, indicating formation of a further permanent gas (presumably hydrogen). Thus, it would appear that, under the reaction conditions, direct thermal decomposition of the "intermediate" $[(\eta^5\text{-}C_5H_5)_2ZrB_{10}H_{12}]$ also occurs, in addition to the rearrangement/disproportionation reaction given in (5) above, which may be written:

$$[Cp_2ZrB_{10}H_{12}] \rightarrow Cp_2ZrB_{10}H_{10} + H_2. \quad (6)$$

Reactions (5) and (6) would, therefore, appear to be competing reactions, leading to the observed yields of $(\eta^5\text{-}C_5H_5)_2ZrB_{10}H_{10}$ and H_2. Analogous reactions presumably occur when $B_{10}H_{14}$ reacts with $(\eta^5\text{-}C_5H_5)_2Zr(CH_3)_2$ in a 1 : 2 stoichiometry, although in this case C_2H_6 is also a likely product according to the equation:

$$2(\eta^5\text{-}C_5H_5)_2Zr(CH_3)_2 + B_{10}H_{14} \rightarrow [(\eta^5\text{-}C_5H_5)_2Zr(H)]_2B_{10}H_{10} + 2CH_4 + C_2H_6. \quad (7)$$

However, attempts to identify C_2H_6 in the presence of excess CH_4 by IR spectroscopy were not definitive in this case.

$(\eta^5\text{-}C_5H_5)_2Zr(BH_4)_2$, $(\eta^5\text{-}C_5H_5)_2Zr(H)BH_4$ *and* $(\eta^5\text{-}C_5H_5)_2Zr(BH_4)CH_3$: *reactions at* 80–110°C; *borane cluster enlargement*

When the reactions between $(\eta^5\text{-}C_5H_5)_2Zr(BH_4)_2$, $(\eta^5\text{-}C_5H_5)_2Zr(H)BH_4$ and $(\eta^5\text{-}C_5H_5)_2Zr(BH_4)CH_3$ with $B_{10}H_{14}$ were performed in refluxing benzene or toluene over an extended period, an orange solid always formed in each case. The IR spectra of these materials [see Fig. 1(d) for a typical spectrum] were essentially identical to that of $(\eta^5\text{-}C_5H_5)_2ZrB_{10}H_{10}$, except for an increase in the size of the Zr—H—B stretching mode(s)

relative to that of the B—H_{ter} stretch. This again indicates strong interactions between zirconium and the product borane anions. The $^{11}B\{^1H\}$ NMR spectra of these solids in DMF or DMSO indicated the presence of $B_{10}H_{10}^{2-}$ as well as two resonances at −15.8 and −16.9 ppm. The relative intensities of these two peaks were dependent on the temperature at which the reaction was performed as well as the time scale. These resonances, therefore, belong to different species and are not attributable to $B_{11}H_{14}^-$, which has two resonances of equal intensity at similar chemical shifts [for $B_{11}H_{14}^-$ in glyme; δ ppm (intensity): −12.5(1), −14.1(5) and −14.9(5)[47]]. The two resonances may be assigned to $B_{12}H_{12}^{2-}$ (−15.8 ppm) and $B_{11}H_{11}^{2-}$ (−16.9 ppm)[48,49] and likely arise from the initial formation of $B_{11}H_{13}^{2-}$ (or $B_{11}H_{14}^-$), followed by decomposition to $B_{11}H_{11}^{2-}$ and H_2, with $B_{10}H_{10}^{2-}$ and $B_{12}H_{12}^{2-}$ formed either directly from $B_{11}H_{13}^{2-}$ (or $B_{11}H_{14}^-$) or by thermal decomposition of $B_{11}H_{11}^{2-}$. Indeed, the method reported for the preparation of $B_{11}H_{11}^{2-}$ involves the pyrolysis of solid $Cs_2B_{11}H_{13}$ above 250°C, followed by repeated recrystallizations from aqueous solution to remove $Cs_2B_{10}H_{10}$ and $Cs_2B_{12}H_{12}$.[49,50] The salt, $Cs_2B_{11}H_{11}$, is itself stable to 400°C but decomposes at 600°C to give $Cs_2B_{10}H_{10}$ and $Cs_2B_{12}H_{12}$.[50] The data on $B_{11}H_{14}^-$ are less accessible, but this anion (as the Cs^+ salt) appears to be pyrolytically unstable above 185°C, giving $B_nH_n^{2-}$ (where $n = 12, 10, 9$).[51] The reaction behaviour described above for the simple caesium salts parallels that observed in the present study, but at considerably higher temperatures. The markedly reduced decomposition temperatures (in solution) observed in this work may be associated with the presence of $(\eta^5\text{-}C_5H_5)_2Zr^{2+}$, that is, to a metal-mediated decomposition process(es). This is likely associated with Zr—H—B interactions between $(\eta^5\text{-}C_5H_5)_2Zr^{2+}$ and the proposed intermediate borane anions (i.e. $B_{11}H_{13}^{2-}$ or, less likely, $B_{11}H_{14}^-$, based on the products formed) of the type established in the compounds described in the two previous sections. While metal-mediated decomposition reactions of the boranes have not previously been reported, metal-mediated oligomerization reactions involving a $(\eta^5\text{-}C_5H_5)_2Mo$ moiety are known leading to metallaboranes containing two, five and nine boron atoms from a [BH_3·THF] substrate.[52]

Zr—H—B *bonding interactions and the* $(\eta^5\text{-}C_5H_5)_2Zr$ *group as a cluster vertex*

The three lowest-lying frontier orbitals of an $(\eta^5\text{-}C_5H_5)_2M$ group with local C_{2v} symmetry (the cyclopentadienyl groups being eclipsed) are, as described by Lauher and Hoffmann,[35] primarily metal based and are, in order of increasing energy, $1a_1$ (58% $d_{x^2-y^2}$ and 30% d_{z^2}), b_2 (73% d_{xz}) and $2a_1$ [35% d_{z^2}, 19% $d_{x^2-y^2}$, 17% s and 16% p_z; data calculated for $(\eta^5\text{-}C_5H_5)_2Zr^{2+}$]. The three orbitals are located in the plane bisecting the two cyclopentadienyl groups and do not transform as do the three frontier orbitals of a BH or $Fe(CO)_3$ skeletal vertex ($A_1 + E$, local C_{3v} symmetry), so that a $(\eta^5\text{-}C_5H_5)_2M$ group and a BH [or $Fe(CO)_3$] vertex are not isolobal. Disregarding skeletal electron contributions the $(\eta^5\text{-}C_5H_5)_2M$ group can be like, for example, an $Mn(CO)_4$ fragment if only two of the three frontier orbitals of the $(\eta^5\text{-}C_5H_5)_2M$ group are used in bonding. An $Mn(CO)_4$ group is actually isolobal with BH_2 or $Cu(PR_3)_2$ and would be expected to bridge two atoms in a cluster provided that the "bite" angle of the frontier orbitals was commensurate with the separation of the two cluster atoms and their (unused) attendant orbitals and that these orbitals were of the appropriate symmetry (and energy) to interact with the frontier orbitals of the $Mn(CO)_4$ group. An $(\eta^5\text{-}C_5H_5)_2M$ fragment is really more complex in that there are three, not two, frontier orbitals. However, true 16-electron systems are quite common for group IV elements and may involve, for example, the $(\eta^5\text{-}C_5H_5)_2Zr^{2+}$ group. Examples using just σ-bonding ligands (which removes the possibility of π-bonding through higher energy ligand donor orbitals) include $(\eta^5\text{-}C_5H_5)_2Zr(CH_3)_2$, $(\eta^5\text{-}C_5H_5)_2Zr(CH_2CMe_3)_2$ and $(\eta^5\text{-}C_5Me_5)_2ZrH_2$. The effective "bite" angle [as given by the X—M—X angle in $(\eta^5\text{-}C_5H_5)_2MX_2$ compounds], which gives rise to the most favourable overlaps of the three frontier orbitals with those of the two X groups (interaction with b_2 and some combination of $1a_1$ and $2a_1$), actually varies depending on the d-orbital population.[35] This angle is 94–97° for d^0, 85–88° for d^1 and 76–82° for d^2 systems. Assuming an average "bite" angle of 96° for $(\eta^5\text{-}C_5H_5)_2Zr^{2+}$ (a d^0 system) and covalent radii for zirconium and boron of 1.45 and 0.79 Å, respectively, the B—B distance in a borane cluster required to support two two-centre/two-electron Zr—B bonds would be 3.32 Å, well in excess of any two adjacent boron atoms in such a species, even though these atoms may be linked by a three-centre/two-electron B—B bond. Considering the distance required an $(\eta^5\text{-}C_5H_5)_2Zr^{2+}$ fragment is thus likely to bond symmetrically along one side of a formal $B_{10}H_{12}^{2-}$ fragment, if the latter is derived from $B_{10}H_{14}$ by loss of two bridging protons from just one side of the parent molecule. This type of interaction is observed in the $[M(B_{10}H_{12})_2]^{2-}$ ions, where M = zinc(II) and nickel(II),[53,54] and the $B_{10}H_{12}^{2-}$ group can be regarded as acting as a

tetrahapto ligand. In the present study, however, $B_{10}H_{12}^{2-}$ was not observed as a boron-containing product. Rather, boron-containing anionic species were obtained which exhibited three-centre/two-electron bonding interactions with $(\eta^5\text{-}C_5H_5)_2Zr^{2+}$ through their terminal hydrogen atoms. The extent of actual Zr—B interaction in these linkages was investigated using extended-Hückel LCAO–MO calculations for an axial–equatorial interaction of $(\eta^5\text{-}C_5H_5)_2Zr^{2+}$ with $B_{10}H_{10}^{2-}$, as is likely to occur in the case of $(\eta^5\text{-}C_5H_5)_2ZrB_{10}H_{10}$. An idealized ($D_{4d}$) geometry for the $B_{10}H_{10}^{2-}$ ion was assumed,[55] taken from that found in $[(PPh_3)_2Cu]_2B_{10}H_{10}$, together with a $(\eta^5\text{-}C_5H_5)_2Zr^{2+}$ fragment so that the H—Zr—H angle was 96°. With Zr—H distances of 1.91 and 2.08 Å, not too different to those found in the three-centre/two-electron Zr—H—Zr bonds in $[(\eta^5\text{-}C_5H_4Me)_2Zr(\mu\text{-}H)H]_2$ (1.94 and 2.05 Å), this gave equal Zr—B distances of 2.39 Å to the axial and equatorial boron atoms, an arrangement similar to that observed for the Cu—B distances (in this case both 2.30 Å) in $[(PPh_3)_2Cu]_2B_{10}H_{10}$.[42] The resulting Zr—B orbital overlaps (absolute values) varied from 0.393 to 0.023, disregarding those restricted to zero by symmetry constraints, and involved all of those orbitals indicated above that contribute strongly to the three lowest-lying frontier orbitals of the $(\eta^5\text{-}C_5H_5)_2Zr^{2+}$ group. In comparison, the Zr—H orbital overlaps varied from 0.331 to 0.039 with the major overlap occuring between $Zr(5p_y)$ and $H(1s)$—the y direction being perpendicular to the vector from zirconium to the middle of the B_a—B_e bond and in the plane bisecting the two cyclopentadienyl groups. Thus, the bonding between zirconium and the borane anion is best described using the following representation:

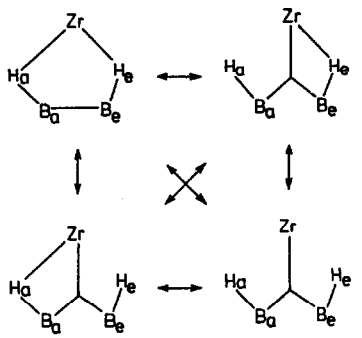

Scheme 1.

A similar array of interactions has been proposed previously in the case of $[(PPh_3)_2Cu]_2B_{10}H_{10}$, although as pointed out in that study the relative contributions of the Cu—H and Cu—B interactions cannot be extracted from the interatomic distances themselves.[42] The $(\eta^5\text{-}C_5H_5)_2Zr^{2+}$ and $(PPh_3)_2Cu^+$ groups are effectively acting like a BH_2 vertex, a commonly found feature in *arachno*-boranes, although in each case they require electron supplementation from the terminal B—H two-centre/two-electron bonds of $B_{10}H_{10}^{2-}$ to create the three-centre/two-electron M—H—B bonds, while a (neutral) BH_2 vertex is a source of one skeletal electron.

Given the frontier orbitals extant, the likely metal–borane interactions involving an $(\eta^5\text{-}C_5H_5)_2Zr$ fragment are of the type proposed to occur in the compounds obtained in this study. As such, these will involve relatively weak three-centre/two-electron bonds (Zr—H—B with a considerable Zr—B contribution, as pertains to this study). For a general $(\eta^5\text{-}C_5H_5)_2M$ fragment the strength of the M—H—B (and M—B) interactions are likely to vary depending on the transition metal, its formal oxidation state and, therefore, the electron population of the frontier orbitals. This will, in turn, affect the bite angle of the frontier orbitals in their interaction with a borane cluster, which may lead to different types of interactions between the $(\eta^5\text{-}C_5H_5)_2M$ fragments and the borane itself. In general, as the interactions are likely to be relatively weak, as found in this study, the metal atoms should exert little influence on aspects of the chemistry of the neutral borane or borane ion(s) in question. Exceptions include, for example, possible borane reduction of the metal and changes in the site of nucleophilic or electrophilic attack caused by electron density changes as a result of formation of the M—H—B bonds, provided that these are retained in solution. The result, as found in this study, was that in its reactions with the zirconium-containing species used, the chemistry of $B_{10}H_{14}$ was recognizably that of its reactions with free (i.e. ionic) H^- and BH_4^-. Evidence of metal intervention was noted, however, in the proposed metal-promoted disproportionation/rearrangement reaction which always occurred at elevated temperatures (above 80°C) when BH_4^- was present. In the absence of a metal these same reactions only occur at much higher temperatures. It should be noted that in cases where an $(\eta^5\text{-}C_5H_5)_2M$ group does act to alter chemistry, such as in the metal-mediated oligomerization of $[BH_3\cdot THF]$ by $(\eta^5\text{-}C_5H_5)_2MoH_2$,[52] photolysis and thermolysis have been used to promote reaction. The resulting higher borane species actually involved incorporation of one cyclopentadiene ring into the cluster geometry so that the $(\eta^5\text{-}C_5H_5)_2Mo$ fragment no longer remained intact.

Acknowledgement—The authors would like to thank Dr D. Rigby of the CSIRO, Division of Exploration Geoscience, for the loan of the Toepler pump.

REFERENCES

1. *Metal Interactions with Boron Clusters* (Edited by R. N. Grimes). Plenum Press, New York (1982).
2. (a) J. D. Kennedy, *Prog. Inorg. Chem.* 1984, **32**, 519; (b) J. D. Kennedy, *Prog. Inorg. Chem.* 1986, **34**, 211.
3. C. E. Housecroft, *Boranes and Metalloboranes: Structure, Bonding and Reactivity*. Ellis Horwood, Chichester (1990).
4. R. N. Grimes, in *Advances in Boron and the Boranes* (Edited by J. E. Liebman, A. Greenberg and R. E. Williams), Ch. 11, p. 235. VCH, New York (1988).
5. F. Klanberg, E. L. Muetterties and L. J. Guggenberger, *Inorg. Chem.* 1968, **7**, 2272.
6. C. Ting and L. Messerle, *J. Am. Chem. Soc.* 1989, **111**, 3449.
7. R. W. Swisher, E. Sinn and R. N. Grimes, *Organometallics* 1984, **3**, 599.
8. C. G. Salentine and M. F. Hawthorne, *J. Am. Chem. Soc.* 1975, **97**, 426.
9. C. G. Salentine and M. F. Hawthorne, *Inorg. Chem.* 1976, **15**, 2872.
10. F. Y. Lo, C. E. Strouse, K. P. Callahan, C. B. Knobler and M. F. Hawthorne, *J. Am. Chem. Soc.* 1975, **97**, 428.
11. G. A. Guter and G. W. Schaeffer, *J. Am. Chem. Soc.* 1956, **78**, 3546.
12. V. W. Hough and L. J. Edwards, in *Borax to Boranes* (Edited by R. F. Gould), Advances in Chemistry Series, No. 32, p. 184. A.C.S., Washington, DC (1961).
13. P. H. Wilks and J. C. Carter, *J. Am. Chem. Soc.* 1966, **88**, 3441.
14. V. D. Aftandilian, H. C. Miller, G. W. Parshall and E. L. Muetterties, *Inorg. Chem.* 1962, **1**, 734.
15. R. M. Adams, A. R. Siedle and J. Grant, *Inorg. Chem.* 1964, **3**, 461.
16. N. N. Greenwood and N. F. Travers, *J. Chem. Soc. (A)* 1967, 880.
17. N. N. Greenwood and N. F. Travers, *Inorg. Nucl. Chem. Lett.* 1966, **2**, 169.
18. A. J. Wynd, S. E. Robins, D. A. Welch and A. J. Welch, *J. Chem. Soc., Chem. Commun.* 1985, 819.
19. F. A. Cotton and G. Wilkinson, *Advanced Inorganic Chemistry*, 5th edn, Ch. 24, p. 1097. Wiley-Interscience, New York (1988).
20. B. D. James, R. K. Nanda and M. G. H. Wallbridge, *Inorg. Chem.* 1967, **6**, 1979.
21. E. Samuel and M. D. Rausch, *J. Am. Chem. Soc.* 1973, **95**, 6263.
22. B. E. Smith, B. D. James and J. A. Dilts, *J. Inorg. Nucl. Chem.* 1976, **38**, 1973.
23. P. C. Wailes, H. Weigold and A. P. Bell, *J. Organomet. Chem.* 1971, **33**, 181.
24. P. C. Wailes and H. Weigold, *J. Organomet. Chem.* 1970, **24**, 405.
25. J. A. Marsella and K. G. Caulton, *J. Am. Chem. Soc.* 1982, **104**, 2361.
26. R. Hoffmann and W. N. Lipscomb, *J. Chem. Phys.* 1962, **36**, 2179, 3489.
27. R. Hoffmann, *J. Chem. Phys.* 1963, **39**, 1397.
28. K. Tatsumi, A. Nakamura, P. Hofmann, P. Stauffert and R. Hoffmann, *J. Am. Chem. Soc.* 1985, **107**, 4440.
29. R. A. Wheeler, M. H. Whangbo, T. Hughbanks, R. Hoffmann, J. K. Burdett and T. A. Albright, *J. Am. Chem. Soc.* 1986, **108**, 2222.
30. T. J. Marks, W. J. Kennelly, J. R. Kolb and L. A. Shimp, *Inorg. Chem.* 1972, **11**, 2540.
31. P. L. Johnson, S. A. Cohen, T. J. Marks and J. M. Williams, *J. Am. Chem. Soc.* 1978, **100**, 2709.
32. S. B. Jones and J. L. Petersen, *Inorg. Chem.* 1981, **20**, 2889.
33. J. M. Manriquez, D. R. McAlister, R. D. Sanner and J. E. Bercaw, *J. Am. Chem. Soc.* 1976, **98**, 6733.
34. D. G. Bickley, N. Hao, P. Bougeard, B. G. Sayer, R. C. Burns and M. J. McGlinchey, *J. Organomet. Chem.* 1983, **246**, 257.
35. J. Lauher and R. Hoffmann, *J. Am. Chem. Soc.* 1976, **98**, 1729.
36. M. F. Guest and I. H. Hiller, *J. Chem. Soc., Faraday Trans. II* 1974, **70**, 2004.
37. A. R. Siedle, G. M. Bodner and L. J. Todd, *J. Inorg. Nucl. Chem.* 1971, **33**, 3671.
38. W. J. Geary, *Coord. Chem. Rev.* 1971, **7**, 81.
39. E. L. Muetterties, J. H. Balthis, Y. T. Chia, W. H. Knoth and H. C. Miller, *Inorg. Chem.* 1964, **3**, 444.
40. T. E. Paxton, M. F. Hawthorne, L. D. Brown and W. N. Lipscomb, *Inorg. Chem.* 1974, **13**, 2772.
41. G. G. Outterson Jr, V. T. Brice and S. G. Shore, *Inorg. Chem.* 1976, **15**, 1456.
42. J. T. Gill and S. J. Lippard, *Inorg. Chem.* 1975, **14**, 751.
43. R. D. Dobrott and W. N. Lipscomb, *J. Chem. Phys.* 1962, **37**, 1779.
44. Yu. L. Gaft, Yu. A. Ustynyuk, A. A. Borisenko and N. T. Kuznetsov, *Russ. J. Inorg. Chem.* 1983, **28**, 1266.
45. J. C. Carter and P. H. Wilks, *Inorg. Chem.* 1970, **9**, 1777.
46. E. Muetterties, *Inorg. Chem.* 1963, **2**, 647.
47. N. S. Hosmane, J. R. Wermer, Z. Hong, T. D. Getman and S. G. Shore, *Inorg. Chem.* 1987, **26**, 3638.
48. G. R. Eaton and W. Lipscomb, *NMR Studies of Boron Hydrides and Related Compounds*. Benjamin, New York (1969).
49. R. L. Middaugh and R. J. Wiersema, *Inorg. Chem.* 1971, **10**, 423.
50. F. Klanberg and E. L. Muetterties, *Inorg. Chem.* 1966, **5**, 1955.
51. This information may be inferred from the observation that while CsB_3H_8 when pyrolysed at 185°C gives $Cs_2B_{10}H_{10}$, $CsB_{11}H_{14}$ (34% yield), $CsBH_4$ and H_2, at 230°C the products are $Cs_2B_nH_n$ (n = 12, 10, 9) and H_2; data reported by J. M. Makhlouf, W. V. Hough and G. T. Hefferan, *Inorg. Chem.* 1967, **6**, 1196 and ref. 47. The conclusion is also consistent with the observation that no reaction occurs between $Me_3NH^+B_{11}H_{14}^-$ and Et_3N at 180°C, both com-

pounds being recovered unchanged after 1 h, implying that no pyrolysis of $B_{11}H_{14}^-$ occurs at this temperature; H. C. Miller, N. E. Miller and E. L. Muetterties, *Inorg. Chem.* 1964, **3**, 1456.

52. P. D. Grebenik, M. L. H. Green, M. A. Kelland, J. B. Leach and P. Mountford, *J. Chem. Soc., Chem. Commun.* 1989, 1397.
53. N. N. Greenwood, J. A. McGinntey and J. D. Owen, *J. Chem. Soc.* (*A*) 1971, 809.
54. L. J. Guggenberger, *J. Am. Chem. Soc.* 1972, **94**, 114.
55. The assumed geometry of $B_{10}H_{10}^{2-}$ had an axial–equatorial B—B distance of 1.68 Å, with equatorial–equatorial distances of 1.82 Å (within the square planes) and 1.80 Å (between the planes) and a B—H distance of 1.11 Å. The H_a—B_a—B_e and H_e—B_e—B_a angles were 130° and 122°, respectively (where a = axial, e = equatorial). For the $(\eta^5\text{-}C_5H_5)_2Zr^{2+}$ fragment the Zr—Cp(centroid) distance was 2.21 Å, with a Cp(centroid)—Zr—Cp(centroid) angle of 130°.

Polyhedron Vol. 12, No. 18, pp. 2169–2173, 1993
Printed in Great Britain

0277–5387/93 $6.00+.00
© 1993 Pergamon Press Ltd

SIX- AND SEVEN-COORDINATED MANGANESE(II) COMPLEXES OF QUATERPYRIDINE. SYNTHESIS, X-RAY CRYSTAL STRUCTURE AND CATALYST FOR ALKENE EPOXIDATION

CHIN-WING CHAN and CHI-MING CHE†

Department of Chemistry, The University of Hong Kong, Pokfulam Road, Hong Kong

and

SHIE-MING PENG

Department of Chemistry, The National Taiwan University, Taiwan

(*Received* 23 *March* 1993; *accepted* 2 *June* 1993)

Abstract—Reaction of $Mn(ClO_4)_2 \cdot xH_2O$ and $Mn(CH_3CO_2)_3 \cdot xH_2O$ with 2,2′:6′,2″:6″,2‴-quaterpyridine (QP) in acetonitrile or methanol gave the complexes $[Mn(QP)(H_2O)_2](ClO_4)_2$ and $[Mn(QP)(CH_3CO_2)(H_2O)](ClO_4)$, respectively. X-ray crystal structure determination revealed that the manganese atom is six-coordinated in the former, but seven-coordinated in the latter. Both complexes catalysed oxidation of alkenes by PhIO.

The coordination chemistry of polypyridine ligands is an active and important area of research.[1,2] Despite the fact that 2,2′-bipyridine and 2,2′:6′-2″-terpyridine and their substituted derivatives have been subjected to extensive works, there are only a few studies on the ligand 2,2′:6′,2″:6″,2‴-quaterpyridine (QP).[3–5] This ligand is expected to be more oxidation resistant and has a low energy orbital for a metal-to-ligand charge transfer transition to occur in the visible region. As part of our program in the design of new oxidative and photochemical catalysts we explore the coordination chemistry of quaterpyridine with transition metal ions. Herein is described the synthesis and structural determination of six- and seven-coordinated manganese(II) complexes of QP. A preliminary study of catalytic epoxidation will be presented.

EXPERIMENTAL

Materials

$Mn(CH_3CO_2)_3 \cdot xH_2O$ and $Mn(ClO_4)_2 \cdot xH_2O$ from Aldrich were used as received. The ligand QP was prepared by literature methods.[3] All solvents for syntheses and recrystallizations were of analytical grade.

Physical measurements and instrumentation

IR spectra were measured in KBr pellets on a Nicolet 20 SXC FT-IR spectrometer. UV–vis spectra were obtained on a Milton Roy Spectronic 3000 spectrophotometer.

Cyclic voltammograms were measured using a Princeton Applied Research (PAR) model 175 universal programmer, model 173 potentiostat and model 179 digital coulometer coupled to a Houston 2000 *X–Y* recorder. A conventional two-compartment cell was used in electrochemical measurements. A silver–silver nitrate (0.1 M in acetonitrile) reference electrode was used in degassed acetonitrile [0.1 M in $(CH_3(CH_2)_3)_4NPF_6$] with a ferrocenium–ferrocene ($Fc^{+\cdot}/Fc$) couple as the internal standard. The working electrode was glassy carbon, which was pre-treated as described previously.[6]

$[Mn(QP)(CH_3CO_2)(H_2O)](ClO_4)$ (**1**). A mixture of $Mn(CH_3CO_2)_3 \cdot xH_2O$ (0.2 g) and QP (0.1 g) in methanol (30 cm^3) was heated at 50°C for 1/2 h, after which the mixture was filtered. The filtrate was

† Author to whom correspondence should be addressed.

treated with $LiClO_4$ to give a pale yellow solid, which was then filtered and air dried.

$[Mn(QP)(H_2O)_2](ClO_4)_2$ (**2**). Excess $Mn(ClO_4)_2 \cdot xH_2O$ and QP were mixed in acetonitrile (50 cm^3) at 70°C. The resulting solution was stirred for 15 min, filtered and concentrated to *ca* 10 cm^3. Ether diffusion afforded greenish-yellow needles. IR (cm^{-1}): 1597m, 1575m, 1490m, 1466m, 1440m, 1314w, 1249w, 1192w, 1110s, 1088s, 1016w, 777s, 652w, 625m, 429w. UV–vis in CH_3CN (λ_{max}, $10^{-3}\varepsilon$): (235, 35.2), (294, 18.1), (301, 26.1), (332, 16.2), (342, 16.9).

X-ray crystallography

Yellow crystals of $[Mn(QP)(CH_3CO_2)(H_2O)](ClO_4)$ (**1**) and $[Mn(QP)(H_2O)_2](ClO_4)_2$ (**2**) were obtained by diffusion of diethyl ether into the corresponding acetonitrile solution. The intensity data were measured on an Enraf–Nonius CAD4 diffractometer equipped with graphite monochromatized Mo-K_α radiation ($\lambda = 0.7093$ Å) using a θ–2θ scan mode at 297 K with $2\theta_{max} = 50°$. Cell parameters and the space group were obtained from 24 strong reflections with 2θ in the ranges 18–27° and 19–25° for complexes **1** and **2**, respectively. For complex **1** a total of 8678 reflections were measured, 8295 of which were considered unique and 5486 of these had $I > 2\sigma(I)$; while for complex **2** a total of 2233 reflections were collected, in which 592 reflections with $I > 2\sigma(I)$ were considered out of 2142 unique reflections. All data were corrected for Lorentz and polarization effects. Empirical absorption corrections were applied. In the final cycle of refinement convergence was reached at $R = 0.045$, $R_w = 0.033$, $S = 2.56$ for complex **1** and $R = 0.070$, $R_w = 0.070$, $S = 1.99$ for complex **2**. Final difference densities were in the range -0.62–0.86 e $Å^{-3}$ for complex **1** and -0.56–0.70 e $Å^{-3}$ for complex **2**. A summary of crystallographic data is listed in Table 1. Selected bond lengths and bond angles are listed in Table 2.

Alkene oxidation by iodosobenzene catalysed by complex **2**

The reaction was conducted in degassed CH_2Cl_2/CH_3CN solution (3 : 1 volume) and under nitrogen. A mixture of complex **2** (7 mg), alkene (40 mg) and PhIO (30 mg) was stirred for 3–6 h. Excess sodium sulphite (100 mg) was added in water (3 cm^3). After excess PhIO was decomposed the organic layer was separated. The aqueous layer was extracted with 3×2 cm^3 of CH_2Cl_2. The combined organic layer was evaporated to dryness under reduced pressure. 3-Methylbenzoic acid (3 mg) was added as an internal standard. The mixture was extracted with 3×5 cm^3 petroleum ether (40–60°C), filtered through a cotton plug and evaporated under reduced pressure. NMR spectra were taken on the residues obtained.

Table 1. Crystallographic data for $[Mn(QP)(H_2O)_2](ClO_4)_2$ and $[Mn(QP)(H_2O)(CH_3CO_2)](ClO_4)(H_2O)$

Compound	$MnC_{20}H_{18}N_4Cl_2O_{10}$	$MnC_{22}H_{21}N_4ClO_8$
Mol. wt	600.22	559.83
Crystal system	Monoclinic	Triclinic
Space group	$C2/c$	$P\bar{1}$
a (Å)	14.299(2)	13.619(2)
b (Å)	11.164(3)	13.848(2)
c (Å)	15.422(5)	13.865(3)
α (°)	90	81.26(2)
β (°)	99.94(2)	111.94(1)
γ (°)	90	102.82(1)
V ($Å^3$)	2424.9(1)	2358.0(7)
$F(000)$	1220	1148
Z	4	4
D_{calc} (g cm^{-3})	1.644	1.580
R	0.070	0.045
R_w	0.070	0.033
ρ (e $Å^{-3}$)	-0.56, $+0.70$	-0.62, $+0.86$
μ (mm^{-1})	0.80	0.70

Table 2. Selected bond lengths (Å) and bond angles (°) for $[Mn(QP)(H_2O)(CH_3CO_2)](ClO_4)$ (**1**) and $[Mn(QP)(H_2O)_2](ClO_4)_2$ (**2**)

	1	**1**[a]		**2**
Mn—O(5)	2.164(3)	2.193(3)	Mn—O(water)	2.179(5)
Mn—O(1), O(2)	2.323(3), 2.301(3)	2.271(3), 2.300(3)	—	—
Mn—N(1), N(4)	2.360(3), 2.367(3)	2.337(3), 2.347(3)	Mn—N(1), N(1A)	2.282(5)
Mn—N(2), N(3)	2.318(3), 2.311(3)	2.291(3), 2.289(3)	Mn—N(2), N(2A)	2.214(6)
C(15)—C(16)	1.48(1)	1.48(1)	C(5)—C(6)	1.46(1)
C(20)—C(21)	1.49(1)	1.49(1)	C(10)—C(10A)	1.48(1)
N(1)—Mn—N(4)	151.6(1)	149.6(1)	N(1)—Mn—N(1A)	144.5(2)
N(1)—Mn—N(2)	68.5(1)	69.2(1)	N(1)—Mn—N(2)	72.0(2)
N(2)—Mn—N(3)	69.3(1)	69.8(1)	N(2)—Mn—N(2A)	71.4(2)
N(1), (4)—Mn—O(5)	82.4(1), 80.3(1)	81.0(1), 80.9(1)	N(1)—Mn—O(1)	84.3(2)
N(1), (4)—Mn—O(1)	99.6(1), 87.7(1)	95.1(1), 94.7(1)		86.6(2)
N(1)—Mn—O(2)	80.6(1)	79.9(1)	—	—
N(2), (3)—Mn—O(5)	106.7(1), 103.2(1)	102.4(1), 100.4(1)	N(2)—Mn—O(1)	101.6(2)
N(2), (3)—Mn—O(1)	95.9(1), 91.5(1)	92.2(1), 94.1(1)		102.7(2)
N(4)—Mn—O(2)	80.7(1)	81.5(1)	—	—
O(5)—Mn—O(1)	156.2(1)	162.2(1)	O(1)—Mn—O(1A)	150.0(2)
O(5)—Mn—O(2)	100.9(1)	105.0(1)	—	—
N(1)—C(15)—C(16)	115.6(3)	114.9(3)	N(1)—C(5)—C(6)	116.4(6)
N(2)—C(20)—C(21)	115.2(4)	115.4(4)	N(2)—C(10)—C(10A)	114.3(6)

[a] There are two independent manganese complexes in an asymmetric unit of **1**.

RESULTS AND DISCUSSION

X-ray structure determination

The reaction of quaterpyridine with $Mn(CH_3CO_2)_3 \cdot xH_2O$ in methanol or ethanol rapidly gave $[Mn(QP)(CH_3CO_2)(H_2O)]^+$, which was isolated as the perchlorate salt in high yield. A similar reaction with $Mn(ClO_4)_2$ in acetonitrile gave the six-coordinated $[Mn(QP)(H_2O)_2](ClO_4)_2$. The IR spectrum of **1** shows strong absorption bands at 3400 and 3230 cm^{-1}, attributed to $\nu(OH_2)$ stretches. The UV–vis absorption spectrum of **1** or **2** in acetonitrile is featureless, being dominated by the intraligand $\pi \rightarrow \pi^*$ transitions at 342, 333 and 302 nm.

The structures of the manganese complexes **1** and **2** have been determined by X-ray crystallography. There are two independent molecules of complex **1** in an asymmetric unit, but these are not significantly different from each other (see Table 2). A perspective view of one cation of **1** with its atomic numbering scheme is shown in Fig. 1. The central manganese atom adopts the common coordination geometry for seven-coordinated manganese(II) complexes—distorted pentagonal-bipyramidal.[7] The equatorial sites are occupied by the four nitrogen atoms of quaterpyridine and one of two oxygen atoms of the chelating acetate ligand. The N_4O donor set of atoms, which form the pentagon, are approximately co-planar with the acetate oxygen atom slightly deviating from the plane defined by N(1)–N(4). The measured ∠O(1){acetate}—Mn—O(5){water} of 156.2(1)–162.2(1)° is substantially deviated from linearity. Such bending is probably a result of the presence of the chelating

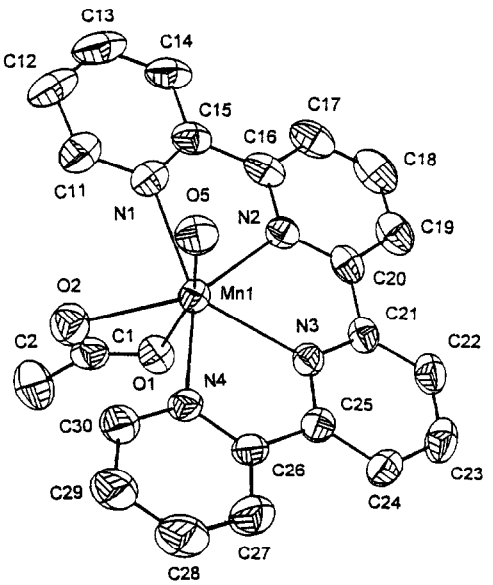

Fig. 1. ORTEP view of $[Mn(QP)(H_2O)(CH_3CO_2)]^+$.

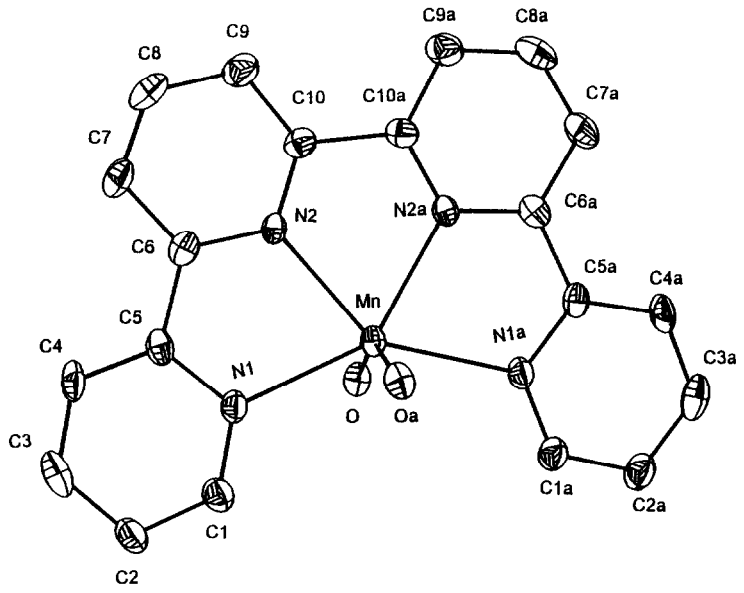

Fig. 2. ORTEP view of $[Mn(QP)(H_2O)_2]^{2+}$.

acetate ligand and the large void angle defined by N(1)—Mn—N(4), similar to the situation in **2**.

A comparison between the reported structure with that of $[Ni(QP)(CH_3CN)_2][PF_6]_2$,[3] $[Pt(QP)](ClO_4)_2$[4b] and $[Co(QP)(H_2O)(SO_3)](NO_3)]\cdot H_2O$[5] reveals much smaller N(1)—M—N(4) void angles for the nickel(II), platinum(II) and cobalt(II) complexes. This is in accord with previous works which indicated that seven-coordinated metal complexes of QP have much larger N(1)—M—N(4) void angles.

The structures of six-coordinated **2** can best be described as a skew-trapezoidal-bipyramid (see Fig. 2). The short edge is comprised of two central pyridyl rings, while the long edge can be imagined as two terminal pyridyl rings and the void between them. Upon coordination the water molecules in the axial positions skew towards the long axis of the trapezoid, i.e. the open end of QP, with ∠O(1)—Mn—O(1A) at 150.0(2)°. Furthermore, the absence of a fifth equatorial coordinated atom in complex **2** allowed closer approach of the axial oxygen atoms and the equatorial nitrogen atoms.

In these structures two mirror planes were retained and the quaterpyridines are essentially coplanar.

The two central Mn—N bonds in both **1** and **2** are slightly shorter than the two outer Mn—N bonds. This may be due to the constrained effect of the quaterpyridine ligand. Nevertheless, these Mn—N distances are normal and comparable to those values of 2.276(4)–2.328(4) Å found in [Mn(dapb)(H_2O)Cl]Cl [dapb = 2,6-diacetylpyridinebis-(benzoylhydrazone)].[6] The Mn—O(5) {water} distance of **1** is somewhat shorter than the average Mn—O(1),(2) {acetate} distance, probably due to the limited ∠O(1)—C(1)—O(2) bite angle of acetate.

As the extent of QP distortions in both **1** and **2** are almost the same [∠N(1)—C(15)—C(16) = 114.9(3)–115.6(3), ∠N(2)—C(20)—C(21) = 115.2(4)–115.4(4); ∠N(1)—C(5)—C(6) = 116.4(6), ∠N(2)—C(10)—C(10A) = 114.3(6)] the almost equal magnitude of void angles in coordinated QP for both seven- and six-coordinate manganese(II) indicates that isolation of the seven-coordinated manganese(II) quaterpyridine complex is possible as long as suitable chelating molecules are present. Furthermore, the larger void angle of complex **2** compared with $[Pt(QP)](ClO_4)_2$[4b] suggests strong interaction of QP with third row transition elements.

Interestingly enough, the quinquepyridine manganese(II) complex was not available from direct synthesis, which was found to be retarded by water.[8] This result was consistent with the fact that manganese(II) generally has a stronger preference for oxygen than nitrogen. The isolation of quaterpyridine manganese(II) complexes again demonstrates the unique chelating strength of four rigidly bridged equatorial pyridyl units.

Electrochemistry

The generation of manganese(III) from complex **2** using the cyclic voltammetric method was unsuccessful as complex **2** was unstable towards decomposition in aqueous solution. A voltammograph was recorded in degassed acetonitrile

Table 3. Epoxidation catalysed by $[Mn(QP)(H_2O)_2](ClO_4)_2$ (**2**)

	Cis-stilbene[a]	*Trans*-stilbene[a]	Styrene[b]	Norbornene[b]
Turnover	1[c] 0.3[f]	4[c]	16[d]	3[e]

[a] Reaction time 6 h.
[b] Reaction time 3 h.
[c] *Trans*-stilbene oxide.
[d] Styrene oxide.
[e] *Exo*-2,3-epoxynorbornane.
[f] *Cis*-stilbene oxide.

solution [0.1 M $(CH_3(CH_2)_3)_4NPF_6$], which can afford an oxidative scan up to +2.5 V. However, no oxidative wave was observed within this condition. Reduction of **2** was observed at *ca* −1.7 V (vs $Fc^{+\cdot}/Fc$), which was believed to be ligand-centre reduction.[9]

Alkene epoxidation by PhIO

Complex **2** was found to catalyse alkene epoxidation by PhIO. A lightly coloured suspension of the reaction mixture turned into a dark green solution within minutes. The reaction was found to be non-stereospecific as *cis*-stilbene gives both *trans*- and *cis*-stilbene oxide with more than 70% *trans*-isomer (see Table 3). Oxo-transfer was more effective with less sterically hindered alkenes as the turnover number for styrene was four times greater than that of *trans*-stilbene and about 20-fold to that of *cis*-stilbene. A small amount of benzaldehyde was detected for styrene oxidation.

Acknowledgements—We acknowledge support from The University of Hong Kong and the National Science Council of Taiwan. CMC acknowledges a visiting professorship, administered by the National Taiwan University.

REFERENCES

1. E. C. Constable, *Adv. Inorg. Chem. Radiochem.* 1986, **30**, 69.
2. E. C. Constable, *Adv. Inorg. Chem. Radiochem.* 1989, **34**, 1.
3. E. C. Constable, S. M. Elder, J. Healy and D. A. Tocher, *J. Chem. Soc., Dalton Trans.* 1990, 1669.
4. (a) C. M. Che, Y. P. Wang, K. S. Yeung, K. Y. Wong and S. M. Peng, *J. Chem. Soc., Dalton Trans.* 1992, 2675; (b) C. W. Chan, C. M. Che, M. C. Cheng and Y. Wang, *Inorg. Chem.* 1992, **31**, 4874.
5. E. N. Maslen, C. L. Raston and A. H. White, *J. Chem. Soc., Dalton Trans.* 1975, 323.
6. C. M. Che, K. Y. Wong and F. C. Anson, *J. Electroanal. Chem.* 1987, **226**, 211.
7. C. Lorenzini, C. Pelizzi, G. Pelizzi and G. Predieri, *J. Chem. Soc., Dalton Trans.* 1983, 721.
8. E. C. Constable, J. Lewis and M. Schröder, *Polyhedron* 1982, **1**, 311.
9. (a) C. W. G. Ansell, J. Lewis, J. N. Ramsden and M. Schröder, *Polyhedron* 1983, **2**, 489; (b) E. C. Constable, S. M. Elder and D. A. Tocher, *Polyhedron* 1992, **11**, 1337.

Polyhedron Vol. 12, No. 18, pp. 2175–2184, 1993
Printed in Great Britain

0277-5387/93 $6.00+.00
© 1993 Pergamon Press Ltd

AN EXAFS STUDY OF GRIGNARD COMPOUNDS IN SOLUTION

T. S. ERTEL* and H. BERTAGNOLLI

Institut für Physikalische Chemie, Universität Stuttgart, Pfaffenwaldring 55, D-7000 Stuttgart 80, F.R.G.

(*Received* 5 *April* 1993; *accepted* 2 *June* 1993)

Abstract—The results of an EXAFS study of the Grignard compounds methyl, ethyl and phenyl magnesium bromide in diethyl ether and vinyl magnesium bromide in tetrahydrofuran are presented in this paper. The degree of molecular association and the local structure around the central magnesium atoms are deduced from the determined distances and coordination numbers.

Grignard compounds in general are probably the most popular organometallic substrates. Since their detection in 1900 by Victor Grignard,[1] their widespread applicability as precursors in synthetic organic and inorganic chemistry have increased over the decades. Grignard reagents can be successfully employed, e.g. in the synthesis of alcohols, aldehydes, ketones, carboxylic acids, esters, amines and mercaptans. The synthesis of ligands or organometallic complexes is also a field of application. Although the Grignard reagents have been used for over 90 years, considerable confusion exists as to their precise nature in solution.[2–8] Almost all methods of physical chemistry have been used to shed some light on the possible equilibria and the species contributing to it.

Molecular weight studies provided the existence of dimeric and oligomeric species in solution.[9] These results, however, are questionable. On the one hand, contamination by oxygen and water was not sufficiently considered.[10–12] On the other hand, this method does not provide any information about the degree of solvation and the geometry of this species.[13]

The question of how dimers are existing, either as R_2MgX_2Mg or $RMgX_2MgR$, was studied by tracer experiments. Former studies showed no exchange of ^{28}Mg.[14] Therefore, the dimer should be written as R_2MgX_2Mg. Recent studies, however, showed a statistical exchange of ^{28}Mg and the former results were not reproduced.[15]

Measurements of the electrolytic conductivity revealed the existence of ionic species.[16–21] The results, however, show that the amount of ions is very small. Therefore, ionic species must not be taken into account for the description of the character of Grignard compounds in solution.

The existence of dimers of the type R_2MgX_2Mg with coordinating diethyl ether was derived from the IR spectroscopic data of CH_3CH_2MgBr.[22,23] C_6H_5MgI in diethyl ether is supposed to be a monomer, besides some small amounts of $(C_6H_5)_2MgI_2$ and $(C_6H_5)_2Mg$. THF solutions of alkyl magnesium bromides and chlorides can be described in terms of an equilibrium between two RMgX and R_2Mg/MgX_2.[24]

^1H NMR studies of alkyl magnesium halogenides in diethyl ether suggest that R_2MgX_2Mg is the predominant species, because their spectra are very similar to those of the corresponding dialkyl magnesium compounds.[25,26] Solutions of aryl magnesium compounds showed a dependence of the equilibrium constant on the type of aryl group. Furthermore, the contribution of the R_2Mg species increases with the coordinating ability of the solvent.[27–29] The only ^{25}Mg NMR study of CH_3CH_2MgBr in THF provided evidence of CH_3CH_2MgBr, $MgBr_2$ and $(CH_3CH_2)_2Mg$.[30] For reasons of completeness ^{13}C NMR studies of various organomagnesium bromides and chlorides should be mentioned.[31–34] However, all these inves-

* Author to whom correspondence should be addressed.

tigations did not provide any information about the possible structures of the species.

Although X-ray diffraction studies have been performed on ethyl and phenyl magnesium bromide dietherates in the solid state,[35-37] only little information is available on structural features such as the intra- and interatomic distances of Grignard reagents in solution. Extended X-ray absorption fine structure (EXAFS) and large angle scattering (LAXS) were used to determine the structure of magnesium bromide and iodide in diethyl ether and THF.[38] The structure of methyl, ethyl and phenyl magnesium bromide in diethyl ether in the concentration range 0.1–1.0 M was also investigated with these two spectroscopic methods.[39]

We decided to perform EXAFS measurements on methyl, ethyl and phenyl magnesium bromide in diethyl ether and vinyl magnesium bromide in THF with concentrations of 3.12, 3.04, 2.96 and 1.56 M. Since in the EXAFS study mentioned above the existence of a second shell could not be observed,[39] we investigated more highly concentrated solutions, thereby increasing the probability of detecting a second or even higher shell, which are a prerequisite for a reasonable structural proposal.

The EXAFS phenomenon is based upon the absorption of X-rays in a particular absorbing atom and the oscillatory variation of the X-ray absorption coefficient μ as a function of the photon energy E beyond an absorption edge. The resulting modulation of $\mu(E)$ provides information about the kind, number and distance of neighbours surrounding the absorbing atom.[40,41]

EXPERIMENTAL

The EXAFS experiment was performed at the bromine K-edge at 13474.0 eV at the beamline RÖMO II at the Hamburger Synchrotronstrahlungslabor (HASYLAB) at DESY, Hamburg, at 20°C, using a Si⟨311⟩ crystal monochromator under ambient conditions (5.4 GeV, beam current 50 mA). Data were collected in the transmission mode with ion chambers. The first ion chamber, monitoring I_0, with a length of 15 cm was continuously flushed with a mixture of 7% argon and 93% nitrogen. The second and third ion chambers, recording I_1 and I_2, respectively, with a length of 30 cm were flushed with 100% argon. The fill of the ion chambers was chosen in such a way that *ca* 10% of the incident X-rays were absorbed in the first ion chamber and about 80% in the sample itself.[42] Energy calibration was monitored with a 30 μm thick anhydrous $MgBr_2$ sample as a reference. All measurements were performed under an inert gas atmosphere. A sample cell suitable for measuring air- and moisture-sensitive compounds was used. We first calculated the sample thickness and, after a test scan, adjusted it to the optimal values depending on the investigated sample.

Data reduction

The common data reduction procedure involves fitting the pre-edge absorption with a Victoreen-type polynomial, extrapolating beyond the edge and subtraction from the total absorption coefficient to give the corrected absorption coefficient. The next step is background removal, which was performed by the use of a modified smoothing spline algorithm, and subsequent normalization with the determined spline. Following Fourier transformation and Fourier filtering in the relevant ranges provides the contribution of one or more backscatterers to these separated coordination shells.[40,41] The background removal of spectra of liquid compounds is very demanding. On the one hand, the high noise level of the data caused by the static disorder is a problem. On the other hand, a high flexibility of the smoothing spline increases the risk of removing part of the few EXAFS oscillations, typical for spectra of liquid compounds. The way of successfully dealing with all the problems and a very detailed description of the used program package with an example of the data analysis for methyl magnesium bromide in diethyl ether are given in ref. 43. In order to determine the coordination number N more accurately, the $\chi(k)$ functions were deconvoluted with the monochromator resolution as a response function. This procedure compensates for the decrease of the $\chi(k)$ amplitude caused by the limited and energy-dependent resolution of the monochromator. In order to determine the degree of association the accuracy to which the coordination number is known plays an important role. The applied weighting scheme and the ranges for Fourier transformation and Fourier filtering for the compounds methyl (MeMgBr), ethyl (EtMgBr), phenyl magnesium bromide (PhMgBr) in diethyl ether and vinyl magnesium bromide (ViMgBr) in THF are shown in Table 1. The background-corrected $k^3\chi(k)$ functions and the Fourier transforms are shown in Fig. 1.

RESULTS

Interpretation and curve fitting with EXCF

The Fourier transforms of all Grignard compounds show a well pronounced first coordination shell (Fourier filtering range 2). It was found that this peak contains the contribution of a single mag-

Table 1. Table of the applied weighting scheme and the ranges of Fourier transformation and Fourier filtering

Compound	MeMgBr	EtMgBr	PhMgBr	ViMgBr
Weighting k^n	3	3	3	3
k range (Å^{-1})	2.55–10.46	2.59–9.95	2.54–11.37	2.50–9.99
Window function	Square	Square	Square	Square
Fourier filtering ranges (Å)				
1	1.56–3.34	1.52–3.38	1.56–3.38	1.52–3.38
2	1.56–2.74	1.52–2.76	1.56–2.60	1.52–2.56
3	2.74–3.34	2.76–3.38	2.60–3.38	2.56–3.38

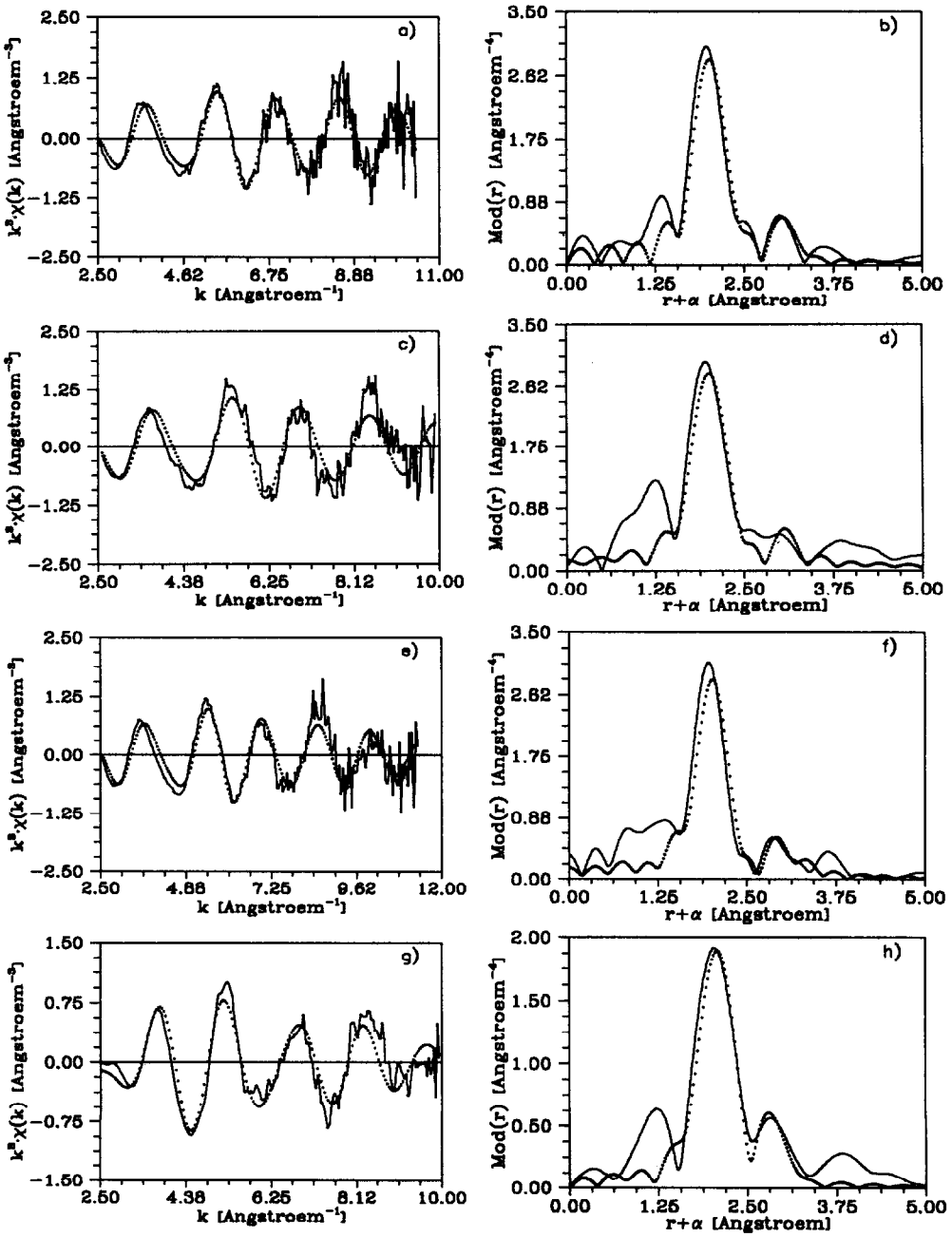

Fig. 1. Experimental (solid line) and theoretically calculated (dots) $k^3\chi(k)$ functions by FEFF, the Fourier transforms and the Fourier transformed best fits (dots) for MeMgBr (a, b), EtMgBr (c, d) and PhMgBr (e, f) in diethyl ether and ViMgBr (g, h) in tetrahydrofuran.

nesium backscatterer to the $k^3\chi(k)$ function. Furthermore, the Fourier transforms show a small second maximum (Fourier filtering range 3). The question now is whether the second peak is an artefact, i.e. a side lobe of the first coordination shell, or a real contribution of other backscatterers. To settle this question the Fourier transforms of the k^n ($n = 0, 1, 2, 3$) weighted $\chi(k)$ functions, multiplied by five different window functions, were compared. The second peak, however, was found in all 20 Fourier transforms of the respective Grignard compound. More proof of the existence of a second coordination shell is that the Fourier filtered ranges of the first peak do not provide a satisfactory description of the $\chi(k)$ functions, i.e. there is a lack of a further frequency component. How many and which kind of backscatterers contribute to this second coordination shell? Only in the case of ViMgBr in THF a single oxygen backscatterer provides the best fit. For all the other compounds the description with a single oxygen backscatterer was insufficient. We tried all reasonable combinations of backscatterer pairs and the oxygen/bromine pair yielded the best results. χ^2, a measure for the agreement of the experimental and theoretically calculated function,[43] was *ca* 200% lower than for other pairs. The improvement reached with a third backscatterer was not significant. Therefore, the existence of a further backscatterer could be ruled out with a high probability. One of the concepts of EXAFS, however, is to achieve a maximum of agreement between theoretically calculated and experimental functions with a mininum of parameters. The curve fitting procedure was performed

Table 2. Summary of the structural parameters—absorber–backscatterer distance r (Å), coordination number N, Debye–Waller factor σ (Å) and the shift of the threshold energy ΔE_0—for the Grignard compounds obtained with the amplitude and phase functions calculated by FEFF and McKale; the coordination number N was corrected for monochromator resolution

	Backscatterer	r (Å)	N	σ (Å)	ΔE_0 (eV)
Methyl magnesium bromide in diethyl ether					
FEFF	Mg	2.475	0.65	0.0571	—
	Br	3.494	0.15	0.1045	—
	O	3.662	0.70	0.0904	—
McKale	Mg	2.476	0.66	0.0670	+3.43
	Br	3.494	0.21	0.1059	+0.01
	O	3.662	0.66	0.0919	−0.01
Ethyl magnesium bromide in diethyl ether					
FEFF	Mg	2.479	0.86	0.0770	—
	Br	3.466	0.30	0.1107	—
	O	3.694	0.84	0.0967	—
McKale	Mg	2.479	0.84	0.0799	+3.43
	Br	3.466	0.37	0.1153	+0.01
	O	3.694	0.86	0.0964	−0.01
Phenyl magnesium bromide in diethyl ether					
FEFF	Mg	2.464	0.71	0.0701	—
	Br	3.472	0.32	0.1116	—
	O	3.695	0.93	0.1077	—
McKale	Mg	2.464	0.73	0.0773	+3.41
	Br	3.469	0.38	0.1227	−0.01
	O	3.679	0.73	0.0981	0.00
Vinyl magnesium bromide in tetrahydrofuran					
FEFF	Mg	2.527	0.74	0.0945	—
	O	3.377	0.79	0.1140	—
McKale	Mg	2.524	0.73	0.0988	+3.41
	O	3.378	0.69	0.1032	+0.04

with theoretical amplitude and phase functions by McKale,[44] as well as with those calculated by the program FEFF (V3.1).[45,46] With McKale phases and amplitudes, $\lambda(k)$ is approximated by the universal curve for inorganic compounds and the amplitude reducing factor $S_0^2(k)$ was set to 1.0. The program FEFF provides the possibility of exactly calculating $\lambda(k)$ and $S_0^2(k)$, which are used in the least-squares refinement to fit the EXAFS data. The first and the second coordination shell were refined separately, as well as in combination. It is a matter of fact that due to the correlation of the shells and termination of series effects caused by the Fourier filtering, the values obtained by both methods differ marginally.

The results of the least-squares refinement for the combination of the first and second coordination shell—with theoretical amplitude and phase functions calculated by FEFF–are shown in Fig. 1. The structural parameters for the Grignard compounds—i.e. absorber–backscatterer distance r (Å), the corresponding coordination number N, the Debye–Waller factor σ (Å) and the shift of the threshold energy ΔE_0 (eV) obtained with the amplitude and phase functions of FEFF and McKale for the combination of the first and second coordination shell—are shown in Table 2.

Curve fitting with EXCURV90

The structural parameters obtained with EXCURV90 are given in Table 3. The first and second coordination shell were refined together. The results obtained with EXCURV90 provide

Table 3. Summary of the structural parameters—absorber–backscatterer distance r (Å), coordination number N and Debye–Waller factor σ^2 (Å^2)—for the Grignard compounds obtained with EXCURV90; furthermore, the shift of the threshold energy ΔE_0 and the fit-index are given

	Backscatterer	r (Å)	N	σ^2 (Å^2)	ΔE_0 (eV)	Fit-index[a]
Methyl magnesium bromide in diethyl ether						
Three shell fit	Mg	2.452	0.91	0.005		
	Br	3.489	0.37	0.010		
	O	3.666	0.59	0.007	13.95	17.81
Four shell fit	Mg	2.447	0.87	0.005		
	Br	3.490	0.29	0.003		
	O	3.664	1.37	0.006		
	O	3.394	0.79	0.003	14.61	11.79
Ethyl magnesium bromide in diethyl ether						
Three shell fit	Mg	2.454	1.23	0.008		
	Br	3.460	0.26	0.010		
	O	3.644	0.62	0.007	13.98	18.40
Four shell fit	Mg	2.452	1.16	0.007		
	Br	3.475	0.50	0.010		
	O	3.681	1.48	0.006		
	O	3.416	0.73	0.004	14.07	12.48
Phenyl magnesium bromide in diethyl ether						
Three shell fit	Mg	2.437	0.97	0.006		
	Br	3.426	0.26	0.010		
	O	3.633	0.67	0.007	14.82	14.60
Four shell fit	Mg	2.437	0.96	0.006		
	Br	3.438	0.23	0.007		
	O	3.636	1.29	0.008		
	O	3.374	0.67	0.010	14.82	12.45
Vinyl magnesium bromide in tetrahydrofuran						
Two shell fit	Mg	2.503	0.97	0.010		
	O	3.345	1.26	0.013	13.21	15.34

[a] Only one shift of the threshold energy ΔE_0 for all backscatterers is calculated within EXCURV90. The fit-index is a measure for the agreement with the experimental data.

additional evidence that the second maximum of the Fourier transform is a real peak. In analogy to the curve-fitting process with EXCF it was tried to describe the Fourier filtered EXAFS functions (Fourier filtering range 1, see Table 1) with one Mg, Br and O backscatterer (MeMgBr, EtMgBr, PhMgBr) or with only one Mg and O backscatterer (ViMgBr). With these backscatterers a good agreement between experimental and theoretically calculated function was achieved. EXCURV90, however, provides the possibility of calculating the significance of added shells when iterations are carried out after adding a new shell. On the contrary to the results of the iterations obtained with EXCF[43] there is a 99% probability for the existence of a further oxygen backscatterer contributing to the second maximum for MeMgBr, EtMgBr and PhMgBr, but not for ViMgBr. For further information concerning the Joyner statistic test see the manual of EXCURV90 and ref. 47.

Curve fitting with model amplitudes and phases

The fit for the experimental data with theoretical amplitude and phase functions yields values of the coordination numbers, which are unexpectedly low, even for the first coordination shell. This is caused by the shortcomings of the used theoretical amplitude and phase functions. Therefore, we tried $MgBr_2$ as a model compound, whose EXAFS spectrum at the bromine *K*-edge was measured as a reference. However, it was impossible to isolate the Br—Mg model amplitude and phase from the first peak in the radial distribution function, because oxygen backscatterers contribute to this peak ($MgBr_2$ is extremely moisture sensitive). Therefore, we decided to use NaBr as a model compound for the Br—Mg pair* for reasons of phase transferability.[48–53] The coordination number for the Br—Na pair was of course corrected for monochromator resolution, too.

With the extracted amplitude and phase functions for the Br—Na absorber–backscatterer pair the number of magnesium atoms in the first shell of bromine in methyl, ethyl, phenyl and vinyl magnesium bromide is 1.60 ± 0.07, 1.62 ± 0.08, 1.33 ± 0.09 and 0.97 ± 0.10. The distances changed to 2.556 ± 0.013, 2.560 ± 0.014, 2.546 ± 0.014 and 2.607 ± 0.015 Å. The deduced standard errors for the distances and coordination numbers are a consequence of possible errors in the extracted model amplitudes and phases.

DISCUSSION

Based upon the structural parameters obtained with the described curve fitting procedures a structural model for the Grignard compounds MeMgBr, EtMgBr and PhMgBr in diethyl ether and ViMgBr in tetrahydrofuran may now be developed. The values of the Br and O coordination numbers will not be discussed, because the contribution of this second coordination sphere to the EXAFS is very small and no model amplitude and phase functions were available. Additionally, the error for the determination of coordination numbers for second shells is *ca* $\pm30\%$.[54] The interpretation of the magnesium coordination numbers, however, is rather reliable. First, the coordination number of the first coordination sphere of the bromine atom calculated with model amplitude and phase functions has considerable confidence. Secondly the first maximum in the radial distribution function contains the contribution of only one kind of backscatterer at a defined distance. With the extracted model amplitude and phase functions for the Br—Na absorber–backscatterer pair, the Mg coordination numbers for methyl, ethyl and phenyl magnesium bromide in diethyl ether and vinyl magnesium bromide in tetrahydrofuran are 1.60 ± 0.07, 1.62 ± 0.08, 1.33 ± 0.09 and 0.97 ± 0.10. The fact that the magnesium coordination numbers are higher than one is an indication of an association of the compounds MeMgBr, EtMgBr and PhMgBr in diethyl ether. This is supported by molecular weight studies.[12,55,56] The existence of a Br—Br pair, as it is deduced from the simulation of the second shell, confirms the association too. However, a Br—Br distance of about the deduced value could also be the result of an equilibrium between $MgBr_2$, MgR_2 and RMgBr. The coordination number of bromine with respect to magnesium, however, would in the case of an equilibrium strictly be one. Considering the structural parameters only, higher associates like oligomers cannot be excluded. However, the following discussion is restricted to monomers and dimers for reasons of clarity. According to the Br—Mg coordination number the percentage of dimers in the ethereal solutions is $60\pm7\%$, $62\pm8\%$ and $33\pm9\%$, respectively. Large angle X-ray scattering (LAXS) investigations revealed a degree of dimerization of 54%, 45% and 34% for 2.7 M, 2.7 M and 1.5 M solutions of methyl, ethyl and phenyl magnesium iodide in diethyl ether, basing upon the

* A normalization of the coordination number of the Br—Br and Br—O pairs seemed to be useless, because the contribution of these pairs to the experimental $k^3\chi(k)$ function is too small. The coordination numbers of these pairs will be discussed only qualitatively and are not used to derive a structure model.

deduced Mg—I coordination numbers.[39] Assuming that the tendency to form associates for organomagnesium ioides is lower than for organomagnesium bromides,[12,55,56] the proposed degree of dimerization of the bromides is in very good agreement with those results. The lower degree of dimerization of phenyl magnesium bromide is caused by the higher steric demands of phenyl groups in common.

Molecular weight studies of organomagnesium bromides in tetrahydrofuran provided no evidence of the existence of associated species, even at very high concentrations.[57,58] The Br—Mg coordination number of 0.97 ± 0.10 for the solution of vinyl magnesium bromide in tetrahydrofuran confirms the existence of monomers, too. Also, no Br—Br absorber–backscatterer pair was found by analysing the EXAFS data.

Summarizing these results, the samples in diethyl ether are mixtures of monomers and dimers. In tetrahydrofuran, however, only monomers are formed. The structure of the monomeric species is now deduced from the obtained Br—Mg and Br—O distances.*

With the results obtained with the programs EXCF (see Table 2) and EXCURV90 (see Table 3) for three backscatterers (Mg, Br, O), Br—Mg—O bond angles of 120.0°, 109.48° and 90.0° and the corresponding Mg—O distances were calculated. The average Mg—O distance in crystalline Grignard compounds is 2.10 ± 0.07 Å.[35–37,59–61] Assuming that there is no considerable change of this distance in solution, the deduced Mg—O distances should be about 2.10 ± 0.30 Å, depending on the calculated Br—Mg—O angle. For the compounds methyl, ethyl and phenyl magnesium bromide in diethyl ether values of Mg—O distances in the mentioned range were reproduced for a Br—Mg—O bond angle of 109.48°. A bond angle of 90° is the only reasonable one for vinyl magnesium bromide in tetrahydrofuran (see Table 4). The conclusion is that the systems in diethyl ether and ViMgBr in tetrahydrofuran are most likely to have tetrahedral or octahedral monomeric structure, respectively.

A Br—Br absorber–backscatterer pair was only found in the etheral solutions, but not for ViMgBr in tetrahydrofuran. Up to now all investigations of Grignard compounds exclude an *inter*molecular Br—Br interaction between monomeric species. In associated structures, the halogen atoms commonly function as bridging atoms. Therefore, we assume that the Br—Br pair belongs to a dimer species. Nevertheless, an EXAFS spectroscopical detection of an intermolecular Br—Br contact is very unlikely due to the high static and thermal disorder in these solutions and the resulting high Debye–Waller factors.[62]

From the experimentally determined values of Br—Mg and Br—Br distances a Br—Mg—Br bond angle of $89.9 \pm 1.6°$ was deduced (see Table 4). Since the compounds in diethyl ether are most likely to have a tetrahedral monomer geometry, the monomer subunits could form distorted tetrahedral dimers. However, such a distorted tetrahedral dimer in solution is very unlikely. X-ray diffraction studies showed that Grignard compounds crystallize as monomer tetrahedral dietherates and do not have any tendency to form distorted tetrahedral dimers.[35–37,60] A more probable structure model with a Br—Mg—Br bond angle of $89.9 \pm 1.6°$ is provided by the formation of octahedral dimers. Assuming such an octahedral dimer, an additional and shorter Br—O distance than this one we found with EXCF should have been detected. Indeed, when we performed iterations with EXCURV90 a further and distinctively shorter Br—O distance with a 99% probability for its existence was determined.

With the results for the Br—Mg and the short Br—O distances, the calculation of Mg—O distances for Br—Mg—O bond angles of 120.0°, 109.48° and 90.0° was repeated. Only a bond angle of 90.0° provides a reasonable Mg—O distance (see Table 4). The determined bond angle favours the proposed octahedral dimers, but does not exclude the existence of octahedral monomers.

The Grignard compounds methyl, ethyl and phenyl magnesium bromide are existing as monomers of the type T_m and O_m as well as dimers of the type O_d (see Fig. 2). The percentage of dimer species is $60 \pm 7\%$, $62 \pm 8\%$ and $33 \pm 9\%$. For methyl and ethyl magnesium bromide the equilibrium is on the side of the dimer and for phenyl magnesium bromide on the side of the monomer species due to steric reasons. The structure of vinyl magnesium bromide in THF can best be described as an octahedral monomer of the type O_m.

It should be noted here that the EXAFS-spectroscopical results do not give any information concerning the *position* of the organic residues at the magnesium atom of the dimers. Therefore, a distinction between octahedral dimers of the types R_2MgBr_2Mg and $RMgBr_2MgR$ (with supporting molecules of solvation) is not possible. The ^1H NMR studies of methyl and ethyl magnesium bromide in diethyl ether[25,26] provided evidence for octahedral dimers of the type R_2MgBr_2Mg,

* The errors for absorber–backscatterer distances of second or higher shells are only *ca* 5%.[54]

Table 4. The derived Br—Mg—Br bond angles and Mg—O distances, deduced from the obtained Br—Mg, Br—Br and Br—O distances (the standard errors, if indicated, are a consequence of the combination of *all* iteration results, i.e. multi-shell fits with EXCF as well as with EXCURV90)

Compound		∠Br—Mg—Br (°)	Mg—O (Å) 120.0°	Mg—O (Å) 109.48°	Mg—O (Å) 90.0°
MeMgBr	Three shell fits	90.3±0.4	1.76±0.01	2.03±0.01	2.73±0.01
	Four shell fit	91.0	1.77	2.03	2.73
			1.43	1.67	2.35
EtMgBr	Three shell fits	89.2±0.4	1.75±0.02	2.02±0.02	2.71±0.02
	Four shell fit	90.2	1.78	2.05	2.75
			1.44	1.70	2.38
PhMgBr	Three shell fits	89.4±0.1	1.76±0.02	2.03±0.03	2.72±0.03
	Four shell fit	89.7	1.74	2.01	2.70
			1.41	1.66	2.33
ViMgBr	Two shell fits	—	1.31±0.01	1.55±0.01	2.24±0.02

whereas phenyl magnesium bromide in diethyl ether exists as a mixture of R_2MgBr_2Mg and $RMgBr_2MgR$.[27-29] Our MOPAC V6.0[63,64] calculations with the Hamilton operator PM3, however, showed that octahedral dimers of the type $RMgBr_2MgR$ are more stable than the R_2Mg Br_2Mg species *independent* from the kind of the organic residue R.

The deduced Mg—O distance for an octahedral geometry (O_m, O_d) is 2.35±0.03 Å for the samples dissolved in diethyl ether, for vinyl magnesium bromide in tetrahydrofuran it is 2.24±0.02 Å. Such an Mg—O distance in tetrahydrofuran can only be assigned to the structure model O_m, whereas this distance for the compounds in diethyl ether can be assigned to the complexes of the type O_m and O_d or O_d only. The structure model O_d is very reasonable

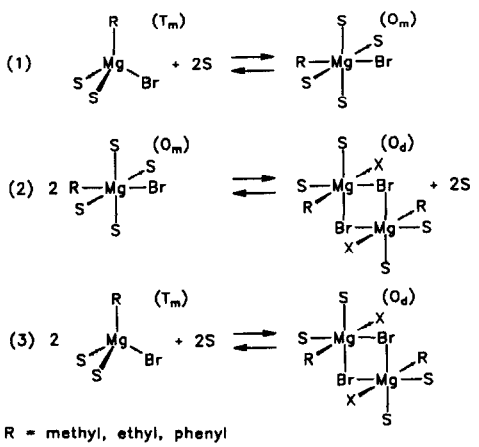

Fig. 2. Proposed equilibria for the compounds methyl, ethyl and phenyl magnesium bromide in diethyl ether.

owing to the determined coordination numbers and the exisence of a Br—Br pair. The structure model for the monomer of the type O_m, however, does not provide an explanation for the increase of 0.11±0.05 Å for the Mg—O distance when the solvent is changed from diethyl ether to tetrahydrofuran. On the contrary, X-ray diffraction studies suggest that the Mg—O distance decreases about 0.08±0.02 Å when changing the coordinated solvent from diethyl ether to tetrahydrofuran.[35-37,59-61] A possible explanation is that the systems in diethyl ether do not have an octahedral monomer (O_m), but only an octahedral dimer geometry of the type O_d. Therefore, the increase of the Mg—O distance is a consequence of the steric demands in the structure model O_d. For the mentioned reasons, a satisfactory description of the systems in diethyl ether is given by the equilibrium 3 in Fig. 2.

A further question is why the monomers in diethyl ether have a tetrahedral structure whereas in tetrahydrofuran they have an octahedral geometry. X-ray diffraction studies reveal that Grignard compounds in diethyl ether preferably crystallize in a tetrahedral geometry.[35-37,60] In tetrahyrofuran, however, mainly five- and six-fold coordination around magnesium is found.[59,61] The authors make the lower steric demand of tetrahydrofuran responsible for that phenomenon.

Considering the structure models T_m and O_d one might ask the question why no contribution of a C backscatterer to the second coordination sphere has been detected. The EXAFS measurements, however, have been performed at 20°C and referring to the results of NMR investigations, there is a very fast exchange of the alkyl and aryl groups at

this temperature. At *ca* −60°C the exchange is slow enough to distinguish between RMgX and R_2Mg species.[27–29] As mentioned before, high exchange rates cause relatively high Debye–Waller factors and, therefore, an EXAFS spectroscopical detection of such near neighbour distances is quite impossible.

The number of organic substituents R is much lower than the number of coordinated solvent molecules. For example, the structure models T_m, O_m and O_d have two, four or six oxygen atoms close to the bromine atom, respectively. Therefore, the detection of oxygen backscatterers in the second coordination sphere is much more probable, although the Debye–Waller factors of these absorber–backscatterer pairs are very high too.

The following section contains some concluding remarks concerning the shift of the threshold energy $\Delta E_0 = E_0^{ref} - E_0$, where E_0^{ref} is the threshold energy of the reference compound $MgBr_2$. These shifts contain some information about the reactivity and the carbanionic character of the respective Grignard compound. The negative shifts of methyl, ethyl and phenyl magnesium bromide (−7.1, −4.6 and −3.3 eV) confirm that the partial negative charge of the bromine atom is partially transferred to the organic group R, thereby increasing the energy required to eject a photoelectron. This fact is supported by UV spectroscopical studies.[65] The carbanionic character and the reactivity of the Grignard compounds increases with Me > Et > Ph, which is in very good agreement with the calculated shifts of the threshold energy. Vinyl magnesium bromide has the lowest reactivity of all the investigated Grignard compounds. This supports the positive shift of 0.4 eV. Assuming that the bromine atom in $MgBr_2$ should have the most negative partial charge, a *positive* shift is very surprising. An explanation can be a stronger +I and +M-effect of the vinyl group compared with the phenyl group. Furthermore, the existence of monomers only in the tetrahydrofuran solution makes a delocalization of the charge more difficult.

CONCLUSION

The structure models, the obtained distances, the deduced degree of dimerization for the Grignard compounds methyl, ethyl and phenyl magnesium bromide in diethyl ether and vinyl magnesium bromide in tetrahydrofuran are summarized in Fig. 3. The standard errors are a consequence of the combination of the results obtained with different theoretical amplitude and phase functions, i.e. McKale, FEFF and those of EXCURV90 and the empirical model amplitude and phase functions.

a)

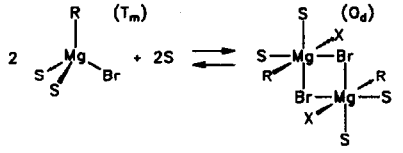

R = methyl, ethyl, phenyl
S = diethyl ether
X = methyl, ethyl, phenyl, diethyl ether

concentrations (mol/l)	methyl	ethyl	phenyl
	3.12	3.04	2.96

dimer O_d (%)	methyl	ethyl	phenyl
	60±7	62±8	33±9

distances (Å)	methyl	ethyl	phenyl
Mg-Br (T_m/O_d)	2.458±0.018	2.462±0.018	2.446±0.019
Br-Br (O_d)	3.492±0.011	3.468±0.012	3.445±0.032
Br-O (T_m)	3.670±0.025	3.671±0.032	3.653±0.052
Br-O (O_d)	3.394±0.021	3.416±0.021	3.374±0.021
Mg-O (T_m)	2.026±0.052	2.023±0.061	2.017±0.088
Mg-O (O_d)	2.340±0.049	2.368±0.049	2.324±0.051

b)

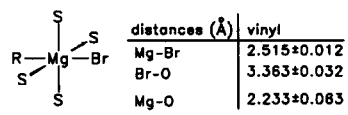

distances (Å)	vinyl
Mg-Br	2.515±0.012
Br-O	3.363±0.032
Mg-O	2.233±0.063

R = vinyl
S = tetrahydrofuran

concentration (mol/l)	vinyl
	1.58

Fig. 3. Summary of the structure models, the obtained distances, the deduced degree of dimerization for the Grignard compounds methyl, ethyl and phenyl magnesium bromide in diethyl ether (a) and vinyl magnesium bromide in tetrahydrofuran (b).

The simulation of the EXAFS spectra of the Grignard compounds with only one of the named amplitude and phase functions would be rather incomplete and of an unscientific nature, because none of them can claim to be the best one.

Acknowledgements—We wish to thank the SFB 347 (Selective Reaktionen Metallaktivierter Moleküle) and the Stipendienfonds des Verbandes der Chemischen Industrie for generous financial support. One of us (T.S.E.) thanks Dr Leni Schöninger-Stiftung for generous financial support.

REFERENCES

1. V. Grignard, *Compt. Rend.* 1900, **130**, 1322.
2. E. C. Ashby, *Q. Rev.* 1967, **21**, 259.
3. E. C. Ashby, *Bull. Soc. Chim. France* 1972, 2133.
4. B. J. Wakefield, *Organomet. Chem. Rev.* 1966, **1**, 131.
5. A. Jutand, PhD thesis, Université de Paris-Nord (1980).
6. E. C. Ashby, *Pure Appl. Chem.* 1980, **52**, 545.
7. M. Lasperas, A. Perez-Rubalcaba and M. L. Quiroga-Feijoo, *Tetrahedron* 1980, **36**, 3403.
8. H. Yamataka, Y. Kawafuji, K. Nagareda, N. Miyano and T. Hanafusa, *J. Org. Chem.* 1989, **54**, 4706.

9. A. P. Terentjew, *Z. Anorg. Allg. Chem.* 1926, **156**, 73.
10. A. D. Vreugdenhil and C. Blomberg, *Rec. Trav. Chim.* 1965, **84**, 39.
11. W. Slough and A. R. Ubbelohde, *J. Chem. Soc.* 1955, 108.
12. S. Hayes, *Bull. Soc. Chim. France* 1963, 1404.
13. J. Toney and G. D. Stucky, *J. Chem. Soc., Chem. Commun.* 1967, 1168.
14. R. E. Dessy, G. S. Handler, J. H. Wotiz and C. A. Hallingsworth, *J. Am. Chem. Soc.* 1957, **79**, 3476.
15. R. E. Dessy, S. E. I. Green and R. M. Salinger, *Tetrahedron Lett.* 1964, **21**, 1396.
16. J. M. Nelson and W. V. Evans, *J. Am. Chem. Soc.* 1917, **39**, 82.
17. F. Kondryew, *Chem. Ber.* 1925, **58**, 459.
18. L. W. Gaddum and H. E. French, *J. Am. Chem. Soc.* 1927, **49**, 1295.
19. W. Zeil, *Z. Electrochem.* 1952, **56**, 789.
20. R. E. Dessy and R. M. Jones, *J. Org. Chem.* 1959, **24**, 1685.
21. W. V. Evans and F. H. Lee, *J. Am. Chem. Soc.* 1933, **55**, 1474.
22. A. Kirrmann, R. Hamelin and S. Hayes, *Bull. Soc. Chim. France* 1963, 1395.
23. R. Hamelin and S. Hayes, *Compt. Rend.* 1961, **252**, 1616.
24. R. M. Salinger and H. S. Mosher, *J. Am. Chem. Soc.* 1964, **86**, 1782.
25. E. C. Ashby, G. E. Parris and F. Walker, *J. Chem. Soc. D.* 1969, **24**, 1464.
26. D. F. Evans and J. P. Maher, *J. Chem. Soc.* 1962, 5125.
27. D. F. Evans and G. V. Fazakerley, *J. Chem. Soc.* 1971, 184.
28. D. F. Evans and G. V. Fazakerley, *J. Chem. Soc., Chem. Commun.* 1968, 1974.
29. P. E. M. Allen, S. Hagias, S. F. Lincoln, C. Mair and E. H. Williams, *Ber. Bunsenges Phys. Chem.* 1982, **86**, 515.
30. R. Benn, H. Lehmkuhl, K. Mehler and A. Rufinska, *Angew. Chem., Int. Edn. Engl.* 1984, **23**, 534.
31. R. Benn and A. Rufinska, *J. Organomet. Chem.* 1982, **239**, C19.
32. M. Schlosser and M. Staehle, *Angew. Chem.* 1982, **94**, 142.
33. M. Schlosser and M. Staehle, *Angew. Chem.* 1980, **92**, 497.
34. R. R. Muslukhov, L. M. Khalilov, A. A. Ibragimov, U. M. Dzhemilev and A. A. Panasenko, *Metalloorg. Khim.* 1988, **1**, 680.
35. L. J. Guggenberger and R. E. Rundle, *J. Am. Chem. Soc.* 1968, **90**, 5375.
36. G. D. Stucky and R. E. Rundle, *J. Am. Chem. Soc.* 1964, **86**, 4825.
37. F. A. Schröder, *Chem. Ber.* 1969, **102**, 2035.
38. A. Ericson and I. Persson, *J. Organomet. Chem.* 1987, **326**, 151.
39. A. Wellmar, A. Hallberg and I. Persson, *J. Organomet. Chem.* 1991, **415**, 167.
40. B. K. Teo, *EXAFS: Basic Principles and Data Analysis*. Springer Verlag, Berlin (1986).
41. D. C. Koningsberger and R. Prins, *X-Ray-Absorption: Principles, Applications, Techniques of EXAFS, SEXAFS and XANES*. J. Wiley & Sons, New York (1988).
42. P. A. Lee, P. H. Citrin, P. Eisenberger and B. M. Kincaid, *Rev. Mod. Phys.* 1981, **53**, 769.
43. T. S. Ertel, H. Bertagnolli, S. Hückmann, U. Kolb and D. Peter, *Appl. Spectrosc.* 1992, **46**, 690.
44. A. G. McKale, B. W. Veal, A. P. Paulikas, S. K. Chan and G. S. Knapp, *J. Am. Chem. Soc.* 1988, **110**, 3763.
45. J. J. Rehr, J. Mustre de Leon, S. I. Zabinsky and R. C. Albers, *J. Am. Chem. Soc.* 1991, **113**, 5135.
46. J. J. Rehr, R. C. Albers and J. Mustre de Leon, *Physica B* 1989,**158**, 417.
47. R. W. Joyner, K. J. Martin and P. Meethan, *J. Phys. C Solid State Phys.* 1987, **20**, 4005.
48. E. A. Stern, D. E. Sayers and F. W. Lytle, *Phys. Rev. B.* 1975, **11**, 4836.
49. S. P. Cramer, T. K. Eccles, F. Kutzler, E. I. Hodgson and S. Doinach, *J. Am. Chem. Soc.* 1976, **98**, 8059.
50. B. Lengeler, *J. Phys. Paris* 1986, **47**, 75.
51. P. H. Citrin, P. Eisenberger and B. M. Kincaid, *Phys. Rev. Lett.* 1976, **36**, 1346.
52. P. A. Lee, B. K. Teo and A. L. Simons, *J. Am. Chem. Soc.* 1977, **99**, 3856.
53. B. K. Teo, P. A. Lee, A. L. Simons, P. Eisenberger and B. M. Kincaid, *J. Am. Chem. Soc.* 1977, **99**, 3854.
54. G. Bunker, S. S. Hasnain and D. Sayers, Report on international workshops on standards and criteria in XAFS, in *X-Ray-Absorption Fine Structure*, p. 751. Ellis Horwood Limited, London (1991).
55. A. D. Vreugdenhil and C. Blomberg, *Rec. Trav. Chim.* 1963, **82**, 453.
56. E. C. Ashby and M. B. Smith, *J. Am. Chem. Soc.* 1964, **86**, 4363.
57. A. D. Vreugdenhil and C. Blomberg, *Rec. Trav. Chim.* 1963, **82**, 461.
58. E. C. Ashby and W. E. Becker, *J. Am. Chem. Soc.* 1963, **85**, 118.
59. M. Vallino, *J. Organomet. Chem.* 1969, **20**, 1.
60. L. M. Engelhardt, S. Harvey, C. L. Raston and A. H. White, *J. Organomet. Chem.* 1988, **341**, 39.
61. N. N. Greenwood and A. Earnshaw, *Chemie der Elemente*, Ch. 5, p. 164. Verlag Chemie, Weinheim (1988).
62. J. E. Penner-Hahn, X-Ray-Absorption Studies of Metallprotein Structure: Cytochrome P-450, Horseradish Peroxidase, Plastocyanin and Laccase, SSRL Report 84/03, p. 104 (1983).
63. J. J. P. Stewart, *J. Comp.-Aided Molec. Design* 1990, **4**, 1.
64. J. J. P. Stewart, *MOPAC Manual*, 6th edn. F. J. Seiler Res. Lab., USAF Academy CO (1990).
65. H. F. Ebel and B. O. Wagner, *Chem. Ber.* 1971, **104**, 307.

Polyhedron Vol. 12, No. 18, pp. 2185–2192, 1993
Printed in Great Britain

0277–5387/93 $6.00+.00
© 1993 Pergamon Press Ltd

STRUCTURE OF IRON(III) AND FORMATION OF IRON(III) THIOCYANATO COMPLEXES IN N,N-DIMETHYLACETAMIDE

KAZUHIKO OZUTSUMI,* EMI HASEGAWA, MAKOTO KURIHARA and TAKUJI KAWASHIMA

Laboratory of Analytical Chemistry, Department of Chemistry, University of Tsukuba, Tsukuba 305, Japan

(*Received* 10 *February* 1993; *accepted* 2 *June* 1993)

Abstract—The solvation structure of the iron(III) ion in N,N-dimethylacetamide (DMA) has been determined by means of EXAFS (extended X-ray absorption fine structure) spectroscopy and the complex formation between iron(III) and thiocyanate ions has been calorimetrically and spectrophotometrically studied in DMA containing $(C_2H_5)_4NClO_4$ (0.4 mol dm^{-3}) as a constant ionic medium at 25°C. The iron(III) ion is surrounded with six DMA molecules and has an octahedral $[Fe(dma)_6]^{3+}$ structure. Calorimetric and spectrophotometric titration data were well explained in terms of the formation of $[Fe(SCN)_n]^{(3-n)+}$ (n = 1–6) and their formation constants, reaction enthalpies and entropies were determined. Electronic spectra of individual iron(III) thiocyanato complexes in DMA were also extracted. The complexation of iron(III) with thiocyanate ions in DMA is more favorable than that in N,N-dimethylformamide (DMF). The favorable formation is mainly due to the more negative reaction enthalpies in DMA than those in DMF, which is resulting from the larger steric interaction between the ligating DMA molecules around the iron(III) ion than the DMF ones.

We have studied calorimetrically and spectrophotometrically the complex formation reactions between iron(III) and thiocyanate ions in water and N,N-dimethylformamide (DMF).[1,2] The $[Fe(SCN)]^{2+}$, $[Fe(SCN)_2]^{+}$, $[Fe(SCN)_3]$, $[Fe(SCN)_4]^{-}$ and $[Fe(SCN)_5]^{2-}$ complexes are formed in DMF,[2] while the formation of only three complexes, $[Fe(SCN)]^{2+}$, $[Fe(SCN)_2]^{+}$ and $[Fe(SCN)_3]$, was observed in water.[1] The complexation in DMF is accompanied by large and positive entropies and is markedly enhanced compared with that in water. The large and positive entropies result from weak solvent–solvent interactions, as generally seen in aprotic solvents.[3,4]

N,N-Dimethylacetamide (DMA) is an aprotic donor solvent and has a molecular structure and solvent properties similar to those of DMF, e.g. relative dielectric constants ε(DMA) = 37.8, ε(DMF) = 36.7; donor numbers D_N(DMA) = 27.8, D_N(DMF) = 26.6; acceptor numbers A_N(DMA) = 13.6, A_N(DMF) = 16.0.[5,6] However, the structure and properties of the metal complexes in DMA are markedly different from those in DMF. The zinc(II) ion has an octahedral structure in DMF, while a solvation equilibrium, $[Zn(dma)_4]^{2+} + 2dma = [Zn(dma)_6]^{2+}$, is established in DMA.[7] The nickel(II) ion has an octahedral structure and forms a series of the $[NiCl_n]^{(2-n)+}$ (n = 1–4) complexes both in DMF and DMA.[7–9] However, the structure of the chloro complexes is significantly different in the two solvents. The octahedral $[NiCl(dmf)_5]^{+}$ and $[NiCl_2(dmf)_4]$ complexes and the tetrahedral $[NiCl_3(dmf)]^{-}$ and $[NiCl_4]^{2-}$ ones are formed in DMF.[8] The tetrahedral $[NiCl_3(dma)]^{-}$ and $[NiCl_4]^{2-}$ complexes are also formed in DMA, while the following equilibria are present for the mono- and dichloro complexes: $[NiCl(dma)_4]^{+} + dma = [NiCl(dma)_5]^{+}$ and $[NiCl_2(dma)_2] + dma = [NiCl_2(dma)_3]$.[9] These strongly indicate that the coordination of DMA molecules to metal ions is sterically hindered by the presence of an acetyl methyl group within a DMA molecule.

* Author to whom correspondence should be addressed.

In this report we describe the complexation of iron(III) with thiocyanate ions in DMA in order to obtain more information on the solvent effect of DMA. The solvation structure of the iron(III) ion in DMA was first determined by means of EXAFS (extended X-ray absorption fine structure) spectroscopy because the solvation structure of metal ions in solution is essential to interpret the thermodynamics of complexation. The thermodynamic parameters for the formation of the iron(III) thiocyanato complexes were then determined in DMA containing $(C_2H_5)_4NClO_4$ (0.4 mol dm^{-3}) as a constant ionic medium by calorimetry and spectrophotometry at 25°C. The thermodynamic parameters thus obtained in DMA are compared with those in water and DMF.

EXPERIMENTAL

Reagents

All chemicals used were of reagent grade. Iron(III) perchlorate was recrystallized once from an aqueous perchloric acid solution. The DMA solvate of iron(III) perchlorate was prepared by dissolving the hydrate of iron(III) perchlorate in DMA and then recrystallized once from DMA and finally dried at room temperature in a vacuum oven. Tetraethylammonium perchlorate was recrystallized once from water. Tetraethylammonium thiocyanate was used without further purification. These compounds were dried at room temperature in vacuum. N,N-Dimethylacetamide was purified as described elsewhere.[7] All DMA solutions were prepared and treated under a dry nitrogen atmosphere.

Calorimetric and spectrophotometric measurements

Calorimetric measurements were carried out by using a fully automatic on-line calorimetry system,[10] consisting of a twin-type calorimeter (Tokyo Riko, Japan). Test solutions contained $(C_2H_5)_4NClO_4$ (0.4 mol dm^{-3}) as a constant ionic medium. An iron(III) perchlorate DMA solution (40 cm^3) was placed in a stainless-steel vessel, the inside wall of which was coated with Teflon, and was titrated with a $(C_2H_5)_4NSCN$ DMA (0.4 mol dm^{-3}) solution using an APB-118 autoburet (Kyoto Electronics, Japan) under a dry nitrogen atmosphere. The vessel was inserted in an aluminum block thermostated at (25.0±0.0001)°C in an air bath. Heats of complexation ranging from 0.2 to 2.0 J at each titration point were measured with a certainty of ±0.02 J and were corrected for heat of dilution of the titrant, which had been determined in advance by separate experiments and was found to be very small.

Electronic spectra were measured at 25°C using a UV-2100 spectrophotometer (Shimadzu, Japan) equipped with a PC-9801VM computer (NEC, Japan), which recorded absorbance data in 1 nm intervals over the wavelength range 300–700 nm. A flow cell with a path-length of 0.5 cm was connected to a titration vessel through Teflon and glass tubes. An iron(III) perchlorate DMA solution placed in the vessel was titrated with a $(C_2H_5)_4NSCN$ DMA (0.4 or 0.04 mol dm^{-3}) solution under a dry nitrogen atmosphere. Spectrophotometric data at 50 selected wavelengths over the range 300–600 nm were employed for the subsequent least-squares calculation.

The overall formation of the $[Fe(SCN)_n]^{(3-n)+}$ complex can be defined as eqs (1) and (2) if the formation of only mononuclear species is assumed.

$$Fe^{3+} + nSCN^- = [Fe(SCN)_n]^{(3-n)+} \quad (1)$$

$$\beta_n = [Fe(SCN)_n^{(3-n)+}]/[Fe^{3+}][SCN^-]^n \quad (2)$$

A heat q_i measured at a titration point i is represented by the overall formation constant β_n and the enthalpy $\Delta H^0_{\beta n}$ of $[Fe(SCN)_n]^{(3-n)+}$ as eq. (3), where V_i denotes the volume of the test solution.

$$q_i = -(V_i \Sigma \beta_n (\Delta H^0_{\beta n})[Fe^{3+}]_i [SCN^-]_i^n - V_{i-1} \Sigma \beta_n (\Delta H^0_{\beta n})[Fe^{3+}]_{i-1}[SCN^-]_{i-1}^n) \quad (3)$$

Similarly, an absorbance A_{ij} measured in a solution i at a given wavelength λ_j is expressed by the formation constant β_n and the molar absorption coefficient $\varepsilon_n(\lambda_j)$ of $[Fe(SCN)_n]^{(3-n)+}$ as eq. (4).

$$A_{ij} = \Sigma \varepsilon_n(\lambda_j) \beta_n [Fe^{3+}]_i [SCN^-]_i^n + \varepsilon_{Fe}(\lambda_j)[Fe^{3+}]_i + \varepsilon_{SCN}(\lambda_j)[SCN^-]_i \quad (4)$$

The concentrations of free Fe^{3+} and SCN^- are related to their total concentrations, $C_{Fe,i}$ and $C_{SCN,i}$, in a solution i by the following mass-balance equations.

$$C_{Fe,i} = [Fe^{3+}]_i + \Sigma \beta_n [Fe^{3+}]_i [SCN^-]_i^n \quad (5)$$

$$C_{SCN,i} = [SCN^-]_i + \Sigma n \beta_n [Fe^{3+}]_i [SCN^-]_i^n \quad (6)$$

Formation constants and enthalpies were obtained simultaneously by minimizing the error-square sum $\Sigma(q_{i,obs} - q_{i,calc})^2$, formation constants and molar absorption coefficients by $\Sigma\Sigma(A_{ij,obs} - A_{j,calc})^2$ using a non-linear least-squares program according to an algorithm proposed by Marquardt.[11]

EXAFS measurements

EXAFS spectra were measured around the iron K edge in the transmission mode using the BL6B

station at the Photon Factory of the National Laboratory for High Energy Physics (KEK).[12] White synchrotron radiations were monochromatized by an Si(111) double crystal. The two crystals were detuned by 50% to the fundamental above the edge in order to eliminate higher order harmonics. Two sample solutions were prepared by dissolving the DMA solvate and hydrate of iron(III) perchlorate in DMA and water, respectively. Concentrations of iron(III) are *ca* 0.2 and *ca* 0.4 mol dm^{-3} in DMA and water, respectively. The aqueous solution contained perchloric acid (3 mol dm^{-3}) in order to prevent the hydrolysis of iron(III). A glass fibre filter, which had been dried at 100°C in an air bath, was immersed in a sample solution and then sealed in a Mylar bag in order to prevent the evaporation of solvent and to avoid moisture. An effective jump at the absorption edge was obtained by changing the number of filters. The apparent absorbance was obtained as $\ln(I_0/I)$, where I and I_0 are X-ray intensities with and without a sample, respectively. The intensities I_0 and I were simultaneously measured by ionization chambers filled with nitrogen and nitrogen(85%)+argon(15%) gas, respectively.

Details of the data reduction procedure of the raw EXAFS spectra have been described elsewhere.[2,7,13–15] The threshold energy of a K-shell electron E_0 was selected as the position of the half-height of the edge jump in each sample and was 7.125 keV in the present study. The structure parameters were finally determined in the k space by comparing the observed EXAFS spectrum and the model function $\chi(k)_{calc}$ according to the single-electron and single-scattering theory.[16–19] The back-scattering amplitude $F(\pi,k)$ and the total scattering phase shift $\alpha(k)$ were quoted from the literature.[20] To minimize the error-square sum $\Sigma k^6(\chi(k)_{obs}-\chi(k)_{calc})^2$, the E_0 value and the mean free path of the photoelectron λ were first evaluated from a standard sample of known structure (an aqueous iron(III) perchlorate solution containing $[Fe(H_2O)_6]^{3+}$).[21] The parameters were then kept constant in the course of the subsequent structural analysis of unknown samples, while the bond length r, the Debye–Waller factor σ and the coordination number n were optimized as variables.

RESULTS

Calorimetry and spectrophotometry

Figure 1 depicts calorimetric titration curves for the iron(III) thiocyanato system in the $(C_2H_5)_4NClO_4$ DMA (0.4 mol dm^{-3}) solution. The heat of complexation q measured at each titration point is normalized with the volume of titrant added δv and the concentration of the ligand in the titrant $C_{SCN,tit}$ and the term $-q/(\delta v C_{SCN,tit})$ is plotted against C_{SCN}/C_{Fe}, where C_{SCN} and C_{Fe} denote the total concentration of the thiocyanate and iron(III) ions, respectively, in solution.

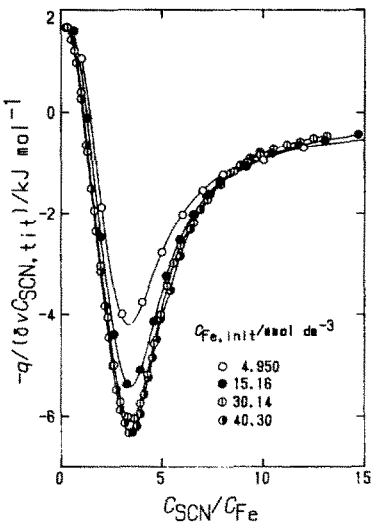

Fig. 1. Calorimetric titration curves for the iron(III) thiocyanato system in N,N-dimethylacetamide containing 0.4 mol dm^{-3} $(C_2H_5)_4NClO_4$ at 25°C. Concentrations of iron(III) ion in initial test solutions, $C_{Fe,init}$ (mmol dm^{-3}), are given. The solid lines are calculated by using constants in Table 1.

The calorimetric titration curves were analysed by assuming the formation of plausible sets of mononuclear complexes and the results are given in Table 1. The calorimetric titration curves were not reproducible by an assumption of the formation of four complexes, i.e. $[Fe(SCN)]^{2+}$, $[Fe(SCN)_2]^+$, $[Fe(SCN)_3]$ and $[Fe(SCN)_4]^-$, because of large R and σ values [see the set (1–4) in Table 1]. The set (1–5), assuming the formation of $[Fe(SCN)]^{2+}$, $[Fe(SCN)_2]^+$, $[Fe(SCN)_3]$, $[Fe(SCN)_4]^-$ and $[Fe(SCN)_5]^{2-}$, gave small R and σ values. The set (1–6), considering the formation of $[Fe(SCN)]^{2+}$, $[Fe(SCN)_2]^+$, $[Fe(SCN)_3]$, $[Fe(SCN)_4]^-$, $[Fe(SCN)_5]^{2-}$ and $[Fe(SCN)_6]^{3-}$, gave appreciably smaller R and σ values than the set (1—5). Furthermore, a significant improvement of uncertainties involved in the formation constants resulted for the set (1–6). Hence, we finally propose the formation of the $[Fe(SCN)]^{2+}$, $[Fe(SCN)_2]^+$, $[Fe(SCN)_3]$, $[Fe(SCN)_4]^-$, $[Fe(SCN)_5]^{2-}$ and $[Fe(SCN)_6]^{3-}$ complexes in DMA. As seen in Fig. 1, the solid lines calculated by using the parameter values for the set (1–6) reproduce well the experimental points over the whole range of C_{SCN}/C_{Fe} examined.

Table 1. Results of least-squares refinements of overall formation constants, $\log(\beta_n/\mathrm{dm}^{3n}\ \mathrm{mol}^{-n})$, and enthalpies, $\Delta H^0_{\beta n}$ (kJ mol^{-1}), of $[Fe(SCN)_n]^{(3-n)+}$ in N,N-dimethylacetamide containing $(C_2H_5)_4NClO_4$ (0.4 mol dm^{-3}) at 25°C[a]

	(1–4)	(1–5)	(1–6)
$\log\beta_1$	3.8(1.3)[b]	5.0(0.5)	5.2(0.3)
$\log\beta_2$	6.5(2.3)	8.9(0.8)	9.3(0.5)
$\log\beta_3$	9.1(2.1)	11.9(0.9)	12.5(0.5)
$\log\beta_4$	10.4(2.2)	14.2(0.9)	14.9(0.5)
$\log\beta_5$	—	15.3(0.9)	16.4(0.6)
$\log\beta_6$	—	—	17.1(0.6)
$\Delta H^0_{\beta 1}$	1.7(0.5)	1.8(0.1)	1.8(0.1)
$\Delta H^0_{\beta 2}$	1.2(5.0)	0.0(0.4)	−0.1(0.2)
$\Delta H^0_{\beta 3}$	−5.9(1.2)	−5.7(0.2)	−5.6(0.1)
$\Delta H^0_{\beta 4}$	−35.2(1.9)	−14.0(0.4)	−14.1(0.3)
$\Delta H^0_{\beta 5}$	—	−34.6(0.6)	−23.6(1.1)
$\Delta H^0_{\beta 6}$	—	—	−36.5(1.2)
R[c]	0.0744	0.0164	0.0085
σ_{obs}[d]	0.0931	0.0208	0.0109

[a] The number of data points is 104.
[b] The values in parentheses refer to three standard deviations.
[c] Hamilton R-factor.
[d] Standard deviation of the observed heats.

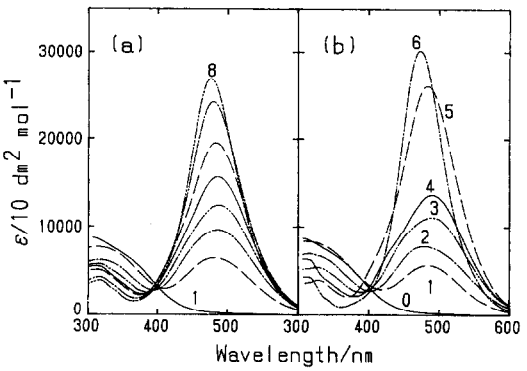

Fig. 2. (a) Typical variation of electronic spectra of iron(III) thiocyanate N,N-dimethylacetamide solutions with varying C_{SCN}/C_{Fe} ratios in the range 300–600 nm. The total concentrations of iron(III) and thiocyanate ions, C_{Fe} and C_{SCN} (mmol dm^{-3}), in measured solutions are (1) 0.3076 and 0, (2) 0.3038 and 0.5004, (3) 0.2965 and 1.466, (4) 0.2734 and 4.505, (5) 0.2121 and 12.58, (6) 0.1025 and 27.02, (7) 0.09500 and 90.34 and (8) 0.04117 and 260.9. (b) Electronic spectra of individual iron(III) thiocyanato complexes in N,N-dimethylacetamide. The number n represents $[Fe(SCN)_n]^{(3-n)+}$.

Figure 2(a) shows the typical variation of electronic spectra measured with varying the C_{SCN}/C_{Fe} mole ratios in the $(C_2H_5)_4NClO_4$ DMA (0.4 mol dm^{-3}) solution, where absorbances were normalized with a unit concentration of the iron(III) ion.

The spectrophotometric titration data were analysed in a similar manner to that employed for the calorimetric data. However, a least-squares calculation failed to derive reliable formation constants because of the monotonous variation of the spectra as shown in Fig. 2(a). We then analysed the spectrophotometric data on the basis of the formation constants calorimetrically obtained and the results are compared in Table 2. As seen in the table, the set (1–6), considering the formation of $[Fe(SCN)]^{2+}$, $[Fe(SCN)_2]^+$, $[Fe(SCN)_3]$, $[Fe(SCN)_4]^-$, $[Fe(SCN)_5]^{2-}$ and $[Fe(SCN)_6]^{3-}$, gave the smallest R and σ values and satisfactorily reproduced variation of the spectra. The spectrophotometric titration data thus confirmed the presence of the $[Fe(SCN)]^{2+}$, $[Fe(SCN)_2]^+$, $[Fe(SCN)_3]$, $[Fe(SCN)_4]^-$, $[Fe(SCN)_5]^{2-}$ and $[Fe(SCN)_6]^{3-}$ complexes in DMA. Figure 2(b) shows the electronic spectra of individual iron(III) thiocyanato complexes extracted.

Figure 3 depicts the species distribution of the iron(III) thiocyanato complexes in the $(C_2H_5)_4NClO_4$ DMA (0.4 mol dm^{-3}) solution, along with that in DMF and water.

EXAFS

The extracted EXAFS oscillations in the form $k^3\chi(k)$ and their Fourier transforms $|F(r)|$ (uncorrected for the phase shift) are shown in Figs 4(A) and (B), respectively. Considering that DMA and

Table 2. Results of least-squares refinements of overall formation constants, $\log(\beta_n/\mathrm{dm}^{3n}\ \mathrm{mol}^{-n})$, of $[Fe(SCN)_n]^{(3-n)+}$ using spectrophotometric data in N,N-dimethylacetamide containing $(C_2H_5)_4NClO_4$ (0.4 mol dm^{-3}) at 25°C[a]

	(1–4)	(1–5)	(1–6)
$\log\beta_1$	3.8[b]	5.0[b]	5.2[b]
$\log\beta_2$	6.5[b]	8.9[b]	9.3[b]
$\log\beta_3$	9.1[b]	11.9[b]	12.5[b]
$\log\beta_4$	10.4[b]	14.2[b]	14.9[b]
$\log\beta_5$	—	15.3[b]	16.4[b]
$\log\beta_6$	—	—	17.1[b]
R[c]	0.0187	0.0164	0.0078
σ_{obs}[d]	0.0137	0.0122	0.0059

[a] The number of data points is 2900.
[b] The values were kept constant.
[c] Hamilton R-factor.
[d] Standard deviation of the observed absorbances.

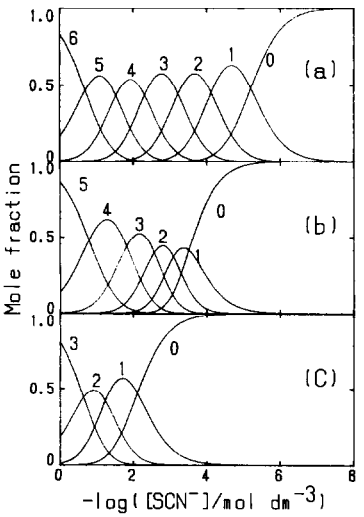

Fig. 3. Species distribution of the iron(III) thiocyanato complexes in (a) N,N-dimethylacetamide, (b) N,N-dimethylformamide and (c) water. The number n represents $[Fe(SCN)_n]^{(3-n)+}$.

water are oxygen-donor solvents, the first intense peaks at 160 pm in the $|F(r)|$ curves are due to Fe—O bonds in the first coordination sphere of the iron(III) ion. The position and height of the first peaks in the $|F(r)|$ curves are virtually the same for the two solutions. The octahedral structure of the hydrated iron(III) ion has been established in water.[21] The iron(III) ion is thus expected to have an octahedral structure in DMA as well as in water.

The structural parameters r, σ and n of the iron(III) ion in DMA were finally determined by a non-linear least-squares calculation. The least-squares method was applied to the Fourier filtered $k^3\chi(k)$ values over the k range 4.0×10^{-2}–13.5×10^{-2} pm^{-1}. The inverse Fourier transformation was performed over the r range 85–210 pm. The E_0 and λ values were estimated in advance from an aqueous iron(III) perchlorate solution involving the $[Fe(H_2O)_6]^{3+}$ ion of known structure.[21] The Fe—O bond length within the $[Fe(H_2O)_6]^{3+}$ ion was also allowed to vary in order to check the reproducibility of the value. The r, σ and n values for the iron(III) ion in DMA were then refined by adopting the E_0 and λ values determined. The best fit values are listed in Table 3. The solid lines calculated using the parameter values thus obtained reproduce well the experimental points, as depicted in Fig. 4(C). The Fe—O bond length within the $[Fe(H_2O)_6]^{3+}$ ion agrees well with the literature values[21] and the E_0 and λ values are well approximated in the present study. The solvation number of nearly six was obtained for the iron(III) ion in DMA and the least-squares calculation thus derived a conclusion that the iron(III) ion has an octahedral $[Fe(dma)_6]^{3+}$ structure.

DISCUSSION

A series of $[Fe(SCN)_n]^{(3-n)+}$ (n = 1–6) complexes are extensively formed in DMA. The stepwise thermodynamic quantities for the formation of the complexes are summarized in Table 4, together with those in DMF and water.

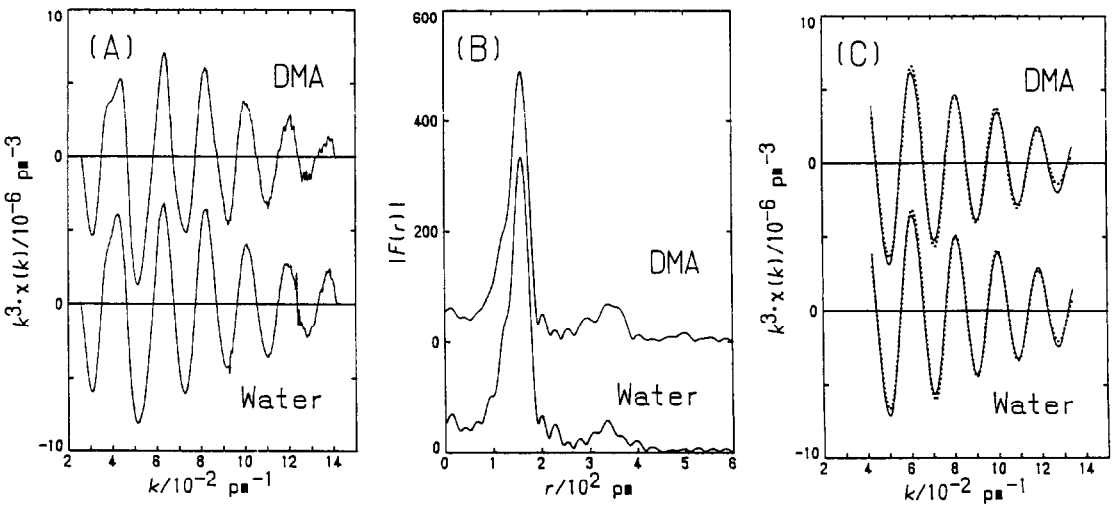

Fig. 4. (A) The EXAFS spectra $\chi(k)$ weighted by k^3 for DMA and aqueous solutions of iron(III) perchlorate. (B) The Fourier transforms $|F(r)|$ of the $k^3\chi(k)$ values shown in (A), uncorrected for the phase shift. (C) The Fourier filtered $k^3\chi(k)$ curves for the samples solutions. The observed values are shown by dots and calculated ones using parameter values in Table 4 are shown by solid lines.

Table 3. The Fe—O bond length r, the Debye–Waller factor σ and the solvation number n for the solvated iron(III) ion in N,N-dimethylacetamide[a,b]

Species	r (pm)	σ (pm)	n
$[Fe(dma)_6]^{3+}$	200(1)	6.0(0.1)	5.9(0.1)
$[Fe(H_2O)_6]^{3+}$	200(1)	5.6(0.1)	6[c]

[a] The values in parentheses refer to standard deviations.

[b] E_0 = 7133.6(2) eV and λ = 646(12) pm.

[c] The values were kept constant during the calculations.

The thiocyanate ion can bind to metal ions through either the nitrogen or sulphur atom, depending on the nature of the metal ions. First-row divalent transition metal ions, which are relatively hard acceptors, prefer a hard nitrogen donor to form N-coordinated isothiocyanato complexes.[22-24] The relatively soft mercury(II) ion prefers a soft sulphur donor to form S-coordinated thiocyanato complexes.[23,24] We expect that the thiocyanate ion binds to the iron(III) ion with its nitrogen donor site in DMA because iron(III) is a hard acceptor.

The iron(III) ion is coordinated with six DMA molecules and has an octahedral $[Fe(dma)_6]^{3+}$ structure in DMA, according to the present EXAFS measurements. The $[Fe(SCN)_6]^{3-}$ complex is also expected to have an octahedral structure. If any of the $[Fe(SCN)_n]^{(3-n)+}$ (n = 1–5) complexes has either a five- or four-coordination structure, extensive desolvation occurs at a certain step of complexation accompanied by large and positive enthalpy and entropy changes. Also, large and negative enthalpy and entropy values should be observed at a higher step of complexation, since the iron(III) ion finally forms the six-coordinate $[Fe(SCN)_6]^{3-}$ complex. However, the stepwise thermodynamic quantities show a monotonous change as seen in Table 4 and thus no structural change occurred at any step of complexation. It is thus concluded that the $[Fe(SCN)_n]^{(3-n)+}$ (n = 1–5) complexes have a six-coordinate octahedral structure like the $[Fe(dma)_6]^{3+}$ ion.

The formation of the iron(III) thiocyanato complexes in aprotic DMA and DMF is more favorable than that in protic water (see Fig. 3 and Table 4). The favorable formation in DMA and DMF than that in water is mainly due to the more positive entropy values in these two solvents. On the other hand, the enthalpy changes are less negative and thus less favorable in the former two solvents than in the latter. The iron(III) ion is octahedrally solvated in the three solvents and the Fe—O bond

Table 4. Thermodynamic quantities, ΔG_n^0 (kJ mol^{-1}), ΔH_n^0 (kJ mol^{-1}) and ΔS_n^0 (J K^{-1} mol^{-1}) for the stepwise formation of $[Fe(SCN)_n]^{(3-n)+}$ in N,N-dimethylacetamide at 25°C

	$(C_2H_5)_4NClO_4$ DMA (0.4 mol dm^{-3})	$(C_2H_5)_4NClO_4$ DMF[2] (0.4 mol dm^{-3})	NH_4ClO_4 water[1] (1 mol dm^{-3})
ΔG_1^0	−29.7(1.5)[a]	−20.0(1.7)	−12.0(0.1)
ΔG_2^0	−23.5(1.2)	−17.7(1.3)	−7.1(0.1)
ΔG_3^0	−18.4(0.7)	−14.7(0.7)	−3.6(0.3)
ΔG_4^0	−13.2(0.3)	−10.4(0.4)	—
ΔG_5^0	−8.7(0.4)	−4.5(0.2)	—
ΔG_6^0	−3.9(0.5)	—	—
ΔH_1^0	1.8(0.1)	3.1(0.1)	−6.2(0.5)
ΔH_2^0	−1.9(0.2)	0.7(0.5)	−4.6(1.3)
ΔH_3^0	−5.5(0.3)	−2.0(0.7)	−12.9(1.8)
ΔH_4^0	−8.5(0.3)	−3.9(0.5)	—
ΔH_5^0	−9.5(1.2)	−14.5(0.7)	—
ΔH_6^0	−12.9(1.6)	—	—
ΔS_1^0	106(5)	77(6)	20(2)
ΔS_2^0	72(4)	62(3)	8(4)
ΔS_3^0	43(2)	42(4)	−31(6)
ΔS_4^0	16(2)	22(3)	—
ΔS_5^0	−3(6)	−34(3)	—
ΔS_6^0	−30(6)	—	—

[a] The values in parentheses refer to three standard deviations.

lengths are all 200 pm.[1,2] The electron-pair donating ability of DMA and DMF [e.g. the donor number D_N(DMA) = 27.8, D_N(DMF) = 26.6] is stronger than that of water (14.8).[5,6] The less negative enthalpy values in DMA and DMF than those in water is thus attributed to the stronger solvation of the iron(III) ion in the former two solvents than in the latter.

The $[Fe(SCN)_n]^{(3-n)+}$ (n = 1–5) complexes are all more stable in DMA than in DMF. However, the enthalpic and entropic contributions to the free energy terms are different in each step.

The formation of $[Fe(SCN)]^{2+}$ in DMA is associated with larger entropy than that in DMF, while the entropy values for the formation of $[Fe(SCN)_2]^+$, $[Fe(SCN)_3]$ and $[Fe(SCN)_4]^-$ are rather similar both in DMA and DMF. The presence of an acetyl methyl group in a DMA molecule causes large steric repulsion between DMA molecules around the iron(III) ion, which restricts the motion of DMA molecules. The DMA molecules in the first coordination sphere of the hexa-solvated iron(III) ion may lose freedom of motion to a greater extent than DMF and thus the formation of $[Fe(SCN)]^{2+}$ in DMA is associated with larger entropy than that in DMF. Once $[Fe(SCN)]^{2+}$ is formed in DMA, DMA molecules in the complex as well as in the higher complexes have similar freedom of motion to the relevant complexes in DMF. Hence, the entropy values for each step of the formation of $[Fe(SCN)_n]^{(3-n)+}$ (n = 2–4) are similar both in DMA and DMF.

The formation of $[Fe(SCN)]^{2+}$, $[Fe(SCN)_2]^+$, $[Fe(SCN)_3]$ and $[Fe(SCN)_4]^-$ in DMA are all enthalpically preferred over DMF. Moreover, the difference in the ΔH_n^0 values increases with increasing the ligand number n. Judging from the electron-pair donating properties of DMA and DMF, energies needed for breaking the Fe—O bonds must be slightly larger for DMA than for DMF. In the crystal the metal—O—C—N torsion angles largely deviate from 180° in a DMA solvate,[25] while in a DMF solvate the metal—O—C—N torsion angles are close to 180°.[26] Hence, DMA molecules are conformationally unstable compared with DMF molecules in the first coordination sphere. As a result of a replacement of a DMA molecule with a thiocyanate ion, the liberated DMA molecule is stabilized in the bulk, which causes the more negative enthalpies in DMA than in DMF. Also, the conformational stabilization of DMA molecules within complexes increases with increasing the ligand number n by the stepwise replacement with the thiocyanate ion. Thus, the stepwise formation of $[Fe(SCN)_n]^{(3-n)+}$ (n = 1–4) in DMA is enthalpically more favorable than in DMF.

In $[Fe(SCN)_4]^-$, in which the coordination of solvent molecules to the central metal ion may not be sterically hindered, the electron-pair donating ability of the solvents may be reflected in the stepwise formation of $[Fe(SCN)_5]^{2-}$. Thus, the more exothermic stepwise formation of $[Fe(SCN)_5]^{2-}$ in DMF than in DMA results.

Acknowledgements—EXAFS measurements were performed under the approval of the Photon Factory Program Advisory Committee (Proposal No. 91-005).

REFERENCES

1. K. Ozutsumi, M. Kurihara, T. Miyazawa and T. Kawashima, *Anal. Sci.* 1992, **8**, 521.
2. K. Ozutsumi, M. Kurihara and T. Kawashima, *Talanta* 1993, **40**, 599.
3. S. Ahrland, *Pure Appl. Chem.* 1979, **51**, 2019.
4. S. Ahrland, *Pure Appl. Chem.* 1982, **54**, 1451.
5. J. A. Riddick, W. B. Bunger and T. K. Sakano, *Organic Solvents*, 4th edn. Wiley-Interscience, New York (1986).
6. V. Gutmann, *The Donor–Acceptor Approach to Molecular Interactions*. Plenum Press, New York (1978).
7. K. Ozutsumi, M. Koide, H. Suzuki and S. Ishiguro, *J. Phys. Chem.* 1993, **97**, 500.
8. S. Ishiguro, K. Ozutsumi and H. Ohtaki, *Bull. Chem. Soc. Japan* 1987, **60**, 531.
9. H. Suzuki and S. Ishiguro, *Inorg. Chem.* 1992, **31**, 4178.
10. H. Suzuki and S. Ishiguro, *Netsu Sokutei* 1988, **15**. 152.
11. D. W. Marquardt, *J. Soc. Ind. Appl. Math.* 1963, **11**, 431.
12. M. Nomura, A. Koyama and M. Sakurai, KEK Report 91-1. National Laboratory for High Energy Physics, Tsukuba, Japan (1991).
13. K. Ozutsumi and T. Kawashima, *Inorg. Chim. Acta* 1991, **180**, 231.
14. K. Ozutsumi, Y. Miyata and T. Kawashima, *J. Inorg. Biochem.* 1991, **44**, 97.
15. K. Ozutsumi and T. Kawashima, *Polyhedron* 1992, **10**, 169.
16. D. E. Sayers, E. A. Stern and F. W. Lytle, *Phys. Rev. Lett.* 1971, **27**, 1204.
17. E. A. Stern, *Phys. Rev. B* 1974, **10**, 3027.
18. E. A. Stern, D. E. Sayers and F. W. Lytle, *Phys. Rev. B* 1975, **11**, 4836.
19. B. Lengeler and P. Eisenberger, *Phys. Rev. B* 1980, **21**, 4507.
20. B.-K. Teo and P. A. Lee, *J. Am. Chem. Soc.* 1979, **101**, 2815.
21. M. Magini, *Chem. Phys. Lett.* 1981, **78**, 106.
22. S. Ishiguro and K. Ozutsumi, *Inorg. Chem.* 1990, **29**, 1117.

23. I. Persson, Å. Iverfeldt and S. Ahrland, *Acta Chem. Scand., Ser. A* 1981, **35**, 295.
24. T. Yamaguchi, K. Yamamoto and H. Ohtaki, *Bull. Chem. Soc. Japan* 1985, **58**, 3235.
25. P. Lemoine and P. Herpin, *Acta Cryst., Sect. B* 1980, **36**, 2772.
26. A. C. M. Young, M. A. Walters and J. C. Dewan, *Acta Cryst., Sect. C* 1989, **45**, 1733.

Polyhedron Vol. 12, No. 18, pp. 2193–2199, 1993
Printed in Great Britain

0277-5387/93 $6.00+.00
© 1993 Pergamon Press Ltd

STUDIES ON CROWN ETHER COMPLEXES—XXX. SYNTHESIS, PROPERTIES AND STRUCTURE OF THE 3:2 COMPLEXES OF HEAVIER LANTHANIDE NITRATES (Sm–Lu) WITH DIBENZO-30-CROWN-10

TONGBU LU, XINMIN GAN* and MINYU TAN

Department of Chemistry, Lanzhou University, Lanzhou 730000, P.R.C.

and

KAIBEI YU

Chengdu Centre of Analysis and Measurement, Academia Sinica, Chengdu 610041, P.R.C.

(*Received* 20 *April* 1993; *accepted* 11 *May* 1993)

Abstract—The heavier lanthanide nitrate complexes with DB30C10 have been prepared in acetonitrile. These new complexes with the general formula $[Ln(NO_3)_2(OH_2)_2(DB30C10)]_2 \cdot [Ln(NO_3)_5] \cdot CH_3CN$ (Ln = Sm–Lu) have been characterized by means of elemental analysis, IR spectra and conductivity measurement. The crystal and molecular structure of $[Lu(NO_3)_2(OH_2)_2(DB30C10)]_2 \cdot [Lu(NO_3)_5] \cdot 5CH_3NO_2$ has been determined by single-crystal X-ray diffraction. The asymmetric unit contains three independent ions: two cations, $[Lu(NO_3)_2(OH_2)_2(DB30C10)]^+$, with nine-coordinate lutetium ions and one anion, $[Lu(NO_3)_5]^{2-}$, with a 10-coordinate lutetium(III) ion. The coordination geometries of the cations and anion are distorted tricapped trigonal prism and distorted bicapped square antiprism, respectively.

Many rare earth-crown ether complexes have been investigated and some have been studied by single-crystal X-ray diffraction methods.[1,2] Among these studies the rare earth complexes with large cavity crown ethers have been less reported.[3] In order to investigate the coordination ways of large cavity crown ethers with rare earth ions we previously synthesized a series of complexes of the heavier lanthanide nitrates with dibenzo-24-crown-8 (DB24C8) and studied their molecular structure.[4] We found that the lanthanide nitrates and DB24C8 formed the hydrogen bonding complexes $[Ln(NO_3)_3(OH_2)_3] \cdot (DB24C8)$ (Ln = Gd–Lu), in which the lanthanide(III) ions were not directly coordinated to the crown ether, but coordinated to three bidentate nitrate groups and three water molecules, the crown ether molecule was hydrogen bonded to the water molecules.[4] As an extension of our previous work we recently synthesized the heavier lanthanide nitrate comlexes with DB30C10 and studied their composition and structure.

EXPERIMENTAL

Reagents

Hydrated lanthanide nitrates were prepared by dissolving Ln_2O_3 (AnalaR) in 1:1 nitric acid. DB30C10 was purchased from TJCRF (China). All other chemicals were AnalaR grade.

Chemical and physical measurements

The metal ion contents was determined by EDTA titration using xylenol-orange as an indicator. Carbon, nitrogen and hydrogen contents were determined using a Carlo–Erba 1106 elemental analyser. The IR spectra were recorded in the 4000–200 cm^{-1} region using KBr pellets and a 170 SX FTR spec-

* Author to whom correspondence should be addressed.

trometer. The crystals data were collected on a R3M/E diffractometer.

Preparation of the complexes

A solution of lanthanide nitrate (0.63 mmol) in acetonitrile (2 cm^3) was added dropwise to a solution of DB30C10 (0.4 mmol) in acetonitrile (2 cm^3). The mixture was stirred at room temperature for 24 h. The precipitated solid complex was filtered, washed with ethylacetate and dried in a desiccator (0.1 mm Hg) over P_4O_{10} for 2 days. All the complexes are powdered solids with the characteristic colour of the corresponding lanthanide nitrates.

All the complexes are hardly soluble in benzene and tetrachloromethane, slightly soluble in ethyl ether and ethyl acetate and soluble in acetonitrile, nitromethane and acetone.

Single crystals of the lutetium complex were obtained by dissolving the powdery solid complex in nitromethane and leaving the solution in a desiccator over $CaCl_2$ at room temperature. After about 1 month the colourless, air-sensitive crystals of the complex formed from the solution.

Crystal structure analysis

X-ray diffraction intensities were collected at 20°C on an R3M/E diffractometer with graphite-monochromated Mo-K_α radiation, using the $\theta/2\theta$ scan technique. The intensities were corrected for Lorentz–polarization effects and for empirical absorption. The crystal data are listed in Table 1.

The structure was solved by the Patterson method and a subsequent difference-Fourier technique and refined by full-matrix least-squares methods with anisotropic thermal factors for all non-hydrogen atoms. All calculations were performed using the SHELXTL system of computer programs.

RESULTS AND DISCUSSION

The composition of the complexes

The analytical data for the newly synthesized complexes, listed in Table 2, indicate that all the complexes conform to a 3:2 metal ion-to-crown ether stoichiometry.

Table 1. Crystal data

Formula	$C_{61}H_{103}N_{14}O_{61}Lu_3$
Molecular weight	2532.63
Crystal dimensions (mm)	$0.20 \times 0.30 \times 0.50$
System	Triclinic
Space group	$P\bar{1}$
Temperature (°C)	20
Lattice parameters	
a (Å)	11.198(2)
b (Å)	18.419(2)
c (Å)	25.707(4)
α (°)	71.00(1)
β (°)	89.45(1)
γ (°)	73.94(1)
Cell volume (Å^3)	4799(1)
Molecules/unit cell	2
D_{calc} (g cm^{-3})	1.75
D_{obs} (g cm^{-3})	1.73
μ (calc.) (cm^{-1})	31.76
Radiation, graphite monochromator	Mo-K_α ($\lambda = 0.71073$)
$F(000)$	2535.43
Standard reflection	$-1, 2, -7$ and $-4, 5, 4$
Scan type and rate (° min^{-1})	$\theta/2\theta$, 8
Collection range	$2° \leqslant 2\theta \leqslant 43°$
Unique data measured	11,817
Observable data with $I \geqslant 3.0\sigma(I)$	8124
No. of variables	1252
Goof (or S)	1.209
Rw	0.0573
R	0.0669

Table 2. Analytical data of the complexes

Compound[a]	C (%) Found (Calc.)	H (%) Found (Calc.)	N (%) Found (Calc.)	Ln (%) Found (Calc.)
$[Sm(NO_3)_3]_3 \cdot L_2 \cdot 4H_2O \cdot CH_3CN$	31.9 (31.6)	4.1 (4.1)	6.9 (6.4)	20.2 (20.5)
$[Eu(NO_3)_3]_3 \cdot L_2 \cdot 4H_2O \cdot CH_3CN$	31.3 (31.6)	4.1 (4.1)	6.4 (6.3)	20.4 (20.7)
$[Gd(NO_3)_3]_3 \cdot L_2 \cdot 4H_2O \cdot CH_3CN$	31.3 (31.3)	4.0 (4.1)	6.6 (6.3)	21.3 (21.3)
$[Tb(NO_3)_3]_3 \cdot L_2 \cdot 4H_2O \cdot CH_3CN$	31.1 (31.3)	3.9 (4.1)	6.3 (6.3)	21.3 (21.4)
$[Dy(NO_3)_3]_3 \cdot L_2 \cdot 4H_2O \cdot CH_3CN$	31.0 (31.1)	3.8 (4.1)	6.1 (6.3)	21.6 (21.8)
$[Ho(NO_3)_3]_3 \cdot L_2 \cdot 4H_2O \cdot CH_3CN$	30.4 (31.0)	3.8 (4.1)	6.0 (6.2)	21.9 (22.1)
$[Er(NO_3)_3]_3 \cdot L_2 \cdot 4H_2O \cdot CH_3CN$	30.9 (30.9)	3.9 (4.0)	6.1 (6.2)	22.1 (22.3)
$[Tm(NO_3)_3]_3 \cdot L_2 \cdot 4H_2O \cdot CH_3CN$	31.0 (30.9)	4.0 (4.0)	6.4 (6.2)	22.8 (22.5)
$[Yb(NO_3)_3]_3 \cdot L_2 \cdot 4H_2O \cdot CH_3CN$	30.7 (30.7)	3.9 (4.0)	5.8 (6.2)	22.8 (22.9)
$[Lu(NO_3)_3]_3 \cdot L_2 \cdot 4H_2O \cdot CH_3CN$	30.6 (30.6)	3.9 (4.0)	5.8 (6.2)	23.0 (23.1)

[a] L = DB30C10.

IR spectra

Compared with those of the free ligand the absorptions of ν(Ar—O—R) and ν(R—O—R) of the complexes showed shifts of -7 to -10 and -17 to -19 cm^{-1}, respectively; this indicates that the crown ether coordinates to the lanthanide(III) ion.

In the IR spectrum of the complexes the absorptions appearing in the 3410–3440, 1629–1633 and 602–603 cm^{-1} regions are clearly due to ν(OH), δ(HOH) and ρ_r(HOH), respectively, indicating that coordinated water molecules exist in the complexes.[5]

The characteristic frequencies of coordinating nitrate groups appear in the 1765–1781 ($\nu_2+\nu_5$), 1730–1734 ($\nu_2+\nu_6$), 1506–1507 (ν_1), 1282–1291 (ν_4), 1047–1051 (ν_2) and 815–863 (ν_3) cm^{-1} regions in the IR spectrum of the complexes; the difference between the two strongest absorptions (ν_1 and ν_4) of nitrate groups is *ca* 200 cm^{-1}, indicating that the nitrate groups in the complexes coordinate to the metal ions as a bidentate ligand.[5] The absence of the absorptions around 1360 cm^{-1} indicates that all the nitrate groups in the complexes coordinate to the lanthanide ions.[5]

Crystal and molecule structure of lutetium(III) *complex*

Selected bond lengths and angles are given in Tables 3 and 4, respectively. Figure 1 shows the

Table 3. Selected bond lengths (Å)

Lu(1)—O(7)	2.404(9)	Lu(2)—O(20)	2.404(9)	Lu(3)—O(37)	2.406(16)
Lu(1)—O(8)	2.388(10)	Lu(2)—O(21)	2.422(8)	Lu(3)—O(38)	2.369(26)
Lu(1)—O(9)	2.382(11)	Lu(2)—O(22)	2.358(12)	Lu(3)—O(40)	2.390(24)
Lu(1)—O(11)	2.394(10)	Lu(2)—O(29)	2.426(9)	Lu(3)—O(41)	2.396(15)
Lu(1)—O(12)	2.425(12)	Lu(2)—O(30)	2.386(10)	Lu(3)—O(43)	2.391(13)
Lu(1)—O(14)	2.354(10)	Lu(2)—O(32)	2.353(10)	Lu(3)—O(44)	2.464(14)
Lu(1)—O(15)	2.439(11)	Lu(2)—O(33)	2.413(10)	Lu(3)—O(46)	2.403(17)
Lu(1)—O(17)	2.285(8)	Lu(2)—O(35)	2.326(11)	Lu(3)—O(47)	2.321(16)
Lu(1)—O(18)	2.281(10)	Lu(2)—O(36)	2.286(8)	Lu(3)—O(49)	2.386(17)
				Lu(3)—O(50)	2.391(18)

Table 4. Selected bond angles (°)

O(7)—Lu(1)—O(8)	67.4(3)	O(7)—Lu(1)—O(9)	134.6(3)
O(8)—Lu(1)—O(9)	67.2(3)	O(7)—Lu(1)—O(11)	73.7(4)
O(8)—Lu(1)—O(11)	73.5(4)	O(9)—Lu(1)—O(11)	91.2(3)
O(7)—Lu(1)—O(12)	123.2(3)	O(8)—Lu(1)—O(12)	108.3(4)
O(9)—Lu(1)—O(12)	70.2(4)	O(11)—Lu(1)—O(12)	52.7(3)
O(7)—Lu(1)—O(14)	91.1(4)	O(8)—Lu(1)—O(14)	71.0(3)
O(9)—Lu(1)—O(14)	76.7(4)	O(11)—Lu(1)—O(14)	144.4(3)
O(12)—Lu(1)—O(14)	143.5(4)	O(7)—Lu(1)—O(15)	71.6(3)
O(8)—Lu(1)—O(15)	107.9(4)	O(9)—Lu(1)—O(15)	125.8(3)
O(11)—Lu(1)—O(15)	141.2(3)	O(12)—Lu(1)—O(15)	143.9(3)
O(14)—Lu(1)—O(15)	53.2(3)	O(7)—Lu(1)—O(17)	143.6(4)
O(8)—Lu(1)—O(17)	139.8(3)	O(9)—Lu(1)—O(17)	78.4(3)
O(11)—Lu(1)—O(17)	129.2(4)	O(12)—Lu(1)—O(17)	77.3(3)
O(14)—Lu(1)—O(17)	81.5(4)	O(15)—Lu(1)—O(17)	75.6(4)
O(7)—Lu(1)—O(18)	77.7(3)	O(8)—Lu(1)—O(18)	139.8(3)
O(9)—Lu(1)—O(18)	142.0(4)	O(11)—Lu(1)—O(18)	78.4(3)
O(12)—Lu(1)—O(18)	74.6(4)	O(14)—Lu(1)—O(18)	130.5(4)
O(15)—Lu(1)—O(18)	77.7(4)	O(17)—Lu(1)—O(18)	80.4(3)
O(20)—Lu(2)—O(21)	66.4(4)	O(20)—Lu(2)—O(22)	133.4(3)
O(21)—Lu(2)—O(22)	67.4(3)	O(20)—Lu(2)—O(29)	124.4(3)
O(21)—Lu(2)—O(29)	113.1(3)	O(22)—Lu(2)—O(29)	70.1(3)
O(20)—Lu(2)—O(30)	76.4(4)	O(21)—Lu(2)—O(30)	73.7(3)
O(22)—Lu(2)—O(30)	85.3(4)	O(29)—Lu(2)—O(30)	53.4(3)
O(20)—Lu(2)—O(32)	92.6(4)	O(21)—Lu(2)—O(32)	70.5(3)
O(22)—Lu(2)—O(32)	77.6(4)	O(29)—Lu(2)—O(32)	141.8(4)
O(30)—Lu(2)—O(32)	144.0(3)	O(20)—Lu(2)—O(33)	72.2(3)
O(21)—Lu(2)—O(33)	106.1(3)	O(22)—Lu(2)—O(33)	127.4(4)
O(29)—Lu(2)—O(33)	140.9(3)	O(30)—Lu(2)—O(33)	145.3(4)
O(32)—Lu(2)—O(33)	53.1(4)	O(20)—Lu(2)—O(35)	77.5(3)
O(21)—Lu(2)—O(35)	139.8(3)	O(22)—Lu(2)—O(35)	141.8(3)
O(29)—Lu(2)—O(35)	73.2(4)	O(30)—Lu(2)—o(35)	81.3(4)
O(32)—Lu(2)—O(35)	130.2(4)	O(33)—Lu(2)—O(35)	77.8(4)
O(20)—Lu(2)—O(36)	143.7(4)	O(21)—Lu(2)—O(36)	138.2(4)
O(22)—Lu(2)—O(36)	79.4(3)	O(29)—Lu(2)—O(36)	76.0(3)
O(30)—Lu(2)—O(36)	129.4(3)	O(32)—Lu(2)—O(36)	78.4(3)
O(33)—Lu(2)—O(36)	74.4(3)	O(35)—Lu(2)—O(36)	81.9(4)
O(37)—Lu(3)—O(38)	47.2(8)	O(37)—Lu(3)—O(40)	148.3(6)
O(38)—Lu(3)—O(40)	143.4(8)	O(37)—Lu(3)—O(41)	141.3(8)
O(38)—Lu(3)—O(41)	150.3(8)	O(40)—Lu(3)—O(41)	51.3(6)
O(37)—Lu(3)—O(43)	76.5(6)	O(38)—Lu(3)—O(43)	122.2(7)
O(40)—Lu(3)—O(43)	79.0(7)	O(41)—Lu(3)—O(43)	81.2(5)
O(37)—Lu(3)—O(44)	72.2(7)	O(38)—Lu(3)—O(44)	93.9(7)
O(40)—Lu(3)—O(44)	76.8(7)	O(41)—Lu(3)—O(44)	115.8(7)
O(43)—Lu(3)—O(44)	50.9(5)	O(37)—Lu(3)—O(46)	104.3(7)
O(38)—Lu(3)—O(46)	71.8(8)	O(40)—Lu(3)—O(46)	71.6(7)
O(41)—Lu(3)—O(46)	114.3(6)	O(43)—Lu(3)—O(46)	120.4(5)
O(44)—Lu(3)—O(46)	72.2(5)	O(37)—Lu(3)—O(47)	123.8(7)
O(38)—Lu(3)—O(47)	76.7(7)	O(40)—Lu(3)—O(47)	79.1(7)
O(41)—Lu(3)—O(47)	85.2(6)	O(43)—Lu(3)—O(47)	158.2(6)
O(44)—Lu(3)—O(47)	123.0(6)	O(46)—Lu(3)—O(47)	51.2(5)
O(37)—Lu(3)—O(49)	85.5(7)	O(38)—Lu(3)—O(49)	72.5(8)
O(40)—Lu(3)—O(49)	124.8(6)	O(41)—Lu(3)—O(49)	79.7(7)
O(43)—Lu(3)—O(49)	121.2(6)	O(44)—Lu(3)—O(49)	157.4(7)
O(46)—Lu(3)—O(49)	118.1(6)	O(47)—Lu(3)—O(49)	72.4(6)
O(37)—Lu(3)—O(50)	70.1(7)	O(38)—Lu(3)—O(50)	97.0(8)
O(40)—Lu(3)—O(50)	119.1(6)	O(41)—Lu(3)—O(50)	72.7(6)
O(43)—Lu(3)—O(50)	69.9(5)	O(44)—Lu(3)—O(50)	115.0(5)
O(46)—Lu(3)—O(50)	167.5(6)	O(47)—Lu(3)—O(50)	121.9(5)
O(49)—Lu(3)—O(50)	51.4(6)		

structure of $[Lu(NO_3)_2(OH_2)_2(DB30C10)]^+$ cations and the $[Lu(NO_3)_5]^{2-}$ anion, whilst Fig. 2 illustrates the molecular packing arrangement in the unit cell.

The structure contains two independent $[Lu(NO_3)_2(OH_2)_2(DB30C10)]^+$ cations, one $[Lu(NO_3)_5]^{2-}$ anion and five uncoordinated nitromethane molecules. In the cations the $Lu_{(1)}^{III}$ and $Lu_{(2)}^{III}$ ions are both nine-coordinated with three crown ether oxygen atoms, two bidentate nitrate groups and two water molecules. The coordination geometries of these two cations are distorted tricapped trigonal prisms[6] (Fig. 3). The distances between lutetium(III) ions and oxygen atoms lie in the ranges: $Lu_{(1)}$—O (crown), 2.382–2.404 (av. 2.395); $Lu_{(2)}$—O (crown), 2.358–2.422 (av. 2.395);

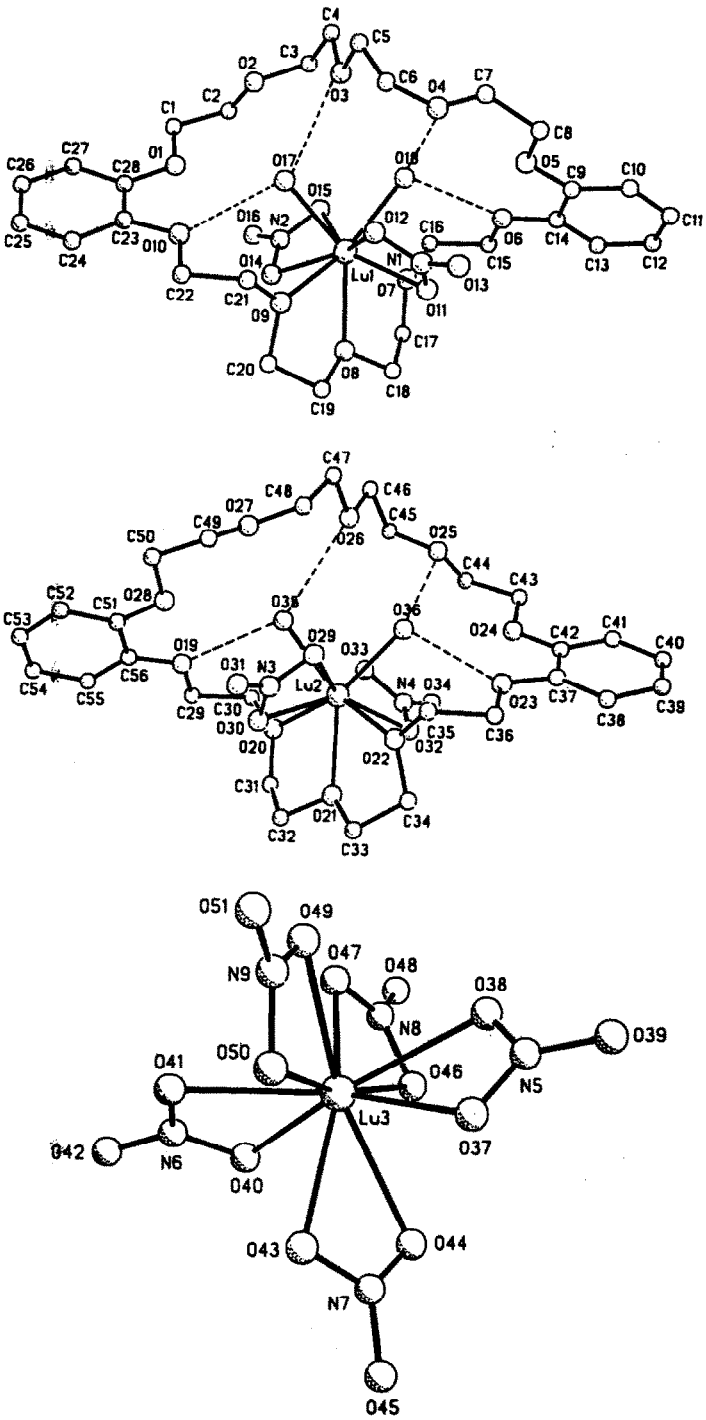

Fig. 1. The structures of the complex cations and complex anion.

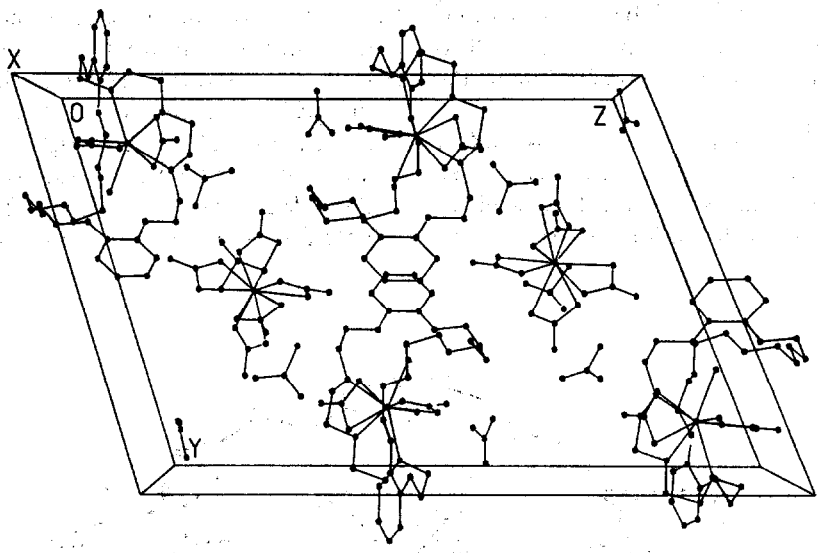

Fig. 2. The molecular packing arrangement in the unit cell.

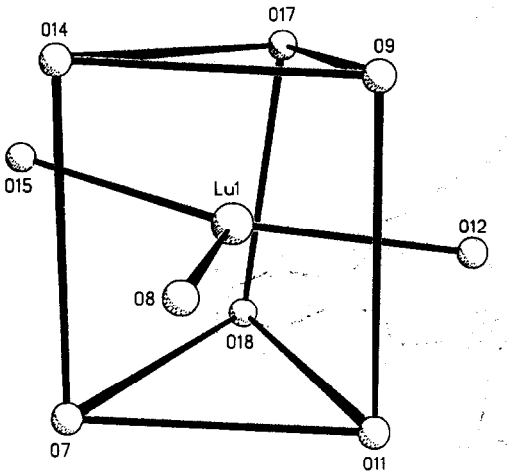

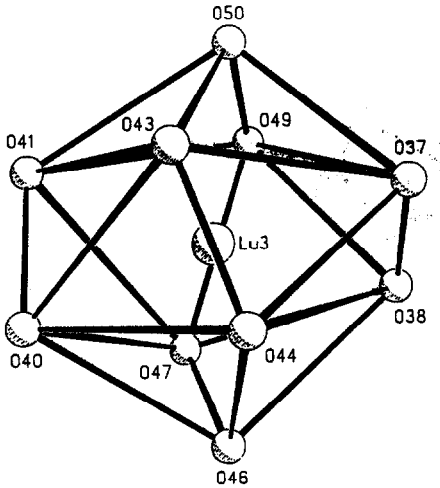

Fig. 3. The coordination geometries of the $Lu_{(1)}^{III}$ cation and $Lu_{(3)}^{III}$ anion.

$Lu_{(1)}$—O (nitrate), 2.354(10)–2.439(11) (av. 2.406); $Lu_{(2)}$—O (nitrate), 2.353(10)–2.426(9) (av. 2.395); $Lu_{(1)}$—O (water), 2.281(10)–2.285(8) (av. 2.283); and $Lu_{(2)}$—O (water), 2.286(8)–2.326(11) Å (av. 2.306 Å). In the anion the 10-coordinated lutetium(III) ion is bonded to five bidentate nitrate groups, forming a distorted bicapped square antiprism[6] (Fig. 3). The $Lu_{(3)}$—O (nitrate) bond lengths lie in the range 2.321–2.464 Å (av. 2.394 Å).

It can be seen from Table 5 that some O(water)···O(crown) distances range from 2.811 to 2.997 Å; these values lie in the range of hydrogen bonding distances.[7] This suggests that the hydrogen bonding occurs between coordinated water molecules and some of the crown ether oxygen atoms.

CONCLUSIONS

In comparison with DB24C8, DB30C10 is more flexible and so it can achieve the correct M—O(crown) distances and directly coordinate to the lanthanide ions. Owing to the too small ionic radius of the lutetium(III) ion the ligand cannot absorb the steric crowding arising from the large

Table 5. Some O(water)···O(crown) distances (Å)

O(17)···O(3)	2.826	O(35)···O(19)	2.889
O(17)···O(10)	2.811	O(35)···O(26)	2.997
O(18)···O(4)	2.867	O(36)···O(25)	2.907
O(18)···O(6)	2.853	O(36)···O(23)	2.812

cavity diameter, so all of the crown ether oxygen atoms in DB30C10 cannot simultaneously coordinate to the metal ion and DB30C10 can only bond to Lu^{3+} ion through part of the ether oxygen atoms.

Acknowledgement—The authors are grateful to the China National Natural Science Foundation for financial support.

REFERENCES

1. J.-C. G. Bunzli, in *Handbook on the Physics and Chemistry of Rare Earths* (Edited by K. A. Gschneidner Jr and L. Eyring), Ch. 60. North Holland Publishing Co., Amsterdam (1987).
2. Y. Inoue and G. W. Gokel, *Cation Binding by Macrocycles Complexation of Cationic Species by Crown Ethers*. Marcel Dekker, Inc., New York (1990).
3. M. Ciampolini and N. Nardi, *Inorg. Chim. Acta* 1979, **32**, L9.
4. T. Lu, X. Gan, M. Tan, C. Li and K. Yu, *Polyhedron* 1993, **12**, 1641.
5. K. Nakamoto, *Infrared and Raman Spectra of Inorganic and Coordination Compounds*, 3rd edn. John Wiley, New York (1978).
6. M. G. B. Drew, *Coord. Chem. Rev.* 1977, **24**, 179.
7. X. M. Gan, N. Tang, X. Wang, Y. Zhu and M. Y. Tan, *J. Coord. Chem.* 1989, **20**, 21.

Polyhedron Vol. 12, No. 18, pp. 2201–2204, 1993
Printed in Great Britain

0277–5387/93 $6.00+.00
© 1993 Pergamon Press Ltd

SYNTHESIS AND CRYSTAL STRUCTURE DETERMINATION OF THE NOVEL COMPOUND IODODIETHYLDITHIOCARBAMATOTELLURIUM(II)

R. KRISHNA KUMAR, G. ARAVAMUDAN,* M. R. UDUPA and M. SESHASAYEE†

Departments of Chemistry and †Physics, Indian Institute of Technology, Madras 600 036, India

and

T. A. HAMOR

School of Chemistry, The University of Birmingham, Edgbaston, Birmingham B15 2TT, U.K.

(*Received* 20 *April* 1993; *accepted* 11 *May* 1993)

Abstract—The title compound $Te^{II}LI$ [L = diethyl dithiocarbamate, $(C_2H_5)_2NCS_2^-$] was synthesized by the reduction of $Te^{IV}L_2I_2$ with elemental tellurium. Its structure has been determined and is found to be polymeric, with I being the bridging ligand. The polymeric chain adopts a helical configuration which runs parallel to the *c*-axis of the tetragonal unit cell. Each tellurium is bonded to two sulphurs of a chelating dithiocarbamate group and to two iodines in a planar configuration. The bond distances of Te—S(1), Te—S(2), Te—I and Te—I′ are 2.536(4), 2.483(5), 3.108(1) and 3.279(1) Å, respectively, and the bond angles of I—Te—S(1), S(1)—Te—S(2), S(2)—Te—I′ and I′—Te—I are 149.6(2), 70.7(2), 151.1(2) and 129.2(2)°, respectively.

During our continuing studies on mixed halide-dithiocarbamate complexes of tellurium in +2 and +4 states we have prepared the novel compound TeLI. Crystal structures of many tellurium(II) bisdithiocarbamates, $Te[R_1(R_2)NCS_2]_2$ [$R_1 = R_2 = C_2H_5$,[1] $(OH)C_2H_4$,[2] C_3H_7,[3] i-C_3H_7[4] and morpholyl,[5] have been determined. In all these cases tellurium(II) exhibits a planar trapezoidal four-fold coordination of sulphur atoms with highly anisobidentate dithiocarbamate chelation. Even though tellurium(II) mixed-ligand complexes of xanthate with dithiocarbamate[6] and halides (Br, Cl and I)[7] have been prepared earlier, preparation of complexes containing both dithiocarbamate and halide was elusive. Recently using suitable synthetic strategies we were able to report on the synthesis and structure determination of adducts of TeLX (where L is a dithiocarbamate group and X a thiocyanate or iodide ion) with TeL_2[8] and TeL_2I_2.[9] In this paper is reported the synthesis and structure of the pure phase iododiethyldithiocarbamato tellurium(II).

The structure determination reveals a novel helical polymeric arrangement of atoms to satisfy the common four-fold coordination of tellurium(II).

EXPERIMENTAL

The title compound was prepared by stirring a solution of $Te^{IV}L_2I_2$ (0.678 g, 1 mmol) with freshly prepared powdered elemental tellurium (0.190 g, 1.5 mmol) for 12 h. The unreacted tellurium powder was filtered and evaporation of the filtrate gave dark brown needle-shaped crystals of TeLI. TeL_2I_2 was prepared by the procedure reported earlier[10] and tellurium powder was obtained by hydrazine reduction of tellurium(IV) chloride in 2 N HCl medium.

* Author to whom correspondence should be addressed.

The composition of the compound was confirmed from elemental analysis results. The percentage weight calculated is given in parentheses. Found: C, 15.0; N, 3.5; H, 2.6; Te, 31.4; I, 31.5. Calc.: C, 14.9; N, 3.5; H, 2.5; Te, 31.7; I, 31.5%.

Crystal data

The crystallographic data are as follows: $Te(C_4H_{10}NCS_2)I$, $Mr = 402.75$, tetragonal, space group $I\bar{4}$, $a = b = 20.107(3)$, $c = 6.283(4)$ Å, $V = 2540.15$ Å^3, $Z = 8$, $D_x = 2.11$, $D_m = 2.14$ mg m^{-3}, λ(Mo-K_α) = 0.71069 Å, $\mu = 4.717$ mm^{-1}, $F(000) = 1471.98$. The density was measured by the flotation method.

Data collection

A single crystal of dimensions $0.5 \times 0.5 \times 0.5$ mm^3 was mounted on an Enraf–Nonius CAD4 diffractometer. Lattice parameters with ESDs were obtained from 24 reflections in the θ range 11.5–15.6°. The intensity data were collected by the ω–2θ scan technique for 2θ range between 4° and 55° with Mo-K_α radiation; the *hkl* range being h: $-17 \rightarrow 18$, k: $0 \rightarrow 26$, l: $0 \rightarrow 8$. Three standard reflections were measured every 2 h for an intensity check and three reflections remeasured after every 200 reflections for an orientation check, which showed no significant variation in the intensity. 3266 reflections were measured, of which 1591 reflections with $I > 3\sigma(I)$ were considered unique. The intensity data were corrected for Lorentz and polarization effects. An absorption correction was applied using the program ABSORB.[11]

Solution and refinement

The structure was solved by the heavy atom method. Tellurium and iodine positions were obtained from the Patterson map and the successive Fourier maps based on tellurium and iodine positions gave the locations of all non-hydrogen atoms. The full-matrix least-squares method using SHELX76[12] gave the positions of non-hydrogen atoms and their anisotropic thermal parameters. Maximum shift per e.s.d. was 0.04 when the refinement was terminated and 286 parameters were refined. Residuals at convergence were $R = 0.057$ and $Rw = 0.056$ for 1591 unique reflections, where $w = 1/[\sigma^2|F_o| + 0.0012|F_o|^2]$. The final difference-Fourier map showed no unusual features with the largest peak maximum being 1.3 e Å^{-3}, which is in proximity to tellurium and has no chemical significance. Hydrogen atoms did not appear in the final difference-Fourier map. Atomic scattering factors for non-hydrogen atoms were taken from Cromer and Mann[13] and anomalous dispersion correction factors were taken from Cromer and Liberman.[14]*

RESULTS AND DISCUSSION

Crystals of the title compound, TeLI, are stable indefinitely under ambient conditions in air. In the characteristic C⟛N IR absorption region for the dithiocarbamates, TeL_2 shows absorptions at 1478, 1446 and 1414 cm^{-1} and TeLI at 1510 and 1420 cm^{-1}. TeLI is highly soluble in dichloromethane, but unlike TeL_2 is very sparingly soluble in carbon tetrachloride. Whereas solutions of TeL_2 in dichloromethane are unaffected by triphenylphosphine, solutions of TeLI in the same solvent undergo immediate decomposition to tellurium on addition of this reagent.

In the tellurium(II) dithiocarbamates generally the coordination around tellurium is four and planar. Tellurium, in the title compound, if it were to exist as a monomer would be coordinately unsaturated, being bound to two sulphur atoms of the dithiocarbamate group and an iodine atom. There are three different possibilities by which four coordination can be attained. In the first possibility the tellurium atom can bind to another tellurium atom to form a dimer having a Te—Te bond. This kind of Te—Te interaction is observed in $Te_2L'_3(SCN)$ [$L' = (OHCH_2CH_2)_2NCS_2^-$],[8] where the "unsaturated" TeL'(SCN) moiety achieves the saturation by bonding to Te of the TeL'_2 group. The inter tellurium bond distance reported therein is 3.221 Å. In the second possibility the dithiocarbamate group(s) can act as a bridging ligand(s), binding to two tellurium atoms. A number of bridged dithiocarbamates have been reported in the complexes of many transition elements, e.g. $(MoL_3)_2$,[15] $(ZnL_2)_2$[16] and $(Ru_2L_5)^+BF_4^-$.[17] In the third possibility the coordination around tellurium can be enhanced by bridging through iodine atoms. Such iodine-bridged structures have been reported for the tellurium(IV) complexes TeL'_2I_2[18] and TeL_2I_2[10] and mixed-valence Te^{II}–Te^{IV} complex, $Te_2L_3I_3$.[9] The present structure determination shows that in the title compound iodine bridging occurs and instead of a dimeric structure, a polymeric structure is obtained. Such halogen-

* Supplementary materials available: Fractional atomic coordinates and equivalent isotropic thermal parameters involving non-hydrogen atoms, anisotropic thermal parameters and bond lengths and angles.

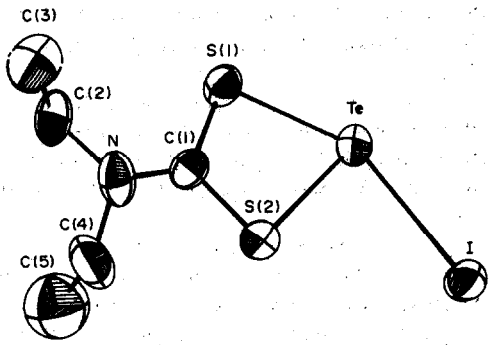

Fig. 1. The ORTEP plot of the fragment of TeLI with 50% probability ellipsoid.

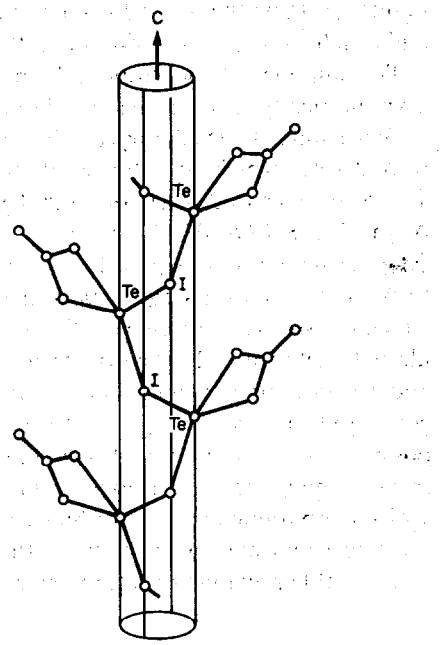

Fig. 2. The helical arrangement of the molecule.

bridged polymeric structures have been found in $[Te(S_2COC_2H_5)Br]_n$[7] and $(OC_4H_8NCSe_3)I$.[19] The ORTEP[20] diagram of the molecule is shown in Fig. 1.

The helical arrangement adopted by the tellurium and iodine atoms, running parallel to the *c*-axis, is shown in Fig. 2, with two pairs of tellurium and iodine atoms forming a repeating unit with a period of 6.283(4) Å. There are four helices within a unit cell, with the shortest separation between two inter-helical tellurium atoms being 9.363(1) Å.

Tellurium atoms in the helix are at a distance of 3.879(2) Å from two other tellurium atoms. This distance is smaller than the sum of the van der Waals radii of 4.12 Å. Similarly two iodine atoms in the helix are at a distance of 5.772 Å from two other iodine atoms.

Each tellurium displays a planar arrangement of two sulphurs and two iodines, the RMS deviation from the mean plane being 0.07 Å. The two pairs of non bonding electrons on the tellurium would lie above and below this plane.

There are two different Te—I bonds (see Table 1), with distances of 3.108(1) and 3.279(1) Å, both being larger than the sum of the individual covalent radii of tellurium and iodine (2.70 Å). This is so because of the appreciable *trans* influence of the dithiocarbamate sulphurs and in addition the bridging of the iodines. The angle subtended at the

Table 1. Bond lengths (Å) and angles (°)

Te—I	3.108(1)	C(1)—N	1.282(19)
Te—I′	3.279(1)	N—C(2)	1.498(19)
Te—S(1)	2.536(4)	N—C(4)	1.532(29)
Te—S(2)	2.483(5)	C(2)—C(3)	1.535(27)
S(1)—C(1)	1.693(15)	C(4)—C(5)	1.552(38)
S(2)—C(1)	1.747(13)		
I—Te—I′	129.2(2)	Te—S(2)—C(1)	87.3(6)
Te—I—Te′	74.7(1)	S(1)—C(1)—N	123.5(9)
I—Te—S(1)	149.6(2)	S(2)—C(1)—N	121.2(9)
I—Te—S(2)	79.3(3)	C(1)—N—C(2)	123(1)
I′—Te—S(1)	80.4(2)	C(1)—N—C(4)	119(1)
I′—Te—S(2)	151.1(2)	C(2)—N—C(4)	118(1)
S(2)—Te—S(1)	70.7(2)	C(3)—C(2)—N	112(1)
S(1)—C(1)—S(2)	115.1(8)	C(5)—C(4)—N	111(2)
Te—S(1)—C(1)	86.7(6)		

(′) = (0.5−*x*, 0.5−*y*, −0.5+*z*).

iodine, bridging the two tellurium atoms, is 74.7(1)° and at tellurium by the iodines is 129.2(2)°.

The sulphurs of the dithiocarbamate group are asymmetrically bound, having bond lengths of 2.536(4) and 2.483(5) Å for Te—S(1) and Te—S(2), respectively, which are shorter than the average Te—S distance of 2.69 Å found in TeL_2[1] and 2.65 Å in $TeL(S_2COC_2H_5)$[6] and other tellurium(II) dithiocarbamate complexes. This may be attributed to the presence of a single dithiocarbamate group which is a stronger complexing ligand than the iodide with tellurium(II). The difference in Te—S(1) and Te—S(2) bond lengths in this compound is less compared with that in TeL_2. In the asymmetrically bound Te—S the shorter Te—S bond is present *trans* to the longer Te—I bond and *vice versa*. The molecular parameters of the dithiocarbamate group are unexceptional and similar to those found in innumerable previous structure determinations.

REFERENCES

1. C. Fabiani, R. Spagna, A. Vaciago and L. Zambonelli, *Acta Cryst.* 1971, **B27**, 1499.
2. G. C. Rout, M. Seshasayee, K. Radha and G. Aravamudan, *Acta Cryst.* 1983, **C39**, 1021.
3. V. Ganesh, M. Seshasayee, SP. Chidambaram, G. Aravamudan, K. Goubitz and H. Schenk, *Acta Cryst.* 1989, **C45**, 1506.
4. V. Kumar, G. Aravamudan, M. Seshasayee, P. Selvam and K. Yvon, *Acta Cryst.* 1990, **C46**, 2081.
5. S. Husebye, *Acta Chem. Scand.* 1970, **24**, 2198.
6. B. F. Hoskins, R. T. E. Tiekink and G. Winter, *Inorg. Chim. Acta* 1985, **105**, 171.
7. W. R. Gable, B. F. Hoskins, R. J. Steen and G. Winter, *Inorg. Chim. Acta* 1983, **72**, 173.
8. K. Radha, G. Aravamudan, A. Rajalakshmi, G. C. Rout and M. Seshasayee, *Aust. J. Chem.* 1986, **39**, 847.
9. V. Ganesh, M. Seshasayee, V. Kumar, SP. Chidambaram, G. Aravamudan, K. Goubitz and H. Schenk, *J. Cryst. Spectrosc. Res.* 1989, **19**, 745.
10. R. Krishna Kumar, G. Aravamudan, M. R. Udupa, M. Seshasayee and T. A. Hamor, *Acta Cryst.* 1993, C49.
11. F. Ugozzoli, *Comput. Chem.* 1987, **11**, 109.
12. G. M. Sheldrick, SHELX76, A Program for Crystal Structure Determination. University of Cambridge, U.K. (1976).
13. D. T. Cromer and J. B. Mann, *Acta Cryst.* 1968, **A24**, 321.
14. D. T. Cromer and D. Liberman, *J. Chem. Phys.* 1970, **53**, 1891.
15. P. C. H. Mitchell and R. D. Scarle, *J. Chem. Soc., Dalton Trans.* 1975, 110.
16. M. Bonamico, G. Mazzone, A. Vaciago and L. Zambonelli, *Acta Cryst.* 1965, **19**, 898.
17. B. M. Mattson, J. R. Heiman and L. H. Pignolet, *Inorg. Chem.* 1976, **15**, 564.
18. G. V. N. Appa Rao, M. Seshasayee, G. Aravamudan and K. Radha, *Acta Cryst.* 1983, **C39**, 1018.
19. F. Bigoli, E. Leporati, M. A. Pellinghelli, G. Crisponi, P. Deplano and E. F. Trogu, *J. Chem. Soc., Dalton Trans.* 1983, 1763.
20. C. K. Johnson, ORTEP Report ORNL-3794. Oak Ridge National Laboratory, Tennessee (1965).

Polyhedron Vol. 12, No. 18, pp. 2205–2213, 1993
Printed in Great Britain

0277–5387/93 $6.00+.00
© 1993 Pergamon Press Ltd

THE REDOX SYNTHESIS, STRUCTURE AND MAGNETIC PROPERTIES OF THE HETEROBIMETALLIC μ-OXO COMPOUND [(py)(TPP)CrOFe(tmtaa)]

PETER J. NICHOLS, GARY D. FALLON, BOUJEMAA MOUBARAKI, KEITH S. MURRAY and BRUCE O. WEST*

Centre of Chemical Synthesis and Department of Chemistry, Monash University, Clayton, Victoria 3168, Australia

(*Received* 20 *April* 1993; *accepted* 11 *May* 1993)

Abstract—The oxidation of Fe^{II}(tmtaa)† by $Cr^{IV}O$(TPP)† in pyridine-tetrahydrofuran solution leads to the formation of the heterobimetallic complex [(py)(TPP)CrOFe(tmtaa)]. Crystal structure determination of the bis-tetrahydrofuran solvate shows that the CrOFe linkage is almost linear [176.6(9)°], while the Fe-tmtaa stereochemistry differs from that previously known for five-coordinate tmtaa complexes. Mössbauer spectra and magnetic data (to 4 K) are reported for the solvent free complex. The $S = 3/2 : S = 5/2$ complex shows strong antiferromagnetic coupling with a $2J$ value of -299 cm^{-1}.

Oxo-bridged heterobinuclear complexes have been prepared[1] by one-electron redox reactions between $Cr^{IV}O$ porphyrin derivatives and a variety of other metal complexes of iron(II),[2–4] molybdenum(IV),[3,5] manganese(II)[3] and vanadium(IV).[6] Heterotrinuclear species can also be formed by two-electron redox reactions between $Ru^{VI}(O)_2$ porphyrins and iron(II)[7] complexes. Ligands used have involved porphyrins, phthalocyanine, salicylaldimines and dithiocarbamates. In contemperaneous work acetate-bridge "supported" heterobinuclear μ-oxo bridged complexes $[(L)M(\mu\text{-}O)(\mu\text{-}CH_3COO)_2M'(L')]^+$ (L and L′ are triazacyclononane type ligands) have also been prepared by Wieghardt *et al.*[8] using hydrolytic procedures in aqueous solution for several combinations of first row transition elements. A number of these compounds have been structurally characterized including $[(L)Cr^{III}(\mu\text{-}O)(\mu\text{-}CH_3COO)_2Fe^{III}(L')]PF_6$[8] (L = 1,4,7-triazacyclononane, L′ = 1,4,7-trimethyl-1,4,7-triazacyclononane). Although an X-ray structural study has been successfully carried out[7] on the trinuclear species Ru^{IV}(TPP)[OFe^{III}(salmah)]$_2$, similar characterizations of singly oxo-bridged compounds have proved elusive because of difficulties in growing suitable single crystals of any of the compounds previously reported.[1–6] One factor contributing to this is their ability to undergo further hydrolysis in the presence of traces of water. Magnetic studies have provided the principal evidence for their constitution so far,[1] since the majority of the complexes show strong to medium antiferromagnetic coupling via the oxo bridge. One incomplete structure determination[2] has been reported for the complex [(py)(TPP)CrOFe(TMP)], which disclosed the gross coordination features of the molecule, including an essentially linear CrOFe linkage, but crystal imperfections prevented refinement of the data to an acceptably low R factor.

A variety of structural studies of metal tmtaa compounds has appeared in recent literature,[9] suggesting that the presence of that ligand may lead to ready crystallization of coordination complexes. Fe^{II}(tmtaa) has been shown[10,11] to react readily with molecular oxygen to form a homobimetallic μ-oxo bridged complex, $[Fe^{III}(tmtaa)]_2O$, and such reactivity has been found to indicate complexes which can reduce $Cr^{IV}O$(P) and form heterobimetallic oxo-bridged complexes.[1] We have accordingly reacted Fe^{II}(tmtaa) with $Cr^{IV}O$(TPP) in the presence

* Author to whom correspondence should be addressed.

† Ligand abbreviations: tmtaa is the dianion of 5,7,12,14-tetramethyldibenzo[b,i][1,4,8,11]tetraazacyclotetradeca-2,4,7,9,11,14-hexaene. TPP is the dianion of 5,10,15,20-tetraphenylporphyrin. TMP is the dianion of 5,10,15,20-tetra-*p*-methoxyphenylporphyrin.

of pyridine and have isolated the complex [(py)(TPP)$Cr^{III}OFe^{III}$(tmtaa)] as a tetrahydrofuran solvate. Crystals of an appropriate quality to enable an X-ray structural study to be completed have been obtained and we wish to report the result of that study. The variation with temperature of the magnetic susceptibility and the Mössbauer spectrum of the complex have also been measured for comparison with CrOFe complexes previously isolated, which have different ligands attached to iron(III).[2,4] There is presently considerable interest in making magnetostructural correlations on heterometallic species not only in order to advance knowledge of superexchange mechanisms, but also because of the occurrence of mixed metal clusters in certain biological systems. Wieghardt and Girerd[8] have recently put forward a superexchange model which has some new features and the magnetic data for the present compound are analysed in this context.

EXPERIMENTAL

Materials and techniques

All manipulations were performed in dry solvents under purified nitrogen as previously described.[2] Spectra were recorded as follows: IR, PE 1600 FTIR; mass, V.G. Micromass; visible, Varian SuperScan 3. (Intensities indicated thus; vs, very strong; s, strong; m, medium; w, weak.)

Microanalyses were performed by the Australian Microanalytical Service and the National Analytical Laboratories Pty Ltd.

Variable-temperature magnetic susceptibility measurements were made using a Quantum Design MPMS Squid magnetometer. The calibrations of field and temperature performed by the manufacturer were also checked against a calibrated palladium sample as well as $Hg[Co(NCS)_4]$ and $CuSO_4 \cdot 5H_2O$. An applied field of 10 kOe was employed for the present measurements. Samples were finely ground and placed in gelatin capsules for measurements. The equipment and procedures for Mössbauer spectral measurements have been described previously.[2]

CrO(TPP) was prepared by the oxidation of Cr(TPP)Cl with iodosylbenzene.[12] Fe^{II}(tmtaa) was prepared following the reported procedure,[11] except that $Fe(py)_4(NCS)_2$ was substituted for Fe(*o*-phenylenediamine)$_2(NCS)_2$. Microanalytical and mass spectral data indicated no incorporation of pyridine or acetonitrile. Selected IR absorption bands (Nujol mull): 1592m, 1566m, 1524m, 1186vs, 1027s, 738vs cm^{-1}. Dry solid Fe(tmtaa) exposed to air overnight gave rise to the following 112 absorption bands (Nujol mull): 1538vs, 1192s, 1027s, 811vs, 742s cm^{-1}. A toluene solution of the complex kept under nitrogen with a slow "leak" of dry oxygen formed the oxo complex $[Fe^{III}(tmtaa)]_2O$, which could be crystallized as a toluene solvate. Found: C, 67.6; H, 5.8; N, 12.3. Calc. for $C_{51}H_{52}Fe_2N_8O$: C, 67.3; H, 5.8; N, 12.4%. Selected IR absorption bands (Nujol mull): 1538vs, 1192s, 1027s, 810vs, 742s cm^{-1}. The 810 cm^{-1} absorption appears most likely to relate to the FeOFe vibration. The band at 890 cm^{-1} assigned to this vibration[10] was not observed and may have been a printing error for 809 cm^{-1}. $\mu_{eff} = 2.5\mu_B$ (lit.[10,11] $1.96\mu_B$). In contrast to the low solubility reported[11] for the analogous CH_3CN adduct the toluene product is soluble in a range of solvents, but these solutions, including that in toluene, decompose rapidly when exposed to moist air forming high-spin iron(III) products showing strong OH IR absorption.

Synthesis of [(py)(TPP)CrOFe(tmtaa)]·2THF

CrO(TPP) (0.36 g, 0.53 mmol) and Fe(tmtaa) (0.21 g, 0.53 mmol) were dissolved in a deoxygenated THF/pyridine (50 : 1; 50 cm^3) solution and stirred at room temperature for 1 h. The red–green solution was filtered, cooled to 0°C and layered with hexane (100 cm^3). After standing at 0°C for 1 week with careful exclusion of air, purple crystals separated and these were collected, washed with hexane and dried under a flow of nitrogen (yield $\approx$ 0.2 g, 30%). A suitable crystal was selected from the batch for an X-ray diffraction study. Found: C, 72.5; H, 5.7; N, 9.5. Calc. for $C_{71}H_{55}CrFeN_9O \cdot 2C_4H_8O$: C, 72.9; H, 5.5; N, 9.7%. UV–vis absorption spectrum (toluene): 380, 436 (Sôret), 548 nm. Selected IR absorption bands (Nujol mull): 1596m, 1562m, 1524m, 1191m, 1068s, 1006vs, 879s, 795s, 746s cm^{-1}. On standing the purple crystalline compound gradually changes to a green powder through loss of THF. Coordinated pyridine is not evolved, however, as is evident from mass spectral examination of the solvent-free residue and its microanalysis. Found: C, 73.5; H, 5.2; N, 10.8. Calc. for $C_{71}H_{55}CrFeN_9O$: C, 73.6; H, 4.8; N, 10.9%. The THF-free compound was used for variable-temperature magnetic and Mössbauer spectral measurements because of the greater reproducibility of the composition of this form of the complex. The loss of THF does not affect the spectral or magnetic properties of the complex.

X-ray crystallography of [py(TPP)CrOFe(tmtaa)]·2THF

A representative purple acicular crystal was used for data collection. Intensity measurements on the

compound were made on a Nicolet R3m/V diffractometer using graphite-monochromated Mo-K_α radiation. Cell parameters were derived by least-squares calculations from 18 angular settings of reflections. The data collection and crystal parameters are given in Table 1. Three standard reflections monitored every 197 reflections did not show any significant variation in intensity over the collection period. Intensity data were processed as described previously.[13] Numerical absorption corrections[14] were applied to each data set. The maximum and minimum transmission factors were 0.959 and 0.936, respectively. The atomic scattering factors for neutral atoms were corrected for anomalous dispersion.[15] All calculations were performed on a MicroVax 2000 computer using the program due to Sheldrick[14] for least-squares refinement. The structure was solved by direct methods. Full-matrix least-squares refinement employing anisotropic thermal parameters for iron, chromium and the oxygen and carbon atoms of the THF solvate molecules and isotropic thermal parameters for all other atoms (single isotropic thermal parameter for hydrogen fixed at 0.08 Å^2—positioned in geometrically idealized positions: C—H 0.96 Å) reduced R to 0.076 and R_w to 0.099, respectively, at convergence, where $R_w = (\Sigma w(||F_o|-|F_c||)^2/\Sigma w|F_o|^2)^{1/2}$ and $w = [\sigma^2(F_o)+0.00040F_o^2]^{-1}$. The highest peak in the difference-Fourier synthesis was 1.07 e Å^{-3}.

RESULTS AND DISCUSSION

Syntheses

Fe^{II}(tmtaa) undergoes ready reaction with Cr^{IV}(O)(TPP) in THF solution to yield the heterobimetallic oxo-bridged complex [(TPP)Cr^{III}OFe^{III}(tmtaa)]. In the presence of pyridine the complex [(py)(TPP)CrOFe(tmtaa)] is formed, which can be isolated from solution as a di-tetrahydrofuran solvate. IR spectral bands indicating the presence of both porphyrin and tmtaa ligands are observed for the compound, while a strong band at 879 cm^{-1} which has no counterpart in the spectra of the reactants is tentatively assigned to the asymmetric CrOFe stretching vibration. The electronic absorption spectrum is dominated by the absorption of the porphyrin with a Sôret band at 436 nm.

The structure of [(py)(TPP)Cr^{III}OFe^{III}(tmtaa)]·2THF

A diagram of the molecular structure of [(py)(TPP)CrOFe(tmtaa)] is given in Fig. 1 with a list of relevant bond distances and angles in Table 2. The molecule consists of a six-coordinate chromium porphyrin unit with a pyridine molecule coordinated to the metal linked by an oxo group to a five-coordinate Fe-tmtaa unit. Tetrahydrofuran

Table 1. Crystallographic data for [(py)(TPP)CrOFe(tmtaa)]·2THF

Molecular formula	$C_{79}H_{71}N_9O_3CrFe$
Mol. wt	1302.3
Crystal system; space group	Monoclinic, $P21/a$
Temperature (°C)	−80(1)
Cell dimensions	
a (Å)	18.500(8)
b (Å)	17.272(12)
c (Å)	22.707(10)
β (°)	110.91(3)
Z	4
V (Å^3)	6778(7)
Density (g cm^{-3}): observed (calc.)	1.29(1) (1.28)
F(000)	2728
μ (cm^{-1})	4.2
λ(Mo-K_α)	0.71073
Crystal dimensions (mm)	0.11 × 0.15 × 0.30
Scan speed (° s^{-1})	0.066–0.326
2θ limits (°)	$3.5 < 2\theta < 45$
Scan range (°)	0.70
Data collected	8919 ($\pm h$, $+k$, $+l$)
No. unique data [$I \geqslant 3\sigma(I)$]	2878
Goodness of fit	1.17
R (R_w)	0.076 (0.099)

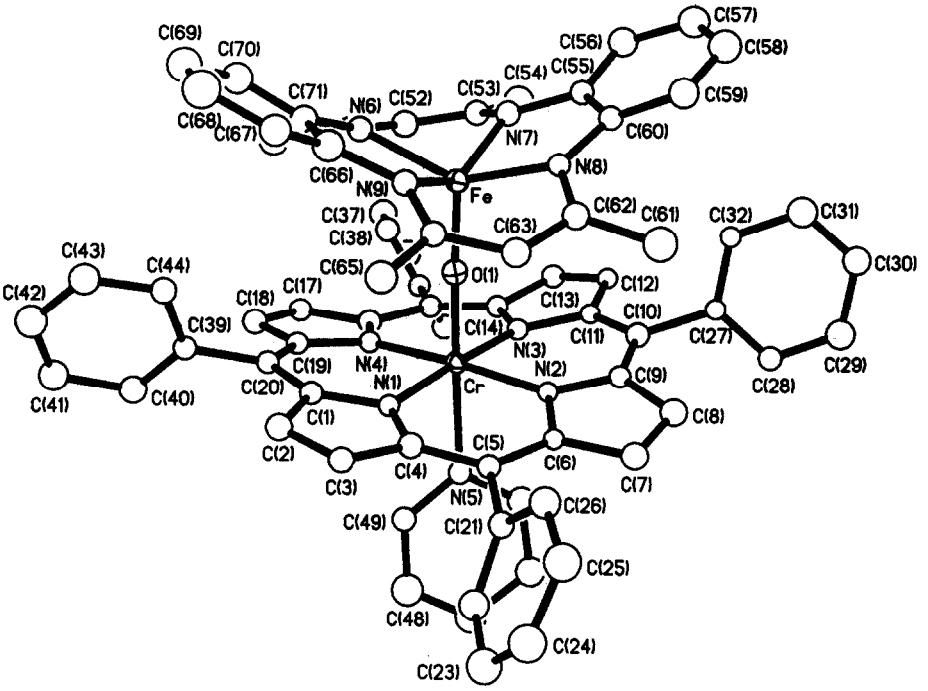

Fig. 1. ORTEP diagram of the structure of [(py)(TPP)CrOFe(tmtaa)] showing 50% probability ellipsoids and the labelling scheme.

molecules occupy lattice cavities formed by the loose packing of the complex molecules and there is no bonding interaction between either of the THF molecules and a molecule of [(py)(TPP)CrO Fe(tmtaa)]. The closest distance of approach between any atom of the tetrahydrofuran molecules and any atom of the complex is 3.619 Å between a carbon atom of a THF molecule and N(7) of the tmtaa ring. Only nine other interatomic contacts are at less than 3.8 Å. The porphyrin ring is ruffled with two of the four *meso*-carbons, C(20) and C(10), displaced from the N_4 plane towards the bridging oxygen atom and the remaining two, C(5) and C(15), displaced away from the oxygen. The coordinated pyridine molecule lies in the fold created by the displacements of C(20) and C(10) at an angle to the line between them. The torsion angle N(1)—Cr—[N(5)—C(49)] is 35.2°. Even with an excess of pyridine in the reaction mixture the iron(III) ion appears unable to accept a further ligand. $[Fe(tmtaa)]_2O$ has been previously shown[11] to be unable to coordinate additional Lewis bases, as has been observed with many other iron(III) μ-oxo compounds involving tetradentate ligands.[16] The earlier[2] incomplete crystallographic study of [(py)(TPP)CrOFe(TMP)] also showed pyridine attached to chromium but not to iron when porphyrin ligands were attached to both metals. The phenyl rings of tetraphenylporphyrin are inclined to the N_4 plane of the porphyrin ring in the propellor form well established for such tetraaryl derivatives. The angles are greatest for the phenyl groups overlain by the benzenoid rings of tmtaa (118° and 116°) and least for those nearer the pentanediimino segments (106° and 108°).

The CrOFe bridge is virtually linear with an angle of 176.6(9)°. Other homobimetallic $Cr^{III}OCr^{III}$ derivatives have shown essentially linear oxo bridges whereas FeOFe compounds display a range of angles from *ca* 140° to 180°. (Table 3 lists a selection of data. Additional references may be found in Table 1 of ref. 1.) The value observed for a particular Fe_2O complex is mainly influenced by inter-ligand steric interactions.[16] While we shall proceed to analyse the magnetic data of the CrOFe and FeOFe molecules in terms of the essentially non-bonding Heisenberg ($-2J\bar{S}_1 \cdot \bar{S}_2$) model (*vide infra*) it is nevertheless interesting to examine an alternative structural correlation developed on the assumption that π-bonding occurs in oxo-bridged species. Thus, such a molecular orbital picture of the bonding in MOM systems first put forward by Dunitz and Orgel[18] and extended by others[19–21] has been successful in correlating linear or bent MOM bonds with the total number of electrons which needs to be accommodated in the available

Table 2. Selected bond distances (Å) and angles (°) for [(py)(TPP)CrOFe(tmtaa)]·2THF

Cr—O(1)	1.776(11)	Fe—O(1)	1.759(11)
Cr—N(1)	2.030(11)	Fe—N(6)	2.036(14)
Cr—N(2)	2.008(15)	Fe—N(7)	2.044(12)
Cr—N(3)	2.018(11)	Fe—N(8)	2.038(14)
Cr—N(4)	2.020(15)	Fe—N(9)	2.040(12)
Cr—N(5)	2.188(18)	Cr···Fe	3.534
Cr to N(2)—N(4) plane	0.0753	Fe to N(6)—N(9) plane	0.646
		Cr—O(1)—Fe	176.6(9)
N(1)—Cr—N(2)	90.6(5)	N(6)—Fe—N(7)	87.6(5)
N(2)—Cr—N(3)	89.5(5)	N(7)—Fe—N(8)	81.0(5)
N(1)—Cr—N(4)	90.3(5)	N(6)—Fe—N(9)	81.8(5)
N(3)—Cr—N(4)	89.4(5)	N(8)—Fe—N(9)	86.5(5)
N(1)—Cr—N(3)	176.1(5)	N(6)—Fe—N(8)	143.0(5)
N(2)—Cr—N(4)	175.3(5)	N(7)—Fe—N(9)	143.1(5)
O(1)—Cr—N(1)	92.7(5)	O(1)—Fe—N(6)	108.0(6)
O(1)—Cr—N(4)	92.2(6)	O(1)—Fe—N(9)	108.4(5)
O(1)—Cr—N(2)	92.4(6)	O(1)—Fe—N(7)	108.5(5)
O(1)—Cr—N(3)	91.3(5)	O(1)—Fe—N(8)	109.0(6)
Torsion angles			
N(1)—Cr—Fe—N(9)	8.7	N(4)—Cr—Fe—N(6)	11.8
N(2)—Cr—Fe—N(8)	10.0	N(1)—Cr—[N(5)—C(49)]	35.2
N(3)—Cr—Fe—N(7)	6.9		

bonding, *anti*-bonding and non-bonding orbitals of the system. For complexes with up to eight metal electrons to be placed in the bonding and non-bonding levels a linear bond structure results as found for d^3–d^3 $Cr^{III}OCr^{III}$ and d^4–d^4 $Ru^{IV}ORu^{IV}$ compounds, whether containing large or small ligands (Table 3). $Fe^{III}OFe^{III}$ derivatives with a total of 10 metal electrons to be accommodated will require the use of anti-bonding levels for placement of the additional electrons and this causes the resultant bond systems to be bent.[16] If, however, interligand steric interactions are sufficiently great the FeOFe bond can approach linearity as in $[Fe(TPP)]_2O$[17b] and $[Fe(3\text{-}^t\text{Busaltmen})]_2O$.[17c] Application of this correlation to the present heterobimetallic $Cr^{III}OFe^{III}$ system with eight electrons to be accommodated would predict an essentially linear system as observed.

The Cr—O and Fe—O bond lengths are each comparable to those observed in homobimetallic

Table 3. Structural parameters for some binuclear oxo bridged complexes

Compound	M—μ-O (Å)	MOM (°)	Ref.
$[Fe(salen)]_2O$[a]	1.78(1)	144.6	17a
$[Fe(tmtaa)]_2O\cdot CH_3CN$	1.793(1)	142.75(9)	12
$[Fe(TPP)]_2O$	1.753(1)	174.5(1)	17b
$[Fe(3\text{-}^t\text{Busaltmen})]_2O$	1.779	173.4	17c
[(py)(TPP)CrOFe(tmtaa)]·2THF	1.759(11) 1.776(9)	176.6(9)	This work
$\{[Cr(NH_3)_5]_2O\}Cl_4$	1.821(3)	180	17d
$\{[Cr(TpyEA)NCS]_2O\}(BPh_4)_2$	1.82(1)	176.5(6)	17e
$K_4\{[RuCl_5]_2O\}$	1.80(2)	180	17f
$[Ru(TPP)(O\text{-}p\text{-}CH_3C_6H_5)]_2O$	1.789(11)	177.8(7)	17g

[a] salen: dianion of N,N′-ethylenebis(salicylaldimine); 3-^{t}Busaltmen: dianion of N,N′-1-2-tetramethylethylene bis(3-^{t}butylsalicylaldimine); TpyEA: tris(2-pyrazol-1-ylethyl)amine.

derivatives of those elements (Table 3). While the chromium ion is essentially located in the plane of the porphyrin ring (0.075 Å towards the oxo bridge from the N_4 plane of the porphyrin) the iron ion is displaced 0.646 Å from the N_4 plane of tmtaa towards the bridging oxygen. Such displacements towards the bridging oxo group are commonly found for five-coordinate iron(III)-μ-oxo complexes,[16] including the homobinuclear compound $[Fe(tmtaa)]_2O$[11] where the displacement is 0.698 Å.

The tmtaa ligand has a "saddle-shaped" conformation in the complex with the pentanediimine rings directed towards the porphyrin ligand and the benzenoid rings directed away (Fig. 2). The displacement of the iron atom from the N_4 plane towards the oxo group thus places it between the pentanediimine rings rather than the benzenoid, an arrangement which is opposite to that found in all other tmtaa coordination compound structures so far determined.[9] In the FeOCr complex the angles between the tmtaa N_4 plane and the pentanediimino planes are considerably smaller by about 13–16°, while the benzenoid rings lie at angles approximately 10° greater than their $[Fe(tmtaa)]_2O$ counterparts (Table 4; the planes being compared are identified in Fig. 3). The particular conformation found in the FeOCr complex allows the close fitting of the porphyrin and tmtaa ligands at the relatively short approach distance required by the oxo bridge, whereas a "normal" conformation of the tmtaa ligand with benzenoid rings directed towards the porphyrin would result in such intermolecular repulsion that the oxo-bridged assembly could probably not form. In $[Fe(tmtaa)]_2O$[11] the benzenoid rings lie towards the oxo group with iron out of the N_4 plane also towards oxygen, but the combination of a bent FeOFe bond and a rotation of the tmtaa molecules about each Fe—O axis allows the ligands to "fit" together without strain. The relative rigidity of the porphyrin molecule and the orientations of its phenyl substituents prevents any such arrangement in the case of the FeOCr complex. The resulting conformation indicates that tmtaa is capable of utilizing its nitrogen lone pairs in a much more flexible manner than has been recognized hitherto. There is further evidence of the minimization of steric interactions between the two ligands in this compound in that each tmtaa nitrogen atom is rotated about the Fe—Cr axis with respect to the eclipsed position with the corresponding porphyrin nitrogen by small angles in the range 6–12° (Table 2). The

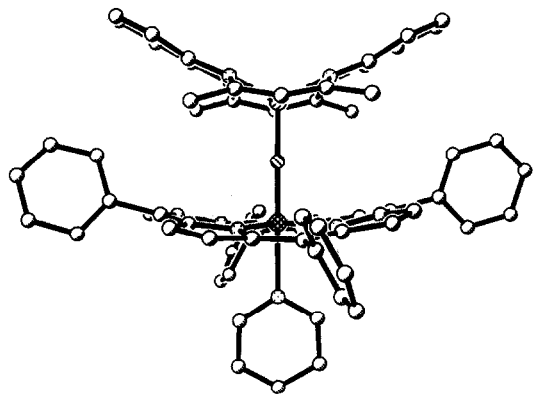

Fig. 2. View of the structure of [(py)(TPP)CrOFe(tmtaa)] showing conformation of the tmtaa system.

Table 4. Angles between selected planes in segments of [(py)(TPP)CrOFe(tmtaa)]·2THF (corresponding angles in $[Fe(tmtaa)]_2O \cdot CH_3CN$[11] are given in parentheses

Defining planes	Angles (°)	Plane[a]
Fe(tmtaa)—N(6)N(7)N(8)N(9) and		
N(6)C(51)C(52)C(53)N(7)	20.6(36.28)	a
N(6)C(51)C(53)N(7)	19.5(36.69)	b
N(8)C(62)C(63)C(64)N(9)	20.8(34.37)	a′
N(8)C(62)C(64)N(9)	19.3(34.99)	b′
N(7)C(55)C(60)N(8)	23.2(13.63)	c
C(55)C(56)C(57)C(58)C(59)C(60)	28.8(19.28)	d
N(6)C(66)C(71)N(9)	25.2(14.41)	c′
C(66)C(67)C(68)C(69)C(70)C(71)	29.5(19.57)	d′
Cr(TPP)—N(1)N(2)N(3)N(4) and		
C(21)C(22)C(23)C(24)C(25)C(26)	118.2	
C(27)C(28)C(29)C(30)C(31)C(32)	105.0	
C(33)C(34)C(35)C(36)C(37)C(38)	116.2	
C(39)C(40)C(41)C(42)C(43)C(44)	108.6	

[a] Planes as in Fig. 3.

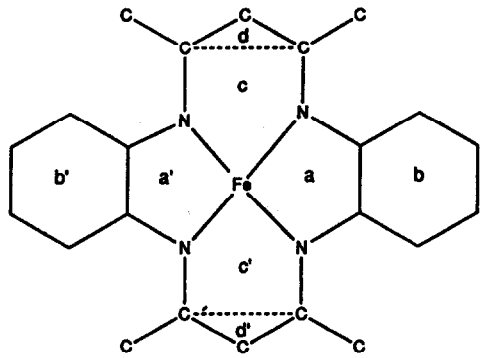

Fig. 3. Diagram of ligand planes for tmtaa showing the numbering scheme.

Cr^{IV}—O distance[22] of 1.62(2) Å in the parent molecule CrO(TPP) is shorter, as expected, than the Cr^{III}—O distance in the heterobimetallic product of 1.776(11) Å.

Mössbauer effect spectra and magnetism

The Mössbauer spectral parameters are shown in Table 5. Sharp, symmetrical quadrupole doublets are observed at 4.2 and 77 K, while a slight asymmetry is evident at 295 K. The parameters are typical of those expected for an $S = 5/2$ iron(III) ion having five-coordinate geometry, as disclosed by the structural data.

The compound shows a magnetic moment of $3.51\mu_B$ at room temperature, considerably reduced from the spin-only value of $7.07\mu_B$ expected for an uncoupled $S = 3/2 : S = 5/2$ system of chromium(III), d^3 and iron(III), d^5 ions (assuming $g_{Cr} = g_{Fe} = 2.0$). A study of the variation of magnetic susceptibility with temperature down to 4.2 K shows the same type of antiferromagnetic behaviour, as was observed with other [(TPP)CrO Fe(Lig)] complexes.[2,4] Thus, the magnetic moment decreases gradually from $3.51\mu_B$ at 300 K to $3.25\mu_B$ at *ca* 120 K and then remains constant until 20 K at which point it decreases rapidly, because of zero-field splitting effects, reaching a value of $2.82\mu_B$ at 4.2 K (Fig. 4). The plateau value of $3.25\mu_B$ corresponds to population of the ground $S' = 1$ spin-state, but is higher than expected (viz. $2.83\mu_B$). We have experienced this before in a few other CrOFe systems, including [(TPP)CrOFe(TMP)],[2] which required $g_{Fe} = 2.05$ to fit the observed μ_{eff} value. Most other examples that have been studied, e.g. [(N–Me–Im)Cr(TPP)OFe(salmah)],[4] as well as the recently reported μ-oxo-di-μ-carboxylato Cr—Fe triazacyclonane compounds of Wieghardt,[8] show plateau values of *ca* $2.9\mu_B$ with a gradual

Table 5. Mössbauer spectral parameters for [(py)(TPP)CrOFe(tmtaa)]

Temperature (K)	Isomer shift[a] δ(mm s^{-1})	Quadrupole splitting ΔE_Q (mm s^{-1})	Line width[b] (mm s^{-1})
295	0.24	0.99	0.24, 0.21
77	0.37	1.05	0.26, 0.26
4.2	0.37	1.06	0.18, 0.18

[a] Calibrated relative to α-Fe.

[b] Half-width at half-maximum height, low velocity and high velocity component.

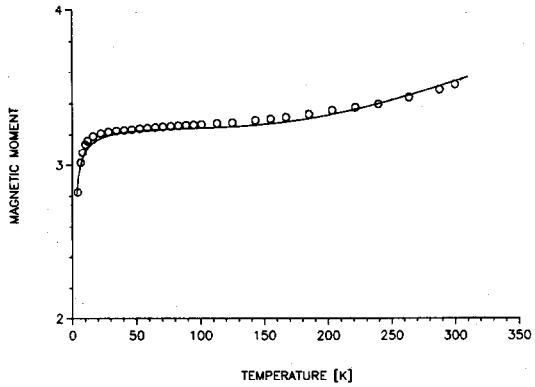

Fig. 4. Variable-temperature magnetic moment data for [(py)(TPP)CrOFe(tmtaa)]. The solid line is that of best-fit using the parameters described in the text.

increase in the μ_{eff} then occurring at higher temperatures, eventually reaching *ca* $3.2\mu_B$ at room temperature. It is possible that a fraction of a further paramagnetic species showing Curie-like behaviour is present in the present complex and is responsible for the slightly enhanced μ_{eff} values. The Mössbauer spectra of the samples used for magnetic susceptibility studies did not show any evidence for an additional, monomeric iron(III) species which might have resulted from a degree of hydrolysis of the samples examined, but the presence of small quantities of chromium(III) and iron(III) monomers arising from such a process cannot be completely ruled out. The microanalytical data for the samples examined also indicated that the samples were "pure", but a hydrolytic process leaving equimolar amounts of Cr(TPP) and Fe(tmtaa) units in the samples would not be detected by such analyses. Despite this problem with the magnitude of "plateau" μ_{eff} values, it was possible to fit the data well to the sample $S = 3/2 : S = 5/2$ dimer model of the type used by Wieghardt *et al.*[8] A best-fit value of $2J = -299$ cm^{-1} was obtained, similar in value to those obtained for (P)CrOFe(P′)[2] compounds (-274 to -300 cm^{-1}), and for triply-bridged, μ-oxo, di-μ-carboxylato complexes[8] (-275 cm^{-1}). The best-fit g value of 2.30 for the present compound is higher than the expected 2.0 because the g acts as a scaling factor, taking into account the factors discussed above. The rapid decrease in μ_{eff} at very low temperatures could be simulated by the incorporation of a $(T-\theta)$ term into the χ equation. A best-fit θ value of -1.2 K was indicative of zero field splitting or perhaps intermolecular exchange effects occurring.

It is interesting to briefly consider the similarities of the $2J$ values in the linear CrOFe complexes and

the "non-linear" $Cr(O)(O_2CR)_2Fe$ compounds in terms of the recent localized "magnetic" orbital model proposed by Wieghardt *et al.*[8] In their treatment the short M—O direction was defined as z and the M—O—M′ pathway was considered to be the principal magnetic exchange pathway. In order of increasing energy the electronic configurations of the localized metal orbitals are iron(III)—$(x^2-y^2, xz, yz, xy, z^2)$, each singly occupied, and chromium(III)—(x^2-y^2, xz, yz), also singly occupied. The strong overall antiferromagnetism in $Cr(O)(O_2CR)_2Fe$ compounds was ascribed[8] to the antiferromagnetic pathways $Fe(z^2)$—$Cr(xz)$ and $Fe(yz)$—$Cr(yz)$ dominating over the ferromagnetic pathways $Fe(xz)$—$Cr(yz)$, $Fe(xz)$—$Cr(xz)$ and $Fe(xz)$—$Cr(x^2-y^2)$. In opening the CrOFe angle from 121° in the $Cr(O)(O_2CR)_2Fe$ system[8] to 177° in the present CrOFe system the yz-yz overlap will be unaffected, but the z^2-xz overlap will decrease towards zero. The xz-xz overlap should correspondingly increase. All of this would suggest that the angle change should also lead to a J value change, unless there is an accidental cancelling out of the constituent J(AF) and J(F) values. An additional influence due to the bridging ligand has been observed in studies on the homobinuclear doubly-bridged species $[(tpa)M(O)(O_2CR)M(tpa)]^{3+}$, where M = Cr^{III}[21] or Fe^{III}[23] and tpa = tris(2-pyridylmethyl)amine. The J values in the Cr···Cr series are very sensitive to changes in the RCO_2^- group as well as to the CrOCr bridge angle and this has been interpreted[21] in terms of a molecular-orbital model with significant π-bonding in the CrOCr unit being affected by variations in the $Cr(O_2CR)Cr$ moiety.

Thus, it can be seen from the above discussion that some of the Wieghardt–Girerd proposals are supported by some studies while others, e.g. ignoring the influence of μ-RCO_2^-, are not. In the case of linear μ-oxo species recent results from our laboratories on Mn^{III}—O—Mn^{III} phthalocyanine complexes[24] and from Holwerda *et al.*[25] on $[X(tpa)CrOCr(tpa)X]^{2+}$ compounds show very large negative J values. Indeed, room-temperature diamagnetism is displayed by the Cr···Cr complex, where X = NCSe. These various pieces of data suggest that while the Wieghardt–Girerd model[8] provides a good guide to the sign of J, effects due to the non-bridging ligands and from π-bonding within the μ-oxo bridge will combined to "fine-tune" the actual values of J. It is noteworthy that Gorun and Lippard[26] were unable to obtain a correlation between J and the superexchange distance in FeOFe systems, but were able to do so for complexes with a "supported" oxo linkage Fe(O)(Y)Fe, where Y = RCO_2^-, etc.

$[Fe(tmtaa)]_2O \cdot$ *toluene*. In the course of this work a new toluene solvate of the homobinuclear compound $[Fe(tmtaa)]_2O$ was isolated and is magnetic susceptibility vs temperature behaviour recorded, since only a room-temperature moment per iron ion of $\mu_{eff} = 1.96\mu_B$ had previously been reported for the CH_3CN adduct.[10] This value is comparable with that found for most μ-oxo iron(III) complexes.[16] Despite many preparations of the toluene solvate in the present work it was not possible to isolate a sample with a moment lower than $2.5\mu_B$ and many samples gave higher values. It is concluded that the ease of hydrolysis of the oxo complex referred to in the Experimental prevented the isolation of a sample of the oxo complex completely free of a high spin Fe—OH species. Confirmation of a monomer impurity is seen in the variable-temperature magnetic data which showed a Curie–Weiss-like increase in χ as the temperature decreases, rather than the anticipated decrease.[27] Even at 4.2 K the μ_{Fe} value had only decreased to *ca* $1\mu_B$, rather than zero, indicative of the presence of *ca* 8% of an $S = 5/2$ monomeric species. The data could be fitted well to an $S = 5/2$ dimer model using the parameters $g = 1.88$, $J = -80$ cm^{-1}, % monomer = 8.3 and $\theta = -4.4$, where θ in the $(T-\theta)$ term allows for possible weak intermolecular effects. The value of J is close to that in $[Fe\ salen]_2O$, which has a very similar FeOFe angle.

Acknowledgements—This work was supported by grants from the Australian Research Council (to B.O.W. and K.S.M.) and the award of an ARC Postdoctoral Research Fellowship (to B.M.). The authors are grateful to Professor J. Cashion. for providing access to Mössbauer spectral facilities and to Yasser Korbatieh for recording and fitting the spectra.

REFERENCES

1. B. O. West, *Polyhedron* 1989, **8**, 219.
2. D. J. Liston, B. J. Kennedy, K. S. Murray and B. O. West, *Inorg. Chem.* 1985, **24**, 1561.
3. R. L. Elliott, P. J. Nichols and B. O. West, *Aust. J. Chem.* 1986, **39**, 975.
4. E. N. Bakshi, R. L. Elliott, K. S. Murray, P. J. Nichols and B. O. West, *Aust. J. Chem.* 1990, **43**, 707.
5. R. L. Elliott, P. Kruger, K. S. Murray and B. O. West, *Aust. J. Chem.* 1992, **45**, 889.
6. R. L. Elliott and B. O. West, *Aust. J. Chem.* 1988, **41**, 1417.
7. L. D. Schulz, G. D. Fallon, B. Moubaraki, K. S. Murray and B. O. West, *J. Chem. Soc., Chem. Commun.* 1992, 971.
8. R. Hotzelmann, K. Wieghardt, U. Flörke, H. J. Haupt, D. C. Weatherburn, J. Bonvoisin, G. Blondin and J. J. Girerd, *J. Am. Chem. Soc.* 1992, **114**, 1681.

9. F. A. Cotton and J. Czuchajowska, *Polyhedron* 1990, **9**, 2553.
10. V. L. Goedken and Y.-A. Park, *J. Chem. Soc., Chem. Commun.* 1975, 214.
11. M. C. Weiss and V. l. Goedken, *Inorg. Chem.* 1979, **18**, 819.
12. J. T. Groves, W. J. Jr Kruper, R. C. Haushalter and W. M. Butler, *Inorg. Chem.* 1982, **21**, 1363.
13. G. D. Fallon and B. M. Gatehouse, *J. Solid State Chem.* 1980, **34**, 193.
14. G. M. Sheldrick, SHELXTL PLUS: Revision 3.4. Seimens Analytical X-Ray Instruments Inc., Madison, Wisconsin, U.S.A. (1988).
15. J. A. Ibers and W. C. Hamilton (Eds), *International Tables for X-ray Crystallography*. Kynoch Press, Birmingham (1974).
16. D. M. Kurtz, *Chem. Rev.* 1990, **90**, 585.
17. (a) J. E. Davies and B. M. K. Gatehouse, *Acta Cryst.* 1973, **B29**, 1934; (b) A. B. Hoffman, D. M. Collins, V. W. Day, E. B. Fleischer, T. S. Srivastava and J. L. Hoard, *J. Am. Chem. Soc.* 1972, **94**, 3620; (c) R: N. Mukherjee, T. D. P. Stack and R. H. Holm, *J. Am. Chem. Soc.* 1988, **110**, 1850; (d) M. Yevitz and J. A. Stanko, *J. Am. Chem. Soc.* 1971, **93**, 1512; (e) M. Di Vaira and F. Mani, *Inorg. Chem.* 1984, **23**, 409; (f) A. M. Mathieson, D. P. Mellor and N. C. Stephenson, *Acta Cryst.* 1952, **5**, 185; (g) J. P. Collman, C. E. Barnes, P. J. Brothers, T. J. Collins, T. Ozawa, J. C. Gallucci and J. A. Ibers, *J. Am. Chem. Soc.* 1984, **106**, 5151.
18. J. D. Dunitz and L. E. Orgel, *J. Chem. Soc.* 1953, 2594.
19. B. Jezowska-Trzebiatowska, *Coord. Chem. Rev.* 1968, **3**, 255; *Pure Appl. Chem.* 1971, **27**, 89.
20. K. Tatsumi and R. Hoffman, *J. Am. Chem. Soc.* 1981, **103**, 3328.
21. B. G. Gafford, R. E. Marsh, W. P. Schaefer, J. H. Zhang, C. J. O'Connor and R. A. Holwerda, *Inorg. Chem.* 1990, **29**, 4562.
22. J. R. Budge, B. M. K. Gatehouse, M. C. Nesbit and B. O. West, *J. Chem. Soc., Chem. Commun.* 1981, 370.
23. R. E. Norman, R. C. Holt, S. Ménage, C. J. O'Connor, J. H. Zhang and L. Que Jr, *Inorg. Chem.* 1990, **29**, 4629.
24. H. Homborg, B. Moubaraki, K. S. Murray and S. Sievertsen, unpublished data.
25. T. F. Tekut, C. J. O'Connor and R. A. Holwerda, *Inorg. Chem.* 1993, **32**, 324.
26. S. M. Gorun and S. J. Lippard, *Inorg. Chem.* 1991, **30**, 1625.
27. K. S. Murray, *Coord. Chem. Rev.* 1974, **12**, 1.

Polyhedron Vol. 12, No. 18, pp. 2215–2219, 1993
Printed in Great Britain

0277–5387/93 $6.00+.00
© 1993 Pergamon Press Ltd

SYNTHESIS, CHARACTERIZATION AND REACTIVITY OF THE PROPIONITRILE COMPLEXES OF RUTHENIUM(II) AND RUTHENIUM(III)

JANETE JANE FERNANDES ALVES, ANA MARIA DE GUZZI PLEPIS, CELSO ULYSSES DAVANZO and DOUGLAS WAGNER FRANCO*

Instituto de Física e Química de São Carlos-USP, Cx. Postal 369, 13560-970 São Carlos-SP, Brazil

(*Received* 20 *April* 1993; *accepted* 11 *May* 1993)

Abstract—The complexes $[Ru(NH_3)_5(NCC_2H_5)](PF_6)_n$ ($n = 2, 3$) have been isolated and characterized by microanalysis, cyclic voltammetry, UV–vis and IR spectroscopies. In acidic media, $C_{H^+} = 1 \times 10^{-3}$ M, $\mu = 0.10$ M ($NaCF_3COO$) at (25.0 ± 0.1)°C, the complex ion $[Ru(NH_3)_5(NCC_2H_5)]^{2+}$ undergoes aquation yielding the *trans*-$[Ru(NH_3)_4(NCC_2H_5)(H_2O)]^{2+}$ ion, with k_{-NH_3} equal to $(1.2 \pm 0.1) \times 10^{-5}$ s^{-1}. The specific rates k_1, k_{-1} and K_{eq} for the reaction:

$$trans\text{-}[Ru(NH_3)_4(NCC_2H_5)(H_2O)]^{2+} + pz \underset{k_{-1}}{\overset{k_1}{\rightleftharpoons}} trans\text{-}[Ru(NH_3)_4(NCC_2H_5)(pz)]^{2+} + H_2O$$

are, respectively, 8.6×10^{-3} M^{-1} s^{-1}, 1.6×10^{-5} s^{-1} and 5.4×10^2 M^{-1}, under the same experimental conditions described above. The value for the pK_a of the acid *trans*-$[Ru(NH_3)_4(NCC_2H_5)(pzH)]^{3+}$ was calculated as (1.6 ± 0.1), $\mu = 0.1$ M ($NaCF_3COO$) at (25.0 ± 0.1)°C. The complex ion $[Ru(NH_3)_5(NCC_2H_5)]^{3+}$ undergoes hydrolysis in alkaline medium yielding the propanamide complex of pentaammineruthenium(III), with k_{OH} equal to $(1.9 \pm 0.1) \times 10^2$ M^{-1} s^{-1}.

Using ruthenium(II),(III) tetraammines as probes we are carrying out a systematic study[1,2] in order to understand the metal–ligand interactions. Besides the interest in the *trans* effect and *trans* influence of the ligands, we are spending a considerable effort to learn how the perturbation of charge density in the metal centre and ligands as a consequence of coordination is reflected in their chemical reactivities.

As part of this work it appears particularly attractive to investigate the ruthenium(II),(III) nitrile systems. This paper describes the behaviour of propionitrile as a ligand in ruthenium(II) and ruthenium(III) tetraammines.

* Author to whom correspondence should be addressed.

EXPERIMENTAL

Chemicals

The solvents employed were freshly distilled before use. Propionitrile (Aldrich) was purified by treatment with phosphorus pentoxide followed by distillation.[3] Doubly distilled water was used throughout. Pyrazine, pz (Aldrich Puriss Grade), was used as supplied.

All of the preparations were carried out under argon. The argon (White Martins S.A.) was purified using $Cr(ClO_4)_2$ solutions and zinc amalgam.

Synthesis of ruthenium compounds

$[Ru(NH_3)_5Cl]Cl_2$ and $[Ru(NH_3)_5(H_2O)](PF_6)_2$ were prepared as described in the literature.[4–6]

$[Ru(NH_3)_5(NCC_2H_5)](PF_6)_2$ (**I**) was prepared by adding $[Ru(NH_3)_5Cl]Cl_2$ (0.2 mmol) to trifluoracetic acid (0.2 M, 9 cm^3) in the presence of zinc amalgam. The zinc amalgam reduces the ruthenium(III) to ruthenium(II) and the chloride ion is fastly aquated,[6] generating the $[Ru(NH_3)_5(H_2O)]^{2+}$ species "*in situ*". When all the $[Ru(NH_3)_5Cl]^{3+}$ species was converted to $[Ru(NH_3)_5(H_2O)]^{2+}$ (*ca* 30 min), propionitrile (3.0 mmol in 0.5 cm^3 methanol) was added to the reaction flask. The mixture was allowed to react in the dark for *ca* 30 min. The complex (**I**) was precipitated by the addition of saturated NH_4PF_6 solution (2 cm^3) and cooling. The resulting yellow solid was filtered and washed with chloroform to remove the excess ligand. Yields better than 80% Found: C, 6.5; N; 15.8; H, 3.8. Calc.: C, 6.8; N, 15.8; H, 3.8%.

$[Ru(NH_3)_5(NCC_2H_5)](PF_6)_3$ (**II**) was obtained by exhaustive electrochemical oxidation of $[Ru(NH_3)_5(NCC_2H_5)]^{2+}$ in aqueous solution. In a typical preparation the $[Ru(NH_3)_5(NCC_2H_5)](PF_6)_2$ salt (40–50 mg) was dissolved in degassed 10^{-3} M CF_3COOH (20–30 cm^3) aqueous solution. Electrochemical oxidation was performed at +0.26 V (vs. S.C.E.). When the oxidation was complete the volume of the solution was reduced through rotaevaporation to 4–5 cm^3. A solid was obtained upon the addition of saturated NH_4PF_6 solution (1 cm^3). The solid was filtered off and washed with cold degassed dry ether (5 cm^3). The yield was better than 60%. Found: C, 5.3; N, 12.0; H, 2.9. Calc.: C, 5.3; N, 12.4; H, 2.9.

Apparatus and techniques

UV and visible spectra were recorded using a Hewlett–Packard Model 8452A Diode Array spectrophotometer. IR spectra were recorded on KBr pellets using a Nicolet Model 5SXC-FT-IR spectrophotometer.

The ^1H NMR spectra were recorded at 200 MHz on a Bruker AC200 instrument; the spectra of the ligand and complexes were obtained in CD_3COCD_3.

The TG/DTG and DSC curves were obtained using a Du Pont Thermal Analyser Model 9900 combined with a Du Pont TGA 951 and DSC 910. The measurements were performed using a dynamic nitrogen atmosphere at a flow rate of 60 $cm^3\ min^{-1}$ up to 600°C. The heating rate was 10°C min^{-1} and sample sizes ranged in mass from 9 to 10 mg.

Electrochemical measurements were made vs the saturated potassium chloride calomel electrode (S.C.E.). The measurements were performed using a Parc Modal 173 potentiostat, a Parc Model 175 universal programmer and a model RE-0091 *X–Y* recorder. A glassy carbon electrode (area 0.51 cm^2), platinum wire and S.C.E. were used in cyclic voltammetric experiments as the working, auxiliary and reference electrodes, respectively. During the electrolysis a platinum net (area 13.6 cm^2) was used as the working elecrode. The number of moles of electrons transferred per mole of complex in an exhaustive electrolysis, at constant potential, was calculated by measuring the total area under the current vs time curves for complete electrolysis. The reversibility of the Ru^{III}/Ru^{II} redox couple was verified on the basis of the ratio of cathodic to anodic peak currents (i_{pa}/i_{pc})[7] and the peak-to-peak potential separation ($\Delta E_{p/a,c}$)[8].

A Corning model 130 pH meter and a Methron EA 147 microglass electrode were used for the pH determinations.

All the measurements were performed at 25.0 ± 0.1°C.

Kinetic measurements

The reactions were followed by monitoring changes in absorbance at fixed wavelengths as a function of time. Pseudo-first-order rate constants (k_{obs}) were determined graphically from plots of $\ln(A_\infty - A_t)$ vs time. The k_{obs} were then used to determine k_1, k_{-1} and K_{eq}, by substitution into the following equation:

$$k_{obs} = k_{-1}[L] + k_{-1} \text{ and } K_{eq} = k_1/k_{-1}.$$

The rate of loss of NH_3 from $[Ru(NH_3)_5(NCC_2H_5)]^{2+}$, k_{-NH_3}, was measured using a high concentration (1.0 M) of a competitor ligand (pz). The study was performed by dissolving **I** in a concentrated aqueous solution of pyrazine (with the pH, ionic strength and temperature previously adjusted) and monitoring the formation of the pz derivative spectrophotometrically at 440 nm.

The hydrolysis of the coordinated propionitrile from $[Ru(NH_3)_5NCC_2H_5)]^{3+}$ to give the propanamide complex was studied in slightly basic solution at 25.0 ± 0.1°C over a range of pH values controlled with $[CO_3^{2-}/HCO_3^-]$ buffer mixtures according to Zanella's procedure.[9]

pK_a *determination*

The pK_a of the acid *trans*-$[Ru(NH_3)_4(NCC_2H_5)(pzH)]^{3+}$ (**III**) was determined spectrophotometrically. The elecronic spectra of **III** (4.8×10^{-4} M) solution at constant ionic strength ($NaCF_3COO/CF_3COOH$, $\mu = 0.10$ M) were recorded as a function of the solution hydrogen ion concen-

tration. The pK_a values were calculated using the relationship:[10]

$$pK_a = pH + \log \frac{A' - A}{A - A^0},$$

where A', A^0 and A are, respectively, the absorbances of the fully protonated complex, the deprotonated complex and a mixture of both at 534 nm (where the protonated species absorbs) at a given pH.

RESULTS AND DISCUSSION

The identity of the propionitrile complex (**I**) has been established through microanalysis, electronic, vibrational and nuclear magnetic resonance spectroscopies and cylic voltammetry.

The electronic spectrum of solutions of **I** shows absorptions at $\lambda_{max} = 262$ ($\varepsilon = 1.5 \times 10^4\ M^{-1}\ cm^{-1}$) and $\lambda_{max} \cong 350$ nm ($\varepsilon = 2.4 \times 10^2\ M^{-1}\ cm^{-1}$), attributed to metal-to-ligand charger-transfer (MLCT) and ligand-field (LF) transitions, respectively (see Table 1). The electronic spectrum of the **II** ion in aqueous solutions exhibits one intense band at 238 nm, attributable to ligand-to-metal charge transfer (LMCT) (see Table 1). These attributions have been proposed by analogy with those described for related complexes.[11]

The cyclic voltammogram of aqueous solutions of **I** or **II** shows a reversible, one-electron process corresponding to the Ru^{III}/Ru^{II} couple at $E^{0\prime} = 0.19 \pm 0.01$ V vs S.C.E.; $\mu = 0.10$ ($(NaCF_3COO)/(CF_3COOH)$), 25.0 ± 0.1°C.

The IR spectra of **I** displays one intense band in the nitrile region at 2260 cm^{-1}, attributed to the stretching frequency ν(CN), which is shifted [$\Delta\nu(CN) = +14\ cm^{-1}$] from the free ligand value.

There has been some controversy in the literature regarding the position of ν(CN) for ruthenium(II) complexes. Ford *et al.*[11] reported that ν(CN) is shifted to lower energy when nitriles are coordinated to the $Ru(NH_3)_5^{2+}$ moiety and ascribed his results to $Ru^{II} \rightarrow NCR$ back-bonding. Chatt *et al.*[12] reported ν(CN) shifts to higher energies for nitriles coordinated to a ruthenium(II) centre. These authors[11] pointed out that besides back-bonding arguments the polarization ability of the counter-ion should also be considered. This seems to be the case for our compound.

For complex **II** ν(CN) is observed at 2294 cm^{-1} [$\Delta\nu(CN) = +48\ cm^{-1}$]. This shift of ν(CN) is expected as a consequence of the σ-bond $Ru^{III} \leftarrow NCR$ and is in agreement with the ν(CN) values reported for related systems in the literature.[11]

The proton magnetic resonance spectrum of propionitrile coordinated to pentaammineruthenium(II) is characterized by a decrease in chemical shielding[13] for the nitrile protons relative to the free ligand. The methyl protons are deshielded much less than the methylene (0.07 and 0.50 ppm, respectively).

As judged from TG/DTG data complex **I** is stable up to 140°C. A small loss of weight (1.17%) is observed before 140°C, probably due to the escape of adherent moisture present in the sample. At temperatures higher than 140°C samples of **I** exhibit a two-step weight loss. The first step, *ca* 9% weight loss, occurs in the range 140–250°C and is enveloped by a well defined second step 250–500°C corresponding to a weight loss of 54%.

Table 1. Band maxima, molar absorption[a] and formal reduction potential[a]

Complex	λ_{max} (nm)[b]	ε ($M^{-1}\ cm^{-1}$)	$E^{0\prime}$ (V vs S.C.E.)
$[Ru(NH_3)_5(NCC_2H_5)]^{2+}$	262	1.5×10^4	0.19 ± 0.01
	$\cong 350$	2.4×10^2	
Trans-$[Ru(NH_3)_4(NCC_2H_5(H_2O)]^{2+}$	262	4.4×10^3	0.20 ± 0.01
	378[b]	3.6×10^2	
Trans-$[Ru(NH_3)_4(NCC_2H_5)(pz)]^{2+}$	442[b]	8.0×10^2	0.64 ± 0.01
$[Ru(NH_3)_5(NCC_2H_5)]^{3+}$	238	1.2×10^3	
	$\cong 290$	4.0×10^3	0.19 ± 0.01
	382	2.6×10^2	
$[Ru(NH_3)_5(NHCOC_2H_5)]^{2+}$	238	3.3×10^3	0.74 ± 0.01[c]
	382[b]	2.4×10^3	

[a] Hexafluorophosphate salt.
[b] ± 2 nm.
[c] Irreversible E_{pa}.

The reaction:

$$[Ru(NH_3)_5NCC_2H_5]^{2+} + H_2O \xrightarrow{k_{-NH_3}} trans\text{-}[Ru(NH_3)_4(NCC_2H_5)(H_2O)]^{2+} + NH_3$$

has been followed spectrophotometrically, using pyrazine as an auxiliary ligand, and the decrease in the solution hydrogen ion concentration was potentiometrically monitored. A good agreement was observed for the specific rate k_{-NH_3} measured by both techniques: $(1.2 \pm 0.1) \times 10^{-5}$ s^{-1}; at 25.0 ± 0.1°C, $\mu = 0.10$ M ($NaCF_3COO/CF_3COOH$).

The characteristics of the electronic spectra of the *trans*-$[Ru(NH_3)_4(NCC_2H_5)(H_2O)]^{2+}$ ion in aqueous solutions are summarized in Table 1. The absorptions at 262 and 378 nm have been attributed to MLCT and LF transitions, respectively.

The cyclic voltammogram of the *trans*-$[Ru(NH_3)_4(NCC_2H_5)(H_2O)]^{3+/2+}$ system in aqueous solution is reversible and the formal potential, $E^{0\prime}$, for the Ru^{III}/Ru^{II} couple in this complex is (0.20 ± 0.01) V vs S.C.E., $\mu = 0.10$ ($NaCF_3COO/CF_3COOH$), $C_{H^+} = 3.0 \times 10^{-4}$ M; at 25.0 ± 0.1°C.

The reaction:

$$trans\text{-}[Ru(NH_3)_4(NCC_2H_5)(H_2O)]^{2+} + pz \underset{k_{-1}}{\overset{k_1}{\rightleftharpoons}} trans\text{-}[Ru(NH_3)_4(NCC_2H_5)(pz)]^{2+} + H_2O$$

has been studied kinetically as a function of the pyrazine concentration, see Table 2.

From the data in Table 2, it is possible to calculate values for k_1, k_{-1} and K_{eq} of 8.6×10^{-3} M^{-1} s^{-1}; 1.6×10^{-5} s^{-1} and 5.4×10^{-2} M^{-1}, respectively.

Evidence for rate saturation was observed in plots at k_{obs} vs C_{pz} for $C_{pz} > 1.0 \times 10^{-1}$ M, suggesting that the substitution reaction is controlled by a dissociative pathway.[1] The same behaviour has been described before for substitution reactions on ruthenium(II) tetra- and pentaammine centres.[1,14,15]

Table 2. Substitution in *trans*-$[Ru(NH_3)_4(NCC_2H_5)(H_2O)]^{2+}$ by pyrazine (pz)[a]

10^2 [pz] (M)	$10^4 k_{obs}$ (s^{-1})
0.50	0.60
1.6	1.6
4.0	3.6
5.0	4.5
6.0	5.3
7.5	6.4
8.0	6.8
10.0	9.0
15.0	9.8
20.0	10.0

[a] $\mu = 0.10$ ($NaCF_3COO$), $C_{H^+} = 3.0 \times 10^{-4}$ M, $C_{Ru^{II}} = 5.0 \times 10^{-4}$ M, each value a mean of at least three independent determinations, agreeing within ±4%.

When the NH_3 ligand in a *trans* position to H_2O, in the coordination sphere of $[Ru(NH_3)_5(H_2O)]^{2+}$, is replaced by propionitrile the substitution rate of the water molecule by pz is reduced about seven fold. Based on the second-order specific rate data for water substitution by pyrazine (k_1) in the *trans*-$[Ru(NH_3)_4L(H_2O)]^{2+}$ complexes, see Table 3, the relative *trans* effect series of L[1] can be written as follows:

$$NCC_2H_5 < SbPh_3 < NH_3 \cong AsPH_3 < SO_2 < PPh_3 < P(OEt)_3 < SO_3^{2-}.$$

The position of the propionitrile in the above series is in agreement with the good π-acid and weak σ-base properties of the NCC_2H_5 molecule. As reported by Isied in a related work[15] this class of ligand exhibits weak *trans* labilizing effects.

Assuming $k_{-1}/k_1 = 1/K_{eq}$ as an indicator of the relative *trans* influence of L[1] and based on the data of Table 3 the following series can be deduced:

$$NH_3 \ll SO_3^{2-} < SbPh_3 < AsPh_3 \leqslant NCC_2H_5 < SO_2 < PPh_3 \ll P(OEt)_3.$$

The extent of the $Ru^{II} \rightarrow$ pz back-bonding is well accepted[1,14-18] and is an indicator of the degree of the competition between L and pz for the 4*dπ*-electrons. Therefore, the stronger the back-bonding interaction $Ru^{II} \rightarrow L$, the weaker will be the $Ru^{II} \rightarrow$ pz bond. The above *trans* influence series of ligands L suggests that NCC_2H_5 is a π-acid as good as $AsPh_3$, but weaker than SO_2.

Another parameter used[1,14,15,17] to evaluate the 4*d*-electron availability upon coordination of the metal centre to L is the pK_a value for *trans*-$[Ru(NH_3)_4L(pzH)]^{3+}$ species. In strongly acidic solution it is possible to protonate reversibly the pyrazine ligand in the *trans*-$[Ru(NH_3)_4(NCC_2H_5)(pz)]^{2+}$ complex. The pK_a value for the *trans*-$[Ru(NH_3)_4(NCC_2H_5)(pzH)]^{+}$ acid was determined as equal to 1.6 ± 0.1, see Experimental.

This pK_a value, between the pK_a[17] of the free pyrazine molecule (0.50) and that[17] for the pyrazine coordinated to the $[Ru(NH_3)_5]^{2+}$ moiety (2.5), reflects the competition for the 4*dπ*-electrons between NCC_2H_5 and pz (see Table 3).

Based on the pK_a values of Table 3, the position of propionitrile in the increasing series of π-acidity for selected ligands is as follows: $NH_3 < SbPh_3 < AsPh_3 < NCC_2H_5 < PPh_3$.

At this point some comments seem in order regarding the reactivity of species **II**.

Table 3. Data on substitution reactions:

trans-$[Ru(NH_3)_4L(H_2O)]^{2+}$ [a] + pz $\rightleftharpoons$ *trans*-$[Ru(NH_3)_4Lpz]^{2+,0} + H_2O$

and pK_a for *trans*-$[Ru(NH_3)_4L(pzH)]^{3+}$ acids

L	k_1 (M^{-1} s^{-1})	k_{-1} (s^{-1})	K_{eq} (M^{-1})	pK_a	Ref.
PPh_3	1.15	3.9×10^{-2}	29.5	1.3	16
$AsPh_3$	5.6×10^{-2}	9.2×10^{-5}	6.1×10^{2}	1.9	16
$SbPh_3$	4.6×10^{-2}	4.8×10^{-5}	9.6×10^{2}	2.1	16
NH_3	5.6×10^{-2}			2.5	17
SO_2	3.0×10^{-2}	8.0×10^{-4}	40	—	15
SO_3^{2-}	13	4.5×10^{-3}	2.9×10^{3}	—	15
$P(OEt)_3$	3.8	2.0×10^{-1}	2.0×10^{-1}	—	18
NCC_2H_5	8.6×10^{-3}	1.6×10^{-5}	5.4×10^{2}	1.6	This work

[a] At 25 ± 0.2°C; $\mu = 0.10$.

Species **I**, in basic medium in the absence of oxygen, only undergoes the aquation reaction described earlier in this paper. If oxygen is present the oxidation of the ruthenium(II) centre occurs followed by the formation of the amide complex:

$$[Ru(NH_3)_5(NCC_2H_5)]^{3+} \xrightarrow[k_{OH}]{[B]} [Ru(NH_3)_5(NHCOC_2H_5)]^{2+}.$$

The k_{OH} for the above reaction $(1.9\pm0.1)\times10^2$ M^{-1} s^{-1} ($\mu = 1.0$ M, $NaClO_4$, $[B] = [CO_3^{2-}/HCO_3^-]$, at 25.0 ± 0.1°C) is very close to those reported in the literature[9] for related ligands.

Fast aquation of the ligand $NHCOC_2H_5$ is observed if the metal centre is reduced to ruthenium(II):

$$[Ru(NH_3)_5(NHCOC_2H_5)]^{2+} \xrightarrow[\text{Fast}]{Zn/Hg} [Ru(NH_3)_5(H_2O)]^{2+} + NH_2COC_2H_5.$$

The ruthenium complex is quantitatively regenerated as $[Ru(NH_3)_5(H_2O)]^{2+}$ and the coordinated nitrile quantitatively converted in the corresponding amide.

Work on related systems is in progress at our Laboratory and results will be reported later.

Acknowledgements—The authors thank the Brazilian agencies CNPq, CAPES and PRONAC-Cat for financial support and to Robert A. Metcalfe and Dr Duncan W. Bruce for reading the English manuscript.

REFERENCES

1. J. C. Nascimento Filho, J. M. de Rezende, B. S. Lima Neto and D. W. Franco, *Inorg. Chim. Acta* 1988, **145**, 111 and refs therein.
2. R. L. Sernaglia and D. W. Franco, *Inorg. Chem.* 1989, **28**, 3485 and refs therein.
3. D. D. Perrin and W. L. F. Almarego, *Purification of Laboratory Chemicals*. Pergamon Press, New York (1983).
4. A. D. Allen, F. Bottomley, R. O. Harris, V. P. Reinslau and C. V. Senoff, *Inorg. Synth.* 1970, **12**, 2.
5. J. A. Marchant, T. Matsubara and P. C. Ford, *Inorg. Chem.* 1977, **16**, 2160.
6. C. G. Kuehn and H. Taube, *J. Am. Chem. Soc.* 1976, **98**, 689.
7. R. S. Nicholson, *Analyt. Chem.* 1966, **38**, 1406.
8. H. S. Lim, D. J. Barclay and F. Anson, *Inorg. Chem.* 1972, **11**, 1460.
9. A. Zanella and P. C. Ford, *Inorg. Chem.* 1975, **14**, 42.
10. A. Albert and E. P. Serjeant, *The Determination of Ionization Constants*. Chapman and Hall Ltd, London (1971).
11. P. C. Ford and R. E. Clarke, *Inorg. Chem.* 1970, **9**, 227.
12. J. Chatt, G. J. Leigh and N. Thankarajan, *J. Chem. Soc.* 1971, **A**, 3168.
13. R. D. Foust Jr and P. C. Ford, *J. Am. Chem. Soc.* 1972, **94**, 5686.
14. H. Taube, *Comm. Inorg. Chem.* 1981, **1**, 17.
15. S. S. Isied and H. Taube, *Inorg. Chem.* 1976, **12**, 3070.
16. D. W. Franco and J. M. de Rezende, manuscript in preparation.
17. P. C. Ford, P. Rudd, R. Gaunder and H. Taube, *J. Am. Chem. Soc.* 1968, **90**, 1187.
18. D. W. Franco and H. Taube, *Inorg. Chem.* 1978, **17**, 571.

Polyhedron Vol. 12, No. 18, pp. 2221–2226, 1993
Printed in Great Britain

0277–5387/93 $6.00+.00
© 1993 Pergamon Press Ltd

FOUR-COORDINATE COPPER(I) IODIDE COMPLEXES WITH TRIPHENYLPHOSPHINE AND HETEROCYCLIC THIONE LIGANDS. THE CRYSTAL STRUCTURE OF $[Cu(PPh_3)_2(pymtH)I]$

P. ASLANIDIS,* S. K. HADJIKAKOU and P. KARAGIANNIDIS

University of Thessaloniki, Faculty of Chemistry, General and Inorganic Chemistry Department, P.O. Box 135, GR-540 06 Thessaloniki, Greece

and

M. GDANIEC and Z. KOSTURKIEWICZ

Department of Crystallography, A. Mickiewicz University, Poznan, Poland

(*Received* 7 *April* 1993; *accepted* 11 *May* 1993)

Abstract—$[Cu(PPh_3)I]_4$ reacts with heterocyclic thiones (L) [L = pyrimidine-2-thione (pymtH), 1,3-thiazoline-2-thione (tzdtH), 1,3-imidazoline-2-thione (imtH), benz-1,3-imidazoline-2-thione ($bzimtH_2$) and benz-1,3-thiazoline-2-thione (bztztH)] in the presence of triphenylphosphine to give mononuclear complexes of the general formula $[Cu(PPh_3)_2(L)I]$. These complexes have been characterized by various physicochemical methods. The crystal structure of $[Cu(PPh_3)_2(pymtH)I]$ has been determined by single-crystal X-ray diffraction methods. The molecule is mononuclear, with a distorted tetrahedral geometry and bond lengths Cu—S = 2.338(4), Cu—I = 2.674(2), Cu—P = 2.296(4) and 2.303(4) Å.

A considerable amount of work has been done in the past two decades on the synthesis and characterization of metal complexes containing heterocyclic thiones as ligands.[1] In particular, owing to the high tendency of copper(I) to form metal–sulphur bonds, a large set of compounds resulting from copper(I) halides and heterocyclic thiones were presented.[2] During our previous studies in this area much attention has been given to understanding the factors that govern the coordination geometry of the metal atom. Working on this problem we used various arylphosphines as a second bulky π-acceptor ligand to induce changes on copper geometry.[3] The structures of the copper(I) complexes we have obtained consist generally of monomeric or dimeric species constructed by bridging halogen or thione ligands. In the case of monomerics triphenylphosphine has been shown to form four-coordinate complexes, while the size of the thione ligand seemed not to play a significant role. Thus, it was believed that three-coordinate complexes should be possible to prepare if more bulky tertiary phosphines were to be employed. Indeed, that has been observed using the sterically more hindered triorthotolylphosphine, as exemplified by the structures of $[Cu(totp)(tzdtH)Br]$[3f] and $[Cu(totp)(pymtH)Cl]$[3h]. In general it has been shown that the geometry of complexes of univalent coinage metals is determined by steric rather than by electronic properties of the phosphine ligands.[4] On the other hand, the reasons for the formation of dimeric complexes as well as the cause of the bridging of the two copper(I) centres either by halogen or by thione-S atoms was not fully understood. As a contribution towards the elucidation of the questions about the stereochemical properties of this very interesting class of complexes, we report here the syntheses and characterization of a new series of mononuclear complexes of the general formula $[Cu(PPh_3)_2(L)I]$.

* Author to whom correspondence should be addressed.

EXPERIMENTAL

Materials and instruments

CuI and PPh_3 were purchased from Merck and used as received. All thiones (Merck or Aldrich) used in this work were recrystallized from hot ethanol, while the solvents were of reagent grade and were used without further purification. $[Cu(PPh_3)I]_4$ was prepared by the method of Costa *et al.*[5]

IR, electronic and NMR spectra, conductivities, melting points, magnetic susceptibility measurements and elemental analyses of carbon, nitrogen and hydrogen were performed as described previously.[3d] Thermogravimetric analyses were performed on a TGS-2 Perkin–Elmer DTG/TG thermobalance in air with a heating rate of 10°C min^{-1}. Sample sizes were *ca* 10 mg.

Preparation of the complexes

A solution of $[Cu(PPh_3)I]_4$ (1 mmol) in acetonitrile (20 cm^3) was treated with a solution (50 cm^3) of the appropriate thione (4 mmol) in the same solvent. The reaction mixture was stirred for 2 h at 40–50°C, filtered and allowed to evaporate slowly at room temperature. The microcrystalline solid thus formed was collected by filtration, washed with small amounts of ethanol and ether and dried *in vacuo*. The yields observed were 35–40%.

All prepared complexes, with their elemental analyses and some physical properties, are given in Table 1.

Crystal structure determination

A crystal of size $0.1 \times 0.2 \times 0.4$ mm was used for the measurement on a Syntex $P2_1$ diffractometer. Cell parameters were obtained from least-squares treatment of setting angles of 15 reflections in the range $19 \leqslant 2\theta \leqslant 22°$. Intensities were collected using graphite monochromatized Mo-K_α radiation in the θ–2θ scan mode and peak profile analysis according to Lehman and Larsen.[6] Only reflections with $I \geqslant 4\sigma(I)$ were classified observed. Intensities were corrected for Lorentz and polarization factors. The structure has been solved by the heavy atom method and refined by full-matrix least-squares calculations on *F*s, with atomic scattering factors from SHELX76.[7] The refinement was carried out, first with isotropic and then with anisotropic temperature factors. Positions of hydrogen atoms were calculated from geometric conditions and refined using a riding model with fixed isotropic *U*. Molecular illustrations were drawn using the ORTEP program.[8] Other experimental conditions and residual factors are listed in Table 2. Main bond distances and angles are given in Table 3. See also "supplementary material".

RESULTS AND DISCUSSION

In previous work monomeric mixed-ligand complexes of copper(I) halides were generally prepared by the simple reaction between the heterocyclic thiones and a 1:2 mixture of CuX and PPh_3 in chloroform or acetone solutions. On the other hand, when a "cubane-like" complex, $[Cu(PPh_3)X]_4$ or $Cu_2X_2(ttp)_n$ (ttp = tritolylphosphine, $n = 2$ or 3),[9] was used as a starting material the reactions resulted, under the same conditions, in the formation of dimers with either sulphur or halogen as bridging atoms. However, compositions and spectroscopic investigations of the compounds discussed here confirm their monomeric nature, although they were synthesized using the method for preparing the dimeric complexes in acetonitrile solution as the only modification. Since CuI forms weak complexes with acetonitrile,[10] it can be suggested that such an unstable complex, probably formed by dissolving $[Cu(PPh_3)I]_4$ in acetonitrile, acts as an intermediate in which CH_3CN ligands

Table 1. Analytical data and some physical properties of the complexes

Complex	Φ_i max[a]	Colour	Melting point (°C)	Elemental analysis: found (calc.) (%) C	H	N
1 $[Cu(PPh_3)_2(pymtH)I]$	0.164	Yellow	209	57.6 (58.1)	4.0 (4.1)	3.5 (3.4)
2 $[Cu(PPh_3)_2(tztH)I]$	0.119	Pale yellow	174	56.3 (56.2)	4.3 (4.2)	1.8 (1.7)
3 $[Cu(PPh_3)_2(imtH)I]$	0.010	Pale yellow	193	57.8 (57.5)	4.3 (4.2)	3.6 (3.5)
4 $[Cu(PPh_3)_2(bzimtH_2)I]$	0.387	White	210	58.6 (59.7)	4.0 (4.2)	3.5 (3.3)
5 $[Cu(PPh_3)_2(bztztH)I]$	0.411	Yellow	199	57.8 (58.6)	4.0 (4.0)	1.6 (1.6)

[a] Φ_i max = quantum yields of *i* complex irradiated at the maximum of the band in the region 290–335 nm.

Table 2. Details of data collection and structure refinement

Formula	$C_{40}H_{34}IN_2P_2SCu$
Formula weight	827.1
a (Å)	9.708(2)
b (Å)	19.838(4)
c (Å)	19.893(4)
β (°)	92.53(3)
V (Å^3)	3827(1)
D_{calc}(Mg m^{-3})	1.434
Z	4
Crystal system	Monoclinic
Space group	$P2_1/n$
Absorption coefficient (mm^{-1})	1.533
No. of reflections for cell determination	15
Radiation	Mo-K_α (λ = 0.71069 Å)
$h\,k\,l$ limits	0°+10, 0°+22, −22°+22
Total reflections	5250
Significant reflections [$I > 4\sigma(I)$]	3089
Refined parameters	425
R, Rw, G.O.F.	0.063, 0.070, 1.63
Weighting scheme	$w^{-1} = \sigma^2(F)+0.0001F^2$

may be readily displaced by thione and phosphine ligands.

All the complexes are microcrystalline solids soluble in chloroforom, methanol, ethanol, acetone and acetonitrile. According to the analytical results, the composition of the complexes is CuI · 2PPh$_3$ · L. Their solutions are non-conducting in acetone and chloroform. Room-temperature magnetic measurements confirmed the diamagnetic nature of the compounds studied.

Table 3. Interatomic distance (Å) and angles (°) for [Cu(PPh$_3$)$_2$(pymtH)I] with ESDs given in parentheses

Cu—I	2.674(2)	P(2)—C(1F)	1.829(12)
Cu—P(1)	2.296(4)	S—C(2)	1.662(13)
Cu—P(2)	2.303(4)	N(2)—C(2)	1.313(17)
Cu—S	2.338(4)	C(2)—N(3)	1.418(18)
P(1)—C(1A)	1.822(13)	N(1)—C(6)	1.375(20)
P(1)—C(1B)	1.829(12)	N(3)—C(4)	1.363(22)
P(1)—C(1C)	1.819(12)	C(4)—C(5)	1.368(22)
P(2)—C(1D)	1.841(13)	C(5)—C(6)	1.335(21)
P(2)—C(1E)	1.811(12)		

I—Cu—S	116.5(1)	C(4)—C(5)—C(6)	119.6(15)
I—Cu—P(1)	103.5(1)	Cu—P(1)—C(1A)	116.0(4)
I—Cu—P(2)	103.6(1)	Cu—P(1)—C(1B)	112.8(4)
S—Cu—P(1)	105.4(1)	Cu—P(1)—C(1C)	114.7(4)
S—Cu—P(2)	103.4(1)	Cu—P(2)—C(1D)	113.7(4)
P(1)—Cu—P(2)	125.3(1)	Cu—P(2)—C(1E)	113.9(4)
Cu—S—C(2)	114.6(5)	Cu—P(2)—C(1F)	118.2(4)
S—C(2)—N(1)	123.8(10)	C(1A)—P(1)—C(1B)	101.7(6)
S—C(2)—N(3)	123.8(10)	C(1B)—P(1)—C(1C)	106.5(6)
C(2)—N(1)—C(6)	129.5(12)	C(1A)—P(1)—C(1C)	117.1(10)
C(2)—N(3)—C(4)	121.1(12)	C(1D)—P(2)—C(1E)	105.2(5)
N(1)—C(2)—N(3)	112.2(12)	C(1E)—P(2)—C(1F)	102.2(5)
N(3)—C(4)—C(5)	121.2(13)	C(1D)—P(2)—C(1F)	101.9(6)
N(1)—C(6)—C(5)	116.2(14)		

Information concerning the structure of the investigated complexes, as well as the coordination mode of the ligands, can be provided on the basis of IR spectra. The presence of ν(NH) bands at 3200–3130 cm^{-1},[11a] the absence of ν(SH) absorptions in the 2500–2600 cm^{-1} region[11b] and the production of characteristic "thioamide" bands[11c] in the solid state IR spectra of both complexes and the corresponding free ligands exhibit the dominance of the thione form of the ligands investigated. The coordination through the sulphur atom is indicated by the shifts of the "thioamide" vibrations upon metal coordination.[3b]

The UV–vis spectra of the complexes in chloroform solutions show two main broad bands in the regions 255–262 and 290–335 nm, respectively, accompanied by another one at 280 nm. The two higher energy bands can be attributed to intraligand transitions of the phosphine ligand, since the spectrum of the free phosphine consists of three bands, at 287, 280 and 262 nm, for which the bands at 262 and 280 nm are found to have log ε values similar to their counterparts in the complexes.

The ^{1}H NMR spectra of the complexes are diagnostically of minor importance, since the protons of the heterocyclic thiones fall in the region of the triphenylphosphine peaks. However, the dominance of the thione form of the ligands in all complexes under investigation can be deduced by the presence of a broad peak in the region 10–14 ppm, assigned to the NH group, connected with the absence of the peak for the thiol (SH) proton at δ = 3–5 ppm.

Thermal analysis in flowing air shows the complexes decompose in two or three stages. Figure 1 illustrates TG and DTG data curves for the complex [Cu(PPh_3)$_2$(pymtH)I]. The thermal decomposition of the compound is a typical example of a two-stage process. The first stage (250–345°C) is connected with two very strong endothermic effects and involves a 76% mass loss, consistent with the evolution of the thione and the two PPh_3 molecules (theoretical mass loss 77%). The second stage (470–570°C) is accompanied by a strong endothermic effect and involves a 14% mass loss corresponding to the evolution of the iodine atom and oxidation of the copper(I) to CuO (theoretical mass loss 13.4%).

Room temperature irradiation of the complexes in chloroform at the maximum of the band in the region 290–335 nm causes the decomposition of the complexes in two photoproducts, as we can estimate according to Coleman's method.[12] The decomposition occurs within minutes and can be checked periodically by comparison of the intensities of the bands in the UV spectra, since no evolution of new bands or significant shifts could be observed during the experiment. In accordance with our earlier observations in mixed-ligand complexes there is no difference in the decomposition mechanism of the complexes, on the grounds of the lability of the phosphine ligand in solution.[13–15] Quantum yields of these complexes have been determined at room temperature and are reported in Table 1.

Description of the structure

Main bond lengths and angles are given in Table 3. Figure 2 shows a view of the molecular structure with hydrogen atoms omitted; molecular packing is shown in Fig. 3. The crystal structure of [Cu

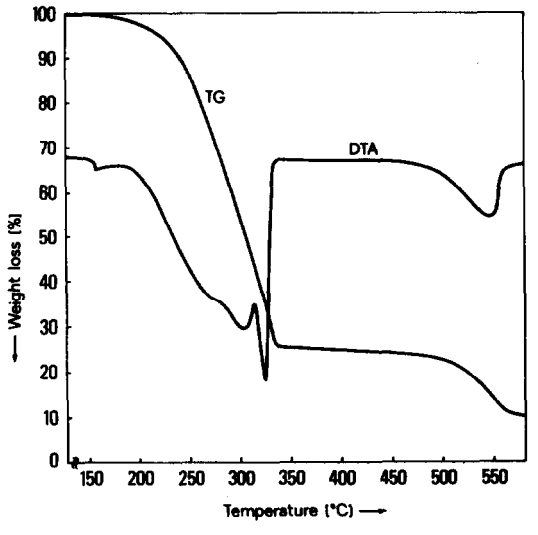

Fig. 1. TG and DTG curves for [Cu(PPh_3)$_2$(pymtH)I].

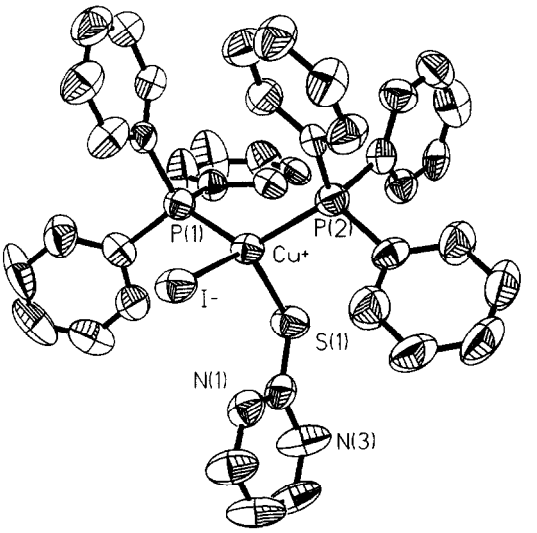

Fig. 2. An ORTEP drawing showing the main atom numbering scheme.

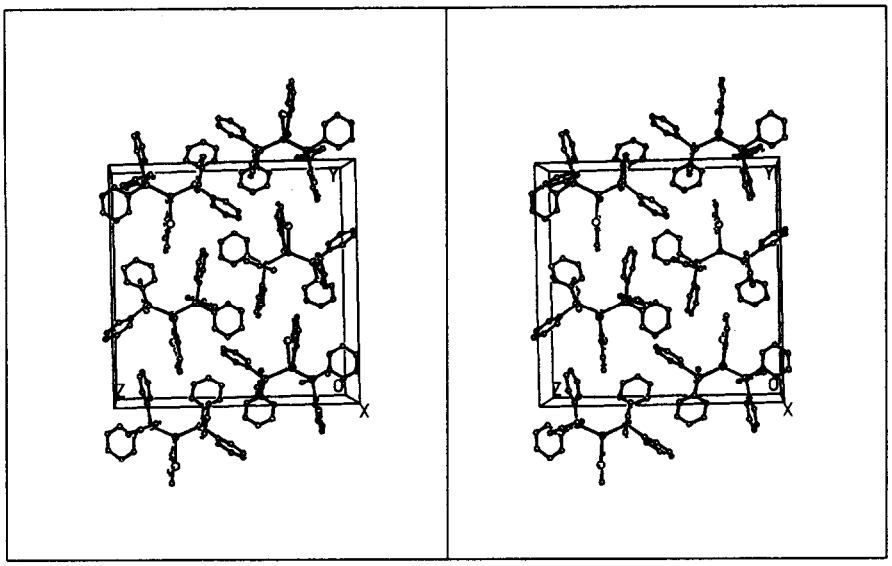

Fig. 3. Packing diagram. A stereoview down the *a*-axis.

$(PPh_3)_2(pymtH)I]$ is built up from well-separated discrete molecules with no crystallographically imposed symmetry. The coordination around the metal is tetrahedral with two phosphorus atoms of the phosphine, one sulphur of the thione and one iodine atom. According to the Cambridge Structural Database this is the first known structure with a $CuIP_2S$ core. This arrangement is considerably distorted since the phosphorus angle at the metal site, P(1)—Cu—P(2) with a value of 125.3(1)°, is much larger than the tetrahedral value, 109.4°. This higher angle is counterbalanced by the bond angles I—Cu—P(1), I—Cu—P(2) and S—Cu—P(2), whose values are lower than 109.4° [103.5(1), 103.6(1) and 103.4(1)°, respectively]. The tetrahedral distortion is due to steric imposition of the bulky phosphine ligands and was previously observed in a series of analogous complexes, e.g. in $[Cu(PPh_3)_2(meimtH)Br]$ [P—Cu—P = 130.9(0)°][3c] and in $[Cu(PPh_3)_2(pymtH)Br]$ [P—Cu—P = 125.0(2)°].[3a]

The Cu—S distance of 2.338(4) Å is somewhat longer than in the bromine isomorph [2.302(4) Å],[3a] but shorter than in $[Cu(PPh_3)_2(meimtH)Br]$ [2.375(1) Å][3c] or in $[Cu(PPH_3)_2(bzimtH_2)Cl]$ and $[Cu(PPh_3)_2(nbzimtH_2)Cl]$ [2.377(1) and 2.381(2) Å, respectively].[3e] This shortening of the Cu—S distance upon coordination reflects the increase of the π-character in this bond. The Cu—P(1) and Cu—P(2) distances of 2.296(4) and 2.303(4) Å, respectively, are significantly longer than those observed in the isomorphous structure of $[Cu(PPh_3)_2(pymtH)Br]$ [2.263(4) and 2.267(4) Å], but closer to those found in other triphenylphosphine complexes.[16,17] The Cu—I distance of 2.674(2) Å is within the range of values (2.622–2.785 Å) previously reported for copper(I) complexes[18] and exactly the same found in $[Cu(py2SH)_2I]_2$.[2c] The short non-bonding distance in the molecule H(1A)···I(1) can be accepted as an intramolecular hydrogen bond with the geometry: N(1)···I(1) = 3.549 Å, H(1A)···I(1) = 2.65 Å and N(1)—H(1A)—I(1) = 176°.

Supplementary material. List of atomic coordinates, positional and isotropic thermal parameters of the hydrogen atoms, the bond lengths and angles and the anisotropic thermal parameters are available from the authors on request.

REFERENCES

1. E. S. Raper, *Coord. Chem. Rev.* 1985, **61**, 115.
2. (a) L. P. Battaglia, A. Bonamartini Corradi, F. A. Devillanova and G. Verani, *Trans. Met. Chem.* 1979, **4**, 264; (b) D. Mentzafos, A. Terzis, P. Karagiannidis and P. Aslanidis, *Acta Cryst.* 1989, **C45**, 54.
3. (a) P. Karagiannidis, P. Aslanidis, D. P. Kessissoglou, B. Krebs and M. Dartmann, *Inorg. Chim. Acta*, 1989, **156**, 47; (b) C. Lecomte, S. Skoulika, P. Aslanidis, P. Karagiannidis and S. Papastefanou, *Polyhedron* 1989, **8**, 1103; (c) P. Karagiannidis, P. Aslanidis, S. Papastefanou, D. Mentzafos, A. Hountas and A. Terzis, *Polyhedron* 1990, **9**, 981; (d) P. Karagiannidis, S. K. Hadjikakou, P. Aslanidis and A. Hountas, *Inorg. Chim. Acta.* 1990, **178**, 27; (e) S. Skoulika, A. Aubry, P. Karagiannidis, P. Aslanidis and S. Papastefanou, *Inorg. Chim. Acta.* 1991, **183**, 207; (f) S. K. Hadjikakou, P. Aslanidis, P. Karagiannidis, D. Mentzafos and A. Terzis, *Inorg.*

Chim. Acta 1991, **186**, 199; (g) S. K. Hadjikakou, P. Aslanidis, P. Karagiannidis, D. Mentzafos and A. Terzis, *Polyhedron* 1991, **10**, 835; (h) S. K. Hadjikakou, P. Aslanidis, P. Karagiannidis, A. Aubry and S. Skoulika, *Inorg. Chim. Acta* 1992, **193**, 129; (i) S. K. Hadjikakou, P. Aslanidis, P. Akrivos, P. Karagiannidis, B. Kojic-Prodic and M. Luic, *Inorg. Chim. Acta* 1992, **197**, 31.

4. (a) A. Baiada, F. H. Jardine and D. Willett, *Inorg. Chem.* 1990, **29**, 4805; (b) A. Baiada, F. H. Jardine and D. Willett, *Inorg. Chem.* 1990, **29**, 3042.
5. C. Costa, E. Reisenhofer and L. Stefani, *J. Inorg. Nucl. Chem.* 1965, **27**, 2581.
6. M. S. Lehmann and F. K. Larsen, *Acta Cryst.* 1974, **A30**, 580.
7. G. M. Sheldrick, SHELX76, Program for Crystal Structure Determination. University of Cambridge, U.K. (1976).
8. C. K. Johnson, ORTEP II, ORNL-1538. Oak Ridge National Laboratory, Tennessee, U.S.A. (1976).
9. S. K. Hadjikakou, P. D. Akrivos, P. Karagiannidis, D. Mentzafos and A. Terzis, *Inorg. Chim. Acta* 1993, **206**, 163.
10. (a) I. Csoregh, P. Kierkegaard, R. Norrestam, *Acta Cryst.* 1975, **B31**, 314; (b) G. Jones, W. Clegg, G. M. Sheldrick, *Acta Cryst.* 1985, **B36**, 141.
11. (a) P. P. Singh and R. Rivest, *Can. J. Chem.* 1968, **46**, 2361; (b) E. S. Raper and J. L. Brooks, *J. Inorg. Nucl. Chem.* 1977, **39**, 2163; (c) C. N. R. Rao and P. Vankataraghavan, *Spectrochim. Acta* 1962, **18**, 541.
12. J. S. Coleman, L. P. Varga and S. H. Mastin, *Inorg. Chem.* 1970, **9**, 1015.
13. D. J. File, W. M. More and K. W. Morse, *Inorg. Chem.* 1984, **23**, 1545.
14. E. L. Muetterties and C. W. Alegranti, *J. Am. Chem. Soc.* 1970, **92**, 4114.
15. P. Aslanidis, P. Karagiannidis and S. Hadjikakou, *Book of Abstr., 1st Chemistry Conf. Cyprus–Greece*, p. 90. Nicosia, Cyprus (1988).
16. J. T. Gill, J. J. Mayerle, P. S. Welker, D. F. Lewis, D. A. Ucko, D. J. Barton, D. Stowens and S. J. Lippard, *Inorg. Chem.* 1976, **15**, 1155.
17. A. P. Gaughan, Z. Dori and J. A. Ibers, *Inorg. Chem.* 1971, **10**, 1322.
18. (a) N. P. Rath, E. M. Holt and K. Tanimura, *J. Chem. Soc., Dalton Trans.* 1986, 2303; (b) J. M. Dyason, L. M. Engelhardt, P. C. Healy and A. H. White, *Aust. J. Chem.* 1986, **39**, 1043.

Polyhedron Vol. 12, No. 18, pp. 2227–2234, 1993
Printed in Great Britain

0277–5387/93 $6.00+.00
© 1993 Pergamon Press Ltd

A SECONDARY REACTION IN THE OXIDATION OF L-METHIONINE BY CHROMIUM(VI) IN ACIDIC MEDIUM*

L. F. SALA,† C. PALOPOLI, V. ALBA and S. SIGNORELLA

Departamento de Ciencias Exactas, Facultad de Ciencias Bioquímicas (UNR), Suipacha 531, 2000 Rosario, Argentina

(*Received* 22 *February* 1993; *accepted* 11 *May* 1993)

Abstract—The reaction mechanism of the oxidation of L-methionine by chromium(VI) in perchloric acid has been reviewed. Secondary reaction products formed by methionine C(1)—C(2) bond scission were observed, besides the major oxidation product: methionine sulphoxide. Methionine sulphoxide and methional (3-[methylthio]-propionaldehyde) were found to be produced by two parallel redox steps. Ammonia and carbon dioxide have been identified and their yields determined. Free radicals were detected during the reaction course and the yield of carbon dioxide was found to be independent of the amount of free radical scavenger. When the amino group was blocked by an acetyl group the N-acetylmethionine sulphoxide was the only oxidation product. The mechanism with the associated reaction kinetics are presented and discussed.

In recent years several studies have reviewed the toxicity and carcinogenicity of chromium compounds.[1–3] Chromium(VI) compounds pose serious dangers to biological systems and many small molecules found within the cell are redox active and should be able to reduce them. These compounds may be important to the cellular metabolism of chromium(VI).[4,5]

Amino acids containing a thiol group are strong reductants of chromium(VI).[6] We have undertaken a study of the reaction between chromium(VI) and methionine, which contains a thio ether group, under acidic conditions. These reactions had previously been investigated[7,8] and the N-methionine sulphoxide was the only product detected by the authors. In this work we demonstrate that C—C scission occurs leading to the formation of carbon dioxide and ammonium ions by a competitive reaction path and that carbon dioxide yield increases as the pH rises. This parallel reaction implies a reformulation of the kinetic law and mechanism with respect to those proposed previously and suggests that amino and carboxylic groups should be coordinated to chromium(VI) to form an intermediate ester, previous to the slow redox step.

EXPERIMENTAL

Materials

(−)-L-methionine (Sigma), potassium dichromate (Cecarelli), sodium perchlorate (Sigma), perchloric acid (Merck, 70% reagent), acetic anhydride (Merck) and 2,4-dinitrophenylhydrazine (Aldrich) were used without further purification. N-acetylmethionine and methionine sulphoxide were synthesized by methods described in the literature.[9,10] Mixtures of sodium perchlorate and perchloric acid were used to maintain a constant ionic strength of 0.4 M at different hydrogen ions concentrations.

Kinetic measurements

Reaction rates were determined spectrophotometrically by monitoring chromium(VI) decay at 350 nm on a Guildford Response II recording spectrophotometer with a thermostated cell-holder. No chromium(V) was observable by EPR spectroscopy under the experimental conditions used, indicating that changes in absorbance at

*The present work has been presented at the XIX Latin American Meeting on Chemistry, Buenos Aires, Argentina (1990).

† Author to whom correspondence should be addressed.

350 nm reflected changes in chromium(VI) concentrations without interference from chromium(V). Rate constants obtained from multiple determinations were within ±5% of each other.

For all the kinetic measurements the concentration of chromium(VI) was kept constant at 6×10^{-4} M, while the L-methionine and N-acetylmethionine concentrations were varied from 1.75×10^{-2} to 0.14 M and from 7.3×10^{-3} to 0.172 M, respectively, at a constant ionic strength of 0.4 M. The reactants were found to be stable over the time course of the kinetic measurements. In every experiment perchloric acid was used as a source of hydrogen ions. Over the course of the reactions the pH was constant to within 0.1 pH unit. In the range of pH used the protonated form of L-methionine ($pK_{a_1} = 2.28$)[11] is the main species in solution.

Test for free radicals

A solution of potassium dichromate (1.2×10^{-3} M, 2 cm^3) in 0.01 M $HClO_4$ was added to a mixture of 0.1 M methionine in 0.01 M $HClO_4$ and 23% p/p acrylonitrile (0.5 cm^3), at 60°C. After 30 min a white precipitate of a polymer appeared slowly. Under the same conditions in a reaction mixture of N-acetylmethionine, potassium dichromate and acrylonitrile a white precipitate appeared after 50 min. The blank experiments in the absence of methionine, N-acetylmethionine or potassium dichromate did not show the formation of any such precipitate.

In a series of experiments increasing amounts of acrylonitrile (11 to 22 mmol) were added to a mixture of L-methionine and potassium dichromate in $HClO_4$ (the same conditions as above) and the carbon dioxide yielded was measured. For all the experiments the yield of carbon dioxide was found to be constant (*ca* 30%), indicating that carbon dioxide radicals should not be formed over the course of the methionine oxidation.

Products analysis

In excess of oxidant. In a typical experiment a solution (25 cm^3) of methionine (0.123 M) in 1 M $HClO_4$ was added to a potassium dichromate solution (25 cm^3, 0.611 M) in 1 M $HClO_4$, at 60°C. The solution was continuously flushed with pure nitrogen. The gaseous products were taken in a 0.3% 2,4-dinitrophenylhydrazine acid solution and in a sodium hydroxide solution.

After 6 h the 2,4-dinitrophenylhydrazone acid solution was filtered out and the yellow residue was analysed by ^1H and ^{13}C NMR. The compound was identified as the 2,4-dinitrophenyl hydrazone of acetaldehyde by comparing the spectra with those of an authentic sample.

The sodium hydroxide solution was titrated against 0.07 N HCl solution to determine the carbon dioxide yielded. Quantitative amounts of carbon dioxide were obtained.

A sample of the reaction mixture (10 cm^3) was alkalinized with NaOH and heated. Distilled ammonia was swept into a 0.2 N HCl solution and titrated against standard NaOH solution. In this way a quantitative yield of ammonia was found.

Unreacted chromium(VI) was determined spectrophotometrically at 350 nm after complete degradation of the organic compound; 2 mol of chromium (VI) were consumed per mole of methionine.

From these experimental data the stoichiometry for the total oxidative degradation of methionine by chromium(VI) is:

$$CH_3S(CH_2)_2CH(NH_3^+)COOH + 2Cr^{VI} \rightarrow (CH_3)_2SO + CH_3CHO + NH_4^+ + CO_2 + 2Cr^{III}. \quad (1)$$

No attempt was made to determine dimethylsulphoxide in the reaction mixture.

In excess of organic substrate. A mixture (25 cm^3) of L-methionine (0.598 M) and potassium dichromate (0.010 M) in 0.78 M $HClO_4$ was allowed to react at 60°C. After the reaction proceeded to completion the mixture was used to charge a Dowex 50W-X8, 100–200 mesh cation exchange column. Continued elution with increasing amounts of $HClO_4$–$NaClO_4$ mixtures resulted in the separation of two fractions. The first was purple in colour and could be eluted with 1 M $HClO_4$. The second had a blue colour and was eluted with 2 M $HClO_4$.

For the blue fraction bands at 410 and 570 nm were observed ($\varepsilon = 13$ and 16 M^{-1} cm^{-1}, respectively), attributable to the octahedral $^4A_{2g} \rightarrow {}^4T_{1g}$ and $^4A_{2g} \rightarrow {}^4T_{2g}$ transitions in O_h symmetry, respectively which are distinctive of the free chromium(III) aqua-ion.

Given the close agreement (*vide infra*) of both visible and UV spectral maxima and the intensities between the observed species in the purple fraction and those of authentic samples independently prepared,[12,13] this fraction might consist of a mixture of binary complexes of methionine/chromium(III) (395 nm, $\varepsilon = 40.5$ and 530 nm, $\varepsilon = 33$) and methionine sulphoxide/chromium(III) (410 nm, $\varepsilon = 25$ and 561 nm $\varepsilon = 24$). Since these absorption bands are strongly pH dependent,[13] absorbances of the synthesized samples were measured in $HClO_4$ solutions of the same concentration as those of the reaction products in the purple fraction.

Carbon dioxide and ammonia were determined

Table 1. Yields of CO_2 (NH_3) in the oxidation of L-methionine by chromium(VI) at different pH. $[Cr^{VI}]_0 = 0.075$ M; $[Met]_0 = 0.7621$ M, $T = 60°C$

pH	$\%CO_2$ (NH_3)
0.77	24
1.23	31
1.55	35
2.51	48

by the same method as described before. Table 1 shows CO_2 (NH_3) yields at different pH, under excess organic substrate.

In a parallel reaction set methionine sulphoxide was determined by the same method described by Olatunji *et al.*[8] However, the yield obtained was substantially lower than reported because of the co-precipitation of unreacted methionine, even when the same conditions described by the authors were employed.

2,4-Dinitrophenylhydraqzine (1 cm^3) in HCl (2 N) was added to the reaction mixture (3 cm^3) and extracted with ethyl acetate. After adding a solution of Na_2CO_3 the aqueous layer was made alkaline with NaOH and methional was detected spectrophotometrically as the 2,4-dinitrophenylhydrazone ($\lambda_{max} = 432$ nm).[14]

RESULTS AND DISCUSSION

Rate studies

Over the whole range of pH used in the kinetic measurements UV–vis studies showed that the reaction of methionine and chromium(VI) resulted in an absorption band at 350 nm and a shoulder at 420–500 nm, characteristic of the $Cr_2O_7^{2-}$ ion.[15] Under our experimental conditions no spectral evidence of a methionine-chromium(VI) ester was obtained.

The observed rate constants were calculated from the absorbance data obtained at 350 nm. The pseudo-first-order rate constants were calculated at various $[Cr^{VI}]_0$, but at constant $[S]_0$, $[H^+]_0$, ionic strength ($I = 0.4$ M) and temperature. The rate was found to be constant with increasing amounts of $[Cr^{VI}]_0$ (Table 2), indicating that the total chromium(VI) concentration must be used in the rate law.

Table 3 summarizes values of k_{obs} for various concentrations of L-methionine at a fixed concentration of perchloric acid. Plots of k_{obs} vs [methionine] at constant acidity gave straight lines (Fig. 1), from which values of k_1 were determined (Table 3). The plot of k_1 vs $[HClO_4]^2$ gave a straight line with a positive intercept, showing that the first-order rate constant k_1 may be expressed as consisting of an acidity independent and an acidity dependent term:

$$k_1 = a + b[H^+]^2, \quad (2)$$

where $a = 0.01402\ M^{-1}\ s^{-1} \pm 8.66 \times 10^{-3}$ and $b = 26.34\ M^{-3}\ s^{-1} \pm 2.02$.

The complete rate law is then given by:

$$-d[Cr^{VI}]/dt = k_{obs}[Cr^{VI}] = (a + b[H^+]^2)[Met][Cr^{VI}] \quad (3)$$

where Cr^{VI} represents the total chromium(VI) concentration and Met = L-methionine.

For the N-acetylmethionine derivative (NAM) a different kinetic law was derived. k'_{obs} values obtained for different $[HClO_4]$ at fixed NAM concentrations are summarized in Table 4. Plots of k'_{obs} vs $[HClO_4]^2$ gave a good straight line (Fig. 2), from which k_2 values were obtained (Table 4). The plot of k_2 vs [NAM] gave a straight line with a positive intercept, showing that k_2 may be expressed as consisting of a term independent of [NAM] and of another with a first-order dependence. The complete rate law is then given by:

$$-d[Cr^{VI}]/dt = k'_{obs}[Cr^{VI}] = (c + d[NAM])[H^+]^2[Cr^{VI}], \quad (4)$$

where $c = 2.53 \times 10^{-3}\ M^{-2}\ s^{-1} \pm 3.4 \times 10^{-4}$ and $d = 9.48\ M^{-3}\ s^{-1} \pm 0.74$ and Cr^{VI} refers to the total chromium(VI) concentration.

Mechanism

A mechanism consistent with all experimental data obtained for the oxidation of methionine with

Table 2. Observed pseudo-first-order rate constants for different $[Cr^{VI}]_0 = 6 \times 10^{-4}$; $T = 30°C$; [Met] = 0.07 M; $I = 0.4$ M

$10^4 \times k_{obs}$ (s^{-1})	9.80	9.78	9.83	9.79	9.76	9.84
$10^4 \times [Cr^{VI}]$ (M)	4.0	5.0	6.0	7.5	10.0	15.0

Table 3. Rate constants for the oxidation of L-methionine by chromium(VI); T = 30°C; I = 0.4 M; $[Cr^{VI}]_0 = 6 \times 10^{-4}$ M

[Met] (M)	$k_{obs} \times 10^4$ (s^{-1}) at [$HClO_4$] 0.01 M	0.03 M	0.055 M	0.075 M
0.0175	2.65	5.88	20.30	27.2
0.0350	4.71	12.30	38.43	55.6
0.0525	7.11	18.4	56.4	83.7
0.0700	9.80	25.4	74.7	112.0
0.0875	12.6	31.0	92.5	136.0
0.1050	15.5	36.1	112.0	—
0.1400	19.3	—	—	—
k_1 ($M^{-1} s^{-1}$)	0.0141	0.0350	0.104	0.157

chromium(VI) is given in Scheme 1:

$$Cr_2O_7^{2-} + H_3CS(CH_2)_2CH(NH_3^+)COOH \underset{\text{(Met)}}{\overset{K_5}{\rightleftharpoons}}$$

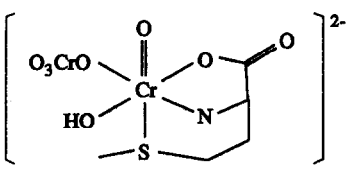

(5)

I

$$I + Met \xrightarrow[\text{slow}]{k_6} Cr^{IV} + H_3CS(CH_2)_2CHO + NH_4^+ + CO_2 + HCrO_4^- \quad (6)$$

$$I + 2H^+ + Met \xrightarrow[\text{slow}]{k_7} Cr^V + HCrO_4^- + H_3S^{\cdot+}(CH_2)_2CH(NH_3^+)COOH \quad (7)$$

(Met$^{\cdot+}$)

$$Met^{\cdot+} + Cr_2O_7^{2-} \rightarrow H_3CSO(CH_2)_2CHNH_3^+COOH + Cr^V + HCrO_4^- \quad (8)$$

(MetSO)

$$2HCrO_4^- \rightleftharpoons Cr_2O_7^{2-} + H_2O \quad (9)$$

Scheme 1.

The first step represents the formation of an anionic complex between chromium(VI) and L-methionine acting as a tridentate ligand.[16] This complex may decompose to the aldehyde, ammonium ion and carbon dioxide assisted by another molecule of L-methionine, or may be protonated to a new complex which interacts with another molecule of methionine in the slow step to yield the sulphoxide.

According to the proposed mechanism the full rate law for the chromic oxidation of L-methionine, under conditions studied in the kinetic measurements, can be derived:

$$-\frac{d[Cr^{VI}]}{dt} = k_6[Met][I] + k_7[Met][I][H^+]^2$$

$$= (k_6K_5[Met]^2 + k_7K_5[Met]^2[H^+]^2)[Cr_2O_7^{2-}] \quad (10)$$

since

$$[Cr^{VI}]_T = [Cr_2O_7^{2-}] + [I]$$

$$= [Cr_2O_7^{2-}](1 + K_5[Met]). \quad (11)$$

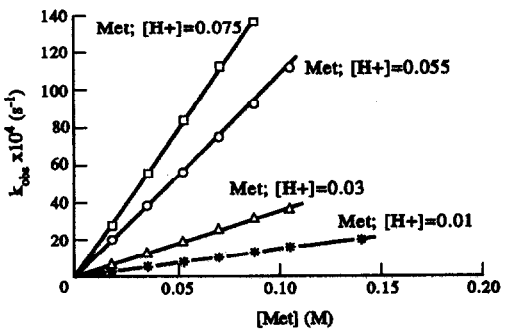

Fig. 1. k_{obs} as a function of [Met] at different [$HClO_4$]; T = 30°C; I = 0.4 M; $[Cr^{VI}]_0 = 6 \times 10^{-4}$ M.

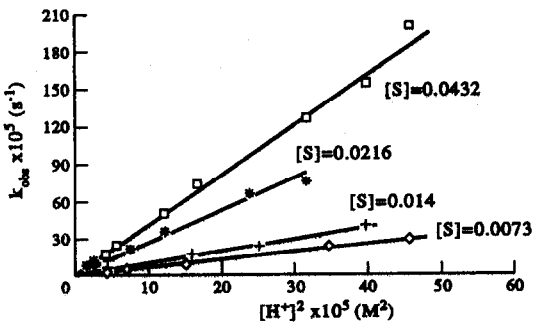

Fig. 2. k'_{obs} as a function of $[HClO_4]^2$ at different [NAM]; T = 30°C; I = 0.4 M; $[Cr^{VI}]_0 = 6 \times 10^{-4}$ M.

Table 4. Observed pseudo-first-order rate constants and calculated k_2 for the oxidation of N-acetyl-L-methionine by chromium(VI); $T = 30°C$; $I = 0.4$ M, $[Cr^{VI}]_0 = 6 \times 10^{-4}$ M

$[HClO_4]$ (M)	$k_{obs} \times 10^5$ (s^{-1}) at [NAM] (M) 0.0073	0.014	0.0216	0.0432	0.0644
0.0107			6.81		
0.0158			10.23		
0.0199				16.7	
0.0204	2.51	4.33			
0.0224					23.29
0.0234				24.3	
0.0263	3.85				35.15
0.0271			22.56		
0.0346				49.8	
0.035			35.03		
0.0364					72.25
0.0389	8.71				
0.0398		14.9			
0.0407				73.7	
0.0437					108.77
0.0489			65.21		
0.0501		23.1			
0.0562			75.68	126.0	185.30
0.0589	23.2				
0.0631		39.5		154.0	
0.0676	29.0			200.0	
0.0692		48.1			
0.0724	34.0				
k_2 (M^{-2} s^{-1}) $\times 10^3$	65.85	101.20	255.96	411.50	605.80

Replacing $[Cr_2O_7^{2-}]$ in (10):

$$-\frac{d[Cr^{VI}]}{dt} = \frac{(k_6 + k_7[H^+]^2) K_5 [Met]^2}{1 + K_5 [Met]} [Cr^{VI}]_T. \quad (12)$$

If K_5 [Met] $\gg$ 1, eq. (12) becomes:

$$-\frac{d[Cr^{VI}]}{dt} = (k_6 + k_7[H^+]^2)[Met][Cr^{VI}]_T$$

$$= k_{obs}[Cr^{VI}]_T, \quad (13)$$

eq. (13) is in full agreement with the experimental findings.

In Scheme 1 the intermediate I differs from those reported previously by other authors who proposed the sulphur atom as the only coordination site.[7,8] The two different oxidation products observed in this work, methionine sulphoxide (oxidation of the sulphur atom) and methyl-3-propionaldehyde thioether [C(1)—C(2) bond scission], suggest that the amino and carboxylate groups should bind chromium(VI) in the intermediate complex. Moreover, the presence of the sulphur function seems to be necessary for amino and carboxylate group coordination and further oxidation. A precedent for suggesting a six-coordinate chromium(VI) intermediate has already been reported for oxidation processes where chromium(VI) acts as a catalyst.[16] To verify the last assumption the reactivity of two structurally related amino acids was checked. Homoserine (4-hydroxy-2-amino-butanoic acid) and isoleucine (3-methyl-2-amino-pentanoic acid) were reacted with chromium(VI) under the same experimental conditions employed to oxidize methionine. As expected, no reaction was detected with either homoserine or isoleucine, indicating that sulphur is essential to yield the redox products.

Sulphur-containing amino acids have been proposed to react by a thioester intermediate with the sulphur as the only atom bound to chromium(VI). However, the possibility of binding by the three coordination sites should not be discarded, even when the main redox product arises from oxidation of the sulphur atom.

The alternative mechanism in Scheme 2 provides another suitable explanation for the formation of

two different oxidation products and also fits the experimental kinetic law well.

$$\text{Met} + Cr_2O_7^{2-} \overset{K_{14}}{\rightleftharpoons} \text{II} \quad (14)$$

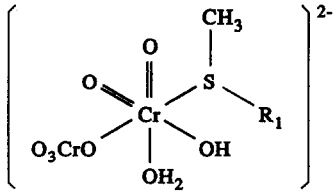

where R_1 is $(CH_2)_2CH(NH_2)COOH$

$$\text{II} + 2H^+ + \text{Met} \xrightarrow[\text{slow}]{k_{15}} H_3CS^{\cdot+}(CH_2)_2CH(NH_3^+)COOH + Cr^V + HCrO_4^- \quad (15)$$

$$\text{II} \overset{K_{16}}{\rightleftharpoons} \text{I} \xrightarrow[\text{Met (slow)}]{k_{16}} H_3CS(CH_2)_2CHO + NH_4^+ + CO_2 + Cr^{IV} \quad (16)$$

Scheme 2.

By this mechanism two intermediate complexes between methionine and chromium(VI) are formed. In complex **II** methionine binds chromium(VI) through the sulphur atom. This complex decomposes towards the sulphoxide in the acid catalysed step. Complex **II** is in equilibrium with complex **I**, in which methionine acts as a tridentate ligand, which slowly yields the decarboxylated-deaminated product. Equations (8) and (9) also constitute this mechanism.

If this second scheme is correct those sulphur-containing amino acids for which K_{16} is negligible should produce the sulphur-oxidized product through complex **II**, e.g. penicillamine[17] and cysteine.[18] In this way this second scheme should represent a more general mechanism which comprises those reported previously.

The fact that the yield in CO_2 increases with pH is in agreement with the formation of CO_2 by a path independent of pH, whereas methionine sulphoxide is formed by an acid catalysed step, such as proposed in both mechanisms.

Two consecutive steps involving oxidation of methionine to methionine sulphoxide and further oxidation to the methional sulphoxide may be ruled out on the basis of the absence of reaction when methionine sulphoxide was reacted with chromium(VI) under the same experimental conditions employed to oxidized methionine.

To explain the decarboxylation path it might be thought that the oxidized sulphur function oxidizes the amino group in a subsequent fast step. This N-oxidation might be sterically assisted with the participating sulphur and nitrogen centres adopting a favourable five-membered ring configuration. The oxidized amino radical, regarded as a protonated imine, may be subject to hydrolysis forming the corresponding aldehyde and ammonia. Two reasons may be given to rule out this intramolecular oxidation. First, this oxidation is favoured in basic or slightly acid solutions and no longer takes place in strong acid solutions.[19] This is in clear contrast with the increasing amounts of carbon dioxide observed as the pH rises. Second, if decarboxylation was assisted by the oxidized sulphur function, yield of carbon dioxide should be affected by adding increasing amounts of acrylonitrile to the reaction mixture. On the contrary, the yield of carbon dioxide remained constant.

The spectrophotometric analysis of the chromium(III) products showed a mixture of chromium(III)-methionine and chromium(III)-methionine sulphoxide binary complexes. Some authors[20] have concluded that initial one-electron reduction of chromium(VI) leads to chromium(III) entrapment of the oxidized substrate, whereas initial two-electron reduction leads to chromium(III) entrapment of excess substrate. If this generalization were accepted then the spectrophotometric observation of the chromium(III)-methionine complex as a product would imply an initial two-electron reduction of chromium(VI) by methionine; whereas the chromium(III)-methionine sulphoxide complex suggests an initial one-electron reduction of chromium(VI) by methionine in the acid catalysed pathway.

The constant yield of carbon dioxide observed after adding increasing amounts of acrylonitrile, and radicals observed in the N-acetyl-methionine-$Cr_2O_7^{2-}$ mixtures (in this case the sulphoxide is the only reaction product, as discussed below), lead us to suggest that radicals formed in the oxidation of methionine might take part in the sulphoxide formation, presumably through a sulphur-centred radical-cation.[19] This radical ion may react with another molecule of $Cr_2O_7^{2-}$ in a fast step [eq. (8)] to yield the methionine sulphoxide and chromium(V). $HCrO_4^-$ produced in the slow redox steps rapidly associates to another $HCrO_4^-$ to form $Cr_2O_7^{2-}$, the predominant species of chromium(VI) in the solution [eq. (9)].[15] Finally, intermediate chromium(V) may react with excess methionine in later steps to yield chromium(III) and the oxidation products.

From the experimental data obtained for the oxidation of NAM with chromium(VI) the mechanism in Scheme 3 was deduced:

$$CrO_7^{2-} + NAM \overset{K_{17}}{\rightleftharpoons} \left[\text{III} \right]^{2-}$$

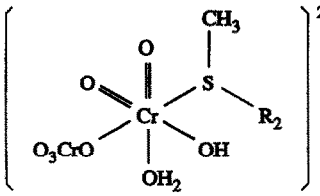

III

(17)

where R_2 is $(CH_2)_2CH(NOAc)COOH$.

$$\text{III} + 2H^+ \xrightarrow[\text{slow}]{k_{18}} H_3CS^{\cdot+}(CH_2)_2CH(NHOAc)COOH + Cr^V \quad (18)$$

$$\text{III} + NAM + 2H^+ \xrightarrow[\text{slow}]{k_{19}} \underset{(NAM^{\cdot+})}{H_3CS^{\cdot+}(CH_2)_2CH(NHOAc)COOH} + Cr^V + NAM \quad (19)$$

$$NAM^{\cdot+} + Cr_2O_7^{2-} \rightarrow H_3CSO(CH_2)_2CH(NHOAc)COOH + Cr^V + HCrO_4^- \quad (20)$$

$$NAM + Cr^V \rightarrow H_3CSO(CH_2)_2CH(NHOAc)COOH + Cr^{III} \quad (21)$$

Scheme 3.

In this case the N-acetyl group blocks the amino group and enables the coordination site at the nitrogen atom. NAM acts then as a monodentate ligand bound to chromium(VI) through the sulphur atom to yield $NAM^{\cdot+}$, through two competitive pathways [eqs (18) and (19)]. Chromium(V) and $NAM^{\cdot+}$, formed in the slow steps, yield the final chromium(III) and the sulphoxide by two later fast steps [eqs (20) and (21)]. This is in agreement with radicals observed when acrylonitrile was added to a reaction mixture. However, the sulphoxide might be formed by a two-electron step, followed by a fast reaction between chromium(IV) and NAM to yield chromium(III) and sulphur-centred radicals responsible for the white precipitate observed with acrylonitrile.

CONCLUSIONS

Methionine reacts with chromium(VI) at a significant rate only at pH < 2; e.g. at pH = 7 it reacts only after prolonged incubation at 37°C.[21] This suggests that the reductant reacts with chromium(VI) especially when protonated to form the intermediate ester, with the ammonium group playing an important role in its rate of formation.[6] At higher pH the rate of formation of this ester is too slow and the oxidation is not significant. At low pH the ester is formed rapidly and the redox steps are rate limiting.

Since decarboxylation viewed as a later oxidation by the oxidized sulphur function was ruled out (discussed above), methionine C(1)—C(2) bond scission reveals that the nitrogen and oxygen atoms might participate in the ester formation. This secondary reaction becomes more important as pH rises and its competitive path becomes slow. It seems reasonable to suppose that this secondary reaction should be more evident for methionine, or any other sulphur-containing amino acid with appropriate structural and configurational characteristics, able to form a strain-free tricyclic intermediate complex with the chromium metal centre.

Acknowledgements—Support for this work by the National Research Council of Argentine (CONICET) and the National University of Rosario is gratefully acknowledged. Pharmacist Palopoli thanks the Research Council of the National University of Rosario (CIURN) for a fellowship. We also thank D. Gomez for technical work.

REFERENCES

1. D. M. L. Goodgame and A. Martin Joy, *J. Inorg. Biochem.* 1986, **26**, 219.
2. D. M. L. Goodgame and A. Martin Joy, *Inorg. Chim. Acta* 1987, **135**, L5.
3. A. Standeven and K. Wetterhahn, *J. Am. Chem. Coll. Toxicol.* 1989, **8**, 1275.
4. M. Branca, A. Dessi, M. Kolowski, G. Micera and J. Swiatek, *J. Inorg. Biochem.* 1990, **39**, 217.
5. S. Brauer and K. Wetterhahn, *J. Am. Chem. Soc.* 1991, **113**, 3001.
6. P. Connett and K. Wetterhahn, *J. Am. Chem. Soc.* 1985, **107**, 4282.
7. K. Goswami, G. Chandra and S. Srivastava, *J. Ind. Chem. Soc.* 1981, **LVIII**, 252.
8. M. Olatunji and G. Ayoko, *Polyhedron* 1988, **7**, 11.
9. G. Wheeler and A. Ingersol, *J. Am. Chem. Soc.* 1951, **73**, 4604.
10. J. Greenstein and M. Winitz, *Chemistry of the Amino Acids*, Vol. 3, p. 2145. R. Krieger Publishing, Malbar (1961).
11. *Handbook of Chemistry and Physics* (Edited by R. C. Weast), 68th edn. CRC Press, Florida (1987).
12. C. McAuliffe, J. Quagliano and L. Vallarino, *Inorg. Chem.* 1966, **5**, 1996.
13. A. Calafat, J. Fiol, A. Terron, V. Moreno, D. Goodgame and I. Hussain, *Inorg. Chim. Acta* 1990, **169**, 133.
14. F. Snell and C. Snell, *Colorimetric Methods of Analysis*, Vol. IIIB, pp. 353–357. Van Nostrand, New York (1961).

15. M. Cieslak-Golonka, *Coord. Chem. Rev.* 1991, **109**, 223.
16. J. Muzart, *Chem. Rev.* 1992, **92**, 113.
17. A. McAuley and M. Olatunji, *Can. J. Chem.* 1977, **55**, 3335.
18. J. McCann and A. McAuley, *J. Chem. Soc., Dalton Trans.* 1975, 784.
19. K. Hiller, B. Masloch, M. Göbl and K. Asmus, *J. Am. Chem. Soc.* 1981, **103**, 2734.
20. D. Kwong and D. Pennington, *Inorg. Chem.* 1984, **23**, 2528.
21. M. Samitz and S. Katz, *J. Invest. Dermatol.* 1964, **43**, 35.

Polyhedron Vol. 12, No. 18, pp. 2235–2239, 1993
Printed in Great Britain

0277–5387/93 $6.00+.00
© 1993 Pergamon Press Ltd

TRANS-2-STYRYLBENZOTHIAZOLE COMPLEXES WITH MERCURY(II) HALIDES. SYNTHESIS, CHARACTERIZATION AND X-RAY CRYSTAL STRUCTURE OF DIIODOBIS(*TRANS*-2-STYRYLBENZOTHIAZOLE)MERCURY(II)

LUIGI PIETRO BATTAGLIA

Istituto di Chimica Generale ed Inorganica, Centro di Studio per la Strutturistica Diffrattometrica del C.N.R., Università di Parma, Viale delle Scienze 78, 43100 Parma, Italy

and

ANNA BONAMARTINI CORRADI, MARIA RITA CRAMAROSSA and IDA MARIA VEZZOSI*

Dipartimento di Chimica, Università di Modena, Via G. Campi 183, 41100 Modena, Italy

and

JOLANDA GELSOMINI GIUSTI

Dipartimento di Chimica, Università di Firenze, Via Maragliano, 75/77, 50144 Firenze, Italy

(*Received* 6 *April* 1993; *accepted* 10 *May* 1993)

Abstract—The synthesis of *trans*-2-styrylbenzothiazole (L) and of its complexes with mercury(II) halides is reported. Complexes with the formulae $[Hg_2(L)Cl_4]$, $[Hg(L)Br_2]$, $[Hg(L)_2I_2]$ and $[Hg(L)I_2]$ were isolated and characterized by conventional chemical analysis, electronic and IR spectra and by thermal analysis. For one of these complexes, $[Hg(L)_2I_2]$, the X-ray crystal structure was also determined. The complex consists of discrete $[Hg(L)_2I_2]$ units in which mercury, located on a two-fold axis, shows a distorted tetrahedral coordination and the ligand molecules are bonded via nitrogen atoms with Hg—I = 2.61(2) Å and Hg—N = 2.36(1) Å bond distances.

A large number of benzothiazole derivatives are of considerable biological and chemical interest. Their pharmaceutical and agrochemical applications are of particular relevance and they have attained technological importance in the field of thermoplastic polymers having high thermal stability.[1] This class of compounds is also interesting from a coordinative point of view, since these molecules contain both S and N heteroatoms and a π-donor aromatic system showing a wide variety of complexes.[2–12] This paper reports the synthesis of *trans*-2-styrylbenzothiazole (L) and the results of a study on its coordinating ability with some mercury(II) halides.

EXPERIMENTAL

Physical measurements

Carbon, nitrogen, hydrogen and sulphur were determined with a Carlo–Erba 1106 elemental analyser; IR spectra were recorded in the solid state with a Bruker IFS 113v Fourier-transform spectro-

* Author to whom correspondence should be addressed.

photometer using KBr pellets (4000–400 cm^{-1}) and polythene pellets (500–50 cm^{-1}). Electronic spectra were recorded at room temperature with a Shimadzu MPS 50L spectrophotometer with solid samples on filter paper or on polythene sheets or as Nujol mulls. Differential scanning calorimetric analyses were performed on a Perkin–Elmer DSC-2C calorimeter equipped with IBM PS 2/30 automatic data acquisition and processing software using sealed aluminium pans.

Syntheses

2-*Styrylbenzothiazole.* Sodium (0.1 mol) was slowly added to absolute ethanol (25 cm^3) in a 100 cm^3 flask and refluxed for *ca* 1 h with stirring. Absolute ethanol (15 cm^3) was then added to complete the reaction; benzaldehyde (10.6 cm^3, 0.1 mol) and 2-methyl-benzothiazole (12.7 cm^3, 0.1 mol) were then added dropwise. The stirred mixture became yellow and upon heating a yellow–orange solid precipitated. The solution was then left at room temperature for 14 h and the solid 2-styryl-benzothiazole was collected by vacuum filtration. The solid was suspended in water (10 cm^3) and acetic acid was added to pH 6.5, the pale yellow solid was filtered again and dried at 50°C for 4 h *in vacuo*. The product was twice recrystallized from ethanol/water (1.5/1), filtered by vacuum and dried at 50°C *in vacuo* (yield 6.21 g, 27%); m.p. 111–112°C. Found: C, 75.9; H, 4.7; N, 5.9. Calc. for $C_{15}H_{11}NS$: C, 75.9; H, 4.7; N, 5.9%.

$[Hg_2(L)Cl_4]$. The complex, as a microcrystalline ivory product, was obtained by mixing warm chloroform solutions of mercury(II) chloride and of the ligand with molar ratios ranging from 2/1 to 1/2; m.p. 204°C; λ_{max} = 390 nm. Found: C, 23.2; H, 1.4; N, 1.9; S, 4.0. Calc. for $C_{15}H_{11}NSCl_4Hg_2$: C, 23.1; H, 1.4; N, 1.8; S, 4.1%.

$[Hg(L)Br_2]$. The compound, as a microcrystalline pale yellow powder, was precipitated by adding with stirring a small amount of n-hexane to a warm ethylbenzene solution of mercury(II) bromide and of the ligand in molar ratios as above; m.p. 183°C; λ_{max} = 395 nm. Found: C, 29.9; H, 1.8; N, 2.4; S, 5.1. Calc. for $C_{15}H_{11}NSBr_2Hg$: C, 30.1; H, 1.8; N, 2.3; S, 5.4%.

$[Hg(L)_2I_2]$. The complex was obtained by slow addition with stirring of warm ethanolic solutions of mercury(II) iodide and the ligand with metal/ligand ratios ranging from 1/2 to 1/3. After some days yellow prisms separated; m.p. 130°C; λ_{max} = 400 nm. Found: C, 38.6; H, 2.4; N, 3.0; S, 6.8. Calc. for $C_{30}H_{22}N_2S_2I_2Hg$: C, 38.8; H, 2.4; N, 3.0; S, 6.9%.

$[Hg(L)I_2]$. The synthesis was performed as above with a 1/1 molar ratio; yellow powder; m.p. 150°C; λ_{max} = 410 nm. Found: C, 25.9; H, 1.6; N, 2.1; S, 4.6. Calc. for $C_{15}H_{11}NSI_2Hg$: C, 26.0; H, 1.6; N, 2.0; S, 4.6%.

Crystal data, solution of the structure and refinement

The crystal of the $[Hg(L)_2I_2]$ compound was mounted in a random orientation on the diffractometer: the resulting crystal data with the details of the intensity data collection and refinements are quoted in Table 1. Intensity data were corrected for Lorentz and polarization effects and an empirical correction for absorption was applied.[13] The structure was solved by Patterson and Fourier methods and refined by full-matrix least-squares with iso-

Table 1. Experimental data for the crystallographic analysis

Formula	$C_{30}H_{22}HgI_2N_2S_2$
M	929.04
Space group	$C\,2/c$
a (Å)	14.443(7)
b (Å)	13.263(6)
c (Å)	15.340(7)
β°	110.10(7)
U (Å^3)	2759(2)
Z	4
D_c	2.236
D_m	2.30
Reflections for number	16
Lattice parameters, θ range	10.5–16.4
$F(000)$	1736
Temperature (K)	294
Diffractometer	Philips PW 1100
Crystal size (mm)	$0.46 \times 0.49 \times 0.82$
Radiation, λ (Å)	Mo-K_α, 0.7107
μ (cm^{-1})	79.6
Scan speed (° min^{-1})	4.2
Scan width (°)	1.8
θ range (°)	3.0–22.0
h range	±14
k range	0, 13
l range	0, 16
Standard reflection	2 0 6
Max. intensity variation (%)	3.3
Scan mode	ω–2θ
No. of measured reflections	1842
No. of reflections used in the refinement	1359
No. of refined parameters	88
Absorption correction (min.–max.)	1.00–1.10
$R = \Sigma\|\Delta F\|/\Sigma\|F_0\|$	0.0506
$R' = [\Sigma w(\Delta F^2)/\Sigma w F_0^2]^{1/2}$	0.0564
k, g in $w = k/[\sigma^2(F_0)+gF_0^2]$	1.8, 1.2×10^{-3}
Max., min. height in final ΔF map (e Å^{-3})	1.00, −0.64

tropic and anisotropic (for Hg, I and S atoms) thermal parameters. Hydrogen atoms were not located but were introduced at the calculated positions only in the final geometrical calculations. Final atomic coordinates and thermal parameters are quoted in the supplementary material; the atomic scattering factors with the anomalous scattering coefficients were taken from International Tables.[14] The calculations were performed on the Gould 32/77 computer of the Centro di Studio per la Strutturistica Diffrattometrica del C.N.R. (Parma) using the SHELX76,[15] ORTEP[16] and PARST[17] programs.

RESULTS AND DISCUSSION

DSC measurements show that all the complexes are very stable up to melting points, following immediately the decomposition, and, therefore, their melting enthalpies are not experimentally accessible. The electronic spectra of the solid complexes show a distinct broad band in the range 390–416 nm, which may be assigned to the CT transition (ligand to metal). The IR spectra of benzothiazoles in the range 1650–1470 cm^{-1} can only be associated with the overall ring-skeleton vibrations, no other specific assignments are possible.[18–20] The identification of the bands in the complexes reported here are made more difficult by the presence of the olefinic double bond of the styryl unit and the possible shifts due to the ligand coordination, therefore, no clear evidence of this fact can be obtained. In the 1320–850 cm^{-1} range, into which fall the CH in-plane deformation and ring-breathing,[19] the spectra of the free ligand and its complexes do not show marked differences. The strong band at 755 cm^{-1} attributable to the CH out-of-plane deformation and the ν(C—S) stretching frequency at 682 cm^{-1} for the free ligand are unchanged in all the complexes, indicating that the metal is not coordinated through the sulphur atom. The far-IR spectrum (500–50 cm^{-1}) of the free ligand exhibits bands at 480, 434, 361, 264, 210, 177 and 100 cm^{-1}: in all the complexes the bands at 480, 430 and 210 cm^{-1}, assignable to the "ring out-of-plane" frequencies, are unchanged. In the chloride and bromide compounds the bands at 339 and 229 cm^{-1}, respectively, are attributable to the mercury–halogen terminal stretching and the band at 361 cm^{-1} of the ligand shifts to 370 cm^{-1}, but no correlation with the structure may be made. $[Hg_2(L)Cl_4]$ shows a band at 353 cm^{-1} which, in agreement with the literature,[21] could suggest the presence of a linear $HgCl_2$ unit and of two non-equivalent $HgCl_2$ molecules. A very strong band at 162 cm^{-1} for the two HgI_2 compounds falls in the region typically associated with the terminal Hg—I vibrations in tetrahedral complexes. All compounds show a band at 270–272 cm^{-1} of medium intensity and absent in the free ligand, tentatively assigned to a ν(Hg—N) mode.

The structure of the complex molecule $[Hg(L)_2I_2]$ is shown in Fig. 1: the mercury atom, located on a two-fold axis is bonded with two iodines and two nitrogen atoms of the ligands. The resulting geometry is very distorted tetrahedral with the angles at the metal N—Hg—N′ 89.9(4)°, I—Hg—I′ 127.4(1)° (′ = $-x,y,1/2-z$) and I—Hg—N 104.5(3)° (Table 2); these values appear to be influenced mainly by the steric hindrance of the bulky iodine atoms. The values found in some tetrahedral N,I-containing mercury compounds are: I—Hg—I 142.7(1), 128.9(1), 122.5(1)° and N—Hg—N 93.7(5), 72.9(5), 102.3(5)°, respectively, in diiodobis(pyridine)mercury(II),[22] (N,N,N′,N′-tetra-

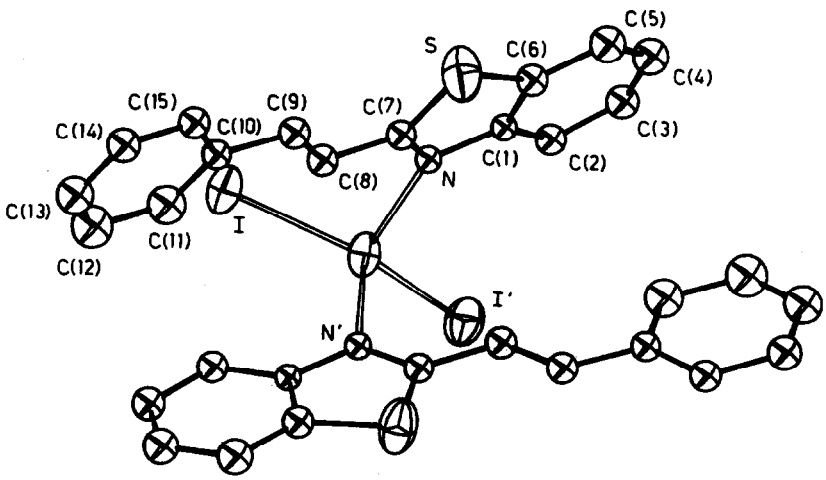

Fig. 1. Perspective view of the complex.

Table 2. (a) Bond distances (Å) and angles (°) with ESDs in parentheses

Hg—I	2.61(2)	C(5)—C(6)	1.39(2)
Hg—N	2.36(1)	C(7)—C(8)	1.46(2)
S—C(6)	1.71(2)	C(8)—C(9)	1.28(2)
S—C(7)	1.67(2)	C(9)—C(10)	1.45(2)
N—C(1)	1.38(2)	C(10)—C(11)	1.37(3)
N—C(7)	1.30(2)	C(10)—C(15)	1.36(2)
C(1)—C(2)	1.36(2)	C(11)—C(12)	1.42(3)
C(1)—C(6)	1.34(2)	C(12)—C(13)	1.36(3)
C(2)—C(3)	1.35(2)	C(13)—C(14)	1.34(3)
C(3)—C(4)	1.39(3)	C(14)—C(15)	1.37(2)
C(4)—C(5)	1.34(2)		

I—Hg—N	104.5(3)	S—C(6)—C(5)	127(1)
I—Hg—I^i	127.4(1)	S—C(6)—C(1)	110(1)
I—Hg—N^i	112.1(3)	S—C(7)—N	116(1)
N—Hg—N^i	89.9(4)	N—C(7)—C(8)	121(1)
C(6)—S—C(7)	89.5(8)	S—C(7)—C(8)	123(1)
Hg—N—C(7)	125(1)	C(7)—C(8)—C(9)	121(2)
Hg—N—C(1)	125(1)	C(8)—C(9)—C(10)	124(2)
C(1)—N—C(7)	109(2)	C(9)—C(10)—C(15)	119(1)
N—C(1)—C(6)	115(1)	C(9)—C(10)—C(11)	120(2)
N—C(1)—C(2)	126(1)	C(11)—C(10)—C(15)	122(2)
C(2)—C(1)—C(6)	119(1)	C(10)—C(11)—C(12)	118(2)
C(1)—C(2)—C(3)	121(2)	C(11)—C(12)—C(13)	118(2)
C(2)—C(3)—C(4)	118(2)	C(12)—C(13)—C(14)	124(2)
C(3)—C(4)—C(5)	124(2)	C(13)—C(14)—C(15)	118(2)
C(4)—C(5)—C(6)	114(2)	C(10)—C(15)—C(14)	120(2)
C(1)—C(6)—C(5)	124(2)		

(b) Relevant contacts (Å)

C(2)···C(11^i)	3.52(2)	C(8)···C(9^{ii})	3.63(2)
C(1)···C(15^{ii})	3.54(2)	C(14)···C(10^{iii})	3.38(2)
C(2)···C(14^{ii})	3.56(2)	C(14)···C(15^{iii})	3.48(2)
C(7)···C(9^{ii})	3.56(2)	N···C(15^{ii})	3.55(2)
C(7)···C(10^{ii})	3.61(2)	C(15)···C(15^{iii})	3.54(2)

Symmetry equivalents
$i = -x, y, 1/2-z$
$ii = -x, -y, -z$
$iii = -x-1/2, 1/2-y, -z$

methyl - *o* - phenylenediamine - N,N′)diiodomercury(II)[23] and diiodo(2,3 : 12,13-dibenzo-1,14,17 - trioxa - 5,10 - diaza - 2,3 : 4,5 : 10,11 : 12,13 - cycloenneadecatetraene)mercury(II).[24] The two Hg—I bond distances, 2.61(2) Å, compare favourably with those found in a relevant number of compounds: an inspection carried out using the Cambridge Structural Database (CSD) system[25] considering only the compounds with Hg—I bonds falling in the range 2.50–270 Å gave the result of 37 crystal structures, in which some of the closely related values are 2.603(4) and 2.611(4) Å in (μ_2-tetramethylthiotetrathia - fulvalene - S,S′,S″,S‴)bis [diiodomercury(II)];[26] 2.623(5) Å in 1,4,7,10,13, 16 - hexaoxa - cyclooctadecanediiodomercury (II);[27] and 2.594(4) and 2.605(4) Å in 1-acetyl-1-methyl-2-[1-(2)-iodomercury-2,2-dimethyl-2-silapropylidene]cyclopentene.[28] Also for the Hg—N bonds 2.36(1) Å similar distances are found in 27 crystal structures of CSD (range 2.33–2.39 Å); some of the close related examples are 2.376(6) and 2.379(6) Å in chloro(1,4,8,11-tetraazacyclotetradecane) mercury (II) tetrachloromercury (II)[29] and 2.369(5) Å in bis(μ_2-5-nitro-1,2,3,4-tetrathiazole-N^1,N^3,N^6,N^9-)mercury.[30] Bond distances and angles in the organic molecule show no abnormal features, in particular those related to the five-membered ring are in good agreement with the mean values calculated using 145 observations obtained from CSD: C=S = 1.745(3), 1.743(3) Å;

C—N = 1.328(4) Å, N—C = 1.396(3) Å and C—S—C = 89.7(2)°. The 2-styrylbenzothiazole molecule is only roughly planar [maximum deviation from the least-squares plane 0.08(1) Å; mercury is out of this plane, 0.214(2) Å]; the dihedral angle formed by the phenyl ring and the benzothiazole moiety is only 2.3(4) Å. Styrylbenzothiazoles show different behaviour because of the free rotation of the aromatic ring. Compounds in which the ligand is nearer to the planarity, as in the present structure, include tetraethylammonium tribromo[2 - (2′ - chloro - 4′ - nitrosil) - 6 - methoxybenzothiazole]platinate(II) with a dihedral angle between the aromatic ring and benzothiazole of 6(4)° and 6.7(2)° in 2-(2′-chlorostyryl) benzothiazole;[31] the reasons for these differences could be due to packing forces.

Acknowledgements—Thanks are due to the Ministero dell'Università e della Ricerca Scientifica e Tecnologica (MURST) of Italy for financial support (60%).

REFERENCES

1. J. V. Metzger, *Comprehensive Heterocyclic Chemistry* (Edited by K. T. Potts), Vol. VI. Pergamon Press, Oxford (1984).
2. E. J. Duff, M. N. Hughes and K. J. Rutt, *J. Chem. Soc.* (*A*) 1968, 2354.
3. E. J. Duff, M. N. Hughes and K. J. Rutt, *J. Chem. Soc.* (*A*) 1969, 2101.
4. L. F. Lindoy and S. E. Livingstone, *Inorg. Chim. Acta* 1968, **2**, 119.
5. P. S. K. Chia and S. E. Livingstone, *Inorg. Chim. Acta* 1968, **2**, 427.
6. P. S. K. Chia, L. F. Lindoy and S. E. Livingstone, *Inorg. Chim. Acta* 1968, **2**, 459.
7. M. J. M. Campbell, D. W. Card and R. Grzeskowiak, *J. Chem. Soc.* (*A*) 1970, 672.
8. S. Jeannin, Y. Jeannin and G. Lavigne, *Inorg. Chem.* 1979, **18**, 3528.
9. R. Abdel-Amid, A. A. El-Samahy, A. H. El-Taher and H. El-Sagher, *Can. J. Chem.* 1987, **65**, 468.
10. R. Abdel-Amid, A. A. El-Samahy, M. A. Abdel-Rahman and H. El-Sagher, *Spectrochim. Acta* 1987, **43A**, 497.
11. R. M. Ramadan, A. M. El-Atrash and A. M. A. Ibrahim, *Spectrochim. Acta* 1990, **46A**, 1305.
12. N. S. Neelam Jalil, *Synth. React. Inorg. Met.-Org. Chem.* 1990, **20**, 1285.
13. A. C. T. North, D. C. Phillips and F. Scott Mathews, *Acta Cryst.* 1968, **A24**, 351.
14. *International Tables for X-ray Crystallography*, Vol. IV, pp. 99 and 150. Kynoch Press, Birmingham (1974).
15. G. M. Sheldrick, SHELX76, a Program for Crystal Structure Determination. University of Cambridge, U.K. (1976).
16. C. K. Johnson, ORTEP, Report ORNL-3794. Oak Ridge National Laboratory, Tennessee (1965).
17. M. Nardelli, *Comput. Chem.* 1983, **7**, 95.
18. C. N. R. Rao, *Applications of Infrared Spectroscopy*. Academic Press, New York (1963).
19. C. N. R. Rao and R. Venkataraghavan, *Can. J. Chem.* 1964, **42**, 43.
20. L. J. Bellamy, *The Infrared Spectra of Complex Molecules*. Chapman and Hall, London (1975).
21. P. A. W. Dean, *Prog. Inorg. Chem.* 1978, **24**, 109.
22. I. Persson, M. Sandstrom, P. L. Goggin and A. Mosset, *J. Chem. Soc., Dalton Trans.* 1985, 1597.
23. C. M. Hughes, M. C. Favas, B. W. Skelton and A. H. White, *Aust. J. Chem.* 1985, **38**, 1521.
24. L. P. Battaglia, A. Bonamartini Corradi and A. Mangia, *Inorg. Chim. Acta* 1980, **42**, 191.
25. F. H. Allen, S. Bellard, M. D. Brice, B. A. Cartwright, A. Doubleday, H. Higgs, T. Hummelink-Peters, O. Kennard, W. D. S. Motherwell, J. N. Rogers and D. G. Watson, *Acta Cryst.* 1979, **B35**, 2331.
26. H. Endres, *Z. Naturforsch.* 1986, TEIL B, **41**, 1351.
27. D. A. Pears, J. F. Stoddart, J. Crosby, B. L. Allwood and D. J. Williams, *Acta Cryst.* 1986, **C42**, 51.
28. A. Bonaventura, J. Drouin, F. Theobald and N. Rodier, *Bull. Soc. Chim. Fr.* 1987, 1006.
29. N. W. Alcock, E. H. Curson, N. Herron and P. Moore, *J. Chem. Soc., Dalton Trans.* 1979, 1987.
30. J. Xianglin, S. Meicheng, H. Haochua, W. Jinming and Z. Yu, *Hua Hsueh Tung Pao* (*Chem. Bull.*) 1982, 336.
31. M. M. Muir, G. M. Gomez, M. E. Cadiz and J. A. Muir, *Inorg. Chim. Acta* 1990, **168**, 47.

Polyhedron Vol. 12, No. 18, pp. 2241–2247, 1993
Printed in Great Britain

0277–5387/93 $6.00+.00
© 1993 Pergamon Press Ltd

ELECTROCHEMICAL SYNTHESIS OF BENZOTHIAZOLE-2-THIONATO COMPLEXES OF NICKEL(II), ZINC(II) AND CADMIUM(II): THE CRYSTAL STRUCTURE OF 2,2′-BIPYRIDINE BIS(BENZOTHIAZOLE-2-THIONATO)ZINC(II)

ROSA CASTRO, JOSE A. GARCIA-VAZQUEZ, JAIME ROMERO and ANTONIO SOUSA*

Departamento de Química Inorgánica, Universidad de Santiago, 15706 Santiago de Compostela, Spain

and

CHARLES A. McAULIFFE and ROBIN PRITCHARD

Department of Chemistry, University of Manchester, Institute of Science and Technology, PO Box 88, Manchester M60 1QD, U.K.

(*Received* 5 *April* 1993; *accepted* 10 *May* 1993)

Abstract—The electrochemical oxidation of anodic metal (nickel, zinc or cadmium) in acetonitrile solutions of benzothiazole-2-thione (Hbztz) gave the compounds $[M(bztz)_2]$ [M = nickel(II), zinc(II) and cadmium(II)]. When the oxidations were repeated in the presence of neutral ligands L′ (2,2′-bipyridine or 1,10-phenanthroline) the complexes $[M(bztz)_2L']$ were obtained. The crystal structure of 2,2′-bipyridine bis(benzothiazole-2-thionato)zinc(II) was determined by X-ray diffraction. This compound consists of monomeric molecules in which the central ZnS_2N_2 unit has a slightly distorted tetrahedral environment. The electronic, IR and ^1H and ^{13}C NMR spectra of the complexes are discussed and related to their structure.

Electrochemical procedures have been widely used for the synthesis of metallic complexes, especially those with weakly acid organic ligands, in which the acidic group is usually a hydroxyl,[1,2] pyrrole NH[3,4] or thiol group.[5,6] Of particular relevance to the present work are metal thiolates obtained starting from thiols or disulphides.[2,7] Metallic complexes of these ligands are of interest in a wide range of fields, which in the case of nickel, zinc and cadmium compounds include biochemical applications.

As part of our continuing interest in thiolate complexes, in this work we prepared electrochemically a series of nickel(II), zinc(II) and cadmium(II) complexes with benzothiazole-2-thione (Hbztz), a versatile molecule that can behave either (a) as a neutral ligand through the exocyclic sulphur atom (1),[8] or (b) as an anionic ligand, in which case it can act as a monodentate through the exocyclic sulphur atom (2)[9] or through its nitrogen atom (3),[10] and (c) as a chelating ligand (4)[11] and as a two- (5)[12] or three-way (6)[13] bridging ligand through its nitrogen and exocyclic sulphur atoms. We also prepared mixed complexes containing $bztz^-$ and either 2,2′-bipyridine(bipy) or 1,10-phenanthroline (phen) and determined the crystal of 2,2′-bipyridine bis(benzothiazole-2-thionato)zinc(II).

Although $[M(bztz)_2]$ compounds have been prepared before by non-electrochemical methods, the other compounds reported in this article have not, as far as we know, been synthesized before.

* Author to whom correspondence should be addressed.

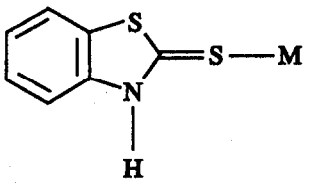

1

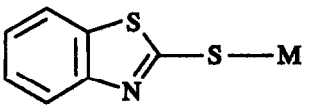

2

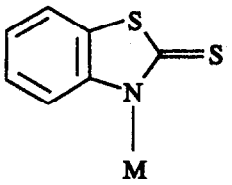

3

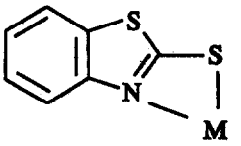

4

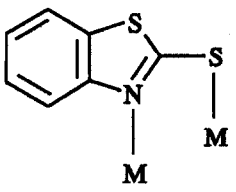

5

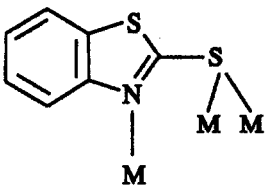

6

EXPERIMENTAL

All solvents, benzothiazole-2-thione, 2,2′-bipyridine and 1,10-phenanthroline were commercial products used without further purification. The metals (Ega Chemie) were used as plates (*ca* 2 × 2 cm).

Preparation of the complexes

The electrochemical method used in the synthesis of the compounds is similar to that described by Tuck.[14] The cell was a 100 cm^3 tall-form beaker fitted with a rubber bung through which the electrochemical leads entered into the cell. The anode, in foil form, was suspended from a platinum wire and the cathode was another platinum wire. The benzothiazole-2-thione was dissolved in acetonitrile (*ca* 50 cm^3) and a small amount of tetramethylammonium perchlorate (*ca* 10 mg) was added to the solution. For the synthesis of mixed compounds, 2,2′-bipyridine or 1,10-phenanthroline was added. Hydrogen was evolved at the cathode and the formation of an insoluble compound was generally visible in a few minutes. At the end of electrolysis, the solid product was collected, washed with acetonitrile and dried *in vacuo*.

The cells can be summarized as Pt(−)/CH_3N+Hbztz/M(+) and Pt(−)/CH_3CN+Hbztz+L′/M(+), where L′ is bipy or phen and M nickel, zinc or cadmium. Details of solution composition and electrochemical conditions are given in Table 1.

Physical measurements

Microanalyses were performed using a Carlo–Erba EA1108 microanalyser and the results are given in Table 2. IR spectra were recorded in KBr mulls on a Perkin–Elmer 180 spectrophotometer and the optical spectra on a Perkin–Elmer Lambda 9 spectrophotometer. ^1H and ^{13}C NMR spectra were recorded on a Bruker WM 250 MHz spectrometer using DMSO-d_6 as solvent; chemical shifts were determined against TMS as an internal standard. Magnetic measurements were performed using a SQUID.

Crystal structure determination

Crystal data for [Zn(bztz)$_2$bipy)]. $C_{24}H_{16}N_4S_4Zn$, $M = 554.04$, triclinic, space group $P\bar{1}$, $a = 11.27(1)$, $b = 14.14(1)$, $c = 8.64(1)$ Å, $\alpha = 105.60(8)$, $\beta = 106.37(9)$, $\gamma = 102.29(8)°$, $V = 1208(2)$ Å^3, $Z = 2$, $D_c = 1.524$ g cm^{-3}, $F(000) = 564$, λ(Mo-K_α) = 0.71069, $\mu = 13.93$ cm^{-1}.

Data collection and processing. A yellow block

Table 1. Experimental conditions for the electrochemical synthesis

Compound	Amount of bztzH (g)[a]	Amount of ligand (g)	Initial voltage (V)[b]	Time (h)	Metal dissolved (mg)	*Ef* (mol F^{-1})
$[Ni(bztz)_2]$	0.38		27	2.5	53.0	0.48
$[Ni(bztz)_2bipy \cdot H_2O$	0.38	0.18	14	3	61.2	0.47
$[Ni(bztzt)_2phen]$	0.38	0.22	25	3	59.9	0.46
$[Zn(bztzt)_2] \cdot H_2O$	0.38		27	2.5	68.0	0.47
$[Zn(bztzt)_2bipy]$	0.38	0.18	20	3	59.5	0.41
$[Zn(bztzt)_2phen]$	0.38	0.22	18	3	64.1	0.44
$[Cd(bztzt)_2]$	0.38		17	2.5	88.5	0.42
$[Cd(bztzt)_2bipy] \cdot H_2O$	0.38	0.18	15	2.3	89.9	0.46
$[Cd(bztzt)_2phen]$	0.38	0.22	16	3	119.8	0.48

[a] Plus Et_4NClO_4 (*ca* 20 mg).
[b] Voltage to produce a current of 20 mA.

crystal of approximate dimensions $0.25 \times 0.20 \times 0.20$ mm was mounted on a glass fibre. All measurements were made on a Rigaku AFC5R diffractometer with graphite monochromated Mo-K_α radiation. Cell constants and an orientation matrix for data collection (obtained from a least-squares refinement using the setting angles of 19 carefully centred reflections in the range $9.45 < 2\theta < 21.12°$) corresponded to a triclinic cell.

The data were collected at room temperature using the $\omega/2\theta$ scan technique with scan widths $(1.15+0.30 \tan \theta)°$ and a scan speed of 4.0° min^{-1} (in omega).

Of the 4488 reflections collected 4253 were unique ($R_{int} = 0.053$). An empirical absorption correction applied using the program DIFABS[15] resulted in transmission factors ranging from 0.87 to 1.00. The data were corrected for Lorentz and polarization effects.

Structure solution and refinement. The structure was solved by direct methods.[16] The non-hydrogen atoms were refined anisotropically. Hydrogen atoms were included in idealized positions. The final cycle of full-matrix least-squares refinement was based on 1672 observed reflections [$I > (2.00\sigma(I)$] and 298 variable parameters and converged to $R = \Sigma(|F_o| - |F_c|)/\Sigma|F_o| = 0.047$ and $Rw = [(\Sigma w (|F_o| - |F_c|)^2/\Sigma w|F_o|^2]^{1/2} = 0.053$. The maximum and minimum peaks on the final difference Fourier map were to 0.43 and -0.37 e $Å^{-3}$.

Neutral atom scattering factors were taken from Cromer and Waber.[17] Anomalous dispersion effects were those of Cromer.[18] All calculations were performed using the TEXSAN[19] crystallographic software package of Molecular Structure Corporation. The atomic positions full lists of bond lengths and angles and other crystallographic data have been deposited as Supplementary Publication No. CSD 57074. Copies can be obtained through the Fachinformation-zentrum Energie Physik Mathematik, D-7514 Eggenstein-Leopoldshafen.

RESULTS AND DISCUSSION

The electrochemical method successfully produced the complexes $[M(bztz)_2]$ and $[M(bztz)_2L']$ (M = Ni, Zn or Cd; L′ = bipy or phen). All these compounds are solid, insoluble in common non-

Table 2. Analytical data

Complex	Found (calc.) (%) C	N	H
$[Ni(bztzt)_2]$	42.5(42.7)	7.3(7.1)	2.4(2.6)
$[Ni(bztzt)_2bipy \cdot H_2O$	50.7(50.5)	10.5(10.7)	3.3(3.1)
$[Ni(bztzt)_2phen]$	54.4(54.7)	9.8(9.8)	2.6(2.8)
$[Zn(bztzt)_2 \cdot H_2O$	39.9(40.2)	7.0(6.7)	2.3(2.8)
$[Zn(bztzt)_2bipy]$	51.5(52.0)	9.6(9.5)	3.0(2.9)
$[Zn(bztzt)_2phen]$	53.1(53.3)	9.9(9.7)	3.1(3.1)
$[Cd(bztzt)_2]$	37.2(37.8)	6.2(6.3)	1.6(1.8)
$[Cd(bztzt)_2bipy] \cdot H_2O$	46.9(46.6)	8.9(9.0)	2.8(2.9)
$[Cd(bztzt)_2phen]$	49.1(49.9)	8.5(8.9)	2.3(2.6)

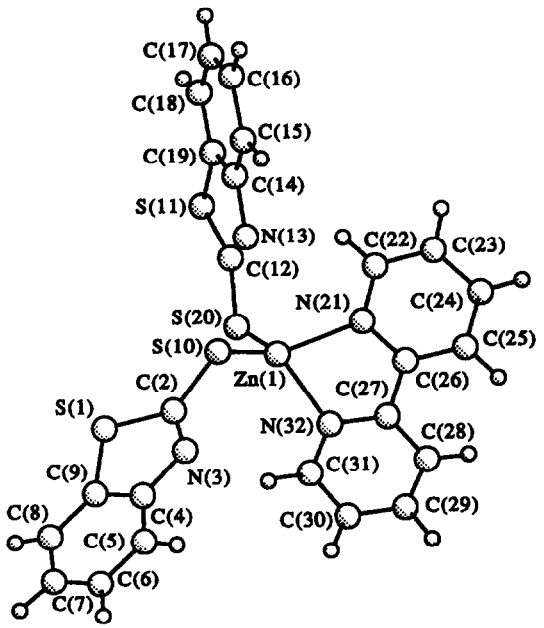

Fig. 1. The molecular structure of $[Zn(bztz)_2bipy]$.

polar organic solvents (including chloroform and acetonitrile) and soluble in more polar solvent such as DMSO.

The electrochemical efficiency, *Ef*, defined as the amount of metal dissolved per Faraday of charge, was found to be *ca* 0.5 mol F^{-1} in all cases. This and the evolution of hydrogen at the cathode suggest that the reaction mechanism can be written as:

$$\textit{Cathode}\quad 2\,Hbztz + 2e^- \rightarrow 2bztz^- + H_2(g)$$

$$\textit{Anode}\quad 2bztz^- + M \rightarrow [M(bztz)_2] + 2e^-$$

$$2bztz^- + M + L' \rightarrow [M(bztz)_2L'] + 2e^-$$

$$M = Ni, Zn \text{ or } Cd;\ L' = phen \text{ or } bipy.$$

Structure of $[Zn(bztz)_2(bipy)]$

$[Zn(bztz)_2(bipy)]$ crystals consist of monomeric units in which a tetra-coordinate zinc atom is bound to the exocyclic sulphur atoms of two monodentate thiolate ligands and to the two nitrogen atoms of a bidentate chelating bipyridine molecule (Fig. 1). The tetrahedral environment of the zinc atom is distorted due to the small bite of the bipyridine [N(21)—Zn—N(32) = 78.9°; see Table 3], which also results in secondary deviation of the other perinuclear angles from the ideal value of 109°.

The $Zn—N_{bipy}$ bond lengths, 2.100(8) and 2.088(7) Å, are very similar to those found in another complex containing tetrahedral zinc and bipyridine, $[Zn(S\text{-}2,4,6\text{-}Pri_3C_6H_2)_2bipy]$.[20] The Zn—S distances, 2.294(5) and 2.321(4) Å, are within the range found in other thiolates with distorted

Table 3. Selected bond distances (Å) and angles (°) for $[Zn(bztzt)_2bipy]$

Zn(1)—S(10)	2.294(5)	C(14)—C(15)	1.38(1)
Zn(1)—S(20)	2.321(4)	C(14)—C(19)	1.41(1)
Zn(1)—N(21)	2.1000(8)	C(15)—C(16)	1.38(1)
Zn(1)—N(32)	2.088(7)	C(16)—C(17)	1.38(2)
S(1)—C(2)	1.76(1)	C(17)—C(18)	1.36(1)
S(1)—C(9)	1.74(1)	C(18)—C(19)	1.40(1)
C(2)—N(3)	1.31(1)	N(21)—C(22)	1.32(1)
C(2)—S(10)	1.69(1)	N(21)—C(26)	1.36(1)
N(3)—C(4)	1.36(1)	C(22)—C(23)	1.36(1)
C(4)—C(5)	1.38(1)	C(23)—C(24)	1.38(1)
C(4)—C(9)	1.39(1)	C(24)—C(25)	1.35(1)
C(5)—C(6)	1.39(2)	C(25)—C(26)	1.39(1)
C(6)—C(7)	1.35(2)	C(26)—C(27)	1.46(1)
C(7)—C(8)	1.34(2)	C(27)—C(28)	1.40(1)
C(8)—C(9)	1.35(2)	C(27)—N(32)	1.34(1)
S(11)—C(12)	1.762(9)	C(28)—C(29)	1.38(1)
S(11)—C(19)	1.73(1)	C(29)—C(30)	1.37(1)
C(12)—N(13)	1.29(1)	C(30)—C(31)	1.38(1)
C(12)—S(20)	1.71(1)	C(31)—N(32)	1.33(1)
N(13)—C(14)	1.39(1)		
S(10)—Zn—S(20)	119.3(1)	Zn—S(10)—C(2)	96.5(4)
S(10)—Zn—N(21)	108.9(2)	S(11)—C(12)—S(20)	121.6(6)
S(10)—Zn—N(32)	121.0(2)	N(13)—C(12)—S(20)	124.8(7)
S(20)—Zn—N(21)	117.7(2)	Zn—S(20)—C(12)	90.6(3)
S(20)—Zn—N(32)	104.8(2)	Zn—N(21)—C(22)	127.2(7)
N(21)—Zn—N(32)	78.9(3)	Zn—N(21)—C(26)	118.7(8)
S(1)—C(2)—S(10)	119.7(6)	Zn—N(32)—C(27)	114.7(7)
N(3)—C(2)—S(10)	127.9(8)	Zn—N(32)—C(31)	119.4(8)

tetrahedral geometry, 2.25–2.36 Å.[21,22] Note that both the Zn—N and Zn—S distances are very similar to those found in [Zn(S-*p*-tolyl)$_2$phen],[22] which in a recent EXAFS study[23] has been used as a model of the zinc centre of Transcription factor IIIA (TFIIIA); this raises the possibility that [Zn(bztz)$_2$(bipy)] might likewise be considered as a model of this protein.

The bipyridine ligand is essentially planar, with no atom deviating from the least-squares plane by more than 0.011 Å. The bond lengths and angles within the ligand are similar to those found in other bipyridine complexes.[4,5,24] The benzothiazole portion of the benzothiazole-2-thionate ligands is also planar, with the largest deviations from the least-square planes being 0.016 Å and the deviations of the exocyclic sulphur atoms from this plane being 0.15 Å for S(10) and just 0.005 Å for S(20). The zinc atom is also practically on the plane of the benzothiazole group to which S(20) it is bound, the deviation being only 0.037 Å, but lies 0.303 Å above the plane of the other benzothiazole portion.

The N—C distances of benzothiazole-2-thionate are shorter in the complex than in the free ligand.[25] The C—S_{exo} distances, on the contrary, are longer in the complex, 1.70(1) Å as against the 1.662 Å that in the free ligand has been considered as indicating a degree of double bond character. The two bztz$^-$ ligands, therefore, appear to have a greater degree of thiolate character in the complex than in the free ligand.

Vibrational spectra

The IR spectra of the complexes (Table 4) lack the bands at *ca* 3100 and 750 cm^{-1}, which in the spectrum of Hbztz are attributed to ν(NH) and δ(NH), respectively.[26] Of the bands appearing at 1032, 1011, 605, 527, 393 and 300 cm^{-1} in the spectrum of the free ligand, i.e. those which on the basis of an S_{exo}-selenation study[26] (substitution of thioketonic sulphur with selenium) have been attributed the greatest ν(C=S) character, only those at 1032 and 1011 cm^{-1} show, in the spectra of the complexes, the shift to smaller wave numbers expected to result from reduction of the C—S bond order. The shift is greater for the 1032 cm^{-1} band, probably due to its having a greater ν(C=S) contribution.

In addition, the spectra show bands due to ν(M—S)[27] in the 380–320 cm^{-1} region. All the mixed complexes exhibit IR bands typical of coordinated bipy and phen.[28,29]

NMR spectra

The ^{1}H NMR spectra of the complexes (Table 5) show signals for all the bztz$^-$ hydrogen atoms except the NH proton, which in the spectrum of the free ligand appears as a broad signal at *ca* 13.4 ppm. This confirms the deprotonation of the ligand during electrosynthesis of the complex. In the spectra of some of the complexes the signals for several different protons appear jointly as a multiplet (as do the signals for H_5, H_6 and H_7 in the spectrum of the free ligand), whereas in those of other complexes the same signals are well differentiated and have the expected multiplicities.

The mixed complexes containing bipy have the expected four bipy signals, all of them shifted downfield, as a result of coordination, with respect to their position in the spectrum of the free ligand. This finding is in keeping with the X-ray diffraction results for [Zn(bztz)$_2$(bipy)]. Similarly, the mixed complexes containing phen show the expected signals, of which those for $H_{2,9}$ and $H_{3,8}$ are shifted downfield as a result of deshielding due to coordination to the metal.[30]

The ^{13}C NMR spectra (Table 6) also show all of the expected signals. The bztz$^-$ C_2 signal is shifted upfield in the spectra of all the complexes as a result of reduced C—S bond order,[31] which is further

Table 4. Select IR spectroscopic data for compounds (cm^{-1})

Compounds	ν(C=N)	ν(C=S)	ν(M—S)
Ni(bztzt)$_2$]	1580	1025, 1010	320
[Ni(bztzt)$_2$bipy]·H$_2$O	1600	1030, 1010	
[Ni(bztzt)$_2$phen]	1600	1028, 1009	
[Zn(bztzt)$_2$]·H$_2$O	1580	1025, 1012	325
[Zn(bztzt)$_2$bipy]	1600	1020, 1015	
[Zn(bztzt)$_2$phen]	1600	1015	
[Cd(bztzt)$_2$]	1585	1025, 1010	380
[Cd(bztzt)$_2$bipy]·H$_2$O	1600	1025, 1010	385
[Cd(bztzt)$_2$phen]	1590	1020, 1008	380

Table 5. ^{1}H NMR data for complexes (ppm)[a]

Compound	bztzt$^-$	phen (bipy) $H_{2,9(6,6')}$	$H_{4,7(3,3')}$	$H_{5,6(4,4')}$	$H_{3,8(5,5')}$
Hbztzt	7.69d(1)(H_4); 7.34m(3)($H_{5,6,7}$)				
[Zn(bztzt)$_2$]	7.61d(2)($H_{4,7}$); 7.22t(1), 7.12t(1)($H_{5,6}$)				
[Zn(bztzt)$_2$bipy]	7.59d(1)(H_4); 7.45d(1)(H_7); 7.20td(1), 7.09td(1)($H_{5,6}$)	8.78br	8.62br	8.19br	7.67br
[Zn(bztzt)$_2$phen]	7.54d(1)(H_4); 7.30br(1)(H_7); 7.14t(1), 7.04t(1)($H_{5,6}$)	9.25br	8.91d	8.28s	8.10br
[Cd(bztzt)$_2$]	7.67d(1)(H_4); 7.41dd(1)(H_7); 7.23td(1), 7.12td(1)($H_{5,6}$)				
[Cd(bztzt)$_2$bipy]	7.63m(1)(H_4); 7.12m(3)($H_{5,6,7}$)	8.87d	8.52d	8.10td	7.63m
[Cd(bztzt)$_2$phen]	7.55m(1)(H_4); 7.29m(2), 6.83br(1)($H_{5,6,7}$)	9.27d	8.79dd	8.18s	8.05m

[a] Integrated relative intensities in parentheses.

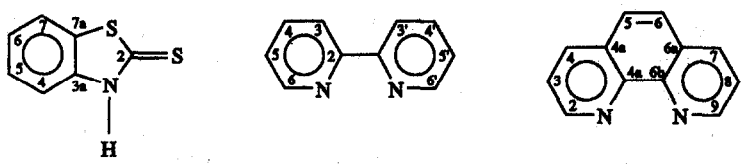

evidence that bztz$^-$ is closer to its thiolate form in the complexes than in Hbztz.

Magnetic moments and electronic spectra

The magnetic moment of the [Ni(bztz)$_2$] complex shows that this compound is essentially diamagnetic and is consistent with square-planar coordination around the nickel(II) centre. This interpretation is compatible with the solid-state electronic spectrum of this compound, which shows two bands at *ca* 16,950 and 21,700 cm^{-1} which can be attributed to $^1B_{1g} \rightarrow {}^1A_{1g}$ and $^1E_{1g} \rightarrow {}^1A_{1g}$ transitions, respectively, in a square-planar field.[32]

The effective room-temperature magnetic moments, μ_{eff}, of [Ni(bztz)$_2$bipy] and [Ni(bztz)$_2$phen], 3.4 and 2.9, respectively, lie in the range expected for octahedral nickel(II) complexes.[33] The diffuse reflectance spectra of these complexes show two *d–d* bands at *ca* 8800 and 16,500 cm^{-1} with a clearly discernible shoulder at *ca* 8000 cm^{-1}. These bands can be respectively attributed to the $^3A_{2g} \rightarrow {}^3T_{2g}$ and $^3A_{2g} \rightarrow {}^3T_{1g}$(F) transitions in an octahedral field.[32] The shoulder may be due to the low energy

Table 6. ^{13}C NMR data for complexes (ppm)

Compound	bztzt$^-$ C_2	C_{3a}	C_{7a}	C_5	C_6	C_4	C_7	phen (bipy) $C_{2(2)}$	$C_{4b(6)}$	$C_{4(4)}$	$C_{4a(5)}$	$C_{5(3)}$	C_3
Hbztzt	189.9	141.3	129.4	127.1	124.2	121.7	112.4						
[Zn(bztzt)$_2$]		151.6	135.4	125.5	122.6	120.5	117.4						
[Zn(bztzt)$_2$bipy]	184.2	151.8	135.8	125.5	122.4	120.5	117.0	153.8	148.8	140.1	126.2	121.9	
[Zn(bztzt)$_2$phen]	184.2	152.2	135.9	125.3	122.2	120.4	116.9	149.3	140.2		128.8	127.2	125.3
[Cd(bztzt)$_2$]	181.6	151.8	137.6	125.7	122.6	120.9	117.6						
[Cd(bztzt)$_2$bipy]	180.4	152.2	137.4	125.6	122.5	120.7	117.5	151.2	149.4	139.4	125.5	121.8	
[Cd(bztzt)$_2$phen]	179.6	152.5	137.2	125.1	122.3	120.5	117.4	149.9	140.4	139.3	128.8	127.0	125.1

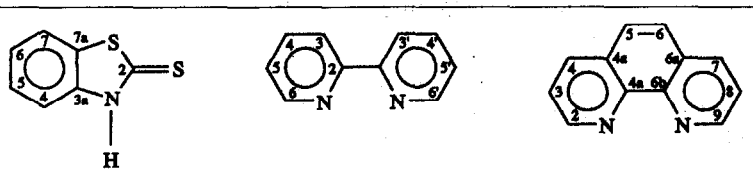

band splitting as a consequence of the distorted octahedral nature of the complexes.

Acknowledgements—We thank the Xunta de Galicia (XUGA20306B91), Spain, for financial support.

REFERENCES

1. A. Castiñeiras, J. A. Castro, M. L. Durán, J. A. García-Vázquez, A. Macías, J. Romero and A. Sousa, *Polyhedron* 1989, **8**, 2543; J. A. Castro, J. Romero, J. A. García-Vázquez, A. Castiñeiras and A. Sousa, *Z. Anorg. Allg. Chem.* 1993, **619**, 601.
2. E. Labisbal, A. de Blas, J. A. García-Vázquez, J. Romero, M. L. Durán, A. Sousa, N. A. Bailey, D. E. Fenton, P. B. Leeson and R. V. Parish, *Polyhedron* 1992, **11**, 227; E. Labisbal, J. A. García-Vázquez, C. Gomez, A. Macias, J. Romero, A. Sousa, U. Englert and D. E. Fenton, *Inorg. Chim. Acta* 1993, **203**, 67.
3. J. A. Castro, J. Romero, J. A. García-Vázquez, M. L. Durán, A. Sousa, E. E. Castellano and J. Zukerman-Schpector, *Polyhedron* 1992, **11**, 235; J. A. Castro, J. Romero, J. A. García-Vázquez, A. Sousa, E. E. Castellano and J. Zukerman-Schpector, *Polyhedron* 1993, **12**, 31.
4. J. A. Castro, J. E. Vilasánchez, J. Romero, J. A. García-Vázquez, M. L. Durán and A. Sousa, *Z. Anorg. Allg. Chem.* 1992, **612**, 83.
5. R. Castro, M. L. Durán, J. A. García-Vázquez, J. Romero, A. Sousa, A. Castiñeiras, W. Hiller and J. Strähle, *J. Chem. Soc., Dalton Trans.* 1990, 531.
6. R. Castro, M. L. Durán, J. A. García-Vázquez, J. Romero, A. Sousa, A. Castiñeiras, W. Hiller and J. Strähle, *Z. Naturforsch.* 1992, **47b**, 1067; R. Castro, M. L. Durán, J. A. García-Vázquez, J. Romero, A. Sousa, E. E. Castellano and J. Zukerman-Schpector, *J. Chem. Soc., Dalton Trans.* 1992, 2559.
7. J. A. Castro, J. Romero, J. A. García-Vázquez, M. L. Durán, A. Castiñeiras, A. Sousa and D. E. Fenton, *J. Chem. Soc., Dalton Trans.* 1990, 3255.
8. S. Jeannin, Y. Jeannin and G. Lavigne, *Inorg. Chem.* 1979, **18**, 3528.
9. E. W. Ainscough, E. N. Baker, A. G. Bingham, A. M. Brodie and C. A. Smith, *J. Chem. Soc., Dalton Trans.* 1989, 2167; J. Bravo, J. S. Casas, M. V. Castaño, M. Gayoso, Y. P. Mascarenhas, A. Sánchez, C. de O. P. Santos and J. Sordo, *Inorg. Chem.* 1985, **24**, 3435.
10. J. A. McCleverty, N. J. Morrison, N. Spencer, C. C. Ashworth, N. A. Bailey, M. R. Johnson, J. M. A. Smith, B. A. Tabbiner and C. R. Taylor, *J. Chem. Soc., Dalton Trans.* 1980, 1945.
11. I. G. Dance and D. Isaac, *Aust. J. Chem.* 1977, **30**, 2425; E. S. Raper, A. M. Britton and W. Clegg, *J. Chem. Soc., Dalton Trans.* 1990, 3341.
12. M. A. Ciriano, J. J. Pérez-Torrente, F. J. Lahoz and L. A. Oro, *Inorg. Chem.* 1992, **31**, 969.
13. M. A. Ciriano, J. J. Pérez-Torrente, F. Viguri, F. J. Lahoz, L. A. Oro, A. Tiripicchio and M. Tiripicchio-Camellini, *J. Chem. Soc., Dalton Trans.* 1990, 1493.
14. J. J. Habeeb, D. G. Tuck and F. H. Walters, *J. Coord. Chem.* 1978, **8**, 27.
15. N. Walker and D. Stuart, *DIFABS*: *Acta Cryst.* 1983, **A39**, 158.
16. C. J. Gilmore, *J. Appl. Cryst.* **17**, 42. University of Glasgow, Scotland (1986); P. T. Beurskens; DIRFIB: Direct Methods for Difference Structures—an Automatic Procedure Phase Extension and Refinement of Difference Structure Factors. Technical report 1984/1 Crystallography Laboratory Toernooireld, 6525 Ed Nigmegen, Netherlands.
17. D. T. Cromer and J. T. Waber, *International Tables for X-ray Crystallography*, Vol. IV, Table 2.2A. The Kynoch Press, Birmingham (1974).
18. D. T. Cromer, *International Tables for X-ray Crystallography*, Vol. IV, Table 2.3.1. The Kynoch Press, Birmingham (1974).
19. TEXSAN–TEXRAY Structure Analysis Package. Molecular Structure Corporation. MSC, 3200 A A Research Forest Drive, The Woodlands, TX 77381, USA (1985).
20. D. T. Corwin Jr and S. A. Koch, *Inorg. Chem.* 1988, **27**, 493.
21. D. Swenson, N. C. Baenziger and D. Coucouvanis, *J. Am. Chem. Soc.* 1978, **100**, 1933; N. Ueyama, T. Sugawara, K. Sasaki, A. Nakamura, S. Yamoshita, Y. Watatsuki, H. Yamazaki and N. Yasuoka, *Inorg. Chem.* 1988, **27**, 741.
22. T. L. Cremers, D. R. Bloomquist, R. D. Willet and G. A. Crosby, *Acta Cryst.* 1980, **B36**, 3097.
23. G. P. Diakun, L. Fairall and A. Klug, *Nature* (*London*) 1986, **324**, 698.
24. R. Castro, M. L. Durán, J. A. García-Vázquez, J. Romero, A. Sousa, A. Castiñeiras, W. Hiller and J. Strähle, *Z. Naturforsch.* 1990, **45b**, 1632.
25. J. P. Chesik and J. Donohue, *Acta Cryst.* 1971, **27B**, 1441.
26. F. A. Devillanova and G. Verani, *Aust. J. Chem.* 1980, **33**, 279.
27. S. Banerji, R. E. Byrne and S. E. Livingstone, *Trans. Met. Chem.* 1982, **7**, 5.
28. R. G. Inskeep, *J. Inorg. Nucl. Chem.* 1962, **24**, 763.
29. A. A. Schilt and R. C. Taylor, *J. Inorg. Nucl. Chem.* 1959, **9**, 211.
30. S. Yamazaki, *Polyhedron* 1985, **4**, 1915; T. A. Annan, R. K. Chadha, D. G. Tuck and K. D. Watson, *Can. J. Chem.* 1987, **65**, 2670.
31. J.-M. Bret, P. Castan, G. Commenges and J.-P. Laurent, *Polyhedron* 1983, **2**, 901.
32. A. B. P. Lever, *Inorganic Electronic Spectroscopy*, 2nd edn. Elsevier, Amsterdam (1984).
33. B. N. Figgis, *Introduction to Ligand Fields*. Interscience, New York (1967).

Polyhedron Vol. 12, No. 18, pp. 2249–2259, 1993
Printed in Great Britain

0277–5387/93 $6.00+.00
© 1993 Pergamon Press Ltd

BONDING PROPERTIES OF PENTA-COORDINATE Cu^{II}–N CHROMOPHORES: STRUCTURES AND ELECTRONIC SPECTRA OF COPPER(II) COMPLEXES OF TRIS(2-AMINOETHYL)AMINE (tren). MOLECULAR STRUCTURES OF [Cu(tren)(N-ACETYLHISTAMINE)]$(ClO_4)_2$ AND [Cu(tren)(2-METHYLIMIDAZOLE)]$(ClO_4)_2$

CHAN-CHENG SU,† WEN-SHUH LU, TSY-YAN HUI and TSUNG-YI CHANG

Department of Chemistry, National Taiwan Normal University, Taipei 11718, Taiwan, R.O.C.

and

SUE-LEIN WANG and FEN-LING LIAO

Department of Chemistry, National Tsing Hua University, Hsinchu, Taiwan, R.O.C.

(*Received* 3 *March* 1993; *accepted* 5 *May* 1993)

Abstract—Tris(2-aminoethyl)aminecopper(II) perchlorate complexes, $[Cu(tren)L](ClO_4)_2$ [tren is tris(2-aminoethyl)amine and L are neutral N-donor ligands including imidazoles, pyridines and amines], have been synthesized and characterized. The X-ray crystal structures of $[Cu(tren)(achmH)](ClO_4)_2$ (**1**) and $[Cu(tren)(2MImH)](ClO_4)_2$ (**2**) (achmH = N-acetylhistamine; 2MImH = 2-methylimidazole) have been determined. Their structures consist of discrete perchlorate anions and distorted trigonal-bipyramidal $[Cu(tren)(N\text{-donor})]^{2+}$ cations with the three primary amine groups of the tren ligand forming the equatorial plane, where one of the equatorial angles is larger than the other two and the Cu—N bond opposite the largest equatorial N—Cu—N angle is significantly longer than the other two. Electronic and EPR spectra are reported for these complexes. The LF spectra are analysed in trigonal-bipyramidal symmetry with the Jahn–Teller effect being considered in the excited state and the effect of geometric distortions. The *d*-orbitals are assigned in a sequence of $d_{z^2} \gg d_{x^2-y^2} > d_{xy} > d_{xz} \sim d_{yz}$. The bonding properties of the CuN_5 chromophores are elucidated and discussed with reference to the electronic structures of the complexes, suggesting no π-interaction in the axial Cu—N bonds.

Penta-coordinate copper(II) complexes exhibit a wealth of stereochemistry[1] and lead to difficulties in correlating the electronic properties and the geometries of the complexes.[2,3] The [tris(2-aminoethyl)amine]copper(II) diperchlorate complex $[Cu(tren)(NH_3)](ClO_4)_2$,[4] which exhibits a nearly regular trigonal-bipyramidal structure, is ideal for electronic structure studies, because complications due to possible π-bonding between the central copper ion and the ligands, and due to non-equivalent donor atoms of the ligands, are eliminated. In these studies difficulties are usually encountered in deciding the effective symmetry group for the complexes,[5] particularly when chelating ligands are in use. However, by analysis of the electronic spectra, the electronic structures are usually assignable with proper effective local symmetry for the complexes. The NH_3 complex was suggested having a D_{3h} symmetry with the *d*-orbital sequence as $d_{z^2} > d_{x^2-y^2}$, $d_{xy} > d_{xz}$, d_{yz} to account for the two *d–d* bands observed. An angular-overlap model analysis for this complex by reproducing the two band maxima was reported.[6]

† Author to whom correspondence should be addressed.

In a theoretical paper by Hoffmann *et al.*[7] the π-substituent effects on penta-coordinate complexes have been elucidated. In our investigation of bonding properties of Cu—N chromophores in trigonal-bipyramidal complexes we feel that with reference to the electronic structure of the NH_3 complex it would be beneficial to study the π-interactions between the central copper ion and the axial ligand by introducing a neutral N-donor, single-faced π-ligand to the fifth site of the tren-copper(II) moiety. We anticipate that the energy level of one of the d_π-orbitals, d_{xz} or d_{yz}, should be decreased or increased by a π-acceptor or a π-donor, respectively, with respect to the degenerate d_{xz} and d_{yz} orbitals of the NH_3 complex. In this regard Gaussian analyses were performed to assure the *d–d* component band positions for these complexes including the NH_3 complex. Surprisingly, we found that there were three, rather than two, *d–d* components for the NH_3 complex. Herein, we report the stereochemistry and the electronic spectra for tren-copper(II) complexes containing amines, imidazoles and pyridines and elucidate their electronic structures and bonding properties.

EXPERIMENTAL

Materials and preparations

N-Methylimidazole (Merck), 2-methylimidazole (Merck), 4-methylimidazole (Aldrich), imidazole (Merck), N-acetylhistamine (Aldrich), pyridine (Merck), 4-methylpyridine (Merck), piperidine (Merck), pyrrolidine (Merck), $Cu(ClO_4)_2 \cdot 6H_2O$ (Merck) and organic solvents of reagent grade and spectrograde were used as received. The tren complexes were prepared by the following general procedure: To a methanol solution of $Cu(ClO_4)_2 \cdot 6H_2O$ and the unidentate ligand (molar ratio 1 : 3) was added dropwise a stoichiometric amount of tren in methanol. The reaction mixture was stirred at room temperature for 2 h. The blue precipitates were filtered and washed with ether and then dried *in vacuo* over P_4O_{10}. The crystals of the title complexes suitable for X-ray structure determination were obtained from a CH_3CN and CH_3OH solution containing an excess amount of the imidazole derivatives and $NaClO_4$.

[Cu(tren)(achmH)]$(ClO_4)_2$ (**1**). Yield 79%, m.p. 224°C (dec.). IR: ν(N—H, tren) 3344s, 3290s; ν[Cu—N(3°)] 533s; ν(Cl—O) 1092vs,br. Found: C, 28.0; H, 5.1; N, 17.4. Calc. for $C_{13}H_{29}N_7O_9Cl_2Cu$: C, 27.8; H, 5.2; N, 17.4%.

[Cu(tren)(2MImH)]$(ClO_4)_2$ (**2**). Yield 92%, m.p. 235°C (dec). IR: ν(N—H, tren) 3345s, 3298s; ν[Cu—N(3°)] 532s; ν(Cl—O) 1090vs, br. Found: C, 24.5; H, 4.7; N, 16.9. Calc. for $C_{10}H_{24}N_6O_8Cl_2Cu$: C, 24.5; H, 4.9; N, 17.1%.

[Cu(tren)(ImH)]$(ClO_4)_2$. Yield 84%, m.p. 256°C (dec.). IR: ν(N—H, tren) 3352s, 3300s; ν[Cu—N(3°)] 528s; ν(Cl—O) 1090vs,br. Found: C, 22.6; H, 4.5; N, 17.5. Calc. for $C_9H_{22}N_6O_8Cl_2Cu$: C, 22.7; H, 4.6; N, 17.6%.

[Cu(tren)(NMIm)]$(ClO_4)_2$. Yield 89%, m.p. 242°C (dec.). IR: ν(N—H, tren) 3347s, 3293s; ν[Cu—N(3°)] 536s; ν(Cl—O) 1090vs,br. Found: C, 24.3; H, 4.8; N, 16.9. Calc. for $C_{10}H_{24}N_6O_8Cl_2Cu$: C, 24.5; H, 4.9; N, 17.1%.

[Cu(tren)(4MImH)]$(ClO_4)_2$. Yield 52%, m.p. 234°C (dec.). IR: ν(N—H, tren) 3350s, 3296s; ν[Cu—N(3°)] 536s; ν(Cl—O) 1090vs,br. Found: C, 24.6; H, 4.7; N, 17.3. Calc. for $C_{10}H_{24}N_6O_8Cl_2Cu$: C, 24.5; H, 4.9; N, 17.1%.

[Cu(tren)(py)]$(ClO_4)_2$. Yield 94%, m.p. 240°C (dec.). IR: ν(N—H, tren) 3339s, 3286s; ν[Cu—N(3°)] 536s; ν(Cl—O) 1090vs,br. Found: C, 26.6; H, 4.5; N, 14.2. Calc. for $C_{11}H_{23}N_5O_8Cl_2Cu$: C, 27.1; H, 4.7; N, 14.4%.

[Cu(tren)(4Mpy)]$(ClO_4)_2$. Yield 85%, m.p. 244°C (dec.). IR: ν(N—H, tren) 3345s, 3289s; ν[Cu—N(3°)] 540s; ν(Cl—O) 1090vs,br. Found: C, 28.6; H, 4.6; N, 13.7. Calc. for $C_{12}H_{25}N_5O_8Cl_2Cu$: C, 28.7; H, 5.0; N, 14.0%.

[Cu(tren)(pip)]$(ClO_4)_2$. Yield 32%, m.p. 225°C (dec.). IR: ν(N—H, tren) 3339s, 3289s; ν[Cu—N(3°)] 532s; ν(Cl—O) 1097vs,br. Found: C, 26.7; H, 5.6; N, 14.1. Calc. for $C_{11}H_{29}N_5O_8Cl_2Cu$: C, 26.7; H, 5.9; N, 14.4%.

[Cu(tren)(prld)]$(ClO_4)_2$. Yield 59%, m.p. 180°C (dec.). IR: ν(N—H, tren) 3337s, 3288s; ν[Cu—N(3°)] 530s; ν(Cl—O) 1098vs,br. Found: C, 25.0; H, 5.6; N, 15.2. Calc. for $C_{10}H_{27}N_5O_8Cl_2Cu$: C, 25.0; H, 5.6; N, 14.6%.

[Cu(tren)(NH_3)]$(ClO_4)_2$. Yield 80%, m.p. 255°C (dec.). IR: ν(N—H, tren) 3352s, 3294s; ν[Cu—N(3°)] 529s; ν(Cl—O) 1095vs,br. Found: C, 16.9; H, 4.8; N, 16.4. Calc. for $C_6H_{21}N_5O_8Cl_2Cu$: C; 16.9; H, 4.9; N, 16.4%.

Physical measurements

Electronic spectra were recorded on a Perkin–Elmer Lambda 9 spectrophotometer. Solid samples were measured as Nujol mulls on Whatman No. 1 filter paper. The deconvolution of the visible spectra into Gaussian component bands was performed on a VAX 6510 computer using the profile-fitting program CUVFIT.[8] EPR spectra were obtained using a Bruker ER 200D spectrometer and calibrated with DPPH ($g = 2.0037$). IR spectra were recorded as Nujol mulls or KBr pellets on a BIO-RAD FTS-40 FTIR spectrometer. A Micro Vax II computer-

controlled Siemens R3m/V diffractometer was used for crystal and molecular structure determination. Elemental analyses were performed by the microanalysis laboratories of Taiwan University, Taipei.

Structure determination and refinement

Details of crystal data and intensity collection are summarized in Table 1. 16 independent reflections with $8° \leqslant 2\theta \leqslant 29°$ for complex **1** and 15 with $9° \leqslant 2\theta \leqslant 25°$ for complex **2** were used for least-squares determination of the cell constants. Diffractometer examination of the the reciprocal lattice showed the space group to be $P2_1$ for **1** from the systematic absences $0k0$, $k \neq 2n+1$, and *Pnma* for **2** from the systematic absences $0kl$, $k+l \neq 2n+1$; $hk0$, $h \neq 2n+1$. Intensity data ($\theta/2\theta$ scan, $2.5° \leqslant 2\theta \leqslant 50.0°$, $(\sin\theta/\lambda)_{max} \simeq 0.6$) were collected at 296 K for two octants of the sphere ($-13 \leqslant h \leqslant 12$, $0 \leqslant k \leqslant 9$, $0 \leqslant l \leqslant 15$, for **1** and $0 \leqslant h \leqslant 18$, $0 \leqslant k \leqslant 9$, $0 \leqslant l \leqslant 18$ for **2**) and corrected for Lorentz and polarization effects, but not for absorption. Three standard reflections were monitored every 50 reflections and showed no signs of crystal deterioration. The structures were solved by direct methods using the SHELXTL PLUS program[9] and refined by full-matrix least-squares on F values. Scattering form factors and anomalous dispersion correction terms were taken from the International Tables for X-ray Crystallography.[10] All hydrogen atoms included in the refinement were placed in idealized positions (C—H = 0.96 Å, H—C—H = 109.4°) after non-hydrogen atoms were refined anisotropically. All calculations were done on a Micro Vax II-based Nicolet SHELXTL PLUS system. Additional material deposited comprises structure factors, atomic coordinates, anisotropic thermal parameters, hydrogen atom coordinates and a full list of bond lengths and angles.

RESULTS AND DISCUSSION

X-ray structure of $[Cu(tren)(achmH)](ClO_4)_2$ (**1**)

The unit cell contains two $[Cu(tren)(achmH)]^{2+}$ cations and four $[ClO_4]^-$ anions interconnected by hydrogen bonds. The structure of the N-acetylhistamine complex is shown in Fig. 1 and the unit cell arrangement in Fig. 2. Selected bond lengths and angles are listed in Table 2.

The copper ion is in a distorted trigonal-bipyramidal geometry with the three primary amine groups of the tren ligand forming the equatorial plane and the tertiary amine and the imidazole moiety of the achmH ligand on the apical positions. The equatorial plane is not strictly triangular; one of the N—Cu—N angles of 129.7(6)° is significantly larger than the other two; the distance of the Cu—N(4) bond [2.137(9) Å] opposite the largest N—Cu—N angle is somewhat longer than the other

Table 1. Summary of crystal data and inensity collection for $[Cu(tren)(achmH)](ClO_4)_2$ and $[Cu(tren)(2MImH)](ClO_4)_2$

Formula	$C_{13}H_{29}N_7O_9Cl_2Cu$	$C_{10}H_{24}N_6O_8Cl_2Cu$
fw	561.9	490.8
Crystal size (mm)	$0.28 \times 0.22 \times 0.18$	$0.48 \times 0.30 \times 0.22$
Space group	$P2_1$, monoclinic	*Pnma*, orthorhombic
a (Å)	11.177(5)	15.122(4)
b (Å)	8.359(3)	8.263(2)
c (Å)	13.237(5)	15.860(3)
β (°)	110.39(3)	90.00
V (Å^3)	1152.3(8)	1981.8(8)
Z	2	4
ρ_{calc} (g cm^{-3})	1.610	1.645
μ (mm^{-1})	1.231	1.423
Radiation (λ, Å)	Mo-K_α (0.71073)	Mo-K_α (0.71073)
Independent reflections	2205 ($1357 \geqslant 3.0\sigma(I)$)	1885 ($1146 \geqslant 3.0\sigma(I)$)
Extinction correction	—	$F^* = F[1+0.002\chi F^2/\sin(2\theta)]^{-1/4}$ $\chi = 0.0011(3)$
Weighting scheme	$w^{-1} = \sigma^2F+0.0045F^2$	$w^{-1} = \sigma^2F+0.0007F^2$
Final R, Rw	0.0518, 0.0570	0.0729, 0.0751
Largest and mean Δ/σ	0.009, 0.001	0.006, < 0.001
Largest difference peak (e Å^{-3})	0.61	1.14
Largest difference hole (e Å^{-3})	−0.39	−0.55

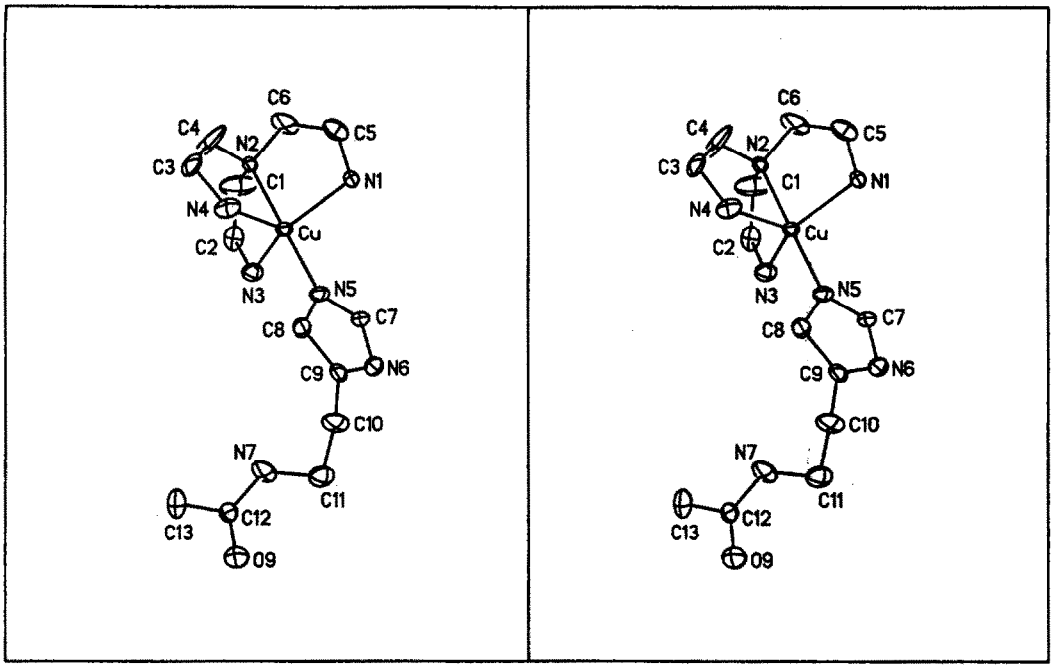

Fig. 1. Stereoscopic drawing of the copper coordination of $[Cu(tren)(achmH)]^{2+}$.

two Cu—N bonds. The copper atom is removed from the equatorial plane towards the imidazole ligand because the tren chelate bite angles are less than 90°. The axial Cu—N(2) bond is shorter than the equatorial Cu—N bonds, while the axial Cu—N(5) bond is even shorter. The tren ligand has one λ [N(4)] and two δ [N(1) and N(3)] chelate rings with small torsion angles (7.4°, 3.6° and 6.7°, respectively) and exhibits large thermal vibrations on the C(1), C(4) and C(6) atoms. The bond lengths and angles of the tren ligand are generally normal, except the ethylene C—C bonds which are shorter than the normal C—C single bond, probably due to anisotropic thermal motion effects.

The amide moiety of the N-acetylhistamine is in the "*trans*" configuration[11] and the C(11)—N(7)—C(12)—O(9) skeleton is co-planar. The imidazole moiety has normal bond distances and

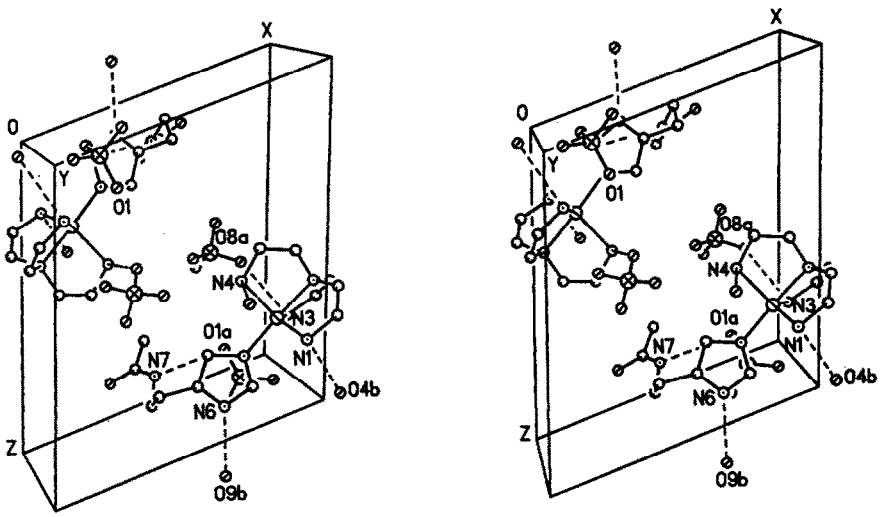

Fig. 2. Stereoscopic drawing of the molecular packing of $[Cu(tren)(achmH)](ClO_4)_2$ in the unit cell. Hydrogen bonds: N(1)···O(4b) 3.077, N(3)···O(8a) 3.078, N(4)···O(6b) 3.184, N(6)···O(9b) 2.884 and N(7)···O(1a) 3.212 Å.

Table 2. Bond lengths (Å) and angles (°) for $[Cu(tren)(achmH)](ClO_4)_2$ and $[Cu(tren)(2MImH)](ClO_4)_2$

	$[Cu(tren)(achmH)](ClO_4)_2$		
Cu—N(1)	2.046(13)	Cu—N(2)	2.062(13)
Cu—N(3)	2.105(16)	Cu—N(4)	2.137(9)
Cu—N(5)	1.957(13)		
N(1)—Cu—N(2)	82.8(6)	N(1)—Cu—N(3)	129.7(6)
N(1)—Cu—N(4)	110.1(7)	N(1)—Cu—N(5)	97.0(6)
N(2)—Cu—N(3)	84.8(7)	N(2)—Cu—N(4)	83.2(4)
N(2)—Cu—N(5)	177.8(4)	N(3)—Cu—N(4)	116.5(7)
N(3)—Cu—N(5)	93.6(7)	N(4)—Cu—N(5)	98.9(4)
	$[Cu(tren)(2MImH)](ClO_4)_2$		
Cu—N(1)	2.001(12)	Cu—N(3)	2.137(13)
Cu—N(4)	2.041(10)	Cu—N(5)	2.024(11)
N(1)—Cu—N(3)	106.8(5)	N(1)—Cu—N(4)	172.3(5)
N(1)—Cu—N(5)	94.1(4)	N(3)—Cu—N(4)	80.8(5)
N(3)—Cu—N(5)	110.9(4)	N(4)—Cu—N(5)	82.9(4)
N(5)—Cu—N(5A)	132.7(7)	Cu—N(1)—C(5)	135.8(11)

angles with short C(7)—N(5) and C(9)—N(6) bonds. The dihedral angle between the imidazole ring and the N(4)—Cu—N(2) plane is 13.4°. The imidazole N(6) is connected to the amide O(9) of the neighboring molecule by a hydrogen bond. The perchlorate anions are in tetrahedral geometry with large thermal vibrations.

X-ray structure of $[Cu(tren)(2MImH)](ClO_4)_2$ (**2**)

The unit cell contains four $[Cu(tren)(2MImH)]^{2+}$ cations and eight $[ClO_4]^-$ anions. The structure of the 2-methylimidazole complex is shown in Fig. 3 and the cell arrangement in Fig. 4. Selected bond lengths and angles are listed in Table 2.

The copper(II) ion is in a distorted trigonal-bipyramidal geometry with the equatorial sites occupied by the primary amine groups of the tren ligand and the axial sites by the tertiary amine and the 2-methylimidazole. The distorted equatorial plane contains the longest Cu—N(3) bond [2.137(13) Å] opposite the largest N(5)—Cu—N(5a) angle [132.7(7)°] and the Cu—N(3) bond is tilted towards the tertiary amine with a bite angle of 80.8(5)°. This

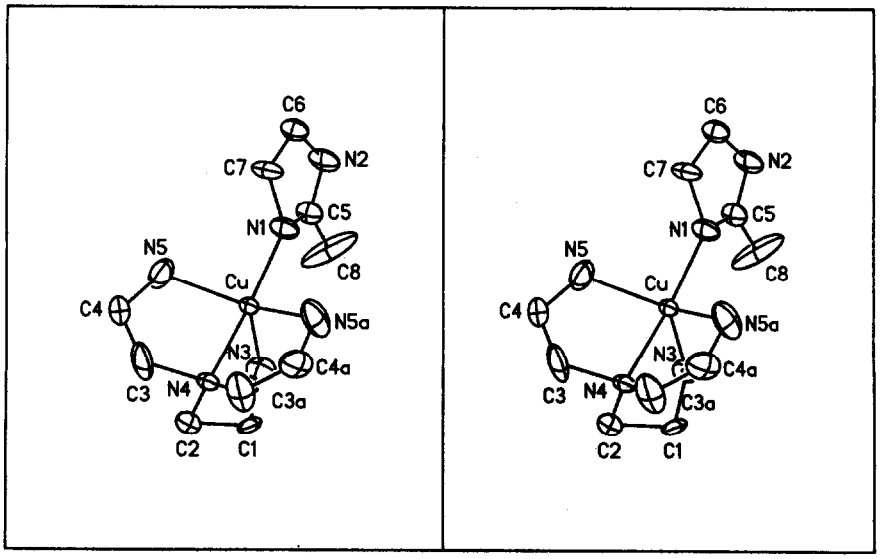

Fig. 3. Stereoscopic drawing of the copper coordination of $[Cu(tren)(2MImH)]^{2+}$.

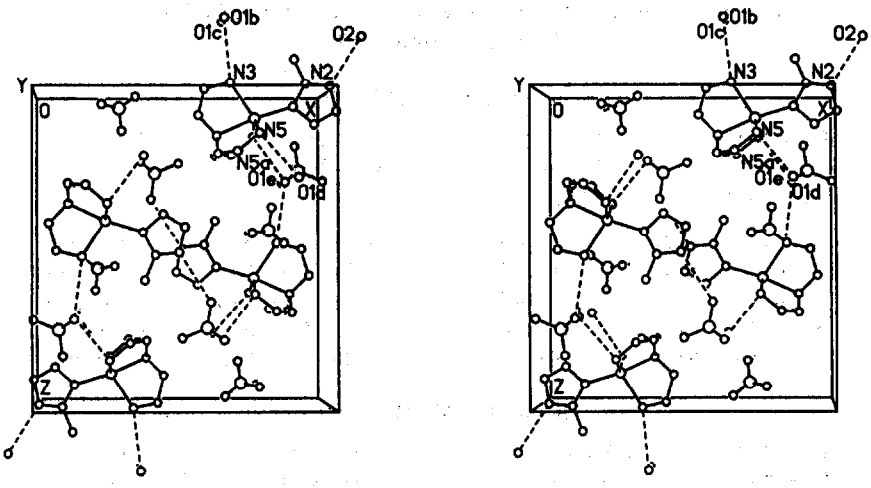

Fig. 4. Stereoscopic drawing of the molecular packing of $[Cu(tren)(2MImH)](ClO_4)_2$ in the unit cell. Hydrogen bonds: N(2)···O(2) 2.966, N(5)···O(1d) 3.179 and N(5a)···O(1e) 3.179 Å, and bifurcated hydrogen bonds, N(3)···O(1b) 3.256 and N(3)···O(1c) 3.256 Å.

chelate ring, in λ conformation with a torsion angle of 29.7°, is seriously disordered so that a mirror plane through Cu—N(3)—N(4) is effected. The other two chelates related by this mirror plane have one λ and one δ conformation with small torsion angles of 4.6°. The N(5), C(3), N(5a) and C(3a) atoms have large thermal parameters, suggesting that the chelate rings are fluctional. The dihedral angle between the 2-methylimidazole ring and the Cu—N(3)—N(4) plane is 14.1°. The dimensions of the 2-methylimidazole ligand are generally normal, except that the C(8) atom is in serous disorder. Note that the 2-methyl group is sitting close to the $N(3)H_2$ group. The ClO_4^- anions have expected tetrahedral geometry although some degree of disorder is apparent. The cations and the anions are interconnected by hydrogen bonds, as shown in Fig. 4.

Electronic and EPR spectroscopy

The visible and EPR spectral data of the tren complexes are listed in Table 3. It is noteworthy that the spectral contours of both the solid state and the solution visible spectra are extremely similar for the tren complexes containing a neutral N-donor unidentate ligand including the NH_3 complex, as illustrated in Fig. 5. This fact suggests that no dissociation of the neutral ligands occurs in solution. The spectra feature a broad band with λ_{max} at 780–810 nm, an apparent flanking high energy shoulder at 650 nm and a low energy shoulder at 900–950 nm. With the exception of the NH_3 complex, which exhibits an isotropic powder EPR spectrum, the powder EPR spectra of the tren complexes are of the reversed type with $g_\perp > g_\parallel \sim 2.00$. However, all of the complexes showed the reversed glass spectra with resolved hyperfine coupling in the $g_\perp$ and $g_\parallel$ regions.

Stereochemistry and bonding properties

The structures of the tripod tren complexes **1** and **2** are not strictly trigonal-bipyramidal. Rather, they are distorted towards a square-pyramidal structure with approximate C_{2v} local symmetry. In fact, among the structurally confirmed tren-copper(II) complexes compiled in Table 4 $[Cu(tren)(NH_3)](ClO_4)_2$[4] is the only compound having regular tbp geometry. It is obvious that the nature of the unidentate ligand plays an important role here. Since the pK_a values of the unidentate ligands in Table 4 vary considerably and randomly with respect to the distortion angles, distortion of the tbp structure due to the σ-donating abilities of the unidentate ligands can be ruled out. It is, then, necessary to consider the effects of π-interactions.

Two structural features of complexes **1** and **2** relevant to π-interactions are discussed here. First, the bond distance of the axial Cu—N(2MImH) [2.001(12) Å] bond of complex **2** obviously resulted from steric congestion, as is evident from the short C(8)—N(3) distance [3.407 Å] and the large bond angles of ∠Cu—N(1)—C(5) [135.8(11)°] and ∠N(1)—Cu—N(3) [106.8(5)°]. One may suspect that in complex **1** π-interactions may participate in the short Cu—N(achmH) bonding [1.957(13) Å], which lies at the short limit of the previously reported Cu—N(imidazole) distances of imidazole copper(II) complexes.[17] However, the short axial

Table 3. Visible and EPR spectral data for tren-copper(II) complexes

Compound[a]	λ_{max} (ε) (nm)[b]	$g_\perp$; $A_\perp$	$g_\parallel$; $A_\parallel$[c]
$[Cu(tren)(achmH)](ClO_4)_2$	650sh 790 900sh/mull 650sh 790(171) 900sh/CH_3CN	2.170; 118	2.000; 58
$[Cu(tren)(2MImH)](ClO_4)_2$	650sh 795 930sh/mull 650sh 795(157) 930sh/CH_3CN	2.181; 122	2.000; 52
$[Cu(tren)(ImH)](ClO_4)_2$	650sh 795 930sh/mull 650sh 790(180) 920sh/CH_3CN	2.161; 111	2.001; 62
$[Cu(tren)(NMIm)](ClO_4)_2$	650sh 790 930sh/mull 650sh 790(179) 920sh/CH_3CN	2.168; 116	2.000; 60
$[Cu(tren)(4MImH)](ClO_4)_2$	650sh 780 930sh/mull 650sh 790(198) 920sh/CH_3CN	2.169; 113	2.001; 62
$[Cu(tren)(py)](ClO_4)_2$	650sh 800 950sh/mull 650sh 800(160) 940sh/CH_3CN	2.178; 130	2.001; 51
$[Cu(tren)(4Mpy)](ClO_4)_2$	650sh 800 930sh/mull 650sh 797(180) 950sh/CH_3CN	2.176; 125	2.003; 51
$[Cu(tren)(pip)](ClO_4)_2$	650sh 790 930sh/mull 650sh 790(165) 920sh/CH_3CN	2.185; 103	2.000; 65
$[Cu(tren)(prld)](ClO_4)_2$	650sh 780 930sh/mull 650sh 780(180) 900sh/CH_3CN	2.190; 108	2.001; 60
$[Cu(tren)(NH_3)](ClO_4)_2$	650sh 810 950sh/mull 650sh 790(141) 910sh/CH_3CN	2.170; 118	2.003; 60

[a] Tren = tris(2-aminoethyl)amine, achmH = N-acetylhistamine, 2MImH = 2-methylimidazole, ImH = imidazole, NMIm = N-methylimidazole, 4MImH = 4-methylimidazole, py = pyridine, 4Mpy = 4-methylpyridine, pip = piperidine, prld = pyrrolidine.

[b] Powder spectra are measured as Nujol mulls on Whatman No. 1 filter paper.

[c] Measured as $H_2O:CH_3OH$ (1 : 1) glass at 77 K. $A_\parallel$ and $A_\perp$ in 10^{-4} cm^{-1}.

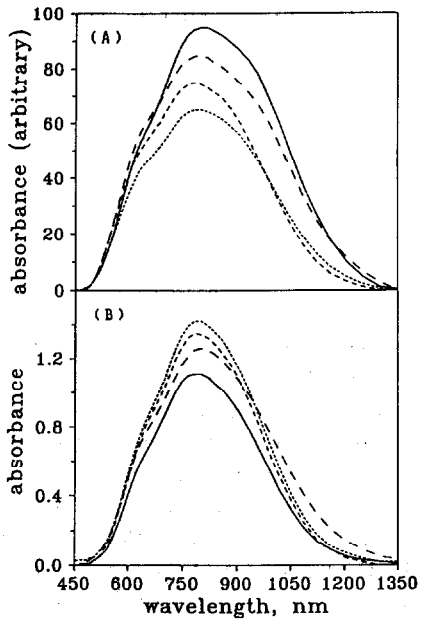

Fig. 5. The LF spectra of (1) $[Cu(tren)(NH_3)](ClO_4)_2$ (———), (2) $[Cu(tren)(py)](ClO_4)_2$ (— — —), (3) $[Cu(tren)(achmH)](ClO_4)_2$ (– – –) and (4) $[Cu(tren)(ImH)](ClO_4)_2$ (----), measured as (A) Nujol mulls and (B) CH_3CN solution, $[Cu^{2+}] = 7.86 \times 10^{-3}$ M.

bond lengths usually observed for tren complexes are attributable to the occupancy of a single electron in the d_{z^2} orbital. Secondly, the imidazole rings of complexes **1** and **2** are offset by 13.4° and 14.1°, respectively, to the longest equatorial Cu—N bond. Geometrically, π-interactions between the metal d_π orbitals and the ligand π-orbitals cannot be ruled out if the *x*- or *y*-axis must coincide with the elongated equatorial Cu—N bond. Nevertheless, based on the structural features π-interactions cannot be unambiguously clarified.

In order to reveal the bonding properties of the tren complexes the visible spectra were deconvoluted into their Gaussian component bands. Starting from a set of three or four trial peaks, computer iteration processes were performed until a minimum value of the reliability factor, *R*,[18] was reached. Each complex had an excellent fit, with the *R* factor ranging from 0.23% to 0.67%, and showed a resulting set of three Gaussian component peaks as typical examples, shown in Fig. 6; the peak positions and their half-height widths and relative peak areas are listed in Table 5. Attempts to fit with two component bands were unsuccessful. In order to

Table 4. Selected bond lengths (Å) and angles (°) for some tren-copper(II) complexes

Compound[a]	∠N—Cu—N; Cu—N[b]	Cu—N(3°)[c]	Cu—L[d]	Ref.
$[Cu(tren)(NH_3)](ClO_4)_2$	119.21(3); 2.082(6) 119.21(3); 2.082(6) 119.21(3); 2.082(6)	2.041(8)	2.023(11)	4
$[Cu(tren)(Im)Zn(tren)]^{3+}$	122.0(7); 2.076(17) 118.2(6); 2.053(15) 115.6(8); 2.075(12)	2.045(11)	1.954(10)	12
$[Cu(tren)(CN)]_2(BPh_4)_2$	122.6(2); 2.119(5) 120.4(2); 2.090(5) 112.5(2); 2.083(5)	2.076(5)	1.967(7)	13
$[Cu(tren)Cl]_2(BPh_4)_2$	123.8(1); 2.107(3) 119.9(1); 2.099(3) 112.3(1); 2.066(3)	2.081(3)	2.253(1)	14
$[Cu(tren)(NCS)]_2(BPh_4)_2$	123.8(2); 2.088(6) 120.4(2); 2.060(5) 112.3(2); 2.075(6)	2.047(6)	1.946(7)	14
$[Cu(tren)(NCO)]_2(BPh_4)_2$	124.2(5); 2.10(1) 120.8(4); 2.08(1) 111.6(4); 2.08(1)	2.06(1)	1.87(1)	14
[Cu(tren)(NCS)](SCN)	129.6(2); 2.144(4) 114.3(2); 2.055(4) 112.9(2); 2.055(4)	2.033(4)	1.959(5)	15
$[Cu_2(tren)_2(BZD)](NO_3)_4$	141.2(4); 2.177(10) 111.4(4); 2.026(11) 104.6(4); 2.041(11)	2.041(10)	2.032(8)	16
$[Cu(tren)(achmH)](ClO_4)_2$	129.7(6); 2.137(9) 116.5(7); 2.046(13) 110.1(7); 2.105(16)	2.062(13)	1.957(13)	This work
$[Cu(tren)(2MImH)](ClO_4)_2$	132.7(7); 2.137(13) 110.9(4); 2.024(11) 110.9(4); 2.024(11)	2.041(10)	2.001(12)	This work

[a] Im = imidazolate, BZD = benzidine.
[b] Equatorial ∠N—Cu—N angle and the opposite Cu—N bond length.
[c] Axial Cu—N(tren).
[d] L is the axial fifth ligand.

assure the reliability of the computer-fitting processes for the solid-state visible spectra the corresponding solution spectra were also deconvoluted into the Gaussian component peaks. The results are given in Table 5 and some examples are shown in Fig. 7.

The three component peaks resolved for the NH_3 complex are consistent with the single-crystal polarized spectra observed for the trigonal-bipyramidal $Cu(NH_3)_2Ag(SCN)_3$.[19] The appearance of three bands has been explained mainly by the effect of spin-orbit coupling.[19-21] However, the spin-orbit coupling cannot properly account for the resolved peaks of the NH_3 complex here. First, the energy difference between the two low energy peaks (corresponding to the $^2\Gamma_9$ and $^2\Gamma_7$ energy levels[19]) of 2.17 kK is much too large for the anticipated $2k\lambda$, where λ is the spin-orbit coupling constant, -0.829 kK, and k is the spin-orbit reduction parameter and is numerically < 1. An average value of 2.09(8) kK is observed for the tren complexes studied here. Secondly, the peak area of the highest energy peak is nearly the same as the sum of the two low energy peaks, suggesting that the highest energy peak consists of two degenerate bands and does not split at all in contrast to the anticipated splitting by a value of $\sim k\lambda$. Moreover, the highest energy peak of each of the other tren complexes studied here also shows

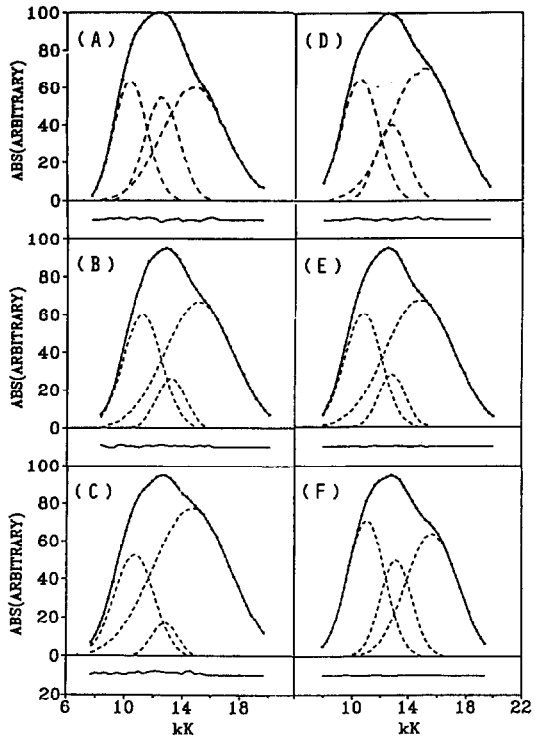

Fig. 6. The solid-state visible spectra and Gaussian lineshape analysis with difference plots of (A) [Cu(tren)(NH_3)]$(ClO_4)_2$, $R = 0.67\%$; (B) [Cu(tren)(achmH)]$(ClO_4)_2$, $R = 0.35\%$; (C) [Cu(tren)(2MImH)]$(ClO_4)_2$, $R = 0.23\%$; (D) [Cu(tren)(py)]$(ClO_4)_2$, $R = 0.44\%$, (E) [Cu(tren)(4Mpy)]$(ClO_4)_2$, $R = 0.32\%$; and (F) [Cu(tren)(prld)]$(ClO_4)_2$, $R = 0.36\%$. (•) profile-fitting points; (---) Gaussian components; (——) observed spectrum.

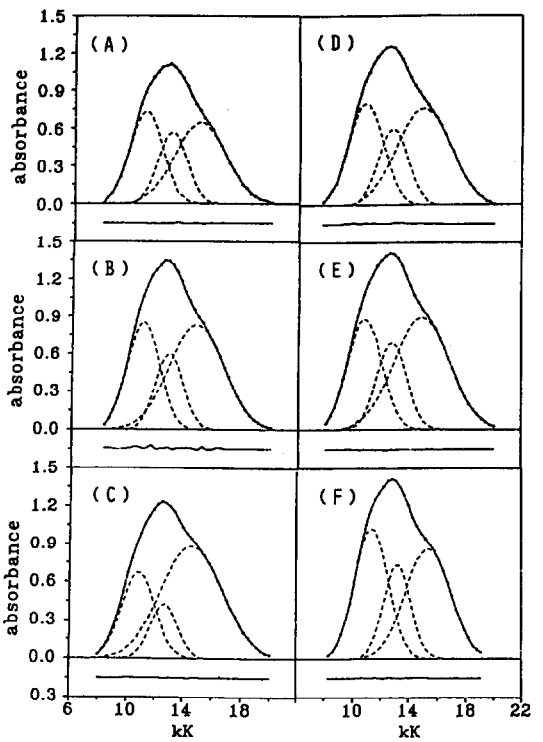

Fig. 7. The visible spectra in CH_3CN and Gaussian lineshape analysis with difference plots of (A) [Cu(tren)(NH_3)]$(ClO_4)_2$, $R = 0.19\%$; (B) [Cu(tren)(achmH)]$(ClO_4)_2$, $R = 0.20\%$; (C) [Cu(tren)(2MImH)]$(ClO_4)_2$; $R = 0.08\%$; (D) [Cu(tren)(py)]$(ClO_4)_2$, $R = 0.36\%$; (E) [Cu(tren)(4Mpy)]$(ClO_4)_2$, $R = 0.28\%$; and (F) [Cu(tren)(prld)]$(ClO_4)_2$, $R = 0.14\%$. (•) profile-fitting points; (---) Gaussian components; (——) observed spectrum.

a large peak area, which is greater than the sum of the other two peaks and likely consists of two component bands. These results suggest that the large highest energy peak of the NH_3 complex and other tren complexes as well is the degenerate d_{xz}, $d_{yz} \rightarrow d_{z^2}$ transition.

We propose that the Jahn–Teller effect in the excited states is more appropriate for interpretation of the spectra here.[22] The five *d*-orbitals are subject to the tbp symmetry field to give a sequence of $d_{z^2} \gg d_{x^2-y^2}$, $d_{xy} > d_{xz}$, d_{yz}, where the d_{z^2} ground state is consistent with the EPR spectral data. The in-plane degenerate $d_{x^2-y^2}$ and d_{xy} orbitals are further affected by the Jahn-Teller instability in the excited states, whilst this effect on the out-of-plane d_{xz} and d_{yz} orbitals is not apparently observable. The areas of the two low energy peaks are nearly equal for the NH_3 complex. However, for other tren complexes the intensity of the central peak is less than half of that of the lower energy peak. This fact is attributable to the geometric distortion towards C_{2v} local symmetry. Accordingly, the *d*-orbital sequence is best arranged in $d_{z^2} \gg d_{x^2-y^2} > d_{xy} > d_{xz} \sim d_{yz}$.

In the trigonal-bipyramidal tren-copper(II) complexes the d_{xz} and d_{yz} orbitals are degenerate if the fifth axial ligand has no π-orbital, such as NH_3. However, for complexes with a single-faced π-ligand at the fifth axial site, π-interaction between the central copper and the ligand should cause one of the d_π-orbitals, d_{xz} or d_{yz}, to ascend or descend, depending on the ligand being a π-donor or a π-acceptor, respectively. In other words, π-interaction should result in lifting the degeneracy of the d_{xz} and d_{yz} orbitals. Here, all of the complexes showed a slightly broadened highest energy peak corresponding to the transition of d_{xz}, d_{yz} to d_{z^2}, irrespective of the difference of the π-bonding capabilities of the axial unidentate ligands, i.e. pyridines are generally considered as π-acceptors and imidazoles are π-donors.[7,23–25] It is, therefore, conceivable that no π-interaction is involved in the axial bonding for the trigonal-bipyramidal tren-copper(II) complexes.

Table 5. Gaussian component bands for the visible spectra of tren-copper(II) complexes[a]

Band	ν (kK)	Area[b]	$\delta_{1/2}$[c]	ν (kK)	Area[b]	$\delta_{1/2}$[c]	Assignment
[Cu(tren)(NH_3)](ClO_4)$_2$							
	/mull (R = 0.67%)[d]			/CH_3CN (R = 0.19%)			
I	10.4	2.67	2.69	11.05	3.31	2.74	$d_{x^2-y^2}$
II	12.6	2.39	2.81	12.95	2.23	2.40	d_{xy}
III	14.9	4.94	5.31	14.9	4.46	4.19	$d_{xz}d_{yz}$
[Cu(tren)(achmH)](ClO_4)$_2$							
	/mull (R = 0.35%)			/CH_3CN (R = 0.20%)			
I	11.2	3.06	3.13	11.0	3.17	2.68	$d_{x^2-y^2}$
II	13.2	1.11	2.36	12.9	1.83	2.29	d_{xy}
III	15.1	5.83	5.60	14.8	5.00	4.47	$d_{xz}d_{yz}$
[Cu(tren)(2MImH)](ClO_4)$_2$							
	/mull (R = 0.23%)			/CH_3CN (R = 0.08%)			
I	10.7	2.47	3.24	10.85	2.61	2.77	$d_{x^2-y^2}$
II	12.8	0.55	2.12	12.7	1.30	2.29	d_{xy}
III	14.7	6.98	6.24	14.6	6.09	5.04	$d_{xz}d_{yz}$
[Cu(tren)(ImH)](ClO_4)$_2$							
	/mull (R = 0.26%)			/CH_3CN (R = 0.26%)			
I	10.9	2.81	3.04	11.0	3.05	2.64	$d_{x^2-y^2}$
II	12.9	1.01	2.31	12.8	2.03	2.32	d_{xy}
III	14.9	6.18	5.76	14.75	4.92	4.45	$d_{xz}d_{yz}$
[Cu(tren)(NMIm)](ClO_4)$_2$							
	/mull (R = 0.27%)			/CH_3CN (R = 0.20%)			
I	10.7	3.23	3.11	11.0	3.24	2.72	$d_{x^2-y^2}$
II	12.9	1.42	2.54	12.9	1.76	2.24	d_{xy}
III	15.05	5.35	5.14	14.7	5.00	4.48	$d_{xz}d_{yz}$
[Cu(tren)(4MImH)](ClO_4)$_2$							
	/mull (R = 0.26%)			/CH_3CN (R = 0.18%)			
I	10.9	3.15	3.07	11.1	3.22	2.73	$d_{x^2-y^2}$
II	13.1	1.29	2.45	12.9	1.71	2.24	d_{xy}
III	15.1	5.56	5.13	14.7	5.07	4.49	$d_{xz}d_{yz}$
[Cu(tren)(py)](ClO_4)$_2$							
	/mull (R = 0.44%)			/CH_3CN (R = 0.36%)			
I	10.55	2.90	3.03	10.7	3.26	2.98	$d_{x^2-y^2}$
II	12.75	1.55	2.60	12.7	2.07	2.52	d_{xy}
III	15.0	5.55	5.38	14.9	4.67	4.53	$d_{xz}d_{yz}$
[Cu(tren)(4Mpy)](ClO_4)$_2$							
	/mull (R = 0.32%)			/CH_3CN (R = 0.28%)			
I	10.8	2.95	3.04	10.75	3.00	2.82	$d_{x^2-y^2}$
II	12.8	0.99	2.22	12.7	2.06	2.47	d_{xy}
III	14.75	6.06	5.61	14.8	4.94	4.60	$d_{xz}d_{yz}$
[Cu(tren)(pip)](ClO_4)$_2$							
	/mull (R = 0.49%)			/CH_3CN (R = 0.30%)			
I	11.2	3.64	3.05	11.2	3.49	2.76	$d_{x^2-y^2}$
II	13.0	1.02	1.99	13.0	2.05	2.25	d_{xy}
III	15.2	5.34	4.76	15.2	4.46	3.86	$d_{xz}d_{yz}$
[Cu(tren)(prld)](ClO_4)$_2$							
	/mull (R = 0.36%)			/CH_3CN (R = 0.14%)			
I	11.0	3.54	3.10	11.35	3.71	2.81	$d_{x^2-y^2}$
II	13.15	2.12	2.64	13.2	2.17	2.28	d_{xy}
III	15.65	4.34	4.22	15.35	4.12	3.72	$d_{xz}d_{yz}$

[a] For abbreviations, see footnote a of Table IV.
[b] Relative peak area in arbitrary scale based on a sum of 10.
[c] Half-width at $E_{max}/2$.
[d] Reliability factor defined as $R = \Sigma|y_{obs,i} - y_{calc,i}|/\Sigma y_{obs,i}$.

In conclusion, we have demonstrated the importance of utilizing Gaussian deconvolution techniques to analyse the LF spectra of the tren-copper(II) complexes and to elucidate the sequence of the *d*-orbitals. The weak d_{xy} to d_{z^2} transition peak can only be revealed from the resolved Gaussian component peaks. We have further explored the π-bonding capabilities of the ligands by comparison of the energy levels of the d_π-orbitals of a series of structurally analogous complexes and concluded that no π-interaction participates in the axial Cu—N bonding for the tren complexes, despite the fact that such an interaction is symmetry allowed. Moreover, unlike the generally recognized copper(II) complexes, the axial ligand is not labile. Finally, the deviation of the tren-copper(II) complexes from regular tbp structure is possibly due to the non-cylindrically symmetric unidentate ligand, which effectively lifts the C_3 axis in the tbp geometry.

Acknowledgements—We thank the National Science Council of the Republic of China for financial support (NSC81-0208-M003-15) and Prof. T.-Y. Dong for use of the Perkin–Elmer Lambda 9 spectrophotometer and valuable discussion.

REFERENCES

1. B. J. Hathaway, in *Comprehensive Coordination Chemistry* (Edited by G. Wilkinson, R. E. Gillard and J. A. McCleverty), Vol. 5, pp. 594–774. Pergamon, Oxford (1987).
2. B. J. Hathaway, *Struct. Bonding* 1984, **57**, 55.
3. N. J. Ray, L. Hulett, R. Sheahan and B. J. Hathaway, *J. Chem. Soc., Dalton Trans.* 1981, 1463.
4. For abbreviations, see footnote a of Table 3. M. Duggan, N. Ray, B. J. Hathaway, G. Tomlinson, P. Brint and K. Pelin, *J. Chem. Soc., Dalton Trans.* 1980, 1342.
5. N. S. Hush and R. J. M. Hobbs, *Prog. Inorg. Chem.* 1968, **10**, 259.
6. R. J. Deeth and M. Gerloch, *Inorg. Chem.* 1985, **24**, 4490.
7. A. R. Rossi and R. Hoffmann, *Inorg. Chem.* 1975, **14**, 365.
8. S.-L. Wang, P. C. Wang and Y. P. Nieh, *J. Appl. Cryst.* 1990, **23**, 520.
9. G. M. Sheldrick, SHELXTL PLUS User Manual, Nicolet XRD Corporation, Madison, WI (1986).
10. *International Tables of X-ray Crystallography*, Vol. IV. Kynoch Press, Birmingham (1974).
11. S.-I. Mizushima, T. Simanouti, S. Nagakura, K. Kuratani, M. Tsuboi, H. Baba and O. Fujioka, *J. Am. Chem. Soc.* 1950, **72**, 3490.
12. Q. Lu, Q. H. Luo, A. B. Dai, Z. Y. Zhou and G. Z. Hu, *J. Chem. Soc., Chem. Commun.* 1990, 1429.
13. D. M. Duggan and D. N. Hendrickson, *Inorg. Chem.* 1974, **13**, 1911.
14. E. J. Laskowski, D. M. Duggan and D. N. Hendrickson, *Inorg. Chem.* 1975, **14**, 2449.
15. P. C. Jain and E. C. Lingafelter, *J. Am. Chem. Soc.* 1967, **89**, 6131.
16. T. R. Felthouse, E. N. Duesler, A. T. Christensen and D. N. Hendrickson, *Inorg. Chem.* 1979, **18**, 245.
17. C.-C. Su, H.-L. Tsai, F.-H. Ko, S.-L. Wang and C.-Y. Cheng, *Inorg. Chim. Acta* 1991, **186**, 171.
18. See footnote d, Table 5.
19. B. J. Hathaway, D. E. Billing, R. J. Dudley, R. J. Fereday and A. A. G. Tomlinson, *J. Chem. Soc. (A)* 1970, 806.
20. D. M. Duggan, R. G. Jungst, K. R. Mann, G. D. Stucky and D. N. Hendrickson, *J. Am. Chem. Soc.* 1974, **96**, 3443.
21. D. M. Duggan and D. N. Hendrickson, *Inorg. Chem.* 1974, **13**, 2929.
22. F. A. Cotton and G. Wilkinson, *Advanced Inorganic Chemistry*, 4th edn, pp. 678–682. John Wiley & Sons, New York (1980).
23. C.-C. Su, J. H. Chen, K.-Y. Hwang, S.-J. Liu, S.-W. Wang, S.-L. Wang and S.-N. Liu, *Inorg. Chim. Acta* 1992, **196**, 231.
24. C.-C. Su, Y.-L. Lin, S.-L. Wang and W.-C. Chou, *Trans. Met. Chem.* 1993, **18**, 113.
25. C.-C. Su, T.-T. Hwang, O. Y.-P. Wang, S.-L. Wang and F.-L. Liao, *Trans. Met. Chem.* 1992, **17**, 91.

Polyhedron Vol. 12, No. 18, pp. 2261–2264, 1993
Printed in Great Britain

0277–5387/93 $6.00+.00
© 1993 Pergamon Press Ltd

SYNTHESIS AND X-RAY CRYSTAL STRUCTURE OF A MIXED-VALENT COBALT COMPLEX, $Co_2Cl_5(py)_5$

HAO XU, JINYU LI, ZHONGZHI WU, JIANZHONG ZOU, ZHENG XU* and XIAOZENG YOU

Coordination Chemistry Institute and the National Key Laboratory of Coordination Chemistry, Najing University, Nanjing 210008, Jiangsu, P.R.C.

and

ZHENGCHAO DONG

Fujian Institute of Research on the Structure of Matter, Chinese Academy of Science, Fuzhou 350002, Fujian, P.R.C.

(*Received* 5 *January* 1993; *accepted* 5 *May* 1993)

Abstract—A new complex, $Co_2Cl_5(py)_5$ was obtained by the reaction of $CoCl_2 \cdot 6H_2O$ with $Bu^n_4NMnO_4$ in pyridine in the presence of benzoic acid. The structure consists of a discrete octahedral $[Co^{III}Cl_2(py)_4]^+$ cation and a tetrahedral $[Co^{II}Cl_3py]^-$ anion. The compound was also characterized by elemental analyses, IR, XPS spectra and variable-temperature magnetic susceptibility measurements. The reaction conditions indicate that when the molar ratio of benzoic acid : $CoCl_2 \cdot 6H_2O$ is below 0.75 the title complex cannot be obtained.

An important current area of research is the development of synthetic methodologies for preparing new inorganic compounds. Recently, Vincent *et al.* have reported that the $Bu^n_4NMnO_4$ is a useful oxide reagent for the synthesis of mixed-valent polynuclearmanganese complexes in non-aqueous solvents.[1–4] In order to enlarge the applied scope of this reagent and to prepare the mixed-valent polynuclear cobalt complexes, we herein first report the synthesis and X-ray crystal structure of the mixed-valent cobalt complex $Co_2Cl_5(py)_5$ using $Bu^n_4NMnO_4$ as an oxide reagent in pyridine.

EXPERIMENTAL

Material and measurements

Benzoic acid, $CoCl_2 \cdot 6H_2O$, pyridine, absolute ethanol and CH_3CN were used as received. $Bu^n_4NMnO_4$ was prepared from $KMnO_4$ and Bu_4NBr as described earlier[5] and used without recrystallization. All operations were performed under aerobic conditions at ambient temperature.

The elemental analyses for carbon, hydrogen and nitrogen were performed on a Perkin–Elmer 240C analyser. The metal analysis for cobalt was measured on a Jarrell–Ash 1100+2000 ICP apparatus. The chlorine analysis was performed using Volhard's method. IR spectra were obtained on a Nicolet FT 170SX spectrometer using KBr pellets. X-ray photoelectron spectra were performed on a VG MK II spectrometer using Mg-K_α radiation and a charge-transfer correction referred to the binding energy of C_{1s}. The variable-temperature (74–300 K) magnetic susceptibility measurements of crystal samples of the title complex (75.24 mg) were obtained on a Shimadzu MB-2 magnetic balance at 1.2 T magnetic field.

Synthesis of $Co_2Cl_5(py)_5$

$CoCl_2 \cdot 6H_2O$ (1.94 g, 8.15 mmol) and benzoic acid (1.00 g, 8.15 mmol) were dissolved in pyridine (40 cm^3) to give a violet–red solution. This was stirred while solid $Bu^n_4NMnO_4$ (1.14 g, 3.15 mmol)

* Author to whom correspondence should be addressed.

was added in small portions over approximately 20 min; the reaction solution turned deep brown. After stirring for 20 min the reaction solution was evaporized to remove the pyridine solvent and a brown oil product was obtained, which was redissolved in absolute ethanol (70 cm^3). The ethanol solution was concentrated by evaporization and stood overnight in a refrigerator at *ca* 5°C to give a green solid product, which was collected by filtration, washed three times with small portions of ethanol and dried in air to give the product (1.10 g, yield 39.1%). This material was redissolved in CH_3CN and stood in air, for 3 days, to give green crystals of the title complex which were suitable for X-ray structure studies. Found: C, 43.0; H, 3.6; N, 10.1; Co, 17.2; Cl, 25.0. Calc. for $C_{25}H_{25}N_5Cl_5Co_2$: C, 43.4; H, 3.6; N, 10.1; Co, 17.0; Cl, 25.6%. IR data: 3112w, 3048w, 1605s, 1489m, 1445s, 1212s, 1149w, 1063s, 1016m, 759s, 695s, 641w, 467w, 423w, 353w. XPS (eV) data: N_{1s} (399.0), $Co2P_{3/2}$ (779.0).

X-ray crystallography

A prismatic green crystal (0.4 × 0.2 × 0.2 mm) was used for X-ray diffraction. Data were collected on a Rigaku AFC5R diffractometer at room temperature using graphite monochromated Mo-K_α (0.71069 Å) radiation. The intensities were corrected for the Lp factor and empirical absorption. A summary of data collection parameters is given in Table 1.

The structure was solved by direct methods. Successive Fourier syntheses gave the coordinates of all the non-hydrogen atoms refined with anisotropic thermal parameters. The hydrogen atoms were placed in geometrically calculated positions with a C—H distance of 0.95 Å and refined with isotropic thermal parameters. The final cycle of refinement led to a final convergence at $R = 0.041$. All calculations were performed on a Micro VAXII computer using TEXSAN programs. Atomic coordinates and thermal parameters, together with observed and calculated structure factors, have been deposited with the Editor, from whom copies are available on request; copies have also been deposited with the Cambridge Crystallographic Data Center.

Table 1. Summary of crystal and intensity collection parameters

Formula	$Co_2Cl_5(py)_5$
Fw	690.64
Crystal dimensions (mm)	0.4 × 0.2 × 0.2
Crystal system	Monoclinic
Space group	$P2_1/n$
Unit cell constants	
a (Å)	28.652(5)
b (Å)	14.108(4)
c (Å)	7.108(4)
β (°)	90.09(1)
V (Å^3)	3001(2)
Z	4
D_c (g cm^{-3})	1.53
μ (cm^{-1})	15.8
F(000)	1396
Scan mode	ω–2θ
Scan speed (° min^{-1})	16
$2\theta_{max}$ (°)	50
hkl ranges	0–34, 0–16, −8–8
Total unique data	5560
Data used in refinement with $I > 3\sigma(I)$	3416
Parameters refined	409
R^a	0.041
Rw^b	0.046
GOF	1.66
w	$1/\sigma^2F$
$\Delta\rho_{max}$, $\Delta\rho_{min}$ (e Å^{-3})	0.7(1), −0.4(1)

$^a R = \Sigma[|F_o| - |F_c|]/\Sigma|F_o|$.
$^b Rw = [w(F_o - |F_c|)^2/\Sigma w(F_o)^2]^{1/2}$.

RESULTS AND DISCUSSION

The use of permanganate for inorganic syntheses in aqueous solvents is common. In recent years $Bu^n_4NMnO_4$ has been successfully used for preparing the mixed-valent polynuclear manganese complexes in non-aqueous solvents.[1–4] We attempt to synthesize the mixed-valent cobalt polynuclear complex by using $Bu^n_4NMnO_4$ to oxidize the divalent cobalt salt $CoCl_2 \cdot 6H_2O$ in pyridine in the presence of benzoic acid. However, the unexpected product $Co_2Cl_5py_5$ was obtained instead of the desired polynuclear complex. Apparently, the benzoic acid does not actually play an important role in this reaction. Although the reaction is not particularly sensitive to the amount of benzoic acid, it is to the molar ratio of benzoic acid: $CoCl_2 \cdot 6H_2O$ used. When the ratio was lower than 0.75 the title complex could not be obtained. Other organic acids are not suitable for the synthesis of the title complex.

Description of the X-ray crystal structure of $Co_5Cl_5(py)_5$

Figure 1 shows a view of the complex molecule $Co_2Cl_5(py)_5$. Selected bond distances and angles are listed in Table 2. The structure contains the crystallographically discrete cation $[Co^{III}Cl_2(py)_4]^+$ and anion $[Co^{II}Cl_3py]^-$ in the ratio 1:1. The six-

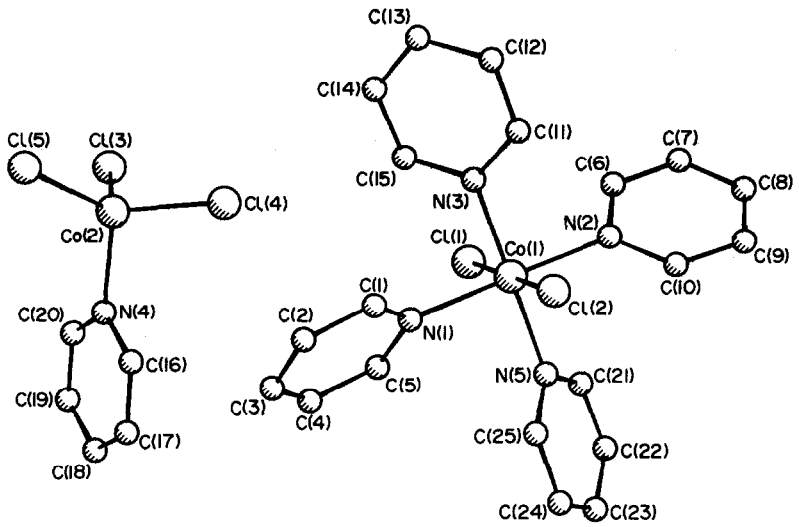

Fig. 1. The structure of $Co_2Cl_5(py)_5$.

coordinated cobalt(III) atom in the cation is bonded to the nitrogen atoms from four pyridine molecules, with Co—N distances of 1.974(5)–1.984(4) Å (average 1.978 Å), and to the two chlorine atoms, with Co—Cl bonds of 2.253(2) and 2.249(2) Å, forming a tetragonal-bipyramid with the chloride atoms in axial directions and nitrogen atoms on the equatorial plane. The four-coordinate cobalt(II) atom in the anion is bonded to three chloride atoms at distances of 2.243(2)–2.258(2) Å (average 2.251 Å) and to the nitrogen atom of the pyridine molecule at a bond length of 2.039(5) Å. The coordination geometry around the cobalt(II) atom is a tetrahedron.

The Co(2)—N(4) bond distance [2.039(5) Å] is longer than Co(1)—N_{av} [N(1)—N(3) and N(5)] [1.978(4) Å] due to the larger radius for Co^{II} vs Co^{III}. This result can be confirmed by a comparison of the Co—N(py) bond lengths in some different valent cobalt–pyridine complexes, such as $[Co^{I}(py)_2(Bph_4)]$, 2.096(9) Å;[6] $[Co^{II}(S\text{-}2.4.6\text{-}Pr_3C_6H_2)_2(py)_2]$, 2.038(9) Å;[7] $[Co^{III}(dpgH)_2Cl(py)]\cdot CH_3OH$, 1.965(3) Å.[8] By comparison, one can find that the Co—Cl bond lengths in the two kinds of ions are similar. Taking the difference in the metal ion radius into account, however, the Co^{II}—Cl bond distance should be longer than the Co^{III}—Cl bond. The reason for this can be ascribed to the

Table 2. Selected bond distances (Å) and angles (°)

Co(1)—Cl(1)	2.253(2)	Co(1)—N(1)	1.984(4)
Co(1)—Cl(2)	2.249(2)	Co(1)—N(2)	1.978(4)
Co(2)—Cl(3)	2.258(2)	Co(1)—N(3)	1.974(5)
Co(2)—Cl(4)	2.258(2)	Co(1)—N(5)	1.976(5)
Co(2)—Cl(5)	2.243(2)	Co(2)—N(4)	2.039(5)
Cl(1)—Co(1)—C(12)	178.59(7)	Cl(3)—Co(2)—Cl(4)	113.95(7)
Cl(1)—Co(1)—N(1)	89.5(1)	Cl(3)—Co(2)—Cl(5)	113.02(7)
Cl(1)—Co(1)—N(2)	90.3(1)	Cl(3)—Co(2)—N(4)	101.5(1)
Cl(1)—Co(1)—N(3)	89.7(1)	Cl(4)—Co(2)—Cl(5)	110.09(8)
Cl(1)—Co(1)—N(5)	90.9(1)	Cl(4)—Co(2)—N(4)	103.9(1)
Cl(2)—Co(1)—N(1)	89.6(1)	Cl(5)—Co(2)—N(4)	114.0(1)
Cl(2)—Co(1)—N(2)	90.7(1)	Cl(2)—Co(1)—N(3)	89.3(1)
Cl(2)—Co(1)—N(5)	90.2(1)	N(1)—Co(1)—N(2)	178.4(2)
N(1)—Co(1)—N(3)	90.7(2)	N(1)—Co(1)—N(5)	89.2(2)
N(2)—Co(1)—N(3)	90.9(2)	N(2)—Co(1)—N(5)	89.3(2)
N(3)—Co(1)—N(5)	179.4(2)		

following. Since the coordination ability of pyridine is stronger than the chlorine anion and four pyridine molecules coordinate to the cobalt(III) ion, compared with one to the cobalt(II) ion, the effective nuclear charge of the cobalt(III) ion should decrease more than that of the cobalt(II) ion. Therefore, the attraction between the cobalt (III) ion and chlorine anion will be weakened more compared with the Co^{II}—Cl bond, thus leading to the lengthening of the Co^{III}—Cl bond and similar distances of Co—Cl bonds in the two kinds of ions. This result has been confirmed by the XPS studies below.

Spectroscopic characterization and magnetic properties of $Co_2Cl_5(py)_5$

The IR spectra of the title complex has been measured. It displays the characteristic absorption peaks of pyridine molecules at 3048w, 1605s, 1498m, 1445s, 1016s, 759s, 641w and 423w cm^{-1} and an absorption at 353 cm^{-1} for Co—Cl bond stretching.[9] The Co—N bond stretching occurs at 256 cm^{-1}.[9] It is well known that upon complex formation the pyridine vibrations in the high frequency region are not shifted appreciably, whereas those at 604 (in-plane ring deformation) and 405 cm^{-1} (out-of-plane ring deformation) are shifted to higher frequencies.[9] In the IR spectra of the title complex the frequencies of these two bands (641 and 423 cm^{-1}) are higher than those of free pyridine molecule, indicating the presence of coordinated pyridine molecules in the complex.

The nature of the complex also was verified by XPS spectra. In view of the XPS data we found that the N_{1s} binding energy of the nitrogen atom of pyridine molecules increased compared with that of the free pyridine molecule (398.6 eV). This shows that the electrons in the nitrogen atoms partially shift to the cobalt atoms due to coordination. This result is consistent with that mentioned in the IR spectra. Due to the presence of cobalt(II) and cobalt (III) ions in the complex the XPS spectra usually display two peaks of $Co2P_{3/2}$ binding energy. However, in the spectra of the title complex only one peak was found. We suppose that this is probably due to the presence of four-coordinate pyridine molecules around the cobalt(III) ion, whereas only one pyridine molecule coordinates to the cobalt(II) ion. Thus, the binding energy of the cobalt(III) ion should decrease much more than that of cobalt(II) ion, thus leading to the similar binding energy of cobalt(III) and cobalt(II) ions.

The variable-temperature magnetic susceptibility measured at 1.2 T in the range 78–300 K for a polycrystalline sample of the title complex obeys the Curie–Weiss expression $\chi = C/(T-\theta)$, with $\theta = 0$, suggesting no magnetic-exchange interaction between the two cobalt ions. The effective magnetic moment of the complex is consistent with that of the cobalt(II) ion. This further verified the composition of the mixed-valent cobalt complex.

Acknowledgement—This research was supported by a grant for the key project from the State Science and Technology Commission and the National Science Foundation of China.

REFERENCES

1. J. B. Vincent, K. Folting, J. C. Huffman and G. Christou, *Inorg. Chem.* 1986, **25**, 996.
2. J. B. Vincent, C. Christmas, J. C. Huffman, G. Christou, H. R. Chang and D. N. Hendrichson, *J. Chem. Soc., Chem. Commun.* 1987, 236.
3. J. B. Vincent, H. R. Chang and K. Folting, *J. Am. Chem. Soc.* 1987, **109**, 5703.
4. P. O. W. Boyd, Q. Y. Li and J. B. Vincent, *J. Am. Chem. Soc.* 1988, **110**, 8537.
5. T. Sala and M. V. Sargent, *J. Chem. Soc., Chem. Commun.* 1978, 253.
6. G. Fachinetti, T. Funaioli and P. F. Zanazzi, *J. Chem. Soc., Chem. Commun.* 1988, 1100.
7. D. T. Corwin Jr, E. S. Gruff and S. A. Koch, *J. Chem. Soc., Chem. Commun.* 1987, 966.
8. C. Lopez, S. Alrarez, M. Aguilo, X. Solans and M. F. Altaba, *Inorg. Chim. Acta* 1987, **127**, 153.
9. K. Nakamoto, *Infrared and Raman Spectra of Inorganic and Coordination Compounds*, 4th edn, pp. 110, 206. Wiley Interscience, New York (1986).

Polyhedron Vol. 12, No. 18, pp. 2265–2269, 1993
Printed in Great Britain

0277–5387/93 $6.00+.00
© 1993 Pergamon Press Ltd

STUDIES ON ORGANOLANTHANIDE COMPLEXES—XLIX.* SYNTHESIS OF MIXED TRIS-CYCLOPENTADIENYL LANTHANIDE COMPLEXES, $(CH_3OCH_2CH_2C_5H_4)Ln(C_5H_5)_2$, CONTAINING ONE INTRAMOLECULAR COORDINATION BOND, CRYSTAL STRUCTURE OF $(CH_3OCH_2CH_2C_5H_4)Y(C_5H_5)_2$

CHANGTAO QIAN,† BING WANG and DAOLI DENG

Laboratory of Organometallic Chemistry, Shanghai Institute of Organic Chemistry, Chinese Academy of Sciences, 345 Lingling Lu, Shanghai 200032, China

and

XIANGLIN JIN

Institute of Physical Chemistry, Peking University, Beijing 100871, China

(*Received* 18 *December* 1992; *accepted* 5 *May* 1993)

Abstract—By the one-pot reaction of lanthanide trichloride with 2 equivalents of sodium cyclopentadienyl and 1 equivalent of sodium 2-methoxyethylcyclopentadienyl in THF, the mixed tricyclopentadienyl lanthanide complexes $(C_5H_5)_2Ln(CH_3OCH_2CH_2C_5H_4)$ (Ln = La, Sm, Gd, Er, Yb, Y) were obtained. The compound $(CH_3OCH_2CH_2C_5H_4)Y(C_5H_5)_2$ (**6**) crystallized from THF. The central metal Y is coordinated to three cyclopentadienyl ring centroids and the ether oxygen forming a distorted tetrahedron. The average Y—C(η^5) bond distance and Y—O bond distance of **6** are 2.702 and 2.414 Å, respectively.

Tris-cyclopentadienyl lanthanide complexes were first reported by Birmingham and Wilkinson in 1956.[1] The X-ray structure study shows that the solid-state structure of trivalent lanthanide metallocenes, $(C_5H_5)_3Ln$, are polymeric involving μ-$\eta^5:\eta^2$-C_5H_5 or μ-$\eta^5:\eta^1$-C_5H_5 units.[2–6] The polymers can be destroyed by Lewis bases to form monomeric Lewis base adducts with a formal coordination number 10[7] or 11.[8,9] Recently, using 2-methoxyethylcyclopentadienyl ($CH_3OCH_2CH_2C_5H_4^-$) as a ligand we have successfully prepared the solvent-free monomeric tris-cyclopentadienyl lanthanides $(CH_3OCH_2CH_2C_5H_4)_3Ln$,[10] in which only two of the ether oxygen atoms coordinate to the metal, whose coordination number is 11. Moreover, the studies on crystal structure of the above compounds show that the average bond lengths of Ln—O are longer than the related bond lengths of the compound $(C_5H_5)_3Ln \cdot THF$.[7,11–13] This result prompted us to propose that the solvent-free monomeric tris-cyclopentadienyl lanthanides might also be obtained by forming one intramolecular coordination bond. Therefore, we have investigated the syntheses of the new mixed tris-cyclopentadienyl lanthanide complexes $(CH_3OCH_2CH_2C_5H_4)Ln(C_5H_5)_2$ and the X-ray crystal structure of $(CH_3OCH_2CH_2C_5H_4)Y(C_5H_5)_2$ has been determined.

Although a few mixed tris-cyclopentadienyl lanthanides have been reported,[14–16] to our knowledge the structural information on mixed tris-cyclopentadienyl lanthanides containing intramolecular coordination bond has not been reported up to now.

* For part XLIIX see ref. 24.

† Authors to whom correspondence should be addressed.

EXPERIMENTAL

All operations were performed under purified argon by using Schlenk techniques. All solvents were refluxed and distilled either over finely divided $LiAlH_4$ or over blue sodium benzophenone under argon immediately before use. C_5H_5Na was prepared by the usual method. IR spectra were recorded on Perkin–Elmer 983 and Digilab FTIS-20/E Fourier-transform IR spectrometers with Nujol and fluorolube mulls and were examined between disc-shaped CsI crystals. Mass spectra were recorded on a Finnigan 4021 spectrometer at E.I., $T = 50$–$300°C$, E.M. = 1.3 kV. ^1H NMR spectra were obtained on a FX-90Q (90 MHz) spectrometer referenced to external Me_4Si in THF-d_8.

Metal analyses of the complexes were accomplished using a direct complexometric titration procedure with disodium EDTA.[14] Carbon and hydrogen analyses were performed by the combustion method in an aluminium tude.

Preparation of $CH_3OCH_2CH_2C_5H_4Na$ (7)

The sodium 2-methoxyethylcyclopentadienyl was prepared according to the previous description.[23] ^1H NMR (90 MHz, C_4D_8O) δ: 2.50 (t,2H), 3.05 (s,3H), 3.28 (t,2H), 5.18 (t,2H), 5.31 (t,2H). IR (cm^{-1}): 3060(m), 2922(s), 1458(v), 1095(s), 1077(s), 1022(m), 786(v), 677(s), 385(w), 340(w), 250(m), 225(s).

Preparation of $(CH_3OCH_2CH_2C_5H_4)La(C_5H_5)_2$ (1)

A THF solution of 1 equivalent of $(CH_3OCH_2CH_2C_5H_4)Na$ (0.45 M, 9.3 cm^3) and 2 equivalents of C_5H_5Na (1.07 M, 7.9 cm^3) were, respectively added to a suspension of $LaCl_3$ (1.05 g, 4.2 mmol) in THF (15 cm^3), which had been cooled to $-50°C$. The reaction mixture was warmed to room temperature and stirred overnight. The solvent was removed *in vacuo* and the residue was sublimed at 170–$220°C/4 \times 10^{-4}$ mm Hg giving 0.75 g of a white solid of $(CH_3OCH_2CH_2C_5H_4)La(C_5H_5)_2$ (1) in 45% yield. ^1H NMR (90 MHz, C_4D_8O) δ: 2.48 (t,2H), 3.45 (s,3H), 3.73 (t,2H), 5.57 (s,10H), 5.78 (s,4H). IR (cm^{-1}): 3069(s), 2920(vs), 2851(s), 1452(s), 1439(s), 1043(s), 1035(s), 1009(s), 963(m), 829(m), 780(s), 760(s), 665(m), 395(m), 321(vw), 250(w), 220(m). Found: C, 55.0; H, 5.3; La, 35.4. Calc. for $C_{18}H_{21}OLa$ (1): C, 55.1; H, 5.4; La, 35.4%. MS (E.I., 50–300°C): *m/z* 392 (21.77) M^+, 327 (100) $[M-C_5H_5]^+$, 124 (7.76) $[CH_3OCH_2CH_2C_5H_5]^+$, 66 (26.15) $[C_5H_6]^+$.

Preparation of $(CH_3OCH_2CH_2C_5H_4)Sm(C_5H_5)_2$ (2)

A THF solution of 1 equivalent of $(CH_3OCH_2CH_2C_5H_4)Na$ (0.45 M, 7.8 cm^3) and 2 equivalents of C_5H_5Na (1.07 M, 6.6 cm^3) were, respectively added to a suspension of $SmCl_3$ (0.91 g, 3.54 mmol) in THF (15 cm^3), which had been cooled to $-20°C$. The reaction mixture was warmed to room temperature and stirred overnight. The solvent was removed *in vacuo* and the residue was sublimed at 170–$220°C/4 \times 10^{-4}$ mm Hg giving 0.83 g of a yellow solid of $(CH_3OCH_2CH_2C_5H_4)Sm(C_5H_5)_2$ (2) in 58% yield. IR (cm^{-1}): 3078(s), 2924(vs), 2831(vs), 1437(s), 1057(s), 1045(s), 1032(m), 1011(s), 965(s), 834(s), 785(s), 761(s), 660(m), 382(m), 321(m), 240(m), 210(s). Found: C, 53.7; H, 5.3; Sm, 37.3. Calc. for $C_{18}H_{21}OSm$ (2); C, 53.5; H, 5.2; Sm, 37.2%. MS (E.I., 50–300°C): *m/z* 405 (6.16) $[M]^+$, 340 (100) $[M-C_5H_5]^+$, 124 (5.50) $[CH_3OCH_2CH_2C_5H_5]^+$, 66 (32.82) $[C_5H_6]^+$.

Preparation of $(CH_3OCH_2CH_2C_5H_4)Gd(C_5H_5)_2$ (3)

The procedure followed was similar to that for **2**. A white solid (**3**) was obtained by sublimation (170–$220°C/4 \times 10^{-4}$ mm Hg) in 50% yield. IR (cm^{-1}): 3078(vs), 2937(vs), 2833(s), 1477(s), 1437(s), 1057(s), 1043(s), 1033(s), 1011(s), 963(vs), 836(m), 785(s), 772(s), 670(m), 390(w), 321(vs), 245(m), 220(s). Found: C, 52.6; H, 5.1; Gd, 38.4. Calc. for $C_{18}H_{21}OGd$ (3): C, 52.6; H, 5.2; Gd, 38.3%. MS (E.I., 50–300°C): *m/z* 411 (10.56) $[M]^+$, 346 (100) $[M-C_5H_5]^+$, 124 (5.65) $[CH_3OCH_2CH_2C_5H_5]^+$, 66 (4.30) $[C_5H_6]^+$.

Preparation of $(CH_3OCH_2CH_2C_5H_4)Er(C_5H_5)_2$ (4)

The procedure followed was similar to that for **2**. A pink solid (**4**) was obtained by sublimation (170–$220°C/4 \times 10^{-4}$ mm Hg) in 40% yield. IR (cm^{-1}): 3080(s), 2930(s), 2840(s), 1452(s), 1437(s), 1060(s), 1045(s), 1035(m), 1011(s), 965(m), 837(m), 770(sh), 665(s), 391(s), 321(s), 240(w), 220(m). Found: C, 51.3; H, 4.9; Er, 40.0. Calc. for $C_{18}H_{21}OEr$ (4): C, 51.4; H, 5.0; Er, 39.8%. MS (E.I., 50–300°C): *m/z* 419 (1.69) $[M]^+$, 354 (100) $[M-C_5H_5]^+$, 124 (6.30) $[CH_3OCH_2CH_2C_5H_5]^+$, 66 (4.30) $[C_5H_6]^+$.

Preparation of $(CH_3OCH_2CH_2C_5H_4)Yb(C_5H_5)_2$ (5)

The procedure followed was similar to that for **2**.

A dark green solid (**5**) was obtained by sublimation (170–220°C/4×10^{-4} mm Hg) in 46% yield. IR (cm^{-1}): 3074(vs), 2935(s), 2833(s), 1453(s), 1440(s), 1060(sh), 1045(s), 1035(m), 1011(s), 965(m), 837(m), 769(s,sh), 665(s), 391(s), 321(vw), 240(w), 220(m). Found: C, 50.0; H, 4.8; Yb, 40.9. Calc. for $C_{18}H_{21}OYb$ (**5**): C, 50.7; H, 5.0; Yb, 40.6%. MS (E.I., 50–300°C): 427 (5.29) $[M]^+$, 362 (100) $[M-C_5H_5]^+$, 124 (19.85) $[CH_3OCH_2CH_2C_5H_5]^+$, 66 (86.74) $[C_5H_6]^+$.

factors for non-hydrogen atoms were refined anisotropically.

RESULTS AND DISCUSSION

Synthesis

The new mixed tris-cyclopentadienyl lanthanide complexes (**1–6**) were synthesized by a one-pot reaction as shown in eq. (1).

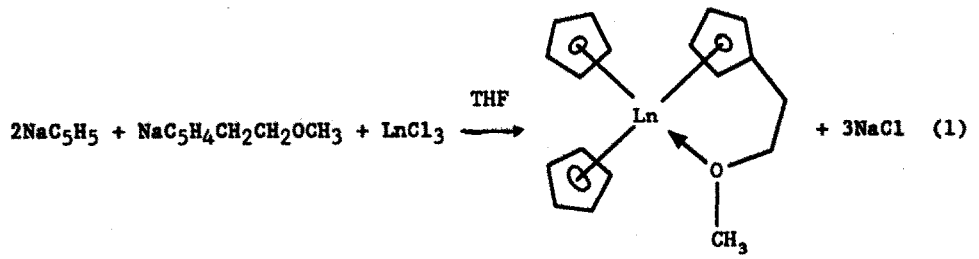

Ln = La(1), Sm(2), Gd(3), Er(4), Yb(5), Y(6)

Preparation of $(CH_3OCH_2CH_2C_5H_4)Y(C_5H_5)_2$ (**6**)

The procedure followed was similar to that for **2**. A white solid (**6**) was obtained by sublimation (170–220°C/4×10^{-4} mm Hg) in 46% yield. ^1H NMR (90 MHz, C_4D_8O) δ: 2.60 (t,2H), 3.45 (s,3H), 3.73 (t,2H), 5.37 (s,10H), 5.89 (t,2H), 6.00 (t,2H). IR (cm^{-1}): 3081(s), 2939(s), 2833(s), 1452(s), 1437(s), 1054(s), 1042(s), 1035(m), 1011(s), 965(m), 837(m), 790(s), 765(s), 632(m), 394(m), 330(w), 259(s), 214(m). Found: C, 62.9; H, 6.1; Y, 25.9. Calc. for $C_{18}H_{21}OY$ (**6**): C, 63.2; H, 6.2; Y, 26.0%. MS (E.I., 50–300°C): 342 (5.60) $[M]^+$, 277 (100) $[M-C_5H_5]^+$, 124 (8.19) $[CH_3OCH_2CH_2C_5H_5]^+$, 66 (39.61) $[C_5H_6]^+$.

X-ray structure analysis

A suitable single crystal, which was obtained through recrystallization from a THF solution of sublimate **6**, was sealed under argon in a thin-walled glass capillary. Intensity data were collected on a Siemens R3m/v diffractometer with Mo-K_α ($\lambda = 0.71073$ Å) radiation in the 2θ–θ scan mode. Final lattice parameters were obtained by a least-squares refinement of the values of reflections. The space group $P21/c$ for compound **6** was identified from the systematic absences. The crystallographic parameters are listed in Table 1. The intensities were corrected for Lorentz and polarization, but not for absorption effects. The Y atom was located by direct methods and all non-hydrogen atoms were obtained from successive Fourier syntheses. Hydrogen atoms were added according to theoretical models. All positional parameters and temperature

All of the new complexes are easily purified by sublimation at 170–220°C/10^{-4} mm Hg, to give solids which were moderately soluble in toluene and very soluble in THF.

In the E.I. mass spectra all of the complexes showed a parent molecular ion, M^+, and related

Table 1. Crystallographic parameters for **6**

Compound	$C_{18}H_{21}OY$
Molecular weight	342.3
Temperature (K)	293
Crystal size (mm)	$0.35\times0.25\times0.10$
Crystal system	Monoclinic
Space group	$P21/c$
Cell constants:	
a (Å)	13.235(7)
b (Å)	8.530(3)
c (Å)	13.829(4)
β (°)	94.13(3)
V (Å^3)	1557.2(11)
Z	4
D_{calc} (g cm^{-3})	1.460
Scan technique	2θ–θ
Data collected	$+h, +k, \pm l$
2θ range (°)	3.0–50.0
μ (Mo-K_α) (cm^{-1})	37.60
Total reflections	3089
Independent reflections	2756
Observed reflections	2186 ($F > 4\sigma(F)$)
F(000)	704
No. of variables	181
R	0.0761
Rw	0.0855
Goodness of fit	2.76

fragments; no m/z greater than M^+ was detected. This indicates that the complexes are monomeric and the Ln—C_5H_5 bond is first cleaved, giving the base peak of $[M-C_5H_5]^+$.

The IR spectra of these new complexes exhibit absorption peaks typical of η^5-cyclopentadienyl at *ca* 775, 1020, 1440 and 3085 cm^{-1}.[17–19] Moreover, the IR spectrum analyses imply the presence of an intramolecular coordination bond from the oxygen atom of the ether-substituted cyclopentadienyl to the lanthanide metal, because the absorption peak of the C—O—C asymmetric stretching vibration in the new complexes is shifted to lower frequency ($\Delta\nu = 35$–53 cm^{-1}) compared with those of $NaC_5H_4CH_2CH_2OCH_3$ (**7**).[14–20]

The ^1H NMR data of complexes **1**, **6** and **7** were measured in perdeuterotetrahydrofuran. It is noteworthy that the proton signals of OCH_3 and OCH_2 shift to lower field compared with those of the sodium salt (**7**). These results show that an intramolecular coordination bond, Ln—O, is formed.[20,21]

Structure

The crystallographic parameters, selected bond lengths and angles of complex **6** are listed in Tables 1 and 2. The molecular and crystal structure of **6** is shown in Fig. 1.

The crystal structure analysis shows that the distorted tetrahedron around the yttrium ion is formed with three centroids of the cyclopentadienyl rings and the oxygen atom of the ligand. Complex **6** is a monomer with an intramolecular coordination bond. However, the formal coordination number of Y^{3+} is 10. The Y—C(η^5) bond distances range from 2.535(20) to 2.793(26) Å and average 2.702 Å. This is similar to the value reported for $(C_5H_5)_3Y$ THF (**8**), 2.71(3) Å.[13] The Y—O bond length in **6** is 2.414(13) Å, which is 0.04 Å shorter than that in **8**. Since the coordination environment of the metal ion in **6** is different from that in $(CH_3OCH_2CH_2C_5H_4)_3Pr$ (**9**),[10] the Y—O distance is significantly shorter than the mean Pr—O distance in **9**, even if the difference in metal ion size is taken

Table 2. Selected bond lengths (Å) and angles (°) for **6**

Y(1)—O(1)	2.414(13)	Y(1)—C(4)	2.736(21)
Y(1)—C(5)	2.669(22)	Y(1)—C(6)	2.640(20)
Y(1)—C(7)	2.693(22)	Y(1)—C(8)	2.765(19)
Y(1)—C(9)	2.700(26)	Y(1)—C(10)	2.793(26)
Y(1)—C(11)	2.788(24)	Y(1)—C(12)	2.727(24)
Y(1)—C(13)	2.744(28)	Y(1)—C(14)	2.737(25)
Y(1)—C(15)	2.535(51)	Y(1)—C(16)	2.716(31)
Y(1)—C(17)	2.640(40)	Y(1)—C(18)	2.665(24)
O(1)—C(1)	1.439(27)	O(1)—C(2)	1.408(26)
C(2)—C(3)	1.515(33)	C(3)—C(4)	1.486(27)
C(4)—C(5)	1.428(31)	C(4)—C(8)	1.395(27)
C(5)—C(6)	1.397(27)	C(6)—C(7)	1.456(30)
C(7)—C(8)	1.422(31)	C(9)—C(10)	1.404(47)
C(9)—C(13)	1.404(40)	C(10)—C(11)	1.364(37)
C(11)—C(12)	1.421(40)	C(12)—C(13)	1.402(44)
C(14)—C(15)	1.412(57)	C(14)—C(18)	1.421(39)
C(15)—C(16)	1.412(57)	C(16)—C(17)	1.391(50)
C(17)—C(18)	1.427(45)	Y(1)—Cent(1)[a]	2.416
Y(1)—Cent(2)	2.481	Y(1)—Cent(3)	2.375
C(1)—O(1)—C(2)	111.4(16)	O(1)—C(2)—C(3)	113.4(18)
C(2)—C(3)—C(4)	110.7(18)	C(3)—C(4)—C(5)	129.0(19)
C(3)—C(4)—C(8)	123.7(20)	C(5)—C(4)—C(8)	107.1(16)
C(4)—C(5)—C(6)	110.0(17)	C(5)—C(6)—C(7)	104.9(18)
C(6)—C(7)—C(8)	108.7(18)	C(4)—C(8)—C(7)	108.3(18)
C(10)—C(9)—C(13)	112.9(25)	C(9)—C(10)—C(11)	98.8(24)
C(10)—C(11)—C(12)	118.9(28)	C(11)—C(12)—C(13)	99.9(23)
C(9)—C(13)—C(12)	108.5(25)	C(15)—C(14)—C(18)	107.1(27)
C(14)—C(15)—C(16)	104.1(32)	C(15)—C(16)—C(17)	111.4(32)
C(16)—C(17)—C(18)	103.8(28)	C(14)—C(18)—C(17)	109.2(24)
Cent(1)—Y—Cent(2)	117.9	Cent(2)—Y—Cent(3)	115.4
Cent(1)—Y—Cent(3)	120.4	Cent(1)—Y—O(1)	91.3
Cent(2)—Y—O(1)	101.3	Cent(3)—Y—O(1)	102.8

[a] Cent(1) is the centroid of the cyclopentadienyl ring defined by C(4)–(8); Cent(2), C(9)–(13); Cent(3), C(14)–(18).

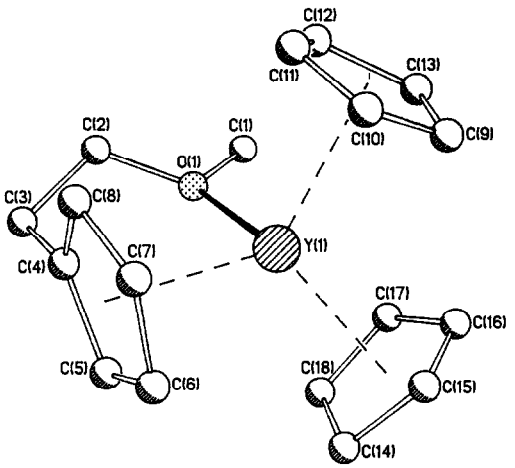

Fig. 1. Molecular structure of $(CH_3OCH_2CH_2C_5H_4)Y(C_5H_5)_2$ (**6**).

into account.[22] This reveals that coordination of the central metal is saturated in the new monomeric complexes $(CH_3OCH_2CH_2C_5H_4)Ln(C_5H_5)_2$, but is over-saturated in the complexes $(CH_3OCH_2CH_2C_5H_4)_3Ln$, resulting in the longer Ln—O distance in the latter.

Three cent—Y—cent angles are 120.4, 117.9 and 115.4°, respectively, and the sum of three angles is 353.7° in **6**, which are comparable with the angles 119.2, 117.5, 115.4 and 352.1° in **8**, respectively. This shows that the arrangement of three cyclopentadienyl rings in **6** is analogous to the arrangement in **8**. The angles of O(1)—Y—cent(1), O(1)—Y—cent(2) and O(1)—Y—cent(3) are 91.3, 101.3 and 102.8° in **6**, respectively. It is noteworthy that the smallest angle O(1)—Y—cent(1) (91.3°) is 5.1° smaller than that of O—Y—cent in **8**. The difference is the result of forming an intramolecular coordination bond.

Acknowledgements—We thank the National Natural Science Foundation of China and Chinese Academy of sciences for financial support.

REFERENCES

1. J. M. Birmingham and G. Wilkinson, *J. Am. Chem. Soc.* 1956, **78**, 42.
2. C. H. Wong, T. Lee and Y. Lee, *Acta Cryst., Sect. B* 1969, **25**, 2580.
3. J. L. Atwood and K. D. Smith, *J. Am. Chem. Soc.* 1973, **78**, 1488.
4. J. H. Burns, W. H. Baldwin and F. H. Fink, *Inorg. Chem.* 1974, **13**, 1916.
5. W. Hinrichs, D. Melzer, M. Rehwoldt, W. Jahn and R. D. Fischer, *J. Organomet. Chem.* 1983, **251**, 299.
6. S. H. Eggers, J. Kopf and R. D. Fischer, *Organometallics* 1986, **5**, 383.
7. H. Schumann and W. Genthe, in *Handbook on the Physics and Chemistry of Rare Earths* (Edited by K. A. Gschneidner Jr and L. Eyring), Vol. 7, Ch. 53. Elsevier, Amsterdam (1985) and refs therein.
8. M. R. Spiret, J. Rebizant, C. Apostolidis and B. Kanellakopulos, *Acta Cryst., Sect. C* 1987, **43**, 2322.
9. X. Li, S. Eggers, J. Kopf, W. Jahn, R. D. Fischer, C. Apostolidis, B. Kanellakopulos, F. Benetello, A. Polo and G. Bombieri, *Inorg. Chim. Acta* 1985, **100**, 183.
10. C. Qian, B. Wang, D. Deng, G. Wu and P. Zheng, *J. Organomet. Chem.* 1992, **427**, C29.
11. F. Benetollo, G. Bombieri, C. Bisicastellani, W. Jahn and R. D. Fischer, *Inorg. Chim. Acta* 1984, **95**, L7.
12. Y. Fan, P. Lu, Z. Jin and W. Chen, *Scient. Sin. B* 1984, **27**, 993.
13. R. D. Rogers, J. L. Atwood, A. Emad, D. J. Sikora and M. D. Rausch, *J. Organomet. Chem.* 1981, **216**, 383.
14. C. Qian, Z. Xie and Y. Huang, *J. Organomet. Chem.* 1990, **398**, 251.
15. C. Qian, C. Ye, H. Lu, Y. Li, J. Zhou, Y. Ge and M. Tsutsui, *J. Organomet. Chem.* 1983, **247**, 161.
16. W. J. Evans and T. A. Ulibarri, *J. Am. Chem. Soc.* 1987, **109**, 4292.
17. C. Qian, C. Ye, H. Lu, Y. Li and Y. Huang, *J. Organomet. Chem.* 1984, **263**, 161.
18. F. W. Siegert and H. J. D. Meijer, *J. Organomet. Chem.* 1969, **20**, 141.
19. H. P. Fritz in *Advances in Organometallic Chemistry* (Edited by F. G. A. Stone and R. West), Vol. 1, p. 239, Academic Press Inc., New York (1966).
20. C. Qian, Z. Xie and Y. Huang, *J. Organomet. Chem.* 1987, **323**, 285.
21. H. Schumann, J. Loebel, J. Pickort, C. Qian and Z. Xie, *Organometallics* 1991, **10**, 215.
22. R. D. Shannon, *Acta Cryst., Sect. A* 1976, **32**, 751.
23. Q. Huang, Y. Qian, W. Xie, M. Shou and E. Tang, *J. Inorg. Chem. (China)* 1985, 166.
24. C. Qian and D. Zhu, *Youji Huaxue*, in press.

Polyhedron Vol. 12, No. 18, pp. 2271–2277, 1993
Printed in Great Britain

0277–5387/93 $6.00+.00
© 1993 Pergamon Press Ltd

KINETICS OF THE SUBSTITUTION REACTION BETWEEN AQUAOXOTETRACYANOMOLYBDATE(IV) AND CYANIDE/HYDROGEN CYANIDE

JAAP P. SMIT, WALTER PURCELL, ANDREAS ROODT* and JOHANN G. LEIPOLDT

Department of Chemistry, University of the Orange Free State, Bloemfontein 9300, South Africa

(*Received* 28 *January* 1993; *accepted* 20 *April* 1993)

Abstract—The kinetics of the substitution reaction between aquaoxotetracyanomolybdate (IV) ions and CN^- and HCN, as an important intermediate step in the formation of the $[Mo(CN)_8]^{4-}$ complex, was studied by stopped-flow spectrometry. The aqua ligand in the $[MoO(H_2O)(CN)_4]^{2-}$ complex is substituted by both CN^- ions and hydrogen cyanide according to the reaction:

$$[MoO(H_2O)(CN)_4]^{2-} + CN^-/HCN(L) \underset{k_{-L}}{\overset{K_L, k_L}{\rightleftharpoons}} [MoO(L)(CN)_4]^{n-} + H_2O.$$

At 15.0°C and $\mu = 1.0$ M (KNO_3) the equilibrium, forward and reverse rate constants of the reaction with CN^- ions were determined as 92(5) M^{-1}, 83(1) $M^{-1}\,s^{-1}$ and 0.87(3) s^{-1}, and for HCN as 3(1) M^{-1}, 458(5) $M^{-1}\,s^{-1}$ and 140(30) s^{-1}, respectively. Coordination of the HCN to the metal centre results in a decrease in the pK_a value of hydrogen cyanide by approximately 1.5 pH units to *ca* 7.6(2).

It was shown over the past few years that the protonation of the dioxotetracyano complexes of molybdenum(IV), tungsten(IV), rhenium(V) and technetium(V) results in the formation of the $[MO(OH)(CN)_4]^{(n+1)-}$ and $[MO(H_2O)(CN)_4]^{n-}$ complexes.[1] These protonated species undergo substitution reactions with mono- (aqua substitution) and bidentate[2] (aqua and cyano substitution) ligands. The protonation behaviour of these systems has recently been the subject of carbon-13 and oxygen-17 NMR[3,4] studies in order to investigate the water exchange of these complex ions.

Previous studies of monodentate substitution reactions on the $[MO(H_2O)(CN_4]^{n-}$ complexes for the tungsten(IV) and rhenium(V) systems[1] included different ligands such as F^-, N_3^- and NCS^- ions, pyridine and substituted thioureas. However, for the molybdenum(IV) system the only monodentate ligand substitution reaction that could be studied was that of fluoride ions as a result of the high lability of the coordinated aqua in the $[MoO(H_2O)(CN)_4]^{2-}$ ion. Although it is known that the HCN entity can act as a monodentate ligand,[5–8] this fact was only recently observed in our laboratory for these dioxotetracyano systems. We have therefore, taken interest in the substitution behaviour of these systems in CN^-/HCN medium in order to investigate the formation of the higher coordinated cyano complexes {i.e. $[M(CN)_8]^{4-}$ (for M = Mo^{IV} and W^{IV})} since the mechanism of such a process is not known at this stage. The results of the kinetic study of the molybdenum(IV) system in aqueous CN^-/HCN medium, forming the oxopentacyanomolybdate(IV) complex as an important intermediate in the formation of the octacyano species, is reported herein.

EXPERIMENTAL

General

All chemicals used were of analytical reagent grade and double distilled water was used in all

* Author to whom correspondence should be addressed.

these experiments. All pH measurements were obtained on an Orion 701 pH meter with a combined glass/calomel electrode.

CAUTION. Cyanide is extremely toxic and HCN is generated throughout these experiments. Care should therefore be taken to perform all manipulations in a fume hood as far as possible.

Preparation of the starting complex

$K_3Na[MoO_2(CN)_4]\cdot 6H_2O$ was prepared in the following way: $Na_2MoO_4\cdot 2H_2O$ (7.0 g, 0.03 mol), KBH_4 (3.0 g, 0.063 mol) and KCN (5.0 g, 0.077 mol) were dissolved in water (100 cm^3) and cooled to *ca* 5°C, followed by the dropwise addition of acetic acid (5 cm^3, 0.08 mol) over *ca.* 10 min. More KCN (5.0 g, 0.077 mol) was then added, followed by the dropwise addition of another aliquot of acetic acid (5 cm^3, 0.007 mol) over *ca* 10 min. A mixture of NaOH (10 g, 0.25 mol) and KOH (14 g, 0.25 mol) (as solids) was added slowly to the molybdenum(IV) solution followed by the slow addition of ethanol (30 cm^3). The pink crystals were washed successively in small portions with an ethanol/water (9:1) (600 cm^3) mixture. Recrystallization was performed by dissolving the crystals in a minimum of water, addition of NaOH and KOH (*ca* 1 g of each) and precipitation of $K_3Na[MoO_2(CN)_4]\cdot 6H_2O$ by the slow addition of ethanol (yield 7.5 g, >50%). The purity was confirmed as described previously.[1]

Data collection and other measurements

The kinetics were obtained at 600 nm on a Durrum D-110 stopped-flow spectrophotometer coupled with a personal computer capable of performing least-squares analyses on the absorbance vs time data obtained from the kinetic runs. All kinetic runs were performed under pseudo-first-order conditions in carbonate/bicarbonate buffer medium with $\mu = 1.0$ M (KNO_3). Selective variation of the molybdenum(IV) concentration throughout these experiments showed no detectable changes in the rate constants observed. Other spectrophotometric measurements were performed on a Hitachi 150-20 double beam instrument, while all temperatures are reported to ±0.1°C accuracy. The solid lines in Figs 1–6 represent the computer least-squares fits of the data to the respective functions. In all calculations the acid dissociation constant for HCN has been taken as 9.20(6), which was confirmed potentiometrically at 10.0°C in $\mu = 1.0$ M (KNO_3). The reported value in 0.1 ionic strength is 9.20[5–9] at 25°C.

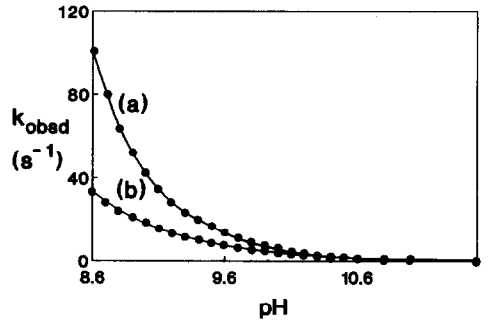

Fig. 1. pH dependence of pseudo-first-order rate constant at 10.0°C, $[Mo^{IV}] = 4.22\times10^{-3}$ M, $\mu = 1.0$ M (KNO_3), for (a) $[CN^-] = 0.05$ M and (b) $[CN]_{tot} = 0.050$ M.

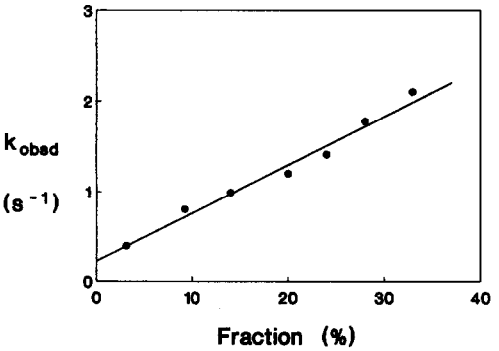

Fig. 2. Dependence of the pseudo-first-order rate constant on the fraction of $[MoO(H_2O)(CN)_4^{2-}]$ as a function of $[Mo^{IV}]_{tot}$ at 10.0°C, $\mu = 1.0$ M (KNO_3), $[CN^-] = 0.050$ M and $[Mo^{IV}] = 4.22\times10^{-3}$ M.

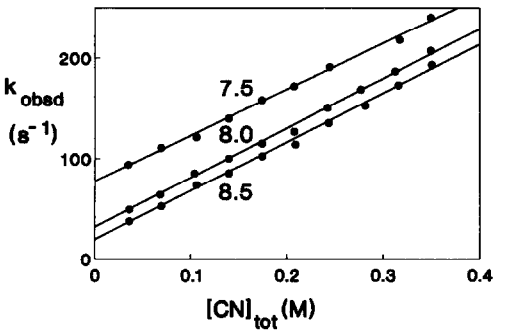

Fig. 3. Dependence of pseudo-first-order rate constant on $[CN]_{tot}$ at pH (a) 7.5, (b) 8.0 and (c) 8.5, at 15.0°C, $[Mo^{IV}] = 4.22\times10^{-3}$ M $\mu = 1.0$ M (KNO_3).

RESULTS

We have taken care to perform the different experiments described here in such a way as to ensure the most complete analysis of this complex system. The following important results from previous research on these systems have to be kept in

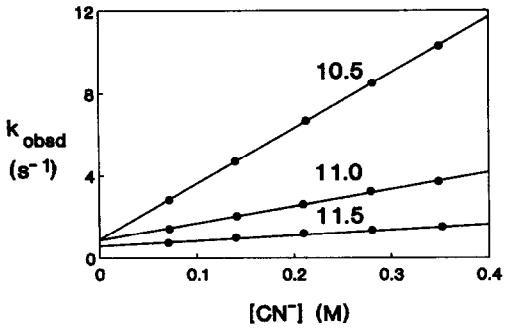

Fig. 4. Dependence of pseudo-first-order rate constant on [CN^-] at pH (a) 10.5, (b) 11.0 and (c) 11.5, at 15.0°C, $[Mo^{IV}] = 4.22 \times 10^{-3}$ M, $\mu = 1.0$ M (KNO_3).

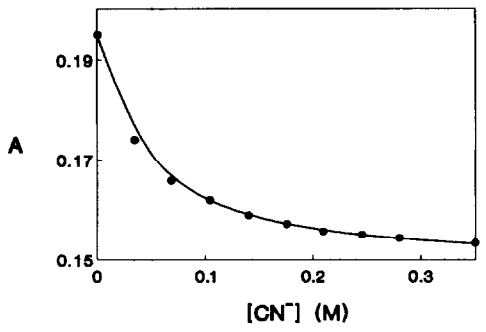

Fig. 6. Absorbance change ($\lambda = 600$ nm) dependence on [CN^-] at 15.0°C, $[Mo^{IV}] = 4.22 \times 10^{-3}$ M, $\mu = 1.0$ M (KNO_3), pH = 10.5.

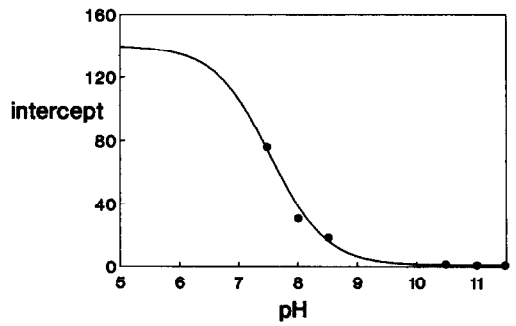

Fig. 5. pH dependence of y-intercept [eqs (4) and (5)] at 15.0°C, $[Mo^{IV}] = 4.22 \times 10^{-3}$ M, $\mu = 1.0$ M (KNO_3), $[CN]_{tot} = 0.050$ M.

mind: (1) The $[MO(H_2O)(CN)_4]^{n-}$ complex is the only protonated species of the dioxotetracyano complexes of molybdenum(IV), tungsten(IV), technetium(V) and rhenium(V) which is reactive towards monodentate substitution, i.e. no replacement of the hydroxo ligand in the $[MO(OH)(CN)_4]^{m-}$ complexes was observed in all the systems studied.[1] (2) In the rhenium(V) system, and some other complexes studied, protonated forms of different ligands, for example, HN_3[10] and specifically HCN,[5-8] can act as monodentate ligands. (3) The oxopentacyanomolybdate(IV) complex, $[MoO(CN)_5]^{3-}$,[11,12] and very recently also the HCN complex, $[MoO(CN)_4(HCH\text{-}\kappa N)]^{2-}$,[13] have already been isolated as the PPh_4^+ salts and characterized crystallographically, confirming the formulation of the reaction products.

These observations, coupled with the fact that the $[MoO(H_2O)(CN)_4]^{2-}$ complex reacts with cyanide at pH values below the pK_a value of HCN (9.2), enables the construction of Scheme 1 for the ligation of $[MoO(H_2O)(CN)_4]^{2-}$ by CN^-/HCN. The coordination mode of the HCN in the $[MoO(HCN)(CN)_4]^{2-}$ complex is via the nitrogen atom,[12,14-16] which has been confirmed recently by the crystal structure determination of $(PPh_3)_2[MoO(NCH\text{-}\kappa N)(CN)_4]\cdot H_2O$.[13] The effect of isomerization is not addressed separately in this system and is assumed to be incorporated in the K_{aNCH} value. It is, however, reasonable to assume that the isomerization is rapid since no deviation from first-order kinetics was observed. This is in agreement with the fast isomerization observed for cobalt(III) ($[Co(CN)_5NC]^{3-} \rightarrow [Co(CN)_6]^{3-}$, $k_{iso} = 0.2$ s^{-1}), even though the normal substitution reactions on the cobalt(III) centre are very slow.[14]

Figure 1(a) illustrates the effect of pH on the observed reaction rate constant for the reaction between $[MoO(H_2O)(CN)_4]^{2-}$ and CN^-/HCN in the pH range 8–12, at constant [CN^-] = 0.05 M (calculated, pK_{aHCN} = 9.20). Similarly, Fig. 1(b) shows the pH dependence of k_{obs} at constant *total* cyanide concentration, i.e. $[CN]_{tot} = 0.050$ M.

The rapid increase in k_{obs} below the pK_a value of HCN from both plots in Fig. 1 is quite obvious. It

$$[MoO(H_2O)(CN)_4]^{2-} + CN^- \underset{k_{-1}}{\overset{k_1}{\rightleftharpoons}} [MoO(CN)_5]^{3-} + H_2O$$

$$+H^+ \; \updownarrow \; -H^+, K_{aHCN} \qquad +H^+ \; \updownarrow \; -H^+, K_{aNCH}$$

$$[MoO(H_2O)(CN)_4]^{2-} + HCN \underset{k_{-2}}{\overset{k_2}{\rightleftharpoons}} [MoO(HCN)(CN_4]^{2-} + H_2O$$

Scheme 1.

is clear that the concentration of the aqua complex increases with a decrease in pH from 12 to 9. Using the data in Fig. 1, and the definition of the acid dissociation constant for the $[MoO(H_2O)(CN)_4]^{2-}$ complex ($pK_{a1} = 10.0$[1]), the fraction concentration of the *aqua* complex in the pH range 10.3–11.5 can be calculated. Figure 2 shows the relationship between the observed rate constant and the fraction of the $[MoO(H_2O)(CN)_4{}^{2-}]$ ion with respect to the total $[Mo^{IV}]$, clearly illustrating a negligible contribution of $[MoO(OH)(CN)_4]^{3-}$ to the observed rate constant (*y*-intercept represents only the contribution of the reverse step, k_{-1}, see Discussion). This observation is in direct correlation with the proposed reaction in Scheme 1, i.e. that the aqua $[MoO(H_2O)(CN)_4]^{2-}$ complex is the only reactive species towards substitution by CN^-/HCN.

The rate law for the complete reaction in Scheme 1 is given by eq. (1)

$$\text{Rate} = k_1[MoH_2O][CN^-] + k_2[MoH_2O][HCN] - k_{-1}[MoCN] - k_{-2}[MoNCH] \quad (1)$$

In eq. (1) MoH_2O, MoCN and MoNCH represent the $[MoO(H_2O)(CN)_4]^{2-}$, $[MoO(CN)_5]^{3-}$ and $[MoO(NCH)(CN)_4]^{2-}$ species, respectively. Before integration of the rate equation the total concentration of molybdenum(IV) reactant ($[Mo^{IV}]_{tot} = [MoO(H_2O)(CN)_4{}^{2-}] + [MoO(OH)(CN_4{}^{3-}]$) and that of the products ($[MoCN]_{tot} = [MoO(CN)_5{}^{3-}] + [MoO(NCH)(CN)_4{}^{2-}]$) was incorporated in eq. (1). The definitions of the first acid dissociation of $[MoO(H_2O)(CN)_4]^{2-}$, K_{a1}, as well as the acid dissociation constant of HCN, K_{aHCN}, and that of the coordinated hydrogen cyanide, K_{aNCH}, were also included. Expressions for the observed first-order rate constant, k_{obs}, were consequently obtained upon integration of the rate law ($[CN^-]$, $[CN^-]_{tot} \gg [Mo]_{tot}$) in terms of the total cyanide concentration, $[CN]_{tot} = ([CN^-] + [HCN])$ [eq. (2)], or in terms of $[CN^-]$ [eq. (3)].

$$k_{obs} = \frac{[(k_1 K_{aHCN}/[H^+]) + k_2][CN]_{tot}}{(1 + K_{a1}/[H^+])(1 + K_{aHCN}/[H^+])} + \frac{k_{-2} + k_{-1}K_{aNCH}/[H^+]}{1 + K_{aNCH}/[H^+]} \quad (2)$$

$$k_{obs} = \frac{[(k_1 K_{aHCN}/[H^+]) + k_2](1 + [H^+]/K_{aHCN})[CN^-]}{(1 + K_{a1}/[H^+])(1 + K_{aHCN}/[H^+])} + \frac{k_{-2} + k_{-1}K_{aNCH}/[H^+]}{1 + K_{aNCH}/[H^+]} \quad (3)$$

The solid line in Fig. 1(b) represents the least-squares fit of the k_{obs} vs pH data to eq. (3) (constant $[CN]_{tot} = 0.050$ M). Similarly, the solid line in Fig. 1(a) gives the least-squares fit of the k_{obs} vs pH data to eq. (2) (constant $[CN^-] = 0.050$ M). The approximate values obtained from both computer fits in Fig. 1 for k_1, k_{-1}, k_2, k_{-2} and K_{aNCH} are 140(20) M^{-1} s^{-1}, $-0.2(2)$ s^{-1}, 300(50) M^{-1} s^{-1}, 180(70) s^{-1} and $2(1) \times 10^{-8}$. Equation (3) has too many parameters to produce accurate results from a single fit to the data in Fig. 1, but good estimates for the different constants could nevertheless be obtained therefrom. More accurate values for the different constants were determined as described below.

At pH values 7–8, where $[H^+] \gg K_{a1}$, K_{aHCN}, eq. (2) simplifies to eq. (4).

$$k_{obs} = k_2[CN]_{tot} + \frac{k_{-2} + k_{-1}K_{aNCH}/[H^+]}{1 + K_{aNCH}/[H^+]} \quad (4)$$

Figure 3 illustrates the dependence of the pseudo-first-order rate constant on the total cyanide concentration (primarily in the form of HCN) at pH values 7.5–8.5 (lower pH values could not be studied due to the small effective equilibrium constant, see Fig. 3). It is clear that the increase in k_{obs} is primarily a result of the increase in the intercept, i.e. the reverse rate constant, and that the kinetics at these pH values are adequately described by eq. (4). It is further obvious that the value of k_2 can be obtained from the slope of the lines in Fig. 3 and the average value obtained from the three pH values is reported in Table 1.

At pH values 11–11.5, where $[H^+] \ll K_{a1}$, K_{aHCN}, eq. (2) simplifies to eq. (5).

$$k_{obs} = \frac{k_1[H^+][CN]_{tot}}{K_{a1}} + \frac{k_{-2} + k_{-1}K_{aNCH}/[H^+]}{1 + K_{aNCH}/[H^+]} \quad (5)$$

Figure 4 shows the dependence of k_{obs} on the total cyanide (primarily in the form of CN^- ions) at pH values 10.5–11.5. It is clear from eq. (5) that k_1 is obtained from the slope upon incorporation of the pH and K_{a1}. The average value for k_1 thus obtained is given in Table 1.

The contribution to the total pseudo-first-order rate constant provided by the reverse path, given in eqs (4) and (5), is at lower pH values, primarily as a function of the acid dissociation constant of the coordinated HCN, i.e. K_{aNCH}. Assuming $pK_{aNCH} < 8$ the reverse reaction in eq. (5) can be simplified even further ($k_{-1} > k_{-2}[H^+]/K_{aNCH}$, as confirmed by the similarity in the intercepts of the lines in Fig. 4) and the expression for the pseudo-first-order rate constant (pH *ca* 11) is given by eq. (6).

$$k_{obs} = \frac{k_1[H^+][CN]_{tot}}{K_{a1}} + k_{-1} \quad (6)$$

At high pH values the intercept in eq. (6), therefore, provides values for the reverse rate constant for the

Table 1. Kinetic and equilibrium data at different temperatures, $\mu = 1.0$ M (KNO_3), $[Mo^{IV}]_{tot} = (4.2-13)\times 10^{-3}$ M

Constant	Temperature (°C)	Result
k_1 ($M^{-1}\,s^{-1}$)	10.0	80(9)[a]
	10.0	57(1)[b]
	15.0	83(1)[b]
	15.0	84(2)[c]
	20.0	116(2)[b]
ΔH^* (k_1) (kJ mol^{-1})	—	51(4)
ΔS^* (k_1) (J K mol^{-1})	—	−53(14)
k_2 ($M^{-1}\,s^{-1}$)	5.0	$3.1(1)\times 10^{2}$[d]
	10.0	$3.80(8)\times 10^{2}$[d]
	15.0	$4.58(5)\times 10^{2}$[d]
	15.0	$4.8(2)\times 10^{2}$[e]
ΔH^* (k_2) (kJ mol^{-1})	—	35(1)
ΔS^* (k_2) (J K mol^{-1})	—	−80(4)
k_{-1} (s^{-1})	10.0	0.37(3)[f]
	10.0	0.40(2)[g]
	15.0	0.87(2)[g]
	20.0	1.20(5)[g]
k_{-2} (s^{-1})	5.0	61(15)[h]
	10.0	$1.0(2)\times 10^{2}$[h]
	15.0	$1.4(3)\times 10^{2}$[h]
K_1 (M^{-1})	15.0	95(5)[i]
	15.0	88(8)[j]
K_2 (M^{-1})	15.0	3(1)[k]
pK_{aNCH}	10.0	7.6(2)[l]

[a] Figure 2, k_1 = slope ($[Mo]_{tot}/[CN^-]$).
[b] Temperature study at pH = 11, k_1 = slope ($K_{a1}/[H^+]$), eq. (5).
[c] Figure 4, k_1 = slope ($K_{a1}/[H^+]$), eq. (5).
[d] Temperature study at pH = 7.5, eq. (4).
[e] Figure 3, eq. (4).
[f] Figure 2, intercept.
[g] Temperature study at pH = 11, eq. (6).
[h] Figure 3, calculated from intercepts assuming $pK_{aNCH} = 7.6$.
[i] Kinetically, $K_1 = k_1/k_{-1}$.
[j] Figure 6, eq. (8).
[k] Kinetically, $K_2 = k_2/k_{-2}$.
[l] Average from computer fits to eqs (2), (3) and (7) (data Figs 1 and 5).

CN^- pathway, of which the results obtained for k_{-1} are given in Table 1.

The pH dependence of the intercept at lower pH values is described by eq. (7), with the contribution of k_{-1} being relatively small at pH < 10 and the intercept is primarily determined by k_{-2}.

$$\text{Intercept} = \frac{k_{-2}[H^+] + k_{-1}K_{aNCH}}{[H^+] + K_{aNCH}} \qquad (7)$$

The pH dependence of the intercept is shown in Fig. 5 [the least-squares fit to eq. (7) given by the solid line], from which a fairly accurate estimated pK_a value of the coordinated HCN could be determined, see Table 1.

A more accurate definition of the complete curve in Fig. 5 is restricted by the decrease in the reaction yield at pH < 7.5. The accurate determination of k_{-2} is limited accordingly.

The equilibrium constants for neither the HCN nor the CN^- pathways can be determined individually as a result of the complexity of the equation defining the reaction equilibria, see Scheme 1. However, at high pH the CN^- pathway dominates and the absorbance dependence on $[CN^-]$ for this system (pH = 10.5), upon incorporation of Beer's law,

mass balance and the definitions of K_1 ($= k_1/k_{-1}$) and K_{a1}, can be described by eq. (8). The results are shown in Fig. 6 and the K_1 value obtained is reported in Table 1.

$$A = \frac{A_m + A_{ml}K_1[CN^-]}{(1+K_{a1}/[H^+])(1+K_1[CN^-])} \quad (8)$$

In eq. (8) A_m and A_{ml} represent the absorbance contributions due to the unsubstituted and substituted complexes, respectively.

A temperature dependence study was undertaken to determine the activation parameters for both the HCN (at pH = 7.5) and CN^- (at pH = 11.0) pathways. The results of the studies showed the normal dependence similar to that given in Figs 3 and 4 and the forward and reverse rate constants and the activation parameters calculated therefrom are given in Table 1. The temperature changes in the pK_a values of the molybdenum(IV) complexes were assumed to be negligible compared with that of the other parameters.

DISCUSSION

The oxopentacyanomolybdate(IV) complex has been obtained previously and is well characterised,[11,12] while reactions of HCN as a ligand have been described previously in aqueous systems such as $[Ni(CN)_4]^{2-}$, $[Ni(trien)]^{2+}$ (trien = triethylenetetramine),[5] $[Ni(daco)_2]^{2+}$ [8] (daco = 1,5-diazicyclooctane), $[Ni(EDTA)]^{2-}$,[8] aqua-cobalamin[7] and [Rh(TPPS)$(H_2O)_2$] [TPPS = tetrakis(4-sulphonatophenyl)porphyrin].[6] It was found that CN^- ions may react more rapidly than HCN,[6] but the opposite also holds true.[8] The HCN coordinates to the metal centre via the nitrogen, as has very recently been crystallographically verified by the structure determination of $(PPh_4)[MoO(CN)_4(NCH\text{-}\kappa N)]\cdot H_2O$.[13] Evidence from the literature concerning the coordination ability of the nitrogen atom in the HCN entity is quite abundant, i.e. the crystal structure determination of $[(NH_3)_5Co NCCo(CN)_5]\cdot H_2O$[15] showed that CN^- can act as an ambidentate ligand, i.e. coordinate with either the carbon or nitrogen atom; the structure determinations of, for example, $[(NH_3)Co(NCacac)](Cl)(ClO_4) \cdot 2H_2O$[16] (NCacac = 3-cyanoacetylacetonato) and $[(PPh_3)_2N]_2[MoO(CN)_4(NCCH_3)]$[12] showed that cyanide can in principle coordinate to a metal centre via the nitrogen atom; the existence of dimeric $[(CN)_6W—NC—W(CN)_6]^-$ and trimeric $[(CN)_7W—CN—W(CN)_6—CN—W(CN)_7]^{6-}$ ions, as has been suggested recently,[17] further illustrates this point.

It is of significance that hydrogen cyanide has been found to react in the case of the $[MoO(H_2O)(CN)_4]^{2-}$ system, providing a possible route for the formation of the octacyano complexes at lower acidity values. Equally important, however, is the fact that in spite of the HCN reacting with the aquaoxotetracyanomolybdate(IV) complex, the stability constant of the pentacyano-oxo complex at pH values less than 8.5 is too low to ensure appreciable amounts of $[MoO(CN)_5]^{3-}$ present, a prerequisite for the formation of the $[Mo(CN)_8]^{4-}$ complex. This is in agreement with the observed fact that the octacyanomolybdate(IV) does not form around these pH values.

In the molybdenum(IV) system it is of significance that the HCN actually reacts approximately five times more rapidly than the CN^- ion, see k_2 and k_1 in Table 1. Since a dissociative mechanism has been assumed for the tungsten(IV) system based on the high pressure kinetic study for the reaction between the $[WO(H_2O)(CN)_4]^{2-}$ complex and N_3^- ions ($\Delta V^* = +10.6$ cm^3 mol^{-1}),[1] a similar mechanism is anticipated for the molybdenum(IV) system. Furthermore, the large *trans* influence of the oxo ligand as observed in the metal–aqua bond distances in the $[MO(H_2O)(CN)_4]^{n-}$ complexes, as well as the mode of distortion (displacement of the central metal atom by 0.3 Å towards the oxo from the plane formed by the four cyano carbon atoms), will promote a dissociative activation.[1] In the aforementioned tungsten(IV) system the difference between the ligation constants for the monodentate ligands NCS^-, N_3^- and py is only a factor of 2 (2.9, 4.1 and 6 M^{-1} s^{-1} at 25°C, respectively) and an acceptable linear free energy relationship was obtained for these three ligand systems. The anation rate constant for the reaction with fluoride ions was, however, only 0.14 M^{-1} s^{-1}, in which case a contribution from hydrogen bonding was assumed. In the case of the tungsten(IV) system the reaction with F^- ions was *ca* 20–40 times slower than the average of the other three ligands. In the case of the molybdenum(IV) system in the present study the reaction with F^- ions is only 10 times slower than the reaction with CN^- ions, but 50 times slower than the reaction with HCN.

By considering the reaction between $[MoO(H_2O)(CN)]^{2-}$ and HCN/CN^- ions in the present study, it is clear that the reverse rate constants (i.e. hydrolysis) differ by more than two orders of magnitude where there is only a five times difference in the aqua substitution rate constants. This is in direct agreement with a dissociative mechanism. The five-fold increase in reaction rate with

the HCN (compared with that of the CN^- ions) observed in this study might be attributed to a better association capability, being a neutral entity, and experiencing less electrostatic repulsion than the negatively charged CN^- ion during the rate-determining step. In fact, slightly increases rates were observed in both the tungsten(IV) (py compared to NCS^- and N_3^-, see previous paragraph) and rhenium(V)[2] (k_1 for the neutral ligands thiourea and hydrazoic acid were between 2 and 10 times larger than the reaction with NCS^- ions) systems when less negative incoming ligands were used. Although negative activation entropy values for both the HCN and CN^- pathways were calculated, this does not necessarily imply an associative mechanism, as has been shown previously on a number of occasions by high pressure kinetic studies.

The fact that the HCN does coordinate in this present system poses similar problems to those observed previously,[5] i.e. the coordination mode and the behaviour of the hydrogen cyanide once coordinated. According to that proposed in Scheme 1 the acid dissociation of the coordinated HCN results in the almost simultaneous isomerization to the carbon-coordinated cyano complex. It might be anticipated that the combination of this dissociation/isomerization still can result in a pK_a value for the coordinated HCN that is more acidic than the free acid in aqueous solution, since the coordination of the HCN via the nitrogen atom is expected to weaken the H—C bond, resulting in a stronger acid.

This study has confirmed the reaction of both free cyanide ions and hydrogen cyanide with the $[MoO(H_2O)(CN)_4]^{2-}$ complex and has described the kinetics of this complex system, which is an important step in the elucidation of the mechanism by which the octacyanometalate complexes form. We are currently in the process of extending these studies to the other dioxotetracyano systems already studied in our laboratories, i.e. tungsten(IV) and also rhenium(V) and technetium(V). The $[TcO(CN)_5]^{3-}$ complex is already known, but no formation kinetics have been reported.[18] The cyanide exchange on these systems by high-field NMR and the formation of higher-coordinated cyano complexes are also under investigation.

Acknowledgement—Financial support by the South African FRD and the Research Fund of the University of the Orange Free State is gratefully acknowledged.

REFERENCES

1. (a) A. Roodt, J. G. Leipoldt, E. A. Deutsch and J. C. Sullivan, *Inorg. Chem.* 1992, **31**, 1080; (b) A. Roodt, J. G. Leipoldt, S. S. Basson and I. M. Potgieter, *Trans. Met. Chem.* 1988, **13**, 336; (c) A. Roodt, J. G. Leipoldt, S. S. Basson and I. M. Potgieter, *Trans. Met. Chem.* 1990, **15**, 439 and refs therein; (d) I. M. Potgieter, S. S. Basson, A. Roodt and J. G. Leipoldt, *Trans. Met. Chem.* 1988, **13**, 209 and refs therein; (e) W. Purcell, A. Roodt, S. S. Basson and J. G. Leipoldt, *Trans. Met. Chem.* 1989, **14**, 224; (f) W. Purcell, A. Roodt, S. S. Basson and J. G. Leipoldt, *Trans. Met. Chem.* 1989, **14**, 369.
2. (a) I. M. Potgieter, S. S. Basson, A. Roodt and J. G. Leipoldt, *Inorg. Chem.* 1987, **26**, 57; (b) A. Samotus, A. Kanas, W. Glug and J. Szklarzewicz, *Trans. Met. Chem.* 1991, **16**, 614.
3. A. Roodt, J. G. Leipoldt, L. Helm and A. E. Merbach, *Inorg. Chem.* 1992, **31**, 2864.
4. A. Roodt, J. G. Leipoldt, L. Helm and A. E. Merbach, *Inorg. Chem.* submitted.
5. (a) G. B. Kolski and D. W. Margerum, *Inorg. Chem.* 1968, **7**, 2230; (b) G. B. Kolski and D. W. Margerum, *Inorg. Chem.* 1969, **8**, 1125.
6. P. Hambright and R. Langley, *Inorg. Chim. Acta* 1987, **137**, 209.
7. W. W. Reenstra and W. P. Jencks, *J. Am. Chem. Soc.* 1979, **101**, 5780.
8. (a) E. J. Billo, *Inorg. Chem.* 1973, **12**, 2783; (b) D. Margerum, G. Caley, D. Weatherburn, I. N. Pagenkopf and A. E. Martell (Editors) *Coordination Chemistry*, Ch. 1. ACS Monograph 174, Washington, DC (1978).
9. D. Dobos, *Electrochemical Data.* Elsevier, London (1975).
10. W. Purcell, A. Rood and J. G. Leipoldt, *Trans. Met. Chem.* 1991, **17**, 339.
11. K. Wieghardt, G. Backes-Dahman, W. Holzbach, W. J. Swiridoff and J. Weiss, *Z. Anorg. Allg. Chem.* 1983, **499**, 44.
12. H. Arzoumanian, M. Pierrot, F. Ridouane and J. Sanchez, *Trans. Met. Chem.* 1991, **16**, 422.
13. J. P. Smit, A. Roodt, W. Purcell, J. G. Leipoldt, *J. Chem. Soc., Chem. Commun.* submitted.
14. (a) J. H. Espenson and J. P. Birk, *J. Am. Chem. Soc.* 1965, **87**, 3280; (b) J. Halpern and S. Nakamura, *J. Am. Chem. Soc.* 1965, **87**, 3002.
15. B.-C. Wang, W. P. Schaefer and R. E. Marsh, *Inorg. Chem.* 1971, **10**, 1492.
16. R. J. Balahura, G. Ferguson, A. Johnson and B. L. Ruhl, *Polyhedron* 1986, **5**, 2075.
17. B. Sieklucka, R. Dziembaj and S. Witkowski, *Inorg. Chim. Acta* 1991, **187**, 5.
18. H. S. Trop, A. Jones and A. Davison, *Inorg. Chem.* 1980, **19**, 1993.

Polyhedron Vol. 12, No. 18, pp. 2279–2289, 1993
Printed in Great Britain

0277–5387/93 $6.00+.00
© 1993 Pergamon Press Ltd

REACTIONS OF 1-ADAMANTYLPHOSPHINE AND BIS-(1-ADAMANTYL)PHOSPHINE WITH CARBONYLS OF GROUP 6, 8 AND 10 METALS. REACTIVITY OF THE P—H BOND IN 1-ADAMANTYLPHOSPHINE COMPLEXES*

JENS R. GOERLICH, AXEL FISCHER, PETER G. JONES and REINHARD SCHMUTZLER†

Institut für Anorganische und Analytische Chemie der Technischen Universität, Postfach 3329, D-38023 Braunschweig, F.R.G.

(*Received* 4 *January* 1993; *accepted* 19 *April* 1993)

Abstract—The reactions between $(1\text{-Ad})_nPH_{3-n}$ (1-Ad = 1-adamantyl; $n = 1, 2$) and $M(CO)_6$ (M = Cr; Mo, W), $Fe_2(CO)_9$ and $Ni(CO)_4$ led to mononuclear derivatives of the type $(OC)_mM[(1\text{-Ad})_nPH_{3-n}]$ ($m = 5$, M = Cr, Mo, W; $m = 4$, M = Fe; $m = 3$, M = Ni; $n = 1, 2$). Although rather unreactive, as a result of the 1-adamantyl substitution, some of these compounds were employed for further synthesis under more vigorous conditions. Thus, pyrolysis of $(1\text{-AdPH}_2)Fe(CO)_4$ (**7**) furnished the binuclear cluster $(1\text{-AdPH})_2Fe_2(CO)_6$ (**11**), whereas substitution of a PH proton in the chromium complex $(1\text{-AdPH}_2)Cr(CO)_5$ (**1**) by a diisopropylphosphino group led to the diphosphine complex $(OC)_5Cr(1\text{-AdPH—P}^i\text{Pr}_2)$ (**15**), which isomerized at elevated temperatures to $(1\text{-AdPH—P}^i\text{Pr}_2)Cr(CO)_5$ (**15a**) with liberation of the diphosphine $1\text{-AdPH—P}^i\text{Pr}_2$ (**16**). The crystal structure of **15** is described; the P—P bond length is 223.6(1) pm. 1-AdPH_2 reacted with $Fe_3(CO)_{12}$ with the formation of a mixture of bi- and trinuclear iron carbonyl clusters.

Primary and secondary phosphines resemble the majority of phosphorus(III) compounds in that they react with metal carbonyls, substituting carbon monoxide.[1] As a result of the reactivity of the $—PH_2$ or the —PH group these compounds can serve as versatile precursors in the synthesis of new compounds. The synthesis of species that are unknown or unstable in an uncoordinated state may be realized in the coordination sphere of a transition metal. Thus, based on phosphine complexes, Treichel and his co-workers[2–4] have described the synthesis of phosphido complexes; Stelzer and his co-workers[5] have synthesized di-, tri- and tetraphosphines coordinated to metal carbonyl fragments; Mathey and his co-workers[6–9] have reported the synthesis of phosphaalkene and phosphirane complexes from coordinated phosphine precursors. Complexes involving PH phosphines have also been used in the synthesis of oligonuclear transition metal clusters.[10,11]

A variety of metal complexes involving primary and secondary phosphines as ligands are known, but the substituents were always aromatic or sterically undemanding alkyl groups. In the course of our studies on tertiary, bulky hydrocarbon group substituents at phosphorus[12–14] the question arose whether the comparatively unreactive 1-adamantyl-substituted phosphines of the type $(1\text{-Ad})_nPH_{3-n}$ ($n = 1, 2$) could be employed as ligands and, if so, whether further chemical reactions at the coordinated phosphine ligands would be possible.

RESULTS AND DISCUSSION

Reactions of 1-adamantylphosphine and bis-(1-adamantyl)phosphine with carbonyls of group 6, 8 and 10 metals

The reaction of 1-adamantyl- and bis-(1-adamantyl)phosphine with a slight excess of the hexa-

* Dedicated to Professor R. W. Parry on the occasion of his 75th birthday.

† Author to whom correspondence should be addressed.

carbonyls of chromium(0), molybdenum(0) and tungsten(0) in high-boiling solvents at 110–140°C was found to lead, selectively, to the monosubstituted derivatives with the loss of carbon monoxide [eq. (1)]. Reactivities and yields were found to decrease from chromium to tungsten carbonyl.

$$R^1R^2PH + M(CO)_6 \xrightarrow[-CO]{\Delta} (R^1R^2PH)M(CO)_5 \quad (1)$$

R^1	R^2	Cr	Mo	W
1-Ad	H	**1**	**2**	**3**
1-Ad	1-Ad	**4**	**5**	**6**

Products **1–6** are colourless solids that are stable in air for hours. They may be purified by recrystallization from THF. The $\delta(^{31}P)$ values of **1–6** exhibit a significant low-field shift from those of the starting phosphines [1-$AdPH_2$, −81.6 ppm and $(1\text{-Ad})_2PH$, 18.71 ppm] (Table 1).

The deshielding effect increases from the tungsten to the chromium complexes. This could be a result of the decrease in the number of electrons at the metal atom and, consequently, a weakened shielding effect. In the ^1H NMR spectra of **1–6**, besides the signals due to the 1-adamantyl groups, the resonances of the phosphine protons are observed in the region 3.81–4.08 ppm (Table 1). Both $\delta(^{31}P)$ and $^1J(PH)$ (302.50–321.00 Hz)[15] lie in the expected region. In the ^{13}C NMR-spectra the *cis*- and *trans*-CO groups may be distinguished on the basis of

Table 1. ^1H, ^{31}P NMR and IR data of compounds **1–10**, **12** and **13**

	δ_P	$\delta_H(PH)$ $^1J(PH)$ $\delta_H(C_{10}H_{15})$	IR (hexane) $\nu(CO)$ $\nu(PH)$
		4.04	2066(s), 1985(s),
$(1\text{-AdPH}_2)Cr(CO)_5$	0.54	312.81	1945(vs)
1		1.71–2.03	2315(w)
		4.08	2074(s), 1987(m),
$(1\text{-AdPH}_2)Mo(CO)_5$	−28.51	308.16	1952(vs)
2		1.66–2.06	2317(w)
		4.44	2075(s), 1980(m),
$(1\text{-AdPH}_2)W(CO)_5$	−47.59	321.00	1945(vs)
3	$^1J(PW) = 212.53$	1.66–2.07	2321(vw)
		3.81	2058(m), 1985(s),
$(1\text{-Ad}_2PH)Cr(CO)_5$	70.39	307.18	1937(vs)
4		1.74–2.07	2300(w)
		3.89	2069(s), 1978(m),
$(1\text{-Ad}_2PH)Mo(CO)_5$	53.46	302.50	1941(vs)
5		1.74–2.06	2300(w)
		4.21	2065(s), 1989(vs),
$(1\text{-Ad}_2PH)W(CO)_5$	39.15	314.32	1934(vs)
6	$^1J(PW) = 216.15$	1.73–2.07	2301(vw)
		4.65	2056(s), 1983(s),
$(1\text{-AdPH}_2)Fe(CO)_4$	14.03	343.69	1949(vs)
7		1.75–2.09	2325(w)
		3.98	2048(s), 1985(s),
$(1\text{-Ad}_2PH)Fe(CO)_4$	81.83	328.04	1947(vs)
8		1.72–2.02	2310(w)
		$\delta_H(H_2) = -24.09$	2091(m), 2058(s),
$(1\text{-AdP})Fe_3(CO)_9H_2$	458.95	$^2J(PH) = 27.41$	2029(vs), 2003(s),
9		1.95–2.18	1983(m), 1974(w)
			2032(vs), 2013(vs),
$(1\text{-AdP})_2Fe_3(CO)_9$	400.85	1.77–2.13	1995(vs), 1984(s),
10		3.85	1970(w)
			2075(s), 2002(vs),
$(1\text{-AdPH}_2)Ni(CO)_3$	−35.03	298.11	
12		1.78–2.04	2319(m)
		3.66	2064(s), 1990(vs),
$(1\text{-Ad}_2PH)Ni(CO)_3$	59.92	301.14	
13		1.70–1.96	2299(m)

Table 2. ^{13}C NMR data of compounds **1–10**, **12** and **13**

	$\delta_C(C^1)$ $^1J(PC)$	$\delta_C(C^2)$ $^2J(PC)$	$\delta_C(C^3)$ $^3J(PC)$	$\delta_C(C^4)$ $^4J(PC)$	$\delta_C(CO)_{cis}$[a] $^2J(PC)$	$\delta_C(CO)_{trans}$[a] $^2J(PC)$
$(1\text{-AdPH}_2)Cr(CO)_5$	33.15	41.85	28.54	35.98	216.71	220.90
1	24.55	—	9.32	—	13.17	6.58
$(1\text{-AdPH}_2)Mo(CO)_5$	31.73	42.09	28.54	35.99	205.44	208.34
2	25.22	1.21	9.50	1.22	8.87	21.99
$(1\text{-AdPH}_2)W(CO)_5$	32.09	41.94	28.52	35.99	195.93	196.93
3	28.62	—	9.80	—	6.87	21.82
$(1\text{-Ad}_2PH)Cr(CO)_5$	40.09	42.44	28.98	36.21	218.59	222.00
4	10.52	—	8.21	—	12.00	5.82
$(1\text{-Ad}_2PH)Mo(CO)_5$	32.33	42.68	28.92	36.27	207.23	210.49
5	11.22	1.25	8.40	—	8.28	22.31
$(1\text{-Ad}_2PH)W(CO)_5$	39.04	42.77	28.94	36.26	198.31	198.90
6	14.86	—	8.41		6.58	21.79
$(1\text{-AdPH}_2)Fe(CO)_4$	34.08	40.99	28.41	35.92		213.22
7	28.83	—	9.95	—		19.37
$(1\text{-Ad}_2PH)Fe(CO)_4$	39.68	41.96	28.85	36.29		219.36
8	15.57	—	8.64	—		13.45
$(1\text{-AdP})Fe_3(CO)_9H_2$	47.55	36.12	29.44	44.70		208.34
9	6.81	1.93	10.42	—		—
$(1\text{-AdP})_2Fe_3(CO)_9$	48.94	35.93	29.80	43.20		213.90
10	[b]	—	[b]	—		—
$(1\text{-AdPH}_2)Ni(CO)_3$	29.98	42.12	28.56	36.17		195.98
12	24.97	2.00	9.35	—		—
$(1\text{-Ad}_2PH)Ni(CO)_3$	36.32	42.04	28.72	36.51		197.47
13	12.92	2.82	8.46	—		—

[a] *Cis/trans* only for the octahedral complexes **1–6**.
[b] X-part of an ABX spectrum.

their $\delta(^{13}C)$ and $^2J(PC)$ values:[16] the $\delta(^{13}C)$ values of *trans*-CO groups are observed consistently at lower field than those of the *cis*-CO groups. In the case of the molybdenum and tungsten complexes $^2J(PC)_{trans}$ is always larger than $^2J(PC)_{cis}$, while the opposite is true for the chromium complexes **1** and **4** (Table 2), in accord with expectation.[16]

Belonging to the point group C_{4v}, for complexes **1–6** in the IR spectra three IR-active bands are expected in the CO region[17] and are indeed observed. ν(PH) is observed in all IR spectra in the region 2299–2321 cm^{-1} (Table 1).[18] The mass spectra of **1–6** are found to exhibit the molecular ion peaks resulting from the successive loss of five CO groups and a peak at m/z 135 from the 1-adamantyl fragment. In the mass spectra of **4–6** signals from the free ligand, $(1\text{-Ad})_2PH$, are observed.

The mononuclear derivatives of iron pentacarbonyl, **7** and **8**, were synthesized from $(1\text{-Ad})_nPH_{3-n}$ and $Fe_2(CO)_9$ in toluene as an inert solvent at room temperature [eq. (2)]. The products are orange–brown solids, melting with decomposition.

$$R^1R^2PH + Fe_2(CO)_9 \xrightarrow[-Fe(CO)_5]{\text{toluene}} (R^1R^2PH)Fe(CO)_4 \quad (2)$$

$R^1 = 1\text{-Ad}, \quad R^2 = H$: **7**

$R^1 = R^2 = 1\text{-Ad}$: **8**

For **7** $\delta(^{31}P)$ is shifted by *ca* 86 ppm and for **8** by *ca* 64 ppm to high field, compared with the free ligands. The $\delta(^1H)$ and $^1J(PH)$ values of the phosphine protons are in accord with expectation and are closely similar to those of **1–6** (Table 1). In the ^{13}C NMR spectra of both compounds only one resonance, a doublet due to $^{31}P—^{13}C$ coupling, is observed for the carbonyl groups (Table 2). Assuming trigonal-bipyramidal geometry at Fe(0) a pseudo-rotation process, too fast to be followed by ^{13}C NMR spectroscopy, would account for this observation. The mass spectra of **7** and **8** exhibit the molecular ion with low intensity and the successive loss of the four carbonyl groups is seen. The IR spectra of **7** and **8** display the expected three bands in the carbonyl region, consistent with the

C_{3v} point group[17] and ν(PH) bands at 2325 (**7**) and 2310 cm^{-1} (**8**).

The reaction of primary phosphines with $Fe_3(CO)_{12}$ and $Ru_3(CO)_{12}$ has been studied.[10,19,20] In all cases oligonuclear phosphinidene clusters were obtained. In the case of osmium the primary reaction product, $Os_3(CO)_{11}(RPH_2)$ (R = Ph, *c*-C_6H_{11}) is well known.[20,21] It was thus of interest to determine whether the comparatively unreactive 1-$AdPH_2$ would yield products analogous to the osmium complexes in its reaction with $Fe_3(CO)_{12}$. Three signals in the ^{31}P NMR spectra of the reaction mixture [$\delta(^{31}P)$ 458.95, 400.85 and 150.88 in a 3 : 8 : 1 ratio] were assigned to the clusters **9**, **10** and **11**. These assignments are based on those of the analogous ^{t}butyl-substituted compounds, from the work of Huttner,[10,23] Vahrenkamp[11] and Stelzer[22] [eq. (3)]. There was no evidence for a primary substitution product, $Fe_3(CO)_{11}$(1-$AdPH_2$). Of the three components of the reaction mixture **9** and **10** could be isolated in a pure state. The phosphido cluster (**11**), present here solely as one of the symmetric isomers, was subsequently synthesized by a different method (*vide infra*).

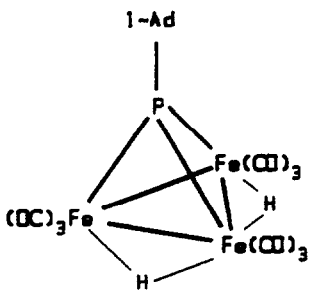

9

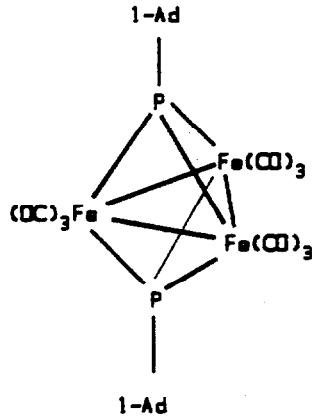

10

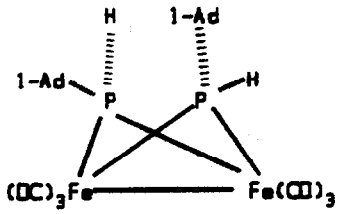

11

$$1\text{-}AdPH_2 + Fe_3(CO)_{12} \xrightarrow[-CO,\,-H_2]{\Delta} \mathbf{9} + \mathbf{10} + \mathbf{11} \quad (3)$$

The singlet absorption at 458.95 ppm in the ^{31}P NMR spectrum of **9** is typical of a μ^3-phosphido ligand. Compared with the signal of the analogous ^{t}butyl compound[10] there is a high-field shift of *ca* 8 ppm. A difference of this magnitude in $\delta(^{31}P)$ between analogous ^{t}butyl- and 1-adamantyl-phosphorus compounds is almost always observed, irrespective of the coordination number of phosphorus.[13] $\delta(^1H)$ for the bridging hydrogen atoms is −24.09 ppm, with $^2J(PH)$ = 27.41 Hz. In the ^{13}C NMR spectra of **9** only one signal is observed for the resonance of the carbonyl groups, suggesting a dynamic structure. For the 1-adamantyl cage the expected four signals are observed, with an unusually small value for $^1J(PC)$ of 6.81 Hz, as against a larger $^3J(PC)$ value of 10.42 Hz. The mass spectrum exhibits the molecular ion at *m/z* 588, fragments from the successive loss of nine carbonyl groups and the fragments $[Fe_3PH]^+$, $[Fe_3P]^+$ and $[Ad]^+$. The IR spectrum, similar to that of the analogous ^{t}butyl compound,[10] shows six bands in the carbonyl region, suggesting a similar structure.

A resonance, $\delta(^{31}P)$ = 400.85 ppm, shifted by *ca* 5 ppm to high field, relative to the analogous ^{t}butyl compound,[23] is observed for **10** in the region typical of μ^3-phosphido ligands. Stelzer and his co-workers have obtained such compounds as stable products of the thermally initiated reaction of primary phosphines with $Fe(CO)_5$.[22] The ^{13}C NMR spectrum of **10** in the carbonyl region shows a single line for the carbonyl groups at 213.90 ppm. The ^{13}C NMR resonances of the atoms C^1 and C^3 of the 1-adamantyl cage appear as X parts of ABX spectra, as a result of coupling with the two non-equivalent phosphorus atoms of the molecule. The mass spectrum of **10** shows a low intensity molecular ion at *m/z* 752 and fragments originating from successive loss of the nine carbonyl groups. In addition, signals due to the fragments $[Fe_3P_2Ad]^+$, $[Fe_2P_2Ad]^+$, $[Fe_3P_2]^+$, $[Fe_3P]^+$ and $[Ad]^+$ are observed.

As for the analogous ^{t}butyl compound[23] five bands are observed in the carbonyl region of the IR spectrum of **10**, their wave numbers differing only slightly from those of the ^{t}butyl analogue. The number and position of these bands confirm the assumed structure.

For the synthesis of mononuclear nickel(0)-phosphine derivatives a large excess of $Ni(CO)_4$ was added to solutions of the phosphines $(1\text{-}Ad)_nPH_{3-n}$ (n = 1, 2) in THF. The reaction mixtures were

stirred at room temperature until the evolution of carbon monoxide ceased [eq. (4)].

$$R^1R^2PH + Ni(CO)_4 \xrightarrow[-CO]{\text{THF, room temperature}} (R^1R^2PH)Ni(CO)_3 \quad (4)$$

R^1 = 1-Ad, R^2 = H: **12**

$R^1 = R^2$ = 1-Ad: **13**

Compound **12** was obtained as a colourless oil, crystallizing at −18°C, while **13** was a colourless solid. As expected there is a marked low-field shift of $\delta(^{31}P)$ (Table 1). In the ^1H NMR spectra signals typical of P*H* protons are observed at 3.85 (**12**) and 3.66 ppm (**13**), with $^1J(PH)$ = 298.11 and 301.14 Hz, respectively (Table 1). In the ^{13}C NMR spectra of both complexes only single resonances are observed for the carbonyl groups. There is a conspicuous high field shift of the ^{13}C NMR resonances of the C^1 atoms of the 1-adamantyl group. In the mass spectrum of **12** the molecular ion is seen at *m/z* 310, whereas for **13** the heaviest fragment arises from the loss of one carbonyl group from the parent molecule. Further characteristic fragments are the result of the successive loss of carbon monoxide. The base peak, in both cases, is the adamantyl cation (*m/z* 135). The IR spectra (C_{3v} molecular symmetry) reveal two bands[17] in the carbonyl region, in agreement with reports on mononuclear nickel carbonyl complexes of other phosphines.[24] IR absorptions due to ν(PH) are seen at 2319 (**12**) and 2299 cm^{-1} (**13**).[18]

Reactions of metal carbonyl-phosphine complexes

As mentioned above, we succeeded in isolating the two trinuclear iron(0) clusters **9** and **10** from the reaction mixture of 1-$AdPH_2$ and $Fe_3(CO)_{12}$, whereas the isolation of a third product [$\delta(^{31}P)$ 150.88] failed. Based on the comparison of the $\delta(^{31}P)$ values to those of other, structurally analogous compounds,[11,22] this signal is assigned to an isomer of the phosphido cluster (**11**). In order to ascertain its identity an alternative synthesis of **11** was realized, following a previously reported procedure,[11] by refluxing a solution of the phosphine complex **7** in toluene [eq. (5)]. A 1 : 1 ratio of **7** : **11** was determined (^{31}P NMR) after a 6 h reflux period.

$$\underset{\mathbf{7}}{2(1\text{-}AdPH_2)Fe(CO)_4} \xrightarrow[-2CO,\ -H_2]{\text{toluene, reflux}} \underset{\mathbf{11}}{(1\text{-}AdPH)_2Fe_2(CO)_6} \quad (5)$$

This ratio remained unchanged upon continued refluxing. Upon work-up by column chromatography **11** was obtained as a yellow solid, consisting of a 1 : 1 mixture of the isomers **11a** and **11b**. From the $\delta(^{31}P)$ value of **11a** (150.88 ppm) it was concluded that it was one of the products obtained in the reaction of 1-$AdPH_2$ with $Fe_3(CO)_{12}$. The ^{31}P NMR spectrum of **11b**, due to the non-equivalence of the two phosphorus atoms, shows a higher order AB type NMR pattern. Presumably as a result of the steric demand of the bulky 1-adamantyl group, isomer **11c** is not observed (Fig. 1).

In contrast, Stelzer and his co-workers obtained a mixture of all three possible isomers[22] from the reaction of $Fe(CO)_5$ with $PhPH_2$, presumably because of the lower steric demand of the phenyl group. The ^1H NMR spectrum of our mixture of isomers, **11a** and **11b**, is found to exhibit numerous lines in the region 2.81–5.15 ppm, which originate

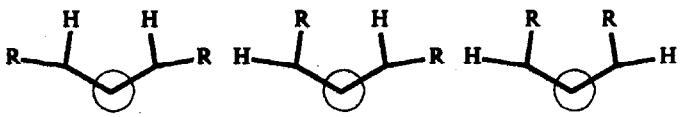

Point Group [2]	C_{2v}	C_s	C_{2v}
R= 1-Ad	**11a**	**11b**	**11c**
	δ_P= 150.88	$\delta_P(P_a)$= 125.99 $\delta_P(P_b)$= 134.62 $^2J(P\text{-}P)$= 129.11	not observed
R= Ph[22]	δ_P= 80.5	$\delta_P(P_a)$= 67.7 $\delta_P(P_b)$= 70.9 $^2J(P\text{-}P)$= 164	δ_P= 68.5

Fig. 1. Newman projection of compounds **11a**, **11b** and **11c**.

from the higher order spectra to be expected for the protons of the phosphido bridges. A precise assignment of the partially overlapping signals was unsuccessful. The mass spectrum of **11a/11b** shows the molecular ion at *m/z* 614, fragments originating from the successive loss of six CO groups and the ions $[Fe_2P_2]^+$ and $[Ad]^+$. Four bands are observed in the carbonyl region of the IR spectrum; they are shifted to slightly lower wave numbers than those of the analogous ^{t}butyl compound.

The formation of heterometallic clusters in the reaction of coordinated phosphines with oligonuclear metal carbonyls has been described in the literature.[10,11,25-27] Employing the conditions described by Huttner and his co-workers,[10] an equimolar mixture of $Fe_3(CO)_{12}$ and **1** in toluene was heated for 12 h at 80°C. An inspection by ^{31}P NMR spectroscopy revealed only the signal of **1** and there was no indication of possible product signals[27] after another 3 h reflux period. The reason for the failure of this reaction under the conditions employed may be the comparatively low reactivity of 1-adamantyl-substituted phosphorus compounds.

In analogy to reports by Stelzer and his coworkers[5] an attempt was made to substitute one or two of the phosphino protons in **2** by diphenylphosphino groups, forming coordinated di- or triphosphines. However, ^{31}P NMR gave no evidence for any reaction, either after stirring a mixture of **2** and diphenylchlorophosphine in toluene in the presence of triethylamine for several days at room temperature or after a 5 h reflux period. The failure of the reaction, in contrast to the analogous reaction of the phenylphosphine-substituted molybdenum pentacarbonyl derivative, is again thought to be due to the reduced reactivity of the 1-adamantyl phosphine derivative **2**.

A successful attempt at the formation of a PP bond in the coordination sphere of a metal was based on the reaction of $(1\text{-AdPH}_2)Cr(CO)_5$ (**1**) with n-butyl lithium, forming the yellow lithium phosphido complex **14**; subsequent addition of diisopropylchlorophosphine gave compound **15**, the chromium pentacarbonyl derivative of the unknown unsymmetrical diphosphine **16**, in high yield [eqs (6) and (7)]. The ^{31}P NMR spectrum of **15** is found to exhibit a higher order pattern, with $\delta(^{31}P)$ ($^iPr_2P$) = 6.22 ppm, $\delta(^{31}P)$ (1-Ad*P*H) = 2.45 ppm, $^1J(PP)$ = 245.97 Hz.[28] The ^{1}H NMR spectrum shows a doublet at 3.92 ppm

$$\underset{\mathbf{1}}{(1\text{-AdPH}_2)Cr(CO)_5} + {}^n\text{BuLi} \xrightarrow[-{}^n\text{BuH}]{-78°C} \underset{\mathbf{14}}{(1\text{-AdPHLi})Cr(CO)_5} \quad (6)$$

$$1\text{-Ad(H)PLi} + {}^i\text{Pr}_2\text{PCl} \xrightarrow[-\text{LiCl}]{} 1\text{-Ad(H)P—P}^i\text{Pr}_2$$
$$\downarrow \qquad\qquad\qquad\qquad \downarrow$$
$$\underset{\mathbf{14}}{Cr(CO)_5} \qquad\qquad \underset{\mathbf{15}}{Cr(CO)_5} \quad (7)$$

[^1J(PH) = 297.49 Hz]. A ^2J(PH) coupling constant cannot be discerned in the spectrum. The protons of both isopropyl groups in the ^{1}H NMR spectrum give rise to partially overlapping higher-order spin systems and while an exact assignment is impossible, the isopropyl groups appear to be non-equivalent. This finding is supported by the observation of six lines for the two isopropyl groups in the ^{13}C {^{1}H, ^{31}P} NMR spectrum. For the carbon atoms of the carbonyl groups two resonances at $\delta(^{13}C)$ = 217.26 ppm, $^2J(PC)$ = 9.39 Hz (*cis*-CO), and $\delta(^{13}C)$ = 221.23 ppm, $^2J(PC)$ = 4.36 Hz (*trans*-CO), are observed. The mass spectrum exhibits the molecular ion at *m/z* 476, fragment ions caused by the successive loss of carbonyl groups and the fragments $[1\text{-AdP(H)P}^i\text{Pr}_2]^+$, $[1\text{-AdP(H)P}]^+$ and $[Ad]^+$. IR bands are observed for ν(PH) at 2307 cm^{-1} and in the carbonyl region at 2060, 1979 and 1937 cm^{-1}.

In order to confirm the structure and identity of **15**, and to exclude the possibility of a migration of the $Cr(CO)_5$ group to the more nucleophilic diisopropyl-substituted phosphorus atom, a single-crystal X-ray diffraction study of **15** was conducted (Fig. 2, Table 3). This confirms the presence of an adamantyl-substituted and pentacarbonyl-chromium-coordinated diphosphine. The main distortion from ideal octahedral coordination geometry

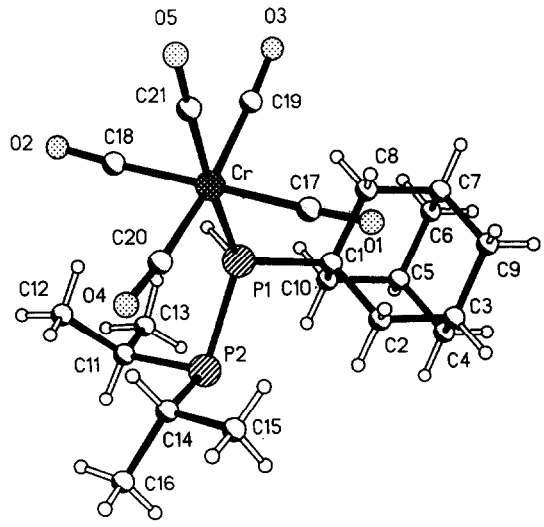

Fig. 2. X-ray crystal structure of compound **15**.

Table 3. Selected bond lengths (pm) and angles (°) for compound **15**

Cr—P(1)	245.9(1)	Cr—C(17)	190.7(2)
Cr—C(18)	189.9(2)	Cr—C(19)	189.9(2)
Cr—C(20)	190.9(2)	Cr—C(21)	185.7(2)
P(1)—P(2)	223.6(1)	P(1)—C(1)	188.4(2)
P(2)—C(11)	186.5(2)	P(2)—C(14)	185.2(2)
O(1)—C(17)	113.9(2)	O(2)—C(18)	113.8(2)
O(3)—C(19)	113.8(2)	O(4)—C(20)	113.6(3)
O(5)—C(21)	114.7(2)		

P(1)—Cr—C(17)	91.6(1)	P(1)—Cr—C(18)	89.1(1)
C(17)—Cr—C(18)	178.9(1)	P(1)—Cr—C(19)	88.5(1)
C(17)—Cr—C(19)	91.7(1)	C(18)—Cr—C(19)	89.2(1)
P(1)—Cr—C(20)	100.6(1)	C(17)—Cr—C(20)	89.6(1)
C(18)—Cr—C(20)	89.5(1)	C(19)—Cr—C(20)	170.8(1)
P(1)—Cr—C(21)	172.3(1)	C(17)—Cr—C(21)	90.0(1)
C(18)—Cr—C(21)	89.4(1)	C(19)—Cr—C(21)	83.9(1)
C(20)—Cr—C(21)	86.9(1)	Cr—P(1)—P(2)	128.3(1)
Cr—P(1)—C(1)	119.2(1)	P(2)—P(1)—C(1)	100.2(1)
P(1)—P(2)—C(11)	103.8(1)	P(1)—P(2)—C(14)	102.7(1)
C(11)—P(2)—C(14)	103.1(1)	P(1)—C(1)—C(2)	110.9(1)
P(1)—C(1)—C(8)	109.4(1)	P(1)—C(1)—C(10)	110.2(1)
P(2)—C(11)—C(12)	116.9(1)	P(2)—C(11)—C(13)	111.1(1)
C(12)—C(11)—C(13)	112.0(1)	P(2)—C(14)—C(15)	109.0(1)
P(2)—C(14)—C(16)	109.4(1)	Cr—C(17)—O(1)	177.9(1)
Cr—C(18)—O(2)	176.3(1)	Cr—C(19)—O(3)	173.4(1)
Cr—C(20)—O(4)	173.2(1)	Cr—C(21)—O(5)	177.3(2)

is indicated by the angles P(1)—Cr—C(20) [100.6(1)°] and C(19)—Cr—C(20) [170.8(1)°]. These wide angles are probably caused by the bulky isopropyl substituents at P(2), which lie approximately synclinal (skew) and synperiplanar (partially eclipsed) relative to the pentacarbonyl-chromium grouping [torsion angles: Cr—P(1)—P(2)—C(11) 93.7°; Cr—P(1)—P(2)—C(14) −13.4°]. The P(1)—P(2) bond length is normal [223.6(1) pm]. The P(1)—C(1) bond length [188.4(2) pm] is slightly greater than P—C bonds in species involving less bulky alkyl substituents, but is comparable with P—C bond lengths in other adamantyl phosphines.[13] The adamantyl group shows, as expected, a narrow range of values for the C—C bond lengths [152.1(2) C(6)—C(7) to 154.6(3) C(5)—C(10); av. 153.2 pm]. P(1) shows a considerably distorted tetrahedral coordination geometry associated with the bulky substituents $Cr(CO)_5$ and $P(^iPr)_2$, which effect a widening of the angle Cr—P(1)—P(2) [128.3(1)°]. The less bulky part of the diisopropylphosphine substituent faces the adamantyl substituent and the angle P(2)—P(1)—C(1) is thus small [100.2(1)°]. The coordination geometry at P(2) is pyramidal; the average angle at P(2) is 103.2°.

Finally, a solution of **15** in methylcyclohexane was heated to 80°C. Within 1 h the resonances of compound **15** disappeared in the ^{31}P NMR spectrum and a new AB spin system was observed. This was assigned to the isomeric complex **15a**, the result of the migration of the $Cr(CO)_5$ group to the diisopropyl-substituted phosphorus atom. The following ^{31}P NMR parameters are observed for **15a**: $\delta(^{31}P)$ (1-Ad*P*H) = 5.03 ppm, $\delta(^{31}P)$ ($^iPr_2P$) = 6.89 ppm, $^1J(PP) = 244.65$ Hz.[28] Additional doublets at $\delta(^{31}P) = -46.61$ and 69.33 ppm [$^1J(PP) = 295.92$ Hz] are assigned to the thermally liberated free ligand 1,1-diisopropyl-2-(1-adamantyl)diphosphine **16**; the signal at lower field

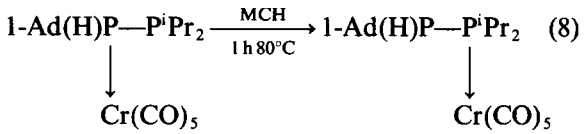

(8)

15 **15a**

+ 1-Ad(H)P—P^{i}Pr$_2$

16

	δ_P(1-Ad(H)*P*)	δ_P($^iPr_2P$)	^1J(PP)
15	2.45	6.22	245.97
15a	5.03	6.89	244.65
16	−46.61	69.33	295.92

arises from the $^{i}Pr_2P$ group, the one at higher field from the 1-Ad*P*H group [eq. (8)]. After a 6 h heating period (80°C) ^{31}P NMR signals of **15a** and **16** are no longer observed. Instead complicated, partially overlapping patterns due to higher order spectra are seen and the signals can no longer be unambiguously assigned.

EXPERIMENTAL

All experiments were conducted in an atmosphere of dry, oxygen-free nitrogen in conventional glass apparatus.[29] Solvents were purified by standard procedures, dried and stored over molecular sieves.[30,31] The following compounds were synthesized according to procedures given in the literature: 1-adamantylphosphine,[32] bis-(1-adamantyl)-phosphine,[33] diiron enneacarbonyl,[34] triiron dodecacarbonyl,[35] diphenylchlorophosphine[36] and diisopropylchlorophosphine.[37]

NMR spectra ($CDCl_3$). Bruker AC-200 (^1H at 200.1 MHz, ^{13}C at 50.3 MHz, ^{31}P at 81.0 MHz). Chemical shifts are given in ppm vs int. $CDCl_3$ (^1H, ^{13}C) and 85% H_3PO_4 ext. (^{31}P), coupling constants are listed in Hz. Chemical shift values were given a positive sign when the absorption, relative to the standard, was at low field and *vice versa*. Multiplicities: s = singlet, d = doublet, m = multiplet.

IR spectra. Beckman IR 4260 and Nicolet FT-IR 740. Except for **15** (solution in chloroform), the IR spectra were recorded on hexane solutions. Absorption frequencies are quoted in wave numbers (cm^{-1}). Intensities: vw = very weak, w = weak, m = medium, s = strong, vs = very strong.

Mass spectra. Finnigan MAT 8430. Samples were introduced into the mass spectrometer via a direct inlet septum (EI ionization).

Analyses. Microanalytical Laboratory Beller (Göttingen) and Analytical Laboratory of the Institut für Anorganische und Analytische Chemie der Technischen Universität, Braunschweig.

Abbreviations. MCH = methylcyclohexane. THF = tetrahydrofuran.

Synthesis of the phosphine complexes **1–6** (*Table* 4)

General procedure. Approximately equimolar amounts of the phosphine and of the appropriate metal carbonyl were dissolved or suspended in the

Table 4. Preparation of compounds **1–6**

	Educts	Solvent Reaction conditions Melting point Yield	Analytical data
1	1-AdPH_2	Diglyme (40 cm^3)	$C_{15}H_{17}CrO_5P$ (360.266)
	(1.63 g, 9.7 mmol)	130°C/7 h	Found: C, 50.07; H, 4.81;
	$Cr(CO)_6$	146°C	P, 8.48. Calc.: C, 50.01;
	(2.31 g, 10.5 mmol)	2.87 g (82.3%)	H, 4.76; P, 8.60%.
2	1-AdPH_2	Decaline (30 cm^3)	$C_{15}H_{17}MoO_5P$ (404.210)
	(1.68 g, 10.0 mmol)	100°C/10 h	Found: C, 44.54; H, 4.41;
	$Mo(CO)_6$	121°C	P, 7.65. Calc.: C, 44.57;
	(3.90 g, 14.8 mmol)	2.97 g (73.5%)	H, 4.24; P, 7.66%.
3	1-AdPH_2	Decaline (30 cm^3)	$C_{15}H_{17}O_5PW$ (490.104)
	(1.68 g, 10.0 mmol)	100°C/12 h	Found: C, 36.95; H, 3.43;
	$W(CO)_6$	128°C	P, 6.28. Calc.: C, 36.76;
	(5.82 g, 16.5 mmo)l	2.59 g (52.9%)	H, 3.08; P, 6.32%.
4	1-Ad_2PH	Diglyme (60 cm^3)	$C_{25}H_{31}CrO_5P$ (494.487)
	(1.57 g, 5.2 mmol)	130°C/6 h	Found: C, 60.95; H, 6.50;
	$Cr(CO)_6$	206°C (dec.)	P, 6.20. Calc.: C, 60.72;
	(1.27 g, 5.8 mmol)	2.22 g (86.3%)	H, 6.32; P, 6.26%.
5	1-Ad_2PH	Diglyme (60 cm^3)	$C_{25}H_{31}MoO_5P$ (538.431)
	(1.51 g, 5.0 mmol)	130°C/7 h	Found: C, 55.91; H, 5.90;
	$Mo(CO)_6$	168°C (dec.)	P, 5.78. Calc.: C, 55.77;
	(1.49 g, 5.6 mmol)	1.94 g (72.1%)	H, 5.80; P, 5.75%.
6	1-Ad_2PH	Diglyme (70 cm^3)	$C_{25}H_{31}O_5PW$ (626.341)
	(1.60 g, 5.3 mmol)	140°C/9 h	Found: C, 48.60; H, 5.36;
	$W(CO)_6$	178°C (dec.)	P, 5.03. Calc.: C, 47.94;
	(1.92 g, 5.5 mmol	1.81 g (54.4%)	H, 4.99; P, 4.95%.

degassed solvent and heated until the evolution of CO ceased. Subsequently, the reaction mixtures were kept at −18°C overnight. The precipitate thus obtained was collected by filtration and was purified by recrystallization from THF.

Mass spectra. **1**: 360 (10) $[M]^+$, 332 (1) $[M-CO]^+$, 304 (6) $[M-2CO]^+$, 276 (10) $[M-3CO]^+$, 248 (30) $[M-4CO]^+$, 220 (100) $[M-5CO]^+$, 135 (10) $[Ad]^+$. **2**: 406 (24) $[M]^+$, 378 (20) $[M-CO]^+$, 350 (60) $[M-2CO]^+$, 322 (38) $[M-3CO]^+$, 294 (100) $[M-4CO]^+$, 266 (60) $[M-5CO]^+$, 135 (85) $[Ad]^+$. **3**: 492 (6) $[M]^+$, 464 (12) $[M-CO]^+$, 436 (100) $[M-2CO]^+$, 408 (14) $[M-3CO]^+$, 380 (16) $[M-4CO]^+$, 352(6) $[M-5CO]^+$, 15 (12) $[Ad]^+$. **4**: 494 (4) $[M]^+$, 466 (3) $[M-CO]^+$, 438 (3) $[M-2CO]^+$, 410 (6) $[M-3CO]^+$, 382 (20) $[M-4CO]^+$, 354 (100) $[M-5CO]^+$, 302 (10) $[Ad_2PH]^+$, 135 (70) $[Ad]^+$. **5**: 540 (1) $[M]^+$, 512 (2) $[M-CO]^+$, 484 (5) $[M-2CO]^+$, 456 (3) $[M-3CO]^+$, 428 (1) $[M-4CO]^+$, 400 (1) $[M-5CO]^+$, 302(18) $[Ad_2PH]^+$, 135 (100) $[Ad]^+$. **6**: 626 (10) $[M]^+$, 598 (25) $[M-CO]^+$, 570 (40) $[M-2CO]^+$, 542 (8) $[M-3CO]^+$, 514 (6) $[M-4CO]^+$, 486 (10) $[M-5CO]^+$, 302 (4) $[Ad_2PH]^+$, 135 (100) $[Ad]^+$.

Synthesis of **7** *and* **8** *(data for* **8** *in square brackets)*

A mixture of $Fe_2(CO)_9$ (5 g, 13.7 mmol) [0.55 g, 1.5 mmol] and 2.25 g/13.3 mmol (0.45 g/1.5 mmol) of the appropriate phosphine in degassed toluene (60 cm^3) [70 cm^3] was stirred for 16 h [96 h] at room temperature. Subsequently, the reaction mixtures were filtered and the solvent removed *in vacuo* (0.1 mm). The crude products thus left were recrystallized from THF.

7: Yield: 3.94 g (88.1%): m.p.: 92°C (dec.). Found: C, 50.1; H, 5.4; Fe, 16.7. Calc. for $C_{14}H_{17}FeO_4P$ (336.107): C, 50.0; H, 5.1; Fe, 16.6%. Mass spectrum: 336 (12) $[M]^+$, 308 (12) $[M-CO]^+$, 280 (10) $[M-2CO]^+$, 252 (90) $[M-3CO]$, 224 (100) $[M-4CO]^+$, 135 (40) $[Ad]^+$. **8**: Yield: 0.52 g (73.7%); m.p.: 117°C. Found: C, 61.5; H, 6.7; Fe, 12.0. Calc. for $C_{24}H_{31}FeO_4P$ (470.327): C, 61.3; H, 6.6; Fe, 11.9%. Mass spectrum: 470 (3) $[M]^+$, 442 (5) $[M-CO]^+$, 414 (1) $[M-2CO]^+$, 386 (60) $[M-3CO]^+$, 358 (40) $[M-4CO]^+$, 302 (14) $[Ad_2PH]^+$, 279 (10) $[M-2CO-Ad]^+$, 135 (100) $[Ad]^+$.

Preparation of **9**, **10** *and* **11**

A mixture of 1-AdPH$_2$ (5 g, 29.7 mmol) and $Fe_3(CO)_{12}$ (15 g, 29.8 mmol) in toluene (170 cm^3) was heated at 100°C for 14 h. The reaction mixture was allowed to cool to room temperature and was filtered through 5 g of silica gel. The solvent was removed from the filtrate at 0.1 mm. A ^{31}P NMR spectrum ($CDCl_3$) showed signals due to **9**, **10** and **11**. This material was sublimed at 100°C (0.1 mm) until no more **9** was deposited on the cold finger. The residue was twice recrystallized from hexane and **11** was obtained as dark red rhombohedral crystals.

9: Yield: 3.54 g (20.3%, based on 1-AdPH$_2$): m.p.: 200°C (dec.). Found: C, 38.7; H, 3.1: Fe, 28.4. Calc. for $C_{19}H_{17}Fe_3O_9P$ (587.853): C, 38.8, H. 2.9; Fe, 28.5. Mass spectrum: 588 (22) $[M]^+$, 560 (12) $[M-CO]^+$, 532 (16) $[M-2CO]^+$, 504 (100) $[M-3CO]^+$, 474 (44) $[M-4CO]^+$, 446 (38) $[M-5CO]^+$, 418 (90) $[M-6CO]^+$, 390 (20) $[M-7CO]^+$, 362 (12) $[M-8CO]^+$, 334 (30) $[M-9CO]^+$, 200 (36) $[Fe_3PH]^+$, 199 (34) $[Fe_3P]^+$, 135 (14) $[Ad]^+$. **10**: Yield: 7.26 g (65.0%, based on 1-AdPH$_2$); m.p.: >240°C. Found: C, 46.9; H, 4.0; Fe, 21.8. Calc. for $C_{29}H_{30}Fe_3O_9P_2$ (752.039): C, 46.3; H, 4.0; Fe, 22.3%. Mass spectrum: 752 (<1) $[M]^+$, 724 (5) $[M-CO]^+$, 696 (12) $[M-2CO]^+$, 668 (10) $[M-3CO]^+$, 640 (<1) $[M-4CO]^+$, 612 (14) $[M-5CO]^+$, 584 (16) $[M-6CO]^+$, 556(10) $[M-7CO]^+$, 528(8) $[M-8CO]^+$, 500 (24) $[M-9CO]^+$, 444 (12) $[Fe_2P_2Ad_2]^+$, 365 (13) $[Fe_3P_2Ad]^+$, 309 (6) $[Fe_2P_2Ad]^+$, 230 (11) $[Fe_3P_2]^+$, 199 (5) $[Fe_3P]^+$, 135 (100) $[Ad]^+$.

Synthesis of **12** *and* **13** *(data for* **13** *in square brackets)*

A mixture of $Ni(CO)_4$ (2.07 g, 12 mmol) [2.55 g, 15 mmol] and 1-AdPH$_2$ [1.69 g, (10 mmol)] or (1-Ad)$_2$PH) [1.51 g, 5 mmol] was stirred in THF (40 cm^3) over 5 h at room temperature until the evolution of CO had ceased. Upon removal of the solvent *in vacuo* (0.1 mm) **12** was left as a colourless oil, **13** as a colourless solid.

12: Yield: 2.17 g (69.9%). Found: C, 49.8; H, 5.5; P, 10.1. Calc. for $C_{13}H_{17}NiO_3P$ (310.949): C, 50.2; H, 5.5; P, 10.0%. Mass spectrum: 310 (1) $[M]^+$, 282 (12) $[M-CO]^+$, 254 (20) $[M-2CO]^+$, 226 (28) $[M-3CO]^+$, 168 (4) $[AdPH_2]^+$, 135 (100) $[Ad]^+$. **13**: Yield: 1.51 g (67.8%); m.p.: 94–96°C. Found: C, 61.8; H, 7.4; P, 7.0. Calc. for $C_{23}H_{31}NiO_3P$ (445.170): C, 62.1; H, 7.0: P, 7.0%. Mass spectrum: 416 (6) $[M-CO]^+$, 388 (10) $[M-2CO]^+$, 360 (16) $[M-3CO]^+$, 302 (10) $[Ad_2PH]^+$, 135 (100) $[Ad]^+$.

Preparation of **11a**/**11b**

A solution of **7** (1.35 g, 4 mmol) in toluene (70 cm^3) was refluxed for 6 h. A product/educt ratio

of 1 : 1 was determined by ^{31}P NMR spectroscopy. This ratio was unchanged after a further 2 h reflux period. The reaction mixture was cooled to room temperature, filtered through 2 g of silica gel and the solvent removed *in vacuo* (0.1 mm). The reaction mixture was separated by column chromatography (10 g of silica gel; mobile phase n-pentane). The mixture of **11a/11b** was obtained as the first, bright yellow fraction. Unreacted **7** (orange–brown) was recovered as a second fraction. Subsequently, the solvent was removed from both fractions *in vacuo* (0.1 mm).

11a/11b: Yield: 0.53 g (43.1%); m.p.: 140°C (dec). Found: C, 50.9; H, 5.4; Fe, 18.2. Calc. for $C_{26}H_{32}Fe_2O_6P_2$ (614.177): C, 50.8; H, 5.2; Fe, 18.2%. ^1H NMR: δ 1.67–2.07 [m, 1-Ad], 2.82–5.15 [m, P—H]. IR spectrum: ν = 2052 (m), 2015 (vs), 1983 (s), 1973 (s). Mass spectrum: 614 (16) $[M]^+$, 586 (14) $[M-CO]^+$, 558 (40) $[M-2CO]^+$, 530 (50) $[M-3CO]^+$, 502 (12) $[M-4CO]^+$, 474 (4) $[M-5CO]^+$, 446 (60) $[M-6CO]^+$, 394 (18) $[M-3CO-AdH]^+$, 366 (22) $[M-4CO-AdH]^+$, 338 (23) $[M-5CO-AdH]^+$, 310 (22) $[M-6CO-AdH]^+$, 174 (100) $[Fe_2P_2]^+$, 135 (24) $[Ad]^+$.

Attempted reaction of **7** *with* $Fe_3(CO)_{12}$

A mixture of **7** (1.8 g, 5.7 mmol) and $Fe_3(CO)_{12}$ (2.52 g, 5 mmol) in toluene (60 cm^3) was heated, first at 80°C for 12 h, then refluxed for a further 3 h. At both stages only the signal of unchanged **7** was observed in the ^{31}P NMR spectrum.

Attempted reaction of **2** *with* Ph_2PCl/NEt_3

A mixture of **2** (1.01 g, 2.5 mmol), Ph_2PCl (1.20 g, 5.4 mmol) and NEt_3 (1.1 g, 11 mmol) in toluene (60 cm^3) was stirred, first at room temperature for 7 days, then heated at reflux for a further 5 h. No precipitation of $[HNEt_3]Cl$ was observed, nor was there a change in the ^{31}P NMR spectrum.

Preparation of **15**

To a suspension of **1** (0.75 g, 2.1 mmol) in a mixture of 10 cm^3 each of diethyl ether and toluene, held at −196°C, was added a 15% solution of ^nBuLi (0.9 g, 2.1 mmol) in hexane *ca* 6 g of a 15% solution via a syringe. The temperature of the reaction mixture was allowed to increase to −78°C. During 0.5 h of stirring the reaction mixture turned orange, accompanied by evolution of a gaseous product (^nBuH). Subsequently, $^iPr_2PCl$ (0.4 g, 2.6 mmol) in toluene (5 cm^3) was added dropwise over 5 min. The mixture was warmed to room temperature, stirred for 2 h and filtered to remove the LiCl. The solvent was removed from the filtrate *in vacuo* (0.1 mm) and the remaining yellow product recrystallized from hexane, giving crystals suitable for the X-ray crystal structure determination.

15: Yield: 0.77 g (77%); m.p.: 121–124°C. Found: C, 53.0; H, 6.4; P, 12.8. Calc. for $C_{21}H_{30}CrO_5P_2$ (476.41): C, 52.9; H, 6.3; P, 13.0%. NMR spectra: ^1H: δ 1.10–1.29 [m, —CH_3], 1.71–2.10 [m, 1-Ad], 2.12–2.32 [m, —$CH(CH_3)_2$], 3.92 [d, P*H*, ^1J(PH) = 297.49]. $^{13}C\{^1H, ^{31}P\}$: δ 20.19, 23.25 [s, —*C*H$(CH_3)_2$], 20.40, 21.09, 22.41, 24.28 [s, —CH(*C*$H_3)_2$], 29.11 [s, C^3 (1-Ad)], 35.94 [s, C^1(1-Ad)], 36.17 [s, C^4(1-Ad)], 41.89 [s, C^2(1-Ad)], 217.29 [s, CO_{cis}], 221.20 [s, CO_{trans}]. $^{13}C\{^1H\}$: δ 19.89–24.51 [m, {*C*$H_3)_2$*C*H—], 28.98–35.88 [m, C^1(1-Ad), C^3(1-Ad)], 36.14 [s, C^4(1-Ad)], 41.83 [d, C^2(1-Ad), ^2J(PC) = 7.09], 217.26 [d, CO_{cis}, ^2J(PC) = 9.39], 221.23 [d, CO_{trans}, ^2J(PC) = 4.36]. IR spectrum: ν = 2307 (w), 2060 (s), 1979 (m), 1937 (vs). Mass spectrum: 476 (3) $[M]^+$, 448 (19) $[M-CO]^+$, 364 (32) $[M-4CO]^+$, 336 (100) $[M-5CO]^+$, 284 (9) $[M-5CO-Cr]^+$, 242 (6) $[M-5CO-Cr-C_3H_6]^+$, 200 (52) $[M-5CO-Cr-2C_3H_6]^+$, 135 (31) $[Ad]^+$.

X-ray crystal structure determination of **15**: Crystal data: $C_{21}H_{30}CrO_5P_2$. M = 476.4, triclinic, space group $P\bar{1}$, a = 1019.2(3), b = 1077.7(3), c = 1125.7(3) pm, α = 84.10(3), β = 74.61(3), γ = 78.10(3), U = 1.165 nm^3, Z = 2, D_x = 1.358 mg m^{-3}. λ(Mo-K_α) = 0.71069 Å, μ = 0.66 mm^{-1}, T = 173 K, F(000) = 500.

Data collection and reduction. A cut yellow prism 1.0 × 0.65 × 0.50 mm was mounted on a glass fibre and transferred to the cold gas stream of the diffractometer (Siemens R3 with LT-2 low-temperature attachment). Data were collected to $2\theta_{max}$ 55°. Cell constants were refined from setting angles of 50 reflections in the range 2θ 20–23°. An absorption correction based on ψ-scans was applied (transmission factors: 0.62–0.66). Of 9018 reflections 5374 were unique (R_{int} = 0.025) and 4727 > $4\sigma(F)$ were used for all calculations (Program system "Siemens SHELXTL PLUS").

Structure solution and refinement. The structure was solved by direct methods. All non-hydrogen atoms were refined anisotropically. Hydrogen atoms were included using a riding model. The hydrogen bonded to phosphorus was then the second largest peak in a difference Fourier synthesis and was kept fixed at the peak position during the final cycles. Refinement proceeded to R = 0.030, wR = 0.041. The weighting scheme was $w^{-1} = \sigma^2(F) + 0.0002F^2$. 262 parameters; S = 1.8; max, Δ/σ = 0.003; max, $\Delta\rho = 0.8 \times 10^{-6}$ e pm^{-3}. Full details of the structure determination have

been deposited at the Fachinformationszentrum Karlsruhe, Gesellschaft für Wissenschaftlich-technische Information mbH, D-76344 Eggenstein-Leopoldshafen 2, Federal Republic of Germany. Any request for this material should quote a full literature citation and the reference number CSD 57330.

Thermolysis of **15**, *formation of* **15a** *and* **16**

A solution of **15** (50 mg, 0.1 mmol) in MCH (6 cm^3) was heated at 80°C for 6 h. ^{31}P NMR spectra of the reaction mixture were recorded at the beginning of the heating period, after 1 h and after 6 h. The experiment was terminated after 6 h because signals from unknown decomposition products were observed.

Acknowledgements—We are grateful to BASF AG, Bayer AG and Hoechst AG, for generous supplies of chemicals used in this research and to the Fonds der Chemischen Industrie for financial assistance.

REFERENCES

1. C. A. McAuliffe and W. Levason, *Phosphine, Arsine and Stibine Complexes of the Transition Elements*. Elsevier, Amsterdam (1979).
2. P. M. Treichel, W. K. Dean and W. M. Douglas, *Inorg. Chem.* 1972, **11**, 1609.
3. P. M. Treichel, W. K. Dean and W. M. Douglas, *Inorg. Chem.* 1972, **11**, 1615.
4. P. M. Treichel, W. K. Dean and J. C. Calabrese, *Inorg. Chem.* 1973, **12**, 2908.
5. M. Baacke, S. Morton, G. Johannsen, N. Weferling and O. Stelzer, *Chem. Ber.* 1980, **113**, 1328.
6. F. Mathey, A. Marinetti, S. Bauer and P. Le Floch, *Pure Appl. Chem.* 1991, **63**, 855.
7. A. Marinetti, S. Bauer, L. Ricard and F. Mathey, *Organometallics* 1990, **9**, 793.
8. S. Bauer, A. Marinetti and F. Mathey, *Heteroatom Chem.* 1991, **2**, 277.
9. A. Marinetti, L. Ricard and F. Mathey, *Synthesis* 1992, 157.
10. G. Huttner, J. Schneider, G. Mohr and J. von Seyerl, *J. Organomet. Chem.* 1980, **191**, 161.
11. H. Vahrenkamp, E. J. Wucherer and D. Wolters, *Chem. Ber.* 1983, **116**, 1219.
12. M. Fild and R. Schmutzler, *J. Chem. Soc.* (*A*) 1970, 2359.
13. J. R. Goerlich, J. V. Weiss, P. G. Jones and R. Schmutzler, *Phosphorus, Sulfur and Silicon* 1992, **66**, 223.
14. J. R. Goerlich, V. Plack, A. Fischer, P. G. Jones and R. Schmutzler, *Z. Naturforsch.* 1993, **48b**, 341.
15. L. C. Thomas, *The Identification of Functional Groups in Organophosphorus Compounds*, p. 78. Academic Press, London (1974).
16. M. F. Guns, E. G. Claeys and G. P. van der Kelen, *J. Molec. Struct.* 1979, **53**, 45.
17. C. Elschenbroich and A. Salzer, *Organometallchemie*, p. 241. Teubner Verlag, Stuttgart (1986).
18. L. C. Thomas, *The Identification of Functional Groups in Organophosphorus Compounds*, p. 73. Academic Press, London (1974).
19. K. Natarjan, O. Scheidsteger and G. Huttner, *J. Organomet. Chem.* 1981, **221**, 301.
20. F. Iwasaki, M. J. Mays, P. R. Raithby, P. L. Taylor and P. J. Wheatley, *J. Organomet. Chem.* 1981, **213**, 185.
21. K. Natarjan, L. Zsolnai and G. Huttner, *J. Organomet. Chem.* 1981, **220**, 365.
22. R. Bartsch, S. Hietkamp, S. Morton and O. Stelzer, *J. Organomet. Chem.* 1981, **222**, 263.
23. H. Lang, L. Zsolnai and G. Huttner, *J. Organomet. Chem.* 1985, **282**, 23.
24. C. A. Tolman, *J. Am. Chem. Soc.* 1970, **92**, 2953.
25. J. Schneider, L. Zsolnai and G. Huttner, *Chem. Ber.* 1982, **115**, 989.
26. G. Huttner and K. Knoll, *Angew. Chem.* 1987, **99**, 765; *Angew. Chem., Int. Edn. Engl.* 1987, **26**, 743.
27. G. Huttner, G. Mohr and P. Friedrich, *Z. Naturforsch.* 1978, **33b**, 1254.
28. H. Günther, *NMR-Spektroskopie*, 2nd edn, p. 148. Georg Thieme Verlag, Stuttgart (1983).
29. D. F. Shriver, *The Manipulation of Air-sensitive Compounds* (Reprint), p. 139. R. E. Krieger Publishing Co., Malabar, Florida (1982).
30. Autorenkollektiv, *Organikum*, 15th edn, p. 783 ff VEB Deutscher Verlag der Wissenschaften, Leipzig (1977).
31. D. D. Perrin and W. L. F. Armarego, *Purification of Laboratory Chemicals*, 3rd edn, Pergamon Press, Oxford (1988).
32. H. Stetter and W. D. Last, *Chem. Ber.* 1969, **102**, 3364.
33. B. I. No, Yu. L. Zotov and V. N. Karev, *Zh. Obshch. Khim.* 1990, **60**, 1795.
34. E. H. Braye and W. Hübel, *Inorg. Synth.* 1966, **8**, 178.
35. W. McFarlane and G. Wilkinson, *Inorg. Synth.* 1966, **8**, 181.
36. L. Horner, P. Beck and V. G. Toscano, *Chem. Ber.* 1961, **94**, 2122.
37. W. Voskuil and J. F. Arens, *Rec. Trav. Chim. Pays-Bas* 1963, **82**, 302.

Polyhedron Vol. 12, No. 19, pp. 2291–2296, 1993
Printed in Great Britain

0277–5387/93 $6.00+.00
© 1993 Pergamon Press Ltd

CRYSTAL STRUCTURE OF HEXAFLUORO-2,4-PENTANEDIONATO COMPLEXES OF COBALT(III). $[Co(hfac)(en)_2](ClO_4)_2$ AND β-$[Co(hfac)(trien)](ClO_4)_2$

N. AZUMA* and T. OZAWA

Department of Chemistry, Faculty of General Education, Ehime University, Matsuyama 790, Japan

and

A. SHIBATA and Y. KITAMURA*

Department of Chemistry, Faculty of Science, Ehime University, Matsuyama 790, Japan

(*Received* 27 *April* 1993; *accepted* 8 *June* 1993)

Abstract—The crystal structures of $[Co(hfac)(en)_2](ClO_4)_2$ (**I**) and β-$[Co(hfac)(trien)](ClO_4)_2$ (**II**) have been determined by X-ray diffraction at ambient temperature, where Hhfac = hexafluoro-2,4-pentanedione, en = ethylenediamine and trien = 1,8-diamino-3,6-diazaoctane. The relative configuration of the cation in **II** is *rel*-Δ-β-*RR*. Their molecular structures are compared with those previously reported for $[Co(hfacOH)(en)_2]^+$, $[Co(hfacOH_3)(en)_2]^+$ and β-$[Co(hfacOCH_3)(trien)]^+$, in which an OH^- or OCH_3^- anion is covalently combined with one of the carbonyl carbon atoms on the hfac ligand. The quasiaromaticity of the coordinating hfac ligand in **I** and **II** was structurally characterized.

A cobalt(III) complex with a bidentate hfac ligand shows a pH dependent rapid and reversible colour change in water and in methanol.[1,2] This phenomenon was studied by UV and NMR spectroscopy and a reversible addition of a lyate anion onto one of the carbonyl carbon atoms in the hfac ligand was proposed

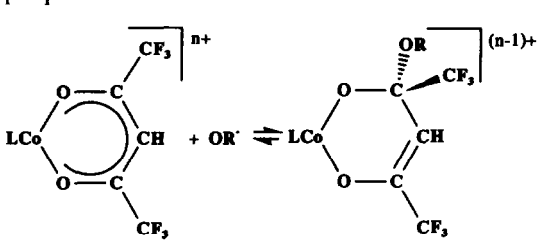

(1)

where L represents ligands occupying the residual four coordination sites and $R = H$ in water and $R = CH_3$ in methanol.[3,4] This mechanism was unequivocally underlined by the X-ray structure analysis of crystals obtained from basic solutions. In $[Co(hfacOH)(en)_2]Br \cdot H_2O$,[5] $[Co(hfacOCH_3)(en)_2]ClO_4$[6] and β-$[Co(hfacOCH_3)(trien)]ClO_4$,[4] an OH^- or OCH_3^- anion is combined with the hfac ligand by a covalent bond as shown on the right side of eq. (1). In the present report, we carry out the X-ray structure analysis for $[Co(hfac)(en)_2](ClO_4)_2$ (**I**) and β-$[Co(hfac)(trien)](ClO_4)_2$ (**II**). We compare their molecular structures with those of the corresponding OR^- combined complexes. We are also interested in the two possible configurations of β-$[Co(hfac)(trien)]^{2+}$; *rel*-Δ-β-*RR* and *rel*-Δ-β-*RS* where the meridional secondary NH proton is remote from or adjacent to a coordinated hfac oxygen atom. In a previous ^{19}F NMR study of **II**, it was indicated that the solid sample was composed of unspecified single isomer.[7]

EXPERIMENTAL

Compounds **I** and **II** were prepared as described elsewhere and recrystallized from water by addition of a slight excess of sodium perchlorate.[1,8]

* Authors to whom correspondence should be addressed.

Structure determination

Crystal data, details of data collection and structure refinement are listed in Table 1. The intensity data were collected using an automated Rigaku four-circle diffractometer AFC5R with graphite monochromatized Mo-K_α radiation ($\lambda = 0.71069$ Å) at the Advanced Instrumentation Center for Chemical Analysis, Ehime University. The cell dimensions for **I** and **II** were obtained using 22 reflections ($28.3° \leqslant 2\theta \leqslant 29.6°$) and 25 ones ($29.4° \leqslant 2\theta \leqslant 29.9°$), respectively. The ω–2θ scan mode with a scan rate 16°/min (in ω) was employed. Corrections were made for the Lorentz and polarization factor. Empirical correction for the absorption was made based on azimuthal (ψ) scans of three reflections.[9]

The structures were solved by a combination of Patterson method and direct methods. During the refinement the structures showed orientational disorder at perchlorate anions in **I** and at trifluoromethyl group in **II**. Partial occupancy factors for these disordered atoms were refined. The coordinates and anisotropic thermal parameters for the non-hydrogen atoms were refined by the full-matrix least-squares procedure based on F with weight $w = 1/\sigma^2(F_o)$. The positions of the hydrogen atoms were calculated from those of the non-hydrogen atoms and were included in F_c calculation. All calculations were performed on a VAXstation 3200 computer with TEXSAN program[10] which used the atomic scattering factors taken from "International Tables for X-ray Crystallography".[11] Anomalous dispersion effects were included in the F_c calculation. The final atomic parameters, together with observed and calculated structure factors have been deposited with the Editor, from whom copies are available on request. Atomic coordinates have also been deposited with the Cambridge Crystallographic Data Centre.

RESULTS AND DISCUSSION

Structure of $[Co(hfac)(en)_2](ClO_4)_2$ **(I)**

There are four $[Co(hfac)(en)_2]^{2+}$ cations and eight ClO_4^- anions in the unit cell. The anions showed an orientational disorder. Large thermal parameters for trifluoromethyl groups suggested similar disorder, but they could not be modelled with split sites. A perspective view of the cation and the atom labelling scheme are shown in Fig. 1.

The quasiaromatic ring is coplanar, Co(1) deviating by 0.094 Å from the plane defined by O(1), C(1), C(2), C(3) and O(2), whereas trifluoromethyl carbon atoms, C(4) and C(5), deviate by 0.043 Å and −0.180 Å from this plane, respectively. The deviations of Co(1) from the xy, yz and zx coordination plane were less significant, where each of the planes is defined by four atoms binding to Co(1). Selected bond distances and angles are summarized in Tables 2 and 3.

Table 1. Crystal data, experimental conditions, and refinement details of $[Co(hfac)(en)_2](ClO_4)_2$ **(I)** and β-$[Co(hfac)(trien)](ClO_4)_2$ **(II)** complex

Compound	I	II
Formula weight	585.08	611.12
Crystal system	Monoclinic	Monoclinic
a (Å)	11.966(3)	16.500(4)
b (Å)	13.358(2)	15.501(3)
c (Å)	13.354(3)	18.729(5)
β (°)	106.90(2)	113.98(2)
Volume (Å^3)	2042.4(8)	4377(4)
Space group and Z	$P2_1/c$, 4	$P2_1/a$, 8
D_c (g cm^{-3})	1.903	1.855
μ(Mo-K_α) (cm^{-1})	12.08	11.32
Colour of crystal	Red	Orange
Range of 2θ(°)	4.5–55.0	4.5–55.0
Number of reflections		
measured	5137	10,760
unique (R_{int})	4913 (0.051)	10,412 (0.043)
observed [$I \geqslant 3\sigma(I)$]	1929	4661
Final R, R_w	0.049, 0.052	0.056, 0.055
Final goodness of fit	1.38	1.83
Residual electron density (e Å^{-3})	−0.30–0.39	−0.48–0.51

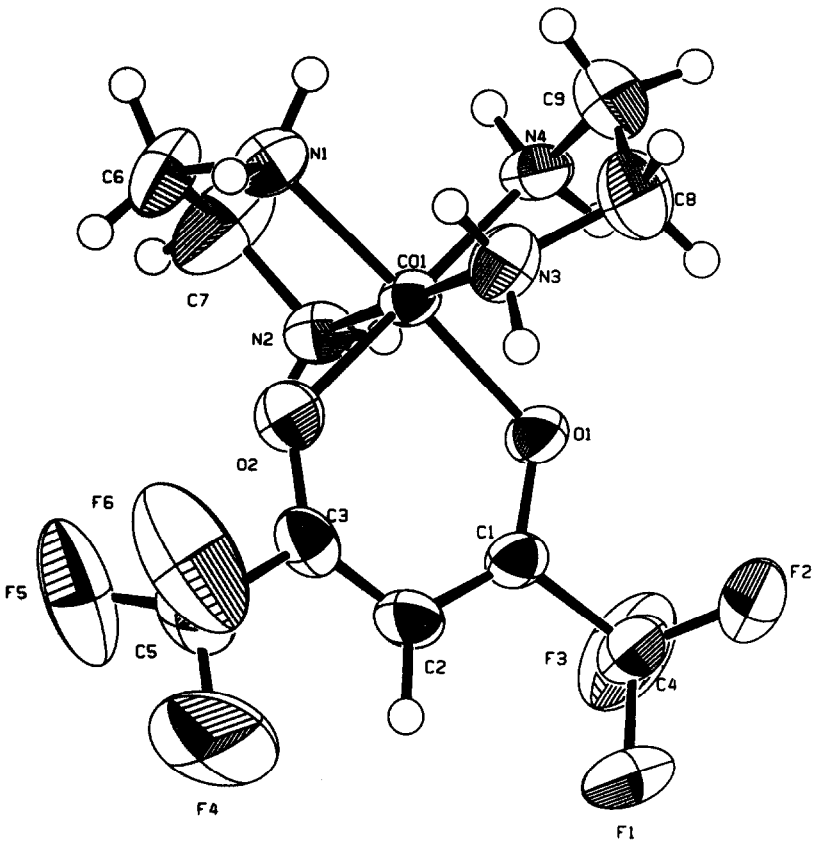

Fig. 1. Perspective view of $[Co(hfac)(en)_2]^{2+}$ cation. Open circles represent hydrogen atoms. Ellipsoids have been drawn at 50% probability.

All the amino groups are hydrogen bonded to the perchlorate ions. The shortest N—H···O bond distance is 2.86(2) Å for N(3). There are nine hydrogen bonds with the distance shorter than 3.30 Å. All the other intermolecular distances are in ordinary van der Waals contacts.[12]

Structure of $[Co(hfac)(trien)](ClO_4)_2$ **(II)**

There are two crystallographically independent cations of β-$[Co(hfac)(trien)]^{2+}$, or **1** and **2**. One of them contains Co(1) and the other cation Co(2). A perspective view of the cations and the atom labelling scheme are shown in Figs 2 and 3. The configurations of **1** are Δ-β-*RR* and Λ-β-*SS* and those of **2** are also Λ-β-*SS* and Δ-β-*RR*. Thus, the relative configuration of this complex is *rel*-Δ-β-*RR*.

The structure of **2** with Λ-β-*SS* configuration is essentially the same as the reflected structure of **1** with Δ-β-*RR* configuration. The noticeable difference stems from the rotation of the trifluoromethyl groups containing C(4) or C(24). The trifluoromethyl group with larger occupancy factor (0.870) in **1** occupies at the position which is rotated around the C—C bond by 120° from that in **2**. Pertinent bond lengths and bond angles are shown in Tables 2 and 3.

The atomic deviations of Co(1) and Co(2) from the respective *xy*, *yz* and *zx* coordination plane range from 0.017 to 0.023 Å, except for one deviation of 0.008 Å. The former values are small but significant. These deviations may be attributed to the existence of the tetradentate ligand trien.

All the nitrogen atoms are hydrogen bonded with the perchlorate oxygen atoms. The shortest hydrogen bond distances are 2.954(9) Å and 2.946(8) Å for N(4) and N(23) atom, respectively. There are fourteen hydrogen bonds with distances shorter than 3.30 Å. All the other intermolecular distances are ordinary van der Waals contacts,[12] except for 2.640(7) Å and 2.95(1) Å for the contacts between F(4) and F(23) and between F(24) and the perchlorate oxygen.

Comparison with the structure of the OR^- *combined complex*

The $[Co(hfac)(en)_2]^{2+}$ is approximately of C_2 symmetry. The average length of the equivalent bonds [i.e. N(1)—C(6) and N(4)—C(9)] was com-

Table 2. Selected bond lengths (Å) of $[Co(hfac)(en)_2]^{2+}$ and β-$[Co(hfac)(trien)]^{2+}$ complex cation

$[Co(hfac)(en)_2]^{2+}$		β-$[Co(hfac)(trien)]^{2+}$	Cation **1**	Cation **2**
Co(1)—O(1)	1.891(4)	Co(1/2)—O(1/21)	1.918(4)	1.918(4)
Co(1)—O(2)	1.892(5)	Co(1/2)—O(2/22)	1.903(4)	1.905(4)
Co(1)—N(1)	1.947(5)	Co(1/2)—N(1/21)	1.944(6)	1.963(6)
Co(1)—N(2)	1.950(5)	Co(1/2)—N(2/22)	1.924(6)	1.921(5)
Co(1)—N(3)	1.954(6)	Co(1/2)—N(3/23)	1.943(6)	1.960(6)
Co(1)—N(4)	1.939(6)	Co(1/2)—N(4/24)	1.938(5)	1.937(5)
O(1)—C(1)	1.266(8)	O(1/21)—C(1/21)	1.255(8)	1.254(7)
C(1)—C(2)	1.37(1)	C(1/21)—C(2/22)	1.37(1)	1.385(9)
C(2)—C(3)	1.36(1)	C(2/22)—C(3/23)	1.382(9)	1.359(9)
C(3)—O(2)	1.253(8)	C(3/23)—O(2/22)	1.257(7)	1.267(7)
N(1)—C(6)	1.482(9)	N(1/21)—C(6/26)	1.48(1)	1.480(9)
C(6)—C(7)	1.44(1)	C(6/26)—C(7/27)	1.49(1)	1.50(1)
C(7)—N(2)	1.46(1)	C(7/27)—N(2/22)	1.47(1)	1.489(9)
N(3)—C(8)	1.48(1)	N(2/22)—C(8/28)	1.45(1)	1.485(9)
C(8)—C(9)	1.47(1)	C(8/28)—C(9/29)	1.52(1)	1.50(1)
C(9)—N(4)	1.49(1)	C(9/29)—N(3/23)	1.50(1)	1.507(9)
		N(3/23)—C(10/30)	1.494(9)	1.479(8)
		C(10/30)—C(11/31)	1.52(1)	1.504(9)
		C(11/31)—N(4/24)	1.480(9)	1.500(8)
C(1)—C(4)	1.54(1)	C(1/21)—C(4/24)	1.53(1)	1.52(1)
C(3)—C(5)	1.53(1)	C(3/23)—C(5/25)	1.52(1)	1.529(9)

pared with the corresponding bond length in the $[Co(hfacOR)(en)_2]^+$, where we assumed OR^- is combined with the carbon atom corresponding to C(3) in **I** (Fig. 1). The β-$[Co(hfac)(trien)]^{2+}$ is apparently of C_1 symmetry. In the previously presented structure of *rel*-Δ-*β*-*RR*-$[Co(hfacOCH_3)(trien)]ClO_4$, the OCH_3^- is combined with the carbon atom corresponding to C(3) in cation **1** or to C(23) in cation **2**. The average length of the corresponding bonds in cations **1** and **2** [i.e. C(6)—C(7) and C(26)—C(27)] is compared with the corresponding bond length in the *rel*-Δ-*β*-*RR*-$[Co(hfacOH_3)(trien)]^+$. The significant differences are summarized in Table 4.

Table 3. Pertinent bond angles (°) of $[Co(hfac)(en)_2]^{2+}$ and β-$[Co(hfac)(trien)]^{2+}$ complex cation

$[Co(hfac)(en)_2]^{2+}$		β-$[Co(hfac)(trien)]^{2+}$	Cation **1**	Cation **2**
O(1)—Co(1)—O(2)	94.6(2)	O(1/21)—Co(1/2)—O(2/22)	92.6(2)	93.1(2)
O(1)—Co(1)—N(1)	175.5(2)	O(1/21)—Co(1/2)—N(1/21)	90.3(2)	88.2(2)
O(1)—Co(1)—N(2)	89.8(2)	O(1/21)—Co(1/2)—N(2/22)	88.8(2)	87.9(2)
O(1)—Co(1)—N(3)	89.6(2)	O(1/21)—Co(1/2)—N(3/23)	90.1(2)	91.4(2)
O(1)—Co(1)—N(4)	86.6(2)	O(1/21)—Co(1/2)—N(4/24)	175.4(2)	176.0(2)
O(2)—Co(1)—N(1)	84.7(2)	O(2/22)—Co(1/2)—N(1/21)	92.0(2)	93.7(2)
O(2)—Co(1)—N(2)	90.7(2)	O(2/22)—Co(1/2)—N(2/22)	178.0(3)	178.9(2)
O(2)—Co(1)—N(3)	90.4(3)	O(2/22)—Co(1/2)—N(3/23)	94.9(2)	93.7(2)
O(2)—Co(1)—N(4)	176.0(2)	O(2/22)—Co(1/2)—N(4/24)	84.5(2)	83.7(2)
N(1)—Co(1)—N(2)	85.8(2)	N(1/21)—Co(1/2)—N(2/22)	86.5(3)	85.9(2)
N(1)—Co(1)—N(3)	94.8(2)	N(1/21)—Co(1/2)—N(3/23)	173.0(3)	172.6(2)
N(1)—Co(1)—N(4)	94.4(2)	N(1/21)—Co(1/2)—N(4/24)	93.4(2)	94.4(2)
N(2)—Co(1)—N(3)	173.8(3)	N(2/22)—Co(1/2)—N(3/23)	86.6(3)	86.8(2)
N(2)—Co(1)—N(4)	93.1(2)	N(2/22)—Co(1/2)—N(4/24)	94.2(2)	95.3(2)
N(3)—Co(1)—N(4)	85.8(3)	N(3/23)—Co(1/2)—N(4/24)	86.6(2)	86.5(2)

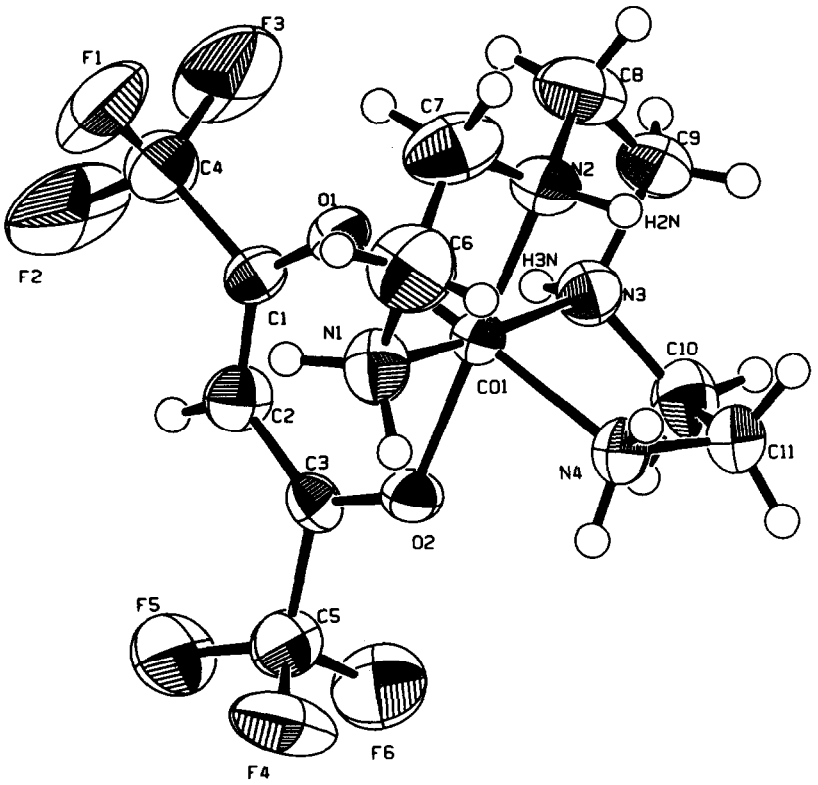

Fig. 2. Perspective view of cation **1** in β-[Co(hfac)(trien)]$(ClO_4)_2$. The fluorine atoms with smaller occupancy factor were omitted for the sake of clarity. Open circle represents hydrogen atom. The hydrogen atom with label is binding to the chiral nitrogen atom. Ellipsoids have been drawn at 50% probability.

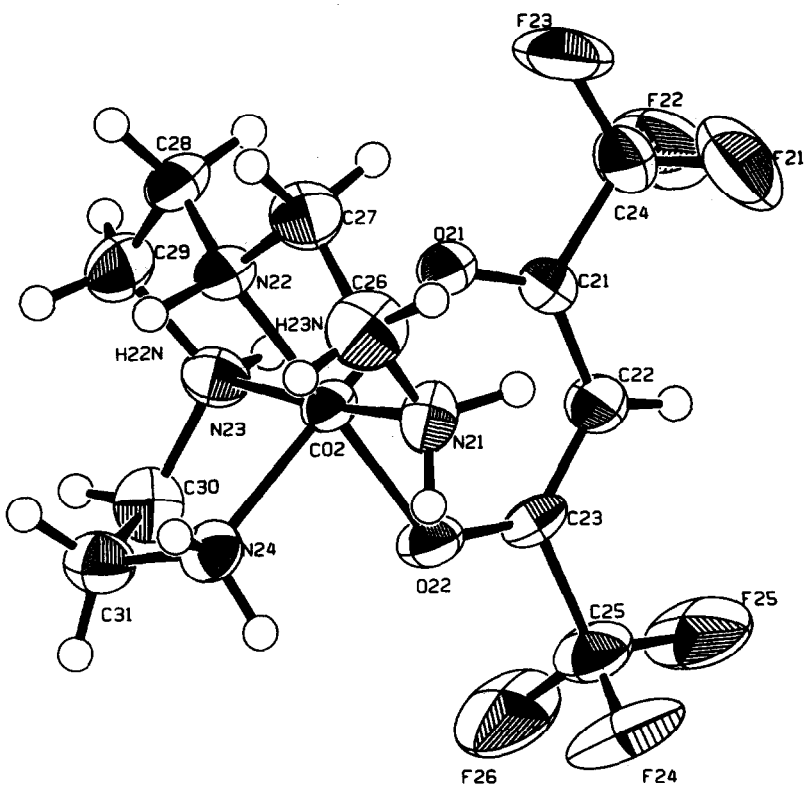

Fig. 3. Molecular structure of cation **2** in β-[Co(hfac)(trien)]$(ClO_4)_2$. Open circles show hydrogen atoms. The hydrogen atoms binding to the chiral nitrogen atom are labelled. Ellipsoids have been drawn at 50% probability.

Table 4. Difference of the average bond length (Å) from the corresponding one in the OR^- combined complex

Bond[a]	$[Co(hfac)(en)_2]^{2+}$ $R = CH_3$[6]	$R = H$[5]	β-$[Co(hfac)(trien)]^{2+}$ $R = CH_3$[4]
Co(1)—O(1)			0.03
Co(1)—O(2)			0.03
Co(1)—N(4)		−0.03	−0.03
O(1)—C(1)	−0.06	−0.04	−0.05
O(2)—C(3)	−0.08	−0.09	−0.09
N(1)—C(6)		0.05	
N(4)—C(9)	−0.03		
N(2)—C(7)	−0.03		
N(2)—C(8)			−0.04
N(3)—C(8)	−0.03		
C(1)—C(2)	0.03	0.04	0.03
C(1)—C(4)	0.04		0.03
C(2)—C(3)	−0.14	−0.13	−0.13
C(3)—C(5)		0.03	−0.06
C(6)—C(7)		0.09	−0.05
C(8)—C(9)	−0.06	−0.04	−0.03

[a] See text. The composite standard deviation for the difference is below 0.01.

The Co—O bond lengths of **I** and, in particular, **II** are longer than those of the corresponding OR^- combined complexes. In contrast the Co—N bond lengths of **I** and **II** are shorter than those of the OR^- combined complexes. The O(1)—C(1), C(2)—C(3) and O(2)—C(3) bonds are significantly shorter and C(1)—C(2) bond is slightly longer than the corresponding one in the OR^- combined complexes. This is consistent with the disappearance of the pseudoaromaticity of the hfac ligand on the right side of eq. (1). In the OR^- combined complex, the bonds corresponding to the O(1)—C(1), C(2)—C(3) and O(2)—C(3) bond are single bonds and that corresponding to C(1)—C(2) is a localized double bond. The differences for the other bonds cannot be attributed clearly to the intramolecular electronic interaction, because the same extent of variation in the bond length will be caused by the intermolecular interaction. Nevertheless these differences might be related to the fact that the equilibrium constant of eq. (1) depends significantly on the variation of L ligand and that for certain L ligands the OR^- combined complexes are labile.[2,13] Most bond angles are similar to the corresponding ones in the OR^- combined complex. Only the N(2)—Co(1)—N(3) angle in **I** (173.8°) is slightly smaller than the corresponding angles in the OR^- combined complexes (177.8° and 178.4°).

REFERENCES

1. K. Kuroda, *Chem. Lett.* 1979, 93.
2. Y. Kitamura and A. Shibata, *Inorg. Chim. Acta* 1993, **203**, 37.
3. Y. Fukuda, M. Ishige, T. Ito, K. Kuroda, K. Sone, Y. Suzuki, S. Yano and S. Yoshikawa, *Chem. Lett.* 1981, 1699.
4. Y. Kitamura, J. G. Leipoldt and A. Roodt, *Inorg. Chim. Acta* 1988, **149**, 125.
5. S. Aygen, E. F. Paulus, Y. Kitamura and R. van Eldik, *Inorg. Chem.* 1987, **26**, 769.
6. W. Purcell, J. G. Leipoldt and Y. Kitamura, *Inorg. Chim. Acta* 1990, **177**, 151.
7. Y. Kitamura and A. Shibata, *Polyhedron* 1992, **19**, 2441. The isomeric designations Δ-β-*SR* and Δ-β-*SS* in this reference are errors. They should read *rel*-Δ-β-*RR* and *rel*-Δ-β-*RS*. The conclusions of the paper are not affected by this change.
8. S. Aygen, Y. Kitamura, K. Kuroda, R. Kume, H. Kelm and R. van Eldik, *Inorg. Chem.* 1985, **24**, 423.
9. A. C. T. North, D. C. Phillips and F. S. Mathews, *Acta Cryst. Sect. A* 1968, **24**, 351.
10. TEXSAN—Texray Structure Analysis Package, Version 5.0, Molecular Structure Corporation, The Woodlands, TX 77381 (1989).
11. *"International Tables for X-Ray Crystallography"*. Vol. IV, Kynoch Press, Birmingham (1974).
12. A. Bondi, *J. Phys. Chem.* 1964, **68**, 443.
13. Y. Kitamura and A. Shibata, *Polyhedron*, in press.

Polyhedron Vol. 12, No. 19, pp. 2297–2305, 1993
Printed in Great Britain

0277–5387/93 $6.00+.00
© 1993 Pergamon Press Ltd

SYNTHESIS AND CHARACTERIZATION OF SOME NOVEL PENTAGONAL BIPYRAMIDAL 2,6-DIACETYLPYRIDINE BIS(BENZOYLHYDRAZONE) ($DAPBH_2$) COMPLEXES OF RHENIUM(III) AND MOLYBDENUM CRYSTAL AND MOLECULAR STRUCTURE OF [ReCl(DAPB)(PPh_3)]. AN INVESTIGATION OF THE MÖSSBAUER SPECTROSCOPY OF [$Fe^{II}Cl_2(DAPBH_2)$]·H_2O AND [Fe^{III}Cl(DAP-Me-B)(H_2O)]*

AYED S. M. AL-SHIHRI, JONATHAN R. DILWORTH,† STUART D. HOWE, JACK SILVER and RUSSELL M. THOMPSON

Department of Chemistry and Biological Chemistry, University of Essex, Wivenhoe Park, Colchester, Essex CO4 3SQ, U.K.

and

JONATHAN DAVIES and DAVID C. POVEY

Department of Chemistry, University of Surrey, Guildford, Surrey GU2 5XH, U.K.

(*Received* 20 *April* 1993; *accepted* 4 *June* 1993)

Abstract—Reaction of [$ReCl_3$(MeCN)(PPh_3)$_2$] with the planar pentadentate diacetylpyridinebis(benzoylhydrazone) ligands $DAPBH_2$ and DAP-Me-BH_2 and triethylamine in isopropanol under reflux gave the dark brown seven-coordinate complexes [ReCl(L)PPh_3], containing the doubly deprotonated pentadentate ligand [L = DAPB(2−) (**1**); L = DAP-Me-B(2−) (**2**)]. Complex **1** has been characterized by crystallography. The central rhenium atom in **1** is seven-coordinate, with pentagonal bipyramidal geometry with the axial positions being occupied by the chloride ion and the triphenylphosphine ligand. The DAPB coordinates in a pentadentate manner in the equatorial plane of the complex and the five donor atoms of the doubly deprotonated DAPB(2−) ligand form an approximately planar pentagon. The rhenium atom is slightly displaced out of the ligand plane towards the phosphorus atom. Reaction of **2** with Ag[BF_4] in CH_2Cl_2 at room temperature gave a black complex of stoichiometry [Re(DAP-Me-B)(PPh_3)][BF_4] (**3**). Reaction of [$MoCl_4$(MeCN)$_2$] with DAP-Me-BH_2 and Et_3N in dry CH_2Cl_2 under reflux gave deep green [$MoCl_2$(DAP-MeB_2)] (**4**), formulated as a seven-coordinate molybdenum(II) complex containing the doubly deprotonated pentadentate DAP-$MeBH_2$ ligand in the equatorial plane of the complex. The Mössbauer spectra of the complexes [$FeCl_2(DAPBH_2)$]·H_2O (**5**) and [FeCl(DAPMe-B)(H_2O)] (**6**) were investigated as a function of temperature. The spectrum of **5** was consistent with high-spin seven-coordinate iron(II) and **6** was shown to contain two distinct iron(III) sites; possible structures are discussed.

The planar pentadentate 2,6-diacetylpyridine bis(benzoylhydrazone) ligands ($DAPBH_2$ and DAP-Me-BH_2, Fig. 1) and similar ligands formed from DAP and a variety of other aroylhydrazines have the ability to behave as neutral or deprotonated ligands and produce stereochemistries with

* Chloro(triphenylphosphine)(2,6 - diacetylpyridinebis[benzoylhydrazonato(2−)]rhenium(III), dichloro-2,6-diacetylpyridinebis(benzoylhydrazone)iron(II), monohydrate, aquochloro-2,6-diacetylpyridinebis[4-methylbenzoylhydrazonato(2−)]iron(III).

† Author to whom correspondence should be addressed.

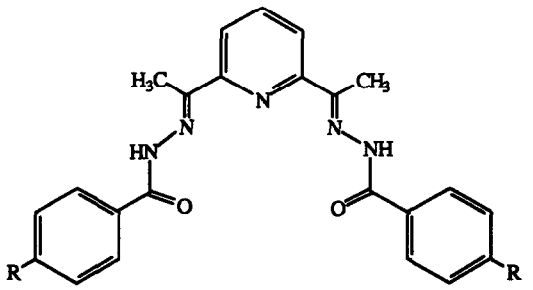

R = H, $DAPBH_2$

R = Me, $DAPMeBH_2$

Fig. 1. The structures of the ligands $DAPBH_2$ and DAP-Me-BH_2.

high coordination numbers.[1,2] The coordination chemistry of these interesting ligands has been extensively studied with first row transition metals and some main group elements, but comparatively little with second and third row transition metals. It is not straightforward to predict the capacity of such metal ions to accommodate pentagonal bipyramidal geometry, or the ways in which multidentate ligands of varying conformational flexibility will respond to the stereochemical preferences of different metal ions. We report here the synthesis and characterization of some rhenium(III) and molybdenum(II) complexes of these ligands, and in order to investigate the detailed coordinate geometry of these complexes we have determined the crystal structure of the seven-coordinate rhenium(III) complex [ReCl(DAPB)(PPh_3)] (**1**). We have also investigated the Mössbauer spectroscopy of the iron(II) and iron(III) complexes **5** and **6** of these ligands.

RESULTS AND DISCUSSION

Preparation and properties of $DAPBH_2$ *and* DAP-Me-BH_2 *complexes*

Table 1 gives analytical and spectroscopic data for the pentadentate ligands and the complexes of rhenium, molybdenum and iron. The rhenium(III) complexes **1** and **2** were prepared in good yield by heating [$ReCl_3$(MeCN)(PPh_3)$_2$] and the appropriate pentadentate ligand in isopropanol under reflux in the presence of triethylamine. The seven-coordinate complexes are non-electrolytes and are soluble in most of the common organic solvents with the exception of alcohols, ethers and alkanes. There is no evidence in the IR spectrum for ν(NH) or ν(C=O), which suggests that the coordinated planar pentadentate ligands are doubly deprotonated in these rhenium(III) complexes. The imino stretching frequency, ν(C=N), for the coordinated ligand appears at 1520 and 1580 cm^{-1} for **1** and **2**, respectively, indicative of coordination by the imino nitrogens. Characteristic bands for coordinated triphenylphosphine appear at 700–750 cm^{-1}. The ^1H

Table 1. Analytical and spectroscopic data for complexes of pentadentate ligands

Compound	Elemental analysis[a] C	H	N	Cl	P	IR data (cm^{-1})[b] ν(OH)	ν(NH)	ν(C=O)	ν(C=N)
$DAPBH_2$	68.7 (69.1)	5.3 (5.3)	17.3 (17.3)	—	—	3400	3170	1660	1600
DAP-Me-BH_2	68.2 (67.4)	6.1 (6.1)	15.6 (15.7)	—	—	3500	3200	1635	1605
[ReCl(DAPB)(PPh_3)] (**1**)	57.1 (55.9)	4.0 (3.9)	8.8 (8.0)	4.2 (4.0)	—	—	—	—	1520
[ReCl(DAP-Me-B)(PPh_3)] (**2**)	54.8 (54.8)	4.2 (4.1)	6.8 (7.3)	5.8 (7.4)	3.7 (3.2)	—	—	—	1580
[Re(DAP-Me-B)(PPh_3)]BF_4 (**3**)	54.9 (53.8)	4.1 (4.0)	5.9 (7.2)	—	3.7 (3.2)	—	—	—	1600
[$MoCl_2$(DAP-Me-B)] (**4**)	51.0 (51.5)	6.3 (4.3)	10.8 (11.7)	10.8 (11.9)	—	—	—	—	1640
[$FeCl_2$($DAPBH_2$)]·H_2O (**5**)	50.1 (50.7)	4.7 (4.3)	13.3 (12.9)	12.3 (13.0)	—	3300	3200	1620	1610
[FeCl(DAP-Me-B)(H_2O)] (**6**)	53.0 (52.1)	4.8 (4.4)	14.0 (12.1)	7.4 (6.2)	—	—	—	—	1600

[a] Calculated values in parentheses.

[b] Recorded as Nujol mulls.

NMR spectra of the two pentadentate ligands are generally little changed on coordination to the rhenium(III). The $^{31}P\{^1H\}$ NMR spectra of the rhenium(III) complexes in $CH_2Cl_2/CDCl_3$ (80 MHz, δ TMP) consist of singlet resonances at -9.0 (**1**) and -9.2 ppm (**2**), respectively, corresponding to the singly coordinated triphenylphosphine ligand.

The black rhenium(III) complex formulated as $[Re(DAP\text{-}Me\text{-}B)(PPh_3)][BF_4]$ (**3**) was prepared in virtually quantitative yield by reacting [ReCl(DAP-Me-B)(PPh_3)] (**2**) with excess $Ag[BF_4]$ under inert atmosphere in dry CH_2Cl_2. The elemental analysis of **3** confirms the absence of chlorine and suggests the formulation $[Re(DAP\text{-}Me\text{-}B)(PPh_3)][BF_4]$. The product is soluble in chlorinated solvents, DMF, DMSO and acetone. The ^1H NMR spectrum of (**3**) was rather broad, but the integral ratio of the barely resolved singlets (CH_3—) vs the aromatic proton multiplet agreed with the formulation for **3** above. The $^{31}P\{^1H\}$ spectrum of **3** shows a single resonance at -1.8 ppm, which indicates a downfield shift in the ^{31}P spectrum of **3** vs that of complex **2**, and indicates retention of a single PPh_3 group. Complex **3** was found to be a 1 : 1 electrolyte in DMF solution by determination of conductivity measurements over a concentration range; the results compare favourably with those obtained for other 1 : 1 electrolytes. The IR spectrum of **3** shows no evidence of ν(NH) or ν(C=O) and bands due to η(C=N) appear at 1600 and 1580 cm^{-1}, which suggests that the planar pentadentate ligand has been retained. The structure of this complex is uncertain and a six-coordinate structure appears to be unlikely since there is no precedent in the literature. So far attempts to grow crystals suitable for an X-ray structure determination have not been successful.

Reaction of $[MoCl_4(MeCN)_2]$ with DAP-Me-BH_2 and Et_3N in CH_2Cl_2 under reflux gave $[MoCl_2$(DAP-Me-B)] (**4**) in good yield. The neutral complex $[MoCl_2$(DAP-Me-B)] (**4**) is hygroscopic and soluble in DMF, DMSO, CH_2Cl_2, $CHCl_3$ and acetone. The product gave a single HPLC peak (retention time 5.6 min). This complex is related to the Schiff's base derivative $[MoCl_2(sal)_2]$ (sal = 2-OC_6H_4CH=NPh), which is six-coordinate.[3] The diamagnetism of the seven-coordinate molybdenum(IV) (d^2) complex is not unexpected and has precedent in $[MoCl(S_2CNMe_2)_3]$.[4]

The neutral dark green complex $[FeCl_2(DAPBH_2)]\cdot H_2O$ (**5**) was prepared from anhydrous $FeCl_2$ and $DAPBH_2$ in dry methanol. It is soluble in DMF, DMSO and slightly soluble in $CHCl_3$, CH_2Cl_2 and acetone, and conductivity measurements in DMF showed the complex to be neutral. The IR spectrum shows the presence of ν(OH) at 3340 cm^{-1}, indicative of the presence of water. The shift of the amide ν(C=O) band by 30 cm^{-1} to lower wave number compared with the free ligand $DAPBH_2$ and the appearance of ν(NH) bands suggest that the ligand is coordinating as a neutral doubly protonated pentadentate yielding a seven-coordinate pentagonal bipyramidal iron(II) complex with the two chlorides occupying axial positions. $DAPBH_2$ ligands are known to coordinate in this fashion in other $[M^{II}Cl_2(DAPBH_2)]$ (M = Mn, Co, Ni, Zn) complexes. The magnetic moment of 5.46 B.M. and the Mössbauer data for **5** are consistent with the formulation as a high-spin iron(II) species. The elemental analysis is in reasonable agreement with the stoichiometry containing a water of crystallization.

The brown complex [FeCl(DAP-Me-B)(H_2O)] (**6**) was prepared by reaction of anhydrous $FeCl_3$ with DAP-Me-BH_2 in absolute ethanol in the presence of triethylamine as base. Elemental analysis suggests the formulation as the iron(III) complex [FeCl(DAP-Me-B)(H_2O)]. The neutral complex **6** is soluble in DMF, DMSO and slightly soluble in CH_2Cl_2. There is no ν(NH) nor ν(C=O) in the IR spectrum, which suggests that the ligand in complex **6** is doubly deprotonated and coordinating in a pentadentate(2−) manner. Peaks at 3160, 3240, 3300 and 3410 cm^{-1} can be assigned to OH stretches of a water molecule. The Mössbauer spectrum and magnetic moment of 5.65 B.M. confirms the assignment as high-spin iron(III). The suggested structure based on Mössbauer studies (see below) is dimeric, with one pentagonal bipyramidal iron with one chloride and the oxygen of another FeCl(DAPMe-B) unit in the axial sites.

Description of the molecular structure of [ReCl(DAPB)(PPh_3)]

The molecular structure of [ReCl(DAPB)(PPh_3)] is shown in Fig. 2 and important bond lengths and angles are given in Table 2. The coordination about the central rhenium atom is essentially pentagonal bipyramidal, with the axial positions being occupied by one chloride ion and the triphenylphosphine ligand. The $DAPBH_2$ ligand on being doubly deprotonated, therefore, coordinates as a planar pentadentate ligand. The pentagonal bipyramidal nature of the complex is more apparent from Fig. 3, which gives a representation of the equatorial ligand with the axial ligands omitted for clarity. The five donor atoms N(2), N(12), N(23), O(1) and O(3) form an approximately planar pentagon around the metal atom. The angles at the metal in the plane are O(1)—Re—N(12), 72.3(1)°; N(12)—Re—N(2), 70.9(1)°; N(2)—Re—N(23), 71.4(1)°; N(23)—Re—O(3), 72.4(1)°; O(1)—Re—O(3), 72.9(1)°; which

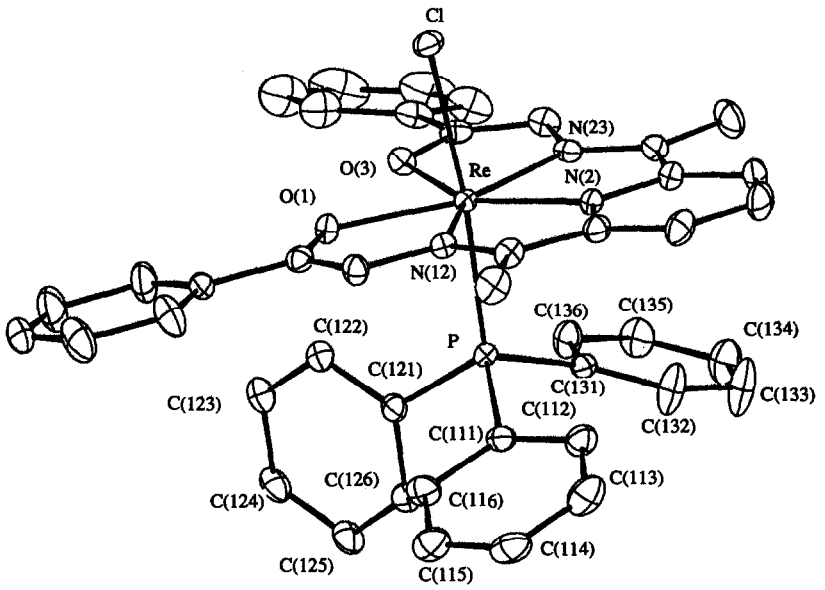

Fig. 2. A representation of the molecular structure of [ReCl(DAPB)(PPh_3)], showing a partial atom-labelling scheme.

confirms the symmetrical, approximately planar pentagonal coordination of the pentadentate ligand. There is no evidence for a water of crystallization or other solvent molecule in the structure.

The pentadentate doubly deprotonated equatorial ligand in complex **1** appears reasonably coplanar on the basis of the bond angle data. However inspection of the data for the least squares plane through the ligand donor atoms reveals small but significant deviations of the five donor atoms in the ligand from planarity. The rhenium atom lies 0.054 Å below the O(1)—N(12)—N(2)—N(23)—O(3) plane.

In the X-ray structure of [Mn(DAPBH$_2$)Cl

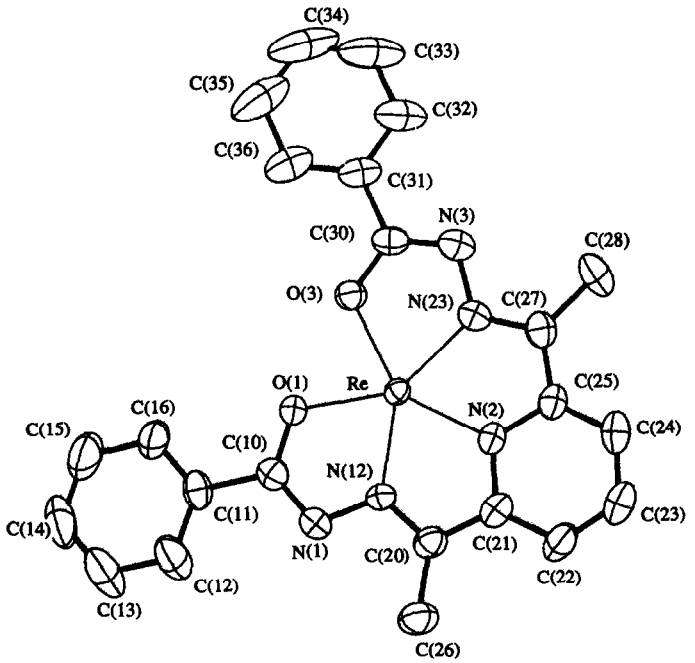

Fig. 3. A view of the structure of complex **1** with the axial ligands omitted for clarity and a further atom-labelling scheme.

Table 2. Selected bond lengths (Å) and angles (°) for [ReCl(DAPB)(PPh_3)]

Re—Cl	2.438(1)	C(30)—O(3)	1.295(5)
Re—P	2.364(1)	C(30)—N(3)	1.292(5)
Re—O(1)	2.063(3)	N(3)—N(23)	1.388(5)
Re—O(3)	2.071(3)	N(23)—C(27)	1.310(6)
Re—N(2)	2.063(3)	C(27)—C(25)	1.406(6)
Re—N(12)	2.074(3)	C(25)—N(2)	1.393(5)
Re—N(23)	2.071(3)	N(1)—N(12)	1.390(5)

Cl—Re—P	173.11(4)	O(3)—Re—N(12)	145.3(1)
O(1)—Re—O(3)	72.9(1)	O(3)—Re—N(23)	72.4(1)
O(1)—Re—N(2)	143.1(1)	N(2)—Re—N(12)	70.9(1)
O(1)—Re—N(12)	72.3(1)	N(2)—Re—N(23)	71.4(1)
O(1)—Re—N(23)	145.0(1)	N(12)—Re—N(23)	142.2(1)
O(3)—Re—N(2)	143.8(1)		

$(H_2O)]Cl$,[1c] where the fully protonated ligand coordinates as a neutral pentadentate ligand, the N_3O_2 donor set of atoms which form the pentagon are also approximately co-planar, the maximum deviation from the least squares plane being 0.13 Å, the manganese atom being 0.12 Å above this plane. Other seven-coordinate, pentagonal bipyramidal $DAPBH_2$ complexes which may be compared with the present one are $[Co(DAPBH_2)(H_2O)(NO_3)]NO_3$ and $[Ni(DAPBH_2)(H_2O)_2][NO_3]_2\cdot 2H_2O$.[5] Small structural differences involve mainly the N—N bond distances, which are longer in the rhenium compound [N(3)—N(23), 1.388(5) and N(1)—N(12), 1.390(5) Å] than in those of the manganese compound [1.380(5) and 1.390(5) Å], and in those of the cobalt [1.365(4) and 1.376(4) Å] and nickel compounds [1.369(6) and 1.366(6) Å]. The two $M—O_{ligand}$ bonds differ by 0.050, 0.079 and 0.195 Å in the compounds of manganese, cobalt and nickel, respectively. In the rhenium complex this difference is much smaller at 0.008 Å. The geometry of the doubly deprotonated ligand in [ReCl(DAPB)(PPh_3)] thus compares quite well with that found for the smaller first row transition metal ions.

Calculated least-squares planes through the two phenyl rings of the ligands (not given in this work) show that the two phenyl rings are not in the equatorial plane of the pentadentate ligand but are rotated some 15–16° from the equatorial plane and about 16° from each other. This may well be a function of crystal packing constraints.

Mössbauer spectroscopic studies of **5** *and* **6**

Mössbauer data and magnetic measurements are given in Table 3. Compound **5** has Mössbauer parameters consistent with a high-spin iron(II) elec-

Table 3. Mössbauer spectroscopic data and magnetic moments for iron complexes

Compound		T (K)	δ(Fe) (mm s^{-1})	QS (mm s^{-1})	Coordination No.	μ_{eff} (B.M.)	Ref.
$[FeCl_2(DABH_2)]\cdot H_2O$		298	1.25(1)	1.91(1)	7	5.46	This work
		78	1.28(1)	2.51(1)	7	—	This work
[FeCl(DAPMe-B)(H_2O)]	A	298	0.54(1)	0.91(3)	7	5.65	This work
	B	298	0.52(1)	0.38(2)			
	A	78	0.63(1)	0.90(1)			
	B	78	0.60(1)	0.35(1)			
[Fe(EDTAH)(H_2O)]		298	0.371	0.498	6	6.16	6
		78	0.457	0.422			
$Li[Fe(EDTA)(H_2O)]\cdot 2H_2O$		298	0.456	0.700	7	6.16	6
$Rb[Fe(EDTA)(H_2O)]\cdot H_2O$		298	0.455	0.521	7	5.82	6
$NH_4[Fe(DTPAH)]\cdot H_2O$		298	0.358	1.095	7	6.21	7
$Li_2[Fe(DTPA)]\cdot 2H_2O$		298	0.386	0.829	8	5.96	7

Table 4. Summary of crystal data, data collection and structure refinement for X-ray diffraction study of [ReCl(DAPB)(PPh_3)]

1. Crystal data	
Empirical formula	$C_{39}H_{36}ClN_5O_2PRe$
Colour, habit	Orange–red, laths
Crystal size (mm)	$0.4 \times 0.15 \times 0.05$
Crystal system	Monoclinic, space group $P2_1/n$
Unit cell dimensions	
a (Å)	11.6278(27)
b (Å)	16.6610(60)
c (Å)	18.2782(33)
α (°)	90
β (°)	9185(2)
γ (°)	90
Volume (Å^3)	3539
Z	4
Density (calc) (g cm^{-3})	1.613
Absorption coefficient (cm^{-1})	36.4
F(000)	1712
2. Data collection	
Diffractometer	Enraf–Nonius CAD 4
Radiation	Mo-K_α
Temperature (K)	298
Monochromator	Graphite
2θ range (°)	2–48
Scan speed (° min^{-1})	4
Background measurement (s)	90
Standard reflections	400
Index ranges	0 −13, 0 −19, −20 20
Reflections collected	6087
Reflections observed	$4794 > 3\sigma$
Absorption correction	None
3. Solution and refinement	
System used	Enraf–Nonius SDP v1-1a
Solution	Heavy atm.
Refinement method	Full matrix
Quantity minimized	$F_o - F_c$
Hydrogen atoms	Calculated
Weighting scheme	$w^{-1} = (\sigma F)^2 + (0.025)^2 + 2.5$
Final R index (obs data)	0.023
R_w	0.038
Goodness-of-fit	0.943
Absorption correction	Difabs

tronic environment. The isomer shift of 78 K is 1.28(1) mm s^{-1} and quadrupole splitting (QS) of 2.51(1) mm s^{-1} would not be inconsistent with a seven-coordinate environment as assumed for **5**. The change in the QS at room temperature is consistent with a thermal population of one or more of the four singly electron-occupied 3d orbitals by the sixth electron originally lying in the lowest energy orbital of an ^{5}A state. There is some evidence from the Mössbauer spectra of **5** for the presence of a small iron(III) impurity.

Complex **6** poses more of a problem, as there are clearly two distinct iron sites A and B at both 298 and 78°, and the computer fit is consistent with two symmetric doublets. The last is consistent with two iron sites that are antiferromagnetically coupled. However, the magnetic moment is only slightly lower than the values found for other high-spin

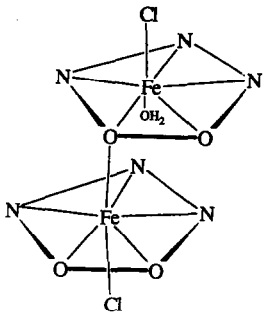

Fig. 4. The proposed structure for $[FeCl(DAPB)]\cdot H_2O$.

iron(III) systems and suggests that any coupling must be small.

There is little data in the literature on seven-coordinate iron(III) complexes for comparison. However, some data on six-, seven- and eight-coordinate complexes with ethylenediaminetetraacetic acid (H_4EDTA) and diethylenetriaminepentaacetic acid (H_5DTPA) have appeared[6,7] and are also summarized in Table 3. The isomer shift values for both sites are consistent with high-spin iron(III). The assignment of coordination number is more difficult as there is no obvious correlation with the isomer shift values and the quadrupole splittings also reflect the changes in symmetry as the donor atoms are varied. Nevertheless, the parameters for site A are in accord with seven-coordination, while those for B are more suggestive of an octahedral geometry.[8-14]

The observation of two different sites is intriguing and as indicated above, the symmetry of the peaks suggests antiferromagnetic coupling. We therefore tentatively assign the complex the dimeric structure shown in Fig. 4 in which an oxygen provides a bridge between the two iron atoms. The chloride analysis corresponding to one chlorine per iron would appear to rule out structures involving bridging oxo- or hydroxo-ligands.

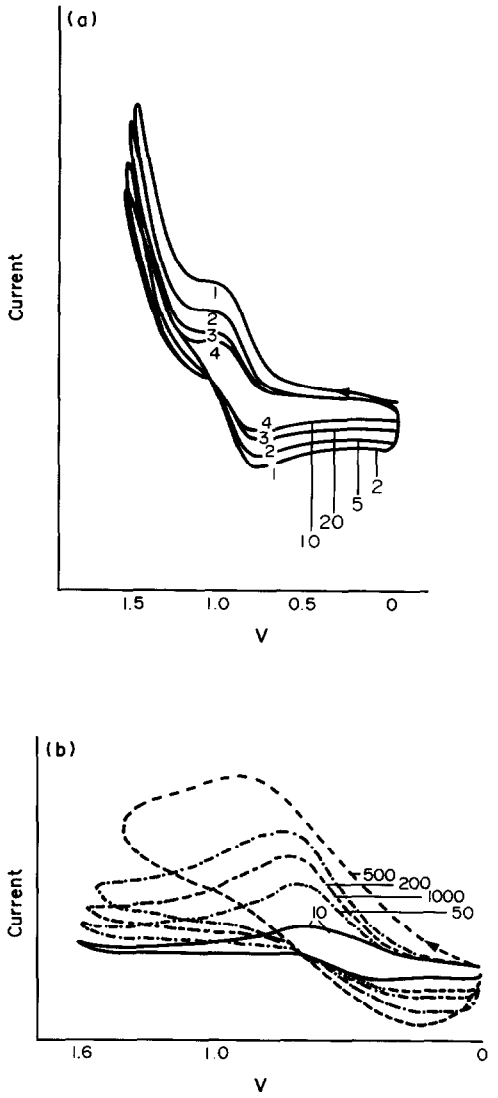

Fig. 5. The cyclic voltammograms of complexes (a) **1** and (b) **5** recorded in CH_2Cl_2 at a gold working electrode vs a silver wire pseudo-reference electrode with $[Bu^n{}_4N][BF_4]$ as a supporting electrolyte at various scan rates ($mV\ s^{-1}$, indicated on the voltammograms).

Redox properties of **2** *and* **5**

The redox properties of the seven-coordinate rhenium(III) complex **1** was studied in 0.2 M $[Bu_4N][BF_4]$/DMF at a gold disc electrode. Figure 5 shows the cyclic voltammograms of the observed single reversible oxidation process at various scan rates. The oxidation ($E_{1/2} = +0.87$ V vs S.C.E.) corresponds to the formation of the cation $[ReCl(DAP\text{-}Me\text{-}B)(PPh_3)]^+$ and lies close to the oxidation limit accessible for a gold electrode.

The electrochemistry of $[FeCl_2(DAPBH_2)]\cdot H_2O$ (**5**) was studied in 0.2 M $[Bu_4N][BF_4]$/DMF at a gold disc electrode. Figure 5 shows the oxidation process at various scan rates. The process is more reversible at high scan rates. The very large ΔE_p values (approximately 500 mV at 500 mV s^{-1}) are indicative of slow heterogeneous electron transfer for the iron(II) complex. Ferrocene showed normal ΔE_p values of 65 mV under similar conditions indicating that uncompensated internal cell resistance is not responsible. The overall process corresponds to oxidation of iron(II) to iron(III), but the simultaneous rapid deprotonation of the ligand cannot be ruled out. Since this would be very fast it would not affect the overall cyclic voltammetric processes.

EXPERIMENTAL

Materials and methods

All experimental manipulations were carried out under an atmosphere of dry nitrogen gas unless stated otherwise. Standard Schlenk-tube, vacuum line and syringe techniques were employed throughout where appropriate. Melting points were determined using an electrothermal melting point apparatus. Elemental analyses were carried out by the Microanalytical Laboratories of Manchester and Sussex Universities. IR spectra were recorded on a Perkin–Elmer 1330 IR spectrophotometer in the range 200–4000 cm^{-1} as Nujol mulls on KBr plates. ^1H and ^{13}C NMR spectra were recorded either on Jeol PMX 60SYS or Bruker WP80SY spectrometers with TMS as an internal standard using the solvents indicated. ^{31}P NMR spectra were recorded on the Bruker WP80SY spectrometer using TMP as the internal standard. Electronic spectra were recorded on a Beckman DU-7 spectrophotometer. Conductivity measurements were made either in DMF or CH_2Cl_2 using a Jenway conductivity meter. Magnetic susceptibility determinations were made in the solid state using a Johnson–Matthey automatic recording magnetic susceptibility balance calibrated with mercury cobalt thiocyanate. The solution state values were obtained using the Evans method. Solvents were dried by standard methods. All other materials and reagents were obtained commercially (Fisons, Aldrich) and used without further purification. $[ReOCl_3(PPh_3)_2]$ was prepared from rhenium metal using the published procedure.[15]

Mössbauer measurements

Mössbauer spectroscopic measurements were carried out on solid samples in aluminium holders. The samples were placed into a cryostat under dinitrogen after quenching at 78 K. The spectrometer (previously described) was calibrated with a natural iron absorber 25 μm thick, which was used as zero for the isomer shift measurements. The spectra were computer fitted.[16]

Electrochemical measurements

Cyclic voltammetry experiments were typically carried out in 0.2 M solutions of $[Bu_4N][BF_4]$ in either CH_2Cl_2 or DMF under a nitrogen atmosphere at room temperature using a three-electrode cell configuration. The working electrode was either a gold or platinum disc. The reference electrode was normally a silver wire arranged such that a luggin capillary was in close proximity to the working electrode. $E_{1/2}$ values were quoted vs S.C.E., against which the ferrocene/ferrocinium couple $[Fc/Fc^+]$ has an $E_{1/2}$ value of 0.54 V in THF–0.2 M $[Bu_4N][BF_4]$. Cyclic voltammetric measurements were made on an EG and G Par model 362 scanning potentiostat. The current and potential values were stored on floppy disk via the EG and G twin channel data recorder. The data was manipulated on an OPUS™ microcomputer using EG and G's CONDECON 300™ software.

Determination of X-ray crystal structure

Full details of the data collection and structure solution are summarized in Table 4.

Preparation of the ligands

Benzoylhydrazine and 4-methylbenzoylhydrazine were prepared by boiling under reflux a 1 : 1 mixture of hydrazine hydrate and either methyl benzoate or 4-methyl benzoate.[17] 2,6-Diacetylpyridinebis(benzoylhydrazone) ($DAPBH_2$) and 2,6-diacetylpyridinebis(4-methylbenzoylhydrazone) (DAP-Me-BH_2) were prepared in about 85% yield by condensation of 2,6-diacetylpyridine and 2 equivalents of the corresponding benzoylhydrazine in absolute ethanol under reflux.[1c] Analytical and spectroscopic data for the ligands and complexes are given in Table 1.

Preparation of the complexes

$[ReCl(DAPB)(PPh_3)]$ (**1**). $DAPBH_2$ (0.5 g, 1.25 mmol), $[ReCl_3(MeCN)(PPh_3)_2]$ (1.08 g, 1.25 mmol) and triethylamine (2 cm^3, 27 mmol) in dry isopropanol (50 cm^3) were stirred at 40°C for 13 h. After cooling the dark brown solid was separated by filtration, washed with ether and dried *in vacuo* (yield 0.60 g, 55%). The product was recrystallized from CH_2Cl_2/Et_2O to yield black crystals suitable for X-ray structure determination.

$[ReCl(DAP\text{-}Me\text{-}B)(PPh_3)]$ (**2**). DAP-Me-BH_2 (0.5 g, 1.17 mmol), $[ReCl_3(MeCN)(PPh_3)_2]$ (1 g, 1.17 mmol) and triethylamine (1.5 cm^3, 20 mmol) were heated under reflux in isopropanol (45 cm^3) for 3 h. After cooling and reducing the volume of the mixture to approximately half, the dark brown solid was filtered off, washed with dry ether and dried *in vacuo* (yield 0.73 g, 67%).

$[Re(DAP\text{-}Me\text{-}B)(PPh_3)][BF_4]$ (**3**). Solid $Ag[BF_4]$ (0.09 g, 0.46 mmol) was added to $[ReCl(DAP\text{-}Me\text{-}B)(PPh_3)]$ (0.21 g, 0.22 mmol) in dry CH_2Cl_2 (30 cm^3).

The mixture was stirred at room temperature in the dark for 45 h before filtration into a clean flask. The solvent was evaporated to dryness to yield a black solid (yield 0.2 g, 98%). The product was soluble in DMF, DMSO, CH_2Cl_2, $CHCl_3$ and acetone.

$[MoCl_2(DAP\text{-}Me\text{-}B)]$ (**4**). $[MoCl_4(MeCN)_2]$ (0.37 g, 1.16 mmol) in dry CH_2Cl_2 (30 cm^3) was added to DAP-Me-BH_2 (0.41 g, 1.57 mmol) in dry CH_2Cl_2 (30 cm^3) and triethylamine (0.6 cm^3, 4.3 mmol) was added. The mixture was heated under reflux (3 h) before cooling to room temperature. The deep green product was collected by filtration under nitrogen, washed with CH_2Cl_2 (10 cm^3) and then dried *in vacuo* (yield 0.5 g, 76%).

$[FeCl(DAP\text{-}Me\text{-}B)]\cdot H_2O$ (**5**). Anhydrous $FeCl_3$ (0.3 g, 1.85 mmol) was added to DAP-Me-BH_2 (0.8 g, 1.85 mmol) in dry methanol (20 cm^3) and triethylamine (0.5 cm^3, 3.7 mmol) was added. The mixture was heated under reflux for 3 h. On cooling a brown solid precipitated, which was collected by filtration and recrystallized from $MeOH/CH_2Cl_2$ (yield 0.65 g, 66%).

$[FeCl_2(DAPBH_2)]\cdot H_2O$ (**6**). Freshly made $FeCl_2$ (0.17 g, 1.25 mmol) in dry methanol (20 cm^3) was added to $DAPBH_2$ (0.5 g, 1.25 mmol) in dry methanol (30 cm^3) under nitrogen. The mixture was heated under reflux (3 h). After cooling the green solid was collected by filtration under nitrogen, washed with ether and dried *in vacuo* (yield 0.39 g, 57%).

Acknowledgements—We gratefully acknowledge Hermann Starck GmbH, Berlin, Germany, for their kind gift of rhenium metal powder. We thank Amersham International plc for their interest in this work and for financial support (RMT). We also thank the University of King Saud in Saudi Arabia for their financial support (ASMA1-S).

REFERENCES

1. (a) C. Pellizzi and G. Pellizzi, *J. Chem. Soc., Dalton Trans.* 1980, 1970; (b) C. Pellizzi, G. Pellizzi, G. Predieri and S. Resola, *J. Chem. Soc., Dalton Trans.* 1982, 1349; (c) C. Lorenzini, C. Pellizzi, G. Pellizzi and G. Predieri, *J. Chem. Soc., Dalton Trans.* 1983, 721.
2. F. A. Cotton and G. Wilkinson, *Advanced Inorganic Chemistry*, 4th edn, p. 878. Wiley Interscience, New York (1980).
3. A. van der Bergen, K. S. Murray and B. O. West, *Aust. J. Chem.* 1972, **25**, 705.
4. M. W. Bishop, J. Chatt and J. R. Dilworth, *J. Organomet. Chem.* 1974, **73**, C59.
5. T. J. Giordano, G. J. Palenik, R. C. Palenik and D. A. Sullivan, *Inorg. Chem.* 1979, **18**, 2445.
6. J. J. Spikerman, L. H. Hall and J. L. Lambert, *J. Am. Chem. Soc.* 1966, **90**, 2039.
7. L. H. Hall, J. J. Spikerman and J. L. Lambert, *J. Am. Chem. Soc.* 1966, **90**, 2044.
8. J. L. Hoard, M. Lind and J. V. Silverton, *J. Am. Chem. Soc.* 1961, **83**, 2770.
9. J. L. Hoard, C. H. L. Kennard and G. S. Smith, *Inorg. Chem.* 1963, **2**, 1316.
10. M. D. Lind, M. J. Hamer, T. A. Hamer and J. L. Hoard, *Inorg. Chem.* 1964, **3**, 34.
11. M. Blume, *Phys. Rev. Lett.* 1965, **14**, 96.
12. N. N. Greenwood and T. C. Gibb, *Mössbauer Spectroscopy*, Ch. 6. Chapman and Hall, London (1971).
13. K. S. Murray, *Coord. Chem. Rev.* 1974, **12**, 1.
14. W. M. Reiff, *J. Chem. Phys.* 1971, **54**, 4718.
15. J. Chatt and G. A. Rowe, *J. Chem. Soc.* 1962, 1019.
16. M. Y. Hamed, R. C. Hider and J. Silver, *Inorg. Chim. Acta* 1982, **66**, 13.
17. E. H. Rodd, *Chemistry of Carbon Compounds*, Vol. 3, Part A, p. 558. Elsevier, London (1954).

Polyhedron Vol. 12, No. 19, pp. 2307–2311, 1993
Printed in Great Britain

0277-5387/93 $6.00+.00
© 1993 Pergamon Press Ltd

THE SYNTHESIS AND CHARACTERIZATION OF A BARIUM SILYL-PHOSPHIDE BY A LOW TEMPERATURE ROUTE

SIMON R. DRAKE,* PHILLIP HALL and ROGER LINCOLN

Department of Chemistry, Imperial College of Science, Technology and Medicine, South Kensington, London SW7 2AY, U.K.

(*Received* 7 *May* 1993; *accepted* 3 *June* 1993)

Abstract—The reaction of tetramethylsilane and sodium hydride in a mixed solvent of THF and HMPA (2:1 by volume), at reflux for 40 h, followed by the addition of PCl_3 yielded $(Me_3Si)_3P$ (**1**) in excellent yield by a simple, non-hazardous and facile route. This phosphine was readily converted into the known phosphide $(Me_3Si)_2PH$ (**2**) by controlled hydrolysis. Reaction of this ligand with barium granules in a mixed liquid ammonia-THF solvent system at −40°C yielded the first barium silylphosphide, $[Ba(P\{SiMe_3\}_2)_2(THF)_2]_n$ (**3**), which was characterized by IR, ^1H, ^{13}C and ^{29}Si NMR spectroscopy.

Alkali metal derivatives of organophosphides are well known, and they have found extensive applications as crystalline sources of PR_2^- in both main group and transition metal chemistry.[1,2] Recent studies have focused predominantly on lithiated silyl phosphines complexed with either mono- or polydentate Lewis bases,[3] or alternatively base free.[4] Investigations into several of the heavier alkali metal complexes (e.g. Na or K) have used these materials as building units for iso-tetraphosphines.[5]

In stark contrast to the situation for the alkali metals there have been few reports of group IIA phosphido complexes, save for two early reports on beryllium diorganophosphides.[6] This apparent dearth of synthetic and structural knowledge may be contrasted with recent advances in our understanding of the trimethylsilylamides of the heavier group IIA metals.[7,8] For these amido complexes there is now a rapidly growing reservoir of knowledge both in solution, the vapour phase and also in the solid state.

Silylphosphides have received considerable attention over the last 30 years, since their first synthesis in 1959 via the reaction of alkyl-chlorosilanes and sodium dialkyl-phosphides.[9] Alternative routes have since included the use of sodium phosphide (Na_3P) and Me_3SiCl in monoglyme[10] and Me_3SiCl and Mg in a range of polar solvents,[11,12] but to date, save for the use of Na_3P,[10] there are presently no simple and safe high-yield routes to these useful ligands. Silyl phosphines and phosphides have found extensive applications as starting materials for reaction with lithium alkyls,[13] carbonyl compounds,[14] boranes[15,16] and unsaturated organic substrates.[17]

We have previously utilized our innovative mixed ammonia-ethereal solvent route to prepare a wide range of group IIA organometallic complexes by this low-temperature facile route, including the solvated and homoleptic trimethylsilylamides. In this paper we wish to report a simple new route to $(Me_3Si)_3P$ and an extension of our ammonical-ethereal solvent route to the hitherto unknown alkaline earth trimethylsilylphosphide, $[Ba(P\{SiMe_3\}_2)_2(THF)_2]_n$ (**3**).

EXPERIMENTAL

General procedures

All manipulations were carried out under dry (molecular sieves) argon (using standard dry-box and Schlenk techniques). All hydrocarbon and ethereal solvents were rigorously dried and then distilled from sodium benzophenone ketyl by standard methods. Elemental analyses were performed by the microanalytical departments of Imperial College and Butterworth Laboratories. Combustion aids

* Author to whom correspondence should be addressed.

were used in an effort to discourage carbide formation. The results for carbon, hydrogen and nitrogen analysis were found to be extremely variable and it was found that experimentally determined carbon contents were often low compared with the expected values. The melting points were measured under argon in sealed capillaries and are uncorrected values.

Instrumentation

NMR data were recorded on a Jeol GS 270 NMR spectrometer, using the protio impurities of the deuterated solvent as reference for ^1H spectra and the ^{13}C resonance of the solvent as a reference for ^{13}C spectra. Chemical shifts were also independently referenced to tetramethylsilane (< 1%) added by volume. The NMR samples were prepared in Wilmad 5 mm NMR tubes, equipped with J. Youngs valves to ensure reproducibility of NMR spectra and ensure sample stability. All chemical shifts are positive to high frequency of the standard.

IR spectra were recorded on a Perkin–Elmer FTIR 1720 spectrometer as Nujol mulls between 25 × 4 mm KBr plates. The Nujol was pre-dried with 4 Å molecular sieves prior to use and the Nujol samples were protected from the atmosphere by an O-ring-sealed Presslok holder. The listing of bands observed at 3000 and 1400 cm^{-1} has been omitted due to overlapping with the C—H stretching frequencies of Nujol.

Starting materials

Barium metal granules were purchased from Alfa Chemicals and stored in an inert atmosphere glovebox. Sodium hydride, tetramethyl silane and phosphorus trichloride were obtained from Aldrich Chemicals and used as supplied. The materials described here are all exceptionally air- and moisture-sensitive and as such they should be routinely prepared under dry argon using thoroughly degassed and dry solvents.

Preparation of $P(SiMe_3)_3$ **(1)**

CAUTION: Hexamethylphosphoramide is a carcinogen and phosphorus trichloride is toxic and must be handled in a well ventilated fume-hood.

Tetrahydrofuran (200 cm^3) and hexamethylphosphoramide (100 g, 0.6 M) were transferred into a dry 1 dm^3, three-necked flask by use of a cannula. The flask was also equipped with an overhead mechanical stirrer, pressure-equalized dropping funnel and water cooled coil condenser. Solid NaH (27.2 g, 1.13 M) was then placed into the flask under argon and tetramethylsilane (100 g, 1.13 M) added dropwise over 1 h at 20°C, stirring the mixture at high speed. The resulting reaction mixture was heated to reflux and held at this temperature for 4 h until a yellow–orange solution persists with a deep grey finely divided solid remaining at the bottom of the flask.

The reaction mixture, which now contains the presumably HMPA solvated sodium trimethylsilyl salt $[Me_3SiNa(HMPA)_x]_n$, was allowed to cool to room temperature and PCl_3 (37.8 cm^3, 51.7 g, 0.376 M) added dropwise over 1 h. The reaction flask was then refluxed for 40 h to ensure maximum conversion to the tris-trimethylsilylphosphine. The progress of the reaction was monitored by ^1H and ^{31}P NMR and stopped when peaks due to the intermediate $(Me_3Si)_2PCl$ had all but disappeared (*ca* less than 4–7% of the reaction mixture by NMR).

The THF was then distilled off under an inert atmosphere and the remaining reaction mixture distilled under reduced pressure, collecting the fraction boiling between 45 and 80° at 0.1 mm. This fraction was then redistilled collecting the fraction boiling between 50 and 63° at 0.1 mm, which contained approximately 100 cm^3. To ensure that no HMPA was present in the product (due to very similar boiling points of these compounds) the solution was fractionated two more times using a vacuum-jacketed Vigreux multi-plate column collecting the fraction boiling at 64°C at 0.2 mm. This yielded a colourless product, $(Me_3Si)_3P$ (59.4 g, 81.2%). Found: C, 42.9; H, 10.8. Calc. for $C_9H_{27}Si_3P$: C, 42.7; H, 10.7%. ^1H NMR (270 MHz, C_6D_6, 20°C): δ 2.32 [d, 9.24 Hz, J(PSiCH) of 4.5 ± 0.1 Hz and δ 0.4 lit]. ^{13}C NMR (67.94 MHz, C_6D_6, 20°C): δ 36.25 (d, 3.7 Hz). ^{31}P NMR (109.37 MHz, C_6D_6 at 20°C): δ 251 ± 1 [J(SiCH) of 6.6 ± 0.1 Hz]. ^{29}Si NMR (53.6 MHz, C_6D_6 at 20°C): δ 2.32 [d, 9.24 Hz, J(PCH) of 4.5 ± 0.1 Hz]. Mass spectra (E.I.) molecular ion at 253 a.m.u.

Synthesis of $(Me_3Si)_2PH$ **(2)**

Into a 250 cm^3 two-necked round bottomed flask, flame dried, evacuated and flushed with argon gas, was added THF (50 cm^3) and tris-trimethylsilylphosphine (30 cm^3, 25.8 g, 0.0103 M). To this stirred solution freshly distilled water (11 cm^3) and KOH in THF (50 cm^3) was added at 50°C and Stp. The desired fraction of bistrimethylsilylphosphide, $(Me_3Si)_2PH$, distilled at 79°C and 36 torr pressure (11.3 g, 63.5 mmol), 62%. A second higher fraction was subsequently collected, which was found to be unreacted $(Me_3Si)_3P$. Found: C, 40.3; H, 10.8. Calc. for $C_6H_{19}Si_2P$: C, 40.0; H, 10.5%. ^1H NMR (270 MHz, C_6D_6, 20°C): δ 2.32 [d, 9.24 Hz,

J(PSiCH) of 4.5±0.1 Hz and δ 0.4 lit]. ^{13}C NMR (67.94 MHz, C_6D_6, 20°C): δ 36.25 (d, 3.7 Hz). ^{31}P NMR (270 MHz, C_6D_6, 20°C): δ 251±1 [J(SiCH) of 6.6±0.1 Hz]. ^{29}Si NMR (53.6 MHz, C_6D_6, 20°C): δ 2.32 [d, 9.24 Hz, J(PCH) of 4.5±0.1 Hz]. Mass spectrum (E.I.) shows a molecular ion at 180 a.m.u.

Synthesis of $[Ba(P\{SiMe_3\}_2)_2(THF)_2]_n$ **(3)**

Into a thoroughly flame-dried Schlenk tube (with three vacuum-purge cycles) was placed barium metal granules (1.37 g, 10 mmol) inside a glove-box under a nitrogen atmosphere. The top was then greased and placed on top of the Schlenk tube and the vessel attached to a vacuum line in a well-ventilated fume cupboard. The Schlenk was then evacuated and back-flushed three times with nitrogen.

THF (25 cm^3), toluene (5 cm^3) and bis-trimethylsilylphosphide (5.40 cm^3, 30.0 mmol, 50% excess) were added to the Schlenk tube via a carefully degassed syringe. The top of the Schlenk was then removed under a positive gas flow and quickly replaced with a rubber suba-seal. At this point the *rapidly* stirred suspension was cooled by means of an external dry ice–acetone bath to *ca* −40°C. The fume hood sash was pulled down as far as possible for the remainder of the experiment. Ammonia gas was then slowly bubbled into the solution for 10–12 min, during which time the solution turned a grey colour. The reaction mixture was then slowly allowed to warm to room temperature. Initially, bronze pieces of $Ba(NH_3)_6$ were formed as the metal reacted, but these readily dissolved over a period of 1–2 h. No further flush with NH_3 was necessary.

The rate of stirring of the solution was then reduced to a minimum and the reaction mixture allowed to stir for *ca* 8–12 h at ambient temperature. After this period of time the solution may have a pale grey colour, at this point the stirrer is turned off and the reaction mixture allowed to stand to allow a small amount (*ca* 50 mg) of finely divided metal to settle out. The solution was then carefully filtered through a celite pad and all the solvent removed *in vacuo*. The resulting residue was dissolved in the minimum of n-hexane/THF and left to stand in the freezer at −25°C, which yielded a large amount of white microcrystalline solid. This was isolated using a filter stick and taken into a glove-box. Yield: 2.71 g, 43.2%. Found: C, 38.9; H, 8.6. Calc. for $C_{20}H_{52}P_2O_2Si_4Ba$: C, 39.8; H, 8.7%. IR (Nujol, ν cm^{-1}) 1243 (st), 1246 (vs), 1088 (vs), 1036 (st), 870 (st), 819 (st), 821 (vs), 754 (st), 650 (st), 602 (st). ^1H NMR (270 MHz, C_6D_6, 20°C): δ 0.23 (s, 36H), δ 1.38 (m, 8H), δ 3.52 (m, 8H). ^{13}C NMR (67.94 MHz, C_6D_6, 20°C): δ 5.20 (s, Me), δ 25.46 (s, THF), δ 68.62 (s, THF). $^{29}Si\{^1H\}$ NMR (53.6 MHz, C_6D_6, 20°C): δ −14.88 (refd. TMS).

RESULTS

Synthesis

Prior to this study synthetic routes to tris-trimethylsilylphosphine, $(Me_3Si)_3P$, were rather limited, generally using the hazardous Na_3P as the phosphorus precursor which may then be reacted *in situ* with a trimethylsilyl halide.[9–12] Given these limitations we have developed an alternative high yield synthetic route. Our strategy involves the reaction of tetramethylsilane and sodium hydride in a mixed solvent of THF and HMPA (2 : 1 by volume), these two materials are held at reflux for 40 h to yield a deep yellow–orange solution of presumably $[NaSiMe_3 \cdot x\text{HMPA}]_n$, see eq. (1).

$$Me_4Si + NaH \xrightarrow[\Delta]{\text{THF/HMPA}} [Me_3SiNa(HMPA)_x]_n + CH_4 \quad (1)$$

To the solution is added phosphorus trichloride, dropwise over a period of 1 h at room temperature, which is then followed by a 40 h reflux and the reaction monitored by NMR. It is stopped when peaks due to the intermediate $(Me_3Si)_2PCl$ have virtually disappeared (*ca* less than 5% of the reaction mixture by multinuclear NMR). The product was finally separated by repeated vacuum distillation from the THF and HMPA in > 80% yield, see eq. (2).

$$[Me_3SiNa(HMPA)_x]_n + PCl_3 \longrightarrow (Me_3Si)_3P + 3NaCl + x\text{HMPA} \quad (2)$$

Separation of the residual HMPA from the $(Me_3Si)_3P$ proved to be best accomplished by repeated distillation, which yielded the final product in good yield and high purity. Attempts at reducing the amount of HMPA in the reaction mixture (due to its carcinogenic nature) were unsuccessful and resulted in mixtures of silyl phosphines, which proved very difficult to separate. Therefore, the 2 : 1 ratio of THF to HMPA is the recommended one for the synthesis of the tris-trimethylsilylphosphine.

The tris-trimethylsilylphosphine is readily converted into the bis-trimethylsilylphosphide by controlled hydrolysis in THF to yield $(Me_3Si)_2PH$, 62%, with some unreacted phosphine remaining. Given the ease and comparative safety behind this preparative route, this has now facilitated a preliminary study of the metallation of the phosphide ligand $(Me_3Si)_2PH$ by the heavier alkaline earth

metals, and in particular by barium granules suspended in ammonical-THF.

We have found that barium metal reacts rapidly with trimethylsilylphosphide at temperatures between −35 and −45°C in THF in the presence of ammonia to yield $[Ba\{P(SiMe_3)_2\}_2(THF)_2]_n$ (**3**) in moderate yield and isolated as a white highly air-sensitive crystalline solid. This material is readily soluble in toluene and THF (and other polar coordinating solvents, e.g. dme, CH_3CN, HMPA, etc.).

DISCUSSION

We have previously reported the application of our ammonia-ethereal solvent route to a wide range of alkaline earth organometallic complexes and more recently extended it to related homoleptic compounds, via the use of ammonical-hydrocarbon solvent synthesis.[7] These routes have been shown to operate via the intermediacy of solvated electrons (either at ambient temperature or at −40°C). We have previously noted that liquid ammonia will form a mixed solvent system with a wide range of organic solvents, both above and below its boiling point.[7]

Up to five years ago many of the heavier alkaline earth complexes were thought to be either polymeric or insoluble in most organic solvents. More recent studies[8,18-19] have revealed that this need not be the case, indeed several studies have recently demonstrated that suitably bulky ligands such as $(Me_3Si)_2NH$, OAr′, etc. will solubilize a wide range of group IIA based compounds. A notable feature of these metals is their strong Lewis acidity, which ensures that in the absence of Lewis base solvents they will generally form polymeric insoluble materials. However, on the addition of suitable Lewis base solvents the polymeric ensembles may be cleaved to yield simpler molecular species. A wide variety of molecular geometries are available, provided that judicious choice of ligands and or Lewis bases are used to achieve coordinative saturation of the large M^{2+} cations.

Using a similar aproach to that of Caulton *et al.*[18] with a small modification,[19] we have been able to isolate the related phosphide complex $[Ba\{P(SiMe_3)_2\}_2(THF)_2]$ (**3**). The ^1H and ^{13}C NMR spectra of this material in C_7D_8 reveal the presence of only one methyl environment on the trimethylsilylphosphide ligand. A similar observation is also observed for the ^{29}Si NMR spectrum, implying that this compound either contains only one distinct type of phosphide environment or as seems more likely a rapid fluxional process is occurring, equilibrating the different ligand environments (both THF and phosphide). A similar situation to this has previously been reported by Westerhausen in his variable-temperature NMR study of $[Ba(N\{SiMe_3\}_2)_2(THF)_2]$.[8] Caulton *et al.*[18] have previously shown by single-crystal X-ray crystallography that this barium trimethylsilamide is monomeric with a distorted tetrahedral structure.[18] Attempts to date at cryoscopic molecular mass measurements in benzene have been unsuccessful with this complex due to its exceptional air- and moisture-sensitivity and its rapid decomposition.

CONCLUSIONS

In this work we have demonstrated a novel and efficient route to trimethylsilylphosphide via use of the readily available starting materials tetramethylsilane and sodium hydride in a mixed solvent of THF and hexamethylphosphoramide at reflux. Reaction of the postulated *in situ* intermediate $[Me_3SiNa(HMPA)_x]_n$ with PCl_3 and subsequent work-up yields $P(SiMe_3)_3$ in excellent yield. Such a facile synthesis of a silylphosphine is noteworthy and promises to ensure that the chemistry of this ligand will now be further explored, especially as a precursor ligand for metal phosphides, e.g. Zn_3P_2. Indeed, the possibility of extending this route to other silyl phosphides, i.e. $(R_3Si)_3P$ (where R is Ph, Et, etc.) looks very promising using simple alkyl or aryl silanes as suitable starting materials.

The synthetic strategy used here to prepare the barium phosphide complex $[Ba(P\{SiMe_3\}_2)_2(THF)_2]$ will find further extension to a wide range of other organic substrates with moderately acidic protons and a pK_a of < 30. Careful manipulation of experimental conditions may allow us to eventually isolate the analogous phosphide complexes of $[Ba(N\{SiMe_3\}_2)_2(THF)]_2$ and $[Ba(N\{SiMe_3\}_2)_2]_2$.[18] Indeed, given the dearth of alkaline earth metal phosphide and phosphine based complexes a study of their fundamental coordination chemistry is long overduc.

Acknowledgement—This work was supported by Research Grants from the Nuffield Foundation, the University of London Central Research Fund and the Royal Society.

REFERENCES

1. A. J. Carty, *Adv. Chem. Ser.* 1982, **196**, 163.
2. R. A. Bartlett, M. M. Olmstead and P. P. Power, *Inorg. Chem.* 1986, **25**, 1243.
3. M. Andrianarision, D. Stalke and U. Klingebiel, *J. Organomet. Chem.* 1990, **381**, C38 and refs therein:

E. Hey, P. B. Hitchcock, M. F. Lappert and A. Rai, *J. Organomet. Chem.* 1987, **325**, 1.
4. E. Hey-Hawkins and E. Sattler, *J. Chem. Soc., Chem. Commun.* 1992, 775.
5. M. Andrianarasion, D. Stalke and U. Klingebiel, *Chem. Ber.* 1990, **123**, 71; M. Scheer, S. Gremler, E. Herrmann, U. Grünhagen, M. Dargatz and E. Kleinpeter, *Z. Anorg. Allg. Chem.* 1991, **600**, 203; M. Scheer, S. Gremler, E. Herrmann, M. Dargatz and F. Uhlig, *Z. Anorg. Allg. Chem.* 1991, **606**, 105.
6. N. A. Bell, G. E. Coates and A. H. Fishwick, *J. Organomet. Chem.* 1980, **198**, 113; R. Masthoff, G. Krieg and C. Uieroth, *Z. Anorg. Allg. Chem.* 1969, **364**, 316; E. Hey, C. L. Raston, A. White and L. M. Engelhart, *Angew. Chem., Int. Edn Engl.* 1987, **26**, 81; J. L. Atwood, S. G. Bott, R. A. Jones and S. Koschmieder, *J. Chem. Soc., Chem. Commun.* 1990, 692.
7. S. R. Drake and D. J. Otway, *J. Chem. Soc., Chem. Commun.* 1991, 517; S. R. Drake, D. J. Otway and S. P. Perlepes, *Main Group Met. Chem.* 1992, **14**, 243.
8. M. Westerhausen, *Inorg. Chem.* 1991, **30**, 96; D. C. Bradley, M. B. Hursthouse, A. A. Ibrahim, K. M. A. Malik, M. Motevalli, R. Moseler, H. Powell, J. D. Runnacles and A. C. Sullivan, *Polyhedron* 1990, **9**, 2959; P. B. Hitchcock, M. F. Lappert, G. A. Lawless and B. Royo, *J. Chem. Soc., Chem. Commun.* 1990, 1141.
9. W. Kuchen and H. Buchwald, *Chem. Ber.* 1959, **92**, 227.
10. G. Becker and W. Holderich, *Chem. Ber.* 1975, **105**, 2484.
11. H. Schumann and L. Rosch, *J. Organomet. Chem.* 1973, **55**, 257.
12. H. Schumann and L. Rosch, *Chem. Ber.* 1974, **107**, 854.
13. G. Fritz and W. Holderich, *Z. Anorg. Allg. Chem.* 1976, **422**, 104; E. Hey, P. B. Hitchcock, M. F. Lappert and A. K. Rai, *Organomet. Chem.* 1987, **325**, 1.
14. G. Becker and O. Mundt, *Z. Anorg. Allg. Chem.* 1980, **462**, 130.
15. G. L. Wood, D. Dou, C. K. Narula, E. N. Duesler, R. T. Paine and H. Noth, *Chem. Ber.* 1990, **123**, 1455.
16. G. W. Parshall and R. V. Lindsey Jr, *J. Am. Chem. Soc.* 1959, **81**, 6273.
17. G. Fritz, *Comm. Inorg. Chem.* 1982, **1**, 329.
18. B. A. Vaarstra, J. C. Huffman, W. E. Streib and K. G. Caulton, *Inorg. Chem.* 1991, **30**, 121.
19. S. R. Drake and D. J. Otway, *Polyhedron* 1992, **11**, 745; S. R. Drake, M. B. Hursthouse, K. M. A. Malik and D. J. Otway, *Polyhedron* 1992, **11**, 1995.

Polyhedron Vol. 12, No. 19, pp. 2313–2323, 1993
Printed in Great Britain

0277–5387/93 $6.00+.00
© 1993 Pergamon Press Ltd

MONITORING THE MOEDRITZER–IRANI SYNTHESIS OF AMINOALKYL PHOSPHONATES

PETER B. IVESON, MARK P. LOWE and JOYCE C. LOCKHART*

Department of Chemistry, University of Newcastle upon Tyne,
Newcastle upon Tyne, NE1 7RU, U.K.

(*Received* 5 *May* 1993; *accepted* 3 *June* 1993)

Abstract—Combined ^{31}P, ^{1}H and ^{13}C NMR studies show the course of the reaction of amines with formaldehyde and phosphorous acid in hydrochloric acid solutions. For symmetrical di- and tri-aza macrocycles, piperazine and 1,4,7-triazacyclononane, the products formed according to the stoichiometry, with all nitrogens apparently derivatized at similar rates; partial derivatization is thus not easily achieved. Primary amines once substituted were disubstituted at a much greater rate than the initial substitution. One asymmetric macrocycle, 1,4,8-triazacyclododecane, was substituted sequentially, showing that it is possible to prepare a partially substituted version in some purity. Guanidineacetic acid was the only one of a series of guanidines to react under Moedritzer–Irani conditions. This may have mechanistic significance.

Since the first attempts to prepare azacrown macrocycles with pendant arms,[1] there have been many publications on the subject. The expressive names lariat ether[2] and bibracchial ether[3] were later coined to describe these and similar entities. In this paper we describe the progress of reactions to derivatize NH groups of small aza macrocycles selectively with methylenephosphonate residues. The coordinating properties of aminoalkyl phosphonates[4] (AAP) have been studied in great detail[5] and their suitability as crystallization inhibitors, peroxide stabilisers, herbicides and builders for detergents is now well established. AAP ligands are usually prepared using the Moedritzer–Irani reaction,[4] shown in eq. (1), for the case of a simple primary amine.

$$RNH_2 + 2H_3PO_3 + 2CH_2O \longrightarrow RN(CH_2PO_3H_2)_2 \quad (1)$$

Commercial products made by this route are often very impure. There is no detailed study of the reaction or its mechanism in the literature. It is not established whether or not partial substitution is favoured by any set of conditions. The major advantages of the Moedritzer–Irani reaction are the availability and inexpensive nature of the starting materials, and the one-step procedure, offset somewhat by the difficulty in purifying the final products, which is especially true of water-soluble derivatives. The difficulties arise because of the presence of partially substituted AAP derivatives or unreacted phosphorous acid starting material in the reaction mixture. Qualitative comparison has been made here between the progress of the reaction and the amounts of partially substituted products formed, in selected reactions involving macrocyclic secondary amines and also some involving open-chain primary amine starting materials. If all N—H groups in a molecule react at the same, or closely similar, rates, it should be difficult to obtain pure partially substituted derivatives, but if differential rates are observed then partially substituted derivatives may be isolable.

The amines 1,4,7-triazacyclononane (**1a**), piperazine (**2a**), 1,4,8-triazacyclododecane (**3a**), 1,3-propanediamine (**4a**) and benzylamine (**5a**) were used as the amine starting materials. To the best of our knowledge macrocycle **3a** has not been prepared before. Its synthesis using the Richman and Atkins method[6] and subsequent AAP derivatisation will be reported elsewhere.[7]

* Author to whom correspondence should be addressed.

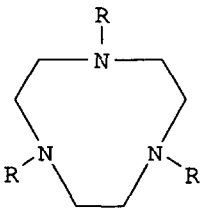

1a. R = H
1b. R = $CH_2PO_3H_2$

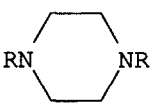

2a. R = H
2b. R = $CH_2PO_3H_2$

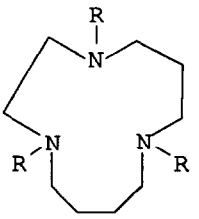

3a. R = H
3b. R = $CH_2PO_3H_2$

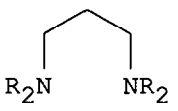

4a. R = H
4b. R = $CH_2PO_3H_2$

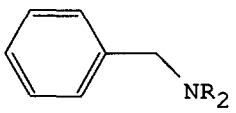

5a. R = H
5b. R = $CH_2PO_3H_2$

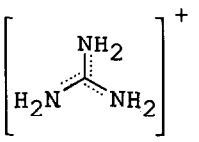

6

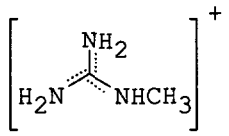

7

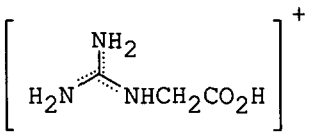

8

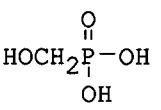

9

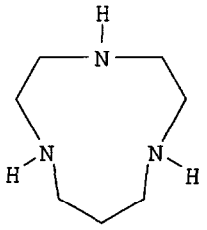

10

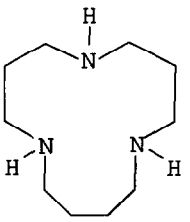

11

EXPERIMENTAL

Monitoring the reaction

An example of the procedure used to follow the reactions is decribed.

Reaction of triazacyclononane **1a**, reaction I. The temperature of a *ca* 5 mol dm^{-3} DCl solution (16 cm^3) under nitrogen, containing the amine trihydrochloride (0.38 g, 1.59 mmol) and phosphorous acid (0.39 g, 4.78 mmol), was initially raised to 92°C using a water bath. Paraformaldehyde (0.29 g, 9.56 mmol) was added in one portion, the flask was shaken vigorously to dissolve the solid and the timing of the reaction was started. Samples were taken by means of a pipette, transferred to an NMR tube and then cooled rapidly in an ice–water bath.

All other reactions were carried out in a similar manner except for that involving **4a**, which was run in an HCl/H_2O solvent and a further reaction IX with **1a**, which was run with aqueous formaldehyde added dropwise over a period of 1 h. Aliquots were removed and cooled, then used directly for NMR. The ^{31}P NMR spectra of the first aliquots taken from each reaction revealed that a significant amount of phosphorous acid had been converted to phosphoric acid,* a side reaction noted in the original Moedritzer–Irani publication.[4] The concentration of H_3PO_4 in the reaction mixture effectively remained constant after the addition of paraformaldehyde and initiation of the AAP forming reaction. The signals are poorly defined and

* The chemical shift of the (internal) H_3PO_4 formed in the reaction is different from that of external standard $H_3PO_4(\delta_P O)$ because of the different acidities of the solutions in which they were measured.

it is difficult to differentiate the multiplicities of overlapping signals. This is probably due to a slower rate of proton exchange between particular ionisable protons. Where convenient, ^1H and ^{13}C spectra were obtained on the same sample, except for reaction VII, for which selected ^1H and ^{13}C spectra were obtained in the following manner. The HCl/H_2O solvent mixture was removed on a rotary evaporator. Repeated additions of D_2O and removals of solvent were carried out in an effort to deuterate the exchangeable protons. As a result, the spectra for each sample cannot be compared directly with the corresponding ^{31}P spectra because the initial warming to remove the HCl/H_2O is likely to have raised the temperature sufficiently to cause the reaction to continue.

Guanidines. The series of guanidines **6–8** was also subjected to similar studies. The only guanidine successfully derivatized was guanidineacetic acid (**8**); the others did not appear to be phosphonated at all.

NMR spectra were run on Brüker WP200, AC200, WB300, AMX500 and JEOL FX90Q spectrometers.

RESULTS AND DISCUSSION

The Moedritzer–Irani reaction [shown in eq. (1)] was monitored for a series of amines **1a–5a** using NMR spectra of quenched samples from the reaction mixtures. One aim of the study was to ascertain if phosphonation was sequential, with subsequent steps of different rate, which could permit partial functionalization. Qualitative inferences may be obtained from the results of this study.

The new ^{31}P signals which appeared during the reaction were assigned using several arguments. The signals present in maximum concentration at the end of a reaction were assigned to the most fully phosphonated product allowed by stoichiometry. Secondly, signals were differentiated in terms of known shielding patterns consequent on protonation.[8–10] The relevant integrals from the phosphorus spectra assisted the assignment of ^1H and ^{13}C NMR signals, together with ^{31}P coupling patterns of the NCH_2P signals. Spectra were normally taken in 5 M acid solutions, but sometimes the pH was raised to neutral to shift the overlapping signals; the latter were also assigned by decoupling experiments and the highest resolution work at 500 MHz for ^1H. Transient signals were also observed and assigned to intermediate species, not identified, and by-products.

In Table 1 are shown the ratios of reagents chosen for each amine studied, together with temperature and an approximate half-life based on the disappearance of initial H_3PO_3. Tables 2 and 3 show the assignment of the signals in ^{31}P and ^1H spectra, respectively, to characteristic groups in the reagents and products, identified in Scheme 1. Results for the several amines are discussed in turn.

Triazacyclononane (**1a**)

For the first amine chosen, triazacyclononane, the reaction was run at three different ratios of

Table 1. Reaction conditions and approximate time-scale

Amine	Reaction[a]	[Amine]	$[H_3PO_3]$	$[CH_2O]^b$	Temperature (°C)	Time-scale[c] (min)
1a	I	0.07	0.02	0.14	90	46
1a	II	0.05	0.04	0.20	92	62
1a	III	0.10	0.21	0.60	92	15
1a	IX[d]	0.07	0.15	0.54	92	12.3
2a	IV	0.30	0.59	1.20	≈ 80	5 hr[e]
3a	V	0.05	0.085	0.30	92	60
3a	VI	0.11	0.48	0.63	92	30
4a	VII	1.18	4.70	9.44	≈ 95[f]	3.5
5a	VIII	0.20	0.34	0.80	87	2 hr[e]

[a] [DCl] = 5 mol dm^{-3}.

[b] Paraformaldehyde expressed as n moles, CH_2O, i.e. $[CH_2O]_n$.

[c] Time taken for 50% reaction of $[H_3PO_3]_0$ except where noted.

[d] CH_2O added dropwise as an aqueous solution over a period of 1 h.

[e] Times correspond to 34 and 32% reaction of $[H_3PO_3]_0$, respectively.

[f] [HCl] = 6 mol dm^{-3}, addition of $(CH_2O)_n$ resulted in a large temperature jump and reaction mixture was under reflux for a few minutes.

Table 2. ^{31}P chemical shifts[a] for reactions I–IX

	H_3PO_3	R_1[b]	R_2[b]	R_3[b]	R_4[b]			9
1a	I 6.19		17.24					24.15
1a	II 6.43		17.43	15.07			23.73	24.04
1a	III[c] 6.48		17.28	15.11		22.06	23.41	23.91
1a	IX 5.87	16.87	16.66	14.43				24.10
2a	IV 6.42	9.78	9.60					
3a	V 6.46	[N(1)] 10.90	[N(2)] 10.50	[N(3)] 12.65				24.03
3a	VI 6.14	[N(1)] 10.71 9.27[d]	[N(2)] 10.38 9.77[d]	[N(3)] 13.80 20.30[d]				19.76
4a	VII[e] 6.15	10.47	10.44	9.85	9.80			
5a	VIII 6.26	13.49	11.06			21.84		23.84

[a] Referenced to internal H_3PO_4; the shifts were measured after ≈ 3 h except in reactions V and VI, where measurements were taken after 24 h.

[b] R_1–R_4 refer to substituents on the appropriate diagram in Scheme 1.

[c] Additional peak at 17.02 ppm.

[d] pD $\approx$ 6.5.

[e] Shifts obtained in HCl/H_2O rather than DCl/D_2O, additional low intensity peaks at 12.26, 16.37, 18.04 and 20.25 ppm.

reagents in an attempt to maximize the amounts of mono-, di- and tri-substituted products, respectively (as shown in Table 1): adventitious oxidation of the phosphorous acid prior to formaldehyde addition altered the ratios originally chosen. The ^{31}P chemical shifts of the signals for mono- and di-substituted 1,4,7-triazacyclononane are very similar and the multiplets are superimposed. The values quoted in Table 2 were obtained from well-resolved spectra from reaction IX.

Peaks observed in the ^1H NMR spectra have been tentatively assigned as shown in Table 3. After 180 min of reaction II the signal for the unsubstituted amine starting material disappeared. The methylene of the R groups appears as a doublet δ_H 3.60, J(P—H) $\approx$ 13.8 Hz. The line-widths of this doublet and the adjacent signal in the final spectrum (after 180 min) suggest that these correspond to R_1 and R_2 of mixtures of partially substituted AAP derivatives (which have non-equivalent protons

Table 3. ^1H chemical shifts[a] for reactions II and IV–VIII

	CH_2CH_2	CH_2*CH_2‡CH_2*	CH_2*CH_2‡CH_2‡CH_2*	CH_2P	ArH	$ArCH_2N$	9
II[b]	3.92[c]						
	3.73[d]			3.60[d]			
IV[b]	3.70[c]						
	3.81[d] 4.05[d]			3.87[d] 3.90[d]			
V[b]	3.69[c]	2.34‡[c] 3.40*[c]	3.40*[c] 2.02‡[c]				
	3.99[d]	2.39‡[d] 3.70*[d]	3.70*[d] 2.17‡[d]	3.70[d]			
VI[b]	4.03[c]	2.67‡[c] 3.74*[c]	3.74*[c] 2.37‡[c]				
	4.19[d]	2.55‡[d] 3.89*[d]	3.89*[d] 2.59‡[d]	3.74[d]			4.21
VII[b]					8.34[c]	5.08[c]	
				4.62[d]	8.43[d]	5.59[d]	4.84
VIII[e]		1.62‡[c] 2.66*[c]					
		1.86‡[d] 3.00*[d]		3.17[d]			3.34

[a] Referenced to external trimethylsilyl propionic acid, centres of multiplets have been quoted where overlapping signals have prevented assignment.

[b] 5 mol dm^{-3} DCl solution.

[c] Amine starting material.

[d] Phosphonate product(s).

[e] pD $\approx$ 1.5.

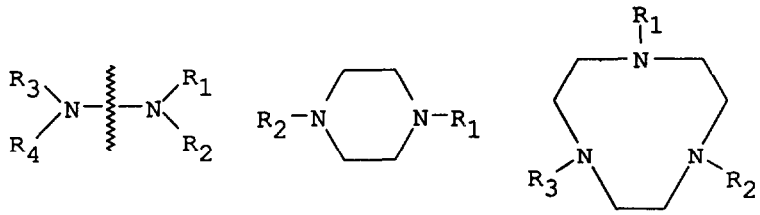

Scheme 1. Definitions of R_1–R_4 for reactions I–IX.

both in the methylenephosphonate groups and the macrocyclic ring).

In the final ^{13}C NMR spectrum from reaction mixture III (after 180 min) remnant formaldehyde appears as a single peak (δ_C 81.77). Two CH_2—P doublets were identified by their J(P—C) coupling constants (Table 4); the most intense doublet was assigned to the tri-substituted product on comparison of this spectrum with the corresponding ^{31}P spectrum [δ_C 51.77, J(P—C) 143.5 Hz]. The macrocyclic ring CH_2 carbon atoms appear as a large single peak (δ_C 50.76) and two much smaller peaks (δ_C 51.63, 49.79). This indicates that most of the amine is fully substituted and in that situation the ring carbon atoms are equivalent. The other ^{13}C spectra are much more difficult to interpret. A number of signals appear upfield from the signals due to ring CH_2 and CH_2—P carbon atoms (δ_C 41.97–45.10). At least four signals are observed at the beginning of the reaction (1–3 min), but only one remains after 180 min (δ_C 45.06). A number of unidentified signals were also observed upfield of the ring CH_2 and CH_2—P proton peaks in the ^1H spectra obtained from reaction II (δ_H 3.0–3.4). The disappearance of the upfield ^{13}C signals in reaction III suggests that these species may be intermediates in the reaction. If the mechanism proposed by Redmore[12] and Vincens *et al.*[13] applies, these signals may be due to the corresponding methylol derivatives (RNR′) (CH_2OH) and/or iminium ions.

A comparison can be made between the reaction in which formaldehyde was added as solid paraformaldehyde in one portion at the beginning (III) and that in which aqueous formaldehyde was added dropwise over a period of 1 h (IX). The initial ratio of [H_3PO_3]/[amine] was roughly the same in each case. The time-scales shown in Table 1 indicate that the time taken for 50% reaction of H_3PO_3 was similar to reactions III and IX. Although the tri-substituted product was only present as 25% of total ^{31}P after 60 min in reaction IX (compared with 41% in reaction III), the concentrations of the fully substituted product are effectively the same after 3 h ($\approx$ 54% in each case). Therefore, the products obtained in the Moedritzer–Irani reaction are essentially the same, irrespective of whether the formaldehyde is added as an aqueous solution or as solid paraformaldehyde. One ephemeral signal appeared in the ^{31}P NMR spectrum of initial samples; this had disappeared before the end of the reaction and thus may be an intermediate. The phosphorus shift and coupling constant were very similar to those of hydroxymethylphosphonic acid, which in other reactions accumulated at the end of the reaction and was thought not to be an intermediate. The identity of the ephemeral signal was not discovered.

Piperazine (**2a**), *reaction* IV

The di-substituted product was found to precipitate from the samples taken during the latter stages of the reaction; assignment of its NMR signals is thus straightforward. The spectra indicate that the initially formed mono-substituted product is gradually converted to the di-substituted product.

Triazacyclododecane (**3a**)

To circumvent the difficulties of distinguishing the signals for partially substituted products in the ^1H and ^{31}P NMR, the macrocyclic ligand **3a**, which contains three chemically distinct nitrogens and also bridging methylenes with differing chemical shifts, was examined. The formation and decay of the various components, traced via the ^{31}P and ^1H NMR signals at various reaction times, are shown in Figs 1 and 2 and are discussed below. The ^{31}P plot shows the fast incorporation of two methylphosphonate groups (R_1 and R_2, see Scheme 1) with the final one forming much later. The A′B′ signals (see key in Scheme 2) are seen to form more slowly than the composite signal for the rest of the ring protons, from the plot in Fig. 2.

^{31}P *studies*

Three sets of signals (Fig. 3) corresponding to product **3b** are seen in the final spectrum of this stack of low-resolution ^{31}P spectra, obtained at

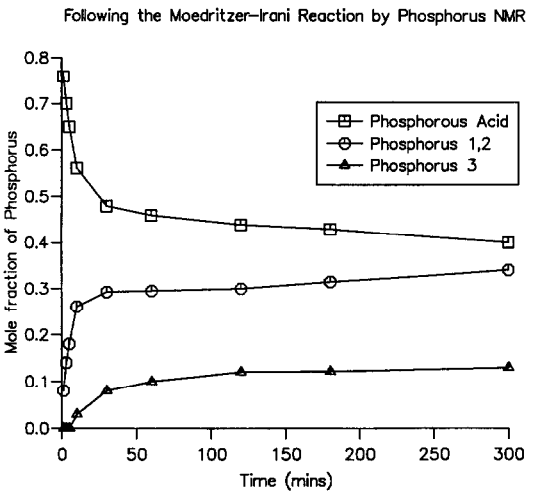

Fig. 1. Decay and build-up of ^{31}P signals for the conversion of **3a** to **3b** (taken from low-resolution 36.2 MHz spectra).

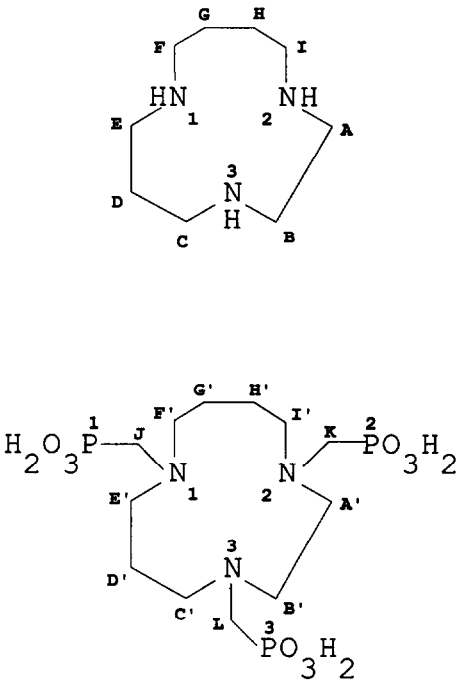

Scheme 2. Labelling scheme for the conversion of **3a** to **3b**.

36.20 MHz. The decay of the phosphorous acid signal in the early stages of the reaction is matched with the rapid increase in signals 1 and 2 as the ligand is phosphonated. The plot shows that one nitrogen of the macrocycle **3a** (labelled as shown in Scheme 2), probably N(1), is slightly more reactive than a second, probably N(2). These undergo rapid reaction in comparison to the third nitrogen, N(3). The assignment of the phosphorus signals was verified by higher resolution spectra and the spectrum of the tri-substituted product, obtained also at neutral pH, together with ^{1}H and ^{31}P decoupling experiments. The evolution of ^{31}P signals (obtained at higher resolution and an RF of 121.496 MHz) with time made clear that several signals with well-resolved triplet couplings to adjacent methylene hydrogens were observed (10.82, 10.70, 10.58 and 10.46 ppm). Downfield, and partly overlapping these signals, was a set of blurred signals, from which accurate coupling constants could not be extracted. There was a third, very blurred, signal, which appeared at 13.5 ppm after a much greater lapse of time. It can be seen (Scheme 3) that the stepwise substitution of **3a** can in principle give three mono-substituted products, of which A1 is more likely than the other two, three di-substituted products of which B12 and B13, are more likely than B23 (which involves substitution of the two least basic nitrogens) and one tri-substituted product C123. The signals in the final spectrum are readily assigned to ligand C123, 13.5, 10.7 and 10.3 ppm to the methylenephosphonate residues on N(3), N(1) and N(2), respectively. The number of sharply resolved multiplets (*ca* 10.9–10.4 ppm) is equal to the number of phosphorous environments expected for N(1) groups on A1, B12, B13 and C123. The number of blurred multiplets (three) is equal to the number of phosphorus environments on N(2) required for B12, A2 and C123. The unique phosphorus environment for N(3) in C123 is at 13.5 ppm in the acid spectra. Since some of the signals [including those for the phosphorus N(1) environments and the remnant phosphorous acid] were quite sharp, it is likely to be a kinetic effect, with

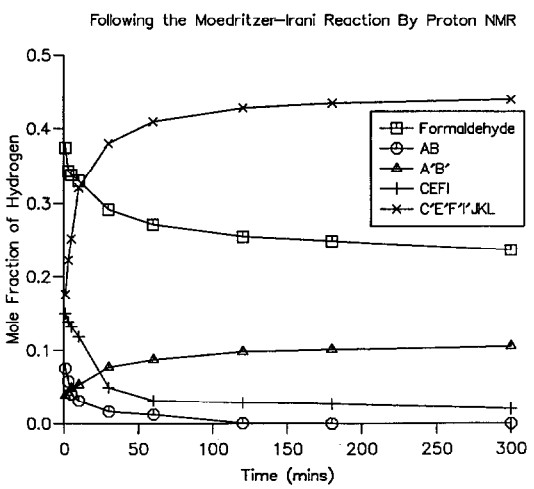

Fig. 2. Decay and build-up of ^{1}H signals for the conversion of **3a** to **3b** (taken from 200 MHz spectra).

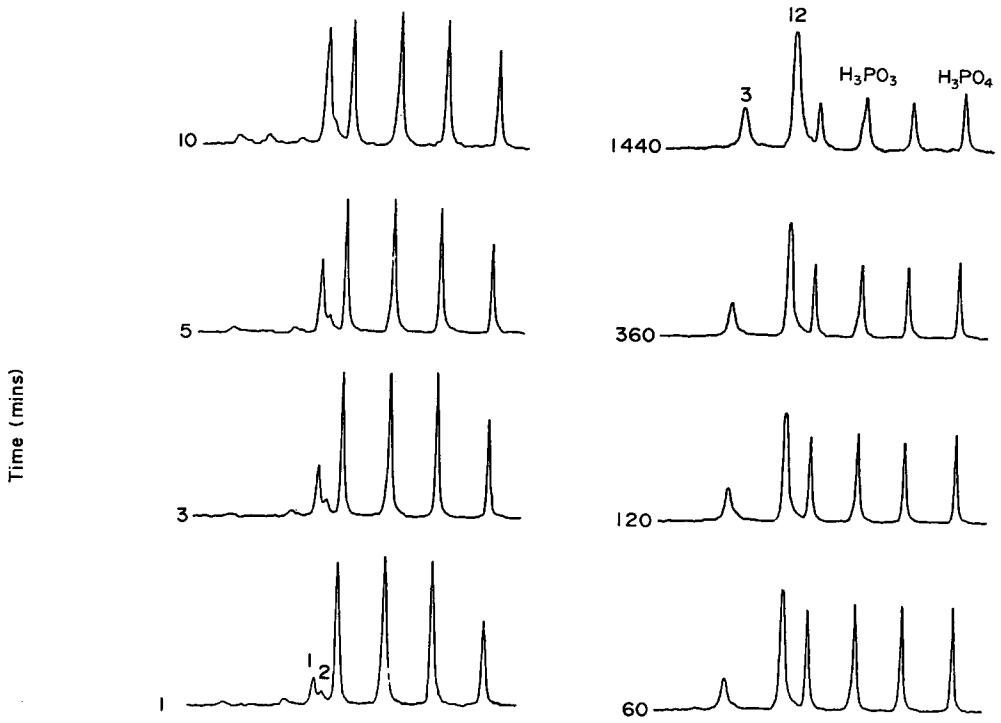

Fig. 3. ^{31}P NMR traces for the conversion of **3a** and **3b** over a period of 24 h (36.2 MHz, ambient temperature).

exchange of protons between particular nitrogens in the macrocyclic ring varying the chemical shifts of attached groups, but with incomplete averaging. This effect was probed in neutral solution, when a sharp triplet was observed for the phosphorus environment attached via N(1).

Most phosphorus spectra were taken in 5.5 M HCl with $H_0 \approx -2$, at which acidity one could expect that the third nitrogen, with a pK_a of *ca* 0–2, although almost fully protonated, would be liable to fast proton exchange which could cause the blurring effect (averaging over sites of different chemical shift) seen in the NMR spectra. The second nitrogen (pK_a *ca* 6) could also be in an intermediate exchange

Table 4. NMR coupling constants[a]

Ligand	^1H ^2J(P—H) (Hz)	^{31}P ^2J(P—H) (Hz)	^{13}C ^1J(P—C) (Hz)
1b[b]		10.34 11.32	143.0 143.5
2b[b]	13.8 13.9	13.4	
3b	(N1) 12.9[b,c] (N2) 12.3[b,c] (N3) 13.6[b,c]	(N1) 13.65[b] 11.54[c,d] 13.9[e]	
4b[b]	13.4	13.5 13.6 13.4 13.5	143.1 142.2
5b[c]	13.3		
8b[d]		12.6	141.3[f]
9[d]	7.1	7.1	159.0[g]

[a] All visible J reported for overlapping multiplets.
[b] 5 mol dm^{-3} DCl.
[c] 500 MHz spectrum.
[d] pD ≈ 6.5.
[e] pD ≈ 10.4.
[f] 6 mol dm^{-3} HCl.
[g] pD ≈ 1.5.

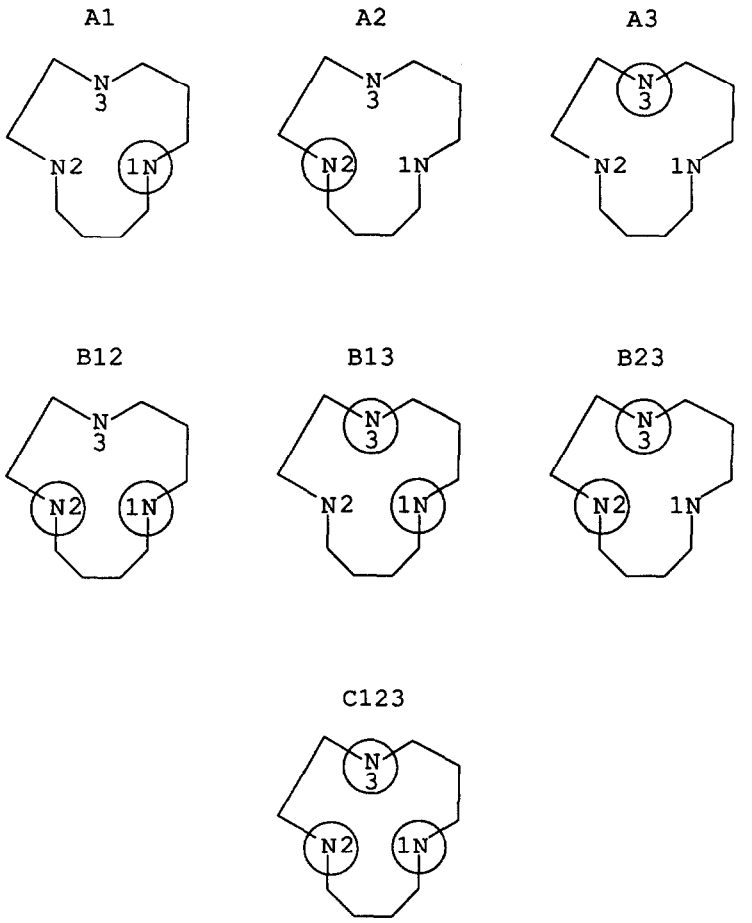

Scheme 3. Possible NMR environments for phosphorus for the conversion of **3a** to **3b**.

region and certainly, for spectra run at pH 7, protons on the two least basic nitrogens would be expected to be in a state of intermediate exchange on a typical NMR time-scale, with resultant effect on NMR signals.

^{1}H *studies*

From the selection of ^{1}H spectra shown in Fig. 4 (and obtained at 200 MHz Rf), initially free ligand is the major component, whose signals are observed. The labels shown on the lowest trace correspond to the proton labels shown in Scheme 2. Similar labels are used for the triphosphonate **3b**, distinguished by a prime where the ring protons are involved. As phosphonate groups are added the DGH/D'G'H' signals lose their fine structure with changing chemical environment. The time-dependent loss of free ligand and growth of phosphonated ligand signals is also quite evident.

The mole fractions of species are plotted against time in Figs 1 and 2, both for the phosphorus and for the proton signals. From the plots of ^{1}H signals (Fig. 2), the decay of the formaldehyde is clearly similar to that of the phosphorous acid in the ^{31}P spectra. It is simpler to consider the growth of the methylene signals on the phosphonated macrocycle A'B', C'E', F'I', J, K, L rather than the decay of the free ligand signals, since the former signals are better resolved. Again the rapid formation of the phosphonate groups on nitrogens N(1), and N(2) is shown by the growth of the C'E'J/F'I'K signal, these being the methylenes adjacent to the nitrogens involved, whereas the A'B' signal does not appear until the 10th minute. This signal only becomes significant after 60 min, subsequent to the first two phosphonations. This appearance at 10 min corresponds to the appearance of the corresponding peak in the ^{31}P spectrum.

These results show a sequential formation of phosphonate groups as hoped, with the phosphonation of the first two nitrogens being clearly faster than that for the third. However there is no large difference in the reactivity of nitrogens N(1) and N(2) (see

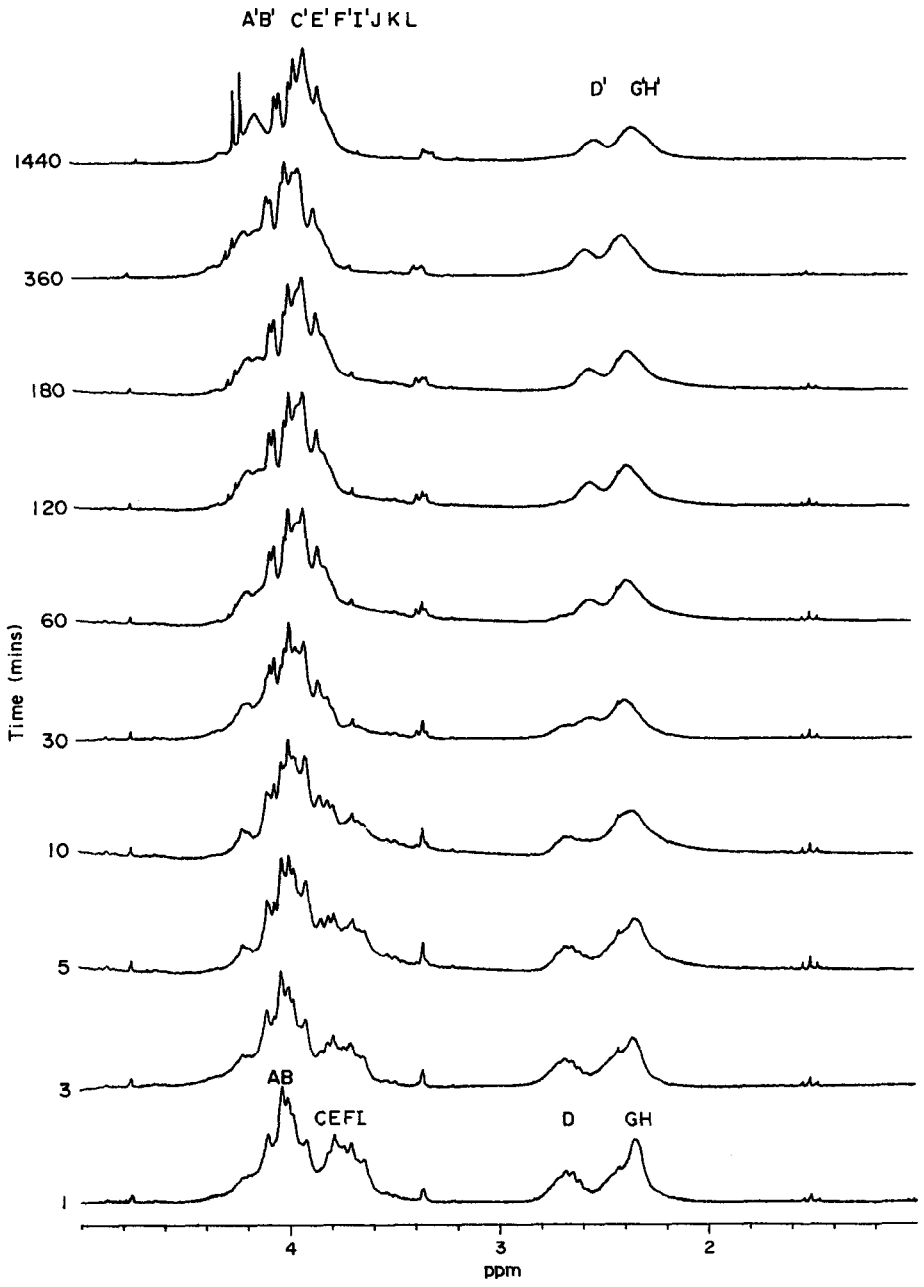

Fig. 4. ^{1}H NMR traces for the conversion of **3a** to **3b** over a period of 24 h (200 MHz, ambient temperature).

Scheme 3 and Fig. 1). The origin of these differences may lie in the pK_a values of the macrocyclic nitrogens. Although no data could be found for ligand **3a**, values from potentiometric studies on similar ligands **1a**, **10** and **11**[14–16,20,21] are shown in Table 5, along with the collected pK_a data for all the amines and guanidines used, where available from the literature.[17–19] For each of the macrocycles, two of the nitrogens are much more basic than the third. This is thought to be caused[7] by a combination of electrostatic repulsion and hydrogen bonding, i.e. the second protonated nitrogen is able to form a hydrogen bond with the unprotonated third nitrogen leaving it less susceptible to protonation. The close proximity of the protonated nitrogen also gives rise to electrostatic repulsion of an incoming proton. These factors make the third nitrogen much more difficult to protonate. In the early stages of the reaction the first two nitrogens are much more reactive to phosphonation. However, once the first two become phosphonated the chemical environment around the third nitrogen will have changed,

Table 5. pK_a values of amine starting materials

Ligand	pK_{a1}	pK_{a2}	pK_{a3}
1a[14]	11.03	7.37	0.7
1a[15]	10.42	6.82	
1a[16]	10.59	6.88	
2a[17]	9.81	5.55	
4a[17]	10.30	8.29	
5a[17]	9.35		
6a[18]	13.65	−10.9	
7a[17]	13.4		
8a[19]	10.85	2.59	
10[20]	13.2	6.96	0.1
10[15]	12.02	6.59	
10[16]	10.85	6.76	
11[14]	12.2	8.79	4.76
11[21]	9.79	8.13	4.18

which will in turn change the basicity and therefore reactivity towards phosphonation. The knowledge of the higher reactivity of the first two nitrogens could be very beneficial in reactions where basicity of the nitrogens is a factor. It should also allow the functionalization of two nitrogens leaving the third one free.

Also relevant are the guanidine reactions. In general guanidine reactions gave no N-methylene phosphonate derivatives by this route, although it is known that guanidines react with formaldehyde under acid conditions.[22] From the pK_as quoted in Table 5 it may be seen that guanidineacetic acid alone has a first pK_a value in the range of the macrocyclic amines, while guanidine is much more basic than any of the amines studied. The fact that guanidine **8** does not undergo the Moedritzer–Irani reaction may be associated with its very high pK_a or with the double-bond character of the C—N links, which may prevent formation of an imine from the methylol as required in the Vincens mechanism.[13]

Primary amines

The Moedritzer–Irani reaction was followed using both 1,3-diaminopropane (**4a**) (reaction VII) and benzylamine (**5a**) (reaction VIII) as the amine starting materials. The diamine was selected because the AAP derivatives were found to be very soluble, permitting the reaction to be carried out at high concentration without problems of precipitation in quenched samples. Six new signals, falling into two shift ranges, observed in the ^{31}P NMR spectra are quoted in Table 2.

The first sample taken after $1\frac{1}{2}$ min shows the presence of a tri- and/or tetra-substituted product, but there is no detectable signal for a mono- or di-substituted AAP derivative. The rapid build-up of signals for R_3 and R_4 (in comparison to those for R_1 and R_2) provides evidence for the increased rate of reaction of a mono- or di-phosphonomethylated primary amine nitrogen atom relative to the precursor amine. The final sample, taken after 1 day, indicated 22% of the mono- and di-substituted and 70% of the tri- and tetra-substituted AAP derivatives. Two signals were observed for the methylene protons in the ^1H spectrum of 1,3-diamino-propane tetrahydrochloride [δ_H: $CH_2CH_2CH_2$ 1.62 (p), $CH_2CH_2CH_2$ 2.66 (t)] and two singlets were observed in the corresponding ^{13}C spectrum (δ_C: $CH_2CH_2CH_2$ 28.81, $CH_2CH_2CH_2$ 38.54). The ^{13}C signal due to the CH_2 group in the middle of the propane diamine chain appears to be split into at least three peaks in all samples taken from the reaction, becoming sharper and less broad towards the end of the reaction as most of the amine starting material is converted to the tri- and tetra-substituted AAP derivatives.

Characteristic C—P coupling constants for all the spectra taken are shown in Table 4. The presence of hydroxy methylphosphonic acid (**9**) in the later samples from several reactions was confirmed by characteristic doublets in both the ^{13}C and ^1H spectra [δ_H: 3.34 J(P—H) 7.1 Hz, δ_C: 57.62 J(P—C) 159.0 Hz]. The significant amount of hydroxymethylphosphonic acid still present after ≈80% of reaction VII provides further evidence that this species is formed as a by-product.

Benzylamine **5a**

Reaction VIII was undertaken in an attempt to obtain simpler, more easily interpretable ^1H spectra. The first products were observed in the ^{31}P spectra after 20 min. Four new species appear to have been formed in the reaction. After 30 min the mono- and di-substituted AAP derivatives are both present as ≈ 0.5% of the total phosphorus in the sample (δ_P: mono- 13.03, di- 10.59 ppm). The amount of the di-AAP derivative then increases until it is present as 32% (of total ^{31}P) after 5 h. The concentration of the mono-AAP derivative is at a maximum after 3 h (1.8%) and this decreases to 1.1% after 5 h. This indicates that, once formed, the mono-AAP derivative is *rapidly* converted to the fully substituted derivative. These results are in agreement with those obtained by Redmore *et al.*[23] These workers detected only trace amounts of the mono-substituted benzylamine derivative after reacting 1 mole equivalent of benzylamine, phosphorous acid and formaldehyde. The amount of hydroxymethylphosphonic acid (**9**) increases

throughout the reaction and it is present as 2.5% (of total ^{31}P) after 5 h ($\delta_P = 23.37$ ppm). The di-substituted AAP derivative was found to be poorly soluble, precipitating from some of the later samples taken from the reaction mixture. This facilitated the assignments of the spectra.

The reaction between benzylamine, H_3PO_3 and formaldehyde (in the ratio 1:2:4) resulted in the almost exclusive formation of the fully substituted derivative (32%) relative to that of the mono-substituted product (1.1%). It was concluded that the rate of reaction of a mono-phosphonomethylated primary amine nitrogen atom was faster than that of the precursor amine. This is probably due to the increased positive charge on the nitrogen atom in the mono-substituted AAP derivative. The amount of partially substituted products (mono- and di-) formed in the reaction between 1,3-diaminopropane, H_3PO_3 and formaldehyde (1:4:8) was greater than the amount formed in the above reaction but tri- and tetra-substituted AAP derivatives were always present at higher concentrations, finishing at 70% of the total phosphorus in the reaction mixture.

In the reaction between piperazine (**2a**), phosphorous acid and formaldehyde (in the ratio 1:2:2), the ratio of fully to partially substituted products was $\approx 1.5:1$, which is much lower than that obtained in the reaction using benzylamine as the amine starting material. All three reactions using 1,4,7-triazacyclononane were carried out using a deficit of phosphorous acid. No fully substituted AAP derivative was formed in reaction I (0.34 mole equivalent of H_3PO_3). The amount of fully substituted product was found to increase with an increase in H_3PO_3, but significant concentrations of partially substituted products were still present in reactions II and III (0.78 and 2.06 mole equivalents of H_3PO_3, respectively). This increase in rate is not as large as that observed with the primary amines. This is probably because the substitutions are occurring on different nitrogen atoms in the secondary amines rather than the same nitrogen atom in the primary amines. With the triazacyclododecane, the differential basicities of the three nitrogens permit sequential formation of phosphonates with the first two nitrogens phosphonating on a shorter time-scale than the third.

Acknowledgements—The authors are grateful to SERC and Courtaulds Coatings for financial support (to MPL and PBI) and to SERC for provision of NMR facilities. Prof. W. MacFarlane and Dr M. N. S. Hill are thanked for NMR spectra and Miss L. G. Wrench for help with experiment II.

REFERENCES

1. J. C. Lockhart and M. E. Thompson, *J. Chem. Soc., Perkin Trans. 1* 1977, 202; J. R. Blackborow, J. C. Lockhart, D. E. Thompson and M. E. Thompson, *J. Chem. Res. (S)* 1978, 53; *J. Chem. Res. (M)* 1978, 0638.
2. G. W. Gokel, D. M. Dishong and C. J. Diamond, *J. Chem. Soc., Chem. Commun.* 1980, 1053.
3. V. J. Gatto and G. W. Gokel, *J. Am. Chem. Soc.* 1984, **106**, 8240.
4. K. Moedritzer and R. R. Irani, *J. Org. Chem.* 1966, **31**, 1603.
5. M. I. Kabachnik, T. Ya. Medved', N. M. Dyatlova and M. V. Rudomino, *Usp. Khim.* 1974, **43**, 1554.
6. T. J. Atkins, J. E. Richman and W. F. Oettle, *Org. Synth.* 1978, **58**, 86.
7. M. P. Lowe and L. G. Wrench, personal communication.
8. C. F. G. C. Geraldes, A. D. Sherry and W. P. Cacheris, *Inorg. Chem.* 1989, **28**, 3336.
9. T. G. Appleton, J. R. Hall and I. J. McMahon, *Inorg. Chem.* 1986, **25**, 726.
10. T. G. Appleton, J. R. Hall, A. D. Harris, H. A. Kimlin and I. J. McMahon, *Aust. J. Chem.* 1984, **37**, 1833.
11. W. C. Clegg, P. B. Iveson and J. C. Lockhart, *J. Chem. Soc., Dalton Trans.* 1992, 3291.
12. D. Redmore, *Topics in Phosphorus Chemistry* (Edited by M. Grayson and E. J. Griffith), Vol. 8, pp. 515–585. J. Wiley & Sons, Inc., New York (1976).
13. H. Mollier, M. Vincens, M. Vidal, R. Pasqualini and M. Duet, *Bull. Soc. Chim. Fr.* 1991, **128**, 787.
14. M. Briellmann, S. Kaderli, C. J. Meyer and A. D. Zuberbühler, *Helv. Chim. Acta* 1987, **70**, 680.
15. L. J. Zompa, *Inorg. Chem.* 1978, **17**, 2531.
16. M. Kodama and E. Kimura, *J. Chem. Soc., Dalton Trans.* 1978, 1081.
17. D. D. Perrin, *Dissociation Constants of Organic Bases in Aqueous Solution*. Butterworths, London (1965).
18. M. L. Hardy and G. Williams, *J. Chem. Soc.* 1953, 2560.
19. R. K. Mittal, M. Chandra and A. K. Dey, *Monatsh. Chem.* 1978, **109**, 953.
20. T. J. Riedo and T. A. Kaden, *Chimia* 1977, **31**, 220; *Helv. Chim. Acta* 1979, **62**, 1089.
21. E. Kimura and T. Yatsunami, *Chem. Pharm. Bull.* 1980, **28**, 994.
22. H. Fraenkel-Conrat and H. S. Olcott, *J. Am. Chem. Soc.* 1946, **68**, 34.
23. D. Redmore and B. Dhawan, *Phosphorus Sulfur* 1983, **16**, 233.

Polyhedron Vol. 12, No. 19, pp. 2325–2329, 1993
Printed in Great Britain

0277–5387/93 $6.00+.00
© 1993 Pergamon Press Ltd

NICKEL COMPLEXES OF TRIDENTATE LIGANDS INCORPORATING THIOETHER AND TRIAZENE-1-OXIDE FUNCTIONS. SYNTHESIS, STRUCTURE AND METAL REDOX

SOMA KARMAKAR, SURANJAN BHANJA CHOUDHURY, DEBASHIS RAY and ANIMESH CHAKRAVORTY*

Department of Inorganic Chemistry, Indian Association for the Cultivation of Science, Calcutta 700 032, India

(*Received* 20 *April* 1993; *accepted* 3 *June* 1993)

Abstract—The reaction of nickel(II) acetate with $RN(O)NNHC_6H_4SMe$ (HL^1: R = Me; HL^2: R = Pr^n; general abbreviation HL) in aqueous ethanol affords $[NiL_2]$ as brown crystalline solids. The X-ray structure of $[NiL^2{}_2]$ is reported. Each ligand acts in the tridentate meridional SNO fashion. The $Ni(SNO)_2$ coordination sphere is severely distorted from octahedral geometry. The Ni—S distances, 2.519(2) and 2.549(2) Å, constitute the longest nickel(II)–thioether bonds reported so far. Due to low symmetry, the octahedral ν_1 band of the complexes are split into components lying at *ca* 1400 and 1000 nm. The complexes display quasireversible cyclic voltammograms corresponding to the metal redox couple $[Ni^{III}L_2]^+/[Ni^{II}L_2]$, $E_{1/2} \sim 0.75$ V (vs S.C.E.). Coulometrically generated $[Ni^{III}L_2]^+$ displays rhombic EPR spectra, the g values of the perpendicular components being larger than that of the parallel component corresponding to the $(d_{z^2})^1$ ground state.

This work forms part of our programme on the synthesis, structure and redox behaviour of nickel(II) complexes incorporating thioether ligation.[1–4] The nickel(II)–thioether link is intrinsically weak[5–7] and we have used polydentate ligation as the stabilizing principle. Ligands having both thioether and triazene-1-oxide functions are well-suited[8] for nickel(II) binding and we have recently reported the case of hexadentate coordination (**1**).[4] In this concluding study on the thioether triazene-1-oxide complexes we examine the case of tridentate ligands, which have two disadvantages compared with hexadentate ligands: diminished chelate effect and potentially easier dissociation of the terminally placed thioether site. Nevertheless, complexes of coordination type **2** have, however, been isolated and one of these has been structurally characterized. Redox activity of nickel–sulphur complexes are of bioinorganic interest.[9,10] The present complexes are oxidisable in solution affording EPR-active nickel(III) species.

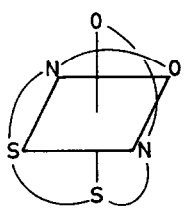

(1)

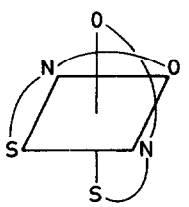

(2)

EXPERIMENTAL

Materials

2-Methylthioaniline was prepared by methylating 2-aminothiophenol by methyl iodide in alkaline media. The hydroxylamines were made by reduction of the corresponding nitro compounds.[11] All reagents used were of commercial grade. Tetraethylammonium perchlorate and pure dichloromethane for electrochemical and spectroscopic work were obtained as before.[12]

* Author to whom correspondence should be addressed.

Physical measurements

Electronic and IR spectra were measured with Hitachi model 330 and Perkin–Elmer model 783 spectrometers. Electrochemical data were collected with a PAR 370-4 electrochemistry system as before.[13] Magnetic measurements were performed with a PAR-155 vibrating sample magnetometer and EPR spectra were recorded with a Varian E-109 C spectrometer (*X*-band) fitted with a quartz Dewar.

Synthesis of ligands and complexes

The ligands HL^1 and HL^2 were synthesized by similar methods and details are given for HL^2, *o*-(1-*n*-propyl triazene-1-oxide)methyl thiobenzene. A solution of 2-(methylthio)aniline (1.39 g) in concentrated HCl (1.7 cm^3) and water (2 cm^3) was diazotized at 0°C with $NaNO_2$ (1.38 g) dissolved in water (5 cm^3). The diazotized solution was added with stirring to 1.12 g of N-*n*-propylhydroxylamine hydrochloride in water (15 cm^3) and cooled to 0°C. The pH of the reaction mixture was kept in the range 3–5 by gradual addition of an aqueous solution (20 cm^3) of sodium acetate (6 g). The ligand separated out as a pale yellow precipitate. This was filtered and recrystallized from alcohol to yield pale yellow needles. Yield: 75%. Found: C, 53.2; H, 6.6; N, 18.8. Calc. for $C_{10}H_{15}N_3OS$: C, 53.3; H, 6.7; N, 18.7%. The ligand HL^1 was synthesized in 68% yield. Found: C, 48.8; H, 5.6; N, 21.2. Calc. for $C_8H_{11}N_3OS$: C, 48.7; H, 5.6; N, 21.3%.

To a hot ethanolic solution of the ligand HL^2 (388 mg, 2.0 mmol) was added an aqueous solution of nickel(II) acetate tetrahydrate (250 mg, 1.0 mmol). The mass was then refluxed for 30 min and on concentration $[NiL^2_2]$ was precipitated as a brown crystalline solid, which was collected by filtration, washed successively with alcohol and water and finally dried over P_4O_{10}. Yield: 72%. Found: C, 47.4; H, 5.6; N, 16.7. Calc. for $C_{20}H_{28}N_6O_2S_2Ni$: C, 47.3; H, 5.5; N, 16.6%. The complex $[NiL^1_2]$ was synthesized similarly and obtained in 70% yield. Found: C, 42.6; H, 4.5; N, 18.4. Calc. for $C_{16}H_{20}N_6O_2S_2Ni$: C, 42.6; H, 4.4; N, 18.6%.

X-ray structure determination of $[NiL^2_2]$

Single crystals of $[NiL^2_2]$ were grown by slow diffusion of hexane into the dichloromethane solution. Cell dimensions were determined with the help of 25 machine centred reflections. Data were collected at 296 K on a Nicolet R3m/V diffractometer with graphite monochromated Mo-K_α (λ = 0.71073 Å) radiation in the ω–2θ scan mode. Two check reflections measured after every 98 reflections showed no significant variations. Lorentz and polarization corrections and semi-empirical absorption correction[14] were performed.

The structure was solved by direct methods and was refined by full-matrix least-squares procedures. All the non-hydrogen atoms were refined anisotropically. Hydrogen atoms were included at the calculated positions in the final refinement cycle with an isotropic thermal parameter (0.08 $Å^2$). Crystal data and other details are collected in Table 1. Computations were performed on a MicroVAX II computer using the SHELXTL-PLUS program system.[15]

Tables of atomic coordinates, anisotropic thermal parameters, full listing of bond lengths and angles and observed and calculated structure factors are available as supplementary material from the Editor.

Table 1. Crystal data, intensity data collection and structural refinement for $[NiL^2_2]$

Compound	$[NiL^2_2]$
Formula	$C_{20}H_{28}N_6O_2S_2Ni$
Crystal size (mm)	0.36 × 0.38 × 0.38
Crystal system	Monoclinic
Space group	$P2_1/a$
a (Å)	10.574(5)
b (Å)	15.703(6)
c (Å)	14.582(5)
β (°)	96.98(3)
U ($Å^3$)	2403(1)
Z	4
M	507.3
D_c (g cm^{-3})	1.405
μ(Mo-K_α) (cm^{-1})	10.11
F(000)	1064
2θ range (°)	2–52
Total no. of reflections	5182
No. of unique reflections	4756
No. of observed reflections [$I > 3\sigma(I)$]	2175
Transmission factors	0.6937–1.0
Weighing scheme g in $w = 1/[\sigma^2(F)+gF^2]$	0
No. of parameters refined	281
Final R	0.0386
Final R_w	0.0397
Goodness-of-fit	1.47
Largest and mean Δ/σ	0.020, 0.001
Data-to-parameter ratio	7.7 : 1
Largest difference peak (e $Å^{-3}$)	0.37
Largest difference hole (e $Å^{-3}$)	−0.30

RESULTS AND DISCUSSION

Synthesis and structure

The ligands (3) used in the present work are HL^1 and HL^2 (general abbreviation HL). The brown crystalline $[NiL_2]$ complexes were prepared in high

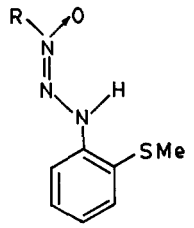

R

HL^1 Me

HL^2 n-Pr

(3)

yields by reacting HL with nickel(II) acetate tetrahydrate in aqueous ethanol. Selected characterization data, shown in Table 2, will be considered further in a later section. For the present we note that the complexes are paramagnetic with two unpaired electrons. The characteristic N_3 and NO vibrations[16] of the chelate rings are present.

The X-ray structure of $[NiL^2_2]$ has been determined. A view of the molecule is shown in Fig. 1 and selected bond distances and angles are listed in Table 3. Each ligand acts in the tridentate meridional SNO fashion. The angle between the two

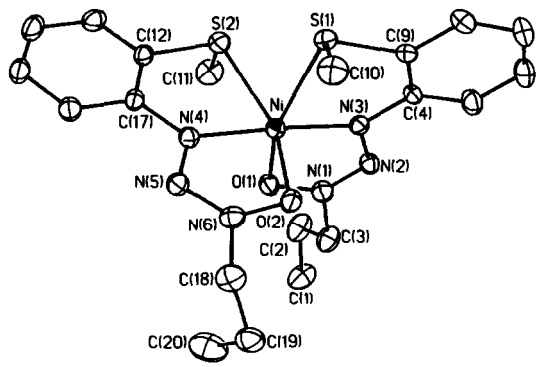

Fig. 1. Perspective view and atom labelling scheme of $[NiL^2_2]$. Atoms are shown as 50% thermal probability ellipsoids.

meridional planes formed by the two ligands is 91.3(2)°. The $Ni(SNO)_2$ coordination sphere is, however, severely distorted from octahedral geometry, the *trans* S—Ni—O angles being 157.7(1)° and 158.2(1)°. The interchelate N(3)—Ni—N(4) *trans* angle, 176.2(2)° is, however, close to 180°. The distortions are created mainly by the constraints of ligand chelation. All the five-membered chelate rings are good planes with mean deviations lying in the range 0.01–0.05 Å. The sulphur atoms are pyramidal and the non-bonded S···S length is 3.519(2) Å.

In nickel(II)–thioether complexes the Ni—S distances usually lie in the range 2.39–2.44 Å.[1,2,17] In a hexadentate thioether triazene-1-oxide complex

Table 2. Magnetic moments,[a] electronic spectra,[b] IR spectra,[c] electrochemical data[d] and EPR data[e] of $[NiL_2]$

Compound	μ_{eff} (B.M.)	λ(nm) [ε (dm^3 mol^{-1} cm^{-1})]	ν(NO) (cm^{-1})	$\nu(N_3)$ (cm^{-1})	Ni^{III}—Ni^{II} couple $E_{1/2}$(V)[f] (ΔE_p(mV))[g]	n[h] (E(V))[i]	g_1	g_2	g_3
$[NiL^1_2]$	3.32	1400[j](39), 1000(88), 625(61), 350(33,775)	1220	1460	0.75(170)	0.97(1.04)	2.217	2.082	2.076
$[NiL^2_2]$	3.18	1400(38), 1000(91), 625(51), 350(38,530)	1275	1450	0.76(170)	0.98(1.05)	2.221	2.083	2.078

[a] In the solid state at 298 K.
[b] In dichloromethane.
[c] In KBr discs.
[d] In CH_2Cl_2 (0.1 M TEAP) at a platinum electrode with an S.C.E. reference.
[e] In frozen (77 K) dichloromethane solution.
[f] From cyclic voltammetry at a scan rate of 50 mV s^{-1}.
[g] Peak-to-peak separation.
[h] n is the ratio of observed : calculated coulomb counts for one-electron transfer.
[i] Potential used for coulometry of $[NiL_2]$.
[j] Shoulder.

Table 3. Selected bond distances (Å) and angles (°)[a] for $[NiL^2_2]$

Ni—S(1)	2.519(2)	Ni—S(2)	2.549(2)
Ni—N(3)	1.972(4)	Ni—N(4)	1.970(4)
Ni—O(1)	2.051(4)	Ni—O(2)	2.048(4)
N(1)—N(2)	1.285(7)	N(1)—O(1)	1.319(6)
N(2)—N(3)	1.321(6)	N(4)—N(5)	1.317(6)
N(5)—N(6)	1.292(6)	N(6)—O(2)	1.339(6)
S(1)—Ni—S(2)	87.9(1)	S(1)—Ni—N(3)	80.8(1)
S(2)—Ni—N(3)	103.4(1)	S(1)—Ni—N(4)	100.1(1)
S(2)—Ni—N(4)	80.4(1)	N(3)—Ni—N(4)	176.2(2)
S(1)—Ni—O(1)	157.7(1)	S(2)—Ni—O(1)	93.1(1)
N(3)—Ni—O(1)	77.3(2)	N(4)—Ni—O(1)	102.0(2)
S(1)—Ni—O(2)	93.2(1)	S(2)—Ni—O(2)	158.2(1)
N(3)—Ni—O(2)	98.3(2)	N(4)—Ni—O(2)	77.9(2)
O(1)—Ni—O(2)	94.0(1)		

[a] Estimated standard deviations are given in parentheses.

of type **1** the Ni—S lengths, 2.494(4) and 2.526(3) Å, were found to lie outside the above range.[4] In the present complex the distances are even longer, 2.519(2) and 2.549(2) Å. There is thus a subtle weakening of the Ni—S(thioether) bond due to a diminished chelate effect on going from **1** (five chelate rings) to **2** (four chelate rings). To our knowledge the average Ni—S length in $[NiL^2_2]$ represents the longest nickel(II)–thioether bond reported so far.

In the triazene-1-oxide chelate rings the N(1)—N(2) and N(5)—N(6) distances are *ca* 0.03 Å shorter than the N(2)—N(3) and N(4)—N(5) distances, respectively. Thus, in the π-delocalization of the N_3O ligand frame, the triazene-1-oxide valence form —N(O)=N—$\bar{N}$— has higher weightage than the hydroxy triazene, —N($\bar{O}$)—N=N—. Consistent with this the Ni—N lengths are *ca* 0.07 Å shorter than the Ni—O lengths.

Spectra and metal redox

The highly distorted coordination sphere observed in the X-ray structure is directly reflected in the ligand field spectra of the complexes, Table 2. Thus, the octahedral ν_1 band is split into two components lying at *ca* 1400 and 1000 nm (Fig. 2).

The complexes are electroactive at platinum and a quasireversible cyclic voltammetric response corresponding to the metal redox couple of eq. (1) is observed (dichloromethane solution). The reduction potentials (Table 2) lie at the higher end of the range observed for thioether ligated nickel complexes.[1-3,18] The brown trivalent cation $[NiL_2]^+$ has been generated in solution coulometrically and such solutions display the same cyclic peaks as $[NiL_2]$, showing that no immediate decomposition occurs.

$$[Ni^{III}L_2]^+ + e \rightleftharpoons [Ni^{II}L_2] \quad (1)$$

The description of $[NiL_2]^+$ as a nickel(III) complex is corroborated by the frozen glass (77 K) EPR spectra of the electrooxidized solutions. The representative case of $[NiL^2_2]^+$ is displayed in Fig. 2. Three signals are observed at $g_1 = 2.221$, $g_2 = 2.083$ and $g_\parallel = 2.078$, the latter two overlapping seriously. To achieve consistency with the spectra of the hexadentate complexes,[4] we assign g_1 and g_2 to components of $g_\perp$ and g_3 to $g_\parallel$. The rhombic splitting is larger in the present tridentate complexes compared with the reported[4] hexadentate case ($g_\perp$ components of 2.199, 2.138, $g_\parallel = 2.035$). The $g_\perp > g_\parallel$ inequality corresponds to a $(d_{z^2})^1$ ground state.[19,20] The EPR parameters of $[NiL^1_2]^+$ with $g_\perp$ components of 2.217, 2.082 and $g_\parallel = 2.076$ are similar to those of $[NiL^2_2]^+$.

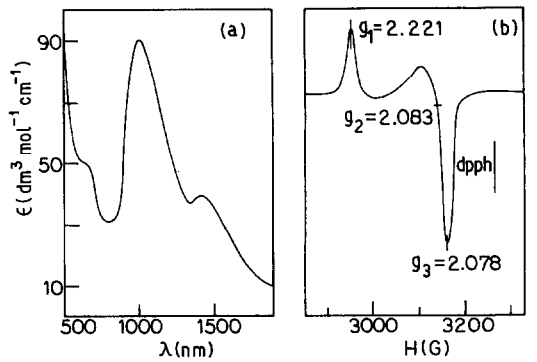

Fig. 2. (a) Electronic spectrum of $[NiL^2_2]$ in dichloromethane solution. (b) *X*-band (9.11 GHz) EPR spectrum of $[NIL^2_2]^+$ in frozen (77 K) dichloromethane.

CONCLUSIONS

Two tridentate ligands (HL) having thioether and triazene-1-oxide functions have afforded nickel(II) complexes of the type $[NiL_2]$. The octahedral ν_1 band shows a large splitting. Structure determination in one case has revealed the presence of a highly distorted $Ni(SNO)_2$ coordination sphere. The Ni—S (thioether) bonds are the longest observed so far among thioether complexes. The bonds are weaker in $[NiL_2]$ compared with those in complexes of hexadentate ligands bearing the same functions. Electrochemical oxidation of $[NiL_2]$ affords $[NiL_2]^+$, which has a $(d_{z^2})^1$ ground state with a large rhombic distortion.

Acknowledgements—Crystallography was performed in the National Single Crystal Diffractometer Facility established at the Department of Inorganic Chemistry, Indian Association for the Cultivation of Science, by the Department of Science and Technology, New Delhi. Financial support received from the Council of Scientific and Industrial Research is also acknowledged.

REFERENCES

1. S. Bhanja Choudhury, D. Ray and A. Chakravorty, *J. Chem. Soc., Dalton Trans.* 1992, 107.
2. S. Bhanja Choudhury, D. Ray and A. Chakravorty, *Inorg. Chem.* 1991, **30**, 4354.
3. D. Ray, S. Pal and A. Chakravorty, *Inorg. Chem.* 1986, **25**, 2674.
4. S. Karmakar, S. Bhanja Choudhury, D. Ray and A. Chakravorty, *Polyhedron* 1993, **12**, 291.
5. S. G. Murrey and F. R. Hartley, *Chem. Rev.* 1981, **81**, 365.
6. S. R. Cooper and S. C. Rawle, *Struct. Bonding* 1990, **72**, 1.
7. A. J. Blake and M. Schröder, *Adv. Inorg. Chem.* 1990, **35**, 1.
8. (a) R. N. Mukherjee and A. Chakravorty, *Inorg. Chem.* 1984, **23**, 4753 and refs therein; (b) P. S. Zacharias and A. Chakravorty, *Inorg. Chem.* 1971, **10**, 1961.
9. J. R. Lancaster Jr, *The Bioinorganic Chemistry of Nickel.* VCH Publishers, New York (1988).
10. R. Cammack, *Adv. Inorg. Chem.* 1988, **32**, 297.
11. A. Chakravorty, B. Behera and P. S. Zacharias, *Inorg. Chim. Acta* 1968, **2**, 85.
12. G. K. Lahiri, S. Bhattacharya, B. K. Ghosh and A. Chakravorty, *Inorg. Chem.* 1987, **26**, 4324.
13. P. Basu, S. Bhanja Choudhury, S. Pal and A. Chakravorty, *Inorg. Chem.* 1989, **28**, 2680.
14. A. C. T. North, D. C. Philips and F. S. Mathews, *Acta Cryst.* 1968, **A24**, 351.
15. G. M. Sheldrick, SHELXTL-Plus 88, Structure Determination Software Programs. Nicolet Instrument Corporation, Madison (1988).
16. R. L. Dutta and R. Sharma, *J. Inorg. Nucl. Chem.* 1980, **42**, 1204.
17. S. R. Cooper, S. C. Rawle, J. A. R. Hartman, E. J. Hintsa and G. A. Admans, *Inorg. Chem.* 1988, **27**, 1209.
18. (a) K. Wieghardt, H.-J. Küppers and J. Weiss, *Inorg. Chem.* 1985, **24**, 3067; (b) D. Fortier and A. McAuley, *Inorg. Chem.* 1989, **28**, 655; (c) L. Fabbrizzi and D. M. Proserpio, *J. Chem. Soc., Dalton Trans.* 1982, 229.
19. S. Bhattacharya, R. N. Mukherjee and A. Chakravorty, *Inorg. Chem.* 1986, **25**, 3448.
20. S. A. Jacobs and D. W. Mergerum, *Inorg. Chem.* 1984, **23**, 1195.

Polyhedron Vol. 12, No. 19, pp. 2331–2334, 1993
Printed in Great Britain

0277–5387/93 $6.00+.00
© 1993 Pergamon Press Ltd

SYNTHESIS AND REACTIVITY OF DIHYDROXORUTHENIUM(IV) COMPLEX OF TETRAMESITYLPORPHYRIN. AEROBIC EPOXIDATION OF NORBORNENE BY RUTHENIUM PORPHYRINS

WA-HUNG LEUNG

Chemistry Department, Hong Kong University of Science and Technology, Clear Water Bay, Kowloon, Hong Kong

and

CHI-MING CHE,* CHI-HUNG YEUNG and CHUNG-KWONG POON†

Department of Chemistry, The University of Hong Kong, Pokfulam Road, Hong Kong

(*Received* 20 *April* 1993; *accepted* 2 *June* 1993)

Abstract—Treatment of Ru(TMP)(CO) with *m*-CPBA in CH_2Cl_2/EtOH afforded Ru(TMP)$(OH)_2$, isolated as air-stable violet crystals. Ru(TMP)$(OH)_2$ is paramagnetic (μ_{eff} *ca* 2.7 B.M.) and displays broad ^{1}H NMR signals with paramagnetic isotropic shifts. The IR spectrum shows a band at 760 cm^{-1} assignable to the Ru—O stretch. Ru(TMP)$(OH)_2$ is capable of catalysing aerobic epoxidation of alkenes under mild conditions.

Oxo complexes of ruthenium porphyrins have received much attention because of their resemblance to active species of mono-oxygenase enzymes[1] and their applications in organic oxidations.[2–4] Recently, Groves and co-workers reported that Ru(TMP)O_2 (TMP = tetramesitylporphyrin dianion) is able to catalyse the aerobic epoxidation of alkenes under mild conditions. The suggested mechanism involves the intermediacy of an unstable oxo-ruthenium(IV) species, which disproportionates to dioxo-ruthenium(VI) and ruthenium(II).[2] The Ru(TMP)O intermediate, which was characterized by ^{1}H NMR spectroscopy, could be obtained by reaction of Ru(TMP)O_2 with 1 equivalent of PPh_3 or aerial oxidation of Ru(TMP)$(MeCN)_2$.[2b] However, attempts to isolate pure Ru(TMP)O have so far been unsuccessful. In a previous paper, we described the synthesis of Ru(OEP)O(EtOH) (OEP = octaethylporphyrin dianion) which was, however, incapable of catalysing the aerobic oxidation of alkenes due to rapid dimerization in non-polar solvents. In our continuing effort to develop metal catalysts for organic oxidation we herein report the synthesis and reactivity of Ru(TMP)$(OH)_2$, which could be a key intermediate in the Ru(TMP)-based oxidations.

EXPERIMENTAL

Ru(TMP)CO was prepared according to the literature method.[1b] *m*-Chloroperoxybenzoic acid (*m*-CPBA) was purchased from Merck and used as received. Tetrakis(2,6-dichlorophenyl)porphyrin, H_2(2,6Cl_2TPP), was synthesized by a modified procedure of Rothemund's method using 1-methyl-2-pyrrolidinone instead of pyridine.[4] All solvents used were of analytical grade. ^{1}H NMR spectra were obtained on a Jeol EX 270 NMR spectrometer and chemical shifts (δ, in ppm) were reported referenced to Me_4Si. IR spectra (Nujol) were obtained on a Nicolet Model 20 FXC FT-IR spectrometer. Reduction potential was determined by cyclic voltammetry using a Princeton PAR 173/179 potentiostat equipped with a model 175 universal pro-

* Author to whom correspondence should be addressed.
† Present address: Department of Applied Biology and Chemical Technology, Hong Kong Polytechnic, Hunghom, Kowloon, Hong Kong.

grammer. A glassy carbon electrode was used as the working electrode and the reduction potential was reported referenced to the ferrocenium/ferrocene couple.

Preparation of Ru(TMP)$(OH)_2$ (**1**)

To a CH_2Cl_2/EtOH (1:2, 25 cm^3) solution of Ru(TMP)CO (50 mg) was added *m*-CPBA (50 mg). The resulting solution was filtered and left to stand at room temperature overnight. The dark violet crystals formed were collected and washed with a small amount of cold ethanol (yield: 25 mg). Concentration of the filtrate gave a second crop of product, which was contaminated with some unreacted *m*-CPBA. ^1H NMR (CD_2Cl_2/CD_3OD, 1:1): 2.62 (*p*-Me), 3.09 (*o*-Me), 7.54 (*meta*-phenyl), −30.58 (pyrrolic); all broad singlets. UV–vis (CH_2Cl_2/EtOH), λ_{max}/nm ($\varepsilon/10^3\ M^{-1}\ cm^{-1}$): 660 (1.29), 600 sh (2.66), 522 (9.33), 408 (93.3), 320 (15.8).

Preparation of Ru(2,6-Cl_2TPP)CO(EtOH) (**2**)

A mixture of $Ru_3(CO)_{12}$ (100 mg), H_2(2,6-Cl_2-TPP) (100 mg) and naphthalene was heated at 220°C under a nitrogen atmosphere for 72 h. After cooling to room temperature the solidified melt was dissolved in toluene and loaded onto a column of neutral alumina. Naphthalene, unreacted $Ru_3(CO)_{12}$ and free porphyrin were eluted with toluene. The ruthenium porphyrin was eluted with $CHCl_3$/EtOH (yield: 20%). ^1H NMR ($CDCl_3$): −1.07 (s br, 2H, H_3CH_2OH), 0.93 (s br, 3H, CH_3CH_2OH), 7.73 (m, 12H, *para*- and *meta*-phenyl), 8.44 (s, 8H, pyrrolic). UV–vis (CH_2Cl_2), λ_{max} (nm) ($\varepsilon/10^3\ M^{-1}\ cm^{-1}$): 410 (252), 530 (20), 558 sh (4.6).

Preparation of Ru(2,6-Cl_2TPP)O_2 (**3**)

To a solution of **2** (50 mg) in CH_2Cl_2 (50 cm^3) at room temperature was added *m*-CPBA (50 mg). After stirring at room temperature for 3 min the resulting solution was loaded onto a column of neutral alumina. The purple product was eluted with CH_2Cl_2 and was recrystallized from CH_2Cl_2/hexane (yield: 40%). ^1H NMR ($CDCl_3$): 7.81 (m, 12H, *para*- and *meta*-phenyl), 8.88 (s, 8H, pyrrolic). UV–vis (CH_2Cl_2), λ_{max} (nm) ($\varepsilon/10^3\ M^{-1}\ cm^{-1}$): 420 (309), 511 (14.4), 566 sh (4.0).

Aerobic epoxidation with ruthenium porphyrins

Typically a mixture of ruthenium porphyrin (3 mg) and norbornene (0.3 cm^3) in benzene (5 cm^3) was stirred under oxygen (4 bar) in an autoclave. After reaction, the organic products were analysed and quantified by gas chromatography using the internal standard method.

RESULTS AND DISCUSSION

Oxidation of Ru(TMP)CO with excess *m*-CPBA in CH_2Cl_2/EtOH afforded Ru(TMP)$(OH)_2$ (**1**), isolated in its pure form. It seems likely that the oxidation of Ru(TMP)CO by *m*-CPBA initially gave Ru(TMP)O_2, which is soluble in CH_2Cl_2 and is gradually reduced by EtOH to give Ru(TMP)$(OH)_2$ (Scheme 1).

Compound **1** was found to be unstable in non-polar solvents such as CH_2Cl_2, in which it is air-oxidized to diamagnetic Ru(TMP)O_2, as indicated by ^1H NMR spectroscopy. However, in the presence of alcohol aerobic oxidation of **1** is completely inhibited presumably because the alcohol molecule blocks the vacant coordination site of Ru^{IV}-TMP (see later section), which is essential for aerobic oxidation of the complex. It might be noted that the dimerization of the related Ru(OEP)O(EtOH) complex can also be inhibited by alcohol.[3a] Therefore, the following studies and characterization of **1** were performed in the presence of alcohol.

The measured magnetic moment of *ca* 2.7 B.M. (by Evans' method[5] in $CDCl_3/CD_3OD$) for **1** is close to the spin-only value for two unpaired electrons, suggesting an $S = 1$ ground-state configuration. Similar magnetic moments have been found for other related paramagnetic ruthenium(IV) porphyrins with π-donating axial ligands such as O^{2-}, Br^- and Cl^-. Ru(porph)R_2 (porph = OEP, TPP; R = Me, Ph) are, however, diamagnetic.[6] The ^1H NMR spectrum of **1** in CD_2Cl_2/CD_3OD shown in Fig. 1 consists of four paramagnetically shifted broad resonance signals assignable to the *para*- and *ortho*-methyl and *meta* protons of the *meso*-phenyl groups and the pyrrolic protons. Peaks at *ca* 1.2 (t) and 3.7 (q) ppm due to unligated EtOH molecules were also found. The observation of a single *ortho*-methyl resonance (down to −50°C) is indicative of the D_{4h} symmetry of the molecule. Formulation of the prepared complex to be Ru(TMP)O(EtOH) or Ru(TMP)O(OH_2) is therefore not preferred. According to our previous work Os(porph)$(OEt)_2$ (porph = OEP, TPP) show paramagnetically shifted ^1H NMR signals for the coordinated ethoxy ligands.[7] No signals due

$$\text{Ru(TMP)CO} + 2m\text{-CPBA} \longrightarrow \text{Ru(TMP)O}_2$$

$$\text{Ru(TMP)O}_2 \xrightarrow{\text{EtOH, H}_2\text{O}} \text{Ru(TMP)(OH)}_2$$

Scheme 1.

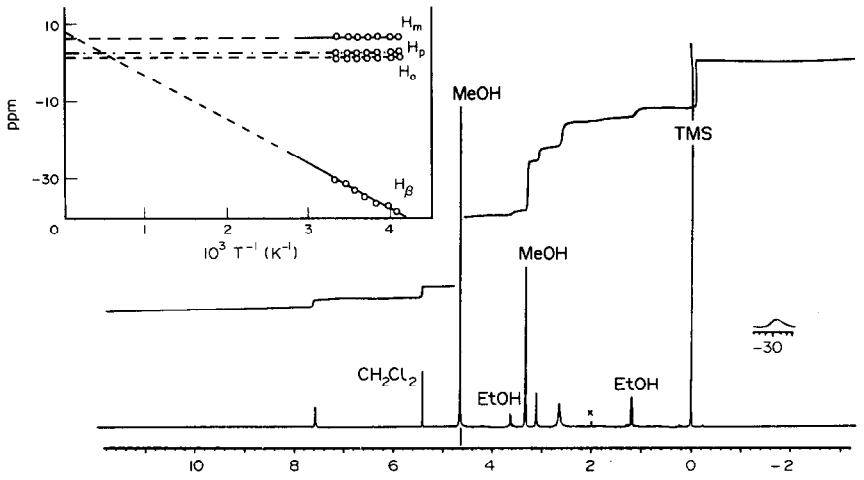

Fig. 1. ^{1}H NMR spectrum of Ru(TMP)$(OH)_2$ in CD_2Cl_2/CD_3OD.

to the coordinated ethoxy group have been found for **1**, thus excluding the possibility of the prepared complex to be Ru(TMP)(OEt)(OH) or Ru(TMP)$(OEt)_2$.

Similar to Ru(TMP)O,[2b] the paramagnetic isotropic shifts for **1** vary inversely with temperature from +50 to −40°C (inset of Fig. 1). The extrapolated intercepts to $T^{-1} = 0$ for all of the resonances are very close to the respective positions expected for diamagnetic TMP complexes. Since there is no evidence for anti-ferromagnetic coupling, the possibility of a dimeric structure for **1** is ruled out. The adherence to the Curie relationship is indicative of the existence of a single spin state throughout the temperature range. The upfield pyrrolic shift (at *ca* −30 ppm), which is typical for paramagnetic ruthenium(IV) porphyrins, suggests that the isotropic shift mainly results from π-delocalization.[6b]

The IR spectrum of **1** does not show any intense band around the 800 cm^{-1} region,[2b] suggesting that no oxo group is present. A new band which is absent in the starting Ru(TMP)CO appears at 760 cm^{-1}. This band is assigned to the Ru—OH stretch. In accordance with this assignment this band shifts to 726 cm^{-1} after isotopic labelling of the compound with ^{18}O.[8] The oxidation-state marker[9] at 1011 cm^{-1} is consistent with the IV oxidation state.[2b,3a]

In order to unambiguously confirm the structure of **1** an X-ray diffraction study was performed. The result indicated that **1** is a Ru^{IV}-TMP complex with an average Ru—O bond distance of 1.929(9) Å.[10] Unfortunately, we have not been able to solve the crystal structure completely due to disorder of the two axial ligands and solvent molecules.

The cyclic voltammogram of **1** in CH_2Cl_2/MeOH (1 : 1) shows a quasi-reversible couple at −0.8 V and an irreversible oxidation wave at 0.80 V vs $Cp_2Fe^{+/0}$. The reduction couple was tentatively assigned to the metal-centred $Ru^{IV}/^{III}$ couple.

Aerobic epoxidation with **1**

Compound **1** is an active catalyst for aerobic epoxidation of alkenes under mild conditions. For example, *ca* 20 equivalents of *exo*-norbornene oxide (determined by GLC) along with an unidentified paramagnetic ruthenium compound were obtained when a benzene solution of **1** and norbornene was stirred at room temperature under 4 bars of oxygen for 35 min (entry 1, Table 1). Consistent with the observation by Groves and co-workers,[2a] the yield of epoxide is rather insensitive to oxygen pressure. It is noteworthy that Ru(TMP)$(OH)_2$ is a more efficient aerobic epoxidation catalyst than Ru(TMP)O_2, although the overall yields for both systems are more or less identical.

We believe that Ru(TMP)O, which is equilibrium with **1**, is the active intermediate for the catalytic aerobic epoxidation. In fact, the conversion of $Ru^{IV}(OH)_2$ to Ru^{IV}=O (possibly catalysed by water) is not without precedence. Previously, we have established a similar equilibrium between $Ru^{IV}(OH)_2$ and $Ru^{IV}O(OH_2)$ for a cationic ruthenium(IV) compound of a non-porphyrinic macrocycle.[11] Of note, recrystallization of [Ru{3,4,5-$(MeO)_3$TPP}$(OH)_2$] from CH_2Cl_2/ETOH solution in air led to the isolation of a structurally characterized ruthenium(III)-aquo(hydroxo) compound, Ru[3,4,5-$(MeO)_3$TPP](OH)(OH_2) [3,4,5-$(MeO)_3$TPP = tetrakis(3,4,5-trimethoxyphenyl)porphyrin dianion].[12] This indicates that oxo and hydroxo ligands of ruthenium porphyrins can be protonated and deprotonated quite easily and exchange rapidly with water in solvent.

Table 1. Aerobic epoxidation of alkenes by ruthenium porphyrins[a]

Catalyst	Reaction time[b]	Substrate	Product (turnover)[c]
1. $Ru(TMP)(OH)_2$	35 min	Norbornene	*Exo*-norbornene oxide (20)
2. $Ru(TMP)O_2$	2.5 h	Norbornene	*Exo*-norbornene oxide (22)
3. $Ru(2,6\text{-}Cl_2\text{-}TPP)O_2$	6 h	Norbornene	*Exo*-norbornene oxide (19)

[a] Reaction conditions: ruthenium porphyrin (3 mg) and norbornene (300 mg) were stirred in benzene (5 cm^3) at room temperature.

[b] Time required for completion of reaction (monitored by GLC).

[c] Turnover based on ruthenium porphyrins used.

In an attempt to develop a long-lived and robust aerobic oxidation catalyst we have also investigated the aerobic oxidation of alkenes catalysed by $Ru(2,6\text{-}Cl_2TPP)O_2$ [2,6-Cl_2TPP = tetrakis(2,6-dichlorophenyl)porphyrin dianion] (entry 3, Table 1). Although the overall turnover of *ca* 19 is similar to that found for the TMP analogues, the rate of aerobic epoxidation by $Ru(2,6\text{-}Cl_2TPP)O_2$ is rather slow. It seems likely that the ruthenium(II) complex of 2,6-Cl_2TPP is so electron-deficient that it is reluctant to undergo aerobic oxidation to dioxo-ruthenium(VI). Therefore, two stereoelectronic factors seem to be critical to aerobic epoxidation catalysed by ruthenium porphyrins. First, the porphyrin must be sterically encumbered so as to prevent bimolecular reactions such as μ-oxo formation. Previously, we have shown that the oxo-ruthenium(IV) compounds of non-sterically demanding OEP are incapable of aerobic oxidation due to rapid dimerization of oxo-ruthenium(IV). Second, the porphyrin must be electron-rich so that aerobic oxidation to dioxo-ruthenium(VI) is energetically favourable. The delicate balance between these two factors in the TMP system makes Ru(TMP) a unique catalyst for aerobic epoxidation.

In summary, we have successfully isolated a monomeric ruthenium(IV)-dihydroxo compound of tetramesitylporphyrin, which catalyses aerobic epoxidation of alkenes via $Ru(TMP)O_2$. The observation of direct interaction of dioxygen with ruthenium(IV) porphyrin provides evidence for a new mechanism for the Ru(TMP)-based aerobic oxidation that involves interconversion of oxo-ruthenium(IV) and dioxo-ruthenium(VI).

Acknowledgement—We acknowledge support from The University of Hong Kong, The Hong Kong University of Science and Technology, and the Hong Kong Research Grants Council.

REFERENCES

1. (a) T. J. McMurry and J. T. Groves, in *Cytochrome P-450: Structures, Mechanisms and Biochemistry* (Edited by P. R. Oritz de Montellano), p. 1. Plenum Publishing Co., New York (1986); (b) J. T. Groves and R. Quinn, *Inorg. Chem.* 1984, **23**, 3844.
2. (a) J. T. Groves and R. Quinn, *J. Am. Chem. Soc.* 1985, **107**, 5790; (b) J. T. Groves and K.-H. Ahn, *Inorg. Chem.* 1987, **26**, 3831; (c) Y. Tokita, K. Yamaguchi, Y. Watanabe and I. Morishima, *Inorg. Chem.* 1993, **32**, 329.
3. (a) W. H. Leung and C. M. Che, *J. Am. Chem. Soc.* 1989, **111**, 8812; (b) C. Ho, W. H. Leung and C. M. Che, *J. Chem. Soc., Dalton Trans.* 1991, 2933; (c) W. H. Leung, C. Ho and C. M. Che, Abstracts of Papers, 203rd National Meeting of the American Chemical Society, San Francisco, INORG 271; (d) H. Ohtake, T. Higuchi and M. Hirobe, *J. Am. Chem. Soc.* 1992, **114**, 10,660.
4. G. M. Badger, R. A. Jones and R. L. Laslett, *Aust. J. Chem.* 1964, **17**, 1028.
5. (a) D. F. Evans, *J. Chem. Soc.* 1959, 2003; (b) D. H. Lives and S. I. Chan, *Analyt. Chem.* 1970, **42**, 791.
6. (a) C. Sishta, M. Ke, B. R. James and D. Dolphin, *J. Chem. Soc., Chem. Commun.* 1986, 787; (b) M. Ke, C. Sishta, B. R. James, D. Dolphin, J. W. Sparapany and J. A. Ibers, *Inorg. Chem.* 1991, **30**, 4766 and refs therein.
7. C. M. Che, W. H. Leung and W. C. Chung, *Inorg. Chem.* 1990, **29**, 1841.
8. $Ru(TMP)(^{18}OH)_2$ was prepared by recrystallization of $Ru(TMP)(OH)_2$ from $CH_2Cl_2/EtOH/H_2{}^{18}O$ (20:20:1). Theoretical shift = 32 cm^{-1}.
9. J. D. Alben, in *The Porphyrins* (Edited by D. Dolphin), Vol. III, Ch. 7. Academic Press, New York (1978).
10. W. H. Leung, C. M. Che, W. T. Wong and T. F. Lai, unpublished results.
11. C. M. Che, W. T. Tang, W. T. Wong and T. F. Lai, *J. Am. Chem. Soc.* 1989, **111**, 9048.
12. C. M. Che and S. M. Peng, results to be published.

Polyhedron Vol. 12, No. 19, pp. 2335–2341, 1993
Printed in Great Britain

0277–5387/93 $6.00 + .00
© 1993 Pergamon Press Ltd

THE SYNTHESIS AND CRYSTAL STRUCTURE OF $[CrF(NH_3)_5]ZnCl_4$

DONALD A. HOUSE*

Chemistry Department, University of Canterbury, Christchurch, New Zealand

and

VICKIE McKEE*

Chemistry Department, Queen's University, Belfast BT9 5AG, Northern Ireland

(*Received* 6 *April* 1993; *accepted* 2 *June* 1993)

Abstract—Salts of $[CrF(NH_3)_5]X_2$ (X = NO_3, $1/2ZnCl_4$) are readily prepared from the reaction between $[Cr(NCO)(NH_3)_5](NO_3)_2$ and 40% HF. The structure of $[CrF(NH_3)_5][ZnCl_4]$ has been determined by single-crystal X-ray analysis.

We are currently interested in the trends observed for Cr—X (X = halide ion) bond lengths in chromium(III) ammine and polyamine complexes. In particular, the observed trends in Cr—Cl bond lengths in $[CrCl(RNH_2)_5]^{2+}$ (R = H, Me, Et) have been correlated with acid hydrolysis rates[1,2] and there is much current debate on the mechanism of the substitution.[3]

Although salts of $[CrF(NH_3)_5]^{2+}$ have been known for many years, the synthetic route via fluoride anation of $[Cr(NH_3)_5(OH_2)](NO_3)_3 \cdot NH_4NO_3$[4,5] is often poorly described[6] and gives variable yields.[7,8]

We describe here a simple, high yield preparation of the $[CrF(NH_3)_5]^{2+}$ cation and the single-crystal X-ray structural analysis of $[CrF(NH_3)_5]ZnCl_4$.

EXPERIMENTAL

$[Cr(NCO)(NH_3)_5](NO_3)_2$ was synthesized by the method of Schmidtke and Schönherr.[9,10] We obtained a 60% yield, with equal weights of urea and $Cr(NO_3)_3 \cdot 9H_2O$ (15 g each) in an aluminium foil covered beaker (250 cm^3) and an oven temperature of 135–140°C for 42 h. A green residue was separated from the orange crystals by washing the solid with warm (40°C) 50:50 ethanol:water (50 cm^3). Decantation of this wash solution gave the crude product, quite suitable for the next step, without further purification.

Fluoropentaamminechromium(III) *nitrate*, $[CrF(NH_3)_5](NO_3)_2$

The orange $[Cr(NCO)(NH_3)_5](NO_3)_2$ (5 g, crude) was suspended in 40% HF (20 cm^3) in a plastic beaker and the mixture was heated at 80°C (water bath) for *ca* 10 min, until all effervescence ceased and a clear, wine-red solution was obtained. **CAUTION:** Use gloves and an efficient fume hood. HF(g) can cause serious burns on contact with wet skin. Solid $NaNO_3$ (3 g) was added and ethanol (20 cm^3) added dropwise to the hot solution giving a pink precipitate. The product was collected from the ice cooled solution and recrystallized from water (25 cm^3, 80°C) by addition of $NaNO_3$ (3 g) and ethanol (25 cm^3), as above. Slow cooling to room temperature and then in ice gave 4.2 g (92%) of $[CrF(NH_3)_5](NO_3)_2$ as orange needles, which were washed with ethanol and air dried.

Fluoropentaammine chromium(III) *tetrachlorozincate*(II), $[CrF(NH_3)_5]ZnCl_4$

The nitrate salt (0.2 g) was dissolved in 0.01 M HCl (10 cm^3) at room temperature and a solution of $ZnCl_2$ (0.5 g) in HCl (5 cm^3, 1 M) was added.

* Authors to whom correspondence should be addressed.

An orange–red microcrystalline precipitate formed immediately (0.24 g, 90%) and this was collected, washed with ethanol and air dried. This solid was dissolved in water (10 cm^3) and X-ray quality, orange–red crystals formed as the solution evaporated at room temperature (3 days).

Visible absorption (Perkin–Elmer λ-2) spectral data in 0.01 M $HClO_4$: λ (nm) [ε, $M^{-1}\,cm^{-1}$]: 366 max [20.3], 420 min [9.1]; 501 max [40.2], Lit.[7] (as perchlorate salt in 0.1 M $HClO_4$): 366 max [20.4], 503 max [41.7]. Lit.[8] (as nitrate monohydrate salt in water): 370 max [21.9], 500 max [42.6].

Table 1. Structure determination summary for $[CrF(NH_3)_5]ZnCl_4$

Crystal data	
Empirical formula	$H_{15}Cl_4CrFN_5Zn$
Colour; habit	Orange irregular block
Crystal size (mm)	$0.54 \times 0.58 \times 0.26$
Crystal system	Orthorhombic
Space group	$Cmc2_1$
Unit cell dimensions	
a (Å)	7.849(2)
b (Å)	17.071(5)
c (Å)	9.061(2)
Volume	1214.0(5)
Z	4
Formula weight	363.3
Density (calc.) ($Mg\,m^{-3}$)	1.999
Absorption coefficient (mm^{-1})	3.790
$F(000)$	724
Data collection	
Diffractometer used	Nicolet R3m
Radiation	Mo-K_α ($\lambda = 0.71073$ Å)
Temperature (K)	193
Monochromator	Hightly oriented graphite crystal
2θ range (°)	4.0–52.0
Scan type	ω
Scan speed (° min^{-1})	Constant; 4.88 in ω
Background measurement	Stationary crystal and stationary counter at beginning and end of scan, each for 20.0% of total scan time
Standard reflections	3 measured every 97 reflections
Index ranges	$0 \leqslant h \leqslant 9,\ -20 \leqslant k \leqslant 3,\ 0 \leqslant l \leqslant 11$
Reflections collected	1331
Independent reflections	687 ($R_{int} = 1.39\%$)
Observed reflections	668 ($F > 6.0\sigma(F)$)
Absorption correction	Empirical ($T_{max} = 0.95$ $T_{min} = 0.57$)
Solution and refinement	
System used	Siemens SHELXTL PLUS (PC Version)
Solution	Direct methods
Refinement method	Full-matrix least-squares
Quantity minimized	$\Sigma w(F_o - F_c)^2$
Hydrogen atoms	Riding model, fixed isotropic U
Weighting scheme	$w^{-1} = \sigma_2(F) + 0.0010F^2$
Numbers of parameters refined	63
Final R indices (obs. data)	$R = 2.71\%$, $wR = 3.78\%$
R indices (all data)	$R = 2.79\%$, $wR = 3.82\%$
Goodness-of-fit	1.13
Largest and mean Δ/σ	0.000, 0.000
Data-to-parameter ratio	10.6:1
Largest difference peak (e $Å^{-3}$)	0.40
Largest difference hole (e $Å^{-3}$)	−0.75

Fluoropentaamminecobalt(III) *tetrachlorozincate*(II), $[CoF(NH_3)_5]ZnCl_4$

Fluoropentaamminecobalt(III) nitrate (1 g)[11] was dissolved in warm (60°C) 0.01 M HCl (50 cm^3 and saturated $ZnCl_2$ solution (3 cm^3) was added. Sparkling, rose-red, crystalline platelets deposited from the warm solution and these were collected after 14 h at room temperature.

Visible absorption spectral data in 0.01 M $HClO_4$: λ (nm), [ε, (M^{-1} cm^{-1})]: 352 max [38.9], 402 min [7.7], 512 max [45.6].

The X-ray powder diffraction patterns (Phillips PW1729) of $[CoF(NH_3)_5]ZnCl_4$ and $[CrF(NH_3)_5]ZnCl_4$ show that these compounds are isomorphous. Positions ($2\theta°$) for several of the major peaks are, Co(Cr, Cr_{calc}): 10.35 (10.43, *10.36*), 15.95 (15.90, *15.81*), 20.88 (20.81, *20.81*), 21.79 (21.68, *21.64*), 27.02 (26.87, *26.87*), 29.07 (28.79, *28.74*), 31.56 (31.35, *31.94*), 44.44 (44.68, *44.10*). Numbers in italics are those predicted[11a] from the crystallographic parameters obtained for $[CrF(NH_3)_5]ZnCl_4$.

X-ray structure determination (Table 1)

X-ray diffraction data for an orange–red crystal of $[CrF(NH_3)_5]ZnCl_4$ were collected under the conditions described in Table 1. The space group was determined by systematic absences and confirmed by the structure analysis. The non-unique data were averaged and the resulting data were corrected for Lorentz polarization, anomalous dispersion, check reflection fluctuations and adsorption effects (Table 1).

The structure was solved by direct methods. In the final cycles of refinement, and in the structure factor calculations (supplementary tables), hydrogen atoms were included in idealized calculated positions (supplementary tables). Bond lengths and angles are listed in Table 2. Tables of supplementary data have been deposited with the Editor and are available from the authors on request. Coordinates have also been deposited with the Cambridge Crystallographic Data Centre.

RESULTS AND DISCUSSION

$[Cr(NCO)(NH_3)_5](NO_3)_2$ is easily prepared by thermal decomposition of urea in the presence of $Cr(NO_3)_3 \cdot 9H_2O$.[9,10] This has proved to be a most useful precursor for several $[CrX(NH_3)_5]^{n+}$ complexes, e.g. X = Cl or NH_3[12] and we have now extended the series to include X = F. In this regard, it should be noted that the decomposition of $[Cr(NCO)(NH_3)_5](NO_3)_2$ in > 6 M HCl gives $[CrCl(NH_3)_5]Cl_2$ and not $[CrCl(NH_3)_4(OH_2)]Cl_2$ as previously reported.[12]

The nature of the product resulting from the hydrolysis of the coordinated cyanate is markedly acid dependent as dilute acids give mainly $[Cr(NH_3)_6]^{3+}$,[9,12] while higher acid concentrations result in complete cyanate loss and anion anation, possibly via $[Cr(NH_3)_5(OH_2)]^{3+}$. We cannot, however, completely eliminate some sort of associative or strong ion-pair pathway in the presence of such high anion concentrations. This is not the first time that acid dependent products have been observed in chromium(III) ammine chemistry, as $[Cr(ox)(NH_3)_4]^+$ forms $[Cr(ox)(NH_3)_3(OH_2)]^+$ in

Table 2. Bond lengths (Å) and angles (°) for $[CrF(NH_3)_5]ZnCl_4$[a]

Cr—F	1.863(4)	Cr—N(1)	2.060(4)
Cr—N(2)	2.099(6)	Cr—N(3)	2.093(4)
Cr—N(1′)	2.060(4)	Cr—N(3′)	2.093(4)
Zn—Cl(1)	2.306(2)	Zn—Cl(2)	2.267(2)
Zn—Cl(3)	2.266(2)	Zn—Cl(3′)	2.266(2)
F—Cr—N(1)	89.7(1)	F—Cr—N(2)	180.0(2)
N(1)—Cr—N(2)	90.3(2)	F—Cr—N(3)	88.6(1)
N(1)—Cr—N(3)	177.8(1)	N(2)—Cr—N(3)	91.3(2)
F—Cr—N(1′)	89.7(1)	N(1)—Cr—N(1′)	88.8(2)
N(2)—Cr—N(1′)	90.3(2)	N(3)—Cr—N(1′)	89.8(1)
F—Cr—N(3′)	88.6(1)	N(1)—Cr—N(3′)	89.8(1)
N(2)—Cr—N(3′)	91.3(2)	N(3)—Cr—N(3′)	91.5(2)
N(1′)—Cr—N(3′)	177.8(1)	Cl(1)—Zn—Cl(2)	110.2(1)
Cl(1)—Zn—Cl(3)	104.5(1)	Cl(2)—Zn—Cl(3)	111.3(1)
Cl(1)—Zn—Cl(3′)	104.5(1)	Cl(2)—Zn—Cl(3′)	111.3(1)
Cl(3)—Zn—Cl(3′)	114.6(1)		

[a] The atom numbering system adopted is shown in Fig. 1.

Table 3. Cr—F distances (Å) in Cr^{III}—F amine complexes

Complex	Cr—F (Å)	Ref.
Trans-$[CrF_2(en)_2]Cl$	1.904	36
Trans-$[CrF(tn)_2(OH_2)][CrF(OH)(tn)_2](ClO_4)_3$	1.900(8)	37, 38
$[enH_2][CrF_4(en)]Cl$	1.90(2)	39
Trans-$[CrF_2(NH_3)_4]I \cdot H_2O$	1.894(3)	40
Trans-$[CrF_2(en)_2]ClO_4$	1.887(6)	41
Cis-$[CrF_2(NH_3)_4]ClO_4$	1.887(6)	40
Trans-$[CrF_2(en)_2]Cl$	1.886	36
Cis-$[CrF_2(en)_2]ClO_4$	1.882(3)	42
Trans-$Li[CrF_2(1,3\text{-pdda})] \cdot 2H_2O$	1.878(2)	43
Trans-$[CrF_2(tn)_2]ClO_4$	1.876(3)	44
Trans-$[CrF(NH_3)(tn)_2](ClO_4)_2$	1.872(3)	48
Cis-$[CrF_2(en)_2]ClO_4 \cdot NaClO_4 \cdot H_2O$	1.868(4)	46
$[CrF(NH_3)_5]ZnCl_4$	1.863(4)	This work
Trans-$[CrF(NH_3)(en)_2](ClO_4)_2$	1.862(3)	45
Trans-$[CrF_2(py)_2]PF_6$	1.853(2)	47
Trans,trans-$[Cr(en)_2(OH_2)_2][CrF(OH)(en)_2]_2(ClO_4)_5 \cdot 2H_2O$	1.854(4)	31, 38
Trans,trans-$[CrF(tn)_2(OH_2)][CrF(OH)(tn)_2](ClO_4)_3$	1.829(8)	37, 38

dilute acid and $[CrX(NH_3)_4(OH_2)]X_2$ (X = Cl, Br) in > 6 M HX.[8,13,14]

Although the Cr—F bond distance[15] has been measured in a number of fluorochromium(III) amine complexes (Table 3) this is the first time, to our knowledge, that a salt of fluoropentaamminechromium(III) has been structurally characterized by a single-crystal X-ray analysis.

The salt consists of octahedral $[CrF(NH_3)_5]^{2+}$ cations and tetrahedral $ZnCl_4^{2-}$ anions (Figs 1 and 2). The mean Cr—NH_3 distance, 2.081(19) Å, lies within the range observed for other $[CrX(NH_3)_5]^{n+}$ complexes, e.g. 2.074(4) Å in $[CrCl(NH_3)_5]Cl_2$

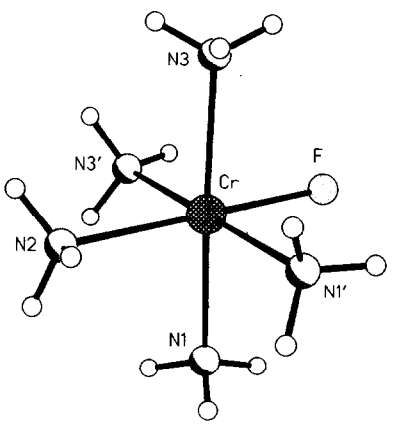

Fig. 1. A view of the $CrF(NH_3)_5^{2+}$ cation showing the numbering scheme used in Tables 2 and 3.

Table 4. M—X distances (Å) in $M^{III}X(NH_2R)_5^{2+}$ complexes (X = halide ion)

Complex	M—X	Ref.
$[CrF(NH_3)_5]ZnCl_4$	1.863(4)	This work
$[CrCl(NH_3)_5]Cl_2$	2.327(1)	49
$[CrCl(NH_2Me)_5]Cl_2$	2.299(1)	50
$[CrCl(NH_2Et)_5]Cl_2$	2.290(1)	51
$[CoCl(NH_3)_5]Cl_2$	2.286(2)	49
$[CoCl(NH_3)_5]SiF_6$	2.306	52
$[CoCl(NH_2Me)_5](NO_3)_2$	2.283(1)	50
$[RhCl(NH_3)_5]Cl_2$	2.356(1)	49
$[RhCl(NH_2Me)_5]Cl_2$	2.339(1)	51
$[RhCl(NH_2Et)_5]Cl_2$	2.343(2)	51
$[InCl(NH_3)_5]Cl_2$	2.371(2)	49
$[RuCl(NH_3)_5]Cl_2$	2.346(1)	49
$[OsCl(NH_3)_5]Cl_2$	2.369(2)	49

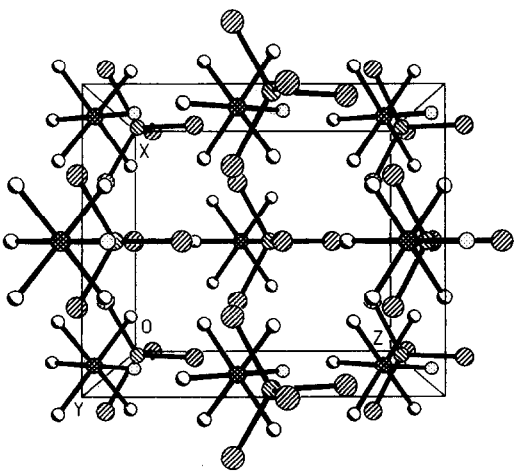

Fig. 2. A packing diagram for $[CrF(NH_3)_5]ZnCl_4$.

(Table 4) or from 2.0592(57) to 2.080(4) Å in various salts of $[Cr(NH_3)_6]^{3+}$.[16] There may be a hint of a solid-state *trans* effect insofar as the Cr—N(2) distance (Fig. 1) is long at 2.099(6) Å, but there are other *cis*-Cr—NH_3 distances of 2.093(4) Å. The Cr—F distance of 1.863(4) Å is one of the shortest observed for a fluoro ligand *trans* to a coordinated nitrogen donor (Table 3), but is similar to that found in *trans*-$[CrF(NH_3)(en)_2]^{2+}$ [Cr—F = 1.862(4)]. Bond lengths and angles in the $ZnCl_4^{2-}$ anion (Fig. 2) are quite within the range observed for other tetrachlorozincate(II) salts with complex ion cations.[17–29]

In view of the current debate[1–3] with regard to

Table 5. Acid hydrolysis rates for some fluoroaminechromium(III) complexes

	T (°C)	k_1[a] (s^{-1})	$\Delta H^{\#}$ (kJ mol^{-1})	$\Delta S^{\#}$ (J K^{-1} mol^{-1})	Ref.
$CrF(NH_3)_5^{2+}$	25.0	2.48×10^{-7}	103	−26	53
	45.0	3.5×10^{-6}			
	55.0	1.14×10^{-5}			
	60.0	2.45×10^{-5}			
	65.0	3.78×10^{-5}			
	72.4	8.2×10^{-5}			
	80.0	1.82×10^{-4}			
	25.0	8.3×10^{-8}	114	+2	54
	54.9	6.0×10^{-6}			
	59.5	1.03×10^{-5}			
	65.5	2.67×10^{-5}			
	70.1	3.67×10^{-5}			
	25.0	1.2×10^{-7}			55
Cis-$CrF_2(en)_2^{+}$[b]	10.13	7.8×10^{-7}			56
	24.96	5.3×10^{-6}			
	25.0	5.4×10^{-6}	87	−54	
	34.93	2.1×10^{-5}			
	40.5	3.1×10^{-5}			
	49.78	7.9×10^{-5}			
	25.0	5.7×10^{-6}	91	−41	57
	42.0	5.04×10^{-5}			
	55.0	1.86×10^{-4}			
	70.0	8.19×10^{-4}			
Cis-$CrF(en)_2(OH_2)^{2+}$	25.0	2.1×10^{-6}	83.3	−74[c]	57
	40.0	1.08×10^{-5}			
	55.0	5.12×10^{-5}			
	65.0	1.30×10^{-4}			
	70.0	1.88×10^{-4}			
Trans-$CrF_2(en)_2^{+}$	Only Cr—N bond rupture				58
	50.0[d]	3.2×10^{-4}			59
Trans-$CrF(en)_2(OH_2)^{2+}$	Only Cr—N bond rupture				60, 62
Trans-$CrF_2(tn)_2^{+}$	35.0[e]	3.9×10^{-5}			59, 61
	50.0[e]	2.65×10^{-4}			
	65.0[e]	1.79×10^{-3}			
	50.0[e]	5.05×10^{-4}			59

[a] Rate law is $k_{obs} = k_1k_2[H^+]$.
[b] In *ca* 0.1 M $HClO_4$.
[c] The sign of $\Delta S^{\#}$ is correctly cited in ref. 57.
[d] k_{obs} in 2.0 M $HClO_4$, ref. 59.
[e] k_{obs} in 1.0 M $HClO_4$, ref. 59.

the relationship between $MX(N_5)^{2+}$ bond length and the mechanism of M—X solvolysis, we have attempted to correlate Cr—F bond distances with reactivity (Table 5). The analysis is complicated by the paucity of data for Cr—F solvolysis rates and the fact that Cr—F solvolysis is an acid-catalysed process.

The normal rate law is $k_{obs} = k_1 + k_2[H^+]$ and plots of k_{obs} vs $[H^+]$ are used to determine k_1 (Table 5) from the intercept. Unfortunately, these systems are difficult to work with (two detailed studies on the solvolysis of $[CrF(NH_3)_5]^{2+}$ give conflicting results at high temperatures[30,31]) as Cr—N bond rupture is competitive with Cr—F bond rupture.[32–34]

Despite the lack of comparative kinetic information, it is evident from the data in Table 5 and the literature[35] that *trans*-difluorochromium(III) systems are very inert to solvolytic fluoride loss; much more so than their *cis*-difluoro analogues. This difference in kinetic lability is not reflected in any pattern of Cr—F bond length in Table 5, as Cr—F distances in *cis* and *trans*-isomers seem to be randomly distributed throughout.

Acknowledgement—We thank the University Grants Committee for funds to purchase instruments used in this research.

REFERENCES

1. P. W. Lay, *Coord. Chem. Rev.* 1991, **110**, 213.
2. P. W. Lay, *Comm. Inorg. Chem.* 1991, **11**, 235.
3. T. W. Swaddle, *Comm. Inorg. Chem.* 1991, **12**, 237.
4. M. Mori, *Inorg. Synth.* 1957, **5**, 131.
5. G. G. Schlessinger, *Inorganic Laboratory Preparations*, p. 199. Chemical Publishing Co., N.Y. (1960).
6. S. C. Chan and K. Y. Hui, *Aust. J. Chem.* 1967, **20**, 893.
7. E. Zinato, R. Lindholm and A. W. Adamson, *J. Inorg. Nucl. Chem.* 1969, **31**, 449.
8. E. Kyuno, M. Kamada and N. Tanaka, *Bull. Chem. Soc. Japan* 1967, **40**, 1848.
9. H. H. Schmidtke and T. Schönherr, *Z. Anorg. Allg. Chem.* 1978, **443**, 225.
10. T. Schönherr, *Inorg. Chem.* 1986, **25**, 171.
11. Ref. 5, p. 216; (a) G. M. Sheldrick, SHELXTL-PLUS (PC version). Siemens Analytical X-ray Instruments Inc., Madison, WI 53719 (1989).
12. D. Yang and D. A. House, *Polyhedron* 1983, **2**, 1267.
13. C. S. Garner and D. A. House, *Trans. Met. Chem.* (N.Y.) 1970, **6**, 59.
14. D. A. House, *Acta Chem. Scand.* 1972, **26**, 2847.
15. D. A. House, in *Mechanisms of Inorganic and Organometallic Reactions* (Edited by M. V. Twigg), Vol. 5, p. 140. Plenum Press, New York (1988).
16. D. A. House, in *Comprehensive Coordination Chemistry* (Edited by G. Wilkinson), Vol. 2, p. 23. Pergamon Press, Oxford (1987).
17. W. Clegg, *Acta. Cryst. B* 1976, **32**, 2907.
18. P. R. Ireland, D. A. House and W. T. Robinson, *Inorg. Chim. Acta* 1970, **4**, 137.
19. A. R. Gainsford, D. A. House and W. T. Robinson, *Inorg. Chim. Acta* 1971, **5**, 595.
20. B. F. Anderson, J. D. Bell, A. R. Gainsford and D. A. House, *Inorg. Chim. Acta* 1978, **30**, 59.
21. D. A. House, G. Hall, A. J. Matheson, W. T. Robinson, Foo Chuk Ha and C. B. Knobler, *Inorg. Chim. Acta* 1980, **39**, 257.
22. G. Bombieri, F. Benetollo, A. Del Pra, M. L. Tobe and D. A. House, *Inorg. Chim. Acta* 1981, **50**, 89.
23. A. R. Gainsford, G. J. Gainsford and D. A. House, *Cryst. Struct. Commun.* 1981, **10**, 365.
24. G. J. Gainsford, D. A. House, P. Comba and W. Marty, *Cryst. Struct. Commun.* 1982, **11**, 215.
25. V. McKee, M. Harnett and D. A. House, *Inorg. Chim. Acta* 1985, **102**, 83.
26. M. Harnett, D. A. House and W. T. Robinson, *Inorg. Chim. Acta* 1985, **102**, 87.
27. A. Reisen, M. Zehnder and D. A. House, *Inorg. Chim. Acta* 1986, **113**, 163.
28. D. A. House and W. T. Robinson, *Inorg. Chim. Acta* 1988, **141**, 211.
29. V. Ugalde-Saldivar, M. A. Luna-Canut, M. E. Sosa-Torres, M. J. Rosales-Hoz, R. A. Toscano and M. L. Tobe, *J. Chem. Soc., Dalton Trans.* 1990, 3629.
30. S. C. Chan and K. Y. Hui, *Aust. J. Chem.* 1967, **20**, 893.
31. T. P. Jones and J. K. Phillips, *J. Chem. Soc. (A)* 1968, 674.
32. B. Herbert, P. Reinhard, M. J. Saliby and P. S. Sheridan, *Inorg. Chem.* 1987, **26**, 4024.
33. S. Pyke and R. G. Linck, *Inorg. Chem.* 1971, **10**, 244.
34. R. G. Linck, *Inorg. Chem.* 1977, **16**, 3143.
35. L. G. Vanquickenborne, B. Coussens, D. Postelmans, A. Ceulemans and K. Pierloot, *Inorg. Chem.* 1991, **30**, 2978; 1992, **31**, 539.
36. J. V. Brencic and I. Leban, *Vestn., Stov. Kem. Durs.* 1985, **32**, 209; *Chem. Abstr.* 1985, **104**, 13,305.
37. X. Solans, M. Font-Altaba, J. L. Brianso, A. Solans, J. Casabo and J. Ribas, *Cryst. Struct. Commun.* 1982, **11**, 1199.
38. R. F. Marsh and F. H. Herstein, *Acta Cryst.* 1988, **44B**, 77.
39. C. Diaz, A. Segui, J. Ribas, X. Solans and M. Font-Altaba, *Trans. Met. Chem.* 1984, **9**, 464.
40. J. V. Brencic, B. Ceh and I. Leban, *Monatsh. Chem.* 1981, **112**, 1359.
41. J. V. Brencic and I. Leban, *Z. Anorg. Allg. Chem.* 1981, **480**, 213.
42. J. V. Brencic, I. Leban and I. Polanc, *Acta Cryst.* 1987, **43C**, 885.
43. R. J. Bianchini, U. Geiser, H. Place, S. Kaizaki, Y. Morita and J. I. Legg, *Inorg. Chem.* 1986, **25**, 2129.
44. J. W. Vaughn and R. D. Rogers, *J. Cryst. Spect. Res.* 1985, **15**, 281.
45. K. A. Beveridge, G. W. Bushnell and A. D. Kirk, *Acta Cryst.* 1985, **41C**, 899.

46. J. V. Brencic, I. Leban and O. Polanc *Z. Anorg. Allg. Chem.* 1987, **551**, 109.
47. G. Fochi, J. Strähle and F. Ging, *Inorg. Chem.* 1991, **30**, 4669.
48. J. W. Vaughn, *Inorg. Chem.* 1981, **20**, 2397.
49. T. W. Hambley and P. A. Lay, *Inorg. Chem.* 1986, **25**, 4553.
50. B. M. Foxman, *Inorg. Chem.* 1978, **17**, 1932.
51. A. M. T. Bygott, T. W. Hambley, P. A. Lay and K. W. Nugent, *Inorg. Chem.*, submitted.
52. J. A. Stanko and I. C. Paul, *Inorg. Chem.* 1967, **6**, 486.
53. T. P. Jones and J. K. Phillips, *J. Chem. Soc. A.* 1968, 674.
54. S. C. Chan and K. Y. Hui, *Aust. J. Chem.* 1967, **20**, 893.
55. A. E. Ogard and H. Taube, *J. Am. Chem. Soc.* 1958, **80**, 1084.
56. K. R. A. Fehrmann and C. S. Garner, *J. Am. Chem. Soc.* 1961, **83**, 1276.
57. B. Herbert, D. Reinhard, M. J. Saliby and P. S. Sheridan, *Inorg. Chem.* 1987, **26**, 4024.
58. S. Pyke and R. G. Linck, *Inorg. Chem.* 1971, **10**, 2445.
59. J. M. DeJovine, W. R. Mason and J. W. Vaughn, *Inorg. Chem.* 1974, **13**, 66.
60. R. G. Linck, *Inorg. Chem.* 1977, **16**, 3143.
61. J. J. Chung, H. T. Kim and S. O. Bek, *Chem. Abs.* 1989, **111**, 45,922.
62. S. O. Oh, S. H. Lee and J. W. Lim, *Chem. Abs.* 1986, **104**, 231,435.

Polyhedron Vol. 12, No. 19, pp. 2343–2350, 1993
Printed in Great Britain

0277–5387/93 $6.00+.00
© 1993 Pergamon Press Ltd

RUTHENIUM(II) COMPLEXES OF O,N-DONOR SCHIFF BASE LIGANDS AND THEIR USE AS CATALYTIC ORGANIC OXIDANTS

AHMED M. EL-HENDAWY* and ABDULLA H. ALKUBAISI

Chemistry Department, Faculty of Science, University of Qatar, Doha, P.O. Box 2713, Qatar

and

ABD EL-GHANY EL-KOURASHY and MAI M. SHANAB

Chemistry Department, Faculty of Science, Damietta, Egypt

(*Received* 6 *April* 1993; *accepted* 2 *June* 1993)

Abstract—A number of new ruthenium(II) complexes, $[Ru(PPh_3)_2L_2]$ (L = monoanions of Schiff bases formed from 2,3-dihydroxybenzaldehyde, 3,5-dibromosalicylaldehyde and salicylaldehyde with aniline or its *p*-substituents), have been prepared. They were characterized by spectroscopic techniques and investigated by cyclic voltammetry. The effective catalytic oxidation of alcohols by these complexes in the presence of N-methylmorpholine-N-oxide or molecular oxygen gas as co-oxidants is reported.

Reaction of dichlorotris(triphenylphosphine) ruthenium(II) with the sodium salts of various Schiff bases, L, derived from aliphatic dianions and β-diketones or aromatic aldehydes gives the octahedral species *trans*-$[Ru^{II}(PPh_3)_nL_m]$ (n = 2, m = 1, 2).[1] It has been briefly noted[2] that the bidentate salicylaldimine Schiff bases *o*-$HOC_6H_4CH{=}NR$ [R = Ph, Bz, *o*- or *p*-$Y \cdot C_6H_4$ (Y = Me, Cl, Br or NO_2)] react with $[RuCl_2(PPh_3)_3]$ under anaerobic conditions and in the presence of triethylamine to give the complexes $[Ru^{II}(PPh_3)_2(OC_6H_4CH{=}NR)_2]$. Recently,[3] the complexes $[Ru^{III}X_2(AsPh_3)_2(HL)]$ (X = Cl, Br; H_2L = Schiff base ligand formed from 2,3-dihydroxybenzaldehyde and aniline or its *o*- and *p*-substituted derivatives, H_2R-Phb) have been prepared and characterized and their use as catalytic oxidants of both alcohols and 3,5-di(tert-butyl)catechol has also been studied.

In continuation of work on catechol Schiff base ligands, H_2L (H_2R-Phb),[3] we now report the preparation of the complexes $[Ru^{II}(PPh_3)_2(HL)_2]$ and also of other Schiff bases derived from 3,5-dibromosalicylaldehyde (HR-BPhSal) or salicylaldehyde (HR-PhSal; R = H, *p*-Me, *p*-MeO, *p*-Cl, *p*-Br or *p*-NO_2). We also report their spectroscopic and electrochemical behaviour and study the catalytic oxidation of alcohols by such complexes in the presence of N-methylmorpholine-N-oxide (NMO) or dioxygen as co-oxidants, since $[RuCl_2(PPh_3)_3]$[4] and $[Ru^{II}Cl_2(PPh_3)_2L]$[5] (L = O,N-neutral donor ligand) have been previously used in this way.

RESULTS AND DISCUSSION

Schiff base ligands are prepared by condensation of aniline (or *p*-substituted aniline) with the corresponding aldehyde in ethanol. Salicylaldimine Schiff bases, HR-PhSal (R = H, *p*-Me, *p*-MeO, *p*-Cl, *p*-Br and *p*-NO_2) were reacted under nitrogen gas with $[RuCl_2(PPh_3)_3]$ in refluxing degassed benzene and in the presence of Et_3N with a 1 : 3 metal : ligand molar ratio. Brown or red solutions were formed during 1–2 h. Evaporation of the solution to low bulk under nitrogen, followed by the addition of degassed methanol gave red–brown

* Author to whom correspondence should be addressed.

microcrystals of the corresponding complexes, which were then thoroughly washed with methanol to remove Et_3NHCl salt. The complexes of the salicylaldimine Schiff bases derived from *p*-methoxyaniline and *p*-nitroaniline were formed during reaction in refluxing benzene as brown or green compounds, respectively. Analytical data (Table 1) indicate that the formulae of these complexes are identical with previously mentioned[2] species, $[Ru(PPh_3)_2(R\text{-}PhSal)_2]$. The complexes of Schiff bases derived from 3,5-dibromosalicylaldehyde (HR-BPhSal) or 2,3-dihydroxybenzaldehyde (H_2R-Phb) were similarly prepared and the analyses are also consistent with the formulae $[Ru(PPh_3)_2(R\text{-}BPhSal)_2]$ and $[Ru(PPh_3)_2(HR\text{-}Phb)_2]$. The tropolonato complex $[Ru^{II}(PPh_3)_2(trop)_2]$ (Htrop- = tropolone, 2-hydroxy-2,4,6-cycloheptatrienone) prepared previously[6] from $[RuH_2(PPh_3)_4]$ is now obtained easily by the same procedure. Most of the complexes are fairly soluble in CH_2Cl_2 and their molar conductivities in this solvent are very low; the complexes are found to be diamagnetic at room temperature.

Spectroscopic properties

The IR spectra of the Schiff bases HR-PhSal and HR-BPhSal show boad bands near 3450 cm^{-1} and strong bands near 1620 cm^{-1}, attributed to ν(O—H) and ν(C=N) vibrations, respectively. The former band was found to disappear, while the latter was shifted to lower wave numbers (10–40 cm^{-1}) in the corresponding complexes. The catecholato Schiff base ligands, H_2R-Phb, show two medium bands near 3400 and 3300 cm^{-1}, due to the ν(O—H) vibrations of the free and hydrogen bonded

Table 1. Analytical and IR spectroscopic data of complexes

	Compound	Analysis Found (Calc.) (%) C	H	N	IR data, wave numbers (cm^{-1})[a] ν(O—H)	ν(C=N)	Other bands	Assignments
Ia	$[Ru(PPh_3)_2(PhSal)_2]$	73.0	4.8	2.7	—	1600 vs		
		(73.2)	(4.9)	(2.8)	3460 b	1614 vs		
Ib	$[Ru(PPh_3)_2(p\text{-}MePhSal)_2]$	72.6	5.1	2.6	—	1605 s		
		(73.5)	(5.2)	(2.7)	3450 b	1622 s		
Ic	$[Ru(PPh_3)_2(p\text{-}MeOPhSal)_2]$	71.0	4.8	2.5	—	1602 s		
		(71.3)	(5.0)	(2.6)	3320 b	1625 s		
Id	$[Ru(PPh_3)_2(p\text{-}ClPhSal)_2]$	67.3	4.4	2.5	—	1604 s		
		(68.4)	(4.4)	(2.6)	3464 b	1650 vs		
Ie	$[Ru(PPh_3)_2(p\text{-}BrPhSal)_2]$	63.1	4.0	2.3	—	1604 s		
		(63.4)	(4.1)	(2.4)	3472 b	1615 s		
If	$[Ru(PPh_3)_2(p\text{-}NO_2PhSal)_2]$	67.1	4.2	5.0	—	1603 s		
		(67.1)	(4.3)	(5.1)	3362 b	1631 s		
IIa	$[Ru(PPh_3)_2(BPhSal)_2]$	55.6	3.2	2.1	—	1587 s		
		(55.8)	(3.5)	(2.1)	3481 b	1616 vs		
IIb	$[Ru(PPh_3)_2(p\text{-}MeBPhSal)_2]$	56.0	3.6	2.1	—	1609 s		
		(56.4)	(3.7)	(2.1)	3482 b	1614 s		
IIc	$[Ru(PPh_3)_2(p\text{-}MeOBPhSal)_2]$	54.7	3.5	1.8	—	1606s		
		(55.1)	(3.6)	(2.0)	3468 b	1613 s		
IIIa	$[Ru(PPh_3)_2(HPhb)_2]$	70.4	4.5	2.5	3426 m	1618 s	1382 m, 1365 m	δ(OH)
		(70.9)	(4.8)	(2.7)	3410 m,b	1625 s	1262 m, 1242 s	ν(C—O)
					3320 b		1215 vs, 1270 s	
IIIb	$[Ru(PPh_3)_2(Hp\text{-}MePhb)_2]$	71.2	4.8	2.3	3400 sh	1615 s	1369 sh. 1370 m	δ(OH)
		(71.3)	(5.0)	(2.6)	3498 m	1622 s	1217 s, 1239 s	ν(C—O)
					3386 m		1268 s	
IIIc	$[Ru(PPh_3)_2(Hp\text{-}BrPhb)_2]$	61.3	4.0	2.2	3416 m	1618 s	1380 m, 1367 m	δ(OH)
		(61.7)	(4.0)	(2.3)	3456 s,b	1620 s	1222 s, 1242 s	ν(C—O)
							1280 s	
IIId	$[Ru(PPh_3)_2(Hp\text{-}ClPhb)_2]$	66.2	4.2	2.4	3402 m	1616 s	1377 sh, 1367 m	δ(OH)
		(66.5)	(4.3)	(2.5)	3456 s,b	1619 s	1218 s, 1237 s	ν(C—O)
							1280 s	

[a] Underlined data refer to the corresponding free Schiff base ligands.

hydroxyl groups,[3] respectively. The lower wave number ν(O—H) vibration disappears in the present complexes as do those found for $[Ru^{III}X_2(AsPh_3)_2(HR\text{-}Phb)]$ (X = Cl, Br).[3] The ν(C=N) vibration is also shifted to lower wave numbers, which is contrary to the case for higher oxidation state metal complexes, $[RuX_2(AsPh_3)_2(HR\text{-}Phb)]$ and $[M^{VI}O_2(HR\text{-}Phb)_2]$ (M = Mo, U).[3] This is due to d_π–p_π back-bonding between ruthenum-d_π and azomethine-p_{π^*} orbitals, since ruthenium(II) is well known to be a strong π-donor.[7] The band observed near 1365 cm^{-1} in the free ligand (H_2R-Phb) assigned to δ(OH)[3] does appear in the corresponding ruthenium(II) complexes, while its disappearance was noted in catecholato[8–10] and naphthalene-2,3-diolato[11] complexes. Distinct bands are also observed in the complexes $[Ru(PPh_3)_2(HR\text{-}Phb)_2]$ and lie in the range 1220–1265 cm^{-1}, consistent with the phenolic ν(C—O) vibration.[12,13] This confirms the participation of the azomethine nitrogen and C(2) hydroxyl oxygen atoms in coordination. Also all of the complexes show bands due to coordinated triphenylphosphine and there are no bands attributed to ν(Ru—Cl) modes around 300 cm^{-1}. The most important IR bands are listed in Table 1; the deep colour of the complexes makes them unsuitable for Raman studies.

The UV–vis spectra of the ruthenium(II) complexes were obtained in CH_2Cl_2 (Table 1) in the concentration range 10^{-3}–10^{-5} M at ambient temperature. A broad band near 700 nm of low molar absorptivity (ε = 300 M^{-1} cm^{-1}) is observed in some complexes within the concentrations used. This band is probably assigned to *d–d* transitions of ruthenium(II), as expected, since a low intensity band near 600 nm characteristic of ruthenum(III) was reported in similar complexes.[14–18] For the green ruthenium complexes derived from the catecholato Schiff base ligands, $[Ru(PPh_3)_2(HR\text{-}Phb)_2]$, an intense band around 700 nm is found, due to ligand(π)–metal(*d*) charge-transfer while the weaker ligand field may be obscured by such transitions.[14–16,19] The peak near 370 nm is likely to be due to metal (*d*)–ligand(π^*) charge transfer.[3,20–24] The bands or shoulders below 300 nm are of the interligand π–π^* type.[3,19,23,24]

The ^{1}H NMR for $[Ru(PPh_3)_2(p\text{-}ClPhSal)_2]$ in $CDCl_3$ showed a multiplet at δ 6.75–7.25 ppm, attributed both to protons of triphenylphosphine and two protons of the coordinated Schiff base ligand; the remaining protons of the latter, including those of the azomethine group, appear as a broad doublet at δ 7.45–7.75 ppm. The proton resonances of the same ligand (*p*-ClPhSal) have been found in the same shift range as for $[Ru^{II}Cl(\eta^6\text{-}p\text{-cymene})(p\text{-}ClPhSal)]$.[25] The ^{31}P NMR spectra[26] of the complexes $[Ru^{II}(PPh_3)_2(R\text{-}PhSal)_2]$ prepared similarly by our method showed a singlet resonance at δ 31–32 ppm, indicating a *trans*-phosphine geometry. A recent study on the X-ray crystal structure of the complex $[Ru^{II}(PPh_3)_2(o\text{-}Cl_4SQ)_2]$ [o-Cl_4SQ = tetrachloro-*o*-benzosemiquinonate(−1)] revealed a *trans*-geometry of the phosphine ligands.[7] On the basis of spectroscopic data and by analogy with related complexes[1,2,26] we tentatively assign the structure shown below for these ruthenium(II) complexes.

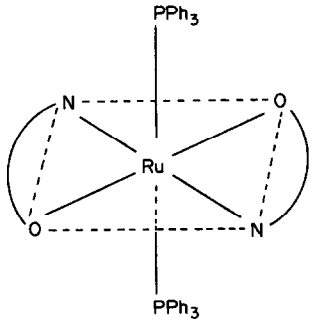

O – N = Schiff base anion (−1)

Redox properties

The electrochemistry of the complex was investigated by cyclic voltammetry. Voltammetric data vs the silver electrode for 0.1 M $(Bu^n_4N)PF_6$–CH_2Cl_2 solution (containing *ca* 10^{-3} M of the complex) are presented in Table 2. The voltammograms of the complexes $[Ru(PPh_3)_2(R\text{-}PhSal)_2]$ do not show any reduction wave (or peak) at negative potentials, but do show two oxidation waves and the current height of the second wave is twice that of the first wave which is reversible (ΔE = 60–80 mV), close to that anticipated for a Nernstian one-electron process [ΔE = 59 mV).[27] The second wave was quasi-reversible (ΔE = 140–160 mV) and is comparable to that observed for $[Ru^{III}Br_2(AsPh_3)_2(8\text{-}hq)]$ (H8-hq = 8-hydroxyquinoline).[5] These two oxidation waves probably correspond to Ru^{II}/Ru^{III} and Ru^{III}/Ru^{IV} oxidation, respectively. The complexes $[Ru(PPh_3)_2(R\text{-}BPhSal)_2]$ show similar voltammograms, but the two oxidation waves have similar current height, presumably due to Ru^{II}/Ru^{III} and Ru^{III}/Ru^{IV} oxidations, respectively. An irreversible oxidation peak at a positive potential due to Ru^{II}/Ru^{III} oxidation was found for $[Ru^{II}(PPh_3)_2(HR\text{-}Phb)_2]$, similar to those observed for $[Ru^{II}Cl_2(HA)]$ (HA = arylazo-oxime),[28] $[Ru^{II}Cl_2(PPh_3)_2L]$ (L = phenylacetic hydrazide)[5] and $[Ru^{II}H(terpy)(PPh_3)_2](Sal)$ [terpy = 2,2′,2″-terpyridine; Sal = salicylate anion(−1)].[29]

Table 2. UV–vis spectroscopic and cyclic voltammetric data of ruthenium(II) complexes

Compound	UV–vis data λ_{max} (ε, M^{-1} cm^{-1})	Voltammetric data (V) oxidations E_{pc}	E_{pa}	ΔE	Scan rate ($mV\ s^{-1}$)
Ia	710(195), 486(2380), 382sh(6550) 346(10,130), 260sh(37,465), 225(73,670)	0.02 1.12	0.10 1.26	0.080 0.140	20, 50
Ib	470(3050), 382(8560), 342(9800) 268sh(36,200), 224(77,400)	0.03 1.12	0.11 1.26	0.080 0.140	20, 50, 100
Ic	554(2370), 435sh(4820), 375(8800) 252(37,700), 223(61,100)	0.34	0.40	0.060	20, 50
Id	720(190), 484(3025), 392(7990) 310(10,950), 262(45,450), 226(89,550)	0.04 1.10	0.10 1.26	0.060 0.160	20, 50
Ie	710(280), 488(27,800, 393(7420) 346(12,980), 268sh(39,600), 226(73,800)	0.16 1.20	0.21 1.34	0.050 0.140	20, 50
If	554(4770), 431sh(6820), 364(32,900) 275sh(45,700), 225(103,000)	0.22 —	0.30 1.44	0.080	20, 50
IIa	735(365), 488(2850), 352(15,670) 395(10,700), 270(10,200), 225(225,200)	0.16 1.24	0.24 1.34	0.080 0.100	20, 50, 100
IIb	490(2750), 398(9070), 350(15,840) 270(18,800), 226(92,200)	0.12 1.22	0.20 1.30	0.080 0.080	20, 50
IIc	700(290), 488(2770), 395(8480), 355(13,970), 271(37,300), 226(94.800)	0.10 1.16	0.17 1.24	0.070 0.080	20, 50
IIIa	670(3200), 375(10,950), 319sh(9650), 297sh(17,200), 224(73,950)	—	1.34	—	50
IIIb	715(2320), 370(7460), 296(8250) 270(17,500), 286(18,300), 220(39,850)	—	1.10	—	20, 5, 100
IIIc	734(1700), 373(7650), 284(19,600) 262(26,800), 227(51,600)	—	1.08	—	20, 50, 100
IIId	732(5650), 366(10,930), 281(21,600) 267(29,500), 225(65,100)	—	1.40	—	20, 50, 100

For scan rates (SR) between 20 and 100 $mV\ s^{-1}$ the ratio $i_p/(SR)^{1/2}$ (i_p = peak current) was constant and the ratio of anodic to cathodic current (i_{p_c}/i_{p_a}) was approximately one, the peak separation being independent of the scan rate. This indicates that the electron transfer is reversible or approaches reversibility and that mass transfer is limited. However, at slow scan rates (e.g. 5 $mV\ s^{-1}$) the current function $i_{p_a}/(SR)^{1/2}$ is larger than the constant value found at faster scan rates and i_{p_c}/i_{p_a} is smaller than unity. The electrochemical behaviour of the complex $[Ru(PPh_3)_2(p\text{-MeBPhSal})_2]$ (**IIb**) was studied on adding 2-propanol (2% v/v), Table 3 and Fig. 1(a). At slow scan rate the anodic peak current is larger than that found in the absence of 2-propanol and the current ratio (i_{p_c}/i_{p_a}) reduces more with decreasing the scan rates, as in the case for $[Ru^{III}Cl_2(TMEA)_2][ClO_4]$ (TMEA = N,N,N′,N′-tetramethyl-1,2-ethanediamine).[30] These results (Table 3) are much more pronounced for the Ru^{III}/Ru^{IV} couple than that for Ru^{II}/Ru^{III} and show that 2-propanol could be catalytically oxidized by complex **IIb** at the electrode surface. For the complex $[Ru^{II}(PPh_3)_2(trop)_2]$ (**IV**), whose cyclic voltammogram[6] is similar to that of **IIb**, we found that its Ru^{III}/Ru^{IV} couple completely disappeared on adding 2-propanol, while the Ru^{II}/Ru^{III} oxidation couple is still displayed [Fig. 1(b)]. This study can be used as a test for the applicability of ruthenium complexes as useful electrochemical oxidative catalysts, since complex **IIb** was found to be an effective catalytic oxidant for alcohols (as shown below) while the tropolonato complex (**IV**) is weak and considered to be an inert catalytic oxidant over several hours in CH_2Cl_2.[6]

Catalytic oxidation

In continuing attempts to find new ruthenium(II) and ruthenium(III) complexes that act as efficient

Table 3. Voltammetric data for the oxidation of $[Ru^{II}(PPh_3)_2(p\text{-MeBPhSal})_2]$ (**IIb**) with or without the addition of 2-propanol

Scan rate ($mV\ s^{-1}$)	Ru^{II}/Ru^{III} without 2-propanol		Ru^{II}/Ru^{III} with 2-propanol (2% v/v)		Ru^{III}/Ru^{IV} without 2-propanol		Ru^{III}/Ru^{IV} with 2-propanol (2% v/v)	
	i_{pa}, μA	i_{pc}/i_{pa}	i_{pa}, μA	i_{pc}/i_{pa}	i_{pa}, μA	i_{pc}/i_{pa}	i_{pa}, μA	i_{pc}/i_{pa}
5	9.0	0.94	9.0	0.90	10.0	0.86	13.0	[a]
10	12.0	0.96	12.5	0.92	13.5	0.89	15.5	0.67
20	17.0	0.97	17.5	0.94	18.5	0.93	20.0	0.82
50	27.0	0.98	29.0	0.97	28.0	0.95	29.0	0.85

[a] No cathodic peak.

catalysts in the presence of N-methylmorpholine-N-oxide (NMO) for selective oxidation of primary alcohols to aldehydes and secondary alcohols to ketones.[3,5,14,19] we find that these ruthenium complexes are better catalytic oxidants than those of dioxo-ruthenium,[31-34] as they are easy to prepare in high yields. They are also less expensive, selective towards catalytic oxidation of alcohols and more efficient catalysts to achieve high turnovers. It has been reported that the complexes $[Ru^{II}Cl_2(PPh_3)_3]$ and $[Ru^{III}Cl_2(EPh_3)_2L]$ [E = As or P; L = O,O-donor ligand anion (−1)] in the presence of excess NMO are good catalytic oxidants for alcohols with turnovers 50–100.[4,14,19] The present Schiff base ruthenium(II) complexes have been used for such catalytic activity in the presence of NMO or O_2 gas as co-oxidants and results are summarized in Table 4. The oxidations were performed at room temperature in CH_2Cl_2, from which water was removed using powdered molecular sieves. Acetonitrile was also used instead of CH_2Cl_2 for the oxidation of *p*-methoxybenzyl alcohol and a similar yield was obtained. There was no detectable oxidation of alcohol in the absence of any ruthenium complex. All complexes (using NMO as a co-oxidant) oxidize primary alcohols to the corresponding aldehydes and secondary alcohols to ketones with high yield and turnovers (up to 160). Also, the catalysts in the presence of NMO are effective towards oxidation of unsaturated alcohol, e.g. cinnamyl alcohol without competing double bond attack. It is clear from the oxidation of *p*-methoxybenzyl alcohol (Table 4) that the coordinated Schiff base derived from salicylaldehyde (R-PhSal) which contains an electron attracting group (R = *p*-Cl) increases the rate of oxidation, contrary to those obtained with the electron repelling group (R = *p*-Me), although the $E_{1/2}$ values of the oxidation waves for their corresponding ruthenium(II) are close. This observation is similar to that found for the $[Ru^{II}Cl_2(PPh_3)_2L]$/NMO system (L = O,N-neutral donor ligand).[5] These ruthenium(II) complexes in the presence of oxygen gas as co-oxidant also effect such oxidations of primary alcohol to aldehyde

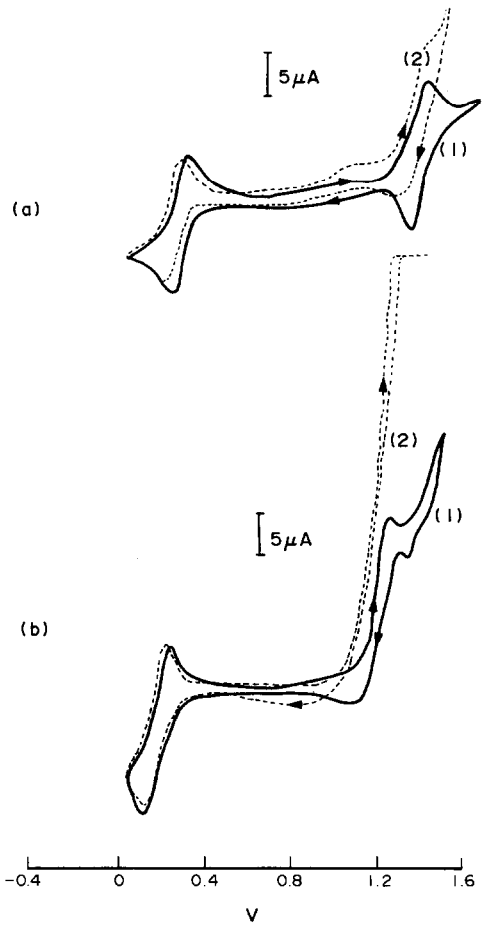

Fig. 1. Cyclic voltammogram in CH_2Cl_2 with 0.1 M $(Bu^n_4N)PF_6$ as the supporting electrolyte; V vs Ag electrode; scan rate 5 mV s^{-1} in the absence of 2-propanol (1) —— and in presence of 2-propanol (2% v/v) (2) ···· for: (a) $[Ru(PPh_3)_2(p\text{-MeBPhSal})_2]$ (10^{-3} M) and (b) $[Ru(PPh_3)_2(trop)_2]$ (10^{-3} M).

Table 4. Catalytic oxidation of alcohols by ruthenium(II) complexes/NMO

Complex	Alcohol	Product[a]	Time (h)	Yield (%)	Turnover[b]
Id	*p*-Methoxybenzyl	A	3	85	130
		A	24	85	15
Ia		A	3	80	100
Ib		A	3	70	100
IIb		A	3	75	75
IIId		A	3	75	120
		A	24	85	25
Id	Benzyl	A	3	40	50
Id	Piperonyl	A	3	90	160
		A	24	90	15
IIb		A	3	90	100
IIId		A	3	85	100
		A	24	90	25
Id	Cinnamyl	A	3	85	80
IIId		A	3	70	80
Id	α-Tetralol	K	3	75	80
IIb		K	3	80	55
IIId		K	3	65	80
		K	72	40	05
Id	Benzohydrol	K	3	80	80
IIb		K	3	55	50
IIId		K	3	60	70

Underlined data refer to catalytic oxidation by the complexes/O_2.
[a] A = corresponding aldehyde, K = corresponding ketone.
[b] Turnover = moles of product/moles of catalyst.

while secondary alcohols, α-tetralol, are hardly oxidized. The complex derived from the catechol Schiff base ligand **IIId** is a better catalyst towards such oxidation. Turnovers of 25 were obtained with the complex **IIId** when oxygen gas was bubbled through solutions of the primary alcohol overnight, similar to those found by *trans*-dioxo-ruthenium(VI) complexes $[RuO_2Cl_3(4\text{-}t\text{-But-py})]^-$ and $[Ru_2O_6py_4]$.[31] Reaction of ruthenium(III) Schiff base complexes with O_2[35–37] or PhIO (iodosobenzene)[37] was suggested to form ruthenium(IV) superoxo complexes[35,36] or oxo-ruthenium(V) complexes.[37] The formation of oxo-ruthenium(V) species was also reported for $RuCl_3$/NMO[38,39] or PhIO[40] systems and the mechanism was mentioned for the oxidation of alcohols, where ruthenium(III) is regenerated.[38]

It is interesting to note that the complexes $[Ru(PPh_3)_2(R\text{-}PhSal)_2]$ (**I**) are more efficient oxidants than those of **III** and **II**. The efficiency of such catalysts increases in the order **II** < **III** < **I**, which is consistent with their difference in electrochemical behaviour. Although the complexes **II** and **I** have a similar reversible wave (due to Ru^{II}/Ru^{III} oxidation), their second oxidation wave is reversible (due to Ru^{III}/Ru^{IV}) and irreversible (due to Ru^{III}/Ru^{V}), respectively. Complex **III** has only an irreversible oxidation peak, as described above. We believe that this lack of reversibility for such oxidation waves reflects the reason for the more efficient catalytic cycle of oxidation[5,6] and consequently the ease of the oxidation reaction with high turnovers. It is relevant from the cyclic voltammetric data that oxidation effected by catalysts is likely to occur via ruthenium high oxidation states (Ru^{IV} or Ru^{V}), which should be accessible through chemical oxidation with the common co-oxidants.[14,15,19,41]

EXPERIMENTAL

Preparation of complexes

Preparation of $[Ru(PPh_3)_2(R\text{-}PhSal)_2]$ (**I**). The complex $[RuCl_2(PPh_3)_3]$[42] (0.25 mmol) was dissolved in dry benzene (20 cm^3) under nitrogen and

then the Schiff base ligand, HR-PhSal (0.65 mmol) and Et_3N (0.5 cm^3) were added, respectively. The mixture was refluxed under nitrogen for 2 h forming a red–brown solution, then evaporated to low bulk under nitrogen, followed by the addition of degassed methanol (20 cm^3) after which time red microcrystals were isolated for the corresponding compounds of R = H, *p*-Me, *p*-Cl and *p*-Br. In the case of the derivatives, R = *p*-MeO and *p*-NO_2, the corresponding brown and green complexes are precipitated after 1–1.5 h during reflux of the benzene solution. The products were filtered off, washed with degassed methanol (3×25 cm^3) to remove triethylamine hydrochloride and finally dried *in vacuo* for a few days after grinding. Some compounds appeared to retain considerable amounts of benzene solvent before they became sufficiently dry (as shown by ^1H NMR spectroscopy).

Similar procedures were used to prepare red–brown microcrystals of $[Ru(PPh_3)_2(R\text{-}BPhSal)_2]$ and $[Ru(PPh_3)_2(trop)_2]$[6] and the green complexes $[Ru(PPh_3)_2(HR\text{-}Phb)_2]$.

Catalytic oxidation by complexes. The oxidation of piperonyl alcohol by $[Ru(PPh_3)_2(Hp\text{-}ClPhb)_2]$ (**IIId**) is typical. To a solution of piperonyl alcohol (1 mmol) was added NMO in CH_2Cl_2 (20 cm^3) and 10^{-2} mmol of compound **IIId**. The solution was stirred for 3 h in the presence of 4 Å molecular sieves (0.5 g). The mixture was then evaporated to dryness and extracted with ether (2×25 cm^3). The combined ethereal extracts were filtered and evaporated to give piperonal which was characterized and quantified as its 2,4-dinitrophenylhydrazone derivative.

A similar procedure was used for aerobically assisted oxidation using molecular oxygen as the co-oxidant instead of NMO. Oxygen gas was bubbled through the solution of piperonyl alcohol (1 mmol) and compound **IIId** (4×10^{-2} mmol) in CH_3CN (20 cm^3). The reaction continued for 24 h.

IR spectra were measured on a Perkin–Elmer 883 spectrometer as paraffin mulls between CsI plates and KBr discs. ^1H NMR spectra were measured on a Brucker AT-FT 100. The electronic spectra were measured on a Varian 634 UV–vis spectrophotometer. Cyclic voltammetric studies were carried out on a potentiostat/wave generator (Oxford Electrodes) using a platinum working electrode in conjunction with a Philips PM8043 *X–Y* recorder. Magnetic measurements were made on a Johnson–Matthey magnetic susceptibility balance.

Acknowledgements—We thank Dr W. P. Griffith for helpful advice and also Johnson–Matthey Ltd for the loan of ruthenium trichloride.

REFERENCES

1. J. R. Thornback and G. Wilkinson, *J. Chem. Soc., Dalton Trans.* 1978, 110.
2. V. Alteparmakian and S. D. Robinson, *Inorg. Chim. Acta* 1986, **116**, L37.
3. A. M. El-Hendawy, A. El-Kourashy and M. M. Shanab, *Polyhedron* 1992, **11**, 523.
4. K. B. Sharpless, K. Akashi and K. Oshima, *Tetrahedron Lett.* 1976, 2503.
5. A. M. El-Hendawy, *Polyhedron* 1991, **10**, 2137.
6. A. M. El-Hendawy, *Trans. Met. Chem.* 1992, 250.
7. N. Bag, G. K. Lahiri and A. Chakravorty, *J. Chem. Soc., Dalton Trans.* 1992, 113.
8. W. P. Griffith, C. A. Pumphrey and T. A. Rainey, *J. Chem. Soc., Dalton Trans.* 1986, 1125.
9. P. A. Wickland and D. G. Brown, *Inorg. Chem.* 1976, **15**, 396.
10. L. Que and R. H. Heistand, *J. Am. Chem. Soc.* 1979, **101**, 2219.
11. A. M. El-Hendawy, W. P. Griffith, C. A. O. Mahoney and D. J. Williams, *Polyhedron* 1989, **8**, 519.
12. J. E. Kovacic, *Spectrochim. Acta* 1967, **23A**, 183.
13. M. R. Mohmoud and M. T. El-Haty, *J. Inorg. Nucl. Chem.* 1980, **42**, 349.
14. A. M. El-Hendawy and M. El-Shahawi, *Polyhedron* 1989, **8**, 2813.
15. A. M. El-Hendawy, *Polyhedron* 1990, **9**, 2309.
16. O. K. Medhi and U. Agarwala, *J. Inorg. Nucl. Chem.* 1980, 1413.
17. K. Natarajan, R. K. Poddar and U. Agarwala, *J. Inorg. Nucl. Chem.* 1977, 431.
18. B. A. Moyer and T. J. Meyer, *Inorg. Chem.* 1981, **20**, 436.
19. A. M. El-Hendawy, *Polyhedron* 1990, **10**, 2511.
20. A. M. El-Hendawy, *Inorg. Chim. Acta* 1991, **179**, 223.
21. S. P. Cooper, Y. B. Koh and K. N. Raymond, *Inorg. Chem.* 1982, **104**, 5092.
22. R. B. Van Dreele and R. C. Fay, *J. Am. Chem. Soc.* 1972, **94**, 7935.
23. T. W. Hambley, C. J. Hawkins and T. A. Kabanos, *Inorg. Chem.* 1987, **26**, 3740.
24. C. J. Hawkins and T. A. Kabanos, *Inorg. Chem.* 1989, **28**, 1084.
25. S. K. Mandal and A. R. Chakravarty, *Polyhedron* 1992, **11**, 823.
26. D. S. Moore and S. D. Robinson, *Inorg. Chem.* 1979, **18**, 2307.
27. R. Nicholson and I. Shain, *Analyt. Chem.* 1964, **36**, 706.
28. A. R. Chakravarty, A. Chakravorty, F. A. Cotton, L. R. Falvello, B. K. Ghosh and M. Tomas, *Inorg. Chem.* 1983, **22**, 1892.
29. A. Pramanik, N. Bag and A. Chakravorty, *J. Chem. Soc., Dalton Trans.* 1992, 97.
30. C. M. Che, K. Y. Wong and C. K. Poon, *Inorg. Chem.* 1986, **25**, 1809.
31. A. C. Dengel, A. M. El-Hendawy, W. P. Griffith, C. O. Mahoney and D. J. Williams, *J. Chem. Soc., Dalton Trans.* 1990, 737.

32. A. C. Dengel, A. M. El-Hendawy, W. P. Griffith and J. Jolliffe, *Polyhedron* 1990, **9**, 1751.
33. A. M. El-Hendawy, W. P. Griffith, B. Piggott and D. J. Williams, *J. Chem. Soc., Dalton Trans.* 1988, 1983.
34. A. M. El-Hendawy, W. P. Griffith, M. N. Moussa and F. I. Taha, *J. Chem. Soc., Dalton Trans.* 1989, 901.
35. M. M. Taqui Khan, N. H. Khan, R. I. Kureshy and A. B. Boricha, *Inorg. Chim. Acta* 1990, **174**, 175.
36. M. M. Taqui Khan, S. A. Mirza, Z. A. Shaikh, C. Sreelatha, P. Paul, R. Shukla, D. Srinivas, A. Rao, S. H. Abdi, S. D. Bhatt and G. Ramachandraiah, *Polyhedron* 1992, **11**, 1821.
37. M. M. Taqui Khan, C. Sreelatha, S. A. Mirza, G. Ramachandraiah and S. H. Abdi, *Inorg. Chim. Acta* 1988, **154**, 103.
38. K. Vijayari, J. Rajaram and J. C. Kuriacose, *J. Molec. Catal.* 1987, **39**, 203.
39. K. Vijayari, J. Rajaram and J. C. Kuriacose, *Proc. Ind. Acad. Sci.* 1986, **97**, 125.
40. D. D. Agarwal, R. Jain, A. Chakravorty and R. Rastogi, *Polyhedron* 1992, **11**, 463.
41. W. H. Leung and C. M. Che, *Inorg. Chem.* 1989, **28**, 4619.
42. T. A. Stephenson and G. Wilkinson, *J. Inorg. Nucl. Chem.* 1966, **28**, 945.

Polyhedron Vol. 12, No. 19, pp. 2351–2354, 1993
Printed in Great Britain

0277–5387/93 $6.00+.00
© 1993 Pergamon Press Ltd

DIOXOURANIUM(VI) AND ZINC(II) COMPLEXES OF BIS(*o*-HYDROXYNAPHTHALDE)OXALOYLDIHYDRAZONE: SYNTHESIS AND SPECTRAL CHARACTERIZATION

RAM A. LAL,* LALIT M. MUKHERJEE, (Mrs) ALAKNANDA N. SIVA, ASIM PAL and SYAMAL ADHIKARI

Department of Chemistry, Tripura University, Agartala-799 004, Tripura, India

and

KRISKAN K. NARANG and (Mrs) MEENA K. SINGH

Department of Chemistry, Banaras Hindu University, Varanasi-221 005, (UP), India

(*Received* 6 *April* 1993; *accepted* 2 *June* 1993)

Abstract—The monometallic complexes $[M(napoxlhH_2)(H_2O)_2]_n \cdot 2nH_2O$ [where $M = UO_2^{2+}$ and Zn^{2+}, and $napoxlhH_4$ = bis(*o*-hydroxynaphthalde)oxaloyldihydrazone] have been synthesized and characterized on the basis of the results obtained from molar conductance data, electronic, IR and ^1H NMR spectral studies. It is proposed that the complex $[UO_2(napoxlhH_2)(H_2O)_2]_n \cdot 2nH_2O$ involves eight coordinated uraniums with six ligand atoms arranged in the equatorial plane perpendicular to the linear uranyl group involving dihydrazone in the enolic form with *cis* configuration, whereas $[Zn(napoxlhH_2)(H_2O)_2]_n \cdot 2nH_2O$ is octahedral involving enolic dihydrazone in the staggered configuration. The phenolic-OH groups remain uncoordinated.

Acyl-, aroyl- and phthaloyldihydrazones containing azomethine, amide and phenolic functions are polyfunctional ligands.[1] These are capable of yielding polymeric polynuclear complexes involving ligand bridging and oxo-bridging.[2,3] Metal complexes of salicylaldehyde dihydrazones, which yield high molecular weight oligomeric products by polymerization, have been studied in some detail, but those containing relatively bulkier aromatic aldehydes and ketones have been much less studied. By the introduction of bulky fragments into the dihydrazone skeleton[4] it is possible to prepare polynuclear homo- and heterobimetallic complexes of dihydrazones having discrete molecularity. Bis (*o*-hydroxynaphthaldehyde)oxaloyldihydrazone is one such ligand capable of holding two or more metal atoms in close proximity, depending upon the preparation conditions. To the best of our knowledge, there is no report on a single complex formed by this ligand. The present paper reports the results of an investigation into the reaction of uranyl acetate and zinc acetate with bis(*o*-hydroxynaphthaldehyde)oxaloyldihydrazone, capable of existing in the staggered (A) and *cis* (B) conformations, and the structural assessment of the resultant products.

RESULTS AND DISCUSSION

The complexes isolated in the present study (Table 1) are air stable and decompose above 300°C. They are soluble in DMSO and DMF only. The complexes showed weight loss corresponding to two water molecules at *ca* 110°C and two water molecules at *ca* 180°C, respectively. The water molecules lost at *ca* 110°C suggest that they are part of the lattice structure, while those lost at 180°C suggest that they are part of the coordination sphere. Their molar conductance values in DMSO are 2.5

* Author to whom correspondence should be addressed.

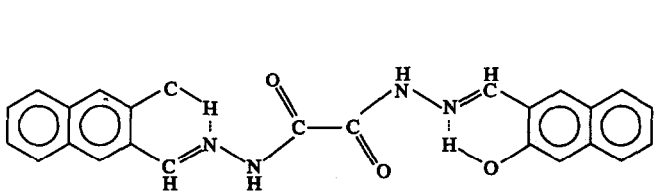

Staggered A

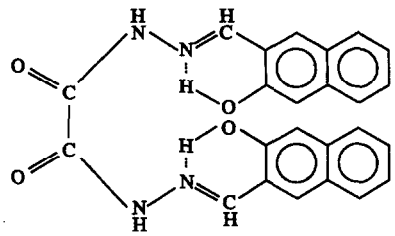

Cis B

and 1.2 Ω^{-1} cm^2 mol^{-1}, indicating that they are non-electrolytes in this solvent.[5] The fact that the complexes are single-phase species has been confirmed by the fact that the DMSO solutions of all the complexes show a uniform spot on a TLC plate covered with silica gel and developed using a mixture of petroleum ether, ether and methanol in the ratio 2 : 2 : 1.

The dihydrazone shows bands at 330 and 370 nm in DMSO solution. A DMSO solution of the zinc complex shows bands at 320, 329, 375 and 450 nm, while the uranyl complex shows two bands at 340 and 405 nm, respectively. The bands in the region 320–375 nm have their origin due to electronic transitions within the ligand, while those in the region 400–450 nm have their origin due to ligand-to-metal charge transfer transitions. In the uranyl complex the band characteristic of the uranyl ion is obscured by ligand-to-metal charge transfer transitions.[6]

The IR and ^{1}H NMR spectral data for the dihydrazone and its complexes are summarized in Table 2. The IR spectrum of the napoxlhH_4 shows bands in the regions 3500–3300sbr, 3382s, 3332s, 3278s, 1655vs, 1616s and 1528 cm^{-1} due to ν(NH)+ν(OH), ν(C=O), ν(C=N) and amide II+ν(C—O)(phenolic). The ^{1}H NMR spectrum of the free ligand in DMSO-d_6 exhibits four and two proton signals at δ 12.72 and 9.75 ppm downfield of TMS, assigned to δ(NH)+δ(OH) and δ(—C=N), respectively.[3] The multiplet due to the naphthyl protons appears in the region δ 7.15–8.20 ppm. The signal at δ 12.72 ppm is relatively broad, indicating the presence of hydrogen bonding in the free dihydrazone.

The absence of the strong amide I band and the appearance of a strong to very strong band in the region 1602–1580 cm^{-1} and a very strong band in the region 1535–1533 cm^{-1} confirm the enolization of the ligand on complexation. The C=N band shows a negative shift by *ca* 14–36 cm^{-1}, indicating azomethine nitrogen coordination. The $[UO_2(napoxlhH_2)(H_2O)_2]_n \cdot 2nH_2O$ complex shows a strong band at 937 cm^{-1} corresponding to the ν_3 stretching frequency of UO_2^{2+}.

The complex $[UO_2(napoxlhH_2)(H_2O)_2]_n \cdot 2nH_2O$ shows doublets at δ 12.65, 12.79 ppm and 9.79, 9.97 ppm, corresponding to two phenolic-OH and two azomethine protons; the corresponding peaks in $[Zn(napoxlhH_2)(H_2O)_2]_n \cdot 2nH_2O$ appear as singlets at δ 12.70 ppm and δ 9.70 ppm. The average δOH peak position in $[UO_2(napoxlhH_2)(H_2O)_2]_n \cdot 2nH_2O$ remains almost at the same position or slightly upfield shifted in the $[Zn(napoxlhH_2)(H_2O)_2]_n \cdot 2nH_2O$ complex compared with that in

Table 1. Analysis, decomposition point, molar conductance data and per cent yields of dioxouranium(VI) and zinc(II) complexes of bis(*o*-hydroxynaphthaldehyde)oxaloyldihydrazone

S. No.	Complex and colour	D.P. (°C)	Yield (%)	Analysis: Found (calc.) % M	C	H	N	Molar conductance (Ω^{-1} cm^2 mol^{-1})
1	$[UO_2(napoxlhH_2)(H_2O)_2]_n \cdot 2nH_2O$	> 300	85	32.3 (31.1)	37.1 (37.6)	3.2 (3.1)	7.3 (7.3)	2.5
2	$[Zn(napoxlhH_2)(H_2O)_2]_n \cdot 2nH_2O$	> 300	90	11.3 (11.6)	51.8 (51.3)	4.3 (4.3)	9.7 (10.0)	1.3

Table 2. Important IR spectral bands and ^1H NMR spectral data (in δ) for napoxlhH_4 and its complexes

S. No.	Complex/ligand	IR spectral data						^1H NMR spectral data		
		ν(OH) + ν(NH)	ν(C=N)	Amide II + ν(C—O) (phenolic)	ν(NCO$^-$)	ν_3	ν(U—O) (carbonyl)	Naphthyl	H —C=N	OH + NH
	napoxlhH_4	3500–3300sbr 3382s 3332s 3278s	1616s	1528s	—	—	—	7.15–8.20(m)	9.75(s)	12.72(s,br)
1	$[UO_2(napoxlhH_2)(H_2O)_2]_n \cdot 2nH_2O$	3550–3000mbr	1602vs	—	1535vs	937vs	466w	7.20–8.65(m)	9.79 9.97(d)	12.65 12.79(d)
2	$[Zn(napoxlhH_2)(H_2O)_2]_n \cdot 2nH_2O$	3550–3000sbr	1594vs	—	1533vssh	—	436w	7.00–8.35(m)	9.70(s)	12.70(s)

the free ligand, thus ruling out the possibility of involvement of the phenolic-OH group in coordination.[7] The average azomethine proton peak position in uranyl complex is downfield shifted by *ca* 0.13 ppm, while in the zinc complex it is slightly upfield shifted by *ca* 0.05 ppm. Such a feature associated with the δ —C=N signal in the complexes indicates coordination through the nitrogen atom of the azomethine group to the metal centre. The downfield shift of δ —C=N in the uranyl complex suggests that there is a drainage of electron density from the nitrogen atom of the azomethine grouping to the metal centre, while in the zinc complex the naphthyl ring electron density flows through the azomethine nitrogen atom to the metal centre.

The splitting of the δ OH and δ —C=N signals into doublets in the uranyl complex is related to the ability of the UO_2^{2+} ion to assemble the dihydrazone in the equatorial plane, which forces a *cis* conformation on the dihydrazone,[8] whereas the zinc ion is unable to do so and the dihydrazone coordinates to the zinc centre in the staggered configuration.

On the basis of the physicochemical data presented and discussed above the uranyl complex maybe suggested to involve an eight-coordinate uranium atom[9] with dihydrazone in *cis* conformation in the enolic form, while the zinc complex may be proposed to be octahedral involving a staggered arrangement of the dihydrazone in the enolic form around the zinc ion, respectively.

EXPERIMENTAL

$UO_2(OAc)_2 2H_2O$, $Zn(OAc)_2 2H_2O$, diethyl oxalate, hydrazine hydrate and *o*-hydroxynaphthaldehyde were BDH, AR or E Merck grade reagents. Oxaloyldihydrazine was prepared by reacting diethyl oxalate (1 mol) with hydrazine hydrate (2 mol). Bis(*o*-hydroxynaphthaldehyde)oxaloyldihydrazone was prepared by refluxing a hot dilute ethanol solution of oxaloyldihydrazine (1 mol) with *o*-hydroxynaphthaldehyde (2 mol). The yellow precipitate obtained was recrystallized from ethanol and dried in an electric oven at *ca* 70°C, m.p. > 300°C. Found: C, 68.0; H, 4.2; N, 13.3. Calc. for $C_{24}H_{18}N_4O_4$: C, 67.6; H, 4.2; N, 13.1%.

Uranium and zinc in the complexes were determined by standard literature methods. Carbon, hydrogen and nitrogen were determined by microanalysis. Water molecules were determined by heating the samples in an electric oven at *ca* 110°C

and 180°C, respectively, and passing the vapour through a trap containing anhydrous copper sulphate, which turned blue, and estimating the weight loss. The molar conductance of the complexes at 10^{-3} M dilution in DMSO was measured using a Direct Reading Conductivity meter 303 with a dip-type conductivity cell. IR spectra were recorded on a Perkin–Elmer 983 spectrophotometer in the range 4000–180 cm^{-1} using KBr discs. The ^1H NMR spectra were recorded on a CFT-20, 90 MHz spectrometer using DMSO-d_6 solution. Electronic spectra were recorded on a Shimadzu MPS-5000 multipurpose spectrophotometer in DMSO.

Preparation of the complexes

The complexes were prepared by the following general method. $M(OAc)_2 \cdot 2H_2O$ (UO_2^{2+}, Zn^{2+}) (0.05 M, 50 cm^3) in ethanol containing a trace of acetic acid was dissolved by gentle heating and stirring. Oxaloyldihydrazine (0.05 M, 55 cm^3) in hot distilled water was added to the above solution accompanied by stirring for a period of 10 min. The reaction mixture was refluxed for 1 h and then filtered under hot conditions, washed with hot water, ethanol and finally with ether.

The precipitate obtained above was suspended in ethanol, to which *o*-hydroxynaphthaldehyde solution (0.1 M, 75 cm^3) in ethanol was added. The reaction mixture was refluxed. The progress of the reaction was followed with the help of TLC. The reaction was complete after 6 h in the case of the uranyl complex, while it required 20 h in the case of the zinc complex. The product was filtered in hot conditions, washed with hot ethanol, ether and dried in an air oven at *ca* 70°C.

Acknowledgements—The authors thank the Department of Atomic Energy, Government of India, Bombay, for financial assistance, the Head, Regional Sophisticated Instrumentation Centre, Lucknow, for providing carbon, hydrogen and nitrogen analytical data and ^1H NMR spectra and the Head, Regional Sophisticated Instrumentation Centre, North-Eastern Hill University, Shillong, for IR spectra.

REFERENCES

1. R. L. Dutta and Md. M. Hossain, *J. Sci. Ind. Res.* 1985, **44**, 635; F. C. J. M. Van Veggel, M. Bos, S. Harkema, H. Vande Bovenkamp, W. Verboom, J. Reedijk and D. N. Reinhoudt, *J. Org. Chem.* 1991, **56**, 225.
2. K. Lal, S. P. Gupta and S. K. Sahni, *Polyhedron* 1986, **5**, 1499; R. A. Lal, R. K. Thapa and S. Das, *Inorg. Chim. Acta* 1989, **132**, 129.
3. G. Paolucci, P. A. Vigato, G. Rossetto, U. Casellato and M. Vidali, *Inorg. Chim. Acta* 1982, **65**, L71; A. Yacouta-Nour, M. M. Mostafa and A. K. T. Maki, *Trans. Met. Chem.* 1990, **15**, 34; *Spectrochim. Acta* 1988, **44A**, 1291.
4. V. Sanz, T. Picher, P. Palanca, P. Gomez-Romero, E. Llopis, J. A. Ramirez, D. Beltran and A. Cervilla, *Inorg. Chem.* 1991, **30**, 3113.
5. W. J. Geary, *Coord. Chem. Rev.* 1971, **7**, 81.
6. B. I. Kim Bong, C. Miyake and S. Imoto, *J. Inorg. Nucl. Chem.* 1975, **37**, 763; I. S. Ahuja, C. L. Yadava and S. Tripathi, *Ind. J. Chem.* 1988, **27A**, 171.
7. R. A. Lal, M. Husain, K. B. Singh and S. S. Bhattacharjee, *Polyhedron* 1991, **10**, 779.
8. R. L. Lintvedt, W. E. Lynch and J. K. Zehetmair, *Inorg. Chem.* 1990, **29**, 3009.
9. A. F. Wells, *Structural Inorganic Chemistry*, 3rd edn. Oxford University Press, Oxford (1966); C. Cattalini, U. Croatto, S. Degetto and E. Tandello, *Inorg. Chim. Acta* 1971, **5**, 19.

Polyhedron Vol. 12, No. 19, pp. 2355–2358, 1993
Printed in Great Britain

0277–5387/93 $6.00+.00
© 1993 Pergamon Press Ltd

^1H AND ^{13}C NMR RELAXATION INVESTIGATION OF THE COPPER(II) COMPLEX OF AMITRAZ, A FORMAMIDINE PESTICIDE

ELENA GAGGELLI, NICOLA GAGGELLI and GIANNI VALENSIN*

Department of Chemistry, University of Siena, Siena 53100, Italy

and

ALESSANDRO FRANCHI

USL 30, Siena, Siena 53100, Italy

(*Received* 23 *March* 1993; *accepted* 2 *June* 1993)

Abstract—The copper(II) complex of amitraz, a formamidine pesticide, was investigated by measuring ^1H NMR spin-lattice relaxation rate enhancements (PRRE) in [$^2H_6$]-DMSO solution. The occurrence of fast exchange conditions was demonstrated by the temperature dependence of the PRRE. The PRRE was interpreted by the Solomon–Bloembergen–Morgan approach; the number of solvent molecules in the coordination shell was calculated at $q = 2$; the reorientational correlation time in the 1 : 1 metal complex was assumed to be the same as in the free ligand and calculated at $\tau_c = 69$ ps. The metal ion was shown to stabilize a *cisoid* conformation of the ligand.

Amitraz, {N,N′[(methylimino)dimethylidyne]di-2,4-xylidine} (Fig. 1), is a formamidine acaricide and insecticide effective against a wide variety of phytophagous mites and insects. It is synthesized from 2,4-dimethylaniline and it reverts to several products on mammalian metabolism and environmental degradation.[1–3]

Extensive use in agriculture has raised the question of its toxicity, especially in light of its interaction with the hepatic mixed-function oxidase systems[1] and also with components of the biogenic amine system.[4]

In this communication we present NMR evidence that amitraz can act as an effective ligand for metal ions, such as Cu^{2+}, forming stable complexes that may play a significant role in eliciting the biochemical activity.

EXPERIMENTAL

Materials

Amitraz (standard analysis reagent) was obtained from Ehrenstorfer Lab. (Augsburg) and used without further purification. Solutions were made in [$^2H_6$]-DMSO or in H_2O and carefully deoxygenated by bubbling nitrogen gas through. The desired copper concentration was obtained using stock solutions of $Cu(ClO_4)_2$ in [$^2H_6$]-DMSO or in H_2O.

Methods

NMR experiments were performed on a Varian VXR-200 spectrometer at controlled temperature (±1 K). Chemical shifts were referenced to internal TMS. Spin-lattice relaxation rates were measured with inversion recovery pulse sequences. Spin–spin relaxation rates were measured with the Carr–Purcell–Meiboom–Gill pulse sequence. The rate values were calculated, in both cases, by linear regression analysis of the recovery or decay curves of longitudinal or transverse magnetization components. $^{13}C\{^1H\}$ nuclear Overhauser effects were measured with gated decoupling techniques.

RESULTS AND DISCUSSION

Different proton spin-lattice relaxation rate enhancements (PRRE) were measured in the pres-

* Author to whom correspondence should be addressed.

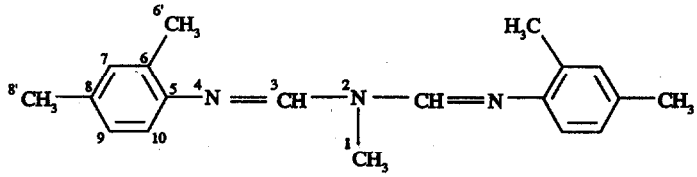

Fig. 1. Molecular formula of amitraz.

ence of copper(II) ions (Table 1). The experimental paramagnetic contributions to the relaxation rates, R_{ip}, were calculated by:

$$R_{ip} = R_{iobs} - R_{if} \quad (i = 1, 2), \tag{1}$$

where R_{iobs} and R_{if} are the rate values measured in the presence and in the absence, respectively, of relatively small concentrations of the paramagnetic ion.

Consideration of the temperature dependence of such PRRE (Fig. 2) suggests that fast exchange conditions apply, such that:

$$R_{ip} = qfR_{iM} \quad (i = 1, 2), \tag{2}$$

where q is the number of coordinated ligand molecules and f is the fraction of bound ligand, the relaxation rate of which is given by R_{iM}. In such situations the PRRE can be interpreted in terms of the Solomon–Bloembergen–Morgan theory;[5–7] since $R_{2p} \gg R_{1p}$ was measured (Table 1) it was concluded that R_{2p} is contributed by the scalar interaction, whereas the paramagnetic contribution to the spin-lattice relaxation rate, R_{1p}, is mainly determined by the dipolar electron spin–nuclear spin interaction given by:[8,9]

$$R_{ip} = \frac{1}{10} qf \frac{\gamma_H^2 g_e^2 \beta_e^2}{r^6} \left\{ \frac{3\tau_c}{1 + \omega_H^2 \tau_c^2} \right\}, \tag{3}$$

where r is the ion-proton distance measured in Å; $\omega_H = 1.257 \times 10^9$ rad s^{-1} is the proton Larmor frequency; τ_c is the correlation time modulating the nuclear spin–electron spin dipole–dipole interaction; $\gamma_H = 2.6753 \times 10^4$ rad s^{-1} G^{-1} is the proton magnetogyric ratio; $g_e = 2.002322$ is the electronic g factor; $\beta_e = 0.92731 \times 10^{-20}$ erg G^{-1} is the Bohr magneton.

The motional correlation time, in the case of copper(II) complexes with small ligands, is a rotational correlation time[8,9] which can be reasonably assumed to be the same as for the free ligand. The validity of this assumption might be questioned but only at a superior level of accuracy, which is not required in this case (a large error in τ_c in fact only yields small uncertainties in evaluating distances). The motional correlation time was, therefore, calculated by measuring the ^{13}C spin-lattice relaxation rates of the free ligand, summarized in Table 2. Since the ^{13}C—^{1}H dipolar interaction may not provide the unique relaxation mechanism, especially for methyls, the spin-lattice relaxation rates were scaled down with the measured nuclear Overhauser effect (n.O.e.) through:

$$R_1^{dip} = R_{1obs} \frac{\eta_{obs}}{\eta_{max}}, \tag{4}$$

where η_{max} (the maximum observable n.O.e. when

Table 1. Paramagnetic proton relaxation rates for amitraz (0.1 mol dm^{-3}) in [^{2}H$_6$]-DMSO at $T = 295$ K in the presence of [Cu^{2+}] = 4.3×10^{-4} mol dm^{-3} and calculated ion-proton distances

Proton	δ (ppm)	R_{1p} (s^{-1})	R_{2p} (s^{-1})	r(Cu—H)^a (Å)	r(Cu—H)^b (Å)
N—CH$_3$	3.31	1.10	6.87	4.0	2.8
H$_3$	8.29	1.98	9.44	3.6	
CH$_3$(6′)	2.21	0.75	4.86	4.2	2.7
H$_7$	6.97	1.25	7.31	3.9	
CH$_3$(8′)	2.18	—	2.21	—	
H$_9$	6.90	0.22	7.11	5.2	
H$_{10}$	6.82	1.76	9.04	3.7	

[a] Calculated from eq. (3) with $\tau_c = 69$ ps.
[b] Calculated from eq. (3) with $t_c = 8$ ps.

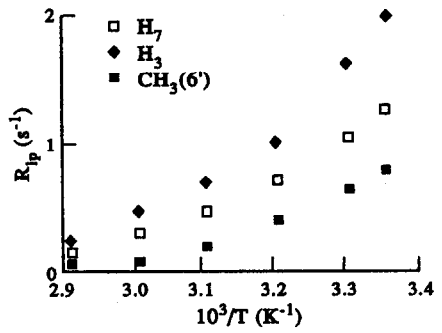

Fig. 2. Temperature dependence of PRRE for selected protons of amitraz (0.1 mol dm^{-3}) in [$^2H_6$]-DMSO.

the relaxation rate is dominated by the dipolar interaction) = 1.98.

From the calculated dipolar relaxation rates, R_1^{dip}, an effective reorientational correlation time of 69.3 ± 15.3 ps for modulation of the internuclear vectors of the four methynes was calculated.[10] As for the methyls the same calculations yield correlation times in the range 6.1–8.5 ps, suggesting "unlocked" free rotation.[11]

The number of ligands in the coordination sphere was evaluated by measuring the solvent proton relaxation rates, shown in Table 3. A large PRRE (R_{1p} = 3.88 s^{-1}) is measured for DMSO protons in the presence of [Cu^{2+}] = 0.43 mmol dm^{-3}, which is reduced (R_{1p} = 1.64 s^{-1}) by the presence of ligand (0.1 mol dm^{-3}). The reduction is due to a decreased number of solvent molecules in the metal coordination sphere. Application of eq. (3) would yield q = 2.5, as compared with q = 6 for the free solvated ion, suggesting that speciation may occur in DMSO. However, repetition of the measurements in H_2O, where the presence of the ligand (0.1 mol dm^{-3}) lowered the solvent PRRE from its free hexaaquo ion value (R_{1p} = 20.6 s^{-1}) to R_{1p} = 13.7 s^{-1}, yields q = 4.0 for the complex. It is concluded that the major species existing in water solution is a metal complex, $ML(H_2O)_4$, having four solvent molecules in the first coordination shell and that preferential solvation by water molecules gives, in the partially hydrated DMSO solvent, metal complexes having mixed solvation shells, $ML(DMSO)_x(H_2O)_{4-x}$.

Since q = 2 for the amitraz molecule that contains pairs of symmetric protons, we can conclude that the main species is a chelated ML complex in which the two imino nitrogens of one ligand molecule coordinate the copper ion. The effective formation of a predominant ML_2 species, in which the coordinating atom is the methylamino nitrogen, can be excluded with the aid of computer graphics molecular modelling. If coordination were occurring via the sp^3 nitrogen there would be no possibility of bringing the aromatic protons close enough to the metal to account for the observed PRRE.

These observations were ratified by calculating ion–proton distances (Table 1). Agreement with the proposed structure becomes very good, especially if the calculations are performed taking into account the correlation time for methyls as in the free state. It is concluded that the ligand retains the same motional flexibility in the bound and in the free state.

Metal binding evidently stabilizes a *cisoid* conformation around the N_4—C_5 bond, thus bringing H_3 and H_{10} quite close to each other. In order to ascertain whether this conformation was also somehow stabilized in the free state selective and double-selective proton spin-lattice relaxation rates were measured for H_3 and H_{10} in order to obtain the dipolar cross-relaxation rate ($\sigma_{3,10}$) between the two:[12,13]

$$\sigma_{3,10} = \sigma_{10,3} = R_3^{3,10} - R_3^{sel} = R_{10}^{3,10} - R_{10}^{sel}, \quad (5)$$

Table 2. ^{13}C NMR parameters of amitraz (0.1 mol dm^{-3}) in [$^2H_6$]-DMSO at T = 295 K

Carbon	δ (ppm)	R_1 (s^{-1})	n.O.e. (η units)	τ_c (ps)
C_1	28.49	0.59	1.75	8.5
C_3	130.63	1.14	1.89	53.9
C_5	145.93	0.11	1.12	—
C_6, C_8	132.56	0.22	1.19	—
C_7	150.74	1.49	1.93	71.6
C_9	126.90	1.53	1.95	74.6
C_{10}	118.37	1.78	1.91	85.0
$C_{6'}$	20.34	0.64	1.62	8.5
$C_{8'}$	17.53	0.46	1.59	6.1

Table 3. Proton spin-lattice relaxation rates (R_1) of water and DMSO in the free solvent and in the presence of amitraz (0.1 mol dm^{-3}) or $Cu(ClO_4)_2 \cdot 6H_2O$ (4.30×10^{-4} mol dm^{-3}) or both at T = 295 K

Solvent	Amitraz (mol dm^{-3})	Cu^{2+} (mol dm^{-3})	R_1 (s^{-1})
DMSO	—	—	0.04
	0.1	—	0.08
	—	4.3×10^{-4}	3.92
	0.1	4.3×10^{-4}	1.72
H_2O	—	—	0.41
	0.1	—	0.75
	—	4.3×10^{-4}	21.06
	0.1	4.3×10^{-4}	14.47

where R_i^{sel} is the spin-lattice relaxation rate after selective excitation of the i resonance and $R_i^{i,j}$ is the rate measured for proton i after double-selective excitation of i and j resonances. The H_3—H_{10} internuclear distance was calculated at 2.54 Å for amitraz in the free state using the measured value of $\sigma_{3,10}$ ($\sigma_{3,10} = 0.07\ s^{-1}$) in the following equation:[14]

$$\sigma_{3,10} = \frac{1}{10}\frac{\gamma_H^4 h^2}{r_{3,10}^6}\left\{\frac{6\tau_c}{1+4\omega_H^2\tau_c^2} - \tau_c\right\}, \qquad (6)$$

where $\tau_c = 69.2$ ps was assumed. From the molecular model it is calculated that, at values of 0° and 90° for the C_3—N_4—C_5—C_{10} torsional angle, the H_3—H_{10} distance is found at 2.1 and 3.5 Å, respectively, whereas a distance of 2.5 Å corresponds to a torsional angle of about 45°. It is concluded that the free ligand in solution exists in some "preferential" conformation, which is further stabilized by coordination with divalent copper ions.

REFERENCES

1. E. C. Kimmel, J. E. Casida and L. O. Ruzo, *J. Agric. Food. Chem.* 1986, **34**, 157.
2. C. O. Knowles and H. J. Benezet, *J. Environ. Sci. Health* 1981, **B16**, 547.
3. R. E. Hornish, *J. Agric. Food. Chem.* 1984, **32**, 114.
4. H. J. Benezet, K. M. Chang and C. O. Knowles, *Pesticides and Venom Neurotoxicity* (Edited by D. L. Shankland, R. M. Hollingworth and T. Smyth), p. 189. Plenum Publishing Corporation, New York (1978).
5. I. Solomon, *Phys. Rev.* 1955, **99**, 559.
6. N. Bloembergen, *J. Chem. Phys.* 1957, **27**, 572.
7. A. W. Nolle and L. O. Morgan, *J. Chem. Phys.* 1957, **26**, 642.
8. I. Bertini and C. Luchinat, *NMR of Paramagnetic Species in Biological Systems*. Benjamin Cummings, Menlo Park (1986).
9. G. Valensin and G. Navon, in *Metal Ions in Biological Systems* (Edited by H. Sigel), Vol. 21, p. 1. Marcel Dekker, New York and Basel (1987).
10. A. Allerhand, D. Doddrell and R. Komoroski, *J. Chem. Phys.* 1971, **55**, 189.
11. F. W. Wehrli and T. Wirthlin, *Interpretation of Carbon-13 NMR Spectra*, p. 255. Heyden, London (1980).
12. L. D. Hall and H. D. W. Hill, *J. Am. Chem. Soc.* 1976, **98**, 1269.
13. E. Gaggelli and G. Valensin, *J. Chem. Soc., Perkin Trans. 2* 1990, 401.
14. J. H. Noggle and R. E. Schirmer, *The Nuclear Overhauser Effect*. Academic Press, New York (1971).

Polyhedron Vol. 12, No. 19, pp. 2359–2361, 1993
Printed in Great Britain

0277–5387/93 $6.00+.00
© 1993 Pergamon Press Ltd

NOVEL μ-TEREPHTHALATO OXOVANADIUM(IV) BINUCLEAR COMPLEXES WITH AN ANTIFERROMAGNETIC EXCHANGE INTERACTION

SHU-LIN MA,* JUAN SHI, DAI-ZHENG LIAO,† ZONG-HUI JIANG, SHI-PING YAN and GENG-LIN WANG

Department of Chemistry, Nankai University, Tianjin 300071, P.R.C.

(*Received* 23 *March* 1993; *accepted* 2 *June* 1993)

Abstract—Three novel oxovanadium(IV) binuclear complexes have been synthesized, namely $[(VO)_2(TPHA)(H_2O)_2(L)_2](Ac)_2$ [L = 2,2′-bipyridyl (bipy), 4,4′-dimethyl-2,2′-bipyridyl (Me_2bipy) and 1,10-phenanthroline (phen); TPHA is the dianion of terephthalic acid]. Based on IR, elemental analyses and magnetic moments at room temperature these complexes are proposed to have extended TPHA-bridged structures and consist of two vanadium(IV) atoms in a distorted square-pyramidal environment. The temperature dependence of the magnetic susceptibility of $[(VO)_2(TPHA)(H_2O)_2(L)_2](Ac)_2$ has been studied, giving the exchange integral $J = -47.75$ cm^{-1}. This indicates an antiferromagnetic exchange interaction between the VO^{2+} ions.

Binuclear metal complexes with extended bridged structure are of current interest due to spin-exchange and charge-transfer between metal ions and in the domains of metalloenzymes and novel magnetic materials.[1] Many works have been published on binuclear copper(II) complexes containing the μ-terephthalato ligand.[2–7] The bridging function of terephthalate dianions and the long-distance antiferromagnetic exchange interactions of these complexes have been revealed by single-crystal X-ray and magnetic analyses.[2,6,7] Recently complexes of this kind with various terminal ligands and other metal ions, such as $[M_2(TPHA)(L)_4](ClO_4)_2$ (M = Ni, Co, L = bipy, phen and Me_2bipy),[8–10] were synthesized in our laboratory and their magnetic properties and some crystal structures were studied. As an extension of that investigation in this paper we report the synthesis, characterization and magnetism of three new complexes, $[(VO)_2(TPHA)(H_2O)_2(L)_2](Ac)_2$ [L = 2,2′-bipyridyl (bipy), 4,4′-dimethyl-2,2′-bipyridyl (Me_2bipy) and 1,10-phenanthroline (phen); TPHA is the dianion of terephthalic acid].

EXPERIMENTAL

Preparation of $[(VO)_2(TPHA)(H_2O)_2(bipy)_2](Ac)_2$

Piperidinium terephthalate was synthesized by the literature method.[2] Bipy, Me_2bipy and phen were of analytical grade.

A solution of piperidinium terephthalate salt (134.4 mg, 0.4 mmol) and 2,2′-bipyridyl (125 mg, 0.8 mmol) in methanol (10 cm^3) was added slowly to a methanol solution (10 cm^3) of $VO(Ac)_2$ (148 mg, 0.8 mmol). After further stirring for 24 h at 60°C. A yellow powder formed with diethyl ether and was dried *in vacuo*. Found: C, 50.0; H, 3.6; N, 7.7. Calc. for $C_{32}H_{30}N_4O_{12}V_2$: C, 50.3; H, 3.7; N, 7.3%.

Preparation of $[(VO)_2(TPHA)(H_2O)_2(Me_2bipy)_2](Ac)_2$

This complex was obtained as a yellow powder by the same procedure as above, but using Me_2bipy

* Tianjin College of Commerce.
† Author to whom correspondence should be addressed.

instead of bipy. Found: C, 52.7; H; 4.8; N, 7.1. Calc. for $C_{36}H_{38}N_4O_{12}V_2$: C, 52.7; H, 4.7; N, 6.8%.

Preparation of $[(VO)_2(TPHA)(H_2O)_2(phen)_2](Ac)_2 \cdot 0.5H_2O$

This complex was obtained as an apricot–yellow powder by the same procedure as above, but using phen instead of bipy. Found: C, 52.5; H, 3.5; N, 7.4. Calc. for $C_{36}H_{30}N_4O_{12}V_2 \cdot 0.5H_2O$: C, 52.6; H, 3.8; N, 6.8%.

Measurements

Analyses for carbon, hydrogen and nitrogen were performed on a Perkin–Elmer analyser, Model 240. The IR spectra were recorded with an IR-408 IR spectrophotometer on KBr disks. Room-temperature magnetic susceptibilities were measured by the Gouy method; the apparatus was calibrated with $[Ni(en)_3]S_2O_3$. Variable-temperature magnetic susceptibility was measured on a vibrating sample magnetometer, Model CF-1. Diamagnetic corrections were made with Pascal's constants for all the constituent atoms and the magnetic moments were calculated using the equation $\mu_{eff} = 2.828(\chi T)^{1/2}$.

RESULTS AND DISCUSSION

General characterization

Elemental analyses have indicated that the reaction of TPHA with $VO(Ac)_2$ and bipy, Me_2bipy or phen yielded the binuclear complexes. For the three $[(VO)_2(TPHA)(H_2O)_2(L)_2(Ac)_2$ complexes the significant bands in the IR spectra are given in Table 1. In the IR region of the spectrum the complexes exhibited the two characteristic strong and broad bands in the 1700–1300 cm^{-1} region, attributed to the $\nu_{as}(COO^-)$ and $\nu_s(COO^-)$ stretching vibrations of the carboxylato groups. An asymmetrical stretching vibration (ν_{as}) of the carboxylato group at 1575 cm^{-1} for the terephthalato was shifted to higher frequencies in the binuclear complexes. However, the symmetrical stretching vibration (ν_s) of the carboxylato group at 1400 cm^{-1} for the terephthalato was shifted to lower frequencies in the binuclear complexes. In addition, the separation between $\nu_{as}(COO^-)$ and $\nu_s(COO^-)$ has often been used to diagnose the coordination modes of the carboxylato groups, that is, bidentate carboxylato groups show a separation smaller than 200 cm^{-1} whereas unidentate carboxylato groups show a separation larger than 200 cm^{-1}. The $\nu_{as}(COO^-) - \nu_s(COO^-)$ values for the present complexes are larger than 200 cm^{-1}, suggesting a unidentate coordination mode for both carboxylato groups.[3] Based on the discussion above these complexes are proposed to have an extended TPHA-bridged structure, in which the TPHA ligand bridges in a bis-unidentate fashion and each vanadium(IV) is in a distorted square-pyramidal environment, as shown in Fig. 1.

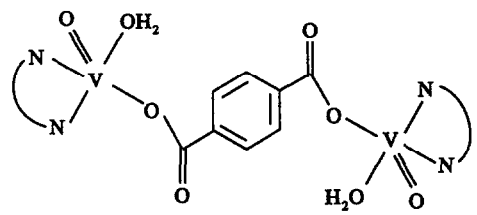

Fig. 1. Proposed chemical structure of the complexes.

Magnetic properties

The observed magnetic moment for the binuclear complexes at room temperature (see Table 1) is considerably less than the spin-only value (2.45 B.M.). This suggests the operation of an antiferromagnetic spin-exchange interaction in these complexes.[10] Variable-temperature (4.2–300 K)

Table 1. Physical data for the complexes

Compounds[a]	Colour	IR (cm^{-1}) $\nu_{as}(COO^-)$	$\nu_s(COO^-)$	$(\nu_{as} - \nu_s)$	μ_{eff} (B.M.) (per dimer unit)
1	Yellow	1630	1325	305	2.06
2	Yellow	1620	1330	290	2.18
3	Apricot–yellow	1625	1345	280	2.18

[a] **1** = $[(VO)_2(TPHA)(H_2O)_2(bipy)_2](Ac)_2$; **2** = $[(VO)_2(TPHA)(H_2O)_2(Me_2bipy)_2](Ac)_2$; **3** = $[(VO)_2(TPHA)(H_2O)_2(phen)_2](Ac_2 \cdot 0.5H_2O$.

magnetic susceptibility data were collected for $[(VO)_2(TPHA)(H_2O)_2(bipy)_2](Ac)_2$ and the magnetic analysis was performed using the susceptibility equation based on the Heisenberg spin operator ($\hat{H} = -2J\hat{S}_1\hat{S}_2$, $S_1 = S_2 = 1/2$):[11]

$$\chi_M = \frac{2N\beta^2g^2}{KT}\left[3+\exp\left(-\frac{2J}{KT}\right)\right]^{-1}, \qquad (1)$$

where χ_M denotes the susceptibility per binuclear complex and the remaining symbols have their usual meanings. As shown in Fig. 2 good fits to the experimental data are attained with eq. (1). The magnetic parameters thus determined are $J = -47.75\ cm^{-1}$ and $g = 2.01$. The agreement factor F, defined here as $\Sigma[(\chi_M)_{obs}-(\chi_M)_{calc}]^2/\Sigma(\chi_M)_{obs}$, is then equal to 9.49×10^{-6}. This result ($J < 0$) indicates that the complexes undergo a moderately strong antiferromagnetic spin-exchange interaction between the VO^{2+} ions.

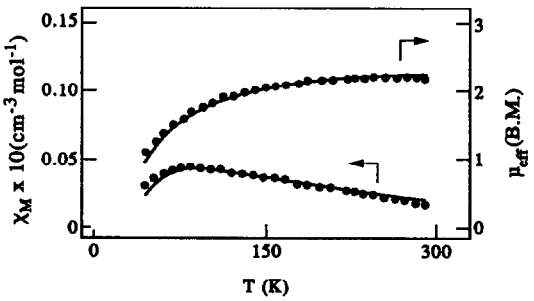

Fig. 2. Temperature variations of the magnetic susceptibility and magnetic moment for $[(VO)_2(TPHA)(H_2O)_2(bipy)_2](Ac)_2$. The curve is drawn based on eq. (1), using the magnetic parameters given in the text.

REFERENCES

1. R. D. Willett, D. Gatteschi and O. Kahn (Editor), *Magneto-Structural Correlation in Exchange-Coupled Systems*, pp. 523–554. NATO ASI Series, Reidel, Dordrecht, The Netherlands (1985).
2. M. Verdaguer, J. Gouteron, S. Jeannin, Y. Jeannin and O. Kahn, *Inorg. Chem.* 1984, **23**, 4291.
3. E. Bakalbassis, J. Mrozinski and C. A. Tsipis, *Inorg. Chem.* 1986, **25**, 3684.
4. E. G. Bakalbassis, A. P. Bozopoulos, J. Mrozinski, P. J. Renyzeperis and C. A. Tsipis, *Inorg. Chem.* 1988, **27**, 529.
5. C. A. Tsipis, P. D. Akvivos and J. Mrozinski, *Inorg. Chim. Acta* 1988, **145**, 121.
6. E. G. Bakalbassis, A. P. Bozopoulos, W. G. Drcissig, H. Hartl and J. Mrozinski, *Inorg. Chem. Acta* 1991, **186**, 113.
7. P. Chaudhuri, K. Oder, K. Wieghardt, S. Gehring, W. Haase, B. Nuber and J. Weiss, *J. Am. Chem. Soc.* 1988, **110**, 3657.
8. Z. L. Deng, J. Shi, Z. H. Jiang, D. Z. Liao, S. P. Yan and G. L. Wang, *Polyhedron* 1992, **10**, 885.
9. S. L. Ma, D. Z. Liao, Z. H. Jiang, S. P. Yan, F. C. Xue and G. L. Wang, *Synth. React. Inorg. Met-Org. Chem.* 1993, **23**, 239.
10. S. D. Lambert, C. L. Spiro, R. R. Gagne and D. N. Hendrickson, *Inorg. Chem.* 1982, **21**, 68.
11. B. Bleaney and K. D. Bowers, *Proc. R. Soc. London, Ser. A* 1952, **24**, 451.

Polyhedron Vol. 12, No. 19, pp. 2363–2369, 1993
Printed in Great Britain

0277–5387/93 $6.00+.00
© 1993 Pergamon Press Ltd

SYNTHESIS AND CHARACTERIZATION OF PLATINUM(II) AZOPHENOLATES INCORPORATING THIOETHER/SULPHINYL DONOR SITES

CHITTARANJAN SINHA

Department of Chemistry, University of Burdwan, Burdwan 713 104, India

(*Received* 27 *January* 1993; *accepted* 2 *June* 1993)

Abstract—Oxygen insertion into the Pt—C bond has been examined. Both thioether and sulphinyl azobenzene platinum(II) complexes (**5** and **6**) undergo metalloxylation by *m*-chloroperbenzoic acid (*m*-CPBA) when stirred in acetonitrile solution for a long time. Usually the reactions in chlorocarbon solvents form platinum(IV) organometallics, unlike isomorphous palladium(II) complexes. The reaction was confirmed by non-oxidative synthesis using hydroxyazobenzenes (**9** or **10**) liberated via reductive elimination of the metal from the corresponding palladium(II) complexes. Platinum(II) azophenolates (**7** or **8**) were characterized by spectroscopic techniques.

There has been growing interest in the chemotherapeutic treatment of platinum compounds, particularly *cis*-platin, *cis*-$Pt(NH_3)_2Cl_2$ and related systems.[1] Currently it is believed that the formation of Pt—S bonds by sulphur containing biomolecules like proteins or peptides is responsible for the inactivation of *cis*-platin and for the observed nephrotoxocity.[2,3]

Our current interest is in designing sulphur coordinated platinum(II) cyclometallates and their interaction with peracids.[4] The platinacycles of coordination type **1**, Pt(C,N,S)Cl, are susceptible to oxidative addition by halogens/peracids in chlorocarbon solvents to form cyclometallated platinum(IV) systems **2**. Herein we describe the reaction of **1** with *m*-chloroperbenzoic acid (*m*-CPBA) in acetonitrile for a long period of time to lead to oxygen insertion into the Pt—C bond giving azophenolato Pt(O,N,S)Cl. These have been structurally characterized with the help of spectroscopic techniques.

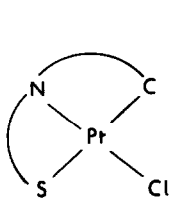

1

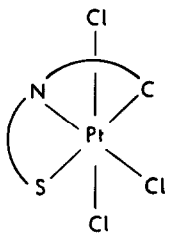

2

RESULTS AND DISCUSSION

Synthesis

The azobenzenes and complexes described in this work are shown in Scheme 1, along with the methods used for synthesis. The azobenzenes contain the donor substituents —SR or —S(O)R at the *ortho* position to the azo function. They are effective tridentate chelating ligands of (C,N,S) types. The thioazobenzenes are formed by the condensation of nitrosoaromatics with anilines and the sulphinyl analogous are synthesized by oxidizing the corresponding sulphides with hydrogen peroxide in acetic acid.

The reaction of azobenzenes with K_2PtCl_4 proceeds smoothly in hot aqueous methanol to give brown coloured platinum(II) complexes in excellent yields. These compounds have been structurally characterized previously.[4]

Upon addition of *m*-CPBA to solutions of **5** (or **6**) in acetonitrile the colour changes immediately from brown to orange–yellow and finally to pink–violet after 5 days of continuous stirring. Removal of the solvents followed by chromatographic purification afforded **7** (or **8**) in high yield. Characterization of the orange–yellow substance has been unsuccessful.

The reaction results in metalloxylation, which is confirmed by non-oxidative synthesis using the

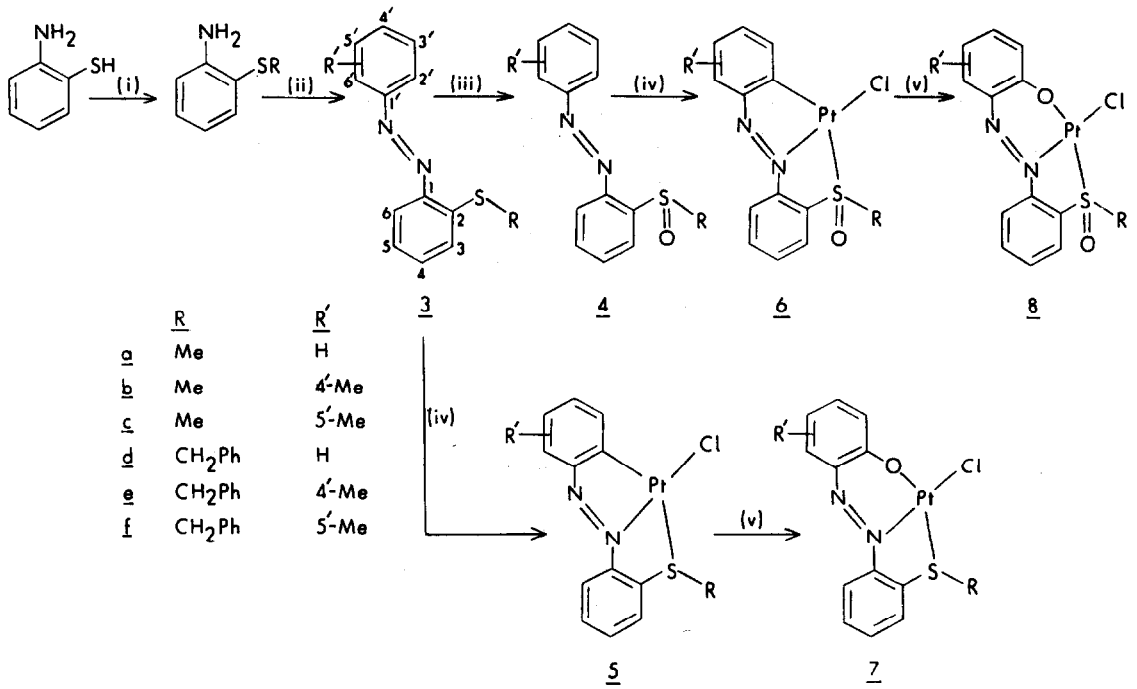

Scheme 1. (i) CH_3I or $PhCH_2Cl/Na/EtOH$; (ii) *m*-/*p*-$RC_6H_4NO/AcOH$; (iii) $H_2O_2/AcOH$; (iv) $K_2PtCl_4/MeOH–H_2O$; (v) *m*-CPBA/MeCN.

hydroxyazobenzene ligand **9** (or **10**) liberated via the demetallation of palladium(II) azophenols by hydrazine hydrate.[5]

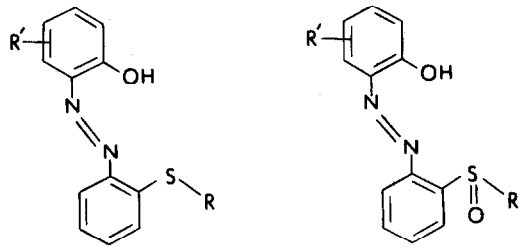

9 10

An interesting feature of the reaction is that the coordinated thioether function is unaffected by peracid, even when the latter is present in excess. The coordinated chloride is also inactive, as in other cases,[4,5] although the free chloride is highly reactive.[6] Free thioethers are easily oxidized by peroxo reagents, yielding sulphoxides and sulphones via nucleophilic attack on the peroxo group by sulphur.[7,8]

Spectral and binding mode

IR and UV–vis spectra. The IR spectra of these complexes display a single N=N stretch around 1380–1390 cm^{-1} and a Pt—Cl stretch near 340 cm^{-1} (Table 1). In the free ligands ν(N=N) occurs in the range 1450–1475 cm^{-1}. The decrease in ν(N=N) on complex formation is characteristic of Pt-azo π-back-bonding.[5,9] Sulphinylazophenolato complexes exhibit another strong band at *ca* 1140–1155 cm^{-1}. This is characteristic of the S=O group.[4,5] The free ligands show the strong band near 1040 cm^{-1} and upon complexation this is shifted to higher frequencies. The specific frequencies are: 1140 in **8a**, 1145 in **8b**, 1145 in **8c**, 1145 in **8d**, 1155 in **8e** and 1155 cm^{-1} in **8f**. The shift to higher energies is an indication of S-bonding. The O-binding shifts ν(S=O) to lower energies (*ca* 900 cm^{-1}).[5,10–12] Confirmatory NMR evidence is presented below.

The complexes afford pink–violet solutions in organic solvents and display characteristic spectra in the UV–vis region (Table 1). The spectra of cyclometallated and azophenolato platinum(II) complexes in the UV–vis region are significantly different (Fig. 1). The spectral differences are diagnostic of the binding mode in the complexes, as in the case of isomorphous palladium complexes.[5]

High-resolution ^1H *NMR spectra.* Sulphur coordination of thioether and sulphinyl ligands to metals in cyclometallated platinum(II) and platinum(IV) complexes is well established.[4] In the present case the hydroxy-azobenzene platinum(II)

Table 1. Elemental analysis, electronic and IR spectral data

Compound	Elemental analysis[a] C (%)	H (%)	N (%)	UV–vis spectra λ_{max} (nm) (ε, mol dm^3 cm^{-1})						IR spectra[b] ν(N=N) (cm^{-1})	ν(Pt—Cl) (cm^{-1})
7a	32.9	2.3	6.0	550,	525,[c]	370,	350,	335,[c]	285[c]	1380	340
	(32.9)	(2.3)	(5.9)	(7633)	(7328)	(11,882)	(12,336)	(10,992)	(5954)		
7b	34.4	2.6	5.7	538,	520,[c]	375,	350,	335,[c]	285[c]	1385	340
	(34.5)	(2.7)	(5.7)	(8450)	(8130)	(13,870)	(12,580)	(10,160)	(5800)		
7c	34.5	2.7	5.6	560,	540,[c]	375,	350,	335,[c]	290[c]	1385	335
	(34.5)	(2.7)	(5.7)	(8995)	(8516)	(13,390)	(14,066)	(12,344)	(6985)		
7d	41.4	2.7	5.2	545,	525,[c]	375,	350,	335,[c]	290[c]	1380	340
	(41.5)	(2.7)	(5.1)	(8426)	(8060)	(14,105)	(15,570)	(13,739)	(9159)		
7e	42.6	2.9	5.0	540,	515,[c]	375,	350,	330,[c]	285[c]	1380	335
	(42.6)	(3.0)	(5.0)	(8800)	(8404)	(15,720)	(11,086)	(10,677)	(6920)		
7f	42.5	3.0	4.9	560,	540,[c]	375,	350,	335,[c]	290[c]	1385	340
	(42.6)	(3.0)	(5.0)	(6929)	(6620)	(10.932)	(11.086)	(9854)	(6467)		
8a	31.9	2.2	5.7	548,	520,[c]	370,	345,	330,[c]	290c	1385	340
	(31.9)	(2.3)	(5.7)	(7800)	(7425)	(12,650)	(13,200)	(11,360)	(6620)		
8b	33.4	2.6	5.6	550,	520,[c]	375,	345,	330,[c]	280[c]	1390	340
	(33.4)	(2.6)	(5.6)	(8725)	(8380)	(14,360)	(13,600)	(11,250)	(6400)		
8c	33.4	2.6	5.5	560,	535,[c]	380,	350,	335,[c]	285[c]	1390	340
	(33.4)	(2.6)	(5.6)	(9010)	(8940)	(14,020)	(13,980)	(12,390)	(6400)		
8d	40.2	2.7	4.5	555,	530,[c]	375,	350,	335,[c]	290[c]	1385	345
	(40.3)	(2.7)	(5.0)	(8850)	(8345)	(14,360)	(15,695)	(14,010)	(9890)		
8e	41.5	2.9	4.9	550,	520,[c]	380,	350,	330,[c]	285[c]	1390	350
	(41.4)	(2.9)	(4.8)	(9200)	(8760)	(15,820)	(11,310)	(11,040)	(7115)		
8f	41.3	2.9	4.8	565,	540,[c]	380,	350,	335,[c]	290[c]	1390	345
	(41.4)	(2.9)	(4.8)	(7640)	(7250)	(11,480)	(11.520)	(10,340)	(6750)		

[a] Calculated values are in parentheses.
[b] In KBr disks.
[c] Shoulder.

complexes are classified in two ways:

(1) S—Me *cases*. The S-binding is reflected in high-resolution ^1H NMR spectra by downfield shifting of the S—Me signal from the free ligand position and the presence of coupling between ^{195}Pt and ^1H(SMe). Selected chemical shift data ($CDCl_3$ solvent) are collected in Table 2. The S—Me signal of **7c** occurs at *ca* 0.45 ppm downfield from those of **9c** and of **8c** at *ca* 1.00 ppm downfield from those of **10c**. This again undergoes a downfield shift by *ca* 0.8 ppm in the sulphinyl complexes, **8a–c**, from thioether complexes, **7a–c**. This may be due to the electron-withdrawing effect of the S=O function.[4] Although sulphur centre oxidation supports the downfield shift of the S—Me signal (by *ca* 0.25 ppm), it is to a lesser extent than their corresponding platinum complexes (by *ca* 0.80 ppm). The coupling between ^{195}Pt ($I = 1/2$, abundance 33.7%) and ^1H (S—Me) is another strong indication of sulphur coordination to the metal centre.[4,13] The coupling constant ^3J(Pt—H) of thioazophenolates (50 Hz) is *ca* 2.5 times that of the sulphinylazophenolates (20 Hz) (Table 2). The coupling constant [^3J(Pt—H)] is largely reduced in cycloplatinates than in the analogous azophenolato complexes (cf. **5b**, 20.1;[4] **7b**, 50 Hz), possibly due to the *trans* influence of the Pt—C bond. The protons of the phenolate ring suffer sizeable upfield shifts compared with the other ring. The differences in δ values of **5b** and **7b** are 3-H, 0.08; 4-H, 0.04; 5-H, 0.04; 6-H, 0.06; 3′-H, 0.52; 5′-H, 0.34 and 6′-H, 0.01, respectively. This is expected in view of the electron releasing effect of the phenolic ring.[5]

All aromatic signals of **7a–c** and **8a–c** have been completely assigned on the basis of chemical shifts; spin–spin structures and the effect of substituents (Table 2). The aromatic protons are systematically deshielded in going from **7** to **8**; the effect being particularly prominent in the case of 3-H, 4-H and 5-H. Assignments are shown schematically in Fig. 2.

(2) S—CH_2Ph *cases*. Evidence in support of S-

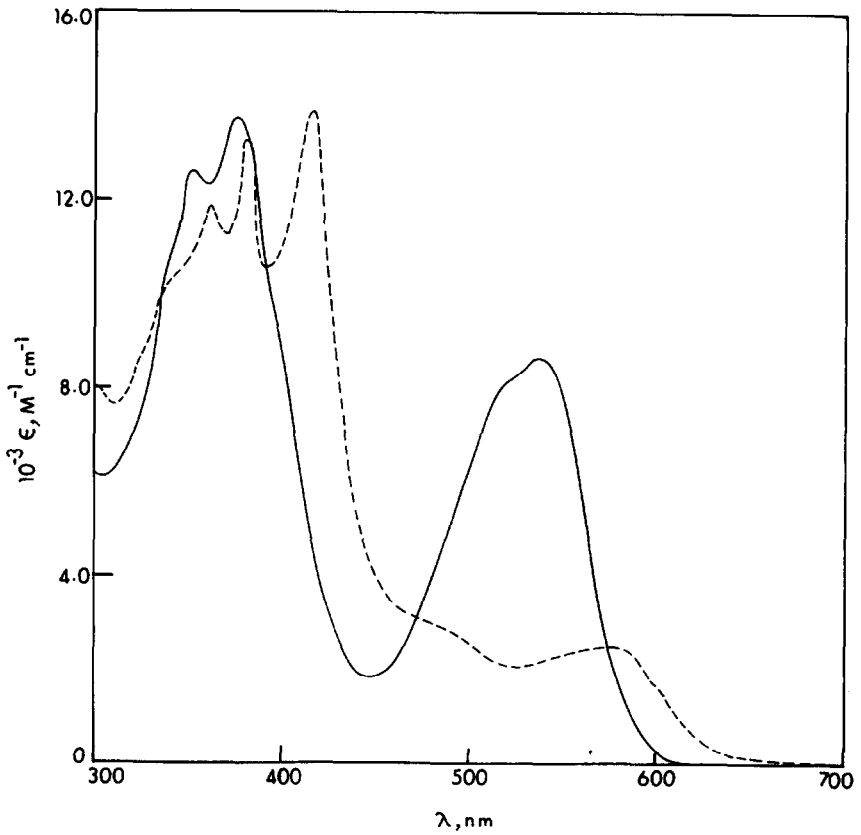

Fig. 1. UV–vis spectra of **5b** (– – –) and **7b** (——) in dichloromethane solution at 300 K (spectral data for **5b** see ref. 4).

binding to metals is the appearance of the inequivalence of the methylene protons of S—CH_2Ph and its increase compared with the free ligand value.[5] The methylene protons of the complexes appear as AB quartets (Table 3). The geminal coupling constant is 13.5 Hz. The quartets display greater separation in the thio compared with the sulphinyl azophenolato complexes (cf. **7d–f**, 0.3 ppm; **8d–f**, 0.2 ppm). This is shown in Fig. 3. The coupling constant ^3J(Pt—H) of the thioazophenolates (**7d–f**,

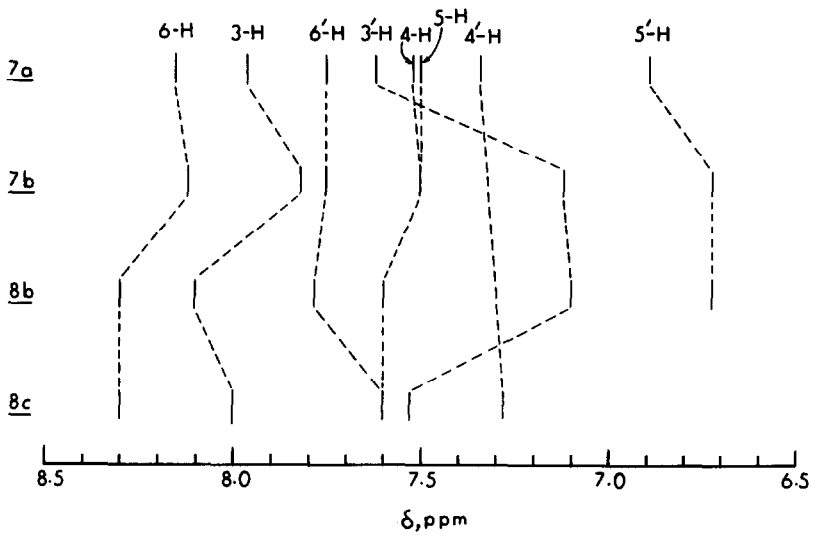

Fig. 2. Schematic ^{1}H NMR spectra of **7a**, **7b**, **8b** and **8c**.

Table 2. ^1H NMR spectral data of **7a–c**, **8a–c**, **9a–c** and **10a–c** in $CDCl_3$

Compound	δ (ppm) J (Hz) 3-H[a]	4-H[b]	5-H[b]	6-H[a]	3′-H	4′-H	5′-H	6′-H	Ar—Me[d]	S—Me	^3J(Pt—H) (Hz)
7a	7.96	7.52	7.50	8.15	7.62[a]	7.34[b]	6.89[b]	7.75[a]		3.05	49.5
	(8.0)	(8.0)	(8.0)	(7.8)	(7.6)	(8.0)	(8.0)	(8.0)			
7b	7.82	7.50	7.50	8.12	7.12[c]		6.72[a]	7.75[a]	2.17	3.02	49.5
	(8.0)	(8.0)	(8.0)	(7.8)			(8.0)	(8.0)			
7c	7.80	7.50	7.52	8.12	7.40[a]	7.24[a]		7.53[c]	2.40	3.00	50.0
	(8.0)	(8.0)	(8.0)	(8.0)	(8.0)	(8.0)					
8a	8.13	7.73	7.70	8.37	7.70[a]	7.45[b]	6.90[b]	7.98[a]		3.87	20.0
	(8.0)	(8.0)	(8.0)	(8.0)	(7.8)	(8.0)	(8.0)	(8.0)			
8b	8.10	7.60	7.60	8.30	7.10[c]		6.72[a]	7.78[a]	2.18	3.83	20.0
	(8.0)	(8.0)	(8.0)	(8.0)			(8.0)	(8.0)			
8c	8.0	7.60	7.60	8.30	7.53[a]	7.28[a]		7.60[c]	2.36	3.84	22.5
	(8.0)	(8.0)	(8.0)	(7.0)	(8.0)	(8.0)					
9a	7.48	7.42	7.42	8.0	7.08[a]	6.72[b]	6.96[b]	7.54[a]		2.56	
	(8.0)	(7.5)	(7.5)	(8.0)	(8.0)	(7.5)	(7.5)	(8.0)		12.64[e]	
9b	7.32	7.40	7.40	7.84	6.88[c]		6.82[a]	7.46[a]	2.40	2.56	
	(8.0)	(7.5)	(7.5)	(8.0)			(8.0)	(8.0)		12.76[e]	
9c	7.40	7.36	7.36	7.84	7.00[a]	6.62[a]		7.45[c]	2.36	2.56	
	(8.0)	(7.5)	(7.5)	(8.0)	(8.0)	(8.0)				12.52[e]	
10a	8.02	7.78	7.78	8.30	7.10[a]	7.42[b]	7.10[b]	8.02[a]		2.82	
	(8.0)	(8.0)	(8.0)	(8.0)	(8.0)	(8.0)	(8.0)	(8.0)		11.92[e]	
10b	8.00	7.71	7.71	8.22	6.92[c]		7.00[a]	7.88[a]	2.44	2.82	
	(8.0)	(8.0)	(8.0)	(8.0)			(8.0)	(8.0)		12.00[e]	
10c	8.00	7.73	7.73	8.22	7.28[a]	7.00[a]		7.76[c]	2.36	2.80	
	(8.0)	(8.0)	(8.0)	(8.0)	(8.0)	(8.0)				11.76[e]	

[a] Doublet.
[b] Triplet.
[c] Singlet.
[d] For **7b–10b**, 4′-Me; **7c–10c**, 5′-Me.
[e] 2′-OH.

ca 80 Hz) is larger than for the sulphinyl azophenolates (**8d–f**, *ca* 52 Hz) (Table 3). The origin of the differences is unclear at present, but the larger steric demand[10] of the sulphinyl function (compared with the thioether function) may have a role to play. The methylene chemical shifts of the azophenolato platinum(II) complexes (**8d–f**) lie *ca* 0.7 ppm downfield from analogous thioazophenolato platinum(II) complexes (Table 3).

The platinacycles display a very small separation

Table 3. Proton chemical shifts of methylene group of (**7d–f**) and (**8d–f**)

Compound	δ CH_2 (ppm)[a]		^3J(Pt—H) (Hz)
7d	4.38	4.67	78
7e[b]	4.37	4.67	81
7f[b]	4.37	4.68	84
8d	5.10	5.29	52
8e[b]	5.09	5.27	50
8f[b]	5.10	5.30	54

[a] Geminal coupling constant for all 13.5 Hz.
[b] **7e**: 4′-Me, 2.16; **7f**: 5′-Me, 2.36; **8e**: 4′-Me, 2.17; **8f**: 5′-Me, 2.39 ppm.

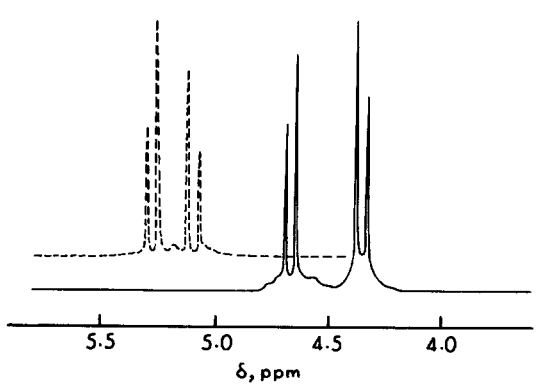

Fig. 3. Methylene ^1H NMR spectra of **7e** (——) and **8e** (– – –) at 270 MHz in $CDCl_3$.

[*ca* 0.05 ppm ^3J(Pt—H) *ca* 13 Hz] of AB quartets for the $PhCH_2S(O)$-coordinated complexes **6d–e** and a broad band for **5d–e**,[4] which are significantly large in the phenolato complexes. This is because of the *trans* influence of the Pt—C bonds in the former, which is absent in phenolato systems. The aromatic region is complicated by signals from the CH_2Ph substituent and hence is not assigned.

EXPERIMENTAL

Dipotassium tetrachloroplatinate was prepared by a published procedure.[4] 2-(Alkylthio) azobenzenes, their sulphinyl derivatives and platinum(II) complexes were prepared as previously described.[4] 2-Hydroxy-azobenzenes were liberated via the demetallation of palladium azophenolates by 99% hydrazine hydrate.[5] *m*-Chloroperbenzoic acid and hydrazine hydrate (99%) were commercially available. The active oxygen content of *m*-CPBA was measured iodometrically.[14] All other common chemicals were reagent grade and were used as received. Commercially available BDH silica gel (60–120 mesh) was used for column chromatography.

Physical measurements

IR and UV–vis spectra were recorded on Perkin–Elmer 783 and Hitachi 333 spectrophotometers, respectively. ^{1}H NMR data were collected in $CDCl_3$ solvent using Varian XL 200 and Brcker 270 MHz FT NMR spectrometers.

Synthesis of 2-(*methylthio*)*azophenolato platinum*(II) (**7a**)

Direct synthesis. To an aqueous methanolic solution of 2-(methylthio)-2′-hydroxyazobenzene (**9a**) (0.05 g, 0.21 mmol) was added an aqueous solution of K_2PtCl_4 (0.1 g, 0.24 mmol) dropwise with continuous stirring at room temperature. The stirring was continued for 2 h. The colour of the solution was changed from light yellow to pink–violet. The reaction mixture was then evaporated to dryness *in vacuo*. The residue was thoroughly washed with 50% (v/v) water–methanol (5×5 cm^3). The residue was dissolved in dichloromethane (5 cm^3) and chromatographed over a silica gel column (45×1 cm) prepared in benzene. Acetonitrile-benzene (10%, v/v) eluted the desired pink–violet compound. Evaporation of the solvent *in vacuo* afforded the pure crystalline product in 80% yield.

Other complexes were also prepared similarly with 75–85% yield.

By m-*CPBA oxidation*: **5a** → **7a**. A solution of *m*-CPBA (0.052 g, 0.30 mmol) in degassed acetonitrile (10 cm^3) was added dropwise to a magnetically stirred solution of complex **5a** (0.12 g, 0.26 mmol) in the same solvent (25 cm^3). The solution colour immediately changed from brown–red to orange–yellow. The stoppered degassed solution was magnetically stirred continuously for 5 days. The orange–yellow solution very slowly changed to pink–violet. The reaction mixture was then evaporated to dryness *in vacuo*. The residue was thoroughly washed with 50% (v/v) water–ethanol (5×8 cm^3) and then chromatographed using dichloromethane solution over a silica gel column (45×1 cm) prepared in petroleum ether. A small amount of an orange–yellow band was eluted first by benzene and then rejected. The desired pink–violet band was eluted by acetonitrile–benzene (10%, v/v) and evaporated to dryness *in vacuo*. Evaporation of the solvent yielded a pure crystalline compound in 50% yield. Recrystallization from a dichloromethane–hexane layer yielded shining needle-shaped crystals.

Other complexes were also prepared similarly with 45–65% yield. Microanalytical data are given in Table 1.

Acknowledgements—I am deeply grateful to Professor A. Chakravorty, Indian Association for the Cultivation of Science, Calcutta, India, for his encouragement and helpful discussion.

REFERENCES

1. W. I. Sundquist and S. J. Lippard, *Coord. Chem. Rev.* 1990, **100**, 293; *Cisplatin, Current Status and New Developments* (Edited by A. W. Prestayko, S. T. Crooke and S. K. Carter). Academic Press, New York (1980).
2. E. L. M. Lempers and J. Reedjik, *Inorg. Chem.* 1990, **29**, 217, 1880; A. Eastman and M. A. Barry, *Biochemistry* 1987, **26**, 3303.
3. T. G. Appleton, J. W. Connor, J. R. Hall and P. D. Prenzler, *Inorg. Chem.* 1989, **28**, 2030; T. G. Appleton, J. W. Connor and J. R. Hall, *Inorg. Chem.* 1988, **27**, 130.
4. S. Chattopadhyay, C. Sinha, P. Basu and A. Chakravorty, *Organometallics* 1991, **10**, 1135; S. Chattopadhyay, C. Sinha, P. Basu and A. Chakravorty, *J. Organomet. Chem.* 1991, **414**, 421.
5. C. Sinha, D. Bandyopadhyay and A. Chakravorty, *Inorg. Chem.* 1988, **27**, 1173; A. K. Mahapatra, D. Bandyopadhyay, P. Bandyopadhyay and A. Chakravorty, *Inorg. Chem.* 1986, **25**, 2214; S. Chattopadhyay, C. Sinha, S. B. Chowdhury and A. Chakravorty, *J. Organomet. Chem.* 1992, **427**, 111.

6. J. E. Hoots, D. A. Lesch and T. B. Ranchfuss, *Inorg. Chem.* 1984, **23**, 3130.
7. H. O. House, *Modern Synthetic Reactions*, p. 334, Benjamin, Mento Park, U.S.A. (1972).
8. R. Cruci, R. A. Diperte, J. O. Edwards and G. Modena, *J. Org. Chem.* 1970, **35**, 740; D. Barnard, *J. Chem. Soc.* 1956, 489.
9. S. Goswami, A. R. Chakraborty and A. Chakravorty, *Inorg. Chem.* 1981, **20**, 2246; R. A. Krause and K. Krause, *Inorg. Chem.* 1982, **21**, 1914.
10. A. J. Davies, *Adv. Inorg. Chem. Radio Chem.* 1981, **24**, 115.
11. J. H. Price, A. N. Williamson, R. F. Schramm and B. B. Wayland, *Inorg. Chem.* 1972, **11**, 1280.
12. G. Anibak, L. Cattalini, L. Canoverse, B. Pitteri, A. Tiripicchio, M. T. Camellini and M. L. Tobe, *J. Chem. Soc., Dalton Trans.* 1986, 1101.
13. E. Wehman, G. Van Koten, C. T. Knaap, H. Ossor, M. Pfeffer and A. L. Spek, *Inorg. Chem.* 1988, **27**, 4409; U. Frey, L. Helm, A. E. Merbach and R. Romeo, *J. Am. Chem. Soc.* 1989, **111**, 8161.
14. A. I. Vogel, *A Text Book of Practical Organic Chemistry*, 2nd edn, p. 809. Longman, Green, London (1956).

Polyhedron Vol. 12, No. 19, pp. 2371–2375, 1993
Printed in Great Britain

0277–5387/93 $6.00+.00
© 1993 Pergamon Press Ltd

SYNTHESIS OF NEW MIXED-ALKYL RHENIUM(VII) ORGANOIMIDO COMPLEXES AND A NEW FACILE ROUTE TO $Me_3SiORe(NBu^t)_3$*

JANOS TAKACS†

Research Group for Petrochemistry of the Hungarian Academy of Sciences, University of Veszprem, H-8200 Veszprem, Hungary

and

WOLFGANG A. HERRMANN†

Anorganisch-chemisches Institut der Technischen Universität München, D-8046 Garching 84747, Lichtenbergstrasse 4, Germany

(*Received* 19 *February* 1993; *accepted* 19 *May* 1993)

Abstract—Alkylation of the rhenium(VII) dichloro compound of the formula $MeRe(NR')_2Cl_2Py$ (**1**) with MeMgCl, Et_2Zn and Pr^iMgCl yields the d^0 trialkyl diimido complexes of the formula $MeR_2Re(NR')_2$ (**2a–c**) (R = Me, Et, Pr^i; R′ = 2,6-dimethylphenyl). Compound **2a** is stable at 25°C, while compounds **2b** and **c** decompose within a few hours. In a similar manner the alkylation of the new tert-butyl imido derivative $MeRe(NBu^t)_2Cl_2$ (**4**) [prepared from $MeRe(NBu^t)_3$ (**3**) by hydrochlorination] yields the trialkyl complexes of the formula $MeR_2Re(NBu^t)_2$ (**5a–c**) (R = Me, Et and Pr^i), of which the mixed-alkyl species are again thermolabile. Analysis of the gas-phase decomposition products revealed a rather complex decomposition pathway, in which the β-hydrogen elimination is likely to play a minor role. Reaction of the polymeric oxo species of the formula $Me_3SnOReO_3$ (**6**) with the silylamine $Bu^tNHSiMe_3$ gives, surprisingly cleanly, the monomeric tris-imido compound of the formula $Me_3SiORe(NBu^t)_3$ (**7**) in 93% yield.

High oxidation state alkyl rhenium complexes containing multiply-bonded ligands such as oxo (=O) or organoimido (=NR) functionalities have received increased attention in the past few years.[1] The stability of these compounds often depends on the nature of the alkyl group. However, it is not yet a settled question as to which decomposition pathways apply for d^0 metal alkyl complexes.[2] Organorhenium(VII) oxides have been shown to catalyse olefin epoxidation and olefin metathesis very efficiently.[3] However, it is not clear how a rhenium-alkylidene unit (Re=CH_2)—known to induce olefin metathesis[4]—is being formed in this system.[5] While several alkyl rhenium oxo and imido compounds are in the literature, very little is known about mixed-alkyl metal derivatives. It was therefore necessary to prepare and study mixed-alkyl rhenium complexes containing alkyl groups with and without β-hydrogen atoms.

RESULTS AND DISCUSSION

Synthesis of trialkyl diimido rhenium(VII) *complexes*

Alkylation of $MeRe(NR')_2Cl_2Py$ (**1**) with neopentyl magnesium chloride yields the mixed-alkyl species $Me(Np)_2Re(NR')_2$ (R′ = 2,6-dimethylphenyl, Np = CH_2CMe_3), which exists in two isomeric forms.[6] One of the isomers was structurally

* Dedicated to Prof. László Markó on the occasion of his 65th birthday. Communication 119, on *Multiple Bonds between Transition Metals and Main-Group Elements*. Preceding paper in this series: J. Mink, A. Stirling, G. Keresztury, W. A. Herrmann, U. N. Flessner and P. Kiprof, *J. Spectrosc.*, in press.

† Authors to whom correspondence should be addressed.

characterized. It exhibits a *tbp* structure with equatorial imido ligands as well as axial neopentyl groups. The compound is stable at ambient temperature. Alkylation of **1** with MeMgCl, Et_2Zn and Pr^iMgCl in a similar manner yields the corresponding species of the formula $MeR_2Re(NR')_2$ (R = Me, Et, Pr^i) (**2a–c**) in 70–80% isolated yield according to Scheme 1.

The trimethyl species **2a** is a low-melting solid which is indefinitely stable at room temperature, like the known imido congener $Me_3Re(NBu^t)_2$.[7] However, the mixed-alkyl derivatives **2b** and **c** decompose within a few hours at room temperature. Although ^1H NMR spectroscopy has its limitations and cannot always be used unambiguously for the determination of organoimido structures,[8,9] the following structures can be proposed for complexes **2a–c**: Since the 2,6-dimethylphenylimido groups are equivalent in all three penta-coordinated compounds, their equatorial position seems likely in the light of the strong competition of these ligands (through the π-bonding) for the empty *d*-orbitals of the metal.[10] The two methyl signals of **2a** (ratio 2/1) give proof of inequivalent methyl groups, two of which must occupy the axial positions of the trigonal-bipyramid while the third is in the equatorial position (Scheme 1). Compound **2b** is a yellow oil that contains two inequivalent ethyl groups (^1H NMR) corresponding to a *tbp* structure with *one* axial and *one* equatorial ethyl ligand. Interestingly, **2c** has two *equivalent* Pr^i ligands that must then occupy the axial positions of the trigonal-bipyramid. This structural difference between **2b** and **2c** can possibly be explained by the bulkiness of the isopropyl as compared with the ethyl group. It is reasonable to assume that two isopropyl groups favour positions *trans* to each other in order to minimize steric repulsion. Although square-pyramidal structures are, in principle, possible for compounds **2a–c**, their close similarity with $Me(Np)_2Re(NR')_2$ (where Np = CH_2CMe_3, R′ = 2,6-dimethylphenyl) of a crystallographically determined *tbp* solid-state structure[6] makes this possibility unlikely. As far as penta-coordinate d^0 rhenium(VII) complexes are concerned, there is a surprisingly great number of species with *tbp* ground-state geometry, e.g. $(Bu^tN)_2ReCl_3$ and $(Bu^tN)_2ReCl_2Ph$,[9] $ReO_2(CH_2CMe_3)_3$,[11a] $MeReO_2(1,2\text{-}O_2C_2Me_4)$,[11b] $RReO_3$(quinuclidine) (R = Et, CH_2SiMe_3),[11c] $[MeReO_3Cl]^-$[11d] and $MeReO_3(H_2NC_6H_5)$.[11e] However, the square-pyramidal geometry does not occur frequently, cf. $(Bu^tN)_2ReCl_2(2\text{-}MeC_6H_4)_2$,[8] $Re(NPPh_3)(SPh)_4$[12a] and $Re(CHBu^t)(N\text{-}2,6\text{-}C_6H_3Pr^i_2)(O\text{-}2,6\text{-}C_6H_3Cl_2)$.[12b] On the other hand, some penta-coordinated d^2-oxo alkyl complexes, e.g. $O{=}Os(CH_3)_4$[13] and $O{=}Os(CH_2CHMe_2)_4$,[14] exhibit even a rigid non-dynamic square-pyramidal geometry.

Reaction of **1** with mesityl- and 2-methylallyl Grignard reagents did not cleanly yield the expected mixed-alkyl compounds of the formula $MeR_2Re(NR')_2$. Instead, decomposition was observed, although neither the alkyl group nor the mesityl group contains a β-hydrogen.

In a similar manner the alkylation of the new di(t-butylimido) dichloro rhenium(VII) complex $MeRe(NBu^t)_2Cl_2$ (**4**) [synthesized from $MeRe(NBu^t)_3$[15] and dry etheral HCl (3 mol)] with MeMgCl, Et_2Zn and Pr^iMgCl gives the corresponding trialkyl diimido rhenium species $MeR_2Re(NBu^t)_2$ (**5a–c**) (R = Me, Et, and Pr^i) in 70–80% yield according to Scheme 2.

Compound **5a** has already been isolated from the reaction of $Re(NBu^t)_2Cl_3$ and $AlMe_3$[7] and a monomeric *tbp* structure was proposed. In contrast, the mixed-alkyl species **5b** and **c** are again thermolabile. Nevertheless, their structure can be assigned on the basis of the ^1H NMR spectra. Thus, the spectrum of **5b** shows *one* Bu^t signal assigned to equivalent t-butylimido groups in equatorial positions as well as *two* different ethyl signals for axial and equatorial positions at the trigonal bipyramid. The ^1H NMR spectrum of **5c** contains *one* Bu^t signal and *two* inequivalent Pr^i signals, indicating a *tbp* structure where the Pr^i groups occupy an equatorial as well as an axial position (Scheme 2). The difference in the configurations of **2c** and **5c** (e.g. *trans* and *cis* Pr^i groups, respectively) is likely

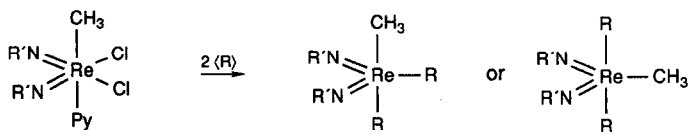

1
R′= 2,6-$C_6H_3(CH_3)_2$

2a: R = CH_3
2b: R = C_2H_5

2c: R = $^iC_3H_7$

Scheme 1. R represents the alkylating reagents CH_3MgCl (for **2a**), $(C_2H_5)_2Zn$ (for **2b**) and $^iC_3H_7MgBr$ (for **2c**).

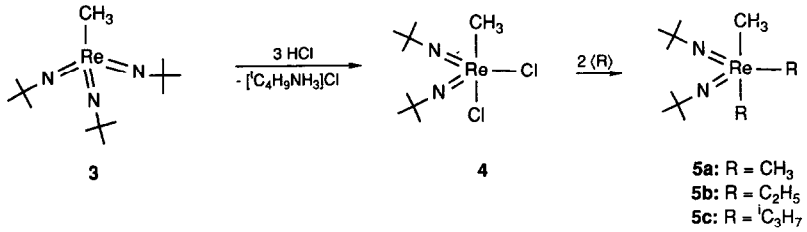

Scheme 2. For R, see Scheme 1.

to arise from the different steric demand of the *aryl*- and *alkyl*imido ligands. The t-butylimido group is spherically bulkier than the disk-shaped 2,6-dimethylphenylimido group, therefore, one of the isopropyl groups is positioned in the equatorial plane (where it is further away from the t-butylimido groups than in the axial position). Steric constraint is thus relieved. This reasoning only holds if the Pr^i group is smaller than the t-butylimido group, which is probably the case.

Decomposition of the mixed-alkyl rhenium(VII) *complexes*

GC analysis of the gaseous decomposition products of neat **2b** and **c** and **5b** and **c** at 25°C (*ca* 4 h) revealed a rather complex decomposition pattern. In all cases except **2c** the main product is the corresponding C_2 or C_3 alkane (ethane, propane), respectively. The C_2 and C_3 alkene is also formed (20–50% of alkane). The amount of methane is smaller. These results suggest that the homolytic cleavage of the Re—C bond, with concomitant reduction of rhenium(VII) to rhenium(VI), followed by disproportionation of the alkyl radical is not the dominant decomposition pathway, since in this case the amount of alkanes and alkenes should be equal. The β-hydrogen elimination-type decomposition pathway does not play a significant role either, since C_2 or C_3 alkenes, respectively, were expected in this case as the main products.

Note that the decomposition was studied without solvent (neat samples). This means that the possibility of hydrogen abstraction from the solvent can be excluded. Also note that **2c** was the only case where more alkene (e.g. propene) than alkane was detected; here, the two isopropyl groups are probably *trans* to each other (^{1}H NMR evidence), a situation that is less likely to result in α-hydrogen abstraction from the other isopropyl group. In this case β-hydrogen elimination could explain the dominant formation of the propene. The ^{1}H NMR spectra of the solid decomposition products gave no clarifying results. It seems obvious that the decomposition behaviour of these mixed alkyl rhenium species is complex. Further efforts must be made to obtain a clear, unambiguous picture. We believe, however, that β-hydrogen elimination is not the major pathway here since the metal (although in its highest oxidation state) is electronically saturated through the strongly π-donating imido ligands.

Synthesis of $MeRe(NBu^t)_2Cl_2$ (**4**) *and* $Me_3SiORe(NBu^t)_3$ (**7**)

The new compound $MeRe(NBu^t)_2Cl_2$ (**4**), used for the preparation of **5a–c**, was synthesized from $MeRe(NBu^t)_3$[15] and 3 equivalents of dry etheral HCl (Scheme 2). The ^{1}H NMR spectrum shows equivalent t-butylimido groups. Since organoimido groups are strong π-donor ligands, we assign them equatorial positions. In contrast to the compound $[R'NH_3]^+[MeRe(NR')_2Cl_3]^-$, formed by hydrochlorination of $MeRe(NR')_3$ (R = 2,6-dimethylphenyl),[6] **4** does not form chloride adducts with the alkylammonium salt formed in the reaction. This result reflects the more electrondonating and/or sterically more demanding character of the t-butylimido group in **4** as compared with the 2,6-dimethylphenylimido ligand.

The synthesis of $MeReO_3$ starting from Re_2O_7 and Me_4Sn also yields the stannoxy complex $Me_3SnOReO_3$ (**6**).[16] The chemistry of this compound is underdeveloped as compared with the siloxy congener, which is mainly due to the polymeric structure of **6**.[17] A facile, simple reaction has now been found to convert this by-product to the more useful tris-imido rhenium(VII) derivative $Me_3SiORe(NBu^t)_3$ (**7**)[18] in excellent yield [eq. (1)].

The other products of this reaction are Bu^tNH_2, $Me_3SiOSiMe_3$ (identified by GC–MS) and a hardly tractable waxy solid that has not been identified due to the difficulty of purification. In theory the stoichiometric reaction of **6** with $Bu^tNHSiMe_3$ (6 mol) produces **7**, Bu^tNH_2 (3 mol), $Me_3SiOSiMe_3$ (2 mol) and "$Me_3SiOSnMe_3$" (1 mol). The ^{1}H NMR spectrum of the waxy solid shows two signals at 1.59 ppm and 3.4 ppm, as in the ^{13}C NMR

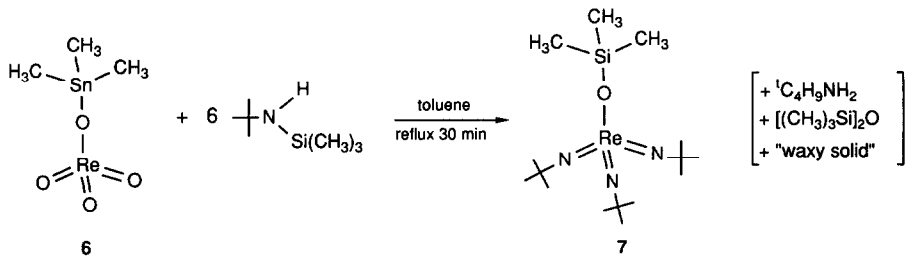

6 7

Equation 1. New synthesis of $(CH_3)_3SiORe[N(^tC_4H_9)]_3$(**7**) from (polymeric) $(CH_3)_3SnOReO_3$ (**6**). The "waxy solid" (unidentified) contains the tin introduced through **6**.

spectrum (26.5 and 70.6 ppm). However, further characterization by MS and elemental analysis gave ambiguous results. The only other known reaction of **6** is conversion to $MeReO_3$ by consecutive treatment with trifluoro or trichloroacetic anhydride and tetramethyltin in acetonitrile.[19,20]

EXPERIMENTAL

General data

All experiments were performed under nitrogen or argon atmosphere using standard Schlenk techniques. Solvents were dry and oxygen-free. The starting compounds $MeRe(NR')_2Cl_2Py$ (**1**), $MeRe(NBu^t)_3$ (**3**) and $Me_3SnOReO_3$ (**6**) were prepared according to the literature methods.[6,15,16] Complexes **2a**, **4**, **5a** and **7** gave satisfactory elemental analysis, while in the case of the mixed-alkyl species the results were influenced by the decomposition and also by the high solubility of these oils which made purification difficult. ^{1}H NMR spectra were recorded at 25°C, 400 MHz (JEOL JNM GX-400) and 300 MHz (Varian Unity 300). The amount of the gaseous decomposition products are expressed as the percentage of the total C_1–C_4 fraction.

Preparations

2a–c. To **1** (510 mg, 1.0 mmol) in toluene (15 cm^3) was added at −78°C MeMgCl (2.0 mmol, 1.0 cm^3, 2.0 M Et_2O solution), Et_2Zn (1.0 mmol, 0.8 cm^3, 1.25 M hexane solution) or Pr^iMgCl (2.0 mmol, 2.0 cm^3, 1.0 M THF solution). The mixture was stirred and the temperature was raised slowly to 25°C. Stirring was continued for 1 h and then the solvents were evaporated *in vacuo*. The residue was extracted with pentane. The pentane solution was filtered and evaporated to dryness *in vacuo* yielding compounds **2a–c** as viscous yellow oils. Compound **2a** solidified to an amorphous "semi-solid".

2a. ^{1}H NMR ($CDCl_3$): δ 1.62 (s, 3H, CH_3); 2.04 (s, 6H, CH_3); 2.30 [s, 12H, 2,6-$C_6H_3(CH_3)_2$]; 6.95–7.05 (m, 6H, 2,6-$C_6H_3Me_2$). IR (cm^{-1}, KBr): 2968 m, 2915 m, 1463 m, 1306 vs, 772 vs. MS (*m/z*, rel. int. %): 455 ($[M-CH_3]^+$, 100).

2b. ^{1}H NMR ($CDCl_3$): δ 1.73 [t, J(H—H) = 7 Hz, 3H, CH_2CH_3], 1.96 [t, J(H—H) = 7 Hz, 3H, CH_2CH_3], 2.14 (s, 3H, CH_3), 2.33 [s, 12H, 2,6-$C_6H_3(CH_3)_2$], 2.44 [q, J(H—H) = 7 Hz, 2H, CH_2CH_3], 3.22 [q, J(H—H) = 7 Hz, 2H, CH_2CH_3], 6.95–7.05 [m, 6H, 2,6-$C_6H_3(CH_3)_2$]. GC analysis: CH_4 8%, C_2H_6 68%, C_2H_4 12%.

2c. ^{1}H NMR ($CDCl_3$): δ 1.78 [d, J(H—H) = 7 Hz, 12H, $CH(CH_3)_2$], 1.96 (s, 3H, CH_3), 2.45 [s, 12H, 2,6-$C_6H_3(CH_3)_2$], 3.77 [septet, J(H—H) = 7 Hz, 2H, $CH(CH_3)_2$], 6.95–7.05 [m, 6H, 2,6-$C_6H_3(CH_3)_2$]. GC analysis: CH_4 8%, C_3H_8 34%, C_3H_6 51%.

4. To **3** (830 mg, 2.0 mmol) in Et_2O (15 cm^3) was added dry HCl (3.1 mmol, 3.1 cm^3, 1.0 M Et_2O solution) at −78°C, with stirring. A yellowish precipitate separated and the mixture was allowed to warm slowly to room temperature. After 1 h of stirring the mixture was filtered and the filtrate was concentrated *in vacuo* until most of the product separated as a yellow solid. The remaining small amount of ether was decanted while it was still cold and the product was dried *in vacuo*. Yield 73%. ^{1}H NMR ($CDCl_3$): δ 1.50 [s, 18H, $C(CH_3)_3$], 1.9 (s, 3H, CH_3). ^{13}C NMR ($CDCl_3$): δ 23.6 (s, $ReCH_3$), 28.9 [s, $C(CH_3)_3$], 75.2 [s, $C(CH_3)_3$]. IR (KBr, cm^{-1}): 2960 s, 2905 m, 1440 m, 1360 m, 1255 m (Re=NR), 1290 s.

5a–c. These species were prepared in an analogous manner to **2a–c**, starting from **4** (414 mg, 1.0 mmol) and MeMgCl (2.0 mmol), Et_2Zn (1.0 mmol) as well as Pr^iMgCl (2.0 mmol), respectively.

5a. Identical to $Me_3Re(NBu^t)_2$ reported in the literature.[7]

5b. ^{1}H NMR ($CDCl_3$): δ 1.30 [s, 18H, $C(CH_3)$], 1.45 (s, 3H, CH_3), 1.61 [t, J(H—H) = 7 Hz, 3H, CH_2CH_3], 1.69–1.79 (m, 5H, CH_2CH_3 and

CH_2CH_3), 2.6 [q, J(H—H) = 7 Hz, 2H, CH_2CH_3]. GC analysis: CH_4 14%, C_2H_6 53%, C_2H_4 24%.

5c. ^{1}H NMR ($CDCl_3$): δ 1.3 [s, 18H, $C(CH_3)$], 1.45 (s, 3H, CH_3), 1.71 [d, J(H—H) = 7 Hz, 6H, $CH(CH_3)_2$], 1.79 [d, J(H—H) = 7 Hz, 6H, $CH(CH_3)_2$], 2.5 [septet, J(H—H) = 7 Hz, 1H, $CH(CH_3)_2$], 3.1 [septet, J(H—H) = 7 Hz, 1H, $CH(CH_3)_2$]. GC analysis: CH_4 8%, C_3H_8 60%, C_3H_6 27%.

7. To a suspension of **6** (4.14 g, 10 mmol) in toluene (40 cm^3) was added $Bu^tNHSiMe_3$ (12 cm^3, 63 mmol). The reaction mixture was then refluxed for 30 min. The clear yellow solution was cooled to room temperature and evaporated to dryness *in vacuo*. The residue was extracted with pentane, filtered and the pentane was removed *in vacuo* leaving a yellow oil which quickly crystallized. Yield 93%. The compound is identical to the one prepared by Nugent from $Me_3SiOReO_3$ and $Bu^tNHSiMe_3$.[18] ^{1}H NMR ($CDCl_3$): δ 0.07 [s, 9H, $Si(CH_3)_3$], 1.33 [s, 27H, $C(CH_3)_3$]. MS (m/z, %) 489 ($[M]^+$, 10), 474 ($[M-CH_3]^+$, 98), 418 ($[M-CH_3-C_4H_8]^+$, 35), 362 ($[M-CH_3-2C_4H_8]^+$, 80), 57 ($[C_4H_9]^+$, 100).

Acknowledgements—We thank the Hungarian National Scientific Research Foundation (Project Nr. OTKA F-4059) and Deutsche Forschungsgemeinschaft for financial support. DEGUSSA AG is acknowledged for a generous gift of rhenium compounds.

REFERENCES

1. (a) K. Mertis and G. Wilkinson, *J. Chem. Soc., Dalton Trans.* 1976, 1488; (b) A. D. Horton and R. R. Schrock, *Polyhedron* 1988, **7**, 1841; (c) W. A. Herrmann, J. G. Kuchler, W. Wagner, J. K. Felixberger and E. Herdtweck, *Angew. Chem., Int. Edn Engl.* 1988, **27**, 294; (d) Review: W. A. Herrmann, *J. Organomet. Chem.* 1990, **382**, 1.
2. A. Yamamoto, *Organotransition Metal Chemistry*, pp. 286–294. Wiley Interscience, New York (1986).
3. W. A. Herrmann, W. Wagner, U. N. Flessner, U. Volkhardt and H. Komber, *Angew. Chem., Int. Edn Engl.* 1991, **30**, 1636–1643.
4. R. R. Schrock, in *Reactions of Coordinated Ligands* (Edited by P. R. Braterman). Plenum Press, New York (1986).
5. R. Buffon, A. Choplin, M. Leconte, J. M. Basset, R. Touroude and W. A. Herrmann, *J. Molec. Catal.* 1992, **72**, L7.
6. M. R. Cook, W. A. Herrmann, P. Kiprof and J. Takacs, *J. Chem. Soc., Dalton Trans.* 1991, 797.
7. D. S. Edwards, L. V. Biondi, J. W. Ziller, M. R. Churchill and R. R. Schrock, *Organometallics* 1983, **2**, 1505.
8. C. J. Longley, P. D. Savage, G. Wilkinson, B. Hussain and M. B. Hursthouse, *Polyhedron* 1988, **7**, 1079.
9. A. A. Danopoulos, C. J. Longley, G. Wilkinson, B. Hussain and M. B. Hursthouse, *Polyhedron* 1989, **8**, 2657.
10. W. A. Nugent, in *Metal–Ligand Multiple Bonds*. Wiley Interscience, New York (1986).
11. (a) S. Cai, D. M. Hoffman and D. A. Wierda, *J. Chem. Soc., Chem. Commun.* 1988, 313; (b) W. A. Herrmann, P.Watzlowik and P. Kiprof, *Chem. Ber.* 1991, **124**, 1101; (c) W. A. Herrmann, C. C. Romao, R. W. Fischer, P. Kiprof and C. M. Bellefon, *Angew. Chem., Int. Edn Engl.* 1991, **30**, 185; (d) W. A. Herrmann, J. G. Kuchler, P. Kiprof and J. Riede, *J. Organomet. Chem.* 1990, **395**, 55; (e) W. A. Herrmann, G. Weichselbaumer and E. Herdtweck, *J. Organomet. Chem.* 1989, **372**, 371.
12. (a) J. R. Dilworth, B. D. Neaves, J. P. Hutchinson and J. A. Zubieta, *Inorg. Chim. Acta* 1982, **65**, L223; (b) M. H. Schofield, R. R. Schrock and L. Y. Park, *Organometallics* 1991, **10**, 1844.
13. W. A. Herrmann, S. J. Eder, P. Kiprof, K. Rypdal and P. Watzlowik, *Angew. Chem.* 1990, **102**, 1460.
14. W. A. Herrmann, S. J. Eder and W. Scherer, *J. Organomet. Chem.*, in press.
15. W. A. Herrmann, G. Weichselbaumer, R. A. Paciello, R. A. Fischer, E. Herdtweck, J. Okuda and D. W. Marz, *Organometallics* 1990, **9**, 489.
16. W. A. Herrmann, J. G. Kuchler, J. K. Felixberger, E. Herdtweck and W. Wagner, *Angew. Chem., Int. Edn Engl.* 1988, **27**, 394.
17. E. Herdtweck, P. Kiprof, W. A. Herrmann, J. G. Kuchler and I. Degnan, *Z. Naturforsch.* 1990, **45b**, 937.
18. W. A. Nugent, *Inorg. Chem.* 1983, **22**, 965.
19. W. A. Herrmann, F. E. Kühn, R. W. Fischer, W. R. Thiel and C. C. Romao, *Inorg. Chem.* 1992, **31**, 4431.
20. W. A. Herrmann, R. W. Fischer, M. V. Rauch and W. Scherer, *J. Molec. Catal.*, in press.

Polyhedron Vol. 12, No. 19, pp. 2377–2385, 1993
Printed in Great Britain

0277–5387/93 $6.00+.00
© 1993 Pergamon Press Ltd

SYNTHESIS AND CHARACTERIZATION OF TRIMETHYLPLATINUM(IV) COMPLEXES WITH (2-DIMETHYLAMINOETHYL)ORGANOCHALCOGENIDES ($Me_2NCH_2CH_2ER$; E = S, Se, Te). X-RAY CRYSTAL STRUCTURE OF [$PtMe_3Br(Me_2NCH_2CH_2SC_6H_4Me$-4)]

VIMAL K. JAIN*

Chemistry Division, Bhabha Atomic Research Centre, Trombay, Bombay 400 085, India

and

SATYAJEET CHAUDHURY

Fuel Chemistry Division, Bhabha Atomic Research Centre, Trombay, Bombay 400 085, India

and

RAKESH BOHRA

Department of Chemistry, University of Rajasthan, Jaipur 302 004, India

(*Received* 20 *April* 1993; *accepted* 11 *May* 1993)

Abstract—Trimethylplatinum(IV) complexes of the type [$PtMe_3X(Me_2NCH_2CH_2ER)$] (X = Cl, Br, I; ER = SBu^t, SC_6H_4Me-4, SPh, SePh, TePh) have been prepared and characterized by elemental analysis and NMR (^1H and ^{13}C) spectral data. The structure of [$PtMe_3Br(Me_2NCH_2CH_2SC_6H_4Me$-4)] has been determined by single-crystal X-ray diffraction. The central platinum atom is coordinated by three *fac*-methyl groups and nitrogen, sulphur and bromine atoms. The five-membered chelate ring PtNCCS is non-planar.

The chemistry of organoplatinum(IV) has attracted much attention in recent years.[1] A wide variety of complexes with nitrogen donors[2–6] and organochalcogenides[7–12] have been synthesized and studied. The organochalcogenide complexes possess interesting dynamic stereochemistries[13,14] and in several cases chalcogen inversion energies have been determined by NMR spectroscopy. However, complexes with hybrid ligands containing one nitrogen and a chalcogen donor have received little attention.[1,15] In this paper we report the synthesis of bidentate hybrid ligands and their complexes with trimethylplatinum halides.

RESULTS AND DISCUSSION

Treatment of trimethylplatinum halides with stoichiometric quantities of $Me_2NCH_2CH_2ER$ gave complexes of the type [$PtMe_3X(Me_2NCH_2CH_2ER)$] (X = Cl, Br, I; ER = SBu^t, SC_6H_4Me-4, SPh, SePh, TePh). ^1H and ^{13}C NMR data are given in Tables 1 and 2. Assignments of NMR chemical shifts and coupling constants are made by comparison with those of the free ligand and complexes of the types [$PtMe_3X(NN)$][2,3,6] and [$PtMe_3X(RE\ ER)$][7,8,10] (E = chalcogen atom). The ^1H and ^{13}C NMR spectra exhibited three Pt—Me resonances in a 1 : 1 : 1 ratio, each flanked with platinum satellites. This suggests that either only one isomer having all three Pt—Me groups *trans* to

* Author to whom correspondence should be addressed.

Table 1. ^{1}H NMR data for $[PtMe_3(X)(Me_2NCH_2CH_2ER)]$ in $CDCl_3$

Complex	Pt—Me			Ligand protons[a]
	Trans to X (X = Cl, Br,I)	*Trans* to N	*Trans* to E (E = S, Se, Te)	
$[Me_2NCH_2CH_2Cl]$	—	—	—	2.20 (s, 6H, NMe_2); 2.60 (t, 7 Hz, 2H, NCH_2—); 3.49 (t, 7 Hz, 2H, —CH_2Cl)
$[Me_2NCH_2CH_2SBu^t]$	—	—	—	1.30 (s, 9H, Bu^t); 2.25 (s, 6H, NMe_2); 2.45 (m, 2H, SCH_2); 2.62 (m, 2H, CH_2N)
$[PtMe_3Cl(Me_2NCH_2CH_2SBu^t)]$	0.68(72.1)	1.12(70.9)	1.28(72.1)	1.52 (s, 9H, Bu^t); 2.26 [s, 3H, J(Pt—H) = 15 Hz, NMe]; 2.80 (m, NMe+CH_2CH_2)
$[PtMe_3Br(Me_2NCH_2CH_2SBu^t)]$	0.80(72.1)	1.25(70.9)	1.38(73.4)	1.52 (s, 9H, Bu^t); 2.26 [s, 3H, J(Pt—H) = 15 Hz, NMe]; 2.90 [s, 3H, J(Pt—H) = 9 Hz, NMe]; 2.85 (m, CH_2CH_2)
$[PtMe_3I(Me_2NCH_2CH_2SBu^t)]$	1.00(70.9)	1.45(72.5)	1.60(73.4)	1.52 (s, 9H, Bu^t); 2.30 [s, 3H, J(Pt—H) = 15 Hz, NMe]; 3.05 [s, 3H, J(Pt—H) = 10 Hz, NMe]; 2.85 (m, CH_2CH_2)
$[Me_2NCH_2CH_2Stol]$	—	—	—	2.21 (s, 6H, NMe_2); 2.30 (s, 3H, tol-Me); 2.50 (m, 2H, CH_2S); 2.90 (m, 2H, CH_2N); 7.00–7.35 (m, 4H, C_6H_4)
$[PtMe_3Cl(Me_2NCH_2CH_2Stol]$	0.55(72.1)	1.24(70.9)	1.28(72.1)	2.40 (s, 3H, tol-Me); 2.44 [s, 3H, J(Pt—H) = 14 Hz, NMe]; 2.87 [s, J(Pt—H) = 10 Hz, NMe, +CH_2]; 3.35 (m, CH_2); 7.30 (br, C_6H_4)
$[PtMe_3Br(Me_2NCH_2CH_2Stol)]$	0.58(72)	1.30(70)	1.35(71.3)	2.36 (s, 3H, tol-Me); 2.39 [s, 3H, J(Pt—H) = 14.6 Hz, NMe]; 2.94 [s, 3H, J(Pt—H) = 10.3 Hz, NMe]; 2.85 (d), 3.34 (br, m) (CH_2CH_2); 7.10–7.30 (C_6H_4)
$[PtMe_3I(Me_2NCH_2CH_2Stol)]$	0.67(69.6)	1.46(70.5)	1.55(71.9)	2.37 (s, 3H, tol-Me); 2.39 [s, 3H, J(Pt—H) = 14.5 Hz, NMe]; 3.11 [s, 3H, J(Pt—H) = 10.6 Hz, NMe]; 2.94 (d), 3.38 (br, m) (CH_2CH_2); 7.11–7.26 (m, C_6H_4)
$[Me_2NCH_2CH_2SPh)]$	—	—	—	2.15 (s, 6H, NMe_2); 2.45 (m, 2H, SCH_2); 2.90 (m, 2H, NCH_2); 7.15 (br, 5H, Ph)
$[PtMe_3Cl(Me_2NCH_2CH_2SPh)]$	0.46(68.9)	1.22(68.9)	1.28(71.1)	2.38 [s, 3H, J(Pt—H) = 15 Hz, NMe]; 2.81 [s, 3H, J(Pt—H) = 9 Hz, NMe]; 3.29–3.42 (m), 2.80 (merged with NMe) (CH_2CH_2); 7.35 (m, 5H, Ph)
$[PtMe_3Br(Me_2NCH_2CH_2SPh)]$	0.58(71)	1.30(68.9)	1.37(71.1)	2.39 [s, 3H, J(Pt—H) = 15 Hz, NMe]; 2.94 [s, 3H, J(Pt—H) = 9 Hz, NMe]; 2.83 (m), 3.38–3.49 (m) (CH_2CH_2); 7.35 (m, 5H, Ph)
$[PtMe_3I(Me_2NCH_2CH_2SPh)]$	0.66(69.3)	1.48(71.9)	1.57(72.1)	2.39 [s, 3H, J(Pt—H) = 14 Hz, NMe]; 3.12 [s, 3H, J(Pt—H) = 10 Hz, NMe]; 2.94 (m), 3.38 (d, 11 Hz); 3.54 (m) (CH_2CH_2); 7.24 (d, 7.8 Hz, 2H, 2,6-H, Ph); 7.31 (t, 7.3 Hz, 1H, 4-H, Ph); 7.43 (t, 7.6 Hz, 2H, 3,5-H, Ph)
$[Me_2NCH_2CH_2SePh]$	—	—	—	2.26 (s, 6H, NMe_2); 2.63 (t, 2H, $SeCH_2$); 3.05 (t, 2H, NCH_2); 7.30–7.60 (m, Ph)

Table 1—*continued*

Complex	Pt—Me *Trans* to X (X = Cl, Br,I)	Pt—Me *Trans* to N	Pt—Me *Trans* to E (E = S, Se, Te)	Ligand protons[a]
$[PtMe_3Cl(Me_2NCH_2CH_2SePh)]$	0.45(72.1)	1.22(70.9)	1.30(72.1)	2.30 [s, 3H, J(Pt—H) = 15 Hz, NMe]; 2.75 [s, 3H, J(Pt—H) = 10 Hz, NMe]; 3.25 (br, m, CH_2CH_2); 7.32 (br, 5H, Ph)
$[PtMe_3Br(Me_2NCH_2CH_2SePh)]$	0.55(72.1)	1.35(70.9)	1.44(72.1)	2.32 [s, 3H, J(Pt—H) = 15 Hz, NMe]; 2.88 [s, 3H, J(Pt—H) = 10 Hz, NMe]; 3.35 (m, br, CH_2CH_2); 7.35 (br, 5H, Ph)
$[PtMe_3I(Me_2NCH_2CH_2SePh)]$	0.68(72.1)	1.52(70.9)	1.65(72.1)	2.35 [s, 3H, J(Pt—H) = 15 Hz, NMe]; 3.08 [s, 3H, J(Pt—H) = 10 Hz, NMe]; 3.40 (br, m, CH_2CH_2); 7.40 (br, Ph)
$[Me_2NCH_2CH_2TePh]$	—	—	—	2.28 (s, 6H, NMe_2); 2.76 (t, 2H, $TeCH_2$); 3.06 (t, 2H, NCH_2); 7.19–7.72 (m, 5H, Ph)
$[PtMe_3Cl(Me_2NCH_2CH_2TePh)]$	0.69(74.7)	1.25(67)	1.44(72.6)	2.32 [s, 3H, NMe, ^3J(Pt—H) = 14.5 Hz]; 2.72 [s, 3H, NMe, ^3J(Pt—H) = 10 Hz]; 2.82 (m), 3.05 (m), 3.30 (m), 3.80 (m) (CH_2CH_2); 7.34 (br, 5H, Ph)
$[PtMe_3Br(Me_2NCH_2CH_2TePh)]$	0.77(74.7)	1.34(68)	1.53(73)	2.31 [s, 3H, NMe, ^3J(Pt—H) = 14 Hz]; 2.81 [s, 3H, NMe, ^3J(Pt—H) = 9.6 Hz]; 2.90 (br), 3.10 (m), 3.33 (m), 3.85 (m) (CH_2CH_2); 7.34 (br, 5H, Ph)
$[PtMe_3I(Me_2NCH_2CH_2TePh)]$	0.89(72)	1.50(69)	1.67(71)	2.29 [s, 3H, NMe, ^3J(Pt—H) = 14 Hz]; 2.93 [s, 3H, NMe, ^3J(Pt—H) = 9 Hz]; 2.80 (m), 3.20 (m), 3.35 (m), 3.90 (m) (CH_2CH_2); 7.34 (br, 5H, Ph)

[a] s = singlet; d = doublet; t = triplet; m = multiplet; br = broad.

three different ligands, *i.e.* N, E and X, exist at room temperature or interconversion between different isomers is rapid on the NMR time scale. The most shielded resonance in the ^1H NMR spectrum was assigned to the Pt—Me *trans* to halide, while the most deshielded resonance was attributed to the methyl group *trans* to the chalcogen atom. The remaining third resonance appearing between these two resonances was assigned to Pt—Me *trans* to nitrogen. The $^2J(^{195}Pt—^1H)$ lies in the range 69–73 Hz.

The ^1H NMR spectra of the free ligand exhibited a singlet for NMe_2 protons, two triplets or multiplets for methylene protons and expected resonances for ER residue. On complexation the methyl groups of the NMe_2 moiety became anisochronous, since two signals flanked with platinum satellites were observed. One of the methyl signals was little affected in its position from the free ligand and showed larger $^3J(^{195}Pt—^1H)$ (*ca* 15 Hz). The other resonance with a smaller value of $^3J(^{195}Pt—^1H)$ (*ca* 10 Hz) was considerably deshielded; it showed marked halogen dependence and moved to higher frequencies with increasing size of the halogen atom. The magnitude of $^3J(^{195}Pt—^1H)$ has been reported in the range 10–28 Hz, depending on the nature of the ligand.[6,12,16] The ligand methylene protons appeared as a complex multiplet.

For six-coordinate *fac*-$PtMe_3XNE$ complexes two enantiomers (**A** and **B**) with opposite configuration around the metal centre are possible; each one can exist in two isomeric forms (**A**, **C** and **B**, **D**) depending on the orientation of the R group on the chalcogen atom. The room-temperature NMR data discussed above indicate that only one form is present in solution. However, at room temperature a rapid interconversion between these forms is likely. Thus, the low-temperature ^1H NMR spectrum of $[PtMe_3I(Me_2NCH_2CH_2SBu^t)]$ was recorded in CD_2Cl_2 at 500 MHz (Fig. 1). Except the PtMe resonance *trans* to N, all the resonances

Table 2. ^{13}C NMR spectral data for $[PtMe_3X(Me_2NCH_2CH_2ER)]$ in $CDCl_3$

Complex	Pt—Me carbons[a]			Ligand carbon			
	Trans to X	*Trans* to N	*Trans* to E	NMe_2	N—CH_2	E—CH_2	ER
$[PtMe_3I(Me_2NCH_2CH_2SBu^t)]$	11.2(719)	−9.6(642)	7.2(664)	46.9 54.3	65.3	28.7	29.7 (Me) 51.3 (C)
$[PtMe_3I(Me_2NCH_2CH_2Stol)]$	12.9	−9.2	4.4	47.7 54.9	63.8	32.4	21.0 (Me) 125.0 127.2 (*o*/*m*) 130.1 (*o*/*m*) 138.5
$[PtMe_3Cl(Me_2NCH_2CH_2SPh)]$	6.6(744)	−8.3(658)	7.2(683)	47.5 49.7	62.7	32.6	127.7 128.3 129.3
$[PtMe_3Br(Me_2NCH_2CH_2SPh)]$	4.9(731)	−8.6(659)	5.9(683)	47.6 51.4	62.8	32.3	127.3 128.2 129.3
$[PtMe_3I(Me_2NCH_2CH_2SPh)]$	12.9(717)	−9.2(650)	4.6(672)	47.7 54.8	63.2	32.1	127.1 128.2 129.3
$[Me_2NCH_2CH_2SePh]$				44.2	58.5	24.7	125.6 126.7 130.5 131.2
$[PtMe_3I(Me_2NCH_2CH_2SePh)]$	12.9(713)	−11.1(650)	6.6(669)	48.0 54.7	64.2	26.4	125.6 128.5 128.9 129.8
$[PtMe_3I(Me_2NCH_2CH_2TePh)]$	12.7	−13.6	10.1	47.3 53.1	65.4	9.1	128.2 129.1 132.7

[a] Values in parentheses are $^1J(^{195}Pt—^{13}C)$ in H_3.

showed broadening at various temperatures and on further lowering the temperature resonances separated into two peaks attributable to two isomeric forms, which are present in a 2:3 ratio. Room-temperature ^1H NMR in CD_2Cl_2: δ 1.00 [^2J(Pt—H) = 70.0 Hz, *trans* to I]; 1.40 [^2J(Pt—H) = 70.9 Hz, *trans* to N], 1.52 [^2J(Pt—H) = 72.3 Hz, *trans* to S] (Pt—Me); 1.50 (s, SBu^t); 2.29 [^3J(Pt—H) = 14.6 Hz], 3.02 [^3J(Pt—H) = 11.0 Hz] (NMe_2). At −60°C, isomer **I** (40%): 1.15 [^2J(Pt—H) = 72.5 Hz *trans* to I], 1.25 [^2J(Pt—H) = 71.0 Hz *trans* to N], 1.34 [^2J(Pt—H) = 71.6 Hz *trans* to S] (Pt Me); 1.33 (s, Bu^t); 2.31 [^3J(Pt—H) = 14.8 Hz], 2.86 (NMe_2). Isomer **II** (60%): 0.75 [^2J(Pt—H) = 69.4 Hz, *trans* to I]; 1.25 [^2J(Pt—H) = 71.0 Hz *trans* to N]; 1.32 [^2J(Pt—H) = 71.5 Hz *trans* to S] (Pt Me); 1.46 (s, Bu^t); 2.13 [^3J(Pt—H) = 14.8 Hz], 3.00 (NMe_2). This suggests that these molecules have dynamic stereochemistry in solution and interconversion between two forms is rapid on the NMR time scale at room temperature. The Pt—Me signal *trans* to N did not broaden in the temperature range 27 to −60°C, but was gradually shielded by 0.15 ppm on cooling the solution down to −60°C. For both the isomers the Pt—Me *trans* to N has the same chemical shift.

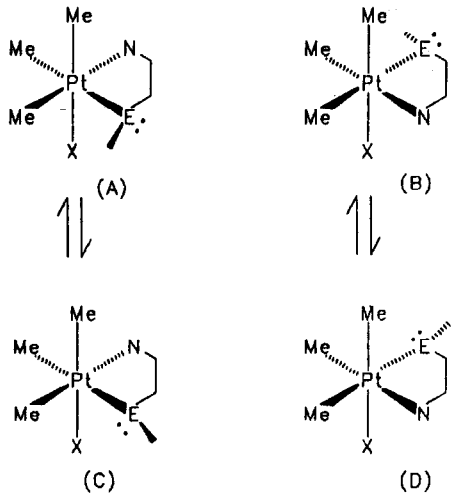

As is evident from Table 2 the platinum–methyl

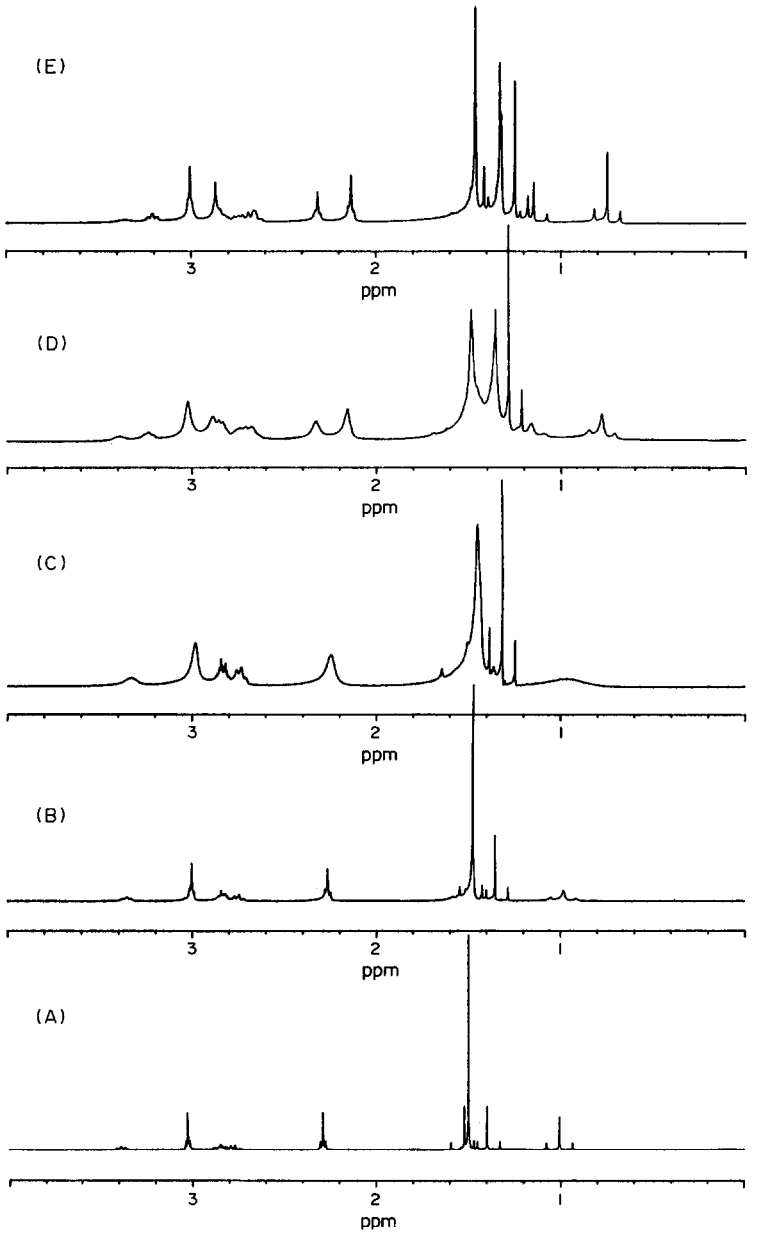

Fig. 1. Variable-temperature ^1H NMR spectra of [$PtMe_3I(Me_2NCH_2CH_2SBu^t)$] in CD_2Cl_2; (A) 27°C; (B) 0°C; (C) −20°C; (D) −40°C; (E) −60°C.

carbon resonances show halogen dependence. The magnitude of $^1J(^{195}Pt—^{13}C)$ for the methyl group *trans* to X is significantly greater than the value observed for the methyl group *trans* to nitrogen or *trans* to the chalcogen atom. The observed values of ^1J(Pt—C) reflect the *trans* influence of various ligands.[17] The magnitude of ^1J(Pt—C) for the methyl group *trans* to halogen also varies with the nature of the halogen atom and follows a trend of ^1J(*trans*-Cl) > ^1J(*trans*-Br) > ^1J(*trans*-I). This is consistent with the *trans* influence of the halogen atoms.[6,10,17]

As with the ^1H NMR spectra $^{13}C\{^1H\}$ displayed two resonances for the NMe_2 carbons with vanishingly small $^2J(^{195}Pt—^{13}C)$. The magnitude of ^2J(Pt—C) in platinum(IV) complexes varies between 3.4 and 108 Hz.[8,10,16] The methylene carbon attached to the ER group was progressively shielded on going from sulphur to selenium to tellurium. This is consistent with the trend of higher shielding with decreasing electronegativity of the atom in analogous compounds.[18]

The structure deduced from NMR data has been established by a single-crystal X-ray study of one

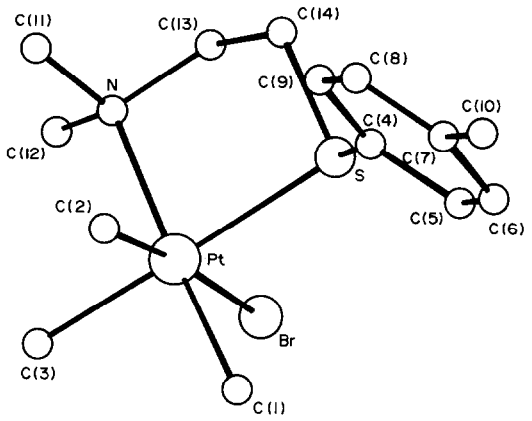

Fig. 2. PLUTO plot of $[PtMe_3Br(Me_2NCH_2CH_2SC_6H_4Me\text{-}4)]$.

representative molecule. The structural analysis of $[PtMe_3Br(Me_2NCH_2CH_2SC_6H_4Me\text{-}4)]$, shown in Fig. 2, revealed that the molecule crystallizes in isomeric form **C**. The central platinum atom is coordinated by three *fac* methyl groups and the nitrogen, sulphur and bromine atoms with the SC_6H_4Me-4 group *cis* to bromide. The configuration about platinum is distorted octahedral with interbond angles in the range 83.9(2)–96.8(4)° for right angles and 174.8(4)–177.4(4)° for linear arrays. The geometry around sulphur is distorted tetrahedral, angles being CH_2SPt 97.7°, CH_2S—tol 104.3° and tol—S—Pt 113.6°. Selected bond lengths and angles are given in Table 3.

The Pt—C distances *trans* to sulphur or bromide are essentially identical, however, the Pt—C distance *trans* to N is shorter. The Pt—C distances are in agreement with those reported earlier for methylplatinum(IV) complexes.[2,10,19,20] The Pt—S distance [2.437(3) Å] is similar to the values found for the trimethyl platinum(IV) complexes with thioether ligands.[10,21] The Pt—N distance [2.310(9) Å] is significantly longer than the values reported for $[PtMe_3I\{(Me_2pz)_2CH_2\}]$ [2.236(4) Å][2] and $[PtMe_3(SSPPh_2)(py)]$ [2.239(9) Å].[20] The Pt—Br distance [2.618(2) Å] is slightly shorter than the distance reported in $[(PtMe_3Br)_2(MeSeSeMe)]$ (mean value 2.629 Å).[22]

The plane defined by PtC(1)C(3)NS atoms (plane **I**) is nearly planar. The five-membered PtNC(13)C(14)S ring (plane **II**) is distinctly non-planar; the maximum deviation of one of the atoms being −0.358 Å. This lies more or less perpendicular to the planar tolyl ring (dihedral angle 78.0°). The dihedral angle between planes **I** and **II** is $4.71 \pm 1.22°$.

EXPERIMENTAL

Trimethylplatinum iodide,[23] $[PtMe_3X]_4$,[24] Ph TeTePh[25] and MeC_6H_4SH were prepared as described in the literature. Diphenyldiselenide (PhSeSePh) (Aldrich), PhSH (Fluka), Bu^tSH (Fluka) and $Me_2NCH_2CH_2Cl \cdot HCl$ were obtained from commercial sources. Analytical grade solvents were used throughout. ^1H NMR spectra were re-

Table 3. Selected bond distances (Å) and angles (°) with e.s.d.s for $[PtMe_3Br(Me_2NCH_2CH_2Stol)]$

Pt—Br	2.618(2)	S—C(4)	1.78(1)
Pt—S	2.437(3)	S—C(14)	1.79(1)
Pt—N	2.310(9)	N—C(11)	1.53(1)
Pt—C(1)	2.05(1)	N—C(12)	1.50(1)
Pt—C(2)	2.07(1)	N—C(13)	1.51(1)
Pt—C(3)	2.07(1)	C(13)—C(14)	1.53(2)
Br—Pt—S	86.45(7)	C(1)—Pt—C(3)	89.1(5)
Br—Pt—N	89.9(2)	C(2)—Pt—C(3)	85.6(5)
Br—Pt—C(1)	90.0(4)	Pt—S—C(4)	113.6(4)
Br—Pt—C(2)	174.8(4)	Pt—S—C(14)	97.7(4)
Br—Pt—C(3)	91.4(3)	C(4)—S—C(14)	104.3(5)
S—Pt—N	83.9(2)	Pt—N—C(11)	113.7(6)
S—Pt—C(1)	93.6(4)	Pt—N—C(12)	112.6(7)
S—Pt—C(2)	96.8(4)	Pt—N—C(13)	105.8(6)
S—Pt—C(3)	176.6(3)	C(11)—N—C(12)	107.1(9)
N—Pt—C(1)	177.4(4)	C(11)—N—C(13)	110.2(9)
N—Pt—C(2)	94.4(4)	C(12)—N—C(13)	107.4(8)
N—Pt—C(3)	93.6(4)	N—C(13)—C(14)	111.7(8)
C(1)—Pt—C(2)	85.8(5)	S—C(14)—C(13)	109.0(8)

corded on a Bruker AC-200 or Bruker AMX-500 NMR spectrometer. Variable-temperature ^1H NMR experiments were performed in CD_2Cl_2 on a Bruker AMX-500 NMR spectrometer. ^{13}C NMR spectra were recorded on a Bruker AC-200 NMR spectrometer operating at 50 MHz. Chemical shifts are relative to an internal chloroform peak (δ 7.26 ppm for ^1H and δ 77.0 ppm for ^{13}C). Microanalyses were provided by the Analytical Chemistry Division of B.A.R.C. Melting points were determined in capillary tubes and are uncorrected.

Synthesis of $Me_2NCH_2CH_2SPh$

To a solution of NaSPh [prepared from sodium (427 mg, 18.6 mmol) in methanol and thiophenol (2 cm^3, 19.5 mmol)] was added freshly distilled and dried $Me_2NCH_2CH_2Cl$ (2.01 g, 18.7 mmol)[26] with vigorous stirring under nitrogen atmosphere. This was stirred at room temperature for 15 h and filtered. The filtrate was dried *in vacuo* to give a pale yellow liquid which was stored in the fridge. Similarly $Me_2NCH_2CH_2SBu^t$ and $Me_2NCH_2CH_2SC_6H_4Me$-4 were prepared.

Synthesis of $Me_2NCH_2CH_2TePh$

To a benzene–methanol solution of NaTePh [prepared from PhTeTePh (786 mg, 1.92 mmol) and methanaolic $NaBH_4$ solution[25]] was added an excess of $Me_2NCH_2CH_2Cl$ (622 mg, 5.79 mmol) with stirring under nitrogen atmosphere. The reactants were stirred at room temperature for 3 h. The solvents were evaporated *in vacuo*. The residue was extracted with hexane and filtered under a nitrogen atmosphere. The solvent was stripped off *in vacuo*

Table 4. Analysis, m.p.s and yield of [$PtMe_3X(Me_2NCH_2CH_2ER)$]

Complex	Yield[a] (%)	M.p. (°C)	Analysis: Found (Calc.) (%) C	H	N
[$PtMe_3Cl(Me_2NCH_2CH_2SBu^t)$]	47	115	30.1 (30.2)	6.4 (6.5)	3.0 (3.2)
[$PtMe_3Br(Me_2NCH_2CH_2SBu^t)$]	53	123	27.3 (27.4)	5.9 (5.9)	2.7 (2.9)
[$PtMe_3I(Me_2NCH_2CH_2SBu^t)$]	36	128	24.8 (25.0)	5.2 (5.3)	2.3 (2.6)
[$PtMe_3Cl(Me_2NCH_2CH_2Stol)$]	35	158	35.6 (35.7)	5.5 (5.6)	2.7 (3.0)
[$PtMe_3Br(Me_2NCH_2CH_2Stol)$]	29	161	32.3 (32.6)	5.0 (5.1)	2.2 (2.7)
[$PtMe_3I(Me_2NCH_2CH_2Stol)$]	23	185	29.4 (29.9)	4.6 (4.7)	2.1 (2.5)
[$PtMe_3Cl(Me_2NCH_2CH_2SPh)$]	29	133	34.4 (34.2)	5.6 (5.3)	3.0 (3.1)
[$PtMe_3Br(Me_2NCH_2CH_2SPh)$]	51	140	30.9 (31.1)	4.8 (4.8)	2.4 (2.8)
[$PtMe_3I(Me_2NCH_2CH_2SPh)$]	47	155	28.2 (28.5)	4.4 (4.4)	2.4 (2.5)
[$PtMe_3Cl(Me_2NCH_2CH_2SePh)$]	40	123	30.8 (31.0)	4.8 (4.8)	2.6 (2.8)
[$PtMe_3Br(Me_2NCH_2CH_2SePh)$]	40	145	28.7 (28.5)	4.4 (4.4)	2.5 (2.5)
[$PtMe_3I(Me_2NCH_2CH_2SePh)$]	23	163	26.0 (26.2)	4.1 (4.1)	2.0 (2.3)
[$PtMe_3Cl(Me_2CH_2CH_2TePh)$]	29	126	28.3 (28.3)	4.1 (4.4)	2.1 (2.5)
[$PtMe_3Br(Me_2NCH_2CH_2TePh)$]	38	148	26.0 (26.2)	4.1 (4.0)	2.1 (2.3)
[$PtMe_3I(Me_2NCH_2CH_2TePh)$]	40	115	24.6 (24.2)	3.7 (3.8)	1.9 (2.2)

[a] All complexes were recrystallized from an acetone–diethylether–hexane mixture at 0°C as white or cream coloured solids.

to give an orange–red liquid, which was used immediately. $Me_2NCH_2CH_2SePh$ was similarly prepared, however, only 1 equivalent of 2-dimethylaminoethylchloride was used.

Synthesis of $[PtMe_3I(Me_2NCH_2CH_2SPh)]$

To a benzene solution of $[PtMe_3I]_4$ (107 mg, 0.073 mmol) was added a solution of $Me_2NCH_2CH_2SPh$ (53 mg, 0.29 mmol) with stirring. The reactants were stirred for 4 h and the solvent was evaporated under vacuum. The residue was dissolved in an acetone–ether–hexane mixture (1 : 1 : 2 v/v), which on cooling at 0°C afforded cream-coloured crystals of the title complex in 47% yield. Other complexes were prepared similarly and pertinent data are summarized in Table 4.

Crystallography

All diffraction measurements were performed at room temperature on an Enraf–Nonius CAD-4 diffractometer using graphite monochromatised Mo-K_α radiation, $\lambda = 0.71069$ Å. The unit cell was determined from 25 ($6° < \theta < 11°$) randomly selected reflections using the automatic search, index and least-squares routines. The refined cell constants and other relevant crystal data for the colourless plates of $[PtMe_3Br(Me_2NCH_2CH_2SC_6H_4Me\text{-}4)]$ (size $0.15 \times 0.30 \times 0.30$ mm) are presented in Table 5. All the data were corrected for Lorentz and polarization effects. An empirical absorption correction was applied to the data by measuring the intensities of four reflections with θ near 90° for different ψ values ($0° < \psi < 360°$, every 10°) and using the EAC program, from the Enraf–Nonius package. The maximum and minimum transmission were 0.99 and 0.23, respectively. Two standard reflections (2, 2–27 and 4, 2–7) measured every 1800 s showed no intensity variation.

Table 5. Crystal data and refinement details for $[PtMe_3Br(Me_2NCH_2CH_2Stol)]$

Formula	$C_{14}H_{26}NSBrPt$
Molecular weight	515.4
Crystal system	Monoclinic
Space group	$P2_1/c$
a (Å)	17.232(5)
b (Å)	7.858(3)
c (Å)	12.690(2)
β (°)	101.44(2)
V (Å^3)	1684.2
Z	4
D_c (g cm^{-3})	2.031
$F(000)$	984
μ (cm^{-1})	108.64
θ limits (°)	$2 < \theta < 25$
No. of data collected	3328
No. of unique data	3195
No. of unique reflections used with $I > 3\sigma(I)$	2484
$R = [\Sigma w(\|F_o\| - \|F_c\|)/\Sigma\|F_o\|$	0.043
$R_w = [\Sigma w(\|F_o\| - \|F_c\|)^2/\Sigma w\|F_o\|^2]$	0.059
Scan technique	θ–2θ

The structure was solved by routine heavy-atom methods and refined by full-matrix least-squares with non-hydrogen atoms anisotropic. Hydrogen atoms were omitted. The weighting scheme was $w = 1/\sigma^2(F)$. A final difference map had a maximum density of 1.37 e Å^{-3} near platinum. Programs from the Enraf–Nonius SDP plus package[27] were run on a PDP 11/73 computer.

Acknowledgements—Thanks are expressed to Drs J. P. Mittal and D. D. Sood for their interest in the work. We are grateful to the Head Analytical Chemistry Division for microanalyses and the National NMR facility at TIFR for providing ^{1}H NMR spectra. R.B. thanks U.G.C., New Delhi, for providing X-ray diffraction facilities at the University of Rajasthan, Jaipur.

REFERENCES

1. V. K. Jain, G. S. Rao and L. Jain, *Adv. Organomet. Chem.* 1987, **27**, 113.
2. H. C. Clark, G. Ferguson, V. K. Jain and M. Parvez, *J. Organomet. Chem.* 1984, **270**, 365.
3. V. K. Jain, *Ind. J. Chem.* 1987, **26.A**, 1019.
4. P. K. Monaghan and R. J. Puddephatt, *J. Chem. Soc., Dalton Trans.* 1988, 595.
5. P. K. Byers, A. J. Canty, B. W. Skelton and A. H. White, *Organometallics* 1990, **9**, 826.
6. V. K. Jain and S. Chaudhury, *J. Coord. Chem.* 1992, **26**, 63.
7. E. W. Abel, S. K. Bhargava, K. Kite, K. G. Orrell, V. Sik and B. L. Williams, *J. Chem. Soc., Dalton Trans.* 1982, 583.
8. E. W. Abel, K. G. Orrell and E. W. G. Platt, *J. Chem. Soc., Dalton Trans.* 1983, 2345.
9. E. W. Abel, P. K. Mittal, K. G. Orrell and V. Sik, *J. Chem. Soc., Dalton Trans.* 1986, 961.
10. E. W. Abel, I. Moss, K. G. Orrell, V. Sik, D. Stephenson, P. A. Bates and M. B. Hursthouse, *J. Chem. Soc., Dalton Trans.* 1988, 521.
11. E. W. Abel, T. P. J. Coston, K. G. Orrell and V. Sik, *J. Chem. Soc., Dalton Trans.* 1989, 711.
12. E. W. Abel, K. G. Orrell, S. P. Scanlan, D. Stephenson, T. Kemmitt and W. Levason, *J. Chem. Soc., Dalton Trans.* 1991, 591.
13. E. W. Abell, S. K. Bhargava and K. G. Orrell, *Prog. Inorg. Chem.* 1984, **32**, 1.
14. K. G. Orrell, *Coord. Chem. Rev.* 1989, **96**, 1.

15. M. A. Ali and S. E. Livingstone, *Coord. Chem. Rev.* 1974, **13**, 101.
16. H. C. Clark, L. E. Manzer and J. E. Ward, *Can. J. Chem.* 1974, **52**, 1973.
17. T. G. Appleton, H. C. Clark and L. E. Manzer, *Coord. Chem. Rev.* 1973, **10**, 335.
18. J. Mason, *Multinuclear NMR*, Ch. 3. Plenum Press, New York (1987).
19. H. C. Clark, G. Ferguson, V. K. Jain and M. Parvez, *Organometallics* 1983, **2**, 806.
20. S. Chaudhury, V. K. Jain, V. S. Jakkal and K. Venkatasubramanian, *J. Organomet. Chem.* 1992, **424**, 115.
21. E. W. Abel, M. Booth, K. G. Orrell, G. M. Pring and T. S. Cameron, *J. Chem. Soc., Chem. Commun.* 1981, 29.
22. E. W. Abel, A. R. Khan, K. Kite, K. G. Orrell, V. Sik, T. Stanley and R. Cordes, *J. Chem. Soc., Chem. Commun.* 1979, 713.
23. J. C. Baldwin and W. C. Kaska, *Inorg. Chem.* 1975, **14**, 2020.
24. D. E. Clegg and J. R. Hall, *J. Organomet. Chem.* 1970, **22**, 491.
25. V. K. Jain and S. Kannan, *J. Organomet. Chem.* 1991, **418**, 349.
26. H. Gurien, *J. Org. Chem.* 1963, **28**, 878.
27. SDP programs for PDP-11/73. Enraf–Nonius Ltd, Delft, Holland (1983).

Polyhedron Vol. 12, No. 19, pp. 2387–2394, 1993
Printed in Great Britain

0277–5387/93 $6.00+.00
© 1993 Pergamon Press Ltd

SPECTROSCOPY OF LANTHANIDE SINGLE CRYSTALS WITH GLYCYLGLYCINE, $Ln(Gly–Gly)_2(ClO_4)_3 \cdot 4H_2O$ (Ln = Nd, Eu)

E. HUSKOWSKA and J. LEGENDZIEWICZ*

Institute of Chemistry, University of Wrocław, 50-383 Wrocław, Poland

(*Received* 27 *April* 1993; *accepted* 7 *May* 1993)

Abstract—The lanthanide(III) compound with a simple dipeptide (glycylglycine) of the formula $Ln(Gly–Gly)_2(ClO_4)_3 \cdot 4H_2O$ was obtained in the form of mono-crystals. These are the first known single crystals of lanthanides with a dipeptide. Well-resolved absorption and luminescence spectra at room and helium temperatures are reported and analysed. The bonding mode of the Ln^{3+} ions with a simple peptide is compared with the available X-ray data for the calcium compounds with diglycine and triglycine. Absorption spectra were measured along the *a*-axis in the region 9000–40,000 cm^{-1}. The probabilities of *f–f* transitions were analysed and the temperature effect on the intensities considered. Single-ion relaxation processes and cooperative effects are discussed. Stark components were determined and point symmetry was assigned. Energy level diagrams for $^4I_{9/2}$ and $^4I_{11/2}$ states are proposed. Spectroscopy results are compared with the X-ray data.

The lanthanide ions are used as isomorphic substitutes for the Ca^{2+} ion in studies of biological systems. Our recent X-ray data and spectroscopic results of model systems (Ln—amino acids), however, show that this kind of substitution could sometimes not be isomorphic.[1]

In all the cases presented the lanthanide ions create the dimeric or polymeric forms in the structure.[1–10] The type of polymer depends on the Ln : A (A = amino acid) ratio in the compounds and on the amino acid (mono-carboxylate or di-carboxylate). No similar data for lanthanide mono-crystals with simple peptides have been reported as yet. It is of course extremely important to establisih what changes, if any, occur upon metal ion substitution in systems of biological importance. In the studies of calcium bonding proteins the rather isomorphic substitution of Ca^{2+} ions by Ln^{3+} ions was stated in few cases.[11]

To solve the problem of the interaction of lanthanide ions with a simple peptide in detail we have undertaken the X-ray[1–3] and spectroscopic studies of mono-crystals with diglycine. A comparison of Ca^{2+} and Nd^{3+} ion interaction with simple peptides is made.

* Author to whom correspondence should be addressed.

EXPERIMENTAL

Mono-crystals of the title compounds were obtained from $Ln(ClO_4)_3$ aqueous solutions at pH ≈ 4; the glycylglycine concentration was maintained well below the lanthanide concentration in accordance with the method described in ref. 4. Mono-crystals of composition $Ln(Gly–Gly)_2(ClO_4)_3 \cdot 4H_2O$ precipitated from the solutions.

The concentration of the lanthanide ions in the mono-crystals was determined complexometrically. The density D_m (g cm^{-3}) = 2.089 was found using the flotation method in a mixture of 1,2-dibromoethane and chloroform.

Spectroscopic measurements

Absorption spectra of the neodymium single crystal were measured using a Cary–Varian spectrophotometer at 300 and 5 K. Stark components were determined in the spectra obtained at 5 K. The absorption spectra obtained at room temperature were used for the *f–f* transition intensity analysis. Oscillator strength values of the electronic transitions were calculated over the measured spectral range by the graphical integration method. These values were used in the calculation of τ_λ parameters

Table 1. Oscillator strength values of f–f transitions for a single crystal of Nd(Gly–Gly)$_2$(ClO$_4$)$_3$·4H$_2$O

S'L'J'	Spectral region (Å)	$P_{exp} \times 10^8$ $T = 295$ K	$T = 123$ K	$T = 5$K
$^4F_{3/2}$	8420–9200	232.5	207.2	
$^4F_{5/2}$, $^2H_{9/2}$	7730–8400	955.5[a]	783.5	508.3
$^4F_{7/2}$, $^4S_{3/2}$	7140–7730	995.8[a]	876.3	547.7
$4F_{9/2}$	6540–7040	91.6	85.2	
$2H_{11/2}$	6160–6540	22.9	18.9	
$^2G_{5/2}$, $^2G_{7/2}$	5500–6100	1497.1[a]	1047.9	838.4
$^4G_{7/2}$, $^2K_{13/2}$, $^4G_{9/2}$	4930–5450	762.2	701.7	
$^2G_{9/2}$, $^2D_{3/2}$, $^4G_{11/2}$, $^2K_{15/2}$	4500–4930	253.5	240.8	
$^2P_{1/2}$, $^2D_{5/2}$	4100–4400	41.4	39.1	
$^4D_{3/2}$, $^4D_{5/2}$, $^4D_{1/2}$, $^2I_{11/2}$	3370–3740	828.5	761.7	
$^2L_{15/2}$, $^4D_{7/2}$, $^2I_{13/2}$, $^2L_{17/2}$	3200–3370	242.0	230.0	

$\tau_2 = 5.49 \pm 0.71 \times 10^{-9}$, $\tau_4 = 4.43 \pm 0.61 \times 10^{-9}$, $\tau_6 = 12.13 \pm 0.94 \times 10^{-9}$.
[a]Mean value from two orientations of crystals.

from the Judd relation.[12] The calculation procedure is described in refs 7–9.

The fluorescence spectra of the neodymium and europium compounds were measured using a GDM 100 grating monochromator with a cooled photomultiplier tube. An ILA 120 argon laser was used as the excitation source (λ_{exc} = 488, 514 nm); Eu^{3+} ions were excited by a xenon lamp (λ_{exc} = 395 nm); the spectrum were recorded at 77 K on an SLM "Aminco" SPF 500 spectrofluorometer.

RESULTS AND DISCUSSION

The results of the spectroscopic studies of the monocrystals of the title compounds are presented in Tables 1–3 and Figs 1–4. The problems we

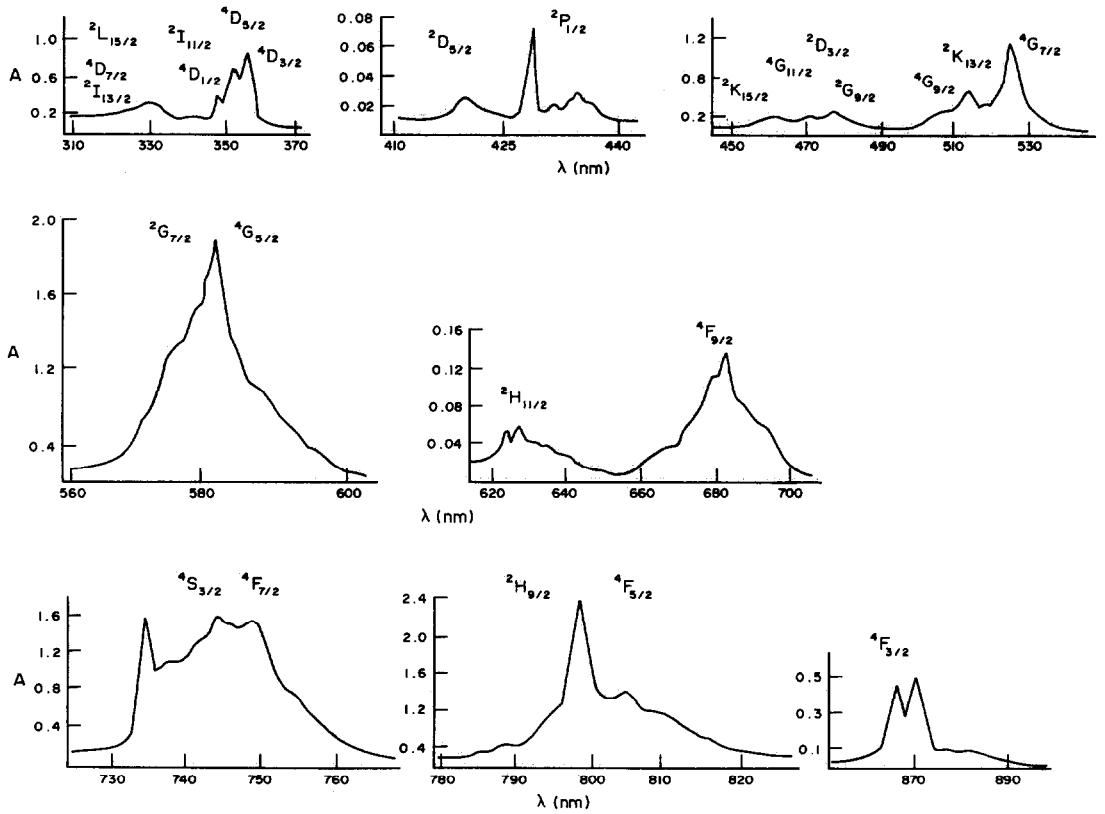

Fig. 1. Absorption spectrum of the Nd(Gly–Gly)$_2$(ClO$_4$)$_3$·4H$_2$O single crystal at room temperature.

Table 2. Experimental energy levels of Nd^{3+} in the $Nd(Gly–Gly)_2(ClO_4)_3 \cdot 4H_2O$ crystal

Term	E (cm^{-1})	Term	E (cm^{-1})	Term	E (cm^{-1})	Term	E (cm^{-1})
$^4I_{9/2}$	0	$^4F_{7/2}$	13,436	$^2K_{13/2}$	19,468	$^2P_{1/2}$	23,312
	90		13,490		19,532		
	196	$^4S_{3/2}$	13,554	$^4G_{9/2}$	19,544	$^2D_{5/2}$	23,805
	288		13,563		19,553		23,873
	381	$^4F_{7/2}$	13,611		19,578		23,952
			13,618		19,596		
$^4I_{11/2}$	1999				19,614	$^2P_{3/2}$	26,198
	2032	$^4F_{9/2}$	14,732		19,630		26,267
	2128		14,763		19,657		
	2136		14,792		19,669	$^4D_{3/2}$	28,063
	2157		14,820		19,694		28,144
	2171		14,877		19,734		
					19,871	$^4D_{5/2}$	28,280
$^4I_{15/2}$	5857	$^2H_{11/2}$	15,930		13,436		28,342
	5912		15,947	$^2G_{9/2}$	21,054		28,399
	6011		15,975		21,070		
	6098		16,019		21,088	$^4D_{1/2}$	28,690
	6129		16,033		21,097		
	6381		16,062		21,156	$^2I_{11/2}$	29,181
	6398						29,289
	6461	$^4G_{5/2}$	17,163	$^2D_{3/2}$	21,222		29,380
			17,199		21,276		29,419
$^4F_{3/2}$	11,488	$^2G_{7/2}$	17,274				29,531
	11,554		17,331	$^4G_{11/2}$	21,414		
			17,373		21,482	$^2L_{15/2}$	30,004
$^4F_{5/2}$	12,512		17,391	$^2K_{15/2}$	21,531		30,127
	12,536		17,464		21,570	$^4D_{7/2}$	30,211
	12,565				21,598		30,294
		$^2L_{15/2}$			21,633	$^2I_{13/2}$	30,406
$^2H_{9/2}$	12,591				21,650		30,493
	12,622	$^4G_{7/2}$	19,043		21,700		30,551
	12,694		19,084		21,739		30,600
	12,750		19,116		21,800		30,675
	12,783		19,195		21,847		30,812
					21,886		30,915

wanted to solve by spectroscopic studies and by comparison with the results from the X-ray analysis in this paper are the following: (1) To elucidate how possible changes in the structure are reflected in such spectroscopic properties of a single crystal as intensity of the hypersensitive transition, point symmetry of the lanthanide ions, splitting and broadening of the electronic lines, the appearance of sidebands of the main electronic lines, etc. (2) Discussion of similarities and differences between the title compound and other lanthanide systems with amino acids. (3) Finally, we would like to consider the mechanism of the radiative transition intensity, based on the room and helium temperature measurements, vibronic coupling and cooperative effect.

Before analysing the spectroscopic results of the title compound let us recall the X-ray data. We obtained a series of single crystals of lanthanides with amino acids[1–10] and found the dimeric or polymeric forms in the solid state, although none involved the hydroxide linkages. The reason for such a situation was probably precipitation from the solution at $pH \leqslant 4$. The results of the lanthanide interaction with glycine and polyglycine in solution were reported recently by Brittain.[13] He found that the degree of association by hydroxide linkages was less for complexes with diglycine compared with those of glycine and also suggested that the steric nature of the amino acid ligand played a dominant role in determining the degree of association.

In our studies of the formation of polymeric

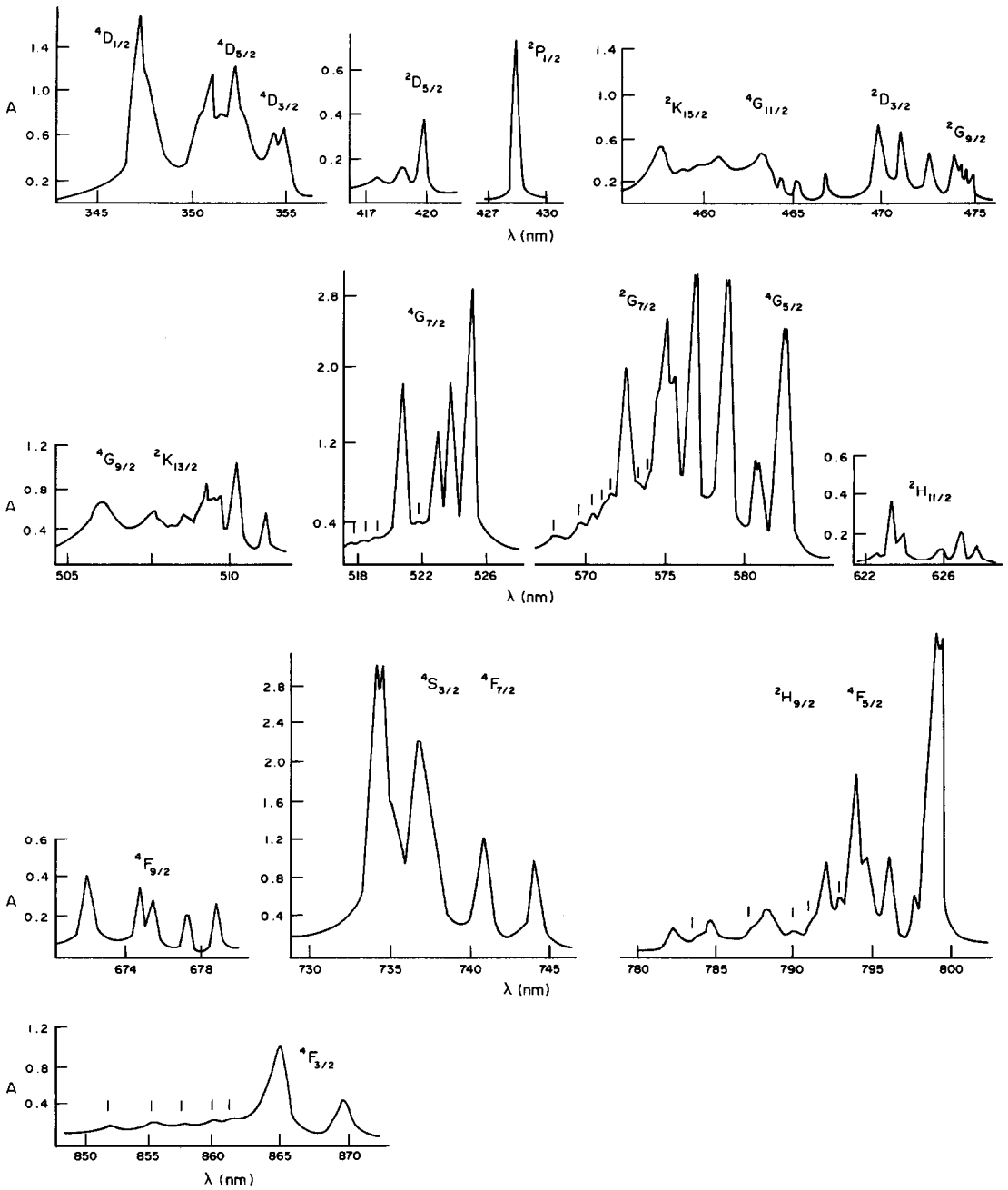

Fig. 2. Absorption spectrum of the neodymium single crystal at 5 K (|—vibronic lines).

species (even in the case of mono-carboxylate amino acids) the carboxyl bridges of Ln—O—C—O—Ln or

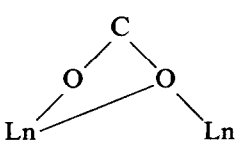

types always participate.[4]

Comparison of the available crystal structure data for Ca^{2+} complexes with glycylglycylglycine[14] with the respective data of $Nd(Gly–Gly)_2(ClO_4)_3 \cdot 4H_2O$[1–3,15] leads to the following statement: in both mono-crystals containing the peptide the Ca^{2+} and Ln^{3+} ions are bonded by the carboxyl and carbonyl group oxygens. However, the coordination numbers are different. The Ca^{2+} ions are bonded to seven oxygen atoms forming approximately a pentagonal bipyramid, but the Ln ions

Table 3. Vibronic components in the absorption spectrum of $Nd(Gly–Gly)_2(ClO_4)_3 \cdot 4H_2O$ ($T = 5K$)

Transition	Energy (cm^{-1})	ΔE (from O-phonon line) (cm^{-1})	
$^4I_{9/2} \rightarrow {}^4F_{3/2}$	11,488		
	11,602	114	δ(ONdO)
	11,631	143	
	11,652	164	
	11,684	196	
	11,731	243	ν(NdO)
$^4I_{9/2} \rightarrow {}^4F_{5/2}$	12,512		
	12,630	118	δ(ONdO)
	12,660	145	
	12,713	198	
	12,760	244	ν(NdO)
	12,565		
	12,683	118	δ(ONdO)
	12,760	195	
$^4I_{9/2} \rightarrow {}^2H_{9/2}$	12,594		
	12,792	198	δ(ONdO)
$^4I_{9/2} \rightarrow {}^4G_{5/2}$	17,163		
	17,406	243	ν(NdO)
	17,490	327	
	17,199		
	17,396	197	δ(ONdO)
	17,438	239	
	17,529	330	ν(NdO)
	17,279		
	17,422	143	δ(ONdO)
	17,520	241	ν(NdO)
$^4I_{9/2} \rightarrow {}^2G_{7/2}$	17,331		
	17,445	114	δ(ONdO)
	17,576	245	ν(NdO)
	17,373		
	17,494	121	δ(ONdO)
	17,513	140	
$^4I_{9/2} \rightarrow {}^4G_{7/2}$	19,045		
	19,161	116	δ(ONdO)
	19,238	193	
	19,278	243	ν(NdO)
	19,316	271	

δ = stretching, ν = bending.

create the nine-coordinate polyhedra with oxygen atoms which belong to the carboxyl groups of different peptides, carbonyl groups and water molecules.[3] Although in both compounds similar carboxyl bridges of the (a) type bond to two different

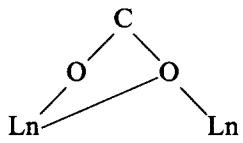

metal ions, the addition of two Ln—O—C—O—Ln (b) type bridges strengthens the bonding between the two lanthanide ions.[1–3] Such a situation can influence the rate of the exchange of lanthanide ions in the peptide and can lead to differences in exchange rates for Ca^{2+} and Ln^{3+} ions. It could also explain the immediate exchange of Ca^{2+} ions by Ln^{3+} ions after their addition to the calcium binding protein. However, in the case of diglycine calcium ions are coordinated in a different manner and the coordination number is 6.

The X-ray studies of lanthanide compound with diglycine indicate the formation of polymeric forms in the structure involving the carboxyl bridge and the carbonyl group in coordination, thus forming the infinite polymeric chains.[1,3] In such a way the fragments of lanthanide ion pairs, coordinated as in single crystals of complexes with glycine and glutamic acid,[4,8] are repeated in the structure. The differences are given by the chelating properties of the carboxyl and carbonyl oxygens existing in the dipeptide simultaneously.

Since lanthanide ions are treated as spectroscopic probes in studies of biological systems in solution and the solid state, it seemed important to study how those structural factors would influence the spectroscopic properties of the lanthanide ion. The intensity analysis data presented in Table 1 show that the oscillator strength values for some f–f transitions remain almost unchanged in comparison to other lanthanide systems with amino acids[1–10] and aqua ions, but a significant increase was observed for hypersensitive transitions (that obey the selection rule $\Delta J \leqslant 2$ and $\Delta S = 0$) and some transitions observed in the IR region ($^4I_{9/2} \rightarrow {}^4F_{5/2}$, $^2H_{9/2}$; $^4S_{3/2}$, $^4F_{7/2}$), see Table 1. The oscillator strength of the hypersensitive transition is similar to that in the single crystal spectra (in one orientation) of the glutamic acid complex.[1,5] This means that although there are differences observed in the coordination of the Nd^{3+} ion, bonding lengths and point symmetry remain similar. However, a precise comparison will be achieved when a big enough single crystal of the title compound is obtained and spectroscopic data at the different crystal orientations can be measured (since the crystals are biaxial). Up to now, however, we have not been able to obtain a crystal suitable for such studies.

The bonding mode of the carboxyl group in both cases remains the same. The additional chelate

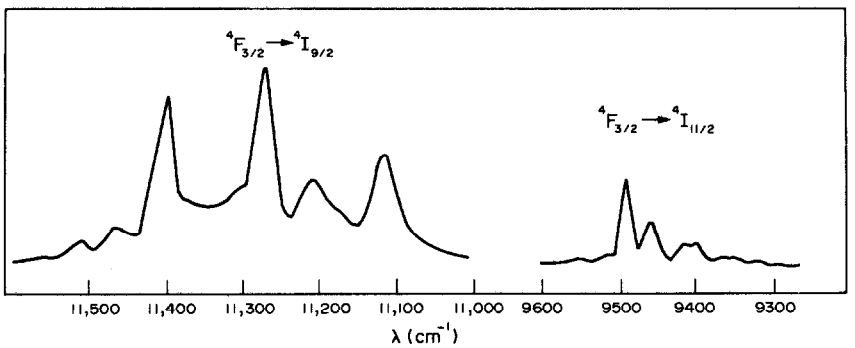

Fig. 3. Fluorescence spectrum of the neodymium single crystal at 5 K.

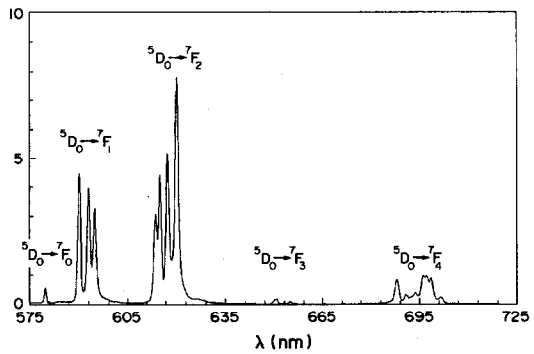

Fig. 4. Fluorescence spectrum of the europium compound at 77 K.

coordination of the CO group of the peptide, however, does not cause a significant change in the direct Nd^{3+} ion environment, so the spectroscopic properties and intensity of these two systems are comparable at room temperature. A subtle distortion of molecular symmetry for four sites of Nd^{3+} in the glutamic acid compounds is not detectable in the room temperature spectra.[5,8]

It is worth noting that in both the absorption and luminescence spectra significant broadening of the optical lines is observed, being, however, less than that observed in the spectra of single crystals with DL-alanine[5,6,15] (Figs 2–4). The differences between the structures are as follows: in the former structure the polymeric chain is formed by linking the dimeric subunits; in the latter dimers are only formed with equivalent lanthanide ions positions, so only one site is occupied. Ln—Ln distances are 3.996 and 4.439 Å, respectively. In both systems the ion pair interactions could lead to the broadening of the optical lines or to the appearance of additional lines (see Figs 2–4).

Regarding the subject of the splitting patterns of luminescence bands (see Fig. 4), $^5D_0 \rightarrow {}^7F_J$ transitions show the C_{2v} point symmetry[16] for the Eu^{3+} ion and also for the Nd^{3+} ion, since the neodymium and europium single crystals are isomorphic. Figure 4 pictures the luminescence spectrum in the region 5780–7500 Å with the Stark components found for 0–0, 0–1, 0–2, 0–3 and 0–4 transitions. The group theory consideration allowed us to assign for 0–0 A_1, 0–1 A_2, B_1, B_2, 0–2 $2A_1$, B_1, B_2, 0–3 A_1, $2B_1$, $2B_2$ and for 0–4 $3A_1$, $2B_1$, $2B_2$ components.[16] The spectroscopy data obtained at 5 K in the region of the $^4I_{9/2} \rightarrow {}^2P_{1/2}$ transition indicate that only one position is occupied by the Nd^{3+} ion, thus confirming the X-ray crystallography data (Fig. 2). These results differ significantly from those for the glycine complex with neodymium, where two different symmetry positions were stated, and for the L-glutamic acid complex with neodymium, where four symmetry sites were found at 5 K.[1,15] Those four positions were not exhibited in the spectra at 77 K.[8]

On the basis of absorption spectra at 300 and 5 K and luminescence spectra at 5 K (see Fig. 3) the energy level diagrams are proposed (Table 2). It was found that splitting of the $^4I_{9/2}$ ground state is equal to 378 cm^{-1} and is almost the same as for other systems with coordination number = 9.[17] Table 2 includes the Stark components of transitions observed in measured spectral regions. The

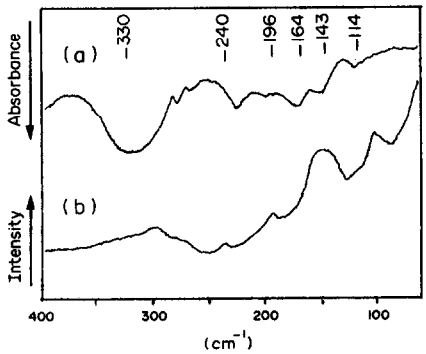

Fig. 5.(a) IR and (b) Raman spectra of the Nd(Gly–Gly)$_2$(ClO$_4$)$_2$·4H$_2$O crystal.

splitting pattern corresponds to the energy level scheme determined by Carnall *et al.* in the absorption spectra of Nd^{3+} ions doped into single crystals of LaF_3 with C_{2v} point symmetry.[18] Figure 2 shows the absorption spectrum of a single crystal of $Nd(Gly–Gly)_2(ClO_4)_3 \cdot 4H_2O$ at 5 K. The complex structure of bands is striking, mainly of those related to the transitions which obey the selection rule $|\Delta J| = 2, 0$; $^4I_{9/2} \rightarrow {}^4G_{5/2}$, $^2G_{7/2}$; $^4F_{5/2}$, $^2H_{9/2}$. This structure is accompanied by the greatest intensity differences as a function of temperature (Table 1).

The weak satellite lines in the high energy range of these bands result from vibronic coupling and ion pair interactions. The electron–phonon interactions were observed in the spectra of coordination compounds with organic ligands by Caro *et al.*[19,20] and by us.[15,21–23] The mechanisms of these transitions were interpreted as interference between respective energy differences of Stark components and phonons of organic molecules. The vibronic components in emission and excitation spectra of europium and gadolinium inorganic systems were widely investigated by Blasse and co-workers.[24–26] They discussed the vibronic transition probabilities in the systems under investigation in terms of the existing theories.

The ion pair interaction has been experimentally studied for lanthanide ionic compounds by Buisson,[27] Malinowski,[28,29] Stręk,[30] Blasse[31,32] and others, but lanthanide molecular systems only by Güdel[33] and by us.[15,21–23,34] Theoretical investigation of this phenomenon was reported by Dahl[35] in the PrF_3 system. Elucidation of the two effects (cooperative effect and vibronic coupling) needs spectroscopic studies of diluted $La_{1-x}Nd_x(Gly–Gly)_2(ClO_4)_3 \cdot 4H_2O$ single crystals. In spite of our efforts up to now we have not been successful in preparing this type of crystal.

Let us analyse the results of the spectroscopic data of fully concentrated single crystals. In the energy region of $^4I_{9/2} \rightarrow {}^2G_{7/2}$, $^4G_{5/2}$; $^4F_{5/2}$, $^2H_{9/2}$; $^4F_{3/2}$; $^4G_{7/2}$ transitions the vibronic sidebands corresponding to the transitions described in Table 3 appear. We have attributed only those lines which were repeated in the composition with all the Stark components observed in the analysed transition. These results correspond quite well to the phonons observed in the IR and Raman spectra (Fig. 5). All bands below *ca* 100 cm^{-1} should be assigned to the odd phonon transitions connected with librational and torsional vibrations of the Ln—O—C—O—Ln ribbon. Besides these sidebands additional strong lines appear for the $^4I_{9/2} \rightarrow {}^4G_{5/2}$, $^2G_{7/2}$ and $^4I_{9/2} \rightarrow {}^4F_{5/2}$, $^2H_{9/2}$ transitions. Their number is irrelevant to the one symmetry site of the Nd^{3+} ions. They result from Davydov splitting. The mechanism of interaction between the Ln^{3+} ion pair can be different: EPI, EMI, MDD, EDD or EX.[35] Vial and Buisson[36] have found exchange to be the most important mechanism for the excitations with higher energies. Dahl and Schaack have reported the magnetoelastic effect in the PrF_3 crystal.[35] At this stage it is difficult to decide which mechanism is predominant. A doublet structure was observed by Caro in neodymium complexes with organic ligands[19] and by us in almost all the polymeric single crystals, thus confirming the close relationship between polymeric structures and the nature of this kind of spectra.[15] This means that two mechanisms are most probable, EPI or EX. The former is close to that proposed by Davydov in polymeric biological systems, and called the solitons mechanism.[37]

A comparison of the neodymium complex with glycine and diglycine leads to the following statements: the Nd^{3+} ion creates, with glycine, triclinic mono-crystals of the formula $Nd(Gly)_3(ClO_4)_3 \cdot 4.5H_2O$.[5] Although in the structure similar coordination modes of carboxyl groups were found and the coordination number of 9 for Nd^{3+} ions is identical to the diglycine complex, only linear polymers in the structure are formed to engage the dimeric pairs of type (a) linked by the weaker bridge of type (b). The point symmetry of Nd^{3+} seems to be C_{2v}, similar to the case of diglycine mono-crystal.

Note that the type of lanthanide coordination in the dipeptide remains the same as in glycine. A similar rule can be found in another complex with glycyl-L-tyrosine.[38] Probably the coordination of the Ln^{3+} ion with particular amino acid residues of peptides will be the same as by a single amino acid.[3,4,7,15]

REFERENCES

1. J. Legendziewicz and E. Huskowska, *Excited States of Transition Elements*, p. 228. World Scientific Publishing Co. Pte. Ltd, Singapore (1989).
2. J.Legendziewicz, I. Csöregh, E. Huskowska and P. Kierkegaard, 12th European Crystallographic Meeting, Moscow (1989), Vol. 2, 388.
3. I. Csöregh, E. Huskowska and J. Legendziewicz, *Acta Cryst.* 1992, C48, 1030.
4. J. Legendziewicz, E. Huskowska, A. Waśkowska and Gy. Argay, *Inorg. Chim. Acta* 1984, **92**, 151.
5. J. Legendziewicz, E. Huskowska, Gy. Argay and A. Waśkowska, *Inorg. Chim. Acta* 1984, **95**, 57.
6. C. N. Dao, T. Głowiak, E. Huskowska and J. Legendziewicz, *J. Less-Comm. Met.* 1988, **136**, 339.
7. C. N. Dao, T. Głowiak, E. Huskowska and J. Legendziewicz, *J. Less-Comm. Met.* 1988, **136**, 339.
8. I. Csöregh, M. Czugler, P. Kierkegaard, J. Legend-

ziewicz and E. Huskowska, *Acta Chim. Scand.* 1989,**43**, 735.
9. I. Csöregh, P.Kierkegaard, J. Legendziewicz and E. Huskowska, *Acta Chim. Scand.* 1987, **41**, 453.
10. J. Legendziewicz, T. Głowiak, E. Huskowska and C. N. Dao, *Polyhedron* 1988, **7**, 2495.
11. C. H. Evans, *Biochemistry of the Lanthanides*. Plenum Press, New York (1990).
12. B. R. Judd, *Phys. Rev.* 1962, **127**, 750.
13. H. G. Brittain and Z. Konteatis, *J. Inorg. Nucl. Chem.* 1981, **43**, 1719; 1981, **43**, 1675 (notes).
14. D. Van Der Helm and T. V. Willoughby, *Acta Cryst.* 1969, **B25**, 2317.
15. J. Legendziewicz, *Excited States of Transition Elements*, p. 149. World Scientific Publishing Co. Pte. Ltd, Singapore (1992).
16. J. H. Forsberg, *Coord. Chem. Rev.* 1973, **10**, 195.
17. E. Huskowska, unpublished results.
18. W. T. Carnall, G. L. Goodman, K. Rajnak and R. S. Rana, A Systematic Analysis of the Spectra of the Lanthanides Doped into Single Crystal LaF_3, report, Argonne National Laboratory (1988).
19. P. Caro, O. K. Moune, E. Antic-Fidancev and M. Lemaitre-Blaise, *J. Less-Comm. Met.* 1985, **112**, 153.
20. P. Caro, *J. Less-Comm. Met.* 1986, **126**, 239.
21. J. Legendziewicz, G. Oczko and G. Meyer, *Polyhedron* 1991, **10**, 1921.
22. G. Oczko, J. Legendziewicz, W. Stręk and J. Hanuza, *Excited States of Transition Elements*. World Scientific Publishing Co. Pte. Ltd, Singapore (1992).
23. E. Huskowska, J. Legendziewicz and J. Hanuza, *Polyhedron* 1990, **9**, 659.
24. G. Blasse and L. H. Brixner, *Inorg. Chim. Acta* 1990, **169**, 25.
25. G. Blasse, *Inorg. Chim. Acta* 1990, **167**, 33.
26. J. Sytsma, W. van Shaik and G. Blasse, *J. Luminesc.* 1991, **48** and **49**, 494.
27. R. Buisson and J. Q. Liu, *J. Phys.* 1984, **45**, 1523.
28. M. Malinowski, R. Wolski and W. Woliński, *J. Luminesc.* 1986, **35**, 1.
29. M. Malinowski and W. Stręk, *J. Phys. C. Solid Phys.* 1987, **20**, 2595.
30. M. Gałczyński, M. Błażej and W. Stręk, *Mat. Chem. Phys.* 1992, **31**, 175.
31. M. Buijs and G. Blasse, *Chem. Phys. Lett.* 1987, **137**, 381.
32. M. Buijs and G. Blasse, *J. Luminesc.* 1988, **39**, 323.
33. M. P. Hehlen, H. Riesen and H. W. Güdel, *Inorg. Chem.* 1991, **30**, 2273.
34. E. Huskowska, J. Legendziewicz, Th. Schleid and G. Meyer, *Mat. Chem. Phys.* 1992, **31**, 111.
35. M. Dahl and G. Schaack, *Phys. Rev. Lett.* 1986, **56**, 232.
36. C. Vial and R. Buisson, *J. Phys. (Paris) Lett.* 1982, **43**, L339, 745.
37. A. S. Davydov, in *Solitons* (Edited by S. E. Trullinger, V. E. Zakharov and V.L. Pokrovsky). Elsevier Science Publishers, Amsterdam (1986).
38. T.Głowiak, E. Huskowska and J. Legendziewicz, *Polyhedron* 1992,**11**, 2897.

Polyhedron Vol. 12, No. 19, pp. 2395–2401, 1993
Printed in Great Britain

0277–5387/93 $6.00+.00
© 1993 Pergamon Press Ltd

STUDIES ON MIXED LIGAND COMPLEXES OF RUTHENIUM(II) CHIRAL SCHIFF BASES WITH NITROGEN DONORS

R. I. KURESHY† and N. H. KHAN

Discipline of Coordination Chemistry and Homogeneous Catalysis,
Central Salt and Marine Chemicals Research Institute, Bhavnagar 364002, India

(*Received* 23 *March* 1993; *accepted* 5 *May* 1993)

Abstract—Mixed ligand complexes of the ruthenium(II) ion using chiral Schiff bases derived from salicylaldehyde, chloro- and methoxysalicylaldehyde and L-histidine with mono- or bidentate nitrogen bases such as azide, imidazole and 2,2-bipyridyl have been synthesized. The characterization was performed by microanalysis, IR, UV–vis $\{^1H\}$, $^{13}C\{^1H\}$ and $^{31}P\{^1H\}$ NMR spectroscopy, conductance measurement, optical rotation, CD spectral studies and electrochemistry. The conformational aspects regarding the asymmetric carbon atom and the nitrogen containing ligands around the ruthenium(II) metal ion have been discussed. The complexes show quasi-reversible behaviour in cyclic voltammetry and the redox potentials of the Ru^{II}/Ru^{I} couplies lie in the range -0.12 to -0.29 V.

The study of mixed ligand complexes is relevant in the field of analytical chemistry, where the use of mixed ligand complexes allows the development of increased selectivity and sensitivity; also it has great importance in the fields of biological and environmental chemistry. Metal chelates of aminoalcohols play important roles in nature, e.g. in the hormones adrenaline and noradrenaline and in amino polysaccharide chemistry.[1] Orthohydroxycarboxylic acid has biological significance and is considered as a model compound in the study of humic and fulvic acids in soils.[2,3] They also have pharmaceutical applications[4,5] owing to the anti-inflammatory properties of their transition metal complexes.[6,7] Mixed ligand complexes of platinum,[8] palladium,[9] ruthenium(II) and ruthenium(III), such as $[(DMSO)_4RuCl_2]$[10] and $[(NH_3)_4RuCl_2]Cl$,[11] are known to possess anti-tumour and antibacterial activity. In view of the importance of these ruthenium complexes we have undertaken the studies of mixed ligand complexes of ruthenium(II) using chiral ligands derived from L-histidine and salicylaldehyde, 5-chloro- and 5-methoxysalicylaldehyde with mono- and bidentate nitrogen bases, viz. azide imidazole and 2,2-bipyridyl with the exception that both types of ligand may deeply affect the known properties, viz. electronic and dichroic behaviour of these mixed ligand complexes.

RESULTS AND DISCUSSION

The complexes were prepared by the replacement of water molecules in terdentate (ONO) chiral ruthenium(II) Schiff base complexes by mono- or bidentate nitrogen denors, such as azide, imidazole and 2,2-bipyridyl (Scheme 1), with a colour change from green to brown or brownish-red for the complexes **1–3** and **7–9**, while **4–6** are all dark green. The analytical and molar conductance data are presented in Table 1. Complexes **1–3** are 1 : 1 electrolytes in methanol, while complexes **4–9** are non-electrolytic in nature.

The IR spectra of the complexes show intense bands near 1605–1590 cm^{-1}, due to the coordinated azomethine group which overlaps with the $(COO^-)_{asym}$ stretching mode. The $(COO^-)_{sym}$ stretching mode lies at 1440 cm^{-1}. A broad band at 3300–3400 cm^{-1} in complexes **1–6** is due to coordinated water occupying the axial position and the bands due to coordinated linear azide appear near 2030, 1325, 630 and 425 cm^{-1}, which are assigned to the asymmetric, symmetric, N_3^- stretching, N_3^- bending and Ru—N_3^- stretching

† Author to whom correspondence should be addressed.

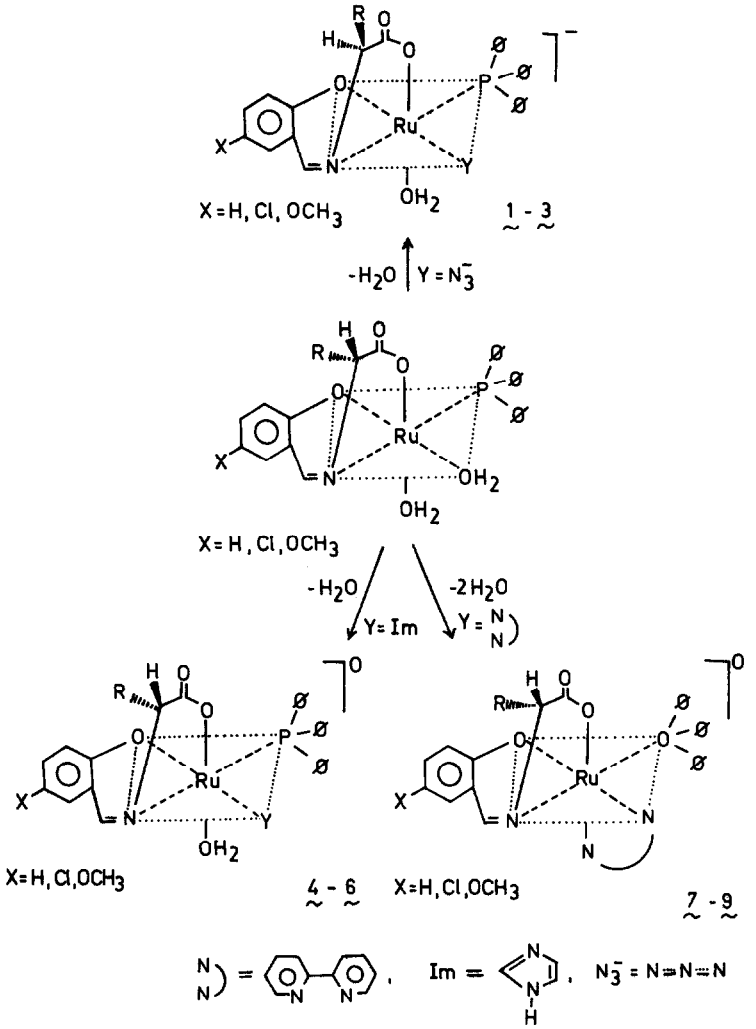

Scheme 1.

modes, respectively,[12] in **1–3**. However, the mixed ligand complexes **4–6** show bands at 618, 650 and 1060 cm^{-1}, due to coordinated imidazole (Table 2). Complexes **7–9** show bands near 1600, 1575, 1460, 1242, 1160 and 770 cm^{-1} due to the coordinated 2,2 bipyridyl ligand.[13] Some of the bands are merged with IR bands of the symmetric or asymmetric COO^- group, azomethine group and ring vibrations. In the far-IR region bands at 550 and 345 cm^{-1} are assigned to ν(Ru—P) and ν(Ru—N), respectively.

The electronic spectra of the complexes recorded in methanol show a high intensity charge-transfer band at 372 ($\varepsilon = 2162$) to 395 nm ($\varepsilon = 2500$) along with the intraligand bands at 320 nm ($\varepsilon = 2500$). The $d \rightarrow \pi^*$ L band in all the complexes lies in the range 604 ($\varepsilon = 878$) to 798 ($\varepsilon = 1171$) nm (Table 3). The position of this band depends on the donating nature of the substituents attached to the metal ion in the chelating ring.[14] The energy of this band decreases in the order N_3^- > Im > 2,2 bipy.

Since complexes **1–6** have an optical centre at metal also so it is possible to investigate the dichroic behaviour of LMCT and *d-d* transitions.

The CD spectra of the complexes in methanol show CD λ_{max} LMCT bands red shifted with respect to the electronic absorption maximum (Table 3). The large red shifts are accompanied by a marked increase in dichroic behaviour. In equatorial binding a blue shift in the *d-d* bands is seen (Table 3) with increased intensity due to substituted azide and imidazole as compared with 2,2-bipyridyl, because the ligand-field transition borrows intensity from the low energy azide or imidazole-to-ruthenium(II) LMCT transition.

Two representative CD spectra, Fig. 1(A), of 5MeOSal[L-hisazidotriphenylphosphinoaquoruthenate(II) and 5ClSal[L-histriphenylphosphino-2,2-

Table 1. Microanalysis, molar conductance of chiral ruthenium(II) mixed ligand complexes

S. No.	Complexes	Yield	Colour	Analysis (%) C	H	N	Molar conductance (Λ_M) (Ω^{-1} cm^2 mol^{-1})
1	$Na^+[(C_{13}H_{11}N_3O_3)(PPh_3)(H_2O)(N_3^-)Ru]$	62	Blackish brown	52.5 (52.8)	4.0 (4.1)	11.5 (11.9)	85
2	$Na^+[(C_{13}H_{10}N_3O_3Cl)(PPh_3)(H_2O)(N_3^-)Ru]$	61	Dark brown	50.2 (50.4)	3.6 (3.8)	11.2 (11.4)	90
3	$Na^+[(C_{14}H_{13}N_3O_4)(PPh_3)(H_2O)(N_3^-)Ru]$	62	Dark brown	52.2 (52.3)	4.4 (4.5)	5.6 (5.7)	95
4	$[(C_{13}H_{11}N_3O_3)(PPh_3)(H_2O)(C_3H_4N_2)Ru]$	74	Dark green	57.5 (57.7)	4.6 (4.7)	9.8 (9.9)	6
5	$[(C_{13}H_{10}N_3O_3Cl)(PPh_3)(H_2O)(C_3H_4N_2)Ru]$	75	Dark green	55.0 (55.0)	4.3 (4.5)	9.4 (9.3)	5
6	$[(C_{14}H_{13}N_3O_4)(PPh_3)(H_2O)(C_3H_4N_2)Ru]$	74	Dark green	56.7 (56.9)	4.3 (4.8)	9.2 (9.5)	4
7	$[(C_{13}H_{11}N_3O_3)(PPh_3)(C_{10}H_8N_2)Ru]$	63	Redish brown	64.6 (64.8)	4.5 (4.6)	9.1 (9.2)	3
8	$[(C_{13}H_{10}N_3O_3Cl)(PPh_3)(C_{10}H_8N_2)Ru]$	62	Redish brown	60.5 (60.6)	4.1 (4.2)	8.5 (8.6)	6
9	$[(C_{14}H_{13}N_3O_4)(PPh_3)(C_{10}H_8N_2)Ru]$	60	Redish brown	62.3 (62.4)	4.5 (4.6)	8.6 (8.7)	4

bipyruthenate(II), [Fig. 1(B)] in methanol show that complexes **A** and **B** have different geometrical configurations and that complex **A** is stereospecifically coordinated to ruthenium metal ion so that the *gauche* chelate ring is located in the λ form, while complex **B** is an equilibrium mixture of the two isomers (λ and δ) with more of the δ-form. Molecular model construction reveals that complexes **1–3** tend to acquire the *S* configuration because of the steric hindrance created by the free rotation of azide with that of the —CH_2 group of the histidine moiety on one side and PPh_3 on the other (Fig. 2), which is also evidenced by the presence of a positive value of the optical rotation (Table 3), while no such steric interaction occurs in the case of complexes **4–9** and they acquire the *R* configuration. Similar interactions were also reported earlier.[15,16]

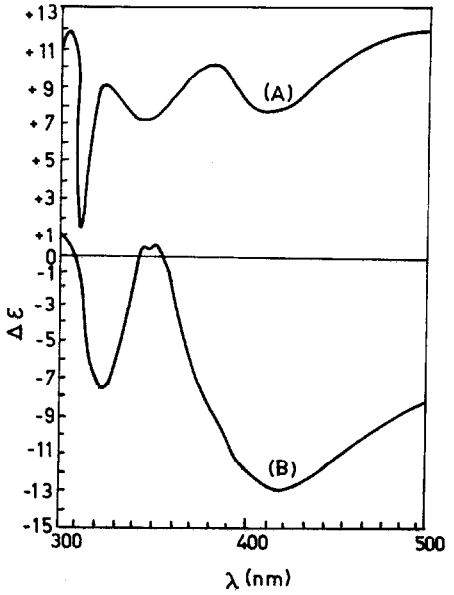

Fig. 1. CD spectra of (A) 5MeOSal[L-hisazidotriphenyl phosphinoaquoruthenate(II)] and (B) 5ClSal[L-histriphenyl phosphino-2,2-bipyridylruthenate(II)] in MeOH.

^{1}H NMR spectra of the complexes in DMSO-d_6 show resonance signals at 2.5–2.04 and 1.13–1.15 ppm due to the proton on the asymmetric carbon and —CH_2 protons. The resonance signal due to the OCH_3 protons is merged with the signal of DMSO-d_6 at 3.39 ppm in complexes **3**, **6** and **9**, while the signals near 6.10–7.00 and 8.12–8.20 ppm are due to aromatic and azomethine protons. A singlet at 14.10–14.50 ppm is due to the NH proton of imidazole, which is confirmed on shaking complexes **4–6** with D_2O; this signal disappears due to fast exchange of protons. Complexes **7–9** show resonance signals around 9.6–10.2 ppm due to the coordinated 2,2-bipyridyl ligand, which is also reported elsewhere.[17]

$^{13}C\{^1H\}$ NMR spectra of the complexes in DMSO show signals at 48.94 and 55–55.9 ppm due to carbon atoms of the —CH_2 and —CH groups, while complexes **3**, **6** and **9** show a singlet at 85.83

Table 2. Selected IR absorption bands in chiral ruthenium(II) mixed ligand complexes

S.No.	Complexes	ν(H—C=N) + asym ν(COO^-)	ν(Ru—P)	ν(Ru—N)	Bands due to N containing ligands
1	Sal[L-hisazidotriphenylphosphinoaquoruthenate(II)]	1595	550	340	2030(s), 1325(s), 630(s), 420
2	5ClSal[L-hisazidotriphenylphosphinoaquoruthenate(II)]	1605	545	340	2030, 1330(s), 635(s), 425
3	5MeOSal[L-hisazidotriphenylphosphinoaquoruthenate(II)]	1600	550	340	2035, 1335(s), 630, 426
4	Sal[L-histriphenylphosphinoimidoaquoruthenate(II)]	1610	540	340	618, 650(s), 1060(s)
5	5ClSal[L-histriphenylphosphinoimidoaquoruthenate(II)]	1600	540	355	620(s), 655(s), 1070(s)
6	5MeOSal[L-histriphenylphosphinoimidoaquoruthenate(II)]	1595	550	340	620(s), 650(s), 1080(s)
7	Sal[L-histriphenylphosphino-2,2-bipyruthenate(II)]	1590	550	340	1460(s), 1440(s), 1160(s), 768(s), 700(s), 405
8	5ClSal[L-histriphenylphosphino-2,2-bipyruthenate(II)]	1605	545	345	1466(s), 1440(s), 1150(s), 760, 700, 408
9	5MeOSal[L-histriphenylphosphino-2,2-bipyruthenate(II)]	1600	550	350	1460(s), 1150(s), 840(s), 725(s), 630(s)

Table 3. Electronic absorption, CD spectral data, absolute configuration and optical rotation of chiral ruthenium(II) mixed ligand complexes

S.No.	Complexes	Absorption λ_{max} (ε M^{-1} cm^{-1})	CD λ_{max} ($\Delta\varepsilon$ M^{-1} cm^{-1})	Absolute configuration	$[\alpha]_D$ ($^\circ$ cm^{-2} g^{-1}) (MeOH)
1	Sal[L-hisazidotriphenylphosphinoaquoruthenate(II)][a]	330(2500), 395(2500), 604(878)	376(+15), 411(+4.5), 584(+16.5)	*S*	+63.6
2	5ClSal[L-hisazidotriphenylphosphinoaquoruthenate(II)][a]	325(2499), 377(2233), 684(684)	295(+1.3), 315(+6.7), 482(+10.4)	*S*	+21.7
3	5MeOSal[L-hisazidotriphenylphosphinoaquoruthenate(II)][a]	330(2499), 372(2162), 759(801)	330(+1.2), 380(+8.2), 480(+8.5)	*S*	+24.3
4	Sal[L-histriphenylphosphinoimidoaquoruthenate(II)][a]	319(2500), 381(2103), 654(903)	308(+8.1), 331(−6.6), 371(+6.0), 450(−10.5)	*R*	−95.5
5	5ClSal[L-histriphenylphosphinoimidoaquoruthenate(II)][a]	320(2500), 378(2127), 668(678)	299(−14.3), 317(−14.6), 362(−14.2), 460(−15.0)	*R*	−27.7
6	5MeOSal[L-histriphenylphosphinoimidoaquoruthenate(II)][a]	340(2500), 381(2376), 781(1077)	340(−12.0), 376(−6.4), 450(−21.3)	*R*	−46.4
7	Sal[L-histriphenylphosphino-2,2-bipyruthenate(II)][a]	385(2370), 447(2351), 652(722)	325(+5.2), 355(+8.0), 465(−3.0)	*R*	−43.5
8	5ClSal[L-histriphenylphosphino-2,2-bipyruthenate(II)][a]	326(2500), 478(2499), 696(437)	333(−6.8), 378(+0.9), 490(−12.0)	*R*	−29.6
9	5MeOSal[L-histriphenylphosphino-2,2-bipyruthenate(II)][a]	320(2500), 499(2499), 798(1171)	370(+2.0), 420(+22.0), 485(−11.0)	*R*	−33.7

[a]Solvent is MeOH.

Table 4. {^{1}H} and ^{13}C{^{1}H} NMR data chiral ruthenium(II) mixed ligand complexes

S. No.	Complexes	^{1}H NMR assignment —CH	—CH=N	Aromatic/signal due to N containing ligands	^{13}C{^{1}H} NMR assignment (ppm) —CH	COO^-	Aromatic/signal due to N containing ligands
1	Sal[L-hisazidotriphenylphosphinoaquoruthenate(II)]	2.46(t)	8.18	6.25–7.50/–	55.87	198.10	132, 129.2, 127/–
2	5ClSal[L-hisazidotriphenylphosphinoaquoruthenate(II)]	2.50(t)	8.27	6.15–7.60, 7.80/–	55.90	200.22	132.42, 130, 128/–
3	5MeOSal[L-hisazidotriphenylphosphinoaquoruthenate(II)]	2.44(t)	8.22	6–7.20, 7.45/–	55.28	197.00	131.2, 129.21, 127.14/–
4	Sal[L-histriphenylphosphinoimidoaquoruthenate(II)]	2.07(t)	8.10	6.11–7.25, 7.67/14.2	55.30	197.30	133.1, 132, 129, 128/–
5	5ClSal[L-histriphenylphosphinoimidoaquoruthenate(II)]	2.26(t)	8.22	6.20–7.35, 7.71/14.5	55.40	199.00	134.20, 132, 130, 128/–
6	5MeOSal[L-histriphenylphosphinoimidoaquoruthenate(II)]	2.04(t)	8.04	6.18–7.31, 7.60/14.10	55.00	197.00	132, 130.32, 129, 127/–
7	Sal[L-histriphenylphosphino-2,2-bipyruthenate(II)]	2.46(t)	8.22	6.15–7, 7.39/9.24, 9.17, 9.6	55.30	197.14	133.25, 129, 127.12, 126.61/124.4, 154.3
8	5ClSal[L-histriphenylphosphino-2,2-bipyruthenate(II)]	2.48(t)	8.30	6.22–7.17, 7.40/10.2, 9.6, 9.26	55.72	198.11	134.35, 131, 129, 127/124.3, 151.9
9	5MeOSal[L-histriphenylphosphino-2,2-bipyruthenate(II)]	2.45(t)	8.19	6.10–7.7, 7.35/9.18, 9.24, 9.62	55.12	197.00	131.67, 129, 127, 126/124.6, 151.3

Table 5. Electrochemical data of chiral ruthenium(II) mixed ligand complexes

S. No.	Complexes	Oxidation (V) (ΔE_p, mv)[a] Ru^{II}/Ru^{III}	Reduction (V) (ΔE_p, mv)[a] Ru^{II}/Ru^{I}
1	Sal[L-hisazidotriphenylphosphinoaquoruthenate(II)]	+0.76(120)	−0.16(100)
2	5ClSal[L-hisazidotriphenylphosphinoaquoruthenate(II)]	+0.65(80)	−0.12(90)
3	5MeOSal[L-hisazidotriphenylphosphinoaquoruthenate(II)]	+0.78(90)	−0.18(90)
4	Sal[L-histriphenylphosphinoimidoaquoruthenate(II)]	+0.90(110)	−0.23(125)
5	5ClSal[L-histriphenylphosphinoimidoaquoruthenate(II)]	+0.73(110)	−0.19(115)
6	5MeOSal[L-histriphenylphosphinoimidoaquoruthenate(II)]	+0.94(140)	−0.20(120)
7	Sal[L-histriphenylphosphino-2,2-bipyruthenate(II)]	+0.80(85)	−0.18(90)
8	5ClSal[L-histriphenylphosphino-2,2-bipyruthenate(II)]	+0.68(116)	−0.16(112)
9	5MeOSal[L-histriphenylphosphino-2,2-bipyruthenate(II)]	+0.81(90)	−0.21(110)

[a]A platinum electrode is the working electrode, the solvent is MeOH, the supporting electrolyte is tetrabutyl ammonium perchlorate (0.001 M), the reference electrode is Ag/AgCl and the scan rate is 200 mV s^{-1}.

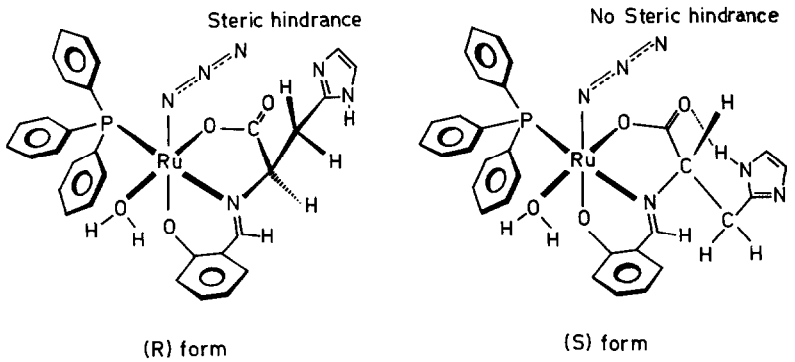

Fig. 2. Configurational aspects regarding azide in the vicinity of the complexes **1–3**.

ppm due to the carbon atom of the methoxy group. The resonance signals in the range 126.31–132.00 ppm are due to carbon atoms of the aromatic rings and a signal at 197.21–200.22 ppm is due to the carbon atom of the coordinated carboxylato group (Table 4). Signals in the range 151–154 ppm are due to the carbon atom directly attached to the nitrogen of 2,2-bipyridyl[18] and resonance signals near 124.6 ppm are due to other carbon atoms in complexes **7–9** (Table 4).

$^{31}P\{^{1}H\}$ NMR spectra of the complexes in DMSO show a singlet in the region 32 ppm due to the presence of only one triphenylphosphino group *trans* to the nitrogen of the azomethine group.[19,20]

The cyclic voltammogram of the complexes in methanol show quasi-reversible (Table 5) one-electron Ru^{II}/Ru^{III} oxidation couples in the potential range +0.65 to +0.94 V vs Ag/AgCl. From the cyclic voltammogram and differential pulse voltammogram the $E_{1/2}$ values of the Ru^{II}/Ru^{I} couple lie in the range −0.12 to −0.29 V. The shift in the redox couple is due to the coordinated nitrogen containing ligands to the ruthenium metal ion.

EXPERIMENTAL

$RuCl_3 \cdot 3H_2O$ was obtained from Johnson Matthey; triphenylphosphine, sodium azide, imidazole, 2,2-bipyridyl (Sisco), salicylaldehyde, 5-chlorosalicylaldehyde, 5-methoxysalicylaldehyde and L-histidine (Aldrich) were used as received. All the chiral Schiff bases were synthesized by a reported procedure.[21] The metal complex $[RuCl_2(PPh_3)_3]$[22] and the chiral ruthenium(II) Schiff base complexes were synthesized by a reported method.[23]

Microanalyses of the complexes were performed on a Carlo Erba Analyser model 1106. Molar conductance was measured at room temperature on a Digisun electronic conductivity bridge DI-909. The IR spectra were recorded on a Carl–Zeiss Specord M-80 spectrophotometer in Nujol mulls/KBr. Electronic spectra were recorded in a Shimadzu UV–vis recording spectrophotometer model 160. ^{1}H, $^{13}C\{^{1}H\}$ and $^{31}P\{^{1}H\}$ NMR spectra were obtained on a Jeol FX-100 NMR spectrometer in DMSO-d_6 and DMSO using $[Si(CH_3)_4]$ as an internal standard and operating at 99.55, 24.99 and 40.27 MHz, respectively. Cyclic voltammograms, and differential pulse voltammograms were recorded with a Princeton Applied Research (PAR) instrument using tetrabutylammonium perchlorate as the supporting electrolyte in methanol. The optical rotation of the complexes in methanol was measured using a polarimeter (Atago Japan). The CD spectra were recorded in methanol by Jasco Machine Model J-20, Japan.

Synthesis of $[RuL(PPh_3)(N_3)^-(H_2O)]^-Na^+$ (1–3)

A hot solution of the complexes $[RuL(PPh_3)(H_2O)_2]$ (0.01 mmol) in dichloromethane/methanol was refluxed with sodium azide (0.013 mmol) for 8–10 h under constant stirring. After completion of reaction the solutions were filtered and concentrated on a rotaevaporator to a small volume and then precipitated by diethyl ether. They were filtered, washed and dried *in vacuo*; yield 60–62%.

$[RuL(PPh_3)(Im)(H_2O)]$ (4–6) *and* $[RuL(PPh_3)(2,2\text{-bipy})]$ (7–9)

Complexes $[RuL(PPh_3)(H_2O)_2]$ (0.01 mmol) were dissolved in dichloromethane/methanol and refluxed with imidazole or 2,2-bipyridyl (0.01 mmol) for 8–9 h. The resulting solutions were filtered, concentrated on a rotaevaporator and precipitated by diethyl ether. They were filtered, recrystallized in CH_2Cl_2/MeOH and dried *in vacuo*; yield 74–75%.

Acknowledgement—We sincerely thank Prof. P. Natarajan, Director, Central Salt and Marine Chemicals Research Institute, for allowing us to send the paper for publication.

REFERENCES

1. C. J. Hawkins and J. A. Palmer, *Aust. J. Chem.* 1978, **31**, 1689.
2. F. M. Morel, J. C. Westall, C. R. O'Melia and J. J. Morgan, *Environ. Sci. Technol.* 1975, **9**, 757.
3. W. Stumm and J. J. Morgan, *Aquatic Chemistry, An Introduction Emphasizing Chemical Equilibria in Natural Waters*. Wiley Interscience, New York (1981).
4. G. E. Jackson, P. M. May and D. R. Williams, *J. Inorg. Nucl. Chem.* 1978, **40**, 1189.
5. G. E. Jackson, P. M. May and D. R. Williams, *J. Inorg. Nucl. Chem.* 1978, **40**, 1227.
6. J. R. J. Sorenson, *Prog. Med. Chem.* 1978, **15**, 211.
7. W. M. Willingham and J. R. J. Sorenson, *Trace Elem. Med.* 1986, **3**, 139.
8. M. J. Cleare and J. D. Hoeshele, *Platinum Met. Rev.* 1973, **15**, 42.
9. B. Rosenberg, in *Nucleic Acid Metal Ion Interactions* (Edited by T. G. Spiro), Vol. 1, p. 127. Marcel Dekker, New York (1979).
10. S. Giraldi, G. Sava, G. Bertouli, G. Mestronic and G. Zassinovich, *Cancer Res.* 1977, **37**, 2662.
11. M. J. Clarke, *Inorg. Chem. Biol. Med., ACS Symp. Ser.* 1980, **140**, 157.
12. H. Ogoshi, E. Watanabe, Z. Yoshida, J. Kincaid and K. Nakamoto, *J. Am. Chem. Soc.* 1973, **95**, 2845.
13. U. C. Sharma, S. C. Sarkar, B. C. Paul and R. K. Poddar, *Inorg. Chim. Acta* 1990, **173**, 195.
14. K. Nakajima, K. Kojima, M. Kojima and J. Fujita, *Bull. Chem. Soc., Japan* 1990, **63**, 2620.
15. L. J. Boucher and C. G. Coe, *Inorg. Chem.* 1976, **15**, 531.
16. K. Okamoto, M. Takari, T. Yonemura, T. Konno and J.Hidaka, *Inorg. Chim. Acta.* 1990, **175**, 31.
17. E. C. Constable, R. P. G. Henney, T.A. Leese and D. A. Tocher, *J. Chem. Soc., Dalton Trans.* 1990, 443.
18. M. J. Cook, A. P. Lewis, C. S. G. McAuliffe and A. J. Thomson, *Inorg. Chim. Acta* 1982, **64**, L-25.
19. F. M. Conroy-Lewis, A. D. Redhouse and S.J. Simpeen, *J. Organomet. Chem.* 1990, 399, 307.
20. C. Bianchini, P. J. Perez, M. Peruzzine, F. Zanobini and A. Vacca, *Inorg. Chem.* 1991, **30**, 279.
21. M. M. Taqui Khan, R. I. Kureshy and N. H. Khan, *Tetrahedron Asym.* 1992, **3**, 307.
22. T. F. Calson and S. D. Robinson, *Inorg. Chim. Acta* 1988, **149**, 13.
23. R. I. Kureshy and N.H. Khan, *Polyhedron* 1993, **12**, 195.

Polyhedron Vol. 12, No. 19, pp. 2403–2409, 1993
Printed in Great Britain

0277–5387/93 $6.00+.00
Pergamon Press Ltd

MIXED HALO/HEXAMETHYLPHOSPHORAMIDE COMPLEXES OF INDIUM(III). ^{115}In, ^{31}P, ^{19}F AND ^{1}H NMR STUDIES OF INDIUM(III) SPECIES IN HEXAMETHYLPHOSPHORAMIDE SOLUTION. X-RAY STRUCTURE OF *TRANS*-DIIODOTETRAKIS(HEXAMETHYLPHOSPHORAMIDE)INDIUM(III) IODIDE

M. A. MALYARICK,* A. B. ILYUHIN and S. P. PETROSYANTS

Kurnakov Institute of General and Inorganic Chemistry, Russian Academy of Sciences, Leninsky Prospect 31, Moscow 117907, Russia

(*Received* 5 *March* 1993; *accepted* 5 *May* 1993)

Abstract—^{115}In NMR studies are reported for InX_3 (X = Cl, Br, I) solutions in hexamethylphosphoramide (HMPA). The resonances of InX_4^- anions are observed for tribromide and triiodide solutions. Mixed $InBr_{4-n}I_n^-$ anions may be obtained for the mixtures of InI_3 and $InBr_3$. A trigonal-bipyramidal complex, $InCl_3(HMPA)_2$, is formed from $InCl_3$–HMPA solutions. Diiodotetrakis(hexamethylphosphoramide)indium(III) iodide has been prepared from an InI_3–HMPA system and fully characterized by elemental analysis, IR and NMR spectroscopy and X-ray crystallography. The cation is *trans*-octahedral. ^{19}F NMR spectra of $In(NO_3)_3$–F^-–HMPA systems demonstrate the formation of six-coordinate mixed $InF_n(HMPA)_m(H_2O)_{6-n-m}^{3-n}$ species.

The high donor number (DN_{SbCl_5} = 38.8) of hexamethylphosphoramide (HMPA) makes it a strong ionizing solvent. Besides this, the shape and dimensions of the HMPA molecule cause different steric interactions in the adducts solvated by it and so complexes with unusual stereochemistry may be formed.

The coordination chemistry of indium(III) halide compounds with HMPA has not been studied intensively. There are no data on solution chemistry of indium species in HMPA and only two works are devoted to the solid-state chemistry of indium adducts with HMPA.[2,3] When studying coordination compounds of aminophosphine oxides Bolster obtained a number of indium(III) halide adducts with HMPA–$InX_3(HMPA)_2$ (X = Cl^-, Br^-, I^-).[2] Based on the data of vibrational spectroscopy Bolster proposed a dimeric structure for these compounds, $[InX_2(HMPA)_4]^+[InX_4]^-$ with *trans*-geometry of the cation. Later, a chloride complex with the same composition was characterized by X-ray crystallography.[3] Indium was shown to be in a trigonal-bipyramidal arrangement with hexamethylphosphoramide molecules in axial positions and three chloride ions in equatorial positions.

The present paper concerns the investigation of a number of complexes formed from InX_3–HMPA (X = Cl^-, Br^-, I^-) and $In(NO_3)_3$–F^-–HMPA–H_2O systems, both in solution and in the solid state, and also continues the consideration of the stereochemical aspects and mutual influence of ligands in mixed halo species of indium(III).

EXPERIMENTAL

Materials

Indium trichloride was prepared by chlorination of indium(III) oxide with CCl_4 at *ca* 450°C. Indium triiodide was obtained according to the literature procedures.[4,5] $(C_4H_9)_4NInX_4$ salts were prepared as insoluble precipitates when mixing aqueous solutions of InX_3 and $(C_4H_9)_4NX$ and their subsequent

* Authors to whom correspondence should be addressed.

recrystallization was achieved from acetonitrile followed by drying *in vacuo*. Indium trinitrate was obtained by dissolving indium(III) oxide of a stoichiometric quantity of nitric acid.

The salts of $InBr_3$, $InF_3 \cdot 3H_2O$, NH_4F and $(CH_3)_4NF$ were obtained from commercial sources without further purification.

Hexamethylphosphoramide was rigorously dried and distilled by standard methods and was used as a solvent for preparing the solutions. All operations with InX_3 ($X = Cl^-$, Br^-, I^-) salts and HMPA were performed under nitrogen.

Preparation of the compounds

X-ray quality crystals of **I** and **II** were grown by slow evaporation of $InCl_3$ and InI_3 solutions, respectively, in HMPA in a vacuum desiccator. The crystals were washed with a small amount of CCl_4 to remove the excess HMPA. The crystals of both **I** and **II** are colourless and transparent. The crystals of **II** are very unstable and completely decompose in air in a few minutes.

Spectra

IR spectra of samples **I** and **II** were run on a Specord 715 IR spectrometer between 400 and 4000 cm^{-1}. ^{115}In, ^{31}P, ^{19}F and ^{1}H NMR spectra were obtained with a Bruker AC-200 P spectrometer. All samples were run as solutions. The main experimental conditions are given in Table 1.

X-ray structure determinations

An Enraf–Nonius CAD-4 diffractometer using graphite-monochromated Mo-K_α radiation was used for structure determinations.

The unit cell parameters of crystals of **I** indicated absolute similarity with the penta-coordinated complex $InCl_3(HMPA)_2$ described in ref. 3.

For preserving, a single crystal of **II** was cemented to a glass fibre and mounted into a sealed Pyrex capillary (under nitrogen) and was then examined on a diffractometer.

Data were collected at 200(2) K for $2\theta_{max} = 50°$. The crystals of **II** belong to the triclinic space group $P\bar{1}$. The unit cell parameters and other crystal data for **II** are: $a = 14.053(3)$, $b = 17.621(3)$, $c = 20.920(4)$ Å; $\alpha = 73.89(1)$, $\beta = 89.25(2)$, $\gamma = 80.05(2)°$; $V = 4899(2)$ Å^3; $Z = 4$, $\mu = 25.1$ cm^{-1}. A total of 8104 independent reflections were measured, of which 6213 with $I \geqslant 2\sigma$ were used for calculation.

The positions of indium and iodine atoms were derived from the heavy-atom procedure; the positions of the remaining non-hydrogen atoms were revealed by a sequence of the difference-Fourier syntheses. The coordinates of the hydrogen atoms were determined for geometrically idealized positions (C—H, 1 Å). Block-diagonal least-squares anisotropic refinement for all non-hydrogen atoms (866 refined parameters) with regard to the hydrogen atoms ($U_{eq} = 0.06$ Å^2) converged to values of $R = 0.057$, $R_w = 0.056$, GOOF = 1.97, $w = (\sigma^2(F_0) + 0.0001F_0^2)^{-1}$.

RESULTS AND DISCUSSION

The ^{115}In NMR spectra of InX_3 ($X = Br^-$, I^-) solutions in HMPA show bands almost identical in frequencies to those found for the corresponding InX_4^- anions (Table 2). A similar situation has been observed when dealing with acetonitrile solutions of indium trihalides also displaying resonances of InX_4^- ($X = Cl^-$, Br^-, I^-) species (Table 2).[6] This was interpreted as being a result of a disproportionation reaction which leads to mixed six-coordinate cationic complexes that share the same anion InX_4^-. As for acetonitrile solutions, no bands for the cationic complexes were observed for InX_3–HMPA systems. It seems reasonable that lowering of the symmetry of the cations causes large quadrupole broadening[7] and thus they are undetectable in ^{115}In NMR. Therefore, it might be assumed that the balance between the ionic charges of the species in solutions of HMPA is reached by forming only unsymmetrical $InX_n(HMPA)_{6-n}^{(3-n)+}$ ($X = Br^-$, I^-; $n = 1, 2$) cationic species because $In(HMPA)_6^{3+}$ could be detected as $In(H_2O)_6^{3+}$.[8]

Table 1. Experimental conditions of running NMR spectra

	^{1}H	^{19}F	^{31}P	^{115}In
Frequence (MHz)	200.00	188.31	81.01	43.86
Lock	$(CD_3)_2CO$	$(CD_3)_2CO$	$(CD_3)_2CO$	D_2O
Tube (o.d.)	5	5	5	10
Standard	$(CH_3)_4Si$	SiF_6^{2-}	H_3PO_4	$(C_4H_9)_4NInCl_4$
Temperature (K)	298	253–298	298	298

Table 2. ^{115}In NMR resonances in HMPA solution of indium salts (0.1 M)

X	HMPA InX_3	δ (ppm) ($\Delta H_{1/2}$, Hz) CH_3CN InX_3^6	CH_3CN $[(C_4H_9)_4N]InX_4^6$	$RInX_4^{7,a}$
Cl	—	8 (1300)	0 (290)	0 ± 2 (310)
Br	−279 (1500)	−254 (580)	−261 (220)	−258 (180)
I	−1021 (730)	−999 (430)	−1007 (240)	−989 (250)

[a] R = $(C_6H_5)_4P$ for $InCl_4^-$ and $InBr_4^-$; $(C_4H_9)_4N$ for InI_4^-.

The formation of InX_4^- anions in InX_3–HMPA ($X = Br^-$, I^-) systems allowed us to obtain $InBr_nI_{4-n}^-$ species when mixing $InBr_3$ and InI_3 solutions. The case of an equimolar mixture of $InBr_3$ and InI_3 solutions illustrates well these findings; the spectrum consists of five distinct lines with chemical shifts (−278, −439, −619, −813 and −1018 ppm) corresponding to the ^{115}In NMR frequencies in $InBr_nI_{4-n}^-$ anions.[6,7]

In view of the much better electron donor properties of HMPA compared with acetonitrile (DN_{SbCl_5} = 38.8 and 14.1, respectively) it is somewhat surprising that no ^{115}In NMR resonances are observed for $InCl_3$ solutions in HMPA in contrast to CH_3CN (Table 2). It is apparent that, in this case, interaction between indium trichloride and the solvent does not lead to salt disproportionation to $InCl_n(HMPA)_{6-n}^{(3-n)+}$ and $InCl_4^-$ complex ions. We can assume that some uncharged mixed $InCl_3(HMPA)_n$ solvates, with thermodynamic stabilities appreciably greater than the ionic complexes, are formed. Taking into account the tendency of indium(III) to form complexes with high coordination numbers with oxygen-donor ligands species with $n = 2$ and 3 seem to be preferred.

This was indeed confirmed when compound **I** was prepared from $InCl_3$–HMPA solution. Elemental analyses (Table 3), IR spectrum and X-ray diffraction of sample **I** indicated it to be the penta-coordinated complex *trans*-$InCl_3(HMPA)_2$.[3] Thus, in spite of the difference in preparative techniques (ours and ref. 3) only one product from the interaction of $InCl_3$ and HMPA is formed. Usually small changes in preparative conditions cause the formation of different products because of the lability of indium(III) complexes. The case of $InCl_3(HMPA)_2$ is an exception to this rule. The trigonal-bipyramidal arrangement of ligands with three halide atoms in equatorial positions is not rare for indium(III) chemistry. Compounds with this type of structure InX_3L_2, where L = $(CH_3)_3N$,[9] $(CH_3)_4N_2CO$,[10] $\{(CH_3)_2N\}_3PO$,[3] $(CH_3)_4N_2CS$,[10] $(CH_3)_3PS$, $(CH_3)_3AsS$,[11] $(CH_3)_3P$, $Ph_2P(CH_2)_2PPh_2$[12] and $(C_6H_5)_3P$,[13] are known. Among a total of 11 complexes, eight are chlorides. Moreover, a comparison of the bond lengths between indium and atoms in the axial positions for complexes with different X indicates that the distances for chloride species are significantly shorter. Considering all these facts we must assume that $InCl_3L_2$ species are more stable compared with other halides, which can circumstantially explain the formation of $InX_3(HMPA)_2$ only for the $InCl_3$–HMPA system.

^{115}In NMR resonances of InX_4^- species for indium tribromide and triiodide solutions in HMPA, together with the data indicating an ionic dimeric structure of $InX_3(HMPA)_2$ adducts,[2] led us to expect the formation of $[InX_2(HMPA)_4]^+$ $[InX_4]^-$ complexes from InX_3–HMPA ($X = Br^-$, I^-) systems.

No crystal phase was yielded from $InBr_3$ solution in HMPA due to glass formation.

Crystals of **II** were obtained from the InI_3–HMPA system. Table 3 indicates that the elemental analysis of this compound differs from that expected for $InI_3(HMPA)_2$.

The IR spectrum of sample **II** contains characteristic bands due to coordinated HMPA molecules and indicates that coordination occurs via the oxygen atom (Table 4).[2,3]

The structure of **II** involves the complex cations $[InI_2(OP\{N(CH_3)_2\}_3)_4]^+$ and I^- anions. The two crystallographically independent cations (a and b) have the same configuration, which is illustrated in Fig. 1. The indium atoms are hexa-coordinated to four HMPA molecules via oxygen and to two *trans*-

Table 3. Elemental analysis of samples **I** and **II**

	$InCl_3(HMPA)_2$ (I) Found	Calc.	$InI_3(HMPA)_4$ (II) Found	Calc.
N	14.1	14.5	13.2	13.9
C	25.3	24.9	23.9	23.8
H	5.7	6.3	6.0	5.9

Table 4. IR spectral data

Mode description	Species	Frequency (cm^{-1})[a] HMPA, liquid	$InI_3(HMPA)_4$
PO stretch	a_1	1218	1190
PN stretch	a_1	740	740
PN stretch	e	982	980
PO bend	e	481	475
CN stretch	a''	1150, 1174	1130

arranged iodine atoms in an octahedral geometry (Fig. 1, Table 5). The packing of **II** is extraordinarily loose; for one non-hydrogen atom there is a value of 25.5 $Å^3$. The shortest contacts are I···I = 7.20, I···C = 3.45, C···C = 3.45 Å.

Careful analyses of the solid phase from InI_3–HMPA solution demonstrates that compound **II** is the only product formed in this system. We can, therefore, conclude that despite the unequivocal formation of the InI_4^- anion in solution the balance between the ionic charges in the solid is reached by iodide ions which are displaced by HMPA molecules from the inner coordination shell of indium.

To date all known ionic structures containing the six-coordinate indium cation $InX_2L_4^+$, where L = Me_3PO for X = Cl^-, Br^-; Ph_2MePO for X = Br^-; Ph_3PO for X = Cl^-, Br^-; Ph_3AsO for X = Cl^- [14] and Me_2SO for X = I,[15] have InX_4^- species as an anion and thus compound **II** is the first example of mixed indium(III) complexes containing an acido ligand in the outer coordination sphere.

Previous authors[14] have tried to analyse reasons for the appearance of ionic structures and assumed preferential formation of ionic derivatives by a heavier halogen and the structure of $InI_3(HMPA)_4$ verifies this assumption.

One more interesting feature of the structure of $InI_3(HMPA)_4$ is the *trans* configuration of the cation. Recently we analysed the stereochemical features of pseudo-octahedral complexes of indium(III) halides.[16] Both VSEPR (valence-shell electron-pair repulsion)[17] and electronic-vibrational[18] concepts predict stabilization of the *trans* isomer for InX_2L_4 species when the difference between the electronegativity and geometrical parameters of donor atoms X and L are significant.

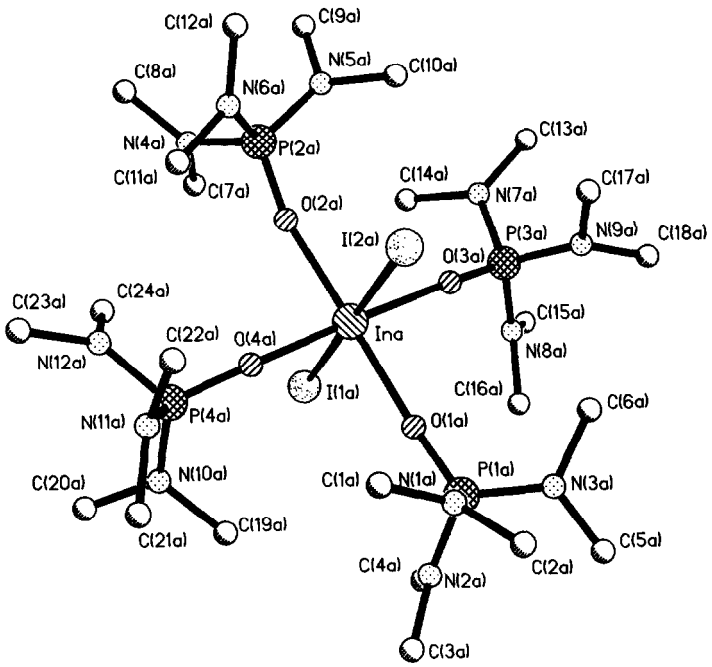

Fig. 1. The $[InI_2(OP\{N(CH_3)_2\}_3)_4]^+$ cation of **II**.

Table 5. Selected bond lengths (Å) and angles (°) for complex cations of **II**

	Molecule a	Molecule b
In—I(1)	2.812(2)	2.794(2)
In—I(2)	2.811(2)	2.803(2)
In—O(1)	2.16(1)	2.15(1)
In—O(2)	2.18(1)	2.17(1)
In—O(3)	2.16(2)	2.16(1)
In—O(4)	2.09(2)	2.14(1)
I(1)—In—I(2)	179.71(9)	179.19(8)
I(1)—In—O(1)	89.1(4)	90.5(4)
I(1)—In—O(2)	89.2(4)	90.1(4)
I(1)—In—O(3)	88.9(4)	89.2(4)
I(1)—In—O(4)	91.0(4)	88.0(4)
I(2)—In—O(1)	90.8(4)	89.6(4)
I(2)—In—O(2)	90.8(4)	89.8(4)
I(2)—In—O(3)	90.8(4)	91.6(4)
I(2)—In—O(4)	89.2(4)	91.2(4)
O(1)—In—O(2)	178.1(5)	179.3(5)
O(1)—In—O(3)	88.2(5)	90.1(5)
O(1)—In—O(4)	90.1(5)	90.8(5)
O(2)—In—O(3)	92.6(5)	89.6(5)
O(2)—In—O(4)	89.1(5)	89.5(5)
O(3)—In—O(4)	178.3(6)	177.1(5)
In—O(1)—P(1)	169.2(9)	159.3(9)
In—O(2)—P(2)	161.1(9)	166.2(9)
In—O(3)—P(3)	167(1)	162.6(9)
In—O(4)—P(4)	163(1)	161.2(9)

According to these approaches the arrangement of iodide ions in $[InI_2(HMPA)_4]^+$ should also be *trans*. It should, however, be noted that the same composition of donor atoms in the coordination sphere (I and O) gives the *cis* isomer for the cation in $[InI_2(Me_2SO)_4]^+[InI_4]^-$.[15] Authors[19] have assumed the dominant role of steric effects of ligands. Calculations of the steric angles of donor iodine and oxygen atoms (based on average bond lengths In—I 2.80 and In—O 2.18 Å) give values of 91° and 80°, respectively. Sums of the steric angles show that the *trans* isomer is destabilized since two of three octahedral planes, in contrast to one for *cis*, contain the larger iodine atoms. In—I and In—O distances in $[InI_2(HMPA)_4]^+$ (Table 5) are almost the same and so the values of the steric angles are equal, but the configuration is *trans* nevertheless. There seems to be two reasons influencing the geometry of the cation, notably (1) that the stabilization of the isomer is a function of the anion present in the lattice (I^- or InI_4^-) and (2) that, as was pointed out in ref. 19, steric stabilization of the *cis* species may disappear for bulky ligands where L—L non-bonded repulsions become predominant and *trans*-ML_2X_4 species may become favoured. HMPA should be undoubtedly considered as a bulky ligand due to the downwards-spreading umbrella geometry of the $\{(CH_3)_2N\}_3PO$ molecule, which invalidates the above arguments by producing an effective steric angle greater than that of the monatomic donor.

The arrangement of four bulky HMPA molecules in one plane and thus the contribution to the cation stability is enabled by an increase in the P—O—In angles, to *ca* 164° in $InI_2(HMPA)_4^+$ compared with 153° for $InCl_3(HMPA)_2$.[3] This oxygen angle value is the greatest for known oxo ligands coordinated to indium and even larger than that for *trans*-$[InCl_2(Ph_3PO)_4]^+$ (160°) with a ligand as large as triphenylphosphine oxide,[14] which indicates the more ionic nature of the indium–oxygen linkage in the adduct with HMPA.

The last assumption can be circumstantially confirmed by ^1H and ^{31}P NMR values. The coordination of HMPA molecules to indium [benzene solution of $InI_3(HMPA)_4$ was analysed] causes a small high-field shift of the NMR lines of both ^1H [1.38 ppm, J(H—H) = 9.5 Hz compared with 1.44 ppm and 9.3 Hz, respectively, for HMPA–C_6H_6 solution] and ^{31}P (22.86 ppm compared to 24.49 ppm for HMPA–C_6H_6 solution). This sharply contrasts with ^{31}P lines of phosphine oxide[14] and phosphate[20] molecules in indium complexes, which are usually shifted downfield by *ca* 5–13 ppm.

In a number of recent papers concerning complex fluorides of group III(13) metals—aluminium, gallium and indium—with various O- and N-donor molecular ligands we have suggested some relation between shielding of the ^{19}F nucleus and the electronegativity of an atom in the *trans* position to fluorine.[21,22] It has been shown that oxygen causes greater transfer of electron density than nitrogen from the ligand donor atom through metal to fluorine, leading to a high-field shift. A similar situation seems to be observed for $InI_3(HMPA)_4$ because the complex cation comprises oxygen atoms in O—In—O fragments, which results in a strong *trans* effect and an increase in electron density on all atoms of the HMPA molecule.

Regarding ^{31}P NMR spectroscopy of indium complexes it should be noted that in contrast to aluminium, for which $Al(HMPA)_4^{3+}$ displays a sharp quintet by ^{27}Al NMR and a sextet for ^{31}P showing clear evidence for a tetrahedral arrangement of four HMPA ligands around Al^{3+},[23] it is not possible to observe couplings between ^{115}In and ^{31}P nuclei. Line broadening must be attributed in the first place to quadrupolar relaxation of the metallic nucleus and then to the low symmetry of the complex.

We have not managed to prepare adducts of InF_3 with HMPA due to the insolubility of $InF_3 \cdot 3H_2O$ in this solvent. In spite of this some interesting information about indium complexes with such

ligands as F^- and HMPA may be obtained when investigating the $In(NO_3)_3$–F^-(NH_4F, $(CH_3)_4NF$)–HMPA–H_2O systems using ^{19}F NMR spectroscopy.

Fast exchange between various indium fluoride species slowed down only at *ca* 258 K, allowing the observation of the separate ^{19}F lines (40–80 Hz) of individual complexes. Varying the HMPA/$In(NO_3)_3$ molar ratio over the range 6–10 when $F^-/In(NO_3)_3$ was kept close to 1 allowed us to detect eight resonances of mixed-fluoro/HMPA/aqua species. We have no direct evidence for the coordination number of indium in these complexes, but the number of bands observed together with the results we obtained when dealing with ^{19}F NMR spectra of In^{3+}–F^-–L–H_2O [L = Cl^-, Br^-, I^-, NCO^-, NCS^-,[24] $(NH_2)_2CO$, NH_2CH_3CO, $(NH_2)_2CS$ and NH_2CH_3CS[25]] systems allowed us to consider the interval of chemical shifts (−150 to −175 ppm) corresponding to the six-coordinate species. The assignment of lines (Table 6) was performed in accordance with both the tendency of the ligands to cause deshielding of ^{19}F nuclei in the complex and the dependence of the integration curves on HMPA concentration. Chemical shifts (δ) of the complexes show the additivity of δ when substituting water molecules in $InF_n(H_2O)_6^{3-n}$ by HMPA (*ca* 2.5 ppm per substitution). The corresponding values for acido ligands (17, Cl^-; 15, Br^-; 7, NCS^-) are significantly higher and demonstrate a stronger influence of ionic ligands compared with neutral molecules on coordinated fluoride.

The consideration of interactions of various indium halide salts with hexamethylphosphoramide leads to several conclusions, notably: HMPA molecules can be combined with atoms of all halides (from F to I) in the coordination sphere of indium(III).

The coordination numbers of indium in mixed-halide complexes with HMPA differ. The same preparative technique leads to five-coordinate chloride species, whereas the coordination number for the iodide complex cation is six. This result is rather unexpected because the opposite situation should be more likely. The reasons for the preference of trigonal-bipyramidal chloride structure has been discussed earlier. It can be assumed that the formation of similar iodide species is hindered by the arrangement of three large iodine atoms in the equatorial plane. The systematic discussion of this observation needs more structural information and quantitative thermodynamic data on mixed indium complexes. Work on this is proceeding.

Table 6. ^{19}F resonances for mixed $InF_n(HMPA)_m(H_2O)_{6-n-m}^{3-n}$ species in aqueous solution

Complex	$-\delta$ (ppm)
$InF(HMPA)(H_2O)_4^{2+}$	174.2
$InF(HMPA)_2(H_2O)_3^{2+}$	171.4
$InF(HMPA)_3(H_2O)_2^{2+}$	169.2
$InF(HMPA)_4(H_2O)^{2+}$	167.0
$InF(HMPA)_5^{2+}$	164.7
$InF_2(HMPA)(H_2O)_3^+$	163.6
$InF_2(HMPA)_2(H_2O)_2^+$	160.6
$InF_2(HMPA)_3(H_2O)^+$	157.3

REFERENCES

1. V. Gutman, *Coordination Chemistry in Non-Aqueous Solutions*. Springer-Verlag, F.R.G. (1968).
2. M. W. G. de Bolster, PhD Thesis, The coordination chemistry of aminophosphine oxides and related ligands. Leiden (1972).
3. S. P. Sinha, T. T. Pakkanen, T. A. Pakkanen and L. Niinisto, *Polyhedron* 1982, **1**, 355.
4. A. J. Carty and D. G. Tuck, *J. Chem. Soc. A.* 1966, 1081.
5. M. J. S. Gynane, M. Wilkinson and I. J. Worral, *Inorg. Nucl. Chem. Lett.* 1973, **9**, 765.
6. M. A. Malyarick and S. P. Petrosyants, *Inorg. Chem.* 1993, **32**, in press.
7. B. R. McGarvey, C. O. Trudell, D. G. Tuck and L. Victoriano, *Inorg. Chem.* 1980, **19**, 3432.
8. A. Fraticllo, D. D. Davis, S. Peak and R. E. Schuster, *Inorg. Chem.* 1971, **10**, 1627.
9. R. Karia, G. R. Willey and M. G. B. Drew, *Acta Cryst.* 1986, **C42**, 558.
10. R. L. Beddoes, D. Collison, F. E. Mabbs and J. Temperley, *Acta Cryst.* 1991, **C47**, 58.
11. W. T. Robinson, C. J. Wilkins and Z. Zeying, *J. Chem. Soc., Dalton. Trans.* 1988, 2187.
12. I. A. Degnan, N. W. Alcock, S. M. Roe and M. G. H. Wallbridge, *Acta Cryst.* 1992, **C49**, 995.
13. M. V. Veidis and G. J. Palenik, *J. Chem. Soc., Chem. Commun.* 1969, 586.
14. W. T. Robinson, C. J. Wilkins and Z. Zeying, *J. Chem. Soc., Dalton. Trans.* 1990, 219.
15. F. W. B. Einstein and D. G. Tuck, *J. Chem. Soc., Chem. Commun.* 1970, 1182.
16. M. A. Malyarick, S. P. Petrosyants and A. B. Ilyuhin, *Polyhedron* 1992, **11**, 1067.
17. R. G. Gillespie, *J. Chem. Educ.* 1970, **47**, 18.
18. A. A. Levin and P. N. Dyachkov, *Electronic Structure, Geometry, Isomerism and Transformation of Heteroligand Molecules*. Nauka, Moscow (1990) (in Russian).
19. A. J. Carty and D. G. Tuck, *Prog. Inorg. Chem.* 1975, **19**, 243.
20. L. Rodenuser, P. R. Rubini and J.-J. Delpuech, *Inorg. Chem.* 1977, **16**, 2837.

21. S. P. Petrosyants, M. A. Malyarick and E. R. Buslaeva, *Zh. Neorg. Khim.* 1991, **36**, 2854.
22. M. A. Malyarick, S. P. Petrosyants, A. B. Ilyuhin and Yu. A. Buslaev, *Zh. Neorg. Khim.* 1991, **36**, 2816.
23. J.-J. Delpuech, M. R. Khaddar, A. Peguy and P. Rubini, *J. Chem. Soc., Chem. Commun.* 1974, 155.
24. S. P. Petrosyants, M. A. Malyarick and Yu. A. Buslaev, *Koord. Khim.* 1989, **15**, 1493.
25. M. A. Malyarick, S. P. Petrosyants and Yu. A. Buslaev. *Zh. Neorg. Khim.* 1990, **35**, 2057.

Polyhedron Vol. 12, No. 19, pp. 2411–2415, 1993
Printed in Great Britain

0277–5387/93 $6.00+.00
© 1993 Pergamon Press Ltd

SYNTHESIS AND CHARACTERIZATION OF SOME LANTHANIDE(III) PERCHLORATO COMPLEXES OF HYDRAZONES OF ISONICOTINIC ACID HYDRAZIDE

RAM K. AGARWAL* and RAJENDRA K. SARIN

Department of Chemistry, Lajpat Rai (Post-Graduate) College, Sahibabad 201005 (Ghaziabad), India

(*Received* 28 *January* 1993; *accepted* 27 *April* 1993)

Abstract—The lanthanide(III) perchlorato complexes of hydrazones of isonicotinic acid hydrazide, viz. N-isonicotinamido-*p*-dimethylaminobenzalaldimine (INH-PDAB) and N-isonicotinamido-3-methoxy-4-hydroxybenzalaldimine (INH-VAN) of the type $Ln(ClO_4)_3 \cdot 4$(INH-PDAB) or $Ln(ClO_4)_3 \cdot 4$(INH-VAN) (Ln = La, Pr, Nd, Sm, Gd, Tb or Dy) have been synthesized and characterized by analytical, magnetochemical, IR and UV–vis spectral methods. The thermal stabilities of these compounds have also been investigated.

The remarkable biological activity of acid hydrazides, R—CO—NH—NH_2, their corresponding aroylhydrazones, R—CO—NH—N=CH—R′ and the dependence of their mode of chelation with transition metal ions present in the living system have been of significant interest in recent years.[1–4] The coordination compounds of aroylhydrazones have been reported to act as enzyme inhibitors[5] and are useful due to their pharmacological applications.[6–8] In view of the increasing interest in hydrazones, on account of the structural, analytical and pharmacological importance of their metal complexes, the synthesis of two hydrazones, i.e. N-isonicotinamido-*p*-dimethylaminobenzalaldimine (INH-PDAB) (I) and N-isonicotinamido-3-methoxy-4-hydroxybenzalaldimine (INH-VAN) (II) and their lanthanide(III) perchlorato complexes are described.

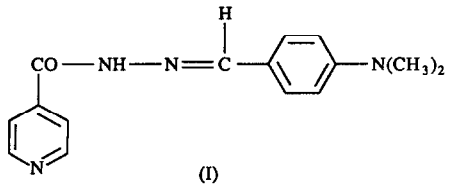

(I)

N-Isonicotinamido-p-Dimethylaminobenzalaldimine (INH-PDAB) (m.f. $C_{15}H_{16}N_4O$)

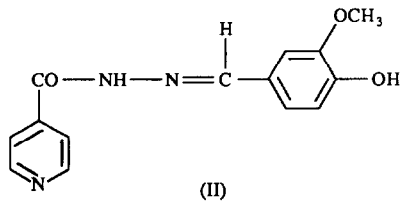

(II)

N-Isonicotinamido-3-Methoxy-4-Hydroxybenzalaldimine (INH-VAN) (m.f. $C_{14}H_{13}N_2O_3$)

EXPERIMENTAL

Reagents

The lanthanide oxides were obtained from Rare Earths Products Ltd (India) and were used without further purification. The perchlorates were prepared by heating the corresponding oxides with perchloric acid (A.R.) and evaporating off the excess acid.[9] The ligands INH-PDAB and INH-VAN were synthesised in the laboratory as follows: isonicotinic acid hydrazide (0.01 mol) was dissolved in 95% ethanol (30 cm^3). To this solution was added the aromatic aldehyde *p*-dimethylaminobenzaldehyde or vanillin (0.01 mol) in 95% ethanol (40 cm^3). The reaction mixture was refluxed on a water bath for *ca* 2 h. The partial removal of solvent on a water bath followed by cooling produced a crystalline product, which was suction filtered, washed with cold alcohol and dried *in vacuo*. The purity of the ligands was checked by elemental analysis, TLC and m.p. determination (INH-PDAB, $C_{15}H_{16}N_4O$,

* Author to whom correspondence should be addressed.

yellow, m.p. 209°C; INH-VAN, $C_{14}H_{13}N_3O_3$, yellow, m.p. 191°C).

Synthesis of the complexes

$[Ln(ClO_4)_3 \cdot 4(INH\text{-}PDAB)]$ (Ln = La, Pr, Nd, Sm, Gd, Tb or Dy). All the perchlorato complexes were prepared by mixing hot ethanolic solutions of ligand and metal perchlorate in a 4:1 molar ratio. The mixture was refluxed on a water bath for 2 h and then concentrated. On cooling the complexes were filtered, washed with ethanol and diethyl-ether and dried *in vacuo* over anhydrous $CaCl_2$.

$[Ln(ClO_4)_3 \cdot 4(INH\text{-}VAN)]$ (Ln = La, Pr, Nd, Sm, Gd, Tb or Dy). Lanthanide(III) perchlorate (2 mmol) and INH-VAN (8.1 mmol) were dissolved separately in hot ethanol (20 cm^3 each). The reaction mixture was refluxed for *ca* 3 h and the solution was concentrated to a viscous mass, which was washed several times with small portions of hot benzene to remove the excess ligand. The finely divided solid mass was finally washed with diethyl-ether and collected and dried *in vacuo* over P_4O_{10}.

Analytical methods

The complexes were analysed for the metals by the conventional method.[10] Microanalyses for carbon, hydrogen and nitrogen were performed on a Perkin–Elmer 23 CHN elemental analyser. The perchlorate was estimated by the Kurz method.[11] The molecular weight of the complexes was determined cryoscopically in freezing nitrobenzene using a Beckmann thermometer of accuracy ± 0.01°C in the laboratory. The conductivity measurements were obtained using a Toshniwal conductivity bridge (type CL 01/01) and a dip-type cell operating at 220 V on an AC mains. All the measurements were performed at room temperature in $PhNO_2$. The magnetic measurements were obtained at room temperature with a Gouy's balance and $[HgCo(SCN)_4]$ was used as a calibrant. The IR spectra of the complexes were recorded on a Perkin–Elmer IR spectrophotometer model-521 in CsI_2 in the range 4000–200 cm^{-1}. A Hilger Uvispek spectrophotometer with a 1 cm quartz cell was employed for recording the visible spectra of these complexes. TG analyses were performed in static air with open sample holders and a small platinum boat; the heating rate was 6°C min^{-1}.

RESULTS AND DISCUSSION

The reaction of non-aqueous solutions of lanthanide(III) perchlorate with INH-PDAB and INH-VAN resulted in the formation of complexes of the composition $Ln(ClO_4)_3 \cdot 4L$ (L = INH-PDAB or INH-VAN; Ln = La, Pr, Nd, Sm, Gd, Tb or Dy). The analytical data of the present complexes are summarized in Table 1. Most of the complexes are fairly stable and could be stored for a long time and are non-hygroscopic in nature. All the complexes are generally soluble in common organic solvents, but partially soluble in diethyl-ether. TG curves indicate no changes up to 130°C, suggesting the absence of coordinated or uncoordinated water molecules in these complexes. The molar conductivity values in nitrobenzene fall in the range 76–82 $\Omega_m\ \Omega^{-1}\ cm^2\ mol^{-1}$, suggesting that these complexes behave as 1:3 electrolytes. Data on the molecular weight of the complexes in nitrobenzene are presented in Table 1, along with values calculated on the basis of established formulae of the complexes. The ratio of molecular weight observed for $Ln(ClO_4)_3 \cdot 4L$ to that calculated is found to be 0.25. This data provide further support that four species are formed in these complexes.

IR spectra

A study and comparison of the IR spectra of the ligands and its complexes imply that both the ligands are bidentate with the carbonyl-oxygen and azomethine-nitrogen as the two coordination sites. In INH-VAN the —OH group is not taking part in the coordination. The presence of various ring vibrations and C—H absorption makes the spectra fairly complicated for complete assignments of individual bands. Tentative assignments to several absorptions associated with C—H, C=C, C—N and ring stretchings have been made; these absorptions are a little sensitive to complexation. Similarly, the absorption and ring breathing mode in the ligands and their Ln^{3+} complexes are very close to each other.

The ligands are expected to be tridentate, the possible coordination sites being the pyridine-nitrogen, the azomethine-nitrogen and the amide group. The amide-I band in the INH derivatives appears at 1660–1640 cm^{-1}. In the IR spectra of the complexes a considerable negative shift in ν(C=O) is observed, indicating a decrease in the stretching force constant of C=O as a consequence of coordination through the carbonyl-oxygen atom of the free base. The amide-II band appears at the normal position in the NH deformation rather than the C—N link. In the INH derivatives the absorption in the 1565–1560 cm^{-1} region has been assigned to amide-II absorption. The NH stretching absorption[12] in the free ligands occurs at *ca* 3290 and 3220 cm^{-1}, which remains unaffected after complexation. This precludes the possibility of coordination

Table 1. Analytical, conductivity, molecular weight and magnetic moment data of lanthanide(III) perchlorato complexes

Complex	Analysis: Found (Calc.) (%) M	C	H	N	Anion	Ω_M ($\Omega^{-1}cm^2$ mol^{-1})	Average Mol. wt (formula weight)	μ_{eff} (B.M.)
$La(ClO_4)_3 \cdot 4$(INH-PDAB)	9.3	47.8	4.2	14.9	19.9	74.9	376	Diamagnetic
	(9.2)	(47.7)	(4.2)	(14.8)	(19.8)		(1509.5)	
$Pr(ClO_4)_3 \cdot 4$(INH-PDAB)	9.4	47.8	4.2	14.9	19.85	75.9	378	3.69
	(9.3)	(47.6)	(4.2)	(14.8)	(19.7)		(1511.5)	
$Nd(ClO_4)_3 \cdot 4$(INH-PDAB)	9.3	47.6	4.2	14.8	19.8	76.3	379	3.58
	(9.2)	(47.5)	(4.2)	(14.8)	(19.7)		(1514.5)	
$Sm(ClO_4)_3 \cdot 4$(INH-PDAB)	9.95	47.4	4.2	14.8	19.7	77.1	382	1.82
	(9.9)	(47.35)	(4.2)	(14.6)	(19.6)		(1520.5)	
$Gd(ClO_4)_3 \cdot 4$(INH-PDAB)	10.3	47.2	4.2	14.7	19.6	78.1	383	7.77
	(10.3)	(47.1)	(4.2)	(14.7)	(19.5)		(1527.5)	
$Tb(ClO_4)_3 \cdot 4$(INH-PDAB)	10.5	47.1	4.2	14.7	19.6	79.7	384	9.39
	(10.4)	(47.1)	(4.2)	(14.6)	(19.5)		(1529.5)	
$Dy(ClO_4)_3 \cdot 4$(INH-PDAB)	10.7	47.1	4.2	14.7	19.5	77.3	385	10.50
	(10.6)	(47.1)	(4.2)	(14.4)	(19.8)		(1533.0)	
$La(ClO_4)_3 \cdot 4$(INH-VAN)	9.25	44.3	3.4	11.1	19.5	76.3	376	Diamagnetic
	(9.1)	(44.2)	(3.4)	(11.0)	(19.6)		(1521.5)	
$Pr(ClO_4)_3 \cdot 4$(INH-VAN)	9.3	44.2	3.45	11.1	19.5	77.4	378	3.71
	(9.25)	(44.1)	(3.4)	(11.0)	(19.6)		(1523.5)	
$Nd(ClO_4)_3 \cdot 4$(INH-VAN)	9.5	44.1	3.4	11.1	19.5	78.2	379	3.60
	(9.4)	(44.0)	(3.4)	(11.0)	(19.55)		(1526.5)	
$Sm(ClO_4)_3 \cdot 4$(INH-VAN)	9.9	44.0	3.4	11.0	19.4	79.0	380	1.58
	(9.8)	(43.8)	(3.4)	(11.0)	(19.5)		(1532.5)	
$Gd(ClO_4)_3 \cdot 4$(INH-VAN)	10.3	43.8	3.4	11.0	19.3	80.3	381	7.96
	(10.2)	(43.65)	(3.4)	(11.0)	(19.4)		(1539.5)	
$Tb(ClO_4)_3 \cdot 4$(INH-VAN)	10.4	43.7	3.4	11.0	19.3	81.4	383	9.51
	(10.3)	(43.6)	(3.4)	(10.9)	(19.4)		(1541.5)	
$Dy(ClO_4)_3 \cdot 4$(INH-VAN)	10.6	43.6	3.4	10.9	19.2	77.2	385	10.63
	(10.51)	(43.5)	(3.4)	(10.9)	(19.3)		(1545.0)	

through the imine nitrogen atom. Another important band occurs at *ca* 1590 cm^{-1}, attributed to ν(C=N) (azomethine mode[13,14]). In the spectra of all the complexes this band is shifted to a lower wave number and appears in the 1550–1530 cm^{-1} region, indicating the involvement of the nitrogen atom of the azomethine group in coordination.[13,14] The strong bands observed at 1575–1520 cm^{-1} and 1080–1000 cm^{-1} are tentatively assigned[14–16] to antisymmetric and symmetric ν(C=C)+ν(C=N) bands of the pyridine ring, but the pyridine ring breathing and deformation bands remain practically unchanged in frequency and band intensities, thus revealing the non-involvement of the pyridine nitrogen in coordination. However, this assignment[17] is not unambiguous because the N—N group of the ligands also absorbs in the region 1000–890 cm^{-1}. In the spectra of INH-VAN the stretching frequency around 3400–3200 cm^{-1} is attributed to ν(OH). In the complexes of INH-VAN the —OH group frequency appears in the same region as in the free ligand, clearly indicating that the —OH group is not taking part in coordination. The overall IR spectral evidence suggests that both the ligands act as bidentate ligands and coordinate through the amide-oxygen and azomethine-nitrogen atoms, forming a five-membered chelate ring. The bands in the region 440–360 cm^{-1} in the complexes under study are tentatively assigned to ν(Ln—O)/ν(Ln—N) modes.[17–19]

In all the complexes only two strong ν_3 and ν_4 bands are observed in the regions 1110–1080 cm^{-1} and 630–620 cm^{-1}, respectively, for the perchlorate ion, indicating that tetrahedral symmetry has not been disturbed on complexation and the perchlorate ions are not bonded to the metal ions.[20,21] This conclusion is also supported by conductance and molecular weight data.

Table 2. Electronic spectral data (cm^{-1}) and related bonding parameters of lanthanide(III) perchlorato complexes of INH-PDAB and INH-VAN

Complex	Complex electronic spectral bands	J Levels	$(1-\beta)$	β	$b^{1/2}$	$\delta(\%)$	η
$Pr(ClO_4)_3 \cdot 4$(INH-PDAB)	22,285	$^3H_4 \rightarrow {}^3P_2$	0.0082	0.9917	0.0640	0.8268	0.0041
	21,110	$^3H_4 \rightarrow {}^3P_1$	0.0100	0.9899	0.0707	1.0102	0.0050
	20,605	$^3H_4 \rightarrow {}^3P_0$	0.0072	0.9927	0.0600	0.7252	0.0036
	16,805	$^3H_4 \rightarrow {}^1D_2$	0.0117	0.9882	0.0764	1.1839	0.0059
$Nd(ClO_4)_3 \cdot 4$(INH-PDAB)	19,470	$^4I_{9/2} \rightarrow {}^2G_{9/2}$	0.0043	0.9956	0.0463	0.4319	0.0022
	17,200	$^4I_{9/2} \rightarrow {}^4G_{5/2}, {}^2G_{7/2}$	0.0095	0.9904	0.0689	0.9592	0.0048
	13,330	$^4I_{9/2} \rightarrow {}^2S_{3/2}, {}^4F_{7/2}$	0.0245	0.9754	0.1106	2.5117	0.0125
	12,400	$^4I_{9/2} \rightarrow {}^4F_{5/2}, {}^4H_{9/2}$	0.0060	0.9939	0.0547	0.6036	0.0030
$Sm(ClO_4)_3 \cdot 4$(INH-PDAB)	24,770	$^6H_{5/2} \rightarrow {}^4F_{9/2}$	0.0040	0.9959	0.0447	0.4016	0.0020
	23,700	$^6H_{5/2} \rightarrow {}^6P_{5/2}$	0.0125	0.9875	0.0790	1.2658	0.0063
	21,500	$^6H_{5/2} \rightarrow {}^4I_{13/2}$	0.0025	0.9974	0.0353	0.2506	0.0013
$Pr(ClO_4)_3 \cdot 4$(INH-VAN)	22,370	$^3H_4 \rightarrow {}^3P_2$	0.00445	0.99554	0.04716	0.44699	0.00223
	21,210	$^3H_4 \rightarrow {}^3P_1$	0.00539	0.99460	0.05191	0.54192	0.00271
	20,610	$^3H_4 \rightarrow {}^3P_0$	0.00674	0.99325	0.05805	0.67858	0.00339
	16,870	$^3H_4 \rightarrow {}^1D_2$	0.00764	0.99235	0.06180	0.76988	0.00384
$Nd(ClO_4)_3 \cdot 4$(INH-VAN)	19,500	$^4I_{9/2} \rightarrow {}^2G_{9/2}$	0.00510	0.99489	0.05049	0.51261	0.00256
	17,260	$^4I_{9/2} \rightarrow {}^4G_{5/2}, {}^2G_{7/2}$	0.00690	0.99309	0.05873	0.69480	0.00347
	13,620	$^4I_{9/2} \rightarrow {}^2S_{3/2}, {}^4F_{7/2}$	0.00438	0.99562	0.04679	0.43992	0.00219
	12,420	$^4I_{9/2} \rightarrow {}^4F_{5/2}, {}^4H_{9/2}$	0.00400	0.99599	0.04472	0.40161	0.00201
$Sm(ClO_4)_3 \cdot 4$(INH-VAN)	24,740	$^4H_{5/2} \rightarrow {}^4F_{9/2}$	0.00522	0.99477	0.05108	0.52474	0.00262
	23,700	$^4H_{5/2} \rightarrow {}^6P_{5/2}$	0.01250	0.98750	0.07905	1.2658	0.00630
	21,500	$^4H_{5/2} \rightarrow {}^4I_{13/2}$	0.00232	0.99767	0.03405	0.2325	0.00116

Electronic spectra

The electronic spectra in the visible region of the solid lanthanide(III) complexes exhibit changes in the intensity and shifts in position of the absorption bands relative to the solid lanthanide(III) salts. These shifts have been ascribed to a nephelauxetic effect. The extent of the red shifts of the hypersensitive bands is related to covalance in the metal–ligand bonds and is assessed by the nephelauxetic ratio (β), bonding parameter ($b^{1/2}$), Sinha's parameter [$\delta(\%)$] and covalency angular overlap parameter (η).[22–24] The values of the covalent parameters are presented in Table 2. The values of the nephelauxetic ratio (β) are smaller than 1 and the positive values of the bonding parameter ($b^{1/2}$) and Sinha's parameter indicate the occurrence of some covalent character in the metal–ligand bond.[25] The comparatively smaller magnitude of the $b^{1/2}$ values also show the involvement of the 4*f*-orbital in the metal–ligand bond to a very small degree.[24]

Thermal studies

The analyses of the thermolysis curves suggest that these complexes do not show the presence of water molecules either in or out of the coordination sphere. There is a change in the curves within the temperature region 285–330°C, due to the loss of mass corresponding to 2.5 mol of organic ligands and at 440°C all the organic ligands are lost. Finally, at *ca* 810°C stable lanthanide oxides are formed.[26]

Stereochemistry

The solution studies in $PhNO_2$ suggest the ionic nature of these complexes. They behave as 1 : 3 electrolytes on $PhNO_2$. The molecular weight determined cryoscopically in freezing $PhNO_2$ suggests that four species are formed in these complexes. This is further confirmed by IR data. IR spectra and TG studies of all the complexes further indicate the absence of water. Thus, in these complexes the central metal ion is surrounded by four oxygen atoms and four nitrogen atoms and thus the coordination number eight applies to these complexes.[27] This is in analogy with other lanthanide perchlorato complexes of 2,2′-bipyridine-1,1′-dioxide,[28] $[Ln(BipyO_2)_4]\ (ClO_4)_3$, or octamethylpyrophosphoramide,[29] $[La(OMPA)_4]\ (ClO_4)_3$. Based on the elemental analyses and various physicochemical

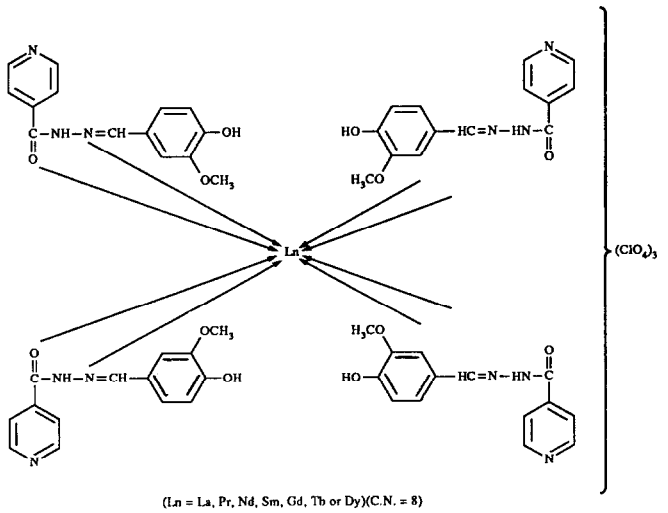

Fig. 1. Probable structures of lanthanide(III) perchlorato complexes of INH-VAN.

studies the following structure may be tentatively proposed for the present complexes (Fig. 1).

Acknowledgement—One of us (R.K.A.) is thankful to the University Grants Commission, New Delhi, for financial support of this work.

REFERENCES

1. I. A. Tossidis, C. A. Bolos, P. N. Aslanidis and G. A. Katsoulos, *Inorg. Chim. Acta* 1987, **133**, 275.
2. J. A. Anten, D. Nicholis, J. M. Markopoulos and O. Markopoulou, *Polyhedron* 1987, **6**, 1075.
3. A. Maiti and S. Ghosh, *Ind. J. Chem.* 1989, **28A**, 980.
4. R. C. Aggarwal, N. K. Singh and R. P. Singh, *Inorg. Chem.* 1981, **29**, 2794.
5. J. C. Craliz, J. C. Rub, D. Willis and J. Edger, *Nature* 1955, **34**, 176.
6. J. R. Dilworth, *Coord. Chem. Rev.* 1976, **21**, 29.
7. J. R. Merchant and D. S. Clothia, *J. Med. Chem.* 1970, **13**, 335.
8. N. S. Biradar and B. R. Havinale, *Inorg. Chim. Acta* 1976, **17**, 157.
9. S. S. Sandhu and G. S. Aulakh, *Ind. J. Chem.* 1974, **12**, 1102.
10. I. M. Kolthoff and P. S. Elving, *Treatise on Analytical Chemistry*, Vol. 8, Part II. Interscience, New York (1963).
11. E. Kurz, G. Kober and M. Berl, *Analyt. Chem.* 1958, **30**, 1983.
12. L. J. Bellamy, *Infrared Spectra of Complex Molecules* Methuen, London (1954).
13. P. K. Radhakrishnan, P. Indrasenan and C. G. R. Nair, *Polyhedron* 1984, **3**, 67.
14. Y. Kumar, P. D. Sethi and C. L. Jain, *J. Ind. Chem. Soc.* 1990, **67**, 796.
15. G. R. Burns, *Inorg. Chem.* 1968, **7**, 277.
16. K. Swaminathan and N. H. Irving, *J. Inorg. Nucl. Chem.* 1964, **26**, 1291.
17. P. S. Radhakrishnan and P. Indrasenan, *Ind. J. Chem.* 1989, **28A**, 234.
18. R. K. Agarwal and S. K. Gupta, *Ind. J. Chem.* 1986, **25A**, 597.
19. P. S. Radhakrishnan and P. Indrasenan, *J. Ind. Chem. Soc.* 1990, **67**, 243.
20. K. Nakamoto, *Infrared Spectra of Inorganic and Coordination Compounds*. Wiley, New York (1970).
21. D. M. Adams, *Metal–Ligand and Related Vibrations*. Arnold, London (1967).
22. C. K. Jorgensen, *Prog. Inorg. Chem.* 1962, **4**, 73.
23. S. P. Sinha, *Spectrochim. Acta* 1966, **22**, 57.
24. J. Mohan, J. P. Tandon and N. S. Gupta, *Inorg. Chim. Acta* 1986, **111**, 187.
25. K. S. Ashok and M. B. Akshya, *J. Inorg. Nucl. Chem.* 1979, **41**, 1311.
26. G. Vicentini, K. Umeda and I. Giolito, *An. Acad. Brasil. Cienc.* 1977, **49**, 143.
27. D. K. Koppikar, P. V. Sivapulliah, L. Ramakrishnan and S. Soundararajan, *Struct. Bonding* 1978, **34**, 135.
28. D. M. Mehs and S. K. Madan, *J. Inorg. Nucl. Chem.* 1968, **30**, 3017.
29. M. D. Joesten and R. A. Jacob, *Adv. Chem. Ser.* 1967, **71**, 13.

Polyhedron Vol. 12, No. 19, pp. 2417–2420, 1993
Printed in Great Britain

0277–5387/93 $6.00+.00
© 1993 Pergamon Press Ltd

SYNTHESIS AND X-RAY CRYSTAL STRUCTURE OF THE ORGANOTUNGSTEN(V) *o*-PHENYLENE DIAMIDO COMPLEX, $(\eta\text{-}C_5Me_5)WCl_2\{1,2\text{-}(HN)_2C_6H_4\}$

CARL REDSHAW and GEOFFREY WILKINSON†

Johnson Matthey Laboratory, Chemistry Department, Imperial College, London SW7 2AY, U.K.

and

TRACY K. N. SWEET and MICHAEL B. HURSTHOUSE†

School of Chemistry and Applied Chemistry, University of Wales Cardiff, P.O. Box 912, Cardiff CF1 3TB, U.K.

(*Received* 5 *April* 1993; *accepted* 22 *April* 1993)

Abstract—The paramagnetic tungsten(V) complex $Cp^*WCl_2[1,2\text{-}(HN)_2C_6H_4]$, $Cp^* = C_5Me_5$, has been obtained by interaction of Cp^*WCl_4 with *o*-phenylenediamine (1,2-diaminobenzene, *o*-pdaH$_2$). The X-ray crystal structure shows a pseudo-square pyramidal geometry with the chelating diamido group and chlorine atoms forming the base and a slipped (3e) Cp* group occupying the axial site.

A number of tungsten complexes with deprotonated ligands derived from 1,2-diaminobenzene were obtained during unsuccessful attempts[1] to obtain the still unknown $W[1,2\text{-}(HN)_2C_6H_4]_3$, which would be isoelectronic with the rhenium(VII) cation $\{Re[1,2\text{-}(HN)_2C_6H_4]_3\}^+$.[2] A number of diamagnetic monoimido compounds with C_5Me_5(Cp*) ligands have been made for niobium and tantalum,[3] $Cp^*M(NR)Cl_2$, R = Me, $C_6H_3Pr^i_2$-2,6, molybdenum and tungsten,[4] $Cp^*M(NBu^t)_2Cl$, rhenium,[5] $Cp^*Re(NR)Cl_2$, R = Me, Bu^t, and iridium, $Cp^*Ir(NBu^t)$.[6]

The paramagentic tungsten (d^1) 1,2-diamido complex $Cp^*WCl_2[1,2\text{-}(HN)C_6H_4]$ (**1**) is obtained by interaction of Cp^*WCl_4[7] with 2 equivalents of *o*-phenylenediamine in refluxing toluene. Alternatively Cp^*WCl_4 and the hydrochloride, *o*-pdaH$_2$ · 2HCl in toluene containing excess NEt_3 are refluxed as before. The EPR spectrum of **1** (*X*-band, 25°C in THF) is sharp with $g = 1.933$, a value typical for tungsten(V);[8] coupling to ^{183}W was observable (82 G), but no hyperfine isotopic coupling due to nitrogen. The IR spectrum has a sharp NH band at *ca* 3300 cm^{-1}. Compound **1** is soluble in polar solvents such as THF and MeCN, but is insoluble in hydrocarbons.

A diagram of the molecule is shown in Fig. 1; selected bond lengths and angles are given in Table 1. The coordination geometry is best described as pseudo-square pyramidal with the Cp* ligand occupying the axial site. The molecule lies on a crystallographic mirror plane through W(1), C(4) and C(7).

The diamido ligand chelates symmetrically (by symmetry) and the metal atom lies close to the least-squares plane of the ligand; the displacement from the plane of 0.21 Å gives an envelope fold about the N···N vector of *ca* 8°. Apart from this small amount of bending the nitrogens are essentially planar,[9a] as is commonly found for amido ligands; indeed, pyramidal amides are quite rare.[9b] On this basis it would be usual to look for evidence of $p\pi$–$d\pi$ donation of the nitrogen lone pairs to the metal, but in the present case the W—N distances of 1.998(8) Å are not unusually short. For example, they are longer than the W^V—N (amido) bond [1.924(14) Å] in $\{WCl_3[1\text{-}(HN)2\text{-}(H_2N)C_6H_4]\}_2\{\mu\text{-}1,2\text{-}(N)_2C_6H_4\}$.[1] There is, however, some indication

* Authors to whom correspondence should be addressed.

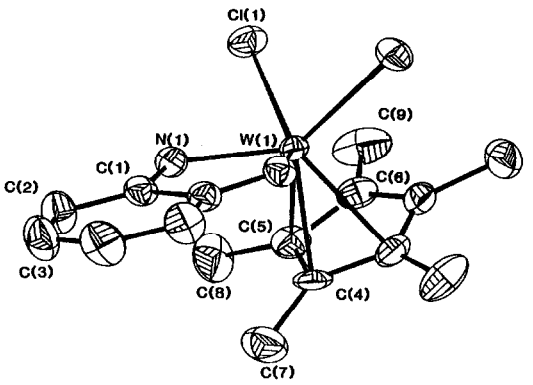

Fig. 1. The structure of $(C_5Me_5)WCl_2[1,2\text{-}(HN)_2C_6H_4]$.

of delocalization of the nitrogen lone pairs into the aromatic ring, since the unique C—N distance is quite short at 1.37(1) Å, but there seems to be little disturbance of the ring aromaticity, with the bonds all within the range 1.38–1.42(2) Å.

One interesting feature of the structure is the bonding of the Cp* ring, for which the W—C distances differ significantly, from 2.27 to 2.46(1) Å. Such distortions may be described in terms either of "tilting"[10] or "slippage".[11] In many instances the two descriptions refer to the same feature, which is fundamentally characterized by a non-orthogonal angle between the vector for the metal atom to the centroid of the Cp (or Cp* or indenyl-C_5) ring and the ring plane. Thus, we defined[10] a "tilt angle" τ as in structure **1(a)**, whilst various authors have proposed alternative ways[11] of measuring slippage; a typical definition is that of Atwood,[11b] as shown in structure **1(b)**.

1a

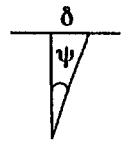

1b

Table 1. Selected bond lengths (Å) and angles (°) for compound **1**

Cl(1)—W(1)	2.413(4)
N(1)—W(1)	1.998(8)
C(5)—W(1)	2.327(9)
C(4)—W(1)	2.273(10)
C(6)—W(1)	2.461(9)
N(1)—W(1)—Cl(1)	82.5(3)
N(1)—W(1)—Cl(1a)	134.4(3)
C(4)—W(1)—Cl(1)	128.6(2)
C(4)—W(1)—N(1)	91.6(4)
C(6)—W(1)—Cl(1)	80.1(3)
C(6)—W(1)—N(1)	118.4(3)
C(5)—W(1)—Cl(1)	92.5(3)
C(5)—W(1)—N(1)	89.0(4)
C(5)—W(1)—C(4)	36.2(2)
C(6)—W(1)—C(5)	34.1(3)
Cl(1)—W(1)—Cl(1a)	86.1(2)
C(1)—N(1)—W(1)	120.4(5)
N(1)—W(1)—N(1a)	74.8(4)
C(6)—W(1)—C(6a)	33.4(3)
C(5)—W(1)—C(5a)	58.9(5)

Key to symmetry operations relating designated atoms to reference atoms at (x, y, z): (a) $1.0+x, y, z$.

Geometrically, Atwood's Ψ angle is equivalent to our τ. In fact, simple geometrical considerations show that slippage must also be accompanied by tilting. The origin and importance of "slippage" has been much discussed in terms of electronic effects and the importance of the feature to fluxional systems, particularly in indenyl complexes. We ascribed the tilting in our manganese complexes[10] to steric interactions in a rather crowded coordination sphere, but this may not always be the case.

One important factor is the electron count on the metal in the complex in question and the potential ability of the Cp type ligand to act as a 5,3 or 1 electron ligand. Slippage is then associated with the lower electron provision, with a $1e,\eta^1$ ligand—essentially a simple alicyclic sigma ligand—as the limiting extreme. However, the η^3 case is not so straightforward. On the one hand we have a clear $3e,\eta^3$ bonding mode characterized by a C_5 ring, which is not only slipped but also folded, such as the classic structure described by Huttner *et al.*[12] Here the C—C bond geometry was also consistent with a disruption of the fully delocalized pi-system to give a form as in structure **2**.

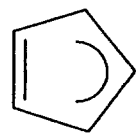

2

On the other hand there are numerous examples of slipped rings in which the planarity and delocalization of the C_5 ring is preserved. The much studied Cp_2Be[13] structure is a classical example and many others are found both within main group and transition metal chemistry.

Our complex is an example of the latter type. The

slippage of the ring is well defined ($\delta = 0.22$ Å, τ or $\Psi = 6.2°$), but the ring remains accurately planar (maximum deviation 0.011 Å) and the C—C distances are equal [1.41–1.43(1) Å] within the limits of experimental error. In view of the presence of different kinds of ligand atoms in the base of the suggested square pyramidal geometry ($2x$ amide N+$2x$Cl) it is difficult to define the true "axial direction" and thus provide the slippage, or tilt, with a firmer reference axis.

Our discussion of slippage here is pertinent since we have a case of "competitive π-donation", as indeed has been featured in previous discussions of the phenomenon.[14] Thus, we have a basic W^V electron count of 11—one metal *d*-electron, two W—N, two W—Cl and one "W—Cp" sigma bonding pairs. Supplementation may then occur via $2x$N—W $p\pi$–$d\pi$ donation, as discussed above, plus a further two or four electrons from the Cp* corresponding to Cp* acting as η^3 or η^5. The latter case would lead to a 19e configuration.

A similar situation occurs in the complex 1,2-W_2(indenyl)$_2$$(NMe_2)_4$, where the indenyl is distinctly η^3 and for which the authors assigned a greater π-donating ability to the NMe_2 group vs the indenyl.[14] It is intriguing to note that in the directly related W(η-$C_5H_4Pr^i$)Cl_4[15] the ($C_5H_4Pr^i$) group is close to η^5, with W—C(Cp) distances differing by no more than 0.033 Å. The balance between various electronic and indeed steric factors is clearly very fine.

EXPERIMENTAL

Analyses were by Imperial College and University College, London, laboratories. General techniques and instrumentation are as described previously.[1]

Synthesis of *CpWCl_2{1,2-$(HN)_2C_6H_4$}

In a typical reaction *$CpWCl_4$ (0.3 g, 0.65 mmol) and *o*-pdaH_2 (0.15 g, 1.38 mmol) in toluene (*ca* 20 cm^3) were refluxed for 12 h. The collected dark precipitate was washed with degassed water (*ca* 10 cm^3), Et_2O (2×15 cm^3) and dried in vacuum (yield *ca* 40%). X-ray quality, black, needle crystals were grown from MeCN. Found: C, 38.7; H, 4.2; N, 5.7. Calc. for $WCl_2N_2C_{16}H_{21}$: C, 38.7; H, 4.3; N, 5.6%. MS(E.I): $m/z = 497$, M^+.

X-ray crystallography

X-ray data were recorded at 298 K on a FAST TV area detector diffractometer with Mo-K_α radiation ($\lambda = 0.71069$ Å), as previously described,[16] using a crystal of dimensions $0.22 \times 0.18 \times 0.04$ mm^3. The structure was solved via the heavy atom method and refined by full-matrix least-squares. The data were corrected for absorption using the DIFABS[17] method at the isotropic refinement stage. All non-hydrogen atoms were refined in the anisotropic approximation whilst hydrogens were identified from the difference map and different U_{iso} values were assigned. Crystal data and experimental details are as follows.

Formula: $C_{16}H_{19}Cl_2N_2W$, $M_r = 494.096$, orthorhombic, $a = 8.105(1)$, $b = 16.001(2)$, $c = 12.939(1)$ Å, $V = 1680.95$ $Å^3$, space group *Pnam* (no. 53, non-standard), $Z = 4$, $D_c = 1.9524$ g cm^{-3}, $F(000) = 948$, μ(Mo-K_α) = 73.363 cm^{-1}. From the ranges scanned 10,447 data were recorded and merged to give 2269 unique ($R_{int} = 0.057$), 1780 observed [$F_o > 3(F_o)$]. $R = 0.0306$, $R_w = 0.0365$, 146 parameters. Tables of atomic coordinates, displacement factor coefficients, full lists of bond lengths and angles and F_o/F_c values have been deposited as supplementary material with the Editor. Atomic coordinates have also been deposited with the Cambridge Crystallograpohic Data Centre.

REFERENCES

1. C. Redshaw, G. Wilkinson, B. Hussain-Bates and M. B. Hursthouse, *J. Chem. Soc., Dalton Trans.* 1992, 555.
2. A. A. Danopoulos, A. C. C. Wong, G. Wilkinson, B. Hussain-Bates and M. B. Hursthouse, *J. Chem. Soc., Dalton Trans.* 1990, 315.
3. D. N. Williams, J. P. Mitchell, A. D. Poole, U. Siemeling, W. Clegg, D. C. R. Hockless, P. A. O'Niel and V. C. Gibson, *J. Chem. Soc., Dalton Trans.* 1992, 739.
4. J. Sundermeyer, U. Radius and C. Burschka, *Chem. Ber.* 1992, **125**, 2379.
5. W. A. Herrmann, G. Weichselbaumer, P. A. Paciello, R. A. Fischer, E. Herdtweck, J. O'Kuda and D. W. Marz, *Organometallics* 1990, **9**, 489.
6. D. S. Glueck, F. J. Hollander and R. G. Bergman, *J. Am. Chem. Soc.* 1989, **111**, 2719.
7. R. C. Murrey, L. Blum, A. H. Liu and R. R. Schrock, *Organometallics* 1985, **4**, 953.
8. W. E. Lindsell, *J. Chem. Soc., Dalton Trans.* 1975, 2528; cf. also, N. Ueyama, H. Oku and A. Nakamura, *J. Am. Chem. Soc.* 1992, **114**, 7310. Note that some W^V compounds may be EPR silent and have low magnetic moments: see V. Saboonchian, G. Wilkinson, B. Hussain-Bates and M. B. Hursthouse, *Polyhedron* 1991, **10**, 595 and refs therein.
9. (a) For discussion of structures and oxidation state for 1,2-diaminobenzene derivatives see O. Caringo, K. Djinovic, M. Rizzi and C. B. Castellani, *J. Chem. Soc., Dalton Trans.* 1991, 1551; cf. also H. Masui,

A. B. P. Lever and E. S. Dodsworth, *Inorg. Chem.* 1993, **32**, 258; (b) M. A. Dewey, A. M. Arif and J. A. Gladysz, *J. Chem. Soc., Chem. Commun.* 1991, 712 and refs therein.

10. C. G. Howard, G. S. Girolami, G. Wilkinson, M. Thornton-Pett and M. B. Hursthouse, *J. Am. Chem. Soc.* 1984, **106**, 2033.
11. (a) J. W. Fuller, R. H. Crabtree and A. Habib, *Organometallics* 1985, **4**, 929; (b) J. L. Atwood, W. E. Hunter, D. C. Hrneir, E. Samuel, H. Alt and M. D. Rausch, *Inorg. Chem.* 1975, **14**, 1757; (c) J. M. O'Connor and C. P. Casey, *Chem. Rev.* 1987, **87**, 307; (d) A. Habib, R. S. Tanke, E. M. Holt and R. H. Crabtree, *Organometallics* 1989, **8**, 1225.
12. G. Huttner, H. H. Brintzinger, L. G. Bel, P. Friedrich, V. Benjenke and D. J. Neugebauer, *J. Organomet. Chem.* 1978, **145**, 329.
13. J. K. Beattie and K. W. Nugent, *Inorg. Chim. Acta* 1992, **198–200**, 309.
14. M. H. Chisholm, M. J. Hampden-Smith, J. C. Huffman, J. D. Martin, K. A. Stahl and K. G. Moodley, *Polyhedron* 1988, **7**, 1991.
15. M. L. H. Green, J. D. Hubert and P. Mountford, *J. Chem. Soc., Dalton Trans.* 1990, 3793.
16. A. A. Danopoulos, G. Wilkinson, B. Hussain-Bates and M. B. Hursthouse, *J. Chem. Soc., Dalton Trans.* 1991, 1855.
17. N. P. C. Walker and D. Stuart, *Acta Cryst., Sect. A* 1983, **39**, 158.

Polyhedron Vol. 12, No. 19, pp. 2421–2423, 1993
Printed in Great Britain

0277–5387/93 $6.00+.00
© 1993 Pergamon Press Ltd

CRYSTAL STRUCTURE OF POLY[{TRIS-μ-IODO-BIS⟨(2,2′,2″-NITRILODIETHOXYETHANOL)DILEAD(II)⟩}-μ-IODO] OBTAINED BY DIRECT METHODS USING LEAD(II) OXIDE AS A STARTING MATERIAL

VLADIMIR KOKOZAY* and ALEXANDER SIENKIEWICZ

Department of Chemistry, University of Kiev, Kiev 252017, Ukraine

(*Received* 4 *January* 1993; *accepted* 7 *April* 1993)

Abstract—A direct method of obtaining $(Pb_4I_4L_2)_n$, where L is twice deprotonated 2,2′,2″-nitrilotriethanol (triethanolamine), is reported. The crystal structure of the compound was determined by X-ray techniques. The crystallographically independent fragments of $Pb_4I_4L_2$ are associated by bridging oxygen and iodine atoms in endless layers parallel to the *bc*-plane of the crystal. Tetradentate twice deprotonated triethanolamine is coordinated to lead(II) via oxygen and nitrogen atoms.

It was reported[1] that the direct method of synthesis leads to the preparation of coordination compounds of unusual composition and original crystal structure, for example, $Cuen_2I_2 \cdot 0.33DMF$ (where en = ethylendiamine, DMF = N,N-dimethylformamide).

The present paper describes the preparation and X-ray investigation of PbI · 0.5L, which assumes an unusual crystal structure.

EXPERIMENTAL

For the preparation of this complex the following method was used: PbO (2.23 g, 0.01 mol), NH_4I (1.45 g, 0.01 mol), DMFA (15 cm^3) and triethanolamine (1.33 cm^3, 0.01 mol) were heated to boiling and stirred until total dissolution of PbO was observed (3–5 min). The clear colourless solution obtained was allowed to stand at room temperature for 2 h after which crystals separated from the solution. The crystals were filtered, washed with dry isopropanol and finally dried *in vacuo* at room temperature; yield 3.0 g (74%). The colourless crystalline compound obtained is sparingly soluble in water and organic solvents. Found: C, 8.7; H, 1.6; Pb, 49.9; I, 31.0; N, 1.6. Calc. for PbI · 0.5L: Pb, 50.7; I, 31.1; N, 1.7; C, 8.8; H, 1.7%.

Crystallographic measurements were obtained at 20°C using an Enraf–Nonius CAD-4 diffractometer operating in the $\omega/2\theta$ scan mode (the ratio of the scanning rates was $\omega/\theta = 1.2$). The intensity data were collected within the range $1 \leqslant \theta \leqslant 27°$ using graphite-monochromated Mo-K_α radiation ($\lambda = 0.71073$ Å). Intensities of 3348 unique reflections were measured. The structure was solved by direct methods and refined by full-matrix least-squares techniques in the anisotropic approximation. In the refinement 2206 reflections with $I > 3\sigma(I)$ were used. About 40% of the hydrogen atoms were located in the Fourier maps; the positions of the remaining atoms were calculated. All hydrogen atoms were included in the final refinements with the fixed positional and thermal ($B_{iso} = 5$ Å^2) parameters. Convergence was obtained at $R = 0.036$ and $R_w = 0.0357$, G.O.F. = 1.15 (252 refined parameters; largest shift/ESD after final cycle < 0.29; the largest peak in the final difference map was 1.17 e Å^3). For the inverted structure $R = 0.0374$, $R_w = 0.0445$, G.O.F. = 1.15. The weighting scheme $w = (\delta^2 F + 0.0016\ F^2)^{-1}$ was used. Corrections for the Lorentz and polarization effects as well as the empirical correction for absorption using the DIFABS program[2] were applied. All structural calculations were performed with a PDP-11/23+ computer using the SDP-PLUS program package.[3] Full crystallographic data have been deposited at the Cambridge Crystallographic Data Centre.

* Author to whom correspondence should be addressed.

Table 1. Bond lengths (Å)

Pb(1)—O(1)	2.29(2)	Pb(3)—O(4)	2.29(2)	N(1)—C(3)	1.51(4)
Pb(1)—O(2)	2.77(2)	Pb(4)—O(4)	2.30(2)	N(1)—C(5)	1.43(3)
Pb(1)—O(3)	2.33(2)	Pb(4)—O(5)	2.37(2)	N(2)—C(7)	1.47(3)
Pb(1)—N(1)	2.54(2)	Pb(4)—O(6)	2.80(2)	N(2)—C(9)	1.46(3)
Pb(2)—I(1)	3.429(2)	Pb(4)—N(2)	2.53(2)	N(2)—C(11)	1.45(3)
Pb(2)—I(2)	3.463(3)	O(1)—C(2)	1.39(3)	C(1)—C(2)	1.34(4)
Pb(2)—I(3)	3.233(3)	O(2)—C(4)	1.41(4)	C(3)—C(4)	1.55(4)
Pb(2)—I(4)	3.171(3)	O(3)—C(6)	1.46(3)	C(5)—C(6)	1.51(3)
Pb(2)—O(1)	2.27(2)	O(4)—C(8)	1.40(3)	C(7)—C(8)	1.53(3)
Pb(3)—I(1)	3.486(2)	O(5)—C(10)	1.42(3)	C(9)—C(10)	1.60(4)
Pb(3)—I(2)	3.376(2)	O(6)—C(12)	1.43(4)	C(11)—C(12)	1.49(5)
Pb(3)—I(3)	3.404(3)	N(1)—C(1)	1.48(3)		

Crystal data for compound of composition $C_{12}H_{30}I_4N_2O_6Pb_4$: $Fw = 1634.8$, orthorombic, $a = 18.555(2)$, $b = 17.914(1)$, $c = 8.119(1)$ Å, $V = 2698.7$ Å^3, $Z = 4$, $d = 4.02$ g cm^{-3}, space group $Pna2_1$; $\mu = 296.3$ cm^{-1}, $F(000) = 2816$.

Bond distances and angles are given in Tables 1 and 2. Atomic coordinates, anisotropic thermal parameters, observed and calculated structure factors and torsion angles are given in the supplementary material.

DISCUSSION

The complex forms an inorganic polymer of composition $(Pb_4I_4L_2)_n$: crystallographically independent units [fragment of Fig. 1 without I(4a), O(5b) and O(3c) atoms] are associated by bridging oxygen and iodine atoms in endless layers parallel to the *bc*-plane (Fig. 2). The coordination of the lead atoms is clear from Fig. 1 and Tables 1 and 2.

Unsymmetrical five-coordination of Pb(1) and Pb(4) atoms is induced by ligand constraints, different functions of oxygen atoms [only O(2) and O(6) are terminal atoms, others are bridging] and the influence of stereochemically-active lone pairs of electrons. Close contacts of atoms O(5b) [$0.5-x$, $y-0.5$, $z-0.5$) and O(3c) ($0.5-x$, $0.5+y$, $0.5+z$) with Pb(1) and Pb(4) are $r\langle$Pb(1)—O(5b)$\rangle = 2.695$ Å and $r\langle$Pb(4)—O(3c)$\rangle = 2.725$ Å; the angles N(1)—Pb(1)—O(5b) and N(2)—Pb(4)—O(3c) are approximately equal at 128 and 120°, respectively.

Conditionally it is possible to divide the co-

Table 2. Bond angles (°)

O(1)—Pb(1)—O(2)	133.0(5)	O(4)—Pb(4)—O(5)	101.0(7)	C(1)—N(1)—C(3)	105(2)
O(1)—Pb(1)—O(3)	89.1(6)	O(4)—Pb(4)—O(6)	126.4(5)	C(1)—N(1)—C(5)	115(2)
O(1)—Pb(1)—N(1)	71.3(6)	O(4)—Pb(4)—N(2)	69.0(6)	C(3)—N(1)—C(5)	115(2)
O(2)—Pb(1)—O(3)	92.0(7)	O(5)—Pb(4)—O(6)	92.8(5)	Pb(4)—N(2)—C(7)	105(1)
O(2)—Pb(1)—N(1)	64.4(6)	O(5)—Pb(4)—N(2)	73.0(5)	Pb(4)—N(2)—C(9)	102(1)
O(3)—Pb(1)—N(1)	73.1(7)	O(6)—Pb(4)—N(2)	66.2(6)	Pb(4)—N(2)—C(11)	118(1)
I(1)—Pb(2)—I(2)	100.07(5)	Pb(2)—I(1)—Pb(3)	67.54(3)	C(7)—N(2)—C(9)	111(2)
I(1)—Pb(2)—I(3)	91.19(5)	Pb(2)—I(2)—Pb(3)	68.39(4)	C(7)—N(2)—C(11)	111(2)
I(1)—Pb(2)—I(4)	82.29(6)	Pb(2)—I(3)—Pb(3)	70.72(5)	C(9)—N(2)—C(11)	109(2)
I(1)—Pb(2)—O(1)	162.5(4)	Pb(1)—O(1)—Pb(2)	116.4(6)	N(1)—C(1)—C(2)	120(2)
I(2)—Pb(2)—I(3)	83.31(5)	Pb(1)—O(1)—C(2)	117(3)	O(1)—C(2)—C(1)	121(3)
I(2)—Pb(2)—I(4)	86.93(5)	Pb(2)—O(1)—C(2)	127(3)	N(1)—C(3)—C(4)	111(3)
I(2)—Pb(2)—O(1)	97.5(4)	Pb(1)—O(2)—C(4)	116(2)	O(2)—C(4)—C(3)	107(2)
I(3)—Pb(2)—I(4)	167.15(6)	Pb(1)—O(3)—C(6)	112(1)	N(1)—C(5)—C(6)	115(2)
I(3)—Pb(2)—O(1)	91.1(6)	Pb(3)—O(4)—Pb(4)	114.8(6)	O(3)—C(6)—C(5)	112(2)
I(4)—Pb(2)—O(1)	98.4(5)	Pb(3)—O(4)—C(8)	123(1)	N(2)—C(7)—C(8)	111(2)
I(1)—Pb(3)—I(2)	100.67(6)	Pb(4)—O(4)—C(8)	122(1)	O(4)—C(8)—C(7)	112(2)
I(1)—Pb(3)—I(3)	87.41(5)	Pb(4)—O(5)—C(10)	118(1)	N(2)—C(9)—C(10)	114(2)
I(1)—Pb(3)—O(4)	170.0(5)	Pb(4)—O(6)—C(12)	107(1)	O(5)—C(10)—C(9)	109(3)
I(2)—Pb(3)—I(3)	82.16(5)	Pb(1)—N(1)—C(1)	104(1)	N(2)—C(11)—C(12)	113(2)
I(2)—Pb(3)—O(4)	89.4(5)	Pb(1)—N(1)—C(3)	111(2)	O(6)—C(12)—C(11)	115(2)
I(3)—Pb(3)—O(4)	94.7(4)	Pb(1)—N(1)—C(5)	108(1)		

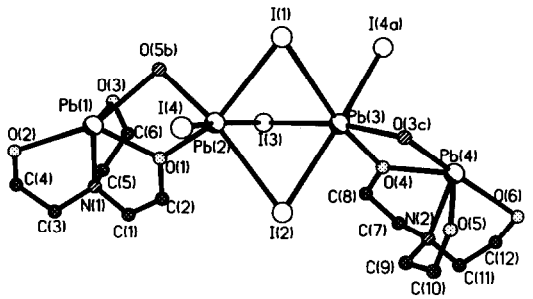

Fig. 1. A fragment of the crystal structure (hydrogen atoms were omitted for clarity).

ordination of Pb(2) and Pb(3) atoms into two spheres. The inner sphere is formed by atoms O(1) and O(5b) $(0.5-x,\ y-0.5,\ z-0.5)$ for Pb(2) [$r\langle$Pb(2)—O(5b)$\rangle$ = 2.468 Å] or O(4) and O(3c) $(0.5-x,\ 0.5+y,\ 0.5+z)$ for Pb(3) [$r\langle$Pb(3)—O(3c)$\rangle$ = 2.442 Å]; hence, the two-coordinate "bent" geometry occurs or, in other words, coordination of the named lead atoms possess ψ-trigonal configuration,[4] where a lone pair occupies one equatorial coordination site. The angles O(1)—Pb(2)—O(5b) and O(4)—Pb(3)—O(3c) are approximately equal (73° and 74°). Outer coordination spheres of Pb(2) and Pb(3) are comprised

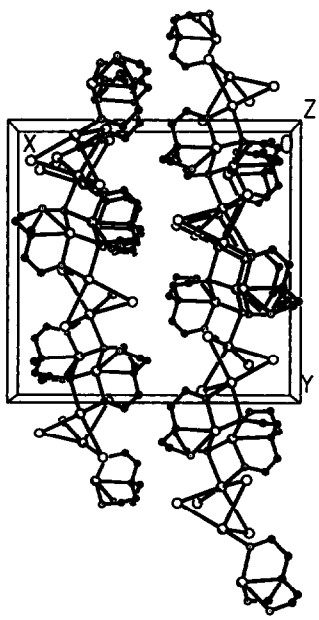

Fig. 2. Perspective view of the packing in the unit cell along the normal to the *ab*-plane.

of iodine atoms, as seen in Fig. 1; $r\langle$Pb(3)—I(4a) $(x,\ y,\ 1+z)\rangle$ = 3.111 Å. From this point of view the coordination polyhedra of atoms Pb(2) and Pb(3) are strongly distorted octahedra.

The atom I(4), as with other iodine atoms, shown in Fig. 1, possesses a bidentate-bridging nature and connects the atoms Pb(2) and Pb(3d) $(x,\ y,\ z-1)$, the latter not being marked in Fig. 1. The atom I(4a) $\{x,\ y,\ 1+z\}$ completes the same function for Pb(3) and Pb(2a), also omitted in Fig. 1.

Metal–metal interatomic close contacts in the complex are equal: $r\langle$Pb(1)—Pb(2)$\rangle$ = 3.866, $r\langle$Pb(2)—Pb(3)$\rangle$ = 3.844 and $r\langle$Pb(3)—Pb(4)$\rangle$ = 3.869 Å; these values exceed the nearest neighbouring lead–lead distance (3.49 Å) in the crystal lattice of lead metal.

Tetradentate twice deprotonated triethanolamine is coordinated to lead via oxygen and nitrogen atoms. Although the coordinates of hydrogen were not refined, the composition of the complex and the structural data [in particular, Pb—O—bond lengths, non-bridging nature of O(2) and O(6) atoms] indicate that the hydroxylic hydrogen atoms are attached to O(2) and O(6).

Puckered five-membered PbOCCN rings possess the *gauche* conformation, with the exception of O(1) and O(4)-containing rings which have envelope conformations. Each PbL of crystallographically independent units have opposite rotational configurations looking along the N—Pb bond. In certain cases the carbon–carbon interatomic distances in the rings are shorter than the normal aliphatic C—C bond length (1.54 Å).[5] This is a common property of chelate complexes containing five-membered rings.

REFERENCES

1. O. Yu. Vasilieva, V. N. Kokozay and Yu. A. Simonov, *Zh. Neorg. Khim.* (*J. Inorg. Chem. Russia*) 1991, **36**, 3119 (in Russian).
2. N. Walker and D. Stuart, *Acta Cryst.* (*A*) 1983, **39**, 158.
3. B. A. Frenz, in *Computing in Crystallography* (Edited by H. Schenk, R. Olthof-Haselkamp, H. van Koningsveld and G. C. Bussi), Delft University Press, Delft (1976).
4. *Comprehensive Coordination Chemistry: The Synthesis, Reaction, Properties & Applications of Coordination Compounds* (Edited by G. Wilkinson), 1st edn. Pergamon Press, Oxford (1987).
5. A. F. Wells, *Structural Inorganic Chemistry*, 5th edn. Clarendon Press, Oxford (1986).

Polyhedron Vol. 12, No. 19, pp. 2425–2428, 1993
Printed in Great Britain

0277–5387/93 $6.00+.00
© 1993 Pergamon Press Ltd

COMMUNICATION

DICOPPER(I) COMPLEXES OF THE NOVEL PHOSPHORUSBIPYRIDYL LIGAND 6-DIPHENYLPHOSPHINO-2,2′-BIPYRIDYL

JOHN S. FIELD, RAYMOND J. HAINES,† CAMPBELL J. PARRY and SADESH H. SOOKRAJ

Department of Chemistry, University of Natal, P.O. Box 375, Pietermaritzburg 3200, Republic of South Africa

(*Received* 1 *April* 1993; *accepted* 19 *July* 1993)

Abstract—Reaction of 6-diphenylphosphino-2,2′-bipyridine (Ph_2Pbipy) with copper(I) precursors such as $[Cu(MeCN)_4]^+$ and $[Cu(2,2'\text{-bipy})(MeCN)_2]^+$ affords dinuclear phosphorusbipyridyl ligand-bridged dicopper products and in particular $[Cu_2(\mu\text{-}Ph_2Pbipy)_2(MeCN)_2]^{2+}$ (**1**) and $[Cu_2(2,2'\text{-bipy})(\mu\text{-}Ph_2Pbipy)_2]^{2+}$ (**2**), respectively. The ligand coordinates head-to-tail in **1**, and head-to-head in **2**, as established by single crystal X-ray diffraction studies.

Transition metal complexes of polypyridyl ligands have been widely investigated as homogeneous electrocatalysts for the reduction of carbon dioxide.[1] Mechanistic studies have indicated that the low-lying and vacant π^*-orbitals of the polypyridyl ligand provide the site for the initial reduction and at relatively low cathodic potentials, i.e. the ligand mediates in the transfer of electrons from the electrode surface to a CO_2 molecule bound to a metal atom. As part of a programme for the development of dinuclear, rather than mononuclear, homogeneous electrocatalysts for CO_2 reduction we have synthesised the hitherto unreported phosphorusbipyridyl ligand, 6-diphenylphosphino-2,2′-bipyridine (Ph_2Pbipy),‡ and have studied its coordination behaviour towards a variety of metal-containing precursors. Electronically this ligand can be considered as being derived from the ubiquitous triphenylphosphine and the equally ubiquitous 2,2′-bipyridine.[3] Alternatively, in terms of its coordination properties, it can be considered as a tridentate equivalent of the widely studied bridging phosphoruspyridyl ligand 2-diphenylphosphinopyridine.[4] As such, the ligand not only contains a chelating bipyridyl fragment, but overall will preferentially adopt a bridging coordination mode thereby stabilizing dinuclear compounds to fragmentation. This communication reports the results of an investigation of the coordination behaviour of this ligand towards two copper(I) precursors.

Treatment of $[Cu(MeCN)_4]PF_6$[5] with one mole equivalent of Ph_2Pbipy in acetonitrile was indeed found to lead to the formation in high yield of a yellow dinuclear product characterized by X-ray

† Author to whom correspondence should be addressed.

‡ The synthesis of the ligand involved the treatment of 2,2′-bipyridine with methyl iodide to produce N-methyl-2,2′-bipyridyl iodide, oxidation of the latter with ferricyanide ions in the presence of sodium hydroxide to give *N*-methyl-2,2′-bipyridin-6-one, chlorination of the oxidized product with phosphoryl chloride and phosphorus pentachloride to afford 6-chloro-2,2′-bipyridine and reaction of the latter with $LiPPh_2$ to give the final product in *ca* 25% overall yield. Details of this synthesis have been reported elsewhere.[2]

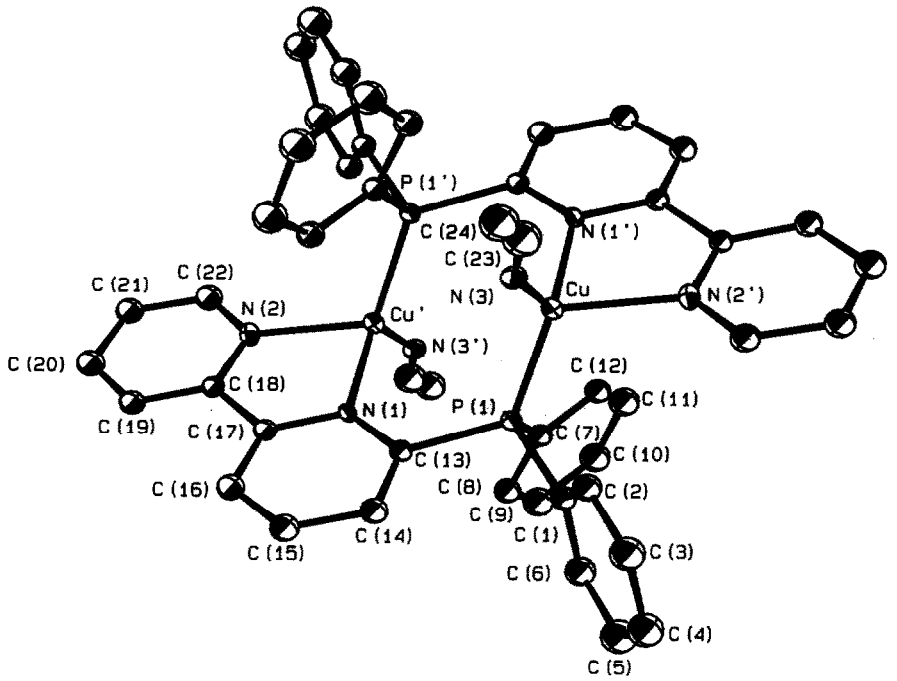

Fig. 1. ORTEP plot (20% probability) of the cation of $[Cu_2(\mu\text{-}Ph_2Pbipy)_2(MeCN)_2](PF_6)_2$ {**1**,$(PF_6)_2$}. Selected interatomic distances (Å) and angles (°): Cu···Cu', 3.941(2); Cu—P(1), 2.191(3); Cu—N(1'), 2.070(9); Cu—N(2'), 2.106(9); Cu—N(3), 2.073(9); P(1)—Cu—N(1'), 123.3(2); P(1)—Cu—N(2'), 113.9(2); P(1)—Cu—N(3), 116.5(2); N(1')—Cu—N(2'), 79.9(3); N(1')—Cu—N(3), 114.7(3); N(2')—Cu—N(3), 98.7(3).

crystallography† as well as by conventional methods‡ as $[Cu_2(\mu\text{-}Ph_2Pbipy)_2(MeCN)_2](PF_6)_2$ {**1**,$(PF_6)_2$}. The stereochemistry of the dication is illustrated in Fig. 1. The two copper atoms which are separated by a non-bonding distance of 3.941(2) Å, are bridged by the two Ph_2Pbipy ligands coordinated head-to-tail; the two ligands are in fact related through a crystallographically imposed centre of symmetry. Each copper atom has coordinated to it a phosphorus atom of the one bridging ligand, a chelating bipyridyl fragment of the other bridging ligand and an acetonitrile molecule. The stereochemistry about each copper atom is considerably distorted from tetrahedral as reflected by the P(1)—Cu—N(1') and N(1')—Cu—N(2') angles of 123.3(2) and 79.9(5)°, respectively. The acetonitriles are very weakly bound and are readily displaced by a wide range of neutral and anionic ligands including water, alcohols, hydrogen sulphide, diphenylphosphine, bis(diphenylphosphino)methane and -ethane, benzonitrile, pyridine and various substituted pyridines, 2,2'- and 4,4'-bipyridine, 1,10-phenanthroline, pyrido[2,3-b]pyrazine, 7-azaindole and halide, cyanide, thiocyanate, hydrogensulphido, dithiocarbamate, carboxylate and borohydride ions.[7] The dication **1** exhibits two reversible one-electron reduction waves at $E_{1/2} = -1.34$ and -1.55 V, vs Ag/AgCl, in its cyclic voltammogram recorded in benzonitrile at a platinum electrode. Significantly, the neutral species formed at the latter potential has been shown to catalyse the electrochemical reduction of CO_2 to CO and CO_3^{2-}. Details are being reported separately.[8]

Reaction of the copper(I) bipyridyl derivative

† *Crystal Data*: $C_{48}H_{40}N_6P_4F_{12}Cu_2$, $M = 1179.85$, monoclinic, space group $P2_1/c$, $a = 11.671(8)$, $b = 9.424(5)$, $c = 22.885(8)$ Å, $\beta = 93.71(6)°$, $U = 2511.8$ Å^3, $D_c = 1.56$ g cm^{-3} for $Z = 2$, $F(000) = 596$, λ(Mo-K_α) = 0.71069 Å, μ(Mo-K_α) = 11.17 cm^{-1}. 3027 unique reflection intensities were measured on a Nonius CAD-4 diffractometer using the ω–2θ scan mode in the range $3 < \theta < 23°$, 2386 of which were classed as observed [$I > 3\sigma(I)$]. These data were corrected for Lorentz and polarization effects and for absorption using the empirical method. The structure was solved by using standard Patterson and Fourier techniques and refined (SHELX-76[6]) by full-matrix least-squares methods (265 parameters) to $R = 0.0777$ {$R' = 0.0853$, $w = 1.0/[\sigma^2(F) + 0.003F^2]$, max. (shift/ESD) = 0.13} with anisotropic thermal factors assigned to all the non-hydrogen atoms except for the phenyl carbon atoms. Hydrogen atoms were not located. Atomic co-ordinates, thermal parameters and interatomic distances and angles have been deposited as supplementary material at the Cambridge Crystallographic Data Centre.

‡ Satisfactory microanalytical data were obtained for the new compounds synthesised.

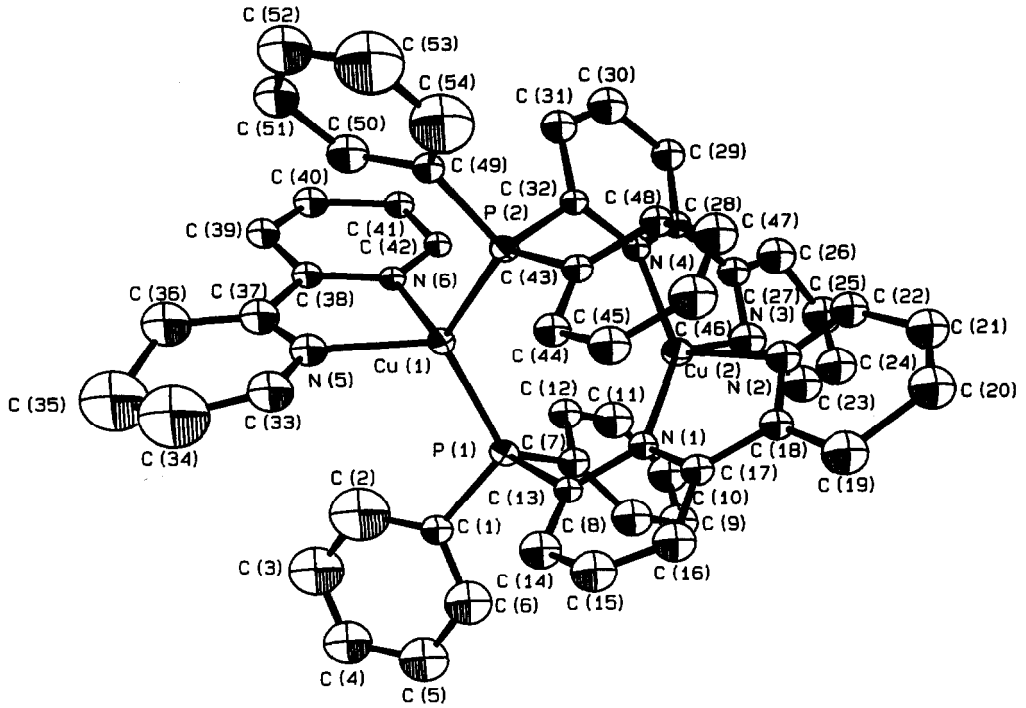

Fig. 2. ORTEP plot (20% probability) of the cation of $[Cu_2(\mu\text{-}Ph_2Pbipy)_2(2,2'\text{-bipy})](PF_6)_2$ {**2,(PF$_6$)$_2$**}. Selected interatomic distances (Å) and angles (°): Cu(1)···Cu(2), 3.692(2); Cu(1)—P(1), 2.234(6); Cu(1)—P(2), 2.237(6); Cu(1)—N(5), 2.03(2); Cu(1)—N(6), 2.14(2); Cu(2)—N(1), 1.96(2); Cu(2)—N(2), 2.10(2); Cu(2)—N(3), 2.13(3); Cu(2)—N(4), 2.03(2); P(1)—Cu(1)—P(2), 121.7(2); P(1)—Cu(1)—N(5), 113.0(6); P(1)—Cu(1)—N(6), 118.3(5); P(2)—Cu(1)—N(5), 112.3(4); P(2)—Cu(1)—N(6), 104.5(6); N(5)—Cu(1)—N(6), 79.3(7); N(1)—Cu(2)—N(2), 81.9(8); N(1)—Cu(2)—N(3), 130.5(9); N(1)—Cu(2)—N(4), 143.8(7); N(2)—Cu(2)—N(3), 96.8(9); N(2)—Cu(2)—N(4), 119.0(8); N(3)—Cu(2)—N(4), 79.2(9).

$[Cu(2,2'\text{-bipy})(MeCN)_2]PF_6$[9] with an equimolar amount of Ph_2Pbipy was found to lead, on the other hand, to the formation of $[Cu_2(\mu\text{-}Ph_2Pbipy)_2(2,2'\text{-bipy})](PF_6)_2$ {**2,(PF$_6$)$_2$**} in which, as established by X-ray crystallography† (Fig. 2), the bridging phosphorusbipyridyl ligands are coordinated head-

† *Crystal data*: $C_{54}H_{42}N_6P_4F_{12}Cu_2$, $M = 1253.93$, monoclinic, space group $C2$, $a = 23.212(2)$, $b = 19.333(3)$, $c = 13.717(2)$ Å, $\beta = 100.06(1)°$, $U = 5799.6$ Å^3, $D_c = 1.44$ g cm^{-3} for $Z = 4$, $F(000) = 634$, $\lambda(\text{Mo-}K_\alpha) = 0.71069$ Å, $\mu(\text{Mo-}K_\alpha) = 9.569$ cm^{-1}. 3888 unique reflection intensities were measured on a Nonius CAD-4 diffractometer using the ω–2θ scan mode in the range $3 < \theta < 23°$, 2948 of which were classed as observed $[I < 3\sigma(I)]$. These data were corrected for Lorentz and polarization effects and for absorption using the empirical method. The systematic absences $h+k = 2n+1$ for all *hkl* in the monoclinic system indicated the space group to be $C2$, Cm, or $C2/m$. Analysis of the intensity distribution strongly suggested that the space group is non-centrosymmetric i.e., $C2$ or Cm. The Patterson showed intense vectors corresponding to copper atoms in different asymmetric units being related by a two-fold axis (but not by a mirror plane); accordingly solution of the structure proceeded in $C2$. Solution of the Patterson allowed the location of the copper and phosphorus atoms of the cation and a difference Fourier synthesis phased on these atoms revealed the positions of the remaining non-hydrogen atoms of the cation. A difference Fourier phased on all the non-hydrogen atoms of the cation indicated that the distribution of PF_6^- anions is as follows: one on a general equivalent position, a second on a two-fold axis and a third on a general equivalent position but disordered such that the site occupation factor is 0.5. The structure was refined (SHELX-76[7]) by full-matrix least-squares techniques (313 parameters) to $R = 0.1075$ $\{R' = 0.1146$, $w = 1.00/[\sigma^2(F) + 0.019F^2]$, max. (shift/ESD) $= 0.09\}$ with anisotropic thermal factors assigned to the copper and phosphorus atoms and isotropic temperature factors to the remaining non-hydrogen atoms. The phenyl rings were refined as rigid groups. Hydrogen atoms were not located. Refinement of the structure in the other hand of $C2$ gave a higher R' value. Some of the isotropic thermal factors of the lighter atoms are very high suggesting that they are partially disordered and that their positional parameters should be treated with circumspection; nevertheless the main features of the structure are correct. Attempts to grow crystals which give a better-defined diffraction pattern are continuing; lack of facilities precluded a data collection at a lower temperature. Atomic coordinates, thermal parameters and bond lengths and angles have been deposited at the Cambridge Crystallographic Data Centre.

to-head. The two copper atoms which are separated by a non-bonding distance of 3.692(2) Å again adopt irregular tetrahedral geometries (see caption to Fig. 2). By careful control of the reaction conditions an intermediate in the formation of **2,$(PF_6)_2$**, viz. $[Cu(bipy)(\eta^1\text{-}Ph_2Pbipy)_2]PF_6$, could be isolated. This compound reacts readily with $[Cu(MeCN)_4]PF_6$ to produce **2,$(PF_6)_2$** and is, in fact, an ideal precursor for the synthesis of a wide range of asymmetric dinuclear compounds. The dication **2** exhibits two reversible one-electron reduction waves at $E_{1/2} = -1.24$ and -1.48 V, and a third partly reversible ($i_{pa}/i_{pc} < 1.0$) wave at $E_{1/2} = -1.85$ V, *vs* Ag/AgCl, in its cyclic voltammogram recorded in benzonitrile under argon at a platinum electrode. When the cyclic voltammogram is recorded under an atmosphere of CO_2 again a significant current enhancement of the second reduction wave is observed indicating that, similar to that observed for **1**, species produced by the reduction of **2** catalyse the electrochemical reduction of CO_2.

Studies of the coordination chemistry of the Ph_2Pbipy ligand are continuing with the eventual aim of producing a range of dinuclear Ph_2Pbipy ligand-bridged complexes which are effective electrocatalysts for the reduction of CO_2 to useful products. Indeed, the efficacy of this ligand for affording dinuclear compounds is illustrated by the range of dinuclear compounds that we have thus far isolated and characterized crystallographically and which include $[Ru_2\{\mu\text{-}OC(Me)O\}(CO)_2(\mu\text{-}Ph_2Pbipy)_2]PF_6$,[10] $[\{Ag_2(\mu\text{-}Ph_2Pbipy)_2\}(\mu'\text{-}4,4'\text{-}bipy)]_n(PF_6)_{2n}$[10] and $[Ni_2(CO)_2(\mu\text{-}Ph_2Pbipy)_2](BF_4)_2$.[11]

Acknowledgements—The authors express their sincere thanks to the Foundation for Research Development and the University of Natal for financial support.

REFERENCES

1. W. M. Ayers, Ed. *Catalytic Activation of Carbon Dioxide*; ACS Symposium Series No. 363; Ch. 6. American Chemical Society; Washington, DC (1988).
2. J. S. Field, R. J. Haines, C. J. Parry and S. H. Sookraj, *S. Afr. J. Chem.*, submitted.
3. F. A. Cotton and G. Wilkinson, *Advanced Inorganic Chemistry*, 5th Edn., Wiley Interscience, New York (1988).
4. See for example: S. Lo Schiavo, E. Rotondo, G. Bruno and F. Faraone, *Organometallics* 1991, **10**, 1613; L. J. Tortorelli, C. A. Tucker, C. Woods and J. Bordner, *Inorg. Chem.* 1986, **25**, 3534; J. P. Farr, M. M. Olmstead and A. L. Balch, *Inorg. Chem.* 1983, **22**, 1229.
5. D. F. Shriver, Ed. *Inorganic Synthesis*, p. 90. Wiley Interscience, New York (1979).
6. G. M. Sheldrick, SHELX 76, Program for Crystal Structure Determination, University of Cambridge (1976).
7. S. H. Sookraj, unpublished results.
8. R. J. Haines, C. P. Kubiak and R. E. Wittrig, *Inorg. Chem.*, submitted.
9. D. L. Reger and M. F. Huff, *Organometallics* 1992, **11**, 69.
10. C. J. Parry, unpublished results.
11. C. Landsberg, unpublished results.

Polyhedron Vol. 12, No. 19, p. 2429, 1993
Pergamon Press Ltd. Printed in Great Britain

ERRATUM

Borosilicate compounds of the type $H_2N(CH_2)_3OB(R)(OSiR'_3)$; the structure of 2-(dimethylphenylsiloxy)-2-phenyl-1,3,2-oxazaborinane. George Ferguson, John F. Gallagher, Denis Murphy, James P. Sheenan and Trevor R. Spalding (*Polyhedron*, Vol. 12, No. 8, pp. 859–864).

It is regretted that Figures 1 and 2 of the above paper were published incorrectly. The correct versions of Figures 1 and 2 appear below.

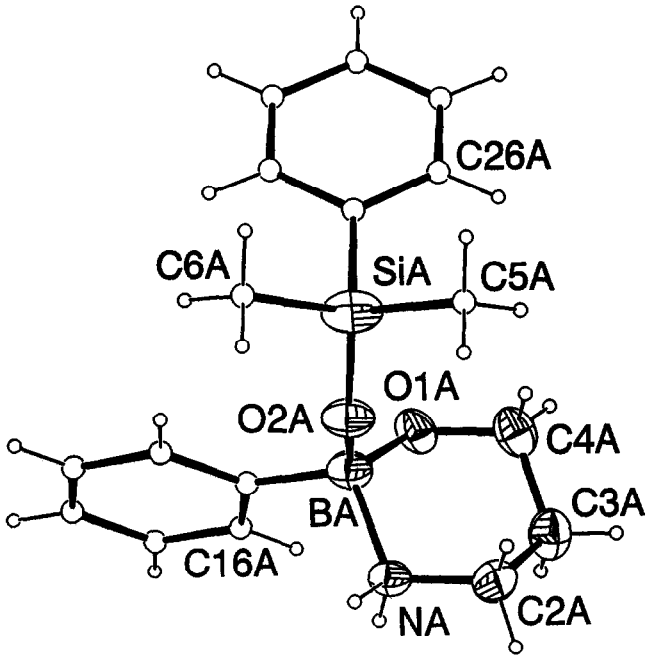

Fig. 1. A view of one of the two independent molecules of **2**, showing conformation and the numbering scheme.

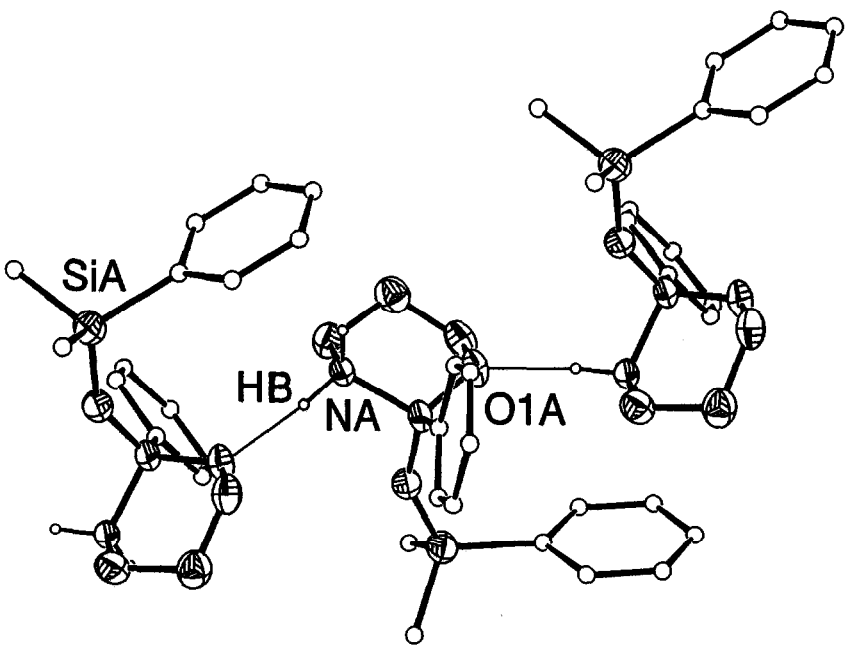

Fig. 2. Part of a hydrogen-bonded chain in **2**.

Polyhedron Vol. 12, No. 20, pp. 2431–2446, 1993
Printed in Great Britain

0277–5387/93 $6.00+.00
Pergamon Press Ltd

POLYHEDRON REPORT NUMBER 49

STABLE COMPOUNDS OF THE HEAVIER GROUP 14 AND 15 ELEMENTS INVOLVING $p\pi$—$p\pi$ MULTIPLE BONDING: AN OVERVIEW OF THE FIRST DECADE

NICHOLAS C. NORMAN

The University of Newcastle upon Tyne, Department of Chemistry,
Newcastle upon Tyne NE1 7RU, U.K.

CONTENTS

1. INTRODUCTION 2431

2. ASPECTS OF SINGLE AND DOUBLE BOND ENERGIES 2432

3. STERIC PROTECTION 2434

4. GROUP 14 2435
4.1. Compounds involving double bonds to a first row element 2435
(i) Silenes (Si=C) and their heavier congeners 2435
(ii) Silanimines (Si=N) and their heavier congeners 2436
4.2. Compounds involving double bonds without a first row element 2437
(i) Disilenes (Si=Si) and their heavier congeners 2437
(ii) Silaphosphenes (Si=P) and their heavier congeners 2438
(iii) Thiosilanones or silanethiones (Si=S) 2439

5. GROUP 15 2439
5.1. Compounds involving double and triple bonds to a first row element 2439
(i) Phospha-alkenes (P=C), phospha-alkynes (P≡C) and related compounds . . . 2439
(ii) Phospha-imines (P=N) 2441
5.2. Compounds involving double bonds without a first row element 2441
(i) Diphosphenes (P=P) and their heavier congeners 2441

6. CONCLUSION AND GENERAL FEATURES 2443

ACKNOWLEDGEMENTS 2444

REFERENCES 2444

1. INTRODUCTION

In Dasent's 1965 monograph entitled *"Nonexistent Compounds"*,[1] molecules of the heavier main group elements containing $p\pi$—$p\pi$ multiple bonds warranted a chapter to themselves, the point being made that whilst multiple bonding was common for the first row elements carbon, nitrogen and oxygen, it was conspicuous by its absence in the chemistry of the heavier congeners (with the exception, to some extent, of sulphur). This was the situation not for lack of effort on the part of synthetic chemists, but rather because many of the compounds which had been described in the early literature as having multiple bonds were later shown to be cyclic oligomeric species containing only single bonds. For example, the compound, described in 1877 by Köhler and Michaelis as

"phosphobenzene", was formulated as PhP=PPh by analogy with the well known azobenzene, PhN=NPh, but it was later shown to adopt cyclic pentameric and hexameric forms in the solid state.[2] Similarly, compounds which were once thought to contain As=As, Si=Si and Si=C double bonds were also later shown to be oligomeric. Not surprisingly, perhaps, these results led to a belief in a "double bond rule" whereby elements of the second and subsequent rows were deemed not to form stable $p\pi$—$p\pi$ multiple bonds.[3] This was the state of affairs which existed until a little over ten years ago and it is possible that it was the belief in a double bond rule which was largely responsible for the stagnation in this field. In this regard, the parallel with the stories of perbromate[4] and noble gas chemistry[5] are illuminating since the important discoveries in each of these cases were preceded by a period in which many reasons for their nonexistence were advanced; it is also noteworthy how many of the compounds in Dasent's book have, in fact, now been synthesized.

The situation changed dramatically, however, in the early 1980s with the synthesis and characterization of the first stable* compounds with a phosphorus–phosphorus (diphosphenes, RP=PR) and a silicon–silicon (disilenes, $R_2Si{=}SiR_2$) double bond, (**1**)[6] and (**2**),[7] respectively, together with examples of stable phospha-alkenes ($RP{=}CR_2$)[8] and silenes ($R_2Si{=}CR_2$).[9]

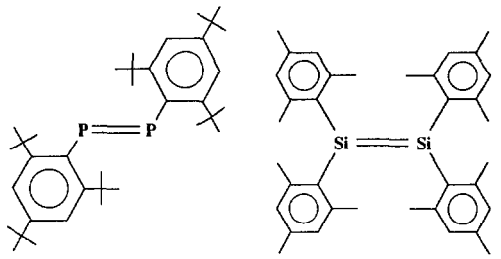

1 2

The area has expanded considerably since this time and is very much part of the renaissance of main-group chemistry which has occurred during this same period. In this review, we shall look back over the first decade of the subject addressing first some thermodynamic aspects regarding the strengths of single and double bonds for the *p*-block elements, followed by an overview of some of the important compounds which have been synthesized, specifically, those in groups 14 and 15 which contain isolated (i.e. non-conjugated) multiple bonds which can be described as of the $p\pi$—$p\pi$ type. Conjugated compounds and the extensive chemistry of multiply bonded sulphur species will not be discussed. Particular emphasis is given to structure and bonding; details on the methods of synthesis and on reactivity studies can be found in the various review articles which are referenced.

2. ASPECTS OF SINGLE AND DOUBLE BOND ENERGIES

In seeking an explanation for the varying stability of $p\pi$—$p\pi$ multiple bonds between the *p*-block elements, we must look first at the strengths of the various bonds involved and an illuminating way in which this can be done is to examine the σ and π-bond increments for particular pairs of atoms. Table 1 lists such increments for several pairs of elements, and is derived largely from the recent work of Kutzelnigg,[10] although the origin of this approach goes back to Pauling.[11] The values in Table 1 are defined such that the first value is that for a typical E—E single or σ-bond; for example the value of 335 kJ mol^{-1} for carbon is that of the C—C bond in ethane. The second value is the difference in energy between a double, or $\sigma+\pi$-bond and that of the single bond given by the first value and this can be taken as a measure of the strength of the π-bond. For carbon, the difference is that between the bond energy of the C=C double bond in ethene (630 kJ mol^{-1}) and the single C—C bond in ethane. Clearly the σ-bond in ethane is not the same as the σ-bond in ethene but the

* The term "stable" is used here to imply that the compounds can be isolated, characterized and stored under ambient conditions of temperature and pressure; in other words, that they are stable with respect to dimerization or oligomerization and/or other facile reaction types.

Table 1. Approximate bond increments (kJ mol^{-1}) for σ/π bonds adapted from ref. 10

C—C	N—N	O—O	C—O	N—O
(335/295)	(160/395)	(145/350)	(335/380)	(190/370)
Si—Si	P—P	S—S	Si—O	P—O
(195/120)	(200/145)	(270/155)	(420/170)	(335/150)
Ge—Ge	As—As	Se—Se	C—S	S—O
(165/110)	(175/120)	(210/125)	(280/265)	(275/250)

differences are likely to be small; moreover, it is broad comparisons between different types of bonds that are important rather than a means of quantitatively predicting particular bond energies.

If we first consider homonuclear bonds, an important point to emerge from Table 1 is that the π-bond increment for the first row or $2p$ elements is considerably greater than that for the elements of the second and subsequent rows. In other words, π-bond strengths are much larger for the first row elements and by a factor of between two and three. The standard explanation for this feature is that the second and subsequent row elements, being larger, have correspondingly larger and therefore more diffuse orbitals. Overlap between these bigger orbitals is poorer which results in weaker bonds, particularly in the case of π-bonds in which the atomic orbitals overlap side-on rather than the head-on overlap of σ-orbitals. Whilst this is probably broadly correct, and is an example of a defining feature of p-block chemistry, wherein bond strengths generally decrease down a group, it is only part of the explanation for the absence of extensive π-bonding in the chemistry of the heavier elements. The other aspect which we must consider is the strengths of the single or σ-bonds between the first row elements. Thus for nitrogen and oxygen, the N—N and O—O single bonds (like the F—F bond) are exceptionally weak as is clear from Table 1. This feature is usually associated with the small size of the first row atoms, leading to significant repulsions between nonbonded pairs of electrons, and to the fact that relatively high energy π^*-orbitals are occupied. These factors are of much lesser importance for the larger, heavier elements, the latter in particular since any factors which result in weak π bonding will also mitigate the effects of occupation of π^*-orbitals. As a result, P—P and S—S single bonds are considerably stronger than N—N and O—O bonds, respectively. In considering both of these factors, it is therefore apparent that for groups 15 and 16, as the values in Table 1 clearly indicate, the combination of a $\sigma+\pi$ bond is more stable than two σ-bonds for the first row elements whereas the reverse is true for the elements of the second and subsequent rows.

In group 14 the comparison is a little different in that the strength of the C—C single bond is greater than that of the Si—Si bond since there are no nonbonded electron pairs associated with the carbon atoms. The absence of an extensive chemistry of multiply bonded silicon compounds is due, as before, to the weakness of π-bonding for this element (two σ-bonds are stronger than one σ and one π-bond) and it is noteworthy that Si—Si π-bonding is the weakest of the $3p$ elements (see Table 1) consistent with the larger size of the silicon atom (vs P or S). The occurrence of π-bonding in carbon chemistry, however, is not associated with any weakness of the C—C σ-bond but much of the extensive and rather special organic chemistry of carbon is the result of the similarity in the strengths of the C—C σ and π-bonds. With this final point in mind, it is also clear from the values for group 14 in Table 1 that, in absence of factors which weaken the first row σ-bond, the ratio of the σ/π bond strengths drops markedly between the first and second row (0.88 vs 0.61) but then remains nearly constant for the second and third row (0.61 vs 0.66).

An examination of σ and π increments for heteronuclear bonds is also instructive. For example, Table 1 reveals that the π-bond increment is large where both elements are from the first row although the σ-bond strengths are also large where one of the elements is carbon. Heteronuclear bonds where a second row element is involved, for example Si—O and P—O, are similar to the homonuclear second row element cases in having a small π increment but we should note the rather special case of sulphur wherein the σ and π increments for both C—S and S—O bonds are about equal. This is mainly the result of a large π increment (as opposed to weak σ-bonding, cf. C—C) and in this sense, sulphur is acting (as far as π-bonding is concerned) more like a first row element. This is undoubtedly due to the relatively small size of the sulphur atom and the consequent better

π overlap, and it is therefore not surprising that $p\pi$—$p\pi$ multiple bonding is important in the chemistry of this element.

3. STERIC PROTECTION

In the previous section it was shown, on the basis of bond energy considerations, why single bonding is expected to be much more common than $p\pi$—$p\pi$ multiple bonding for the heavier *p*-block elements. However, an analysis which deals only with strengths of particular bonds does not encompass other important features. The synthesis of stable compounds containing isolated multiple bonds, which are the subject of this report, was, in fact, achieved by employing sterically bulky substituents, typical examples of which are $C_6H_2R_3$-2,4,6 (R = Me, Et, Pr^i, Bu^t, CF_3), $(Me_3Si)_3C$, $(Me_3Si)_2CH$ and Ph_3Si as shown below.

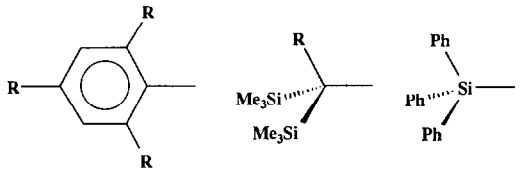

R = Me, Et, Pr^i, Bu^t, CF_3 R = Me_3Si, H

The efficacy of such groups in this regard has often been stated to be kinetic in origin with the implication that they protect an unstable functional group from oligomerization by means of their size. However, whilst there is much truth in this assertion, it is not really kinetic stabilization. If we take as an example some compounds which have already been mentioned, then for the RP or phosphinidene unit, when R is phenyl, cyclic pentameric and hexameric species are formed whereas when R is the much more bulky aryl substituent $C_6H_2Bu^t_3$-2,4,6 (hereafter Ar′ and often referred to as supermesityl), it is a diphosphene which is obtained. If we now consider various possible ring sizes and also that a diphosphene can be thought of, albeit somewhat perversely, as a two-membered ring, it is clear from the diagrams below that more bulky substitutents will favour smaller ring sizes since the R—P—P angle(s), and hence the R···R separation, increase as the ring size decreases. This argument assumes that the P_n rings are planar and that the bonded atoms of the R groups are coplanar with the P_n ring which will not generally be the case, but the basic point of the argument remains in that smaller rings will more readily accommodate larger R groups.

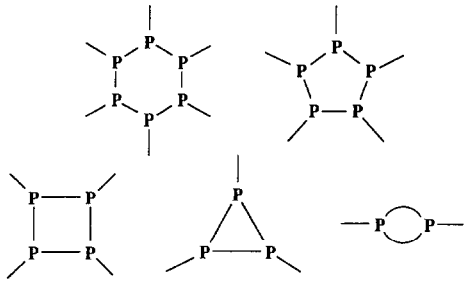

On this basis, it is apparent that the stabilization of a diphosphene by sterically demanding substituents is not really kinetic stabilization but it is a form of thermodynamic stabilization since it is certainly not the case that **1** is a kinetic product which is somehow prevented (by a large activation energy) from forming a larger, and thermodynamically more stable, P_n ring. Thus, π-bonded compounds (two membered rings) can be rendered quite stable if the σ-bonded alternatives (larger rings) are made less stable by using large and bulky side groups; in effect, these large groups exert thermodynamic control over oligomerization and kinetic control over other reactions which may occur at the double bond.

There is an interesting parallel to note here between the use of sterically demanding groups used to stabilize P=P and Si=Si double bonds in diphosphenes and disilenes, respectively, and the

similar use of such groups to stabilize element–element single bonds in group 13 chemistry. Thus compounds of the type R_2E—ER_2 containing two-centre, two-electron E—E single bonds are particularly uncommon in the chemistry of the group 13 elements, especially for the heavier elements. This instability is likely to be associated with the presence of a vacant *p*-orbital at each element centre rather than with any inherent weakness of the E—E bonds; the B—B single bond, for example, has a substantial bond energy of about 300 kJ mol^{-1}. For boron, the use of strong π-donors is efficacious in this regard[12] whereas for aluminium, gallium and indium, the sterically demanding group $(Me_3Si)_2CH$ has been utilised by Uhl and co-workers[13] to effect the isolation of such compounds; Cowley *et al.* have also described a di-indium compound stabilized by four $C_6H_2(CF_3)_3$-2,4,6 groups.[14]

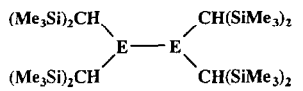

E = Al, Ga, In.

In this case, the sterically bulky $(Me_3Si)_2CH$ groups probably are effective in stabilizing the E—E bond for kinetic reasons in that they inhibit reactions which would degrade the E—E bond, particularly disproportionation reactions.

Having looked at some general properties which affect the stability of multiply bonded compounds in the *p*-block, we will now look at some specific examples. This is certainly not a comprehensive or exhaustive list but the compounds described serve to illustrate some of the general features associated with this subject.

4. GROUP 14

4.1. *Compounds involving double bonds to a first row element*

(i) *Silenes* (Si=C) *and their heavier congeners.* The first stable compound in this class to be structurally characterized was $(Me_3Si)_2Si{=}C(OSiMe_3)$(1-ad) (**3**) (ad = adamantyl) described by Brook and co-workers[15] in 1982. Key features of this compound include a Si=C bond which is approximately 10% shorter than a typical Si—C single bond, and the near coplanarity of the Si=C unit and the atoms to which it is bonded. Other important features, derived from NMR spectroscopy, are the inequivalence of the Me_3Si groups, which indicates hindered rotation about the Si=C bond, a deshielded ^{29}Si NMR chemical shift and a large ^1J(SiC) coupling constant. All of these features are important in establishing the presence of double bonding akin to that commonly encountered for the first row elements.

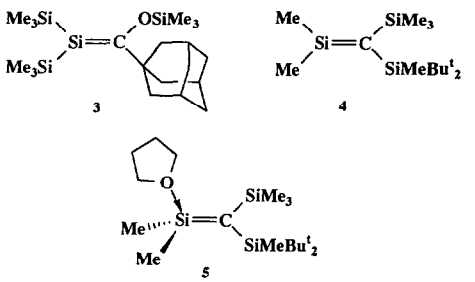

An additional and important structural feature of **3** is the presence of four bulky groups surrounding the Si=C unit which is undoubtedly responsible, in large part, for the stability of **3** with regard to dimerization, a usually facile reaction for less hindered silenes. However, the subsequent isolation and structural characterization of complex **4** by Wiberg and co-workers[16a] shows that massive steric protection is not always a necessary condition, at least as far as the silicon

centre is concerned, for stability towards dimerization; there are other examples of complexes (see later) where steric factors alone are unlikely to prevent dimerization. It is also noteworthy that the silicon centre in **4** is quite Lewis acidic and readily accommodates a coordinated thf (tetrahydrofuran) molecule to give complex **5**.[16b] Lewis acidity is commonly associated with three-coordinate, multiply bonded silicon centres in silenes, silanimines (see later) and in transition metal silylene complexes, $L_nM{=}SiR_2$.[17]

Compounds containing Ge=C double bonds (germenes) are fewer in number and have been reviewed by Barrau *et al.*[18] Two examples, **6**[19] and **7**[20,21] have been structurally characterized and both contain Ge=C bonds which are significantly shorter than typical Ge—C single bonds in accord with that found for silenes. However, whilst in **6** the atoms to which the Ge=C unit is bonded are nearly coplanar, in **7** the average twist angle, ϕ, defined in the diagram below, is 36°. Relatively large twist angles are sometimes encountered in complexes of this and related types (see later) which reflects the relative weakness of the π-bond. It should also be noted that in both **6** and **7** there is the possibility of π-conjugation with the substituents which may enhance their stability.

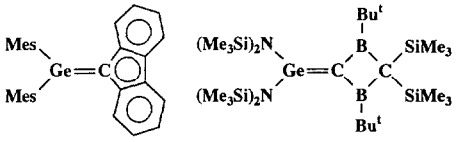

6 7

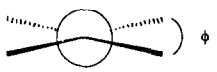

Stannenes (compounds with Sn=C double bonds) related to **6**[22] and **7**[23] have also been reported (the latter characterized by X-ray crystallography) together with the stannaketenimine $(C_6H_2(CF_3)_3$-2,4,6$)_2$Sn=C=N(mes) (**8**),[24] the structure of which will be discussed later.

(ii) *Silanimines* (Si=N) *and their heavier congeners.* The first stable silanimine $(Bu^t)_2Si{=}N(SiBu^t_3)$ (**9**) was described by Wiberg and co-workers[25] in 1986. The Si=N bond distance (1.568 Å) is significantly shorter than typical Si—N single bonds and is also shorter than the N—$SiBu^t_3$ bond length in **9** (1.695 Å), but of more interest is the almost linear coordination about the nitrogen atom (Si=N—Si 177.8°). Such a geometry is clearly inconsistent with a bonding scheme as represented in **A** with a localized lone pair on the nitrogen atom; some degree of delocalization involving a vacant orbital on the $SiBu^t_3$ silicon centre, as shown in **B**, is implied and in which the nitrogen is better described as *sp* hybridized rather than sp^2. Delocalization of nitrogen lone pairs onto adjacent silicon centres is not uncommon and is seen, for example, in the planar structure of silyl substituted amines such as $N(SiMe_3)_3$ and related compounds.[26] As with the silenes, the three-coordinate silicon centres in silanimines are appreciably Lewis acidic and readily coordinate (albeit weakly) a Lewis base. The structure of the thf adduct Me_2(thf)Si=N($SiBu^t_3$) (**10**)[25] reveals a Si=N bond (av. 1.581 Å for two independent molecules) slightly lengthened compared to **9** due to the fact that the acceptor orbital on silicon is probably the Si=N π^*-orbital, and also that the nitrogen centre is now noticeably bent (Si=N—Si av. 161.3°). Additional structures of Lewis base adducts (with Si=N distances and Si—N—Si angles in parentheses) are $Bu^t_2(Ph_2CO)$Si=N($SiBu^t_3$) (**11**) (1.601 Å, 169.3°)[27] and Bu^t_2(thf)Si=N($SiBu^t_2$Me) (**12**) (1.596 Å, 174.3°).[28] Moreover, it is apparent when comparing the structures of the similarly substituted compounds **11** and **12**, that a longer Si=N bond correlates with a smaller Si—N—Si angle which is in accord with a limiting, zwitterionic structure **C**.

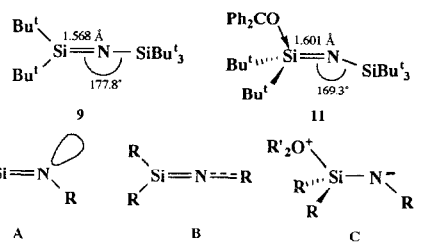

9 11

A B C

Many stable germanimines (Ge=N) have been described and the topic has been reviewed[18] although the only crystal structure determinations that have been reported are those for $\{(R)(Me_3Si)N\}_2Ge{=}N(R)$ (R = mes, $C_6H_3Pr^i_2$-2,6).[29] Both compounds have short Ge=N bonds and planar structures consistent with the presence of $p\pi$—$p\pi$ Ge=N bonds.

4.2. *Compounds involving double bonds without a first row element*

(i) *Disilenes*[30] (Si=Si) *and their heavier congeners.* The first stable disilene **2** was reported in 1981 by West, Fink and Michl[7] and the crystal structure determination of **2** was reported in 1984[31] together with that of the *E* isomer of (mes)(Bu^t)Si=Si(mes)(Bu^t) (mes = $C_6H_2Me_3$-2,4,6) (**13**),[31] the structures of $(C_6H_3Et_2\text{-}2,6)_2Si{=}Si(C_6H_3Et_2\text{-}2,6)_2$ (**14**)[32] and (*E*)-$(C_6H_2Pr^i_3\text{-}2,4,6)$(R)Si=Si$(C_6H_2Pr^i_3\text{-}2,4,6)$(R) (**15**) (R = Bu^t, $SiMe_3$) have also been described[33] together with those of the air stable compound $(C_6H_2Pr^i_3\text{-}2,4,6)_2Si{=}Si(C_6H_2Pr^i_3\text{-}2,4,6)_2$[34] and *E*-(mes)(1-ad)Si=Si(mes)(1-ad).[35] In all complexes, the Si=Si bond length is around 2.15±0.01 Å which is about 10% shorter than typical Si—Si single bond lengths consistent with double bond character for the Si=Si unit (C=C bonds are typically about 10–12% shorter than C—C bonds with comparably sized substituents). Moreover, in complexes **13** and **15**, the Si=Si unit and the atoms to which it is bonded are coplanar where the twist angle ϕ and the pyramidalization angle θ are zero (θ is defined as the angle made by the E—E′ vector to the RRE plane as shown in the diagram below). Maximum deviations from planarity are found in **2** for which θ is 18° and in **14** for which ϕ is 10°.

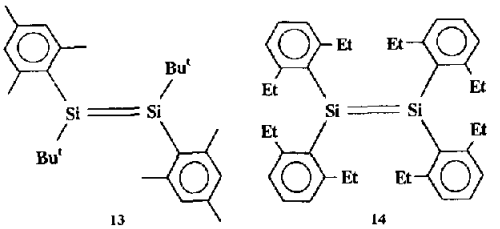

13 14

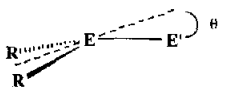

Other factors consistent with a double bond formulation for disilenes are the deshielded ^{29}Si NMR chemical shifts and large ^1J(SiSi) coupling constants. Moreover, for **13**, *E* and *Z* isomers can be isolated (although these equilibrate in solution, especially under photochemical conditions), NMR data for which establish a barrier to rotation about the Si=Si bond of 131 kJ mol^{-1}. This can be compared with the rotational barrier in stilbene which is 179 kJ mol^{-1}, i.e. about 30% larger.

Tetra-alkylated disilenes are $\{(Me_3Si)_2CH\}_2Si{=}Si\{CH(SiMe_3)_2\}_2$[36] and $Bu^t_2Si{=}SiBu^t_2$[37] the former being air stable and rather unreactive due to the extremely large substituents.

Digermenes which have been structurally characterized are $(C_6H_3Et_2\text{-}2,6)_2Ge{=}Ge(C_6H_3Et_2\text{-}2,6)_2$ (**16**)[38] and (mes)$(C_6H_3Et_2\text{-}2,6)$Ge=Ge$(C_6H_3Et_2\text{-}2,6)$(mes) (**17**)[39] by Masamune *et al.*, together with $\{(Me_3Si)_2CH\}_2Ge{=}Ge\{CH(SiMe_3)_2\}_2$ (**18**)[40] and the distannene, $\{(Me_3Si)_2CH\}_2Sn{=}Sn\{CH(SiMe_3)_2\}_2$ (**19**)[40] which have been described by Lappert and co-workers.

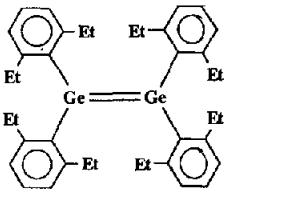

16

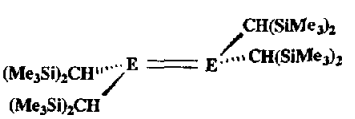

18, E = Ge; **19**, E = Sn.

In **16**,[38,39] the twist angle, ϕ, is 10° and the pyramidalization angle, θ, is 12° neither of which is significantly larger than those found in disilenes. In **17**, however, the germanium atoms are markedly pyramidal ($\theta = 36°$, $\phi = 7°$)[39] and compounds **18** and **19** are significantly distorted from a planar geometry such that whilst ϕ is zero in both cases, they adopt strongly *trans* bent structures, where θ is 32° and 41°, respectively.[40] Clearly a standard $\sigma+\pi$ bonding description applicable to olefins is reasonable for the disilenes and the digermene **16** but is not appropriate for the digermenes **17** and **18** and the distannene **19**. The bonding in these latter two species has been addressed by Lappert *et al.*[40] Pauling[41] and in a series of papers by Trinquier and co-workers.[42] The basis of the argument is that a planar structure as shown in **D** is only feasible if the triplet state of the ER_2 fragment is energetically accessible. For carbon, this is certainly the case (the triplet state of CH_2 is slightly lower in energy than the singlet state) but as the group is descended (C, Si, Ge, Sn), not only is the singlet state more stable, but the singlet–triplet energy separation, ΔE_{ST}, increases. In the situation where $\Delta E_{ST} > 1/2E—E(\sigma+\pi)$, where $E—E(\sigma+\pi)$ is the double bond energy, a *trans* bent structure should be preferred. For germanium and certainly for tin, ΔE_{ST} is sufficiently large and the planar structure of type **D** is no longer the energy minimum. The bonding in the resultant *trans* bent structure may therefore be represented as an interaction of two singlet states as shown in **E**.

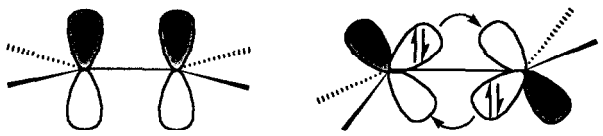

D **E**

In the stannaketenimine **8**,[24] the tin atom is also markedly pyramidal (sum of angles = 290.9°) and this compound may be thought of as linked, singlet stannylene (R_2Sn) and isocyanide (C≡NR) species as shown in the diagram below. Consistent with this view is the bent geometry at the carbon atom (153.9°) and the near linear coordination (175.0°) at nitrogen.

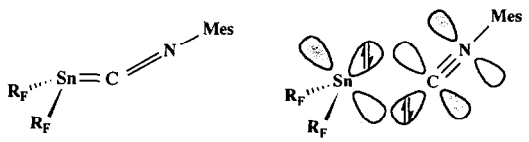

8, $R_F = C_6H_2(CF_3)_3$-2,4,6

An alternative, although complementary, description is provided by Albright, Burdett and Whangbo[43] wherein the change in structure from type **D** to type **E** as group 14 is descended, is considered in terms of a second order Jahn–Teller distortion due to mixing of the $b_{1u}\pi$ and $b_{2g}\pi^*$ levels with the $3b_u\sigma^*$ and $3a_g\sigma^*$ levels, respectively. These levels become closer in energy as the group is descended leading to greater mixing and hence to a larger *trans* bent distortion. In this sense, the increasing pyramidalization is seen as a special case of pyramidalization in eight-electron EX_3 species reasons for which are also discussed. Similar reasons for an increase in bending for six-electron EX_2 species with a concomitant increase in ΔE_{ST} are also addressed. The % bond shortenings in **18** and **19** compared with typical single bond values are 4 and 2%, respectively which also indicates that the standard $\sigma+\pi$ double bonding model is not appropriate in these cases.

(ii) *Silaphosphenes* (Si=P) *and their heavier congeners.* The following compounds which are examples of silaphosphenes, germaphosphenes (Ge=P) and stannaphosphenes (Sn=P) have been described: RR′Si=PAr′ (R = R′ = $C_6H_2R''_3$-2,4,6 for R″ = Me, Et, Pr^i; R = $C_6H_2Pr^i_3$-2,4,6, R′ = Ph, mes, Bu^t),[44a–c] $(mes)_2Ge$=PAr′ (**20**)[45] and $\{(Me_3Si)_2CH\}_2Sn$=PAr′[46] together with the cumulene Ar′P=Si=PAr′.[47] Compound **20** has been structurally characterized[45] and has a Ge=P bond length which is about 8% shorter than a typical Ge—P single bond. Moreover, the coordination around the Ge=P unit is essentially planar with important interbond angles as shown below, and it is noteworthy that there is no appreciable pyramidalization at the germanium centre, similar to the situation found for **16**; the uneven angles to the mesityl groups are clearly a consequence of the

supermesityl *cis* to one mesityl group. There has been one report of a sila-arsene, $(C_6H_2Pr^i_3$-2,4,6)$_2$Si=AsSiPr^i_3[48] which has been characterized spectroscopically.

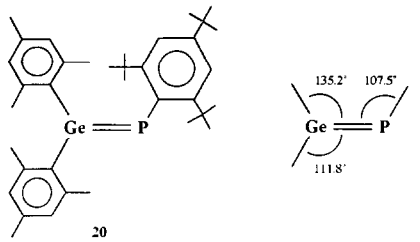

20

(iii) *Thiosilanones or silanethiones* (Si=S). The only compounds to have been reported in this class[49] are of the form shown below in which the silicon centre is additionally coordinated, intramolecularly, by an amine function; the electrophilic nature of three-coordinate silicon was encountered with silenes and silanimines. Possible canonical forms are also represented.

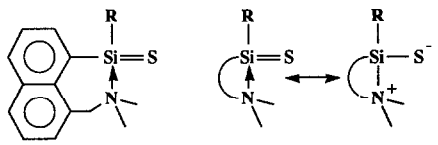

R = Ph, Naphthyl

Compounds of this type have also been isolated with Si=NBu^t and Si=PPh units[50] and brief mention should also be made of a compound containing a base stabilized Ge=S bond, **21** see below,[51] and also of ESR evidence for the radical anion species $[Bu^t_2Si{=}O]^{-\bullet}$[52] although no data is yet available for stable neutral silanones, $R_2Si{=}O$.

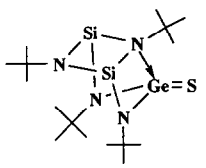

21

5. GROUP 15

5.1. *Compounds involving double and triple bonds to a first row element*

(i) *Phospha-alkenes* (P=C), *phospha-alkynes* (P≡C) *and related compounds.* Phospha-alkenes[8] are one of the most extensively studied class of compound containing multiply bonded phosphorus. The first report of stable non-conjugated phospha-alkenes was by Becker in 1976[53] who described the complexes RP=CR′(OSiMe$_3$) (R = R′ = Bu^t; R = *c*-hexyl, R′ = Bu^t; R = Ph, R′ = Bu^t) and examples of complexes which have subsequently been structurally characterized are (mes)P=CPh_2 (**22**)[54] and Ar′P=C$(SiMe_3)_2$ (**23**)[55] which are shown below. Of particular interest are the structures of the *E* and *Z* isomers of Ar′P=CH(Ph) (**24**);[56a–c] both of these isomers are also configurationally rigid in solution under ambient conditions indicating hindered rotation about the P=C bond.

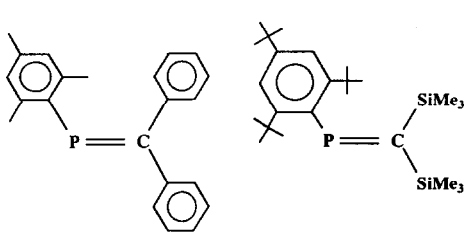

22 23

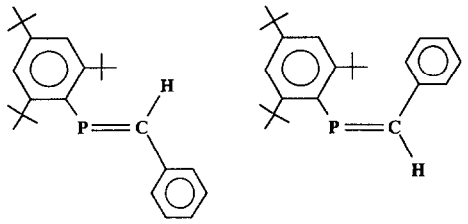

E, 24a *Z*, 24b

In general, a degree of steric protection is required in order for compounds containing isolated P=C bonds to be stable (with respect to dimerization) but this condition is relaxed somewhat when the P=C unit is part of a conjugated system or when the phosphorus is bonded to an electronegative atom or group. Examples of the former class of compound are the phosphabenzenes $C_5H_2R_3$-2,4,6-P (R = H and Ph)[57] whilst the latter is exemplified by $ClP{=}C(SiMe_3)_2$ (**25**).[58] In **25**, and a series of related compounds, the chlorine atom, by virtue of its electronegativity, probably leads to a phosphorus centre with a greater δ^+ charge which in turn results in a contraction of the phosphorus *p*-orbital which overlaps more effectively with the carbon *p*-orbital.

An important class of phospha-alkene is the metalla-phospha-alkene of which two basic types have been characterized depending on the position of the organotransition metal fragment, viz $(L_nM)P{=}CR_2$ and $RP{=}CR(ML_n)$. Structurally characterized examples are $(\eta\text{-}C_5Me_5)(CO)_2Fe{-}P{=}C(SiMe_3)_2$ (**26**)[59] and $Bu^tP{=}C(OSiMe_3)\{Re(CO)(NO)(\eta\text{-}C_5Me_5)\}$ (**27**)[60] in which the metal atoms are bonded to phosphorus and carbon, respectively.

Further derivatives of this class of compound are the phosphavinylidene complex $(\eta\text{-}C_5H_5)(CO)_2Mo{=}P{=}C(SiMe_3)_2$ (**28**)[61] reported by Cowley *et al.* which is an example where the phosphorus is multiply bonded to the metal atom as well as to carbon, and the arsa-alkene complex $(\eta\text{-}C_5H_5)(CO)_2Fe{-}As{=}CBu^t(OSiMe_3)$ (**29**)[62] described by Weber and co-workers, one of only very few examples of an arsenic–carbon double bond.

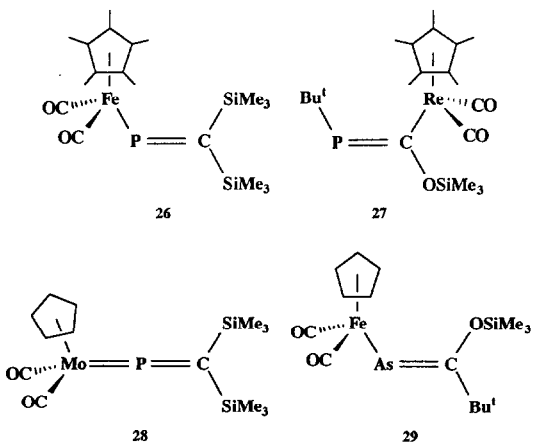

26 **27**

28 **29**

Important structural features associated with all the phospha-alkenes are a P=C bond length which is about 8–10% shorter than a P—C single bond and the coplanarity of the atoms bonded to the P=C unit. Angles at phosphorus are usually about 100°, except for some of the P-bonded metalla-phospha-alkenes in which these angles are often a little larger. NMR parameters are also consistent with the presence of a P=C double bond.

The first phospha-alkyne stable to polymerization, $Bu^tC{\equiv}P$ (**30**) was described in 1981 by Becker[63] and the chemistry of this and related species has been extensively reviewed.[64] The structure of **30** and other compounds RC≡P (R = H, Me, Ph) have been determined by microwave spectroscopy[65] whilst the structure of the crystalline compound $Ar'C{\equiv}P$ (**31**) has been determined by X-ray crystallography;[66] in all cases, the P≡C bond distances are short and consistent with a P≡C triple bond. The arsenic analogue of **31**, $Ar'C{\equiv}As$, has been reported by Märkl[67] although no structural details are available.

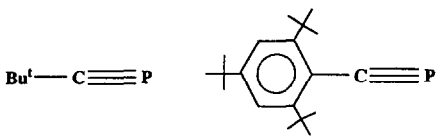

30 31

Finally in this section, it is important to mention a number of cumulenes involving P=C double bonds. This area, which has been reviewed by Appel,[8] has developed to include a large range of compounds, examples of which are 1,3-phospha-allenes RP=C=PR, 1-phospha-allenes RP=C=CR_2 and phosphaketenes RP=C=O.

(ii) *Phospha-imines* (P=N). The chemistry of phospha-imines has a slightly longer history than many of the other classes of compound described in this review, dating back to 1973, and the subject has recently been reviewed by Niecke.[68] Of particular interest are the structures of these compounds (all of which contain at least one bulky group) which can be classified according to three general classes. The first type, **F**, involves a *trans* and planar arrangement about the P=N bond and is defined by a RP=NR torsion angle of about 180°. The P=N bond distances are all close to 1.55 Å with the angle at phosphorus (α) typically between 100 and 110° and the angle at nitrogen (β) between 115 and 125°. The second type, **G**, has a *cis* configuration for which the RP=NR torsion angle is close to 0°. Compounds of this type have similar P=N bond lengths to those of type **F** and also similar values for the angle α, but values for β are larger falling in the range 130–145°. In the final type, **H**, the nitrogen atom adopts a nearly linear coordination in which β ranges from 155 to 180°. An examination of the structural data indicates that there is essentially a continuum between types **G** and **H** in which the angle at nitrogen increases from 130 to 180°. Moreover, this increase in β correlates with a decrease in the P=N bond length from about 1.55 to 1.48 Å. This latter observation is consistent with the view that type **H** compounds are best represented as incipient ionic species of the form $[RN{\equiv}P]^+[R]^-$ in which the PN linkage has substantial triple bond character. Not surprisingly, therefore, type **H** compounds are found when the $[R]^-$ group is electron withdrawing such as halide, $Bu^t{}_3CO$ or $Bu^t{}_2HCO$ and complete ionization occurs in the complex $[Ar'N{\equiv}P]^+[AlCl_4]^-$ (**32**). Compound **32** and related species are analogous to organic diazonium cations and isoelectronic with phospha-alkynes.

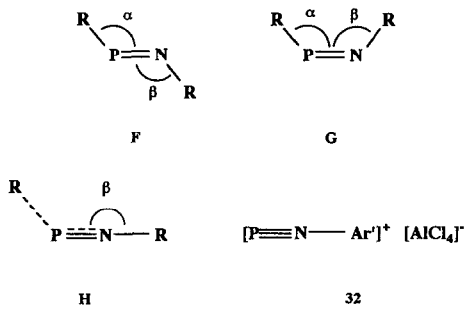

F G

H 32

5.2. *Compounds involving double bonds without a first row element*

(i) *Diphosphenes* (P=P) *and their heavier congeners.* The first stable diphosphene, **1**, was reported in 1981 by Yoshifuji[6] and the subject has been reviewed a number of times by Cowley,[69] Yoshifuji[70] and Weber.[71] In all cases, sterically bulky groups on at least one of the phosphorus atoms (mostly both) are required in order to stabilize these compounds with salient structural features being a P=P bond length of about 2.03 Å, which is 8–10% shorter than typical P—P single bonds, and angles at the phosphorus atoms which range from 100 to 110° (c.f. phospha-imines). In **1**, for example, the C—P—P angle is 102.8° which is considerably smaller than an angle of 120° which might be anticipated from a bonding model involving sp^2 hybridization at the phosphorus centre. Such a model is much more appropriate for the diazo analogue of **1**, Ar'N=NAr' (**33**),[72] for which the bond angles at nitrogen are 113.5° (av.), and for the nitrogen centres in some phospha-imines.

In fact, a trend wherein the bond angles decrease as the group is further descended is apparent when diarsenes are considered (see below).

Most of the diphosphenes which have been structurally characterized to date, including the metalla-diphosphene (η-C_5Me_5)$(CO)_2$Fe—P=PAr′ (**34**)[73] adopt a *trans* or *E* configuration analogous to **1** and for a long time it was considered that this was the only isomer which was likely to be observed since a *cis* or *Z* form would present no obvious steric barrier to dimerization. The first indication of a *cis* diphosphene was obtained by Koenig and co-workers[74] from laser irradiation studies of **1**, and also by Yoshifuji *et al.*[75] who isolated the $Cr(CO)_5$ complex Ar′P=P[$Cr(CO)_5$](mes) (**35**), but subsequently, the uncoordinated *cis* diphosphenes Ar′P=PR (R = Bu^{t}NH, 1-adNH) were isolated and structurally characterized by Niecke and co-workers who later reported the structural characterization of both the *cis* and *trans* isomers of Ar′P=P{N($SiMe_3$)[N($SiMe_3$)$_2$]} (**36a,b**).[76]

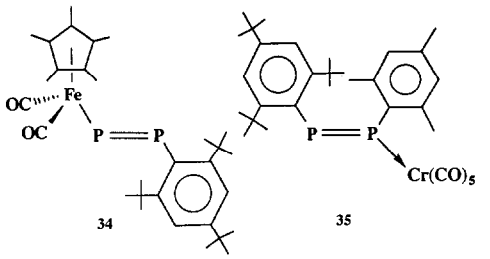

34 35

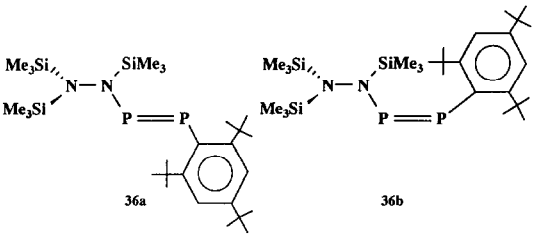

36a 36b

If one considers the stabilization of diphosphenes to be due to steric protection alone, then the isolation of uncoordinated *cis* isomers, which are also stable in solution albeit in equilibrium with the *trans* form,[76] presents a difficulty since, as mentioned above, the attached groups present no obvious barrier to dimerization. The reason for their stability undoubtedly lies not so much with steric effects but with electronic factors. For example, in **36b**, the nitrogen atom to which one of the phosphorus atoms is bonded adopts a trigonal planar geometry in which this plane is coplanar with the NPP plane. There is, therefore, the possibility of conjugation between the nitrogen lone pair and the P=P bond giving rise to a three-centre, four-electron system which is undoubtedly associated with their stability. Nevertheless, the consequences of having two large groups *cis* to each other is evident from a comparison of the angles at phosphorus in compounds **36a** and **36b**. In **36a** the two angles N—P—P and P—P—C are 106.1 and 97.6°, respectively whereas in **36b** they are 126.3 and 121.4°.

The angle of 97.6° in **36a** is one of the smallest observed for a diphosphene, but even smaller angles are found in diarsenes in which the relevant bond angles are usually a few degrees less than those in the analogous phosphorus compounds. Two diarsenes $(Me_3Si)_3CAs{=}AsC(SiMe_3)_3$ (**37**)[77a] and Ar′As=AsCH($SiMe_3$)$_2$ (**38**)[77b] and a phospha-arsene Ar′P=AsCH($SiMe_3$)$_2$ (**39**)[77c] prepared by Cowley and co-workers have been structurally characterized, important angles for which are shown below and which illustrate the trend to decreasing interbond angles as the group is descended. This trend to smaller angles on descending the group is not unexpected and can be considered as a special case of the same trend observed in other EX_2 species. The rationale for this effect is similar to that offered for the increasing pyramidalization in compounds of group 14 and is described in detail in ref. 43. It is important to note, however, that in the group 15 compounds, the π-bonding orbitals are not involved in the orbital mixing associated with the change in geometry. Thus, whereas in group 14 the increase in pyramidalization leads to a weakening of the E—E bond and a decrease in the per cent bond shortening (compared to a single bond), in group 15 no such weakening occurs

and the bond lengths found in phospha-arsenes and diarsenes are, like diphosphenes, 8–10% shorter than typical single bonds.

No structural data is available for an antimony containing compound although spectroscopic data have been reported for $Ar'P{=}SbCH(SiMe_3)_2$.[77c]

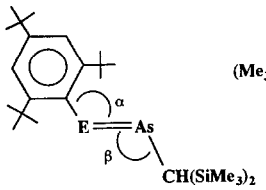

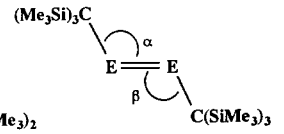

E = P, $\alpha = 101.2$, $\beta = 96.4°$ E = P, $\alpha,\beta = 108.5°$ (av.)
E = As, $\alpha = 99.9$, $\beta = 93.6°$ E = As, $\alpha,\beta = 106.3°$ (av.)

6. CONCLUSION AND GENERAL FEATURES

In concluding this perspective, it will be useful to recapitulate briefly the salient features associated with the multiply bonded compounds described herein. In the early years of the subject there was much discussion as to whether "true" double bonds were really present. In most cases, the answer to this question must now be seen to be yes inasmuch as the spectroscopic and structural features are those expected for multiply bonded species. For example, in all compounds where a suitable NMR nucleus is available, the chemical shifts and coupling constants are usually consistent with the presence of a multiple bond; the solid state NMR studies of Zilm and co-workers[78] are a particularly elegant example in this regard.

Moreover, the structural studies on which this report has focused are also consistent with multiple bonding in that percentage bond shortenings of between 8 and 10% (for double bonds) are commonly observed in conjunction with a planar or near planar environment around the E=E unit. The only major exceptions are found for the digermenes and distannenes (and other tin containing species) in which the standard $\sigma + \pi$ model is clearly not appropriate in most cases. Some of the structural features of the silanimines and the phospha-imines are also unusual. Nevertheless, we must exercise a little caution in the discussions of bond lengths particularly with respect to the percentage shortenings observed. Thus, in an insightful paper, Power *et al.*[79] have shown that comparisons between bond lengths must take due account of the formal hybridizations of the elements involved. For example, typical P—P single bonds in compounds such R_2P—PR_2 are about 2.2 Å whereas the P=P bonds in diphosphenes are about 2.03 Å, a shortening of about 8%. However, the phosphorus hybridization in diphosphines and diphosphenes is sp^3 and sp^2, respectively and Power has estimated that a bond shortening of about 0.1 Å (i.e. about 4%) is due to this change in hybridization alone. It is therefore likely that only half of the shortening observed for P=P bonds is due to the presence of the π-bond, the other half being due simply to the different hybridization of the phosphorus atoms. Analogous examples from nitrogen chemistry, however, suggest that the shorter distances found for N=N double bonds vs N—N single bonds are mostly due to the presence of the π-bond (about 75%) and less to the different hybridization of the nitrogen (25%). These observations are consistent with the relatively stronger π-bonding expected for nitrogen vs phosphorus as outlined earlier.

Finally, it is worth mentioning some of the types of compound which have yet to be synthesized. Clearly there is a paucity of data for species involving the heaviest elements, particularly the 6*p* elements lead and bismuth although it is likely that even more sterically bulky ligands will be needed to afford stability in these cases. An alternative strategy is to exploit the Lewis acidity of these elements and to use groups which are both bulky and which contain Lewis basic sites in order to form intramolecular acid–base complexes. However, the concomitant increase in coordination number means that a description of the bonding in terms of a pure $p\pi$—$p\pi$ interaction is no longer entirely appropriate.

In the chemistry of the group 14 elements, the isolation of triply bonded compounds has so far eluded researchers in the field. Thus whilst C≡C and C≡N bonds are well characterized, there are no stable examples of sila-alkynes, RSi≡CR, silanitriles, RSi≡N, disilyenes, RSi≡SiR or analogous

compounds involving the heavier congeners. This is in contrast to group 15 where the chemistry of phospha-alkynes is now well established and this probably reflects the fact that phosphorus forms somewhat more stable π bonds than silicon due to its smaller size. Success in the field of heavier element triple bonds is also likely to require new and even more bulky ligands, particularly those with the ability to stabilize what are likely to be extremely electrophilic silicon centres. It is probable that conjugatively stabilized compounds and transition metal complexes will be prepared before uncoordinated compounds are isolated as has happened before in this field.

Note added at proof

Since the submission of the manuscript, X-ray crystal structures have been reported for the stannaimine complex $\{(Me_3Si)_2N\}_2Sn{=}N(C_6H_3Pr^i_2\text{-}2,6)$[80] and for the phosphasilene complex $(C_6H_2Bu^t_3\text{-}2,4,6)P{=}Si(Bu^t)\{P(C_6H_2Bu^t_3\text{-}2,4,6)(PPh_2)\}$.[81]

Acknowledgements—I would like to thank Drs Paul D. Lickiss and A. Guy Orpen and Professor Alan H. Cowley FRS for their comments and advice in preparing this manuscript.

REFERENCES

1. W. E. Dasent, *Nonexistent Compounds*. Marcel Dekker, New York (1965).
2. H. Köhler and A. Michaelis, *Ber. Dtsch. Chem. Ges.* 1877, **10**, 807; J. J. Daly and L. Maier, *Nature (London)* 1964, **203**, 1167 and 1965; **208**, 383; J. J. Daly, *J. Chem. Soc.* 1964, 6147 and 1965, 4789.
3. P. Jutzi, *Angew. Chem. Int. Ed. Engl.* 1975, **14**, 232; L. E. Gusel'nikov and N. S. Nametkin, *Chem. Rev.* 1979, **79**, 529. See also K. S. Pitzer, *J. Am. Chem. Soc.* 1948, **70**, 2140; R. S. Mulliken, *J. Am. Chem. Soc.* 1950, **72**, 4493 and 1955, **77**, 884.
4. E. H. Appelman, *Acc. Chem. Res.* 1973, **6**, 113.
5. P. Laszlo and G. J. Schrobilgen, *Angew. Chem. Int. Ed. Engl.* 1988, **27**, 479.
6. M. Yoshifuji, I. Shima, N. Inamoto, K. Hirotsu and T. Higuchi, *J. Am. Chem. Soc.* 1981, **103**, 4587.
7. R. West, M. J. Fink and J. Michl, *Science* 1981, **214**, 1343.
8. R. Appel and F. Knoll, *Adv. Inorg. Chem.* 1989, **33**, 259; R. Appel, in *Multiple Bonds and Low Coordination in Phosphorus Chemistry* (Edited by M. Regitz and O. J. Scherer). Georg Thieme Verlag, Stuttgart (1990).
9. A. G. Brook and K. M. Baines, *Adv. Organomet. Chem.* 1986, **25**, 1; G. Raabe and J. Michl, *Chem. Rev.* 1985, **85**, 419; G. Raabe and J. Michl, in *The Chemistry of Organic Silicon Compounds* (Edited by S. Patai and Z. Rappoport). Wiley, Chichester (1989).
10. W. Kutzelnigg, *Angew. Chem. Int. Ed. Engl.* 1984, **23**, 272.
11. L. Pauling, *The Nature of the Chemical Bond*. Cornell University Press, Ithaca, New York (1960).
12. A. Moezzi, M. M. Olmstead and P. P. Power, *J. Chem. Soc., Dalton Trans.* 1992, 2429; A. Moezzi, M. M. Olmstead, R. A. Bartlett and P. P. Power, *Organometallics* 1992, **11**, 2383 and refs. therein.
13. (a) W. Uhl, *Z. Naturforsch., Teil B* 1988, **43**, 1113; (b) W. Uhl, M. Layh and T. Hildenbrand, *J. Organomet. Chem.* 1989, **364**, 289; (c) W. Uhl, M. Layh and W. Hiller, *J. Organomet. Chem.* 1989, **368**, 139.
14. R. D. Schluter, A. H. Cowley, D. A. Atwood, R. A. Jones, M. R. Bond and C. J. Carrano, *J. Am. Chem. Soc.* 1993, **115**, 2070.
15. A. G. Brook, S. C. Nyburg, F. Abdesaken, B. Gutekunst, G. Gutekunst, R. K. M. R. Kallury, Y. C. Poon, Y.-M. Chang and W. Wong-Ng, *J. Am. Chem. Soc.* 1982, **104**, 5667. See also K. M. Baines, A. G. Brook, R. R. Ford, P. D. Lickiss, A. K. Saxena, W. J. Chatterton, J. F. Sawyer and B. A. Behnam, *Organometallics* 1989, **8**, 693.
16. (a) N. Wiberg, G. Wagner and G. Müller, *Angew. Chem., Int. Ed. Engl.* 1985, **24**, 229; (b) N. Wiberg, G. Wagner, G. Müller and J. Riede, *J. Organomet. Chem.* 1984, **271**, 381.
17. P. D. Lickiss, *Chem. Soc. Rev.* 1992, **25**, 271.
18. J. Barrau, J. Escudié and J. Satgé, *Chem. Rev.* 1990, **90**, 283.
19. M. Lazraq, J. Escudié, C. Couret, J. Satgé, M. Dräger and R. A. Dammel, *Angew. Chem. Int. Ed. Engl.* 1988, **27**, 828.
20. H. Meyer, G. Baum, W. Massa and A. Berndt, *Angew. Chem. Int. Ed. Engl.* 1987, **26**, 798.
21. A. Berndt, H. Meyer, G. Baum, W. Massa and G. Berger, *Pure Appl. Chem.* 1987, **59**, 1011.
22. G. Anselme, H. Ranaivonjatovo, J. Escudié, C. Couret and J. Satjé, *Organometallics* 1992, **11**, 2748.
23. H. Meyer, G. Baum, W. Massa, S. Berger and A. Berndt, *Angew. Chem. Int. Ed. Engl.* 1987, **26**, 546.
24. H. Grützmacher, S. Freitag, R. Herbst-Irmer and G. M. Sheldrick, *Angew. Chem. Int. Ed. Engl.* 1992, **31**, 437.
25. N. Wiberg, K. Schurz, G. Reber and G. Müller, *J. Chem. Soc., Chem. Commun.* 1986, 591.
26. N. Mitzel, A. Schier and H. Schmidbaur, *Chem. Ber.* 1992, **125**, 2711 and refs. therein.

27. N. Wiberg, K. Schurz, G. Müller and J. Riede, *Angew. Chem. Int. Ed. Engl.* 1988, **27**, 935.
28. S. Walter, U. Klingebiel and D. Schmidt-Bäse, *J. Organomet. Chem.* 1991, **412**, 319.
29. A. Meller, G. Ossig, W. Maringgele, D. Stalke, R. Herbst-Irmer, S. Freitag and G. M. Sheldrick, *J. Chem. Soc., Chem. Commun.* 1991, 1123.
30. R. West, *Angew. Chem. Int. Ed. Engl.* 1987, **26**, 1201; R. West, *Pure Appl. Chem.* 1984, **56**, 163.
31. M. J. Fink, M. J. Michalczyk, K. J. Haller, R. West and J. Michl, *Organometallics* 1984, **3**, 793.
32. S. Masamune, S. Murakami, J. T. Snow, H. Tobita and D. J. Williams, *Organometallics* 1984, **3**, 333.
33. R. S. Archibald, Y. van den Winkel, A. J. Millevolte, J. M. Desper and R. West, *Organometallics* 1992, **11**, 3276.
34. H. Watanabe, K. Takeuchi, N. Fukawa, M. Kato, M. Goto and Y. Nagai, *Chem. Lett.* 1987, 1341.
35. B. D. Shepherd, D. R. Powell and R. West, *Organometallics* 1989, **8**, 2664.
36. S. Masamune, Y. Eriyama and T. Kawase, *Angew. Chem. Int. Ed. Engl.* 1987, **26**, 584.
37. M. Weidenbruch, B. Flintjer, S. Pohl and W. Saak, *Angew. Chem. Int. Ed. Engl.* 1989, **28**, 95.
38. J. T. Snow, S. Murakami, S. Masamune and D. J. Williams, *Tetrahedron Lett.* 1984, **25**, 4191.
39. S. A. Batcheller, T. Tsumuraya, O. Tempkia, W. M. Davis and S. Masamune, *J. Am. Chem. Soc.* 1990, **112**, 9394.
40. D. E. Goldberg, P. B. Hitchcock, M. F. Lappert, K. M. Thomas, T. Fjeldberg, A. Haaland and B. E. R. Schilling, *J. Chem. Soc., Dalton Trans.* 1986, 2387.
41. L. Pauling, *Proc. Natl. Acad. Sci. U.S.A.* 1983, **80**, 3871.
42. (a) G. Trinquier and J.-P. Malrieu, *J. Am. Chem. Soc.* 1987, **109**, 5303; (b) J.-P. Malrieu and G. Trinquier, *J. Am. Chem. Soc.* 1989, **111**, 5916; (c) G. Trinquier, *J. Am. Chem. Soc.* 1990, **112**, 2130.
43. T. A. Albright, J. K. Burdett and M. H. Whangbo, *Orbital Interactions in Chemistry*. Wiley, New York (1985).
44. (a) C. N. Smit, F. M. Lock and F. Bickelhaupt, *Tetrahedron Lett.* 1984, **25**, 3011; (b) C. N. Smit and F. Bickelhaupt, *Organometallics* 1987, **6**, 1156; (c) Y. van der Winkel, H. M. M. Bastiaans and F. Bickelhaupt, *J. Organomet. Chem.* 1991, **405**, 183.
45. M. Dräger, J. Escudié, C. Couret, H. Ranaivonjatovo and J. Satgé, *Organometallics* 1988, **7**, 1010.
46. C. Couret, J. Escudié, J. Satgé, A. Rahainirina and J. D. Andriamizaka, *J. Am. Chem. Soc.* 1985, **107**, 8280.
47. K. Hassler, F. Mitter and B. Reiter, *J. Organomet. Chem.* 1989, **376**, C1.
48. M. Driess and H. Pritzkow, *Angew. Chem. Int. Ed. Engl.* 1992, **31**, 316. See also M. Driess, H. Pritzkow and M. Sander, *Angew. Chem. Int. Ed. Engl.* 1993, **32**, 283.
49. P. Arya, J. Boyer, F. Carré, R. Corriu, G. Lanneau, J. Lapasset, M. Perrot and C. Priou, *Angew. Chem. Int. Ed. Engl.* 1989, **28**, 1016.
50. R. Corriu, G. Lanneau and C. Priou, *Angew. Chem. Int. Ed. Engl.* 1991, **30**, 1130.
51. M. Veith, S. Becker and V. Huch, *Angew. Chem. Int. Ed. Engl.* 1989, **28**, 1237.
52. A. G. Davies and A. G. Neville, *J. Organomet. Chem.* 1992, **436**, 255.
53. G. Becker, *Z. Anorg. Allg. Chem.* 1976, **423**, 247.
54. T. A. van der Knaap, L. Jenneskens, H. J. Meenwissen, F. Bickelhaupt, D. Walther, E. Dinjus, E. Uhlig and A. L. Spek, *J. Organomet. Chem.* 1983, **254**, C33.
55. A. H. Cowley, R. A. Jones, J. G. Lasch, N. C. Norman, C. A. Stewart, A. L. Stuart, J. L. Atwood, W. E. Hunter and H.-M. Zhang, *J. Am. Chem. Soc.* 1984, **106**, 7015.
56. (a) R. Appel, J. Menzel, F. Knoch and P. Volz, *Z. Anorg. Allg. Chem.* 1986, **534**, 100; (b) M. Yoshifuji, K. Toyota, K. Shibayama and N. Inamoto, *Chem. Lett.* 1983, 1153; (c) M. Yoshifuji, K. Toyota and N. Inamoto, *Tetrahedron Lett.* 1985, **26**, 1727.
57. (a) A. J. Ashe, *J. Am. Chem. Soc.* 1971, **93**, 3293; (b) G. Märkl, *Angew. Chem. Int. Ed. Engl.* 1966, **5**, 846.
58. R. Appel and A. Westerhaus, *Tetrahedron Lett.* 1981, **22**, 2159.
59. D. Gudat, E. Niecke, A. M. Arif, A. H. Cowley and S. Quashie, *Organometallics* 1986, **5**, 593.
60. L. Weber, K. Reizig, R. Boese and M. Polk, *Organometallics* 1986, **5**, 1098.
61. A. M. Arif, A. H. Cowley, C. M. Nunn, S. Quashie, N. C. Norman and A. G. Orpen, *Organometallics* 1989, **8**, 1878.
62. (a) L. Weber, G. Meine and R. Boese, *Angew. Chem. Int. Ed. Engl.* 1986, **25**, 469; (b) L. Weber, G. Meine, R. Boese and D. Bungardt, *Z. Anorg. Allg. Chem.* 1987, **549**, 73.
63. G. Becker, G. Gresser and W. Uhl, *Z. Naturforsch., Teil B*, 1981, **36**, 16.
64. (a) M. Regitz, in *Multiple Bonds and Low Coordination in Phosphorus Chemistry* (Edited By M. Regitz and O. J. Scherer). Georg Thieme Verlag, Stuttgart (1990); (b) P. Binger, *ibid*; (c) M. Regitz, *Chem. Rev.* 1990, **90**, 191; (d) J. F. Nixon, *Chem. Rev.* 1988, **88**, 1327.
65. H. W. Kroto, *Chem. Soc. Revs.* 1982, **11**, 435.
66. A. M. Arif, A. R. Barron, A. H. Cowley and S. W. Hall, *J. Chem. Soc., Chem. Commun.* 1988, 171 and refs therein.

67. G. Märkl and H. Sejpka, *Angew. Chem. Int. Ed. Engl.* 1986, **25**, 264.
68. E. Niecke, in *Multiple Bonds and Low Coordination in Phosphorus Chemistry* (Edited by M. Regitz and O. J. Scherer). Georg Thieme Verlag, Stuttgart (1990). See also E. Niecke, R. Detsch, M. Nieger, F. Reichert and W. W. Schoeller, *Bull. Soc. Chim. Fr.* 1993, **130**, 25 and refs therein.
69. (a) A. H. Cowley, J. E. Kilduff, J. G. Lasch, S. K. Mehrotra, N. C. Norman, M. Pakulski, B. R. Whittlesey, J. L. Atwood and W. E. Hunter, *Inorg. Chem.* 1984, **23**, 2582; (b) A. H. Cowley and N. C. Norman, *Prog. Inorg. Chem.* 1986, **34**, 1; (c) A. H. Cowley, *Acc. Chem. Res.* 1984, **17**, 386; (d) A. H. Cowley, *Polyhedron* 1984, **3**, 389; (e) A. H. Cowley, *J. Organomet. Chem.* 1990, **400**, 71.
70. M. Yoshifuji, in *Multiple Bonds and Low Coordination in Phosphorus Chemistry* (Edited by M. Regitz and O. J. Scherer). Georg Thieme Verlag, Stuttgart (1990).
71. L. Weber, *Chem. Rev.* 1992, **92**, 1839.
72. Y. LePage, E. J. Gabe, Y. Wang, L. R. C. Barclay and H. L. Holm, *Acta Cryst., Sect. B* 1980, **36**, 2846.
73. L. Weber and K. Reizig, *Angew. Chem. Int. Ed. Engl.* 1985, **24**, 865.
74. A.-M. Caminade, M. Verrier, C. Ades, N. Paillous and M. Koenig, *J. Chem. Soc., Chem. Commun.* 1984, 875.
75. M. Yoshifuji, T. Hashida, N. Inamoto, K. Hirotsu, T. Horiuchi, T. Higuchi, K. Ito and S. Nagase, *Angew. Chem. Int. Ed. Engl.* 1985, **24**, 211.
76. (a) E. Niecke, B. Kramer and M. Nieger, *Angew. Chem. Int. Ed. Engl.* 1989, **28**, 215; (b) E. Niecke, O. Altmeyer and M. Nieger, *Angew. Chem. Int. Ed. Engl.* 1991, **30**, 1136.
77. (a) A. H. Cowley, N. C. Norman and M. Pakulski, *J. Chem. Soc., Dalton Trans.* 1985, 383; (b) A. H. Cowley, J. G. Lasch, N. C. Norman and M. Pakulski, *J. Am. Chem. Soc.* 1983, **105**, 5506; (c) A. H. Cowley, J. G. Lasch, N. C. Norman, M. Pakulski and B. R. Whittlesey, *J. Chem. Soc., Chem. Commun.* 1983, 881.
78. (a) K. W. Zilm, G. G. Webb, A. H. Cowley, M. Pakulski and A. Orendt, *J. Am. Chem. Soc.* 1988, **110**, 2032; (b) J. C. Duchamp, M. Pakulski, A. H. Cowley and K. W. Zilm, *J. Am. Chem. Soc.* 1990, **112**, 6803.
79. D. C. Pestana and P. P. Power, *Inorg. Chem.* 1991, **30**, 528.
80. G. Ossig, A. Meller, S. Freitag and R. Herbst-Irmer, *J. Chem. Soc., Chem. Commun.* 1993, 497.
81. H. R. G. Bender, E. Niecke and Nieger, *J. Am. Chem. Soc.*, 1993, **115**, 3314.

Polyhedron Vol. 12, No. 20, pp. 2447–2451, 1993
Printed in Great Britain

0277–5387/93 $6.00+.00
© 1993 Pergamon Press Ltd

SYNTHESIS AND CHARACTERIZATION OF ALKYL-2,2,2-TRIFLUOROETHYL SULPHITES

SURAJ P. NARULA,* SUKHJEEVAN KAUR, RAVI SHANKAR and SURINDER K. SHARMA

Department of Chemistry, Panjab University, Chandigarh-160014, India

(*Received* 2 *June* 1993; *accepted* 7 *July* 1993)

Abstract—Some new asymmetric organic sulphites, $R'CH_2OS(O)OCH_2CF_3$ ($R' = H$, CH_3, CH_2Cl, C_2H_5 or C_3H_7) were prepared and characterized by elemental analyses, IR, mass and multinuclear (^1H, ^{13}C, ^{19}F) NMR spectral studies. The quantitative increase of ^1H NMR chemical shift difference of non-equivalent protons with bulk of the R′ substituent is reported.

Organic sulphites have such practical uses as: (i) insecticides;[1] (ii) non-aqueous solvents[2] and (iii) polymerization catalysts.[3] These compounds have also been investigated for reasons of their chemical reactivity[4–8] and structural features.[4,9–13] The structure of these compounds has been studied from the standpoint of non-equivalence of α-methylene protons located in the vicinity of oxygen atoms, linked to the asymmetric centre S=O. In these studies attention has mainly been focussed on the structure of cyclic sulphites while only a few acyclic organic sulphites are characterized;[10–12] and even amongst them very little is known about the nature of asymmetrical sulphites, ROS(O)OR′. Therefore, alkyl-2,2,2-trifluoroethyl sulphites $R'CH_2OS(O)OCH_2CF_3$ ($R' = H$, CH_3, CH_2Cl, C_2H_5, C_3H_7) are isolated, characterized by molecular spectroscopy and the results obtained are reported in this paper.

EXPERIMENTAL

All reactions were performed under dry nitrogen. Thionyl chloride (Fluka) was distilled over mercury before use. Methyl/ethyl/n-propyl/n-butyl alcohols were dried by standard methods given in the literature.[14]

2-Chloroethyl/2,2,2-trifluoroethyl alcohols (Fluka) were used as such. Sulphur and chlorine were estimated by gravimetric methods.[15]

Elemental analyses of the samples were obtained using a Perkin–Elmer (Model 2400) CHN Analyser. Gas Chromatographic analyses were performed on a Perkin–Elmer (Sigma 300) instrument using 6m × 1/8″ long SE-52 column and helium as carrier gas with recorder rate 0.5 cm min^{-1}. IR spectra were recorded as thin films using KBr optics on a Perkin–Elmer 1430 ratio recording spectrophotometer. ^1H and ^{13}C NMR spectra were obtained on Brüker AMX-400 instrument using TMS as internal standard; while ^{19}F NMR spectra were recorded on Varian EM-390 with Freon-11 as external reference. Mass spectra were recorded at 70 eV on VG-Analytical 70-S Spectrometer.

Preparative methods

Methyl/ethyl/2-chloroethyl/n-propyl/n-butyl chlorosulphites were prepared by the reaction of thionyl chloride (40.0 mmol) and the corresponding alcohol (40.0 mmol) as reported earlier.[4] The purity of these compounds was checked by elemental analyses, IR and ^1H NMR spectral data.

Preparation of methyl/ethyl/2-chloroethyl/n-propyl/n-butyl-2,2,2-trifluoroethyl sulphite

A slow addition of 2,2,2-trifluoroethanol (13.7 mmol) was carried out separately into methyl/ethyl/2-chloroethyl/n-propyl or n-butyl chlorosulphite (13.7 mmol) at 50–60°C with constant stirring. A slow stream of dry nitrogen was bubbled into the reaction mixture to expel the HCl gas

* Author to whom correspondence should be addressed.

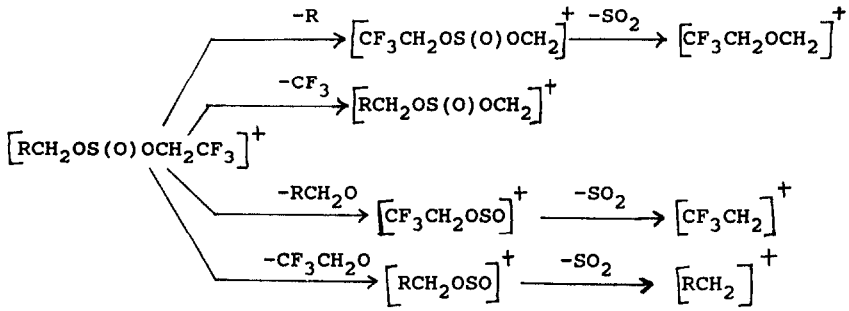

Scheme 1.

formed. After the addition was complete, the contents were heated at 80–90°C for 8–10 h until evolution of HCl gas ceased. The crude mixture was distilled under partial vacuum using a 2 ft long silvered glass column containing glass helices. The constant boiling fractions at 28, 43, 74, 48, 54°C/2 mm Hg, respectively, were collected (% Yield: 70.2, 74.0, 80.7, 82.0, 85.0, respectively) and analysed. Found: C, 20.6; H, 2.7; S, 18.2. Calc. for $C_3F_3H_5O_3S$: C, 20.2; H, 2.8; S, 18.0%. Found: C, 24.9; H, 3.7; S, 16.1. Calc. for $C_4F_3H_7O_3S$: C, 25.0; H, 3.7; S, 16.7%. Found: C, 21.4; H, 2.6; S, 14.4. Calc. for $C_4ClF_3H_6O_3S$: C, 21.2; H, 2.7; S, 14.1%. Found: C; 29.3; H, 4.6; S, 15.1. Calc. for $C_5F_3H_9O_3S$: C, 29.1; H, 4.4; S, 15.5%. Found: C, 32.9; H, 5.2; S, 14.8. Calc. for $C_6F_3H_{11}O_3S$: C, 32.7; H, 5.0; S, 14.5%.

RESULTS AND DISCUSSION

Methyl/ethyl/2-chloroethyl/n-propyl/n-butyl-2,2,2-trifluoroethyl sulphites were prepared separately by the reaction of 2,2,2-trifluoroethanol with the appropriate alkyl chlorosulphite.[4] This

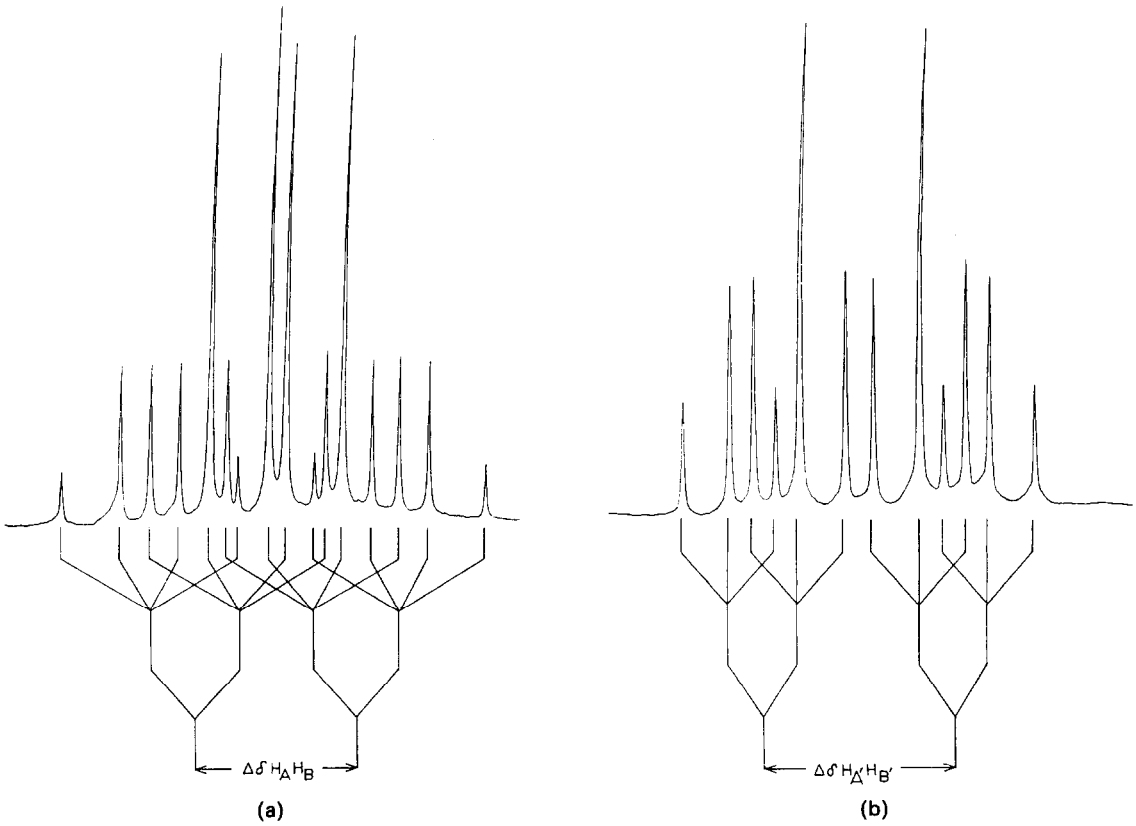

Fig. 1. (a) Splitting pattern for the α-methylene protons of 2,2,2-trifluoroethyl group in $C_3H_7OS(O)OCH_2CF_3$. (b) Splitting pattern for the α-methylene protons of n-propyl group in $C_3H_7OS(O)OCH_2CF_3$.

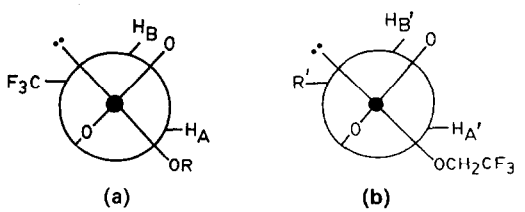

Fig. 2. (a and b) The central atom represents sulphur atom with the lines connecting the oxygen, the lone pair, alkoxy/2,2,2-trifluoroethoxy groups. The large circle represents the α-methylene carbon bonded with two hydrogens, the oxygen and the CF_3/R′ groups.[20]

direct method gives higher yields (70–85%) of the products than the one in which "alcohol–amine"[16] adduct is used (30–40%). All these compounds are colourless, distillable liquids and contain only minor amounts (< 1%) of dialkyl sulphites as evidenced by GLC.

Spectral data

Infrared spectra of these sulphites give important absorptions at 1270–1260, 1215–1210, 1180–1160, 960–920 and 550–530 cm^{-1} assignable to $\nu_{as}CF_3$, $\nu S{=}O$, $\nu_{sy}CF_3$, $\nu SO(C)$ and δSO_2 modes, respectively.[13,17]

Mass spectra of these compounds show molecular ion peak M^+ in each case. The major fragments and their origin (Scheme 1) suggest that the titled sulphites fragment in the manner partially similar to both the symmetrical analogs.[13,18]

^1H NMR spectra of the compounds give the distinct quartets/triplets in the region 4.4–4.2 and 4.2–4.0 ppm (Fig. 1a,b). The spectral pattern can be rationalized on the basis of non-equivalence of α-methylene protons of CF_3CH_2O and $R'CH_2O$ groups (R′ = H, CH_3, C_2H_5 and C_3H_7), respectively.[12,19] The chemical environments of each set of protons may be diagrammatically represented as shown in Fig. 2a,b. The assignments of the chemical shift values are made in accordance with the reported trends[21,22] and are recorded in Table 1. The spectrum of 2-chloroethyl 2,2,2-trifluoroethyl sulphite could not be analysed unambiguously due to extensive overlapping of signals.

A perusal of Table 1 reveals that the chemical shift difference of each set of non-equi-

Table 1. ^1H NMR spectral data of methyl/ethyl/n-propyl/n-butyl-2,2,2-trifluoroethyl sulphites

Compound	Chemical shift[a] (δ) ppm	$\Delta\delta H_A$-$H_{B'}$/ $\Delta\delta H_A H_B$ ppm	^nJ(H-H/F) Hz
$\overset{a}{C}H_3OS(O)OCH_2CF_3$	a = 3.722(3H,s) A = 4.257(1H,dq) B = 4.313(1H,dq)	—/0.056	$^2J(H_A{-}H_B) = 12.7$ $^3J(H_A{-}F) = 8.3$ $^3J(H_B{-}F) = 8.4$
$\overset{a}{C}H_3CH_2OS(O)OCH_2CF_3$	a = 1.401(3H,t) A′ = 4.158(1H,dq) B′ = 4.224(1H,dq) A = 4.272(1H,dq) B = 4.342(1H,dq)	0.066/0.070	$^2J(H_A{-}H_{B'}) = 10.2$ $^3J(H_A{-}H_a) = 7.2$ $^3J(H_{B'}{-}H_a) = 7.3$ $^2J(H_A{-}H_B) = 12.6$ $^3J(H_A{-}F) = 8.3$ $^3J(H_B{-}F) = 8.4$
$\overset{a}{C}H_3\overset{b}{C}H_2CH_2OS(O)OCH_2CF_3$	a = 0.969(3H,t) b = 1.897(2H,m) A′ = 4.033(1H,dt) B′ = 4.124(1H,dt) A = 4.272(1H,dq) B = 4.350(1H,dq)	0.091/0.078	$^2J(H_A{-}H_B) = 10.1$ $^3J(H_A{-}H_b) = 6.6$ $^3J(H_B{-}H_b) = 6.6$ $^2J(H_A{-}H_B) = 12.6$ $^3J(H_A{-}F) = 8.3$ $^3J(H_B{-}F) = 8.3$
$\overset{a}{C}H_3\overset{b}{C}H_2\overset{c}{C}H_2CH_2OS(O)OCH_2CF_3$	a = 0.969(3H,t) b = 1.441(2H,m) c = 1.711(2H,m) A′ = 4.056(1H,dt) B′ = 4.148(1H,dt) A = 4.250(1H,dq) B = 4.332(1H,dq)	0.092/0.082	$^2J(H_A{-}H_{B'}) = 10.2$ $^3J(H_A{-}H_c) = 6.6$ $^3J(H_B{-}H_c) = 6.5$ $^2J(H_A{-}H_B) = 12.6$ $^3J(H_A{-}F) = 8.3$ $^3J(H_B{-}F) = 8.3$

[a] A,B and A′,B′ denotes the two non-equivalent α-methylene protons of —OCH_2CF_3 and —OCH_2R' groups, respectively. a,b,c denotes different hydrogen atoms as specified.

Table 2. ^{13}C and ^{19}F NMR spectral data of methyl/ethyl/2-chloroethyl/n-propyl/n-butyl-2,2,2-trifluoroethyl sulphites

Compound	Chemical shift[a] ($\delta^{13}C$)[b] ppm	$^{n}J(^{13}C-^{19}F)$ Hz	Chemical shift ($\delta^{19}F$)[c] ppm	$^{n}J(^{19}F-H)$ Hz
$\overset{a}{CH_3}OS(O)O\overset{A}{CH_2}\overset{B}{CF_3}$	a = 49.4(s) A = 57.8(q) B = 123.4(q)	$^{1}J(^{13}C-^{19}F) = 278.2$ $^{2}J(^{13}C-^{19}F) = 38.2$	−74.3(t)	$^{3}J(^{19}F-H) = 8.3$
$\overset{a}{CH_3}\overset{b}{CH_2}OS(O)O\overset{A}{CH_2}\overset{B}{CF_3}$	a = 15.5(s) b = 60.2(s) A = 57.8(q) B = 123.3(q)	$^{1}J(^{13}C-^{19}F) = 277.6$ $^{2}J(^{13}C-^{19}F) = 37.6$	−74.3(t)	$^{3}J(^{19}F-H) = 8.3$
$Cl\overset{a}{CH_2}\overset{b}{CH_2}OS(O)O\overset{A}{CH_2}\overset{B}{CF_3}$	a = 42.1(s) b = 63.1(s) A = 58.3(q) B = 123.2(q)	$^{1}J(^{13}C-^{19}F) = 277.4$ $^{2}J(^{13}C-^{19}F) = 37.6$	−74.5(t)	$^{3}J(^{19}F-H) = 8.4$
$\overset{a}{CH_3}\overset{b}{CH_2}\overset{c}{CH_2}OS(O)O\overset{A}{CH_2}\overset{B}{CF_3}$	a = 10.3(s) b = 23.0(s) c = 65.5(s) A = 57.8(q) B = 123.4(q)	$^{1}J(^{13}C-^{19}F) = 276.9$ $^{2}J(^{13}C-^{19}F) = 37.2$	−74.2(t)	$^{3}J(^{19}F-H) = 8.3$
$\overset{a}{CH_3}\overset{b}{CH_2}\overset{c}{CH_2}\overset{d}{CH_2}OS(O)O\overset{A}{CH_2}\overset{B}{CF_3}$	a = 13.2(s) b = 18.9(s) c = 31.4(s) d = 63.5(s) A = 57.7(q) B = 123.3(q)	$^{1}J(^{13}C-^{19}F) = 277.6$ $^{2}J(^{13}C-^{19}F) = 37.2$	−74.2(t)	$^{3}J(^{19}F-H) = 8.4$

[a] a,b,c,d and A,B denotes different carbon atoms as specified.
[b] Solvent $CDCl_3$ ($\delta^{13}C = 77.5$ ppm).
[c] Freon-11 as external reference.

valent protons, i.e. $\Delta\delta H_AH_B/\Delta\delta H_A'H_B' = \delta(H_B-H_A)/\delta(H_B'-H_A')$ increases with increasing the size of R′ group. The variation of anisochronism with the bulk of R group in symmetrical sulphites, $(RCH_2O)_2SO$ is reported;[23] however, quantitative assessment of the steric effect of straight chain alkyl groups on the non-equivalent protons of both the α-methylene groups separately are being reported for the first time.

^{13}C and ^{19}F NMR chemical shifts along with the observed coupling constant data[13,24] (Table 2) are also consistent with the structure of these compounds.

Acknowledgements—Authors are grateful to Professor (Dr) D. Kummer, Inst. F. Anorg. Chemie de Univ., Karlsruhe, Germany and Professor C. L. Khetrapal, I.I.Sc, Bangalore for NMR spectra. RS and SK are grateful to UGC and CSIR, respectively for the award of Research Scientist "A" and SRF, respectively.

REFERENCES

1. R. A. Covey and R. E. Grahame, *Ger. Patent*, 2,453,138 1975; *Chem. Abstr.* 1975, **83**, 131317v.
2. E. Plichta, M. Salomon, S. Slane and M. Uchiyamna, *J. Solution Chem.* 1986, **15**, 663.
3. Asahi Chemical Industry Co, Ltd., *Jpn. Patent*, 8,126,906 1981; *Chem. Abstr.* 1981, **95**, 43957w.
4. H. F. Van Woerden, *Chem. Rev.* 1963, **63**, 557.
5. R. C. Kumar, S. A. Kinkead and J. M. Shreeve, *Inorg. Chem.* 1984, **23**, 3112.
6. C. G. Krespan and B. E. Smart, *J. Org. Chem.* 1986, **51**, 320.
7. Y. Tamaru, K. Nagao, T. Bando and Z. Yoshida, *J. Org. Chem.* 1990, **55**, 1823.
8. H. Eibisch, *Z. Chem.* 1986, **26**, 375; *Chem. Abstr.* 1987, **106**, 101715z.
9. H. Faucher, A. C. Guimaraes, J. B. Robert, F. Sauriol and M. St-Jacques, *Tetrahedron* 1981, **37**, 689.
10. A. J. Baines and B. J. Vander Veken, *J. Mol. Struct.* 1987, **157**, 119.
11. J. G. Tillet, *Int. J. Sulfur Chem.* 1973, **3**, 289; *Chem. Abstr.* 1973, **79**, 136013v.
12. J. S. Waugh and F. A. Cotton, *J. Phys. Chem.* 1961, **65**, 562.
13. R. A. De Marco, A. T. Kovacina and W. B. Fox, *J. Fluorine Chem.* 1975, **5**, 221.
14. J. A. Riddick and W. B. Bunger, "Techniques of Chemistry", *Organic Solvents*, 3rd edn, Vol. 2 Wiley-Interscience, New York (1970).

15. A. I. Vogel, *Textbook of Quantitative Inorganic Analysis*, 4th edn, English Language Book Society, Longmans, London (1986).
16. T. A. Kovacina, R. A. De Marco, W. B. Fox, D. E. Young and L. R. Anderson, *Inorg. Nucl. Chem. Lett.* 1974, **10**, 763.
17. P. V. Huong and E. Raducanu, *J. Mol. Struct.* 1974, **23**, 81.
18. A. A. Gamble, J. R. Gilbert, J. G. Tillet, R. E. Coombs and A. J. Wilkinson, *J. Chem. Soc.* (*B*) 1969, 655.
19. M. Oki and H. Iwamura, *Bull. Chem. Soc. Jpn* 1962, **35**, 1428.
20. R. S. Drago, *Physical Methods in Chemistry*, p. 215, W. B. Saunders, Company Press, Philadelphia, PA (1977).
21. J. G. Pritchard and P. C. Lauterbur, *J. Am. Chem. Soc.* 1961, **83**, 2105.
22. H. Finegold, *J. Phys. Chem.* 1968, **72**, 3244.
23. A. G. Yurchenko, P. A. Krasutskii, A. N. Vlasova and Kh. E. Dzhuva, *Ser. Khim. Mashinobuduv. Tekhnol.* 1977, **14**, 15; *Chem. Abstr.* 1978, **89**, 107104b.
24. J. B. Stothers, *Carbon-13 NMR Spectroscopy, Organic Chemistry*, A series of Monographs (Edited by A. T. Blomquist and H. Wasserman), Vol. 24, p. 363. Academic Press, New York (1972).

Polyhedron Vol. 12, No. 20, pp. 2453–2458, 1993
Printed in Great Britain

0277–5387/93 $6.00+.00
© 1993 Pergamon Press Ltd

THE OXIDATION OF TETRAPHENYLPORPHYRINATOIRON(III)HEXAFLUOROANTIMONATE WITH PEROXYLAURIC ACID AND *t*-BUTYL HYDROPEROXIDE

GUDMUNDUR G. HARALDSSON

Science Institute, University of Iceland, Dunhaga 3, 107 Reykjavik, Iceland

and

JACK E. BALDWIN*

The Dyson Perrins Laboratory, University of Oxford, South Parks Road, Oxford OX1 3QY, England, U.K.

and

JOHN G. JONES

The Chemistry Department, N.U.U., Coleraine, U.K.

and

JOHN DEBERNARDIS

Chemistry Department, Massachusetts Institute of Technology, Cambridge, MA 02139, U.S.A.

(*Received* 23 *June* 1993; *accepted* 1 *July* 1993)

Abstract—The treatment of tetraphenylporphyrinatoiron(III)hexafluoroantimonate (**1**), $FeTPPSbF_6$, with peroxylauric acid, to form high-valent μ-oxo dimers of FeTPP, and *t*-butylhydroperoxide, leading to the isolation of μ-oxo bridged high-valence iron(IV) porphyrin and a *t*-butylperoxo substituted isoporphyrin cation, is described.

Cytochrome P-450 is a family of remarkable heme-containing proteins that perform a number of monooxygenation transformations on a great variety of substrates.[1–3] These include the insertion of an oxygen atom into an alkane C—H bond, hydroxylation of arenes, epoxidation of olefins and oxidation as well as dealkylation of heteroatoms.[3] It is now widely accepted that the nature of the active species responsible for the oxygenations by cytochrome P-450 is an oxo-ferryl porphyrin π-cation radical.[4] This is formally an oxoferryl intermediate, Fe(V)=O, two oxidation equivalents above the native ferric heme, similar to compound I species of horse-radish peroxidase whose structures have been established as Fe(IV)-oxo porphyrin π-cation radicals.[5] Extensive model studies of simple synthetic hemins with various oxygen atom transfer agents such as iodosylbenzene, peracids and hydroperoxides have not only accomplished the oxygen atom transfer reactions performed by cytochrome P-450, but also strongly support the above formalization of the active oxidant.[4,6–11]

We have described the generation of tetraphenylporphyrinatoiron(III)hexafluoroantimonate, (**1**), $FeTPPSbF_6$, along with some of its properties.[12] It was anticipated that such an iron(III) porphyrin system free of axial ligands might be reactive toward superoxide ion and peroxides and thus serve as a possible model for the

* Author to whom correspondence should be addressed.

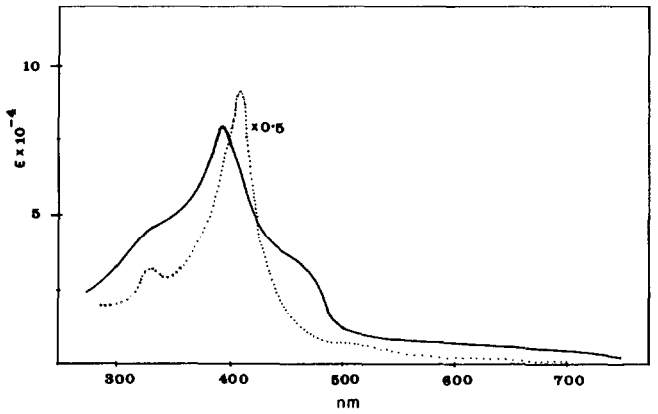

Fig. 1. The electronic spectra of **2** (solid line) and **3** (broken line) in dichloromethane.

active sites of biological systems responsible for oxygen activation, such as cytochrome P-450, peroxidase[5,13] and catalase.[5,13] The reactions of **1** with superoxide ion has previously been described,[12] but in the present report the treatment of **1** with peroxylauric acid and *t*-butylhydroperoxide is described.

RESULTS AND DISCUSSION

When **1** was treated with an excess of peroxylauric acid in benzene at 0°C a black glistening solid, **2**, was isolated by centrifugation in 62% yield. The material was insoluble in hydrocarbon solvents, but dissolved readily in dichloromethane. Its electronic absorption spectrum in this solvent displayed a very broad Soret band at 396 nm with shoulders at 325 and 450 nm as demonstrated in Fig. 1. After dithionite reduction of **2** in pyridine the pyridine hemochrome, $FeTPP(pyr)_2$, spectrum[12] was observed confirming the presence of an iron porphyrin moiety in the compound. Thin-layer chromatography of **2** on alumina produced a μ-oxo dimer, FeTPP-O-FeTPP,[14] again suggesting the presence of an iron porphyrin. The infrared spectrum of the solid had absorption bands appropriate to the TPP skeleton, to SbF_6^- (655 and 290 cm^{-1})[15] and a very strong Fe–O stretch[14] at 860 cm^{-1}, all indicative of a possible oxidized form of a μ-oxo dimer, $[Fe(TPP\text{-}O\text{-}FeTPP]^{+n}(SbF_6^-)_n$. Treatment of μ-oxo dimer, $(FeTPP)_2O$, with silverhexafluoroantimonate in dichloromethane solution at room temperature resulted in a solution showing an identical electronic spectrum to that of **2**, providing further evidence for the presence of an oxidized μ-oxo dimer adduct and demonstrating that silver ions are capable of oxidizing $(FeTPP)_2O$ to **2**.

Electrochemical oxidation of the μ-oxo dimer, $(FeTPP)_2O$, is known to proceed in two one-electron steps.[16] The first oxidation step was assigned as the production of a mixed-valence oxidation state μ-oxo dimer of iron(III) and iron(IV), which could be isolated as a perchlorate salt, [Fe(III)TPP-O-

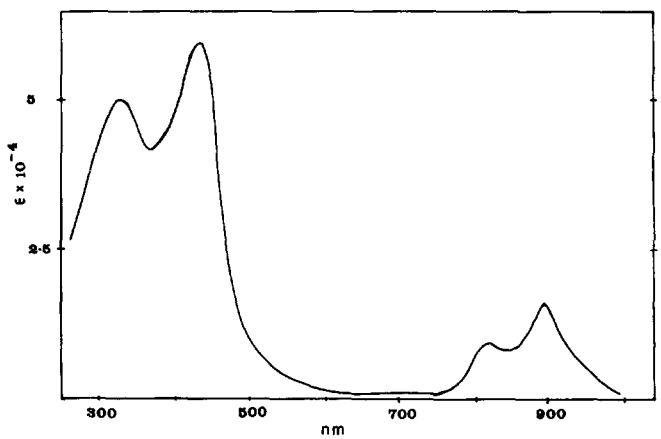

Fig. 2. The electronic spectrum of **4** in dichloromethane.

Fe(IV)TPP]$^{+}ClO_4^{-}$, and the second was assigned as the bis-oxidized dimer of two iron(IV) centres, which has also, more recently,[17] been isolated as a perchlorate salt, [Fe(IV)TPP-O-Fe(IV)TPP]$^{+2}$ $(ClO_4^{-})_2$. Strong evidence supporting Fe(III) porphyrin π-cation radical assignments for these high-valent dimers has been put forward.[18] The electronic spectrum of **2** (Fig. 1) was found to be identical to that of the bis-oxidized μ-oxo bridged dimers described above. Polarographic studies of **2** and the μ-oxo dimer with tetra(n-hexyl) ammonium hexafluoroantimonate as supporting electrolyte further strengthened the assignment of **2** as the bis-oxidized μ-oxo dimer, [Fe(IV)TPP-O-Fe(IV)TPP]$^{+2}(SbF_6^{-})_2$. Two reversible oxidation waves at 0.70 and 1.00 V were observed of equal height and a wave double that height at 1.54 V for the μ-oxo dimer. The first two waves were ascribed to the formation of [Fe(III)TPP-O-Fe(IV)TPP]$^{+}$ and [Fe(IV)TPP-O-Fe(IV)TPP]$^{+2}$, respectively, but the two-electron wave must either correspond to the iron centres going to iron(V) simultaneously, or more accurately, both porphyrin rings being oxidized to radical π-cations simultaneously with both metals remaining at the Fe(IV) oxidation state. When **2** was subjected to polarography under the same conditions, reduction waves were observed at 0.65–0.70 V and 0.96–1.10 V, and an oxidation wave at 1.55 V. These results are therefore consistent with the proposed structure, and agree with the similar polarographic studies of Felton *et al.*[16] and Phillippi and Goff.[17,18]

The compound was stable for 24 h in solution under anhydrous aprotic conditions. Attempted crystallizations of **2** failed due to the reduction of the compound to the mixed-valence dimer or the μ-oxo dimer. When the peroxylauric acid oxidation was carried out in refluxing benzene a different compound, **3**, was obtained as a brown solid in reduced yields. This compound, readily soluble in dichloromethane, was substantially more stable both in solution and in the solid state than **2**. Electron absorption spectroscopy in dichloromethane showed the presence of a Soret band at 408 nm, a band at 330 nm and a very broad band centred around 500 nm as shown in Fig. 1. This spectrum was identical to that of the mixed-valence μ-oxo dimer,[16-18] [Fe(III)TPP-O-Fe(IV)TPP]$^{+}ClO_4^{-}$. That **3** was indeed the mixed-valence oxidation state dimer, [Fe(III)TPP-O-Fe(IV)TPP]$^{+}SbF_6^{-}$, was further supported by polarographic studies of the compound which were consistent with those cited above for [Fe(III)TPP-O-Fe(IV)TPP]$^{+}ClO_4^{-}$: a reduction wave at 0.70 V, an oxidation wave of a similar height at 1.00 V and another oxidation wave twice that height as expected at 1.55 V. Field desorption mass spectrometry provided the required molecular ion of **3** at m/z 1587 and another more stable one at 1352 amu corresponding to [Fe(III)TPP-O-Fe(IV)TPP]$^{+}$. Infrared spectroscopy showed the characteristic Fe–O stretching frequency at 865 cm^{-1} as well as bands characteristic of SbF_6^{-}.

Further support for the mixed-valence formulation came from the reaction of equimolar amounts of $(FeTPP)_2O$ with **2** in dichloromethane at room temperature. The product displayed an electronic spectrum identical to that of **3**. When the peroxylauric acid oxidation was carried out at room temperature, a mixture of **2** and **3** was afforded as detected by optical absorption spectroscopy and polarographic studies. By varying the temperature of the reaction it became possible to control the preparation of either of these compounds in pure state. All this, together with the fact that attempted recrystallizations of **2** normally failed and a product having an optical spectrum identical to **3** resulted, highlights the close relationship between the μ-oxo dimer, **2** and **3**.

Excess *t*-butylhydroperoxide reacted with **1** in benzene at 0°C to provide a pale-brown precipitate, **4**, which was isolated by centrifugation in almost quantitative yield. Its optical spectrum in dry dichloromethane as shown in Fig. 2 displayed a Soret band at 415 nm, another maximum at 320 nm and the near-infrared region had absorption bands at 898 and 815 nm, characteristic of isoporphyrin cations.[19] Attempted crystallization of **4** in various solvents was unsuccessful and resulted in conversion variously to the postulated adducts [Fe(IV)TPP-O-Fe(IV)TPP]$^{+2}(SbF_6^{-})_2$ and [Fe(IV)TPP-O-Fe(III)TPP]$^{+}SbF_6^{-}$, the μ-oxo dimer, $(FeTPP)_2O$, and an FeTPPX-type adduct. Spectroscopic studies showed that both [Fe(IV)TPP-O-Fe(IV)TPP]$^{+2}(SbF_6^{-})_2$ and [Fe(IV)TPP-O-Fe(III)TPP]$^{+}SbF_6^{-}$, but also $(FeTPP)_2O$, could be converted to **4** upon addition of *t*-butylhydroperoxide in dichloromethane at room temperature, indicating a higher oxidation state and further highlighting the structural resemblance between the μ-oxo dimer, **2** and **3**, and also **4**. Reduction of **4** by dithionate/pyridine resulted in the pyridine hemochrome[12] and reduction by aqueous iodide solution resulted in the formation of $(FeTPP)_2O$. Atomic absorption spectroscopic results showed an Fe : Sb ratio of 1 : 1 within experimental error.

On the basis of this evidence the structure shown in Fig. 3 is proposed for **4**. This is an iron(III) *t*-butylperoxide substituted isoporphyrin cation bridged to an iron(IV) porphyrin unit by a μ-oxo bridge. This structure was further supported by gas

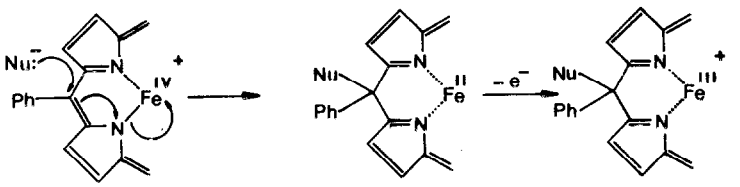

Scheme 1.

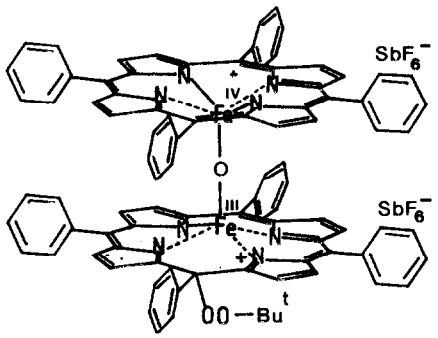

Fig. 3. The proposed structure for **4**.

chromatography studies indicating that **4**, when reduced with ethane thiol produces *t*-butyl alcohol. Cyclic voltammetry conducted on **4** in dichloromethane with tetra(n-hexyl)ammonium hexafluoroantimonate as supporting electrolyte showed the compound to behave quite differently electrochemically from the family based on $(FeTPP)_2O$. Two reduction waves of equal height were observed with $E_{1/2}$-values of -0.05 and 0.26 V, together with an oxidation wave at 1.54 V. It is thus a much less powerful oxidant in free-energy terms than $[Fe(IV)TPP\text{-}O\text{-}Fe(IV)TPP]^{+2}$, though more powerful in terms of oxidizing equivalents for the conversion of iodide to iodine in aqueous solution.

An isoporphyrin of the type reported here has not previously been prepared. The mechanism for its formation is coherently believed to involve the formation of the bis-oxidized μ-oxo adduct, $[Fe(IV)TPP\text{-}O\text{-}Fe(IV)TPP]^{+2}(SbF_6^-)_2$, formed in a similar manner to that of the peroxylauric acid case. *t*-Butylhydroperoxide, a substantially better nucleophile than peroxylauric acid, attacks at the *meso*-position of one of the $Fe(IV)TPP^+$-units of the dimer. The excess *t*-butylhydroperoxide oxidizes the resulting iron(II) species to iron(III) as demonstrated in Scheme 1.

Finally, Scheme 2 illustrates the proposed mechanism for the formation of **2**, **3** and **4**. Although this mechanism has not been well established it has features similar to the mechanism proposed by LaMar and co-workers[20,21] for the irreversible μ-oxo dimer formation of ferrous porphyrins in the presence of dioxygen. It involves a heterolytic cleavage of a peroxo bond in the intermediate peroxy iron(III) species, resulting in the formation of an electron deficient oxygen species which is formally equivalent to an iron(V) ferryl intermediate,[22-24] Fe(V)=O. This intermediate would presumably be stabilized by the π-cation radical assignment orig-

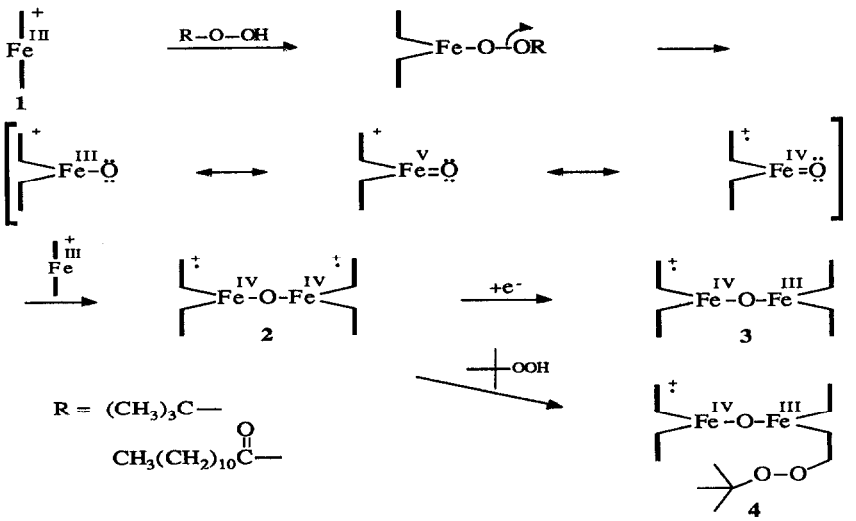

Scheme 2.

inally postulated by Dolphin *et al.*[25-27] but should be a far more potent oxidizing agent than the corresponding Fe(IV)=O intermediate proposed by LaMar *et al.* (*vide supra*). It also lacks a stabilizing electron-donating axial ligand. Consequently, its concentration would never be expected to reach any detectable levels and it reacts instantaneously with a second free cation, $FeTPP^+$, to form the bis-oxidized μ-oxo dimer.

EXPERIMENTAL

Electronic absorption spectra were measured on a Perkin–Elmer 555 UV–VIS spectrophotometer. When included, $\log\varepsilon$ follows each λ_{max} in parentheses. Infrared spectra were recorded on either a Perkin–Elmer 521 Grating IR spectrophotometer or a Perkin–Elmer 297 IR spectrophotometer. Field desorption mass spectra were recorded on a VG-16F instrument. All solvents were Analytical Reagent grade or redistilled commercial grade and were always dried. Measurements at stationary and rotating platinum electrodes were carried out in dry dichloromethane using 0.01 M $(n\text{-hexyl})_4N^+SbF_6^-$ as supporting electrolyte and a Princeton Applied Research 174 polarographic analyser. Gas chromatography was performed on a Varian instrument under the following conditions: injector 250°C, detector 275°C; H_2 5 lbs, He 40 lbs, air 40 lbs; column SE 30 $12' \times 1/8''$, 40°C. Iodometric titrations were performed using standard procedures with $KI/Na_2S_2O_3$ and starch as an indicator. Peroxylauric acid was prepared according to the procedure of Swern.[28] *t*-Butylhydroperoxide (90%) (Aldrich) was dried by the procedure of Sharpless *et al.*[29]

The preparation of the proposed μ-oxo-bis(tetraphenylporphyrinatoiron(IV) bishexafluorantimonate, $[Fe(IV)TPP\text{-}O\text{-}Fe(IV)TPP]^{+2}(SbF_6^-)_2$, **2**

To a stirred ice-cooled dry benzene solution (35 cm^3) of peroxylauric acid (0.2 g, 0.93 mmol) under nitrogen was added $FeTPPSbF_6$, **1**, (0.05 g, 0.55 mmol) dissolved in minimum amount of dry dichloromethane (1–2 cm^3). No effervescence was noted and after stirring for 15 min at 0°C a solid precipitated from solution. Centrifugation afforded a black glistening solid, which was washed twice with dry benzene and twice with pentane. The product was dried *in vacuo* for 3 h to yield an initial product (22 mg). A second crop was obtained by adding pentane to the centrifugate (8 mg; total 31 mg, 62%). [Found: C, 54.8; H, 3.4; N, 5.7; F, 11.7; Fe, 5.8. Calc. for $C_{88}H_{56}N_8OF_{12}Fe_2Sb_2$: C, 57.9; H, 3.1; N, 6.1; F, 12.5; Fe, 6.1%. λ_{max} (CH_2Cl_2) 325 (sh, 4.63), 396 (4.90), 450 (sh, 4.53) nm. ν_{max} (KBr) 3040 (s, C—H), 1595 (s, C=N), 860 (s, Fe—O—Fe), 655 (s, SbF_6^-), 290 (s, SbF_6^-) cm^{-1}. Polarographic results: reduction waves recorded at 0.65–0.70 and 0.96–1.10 V and an oxidation wave at 1.54 V.]

The preparation of the proposed μ-oxo-[5,10,15,20-tetraphenylporphyrinatoiron(III), 5,10,15,20-tetraphenylporphyrinatoiron(IV)] hexafluoroantimonate, $[Fe(III)TPP\text{-}O\text{-}Fe(IV)TPP]^+SbF_6^-$, **3**

The same procedure as for **2** was followed, but after the addition of $FeTPPSbF_6$ at 0°C the stirred solution was transferred to a steam-bath and stirred for 30 min at 65°C. A brown solid precipitated from solution, which after cooling was centrifuged, washed with cold benzene and pentane and finally dried *in vacuo* for 3 h. **3** was obtained as a brown solid (20 mg, 46%). [λ_{max} (CH_2Cl_2) 330 (4.78), 408 (5.25), 500 (sh, 4.24) nm. ν_{max} (KBr) 3040 (s, C—H), 1595 (s, C=N), 865 (s, Fe—O—Fe), 660 (s, SbF_6^-), 290 (s, SbF_6^-) cm^{-1}. *m/z* (FD) 1587 (M^+), 1352 (M—SbF_6^-). Polarographic results: reduction waves recorded at 0.70 V and oxidation waves at 1.00 and 1.55 V.]

The preparation of the proposed μ-oxo-[5-t-butylperoxide-5,10,15,20-tetraphenylisoporphyrinatoiron (III), 5,10,15,20-tetraphenylporphyrinatoiron(IV)], bishexafluorantimonate, **4**

To an ice-cooled stirred solution of dry benzene (500 cm^3) and dry 90% *t*-butylhydroperoxide [13.3 g (12.0 cm^3), 133 mmol] was added $FeTPPSbF_6$ (1.61 g, 1.78 mmol) dissolved in a minimum amount of dry dichloromethane (40 cm^3). Effervescence was noted and the reaction mixture was stirred for approximately 5 min. A precipitate appeared and the reaction mixture was filtered. The residue was washed with benzene and then with pentane, air dried momentarily and finally dried *in vacuo* for several hours affording **4** as a brown solid (1.64 g, 96%). [λ_{max}(CH_2Cl_2) 320 (4.69), 415 (4.78), 815 (3.89), 898 (4.07) nm. λ_{max}(benzene) 320, 385, 420 nm. ν_{max}(nujol) 860 (m, Fe—O—Fe), 655 (m, SbF_6^-), 290 (m, SbF_6^-) cm^{-1}. Atomic absorption: Fe:Sb ratio of 1:1.12, equivalent to 1:1 within experimental error. Polarographic results: reduction waves recorded at −0.05 and 0.25 V and an oxidation wave at 1.54 V.]

Thiol reduction of **4**

The isoporphyrin **4** (20 mg) was dissolved in chloroform (2 cm^3) and ethanethiol was added (20

drops). The mixture was stirred at room temperature for 20 min at which time the solution was injected into the gas chromatograph. *t*-Butyl alcohol was detected in accordance with the proposed structure.

Acknowledgements—The authors wish to thank Dr R. T. Aplin for mass spectral determinations and the U.S. Public Health Service and the Science Research Council for financial support.

REFERENCES

1. P. Ortiz de Montellano, ed., *Cytochrome P-450: Structure, Mechanism and Biochemistry*. Plenum Press, New York (1986).
2. R. E. White and M. J. Coon, *Ann. Rev. Biochem.* 1980, **49**, 315.
3. F. P. Guengerich and T. L. Macdonald, *Acc. Chem. Res.* 1984, **17**, 9.
4. T. J. McMurry and J. T. Groves, in *Cytochrome P-450: Structure, Mechanism and Biochemistry*, P. Ortiz de Montellano, ed., Ch. 1. Plenum Press, New York (1986).
5. L. K. Hanson, C. K. Chang, M. S. Davis and J. Fajer, *J. Am. Chem. Soc.* 1981, **103**, 663.
6. J. T. Groves, T. E. Nemo and R. S. Myers, *J. Am. Chem. Soc.* 1979, **101**, 1032.
7. J. T. Groves and Y. Watanabe, *J. Am. Chem. Soc.* 1988, **110**, 8443.
8. J. P. Collman, P. D. Hampton and J. I. Brauman, *J. Am. Chem. Soc.* 1990, **112**, 2977.
9. K. Murata, R. Panicucci, E. Gopinath and T. C. Bruice, *J. Am. Chem. Soc.* 1990, **112**, 6072.
10. T. G. Traylor and F. Xu, *J. Am. Chem. Soc.* 1990, **112**, 178.
11. H. Sugimoto, H.-C. Tung and T. Sawyer, *J. Am. Chem. Soc.* 1988, **110**, 2465.
12. J. E. Baldwin, G. G. Haraldsson and J. G. Jones, *Inorg. Chim. Acta* 1981, **51**, 29.
13. W. D. Hewson and C. P. Hager, in *The Porphyrins*, D. Dolphin ed. Vol. VII, pp. 295–332. Academic Press, New York (1979).
14. E. M. Fleischer and T. S. Srivasta, *J. Am. Chem. Soc.* 1969, **91**, 2403.
15. D. W. A. Sharp and R. D. Peacock, *J. Chem. Soc.* 1959, 2762.
16. R. H. Felton, G. S. Owen, D. Dolphin, A. Forman, D. C. Borg and J. Fajer, *Ann. N.Y. Acad. Sci.* 1973, **206**, 504.
17. M. A. Phillippi and H. M. Goff, *J. Am. Chem. Soc.* 1979, **101**, 7641.
18. M. A. Phillippi and H. M. Goff, *J. Am. Chem. Soc.* 1982, **104**, 6026.
19. D. Dolphin, R. H. Felton, D. C. Borg and J. Fajer, *J. Am. Chem. Soc.* 1970, **93**, 743.
20. D.-H. Chin, G. N. LaMar and A. L. Balch, *J. Am. Chem. Soc.* 1980, **102**, 4344.
21. L. Latos-Grazynski, R. J. Chang, G. N. LaMar and A. L. Balch, *J. Am. Chem. Soc.* 1982, **104**, 5992.
22. V. Ullrich, *Angew. Chem. Int. Ed.* 1971, **11**, 701.
23. G. A. Hamilton, *J. Am. Chem. Soc.* 1964, **86**, 3391.
24. J. T. Groves and T. E. Nemo, *J. Am. Chem. Soc.* 1983, **105**, 5786 and references cited therein.
25. D. Dolphin, A. Forman, D. C. Borg, J. Fajer and R. H. Felton, *Proc. Nat. Acad. Sci. U.S.A.* 1971, **68**, 614.
26. D. Dolphin and R. H. Felton, *Acc. Chem. Res.* 1974, **7**, 26.
27. R. K. Dinello, R. P. Farell, B. R. James and C. Welborn, *Int. J. Quantum Chemistry* 1979, **26**, 311.
28. D. Swern, *Organic Peroxides*, Vol. I, p. 484. Wiley-Interscience (1970).
29. M. A. Umbreit and K. B. Sharpless, *J. Am. Chem. Soc.* 1977, **99**, 5526.

Polyhedron Vol. 12, No. 20, pp. 2459–2463, 1993
Printed in Great Britain

0277–5387/93 $6.00+.00
© 1993 Pergamon Press Ltd

THE STRUCTURE AND MAGNETIC PROPERTIES OF μ_3-OXOTRIIRON(III) COMPLEX $[Fe_3O(OBZ)_6(CH_3OH)_3](NO_3)(CH_3OH)_2$ (HOBZ = BENZOIC ACID)

FU DEGANG, WANG GUOXIONG and TANG WENXIA*

Coordination Chemistry Institute, Nanjing University, Nanjing, 210008, P.R.C.

and

YU KAIBEI

Analysis Center, Chengdu Branch of Chinese Academy of Science, Chengdu, 610015, P.R.C.

(*Received* 10 *May* 1993; *accepted* 1 *July* 1993)

Abstract—A new μ_3-O triiron(III) complex $[Fe_3O(OBZ)_6(CH_3OH)_3](NO_3)(CH_3OH)_2$ (HOBZ = benzoic acid) has been synthesized, its structure has been determined and variable temperature magnetic susceptibility has been measured. In the cation of the complex, three iron atoms form an equilateral triangle with μ_3-O in the centre. An intramolecular antiferromagnetic exchange interaction occurs with $J = -27.06$ cm^{-1}, and a weaker intermolecular antiferromagnetic exchange interaction occurs with $zJ' = -2.59$ cm^{-1}.

Trinuclear basic carboxylate complexes $[M_3^{III}O(RCO_2)_6L_3]^+$ (M = Fe, Mn, Cr) have been used as the materials for synthesis of high nuclearity spin clusters, such as Fe_6, $Fe_{16}M$ (M = Co, Mn), Mn_4, Mn_{12},[1–4] and they also occupy a special place in magnetochemistry.[5] So the studies of their structures, bonding properties and magnetism are a current topic of research. To date the structures of $[Fe_3O(RCO_2)_6L_3]^+$ for R = CH_3, L = H_2O;[6] R = $C(CH_3)_3$, L = CH_3OH;[7] R = $CH_2(NH_2)$, L = H_2O;[8] and $[Fe_3O(MeCO_2)_3(EtCO_2)_3(H_2O)_3]^+$,[9] have been reported, but where R = phenyl have not been reported. In this paper, we report the structure and magnetic properties of the title compound for which R = Ph, L = CH_3OH.

EXPERIMENTAL

Preparation

Basic iron(III) benzoate (which was synthesized by literature procedures[10]) (0.5 g, *ca* 0.5 mmol) was mixed with equiv. nitrate (such as $Ni(NO_3)_2 \cdot 6H_2O$) in 40 cm^3 methanol and refluxed for 20 min, cooled to room temperature and filtered. The filtrate slowly evaporated in the air to give brown–red crystals. The crystals exposed in air lost solvent molecules. Found: C, 49.3; H, 3.6; N, 1.1; Fe, 14.6. Calc. for $C_{46}H_{46}NO_{20}Fe_3$: C, 50.6; H, 3.9; N, 1.3; Fe, 15.3.%.

X-ray crystallography

Cell dimensions were determined on an R3M/E four-circle diffractometer and reflection intensities measured in the ω–2θ scan mode with graphite monochromated Mo-K_α radiation ($\lambda = 0.71069$ Å). The data were not corrected for absorption. The atomic coordinates of the metal atoms were first obtained by analysing the Patterson function. The other non-hydrogen atom coordinates were gradually obtained by Fourier synthesis. After all the coordinates of the non-hydrogen atoms were refined, the hydrogen atom coordinates were obtained from difference Fourier synthesis and analysis of geometry. Finally, the coordinates, anisotropic thermal parameters for non-hydrogen atoms and

*Author to whom correspondence should be addressed.

Table 1. Crystal data for the title complex

Formula	$C_{47}H_{50}NO_{21}Fe_3$
Formula weight	1132.45
Space group	*P*21/N
a (Å)	14.747(3)
b (Å)	22.607(5)
c (Å)	15.893(3)
α (°)	90.00(0)
β (°)	95.44(2)
γ (°)	90.00(0)
V (Å^3)	5275(2)
Z	4
F(000)	2327.65
D_{calc} (g cm^{-3})	1.42
Crystal size (mm)	0.37 × 0.44 × 0.50
μ(Mo-K_α) (cm^{-1})	8.86
Data collection instrument	R3M/E
Radiation monochromated in incident beam (Mo-K_α Å)	0.71073
Scan type and rate	θ–2θ, 8°/min
Data collection range, 2θ(°)	$2° < 2\theta < 43°$
Number of unique data, total with $[I > 1.5\sigma(I)]$	6682 3844
Number of parameters refined	650
R^a	0.0725
$R_w{}^b$	0.0610
Largest shift/ESD	0.127

$^a R = [\Sigma|F_o - F_c|]/\Sigma F_o$.
$^b R_w = \Sigma[|F_o - F_c| \cdot w^{1/2}]/\Sigma[|F_o| \cdot w^{1/2}]$.
$w = 1/(\sigma^2(F) + |g| \cdot F^2)$.

the isotropic thermal parameters for hydrogen atoms were refined by block diagonal matric least-squares methods. Crystal data for the title complex are given in Table 1.

Mössbauer spectroscopy and magnetic susceptibility measurement

The Mössbauer spectrum of a polycrystalline sample was obtained on a S-600 type spectrometer at room temperature, the quadrupole splitting ΔE_Q and the isomer shift δ were measured relative to iron.

Solid state magnetism measurement of powdered sample was carried out with a CF-1 type extracting sample magnetometer at 50 KOe in the temperature range 1.8–300 K. The diamagnetism has been corrected.

RESULTS AND DISCUSSION

Structure description

The structure of title complex consists of one cation $[Fe_3O(OBZ)_6(CH_3OH)_3]^+$, one NO_3^- anion and two methanol molecules. The structure of the complex is shown in Fig. 1. Selected bond lengths and angles are given in Tables 2 and 3, respectively.

In the cation, the distances of Fe(1)—Fe(2).

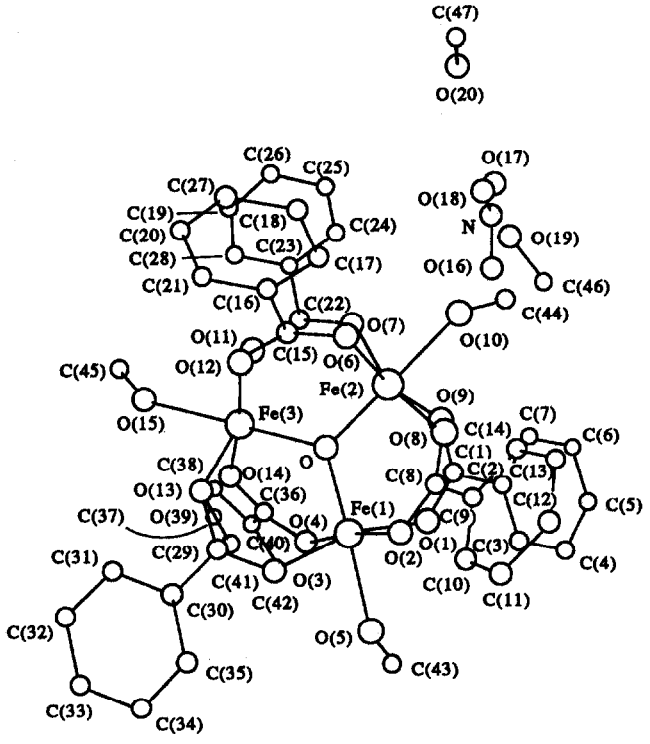

Fig. 1. Structure of the complex.

Table 2. Selected bond lengths (Å)

Fe(1)—O	1.895(5)	Fe(2)—O	1.890(5)
Fe(3)—O	1.907(5)	Fe(1)—O(1)	2.018(6)
Fe(1)—O(2)	2.015(5)	Fe(1)—O(3)	2.005(6)
Fe(1)—O(4)	1.994(6)	Fe(1)—O(5)	2.084(5)
Fe(2)—O(8)	2.000(5)	Fe(2)—O(10)	2.095(6)
Fe(3)—O(11)	2.001(6)	Fe(3)—O(15)	2.090(5)
O(2)—C(8)	1.279(9)	O(8)—C(8)	1.249(10)
C(8)—C(9)	1.500(12)	C(9)—C(10)	1.367(14)
C(9)—C(14)	1.351(14)	C(10)—C(11)	1.389(19)
C(11)—C(12)	1.358(21)	C(12)—C(13)	1.372(22)
C(13)—C(14)	1.408(18)	N—O(18)	1.233(12)
O(10)—C(44)	1.390(17)	O(19)—C(46)	1.369(16)

Table 4. Oxygen–oxygen distances in the complex (Å)

O(1)—O(5)	2.760	O(2)—O(6)	2.820
O(3)—O(5)	2.675	O(4)—O(5)	2.828
O(6)—O(10)	2.835	O(7)—O(10)	2.656
O(8)—O(10)	2.822	O(9)—O(10)	2.748
O(10)—O(16)	2.867	O(10)—O(18)	3.000
O(11)—O(15)	2.720	O(12)—O(15)	2.819
O(13)—O(15)	2.668	O(14)—O(15)	2.816
O(17)—O(19)	2.695	O(17)—O(20)	2.756

Fe(1)—Fe(3) and Fe(2)—Fe(3) are 3.274, 3.300 and 3.284 Å, respectively. Three iron atoms define an equilateral triangle with the μ_3-O atom in the centre; the μ_3-O atom is within the same plane (ΣFe—O—Fe′ = 359.9°), three methanol O atoms also are located on this plane. Two OBZ^- anions which bridge the same pair of iron atoms lie on each side of the 3Fe—μ_3-O plane, their angles with 3Fe—μ_3-O plane are not equal.

Each iron has an octahedral coordination. The values of $\angle\mu_3$-O—Fe—methanol O are close to 180°. The angles in the plane constructed from coordinated benzoate O atoms, such as $\angle$O(1)—Fe(1)—O(2), are close to 90°, but the values of $\angle\mu_3$-O—Fe—benzoate O are (in the range of 91.8–97.8) larger than 90°. The bond lengths of Fe—benzoate O(1.994–2.030 Å), Fe—μ_3-O(1.890–1.907 Å), Fe—methanol O(2.084–2.015 Å) are in the normal range.[11] The average bond length of Fe—μ_3-O is about 0.2 Å shorter than that of Fe—benzoate O, thus Fe atoms are positioned out from the plane constructed from coordinated benzoate O atoms and towards μ_3-O atom. The fact that three Fe atoms and μ_3-O atoms are coplanar and the distances of Fe—μ_3-O are shorter than Fe—benzoate O indicate that in $[Fe_3O(OBZ)_6(CH_3OH)_3]^+$, there is not only a σ bond, but also a delocalized π interaction around the three iron atoms and μ_3-O atom.

Table 4 shows the oxygen–oxygen distances in the complex. These distances vary from 2.656 Å to 3.000 Å, within the range of hydrogen bond lengths. There are no intermolecular hydrogen bonds.

Table 3. Selected bond angles (°)

O—Fe(1)—O(1)	97.2(2)	O—Fe(1)—O(2)	93.5(2)
O(1)—Fe(1)—O(2)	90.2(2)	O—Fe(1)—O(3)	96.6(2)
O(1)—Fe(1)—O(3)	166.2(2)	O(2)—Fe(1)—O(3)	88.1(2)
O—Fe(1)—O(4)	91.9(2)	O(1)—Fe(1)—O(4)	87.0(2)
O(2)—Fe(1)—O(4)	174.2(2)	O(3)—Fe(1)—O(4)	93.4(2)
O—Fe(1)—O(5)	178.2(2)	O(1)—Fe(1)—O(5)	84.5(2)
O(2)—Fe(1)—O(5)	87.0(2)	O(3)—Fe(1)—O(5)	81.7(2)
O(4)—Fe(1)—O(5)	87.7(2)	O—Fe(2)—O(10)	177.4(2)
O—Fe(3)—O(15)	178.7(2)	O(17)—N—O(18)	121.0(8)
Fe(1)—O—Fe(2)	119.7(3)	Fe(1)—O—Fe(3)	120.4(2)
Fe(2)—O—Fe(3)	119.8(2)	Fe(1)—O(1)—C(1)	131.7(5)
Fe(1)—O(2)—C(8)	128.6(5)	Fe(1)—O(5)—C(43)	129.0(6)
O(1)—C(1)—O(9)	126.9(8)	O(1)—C(1)—C(2)	115.6(7)
O(9)—C(1)—C(2)	117.5(8)	C(1)—C(2)—C(3)	121.3(9)
C(1)—C(2)—C(7)	119.6(9)	C(3)—C(2)—C(7)	119.1(10)
C(2)—C(3)—C(4)	121.6(11)	C(3)—C(4)—C(5)	117.5(13)
C(4)—C(5)—C(6)	123.3(15)	C(5)—C(6)—C(7)	119.4(15)
C(2)—C(7)—C(6)	119.2(11)	O(2)—C(8)—O(8)	123.6(7)
O(6)—C(15)—O(12)	123.7(7)	O(7)—C(22)—O(11)	126.0(8)
O(3)—C(29)—O(13)	122.2(7)	O(4)—C(36)—O(14)	123.4(7)

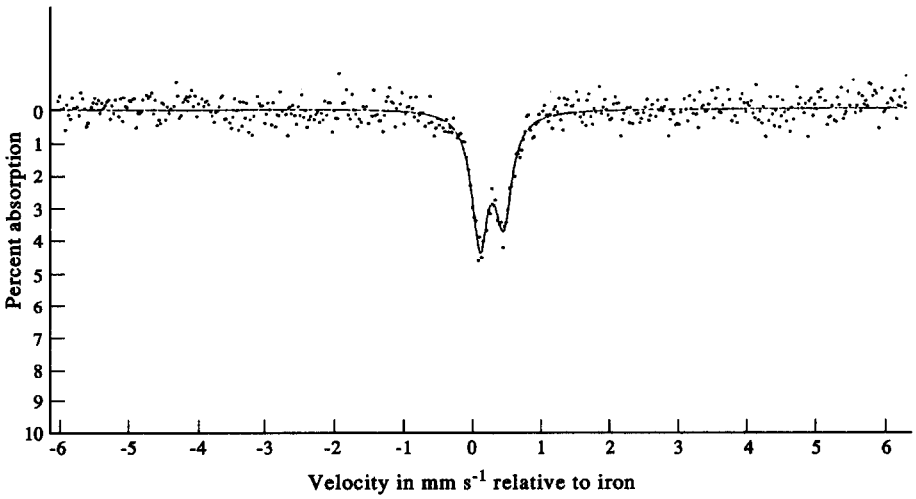

Fig. 2. Mössbauer spectrum of the complex.

Magnetic properties

The Mössbauer spectrum of title complex at room temperature is presented in Fig. 2. A least-squares fit (solid line) to the experiment points, assuming a Loentzian line shape, gives an isomer shift value $\delta = 0.31$ mm s^{-1}, within the range of 0.3–0.6 mm s^{-1} typically observed for high-spin iron(III) complexes.[12] The quadrupole splitting value $\Delta E_Q = 0.346$ mm s^{-1}, which is outside the range of 0.45–0.71 mm s^{-1} that are found for other basic iron carboxylates, shows the title complex is high symmetrical. The other feature of the spectrum which is the asymmetry in intensity that is also observed in other triiron complexes, may be explained by the Goldanskii Karayagin effect.[13,14]

The magnetic properties of $[M_3O(RCO_2)_6L_3]^+$ (R = H, CH_3) have been studied by many people,[14–16] though their structure can be described as consisting of a central oxygen atom surrounded by an equilateral triangle of metal atoms. However, their magnetic behaviour cannot be satisfactorily explained in terms of an intracluster isotropic exchange interaction, involving equivalent coupling constants. Other models such as the isosceles triangle and biquadratic model have been proposed. In the isosceles triangle model, isotropic exchange is also assumed, but one coupling constant is allowed to differ from the other two. This model provides good agreement with experimental data but is in conflict with the crystal structure of an equilateral triangle of metal atoms. The biquadratic exchange model only gives a good fit to the experimental data when it is allowed to be non-Hermitian, however the physical significance of biquadratic exchange is far from clear. The magnetic property of $[Fe_3O(OBZ)_6(H_2O)_3](OBZ)\cdot 6H_2O$ has also been studied, but their is no reasonable fitting of the data.[15] In this paper, we consider intracluster interaction with the isotropic exchange Hamiltonian which involves equivalent coupling constant J[17] [eq. (1)],

$$H = -2J(S_2S_2+S_2S_3+S_1S_3). \tag{1}$$

Then the paramagnetic susceptibility per mole χ_M can be expressed as eq. (2):

$$\chi_M = \frac{Ng^2\beta^2A}{4kTB}, \tag{2}$$

where $A = 1+20\exp(3x)+105\exp(8x)+210\exp(15x)+330\exp(24x)+429\exp(35x)+455\exp(48p)+340\exp(63x)$

$B = 1+4\exp(3x)+9\exp(8x)+10\exp(15x)+10\exp(24x)+9\exp(35x)+7\exp(48x)+4\exp(63x)$

$\chi = J/kT.$

In addition, we also consider intercluster interation with molecular field model[18] which involves intercluster coupling constant zJ' [eq. (3)],

$$\chi' = \frac{\chi_M}{1-(2zJ'/Ng^2\beta^2)\chi_M}. \tag{3}$$

The above mentioned model gives an excellent fit (see Fig. 3) with $g = 2.00$ (not varied in fitting), $J = -27.06$ cm^{-1}, $zJ' = -2.59$ cm^{-1} and $R = 5.9\times10^{-3}$ ($R = \Sigma(\chi_c-\chi_c)^2/\Sigma\chi_c^2$). This J value is consistent with the values obtained from other triiron complexes. These results indicate that the

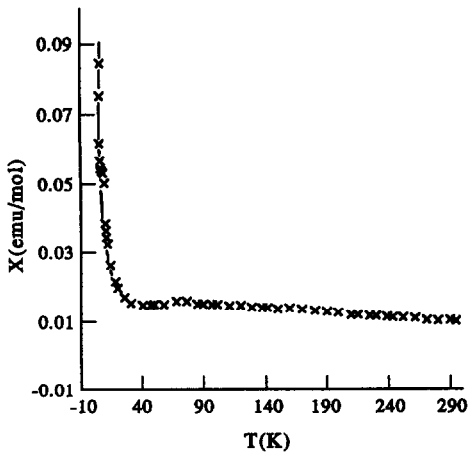

Fig. 3. The fitting of magnetic susceptibility.

J value for $[Fe_3O(RCO_2)_6]^+$ have no apparent relationship with the substituted R group, and also confirm that in these complexes the path of exchange interaction is through μ_3—O.

The intercluster interaction has been considered for complex $[FeO(CH_3CO_2)_6(H_2O)_3](ClO_4)\cdot 2H_2O$, and the resulting slightly positive value of zJ' has been explained by weak exchange occurring through the hydrogen bond network, but there is no structural evidence.[17] In this study, we found slightly negative value of zJ', but the crystal structural data shows no hydrogen bond linkage between clusters. This means that the pathway for intermolecular spin exchange interaction may be not through hydrogen bond network, the interaction between molecules may have another mechanism, such as phase transition in low temperature. However, intensive study on the magnetic properties of these complexes need more structural data, especially at low temperatures.

REFERENCES

1. W. Micklitz and S. J. Lippard, *Inorg. Chem.* 1988, **27**, 3069; W. Micklitz, S. G. Bott, J. G. Bentsen and S. J. Lippard, *J. Am. Chem. Soc.* 1989, **111**, 372.
2. W. Micklitz and S. J. Lippard, *J. Am. Chem. Soc.* 1989, **111**, 6856.
3. J. B. Vincent, C. Christmas, H. R. Chang, Q. Y. Li, P. D. W. Boyd, J. C. Huffman, D. N. Hendrickson and G. Christou, *J. Am. Chem. Soc.* 1989, **111**, 2086.
4. P. D. W. Boyd, Q. Li, J. B. Vincent, K. Floting, H. R. Chang, W. E. Streib, J. C. Huffman, G. Christou and D. N. Hendrickson, *J. Am. Chem. Soc.* 1988, **110**, 8537.
5. A. B. Blake, A. Yavari, W. E. Hatfield and C. N. Sethulekshmi, *J. Chem. Soc., Dalton Trans.* 1985, 2509.
6. K. Anzenhofer and J. J. Deboer, *Rec. Trav. Chim.* 1969, **88**, 286.
7. A. B. Blake and L. R. Frase, *J. Chem. Soc., Dalton Trans.* 1975, 193.
8. R. V. Thundathil, E. M. Holt, S. J. Holt and K. J. Watson, *J. Am. Chem. Soc.* 1977, **99**, 1818.
9. H. H. Zhang and X. F. Yu, *J. Struct. Chem.* (Chinese) 1990, **9**, 6.
10. R. F. Weinland and A. Herz, *Ber. Btsch. Chem. Ges.* 1912, **45**, 2662.
11. Q. H. Chen, J. B. Lynch, P. Gomez-Romero, A. Ben-Hussein, G. B. Jameson, C. J. O'Connor and L. Que Jr, *Inorg. Chem.* 1988, **27**, 2673; G. C. Papaefthymious, S. M. Gorun, R. B. Frankel and S. J. Lippard, *J. Am. Chem. Soc.* 1987, **109**, 3337.
12. S. M. Gorun, G. C. Papaefthymious, R. B. Frankel and S. J. Lippard, *J. Am. Chem. Soc.* 1987, **109**, 4244.
13. M. Takano, *J. Phys. Soc. Japan* 1972, **33**, 1314.
14. G. J. Long, W. T. Robinson, W. P. Tappmeyer and D. L. Bridges, *J. Chem. Soc., Dalton Trans.* 1973, 573.
15. A. Earnshaw, B. N. Figgis and J. Lewis, *J. Chem. Soc.* (*A*), (*Inorg. Phys. Theor.*) 1966, 1657.
16. C. T. Dziobkowski, J. T. Wrobleski and D. B. Brown, *Inorg. Chem.* 1981, **20**, 671.
17. K. Kambe, *J. Phys. Soc. Japan* 1950, **5**, 48.
18. B. E. Myers, L. Berger and S. A. Friedberg, *J. Appl. Phys.* 1969, **40**, 1149.

Polyhedron Vol. 12, No. 20, pp. 2465–2470, 1993
Printed in Great Britain

0277–5387/93 $6.00+.00
© 1993 Pergamon Press Ltd

IRON(III) COMPLEXES OF HEXADENTATE NSO-DONOR LIGANDS, 1,3-di(*o*-SALICYLALDIMINOPHENYLTHIO)PROPANE AND 1,2-di(*o*-SALICYLALDIMINOPHENYLTHIO)XYLENE

SHEFALI PAL and SAILENDRA NATH PODDAR*

Department of Inorganic Chemistry, Indian Association for the Cultivation of Science, Calcutta 700 032, India

and

GURUCHARAN MUKHERJEE

Department of Chemistry, Durgapur Government College, Durgapur 713 214, India

(*Received* 16 *June* 1993; *accepted* 28 *June* 1993)

Abstract—Iron(III) complexes of hexadentate Schiff base $N_2S_2O_2$ donor ligands, 1,3-di(*o*-salicylaldiminophenylthio)propane (H_2DSALPTP) and 1,2-di(*o*-salicylaldiminophenylthio)xylene (H_2DSALPTX) have been synthesized and characterized. The ligands gave dark green iron(III) complexes [Fe(DSALPTP)]$FeCl_4$ and [Fe(DSALPTX)]$FeCl_4$ when reacted with anhydrous $FeCl_3$. The Mössbauer data of these two complexes suggest the presence of two iron sites, one of which is octahedral and the other tetrahedral. The octahedral site is the complex cationic species and the tetrahedral site is the anion $FeCl_4^-$. On the other hand, $Fe(ClO_4)_3 \cdot 6H_2O$ reacted with the ligands to give the complexes [Fe(DSALPTP)]ClO_4 and [Fe(DSALPTX)]ClO_4. The iron(III) centre in the complex cationic species of the first two complexes are low-spin and for the latter two complexes high-spin. Though a colour change from yellow to green occurred when the ligands reacted with $Fe(NO_3)_3 \cdot 9H_2O$, no compound could be isolated in the solid state from the solution.

Hexadentate ligands, capable of octahedral coordination to a transition metal ion, may encapsulate it in a 1:1 complex whose exterior exhibits the properties of an organic material. Such species generated interest particularly in the production of the metal containing pharmaceuticals and the formation of selective metal ion extractants.[1]

The hexadentate ligand, 1,2-di(*o*-salicylaldiminophenylthio)ethane (abbreviated as H_2DSALPTE), a condensation product of 1,2-di(*o*-aminophenylthio)ethane and salicylaldehyde was first reported by Dwyer and his co-workers,[2] later by Cannon *et al.*[3] Rothin *et al.*[1] and by us.[4] Recently, complexes of iron(II) and iron(III) with certain hexadentate ligands have aroused much interest because of their anomalous magnetic behaviour. The equilibria between high and low spin states in the solid state and in solution have been investigated by variable temperature magnetic moment and Mössbauer spectroscopic measurements.[5–8] Though certain complexes of 1,3-di(*o*-aminophenylthio)propane were studied,[9] and nickel(II) complexes of 1,2-di(*o*-aminophenylthio)xylene prepared through the reaction of the *o*-aminothiophenolato complex with α,α′-dibromo-*o*-xylene,[10] no work was carried out with the Schiff base ligands derived from them through condensation with salicylaldehyde. As a part of our studies with N,S and N,S,O donor ligands and their metal complexes,[4,11–14] we have synthesized the hexadentate ligands (Fig. 1) 1,3-di(*o*-salicylaldiminophenylthio)propane (abbreviated as H_2DSALPTP) and 1,2-di(*o*-salicylaldiminophenylthio)xylene (abbreviated as H_2DSALPTX) and characterized their iron(III) complexes.

* Author to whom correspondence should be addressed.

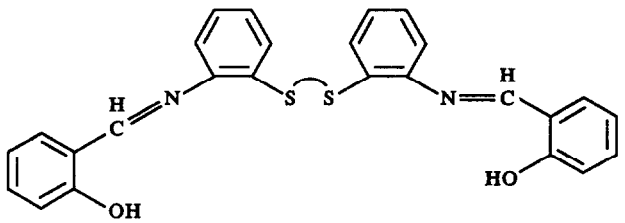

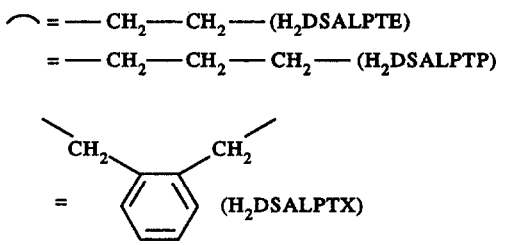

Fig. 1. Structure of the ligands.

EXPERIMENTAL

Synthetic procedures

1,3-*di*(o-*aminophenylthio*)*propane*. This ligand was prepared by a method published earlier.[3]

1,2-*di*(o-*aminophenylthio*)*xylene*. The same preparative procedure as above was adopted, except that α,α′-dibromo-*o*-xylene was used as the difunctional alkylating agent.

1,3-*di*(o-*salicylaldiminophenylthio*)*propane* (*H_2-DSALPTP*). The ligand was prepared by adding an alcoholic solution of 1,3-di(*o*-aminophenylthio)propane (one molecular proportion) to an alcoholic solution of salicylaldehyde (two molecular proportions) and refluxing the mixture for 1/2 h. On cooling the mixture after reflux, yellow crystals separated out. The product was filtered and recrystallized from $CHCl_3$-Pet.ether. (yield 90%, m.p. 70°C)).

1,2-*di*(o-*salicylaldiminophenylthio*)*xylene* (*H_2-DSALPTX*). The ligand was prepared following the same procedure as the previous one, except that 1,2-di(*o*-aminophenylthio)xylene was condensed with salicylaldehyde. Yellow crystals were obtained after recrystallization (yield 90%, m.p. 135°C).

[Fe(*DSALPTP*)][$FeCl_4$] (**1**). A solution of anhydrous $FeCl_3$ (0.162 g, 1 mmol) in dry methanol was added to a stirred solution of H_2DSALPTP (0.498 g, 1 mmol) in chloroform. After the addition, the stirring was further continued for 10 h. Green crystals separated out on adding petroleum ether to the reaction-mixture. The product was filtered and recrystallized from methanol (yield 65%).

[Fe(*DSALPTP*)]ClO_4 (**2**). This was obtained as green crystals by applying the same procedure as above, excepting that $Fe(ClO_4)_3 \cdot 6H_2O$ (0.46 g, 1 mmol) was taken as the starting metal salt (yield 60%).

[Fe(*DSALPTX*)][$FeCl_4$] (**3**). To an ethanolic suspension of H_2DSALPTX (0.56 g, 1 mmol), an ethanolic solution of anhydrous $FeCl_3$ (0.162 g, 1 mmol) was added with stirring. The mixture was further stirred for 8 h, when a green precipitate formed. This was filtered, washed with ether and recrystallized from methanol (yield 70%).

[Fe(*DSALPTX*)]ClO_4 (**4**). This complex was prepared by the similar method as the previous one with $Fe(ClO_4)_3 \cdot 6H_2O$ (0.46 g, 1 mmol) as the starting metal salt. It formed green crystals on recrystallization from methanol. (Yield 80%).

Physical measurements. The analyses of C, H and N of the compounds were carried out in a Perkin–Elmer Model 240C elemental analyser. Elemental analyses of iron were done by conventional method after decomposing the compounds with concentrated mineral acids. Infrared spectra (4000–200 cm^{-1}) in KBr discs were recorded with a Perkin–Elmer 783 spectrophotometer. Electronic spectra were recorded in a Hitachi 330 spectrophotometer. ^{1}H NMR spectra were recorded using a Varian XL-200 spectrometer with tetramethylsilane as the internal standard. The magnetic susceptibility measurements at room temperature were made in a PAR 155 vibrating-sample magnetometer. Mössbauer spectra were recorded in a 2 × 256 channel multiscalar confined to constant acceleration drive system. The source used was 10 mci ^{57}Co in Rh-matrix. A least squares fit programme[15] (LGFIT2) has been used to fit the experimental

data. The data were calculated relative to metallic iron. All the chemicals and solvents used were of A.R. or G.R. grade.

RESULTS AND DISCUSSION

The iron(III) salts react smoothly with the ligands to form the complexes [Fe(DSALPTP)][$FeCl_4$] (**1**), [Fe(DSALPTP)]ClO_4 (**2**), [Fe(DSALPTX)][$FeCl_4$] (**3**) and [Fe(DSALPTX)]ClO_4 (**4**). The ligands function as dibasic hexadentate ones, losing two protons from the two phenolic groups present in them. The anions of the starting salts have a marked influence on the composition of the complexes. Complexes are formed with anhydrous $FeCl_3$ or $Fe(ClO_4)_3 \cdot 6H_2O$, but no stable complex could be isolated with $Fe(NO_3)_3 \cdot 9H_2O$ as the starting metal salt, though there is a distinct colour change from yellow to green during the course of the reaction. Examples where $Fe(NO_3)_3$ does not give isolable products with hexadentate ligands have also been reported earlier.[1] The presence of comparatively larger sulphur atom in the ligand structure places limitations on their ability to fully coordinate to a single metal ion.[1,16] The complexes isolated in the present study are unstable in solution and slowly change colour from deep green to pale yellow after several hours. Elemental analyses for the complexes are given in Table 1.

The ^1H NMR spectrum of H_2DSALPTP shows a singlet at δ 8.6 ppm (2H) attributed to the phenolic protons. The signals for the aromatic and HC=N protons appear as a multiplet at δ 6.9–7.5 ppm (18H), —S—CH_2— protons as a triplet at δ 3.06 ppm (4H) and —CH_2— protons as a quintet at δ 2.05 ppm (2H). For H_2DSALPTX, the signal for the phenolic protons appear at δ 8.46 ppm (2H), aromatic and HC=N protons as a multiplet at δ 6.85–7.4 ppm (22H) and —S—CH_2 protons as a singlet at δ 4.22 ppm (4H).

The IR spectra of the free ligands contained bands at 1610–1600 cm^{-1} which may be assigned to the C=N stretching frequency. A broad band at 3500 cm^{-1} for H_2DSALPTP and 3440 cm^{-1} for H_2DSALPTX may be attributed to ν(OH).[17] The ν(C—O) (aromatic carbon and phenolic oxygen) is observed at 1350 and 1365 cm^{-1} for H_2DSALPTP and H_2DSALPTX, respectively. The ν(—S—CH_2) modes for the free ligands appear at 700–640 cm^{-1}. The ν(C=N) modes in the ligands are lowered by 5–15 cm^{-1} in the complexes which indicates the coordination of the azomethine nitrogen atom to the metal centre.[17] The ν(C—O) modes are shifted by 20–30 cm^{-1} in the higher region in the complexes suggesting thereby Fe—O linkage. Moreover, —S—CH_2— frequencies of the free ligands are lowered by 10–15 cm^{-1} upon complexation suggesting that the thioether moieties take part in coordination. Fe—S linkage in the complexes is substantiated by the appearance of bands below 400 cm^{-1} which are absent in the ligands (generally ν(M—S) appears[17–19] between 350–250 cm^{-1}).

Appearance of strong broad band centred at 1100 cm^{-1} (ν_3), a weak one at 950 cm^{-1} (ν_1) and a sharp one at 625 cm^{-1} (ν_4) for both complexes (**2**) and (**4**) indicate the presence of ionic perchlorates.[19–22] Intense band found at 390 cm^{-1} for both (**1**) and (**3**) is attributed to $\nu_3(FeCl_4)$.[17] However, a very slight shoulder is observed at 375 cm^{-1} for both of these bands, which may be due to steric factors reducing the symmetry from T_d.

Electronic spectral data for the complexes are set out in Table 2. For complexes (**3**) and (**4**), there is no significant difference between band energies, indicating that the electronic transitions of the cations dominate the spectra. A band at 16,949 cm^{-1} ($\varepsilon = 861$) is assigned to $^6A_{1g} \rightarrow {}^4T_{2g}(G)$ transition for octahedral, high-spin iron(III) centre present in complex (**4**). Complex (**3**), shows this band at 15,723 cm^{-1} ($\varepsilon = 2243$). Probably, the band due to cationic species is overlapped with the spin-forbidden transition expected[23] for $[FeCl_4]^-$ between 16,000 and

Table 1. Analytical data[a] of the complexes

Complex	C	H	N	M
[Fe(DSALPTP)][$FeCl_4$] (**1**)	46.6	3.3	3.7	15.2
	(46.4)	(3.2)	(3.7)	(14.9)
[Fe(DSALPTP)](ClO_4) (**2**)	53.8	3.6	4.4	8.8
	(53.4)	(3.7)	(4.3)	(8.6)
[Fe(DSALPTX)][$FeCl_4$] (**3**)	50.3	3.3	3.8	14.0
	(50.3)	(3.2)	(3.5)	(13.8)
[Fe(DSALPTX)]ClO_4 (**4**)	57.2	3.6	4.0	8.0
	(57.2)	(3.6)	(3.9)	(7.9)

[a] Found (Calcd.) %.

13,700 cm^{-1}. The cationic part of (**1**) and (**2**) are low-spin. Unfortunately, the electronic spectra of low-spin iron(III) complexes have not been adequately characterized.[24] This is often due to strong charge transfer bands dominating the visible portion of the electronic spectrum. Bands between 15,000 cm^{-1} and 22,000 cm^{-1} in the spectrum are likely due to $d \rightarrow \pi^*$ metal-to-ligand bands[25] as well as sulphur to iron(III) transitions.[26,27] The bands below 15,000 cm^{-1} which can be assigned to *d–d* transitions of the spin-paired cations could not be detected. However, the spin-forbidden transition for $[FeCl_4]^-$ (high-spin anion) may be overlapped within this region in complex (**1**). Bands are observed at 16,393 cm^{-1} ($\varepsilon = 1754$) for complex (**2**) and 18,181 cm^{-1} ($\varepsilon = 352$) and 22,321 cm^{-1} ($\varepsilon = 1950$) in complex (**1**). The higher energy band in complex (**1**) which is not observed in (**2**) may arise because of $^6A_1 \rightarrow {}^4E(D)$ transition.[23(a)]

The electrical conductivity measurements (Table 2) are in conformity with 1:1 electrolytes. The slight lower values observed for (**1**) and (**3**) may probably arise because of ion-association of $[FeCl_4]^-$ anions with solvent molecules.[27] The magnetic moment values at room temperature of the complexes are given in Table 2. It is seen that complex (**2**) is low-spin with a value of 2.03 B.M. Therefore complex (**1**) which has the same complex cation part must involve a low-spin cationic part and a high-spin anionic $[FeCl_4]^-$ part. Thus the magnetic moment observed (4.21 B.M. per iron atom) may be rationalized as an average contribution from low-spin iron(III) site and a high-spin iron(III) site. Direct support for the proposed formulation is provided by the Mössbauer spectrum (Fig. 2) which shows clearly the presence of two iron sites. Complex (**4**) on the other hand has a high-spin iron(III) centre with a magnetic moment of 5.63 B.M. Therefore complex (**3**) has both the cationic part and the anionic part in high-spin states. The measured magnetic moment is 4.82 B.M. per iron atom; the low-value possibly indicating some interaction involving the anionic species. The Mössbauer spectrum (Fig. 3) clearly indicates two iron centres.

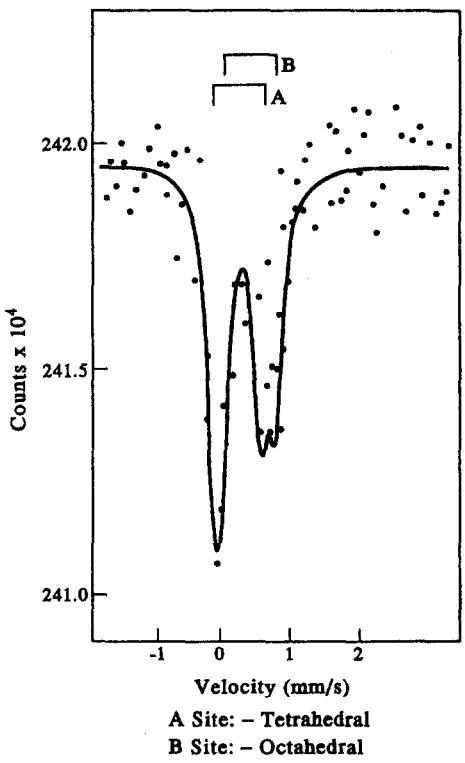

Fig. 2. Mössbauer spectrum of [Fe(DSALPTP)][$FeCl_4$] (**1**).

The Mössbauer spectrum of (**1**) shows a doublet with large bandwidths. Two doublets were fitted to the experimental data; a reasonably good fit is

Table 2. Electrical conductivity, magnetic moment and electronic spectral data

Complex	Λ_M (ohm^{-1} cm^2 mol^{-1})	Room temperature magnetic moment (B.M.)	λ_{max} (ε), cm^{-1}, ($lmol^{-1}$ cm^{-1})
[Fe(DSALPTP)][$FeCl_4$] (**1**)	46.7[a]	4.21 (per iron atom)	18,181(352), 22,321(1950)[b]
[Fe(DSALPTP)]ClO_4 (**2**)	80.6[a]	2.03	16,393(1754), 31,746(sh), 39,370(18,111)[c]
[Fe(DSALPTX)][$FeCl_4$] (**3**)	45.7[a]	4.82 (per iron atom)	15,723(2243), 27,777(20,059), 32,786(32,689), 43,478(54,814)[b]
[Fe(DSALPTX)]ClO_4 (**4**)	84.4[a]	5.63	16,949(861), 28,571(20,086), 32,258(25,824), 37,037(43,041), 43,478(78,909)[b]

[a] In $MeNO_2$.
[b] In CH_2Cl_2.
[c] In DMF.

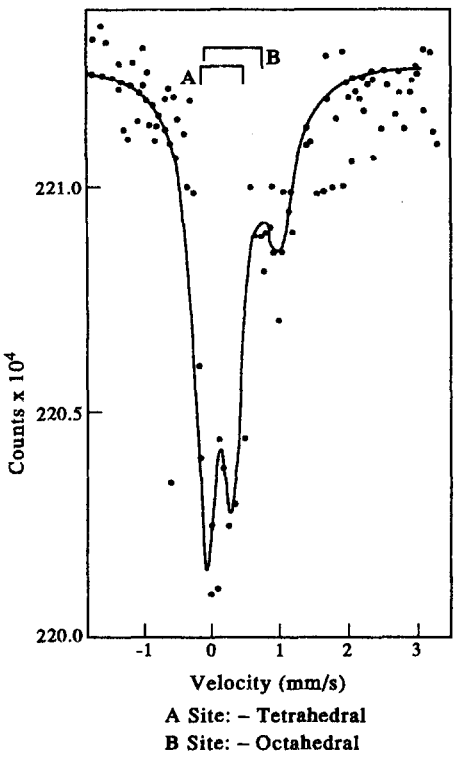

Fig. 3. Mössbauer spectrum of [Fe(DSALPTX)][$FeCl_4$] (**3**).

obtained. The doublet with isomer shift of 0.25 mm s^{-1} and quadrupole-splitting value of 0.67 mm s^{-1} is ascribed to iron(III) centre in tetrahedral environment. The two values are very well in agreement with data available for $[FeCl_4]^-$ ions.[28] The higher q.s. value indicates that $[FeCl_4]^-$ anion is slightly distorted from perfect tetrahedral symmetry, an observation in conformity with the IR spectra. The other doublet has I.S. value of 0.37 mm s^{-1} and q.s. value of 0.71 mm s^{-1} and indicate that this iron(III) centre has an octahedral environment.[28,29] Moreover, assuming same Lamb–Mössbauer factors for both sites, the population ratio of iron(III) centres has been calculated from the corresponding resonance areas and are found to be Fe^{III}_{tet} : Fe^{III}_{oct} = 1 : 1, in fair agreement with the formulation suggested. No spectrum was obtained for (**2**), the reason for which is not clearly understood. For complex (**3**) again, a "two doublet" fit gives good results. The doublet with I.S. value of 0.12 mm s^{-1} and q.s. value of 0.38 mm s^{-1} is in agreement with tetrahedral iron(III) centres and therefore ascribed to $[FeCl_4]^-$. The other doublet with I.S. value of 0.46 mm s^{-1} and q.s. value of 0.91 mm s^{-1} is due to the complex cationic part in octahedral geometry. The population ratio of Fe^{III}_{tet} : Fe^{III}_{oct} = 1 : 1.17. The spectrum of complex (**4**) shows a symmetrical doublet. I.S. value obtained is 0.49 mm s^{-1} and q.s. value 0.64 mm s^{-1}; these indicate iron(III) centre in octahedral geometry.[28] The bandwidth in this spectrum is found to be a bit larger (0.71 mm s^{-1}): but from analytical data, more than one iron(III) site is not possible. This broadening is most probably due to ultrafine nature[28] of (**4**).

Acknowledgement—The authors thank Dr Dipankar Das, Department of Solid State Physics, IACS, for recording the Mössbauer spectra.

REFERENCES

1. A. S. Rothin, H. K. Banbery, F. J. Berry, T. A. Hamor, C. J. Jones and J. A. McCleverty, *Polyhedron* 1989, **8**, 491.
2. F. P. Dwyer, N. S. Gill, E. C. Gyarfas and F. Lions, *J. Am. Chem. Soc.* 1954, **76**, 383.
3. R. D. Cannon, B. Chiswell and L. M. Venanzi, *J. Chem. Soc. A* 1967, 1277.
4. G. Mukherjee, S. N. Poddar and K. Dey, *Ind. J. Chem. Sect. A* 1986, **21**, 278.
5. M. H. Hosetton, L. J. Wilson and R. S. Drago, *J. Am. Chem. Soc.* 1975, **97**, 1722.
6. E. Sinn, G. Sim, E. V. Dose, M. F. Tweedle and L. J. Wilson, *J. Am. Chem. Soc.* 1978, **100**, 3375.
7. E. V. Dose, K. M. M. Murphy and L. J. Wilson, *Inorg. Chem.* 1976, **15**, 2622.
8. J. A. Broomhead and D. J. Robinson, *Aust. J. Chem.* 1968, **21**, 1365.
9. C. A. McAuliffe, F. P. McCullough and A. Werfalli, *Inorg. Chim. Acta* 1978, **29**, 57.
10. R. W. Hay, A. L. Galyer and G. A. Lawrance, *J. Chem. Soc., Dalton Trans.* 1976, 942.
11. G. Mukherjee, S. N. Poddar and K. Dey, *Trans. Met. Chem.* 1987, **12**, 323.
12. G. Mukherjee, S. N. Poddar, K. Choudhury and K. Dey, *Trans. Met. Chem.* 1988, **13**, 58.
13. S. Pal, G. Mukherjee and S. N. Poddar, *Trans. Met. Chem.*, in press.
14. G. Mukherjee, S. Pal, S. N. Poddar and K. Dey, *Proc. Ind. Acad. Sci. (Chemical Sciences)* 1993, **105**, 1.
15. E. Von Meerwall, *Comp. Phys. Commun.* 1975, **9**, 117.
16. H. J. Banbery, F. McQuillan, T. A. Hamor, C. J. Jones and J. A. McCleverty, *Polyhedron* 1989, **8**, 559.
17. K. Nakamoto, *Infrared and Raman Spectra of Inorganic and Coordination Compounds*. John Wiley, New York (1978).
18. M. T. H. Tarafder, M. A. Jalil Miah and R. N. Bose, *J. Inorg. Nucl. Chem.* 1981, **43**, 3151.
19. N. S. Bhave and R. B. Kharat, *J. Inorg. Nucl. Chem.* 1981, **43**, 414.
20. C. H. Perry, D. P. Athans, E. F. Young, J. R. Durig and B. R. Mitchell, *Spectrochim. Acta* 1967, **23A**, 1967.

21. K. Nakamoto, P. J. McCarthy, J. Fujita, R. A. Condrate and G. T. Behake, *Inorg. Chem.* 1965, **4**, 36.
22. J. S. Coe and J. R. Lyons, *Inorg. Chem.* 1970, **9**, 1775.
23. (a) A. P. Ginsberg and M. B. Robin, *Inorg. Chem.* 1963, **2**, 817; (b) B. J. Hathaway and D. G. Holah, *J. Chem. Soc.* 1964, 2408.
24. D. Nicholls, in *Comprehensive Inorganic Chemistry*, (Edited by J. C. Bailan, Jr, H. J. Emeleus, R. S. Nyholm and A. F. Trotman-Dickenson), Vol. 3, p. 1049. Pergamon Press, London.
25. (a) R. Raina and T. S. Srivastava, *Inorg. Chim. Acta* 1982, **67**, 83; (b) R. Raina and T. S. Srivastava, *Ind. J. Chem. Soc. A* 1983, **22**, 701; (c) R. Raina and T. S. Srivastava, *Inorg. Chim. Acta* 1984, **91**, 137.
26. H. Beraldo and L. Tosi, *Inorg. Chim. Acta* 1983, **75**, 249.
27. D. X. West, P. M. Ahrweiler, G. Ertem, J. P. Scovill, D. L. Klayman, J. L. Flippen-Anderson, R. Gilardi, C. George and L. K. Pannell, *Trans. Met. Chem.* 1985, **10**, 264.
28. N. N. Greenwood and T. C. Gibb, *Mössbauer Spectroscopy*, Ch. 6, Chapman and Hall, London (1971).
29. I. S. Gruverman and C. W. Siedel, *Mössbauer Effect Methodology*, Vol. 8, Plenum Press, New York (1973).

Polyhedron Vol. 12, No. 20, pp. 2471–2475, 1993
Printed in Great Britain

0277–5387/93 $6.00+.00
© 1993 Pergamon Press Ltd

SYNTHESIS AND COMPLEXATION CHEMISTRY OF THE NOVEL (1,3)-BIFUNCTIONAL ORGANOPHOSPHORUS(III) ESTERS $[(RO)_2PO]_4Si$ (R = Me, Et)

NIGEL GREENE and TERENCE P. KEE*

School of Chemistry, University of Leeds, Leeds LS2 9JT, U.K.

(*Received* 3 *June* 1993; *accepted* 28 *June* 1993)

Abstract—The new, silylated tetraphosphite compounds $[(RO)_2PO]_4Si$ (R = Me, Et) have been synthesised in high yield from the reactions between $SiCl_4$ and $(RO)_2P(=O)H$ in the presence of NEt_3. These compounds can bridge two metal centres in the form of a bis-bidentate, chelating ligand such as in the compounds $\{M\}\{[P(OMe)_2O]_2Si[O(OMe)_2P]_2\}\{M\}$ $\{M = [Mo(CO)_4]$ and $[PtCl_2]\}$.

We are currently investigating the coordination and organic chemistry of main-group and transition metal phosphito compounds of the general form $[(RO)_2PO]_nM$ where R is an organic residue and M is a main-group or transition metal atom. These types of molecule combine both electrophilic (M) and nucleophilic (P) centres connected via an electronically conducting single atom spacer and as such belong to the general class of 1,3-bifunctional compounds. Consequently, we have found that phosphito compounds are reactive towards both electrophilic and nucleophilic reagents and display chemistries which make them desirable both as ligands to transition metals[1] and as reagents for organic, and in particular asymmetric, synthesis.[2] This paper extends further the uses of main-group phosphito compounds as ligands through the synthesis of novel silylated tetraphosphite esters.

During the course of our investigations we have studied the reactions between secondary phosphites, $(RO)_2P(=O)H$, and mixed organochlorosilanes (eq. 1) which have facilitated access to a range of silylated polyphosphite esters.[1]

$$(R^1O)_2P(O)H + 1/nCl_nSiR^2_{4-n} \xrightarrow{NEt_3} 1/n[(R^1O)_2PO]_nSiR^2_{4-n} + NHEt_3Cl \quad (1)$$

R^1 = Me, Et; R^2 = Me, Ph, CH=CH_2

We have shown that the reaction in eq. (1) can be used to prepare (1,3)-bifunctional monophosphite esters [1a] ($n = 1$), diphosphite esters[1b,c] ($n = 2$) and triphosphite esters[1d] ($n = 3$) and here wish to report the extension of this methodology to the synthesis of (1,3)-bifunctional tetraphosphite esters ($n = 4$).

RESULTS AND DISCUSSION

Synthesis and characterisation of the tetraphosphites $[(RO)_2PO]_4Si$ (R = Me, Et)

The tetraphosphites $[(RO)_2PO]_4Si$ (R = Me **1**, Et **2**) are synthesised in high yields as colourless liquids according to the reaction in eq. (1) ($n = 4$). In practice, since the reactions are slower than those required for diphosphites ($n = 2$) and triphosphites ($n = 3$), we find that the use of five equivalents of the secondary phosphite leads to more reasonable reaction times (Scheme 1).

Mass spectrometry of **1** and **2** locates the molecular ions at m/z 464 and m/z 576, respectively. Infrared spectroscopy reveals no evidence for ν(P=O) vibrations {cf. 1265 cm^{-1} for $(MeO)_2P(=O)H$ and 1255 cm^{-1} for $(EtO)_2P(=O)H$} and NMR spectroscopic data are comparable to those found for other silylated phosphites.[1] Particularly characteristic is the high frequency value[3] of the ^{31}P NMR resonances for **1** and **2**; δ 124.8 and δ 123.4, respectively. Moreover, the observation of quintet resonances in the ^{29}Si NMR spectra of **1** and **2** at δ −108.3 ($^2J_{PSi}$ 6.7; *ca* 1.5 M solution in toluene at 298 K) and δ −109.0 ($^2J_{PSi}$ 5.5; *ca* 1.5 M solution in $CDCl_3$ at 298 K), respectively indicate that four phosphito residues are coordinated to silicon (Fig. 1). These chemical shifts are in the region expected

* Author to whom correspondence should be addressed.

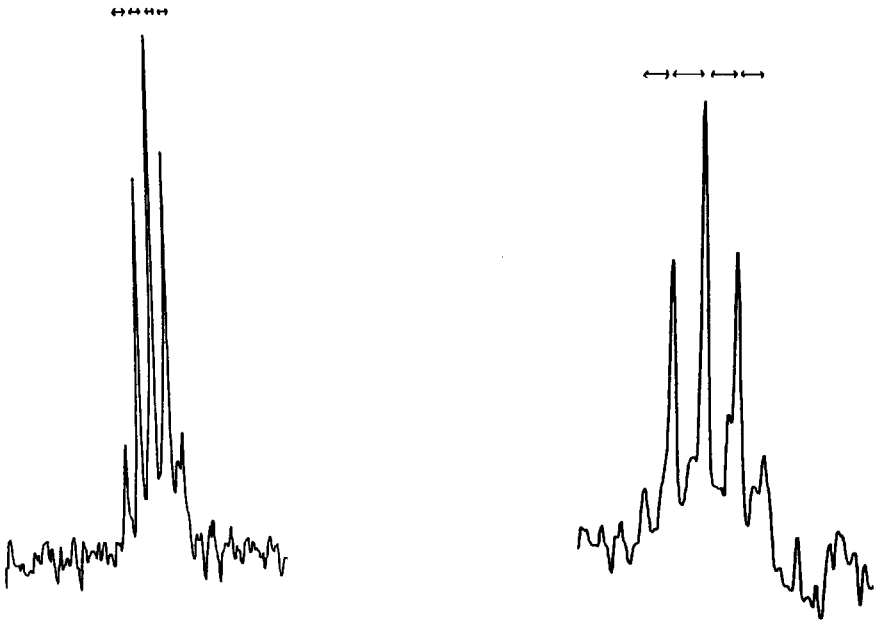

(a)
$[(MeO)_2PO]_4Si$, (1.5 M in toluene, 298 K)
δ–108.3 ppm, $^2J_{PSi}$ 6.7 Hz

(b)
$[(EtO)_2PO]_4Si$, (1.5 M in $CDCl_3$, 298 K)
δ–109.0 ppm, $^2J_{PSi}$ 5.5 Hz

Fig. 1. ^{29}Si NMR spectra (17.8 MHz) of **1** and **2** emphasising the quintet coupling patterns expected for systems containing four equivalent phosphito residues. The two spectra are not on the same scale.

for siloxanes containing four coordinated oxygen atoms.[4] Furthermore, the $^2J_{PSi}$ values of 6.7 and 5.5 Hz, respectively are also within the range normally observed (+1 to +27 Hz).[4]

In a similar manner to analogous diphosphites and triphosphites, the tetraphosphites **1** and **2** are sensitive to hydrolysis, decomposing to the constituent secondary phosphites upon exposure to moist air at room temperature.

The synthetic strategy outlined in eq. (1) has now been used to prepare silylated mono-, di-, tri- and tetra-phosphites readily and in high yields. With this in mind we have sought to extend the strategy to incorporate elements other than silicon in the backbone of the polyphosphite. We have investigated the reactions of PCl_3, $S(=O)Cl_2$, $S(=O)_2Cl_2$, and $SnCl_4$ with stoichiometric quantities of $(MeO)_2P(=O)H$ and NEt_3 at room temperature. In each case, reaction occurred readily as evidenced by the precipitation of $NHEt_3Cl$ however, in no case could a clean product be isolated. With PCl_3, a pentane soluble liquid was isolated which displayed several resonances in the δ 129–131 region expected for a phosphito compound but we were unable to isolate a pure material.

Reactions of $[(MeO)_2PO]_4Si$ *with transition metals*

The tetraphosphites **1** and **2** have the potential to complex to two transition metal atoms in two different ways, illustrated in Fig. 2 (this does not include the several ways in which such tetradentate ligands can bridge more than two metals) and exemplified by the coordination chemistry of the tetraphosphines $[Ph_2PCH_2]_4C$[5] and $[Ph_2PCH_2]_2CH_2CH_2[CH_2PPh_2]_2$.[6] We were particularly interested to promote bis-bidentate bridging be-

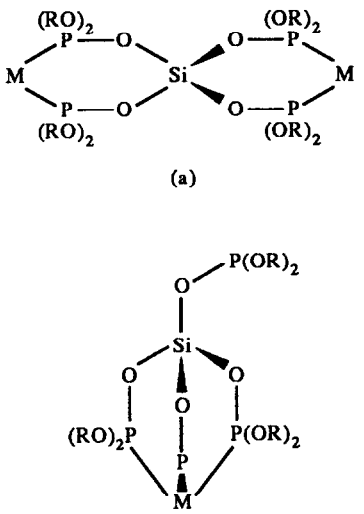

(a)

(b)

Fig. 2. Possible coordination modes of silylated tetraphosphites to two metal centres.

tween two metal centres (Fig. 2a) and in an effort to do so have examined the reactivity between **1** and $Mo(CO)_4$(NBD) and PtX_2(COD) (X = Cl, Me).

A 2 : 1 mixture of $Mo(CO)_4$(NBD) and **1** react at room temperature to afford product mixtures which are dependent upon the order and rate of addition of the reactants. When $Mo(CO)_4$(NBD) is added to **1**, a mixture of compounds is obtained from which it has not been possible to isolate a pure compound. However, when the order of addition of reagents is reversed, a white solid can be isolated in low yield (**3**) which, by ^{31}P NMR analysis, appears to consist of a single phosphorus-containing compound. Specifically, a single resonance at δ 153.7 is consistent with the presence of metal-bound phosphito groups.[1] Infrared spectroscopy reveals ν(CO) stretching vibrations characteristic of a tetracarbonyl system leading to the conclusion that **3** is the dimeric bridged complex, $\{Mo(CO)_4\}_2\{\mu$-$[P(OMe)_2O]_4Si\}$ (Scheme 1). This is further supported by elemental analysis, mass spectrometry and ^{13}C NMR spectroscopy which reveals two carbonyl carbon resonances, an AXX′ multiplet at δ 211.52 due to the carbonyl groups *trans* to phosphorus and a triplet at δ 206.72 ppm due to the carbonyls *cis* to phosphorus, respectively. This pattern is characteristic of the [*cis*-$Mo(CO)_4L_2$] moiety. Interestingly, the ^{13}C resonance for the carbonyls *trans* to the phosphorus atoms is very slightly lower in frequency than those of related diphosphite complexes[1c] of the form $[Mo(CO)_4\{P(OMe)_2O\}_2SiR^1R^2]$ where R^1, R^2 are variously Me, Ph, CH=CH_2 (Table 1) suggesting that the ligands $[P(OMe)_2O]_2Si[OP(OMe)_2]_2$ are slightly less electron-donating towards molybdenum than $[P(OMe)_2O]_2SiR^1R^2$. This result is consistent with the more electronegative coordination environment around silicon in the tetraphosphites.[7]

Table 1. Comparitive $\delta(CO)_{trans}$ values for selected $Mo(CO)_4$(L—L) species

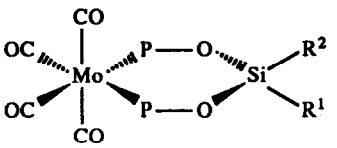

R^1, R^2 = variously, Me, Ph, CH=CH_2, $OP(OMe)_2$
(Methoxo groups on phosphorus omitted for clarity)

Ligand	δ(CO)*trans*
$[P(OMe)_2O]_2SiMe_2$	212.91
$[P(OMe)_2O]_2SiMePh$	212.82
$[P(OMe)_2O]_2SiMeVn$	212.82
$[P(OMe)_2O]_2SiPh_2$	212.68
1	211.52

[a] Vn is CH=CH_2.
[b] ppm in C_6D_6.

Reaction between **1** and $Mo(CO)_4$(NBD) in a 1 : 1 stoichiometric ratio again afforded a mixture of products, but the presence of ^{31}P NMR res-

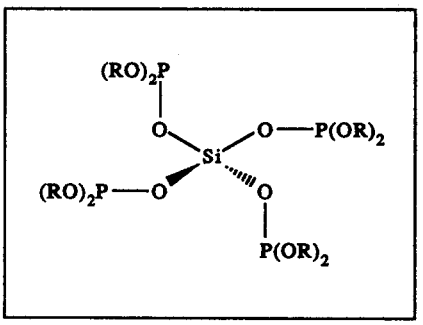

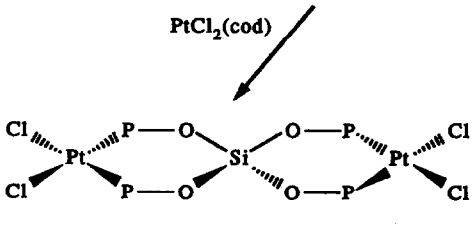

4; substituents on phosphorus omitted for clarity

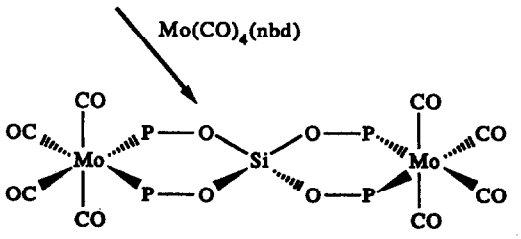

3; substituents on phosphorus omitted for clarity

Scheme 1. Some reactions of $[(RO)_2P]_4Si$.

onances in the regions δ 154–152 and δ 126–124 suggest that not all phosphorus atoms are metal-bound, the latter resonances being indicative of uncoordinated phosphito residues.[1]

$PtCl_2$(COD) reacted smoothly with **1** at room temperature to afford a white, microcrystalline product which was insufficiently soluble in common non-coordinating organic solvents for NMR analysis and apparently decomposed in pyridine. Nevertheless, elemental analysis supports the formulation $\{PtCl_2\}_2\{[P(OMe)_2O]_4Si\}$ **4** in which the tetraphosphite ligand presumably coordinates to both metal atoms as a bis-bidentate bridging ligand (Scheme 1). In an attempt to increase both solubility and crystallinity we subsequently examined the reaction of **1** with $PtMe_2$(COD), but although this did produce products containing platinum-coordinated phosphorus atoms, no pure product was isolated.

We believe that although ligation proceeds readily for the tetraphosphite ester **1**, the degree of flexibility in the backbone permits the compound to coordinate to metal centres in a variety of modes, such as bridging more than two metal centres, thus leading to mixtures of oligomeric products of low solubility which prove difficult to characterise. Consequently, we are currently shifting our attention to more robust, geometrically constrained phosphorus(III) esters which have more electron-releasing properties and these systems will form the basis of future reports.

EXPERIMENTAL

All syntheses were performed under dry dinitrogen using Schlenk and cannula techniques or in an inert-atmosphere filled dry-box. Solvents were dried over either sodium wire, calcium chloride or 4 Å molecular sieves before reflux and subsequent distillation, under dinitrogen, from a suitable drying agent (given in parentheses); pentane (sodium benzophenone ketyl), toluene (sodium metal), dichloromethane (calcium hydride). Deuterated solvents were dried by passage down a column of basic alumina (Brockmann Grade I). All solvents were deoxygenated before use. Elemental analyses and molecular weight measurements were performed by the Microanalytical Laboratory of this department, the latter on a Hitachi Perkin–Elmer 215 Apparatus. IR spectra were recorded between KBr windows on a Perkin–Elmer 257 grating spectrophotometer. NMR spectra were obtained on JEOL FX90Q, JEOL FX100 and Bruker AM 400 instruments; the ^{31}P and ^{13}C spectra being recorded under conditions of broad-band decoupling. Spectra are referenced to TMS or residual $CHCl_3$, C_6D_5H solvent resonances (^1H, ^{13}C, ^{29}Si) or 85% $H_3PO_{4(aq)}$ as 0 ppm. Mass spectra were recorded either in the electron impact (E.I.) or F.A.B. modes on a VG Autospec instrument. The compounds $SiCl_4$, $SOCl_2$, SO_2Cl_2 and $SnCl_4$, were purchased from commercial sources and were used as received. $(RO)_2P(=O)H$ (R = Me, Et) and NEt_3 were purified by passage down a short column of basic alumina (Brockmann Grade I). $Mo(CO)_4$(NBD)[8] and $PtCl_2$(COD)[9] were prepared using published procedures. NBD = norborna-2,5-diene, COD = cycloocta-1,5-diene.

Synthesis of $[(RO)_2PO]_4Si$ (R = Me **1**, Et **2**)

$SiCl_4$ (0.45 g, 2.62 mmol) was added dropwise at room temperature to a stirred mixture of $(RO)_2P(=O)H$ (1.44 g, 13.09 mmol R = Me; 1.81 g, 13.09 mmol R = Et) and NEt_3 (2.2 cm^3, 15.71 mmol) in pentane solvent (40 cm^3). The initially clear solutions became cloudy within seconds of adding the silicon reagent due to the precipitation of $NHEt_3Cl$. After stirring for 72 h, the mixture was filtered, the residue washed with pentane (10 cm^3) and all the volatiles removed under reduced pressure to leave a colourless liquid in which was suspended a small amount of $NHEt_3Cl$. Subsequent extraction into pentane (15 cm^3), re-filtration and removal of the volatiles *in vacuo* afforded the products as clear, mobile liquids. Yields, **1** 1.1 g, (88%); **2** 1.2 g (77%). For **1**: ^1H ($CDCl_3$) 3.46 (m, 24H, J_{PH} 9, CH_3O). ^{13}C ($CDCl_3$) 48.3 (m, J_{PC}, 9 CH_3O). ^{31}P ($CDCl_3$) 124.8 (s). ^{29}Si (toluene) −108.3 (quin, $^2J_{PSi}$ 6.7) i.r. (thin film, cm^{-1}) 979 {s, br, ν(POSi)}. *m/z*; 464 $(M)^+$, 434 $(M-2CH_3)^+$, 356 $[M-OP(OMe)_2]^+$, 246 $[M-2OP(OMe)_2]^+$.

For **2**: ^1H ($CDCl_3$) 3.86 (m, 16H, $^3J_{HH}$ 7, CH_3CH_2O), 1.17 (t, 24H, $^3J_{HH}$ 7, CH_3CH_2O). ^{13}C ($CDCl_3$) 57.2 (m, J_{PC} 6, CH_3CH_2O), 16.6 (s, CH_3CH_2O): ^{31}P ($CDCl_3$) 123.4 (s). ^{29}Si ($CDCl_3$) −109.0 (quin, $^2J_{PSi}$ 5.5) i.r. (thin film, cm^{-1}) 935 {s, br, ν(POSi)}. *m/z*; 576 $(M)^+$, 440 $[M-OP(OEt)_2]^+$.

Reaction of $[(MeO)_2PO]_4Si$ *with* $Mo(CO)_4$(NBD)

A solution of $[(MeO)_2PO]_4Si$ (0.49 g, 1.07 mmol) in pentane (30 cm^3) was added dropwise to a suspension of $Mo(CO)_4$(NBD) (0.64 g, 2.12 mmol) in pentane (30 cm^3) cooled to −78°C. After the addition was complete (*ca* 1 h) the mixture was allowed to warm to room temperature and stirred thus for a further 3 h. During this period a white, free-flowing suspension formed in the reaction vessel along with a small quantity of brown material lining the flask. The mixture was allowed to settle

and the pentane solution decanted off carefully. The residue was washed with a further portion of pentane (10 cm^3) and all extracts combined. Concentration of the pentane solution to *ca* one third volume resulted in precipitation of $\{Mo(CO)_4\}\{\mu\text{-}[P(OMe)_2O]_4Si\}$ **3** as a white crystalline compound in low (< 10%) yield. (Found: C, 22.0; H, 2.7; $C_{16}H_{24}O_{20}MoP_4Si$ requires: C, 21.8; H, 2.8%. ^1H (C_6D_6) 3.29 (m, 24H, J_{PH} 12, CH_3O—); ^{13}C (C_6D_6) 211.52 (m, J_{PC} 24.7, CO_{trans}), 206.72 (t, $^2J_{PC}$ 13.7, CO_{cis}), 49.97 (s, CH_3O—); ^{31}P (C_6D_6) 153.7 (s). i.r. (CH_2Cl_2 solution, cm^{-1}) 2035 {s, ν(CO)}, 1962 {s sh, ν(CO)}, 1942 {s br, ν(CO)}. *m/z*; 879 $[M]^+$.

The same procedure as described above was used with a 1:1 stoichiometric mixture of $Mo(CO)_4$ (NBD) and $[(MeO)_2PO]_4Si$ except that the addition of reagents was reversed; where upon an oily mixture was obtained and analysed by ^{31}P NMR spectroscopy (see text).

Reaction of $[(MeO)_2PO]_4Si$ *with* $PtCl_2(COD)$

A solution of $[(MeO)_2PO]_4Si$ (0.22 cm^3, 0.92 M, 0.20 mmol) in THF was added at room temperature to a solution of $PtCl_2(COD)$ (0.15 g, 0.40 mmol) in THF (15 cm^3). The mixture quickly became cloudy due to a precipitate. After 16 h at ambient temperature, the mixture was allowed to settle and the fine-grained white precipitate, compound **4**, isolated by filtration, washed with pentane (2×5 cm^3) and dried *in vacuo*. (Found: C, 10.0; H, 2.8; Cl, 15.3. Calc. for $C_8H_{24}Cl_4O_{12}P_4Pt_2Si$: C, 9.6; H, 2.4; Cl, 14.2%.

Acknowledgements—We thank the S.E.R.C. and B. P. Chemicals Ltd. for financial support.

REFERENCES

1. (a) K. M. Cooke, T. P. Kee, A. L. Langton and M. Thornton-Pett, *J. Organomet. Chem.* 1991, **419**, 171; (b) T. P. Kee and M. T. Patel, *Polyhedron* 1992, **11**, 135; (c) V. Sum, M. T. Patel, T. P. Kee and M. Thornton-Pett, *Polyhedron* 1992, **11**, 1743; (d) V. Sum, T. P. Kee and M. Thornton-Pett, *J. Organomet. Chem.* 1992, **438**, 89; (e) N. Greene, H. Taylor, T. P. Kee and M. Thornton-Pett, *J. Chem. Soc., Dalton Trans.* 1993, 821.
2. (a) V. Sum, A. J. Davies and T. P. Kee, *J. Chem. Soc., Chem. Commun.* 1992, 1771; (b) I. F. Pickersgill, P. G. Devitt and T. P. Kee, *Synth. Commun.* 1993, **23**, 1643; (c) N. Greene and T. P. Kee, *ibid*, 1993, **23**, 1651; (d) V. Sum and T. P. Kee, *J. Chem. Soc., Perkin Trans. I* 1993, 1369.
3. D. G. Gorenstein (Ed.), *Phosphorus-31 NMR: Principles and Applications*, Ch. 18. Academic Press, New York (1984).
4. R. K. Harris, J. D. Kennedy and W. McFarlane, in *NMR and The Periodic Table*, Ch. 10. R. K. Harris and B. E. Mann (Eds.), Academic Press, London (1978).
5. H. G. Schmidbaur, A. Stutzer and P. Bissinger, *Z. Naturforsch.* 1992, **47b**, 640.
6. M. R. Mason, C. M. Duff, L. L. Miller, R. A. Jacobson and J. G. Verkade, *Inorg. Chem.* 1992, **31**, 2746.
7. G. M. Bodner and L. J. Todd, *Inorg. Chem.* 1974, **13**, 1335.
8. M. A. Bennett, L. Pratt and G. Wilkinson, *J. Chem. Soc.* 1961, 2037.
9. D. Drew and J. R. Doyle, *Inorg. Synth.* 1972, **13**, 47.

Polyhedron Vol. 12, No. 20, pp. 2477–2487, 1993
Printed in Great Britain

0277–5387/93 $6.00 + .00
© 1993 Pergamon Press Ltd

GAS PHASE REACTIONS OF THE NEGATIVE AND POSITIVE IONS OF GOLD AND PLATINUM WITH AROMATIC HYDROCARBONS, THIOLS AND H_2S

JOHN H. EL-NAKAT, IAN G. DANCE,* KEITH J. FISHER* and GARY D. WILLETT

School of Chemistry, University of New South Wales,
PO Box 1, Kensington, NSW 2033, Australia

(*Received* 2 *June* 1993; *accepted* 14 *June* 1993)

Abstract—The negative and positive ions of gold and platinum, Au^-, Pt^-, Au^+ and Pt^+, generated by the direct laser ablation of the metals, were reacted with benzene, alkyl substituted benzenes, benzenethiol, H_2S, n-propanethiol and the four butanethiols in a Fourier Transform Ion Cyclotron Resonance Mass Spectrometer (FT–ICR–MS). Reactions were carried out with ions collisionally cooled, to reduce their kinetic energy and deactivate electronic excited states, and with "hot" ions directly after production by the laser. The negative ions of both metals react at a slower rate than the positive ions and their spectra show fewer products. No products were observed for the reaction of metal negative ions with the aromatic hydrocarbons except for the reaction of Pt^- ions with mesitylene to give the $(CH_3)_2C_6H_3CH_2^-$ anion as the major product. The reactions of Au^- ions with most of the aryl and the alkyl thiols produced the SR^- anion as the major product. The reactions of both Au^+ and Pt^+ ions with benzene and the substituted benzenes gave the charge transfer ions L^+ (e.g. $C_6H_6^+$) as the major products. Collisionally cooled Pt^+ ions gave minor product ions identified as Pt-benzyne species ($PtC_6H_4^+$), while "hot" Pt^+ ions gave the Pt-benzyne species as the major ions. Benzenethiol reacted with both Au^+ and Pt^+ to yield the charge transfer ion $C_6H_5SH^+$ as the major product, while the reactions of Au^+ and Pt^+ ions with H_2S both gave addition complexes MH_2S^+ and $M(H_2S)_2^+$, similar to the reactions of Ag^+ and Cu^+. The reactions of n-propanethiol and the four butanethiols with Au^+ and Pt^+ ions generally gave the protonated thiol as the major ion with significant quantities of other ions including addition complexes. These results are different from the previously reported reactions of Cu^+ and Ag^+ ions which gave the addition ions as the major products.

The production of metal ions by laser ablation of a pure metal generally yields[1] the mono cation M^+, which may not be the common positive ion observed in condensed phase chemistry: an example is Pt^+. Further, the ions produced often are in electronically excited states. A few metals also produce negative ions M^- which are in very unusual oxidation states. Gold and platinum form both negative and positive mono-ions, $M^+(g)$ and $M^-(g)$. The Au^+ ion may be considered to be in a normal oxidation state, but the other three ions are in unusual oxidation states.

Our studies of the reactions of metal ions with thiols have included the reactions of $Cu^+(g)$ and $Ag^+(g)$, reported earlier.[2] Now we report the reactions of Au^+ for comparison with those of Cu^+ and Ag^+, and extend to the monoanion of Au. We have also studied the reactions of the positive and negative ions of Pt, for comparison with Au.

An extensive study of the reactions of gold cations with aromatic and aliphatic hydrocarbons was carried out by Chowdhury and Wilkins[3] using Fourier Transform mass spectrometry. They found hydride abstraction to be the major reaction of alkanes higher than ethane. The reaction with arenes gave the charge transfer products ArH^+,

* Authors to whom correspondence should be addressed.

some hydride abstraction products Ar^+ and some addition ($AuArH^+$) products. With alkyl halides the methide ion ($AuCH_2^+$) was a major product. Weil and Wilkins[4] studied the reactions of Au^+ with alcohols, and showed that hydride abstraction was the major reaction pathway, and that loss of water to form the gold-alkene ion was the main secondary pathway. Both studies produced ions by laser ablation, used collisional cooling to reduce the translational energy of the ions and allow excited states of the metal ion to decay to the ground state or be removed by rapid reaction.

In two papers Grady and Bursey[5,6] used a spark source to produce high energy Au^+, and reacted the ions with various hydrocarbons and carbonyl compounds, concluding that there was evidence of the intervention of excited states of the ion in the chemical reactions observed. The simple catonized ion AuL^+ was not observed, and also more fragmentation of the organic species occurred if the metal had low lying excited states. Recently greater attention has been given to how the reactivity of an ion might change if ions in excited states are produced during ionization.[7] Various studies have been undertaken to determine the amounts of excited state ions present after ionization.[7-9] Excited state ions are potentially more important for Au^+ than for Cu^+ and Ag^+, as the first excited state for Au^+ is 1.9 eV above the ground state whereas the energy gap values for Cu^+ and Ag^+ are 2.8 eV ($3d^94s^1$) and 4.9 eV ($4d^95s^1$), respectively.[10]

Only one previous study of the reactions of Pt^+ has been reported, this was with methane,[11] as part of a study of the reactions of third row transition metal ions. Pt^+ has a ground state of ^2D ($5d^9$) but several excited states less than 2 eV above the ground state [^4F 0.59 eV, ^2D ($J = 3/2$) 1.04 eV, ^4F 1.16 eV, ^4P 1.65 eV]. Our principal interest is in the reactions of thiols with these metal ions. Because a thiol can react with gaseous metal ions at either the SH function or the hydrocarbon function, we have included studies of reactions with H_2S and with hydrocarbons for reference purposes in this paper.

EXPERIMENTAL

Mass spectra were obtained using a Spectrospin CMS-47 (FT-ICR) mass spectrometer, equipped with a 4.7T superconducting magnet.[12] The metal was secured to a satellite probe tip and introduced into the ICR cell using a direct insertion probe. A cylindrical ICR cell (radius 30 mm × 60 mm) with six titanium single section plates was used in an ultra high vacuum chamber maintained at a base pressure of 10^{-9} mbar by a turbomolecular pump.

Laser-ablation was performed using a Nd-YAG laser (1064 nm, Spectra Physics DCR-11) focused to an area of 0.1 mm^2 on the metal at the end of the cell, flush and in contact with the ICR trapping plate. The laser was used in the Q-switched mode producing a pulse for 8 ns and a maximum energy at the sample of ~ 1600 MW cm^{-2}. The pulse energy at the sample was modified using neutral density filters; energies of 340 and 150 MW cm^{-2} were most commonly used.[13]

Ions were isolated using an ejection pulse, and a minimum delay of 100 ms was used to allow collisional cooling before the reaction was observed. Positive or negative ions were trapped in the cell by potentials of +4 V or −4 V, respectively. A typical pulse program and the treatment of data have previously been reported.[2] The reactants were degassed by repeated freeze–thawing and introduced through a heated inlet system. The reactants were admitted to give a background pressure of 6.5×10^{-8} mbar (uncorrected) and ablation was performed in the presence of the reactant.

RESULTS

In the following, the symbols Au^+ and Pt^+ are used for the positive ions which were selected and collisionally cooled in the presence of the reactant for 100 ms before the reactions were monitored. Some experiments were carried out without collisional cooling, and the metal ions reacted directly after laser production and are denoted $*Au^+$ and $*Pt^+$.

The principal reaction types observed in this study are listed below. The symbol L is used for the reactant where the reaction does not involve fragmentation. For other reactions we use the symbol HXYH such that for the hydrocarbons XY is the doubly deprotonated species (e.g. $C_6H_6 = HC_6H_4H$), and for the thiols X = S and YH = R where R is the alkyl or aryl substituent.

Mono-complex formation;

$$M^+ + L \rightarrow ML^+ \text{ or } M^- + L \rightarrow ML^-, \quad (1)$$

Bis-complex formation;

$$ML^+ + L \rightarrow ML_2^+ \text{ or } ML^- + L \rightarrow ML_2^-, \quad (2)$$

Charge transfer;

$$M^+ + L \rightarrow M + L^+, \quad (3)$$

Hydride abstraction;

$$M^+ + HXYH \rightarrow HXY^+ + MH \text{ or}$$
$$M^- + HXYH \rightarrow HXY^- + MH, \quad (4)$$

Elimination of H_2;

$$M^+ + HXYH \rightarrow MXY^+ + H_2, \quad (5)$$

Table 1. Charged products of reactions of the negative ions Au^- and Pt^-

Reactant	Au^- major	Au^- minor	Pt^- major	Pt^- minor
C_6H_6	—	—	—	—
C_7H_8 (toluene)	—	—	—	—
C_8H_{10} (p-xylene)	—	—	—	—
C_9H_{12} (mesitylene)	—	—	$C_9H_{11}^-$	$PtC_9H_{12}^-$
C_6H_5SH	$C_6H_5S^-$	—	$C_6H_5S^-$	—
H_2S	—	—	PtH_2S^-	$Pt(H_2S)_2^-$, HS^-
n-C_3H_7SH	—	—	$C_3H_7S^-$	—
n-C_4H_9SH	$C_4H_9S^-$	S_3^-	$C_4H_9S^-$	PtS^-, $PtS(SC_4H_9)^-$
i-C_4H_9SH	$C_4H_9S^-$	S_3^-	$C_4H_9S^-$	PtS^-, $PtS(SC_4H_9)^-$
s-C_4H_9SH	$C_4H_9S^-$	S_3^-	$C_4H_9S^-$	PtS^-, $PtS(SC_4H_9)^-$
t-C_4H_9SH	S_3^-	—	$C_4H_9S^-$	PtS^-, $PtS(SC_4H_9)^-$

A dash signifies that no ions were detected.

Elimination of H_2Y;

$$M^- + HXYH \rightarrow MX^- + H_2Y, \quad (6)$$

Elimination of H_2X;

$$M^+ + HXYH \rightarrow MY^+ + H_2X, \quad (7)$$

Elimination of Y;

$$M^+ + HXYH \rightarrow MH_2X^+ + Y, \quad (8)$$

Abstraction of HX^-;

$$M^+ + HXYH \rightarrow YH^+ + MHX. \quad (9)$$

The reactions of Au^- *and* Pt^-

The reactions of the anions Au^- and Pt^- are shown in Table 1.

The aromatic hydrocarbons were unreactive towards the metal anions with the exception of mesitylene which reacted with Pt^- by hydride abstraction (eq. 4) to give the anion $C_9H_{11}^-$. There was also a trace of the addition reaction to form the mono-complex (eq. 1).

The reaction of the metal anions with the thiols was hydride abstraction to form MH (eq. 4) in almost all cases, the exceptions being the non-reactivity of Au^- with n-C_3H_7SH, and the reaction of Au^- with t-C_4H_9SH to give mainly S_3^- after long reaction times, S_3^- is a quite stable anion also observed as a minor product in other reactions. Minor pathways in the Pt^- plus thiol reactions involved sulfur abstraction (eq. 6) to form PtS^-, and subsequent addition of the dehydrogenated thiol to give $PtS(SC_4H_9)^-$.

H_2S was unreactive with Au^- but reacted with Pt^- to give the addition products (eqs 1 and 2).

The reactions of Au^+

The major reaction of the collisionally cooled Au^+ ions with the hydrocarbons was the charge transfer reaction (eq. 3). The reactive toluene also gave by hydride abstraction the stable ion $C_7H_7^+$ (eq. 4). This ion was also observed in the reaction of xylene by loss of a methyl group. The reactions of hydrocarbons with $*Au^+$ ions (not collisionally cooled) were studied for benzene and toluene. In both cases the charge transfer reaction (eq. 3) was a secondary pathway and for benzene the addition reactions (eqs 1 and 2) produced the major products, whereas for toluene $C_7H_7^+$ (eq. 4) was the major product ion.

The reaction of benzenethiol with Au^+ ions gave the charge transfer reaction (eq. 3) as the major pathway and the formation of the mono-complex (eq. 1) as the secondary pathway. The reaction of $*Au^+$ with benzenethiol did not alter the main pathway, but one minor product indicated S abstraction

Table 2. The reactions of gold cations

Reactant	Au^+ major	Au^+ minor	$*Au^+$ major	$*Au^+$ minor
C_6H_6	$C_6H_6^+$	—	$Au(C_6H_6)^+$	$C_6H_6^+$, $Au(C_6H_6)_2^+$
C_7H_8	$C_7H_8^+$	$C_7H_7^+$	$C_7H_7^+$	$C_7H_8^+$
C_8H_{10}	$C_8H_{10}^+$	$C_7H_7^+$	[a]	[a]
C_9H_{12}	$C_9H_{12}^+$	$AuC_9H_{12}^+$	[a]	[a]
C_6H_5SH	$C_6H_5SH^+$	$AuC_6H_5SH^+$	$C_6H_5SH^+$	$AuC_6H_5SH^+$, $AuS(C_6H_5SH)^+$, $AuC_4H_4^+$
H_2S	AuH_2S^+	$Au(H_2S)_2^+$	[a]	[a]
n-C_3H_7SH	$C_3H_7SH_2^+$	$AuC_3H_7SH^+$, $C_3H_7^+$, $Au(H_2S)^+$, $AuC_3H_6^+$	$C_3H_7SH_2^+$	$AuC_3H_7SH^+$, $C_3H_7^+$, $Au(C_3H_7SH)_2^+$, AuH_2S^+, $Au(H_2S)C_3H_7SH^+$, $AuC_3H_6^+$, $AuC_3H_8^+$
n-C_4H_9SH	$C_4H_9SH_2^+$	$AuC_4H_9SH^+$, $C_4H_9^+$, $Au(C_4H_9SH)_2^+$, AuH_2S^+, $Au(H_2S)C_4H_9SH^+$	[a]	[a]
i-C_4H_9SH	$C_4H_9^+$	$C_4H_9SH_2^+$ $C_4H_9SH^+$	$C_4H_9^+$	$C_4H_9SH_2^+$, $C_4H_9SH^+$, $AuC_2H_4^+$
s-C_4H_9SH	$C_4H_9SH_2^+$	$C_4H_9^+$, $Au(C_4H_9SH)^+$, $Au(C_4H_9SH)_2^+$	[a]	[a]
t-C_4H_9SH	$C_4H_9SH_2^+$	$C_4H_9SH^+$, $C_4H_9^+$	$C_4H_9SH_2^+$	$C_4H_9^+$, $AuC_2H_4^+$

[a] Signifies that the reaction was not investigated.

from the thiol. Only the addition reaction was observed for Au^+ with H_2S (eqs 1 and 2). The reactions of Au^+ with the alkyl thiols gave many similar products not involving Au, namely the protonated thiol RSH_2^+, the charge transfer product RSH^+, and $C_4H_9^+$ formed by the abstraction of SH^- (eq. 9). Two of the thiols were reacted with $*Au^+$ and gave the same major ions but the minor ion $AuC_2H_4^+$ indicated C—C bond cleavage.

The reactions of Pt^+

The major product of the reaction of Pt^+ with the hydrocarbons was the charge transfer ion, RH^+ (eq. 3). Another significant ion (about 15%) was the hydride abstraction product R^+ (eq. 4). Although the major ions contributed ~ 90% of the products, examination of the minor ions using narrow band spectra revealed some interesting products.

In order to establish the compositions of some of the unusual product ions in our reactions we report and interpret representative spectra. For reference, Fig. 1 shows the spectrum of Pt^+ as obtained by our broad band ejection procedure: the ions present agree with the theoretical isotopic distribution (relative to the most abundant isotope) of platinum (^{194}Pt 97%, ^{195}Pt 100%, ^{196}Pt 75%, ^{198}Pt 21%).

After collisionally cooled Pt^+ had reacted with benzene for 2 s, part of the isotopic pattern of the addition products was as shown in Fig. 2. The intensity distribution of the ions at *m/z* of 270, 271, 272 and 274 agree with and can only be due to the benzyne product $PtC_6H_4^+$, while the phenyl addition product $PtC_6H_5^+$ and the benzene

Table 3. The reactions of platinum cations

Reactant	Pt^+ major	Pt^+ minor	$*Pt^+$ major	$*Pt^+$ minor
C_6H_6	$C_6H_6^+$	$C_6H_5^+$, PtL^+, PtL_2^+, PtL_3^+	$PtC_6H_4^+$	$C_6H_6^+$, PtL^+, PtL_2^+, PtL_3^+
Toluene, C_7H_8	$C_7H_8^+$	$C_7H_7^+$, PtL^+, PtL_2^+, PtL_3^+	$PtC_7H_6^+$	$C_7H_7^+$, PtL_2^+, PtL_3^+
p-xylene, C_8H_{10}	$C_8H_{10}^+$	$C_8H_9^+$, $C_7H_7^+$, PtL^+	[a]	[a]
Mesitylene C_9H_{12}	$C_9H_{12}^+$	$C_9H_{11}^+$, PtL^+	$PtC_9H_{10}^+$	$C_9H_{12}^+$, $C_9H_{11}^+$
C_6H_5SH	$C_6H_5SH^+$	$PtC_6H_5SH^+$	$C_6H_5SH^+$	PtL^+, PtL_2^+, $PtSL^+$, PtS_2L^+, $PtSL_2^+$, $PtS_2L_2^+$, $PtSL_3^+$
H_2S	PtH_2S^+	$Pt(H_2S)_2^+$	[a]	[a]
n-C_3H_7SH	$C_3H_7SH_2^+$	$C_3H_7SH^+$, $C_3H_7S^+$	[a]	[a]
n-C_4H_9SH	$C_4H_9SH_2^+$	$PtC_4H_7^+$, $PtC_4H_8S^+$	[a]	[a]
i-C_4H_9SH	$C_4H_9SH_2^+$	$PtC_4H_7^+$, $PtC_4H_8S^+$	[a]	[a]
s-C_4H_9SH	$C_4H_9SH_2^+$	$C_4H_9^+$, $PtC_4H_7^+$, $PtC_4H_8S^+$	[a]	[a]
t-C_4H_9SH	$C_4H_9^+$	$C_4H_9SH_2^+$, $C_4H_9SH^+$, $PtC_4H_7^+$	[a]	[a]

Where L is used there are several products, see text.

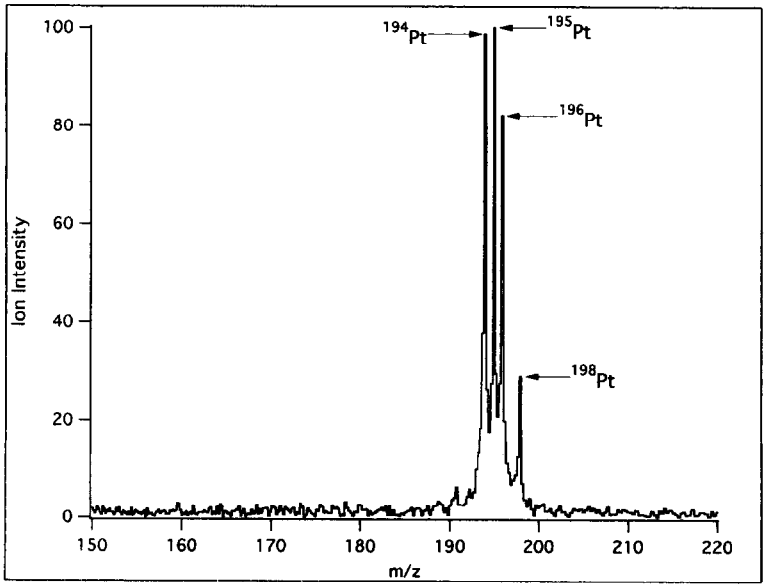

Fig. 1. The spectrum of collisionally cooled Pt^+ ions, obtained by broad-band ejection of all other ions from laser ablated platinum.

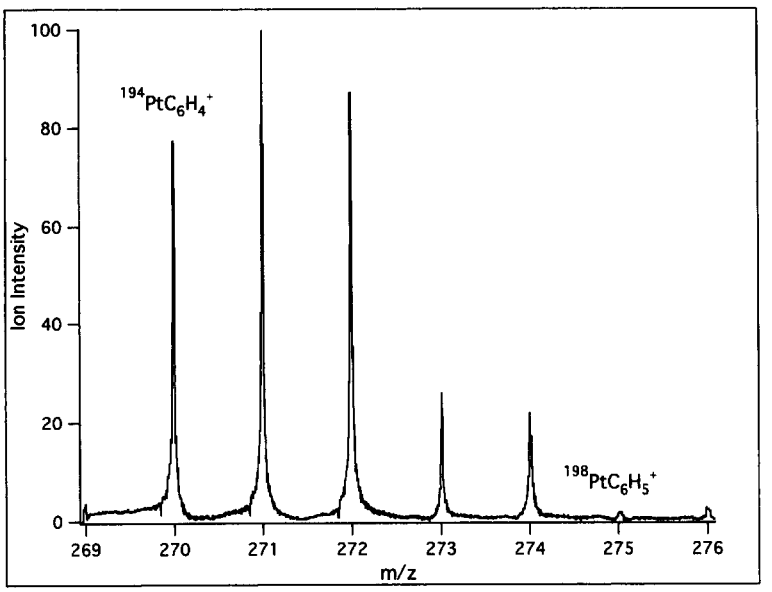

Fig. 2. The narrow band spectrum of the products of reaction of collisionally cooled Pt^+ ions with benzene after 2 s.

addition product, $PtC_6H_6^+$, are unambiguously proven as minor products by the low intensity ions at *m/z* 275 and 276. Thus the peaks at *m/z* 271, 272, 273 and 274 are due to more than one ion, e.g. *m/z* 274 is a mixture of $^{196}PtC_6H_6^+$ and $^{198}PtC_6H_4^+$.

Continuation of the same reaction for 10 s yielded two other sets of minor products, for which the spectra are shown in Figs 3 and 4. The products in Fig. 3 are the bis addition products and involve both benzyne and benzene ligands. For instance the peak at *m/z* 346 is the bis-benzyne product $^{194}Pt(C_6H_4)_2^+$. The peaks at *m/z* 353 and *m/z* 354 indicate the presence of $^{198}Pt(C_6H_6)(C_6H_5)^+$ and $^{198}Pt(C_6H_6)_2^+$, respectively. The other peaks are overlaps and mixed ligand ions.

The spectrum of the tris-complexes shown in Fig.

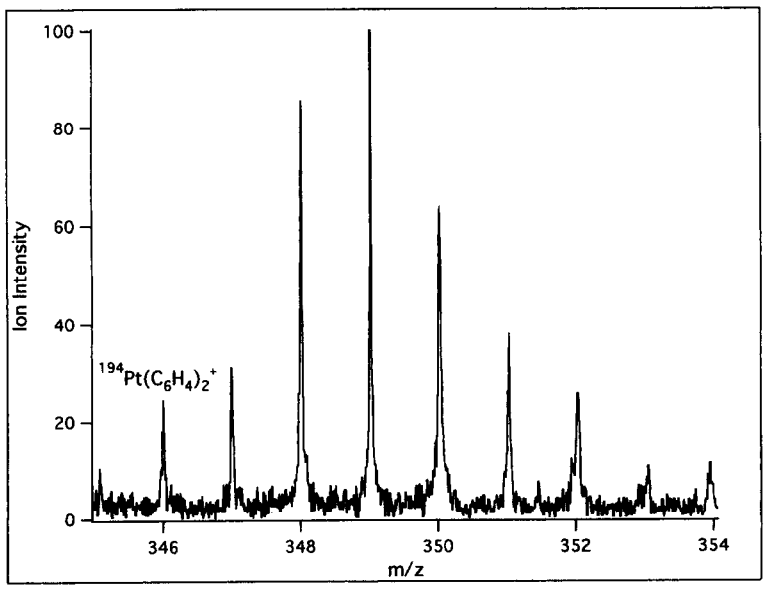

Fig. 3. The narrow band spectrum of the minor products of reaction of collisionally cooled Pt^+ ions with benzene after 10 s.

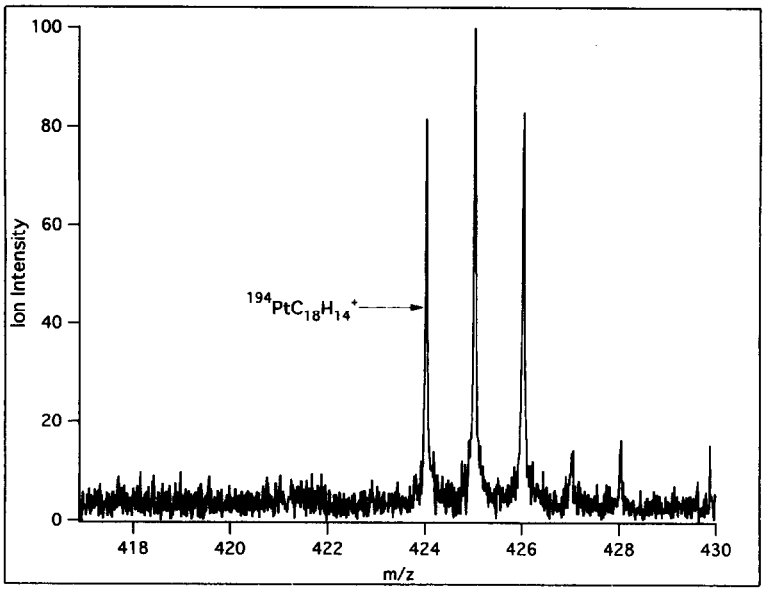

Fig. 4. The narrow band spectrum of the minor products of reaction of collisionally cooled Pt^+ ions with benzene after 10 s.

4 is much simpler and suggests that the ion at m/z 424 is $^{194}Pt(C_6H_4)_2(C_6H_6)^+$ or $^{194}Pt(C_6H_4)(C_6H_5)_2^+$. The isotope pattern in Fig. 4 is similar to the isotope pattern in Fig. 1. The reaction of Pt^+ with toluene gave the charge transfer ion $C_7H_8^+$ as the major product with approximately 15% of the hydrogen transfer product $C_7H_7^+$. Other minor addition products were observed as shown in the narrow band spectra Figs 5 and 6. The mono- and bis-benzyne products $PtC_7H_6^+$ and $Pt(C_7H_6)_2^+$ are at m/z 284 and 374, respectively for the ^{194}Pt ion. The peaks at m/z 283, 372 and m/z 373 indicate the presence of ions having further losses of hydrogen such as $^{194}Pt(C_7H_5)_2^+$ (m/z 372) compared to $^{194}Pt(C_7H_6)_2^+$ (m/z 374).

The reaction of $*Pt^+$ ions afforded greater concentrations of the addition complexes and the hydrogen transfer product. The mono-addition

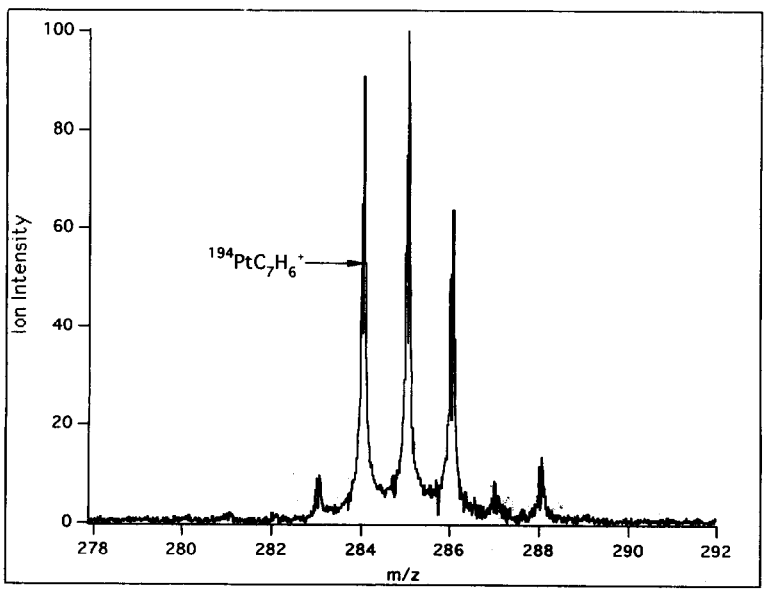

Fig. 5. Narrow band spectrum of the reaction of collisionally cooled Pt^+ ions with toluene, after 1.5 s.

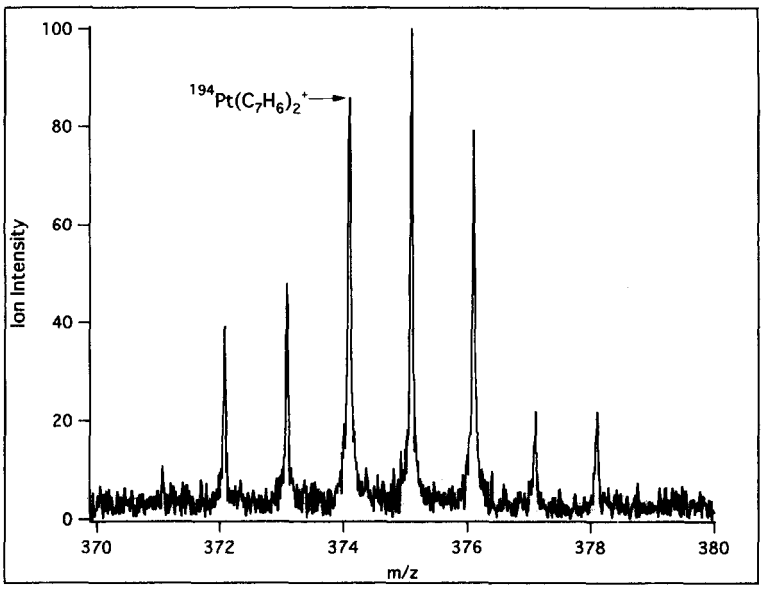

Fig. 6. Narrow band spectrum of the reaction of collisionally cooled Pt^+ ions with toluene, after 1.5 s.

products were the initial major ions rather than the charge transfer product or the hydride transfer product, the $C_7H_7^+$ ion.

The reaction of Pt^+ ions with p-xylene gave the charge transfer product $C_8H_{10}^+$ as the major ion and $C_8H_9^+$ as the second most intense ion, with smaller amounts of $C_7H_7^+$. The addition products were observed in the narrow band spectrum, shown in Fig. 7. The ions at *m/z* 296, 297 and 298 are most probably $^{194}PtC_8H_6^+$, $^{194}PtC_8H_7^+$ and $^{194}PtC_8H_8^+$, respectively with the peaks at *m/z* 297 and 298 having contributions from $^{195}PtC_8H_6^+$ and $^{195}PtC_8H_7^+$, respectively.

The reaction of Pt^+ with mesitylene gave the charge transfer product $C_9H_{12}^+$ as the major ion, and the addition products shown in Fig. 8 as minor products. The ions at *m/z* 310, 311 and 312 are identified as $^{194}PtC_9H_8^+$, $^{194}PtC_9H_9^+$ and $^{194}PtC_9H_{10}^+$, respectively, while *m/z* 311 and 312 have contributions from $^{195}PtC_9H_8^+$ and $^{195}PtC_9H_9^+$, respectively.

Pt^+ reacted cleanly with benzenethiol to produce

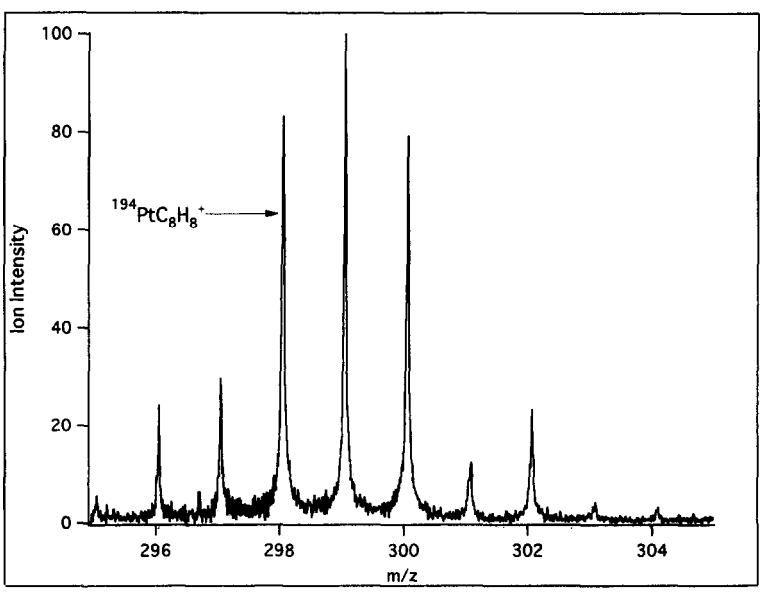

Fig. 7. Part of the spectrum of the reaction of collisionally cooled Pt^+ ions with p-xylene, after 1.5 s.

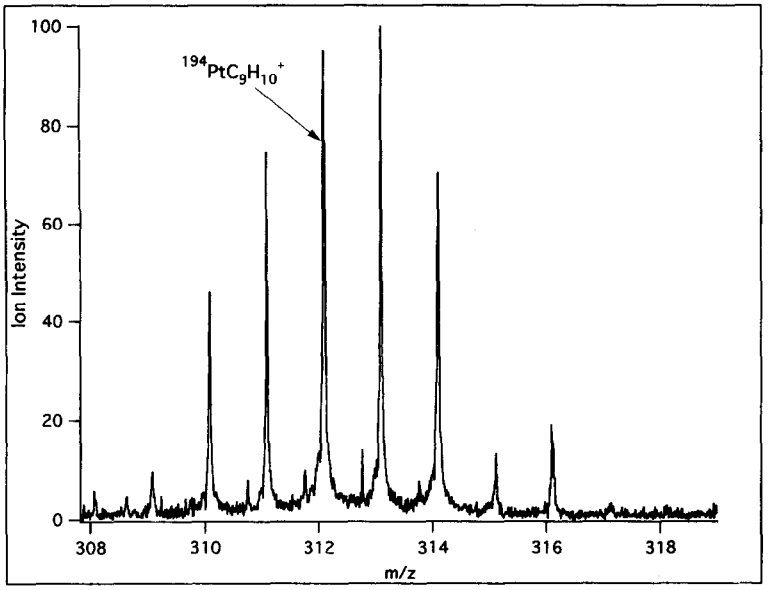

Fig. 8. The narrow band spectrum of the reaction of collisionally cooled Pt^+ ions with mesitylene, after 0.2 s.

the charge transfer ion $C_6H_5SH^+$ as the major product, while the mono-complex ion $PtC_6H_5SH^+$ was a trace product.

*Pt^+ ions were more reactive and this was shown in the variety of products which were obtained at low intensity levels (< 4%). The charge transfer product L^+ was a major ion, and the mono- and bis-complex ions $PtC_6H_5SH^+$ and $Pt(C_6H_5SH)_2^+$ were observed together with other species such as $PtS_n(C_6H_5SH)_m^+$ where n = 1, 2 and m = 1, 2 and $PtS(C_6H_5SH)_3^+$. The reaction of Pt^+ with H_2S gave only the addition products PtH_2S^+ (eq. 1) and $Pt(H_2S)_2^+$ (eq. 2).

The reactions of Pt^+ with all the alkyl thiols (except t-butanethiol) gave the protonated thiol RSH_2^+ as the major ion. The removal of HS^- (eq. 9) to give $C_4H_9^+$ as the major ion occurred for t-butanethiol. An unusual minor ion observed in the reactions of all the butanethiols was $PtC_4H_7^+$ produced by the loss of H_3S.

DISCUSSION

The production of bare metal ions using the laser method is expected to produce ions with high translational energy and also ions in excited electronic states. Collisional cooling using an inert gas or the reacting molecule might be expected to significantly reduce translational energy but may not provide pathways for the deactivation of excited state ions to ground state ions. The excited state ions often have long lifetimes as shown by Ridge[15] or react differently as shown recently by Russell.[7] Russell has used the different reactivity to investigate Fe^+ formed by Electron Impact and found that 65% of the ions formed were in excited states. The production of high energy Au^+ using a spark source[5,6] is obviously a guide to the reactivity of Au^+ in excited states.

The metal negative ions were markedly less reactive than the positive ions. Au^- ($d^{10}s^2$) was a particularly unreactive ion. The major reaction of Au^- and Pt^- with the thiols was the hydride abstraction reaction, eq. 4. The exception was with H_2S, which from solution chemistry would be expected to be more acidic than the thiols, but was unreactive towards Au , and underwent simple addition with the more reactive Pt^-. The time course of the $Pt^- + H_2S$ reactions is shown in Fig. 9.

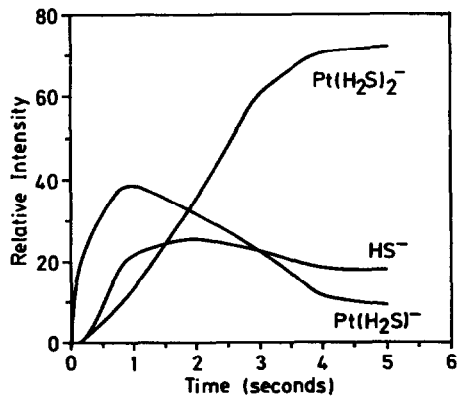

Fig. 9. Time course of the reaction of Pt^- with H_2S.

The ionization energy of Au, 9.225 eV is slightly lower than that of benzene (9.25 eV) but the reaction of collisionally cooled Au^+ with benzene gave the charge transfer reaction. The formation of the addition complexes $AuC_6H_6^+$ and $Au(C_6H_6)_2^+$ with "hot" $*Au^+$ suggests that excited state ions may be reacting to give different products than the charge transfer product produced by the ground state ions. Sato *et al.*[16] using laser ablation and a molecular beam method had observed the addition products and $Au(C_6H_6)_2^+$, but their reactions were carried out at benzene pressures of 60 torr.

The observation of only 30% charge transfer reaction with "hot" Au^+ ions suggest that the excited state ions may be at twice the concentration of the ground state ions, or that ions with higher translational energy may undergo the addition reaction in preference to the charge transfer reaction.

The ionization potentials of the methyl substituted benzenes studied ($\sim$ 8.4–8.8 eV)[17] are significantly lower than the ionization potential of benzene. In the case of toluene the reaction with collisionally cooled Au^+ was the charge transfer reaction as expected. The minor product was the very stable ion $C_7H_7^+$ which involved hydride abstraction (eq. 4).

With "hot" Au^+ ions the major product ion was $C_7H_7^+$ and the minor product ion was the charge transfer ion $C_7H_8^+$. After a reaction time of 2 s the ratio of the ions $C_7H_7^+ : C_7H_8^+$ was approximately 3 : 1. If $C_7H_7^+$ ions were formed by the reaction of excited state Au^+ ions present directly after laser ablation, then the ground state ions were only about 25% of the total ions. The charge transfer ions were the major species observed in the reactions of collisionally cooled Au^+ with xylene and mesitylene as expected from the ionization potentials.[17]

Our results differ in detail from those of Chowdhury and Wilkins who observed the major product of the reaction of Au^+ with benzene to be the addition product $AuC_6H_6^+$ and the charge transfer ion to be the major product for the reaction of toluene.

The reactions of Au^+ with benzene and substituted benzenes also contrast with the reactions of Cu^+ and Ag^+,[2] where the major ions formed were the addition complexes ML^+ and ML_2^+. The ionization potentials of Cu and Ag (7.73 and 7.58 eV, respectively) are significantly lower than the ionization potential of Au, thus the charge transfer process would be highly endothermic for ground state Cu^+ and Ag^+.

The reaction rates of Pt^+ with benzene and the substituted benzenes indicate that this metal ion is more reactive than Au^+. This is possibly due to the filled shell electronic configuration of Au^+ (d^{10}) being a more stable, less reactive species compared with Pt^+ (d^9), but may also be due to long lived excited states of Pt^+. The ionization energy of Pt (9.0 eV) is significantly lower than that of benzene and yet the charge transfer ion and the hydride transfer ion are formed in the reaction of Pt^+ with benzene. This suggests that although the ground state reaction to form the charge transfer products may be endothermic, the participation of excited state Pt^+ ions may involve exothermic reactions. The observation of the benzyne product and other similar products with the substituted benzenes, and the increase in the proportion of these ions when "hot" $*Pt^+$ was used also indicates the presence of excited state ions.

The formation of addition products was greater for the more reactive toluene than for benzene, and also greater for the more reactive "hot" ions. The "benzyne" products could be formed by removal of two aromatic hydrogens (a real benzyne), or involve removal of one or two of the methyl protons: our current experiments cannot distinguish these mechanisms. There was also evidence of the further removal of hydrogens from the benzene ring in the formation of products such as $Pt(C_7H_5)_2^+$ in the reaction of Pt^+ with toluene. It is possible for p-xylene to form a benzyne, but mesitylene cannot easily form a benzyne derivative and so loss of methyl protons must take place in the formation of the products giving ions such as m/z 310, $^{194}PtC_9H_8^+$.

Reactions involving the formation of metal-benzyne complexes from aryl halides have been reported previously, principally with Sc^+, Ti^+, V^+ and Fe^+.[18,19] Platinum benzyne and other metal benzyne compounds have also been prepared in the condensed phase.[20]

The ionization potential of benzenethiol, 8.32 eV suggests that both Au^+ and Pt^+ should give the charge–transfer reaction, as was observed. The production of minor ions particularly with $*Pt^+$ suggests the reactions involve excited state ions. The higher ionization potentials of Au and Pt compared with Cu and Ag are the reason for the completely different reaction pathways in the gas phase reactions of their mono-cations.

H_2S has a high ionization potential (10.5 eV) and so the only reaction observed with the positive ions Au^+, Pt^+ and Cu^+ was the addition reaction. In all cases there was no evidence of metal sulphide formation in contrast to well known solution reactions.

The alkyl thiols have higher ionization potentials (9.2–8.7 eV), but the major ion observed for both Au^+ and Pt^+ was the protonated ligand, which may

arise from the initial charge transfer ion RSH^+ reacting further with the neutral thiol. The minor products formed arise mainly from the rupture of the C—S bond and the elimination of H_2S which may add to the reacting metal ion or be pumped away as a neutral molecule. Pt^+ gave the unusual minor ions $PtC_4H_8S^+$ and $PtC_4H_7^+$ which involve the loss of H_2 (eq. 5) and H_3S, respectively.

In contrast to our previous study of the reactions of Cu^+ and Ag^+ where the formation of addition products with similar molecules was the principal reaction, the reactions of Au^+ and Pt^+ indicated above are very different.

Acknowledgements—This research is supported by the Australian Research Council. J.H.ElN. acknowledges an Australian Postgraduate Research Award. K.J.F. acknowledges a National Research Fellowship.

REFERENCES

1. R. B. Cody, R. C. Burnier, W. D. Reents Jr, T. J. Carlin and D. A. McCrery, *Int. J. Mass Spect. Ion Phys.* 1980, **33**, 37; S. W. Buckner and B. S. Freiser, *Gas Phase Inorganic Chemistry* (Edited by D. H. Russell), Ch. 9, pp. 279–323. Plenum Press, New York (1989).
2. J. H. El-Nakat, I. G. Dance, K. J. Fisher and G. D. Willett, *Polyhedron* 1992, **11**, 1125.
3. A. K. Chowdhury and C. L. Wilkins, *J. Am. Chem. Soc.* 1987, **109**, 5336.
4. D. A. Weil and C. L. Wilkins, *J. Am. Chem. Soc.* 1985, **107**, 7316.
5. W. L. Grady and M. M. Bursey, *Int. J. Mass Spectrom. Ion Phys.* 1983, **52**, 247.
6. W. L. Grady and M. M. Bursey, *Int. J. Mass Spectrom. Ion Phys.* 1983, **52**, 259.
7. J. V. B. Oriedo and D. H. Russell, *J. Phys. Chem.* 1992, **96**, 5314.
8. P. B. Armentrout, *Annu. Rev. Phys. Chem.* 1990, **41**, 313.
9. P. R. Kemper and M. T. Bowers, *J. Phys. Chem.* 1991, **95**, 5134.
10. C. E. Moore, Atomic Energy Levels, *Nat. Stand. Ref. Data Ser. Nat. Bur. Stand.* (U.S.A.) 35, (1971).
11. K. K. Irikura and J. L. Beauchamp, *J. Am. Chem. Soc.* 1991, **113**, 2769.
12. P. F. Greenwood, M. G. Strachan, G. D. Willett and M. A. Wilson, *Org. Mass Spect.* 1990, **25**, 353.
13. J. H. El-Nakat, I. G. Dance, K. J. Fisher, D. Rice and G. D. Willett, *J. Am. Chem. Soc.* 1991, **113**, 5141.
14. K. Eller and H. Schwartz, *Chem. Rev.* 1991, **91**, 1121.
15. W. D. Reents Jr, F. Strobel, R. B. Freas III, J. Wronka and D. P. Ridge, *J. Phys. Chem.* 1985, **89**, 5666.
16. H. Higashide, T. Kaya, M. Kobayashi, H. Shinohara and H. Sato, *Chem. Phys. Lett.* 1990, **171**, 297.
17. Ionization potentials taken from J. Physical and Chemical Reference Data 1977, **6**, Supplement 1. Benzene 9.25 eV, toluene 8.82 eV, p-xylene 8.45 eV, mesitylene 8.4 eV, benzenethiol 8.32 eV, hydrogen sulphide 10.47 eV, n-propanethiol 9.2 eV, n-butanethiol 9.14 eV and i-butanethiol 8.7 eV.
18. T. G. Dietze, D. S. Chatellier and D. P. J. Ridge, *J. Am. Chem. Soc.* 1978, **110**, 4905.
19. A. Bjarnason, *Organometallics* 1991, **10**, 1244.
20. M. A. Bennett and H. P. Schwenlein, *Angew. Chem. Int. Ed. Engl.* 1989, **28**, 1296.

Polyhedron Vol. 12, No. 20, pp. 2489–2497, 1993
Printed in Great Britain

0277–5387/93 $6.00+.00
© 1993 Pergamon Press Ltd

STRUCTURES OF NICKEL(II) AND COPPER(II) COMPLEXES OF 2-ACETYLPYRIDINE AZACYCLOTHIOSEMICARBAZONES

DOUGLAS X. WEST* and HAILESELASSIE GEBREMEDHIN

Department of Chemistry, Illinois State University, Normal, IL 61761, U.S.A.

and

RAY J. BUTCHER

Department of Chemistry, Howard University, 2400 Sixth Street N.W., Washington, D.C. 20059, U.S.A.

and

JERRY P. JASINSKI

Department of Chemistry, Keene State College, Keene, NH 03431, U.S.A.

and

ANTHONY E. LIBERTA

Department of Biological Sciences, Illinois State University, Normal, IL 61761, U.S.A.

(*Received* 11 *February* 1993; *accepted* 9 *June* 1993)

Abstract—Anions (loss of ^{3}N hydrogen) of 2-acetylpyridine azacyclothiosemicarbazones coordinate in a planar conformation to a central nickel(II) or copper(II) ion through the pyridyl N, azomethine N and thiolato S atoms. The fourth coordination site is occupied by a bromo ligand. Their ability to inhibit the growth of two fungi is compared to their structural differences.

Heterocyclic thiosemicarbazones, as well as their metal complexes, are important series of compounds because of potentially beneficial, biological activity.[1] In particular, copper(II) thiosemicarbazone complexes have shown enhanced biological activity compared to uncomplexed thiosemicarbazones.[2] Although there has been considerable effort directed toward the isolation of new complexes and their spectral and magnetic characterization,[3,4] comparatively few crystal structures of nickel(II) and copper(II) thiosemicarbazones have, as yet, been determined. Ferrari *et al.* reported the crystal structure of 3-hydroxy-5-hydroxymethyl-4-formyl-2-picoline thiosemicarbazone, H_2Pictsc, as well as the copper(II) complex, $[Cu(HPictsc)H_2O]Cl \cdot H_2O$, derived from aqueous copper(II) chloride.[5] Bell and Theocharis[6] and Muller *et al.*[7] both reported the crystal structure of the dimeric copper(II) complex derived from 2-formylpyridine thiosemicarbazone and copper(II) acetate. Ainscough *et al.* determined the crystal structure of a monomeric copper(II) complex formed from this dimeric copper(II) acetate complex and saccharin.[8] More recently this same group reported additional copper(II) complexes of 2-formylpyridine thiosemicarbazone.[9]

Few crystal structures have been reported of complexes formed from 2-acetylpyridine ^{4}N-substituted thiosemicarbazones, which may possess more beneficial biological activity than their 2-formylpyridine analogues.[10] The structure of a

*Author to whom correspondence should be addressed.

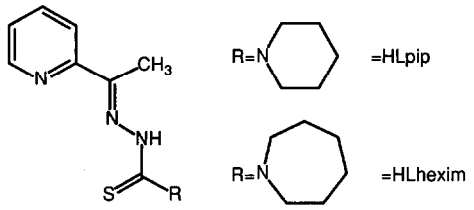

Fig. 1. The E isomer of 2-acetylpyridine piperidinyl- and hexamethyleneiminylthiosemicarbazones, HLpip and HLhexim, respectively.

nickel(II) complex of 2-acetylpyridine azabicyclo [3.2.2]nonylthiosemicarbazone, [Ni(Lbcn)NCS], was reported a few years ago.[11] More recently, we have reported the molecular structure[12] of a copper(II) complex of 2-acetylpyridine hexamethyleneiminylthiosemicarbazone, HLhexim (Fig. 1), which is one of the more active growth inhibitory agents against *Aspergillus niger* and *Paecilomyces variotii*.[13] Also, a structural study of two nickel(II) complexes of acetylpyrazine N-substituted thiosemicarbazones has just been completed.[14] Here we report the nickel(II) complex of HLhexim, [Ni(Lhexim)Br] and the copper(II) complex of the related 2-acetylpyridine piperidinylthiosemicarbazone (Fig. 1), [Cu(Lpip)Br].

EXPERIMENTAL

HLpip and HLhexim were synthesized according to the method recently reported by Scovill.[15] [Ni(Lhexim)Br] and [Cu(Lpip)Br] were prepared in boiling ethanol and the antifungal studies were carried out as described previously[14] and the crystals were grown by slow evaporation of dimethyl sulphoxide solutions at 35°C. The crystals, a light brown prism of approximate dimensions $0.40 \times 0.30 \times 0.60$ mm for [Ni(Lhexim)Br] and an orange–brown prism of approximate dimensions $0.30 \times 0.15 \times 0.35$ mm for [Cu(Lpip)Br], were measured on a Siemens R3m/V Diffractometer using a 2θ range of 4 to 55°. The structures were solved with a Siemens SHELXTL PLUS (VMS) using direct methods. All non-hydrogen atoms were refined anisotropically. Hydrogen atoms were included in structure factor calculations in their calculated positions. Refinement of the parameters was accomplished by full-matrix least-squares using a riding model for hydrogen atoms and converged with $R = 0.069$ and $R_w = 0.090$ for the 3782 observed reflections and $R = 0.085$ and $R_w = 0.092$ for the 5358 observed reflections [Ni(Lhexim)Br] and [Cu(Lpip)Br], respectively. The goodness-of-fits were 2.99 and 2.20. For a summary of crystal data, see Table 1.

RESULTS AND DISCUSSION

Interatomic distances and bond angles are compiled in Tables 2 and 3 for [Ni(Lhexim)Br] and [Cu(Lpip)Br], respectively. The supplementary material contains a list of the final positional and equivalent isotropic thermal parameters of the non-H atoms. H-atom coordinates and isotropic displacement coefficients are also included in the supplementary material as are the packing diagrams,

Table 1. Crystallographic data for [Ni(Lhexim)Br] and [Cu(Lpip)Br]

Empirical formula	$C_{14}H_{19}BrN_4SNi$	$C_{13}H_{17}BrN_4SCu$
Colour; habit	light brown prism	orange brown prism
Crystal size (mm)	$0.40 \times 0.30 \times 0.60$	$0.30 \times 0.15 \times 0.35$
Crystal system	Monoclinic	Monoclinic
Space group	$P2_1/n$ (# 14)	$P2_1/c$ (# 14)
Unit cell dimensions		
a (Å)	7.244(2)	11.251(2)
b (Å)	24.905(3)	15.124(3)
c (Å)	9.1769(8)	8.959(2)
β (°)	104.24(1)	90.09(2)
V (Å^3)	1604.8(9)	1524.4(9)
Z	4	4
Formula weight	418.8	404.8
Density (calc.) (g cm^{-3})	1.705	1.777
Absorption coefficient (mm^{-1})	3.803	4.159
F(000)	840	812

Table 2. Bond lengths and bond angles for [Ni(Lhexim)Br]

Bond lengths (Å)			
Ni—Br	2.308(1)	Ni—S	2.155(4)
Ni—N(1)	1.91(1)	Ni—N(2)	1.857(8)
S—C(9)	1.76(1)	N(1)—C(2)	1.36(1)
N(1)—C(6)	1.37(1)	N(2)—N(3)	1.37(1)
N(2)—C(7)	1.33(1)	N(3)—C(9)	1.31(1)
C(2)—C(3)	1.38(2)	C(3)—C(4)	1.36(2)
C(4)—C(5)	1.39(2)	C(5)—C(6)	1.38(2)
C(6)—C(7)	1.41(2)	C(7)—C(8)	1.47(1)
C(9)—N(4)	1.33(1)	N(4)—C(10)	1.45(1)
N(4)—C(15)	1.52(2)	C(10)—C(11)	1.49(2)
C(11)—C(12)	1.48(3)	C(12)—C(13)	1.46(4)
C(13)—C(14)	1.46(4)	C(14)—C(15)	1.46(3)

Bond angles (°)			
Br—Ni—S	91.7(1)	Br—Ni—N(1)	97.9(2)
S—Ni—N(1)	170.4(3)	Br—Ni—N(2)	176.5(3)
S—Ni—N(2)	87.9(3)	N(1)—Ni—N(2)	82.6(3)
Ni—S—C(9)	94.8(4)	Ni—N(1)—C(2)	129.7(7)
Ni—N(1)—C(6)	112.8(7)	C(2)—N(1)—C(6)	117(1)
Ni—N(2)—N(3)	122.2(7)	Ni—N(2)—C(7)	117.5(7)
N(3)—N(2)—C(7)	120.3(8)	N(2)—N(3)—C(9)	113.0(8)
N(1)—C(2)—C(3)	122(1)	C(2)—C(3)—C(4)	121(1)
C(3)—C(4)—C(5)	118(1)	C(4)—C(5)—C(6)	120(1)
N(1)—C(6)—C(5)	122(1)	N(1)—C(6)—C(7)	114(1)
C(5)—C(6)—C(7)	124(1)	N(2)—C(7)—C(6)	112.7(9)
N(2)—C(7)—C(8)	120.7(9)	C(6)—C(7)—C(8)	127(1)
S—C(9)—N(3)	122.1(9)	S—C(9)—N(4)	119.9(9)
N(3)—C(9)—N(4)	118(1)	C(9)—N(4)—C(10)	121(1)
C(9)—N(4)—C(15)	123(1)	C(10)—N(4)—C(15)	114.6(9)
N(4)—C(10)—C(11)	115(1)	C(10)—C(11)—C(12)	121(1)
C(11)—C(12)—C(13)	119(2)	C(12)—C(13)—C(14)	115(2)
C(13)—C(14)—C(15)	120(2)	N(4)—C(15)—C(14)	115(1)

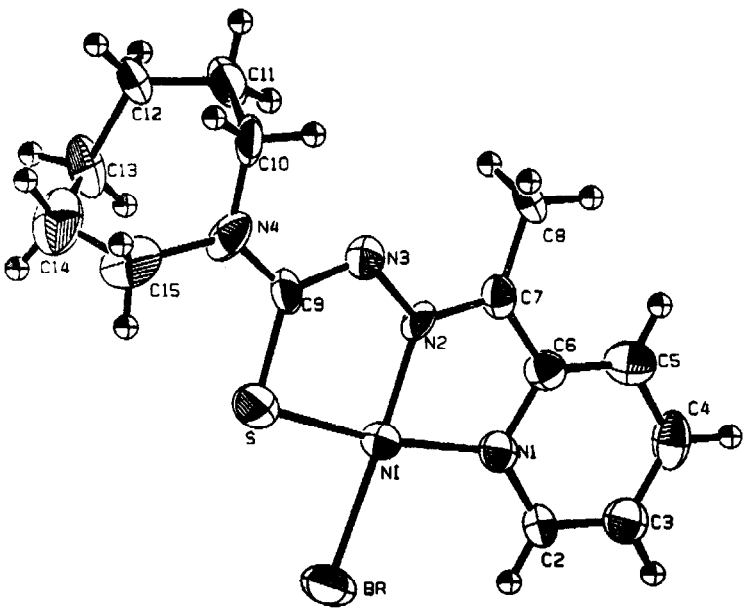

Fig. 2. Ortep diagram for [Ni(Lhexim)Br].

Table 3. Bond lengths and bond angles for [Cu(Lpip)Br]

Bond lengths (Å)			
Cu—Br	2.344(3)	Cu—S	2.230(5)
Cu—N(1)	1.98(1)	Cu—N(2)	2.00(1)
S—C(9)	1.71(2)	N(1)—C(2)	1.35(2)
N(1)—C(6)	1.42(2)	N(2)—N(3)	1.39(2)
N(2)—C(7)	1.28(2)	N(3)—C(9)	1.31(2)
C(2)—C(3)	1.46(2)	C(3)—C(4)	1.30(2)
C(4)—C(5)	1.40(2)	C(5)—C(6)	1.35(2)
C(6)—C(7)	1.44(2)	C(7)—C(8)	1.48(2)
C(9)—N(4)	1.37(2)	N(4)—C(10)	1.47(2)
N(4)—C(14)	1.44(2)	C(10)—C(11)	1.53(2)
C(11)—C(12)	1.59(2)	C(12)—C(13)	1.50(2)
C(13)—C(14)	1.45(2)		

Bond angles (°)			
Br—Cu—S	97.4(1)	Br—Cu—N(1)	98.2(4)
S—Cu—N(1)	162.5(4)	Br—Cu—N(2)	175.8(4)
S—Cu—N(2)	84.3(5)	N(1)—Cu—N(2)	80.6(6)
Cu—S—C(9)	96.2(6)	Cu—N(1)—C(2)	129(1)
Cu—N(1)—C(6)	114(1)	C(2)—N(1)—C(6)	117(1)
Cu—N(2)—N(3)	121(1)	Cu—N(2)—C(7)	116(1)
N(3)—N(2)—C(7)	123(1)	N(2)—N(3)—C(9)	112(1)
N(1)—C(2)—C(3)	121(2)	C(2)—C(3)—C(4)	121(2)
C(3)—C(4)—C(5)	119(2)	C(4)—C(5)—C(6)	121(2)
N(1)—C(6)—C(5)	121(2)	N(1)—C(6)—C(7)	112(1)
C(5)—C(6)—C(7)	127(2)	N(2)—C(7)—C(6)	118(2)
N(2)—C(7)—C(8)	120(2)	C(6)—C(7)—C(8)	122(1)
S—C(9)—N(3)	126(1)	S—C(9)—N(4)	118(1)
N(3)—C(9)—N(4)	116(1)	C(9)—N(4)—C(10)	117(1)
C(9)—N(4)—C(14)	128(1)	C(10)—N(4)—C(14)	113(1)
N(4)—C(10)—C(11)	111(1)	C(10)—C(11)—C(12)	110(1)
C(11)—C(12)—C(13)	108(1)	C(12)—C(13)—C(14)	111(2)
N(4)—C(14)—C(13)	110(1)		

which show no indication of interaction between metal centres. Perspective views of [Ni(Lhexim)Br] and [Cu(Lpip)Br] are shown in Figs 2 and 3.

The anionic thiosemicarbazones each act as a tridentate ligand and coordinate to the central metal atom via the pyridyl nitrogen, N(1); the azomethine nitrogen, N(2); and the thiolato sulphur atom with the fourth coordination site occupied by a bromine atom in each compound, Figs 2 and 3. The hexamethyleneiminyl and pyridinyl rings are bent away from the remainder of the molecule. This is shown in the packing diagrams (Figs 4 and 5): the two

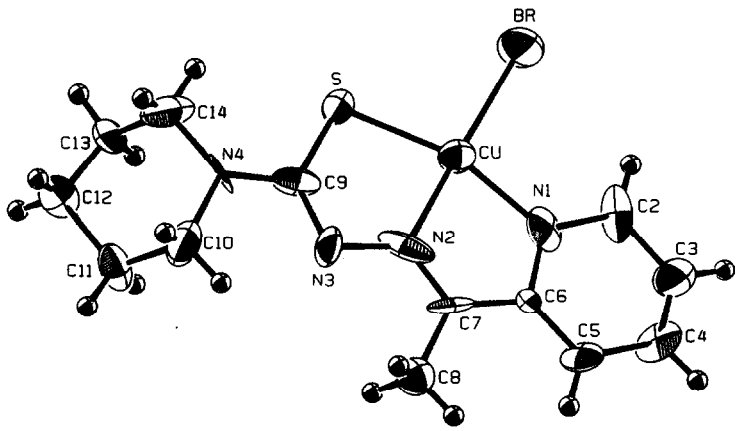

Fig. 3. Ortep diagram for [Cu(Lpip)Br].

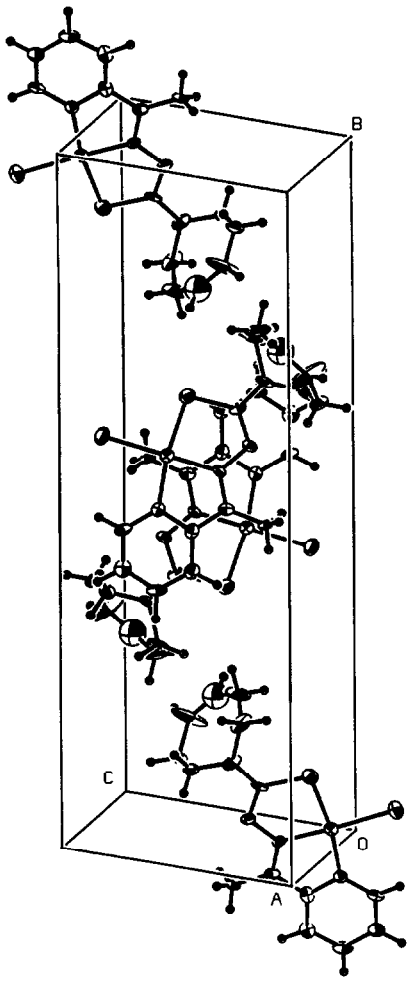

Fig. 4. Packing arrangement for [Ni(Lhexim)Br].

[Ni(Lhexim)Br] molecules in the centre of the cube are rotated 180° from each other to avoid steric interaction, while molecules on the corner have an eclipsed appearance. The bend out of the coordination plane is considerably less for the smaller piperidinyl group in [Cu(Lpip)Br], Fig. 3. For both complexes there seems to be minimal interaction between adjacent metal(II) centres via bromine or sulphur atoms.

In Table 4 is a comparison of the bond lengths for the thiosemicarbazone moiety for [Ni(Lhexim)Br] and [Cu(Lpip)Br] with previously studied copper(II) and nickel(II) thiosemicarbazone complexes. Most of the complexes, except those studied by West *et al.*[11,12,14] involve unsubstituted thiosemicarbazones with two hydrogens attached to ^{4}N in contrast to ^{4}N being a part of a ring. There is little difference in the bond lengths of C=^{2}N between the various thiosemicarbazone complexes although [Ni(Lhexim)Br] has the longest bond, and the nickel(II) complexes generally have longer C=^{2}N bonds than the copper(II) complexes. Comparatively, the 2-acetylpyridine azacyclothiosemicarbazone complexes have long ^{2}N—^{3}N bonds, short ^{3}N—^{9}C bonds, and long ^{9}C—S bonds. This is indicative of the coordinated ligand's greater conjugation and therefore, more delocalized electron density. It then follows that this coordinated ligand also possesses lower energy bonding acceptor orbitals (π^*) and has lower energy metal---→ligand charge transfer bands. [Ni(Lhexim)Br] and [Cu(Lpip)Br] have bands which can be assigned to thiosemicarbazone

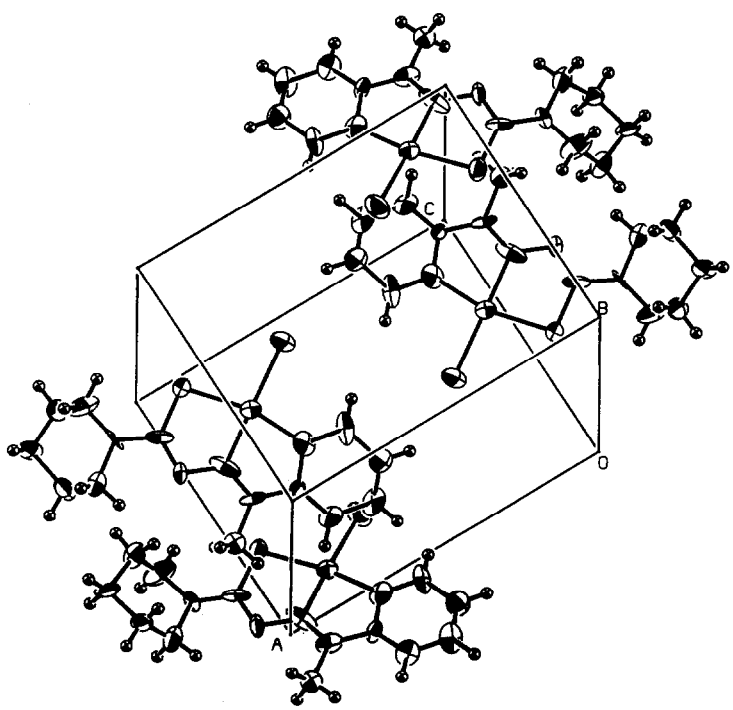

Fig. 5. Packing arrangement for [Cu(Lpip)Br].

Table 4. Comparison of thiosemicarbazone moiety bond lengths (Å) for copper(II) complexes

Compound	C=^{2}N	^{2}N—^{3}N	^{3}N—^{9}C	^{9}C—S	^{9}C—^{4}N	Reference
$\{[Cu(Hpt)Cl]\cdot 2H_2O\}_n$[a]	1.291	1.358	1.355	1.710	1.301	18
$[Cu(ept)Cl]_2$[b]	1.297	1.346	1.327	1.745	1.321	18
$[Cu(Pydox)OH_2]Cl$[c]	1.298	1.368	1.324	1.719	1.333	5
$[Cu(4DH)OAc)]_2$[d]	1.290	1.359	1.335	1.725	1.333	7
$[Cu(4DH)sacc(H_2O)]$	1.285	1.358	1.340	1.721	1.327	8
[Cu(4DH)bipy]sacc	1.292	1.358	1.329	1.736	1.338	8
$[Cu(H4DH)(SO_4)]_2$[e]	1.277	1.366	1.362	1.703	1.309	8
$[\{CuH4DH(CF_3CO_2)\}_2]^{2+}$	1.293	1.345	1.342	1.716	1.316	9
[Cu(Lpip)Br]	1.28	1.39	1.31	1.71	1.37	This work
[Cu(Lhexim)Br]	1.275	1.373	1.301	1.759	1.377	11
[Ni(Lhexim)Br]	1.33	1.37	1.31	1.76	1.33	This work
[Ni(Lbcn)NCS)][f]	1.300	1.373	1.317	1.764	1.346	15
[Ni(Pz4M)Cl][g]	1.312	1.376	1.317	1.756	1.327	13
[Ni(Pz4DM)Cl][h]	1.304	1.370	1.320	1.756	1.342	13
$[Ni(Sal4Ph)NH_3]$[i]	1.316	1.393	1.333	1.717	1.357	19

[a] Hpt = anion (loss of ^{3}N proton) of pyruvic acid thiosemicarbazone.
[b] ept = anion (loss of ^{3}N proton) of ethyl pyruvatethiosemicarbazone.
[c] Pydox = anion (loss of ^{3}N proton) of pyridoxal thiosemicarbazone.
[d] 4DH = anion (loss of ^{3}N proton) of 2-formylpyridine thiosemicarbazone.
[e] H4DH = 2-formylpyridine thiosemicarbazone.
[f] Lbcn = anion (loss of 3N proton) of 2-acetylpyridine 3-azabicyclo[3.2.2]nonylthiosemicarbazone.
[g] Pz4M = anion (loss of ^{3}N proton) of acetylpyrazine ^{4}N-methylthiosemicarbazone.
[h] Pz4DM = anion (loss of ^{3}N proton) of acetylpyrazine ^{4}N-dimethylthiosemicarbazone.
[i] Sal4Ph = dianion (loss of hydroxy and ^{3}N proton) of salicylaldehyde ^{4}N-phenylthiosemicarbazone.

moiety---→metal charge transfer bands as low as 20,620 and 22,520 cm^{-1}, respectively.[16,17]

Table 5 shows the metal(II)-donor atom bond lengths for the nickel(II) and copper(II) complexes of tridentate thiosemicarbazones; most have a heterocyclic nitrogen as the third donor atom. Although [Cu(Lhexim)Br] is comparable,[11] [Cu(Lpip)Br] has the shortest Cu—S bond indicating strong bonding of this donor atom. Further, it is the only copper(II) thiosemicarbazone that has a shorter pyridine Cu—N bond than azomethine Cu—N bond although the two bonds are similar in

Table 5. Comparison of copper- and nickel-donor atom bond lengths (Å) for heterocyclic (i.e. pyridine) thiosemicarbazone copper(II) and nickel(II) complexes

Compound	Cu/Ni—S	Cu/Ni—^{2}N	Cu/Ni—^{1}N	Cu/Ni—Br	Reference
$[Cu(4DH)(OAc)]_2$[d]	2.274	1.970	2.059	—	7
$[Cu(4DH)sacc(H_2O)]$	2.264	1.956	2.020	—	8
[Cu(4DH)bipy]sacc	2.277	1.949	2.042	—	8
$[Cu(H4DH)(SO_4)]_2$[e]	2.279	1.953	2.024	—	8
$[\{CuH4DH(CF_3CO_2)\}_2]^{2+}$	2.273	1.953	2.037	—	9
[Cu(Lpip)Br]	2.230	2.00	1.98	2.344	This work
[Cu(Lhexim)Br]	2.236	1.963	2.016	2.359	11
[Ni(Lhexim)Br]	2.155	1.858	1.91	2.308	This work
[Ni(Lbcn)NCS)][f]	2.138	1.846	1.912	—	15
[Ni(Pz4M)Cl][g]	2.169	1.852	1.923	—	13
[Ni(Pz4DM)Cl][h]	2.141	1.855	1.918	—	13
$[Ni(Sal4Ph)NH_3]$[i]	2.166	1.844	—	—	19

See footnotes for Table 4 for identification of ligands.

Table 6. Comparison of thiosemicarbazone moiety and coordination site bond angles (°) for copper(II) and nickel(II) complexes

Compound	S—Cu—^{1}N	S—Cu—^{2}N	^{1}N—Cu—^{2}N	Cu—S—^{9}C	Cu—^{2}N—^{3}N	References
$\{[Cu(Hpt)Cl]\cdot 2H_2O\}_n$[a]	—	85.1	—	96.4	119.9	16
$[Cu(ept)Cl]_2$[b]	—	84.7	—	96.4	119.9	16
$[Cu(Pydox)OH_2]Cl$[c]	—	86.3	—	94.3	121.0	6
$[Cu(4DH)(OAc)]_2$[d]	162.6	83.2	80.6	95.8	124.3	8
$[Cu(4DH)sacc(H_2O)]$	162.3	82.6	81.2	96.3	125.9	9
[Cu(4DH)bipy]sacc	159.9	83.5	81.2	94.9	124.7	9
$[Cu(H4DH)(SO_4)]_2$[e]	160.1	85.1	80.2	96.4	120.0	9
$[\{CuH4DH(CF_3CO_2)\}_2]^{2+}$	163.9	84.3	80.2	96.3	121.6	10
[Cu(Lpip)Br]	162.5	84.3	80.6	96.2	121.0	This work
[Cu(Lhexim)Br]	165.3	85.1	80.5	94.5	122.7	11
[Ni(Lhexim)Br]	170.4	87.8	82.7	94.9	122.3	This work
[Ni(Lbcn)NCS][f]	171.0	87.0	84.0	95.5	124.4	15
[Ni(Pz4M)Cl][g]	170.0	86.7	83.3	95.2	124.1	13
[Ni(Pz4DM)Cl][h]	170.6	87.3	83.4	95.3	123.8	13
$[Ni(Sal4Ph)NH_3]$[i]	—	87.7	—	95.9	121.5	19

See footnotes for Table 4 for identification of ligands.

length to the complexes of 2-formylpyridine thiosemicarbazone.[8,9] The Cu—Br bonds for [Cu(Lpip)Br] is shorter than that of [Cu (Lhexim)Br] which may be due to the reduced bulkiness of the 6-membered piperidinyl ring compared to the 7-membered hexamethyleneiminyl ring.[11]

The nickel(II) thiosemicarbazone complexes have significantly shorter metal–ligand bonds than the copper(II) complexes which is likely due to nickel's smaller number of *d*-electrons and vacant *d* orbital. Comparing [Ni(Lhexim)Br] with [Cu(Lhexim)Br] shows that the bond distances for the two harder donor atoms, the nitrogens, differ the most in the two complexes. This is likely due to the harder nickel(II) center forming stronger bonds with the hard nitrogen donors. Alternatively, back π-bonding of the copper(II) electron to empty *d* orbitals on the bromo and thiol donor atoms may provide some added strength to these ligand–copper(II) bonds. This is evidently not a factor in copper bonding to the pyridyl nitrogen.

A comparison of bond angles of the metal ligand bonds for various thiosemicarbazone complexes is shown in Table 6. The nickel(II) complexes have larger bond angles than the copper(II) complexes for each of the following: S—Cu—^{1}N, S—Cu—^{2}N and ^{1}N—C—^{2}N, which is consistent with the nickel–ligand bonds being shorter. The larger angles reduce interelectronic repulsion for these shorter bonds. Of the angles involving the bromo ligands in [Ni(Lhexim)Br] and [Cu(Lhexim)Br][11] only Br—Cu—S (97.4°) is significantly different from Br—Ni—S (91.6°), so that the only nickel(II) complex's bond angle which is smaller than the copper(II) complex's angle is the one between the two longest metal ligand bonds. Table 6 shows fairly consistent bond angles for the different thiosemicarbazones for both the copper(II) and nickel (II) complexes. Bond angles seem to be less useful in identifying aspects of a complex that would indicate biological activity.

The greater biological activity of copper(II) thiosemicarbazones compared to the uncomplexed ligands, Table 7, is likely due to the extent of conjugation of the coordinated thiosemicarbazone anion. Since the copper(II) complex is more active against both fungi than the analogous nickel(II) complex, which has comparable activity to the uncomplexed ligand, it is likely that the ease of reduction of copper(II) is also significant. Electrochemical studies[20] have shown that the best antifungal agents in this series of compounds are those which have the lowest reduction potential for the copper(II) and for the coordinated thiosemicarbazone. The voltage vs Ag/AgCl for the reduction of the copper(II) in both complexes is -0.425 and for the coordinated thiosemicarbazone -1.225 V and -1.275 V for [Cu(Lpip)Cl] and [Cu(Lhexim)Cl], respectively.[20] Spectroscopic studies[13] indicate that the effectiveness of fungal growth inhibition of these thiosemicarbazone complexes is inversely related to the magnitude of $g_\parallel$ (i.e. inhibition increases with increasing covalency of ligand bonding). The room temperature powder $g_\parallel$ values are 2.159 and 2.145 for [Cu(Lpip)

Table 7. Antifungal activity of some metal thiosemicarbazone complexes

Compound	200[a]	400	600	1000	1600
Aspergillus niger					
HLpip	6.0[b]	6.0	6.0	7.3	7.7
[Cu(Lpip)Br]	15.6	16.4	18.6	19.8	19.3
HLhexim	7.7	8.3	9.5	10.5	10.8
[Cu(Lhexim)Br]	18.8	17.8	21.7	21.8	22.7
[Ni(Lhexim)Br]	8.2	9.2	11.2	11.3	10.3
Paecilomyces variotii					
HLpip	6.0	6.0	6.0	9.8	16.8
[Cu(Lpip)Br]	30.2	32.5	33.5	34.3	34.8
HLhexim	7.8	12.2	16.5	17.3	19.2
[Cu(Lhexim)Br]	25.3	26.0	26.2	26.3	26.3
[Ni(Lhexim)Br]	13.2	13.5	15.2	14.7	16.2

[a] $\mu g\ cm^{-3}$.
[b] mm diameter of growth inhibition zone (6.0 = no inhibition).

Cl][17] and [Cu(Lhexim)Cl],[16] respectively, and they are among the lowest for thiosemicarbazone complexes having the general formula (Cu(NNS)Cl]. A further indication of biological activity from this paper study appears to be the short $^{3}N—^{9}C$, long $^{9}C—S$, long $^{9}C—^{4}N$ and short Cu—S bond lengths for [Cu(Lpip)Br] and [Cu(Lhexim)Br] since these two compounds are among the most active antifungal agents of the more than 50 copper thiosemicarbazone complexes tested in this laboratory to date. All are related to the strength of coordination of the thiol sulphur. Further, a copper(II) complex with its weaker metal–ligand bonding compared to the analogous nickel(II) complex would be a stronger Lewis acid, which may be important to the biological activity. For example, the copper(II) complex, through its Lewis acidity, may be able to place the ligand in close proximity to the site of the thiosemicarbazone's inhibitory action against ribonucleotide reductase.[21]

Supplementary material

Atomic coordinates have been deposited with the Director, Cambridge Crystallographic Data Centre.

Acknowledgement—Acknowledgement is made to the Donors of the Petroleum Research Fund, administered by the American Chemical Society for the partial support of this research.

REFERENCES

1. J. P. Scovill, D. L. Klayman and C. F. Franchino, *J. Med. Chem.* 1982, **25**, 1261.
2. D. X. West, C. S. Carlson, C. P. Galloway, A. E. Liberta and C. R. Daniel, *Trans. Met. Chem.* 1990, **15**, 43.
3. D. X. West, C. S. Carlson, A. E. Liberta, J. N. Albert and C. R. Daniel, *Trans. Met. Chem.* 1990, **15**, 341 and references therein.
4. B. S. Garg, M. R. P. Kurup, S. K. Jain and Y. K. Bhoon, *Trans. Met. Chem.* 1988, **13**, 247 and references therein.
5. M. B. Ferrari, G. G. Fava, C. P. Pelizzi, P. Tarasconi and G. Tosi, *J. Chem. Soc., Dalton Trans.* 1987, 227.
6. C. F. Bell and C. R. Theocharis, *Acta Cryst.* 1987, **C43**, 26.
7. A. G. Bingham, H. Bogge, A. Muller, E. W. Ainscough and A. M. Brodie, *J. Chem. Soc., Dalton Trans.* 1987, 493.
8. E. W. Ainscough, E. N. Baker, A. M. Brodie, R. J. Cresswell, J. D. Ranford and J. M. Waters, *Inorg. Chim. Acta* 1990, **172**, 185.
9. E. W. Ainscough, A. M. Brodie, J. D. Ranford and J. M. Waters, *J. Chem. Soc., Dalton Trans.* 1991, 2195.
10. D. X. West, D. L. Huffman, J. S. Saleda and A. E. Liberta, *Trans. Met. Chem.* 1991, **16**, 565.
11. D. X. West, J. P. Scovill, J. V. Silverton and A. Bavoso, *Trans. Met. Chem.* 1986, **11**, 123.
12. R. J. Butcher and D. X. West, *Trans. Met. Chem.*, in press.
13. D. X. West, C. S. Carlson, K. J. Bouck and A. E. Liberta, *Trans. Met. Chem.* 1991, **16**, 271; A. E. Liberta and D. X. West, *Biometals* 1992, **5**, 121.

14. D. X. West, M. A. Lockwood, A. E. Liberta, X. Chen and R. D. Willett, *Trans. Met. Chem.*, in press.
15. J. P. Scovill, *Phosphorus, Sulfur and Silicon* 1991, **60**, 15.
16. D. X. West and D. S. Galloway, *Trans. Met. Chem.* 1988, **13**, 410.
17. D. X. West, D. S. Galloway and D. A. Case, *Trans. Met. Chem.* 1988, **13**, 415.
18. M. B. Ferrari, G. G. Fava, P. Tarasconi and C. Pelizzi, *J. Chem. Soc., Dalton Trans.* 1989, 361.
19. J. Valdez-Martinez, R. A. Toscano, M. Soriano-Garcia, M. Rubio, J. Gomez-Lara, M. A. Vazquez-M. and S. Carranza, *Polyhedron* 1989, **8**, 727.
20. A. S. Kumbhar, S. B. Padhye, D. X. West and A. E. Liberta, *Trans. Met. Chem.* 1991, **16**, 271; A. S. Kumbhar, S. B. Padhye, D. X. West and A. E. Liberta, *Trans. Met. Chem.* 1992, **17**, 446.
21. C. Chan-Stier, D. T. Minkel and D. H. Petering, *Bioinorganic Chem.* 1976, **6**, 203; W. E. Antholine, J. M. Knight and D. H. Petering, *J. Med. Chem.* 1976, **19**, 339; L. A. Saryan, E. Ankel, C. Krishnamurti, D. H. Petering and H. Elford, *J. Med. Chem.* 1979, **22**, 1218.

Polyhedron Vol. 12, No. 20, pp. 2499–2506, 1993
Printed in Great Britain

0277–5387/93 $6.00+.00
© 1993 Pergamon Press Ltd

HALOCUPRATES(II) OF TRIAMTERINIUM, A DIPROTONATED PTERIDINE DERIVATIVE. CRYSTAL STRUCTURE OF (TRIAMTERINIUM)$CuCl_4$. ELECTRONIC AND EPR CHARACTERIZATION OF (TRIAMTERINIUM)CuX_4 (X = Cl, Br)

M. J. LLOPIS, G. ALZUET, A. MARTIN and J. BORRÁS†

Dpto. Q. Inorgánica, Fac. Farmacia, Univ. Valencia, Spain

and

S. GARCÍA-GRANDA and R. DÍAZ

Dpto. Q. Física y Analítica, Fac. Química, Univ. Oviedo, Spain

(*Received* 20 *April* 1993 ; *accepted* 8 *June* 1993)

Abstract—The crystal structure of triamterinium tetrachlorocuprate(II), $(C_{12}H_{13}N_7)CuCl_4$, was determined by X-ray diffraction. The crystals are monoclinic, $P2_1/n$, with $a = 13.959(3)$, $b = 7.118(2)$, $c = 17.280(5)$ Å, $\beta = 99.99(2)°$, $V = 1690.9(9)$ Å^3 and $Z = 4$. A final R value of 0.031 was obtained. The structure consists of the $[CuCl_4]^{2-}$ anion and a triamterinium diprotonated cation. The $[CuCl_4]^{2-}$ anion shows a flattened tetrahedral geometry, the two larger Cl—Cu—Cl angles being 133.83 and 143.71°; the dihedral angle is 31.13°. The Cu—Cl distances range from 2.23 to 2.29 Å. The spectroscopic and magnetic results of $[CuCl_4]^{2-}$ and $[CuBr_4]^{2-}$ are in agreement with a high distortion of these ions from the tetrahedral configuration. According to the sites of protonation of the triamterene, the best donor atoms are the endocyclic N(3) and N(8) atoms.

Natural pteridine derivatives such as folic acid and biopterin are important co-factors in biological redox reactions.[1] Pteridines are fused-ring nitrogen heterocyclic compounds that function as co-factors for enzymes involved in hydroxylation[2] and methyl transfer[3] and as redox mediators. Variation of the substituents of the core of the folates has provided a synthetic anticancer drug, methotrexate.[4,5] At this time, two pterin co-factors are known for enzymes that also require a metal for a catalytic activity. Since pterins as co-factors in biological redox reactions are thus associated with metal ions and contribute to electron transfer in biological processes, information on pterin–metal interactions may give clues to the roles of metal ions in the utilization of dioxygen and concomitant electron transfer in relevant enzymatic reactions.

From the pteridine derivatives we have chosen triamterene(triam) (2,4,7-triamino-6-*o*-tolylpteridine ; Fig. 1), which is a potassium retaining diuretic which is widely used in the therapy of hypertension, mainly to prevent the K^+ losses which are caused by stronger natriuretic compounds like thiazides or loop diuretics.[6]

The structure activity relationship of the pteridine diuretics may be rationalized by assuming that the pteridines bind to some active sites at two points. The more important site involves a basic centre which in triamterene may be the N(1) and N(8) atoms. The other site probably involves the

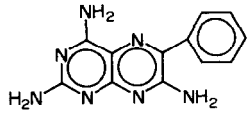

Fig. 1. Triamterene.

† Author to whom correspondence should be addressed.

phenyl substituent of triamterene and may be hydrophobic in nature.[7]

Triamterene has several nitrogen atoms which can behave as donors with metallic ions. The basic centre may be modified by the interaction of the metallic ions and these can increase or diminish the therapeutic activity of the drug. Another important point is that the complex formation can increase the solubility of these insoluble compounds.

Various recent reports exist in the literature for metal interactions with pteridine derivatives,[8–13] but the synthesis and characterization of metal–triam complexes have not yet been reported. On the other hand, there is great interest in the tetrahalocuprates(II) due to the fact that they show a high variety of coordination numbers and geometries[14–17] and, in some cases, a discontinuous reversible thermochromic behaviour.

We have initiated the synthesis and characterization of metal–triam complexes ; in this paper we report the first instance of metal compounds of triam, including the crystal structure of the triamterinium tetrachlorocuprate.

EXPERIMENTAL

Triam was kindly supplied as a powder material by Almirall Laboratories. All reagents used were of analytical grade. Due to the insolubility of triam, the complex formation reactions were investigated in acid media.

Synthesis of $[H_2triam][CuCl_4]$

Solid triam (1 mmol) was dissolved in concentrated HCl (25 cm^3) (35%) with continuous stirring by heating at 35°C. $CuCl_2 \cdot 2H_2O$ (3 mmol) was then added. When the mixture was stirred for *ca* 5 min, an orange microcrystalline precipitate appeared. The solid was collected by filtration and washed with benzene. After a few days single crystals, which were suitable for X-ray diffraction, were obtained in the filtrate. Yield : 68%. Found : C, 32.0 ; H, 3.1 ; N, 21.8 ; Cl, 29.3 ; Cu, 13.6. Calc. for $[H_2triam][CuCl_4]$: C, 31.3 ; H, 2.8 ; N, 21.3 ; Cl, 30.8 ; Cu, 13.8%.

Synthesis of $[H_2triam][CuBr_4]$

To a bromohydric solution of triam [1 mmol in 50 cm^3 of concentrated HBr (48%)] was added $CuBr_2$ (3 mmol) with continuous stirring. From the purple solution a microcrystalline solid precipitated. The precipitate was filtered, washed with benzene and dried at 70°C to constant weight. Yield : 45%. Found : C, 22.8 ; H, 1.9 ; N, 16.2 ; Cu, 10.0. Calc. for $[H_2triam][CuBr_4]$: C, 22.6 ; H, 2.0 ; N, 15.4 ; Cu, 9.9%.

Analyses were performed by elemental analyses for C, H and N and by AAS for copper.

Physical measurements

IR spectra of KBr/CsI pellets were recorded on a Perkin–Elmer 843 instrument. Electronic spectra in the UV–vis range were obtained with a Perkin–Elmer Lambda 15 spectrophotometer. Electronic spectra in the NIR region were registered with a Perkin–Elmer Lambda 9 spectrophotometer. EPR spectra of polycrystalline samples were recorded at *X*-band frequencies with a Bruker ER 200D spectrometer equipped with a liquid nitrogen continuous flow cryostat. Magnetic susceptibility data were collected on powdered samples for the compounds with the use of a Faraday-type magnetometer fitted with a liquid nitrogen continuous flow cryostat. Mercury tetrakis(thiocyanato) cobaltate was used as a susceptibility standard. All data were corrected for diamagnetism with the appropriate Pascal constants.

X-ray powder diffraction patterns were obtained through a Kristalloflex 810 Siemens diffractometer using Cu-K_α radiation.

Crystallographic data collection

Red crystal, size 0.43 × 0.26 × 0.13 mm. Throughout the experimental Mo-K_α radiation was used with a graphite crystal monochromator on an Enraf–Nonius CAD-4 single-crystal diffractometer ($\lambda = 0.71073$ Å). The unit cell dimensions were determined from the angular settings of 25 reflections with θ between 14 and 19°. The space group was determined to be $P2_1/n$ from the systematic absences. The intensity data of 3482 reflections, in the *hkl* range (16, 8, 20) to (0, 0, −20) and θ limits ($0 < \theta < 25°$) were measured using the ω–2θ scan technique and a variable scan rate with a maximum scan time of 60 s per reflection. The intensity of the primary beam was checked throughout the data collection by monitoring three standard reflections every 60 min. The final drift correction factors were between 1.01 and 0.99. On all reflections profile analysis was performed ;[18,19] an empirical absorption correction was applied, using Ψ scans[20] μ(Mo-K_α) = 1.94 mm^{-1} (correction factors were in the range 1.00–0.76). Symmetry equivalent reflections were averaged, $R_{int} = \Sigma(I - \langle I \rangle)/\Sigma I = 0.020$, resulting in 2967 unique reflections, of which only 2414 were observed with $I > 3\sigma(I)$. Lorentz and polarization corrections were applied and the data were reduced to $|F_o|$ values. The structure was solved by

Patterson interpretation using the program SHELXS86[21] and Fourier synthesis. Isotropic least-squares refinement, using SHELXS76,[22] converged to $R = 0.097$. At this stage an additional empirical absorption correction was applied,[23] resulting in a further decrease of R to 0.085. The maximum and minimum absorption correction factors were 1.28 and 0.88, respectively. Further anisotropic refinements followed by a difference-Fourier synthesis allowed the location of all the hydrogen atoms.

During the final stages of the refinement the positional parameters and the anisotropic thermal parameters of the non-hydrogen atoms were refined. All hydrogens were refined isotropically. The final conventional agreement factors were $R = 0.031$ and $wR = 0.031$ for the observed reflections and variables. The function minimized was $\Sigma w(F_o - F_c)^2$, $w = 1/[\sigma^2(F_o) + 0.00010F_o^2]$ with $\sigma(F_o)$ from counting statistics. The maximum shift-to-ESD ratio in the last full-matrix least-squares cycle was less than 0.1. The final difference-Fourier map showed no peaks higher than 0.35 e $Å^{-3}$ or deeper than -0.54 e $Å^{-3}$. Atomic scattering factors were taken from the International Tables for X-ray Crystallography (1974).[24] The plot was made with PLUTO.[25] Geometrical calculations were made with PARST.[26] All calculations were made on a MicroVAX-3400 at the Scientific Computer Center of the University of Oviedo.

RESULTS AND DISCUSSION

The X-ray powder patterns have been recorded showing that the triamterinium tetrahalocuprates are isomorphous.

Description of the $[H_2triam][CuCl_4]$ *crystal structure*

Molecular geometry data are collected in Table 1. The structure, which is shown in Fig. 2, together with the atomic numbering scheme, consists of one independent H_2triam^{2+} cation and one $CuCl_4^{2-}$ anion. In the anion there is a significant deviation

Table 1. Bond lengths (Å) and angles (°) with ESDs in parentheses

Cu(1)—Cl(1)	2.264(1)	Cu(1)—Cl(2)	2.249(1)
Cu(1)—Cl(3)	2.289(1)	Cu(1)—Cl(4)	2.229(1)
C(1P)—C(2P)	1.404(4)	C(1P)—C(6P)	1.407(4)
C(1P)—C(6)	1.473(4)	C(2P)—C(3P)	1.388(5)
C(3P)—C(4P)	1.397(5)	C(4P)—C(5P)	1.365(6)
C(5P)—C(6P)	1.391(5)	N(1)—C(2)	1.335(4)
N(1)—C(8A)	1.335(4)	C(2)—N(2)	1.309(4)
C(2)—N(3)	1.376(4)	N(3)—C(4)	1.355(4)
C(4)—N(4)	1.307(4)	C(4)—C(4A)	1.427(4)
C(4A)—N(5)	1.353(4)	C(4A)—C(8A)	1.389(4)
N(5)—C(6)	1.317(4)	C(6)—C(7)	1.462(4)
C(7)—N(7)	1.315(4)	C(7)—N(8)	1.340(4)
N(8)—C(8A)	1.374(4)		

Cl(2)—Cu(1)—Cl(1)	143.71(5)	Cl(3)—Cu(1)—Cl(1)	93.37(5)
Cl(3)—Cu(1)—Cl(2)	95.91(5)	Cl(4)—Cu(1)—Cl(1)	100.10(6)
Cl(4)—Cu(1)—Cl(2)	98.42(5)	Cl(4)—Cu(1)—Cl(3)	133.83(5)
C(2P)—C(1P)—C(6P)	118.8(3)	C(6)—C(1P)—C(6P)	122.8(3)
C(6)—C(1P)—C(2P)	118.2(3)	C(5P)—C(6P)—C(1P)	119.8(3)
C(4P)—C(5P)—C(6P)	120.9(3)	C(3P)—C(4P)—C(5P)	120.3(3)
C(2P)—C(3P)—C(4P)	119.8(3)	C(3P)—C(2P)—C(1P)	120.3(3)
N(5)—C(6)—C(1P)	117.1(2)	C(7)—C(6)—C(1P)	123.1(2)
C(7)—C(6)—N(5)	119.7(3)	C(4A)—N(5)—C(6)	119.8(2)
C(4)—C(4A)—N(5)	120.1(2)	C(8A)—C(4A)—N(5)	123.6(2)
C(8A)—C(4A)—C(4)	116.2(3)	N(4)—C(4)—C(4A)	123.1(3)
N(3)—C(4)—C(4A)	116.2(3)	N(3)—C(4)—N(4)	120.6(3)
C(2)—N(3)—C(4)	123.1(2)	N(2)—C(2)—N(3)	117.9(3)
N(1)—C(2)—N(3)	122.3(3)	N(1)—C(2)—N(2)	119.8(3)
C(8A)—N(1)—C(2)	115.2(2)	N(1)—C(8A)—C(4A)	127.0(3)
N(8)—C(8A)—C(4A)	116.0(3)	N(8)—C(8A)—N(1)	117.0(3)
C(7)—N(8)—C(8A)	123.0(3)	N(8)—C(7)—C(6)	117.8(2)
N(7)—C(7)—C(6)	123.7(3)	N(7)—C(7)—N(8)	118.5(3)

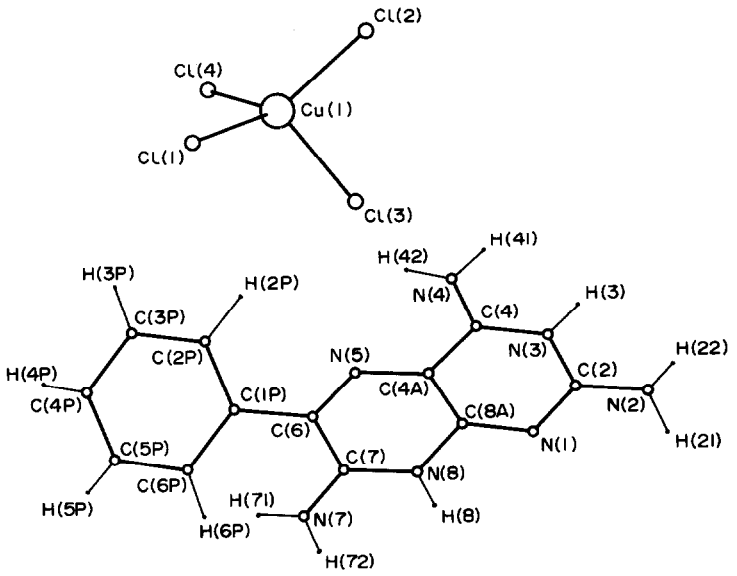

Fig. 2. A perspective view and the atomic numbering scheme of $[H_2triam][CuCl_4]$.

from both of the two ideal geometries, square planar and tetrahedral, so that the Cl—Cu—Cl angles around the metal atom are 143.71(5), 95.91(5), 98.42(5), 93.37(5), 100.10(6) and 133.83(5)°. The Cu—Cl bond lengths are, however, regular at 2.264(1), 2.289(1), 2.249(1) and 2.229(1) Å. Two of the Cu—Cl distances are longer owing to their extensive involvement in hydrogen bonding. Cl(1) is hydrogen bonded to H(N8), Cl(3) is hydrogen bonded to H(N2) and H(N4), Cl(2) is hydrogen bonded to H(N2) and H(N4) and Cl(4) is hydrogen bonded to H(N7) and H(N4), with Cl—H distances of 2.20, 2.40, 2.30 and 2.30, respectively.

In general terms the structure of the $CuCl_4^{2-}$ anion is sensitive to the nature of the cation. Thus, for small cations there is octahedral 4+2 coordination, but with large and non-spherical cations four-coordination, commensurate with a flattened tetrahedral geometry, is found, e.g. [N-(2-ammonioethyl)morpholinium][$CuCl_4$].[27] In a recent publication Halvorson *et al.*[14] have analysed over 60 crystal structure determinations containing the $CuCl_4^{2-}$ anion. Variations in angular deformations of the $CuCl_4^{2-}$ anions between these known structures have been examined from a plot of the *trans*-Cl—Cu—Cl angle against frequency of occurrence, which shows the majority of the structures contain *trans* angles between 125 and 145°. In general, hydrogen bonds tend to remove charge from the chlorine atoms. This reduces the electrostatic repulsions between the chlorine atoms and allows the $CuCl_4^{2-}$ ions to move towards a square planar geometry. Typically values range from 130° for large non-hydrogen bonding cations to 180° for those cations which can form extensive hydrogen bond interactions.

The deformation from the tetrahedral geometry can be expressed by the Cl(1)—Cu—Cl(4)—Cl(2)—Cu—Cl(3) = 31.13(4)° dihedral angle. This dihedral angle indicates a very strong distortion if we take into account that this angle is 90° for tetrahedral geometry and 0° for square planar.[28] The Cl---N interactions may explain the large distortion of the $[CuCl_4]^{2-}$ ion from the tetrahedral configuration.

With respect to the cation, the first aspect to be noted is that the protonation takes place in the endocyclic nitrogen N(3) and N(8) atoms.

Table 2 compares the bond distances and angles of the crystal structure of the triam[29] and the triamterinium cation observed in the structure of the $[H_2triam][CuCl_4]$ compound. We can appreciate an increase of double bond character in the C—NH_2 distances as a consequence of the higher electronic demand of the protonated contiguous endocyclic nitrogen atoms. Furthermore, the protonation increases the C—N—C bond angles (C—N—C 123° in the cation and 117.3°, 116.1° in the triam). Bond angles are less than 120° at the unprotonated N ring atoms.

The torsion angle C(2P)—C(1P)—C(6)—N(5) is 35.4(4)°, similar to that observed in the triamterene. This angle indicates the twist between the phenyl and fused rings and is related to the antifolate activity.[29]

Molecules are linked by an intricate and unusual

Table 2. Comparison of the bond distances of the triam and the triamterinium cation

	Triamterinium	Triam
N(1)—C(8A)	1.335(4)	1.360
C(2)—N(3)	1.376(4)	1.377
C(4)—N(4)	1.307(4)	1.350
C(4A)—N(5)	1.353(4)	1.354
N(5)—C(6)	1.317(4)	1.316
C(7)—N(7)	1.315(4)	1.355
N(8)—C(8A)	1.374(4)	1.358
N(1)—C(2)	1.335(4)	1.327
C(2)—N(2)	1.309(4)	1.351
N(3)—C(4)	1.355(4)	1.320
C(4)—C(4A)	1.427(4)	1.431
C(4A)—C(8A)	1.389(4)	1.398
C(6)—C(7)	1.462(4)	1.441
C(7)—N(8)	1.340(4)	1.338

network of hydrogen bonds (Table 3 and Fig. 3). It is noteworthy that the only intramolecular hydrogen bond in the triamterinium cation is formed by the N(4)—N(5) atoms, the opposite to that found in the triamterene where the stronger hydrogen bonds are formed by N(2) and the N(4) atom forms only one weak hydrogen bond. The cation and anion are linked by strong hydrogen bonding between Cl and the protonated N(3) and N(8) atoms.

As we have indicated the isomorphous character of the tetrabromocuprate complex permits us to suggest a similar distorted tetrahedron around the copper(II) ion.

IR and electronic spectra

The characterization data of the solids can readily be interpreted once the crystal structure is known.

The IR spectra of the dihydrohalide salts show a complex series of absorption bands at 3440–3200 and 2900–2650 cm^{-1}. The first group of bands corresponds to ν(N—H) vibrations and are shifted with respect to those of the ligand, probably due to the different hydrogen bonding arrangement shown in the crystal structures. The second region of bands can be attributed to N—H^+ stretching vibrations; the low frequencies observed is a consequence of the strong hydrogen bonding between the triamterinium cation and the CuX_4^{2-} anion.[28]

The far-IR spectrum of [H_2triam][$CuCl_4$] shows a new band with respect to the ligand at 300 cm^{-1}, which is assigned to a ν(Cu—Cl) vibrations.[28]

The solid reflectance electronic spectrum of [H_2triam][$CuCl_4$] shows two broad *d–d* transitions at 7460 and 10,720 cm^{-1}. The energies of the *d–d* bands are considerably higher than those normally found for flattened tetrahedra and may be explained by the greater distortion toward planarity, which increases the overall splitting of the *d*-orbital energy levels.[30]

Some attempts have been made to correlate

Table 3. Hydrogen bonding and geometrical parameters

Donor—H	Donor···acceptor	H···acceptor	Donor—H···acceptor
N(4)—H(42)	N(4)···N(5)	H(42)···N(5)	N(4)—H(42)···N(5)
0.86(4)	2.821(4)	2.56(3)	99.(3)
N(7)—H(72)	N(7)···Cl(4)(1)	H(72)···Cl(4)(1)	N(7)—H(72)···Cl(4)(1)
0.87(3)	3.239(3)	2.73(4)	118.(3)
N(4)—H(42)	N(4)···Cl(4)(2)	H(42)···Cl(4)(2)	N(4)—H(42)···Cl(4)(2)
0.86(4)	3.369(3)	2.56(4)	157.(3)
N(4)—H(41)	N(4)···Cl(2)(2)	H(41)···Cl(2)(2)	N(4)—H(41)···Cl(2)(2)
0.92(3)	3.326(3)	2.71(3)	125.(2)
N(3)—H(3)	N(3)···Cl(3)(3)	H(3)···Cl(3)(3)	N(3)—H(3)···Cl(3)(3)
0.93(5)	3.080(3)	2.16(5)	169.(5)
N(4)—H(41)	N(4)···Cl(3)(3)	H(41)···Cl(3)(3)	N(4)—H(41)···Cl(3)(3)
0.92(3)	3.483(3)	2.74(3)	138.(2)
N(8)—H(8)	N(8)···Cl(1)(4)	H(8)···Cl(1)(4)	N(8)—H(8)···Cl(1)(4)
0.86(3)	3.054(3)	2.20(3)	172.(3)
N(2)—H(22)	N(2)···Cl(2)(4)	H(22)···Cl(2)(4)	N(2)—H(22)···Cl(2)(4)
0.96(4)	3.294(3)	2.34(4)	170.(4)

Symmetry code: (1) $-x+1/2, +y+1/2, -z-1/2$; (2) $+x, +y+1, +z$; (3) $-x, -y+1, -z$; (4) $+x-1/2, -y+1/2, +z-1/2$.

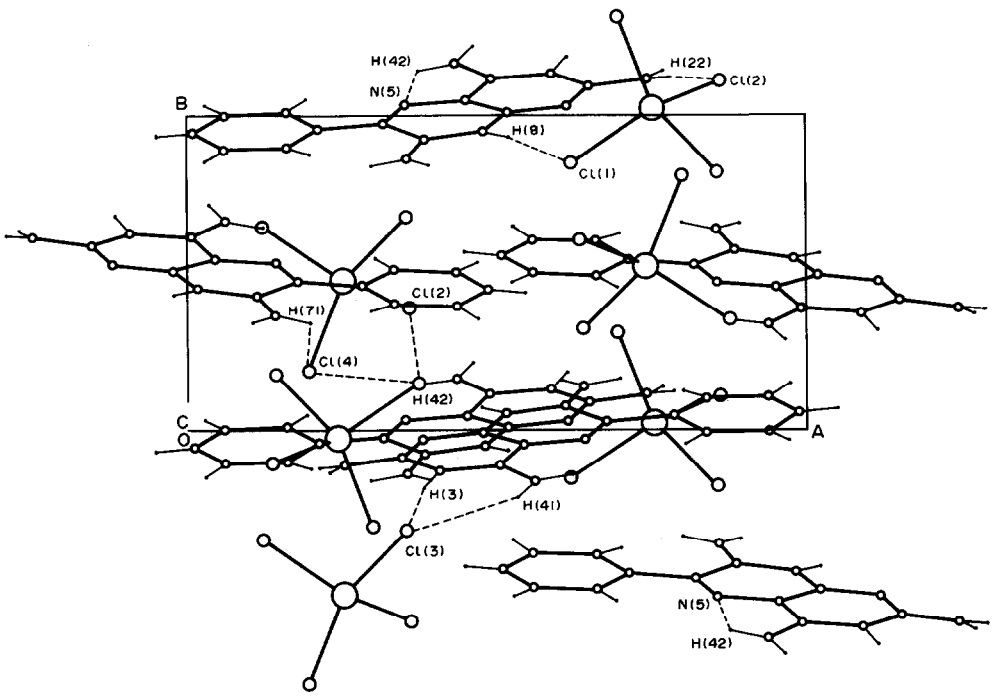

Fig. 3. A view of the molecular packing along the *z*-axis showing the hydrogen bonding network.

empirically the maximum of the *d–d* transition for several tetrachlorocuprate(II) salts with the amount of distortion from T_d symmetry determined from X-ray crystal structure studies. Battaglia *et al.*[28] correlated the maximum *d–d* spectra vs distortion expressed as the Cl—Cu—Cl dihedral angle. Halvorson *et al.*[14] in previously cited work compared the *d–d* electronic absorption energy with the average *trans* angle. If we represent the dihedral angle of $[H_2triam][CuCl_4]$ in the diagram of this work, the value of the maximum energy is 10,800 cm^{-1}, close to 10,720 cm^{-1} observed in the electronic spectrum.

The electronic spectrum of $[H_2triam][CuCl_4]$ also presents broad bands at 21,740, 25,190 and 38,460 cm^{-1} assigned to a $\pi a_2(N) \rightarrow b_2$ MLCT, $\pi \rightarrow \pi^*$(L—L) and $\sigma \rightarrow b_2$ MLCT.[31]

The UV–vis spectrum of $[H_2triam][CuBr_4]$ shows three bands in the visible region at 15,970, 18,830 and 23,580 cm^{-1}. These bands, according to the literature,[32,33] are associated with a ligand-to-metal charge-transfer transition, since the *d–d* transitions are expected in the near-IR region in the case of the $CuBr_4^{2-}$ chromophore.

The *d–d* transitions appear as a broad feature in the 5000–12,500 cm^{-1} region with several peaks. Using a simulation program with Gaussian line shape it was possible to identify all the *d–d* transitions of the $CuBr_4^{2-}$ ion. According to Willet *et al.*[17] the transitions at 10,750, 10,000, 7270 and 6100 cm^{-1} correspond to

$$^2A_{1(dxy)} \longrightarrow {}^2B_{2(dxz)}$$
$$\longrightarrow {}^2A_{2(dx^2-y^2)}$$
$$\longrightarrow {}^2B_{1(dyz)}$$
$$\longrightarrow {}^2A_{1(dz^2)}$$

in the splitting of the ^2E level in the D_{2d} symmetry into non-degenerate $^2B_1$ and $^2B_2$ levels in C_{2v} symmetry due to the orthorhombic distortion.

Magnetism and EPR spectra

The magnetic moment at room temperature of $[H_2triam][CuCl_4]$ is 1.72 B.M., similar to that obtained for other tetrachlorocuprates.[34]

Powder magnetic susceptibility measurements of $[H_2triam][CuBr_4]$ were made in the temperature range 75–300 K. From the plot of the μ_{eff} vs T it can be deduced that the magnetic interactions obey a Curie–Weiss dependence on temperature with $\theta = 24.4$ K.

Figure 4 shows the EPR spectrum of a finely ground powder sample of $[H_2triam][CuCl_4]$ at room temperature. It is an axial copper d^9 EPR spectrum with $g_\parallel = 2.38$ and $g_\perp = 2.09$. No hyperfine structure was observed; the absence of resolved hyperfine structure in the EPR has been attributed to a

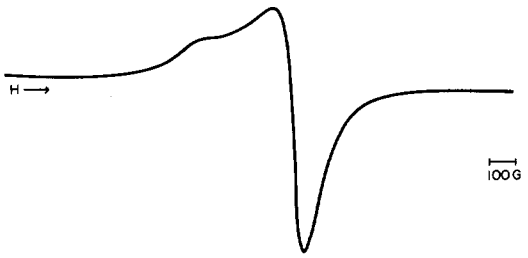

Fig. 4. EPR powder spectrum of $[H_2triam][CuCl_4]$.

strong admixture of the 4*p* state into $3d(t_2)$ orbitals of the copper ion.[35] Sharnoff[36] has reported the EPR spectra of the tetrachlorocuprate(II) ion with a tetrahedral geometry with similar *g* parameters to those found in the EPR of $[H_2triam][CuCl_4]$. Sharnoff has indicated that the values of *g* seem to be those of an octahedral copper(II) polyhedron, in spite of the fact that they are obtained from a distorted copper(II) tetrahedron. This is a result of the presence of the wave functions with a significant amount of central ion orbitals belonging to the 4*p* shell. The LCAO–MO analysis of Cs_2CuCl_4 shows that this orbital contains 70.3% 3*d* character, 11.7% 4*p* character and 18% ligand character. Battaglia *et al.*[37] compared the *g*-values of some tetrachlorocuprates(II) with the *trans* angle and suggest that the discrepancy may be due to that fact that the local pseudo-S_4 axes are not parallel to the tetragonal *c*-axis.

In summary, the resolution of the crystal structure and the study of spectroscopic properties of the tetrahalide salts permits us to identify the best donor atom [endocyclic N(3) and N(8)] of the drug and, as a consequence, to study its behaviour as a ligand.

Supplementary material

Final positional and thermal parameters, anisotropic thermal parameters, hydrogen-atom parameters, distances and angles involving hydrogen atoms, least-squares planes data, principal torsion angles and list of structure amplitudes have been deposited.

Acknowledgement—We greatly appreciate financial support from the Spanish CICYT(FAR 91-197).

REFERENCES

1. R. L. Blakley and S. J. Benkovic (Editors), *Folates and Pterins*. Wiley, New York (1985).
2. S. J. Benkovic, *Ann. Rev. Biochem.* 1980, **49**, 227.
3. P. Van Beelen, J. W. Van Neck, R. M. de Cock, G. D. Vogels, W. Guijt and C. A. G. Hasnoot, *Biochemistry* 1984, **23**, 4448.
4. W. Pfeiderer, in *Biochemical and Clinical Aspects of Pteridines* (Edited by H. Watchter, H. C. Curtius and W. Pfeiderer). DeGruyter, Berlin (1982).
5. R. L. Blakley and L. Cocco, *Biochemistry* 1985, **24**, 4702.
6. H. Priewer, H. Kraft and E. Mutschler, *Arzneim.-Forsch/Drug Res.* 1986, **36**, 213.
7. M. E. Wolff, in *Burger's Medicinal Chemistry*, Part III, 4th edn. John Wiley and Sons, New York (1981).
8. S. J. Nieter Burgmayer and E. I. Stiefel, *Inorg. Chem.* 1988, **27**, 4059.
9. T. Kohzuma, A. Odani, Y. Morita, M. Takani and O. Yamauchi, *Inorg. Chem.* 1988, **27**, 3854.
10. E. C. Taylor, P. S. Ray and I. S. Darwish, *J. Am. Chem. Soc.* 1989, **111**, 7664.
11. R. Hille, G. N. George, M. K. Eidsness and S. P. Cramer, *Inorg. Chem.* 1989, **28**, 4018.
12. A. Abelleira, R. D. Galang and M. H. Clarke, *Inorg. Chem.* 1990, **29**, 633.
13. T. Manfredini, G. C. Pellacani, A. Bonamartini-Corradi, L. P. Battaglia, G. G. T. Guarini, J. G. Giusti, G. Pont, R. D. Willett and D. X. West, *Inorg. Chem.* 1990, **29**, 2221.
14. K. E. Halvorson, C. Patterson and R. D. Willet, *Acta Cryst.* 1990, **B46**, 508.
15. J. G. H. Du Preez, B. A. M. Van Brecht and I. Warden, *Inorg. Chim. Acta* 190, **171**, 121.
16. M. R. Sundberg, R. Kivekas, J. Ruiz, J. M. Moreno and E. Colacio, *Inorg. Chem.* 1992, **31**, 1062.
17. A. C. Massabni, O. R. Nascimento, K. Halvorson and R. D. Willet, *Inorg. Chem.* 1992, **31**, 1779.
18. M. S. Lehman and F. K. Larsen, *Acta Cryst.* 1974, **A30**, 580.
19. D. F. Grant and E. J. Gabe, *J. Appl. Cryst.* 1978, **11**, 114.
20. A. C. T. North, D. C. Phillips and F. S. Mathews, *Acta Cryst.* 1968, **A24**, 351.
21. G. M. Sheldrick, SHELXS86, in *Crystallographic Computing 3* (Edited by G. M. Sheldrick, C. Kruger and R. Goddard), p. 175. Clarendon Press, Oxford (1985).
22. G. M. Sheldrick, SHELX76. Program for Crystal Structure Determination. University of Cambridge, U.K. (1976).
23. N. Walker and D. Stuart, *Acta Cryst.* 1983, **A39**, 158.
24. *International Tables for X-ray Crystallography*, Vol. IV. Kynoch Press, Birmingham (Present distributor Kluwer Academic Publishers, Dordrecht) (1974).
25. W. D. S. Motherwell and W. Clegg, PLUTO, Program for Plotting Molecular and Crystal Structures. University of Cambridge, U.K. (1978).
26. M. Nardelli, *Comp. Chem.* 1983, **7**, 95.
27. L. P. Battaglia, A. Bonammartini Corradi, G. Marcotrigiano, L. Menabue and G. C. Pellacani, *Inorg. Chem.* 1982, **21**, 3919.
28. L. P. Battaglia, A. Bonammartini Corradi, G. Marcotrigiano, L. Menabue and G. C. Pellacani, *Inorg. Chem.* 1979, **18**, 148.

29. C. H. Schwalbe and G. J. B. Williams, *Acta Cryst.* 1987, **C43**, 1097.
30. R. L. Harlow, W. J. Wells, G. W. Watt and S. H. Simonsen, *Inorg. Chem.* 1975, **14**, 1768.
31. R. D. Willett, O. L. Liles and C. Michelson, *Inorg. Chem.* 1967, **10**, 1885.
32. P. S. Braterman, *Inorg. Chem.* 1963, **2**, 448.
33. G. Marcotrigiano, L. Menabue, G. C. Pellacani and M. Saladini, *Inorg. Chim. Acta* 1979, **34**, 43.
34. E. A.Boudreaux and L. N. Mulay, *Theory and Applications of Molecular Paramagnetism*, John Wiley and Sons, New York (1976).
35. C. A. Bates, W. S. Moore, K. J. Standley and K. W. H. Stevens, *Proc. Fis. Soc.* 1962, **79**, 73.
36. M. Sharnoff, *J. Chem. Phys.* 1965, **42**, 3383.
37. A. Bonamartini-Corradi, L. P. Battaglia, J. Rubenacker, R. D. Willet, T. E. Grigereit, P. Zhou and J. E. Drumheller, *Inorg. Chem.* 1992, **31**, 3859.

Polyhedron Vol. 12, No. 20, pp. 2507–2511, 1993
Printed in Great Britain

0277–5387/93 $6.00+.00
© 1993 Pergamon Press Ltd

DINUCLEAR OXOVANADIUM(IV) COMPOUND WITH ALKOXYALCOHOL: SYNTHESIS AND STRUCTURAL STUDY OF $\{VOCl[OCH(CH_3)CH_2OCH_3]\}_2$

GISELE FOULON, JEAN-DOMINIQUE FOULON and NADINE HOVNANIAN*

Laboratoire de Physicochimie des Matériaux, URA 1312, ENSCM 8 rue Ecole Normale, 34053 Montpellier Cédex 1, France

(*Received* 21 *April* 1993; *accepted* 4 *June* 1993)

Abstract—The reaction between $VOCl_3$ and 3 equivalents of sodium 1-methoxy-2-propanoxide in a mixture of toluene/1-methoxy-2-propanol leads, after removal of the salt and crystallization of the concentrated filtrate, to a vanadium(IV) compound which has been characterized by the usual techniques (elemental analysis, IR, MS, EPR, ^1H and ^{51}V NMR) and X-ray diffraction as a dimeric five-coordinate oxovanadium(IV) chloride dialkoxide, $\{VOCl[OCH(CH_3)CH_2OCH_3]\}_2$. This compound can also be obtained from $VOCl_3$ with 1-methoxy-2-propanol in THF using ammonia gas. One of the two oxygen atoms from each methoxyalkoxo group bridges the vanadium centres yielding a planar V_2O_2 core. Surprisingly, a *cis* configuration around the V—O—V—O ring is adopted both by oxo groups and chlorine atoms.

Oxoalkoxovanadium complexes are attractive sources of molecular oxide precursors for sol–gel processes.[1] They can lead also to vanadium alkoxo compounds of high interest in catalytic and biological applications.[2]

A number of vanadium oxoalkoxides derived from primary, secondary and tertiary monoalcohols have been synthesized from V_2O_5, NH_4VO_3, $VOCl_3$ or by ester-exchange reactions[3]. Some of them have been structurally characterized as polymeric species such as $[VO(OMe)_3]_\infty$[4] or five-coordinate complexes such as $VO(OCH_2CH_2Cl)_3$[5] and $[VO(cyclo\text{-}C_5H_9O)_3]_2$[6]; the main character is that alkoxide ligands often act as bridging groups. The literature also mentions crystallographic data for derivatives with potential polydentate alcohols, particularly diols in dimeric or tetrameric associations. These polymerizations are achieved by two different bridging structural arrangements between the vanadium centre and the diols: either one of the oxygen atoms of each of the diol moieties bridges two vanadium centres[7] or each alkoxide oxygen atom is coordinated to only one metal atom.[8] Note that recently a hydrothermal synthesis based on polyols such as $CH_3C(CH_2OH)_3$ or $CH_3CH_2C(CH_2OH)_3$ yielded hexavanadium polyoxo alkoxide anion clusters.[9]

We have decided to study the reactivity of $VOCl_3$ towards alkoxyalcohols, since these derivatives are used as additives in sol–gel techniques, yielding multicomponent oxides, in order to avoid formation of heterogeneous media, to slow down hydrolysis rates and/or stabilize gels.[10] Alkoxyalcohols have proved to react easily with various transition metals, main group elements or lanthanides yielding stable and highly soluble alkoxide derivatives.[11]

In this paper we describe the synthesis, X-ray crystallographic characterization and spectroscopic study of $\{VOCl[OCH(CH_3)CH_2OCH_3]\}_2$, a five-coordinate oxovanadium (IV) chloride dialkoxide compound obtained from 1-methoxy-2-propanol.

EXPERIMENTAL

All manipulations were routinely performed under argon using Schlenk tubes and vacuum-line techniques with solvents purified by standard methods. $VOCl_3$ was used as received. ^1H and ^{51}V NMR and IR spectra were run on Bruker AC-250 and IR FT Nicolet ZDX spectrometers, respectively. $\delta(^{51}V)$ values are quoted relative to $VOCl_3$ and the

* Author to whom correspondence should be addressed.

spectra in non-deuterated solvents (parent alcohol) were recorded with external lock (D_2O). IR spectra were obtained as Nujol mulls between KBr plates. Mass spectra were recorded on a 300 DX JEOL by Electronic Impact. EPR spectra were recorded on a Bruker ER 200D spectrometer, operating at *X*-band with 100 KHz field modulation; the measurements were made on a solid sample at room temperature. Analytical data were obtained from the Centre de Microanalyses du CNRS.

Synthesis of $\{VOCl[OCH(CH_3)CH_2OCH_3]\}_2$ **(1)**

Pieces of sodium metal rods (1.52 g, 66 mmol) were slowly added under vigorous stirring to a solution of 1-methoxy-2-propanol (8 cm^3, 79.2 mmol) in toluene (15 cm^3). The solution was heated as the reaction slowed down. The mixture was stirred at room temperature overnight until all the sodium metal was consumed. The solution was then cooled at 0°C and vanadium oxytrichloride (2 cm^3, 21.2 mmol) was added dropwise under a slow argon flow. The reaction was exothermic and the colorless solution turned brown–red. The mixture was stirred for 12 h at room temperature and then filtered. After concentration the brown–red filtrate was left to crystallize at 5°C over a few days. Dark blue needle-shaped crystals were formed. Yield: 40% based on vanadium. Found: C, 25.2; H, 4.6; Cl, 17.9; V, 26.3. Calc. for $C_8H_{18}O_6Cl_2V_2$: C, 25.0; H, 4.7; Cl, 18.5; V, 26.6.%. IR (cm^{-1}): 1307, 1258, 1159, 1089, 1019, 962, 864, 801, 723, 674, 541, 462, 354. SM (*m/z*, EI), OR = $OCH(CH_3)CH_2OMe$: $[VOCl(OR)]_2$ (12%), $V_2O_2Cl(OR)_2$ (10%), $V_2OCl(OR)_2$ (7%), $VO_2Cl(OR)_2$ (13%), VO(OR) $Cl(CHCH_2OMe)$ (6%), VO(OR)$(CHCH_2OMe)$ (5%), VO(OR) (5%), $OMeCH_2CH(CH_3)$ (100%), $OMeCH_2$ (30%). ^1H NMR (CD_2Cl_2, ppm): 1.09 m (CH_3, 3H); 3.15 m–3.31 m (CH_2 and CH_3, 5H); 3.9 m (CH, 1H). ^{51}V NMR (1-methoxy-2-propanol, ppm): −573.1 (1); −573.9 (1).

Alternative synthesis of **1**

$VOCl_3$ (2 cm^3, 21 mmol) was added to THF (40 cm^3) immediately yielding a dark red solution. After addition of 1-methoxy-2-propanol (8 cm^3, 79.2 mmol) the dark red solution was stirred. Then ammonia gas was bubbled at intermittent intervals of 2–5 min until the white fog formed above the reaction mixture disappeared. The solution became bright orange, then orange–white. After removal of NH_4Cl by filtration the bright orange filtrate was concentrated and left to crystallize at 5°C. Dark blue crystals were formed.

Crystallographic studies

A suitable crystal of $\{VOCl[OCH(CH_3)CH_2OCH_3]\}_2$ was mounted onto a Siemens P3 automatic diffractometer. Unit cell parameters were obtained from least-squares fit to the automatically centred settings for 20 reflections. The crystal parameters and basic information related to data collection and structure refinement are summarized in Table 1. The profile fitting option of the XDISK program[12] was used during data reduction in order to correct 25% of decay. No correction for absorption was made. All calculations were performed on a VAX 3100. Complex neutral-atom scattering factors were employed. Anomalous dispersion terms were used. Positions for the vanadium and chlorine atoms were obtained from a Patterson syn-

Table 1. Crystallographic data of $\{VOCl[OCH(CH_3)CH_2OCH_3]_2\}$

Compound	$C_8H_{18}O_6Cl_2V_2$
Molecular weight	382.9
Crystal system	Monoclinic
Space group	$P2_1/c$
a (Å)	14.104(7)
b (Å)	10.356(4)
c (Å)	11.388(8)
β (°)	111.75(5)
V (Å^3)	1544(1)
Z	4
D (calc.) (g cm^{-3})	1.647
F(000) (e-)	776
Temperature (K)	293
Radiation	Mo-K_α
Scan type	ω–2θ
Scan width	$1.2+0.35\tan\theta$
hkl limits	$+h, +k, \pm l$
Reference reflections	3 every 100 reflections
Intensity stability	25% of decay (during data collection)
Data collected	1432
Unique data used ($F_0^2 > 3\sigma(F_0)^2$)	940
μ (cm^{-1})	15.7
R^a	0.0463
$R_w{}^a$	0.0545
Weight	$\omega = 1/[\sigma^2(F)+0.0009F^2]$
(Δ/σ) max^b	0.001
Residual electron density (e Å^{-3})	±0.4

[a] The quantity minimized in the least-squares procedure is: $w(|F_0|-|F_c|)^2$. $R = \Sigma||F_0|-F_c||/\Sigma|F_0|$; $R_w = [\Sigma w(|F_0|-|F_c|)^2/\Sigma w(F_0)^2]^{1/2}$.

[b] Maximum ratio of the rms shift to standard deviation observed for the last cycle of refinement.

thesis using SHELXS-86[13] and were confirmed by subsequent development of the structure. All remaining non-hydrogen atoms were found by successive electron density map calculations using SHELX 76.[14] Anisotropic temperature factors were introduced for all non-hydrogen atoms. Hydrogen atoms were placed in calculated positions (C—H = 1.08 Å) and were no further refined, but recalculated after each cycle. Positional parameters and anisotropic thermal parameters are given as supplementary material.

RESULTS AND DISCUSSION

The exothermic reaction of $VOCl_3$ with 3 equivalents of sodium 1-methoxy-2-propanoxide in a mixture of toluene/1-methoxy-2-propanol yielded a dark blue solid, $\{VOCl[OCH(CH_3)CH_2OCH_3]\}_2$ (**1**). This compound was also obtained by reaction between $VOCl_3$ and 1-methoxy-2-propanol in THF using ammonia gas. This compound crystallized from the concentrated reaction medium after removal of NaCl or NH_4Cl.

Despite the bubbling of NH_3 through the solution or the reaction with an alkali alkoxide, chloride ligands are still present and a reaction of reduction has occurred. Since solutions of light-sensitive vanadium(V) compounds when they are exposed to diffuse daylight or UV turn to light blue vanadium(IV) simultaneously with a black powder precipitate, we have carried out the syntheses in the dark and reproducible quantities of $\{VOClOCH(CH_3)CH_2OCH_3]\}_2$ were obtained. According to the literature no reduction products are formed by reaction of $VOCl_3$ with functionalized alcohols when methylene chloride is used as a solvent of reaction or of recrystallization.[15] However, some reduction reactions occurred when vanadium(III) and (IV) carboxylates were previously prepared from $VOCl_3$.[16]

$\{VOCl[OCH(CH_3)CH_2OCH_3]\}_2$ is soluble in polar organic solvents such as parent alcohol or DMSO and insoluble in pentane. Its dissolution in chlorinated solvents (CH_2Cl_2) or in toluene or THF is slow and results in a partially clear and blue solution. The oxidation degree of this oxovanadium chloride alkoxide correlates well with its colour, either in the solid state or in solution. Sol–gel investigations have shown us that in the presence of low or high water concentration, in the parent alcohol, compound **I** yields clear and limpid yellow or green solutions without any precipitation. These solutions become blue after many weeks. This observation (stability towards hydrolysis which seems to generate soluble materials) appears at first surprising, considering the known sensitivity of alkoxides towards water. The study of hydrolysis of this oxoalkoxide (by ^{51}V NMR and IR spectroscopies) is in progress.

In order to confirm the vanadium(IV) oxidation state assignment for the bulk sample of **1** an EPR spectrum of **1** was carried out. It consists of an intense and symmetric broad signal, showing a partially resolved hyperfine structure due to the coupling with the vanadium nucleus ($I = 7/2$; eight lines are distinguishable. The direct measurement of g from the EPR spectrum gives a value of 1.95, which is similar to those previously recorded for a number of oxovanadate(IV) complexes.[17]

IR spectroscopy for **1** is consistent with the formulation provided by the X-ray analysis; it exhibits in particular two bands at 1159 and 1089 cm^{-1} which can be assigned to ν(C—O—V) vibrations, while an intense band at 1019 cm^{-1} is attributed to ν(V=O). In the low energy range the peaks located at 674, 541, 462 and 354 cm^{-1} are typical of ν(V—OR) and ν(C—Cl) vibrations, respectively.

Despite the paramagnetism of compound **1**, a ^1H NMR spectrum reveals the characteristic chemical shifts of the alkoxide groups. Nevertheless, no structural information can be provided because of the broadening of the signals due to quadrupolar and paramagnetic effects. The ^{51}V NMR spectrum of **1** shows two very close signals at −573.1 and −573.9 ppm in a ratio 1:1, which reveals a non-absolute equivalence for the ^{51}V resonances. We note that the weak half-line width of these resonances (45 Hz) is not affected by paramagnetic effects. Due to the lack of ^{51}V NMR information about oxovanadium(IV) compounds,[18] conversely to oxovanadium(V) species, no comparison is possible.

The dimeric nature of the compound was first suggested by mass spectral data, which exhibit the parent molecular ion without any ion of higher molecular mass. It has been definitively confirmed by an X-ray structural study.

The X-ray crystal structure of **1** is shown in Fig. 1. Relevant bond lengths and angles are collected in Table 2. The complex consists of a dimeric unit in which the two independent $VOCl[OCH(CH_3)CH_2OCH_3]$ units are held together by the bridging μ_2-O(1) and μ_2-O(2) oxygen atoms. Although no crystallographic symmetry is imposed, a molecule of **1** exhibits an overall symmetry close to C_2, with the approximate C_2 axis passing through the midpoint of a line joining the vanadium atoms and perpendicular to the V—O—V—O plane. Thus, both oxo groups and chlorine atoms adopt a *cis* configuration around the V—O—V—O ring. Such a configuration is rather rare since the *trans* configuration is more often encountered as

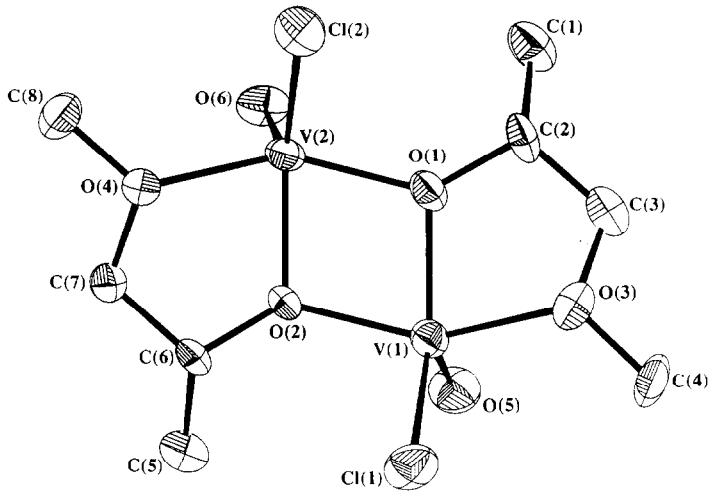

Fig. 1. ORTEP view of the $\{VOCl[OCH(CH_3)CH_2OCH_3]\}_2$ molecule, showing the atomic numbering scheme (thermal ellipsoids drawn at 40% probability level).

in the related vanadium(V) complex $\{VOCl[OC(CH_3)_2]_2\}_2$.[7a] Moreover, the C_2 symmetry of the molecule leads to a boat-like configuration, as evidenced by Fig. 2. This configuration tends to reduce the intramolecular interactions between the alkoxide ligand and both oxo group and chlorine atom. The vanadium atoms are five-coordinate, defining a distorted trigonal bipyramid. Actually, this environment can alternatively be described as a distorted square pyramid. Although important shifts between the ideal angle values and the observed ones are noticed in both descriptions, we tend to prefer the trigonal bipyramid model in the way that deviation from planarity (± 0.17 Å) of the square base in the pyramidal model appear to be consequent. Nevertheless, these two types of environment

Table 2. Selected bond lengths (Å) and angles (°) (standard deviations in parentheses)

V(1)—O(1)	1.952(7)	V(2)—O(2)	1.964(7)
V(1)—O(2)	1.966(7)	V(2)—O(1)	1.948(7)
V(1)—O(3)	2.052(7)	V(2)—O(4)	2.065(7)
V(1)—O(5)	1.590(7)	V(2)—O(6)	1.584(7)
V(1)—Cl(1)	2.282(3)	V(2)—Cl(2)	2.281(3)
O(1)—C(2)	1.454(11)	O(2)—C(6)	1.428(11)
C(1)—C(2)	1.547(14)	C(5)—C(6)	1.536(14)
C(2)—C(3)	1.484(14)	C(6)—C(7)	1.496(14)
C(3)—O(3)	1.452(12)	C(7)—O(4)	1.455(11)
O(3)—C(4)	1.424(11)	O(4)—C(8)	1.435(11)

V . . . V interaction

V(1)—V(2) 3.084(3)

V(2)—O(1)—V(1)	104.5(3)	V(1)—O(2)—V(2)	103.4(3)
O(1)—V(1)—O(2)	76.0(3)	O(2)—V(2)—O(1)	76.1(3)
O(1)—V(1)—O(3)	78.5(3)	O(2)—V(2)—O(4)	77.6(3)
O(1)—V(1)—O(5)	113.8(3)	O(2)—V(2)—O(6)	114.2(3)
O(1)—V(1)—Cl(1)	138.0(2)	O(2)—V(2)—Cl(2)	136.7(2)
O(2)—V(1)—O(3)	148.0(3)	O(1)—V(2)—O(4)	147.2(3)
O(2)—V(1)—O(5)	106.2(3)	O(1)—V(2)—O(6)	106.2(3)
O(2)—V(1)—Cl(1)	94.7(2)	O(1)—V(2)—Cl(2)	95.6(2)
O(3)—V(1)—O(5)	101.5(3)	O(4)—V(2)—O(6)	102.3(3)
O(3)—V(1)—Cl(1)	91.5(2)	O(4)—V(2)—Cl(2)	90.2(2)
O(5)—V(1)—Cl(1)	108.2(3)	O(6)—V(2)—Cl(2)	108.9(3)

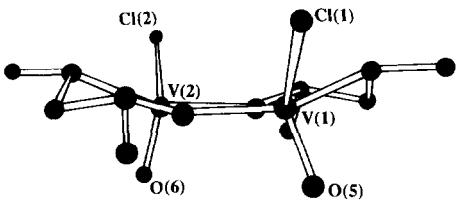

Fig. 2. View of **1** perpendicular to the V—O—V—O ring, showing the boat-like configuration.

are currently encountered in vanadium(IV) complexes.[16a,17a,19]

The V—O and V—Cl bond lengths fall in the range of values previously reported in the literature.[7a,7b,17a]. Worthy of mention is the V—μ_1—O bond length, which is significantly longer than the V—μ_2—O one [average 2.058(7) and 1.957(7) A°, respectively]. This is clearly explained by the fact that the μ_2-O atoms [O(1) and O(2)] are negatively charged, whereas the μ_1-O atoms of the methoxy groups [O(3) and O(4)] are uncharged, allowing a weaker $p\pi$–$d\pi$ donation. The value of the intermetallic distance [V(1)...V(2) = 3.084(3) Å] is in good agreement with the V...V distance observed in the related oxovanadium compounds.[7a,17a,20] At this distance a V—V bonding should not be expected and consequently, the two unpaired electrons should be mainly localized on one V=O unit.

The presence of remaining chloride ligands in complex **1** makes the metal atom functionalizable and may permit the introduction of a second metal (by reaction with a species such as $K[M(OR)_n]$ with salt elimination, for example). Further investigations towards the reactivity of **1** are in progress in this way.

REFERENCES

1. M. Nabavi, C. Sanchez and J. Livage, *Eur. J. Solid State Inorg. Chem.* 1991, **28**, 1173.
2. S. I. Zones, M. R. Palmer, J. G. Palmer, J. M. Doemeny and G. N. Schrauzer, *J. Am. Chem. Soc.* 1978, **100**, 2113.
3. (a) D. C. Crans, H. Chen and R. A. Felty, *J. Am. Chem. Soc.* 1992, **114**, 4543; (b) F. Hillerns and D. Rehder, *Chem. Ber.* 1991, **124**, 2249; (c) R. K. Mittal and R. C. Mehrotra, *Z. Anorg. Allg. Chem.* 1964, **327**, 311; (d) N. F. Orlov and M. G. Voronkov, *Bull. Acad. Sci URSS, Div. Chem. Sci.* 1959, 933; (e) Von H. Funk, W. Weiss and M. Zeising, *Z. Anorg. Allg. Chem.* 1958, **296**, 36.
4. C. N. Caughlan, H. M. Smith and K. Watenpaugh, *Inorg. Chem.* 1966, **5**, 2131.
5. W. Priebsch and D. Rehder, *Inorg. Chem.* 1990, **29**, 3013.
6. F. Hillerns, F. Olbrich, U. Behrens and D. Reher, *Angew. Chem, Int. Edn Engl.* 1992, **31**, 447.
7. (a) D. C. Crans, R. A. Felty and M. M. Miller, *J. Am. Chem. Soc.* 1991, **113**, 265; (b) D. C. Crans, R. W. Marshman, M. S. Gottlieb, O. P. Anderson and M. M. Miller, *Inorg. Chem.* 1992, **31**, 4939.
8. D. C. Crans, R. A. Felty, O. P. Anderson and M. M. Miller, *Inorg. Chem.* 1993, **32**, 247.
9. D. L. Clark, J. G. Watkin and J. C. Huffman, *Inorg. Chem.* 1992, **31**, 1556.
10. (a) D. J. Eichorst and D. A. Payne, *Better Ceramics Through Chemistry III, Material Research Society Symp. Proc.* 1988, **121**, 773; (b) J. T. J. Davies, H. C. Winterton and N. N. Hughes, *Better Ceramics Through Chemistry II* 1986, **73**, 111.
11. (a) O. Poncelet, L. Hubert-Pfalzgraf, J.-C. Daran and R. Astier, *J. Chem. Soc., Chem. Commun.* 1989, 1846; (b) K. G. Caulton, M. H. Chisholm, S. R. Drake and J. C. Huffman, *J. Chem. Soc., Chem. Commun.* 1990, 1498; (c) M.-C. Massiani, R. Papiernik, L. Hubert-Pfalzgraf and J-C. Daran, *J. Chem. Soc., Chem. Commun.* 1990, 301; (d) S. C. Goel, M. A. Matchett, M. Y. Chiang and W. E. Buhro, *J. Am. Chem. Soc.* 1991, **113**, 1844; (e) S. Boulmaaz, R. Papiernik, L. Hubert-Pfalzgraf, J. Vaissermann and J.-C. Daran, *Polyhedron* 1992, **11**, 1331; (f) S. C. Goel, M. Y. Chiang and W. E. Buhro, *Inorg. Chem.* 1990, **29**, 4640.
12. Program XDISK from the commercial package SHELXTL PLUS distributed by Siemens.
13. G. M. Sheldrick, SHELXS-86, Program for the Solution of Crystal Structures. University of Göttingen, F.R.G. (1987).
14. G. M. Sheldrick, SHELX 76, Program for Crystal Structure Determination. University of Cambridge, U.K. (1976).
15. It seems that this solvent stabilizes the oxovanadium(V) alkoxide species. Further reactions in CH_2Cl_2 are, at present, being investigated to confirm this hypothesis.
16. (a) D. Rehder, W. Priebsch and M. von Oeynhausen, *Angew. Chem., Int. Edn Engl.* 1989, **28**, 1221; (b) H. J. Seifert, *Z. Anorg. Allg. Chem.* 1962, **317**, 123; (c) R. C. Paul and A. Kumar, *J. Inorg. Nucl. Chem.* 1965, **27**, 2537.
17. (a) F. A. Cotton, G. E. Lewis and G. N. Mott, *Inorg. Chem.* 1983, **22**, 378; (b) R. R. Reeder and P. H. Rieger, *Inorg. Chem.* 1971, **6**, 1258; (c) N. D. Chasteen and M. W. Hanna, *J. Phys. Chem.* 1972, **76**, 3951; (d) A. T. Casey, B. S. Morris, E. Sinn and J. R. Thackeray, *Aust. J. Chem.* 1972, **25**, 1195.
18. To our knowledge, the only ^{51}V data of vanadium (IV) compounds are published by F. Preuss and L. Ogger in *Z. Naturforsch.* 1982, **37b**, 957.
19. G. Barr-David, T. W. Hambley, J. A. Irwin, R. J. Judd, P. A. Lay, B. D. Martin, R. Bramley, N. E. Dixon, P. Hendry, J.-Y. Ji, R. S. U. Baker and A. M. Bonin, *Inorg. Chem.* 1992, **31**, 4906.
20. S. Gambarotta, F. van Bolhuis and M. Y. Chiang, *Inorg. Chem.* 1987, **26**, 4301.

Polyhedron Vol. 12, No. 20, pp. 2513–2517, 1993
Printed in Great Britain

0277–5387/93 $6.00+.00
© 1993 Pergamon Press Ltd

SYNTHESIS AND MOLECULAR STRUCTURE OF (*t*-BUTYLIMIDO)TRIS(MESITYL)(TRIMETHYLSILOXY)MOLYBDENUM(VI)

RICHARD LAÏ,* VERONIQUE PIASCO, CHRISTINE BELIN and CATHERINE ROS

E.N.S.S.P.I.C.A.M., U.R.A. C.N.R.S. 1410, Faculté des Sciences/Saint-Jérôme, 13013 Marseille, France

and

JANINE FENEAU-DUPONT and JEAN-PAUL DECLERCQ*

Laboratoire de Chimie Physique et de Cristallographie, Université Catholique de Louvain la Neuve, 1348 Louvain la Neuve, Belgium

(*Received* 6 *April* 1993; *accepted* 4 *June* 1993)

Abstract—The reaction of $Mo(O)(NBu^t)(OSiMe_3)Cl$ or $Mo(O)(NBu^t)(OSiMe_3)_2$ with mesMgBr affords the imido complex $[Mo(NBu^t)(mes)_3(OSiMe_3)]$ (**2**); the crystal structure of **2** indicates that the imido and the siloxy ligands are linear, the Mo—N bond of 1.786(10) Å being one of the longest reported to date for a linear molybdenum imido group.

The chemistry of transition metal complexes possessing oxo or imido ligands has been investigated extensively[1] and is still of considerable current interest. In this research field we have been interested in the behaviour of dioxo and diimido molybdenum(VI) complexes with different small molecules such as phosphorus ylides, isocyanates, carbon monoxide and isocyanides.[2] In most cases the differences in reactivity between the dioxo and the diimido compounds are very important and were explained by the better π-donating properties of imido groups with respect to oxo ligands.[2d] Accordingly, we thought it could be interesting to prepare oxo-imido molybdenum(VI) complexes and to study their reactivity in comparison with that of their dioxo and diimido analogues.

Since the interaction of four equivalents of t-butyltrimethylsilylamine, $Bu^tN(SiMe_3)H$, with $Mo(O)_2Cl_2$ yields, almost quantitatively, $Mo(NBu^t)_2(OSiMe_3)_2$,[3] which upon treatment with mesMgBr (mes = 2,4,6-$C_6H_2Me_3$) affords $Mo(NBu^t)_2mes_2$,[4] we anticipated it might be possible to obtain $Mo(O)(NBu^t)mes_2$ via the following synthetic sequence:

$$Mo(O)_2Cl_2 + 2\,Bu^tN(SiMe_3)H \longrightarrow Mo(O)(NBu^t)(OSiMe_3)Cl + [SiMe_3NH_2Bu^t]^+Cl^-$$

$$Mo(O)(NBu^t)(OSiMe_3)Cl + 2\,mesMgBr \longrightarrow Mo(O)(NBu^t)mes_2 + MgBrCl + MgBrOSiMe_3.$$

In this paper we report on the reactivity of oxoimido molybdenum complexes with mesMgBr along with the X-ray crystal structure of $[Mo(NBu^t)(mes)_3(OSiMe_3)]$.

RESULTS AND DISCUSSION

When $Mo(O)_2Cl_2$ was reacted in hexane with 2 equivalents of $Bu^tN(SiMe_3)H$ a yellow solution was obtained after filtration of $[(SiMe_3)H_2NBu^t]^+Cl^-$. Evaporation of this solution afforded a yellow solid characterized by ^1H NMR as $Mo(O)(NBu^t)(OSiMe_3)Cl$ (**1**). It proved to be impossible to isolate this complex analytically pure owing to slow decomposition in solution into oligomeric species. Oligomer formation was supposed to occur by con-

* Authors to whom correspondence should be addressed.

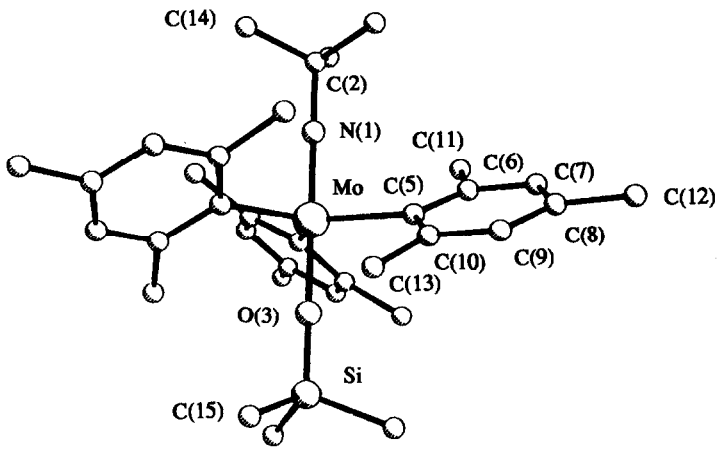

Fig. 1. Molecular structure of [Mo(NBu^t)(mes)$_3$OSiMe$_3$] (**2**) (Program PLUTO[16]). Hydrogen atoms are omitted for clarity.

densation of the $OSiMe_3$ groups to form an oxo bridge and 1 equivalent of $(Me_3Si)_2O$, as shown by the disappearance of the $OSiMe_3$ signal in the NMR spectra of the crystals isolated from solutions containing **1**.

Addition of 2 equivalents of mesMgBr (0.96 M in THF) to freshly prepared **1** dissolved in THF gave a brown–yellow solid after evaporation of the solvent. Crystallization of this solid in Et_2O-hexane afforded yellow crystals. The X-ray structure of this compound has been determined and the molecular structure is shown in Fig. 1 along with the atom numbering scheme. The main bond lengths and angles are given in Table 1. Contrary to our expectations it happened that it was not the hoped-for oxo-imido species, but a t-butylimido(trimesityl) (trimethylsiloxy)molybdenum(VI) complex, [Mo(NBu^t)(mes)$_3$(OSiMe$_3$)] (**2**).

The geometry about the molybdenum atom is a perfect trigonal bipyramid. The three mesityl groups lie in the basal plane of the bipyramid and are twisted with respect to this plane with a 33° angle, as can be seen from the N(1)—Mo—C(5)—C(6) torsional angle of 123°. The existence of a third-order symmetry axis shows that C(2)—N(1)—O(3) and Si are linear. The most striking features of the structure are the following. Although the triply bonded nature of the imido ligand can clearly be seen in the linearity of the Mo—N—C unit, the N(1)—Mo bond length of 1.786(10) Å is expected to be much shorter.[1c,5] It seems to be one of the longest known for a linear imido ligand bound to a high valent transition metal.[4,5] Such a distance of 1.786 Å would imply a Mo—N bond order somewhat smaller than 3.[1c,6] Another striking feature concerns the Mo—O(3) and Si—O(3) distances of 1.904(10) and 1.606(11) Å, the former being shorter and the second slightly longer than normal.[7] This observation provides a clear manifestation of strong oxygen $p\pi$–$d\pi$ donation. The considerable lengthening of the N(1)—Mo bond together with the unprecedented linearity of the Mo—O—Si angle might be due to steric interaction of the bulky mesityl groups with the metal centre. Indeed, short intramolecular contacts (< 2.4 Å) exist between hydrogen atoms of the tert-butyl and of the trimethylsilyl groups and the mesitylene methyl groups:

Table 1. Selected bond lengths (Å) and bond angles (°) for [Mo(NBu^t)(mes)$_3$OSiMe$_3$] (**2**)

Mo—N(1)	1.786(10)	N(1)—C(2)	1.456(14)
Mo—O(3)	1.904(10)	Si—O(3)	1.606(1)
Mo—C(5)	2.138(8)	Si—C(15)	1.815(12)
O(3)—Mo—N(1)	180.0	C(2)—N(1)—Mo	180.0
C(5)—Mo—O(3)	89.6(2)	Mo—C(5)—C(6)	122.1(6)
C(5)—Mo—N(1)	90.4(2)	Mo—C(5)—C(10)	120.1(6)
Mo—O(3)—Si	180.0	N(1)—C(2)—C(14)	110.3(5)
O(3)—Si—C(15)	110.3(4)	C(15)—Si—C(15)	108.6(4)
C(14)—C(2)—C(14)	108.6(4)		

H(C14)---H(C11) 2.18 and 2.28 Å;

H(C15)---H(C13) 2.24 Å.

We observed also that whatever the amount of mesMgBr reacted with $Mo(O)(NBu^t)(OSiMe_3)Cl$ the only compound isolated was **2**. Furthermore, **2** could also be formed upon treatment of mesMgBr with freshly prepared $Mo(O)(NBu^t)(OSiMe_3)_2$ (**3**), obtained by reacting $Mo(NBu^t)_2(OSiMe_3)_2$ with 1 equivalent of H_2O and 1 equivalent of HCl as reported for the synthesis of $Cr(O)(NBu^t)(OSiMe_3)_2$.[8]

The observed reactivity of these oxo-imido complexes is unusual and, to our knowledge, such a behaviour has been reported only once.[9] Indeed, although alkylation of metal-oxo or further alkylation of oxoalkyls is a way to obtain metal alkyls[10] with the loss of the oxo group, in most cases the oxo group is notoriously inactive, particularly when halogeno or siloxo groups are attached to the metal.[11] Here, the presence of the imido seems to render the reactivity of the oxo groups different from other oxo complexes since, under very mild conditions, it is the oxo functionality which is alkylated rather than the $OSiMe_3$ group.

Substitution of the $OSiMe_3$ ligand was cleanly achieved by reacting **2** with $BrSiMe_3$, affording $Mo(NBu^t)(mes)_3Br$ (**4**) in good yields. However, upon treatment with Me_3SiCH_2MgCl, $Mo(NBu^t)(mes)_3Br$ was recovered unchanged (Scheme 1).

Complexes **2** and **4** appear to be rigid on the NMR time scale at room temperature. For both species, the three mesityl ligands are identical and the three methyls of each aromatic ring are magnetically different in the ^1H and ^{13}C NMR spectrum. The principal features which differentiate these two species are that in the ^1H NMR spectrum of **2** the aromatic protons resonate at the same frequency, whereas they appear at two different chemical shifts for **4**. On the other hand, the *ortho* quaternary carbon atoms of the mesityls are differentiated in the ^{13}C NMR spectrum of **2**, whereas they are not in the case of **4**. The ^{13}C NMR shift differences between the α- and β-carbons in the t-butyl groups of **2** and **4** were found to be 38.3 and 42.6, respectively, showing that π-donation from the nitrogen atom is slightly greater for the latter than for **2**.[1c]

EXPERIMENTAL

All reactions were carried out in an atmosphere of purified nitrogen using standard Schlenk techniques. Solvents were dried over and distilled from the sodium ketyl of benzophenone. Instruments: NMR, Bruker AM-200 and AM-400X; IR, FT-IR

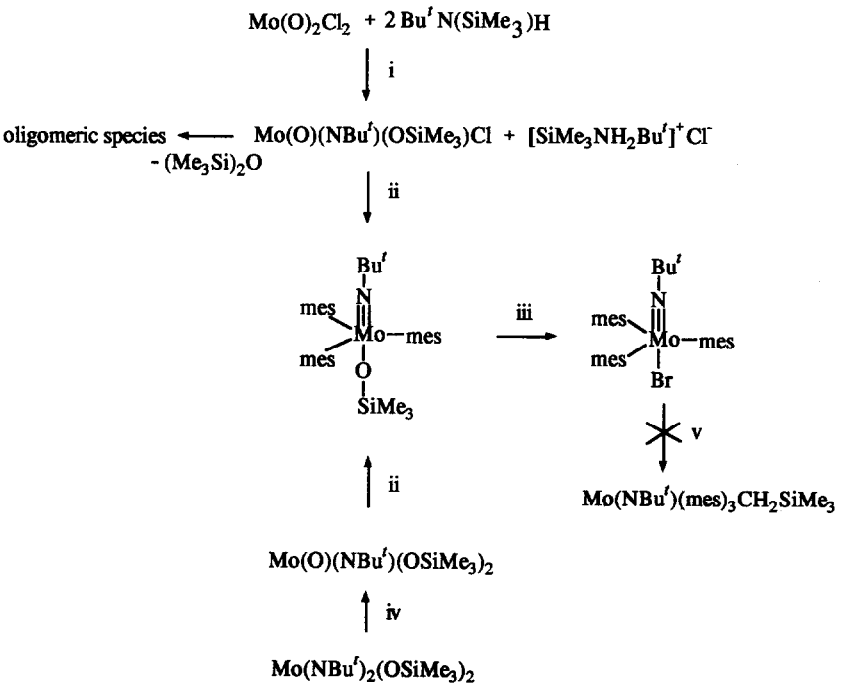

Scheme 1. Synthesis and reactivity of $[Mo(NBu^t)(mes)_3OSiMe_3]$ (**2**). Reagents and conditions: (i) hexane, reflux, 0.5 h; (ii) mesMgBr, THF, −20–23°C, 10 h ; (iii) 1 equivalent of Me_3SiBr in Et_2O, room temperature; (iv) 1 equivalent of H_2O and 1 equivalent of HCl in Et_2O, −78°C; (v) Me_3SiCH_2MgCl, THF, −20–23°C.

Nicolet MX-S. $Mo(O)_2Cl_2$,[12] $Bu^tN(SiMe_3)H$[13] and $Mo(NBu^t)_2(OSiMe_3)_2$[3] were prepared as previously described.

(t-Butylimido)oxo(trimethylsiloxy)chloromolybdenum(VI) (**1**)

A suspension of $Mo(O)_2Cl_2$ (2 g, 10 mmol) in hexane (30 cm^3) was refluxed for 0.5 h in the presence of $NHBu^tSiMe_3$ (3.18 g, 20 mmol). After cooling the yellow solution was filtered, the solid residue was washed with hexane (15 cm^3) and the combined hexane extracts were pumped *in vacuo*, affording crude **1** as a yellow solid. Yield: 2.3 g (75%). NMR: ^1H ($CDCl_3$): δ 1.45 (9H, s, Bu^t), 0.18 (9H, s, $OSiMe_3$).

(t-Butylimido)oxobis(trimethylsiloxy)chloromolybdenum(VI) (**3**)

To a stirred solution of $Mo(NBu^t)_2(OSiMe_3)_2$ (0.49 g, 1.18 mmol) in Et_2O (30 cm^3) at $-78°C$ was successively added water (0.02 cm^3, 1.18 mmol) and ethereal HCl (5.9 cm^3, 0.2 M solution). The solution was allowed to warm to 25°C. Rapid filtration through a medium porosity frit and removal of solvent gave crude **3** as a yellow solid. Yield: 0.297 g, 70%. NMR: ^1H ($CDCl_3$): δ 1.34 (9H, s, Bu^t), 0.06 (18H, s, $OSiMe_3$).

(t-Butylimido)tris(mesityl)(trimethylsiloxy)molybdenum(VI) (**2**)

To a solution of $Mo(O)(NBu^t)(OSiMe_3)Cl$ freshly prepared (2.37 g, 7.7 mmol) in THF (30 cm^3) was added dropwise at $-20°C$ mesMgBr (26.6 cm^3, 0.87 M solution in THF). The yellow solution turned red and was stirred overnight at room temperature. Removal of solvent, extraction of the residue into hexane (3×25 cm^3), filtration and concentration of the orange–brown solution followed by cooling at $-20°C$ afforded yellow crystals of **2**. Yield: 1.19 g, 60%. NMR: ^1H ($CDCl_3$): δ 6.75 [6H, s, 2,4,6-$C_6H_2(CH_3)_3$], 2.46 [9H, s, *2*,4,6-$C_6H_2(CH_3)_3$], 2.31 [9H, s, 2,4,*6*-$C_6H_2(CH_3)_3$], 2.23 [9H, s, 2,*4*,6-$C_6H_2(CH_3)_3$], 1.36 (9H, s, Bu^t), -0.13 (9H, s, $OSiMe_3$). ^{13}C ($CDCl_3$): δ 179.3 (C *ipso*), 140.4, 139.3 (*2*,4,*6*-$C_6H_2CH_3$), 136.5 (2,*4*,6-$C_6H_2CH_3$), 128.9, 129.96 (CH arom), 67.1 [$C(CH_3)_3$], 28.7 [$C(CH_3)_3$], 26.8, 25.2 [*2*,4,*6*-$C_6H_2(CH_3)_3$], 20.9 [2,*4*,6-$C_6H_2(CH_3)_3$], 2.0 [$OSi(CH_3)_3$].

(t-Butylimido)tris(mesityl)bromomolybdenum(VI) (**4**)

To a stirred solution of $Mo(NBu^t)(mes)_3OSiMe_3$ (0.7 g, 1.14 mmol) in hexane (20 cm^3) was added Me_3SiBr (0.15 cm^3, 1.14 mmol) at room temperature. The colour of the solution changed to red

Table 2. Data for crystal structure of **2**

Formula	$C_{34}H_{51}NOMoSi$, $[C_6H_3(CH_3)_3]_{1/2}$
M_r	673.9
Crystal system	Trigonal
a (Å)	13.455(3)
c (Å)	12.167(2)
U (Å^3)	1907.7(8)
Space group	*P*-3
D_x (g cm^{-3})	1.17
(Mo-K_α)	0.71069
Z	2
F(000)	718
μ (cm^{-1})	3.99
θ max (°)	25
Number of unique reflections	2552
Number of observed reflections	1432
Significance test	$F > 2.5\sigma(F)$
Number of parameters	121
Weighting scheme parameters, g	0.00167
Max Δ/σ	0.05
GOF	1.34
Max. and min. density in ΔF map (e Å^{-3})	0.97, -0.91
Final R	0.069
R_w	0.069

$w = 1/(\sigma^2 + gF^2)$; $R = \Sigma|\Delta F|/\Sigma|F_o|$; $R_w = [\Sigma|\Delta F|^2/\Sigma w|F_o^2|]^{1/2}$.

and then to green–brown. After stirring overnight, filtration and removal of the solvent afforded a solid residue, which was extracted into Et_2O (10 cm^3). Addition of hexane (5 cm^3) followed by cooling at −20°C gave yellow crystals of **4**. Yield: 0.3 g, 50%. NMR: ^1H ($CDCl_3$): δ 6.81, 6.76 [2 × 3H, s, 2,4,6-$C_6H_2(CH_3)_3$], 2.48, 2.42 [2 × 9H, s, 2,4,6-$C_6H_2(CH_3)_3$], 2.21 [9H, s, 2,4,6-$C_6H_2(CH_3)_3$], 1.40 (9H, s, Bu^t). ^{13}C ($CDCl_3$): δ 185.7 (C *ipso*), 138.7 (2,4,6-C_6H_2-CH_3), 138.0 (2,4,6-$C_6H_2CH_3$), 131.0, 129.1 (CH arom), 70.2 [$C(CH_3)_3$], 28.4, 26.7 [2,4,6-$C_6H_2(CH_3)_3$], 27.6 [$C(CH_3)_3$], 20.8 [2,4,6-$C_6H_2(CH_3)_3$].

X-ray crystallography

A parallelepiped crystal with dimensions 0.3 × 0.3 × 0.25 mm was used for data collection on a Huber four-circle diffractometer using graphite monochromatized Mo-K_α radiation. Lattice parameters were refined using 24 reflections in the range $4 \leqslant 2\theta \geqslant 27°$. A standard reflection (3 4 −1) was checked every 50 reflections, no significant deviation was observed. The structure was solved by direct methods using SHELXS86.[14] All non-hydrogen atoms were refined with anisotropic displacements factors coefficients (SHELX76[15]). Hydrogen atoms were included in idealized positions and were assigned a common refined temperature factor ($U = 0.14$ Å^2). Atomic scattering factors were calculated from data obtained from ref. 17. Crystal data for **2** are given in Table 2. A disordered mesitylene molecule, statistically distributed on two positions, appears around the symmetry element −3. The occupation factor corresponds to about 1/2 mesitylene for one molecule of complex.

Supplementary material (atomic coordinates, bond lengths and angles, and thermal parameters) have been deposited with the Editor at the Cambridge Crystallographic Data Centre.

REFERENCES

1. (a) W. A. Nugent and J. M. Mayer, *Metal–Ligand Multiple Bonds*. Wiley, New York (1988); (b) F. Bottomley and L. Sutin, *Adv. Organomet. Chem.* 1988, **28**, 339; (c) W. A. Nugent and B. L. Haymore, *Coord. Chem. Rev.* 1980, **31**, 123.
2. (a) H. Arzoumanian, A. Baldy, R. Laï, J. Metzger, M.-L. Nkeng Peh and M. Pierrot, *J. Chem. Soc., Chem. Commun.* 1985, 1151; (b) R. Laï, S. Le Bot, M. Pierrot and H. Arzoumanian, *J. Chem. Soc., Chem. Commun.* 1986, 1208; (c) R. Laï, S. Mabille, A. Croux and S. Le Bot, *Polyhedron* 1991, **10**, 463; (d) R. Laï, S. Le Bot and F. Djafri, *J. Organomet. Chem.* 1991, **410**, 335; (e) R. Laï, O. Desbois, F. Zamkotsian, J. Feneau-Dupont and J. P. Declercq, manuscript in preparation.
3. W. A. Nugent and R. L. Harlow, *Inorg. Chem.* 1980, **19**, 777.
4. A. C. Sullivan, G. Wilkinson, M. Motevalli and M. B. Hursthouse, *J. Chem. Soc., Dalton Trans.* 1988, 53.
5. (a) W. A. Nugent and R. L. Harlow, *J. Am. Chem. Soc.* 1980, **102**, 1759; (b) M. L. H. Green, P. C. Konadiris, P. Mountford and S. J. Simpson, *J. Chem. Soc., Chem. Commun.* 1992, 256; (c) J. C. Green, M. L. H. Green, J. T. James, P. C. Konadiris, G. H. Maunder and P. Mountford, *J. Chem. Soc., Chem. Commun.* 1992, 1361.
6. G. Parkin, A. van Asselt, D. J. Leahy, L. Whinnery, N. G. Hua, R. W. Quan, L. M. Henling, W. P. Schaefer, B. D. Santarsiero and J. E. Bercaw, *Inorg. Chem.* 1992, **31**, 82.
7. T. V. Lubben, P. T. Wolczanski and G. V. Van Duyne, *Organometallics* 1984, **3**, 977.
8. N. Meijboom, C. J. Schaverien and A. G. Orpen, *Organometallics* 1990, **9**, 774.
9. D. Ehrenfeld, J. Kress, B. D. Moore, J. A. Osborn and G. Schottel, *J. Chem. Soc., Chem. Commun.* 1987, 129.
10. (a) K. Mertis and G. Wilkinson, *J. Chem. Soc., Dalton Trans.* 1976, 1488; (b) W. A. Herrmann, *Angew. Chem. Int. Edn Engl.* 1988, **27**, 1297; (c) P. Stavropoulos, P. G. Edwards, T. Behling, G. Wilkinson, M. Motevalli and M. B. Hursthouse, *J. Chem. Soc., Dalton Trans.* 1987, 169.
11. (a) W. A. Herrmann, G. Weichselbaumer, R. A. Paciello, R. A. Fischer, E. Herdtweck, J. Okuda and D. W. Marz, *Organometallics* 1990, **9**, 489; (b) W. A. Herrmann, F. E. Kühn, R. W. Fischer, W. R. Thiel and C. C. Romao, *Inorg. Chem.* 1992, **31**, 4431.
12. L. G. McCullough, R. R. Schrock, J. C. Dewan and J. C. Murdzek, *J. Am. Chem. Soc.* 1985, **107**, 5987.
13. R. M. Pike, *J. Org. Chem.* 1961, **26**, 232.
14. G. M. Sheldrick, in *Crystallographic Computing* 3 (Edited by G. M. Sheldrick, C. Kruger and R. Goddard), pp. 175–189. Oxford University Press, Oxford (1985).
15. G. M. Sheldrick, SHELX76, Program for Crystal Structure Determination. University of Cambridge, U.K. (1976).
16. S. Motherwell and W. Clegg, A Program for Plotting Crystal and Molecular Structures. University of Cambridge, U.K. (1978).
17. *International Tables for X-ray Crystallography*, Vol. IV. Kynoch Press, Birmingham (1974).

Polyhedron Vol. 12, No. 20, pp. 2519–2523, 1993
Printed in Great Britain

0277–5387/93 $6.00+.00
© 1993 Pergamon Press Ltd

COMPLEXES OF TWO MANNOSE α-AMINO ACID DERIVATIVES WITH ZINC AND CADMIUM

M. A. DÍAZ-DÍEZ*

Departamento de Química Analítica y Electroquímica, Facultad de Ciencias, Universidad de Extremadura, 06071 Badajoz, Spain

and

F. J. GARCÍA-BARROS, F. J. HIGES-ROLANDO, A. BERNALTE-GARCÍA and C. VALENZUELA-CALAHORRO

Departamento de Química Inorgánica, Facultad de Ciencias, Universidad de Extremadura, 06071 Badajoz, Spain

(*Received* 7 *May* 1993; *accepted* 3 *June* 1993)

Abstract—Complexes of zinc(II) and cadmium(II) with 2-amino-2-deoxy-D-glycero-D-talo heptonic acid (HMa) and 2-(benzylamino)-2-deoxy-D-glycero-D-talo heptonic acid (BnMa) have been obtained. The complexes were characterized by elemental analysis, IR spectroscopy and X-ray powder diffraction. These complexes have a 1 : 2 metal-to-ligand ratio and an octahedral structure. Coordination occurs through the nitrogen atom of the amino group and oxygen atoms of the bridging carboxylate group. The thermal behaviour of the complexes has also been studied.

Studies of the interactions of carbohydrates and their derivatives with metal ions have increased during the last few years, mainly due to the possible importance of such interactions in a variety of industrial, pharmaceutical and biological processes.[1,2]

The ability of sugar derivatives to sequester metal ions can be utilized for the extraction of metals which are economically important and for the development of new classes of metal-based affinity catalysts. Furthermore, carbohydrates are often highly soluble in water and are usually only weakly immunogenic and of low toxicity. These properties are very useful in developing pharmaceutical agents for the removal of toxic metals or the uptake of essential metals.

Finally, the complexation of metal ions by several carbohydrates derivatives is of great interest in view of their biological role, particularly in the availability of nutrients to plants and in the regulation of the flow of metal ions across cell walls.[3]

It is worth noting that on introduction of a carboxy or amino group (or both) into a sugar molecule the complex-forming ability is enhanced by several orders of magnitude, even in acidic or neutral solution.[4–6]

Our interest in the coordination chemistry of carbohydrate α-amino acids[7–9] prompted us to prepare and characterize the zinc(II) and cadmium(II) complexes of 2-amino-2-deoxy-D-glycero-D-talo heptonic acid (HMa) and 2-(benzylamino)-2-deoxy-D-glycero-D-talo heptonic acid (BnMa) in order to investigate the mode of attachment of the ligand molecules to the metal ions. The ligands used in this study have the structure shown in Fig. 1.

EXPERIMENTAL

Preparation of the ligands and complexes

The ligands 2-amino-2-deoxy-D-glycero-D-talo heptonic acid (HMa) and 2-(benzylamino)-2-deoxy-D-glycero-D-talo heptonic acid (BnMa) were prepared according to the method of Galbis *et al.*[10]

* Author to whom correspondence should be addressed.

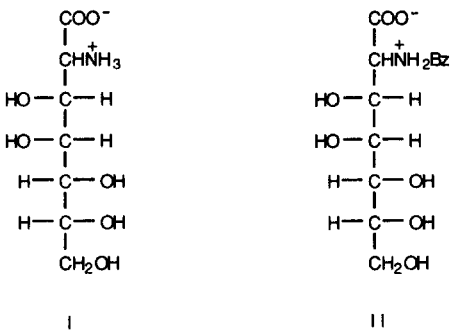

Fig. 1. Structural formulae of the ligands HMa (I) and BnMa (II).

and recrystallized twice from doubly-distilled water. All the remaining chemicals proved to be sufficiently reliable to be used without further purification.

The complexes were synthesized as follows: A freshly prepared aqueous solution of the metal nitrate was added to a hot aqueous solution of the ligand in the metal: ligand stoichiometric ratio of 1:2. The pH of the whole solution was then adjusted at a pH value lower than that of precipitation of the correspondent hydroxide, by dropwise addition of dilute NaOH. When the resulting solutions were stirred during the next few hours and they were either concentrated or cooled, microcrystalline solids were isolated.

All compounds were filtered off by suction, washed consecutively with water, ethanol and diethylether, air-dried and stored *in vacuo* over anhydrous $CaCl_2$

Apparatus and methods

Chemical analysis of carbon, hydrogen and nitrogen were performed by means of microanalytical methods using a Perkin–Elmer 240 microanalyser. The metal content was determined by thermogravimetry.

IR spectra were obtained from KBr pellets (4000–450 cm^{-1}) using a Perkin–Elmer FT-IR 1720 spectrophotometer.

Thermoanalytical data were obtained from TG, DTG and DSC curves. These were recorded on a Mettler TA-3000 system provided with a Mettler TG 50 thermobalance and a Mettler DSC 20 differential scanning calorimeter. The atmospheres used were air (flow = 200 cm^3 min^{-1}) or nitrogen (flow = 200 cm^3 min^{-1}, purity = 99.99% v.v.) for TG and DSC runs. The heating rate was 10°C min^{-1} and the weight of the samples was between 3 and 13 mg.

The X-ray powder diffraction patterns were obtained through a Philips PW-1700 diffractometer using Cu-K_α radiation.

RESULTS AND DISCUSSION

The analytical data and proposed formulae for the complexes are summarized in Table 1. Analyses for nitrate proved negative.

IR spectra

The bonding sites of the ligands that are involved in coordination with the metal ion have been examined by a careful comparison of the IR spectra of the free ligands and their complexes. Besides, the IR spectra of the complexes have been analysed, paying attention to the bands due to the carboxylate and amino groups. The position in the bands corresponding to the stretching vibrations of these groups can illustrate its coordination to the metal ions, because its energy depends on the degree of symmetry of these groups.

The IR spectra of HMa complexes are almost identical, showing their similarity in structure and the type of bonding present. Compared with the spectrum of the free ligand,[11] in the high frequency IR region they show an absorption centred at 3502 [zinc(II) complex] and 3504 cm^{-1} [cadmium(II) complex], which has been identified as being due to the stretching vibrations in hydroxyl groups with intramolecular hydrogen bonds. Besides, the absorption band observed for HMa at 3124 cm^{-1} assigned to the $\nu(NH_3^+)$ stretching vibration is absent in the spectra of the complexes, indicating that the amino group participates in the coordination.

On the other hand, the asymmetric COO^- stretching frequency (ν_{asym}) of the amino acids occurs at 1580–1660 cm^{-1} when the group is coordinated to metals, whereas, a non-coordinated COO^- group

Table 1. Analytical data [Found (Calc.)] and proposed formulae for the complexes

Compound	C(%)	H(%)	N(%)	M(%)
$ZnMa_2$	32.4	5.4	5.3	13.0
	(32.7)	(5.5)	(5.4)	(12.7)
$CdMa_2$	30.5	5.1	4.9	19.7
	(30.0)	(5.0)	(5.0)	(20.0)
$Zn(BnMa)_2 \cdot 2H_2O$	45.6	6.1	3.8	9.2
	(46.1)	(6.1)	(3.8)	(8.9)
$Cd(BnMa)_2 \cdot 2H_2O$	43.0	5.8	3.6	14.5
	(43.3)	(5.7)	(3.6)	(14.5)

has the $\nu_{asym}(COO^-)$ stretching at lower frequencies.[12,13] The bands at 1606 [zinc(II) complex] and 1587 cm^{-1} [cadmium(II) complex] therefore indicates that COO^- is also coordinating in the complexes.

The presence of the coordinated carboxylate group is supported by similar previous assignments[14] in the complexes of analogous α-amino acids with zinc(II) and cadmium(II), in which the amino group and one oxygen of the carboxylate moiety provide a chelate ring in the equatorial plane with carbonyl substituents at axial positions.

It is generally observed that the value of $\Delta\nu$ corresponding to $(\nu_{asym} - \nu_{sym})$ of the carboxylate group change in the order zinc(II) > cadmium(II). In our case the same occurs and thus the values are 185 and 178 cm^{-1} for the zinc(II) and cadmium(II) complexes, respectively. This could be explained on the basis that as the relation charge/ratio decreases for cadmium(II) with regard to zinc(II) the metal–oxygen bond [C—O···M] is weakened and C—O is strengthened and, consequently, $\Delta\nu$ decreases too.

With regard to the IR spectra data of the BnMa complexes with zinc(II) and cadmium(II) it is worth noting that the same criteria: (a) position of $\nu_{asym}(COO^-)$ stretching[15] and (b) $\Delta\nu$ difference between asymmetric and symmetric carboxylate stretching frequencies, are known in order to decide the coordination behaviour of the carboxylate group. On the basis of these criteria, the carboxylate group coordinates as a bridging bidentate ligand in both complexes. Likewise, coordination of the amino group is supported by the disappearance of the absorption band assigned to N—H bonding with respect to same band in the free ligand.

In this case the $\Delta\nu$ values are greater than those observed for HMa complexes. This behaviour is usual in N-protected amino acids with N-protecting groups showing an electron-withdrawing effect, because these groups reduce the basicity of the amino group. This implies a weakness of the nitrogen–metal bond and a concomitant increase in the strength of the oxygen–metal bond C—O···M, therefore, resulting in greater values.[16]

From these considerations it could be concluded that the coordination behaviour of BnMa in these compounds is the same as that of HMa.

Thermal study

The TG and DSC curves of complexes of the same ligand are very similar, which, having in mind the similar molecular structures, also suggests a similar thermal decomposition mechanism. Table 2

Table 2. Thermoanalytical data of the metal complexes

Complex	Process	Temperature (°C)	Weight loss (%)	ΔH ($J\,g^{-1}$)	Residue	Weight (%)	
					Compound	Calc.	Found
$ZnMa_2$	Pyrolysis	200–300	43.0				
		(257, endo)		327			
	Combustion of	300–500	40.6				
	the rest	(355, exo)		251			
		(484, exo)		263	ZnO	15.8	16.4
$CdMa_2$	Pyrolysis	215–294	39.8				
		(255, endo)		330			
	Combustion of	300–550	37.7				
	the rest	(450, exo)		529	CdO	22.9	22.5
$Zn(BnMa)_2 \cdot 2H_2O$	Dehydration[a]	75–160	4.7 (4.9 calc.)				
	Pyrolysis	160–240	35.7				
		(170, 181, endo)		360			
	Combustion of	240–520	48.1				
	the rest	(486, exo)		1057	ZnO	11.1	11.5
$Cd(BnMa)_2 \cdot 2H_2O$	Dehydration[a]	60–154	4.7 (4.6 calc.)				
	Pyrolysis	154–210	23.6				
		(165, endo)		326			
	Combustion of	210–555	55.1				
	the rest	(463, exo)		990	CdO	16.4	16.6

[a] This step overlaps with the start of the pyrolysis.

Table 3. X-ray powder diffraction data of $Zn(BnMa)_2 \cdot 2H_2O$ and $Cd(BnMa)_2 \cdot 2H_2O$

$Zn(BnMa)_2 \cdot 2H_2O$				$Cd(BnMa)_2 \cdot 2H_2O$		
d_{obs}(Å)	d_{calc} (Å)	I/I_0	*hkl*	d_{obs} (Å)	d_{calc} (Å)	I/I_0
11.55	11.56	14	020	11.86	11.84	11
9.94	9.95	100	011	10.00	10.00	100
7.97	7.98	17	021	8.07	8.07	13
			031	6.43	6.42	7
6.26	6.26	12	200	6.24	6.24	19
6.05	6.04	1	210	6.03	6.03	2
5.78	5.78	6	040	5.93	5.92	5
5.51	5.51, 5.51	25	002, 220	5.52	5.52, 5.52	36
5.36	5.36	9	012	5.37	5.37	7
			211	5.32	5.31	6
5.12	5.12	17	041	5.22	5.22	8
4.98	4.98	19	022	5.00	5.00	19
4.91	4.91, 4.90	7	$11\bar{2}$, $22\bar{1}$	4.91	4.92, 4.92	6
4.85	4.86	3	230			
4.48	4.48	15	032	4.52	4.52	14
			231	4.48	4.48	6
4.26	4.27	65	051	4.35	4.35	44
			240	4.29	4.29	3
4.16	4.17	24	202	4.15	4.15	29
			151, $20\bar{2}$	4.11	4.12, 4.11	12
			212	4.06	4.05	3
3.988	3.990	8	042			
3.949	3.951	6	$24\bar{1}$	3.997	3.994	5
3.853	3.854	14	060	3.948	3.946	4
			222	3.906	3.914	3
3.719	3.720	4	250	3.771	3.771	5
3.636	3.639	17	061	3.715	3.716	9
			013	3.636	3.634	3
3.540	3.543	15	052	3.595	3.593	9
			$25\bar{1}$, $16\bar{1}$	3.567	3.563, 3.563	12
			023	3.511	3.512	3
			242, 123	3.394	3.397, 3.387	2
3.317	3.317	9	033	3.333	3.333	12
3.279	3.282	2	260			
			062, 322	3.207	3.209, 3.208	8
3.159	3.159	19	213	3.152	3.150	16
3.100	3.101	17	043	3.121	3.123	21
			420	3.018	3.015	3
2.975	2.975	6	$41\bar{1}$	2.972	2.971	16
2.945	2.946	3	233			
2.877	2.877	11	053	2.907	2.904	17
2.832	2.829	5	271	2.873	2.873	7
			243, $43\bar{1}$	2.800	2.800, 2.800	5
2.770	2.768	5	172			
2.758	2.756	5	004	2.758	2.758	4
2.682	2.684, 2.681	3	$10\bar{4}$, 024	2.687	2.688, 2.686	9
2.627	2.625	12	253	2.642	2.639	7
2.595	2.595	3	034			
2.561	2.560	13	082	2.610	2.608	11
2.502	2.503	7	091	2.560	2.559	8
			$45\bar{1}$	2.532	2.531	3
2.458	2.457	34	073	2.490	2.489	21
			$44\bar{2}$, $22\bar{4}$	2.461	2.461, 2.460	11
2.374	2.375	24	282	2.409	2.409	4
2.329	2.329	8	092			
			$46\bar{1}$	2.386	2.385	7
2.314	2.313	7	0100	2.368	2.368	12
2.294	2.294	3	273	2.317	2.316	5
2.273	2.272, 2.272	5	470, 083			

lists the most important features of these diagrams.

The TG curves of $ZnMa_2$ and $CdMa_2$ show an abrupt weight loss which starts at about 200°C and finishes at 300°C; this effect is accompanied by a sharp endothermic effect, at 257°C, clearly differentiated in the DSC plots of the complexes; the relative values of their energies suggest that such pyrolytic processes are similar. The combustion of the remaining sample, in the 300–500°C temperature range, yields the ZnO and CdO residues, respectively.

The thermal behaviour of the zinc(II) and cadmium(II) complexes with BnMa is very similar to that mentioned above for the HMa complexes. The first pyrolytic effect begins at approximately 70°C, finishing around 230°C; it is centred at 168°C for both complexes and with very similar energy. However, in the TG plots, especially in the one corresponding to cadmium(II), a shoulder of this first main effect can be observed that incorporates a weight loss of the order 4.7%, corresponding to the loss of two H_2O molecules.

At temperatures above this first effect, combustion of the sample takes place, finally giving the corresponding oxides that were characterized by IR spectroscopy and X-ray powder diffraction patterns.

X-ray diffraction

The X-ray powder patterns of $Zn(BnMa)_2 \cdot 2H_2O$ and $Cd(BnMa)_2 \cdot 2H_2O$ (Table 3) show that these compounds are isomorphous and crystallize in the monoclinic system. The systematic extinctions, $(0k0)$ absent for k = odd and $(h0l)$ for l = odd, indicate that the most probable space group is $P2_1/c$. The unit cell data were refined by a classical least-squares method, minimizing the $\Sigma(\sin^2\theta_0 - \sin^2\theta_c)^2$ expression. The refined parameters are: $a = 12.521(4)$, $b = 23.126(4)$, $c = 11.024(2)$ Å; $\beta = 89.23(3)°$; $V = 3192(1)$ Å^3 for $Zn(BnMa)_2 \cdot 2H_2O$; and $a = 12.474(3)$, $b = 23.687(5)$, $c = 11.032(2)$ Å; $\beta = 89.57(2)°$; $V = 3259(1)$ Å^3 for $Cd(BnMa)_2 \cdot 2H_2O$. The greater volume of the unit cell of $Cd(BnMa)_2 \cdot 2H_2O$ is consistent with the greater size of the cadmium(II) ion compared with the zinc(II) ion.

REFERENCES

1. S. Yano, *Coord. Chem. Rev.* 1988, **92**, 113.
2. D. M. Whitfield, S. Stojkovski and B. Sarkar, *Coord. Chem. Rev.* 1993, **122**, 171.
3. V. Sauchelli, *Trace Elements in Agriculture*. Van Nostrand Reinhold, New York (1969).
4. D. T. Sawyer, *Chem. Rev.* 1964, **64**, 633.
5. Z. Tamura and M. Miyazaki, *Chem. Pharm. Bull.* 1965, **13**, 333.
6. G. Micera, S. Deiana, A. Dessi, P. Decock, B. Dubois and H. Kozlowski, *Inorg. Chim. Acta* 1985, **107**, 45.
7. C. Valenzuela-Calahorro, M. A. Díaz-Díez, E. Sabio-Rey, F. J. García-Barros and E. Román Galán, *Polyhedron* 1992, **11**, 563.
8. M. A. Díaz-Díez, F. J. García Barros, E. Sabio Rey and C. Valenzuela Calahorro, *J. Inorg. Biochem.* 1992, **48**, 129.
9. M. A. Díaz-Díez, F. J. García Barros, E. Sabio Rey and C. Valenzuela Calahorro, *J. Inorg. Biochem.*, in press.
10. J. A. Galbis, J. C. Palacios and E. Román, *Carbohydr. Res.* 1983, **114**, 158.
11. M. A. Díaz-Díez, Compuestos de coordinación de iones de metales de transición con α-aminoácidos derivados de Manosa, PhD Thesis. Universidad de Extremadura, Badajoz (1992).
12. M. Chandrasenkharan, M. R. Udupa and G. Aravamudan, *Inorg. Chim. Acta* 1973, **77**, 88.
13. W. Levason and C. A. McAuliffe, *Inorg. Nucl. Chem. Lett.* 1977, **13**, 123.
14. C. A. McAuliffe and W. D. Perry, *J. Chem. Soc.* 1969, **4**, 634.
15. L. P. Battaglia, A. Bonamartini Corradi, G. Marcotrigiano, L. Menabue and G. C. Pellacani, *J. Am. Chem. Soc.* 1980, **102**, 2663.
16. R. Battini, G. G. Battistuzzi, G. Grandi, L. Menabue, G. G. Pellacani, M. Saladini and A. Bonamartini Corradi, *J. Chem. Soc., Dalton Trans.* 1981, **8**, 1665.

Polyhedron Vol. 12, No. 20, pp. 2525–2534, 1993
Printed in Great Britain

0277–5387/93 $6.00+.00
© 1993 Pergamon Press Ltd

THE DISECONDARY PHOSPHINES [PhHP$(CH_2)_n$PHPh] (n = 2–4, 6): IMPROVED SYNTHESES, NMR SPECTRA AND COMPLEXATION BEHAVIOUR WITH GROUP VI TRANSITION METAL HEXACARBONYLS

BRYAN R. KIMPTON, WILLIAM McFARLANE,* ALAN S. MUIR and PALLAVI G. PATEL

Department of Chemistry, University of Newcastle upon Tyne, Newcastle upon Tyne NE1 7RU, U.K.

and

JONATHAN L. BOOKHAM

Department of Chemical and Life Sciences, University of Northumbria, Newcastle upon Tyne NE1 8ST, U.K.

(*Received* 20 *April* 1993; *accepted* 3 *June* 1993)

Abstract—Improved preparations of the disecondary phosphines PhHP$(CH_2)_n$PHPh (n = 2, mppe; n = 3, mppp; n = 4, mppb; n = 6, mpph) by the lithium cleavage of the corresponding ditertiary phosphine $Ph_2P(CH_2)_nPPh_2$ are described and various NMR parameters are reported; a $^{12/13}C$ isotope effect upon $\delta(^{31}P)$ is observed in the case of mppe. Reactions of mppe and mppp with $[M(CO)_6]$ (M = Cr, Mo, W) yield 1:1 complexes; both the *meso* and the *rac* isomers are produced, are separated and are unequivocally characterized by elemental analysis, vibrational spectroscopy and ^1H, ^{13}C and ^{31}P NMR spectroscopy.

The ditertiary phosphines $Ph_2P(CH_2)_nPPh_2$ [e.g. dppm (n = 1) and dppe (n = 2)] have been used for many years as bidentate chelating ligands for a wide range of metal substrates,[1,2] but the relatively high symmetry of these ligands and their complexes limits the data readily available from their ^{31}P, ^{13}C and ^1H NMR spectra. Ligands of lower symmetry are therefore of considerable interest and, hitherto, RR′P$(CH_2)_n$PR′R and $R_2P(CH_2)_n$PR′R [R, R′ = H, alkyl, aryl] have been studied with this in mind.[3–22] Of particular potential value in this regard are the disecondary phosphines PhHP$(CH_2)_n$PHPh, both in view of the small size of the hydrogen substituent on phosphorus and the opportunities offered for further reactions, e.g. with BuLi or various unsaturated species. One published synthesis of mppe, [PhHP$(CH_2)_2$PHPh] (**1**), involves the preparation of Ph(Pr^{i}O)P(O)CH_2 CH_2(O)P(Pr^{i}O)Ph followed by its reduction with $LiAlH_4$ and is somewhat inconvenient,[10,11] although another route via the hydrolysis of $[(Li(thf)_2)_2(PhPCH_2CH_2PPh)]$ yielded 58% of the desired product.[24] A different procedure involving the reaction of either NaPPhH or KPPhH with the appropriate n-dihaloalkane has been used to prepare **1**[7] as well as mppp, [PhHP$(CH_2)_3$PHPh][4] (**2**), mppb, [PhHP$(CH_2)_4$PHPh][4] (**3**), and mpph, [PhHP$(CH_2)_6$PHPh][5] (**4**), but is somewhat cumbersome. An attractive alternative is the lithium cleavage of ditertiary phosphines, $Ph_2P(CH_2)_n$ PPh_2, to give PhLiP$(CH_2)_n$PLiPh, which can then be hydrolysed to the desired disecondary phosphine. Unfortunately, this reaction often yields substantial amounts of alternative products owing to cleavage of a P—CH_2 bond,[25–30] but we find that under suitable conditions the formation of these and the consequent Ph_2PH can be minimized. Thus, the reaction offers a convenient, high-yielding route to **1** and also to **2**, **3** and **4**.

* Author to whom correspondence should be addressed.

Although all of these ligands should form complexes with metal substrates, relatively little work has been reported in this area: the main results are for reactions of **1** with chalcogens,[7,10,31,32] methyl iodide,[7,10] nickel and cobalt halides[11] and the organoelement halides R_2ECl_2 and $RECl_2$.[14,33] Similar reactions of **2** have been studied[4,14,31-33] as well as its reactions with $Ni(CO)_4$, $C_7H_8Mo(CO)_4$ and $Mo(CO)_6$.[19]

We report here the improved syntheses of **1**, **2**, **3** and **4** and present their ^{31}P, ^{13}C and ^{1}H NMR parameters. Preparative, NMR and vibrational spectroscopic studies of the reactions between **1** and **2** and group VI transition metal hexacarbonyls are also reported and individual diastereomers (arising from the presence of the phosphorus chiral centres) of the complexes have been isolated as air-stable, microcrystalline solids.

RESULTS AND DISCUSSION

General

The reaction between a thf solution of dppe and metallic lithium was complete within *ca* 24 h at 300 K, but significant cleavage of P—CH_2 bonds occurred so that after hydrolysis substantial amounts (50%) of Ph_2PH were produced and the subsequent yield of the desired product [mppe, (**1**)] was low.[28] However, at 273 K the P—C bond cleavage was more selective and favoured the formation of $PhLiPCH_2CH_2PLiPh$ so that crude yields (^{31}P NMR evidence) of mppe in excess of 95% were achieved, although the reaction now took *ca* 200 h to complete.[28] With other α,ω-bis(diphenylphosphino)alkanes satisfactory yields of the desired disecondary phosphines [mppp, (**2**); mppb (**3**); mpph, (**4**)] were obtained when the cleavage reaction was conducted at 300 K or above and they were therefore complete more rapidly. For **1** and **2** ^{31}P NMR showed that 1:1 mixtures of diastereomeric products were obtained, but these were not separated; presumably **3** and **4** were also diastereomeric mixtures.

The 1:1 diastereomeric mixtures of mppe (**1**) and mppp (**2**) each reacted smoothly in refluxing $MeOCH_2CH_2OCH_2CH_2OMe$ with $M(CO)_6$ [M = Cr, Mo, W] to yield solutions containing the corresponding complexes $M(CO)_4L$ (**5**–**16**) in each case as diastereomeric pairs in the proportions shown in Table 1. For the mppe complexes it was possible to separate the individual *meso* and *rac* isomers in each case by fractional crystallization, and their melting points and analytical data are in Table 1. With mppp each of the diastereomers of the chromium complex was isolated, but only the *meso* forms were obtained pure for molybdenum and tungsten. Attempts to isolate the *rac* forms were thwarted by polymerization; this is consistent with a previous study of the mppp/$Mo(CO)_6$ system.[19]

Unequivocal identification of the *rac* and *meso* diastereomers was obtained from their ^{13}CO NMR spectra since the former yields a triplet (from the two equivalent axial CO groups) and an ABX multiplet (from the equatorial CO groups), whilst the latter gives *two* triplets (from the inequivalent axial CO groups) and an ABX multiplet.[34,35] Representative spectra are shown in Fig. 1. The formation of unequal proportions of the *rac* and *meso* diastereomers from a 1:1 mixture of the two diastereomers of the ligand indicates that inversion of phosphorus must occur at the reaction temperature (435 K).

NMR spectra

Tables 2 and 3 give ^{13}C, ^{31}P and selected ^{1}H data for the disecondaryphosphines **1**–**4**. For **3** and **4** the

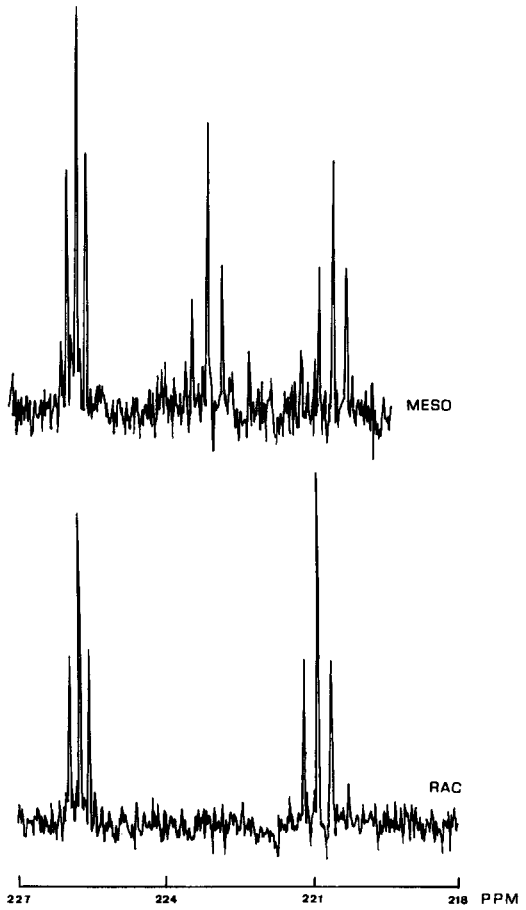

Fig. 1. ^{13}C NMR spectra at 50.3 MHz of carbonyl regions of complexes **11** and **12**.

Table 1. Analytical and other data for the complexes *cis*-[PhHP(CH$_2$)$_n$PHPh]M(CO)$_4$ [n = 2, 3; M = Cr, Mo, W]

No.	Complex	M.p. (°C)	%C		%H		Colour	R.M.M.[a]	Reflux time[b]	%[c]	Isolated yield (%)[d]
			Calc.	Found	Calc.	Found					
5	*Meso*-Cr(CO)$_4$[PhHP(CH$_2$)$_2$PHPh]	130–132	52.7	52.5	3.9	3.9	Pale yellow	410	30	52	14.5
6	*Rac*-Cr(CO)$_4$[PhHP(CH$_2$)$_2$PHPh]	149–151	52.7	52.8	3.9	3.9	Pale yellow	410		48	13.0
7	*Meso*-Mo(CO)$_4$[PhHP(CH$_2$)$_2$PHPh]	146–149	47.6	47.4	3.5	3.4	Ochre	456	15	60	9.4
8	*Rac*-Mo(CO)$_4$[PhHP(CH$_2$)$_2$PHPh]	157–159	47.6	47.4	3.5	3.4	Ochre	456		40	12.7
9	*Meso*-W(CO)$_4$[PhHP(CH$_2$)$_2$PHPh]	137–140	39.9	39.3	2.9	2.9	Brown	542	390	50	10.5
10	*Rac*-W(CO)$_4$[PhHP(CH$_2$)$_2$PHPh]	165–168	39.9	39.8	2.9	2.9	Brown	542		50	22.9
11	*Meso*-Cr(CO)$_4$[PhHP(CH$_2$)$_3$PHPh]	108–111	53.8	53.2	4.3	4.1	Bright yellow	424	90	53	11.3
12	*Rac*-Cr(CO)$_4$[PhHP(CH$_2$)$_3$PHPh]	179–182	53.8	53.5	4.3	4.2	Pale yellow	424		47	18.9
13	*Meso*-Mo(CO)$_4$[PhHP(CH$_2$)$_3$PHPh]	184–187	48.7	48.2	3.9	3.9	Golden brown	468	105	55[e]	27.1
15	*Meso*-W(CO)$_4$[PhHP(CH$_2$)$_3$PHPh]	d > 168	41.0	40.3	3.3	3.1	Reddy brown	556	240	60[e]	16.5

[a] Determined mass spectrometrically.

[b] Reflux time (in min) for the reaction of PhHP(CH$_2$)$_n$PHPh and M(CO)$_6$ in diglyme.

[c] % of particular isomer in unseparated reaction mixture as determined by ^{31}P NMR.

[d] Isomeric purity >95% by ^{31}P NMR.

[e] Although both isomers were observed in the reaction mixture, only the *meso* form proved isolable.

Table 2. NMR parameters for the disecondary phosphines $PhHP(CH_2)_nPHPh$ (n = 2–4, 6)[a]

No.	Phosphine	$\delta(^{31}P)$	$^nJ(^{31}P^{31}P)$	$\delta(^{13}C)$, $J(^{31}P^{13}C)$					$\delta(^1H)$[b]	Literature ref.
				$C_{b\text{-bone}}$	C_{ortho}	C_{meta}	C_{para}	C_{ipso}		
1	$PhHP(CH_2)_2PHPh$ (mppe)	−45.6 −45.9	11.5±0.2	23.0 $^1J = \pm 15.7$ $^2J = \mp 8.8$ $v_0\delta = 4$[d]	134.3(0.08)[c] $^2J = 15.4$ $^5J < 1$	128.4(0.006)[c] $^3J = 5.6$ $^6J \sim 0$	128.0(0.04)[c] $J \sim 0$	136.0(0.01)[c] $^1J = 12.5$ $^4J \sim 0$ $v_0\delta = 3.4$[d]	1.99 (CH_2) 4.29 (PH)	7, 9, 30
2	$PhHP(CH_2)_3PHPh$ (mppp)	−51.9 −52.0	⩽1	25.3 (α) 27.8 (β) $^1J = 12.2$ $^2J = 8.3$ $^3J = 7.4$	134.3 $^2J = 15.8$	129.2 $^3J = 5.5$	128.8 $J \sim 0$	136.4 $^1J = 12.2$	4.21 (Ph) ^3J(HH) = 6.7	4
3	$PhHP(CH_2)_4PHPh$ (mppb)	−52.5	<1	23.8 (α) 30.4 (β) $^1J = 12.2$ $^2J = 7.9$ $^3J = 7.9$	134.4 $^2J = 14.7$	129.2 $^3J = 6.1$	128.8 $J \sim 0$	136.7 $^1J = 13.4$	4.16 (PH) ^3J(HH) = 6.9	4
4	$PhHP(CH_2)_6PHPh$ (mpph)	−51.9	<1	23.5 (α) 28.3 (γ) 30.6 (β) $^1J = 10.8$ $^2J = 7.5$ $^3J = 9.1$	133.7 $^2J = 15.0$	128.6 $^3J = 5.6$	128.2 $J \sim 0$	136.0 $^1J = 11.0$	4.21 (PH) ^3J(HH) = 6.9	5

[a] Chemical shifts are in ppm: for ^{31}P to high frequency of external 85% H_3PO_4, for ^{13}C and ^1H to high frequency of $SiMe_4$. Coupling constants are in Hz.
[b] Selected data shown as phenyl proton resonances were not well resolved.
[c] Chemical shift difference between the two diastereomers indicated in parenthesis.
[d] $v_0\delta$ is the $^{12/13}C$ isotope effect in Hz upon $\delta(^{31}P)$ of the corresponding carbon atom at 11.8 T.

Table 3. ^{31}P parameters for the complexes *cis*-[PhHP(CH$_2$)$_n$PHPh]M(CO)$_4$ [n = 2, 3; M = Cr, Mo, W][a]

No.	Complex	$\delta(^{31}P)$	$\Delta\delta(^{31}P)$[b]	$^1J(^{31}P—^1H)$[c]	$^2J(^{31}P—^{31}P)$[d]
5	*Meso*-Cr(CO)$_4$mppe	48.9	94.6	331	21.9
6	*Rac*-Cr(CO)$_4$mppe	51.5	97.2	322[e]	23.4
7	*Meso*-Mo(CO)$_4$mppe	17.6	63.3	321	16.2
8	*Rac*-Mo(CO)$_4$mppe	20.4	66.1	315[e]	17.6
9	*Meso*-W(CO)$_4$mppe	1.1[f]	46.8	337	12.6
10	*Rac*-W(CO)$_4$mppe	3.7[f]	49.4	335[e]	14.9
11	*Meso*-Cr(CO)$_4$mppp	17.6	69.5	329	15.0
12	*Rac*-Cr(CO)$_4$mppp	21.8	73.7	319	13.7
13	*Meso*-Mo(CO)$_4$mppp	−7.8[g]	44.1	317	14.2
14	*Rac*-Mo(CO)$_4$mppp	−9.8[g,h]	42.1	N.R.	N.R.
15	*Meso*-W(CO)$_4$mppp	−32.2[f]	19.7	328	14.5
16	*Rac*-W(CO)$_4$mppp	−37.3[h]	14.6	N.R.	N.R.

[a] Chemical shifts are in ppm to high frequency of external 85% H_3PO_4. Coupling constants are in Hz.

[b] $\Delta\delta(^{31}P) = \delta(^{31}P)$ complex $-\delta(^{31}P)$ ligand.[36]

[c] Determined from ^{1}H spectrum.

[d] Determined from ^{13}C spectrum.

[e] $^3J(^{31}P—^1H)$: 38 Hz for **6**, 35 Hz for **8** and 38 Hz for **10**.

[f] $^1J(^{31}P—^{183}W)$ values all within 220–222 Hz.

[g] Compared with values of −8.3 and −11.7 ppm.[19]

[h] Values taken from reaction mixture (diglyme). Products not isolated.

N.R. = not recorded.

centres of chirality are sufficiently far apart for no differences between pairs of diastereomers to be apparent; and for **2** $\delta(^{31}P)$ is the only parameter to show any differences. In the case of **1** there are small differences in the chemical shifts, but not in the coupling constants, and this presumably indicates that any conformational imbalances are relatively small as these molecules have no bulky substituents. Under conditions of broad-band proton decoupling the natural abundance ^{13}C spectra of these species are from ABX spin systems [A, B = ^{31}P, X = ^{13}C] and their appearance is therefore dependent upon J(AB), J(AX) and J(BX), as well as $\nu_0\delta$(AB), which arises from the $^{12/13}$C isotope effect upon $\delta(^{31}P)$. In the absence of this effect the spin system is AA′X and would yield a symmetrical five-line pattern for the X sub-spectrum; most such spectra have previously been analysed on this basis. However, for higher values of $B_0V_0\delta_{AB}$ becomes appreciable and this leads to a splitting of the central X resonance so that a six-line pattern is obtained. This is illustrated in Fig. 2 and provides a convenient and precise indirect method of measuring $^{12/13}$C isotope effects upon ^{31}P shieldings, although it does not yield their signs. There appear to be very few *direct* observations of this effect. For the *ipso*-phenyl carbons of **1** the effect is 0.017 ppm and is 0.02 ppm for the directly bonded backbone carbons.

Although the differences in $\delta(^{31}P)$ for the two diastereomers of **1** and **2** are of undoubted diagnostic value, it is not appropriate to comment in detail upon their origin. However, it is noteworthy that in the complexes of these two ligands (*vide infra*), where the two chiral centres are separated by only two chemical bonds, the differences are much larger (*ca* 3 ppm) and are of similar magnitude for both phosphines. Presumably these differences

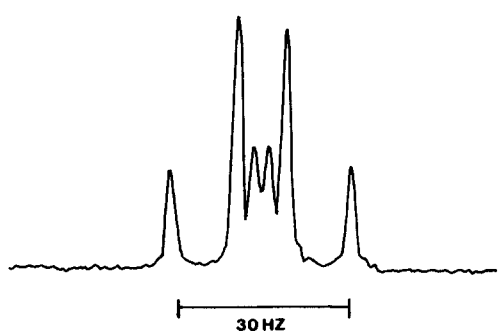

Fig. 2. ^{13}C NMR spectrum of the backbone region of the disecondary phosphine **1** at 50.3 MHz. Equal proportions of the two diastereomers were present, but this had no observable effect upon the spectra, the splitting of the central line being due to the $^{12/13}$C isotope effect upon $\delta(^{31}P)$.

would be retained in similar complexes of $PhHP(CH_2)_nPHPh$ no matter how large the value of n owing to the availability of the two-bond route via the metal atom.

The analysis of the ^{13}C spectra of the ligand parts of the complexes **5–16** proceeded as above and the results are summarized in Table 4. An important feature of this analysis is that it yields $^2J(^{31}P^{31}P)$ [ideally from the $^{13}C_{meta}$ resonances of the phenyl groups for which $^5J(^{31}P^{13}C)$ can be realistically taken as zero] and this then provides the key to the analysis of the carbonyl resonances. For axial carbonyls there are triplets resulting from coupling to the two ^{31}P nuclei and for the equatorial characteristic ABX patterns are obtained. Only in those cases for which the signal-to-noise ratio was sufficient to observe all lines of the X spectrum was it possible to obtain separate values of $^2J(^{31}P^{13}C_{cis})$ and $^2J(^{31}P^{13}C_{trans})$. Although we have previously observed $^{12/13}C$ isotope effects upon $\delta(^{31}P)$ in the carbonyl spectra of metal phosphine complexes[36] the dispersion in the present study was insufficient for this. In a combined NMR and X-ray diffraction study[34] of *meso*-$Ph_2PCHPhCHPhPPh_2Mo(CO)_4$, which has the same local symmetry at molybdenum as **7**, it was possible to make a reasonable assignment of the ^{13}C resonances of the two types of axial carbonyl group on the basis of their large (7.2 ppm) chemical shift difference and a comparison with $[Ph_2P(CH_2)_2PPh_2]Mo(CO)_4$.[35] In the present series the corresponding chemical shift differences are much smaller (*ca* 3 ppm or less) so that no comparable conclusions can be drawn, and the two types of carbonyl are simply styled ax and ax′, with ax being arbitrarily assigned the higher value of $\delta(^{13}C)$.

This study brings out the clear effects of relatively small changes in interbond and dihedral angles upon chemical shifts and particularly coupling constants, since differences in electronic effects should be insignificant between the pairs of diastereomers. In the diphosphines themselves the observed effects are small, presumably because the absence of bulky substituents leads to a high degree of conformational mobility and because the different conformers have approximately equal populations.

The coordination chemical shifts $\Delta\delta(^{31}P)$[37] for the complexes of mppe are less than for dppe[35] with both molybdenum and tungsten, but are more with chromium, whilst those for mppp complexes are greater than for dppp except in the case of the *rac*-$W(CO)_4$ derivative. Coordination chemical shifts in chelate complexes have significant components arising from "ring strain" and the extent to which this can be relieved by ring puckering. This in turn will be affected by the bulk of substituents and should be an easy process in complexes of mppe and mppp; that is the extent of ring strain should be least in these. In conformity with this the differences in various ^{13}C parameters [viz. $\delta(^{13}C)$ and $J(^{31}P^{13}C)$] between diastereomeric pairs are quite small for these complexes and the parameters themselves follow patterns similar to those found for complexes of dppe and dppp.[35] There are, however, interesting differences in certain proton parameters for the members of diastereomeric pairs of the mppe complexes. Specifically, there is a chemical shift difference of *ca* 1.4 ppm in $\delta(^1H)$ for the two types of CH_2 proton in the *rac* isomers, but of only *ca* 0.3 ppm for the *meso* isomers and these are paralleled by values of $^3J(^{31}PCC^1H)$ of *ca* 38 Hz for *one* type of proton in the *rac* isomers. These observations can be understood if account is taken of a high degree of chelate ring puckering, as has been determined for complexes of dppe[38] and $Ph_2PCHPhCHPhPPh_2$.[34] Figure 3 shows four idealized conformers for a $PhHP(CH_2)_2PHPhM(CO)_4$ complex: the two pairs (*a*) and (*b*), and (*c*) and (*d*) represent extremes of the *rac* and *meso* diastereomers, respectively. In the *rac* diastereomer the two conformers have either *both* Ph groups axial or *both* equatorial and will therefore differ in energy so that one form may predominate. Hence, protons A and A′ will be mainly equatorial and B and B′ mainly axial or *vice versa*. In the *meso* diastereomer the two conformers are of equal energy (each has *one* Ph group axial and *one* equatorial) and are thus equally populated; hence, the A,A′ and B,B′ protons will spend equal amounts of time in axial and equatorial positions; thus, the environments are partially averaged and the chemical shift difference is reduced. Also, in the latter diastereomer there will be a greater degree of averaging of dihedral angles relating P and CH_2 and hence smaller values of $^3J(^{31}P^1H)$. Interestingly, this behaviour is also found in the complexes of mppp, despite the presumably greater flexibility of the six-membered chelate ring.

Vibrational spectra

The vibrational characteristics of the dppe derivatives of group VI transition metal hexacarbonyls have previously been reported,[39,40] but no data appear to be available for the mppe homologues. In general, local C_{2v} symmetry in the *cis*-$L_2M[CO]_4$ species leads to four carbonyl stretching modes [$2A_1$, B_1, B_2], each being IR and Raman active. Selected vibrational frequencies for the mppe complexes (**5–10**) are presented in Table 5; the IR solution spectra (in CH_2Cl_2) were all similar with hardly any differences between the cor-

Table 4. Selected ^{13}C and ^{1}H NMR data for the complexes *cis*-[PhHP(CH$_2$)$_n$PHPh]M(CO)$_4$ [n = 2, 3; M = Cr, Mo, W][a]

No.	Complex	$\delta(^{13}C_{ax})$	$\delta(^{13}C_{eq})$	$\delta(^{13}C_{ax'})$	$J(^{31}P^{13}C_{ax})$	$J(^{31}P^{13}C_{ax'})$	$J(^{31}P^{13}C_{eq}) \pm J(^{31}P^{13}C_{eq'})$	$\delta(^{13}C_{bb})$[b]	$J(^{31}P^{13}C_{bb})$[b]	$\delta(^{1}H_{bb})$[b]
5	*Meso*-Cr(CO)$_4$mppe	220.8	227.7	219.3	14.9	12.7	16.7	24.7	$N = 44.1$[c]	2.04, 2.22
6	*Rac*-Cr(CO)$_4$mppe	220.6	227.7	220.6	14.2	14.2	16.4	25.2	$N = 42.1$[c]	1.32, 2.79[d]
7	*Meso*-Mo(CO)$_4$mppe	211.6	216.3	208.7	7.8	N.A.	17.1,[e] 8.3[f]	25.1	$N = 42.6$[c]	2.00, 2.31
8	*Rac*-Mo(CO)$_4$mppe	209.2	216.0	209.2	9.4	9.4	25.9,[e] 9.2[f]	25.1	34.3,[g] 6.5[h]	1.35, 2.83[i]
9	*Meso*-W(CO)$_4$mppe	201.7	206.9	198.9	7.7	5.8	26.0,[e] 7.4[f]	26.0	35.5,[g] 8.4[h]	2.06, 2.38
10	*Rac*-W(CO)$_4$mppe	200.2	206.6	200.2	7.1	7.1	25.4,[e] 7.1[f]	26.6	32.8,[g] 10.3[h]	1.40, 2.90[i]
11	*Meso*-Cr(CO)$_4$mppe	222.8	225.6	220.1	15.6	14.2	19.9	26.7, 23.7	24.4,[j] 2±0.5[k]	[m]
12	*Rac*-Cr(CO)$_4$mppe	220.9	225.6	220.9	9.9	9.9	28.2	26.1, 21.5	25.6,[j] 1.8±0.5[k]	[m]
13	*Meso*-Mo(CO)$_4$mppe	211.6	214.3	208.1	10.1	9.2	13.0	27.9, 23.8	24.0,[j] 5±1[k]	[m]
15	*Rac*-Mo(CO)$_4$mppe	203.3	204.8	199.2	8.5	7.0	14.3	27.7, 23.9	27.4,[j] N.A.[k]	[m]

[a] Chemical shifts in ppm ±0.1 ppm to high frequency of Me_4Si. Coupling constants in Hz ±0.1.
[b] bb = backbone. [c] $N = {}^{1}J(^{31}P^{13}C) + {}^{2}J(^{31}P^{13}C)$. [d] ${}^{3}J(^{31}P^{1}H) = 37.6$ Hz.
[e] ${}^{2}J(^{31}P^{13}C_{trans})$. [f] ${}^{2}J(^{31}P^{13}C_{cis})$. [g] ${}^{1}J$. [h] ${}^{2}J$. [i] ${}^{3}J(^{31}P^{1}H) = 35.0$ Hz. [j] ${}^{1}J + {}^{3}J$.
[k] ${}^{2}J$. [l] ${}^{3}J(^{31}P^{1}H) = 37.8$ Hz.
[m] Behaviour similar to that of the mppe complexes, but aliphatic spectral regions are more complex.
N.A. = not available.

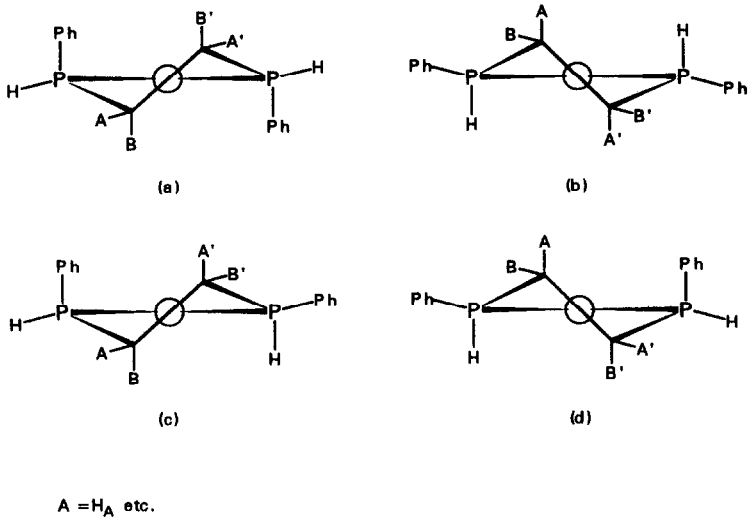

Fig. 3. Four idealized conformers of a $[PhHP(CH_2)_2PHPh]M(CO_4)$ complex: (a) and (b) represent two extremes of the *rac* diastereomer whilst (c) and (d) represent two extremes of the *meso* diastereomer.

responding *rac*/*meso* pairs. In all cases a higher frequency carbonyl band at *ca* 2010–2020 cm^{-1} was observed, together with a group of three overlapping lower frequency carbonyl bands in the 1850–1950 cm^{-1} region. However, the solid-state spectra show marked differences between corresponding *rac* and *meso* pairs in both the ν(CO) and ν(P—H) spectral regions. The carbonyl region spectra were still essentially four-band, but various splittings and shoulders were observed, presumably indicative of differing environments in the crystal. For the chromium complexes **5** (*meso*) and **6** (*rac*), a higher frequency carbonyl mode occurs at 2011 and 2009 cm^{-1}, respectively, in the Raman spectra. The *meso* isomer also has strong bands at 1903, 1899 and 1865 cm^{-1}; the first two of these overlap and are therefore not totally resolved. By contrast, the *rac* isomer (**6**) displays a strong, broad band at 1904 cm^{-1} with a higher frequency shoulder at 1921 cm^{-1}. Additional bands are present at 1881 and

Table 5. Selected vibrational spectroscopic data (cm^{-1}) for the *cis*-$[PhHP(CH_2)PHPh]M(CO)_4$ [M = Cr, Mo, W] complexes

No.	Complex	ν(CO)	ν(PH)
5	*Meso*-$Cr(CO)_4$mppe	2011, 1919, 1896, 1875 (IR)° 2008, 1910, 1903, 1870, 1842, (IR)× 2009, 1903, 1897, 1865 (R)	2317, 2327 (IR)× 2319, 2326 (R)
6	*Rac*-$Cr(CO)_4$mppe	2011, 1922, 1896, 1877, (IR)° 2006, 1918, 1903, 1875, 1864, 1841, (IR)× 2009, 1921, 1904, 1881, 1865 (R)	2327, 2350 (IR)× 2329, 2355 (R)
7	*Meso*-$Mo(CO)_4$mppe	2023, 1927, 1908, 1893 (IR)° 2020, 1917, 1903, 1881, 1870, 1846 (IR)× 2023, 1913, 1906, 1867 (R)	2321, 2333 (IR)× 2320, 2332 (R)
8	*Rac*-$Mo(CO)_4$mppe	2023, 1928, 1908, 1892 (IR)° 2017, 1923, 1910, 1883, 1868, 1844 (IR)× 2018, 1920, 1912, 1887, 1869 (R)	2320, 2334, 2346 (IR)× 2334, 2347 (R)
9	*Meso*-$W(CO)_4$mppe	2018, 1914, 1896, 1873, 1847 (IR)×	2326, 2357 (IR)
10	*Rac*-$W(CO)_4$mppe	2019, 1919, 1899, 1884 (IR)° 2014, 1915, 1901, 1876, 1861, 1846 (IR)× 2016, 1911, 1904, 1881, 1863 (R)	2322, 2336 (IR)

(R) = Raman. × Indicates KBr discs; ° indicates CH_2Cl_2 solution.

1865 cm^{-1}; of these the latter is much less intense than the corresponding one in the spectrum of the *meso* complex. The KBr disc IR spectra of **5** and **6** display similar characteristics, although with much reduced resolution. The molybdenum and tungsten congeners behave similarly and show the same band patterns in both the solid-state IR and Raman spectra. Overall these data indicate that in the solid-state there is undoubtedly some distortion from idealized pseudo-octahedral geometry and there are probably interactions between the phenyl moieties and the equatorial carbonyl groups; such effects have been crystallographically determined for $Ph_2P(CH_2)_2PPh_2Mo(CO)_4$.[38] However, in solution such interactions are presumably much reduced; this would account for the striking similarities between the spectra of corresponding *meso*/*rac* pairs in CH_2Cl_2 solution.

EXPERIMENTAL

^{1}H, ^{13}C and ^{31}P NMR spectra were recorded at room temperature in CH_2Cl_2 solutions contained in either 5 or 10 mm o.d. spinning tubes at field strengths of 2.1 (Jeol FX 90Q), 4.7 (Bruker AC 200F), 7.1 (Bruker WF 300) and 11.8 (Bruker AMX 500) T.

IR spectra were recorded as solutions in CH_2Cl_2 or as KBr discs using either a Perkin–Elmer 1600 or a Nicolet 20 PC FTIR spectrometer. Raman spectra were recorded on solid samples sealed in glass capillaries using a Coderg PHO spectrometer with excitation provided at 514.5 nm by a Coherent Radiation Argon Ion Laser.

All solutions were deaerated prior to use and manipulations were performed under an atmosphere of dry dinitrogen.

1,2-*Bis*(*diphenylphosphino*)*ethane* (*dppe*) *and* 1,3-bis(*diphenylphosphino*)*propane* (*dppp*)

These were prepared by established procedures[3,35,41] involving the reaction of sodium diphenylphosphide and the appropriate dichloroalkane in liquid ammonia. Other α,ω-bis(diphenylphosphino)alkanes were synthesized similarly [yields $>70\%$].

1,2-*Bis*(*phenylphosphino*)*ethane* [*mppe*, (**1**)]

Dppe (70.3 g, 0.176 mol) and thinly cut lithium metal strips (4.9 g, 0.704 mol) were reacted in dry thf (700 cm^3); the mixture was stirred for *ca* 200 h at 273 K when ^{31}P NMR indicated total reaction of the starting diphosphine. To the deep red solution degassed water (250 cm^3) was added (cautiously at first) to hydrolyse the lithiated disecondary phosphine and to remove any dissolved salts. Diethyl ether was added and the organic layer was separated and dried over Na_2SO_4; after filtration, the solvent was removed by distillation. The resulting straw-coloured viscous liquid was distilled [140°C/0.2 mm Hg: literature 161°C/0.8 mm Hg[3,10]] to give a clear product (yield 85%) in which ^{31}P NMR indicated the presence of two diastereomers in a 1:1 ratio, although no separation was attempted.

1,3-*Bis*(*phenylphosphino*)*propane* [*mppe*, (**2**)], 1,4-bis(*phenylphosphino*)*butane* [*mppe*, (**3**)] *and* 1,6-bis(*phenylphosphino*)*hexane* [*mppe*, (**4**)]

These disecondary phosphines were prepared in a similar way to mppe (**1**) using the appropriate bis(diphenylphosphino)alkane; reactions were monitored to completion by ^{31}P NMR. For mppp (**2**), lithiation of dppp was completed within 24 h at room temperature and the product (77% yield) was isolated by distillation [190°C/4.0 mm Hg: literature 196°C/5 mm Hg[3,4]]. The two diastereomers observed by ^{31}P NMR were not separated. The lithiation of dppb to yield mppb (**3**) was effected by stirring at room temperature for 8 h followed by refluxing for 2 h to ensure complete reaction; the product was isolated in *ca* 75% yield by distillation [147°C/0.09 mm Hg; literature 208°C/4.0 mm Hg[3,4]]. Mpph (**4**) was prepared from lithiated dpph (reaction was complete within 8 h at room temperature) and isolated in 80% yield by distillation [165°C/0.05 mm Hg: literature 178°C/0.2 mm Hg[3,5]].

Reactions of mppe (**1**) *and mppe* (**2**) *with* M(CO)$_6$ [M = Cr, Mo, W]

The reactions of either mppe (**1**) or mppe (**2**) with M(CO)$_6$ were conducted in refluxing diglyme. Experimental details are presented in Table 1. After complete reaction (as monitored by ^{31}P NMR) the solvent was removed *in vacuo* and addition of MeOH followed by refrigeration yielded a first crop of crystals (*rac* isomer). Repeated evaporation and refrigeration yielded further crystals (*meso* isomer). Products were recrystallized from CH_2Cl_2/MeOH. From the reactions of mppp (**2**) with molybdenum and tungsten hexacarbonyls only one product—the *meso* isomer—could be isolated.

Acknowledgements—We thank the NAB, the Royal Society, the Leverhulme Trust and the SERC for financial support, the former City of London Polytechnic for facilities, Mr S. Richards and Dr P. N. Gates (Royal

Holloway and Bedford New College) for assistance with vibrational spectroscopy and Dr J. H. Carpenter for helpful comments.

REFERENCES

1. R. J. Puddephat, *Chem. Soc. Rev.* 1983, **12**, 99.
2. C A. McAuliffe and W. Levason, *Phosphine, Arsine and Stibine Complexes of the Transition Elements.* Elsevier, Amsterdam (1979).
3. G. M. Kosolapoff and L. Maier, *Organic Phosphorus Compounds*, Vol. 1. Wiley–Interscience, New York (1972).
4. K. Issleib and D. Jacob, *Chem. Ber.* 1961, **94**, 107.
5. K. Issleib and F. Krech, *Chem. Ber.* 1961, **94**, 2656.
6. K. Issleib and G. Döll, *Chem. Ber.* 1961, **94**, 2664.
7. K. Issleib and K. Staudtke, *Chem. Ber.* 1963, **96**, 279.
8. K. Issleib and G. Döll, *Z. Anorg. Allg. Chem.* 1963, **324**, 259.
9. K. Issleib, K. Krech and K. Gruber, *Chem. Ber.* 1963, **96**, 2186.
10. K. Issleib and H. Weichmann, *Chem. Ber.* 1968, **101**, 2197.
11. K. Issleib and H. Weichmann, *Z. Anorg. Allg. Chem.* 1968, **362**, 33.
12. S. O. Grim, R. P. Molenda and R. L. Keiter, *Chem. Ind.* 1970, 1378.
13. S. O. Grim, J. Del Gaudio, R. P. Molenda, C. A. Tolman and J. P. Jesson, *J. Am. Chem. Soc.* 1974, **96**, 3416.
14. K. Issleib and W. Böttcher, *Z. Anorg. Allg. Chem.* 1974, **406**, 178.
15. S. O. Grim and R. C. Barth, *J. Organomet. Chem.* 1975, **94**, 327.
16. S. O. Grim and J. D. Mitchell, *Inorg. Chem.* 1977, **16**, 1762.
17. S. O. Grim and J. D. Mitchell, *Inorg. Chem.* 1977, **16**, 1770.
18. S. O. Grim and J. D. Mitchell, *Inorg. Chem.* 1977, **16**, 1776.
19. M. Baacke, S. Morton, O. Stelzer and W. S. Sheldrick, *Chem. Ber.* 1980, **113**, 1343.
20. O. Stelzer, S. Hietkamp and H. Sommer, *Phosphorus Sulphur* 1983, **18**, 279.
21. S. Heitkamp, H. Sommer and O. Stelzer, *Chem. Ber.* 1984, **117**, 3400.
22. H. Schmidbaur and S. Schnatterer, *Chem. Ber.* 1986, **119**, 2832.
23. K. P. Langhaus and O. Stelzer, *Chem. Ber.* 1987, **120**, 1707.
24. D. M. Anderson, P. B. Hitchcock, M. F. Lappert and I. Moss, *Inorg. Chem. Acta* 1988, **141**, 157.
25. P. A. Brooks, M. J. Gallagher and A. Sarroff, *Aust. J. Chem.* 1987, **40**, 1341.
26. P. A. Brooks, D. C. Craig, M. J. Gallagher, A. D. Rae and A. Sarroff, *J. Organomet. Chem.* 1987, **323**, C1.
27. I. J. Colquhoun, H. C. E. McFarlane and W. McFarlane, *J. Chem. Soc., Chem. Commun.* 1982, 220.
28. P. G. Patel, PhD Thesis, City of London Polytechnic (1989).
29. W. Hewertson and H. R. Watson, *J. Chem. Soc.* 1962, 1490.
30. K. Sommer, *Z. Anorg. Allg. Chem.* 1970, **376**, 37.
31. B. Walther, R. Schöps and W. Kolbe, *Z. Chem.* 1979, **19**, 417.
32. G. Grossman, B. Walther and U. Gastrock-Mey, *Phosphorus Sulphur* 1981, **11**, 259.
33. K. Issleib and W. Böttcher, *Synth. React. Inorg. Met. Org. Chem.* 1976, **6**, 179.
34. J. L. Bookham, W. McFarlane, M. Thornton-Pett and S. Jones, *J. Chem. Soc., Dalton Trans.* 1990, 3621.
35. G. T. Andrews, I. J. Colquhoun and W. McFarlane, *Polyhedron* 1983, **2**, 783.
36. P. Groves and W. McFarlane, unpublished observations.
37. L. S. Merriweather and J. R. Leto, *J. Am. Chem. Soc.* 1961, **83**, 1113.
38. I. Bernal, G. M. Reisner, G. R. Dobson and C. B. Dobson, *Inorg. Chim. Acta* 1986, **121**, 199.
39. J. Chatt and H. R. Watson, *J. Chem. Soc.* 1961, 4980.
40. F. A. Cotton and C. S. Kraihanzel, *J. Am. Chem. Soc.* 1962, **84**, 4432.
41. I. J. Colquhoun and W. McFarlane, *J. Chem. Soc., Dalton Trans.* 1982, 1915.

Polyhedron Vol. 12, No. 20, pp. 2535–2538, 1993
Printed in Great Britain

0277–5387/93 $6.00+.00
© 1993 Pergamon Press Ltd

COMMUNICATION

SYNTHESIS OF HETEROLEPTIC BIS(AMIDES): CRYSTAL STRUCTURE OF THE REPRESENTATIVE COMPOUND, $[\{Mg[N(Ph)_2][N(Ph)(2\text{-}Pyr)]\}_2]$

KENNETH W. HENDERSON and ROBERT E. MULVEY*

Department of Pure and Applied Chemistry, University of Strathclyde, Glasgow G1 1XL, U.K.

and

WILLIAM CLEGG and PAUL A. O'NEIL

Department of Chemistry, University of Newcastle, Newcastle upon Tyne NE1 7RU, U.K.

(*Received* 12 *July* 1993; *accepted* 11 *August* 1993)

Abstract—Reaction of Ph(2-Pyr)NH with "$Mg(Bu)_2$", followed by addition of amine substrates, gives heteroleptic magnesium bis(amides), one of which, $[\{Mg[N(Ph)_2][N(Ph)(2\text{-}Pyr)]\}_2]$, has been crystallographically characterized and shown to be a dimer with a central, rectangular azamagnesacyclic ring.

Magnesium is generally regarded as having a "diagonal relationship" with lithium,[1,2] its diagonal neighbour in the periodic table, in view of the many chemical similarities between them. However, as yet, very little research has been done on the magnesium front to test the validity of this relationship, with respect to amides (derived from amines). Lithium amide reagents, epitomized by the hindered kinetic base lithium diisopropylamide (LDA),[3,4] are essential to the synthetic chemist's repertoire, and considerable attention has been paid to establishing their natures, both in solution (where they operate)[5] and in the solid state.[6,7] The chemical utility of magnesium amides has been largely unexplored by comparison, though bromo derivatives $[\{Mg[N(R)_2]Br\}_n]$ have been used to promote self-condensation of certain ethers,[8–10] and bis(amido) species $[\{Mg(NR^1R^2)_2\}_n]$ have been used to generate mono(amido)magnesium hydride stereoselective reducing agents.[11] Structural information on magnesium amides is commensurately scarce.[12] There is a particular dearth of reports concerning bis(amides). This stems in part from the failure of certain bis(alkyl)magnesium compounds to undergo two successive aminations;[13] instead reaction can cease after the initial amination step to give mono(amido)magnesium alkyls, $[Mg(NR^1R^2)R^3]$. Recently, however, it has been shown that such compositions are accessible *via* the hydrocarbon-soluble "dibutylmagnesium" (DBM),† though their structures were not investigated.[14] This reagent was previously shown to be a convenient starting material for generating other organomagnesium compounds including aryloxides and cyclopentadienyls.[15]

In a previous study,[16] we reported making the octahedral bis(amide) $[Mg\{N(Ph)(2\text{-}Pyr)\}_2\cdot(THF)_2]$, **1**, by a procedure expected to produce the mono(amido) analogue $[\{Mg[N(Ph)(2\text{-}Pyr)]Bu^n\}_n]$, **2** (Scheme 1). By comparison with tetrahedral

* Author to whom correspondence should be addressed.

† Developed by the FMC corporation and commercially available from the Aldrich Chemical Co., Ltd. It is essentially $Mg(Bu^n)Bu^s$ with a small amount (typically, 5%) of *n*-octyl groups present. See refs 14 and 15 for more details.

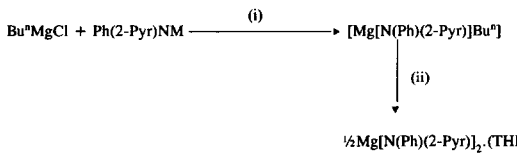

Scheme 1. (i) hexane, THF solvent, M = Li or Na, removal of LiCl or NaCl; (ii) $-1/2[Mg(Bu^n)_2\cdot(THF)_2]$.

$[\{Mg[N(CH_2CH_2NMe_2)CH_2Ph]Bu^n\}_2]$, **3**, made *via* the same Grignard reagent (Bu^nMgCl), we concluded that **1** resulted from the THF-induced disproportionation of the intermediate **2**, which is suspected to be a dimer ($n = 2$) akin to **3**, but with a more sterically exposed Mg centre, accessible to penetration by THF donor solvent molecules. In the belief that intermediates akin to **2** should be open to reaction with other molecules (besides THF), including amines, we substituted DBM for the Grignard reagent, so removing the need for THF, then reacted the resulting solution with different amines. This proved successful and led to the synthesis of hitherto rather elusive heteroleptic bis(amido) magnesium compounds, as reported herein. The crystal structure of a representative compound of this type, $[\{Mg[N(Ph)_2][N(Ph)(2\text{-}Pyr)]\}_2]$, **4**, is also revealed.

EXPERIMENTAL

The general synthetic approach is outlined in Scheme 2. Crystalline **4** was prepared specifically as follows. Freshly standardized dibutylmagnesium (5 mmol in heptane) was introduced to a Schlenk tube under argon gas containing a chilled mixture of the amine Ph(2-Pyr)NH (5 mmol) in hexane. A reaction occurred immediately with evolution of gas. At this stage, for kinetic reasons, the magnesium product is thought to be $[\{Mg[N(Ph)(2\text{-}Pyr)]Bu^s\}_n]$,[17] rather than its isomer $[\{Mg[N(Ph)(2\text{-}Pyr)]Bu^n\}_n]$. Addition of second amine, $(Ph)_2NH$ (5 mmol), caused further gas evolution and the precipitation of a brownish–green solid. The solvent mixture was then removed

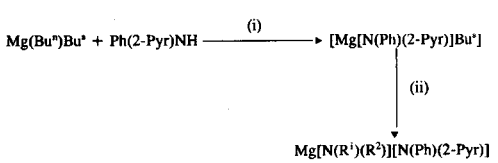

Scheme 2. (i) hexane/heptane solvent, $-Bu^nH\uparrow$; (ii) R^1R^2NH (1 equivalent), R^1, R^2 = Ph, Me; $R^1 = PhCH_2$, $R^2 = Me_2NCH_2CH_2$. $-Bu^sH\uparrow$.

in vacuo and replaced with toluene, which on warming dissolved the solid. Allowing the solution to slowly reach ambient temperature by surrounding it with a water bath gave, after 18 h, a crop of yellow cubic crystals. These crystals were washed with toluene, dried *in vacuo*, isolated in a dry box, and identified as the new compound **4**. Yield of **4**, 82%; m.p. 217–218°C; (Found: C, 76.2; H, 5.6; Mg, 6.6; N, 11.2. Calc. for $C_{23}H_{19}MgN_3$: C, 76.4; H, 5.3; Mg, 6.6; N, 11.6%).

5: ^{1}H NMR (400 MHz in C6D6): 7.71 (*d*, 1H, α-H of Pyr); 7.35 (*t*, 2H, *m*-H of Ph); 7.27 (*d*, 2H, *o*-H of Ph); 7.03 (*m*, 1H/1H, γ-H of Pyr/*p*-H of Ph); 6.94 (*t*, 1H, β′-H of Pyr); 6.03 (*t*, 1H, β-H of Pyr); 1.84 (s, 6H, NMe_2). Yield, 4%; m.p. 125–127°C; (Found: C, 64.9; H, 6.0; Mg, 10.2; N, 18.8. Calc. for $C_{13}H_{15}MgN_3$: C, 65.7; H, 6.4; Mg, 10.2; N, 17.7%).

6: ^{1}H NMR (400 MHz in d^8-Toluene): 7.70 (*d*, 1H, α-H of Pyr); 7.57 (*d*, 2H, *o*′-H of Ph); 7.30 (*m*, 2H/2H, *o*-H, *m*-H of Ph); 7.21 (*t*, 2H, *m*′-H of Ph); 7.08 (*t*, 1H, *p*′-H of Ph); 7.00 (*m*, 1H/1H, *p*-H of Ph and γ-H of Pyr); 6.63 (*d*, 1H, β′-H of Pyr); 6.06 (*t*, 1H, β-H of Pyr); 4.27 (*s*, 2H, CH_2Ph); 2.70 (*m*, 2H, CH_2 of Et); 2.27 (*m*, 2H, CH_2 of Et); 1.75 (*s*, 6H, NMe_2). Yield, 5%; m.p. 141–143°C; (Found: C, 72.0; H, 6.9; Mg, 6.6; N, 15.0. Calc. for $C_{22}H_{26}MgN_4$: C, 71.3; H, 7.1; Mg, 6.6; N, 15.1%).

Due to their high solubility in hydrocarbon solvents compounds **5** and **6** were isolated in small yield as impure powders by crashing them out of solution at low temperature (−35°C). Further experiments are being carried out to attempt to prepare crystalline samples for X-ray analysis studies.

Crystallography

4: $C_{46}H_{38}Mg_2N_6$, $0.48\times0.42\times0.37$ mm, $M = 723.44$, monoclinic, space group $P2_1/n$, $a = 8.794(14)$, $b = 22.298(12)$, $c = 9.915(10)$ Å, $\beta = 99.16(11)°$, $U = 1919.4(38)$ Å^3, $Z = 2$, $D_c = 1.252$ g cm^{-3}, $\mu = 0.877$ mm^{-1} (Cu–K_α radiation, $\lambda = 1.54184$ Å), $F(000) = 760$; $R' = 0.2671$ for 245 parameters, including anisotropic displacement parameters for non-H atoms and isotropic displacement parameters for constrained H atoms, by refinement on F^2 from all 2818 measured unique data ($2\theta_{max}$ 120°) measured at 200 K on a Stoe–Siemens diffractometer; weighting scheme, $w = 1/[\sigma^2(F_o^2)+(0.15p)^2+1.48p]$ where $p = (F_o^2+2F_c^2)/3$; conventional $R = 0.0978$ for F values of 2385 reflections with $F_o^2 > 2\sigma(F_o^2)$.[18,19] The rather high R value is due to the highly air and moisture sensitive nature of the crystals.

Atomic coordinates, displacement parameters

and bond lengths and angles have been deposited with the Editor and the Cambridge Crystallographic Data Centre.

RESULTS AND DISCUSSION

The centrosymmetric molecular structure of **4** in the solid state (Fig. 1) is dimeric. Its principal feature, a central, planar, four-membered azamagnesacyclic ring, is noteworthy for having perfect right-angled internal corners [90.0(2)°]. So far we are unable to explain why this is so. Related MgNMgN rings in other compounds tend to have angles straddling 90°, with the acute angle at N, e.g. in **2**, 87.6(1)° and 92.4(1)°;[16] in [{[*o*-$(Me_3Si)NC_6H_4(SiMe_3)N]Mg\cdot(OEt_2)\}_2$], 86.1(3)° and 93.9(3)°.[15] N atoms in this ring for **4** belong to the Ph_2N^- amido anions. These formally sp^3-hybridized atoms occupy four coordinate, distorted tetrahedral sites [mean bond angle at N(1), 108.9°]. Both sp^2-N atoms within the terminally attached Ph(2-Pyr)N$^-$ amido anions, in contrast, occupy three-coordinate, distorted trigonal planar sites [mean bond angles: N(2), 120.0°; N(3), 119.6°]. Approximately planar MgNCN rings are formed as a consequence of this bidentate chelation. The (amido)N atom interacts more efficiently with the Mg atom than does the (pyridyl)N atom, as evidenced by the wider C(1)N(3)Mg bond angle [93.7(3)° cf. 90.8(2)° for C(1)N(2)Mg] and the shorter Mg—N(3) bond length [2.025(5) Å cf. 2.107(5) Å for Mg—N(2)]. A similar pattern was previously noted in the structure of **1**,[16] though its MgNCN rings are significantly larger [corresponding bond angles, 94.9(1)° and 91.0(1)°, respectively: corresponding bond lengths, 2.105(2) Å and 2.182(2) Å, respectively] due to the higher coordination (six cf. four in **4**) of its Mg atom. Returning to the central MgNMgN ring of **4**, it is interesting that while the internal bond angles at Mg and N are equal as discussed earlier, the Mg—N μ-bonding is unsymmetrical with short edges of 2.080(5) Å [Mg—N(1)] and long edges of 2.119(5) Å [Mg—N(1′)]. This prompts the thought that the origin of the dimeric set-up lies in two monomeric moieties, which combine in a transoid arrangement with respect to its amido substituents with the new bonds formed being Mg—N(1′) and Mg′—N(1) (i.e. the long edges). These bonds may also be the first to cleave in reactions of this compound, giving coordinatively unsaturated, mononuclear Mg intermediates.

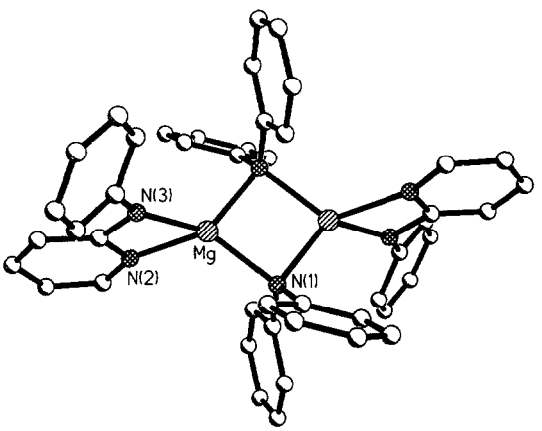

Fig. 1. A view of the structure of **4** with important atoms labelled and hydrogen atoms omitted for clarity. Selected bond lengths (Å) and angles (°): Mg—N(1) 2.080(5), Mg—N(1′) 2.119(5), Mg—N(2) 2.107(5), Mg—N(3) 2.025(5); N(1)—Mg—N(1′) 90.0(2), N(1)—Mg—N(2) 122.2(2), N(1)—Mg—N(3) 134.9(2), N(2)—Mg—N(3) 65.4(2), Mg—N(1)—Mg′ 90.0(2).

Two other heteroleptic bis(amido)magnesium solids were prepared following the synthetic procedure in Scheme 2: [{Mg[N(Me)$_2$][N(Ph)(2-Pyr)]}$_n$], **5** and [{Mg[N(CH$_2$CH$_2$NMe$_2$)CH$_2$Ph][N(Ph)(2-Pyr)]}$_n$], **6**. Produced by adding the amines Me_2NH and $PhCH_2(Me_2NCH_2CH_2)NH$, respectively, at the second stage of the process, both compounds were characterized by microanalysis and by ^{1}H NMR spectroscopy. Structural characterization of **5** and **6** are yet to be carried out. However, the former compound is probably analogous with **4**. The crystal structure of **6**, in contrast, is likely to be monomeric given that both of its amido ligands contain two N atoms, which collectively could saturate the Mg atom in a distorted tetrahedral geometry, obviating the need for aggregation.

Acknowledgements—We thank ICI for generously sponsoring this research and P.J.V. Jones, their representative, for helpful discussions, and the SERC for studentships to K.W.H. and P.A.O.

REFERENCES

1. N. N. Greenwood and A. Earnshaw, *Chemistry of the Elements*, Pergamon Press, Oxford (1984).
2. A. G. Massey, *Main Group Chemistry*, Ellis Horwood, Chichester (1990).
3. D. A. Whiting, *Aldrichimica Acta* 1986, **19**, 31.
4. N. D. R. Barnett, R. E. Mulvey, W. Clegg and P. A. O'Neil, *J. Am. Chem. Soc.* 1991, **113**, 8187.
5. A. S. Galiano-Roth and D. B. Collum, *J. Am. Chem. Soc.* 1989, **111**, 6772.
6. R. E. Mulvey, *Chem. Soc. Rev.* 1991, **20**, 167.
7. K. Gregory, P. v. R. Schleyer and R. Snaith, *Adv. Inorg. Chem.* 1991, **31**, 47.

8. C. R. Hauser and H. G. Walker Jr, *J. Am. Chem. Soc.* 1947, **69**, 295.
9. F. C. Frostick Jr and C. R. Hauser, *J. Am. Chem. Soc.* 1949, **71**, 1350.
10. G. Bradley, J. F. Cavalla, T. Edington, R. G. Shepherd, A. C. White, B. J. Bushell, J. R. Johnson and G. O. Weston, *Eur. J. Med. Chem.* 1980, **15**, 375.
11. E. C. Ashby, J. J. Lin and A. B. Goel, *J. Org. Chem.* 1978, **43**, 1564.
12. M. F. Lappert, P. P. Power, A. R. Sanger and R. C. Srivastava, *Metal and Metalloid Amides.* Ellis Horwood, Chichester (1980).
13. G. Dozzi, G. Del Piero, M. Cesari and S. Cucinella, *J. Organomet. Chem.* 1980, **190**, 229.
14. V. C. Mehta, T. L. Rathman, R. Sanchez and R. C. Morrison, U.S. Patent 4,944,894 (1990).
15. A. W. Duff, P. B. Hitchcock, M. F. Lappert, R. A. Taylor and J. A. Segal, *J. Organomet. Chem.* 1985, **293**, 271.
16. K. W. Henderson, R. E. Mulvey, W. Clegg and P. A. O'Neil, *J. Organomet. Chem.* 1992, **439**, 237.
17. L. M. Engelhardt, B. S. Jolly, P. C. Junk, C. L. Raston, B. W. Skelton and A. H. White, *Aust. J. Chem.* 1986, **39**, 1337.
18. W. Clegg, *Acta Cryst., Sect. A* 1981, **37**, 22.
19. G. M. Sheldrick, SHELXL-92, a program for crystal structure refinement, beta-test version, University of Göttingen (1992).

Polyhedron Vol. 12, No. 20, pp. 2539–2542, 1993
Printed in Great Britain

0277-5387/93 $6.00+.00
© 1993 Pergamon Press Ltd

COMMUNICATION

THE SYNTHESIS OF $[HB[3,5\text{-}(Bu^tph)_2pz]_3]^-$ ($Bu^tph = p\text{-}C_6H_4Bu^t$), A NEW TRIS(PYRAZOLYL)HYDROBORATO LIGAND: THE CRYSTAL AND MOLECULAR STRUCTURE OF $Tl\{\eta^3\text{-}HB[3,5\text{-}(Bu^tph)_2pz]_3\}$

EMANUELA LIBERTINI,* KEUM YOON and GERARD PARKIN†

Department of Chemistry, Columbia University, NY 10027, U.S.A.

(*Received* 22 *June* 1993; *accepted* 6 *August* 1993)

Abstract—The synthesis of a new sterically demanding tris(pyrazolyl)hydroborato ligand, $[HB[3,5\text{-}(Bu^tph)_2pz]_3]^-$ (Bu^tph = *para*-$C_6H_4Bu^t$), is reported. The potassium derivative is prepared by the direct reaction of KBH_4 with 3,5-bis(*para*-tert-butylphenyl)pyrazole. Metathesis with $TlNO_3$ converts the potassium derivative to the thallium complex $Tl\{\eta^3\text{-}HB[3,5\text{-}(Bu^tph)_2pz]_3\}$. The crystal and molecular structures of the pyrazole derivative $[3,5\text{-}(Bu^tph)_2pz]_2ZnI_2$ and the thallium derivative $Tl\{\eta^3\text{-}HB[3,5\text{-}(Bu^tph)_2pz]_3\}$ have been determined.

Since the original report by Trofimenko in 1966,[1] the tris(pyrazolyl)hydroborato ligand system $[HB(3,5\text{-}RR'pz)_3]^-$ (RR'pz = substituted pyrazole), shown in Fig. 1, has found widespread applications.[2,3] Some recent developments have involved the incorporation of a variety of substituents into the 3-position of the tris(pyrazolyl)hydroborato ligand, thereby effectively tailoring the steric environment about a metal centre. For example, the cone angles of the tris(pyrazolyl)hydroborato ligands $[\eta^3\text{-}HB(pz)_3]^-$, $[\eta^3\text{-}HB(3,5\text{-}Me_2pz)_3]^-$ and $[\eta^3\text{-}HB(3\text{-}Bu^tpz)_3]^-$ have been estimated as 184, 224 and 244°, respectively.[4,5] Moreover, the incorporation of substituents such as trifluoromethyl, e.g. $[\eta^3\text{-}HB(3\text{-}CF_3\text{-}5\text{-}Mepz)_3]^-$, may also exert electronic influences.[1]

One of the most appealing attributes of sterically-demanding derivatives such as $[\eta^3\text{-}HB(3\text{-}Bu^tpz)_3]^-$ is that the bulky tert–butyl substituents in the 3-position of the pyrazolyl ring provide a ligand environment that strongly stabilizes four-coordination in preference to higher coordination numbers. Consequently, the ligand has been aptly termed a "tetrahedral enforcer", especially with regard to the first-row transition metals.[4a]

Our specific interest in tris(pyrazolyl)hydroborato ligands has focussed on the use of the sterically-demanding $[HB(3\text{-}Bu^tpz)_3]^-$ [4a] and $[HB(3\text{-}Bu^t\text{-}5\text{-}Mepz)_3]^-$ [6] ligands to stabilize a series of monomeric alkyl, hydride and hydroxide derivatives of the *s*- and *p*-block metals, e.g. Be,[7] Mg,[8] Al,[8a,9] Zn[10] and Cd.[11] Indeed, these ligands sta-

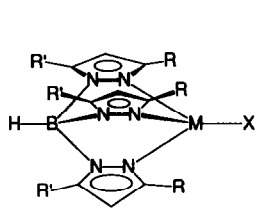

Fig. 1. The tris(pyrazolyl)hydroborato ligand.

* Present address: Dipartimento di Ingegneria e Fisica dell'Ambiente, Universita degli Studi della Basilicata, Via della Tecnica 3, 85100 Potenza, Italy.

† Author to whom correspondence should be addressed.

bilize such derivatives to the extent that their reactivity may be reduced considerably from that observed in other systems. For example, the zinc alkyl derivatives $\{\eta^3\text{-HB(3-Bu}^t\text{pz)}_3\}\text{ZnR}$ are not particularly reactive towards O_2, whereas the dialkyls ZnR_2 are pyrophoric.[10a] In order to promote the reactivity of these systems we required a ligand that was less sterically-demanding than either of the ligands $[\text{HB(3-Bu}^t\text{pz)}_3]^-$ or $[\text{HB(3-Bu}^t\text{-5-Mepz)}_3]^-$. However, less sterically-demanding ligands such as $[\text{HB(3,5-Me}_2\text{pz)}_3]^-$ and $[\text{HB(3,5-Ph}_2\text{pz)}_3]^-$ suffer from the disadvantage that ligand redistribution (eq. 1) may often be facile, resulting in the formation of the corresponding six-coordinate sandwich complexes $\{\eta^3\text{-HB(3,5-R}_2\text{pz)}_3\}_2\text{M}$, such as $\{\eta^3\text{-HB(3,5-Me}_2\text{pz)}_3\}_2\text{Mg}$[12] and $\{\eta^3\text{-HB(3,5-Ph}_2\text{pz)}_3\}_2\text{M}$ (M = Mn, Fe).[13]

$$2\{\eta^3\text{-HB(3,5-R}_2\text{pz)}_3\}\text{MX} \longrightarrow \{\eta^3\text{-HB(3,5-R}_2\text{pz)}_3\}_2\text{M} + \text{MX}_2 \quad (1)$$

Moreover, even the neopentyl (Np) derivative $[\eta^3\text{-HB(3-Nppz)}_3]^-$ also forms a six-coordinate sandwich complex of nickel, $\{\eta^3\text{-HB(3-Nppz)}_3\}_2\text{Ni}$.[14] In this paper we report the synthesis of the $[\text{HB[3,5-(Bu}^t\text{ph)}_2\text{pz]}_3]^-$ (Bu^{t}ph = *para*-C_6H_4Bu^t) ligand which has been designed with the intentions that : (i) the *para*-tert-butyl substituents will be sufficient to inhibit the formation of six-coordinate $\{\eta^3\text{-HB[3,5-(Bu}^t\text{ph)}_2\text{pz]}_3\}_2\text{M}$ sandwich complexes; but yet (ii) the phenyl substituents in the immediate vicinity of the metal centre will provide a coordination environment that is less sterically-demanding than that of the tert-butyl derivative $[\text{HB(3-Bu}^t\text{pz)}_3]^-$.

Although we are interested primarily in controlling the coordination environment at the metal centre, i.e. the 3-position of the pyrazolyl group, the use of a symmetric 3,5-disubstituted pyrazole derivative offers several advantages : (i) substitution at the 5-position also provides a protective environment about the B–H group that will help prevent ligand degradation, (ii) monosubstituted and asymmetric 3,5-disubstituted pyrazoles may give mixtures of tris(pyrazolyl)hydroborato derivatives, depending upon the selectivity of the reaction with the inequivalent nitrogen centres of the pyrazole, and (iii) asymmmetric $\{\eta^3\text{-HB[3,5-RR'}_2\text{pz]}_3\}\text{MX}$ derivatives may rearrange in order to relieve steric congestion. For example, 3,5-Pr^{i}MepzH reacts with BH_4^- to give a mixture of isomers,[15] and $\{\eta^3\text{-HB(3-Nppz)}_3\}_2\text{Ni}$ rearranges to $\{\eta^3\text{-HB(3-Nppz)}_2\text{(3-Nppz)}\}_2\text{Ni}$ upon heating.[14] Clearly, such problems are avoided with the use of symmetric 3,5-disubstitued pyrazoles.

As with the synthesis of the tris(3,5-diphenylpyrazolyl)hydroborato ligand,[16] the starting material for the synthesis of $[\text{HB[3,5-(Bu}^t\text{ph)}_2\text{pz]}_3]^-$ is 3,5-bis(*para*-tert-butylphenyl)pyrazole. The pyrazole 3,5-(Bu^{t}ph)$_2$pzH* is readily obtained by the reaction of $N_2H_4\cdot(H_2O)$ with the diketone $[\text{(Bu}^t\text{ph)C(O)]}_2\text{CH}_2$† via a procedure analogous to that used for the unsubstituted derivative, 3,5-diphenylpyrazole.[16] 3,5-bis(*para*-tert-butylphenyl) pyrazole has also been characterized by X-ray diffraction as its adduct with ZnI_2, $[3,5\text{-(Bu}^t\text{ph)}_2\text{pzH}]_2\text{ZnI}_2$.‡ The molecular structure of $[3,5\text{-(Bu}^t\text{ph)}_2\text{pzH}]_2\text{ZnI}_2$ is shown in Fig. 2.§

The tris[3,5-(*para*-tert-butylphenyl)$_2$pyrazolyl]hydroborato ligand $[\text{HB[3,5-(Bu}^t\text{ph)}_2\text{pz]}_3]^-$ is readily obtained as the potassium derivative by the direct reaction of KBH_4 with 3,5-bis(*para*-tert-butylphenyl)pyrazole at *ca* 280°C (eq. 2).

$$KBH_4 + 3[3,5\text{-(Bu}^t\text{ph)}_2\text{pzH}] \longrightarrow K\{\text{HB[3,5-(Bu}^t\text{ph)}_2\text{pz]}_3\} + 3H_2 \quad (2)$$

In addition to potassium complexes, thallium derivatives are also useful reagents in the synthesis

---

*Data for 3,5-(Bu^{t}ph)$_2$pzH (m.p. 200–202°C). ^{1}H NMR (C_6D_6): *d* 1.18 [18H, s, 2C(CH$_3$)$_3$], 6.72 [1H, s, CH(pz)], 7.19 [4H, d, $^3J_{H\text{-}H}$ = 8.4, 4H of (*para*-C_6H_4Bu^t)$_2$], 7.74 [4H, d, $^3J_{H\text{-}H}$ = 8.4, 4H of (*para*-C_6H_4Bu^t)$_2$], 12.6 [1H, very broad, NH]. Found : C, 82.7; H, 9.0; N, 8.9 : Calc. : C, 83.1 ; H, 8.5 ; N, 8.4%.

†$[\text{(Bu}^t\text{ph)C(O)}]_2\text{CH}_2$ is synthesized by the condensation of (Bu^{t}ph)C(O)CH$_3$ with (Bu^{t}ph)CO$_2$Ph in the presence of NaH. For example, see : A. Magnani and S. M. McElvain, *Organic Syntheses Collective* Vol. 3, 251–253 (1955). $[\text{(Bu}^t\text{ph)C(O)}]_2\text{CH}_2$ exists as the keto–enol isomer, (Bu^{t}ph)C(O)CH=CH(OH)(Bu^{t}ph), m.p. 85–87°C. ^{1}H NMR (C_6D_6): δ 1.14 [18H, s, 2C(CH$_3$)$_3$], 6.84 [1H, s, CH], 7.24 [4H, d, $^3J_{H\text{-}H}$ = 8.4, 4H of 2(*para*-C_6H_4Bu^t)], 7.93 [4H, d, $^3J_{H\text{-}H}$ = 8.4, 4H of 2(*para*-C_6H_4Bu^t)], 18.05 [1H, OH]. Found : C, 81.7; H, 8.9. Calc. : C, 82.1 ; H, 8.4%.

‡Data for $[3,5\text{-[Bu}^t\text{ph)}_2\text{pzH}]_2\text{ZnI}_2$ (m.p. 239–241°C). ^{1}H NMR (C_6D_6): δ 0.92 [18H, s, 3- or 5-C(CH$_3$)$_3$], 1.20 [18H, s, 5- or 3-C(CH$_3$)$_3$], 6.11 [2H, s, CH(pz)], 7.01–7.20 [12H, m, 12H of (*para*-C_6H_4Bu^t)$_2$] 7.68 [4H, d, 4H of (*para*-C_6H_4Bu^t)$_2$], 11.87 [2H, bs, NH]. Found : C, 55.7; H, 5.6; N, 6.2. Calc. : C, 56.1 ; H, 5.7; N, 5.7%.

§Crystal data for $[3,5\text{-(Bu}^t\text{ph)}_2\text{pzH}]_2\text{ZnI}_2$ at room temperature : Monoclinic $P2_1/n$ (No. 14), a = 15.348(5), b = 14,577(4), c = 21.413(3) Å, β = 95.59(2)°, V = 4768(2) Å^3, Z = 4, R = 0.0488, R_w = 0.0543. A complete set of tables of crystal and intensity collection data, atomic coordinates, bond distances and angles, and anisotropic displacement parameters, and an ORTEP drawing have been deposited with the Editor as supplementary materials. The atomic coordinates have also been deposited with the Cambridge Crystallographic Data Centre.

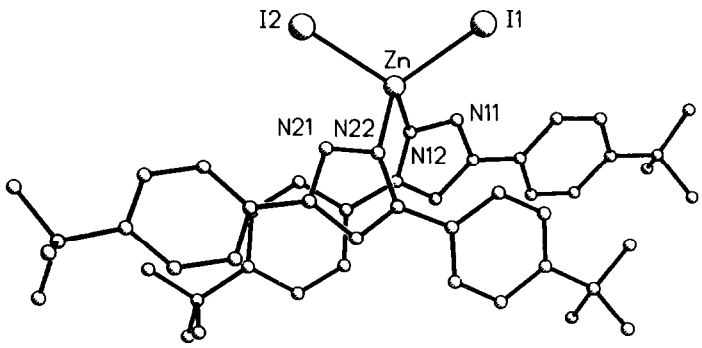

Fig. 2. The molecular structure of $[3,5\text{-}(Bu^t ph)_2pzH]_2ZnI_2$. Other atoms are not labelled for clarity. Selected bond lengths (Å) and angles (°): Zn—I(1) 2.567(2), Zn—I(2) 2.603(2), Zn—N(12) 2.062(7), Zn—N(22) 2.077(8); I(1)—Zn—I(2) 112.2(1), N(12)—Zn—N(22) 99.5(3), I(1)—Zn—N(12) 102.5(2), I(1)—Zn—N(22) 121.7(2), I(2)—Zn—N(12) 120.2(2), I(2)—Zn—N(22) 101.3(2).

of tris(pyrazolyl)hydroborato complexes. Thus, the potassium derivative is readily converted to the thallium reagent $Tl\{\eta^3\text{-}HB[3,5\text{-}(Bu^t ph)_2pz]_3\}$‖ by metathesis with aqueous $TlNO_3$ (eq. 3).

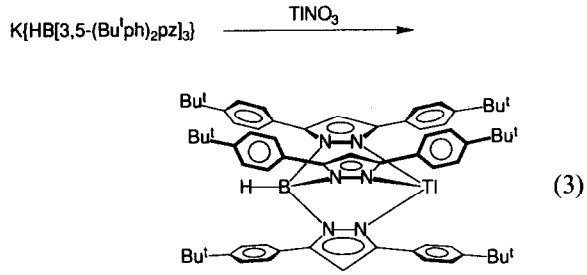

(3)

The molecular structure of $Tl\{\eta^3\text{-}HB[3,5\text{-}(Bu^t ph)_2pz]_3\}$ has been determined by X-ray diffraction, as shown in Fig. 3.¶ The coordination geometry about thallium is similar to that in the related complex $Tl\{\eta^3\text{-}HB(3\text{-}Bu^t pz)_3\}$.[17] For example, the average Tl—N bond length [2.61(5) Å] and N—Tl—N bond angle [77(2)°] in $Tl\{\eta^3\text{-}HB[3,5\text{-}(Bu^t ph)_2pz]_3\}$ compare well with the values of 2.59(1) Å and 78(3)° in $Tl\{\eta^3\text{-}HB(3\text{-}Bu^t pz)_3\}$. The average Tl—N bond length in $Tl\{\eta^3\text{-}HB[3,5\text{-}(Bu^t ph)_2pz]_3\}$ is longer than the sum of the covalent radii (2.31 Å),** and is presumably a reflection of the fact that overall the bonding between Tl and the tris(pyrazolyl) hydroborato ligand is composed of one normal covalent and two dative covalent interactions.[18]

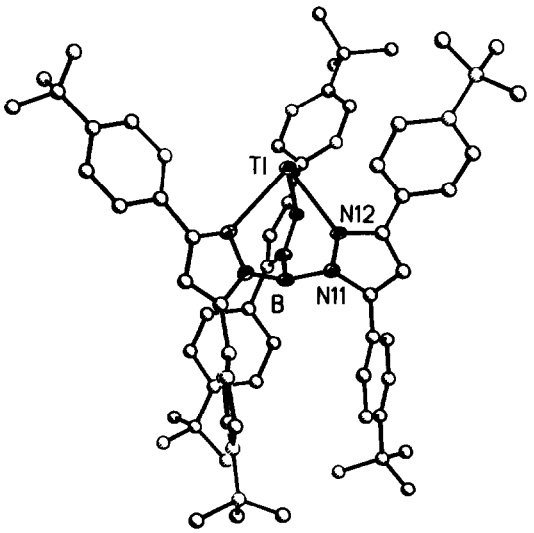

Fig. 3. The molecular structure of $\{\eta^3\text{-}HB[3,5\text{-}(Bu^t ph)_2pz]_3\}Tl$. Other atoms are not labelled for clarity. Selected bond lengths (Å) and angles (°): Tl—N(12) 2.568(10), Tl—N(22) 2.584(10), Tl—N(32) 2.663(15), N(12)—Tl—N(22) 75.2(3), N(12)—Tl—N(32) 77.7(4), N(22)—Tl—N(32) 78.3(4).

‖ Data for $Tl\{\eta^3\text{-}HB[3,5\text{-}(Bu^t ph)_2pz]_3\}$. ^1H NMR (C_6D_6): δ 1.09 [27H, s, $C(CH_3)_3$], 1.29 [27H, s, $C(CH_3)_3$], 6.76 [3H, s, CH(pz)], 6.99–7.23 [18H, m, 18H of *para*-$C_6H_4Bu^t$ groups], 7.69 [6H, d, $^3J_{H-H}$ = 8.2, 6H of *para*-$C_6H_4Bu^t$ groups]. Found: C, 68.4; H, 7.0; N, 7.3. Calc.: C, 68.5; H, 6.8; N, 6.9%.

¶ Crystal data for $Tl\{\eta^3\text{-}HB[3,5\text{-}(Bu^t ph)_2pz]_3\}$ at room temperature: Monoclinic, $P2_1/a$ (No. 14), a = 18.677(5), b = 19.486(5), c = 19.628(4) Å, β = 112.16(2)°, V = 6615(3) Å^3, Z = 4, R = 0.0624, R_w = 0.0825. A complete set of tables of crystal and intensity collection data, atomic coordinates, and bond distances and angles, and an ORTEP drawing have been deposited with the Editor as supplementary materials. The atomic coordinates have also been deposited with the Cambridge Crystallographic Data Centre.

** $r_{cov}(Tl)$ = 1.57 Å, $r_{cov}(N)$ = 0.74 Å. L. Pauling, *The Nature of The Chemical Bond* (3rd edn). Cornell University Press, Ithaca (1960).

In summary, the synthesis of a new tris(pyrazolyl)hydroborato ligand $[\eta^3\text{-HB[3,5-(Bu}^t\text{ph)}_2\text{pz]}_3]^-$ is reported. We believe that this ligand offers considerable potential for supporting metal centres that are less sterically demanding than those obtained by the use of the $[\eta^3\text{-HB(3-Bu}^t\text{pz)}_3]^-$ ligand, while still restricting the formation of sandwich complexes.

Acknowledgements—Acknowledgement is made to the National Science Foundation (Grant CHE 90-07512) for support of this research. G.P. is the recipient of an A.P. Sloan Research Fellowship (1991–1993), a Camille and Henry Dreyfus Teacher–Scholar Award (1991–1996), and a Presidential Faculty Fellowship Award (1992–1997).

REFERENCES

1. S. Trofimenko, *J. Am. Chem. Soc.* 1966, **88**, 1842.
2. S. Trofimenko, *Chem. Rev.* 1993, **93**, 943.
3. (a) S. Trofimenko, *Prog. Inorg. Chem.* 1986, **34**, 115; (b) K. Niedenzu and S. Trofimenko, *Topics Curr. Chem.* 1986, **131**, 1.
4. (a) S. Trofimenko, J. C. Calabrese and J. S. Thompson, *Inorg. Chem.* 1987, **26**, 1507; (b) S. Trofimenko, J. C. Calabrese, P. J. Domaille and J. S. Thompson, *Inorg. Chem.* 1989, **28**, 1091.
5. E. Frauendorfer and H. Brunner, *J. Organomet. Chem.* 1982, **240**, 371.
6. S. Trofimenko, J. C. Calabrese, J. K. Kochi, S. Wolowiec, F. B. Hulsbergen and J. Reedijk, *Inorg. Chem.* 1992, **31**, 3943.
7. (a) R. Han and G. Parkin, *Inorg. Chem.* 1992, **31**, 983; (b) R. Han and G. Parkin, *Inorg. Chem.*, in press.
8. (a) R. Han, A. Looney and G. Parkin, *J. Am. Chem. Soc.* 1989, **111**, 7276; (b) R. Han and G. Parkin, *Organometallics* 1991, **10**, 1010; (c) R. Han and G. Parkin, *J. Am. Chem. Soc.* 1992, **114**, 748; (d) R. Han, M. Bachrach and G. Parkin, *Polyhedron* 1990, **9**, 1775.
9. A. Looney and G. Parkin, *Polyhedron* 1990, **9**, 265.
10. (a) I. B. Gorrell, A. Looney and G. Parkin, *J. Chem. Soc., Chem. Commun.* 1990, 220; (b) R. Han, I. B. Gorrell, A. Looney and G. Parkin, *J. Chem. Soc., Chem. Commun.* 1991, 717; (c) R. Alsfasser, S. Trofimenko, A. Looney, G. Parkin and H. Vahrenkamp, *Inorg. Chem.* 1991, **30**, 4098; (d) A. Looney, G. Parkin, R. Alsfasser, M. Ruf and H. Vahrenkamp, *Angew. Chem. Int. Ed. Engl.* 1992, **31**, 92; (e) R. Han, A. Looney, K. McNeill, G. Parkin, A. L. Rheingold and B. S. Haggerty, *J. Inorg. Biochem.* 1993, **49**, 105; (f) A. Looney, R. Han, K. McNeill and G. Parkin, *J. Am. Chem. Soc.* 1993, **115**, 4690.
11. A. Looney, A. Saleh, Y. Zhang and G. Parkin, *Inorg. Chem.*, submitted.
12. R. Han and G. Parkin, *J. Organomet. Chem.* 1990, **393**, C43.
13. D. M. Eichhorn and W. H. Armstrong, *Inorg. Chem.* 1990, **29**, 3607.
14. J. C. Calabrese and S. Trofimenko, *Inorg. Chem.* 1992, **31**, 4810.
15. M. Cano, J. V. Heras, S. Trofimenko, A. Monge, E. Gutierrez, C. J. Jones and J. A. McCleverty, *J. Chem. Soc., Dalton Trans.* 1990, 3577.
16. (a) N. Kitajima, K. Fujisawa, C. Fujimoto and Y. Moro-oka, *Chem. Lett.* 1989, 421; (b) N. Kitajima, K. Fujisawa, C. Fujimoto, Y. Moro-oka, S. Hashimoto, T. Kitagawa, K. Toriumi, K. Tatsumi and A. Nakamura, *J. Am. Chem. Soc.* 1992, **114**, 1277.
17. A. H. Cowley, R. L. Geerts, C. M. Nunn and S. Trofimenko, *J. Organomet. Chem.* 1989, **365**, 19.
18. A. Haaland, *Angew. Chem. Int. Edn. Engl.* 1989, **28**, 992.

Polyhedron Vol. 12, No. 20, pp. 2543–2544, 1993
Pergamon Press Ltd. Printed in Great Britain

BOOK REVIEWS

Nuclear Chemistry. By O. Navrátil, J. Hála, R. Kopunec, F. Macásek, V. Mikulaj and L. Leseticky (translated by J. Hála and P. Huth). Ellis Horwood Ltd, Chichester, U.K. and Academia (Czech. Academy of Sciences), Prague, Czechoslovakia, 1992. ISBN 0-13-626904-4, £50.00.

It is a pleasure to read a new text on Nuclear Chemistry which covers most aspects of the subject thoroughly and which is written in such a clear and comprehensible way. In composition the book is logical, starting with nuclear structure, nuclear reactions and nucleogenesis, then proceeding on to the interaction of radiation with matter and the detection of radioactivity. Further chapters consider the analytical applications of radiation and radioisotopes, the preparation of labelled compounds and the radiochemical aspects of nuclear power generation. This latter topic leads to a consideration of some of the environmental problems posed by the current exploitation of radioactivity, in medicine and in research. There is, however, one grave omission, which detracts from the overall value of the book: no detailed consideration is given to radiological protection, to the international requirements that control the use and disposal of radioactive materials and to the reasons for these controls.

In all other respects, this book is excellent and the structure of each chapter exemplary. The basic concepts, either physical or chemical, are presented first, followed by a detailed exposition and development. Each chapter is brought to a conclusion by a consideration of a series of examples of applications. Thus, for each topic there is a thorough explanation and the interest of the reader is stimulated and maintained. This reflects well both on the Czech authors of the original text and upon the translators. In this book the problem of uneven structure that besets multi-authored texts and an awkwardness of style that so often accompanies translation have both been very successfully avoided.

Due to the breadth of topics covered (with just one exception) and the depth and thoroughness with which each topic is covered, this book should become a widely-used text. Practising radiochemists and those engaged in nuclear chemistry will start out thinking it useful and end up finding if invaluable. Those about to start work with radioactivity will find it an excellent text from which to learn and a mine of useful information.

Department of Chemistry, **D. S. URCH**
Queen Mary and Westfield College,
Mile End Road
London E1 4NS, U.K.

Gmelin Handbook of Inorganic and Organometallic Chemistry. 8th Ed. Silicon Supplement Volume B7: Binary Species of Silicon and Fluorine. Edited by G. Hönes, H. Keller-Rudek, D. Koschel, P. Merlet, H. Schäfer and F. Schröder. Springer-Verlag, Berlin, 1992, ISBN 3-540-93651-3, 348 + xix pp., DM 1980.

This is the sixth in the ambitious series of updated Gmelin volumes on silicon compounds, the first of which appeared in 1982. As is normal with this series, the book is the result of large-scale collaboration: no less than eleven authors (led by Edwin Hengge and Robert Schlögl) and six editors (with Friedrich Schröder as chief editor) were involved. Literature coverage generally starts where the earlier Main Volume left off, at the end of 1949, although a few earlier key references are included. All relevant references up to January 1992 are included, and even a few later ones, which represents an admirably rapid production schedule.

It needs to be emphasized that this volume deals solely with binary Si_xF_y compounds; species in which elements other than fluorine are bonded to silicon will be dealt with in a forthcoming supplement volume B8. This means that compounds such as $(SiF_3)_2O$ and $SiF_2(NMe_2)_2$ are not covered in detail here, although they are referred to as reaction products derived from SiF_4.

Most chemists would expect to find SiF_2, SiF_4, and Si_2F_6 dealt with in such a volume, and indeed they take up 60% of the book, with 48, 144, and 16 pages devoted to them, respectively. But many other species are here, including neutral SiF_m (m = 1, 3, 5, 6), cations such as SiF^{n+} (n = 1–3) and SiF_m^{n+} (m = 2–4; n = 1,2), anions like SiF_m^- (m = 1–5) and SiF_m^{3-} (m = 1, 5), and various polysilicon derivatives such as $(SiF_2)_n$, $Si_{10}F_{16}$, and Si_mF^+ (m = 2–6). The familiar anion SiF_6^{2-} is treated at some length, and electronic, spectroscopic, structural and chemical properties of hexafluorosilicates with a range of cations are discussed. Possible duplication appears to be an inherent difficulty of the Gmelin system of classification, since Na_2SiF_6, for example, will also appear in the Sodium volumes.

Some of the compounds noted above are only "theoretical"; SiF^- has not been observed experimentally, for instance, but computational methods have provided values for its bond length, dissociation energy, dipole moment and some other properties. Indeed, the book contains numerous impressive illustrations of the power of modern theoretical methods. One striking example involves possible isomers of Si_2F_4: five different computational methods agree in predicting that the most stable arrangement is $(SiF_3)SiF$ rather than $F_2Si{=}SiF_2$.

Besides the expected full accounts of preparations and properties, there are extended discussions of results from more recent and exotic techniques such as multiple photon absorption, ion cyclotron resonance, gas-phase and solid-state NMR, and resonant Auger spectra. It was

Polyhedron Vol. 12, No. 20, pp. 2543–2544, 1993
Pergamon Press Ltd. Printed in Great Britain

BOOK REVIEWS

Nuclear Chemistry. By O. Navrátil, J. Hála, R. Kopunec, F. Macásek, V. Mikulaj and L. Leseticky (translated by J. Hála and P. Huth). Ellis Horwood Ltd, Chichester, U.K. and Academia (Czech. Academy of Sciences), Prague, Czechoslovakia, 1992. ISBN 0-13-626904-4, £50.00.

It is a pleasure to read a new text on Nuclear Chemistry which covers most aspects of the subject thoroughly and which is written in such a clear and comprehensible way. In composition the book is logical, starting with nuclear structure, nuclear reactions and nucleogenesis, then proceeding on to the interaction of radiation with matter and the detection of radioactivity. Further chapters consider the analytical applications of radiation and radioisotopes, the preparation of labelled compounds and the radiochemical aspects of nuclear power generation. This latter topic leads to a consideration of some of the environmental problems posed by the current exploitation of radioactivity, in medicine and in research. There is, however, one grave omission, which detracts from the overall value of the book: no detailed consideration is given to radiological protection, to the international requirements that control the use and disposal of radioactive materials and to the reasons for these controls.

In all other respects, this book is excellent and the structure of each chapter exemplary. The basic concepts, either physical or chemical, are presented first, followed by a detailed exposition and development. Each chapter is brought to a conclusion by a consideration of a series of examples of applications. Thus, for each topic there is a thorough explanation and the interest of the reader is stimulated and maintained. This reflects well both on the Czech authors of the original text and upon the translators. In this book the problem of uneven structure that besets multi-authored texts and an awkwardness of style that so often accompanies translation have both been very successfully avoided.

Due to the breadth of topics covered (with just one exception) and the depth and thoroughness with which each topic is covered, this book should become a widely-used text. Practising radiochemists and those engaged in nuclear chemistry will start out thinking it useful and end up finding if invaluable. Those about to start work with radioactivity will find it an excellent text from which to learn and a mine of useful information.

Department of Chemistry, **D. S. URCH**
Queen Mary and Westfield College,
Mile End Road
London E1 4NS, U.K.

Gmelin Handbook of Inorganic and Organometallic Chemistry. 8th Ed. Silicon Supplement Volume B7: Binary Species of Silicon and Fluorine. Edited by G. Hönes, H. Keller-Rudek, D. Koschel, P. Merlet, H. Schäfer and F. Schröder. Springer-Verlag, Berlin, 1992, ISBN 3-540-93651-3, 348 + xix pp., DM 1980.

This is the sixth in the ambitious series of updated Gmelin volumes on silicon compounds, the first of which appeared in 1982. As is normal with this series, the book is the result of large-scale collaboration: no less than eleven authors (led by Edwin Hengge and Robert Schlögl) and six editors (with Friedrich Schröder as chief editor) were involved. Literature coverage generally starts where the earlier Main Volume left off, at the end of 1949, although a few earlier key references are included. All relevant references up to January 1992 are included, and even a few later ones, which represents an admirably rapid production schedule.

It needs to be emphasized that this volume deals solely with binary Si_xF_y compounds; species in which elements other than fluorine are bonded to silicon will be dealt with in a forthcoming supplement volume B8. This means that compounds such as $(SiF_3)_2O$ and $SiF_2(NMe_2)_2$ are not covered in detail here, although they are referred to as reaction products derived from SiF_4.

Most chemists would expect to find SiF_2, SiF_4, and Si_2F_6 dealt with in such a volume, and indeed they take up 60% of the book, with 48, 144, and 16 pages devoted to them, respectively. But many other species are here, including neutral SiF_m (m = 1, 3, 5, 6), cations such as SiF^{n+} (n = 1–3) and SiF_m^{n+} (m = 2–4; n = 1,2), anions like SiF_m^- (m = 1–5) and SiF_m^{3-} (m = 1, 5), and various polysilicon derivatives such as $(SiF_2)_n$, $Si_{10}F_{16}$, and Si_mF^+ (m = 2–6). The familiar anion SiF_6^{2-} is treated at some length, and electronic, spectroscopic, structural and chemical properties of hexafluorosilicates with a range of cations are discussed. Possible duplication appears to be an inherent difficulty of the Gmelin system of classification, since Na_2SiF_6, for example, will also appear in the Sodium volumes.

Some of the compounds noted above are only "theoretical"; SiF^- has not been observed experimentally, for instance, but computational methods have provided values for its bond length, dissociation energy, dipole moment and some other properties. Indeed, the book contains numerous impressive illustrations of the power of modern theoretical methods. One striking example involves possible isomers of Si_2F_4: five different computational methods agree in predicting that the most stable arrangement is $(SiF_3)SiF$ rather than $F_2Si{=}SiF_2$.

Besides the expected full accounts of preparations and properties, there are extended discussions of results from more recent and exotic techniques such as multiple photon absorption, ion cyclotron resonance, gas-phase and solid-state NMR, and resonant Auger spectra. It was

something of a revelation to this reviewer to learn how much punishment some unlikely species have taken: we find, for example, that not only the IR visible, UV, and ESR spectra of SiF_3 have been determined, but also its thermodynamic parameters, structure, bond dissociation energy, ionization energy and cross-section, electron and proton affinity, polarizability, and even some chemical reactions. Some other highlights were the excellent discussions of SiF_2 reactivity and the use of Si—F species in microelectronic device fabrication.

All this information is clearly and critically displayed; it is particularly helpful that inconsistencies both within and between publications are pointed out. Altogether some 3700 references are cited, although there is a good deal of duplication because references are given for each short section. Apart from a very few infelicitous passages of English, it is almost impossible to fault the volume; it is comprehensive, well structured, and authoritative, and the team of authors and editors are to be congratulated on an excellent achievement (but could an author index be considered in future volumes?). If you ask "Is it worth the money?", just consider the cost of *your* time in collecting, checking, marshalling, and critically assessing even part of this mass of information!

Department of Chemistry,
Queen Mary & Westfield College,
Mile End Road,
London, E1 4NS, U.K.

B. J. AYLETT

Polyhedron Vol. 12, No. 21, pp. 2545–2549, 1993
Printed in Great Britain

0277-5387/93 $6.00+.00
© 1993 Pergamon Press Ltd

TETRAMETHYLUREA ADDUCTS OF THE TRICYCLOPENTADIENYL LANTHANIDE COMPLEXES

ÂNGELA DOMINGOS, NOÉMIA MARQUES* and A. PIRES DE MATOS

Departamento de Química, ICEN, LNETI, 2686 Sacavém Codex, Portugal

and

M. G. SILVA-VALENZUELA and LEA BARBIERI ZINNER

Universidade de S. Paulo, Instituto de Química, Caixa Postal 20780, CEP 01498-970, Sao Paulo, Brazil

(*Received* 10 *May* 1993; *accepted* 12 *July* 1993)

Abstract—The tetramethylurea adducts of tricyclopentadienyl lanthanide(III) complexes, $Cp_3Ln \cdot TMU$ (Ln = La, Ce, Nd, Sm, Eu and Yb, TMU = 1,1,3,3-tetramethylurea), have been isolated by addition of the stoichiometric amount of $(CH_3)_2NCON(CH_3)_2$ to $Cp_3Ln \cdot THF$, in hexane. The compounds were characterized by standard techniques and the molecular structures of $Cp_3Ce \cdot TMU$ and $Cp_3Nd \cdot TMU$ were determined by single crystal X-ray diffraction analysis. The two compounds are isomorphous. The metal centre is tetrahedrally coordinated.

Since the synthesis of the first tricyclopentadienyl lanthanide compounds, Cp_3Ln, by Birmingham and Wilkinson,[1] a large amount of adducts of these complexes with Lewis bases containing C, N, O or P donor ligands have been synthesized. These results have been extensively reviewed.[2] However, oxygen donor adducts are limited to the coordinated solvent where the compounds are prepared, the only exceptions being $Cp_3La \cdot L$ [L = dioxane, DMSO, DMF, $OP(OMe)_3$, $OCMe_2$] reported by Fischer[3] who studied their ^{139}La NMR. In this contribution we describe the synthesis and characterization of some lanthanide tricyclopentadienides with 1,1,3,3-tetramethylurea. The crystal and molecular structures of $CeCp_3 \cdot TMU$ and $NdCp_3 \cdot TMU$ are also reported.

EXPERIMENTAL

Materials and methods

All operations were performed under rigorous oxygen and moisture exclusion in an argon-filled glove-box or using Schlenk and vacuum-line techniques.

Tetrahydrofuran and n-hexane were dried over sodium benzophenone ketyl, under argon, and distilled prior to use. The solvents were degassed on the vacuum line. Deuterated benzene was dried over sodium benzophenone ketyl and distilled. 1,1,3,3-Tetramethylurea was dried with BaO and distilled prior to use. NaCp was prepared by reacting sodium with the stoichiometric amount of cyclopentadiene monomer in THF. The anhydrous lanthanide trichlorides, $LnCl_3$, were prepared according to literature procedures.[4] The compounds $Cp_3Ln \cdot THF$ were synthesized by metathetical reactions of the lanthanide trichlorides with three equivalents of sodium cyclopentadienide in THF.

Metal analyses were carried out by complexometric titration with EDTA. ^1H NMR spectra were recorded using a Bruker SY80FT multinuclear spectrometer and the proton chemical shifts are reported in ppm relative to Me_4Si. IR spectra were recorded on a Perkin–Elmer 577 spectrophotometer using Nujol mulls between CsI plates.

*Author to whom correspondence should be addressed.

X-ray crystallography of $Cp_3Ln \cdot TMU$ (Ln = Ce, Nd)

The crystals for X-ray diffraction were mounted in quartz capillaries in an argon-filled glovebox.

Data were collected at room temperature on an Enraf–Nonius CAD4 diffractometer with graphite-monochromatized Mo-K_α radiation using the ω–2θ scan mode. The pertinent crystallographic parameters are listed in Table 1. Data were corrected for Lorentz-polarization, linear decay, and for absorption (Ψ scans) using the Enraf–Nonius program. The structure was solved by Patterson and Fourier methods and refined by full-matrix least-squares using SHELX-76.[5] All the non-hydrogen atoms were refined anisotropically and the contribution of the hydrogen atoms were introduced in calculated positions, with group U_{iso} values assigned. In the final difference Fourier map the highest peaks were 0.8 e $Å^{-3}$ for Ce and Nd compounds and were located near the Ln atom.

Atomic scattering factors and anomalous scattering terms were taken from International Tables for X-Ray Crystallography.

Tables of final atomic positional and thermal parameters, full lists of bond lengths and angles, equations of mean least-squares planes and tables of F_o/F_c values have been deposited as supplementary material with the Editor.

Syntheses

$Cp_3La \cdot TMU$ (**1**). All the complexes were prepared in a similar way. In a typical experiment $Cp_3La \cdot THF$ (200 mg, 0.49 mmol) in 10 cm^3 of n-hexane was stirred overnight with $(CH_3)_2NCON(CH_3)_2$ (57 mg, 0.49 mmol). The suspension was decanted and the white solid obtained was washed several times with n-hexane and dried in the vacuum-line. Yield, 96%. Sublimation temperature: 170°C/10^{-3} mm Hg. IR (Nujol, ν cm^{-1}): 3060w, 1580s, 1530w, 1258m, 1232w, 1162s, 1062m, 1009s, 909m, 775vs, 742vs, 580m, 418vw, 360w. Found: La, 30.8. Calc. for $LaC_{20}H_{27}N_2O$: La, 30.8%. ^1H NMR (C_6D_6) (δ ppm *vs* TMS): 6.19 (15H), 2.16 (12H).

$Cp_3Ce \cdot TMU$ (**2**). $Cp_3Ce \cdot THF$ (200 mg, 0.49 mmol) in 10 cm^3 of n-hexane was stirred overnight with $(CH_3)_2NCON(CH_3)_2$ (57 mg, 0.49 mmol). A yellow solid was obtained with a yield of 95%. Sublimation temperature: 150°C/10^{-3} mm Hg. IR (Nujol, ν cm^{-1}): 3060w, 1570s, 1525m, 1255w, 1230w, 1155s, 1060m, 1003s, 905m, 775s, 740vs, 572m, 420vw, 355w. Found: Ce, 30.5. Calc. for $CeC_{20}H_{27}N_2O$: Ce, 31.0%. ^1H NMR (C_6D_6) (δ ppm *vs* TMS): 6.85 (15H), −0.59 (12H).

Yellow crystals suitable for X-ray diffraction were obtained by slow diffusion of n-hexane into a saturated solution of $Cp_3Ce \cdot TMU$, in toluene, at room temperature.

Table 1. Crystallographic data for $Cp_3Ce \cdot TMU$ and $Cp_3Nd \cdot TMU$

Compound	$Cp_3Ce \cdot TMU$	$Cp_3Nd \cdot TMU$
Formula	$C_{20}H_{27}N_2OCe$	$C_{20}H_{27}N_2ONd$
Molecular weight	451.56	455.69
Crystal system	Monoclinic	Monoclinic
Space group	$P2_1/c$	$P2_1/c$
a (Å)	10.708(2)	10.709(2)
b (Å)	8.538(1)	8.487(1)
c (Å)	21.188(3)	21.087(5)
β (°)	94.74(1)	94.83(1)
V ($Å^3$)	1930.5(5)	1909.8(6)
Z	4	4
D_{calc} (g cm^{-3})	1.554	1.585
Linear absorbance coefficient (cm^{-1}) (M_o–K_α)	21.44	25.65
2θ range (°)	3.0–56.0	3.0–50.0
Number of reflections ($F_o > 3\sigma(F_o)$	3427	4006
Decay corrections, min., max.	1.00000, 1.00614	1.00010, 1.05744
Range in abs. correction factors	0.7189, 0.9997	0.8662, 0.9994
Number of parameters refined	219	219
Weighting scheme used, $w = [\sigma^2(F_o) + g(F_o^2)]^{-1}$, g	0.00003	0.0008
Final R, R_w	0.045, 0.051	0.041, 0.049

$Cp_3Nd \cdot TMU$ (**3**). $Cp_3Nd \cdot THF$ (200 mg, 0.49 mmol) in 10 cm^3 of n-hexane was stirred with $(CH_3)_2NCON(CH_3)_2$ (57 mg, 0.49 mmol). A pale blue–violet solid was obtained with 96% yield. Sublimation temperature: 145°C/10^{-3} mm Hg. IR (Nujol, ν cm^{-1}): 3062w, 1580s, 1525m, 1249m, 1230w, 1155s, 1062m, 1009s, 910m, 779vs, 745vs, 575s, 410w, 358w. Found: Nd, 31.6. Calc. for $NdC_{20}H_{27}N_2O$: Nd, 31.6%. ^1H NMR (C_6D_6) (δ ppm *vs* TMS): 2.23 (15H), −6.01 (12H).

Crystals suitable for X-ray diffraction were obtained by slow diffusion of n-hexane into a saturated solution of $Cp_3Nd \cdot TMU$, in toluene, at room temperature.

$Cp_3Sm \cdot TMU$ (**4**). An orange solid was obtained from $Cp_3Sm \cdot THF$ (200 mg, 0.48 mmol) and $(CH_3)_2NCON(CH_3)_2$ (54 mg, 0.48 mmol) in 10 cm^3 of n-hexane with a yield of 95%. Sublimation temperature: 122°C/10^{-3} mm Hg. IR (Nujol, ν cm^{-1}): 3080w, 1580s, 1520m, 1260w, 1240w, 1150s, 1060m, 1010s, 900m, 780vs, 740vs, 560m, 420w, 350w. Found: Sm, 33.0. Calc. for $SmC_{20}H_{27}N_2O$: Sm, 32.6%. ^1H NMR (C_6D_6) (δ ppm *vs* TMS): 11.74 (15H), 0.75 (12H).

$Cp_3Eu \cdot TMU$ (**5**). A brown solid was obtained from $Cp_3Eu \cdot THF$ (200 mg, 0.48 mmol) and $(CH_3)_2NCON(CH_3)_2$ (54 mg, 0.48 mmol) in 10 cm^3 of n-hexane with a yield of 94%. Sublimation temperature: 105°C/10^{-3} mm Hg. IR (Nujol, ν cm^{-1}): 3060w, 1578s, 1525m, 1260w, 1232w, 1150s, 1060w, 1009s, 909m, 762s, 745s, 575s, 410vw, 353w. Found: Eu, 32.8. Calc. for $EuC_{20}H_{27}N_2O$: Eu, 32.8%. ^1H NMR (C_6D_6) (δ ppm *vs* TMS): 30.52 (15H), 17.58 (12H).

$Cp_3Yb \cdot TMU$ (**6**). A dark green solid was obtained from $Cp_3Yb \cdot THF$ (200 mg, 0.45 mmol) and $(CH_3)_2NCON(CH_3)_2$ (53 mg, 0.45 mmol) in 10 cm^3 of n-hexane with a yield of 97%. Sublimation temperature; 91°C/10^{-3} mm Hg. IR (Nujol, ν cm^{-1}): 3062w, 1580s, 1530m, 1260w, 1240w, 1150s, 1060m, 1010s, 910m, 740vs, 720vs, 550s, 410w, 350w. Found: Yb, 35.6. Calc. for $YbC_{20}H_{27}N_2O$: Yb, 35.7%. ^1H NMR (C_6D_6) (δ ppm *vs* TMS): −39.85 (15H), 28.06 (12H).

RESULTS AND DISCUSSION

The preparation of the compounds $Cp_3Ln \cdot TMU$ was carried out by adding the stoichiometric amount or a slight excess of TMU to a suspension of $Cp_3Ln \cdot THF$ in hexane.

Complexes were characterized by IR and ^1H NMR spectroscopies and metal analyses.[6] The compounds are air sensitive, especially the cerium compound, and can be stored at room temperature, under argon, during several months without noticeable decomposition; they are soluble in ethers, halogenated and aromatic solvents and slightly soluble in aliphatic solvents. All the compounds can be sublimed without losing the tetramethylurea molecule, suggesting a strong M—O bond in these compounds (see the X-ray crystal structures).

The IR spectra of the complexes are essentially independent of M suggesting similar molecular structures. The bands assigned to Cp ligand appear at 3080–3060, 1010–1003 and 780–762 cm^{-1} indicating a η^5 mode of coordination of the Cp to the metallic centre.[7] The antisymmetric ring stretching frequency located at about 1150 cm^{-1} could not be assigned due to superposition of a strong vibration mode of TMU. Coordination of the base to the lanthanide centre was inferred from the shift to lower frequencies of the band assigned to the ν(C=O) stretching vibration that appears in the 1580–1570 cm^{-1} range (1648 cm^{-1} for the uncoordinated base).

The ^1H NMR spectra of the complexes show one single resonance for the cyclopentadienyl rings and one single resonance for the methyl groups of the TMU ligand.

Crystal structure of $Cp_3Ce \cdot TMU$ *and* $Cp_3Nd \cdot TMU$

The structure analysis shows that the two compounds are isomorphous. Considering that the Cp ligand occupies a single coordination site, the lanthanide centre is four-coordinate with bonding to three η^5-cyclopentadienyl groups and to one σ-bonded TMU and displays a distorted tetrahedral geometry. A PLUTO drawing of $Cp_3Nd \cdot TMU$ molecule is shown in Fig. 1. Selected bond lengths and bond angles are given in Table 2.

The average Ln—C bond length is 2.83(2) Å for the Ce compound and 2.80(2) Å for the Nd compound. The TMU molecule is coordinated to the metal at Ln—O distances of 2.459(7) Å for the Ce compound and 2.437(5) Å for the Nd compound with Ln—O—C(1) angles of 154.8(5)° and 153.6(4)°, respectively. In both compounds the OCN_2 moieties in the TMU are planar with O—C(1) distances of 1.26(1) Å.

Similar tetrahedral structures have been found in the isostructural $Cp_3Ln \cdot THF$ series (Ln = La,[8] Pr,[9] Nd,[9,10] Gd,[11] Dy,[12] Lu[13]). Also in the present case the Ln—O and Ln—C(Cp) distances are in accordance with the general decreasing trend of bond distances as the ionic radius of the metal decreases. A comparison of the structural data of $Cp_3Nd \cdot TMU$ with those of $Cp_3Nd \cdot THF$[9] shows similar average Nd—C distances [2.80(2) and

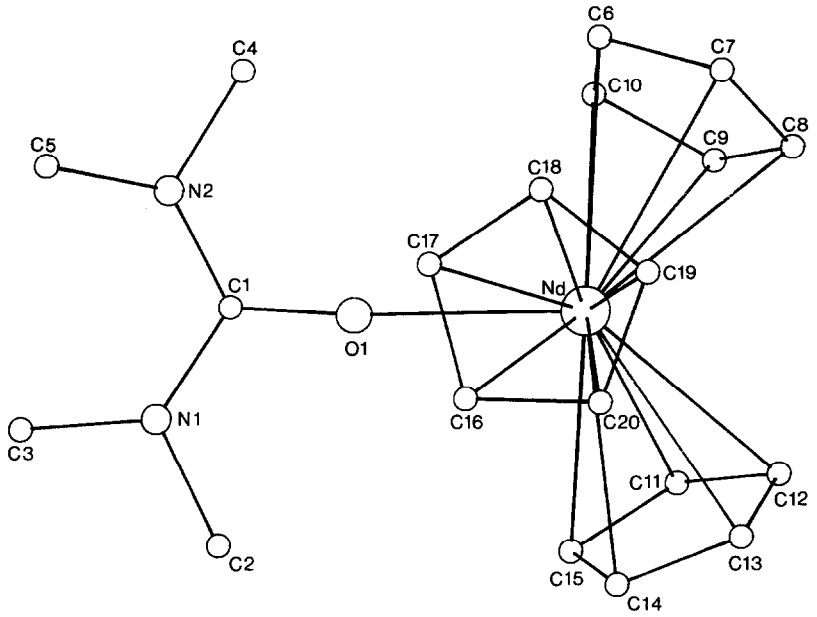

Fig. 1. PLUTO view of $Cp_3Nd \cdot TMU$.

Table 2. Selected bond distances (Å) and angles (°) for $Cp_3Ce \cdot TMU$ and $Cp_3Nd \cdot TMU$

Bond	Ce	Nd	Bond	Ce	Nd
M—C(6)	2.850(11)	2.815(9)	M—O	2.459(7)	2.437(5)
M—C(7)	2.823(11)	2.799(8)	O—C(1)	1.256(10)	1.258(7)
M—C(8)	2.821(11)	2.790(9)	C(1)—N(1)	1.341(10)	1.353(8)
M—C(9)	2.850(10)	2.812(8)	C(1)—N(2)	1.350(11)	1.337(8)
M—C(10)	2.845(11)	2.809(9)	N(1)—C(2)	1.453(11)	1.452(9)
M—Cp_1[a]	2.58(1)	2.54(1)	N(1)—C(3)	1.460(11)	1.463(9)
M—C(11)	2.848(12)	2.808(10)	N(2)—C(4)	1.486(11)	1.464(8)
M—C(12)	2.806(12)	2.778(9)	N(2)—C(5)	1.467(11)	1.461(9)
M—C(13)	2.793(11)	2.753(9)			
M—C(14)	2.803(11)	2.765(9)			
M—C(15)	2.859(12)	2.810(10)			
M—Cp_2	2.57(1)	2.53(1)			
M—C(16)	2.860(10)	2.839(9)			
M—C(17)	2.841(11)	2.812(8)			
M—C(18)	2.813(11)	2.790(8)			
M—C(19)	2.810(11)	2.767(8)			
M—C(20)	2.846(11)	2.817(8)			
M—Cp_3	2.58(1)	2.55(1)			
Angles					
M—O—C(1)	154.8(5)	153.6(4)			
O—M—Cp_1	106.1	105.6			
O—M—Cp_2	103.4	102.7			
O—M—Cp_3	96.3	96.4			
Cp_1—M—Cp_2	114.7	114.8			
Cp_1—M—Cp_3	115.8	116.3			
Cp_2—M—Cp_3	117.0	117.1			

[a] Cp_1 is the centroid of the C(6)—C(10) riong; Cp_2 of the C(11)—C(15) ring and Cp_3 of the C(16)—C(20) ring.

2.78(2) Å, respectively] and a shorter Nd—O bond [2.437(5) and 2.54(1) Å, respectively], indicating a stronger affinity of the tetramethylurea for the lanthanide centre.

REFERENCES

1. J. M. Birmingham and G. Wilkinson, *J. Am. Chem. Soc.* 1956, **78**, 42.
2. (a) H. Schumann and W. Genthe, Organometallic Compounds of the Rare Earths, in: *Handbook of the Physics and Chemistry of Rare Earths* (Edited by K. A. Gschneider, Jr and L. Eyring), Elsevier Science Publishers, Amsterdam (1984); (b) H. Schumann, Organolanthanoids: Review and New Developments, in: *Fundamental and Technological Aspects of Organo-f-Element Chemistry*, NATO ASI Series (Edited by T. J. Marks and I. L. Fragalá), D. Reidel Publishing Company (1985); (c) R. D. Rogers and L. M. Rogers, *J. Organomet. Chem.* 1992, **442**, 83; (b) *ibid.* 1992, **442**, 225.
3. (a) S. H. Eggers, M. Adam, E. T. K. Haupt and R. D. Fischer, *Inorg. Chim. Acta* 1987, **139**, 315; (b) M. Adam, E. T. K. Haupt and R. D. Fischer, *Bull. Magn. Res.* 1990, **12**, 101.
4. G. Meyer, *Inorg. Synth.* 1989, **25**, 146.
5. G. M. Sheldrick, SHELX Crystallographic Program. University of Cambridge, U.K. (1976).
6. Complete elemental analyses have been made but we were not able to get satisfactory results for C, H, and N. However, the metal analysis and the ^{1}H NMR spectra unambiguously identified the complexes.
7. B. Kanellakopulos and K. W. Bagnall (eds), *Inorg. Chem. Series One*, Butterworth & Co. Ltd, 1972, 7, 299.
8. R. D. Rogers, J. L. Atwood, A. Emad, D. J. Sikora and M. D. Rausch, *J. Organomet. Chem.* 981, **216**, 383.
9. Fan Yuguo, Yu Pinzhe, Jin Zhongsheng and Chen Wenqui, *Sci. Sin., Sect. B*, 1984, **1**, 387.
10. F. Benetollo, G. Bombieri, C. Bisi Castellani, W. Jahn and R. D. Fischer, *Inorg. Chim. Acta* 1984, **95**, L7.
11. R. D. Rogers, R. V. Bynum and J. L. Atwood, *J. Organomet. Chem.* 1980, **192**, 65.
12. Zhongwen Ye, Shaowu Wang, Yongfei Yu and Lei Shi, *Inorg. Chim. Acta* 1990, **177**, 97.
13. C. Ni, D. Deng and C. Qian, *Inorg. Chim. Acta* 1985, **110**, L7.

Polyhedron Vol. 12, No. 21, pp. 2551–2556, 1993
Printed in Great Britain

0277–5387/93 $6.00+.00
© 1993 Pergamon Press Ltd

FLEXIDENTATE BEHAVIOUR OF N-(2-HYDROXYETHYL)-1,2-ETHANEDIAMINE(L) IN PALLADIUM(II) HALIDE COMPLEXES. THERMAL, IR AND ^{1}H NMR STUDIES AND SINGLE CRYSTAL X-RAY ANALYSIS OF [PdLCl$_2$]

SUBRATANATH KONER, ASHUTOSH GHOSH* and NIRMALENDU RAY CHAUDHURI†

Department of Inorganic Chemistry, Indian Association for the Cultivation of Science, Calcutta 700 032, India

and

MONIKA MUKHERJEE

Department of Solid State Physics, Indian Association for the Cultivation of Science, Calcutta 700 032, India

and

ALOK K. MUKHERJEE

Department of Physics, Jadavpur University, Calcutta 700 032, India

(*Received* 10 *May* 1993; *accepted* 12 *July* 1993)

Abstract—Tridentate and bidentate coordination behaviour of N-(2-hydroxyethyl)-1,2-ethanediamine(L) with PdX_2 (X = Cl or Br) and their isomerization (N,N,O → N,N coordination) both in the solid state and in the solution have been studied by thermal techniques (DSC and TG-DTA), IR and ^{1}H NMR spectroscopy. One of the isomers [PdLCl$_2$] has been characterized by single crystal X-ray analysis. The palladium(II) ion possesses a square planar geometry with the N_2Cl_2 donor set.

A number of investigations have been reported[1–5] on the nature of the complex formation with N-(2-hydroxyethyl)-1,2-ethanediamine(L). The ligand has three potential donor sites (N,N,O), two nitrogens of the diamine and one oxygen of the hydroxyl group. The hydroxy coordination to metal seems to be weaker than the nitrogen. As a result the ligand is bidentate (via two N) when the other coordination sites of the metal are already occupied by strongly coordinating groups (e.g. NO_2^-, ethylenediamine, triethylenetetramine etc.) but is tridentate when those are weakly coordinating (e.g. H_2O, halogens etc). Moreover, it has been reported that there is a tendency of the bidentate form of this ligand to be transformed into the tridentate form in some complexes.[1]

The above propositions were made on the basis of conductance, spectral (electronic, IR and NMR) data and supported by chemical reaction (acetylation). However, due to lack of single crystal X-ray analysis data, the structures of these complexes as well as the flexidentate behaviour of the ligand remain more or less speculative. Moreover, the coordinating power of hydroxy group (—OH) and that of halogens are not very different. Therefore, it may be expected that interchange between these coordination sites (—OH and halogens) in solid state is possible if the potential barrier of the transformation is not very high.[6]

In this paper we report the syntheses of both bidentate and tridentate form of the ligand (L) in

* Present address: Department of Chemistry, Jhargram Raj College, Jhargram 721 507, India.

† Author to whom correspondence should be addressed.

$PdLX_2$ (X = Cl or Br). Isomerization (tridentacy → bidentacy of L) has also been described along with the crystal structure analysis of $[PdLCl_2]$ where L is bidentate.

EXPERIMENTAL

Materials

All the chemicals used were of AR grade and high purity N-(2-hydroxyethyl)-1,2-ethanediamine (L) was purchased from Fluka AG and distilled before use.

Physical measurements

The instruments used for IR and electronic spectra, thermal investigations [thermogravimetry (TG), differential thermal analysis (DTA) and differential scanning calorimetry (DSC)], elemental analyses, X-ray powder diffraction and conductance measurements were the same as reported earlier.[7] The ^1H NMR spectra were obtained on a 270 MHz Bruker 270 FT NMR spectrometer in DMSO-D_6 with TMS as an internal standard at IISc, Bangalore, India.

Preparation of $PdLCl_2$ (**1**) *and* $PdLBr_2$ (**2**)

These compounds were prepared by following the methods reported earlier.[1,5] Found: C, 17.1; H, 4.5; N, 9.9. Calc. for $C_4H_{12}N_2OCl_2Pd$ (**1**): C, 17.0; H, 4.3; N, 9.9%. Found: C, 13.0; H, 3.3; N, 7.4. Calc. for $C_4H_{12}N_2OBr_2Pd$ (**2**): C, 13.0; H, 3.2; N, 7.6%.

Preparation of $[PdLCl_2]$ (**1a**)

After removing $PdLCl_2$ (**1**), the mother liquor was kept at room temperature for 48 h, when rhomboid, pale-yellow crystals were separated out. These crystals were collected by filtration and dried in a desiccator. Yield 10%. Found: C, 17.2; H, 4.5; N, 10.0. Calc. for $C_4H_{12}N_2OCl_2Pd$ (**1a**): C, 17.0; H, 4.3; N, 9.9%.

Preparation of $[PdLBr_2]$ (**2a**)

The desired dazzling yellow coloured complex was obtained on recrystallization of **2** from water. Yield 40%. Found: C, 12.9; H, 3.1; N, 7.6. Calc. for $C_4H_{12}N_2OBr_2Pd$ (**2a**): C, 13.0; H, 3.2; N, 7.6%.

Crystallography

Crystal data. $C_4H_{12}N_2OCl_2Pd$ (**1a**), M = 281.8, monoclinic, $a = 8.646(2)$, $b = 9.746(2)$, $c = 10.388(3)$ Å, $\beta = 99.33(3)°$, $U = 863.8$ Å^3 (by least-squares refinement on diffractometer angles for 20 automatically centred reflections, $\lambda = 0.71069$ Å), space group $P2_1/c$, $Z = 4$, $D_c = 2.17$ g cm^{-3}, $F(000) = 552$, rhomboid light yellow crystals, dimensions $0.30 \times 0.16 \times 0.12$ mm, μ(Mo-K_α) = 24.9 cm^{-1}, $T = 293$ K.

Structure determination

Intensities for 2523 unique reflections ($1.5 < \theta < 30°$) were collected on a Hilger-Watt diffractometer in ω–2θ scan mode using graphite monochromatised Mo-K_α radiation. Data were corrected for absorption (max., min. transmission factor 0.90, 0.65) according to ref. 8. A total of 2123 reflections with $I > 3\sigma(I)$ was considered observed. The structure was solved by Patterson, Fourier methods and refined by full-matrix least-squares. All hydrogen atoms were located from difference maps. Final refinement with all non-hydrogen atoms anisotropic and hydrogen atoms isotropic (OH hydrogen was kept fixed) converged to $R = 0.047$, $R' = 0.048$. The weighting scheme $w = 1/[\sigma^2(F_o) + 0.001|F_o|^2]$ with $\sigma(F_o)$ from counting statistics gave satisfactory agreement analyses. Programs, computer used and sources of scattering factor data are given in ref. 9.

Supplementary material available.

Tables of positional and thermal parameters, interatomic distances and angles, and prominent lines in the X-ray powder diffraction patterns of **1** and **1a** are available from the authors on request.

RESULTS AND DISCUSSION

Structure of complex $[PdLCl_2]$ (**1a**)

The crystal structure consists of discrete monomeric units. An ORTEP[10] plot of **1a** with atom labelling scheme is shown in Fig. 1. Table 1 gives selected bond lengths and bond angles. Four ligand atoms [Cl(1), Cl(2), N(1), N(2)] around the palladium(II) form a distorted square planar arrangement with one bidentate N-(2-hydroxyethyl)-1,2-ethanediamine molecule and two chlorine atoms in *cis* position. The deviations from the weighted mean plane through the coordinated atoms are Cl(1) 0.001(1), Cl(2) −0.001(1), N(1) 0.015(5), N(2) −0.011(4) Å with the palladium atom 0.004(1) Å

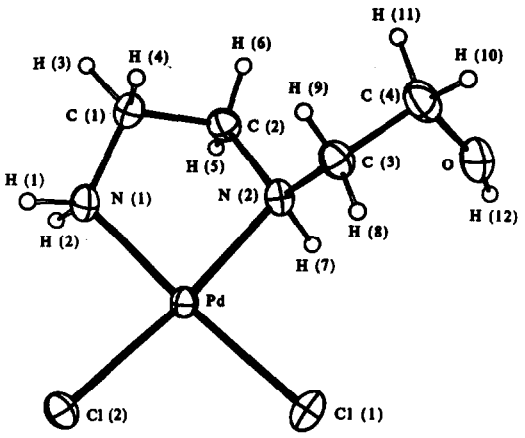

Fig. 1. ORTEP-plot of $[PdLCl_2]$ (**1a**) with atom numbering scheme.

from this plane. The Pd—Cl bond lengths in **1a** [mean value 2.322(1) Å] are in agreement with the values reported for palladium(II) complexes having chloro ligands.[11-13] The Pd—N distances 2.029(4), 2.062(4) Å are comparable to those observed in other palladium amine complexes.[14,15] The bending of Cl(2)—Pd—N(2) angle from linearity [174.2(1)°] can be related to the steric bulk of hydroxyethyl group attached to N(2). Other bond distances and angles are of usual values.

Therefore, it is clearly established that in $PdLCl_2$ (**1a**) the ligand, N-(2-hydroxyethyl)-1,2-ethanediamine in contrast to the earlier reports[1,5] is not tridentate but bidentate (coordinated via two N; the OH group remains uncoordinated).

Synthesis and X-ray powder diffraction study of (**1**)

The X-ray powder diffraction studies of **1** and **1a** reveal that all the prominent lines of **1a** are present in the diffraction pattern of **1** in addition to several other lines. Therefore, it is reasonable to infer that compound **1** which was reported as [PdLCl]Cl by the earlier investigators,[1,5] is not a single compound but admixed with **1a**. In spite of repeated attempts, we could not synthesize **1** in pure form. The relative ratio of these two complexes in the solid phase depends on several procedural factors e.g. temperature, nature of the solvent and even on the time taken for the addition of ligand to the Pd(II) solution during the preparation of the complex **1**. As the temperature of solution of $M_2[PdCl_4]$ (M = Li, Na or K) is lowered during the preparation, the relative percentage of the species [PdLX]X in the mixture is increased and reaches a maximum at *ca* 0–1°C. It is also noticed that the quicker the addition of the ligand to $M_2[PdCl_4]$ solution the lower is the percentage of the $[PdLCl_2]$. However, for the non-aqueous solvent e.g. methanol, ethanol, isopropanol etc. the amount of $[PdLCl_2]$ is always higher than [PdLCl]Cl. The relative ratio of these two species may be qualitatively measured by the relative peak intensity of the powder diffraction lines and the —OH bands appearing in the region 3500–3350 cm^{-1} in the IR spectra as well as by the measurement of the enthalpy change (ΔH) for the isomerization $[PdLCl]Cl \rightarrow [PdLCl_2]$ by DSC in the solid state *vide infra*. Complex **1** having least amounts of **1a** has been used for the following studies.

Isomerization [(**1**) → (**1a**)] *in the solid state and in solution*

Complex **1** on heating undergoes an endothermic irreversible phase transition (peak temp. 180°C) without any mass loss as is evident from the simultaneous TG–DTA and DSC studies (Fig. 2). The species isolated after phase transition appears to be **1a** as is evident from X-ray powder diffraction pattern, IR and NMR spectra. Complex **1a** on the other hand does not show any phase transition before decomposition. Therefore, the enthalpy change for **1** → **1a** non-isothermal transformation, is solely due to isomer **1** and is used to assess the relative amount of the isomers. The structure of

Table 1. Selected bond lengths (Å) and bond angles (°) of $[PdLCl_2]$ (**1a**) with ESDs in parentheses

Pd—Cl(1)	2.327(1)	Pd—Cl(2)	2.318(1)
Pd—N(1)	2.029(4)	Pd—N(2)	2.062(4)
N(1)—C(1)	1.487(7)	N(2)—C(2)	1.506(7)
N(2)—C(3)	1.490(7)	O—C(4)	1.415(9)
Cl(1)—Pd—N(1)	176.3(1)	Cl(2)—Pd—N(2)	174.2(1)
Cl(1)—Pd—Cl(2)	94.0(1)	Cl(1)—Pd—N(2)	91.8(1)
Cl(2)—Pd—N(1)	89.6(1)	N(1)—Pd—N(2)	84.6(2)
Pd—N(2)—C(3)	112.0(3)	C(3)—C(4)—O	107.5(5)

this isomer is proposed to be [PdLCl]Cl where L is tridentate, as is evident from IR and NMR spectra *vide infra*. Earlier reports[1,5] are also in line with this proposed structure.

The **1** → **1a** transformation occurs slowly also at room temperature in presence of high relative humidity (*ca* 70% or more) and becomes complete in one month. However, this transformation has not been found to occur in detectable quantity in a P_4O_{10} desiccator for several months. Complex **1** transforms to **1a** on crystallization from hot water.

Conductance

The electrolytic conductance of the complexes $PdLCl_2$ were measured in DMSO. The complex **1** shows $\Lambda m = 30\ \Omega^{-1}$ mol cm^2 and is very close to the desired value for 1:1 complex,[16] whereas the complex **1a** is non-electrolyte ($\Lambda m = 4\ \Omega^{-1}$ mol cm^2). The conductance value of **1** approaches to that of **1a** on keeping the solution overnight.

Infrared spectra

The complex **1** shows a band at *ca* 3390 cm^{-1} for OH stretching modes (Fig. 3) while in the case of **1a** this band appears at 3458 cm^{-1}. From this shifting it is legitimate to assume that in the former case the hydroxy group is coordinated with palladium but not in the latter case. In the far-IR region, complex **1** shows one strong band for Pd—Cl stretching at *ca* 330 cm^{-1} but the complex [$PdLCl_2$] (**1a**) shows two peaks for Pd—Cl stretching at 350 and 312 cm^{-1}. This splitting is expected as the complex **1a** possesses *cis* gometry.[17,18] From the above discussion it can be assumed that the OH group of the ligand is also coordinated along with the two N in **1**.

Proton NMR spectra

To obtain a greater insight into the mode of coordination of ligand in solid state as well as in solution we studied the palladium(II) halide complexes by ^{1}H NMR spectroscopy.

The [$PdLCl_2$] (**1a**) shows four peaks (Fig. 4) for all the —CH_2— ^{1}H except for —CH_2O— at the region of δ 3.00–2.32, while for —CH_2O— it appears as a multiplet at δ 3.71–3.58. All NH protons appear at lower field than the —CH_2— absorptions (δ 4.75–5.26). The —OH proton appears as a broad peak at δ 5.82. All the —CH_2— including —CH_2—O— in the complexes have the same chemical shift as in the free ligand, whereas the most pronounced change in chemical shift is observed for the protons adjacent to the ligation site, probably due to the decrease in the electron density of the donor atoms on complexation.[19] All the —NH— and —OH protons are almost removed in D_2O.

The complex $PdLCl_2$ (**1**) shows some extra peaks (Fig. 5) in addition to the peaks appearing in the case of [$PdLCl_2$] (**1a**) for the protons attached to the donor atoms. These extra peaks appear at the

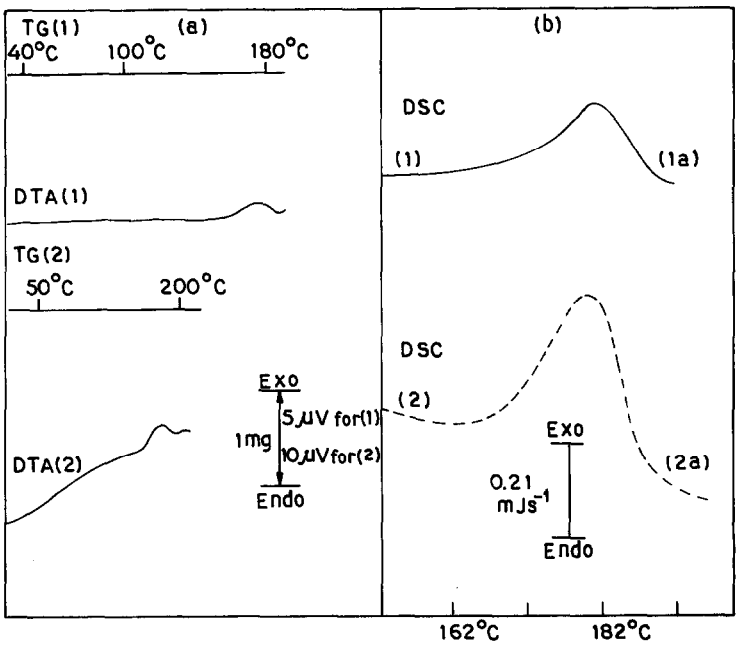

Fig. 2. TG-DTA(a) and DSC(b) runs for the complexes $PdLCl_2$ (**1**) and $PdLBr_2$ (**2**).

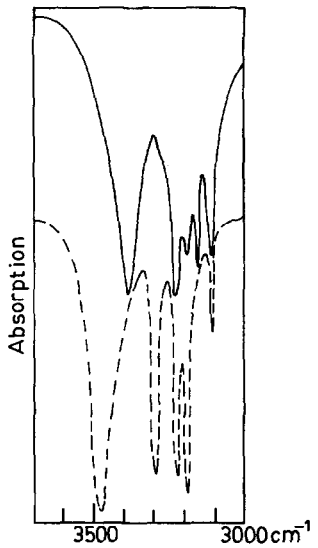

Fig. 3. IR spectra of $PdLCl_2$ (**1**) (——) and $[PdLCl_2]$ (**1a**) (– – –).

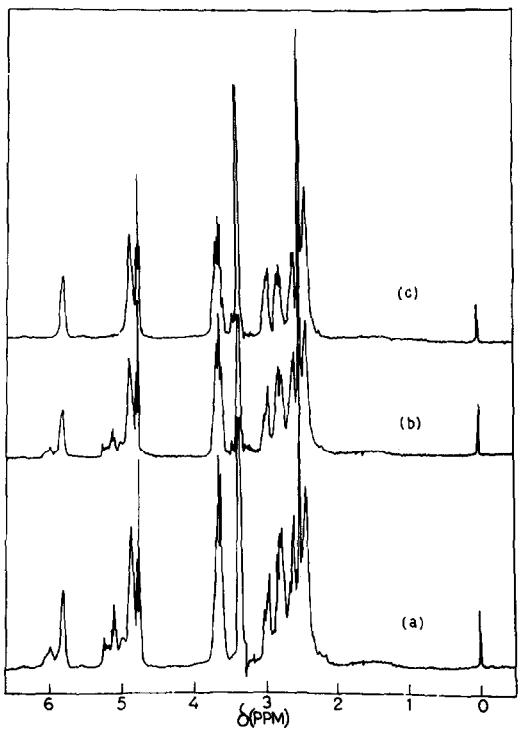

Fig. 5. ^1H NMR spectra of $PdLCl_2$ (**1**) showing the change of positions of the peaks with time, (a) just after dissolving in DMSO-D_6, (b) after 1 h and (c) after 24 h.

lower field than the corresponding peaks appeared in the complex $[PdLCl_2]$ (**1a**). It is interesting to note that these additional peaks are shifted to the higher field with time and ultimately, after *ca* 24 h, they merge with the original peaks of complex **1a** indicating the complete transformation of **1** → **1a**.

The corresponding bromo complex, $PdLBr_2$ behaves quite similarly to chloro complex. However, there are some differences between them which are summarized below. (i) The colour of [PdLBr]Br (**2**) is red and that of $[PdLBr_2]$ (**2a**) is yellow. Therefore on heating of the species **2**, an irreversible thermochromism (red → yellow) is observed along with the endothermic phase transition. (ii) The complex **2** is also not pure. It contains its isomer **2a** as impurity like the corresponding chloro analogue but in higher percentage (evident from X-ray powder diffraction, IR spectra and DSC experiment). (iii) On dissolution in DMSO, complex **2** transforms immediately to **2a** as the NMR spectra of **2** and **2a** in DMSO are observed to be identical.

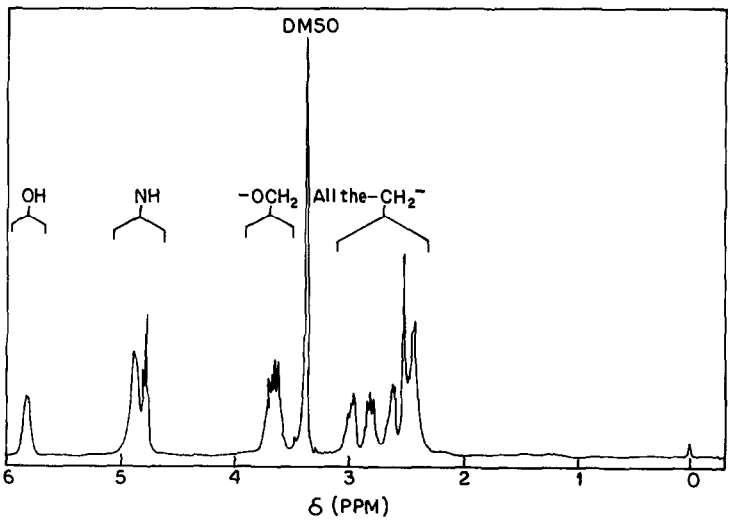

Fig. 4. ^1H NMR spectra of $[PdLCl_2]$ (**1a**).

CONCLUSION

The above studies show that this ligand forms two isomeric 1 : 1 complexes with PdX_2 (X = Cl or Br). One is metastable [PdLX]X and the other is stable $PdLX_2$. The ligand is tridentate in the former and bidentate in the latter. However, the solid product separated immediately after mixing a solution of Pd salt and the ligand (1 : 1) is [PdLX]X admixed with a slight amount of $[PdLX_2]$ indicating that the former is kinetically favoured. The transformation of this metastable [PdLX]X to stable $[PdLX_2]$ can be brought about by three different procedures: (i) on heating in the solid state; (ii) by crystallization/dissolution in suitable solvent and (iii) by keeping the solid complex in the humid atmosphere (relative humidity 70% or more).

Acknowledgement—The authors wish to thank Dr A. R. Chakraborty, Department of Inorganic and Physical Chemistry, IISc, Bangalore for ^1H NMR spectra. We are also grateful to the Department of Physics, University of York, U.K. for allowing two of the authors (AKM, MM) to use the X-ray diffractometer facility.

REFERENCES

1. B. Das Sarma and J. C. Bailar, Jr, *J. Am. Chem. Soc.* 1969, **91**, 5958.
2. R. N. Keller and L. J. Edwards, *J. Am. Chem. Soc.* 1952, **74**, 215.
3. W. C. Drinkard, H. F. Bauer and J. C. Bailer, Jr, *J. Am. Chem. Soc.* 1960, **82**, 2992.
4. B. Das Sarma, G. J. Tennenhouse and J. C. Bailar, Jr, *J. Am. Chem. Soc.* 1968, **90**, 1362.
5. E. I. Karpeiskaya, Yu. N. Kukushkin, V. A. Trofimov, I. P. Yakovlev and R. A. Vlasova, *Russ. J. Inorg. Chem.* 1972, **17**, 1411.
6. D. R. Bloomquist and R. D. Willett, *Coord. Chem. Rev.* 1982, **47**, 125.
7. (a) S. Koner, A. Ghosh and N. Ray Chaudhuri, *J. Chem. Soc., Dalton Trans.* 1990, 1563; (b) S. Koner, A. Ghosh and N. Ray Chaudhuri, *Trans. Met. Chem.* 1900, **15**, 394.
8. A. C. T. North, D. C. Phillips and F. S. Mathews, *Acta Cryst., Sect. A* 1968, **24**, 351.
9. (a) G. M. Sheldrick, SHELX-76, *Programs for Crystal Structure Determination.* University of Cambridge, U.K. (1976); (b) M. Nardelli, PARST, *A System of Computer Programs for Calculating Molecular Parameters from Results of Crystal Structure Analyses*, University of Parma, Italy (1982); (c) Vax Cluster System at the University of York, England; (d) *International Tables for X-ray Crystallography*, Vol. IV. Kynoch Press, Birmingham (1974).
10. C. K. Johnson, ORTEP II, Rep. ORNL-5138, Oak Ridge National Laboratory, Oak Ridge, TN (1976).
11. G. Bruno, M. Cusumano, A. Giannetto, A. Giuffrida and G. Guglielno, *Acta Cryst., Sect. C* 1990, **46**, 192.
12. A. Albinati, C. G. Anklin, F. Ganazzoli, H. Ruegg and P. S. Pregosin, *Inorg. Chem.* 1987, **26**, 503.
13. R. Bertani, M. Mozzon, F. Bauetollo, G. Bombieri and R. A. Michelin, *J. Chem. Soc., Dalton Trans.* 1990, 1197.
14. G. Wilkinson (ed), *Comprehensive Coordination Chemistry*, Vol. 5, p. 1116. Pergamon, Oxford (1987).
15. K. Matsumoto, H. Moriyama and K. Suzuki, *Inorg. Chem.* 1990, **29**, 2096.
16. (a) W. J. Geary, *Coord. Chem. Rev.* 1971, **7**, 81; (b) Y. Fukuda, C. Fujita, H. Miyamae, H. Nakagawa and K. Sone, *Bull. Chem. Soc. Jpn* 1989, **62**, 745.
17. (a) D. M. Adams, *Metal-Ligand and Related Vibrations*, Edward Arnold, Lond (1967); (b) J. R. Ferraro, *Low Frequency Vibrations of Inorganic and Coordination Compounds*, Plenum, New York (1971).
18. P. L. Goggin and J. Mink, *J. Chem. Soc., Dalton Trans.* 1974, 1479.
19. (a) N. J. Mason, W. J. Geary, L. A. Nixon and I. W. Nowell, *J. Chem. Soc., Dalton Trans.* 1986, 1347; (b) D. L. Klayman, J. P. Scovil, J. F. Bartosevich and J. Bruce, *J. Med. Chem.* 1983, **26**, 35; (c) A. C. Fabretti, G. Frauchini, W. Malavasi and G. Peyronel, *Polyhedron* 1985, **4**, 989.

Polyhedron Vol. 12, No. 21, pp. 2557–2561, 1993
Printed in Great Britain

0277–5387/93 $6.00+.00
© 1993 Pergamon Press Ltd

SYNTHESIS, SPECTROSCOPIC AND CRYSTAL STRUCTURE STUDY OF NaMn(PYRAZINATO)$(N_3)_2(H_2O)_2$. A POLYMERIC STRUCTURE CONTAINING (μ-1,1,3)-BRIDGING AZIDO LIGANDS BETWEEN MANGANESE AND SODIUM CENTRED POLYHEDRA

MOHAMED A. S. GOHER*

Department of Chemistry, Faculty of Science, Alexandria University, Alexandria 21321, Egypt

and

FRANZ A. MAUTNER*

Institut für Physikalische und Theoretische Chemie, Technische Universität Graz, A-8010 Graz, Austria

and

ALOIS POPITSCH

Institut für Anorganische Chemie, Karl-Franzens-Universität Graz, A-8010 Graz, Austria

(*Received* 10 *May* 1993; *accepted* 12 *July* 1993)

Abstract—The complex [NaMn(pyrazinato)$(N_3)_2(H_2O)_2$] has been synthesized and characterized by spectroscopic methods and X-ray crystallography. The infrared and Raman spectral results indicate that the complex contains an N,O-bidentate pyrazinato anion, aqua ligands and asymmetric azido groups. The structure of the complex features an octahedrally coordinated manganese atom as well as six-coordinated sodium atom. Each manganese atom, which links a bridging aqua ligand [Mn—O = 2.244(3) Å] and three μ(1,1,3)-bridging azido ligands [Mn—N from 2.137(3) to 2.257(3) Å], is chelated by a pyrazinato anion [*via* its ring nitrogen atom, Mn—N = 2.297(3) Å, and a carboxylato oxygen atom, Mn—O = 2.148(3) Å]. The sodium atom is bonded to three μ(1,1,3)-bridging azido ligands in a facial arrangement [Na–N from 2.415(4) to 2.517(4) Å] and three water molecules [Na–O from 2.368(3) to 2.440(3) Å] in which two of them act as bridges between two sodium octahedra. The manganese and sodium octahedra have a common edge *via* an aqua ligand and an azido group.

Complexes of first-row transition metal ions with pyridine and its derivatives have been extensively studied.[1] With a carboxy substituent at the 2-position on the pyridine ring, several possibilities arise regarding the mode of interaction between the ligands and the metal ions: the carbonyl oxygen may coordinate alone, or along with the nitrogen of the pyridine ring on the central metal ion to form a five-membered ring, the two oxygen atoms of the carboxy group may coordinate by one or two metal atoms, or the nitrogen atom may function alone as a monodentate ligand. In a search of selective extraction reagents for transition metal ions, Elman *et al.*[2,3] and Csoregh *et al.*[4] studied the effects of various substituents on the coordinating properties of pyridine- and quinoline-carboxylic acids and the stereochemistry of the resulting complexes. On the

* Authors to whom correspondence should be addressed.

other hand, pyrazine and pyrazine-2-carboxylic acid (hereafter abbreviated as H-pyz) combine the coordinating features of the pyridine-2-carboxylic acid, plus the fact that the pyrazine moiety may act as bridge and thus aid the formation of polymeric derivatives.[5]

Recently we studied the interaction between pyridine-2-carboxylic acid and manganese(II) ions in the presence of azide ions and described the crystal structure of the resulting complex Mn (picolinato)(N_3)(H_2O).[6] In the present work we employed pyrazine-2-carboxylic acid in preparing the title manganese(II) azide complex and determined its structures by spectroscopic and X-ray crystallographic methods in order to establish its molecular and coordination geometry.

EXPERIMENTAL

Pyrazinic acid was obtained from Aldrich and the other chemicals were of analytical grade quality.

Preparation of the NaMn(*pyrazinato*)(N_3)$_2$(H_2O)$_2$

The NaMn(pyz)(N_3)$_2$(H_2O)$_2$ complex was prepared by dissolving $MnCl_2 \cdot 3H_2O$ (0.71 g, 5 mmol) in distilled water (20 cm^3). Pyrazinic acid (1.24 g, 10 mmol) dissolved in boiled water (*ca* 10 cm^3) was then added. To the clear solution, NaN_3 (0.65 g, 10 mmol) in distilled water (5 cm^3) was also added dropwise with stirring and the mixture became yellow solution. Transparent yellow crystals were obtained by slow evaporation in a desiccator charged with $CaCl_2$ and kept in the dark for several days. Found: C, 18.6; H, 2.4; N, 34.7; Mn, 17.3. Calc.: C, 18.7; H, 2.2; N, 34.9; Mn, 17.1%.

Physical measurements

Raman spectra were obtained using equipment consisting of a Spex 1301 monochromator, C31034 photomultiplier tube, photon counting electronics and a Spectra-Physics Model 2016 argon-ion laser ($\lambda = 514.5$ nm). The power of the laser beam used was approximately 20 mW. The experimental procedures and instruments used for other measurements are as described previously.[7]

X-ray analysis

A modified STOE four circle diffractometer was used for single crystal X-ray measurements. Lattice parameters were obtained by least-squares refinement of the diffraction data from 28 reflections in the 2θ range 8–15°. Data were collected at 300(1) K using graphite crystal-monochromatized Mo–K_α radiation ($\lambda = 0.71069$ Å) and the ω-scan technique. The intensities were corrected for Lorentz and polarization effects, and for absorption by an empirical method.[8] Crystallographic data are given in Table 1.

Table 1. Crystallographic data and processing parameters

Chemical formula	$C_5H_7MnNaN_8O_4$
Molecular weight	321.09
Crystal system	Monoclinic
a (Å)	7.633(3)
b (Å)	15.660(4)
c (Å)	19.379(5)
β (°)	91.37(2)
V (Å^3)	2316(1)
Space group	$I2/a$ (No. 15)
Z	8
$F(000)$	1288
D_{calc} (Mg m^{-3})	1.842
Approx. crystal size (mm)	$0.65 \times 0.15 \times 0.15$
Data collection limits	$\pm h, k, l$; $2\theta < 60°$
Scan mode	ω-scan, $\Delta\omega = 1.4°$
Least squares parameters	191
$F_o > 3\sigma(F_o)$	1973
μ(Mo-K_α) (mm^{-1})	1.16
R	0.042
R_w	0.042
Weighting scheme	$1.347\sigma^{-2}(F_o)$
Residual electron density (e Å^{-3})	+0.73/−0.44

The structure was solved by Patterson methods. Anisotropic displacement parameters were only applied to the non-hydrogen atoms in full-matrix least-squares refinements. The hydrogen atoms were included in the final refinement cycles on calculated positions. The programs DIFABS,[8] SHELX-76,[9] SHELXS-86,[10] PLATON[11] and THE XRAY SYSTEM[12] were used for computations. Analytical expressions of neutral-atom scattering factors were employed, and anomalous dispersion corrections were incorporated.[13] Selected bond distances and bond angles are given in Table 2. Positional parameters, anisotropic displacement parameters, hydrogen atom coordinates, a full list of bond lengths and angles and observed and calculated structure factors have been deposited with the Editor as supplementary material.

DISCUSSION

The principal structural features of the title complex are illustrated in Fig. 1. The coordination environment about each manganese(II) atom is a distorted octahedron. The pyrazinato anion chelates a manganese atom *via* its ring nitrogen atom

Table 2. Selected bond distances (Å) and angles (°)

Mn—O(1)	2.148(3)	Mn—O(3)	2.244(3)
Mn—N(1)	2.297(3)	Mn—N(11)	2.137(3)
Mn—N(21)	2.257(3)	Mn—N(21f)	2.160(3)
Na—O(3)	2.411(3)	Na—N(11)	2.517(4)
Na—O(4)	2.440(3)	Na—N(13)	2.415(4)
Na—N(23)	2.455(4)	Na—O(4c)	2.368(3)
O(1)—C(5)	1.258(4)	O(2)—C(5)	1.231(4)
N(11)—N(12)	1.164(5)	N(12)—N(13e)	1.150(5)
N(21)—N(22)	1.182(4)	N(22)—N(23b)	1.124(5)
O(1)—Mn—O(3)	88.5(1)	O(1)—Mn—N(1)	73.7(1)
O(1)—Mn—N(11)	97.6(1)	O(1)—Mn—N(21)	88.8(1)
O(1)—Mn—N(21f)	158.6(1)	O(3)—Mn—N(1)	85.1(1)
O(3)—Mn—N(11)	86.4(1)	O(3)—Mn—N(21)	175.7(1)
O(3)—Mn—N(21f)	101.8(1)	N(1)—Mn—N(11)	167.9(1)
N(1)—Mn—N(21)	91.0(1)	N(1)—Mn—N(21f)	88.4(1)
N(11)—Mn—N(21)	97.2(1)	N(11)—Mn—N(21f)	101.7(1)
N(21)—Mn—N(21f)	79.8(1)	O(3)—Na—N(11)	75.0(1)
O(3)—Na—O(4)	109.5(1)	O(3)—Na—N(13)	161.1(2)
O(3)—Na—N(23)	78.2(1)	O(3)—Na—O(4c)	85.9(1)
N(11)—Na—O(4)	175.5(1)	N(11)—Na—N(13)	86.6(1)
N(11)—Na—N(23)	95.8(1)	N(11)—Na—O(4c)	94.9(1)
O(4)—Na—N(13)	88.9(1)	O(4)—Na—N(23)	85.2(1)
O(4)—Na—O(4c)	85.7(1)	N(13)—Na—N(23)	100.1(2)
N(13)—Na—O(4c)	99.9(2)	N(23)—Na—O(4c)	157.8(2)
Mn—O(1)—C(5)	119.9(2)	Mn—O(3)—Na	98.5(1)
Na—O(4)—Na(c)	94.2(1)	Mn—N(11)—Na	98.2(1)
Mn—N(11)—N(12)	131.9(3)	Na—N(11)—N(12)	114.8(3)
N(11)—N(12)—N(13e)	178.7(5)	Na—N(13)—N(12d)	145.9(3)
Mn—N(21)—N(2)	121.8(2)	Mn—N(21)—Mn(f)	100.2(1)
N(22)—N(21)—Mn(f)	137.0(3)	N(21)—N(22)—N(23b)	179.2(5)
Na—N(23)—N(22a)	147.1(3)	O(1)—C(5)—O(2)	125.8(3)

Symmetry code: (a) $x-1, y, z$; (b) $x+1, y, z$; (c) $-x-1/2, y, -z$; (d) $x-1/2, 1-y, z$; (e) $x+1/2, 1-y, z$; (f) $1/2-x, 1/2-y, 1/2-z$; (g) $-1/2-x, 1/2-y, 1/2-z$.

N(1) and a carboxylate oxygen atom O(1) to form a five-membered chelate ring. The chelate ring deviates only 0.07(1) Å from planarity, the N(1)···O(1) distance is 2.669(7) Å. The manganese atom is further coordinated by three nitrogen atoms from three μ(1,1,3)-bridging azido ligands in a facial arrangement [Mn—N from 2.137(3) to 2.257(3) Å] and a bridging water molecule at Mn—O(3) bond length of 2.244(3) Å. This water molecule further bridges a sodium atom [Na—O(3) = 2.411(3) Å] which is also six-coordinated. The sodium atom is coordinated by two more aqua ligands [Na—O(4) = 2.440(3) and Na—O(4c) = 2.368(3) Å] and three nitrogen atoms (facial) from three μ(1,1,3)-bridging azido ligands [Na—N from 2.415(4) to 2.517(4) Å]. The last two aqua ligands, O(4) and O(4c) act as bridges between two sodium octahedra. Thus two centrosymmetric related manganese polyhedra have a common edge *via* μ(1,1,3) azido ligands, whereas the manganese and sodium octahedra have their common edge *via* the aqua ligand O(3) and the azido group N(11)—N(12)—N(13e). Conforming to the general characteristics of the coordinated azides,[14-16]

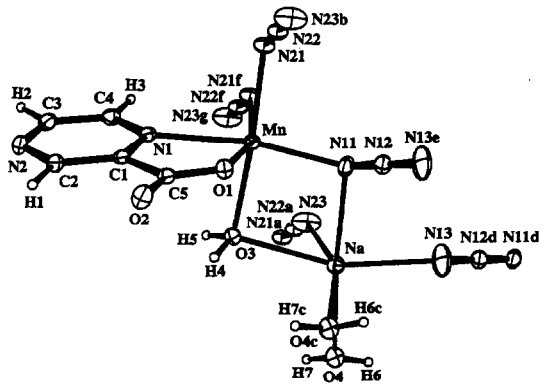

Fig. 1. Molecular structure of NaMn(pyz)$(N_3)_2(H_2O)_2$. Symmetry code according Table 2.

the two $\mu(1,1,3)$ azides are linear, but one of them may be considered as symmetrical within experimental errors [N(11)—N(12) = 1.164(5) and N(12)—N(13e) = 1.150(5) Å] whereas the other is asymmetric [N(21)—N(22) = 1.182(4) and N(22)—N(23b) = 1.124(5) Å]; however, in both of them the longer N—N distance is that between the central nitrogen and the nitrogen coordinated to two metal centres.

The $\mu(1,1,3)$ mode of azide bridging has previously been found in the structures of the polymeric complexes $Cu(NH_3)_2(N_3)_2$,[17] Cu(pyridine)$_2(N_3)_2$[18] and Cu(DENA)$(N_3)_2$ (DENA = diethylnicotinamide).[19] The structure of the title complex, however, is novel in that the $\mu(1,1,3)$ azido bridging occurs between three centres of two different metal atoms (Fig. 2). The Mn—N bond distances given in Table 2 are longer than corresponding values reported for $[(CO_3)Mn(N_3)_3Mn(CO)_3]$ containing only $\mu(1,1)$ azides [2.06(2)–2.11(2) Å],[20] but resemble those reported for polymeric Mn(pyridine)$_2(N_3)_2$ having only $\mu(1,3)$ azides [2.195(5) and 2.217(4) Å].[21]

The present complex differs from that obtained when picolinic acid, also known as 2-pyridinecarboxylic acid, was used instead of pyrazinic acid in a similar reaction, namely Mn(picolinato)$(N_3)(H_2O)$.[6] In the latter complex, the picolinate anion functions differently from the pyrazinate anion, and acts as a tridentate ligand. It chelates a manganese atom *via* its ring nitrogen and carboxylate oxygen atom which is further bridging another manganese atom giving rise to a dimeric Mn_2O_2 unit. The Mn—O distance in the present structure is shorter, whereas the Mn—N distance is little longer than corresponding values in the structure of the picolinato complex [Mn—O(pic) = 2.243(2) and Mn—N(pic) = 2.278(3) Å].[6] In the present structure there are four kinds of hydrogen bonding interactions that consolidate the crystal lattice: O(3)—H(4)···O(2) = 1.81(4) Å and O(4)—H(7)···O(1) = 1.91(4) Å, which link the bridging aqua ligands with coordinated and uncoordinated oxygen atoms, respectively, of a chelated pyrazinato anion, and O(3)—H(5)···N(2) = 1.93(3) Å and O(4)—H(6)···N(13) = 2.23(4) Å which link the same bridging aqua ligands given above with a non-bonded nitrogen atom of a pyz^- anion of an adjacent molecule and a monodentate nitrogen atom of an azido group in the same asymmetric unit, respectively. These hydrogen bonds are non-linear and the O—H···O or O—H···N angles vary from 152(4) to 172(4)°. The Na—N distances of 2.415(4) to 2.517(4) Å within the sodium octahedron (Fig. 1 and Table 2) are shorter than those (2.61–2.64 Å) in other NaN_6 coordination octahedra.[22] Likewise, the Na—O bond lengths of 2.368(3) to 2.440(3) Å found in the present structure are close to those in similar NaO_6 octahedra.[22]

The IR spectrum of free pyrazinic acid exhibits the following absorption bands (cm^{-1}, v = very, m = medium, w = weak, s = strong, br = broad): 1725vs,br [ν(C=O)], 1316vs [ν(C—O)], 1020s, 825m, 789s, 705m, 410/400m (pyrazine ring vibrations).[23] The spectrum of the complex on the other hand shows a substantial decrease of the $\nu_{as}(CO_2^-)$ to 1665s, and an increase of the $\nu_s(CO_2^-)$ to 1377s (IR) and 1377m (Raman). This large separation between the two ν(CO) indicates the unidentate coordination to the metal atom as found for many metal complexes of carboxylic acids.[24–27] Vibrations related to the pyrazine moiety are slightly shifted to higher wave-numbers and appear at 1038m, 855m, 793m, 724m and 432w. These results are indicative of the existence of N,O-bidentate chelate pyrazinate anion. Hydrogen bonding of the type O—H···O in the free acid is indicated by the appearance of broad bands at *ca* 2500 cm^{-1} and at *ca* 1900 cm^{-1}.[28,29] The IR spectrum of the complex shows a strong broad band with several peaks at 3506, 3412, 3354 and 3279 cm^{-1}, due to hydrogen bonded aqua ligands.

The $\nu_{as}(N_3)$ mode appears as a very strong band

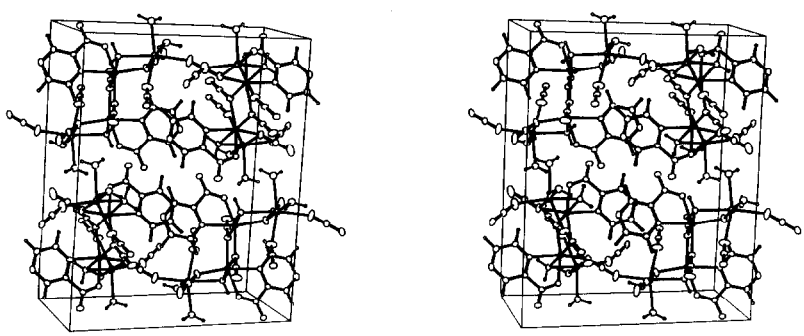

Fig. 2. Stereoplot of the unit cell viewed along the a axis.

at 2086 cm^{-1} together with a shoulder around 2020 cm^{-1}. In the Raman spectrum no band is observed in this region. Considering the significant difference between the two N—N distances (Δd) in each azide group (Table 2), the peak at 2086 cm^{-1} can be assigned to the azide group N(21)—N(22)—N(23b) ($\Delta d = 0.058$ Å) and the shoulder at 2020 cm^{-1} to the more symmetric N(11)—N(12)—N(13e) ($\Delta d = 0.015$ Å) group. The strongest band in the Raman spectrum at 1356 cm^{-1} and the corresponding medium strong band at 1353 cm^{-1} in the IR are associated with the symmetric stretch vibration mode of the azide ligand.[30,31] This is an expected result since the $\nu_s(N_3)$ mode is IR-inactive for entirely symmetrical azide ion. Thus while intensity considerations of such stretch vibration modes are valuable in assigning the slight asymmetric nature of both azide groups, they are of no value in determining the mode of bonding of these azides, i.e. whether they are terminal, $\mu(1,1)$-, $\mu(1,3)$-, or $\mu(1,1,3)$-bridging.

In the far-IR region, we tentatively assign to the metal-ligand vibrations the following frequencies:[32] 407sh and 375vw to ν(Mn—O(H_2O)]; the bands are 291m and 268m to ν(Mn—N(N_3)]; the bands at 314m (at 315 in the Raman spectrum) and 238s to ν[Mn—O(pyz)] and ν[Mn—N(pyz)], respectively. The metal-nitrogen vibrations are also found in the Raman spectrum at 285, 265 and 245 cm^{-1}, respectively.

Acknowledgement—The authors thank Prof. Ch. Kratky for the use of experimental equipment.

REFERENCES

1. J. Reedijk, in *Comprehensive Coordination Chemistry* (Edited by G. Wilkinson, R. D. Gillard and J. A. McCleverty), Vol. II, pp. 79–80. Pergamon Press, Oxford (1987).
2. B. Elman, A. G. S. Hogberg, M. Weber and M. Muhammed, *Polyhedron* 1985, **4**, 1197.
3. B. Elman, A. G. S. Hogberg, C. Moberg and M. Muhammed, *Polyhedron* 1986, **5**, 1917.
4. I. Csoregh, B. Elman, A. G. S. Hogberg, C. Moberg and M. Negren, *Inorg. Chem.* 1988, **27**, 235.
5. R. W. Matthews and R. A. Walton, *Inorg. Chem.* 1971, **7**, 1433.
6. M. A. S. Goher, M. A. M. Abu-Youssef, F. A. Mautner and A. Popitsch, *Polyhedron* 1992, **11**, 2137.
7. M. A. S. Goher, R.-J. Wang and T. C. W. Mak, *Polyhedron* 1992, **11**, 837.
8. N. Walker and D. Stuart, *Acta Cryst.* 1983, **A39**, 158.
9. G. M. Sheldrick, SHELX-76, *A Program for Crystal Structure Determination*. University Chemical Laboratory, Cambridge (1976).
10. G. M. Sheldrick, SHELXS-86. Universität Göttingen, F.R.G. (1986).
11. A. L. Spek, in *Computational Crystallography* (Edited by D. Sayre), p. 528. Clarendon Press, Oxford (1982).
12. J. M. Stuart, The X-RAY SYSTEM, version of 1976, Technical Report TR-466. University of Maryland, College Park (1976).
13. *International Tables for X-Ray Crystallography*, Vol. IV, pp. 99 and 149. Kynoch Press, Birmingham (1974).
14. Z. Dori and R. F. Ziolo, *Chem. Rev.* 1973, **73**, 247.
15. L. Casella, M. Gukkotti, G. Pallanza and M. Buga, *Inorg. Chem.* 1991, **30**, 221.
16. T. Rojo, J. I. R. Larramendi, I. Duran, J. L. Mesa, J. Via and M. I. Arriortua, *Polyhedron* 1990, **9**, 2693; O. L. Casagrande, Jr, S. I. Klein, A. E. Mauro and K. Tomita, *Trans. Met. Chem.* 1989, **14**, 45.
17. I. Agrell, *Acta Chem. Scand.* 1966, **20**, 1281.
18. I. Agrell, *Acta Chem. Scand.* 1969, **23**, 1667.
19. M. A. S. Goher, R.-J. Wang and T. C. W. Mak, *J. Mol. Struct.* 1991, **243**, 179.
20. R. Mason, G. A. Rasholme, W. Beck, H. Engelmann, K. Joos, B. Lindenberg and H. S. Smedal, *J. Chem. Soc., Chem. Commun.* 1971, 496.
21. M. A. S. Goher and F. A. Mautner, *Croat. Chem. Acta* 1990, **63**, 559.
22. M. S. Poonia and A. V. Bajaj, *Chem. Rev.* 1979, **79**, 389 and references therein.
23. J. Bus, Th. J. Liefkens and W. Schwaiger, *Recl. Trav. Chim. Pays-Bas* 1973, **92**, 123.
24. A. L. Magri, A. D. Magri, F. Balestrieri, E. Cardarelli, G. D'Ascenzo and E. Chiacchierini, *Thermochim. Acta* 1980, **38**, 225.
25. J. R. Allan, A. D. Paton, K. Turvey, H. J. Bowley and D. L. Gerrad, *Inorg. Chim. Acta* 1987, **132**, 41.
26. C. L. Klein, L. M. Trefonas, J. C. O'Conner and R. J. Majeste, *Cryst. Struct. Commun.* 1981, **10**, 891.
27. J. C. O'Conner and E. K. K. Sinn, *Inorg. Chem.* 1981, **20**, 545.
28. I. Nakagawa and T. Shimanouchi, *Spectrochim. Acta* 1964, **20**, 429.
29. L. S. Gelfand, L. L. Pytlewsky, A. N. Speca, C. M. Mikulsky and N. M. Karayannis, *J. Inorg. Nucl. Chem.* 1980, **42**, 209; H. Stammreich and K. Forneris, *Spectrochim. Acta* 1960, **16**, 363.
30. I. Agrell, *Acta Chem. Scand.* 1971, **25**, 2965.
31. M. A. S. Goher, *Acta Chim. Hung.* 1990, **127**, 213.
32. K. Nakamoto, *Infrared and Raman Spectra of Inorganic and Coordination Compounds*. J. Wiley, New York (1978).

Polyhedron Vol. 12, No. 21, pp. 2563–2568, 1993
Printed in Great Britain

0277-5387/93 $6.00+.00
© 1993 Pergamon Press Ltd

SYNTHESIS AND CHARACTERIZATION OF BIS(UNDECATUNGSTOCUPRATE) LANTHANATES OF POTASSIUM

WU QINGYIN*

Department of Chemistry, Liaoning University, Shenyang, China

and

WANG ENBO and LIU JINGFU

Department of Chemistry, Northeast Normal University, Changchun, China

(*Received* 30 *April* 1993; *accepted* 12 *July* 1993)

Abstract—The complexes of $K_{17}Ln(CuW_{11}O_{39})_2 \cdot nH_2O$ (Ln = La, Ce, Pr, Nd, Sm, Eu, Gd, Dy, Ho, Yb) have been prepared by the stepwise acidification and the stepwise addition of materials. The products were characterized by elemental analysis, ion-exchange, conductometric titration, IR, UV, X-ray powder diffraction and thermal analysis. The results show that the structure of the products is similar to that of $Cs_{12}U(GeW_{11}O_{39})_2$. The thermal analysis indicated that the complexes with undecatungstocuprate heteropolyanion as a ligand had higher thermal stability than that of saturated Keggin structure dodecatungstocuprate.

The studies on the mixed heteropoly complexes are a frontal work in the basic studies on heteropoly compounds. Lanthanides can react with lacunar heteropolyanions $XW_{11}O_{39}$ (X = Si, P, As, Ga, Ge) to give bisundecatungstolanthanates. The structure of this kind of heteropolyanions is a square antiprism consisted of eight oxygen atoms of two $XW_{11}O_{39}$ heteropolyanions and a lanthanide ion.[1] These triheteropoly complexes containing lanthanide elements are efficient catalysts in some organic synthesis reactions.[2] However, there have been few reports on the heteropoly complexes with subgroup element-centred undecatungstate ligands. We describe here the synthesis and characterization of $K_{17}Ln(CuW_{11}O_{39})_2 \cdot nH_2O$ (Ln = La, Ce, Pr, Nd, Sm, Eu, Gd, Dy, Ho, Yb).

EXPERIMENTAL

Preparation

36.3 g (0.11 mol) of $Na_2WO_4 \cdot 2H_2O$ was dissolved in 200 cm^3 of water and the pH of the solution was adjusted to 6.3 with acetic acid. The solution was then heated to 90°C and a solution of 2.4 g (0.01 mol) $Cu(NO_3)_2 \cdot 3H_2O$ in 30 cm^3 of hot water was added dropwise with stirring. After the reaction proceeded for 35 min, a solution of 2.2 g (0.005 mol) $Ln(NO_3)_3$ in 25 cm^3 of water was added. The pH was readjusted to 5.6 and stirring was continued for 30 min. After cooling, the light yellow oil, which precipitated by adding absolute alcohol, was dissolved in a little water, then 25 g of KCl was added to it and the mixture was stirred for several minutes at room temperature. The oily product was cooled out and was left for a period of time until it solidified. There was no precipitation during the synthesis. The product was recrystallized from warm water three times and kept in a desiccator over P_2O_5. The yields were in the region of 20%.

Chemical analyses

Potassium was determined gravimetrically as the tetraphenylborate. The lanthanides were determined by EDTA volumetry with cresol orange as the indicator.[3] Copper was determined by atomic absorption spectrophotometry.[4] Tungsten was

* Author to whom correspondence should be addressed.

Table 1. The results of elemental analyses

Compound	Found (calc.) (%)				
	K	Ln	Cu	W	H_2O
$K_{17}La(CuW_{11}O_{39})_2 \cdot 33H_2O$	9.8 (9.7)	2.0 (2.0)	1.8 (1.9)	59.5 (59.3)	8.7 (8.7)
$K_{17}Ce(CuW_{11}O_{39})_2 \cdot 36H_2O$	9.7 (9.7)	2.0 (2.0)	1.8 (1.8)	58.9 (58.9)	9.3 (9.4)
$K_{17}Pr(CuW_{11}O_{39})_2 \cdot 30H_2O$	9.8 (9.8)	2.0 (2.1)	1.8 (1.9)	59.8 (59.8)	8.0 (8.0)
$K_{17}Nd(CuW_{11}O_{39})_2 \cdot 28H_2O$	9.8 (9.9)	2.1 (2.1)	1.9 (1.9)	59.9 (60.1)	7.4 (7.5)
$K_{17}Sm(CuW_{11}O_{39})_2 \cdot 34H_2O$	9.7 (9.7)	2.1 (2.2)	1.8 (1.9)	59.0 (59.1)	8.9 (8.9)
$K_{17}Eu(CuW_{11}O_{39})_2 \cdot 35H_2O$	9.7 (9.7)	2.2 (2.2)	1.8 (1.8)	59.0 (58.9)	9.1 (9.2)
$K_{17}Gd(CuW_{11}O_{39})_2 \cdot 28H_2O$	9.9 (9.8)	2.3 (2.3)	1.8 (1.9)	59.9 (60.0)	7.4 (7.5)
$K_{17}Dy(CuW_{11}O_{39})_2 \cdot 31H_2O$	9.7 (9.8)	2.4 (2.4)	1.8 (1.9)	59.4 (59.4)	8.1 (8.2)
$K_{17}Ho(CuW_{11}O_{39})_2 \cdot 30H_2O$	9.8 (9.8)	2.4 (2.4)	1.8 (1.9)	59.5 (59.6)	7.9 (8.0)
$K_{17}Yb(CuW_{11}O_{39})_2 \cdot 29H_2O$	9.8 (9.8)	2.5 (2.5)	1.8 (1.9)	59.6 (59.7)	7.6 (7.7)

determined by 8-hydroxy-quinoline-tannin acid-methylviolet gravimetry.[5] The water content was determined by thermogravimetry. The analytical results are presented in Table 1.

Physical measurements

IR spectra were obtained on an Alpha Centauri FT infrared spectrometer in the range 400–4000 cm^{-1} using KBr pellets. UV spectra were recorded on a DU–8B UV spectrophotometer. X-ray powder diffraction patterns were made with a D/max-IIIC diffractometer. Thermogravimetric experiments were conducted on a Q-Derivatograph thermal analyzer with a rate of temperature increase of 10°C min^{-1}. A P–E 3030 atomic absorption spectrophotometer, a pH S-2 acidimeter and a DDS-11A conductometer were also used.

RESULTS AND DISCUSSION

Stability and basicity

The stability of the solution of heteropoly complex $K_{17}Ce(CuW_{11}O_{39})_2 \cdot 36H_2O$ towards acid and base was investigated by spectrophotometry. The variation of absorbance of $K_{17}Ce(CuW_{11}O_{39})_2 \cdot 36H_2O$ at 253.3 nm under different pH values was measured. If the heteropolyanion was hydrolyzed at a pH value, its concentration and absorbance A would be changed accordingly. It can be seen from A-pH curve that the absorbance A is almost unchanged at pH = 3.6–6.2, indicating that the heteropoly complex is stable under such conditions.

The basicity of the heteropolyanions can be determined by conductometric titration. The conductometric titration curve of $K_{17}La(CuW_{11}O_{39})_2 \cdot 33H_2O$ is shown in Fig. 1. The result shows that at end point of conductometric titration, $Ag^+/La(CuW_{11}O_{39})_2^{17-} = 16.8$. This value is close to the real value of 17. The basicity of $K_{17}La(CuW_{11}O_{39})_2 \cdot 33H_2O$ is 16.8.

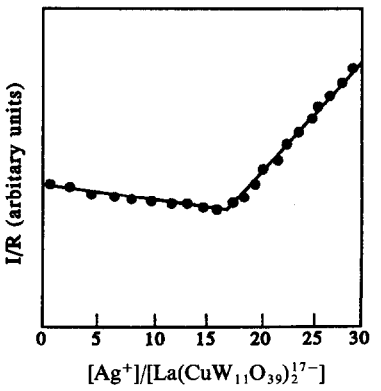

Fig. 1.

Ion-exchange experiment

In order to prove lanthanides to be inside the coordination sphere, we performed ion-exchange experiments. Before and after the experiment of ion-exchange on a column fitted with the resin of K^+ type, the colour of the solution, the characteristic peak of UV and chemical composition were almost unchanged. This indicates that after ion-exchange Ln^{3+} and Cu^{2+} ions are not replaced, showed Ln^{3+} and Cu^{2+} ions to be inside the heteropolyanion, unlike balance ions or free ions. After ion-exchange on a bed fitted with the resin of H^+ type, it was found that the IR spectrum of $K_{17}Pr(CuW_{11}O_{39})_2 \cdot 30H_2O$ before elution is obviously different from that of $K_{17}Pr(CuW_{11}O_{39})_2 \cdot 30H_2O$ after elution (Fig. 2), indicating the heteropolyanions are being decomposed.

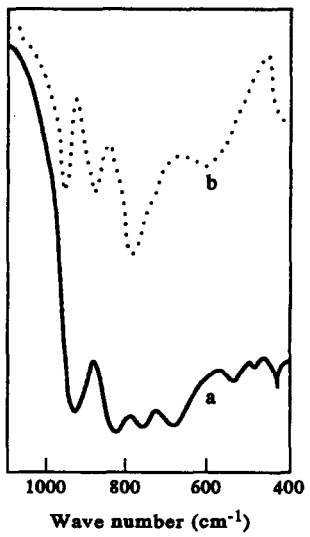

Fig. 2.

IR spectra

The observed frequencies of the complexes and the tentative assignments of the main absorption bands are listed in Table 2.

The following conclusions can be drawn from Table 2.

(i) After the formation of $Ln(CuW_{11})_2$, the structural symmetry is reduced, i.e. from Td of CuW_{12} to D_{4d} due to the coordination effect. In $Ln(CuW_{11})_2$, Ln^{3+} does not occupy the original position, but is bonded to the four oxygen atoms surrounding the hole. The formation of Ln—O bond destroys the symmetry of Keggin structure and a big distortion takes place.

(ii) Comparing $Ln(CuW_{11})_2$ with CuW_{12}, both $\nu_{as}(W—O_d)$ and $\nu_{as}(W—O_b—W)$ are lower, because the coordination of Ln^{3+} by O_b and O_c causes electronic cloud transfer of O_d in the direction of $O_d—W—C_c(O_b)$ and the density reduction of electronic cloud of $O_d—W$ bond, changing the force constant of the bond and making the frequency reduced.[6] Compared with CuW_{12}, $\nu_{as}(W—O_b—W)$ is not split, while $\nu_{as}(W—O_c—W)$ is split, because the unsaturated heteropolyanion is a four-dentate ligand and Ln^{3+} bonds to both O_b and O_c. In addition to the coordination bond, there is also an electrostatic force between Ln^{3+} and O_c (or O_b) due to the higher charges of Ln^{3+}, which attracts the oxygen atoms nearby. In Keggin structure, $W—O_c—W$ does not combine as firmly as $W—O_b—W$ does and under the influence of Ln^{3+}, $W—O_c—W$ distorts easily, so that the symmetry turns lower, causing the split of the band.[7]

(iii) The $\nu_{as}(W—O_d)$ vibrational frequencies of samples are similar to each other but change in

Table 2. IR data (cm^{-1})

Complex	$\nu_{as}(W—O_d)$	$\nu_{as}(W—O_b—W)$	$\nu_{as}(W—O_c—W)$	$\nu_{as}(Cu—O)$ or $\delta(O—Cu—O)$
$La(CuW_{11})_2$	943.1	847.7	791.7, 711.7	538.1, 476.4, 413.7
$Ce(CuW_{11})_2$	936.7	841.7	787.2, 706.9	536.7, 467.9, 417.6
$Pr(CuW_{11})_2$	937.4	843.8	787.9, 712.7	537.1, 476.9, 414.7
$Nd(CuW_{11})_2$	937.4	846.7	789.8, 708.8	538.1, 483.3, 413.3
$Sm(CuW_{11})_2$	941.5	847.1	790.0, 710.4	538.0, 481.6, 418.5
$Eu(CuW_{11})_2$	935.4	844.8	786.9, 705.9	542.0, 483.1, 423.4
$Gd(CuW_{11})_2$	935.1	844.5	786.9, 709.0	535.8, 478.5, 415.9
$Dy(CuW_{11})_2$	936.1	846.1	788.6, 709.6	536.6, 480.5, 417.3
$Ho(CuW_{11})_2$	937.6	846.8	788.1, 710.6	538.2, 478.9, 419.3
$Yb(CuW_{11})_2$	939.1	847.3	788.8, 711.3	540.9, 480.1, 424.1

Table 3. UV data (nm)

Complex	$O_d \rightarrow W$	$O_b/O_c \rightarrow W$
$La(CuW_{11})_2$	193.3	253.6
$Ce(CuW_{11})_2$	193.5	253.3
$Pr(CuW_{11})_2$	197.5	254.1
$Nd(CuW_{11})_2$	195.0	253.5
$Sm(CuW_{11})_2$	201.7	253.3
$Eu(CuW_{11})_2$	195.5	254.1
$Gd(CuW_{11})_2$	198.2	253.5
$Dy(CuW_{11})_2$	196.1	253.4
$Ho(CuW_{11})_2$	197.1	254.1
$Yb(CuW_{11})_2$	197.6	253.8

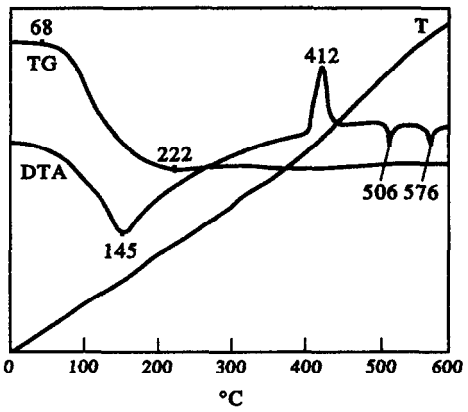

Fig. 3.

fluctuation. The general tendency is that the change of $\nu_{as}(W—O_d)$ increases with the increased atomic number of Ln^{3+}, so does $\nu_{as}(W—O_b—W)$. This is due to the effect of the periodical arrangement of electrons and the lanthanide contract.

UV spectra

There is a strong absorption band in UV region resulting from the $p\pi$–$d\pi$ transition of W—O bonds in polyacid complexes. Two absorption peaks appear in the UV region for $Ln(CuW_{11})_2$, of which one with a higher energy is assigned to $O_d \rightarrow W$ charge transition, and the other wth a lower energy to O_b(or O_c)$\rightarrow$W charge transition.[8] The UV spectra are listed in Table 3.

Compared with those of CuW_{12}, the bands of charge transition are shifted to short wave and high energy field.[9] This is due to the increase of negative charge density.

X-ray powder diffraction

X-ray diffraction analysis is used extensively to study the structure of heteropoly complexes. The data of X-ray powder diffraction of some products synthesized are listed in Table 4.

It can be seen that the data of X-ray diffraction of the products synthesized are similar. The intensities and positions of the diffraction peaks are similar to those of $Cs_{12}U(GeW_{11}O_{39})_2$. This is consistent with the conclusion of reference.[10]

Thermal stability

In general, we take the temperature of the exothermic peak of DTA curves as the sign of thermal

Table 4. XRD data of some products synthesized

$Nd(CuW_{11})_2$			$Sm(CuW_{11})_2$			$Dy(CuW_{11})_2$		
$2\theta°$	d (Å)	I/I_0	$2\theta°$	d (Å)	I/I_0	$2\theta°$	d (Å)	I/I_0
8.60	10.273	15	8.56	10.321	22	8.56	10.321	36
9.44	9.361	21	9.38	9.420	30	9.38	9.420	42
9.92	8.909	37	9.88	8.945	53	9.88	8.945	57
10.10	8.750	49	10.06	8.785	59	10.02	8.820	69
10.50	8.418	21	10.48	8.434	20	10.46	8.450	25
10.84	8.155	46	10.80	8.185	41	10.74	8.230	25
12.38	7.145	30	12.58	7.030	33	11.92	7.418	47
13.30	6.651	100	13.36	6.622	100	13.44	6.582	100
26.80	3.323	26	26.96	3.304	35	27.14	3.282	42
28.22	3.159	12	28.32	3.148	20	28.28	3.153	20
29.42	3.033	39	29.38	3.037	30	29.42	3.033	23
31.46	2.841	40	31.62	2.827	44	31.86	2.806	29
33.68	2.658	22	33.88	2.643	23	34.12	2.625	31

Table 5. DTA data for the complexes (°C)

Complex	Endotherms	Exotherms
$La(CuW_{11})_2$	93, 500, 580	407
$Ce(CuW_{11})_2$	106, 505, 580	407
$Pr(CuW_{11})_2$	96, 500, 574	409
$Nd(CuW_{11})_2$	96, 505, 580	406
$Sm(CuW_{11})_2$	145, 506, 576	412
$Eu(CuW_{11})_2$	98, 500, 580	408
$Gd(CuW_{11})_2$	100, 502, 575	406
$Dy(CuW_{11})_2$	105, 500, 580	406
$Ho(CuW_{11})_2$	97, 501, 575	409
$Yb(CuW_{11})_2$	100, 502, 580	411

stability of heteropoly complexes. The thermogram of $Sm(CuW_{11})_2$ is shown in Fig. 3 and DTA data of $K_{17}Ln(CuW_{11}O_{39})_2 \cdot nH_2O$ are listed in Table 5.

It can be shown from the thermogram that all $Ln(CuW_{11})_2$ show weight loss by one step. Before 250°C there is a continuous weight loss process corresponding to a big endothermal peak. The IR spectra at different temperatures and solubility tests show that under such conditions the heteropoly complexes did not decompose, so the weight loss because of absorbing heat could be assigned to the loss of zeolite water or the water weakly bonded to balancing-ions and the water between $Ln(CuW_{11})_2$. At a higher temperature (above 500°C) the two endothermal peaks on the DTA curve can be assigned to the crystallization or melting of decomposed products.

Both the formation of bridge bond W—O—W and the existence of $W{=}O_d$ with partial double bond are the sign of the formation of heteropoly complexes. The change of these bonds can be tested by IR spectra at different temperatures and by solubility experiments. The IR spectra of $Sm(CuW_{11})_2$ at different temperatures are shown in Fig. 4 and the results of solubility experiments of $K_{17}Sm(CuW_{11}O_{39})_2 \cdot 34H_2O$ at different temperatures are listed in Table 6. The decomposing temperature is 350–400°C. As can be seen from Table 5 the thermal stability of the complexes with undecatungstocuprate heteropolyanion as ligand is higher than that of saturated Keggin structure dodecatungstocuprate.

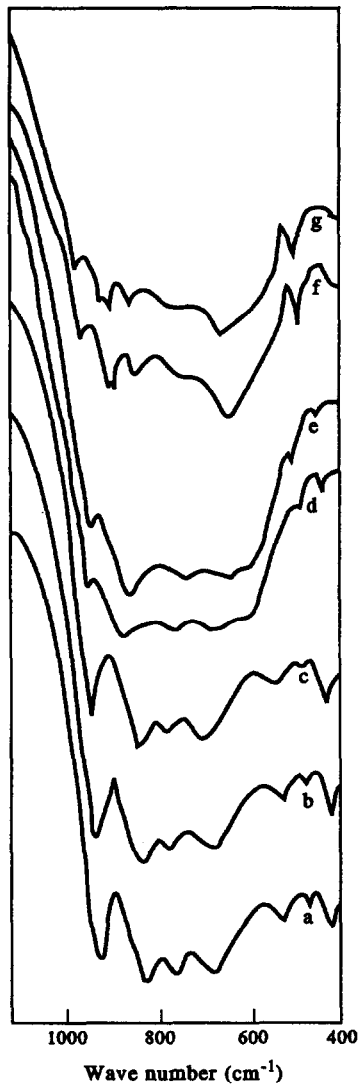

Fig. 4.

Acknowledgement—This work was supported by the National Natural Science Foundation of China.

REFERENCES

1. (a) R. D. Peacock and T. J. R. Weakley, *J. Chem. Soc. (A)* 1971, 1836; (b) S. A. Zubairi, S. M. Ifzal and A. Malik, *Inorg. Chim. Acta* 1977, **22**, L29; (c) Liu Jingfu, Rong Chaoying and Wang Enbo, *Chem. J. Chin. Univ.* 1986, **7**, 565; (d) Rong Chaoying, Liu Jingfu, Chen Xin and Wang Enbo, *Inorg. Chim. Acta*

Table 6. The solubility of $Sm(CuW_{11})_2$ with various temperature

Temperature	100	200	300	320	350	380	400	420
Solubility	sol.	sol.	sol.	sol.	some	some	insolu.	insolu.

1987, **130**, 265; (e) Liu Jingfu, Zu Zhiping, Zhao Benliang and Liu Zhao, *Inorg. Chim. Acta* 1989, **164**, 179.
2. Wu Zhiyun, Zhao Zhongqing, Li Kai and Zheng Qiang, *Chem. J. Chin. Univ.* 1985, **6**, 459.
3. Wu Qingyin, Wang Enbo and Zhou Yanxiu, *J. Chin. Rare Earth Soc.* 1990, **8**, 209.
4. Wang Enbo, Wu Qingyin, Zhang Baojian and Huang Rudan, *Trans. Met. Chem.* 1991, **16**, 478.
5. Wu Qingyin, Wang Enbo and Zhou Yanxiu, *Chin. Sci. Bull.* 1990, **35**, 2052.
6. D. H. Brown, *Spectrochim. Acta* 1963, **19**, 585.
7. M. T. Pope, *Inorg. Chem. Concepts* 1983, 248.
8. H. So and M. T. Pope, *Inorg. Chem.* 1972, **11**, 1441.
9. Wu Qingyin and Wang Enbo, *Zh. Neorgan. Khim.* 1992, **37**, 1547.
10. C. M. Tourne, G. F. Tourne and M. C. Brianso, *Acta Cryst. Sect. B* 1980, **36**, 2012.

Polyhedron Vol. 12, No. 21, pp. 2569–2575, 1993
Printed in Great Britain

0277–5387/93 $6.00+.00
© 1993 Pergamon Press Ltd

PREPARATION OF SOME MIXED CHLORO-CATECHOLATE AND CHLORO-OXO-CATECHOLATE COMPLEXES OF HIGH OXIDATION STATE TUNGSTEN AND MOLYBDENUM

CHRISTINA PERSSON and CARLAXEL ANDERSSON*

Department of Inorganic Chemistry 1, Chemical Centre, University of Lund, P.O. Box 124, S 221 00 Lund, Sweden

(*Received* 27 *April* 1993; *accepted* 12 *July* 1993)

Abstract—9,10-Phenanthrenequinone (phq) reacts with WCl_4(DME) and $MoCl_4(OEt_2)_2$ to give the complexes tetrachloro[9,10-phenanthrenediolato(2−)-O,O′]tungsten(VI) and tetrachloro[9,10-phenanthrenesemiquinonato(1−)-O,O′]molybdenum(V), respectively; and with the oxohalide complexes $MOCl_3$(DME) (M = Mo, W) to give the complexes trichlorooxo[9,10-phenanthrenequinone-O,O′]molybdenum(V) and trichlorooxo[9,10-phenanthrenesemiquinonato(1−)-O,O′]tungsten(VI).

Tetrachloro[3,4,5,6-tetrachloro-1,2-benzenediolato(2−)-O,O′]molybdenum(VI) is obtained in less than 50% yield by reaction of tetrachloro-1,2-benzoquinone (tcq) with $MoCl_5$, and tetrachloro[3,4,5,6-tetrachloro-1,2-benzenediolato(2−)-O,O′]tungsten(VI) is obtained in quantitative yield by reaction of WCl_6 with tcq, concomitant with oxidation of the toluene solvent.

Tetrachloro[9,10-phenanthrenesemiquinonato(1−)-O,O′]molybdenum(V) reacts with *t*-$BuOSiMe_3$ to give dichlorooxo[1,1-oxybis(ethane)][9,10-phenanthrenediolato(2−)-O,O′] molybdenum(VI).

Based on analytical, IR and magnetic data suggested assignments of formal oxidation states of the metal and the quinone ligands in the complexes are presented.

Research in the field of high-valent organometallic chemistry has resulted in the development of highly effective olefin metathesis catalysts of molybdenum,[1,2] tungsten,[3] and rhenium.[4] Hard donors, e.g. oxo, imido, alkoxy, and aryloxy groups, which stabilize the high oxidation state of the metal, are recurrent auxiliary ligands in high valent organometallic complexes. The steric and electronic properties of the auxiliary ligands can to some extent be used to tune the catalytic properties of a particular complex. This is nicely demonstrated by the $(RO)_2M(NR')(=CH-R'')$ [M = Mo, W; R″ = *t*-Bu, NR′ = 2,6-di-*iso*-propylaniline, R = *t*-Bu or $CMe(CF_3)_2$] class of metathesis catalysts.[2,5]

Catechols/quinones are ligands of significance in biological redox systems.[6,7] By their ability to coordinate metal ions in the quinone, semiquinone, or catecholate form[8,9] this class of ligands spans a wide range of electronic properties. Redox properties of the quinones/catechols are also influenced by the ligand substituents. Moreover, the steric requirements of catecholate/quinone ligands can be varied extensively.

Phenoxide complexes of tungsten have been used as catalyst precursors in the metathesis of olefins[10,11] and an alkylation of mixed chloro-phenoxide complexes of tungsten have lead to the isolation of catalytically active tungsten alkylidene complexes.[12–14] Following this line of research we have been interested in the preparation of mixed chloro-catecholate complexes of the type (cat)MCl_4 (M = Mo, W; cat = catecholate, semiquinone, or quinone) and to use these as starting materials for further syntheses. In particular the known method to convert halide complexes to imido complexes[15] or the alkylation of such precursors have been considered of interest. In this paper we present the preparations of some mixed chloro-catecholate and some mixed oxo-chloro catecholate complexes.

* Author to whom correspondence should be addressed.

RESULTS AND DISCUSSION

Known methods to prepare catecholate complexes include alcoholysis of metal-halides with catechol,[16,17] condensation of catechols with metal-oxo groups,[18] and the oxidative addition of quinones to low valent metal complexes.[19,20] The reactions of quinones with homoleptic metal carbonyl complexes have been used frequently to prepare catecholate complexes of tungsten and molybdenum.[21-24] The term oxidative addition is often used for this reaction although the reaction is better characterized as an oxidative substitution since the coordination number remains intact.

We have recently described the syntheses of WCl_4L_2 and $MoCl_4L_2$ (L = monodentate ether; L_2 = bidentate ether).[25] These complexes are labile and the ether ligands are easily displaced by other ligands. Since an oxidation from the +IV oxidation state to the +VI oxidation state seemed within reach using quinones as entering ligands these complexes were considered as suitable starting materials for the syntheses of complexes of the general formulation MCl_4(cat). The present study has been limited to tetrachloro-1,2-benzoquinone and 9,10-phenanthrenequinone as entering ligands. In the following the abbreviations tcq = tetrachloro-1,2-benzoquinone, tcsq = tetrachloro-1,2-benzosemiquinone, tcc = tetrachlorocatecholate and phq = 9,10-phenanthrenequinone, phsq = 9,10-phenanthrenesemiquinone, phc = 9,10-phenanthrenecatecholate are used to denote the oxidation states of these ligands.

$MCl_4(L_2)$ [M = Mo, W, L = THF, Et_2O, L_2 = DME (*dimethoxyethane*)] *as starting material*

WCl_4(DME) and $MoCl_4(OEt_2)_2$ react smoothly in CH_2Cl_2 solution at room temperature with an equimolar amount of phq to furnish the complexes WCl_4(phc) (**1**) and $MoCl_4$(phsq) (**2**) as dark microcrystalline powders. The yields [(**1**) = 79%; (**2**) = 87%] are high and the complexes are obtained in analytically pure state by filtration and washing with diethyl ether. These are the only cases where the oxidative substitution reaction have led to well-defined products.

All attempts to react $WCl_4(THF)_2$ with 9,10-phenanthrenequinone gave crude products showing a strong IR band at 962 cm^{-1}, which is not present in (**1**). Tungsten(V) is very prone to abstract oxygen from THF[25-27] and the IR band at 962 cm^{-1} is most likely a terminal tungsten-oxo stretching vibration resulting from an oxygen abstraction from THF. A reaction path involving an initial substitution and a one-electron oxidation of the tungsten atom with subsequent abstraction of an oxygen atom from THF is a possible reason for the formation of a tungsten–oxygen bond.

Likewise, none of the precursor complexes, i.e. WCl_4(DME), $WCl_4(THF)_2$, $MoCl_4$(DME) or $MoCl_4(OEt_2)_2$ is suitable for reactions with tetrachloro-1,2-benzoquinone. Nothing but an ill-defined mixture of products has been obtained independent of solvent and reaction conditions applied. A more complex reaction pattern than a single oxidative addition is likely and has been observed in a similar context,[28] i.e. in the reaction of the acetylene complex $WCl_4(C_2I_2)$ with tcq.

Syntheses of tetrachloroquinone complexes from $WCl_5(OEt_2)$, $MoCl_5$ *and* WCl_6

The failure of the attempted oxidative substitution reaction to give the target substances in the case of tcq indicate that the redox chemistry involved is complicated. To elaborate somewhat on the redox chemistry some further experiments, with limited prospects of being synthetically useful, were carried out using precursors in oxidation states +V and +VI.

Dark, olive-green crystals of a compound analysing as $MoCl_4$(tcc) (**3**) were obtained in slightly less than 50% yield by reaction of $MoCl_5$ suspended in CH_2Cl_2 with tcq. Similarly, the reaction of $WCl_5(OEt_2)$ with tcq in CH_2Cl_2 gave, after work up, a low yield (< 20%) of a compound which by IR spectroscopy was shown to be identical to WCl_4(tcc) (**4**). The formation of (**4**) in the reaction between $WCl_5(OEt_2)$ and tcq is accompanied by the formation of small amounts of WCl_6. Based on the low yields (less than 50%) of complexes (**3**) and (**4**) together with the identification of WCl_6 in the reaction with $WCl_5(OEt_2)$ it can be suggested that the chemistry involved may be described by the net disproportionation reactions:

$$2WCl_5 + tcq \longrightarrow WCl_4(tcc) + WCl_6 \quad (1)$$

$$2MoCl_5 + tcq \longrightarrow MoCl_4(tcc) + \text{“Mo(VI)”}. \quad (2)$$

Most likely, eqs (1) and (2) do not completely describe the situation. IR spectra run on the solid residues obtained after isolation of the metal complexes show strong absorption peaks in the range 1775–1716 cm^{-1}. C—O stretching frequencies in that range are usually found in organic carbonyl compounds having two chlorine substituents at the α-carbon atom. The observed high frequency peaks may therefore indicate that a reaction involving oxidation of tcq also occurs.

A possible way to make the reactions more synthetically useful i.e. to avoid the disproportionation of the metal and/or the oxidation of tcq would be the use of a solvent with reducing properties which could act as chlorine acceptor. In the case of the M(V) precursors efforts in that direction have been discouraging. A complex, formulated as $MoCl(tcc)_2$ on the basis of elemental analysis, is formed in the reaction of $MoCl_5$ with tcq using toluene as solvent. Based on the diamagnetism of this complex it is most likely a dimer $[MoCl(tcc)_2]_2$ (**5**). The formation of chlorotoluene, as observed by GC–MS analyses on the volatile reaction products, shows that toluene acts as reducing agent. Aromatic compounds, e.g. benzene[29,30] or toluene,[31] have been used previously as reducing agents in the preparation of $MoCl_4$ and complexes thereof.

The synthetic feasibility of the concept of reducing solvents is, however, nicely demonstrated by the preparation of WCl_4(tcc) (**4**) from WCl_6. WCl_6 reacts in toluene suspension at room temperature with an equimolar amount of tcq to give (**4**) in a quantitative yield. This reaction can also be carried out in benzene, although benzene is not as easily oxidized as toluene and the reaction is considerably slower in this solvent. The oxidized products found by GC–MS analyses of the volatile reaction products using toluene or benzene as solvent are chlorotoluene (two isomers) and chlorobenzene, respectively. It is noteworthy that the chlorination of toluene does not give benzylchloride. This indicates that the reducing solvents are not acting as chlorine radical acceptors but that their participation in the reaction sequence follow another reaction pathway.

Reactions of phenanthrenequinone with $MOCl_3$(DME) (M = Mo, W) *and synthesis of* $MoOCl_2$(phc)(OEt_2)

The formal oxidation state (see below) of the metals and thereby of the phenanthrenequinone ligands differs in complexes WCl_4(phc) (**1**) and $MoCl_4$(phsq) (**2**); **1** is a catecholate complex of tungsten(VI) while **2** is a semiquinonate complex of molybdenum(V). This difference prompted attempts to prepare phenanthrenequinone complexes of M(+V) oxohalides from the easily accessible starting materials $WOCl_3$(DME) and $MoOCl_3$(DME). Both starting materials react straightforwardly with phq in CH_2Cl_2 at room temperature affording the complexes $WOCl_3$(phsq) (**6**) and $MoOCl_3$(phq) (**7**) in high to fair yield. The formal oxidation state of the metal and the quinone ligands of these complexes will be discussed below.

Chloro complexes of tungsten and molybdenum in the +V oxidation state are easily converted to the corresponding oxochloride complexes using oxygen transfer reagents as $Me_3SiOSiMe_3$[32,33] or *t*-BuO-$SiMe_3$.[33] It was considered of interest to apply this kind of oxygen-transfer reaction on the catecholate complexes in the present study, especially in relation to the different oxidation states assigned to the metal in complexes (**1**) and (**2**). The molybdenum complex (**2**) reacts smoothly with *t*-$BuOSiMe_3$ in the presence of diethyl ether to give $MoOCl_2$(phc)(OEt_2) (**8**) in high isolated yield. The corresponding reaction using the tungsten complex (**1**) is considerably more sluggish and no well-defined products were isolated despite several attempts. IR spectroscopic investigations of the solids isolated in the reactions of the tungsten complex showed the presence of $OSiMe_3$- groups in the product, indicating that the reaction does not go to completion. This difference in reactivity may be a reflection of the different oxidation states of the starting materials, Mo(V) and W(VI), respectively; the formation of the molybdenum-oxo group in complex (**8**) is accompanied by an oxidation of the molybdenum atom and a reduction of phsq to phc.

Formal oxidation states of the quinone ligands and the metals in the complexes

Elemental analysis data for the complexes (**1–8**) are given in Table 1. The complexes have also been subjected to analysis by mass-spectroscopy. Spectra run in the FAB^+ mode in ethylene glycol matrix are non-informative while fragments of the molecules can be observed in the EI spectra (70 eV) (Table 2). The molecular ion peaks of the complexes, which appear as the $[M+1]^+$ ion, are usually very weak or not at all observable. A ready elimination of chloro ligands and ligand redistribution reactions in the spectrometer are common features observed in the mass spectra of these types of complexes.

The oxidation state of the metal and the quinone, semiquinone, or catecholate character of the ligand is one important question relating to the complexes prepared in the present study. As observed in a large number of structurally characterized catecholate complexes,[8] the oxidation state of the ligand is reflected in the C—O bonding distance of the ligand. X-ray quality single crystals for either of complexes (**1–8**) have, however, not been obtained, so the discussion on oxidation states must be based on other observations.

The stretching frequency of the C—O bond in quinones has been used to distinguish between different modes of quinone coordination.[9] The IR bands observed for complexes (**1–2**) and (**4–8**) are

Table 1. Analytical data

		Analysed % (Calculated %)			
		C	H	Cl	M
1	WCl_4(phc)	31.9 (31.5)	1.6 (1.5)	25.4 (26.6)	34.3 (34.4)
2	$MoCl_4$(phsq)	36.9 (37.7)	1.9 (1.8)	31.3 (31.8)	21.2 (21.5)
3	$MoCl_4$(tcc)	15.2 (14.9)	—	58.2 (58.6)	19.6 (19.8)
4	WCl_4(tcc)	12.6 (12.6)	—	49.1 (49.6)	32.1 (32.2)
5	$[MoCl(tcc)_2]_2$	23.2 (23.1)	—	50.6 (51.2)	15.8 (15.4)
6	$WOCl_3$(phsq)	33.4 (32.7)	1.8 (1.6)	20.8 (20.7)	34.7 (35.6)
7	$MoOCl_3$(phq)	39.5 (39.4)	1.9 (1.9)	24.8 (24.9)	22.9 (22.5)
8	$MoOCl_3$(phc)(OEt_2)	45.8 (46.5)	4.0 (3.9)	15.5 (15.2)	20.3 (20.6)

given in the Experimental section and the values of ν_{M-Cl} and $\nu_{M=O}$ in Table 2. For the complex $MoOCl_3$(phq) (**7**) a band at 1627 cm^{-1} of medium intensity is observed; it is shifted 47 cm^{-1} relative to the C—O stretching frequency of free phq. This band can rather safely be assigned to a C—O stretching band[9] and the phq ligand in complex (**7**) is therefore coordinated in its quinone form giving the metal a formal oxidation state of +V. Complex (**7**) is the only one which by IR criteria can be stated to contain the ligand in its quinone form; the absence of bands at wavenumbers above 1600 cm^{-1} in the IR spectra of all the other complexes indicate that these contain the ligands in their reduced semiquinone or catecholate state.

Magnetic susceptibility and magnetic moments for the complexes are collected in Table 3. The compounds WCl_4(phc) (**1**), $MoCl_4$(tcc) (**3**), WCl_4(tcc) (**4**) and $MoOCl_2$(phc)(OEt_2) (**8**) are diamagnetic and can therefore be formulated as catecholate complexes of molybdenum and tungsten in the +VI oxidation state (d^0). The dimeric complex $[MoCl(tcc)_2]_2$ (**5**) is also diamagnetic, indicating that this is a catecholate complex of

Table 2. Spectroscopic data

		MS [EI (70 eV)]			IR (cm^{-1})	
Compound		Fragment[a]	m/z[b]	(%)	M—Cl	M=O
1	WCl_4(phc)	{WCl(phq)}	429	(10)	394 376 327	
2	$MoCl_4$(phsq)	$\{MoOCl_2(phq)\}$	392	(7)	385 374 328	
		$\{2\text{-}C_6H_5\}$	368	(17)		
		{MoCl(phq)}	339	(3)		
3	$MoCl_4$(tcc)	$\{MoOCl_2(tcc)\}$	428	(2)	No IR spectrum obtained	
4	WCl_4(tcc)	$\{WCl_2(tcc)_2\}$	746	(100)	401 388 349	
		$\{WCl(tcc)_2\}$	712	(8)		
		$\{WCl_4(tcc)\}$	572	(20)		
		$\{WCl_3(tcc)\}$	536	(25)		
		$\{WCl_2(tcc)\}$	500	(70)		
		$\{WOCl_2(tcc)\}$	516	(80)		
		{WCl(tcc)}	465	(25)		
5	$[MoCl(tcc)_2]_2$	No assignable peaks			370	
6	$WOCl_3$(phsq)	$\{WCl_2(phq)_2\}$	672	(35)	366 350 339	995
		$\{WOCl_2(phq)\}$	480	(80)		
7	$MoOCl_3$(phq)	$\{MoOCl_2(phq)\}$	392	(65)	383 376 351 341	993
		{MoOCl(phq)}	357	(8)		
8	$MoOCl_2$(phc)(OEt_2)	$\{MoOCl_2(phq)\}$	392	(15)	358 336	962

[a] In the fragments, the abbreviations phq and tcc are used regardless of the oxidation state of the ligand.

[b] The most significant peak in the cluster of isotope peaks.

Table 3. Magnetic properties[a]

Compound		$\chi_M/10^{-5}$ (m^3/kmol)	μ_{eff}
1	WCl_4(phc)	Diamagnetic	
2	$MoCl_4$(phsq)	3.430	254
3	$MoCl_4$(tcc)	Diamagnetic	
4	WCl_4(tcc)	Diamagnetic	
5	$[MoCl(tcc)_2]_2$	Diamagnetic	
6	$WOCl_3$(phsq)	1.044	1.40
7	$MoOCl_3$(phq)	1.380	1.61
8	$MoOCl_2$(phc)(OEt_2)	Diamagnetic	

[a] No corrections are made for diamagnetism.

molybdenum +V with spin pairing of the two paramagnetic metal ions. $MoCl_4$(phsq) (**2**), $WOCl_3$(phsq) (**6**) and $MoOCl_3$(phq) (**7**) are paramagnetic. The IR spectra discussed above is consistent with a fully oxidized phenanthrenequinone ligand in complex (**7**) thus leaving the unpaired electron localized in a metal orbital. The analogous tungsten complex (**6**) is also paramagnetic with a magnetic moment close to that observed for the molybdenum complex (**7**). For complex (**6**), however, no IR evidence substantiating the formulation of the ligand as a quinone was observed and the unpaired electron is most likely localized in a quinone orbital.

The molybdenum complex (**2**) is paramagnetic with a magnetic moment close to the value expected for two unpaired electrons. Given the composition of complex (**2**) two different possible formulations are in accordance with the observed magnetic moment; a molybdenum(+IV) complex with phenanthrenequinone ligand or a molybdenum(+V) complex with a phenanthrenesemiquinone ligand. The IR spectra of complex (**2**) is, however, inconsistent with a fully oxidized phq ligand. This leaves a formulation involving molybdenum(+V) and a phsq ligand as the most likely one. The difference with regard to electronic structure between complexes (**6**) and (**7**) and between complexes (**1**) and (**2**) is noteworthy and reflects a general trend for molybdenum and tungsten.[9,34]

Complexes (**3**) and (**4**) have also been characterized by ^{13}C-NMR (cf. Experimental section). The low field signals are tentatively assigned to the carbonyl carbon atom. The coordination shift of that atom, δ(free ligand)–δ(complex), is positive for both complexes although the values are substantially lower than for other metal-catecholate complexes.[35,36] The value of the coordination shift for the tungsten complex is greater than for the molybdenum complex. This can be due to a greater catecholate character in the tcc ligand of the tungsten complex. Unfortunately, low solubility precluded NMR measurements on the other complexes.

EXPERIMENTAL

General procedures and chemicals

All preparations were carried out under dried argon using conventional Schlenk technique. Solvents were dried by and stored over activated molecular sieves. Tungsten hexachloride (Aldrich, 99.9%) and molybdenum pentachloride (Aldrich 99.9%) were used as received. Tetrachloro-1,2-benzoquinone and 9,10-phenanthrenequinone (Janssen Chimica) were used as received. WCl_4(DME), $MoCl_4(OEt_2)_2$,[25] $WOCl_3$(DME) and $MoOCl_3$(DME)[33] were prepared as described earlier.

Tungsten and molybdenum were determined gravimetrically as WO_3 and MoO_3, respectively. Elemental analyses were done by Mikro Kemi AB (Uppsala, Sweden) and Analyslaboratoriet (Lund, Sweden).

Infrared spectra were recorded on a Nicolet 20 SXC FT-IR or a PE 580B spectrometer as Nujol mulls between CsI windows. ^{13}C-NMR spectra were recorded on a Varian Unity 300 spectrometer. Magnetic susceptibilities were measured at ambient temperature by Evans's method using a Sherwood Scientific Magnetic Susceptibility Balance.

Preparations

Tetrachloro[9,10-*phenanthrenediolato*(2−)-O,O′] *tungsten*(VI) (**1**). Dichloromethane (20 cm^3) was added to a mixture of WCl_4(DME) (1.3 g, 3.1 mmol) and phenanthrenequinone (0.65 g, 3.1 mmol). Stirring at room temperature gave a green solution which rapidly turned blue as a dark precipitate formed. The solid was isolated by Schlenk-filtration after 20 min, washed once with diethyl ether and dried *in vacuo* giving WCl_4(phc) (**I**) as a dark bluish–black shining solid. Yield: 1.3 g, 79%. IR: 1600s, 1588w, 1557m, 1547w, 1508s, 1494m, 1415s, 1347m, 1329m, 1311s, 1298m, 1257m, 1124m, 1040w, 992m, 960m, 935m, 871w, 760vs, 735sh, 716s, 672w, 651w, 612w, 531ms, 460m, 433m, 394s, 376s, 327vs, 289m.

Tetrachloro[9,10 - *phenanthrenesemiquinonato* (1−)-O,O′]*molybdenum*(V) (**2**). Phenanthrenequinone (1.35 g, 6.48 mmol) in dichloromethane (45 cm^3) was added at room temperature to a stirred suspension of $MoCl_4(OEt_2)_2$ (2.5 g, 6.48 mmol) in dichloromethane (20 cm^3). The solution immedi-

ately turned dark bluish–green and a dark precipitate started to form. The reaction was continued overnight. $MoCl_4$(phsq) (**2**) was isolated as a black solid by Schlenk-filtration, washed with three aliquots of diethyl ether (10 cm^3) and dried *in vacuo*. Yield: 2.5 g, 87%. IR: 1592s, 1571sh, 1548s, 1491ms, 1364s, 1324m, 1304s, 1292sh, 1237w, 1171m, 1159ms, 1124ms, 1098w, 1080w, 1037w, 993m, 974w, 967w, 937m, 885w, 811w, 787m, 773m, 766vs, 735sh, 705s, 684m, 674m, 633w, 527ms, 428ms, 412m, 385s, 374s, 351sh, 328vs.

Tetrachloro[3,4,5,6 - *tetrachloro* - 1,2 - *benzenediolato*(2−)-O,O′]*molybdenum*(VI) (**3**). Tetrachloroquinone (3.28 g, 13.33 mmol) in dichloromethane (30 cm^3) was slowly added to a cooled (−25°C), stirred suspension of $MoCl_5$ (3.65 g, 13.35 mmol) in dichloromethane (60 cm^3). The reddish–brown suspension rapidly turned intensely green and a dark precipitate formed. The reaction was continued at −25°C for 30 min and then at room temperature for 45 min. Cooling and Schlenk-filtration gave dark olive–green crystals of $MoCl_4$(tcc) (**3**) which were washed with diethyl ether and dried *in vacuo*. Yield: 2.7 g, 42%. The substance does not mull in Nujol and, consequently, no IR spectrum was obtained. ^{13}C-NMR (CH_2Cl_2/CD_2Cl_2 3:1): 163.77, 155.97, 111.19 ppm.

Tetrachloro[3,4,5,6 - *tetrachloro* - 1,2 - *benzenediolato*(2−)-O,O′]*tungsten*(VI) (**4**). Solid tetrachloroquinone (1.55 g, 6.30 mmol) was added to a dark blue suspension of WCl_6 (2.5 g, 6.30 mmol) in toluene (40 cm^3) giving a dark green solution and a black precipitate. The reaction mixture was stirred for 24 h at room temperature, causing the precipitate to slowly dissolve. The deep purple solution obtained was cooled at −25°C overnight. Schlenk-filtration and evaporation of the filtrate gave dark green crystals of WCl_4(tcc) (**4**). Yield: 3.52 g, 98%. Minor impurities of $WOCl_4$ were removed by washing with diethyl ether or by sublimation. IR: 1529w, 1400m, 1269w, 1240m, 1017m, 1006w, 819m, 786s, 616m, 582m, 513w, 419ms, 401s, 388s, 349vs, 291ms. ^{13}C-NMR (CH_2Cl_2/CD_2Cl_2 3:1): 153.87, 145.24, 116.06 ppm.

Tetrakis[3,4,5,6 - *tetrachloro* - 1,2 - *benzenediolato*(2−)-O,O′]*dichlorodimolybdenum*(V) (**5**). $MoCl_5$ (1.0 g, 3.66 mmol) and tetrachloroquinone (0.9 g, 3.66 mmol) were treated with toluene (15 cm^3) under stirring at room temperature. An immediate reaction ensued, giving a clear, green solution which turned blue within 20 min. The reaction was allowed to continue for 24 h, resulting in a dark blue solution and a dark precipitate. Schlenk-filtration, washing with diethyl ether and drying *in vacuo* gave a dark reddish–brown compound which according to its IR-spectrum and elemental analysis contained toluene. Toluene was removed by stirring the solid in dichloromethane overnight followed by filtration and drying *in vacuo* giving (**5**) as a red–black powder. Yield: 1.11 g, 49%. IR: 1577w, 1558w, 1511s, 1409s, 1330m, 1299ms, 1269m, 1224vs, 1006s, 1000sh, 898w, 810w, 794s, 730m, 572m, 560m, 495m, 435s, 393w, 370s, 277m.

Trichlorooxo[9,10 - *phenanthrenesemiquinonato*(1−)-O,O′]*tungsten*(VI) (**6**). Phenanthrenequinone (0.92 g, 4.42 mmol) in dichloromethane (25 cm^3) was added to a stirred solution of $WOCl_3$(DME) (1.75 g, 4.42 mmol) in dichloromethane (40 cm^3) at room temperature. The blue solution immediately turned red–violet and a dark precipitate started to form. The reaction was continued for 2 h. $WOCl_3$(phsq) (**6**) was isolated by Schlenk-filtration, washed with two aliquots of diethyl ether (5 cm^3) and dried *in vacuo*. Concentration of the filtrate followed by addition of diethyl ether gave a second crop of (**6**). Total yield: 1.75 g, 77%. IR: 1597ms, 1585s, 1519w, 1494m, 1394ms, 1341m, 1311s, 1290s, 1279s, 1240w, 1230m, 1210s, 1160m, 1125m, 1105m, 1081w, 1037m, 1004w, 995vs (W=O), 986m, 969m, 960w, 938m, 877m, 784m, 766vs, 735m, 710s, 677m, 636m, 531ms, 495m, 417w, 393m, 384m, 366vs, 350s, 339s, 320m, 248m.

Trichlorooxo[9,10 - *phenanthrenequinone* - O,O′]*molybdenum*(V) (**7**). The preparation was carried out as described for (**6**) giving $MoOCl_3$(phq) (**7**) in 48% yield. IR: 1627m (C=O), 1585s, 1573s, 1557s, 1545sh, 1361m, 1325w, 1299s, 1290sh, 1260w, 1246w, 1171m, 1159ms, 1124ms, 993vs (Mo=O), 965w, 938m, 925w, 883w, 822w, 787m, 780m, 766vs, 733sh, 707s, 683mw, 676m, 633w, 531ms, 510m, 476mw, 430m, 399mw, 383s, 376s, 351vs, 341vs, 313m.

Dichlorooxo[1,1 - *oxybis*(*ethane*)][9,10 - *phenanthrenediolato*(2−)-O,O′]*molybdenum*(VI) (**8**). *t*-$BuOSiMe_3$ (1.18 g, 8.07 mmol) was added to a stirred suspension of $MoCl_4$(phsq) (3.6 g, 8.07 mmol) in dichloromethane (100 cm^3) at room temperature. The blue solution rapidly turned purple. Addition of diethyl ether (15 cm^3) after 5 min caused the solid to partly dissolve. The reaction was continued for 24 h and $MoOCl_2$(phc)(OEt_2) (**8**) was collected by Schlenk-filtration and dried *in vacuo*. Concentration and cooling of the filtrate gave a second crop of (**8**). A third crop was obtained by the addition of diethyl ether to the filtrate. Total yield: 3.4 g, 91%. IR: 1598ms, 1573m, 1549w, 1498s, 1408m, 1394s, 1324m, 1317m, 1301ms, 1236m, 1228sh, 1187m, 1165w, 1153w, 1147m, 1124m, 1082m, 1040w, 1012m (C—O—C ether), 985m, 962vs (Mo=O), 941m, 891m, 867w, 862w, 826m, 789m, 771s, 757vs, 713s, 689m, 673m, 640w,

551m, 540ms, 502m, 466m, 444w, 433m, 401m, 393m, 382m, 358vs, 336vs, 291m.

REFERENCES

1. G. Schoettel, J. Kress and J. A. Osborn, *J. Chem. Soc., Chem. Commun.* 1989, 1062.
2. R. R. Schrock, J. S. Murdzek, G. C. Bazan, J. Robbins, M. DiMare and M. O'Regan, *J. Am. Chem. Soc.* 1990, **112**, 3875.
3. R. R. Schrock, R. T. DePue, J. Feldman, K. B. Yap, D. C. Yang, W. M. Davis, L. Park, M. DiMare, M. Schofield, J. Anhaus, E. Walborsky, E. Evitt, C. Krüger and P. Betz, *Organometallics* 1990, **9**, 2262.
4. W. A. Herrmann, J. G. Kuchler, J. K. Felixberger, E. Herdtweck and W. Wagner, *Angew. Chem. Int. Ed. Engl.* 1988, **27**, 394.
5. R. R. Schrock, R. T. DePue, J. Feldman, C. J. Schaverien, J. C. Dewan and A. H. Liu, *J. Am. Chem. Soc.* 1988, **110**, 1423.
6. K. N. Raymond and C. J. Carrano, *Accts Chem. Res.* 1979, **12**, 183.
7. *The Chemistry of the Quinonoid Compounds* (Edited by S. Patai), Parts 1 and 2. Wiley, New York (1974).
8. C. G. Pierpont and R. M. Buchanan, *Coord. Chem. Rev.* 1981, **38**, 45.
9. T. P. Blatchford, M. H. Chisholm and J. C. Huffman, *Inorg. Chem.* 1988, **27**, 2059.
10. H. T. Dodd and K. J. Rutt, *J. Mol. Catal.* 1982, **15**, 103.
11. H. T. Dodd and K. J. Rutt, *J. Mol. Catal.* 1985, **28**, 33.
12. F. Quignard, M. Leconte and J.-M. Basset, *J. Chem. Soc., Chem. Commun.* 1985, 1816.
13. F. Quignard, M. Leconte and J.-M. Basset, *J. Mol. Catal.* 1986, **36**, 13.
14. J.-L. Couturier, C. Paillet, M. Leconte and J.-M. Basset, *Abstr. 8th International Symposium on Homogeneous Catalysis*, Amsterdam (1992).
15. M. H. Chisholm and I. P. Rothwell, *Amido and Imido Metal Complexes, Comprehensive Coordination Chemistry* (Edited by G. Wilkinson, R. D. Gillard and J. A. McCleverty), Vol. 2. Pergamon, Oxford (1987).
16. H. Funk and G. Mohaupt, *Z. Anorg. Allg. Chem.* 1962, **315**, 204.
17. S. M. Beshouri and I. P. Rothwell, *Inorg. Chem.* 1986, **25**, 1962.
18. J. Takacs, P. Kiprof, J. Riede and W. A. Herrmann, *Organometallics* 1990, **9**, 782.
19. L. A. deLearie and C. G. Pierpont, *J. Am. Chem. Soc.* 1986, **108**, 6393.
20. Y. S. Sohn and A. L. Balch, *J. Am. Chem. Soc.* 1972, **94**, 1144.
21. C. G. Pierpont, H. H. Downs and T. G. Rukavina, *J. Am. Chem. Soc.* 1974, **96**, 5573.
22. L. A. deLearie and C. G. Pierpont, *Inorg. Chem.* 1988, **27**, 3842.
23. R. M. Buchanan and C. G. Pierpont, *Inorg. Chem.* 1979, **18**, 1616.
24. C. G. Pierpont and H. H. Downs, *J. Am. Chem. Soc.* 1975, **97**, 2123.
25. C. Persson and C. Andersson, *Inorg. Chim. Acta* 1993, **203**, 235.
26. H. Funk and H.-R. Hoppe, *Z. Chem.* 1968, **8**, 31.
27. C. Persson and C. Andersson, *Polyhedron* 1991, **10**, 2089.
28. K. Stahl and K. Dehnicke, *Z. Naturforsch.* 1987, **42b**, 253.
29. M. L. Larson and F. W. Moore, *Inorg. Chem.* 1964, **3**, 285.
30. S. Herzog, K. Gustav and J. Strähle, *Handbuch der Präparativen Anorganischen Chemie* (Edited by G. Brauer), Vol. 3, 3rd edn, p. 1533. Ferdinand Enke, Stuttgart (1981).
31. E. Hey-Hawkins and H. G. von Schnering, *Z. Naturforsch.* 1991, **46b**, 307.
32. V. C. Gibson, T. P. Kee and A. Shaw, *Polyhedron* 1990, **9**, 2293.
33. C. Persson and C. Andersson, *Polyhedron* 1992, **11**, 847.
34. S. Yu and R. H. Holm, *Inorg. Chem.* 1989, **28**, 4385.
35. S. Bristow, J. H. Enemark, C. D. Garner, M. Minelli, G. A. Morris and R. B. Ortega, *Inorg. Chem.* 1985, **24**, 4070.
36. H. E. Mabrouk and D. G. Tuck, *J. Chem. Soc., Dalton Trans.* 1988, 2539.

Polyhedron Vol. 12, No. 21, pp. 2577–2585, 1993
Printed in Great Britain

0277–5387/93 $6.00+.00
© 1993 Pergamon Press Ltd

SYNTHESIS AND SPECTROSCOPIC PROPERTIES OF DIARYLPOLYSELANES R_2Se_x (x = 2–7) AND OF DIARYLDISELENAPOLYSULPHANES $(RSe)_2S_y$ (y = 1–15) WITH R = 4-Cl-C_6H_4*

MARKUS PRIDÖHL and RALF STEUDEL†

Institut für Anorganische und Analytische Chemie, Technische Universität Berlin, Sekr. C 2, D-10623, Berlin

and

FRANK BAUMGART

Iwan-N. Stranski-Institut für Physikalische und Theoretische Chemie, Technische Universität Berlin, D-10623, Berlin

(*Received* 2 *June* 1993; *accepted* 1 *July* 1993)

Abstract—Reaction of RSeCl (R = 4-Cl-C_6H_4) with titanocene pentasulphide Cp_2TiS_5 affords the novel $RSeS_5SeR$ as a yellow oil which is quite stable at 20°C. Using $Cp_4'Ti_2S_4$ (Cp′ = $CH_3C_5H_4$) as a sulphur transfer reagent the reaction with RSeCl results in a mixture of $(RSe)_2S_n$ molecules with n = 0–10, which on heating produces even longer chains as demonstrated by HPLC analysis. Titanocene pentaselenide Cp_2TiSe_5 reacts with RSeCl at 4°C to give a mixture of R_2Se_x molecules (x = 1–7) and Se_8, the relative concentrations sharply decrease with increasing x. ^{77}Se NMR and UV spectra as well as retention index data of the new molecules are reported.

While organic polysulphanes **1** are known in large numbers,[2] little information on the analogous organic polyselanes **2** is available and the same holds for organic selenasulphanes **3**.

R—S_n—R R—Se_n—R R—Se_nS_m—R
1 **2** **3**

This is due to the fact that the bond energy of SeSe bonds is much lower than that of SS bonds and therefore polyselenium compounds usually decompose rapidly even at 20°C, especially in solution, and often with precipitation of elemental selenium. In the case of R = aryl and $n > 2$ only some triselanes have been prepared (R = substituted phenyl groups).[3] In addition, a cyclic ferrocenyltriselane $Fe(C_5H_4)_2Se_3$ is known.[4]

In recent years a number of polysulphur and polyselenium compounds has been prepared using the titanocene chelate complexes Cp_2TiS_5 and Cp_2TiSe_5 (Cp = C_5H_5) as sulphur and selenium transfer reagents.[5–7] By reaction with SCl or SeCl compounds these reagents transfer the —S_5—, respectively —Se_5— groups in exchange for chlorine atoms. The dinuclear complex $Cp_2'Ti(\mu\text{-}S_2)_2TiCp_2'$ (Cp′ = $C_5H_4CH_3$) reacts in a similar manner as a transfer reagent for —S_2— units.[8]

In this work we report on the attempts to synthesize acyclic diarylpolychalcogen compounds of types **2** and **3** from the above mentioned titanocene complexes by reactions shown in eqs (1)–(4) with R = 4-Cl-C_6H_4:

$$R_2Se_2 + Cl_2 \longrightarrow 2RSeCl, \quad (1)$$

$$2RSeCl + Cp_2TiS_5 \longrightarrow (RSe)_2S_5 + Cp_2TiCl_2, \quad (2)$$

$$4RSeCl + Cp_2'Ti(\mu\text{-}S_2)_2TiCp_2' \longrightarrow 2(RSe)_2S_2 + 2Cp_2'TiCl_2, \quad (3)$$

$$2RSeCl + Cp_2TiSe_5 \longrightarrow R_2Se_7 + Cp_2TiCl_2. \quad (4)$$

* Part 169 of the Series Sulphur Compounds; for Part 168 see ref. 1.

† Author to whom correspondence should be addressed.

The reactions were followed by reversed-phase high-pressure liquid chromatography (HPLC) and ^{77}Se NMR spectroscopy using the natural abundance of ^{77}Se (7.6%, I = 1/2). Both HPLC[9] and ^{77}Se NMR spectroscopy[10,11] have previously been applied successfully to analyse mixtures of organic polyselenium compounds.

EXPERIMENTAL

Materials

Carbon disulphide (techn. grade) was purified and dried by distillation from P_4O_{10}. Cp_2TiS_5 (Cp = C_5H_5) and $Cp'_4Ti_2S_4$ (Cp' = $CH_3C_5H_4$) were prepared according to literature methods.[12] Bis(4-chlorophenyl)diselane (98%, Aldrich) was used as delivered. For chlorination reactions a solution of Cl_2 in CCl_4 was prepared by bubbling dry Cl_2 into 1.5 l of CCl_4 (p.a. Merck). The concentration was determined as 15.2 mg Cl_2/(ml CCl_4) by differential weighing. Technical methanol used as an eluent was distilled from anhydrous magnesium sulphate and degassed under reduced pressure and with application of ultrasound prior to use. Silica gel (Kieselgel 40, Merck Rt. 10181) was used for filtration.

Procedures and instrumentation

HPLC analysis was performed with the following equipment: Millipore Waters Radial-Pak cartridges filled with C18 phase (particle size 5 μm, length 10 cm, inner diameter 8 mm) contained in a compression module (Waters RCM 100); Perkin–Elmer LC 75 (variable wavelength detector with deuterium lamp) for UV detection at 254 nm; Perkin–Elmer Series 2 pump; Rheodyne syringe loading injector 7125 (sixport) with a 10 μl sample loop; electronic integrator HP 3390A for retention time measurements. UV spectra were recorded using a diode array detector (Waters 990) with a resolution of 2 nm controlled by a NEC APC III computer. ^{77}Se NMR spectra were recorded at 68.679 MHz with a Bruker WM 360 spectrometer controlled by an Aspect 3000 computer. Sample tubes of 10 mm outer diameter were used.

The samples were dissolved in CS_2/C_6D_6 (3/1). Neat Me_2Se sealed in an NMR glass tube surrounded by neat C_6D_6 in an outer coaxial NMR tube was used as a standard and chemical shifts refer to this compound. Raman spectra were obtained with a Kr ion laser (Spectra Physics) operating at 647.1 nm, a double monochromator Ramanor U1000 (Jobin Yvon), equipped with a GaAs photomultiplier R943-02 (Hamamatsu) and a data processing and controlling unit MAC 80 A with the software Spectra Control (Spectra Data) under the following conditions: slit width 650 μm, sample temperature, −50°C, laser power 80 mW, wavelength accuracy ± 1 cm^{-1}.

Synthesis of $RSeS_5SeR$ (R = 4-ClC_6H_4)

A solution (16.1 cm^3) of Cl_2 (3.45 mmol) in CCl_4 was added to a stirred solution of 0.982 g R_2Se_2 (2.56 mmol) in 15 cm^3 carbon disulphide to prepare RSeCl. After 25 min the excess of Cl_2 was removed *in vacuo*. Within 2 min the reaction mixture was added dropwise to a stirred solution of 0.868 g Cp_2TiS_5 (2.56 mmol) in 80 cm^3 CS_2. After 5 min the reaction mixture was sucked through a column filled with 10 cm silica gel. The eluate was filtered again. After removing the solvent *in vacuo* 1.39 g (83%) $RSeS_5SeR$ was obtained as a yellow oil. Found: C, 26.9; H, 1.6; S, 29.8. Calc.: C, 26.6; H, 1.5; S, 29.6%.

Vibrational spectra (values in cm^{-1}, relative intensities in brackets): (a) Raman spectrum: 166(m), 233(vw), 250(m),. 334(vw), 372(vs), 403(vw), 430(w), 452(s), 469(s). 626(w), 729(m), 1066(s), 1088(m), 1176(w), 1570(m), 3046(vw), 3062(vw). (b) IR spectrum: 303(w), 330(w), 332(w), 370(w), 400(w), 480(vs), 622(vw), 692(w), 727(s), 807(vs), 947(w), 953(w), 1008(vs), 1058(m), 1062(m), 1087(vs), 1105(s), 1172(s), 1220(w), 1263(m), 1291(m), 1340(vw), 1383(vs), 1424(m), 1470(vs), 1568(s), 1635(m), 1773(w), 1818(vw), 1890(m).

Synthesis of $RSeS_2SeR$ *and* $RSeS_ySeR$ (y = 1–15)

A solution (18.7 cm^3) of Cl_2 (5.19 mmol) in CCl_4 was added to a stirred solution of 1.524 g R_2Se_2 (4.0 mmol) in 16 cm^3 carbon disulphide. After 15 min the excess of Cl_2 was removed *in vacuo*. Within 5 min the cold reaction mixture was added dropwise to a stirred solution of 1.081 g $Cp'_4Ti_2S_4$ (2.00 mmol) in 80 cm^3 CS_2 at 4°C. After 3 min the reaction mixture was sucked through a column filled with 10 cm silica gel. The eluate was filtered again. After removing the solvent *in vacuo* a yellow oil was obtained containing several $RSeS_ySeR$ molecules (y = 1–7) and R_2Se_2 with $RSeS_2SeR$ as the main sulphur containing product. Heating of this mixture resulted in the formation of additional $RSeS_ySeR$ molecules (y = 1–10), strong heating yielded $RSeS_ySeR$ (y = 1–15) and traces of S_8.

Synthesis of R_2Se_x (x = 1–7)

A solution (8.3 cm^3) of Cl_2 (1.8 mmol) in CCl_4 was added to the stirred solution of 0.520 g (1.365

mmol) R_2Se_2 in 10 cm^3 carbon disulphide. After 25 min any excess of Cl_2 was removed *in vacuo*. The reaction mixture was added to a stirred solution of 0.781 g Cp_2TiSe_5 (1.365 mmol) in 80 ml CS_2 at 20°C. After 9 min the mixture was sucked through a column filled with 10 cm of silica gel to remove Cp_2TiCl_2. The eluate was filtered again. After evaporation *in vacuo* a red solid consisting of a mixture of R_2Se_x molecules (x = 1–7) and Se_8 was obtained.

RESULTS

$RSeS_5SeR$

4-Chlorobenzeneselenylchloride reacts with Cp_2TiS_5 at 20°C quantitatively according to eq. (2) to give the mixed polychalcogenide $(RSe)_2S_5$ which was isolated as a yellow oil. The HPLC analysis of the yellow oil showed that the freshly prepared product contained small amounts (*ca* 2 mol%) of the starting material R_2Se_2 but no other $(RSe)_2S_y$ molecules could be detected (Fig. 1a). On standing at 20°C the yellow oil as well as its solution in CS_2/C_6D_6 (for NMR measurements) slowly decomposed yielding new molecules which originate from a sulphur atom exchange reaction; eq. (5).

$$2(RSe)_2S_y \rightleftharpoons (RSe)_2S_{y+n} + (RSe)_2S_{y-n}. \quad (5)$$

The HPLC analysis of such a mixture showed small peaks of almost equal size (by area) for all species with 1–10 sulphur atoms. The natural abundance ^{77}Se NMR spectrum (recording time 12 h) exhibited a major signal for $(RSe)_2S_5$ at 650.9 ppm and in addition signals for other $(RSe)_2S_y$ molecules which are assigned to the species with y = 1, 2, 3 and 4 (Fig. 2). The NMR signals of the species with y = 6–10 are probably hidden in the wing on the left side of the tallest signal. Enhancement of the resolution by data processing showed a triplet with a coupling constant of 2.7 ± 0.1 Hz for the Se—H coupling in $(RSe)_2S_5$ ($^3J_{Se-H}$).

The Raman spectrum of neat $(RSe)_2S_5$ (Fig. 3) exhibits the expected lines for 4 SS stretching vibrations at 430, 452, 469 and 490 cm^{-1} as well as two lines at 372 and 389 cm^{-1} which can be assigned to the SeS stretching modes by comparison with the spectra of other SeS compounds.[13]

R_2Se_2 has its strongest Raman line at 269 cm^{-1} (SeSe stretching mode); this line is not observed in the $(RSe)_2S_5$ spectrum indicating that the concentration of R_2Se_2 is very low. The other Raman lines as well as most of the IR frequencies may be assigned to vibrations of the *para*-substituted benzene ring.

The EI mass spectrum of $(RSe)_2S_5$, as expected, did not show a peak of the molecular ion. The

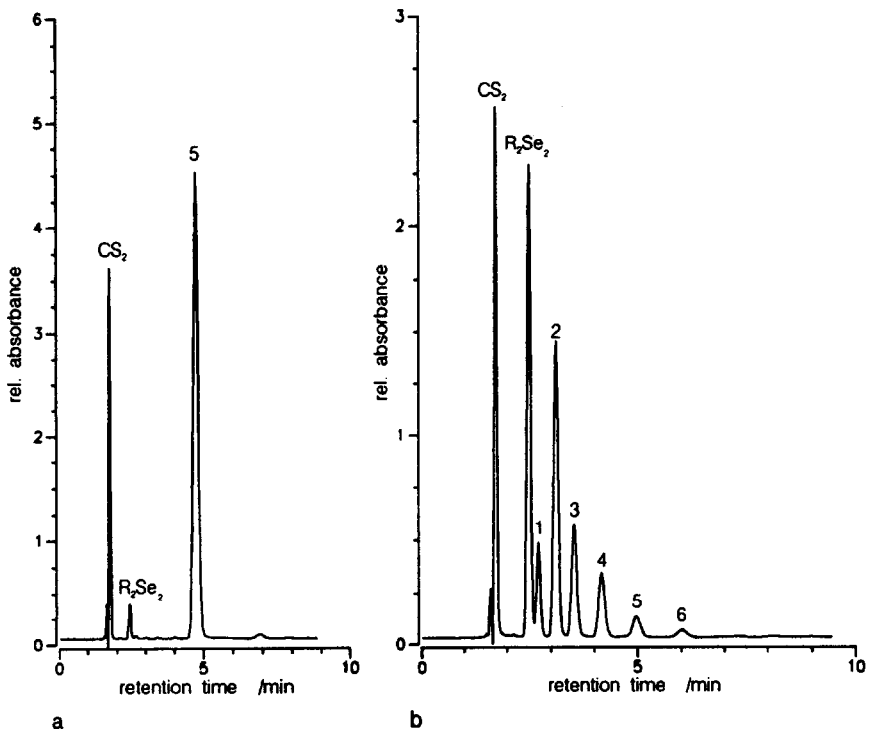

Fig. 1. HPLC analysis of (a) the yellow oil obtained by reaction shown in eq. (2) and (b) of the mixture obtained by reaction in eq. (3). The numbers at the peaks give the number of sulphur atoms in the formula $(RSe)_2S_y$.

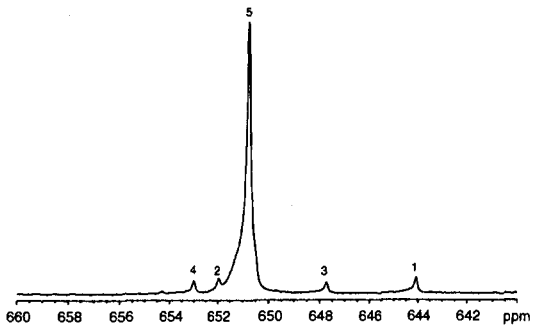

Fig. 2. ^{77}Se NMR spectrum of the yellow oil obtained in reaction shown in eq. (2). Solvent: CS_2/C_6D_6. The numbers at the peaks give the number of sulphur atoms in the formula $(RSe)_2S_y$. The shoulder at the left wing of the tallest peak probably represents molecules with six and more sulphur atoms.

heaviest fragment was observed at $m/z = 414$ and corresponds to $(RSe)_2S^+$. In addition, peaks for $R_2Se_2^+$, R_2Se^+, Se_2^+, and S_y^+ ($y = 2$–8) were observed (sample temperature 100°C; electron energy 60 eV).

$RSeS_2SeR$

When freshly prepared RSeCl was treated with $Cp'_4Ti_2S_4$ in CS_2 at 20°C the primary reaction was the formation of $(RSe)_2S_2$ according to eq. (3). The HPLC analysis after removal of Cp'_2TiCl_2 (Fig. 1b) showed, however, the presence of considerable concentrations of R_2Se_2 as well as of other members of the homologous series $(RSe)_2S_y$. This may be explained by a series of sulphur transfer reactions [eq. (5)] which are probably catalysed by either titanocene complexes or by the silica gel used to remove Cp'_2TiCl_2. Part of the R_2Se_2 observed may stem from the preparation of RSeCl, however (imperfect chlorination).

The ^{77}Se NMR spectrum of the mixture obtained by reaction (3) exhibits large peaks for R_2Se_2 and $(RSe)_2S_2$ as well as smaller ones for the other members of the homologous series with 1–6 sulphur atoms connecting the two RSe units (Fig. 4). From the peak heights in the NMR spectrum the following molecular composition (mol-%) was derived: R_2Se_2 28.5, $(RSe)_2$ 7.8, $(RSe)_2S_2$ (30.6), $(RSe)_2S_3$ 13.5, $(RSe)_2S_4$ 10.4, $(RSe)_2S_5$ 5.7, $(RSe)_2S_6$ 3.6%.

When this mixture was heated to above 100°C for a short time the decomposition according to equation (5) was accelerated and in addition S_8 was formed:

$$(RSe)_2S_{8+n} \longrightarrow (RSe)_2S_n + S_8. \qquad (6)$$

The chromatogram of this decomposed sample shows $(RSe)_2S_{15}$ as the largest molecule present (Fig. 5). The assignment of these peaks is straightforward since members of homologous series show the following dependence of the retention time t_r on the chain-length y (k' = capacity factor, t_0 = dead time):

$$\ln k' = a \cdot y + b,$$

$$k' = (t_r - t_0)/t_0.$$

In Fig. 6 it is shown that for $(RSe)_2S_y$ molecules this relationship holds for $y = 1$–12 with small deviations for $y = 1$ and 2. It is often observed that the first members of a series do not fit the linear equation too well. Since $(RSe)_2S_2$ is the main product

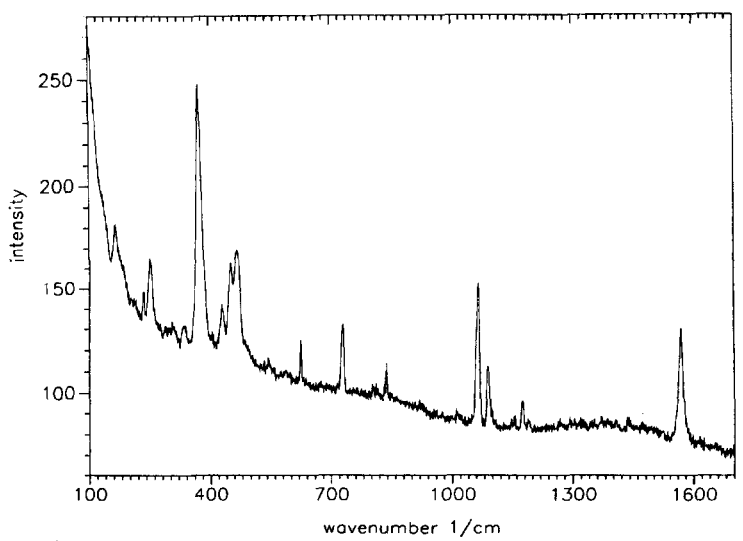

Fig. 3. Raman spectrum of neat $(RSe)_2S_5$ at −50°C.

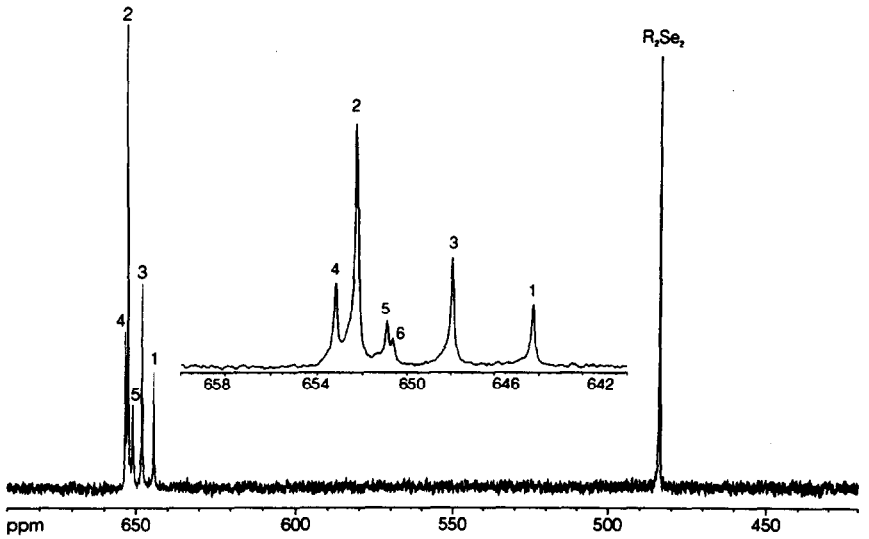

Fig. 4. ^{77}Se NMR spectrum of the mixture obtained by reaction shown in eq. (3). The numbers at the peaks give the number of sulphur atoms in the formula $(RSe)_2S_y$.

in the reactions in eq. (3) and $(RSe)_2S_5$ in eq. (2) the assignment of the peaks in Fig. 5 is straightforward. The correlation coefficient of the linear relationship applying to $(RSe)_2S_y$ with $y > 2$ is better than 0.9999. The retention times are given in Table 1.

This Table also gives the retention index values RS which, like Kovats retention indices in gas chromatography, give the retention relative to the sulphur homocycles S_6, S_8, S_9 and S_{10}. Such RS values are characteristic properties of compounds and independent on the HPLC apparatus used.[2,14]

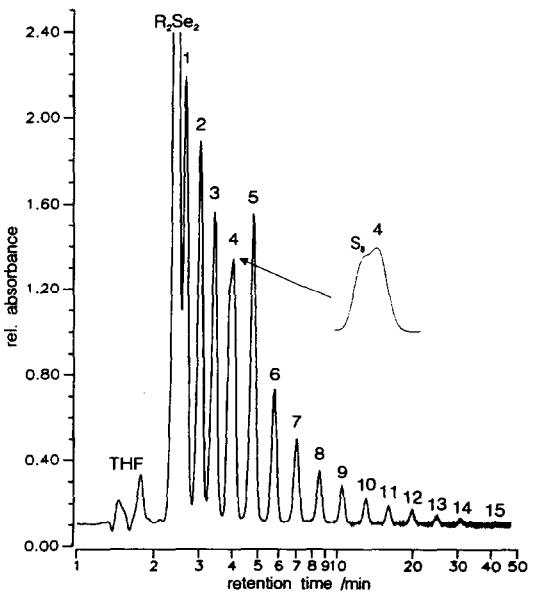

Fig. 5. HPLC analysis of a mixture of $(RSe)_2S_y$ molecules ($y = 0$–15) obtained by heating the products of reaction shown in eq. (3). Note the logarithmic plot of the retention time. The numbering of peaks gives the number of sulphur atoms in the formula. THF was used as a solvent.

The assignment of the NMR signals in Figs 2 and 4 is more complicated but by correlating the NMR peak heights with the HPLC peak areas of various mixtures of $(RSe)_2S_y$ molecules it was possible to assign the signals caused by the first six members of this series ($y = 1$–6). The corresponding chemical shifts are given in Table 2. Using a diode array detector connected to the HPLC apparatus the absorption spectra of freshly separated $(RSe)_2S_y$ molecules ($y = 1$–5) could be recorded on-line in the eluent methanol and in the range 200–600 nm. Two absorption maxima were observed for each compound. No absorbance coefficients can be

Table 1. Retention data of $RSeS_xSeR$ and RSe_xR molecules in reversed-phase HPLC (t_r = retention time (min); RS = sulphur based retention index)

	$RSeS_xSeR$		RSe_xR	
x	t_r	RS	t_r	RS
1	2.676	624	2.078	492
2	3.083	690	2.402	578
3	3.511	745	2.840	666
4	4.162	814	3.424	752
5	4.977	881	4.097	829
6	6.029	949	5.139	918
7	7.390	1019	6.641	1012
8	9.036	1085		
9	11.185	1153		
10	13.833	1220		

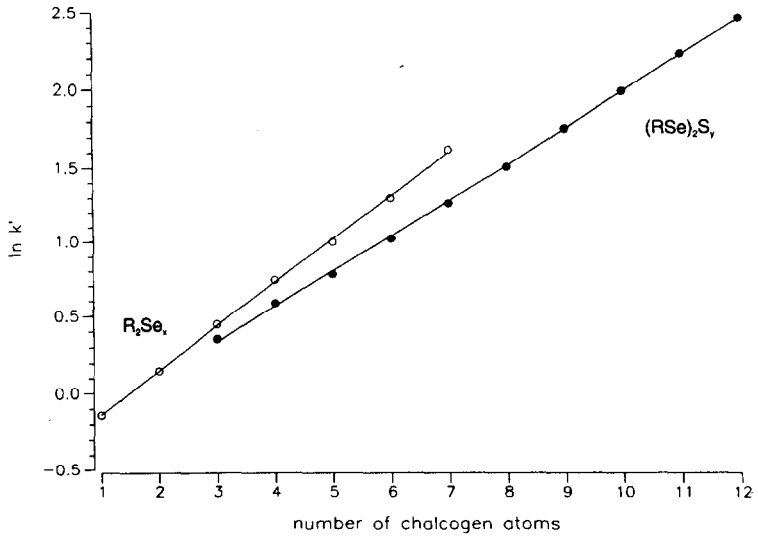

Fig. 6. Linear dependence of the logarithm of the capacity factor k' on the number of chalcogen atoms in R_2Se_x and $(RSe)_2S_y$ molecules.

Table 2. ^{77}Se chemical shifts (ppm) of RSe_xR and $RSeS_ySeR$ molecules (R = 4-Cl—C_6H_4) in CS_2/C_6D_6 solution at 25°C

Substance	$\delta(^{77}Se_\alpha)$	$\delta(^{77}Se_\beta)$	$\delta(^{77}Se_\gamma)$	$\delta(^{77}Se_\delta)$	Substance	$\delta(^{77}Se_\alpha)$
$ArSeAr$	[a]				$ArSe_2Ar$	483.7
$ArSe_2Ar$	480.3				$ArSeSSeAr$	444.3
$ArSe_3Ar$	568.0	763.8			$ArSeS_2SeAr$	652.2
$ArSe_4Ar$	558.2	802.9			$ArSeS_3SeAr$	647.9
$ArSe_5Ar$	566.2	800.5	865.0		$ArSeS_4SeAr$	653.2
$ArSe_6Ar$	565.1	808.5	856.7		$ArSeS_5SeAr$	650.9
$ArSe_7Ar$	561.8	808.9	861.7	857.0[b]	$ArSeS_6SeAr$	650.6

[a] Could not be observed.
[b] Tentative value.

determined in this way but the relative intensities of the two maxima at 248 and 353 ± 2 nm are given in Table 3.

RSe_xR

When RSeCl was reacted with Cp_2TiSe_5 in CS_2 at 20°C the HPLC analysis of the mixture showed that the reaction in eq. (4) had taken place but the expected main product RSe_7R was present in traces only, even when the reaction was carried out at −50°C and with exclusion of light. The precipitation of Se_8 from the reaction mixture shows that decomposition according to eqs (7) and (8) rapidly occurred.

$$2R_2Se_7 \rightleftharpoons R_2Se_{7-n} + R_2Se_{7+n}, \quad (7)$$

$$R_2Se_{7+n} \longrightarrow R_2Se_{n-1} + Se_8. \quad (8)$$

The ^{77}Se NMR spectrum of a sample prepared as described in the Experimental section and the

Table 3. Absorption spectra of RSe_xR and $RSeS_xSeR$ molecules (wavelengths in nm; relative intensities in brackets)

$ArSe_2Ar$	252 (100)	338 (6)
$ArSe_3Ar$	252 (100)	382 (12)
$ArSe_4Ar$	253 (100)	395 (12)
$ArSe_5Ar$	256 (100)	395 (13)
$ArSe_6Ar$	255 (100)	396 (10)
$ArSe_7Ar$	256 (100)	[a]
$ArSeSSeAr$	248 (100)	355 (12)
$ArSeS_2SeAr$	248 (100)	352 (3)
$ArSeS_3SeAr$	248 (100)	352 (3)
$ArSeS_4SeAr$	248 (100)	352 (3)
$ArSeS_5SeAr$	248 (100)	352 (2)

[a] Signal to noise ratio insufficient.

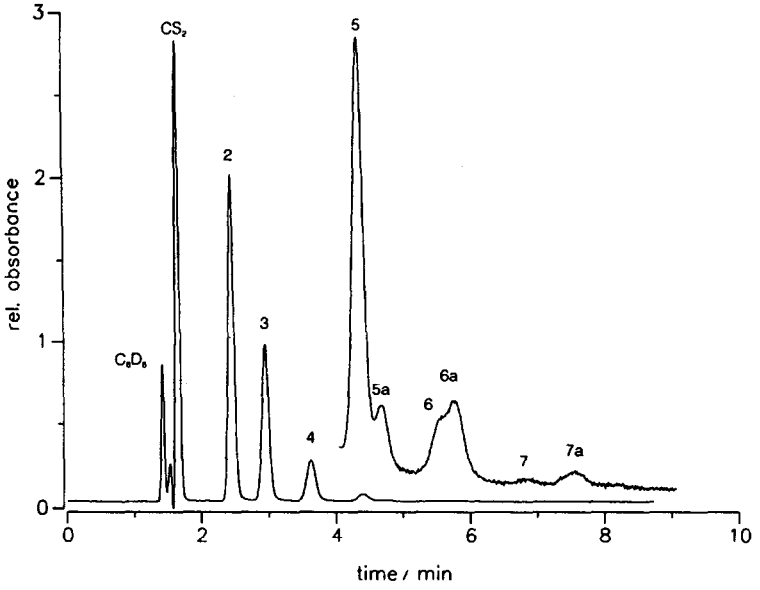

Fig. 7. HPLC analysis of the products of reaction shown in eq. (4) after storage at 20°C for 12 h. The peak numbers give the number of Se atoms in the formula R_2Se_x; peaks 5a, 6a, and 7a have not been identified.

HPLC analysis of this sample are shown in Figs 7 and 8. The chromatogram shows in decreasing concentrations R_2Se_2, R_2Se_3 and R_2Se_4 as the main constituents. Since the molar extinction coefficients must increase with the length of the selenium chain the decrease in concentration is even more dramatic than suggested by the peak areas in Fig. 7. R_2Se_5 is present in trace amounts only. In addition, there are a few very weak peaks (5a, 6, 6a, 7, 7a) of which 6 and 7 can be assigned to R_2Se_6 and R_2Se_7 on the

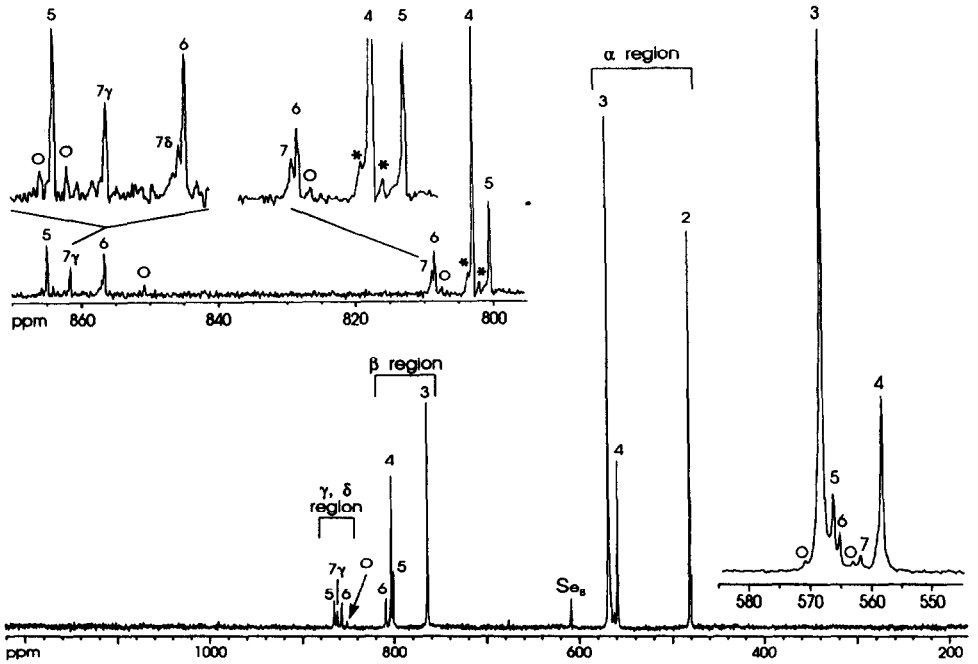

Fig. 8. ^{77}Se NMR spectrum of the mixture of R_2Se_x molecules obtained by reaction shown in eq. (4). The atom numbering α through δ is explained in Fig. 9. The numbers at the peaks give the chain-length x. Open circles indicate signals possibly arising from the minor components R_2Se_8 and R_2Se_9. The two satellites of peak 4 in the β region marked by asterisks arise from Se—Se coupling. For chemical shift data see Table 2.

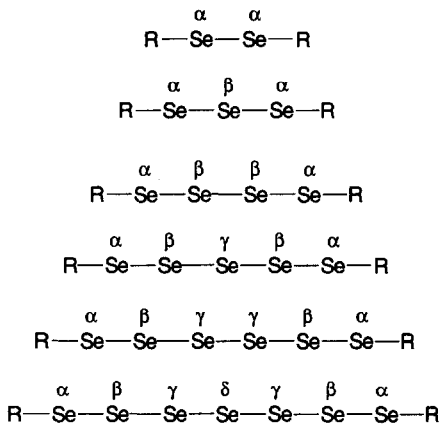

Fig. 9. Labelling of Se atoms in organic polyselanes.

basis of the linear relationship depicted in Fig. 6. The correlation coefficient of this relationship for x = 1–7 amounts to 0.9998. However, peaks 5a, 6a and 7a cannot be explained at present. No HPLC signals for Se_6, Se_7 or Se_8 could be detected. The absorption spectra of R_2Se_x molecules in methanol are characterized by two maxima in the range 200–600 nm occurring near 255 and 390 nm for x = 3–6 while for R_2Se_2 the second maximum is observed at 338 nm (see Table 3).

The complex ^{77}Se NMR spectrum of the mixture obtained by eqs (4), (7) and (8) (Fig. 8) was assigned mainly on the basis of the HPLC peak areas and taking the sparse literature data[10,11] into account. It is common practise to term the terminal Se atoms in R_2Se_x molecules as α, the neighboring atoms as β, and so forth (Fig. 9). The available data indicate that the chemical shift increases in going from α over β to γ Se atoms.[10,11] Data for δ Se atoms are known from Et_2Se_7 only.[11] Consequently, we assign the signals in the range 475–600 ppm to α Se atoms, those in the range 760–820 ppm to β atoms and signals above 820 ppm to γ and δ atoms (see Table 2). The width of the NMR lines at half height will depend on the coupling between ^{77}Se and ^{1}H, ^{13}C and other ^{77}Se atoms.

The latter should result in satellites of 3.8% the intensity of the centre line. Only in one case we observed a Se—Se coupling: the lines arising from the β Se atoms of R_2Se_4 show two satellites with a coupling constant $^2J_{Se-Se}$ of 113 Hz (see Fig. 8). All other couplings were not resolved and will contribute to the line half-width which for α Se atoms increases with the chain-length from 38 Hz for R_2Se_2 to *ca* 55 Hz for R_2Se_7. The typical half-width of the lines of β, γ and δ Se atoms is 30–40 Hz.

DISCUSSION

Our results demonstrate that titanocene polychalcogenide complexes may be used to synthesize organic selenium containing compounds of type **2** and **3**. However, only such species not containing Se—Se bonds seem to be stable enough to be isolated as pure materials. The $RSeS_5SeR$ prepared in this work as a pure material represents the longest mixed chain of chalcogen atoms ever prepared in an acyclic organic compound. And the $(RSe)_2S_y$ molecules with $y = 1$–15 as detected by HPLC form the longest series of Se containing chain-like compounds observed so far. HPLC and ^{77}Se NMR spectroscopy are ideal complementary techniques to elucidate the composition of such mixtures. The longest homoatomic Se chain detected in this work with certainty is R_2Se_7. This species is similar to the $(C_2H_5)_2Se_7$ detected in trace amounts by ^{77}Se NMR spectroscopy in an Et_2Se_x mixture prepared from EtSH and $SeOCl_2$ followed by distillation in a high vacuum; the residue thus obtained contains higher members of the series Et_2Se_x (x = 1–7).[11]

The interconversion reactions [eqs (5)–(8)] are known to be catalysed by traces of nucleophiles[2] and also by titanocene complexes.[15] Therefore, reactions shown in eqs (3) and (4) did not yield the pure compounds $(RSe)_2S_2$ and R_2Se_7 which we had expected. But nevertheless the chromatographic and spectroscopic analysis of the reaction mixtures provided valuable data about the members of the homologous series $(RSe)_2S_y$ and R_2Se_x.

Acknowledgements—Support by the Deutsche Forschungsgemeinschaft, Verband der Chemischen Industrie and Graduiertenkolleg of TU and FU Berlin is gratefully acknowledged.

REFERENCES

1. V. Münchow and R. Steudel, *Z. anorg. allg. Chem.*, in press.
2. R. Steudel and M. Kustos, in *Encyclopedia of Inorganic Chemistry* (Edited by B. King), Vol. 7. Wiley, Sussex, in press.
3. H. Rheinboldt and E. Giesbecht, *Chem. Ber.* 1955, **88**, 1.
4. R. E. Hollands, A. G. Osborne and I. Townsend, *Inorg. Chem. Acta* 1979, **37**, L541.
5. R. Steudel and M. Kustos, *Phosphorus Sulfur Silicon* 1991, **62**, 127.
6. R. Steudel, S. Förster and J. Albertsen, *Chem. Ber.* 1991, **124**, 2357.
7. R. Steudel, in *The Chemistry of Inorganic Ring Systems* (Edited by R. Steudel), Ch. 13, p. 233. Elsevier Science Publ., Amsterdam (1992).

8. M. Kustos, J. Pickardt, J. Albertsen and R. Steudel, *Z. Naturforsch.* 1993, **48b**, 928.
9. H. J. Möckel, F. Höfler and H. Melzer, *Chromatographia* 1985, **20**, 471.
10. H. Eggert, O. Nielsen and L. Henriksen, *J. Am. Chem. Soc.* 1986, **108**, 1725.
11. E. Utzel, Dissertation, Techn. Hochschule Aachen (1985).
12. R. Steudel and R. Strauss, *J. Chem. Soc., Dalton Trans.* 1984, 1775; C. M. Bolinger, J. E. Hoots and T. B. Rauchfuss, *Organometallics* 1982, **1**, 223.
13. R. Laitinen and R. Steudel, *J. Mol. Struct.* 1980, **68**, 19; R. Laitinen, R. Steudel and E.-M. Strauss, *J. Chem. Soc., Dalton Trans.* 1985, 1869.
14. R. Steudel, E.-M. Strauss and D. Jensen, *Z. Naturforsch.* 1990, **45b**, 1282.
15. D. Jensen, Dissertation, Techn. Univ. Berlin (1989).

Polyhedron Vol. 12, No. 21, pp. 2587–2591, 1993
Printed in Great Britain

0277–5387/93 $6.00+.00
© 1993 Pergamon Press Ltd

SYNTHESIS OF PILLARED SMECTITES FROM HYDROUS METAL OXIDE SOL–SMECTITE MIXTURES UNDER REFLUX CONDITIONS

S. SIVAKUMAR, K. G. K. WARRIER* and A. D. DAMODARAN

Regional Research Laboratory (CSIR), Thiruvananthapuram 695 019, India

(*Received* 16 *June* 1993; *accepted* 28 *June* 1993)

Abstract—A novel method for the synthesis of pillared smectites (cross linked intercalated smectites) by refluxing a mixture of bentonite (2 wt%) and nano hydroxy aluminium oxide (boehmite, Al—O—OH) sol in aqueous medium is reported. Mixed sol containing boehmite and hydrous cerium oxide has resulted in mixed oxide pillared smectites. The various conditions of the intercalation are reported and the characteristics of the intercalated smectites have been evaluated using XRD, surface area analysis and thermogravimetric techniques. The present method is shown to be effective in reducing the time of pillaring. High order of intercalation 20 Å and specific surface area of 260 $m^2 g^{-1}$ are achieved by this method. Further, the possibility of handling a higher concentration of the smectite, which has been a limiting factor in the usual methods, is highlighted. The dielectric constants of the dried smectites after intercalation by reflux are compared with those prepared by usual methods. The present technique of refluxing a mixture of mono ion exchanged smectite and hydrous metal oxide sols is novel due to its capability to intercalate smectites having high surface area, increased interlayer spacing and also enhanced thermal stability.

Alumino silicate minerals of the montmorillonite type, generally known as smectites, can be intercalated with suitable large size organic molecules or hydrated metal oxide clusters. Such intercalated alumino silicates have been found to possess large specific surface area and hence have gained commercial importance as catalysts. Specifically when the intercalation is done using hydroxy metal oxide oligomers, they can be dehydroxylated to metal oxide intercalated smectites or also known as pillared intercalated clays (PILC) or cross linked smectites (CLS).[1–4] Usually montmorillonite clays are used as the alumino silicate source. A dilute suspension (about 1 wt%) of the montmorillonite after mono ion exchange is mixed with intercalating species of hydrated metal oxide (aluminium, zirconium, iron etc.) and allowed to stand under constant shaking for 15–40 h. The solid is separated and washed several times and dehydroxylated.[4–6]

Some of the major difficulties involved in the synthesis of such smectites are the low solid content used in the suspension, long reaction times, control of pH and the drying and dehydroxylation.[2] The possibility of using high solid content has been reported through the hydrothermal reaction.[7] Similarly hydrated metal oxide nanosize dispersion such as sols[8,9] have been successfully used as intercalating agents associated with enhanced thermal stability. Further, microwave drying of the intercalated smectites as well as drying under supercritical condition[10] has been successful in reducing the drying time considerably. Recent studies have shown that intercalation at elevated temperature can increase the extent of pillaring.[8]

The present work is on the possibility of conducting intercalation reactions involving hydroxy metal oxide and mixed oxide sols under reflux conditions. Such intercalated smectites have been compared with those derived from sol cross linked smectites (SCLS) at a lower temperature. The rate of intercalation reaction is fast under reflux and such smectites have improved properties. Further, intercalation from a mixed sol system is also possible under reflux conditions.

*Author to whom correspondence should be addressed.

EXPERIMENTAL

The montmorillonite sample was of high purity having a cation exchange capacity of 34.4 meq g^{-1} and was characterized by the usual methods. The montmorillonite was converted to a sodium exchanged one by treating with 0.1 M NaCl under shaking for 12 h followed by centrifugal separation and repeated washing.

A suspension containing 2 wt% sodium exchanged montmorillonite and a boehmite sol[11] containing 0.25 g Al g^{-1} of montmorillonite was refluxed for a period of 2 h and kept for another 12 h. The initial pH was 4.05 which was lowered to 4.0 after the intercalation. The time of reaction was fixed after trials. Similarly, mixtures of sols in a 50 : 50 ratio were made from aluminium and cerium hydroxides and the intercalating mixture contained 2 wt% montmorillonite and 0.25 g metal g^{-1} of montmorillonite. The details of the preparation are presented in the flow chart.

The reaction mixture was centrifuged to remove the solid part and washed repeatedly with distilled water. Intercalated montmorillonite was dried at 60°C in an air oven. Part of this was heated for 2 h at 500 and 700°C. One experiment was conducted with the same mixture at 32°C for comparison. The basal spacings were detected by the XRD technique using a diffractometer (Rigaku, Japan) with Ni filtered Cu-K_α radiation. The specific surface area was measured using the BET technique (Surface Area Analyser, Micromeritics Model 2000). Thermogravimetry of the samples was done at a heating rate of 5°C min^{-1} (TGA Dupont, U.S.A.). Dielectric constants on 10 mm pellets pressed out of air dried samples were measured on an Impedence Analyser (Hewlett Packard, Switzerland).

RESULTS AND DISCUSSION

The montmorillonite sample after sodium exchange had a specific surface area of 77 m^2 g^{-1} which on intercalation with boehmite sol at 32°C gave a value of 160 m^2 g^{-1}. On the other hand, the mixed sol intercalation gave only about 105 m^2 g^{-1}. The reflux method resulted in values as high as 213 m^2 g^{-1} in the case of boehmite sol and a still higher value of 265 m^2 g^{-1} for the boehmite-hydrous ceria sol in a 1 : 1 ratio. The possibility of delamination under the reflux conditions and also control of the optimum pH would have assisted the cationic species to attach themselves in the interlayer space as pillars. The

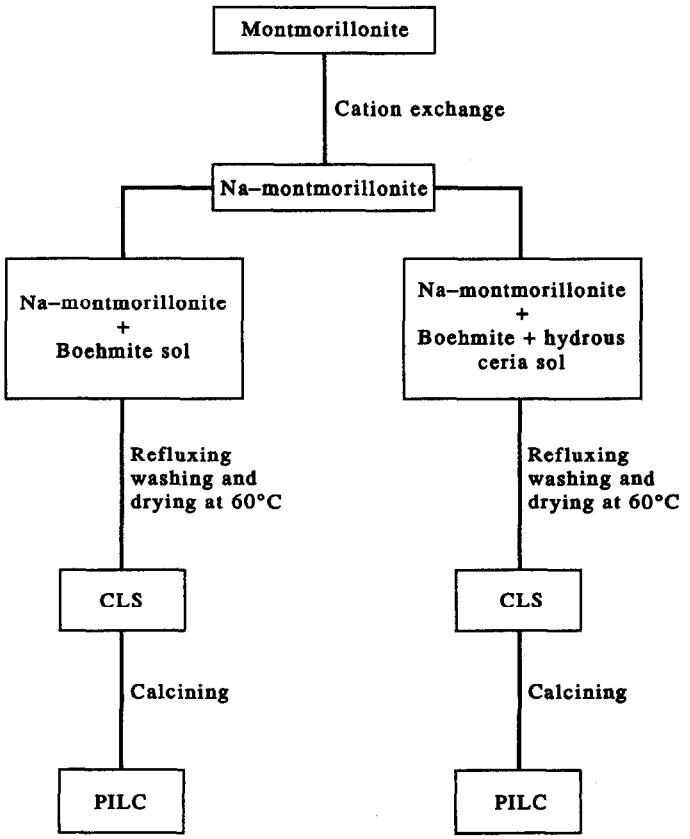

polymerized molecular aggregates of the sol could hold on to the reactive sites in the delaminated montmorillonite layers and thus resulted in high surface areas. From the specific surface area values of intercalated smectites between the reflux and low temperature conditions, it is reasonable to assume a sort of staggered pillaring pattern to prop up the layers of the smectites. The high values also indicate the efficiency of reflux method within short reaction time. Even after heating above 700°C over a fairly long period, these values have remained above 175 $m^2 g^{-1}$ which is quite reasonable for such intercalated smectites.[8,9]

The XRD patterns of the mono ion exchanged montmorillonite, boehmite and boehmite–hydrous ceria sols at 32°C and at reflux conditions are presented in Fig. 1. The relevant XRD peaks characteristic of the basal plane are presented in Table 1. The montmorillonite as received had a basal spacing of 12 Å which increased on sodium exchange to 13.19 Å. Intercalation experiments conducted in the usual manner[8,9] at 32°C resulted in the increase of basal value to 18.03 and 13.99 Å in the case of boehmite and boehmite–ceria mixed sol, respectively. There was only marginal improvement in the mixed sol probably because of the lack of sufficient delamination of the smectite layers to allow the fairly large size mixed cationic species in the aqueous suspension. The possible staggered intercalation is also reflected in the broad XRD peaks in this sample. However, under reflux conditions the intercalation has taken place to considerable extent resulting in an increase of basal spacing to 20.08 and 20.55 Å, respectively for boehmite and boehmite–ceria mixed sol. Further, there was only marginal reduction in the basal spacing of these samples after heat treatment above 500°C to 18.88 and 18.81 Å, respectively, being still fairly stable up to 700°C.

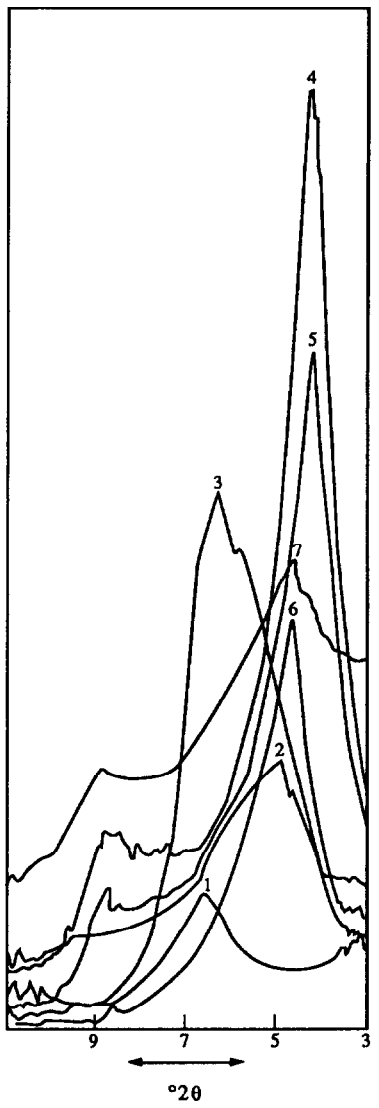

Fig. 1. XRD patterns of: (a) Na-montmorillonite; (2) Boehmite intercalated at 32°C; (3) Boehmite–ceria sol mixed intercalated at 32°C; (4) Boehmite intercalated at reflux condition; (5) Boehmite–ceria intercalated at reflux condition; (6) Boehmite intercalated at reflux condition (500°C) and (7) Boehmite–ceria intercalated at reflux condition (500°C).

Table 1. Basal spacings of intercalated montmorillonite

No.	Sample	Basal spacing (001) Å: As intercalated	Basal spacing (001) Å: After calcination at 500°C
1.	Boehmite intercalated at 32°C	18.03	16.36
2.	Boehmite intercalated at reflux condition	20.08	18.88
3.	Boehmite–ceria sol mixed intercalated at 32°C	13.99	—
4.	Boehmite–ceria sol mixed intercalated at reflux condition	20.55	18.81

The thermal stability and dehydroxylation characteristics have been followed from the data on thermogravimetric analysis presented in Fig. 2. The boehmite and mixed sol intercalated smectite under reflux conditions had total volatiles of about 25 and 22%, respectively, while the one prepared from mixed sol at 32°C had only about 18%. There appears a clear difference in the decomposition between these samples. While the boehmite interca-

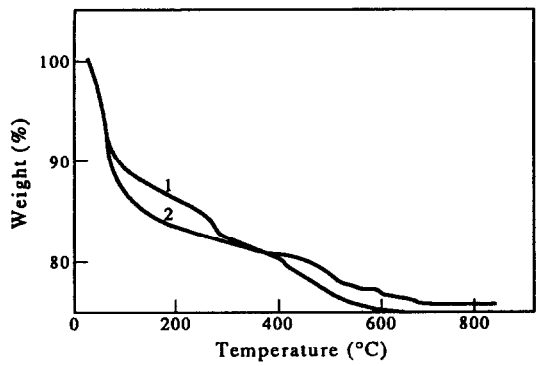

Fig. 2. Thermogravimetric analysis of: (1) Boehmite intercalated at reflux condition and (2) Boehmite–ceria sol mixed at reflux condition.

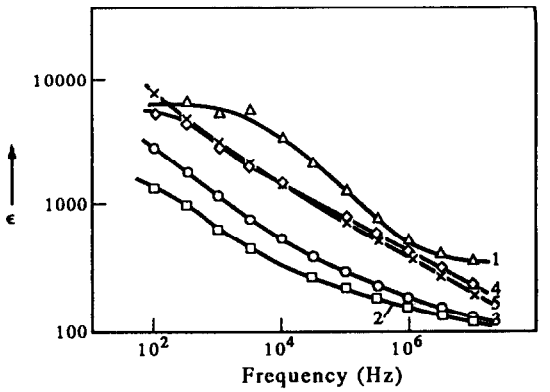

Fig. 3. Dielectric constant (ε) *vs* frequency curve of: (1) Na-montmorillonite; (2) Boehmite intercalated at reflux condition; (3) Boehmite intercalated at 32°C; (4) Boehmite–ceria sol mixed intercalated at reflux condition and (5) Boehmite–ceria sol mixed intercalated at 32°C.

lated one has a two step decomposition pattern, the mixed sol one has those above 600°C. This probably indicates the staggered intercalated pattern. The two major decompositions of the boehmite intercalated smectite are at 280 and 500°C. On the other hand, the mixed sol intercalated montmorillonite eliminates the major portion of the hydroxyls above 600°C indicating the increased stability of the latter. The mixed sol intercalated smectite sample at 32°C has very small loss by weight above 600°C, indicating a relatively low level of intercalation, with reasonable stability. Therefore, intercalation from mixed sols could provide enhanced stability to CLS in any case; which is further supported by the observation that there is only a 20% loss of specific surface area in the case of the mixed sol intercalated samples, in the present experiment.

The dielectric constant is a direct measure of the charge carriers in a material and in the present set of materials the major charge carriers are the hydroxyls and impurity ions. In layered aluminosilicates dipolarity as well as space charge polarization are the major mechanisms of electrical condition and hence the dielectric constant values could be indicative of the intercalated species. It is seen from Fig. 3 that the sodium exchanged montmorillonite has the higher dielectric constant which decreases over a range of temperatures. As usual, the dielectric constant decreases with frequency. This is naturally so, the high order of sodium ions which are also charge carriers, present in the mono ion exchanged smectite result in higher order of dielectric constant. This is true as shown in Fig. 3 on intercalation, the sodium ions are substituted by a hydrogen bonded large hydroxy metal oxide network and hence the number of charge carriers decreases as is evident from Fig. 3. There is only a slight difference in the dielectric constant values corresponding to samples derived from the mixed boehmite and ceria sols, irrespective of the temperature of intercalation. Between the two there is marginal enhancement in loss in the case of refluxed sample compared to that prepared at 32°C. Furthermore, there is a reduction in surface area and line broadening due to the disordered pillaring. On the other hand, the intercalation from a boehmite sol, is distinctly clear because of the maximum substitution of sodium ions by aluminium ions. In this case, there is considerable difference in the extent of intercalation between the samples prepared at 32°C and at reflux condition. All the differences are more pronounced at the low frequency range of 1–10 MHz and the difference slowly narrows down as the frequency increases. This clearly shows that the dipolar and space charge polization effects cause the change in dielectric constant values. The extent of intercalation can thus indirectly be derived based on the electrical measurements.

CONCLUSION

Intercalation reactions under reflux conditions of a mixture of mono ion exchanged smectite and nano dispersed hydroxy metal oxide sol, have shown an enhanced value of specific surface area, thermal stability and interlayer spacing. These values have been compared with those obtained through methods already reported for such intercalation reactions. The possibility of starting with high concentrations of smectite suspension and short reaction time are also highlighted. The method is also convenient to intercalate smectite from mixed sols.

Intercalated smectites using boehmite sol under reflux condition resulted in a specific surface area of 213 $m^2 g^{-1}$ as compared to 159 $m^2 g^{-1}$ obtained through the usual method at 32°C. Similarly, the intercalation done by reflux from a mixed sol system containing 1 : 1 boehmite and hydrous cerium oxide reached a specific surface area of 255 $m^2 g^{-1}$ against 105 $m^2 g^{-1}$ obtained in the usual way. The initial basal spacing of 13.19 Å was elevated to 20.08 and 20.55 Å in the case of boehmite and mixed sols under reflux conditions. Thermal treatment at 700°C brought down the specific surface area to about 22% in the case of boehmite and 25% in the case of mixed sol intercalation. The dielectric constant of the dried intercalated smectite as a function of frequency has been presented and indicated towards the extent of intercalation.

Acknowledgement—This work has been supported by the Department of Science and Technology, Government of India through project number SP/SI/40/2/91. The authors are grateful to Dr Sobhan Ghosh and Dr H. S. Ray of Indian Oil Corporation R&D, Faridabad, India for constant interaction in this work. Thanks are due to Mr K. T. Govindankutty, United Catalyst India Ltd, R&D, Kerala, India for the surface area measurements. One of the authors, S. Sivakumar is thankful to DST for a Research Fellowship.

REFERENCES

1. T. J. Pinnavaia, *Science* 1983, **220**, 365.
2. F. Figueras, *Catal. Rev. Sci. Eng.* 1988, **30**, 457.
3. D. W. E. Vaughan, *Catal. Today* 1988, **2**, 187.
4. T. J. Pinnavaia, M. S. Tzou, S. D. Landau and R. H. Raythatha, *J. Mol. Catal.* 1984, **27**, 195.
5. S. Yamanaka and G. W. Brindley, *Clays and Clay Min.* 1979, **27**, 119.
6. D. H. Doff, N. H. J. Gangast, J. E. M. Allan and J. M. D. Coey, *Clay Min.* 1988, **23**, 367.
7. R. Molina, A. Vieira-Coelho and G. Poncelet, *Clays and Clay Min.* 1992, **40**, 480.
8. Swapankumar Ghosh, P. Mukundan, K. G. K. Warrier and A. D. Domadaran, *J. Mat. Sci. Lett.* 1991, **10**, 1193.
9. S. Yamanaka and M. Hattori, *Chemistry of Microporous Materials* (Edited by T. Inui, S. Namba and T. Tatsumi), pp. 89–96. Elsevier, Tokyo (1991).
10. K. Thakhama, M. Yokoyama and S. Yamanaka, *J. Mater. Sci.* 1992, **27**, 1297.
11. A. C. Pierre, D. R. Uhlmann, John D. Mackenzie and Donald R. Ulrich, Eds. *Ultrastructure Processing of Advanced Ceramics*, pp. 865–871. Wiley Interscience, New York (1988).

Polyhedron Vol. 12, No. 21, pp. 2593–2602, 1993
Printed in Great Britain

0277–5387/93 $6.00+.00
© 1993 Pergamon Press Ltd

AMINE COMPLEXES OF TUNGSTEN(II) AND MOLYBDENUM(II): $M(NH_2R)Cl_2(PMePh_2)_3$ AND $M(NH_2CH_2CH_2NH_2)Cl_2(PMePh_2)_2$

DIANA E. OVER* and JAMES M. MAYER†

Department of Chemistry BG-10, University of Washington, Seattle, WA 98195, U.S.A.

(*Received* 24 *March* 1993; *accepted* 10 *June* 1993)

Abstract—Addition of primary amines or ammonia to solutions of $WCl_2(PMePh_2)_4$ (**1**) or $MoCl_2(PMePh_2)_4$ (**6**) results in the formation of $[M(NH_2R)Cl_2(PMePh_2)_3]$ (M=W (**2**), Mo (**7**); R=H, Me, ^{n}Pr, ^{i}Pr, C_6H_{11}, CH_2CF_3, or $CH_2CH{=}CH_2$). With larger secondary amines, no reaction is observed, except for a transient adduct of aziridine. Ethylenediamine substitutes for two phosphines, forming $M(en)Cl_2(PMePh_2)_2$, but further substitution has not been observed even in neat ligand. Reactions of $[WCl_2(CH_2{=}CH_2)_2(PMePh_2)_2]$ (**4**) with NH_2Me and $NH_2{}^nPr$ yield equilibrium amounts of amine–ethylene complexes $[W(NH_2R)Cl_2(CH_2{=}CH_2)(PMePh_2)_2]$ (**5**) plus ethylene. The characterization of these compounds by paramagnetic NMR, IR, and mass spectra is described. The amine complexes do not lose hydrogen to form imido complexes, in contrast to the analogous reactions of alcohols and thiols with **1** which yield oxo and sulphido complexes. This appears to be related to the lower acidity of amines versus alcohols and thiols.

Amine complexes are the wellspring of coordination chemistry, and have been widely studied for first-row transition metals and for the later second and third row metals (groups 8–11). There has been much less work on amine complexes of the earlier transition metals, particularly for the +2 and +3 oxidation states which dominate the chemistry of first-row transition metal amine compounds.[1–3] The early transition metals in their lower oxidation states have a tendency to form metal–metal bonds and are often quite reducing (in the absence of carbonyl ligands), both of which hinder the formation of monomeric amine complexes.

Our interest in tungsten(II) and molybdenum(II) complexes derives from their reducing nature and their desire to form metal–ligand multiple bonds.[4–13] WCl_2L_4 (**1**, L = $PMePh_2$ throughout this report) removes oxygen atoms from a wide range of substrates, for instance reacting with water to form hydrogen and the tungsten(IV) oxo complex $W(O)Cl_2L_3$ (eq.1).[6] Similarly, reaction of **1** with alcohols forms both oxo and alkoxide compounds and thiols are reduced by **1** to alkanes and a terminal sulfido complex (eqs 2, 3).[6]

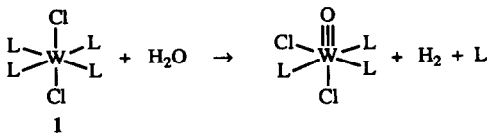
(1)

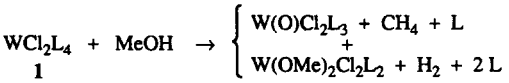
(2)

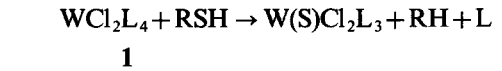
(3)

We report here[14] that the analogous reaction with amines do not yield the imido compounds $W(NR)Cl_2L_3$, even though stable tungsten(IV)–imido complexes are well established for a range of R groups.[15] Instead, novel amine adducts are formed through substitution of a phosphine ligand with an amine. The characterization of these tungsten and molybdenum amine complexes, expecially their paramagnetic ^{1}H NMR spectra, is also described.

EXPERIMENTAL

General considerations

All experiments were performed in a nitrogen atmosphere using standard high vacuum line or Schlenk techniques and a glove box. Solvents were

* Current address: Université René Descarte, Paris, France.

† Author to whom correspondence should be addressed. US NSF Presidential Young Investigator, 1988–1993.

degassed and dried by standard methods,[16] as were the amine reagents (Aldrich) except NH_3, NH_2Me, and $NHMe_2$ (Matheson) which were used without purification directly from their cylinders. NMR spectra were obtained using a Varian VXR-300 Fourier Transform spectrometer. The chemical shifts in ^1H NMR spectra are given in ppm relative to the solvent peak (C_6D_6). Two-dimensional NMR spectra for $Mo(NH_2Me)Cl_2L_3$ (**7b**) and $Mo(en)Cl_2L_2$ (**8**) were obtained from a two-dimensional homonuclear Hartmann–Hahn (HOHAHA) experiment as previously described.[17] IR spectra were obtained as nujol mulls on NaCl plates with a Perkin–Elmer FT1604 spectrometer and are reported in cm^{-1}. FAB-mass spectra were acquired using a VG 70 SEQ tandem hybrid instrument (VG Analytical, Altrincham, U.K.). The instrument was equipped with a standard unheated VG FAB ion source and a standard saddlefield gun (Ion Tech Ltd, Middlesex, U.K.) producing a beam of xenon atoms at 8 keV and 1mA. The mass spectrometer was adjusted to a resolving power of 1000 and spectra were obtained at 8 kV and at a scan speed of 10 s per decade. Either 3-nitrobenzylalcohol or thioglycerol was used as the matrix in the positive ion FAB/MS mode. All apectral data are given in Table 1. Elemental analyses were performed by Canadian Microanalytical Service Ltd. (Delta, British Columbia).

Some reactions were performed in an NMR tube. In a typical procedure, a benzene-d_6 solution of 15 mg (0.014 mmol) WCl_2L_4 was loaded in the glovebox into an NMR tube sealed to a ground glass joint. Ethylenediamine [1×10^{-3} cm^3 (= 1 μl), 0.014 mmol] was added (gases were vacuum transferred on the vacuum line), the NMR tube was capped with a teflon valve, and removed to a vacuum line where the reaction solution was cooled to $-196°C$, evacuated and flame sealed. All spectra were taken at 25°C.

$WCl_2(PMePh_2)_4$ (**1**), $WCl_2(CH_2{=}CH_2)_2(PMePh_2)_2$ (**4**),[18] and $MoCl_2(PMePh_2)_4$ (**6**)[12] we prepared following published procedures.

Syntheses

The following procedure is representative for the preparation of all tungsten- or molybdenum-amine adducts.

$W(NH_2Me)Cl_2(PMePh_2)_3$ (**2b**). To a suspension of 0.25 g (0.24 mmol) WCl_2L_4 (**1**) in 30 cm^3 pentane, a 10-fold excess of NH_2Me (1 cm^3, 2.4 mmol) was added via vacuum transfer. The mixture was stirred at room temperature under an atmosphere of argon overnight. Within the first hour red solids have already formed. The next day the red solids are filtered and washed with fresh pentane and dried *in vacuo*; yielding 0.17 g, 83%. The solids can be recrystallized from toluene and pentane. Isolated yields for the tungsten amine adducts $W(NH_2R)Cl_2L_3$ were as follows: **2a** (NH_3) 79%; **2b** (NH_2Me) 83%; **2c** ($NH_2{}^nPr$) 81%; **2d** ($NH_2{}^iPr$) 84%; **2e** ($NH_2C_6H_{11}$) 81%; **3** (en) 74% Yields for the molybdenum derivatives were: **7a** (NH_3) 76%; **7b** (NH_2Me) 86%; **7c** ($NH_2{}^nPr$) 60%; **7d** ($NH_2{}^iPr$) 65%; **7e** ($NH_2C_6H_{11}$) 95%; **8** (en) 70%. Analytical data: Found for $W(NH_2Me)Cl_2L_3$ (**2b**) $WCl_2NP_3C_{40}H_{44}$: C, 54.5; H, 6.1; N, 1.6. Calc. C, 54.2; H, 5.0; N, 1.6%. Found for $Mo(NH_3)Cl_2L_3$ (**7a**) $MoCl_2NP_3C_{39}H_{42}$: C,60.1; H, 5.4; N, 1.8. Calc.: C, 59.7; H, 5.4; N, 1.8. Found for $Mo(NH_2Me)Cl_2L_3$ **7b**, $MoCl_2NP_3C_{40}H_{44}$: C, 60.3; H, 5.6; N, 1.8. Calc.: C, 60.2; H, 5.6; N, 1.7%.

RESULTS

Syntheses

The tungsten(II) complex $WCl_2(PMePh_2)_4$ (**1**) reacts at ambient temperatures with primary amines and ammonia to form the tungsten(II)–amine adducts $W(NH_2R)Cl_2L_3$ (**2**) (eq. 4).

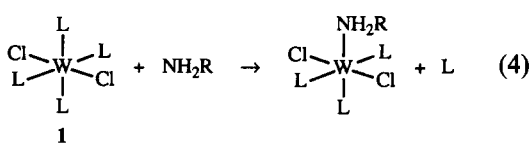

(4)

1

NH_2R = NH_3 (**2a**), NH_2Me (**2b**), $NH_2{}^nPr$ (**2c**) $NH_2{}^iPr$ (**2d**), NH_2–⬡ (**2e**), $NH_2CH_2CF_3$ (**2f**)

The reaction goes to completion in 5–10 min, and the resulting compounds vary in colour from deep orange to bright red depending on the amine. Even in the presence of a large excess of the amine, no further substitution is observed. Monitoring the reactions by NMR show the concurrent formation of one equivalent of free $PMePh_2$. Isolation of **2a–2e** is best accomplished in pentane, a solvent in which the starting material and product are only slightly soluble. The reaction proceeds readily in other solvents, such as toluene or benzene, but the products are usually isolated as oils, typically contaminated with free phosphine. In pentane, the liberated phosphine is in solution and the products precipitate as they are formed—the suspension of **1** slowly becomes a suspension of **2**. Compounds **2a–2e** have been isolated as air sensitive solids in *ca* 80% yield, while the trifluoroethyl amine adduct **2f** has only been observed by NMR. The complexes were identified by ^1H NMR, IR

and FAB/MS spectroscopies and magnetic susceptibility measurements, as described below.

The tungsten(II) amine complexes **2** are stable for a couple of months in the solid state when stored under nitrogen, but decompose in THF in about 2 h, and in benzene solutions over a period of 2 weeks. The decomposition products have not been identified. Generally, decomposition in solution gives dark, paramagnetic solids, which do not give NMR spectra even when dissolved in other solvents. In some cases, small amounts of WCl_3L_3[11] are observed.

One equivalent of *t*-butyl amine does not react with **1** over a week at ambient temperatures. But with 10 equivalents of $NH_2{}^tBu$, the solution turns from the yellow colour of **1** to orange within minutes, and ^1H NMR spectra show peaks characteristic of the tungsten–amine adducts. Allyl amine, $NH_2CH_2CH{=}CH_2$, reacts rapidly with **1** to form a red amine adduct, $W(NH_2CH_2CH{=}CH_2)Cl_2L_3$ (**2g**) from **1** (by NMR), but this is completely decomposed within 15 min in benzene solution. The NMR spectrum indicates that only the nitrogen of the allyl group is coordinated (see below). No reaction has been observed with secondary amines or with aniline (NH_2Ph) at 25°C (heating the solution causes decomposition of **1**, as in the absence of amine). Aziridine, $HNCH_2CH_2$, a very small secondary amine, does rapidly form a red adduct (**2h**), whose NMR is indicative of an amine adduct (Table 1).[19] This species reacts further within minutes at ambient temperatures to form the tungsten(IV) imido products $W(NH)Cl_2L_3$ and $W(NH)Cl_2(CH_2{=}CH_2)L_2$ (eq. 5).[7] Tertiary aziridines $RNCH_2CH_2$ also yield imido products, although more slowly and simple adducts are not observable.[7]

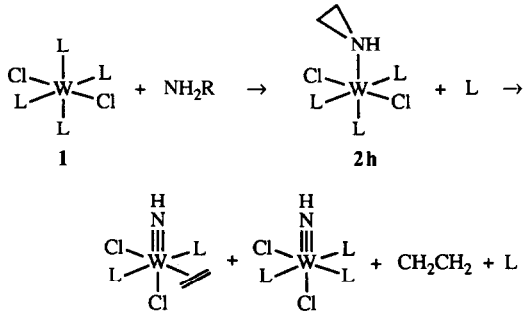

(5)

Complex **1** reacts upon mixing with ethylenediamine ($NH_2CH_2CH_2NH_2$=en) to form $W(NH_2CH_2CH_2NH_2)Cl_2L_2$, **3** (eq. 6), with substitution of two phosphine ligands. This red, paramagnetic complex has been isolated in 74% yield. It displays a greater stability than the other monodentate amine complexes, as benzene and THF solutions are stable for weeks.

$$\underset{\mathbf{1}}{WCl_2L_4} + NH_2CH_2CH_2NH_2 \rightarrow \underset{\mathbf{3}}{W(NH_2CH_2CH_2NH_2)Cl_2L_2} + 2L \quad (6)$$

The tungsten(II) bis-ethylene complex, $WCl_2(CH_2{=}CH_2)_2L_2$ (**4**)[18a] reacts at ambient temperatures with the primary amines NH_2Me and $NH_2{}^nPr$ with loss of one equivalent of ethylene, to form $W(NH_2R)Cl_2(CH_2{=}CH_2)L_2$ (R=Me, **5b**, ^nPr, **5c**; eq. 7). These products are formed in equilibrium with **4** and have not been isolated; they have been characterized by ^1H NMR. The equilibrium in eq. 6 can also be established by addition of excess ethylene to the methylamine adduct **2b**; addition of one equivalent of ethylene to **2c** gives **5c**.

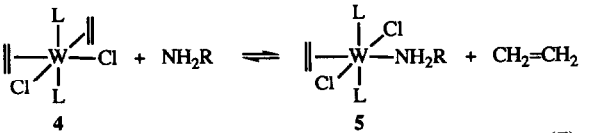

(7)

The molybdenum complex analogous to **1**, $MoCl_2L_4$ (**6**), reacts similarly with primary amines to form bright red molybdenum(II) amine adducts, $Mo(NH_2R)Cl_2L_3$ (**7**), within minutes (eq. 8). These complexes are isolated from pentane in 60–95% yield. Ethylenediamine also displaces two phosphines from molybdenum, producing the complex $Mo(en)Cl_2L_2$ (**8**).

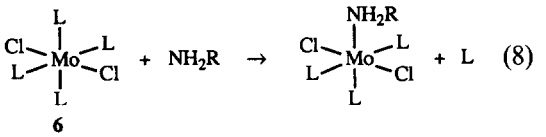

(8)

NH_2R = NH_3 (**7a**), NH_2Me (**7b**), $NH_2{}^nPr$ (**7c**) $NH_2{}^iPr$ (**7d**), NH_2–⬡ (**7e**)

Spectroscopic characterization

The identification of the amine adducts is based primarily on ^1H NMR, IR and mass spectral data, which are given in Table 1. The FAB mass spectra of compounds **2** and **7** typically show a parent ion for $M(NH_2R)Cl_2L_3$ and peaks corresponding to loss of the amine, loss of a phosphine, and loss of both the amine and a phosphine. The $[MCl_2L_2]$ fragment is thus observed in all the spectra (568 for M=Mo; 654, 656 for M=W). The ethylenediamine complexes **3** and **8** show peaks corresponding to M^+ and M^+-$PMePh_2$. In all cases the complex envelope of peaks for each ion matches the calculated isotopic abundances quite well.

The IR spectra of the isolated amine complexes all show two N–H stretches, in the range of 3240–

Table 1. Spectroscopic Data

Compound (L = $PMePh_2$)	^1H NMR[a,b] phenyl resonances[b]	^1H NMR[a,b] methyl resonances	^1H NMR[a,b] amine resonances[e]	IR[c] ν_{NH} (cm^{-1})	FAB–MS[d] M^+ (calc.)
$W(NH_3)Cl_2L_3$ (**2a**)	11.92 (s, 8H), 8.40 (s, 4H) (*ortho*) 8.91 (d, 8H), 10.36 (d, 4H) (*meta*) 10.75 (t, 4H), 10.13 (t, 2H) (*para*)	4.47 (s, 3H) −3.62 (s, 6H)		3340, 3256	871, 873 (871, 873)
$W(NH_2Me)Cl_2L_3$ (**2b**)	11.63 (s, 8H), 8.57 (s, 4H) (*ortho*) 8.85 (d, 8H), 9.95 (d, 4H) (*meta*) 10.72 (t, 4H), 10.26 (t, 2H) (*para*)	3.11 (s, 3H) −3.59 (s, 6H)	5.89 (s, 3H) (CH_3)	3315, 3270	687 (687) (M^+–$PMePh_2$)
$W(NH_2{}^nPr)Cl_2L_3$ (**2c**)	11.38 (s, 8H), 8.51 (s, 4H) (*ortho*) 8.87 (d, 8H), 9.95 (d, 4H) (*meta*) 10.65 (t, 4H), 10.23 (t, 2H) (*para*)	2.59 (s, 3H) −3.61 (s, 6H)	5.25 (t, 3Hz, 3H) (CH_3) 8.16 (s, 2H) (CH_2) 12.00 (s, 2H) (CH_2)	3298, 3265	914, 916[f] (913, 915)
$W(NH_2{}^iPr)Cl_2L_3$ (**2d**)	10.54 (s, 8H), 7.89 (s, 4H) (*ortho*) 8.75 (d, 8H), 9.63 (d, 4H) (*meta*) 10.32 (t, 4H), 10.14 (t, 2H) (*para*)	1.93 (s, 3H) −2.46 (s. 6H)	6.56 (s, 6H) (CH_3) 3.00 (m, 1H) (CH)	3289, 3248	913, 915 (913, 915)
$W(NH_2C_6H_{11})Cl_2L_3$ (**2e**)	10.61 (s, 8H), 7.89 (s, 4H) (*ortho*) 8.77 (d, 8H), 9.66 (d, 4H) (*meta*) 10.36 (t, 4H), 10.15 (t, 2H) (*para*)	1.92 (s, 3H) −2.47 (s, 6H)	2.79 (m, 4H) 4.39 (m, 4H) 4.10 (m, 2H) 9.15 (s, 1H) ($C\underline{H}NH_2$)	3290, 3268	755 (755) (M^+–$PMePh_2$)
$W(NH_2CH_2CF_3)Cl_2L_3$ (**2f**)	10.97 (s, 8H), 7.90 (s, 4H) (*ortho*) 8.81 (d, 8H) (*meta*) 10.60 (t, 4H) (*para*) 10.09 (d, 6H) (*meta and para*)	3.66 (s, 3H) −3.08 (s, 6H)			
$W(NH_2CH_2CH{=}CH_2)Cl_2L_3$ (**2g**)	11.43 (s, 8H), 8.43 (s, 4H) (*ortho*) 8.86 (d, 8H), 10.01 (d, 4H) (*meta*) 10.68 (t, 4H), 10.21 (t, 2H) (*para*)	2.83 (s, 3H) −3.62 (s, 6H)			
$W(H\overline{NCH_2CH_2})Cl_2(PMePh_2)_3$ (**2h**)[g]	10.72 (s, 8H), 7.53 (s, 4H) (*ortho*) 8.98 (s, 8H), 9.84 (s, 4H) (*meta*) 10.21 (s, 4H), 10.28 (s, 2H) (*para*)	4.28 (s, 3H) −1.54 (s, 6H)	7.95 (m, 2H) 6.83 (s, 2H) ($C\underline{H}H'C\underline{H}H'$)		
$W(en)Cl_2L_2$ (**3**)	11.59 (s, 8H) (*ortho*) 9.86 (d, 8H) (*meta*) 11.30 (t, 4H) (*para*)	3.56 (s, 6H)	12.99 (s, 4H) (CH_2CH_2)	3323, 3240	714, 716 (714, 716)

$W(NH_2Me)(CH_2{=}CH_2)Cl_2L_2$ (**5b**)	11.54 (s, 8H) (*ortho*) 8.77 (d, 8H) (*meta*) 10.00 (t, 4H) (*para*)	−8.25 (s, 6H)			
$W(NH_2{}^nPr)(CH_2{=}CH_2)Cl_2L_2$ (**5c**)	11.37 (s, 8H) (*ortho*) 8.76 (d, 8H) (*meta*) 10.00 (t, 4H) (*para*)	−8.42 (s, 6H)			
$Mo(NH_3)Cl_2L_3$ (**7a**)	9.2–10.3 (br s, 12H) (*ortho*) 6.54 (s, 8H), 8.05 (s, 4H) (*meta*) 10.48 (s, 4H), 10.79 (s, 2H) (*para*)	−16.26 (br s, 6H) −8.71 (br s, 3H)		3353, 3270	785 (785)
$Mo(NH_2Me)Cl_2L_3$ (**7b**)	9.1 to 10.4 (br s, 12H) (*ortho*) 6.55 (s, 8H), 7.61 (s, 4H) (*meta*) 10.53 (s,. 4H), 10.81 (s, 2H) (*para*)	−16.45 (br s, 6H) −9.88 and −8.49 (both br s, 3H) ($PC\underline{H}_3$ and $NH_2C\underline{H}_3$)		3325, 3280	799 (799)
$Mo(NH_2{}^nPr)Cl_2L_3$ (**7c**)	9.2 to 10.2 (br s, 12H) (*ortho*) 6.59 (s, 8H), 7.64 (s, 4H) (*ortho*) 10.43 (s, 4H), 10.78 (s, 2H) (*para*)	−16.18 (br s, 6H) −10.36 (br s, 3H)	2.37 (s, 3H) (CH_3)	3307, 3262	828[h] (827)
$Mo(NH_2{}^iPr)Cl_2L_3$ (**7d**)	8.4 to 9.9 (br m, 12 H) (*ortho*) 6.59 (s, 8H), 7.41 (s, 4H) (*meta*) 10.15 (s, 4H), 10.62 (s, 2H) (*para*)	−15.18 (br, 6H) −11.22 (br s, 3H)		3300, 3252	828[h] (827)
$Mo(NH_2C_6H_{11})Cl_2L_3$ (**7e**)	8.1 to 10.1 (br s, 12H) (*ortho*) 6.57 (s, 8H), 7.36 (s, 4H) (*meta*) 10.18 (s, 4H), 10.65 (s, 2H) (*para*)	−15.19 (br s, 6H) −11.41 (br s, 3H)		3287, 3257	867 (867)
$Mo(en)Cl_2L_2$ (**8**)	11.1 to 11.7 (br s, 8H) (*ortho*) 7.08 (s, 8H) (*meta*) 11.76 (s, 4H) (*para*)	−8.28 (br s, 6H)	−4.25 (br s, 4 H) (CH_2CH_2)	3332, 3248	628 (628)

[a] Spectra taken in C_6D_6 solution and reported as chemical shift (multiplicity, coupling constant, # hydrogens), with chemical shifts given in ppm relative to the solvent peak. br = broad, s = singlet, d = doublet, t = triplet, m = mutiplet.

[b] Phenyl resonances reported as chemical shift (multiplicity, # hydrogens); the coupling constants, when observed, are all 6 or 7 Hz and are not listed here.

[c] IR spectra obtained as Nujol mulls.

[d] The largest peak(s) in the highest mass envelope reported, either the parent ion or, when noted, M^+-$PMePh_2$. In all cases, the observed envelope closely matches the calculated isotope abundances.

[e] Not all amine resonances were observed, especially for the molybdenum complexes due to the breadth of some of the peaks.

[f] Observed masses 913.7 and 915.7. The envelope is only very slightly shifted from that of the ^{i}Pr derivative **2d**, and closely matches the calculated isotopic abundances.

[g] Spectrum taken at 5°C.

[h] Observed mass 827.6. The observed envelope closely matches the calculated isotopic abundances.

3350 cm^{-1}. This implies the presence of an NH_2 group in each compound and indicates that the amine ligand is intact, rather than, for instance, having oxidatively added to the metal centre to form an amide–hydride complex.

The amine complexes are paramagnetic, as indicated by the wide range of chemical shifts observed in their ^1H NMR spectra, from $\delta + 12$ to -17. The magnetic susceptibilities of $W(NH_2{}^iPr)Cl_2L_3$ (**2d**), $Mo(NH_2Me)Cl_2L_3$ (**7b**), and $Mo(NH_2{}^iPr)Cl_2L_3$ (**7d**), determined on a Faraday balance, are 1.7, 2.45 and 2.49 BM, respectively. The values are consistent with a description of these molecules as low-spin d^4 octahedral species (four electrons in the "t_{2g} set"), as has been concluded for a number of related d^4 phosphine complexes of the second- and third-row transition metals.[20] The magnetic moments are less than the spin-only value for complexes with two unpaired electrons, 2.83 BM, especially for the tungsten complex, probably due to large spin-orbit coupling.

The ^1H NMR spectra of the amine complexes (Table 1) contain a great deal of information about the composition and structure of these molecules, although the interpretation is complicated by the absence of standard chemical shift information because of the paramagnetic shifting. The tungsten compounds **2**, **3**, and **5** give spectra that are in places sharp enough to see spin–spin coupling, but spectra of the molybdenum analogues are invariably broader (see Fig. 1). This is a typical feature of these paramagnetic, low-spin d^4 octahedral complexes.[11,20] For the tungsten compounds which exhibit sharp peaks, the paramagnetic shifting is an advantage because the resonances are well separated and there is little likelihood of two peaks being accidentally degenerate. Assignments have been made based on integrals and coupling, the latter either observed directly or using two-dimensional NMR spectra with a HOHAHA (homonuclear Hartmann–Hahn) pulse sequence (Fig. 2).[17] The two-dimensional experiments can be of great assistance in assigning these paramagnetic spectra.

The ^1H NMR spectra of the $W(NH_2R)Cl_2L_3$ compounds (**2**) (Table 1) have a distinctive pattern of peaks that are independent of the amine used in the reaction, due to the three $PMePh_2$ ligands (Fig. 1, top), In the range of 8 to 11 ppm, the spectra exhibit two doublets, two broad signlets, and two triplets with intensities 8:4:8:4:4:2. These are due to six phenyl groups in a 4:2 ratio, with less intense triplets for the para hydrogens. Irradiation of the triplets in the spectrum of **2d** causes collapse of the doublets, indicating that the doublets should be assigned as the meta protons. The broadened peaks are therefore the ortho protons, consistent with their closer proximity to the metal centre. There are also two broad singlets due to the phosphine methyl groups (ratio 6:3), the larger having a chemical shift between -2 and -4 ppm and the smaller appearing between 2 and 5 ppm.

The spectra show that two of the three coordinated phosphine ligands are equivalent, and that none of the pairs of phenyl groups are diastereotopic. This is consistent only with the C_{2v} *meridional-trans* structure shown in eqs 4 and 8. The other possible isomers, *meridional-cis* and *facial*, have only C_s symmetry and would show a 2:2:2 ratio of phenyl groups. The similarity of the spectrum of the allyl amine complex **2g** with the spectra of saturated amines complexes (Table 1) indicates a similar structure, with the allyl amine coordinated to tungsten via only the nitrogen.

The analogous molybdenum complexes **7** have broader ^1H NMR spectra, in which no coupling can be resolved (Fig. 1, bottom). But, as in the tungsten case, a characteristic pattern is observed independent of the amine ligand (Table 1). For instance, resonances are found at -8 top -11 and at -15 to -16 in the ratio of 3:6 for each compound, due to the methyl groups on the three phosphines. The phenyl regions are not very well separated and show four distinctive peaks (integral 2:4:4:8) and one broad lump. Despite the broadness in this region, clear cross peaks are observed in the HOHAHA spectrum of **7b** (Fig. 2). The cross peaks between the resonances at 10.81 (2H) and at 7.61 ppm (4H), and between the resonances at 10.53 (4H) and at 6.55 ppm (8H) allow the assignment of these as *para* and *meta* phenyl proton resonances. The former are due to the unique phosphine ligand, the latter due to the *trans* pair of phosphines. The broad lump from 9.1 ppm to 10.4 ppm, too broad to be observed in the two-dimensional NMR spectrum, is thus due to the twelve *ortho* protons. Just as found for the tungsten compounds, these are the closest to the metal centre and their peaks are most broadened. The greater broadening for compounds 7 has often prevented assignment of the resonances for the amine alkyl group.

The spectrum of $W(en)Cl_2L_2$ (**3**) is similar to those of **2**, but shows a single set of phenyl resonances, a single peak at $\delta 3.56$ for the two phosphine methyl groups, and one resonance ($\delta 12.99$) for the methylene groups of the ethylenediamine ligand. A similar (though broader) spectrum is observed for the molybdenum analogue, which was again assigned with the help of a two-dimensional spectrum. Two C_{2v} structures—both *cis–cis–trans*—are consistent with these data (**A** and **B** below), although only one of the isomers is formed. Considering the steric bulk of the $PMePh_2$ ligands, the

isomer with trans phosphines (**B**) might be more likely.

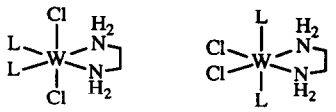

A similar analysis of the spectra of the amine–ethylene complexes **5** also indicates C_{2v} symmetry, which is consistent only with the all-*trans* geometry shown in eq. 7. No resonances are observed for the ethylene protons or the NH_2 protons in any of these compounds. They may be broadened too severely by the paramagnetic metal centre or possibly shifted out of the chemical shift range we examined: a recent report of isoelectronic rhenium(III) amine complexes such as $ReCl_2(en)_2^+$ gives chemical shifts for the amine protons in the range δ134–207.[21]

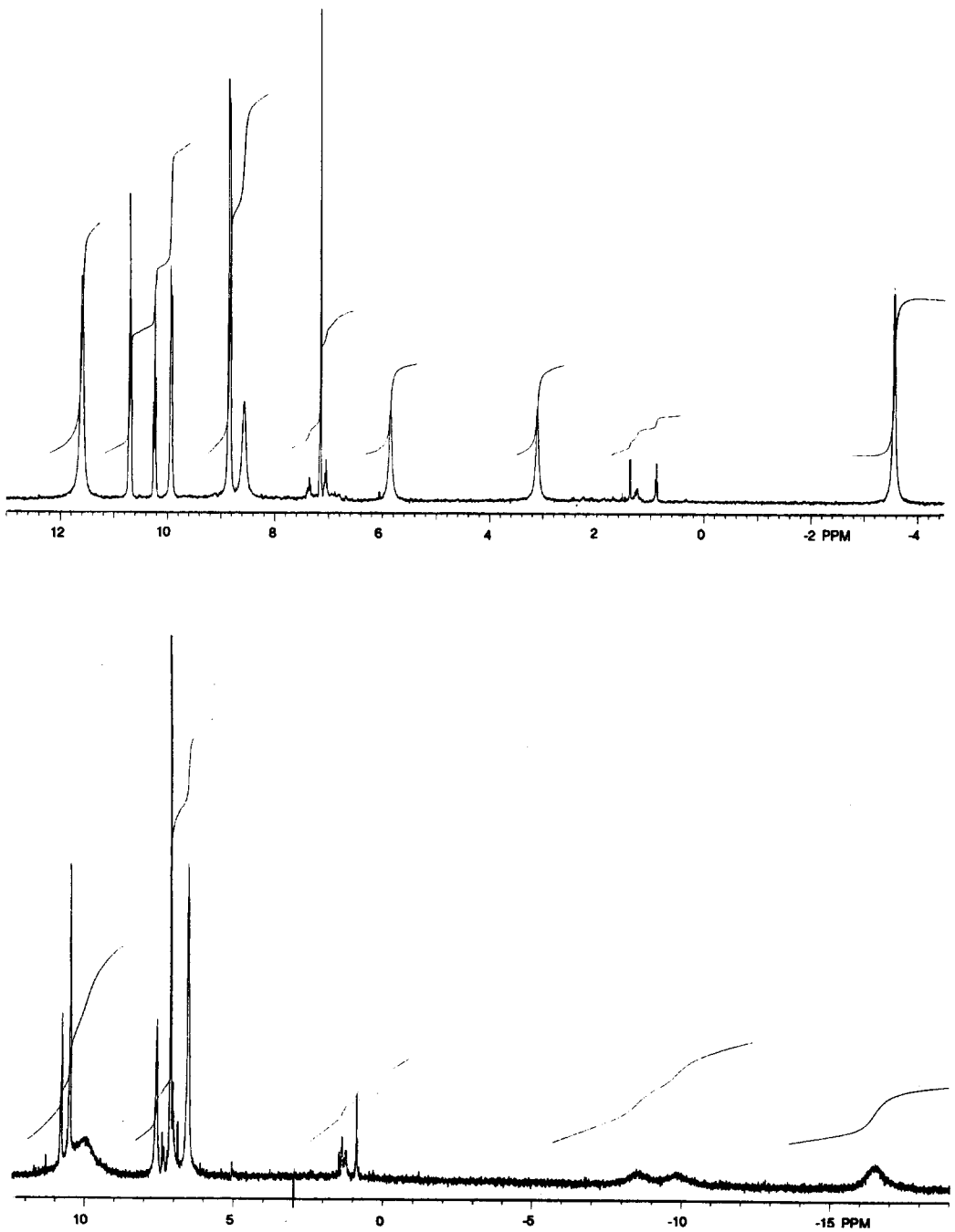

Fig. 1. ^1H NMR spectra for $W(NH_2Me)Cl_2L_3$ **2b** and $Mo(NH_2Me)Cl_2L_3$ **7b**. Solvent or impurity peaks are visible at δ7.15 (C_6D_6), 0.8 and 1.3 (pentane), and 1.4, 7.1, and 7.4 (free $PMePh_2$).

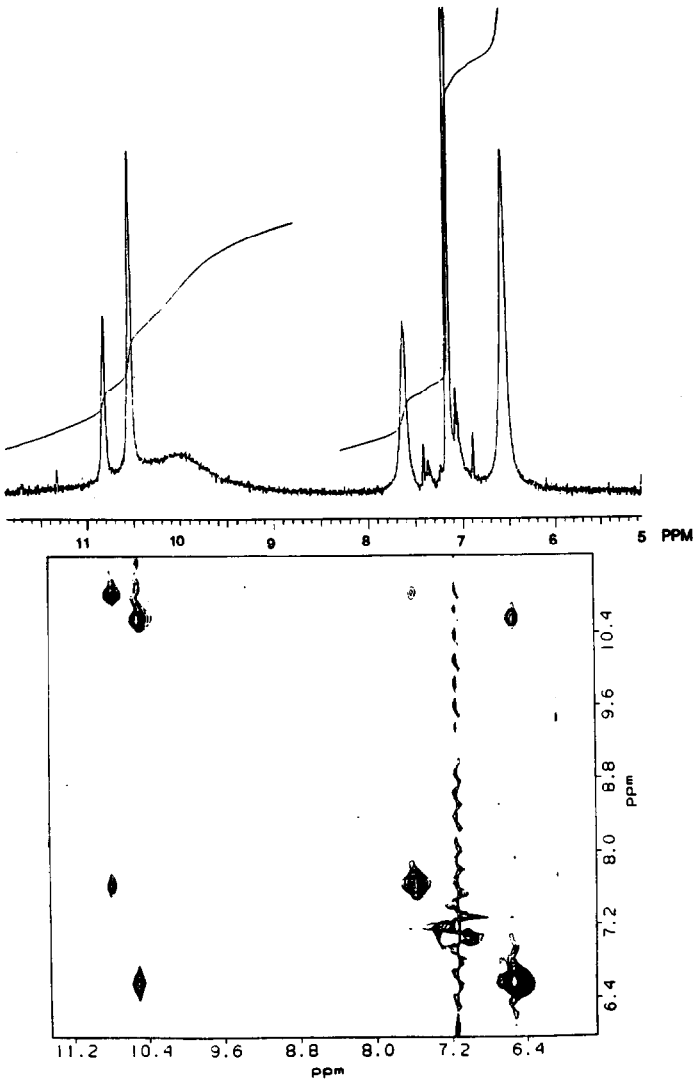

Fig. 2. Two-Dimensional ^{1}H NMR HOHAHA spectrum (δ6–11) of $Mo(NH_2Me)Cl_2L_3$ (**7b**). The normal NMR spectrum in this region is shown above; solvent (δ7.15, C_6D_6) and $PMePh_2$ (δ7.1, 7.4) resonances are also visible.

DISCUSSION

Formation of amine complexes

Addition of amines to the tungsten(II) and molybdenum(II) complexes **1** and **6** forms an apparently equilibrium amount of amine adducts **1** and **6** (eq. 9).

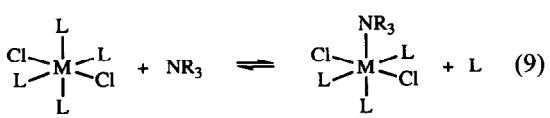

(9)

A similar equilibrium is established between the tungsten ethylene complex **4** and the ethylene–amine adducts **5** (eq. 6 previously). The equilibrium mixtures are rapidly established, consistent with the high lability of the phosphine ligands in **1** and **2**.[12]

The position of the equilibria depend to a large extent on the steric bulk of the amine: with small primary amines the equilibria lie toward the amine adducts, while with *t*-butyl amine adducts can be observed but not formed quantitatively. No reaction is observed with secondary amines (except aziridine). Reaction of one equivalent of *t*-butyl amine with **6** gives an observable molybdenum amine adduct but excess amine is required to form a significant amount of a tungsten adduct from **1**, suggesting that molybdenum has a higher affinity for an amine ligand than tungsten does. The lack of reaction of **1** with aniline is due to its lower basicity rather than steric effects, as aniline is smaller than cyclohexylamine which binds well. In contrast, aziridines bind more strongly than simple secondary amines even though they are somewhat less basic

(the lone pair on aziridines has more s-character and is therefore less basic). In this case, steric effects override the difference in basicity. Similarly, the small $CF_3CH_2NH_2$ ligand binds well, even though it is substantially less basic than simple alkyl amines.[22]

Substitution of more than one phosphine ligand has been achieved only with the chelating ethylenediamine. But even in neat ethylenediamine, no more than two phosphine ligands are replaced. Phosphine loss from the sterically crowded tetrakisphosphine complexes **1** and **6** is quite facile[12] but appears to be less favourable once an amine ligand is present in the coordination sphere. The electron-rich metal centres also seem to prefer a mix of π-acid and σ-donor ligands. The amine complexes **2** substitute a phosphine ligand for ethylene but not for a second amine. One of the two ethylene ligands in **4** is readily substituted by an amine while the phosphines are unaffected. Allyl amine binds to the $WCl_2(PMePh_2)_3$ fragment through the nitrogen rather than the more π-acidic but more sterically hindered alkene. Alkene coordination has been implicated as the initial step in the deoxygenation of allylic alcohols and ethers by **1**,[6,10] but the alcohol and ether groups are not as good ligands as an amine (see below).

Contrast with reactions of alcohols and thiols

The formation of stable amine complexes from **1** contrasts with the deoxygenation of alcohols and desulphurization of thiols by **1** (eqs 1–3, previously). Alcohol and thiol adducts analogous to the amine complexes **2** have not been observed.[23] Phosphine substitution reactions of **1** and **6** are quite rapid: addition of amines, ethylene, ketones, or other phosphines form products or equilibrium mixtures within minutes.[5,8,12,13,18a] The reactions of alcohols and thiols with **1** occur over a much slower timescale (weeks and hours, respectively[6]), so equilibria analogous to the amine reactions (eq. 9) are undoubtedly established but the concentrations of alcohol and thiol adducts are evidently too low to detect. This is consistent with the poorer ligating ability of alcohols and thiols versus amines. Alcohol and thiol adducts, however, are likely to be intermediates in the deoxygenation and desulphurization reactions, although it is also possible that oxidative addition of an O—H or S—H bond occurs without prior coordination of the heteroatom.[24]

The amine complexes are fairly stable in solution and do not decompose to tungsten(IV) imido complexes $W(NR)Cl_2(PMePh_2)_3$, as might have been expected by analogy with the reactions of alcohols and thiols. This is not due to any instability of the imido compounds, as these are readily formed,[15] for instance in the reactions of **1** with aziridines[7] (see previously). The observation that reactions with **1** cleave O—H and S—H bonds but not N—H bonds suggests that the substrate acidity is the key parameter, as the acidities vary in the order RSH > ROH > RNH_2.[25] This trend does not correlate with bond strengths, which vary in the order O—H > N—H > S—H.[25] The importance of acidity is illustrated by the relative rates of reactions with **1**: phenol reacts over a week to make a phenoxide complex, while the more acidic *para*-bromophenol requires only a day to go to completion (aqueous pK_a values: phenol, 10.0; BrC_6H_4OH, 9.4). The less acidic aliphatic alcohols (aqueous $pK_a \cong 16$) require 3 weeks for reaction. pK_a values are much lower for aniline (30.6 in DMSO) and primary amines (aqueous $pK_a > 30$). Even the more acidic $CF_3CH_2NH_2$[22] simply coordinates to tungsten, without formation of an imido complex.

Acknowledgements—We thank Dr S. C. Critchlow, K. A. Hall and Dr L. M. Atagi for helpful suggstions, and K. A. Hall for preparing $MoCl_2L_4$. We also thank Dr T. Pratum for help with the two-dimensional NMR. We are grateful to the US National Science Foundation for financial support.

REFERENCES

1. (a) F. A. Cotton and G. Wilkinson, *Advanced Inorganic Chemistry*, 5th edn, Wiley, New York, (1988); (b) *Comprehensive Coordination Chemistry* (Edited by G. Wilkinson), Pergamon, New York (1987).
2. Molybdenum and tungsten reviews: (a) J. G. Leigh and R. L. Richards in reference 1b, Vol. 3, 1265–1298; (b) C. D. Garner and J. M. Charnock in reference 1b, Vol. 3, 1329–1374; (c) Z. Dori *Prog. Inorg. Chem.* 1981, **28**, 239–307 and in reference 1b, Vol. 3, 973–1022.
3. Monomeric Mo(III) amine complexes: (a) S. P. Ghosh and K. M. Prasad in *Proceedings of the First International Conference on the Chemistry and Uses of Molybdenum* (Edited by P. C. H. Mitchell), Climax Molybdenum Co., Ann Arbor, MI, p. 119, (1974); (b) K. Wieghardt, M. Hahn, W. Swirdoff and J. Weiss *Inorg. Chem.* 1984, **23**, 94; see also K. Wieghardt, M. Guttmann, P. Chaudhuri, W. Gebert, M. Minelli, C. G. Young and J. H. Enemark *Inorg. Chem.* 1985, **24**, 3151. (c) For a recent report of rhenium(III) amine complexes, see reference 21.
4. F.-M. Su, J. C. Bryan, S. Jang and J. M. Mayer, *Polyhedron* 1989, **8**, 1261.
5. J. C. Bryan and J. M. Mayer, *J. Am. Chem. Soc.* 1990, **112**, 2298.
6 S. Jang, L. M. Atagi and J. M. Mayer, *J. Am. Chem. Soc.*1990, **112**, 6413.
7. L. M. Atagi, D. E. Over, D. R. McAlister and J. M. Mayer, *J. Am. Chem. Soc.* 1991, **113**, 870.

8. S. Brock and J. M. Mayer, *Inorg. Chem.* 1991, **30**, 2138.
9. K. A. Hall, S. C. Critchlow and J. M. Mayer, *Inorg. Chem.* 1991, **30**, 3593.
10. L. M. Atagi, S. C. Critchlow and J. M. Mayer, *J. Am. Chem. Soc.* 1992, **114**, 1483.
11. D. E. Over, S. C. Critchlow and J. M. Mayer, *Inorg. Chem.* 1992, **31**, 4643.
12. K. A. Hall and J. M. Mayer, *J. Am. Chem. Soc.* 1992, **114**, 10402.
13. J. C. Bryan, G. K. Cook, J. B. Arterburn and J. M. Mayer, *Organometallics* 1992, **11**, 3965.
14. Part of this work was presented at the 5th Chemical Congress of North America, San Francisco, CA, April 1992, paper INOR468.
15. (a) W. A. Nugent and J. M. Mayer, *Metal–Ligand Multiple Bonds*, Wiley-Interscience, New York, (1988); (b) J. Chatt and J. R. Dilworth, *J. Chem. Soc., Chem. Comm.* 1975, **983**; (c) G. L. Hillhouse and B. L. Haymore, *J. Organomet. Chem.* 1978, **162**, C23; (d) E. A. Maatta and D. D. Devore, *Angew. Chem. Int. Ed. Engl.* 1988, **27**, 569; (e) G. R. Clark, A. J. Nielson, C. E. F. Rickard and D. C. Ware, *Polyhedron* 1990, **9**, 603; (f) J. D. Lichtenhan, S. C. Critchlow and N. M. Doherty, *Inorg. Chem.* 1990, **29**, 439; (g) References 4, 7, and 12.
16. D. D. Perrin and W. L. F. Armarego, *Purification of Laboratory Chemicals*, 3rd edn, Pergamon, New York (1988).
17. See reference 11. Our attention was drawn to the value of this experiment for paramagnetic transition metal complexes by A. Stassinopoulos, G. Schulte, G. C. Papaefthymiou and J. P. Caradonna *J. Am. Chem. Soc.* 1991, **113**, 8686.
18. (a) P. R. Sharp, *Organometallics* 1984, **3**, 1217; (b) P. R. Sharp, J. C. Bryan and J. M. Mayer, *Inorg. Synth.* 1990, **28**, 326.
19. The best spectra of **2h** were obtained at 5°C in benzene. At lower temperatures the NMR resonances are much broader; at 25°C sharp peaks can be observed but **2h** is too transient to obtain good spectra.
20. J. Chatt, G. J. Leigh and D. M. P. Mingos, *J. Chem. Soc. A* 1969, 1674 and reference 18a.
21. S. D. Orth, J. Barrera, M. Sabat, W. D. Harman, *Inorg. Chem.* 1993, **32**, 594.
22. $CF_3CH_2NH_2$($pK_b = 8.3$) is substantially less basic than ethylamine ($pK_b = 3.3$); pK_a values for $CF_3CH_2NH_2$ do not appear to be available, but the low basicity of $CF_3CH_2NH_2$ suggests a higher acidity. (a) D. D. Perrin in IUPAC, Analytical Chemistry Division, Commission of Electroanalytical Chemistry, *Dissociation Constants of Organic Bases in Aqueous Solution*, Butterworths, London, (1965); (b) M. Hudlicky, *Chemistry of Organic Fluorine Compounds*, Halsted Press, Wiley, New York (1976).
23. Similarly, no significant phosphine substitution is observed on dissolving **1** in THF.
24. In the oxidative addition of a C—S bond of thiophene, initial coordination at the sulfur is required (W. D. Jones and L. Dong *J. Am. Chem. Soc.* 1991, **113**, 559) but oxidative addition of a vinyl C—H bond can occur without alkene coordination (P. O. Stoutland and R. G. Bergman, *J. Am. Chem. Soc.* 1988, **110**, 5732).
25. (a) J. March, *Advanced Organic Chemistry*, 3rd edn, Wiley, New York, (1985). Table of pK_a values: pp. 220–223. Table of bond strengths: p. 23. pK_a values for phenols: E. P. Serjeant and B. Dempsey *Ionization Constants of Organic Acids in Aqueous Solution*, Pergamon, New York (1979). pK_a value for aniline: F. G. Bordwell *Pure Appl. Chem.* 1977, **49**, 936.

Polyhedron Vol. 12, No. 21, pp. 2603–2609, 1993
Printed in Great Britain

0277–5387/93 $6.00+.00
© 1993 Pergamon Press Ltd

MOLYBDENUM(VI) DIOXO COMPLEXES WITH MACROCYCLIC AMINE LIGANDS

ABDESSADEK LACHGAR,* PAUL FARRALL and JAMES M. MAYER†

Department of Chemistry BG-10, University of Washington, Seattle, WA 98195, U.S.A.

(*Received* 1 *March* 1993; *accepted* 19 *May* 1993)

Abstract—Reaction of MoO_2Cl_2 with the tetradentate amine ligand 1,4,8,12-tetraazacyclopentadecane ([15]aneN$_4$) yields the molybdenum(VI) dioxo complex [MoO_2([15]aneN$_4$-H)]Cl (**I**), a rare example of a cationic complex containing the MoO_2^{2+} unit. The oxo ligands are *cis* and the macrocyclic amine coordinates in a non-planar fashion, as revealed by X-ray crystal structure and NMR data. One of the nitrogen donors *cis* to the oxo groups has been deprotonated to give an amide ligand (NR_2^-). In contrast, reaction of MoO_2Cl_2 with tetramethylcyclam (1,4,8,11-tetramethyl-1,4,8,11-tetraazacyclotetradecane, TMC) yields the neutral adduct $MoO_2Cl_2(\eta^2$-TMC) (**III**), in which only two of the amine nitrogens are coordinated. An X-ray structure of **III** shows it to have an all-*cis* octahedral geometry, very unusual for $MoO_2X_2L_2$ complexes, with one oxo ligand *trans* to an amine and the other *trans* to a chloride. Compounds [MoO_2([15]aneN$_4$-H)]BPh_4 **II** and **III** are not very stable in solution; **II** is not reduced electrochemically or by PPh_3.

The chemistry of molybdenum oxo complexes has been intensively studied, particularly as models for active sites in metalloenzymes and on heterogeneous catalysts.[1] Yet, despite the large number of molybdenum(VI) oxo complexes,[2] to our knowledge there is only one well-characterized cationic derivative, $[MoO_2Br(tacn)]^+$ (tacn = triazacyclononane),[3] and there are no complexes with tetradentate amine ligands.[2] We report here two complexes formed from reaction of MoO_2Cl_2 with the macrocyclic amine ligands 1,4,8,12-tetraazacyclopentadecane ([15]aneN$_4$) and 1,4,8,11-tetramethyl-1,4,8,11-tetraazacyclotetradecane (tetramethylcyclam, TMC).

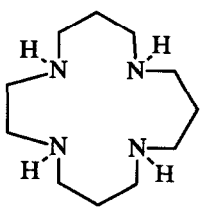

[15]aneN$_4$

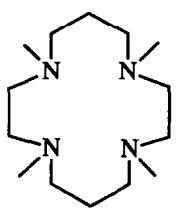

TMC

* Currently at: Department of Chemistry, Wake Forest University, Winston-Salem, NC 27109, U.S.A.

† Author to whom correspondence should be addressed.

EXPERIMENTAL

General considerations

All experiments were performed under a nitrogen atmosphere or under vacuum employing high vacuum-line, Schlenk and standard glove-box techniques, unless otherwise noted. Solvents were dried according to standard procedures.[4] Acetonitrile was first dried over 3 Å molecular sieves and then vacuum transferred into a flask containing CaH_2, from which it was vacuum transferred immediately before use. MoO_2Cl_2 (Aldrich) was sublimed at 50°C under a static vacuum. 1,4,8,12-Tetraazacyclopentadecane (**A**) and 1,4,8,11-tetramethyl-1,4,8,11-tetraazacyclotetradecane (**B**) were sublimed *in vacuo* at 73 and 40°C, respectively, and stored under nitrogen. ^{1}H NMR spectra were acquired at ambient temperatures using a Varian VXR-300 Fourier-transform spectrometer (300 MHz). The ^{1}H NMR spectra are reported in ppm downfield of TMS or DSS and were referenced relative to the residual protons in the solvent or to DSS for spectra in D_2O. The $^{13}C\{^1H\}$ NMR spectra were recorded at 75.43 MHz. Spectra are reported as: δ (ppm) [multiplicity, coupling constants (in Hz), number of hydrogens]. IR spectra were recorded on a Perkin–Elmer 1600 FT-IR spectrometer

as Nujol mulls using NaCl plates and are reported in cm^{-1}. Intensities of IR bands are reported as (s) = strong, (w) = weak or (sh) = shoulder. Elemental analyses were performed by Canadian Microanalytical Services Ltd (Delta, B.C., Canada). Electrochemical measurements were obtained using a Bioanalytical Systems CV-27 with a platinum disk electrode, platinum wire auxiliary electrode and an Ag/AgCl reference electrode. The concentration of **I** in CH_3CN was *ca* 10^{-3} M, with 0.1 M $^nBu_4NPF_6$ as a supporting electrolyte.

$[MoO_2([15]aneN_4\text{-}H)]Cl$ (I)

A solution of [15]aneN$_4$ (67 mg, 0.31 mmol) in CH_2Cl_2 (10 cm^3) was added to a solution of MoO_2Cl_2 (62 mg, 0.31 mmol) in CH_2Cl_2 (10 cm^3). An immediate colour change to yellow was followed quickly by the appearance of solids and a change to a forest green colour. The reaction was stirred for 10 min and then exposed to air and filtered to give a green filtrate, which changed to a bright yellow colour after sitting for 24 h. Filtration, concentration to *ca* 2 cm^3 and addition of diethyl ether (9 cm^3) yielded a bright yellow precipitate, which was collected by filtration and washed with 2×3 cm^3 of Et_2O. Yield: 59.1 mg (0.16 mmol); 51%. X-ray quality crystals were grown by slow evaporation of a CH_2Cl_2 solution at 10°C. Found: C, 35.8; H, 6.9; N, 15.1. Calc. for $MoO_2C_{11}N_4H_{25}Cl$: C, 35.1; H, 6.7; N, 14.9%. ^1H NMR (D_2O): 4.34 (d of t, 13 and 5 Hz, 1 H); 3.98 (t, 13 Hz, 1H); 3.75 (d, 13 Hz, 1H); 3.38 (m, 3H); 3.18 (d, 7 Hz, 1H); 2.85 (m, 11H); 2.35 (br s, 1H); 2.02 (m, 2H); 1.70 (m, 3H); 1.45 (q, 14 Hz, 1H). $^{13}C\{^1H\}$ NMR (D_2O, referenced to DSS at 0 ppm): 72.1, 67.1, 58.4, 55.8, 55.3, 54.3, 52.3, 47.4, 30.9, 30.7, 25.3. IR: 3053 [ν(NH)], 1304, 1112, 1038, 1024, 976, 900 [$\nu(MoO_2)$], 882 [$\nu(MoO_2)$], 815.

$[MoO_2([15]aneN_4\text{-}H)]BPh_4$ (II)

$[MoO_2([15]aneN_4\text{-}H)]Cl$ (28 mg) was dissolved in distilled H_2O (10 cm^3) and filtered on a glass frit in the air. Addition of a saturated aqueous solution of $NaBPh_4$ (15 cm^3) (Aldrich) forms a pale yellow precipitate, which was collected by filtration and washed with H_2O and Et_2O. Recrystallization by vapour diffusion of hexane into a CH_2Cl_2 solution gives the desired yellow crystals and an impurity as white needle-like crystals. The formation of a white solid always accompanies recrystallization of **I** and **II**. ^1H NMR (CD_3CN): 7.30 (s, 8H); 7.00 (t, 8 Hz, 8H); 6.84 (t, 8 Hz, 4H) [BPh_4]; 4.28 (m, 1H); 3.98 (m, 1H); 3.72 (m, 2H); 3.48 (m, 1H); 2.95 (m, 16H); 2.49 (m, 1H); 1.78 (m, 2H); 1.52 (m, 1H). IR: 3053, 1612, 1578, 1303, 1268, 1148, 1033, 910–754, 736, 710, 613.

$MoO_2Cl_2(\eta^2\text{-TMC})$ (III)

Following a procedure similar to that for $[MoO_2([15]aneN_4\text{-}H)]Cl$, a solution of tetramethylcyclam (TMC) (39 mg) in MeCN (2.5 cm^3) was slowly added to a solution of MoO_2Cl_2 (30 mg) in MeCN [$MoO_2Cl_2(MeCN)_2$[5]] in a flow of nitrogen. Removal of solvent from the yellow solution typically yielded a yellow–brown oil; yellow solids were most reproducibly obtained on cooling to −20°C and filtering. The yellow solution and yellow solids are not very stable, turning brown and forming white solids. ^1H NMR spectra of isolated **III** and of a reaction solution containing MoO_2Cl_2 and TMC (1 : 1) in CD_3CN were both broad: 2.65 (br s, 8H, NCH_2), 2.59 (br s, 8H, NCH_2), 2.37 (br s, 12H, NCH_3), 1.78 (br s, 4H, $NCH_2CH_2CH_2N$); a small peak at δ 9.40 was also typically observed.

X-ray crystal structure of $[MoO_2([15]aneN_4\text{-}H)]Cl$ (I)

A rhombus-like single crystal ($0.57 \times 0.45 \times 0.4$ mm^3) was sealed in a glass capillary. Oscillation and zero level Weissenberg photographs gave preliminary unit cell parameters and showed $2/m$ Laue symmetry. This was confirmed by diffraction data collected on a four-circle diffractometer (CAD4) using graphite-monochromated Mo-K_α radiation. Compound **I** was found to crystallize in the monoclinic space group $P2_1/n$ ($Z = 4$) with cell parameters: $a = 7.2147(9)$, $b = 12.3041(11)$, $c = 17.4031(18)$ Å, $\beta = 99.601(16)°$, $V = 1523.1(9)$ Å^3, $Z = 4$, $D_{calc} = 1.63$ g cm^{-3}. Data in two octants ($hk \pm l$) were collected ($2° < 2\theta < 55°$) and three Ψ-scans were used for an empirical absorption correction[6] ($\mu = 10.2$ cm^{-1}, transmission factors = 0.997–0.714, av. = 0.820). 2794 symmetry independent observed reflections [$I/\sigma(I) > 3$] out of 3942 measured were considered in subsequent calculations. Direct methods (SHLEXS-86[7]) provided an initial model, which was successfully completed with the aid of standard least-squares full-matrix refinement and Fourier synthesis. The carbon backbone between N(1) and N(4) shows a flip-flop-like disorder, which was modelled by splitting C(7) into two positions, C(7a) and C(7b), with equal occupancies. Three hydrogen atoms, H(1N) H(2N) and H(4N) were located on a difference-Fourier map and refined; no hydrogen atom could be found on N(3). The hydrogen atoms attached to carbon atoms were calculated and not refined. Anisotropic refinement (scattering factors from ref. 8) of all non-hydrogen atoms (192 par-

ameters) converged with $R = 0.040$ and $R_w = 0.051$ (G.O.F. = 1.73). The final difference-Fourier map was flat with the largest background electron residual being 0.60 e $Å^{-3}$ near the molybdenum atom and 0.30 e $Å^{-3}$ elsewhere.

X-ray crystal structure of $MoO_2Cl_2(\eta^2$-TMC) (**III**)

Tetrahedral shaped yellow crystals of **III** were grown in an NMR tube from a reaction of $MoO_2Cl_2(MeCN)_2$ and TMC in a 1/1 molar ratio. A suitable single crystal ($0.35 \times 0.25 \times 0.25$ mm^3) was mounted and sealed in a thin-walled glass capillary. Preliminary studies using a single-crystal X-ray diffractometer (CAD4) confirmed the orthorhombic *mmm* symmetry obtained from film studies. Unit cell parameters obtained from the least square refinement of 25 reflections are $a = 13.752(1)$, $b = 12.157(2)$, $c = 24.061(4)$ Å, $Z = 8$, $D_{calc} = 1.503$ g cm^{-3}. Analysis of reflection data collected ($h \pm kl$) showed the extinction conditions $0kl$, $k = 2n+1$; $h0l$, $l = 2n+1$; $hk0$, $h = 2n+1$, consistent with space group *Pbca*. A large decay of 58% (probably due to the chemical instability of **III**) was observed as shown by the observation of 1415 unique reflections with $I/\sigma(I) > 3$ out of 7944 measured. A decay correction based on the program CHORT[6a] was applied rather than a linear decay correction. An empirical absorption correction[6] was applied ($\mu = 9.17$ cm^{-1}, transmission factors 0.9988–0.8771, av. = 0.9582). Direct methods (SHLEXS-86[7]) gave the initial atomic positions of Mo, Cl(1), Cl(2), O(1) and O(2) atoms. Subsequent least squares refinement and difference-Fourier map revealed the positions of the carbon and nitrogen atoms. Hydrogen atom positions were calculated and included in the model, but not refined. Anisotropic refinement of all non-hydrogen atoms (208 parameters) converged to $R = 0.057$ and $R_w = 0.068$ (G.O.F. = 1.22). The final difference-Fourier map was featureless with the largest residual electron density of 1.1 e $Å^{-3}$ at 1.1 Å from the molybdenum atom.

Atomic coordinates for compounds **I** and **III** have been deposited with the Cambridge Crystallographic Centre.

RESULTS AND DISCUSSION

Syntheses

Addition of a methylene chloride solution of [15]aneN$_4$ to MoO_2Cl_2 in CH_2Cl_2 results in a yellow solution, from which yellow solid (**I**) can be isolated [eq. (1)]. An X-ray crystal structure (described below) shows **I** to contain MoO_2^{2+} coordinated to a singly deprotonated macrocyclic amine ligand, with a chloride counter-ion: [MoO_2([15]aneN$_4$-H)]Cl. The chloride can be exchanged to give [MoO_2([15]aneN$_4$-H)]BPh_4 (**II**) by addition of a saturated aqueous solution of $NaBPh_4$ to an aqueous solution of **I**.

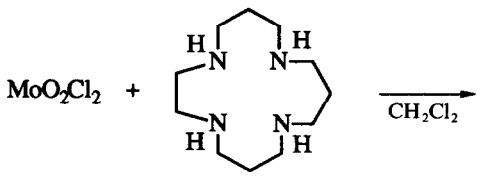

[15]aneN$_4$

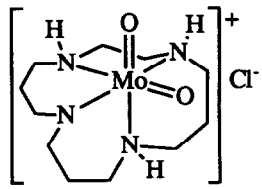

[+ HCl] (1)

I

The NMR spectra for **I** and **II** are consistent with the X-ray structure of **I**. The carbons of the amine ligand give rise to 11 resonances in the $^{13}C\{^1H\}$ NMR, consistent with the lack of molecular symmetry in the solid state. The ^1H NMR spectra of **I** and **II** show a number of complex multiplets for the coordinated amine, including separate resonances for six individual protons, again supporting C_1 symmetry. The IR spectrum of **I** is consistent with a *cis*-MoO_2^{2+} unit, with bands at 900 and 882 cm^{-1}.

Monitoring reaction (1) by ^1H NMR in CD_3CN shows rapid formation of **I** as well as other species. A broad peak at δ 9.4 is observed, suggesting that an aldimine function (—N=CH—) is formed by oxidation of the macrocyclic ligand. Conversion of macrocyclic amine ligands to imines is a common reaction for oxidizing metal centres.[9] Both compounds **I** and **II** are unstable in solution, slowly depositing a white insoluble material; this has hampered efforts to obtain analytically pure material and to investigate their chemistry.

Table 1. Bond distances in [MoO_2([15]aneN$_4$-H)]Cl (**I**) (Å)

Mo—O(1)	1.716(2)	N(1)—C(1)	1.486(4)
Mo—O(2)	1.714(2)	N(1)—C(11)	1.498(4)
Mo—N(1)	2.287(2)	N(2)—C(2)	1.478(4)
Mo—N(2)	2.320(2)	N(2)—C(3)	1.481(4)
Mo—N(3)	1.932(3)	N(3)—C(5)	1.466(4)
Mo—N(4)	2.415(2)	N(3)—C(6)	1.462(4)
N(4)—C(8)	1.489(5)	N(4)—C(9)	1.488(4)

Addition of tetramethylcyclam (TMC) to MoO_2Cl_2 in acetonitrile has also resulted in the formation of X-ray quality crystals, although the yellow product **III** is quite different from **I** [eq. (2)]. Complex **III** is a neutral adduct of MoO_2Cl_2 and TMC with only two of the macrocyclic nitrogen atoms coordinated, $MoO_2Cl_2(\eta^2$-TMC).

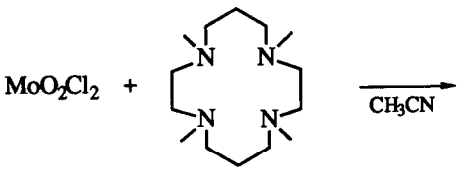

TMC

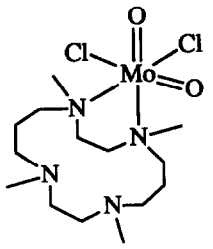

III (2)

The synthesis of **III** is temperamental and solids can be difficult to obtain. The yellow reaction solution begins to deposit white solid within minutes at ambient temperatures and turns brown in a few hours; removal of the acetonitrile typically results in the formation of a yellow–brown oil. ^{1}H NMR spectra of the yellow oil and of reaction solutions in CD_3CN show broad resonances, with a pattern similar to that of free tetramethylcyclam but with different chemical shifts. Spectra of **III** in the presence of excess amine show shifted broad peaks without the sharp resonances for the free ligand, implying facile ligand exchange. Cooling the NMR sample to -30°C does not sharpen the spectra. ^{1}H NMR spectra of **III** always display a small peak at *ca* δ 9.4, similar to that seen in reactions with [15]aneN$_4$, which suggests decomposition via ligand oxidation to an imine (as discussed above).

X-ray structures of $[MoO_2([15]aneN_4\text{-}H)]Cl$ **(I)** *and* MoO_2Cl_2(TMC) **(III)**

The structure of **I** consists of molybdenum-oxo-amine cations and chloride anions, with the chloride forming hydrogen bonds to the hydrogen on N(4) in two different molecules. Bond lengths and angles are listed in Tables 1 and 2. The cation has a distorted octahedral geometry typical of MoO_2^{2+} complexes (Fig. 1), with *trans* angles of 160.4(1)° [O(1)—Mo—N(2)], 162.6(1)° [O(2)—Mo—N(4)] and 156.9(1)° [N(1)—Mo—N(3)]. The large O(1)—Mo—O(2) angle of 109.1(1)° and short Mo=O distances [1.716 and 1.714(2) Å] are also typical of octahedral MoO_2^{2+} complexes.[10]

All four nitrogens of the macrocyclic amine are coordinated to the molybdenum, in a non-planar fashion to allow the preferred *cis*-coordination of the MoO_2^{2+} unit. One of the nitrogens [N(3)] has been deprotonated, forming an amide (NR_2^-) ligand. This is clearly shown by a number of structural features, in addition to the presence of only one chloride counter-ion.[11] The amide distance, Mo—N(3) = 1.932(3) Å, is substantially shorter than the Mo-amine distances (2.287(2) [N(1)], 2.320(2) [N(2)] and 2.415(2) Å [N(4)]). The angles about the amine nitrogens N(1), N(2) and N(4) are all in the range 108.0(3)–118.2(2)°, while those about the amide nitrogen are: 120.4(2)° [Mo—N(3)—C(5)], 125.8(2)° [Mo—N(3)—C(5)] and 113.0(3)° [Mo—N(3)—C(5)]. The sum of the

Table 2. Bond angles in $[MoO_2([15]aneN_4\text{-}H)]Cl$ **I** (°)

O(1)—Mo—O(2)	109.1(1)	Mo—N(1)—C(1)	113.7(2)
O(1)—Mo—N(1)	91.8(1)	Mo—N(1)—C(11)	118.1(2)
O(1)—Mo—N(2)	160.4(1)	C(1)—N(1)—C(11)	111.3(2)
O(1)—Mo—N(3)	104.8(1)	Mo—N(2)—C(2)	109.4(2)
O(1)—Mo—N(4)	83.2(1)	Mo—N(2)—C(3)	144.7(2)
O(2)—Mo—N(1)	89.5(1)	C(2)—N(2)—C(3)	109.3(2)
O(2)—Mo—N(2)	84.5(1)	Mo—N(3)—C(5)	120.4(2)
O(2)—Mo—N(3)	99.8(1)	Mo—N(3)—C(6)	125.8(2)
O(2)—Mo—N(4)	162.6(1)	C(5)—N(3)—C(6)	113.0(3)
N(1)—Mo—N(2)	73.8(1)	Mo—N(4)—C(8)	112.9(2)
N(1)—Mo—N(3)	156.9(1)	Mo—N(4)—C(9)	113.7(2)
N(1)—Mo—N(4)	77.5(1)	C(8)—N(4)—C(9)	108.0(3)
N(2)—Mo—N(3)	86.0(1)		
N(2)—Mo—N(4)	80.8(1)		
N(3)—Mo—N(4)	88.5(1)		

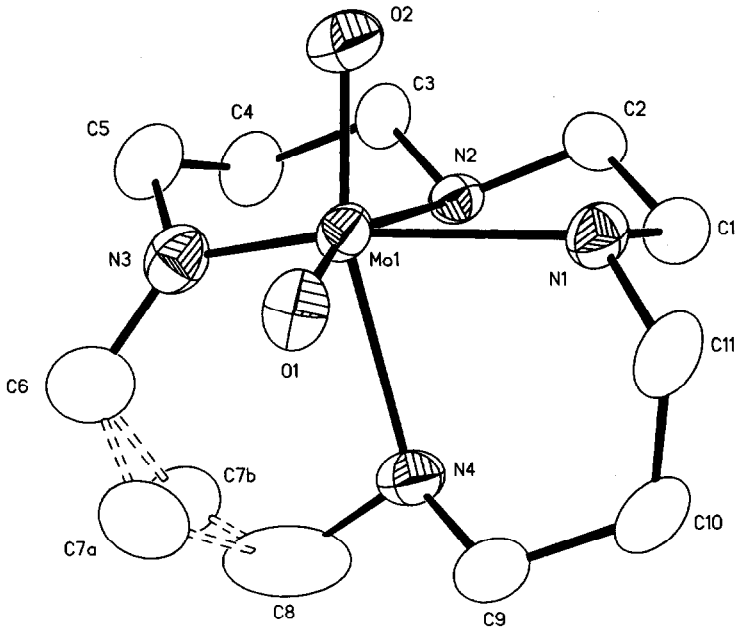

Fig. 1. ORTEP drawing of the cation in $[MoO_2([15]aneN_4\text{-}H)]Cl$ (I). The two equally populated positions of C(7) are shown.

angles about N(3) is thus 359.2°, indicating a trigonal planar(sp^2) nitrogen, while the sums of the angles about N(1), N(2) and N(4) to the non-hydrogen atoms are 343.1°, 333.4° and 334.1°. The difference between the sp^2 and sp^3 nitrogens is even reflected in the N—C distances: the bonds to N(3) are 1.466(4) and 1.462(4) Å, while the bond distances in the amine portions range from 1.478(4) to 1.498(4) Å. Deprotonation of N(3) is favoured by N(3)→Mo π-donation; the facial orientation of O(1), O(2) and N(3) is typical of three π-donors on a d^0 metal centre.[10]

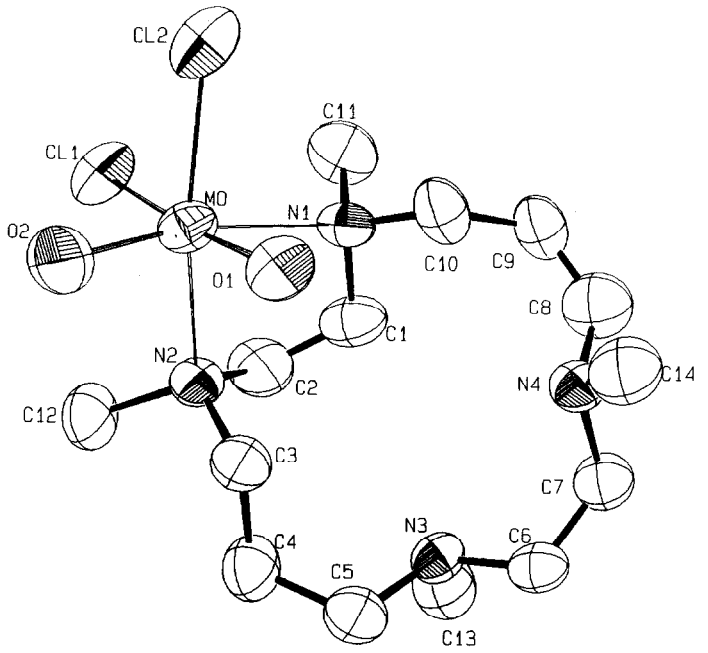

Fig. 2. ORTEP drawing of $MoO_2Cl_2(TMC)$ (III)

Table 3. Bond distances in MoO_2Cl_2(TMC) (**III**) (Å)

Mo—O(1)	1.701(7)	Mo—Cl(1)	2.486(3)
Mo—O(2)	1.673(7)	Mo—Cl(2)	2.331(3)
Mo—N(1)	2.478(8)	Mo—N(2)	2.289(8)

Complex **III** consists of isolated molecules in the solid state, in which only two of the four nitrogen atoms of the macrocycle are coordinated to the molybdenum (Fig. 2, Tables 3 and 4). Complex **III** is, therefore, a member of a rather large class of octahedral $MoO_2X_2L_2$ compounds, including a number of adducts of MoO_2Cl_2.[2] Complex **III** adopts an all-*cis* structure, with a chloride ligand *trans* to one oxo group and an amine nitrogen *trans* to the other, which is very unusual for $MoO_2X_2L_2$ species. In all previous examples, save one, the neutral ligands (L) are found *trans* to the oxo groups and the anionic ligands (X) avoid the strong oxo *trans* influence.[2] While this manuscript was in preparation, a report in this journal[12] described tetramethylethylenediamine adducts of MoO_2Cl_2 and WO_2Cl_2 (**A**). The stereochemistry was indicated by an X-ray crystal structure of the tungsten derivative (as well as NMR data); the molybdenum complex was determined to be isostructural from powder X-ray diffraction data.

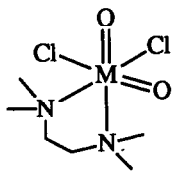

A

The lack of symmetry in the structure of **III** and the large differences in *trans* influence of the ligands lead to substantial disparities in bond lengths. The chloride *trans* to oxo forms a bond 0.15 Å longer than that *trans* to nitrogen [Mo—Cl(1) 2.486(3), Mo—Cl(2) 2.331(3) Å] and the difference in molybdenum–nitrogen distances is almost 0.2 Å (Mo—N1, 2.478(8) Å; Mo—N2, 2.289(8) Å). Even the Mo=O distances of 1.701(7) and 1.673(7) Å are significantly different, although still in the normal range for MoO_2^{2+} complexes, as is the O—Mo—O angle of 101.5(3)°.[10] The tungsten-ethylenediamine complex (**A**, M = W) has very similar bond lengths and angles, except that the two W=O distances are more comparable [1.705(7) and 1.711(7) Å]. The similarity of the two structures is not surprising, as the portion of the macrocycle that coordinates to molybdenum in **III** is essentially tetramethylethylenediamine. However, the fact that these two structures are the only known all-*cis* $MoO_2X_2L_2$ compounds indicates that it is the tertiary amine ligand that is controlling the coordination geometry, perhaps for the reason suggested for **A**:[12] to avoid unfavourable steric interactions between the chelating ligand and the chloride ligands in the more typical, *trans*-halide form.

Reactivity of $[MoO_2([15]aneN_4\text{-}H)]BPh_4$ (**II**)

The instability of **I**, **II** and **III** have hampered our efforts to monitor their reaction chemistry in depth, but preliminary studies indicate that **II** is not a good oxidant. Cyclic voltammograms of **II** in acetonitrile show no evidence of a reduction to −2.0 V (vs Ag/AgCl). Irregular oxidation waves were observed, perhaps due to ligand oxidation. Complex **II** is also inert to PPh_3 in methylene chloride solution for 2 days at ambient temperatures and does not oxidize benzaldehyde under these conditions. These results argue against our initial hypothesis that a cationic derivative might be more easily reduced and show more electrophilic character at oxygen. However, the presence of an amide ligand in **II** provides an additional stabilization for molybdenum(VI) and likely destabilizes molybdenum(V) and molybdenum(IV), because of a π-antibonding interaction with any molybdenum *d*-electrons. The reactivity of $[MoO_2Br(tacn)]^+$[3a] might provide more insight into these issues.

Table 4. Bond angles in MoO_2Cl_2(TMC) (**III**) (°)

O(1)—Mo—O(2)	101.5(3)	O(2)—Mo—Cl(1)	91.1(3)
O(1)—Mo—Cl(1)	166.8(2)	O(2)—Mo—Cl(2)	104.5(3)
O(1)—Mo—Cl(2)	94.6(3)	O(2)—Mo—N(1)	163.9(3)
O(1)—Mo—N(1)	82.6(3)	O(2)—Mo—N(2)	89.1(3)
O(1)—Mo—N(2)	90.9(3)	Cl(2)—Mo—N(1)	90.5(2)
Cl(1)—Mo—Cl(2)	85.8(1)	Cl(2)—Mo—N(2)	163.9(3)
Cl(1)—Mo—N(1)	84.2(2)	N(1)—Mo—N(2)	75.2(3)
Cl(1)—Mo—N(2)	85.5(2)		

Acknowledgements—We are grateful to the Sloan Foundation, the U.S. National Science Foundation and the donors of the Petroleum Research Fund, administered by the American Chemical Society, for financial support. We thank A. L. Shultz for assistance with the electrochemical experiments and Drs S. C. Critchlow and D. Barnhart for help with the crystallography.

REFERENCES

1. T. G. Spiro (Editor), *Molybdenum Enzymes*. Wiley, New York (1985); R. H. Holm, *Coord. Chem. Rev.* 1990, **100**, 183; B. C. Gates, J. R. Katzer and G. C. A. Schuit, *Chemistry of Catalytic Processes*, pp. 325–389. McGraw-Hill, New York (1979); G. W. Keulks, L. D. Krenzke and T. M. Notermann, *Adv. Catal.* 1978, **27**, 183; R. K. Grasselli and J. D. Burrington *et al.*, *Adv. Catal.* 1981, **30**, 133; *Farad. Disc. Chem. Soc.* 1982, **72**, 203; L. C. Glazer, J. F. Bradzil, M. A. Hazle, M. Mehicic and R. K. Grasselli, *J. Chem. Soc., Faraday I* 1985, **81**, 2903; Y. Iwasawa, T. Nakamura, K. Takamatsu and S. Ogasawara, *J. Chem. Soc. Faraday I* 1980, **76**, 939; W. E. Farneth, R. H. Staley and A. W. Sleight, *J. Am. Chem. Soc.* 1986, **108**, 2327.
2. E. I. Stiefel, in *Comprehensive Coordination Chemistry* (Edited by G. Wilkinson), Vol. 3, pp. 1375–1420. Pergamon Press, New York (1987). See also refs 10 and 12.
3. (a) G. Backes-Dahmann, W. Herrmann, K. Wieghardt and J. Weiss, *Inorg. Chem.* 1985, **24**, 485; (b) $[MoO_2(H_2O)_4]^{2+}$ is likely the dominant Mo^{VI} species in water at low pH: A. G. Sykes, in *Comprehensive Coordination Chemistry* (Edited by G. Wilkinson), Vol. 3, p. 1256. Pergamon Press, New York (1987); (c) cationic molybdenum(VI) oxo complexes have also been generated electrochemically, for instance: C.-S. J. Chang and J. H. Enemark, *Inorg. Chem.* 1991, **30**, 683.
4. D. D. Perrin and W. L. F. Armarego, *Purification of Laboratory Chemicals*, 3rd edn. Pergamon Press, New York (1989).
5. R. J. Butcher, H. P. Gunz, R. G. Maclagan, H. Kipton, J. Powell, C. J. Wilkins and Y. S. Hian, *Chem. Soc., Dalton Trans.* 1975, **12**, 1223.
6. (a) SDP Software, Enraf–Nonius Corp., Bohemia, New York; B. A. Frenz, The Enraf–Nonius CAD4-SDP, in *Computing in Crystallography* (Edited by H. Schenk, R. Olthof-Hazencamp, H. Van Koningveld and B. C. Bassi), pp. 64–71. University Press, Delft, Holland (1978); (b) the software calculates an absorption correction, including transmission factors using the Ψ-scans.
7. G. M. Sheldrick, SHELXS-86. Institute für Anorganische Chemie, Universität Göttingen, F.R.G. (1986).
8. D. T. Cromer and J. B. Mann, *Acta Cryst.* 1986, **A24**, 321; D. T. Cromer and J. Libermann, *J. Chem. Phys.* 1970, **53**, 1891.
9. N. F. Curtis, in *Comprehensive Coordination Chemistry* (Edited by G. Wilkinson), Vol. 2, pp. 905–906. Pergamon Press, New York (1987).
10. W. A. Nugent and J. M. Mayer, *Metal–Ligand Multiple Bonds*. Wiley-Interscience, New York (1988); J. M. Mayer, *Inorg. Chem.* 1988, **27**, 3899.
11. Formulation of **I** as a Mo^{V} species such as "$[MoO_2([15]aneN_4)]Cl$" is ruled out by the diamagnetic ^1H and ^{13}C NMR spectra; such a species would also be expected to be darkly coloured and very reactive.
12. K. Dreisch, C. Andersson and C. Stålhandske, *Polyhedron* 1992, **17**, 2143.

Polyhedron Vol. 12, No. 21, pp. 2611–2617, 1993
Printed in Great Britain

0277–5387/93 $6.00+.00
© 1993 Pergamon Press Ltd

SYNTHESIS, SPECTROSCOPIC CHARACTERIZATION AND MOLECULAR STRUCTURE OF DIMERIC (DIETHYLDITHIOPHOSPHINATO)DI(*para*-TOLYL) ANTIMONY(III), $[(p\text{-}CH_3C_6H_4)_2SbS_2P(C_2H_5)_2]_2$, CONTAINING A NOVEL MONOCYCLIC $P_2S_4Sb_2$ INORGANIC RING SYSTEM, FORMED THROUGH Sb...S SEMIBONDING INTERACTIONS

CRISTIAN SILVESTRU and IONEL HAIDUC*

Chemistry Department, Babes-Bolyai University, R-3400 Cluj-Napoca, Roumania

and

ROSE KALLER, KLAUS H. EBERT and HANS J. BREUNIG

Fachbereich 2 der Universität Bremen, Postfach 330440, D-2800 Bremen 33, Germany

(*Received* 27 *April* 1993; *accepted* 8 *June* 1993)

Abstract—The title compound, $(p\text{-}CH_3C_6H_4)_2SbS_2P(C_2H_5)_2$, was obtained in high yield by reacting $(p\text{-}CH_3C_6H_4)_2SbCl$ with $(C_2H_5)_2PS_2Na\cdot 2H_2O$ and was characterized by means of IR, ^1H and ^{31}P NMR and mass spectra. The solid-state structure was determined using the X-ray diffraction method. The compound is a cyclic dimer in which the fragments are held together by weak (semibonding) antimony–sulphur interactions, i.e. Sb(1)—S(1) 2.485, Sb(1)...S(4) 3.556, Sb(2)—S(3) 2.509 and Sb(2)...S(2) 3.318 Å, respectively, to form an eight-membered $P_2S_4Sb_2$ inorganic ring system. The anisobidentate behaviour of the bridging, bimetallic biconnective dithioligand is reflected in the different lengths of the phosphorus–sulphur bonds, which can be considered as single (P—S 2.077 Å) and double (P=S 1.965 Å). The antimony lone pair of electrons seems to be stereochemically active; the coordination geometry around the metal can be described as pseudo-trigonal bipyramidal, with two carbon atoms of the aromatic groups and the lone pair in equatorial positions and sulphur atoms in axial positions (S—Sb...S angle of *ca* 174°).

The interest in the chemistry of organoantimony derivatives of dithiophosphorus ligands arises from their potential biological activity, i.e. antitumor properties,[1–5] and from their frequently displayed unusual coordination geometries and other structural features. Thus, previous studies based on X-ray diffraction have shown that (diphenyldithiophosphinato)diphenylantimony (III), $Ph_2SbS_2PPh_2$,[6] and (di-isopropyldithiophosphato) diphenylantimony (III), $Ph_2SbS_2P(OPr^i)_2$,[7] exhibit basically different structures. Thus, the diphenyldithiophosphinate is a dimer,[6] whereas the di-isopropyldithiophosphate is a polymer.[7] Both are formed by weak Sb...S interactions, leading to interatomic distances longer than expected for a covalent bond (sum of covalent radii Sb—S 2.45 Å),[8] but significantly shorter than the sum of van der Waals radii (Sb 2.20 Å, S 1.80 Å, sum *ca* 4.0 Å).[9] Such interactions are called *semibonding*[10] and this term will be used here to describe them in various structures.

Dithiophosphorus ligands exhibit a broad variety of coordination patterns: monodentate, isobidentate, anisobidentate and bridging.[11] The latter can lead to dimer or polymer formation and different structures are formed, depending on whether the bridge is bimetallic biconnective or bimetallic triconnective. Some examples are illustrated in Fig. 1.

Monodentate coordination **a** is rare; it occurs,

* Author to whom correspondence should be addressed.

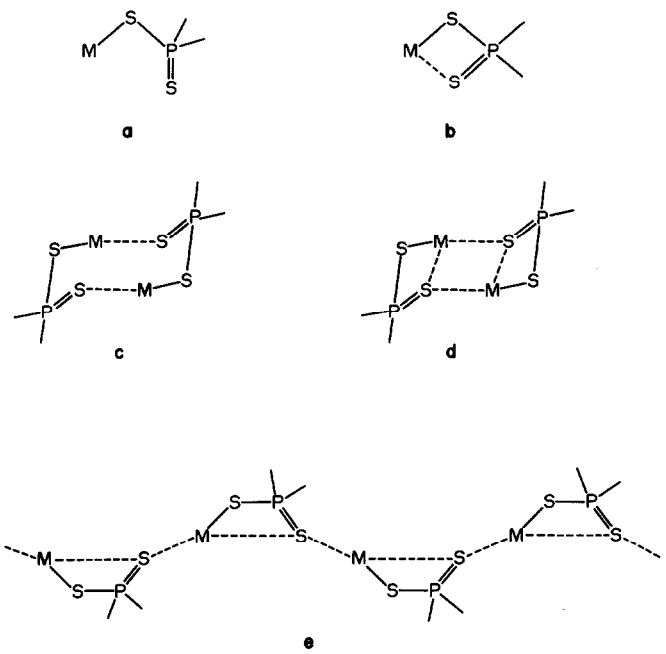

Fig. 1. Some coordination patterns of dithiophosphorus ligands.

for example, in $Ph_3SnS_2P(OEt)_2$[12] and in the germanium compounds $Ph_3GeS_2P(OMe)_2$ and $Ph_2Ge[S_2P(OMe)_2]_2$,[13] but has not been reported for any antimony compound. Anisobidentate coordination **b** is very frequent (for a review see ref. 14); in antimony chemistry it has been well documented.[6,15] The formation of monocyclic dimers based upon an eight-membered ring system **c** is known for zinc,[16] cadmium[17] and mercury[18] compounds, but, so far, has not been found in antimony chemistry. The tricyclic dimer **d**, first reported for $\{Sn^{II}[S_2P(OPh)_2]_2\}_2$,[19] is known in antimony chemistry, e.g. for $[Ph_2SbS_2PPh_2]_2$.[6] The polymeric structure **e** is unique for $\{Ph_2Sb[S_2P(OPr^i)_2]\}_\infty$.[7]

We now report the first example of an antimony compound containing a monocyclic, eight-membered ring system **c**, found by determining the crystal and molecular structure of (diethyldithiophosphinato)di(*p*-tolyl)-antimony(III), $(p\text{-}CH_3C_6H_4)_2SbS_2P(C_2H_5)_2$.

EXPERIMENTAL

Di(*p*-tolyl)antimony(III) chloride was prepared by scrambling at room temperature $(p\text{-tolyl})_3Sb$ and $SbCl_3$ in a 2:1 molar ratio[20] and used without further purification. $Et_2PS_2Na \cdot 2H_2O$ was obtained using a published procedure.[21] The IR spectrum was recorded in the 4000–400 cm^{-1} range on BIORAD spectrometer, using Nujol mulls. ^1H and ^{31}P NMR spectra were recorded in C_6D_6 solutions with a Bruker WH 360 instrument operating at 360 and 146 MHz, respectively, and the mass spectrum was recorded on a FINNIGAN MAT 8222 apparatus. Elemental analyses (carbon and hydrogen) were performed by BELLER Mikroanalytisches Laboratorium (Göttingen).

Preparation of $(p\text{-}CH_3C_6H_4)_2SbS_2P(C_2H_5)_2$

Stoichiometric amounts of $(p\text{-}CH_3C_6H_4)_2SbCl$ (0.68 g, 2 mmol) and $Et_2PS_2Na \cdot 2H_2O$ (0.43 g, 2 mmol) in anhydrous benzene (25 cm^3) were stirred under reflux for 2 h. The resulting sodium chloride was filtered off and the yellow filtrate was evaporated *in vacuo*, leading to a yellow oily product, partially crystallized. This was dissolved in acetonitrile and a small volume of n-hexane was added. Slow evaporation of the solvent mixture allowed the isolation of the title compound as slightly yellowish, prismatic crystals. $C_{18}H_{24}PS_2Sb$ (457.2): Yield: 0.8 g (88%); m.p. 120–122°C. Found: C, 47.3; H, 5.2. Calc.: C, 47.3; H, 5.3%. ^1H-NMR (C_6D_6): 1.05 ppm, dt (6H, CH_3—CH_2—P), $^3J(^{31}PCC^1H) = 22.7$ Hz, $^3J(^1HCC^1H) = 7.6$ Hz; 1.73 ppm, dq (4H, CH_3—CH_2—P), $^2J(^{31}PC^1H) = 13.7$ Hz, $^3J(^1HCC^1H) = 7.6$ Hz; 2.03 ppm, s (6H, *p*-CH_3—C_6H_4); 6.98 ppm, ds (4H, *p*-CH_3—C_6H_4, *meta*), $^3J(^1HCC^1H) = 7.6$ Hz; 7.67 ppm, ds (4H, *p*-CH_3—C_6H_4, *ortho*), $^3J(^1HCC^1H) = 7.6$ Hz. ^{31}P NMR (C_6D_6, H_3PO_4 85%): 76.2 Hz.

Crystal structure determination

Crystal data. $C_{18}H_{24}PS_2Sb$, $M = 457.2$, orthorhombic, $a = 19.907$ (4), $b = 12.293(2)$, $c = 16.285(2)$ Å, $U = 3985.2(10)$ Å^3, $Z = 8$, $D_{calc} = 1.524$ g cm^{-3}, $F(000) = 1840$, space group $Pna2_1$, Mo-K_α radiation, $\lambda = 0.71073$ Å, μ (Mo-K_α) = 1.669 mm^{-1}, crystal size $0.9 \times 0.6 \times 0.4$ mm^3 as a colourless fragment.

Structure determination. Data were collected on a Siemens P4 four-circle diffractometer for 5211 reflections in the 2θ–ω mode, of which 4768 were independent reflections ($R_{int} = 1.16\%$) and 3960 [$F > 4.0\sigma(F)$] were used in the full-matrix least-squares refinement with the SHELXTL PLUS (VMS)[22] program system. The structure was solved by direct methods for the antimony and the difference-Fourier synthesis revealed the positions for the other non-hydrogen atoms. All non-hydrogen atoms were refined anisotropically and hydrogen atoms were calculated as a riding model with isotropic U. The final R values are $R = 4.5\%$ and $wR = 5.59\%$ ($R = 5.58\%$ and $wR = 6.02\%$ for all data) with weights $w^{-1} = \sigma^2(F) + 0.0012F^2$. Our goodness-of-fit (Goof) finished at 1.24. The residual electron density from a final difference-Fourier synthesis was in the range -1.02–1.30 e A^{-3}. Further details of the crystal structure investigation may be obtained from the Fachinformationszentrum Karlsruhe, Gesellschaft fur wissenschaftlich-technische Informations mbH, D-W-7514 Eggenstein-Leopoldshafen 2 (FRG), on quoting the deposit number CSD−57231, the names of the authors and the journal citation.

RESULTS AND DISCUSSION

Di(*p*-tolyl)antimony(III) chloride reacts with sodium diethyldithiophosphinate, in benzene, according to eq. (1):

$$(p\text{-}CH_3C_6H_4)_2SbCl + Et_2PS_2Na \cdot 2H_2O \longrightarrow (p\text{-}CH_3C_6H_4)_2SbS_2PEt_2 + NaCl + 2H_2O \quad (1)$$

(Diethyldithiophosphinato)di(*p* - tolyl)antimony(III) was isolated from the reaction mixture (see Experimental) as slightly yellowish prismatic crystals. The compound is quite soluble in organic solvents, e.g. benzene, acetonitrile and chloroform.

The IR spectrum of the title compound exhibits strong absorptions in the 600–400 cm^{-1} range, i.e. 591 and 479 cm^{-1}, which can be assigned to asymmetric and symmetric PS_2 stretching vibrations, by comparison with those observed for $Et_2P(S)SMe$ (585 cm^{-1} for the P=S bond and 477 cm^{-1} for the P—S bond).[23] The difference $\Delta = \nu_{as}(PS_2) - \nu_s(PS_2) = 112$ cm^{-1} suggests a monodentate coordination of the dithiophosphinato ligand.[24] However, taking into account (a) the affinity of antimony for sulphur, (b) the tendency of antimony to increase its coordination number to five or six and (c) the dimeric structure already established for the related $Ph_2SbS_2PPh_2$,[6] a bridging pattern of the dithiophosphinato ligand, involving weak Sb...S(=P) interactions, cannot be ruled out.

The ^{1}H NMR spectrum confirms the identity of the compound. It contains a doublet of doublets of the same intensity, centred at 7.67 and 6.88 ppm [$^3J(^1HCC^1H) = 7.6$ Hz], as expected for the *ortho* and *meta* protons of the aromatic groups, and a singlet resonance for the methyl protons of the *p*-tolyl groups, at 2.03 ppm. The proton resonances of the ethyl groups attached to phosphorus exhibit the expected pattern, i.e. a doublet of quartets ($\delta = 1.73$ ppm) for methylene protons and a doublet of triplets ($\delta = 1.05$ ppm) for the methyl protons, due to phosphorus–proton and proton–proton couplings. The number and pattern of the proton resonances indicate the equivalence of both aromatic and ethyl groups bound to antimony and phosphorus, respectively. As a consequence, the structure of the compound in solution might be regarded as either monomeric (thus allowing the free rotation of the organic groups and of the whole dithiophosphinato ligand) or dimeric, as found in the solid state (see later). The latter would suggest rapid exchanges in the conformation of the eight-membered $P_2S_4Sb_2$ ring to occur in solution at room temperature.

The ^{31}P NMR spectrum in deuterated benzene shows a singlet resonance at 76.2 ppm, consistent with a unique kind of phosphorus atom.

The DCI(−) mass spectrum of the title compound exhibits some particular features. A dimeric fragment (see the molecular structure description below) was not observed and the monomeric molecular ion $[M—H]^{+\cdot}$ has very low intensity. One of the expected ions of the first fragmentation, i.e. $(p\text{-}CH_3C_6H_4)SbS_2PEt_2^+$, was not observed either (or has a very low intensity). The base peak is $Et_2PS_2^+$. Other ions of the first fragmentation are $(p\text{-}CH_3C_6H_4)_2Sb^+$ and $(p\text{-}CH_3C_6H_4)_2SbS^+$ and could be accounted for by the loss of $Et_2PS_2^{\cdot}$ or $Et_2P(S)^{\cdot}$ radicals, as a result of the cleavage of antimony–sulphur or phosphorus–sulphur bonds, respectively. A tentative fragmentation scheme, with monoisotopic m/z values and relative abundances, is given in Fig. 2.

The crystal and molecular structure of $(p\text{-}CH_3C_6H_4)_2SbS_2P(C_2H_5)_2$ was determined by X-

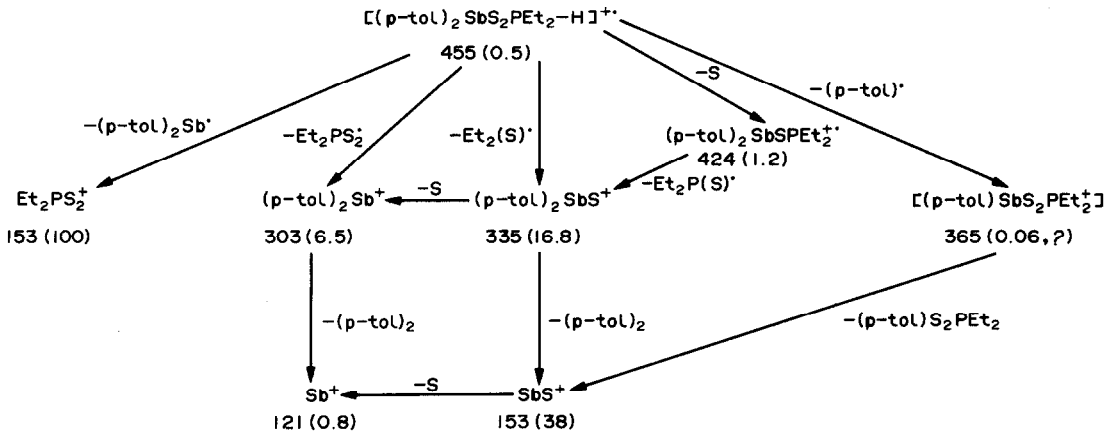

Fig. 2. Fragmentation pattern of $(p\text{-}CH_3C_6H_4)_2SbS_2PEt_2$ ($p\text{-}CH_3C_6H_4$ is abbreviated as *p*-tol).

ray diffraction. Important bond distances and angles are listed in Table 1, and the structure with the numbering atom scheme is shown in Fig. 3.

The two phosphorus–sulphur distances in the ligand unit (averages of two molecules) 2.077 and 1.965 (Å) are close to those reported for $Ph_2P(S)SH$ (2.077 and 1.954 Å)[25] and may be regarded as basically single (long) and double (short) phosphorus–sulphur bonds, in good agreement with the IR data. Comparison of these bond lengths with those observed in the sodium salt, $Et_2PS_2Na \cdot 2H_2O$,[26] i.e. 2.034 and 1.993 Å, provides further evidence concerning the absence of a strong delocalization of the π-electron pair over the PS_2 system in the organometallic compound. The distortion of the tetrahedral environment around the phosphorus atom is reflected in the S—P—S and C—P—C bond angles (av. 115.6 and 105.0°, respectively), which are very close to those found in $Et_2PS_2Na \cdot 2H_2O$ (115.8 and 106.5°, respectively).[26]

If only primary bonded atoms to antimony, i.e. a monodentate behaviour of the dithioligand, are

Table 1. Selected bond lengths (Å) and angles (°) for $(p\text{-}CH_3C_6H_4)_2SbS_2P(C_2H_5)_2$

Sb(1)—C(11)	2.151(8)	Sb(2)—C(31)	2.134(11)
Sb(1)—C(21)	2.140(10)	Sb(2)—C(41)	2.151(10)
Sb(1)—S(1)	2.485(3)	Sb(2)—S(3)	2.509(3)
Sb(1)...S(4)	3.556(3)	Sb(2)...S(2)	3.318(3)
P(1)—S(1)	2.081(3)	P(2)—S(3)	2.072(3)
P(1)—S(2)	1.965(3)	P(2)—S(4)	1.965(4)
P(1)—C(1)	1.809(11)	P(2)—C(5)	1.801(12)
P(1)—C(3)	1.815(11)	P(2)—C(7)	1.835(12)
C(1)—C(2)	1.494(16)	C(5)—C(6)	1.528(17)
C(3)—C(4)	1.540(16)	C(7)—C(8)	1.480(16)
C(11)—Sb(1)—C(21)	95.6(4)	C(31)—Sb(2)—C(41)	95.2(4)
C(11)—Sb(1)—S(1)	93.4(3)	C(31)—Sb(2)—S(3)	94.4(3)
C(21)—Sb(1)—S(1)	92.6(3)	C(41)—Sb(2)—S(3)	88.8(3)
S(1)—Sb(1)...S(4)	173.7		
C(11)—Sb(1)...S(4)	92.4		
C(21)—Sb(1)...S(4)	89.2		
Sb(1)—S(1)—P(1)	98.3(1)	Sb(2)—S(3)—P(2)	100.2(1)
S(1)—P(1)—S(2)	115.1(2)	S(3)—P(2)—S(4)	116.0(2)
S(1)—P(1)—C(1)	102.1(4)	S(3)—P(2)—C(5)	105.6(4)
S(2)—P(1)—C(1)	112.8(4)	S(4)—P(2)—C(5)	112.6(4)
S(1)—P(1)—C(3)	108.9(4)	S(3)—P(2)—C(7)	102.0(4)
S(2)—P(1)—C(3)	111.2(4)	S(4)—P(2)—C(7)	115.2(4)
C(1)—P(1)—C(3)	106.0(5)	C(5)—P(2)—C(7)	104.0(5)

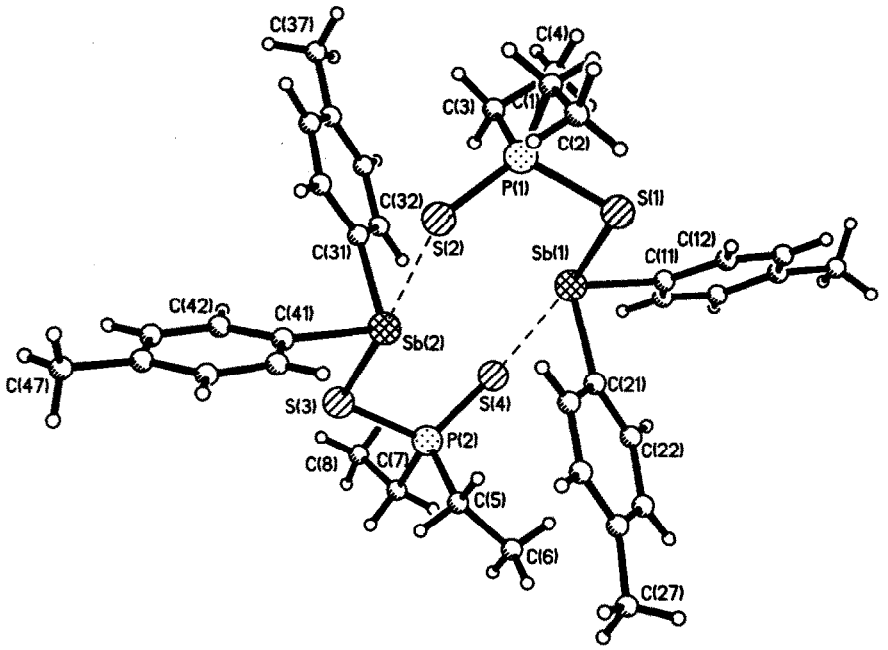

Fig. 3. View of the dimeric molecule of (diethyldithiophosphinato)di(*p*-tolyl)antimony(III), illustrating the atomic numbering.

considered the coordination geometry of the metal atom can be described as pyramidal, with angles at the metal atom ranging between 88.8 and 95.6°. However, each antimony atom forms a longer intermolecular contact, with the sulphur atom doubly bonded to phosphorus of a neighbouring molecule, i.e. Sb(1)...S(4) 3.556 Å, Sb(2)...S(2) 3.318° Å, which are well below the sum of van der Waals radii (*ca* 4.0 Å). This leads to dimeric associations, containing eight-membered inorganic $P_2S_4Sb_2$ rings, as shown in Fig. 3.

As mentioned above, a dimeric structure was reported for $Ph_2SbS_2PPh_2$.[6] However, here further intramolecular interactions between antimony and sulphur (S=P) have been noted (Table 2). Therefore, taking into account the secondary antimony–sulphur bondings, the coordination pattern of the dithiophosphinato ligand is essentially different in these two related compounds, i.e. *bimetallic triconnective* (bridging)[6] in $[Ph_2SbS_2PPh_2]_2$ and *bimetallic biconnective* (bridging) in $[(p\text{-}CH_3C_6H_4)_2SbS_2PEt_2]_2$, respectively.

The eight-membered $P_2S_4Sb_2$ ring has a twist-chair conformation, with the sulphur and antimony atoms almost in the same plane [deviations from the best S_4Sb_2 plane are Sb(1) +0.052, S(1) +0.102, S(2) −0.152, Sb(2) +0.034, S(3) +0.119, S(4) −0.155 Å] and phosphorus atoms lying up and down, respectively, relative to this plane [deviations: P(1) −0.993, and P(2) +0.850 Å] (Fig. 4.).

Table 2. Comparison of antimony–sulphur distances in the dimers of $R_2SbS_2PR'_2$ (in Å)

R = *p*-$CH_3C_6H_4$, R′ = Et (this work)		R = R′ = Ph[6]	
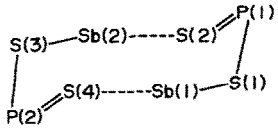		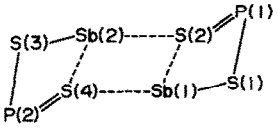	
Sb(1)—S(1)	2.485 (normal covalent)	Sb(1)—S(1)	2.490 (normal covalent)
Sb(1)...S(2)	4.013 (non-bonding)	Sb(1)...S(2)	3.440 (semibonding)
Sb(1)...S(4)	3.556 (semibonding)	Sb(1)...S(4)	3.474 (semibonding)
Sb(2)—S(3)	2.509 (normal covalent)	Sb(2)—S(3)	2.490 (normal covalent)
Sb(2)...S(4)	3.940 (non-bonding)	Sb(2)...S(4)	3.440 (semibonding)
Sb(2)...S(2)	3.318 (semibonding)	Sb(2)...S(2)	3.474 (semibonding)

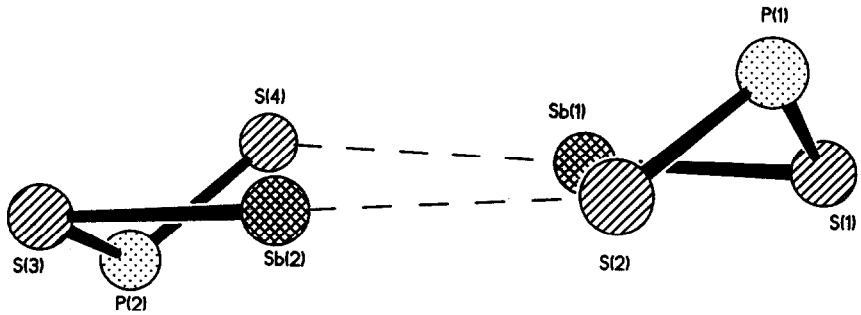

Fig. 4. Schematic illustration of the eight-membered $P_2S_4Sb_2$ inorganic ring system.

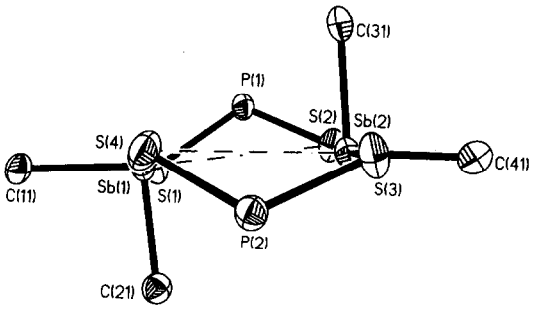

Fig. 5. View of the dimer skeleton along the imaginary phosphorus–phosphorus axis.

If these weaker antimony–sulphur interactions are considered the coordination geometry around the metal atom becomes a distorted square pyramid (with possibly the antimony lone pair of electrons being stereochemically inactive) in $[Ph_2SbS_2PPh_2]_2$ and distorted pseudo-trigonal bipyramidal in the title compound, with the two sulphur atoms in axial positions and carbon atoms of the aromatic groups bound to antimony in equatorial positions. The third equatorial position would be occupied by the stereochemically active lone pair of electrons. A view of the molecule along the imaginary P(1)...P(2) axis (Fig. 5) reveals much apparently free space above Sb(1) and below Sb(2), which could be occupied by the lone pair, if stereochemically active. It would be in an equatorial plane also comprising C(11) and C(21) at Sb(1) and C(31) and C(41) at Sb(2). Both electron pairs should be along a direction bent towards the centre of the ring. This is supported by the bond angles at antimony: S(1)Sb(1)...S(4) 173.7°, C(11)—Sb(1)—C(21) 95.6°, C—Sb(1)—S (range) 89.2–93.4°.

Acknowledgements—Dr Christian Silvestru thanks Bremen University for its hospitality and the financial support provided for a 3 month stay in Bremen.

REFERENCES

1. I. Haiduc and C. Silvestru, *Organometallics in Cancer Chemotherapy. Vol. I. Main Group Metal Compounds*, p. 129. CRC Press, Boca Raton, FL (1989).
2. C. Silvestru, C. Socaciu, A. Bara and I. Haiduc, *Anticancer Res.* 1990, **10**, 803.
3. A. Bara, C. Socaciu, C. Silvestru and I. Haiduc, *Anticancer Res.* 1991, **11**, 1651.
4. C. Socaciu, A. Bara, C. Silvestru and I. Haiduc, *In Vivo* 1991, **5**, 425.
5. B. K. Keppler, C. Silvestru and I. Haiduc, in preparation.
6. C. Silvestru, L. Silaghi-Dumitrescu, I. Haiduc, M. J. Begley, M. Nunn and D. B. Sowerby, *J. Chem. Soc., Dalton Trans.* 1986, 1031.
7. C. Silvestru, M. Curtui, I. Haiduc, M. J. Begley and D. B. Sowerby, *J. Organomet. Chem.* 1992, **426**, 49.
8. J. E. Huheey, *Inorganic Chemistry*, p. 278. Walter de Gruyter, Berlin (1988).
9. A. Bondi, *J. Phys. Chem.* 1964, **68**, 441.
10. N. W. Alcock, *Adv. Inorg. Chem. Radiochem.* 1972, **15**, 1.
11. I. Haiduc, *Rev. Inorg. Chem.* 1981, **3**, 353.
12. K. C. Molloy, M. B. Hossain, D. van der Helm, J. J. Zuckerman and I. Haiduc, *Inorg. Chem.* 1979, **18**, 3507.
13. R. K. Chadha, J. E. Drake and A. B. Sarkar, *Inorg. Chem.* 1985, **24**, 3156.
14. (a) E. R. T. Tiekink, *Main Group Metal Chem.* 1992, **15**, 161; (b) B. P. Singh, G. Srivastava and R. C. Mehrotra, *Coord. Chem. Rev.* 1984, **55**, 207.
15. (a) M. J. Begley, D. B. Sowerby and I. Haiduc, *J. Chem. Soc., Chem. Commun.* 1980, 64; (b) D. B. Sowerby, I. Haiduc, A. Barbul-Rusu and M. Salajan, *Inorg. Chim. Acta* 1983, **68**, 87; (c) R. K. Gupta, A. K. Rai, R. C. Mehrotra, V. K. Jain, B. F. Hoskins and E. R. T. Tiekink, *Inorg. Chem.* 1985, **24**, 3280.
16. (a) S. L. Lawton and G. T. Kokotailo, *Inorg. Chem.* 1969, **8**, 2410; (b) M. Calligaris, G. Nardin and A. Ripamonti, *J. Chem. Soc., A* 1970, 714; (c) H. Wunderlich, *Acta Cryst.* 1982, **B38**, 614.

17. (a) H. Wunderlich, *Acta Cryst.* 1986, **C42**, 631; (b) G. Svensson and J. Albertsson, *Acta Chem. Scand.* 1991, **45**, 820.
18. J. Zukerman-Schpector, E. M. Vazquez-Lopez, A. Sanchez, J. S. Casas and J. Sordo, *J. Organomet. Chem.* 1991, **405**, 67.
19. J. L. Lefferts, M. B. Hossain, K. C. Molloy, D. van der Helm and J. J. Zuckerman, *Angew. Chem., Int. Edn. Engl.* 1980, **19**, 309; *Inorg. Chem.* 1982, **21**, 1410.
20. M. Nunn, D. B. Sowerby and D. M. Wesolek, *J. Organomet. Chem.* 1983, **251**, C45.
21. W. Kuchen, H. Strolenberg and J. Metten, *Chem. Ber.* 1963, **96**, 1733.
22. Siemens, SHELXTL PLUS, Release 4.0 for Siemens R3 Crystallographic Research Systems. Siemens Analytical X-Ray Instruments, Inc., Madison, WI, U.S.A. (1989).
23. A. B. Remizov, I. Ya. Kuramshin, A. V. Aganov and G.G. Butenko, *Dokl. Akad. Nauk SSSR* 1973, **208**, 1118.
24. I. Haiduc, I. Silaghi-Dumitrescu, R. Grecu, R. Constantinescu and L. Silaghi-Dumitrescu, *J. Molec. Struct.* 1984, **114**, 467.
25. B. Krebs and G. Henkel, *Z. Anorg. Allg. Chem.* 1981, **475**, 143.
26. G. Svensson and J. Albertsson, *Acta Cryst.* 1989, **C45**, 395.

Polyhedron Vol. 12, No. 21, pp. 2619–2626, 1993
Printed in Great Britain

0277–5387/93 $6.00+.00
© 1993 Pergamon Press Ltd

THERMAL DECOMPOSITION STUDIES OF TRIS(N,N′-DIALKYLDITHIOCARBAMATO)IRON(III) COMPLEXES BY MÖSSBAUER SPECTROSCOPY

R. B. LANJEWAR and A. N. GARG*

Department of Chemistry, Nagpur University, Nagpur 440 010, India

(*Received* 23 *March* 1993; *accepted* 8 *June* 1993)

Abstract—A series of complexes of the type $[Fe(R'R''NCS_2)_3]$ with $R' = R'' = CH_3$ and C_2H_5; $R' = CH_3$, $R'' = C_2H_5$; $R' = CH_3$, $R'' = i\text{-}C_3H_7$; $R' = CH_3$, $R'' = C_6H_5$ and $R'NR''$ = pyrrolidyl and piperidyl, has been synthesized and their thermal decomposition studied. The complexes have been characterized by elemental analysis, electronic, IR and Mössbauer spectral and magnetic measurements. Mössbauer spectra of all the complexes at room temperature exhibit a quadrupole doublet with $\delta = 0.58$–0.68 mm s^{-1} (w.r. to SNP) and $\Delta E_Q = 0.25$–0.70 mm s^{-1}, except for pyrrolidyl and piperidyl complexes which exhibit $\delta = 0.93$ and 0.42 mm s^{-1}, respectively. Thermal decomposition behaviour can be divided into three groups of volatile, non-volatile and those yielding metal sulphides/oxides. An attempt has been made to identify intermediate and final products. Mössbauer spectra of the complexes at $>650°C$ exhibit six line patterns with $H_{eff} = 515 \pm 5$ kOe, suggesting the formation of $\alpha\text{-}Fe_2O_3$ in all cases.

Sulphur donor ligands are well known for their anticancer, antiviral and antifungal activities as well as widespread industrial applications in the vulcanization of rubber.[1] The dithiocarbamate ligand has coordinating ability to act as a unidentate, bidentate chelating or bridging ligand.[2,3] Cambi *et al.*[4] performed pioneering work on N,N′-dialkyldithiocarbamato iron(III) complexes, which provided a basis for the understanding of the spin state equilibrium in iron(III) complexes. Since then a large number of studies have been reported on the structure and magnetic behaviour of $[Fe(R,R''NCS_2)_3]$ by electronic,[5] IR[6], ESR and Mössbauer spectroscopic[7,8] studies down to liquid nitrogen temperature. The thermal decomposition of metal dithiocarbamates has also been of interest to many workers.[9–11] D'Ascenzo and Wendlendt[10] and Cardwell *et al.*[11] studied the thermal behaviour of $[Fe(S_2CNEt_2)_3]$ by TGA, DTA and found it to be completely volatile. It has been stated that most volatile compounds contain branched groups like i-butyl and i-propyl, while replacement by the benzyl group may lead to a sharp decline in volatility. Earlier we have reported thermal decomposition studies of some mixed-ligand dithiocarbamato iron(III) complexes, where loss of the ligand and/or the formation of Fe_2O_3/Fe_2S_3 was suggested.[12] Willemse *et al.*[13] have reviewed transition metal group complexes and the role of the dithiocarbamate ligand in stabilizing unusual oxidation states.

In this paper we report the synthesis of tris-(dialkyldithiocarbamato)iron(III) complexes with dimethyl, diethyl, methylethyl, i-propylmethyl, phenylmethyl, pyrrolidyl and piperidyl heterocyclic bases and their electronic, IR and Mössbauer spectroscopic studies. Thermal decomposition behaviour of the complexes was studied and its intermediate and final products were identified employing Mössbauer spectral measurements.

EXPERIMENTAL

All the chemicals used were of AR, GR or high purity grade. All solvents were purified before use.

Preparation of the complexes

First sodium salts of the ligands were prepared by the reaction of the respective amine (N-methylaniline, N,N′-dimethylamine, N,N′-methyl-

* Author to whom correspondence should be addressed.

Table 1. Analytical and IR spectral data of tris(dialkyldithiocarbamato)iron(III) complexes

Complex	Found (Calc.) (%) C	H	N	S	Fe	IR bands (cm^{-1}) ν(C=N)	ν(C···S)	ν(M—S)
$Fe(S_2CNMe_2)_3$	22.4	6.9	8.6	40.2	12.3	1520s	970s	230s
	(23.0)	(7.0)	(8.9)	(40.8)	(11.9)			350s
$Fe(S_2CNEt_2)_3$	—	—	—	—	—	1500s	990s	—
$Fe(S_2CNEtMe)_3$	31.4	5.0	8.8	41.7	12.4	1630m	970m	260m
	(31.4)	(5.2)	(8.2)	(41.9)	(12.2)			
$Fe(S_2CNPriMe)_3$	36.8	6.0	8.2	38.9	11.5	1630m	970m	240w
	(36.0)	(6.0)	(8.4)	(38.4)	(11.2)			
$Fe(S_2CNPhMe)_3$	48.0	3.8	6.2	32.0	9.3	1550s	970m	260m
	(47.8)	(4.0)	(6.9)	(31.8)	(9.3)			350m
$Fe[S_2CN(CH_2)_4]_3$	36.4	4.5	8.2	38.3	11.6	1430s	990s	260m
	(36.4)	(4.9)	(8.5)	(38.9)	(11.3)			320s
$Fe[S_2CN(CH_2)_5]_3$	46.3	5.5	7.5	35.8	10.8	1400s	1000s	340w
	(46.3)	(5.6)	(7.8)	(35.8)	(10.4)	1480		

ethylamine, piperidine and pyrrolidine) in dried diethyl ether with carbon disulphide and adding NaOH solution in an equal mole ratio with vigorous stirring. The crude products were recrystallized from chloroform. Sodium diethyldithiocarbamate was of AnalaR (BDH, England) grade. Complexes were prepared by mixing an ethanolic solution of 0.1 M ferric nitrate (GR, S. Merck) with a 0.3 M solution of the respective sodium dialkyldithiocarbamate.[8] Ferric nitrate (4 g) and a calculated amount of sodium dialkyldithiocarbamate were dissolved separately in minimum amounts of absolute ethanol and mixed with thorough stirring at room temperature for 1–2 h. In most cases a black coloured precipitate separated out, which was filtered, washed with water and then with acetone and diethylether and dried in a desiccator over fused $CaCl_2$. The complexes were characterized by the elemental analysis of C, H, N, S and Fe. Analytical data of the complexes are given in Table 1.

Physical measurements

Mössbauer spectra were recorded using a constant acceleration transducer driven Mössbauer spectrometer in conjunction with a PC based 1k multichannel analyser (Nucleonix, Hyderabad). A 5mCi ^{57}Co(Rh) source (procured from the Isotope group, BARC, Bombay) was used. All the spectra were recorded at room temperature and few simple ones were computer fitted with Lorentzian line shape. The spectrometer was calibrated using natural iron foil.[14] Sodium nitroprusside dihydrate (SNP) was used as a standard for isomer shift measurements.

Reflectance spectra were recorded using a Shimadzu Model UV-240 spectrophotometer employing MgO as a reference. IR spectra (4000–200 cm^{-1}) were recorded in KBr medium on a Perkin–Elmer 157 IR spectrophotometer. Thermograms were recorded on a Perkin–Elmer Thermogravimetric analyser System Model TGS-2 and Thermal Analysis Data Station TADS-3600 at a heating rate of 10 and 20°C per min. Magnetic moments were determined from magnetic susceptibility measurements using a Gouy balance and $Hg[Co(SCN)_4]$ as the standard.

The complexes were heated at different temperatures (as ascertained from TGA plot) in an electronically controlled muffle furnace for 3 h and then Mössbauer spectra of quenched samples were recorded.

RESULTS AND DISCUSSION

All the complexes were black coloured solids and stable under normal atmospheric conditions. Characteristic IR frequencies due to C···N, C···S and M—S stretching vibrations are listed in Table 1. Typical Mössbauer spectra of dimethyl, phenylmethyl and piperidyl dithiocarbamato iron(III) complexes at room temperature and after heating at different temperatures are shown in Figs 1, 2 and 3, respectively. Mössbauer parameters at various temperatures and magnetic moments are listed in Table 2. In Figs 4, 5 and 6 are shown the TGA and DTG plots of all the complexes and their respective thermogravimetric data are given in Table 3.

$Fe(dtc)_3$ is likely to have trigonally distorted octahedral geometry with six sulphur donor atoms surrounding it.[13] As a first approximation in O_h symmetry, the electronic configuration in the high

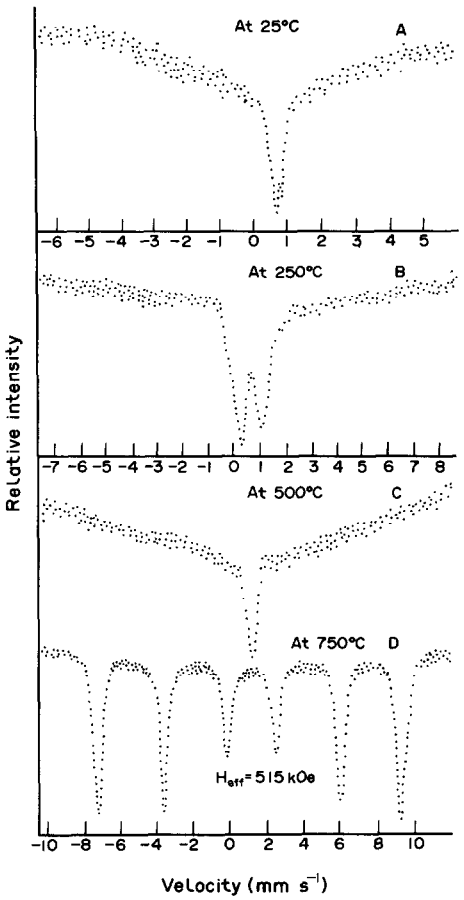

Fig. 1. Mössbauer spectra of tris(dimethyldithiocarbamato)iron(III) at (A) room temperature and after heating at (B) 250°C, (C) 500°C and (D) 750°C for 3 h in air.

spin state will be $t_{2g}^3 e_g^2$ or $^6A_{1g}$. However, in the case of the low spin state the electronic configuration would be t_{2g}^5 or $^2T_{2g}$. Magnetic moments of the complexes at room temperature are in the range 3.81–5.76 B.M. (Table 2) for spin free and spin paired configurations. The magnetic moment of the pyrrolidyldithiocarbamate complex (5.76 B.M.) is comparable to that for one spin free state (5.9 B.M.), while the phenyl methyl, dimethyl and i-propylmethyl substituted dithiocarbamate complexes appear to be in equilibrium between low and high spin states. Mitchell and Parker[15] have suggested that the most probable explanation for such low magnetic moments may be attributed to the presence of iron(III) in the intermediate spin state, $S = 3/2$.

Reflectance spectra of the complexes exhibit three bands of varying intensities at 15,000, 19,500 and 25,000 cm^{-1} corresponding to $^6A_{1g} \rightarrow {}^4T_{1g}$, $^6A_{1g} \rightarrow {}^4T_{2g}$ and $^6A_{1g} \rightarrow {}^4T_{1g}$, ^4E_g transitions,[16] respectively. It is observed that for ethylmethyl, phenylmethyl and i-propylmethyl substituted dithiocarbamate complexes the band at 25,000 cm^{-1} is more intense compared with a symmetric band of low intensity at *ca* 20,000 cm^{-1}. Contrary to this for other complexes the band at 25,000 cm^{-1} is less intense and only a broad intense shoulder is observed at 20,000 cm^{-1}.

IR spectra

Kellner *et al.*[17] attempted to detect the type of metal–ligand bonding from the solid-state vibrational spectra. We have observed a single band at 315 cm^{-1} for the supposedly high spin pyrrolidyl complex, which is in accordance with the earlier observation of 320 cm^{-1} by Ewald *et al*[18]. For the piperidyl complex also a single band observed at 340 cm^{-1} is suggestive of its high spin nature. However, for other complexes two bands at 260 and 350 cm^{-1} are observed. On the basis of these observations an equilibrium between the two spin states or a mixed spin state is expected.

The stretching vibration due to C···N has been observed at 1500 ± 100 cm^{-1}. Interestingly for high spin pyrrolidyl and piperidyl complexes it is

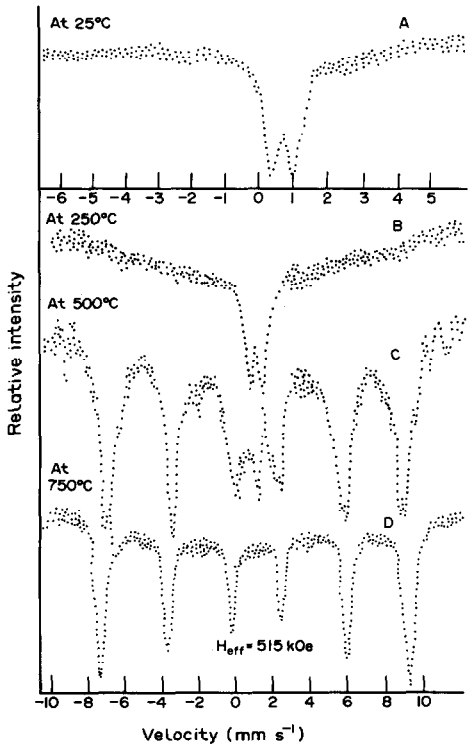

Fig. 2. Mössbauer spectra of tris(phenylmethyldithiocarbamato)iron(III) at (A) room temperature and after heating at (B) 250°C, (C) 500°C and (D) 750°C for 3 h in air.

observed at the lower frequency of 1450 cm^{-1} while for other complexes it is observed at 1500 and 1630 cm^{-1}. Bradley and Gitlitz[19] have found these bands to be insensitive of the nature of the metal or alkyl group. A strong band in the region 1000–970 cm^{-1} due to C=S stretching vibrations is suggestive of the chelating character of the dithiocarbamate ligands in all these cases.

Mössbauer parameters

Room-temperature Mössbauer spectra of dimethyl and diethyl substituted dithiocarbamate complexes show a doublet with $\Delta E_Q = 0.36$ and 0.25 mm s^{-1}, respectively. The corresponding δ values (Table 2) are 0.63 and 0.60 mm s^{-1}, which are in reasonably good agreement with those of $\delta = 0.65$ mm s^{-1} (for both) reported by Fiddy *et al.*[7] In all other cases well-resolved doublets were observed. Our ΔE_Q values for various dithiocarbamate complexes compare well with those reported in the literature.[20]

Since the *zz*-component of the electric field gradient tensor at the iron nucleus is zero for the configuration $t_{2g}^3 e_g^2$ ($^6A_{1g}$), the high spin state is not expected to show any quadrupole splitting and a

Table 2. Magnetic moment and Mössbauer parameters for tris(N,N'dialkyldithiocarbamato)iron(III) complexes and their thermal decomposition products at different temperatures

[Fe(R'R''NCS$_2$)$_3$]	Temperature (°C)	μ_{eff} (B.M.)	Isomer shift[a] δ(mms^{-1})[b]	Quadrupole splitting ΔE_Q (mm s^{-1})[b]	H_{eff} (kOe)[b]
R' = R'' = CH_3	25	3.98	0.63	0.36	
	250		0.65	0.78	
	500		0.63	—	—
	750		0.75	—	515
R' = R'' = C_2H_5	25	4.24	0.60	0.25	
	250		0.63	0.87	
	500		0.72	—	520
R' = CH_3, R'' = C_2H_5	25	4.86	0.68	0.53	
	250		0.63	0.62	
	500		0.72	—	510
			0.95	—	
	750		0.70	—	515
R' = CH_3, R'' = i-C_3H_7	25	3.97	0.68	0.53	
	250		0.65	0.60	
	500		0.68	—	505
			0.86	—	
	750		0.70	—	510
R' = CH_3, R'' = C_6H_5	25	3.81	0.56	0.60	
	250		0.72	0.64	
	500		0.65	—	495
			0.77	—	
	750		0.70	—	515
R' = R'' = —$(CH_2)_4$—	25	5.76	0.93	0.70	
	250		0.60	0.81	
	350		1.63	2.98	
			0.56	0.86	
	600		0.75	—	520
R' = R'' = —$(CH_2)_5$—	25	4.51	0.42	0.70	
	250		0.60	0.74	
	350		1.65	2.95	
			0.58	0.82	
	600		0.72	—	520

[a]w.r. to sodium nitroprusside dihydrate as standard.

[b]Errors are within ± 0.03 mm s^{-1} for δ and ΔE_Q and ± 5 kOe for magnetic field measurements.

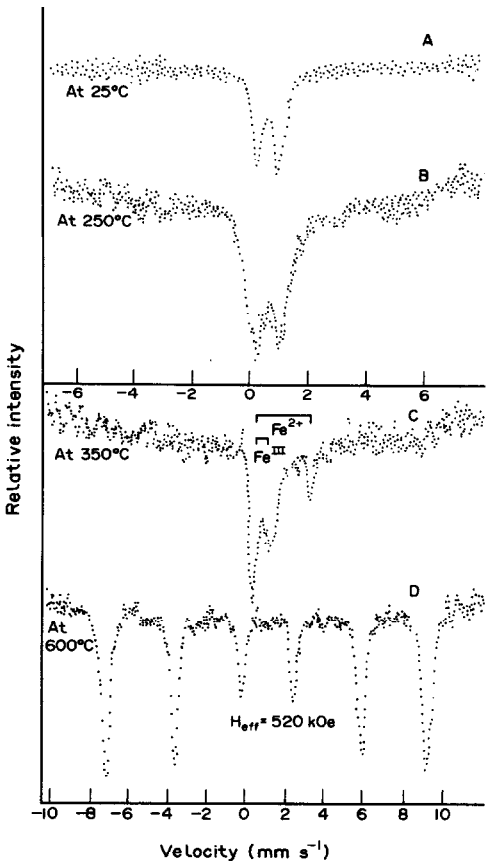

Fig. 3. Mössbauer spectra of tris(pyrrolidyldithiocarbamato)iron(III) at (A) room temperature and after heating at (B) 250°C, (C) 350°C and (D) 600°C for 3 h in air.

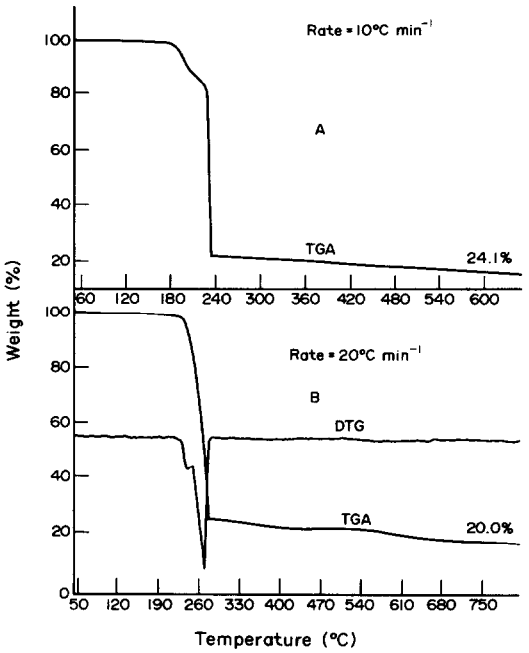

Fig. 4. Thermogravimetric plots of tris (A) (dimethyl-) and (B) (diethyldithiocarbamato)iron(III) complexes.

single absorption peak is expected. On the other hand a well-defined quadrupole doublet is expected for the low spin state ($^2T_{2g}$). The well-resolved doublet in the unsymmetrically substituted dialkyldithiocarbamate complexes with phenylmethyl, ethylmethyl and i-propylmethyl groups is noteworthy. It suggests that the substitution of the

Table 3. Thermogravimetric data of iron(III) tris(N,N'-dialkyldithiocarbamato) complexes

Complex	Initial decomposition temperature (°C)	DTG peak (°C)	Decomposition process	Constant weight temperature (°C)	Final weight (%)	Possible end product
$Fe(S_2CNMe_2)_3$	160	180 240	Fast, single stage	250	24.1	Fe_2S_3
$Fe(S_2CNEt_2)_3$	220	245 270	Fast, single stage	650	20.0	Fe_2S_3
$Fe(S_2CNEtMe)_3$	50	80 240	Fast, two stage	900	77.8	Loss of one ligand
$Fe(S_2CNPriMe)_3$	50	100 250	Slow, continuous	900	75.8	Loss of one ligand
$Fe(S_2CNPhMe)_3$	140	230	Fast, single stage	900	71.5	Loss of one ligand
$Fe[S_2CN(CH_2)_4]_3$	200	200,250 430	Fast, slow three stage	650	1.9	Volatile
$Fe[S_2CN(CH_2)_5]_3$	200	200,245 450	Fast, slow three stage	650	8.4	Volatile

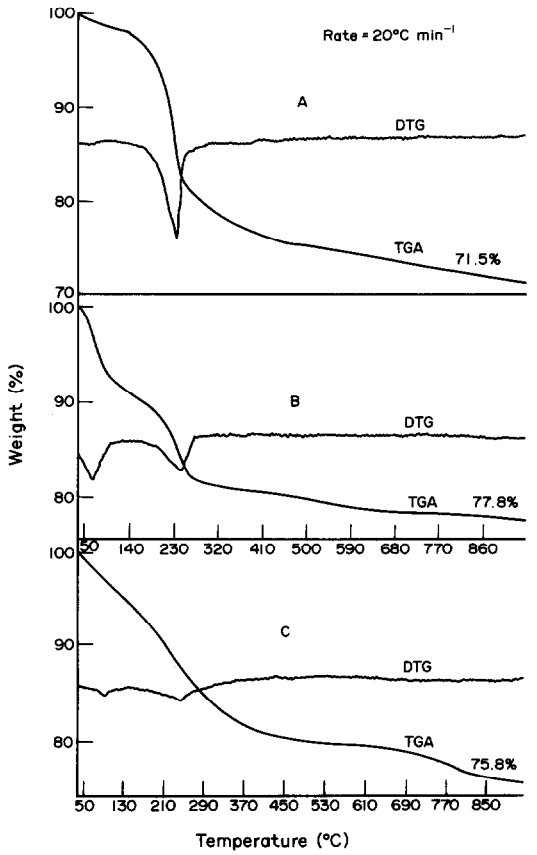

Fig. 5. Thermogravimetric plots of tris (A) (phenylmethyl-), (B) (ethylmethyl-) and (C) (i-propylmethyldithiocarbamato)iron(III) complexes.

stitution of different alkyl groups. In the present study δ values vary in the range 0.56–0.68 mm s^{-1}, except for N-heterocyclic base substituted pyrrolidyl and piperidyl complexes which show $\delta = 0.93$ and 0.42 mm s^{-1}, respectively. The large difference in δ values for the two complexes may possibly be due to the ring structure and size. If the average $\delta = 0.62$ mm s^{-1} is assumed for the dialkyldithiocarbamates, then for pyrrolidyldithiocarbamato iron(III) it is enhanced by 0.20 mm s^{-1}, whereas for piperidyldithiocarbamato iron(III) it is reduced by the same extent. Possibly the ring structure may be playing a role in enhancing or decreasing *s*-electron density at the iron nucleus. Interestingly, both the complexes show similar ΔE_Q values of 0.70 mm s^{-1}, suggesting distortion to the same extent.

Thermal decomposition studies

Thermal decomposition of metal dithiocarbamates has been a subject matter of detailed investigations.[9,10,12] It has been suggested that metal dialkyldithiocarbamates may be divided into two groups; volatile and non-volatile. Decomposition seems to proceed via the formation of metal thiocyanate as an intermediate, which may ultimately yield metal sulphide and/or oxide. However, a perusal of thermogravimetric data in Table 3

inequivalent alkyl groups causes a greater distortion in the axial symmetry of the complex. Interestingly, ΔE_Q values decrease in the order phenylmethyl > ethylmethyl > i-propylmethyl. Recently Terzis *et al.*[21] observed $\Delta E_Q = 0.10$ mm s^{-1} in tris(N-methyl-N′-n-butyldithiocarbamato) iron (III), which is smaller than for all the unsymmetrically substituted dithiocarbamate complexes of this study.

The Mössbauer spectra of pyrrolidyl and piperidyl dithiocarbamate complexes are somewhat complex, but the quadrupole splitting is well defined. High magnetic moments of these complexes suggest the predominance of the high spin state ($^6A_{1g}$) with little contribution from the low spin state ($^2T_{2g}$). Our value of $\mu_{eff} = 4.5$ B.M. for piperidyl substituted complex compares well with 4.04 B.M. reported by Wazda *et al.*[20] In spite of this, large ΔE_Q values may be attributed to the distortion in the octahedral geometry, as already confirmed by X-ray crystal structure.[22] It has been suggested that δ values in these complexes remain fairly constant as *s*-electron density is unduly sensitive to the sub-

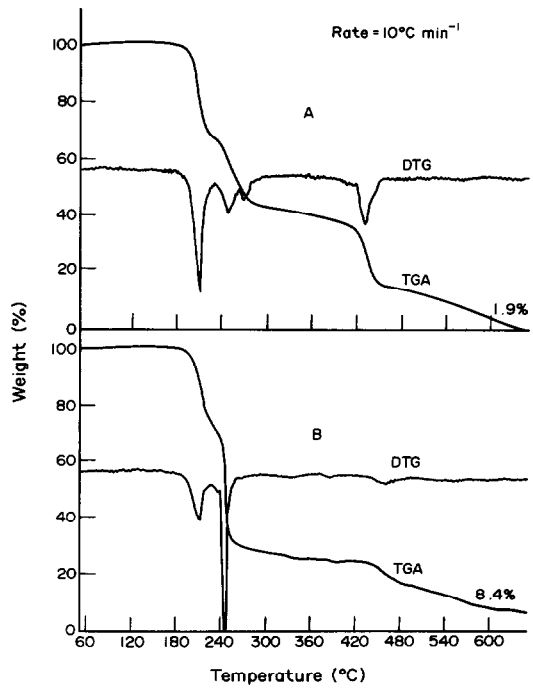

Fig. 6. Thermogravimetric plots of tris (A) (pyrrolidyl-) and (B) (piperidyldithiocarbamato)iron(III) complexes.

shows that the tris(dialkyldithiocarbamato) iron(III) complexes investigated in this study may be divided into three distinct groups:

(A) *Non-volatile complexes of symmetrically substituted dithiocarbamates.* Thermograms of dimethyl and diethyl substituted dithiocarbamate complexes (Fig. 4) show a sharp and single stage decomposition at ~250°C yielding 24.1 and 20.0% residual weights, respectively. These correspond to the formation of Fe_2S_3 (cf. calculated weights 25.0 and 20.8%, respectively, for the two complexes). D'Ascenzo and Wendlendt[10] have reported iron(III) diethyldithiocarbamate as a volatile metal chelate, which is contrary to our observation. In our earlier study of mixed-ligand diethyldithiocarbamates with different chelating ligands, the residual weights of 17.4–55.0% were observed and none of the complexes were found to be volatile.[12]

Mössbauer spectra of dimethyl and diethyl substituted dithiocarbamate complexes heated at 250°C for 3 h exhibit an asymmetric doublet (Fig. 1) with increased ΔE_Q of 0.78 and 0.87 mm s^{-1}, respectively. On further heating at 500°C, Mössbauer spectra of the dimethyl substituted complex show a singlet with $\delta = 0.63$ mm s^{-1}, whereas for the diethyl substituted complex a magnetic hyperfine splitting with $\delta = 0.72$ mm s^{-1} and $H_{eff} = 520$ kOe is observed. It seems on heating up to 250°C either a ligand is lost or iron(III) thiocyanate is formed, giving a doublet in both cases. At 500°C, however, in the case of the dimethyl dithiocarbamate complex, a single line spectrum is suggestive of a highly symmetric environment around the iron atom. When this complex is further heated to 750°C a well defined six-line spectrum is observed with $\delta = 0.75$ mm s^{-1} and $H_{eff} = 515$ kOe (Fig. 1). This difference in behaviour is more intriguing. Fiddy *et al.*[7] have also noted some difference in the low-temperature Mössbauer spectral behaviour of dimethyl and diethyl substituted dithiocarbamates and attributed it to crystallographic phase change. Even though thermogravimetric studies suggest the formation of Fe_2S_3 in both cases, six-line Mössbauer spectra with $H_{eff} = 515$–520 kOe suggest the formation of α-Fe_2O_3. The line separations also match with those reported in the literature.[23,24] In order to further resolve the ambiguity about Fe_2O_3 or Fe_2S_3 we attempted to determine sulphur content in the end product, but could not find any sulphur in it. Therefore, as Mössbauer spectral and elemental analysis evidences, formation of α-Fe_2O_3 is a certainty. Presumably, in TGA studies where a sample is heated at 10°C min^{-1}, Fe_2S_3 is being formed which on prolonged heating in air for 3 h maybe converted to α-Fe_2O_3 to exhibit a six-line spectrum.

(B) *Non-volatile complexes of unsymmetrically substituted dithiocarbamates.* Thermograms of phenylmethyl, ethylmethyl and i-propylmethyl substituted complexes (Fig. 5) yield 71.5, 77.5 and 75.8% residual weights, respectively, at 900°C. The weight losses correspond to approximately one ligand in all three cases. The phenylmethyl dithiocarbamate complex gives a DTG peak at 230°C [Fig. 5(A)], exhibiting fast decomposition up to 300°C and later it decomposes slowly up to 900°C. In the case of the ethylmethyl substituted complex decomposition starts at 50°C, giving a DTG peak at 80°C and another at 240°C. Beyond 300°C it decomposes very slowly. For tris(i-propylmethyldithiocarbamato)iron(III), decomposition is uniformly slow in the entire temperature range up to 900°C. Again two broad DTG peaks are observed at 100 and 250°C. Therefore, not only are these complexes non-volatile but their decomposition behaviour is also complex.

Mössbauer spectra of all the three complexes heated at 250°C exhibit doublets with $\Delta E_Q = 0.60$–0.64 mm s^{-1} and $\delta = 0.63$–0.72 mm s^{-1}. It may be noted that as compared with room temperature ΔE_Q increases insignificantly. It seems that the dithiocarbamate ligand is decomposed partially, whereby the substitutent alkyl group may be eliminated. On further heating at 500°C six-line hyperfine splitting ($H_{eff} = 495$–510 kOe) along with a singlet may correspond to a somewhat symmetric environment around the iron nucleus while the decomposition is still in progress. At the same time a partially magnetic phase as evidenced by hyperfine splitting with $H_{eff} = 510$–515 kOe is observed for all the three complexes. Identical δ values of 0.70 mm s^{-1} and the strength of the magnetic field in all three cases suggest the formation of α-Fe_2O_3.[21]

(C) *Volatile complexes of N-heterocyclic substituted dithiocarbamates.* As evident from thermograms in Fig. 6 pyrrolidyl and piperidyl dithiocarbamate complexes show a three-stage decomposition. In both the complexes two sharp DTG peaks appear at 200 and 250°C and a third broad peak at *ca* 440°C. Ultimately 1.9 and 8.4% residual weights are obtained at 650°C for both the complexes. It clearly suggests the volatile nature of both the complexes because even their metal contents are 11.3 and 10.4%, respectively. Presumably, it represents the removal of the three ligands, one at a time, when part of the iron metal seems to be converted to oxide at 650°C, as evidenced by six-line hyperfine splitting with $H_{eff} = 520$ kOe.

Mössbauer spectra of both the complexes heated at 250°C show a doublet with little increase in quadrupole splitting. It may be due to detachment of

one of the ligands. At 350°C the spectrum consists of three lines of unequal intensities [Fig. 3(C)]. It may be resolved into two sets of doublets. The first set shows a large $\Delta E_Q = 3.0$ mm s^{-1} and $\delta = 1.65$ mm s^{-1}, which may correspond to iron(II) in the high spin state.[25] Another doublet, however, has a smaller $\Delta E_Q = 0.82$ and 0.86 mm s^{-1} with $\delta = 0.58 \pm 0.02$ mm s^{-1}. These are the same as at 250°C and correspond to iron(III) in the low spin state. It seems that after the detachment of the first ligand at 250°C iron(III) is partially reduced to iron(II), giving the complex in the high spin state. On further heating up to 600°C in air the whole complex volatilizes. In this process part of the metal may be oxidized to form a ferromagnetic phase of α-Fe_2O_3. δ values of 0.75 and 0.72 mm s^{-1} and $H_{eff} = 520$ kOe for both complexes clearly suggest the formation of α-Fe_2O_3.[24]

Possibly, these compounds may be of special technical importance in the rubber industry, whereby metal oxides are added during vulcanization thus altering its properties for useful purposes. In view of some of these investigations, the thermal decomposition of dithiocarbamates needs to be reinvestigated (in the absence of air) and more precise identification of thermal decomposition products is essential.

Acknowledgements—Our grateful thanks are due to the Council of Scientific and Industrial Research, New Delhi, for financial assistance. One of the authors (RBL) thanks CSIR for the award of SRF. Thanks are also due to the directors of RSIC, Lucknow, for elemental analysis and IR spectra and of RSIC, Nagpur, for TGA studies.

REFERENCES

1. G. D. Thorn and R. A. Ludwig, *The Dithiocarbamates and Related Compounds*. Elsevier, New York (1980).
2. S. V. Lorionaova, *Zhur. Neorg. Khim.* 1978, **24**, 1446.
3. J. O. Hill and R. J. Magee, *Rev. Inorg. Chem.* 1981, **3**, 141.
4. L. Cambi and A. Cagnasso, *Atti. Accad. Naz. Lincei. Cl Sci Fis Mat. Nat. Rend.* 1931, **13**, 809; L. Cambi and L. Szego, *Ber. Dtsch. Chem. Ges.* 1931, **B64**, 2591.
5. A. H. Ewald, R. L. Martin, E. Sinn and A. H. White, *Inorg. Chem.* 1969, **8**, 1837.
6. G. R. Hall and D. N. Hendrikson, *Inorg. Chem.* 1976, **15**, 607.
7. J. M. Fiddy, I. Hall, F. Grandjean, U. Russo and G. J. Long, *Inorg. Chem.* 1987, **26**, 4138.
8. B. S. Manhas and S. Bala, *Polyhedron* 1988, **24**, 2465.
9. A. K. Sharma, *Thermochim. Acta* 1986, **104**, 339.
10. G. D'Ascenzo and W. W. Wendlendt, *J. Inorg. Nucl. Chem.* 1970, **32**, 2431.
11. T. J. Cardwell, D. L. Desarro and F. C. Uden, *Anal. Chim. Acta* 1976, **85**, 415.
12. R. B. Lanjewar and A. N. Garg. *Ind. J. Chem* 1992, **31A**, 849.
13. J. Willemse, J. A. Cras, J. J. Stegerda and C. D. Keijers, *Struct. Bonding* 1976, **28**, 83.
14. R. B. Lanjewar and A. N. Garg. *Ind. J. Chem.* 1991, **30A**, 166, 350.
15. P. C. H. Mitchell and D. A. Parker, *J. Chem. Soc., Dalton Trans* 1976, 1821.
16. C. J. Ballhausen, *Introduction to Ligand Field Theory*, p. 253. McGraw Hill Book Co., Inc., New York (1962).
17. R. Kellner, G. S. Nikolov and T. Trendafilova, *Inorg. Chim. Acta* 1984, **84**, 233.
18. A. H. Ewald, R. L. Martin, I. G. Ross and A. H. White, *Proc. R. Soc. London.* 1964, **A280**, 235.
19. D. C. Bradley and M. H. Gitlitz, *J. Chem. Soc. A* 1969, 1152.
20. S. Wajda, K. Drabent and A. Ozarowski, *Inorg. Chim. Acta* 1980, **45**, L201.
21. A. Terzis, S. Filippakis, D. Mentzafos, M. V. Petrouleas and A. Malliaris *Inorg. Chem.* 1984, **23**, 334.
22. R. L. Martin, N. H. Rohde, G. B. Robertson and D. Taylor, *J. Am. Chem. Soc.* 1974, **96**, 3647.
23. W. Kundig and H. Bommel, *Phys. Rev.* 1966, **142**, 327.
24. E. Murad and J. H. Johnston, in *Mössbauer Spectroscopy Applied to Inorganic Chemistry* (Edited by G. J. Long), Vol. 2, p. 507. Plenum Press, New York (1987).
25. P. Gutlich, R. Link and A. Trautwein, *Mössbauer Spectroscopy and Transition Metal Chemistry*. Springer-Verlag, Berlin (1978).

Polyhedron Vol. 12, No. 21, pp. 2627–2633, 1993
Printed in Great Britain

0277-5387/93 $6.00+.00
© 1993 Pergamon Press Ltd

COVALENTLY LINKED MOLYBDENUM–MOLYBDENUM QUADRUPLE BONDS. DIOXYPYRIDAZINE DIANION AND 2-IMIDAZOLINETHIONATE AS BRIDGES BETWEEN DIMOLYBDENUM FRAGMENTS

ROGER H. CAYTON, MALCOLM H. CHISHOLM,† ELENA F. PUTILINA and KIRSTEN FOLTING

Department of Chemistry and Molecular Structure Center,
Indiana University, Bloomington, IN 47405, U.S.A.

(*Received* 21 *April* 1993; *accepted* 4 *June* 1993)

Abstract—$[Mo_2(O_2CBu^t)_3(CH_3CN)_2]^+[BF_4]^-$ and the disodium salt of the dioxypyridazine dianion (DOP) react in CH_2Cl_2/CH_3CN/MeOH solution to give the red microcrystalline tetranuclear compound $[Mo_2(O_2CBu^t)_3]_2(\mu$-DOP) (**1**), which is soluble in coordinating solvents such as THF and pyridine (py). Compound **1** shows two oxidation potentials by cyclic voltammetry, $\mathbf{1} \rightarrow \mathbf{1}^+$, $E_{1/2} = -0.15$ V, and $\mathbf{1}^+ \rightarrow \mathbf{1}^{2+}$, $E_{1/2} = +0.28$ V, vs the Cp_2Fe/Cp_2Fe^+ couple. The first oxidation is chemically reversible and the cationic complex $[\mathbf{1}]^+[BF_4]^-$ was isolated. The reaction between $[Mo_2(O_2CBu^t)_3(CH_3CN)_2]^+[BF_4]^-$ and the sodium salt of the dianion derived from deprotonation of 2-imidazolinethione in a CH_2Cl_2/CH_3CN/MeOH solvent mixture gave $Mo_2(O_2CBu^t)_3$(IMT) (**2**), where IMT represents the anion from a single deprotonation of 2-imidazolinethione. Compound **2** was structurally characterized as its pyridine adduct $\mathbf{2}\cdot(py)_2$ and contained a central Mo$\overset{4}{-}$Mo bond, 2.116(1) Å, bridged by three O_2CBu^t ligands and an IMT ligand which forms Mo—N and Mo—S bonds of lengths 2.12(1) and 2.49(1) Å, respectively. The two molecules of pyridine are coordinated along the Mo—Mo axis, one in a rather normal manner, Mo—N = 2.63(1) Å, but the other in a more distant arrangement with Mo---N = 2.97(1) Å. The latter py is coordinated to the molybdenum atom that is bonded to the nitrogen atom of the IMT ligand. These results are compared with those of earlier studies aimed at covalently linking M$\overset{4}{-}$M bonds.

The wide range of optical, magnetic and electrochemical properties associated with complexes containing metal–metal multiple bonds[1] promoted our investigation of macromolecular ordered assemblies (oligomers, polymers and metallomesogens) containing such subunits.[2,3] One of the goals of this research is the preparation of covalently-linked, stiff-chain polymers wherein facile electron transfer is possible between quadruple bonds incorporated along the polymeric backbone.[4] We have concentrated on the use of dimetal tetracarboxylates as the quadruply-bonded subunit and bridging ligands containing conjugated π-systems as the linking moieties. In principle the 1-D polymer can be ordered such that the M—M axis is either perpendicular or parallel to the polymer axis.[2]

The potential conductivity of these targeted polymeric systems can be estimated from the redox chemistry of smaller molecular fragments, such as two dinuclear subunits linked by a single polydentate ligand. This strategy was utilized previously to prepare tetranuclear complexes coupled through dicarboxylate and di-α-oxypyridinato links.[2] The electronic coupling of the quadruple bonds in these complexes was shown to be a function of both the metal (Mo vs W) and the nature of the bridging group. For example, the complexes $[Mo_2(O_2CR)_3]_2$(DOQ) (**A**) and $[Mo_2(O_2CR)_3]_2$(DON) (**B**) (where R = Bu^t, DOQ = dioxyquinoxaline, DON = dioxynaph-

† Author to whom correspondence should be addressed.

thyridine) exhibit different oxidation behaviour. In the drawing three carboxylato ligands were omitted from each Mo–Mo for clarity. Compound **A** displays a 366 mV separation between its first and second oxidation potentials, whereas compound **B** shows more communication with a separation of 373 mV between the same redox couples. Despite the different alignment of the Mo—Mo axes in **A** and **B**, the coupling occurs through the mixing of metal–metal δ-orbitals with those of the π^*-orbitals of the ligands. This was evident from the use of $[p\text{-}O_2C\text{—}C_6F_4\text{—}CO_2]^{2-}$ and the 1,8-anthracene dicarboxylate dianion which yielded tetranuclear compounds stereochemically related to **A** and **B**, but with very small electronic couplings between the Mo_2 centres, i.e. the separation between the first and second oxidation potentials was *ca* 50 mV or less.[2]

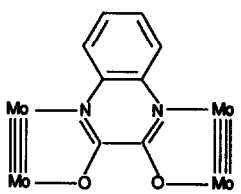

A

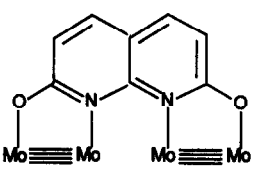

B

In this work we report further studies aimed at the preparation of tetranuclear complexes containing quadruply-bonded dimolybdenum centres linked with bridges that we expected would show even greater electronic communication.

RESULTS AND DISCUSSION

Anticipating that bridging groups that are capable of providing even shorter conjugation paths between the quadruple bonds would lead to greater charge delocalization, we examined the potentially bridging ligands derived from deprotonation of dihydroxypyridazine and 2-imidazolinethione shown in **C** and **D** below.

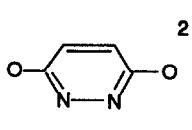

C

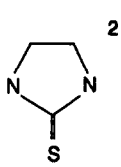

D

The synthetic strategy employed the substitution chemistry of the labile complex $Mo_2(O_2CBu^t)_3(CH_3CN)_2{}^+BF_4{}^-$, which can be prepared via alkylation of $Mo_2(O_2CBu^t)_4$ in CH_3CN.[5] The acetonitrile ligands, as well as the pivalate groups are kinetically labile, such that the equilibrium shown in eq. (1) is established in acetonitrile.

$$Mo_2(O_2CBu^t)_4 + Mo_2(O_2CBu^t)_2{}^{2+} \overset{K}{\rightleftharpoons} 2Mo_2(O_2CBu^t)_3{}^+BF_4{}^- \quad (1)$$

At room temperature K is on the order 60 and most of the material exists as the tris-pivalato cation.

The compound $[Mo_2(O_2CBu^t)_3]_2$(DOP) (**1**) was prepared from the dimolybdenum trispivalato cation as shown in eq. (2).

$$2Mo_2(O_2CBu^t)_3{}^+BF_4{}^- + Na_2DOP \longrightarrow [Mo_2(O_2CBu^t)_3]_2(\mu\text{-DOP}) + 2NaBF_4 \quad (2)$$

1

The ^1H NMR spectrum displays the expected 2 : 1 ratio of the Bu^t resonances along with a doublet in the aromatic region indicative of a symmetrically disubstituted DOP ligand. Assuming the usual coordination mode of α-oxypyridinato ligands,[2] the structure of **1** would be that shown below in **E**.

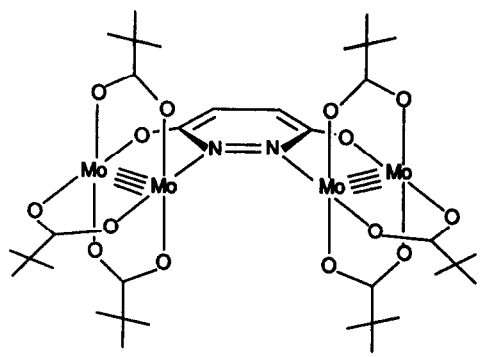

E

In **1** the shortest pathway between the linked quadruple bonds is via the two π-conjugated nitrogen atoms of the DOP ligand. This represents a shorter path than in either of compounds **A** (four atoms) or **B** (three atoms). Although the π-system in this series of compounds is different in each case, we felt that the electronic coupling in **1** may be stronger than for the other tetranuclear complexes because of the shorter pathway available. We carried out the cyclic voltammetry of **1** in THF and the response is depicted in Fig. 1. Two chemically reversible one-electron oxidation waves were observed and the resulting potentials are listed in Table 1, along with those for **A** and **B** and related compounds for comparison. The $E_{1/2}$ values for the redox couples of **1** were determined to be $E_{1/2}{}^1 = -0.15$ V and $E_{1/2}{}^2 = +0.28$ V vs the $Cp_2Fe^{0/1+}$ couple used as an internal standard.

The oxidation processes shown in Table 1 represent successive removal of one-electron from each of the complexes. The magnitude of the separation of the two oxidation processes is indicative of the

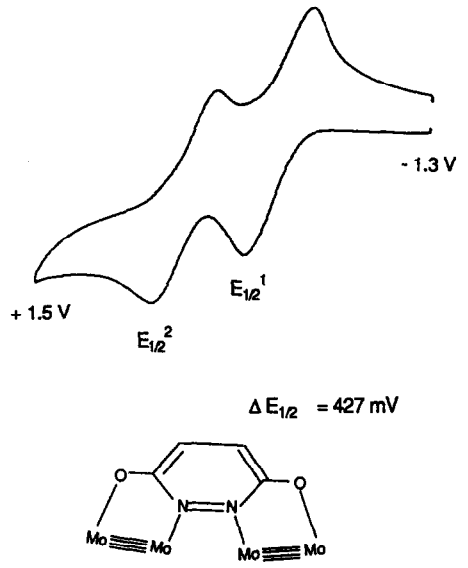

Fig. 1. Cyclic voltammogram of **1** in THF with 2.0 $M[N(Bu^n)_4][PF_6]$ as the supporting electrolyte at 200 mV s^{-1}.

extent of electron delocalization in the singly oxidized radical cation $\mathbf{1}^+$. The greater the separation between the oxidation processes, the more highly delocalized the charge in the radical cation.[8] Compared with the electrochemical behaviour of the compounds **A** and **B**, the DOP ligand does indeed provide for greater electronic communication between the Mo—Mo multiple bonds (see Table 1).

This also results in a more stable radical cation with respect to disproportionation to the neutral and dicationic species. The equilibrium reaction is depicted in eq. (3) as a comproportionation.

$$\mathbf{1} + \mathbf{1}^{2+} \overset{K_c}{\rightleftharpoons} 2[\mathbf{1}]^+ \qquad (3)$$

The comproportionation equilibrium constant can be calculated from the electrochemical data according to the formula $K_c = \exp(\Delta E_{1/2}/25.69)$ and results in a value of 1.7×10^7 for $\mathbf{1}^{1+}$.[8]

With the hope of preparing a linked tetranuclear complex displaying even stronger electronic communication between quadruple bonds, we focused on the potentially single-atom-bridged ligand derived from double deprotonation of 2-imidazolidinethione. However, treatment of the disodium salt of this dianion with 2 equivalents of the tris-pivalato Mo_2 cation resulted in the isolation of the dimolybdenum dinuclear complex **2**, which contains a single deprotonated 2-imidazolinethione ligand. Either we were unsuccessful in deprotonating the ligand twice or the dianion has scavenged a proton in the formation of **2**. The failure of the ligand to link two Mo_2 units was evident in

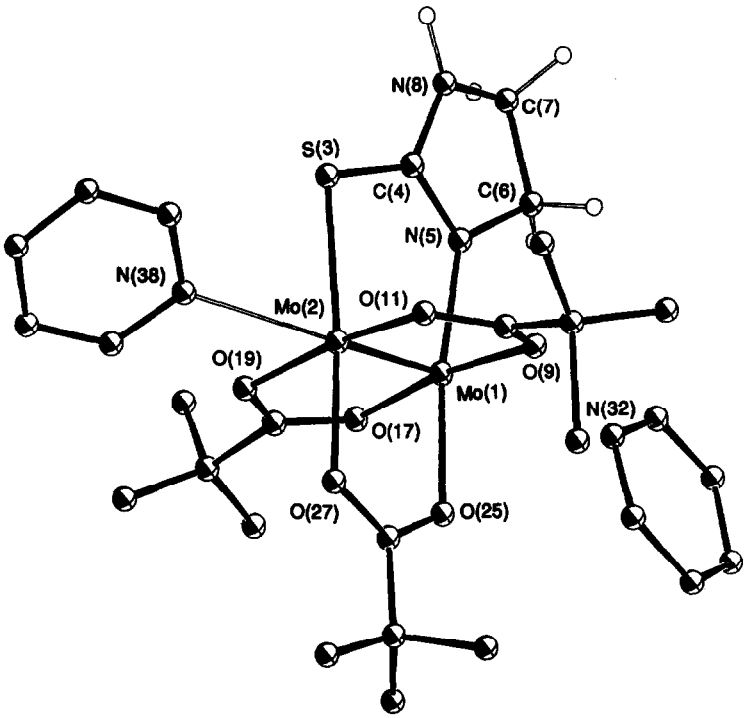

Fig. 2. Ball-and-stick representation of $Mo_2(O_2CBu^t)_3(IMT) \cdot 2py$. The hydrogen atoms of the Bu^t groups have been omitted for clarity.

Table 1. Changes in the redox potentials in compound **1** and related covalently-linked quadruply-bonded complexes together with some mononuclear Ru^{II}-bridged complexes showing how K_c decreases with increasing length of the bridge

Compound	Name	$E_{1/2}^1$ (V)	$E_{1/2}^2$ (V)	$\Delta E_{1/2}$ (mV)	K_c	Ref.
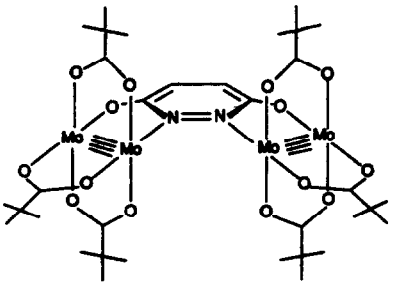	Mo_4DOP	−0.15	+0.28	427	1.7×10^7	This work
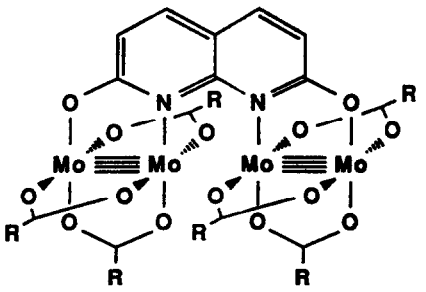	Mo_4DON	−0.08	+0.30	373	2.0×10^6	2
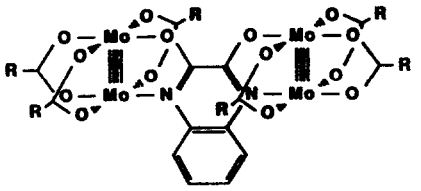	Mo_4DOQ	−0.13	+0.24	366	1.5×10^6	2
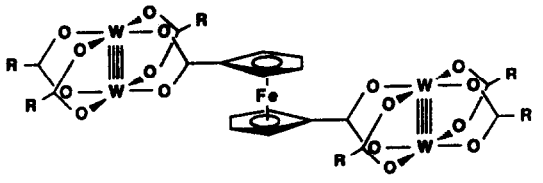	$W_4(FDC)$	−0.81	−0.72	93	37	2
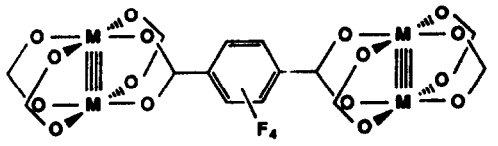	Mo_4PFT	+0.10		65	13	2
Related mononuclear systems						
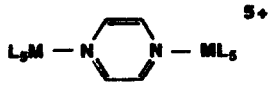	M = Ru L = NH_3	−0.45	−0.06	390	3.9×10^6	6,7
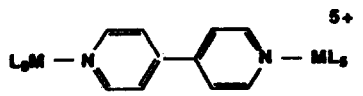	M = Ru L = NH_3				20	6, 7

the ^{1}H NMR spectrum. Two pivalate resonances at 1.50 and 1.62 ppm in a 1 : 2 ratio, a multiplet at 3.55 integrating to one IMT ligand per $[Mo_2piv_3]$ unit and a singlet at 8.18 ppm due to the N—H proton were observed in pyridine-d_5.

Crystals of **2** suitable for a single-crystal X-ray diffraction study were obtained from pyridine and a ball-and-stick diagram of the molecule is shown in Fig. 2. Pertinent bond distances and angles for **2** are provided in Table 2. The compound crystallized with two weakly bound pyridine ligands in the axial sites [Mo—N distances are 2.97(1) and 2.63(1) Å]. The longer Mo—N distance is accompanied by a tilting of the pyridine such that the nitrogen lone pair is not optimized for Mo—py bonding. It appears almost as if a Mo—py bond is being formed or broken. Why pyridine coordination to Mo(2) is preferred relative to Mo(1) could be due to either steric or electronic factors, or both. Inspection of the Mo—O distances reveals that Mo(1) and Mo(2) are equivalently bonded to the pivalate ligands. The Mo—Mo distance of 2.116(2) Å is typical of a quadruple bond. The IMT ligand spans the Mo—Mo bond with the expected N—C—S coordination mode, however, the second nitrogen atom of the IMT ligand is protonated rather than being coordinated to another Mo_2 unit. The bidentate nature of the IMT ligand may be compared with that seen by Constable and Raithby[9] in ruthenium mononuclear complexes involving the anion derived from 2-pyridinethione.

EXPERIMENTAL

^{1}H NMR spectra were recorded on a Varian XL-300 spectrometer in dry and oxygen-free solvents. Electrochemical measurements were obtained with a PAR 173 potentiostat and 175 programmer along with a Houston Instruments 2000 *XY* recorder. The cyclic voltammogram was recorded in an air-free cell under a nitrogen atmosphere in THF with 2.0 M tetra-n-butylammonium hexafluorophosphate as the supporting electrolyte. The working electrode was a glassy carbon electrode and the counter electrode was a platinum-gauze electrode. All potentials reported are relative to the $(C_5H_5)_2Fe/(C_5H_5)_2Fe^+$ couple which occurs at +0.89 V (ΔE = 70 mV) under the conditions specified above when compared with Ag/Ag^+.

Elemental analyses were performed by Oneida Research Services, Whitesboro, New York. All reactions were performed under an atmosphere of dry and oxygen-free nitrogen using standard Schlenk and glove-box techniques. All solvents were dried and degassed by standard methods and distilled prior to use.

Dihydroxypyridazine and 2-imidazolinethione were purchased from Aldrich. $[Mo_2(O_2CBu^t)_3(CH_3$

Table 2. Pertinent bond distances (Å) and bond angles (°) for $Mo_2(O_2CBu^t)_3$(IMT) (**2**)

Mo(1)—Mo(2)	2.1165(19)	Mo(2)—O(27)	2.135(8)
Mo(1)—O(9)	2.115(9)	Mo(2)—N(38)	2.631(12)
Mo(1)—O(17)	2.119(8)	S(3)—C(4)	1.693(16)
Mo(1)—O(25)	2.123(8)	N(5)—C(4)	1.362(19)
Mo(1)—N(5)	2.124(11)	N(5)—C(6)	1.463(17)
Mo(1)—N(32)	2.966(14)	N(8)—C(4)	1.381(17)
Mo(2)—S(3)	2.487(4)	N(8)—C(7)	1.437(20)
Mo(2)—O(11)	2.112(8)	C(6)—C(7)	1.555(22)
Mo(2)—O(19)	2.114(9)		

Mo(2)—Mo(1)—O(9)	92.67(26)	Mo(2)—S(3)—C(4)	101.9(6)
Mo(2)—Mo(1)—O(17)	91.04(27)	Mo(2)—O(27)—C(26)	116.1(9)
Mo(2)—Mo(1)—O(25)	89.97(24)	Mo(1)—N(5)—C(4)	121.1(9)
Mo(2)—Mo(1)—N(5)	98.8(3)	Mo(1)—N(5)—C(6)	130.3(11)
Mo(2)—Mo(1)—N(32)	164.13(23)	C(4)—N(5)—C(6)	107.3(13)
O(9)—Mo(1)—O(17)	172.5(4)	C(4)—N(8)—C(7)	110.8(13)
Mo(1)—Mo(2)—S(3)	95.01(11)	C(39)—N(38)—C(43)	114.8(13)
Mo(1)—Mo(2)—O(11)	90.51(26)	S(3)—C(4)—N(5)	122.7(11)
Mo(1)—Mo(2)—O(19)	92.14(27)	S(3)—C(4)—N(8)	125.9(13)
Mo(1)—Mo(2)—O(27)	92.51(24)	N(5)—C(4)—N(8)	111.3(14)
Mo(1)—Mo(2)—N(38)	164.96(22)	N(5)—C(6)—C(7)	105.7(14)
S(3)—Mo(2)—O(11)	95.2(3)	N(8)—C(7)—C(6)	100.5(11)

$CN)_2]^+BF_4^-$ was prepared according to published procedures.[5]

Synthesis

$[Mo_2(O_2CBu^t)_3]_2(DOP)$ (**1**). A 1:1 mixture of $Mo_2(O_2CBu^t)_4$ and $Mo_2(O_2CBu^t)_2^{2+}$ (total weight of 1.00 g, 1.56 mmol) was dissolved in a mixture of CH_2Cl_2 (30 cm^3) and CH_3CN (5 cm^3) and stirred for 1 h at 60°C. After the initially red solution became orange, it was cooled to room temperature. Dihydroxypyridazine (0.088 g) was dissolved in MeOH (10 cm^3) and deprotonated with 2 equivalents of NaOMe (0.36 cm^3, 1.56 mmol) in MeOH at room temperature to give a colourless solution. This solution was added dropwise to the "$Mo_2(O_2CBu^t)_3^{1+}$" solution. The colour changed upon mixing to deep wine–red. The mixture of solvents was removed and the remaining $Mo_2(O_2CBu^t)_4$ was extracted with CH_2Cl_2. The final product was recrystallized from a small amount of THF at −40°C.

^1H NMR (CD_3OD), δ: 1.32 (s, 18H); 1.37 (s, 36H); 7.21 (d, 2H). Found: C, 37.1; N, 2.5; H, 5.1. Calc. for $Mo_4C_{34}O_{14}N_2H_{56}$: C, 36.9; N, 2.3; H, 4.7%.

$[Mo_2(O_2CBu^t)_3]IMT$ (**2**). $Mo_2(O_2CBu^t)_3^{1+}$ (1.10 mmol) was prepared according to the procedure described above from $Mo_2(O_2CBu^t)_2(CH_3CN)_6(BF_4)_2$ (0.806 g, 1.10 mmol) and $Mo_2(O_2CBu^t)_4$ (0.675 g, 1.10 mmol). 2-Imidazolinethione (0.112 g, 1.10 mmol) was dissolved in MeOH (10 cm^3), deprotonated with NaOMe (0.51 cm^3, 2.20 mmol) in MeOH and added to the "$Mo_2(O_2CBu^t)_3^{1+}$" solution at room temperature. The colour turned brown upon mixing. The mixture of solvents was removed and the product was recrystallized at −40°C from a small amount of pyridine.

^1H NMR (pyridine-d_5) δ: 1.50 (s, 9H); 1.62 (s, 18H); 3.55 (m, 4H); 8.18 (s, 1H).

Crystallographic studies. General operating procedures and listings of programs have been given.[10] A summary of crystal data is given in Table 3.

Table 3. Summary of crystal data for $Mo_2(O_2CBu^t)_3IMT \cdot 2py$ (**2**)

Empirical formula	$C_{28}H_{42}Mo_2N_4O_6S$
Colour of crystal	Amber
Crystal dimensions (mm)	$0.06 \times 0.20 \times 0.28$
Space group	$P2_1/c$
Cell dimensions	
temperature (°C)	−170
a (Å)	15.326(3)
b (Å)	11.161(2)
c (Å)	20.003(4)
β (°)	107.10(1)
Z (molecules/cell)	4
Volume (Å^3)	3270.16
Calculated density (g cm^{-3})	1.533
Wavelength (Å)	0.71069
Molecular weight	754.60
Linear absorption coefficient (cm^{-1})	8.525
Detector to sample distance (cm)	22.5
Sample to source distance (cm)	23.5
Average Ω scan width at half height	0.25
Scan speed (° min^{-1})	6.0
Scan width (° + dispersion)	2.0
Individual background (s)	6
Aperture size (mm)	3.0×4.0
Two-theta range (°)	6–45
Total no. of reflections collected	5423
Number of unique inensities	4387
Number with $I > 0.0$	3664
Number with $I > 2.23 * \sigma(I)$	2320
$R(F)$	0.0610
$Rw(F)$	0.0609
Goodness-of-fit for the last cycle	1.163
Maximum δ/σ for last cycle	0.05

$Mo_2(O_2CBu^t)_3(IMT)$ (**2**). A suitable small crystal was selected from the bulk sample using inert atmosphere handling techniques. The crystal was transferred to the goniostat where it was cooled to −170°C for characterization and data collection. A systematic search of a limited hemisphere of reciprocal space yielded a set of reflections which exhibited monoclinic (2/*m*) symmetry. The systematic extinction of 0*k*0 for $k = 2n+1$ and of *h*01 for $h+1 = 2n+1$ uniquely determined the space group as $P2_1/c$ (No. 14). This choice was confirmed by the successful solution and refinement of the structure. Unit cell dimensions were determined from a least squares fit of the setting angles for 52 carefully centred reflections. The reflections used had two theta values between 19 and 30°.

Data collection was undertaken as detailed in Table 3. It should be noted that the diffraction was not too strong beyond 35° (two theta). The *R* for the averaging was 0.085 for 755 unique reflections observed more than once. A plot of the four standard reflections (4 0 0, 0 2 0, −4 0 8 and 0 0 4) measured every 400 reflections did not show any significant trends. A correction for absorption was carried out.

The structure was solved using the usual combination of direct methods and difference Fourier techniques. The two molybdenum atoms were located in the best *E*-map from MULTAN78. The remaining non-hydrogen atoms were located in successive difference maps. Two of the tertiary butyl groups were found to be disordered. Following the initial refinement a few of the hydrogen atoms were evident in a difference map. Hydrogen atoms were introduced in fixed idealized positions, except on the disordered t-butyl groups. The full-matrix least-squares refinement was completed using anisotropic thermal parameters on all non-hydrogen atoms (except for the two disordered t-butyl groups). The *R*(*F*) for the full data set was 0.082. The limited data set was used for the least-squares refinement, for all other calculations the full data set was used.

The final difference map was essentially featureless, the maximum and minimum electron densities were 1.8 and −1.4 e $Å^{-3}$, respectively. The largest density was observed in the region of the disordered t-butyl groups. Atomic coordinates have been deposited with the Cambridge Crystallographic Data Center.

Acknowledgements—We thank the National Science Foundation for support. R.H.C. was a NSF postdoctoral fellow 1989–1991.

REFERENCES

1. F. A. Cotton and R. A. Walton, *Multiple Bonds Between Metal Atoms*, Wiley Interscience, New York (1982); 2nd edn. Oxford University Press, Oxford (1993).
2. R. H. Cayton, M. H. Chisholm, J. C. Huffman and E. B. Lobkovsky, *J. Am. Chem. Soc.* 1991, **113**, 8709.
3. R. H. Cayton, M. H. Chisholm and F. D. Darrington, *Angew. Chem., Int. Edn Engl.* 1990, **29**, 1481.
4. R. H. Cayton, M. H. Chisholm, J. C. Huffman and E. B. Lobkovsky, *Angew. Chem., Int. Edn Engl.* 1991, **30**, 862.
5. R. H. Cayton, M. H. Chisholm, E. F. Putilina, K. Folting, J. C. Huffman and K. G. Moodley, *Inorg. Chem.* 1992, **31**, 2928.
6. C. Creutz and H. Taube, *J. Am. Chem. Soc.* 1973, **95**, 1086.
7. C. Creutz and H. Taube, *Prog. Inorg. Chem.* 1983, **30**, 1.
8. D. E. Richardson and H. Taube, *Coord. Chem. Rev.* 1984, **60**, 107.
9. E. C. Constable and P. R. Raithby, *Inorg. Chim. Acta* 1991, **183**, 21.
10. M. H. Chisholm, K. Folting, J. C. Huffman and C. C. Kirkpatrick, *Inorg. Chem.* 1984, **23**, 1021.

Polyhedron Vol. 12, No. 21, pp. 2635–2643, 1993
Printed in Great Britain

0277–5387/93 $6.00+.00
© 1993 Pergamon Press Ltd

SYNTHESIS AND CHARACTERIZATION OF IRON(III) COMPLEXES WITH TRIDENTATE LIGANDS CONTAINING N_2O/N_2S DONOR SITES

GITA BATRA and PAVAN MATHUR*

Department of Chemistry, University of Delhi, Delhi 110 007, India

(*Received* 5 *April* 1993; *accepted* 3 *June* 1993)

Abstract—Iron(III) complexes of tridentate ligands bis(2-benzimidazolylmethyl) ether, sulphide and their N-butyl derivatives have been synthesized and characterized. *X*-band EPR spectra in frozen DMF reveal the presence of a number of signals in the region $g_{eff} = ca\ 4$ to $g_{eff} = ca\ 9$. The departure of signals away from $g_{eff} = ca\ 4.3$ is indicative of distortion from purely rhombic to axial geometry. The ^1H NMR spectra of iron(III) depict dipolar, broadened, isotropically contact shifted resonances in the range -10 to $+40$ ppm, with respect to TMS, typical of high spin iron(III). Cyclic voltammograms of these complexes have been recorded which show complexes containing chloride as an inner sphere ligand have a consistently lower redox potential, which suggests that the Cl^- anion is more effective in reducing the Lewis acidity of the iron(III) centre compared with the nitrate anion. These complexes may have relevance to iron coordination sites in phenylalanine hydroxylase and soyabean lipoxygenase.

There has been a growing interest in probing the active site structure of non-haeme oxygenases in order to reveal how the coordination of the iron centre relates to the function of the enzyme.[1,2] Non-haeme iron oxygenases such as phenylalanine hydroxylase and soyabean lipoxygenase catalyse the hydroxylation of phenylalanine to tyrosine and the oxidation of linoleic acid by oxygen to the 9,11-*cis*,*trans*-diene-1,3,5-hydroperoxide, respectively. Both these enzymes have ferric forms that exhibit no visible chromophore.[3,4] EXAFS estimates three to four histidines coordinated to the iron in soyabean lipoxygenase,[5] a ligand also implicated in binding the iron site in phenylalanine hydroxylase.

The present study is directed at the synthesis and characterization of high-spin ferric complexes with tridentate bis(2-benzimidazolylmethyl)ether (DGB), bis(2-benzimidazolylmethyl)sulphide (TGB) and their N-butyl derivatives (BDGB and BTGB). These ligands provide an N_2O/N_2S type of donor environments and incorporate benzimidazole groups, mimetic of histidine imidazoles.

* Author to whom correspondence should be addressed.

EXPERIMENTAL

Chemicals and starting materials

Solvents and reagents were of AR grade and used without further purification. Acetonitrile and THF were dried as described earlier.[6–8] Chloroform was dried over fused calcium chloride before a final reflux and distillation. Diethyl ether was dried first with fused calcium chloride and then refluxed with and stored over sodium.

Synthesis of ligands

Bis(2-benzimidazolylmethyl)ether (DGB), bis(2-benzimidazolylmethyl)sulphide (TGB) and their N-butyl derivatives (BDGB and BTGB) were synthesized as follows.

Diglycolic acid (12.1 g, 90 mmol) for DGB and thiodiglycolic acid (13.5 g, 90 mmol) for TGB were combined with *o*-phenylenediamine (19.5 g, 180 mmol) and powdered. The mixture was heated for *ca* 3 h at a temperature of *ca* 150°C on an oil bath until all efferverscence ceases. The resulting red–blue glass-like solid after cooling was powdered

and was added to 4 M HCl (250 cm^3). Upon scratching the sides of the flask a grey–white precipitate was obtained. This was filtered out and washed by slurrying in acetone several times. The above hydrochloride was dissolved in distilled water (200 cm^3) and the resulting filtrate was then neutralized with 1 : 1 ammonia until a white precipitate was formed. This white precipitate was collected, washed with ether and recrystallized from acetone; yield 14 g, m.p. 280–295°C.

A sample (5 g) of dried ligand (DGB or TGB) was suspended in dry tetrahydrofuran and was stirred overnight with NaOH (1.4 g). Butyl bromide (4 cm^3) was then added and the solution was left stirring for *ca* 72 h. The solvents were stripped off and the resulting residue was dissolved in chloroform and the solution filtered. To the filtrate was added n-hexane and a yellow powder deposited. This yellow powder was washed with hexane. The procedure is similar to that of Reed *et al.*[9]

The ligands were characterized by elemental analysis, NMR spectroscopy and UV spectroscopy. Found: C, 68.2; H, 4.7; N, 20.7. Calc. for $C_{16}H_{14}N_4O$(DGB): C, 69.0; H, 5.0; N, 20.1%. Found: C, 64.8; H, 4.2; N, 18.8. Calc. for $C_{16}H_{14}N_4S$(TGB): C, 65.3; H, 4.7; N, 19.0%. Found: C, 72.9; H, 7.9; N, 13.6. Calc. for $C_{24}H_{30}N_4O$(BDGB): C, 73.8; H, 7.6; N, 14.3%. Found: C, 69.8; H, 7.4; N, 15.2. Calc. for $C_{24}H_{30}N_4S$(BTGB): C, 70.9; H, 7.4; N, 14.3%. ^1H NMR (DMSO-d_6) of $C_{16}H_{14}N_4O$(DGB): δ 7.7 (4H, m), 7.3 (4H, m), 4.95 (4H, s). UV (ethanol), λ_{max} (log ε): 282 (4.18), 272 (4.23), 252 (4.14). ^1H NMR (DMSO-d_6) of $C_{16}H_{14}N_4S$(TGB): δ 7.6 (4H, m), 7.2 (4H, m), 4.05 (4H, s). UV (butanol), λ_{max} (log ε): 286 (4.12), 277 (4.17), 256 (4.12). ^1H NMR (CCl_4) of $C_{24}H_{30}N_4O$(BDGB): δ 7.5 (4H, m), 7.05 (4H, m), 4.6 (4H, s), 3.95 (4H, t), 1.65 (4H, m), 1.55 (4H, m), 0.7 (6H, d). UV (methanol), λ_{max} (log ε): 286 (4.13), 277 (4.18), 258 (4.19). ^1H NMR (CCl_4) of $C_{24}H_{30}N_4S$(BTGB): δ 7.7 (4H, m), 7.2 (4H, m), 4.2 (8H, t), 1.75 (4H, m), 1.45 (4H, m), 1.0 (6H, d). UV (methanol), λ_{max} (log ε): 285 (4.17), 276 (4.16), 246 (4.02).

Synthesis of complexes

The ligand [91 mg (DGB), 129 mg (BDGB), 97 mg (TGB), 133 mg (BTGB); 0.33 mM] was suspended in methanol (5 cm^3) and $FeCl_3$ (53 mg, 0.33 mM) solution (5 cm^3) in methanol and was added to the suspension. The ligand went into solution and turned dark brown. After 15 min of stirring a dark yellow coloured compound precipitated in the cases of DGB, TGB and BTGB iron(III) complexes, while in the case of the reaction between $FeCl_3$ and BDGB a dark reddish-orange coloured precipitate resulted. The solution was left stirring for an additional 3 h. The precipitate was filtered and washed with methanol. The crude product obtained was then recrystallized from a DMF : methanol (1 : 2) mixture.

$[Fe(L)(NO_3)_3]\cdot nH_2O$ (*where* L = BDGB, TGB *and* BTGB). The ligand [129 mg (BDGB), 97 mg (TGB), 133 mg (BTGB); 0.33 mM] was suspended in methanol (5 cm^3) and $Fe(NO_3)_3\cdot 9H_2O$ (133 mg, 0.33 mM) solution (5 cm^3) in methanol was added to the suspension. The ligand went into solution and a clear dark brown coloured solution resulted. A clear solution was obtained after 15 min of stirring at room temperature in all cases, except for the iron(III)TGB reaction, for which a dark yellow coloured precipitate resulted. The solutions were left with stirring for *ca* 2 h. The clear solution was then concentrated to a small volume on a rotary evaporator. The addition of ether to the clear solution precipitated a dark brown coloured powder. This was collected and recrystallized from methanol : ether (1 : 2) mixture. The precipitate formed in the case of TGB was filtered and washed with methanol. The crude product was then recrystallized from a DMF : methanol (1 : 2) mixture. Elemental analyses of all the iron(III) complexes are reported in Table 1.

Table 1. Microanalytical and magnetic moment data of iron(III) complexes

Compound	%C Found (Calc)	%H Found (Calc)	%N Found (Calc)	%Fe Found (Calc)	μ_{eff} B.M./atom
$[Fe(DGB)Cl_3]$	44.8(43.5)	4.3(3.1)	11.8(12.7)	12.2(12.7)	5.45
$[Fe(BDGB)Cl_3]$	48.8(50.3)	5.9(5.7)	10.8(10.1)	8.9(10.1)	5.42
$[Fe(TGB)Cl_3]$	40.7(42.0)	3.8(3.0)	12.8(12.2)	13.3(12.2)	5.62
$[Fe(BTGB)Cl_3]\cdot H_2O$	45.7(45.9)	4.9(5.9)	9.4(9.2)	9.2(9.2)	5.88
$[Fe(BDGB)(NO_3)_3]$	44.8(45.2)	5.2(4.7)	14.9(15.4)	8.4(8.8)	5.79
$[Fe(TGB)(NO_3)_3]$	36.2(35.8)	3.2(2.6)	17.8(18.2)	9.8(10.4)	5.85
$[Fe(BTGB)(NO_3)_3]$	42.2(42.9)	5.2(4.9)	14.6(15.1)	8.2(8.6)	6.22

RESULTS AND DISCUSSION

EPR spectroscopy

Figures 1(a)–(g) illustrate the 9.5 GHz EPR spectra of the iron(III) complexes with DGB, BDGB, TGB and BTGB at 143 K. All the spectra have been recorded in frozen DMF/acetonitrile solution. In the case of $Fe(BDGB)(NO_3)_3$ and $Fe(BTGB)(NO_3)_3$ complexes a $g = ca$ 7.7 signal

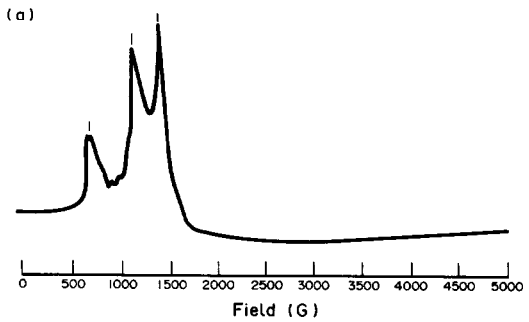

Fig. 1(a). 5000 G scan of frozen DMF solution of $[Fe(DGB)Cl_3]$; conditions: r-gain $= 3.2 \times 10^2$; microwave power 10 mW; microwave frequency 9.2 GHz; 6.3 G modulation amplitude; $T = 143$ K at X-band and centred at 2500 G.

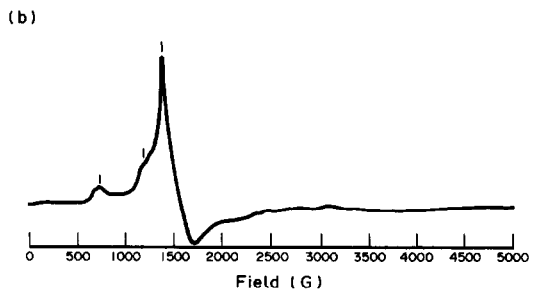

Fig. 1(b). 5000 G scan of frozen acetonitrile solution of $[Fe(BDGB)Cl_3]$; conditions: r-gain $= 3.2 \times 10^2$; microwave power 10 mW; microwave frequency 9.2 GHz; 6.3 G modulation amplitude; $T = 143$ K at X-band and centred at 2500 G.

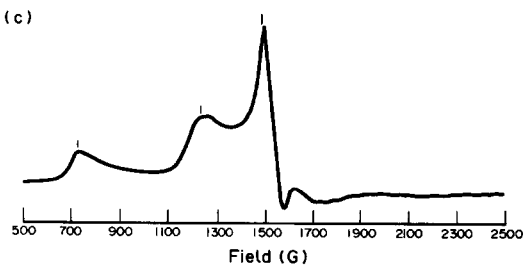

Fig. 1(c). 2000 G scan of frozen DMF solution of $[Fe(TGB)Cl_3]$; conditions: r-gain $= 7.9 \times 10^2$; microwave power 10 mW, microwave frequency 9.2 GHz; 6.3 G modulation amplitude, $T = 13$ K at X-band and centred at 1500 G.

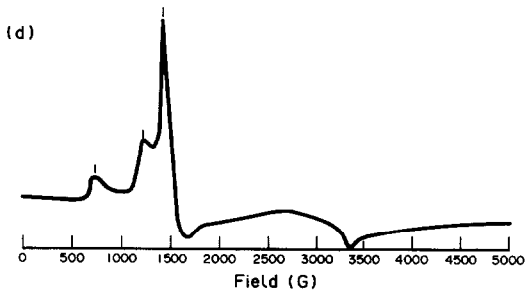

Fig. 1(d). 5000 G scan of frozen DMF solution of $[Fe(BTGB)Cl_3]\cdot H_2O$; conditions: r-gain $= 1.25 \times 10^3$; microwave power 10 mW; microwave frequency 9.19 GHz; 6.3 G modulation amplitude; $T = 143$ K at X-band and centred at 2500 G.

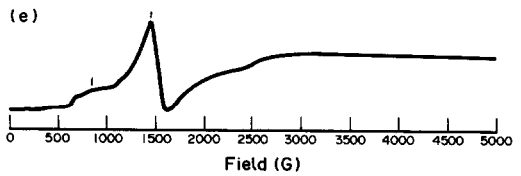

Fig. 1(e). 5000 G scan of frozen DMF solution of $[Fe(BDGB)(NO_3)_3]$; conditions: r-gain $= 10 \times 10^2$; microwave power 10 mW; microwave frequency 9.2 GHz; 6.3 G modulation amplitude, $T = 143$ K at X-band and centred at 2500 G.

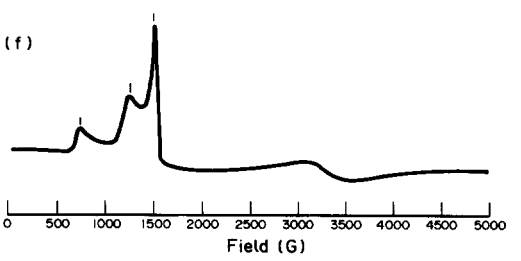

Fig. 1(f). 5000 G scan of frozen DMF solution of $[Fe(TGB)(NO_3)_3]$; conditions: r-gain $= 2 \times 10^3$; microwave power 10 mW; microwave frequency 9.2 GHz; 6.3 G modulation amplitude; $T = 143$ K at X-band and centred at 2500 G.

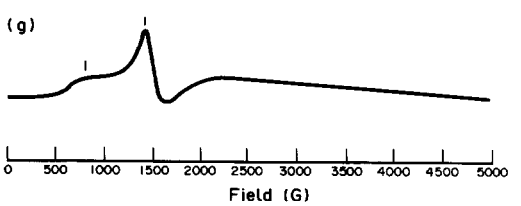

Fig. 1(g). 5000 G scan of frozen DMF solution of $[Fe(BTGB)(NO_3)_3]$; conditions; r-gain $= 10 \times 10^2$; microwave power 10 mW; microwave frequency 9.19 GHz; 6.3 G modulation amplitude; $T = 143$ K at X-band and centred at 2500 G.

Table 2. EPR data of iron(III) complexes

Compound	Observed EPR[a] g-values
$[Fe(DGB)Cl_3]$	8.8, 5.3, 4.1
$[Fe(BDGB)Cl_3]$	9.0, 5.0, 4.0
$[Fe(TGB)Cl_3]$	9.0, 5.2, 4.2
$[Fe(BTGB)Cl_3]\cdot H_2O$	8.7, 5.1, 4.2
$[Fe(TGB)(NO_3)_3]$	8.7, 5.1, 4.3
$[Fe(BDGB)(NO_3)_3]$	7.7, 4.4
$[Fe(BTGB)(NO_3)_3]$	7.5, 4.4

[a] These are effective g values, the real g-value being very close to 2.00.

along with a $g = ca$ 4.4 are observed. The $[Fe(DGB)Cl_3]$, $[Fe(BDGB)Cl_3]$, $[Fe(TGB)Cl_3]$, $[Fe(BTGB)Cl_3]$ and $[Fe(TGB)(NO_3)_3]$ complexes show a $g = ca\,4$ signal accompanied by EPR signals at lower fields (1250 G, 750 G). Dowsing and Gibson[10a] have shown that the absorptions at 1500 G and 700 G are expected if λ is almost equal to 1/3 and D is greater than 0.23 cm^{-1}. The line at 1500 G is known to broaden or split as λ departs from 1/3. Thus, the departure of the absorption away from $g_{eff} = ca$ 4.3 is a signal for distortion from purely rhombic to axial geometry. Recently Collison and Powell[10b] have given computer simulated EPR plots using different λ and D values for FeO_6 tris chelate complexes; these show that a very high value of D (1.8 cm^{-1}) is needed to fit two resonances at *ca* 1500 G and 1100 G; a case found for our $[Fe(L)Cl_3]$ and $[Fe(TGB)(NO_3)_3]$ complexes (Table 2).

^1H *NMR spectroscopy*

Figures 2(a)–(c) depict the dipolar broadened isotropic contact shifted resonances typically in the range -10 to $+40$ ppm with respect to TMS. Figure 2(a) depicts the ^1H NMR spectrum of the $[Fe(TGB)Cl_3]$ complex. The peaks observed are listed in Table 3. In the PMR spectra the broadest peaks (line width 2000 Hz) are observed at $+40$ ppm and $+20$ ppm. Since the paramagnetic relaxation time is proportional to the sixth power of dipolar separation, a pronounced broadening is expected for protons that are in close proximity to the iron centre. We thus tentatively assign these peaks to the 4-H of the benzimidazole nucleus and α-CH_2 of the aliphatic chain, respectively. The spectra also reveal broad upfield shifted peaks at around -4, -10 and -20 ppm. This reflects that besides the dominant σ-spin delocalization, the complex also has a mechanism of π-spin delocalization. We, therefore, tend to assign these peaks to the *meta*-

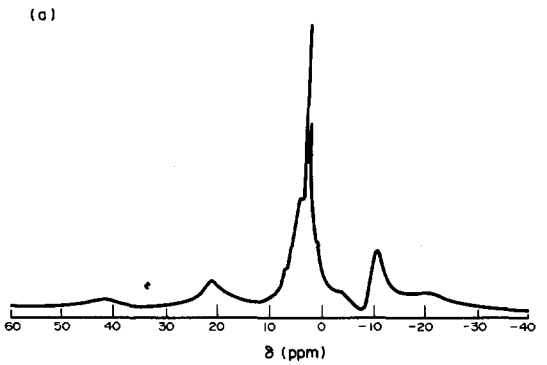

Fig. 2(a). ^1H NMR spectra of $[Fe(TGB)Cl_3]$ complex in d_6-DMSO at room temperature at 400 MHz.

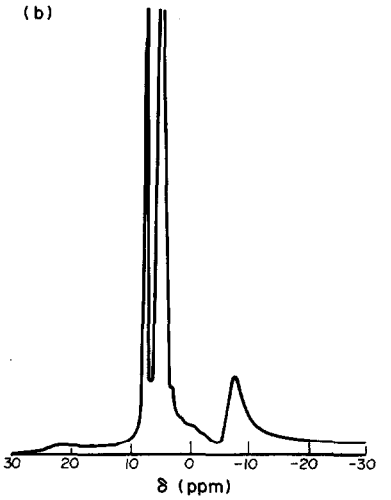

Fig. 2(b). ^1H NMR spectra of $[Fe(DGB)Cl_3]$ complex in d_6-DMSO at room temperature at 400 MHz.

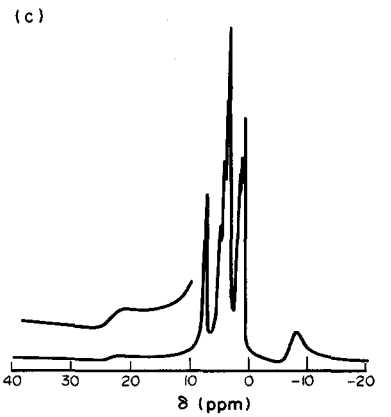

Fig. 2(c). ^1H NMR spectra of $[Fe(BDGB)Cl_3]$ complex in d_6-DMSO at room temperature at 400 MHz.

Table 3. Proton contact shifts of iron(III) complexes in ppm

[Fe(TGB)Cl_3]	[Fe(DGB)Cl_3]	[Fe(BDGB)Cl_3]	Tentative assignments
42.0	—	—	C-4H
21.0	25.0	20.0	α-CH_2
		3.51 1.65 1.20 0.80	N-butyl chain
−10.66	−7.7	−8.2	*Meta*-protons

protons of the benzimidazole nucleus. Such a σ- and π-delocalization mechanism has been invoked to explain the PMR of other paramagnetic metal ion complexes.[11-14]

Upon comparing the ^1H NMR spectrum of the [Fe(TGB)Cl_3] complex with that of the [Fe(DGB)Cl_3] complex [Fig. 2(b)] we find a comparatively simpler spectrum; a weak broad peak can be picked up at around +20 ppm which using the analogy of the above assignment are due to protons of the aliphatic carbon chain (α-CH_2). An upfield shifted peak at −7.7 ppm is observed, which again reinforces the idea of both σ- and π-spin delocalization.

Since it is found that weakly electronegative and strongly π-bonding groups tend to occupy equatorial positions, the [Fe(TGB)Cl_3] complex may adopt a meridonial configuration with the sulphur atom occupying an equatorial site, in contrast to the [Fe(DGB)Cl_3] complex which is likely to be facial. This seems to be borne out from the NMR data. The larger number of peaks observed for the [Fe(TGB)Cl_3] complex in comparison with [Fe(DGB)Cl_3] could be interpreted as arising from inequivalent benzimidazole rings. This is expected in a meridonial isomer as a facial isomer would possess a vertical plane of symmetry.

Figure 2(c) represents the ^1H NMR spectra of [Fe(BDGB)Cl_3] and is similar to that of [Fe(DGB)Cl_3], except that the N-butyl chain protons could be identified as peaks at 0.80, 1.23, 1.65 and 3.5 ppm (Table 3).

Electronic spectroscopy

The present series of iron(III) complexes show UV spectra characteristic of the benzimidazolyl group. The absorption bands and respective extinction coefficients for the above iron(III) complexes are reported in Table 4. The UV bands are in general shifted upon coordination suggesting the binding of iron(III) to the ligand donor atom. In the case of [Fe(DGB)Cl_3], [Fe(BDGB)Cl_3], [Fe(TGB)Cl_3] and [Fe(BTGB)Cl_3] complexes bands appear at 309, 319, 305 and 308 nm. These are assigned as benzimidazole(N) → iron(III) charge-transfer bands.[15] The bands at 356, 354, 362 and 360 nm in the above complexes are predominantly

Table 4. Electronic spectral and cyclic voltammetric data of iron(III) complexes at 298 K

Compound	Solvent	λ_{max} (nm) (log ε)	λ_{max} (nm) in the presence of catechol	λ_{max} (nm) in the presence of *p*-cresol	$E_{1/2}$ (V) vs Ag/AgCl	$E_{1/2}$ (V) vs NHE
[Fe(DGB)Cl_3]	DMF	356(3.52), 309(3.60)	—	—	0.16	(0.38)
[Fe(BDGB)Cl_3]	Acetonitrile	360(2.86), 319(2.96)	756	540	0.15	(0.37)
[Fe(TGB)Cl_3]	DMF	362(3.20), 305(3.20)	—	—	—	—
[Fe(BTGB)Cl_3]·H_2O	DMF	360(3.47), 308(3.79)	685, 450	492	—	—
[Fe(BDGB)$(NO_3)_3$]	DMF	480(2.95)	—	500	0.30	(0.52)
[Fe(TGB)$(NO_3)_3$]	DMF	479(2.10)	—	—	—	—
[Fe(BTGB)$(NO_3)_3$]	DMF	469(2.44)	—	500	0.41	(0.63)

assigned as $Cl^- \rightarrow Fe^{III}$ charge-transfer bands.[16,17]

The corresponding $[Fe(BDGB)(NO_3)_3]$, $[Fe(TGB)(NO_3)_3]$ and $[Fe(BTGB)(NO_3)_3]$ complexes show bands at 479, 469 and 380 nm, respectively. These are assigned to $NO_3^- \rightarrow Fe^{3+}$ charge-transfer bands.

Complexation with catechol and p-*cresol*

The present series of iron complexes were reacted with catechol and *p*-cresol (in equimolar quantities) in DMF solution. The change observed in their absorption spectra is shown in Figs 3(a)–(c) and λ_{max} of the new bands is reported in Table 4. The visible spectra of iron complexes with the above tridentate ligands are characterized by two new absorption features in the ranges 450–460 and 650–750 nm. Since the present iron complexes do not show bands in these regions, these features in the visible region are assigned to catecholate–Fe^{3+} LMCT bands.[18] This implies that catechol binds as a bidentate ligand to yield a distorted octahedral complex[19] for the chloride complexes. The nitrate complexes show no reactivity. A colour change does appear after 48 h.

In contrast to catechol, *p*-cresol is a monodentate ligand and hence its binding need only displace one of the axial ligands already on the iron(III) complex (Fig. 5). The trend for the iron(III)–*p*-cresolate LMCT band is the same as for the catecholate complexes, i.e. the BTGB complex has a higher energy band compared with the BDGB complex (Table 4).

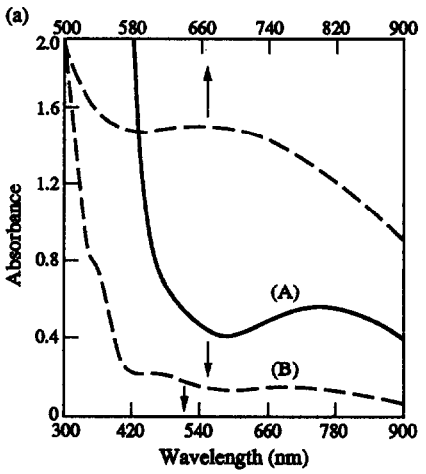

Fig. 3(a). Visible spectrum of (A) $[Fe(BDGB)Cl_3]$ and (B) $[Fe(BTGB)Cl_3]\cdot H_2O$ complexes in the presence of catechol in DMF.

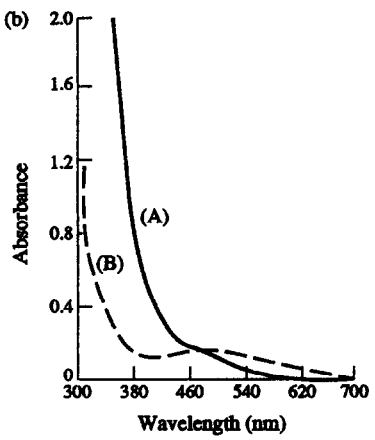

Fig. 3(b). Visible spectrum of (A) $[Fe(BDGB)(NO_3)_3]$ and (B) $[Fe(BTGB)(NO_3)_3]$ complexes in the presence of *p*-cresol in DMF.

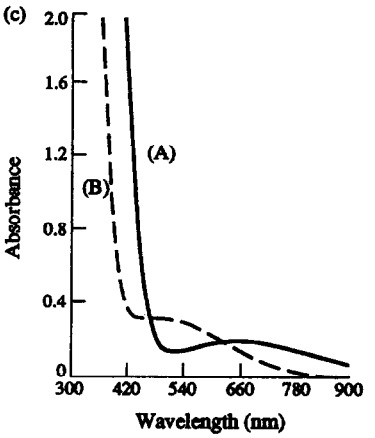

Fig. 3(c). Visible spectrum of (A) $[Fe(BDGB)Cl_3]$ and (B) $[Fe(BTGB)Cl_3]$ complexes in the pressure of *p*-cresol in DMF.

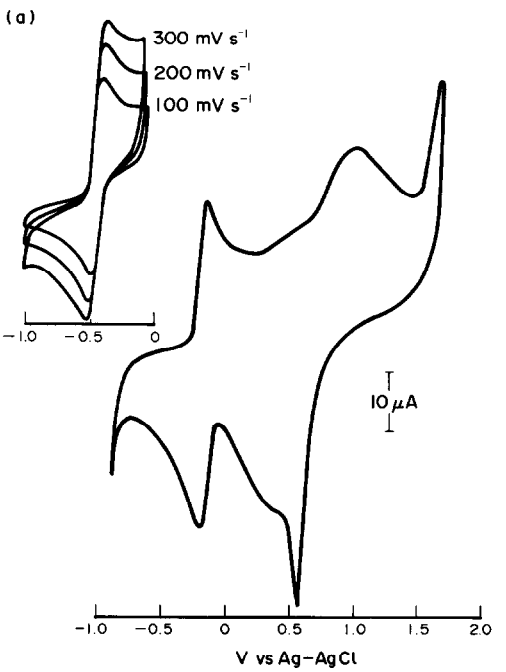

Fig. 4(a). Cyclic voltammogram of $[Fe(DGB)Cl_3]$ complex in DMSO: scan rate 180 mV s^{-1}.

Electrochemistry

Cyclic voltammograms for $[Fe(DGB)Cl_3]$, $[Fe(BDGB)Cl_3]$, $[Fe(BDGB)(NO_3)_3]$ and $[Fe(BTGB)(NO_3)_3]$ are shown in Figs 4(a)–(d). The voltammograms were recorded in DMSO as a solvent, using tetraethyl ammonium perchlorate (0.1 M) as the supporting electrolyte, on a BAS CV-27 voltammograph. All potentials are with respect

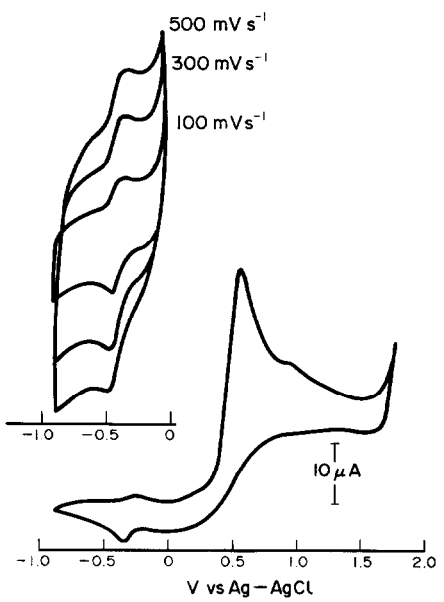

Fig. 4(b). Cyclic voltammogram of $[Fe(BDGB)Cl_3]$ complex in DMSO: scan rate 100 mV s^{-1}.

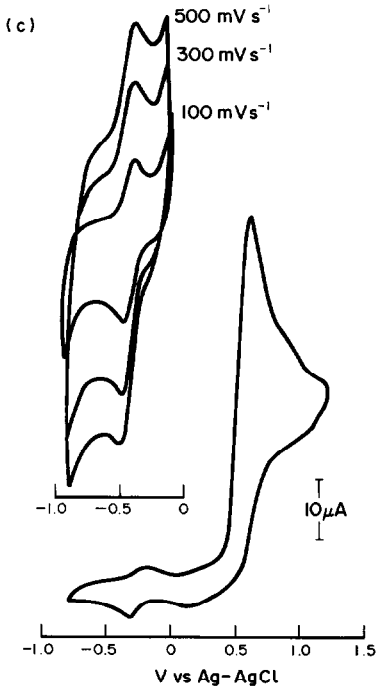

Fig. 4(c). Cyclic voltammogram of $[Fe(BDGB)(NO_3)_3]$ complex in DMSO: scan rate 150 mV s^{-1}.

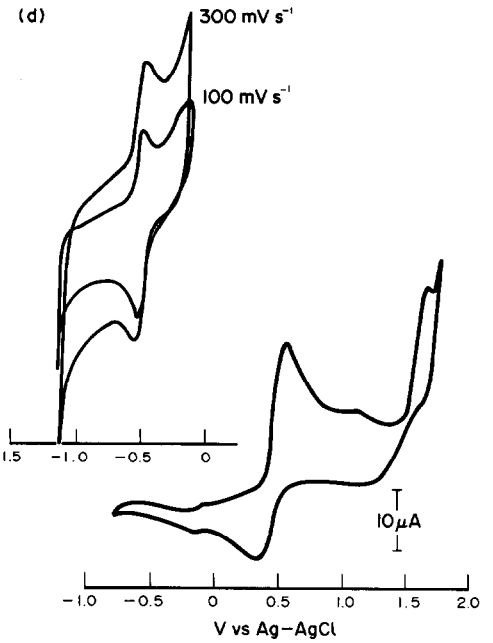

Fig. 4(d). Cyclic voltammogram of $[Fe(BTGB)(NO_3)_3]$ complex in DMSO: scan rate 150 mV s^{-1}.

to an Ag/AgCl electrode. The cyclic voltammograms show a one-electron redox wave, assigned to the Fe^{III}/Fe^{II} redox couple. A scan rate dependence confirms the reversibility of the above redox couple.

The averages of the peak potentials for the oxidation and reduction waves are tabulated in Table 4. The chloride complexes have a consistently lower redox potential; this suggests that the Cl^- anion is more effective in reducing the Lewis acidity of the iron(III) centre compared with the NO_3^- anion.

Magnetic susceptibility

The magnetic susceptibility of all the iron(III) complexes was obtained using a CAHN-2000 magnetic balance and are reported in Table 1. The data incorporates the diamagnetic correction for the ligand in each complex and has been obtained using Pascal's constant. It is found that these magnetic moments are close to the spin-only value of 5.9 B.M./Fe^{3+} atom. This is expected since Fe^{3+} has a $^6A_{1g}$ ground term with negligible temperature-independent paramagnetism. It also does not show any reduction in magnetic moment below the spin-only value due to spin-orbit coupling with higher ligand field terms.

IR spectroscopy

IR spectra of iron(III) complexes have been obtained in Nujol mulls. The band appearing at *ca* 1460 cm^{-1} is assigned to the (C=N—C=C)

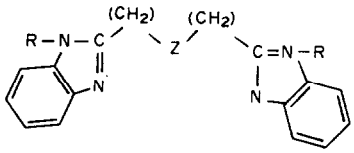

when Z=O, R=H, L=DGB
when Z=S, R=H, L=TGB
when Z=O, R=H, L=BDGB
when Z=S, R=H, L=BTGB

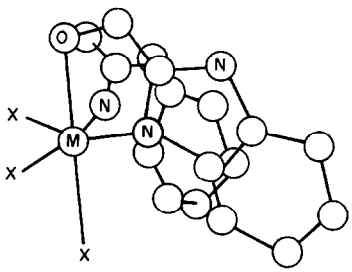

Facial Coordination

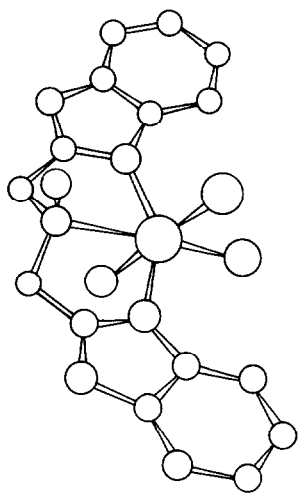

Meridonial Coordination

Fig. 5.

stretching. In our iron(III) complexes the shift is around 10 cm^{-1}. This implies direct coordination of all three imine nitrogen atoms of the ligand to iron(III). This is the preferred nitrogen atom for coordination, as found for other metal complexes with benzimidazoles.[20]

Gatehouse *et al.*[21] have reported earlier that when the nitrate group is bound as a terminal ligand in the unidentate mode IR bands appear at 1420, 1305 and 1008 cm^{-1}, respectively. The separation of the two highest frequency bands is less than 100 cm^{-1} for a chelating bidentate nitrate. In our nitrato complexes bands are found in the same region. Hence, it is likely that we have a monodentate nitrate bound to iron in the ferric complexes. Other examples of monodentate nitrate coordination to iron(III) as studied by X-ray crystallography[22,23] and EXAFS[24] have been reported in the literature. Solution EPR, NMR and CV studies are indicative of the monomeric nature of the complexes. However, in the absence of a crystal structure and in view of their low solubility in weakly polar solvents, the solution structure may be different from the solid-state structure.

The Lewis acidity of the ferric centre in these complexes compares favourably with that displayed by the ferric centre in phenylalanine hydroxylase and soyabean lipoxygenase, as indicated by the catecholate → iron(III) CT bands; thus, the ferric complexes with Cl^- as an inner sphere ligand may have relevance to iron coordination sites in the above enzymes.

Acknowledgement—The authors acknowledge financial support from CSIR; New Delhi, India (Project No. 1/1108/88). They also thank Dr A. P. Bhaduri, RSIC Division, CDRI, Lucknow, for helping in obtaining the ^1H NMR data. They are also grateful to Mr Avinash Kumbhar, Department of Chemistry, University of Pune, Pune, for helping them in the cyclic voltammetric studies.

REFERENCES

1. L. Que Jr, *Struct. Bonding (Berlin)* 1980, **40**, 39.
2. L. Que Jr, *Adv. Inorg. Biochem.* 1983, **5**, 166.
3. D. E. Wallick, L. M. Bloom, B. J. Gaffney and S. J. Benkovic, *Biochemistry* 1984, **23**, 1295.
4. G. A. Veldink and J. F. G. Vliegenthart, *Adv. Inorg. Biochem.* 1984, **6**, 139.
5. M. C. Feilers, J. F. G. Vliegenthart, J. Reedijk and B. G. Malmstrom, *Rec. Trav. Chim.* 1987, **106**, 227.
6. G. Batra and P. Mathur, *Inorg. Chem.* 1992, **31**, 1575.
7. H. N. Pandey, Y. S. Sharma and P. Mathur, *Polyhedron* 1992, **11**, 2631.
8. M. Prasad, H. N. Pandey and P. Mathur, *Trans. Met. Chem.* 1993, **18**, in press.
9. V. McKee, M. Zvagulis, J. V. Dagdigian, M. G. Patch and C. Reed, *J. Am. Chem. Soc.* 1984, **106**, 4765.
10. (a) R. D. Dowsing and J. F. Gibson, *J. Chem. Phys.* 1969, **50**, 294; (b) D. Collison and A. K. Powell, *Inorg. Chem.* 1990, **29**, 4735.
11. R. H. Holm, W. D. Phillips, B. A. Averill, J. J. Mayerle and T. Hers Kovitz, *J. Am. Chem. Soc.* 1974, **96**, 2109.
12. J. G. Reynolds, E. J. Laskowski and R. H. Holm, *J. Am. Chem. Soc.* 1978, **100**, 5315.
13. P. C. Healy, J. M. Patrick, B. W. Skitton and A. H. White, *Aust. J. Chem.* 1983, **36**, 2031.

14. W. M. Reiff, E. H. Witten, K. Mottle, J. F. Brennan and A. R. Garaflo, *Inorg. Chim. Acta* 1983, **77**, L27.
15. S. Holt and R. Dingle, *Acta Chem. Scand.* 1968, **22**, 1091.
16. W. E. Hatfield, *Inorg. Chem.* 1964, **3**, 605.
17. K. Neuenschwander, H. U. Gudel, J. C. Collingwood and P. N. Schatz, *Inorg. Chem.* 1983, **22**, 1712.
18. S. Salama, J. D. Stong, J. B. Neilands and T. G. Spiro, *Biochem.* 1978, **17**, 3781.
19. L. S. White, L. S. Nilson, L. H. Pignolet and L. Que Jr, *J. Am. Chem. Soc.* 1982, **104**, 2789.
20. H. N. Pandey and P. Mathur, *Ind. J. Chem.* 1992, **31A**, 666.
21. B. M. Gatehouse, S. E. Livingstone and R. S. Nyholm, *J. Chem. Soc.* 1957, 422.
22. S. Menage and L. Que Jr, *Inorg. Chem.* 1990, **29**, 4293.
23. Y. Nishida, H. Shimo, K. Takahashi and S. Kida, *Mem. Fac. Sci. Kyushu Univ. Ser. C* 1984, **14**, 301.
24. B. A. Brennan, Q. Chen, C. Juarez-Garcia, A. E. True, C. J. O'Connor and L. Que, *Inorg. Chem.* 1991, **30**, 1937.

Polyhedron Vol. 12, No. 21, pp. 2645–2649, 1993
Printed in Great Britain

0277–5387/93 $6.00+.00
© 1993 Pergamon Press Ltd

^{1}H AND ^{19}F EMR STUDY OF POWDERED SAMPLES OF COPPER(II) ETHYLXANTHATE AND TRIFLUOROETHYLXANTHATE COMPLEXES MAGNETICALLY DILUTED IN THE CORRESPONDING NICKEL(II) HOST LATTICES

MARIETA ZDRAVKOVA and NICOLA D. YORDANOV*

Institute of Kinetics and Catalysis, Bulgarian Academy of Sciences, 1113 Sofia, Bulgaria

and

GEORGI GOCHEV

Department of Chemistry, Sofia University, 1126 Sofia, Bulgaria

(*Received* 26 *February* 1993; *accepted* 2 *June* 1993)

Abstract—Powdered samples of bis(ethyldithiocarbonato)copper(II) and bis(trifluor-ethyldithiocarbonato)copper(II) complexes magnetically diluted in the corresponding nickel(II) host lattices have been studied by ^{1}H and ^{19}F Electron Magnetic Resonance (ENDOR) spectroscopy. The values of isotropic and anisotropic components of electron-nuclear interactions with the CH_2 and CF_3 groups were extracted from the spectra. Interactions with protons from neighbouring molecules of the lattice were also recorded. With the use of computer-aided EMR spectroscopy some aspects of the geometric structure of the copper(II)–xanthate complex studied were found. The structure of the guest molecules of copper complexes appears to accept the nickel(II) host lattice structure.

The metal complexes of xanthates (dithiocarbonates), $[M(ROCS_2)_2]$, are of great interest because of their biological activity, analytical application, as vulcanization accelerators, utilization in flotation, etc. This is the reason why many investigators have concentrated their attention on the structure, properties and reactivity of these complexes using different chemical and physical methods.[1] The bis(*R*-xanthate)copper(II) complexes are known to be unstable in solution and in general do not exist in the solid state due to a "self-redox" reaction[2,3] which makes it impossible to perform X-ray structure analysis on them. In view of this any structural information available about this class of complexes is very important.

In the present paper we make use of the fact that when trapped[2,3] the upper bis-chelates are stable for an unlimited period of time.[2] We report here the results obtained with ^{1}H and ^{19}F Electron Magnetic Resonance—EMR (ENDOR) spectroscopy concerning the structure of bis(ethylxanthate) copper(II), $[Cu(Et\text{-}xant)_2]$, and bis(trifluoroethylxanthate)copper(II), $[Cu(F\text{-}Et\text{-}xant)_2]$, magnetically diluted in the corresponding nickel(II) host lattices. Generally the information obtained by EPR spectroscopy of copper(II) xanthate complexes concerns only the chromophore CuS_4[2,3] because of the limited resolution of the method. Structural information about the remote ligand substituents may be reached only with the use of ENDOR spectroscopy. The studies reported here were performed on powdered samples by the previously described method.[4,5] Many groups working in this field[5–8] have shown that its approach is very useful particularly for the understanding of electronic and geometric structure of samples with a large anisotropy of the EPR parameters such as metal complexes.

* Author to whom correspondence should be addressed.

EXPERIMENTAL

Sodium ethylxanthate was synthesized by the method previously described.[1,9] The nickel(II) complex was obtained by mixing of aqueous solutions of $NiCl_2$ and Na(Et-xant) followed by extraction with chloroform. After evaporation of the chloroform the complex obtained was recrystallized twice from chloroform.

The fluorinated sample of bis(ethyl-xanthato) nickel(II) complex was obtained by the previously described method.[10]

Magnetically diluted samples were prepared by exchange of approximately 2% of nickel(II) by ^{63}copper(II) in chloroform–water, followed by separation of the $CHCl_3$ layer and evaporation of the solvent.

^{1}H and ^{19}F ENDOR spectra were recorded with a Bruker ER 200 D-SRC spectrometer equipped with an Aspect 2000 computer. All measurements were performed at 100 K. Typical experimental conditions were: microwave power 20 mW, radio-frequency power 200–300 W, modulation frequency 12.5 kHz, modulation depth 80–100 kHz. No field modulation was used while the ENDOR spectra were recorded.

Analysis of the experimental data and EMR simulation were performed with a computer programme based on the algorithm described previously.[4]

RESULTS AND DISCUSSION

The EMR (EPR) spectrum of ^{63}Cu(Et-xant)$_2$, magnetically diluted in the corresponding nickel(II) host lattice at 100 K is shown in Fig. 1. Under the same conditions the spectrum of ^{63}Cu(F-Et-xant)$_2$ is not affected by the fluorination. The shape of the EPR spectra as well as the EPR data collected in Table 1 suggest axial symmetry of the complexes. Since the corresponding nickel(II) complexes are known from X-ray structural analysis to have a planar chromophore (NiS_4)[11–14] the conclusion is made that copper(II) chelates are accepting the host lattice structure. This behaviour is very suitable for applying the method of ENDOR study of powdered samples.[4,5] The EMR spectral "windows", as shown in Fig. 1, in which only one EMR transition takes place, were used for recording the ENDOR spectra. The windows were chosen so as to cover the whole range between $0° \leqslant \theta° \leqslant 90°$ (θ is the angle between the direction of the magnetic field and the symmetry axis of the complex).

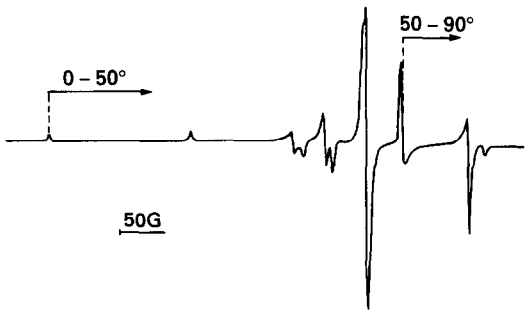

Fig. 1. EMR (EPR) spectrum typical for powdered samples of ^{63}Cu(Et-xant)$_2$ and ^{63}Cu(F-Et-xant)$_2$ magnetically diluted in the corresponding nickel(II) host lattices.

Table 1. EMR parameters of Cu/Ni(Et-xant)$_2$ and Cu/Ni(F-Et-xant)$_2$ samples

Complex	$g_\parallel$[a]	$g_\perp$[a]	$A_\parallel$[b]	$A_\perp$[b]
^{63}Cu(Et-xant)$_2$	2.086	2.027	153	42
^{63}Cu(F-Et-xant)$_2$	2.088	2.025	154	43

[a] ± 0.002.
[b] $\pm 2G$.

The electron–nuclear couplings A_i measured at different settings of the magnetic field and thus choosing different polar angles θ_i[4,5] are related to the anisotropic and isotropic shf couplings by eq. (1):

$$A(\theta_i) = \{\beta_e\beta_n g_n g(\theta_i)[3\cos^2(\theta_i - a) - 1]/r^3\} + A_{iso}, \quad (1)$$

where a is the angle between g_z direction (or the z-axis of the complex) and the line connecting the unpaired electron and the corresponding nucleus.

In the ^{1}H region of the ENDOR spectra of Cu(Et-xant)$_2$ complex we can expect that several ENDOR transitions, due to the electron–nuclear interactions with protons from its own molecule as well as an unknown number of "matrix" ENDOR transitions due to pure dipole–dipole interactions of the copper(II) unpaired electron with protons from neighbouring molecules of the host lattice, will appear. Since all this will complicate the interpretation of the spectra we decided to synthesize and investigate also the partially fluorinated samples and thus to increase the resolution of the method. On the other hand the ratio between the theoretical ^{19}F and ^{1}H isotropic shf couplings ($^{19}Fa_{iso}/{}^1Ha_{iso} = 33.8$) makes the studies more sensitive.[16]

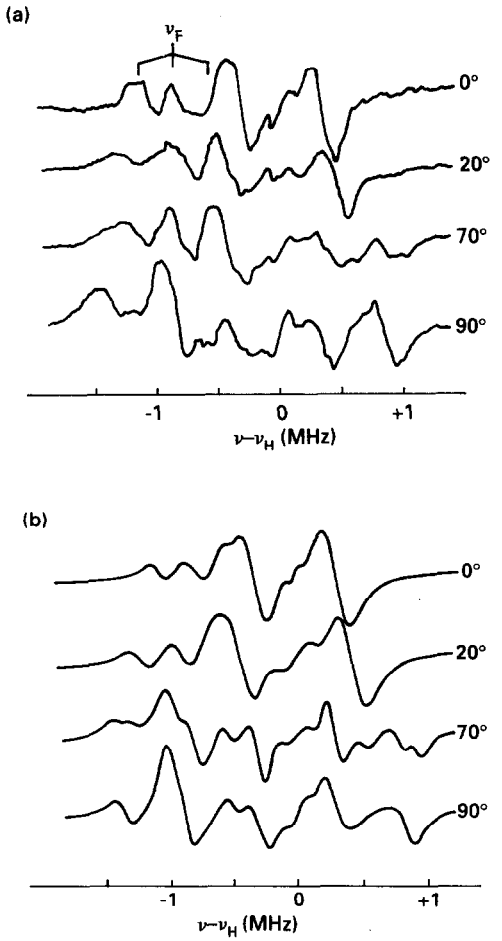

Fig. 2. ^{1}H and ^{19}F EMR (ENDOR) spectra of ^{63}Cu/Ni(F-Et-xant)$_2$ taken and computed at different polar angles θ: (a) experimental spectra, $T = 100$ K; (b) simulated spectra.

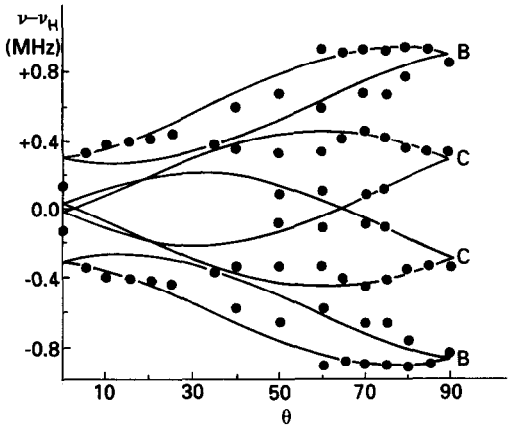

Fig. 3. Angular dependence of ^{1}H EMR (ENDOR) transitions of ^{63}Cu/Ni(F-Et-xant)$_2$. The experimental values are represented by dots. Full lines show the theoretical calculation.

^{1}H *EMR spectroscopy*

^{1}H EMR spectra of ^{63}Cu/Ni(F-Et-xant)$_2$. Some ^{1}H EMR (ENDOR) spectra, recorded at different polar angles θ, are shown in Fig. 2(a). The experimental results obtained for the angular dependence of ^{1}H shf coupling are marked in Fig. 3 with dots, and full lines represent the best fit between experimental data and theoretical calculations using eq. (1).

The central ENDOR lines, which can be seen in all spectra in Fig. 2(a), are due to far "matrix" ENDOR since their splitting of *ca* 0.20 MHz practically does not change with the angle.

The principal value of transition B is situated at an angle of about 80° towards the axis of symmetry of the complex (or g_z). The best fit between experimental and theoretical results is obtained with the following parameters: $A_{aniso} = 0.44$ MHz; $A_{iso} = 0.98$ MHz and $a = 78°$. The isotropic component shows unambiguously that this transition is due to interaction of the unpaired electron of copper(II) with protons of its own molecule. The only possible interaction of this type is with the protons from the CH_2 group.

The distance between the copper atom and these protons can be calculated by using the point-dipole approximation. It is found that $r = 4.76$ Å which is in good agreement with X-ray data for the fluorinated bis(ethyl-xanthate)nickel(II) complex[14]; the protons from the CH_2 group are situated at 4.40 Å away from the copper ion and have a polar angle $a = 78°$ with the symmetry axis.

Transition C can be described by the following parameters: $a = 60°$, $A_{aniso} = 0.46$ and $A_{iso} = 0.00$ MHz. Consequently it is a pure dipole–dipole interaction between the unpaired electron and protons from neighbouring molecules. Using the point dipole approximation the distance Cu—H of 4.67 Å was calculated which can be compared with X-ray data.[14] The molecules in the lattice are arranged in linear layers. Two neighbouring molecules from one layer are oriented with their equal ends and hence interaction with proton of another molecule is possible only between molecules from different layers. From the X-ray data[14] an angle $a = 62°$ is calculated which is in good agreement with the experimental ^{1}H EMR (ENDOR) data.

In order to check our results some ^{1}H EMR spectra were simulated by a computer programme based on the algorithm described in ref. 4 and with the use of the parameters reported here. The simulated spectra [Fig. 2(b)] are compared with the experimental ENDOR spectra taken at the same

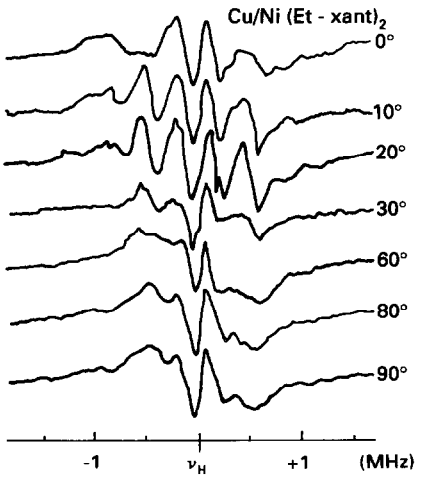

Fig. 4. Some experimental ^{1}H EMR (ENDOR) spectra of ^{63}Cu/Ni(Et-xant)$_2$ taken at different angles θ, T = 100 K.

Table 2. ^{1}H and ^{19}F EMR spectra parameters (MHz), angles (°) and distances Cu—H (Å) for ^{63}Cu(Et-xant)$_2$ and ^{63}Cu(F$_3$-Et-xant)$_2$ complexes

Complex/Fragment	A_{aniso}	A_{iso}	a	r
^{63}Cu/Ni(Et-xant)$_2$				
CH_3 (C)[a]	0.93	0.00	90	3.71
CH_3 (D)[a]	0.44	0.00	90	4.76
^{63}Cu/Ni(F$_3$-Et-xant)$_2$				
CH_2 (B)[b]	0.44	0.98	78	4.76
CH_2 (C)[a]	0.46	0.00	60	4.67
CF_3[b]	0.18	0.74	77	6.27

[a] From neighbouring molecules.
[b] From the same molecule.

angle θ [Fig. 2(a)]. The good agreement between them confirms the correctness of the structural parameters reported above.

^{1}H *EMR spectra of* ^{63}Cu/Ni(Et-xant)$_2$. Some ^{1}H EMR spectra recorded at different angles θ are shown in Fig. 4. The angular dependence of ^{1}H shf coupling is shown in Fig. 5. The two transitions—C and D which can be seen, differ from the analogous dependence for the fluorinated complex.

Transitions C and D are traceless ($A_\parallel = 2A_\perp$) and their principal values are found at an angle of 90°. Therefore these two transitions are due to interaction of the unpaired electron with protons from neighbouring molecules of the matrix, situated in the plane of the copper(II) complex. The best fit between the experimental results and theoretical calculations was obtained using the following parameters: $a^c = 90°$, $A^c_{aniso} = 0.93$ Mhz, $A^c_{iso} = 0.00$ MHz and $a^D = 90°$, $A^D_{aniso} = 0.44$ Mhz, $A^D_{iso} = 0.00$ MHz. Distances between the copper and the protons were also calculated: $r_{Cu—H} = 3.71$ Å for transition C and $r_{Cu—H} = 4.75$ Å for transition D. The data are collected in Table 2.

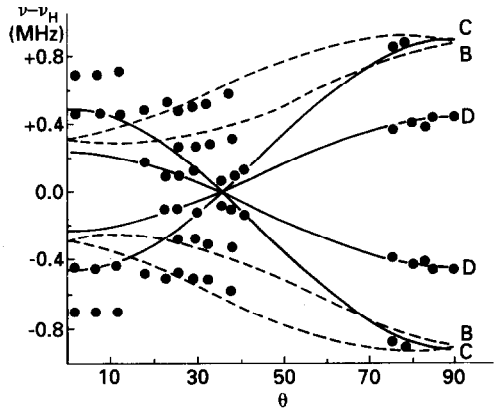

Fig. 5. Angular dependence of ^{1}H EMR (ENDOR) transitions of ^{63}Cu/Ni(Et-xant)$_2$. The experimental values are represented by dots. Full lines show the theoretical calculation.

The existence of equatorially situated protons from neighbouring molecules detected with ^{1}H EMR can be explained with the space structure of the complex. The X-ray studies of the nickel(II) complex[11–14] show that the complex exists in two different modifications—triclinic and rhombic. The only difference between them is the manner of the spacial arrangement of the molecules. Both modifications crystallize simultaneously from chloroform[13] and therefore are present in the powder sample. Thus transition C can be due to the interaction of the unpaired electron with a methyl proton from a neighbouring molecule in the triclinic modification, transition D—being due to the methyl group in rhombic modification.

Transition B, found in the fluorinated ethylxanthate complex, is marked with a dashed line in Fig. 5. As can be seen from the figure, transition B is undetectable without partial fluorination of the ethylxanthate (*vide supra*).

At the moment we are not in a position to explain the origin of some weak ^{1}H EMR lines appearing in the region 0°–10° for the ethylxanthate and in the region 20°–50° for the fluorinated complex.

^{19}F *EMR spectroscopy*

In the ^{19}F EMR spectra of the fluorinated complex a pair of lines are centred at the ^{19}F frequency.

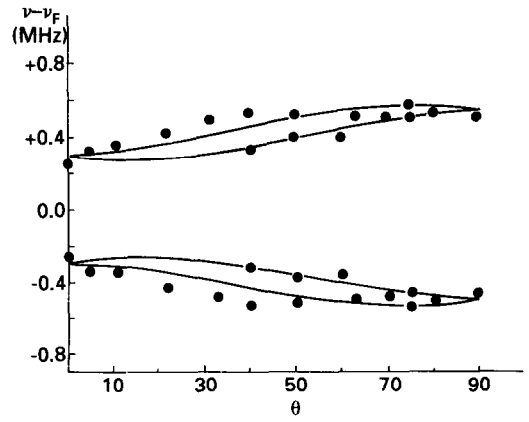

Fig. 6. Angular dependence of ^{19}F EMR (ENDOR) transitions of ^{63}Cu/Ni(F-Et-xant)$_2$.

One of them exists in all spectra and is due to fluorine atoms situated a long distance away from copper. In Fig. 6 the angular dependence of the rest of the lines is shown. Its characteristic parameters are: $a = 77°$, $A_{iso} = 0.74$ MHz and $A_{aniso} = 0.18$ MHz. The values of A_{iso} and A_{aniso} indicate that the interaction of the unpaired electron is with the fluorine atom from the methyl group of its own molecule. This type of interaction is very weak and can be recorded only in the fluorinated complex (*vide supra*). In the ^{1}H-ethylxanthate such an interaction (with the methyl group) will not be observable because the corresponding isotropic shf splitting from the methyl group CH_3 must be 33.7 times weaker—$^{1}Ha_{iso} = 0.02$ MHz. It is obvious that this value is too small for the resolution of the ENDOR spectroscopy of disordered systems.

The angle of 77° is also unexpected. The most likely angle seems to be 90° or near it by analogy with the CH_3 group which is freely rotating and the three protons are equivalent. A similar case is reported for a CF_3 group in ref. 15. In the ^{19}F-ethylxanthate it is very possible that the CF_3 group is not freely rotating and therefore interaction with only one fluorine atom at 77° is registered.

Acknowledgements—Financial support from the National Foundation for Scientific Research (project No. X-137) and the Bulgarian Academy of Sciences is gratefully acknowledged.

REFERENCES

1. S. R. Rao, *Xanthates and Related Compounds*. Dekker, New York (1971).
2. V. Alexiev, V. Iliev and N. D. Yordanov, *J. Mol. Struct.* 1984, **114**, 441; N. D. Yordanov and B. I. Velcheva, *C.R. Acad. Bulg. Sci.* 1990, **43**, 57.
3. N. D. Yordanov, V. Alexiev, J. Macicek, T. Glowiak and D. R. Russell, *Trans. Met. Chem.* 1983, **8**, 261; N. D. Yordanov, V. Alexiev, Ch. Malakova and A. Shishkov, *Trans. Met. Chem.* 1983, **8**, 210.
4. G. Gochev and N. D. Yordanov, *J. Magn. Res. A*, 1993, **102**, 180.
5. N. D. Yordanov, M. Zdravkova and D. Shopov, *Chem. Phys. Lett.* 1986, **124**, 191.
6. B. M. Hoffman, J. Martinsen and R. A. Venters, *J. Magn. Res.* 1984, **59**, 110.
7. G. C. Hurst, T. A. Henderson and R. W. Kreilick, *J. Am. Chem. Soc.* 1985, **107**, 7294.
8. G. J. Baker and J. B. Raynor, *J. Chem. Soc., Faraday Trans. I*, 1988, **84**, 4267.
9. G. H. Morrison and H. Freiser, *Solvent Extraction in Analytical Chemistry*, Wiley, New York (1957); J. Stary, *The Solvent Extraction of Metal Complexes*, Pergamon Press, New York (1964).
10. S. V. Larionov and L. A. Kosareva, *Commun. Siberian Branch Acad. Sci. U.S.S.R.* 1976, 1451.
11. M. Franzini, *Z. Kristallogr.* 1963, **118**, 393.
12. B. F. Hoskins, E. R. T. Ticknik and G. Winter, *Z. Kirstallogr.* 1985, **172**, 257.
13. T. Mizota, Y. Fujii and H. Asahina, *Technol. Rep. Yamaguchi Univ.* 1980, **2**, 389.
14. V. Romanenko, N. V. Podberezkaja and V. Bakakin, *Zh. Strukt. Khim.* 1987, **28**, 98.
15. H. Kurreck, N. H. Bretz, N. Helle, N. Henzel and E. Wulbacher, *J. Chem. Soc., Faraday Trans. I*, 1988, **84**, 3293.
16. H. Kurreck, B. Kirste and W. Lubitz, *Electron Nuclear Double Resonance Spectroscopy of Radicals in Solution: Application to Organic and Biological Chemistry*, VCH Publishers, Weinheim (1988).

Polyhedron Vol. 12, No. 22, pp. 2651–2662, 1993
Printed in Great Britain

0277–5387/93 $6.00+.00
© 1993 Pergamon Press Ltd

ORGANOCHROMIUM π-COMPLEXES—VI.* THE PREPARATION OF Cp′(η^3-ALLYL)$_2$Cr COMPOUNDS AND THEIR REACTIONS WITH DONOR LIGANDS

P. BETZ, A. DÖHRING, R. EMRICH, R. GODDARD, P. W. JOLLY,† C. KRÜGER, C. C. ROMÃO,‡ K. U. SCHÖNFELDER and Y.-H. TSAY

Max-Planck-Institut für Kohlenforschung, D-45466 Mülheim an der Ruhr, Germany

(*Received* 3 *June* 1993; *accepted* 15 *July* 1993)

Abstract—The title compounds have been prepared by reacting a Cp′CrCl$_2$ or a (η^3-allyl)$_2$CrCl species with either an allylmagnesium halide or a substituted cyclopentadienyllithium derivative. The compounds react further at room temperature to give the dinuclear species [Cp′(μ-η^3-allyl)Cr]$_2$, and with P-donor ligands with reductive coupling of the allyl groups to give Cp′(η^2,η^2-1,5-hexadiene)CrPR$_3$ species. Diene exchange is observed upon reacting the hexadiene compounds with butadiene or cyclohexadiene. The crystal structures of [Cp(μ-η^3-C$_3$H$_5$)Cr]$_2$, [(η^5-indenyl)(μ-η^3-C$_3$H$_5$)Cr]$_2$, (η^5-indenyl)(η^2,η^2-1,5-hexadiene)CrP(OMe)$_3$ and three compounds containing a 1,3-diene, *viz.* Cp(η^4-1,3-C$_4$H$_6$)CrPMe$_3$, (η^5-Me$_5$C$_5$)(η^4-1,3-C$_4$H$_6$)CrCO and Cp(η^4-1,3-cyclohexadiene)CrP(OMe)$_3$ have been established by X-ray diffraction.

In this and the following two publications we describe the preparation of a series of paramagnetic Cp′(η^3-allyl)$_2$Cr complexes and discuss their reactions with donor ligands and unsaturated organic compounds. Some of the results have been mentioned in a short communication.[2]

RESULTS AND DISCUSSION

The simplest member of the series, Cp(η^3-C$_3$H$_5$)$_2$Cr (**1**), may be prepared in high yield by reacting [CpCrCl$_2$]$_2$ with *ca* 10% excess of allylmagnesium chloride in ether at −60°C. The yields are lower if the reaction is carried out at higher temperatures, if allylmagnesium bromide is used or if the Grignard reagent is added too quickly. The compound can also be prepared in *ca* 70% yield by reacting [(η^3-C$_3$H$_5$)$_2$CrCl]$_2$ (prepared from (η^3-C$_3$H$_5$)$_3$Cr and HCl; see experimental section) with cyclopentadienyllithium (eq. 1).

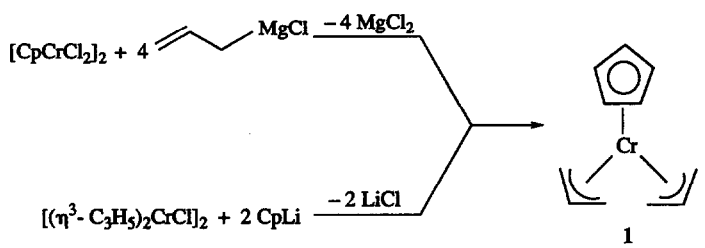

(1)

1

Compound **1** is an orange–red solid which is soluble in all common solvents. Solutions react further above *ca* −15°C (see below) whereas the solid can be handled briefly at room temperature in an inert atmosphere without noticeable decomposition. Samples should, however, be stored at −20°C. The allyl groups are readily displaced as 1,5-hexadiene upon reaction with HCl, CH_2Cl_2 or I_2 and [CpCrX$_2$]$_2$ (X = Cl, I) is formed. Protonation with acetylacetone results in the formation of Cr(acac)$_3$ and the liberation of propene and cyclopentadiene. Treatment with excess triphenylphosphine at 100°C

* For part V see ref. 1.

† Author to whom correspondence should be addressed.

‡ Present address: Centro de Tecnologia Quimica e Biologica, 2780 Oeiras, Portugal.

is accompanied by the release of a mixture of C_6-hydrocarbons. The magnetic moment (μ_B 1.9 B.M.) is consistent with the presence of one unpaired electron and the crystal structure has been confirmed by X-ray diffraction and reported in a preliminary communication.[2]

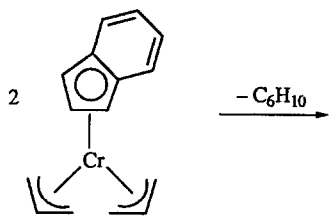

6

The related compounds $(\eta^5\text{-}RC_5H_4)(\eta^3\text{-}C_3H_5)_2Cr$ (R = Me, **2**; R = t-C_4H_9, **3**; R = Me_2PhC, **4**), $(\eta^5\text{-}Me_5C_5)(\eta^3\text{-}C_3H_5)_2Cr$ (**5**) and (η^5-indenyl)$(\eta^3\text{-}C_3H_5)_2Cr$ (**6**) have been prepared by reacting $[(\eta^3\text{-}C_3H_5)_2CrCl]_2$ with the appropriate organolithium derivative. In addition, $Cp(\eta^3\text{-}2\text{-}MeC_3H_4)_2Cr$ (**7**) and (η^5-indenyl)$(\eta^3\text{-}2\text{-}MeC_3H_4)_2Cr$ (**8**) have been prepared from $[(\eta^3\text{-}2\text{-}MeC_3H_4)_2CrCl]_2$. Reaction between $[(\eta^3\text{-}C_3H_5)_2CrCl]_2$ and tritylcyclopentadienyllithium or tetraphenylcyclopentadienyllithium takes a different course: the allyl groups are displaced and the chromocene derivatives **9** (MS: *m/z* 666, M^+) and **10** (MS: *m/z* 792, M^+) are formed

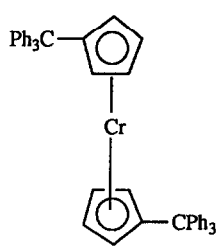

9

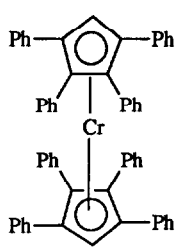

10

in *ca* 20% yield. Both of these compounds are more conveniently prepared directly from $CrCl_2$.[3]

$Cp(\eta^3\text{-}C_3H_5)_2Cr$ (**1**) reacts further in solution above *ca* −15°C to give a brown, paramagnetic (μ_B 4.1) species which had previously been isolated from the reaction between $[CpCrCl_2]_2$ and allylmagnesium chloride in THF at room temperature and identified as the dinuclear species $[Cp(\mu\text{-}\eta^3\text{-}C_3H_5)Cr]_2$ (**11**).[4] The corresponding indenyl derivative **6** reacts similarly to give the dark brown dinuclear compound **12**. The presence of bridging allyl groups in both **11** and **12** has been confirmed by X-ray diffraction (see below).

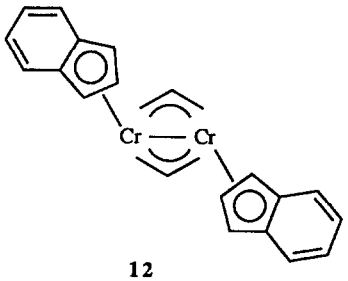

12 (2)

$Cp(\eta^3\text{-}C_3H_5)_2Cr$ (**1**) reacts with a variety of donor ligands with reductive coupling of the allyl groups to give compounds containing metal-bonded 1,5-hexadiene (eq. 3). The products of the reaction with the monodentate ligands CO, PMe_3, $P(OMe)_3$ and $P(OPh)_3$ are the dark green compounds **13–16** in which the hexadiene is bonded as an η^2,η^2-organic ligand. These compounds, which can also be prepared in a one-pot procedure by reacting $[CpCrCl_2]_2$ consecutively with allylmagnesium chloride and the donor ligand, are stable at room temperature and are relatively insensitive towards oxygen. The crystal structures of **14** and **15** have been determined by X-ray diffraction and have been reported earlier.[2] The reaction of **1** with CO or PMe_3 is accompanied by the formation in low yield of species having the composition $Cp_2Cr_2L_5$ (L = CO, PMe_3).

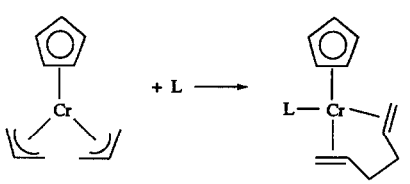

1 (3)

13 L = CO; **14** L = PMe_3;
15 L = $P(OMe)_3$; **16** L = $P(OPh)_3$

In contrast to the examples described above, the adducts formed by reacting **1** with PPh_2Me or PPh_3 are bright yellow and a cryoscopic molecular weight determination of the species containing diphenylmethylphosphine shows it to be dimeric. This, combined with the magnetic moment (two unpaired electrons), suggests a structure (**17**) in which two hexadiene molecules bridge two $CpCr(PPh_2Me)$-fragments. The presence of an uncomplexed double bond (ν 1635 cm^{-1}) in the IR-spectrum of the adduct formed by reacting **1** with the bidentate ligand bis(dimethylphosphino)ethane, suggests that this has a structure (**18**) in which the hexadiene molecule is acting as an η^2-organic ligand. Steri-

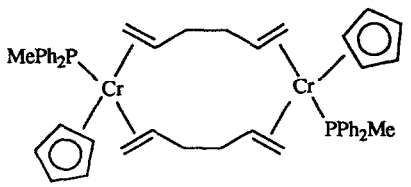

17

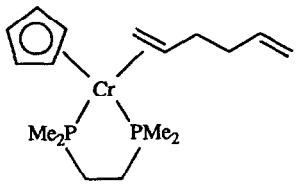

18

cally demanding phosphines such as $P(C_3H_7\text{-}i)_3$, $P(C_4H_9\text{-}t)_3$ and PCy_3 react with **1** much less readily and well defined products could not be isolated.

(η^5-Indenyl)(η^3-C_3H_5)$_2$Cr (**6**) reacts with donor ligands in an analogous manner and the adducts **19** and **20** have been isolated from the reaction with trimethylphosphite or trimethylphosphine (eq. 4). The structure of **19** has been confirmed by X-ray diffraction (see below).

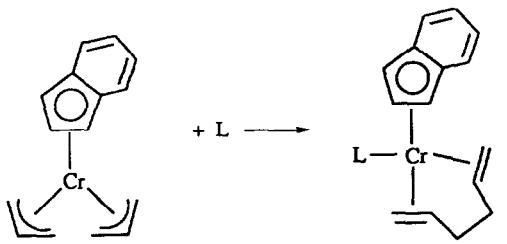

(4)

6

19 L = $P(OMe)_3$;
20 L = PMe_3

The hexadiene molecule in compounds **14**, **15** and **20** can be readily displaced by 1,3-butadiene and Cp(η^4-1,3-C_4H_6)$CrPR_3$ (**21**, R = Me; **22**, R = OMe) and (η^5-indenyl)(η^4-1,3-C_4H_6)$CrPMe_3$ (**23**) have been isolated. Compounds **21** and **22** can also be prepared by reacting $[CpCrCl_2]_2$ with magnesium-butadiene in the presence of the donor ligand and the same procedure has been used to prepare (η^5-Me_5C_5)(η^4-1,3-C_4H_6)$CrPR_3$ (**24**, R = Me; **25**, R = OMe). The reaction of **24** (R = Me) with CO is accompanied by donor-ligand exchange and (η^5-Me_5C_5)(η^4-1,3-C_4H_6)CrCO (**26**) is formed. The *prone* arrangement of the butadiene molecule in **21** and **26** has been established by the crystal structure determinations discussed below and extended-Hückel MO calculations for **26** indicate that this arrangement (**a**)

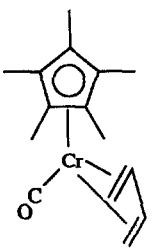

26a

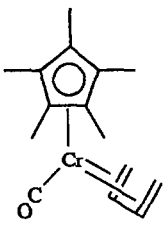

26b

is *ca* 9 kcal mol^{-1} more stable than the *supine* arrangement (**b**).[12] This result is in contrast to that obtained for related compounds containing early transition metals such as Cp(η^4-1,3-C_4H_6)$TaCl_2$ for which it has been calculated that the *supine* arrangement is *ca* 16 kcal mol^{-1} more stable than the *prone* arrangement.[13]

The reaction of **15** with 1,3-cyclohexadiene also results in diene exchange and the η^4-1,3-cyclohexadiene compound **27** is formed as a red, crystalline solid (eq. 5). This reaction is accompanied by the formation of lesser amounts of Cp(η^6-C_6H_6)Cr (**28**) which is the product of the further reaction of **27** in solution at room temperature. This last reaction presumably proceeds by phosphite dissociation followed by Cr-induced dehydrogenation of the cyclohexadiene molecule. A related reaction leading to the formation of **28** has been observed upon reacting Cp(η^3-C_3H_5)$_2$Cr (**1**) with 1,3-cyclohexadiene and has been suggested to involve H-transfer from the diene to the metal followed by homolytic cleavage of the resulting Cr—H bond and the indiscriminant reaction of the H-radical with the reaction media.[5]

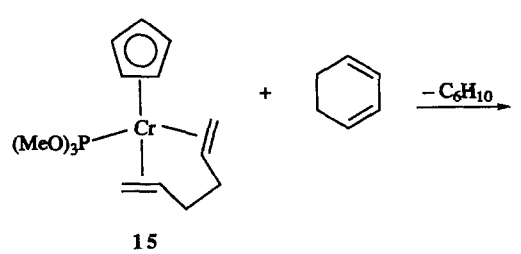

15

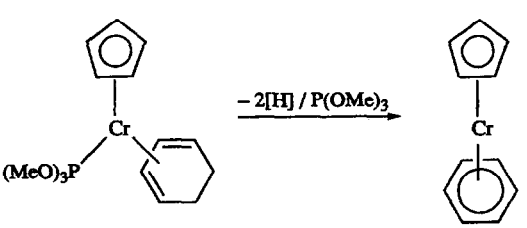

27 28

(5)

CRYSTAL STRUCTURE DETERMINATIONS

We have already discussed in an earlier publication the crystal structure of Cp(η^2,η^2-1,5-hexadiene)CrPMe$_3$ (**14**)[2] and here we report that of the related complex (η^5-indenyl)(η^2,η^2-1,5-hexadiene)CrP(OMe)$_3$ (**19**) the analysis of which was undertaken mainly to determine the hapticity of the indenyl fragment. The molecular structure is shown in Fig. 1 and selected structural parameters are listed in Table 1. The structure is similar to that of **14** with the indenyl group acting as an η^5-organic ligand, i.e. the indenyl group is essentially planar: the fold angle between the five- and six-membered rings is only 1.8°.

The crystal structure of both [Cp(μ-η^3-C_3H_5)Cr]$_2$ (**11**) and [(η^5-indenyl)(μ-η^3-C_3H_5)Cr]$_2$ (**12**) have been determined by X-ray diffraction. **12** contains two independent molecules in the unit cell which differ slightly in the coordination of the indenyl-group to the metal atom. The molecular structure of **11** and **12a** (molecule 1) is shown in Fig. 2 while selected bond distances and angles for **11** and both molecules of **12** are listed in Table 2.

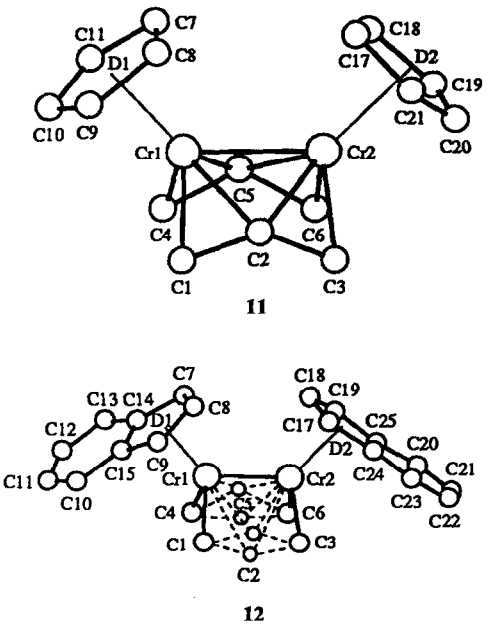

Fig. 2. The molecular structure of [Cp(μ-η^3-C_3H_5)Cr]$_2$ (**11**) and [(η^5-indenyl)(μ-η^3-C_3H_5)Cr]$_2$ (**12**, molecule 1).

In both compounds, two Cr-atoms are bridged by two μ-η^3-allyl groups. In **11**, the two allyl groups adopt a *cis*-configuration with the two meso-C atoms pointing towards the Cr—Cr bond and with a dihedral angle of 54.9° between the two allyl planes (C1/C2/C3 and C4/C5/C6). Three of the four allyl groups in the two independent molecules of **12** are disordered and have been treated accordingly.

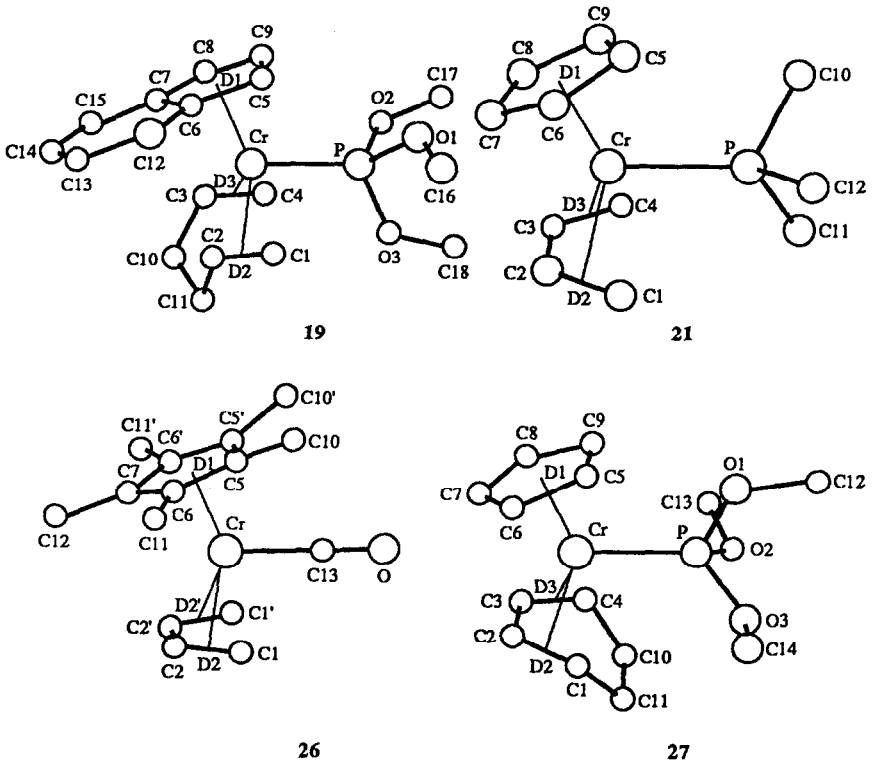

Fig. 1. The molecular structures of (η^5-indenyl)(η^2,η^2-1,5-hexadiene)CrP(OMe)$_3$ (**19**), Cp(η^4-1,3-C_4H_6)CrPMe$_3$ (**21**), (η^5-Me_5C_5)(η^4-1,3-C_4H_6)CrCO (**26**) and Cp(η^4-1,3-cyclohexadiene)Cr P(OMe)$_3$ (**27**).

Table 1. Selected structural parameters for (η^5-indenyl)(η^2,η^2-1,5-hexadiene)CrP(OMe)$_3$ (**19**), Cp(η^4-1,3-C_4H_6)CrPMe$_3$ (**21**), (η^5-Me_5C_5)(η^4-1,3-C_4H_6)CrCO (**26**) and Cp(η^4-1,3-cyclohexadiene)CrP(OMe)$_3$ (**27**)

Distance/ angle (ESD)	**19**[b]	**21**	**26**[c]	**27**[e]
Cr—P	2.243(1)	2.326(1)	1.837(4)[d]	2.265(1)
Cr—C1	2.207(5)	2.156(3)	2.183(3)	2.220(1)
Cr—C2	2.162(5)	2.073(3)	2.095(2)	2.104(1)
Cr—C3	2.190(6)	2.075(2)	—	2.099(1)
Cr—C4	2.172(6)	2.155(2)	—	2.207(1)
Cr—C5	2.245(4)	2.208(2)	2.171(2)	2.177(1)
Cr—C6	2.345(4)	2.219(3)	2.196(2)	2.200(1)
Cr—C7	2.324(4)	2.186(2)	2.218(3)	2.228(1)
Cr—C8	2.226(5)	2.165(2)	—	2.227(1)
Cr—C9	2.213(5)	2.193(3)	—	2.184(1)
Cr—D1[a]	1.926(5)	1.843(3)	1.827(3)	1.841(1)
Cr—D2[a]	2.072(5)	1.994(3)	2.023(3)	2.043(1)
Cr—D3[a]	2.065(6)	1.997(2)	—	2.033(1)
C1—C2	1.387(7)	1.408(4)	1.394(4)	1.422(2)
C2—C3	—	1.402(5)	1.423(4)[d]	1.425(2)
C3—C4	1.407(8)	1.393(4)	—	1.423(2)
C5—C6	1.415(6)	1.388(4)	1.409(3)	1.419(2)
C6—C7	1.424(6)	1.399(3)	1.424(2)	1.418(2)
C7—C8	1.430(7)	1.393(4)	—	1.417(2)
C8—C9	1.394(7)	1.409(3)	—	1.424(2)
C5—C9	1.412(8)	1.410(4)	1.440(3)[d]	1.442(2)
D1—Cr—D2	120.5(1)	131.7(1)	132.3(1)	128.6(1)
D1—Cr—D3	124.0(1)	130.9(1)	—	131.7(1)
D2—Cr—D3	99.2(1)	63.6(1)	63.1(1)[d]	59.7(1)
D3—Cr—P	96.1(1)	105.3(1)	—	105.1(1)
D2—Cr—P	96.9(1)	102.0(1)	101.1(1)[d]	108.1(1)
D1—Cr—P	114.4(1)	112.9(1)	114.8(1)[d]	112.8(1)
C1—C2—C3	—	120.2(3)	119.9(2)	115.0(1)
C2—C3—C4	—	119.8(2)	—	115.3(1)
C1—Cr—C2	37.0(2)	38.8(1)	38.0(1)	38.3(1)
C3—Cr—C4	37.6(2)	38.4(1)	—	38.5(1)
C1—Cr—C4	108.5(2)	81.1(1)	80.2(1)	73.0(1)

[a] Midpoints of C5-ring, C1—C2 and C3—C4, respectively.

[b] C2—C11 1.514(8), C11—C10 1.50(1), C10—C3 1.496(8), C6—C12 1.425(7), C12—C13 1.348(7), C13—C14 1.398(8), C14—C15 1.346(8), C7—C15 1.425(7), C1—C2—C11 123.0(5), C4—C3—C10 121.6(5), C2—C11—C10 108.5(5), C3—C10—C11 110.3(5).

[c] C13—O 1.151(5), C5/6/7—C10/11/12 1.491(5)—1.507(4), Cr—C13—O 178.8(4).

[d] Cr—P ≡ Cr—CO, C2—C2* ≡ C2—C3, C5—C5* ≡ C5—C9, D2—Cr—D2* ≡ D2—Cr—D3, D_n—Cr—P ≡ D_n—Cr—C13.

[e] C1—C11 1.523(2), C4—C10 1.522(2), C10—C11 1.546(2), C2—C1—C11 117.1(1), C3—C4—C10 118.1(1), C1—C11—C10 110.8(1), C4—C10—C11 111.0(1).

Table 2. Selected structural parameters for [Cp(μ-η^3-C_3H_5)Cr]$_2$ (**11**) and [(η^5-indenyl)(μ-η^3-C_3H_5)Cr]$_2$ (**12**)

Distance/angle (ESD)	**11**	**12a** (Mol. 1)	**12b** (Mol. 2)
Cr1—Cr2	2.299(1)	2.171(1)	2.198(1)
Cr1—C1	2.098(3)	2.108(6)	2.095(5)
Cr1—C2	2.303(3)	2.425(8)	2.335(5)
Cr1—C4	2.091(3)	2.089(5)	2.103(6)
Cr1—C5	2.309(3)	2.329(7)	2.426(7)
Cr2—C2	2.308(3)	2.439(8)	2.342(5)
Cr2—C3	2.083(3)	2.106(5)	2.098(5)
Cr2—C5	2.316(3)	2.359(7)	2.442(7)
Cr2—C6	2.081(3)	2.102(5)	2.111(5)
Cr1—C7	2.251(4)	2.281(5)	2.301(7)
Cr1—C8	2.239(3)	2.256(5)	2.255(7)
Cr1—C9	2.285(3)	2.299(5)	2.277(5)
Cr1—C10	2.308(3)	2.450(5)[b]	2.411(5)[b]
Cr1—C11	2.269(3)	2.452(5)[c]	2.441(5)[c]
Cr—D1	1.940(4)[a]	2.021(5)[d]	2.008(7)[d]
Cr—D2	1.938(6)[a]	2.030(6)[d]	2.012(9)[d]
C1—C2	1.405(5)	1.35(1)	1.429(9)
C2—C3	1.428(5)	1.38(1)	1.426(8)
C4—C5	1.419(4)	1.40(1)	1.349(9)
C5—C6	1.427(4)	1.443(9)	1.411(9)
C7—C8	1.407(6)	1.393(8)	1.35(1)
C8—C9	1.399(6)	1.394(8)	1.411(9)
C9—C10	1.359(6)	1.427(7)[e]	1.428(8)[e]
C10—C11	1.380(6)	1.418(7)[f]	1.437(7)[f]
C11—C7	1.388(6)	1.416(7)[g]	1.416(8)[g]
C10—C15	—	1.393(8)	1.412(7)
C10—C11	—	1.33(1)	1.32(1)
C11—C12	—	1.41(1)	1.40(1)
C12—C13	—	1.383(9)	1.39(1)
C13—C14	—	1.433(8)	1.401(8)
D1—Cr1—Cr2	131.2(1)	132.4(1)	132.9(1)
D2—Cr2—Cr1	132.4(1)	132.8(1)	133.3(1)
C1—C2—C3	126.3(3)	133.6(7), 145(1)[h]	125.3(5)
C4—C5—C6	125.5(3)	125.7(6), 165(2)[h]	129.9(6), 151(2)[h]

[a] Midpoints of planes defined by C7—C11 and C17—C21.

[b] Cr1—C15

[c] Cr1—C14

[d] Midpoints of planes defined by C7—C9, C14, C15 and C17—C19, C24, C25.

[e] C9—C15.

[f] C14—C15.

[g] C7—C14.

[h] Disordered at C2 and C5.

No significance should therefore be attached to the associated bonding parameters. The main interest in **12** centres on the hapticity of the indenyl—Cr bond: the indenyl group in both molecules is essentially planar (the fold angle between the five- and six-membered rings are 2.2°/4.7° for molecule 1 and 2.4°/2.4° for molecule 2) while all of the C-atoms of the five-membered ring are within a bonding distance to the metal so that the indenyl group is best regarded as being bonded in an η^5-manner to the metal atom and not in an η^3-manner. In contrast, in (η^3-indenyl)Ir(PMe_2Ph)$_3$ for example, the two C-atoms shared by both the five- and six-membered rings are much further away [3.036/3.014(8) Å] from the metal atom than the other three [2.047(8)–2.236(13) Å] and there is a 20° angle between the planes of the allyl group and the six-membered ring.[6] The slight differences in the indenyl—Cr bond lengths for the two independent molecules of **12** suggest that **12b** has more η^5-character than **12a** and this may well be the result of packing effects within the crystal. **12** is diamagnetic (NMR; see experimental) and this combined with the much shorter Cr—Cr distance observed in the structurally related [(η^3-C_3H_5)(μ-η^3-C_3H_5)Cr]$_2$ [1.97(6) Å] for which a quadruple metal–metal bond has been suggested,[7,8] could be taken as an indication that **12** contains a metal–metal double bond. One ambiguity, however, remains unresolved: [Cp(μ-η^3-C_3H_5)Cr]$_2$ (**11**) is paramagnetic and it remains unclear whether this is an artefact (due to impurities in the bulk sample) or is the result of a difference in the multiplicity of the metal–metal bond.

The crystal structures of two donor-ligand stabilized Cp′(η^4-1,3-C_4H_6)-species (**21** and **26**) have been determined by X-ray diffraction. The molecular structures are shown in Fig. 1 and selected structural parameters are compared in Table 1. In both cases the butadiene molecule has a single-*cis* geometry and is bonded in an η^4-manner to the metal atom. The pentamethylcyclopentadienyl group in **26** is essentially planar with the methyl groups bent by an average of only 1.8° out of the ring-plane away from the metal atom. The Cr—C—O fragment is practically linear [Cr—C13—O 178.8(4)°] with the oxygen atom bent slightly towards the ring.

The crystal structure of Cp(η^4-1,3-cyclohexadiene)CrP(OMe)$_3$ (**27**) has also been determined (Fig. 1) and selected structural parameters are listed in Table 1. The 1,3-cyclohexadiene molecule is bonded as an η^4-organic ligand, the methylenic C-atoms are directed away from the metal atom. Complexation to the metal leads to a delocalization of the electrons within the 1,3-diene fragment (for free 1,3-cyclohexadiene C1—C2 = 1.348 and C2—C3 = 1.465 Å).[14] The cyclopentadienyl ring is planar.

EXPERIMENTAL

All experiments were carried out under an atmosphere of argon. Solvents (diethylether, pentane) were dried and freed from dissolved oxygen by distillation from diethylmagnesium. Chromocene,[9] (η^3-C_3H_5)$_3$Cr and (η^3-2-MeC_3H_4)$_3$Cr[10] were prepared by published procedures. The alkali metal salts of cyclopentadiene, substituted cyclopentadiene and indene were prepared by standard methods either by reaction with n-butyllithium or the alkali metal.

Infrared spectra were recorded with a Nicolet-FT-IR-spectrometer and the magnetic susceptibility was measured using a magnetic balance constructed in the Institute mainly from Varian parts (field strength 9000 G).

[$CpCrCl_2$]$_2$

The following synthesis is a modification of the published procedure.[11] Cp_2Cr (20 g, 110 mmol) was dissolved in pentane (1 l) at 0°C. The resulting red solution was stirred vigorously and treated with dry, gaseous HCl. The product was formed immediately as a green precipitate and the reaction was continued until the pentane became colourless. The compound, a green powder (dec. > 250°C) which is relatively insensitive to air but extremely moisture sensitive, was isolated and washed with pentane (3×100 cm^3) at room temperature. Yield 18.6 g (90% theory).

[(η^3-C_3H_5)$_2$CrCl]$_2$

The following synthesis is a modification of the published procedure.[11] (η^3-C_3H_5)$_3$Cr[10] (6.1 g, 34.9 mmol) was dissolved in diethylether (200 cm^3) and an ethereal solution of HCl (66 cm^3 of a 0.5 N solution, 33 mmol) was added dropwise at −78°C with vigorous stirring to give the product as a red–brown precipitate. Solvent was removed at −25°C under high vacuum and the residue washed with 50 cm^3 aliquots of pentane [to remove unreacted (η^3-C_3H_5)$_3$Cr] until the washings were colourless. The compound, which decomposes above −20°C, was dried at −40°C. Yield 5.33 g (90% theory). Found: C, 42.4; H, 5.9; Cl, 21.0; Cr, 30.7. Calc. for $C_{12}H_{20}Cl_2Cr_2$: C, 42.5; H, 5.9; Cl, 20.9; Cr, 30.7%. MS: *m/z* 296 (M^+-C_3H_6), 221, 210, 185, 175, 134, 93.

$[(\eta^3\text{-}2\text{-}MeC_3H_4)_2CrCl]_2$

$(\eta^3\text{-}2\text{-}MeC_3H_4)_3Cr$ [prepared in an analogous manner to $(\eta^3\text{-}C_3H_5)_3Cr$[10]] (7.6 g, 34.9 mmol) was dissolved in diethylether (200 cm^3) at −78°C and treated with ethereal-HCl (66 cm^3 of a 0.5 N solution, 33 mmol) as described above. The compound was isolated as a red–brown powder which decomposed above −20°C and which inflamed spontaneously in air. Yield 6.23 g (90% theory). Found: C, 48.2; H, 7.6; Cl, 18.0; Cr, 25.8. Calc. for $C_{16}H_{28}Cl_2Cr_2$: C, 48.6; H, 7.1; Cl, 17.9; Cr, 26.3%. MS: *m/z* 394 (M^+), 339 (M^+-C_4H_7), 284, 229, 217, 162, 107.

$Cp(\eta^3\text{-}C_3H_5)_2Cr$ (**1**)

Allylmagnesium chloride (1.06 l of a 0.308 mol l^{-1} ethereal solution, 325.6 mmol) was added dropwise to a suspension of $[CpCrCl_2]_2$ (27.86 g, 74.1 mmol) in diethylether (300 cm^3) at −60°C over 12 h. The reaction mixture was stirred at −60°C for a further 14 h and the solvent removed under high vacuum at −50°C. The residue was dried under high vacuum and then extracted with aliquots of carefully dried pentane at −30°C until the extract was colourless. The combined extract (*ca* 5 l) was cooled to −78°C to give the compound as orange–red crystals. Yield 24.78 g (83.9% theory). The compound can also be prepared (yield *ca* 70%) by reacting $[(\eta^3\text{-}C_3H_5)_2CrCl]_2$ with cyclopentadienyllithium in ether at −35°C. The compound reacts further above −20°C. Found: C, 66.2; H, 7.6; Cr, 26.0. Calc. for $C_{11}H_{15}Cr$: C, 66.3; H, 7.6; Cr, 26.1%. MS (70 eV, 40°): *m/z* 199 (M^+), 171, 158 (M^+-C_3H_5), 117. Magn. moment: μ_{eff} 1.8 BM. IR (KBr, −45°C): *v* 3100, 3000, 1495, 1435, 1370, 1210, 1125, 1060, 1005, 910, 825, 750, 580. Crystal structure: see ref. 2.

Reaction of **1** *with* HCl

$Cp(\eta^3\text{-}C_3H_5)_2Cr$ (1.31 g, 6.57 mmol) was suspended in pentane (40 cm^3) at −50°C and treated with gaseous HCl (306.7 cm^3, 13.69 mmol) from a gas burette. Propene was liberated and determined by GC (98.6% theory) and a turquoise-coloured suspension of $(CpCrCl_2)_2$ was formed. Yield 1.08 g (87.9% theory). The same compound is also formed upon treatment of **1** with CH_2Cl_2 and is accompanied by the liberation of 1,5-hexadiene.

Reaction of **1** *with* I_2

$Cp(\eta^3\text{-}C_3H_5)_2Cr$ (0.95 g, 4.77 mmol) was suspended in pentane (60 cm^3) at −78°C and iodine (1.82 g, 7.17 mmol) in diethylether (5 cm^3) was added. The reaction mixture was allowed to warm to 0°C and stirred overnight. 1,5-Hexadiene (33% theory, GC) was liberated with formation of green $(CpCrI_2)_2$. Yield 1.26 g (71.3% theory). Found: Cr, 13.9; I, 68.6. Calc. for $C_{10}H_{10}Cr_2I_4$: Cr, 14.0; I, 68.4%. MS (CI, 230°): *m/z* 742 (M^+), 615 (M^+—I).

Reaction of **1** *with acetylacetone*

$Cp(\eta^3\text{-}C_3H_5)_2Cr$ (1.69 g, 8.9 mmol) was dissolved in diethylether (100 cm^3) at −78°C and treated with excess acetylacetone (3 cm^3) at −20°C. The reaction mixture became dark red. The solvent was distilled off and shown by GC to contain propane (61.6% theory) and cyclopentadiene (100.4% theory) and the solid identified as $Cr(acac)_3$. Yield 1.98 g (66.8% theory).

Reaction of **1** *with excess* PPh_3

Excess PPh_3 (5.2 g) was added to solid $Cp(\eta^3\text{-}C_3H_5)_2Cr$ (1.23 g, 6.17 mmol) at −78°C and the reaction vessel connected by a glass bridge to a trap. The apparatus was evacuated and closed and the reaction vessel lowered into a bath at 100°C while the trap was cooled in liquid N_2. 0.53 g (103.9% theory) of condensate was liberated and shown to consist of 1,5-hexadiene (60.9% theory) and other C_6-hydrocarbons (33.4% theory).

$(\eta^5\text{-}MeC_5H_4)(\eta^3\text{-}C_3H_5)_2Cr$ (**2**)

Methylcyclopentadienyllithium (1.17 g, 13.6 mmol) was added to a stirred suspension of $[(\eta^3\text{-}C_3H_5)_2CrCl]_2$ (2.1 g, 6.2 mmol) in diethylether (200 cm^3) at −78°C. The reaction mixture was stirred at −35°C for 16 h, evaporated to dryness and the residue extracted with pentane (3 × 100 cm^3). The extract was filtered and cooled to −78°C to give the compound as red, cubic crystals which decomposed at −20°C. Yield 1.85 g (70% theory). Found: C, 67.4; H, 8.1; Cr, 24.4. Calc. for $C_{12}H_{17}Cr$: C, 67.6; H, 8.0; Cr, 24.4%. MS: *m/z* (M^+), 172 (M^+-C_3H_5), 131. Magn. moment: μ_B 1.6 BM. IR (KBr, −45°C): *v* 3080, 2990, 2920, 1495, 1455, 1375, 1210, 1050, 1000, 830, 745, 580.

$(\eta^5\text{-}t\text{-}C_4H_9C_5H_4)(\eta^3\text{-}C_3H_5)_2Cr$ (**3**)

Prepared as above from t-butylcyclopentadienyllithium as yellow crystals which decompose above −20°C. Yield 65% theory. Found: C, 70.1; H, 9.2; Cr, 20.9. Calc. for $C_{15}H_{23}Cr$: C, 70.6; H, 9.1; Cr, 20.4%. MS: the compound decomposed. IR (KBr,

−45°C): *v* 3100, 3000, 2930, 1490, 1380, 1360, 1215, 1045, 1005, 920, 830, 745, 580.

(η^5-$Me_2PhCC_5H_4$)(η^3-C_3H_5)$_2$Cr (**4**)

Prepared as above from 2-phenylisopropylcyclopentadienyllithium as red needles which decompose above −20°C. Yield 65% theory. Found: C, 75.6; H, 7.8; Cr, 16.5. Calc. for $C_{20}H_{25}Cr$: C, 75.7; H, 7.9; Cr, 16.4%. MS: the compound decomposed. IR (KBr, −45°C): *v* 3100, 3060–3040, 2980, 1620, 1590, 1490, 1380, 1205, 1040, 1000, 775, 705, 580.

(η^5-Me_5C_5)(η^3-C_3H_5)$_2$Cr (**5**)

Prepared as above from pentamethylcyclopentadienyllithium as red needles which decompose above −20°C. Yield 65% theory. Found: C, 71.0; H, 9.4; Cr, 19.7. Calc. for $C_{16}H_{25}Cr$: C, 71.3; H, 9.4; Cr, 19.3%. MS. *m/z* 269 (M^+), 187 (M^+-C_6H_{10}), 131. Magn. moment: μ_B 2.0 BM. IR (KBr, −45°C): *v* 3060, 2990, 2920, 1490, 1435, 1375, 1210, 995, 590.

(η^5-*Indenyl*)(η^3-C_3H_5)$_2$Cr (**6**)

[(η^3-C_3H_5)$_2$CrCl]$_2$ (5.1 g, 15 mmol) was suspended in diethylether (400 cm^3) at −78°C and treated with indenyllithium (3.78 g, 31 mmol). The reaction mixture was warmed to −40°C and stirred for 14 h to give an intensive red–brown solution. The solvent was removed at −35°C and the residue extracted with pentane (3 × 100 cm^3). The resulting solution was cooled to −78°C to give the compound as dark brown needles which decompose above −20°C. Yield 5.16 g (69% theory). Found: C, 72.1; H, 7.1; Cr, 20.7. Calc. for $C_{15}H_{17}Cr$: C, 72.3; H, 6.9; Cr, 20.9%. MS (70 eV, 30°C): *m/z* 249 (M^+), 208 (M^+-C_3H_5), 167. Magn. moment: μ_B 1.6/1.8. IR (KBr, −45°): *v* 3090–3040, 1630, 1610, 1490, 1450, 1380, 1350, 1210, 995, 745, 580.

Cp(η^3-2-MeC_3H_4)$_2$Cr (**7**)

[(η^3-2-MeC_3H_4)$_2$CrCl]$_2$ (2.1 g, 5.3 mmol) was suspended in diethylether (200 cm^3) at −78°C and treated with cyclopentadienyllithium (0.79 g, 11 mmol). The reaction mixture was stirred for 16 h at −35°C to give a red–violet solution. The solvent was evaporated at −35°C and the residue extracted with pentane (3 × 100 cm^3). Cooling to −78°C failed to cause precipitation of the compound which was isolated as a red–violet oil (which decomposed at −20°C) by evaporation to dryness. Yield 0.72 g (30% theory). Satisfactory elemental analysis of this thermolabile oil could not be obtained. MS: *m/z* 227 (M^+), 117 (M^+-C_8H_{14}). IR (film): *v* 3080, 2940, 2860, 2810, 1480, 1375, 1095, 1010, 790, 580.

(η^5-*Indenyl*)(η^3-2-MeC_3H_4)$_2$Cr (**8**)

[(η^3-2-MeC_3H_4)$_2$CrCl]$_2$ (2.1 g, 5.3 mmol) was suspended in diethylether (200 cm^3) at −78°C and treated with indenyllithium (1.34 g, 11 mmol). The reaction mixture was stirred for 16 h at −35°C. The solvent was removed and the residue extracted with pentane (3 × 100 cm^3). Removal of the solvent at −40°C gave the product as a violet oil which decomposed above −20°C. Yield 0.88 g (30% theory). Satisfactory analytical data could not be obtained for this thermolabile oil. MS: the compound decomposed. IR (film): *v* 3060, 2960–2860, 1480, 1440, 1375, 1210, 740.

[Cp(μ-η^3-C_3H_5)Cr]$_2$ (**11**)[4]

Cp(η^3-C_3H_5)$_2$Cr (**1**) (1.83 g, 9.19 mmol) was suspended in pentane (50 cm^3) at −78°C and toluene (30 cm^3) was added. The reaction mixture was allowed to slowly warm to −15°C and stirred for 24 h. A brown solid precipitated. Yield 1.01 g (69.8% theory; the yield in the absence of toluene was only *ca* 25%). Found: C, 60.9; H, 6.3; Cr, 32.8. Calc. for $C_{16}H_{20}Cr_2$: C, 60.8; H, 6.4; Cr, 32.9%. Magn. moment: μ_{eff} 4.1 BM. Crystal structure: see Fig. 2.

[(η^5-*Indenyl*)(μ-η^3-C_3H_5)Cr]$_2$ (**12**)

(η^5-Indenyl)(η^3-C_3H_5)$_2$Cr (**6**) (0.60 g, 2.4 mmol) was dissolved in diethylether (50 cm^3) at −30°C in an atmosphere of ethylene and the solution allowed to reach room temperature over 24 h. The solvent was removed and the residue separated from polyethylene (0.6 g) by extraction. The resulting brown solid was treated with Avicel and cooled to −78°C to give the compound as dark brown crystals. Yield 0.21 g (40% theory). The same compound is formed in the absence of ethylene. Found: C, 69.1; H, 5.9; Cr, 25.1. Calc. for $C_{24}H_{24}Cr_2$: C, 69.2; H, 5.8; Cr, 25.0%. MS: *m/z* 374 (M^+-C_3H_6), 334 (M^+-C_6H_{12}), 282, 208, 167. IR (KBr, room temperature): *v* 2040, 1605, 1480, 1335, 1215, 995, 820, 745. ^{1}H NMR (d_8-THF, 30°C): δ 7.01, 6.75 (indenyl); 6.26, 5.91 (indenyl); 4.79, 3.27, 2.28, 1.50 (allyl). Crystal structure: see Fig. 2.

Cp(η^2,η^2-1,5-*hexadiene*)CrCO (**13**)[2]

Cp(η^3-C_3H_5)$_2$Cr (**1**) (2.18 g, 10.94 mmol) was suspended in pentane (40 cm^3) at −78°C and the

reaction vessel connected to a glass burette filled with CO. The reaction mixture was stirred vigorously and warmed to 0°C. CO (12.83 mmol) was absorbed and the solution became dark green. A small amount of a green–grey solid (yield *ca* 4%; presumably $Cp_2Cr_2(CO)_5$, ν(CO) 1945, 1845, 1780, 1730) was filtered off and the solution evaporated to dryness to give the compound as green needles. Yield 2.12 g (85.3% theory). Found: C, 65.1; H, 7.1; Cr, 22.8. Calc. for $C_{12}H_{15}CrO$: C, 63.4; H, 6.7; Cr, 22.8%. MS (70 eV, 30°C): *m/z* 227 (M^+), 144 (M^+-CO), 171, 117. Magn. moment: μ_{eff} 1.61/1.58 BM. IR (KBr, −40°C): ν(CO) 1870vs, 1830sh, 1012, 1002, 820, 803, 590, 556, 546, 487.

Cp(η^2,η^2-1,5-*hexadiene*)CrPMe$_3$ (**14**)[2]

Cp(η^3-C_3H_5)$_2$Cr (**1**) (6.33 g, 31.8 mmol) was suspended in pentane (100 cm^3) at −78°C and PMe_3 (2.42 g, 3.3 cm^3, 31.8 mmol) added slowly with a pipette. The reaction mixture was allowed to warm to 0°C during which the colour changed to dark green. The solution was stirred overnight, filtered to remove a small amount of a grey–green solid [approx. composition $Cp_2Cr_2(PMe_3)_5$] and cooled to −78°C to give the compound as a dark green, crystalline solid which decomposed at 80°C. Yield 7.18 g (82% theory). Found: C; 61.1; H, 8.7; Cr, 18.8; P, 11.3. Calc. for $C_{14}H_{24}CrP$: C, 61.1; H, 8.8; Cr, 18.9; P, 11.3%. MS (70 eV, 50°C): *m/z* 275 (M^+), 193 (M^+-C_6H_{10}), 117. Magn. moment: μ_B 1.9 BM. IR (KBr, room temperature): ν 3100, 3020, 2920, 1470, 1465, 1420, 1120, 950, 800. Crystal structure: see ref. 2.

Cp(η^2,η^2-1,5-*hexadiene*)CrP(OMe)$_3$ (**15**)[2]

Prepared as above as dark green needles in 89% yield. Found: C, 52.1; H, 7.6; Cr, 16.1; P, 9.5. Calc. for $C_{14}H_{24}CrO_3P$: C, 52.0; H, 7.5; Cr, 16.1; P, 9.6%. MS (70 eV, 50°C): *m/z* 323 (M^+), 241 (M^+-C_6H_{10}), 182, 117. Magn. moment: μ_{eff} 1.9/2.0 BM. IR (KBr, room temperature): ν 3100, 3040, 2940, 2840, 1480, 1450, 1440, 1120, 1040, 805, 760, 700. Crystal structure: the structure has been confirmed by an X-ray diffraction study but disorder prevented refinement of the data.

Cp(η^2,η^2-1,5-*hexadiene*)CrP(OPh)$_3$ (**16**)

Prepared as above as a dark green, relatively insoluble compound in 85% yield. Found: Cr, 10.1; P, 6.0. Calc. for $C_{29}H_{30}CrO_3P$: Cr, 10.2; P, 6.1%. MS (70 eV, 110°C): *m/z* 509 (M^+), 428, 427 (M^+-C_6H_{10}), 326, 311, 182, 117. Magn. moment: μ_{eff} 2.2 BM.

[Cp(η^2,η^2-1,5-*hexadiene*)CrPPh$_2$Me]$_2$ (**17**)

Cp(η^3-C_3H_5)$_2$Cr (**1**) (1.50 g, 7.5 mmol) and PPh_2Me (1.60 g, 8 mmol) were dissolved in diethylether (80 cm^3) at −30°C and the mixture warmed to 0°C and stirred overnight. The resulting yellow solution was evaporated, the residue extracted with pentane and the extract cooled to −78°C to give the compound as lemon-yellow crystals which decompose at 80°C. Yield 2.41 g (80% theory). Found: C, 72.1; H, 7.0; Cr, 13.0; P, 7.9. Calc. for $C_{48}H_{56}Cr_2P_2$: C, 72.2; H, 7.1; Cr, 13.0; P, 7.8%. Mol. wt (cryoscopic, C_6H_6): 782 (calc. 799). MS (70 eV, 90°C): *m/z* 317 ([CpCrPPh$_2$Me]$^+$). Magn. moment: μ_{eff} 2.7/2.6 BM. IR (KBr, room temperature): ν 3080, 3000, 2920, 2820, 1540, 1480, 1435, 1270, 815.

Cp(η^2-1,5-*hexadiene*)Cr($Me_2PC_2H_4PMe_2$) (**18**)

Cp(η^3-C_3H_5)$_2$Cr (**1**) (1.50 g, 7.5 mmol) and 1,2-bis(dimethylphosphino)ethane (1.20 g, 8 mmol) were dissolved in diethylether (100 cm^3) at −30°C and the solution allowed to reach 0°C over 16 h. The reaction mixture was evaporated to dryness and the residue extracted with pentane. Filtration and cooling to −78°C gave the compound as a brown, crystalline solid which decomposed at 80°C. Yield 2.36 g (90% theory). Found: C, 58.6; H, 8.6; Cr, 14.7; P, 17.9. Calc. for $C_{17}H_{31}CrP_2$: C, 58.4, H, 8.9; Cr, 14.9; P, 17.7%. MS: *m/z* 349 (M^+), 267 (M^+-C_6H_{10}). Magn. moment: μ_{eff} 1.8 BM. IR (KBr, room temperature): ν 3100, 3060, 2960, 2840, 1635, 1535, 1005, 990, 905.

(η^5-*Indenyl*)(η^2,η^2-1,5-*hexadiene*)CrP(OMe)$_3$ (**19**)

Trimethylphosphite (0.57 g, 4.6 mmol) was added to an ethereal solution of (η^5-indenyl)(η^3-C_3H_5)$_2$Cr (**6**) at −30°C and the solution stirred at −10°C for 12 h. The solution was evaporated to dryness at room temperature in a high vacuum and the residue dissolved in hexane, filtered and the solution cooled to −78°C to give the compound as red, needle-shaped crystals which were dried under high vacuum and which decompose above 70°. Yield 1.16 g (80% theory). Found: C, 57.9; H, 7.0; Cr, 13.9; P, 8.3. Calc. for $C_{18}H_{26}CrO_3P$: C, 58.2; H, 6.9; Cr, 14.2; P, 8.3%. IR (KBr, room temperature): ν 3080, 2940, 2820, 1600, 1480, 1460, 1040. MS: *m/z* 373 (M^+), 291 (M^+-C_6H_{10}), 249 [M^+-P(OMe)$_3$]. Crystal structure: see Fig. 1.

(η^5-*Indenyl*)(η^2,η^2-1,5-*hexadiene*)$CrPMe_3$ (**20**)

Prepared as above by reacting trimethylphosphine with (η^5-indenyl)(η^3-C_3H_5)$_2$Cr (**6**) in diethylether at -10°C. The compound decomposes above 70°C. Yield 80%. Found: C, 66.5; H, 8.1; Cr, 16.0; P, 9.5. Calc. for $C_{18}H_{26}CrP$: C, 66.3; H, 7.9; Cr, 16.2; P, 9.3%. IR (KBr, room temperature): ν 3070, 3030, 2950, 2800, 1600, 1470, 1420, 1340, 1270, 940. MS. m/z 325 (M^+), 249 (M^+-PMe_3), 243 (M^+-C_6H_{10}).

Cp(η^4-1,3-C_4H_6)$CrPMe_3$ (**21**)

Cp(η^2,η^2-1,5-hexadiene)$CrPMe_3$ (**14**) (1.79 g, 6.5 mmol) was dissolved in diethylether (100 cm^3) and treated with a 10-fold excess of 1,3-butadiene at 0°C and stirred for 48 h. The colour of the reaction mixture changed from dark green to orange–red. The solvent was removed under high vacuum and the residue extracted with pentane. The extract was cooled to -78°C to give the compound as ruby red needles which melt at 94°C and decompose above 130°C. Yield 1.45 g (90% theory). The compound can also be prepared in a manner analogous to that described below (yield 61% theory) by reacting [CpCrCl$_2$]$_2$ consecutively with PMe_3 and magnesium-butadiene in THF. Found: C, 57.9; H, 8.0; Cr, 21.2; P, 12.4. Calc. for $C_{12}H_{20}CrP$: C, 58.3; H, 8.2; Cr, 21.0; P, 12.5%. MS: m/z 247 (M^+), 193, 171, 117, 76, 52. IR (KBr): ν 3110, 3040, 2960, 2910, 1445, 1420, 1280, 1210, 1105, 1000, 950, 800. Crystal structure: see Fig. 1.

Cp(η^4-1,3-C_4H_6)$CrP(OMe)_3$ (**22**)

[CpCrCl]$_2$ (1.88 g, 5 mmol) was suspended in THF (300 cm^3) and $P(OMe)_3$ (1.36 g, 11 mmol) was added. The resulting deep blue solution was cooled to -78°C and $C_4H_6Mg(THF)_2$ (2.33 g, 10.5 mmol) was added. The reaction mixture was stirred and allowed to warm to room temperature over 16 h during which time it became red. Solvent was removed under high vacuum and the residue extracted with pentane (3 × 100 cm^3) at room temperature. The resulting red extract was concentrated and cooled to -78°C to give the compound as orange red crystals (m.p. 120°C) which were recrystallized from hexane. Yield 1.77 g (60% theory). The compound can also be prepared as described above (yield 90% theory) by reacting Cp(η^2,η^2-1,5-hexadiene)$CrP(OMe)_3$ (**15**) with excess butadiene in ether. Found: C, 48.7; H, 7.0; Cr, 17.9; P, 10.3. Calc. for $C_{12}H_{20}CrO_3P$: C, 48.8; H, 6.8; Cr, 17.6; P, 10.5%. MS: m/z 295 (M^+), 241, 171, 117, 52. IR (KBr): ν 3105, 3040, 2940, 2830, 1455, 1430, 1110, 1020, 805, 770, 725.

(η^5-*Indenyl*)(η^4-1,3-C_4H_6)$CrPMe_3$ (**23**)

Prepared as described for **21** by reacting (η^5-indenyl)(η^2,η^2-1,5-hexadiene)$CrPMe_3$ with excess butadiene at 0°C. The compound was isolated as dark green needles (m.p. 50°C dec.) in 79% yield. Found: C, 64.7; H, 7.4; Cr, 17.6; P, 10.2. Calc. for $C_{16}H_{22}CrP$: C, 64.6; H, 7.5; Cr, 17.5; P, 10.4%. MS: m/z 243 (M^+-C_4H_6), 221, 167. IR (KBr): ν 3080, 3030, 2960, 2910, 1605, 1470, 1420, 1330, 945.

(η^5-Me_5C_5)(η^4-1,3-C_4H_6)$CrPMe_3$ (**24**)

Cp*Cr(THF)Cl$_2$ (100 cm^3 of a 0.081 molar solution, 8.1 mmol) was treated with PMe_3 (1 cm^3, 9.6 mmol) in THF at room temperature. The solution was cooled to -78°C and a suspension of (C_4H_6)Mg(THF)$_2$ (2 g, 9 mmol) in THF (100 cm^3) was added. The reaction mixture was stirred at -20°C for 7 h, evaporated to dryness and the residue extracted with pentane (210 cm^3) at -10°C. The extract was filtered, concentrated and cooled to -78°C to give the compound as dark red platelets. Yield: 1.85 g (72% theory). Found: C, 63.9; H, 10.2; Cr, 16.2; P, 9.7. Calc. for $C_{17}H_{30}CrP$: C, 64.3; H; 9.5; Cr, 16.4; P, 9.8%. MS (70 eV): m/z 241 (M^+-PMe_3, 60%), 187 (M^+-PMe_3/C_4H_6, 100%). IR (KBr): ν(Cp*) 1460m, 1370s, 1070m, 1020s; (C_4H_6) 1490m, 1230m, 880m, 830m; (PMe_3) 1300m, 1280s, 950s, 720m.

(η^5-Me_5C_5)(η^4-1,3-C_4H_6)$CrP(OMe)_3$ (**25**)

Prepared as above in the presence of $P(OMe)_3$ as a red crystalline compound in 75% yield. Found: C, 55.8; H, 8.7; Cr, 14.2; P, 8.4. Calc. for $C_{17}H_{30}CrO_3P$: C, 55.9; H, 8.3; Cr, 14.2; P, 8.5%. MS (70 eV): m/z 365 (M^+, 10%), 334 (3%), 311 (M^+-C_4H_6, 8%), 241 (M^+-$P(OMe)_3$, 89%), 218 (64%), 187 (M^+-C_4H_6/$P(OMe)_3$, 100%). IR (KBr): ν(Cp*) 1440m, 1370m, 1080m; (C_4H_6) 1490msh, 1230m, 880m; (PR_3) 1470m, 1180m, 1020s, 760m, 720s, 545m.

(η^5-Me_5C_5)(η^4-1,3-C_4H_6)CrCO (**26**)

(η^5-Me_5C_5)(η^4-1,3-C_4H_6)$CrPMe_3$ (**24**) (0.5 g, 1.58 mmol) was dissolved in pentane (50 cm^3), cooled to -70°C and the apparatus connected to a gas-burette filled with CO. The reaction mixture was stirred and allowed to warm to room temperature. The resulting green solution was cooled to -78°C to give the compound as red crystals.

Table 3. Crystal structure data for **19**, **21**, **26** and **27**[a]

	19	**21**	**26**	**27**
Formula	$C_{18}H_{26}CrO_3P$	$C_{12}H_{20}CrP$	$C_{15}H_{21}CrO$	$C_{14}H_{22}CrO_3P$
Molecular weight	373.4	247.3	269.3	321.3
Crystal size [mm]	0.07 × 0.40 × 0.40	0.32 × 0.50 × 0.43	0.25 × 0.47 × 0.40	0.40 × 0.43 × 0.54
Crystal system	orthorhombic	monoclinic	monoclinic	monoclinic
Space group [No.]	*Pbca* [61]	$P2_1/n$ [14]	$P2_1/m$ [11]	$P2_1/a$ [14]
a [Å]	8.657(1)	7.602(1)	7.097(1)	14.474(2)
b [Å]	16.887(2)	15.024(2)	11.664(1)	7.629(1)
c [Å]	24.642(4)	11.724(1)	8.567(1)	14.838(2)
β [°]	—	107.19(1)	96.69(1)	114.48(1)
V [Å^3]	3602(1)	1279(1)	704(1)	1491(1)
Z	8	4	2	4
Calculated density [g cm^{-3}]	1.38	1.28	1.27	1.43
μ [cm^{-1}]	7.17	9.60	7.75	8.54
Mo-K_α radiation [Å]	0.71069	0.71069	0.71069	0.71069
$F(000)$ [e]	1576	524	286	676
Temperature [K]	293	293	293	113
Diffractometer	Enraf–Nonius CAD4	Enraf–Nonius CAD4	Enraf–Nonius CAD4	Enraf–Nonius CAD4
Scan mode	ω–2θ	ω–2θ	ω–2θ	ω–2θ
$[\sin\theta/\lambda]_{max}$ [Å^{-1}]	0.65	0.70	0.70	0.74
Total number of reflections	6053 $(+h, +k, +l)$	3991 $(\pm h, +k, +l)$	2266 $(\pm h, +k, +l)$	10,907 $(\pm h, \pm k, +l)$
Independent reflections	4051	3695	2134	5129
Observed reflections [$I > 2\sigma(I)$]	2250	2820	1858	4505
Refined parameters	208	207	85	260
R, R_w [$w = 1/\sigma^2(F_o)$]	0.055, 0.047	0.030, 0.036	0.045, 0.058	0.025, 0.036
Error of fit	1.8	1.9	2.7	1.9
Residual electron density [e Å^{-3}]	0.39	0.28	0.51	0.38
Method of structure solution (SHELX86)	heavy atom	heavy atom	heavy atom	heavy atom

[a] Further details of the crystal structure investigations and lists of final atomic coordinates, thermal parameters, distances, angles, and structure factors may be obtained from the Cambridge Crystallographic Data Centre (CCDC).

Yield 0.35 g (81% theory). Found: C, 66.7; H, 8.0; Cr, 19.2. Calc. for $C_{15}H_{21}CrO$: C, 66.9; H, 7.8; Cr, 19.3%. MS: m/z 269 (M^+), 241, 187, 52. IR (KBr): ν 3060, 3040, 2980–2920, 2880, 1900 (CrCO), 1480, 1380, 1220, 1180, 880, 860. Crystal structure: see Fig. 1.

Cp(η^4-1,3-*cyclohexadiene*)CrP(OMe)$_3$ (**27**)

Cp(η^2,η^2-1,5-hexadiene)CrP(OMe)$_3$ (**15**) (1.62 g, 5 mmol) in diethylether was treated with a 10-fold excess of 1,3-cyclohexadiene and stirred at room temperature for 4 days. The resulting orange–brown solution was evaporated to dryness and the residue extracted with pentane. Diethylether was added to the extract (ether: pentane 1 : 5) and the compound isolated by fractional crystallization. Yellow crystals of Cp(η^6-C_6H_6)Cr (**28**) (0.25 g, 28% yield[5]) were deposited initially followed by **27** as dark red crystals which decomposed in solution above 25°C. Yield 0.92 g (57% theory). Found: C, 52.4; H, 7.0; Cr, 16.3; P, 9.5. Calc. for $C_{14}H_{22}CrO_3P$: C, 52.3; H, 6.9; Cr, 16.2; P, 9.6%. MS: m/z 321 (M^+), 197, 195, 124, 117, 52. IR (KBr): ν 3080, 2940, 2820, 1460, 1430, 1110, 1020, 800, 755, 710. Crystal structure: see Fig. 1.

Crystal structure determination

Crystal data for **19**, **21**, **26**, and **27** are summarized in Table 3 and those for **11** and **12** in Table 4.

Table 4. Crystal structure data for **11** and **12**[a]

	11	**12**
Formula	$C_{16}H_{20}Cr_2$	$C_{24}H_{24}Cr_2$
Molecular weight	316.3	416.5
Crystal size [mm]	$0.21 \times 0.49 \times 0.39$	$0.18 \times 0.29 \times 0.32$
Crystal system	orthorhombic	monoclinic
Space group [No.]	$Pna2_1$ [33]	$P2_1/a$ [14]
a [Å]	21.618(1)	21.140(5)
b [Å]	8.674(1)	6.972(1)
c [Å]	7.502(1)	27.856(7)
β [°]	—	110.46(2)
V [Å^3]	1407(1)	3847(1)
Z	4	8
Calculated density [g cm^{-3}]	1.49	1.44
μ [cm^{-1}]	14.88	11.07
Mo-K_α radiation [Å]	0.71069	0.71069
$F(000)$ [e]	656	1728
Temperature [K]	293	293
Diffractometer	Enraf–Nonius CAD4	Enraf–Nonius CAD4
Scan mode	ω–2θ	ω–2θ
$[\sin\theta/\lambda]_{max}$ [Å^{-1}]	0.77	0.65
Total number of reflections	5715 ($\pm h$, $\pm k$, $+l$) transformed	9370 ($\pm h$, $+k$, $+l$)
Independent reflections	3976	8652
Observed reflections [$I > 2\sigma(I)$]	3529	5060
Refined parameters	231	466
R, R_w [$w = 1/\sigma^2(F_o)$]	0.033, 0.037	0.051,0.051
Error of fit	1.5	2.3
Residual electron density [e Å^{-3}]	0.71	0.61
Method of structure solution (SHELX86)	heavy atom abs. conf. determined	heavy atom disordered π-allyl-groups

[a] Further details of the crystal structure investigations and lists of final atomic coordinates, thermal parameters, distances, angles, and structure factors may be obtained from the Cambridge Crystallographic Data Centre (CCDC).

REFERENCES

1. P. W. Jolly and U. Zakrzewski, *Polyhedron* 1991, **10**, 1427.
2. K. Angermund, A. Döhring, P. W. Jolly, C. Krüger and C. C. Romão, *Organometallics* 1986, **5**, 1268.
3. M. P. Castellani, S. J. Geib, A. L. Rheingold and W. C. Trogler, *Organometallics* 1987, **6**, 1703.
4. J. Nieman, J. W. Pattiasina and J. H. Teuben, *J. Organomet. Chem.* 1984, **262**, 157.
5. K. Angermund, P. Betz, A. Döhring, P. W. Jolly, C. Krüger and K. U. Schönfelder, *Polyhedron* 1993, **12**, 2663.
6. J. S. Merola, R. T. Kacmarcik and D. V. Engen, *J. Am. Chem. Soc.* 1986, **108**, 329.
7. T. Aoki, A. Furusaki, Y. Tomiie, K. Ono and F. Tanaka, *Bull. Chem. Soc. Jpn* 1969, **42**, 545.
8. F. A. Cotton and R. A. Walton, in *Multiple bonds between metal atoms*, Wiley-Interscience, New York (1982).
9. F. A. Cotton and G. Wilkinson, *Z. Naturforsch.* 1954, **9B**, 417.
10. W. Oberkirch, Dissertation, Techn. Hochschule Aachen, 1963.
11. H. J. Klocke, Dissertation, Ruhr-Universität, Bochum, 1984.
12. R. Emrich, Dissertation Ruhr-Universität, Bochum 1991.
13. H. Yasuda, K. Tatsumi, T. Okamoto, K. Mashima, K. Lee, A. Nakamura, Y. Kai, N. Kanehisa and N. Kasai, *J. Am. Chem. Soc.* 1985, **107**, 2410.
14. H. Oberhammer and S. H. Bauer, *J. Am. Chem. Soc.* 1969, **91**, 10.

Polyhedron Vol. 12, No. 22, pp. 2663–2669, 1993
Printed in Great Britain

0277–5387/93 $6.00+.00
© 1993 Pergamon Press Ltd

ORGANOCHROMIUM π-COMPLEXES—VII.* THE REACTIONS OF Cp(η^3-ALLYL)$_2$Cr COMPOUNDS WITH ALKYNES AND ALKENES

K. ANGERMUND, P. BETZ, A. DÖHRING, P. W. JOLLY,† C. KRÜGER and K. U. SCHÖNFELDER

Max-Planck-Institut für Kohlenforschung, D-45466 Mülheim an der Ruhr, Germany

(*Received* 3 *June* 1993; *accepted* 15 *July* 1993)

Abstract—The compounds (η^5-RC_5H_4)(η^3-C_3H_5)$_2$Cr (R = H, Me, t-C_4H_9) and (η^5-indenyl)(η^3-C_3H_5)$_2$Cr react with alkynes (RC_2R) with displacement of 1,5-hexadiene to give Cp′(η^6-R_6C_6)Cr species. Treatment with cyclooctatetraene gives compounds containing an η^6-C_8H_8 group while the final product of the reaction with cycloheptatriene contains an η^7-cycloheptatrienyl fragment. 1,3-Butadiene reacts with dimerization to give the diamagnetic, dinuclear species (Cp′Cr)$_2$(μ-η^3,η^3-C_8H_{12}). The molecular structures of Cp(η^6-Me_6C_6)Cr, (η^5-indenyl)(η^6-Me_6C_6)Cr and Cp(η^6-C_8H_8)Cr have been confirmed by X-ray diffraction.

In the preceding publication we reported the synthesis of a series of Cp′(η^3-allyl)$_2$Cr compounds by reacting [CpCrCl$_2$]$_2$ or [(η^3-allyl)$_2$CrCl]$_2$ with allylmagnesium chloride or a substituted cyclopentadienyllithium derivative.[1] These compounds react with nucleophiles with reductive coupling of the two allyl groups to give a 1,5-diene which can in turn be readily displaced from the metal atom and they can hence be regarded as a ready source of the [Cp′Cr]-fragment for synthetic purposes. Here we discuss the reaction with alkynes and polyenes.

RESULTS AND DISCUSSION

Perhaps the most interesting reaction reported here is that with alkynes: cyclotrimerization occurs at the metal centre with displacement of 1,5-hexadiene to give species containing an η^6-arene molecule as paramagnetic, orange to red, sublimable solids in 80–90% yield (eq. 1).

$$Cp'(\eta^3\text{-}C_3H_5)_2Cr + 3RC{\equiv}CR \longrightarrow Cp'(\eta^6\text{-}R_6C_6)Cr + C_6H_{10} \quad (1)$$

The reaction appears to be general and provides a convenient access to these systems. Most attention has been given to the reaction involving Cp(η^3-C_3H_5)$_2$Cr but individual compounds have been prepared from systems containing η^5-MeC_5H_4, η^5-t-$C_4H_9C_5H_4$ and η^5-indenyl. Reactions with acetylene, 2-butyne, 3-hexyne and diphenylacetylene are described in the experimental section and in addition the mass spectroscopic data indicate that (η^6-arene)Cr-species are also formed in the reaction between Cp(η^3-C_3H_5)$_2$Cr and 2-pentyne or 1-butyne.

Cp(η^6-C_6H_6)Cr was first isolated over 30 years ago and has been prepared in low yield by reacting $CrCl_3$ with the cyclopentadienyl anion and phenylmagnesium bromide,[2,3] and sporadic attention has been given to its spectroscopic properties and to a description of the bonding.[4–7] In addition it has been reported that (η^5-Me_5C_5)(η^6-Me_6C_6)Cr is the product of a curious reaction involving the reduction of the product of the treatment of $CrCl_3$ with an aluminium alkyl and 2-butyne.[8,9]

Repeated attempts in this institute over the last two decades to confirm the molecular structure of a member of this class of compound by X-ray diffraction have been thwarted by disorder in both rings and although in the case of Cp(η^6-Me_6C_6)Cr disorder in the six-membered ring prevented us from refining the diffraction data (see experimental section), the sandwich structure could be confirmed. Fortunately, (η^5-indenyl)(η^6-Me_6C_6)Cr does not exhibit disorder and the molecular structure and

* For part VI, see ref. 1.

† Author to whom correspondence should be addressed.

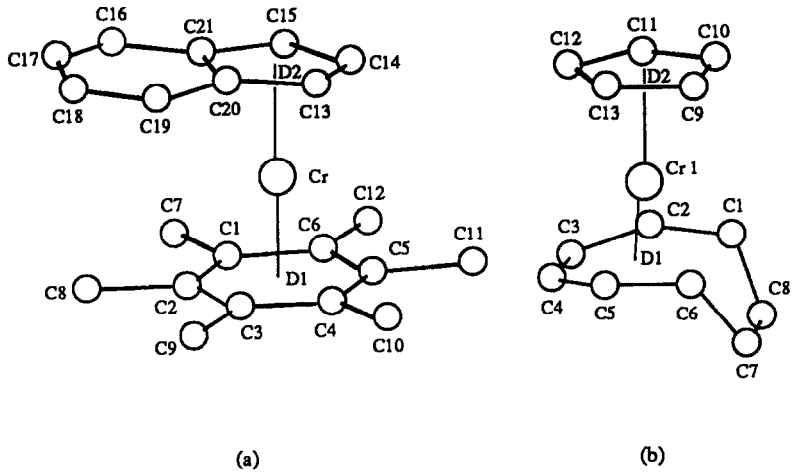

Fig. 1. The molecular structure of (a) (η^5-indenyl)(η^6-Me_6C_6)Cr and (b) Cp(η^6-C_8H_8)Cr.

selected structural parameters are shown in Fig. 1 and Table 1, respectively. There is no evidence for alternation of the bonds within the six-membered ring and both C—C and Cr—C bond distances are similar to those observed for (η^6-C_6H_6)$_2$Cr (1.41 and 2.13 Å, respectively[10]). The six-membered ring is planar (maximum deviation $\pm$0.01 Å). The methyl groups at C7/C8/C11/C12 lie in the ring plane while those at C9 and C10 are bent by 3.4° and 4.8°, respectively towards the Cr-atom. The indenyl group is also planar (maximum deviation $\pm$0.002 Å) supporting its formulation as an η^5-ligand. Although the two chromium-bonded rings are almost parallel to each other, an interplanar angle of 6.3° indicates some steric interference between the methyl groups (C7/C8/C9) and the six-membered ring of the indenyl group.

We have also investigated the reaction of the

Table 1. Structural parameters for (η^5-indenyl)(η^6-Me_6C_6)Cr

Distance (Å) (ESD)			
Cr—D1 (Me_6C_6)	1.573(7)	C4—C5	1.399(9)
Cr—D2 (indenyl)	1.800(9)	C5—C6	1.401(9)
Cr—C1	2.095(6)	C6—C1	1.437(9)
Cr—C2	2.131(6)	C—Me	1.52–1.54(1)
Cr—C3	2.124(7)	C13—C14	1.40(2)
Cr—C4	2.129(7)	C14—C15	1.38(2)
Cr—C5	2.109(6)	C15—C21	1.47(1)
Cr—C6	2.095(7)	C21—C20	1.45(1)
Cr—C13	2.183(8)	C13—C20	1.41(1)
Cr—C14	2.08(1)	C16—C21	1.43(1)
Cr—C15	2.14(1)	C16—C17	1.33(1)
Cr—C20	2.226(6)	C17—C18	1.36(2)
Cr—C21	2.208(7)	C18—C19	1.33(1)
C1—C2	1.387(9)	C19—C20	1.41(1)
C2—C3	1.417(9)		
Angle (°) (ESD)			
D1—Cr—D2	177.9(1)	C17—C18—C19	121.5(9)
C1—C2—C3	120.4(5)	C18—C19—C20	120.3(8)
C3—C4—C5	120.5(6)	C19—C20—C21	117.9(6)
C20—C13—C14	107.0(8)	C21—C20—C13	108.8(6)
C13—C14—C15	111.8(9)	C19—C20—C13	133.2(7)
C14—C15—C21	106.5(8)	C20—C21—C15	105.8(7)
C17—C16—C21	118.8(8)	C16—C21—C15	136.0(7)
C16—C17—C18	122.9(9)	C20—C21—C16	118.1(7)

$Cp'(\eta^3\text{-}C_3H_5)_2Cr$ species with selected polyenes, and in all cases reductive coupling of the two allyl groups and displacement of 1,5-hexadiene is observed. The product of the reaction of the cyclopentadienyl- and indenyl-stabilized species with cyclooctatetraene is $Cp(\eta^6\text{-}C_8H_8)Cr$ and $(\eta^5\text{-indenyl})(\eta^6\text{-}C_8H_8)Cr$, respectively. The first of these is a known compound having been prepared by reacting $[CpCrCl_2]_2$ with isopropylmagnesium and cyclooctatetraene.[11-13] The presence of an absorption at *ca* 1650 cm^{-1} in both compounds supports the suggestion that one double bond of the tetraene is not complexed to the metal atom and this has been confirmed by a crystal structure determination for $Cp(\eta^6\text{-}C_8H_8)Cr$. The molecular structure is shown in Fig. 1(b). There are two independent molecules in the unit cell which have very similar structural parameters and averaged values are listed in Table 2. The planes formed by the Cp-ring and Cl—C6 of the cyclooctatetraene molecule are almost parallel forming an angle of only 4.4° to each other. The planes C1—C6 and C1/C8/C7/C6 lie at 63.7° to each other.

Related reactions have been observed with cyclopentadiene, 1,3-cyclohexadiene and 1,3,5-cycloheptatriene but in these cases the reaction is accompanied by deprotonation of the polyene. The product of the reaction between $Cp(\eta^3\text{-}C_3H_5)_2Cr$ and cyclopentadiene is chromocene (90% yield) while both $Cp(\eta^3\text{-}C_3H_5)_2Cr$ and $(\eta^5\text{-indenyl})(\eta^3\text{-}C_3H_5)_2Cr$ react with 1,3-cyclohexadiene to give $Cp(\eta^6\text{-}C_6H_6)Cr$ and $(\eta^5\text{-indenyl})(\eta^6\text{-}C_6H_6)Cr$, respectively. The initial product of the reaction between $Cp(\eta^3\text{-}C_3H_5)_2Cr$ and cycloheptatriene is the paramagnetic compound $Cp(\eta^6\text{-}C_7H_8)Cr$[14] which reacts further upon heating in solution to the diamagnetic, cycloheptatrienyl-chromium species $Cp(\eta^7\text{-}C_7H_7)Cr$.[14-20] Related species have been isolated from the reaction between cycloheptatriene and $(\eta^5\text{-indenyl})(\eta^3\text{-}C_3H_5)_2Cr$ or $(\eta^5\text{-}Me_5C_5)(\eta^3\text{-}C_3H_5)_2Cr$. In all of these cases, we have confirmed the displacement of the two allyl groups in the starting material as 1,5-hexadiene but in none of them were we able to determine the fate of the H-atoms abstracted from the polyene: since neither propene, hydrogen nor the products of disproportionation of the polyene (e.g. cyclohexene and benzene from 1,3-cyclohexadiene) could be detected, we assume that the reaction proceeds by complexation of the polyene to the Cp'Cr-fragment, followed by H-transfer to the metal, homolytic cleavage of the resulting Cr—H bond and indiscriminant reaction of the H-radical with the reaction media.

1,5-Hexadiene is also eliminated upon reacting

Table 2. Selected structural parameters for $Cp(\eta^6\text{-}C_8H_8)Cr$ (average values)

	Distance (Å) (ESD)		
Cr—D1[a]	1.346(6)	C1—C2	1.44(1)
Cr—D2(Cp)[b]	1.832(5)	C2—C3	1.41(1)
Cr—C1	2.16(1)	C3—C4	1.40(2)
Cr—C2	2.074(7)	C4—C5	1.40(2)
Cr—C3	2.11(1)	C5—C6	1.42(2)
Cr—C4	2.11(2)	C6—C7	1.49(1)
Cr—C5	2.073(3)	C7—C8	1.29(2)
Cr—C6	2.168(6)	C8—C1	1.46(3)
Cr—C9	2.194(5)	C9—C10	1.37(3)
Cr—C10	2.189(5)	C10—C11	1.40(2)
Cr—C11	2.18(2)	C11—C12	1.38(2)
Cr—C12	2.18(1)	C12—C13	1.42(1)
Cr—C13	2.181(6)	C13—C9	1.415(9)
	Angle (°) (ESD)		
D1—Cr—D2	173(1)	C7—C8—C1	119.6(7)
C1—C2—C3	127.0(5)	C8—C1—C2	122.2(5)
C2—C3—C4	131.2(6)	C6—Cr—C5	39.0(6)
C3—C4—C5	130.8(5)	C1—Cr—C2	39.6(4)
C4—C5—C6	127.7(7)	C3—Cr—C4	38.8(3)
C5—C6—C7	122.4(6)	C6—Cr—C1	78.0(2)
C6—C7—C8	118.7(7)		

[a] D1 is the mid-point of the plane defined by C1—C6.
[b] D2 is the mid-point of the plane defined by C9—C13.

$Cp'(\eta^3\text{-}C_3H_5)_2Cr$ (Cp' = Cp, MeC_5H_4, indenyl) with 1,3-butadiene.[21] The product is not, however, the expected $Cp'(\eta^4\text{-}1,3\text{-}C_4H_6)Cr$ species, instead diamagnetic, dinuclear complexes are formed whose NMR spectroscopic data indicate that two diene molecules have coupled to form an η^3,η^3-octadienediyl fragment which bridges both metal atoms (eq. 2).

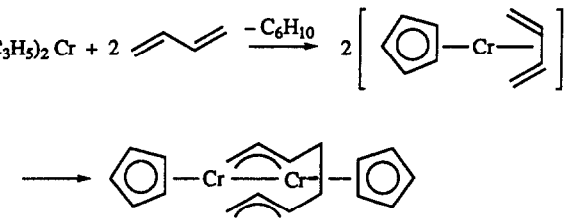

(2)

The intermediate formation of an $(\eta^4\text{-}1,3\text{-}C_4H_6)Cr$-species is suggested by the isolation of $Cp'(\eta^4\text{-}1,3\text{-}C_4H_6)CrPR_3$ complexes when the reaction is carried out in the presence of tertiary phosphines[1] as well as by the formation of $(\eta^5\text{-}Me_5C_5)(\eta^4\text{-}1,4\text{-}Me_2C_4H_4)Cr$ upon reaction of $(\eta^5\text{-}Me_5C_5)(\eta^3\text{-}C_3H_5)_2Cr$ with 2,4-hexadiene.[22] Related dinuclear species containing bridging allyl groups, e.g. $(CpCr)_2(\mu\text{-}C_3H_5)_2$, are the products of the further reaction of the $Cp'(\eta^3\text{-}C_3H_5)_2Cr$ (Cp' = Cp, indenyl) in the absence of nucleophiles and their structures have been confirmed by crystal structure determinations.[1]

EXPERIMENTAL

The preparation of the $Cp'(\eta^3\text{-}C_3H_5)_2Cr$ compounds and the general experimental conditions have been described in ref. 1.

$Cp(\eta^6\text{-}C_6H_6)Cr$[2,3]

$Cp(\eta^3\text{-}C_3H_5)_2Cr$ (0.90 g, 4.52 mmol) was suspended in pentane (70 cm^3) at −78°C and the reaction vessel connected to a gas burette filled with dry acetylene. The reaction mixture was allowed to warm slowly to 0°C and stirred at this temperature for a further 48 h during which time 310.9 cm^3 (13.88 mmol) of acetylene were absorbed. The resulting brown suspension was filtered and the filtrate cooled to −78°C to give the product as an orange–red crystalline solid. Yield: 0.76 g (86.2% theory). The presence of 1,5-hexadiene (85% theory) in the solvent was confirmed by GC. Found: C, 67.6; H, 5.2; Cr, 26.8. Calc. for $C_{11}H_{11}Cr$: 67.7; H, 5.2; Cr, 26.6%. MS (70 eV, 30°C): *m/z* 195 (M^+), 117, 52. The compound may also be prepared (yield: 54%) by reacting $Cp(\eta^3\text{-}C_3H_5)_2Cr$ with 1,3-cyclohexadiene in pentane at 0°C.

$Cp(\eta^6\text{-}Me_6C_6)Cr$

$Cp(\eta^3\text{-}C_3H_5)_2Cr$ (0.74 g, 3.71 mmol) was suspended in pentane at −78°C and 2-butyne (0.69 g, 12.80 mmol) was added. The reaction mixture was stirred and allowed to reach 0°C over 7 h (slow warming is necessary to suppress the catalytic formation of hexamethylbenzene) and held at this temperature for a further 48 h. The reaction mixture was filtered and the filtrate cooled to −78°C to give the product as red needles. Yield: 0.98 g (94.6% theory). The presence of 1,5-hexadiene (86% theory) in the solvent was confirmed by GC. Found: C, 73.3; H, 8.2; Cr, 18.5. Calc. for $C_{17}H_{23}Cr$: C, 73.1; H, 8.3; Cr, 18.0%. MS (70 eV, 60°C): *m/z* 279 (M^+), 147, 117, 52. Magn. moment: μ_{eff} 1.72 BM. IR (KBr, −40°C): *v* 1440, 1380, 1096, 992, 770, 456. Crystal structure: rotational disorder in the Me_6C_6 ring prevented refinement of the data below an R-factor of 0.071 (space group $P2_1/n$, $a = 8.368(1)$, $b = 14.744(1)$, $c = 11.835(1)$, $\beta = 94.281$, $Z = 4$).

$Cp(\eta^6\text{-}Et_6C_6)Cr$

Prepared as described above by reacting 3-hexyne. Orange–brown crystals. Yield: 77.9% theory. The presence of 1,5-hexadiene (40% theory) in the solvent was confirmed by GC. Found: C, 75.9; H, 9.8; Cr, 14.2. Calc. for $C_{23}H_{35}Cr$: C, 76.0; H, 9.8; Cr, 14.3%. MS (70 eV, 50°C): *m/z* 363 (M^+), 231, 117, 52. Binuclear species, $(CpCr)_2(Et_6C_6)$, are detected if the MS is measured at higher temperatures. Magn. moment: μ_{eff} 1.73 BM.

$Cp(\eta^6\text{-}Ph_6C_6)Cr$

Prepared as described above by reacting diphenylacetylene. Yellow solid. Yield: 88.3%. The presence of 1,5-hexadiene (65.2% theory) in the solvent was confirmed by GC. Found: C, 79.6; H, 4.7; Cr, 7.4. Calc. for $C_{47}H_{35}Cr$: C, 86.6; H, 5.4; Cr, 8.0%. The unsatisfactory analytical data are presumably a result of the high stability of hexaphenylbenzene.

MS (70 eV, 100°C): *m/z* 651 (M^+), 586, 534 (Ph_6C_6), 117, 52. Magn. moment: μ_{eff} 2.3 BM. IR (KBr): *ν* 1600, 1497, 1440, 780, 732, 695, 572.

$(\eta^5\text{-}MeC_5H_4)(\eta^6\text{-}Me_6C_6)Cr$

Prepared as described above by reacting $(\eta^5\text{-}MeC_5H_4)(\eta^3\text{-}C_3H_5)_2Cr$ with 2-butyne in diethyl ether. Red crystals. Yield: 61%. The presence of 1,5-hexadiene (67% theory) in the solvent was confirmed by GC. Found: C, 73.6; H, 8.5; Cr, 17.7. Calc. for $C_{18}H_{25}Cr$: C, 73.7; H, 8.6; Cr, 17.7%. MS: *m/z* 293 (M^+), 214, 162, 131, 52. IR (KBr): *ν* 3080, 2860, 1380, 1015.

$(\eta^5\text{-}t\text{-}C_4H_9C_5H_4)(\eta^6\text{-}C_6H_6)Cr$

Prepared as described above by reacting $(\eta^5\text{-}t\text{-}C_4H_9C_5H_4)(\eta^3\text{-}C_3H_5)_2Cr$ with acetylene-saturated diethyl ether. Yellow crystals. Yield: 60% theory. The presence of 1,5-hexadiene (75% theory) in the solvent was confirmed by GC. Found: C 71.5; H, 7.7; Cr, 20.8. Calc. for $C_{15}H_{19}Cr$: C, 71.7; H, 7.6; Cr, 20.7%.

MS: *m/z* 251 (M^+), 173, 157, 78, 52. IR (KBr): *ν* 3100, 3070, 2960, 1390, 1360, 980, 955, 790.

$(\eta^5\text{-Indenyl})(\eta^6\text{-}C_6H_6)Cr$

Prepared as described above by reacting $(\eta^5\text{-indenyl})(\eta^3\text{-}C_3H_5)_2Cr$ with acetylene-saturated diethyl ether. The compound was isolated as a red–brown solid by high-vacuum sublimation at 90°C. Yield: 56% theory. Found: C, 73.3; H, 5.6; Cr, 21.2. Calc. for $C_{15}H_{13}Cr$: C, 73.5; H, 5.3; Cr, 21.2%. MS: *m/z* 245 (M^+), 167. IR (KBr): *ν* 3080, 3050, 1600, 1450, 1330, 1030, 980, 955, 770, 740.

The compounds may also be prepared (yield 51%) by reacting $(\eta^5\text{-indenyl})(\eta^3\text{-}C_3H_5)_2Cr$ with 1,3-cyclohexadiene.

$(\eta^5\text{-Indenyl})(\eta^6\text{-}Me_6C_6)Cr$

Prepared as described above by reacting $(\eta^5\text{-indenyl})(\eta^3\text{-}C_3H_5)_2Cr$ with 2-butyne in diethyl ether. Red needles (dec. > 120°): Yield: 76% theory. Found: C, 76.8; H, 7.6; Cr, 15.7. Calc. for $C_{21}H_{25}Cr$: C, 76.6; H, 7.7; Cr, 15.8%. MS: *m/z* 329 (M^+), 214, 167. IR (KBr): *ν* 3040, 2900, 1600, 1445, 1375, 1325, 1015, 735. Crystal structure: see Fig. 1(a) and Table 1.

$Cp(\eta^6\text{-}C_8H_8)Cr$[11–13]

$Cp(\eta^3\text{-}C_3H_5)_2Cr$ (3.24 g, 16.3 mmol) was suspended in pentane at −78°C and cyclooctatetraene (1.84 g, 17.7 mmol) was added. The reaction mixture was stirred for 3 days at −20°C to give a beige suspension which was evaporated to dryness and the residue sublimed at 60°C under high vacuum to give the compound as a beige–yellow solid. Yield: 3.09 g (85.7% theory). The presence of 1,5-hexadiene (94% theory) in the solvent was confirmed by GC. Found: C, 70.7; H, 5.5; Cr, 23.7. Calc. for $C_{13}H_{13}Cr$: C, 70.6; H, 5.9; Cr, 23.5%. MS (70 eV, 50°C): *m/z* 221 (M^+), 195, 117, 52. Magn. moment: μ_{eff} 1.7 BM. IR (KBr): *ν* (C:C) 1647. Crystal structure: see Fig. 1(b) and Table 2.

$(\eta^5\text{-Indenyl})(\eta^6\text{-}C_8H_8)Cr$

Prepared as described above by reacting $(\eta^5\text{-indenyl})(\eta^3\text{-}C_3H_5)_2Cr$ in diethyl ether. The compound was isolated as a dark-red solid by high vacuum sublimation at 110°C. Yield: 60% theory. Found: Cr, 19.3. Calc. for $C_{17}H_{15}Cr$: Cr, 19.2%. MS: *m/z* 271 (M^+), 258, 245, 167, 115. IR (KBr): *ν* (C:C) 1645; 1515, 1335, 1015, 845, 795, 740.

$Cp(\eta^7\text{-}C_7H_7)Cr$[14–20]

$Cp(\eta^3\text{-}C_3H_5)_2Cr$ (2.96 g, 14.86 mmol) was suspended in pentane (150 cm^3) and treated with cycloheptatriene (1.37 g, 1.53 cm^3, 14.86 mmol). The reaction mixture was allowed to warm to +5°C and stirred for 72 h. The solvent was evaporated and the residue sublimed at 60°C under high vacuum to give the compound as a dark-brown (dark-green![16]) solid. Yield: 1.22 g (39.4% theory). Found: C, 68.9; H, 6.3; Cr, 24.7. Calc. for $C_{12}H_{12}Cr$: C, 68.9; H, 6.3; Cr, 24.9%. MS (70 eV, 50°C): *m/z* 208 (M^+), 182, 131, 117, 91, 52. ^1H NMR (D_8-THF): *δ* 5.61 (s, C_7H_7), 3.84 (s, Cp).[19] ^{13}C NMR (D_8-THF): *δ* 87.5 (C_7H_7, *J*(C,H) 163), 75.2 (Cp, *J*(C,H) 172).[19] The compound can also be prepared (yield 31%) by reacting 1,3-cycloheptadiene.

$(\eta^5\text{-}Me_5C_5)(\eta^7\text{-}C_7H_7)Cr$

Prepared as described above by reacting $(\eta^5\text{-}Me_5C_5)(\eta^3\text{-}C_3H_5)_2Cr$ in diethyl ether and isolated as a dark-red solid by sublimation at 90°C in high vacuum. Yield: 60%. Found: C, 73.5; H, 7.9; Cr, 18.8. Calc. for $C_{17}H_{22}Cr$: C, 73.4; H; 8.0; Cr, 18.7%. MS. *m/z* 278 (M^+, 100%), 187, 91, 52. IR (KBr). *ν* 3020, 2960, 2920, 1375, 960, 850, 820.

$(\eta^5\text{-Indenyl})(\eta^7\text{-}C_7H_7)Cr$

Prepared as described above by reacting $(\eta^5\text{-indenyl})(\eta^3\text{-}C_3H_5)_2Cr$ and isolated as a dark-green solid by high vacuum sublimation at 100°C. Yield:

64%. Found: C, 74.3; H, 5.6; Cr, 20.2. Calc. for $C_{16}H_{14}Cr$: C, 74.4; H, 5.5; Cr, 20.1%. MS. *m/z* 258 (M^+), 167, 143. IR (KBr): *v* 3020, 2980, 2920, 1600, 1335, 1240, 1030, 960, 855, 815, 800, 741. ^1H NMR (D_8-THF): δ 7.65 (m, 2H), 6.90 (m, 2H), 5.05 (m, 2H), 3.90 (s, 1H)-indenyl; 5.50 (s, 7H)-C_7H_7.

$[(\eta^5\text{-Indenyl})Cr]_2(\mu\text{-}\eta^3,\eta^3\text{-}C_8H_{12})$

Prepared as described below by reacting $(\eta^5$-indenyl$)(\eta^3\text{-}C_3H_5)_2Cr$. Green–brown solid (dec. > 140°C). Found: C, 70.3; H, 6.2; Cr, 23.4. Calc. for $C_{26}H_{26}Cr_2$: C, 70.6; H, 5.9; Cr, 23.5%. MS: *m/z* 442 (M^+), 388, 334, 282, 167, 115, 52. IR (KBr): *v* 3090, 3050, 2990–2820, 1605, 1470, 1445, 1330, 1005, 810, 780. ^1H NMR (D_8-toluene): 7.50–6.70 (4H), 6.20/6.10/5.45 (3H)-indenyl; *ca* 3.7 (br. 2-H), 3.05 (m, 1-H, anti), 2.40–2.10/1.95–1.50-C_8H_{12}, assignment provisional.

$(CpCr)_2(\mu\text{-}\eta^3,\eta^3\text{-}C_8H_{12})$[21]

$Cp(\eta^3\text{-}C_3H_5)_2Cr$ (1.0 g, 5 mmol) was dissolved in diethyl ether at −30°C, treated with a 10-fold excess of 1,3-butadiene and the reaction mixture warmed to −5°C over 12 h. Solvent was evaporated and the residue extracted with pentane. Cooling the extract to −78°C gave the compound as dark-brown crystals (dec. > 130°). Yield: 0.62 g (72% theory). The presence of 1,5-hexadiene in the solvent (83% theory) was confirmed by GC. Found: C, 62.7; H, 7.0; Cr, 30.2. Calc. for $C_{18}H_{22}Cr_2$: C, 63.2; H, 6.5; Cr, 30.4%.

MS: *m/z* 342 (M^+), 286, 182, 117, 52. IR (KBr): *v* 3090, 3030, 2960–2820, 1440, 1430, 1105, 1000, 810, 785. ^1H NMR (D_8-toluene, −30°C): δ 4.89/4.75 (s, Cp), 3.76 (brs, 2-H), 2.83/2.54 (br, 4-H), 2.71 (d, 1-H, syn), 2.17 (m, 1-H, anti). Numbering scheme shown below, assignment provisional.

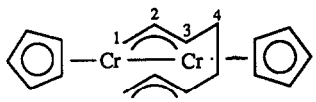

The compound can also be prepared (55% yield) by reacting $(CpCrCl_2)_2$ with (1,3-butadiene)Mg$(THF)_2$ in THF.

$[(\eta^5\text{-}MeC_5H_4)Cr]_2(\mu\text{-}\eta^3,\eta^3\text{-}C_8H_{12})$

Prepared as described above by reacting $(\eta^5$-$MeC_5H_4)(\eta^3\text{-}C_3H_5)_2Cr$. Dark-brown crystals (m.p. 100° dec.). Yield: 60% theory. Found: C, 64.6;

Table 3. Crystal structure determination of $(\eta^5$-indenyl$)(\eta^6\text{-}Me_6C_6)Cr$ and $Cp(\eta^6\text{-}C_8H_8)Cr$

Formula	$C_{21}H_{25}Cr$	$C_{13}H_{13}Cr$
Molecular weight	329.4	221.2
Space group	*Pbca*	$P2_1/n$
a (Å)	25.779(5)	13.749(2)
b (Å)	14.971(2)	11.806(2)
c (Å)	8.945(2)	14.302(1)
α (°)	90	90
β (°)	90	116.44(1)
γ (°)	90	90
V (Å)	3452.1	2078.6
D_{calc} (g cm^{-3})	1.27	1.41
μ (cm^{-1})	6.41	10.28
Z	8	8
λ (Å)	0.71069	0.71069
Measured reflections	5567 ($+h$, $+k$, $+l$)	5107 ($\pm h$, $+k$, $+l$)
$\sin\theta/\lambda_{max}$	0.70	0.65
Independent reflections	4974	4693
Observed reflections	2152	3250
Refined parameters	199	253
R	0.068	0.045
R_w	0.080	0.053
ρ (max), e/Å^3	0.39	0.36

Further details of the crystal structure investigations and lists of final atomic coordinates, thermal parameters, distances, angles and structure factors may be obtained from the Cambridge Crystallographic Data Centre (CCDC).

H, 7.2; Cr, 28.2. Calc. for $C_{10}H_{26}Cr_2$: C, 64.9; H, 7.1; Cr, 28.1%.

MS: *m/z* 370 (M^+), 314, 210, 131, 52. IR (KBr): *ν* 3100, 3030, 2980–2810, 1375, 1105, 810, 790. ^1H NMR (D_8-toluene): *δ* 5.05/4.70 (s, 2H), 4.50 (s, 2H), 1.45 (Me)-MeC_5H_4; 3.65 (br, 2-H), 2.65/2.10 (m, 4-H), 2.45 (br, 1-H, syn.). Numbering scheme shown above.

X-ray diffraction studies

Single crystal structure analyses were carried out using Enraf–Nonius CAD-4 diffractometers. Crystallographic data for (η^5-indenyl)(η^6-Me_6C_6)Cr and Cp(η^6-C_8H_8)Cr and details of the refinement are summarized in Table 3 and in the supplementary material.

REFERENCES

1. P. Betz, A. Döhring, R. Emrich, R. Goddard, P. W. Jolly, C. Krüger, C. C. Romão, K. U. Schönfelder and Y.-H. Tsay, *Polyhedron* 1993, **12**, 2651.
2. E. O. Fischer and H. P. Kögler, *Z. Naturforsch.* 1958, **13b**, 197.
3. E. O. Fischer and S. Breitschaft, *Chem. Ber.* 1966, **99**, 2213.
4. S. Evans, J. C. Green and S. E. Jackson, *J. Chem. Soc. Faraday Trans. II*, 1972, 249.
5. C. Elschenbroich and F. Gerson, *J. Organomet. Chem.* 1973, **49**, 445.
6. D. W. Clack and K. D. Warren, *J. Organomet. Chem.* 1978, **157**, 421.
7. J. Müller, W. Holzinger and W. Kalbfus, *J. Organomet. Chem.* 1975, **97**, 213.
8. H. Benn, G. Wilke and D. Henneberg, *Angew. Chem.* 1973, **85**, 1052.
9. G. Wilke, *Proc. 5th IUPAC Symp. Org. Synth. Freiburg 1984*, 1985, 1.
10. E. Keulen and F. Jellinek, *J. Organomet. Chem.* 1966, **5**, 490.
11. J. Müller and H. Menig, *J. Organomet. Chem.* 1975, **96**, 83.
12. J. Heck and G. Rist, *J. Organomet. Chem.* 1988, **342**, 45.
13. B. Bachmann, F. Hahn, J. Heck and M. Wünsch, *Organometallics* 1989, **8**, 2523.
14. E. O. Fischer and J. Müller, *Z. Naturforsch.* 1963, **18b**, 1137.
15. E. O. Fischer and S. Breitschaft, *Chem. Ber.* 1966, **99**, 2905.
16. R. B. King and M. B. Bisnette, *Tetrahedron Lett.* 1963, 1137.
17. R. B. King and M. B. Bisnette, *Inorg. Chem.* 1964, **3**, 785.
18. E. O. Fischer and S. Breitschaft, *Angew. Chem.* 1963, **75**, 94.
19. C. J. Groenenboom and F. Jellinek, *J. Organomet. Chem.* 1974, **80**, 229; H. O. van Oven, C. J. Groenenboom and H. J. de Liefde Meijer, *J. Organomet. Chem.* 1974, **81**, 379.
20. H. W. Wehner, E. O. Fischer and J. Müller, *Chem. Ber.* 1970, **103**, 2258.
21. K. Angermund, A. Döhring, P. W. Jolly, C. Krüger and C. C. Romão, *Organometallics* 1986, **5**, 1268.
22. A. Döhring, R. Emrich, R. Goddard, P. W. Jolly and C. Krüger, *Polyhedron* 1993, **12**, 2671.

Polyhedron Vol. 12, No. 22, pp. 2671–2680, 1993
Printed in Great Britain

0277–5387/93 $6.00+.00
© 1993 Pergamon Press Ltd

ORGANOCHROMIUM π-COMPLEXES—VIII.† REACTIONS OF THE (η^5-Me_5C_5)Cr-SYSTEM WITH 1,3-DIENES AND ALKYNES

A. DÖHRING, R. EMRICH, R. GODDARD, P. W. JOLLY‡ and C. KRÜGER

Max-Planck-Institut für Kohlenforschung, D-45466 Mülheim an der Ruhr, Germany

(*Received* 3 *June* 1993; *accepted* 15 *July* 1993)

Abstract—Cp*(η^4-1,3-diene)Cr compounds have been prepared either by reacting Cp*(η^3-$C_3H_5)_2$Cr with a diene or by reducing Cp*Cr(THF)Cl_2 with activated-Mg in the presence of the diene. These coordinatively and electronically unsaturated species readily form adducts with CO or P-donor ligands. The reaction of Cp*(η^4-1,3-C_4H_6)Cr with further butadiene leads to the formation of Cp*(η^3,η^3-octadienediyl)Cr which in turn reacts with a disubstitued alkyne (RC_2R) with addition to the 2,7-positions of the octadienediyl chain to give Cp*(η^1,η^2,η^1-$R_2C_{10}H_{12}$)Cr species. The crystal structures of representative compounds have been established by X-ray diffraction.

The isolation of Cp(η^3-$C_3H_5)_2$Cr in 1986 opened a new entry into the chemistry of the CpCr-system and a few typical reactions are shown in the scheme below.[1–3] As part of our attempts to prepare model compounds relevant to the chromium-catalysed oligomerization of alkenes, we have turned our attention to the chemistry of the Cp*-stabilized analogue (Cp* = η^5-Me_5C_5) since it has been well established[4–9] that the introduction of five methyl groups into the five-membered ring has a considerable effect upon the reactivity of the cyclopentadienyl-stabilized species, the increase in the electronic density at the metal centre decreasing the reactivity towards nucleophiles.

Here, we describe the preparation and reaction of Cp*Cr-stabilized 1,3-diene compounds.

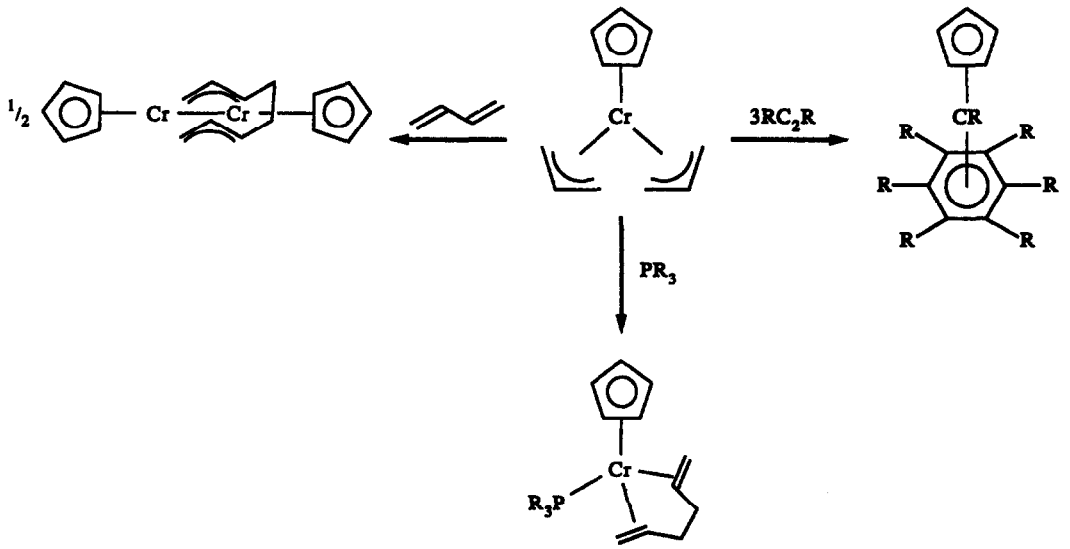

Scheme 1.

† For parts VI and VII see refs. 1 and 2.
‡ Author to whom correspondence should be addressed.

RESULTS AND DISCUSSION

The Cp*(η^4-1,3-diene)Cr complexes **1** and **2** containing butadiene or 1,2,3,4-tetraphenylbutadiene have been prepared by reacting Cp*Cr(THF)Cl_2 with the metallated dienes $(C_4H_6)Mg(THF)_2$ or $Ph_4C_4H_2Li_2$ while the 2,3-dimethylbutadiene analogue **3** is the product of the reaction with active-Mg[10] in the presence of the diene (eq. 1).

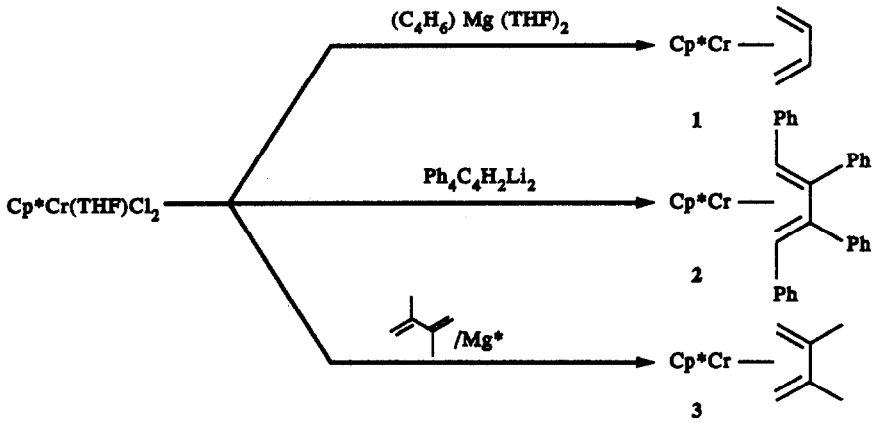

(1)

Compounds of this type, e.g. Cp*(η^4-1,3-C_4H_6)$CrPR_3$ (**8**, R = Me; **9**, R = OMe), can also be prepared by reacting Cp*Cr(THF)Cl_2 with $(C_4H_6)Mg(THF)_2$ in the presence of the donor ligand while **5** is also the product of a ligand exchange reaction between **8** or **9** and CO[1]. The structure of Cp*(η^4-1,3-C_4H_6)CrCO (**5**) has been confirmed by X-ray diffraction and has been discussed with those of related compounds in an earlier publication.[1] The adducts are stable at room temperature.

The 2,4-hexadiene-containing compound **4** (but not the butadiene compound **1**; see Scheme 2 below) is the product of the reaction between the diene and Cp*(η^3-C_3H_5)$_2$Cr (eq. 2).

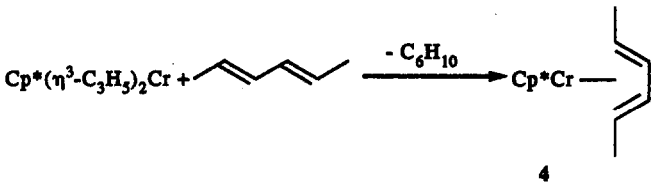

(2)

Compounds **1–4** are isolated as dark red–brown crystals which are stable below −20°C.

The 1,3-diene compounds **1–4** are electronically and coordinatively unsaturated and react readily with CO or P-donor ligands and the adducts **5–7** have been isolated (eq. 3).

Cp*(η^4-1,3-C_4H_6)Cr (**1**) reacts readily with further butadiene with oxidative coupling of the two diene molecules to give Cp*(η^3,η^3-octadienediyl)Cr (**10**). The same compound can also be prepared by reducing Cp*Cr(THF)Cl_2 in the presence of

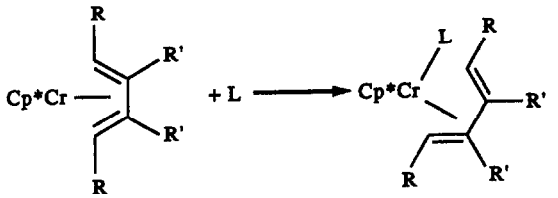

(3)

5 R = R' = H, L = CO

6 R = H, R' = Me, L = CO

7 R = Me, R' = H, L = PMe_3

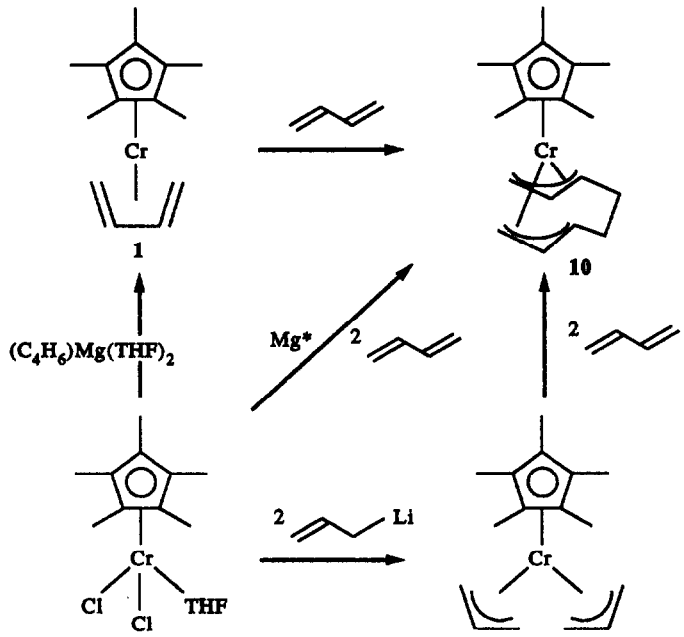

Scheme 2.

butadiene or by reacting $Cp^*(\eta^3\text{-}C_3H_5)_2Cr$ with butadiene (Scheme 2).

Although an analogous reaction between $Cp^*(\eta^3\text{-}C_3H_5)_2Cr$ and *cis*- or *trans*-piperylene leads to the formation of $Cp^*(\eta^3,\eta^3\text{-}1,5\text{-}Me_2C_8H_{10})Cr$ (**11**, eq. 4), 2,4-hexadiene reacts to give the mono-diene compound **4** (eq. 2). This difference in behaviour between the dienes presumably has a steric origin.

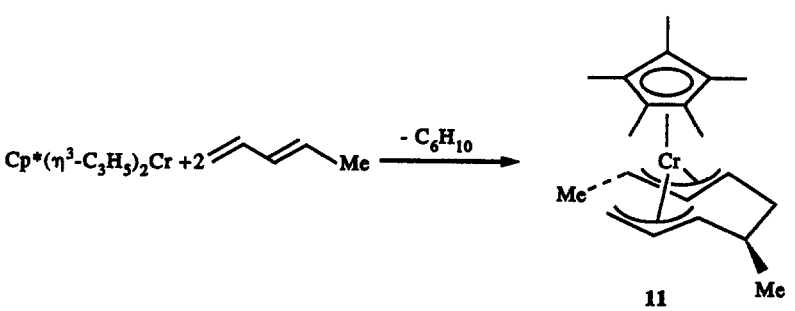

(4)

The crystal structures of **10** and **11** have been determined by X-ray diffraction and are shown in Fig. 1; selected structural parameters are listed in Table 1. Both compounds contain an octadienediyl chain bonded in an η^3,η^3-manner to the chromium atom with the meso-C-atoms of the C_8-chain pointing away from the metal.

The bis-methylene bridge in **10** is disordered. This disorder was resolved during the refinement procedure assuming a 50% occupancy for each C-atom. The Cp*-group is oriented with one C-atom (C1) directed towards the methylene bridge. The η^3-allyl fragments have typical bonding parameters with the planes defined by the allylic C-atoms arranged at an angle of 40° to each other.

The octadienediyl chain in **11** is substituted in the 1,5-position by methyl groups and the compound is thus the product of the head-to-tail coupling of two *trans*-piperylene molecules. The different substitution pattern for the two allyl fragments is reflected in differences in the observed structural parameters. Exactly as observed for **10**, one C-atom of the Cp*-ring (C3) is directed towards the bridging C-atom while the two allyl groups are also arranged at *ca* 40° to each other.

Organotransition metal compounds containing the octadienediyl-group have attracted attention as model compounds for intermediates in the catalytic cyclodimerization of butadiene to 1,5-cyclo-

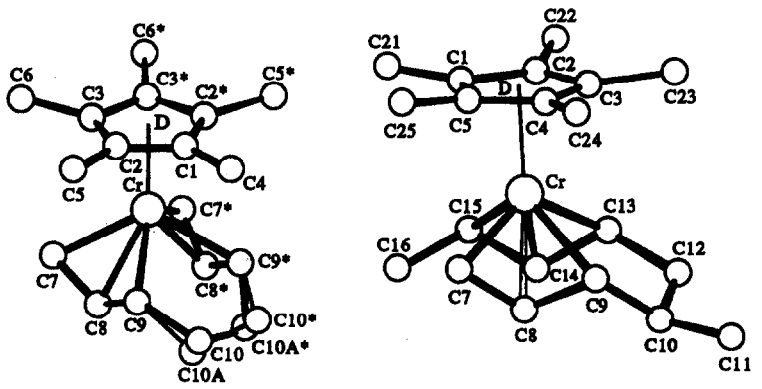

10 **11**

Fig. 1 The molecular structures of Cp*(η^3,η^3-C_8H_{10})Cr (**10**) and Cp*(η^3,η^3-1,5-$Me_2C_8H_8$)Cr (**11**).

octadiene, 4-vinylcyclohexene or 1,2-divinylcyclobutane. A similar arrangement to that observed for **10** has been established by NMR spectroscopy for the nickel compound **12**[11] and has also been proposed for the related vanadium species **13** as well as its Cp*-stabilized analogue.[12]

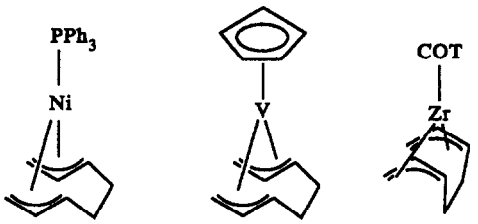

12 **13** **14**

In contrast, the zirconium compound **14** has been shown by NMR spectroscopy to contain an anti-substituted octadienediyl-chain.[13] As far as we are aware, compound **11** is the only known example in which the dimethyl-C_8-fragment is formed by the head-to-tail coupling of two piperylene molecules: nickel-containing species related to **12** have the methyl groups in the 4,5-positions as the result of a tail-to-tail coupling[11] while the crystal structure determination of (cot)(η^3,η^3-1,8-$Me_2C_8H_{10}$)Zr has confirmed the head-to-head coupling of the two diene molecules.[14]

The chromium-atom in the octadienediyl compounds **10** and **11** (as well as in Cp*(η^3-C_3H_5)$_2$Cr) has 17-electrons in its valence shell and as expected

Table 1. Selected structural parameters for Cp*(η^3,η^3-C_8H_{12})Cr (**10**) and Cp*(η^3,η^3-1,5-$Me_2C_8H_{10}$)Cr (**11**)

Bond distance (Å, ESD)	**10**	Bond distance (Å, ESD)	**11**[a]
Cr—C7	2.158(4)	Cr—C7/Cr—C15	2.164(4)/2.183(3)
Cr—C8	2.141(3)	Cr—C8/Cr—C14	2.150(3)/2.134(3)
Cr—C9	2.180(4)	Cr—C9/Cr—C13	2.187(3)/2.162(3)
Cr—D	1.915(4)	Cr—D	1.916(2)
C7—C8	1.379(6)	C7—C8/C15—C14	1.383(5)/1.387(5)
C8—C9	1.388(6)	C8—C9/C14—C13	1.386(6)/1.403(5)
C9—C10	1.54(1)	C9—C10/C13—C12	1.529(5)/1.508(5)
C9—C10a	1.52(1)	C9—C10a	—
C10—C10*	1.48(2)	C10—C12	1.513(6)
C—C(Cp*)	1.404(4)–1.414(3)	C—C(Cp*)	1.404(4)–1.411(3)
C—Me(Cp*)	1.497(4)–1.512(6)	C—Me(Cp*)	1.498(4)–1.514(5)
Bond angles (°, ESD)		Bond angles (°, ESD)	
C7—C8—C9	121.6(3)	C7—C8—C9/C15—C14—C13	122.0(3)/123.5(3)
C8—C9—C10	127.4(6)	C8—C9—C10/C14—C13—C12	116.8(3)/122.7(3)

[a] C15—C16 1.496(6), C10—C11 1.508(7).

these species are paramagnetic. A one-electron reduction should lead to the formation of a diamagnetic, 18-electron system and indeed a cyclic voltammogram of **10** in THF indicates reversible redox behaviour (E_{ox} −0.13 V, E_{red} −0.99 V; Pt-electrode vs SCE). However, the profile of the curve indicates that structural changes occur during both the reduction and oxidation and therefore an attempt was made to reduce **10** chemically. Treatment with Li(naphthalene) in THF followed by the addition of tetramethylethylenediamine led to the formation in high yield of a red crystalline compound having the composition $[Cp^*(C_8H_{12})Cr][Li(Me_2NC_2H_4NMe_2)_2]$. However, a magnetic susceptibility measurement indicates that the species is not diamagnetic as expected but has a value corresponding to two unpaired electrons (2.9 μ_B). Furthermore, the IR spectrum suggests that the species no longer contains η^3-allyl groups and it seems probable that here also rearrangement of the organic group has occurred. Unfortunately, we were unable to obtain crystals of suitable quality for an X-ray diffraction study so that the suggestion that coupling of the allyl groups has occurred to give a $[Cp^*(\eta^2,\eta^2\text{-cod})Cr]^+$-species remains speculation.

Since it is known that η^3-allyl-transition metal compounds react readily with alkynes (examples from our research group are discussed in ref. 15), we have investigated the behaviour of **10**. An unusual reaction occurs in which the alkyne adds to the 2,7-position of the C_8-chain to give the species **15–17** as room temperature stable, red crystalline compounds.

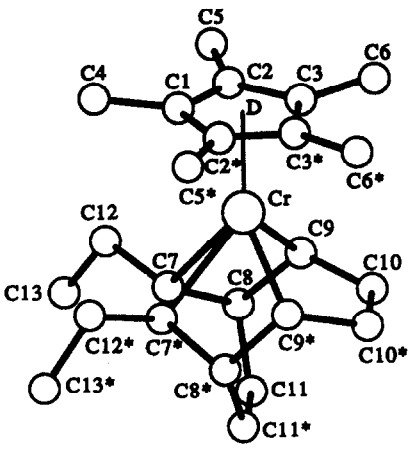

16

Cr—C7 2.341(4), Cr—C9 2.064(5), Cr—D 1.926(6), C7—C8 1.508(6), C8—C9 1.542(7), C9—C10 1.538(7), C10—C10* 1.496(9), C7—C7* 1.364(6), C8—C11 1.533(7), C—C(Cp*) 1.383(6)—1.402(5), C—Me(Cp*) 1.49(1)—1.509(9), C7—Cr—C7* 33.9(2), C9—Cr—C9* 79.4(2), C7—C8—C9 106.6(4), C7—C8—C11 110.0(4), C8—C9—C10 118.2(4), C9—C10—C10* 111.8(4), C8—C11—C11* 112.9(4).

Fig. 2. The molecular structure of $Cp^*(\eta^1,\eta^2,\eta^1\text{-}1,2\text{-}Et_2C_{10}H_{12})Cr$ (**16**) with selected bond distances (Å) and angles (°).

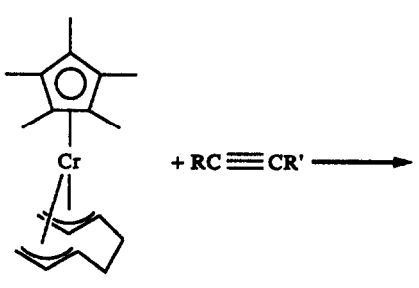

10

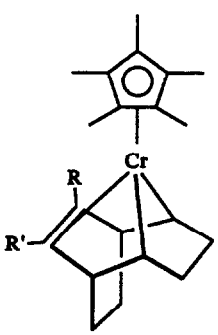

15 R = R' = Me
16 R = R' = Et
17 R = Me, R' = Et

(5)

The mass spectrum of the product of the stoichiometric reaction between **10** and acetylene [*m/z*: 321 (M^+, 30%), 319 (40%), 295 (M^+-HC_2H, 15%), 293 (16%), 187 (100%)] indicates that an analogous reaction has occurred although the compound could not be obtained analytically pure, while in the presence of excess acetylene, *cis/trans*-polyacetylene (IR (KBr): ν 1015, 735 cm^{-1}) is formed. The reaction of **10** with *t*-butylacetylene takes a different course: the C_8H_{12}-fragment is displaced and a brown–green oil is formed which has the composition $Cp^*(t\text{-}C_4H_9C_2H)_4Cr$ and which was not investigated in detail although the liberation of $(t\text{-}C_4H_9)_4C_8H_4$ upon thermolysis (MS) suggests that it may contain a tetra-substituted cyclooctatetraene molecule. The crystal structure of **16** was established by X-ray diffraction and is shown in Fig. 2 along with selected structural parameters. The

bicyclic hydrocarbon fragment is bonded to the chromium atom through σ-bonds to C9/C9* and a π-bond to C7/C7*.

The only reaction which we are aware of which might be related is that shown in eq. (6) in which **18** is formed as the result of a 1,4-addition of the alkyne to a cyclooctadiene molecule.[16]

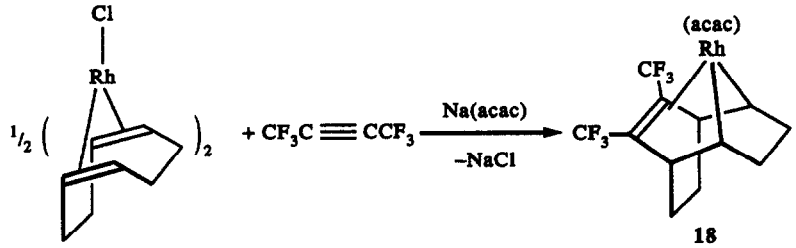

(6)

18

Having determined the crystal structure of both the starting material, Cp*(η^3,η^3-C_8H_{12})Cr, and of the product of the reaction with 1-hexyne, Cp*(η^1,η^2,η^1-1,2-$Et_2C_{10}H_{12}$)Cr, we are in a position to speculate on the mechanism. A possible course is shown below (Scheme 3): the η^3,η^3-C_8H_{12}-fragment rearranges either thermally or under the influence of the alkyne to the related η^1,η^1-form (compounds containing this fragment have been reported for Pd[17] and Pt[18]) which isomerizes by disrotatory rotation about the vinyl axis (a computer simulation indicates that a conrotatory rotation is unlikely since this would bring the meso-H atom and one of the terminal H-atoms to within 0.4 Å of each other) and is followed by a $2_\pi+2_\pi+2_\pi$-cycloaddition involving the second π-bond of the complexed alkyne molecule.

The results of an extended-Hückel MO treatment of the three species involved is shown in simplified form as Fig. 3(i–iii). On the left hand side are shown the relative levels of the Cr-*d*-orbitals for the coordination of the bis(η^3-allyl)fragment to Cr(III). η^3-to-η^1 rearrangement of the allyl groups by disrotatory rotation of the vinyl groups (as discussed above) with maintenance of the symmetry to give (ii) is accompanid by a significant decrease in the energies of the d_{xy} and d_{xz} orbitals as a result of the loss of the antibonding contribution to the atomic orbitals of the terminal allylic-C-atoms. This results in an increase in the acceptor ability of the metal and the HOMO of the alkyne molecule which has the correct symmetry to overlap with the d_{xz}-orbital of the chromium atom (eq. 7).

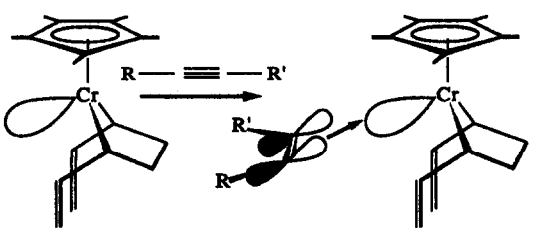

(7)

Additional changes in the *d*-orbital energies upon formation of the product are shown in Fig. 3(iii). Of particular significance is the further stabilization of the d_{xy}-orbital (the degeneracy with the $d_{x^2-y^2}$-orbital is coincidental) as a result of a bonding interaction between the metal orbitals and the π*-orbital (LUMO) of the alkyne. A consequence of Hund's rule is that the metal atom in the product should have a high-spin configuration with three unpaired electrons: the observation of a value of 3.1 μ_B for the magnetic susceptibility of **16** confirms the relevance of this simple MO-description.

EXPERIMENTAL

The general experimental conditions have been described in ref. 1. Cp*Cr(THF)Cl_2 was prepared by reacting $Cr(THF)_3Cl_3$ with Cp*Li[19] in THF or diethyl ether at −30°C to 0°C and reacted further using solutions whose concentrations were

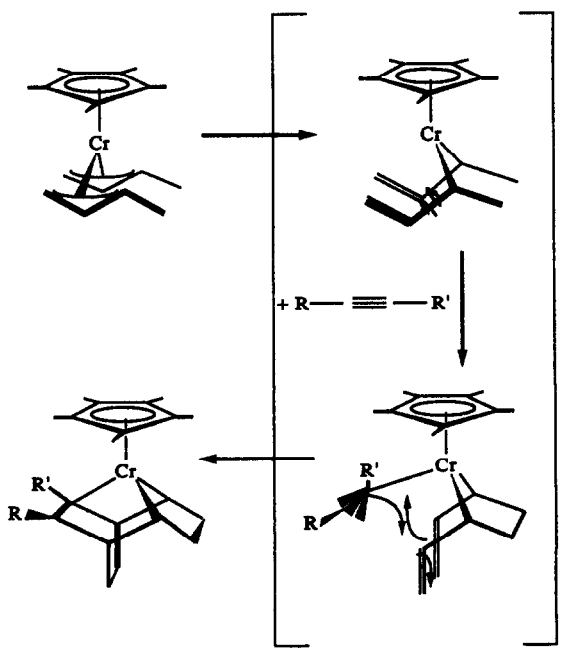

Scheme 3.

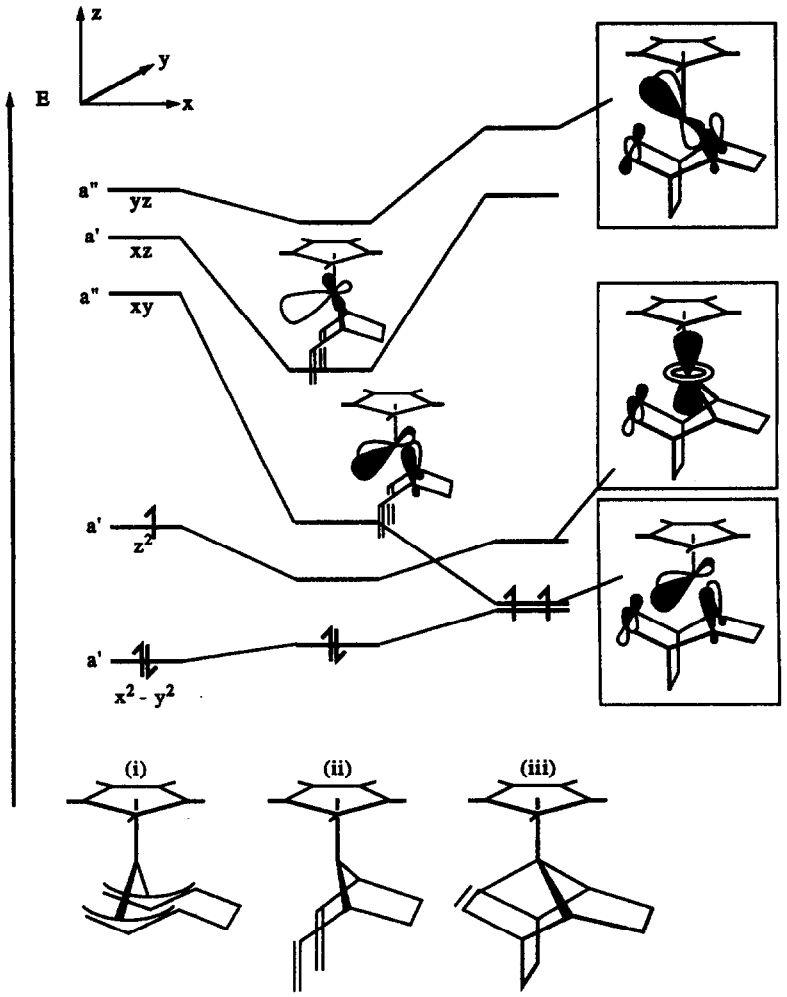

Fig. 3. MO-scheme illustrating the change in the energy of the Cr-*d*-orbitals during the transition from Cp*(η^3,η^3-C_8H_{12})Cr to Cp*(η^1,η^2,η^1-1,2-$C_{10}H_{14}$)Cr.

determined by measuring the intensity of the 670 nm absorption in the UV-spectrum. (C_4H_6)$Mg(THF)_2$ was prepared by reacting Mg-turnings with butadiene in THF.[20] Dilithium-1,2,3,4-tetraphenylbutadiene was prepared by reacting 1,2,3,4-tetraphenylbutadiene with excess lithium in THF at 0°C to 5°C.[21] Cp*(η^3-C_3H_5)$_2$Cr was prepared either by reacting [(η^3-C_3H_5)$_2$CrCl]$_2$ and Cp*Li[1] or by reacting Cp*Cr(THF)Cl_2 with allyllithium in ether at −60°C to −30°C (yield *ca* 85%). Active Mg was kindly supplied by Prof. B. Bogdanović and his co-workers and was prepared by the dehydrogenation of MgH_2 in the presence of $FeCl_2$.

Cp*(η^4-1,3-C_4H_6)Cr (**1**)

An ethereal solution of Cp*Cr(THF)Cl_2 (100 cm^3 of a 0.063 molar solution, 6.3 mmol) was added to a suspension of (C_4H_6)$Mg(THF)_2$ (1.5 g, 6.67 mmol) in ether at −78°C. The reaction mixture was allowed to warm to 5°C and stirred for a further 5 h. The resulting yellow–brown solution was evaporated to dryness and the compound extracted and cooled to −78°C to give the product as red–brown crystals. A further fraction was obtained by concentrating the mother liquor. Yield: 0.86 g (70% theory). Found: C, 69.7; H, 8.8; Cr, 21.5. Calc. for $C_{14}H_{21}Cr$: C, 69.7; H; 8.8; Cr, 21.6%. MS (70 eV): *m/z* 241 (M^+, 47%), 187 (M^+-C_4H_6, 100%). IR (KBr): ν(Cp*) 1460s, 1375s, 1030m; (C_4H_6) 1210s, 1155s, 1040m, 930m.

Cp*(η^4-1,2,3,4-$Ph_4C_4H_2$)Cr (**2**)

Cp*Cr(THF)Cl_2 (65 cm^3 of a 0.081 molar solution, 5.3 mmol) in ether was treated with dilithium-1,2,3,4-tetraphenylbutadiene (150 cm^3 of a 0.037 molar solution, 5.55 mmol) in THF at −55°C. The reaction mixture was allowed to warm to 0°C and stirred for a further 4 h. The resulting brown solu-

tion was evaporated to dryness and the compound extracted with pentane (2×70 cm^3). The filtrate was concentrated and cooled to -78°C to give the product as a dark brown powder. Yield: 1.93 g (67% theory). The compound was contaminated by tetraphenylbutadiene and this could not be completely removed by repeated recrystallization. Found: C, 83.9; H, 7.5; Cr, 8.7. Calc. for $C_{38}H_{37}Cr$: C, 83.6; H, 6.8; Cr, 9.5%. MS (70 eV): *m/z* 545 (M^+, 40%), 187 (M^+-$Ph_4C_4H_2$, 6%). IR (KBr): ν(Cp*) 1440m, 1380m, 1030m.

Cp*(η^4-2,3-$Me_2C_4H_4$)Cr (**3**)

A suspension of activated-Mg (0.12 g, 5 mmol) in THF (20 cm^3) at -78°C was treated with a solution of Cp*Cr(THF)Cl_2 (50 cm^3 of a 0.09 molar solution, 4.5 mmol) in THF and excess 2,3-dimethylbutadiene (15 cm^3). The reaction mixture was stirred at -50°C overnight to give a red–brown solution which was stirred for a further 3 h at room temperature. The solution was filtered and cooled to -78°C to give the compound as red–brown crystals. Yield: 0.73 g (60% theory). Found: C, 70.6; H, 9.5; Cr, 19.8. Calc. for $C_{16}H_{25}Cr$: C, 71.3; H, 9.4; Cr, 19.3%. MS (70 eV): *m/z* 269 (M^+, 50%), 187 (M^+-C_6H_{10}, 100%). IR (KBr): ν(Cp*) 1470m, 1370s, 1065m, 1020s; (diene) 1330m, 1225m, 1180m, 980m.

Cp*(η^4-1,4-$Me_2C_4H_4$)Cr (**4**)

Cp*(η^3-C_3H_5)$_2$Cr (0.9 g, 3.34 mmol) was stirred in pentane (100 cm^3) at -70°C and treated with excess *trans,trans*-2,4-hexadiene (3 cm^3). The reaction mixture was allowed to warm to 0°C and the resulting dark red solution filtered and evaporated to dryness. The residue was extracted with pentane (40 cm^3) at 5°C and the extract concentrated and cooled to -78°C to give the compound as red crystals. Yield: 0.57 g (63% theory). Unsatisfactory analytical data were obtained since the compound was contaminated by an oil which could not be completely removed by repeated recrystallization. Found: C, 70.2; H, 9.2; Cr, 18.6. Calc. for $C_{16}H_{25}Cr$: C, 71.3; H, 9.4; Cr, 19.3%. MS (70 eV): *m/z* 269 (M^+, 3%), 241 (M^+-C_2H_4, 70%), 187 (M^+-C_6H_{10}, 100%). IR (KBr): ν(Cp*) 1440m, 1430s, 1370s, 1020m; (diene) 1495s, 1200s, 795s, 785s.

Cp*(η^4-1,3-C_4H_6)CrCO (**5**)

The compound, which has been reported as the product of the reaction between Cp*(η^4-1,3-C_4H_6)CrPMe$_3$ (**8**) and CO[1], can also be prepared by reacting Cp*(η^4-1,3-C_4H_6)Cr (**1**) with CO in pentane -60°C to 0°C or by reacting [Cp*(η^4-1,3-C_4H_6)Cr]$_2$($Ph_2PC_2H_4PPh_2$) (prepared as a red–brown insoluble compound by reacting Cp*Cr(THF)Cl_2 with (C_4H_6)Mg(THF)$_2$ and bis(diphenylphosphino)ethane in THF) with CO in pentane at room temperature (yield 82%).

Cp*(η^4-2,3-$Me_2C_4H_4$)CrCO (**6**)

Prepared as described above from Cp*(η^4-2,3-$Me_2C_4H_4$)Cr and CO as green crystals in 86% yield. Found: C, 68.1; H, 8.7; Cr, 17.8. Calc. for $C_{17}H_{25}CrO$: C, 68.7; H, 8.5; Cr, 17.5%. MS (70 eV): *m/z* 297 (M^+, 4%), 269 (M^+-CO, 94%), 187 (M^+-CO/C_6H_{10}, 100%). IR (KBr): ν(CO) 1880s; (Cp*) 1960m, 1900m, 1430m, 1380m, 1030m; (C_6H_{10}) 1480m, 1450m, 1380s, 1265m, 880m.

Cp*(η^4-1,4-$Me_2C_4H_4$)CrPMe$_3$ (**7**)

Prepared as described above by reacting Cp*(η^4-1,4-$Me_2C_4H_4$)Cr with PMe$_3$ in pentane at 5°C.

Cp*(η^4-1,3-C_4H_6)CrPMe$_3$ (**8**) *and* Cp*(η^4-1,3-C_4H_6)CrP(OMe)$_3$ (**9**)

These compounds have been reported previously as the product of the reaction between Cp*Cr(THF)Cl_2, PR_3 (R = Me, OMe) and (C_4H_6)Mg(THF)$_2$ in THF at -78°C to -20°C.[1]

Cp*(η^3,η^3-C_8H_{12})Cr (**10**)

Cp*(η^3-C_3H_5)$_2$Cr (1.1 g, 4.1 mmol) was dissolved in pentane (150 cm^3) at -30°C and the solution cooled to -78°C. 1,3-butadiene (35 cm^3) was added and the reaction mixture warmed to 0°C and stirred for 10 h. The solution was filtered and the filtrate cooled to -78°C to give the compound as a dark red crystalline solid which was dried under high vacuum at 0°C. Yield: 1.02 g (84% theory). Found: C, 72.8; H, 9.3; Cr, 17.9. Calc. for $C_{18}H_{27}Cr$: C, 73.2; H, 9.2; Cr, 17.6%. MS (70 eV): *m/z* 295 (M^+, 30%), 263 (32%), 241 (M^+-C_4H_6, 20%), 187 (M^+-C_8H_{12}, 100%). IR (KBr): ν(Cp*) 1430m, 1370s, 1020m; (allyl) 1235m, 1215m, 1195m, 1065m, 945m. Magn. suscept.: 1.9–2.3 μ_B. Crystal structure: see Fig. 1 and Table 1. Treatment with ethereal–HCl leads to the liberation of a mixture of *t,t*-, *t,c*- and *c,c*-2,6-octadiene (1 : 2 : 1) in 75% yield. A pentane solution of the compound reacts with CO at 5°C with displacement of 1,5-cyclooctadiene and 4-vinylcyclohexene (1 : 2) and formation of [Cp*Cr(CO)$_2$]$_2$; ν(CO) 1865vs, 1840vs.

The compound can also be prepared by reacting

$Cp^*Cr(THF)Cl_2$ with active-Mg and 1,3-butadiene in ether at −78°C to −10°C (yield 61%), by reacting $Cp^*Cr(THF)Cl_2$ with $(C_4H_6)Mg(THF)_2$ and 1,3-butadiene in THF at 0°C (yield 57%) or by reacting $Cp^*(\eta^4\text{-}1,3\text{-}C_4H_6)Cr$ with butadiene in pentane at 5°C (yield 88%).

$Cp^*(1,5\text{-}Me_2C_8H_{10})Cr$ (11)

Prepared as described above by reacting *trans,trans*-1,3-pentadiene in the form of red plates in 72% yield. Found: C, 73.8; H, 9.8; Cr, 16.1. Calc. for $C_{20}H_{31}Cr$: C, 74.2; H, 9.7; Cr, 16.1%. MS (70 eV): *m/z* 323 (M^+, 26%), 321 (25%), 255 ($M^+\text{-}C_5H_8$, 36%), 187 ($M^+\text{-}C_{10}H_{16}$, 100%). IR (KBr): ν(Cp*) 1445s, 1370s, 1020s; (allyl) 1485s, 1220m, 860m. Crystal structure: see Fig. 1 and Table 1.

The compound was formed in lower (58%) yield upon reacting a mixture of *cis*- and *trans*-piperylene (7:13). An analogous reaction with *cis*-piperylene led to the formation of a red–brown oil which is presumably a mixture of isomers [MS: *m/z* 323 (M^+)] differing in the arrangement of the methyl groups.

$[Cp^*(C_8H_{12})Cr][Li(Me_2NC_2H_4NMe_2)_2]$

$Cp^*(\eta^3,\eta^3\text{-}C_8H_{12})Cr$ (**10**, 0.9 g, 3.05 mmol) was dissolved in THF (50 cm^3) and the solution cooled to −78°C and treated with Li(naphthalene) (25 cm^3 of a 0.13 mol solution, 3.25 mmol). The reaction mixture was allowed to warm to room temperature and stirred for a further 5 h. The solvent was removed *in vacuo* and the oily residue dissolved in ether (40 cm^3), filtered and the red–brown filtrate treated with tetramethylethylenediamine (2 cm^3, 13.36 mmol). The resulting solution was cooled to −30°C to give the compound as red crystals. Yield: 1.35 g (83% theory). Found: C, 66.6; H, 11.3; Cr, 10.0; Li, 1.1; N, 10.1%. Calc. for $C_{30}H_{59}CrLiN_4$: C, 67.4; H, 11.1; Cr, 9.7; Li, 1.3; N, 10.5%. MS:

Table 2. Crystallographic data for $Cp^*(\eta^3,\eta^3\text{-}C_8H_{12})Cr$ (**10**), $Cp^*(\eta^3,\eta^3\text{-}1,5\text{-}Me_2C_8H_{10})Cr$ (**11**) and $Cp^*(\eta^1,\eta^2,\eta^1\text{-}1,2\text{-}Et_2C_{10}H_{12})Cr$ (**16**)

	10	**11**	**16**
Formula	$C_{18}H_{27}Cr$	$C_{20}H_{31}Cr$	$C_{24}H_{37}Cr$
Mol. wt, g mol^{-1}	295.4	323.5	377.6
Crystal size, mm	0.72 × 0.54 × 0.14	0.32 × 0.18 × 0.61	0.14 × 0.57 × 0.40
a (Å)	14.362(1)	8.270(1)	17.795(2)
b (Å)	13.038(1)	8.648(1)	13.700(1)
c (Å)	8.437(1)	14.284(1)	8.680(1)
α (°)	90.0	75.96(1)	90.0
β (°)	90.0	89.54(1)	90.0
γ (°)	90.0	65.06(1)	90.0
V (Å^3)	1580.0	893.5	2116.0
T (K)	293	293	293
D_{calc} g cm^{-3}	1.24	1.20	1.18
λ (Mo) (Å)	0.71069	0.71069	0.70930
Z	4	2	4
Space group (No.)	*P*nma (62)	$P\bar{1}$(2)	*P*nma (62)
Data collected	$\pm h, +k, +l$	$\pm h, \pm k, +l$	$+h, +k, +l$
Reflns measured	4020	5233	2771
Ind. reflns	2379	5174	2519
Obsd. reflns [$I > 2\sigma(I)$]	1607	3932	1676
No. of variables	137	314	118
R	0.050	0.049	0.071
R_w [$w = I/\sigma^2(F\sigma)$]	0.050	0.048	0.070
Residual electron density (near Cr), (e Å^{-3})	0.47	0.59	0.33

Further details of the crystal structure investigations and lists of final atomic coordinates, thermal parameters, distances, angles, and structure factors may be obtained from the Cambridge Crystallographic Data Centre (CCDC).

m/z 295 ($Cp^*(C_8H_{12})Cr^+$) no parent peak. IR (KBr): $\nu(Cp^*)$ 1380m, 1030s; ($Me_2NC_2H_4NMe_2$) 1460sbr, 1290m, 1020m, 950m, 790m. Magn. suscept.: 2.9 μ_B.

$Cp^*(1,2\text{-}Me_2C_{10}H_{12})Cr$ (**15**)

$Cp^*(\eta^3,\eta^3\text{-}C_8H_{12})Cr$ (**10**, 0.8 g, 2.7 mmol) was dissolved in pentane at −45°C and treated with 2-butyne (0.4 cm^3, 5.12 mmol). The reaction mixture was warmed to 5°C and stirred for 15 h, evaporated to dryness and the residue extracted with pentane (10 cm^3). The extract was cooled to −78°C to give the compound as red crystals. Yield: 0.43 g (46% theory). Found: C, 75.6; H, 9.5; Cr, 14.9. Calc. for $C_{22}H_{33}Cr$: C, 75.3; H, 9.3; Cr, 15.4%. MS (70 eV): *m/z* 349 (M^+, 26%), 347 (56%), 293 (M^+-Me_2C_2, 9%), 187 (100%). IR (KBr): $\nu(Cp^*)$ 1430s, 1370s; (C:C) 1580m, 1485m; 1280m, 1020s.

$Cp^*(1,2\text{-}Et_2C_{10}H_{12})Cr$ (**16**)

Prepared as described above by reacting $Cp^*(\eta^3,\eta^3\text{-}C_8H_{12})Cr$ (**10**) with 1-hexyne in pentane at −78°C to room temperature. The red crystals were recrystallized from pentane. Yield 48% theory. Found: C, 76.4; H, 9.9; Cr, 13.7. Calc. for $C_{24}H_{37}Cr$: C, 76.4; H, 9.9; Cr, 13.8%. MS (70 eV): *m/z* 377 (M^+, 27%), 375 (44%), 321 (14%), 187 (63%). IR (KBr): $\nu(Cp^*)$ 1440m, 1365m, 1020m; 1580m, 1460m, 1050. Magn. suscept.: 3.1 μ_B. Crystal structure: see Fig. 2.

$Cp^*(1,2\text{-}EtMeC_{10}H_{12})Cr$ (**17**)

Prepared as above by reacting $Cp^*(\eta^3,\eta^3\text{-}C_8H_{12})Cr$ (**10**) with 2-pentyne. Yield: 41% theory. Found: Cr, 14.2. Calc. for $C_{23}H_{35}Cr$: Cr, 14.3%. MS (70 eV): *m/z* 363 (M^+, 47%), 361 (90%), 187 (100%). IR (KBr): $\nu(Cp^*)$ 1375m, 1030m; 1550m, 1485m, 1450m, 1375m, 1045m.

X-ray diffraction studies and MO calculations

Single crystal structure analyses were carried out using an Enraf–Nonius CAD-4 diffractometer. Crystallographic data for **10**, **11** and **16** and details of the refinement are summarized in Table 2 and in the supplementary material.

Extended Hückel MO calculations based on the structures of **10** and **16** were carried out using the programme ICON (v. 8, 1974).

REFERENCES

1. P. Betz, A. Döhring, R. Emrich, R. Goddard, P. W. Jolly, C. Krüger, C. C. Romão, K. U. Schönfelder and Y.-H. Tsay, *Polyhedron* 1993, **12**, 2651.
2. K. Angermund, P. Betz, A. Döhring, P. W. Jolly, C. Krüger and K. U. Schönfelder, *Polyhedron* 1993, **12**, 2663.
3. K. Angermund, A. Döhring, P. W. Jolly, C. Krüger and C. C. Romão, *Organometallics* 1986, **5**, 1268.
4. S. P. Nolan, C. D. Hoff and J. T. Landrum, *J. Organomet. Chem.* 1985, **282**, 357.
5. J L. Robbins, N. Edelstein, B. Spencer and J. C. Smart, *J. Am. Chem. Soc.* 1982, **104**, 1882.
6. D. C. Calabro, J. L. Hubbard, C. H. Blevins, A. C. Campbell and D. L. Lichtenberger, *J. Am. Chem. Soc.* 1981, **103**, 6839.
7. P. G. Gassmann, D. W. Macomber and J. W. Hershberger, *Organometallics* 1983, **2**, 1470.
8. E. J. Miller, S. F. Landon and T. B. Brill, *Organometallics* 1985, **4**, 533.
9. A. Grohmann, F. H. Köhler, G. Müller and H. Zeh, *Chem. Ber.* 1989, **122**, 897.
10. E. Bartmann, B. Bogdanović, N. Janke, Sh. Liao, K. Schlichte, B. Spliethoff, J. Treber, U. Westeppe and U. Wilczok, *Chem. Ber.* 1990, **123**, 1517.
11. R. Benn, B. Büssemeier, S. Holle, P. W. Jolly, R. Mynott, I. Tkatchenko and G. Wilke, *J. Organomet. Chem.* 1985, **279**, 63.
12. K. Jonas and V. Wiskamp, *Z. Naturforsch.* 1983, **38b**, 1113; V. Wiskamp, Dissertation Ruhr-Universität, Bochum 1981; W. Rüsseler, Dissertation Ruhr-Universität, Bochum, 1986; K. Jonas, *Angew. Chem.* 1985, **97**, 292.
13. H. J. Kablitz and G. Wilke, *J. Organomet. Chem.* 1973, **51**, 241.
14. D. J. Brauer and C. Krüger, *Organometallics* 1982, **1**, 207.
15. B. Büssemeier, P. W. Jolly and G. Wilke, *J. Am. Chem. Soc.* 1974, **96**, 4726; R. Benn, B. Gabor, P. W. Jolly, R. Mynott and B. Raspel, *J. Organomet. Chem.* 1985, **296**, 443; P. W. Jolly, C. Krüger and U. Zakrzewski, *J. Organomet. Chem.* 1991, **412**, 371.
16. D. R. Russell and P. A. Tucker, *J. Chem. Soc., Dalton Trans.* 1976, 841.
17. P. W. Jolly, *Angew. Chem.* 1985, **97**, 279; G. Schenker, Dissertation Ruhr-Universität, Bochum, 1984.
18. G. K. Barker, M. Green, J. A. K. Howard, J. L. Spencer and F. G. A. Stone, *J. Am. Chem. Soc.* 1976, **98**, 3373.
19. R. S. Threlkel and J. E. Bercaw, *J. Organomet. Chem.* 1977, **136**, 1.
20. K. Fujita, Y. Ohnuma, M. Yasuda and H. Tani, *J. Organomet. Chem.* 1976, **113**, 201.
21. L. I. Smith and H. H. Hoehn, *J. Am. Chem. Soc.* 1941, **63**, 1184.

Polyhedron Vol. 12, No. 22, pp. 2681–2685, 1993
Printed in Great Britain

0277–5387/93 $6.00+.00
© 1993 Pergamon Press Ltd

SYNTHESIS AND STRUCTURE OF η^5-PENTAMETHYLCYCLOPENTADIENYLDICHLORO-IRIDIUMTRIS(2,6-DIFLUOROPHENYL)PHOSPHITE

JOHN H. HOLLOWAY, ERIC G. HOPE, KEVIN JONES and GRAHAM C. SAUNDERS†

Department of Chemistry, University of Leicester, Leicester LE1 7RH, U.K.

and

JOHN FAWCETT, NIGEL REEVES and DAVID R. RUSSELL

Crystallography Laboratory, Department of Chemistry, University of Leicester LE1 7RH, U.K.

and

MALCOLM J. ATHERTON

BNFL Fluorochemicals Ltd., Springfields, Salwick, Preston PR4 0XJ, U.K.

(*Received* 2 *June* 1993; *accepted* 15 *July* 1993)

Abstract—The new fluorine containing ligand, tris(2,6-difluorophenyl)phosphite, prepared from the reaction between 2,6-difluorophenol and phosphorus trichloride, reacts with η^5-pentamethylcyclopentadienyldichloroiridium dimer to give the title compound in high yield. The molecular structure of this compound has been determined by single crystal X-ray crystallography.

We are interested in the properties the presence of fluorine in ligands, particularly phenylphosphines and phenylphosphites, can bestow upon transition-metal complexes of those ligands. Although tris (pentafluorophenyl)phosphite has been reported,[1] there are no reports of metal complexes of phenyl-phosphites containing *ortho* fluorines. Here we report the synthesis and characterization of the new fluorine containing ligand tris(2,6-difluorophenyl) phosphite, **1**, and the complex η^5-pentamethyl-cyclopentadienyliridiumdichlorotris(2,6 - difluoro-phenyl)phosphite, **2**, which has been structurally characterized by X-ray crystallography.

EXPERIMENTAL

$[Cp^*IrCl_2]_2$ (Aldrich), PCl_3 (BDH) and 2,6-difluorophenol (Fluorochem) were used as supplied. Triethylamine was dried by storage over CaH_2 prior to use. THF was dried over sodium wire and then distilled from sodium/benzophenone under dinitrogen. NMR spectra were recorded on a Bruker AM300 spectrometer. ^1H NMR spectra were recorded at 300 MHz and referenced internally using the residual protio solvent resonance relative to tetramethylsilane ($\delta = 0$ ppm). ^{13}C NMR spectra were recorded at 75.47 MHz and referenced internally using the solvent resonance relative to tetramethylsilane ($\delta = 0$ ppm). ^{19}F NMR spectra were recorded at 282.41 MHz and referenced externally to $CFCl_3$ ($\delta = 0$ ppm). ^{31}P NMR spectra were recorded at 121.50 MHz and referenced externally to 85% H_3PO_4 ($\delta = 0$ ppm). All chemical shifts are quoted in δ (ppm) and coupling constants in Hz. Abbreviations used in multiplicities are s = singlet, d = doublet, t = triplet and m = multiplet. IR spectra were recorded as Nujol mulls on a Digilab FTS40 Fourier transform spectrometer. The mass

† Author to whom correspondence should be addressed.

spectrum was recorded on a V.G. Micromass 16B mass spectrometer.

Preparation of tris(2,6-difluorophenyl)phosphite (**1**)

2,6-Difluorophenol (25 g, 0.19 mol) and triethylamine (21.8 g, 0.22 mol) in THF (100 cm^3) were added during 2 h to PCl_3 (7.9 g, 0.06 mol) in THF (200 cm^3) at 0°C. The white solid was separated by filtration and washed with THF (150 cm^3). The filtrate and washings were combined and the solvent removed by rotary evaporation to give a pale yellow oil, which was dried *in vacuo* affording impure product as an off-white solid. No attempts were made to purify **1** as it was found to be amenable for further reactions. Yield 12.85 g (51%). ^1H NMR ($CDCl_3$): δ 6.96 (m, 3H, *para*); 6.91 (m, 6H, *meta*). ^{31}P-{^1H} ($CDCl_3$): δ 131.79 [septet, $^4J(PF) = 34.2$ Hz]. ^{19}F-{^1H} ($CDCl_3$): δ −126.50 [d, $^4J(PF) = 34.2$ Hz]. ^{13}C ($CDCl_3$): δ 154.79 [dd, $^1J(CF) = 249.7$ Hz, $^2J(CH) = 11.6$ Hz, *ortho*]; 127.82 [t, $^2J(CF) = 15.8$ Hz, *ipso*]; 124.00 [dt, $^1J(CH) = 166.0$ Hz, $^3J(CF) = 8.4$ Hz, *para*]; 111.82 [ddd, $^1J(CH) = 166.0$ Hz, $^2J(CF) = 22.0$ Hz, $^2J(CH) = 7.5$ Hz, *meta*]. Mass spectrum *m/z* (%): 420 (0.5), 419 (4.4), 418 (22.0) [{$P(OC_6H_3F_2)_3$}$^+$]; 291 (0.6), 290 (7.7), 289 (56.0) [{$P(OC_6H_3F_2)_2$}$^+$]; 132 (0.5), 131 (6.5), 130 (100) [$(OC_6H_3F_2)^+$]. IR (cm^{-1}, Nujol mull): 2983 (w), 2864 (w), 1604 (m), 1560 (w), 1502 (s,br), 1296 (s), 1244 (m), 1201 (s), 1148 (w), 1064 (m), 1013 (s), 916 (m), 870 (s), 775 (s), 748 (s), 721 (m), 653 (w), 574 (w), 501 (w).

Preparation of η^5*-pentamethylcyclopentadienyldichloroiridiumtris(2,6-difluorophenyl)phosphite* (**2**)

A slurry of $[Cp^*IrCl_2]_2$ (0.10 g, 0.13 mmol) and **1** (0.20 g, 0.48 mmol) in benzene (50 cm^3) was heated under reflux under nitrogen for 2 h. The orange solution was allowed to cool and concentrated by rotary evaporation. Hexane (30 cm^3) was added to afford, on further concentration, a yellow solid. The solid was filtered, washed with hexane (4 × 10 cm^3) and dried *in vacuo*. Yield 0.19 g (90%). Found: C, 41.8; H, 2.8; Cl, 7.8. Calc. for $\{\eta^5\text{-}C_5(CH_3)_5\}IrCl_2\{P(OC_6H_3F_2)_3\} \cdot 1/6\ C_6H_6$: C, 42.0; H, 3.0; Cl, 8.55%. ^1H NMR ($CDCl_3$): 7.37 (s, C_6H_6); 7.03 (m, 3H, *para*); 6.85 (m, 6H, *meta*); 1.81 [d, $J(PH) = 4.0$ Hz, 15H, CH_3]. ^{31}P-{^1H} ($CDCl_3$): 62.80 (m). ^{19}F-{^1H} ($CDCl_3$): −123.07 [d, $^4J(PF) = 3.1$ Hz]. IR (cm^{-1}, Nujol mull): 1606 (m), 1568 (w), 1501 (s), 1480 (m), 1452 (sh), 1378 (m), 1300 (s), 1247 (w), 1229 (w), 1205 (m), 1198 (m), 1150 (w), 1009 (s), 932 (s), 912 (s), 790 (m), 765 (m), 759 (s), 727 (w), 662 (w), 645 (w), 575 (w), 514 (w).

Crystal structure determination

Crystals suitable for a single crystal X-ray crystallographic study were obtained by slow evaporation of solvent from a solution of complex **1** in $CDCl_3$. A crystal with dimensions 0.7 × 0.12 × 0.28 mm was glued to the end of a thin glass fibre using epoxy resin. Unit cell parameters were determined by least squares refinement of omega angles from 24 centred reflections with $15 < 2\theta < 25°$. Intensities of 6083 reflections in the range $4 < 2\theta < 51.7°$ and $-1 \leqslant h \leqslant 11$, $-1 \leqslant k \leqslant 12$, $-27 \leqslant l \leqslant 27$ were measured on a Siemens P4 Diffractometer using a $\theta/2\theta$ technique and graphite monochromated Mo-K_α radiation. No crystal decay was detected from periodically measured check reflections. The data were corrected for Lorentz and polarization effects. The reflections merged to a unique data set of 4380 reflections ($R_{int} = 2.38\%$) with 3205 having $I > 2\sigma(I)$ regarded as observed. An absorption correction was applied to the data set, maximum and minimum transmission factors 0.422 and 0.305, respectively. Crystal data for **2**: $[C_{28}H_{24}Cl_2F_6IrO_3P]$, $M_r = 816.2$, monoclinic, $P2_1/c$, $a = 10.311(2)$, $b = 11.203(2)$, $c = 24.328(5)$ Å, $\beta = 92.13(3)°$, $V = 2808.3(14)$ Å^3, $Z = 4$, $D_{calc} = 1.931$ g cm^{-3}, λ(Mo-K_α) = 0.71073 Å, $\mu = 48.55$ cm^{-1}, $F(000) = 1584$, $T = 293$ K. Structure solution by Patterson methods and refinement were carried out using the SHELXTL-PC programme package.[2] All hydrogen atoms were included in calculated positions (C—H = 0.95 Å) with a common fixed isotropic thermal parameter (0.08 Å^2). All non-hydrogen atoms were refined as anisotropic. Final $R = 0.0336$ and $R_w = 0.0333$, $w = [\sigma^2(F) + 0.0010F^2]^{-1}$, for the 368 parameters refined with largest Δ/σ 0.018. Maximum and minimum peak heights in the difference Fourier map were +0.91 and −0.45 e Å^{-3}. An analysis of the weighting scheme over $|F_o|$ and $\sin\theta/\lambda$ was satisfactory.

RESULTS AND DISCUSSION

Treatment of PCl_3 with 2,6-difluorophenol in the presence of triethylamine yielded impure tris(2,6-difluorophenyl)phosphite, **1**, in *ca* 50% yield as an off-white solid which decomposes slowly in the presence of moisture (Scheme 1). Phosphite **1** was characterized by mass spectrometry, and NMR and IR spectroscopies. In particular the ^{31}P-{^1H} NMR spectrum exhibits a septet at δ 131.79 with a coupling constant, $^4J(PF)$, of 34.2 Hz, and the ^{19}F-{^1H} NMR spectrum exhibits a doublet at δ −126.50 with the same coupling constant. The value of

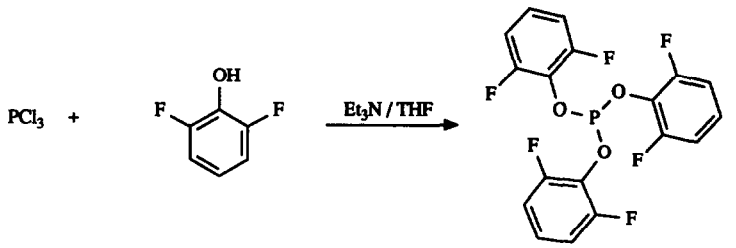

Scheme 1.

^4J(PF) is similar to those of ^3J(PF) for *ortho*-fluorine containing phenylphosphines.[3]

η^5-Pentamethylcyclopentadienyldichloroiridium dimer was treated with an excess of tris(2,6-difluorophenyl)phosphite in refluxing benzene. Concentration of the orange solution and addition of hexane yielded complex **2** as a yellow, air-stable, microcrystalline solid, containing 1/6 mole of solvent of crystallization, in 90% yield. The product was characterized by elemental analysis, and NMR and IR spectroscopies. The ^{31}P-{^{1}H} NMR spectrum, recorded in $CDCl_3$, exhibits a multiplet at δ 62.80, and the ^{19}F-{^{1}H} NMR spectrum exhibits a doublet at δ −123.07 with a coupling constant, ^4J(PF), of 3.1 Hz. This value is significantly lower than ^4J(PF) for the uncomplexed phosphite. This is consistent with the fact that values of ^3J(PF) coupling constants for uncomplexed *ortho*-fluorine containing phenylphosphines are significantly larger than those of the complexed phosphines.[3]

The molecular structure of complex **2** is shown in Fig. 1. The geometry of $Cp^*IrCl_2\{P(OC_6H_3F_2)_3\}$ about the iridium atom is that of a three-legged piano stool with the Ir—P and Ir—Cl bonds being almost orthogonal, as found for $Cp^*IrCl_2(PMe_3)$[4] and the isocyanide complex $Cp^*IrCl_2(CNR)$ (R = $C_5H_5(OCOCH_3)_4O$).[5] Selected bond distances and angles are given in Table 1. The Ir—C distances range from 2.166(8) to 2.247(9) Å with an average of 2.195 Å, which is close to that of 2.194 Å in $Cp^*IrCl_2(CNR)$ and intermediate between those of 2.13 and 2.23 Å for $[Cp^*IrCl(\mu\text{-}Cl)]_2$[6] and $Cp^*IrCl_2(PMe_3)$, respectively. The Ir—Cl distances of 2.363(3) and 2.376(3) Å are slightly shorter than those of $Cp^*IrCl_2(CNR)$ [2.389(6) and 2.391(5) Å] and $Cp^*IrCl_2(PMe_3)$ [2.37(1) and 2.39(1) Å]. The $C(sp^2)$—$C(sp^2)$ distances [1.416(13) to 1.441(12) Å], $C(sp^2)$—$C(sp^3)$ distances [1.471(13) to 1.505(12) Å], internal C—C—C angles [105.6(8) to 110.1(7)°] and C—C—CH_3 angles [123.1(8) to 128.0(8)°] of the Cp* ring are consistent with those of $Cp^*IrCl_2(CNR)$; $Cp^*IrCl_2(PMe_3)$ and $[Cp^*IrCl]_2(\mu\text{-}H)(\mu\text{-}Cl)$.[6] The Ir—P bond distance of 2.211(2) Å is shorter than that of $Cp^*IrCl_2(PMe_3)$ by 0.07 Å. This is consistent with the π-bonding capability of phosphites being greater than that of phosphines.[7]

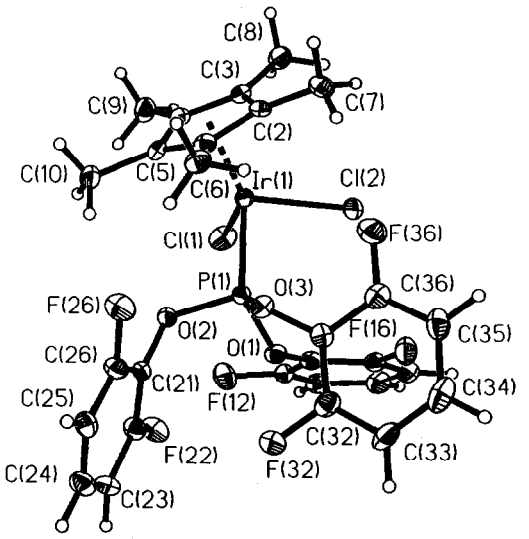

Fig. 1. Molecular structure of $Cp^*IrCl_2\{P(OC_6H_3F_2)_3\}$, **2**.

The coordination about the phosphorus atom may be described as distorted tetrahedral with significant distortions from C_3 symmetry about the axis along the Ir—P bond. The three Ir—P—O angles differ greatly, ranging from 109.2(2) to 126.2(2)°. The three O—P—O angles are similar, but the P—O—C angles range from 125.4(5) to 133.7(5)°, such that the greater than Ir—P—O angle the greater the respective P—O—C angle. All three P—O distances are close to 1.60 Å, and the O—C distances are *ca* 1.38 Å. The C—C bond distances of the phenyl rings range from 1.343(15) to 1.381(12) Å. The O—C—C angles are all slightly greater than 120° with concomittant smaller C—C(O)—C angles. The C—F bond distances range from 1.323(12) to 1.355(11) Å. These values can be compared to those of the iridium(III) triphenylphosphite complex, $IrCl\{P(OPh)_2OC_6H_4\}_2\{P(OPh)_3\}$[8] in which the non-*ortho*-metallated phosphite shows only small deviations from local C_{3v} symmetry about the phosphorus atom. The Ir—P—O angles of the triphenylphosphite ligand are all *ca* 114°, the O—P—O angles of

Table 1. Selected bond lenghs (Å) and bond angles (°) for $Cp^*IrCl_2\{P(OC_6H_3F_2)\}$, **2**[a]

Ir(1)—{$C_5(CH_3)_5$}[b]	1.830	C(12)—F(12)	1.328(11)
Ir(1)—Cl(1)	2.363(3)	C(16)—F(16)	1.355(11)
Ir(1)—Cl(2)	2.376(3)	C(22)—F(22)	1.339(11)
Ir(1)—P(1)	2.211(2)	C(26)—F(26)	1.345(11)
P(1)—O(1)	1.594(6)	C(32)—F(32)	1.354(12)
P(1)—O(2)	1.597(6)	C(36)—F(36)	1.323(12)
P(1)—O(3)	1.598(6)		
O(1)—C(11)	1.382(10)		
O(2)—C(21)	1.384(9)		
O(3)—C(31)	1.387(10)		

Cl(1)—Ir(1)—Cl(2)	87.9(1)	O(1)—C(11)—C(12)	121.7(8)
Cl(1)—Ir(1)—P(1)	90.0(1)	O(1)—C(11)—C(16)	120.1(8)
Cl(2)—Ir(1)—P(1)	92.0(1)	C(11)—C(12)—F(12)	119.2(8)
Cl(1)—Ir(1)—{$C_5(CH_3)_5$}[b]	122.4(1)	C(11)—C(16)—F(16)	118.1(8)
Cl(2)—Ir(1)—{$C_5(CH_3)_5$}[b]	123.1(1)	C(12)—C(11)—C(16)	117.5(8)
P(1)—Ir(1)—{$C_5(CH_3)_5$}[b]	129.9(1)	O(2)—C(21)—C(22)	121.0(7)
Ir(1)—P(1)—O(1)	126.2(2)	O(2)—C(21)—C(26)	121.5(7)
P(1)—O(1)—C(11)	133.7(5)	C(21)—C(22)—F(22)	118.4(7)
Ir(1)—P(1)—O(2)	109.2(2)	C(21)—C(26)—F(26)	117.8(7)
P(1)—O(2)—C(21)	125.4(5)	C(22)—C(21)—C(26)	117.2(7)
Ir(1)—P(1)—O(3)	117.6(2)	O(3)—C(31)—C(32)	121.1(8)
P(1)—O(3)—C(31)	129.7(5)	O(3)—C(31)—C(36)	121.1(8)
O(1)—P(1)—O(2)	102.3(3)	C(31)—C(32)—F(32)	117.7(9)
O(1)—P(1)—O(3)	98.4(3)	C(31)—C(36)—F(36)	118.1(9)
O(2)—P(1)—O(3)	99.0(3)	C(32)—C(31)—C(36)	117.7(9)

[a] ESDs are given in parentheses.
[b] Centroid.

105.5, 102.9 and 105.4° are significantly greater than those of complex **2**, and the P—O—C angles are 128.5, 129.2 and 126.4°. All the O—C—C bond angles are significantly less than 120°, ranging from 114.4 to 119.1°. Thus there are significant differences in the geometries about the phosphorus and oxygen atoms between triphenylphosphite and tris(2,6-difluorophenyl)phosphite coordinated to iridium(III) centres, in particular the Ir—P—O and P—O—C angles. These differences cannot be ascribed solely to the differences between the iridium(III) centres, and are, at least in part, due to the steric and electronic properties bestowed upon the phenyl rings by the *ortho*-fluorine atoms. This is corroborated by the structure of $Cp^*IrCl_2(PMe_3)$, where the Cp^*IrCl_2 moiety does not cause deviations from local C_{3v} symmetry about the phosphorus atom [P—C bond distances are 1.84(3), 1.86(3) and 1.83(4) Å, and the corresponding Ir—P—C bond angles are 113(1), 114(1) and 115(1)°, respectively].[4]

In summary the iridium(III) complex, **2**, has been prepared from the new fluorine containing ligand, tris(2,6-difluorophenyl)phosphite, **1**, and its structure has been determined by single crystal X-ray crystallography. There are significant differences between tris(2,6-difluorophenyl)phosphite and triphenylphosphite coordinated to iridium(III) centres, which are due to the presence of the *ortho*-fluorine atoms.

Acknowledgements—We thank BNFL Fluorochemicals Ltd. for support (to G.C.S.) and Dr G. A. Griffith for assistance in recording the NMR spectra.

REFERENCES

1. S. A. Krupoder, G. G. Furin, G. G. Yakobson, G. N. Dolenko, L. N. Mazalov, A. Sh. Sultanov and I. I. Furley, *J. Fluorine Chem.* 1983, **22**, 305; G. G. Furin, S. A. Krupoder, A. I. Rezvukhin, T. M. Kilina and G. G. Yakobson, *ibid* 1983, **22**, 345.
2. G. M. Sheldrick, SHELXTL-PC RELEASE 4.1, Program for crystal structure determination and refinement. Siemens Analytical X-ray Instruments Inc., Madison, Wisconsin, U.S.A. (1990).
3. D. I. Nichols, *J. Chem. Soc.* (*A*) 1969, 1471.
4. F. W. B. Einstein, X. Yan and D. C. Sutton, *Acta Cryst.* 1991, **C47**, 1975.

5. T. Pill, K. Polborn and W. Beck, *Chem. Ber.* 1990, **123**, 11.
6. M. R. Churchill and S. A. Julias, *Inorg. Chem.* 1977, **16**, 1488.
7. A. D. U. Hardy and G. A. Sim, *J. Chem. Soc., Dalton Trans.* 1972, 1900.
8. J. M. Guss and R. Mason, *J. Chem. Soc., Dalton Trans.* 1972, 2193.

Polyhedron Vol. 12, No. 22, pp. 2687–2696, 1993
Printed in Great Britain

0277–5387/93 $6.00+.00
© 1993 Pergamon Press Ltd

BONDING PROPERTIES OF COPPER(II)—N CHROMOPHORES: MOLECULAR AND ELECTRONIC STRUCTURES OF COPPER(II) COMPLEXES CONTAINING ETHYLENEDIAMINE AND HETEROCYCLIC DIIMINE LIGANDS

CHAN-CHENG SU,* YUH-LAN LIN and SHYH-JIUN LIU

Department of Chemistry, National Taiwan Normal University, Taipei 11718, Taiwan, Republic of China

and

TSU-HSIN CHANG

Department of Chemistry, National Sun Yat-Sen University, Kaoshion, Taiwan, Republic of China

and

SUE-LEIN WANG and FEN-LING LIAO

Department of Chemistry, National Tsing Hua University, Hsinchu, Taiwan, Republic of China

(*Received* 21 *April* 1993; *accepted* 15 *July* 1993)

Abstract—Mixed ligand ethylenediaminecopper(II) perchlorate complexes, [Cu(en)LL$(H_2O)](ClO_4)_2$, en = ethylenediamine and LL stands for 2,2′-bipyridine (bipy), 1,10-phenanthroline (phen), and *N,N,N′,N′*-tetramethylethylenediamine (tmen), have been prepared and characterized by elementary analyses, and electronic, vibrational, and EPR spectroscopic measurements. The crystal and molecular structures of [Cu(en)(bipy)$(H_2O)](ClO_4)_2$ (**1**) and [Cu(en)(phen)$(H_2O)](ClO_4)_2$ (**2**) have been determined from single-crystal, three-dimensional X-ray diffraction data. Both complexes, crystallized in triclinic $P\bar{1}$ group, contain discrete copper(II) cations having a CuN_4 basal plane and a H_2O on the apex. A similar structure was suggested for [Cu(en)(tmen)$(H_2O)](ClO_4)_2$ (**3**). The single-crystal polarized electronic spectra of **1** and **2** were measured and resolved into a set of three Gaussian component peaks for each spectrum. Gaussian analyses performed on the crystal and the powder LF bands for these complexes yielded a one-electron orbital sequence $d_{xy} > d_{z^2} > d_{x^2-y^2} > d_{yz} > d_{xz}$. Bonding properties of the bidentate ligands are elucidated suggesting virtually no π-interactions between the heterocyclic diimine ligands and the central copper(II) ion in these ethylene–diamine complexes.

The complexity of copper(II) stereochemistry has been well documented,[1] and many factors,[2–4] such as ligand field stabilization energies, the Pauling electroneutrality principle, the Jahn–Teller effect, semicoordination, counter ion effects, steric effects, etc., have been invoked to account for the complicated structures of copper(II) complexes. Basically, the energies of the frontier orbitals, which result from coordination of ligands, can reflect the bond strengths and the geometries of the complexes. It is, therefore, valuable to examine the bonding properties of ligands in order to correlate with the stereo-chemistry of the complexes.

Usually, the donor abilities of ligands may be

* Author to whom correspondence should be addressed.

estimated from their pK_a values. However, this often suffers from considerable interference, for instance, the potential π-interactions between the central metal ion and ligands, and the steric congestion between ligands. In addition, it is even more difficult to evaluate the extent of π-interactions. Because the layout of *d* orbitals is a direct response of the strengths of the metal–ligand bonds, it is anticipated that the bonding abilities of ligands, namely, the σ- and π-bonding capabilities, may be elucidated from the energies of the corresponding d_σ and d_π orbitals of the complexes, provided that the structures of the complexes are analogous. Herein, we report the molecular and electronic structures of two mixed ligand ethylenediamine and heterocyclic diimine copper(II) complexes, **1** and **2**, and discuss their bonding properties.

EXPERIMENTAL

Materials and preparations

Ethylenediamine (Fluka), 2,2′-bipyridine (Sigma), 1,10-phenanthroline (Sigma), *N,N,N′,N′*-tetramethylethylenediamine (Aldrich), $Cu(ClO_4)_2 \cdot 6H_2O$ (Aldrich), and organic solvents were used as received. Bis(ethylenediamine)copper(II) diperchlorate[5] was prepared according to the cited literature. The diimine complexes were prepared by the following procedure: to a MeOH solution of $Cu(ClO_4)_2 \cdot 6H_2O$, a stoichiometric amount of the heterocyclic diimine ligand in MeCN was added. After stirring for 30 min, a stoichiometric amount of ethylenediamine in MeCN was added dropwise. The reaction mixture was stirred at room temperature for 3 h. Ether was added to give the blue 2,2′-bipyridine complex, which was further recrystallized from MeCN and ether. For the 1,10-phenanthroline complex, the blue product was obtained from the concentrated reaction mixture, and recrystallized from MeCN. $[Cu(en)(tmen)(H_2O)](ClO_4)_2$[6] (**3**) was prepared by adding a stoichiometric amount of MeOH solution containing equal molar tmen and en to a MeOH solution of $Cu(ClO_4)_2 \cdot 6H_2O$. The blue solids were filtered and washed with ether and dried *in vacuo* over P_4O_{10}.

$[Cu(en)(bipy)(H_2O)](ClO_4)_2$ (**1**), Yield 55%, m.p. 268°C. Found: C, 29.8; H, 3.2; N, 11.4. Calc. for $C_{12}H_{18}N_4O_9Cl_2Cu$: C, 29.0; H, 3.6; N, 11.3%.

$[Cu(en)(phen)(H_2O)](ClO_4)_2$ (**2**), Yield 48%, m.p. 278°C (dec.). Found: C, 32.4; H, 3.2; N, 10.8. Calc. for $C_{14}H_{18}N_4O_9Cl_2Cu$: C, 32.3; H, 3.5; N, 10.8%.

$[Cu(en)(tmen)(H_2O)](ClO_4)_2$ (**3**), Yield 42%, m.p. 180°C (dec.). Found: C; 20.1; H, 5.3; N, 12.4. Calc. for $C_8H_{26}N_4O_9Cl_2Cu$: C; 20.2; H, 5.9; N, 11.8%.

Single crystals suitable for X-ray structure determination were obtained by diffusion of ether into an MeCN solution of complex **1**, and by slow evaporation of an MeCN solution of complex **2**. Crystals suitable for polarized LF spectroscopic measurements were grown by slow crystallization from MeCN between quartz plates.

Physical measurements

Perkin–Elmer lambda 9 and Jasco model 7850 spectrophotometers were used for electronic spectra measurements. Spectra of solid samples were recorded as Nujol mulls on Whatman No. 1 filter paper. The deconvolution of visible spectra into Gaussian component bands was performed on a VAX 6510 computer using the profile-fitting program CUVFIT.[7] The single crystal polarized spectra were recorded at ambient temperature using a Hitachi model 3501 spectrophotometer. The light was polarized with a Glan–Thompson polarizer. Both complexes **1** and **2** had the (001) plane well developed. This was checked by X-ray precession measurements on the crystals, and by trying several possible faces and performing the calculation for each possibility. The extinction directions for the faces were found to lie at angles of $+26.4°$ and $-63.6°$ to the *a* axis for **1** and $+21.3°$ and $-68.7°$ to the *a* axis for **2**. The positive sign corresponds to a rotation of the electric vector into the quadrant containing an obtuse angle. Epr spectra were obtained by using a Bruker ER 200D model spectrometer and calibrated with DPPH (g = 2.0037). IR spectra were recorded as Nujol mulls or KBr pellets on a BIO–RAD FTS-40 FTIR. A Micro VAX II computer-controlled Siemens R3m/V diffractometer was used for crystal and molecular structure determination. Elemental analyses were carried out by the microanalysis laboratories of Taiwan University, Taipei.

Structure determination and refinement

Details of crystal data and intensity collection are summarized in Table 1. Nineteen independent reflections with $11.23° \leqslant 2\theta \leqslant 30.98°$ for complex **1** and thirteen with $13.56° \leqslant 2\theta \leqslant 26.39°$ for complex **2** were used for least-squares determination of the cell constants. Diffractometer examination of the reciprocal lattice revealed no systematic absences. Intensity data [$\theta/2\theta$ scan, $2.5° \leqslant 2\theta \leqslant 50.0°$, $(\sin\theta/\lambda)_{max} \simeq 0.6$] were corrected for Lorentz and polarization effects but not for absorption. Three standard reflections were

Table 1. Summary of crystal data and intensity collection for $[Cu(en)(bipy)(H_2O)](ClO_4)_2$ and $[Cu(en)(phen)(H_2O)](ClO_4)_2$

Formula	$C_{12}H_{18}N_4O_9Cl_2Cu$	$C_{14}H_{18}N_4O_9Cl_2Cu$
Fw	496.7	520.8
Crystal size (mm)	$0.54 \times 0.52 \times 0.38$	$0.84 \times 0.41 \times 0.32$
Space group	$P\bar{1}$, triclinic	$P\bar{1}$, triclinic
a (Å); α (°)	7.358(1); 96.82(1)	7.312(1); 91.25(2)
b (Å); β (°)	10.223(1); 102.22(1)	10.391(2); 105.55(2)
c (Å); γ (°)	12.926(2); 98.86(1)	13.525(3); 103.30(1)
V (Å^3)	927.3(2)	959.6(3)
Z	2	2
D_{calc} (g cm^{-3})	1.779	1.802
μ (mm^{-1})	1.523	1.477
Radiation (λ, Å)	Mo-K_α (0.71073)	Mo-K_α (0.71073)
Independent refl.	3283 ($2764 \geqslant 3.0\sigma(I)$)	3414 ($2922 \geqslant 3.0\sigma(I)$)
Extinction correction	$\chi = 0.0037(7)$	$\chi = 0.0024(5)$
$F^* = F[1+0.002\chi F^2/\sin(2\theta)]^{-1/4}$		
Weighting scheme	$w^{-1} = \sigma^2 F + 0.0017F^2$	$w^{-1} = \sigma^2 F + 0.0024F^2$
Final R, R_w	0.0461, 0.0552	0.0360, 0.0448
Largest and mean Δ/σ	0.002, < 0.001	0.027, 0.004
Largest diff. peak (e Å^{-3})	0.73	0.64
Largest diff. hole (e Å^{-3})	−0.46	−0.43

monitored every 50 reflections and showed no signs of crystal deterioration. The structures were solved by direct methods using SHELXTL PLUS program[8] and refined by full-matrix least-squares on F values. Scattering factors and anomalous dispersion correction terms were taken from the *International Tables for X-ray Crystallography*.[9] The quantity minimized was $\Sigma w(K|F_o| - |F_c|)^2$, with $w = [\sigma^2(F_o) + gF_o^2]^{-1}$, where $g = 0.0017$ for complex **1**, and 0.0024 for complex **2**. All hydrogen atoms included in the refinement were placed in idealized positions (C—H = 0.96 Å, H—C—H = 109.4°) with a fixed U (0.08 Å^2) after the non-hydrogen atoms were refined anisotropically. All calculations were done on a Micro Vax II-based Nicolet SHELXTL PLUS system. Additional material deposited comprises structure factors, atomic coordinates, anisotropic thermal parameters, H atom coordinates, and a full list of bond lengths and angles.

RESULTS AND DISCUSSION

Description of the structures

The molecular and crystal structures of complexes **1** and **2** are shown in Figs 1–4. Selected bond lengths and angles are listed in Table 2. The structures of **1** and **2** consist of ClO_4^- anions and discrete square-pyramidal $CuN_4(H_2O)^{2+}$ cations

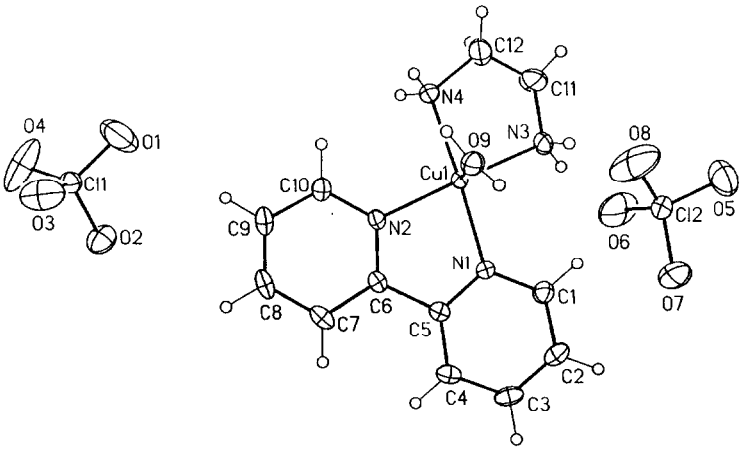

Fig. 1. Molecular structure of $[Cu(en)(bipy)(H_2O)](ClO_4)_2$ with numbering scheme.

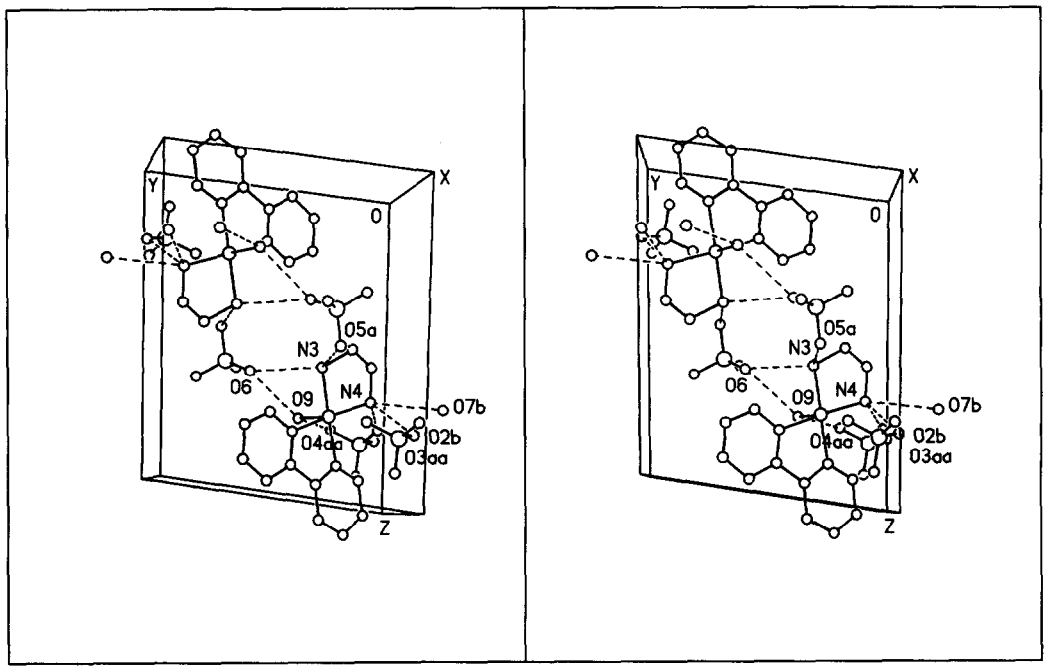

Fig. 2. Stereoscopic drawing of the molecular packing of $[Cu(en)(bipy)(H_2O)](ClO_4)_2$ in the unit cell. Hydrogen bonds: N(3)···O(5a), 3.207 Å, N(3)···O(6), 3.103 Å, N(4)···O(2b), 3.031 Å, N(4)···O(3aa), 3.006 Å, N(4)···O(7b), 3.015 Å, O(9)···O(6), 3.090 Å and O(9)···O(4aa), 3.037 Å.

with one ethylenediamine and one heterocyclic diimine ligand forming the basal plane and a water molecule on the apex [**1**, 2.435(4) Å; **2**, 2.393(3) Å]. Although one of the perchlorate anions is geometrically oriented for potential axial Cu—$OClO_3$ bonding, the shortest Cu—O distance is greater than 2.7 Å, and the axial bonding is considered to be absent. The CuN_4 units are nearly coplanar; the copper atom lies above (**1**, 0.1312 Å, **2**, 0.0772 Å) toward the H_2O. The ethylenediamine ligands bind to the central copper atom with Cu—N distances of ~ 2.0 Å and the N—Cu—N bite angle of ~ 85°, which are typical for ethylenediamine copper(II) complexes.[5,10–12] Disorder on the ethylene carbons of the en chelate is apparent and has been successfully modelled with the presence of both δ and λ conformations to give normal bond lengths and angles. The Cu—N distances of ~ 2.02 Å and the bite angles of ~ 81° of the bipy and phen ligands are close to the average values for bipy[13–15] and

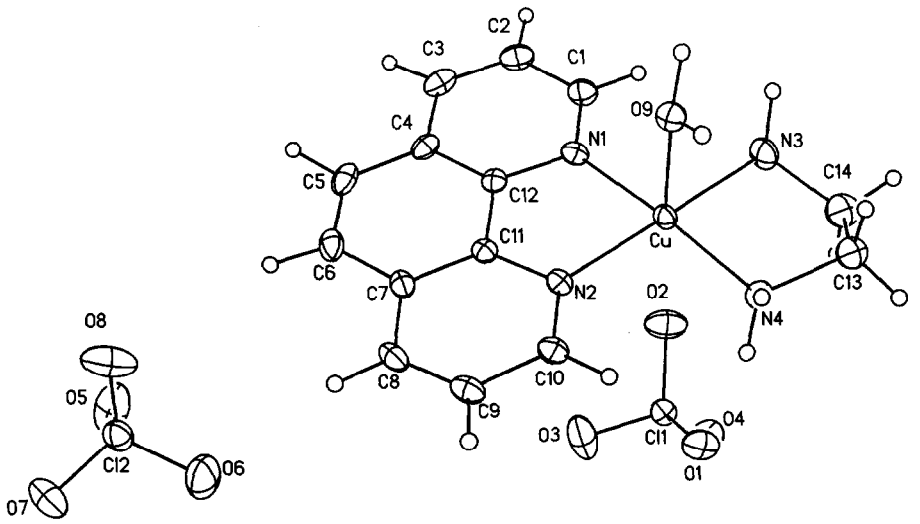

Fig. 3. Molecular structure of $[Cu(en)(phen)(H_2O)](ClO_4)_2$ with numbering scheme.

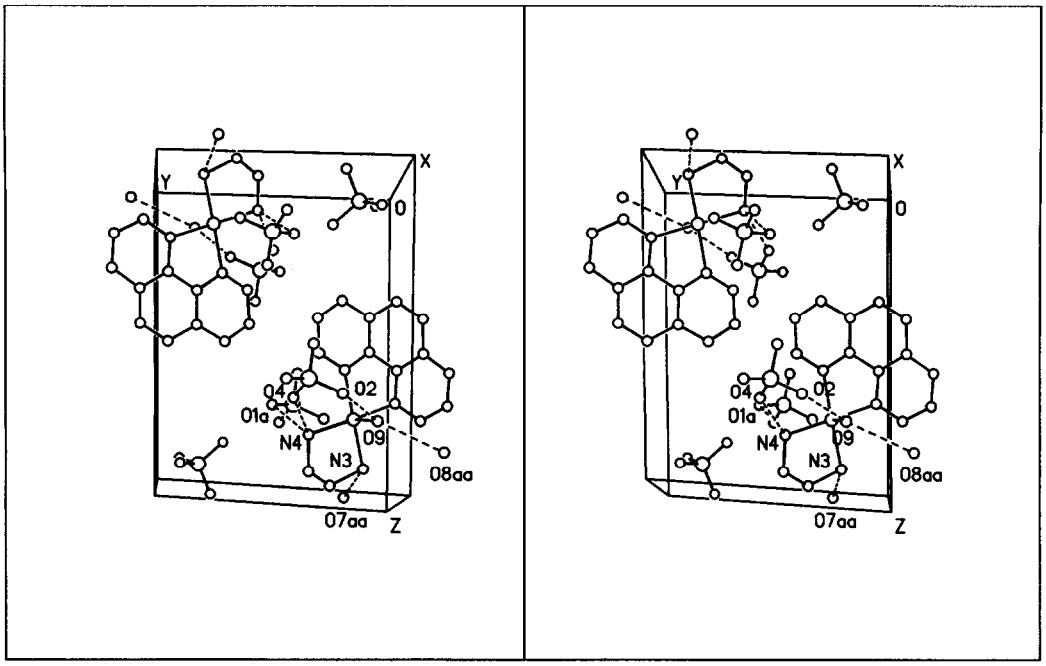

Fig. 4. Stereoscopic drawing of the molecular packing of $[Cu(en)(phen)(H_2O)](ClO_4)_2$ in the unit cell. Hydrogen bonds: N(3)···O(7aa), 3.154 Å, N(4)···O(1a), 3.029 Å, N(4)···O(4), 3.073 Å, O(9)···O(2), 3.037 Å, and O(9)···O(8aa), 2.955 Å.

Table 2. Bond lengths (Å) and angles (°) for $[Cu(en)(bipy)(H_2O)](ClO_4)_2$ and $[Cu(en)(phen)(H_2O)](ClO_4)_2$

$[Cu(en)(bipy)(H_2O)](ClO_4)_2$			
Cu(1)—N(1)	2.016(3)	Cu(1)—N(2)	2.005(3)
Cu(1)—N(3)	2.017(4)	Cu(1)—N(4)	2.005(3)
Cu(1)—O(9)	2.435(4)	N(3)—C(11)	1.517(12)
N(4)—C(12)	1.504(8)	N(3)—C(11a)	1.511(19)
N(4)—C(12a)	1.516(15)	C(11)—C(12)	1.458(21)
C(11a)—C(12a)	1.453(23)		
N(1)—Cu(1)—N(2)	81.0(1)	N(1)—Cu(1)—N(3)	97.0(1)
N(1)—Cu(1)—N(4)	167.5(2)	N(2)—Cu(1)—N(3)	176.8(2)
N(2)—Cu(1)—N(4)	97.0(1)	N(3)—Cu(1)—N(4)	84.4(1)
N(1)—Cu(1)—O(9)	97.4(1)	N(2)—Cu(1)—O(9)	89.7(1)
N(3)—Cu(1)—O(9)	93.0(2)	N(4)—Cu(1)—O(9)	94.9(1)
$[Cu(en)(phen)(H_2O)](ClO_4)_2$			
Cu—N(1)	2.023(2)	Cu—N(2)	2.017(3)
Cu—N(3)	2.012(3)	Cu—N(4)	2.001(3)
Cu—O(9)	2.393(3)	N(3)—C(14)	1.495(7)
N(4)—C(13)	1.493(5)	N(3)—C(14a)	1.493(5)
N(4)—C(13a)	1.494(7)	C(13)—C(14)	1.505(10)
C(13a)—C(14a)	1.504(8)		
N(1)—Cu—N(2)	81.8(1)	N(1)—Cu—N(3)	96.2(1)
N(1)—Cu—N(4)	172.9(1)	N(2)—Cu—N(3)	177.4(1)
N(2)—Cu—N(4)	97.1(1)	N(3)—Cu—N(4)	84.6(1)
N(1)—Cu—O(9)	96.9(1)	N(2)—Cu—O(9)	92.2(1)
N(3)—Cu—O(9)	89.7(1)	N(4)—Cu—O(9)	90.1(1)

phen[16,17] copper(II) complexes. The dimensions of the heterocyclic ligands are normal. The perchlorate ions appear to be loosely held in lattice holes by Coulombic forces and by weak hydrogen bonds to the water hydroxyl and ethylenediamine N—H groups as shown in Figs 2 and 4. The perchlorate bond distances and angles are in the normal ranges. Note that the molecules of both complexes are packed in nearly the same orientations in the unit cells with $P\bar{1}$ space group.

IR, EPR, and LF spectra of en—Cu(II) *complexes*

The IR spectral data are listed in Table 3. The appearance of two relatively sharp O—H stretchings in the region of ~ 3550 cm^{-1} is consistent with the structures of complexes **1** and **2** having a H_2O on the apex. This also suggests a H_2O bonded to the central copper(II) ion in the tmen complex. The very strong ClO_4^- stretching in the region of ~ 1085 cm^{-1} is broad, but not very broad, for each of the three complexes, indicating that the perchlorate anions are not coordinated to the central copper(II) ion in these complexes. Since both en and tmen are much stronger ligands than H_2O, it is conceivable that the structure of the tmen complex is a five coordinate square-pyramid with an apical H_2O. The slight variation of the O—H(H_2O) and N—H(en) vibrations for these complexes is probably mainly due to the hydrogen bonds. The Cu—N(en) stretchings[18,19] are tentatively assigned in the region of 420–320 cm^{-1}, while Cu—N(LL) stretchings are at lower energy.[20–22]

The LF spectral data and the EPR parameters for the mixed ligand ethylenediamine copper(II) complexes are listed in Table 4. The mull LF spectra with λ_{max} appeared in the region of ~ 550 nm and tailing toward the long wavelength region are consistent with the square-pyramidal structure.[23] In aqueous methanol (1 : 1) solution, these complexes likely consist of tetragonal CuN_4 units with one or two H_2O molecules loosely bound on the axial positions. This is consistent with the observations that the *d–d* spectra are red-shifted by ~ 20 nm and the band envelopes are not much changed as compared with their mull spectra. The structures of the solution species are also supported by the glass EPR spectral data, measured in aqueous methanol (1 : 1) matrix at 77 K. These axial EPR spectra are characteristic of tetragonal copper(II) chromophores with CuN_4 coordination plane. The approximately 9-line nitrogen hyperfine splitting on the $g_\perp$ peaks arises from the four N donors, which appear essentially equivalent. The nearly invariant $g_\perp$ parameters for complexes **1**, **2** and **3** either in solid state or in aqueous methanol solution infer that their coordination bond properties are similar. In other words, it is likely that no out-of-plane π-interactions involve in the bipy–copper(II) and phen–copper(II) bonds.

In order to compare the energy levels of the *d* orbitals for these structurally similar mixed ligand en–copper(II) complexes, resolution of the solid state *d–d* spectra is necessary. Starting from a set of three or four trial peaks, the computer iteration processes for curve fitting were carried out until a minimum value of the reliability factor,[24] *R*, was reached. Unfortunately, two final sets with either three or four Gaussian component peaks, both with excellent fit, were obtained for these nearly featureless LF spectra. It is, therefore, necessary to investigate the single crystal polarized spectra. The sets with four Gaussian component bands for the solid state LF spectra of these complexes were

Table 3. Infrared spectral data for en–copper(II) complexes[a]

1[b]	2	3	Assignment
3597m, 3546m	3570m, 3520m	3574m, 3510m	ν(O—H)
3316s, 3273s, 3168m	3335s, 3269s, 3188m	3323s, 3275s, 3158m	ν(N—H)
1610m	1628m	1641m	δ(O—H)
1601s	1589s	1591s	δ(N—H)
1084vs,br	1092vs,br	1080vs,br	ν(Cl—O)
625s	627s	625s	ν(Cl—O)
386m, 330m	374w, 322m	374w, 322w	ν(Cu—N(en))
320m, 285w	310m, 287w	484w, 409m	ν(Cu—N(L))

[a] Measured as Nujol mulls or KBr pellets. vs = very strong; m = medium; w = weak; br = broad.

[b] **1** = [Cu(en)(bipy)(H_2O)](ClO_4)$_2$; **2** = [Cu(en)(phen)(H_2O)](ClO_4)$_2$; **3** = [Cu(en)(tmen)(H_2O)](ClO_4)$_2$. en = ethylenediamine; bipy = 2,2′-bipyridine; phen = 1,10-phenanthroline; tmen = *N,N,N′,N′*-tetramethylethylenediamine.

Table 4. Visible and EPR spectral data for en–copper(II) complexes[a]

Compound[b]	λ_{max}, nm/ mull	$\lambda_{max}(\varepsilon)$, nm/ solution[c]	$g_{\parallel}$	$g_{\perp}$	$A_{\parallel}(Cu)^d$	$A_{\perp}(N)^d$
$[Cu(en)(bipy)(H_2O)](ClO_4)_2$	560	585(74)	2.218 (2.194)	2.055 (2.062)	195	12
$[Cu(en)(phen)(H_2O)](ClO_4)_2$	568	588(77)	2.218 (2.193)	2.055 (2.063)	195	10
$[Cu(en)(tmen)(H_2O)](ClO_4)_2$	545	560(98)	2.205 (2.190)	2.053 (2.064)	200	11
$[Cu(en)_2(ClO_4)_2]$	529	545(66)	2.203	2.050	201	11

[a] X-band EPR spectra measured at 77 K in $H_2O:CH_3OH$ (1 : 1). Powder data in parentheses.
[b] For abbreviations, vide footnote of Table 3.
[c] $CH_3OH:H_2O$ (1 : 1).
[d] In 10^{-4} cm^{-1}.

found more proper for reasoning the spectra (*vide infra*). The spectra accompanying with their Gaussian components are presented in Fig. 5, and the corresponding data are given in Table 5.

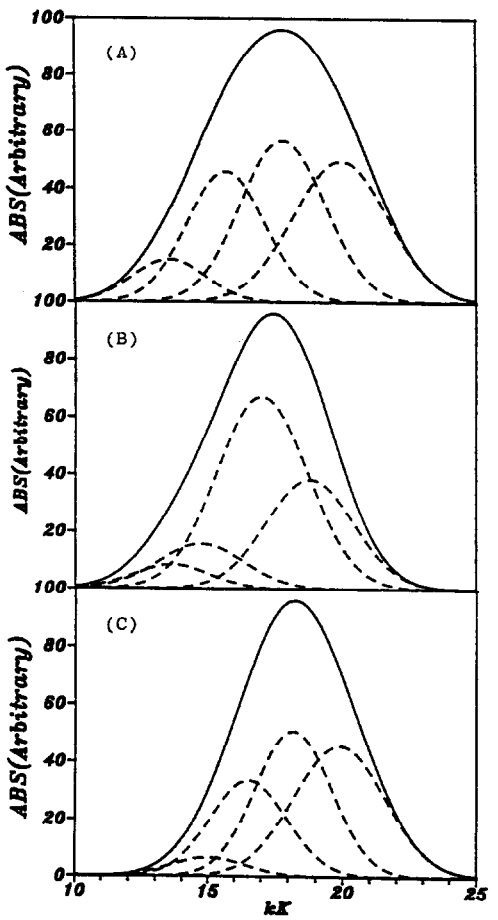

Fig. 5. The solid state visible spectra and Gaussian lineshape analysis of (A) $[Cu(en)(bipy)(H_2O)](ClO_4)_2$, R = 0.478%; (B) $[Cu(en)(phen)(H_2O)](ClO_4)_2$, R = 0.317%; (C) $[Cu(en)(tmen)(H_2O)](ClO_4)_2$, R = 0.531%.

Single-crystal polarized spectra

The single-crystal polarized LF spectra for complexes **1** and **2** are very similar both in peak positions and spectral contours, and accordingly their Gaussian component bands are expected to be very much alike as shown in Figs 6 and 7. It is noteworthy that the optical densities of the parallel spectra are about five times larger than those of the perpendicular spectra in the high energy region and about twice in the low energy region. The observed extinction axes also appear in approximately the same direction for both complexes. This is in agreement with the analogy of their molecular and crystal structures, suggesting that the bonding properties of bipy and phen ligands are highly analogous. For both complexes, each of the spectra was resolved into three Gaussian component peaks with excellent fit. The reliability factors were minimized down to ~ 0.5%. However, the perpendicular spectrum for complex **1** is less reliable owing to its low intensity. Attempts to fit with two peaks were unsuccessful. Attempts to resolve the highest energy peak into two components did not improve the R values. The peak positions for the two low energy peaks are in good agreement for the parallel and the perpendicular spectra for both complexes. The highest energy peaks agree resonably well for complex **2**, but they are significantly off for complex **1**. The one at 18.9 kK in the perpendicular spectrum for complex **1** is less reliable.

The coordinate system used to discuss the spectra was defined with y lying parallel to the least-squares plane of $N_1N_2N_3N_4$ and along the vector from the central copper atom to the midpoint of the two nitrogen atoms of the heterocyclic chelate ring, with x orthogonal to y and lying in the least-squares plane through the copper atom, and with z orthogonal to x and y toward the water oxygen atom.

Table 5. Gaussian components bands for the visible spectra of en–copper(II) complexes

Band	ν, kK	Area[a]	$\delta_{1/2}$[b]	Assignment
$[Cu(en)(bipy)(H_2O)](ClO_4)_2$				
Crystal(//) (R = 0.264%)[c]				
I	13.5	0.295	3.59	d_{z^2}
II	15.9	0.876	4.36	$d_{x^2-y^2}$
III	17.6	5.295	4.17	d_{yz}
Crystal(⊥) (R = 0.475%)				
I	13.55	0.483	3.32	d_{z^2}
II	15.9	1.787	3.54	$d_{x^2-y^2}$
III	18.9	0.819	3.42	d_{yz}
Powder (R = 0.478%)				
I	13.5	0.416	3.25	d_{z^2}
II	15.65	1.35	3.45	$d_{x^2-y^2}$
III	17.8	1.79	3.69	d_{yz}
IV	19.9	1.73	4.10	d_{xz}
$[Ce(en)(phen)(H_2O)](ClO_4)_2$				
Crystal(//) (R = 0.276%)				
I	13.45	1.20	3.41	d_{z^2}
II	14.8	1.45	3.65	$d_{x^2-y^2}$
III	17.6	5.95	3.60	d_{yz}
Crystal(⊥) (R = 0.351%)				
I	13.5	1.63	3.26	d_{z^2}
II	14.8	3.09	3.43	$d_{x^2-y^2}$
III	17.7	3.94	3.01	d_{yz}
Powder (R = 0.317%)				
I	13.6	0.10	3.34	d_{z^2}
II	14.7	0.22	3.79	$d_{x^2-y^2}$
III	17.0	0.98	4.01	d_{yz}
IV	18.8	0.53	3.80	d_{xz}
$[Cu(en)(tmen)(H_2O)](ClO_4)_2$				
Powder (R = 0.531%)				
I	15.0	0.12	3.33	d_{z^2}
II	16.5	0.64	3.38	$d_{x^2-y^2}$
III	18.2	0.94	3.31	d_{yz}
IV	19.9	1.02	3.97	d_{xz}

[a] Relative peak area.
[b] Half-height width.
[c] Reliability factor $R = \Sigma|y_{obs,i} - y_{calc,i}|/\Sigma y_{obs,i}$.

The molecular projections made by a unit electric vector along the extinction directions in the (001) face for each spectrum were calculated. The optical densities of the parallel and perpendicular crystal spectra can be equated to the sum of the molecular projections squared time the extinction coefficients in the molecular coordinate system (eqs 1–4), where the transformation matrices for a vector in crystal

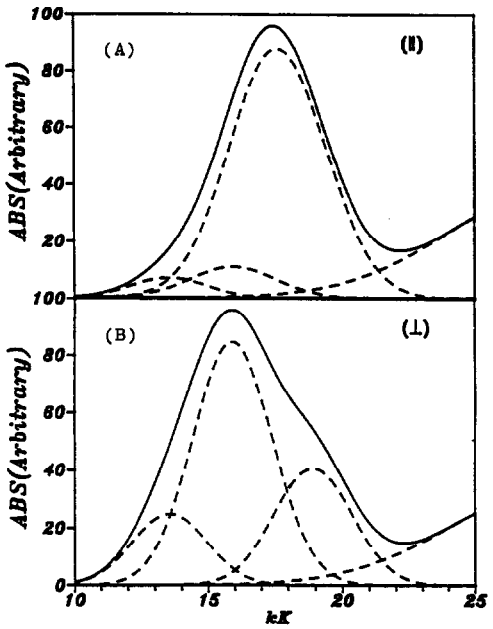

Fig. 6. The polarized spectrum of the (001) face of $[Cu(en)(bipy)(H_2O)](ClO_4)_2$ with the electric vector (A) 26.4° from the a axis and (B) −63.6° from the a axis.

coordinates into molecular coordinates are:

$$\begin{bmatrix} x \\ y \\ z \end{bmatrix} = \begin{bmatrix} 0.6600 & 0.7361 & -0.5490 \\ -0.2028 & -0.2419 & -0.7096 \\ -0.7230 & 0.6320 & 0.4415 \end{bmatrix} \begin{bmatrix} a \\ b \\ c \end{bmatrix}$$

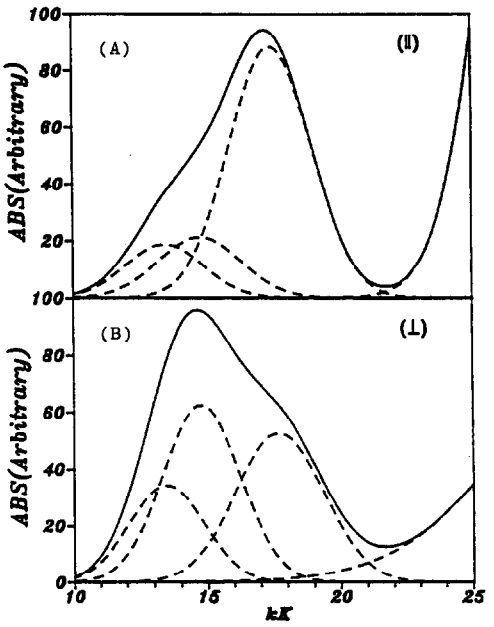

Fig. 7. The polarized spectrum of the (001) face of $[Cu(en)(phen)(H_2O)](ClO_4)_2$ with the electric vector (A) 21.3° from the a axis and (B) −68.7° from the a axis.

and

$$\begin{bmatrix} x \\ y \\ z \end{bmatrix} = \begin{bmatrix} -0.4955 & -0.7120 & 0.4415 \\ 0.0584 & 0.3040 & 0.7278 \\ 0.8043 & -0.6334 & -0.5255 \end{bmatrix} \begin{bmatrix} a \\ b \\ c \end{bmatrix}$$

for **1** and **2**, respectively.

$$0.5928\varepsilon_x + 0.0401\varepsilon_y + 0.4142\varepsilon_z = \mathrm{OD}(//)(\mathbf{1}), \quad (1)$$

$$0.3730\varepsilon_x + 0.0777\varepsilon_y + 0.5329\varepsilon_z = \mathrm{OD}(\perp)(\mathbf{1}), \quad (2)$$

$$0.9375\varepsilon_x + 0.0928\varepsilon_y + 0.1790\varepsilon_z = \mathrm{OD}(//)(\mathbf{2}), \quad (3)$$

$$0.2178\varepsilon_x + 0.0248\varepsilon_y + 0.6287\varepsilon_z = \mathrm{OD}(\perp)(\mathbf{2}). \quad (4)$$

Because the crystal spectra were measured in only one face, transformation of the crystal spectra into molecular spectra[25] was not performed. Inspection of the values of the molecular projections reveals that the parallel spectra are mainly x polarized for both complexes, while the perpendicular spectra are mainly z polarized with some extent of x polarization. This is in agreement with the observed polarized spectra assuming an effective symmetry of C_{2v} for both complexes.

The molecules have C_s symmetry, but the contours of the powder spectra having high intensity in the high energy region suggest the symmetry must be higher to C_{2v} group. The ground state in this point group is $A_2(d_{xy})$. The only allowed d–d transitions by a static electric dipole mechanism are $A_2(d_{xy}) \leftarrow B_2(d_{xz})$ in y polarization and $A_2(d_{xy}) \leftarrow B_2(d_{yz})$ in x polarization. The intense component appeared in the parallel spectra at 17.6 kK for both **1** and **2** can be assigned as $A_2(d_{xy}) \leftarrow B_2(d_{yz})$ and the highest energy peak in the perpendicular spectra at 17.7 kK for **2** also as $A_2(d_{xy}) \leftarrow B_2(d_{yz})$. The peak at 18.9 kK, which is not reliable, must be assigned as $A_2(d_{xy}) \leftarrow B_2(d_{yz})$ in accordance with the above analysis. The two low energy peaks with low intensities are assigned as the statically forbidden $A_2(d_{xy}) \leftarrow A_1(d_{z^2})$ and $A_2(d_{xy}) \leftarrow A_2(d_{x^2-y^2})$ transitions. The sequence of the d orbitals is therefore suggested as $d_{xy} > d_{z^2} > d_{x^2-y^2} > d_{yz}$, where d_{xz} is not observed.

Inspecting the Gaussian components of the crystal and the powder spectra for complexes **1** and **2**, the agreement in peak positions and contours is striking. For the powder spectra, two intense peaks were resolved in the high energy region for the bipy and the phen complexes, corresponding to the d_{yz} and d_{xz} orbitals, and two small peaks as d_{z^2} and $d_{x^2-y^2}$ in the low energy region. The spectra agree with C_{2v} local symmetry and the coordinate system mentioned above for complexes **1** and **2**. The sequence of the d orbitals is $d_{xy} > d_{z^2} > d_{x^2-y^2} > d_{yz} > d_{xz}$.

Since the symmetry group for the tmen complex is similar to that of complexes **1** and **2** and there are also two intense high energy component peaks and two weak low energy peaks for the tmen complex, an effective symmetry of C_{2v} is again appropriate for this square-pyramidal complex and the sequence of the d orbitals is suggested to be $d_{xy} > d_{z^2} > d_{x^2-y^2} > d_{yz} > d_{xz}$.

Finally, it is interesting to consider the energy levels for these complexes. Note that the energy differences between the d_{xz} and the d_{yz} orbitals are nearly the same for the tmen complex and the bipy and the phen complexes, indicating that they are of non-bonding orbitals and are resulted from the geometries of the complexes. Should there by π-interactions between the d_{yz} orbitals and the π-orbitals of the bipy and phen ligands, the d_{yz} orbitals should be ascended or descended with respect to that of the tmen complex, where no π-interaction is possible. We therefore conclude no π-interactions in the bipy–copper(II) and phen–copper(II) bonds in these square-pyramidal complexes. This could be ascribed to the large energy separation between the ligand π orbitals and the copper d_{yz} orbital.

Acknowledgements—We gratefully acknowledge the National Science Council of the Republic of China for financial support (NSC81-0208-M-110-27).

REFERENCES

1. B. J. Hathaway, in G. Wilkinson, R. D. Gillard and J. A. McCleverty (eds), *Comprehensive Coordination Chemistry*, Vol. 5, pp. 594–774, Pergamon, Oxford (1987).
2. B. J. Hathaway, *Structure and Bonding* 1984, **57**, 55.
3. B. J. Hathaway, in J. N. Bradley and R. D. Gillard (eds), *Essays in Chemistry*, pp. 61–92. Academic Press, New York (1971).
4. B. J. Hathaway and D. E. Billing, *Coord. Chem. Rev.* 1970, **5**, 143.
5. I. M. Proctor, B. J. Hathaway and P. Nicholls, *J. Chem. Soc.* (*A*) 1968, 1678.
6. For abbreviations, vide footnote of Table 3.
7. S.-L. Wang, P.-C. Wang and Y. P. Nieh, *J. Appl. Cryst.* 1990, **23**, 52.
8. G. M. Sheldrick, *SHELXTL PLUS User Manual*, Nicolet XRD Corporation, Madison, WI (1986).
9. *International Tables for X-ray Crystallography*, Vol. 4, Kynoch, Birmingham, U.K. (1974).
10. C.-C. Su, Y.-L. Lin, S.-L. Wang and W.-C. Chou, *Transition Met. Chem.* 1993, **18**, 113.
11. D. E. Billing, R. Dudley, B. J. Hathaway, P. Nicholls and I. M. Procter, *J. Chem. Soc.* (*A*) 1969, 312.
12. D. S. Brown, J. D. Lee and B. G. A. Nelson, *Acta Cryst.* 1968, **B24**, 730, and references therein.
13. M. V. Veidis, G. M. Schreiber, T. E. Gough and G. J. Palenik, *J. Am. Chem. Soc.* 1969, **91**, 1859.

14. N. Nakai, *Bull. Chem. Soc. Jpn* 1983, **56**, 1637.
15. J. Foley, D. Kennefiek, D. Phelan, S. Tyagi and B. J. Hathaway, *J. Chem. Soc., Dalton Trans.* 1983, 2333.
16. A. Sedov, M. Dunaj-Jurco, M. Kabesova, J. Gazo and J. Garaj, *Inorg. Chim. Acta* 1982, **64**, L257.
17. C. Escobar and O. Wittke, *Acta Cryst. C* 1983, **39**, 1643.
18. G. W. R. Canham and A. B. P. Lever, *Can. J. Chem.* 1972, **50**, 3866.
19. R. W. Berg and K. Rasmussen, *Spectrochim. Acta* 1974, **30A**, 1881.
20. Y. Saito, J. Takemoto, B. Hutchinson and K. Nakamoto, *Inorg. Chem.* 1970, **11**, 2003.
21. J. Takemoto, B. Hutchinson and K. Nakamoto, *Chem. Commun.* 1971, 1007.
22. R. E. Wilde and T. K. J. Srinivasan, *Inorg. Nucl. Chem.* 1974, **36**, 323.
23. B. J. Hathaway, *J. Chem. Soc., Dalton Trans.* 1972, 1196.
24. See Table 5 footnote c.
25. M. A. Hitchman and R. L. Belford, *Inorg. Chem.* 1971, **10**, 984.

Polyhedron Vol. 12, No. 22, pp. 2697–2704, 1993
Printed in Great Britain

0277–5387/93 $6.00+.00
© 1993 Pergamon Press Ltd

SYNTHESIS, STRUCTURE AND MAGNETIC PROPERTIES OF TRINUCLEAR COMPLEXES OF COPPER(II) WITH DIFFERENT AMINES AS TERMINAL LIGANDS

RAMON COSTA, AUXILIADORA GARCIA, ROSER SANCHEZ and JOAN RIBAS*

Departament de Química Inorgánica, Universitat de Barcelona,
Diagonal 647, 08028-Barcelona, Spain

and

XAVIER SOLANS and VICTOR RODRIGUEZ

Departament de Cristal.lografia i Dipósits Minerals, Universitat de Barcelona,
Martí i Franqués s/n, 08028-Barcelona, Spain

(*Received* 16 *June* 1993; *accepted* 12 *July* 1993)

Abstract—Three new trinuclear copper(II) complexes were synthesized: {[(ettmd)Cu]$_2$[μ-Cu(pba)]}(ClO$_4$)$_2$ (**1**), {[(pmd)Cu]$_2$[μ-Cu(Me$_2$pba)]}(ClO$_4$)$_2$·3H$_2$O (**2**) and {[(bapa)Cu]$_2$[μ-Cu(Me$_2$pba)]}(ClO$_4$)$_2$ (**3**) where Cu(pba) = 1,3-propanediyl-bis(oxamato)cuprate(II), Cu(Me$_2$pba) = 2,2-dimethyl-1,3-propanediyl-bis(oxamato)cuprate(II), ettmd = 4-ethyl-1,1,7,7-tetramethyldiethylenetriamine; pmd = N,N,N′,N″, N″-pentamethyldiethylenetriamine, bapa = bis(3-aminopropyl)amine. The structures of compounds **1**, **2** and **3** were determined by X-ray analysis. The crystals of **1** are monoclinic, space group $P2_1/c$, with a = 18.463(4), b = 14.402(3), c = 16.537(4) Å, β = 109.00(3)°, Z = 4 and R = 0.072 for 2447 reflections observed. The crystals of **2** are triclinic, space group $P\bar{1}$, with a = 19.610(4), b = 16.626(4), c = 16.007(3) Å, α = 115.75(3)°, β = 89.97(3)°, γ = 100.86(4)°, Z = 4 and R = 0.068 for 7342 reflections observed. The crystals of **3** are orthorhombic, space group *Pcba*, a = 40.492(4), b = 16.363(3), c = 10.944(3) Å, Z = 8 and R = 0.034 for 1634 reflections observed. The central copper(II) ions of compounds **1** and **2** are square-pyramidal, the apical positions being occupied by a perchlorate anion. In **3** the central copper ion is square-planar. The terminal copper ions of compounds **1**, **2** and **3** are all pentacoordinated with geometries that are intermediate between square-pyramidal and trigonal-bipyramidal. If the coordination is described in terms of square-pyramidal geometry, the basal plane of each terminal copper atom is approximately perpendicular to the basal plane of the central copper ion. The distortion towards trigonal-bipyramidal geometry is largest for compound **1** and smallest for **3**. Magnetic susceptibility measurements were carried out for this series of complexes. The magnetic data were interpreted using the Heisenberg Hamiltonian and led to J values of −137.1, −128.1 and −92.1 cm^{-1} for **1**, **2** and **3**, respectively. The intensity of the magnetic coupling is discussed in terms of the relative orientation of magnetic orbitals.

Magneto-structural correlations in binuclear copper(II) complexes have been exhaustively investigated[1–5] in the last two decades. It is now well established that $C_2X_2Y_2$ (X, Y = O, N, S) ligands are efficient in propagating the magnetic interaction when they bridge two copper(II) centres, giving antiferromagnetic coupling. It has been shown in binuclear systems that it is possible to tune the magnitude of the interaction by retaining the same bridging ligand and changing only the terminal ones.[2c,3d] In comparison, the literature on magnetic properties of trinuclear systems is rather limited.[6] We have recently studied the influence of terminal ligands on the magnitude of the magnetic exchange

* Author to whom correspondence should be addressed.

interaction through the oxamato bridge in trinuclear copper(II) complexes.[7] With tridentate amine as terminal blocking ligand, the tendency to have bpt or sqp geometry according to the bulkiness of the N-substituents allows us to correlate geometry and magnetic coupling. In order to improve the magneto-structural correlations already found, we have undertaken the synthesis and characterization of new complexes with different terminal tridentate amine ligands, and also with a slightly different central copper(II) ligand. We now present the study of three new trinuclear compounds structurally characterized: $\{[(ettmd)Cu]_2[\mu\text{-}Cu(pba)]\}(ClO_4)_2$ (**1**), $\{[(pmd)Cu]_2[\mu\text{-}Cu(Me_2pba)]\}(ClO_4)_2\cdot 3H_2O$ (**2**) and $\{[(bapa)Cu]_2[\mu\text{-}Cu(Me_2pba)]\}(ClO_4)_2$ (**3**) where Cu(pba) = 1,3-propanediyl-bis(oxamato)cuprate(II), $Cu(Me_2pba)$ = 2,2-dimethyl-1,3-propanediyl-bis(oxamato) cuprate(II), ettmd = 4-ethyl-1,1,7,7-tetramethyldiethylenetriamine; pmd = N,N,N′,N″,N″-pentamethyldiethylenetriamine, bapa = bis(3-aminopropyl)amine.

EXPERIMENTAL

Preparation of the copper(II) complexes

The syntheses of sodium propanediylbis (oxamato)cuprate(II) hexahydrate ($Na_2[Cu(pba)]\cdot 6H_2O$) was carried out according to the literature method.[8] The 2,2-dimethyl-derivative was synthesized in a similar manner, using 2,2-dimethyl-1,3-propanediamine (Aldrich) instead of 1,3-propanediamine.

The compounds $\{[(ettmd)Cu]_2[\mu\text{-}Cu(pba)]\}(ClO_4)_2$ (**1**), $\{[(pmd)Cu]_2[\mu\text{-}Cu(Me_2pba)]\}(ClO_4)_2\cdot 3H_2O$ (**2**) and $\{[(bapa)Cu]_2[\mu\text{-}Cu(Me_2pba)]\}(ClO_4)_2$ (**3**) were synthesized as follows: 1 mmol of the tridentate amine (ettmd, pmd, bapa; Aldrich, without further purification) was added dropwise with stirring to 0.37 g (1 mmol) of copper(II) perchlorate hexahydrate dissolved in 10 cm^3 of water. The solutions turned dark blue. After some minutes, a hot solution of 0.5 mmol of $Na_2[Cu(pba)]\cdot 6H_2O$ or $Na_2[Cu(Me_2pba)]\cdot 3H_2O$ in 10 cm^3 of water was added slowly to the stirred solutions. The resulting blue mixtures were left to stand until dark blue crystals of the complexes were formed. The products were recrystallized in acetonitrile. In all cases the analytical results agree with the formulae proposed.

X-ray data collection and structure determination

Data for compounds **1**, **2** and **3** were collected on a Philips PW-1100 diffractometer, using monochromatic Mo-K_α radiation. Unit cell parameters were determined from 25 automatically centered reflections in the θ-ranges 8–12°. Intensity data were collected in the θ-ranges 2–25°, with the ω-scan technique. The total number of unique reflections recorded was 2447, 7342, and 1634 for compounds **1**, **2** and **3**, respectively. In each case the three reference reflections monitored throughout the data collection showed no significant intensity decay with time. The data were corrected for Lorentz and polarization effects.

Structure **1** was solved by direct methods, using the Multan system[9]; structures **2** and **3** by Patterson synthesis, using SHELXS program.[10] Refinements were performed by least-squares methods minimizing the function $\Sigma w||F_o|-|F_c||^2$, with $w = [\sigma^2(F_o)+k|F_o|^2]^{-1}$, where k = 0.002 for **1**, 0 for **2** and 0.0028 for **3**. The calculations were carried out with the SHELX76 computer program.[11] f,f′,f″ were taken from International Tables of Crystallography.[12] Special aspects of solution and refinement of each structure are described separately as follows.

Compound **1**. Oxygen atoms of perchlorate ions and some carbon atoms of ethyl groups are disordered, the occupancy factor was assumed to be 0.5 according to the height of the peaks of Fourier synthesis. The position of hydrogen atoms linked to carbon atoms was computed and refined with an overall isotropic temperature factor using a riding model. All non-hydrogen and non-disordered atoms were refined anisotropically. The final R factor was 0.072 ($R_w = 0.078$) for all reflections observed. Max. shift/ESD = 0.06 in z of O(102); max and min peaks in the final difference synthesis were 0.4 and −0.2 e $Å^{-3}$, respectively.

Compound **2**. The final R factor was 0.068 ($R_w = 0.074$) for all reflections observed. Number of parameters refined was 1062. Max. shift/ESD = 0.1; max and min peaks in final difference synthesis were 0.4 and −0.4 e $Å^{-3}$, respectively.

Compound **3**. 44 H atoms were computed in its position and refined with an overall isotropic temperature factor using a riding model. The final R factor was 0.034 ($R_w = 0.036$) for all reflections observed. Number of parameters refined was 438. Max. shift/ESD = 0.1; max and min peaks in final difference synthesis were 0.4 and −0.4 e $Å^{-3}$, respectively.

Crystal data for **1**. $C_{27}H_{56}Cu_3N_8O_2(ClO_4)_2$, formula weight = 978.29, monoclinic, a = 18.463(4), b = 14.402(3) c = 16.537(4) Å, β = 109.00(3)°, V = 4158(3) $Å^3$, $P2_1/c$, $D_{calc.}$ 1.562 g cm^{-3}, Z = 4, $F(000)$ = 2028.0, λ(Mo-K_α) = 0.71069, μ(Mo-K_α) = 17.78 cm^{-1}, 298 K.

Crystal data for **2**. $C_{27}H_{56}Cu_3N_8O_6(ClO_4)_2 \cdot 3H_2O$, formula weight = 1032.32, triclinic, a = 19.610(4), b = 16.626(4), c = 16.007(3) Å, α = 115.75(3)°, β = 89.97(3)°, γ = 100.86(4)°, V = 4597(3) Å^3, P-1, D_{calc} = 1.491 g cm^{-3}, Z = 4, $F(000)$ = 2148.0, λ(Mo-K_α) = 0.71069 Å, μ(Mo-K_α) = 16.17 cm^{-1}, 298 K.

Crystal data for **3**. $C_{21}H_{44}Cu_3N_8O_6(ClO_4)_2$, formula weight = 894.2, orthorhombic, a = 40.492(4), b = 16.363(3), c = 10.944(3) Å, V = 7251(4) Å^3, $Pcab$, D_{calc} = 1.638 g cm^{-3}, Z = 8, $F(000)$ = 3672.0, λ(Mo-K_α) = 0.71069 Å, μ(Mo-K_α) = 20.30 cm^{-1}, 298 K.

Physical measurements. Magnetic susceptibility of powdered samples of products **1**, **2** and **3** was measured in a 15 kG field on a MANICS-DSM8 susceptometer equipped with an Oxford Instruments liquid helium cryostat, working down to 4.2 K. The independence of the susceptibility vs the applied field was checked at room temperature for all compounds. Mercury tetrakis(thiocyanato) cobaltate(II) was used as a susceptibility standard.

RESULTS

Description of structures

The structures of compounds **1** and **3** are made up of a cationic trinuclear copper(II) unit and two perchlorate anions. The cation structures are depicted with their labelling schemes in Figs 1 and 2, respectively. For complex **2**, two very similar trinuclear units are present in the crystal net, together with three water molecules. The structure of one of the trinuclear cations with its labeling scheme is shown in Fig. 3. Main bond lengths and angles for compounds **1**, **2** and **3** are listed in Tables 1, 2 and 3, respectively.

The central copper atom of the trinuclear cations of compounds **1** and **2** have approximately square-pyramidal coordinations. In the basal plane they are surrounded by two nitrogen atoms and two oxygen atoms of the oxamato bridges. The apical positions are occupied by oxygen atoms of a perchlorate ion at 2.52 Å (compound **1**) and 2.45 Å (compound **2**, unit **A**) and 2.67 Å (compound **2**,

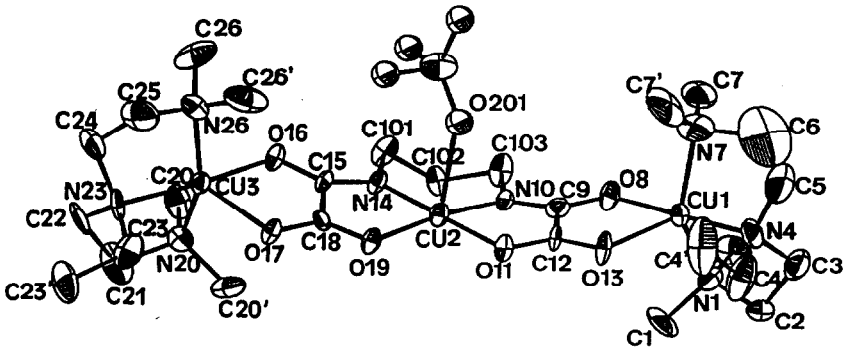

Fig. 1. Plot of the trinuclear cation of $\{[(ettmd)Cu)]_2[\mu\text{-}Cu(pba)]\}(ClO_4)_2$ (**1**), showing the atom numbering scheme.

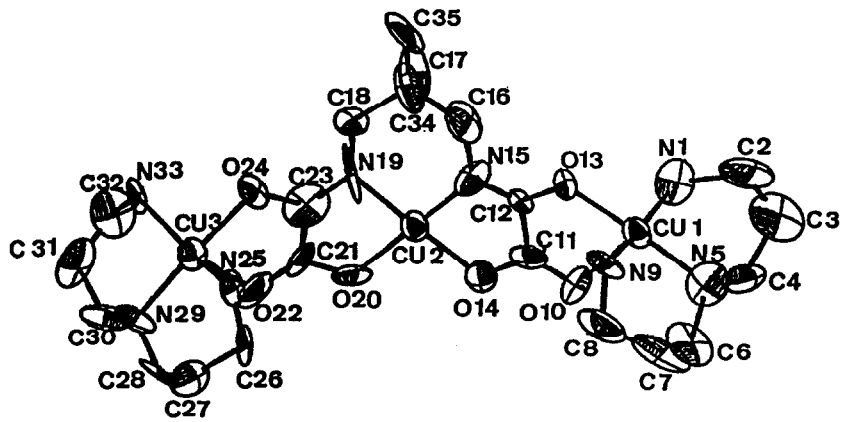

Fig. 2. Plot of the trinuclear cation of $\{[(bapa)Cu]_2[\mu\text{-}Cu(Me_2pba)]\}(ClO_4)_2$ (**3**), showing the atom numbering scheme.

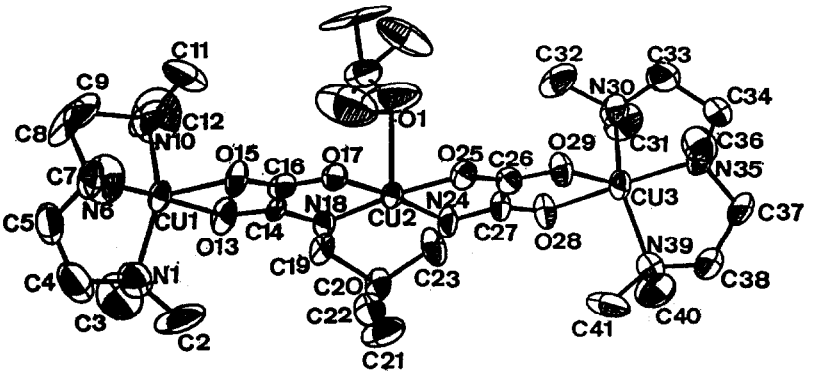

Fig. 3. Plot of the trinuclear cation of $\{[(pmd)Cu]_2[\mu\text{-}Cu(Me_2pba)]\}(ClO_4)_2 \cdot 3H_2O$ (**2**), showing the atom numbering scheme.

unit **B**). In compound **3** the central copper atom has an approximately square planar coordination, surrounded by two nitrogen atoms and two oxygen atoms of the oxamato bridge.

In all cases the terminal copper atoms are in similar environments, intermediate between trigonal-bipyramidal and square-pyramidal coordinations. In the two cases, the equatorial or basal planes, respectively, are orthogonal to the oxamato bridging groups. Deviation from these ideal geometries will be analysed immediately.

RELATIONSHIPS BETWEEN bpt AND sqp GEOMETRIES FOR TERMINAL COPPER(II) IONS

The evolution between the two geometries can be quantified using the τ parameter[13] defined as:

Table 1. Main bond lengths and angles for $C_{27}H_{56}Cu_3N_8O_6(ClO_4)_2$ (**1**)

N(1)···Cu(1)	2.08(2)	O(19)···Cu(2)	1.96(1)
N(4)···Cu(1)	2.01(1)	O(201)···Cu(2)	2.52(3)
N(7)···Cu(1)	2.05(2)	O(201′)···Cu(2)	2.63(5)
O(8)···Cu(1)	1.96(1)	O(16)···Cu(3)	1.98(1)
O(13)···Cu(1)	2.19(1)	O(17)···Cu(3)	2.24(1)
N(10)···Cu(2)	1.91(1)	N(20)···Cu(3)	2.08(2)
O(11)···Cu(2)	1.97(1)	N(23)···Cu(3)	2.04(1)
N(14)···Cu(2)	1.91(1)	N(26)···Cu(3)	2.08(2)
N(4)—Cu(1)—N(1)	88.1(7)	O(201)—Cu(2)—O(11)	83.7(7)
N(7)—Cu(1)—N(1)	139.6(7)	O(201)—Cu(2)—N(14)	96.9(8)
N(7)—Cu(1)—N(4)	86.0(8)	O(201)—Cu(2)—O(19)	95.2(8)
O(8)—Cu(1)—N(1)	91.7(6)	O(201)—Cu(2)—N(10)	110.1(11)
O(8)—Cu(1)—N(4)	178.8(7)	O(201)—Cu(2)—O(11)	94.3(9)
O(8)—Cu(1)—N(7)	93.4(7)	O(201)—Cu(2)—N(14)	86.6(10)
O(13)—Cu(1)—N(1)	110.1(6)	O(201)—Cu(2)—O(19)	78.6(10)
O(13)—Cu(1)—N(4)	101.4(7)	O(17)—Cu(3)—O(16)	80.0(4)
O(13)—Cu(1)—N(7)	110.2(6)	N(20)—Cu(3)—O(16)	94.4(6)
O(13)—Cu(1)—O(8)	79.8(5)	N(20)—Cu(3)—O(17)	98.6(5)
O(11)—Cu(2)—N(10)	84.0(5)	N(23)—Cu(3)—O(16)	172.6(5)
N(14)—Cu(1)—N(10)	94.9(6)	N(23)—Cu(3)—O(17)	107.2(5)
N(14)—Cu(2)—O(11)	178.7(6)	N(23)—Cu(3)—N(20)	86.7(7)
O(19)—Cu(2)—N(10)	171.3(6)	N(26)—Cu(3)—O(16)	89.6(6)
O(19)—Cu(2)—O(11)	95.1(4)	N(26)—Cu(3)—O(17)	104.1(5)
O(19)—Cu(2)—N(14)	85.9(5)	N(26)—Cu(3)—N(20)	157.3(6)
O(201)—Cu(2)—N(10)	93.3(8)	N(26)—Cu(3)—N(23)	86.6(7)

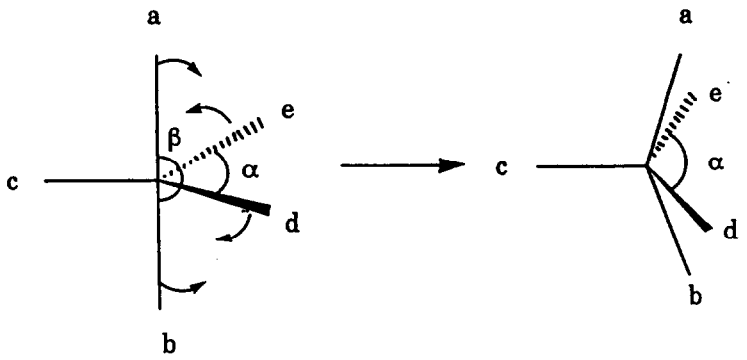

$$\tau = (\beta - \alpha)/60,$$

the angles α and β are defined in the above scheme. The main factor in the distortion is the variation of the α angle going from square-pyramid (sqp, $\alpha = 180°$, $\tau = 0$) to trigonal-bipyramid (bpt, $\alpha = 120°$, $\tau = 1$). The average τ for **1**, **2** and **3** are 0.45, 0.44 and 0.29, respectively. This means that complexes **1** and **2** are really intermediate between sqp and bpt and complex **3** is more pronouncedly sqp. These results agree with literature data on these tridentate amines when they coordinate copper(II) ions: the more N-substituted or the more bulky substituents, the more pronounced is the tendency to bpt geometry.

Magnetic properties

The susceptibility measurements were carried out in the 300–4.2 K temperature range. The $\chi_M \cdot T$ plots vs T are shown in Fig. 4 for all compounds. At room temperature $\chi_M \cdot T$ values are lower than expected for three uncoupled copper(II) ions (1.3 $cm^3\ mol^{-1}\ K$) and are equal to 1.03, 1.07 and 1.10 $cm^3\ mol^{-1} \cdot K$ for **1**, **2** and **3**, respectively. The $\chi_M \cdot T$ product decreases upon cooling and presents a plateau at low temperature with $\chi_M \cdot T$ values equal to 0.44, 0.47 and 0.43 $cm^3\ mol^{-1} \cdot K$ for **1**, **2** and **3**. These values are in the expected range for spin doublet states. At very low temperature, the $\chi_M \cdot T$ product of **1**, **2** and **3** decreases, indicating that an intermolecular antiferromagnetic interaction occurs in these compounds. The experimental data were fitted using the theoretical expression deduced from the following spin Hamiltonian:

$$\hat{H} = -J[\hat{S}_{T1}\hat{S}_C + \hat{S}_C\hat{S}_{T2}] + \beta\vec{H}(g_T[\hat{S}_{T1} + \hat{S}_{T2}] + g_C\hat{S}_C), \quad (1)$$

where T1 and T2 are the two terminal copper(II) ions and C the central one. In this Hamiltonian, the interaction between the terminal ions is assumed to be nil. Using the Van-Vleck formula, the sus-

Table 2. Main bond lengths and angles for $C_{27}H_{56}Cu_3N_8O_6(ClO_4)_2 \cdot 3H_2O$ (**2**)

	Unit A	Unit B
N(1)···Cu(1)	2.062(11)	2.045(10)
N(6)···Cu(1)	2.019(12)	2.004(13)
N(10)···Cu(1)	2.035(9)	2.037(11)
O(13)···Cu(1)	1.970(10)	1.948(10)
O(15)···Cu(1)	2.250(9)	2.236(7)
O(17)···Cu(2)	1.990(9)	1.972(11)
N(18)···Cu(2)	1.938(11)	1.924(9)
N(24)···Cu(2)	1.940(11)	1.930(12)
O(25)···Cu(2)	1.981(8)	1.973(7)
O(1)···Cu(2)	2.448(12)	2.673(7)
O(28)···Cu(3)	1.931(10)	1.936(7)
O(29)···Cu(3)	2.296(11)	2.226(11)
N(30)···Cu(3)	2.091(11)	2.057(10)
N(35)···Cu(3)	2.002(13)	2.017(11)
N(39)···Cu(3)	2.033(12)	2.038(11)
N(6)—Cu(1)—N(1)	86.7(4)	85.1(5)
N(10)—Cu(1)—N(1)	152.2(5)	152.0(4)
N(10)—Cu(1)—N(6)	86.8(4)	87.3(5)
O(13)—Cu(1)—N(1)	91.2(4)	93.7(5)
O(13)—Cu(1)—N(6)	175.5(5)	175.1(4)
O(13)—Cu(1)—N(10)	93.2(4)	91.6(4)
O(15)—Cu(1)—N(1)	107.2(4)	102.5(3)
O(15)—Cu(1)—N(6)	104.3(5)	104.0(4)
O(15)—Cu(1)—N(10)	100.6(4)	105.5(3)
O(15)—Cu(1)—O(13)	80.1(4)	80.9(4)
N(18)—Cu(2)—O(17)	83.9(4)	84.2(4)
N(24)—Cu(2)—O(17)	173.7(3)	178.4(3)
N(24)—Cu(2)—N(18)	94.4(5)	94.5(5)
O(25)—Cu(2)—O(17)	96.9(4)	96.5(4)
O(25)—Cu(2)—N(18)	173.9(3)	178.3(4)
O(25)—Cu(2)—N(24)	84.2(4)	84.9(4)
O(29)—Cu(3)—O(28)	79.4(4)	81.2(4)
N(30)—Cu(3)—O(28)	93.7(4)	91.9(4)
N(30)—Cu(3)—O(29)	100.9(5)	106.4(5)
N(35)—Cu(3)—O(28)	177.0(6)	178.0(5)
N(35)—Cu(3)—O(29)	103.0(5)	100.5(5)
N(35)—Cu(3)—N(30)	87.5(5)	86.7(4)
N(39)—Cu(3)—O(28)	89.5(5)	92.7(4)
N(39)—Cu(3)—O(29)	111.9(4)	107.4(5)
N(39)—Cu(3)—N(30)	147.1(6)	146.1(6)
N(39)—Cu(3)—N(35)	88.0(5)	87.8(5)

Table 3. Main bond lengths and angles for $C_{21}H_{44}Cu_3N_8O_6(ClO_4)_2$ (3)

N(1)···Cu(1)	2.047(7)	N(19)···Cu(2)	1.899(9)
N(5)···Cu(1)	2.010(8)	O(20)···Cu(2)	1.970(6)
N(9)···Cu(1)	2.021(6)	O(22)···Cu(3)	2.310(7)
O(10)···Cu(1)	2.286(7)	O(24)···Cu(3)	1.981(6)
O(13)···Cu(1)	2.057(6)	N(25)···Cu(3)	2.065(8)
O(14)···Cu(2)	1.994(7)	N(29)···Cu(3)	2.018(10)
N(15)···Cu(2)	1.963(11)	N(33)···Cu(3)	2.005(8)
N(5)—Cu(1)—N(1)	94.9(3)	N(19)—Cu(2)—O(14)	178.1(3)
N(9)—Cu(1)—N(1)	149.9(3)	N(19)—Cu(2)—N(15)	91.0(4)
N(9)—Cu(1)—N(5)	94.3(3)	O(24)—Cu(3)—O(22)	79.9(2)
O(10)—Cu(1)—N(1)	112.0(3)	N(25)—Cu(3)—O(22)	95.6(3)
O(10)—Cu(1)—N(5)	92.4(3)	N(25)—Cu(3)—O(24)	87.5(3)
O(10)—Cu(1)—N(9)	96.1(3)	N(29)—Cu(3)—O(22)	100.2(3)
O(13)—Cu(1)—N(1)	84.7(3)	N(29)—Cu(3)—O(24)	176.5(3)
O(13)—Cu(1)—N(5)	171.4(3)	N(29)—Cu(3)—N(25)	89.0(4)
O(13)—Cu(1)—N(9)	90.3(2)	N(33)—Cu(3)—O(22)	100.6(3)
O(13)—Cu(1)—O(10)	79.8(3)	N(33)—Cu(3)—O(24)	89.4(3)
N(15)—Cu(2)—O(14)	87.8(4)	N(33)—Cu(3)—N(25)	162.7(3)
O(20)—Cu(2)—O(14)	96.2(3)	N(33)—Cu(3)—N(29)	94.0(4)
O(20)—Cu(2)—N(15)	174.8(3)		
O(20)—Cu(2)—N(19)	84.9(3)		

ceptibility expression is given as:

$$\chi_M = \frac{N\beta^2}{kT} \cdot \frac{\frac{1}{2}\left(\frac{4g_T - g_C}{3}\right)^2 e^{-J/kT} + \frac{1}{2}g_C^2 + 5\left(\frac{2g_T + g_C}{3}\right)^2 e^{J/kT}}{2e^{-J/kT} + 2 + 4e^{J/kT}} \quad (2)$$

The different g factors of the doublet ground state and the excited doublet and quartet states are taken from Bencini and Gatteschi.[14,15] Minimizing $R = \Sigma[(\chi_M T)^{obs} - (\chi_M T)^{calc}]^2/[(\chi_M T)^{obs}]^2$ by a simplex method leads to the values listed in Table 4. For compound **2**, due to the presence of two different trinuclear entities in the unit cell, the J value corresponds to their average.

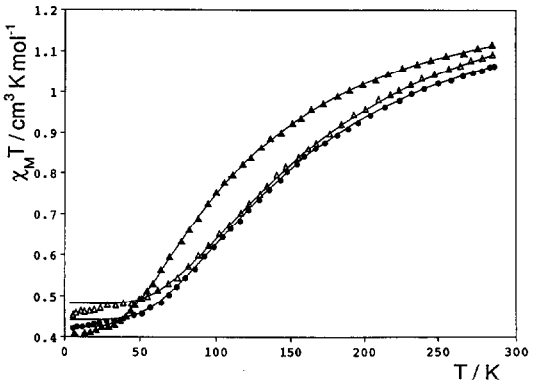

Fig. 4. Plot of the temperature dependence of the product $\chi_M T$ for compounds **1** (●), **2** (△), and **3** (▲).

DISCUSSION

According to the literature data,[7c,16] the variation in the coupling constant J varies approximately as S^2, S being the overlap integral between the magnetic orbitals.

In the series presented here, the coordination around the central copper atoms is either 4 or 4+1. Thus, the magnetic orbitals are well described by the antibonding combination of the $d_{x^2-y^2}$ metallic orbitals with the symmetry adapted molecular orbitals of the oxamato bridge. Concerning the terminal copper atoms, the tridentate amine ligands impose five-coordination which varies between two ideal geometries, trigonal-bipyramidal and square-pyramidal, depending on the bulkiness of the substituents on the nitrogen atoms. Indeed, the bulkier the substituents, the closer the geometry is to the trigonal-bipyramid. The two extreme situations are shown in Fig. 5. In the square-pyramidal case the magnetic orbitals are located in planes orthogonal to the oxamato bridge. When the terminal ligands

Table 4. Least-squares values for the magnetic parameters fitting of the magnetic susceptibility data of compounds **1–3**

Complex	J	g_C	g_T	R
1	−137.1	2.25	2.26	1.2×10^{-4}
2	−128.1	2.25	2.19	2.8×10^{-4}
3	−92.1	2.22	2.15	6.7×10^{-5}

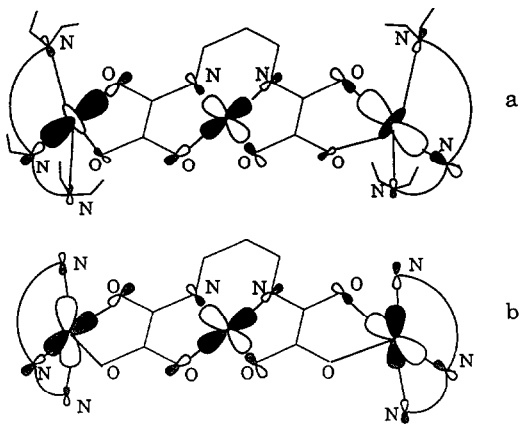

Fig. 5. Relative orientations of the magnetic orbitals when they lie in different planes with trigonal-bipyramidal coordination for both copper(II) terminal ions (a) and square-pyramidal coordination for both copper(II) terminal ions (b).

restrict the geometry in such a way that the magnetic orbitals of the three copper atoms are not in the same place or of the same type, the overlap is reduced and the extent of the interaction is small. J value should be greater when the geometry is bpt than when it is sqp. Structural data for compounds **1**, **2** and **3** present intermediate situations between the two latter cases. Despite the drastic approximation of the model, the J parameter values lie in the expected ranged. Figure 6 shows a simple linear relationship between the values of the experimental J parameter and the average values of the experimentally determined distortion parameter τ. In this figure we also show the average τ for four similar complexes previously reported[7c] together with their J values. This relation confirms that the closer the geometry of the terminal copper(II) ions is to a trigonal-bipyramid the higher is the coupling constant.

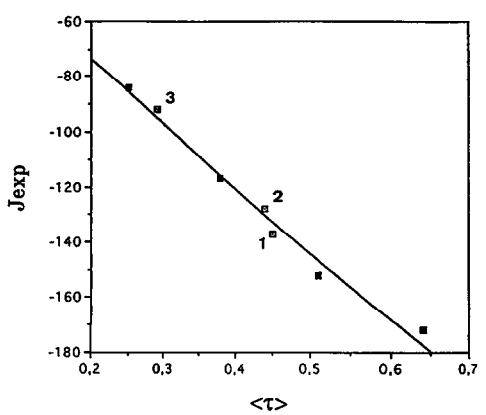

Fig. 6. Representation of the experimental J values for compounds **1**, **2** and **3** vs the average $\langle\tau\rangle$ parameters of their terminal copper(II) ions. $\langle\tau\rangle$ values of the similar complexes reported in reference 7c are also shown.

Supplementary material available

A listing of all bond distances and angles, final atomic coordinates, anisotropic thermal parameters, hydrogen atom coordinates and observed and calculated structure factors has been deposited with the Editor.

Acknowledgement—We are very grateful to DGICYT (grant PB88/197) for financial support.

REFERENCES

1. J. Ribas, A. Garcia, R. Costa, M. Monfort, S. Alvarez, C. Zanchini, X. Solans and M. V. Domenech, *Inorg. Chem.* 1991, **30**, 841.
2. (a) T. R. Felthouse, E. J. Laskowski and D. N. Hendrickson, *Inorg. Chem.* 1977, **16**, 1977; (b) M. Julve, M. Verdaguer, O. Kahn, A. Gleizes and M. Philoche-Levisalles, *Inorg. Chem.* 1984, **22**, 358; (c) M. Julve, M. Verdaguer, A. Gleizes, M. Philoche-Levisalles and O. Kahn, *Inorg. Chem.* 1984, **23**, 3808; (d) M. Julve, J. Faus, M. Verdaguer and A. Gleizes, *J. Am. Chem. Soc.* 1984, **106**, 8306.
3. (a) M. Verdaguer, O. Kahn, M. Julve and A. Gleizes, *Nouv. J. Chim.* 1985, **9**, 325; (b) L. Nonoyama, H. Ojima, K. Ohki and M. Nonoyama, *Inorg. Chim. Acta* 1980, **41**, 155; (c) A. Bencini, C. Benelli, D. Gatteschi, C. Zanchini, A. C. Fabretti and G. C. Franchini, *Inorg. Chim. Acta* 1984, **86**, 169; (d) Y. Journaux, J. Sletten and O. Kahn, *Inorg. Chem.* 1985, **24**, 4063.
4. R. Vicente, J. Ribas, S. Alvarez, A. Segui and M. Verdaguer, *Inorg. Chem.* 1987, **25**, 4004,
5. (a) M. Verdaguer, M. Julve, A. Michalowicz and O. Kahn, *Inorg. Chem.* 1983, **22**, 2624; (b) Y. Pei, M. Verdaguer, O. Kahn, J. Sletten and J. P. Renard, *Inorg. Chem.* 1987, **26**, 138.
6. (a) H. Okawa, M. Kaikawa, S. Kida, D. Luneau and H. Oshio, *J. Chem. Soc., Dalton Trans.* 1990, 469; (b) D. Luneau, H. Oshio, H. Okawa and S. Kida, *J. Chem. Soc., Dalton Trans* 1990, 2283; (c) R. Veit, J. J. Girerd, O. Kahn, F. Robert and Y. Jeannin, *Inorg. Chem.* 1986, **25**, 4175; (d) P. Arrizabalaga, P. Castan and F. Dahan, *Inorg. Chem.* 1983, **22**, 2245; (e) H. Knuutila, *Inorg. Chim. Acta* 1983, **72**, 11; (f) R. Sillanpää and J. Valkonen, *Acta Chem. Scand.* 1992, **46**, 1072.
7. (a) A. García, R. Costa and J. Ribas, *Inorg. Chim. Acta* 1990, **168**, 249; (b) A. García, R. Costa, J. Ribas and M. Monfort, *An. Quim.* 1990, **86**, 524; (c) R. Costa, A. García, J. Ribas, T. Mallah, Y. Journaux, J. Sletten, X. Solans and V. Rodríguez, *Inorg. Chem.* 1993, **32**, 3733.
8. K. Nonoyama, H. Ojima and M. Nonoyama, *Inorg. Chim. Acta* 1976, **20**, 127.
9. MULTAN. A system of computer programs for crystal structure determination from X-ray diffrac-

tion data. University of York, England and University of Louvain, Belgium (1984).
10. G. M. Sheldrick, SHELX. A computer program for crystal structure determination. University of Cambridge, England (1976).
11. G. M. Sheldrick, *Acta Cryst.* 1990, **A46**, 467.
12. *International Tables for X-ray Crystallography*, Vol. IV, 99 (tab. 2.2B). Kynoch Press, Birmingham, England (1974).
13. J. Galy, J. J. Bonnet and S. Anderson, *Acta Chem. Scand., Ser. A* 1979, **A33**, 383.
14. A. Bencini and D. Gatteschi, *EPR of exchange coupled systems*, Springer Verlag, Berlin, Germany (1990).
15. A. Bencini, I. Bertini, D. Gatteschi and A. Scozzafava, *Inorg. Chem.* 1978, **17**, 3194.
16. P. J. Hay, J. C. Thibeault and R. Hoffmann, *J. Am. Chem. Soc.* 1975, **97**, 4884.

Polyhedron Vol. 12, No. 22, pp. 2705–2710, 1993
Printed in Great Britain

0277–5387/93 $6.00+.00
© 1993 Pergamon Press Ltd

FORMATION OF AN UNUSUAL POLYMERIC 24-MEMBERED MACROCYCLIC COMPLEX OF PRASEODYMIUM(III): X-RAY CRYSTAL STRUCTURE OF $[Pr(Ph_3PAuL)_2(NO_3)_3]_n$ (L = SUCCINIMIDE ANION) AND OF ITS $(Ph_3P)AuL$ PRECURSOR

DAVID M. L. GOODGAME,* CAROLINE A. O'MAHONEY, STEVEN D. PLANK and DAVID J. WILLIAMS

Chemistry Department, Imperial College of Science, Technology and Medicine, London SW7 2AY, U.K.

(*Received* 2 *June* 1993; *accepted* 12 *July* 1993)

Abstract—The syntheses and X-ray structures are reported of $(Ph_3P)AuL$, where L = the anion of succinimide, and of the polymeric, macrocyclic array $[Pr(Ph_3PAuL)_2(NO_3)_3]_n$. In the latter compound the Pr atoms are linked by succinimide anions, *via* Pr—O bonding, to produce sheets of fused 24-membered Pr_4L_4 rings.

A variety of gold(I) phosphine complexes exhibit oral anti-inflammatory activity; for example, (1-thio-β-D-glucopyranose-2,3,4,6-tetra-acetato-S)(triethylphosphine)gold(I), "auranofin", is effective in the treatment of rheumatoid arthritis.[1,2] It has also been demonstrated that some gold(I) compounds display anticancer activity.[3]

We have recently reported a range of novel heterometallic, Hg/M, polymeric complexes displaying a diversity of structural types, involving the formation of large metallamacrocycles. These have all included relatively simple ambidentate (N,O donor) ligands, such as β-propiolactam[4,5] (I), 2-pyrrolidone[6] (II), and 2-oxazolidone[5,7] (III). An important, but not necessarily exclusive,[8] component in such systems has been the use of mercury(II) to bind to a deprotonated ring nitrogen atom of the organic ligand, with consequent formation of an essentially linear N—Hg—N arrangement, leaving the exocyclic oxygen atoms free to bind to other metal ions.

In expanding this work, we have sought to replace mercury(II) with gold(I), keeping the other facets of the system essentially unchanged. Attempts to synthesize AuL_2^- species directly analogous to the HgL_2 units used to form the mercury(II)/M polymeric complexes, have so far proved to be unsuccessful. Gold(I) shows a much greater tendency to form complexes with sulphur and phosphorus donor ligands than with those in which O or N are the donor atoms. A correspondingly small number of N-donor complexes, especially with a linear N—Au—N arrangement, have been structurally characterized.[9] The structure of sodium bis(N-methylhydantoinato)gold(I)[10] contains AuL_2^- units (where LH = N-methylhydantoin, IV) analogous to the HgL_2 units of bis(N-methylhydantoinato)mercury(II),[11] but the overall structure is very different. This is due to the presence of the sodium counter ions in the gold compound.

The situation prompted us to investigate complexes of the type $(R_3P)AuL$, where L is an imido-ligand related to those used previously (I–V). Sadler and co-workers[12] have synthesized a range of gold(I) tertiary phosphine complexes with imido-ligands and investigated their anti-inflammatory activity. The synthesis of tertiary phosphine gold(I) derivatives of 2-pyridones has also been reported.[13]

Using succinimide (V) as the imido ligand, the complex $(Ph_3P)AuL$ (where LH = V) (**1**) was readily obtained. This, in turn, has been reacted with praseodymium(III) nitrate to explore its potential as a bridging unit in the formation of macrocyclic compounds. This reaction gave crystals of the polymer $[Pr(Ph_3PAuL)_2(NO_3)_3]_n$ (**2**). We report here the preparation and X-ray structural characterization of both **1** and **2**.

* Author to whom correspondence should be addressed.

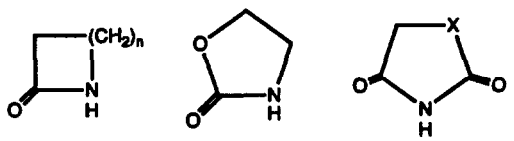

I n = 1
II n = 2

III

IV X = NMe
V X = CH_2

EXPERIMENTAL

Preparation

Ph_3PAuCl. This was prepared by a method analogous to those previously described.[14,15] A solution of Ph_3P (0.77 g) in ether (10 cm^3) was added dropwise, with stirring, to a solution of $HAuCl_4$ (0.5 g) in ether (30 cm^3) at 0°C. After 1 h the initial yellow precipitate turned white. The solution was stirred for a further 2 h and then allowed to warm to room temperature. The white solid was filtered off and dried. Yield 85%. Found: C, 43.8; H, 2.9. Calc. for $C_{18}H_{15}AuClP$: C; 43.6; H, 3.1%.

Ph_3PAuL (LH = *succinimide*) (**1**). To a cooled, stirred solution of Ph_3PAuCl (0.6 g) in methanol (20 cm^3) was added dropwise a solution of succinimide (0.24 g) in methanol (5 cm^3) containing an equimolar amount of NaOH. The solution was stirred for 2 h and the product precipitated by addition of water (*ca* 30 cm^3). The solid was filtered off and recrystallized from methanol (5 cm^3) by the addition of water. The yield of white crystals was 0.535 g (79%). Found: C, 47.1; H, 3.3; N, 2.5. Calc. for $C_{22}H_{19}AuNO_2P$: C, 47.4; H, 3.4; N, 2.5%. The infrared spectrum of **1** shows a single ν(C=O) band at 1650 cm^{-1}. Crystals suitable for X-ray analysis were obtained by slow evaporation of a solution of **1** in methanol.

$[Pr(Ph_3PAuL)_2(NO_3)_3]_n$ (LH = *succinimide*) (**2**). Small pale green crystals of **2** separated over 5 days from a methanolic solution of **1** (0.05 g) and hydrated praseodymium(III) nitrate (0.02 g). These were filtered off, washed with ethanol and ether and recrystallized from methanol six times before a crystal of suitable quality could be obtained for X-ray analysis.

X-ray study

Compound **1**. Crystal data for **1**: $C_{22}H_{19}AuNO_2P$, $M = 557.3$, monoclinic, $a = 10.844(3)$, $b = 7.947(1)$, $c = 22.948(4)$ Å, $\beta = 92.38(2)°$, $V = 1976$ $Å^3$, space group $P2_1/n$, $Z = 4$, $D_{calc} = 1.87$ g cm^{-3}, Cu radiation, $\lambda = 1.54178$ Å, μ(Cu-K_α) = 149 cm^{-1}, $F(000) = 1072$. Data were measured on a Nicolet R3m diffractometer with Cu-K_α radiation (graphite monochromator) using ω-scans. A crystal of dimensions $0.06 \times 0.13 \times 0.30$ mm was used. 2668 independent reflections ($2\theta \leqslant 116°$) were measured, of which 2424 had $|F_o| > 3\sigma(|F_o|)$ and were considered observed. The data were corrected for Lorentz and polarization factors; a numerical absorption correction (face-indexed crystal) was applied; maximum and minimum transmission factors were 0.463 and 0.186.

The structure was solved by the heavy atom method. The non-hydrogen atoms were refined anisotropically. The positions of the hydrogen atoms were idealized, C—H = 0.96 Å, assigned isotropic thermal parameters, $U(H) = 1.2U_{eq}(C)$, and allowed to ride on their parent carbon atoms. Refinement was by block-cascade full-matrix least-squares to $R = 0.028$, $R_w = 0.029$ [$w^{-1} = \sigma^2(F) + 0.00031F^2$]. The maximum and minimum residual electron densities in the final ΔF map were 1.00 and −0.79 e $Å^{-3}$, respectively. The mean and maximum shift/error in the final refinement were 0.001 and 0.003, respectively. Computations for both **1** and **2** were carried out on a 486 PC using the SHELXTL-PC program system.

Selected bond lengths and angles for **1** are listed in Table 1.

Compound **2**. Crystal data for **2**: $C_{44}H_{38}Au_2N_5O_{13}P_2Pr$, $M = 1441.6$, monoclinic, $a = 13.856(3)$, $b = 11.691(2)$, $c = 29.208(6)$ Å, $\beta = 90.99(3)°$, $V = 4731$ $Å^3$, space group $C2/c$, $Z = 4$, $D_{calc} = 2.024$ g cm^{-3}, Cu radiation, $\lambda = 1.54178$ Å, μ(Cu-K_α) = 204 cm^{-1}, $F(000) = 2752$. Data were collected on a Nicolet R3m diffractometer with Cu-K_α radiation (graphite monochromator) using ω-scans. A crystal of dimensions $0.09 \times 0.09 \times 0.17$ mm was used. 2404 independent reflections ($2\theta \leqslant 116°$) were measured, of which 2043 had $|F_o| > 6\sigma(|F_o|)$ and were considered observed. The data were corrected for Lorentz and polarization factors; an empirical absorption correction (ellipsoidal) was applied; maximum and minimum transmission factors were 0.092 and 0.025.

The structure was solved by the heavy atom method. The Pr and Au atoms were refined anisotropically; the remaining non-hydrogen atoms were refined isotropically. The phenyl rings of the triphenylphosphine unit were geometrically optimized and refined as rigid bodies. The nitrate groups were constrained to a trigonal geometry and refined subject to N—O and O···O distance constraints. All hydrogen atoms were placed in calculated positions and assigned fixed isotropic thermal parameters ($U = 0.08$). Refinement was by full-matrix least squares to $R = 0.131$, $R_w = 0.155$ [$w^{-1} = \sigma^2(F) + 0.0007F^2$]. The maximum and minimum residual electron densities in the final ΔF map

Table 1. Selected bond lengths (Å) and angles (°) for **1**

Au—P	2.235(2)	Au—N	2.045(5)
P—C(5)	1.829(6)	P—C(11)	1.816(6)
P—C(17)	1.804(5)	N—C(1)	1.355(8)
N—C(4)	1.375(8)	C(1)—O(1)	1.197(9)
C(4)—O(4)	1.224(9)		

P—Au—N	176.9(1)	Au—P—C(5)	111.4(2)
Au—P—C(11)	111.6(2)	Au—P—C(17)	115.6(2)
Au—N—C(1)	124.8(4)	Au—N—C(4)	122.9(4)
C(5)—P—C(11)	104.8(3)	C(5)—P—C(17)	107.7(2)
C(11)—P—C(17)	105.1(2)	C(1)—N—C(4)	112.2(5)
N—C(1)—O(1)	125.1(6)	N—C(4)—O(4)	124.7(6)
N—C(1)—C(2)	109.6(6)	N—C(4)—C(3)	109.6(6)
O(1)—C(1)—C(2)	125.2(6)	C(3)—C(4)—O(4)	125.6(6)

were 5.50 and −4.43 e $Å^{-3}$, respectively in the regions of the Pr and Au atoms. The mean and maximum shift/error in the final refinement were 0.050 and 0.177, respectively.

Because of the severe twinning in the crystalline sample, the resulting data were of poor quality and the final *R* factors are appreciably higher than we would normally accept, indeed data collections were carried out for three different crystals and the results reported correspond to those from the best of those crystals. Attempts at refining the light atoms anisotropically resulted in several of the atoms becoming non-positive definite, probably due to the inability to correct adequately for absorption. However, the gross structural features, in particular the nature of the polymeric array, are undoubtedly correct.

RESULTS AND DISCUSSION

The X-ray structure of **1** (Fig. 1) confirms the main features expected for this type of compound. The gold is bound to the nitrogen atom of the succinimide and to the phosphine in a linear (176.9°) geometry. The Au—N and Au—P distances [2.045(5) and 2.235(2) Å, respectively] do not differ significantly from those in similar compounds.[9,12,13] The succinimide nitrogen atom retains a trigonal planar geometry. Within the crystal, there are no significant short intermolecular contacts. Despite the fairly close approach of the succinimide oxygen atoms to the gold atom (3.26 and 3.29 Å) the environment of the metal is not as crowded as the bulk of the two ligands might indicate. Approach of another metal to the oxygen atoms would not, therefore, be significantly hindered.

Slow evaporation of a methanolic solution of **1** and praseodymium nitrate resulted in the simultaneous formation of large crystals of **1** and crystals of praseodymium nitrate aggregated with those of a new complex $[Pr(Ph_3PAuL)_2(NO_3)_3]_n$ (**2**). Extensive crystal surgery was only able to provide a partially twinned fragment of **2**. This was adequate to provide a definitive structural characterization of the complex, though severely limited in accuracy.

The praseodymium atom is nine coordinate (Fig. 2) and is bonded to four succinimide oxygen atoms, each from a different succinimide unit, two bidentate nitrates and one monodentate nitrate. The structure has crystallographic C_2 symmetry (the monodentate nitrate is disordered about this axis). The coordination geometry about the Pr atom can best be described as pentagonal bipyramidal with four succinimide oxygen atoms and the oxygen of the monodentate nitrate forming the equatorial plane and the two bidentate groups occupying the axial positions (Fig. 3). (These bidentate nitrates are also disordered about the NO_3—Pr—NO_3 axis, the

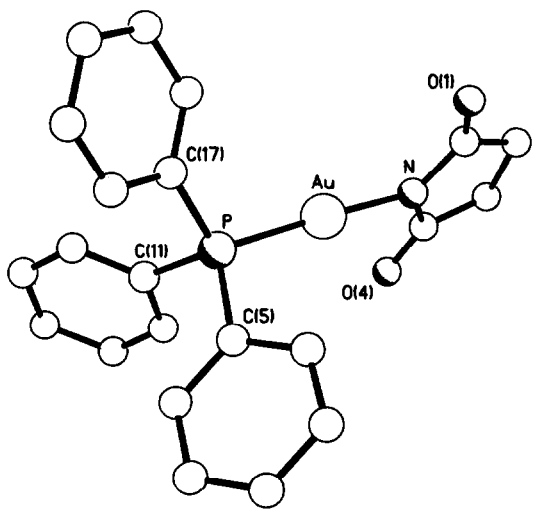

Fig. 1. Perspective view of the structure of **1**.

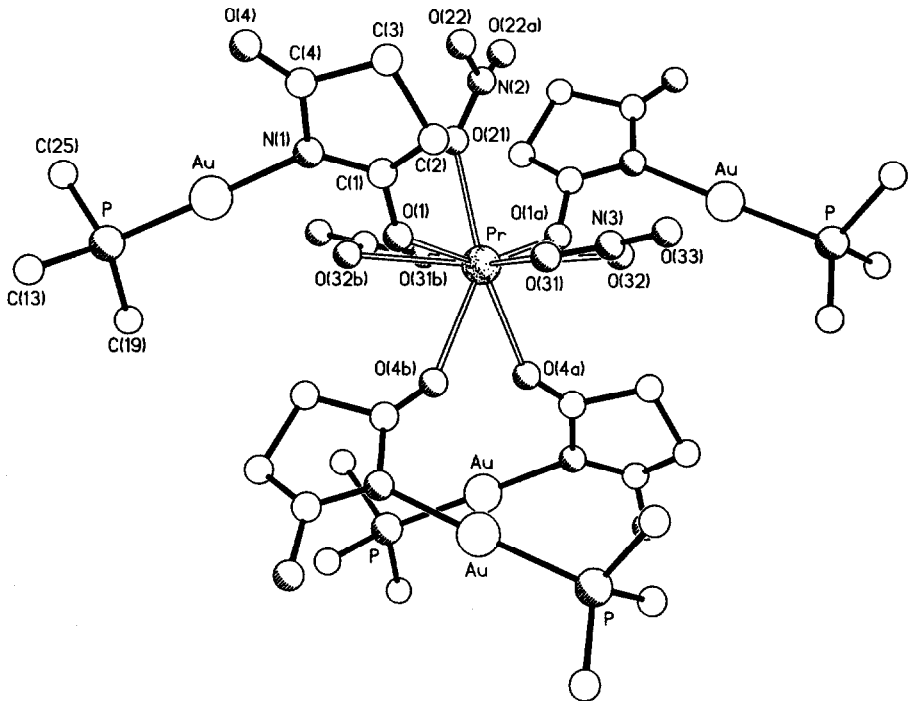

Fig. 2. Molecular environment of each Pr atom in **2**. The phenyl rings on C(13), C(19) and C(25) have been omitted for clarity.

alternate orientation of the nitrates being essentially orthogonal to those depicted.) The in-plane O—Pr—O angles are in the range 63–80° and the axial N—Pr—N angle is 165°. The Pr—O distances lie in the range 2.41(5) to 2.64(3) Å. The Au—P and Au—N distances [2.25(1) and 2.06(3) Å, respectively] do not differ significantly from those observed in **1**.*

The succinimides bridge adjacent Pr centres, thus creating an extended polymeric array comprising fused 24-membered macrocycles, each containing four Pr atoms (Fig. 4a). The periphery of each macrocycle is approximately planar (as is the contiguous array), and the $(Ph_3P)Au$ units and the bidentate nitrates are directed above and below the ring plane (Fig. 4b). The phosphine ligands and the monodentate nitrate groups are all directed in towards the ring centre.

An interesting feature of each 24-membered ring, and of the resulting contiguous array, is their polar nature. However the crystal structure is centrosymmetric and adjacent sheets have opposite polarities.

The result further demonstrates that lanthanide ions can form large macrocyclic arrays without the need for mercury atoms as links between the organic units which bridge the adjacent lanthanide centres. Although the gold atom does not play a direct part in the ring framework, the $(Ph_3P)Au$ unit does appear to play an important role in the macrocycle

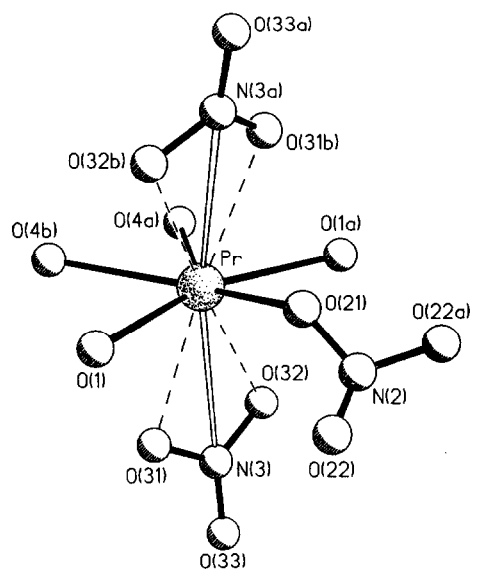

Fig. 3. Pentagonal bipyramidal coordination geometry about Pr in **2**.

* In view of the very limited accuracy of this structure determination, it is not realistic to analyse further in detail aspects of the molecular geometry.

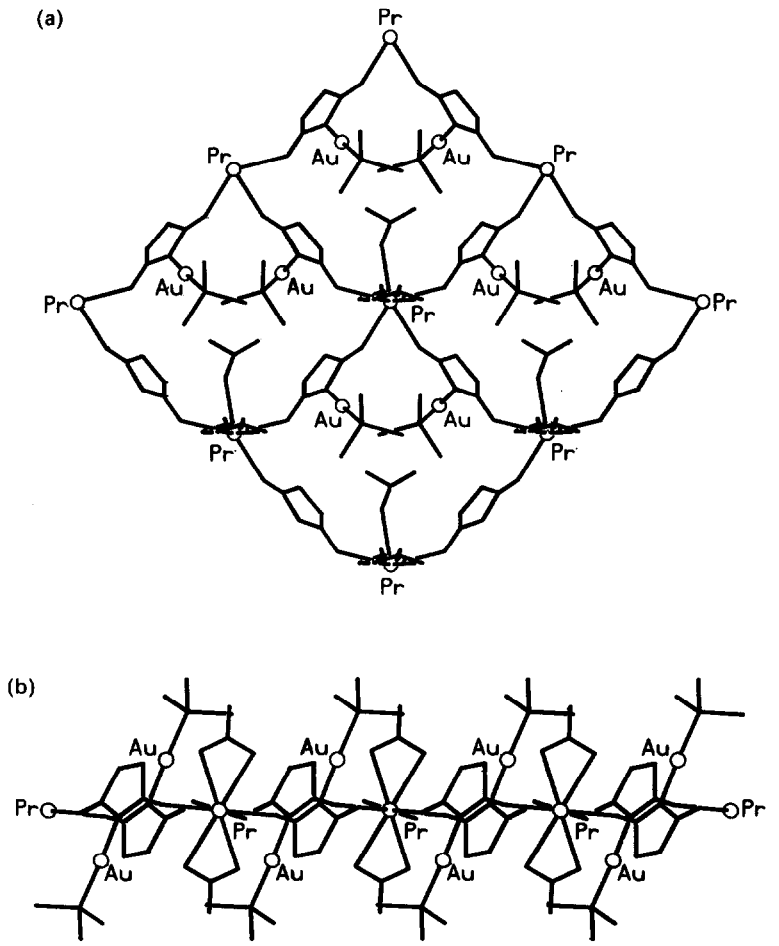

Fig. 4. Part of the contiguous macrocyclic array in the crystals of **2**: (a) plan view; (b) elevation. (In each case, the phenyl rings have been omitted for clarity, and only one set of orientations for the disordered nitrate groups is shown).

formation, as attempts to form such rings using uncomplexed succinimide, its anion, or N-methylsuccinimide have so far been unsuccessful.

Acknowledgements—We thank Johnson Matthey plc for the loan of $HAuCl_4$ and the SERC for funds for the diffractometer and for a Research Studentship (to C.A.O'M).

REFERENCES

1. R. V. Parish and S. M. Cottrill, *Gold Bull.* 1987, **20**, 3.
2. B. M. Sutton, *Gold Bull.* 1986, **19**, 15.
3. (a) C. K. Mirabelli, C-M. Sung, J. P. Zimmerman, D. T. Hill, S. Mong and S. T. Crooke, *Biochem. Pharm.* 1986, **35**, 1427; (b) C. K. Mirabelli, R. K. Johnson, D. T. Hill, L. F. Faucette, G. R. Girard, G. Y. Kuo, C. M. Sung and S. T. Crooke, *J. Med. Chem.* 1986, **29**, 218.
4. D. M. L. Goodgame, A. M. Khaled, C. A. O'Mahoney and D. J. Williams, *J. Chem. Soc., Chem. Commun.* 1990, 851.
5. D. M. L. Goodgame, S. P. W. Hill and D. J. Williams, *Polyhedron* 1992, **11**, 1841.
6. D. M. L. Goodgame, D. J. Williams and R. E. P. Winpenny, *Polyhedron* 1989, **8**, 1913 and refs therein.
7. L. H. Carrad, D. M. L. Goodgame, S. P. W. Hill and D. J. Williams, *J. Chem. Soc., Dalton Trans.* 1993, 1003.
8. G. A. Doyle, D. M. L. Goodgame, S. P. W. Hill and D. J. Williams, *J. Chem. Soc., Chem. Commun.* 1993, 207.
9. P. G. Jones, *Gold Bull.* 1981, **14**, 102.
10. N. A. Malik, P. J. Sadler, S. Neidle and G. L. Taylor, *J. Chem. Soc., Chem. Commun.* 1978, 711.
11. D. M. L. Goodgame, A. M. Khaled, C. A. O'Mahoney and D. J. Williams, *Polyhedron* 1990, **9**, 1765.
12. S. J. Berners Price, M. J. DiMartino, D. T. Hill, R. Kuroda, M. A. Mazid and P. J. Sadler, *Inorg. Chem.* 1985, **24**, 3425.

13. F. Bonati, A. Burini, R. Pietroni and B. Bovio, *J. Organomet. Chem.* 1985, **296**, 301.
14. F. G. Mann, A. F. Wells and D. Purdie, *J. Chem. Soc.* 1937, 1828.
15. M. I. Bruce, B. K. Nicholson and O. Bin Shawkataly, *Inorg. Syn.* 1989, **26**, 324.
16. G. M. Sheldrick, SHELXTL, An integrated system for solving, refining and displaying crystal structures from diffraction data. Revision 4.1. University of Göttingen (1983).

Polyhedron Vol. 12, No. 22, pp. 2711–2717, 1993
Printed in Great Britain

0277–5387/93 $6.00+.00
© 1993 Pergamon Press Ltd

X-RAY STRUCTURE AND BONDING OF 1-PHENYLETHYNYL-2-PHENYL-1,2-DICARBADODECABORANE(12), [1-(PhC≡C)-2-Ph-1,2-$C_2B_{10}H_{10}$], A MODEL ALKYNE COMPLEX CONTAINING A RICH VARIETY OF CARBON–CARBON BOND TYPES

WILLIAM CLEGG

Chemistry Department, Newcastle University, Newcastle upon Tyne NE1 7RU, U.K.

and

ROBERT COULT, MARK A. FOX, WENDY R. GILL, J. A. HUGH MACBRIDE and KENNETH WADE*

Chemistry Department, Durham University Science Laboratories, South Road, Durham DH1 3LE, U.K.

(*Received* 11 *May* 1993; *accepted* 12 *July* 1993)

Abstract—The crystal and molecular structure of 1-phenylethynyl-2-phenyl-1,2-dicarbadodecaborane(12) (**1**), prepared by the reaction between 1,4-diphenylbutadi-yne and the decaborane adduct $B_{10}H_{12}(NCMe)_2$ in boiling toluene, have been established by an X-ray crystallographic study. Evidence of some delocalization of pi-electronic charge in the phenylethynyl ligand towards the carborane cage is provided by the carbon—carbon bond distances [1.431(2), 1.194(2) and 1.433(2) Å, respectively from benzene ring to carborane isocahedron] and Molecular Orbital Bond Index (MOBI) calculations, which also reveal subtle differences in the bonding of the two skeletal carbon atoms to their boron neighbours in the icosahedron. Consideration of (**1**) as an adduct in which one alkyne function of PhC≡CC≡CPh coordinates to an *arachno*-shaped $B_{10}H_{10}$ residue reveals the strong electron-withdrawing capacity of the latter, which is compared with other borane and metal cluster residues.

A recent report[1] of some aryl carboranes, prepared for a study of their second-harmonic generation (SHG) properties, included reference to the new compound 1-phenylethynyl-2-phenyl-1,2-dicarbadodecaborane(12), 1-(PhC≡C)-1-Ph-1,2-$C_2B_{10}H_{10}$ (**1**). We prepared this same compound during our own continuing studies of carborane derivatives for polymer synthesis.[2–6] Our work included a single crystal X-ray study of (**1**) which revealed several features of structural and bonding interest, which we discuss below. They include the rich variety of carbon–carbon bond types; evidence of conjugation between the alkynyl function and the carborane cage; and the presence of an uncoordinated alkynyl unit PhC_2 adjacent to the phenyl-*ortho*-carborane unit $PhC_2B_{10}H_{10}$, which itself can be regarded as an alkyne complex in which a PhC_2 unit coordinates to an *arachno*-shaped $B_{10}H_{10}$ cluster.

RESULTS AND DISCUSSION

Our synthesis of **1**, like that of Mingos and co-workers[1] involved the reaction in boiling toluene between 1,4-diphenylbutadi-yne, PhC≡CC≡CPh, and decaborane. However, instead of carrying out the reaction in the presence of the Lewis base, we used a previously prepared sample of the *arachno* bis(nitrile) adduct $B_{10}H_{12}(NCMe)_2$:

* Author to whom correspondence should be addressed.

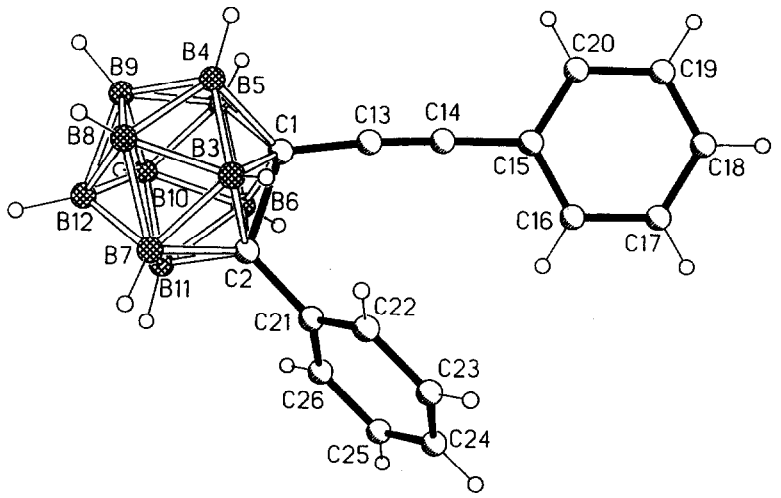

Fig. 1. Structure of compound **1**, 1-PhC≡CC-2-Ph-1,2-$C_2B_{10}H_{10}$, showing atom numbering and highlighting the carbon–carbon links therein.

$$B_{10}H_{14} \xrightarrow[-H_2]{2MeCN} B_{10}H_{12}(NCMe)_2 \xrightarrow[-H_2,\,-2MeCN]{PhC{\equiv}CC{\equiv}CPh} 1\text{-}(PhC{\equiv}C)\text{-}2\text{-}Ph\text{-}1,2\text{-}C_2B_{10}H_{10}\ (\mathbf{1})$$

nido → *arachno* → *closo*

Single crystals of compound **1** suitable for X-ray diffraction were grown from hexane. The molecular structure is shown in Fig. 1. Selected bond lengths and angles are given in Table 1.

One feature of the molecular structure worthy of comment is the orientation of the phenyl groups. If they were oriented so as to minimize intramolecular nonbonded repulsions between them, both would lie in planes perpendicular to the plane of the atoms (C2, 1, 13 and 14) that connect them. In fact, although the phenyl group directly attached to the carborane cage does have roughly the expected orientation [shown in projection in Fig. 2(b)—the

Table 1. Bond lengths (Å) and selected bond angles (°) for **1**

C1—C13	1.433(2)	C1—B4	1.703(2)
C1—B5	1.704(2)	C1—C2	1.710(2)
C1—B6	1.724(2)	C1—B3	1.731(2)
C2—C21	1.503(2)	C2—B11	1.705(2)
C2—B7	1.706(2)	C2—B3	1.741(2)
C2—B6	1.742(2)	B3—B8	1.757(3)
B3—B7	1.770(3)	B3—B4	1.775(3)
B4—B9	1.772(3)	B4—B8	1.773(3)
B4—B5	1.780(3)	B5—B10	1.771(3)
B5—B9	1.772(3)	B5—B6	1.779(3)
B6—B10	1.758(3)	B6—B11	1.775(3)
B7—B11	1.778(3)	B7—B8	1.779(3)
B7—B12	1.782(3)	B8—B12	1.782(3)
B8—B9	1.783(3)	B9—B12	1.777(3)
B9—B10	1.783(3)	B10—B11	1.778(3)
B10—B12	1.787(3)	B11—B12	1.774(3)
C13—C14	1.194(2)	C14—C15	1.431(2)
C15—C16	1.389(2)	C15—C20	1.392(2)
C16—C17	1.388(3)	C17—C18	1.378(3)
C18—C19	1.371(3)	C19—C20	1.373(3)
C21—C26	1.391(2)	C21—C22	1.391(2)
C22—C23	1.384(2)	C23—C24	1.378(3)
C24—C25	1.379(3)	C25—C26	1.384(2)
C13—C1—C2	115.06(12)	C21—C2—C1	117.63(12)
C14—C13—C1	174.6(2)	C13—C14—C15	178.1(2)

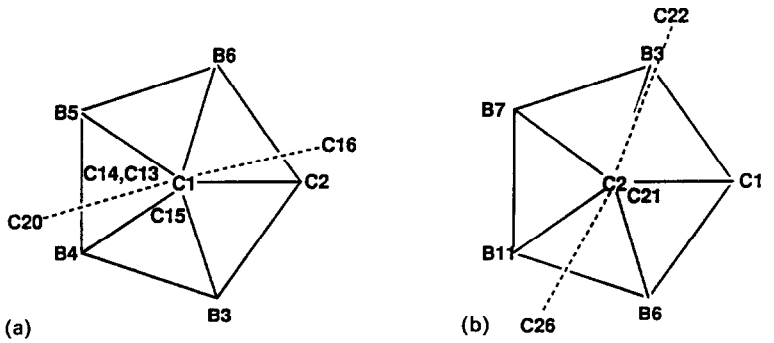

Fig. 2. The pentagonal pyramidal environments of the carboranyl carbon atoms (a) C1 and (b) C2, viewed down their *exo* bonds (C13 to C1, C21 to C2) and showing in projection the orientations of the phenyl groups.

ring plane almost exactly eclipses the link C2—B3, rather than lying parallel to the B3—B6 axis; torsion angle C22—C21—C2—B3 = −0.6°] the other phenyl group [Fig. 2(a)] lies close to the plane of C2, 1, 13, 14 (torsion angle C16—C15···C1—C2 = 13.8°) and the alkyne function bends slightly [by 5.4(2)° at C13 and by 1.9(2)° at C14] *towards* the first phenyl group, as if attracted to it, placing one *ortho* hydrogen atom of the second benzene ring near to the pseudo-6-fold axis of the first ring (H16 lies 3.21 Å from the plane of this ring). These orientations of the phenyl groups have implications for their respective capacities to participate in conjugative interactions with the tangentially-orientated p AO's on the cluster carbon atoms 1 and 2, which in turn are the orbitals through which C1 and C2 bond to their neighbours within the caborane icosahedron (Fig. 3), a point to which we return below.

In principle, significant conjugative interactions involving the phenyl or phenylethynyl ligands should be apparent from their carbon–carbon bond distances. Compound **1** contains an unusually rich variety of carbon–carbon bond types. Their bond distances are given in Table 2, classified according to the connectivities (coordination numbers), k, of the atoms they link. The bonds in the benzene rings, linking atoms for which k = 3, are treated as all of one type, and averaged in this Table, which also lists typical interatomic distances in related compounds for purposes of comparison. From these, it is apparent that the formally single bonds to the ligands (and the bond C14—C15) are a little shorter than might have been expected for single bonds of the connectivities concerned, and both phenyl groups show slight lengthening (by *ca* 0.01 Å) of the bonds to the substituted carbon atoms, i.e. C15—C16/20 and C21—C22/26.

In order to probe the bonding in **1**, we have carried out a Molecular Orbital Bond Index calculation to determine the bond indices (B.I.) which correspond to (though they are typically slightly lower than) formal bond orders.[13] From the bond indices of the carbon–carbon bonds (Table 2) it is

Table 2. Carbon–carbon bond distances (d) and indices (B.I.) in **1**

d/Å	k	B.I.	Carbon atoms involved	Literature values of d/Å
1.710(2)	6–6	0.60	1–2	1.62–1.75[1,9,10a]
1.503(2)	6–3	1.00	2–21	1.49–1.51[1,9,10]
1.433(2)	6–2	1.06	1–13	—
1.383(3)	3–3	1.42	aryl	1.37–1.40[12]
1.431(2)	3–2	1.10	14–15	1.43–1.44[12b]
1.194(2)	2–2	2.69	13–14	1.17–1.20[12c]

[a] Higher values have been found in systems in which the *exo* atoms form strong dative π-bonds to the skeletal atoms (see refs 11, 25, 26).

[b] For single bonds between sp^2 and sp^1 carbon atoms.

[c] For triple bonds in alkynes RC≡CR′.

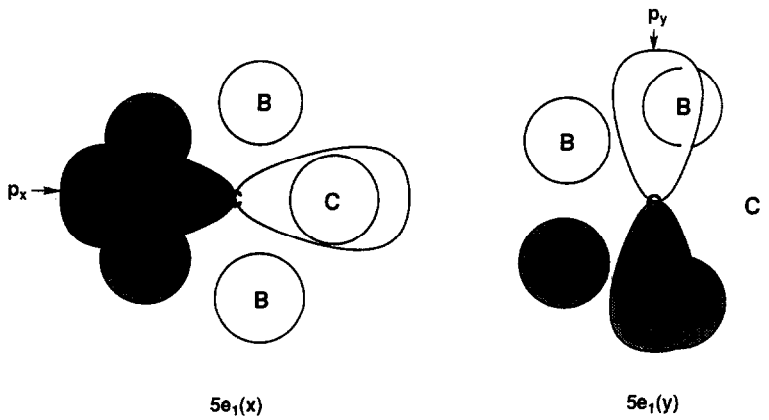

Fig. 3. Frontier orbitals[7,8] through which atoms C1 and C2 bond to their neighbours in the pentagonal faces of the *nido*-shaped CB_{10} residues.

clear that, within the phenylethynyl ligand, the bonds either side of the alkyne unit (particularly that adjacent to the icosahedron) have acquired some multiple bond character at the expense of the triple bond.

Bond indices for all of the links involving the carbon atoms within the carborane icosahedron are shown in Fig. 4. From these it is apparent that atoms C1 and C2 differ subtly but nevertheless significantly in the way they bond to their neighbouring atoms in the icosahedron (C2 and B3, 4, 5 and 6) than does C(2) (whose skeletal neighbours are C1 and B6, 11, 7 and 3), a difference intelligible in that the *exo* π-bonding to C1 referred to above slightly reduces its capacity for cluster bonding compared with C2. A particularly revealing feature of the difference between C1 and C2 in the manner in which they bond to their neighbours within the carborane icosahedron is the pattern of stronger bonds in Fig. 4 (indicated by asterisks), when the environments of C1 [Fig. 4(a)] and C2 [Fig. 4(b)] are compared. Atom C2 is seen to bond some 3–4% more strongly to its four boron neighbours than does C1, and moreover there is stronger bonding between B6 and B11, and between B7 and B3, than is the case between the corresponding atoms adjacent to C1 (B3–B4 and B5–B6).

Comparison of Fig. 4 with Figs 2 and 3 shows that these features are fully in line with the conclusion that conjugative interactions *exo* to the carborane icosahedron involve primarily the p_y orbital on C1 and the p_x orbital on C2, so reducing their contributions to the bonding within the icosahedron, which accordingly is dominated by the p_x orbital on C1 and the p_y orbital on C2.

A further feature of the structure of **1** worthy of comment is prompted by its synthesis from the di-yne PhC≡C—C≡CPh and the *arachno*-borane adduct $B_{10}H_{12}(NCMe)_2$. Compound **1** can be regarded as an adduct in which one of the alkyne functions coordinates to an *arachno*-shaped $B_{10}H_{10}$ residue. The other remains intact as the substituent phenylethynyl unit PhC≡C (Fig. 5); this aspect is also emphasised in Fig. 1 by the representation of open bonds within the $B_{10}H_{10}$ residue and filled bonds in the di-yne residue. Coordination to the

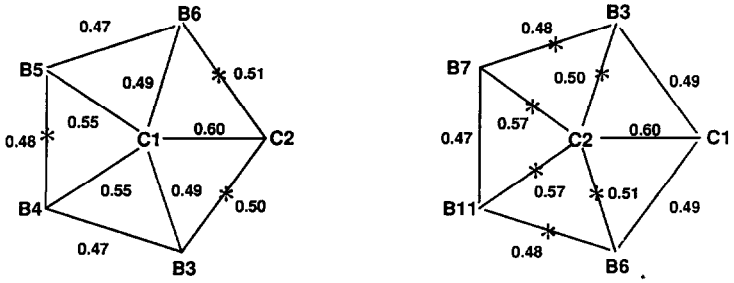

Asterisks mark the stronger bonds when the environments of **C1** and **C2** are compared.

Fig. 4. Bond indices of the cluster bonds near C1 and C2, (a) C1 neighbours, (b) C2 neighbours.

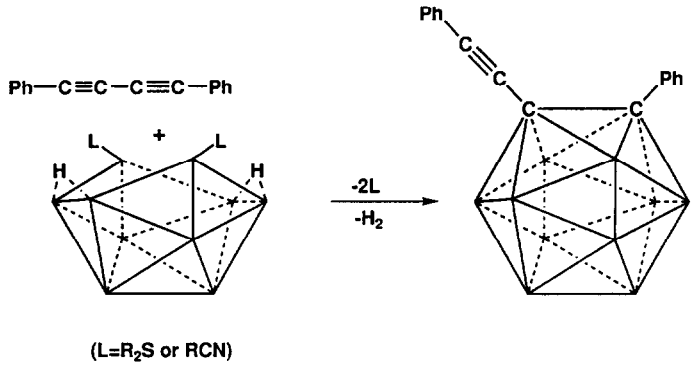

Fig. 5. Formation of **1** represented as the coordination of one alkyne unit of PhC≡CC≡CPh to an *arachno*-shaped $B_{10}H_{10}$ residue.

boat-shaped $B_{10}H_{10}$ residue causes the carbon atoms originally linked by a triple bond of length 1.20 Å in PhC≡CC≡CPh to separate to a distance of 1.71 Å (corresponding to a bond of bond index 0.60) while the C—C—C bond angles at the two carbon atoms [C1 and C2 in **1**] decrease from 180° to 115–118°.

These dramatic changes resemble in kind (though surpassing in extent) those that occur when alkynes coordinate to transition metal clusters. It is usual, for electron book-keeping purposes, to regard the alkynes as 4-electron ligands, donating both pairs of electrons from their pi-systems, when they coordinate to two or more metal atoms, the sigma C—C bond pair being retained by the coordinating alkyne. However, compound **1** provides a reminder that alkynes RC≡CR′ may alternatively be regarded as sources of two carbyne units, RC and R′C, each a source of three electrons. Indeed, in the formation of **1** from $B_{10}H_{12}(NCMe)_2$ and PhC≡CC≡CPh, the loss of two 2-electron ligands (2MeCN) and two 1-electron ligands (2H) from the former is compensated by the provision of two 3-electron units (PhC≡CC and PhC) from the latter, allowing the *arachno* shape of the $B_{10}H_{10}$ residue to be retained. The dramatic reduction in the carbon–carbon bond order of the alkyne effectively results from conversion to a boron–carbon bonding role of the electrons originally forming the alkyne triple bond, sigma as well as pi, even though a weak carbon–carbon link persists.

The effect on the carbon–carbon bond distance of coordination of an alkyne to assorted metal or boron residues is illustrated by the data in Table 3, from which it is apparent that compound **1**, viewed as an η^2-alkyne complex, like other icosahedral carboranes, falls near the upper end of the range of carbon–carbon distances found in such systems.[1,14–24] It is also apparent that the effect on the coordinated alkyne increases with the nuclearity of the system to which it is coordinating, whether metallic (when the carbon–carbon distances can range from *ca* 1.30–1.45 Å, depending on the number of metal atoms and the identity of the other ligands) or boron (when the carbon–carbon distances span the higher range of *ca* 1.43–1.73 Å). Even greater C—C distances have been found in certain other icosahedral carborane systems, such as the anions $[1,2\text{-}X(Ph)C_2B_{10}H_{10}]^-$ (1.86 Å when X = S, 2.00 Å when X = O) in which special circumstances—strong *exo* π-bonding to the substituent sulphur or oxygen atom—apply.[25,26]

EXPERIMENTAL

Synthesis of 1

A solution of 1,4-diphenylbutadi-yne (1.01 g, 5 mmol) in dry toluene (25 cm^3) was added to a suspension of decaborane bis(acetonitrile) adduct (1.01 g, 5 mmol) in toluene (20 cm^3) under nitrogen. After 24 h reflux the red solution was cooled, treated with

Table 3. Carbon–carbon bond lengths in carboranes compared with those in alkyne-metal complexes

Compound	*d*(C—C)/Å	k	References
$1,2\text{-Aryl}_2C_2B_{10}H_{10}$	1.70–1.75	6–6	9, 10
$1,2\text{-}(BrCH_2)_2C_2B_{10}H_{10}$	1.64	6–6	14
$1,2\text{-}H_2C_2B_7H_9$	1.55	4–4	15
$1,2\text{-}H_2C_2B_4H_4$	1.54	5–5	16
$2,3\text{-}H_2C_2B_4H_6$	1.43	4–4	17
$(Et_2C_2)Co_4(CO)_{10}$	1.44	5–5	18
$(Ph_2C_2)_2Fe_3(CO)_8$	1.44	4–4	19
$(Ph_2C_2)Os_3(CO)_{10}$	1.44	4–4	20
$(Ph_2C_2)Fe_3(CO)_9$	1.41	4–5	21
$(Ph_2C_2)Ni_2Cp_2$	1.35	4–4	22
$(Bu^t{}_2C_2)Ta_2Cl_6$	1.35	4–4	23
Various $R_2C_2ML_n$	1.25–1.35	3–3	24

methanol (20 cm^3) then evaporated. The residue was extracted with hexane from which **1** (0.52 g, 33%) crystallized on partial evaporation, m.p. 119–120°C [Found: C, 60.7; H, 6.3%; M_r (mass spectrum) 316–322. Calc. for $C_{16}H_{20}B_{10}$: C, 60.0; H, 6.3%; M_r, 312–322] ν_{max} (KBr disc/cm^{-1}) 3108w, 3086w, 3077w, 3060w, 3044w, (ArH) 2661w, 2649m, 2605s, 2581s, 2577s, (BH) 2239m (C≡C) 756s, 687s (C_6H_5).

NMR spectra of **1** (*solvent* $CDCl_3$)

^1H (300 MHz), $^{11}B\{^1H\}$ (96.25 MHz) and $^{13}C\{^1H\}$ (75.5 MHz) spectra were recorded at the frequencies indicated using $CDCl_3$ as solvent; δ values were identical to, or not significantly different from, those given in ref. 1.

Crystal data for **1**

$C_{16}H_{20}B_{10}$, $M_r = 320.42$, triclinic, space group $P\bar{1}$, $a = 7.2825(10)$, $b = 10.4122(14)$, $c = 12.763(2)$ Å, $\alpha = 74.336(11)$, $\beta = 81.418(10)$, $\gamma = 86.172(10)°$, $V = 921.0(2)$ $Å^3$ at 240 K (Cu–K_α radiation, $\lambda = 1.54184$ Å), $Z = 2$, $D_c = 1.155$ g cm^{-3}, $\mu = 0.405$ mm^{-1}, $F(000) = 332$.

Data collection and processing: crystal size $0.68 \times 0.44 \times 0.24$ mm, Stoe–Siemens diffractometer with Cryostream cooler,[27] cell parameters from 2θ values (44–57°) of 32 reflections measured at $\pm\omega$, intensities from ω/θ scans with on-line profile fitting,[28] 2θ range 7 to 130°, index ranges h 0 to 8, k −12 to 12, l −14 to 14 (Friedel opposites were measured instead for some inaccessible reflections); corrections for 5% intensity decay of 3 standard reflections, no absorption corrections.

Structure solution and refinement:[29] non-hydrogen atoms by direct methods, H atoms constrained [riding model, with C—H 0.94 Å, B—H 1.11 Å, $U(H) = 1.2\ U_{eq}$ (C or B)]; full-matrix least-squares refinement on F^2 for all 3082 measured data, with weighting $W^{-1} = \sigma^2(F_o^2) + (0.0892P)^2 + 0.3378P$, where $P = (F_o^2 + 2F_c^2)/3$; isotropic extinction parameter $\chi = 0.007(1)$, where F_c^2 is multiplied by $(1 + 0.001\chi F_c^2 \lambda^3/\sin 2\theta)^{-1/4}$; all shifts < 0.001 times corresponding parameter ESD; final difference map between +0.211 and −0.252 e $Å^{-3}$. For 236 parameters, $wR2 = [\Sigma w(F_o^2 - F_c^2)^2/\Sigma w(F_o^2)^2]^{1/2} = 0.1517$ for all data, conventional $R = 0.0531$ for unweighted F values of 2804 reflections having $F_o^2 > 2\sigma(F_o^2)$, goodness of fit on $F^2 = 1.037$.

Atomic coordinates, complete bond lengths and angles, and displacement parameters have been deposited as supplementary material at the Cambridge Crystallographic Data Centre.

Acknowledgement—SERC support of this work is gratefully acknowledged.

REFERENCES

1. D. M. Murphy, D. M. P. Mingos, J. L. Hagitt, H. R. Powell, S. A. Westcott, T. B. Marder, N. J. Taylor and D. R. Kanis, *J. Mater. Chem.* 1993, **3**, 139.
2. H. M. Colquhoun, J. A. Daniels, I. R. Stephenson and K. Wade, *Polym. Commun.* 1991, **32**, 272.
3. D. A. Brown, H. M. Colquhoun, J. A. Daniels, J. A. H. MacBride, I. R. Stephenson and K. Wade, *J. Mater. Chem.* 1992, **2**, 793.
4. R. Coult, M. A. Fox, W. R. Gill, P. L. Herbertson, J. A. H. MacBride and K. Wade, *J. Organometal. Chem.* 1993, in press.
5. I. R. Stephenson, Ph.D. Thesis, Durham University (1988).
6. M. A. Fox, Ph.D. Thesis, Durham University (1991).
7. D. M. P. Mingos, *J. Chem. Soc., Dalton Trans.* 1977, 602.
8. H. M. Colquhoun, T. H. Greenhough and M. G. H. Wallbridge, *J. Chem. Soc., Dalton Trans.* 1979, 619.
9. Cambridge Structural Database (CSD), Cambridge University, U.K.
10. S. V. Lindeman, I. A. Khotina, M. M. Teplyakov, Yu. T. Struchkov, V. V. Korshak, *Makromol. Chem.* 1988, **189**, 471.
11. F. Teixidor, C. Viñas, T. Rius, C. Miravitlles and J. Casabo, *Inorg. Chem.* 1990, **29**, 149.
12. F. H. Allen, O. Kennard, D. G. Watson, L. Brammer, A. G. Orpen and R. Taylor, *J. Chem. Soc., Perkin Trans.* II, 1987, S1.
13. D. R. Armstrong, P. G. Perkins and J. J. P. Stewart, *J. Chem. Soc. (A)* 1971, 3674; *J. Chem. Soc., Dalton Trans.* 1973, 838.
14. D. Voet and W. N. Lipscomb, *Inorg. Chem.* 1964, **3**, 1679.
15. T. F. Koetzle, F. E. Scarbrough and W. N. Lipscomb, *Inorg. Chem.* 1968, **7**, 1076.
16. R. A. Beaudet and R. L. Poynter, *J. Chem. Phys.* 1970, **53**, 1899.
17. W. E. Streib, F. P. Boer and W. N. Lipscomb, *J. Am. Chem. Soc.* 1963, **85**, 2331.
18. L. F. Dahl and D. L. Smith, *J. Am. Chem. Soc.* 1962, **84**, 2450.
19. R. P. Dodge and V. Schomaker, *J. Organometal. Chem.* 1965, **3**, 274; G. Maier, S. Pfriem, U. Schäfer, K. Malsch and R. Matusch, *Chem. Ber.* 1981, **114**, 3965.
20. M. Tachikawa, J. R. Shapley and C. G. Pierpoint, *J. Am. Chem. Soc.* 1975, **97**, 7174; G. C. Pierpoint, *Inorg. Chem.* 1977, **16**, 636.
21. J. F. Blount, L. F. Dahl, C. Hoogzand and W. Hubel, *J. Am. Chem. Soc.* 1966, **88**, 292.
22. O. S. Mills and B. W. Shaw, *Acta Cryst.* 1965, **18**, 562; *J. Organometal. Chem.* 1968, **11**, 595.
23. F. A. Cotton and W. T. Hall, *Inorg. Chem.* 1980, **19**, 2354.

24. Various papers cited by M. J. McGeary, A. S. Gamble and J. L. Templeton, *Organometallics* 1988, **7**, 271, and by P. R. Raithby and M. J. Rosales, *Advan. Inorg. Chem. Radiochem.* 1985, **29**, 169.
25. D. A. Brown, W. Clegg, H. M. Colquhoun, J. A. Daniels, I. R. Stephenson and K. Wade, *J. Chem. Soc., Chem. Commun.* 1987, 889.
26. R. Coult, M. A. Fox, W. R. Gill, K. Wade and W. Clegg, *Polyhedron* 1992, **11**, 2717.
27. J. Cosier and A. M. Glazer, *J. Appl. Cryst.* 1986, **19**, 105.
28. W. Clegg, *Acta Cryst., Sect. A* 1981, **37**, 22.
29. G. M. Sheldrick, SHELXTL/PC Manual. Siemens Analytical X-Ray Instruments, Inc., Madison, U.S.A. (1990); SHELXL-92, program for crystal structure refinement, beta-test version, University of Göttingen, Germany (1992).

Polyhedron Vol. 12, No. 22, pp. 2719–2724, 1993
Printed in Great Britain

0277–5387/93 $6.00+.00
© 1993 Pergamon Press Ltd

THE SYNTHESIS AND CRYSTAL STRUCTURES OF 1-PHENYL-3-METHYL-4-BUTANOYLPYRAZOL-5-ONE AND OF TWO PYRAZOLONATO COMPLEXES OF IRON

AUGUSTUS B. UZOUKWU

Department of Pure and Industrial Chemistry, University of Port Harcourt, Nigeria

and

SALIH S. AL-JUAID, PETER B. HITCHCOCK and J. DAVID SMITH†

School of Chemistry and Molecular Sciences, University of Sussex, Brighton BN1 9QJ, U.K.

(*Received* 5 *May* 1993; *accepted* 28 *June* 1993)

Abstract—An X-ray study showed that 1-phenyl-3-methyl-4-butanoylpyrazol-5-one, $RCOC_{10}H_9N_2O$ (abH, R = Pr) (**1**), crystallized in the enol form. It reacted with iron(III) salts to give a dark red complex, $[Fe(ab)_3]$, which crystallized from butanol as the *mer*-isomer. The complex $[Fe(ab)_3]$ (R = Me) was prepared similarly, but the *fac*-isomer was obtained.

Selective extraction is a key step in many hydrometallurgical processes. Among the many reagents which have been examined as extractants the 1-phenyl-3-methyl-4-acylpyrazolones, $RCOC_{10}H_8N_2OH$ (**1–4**) have several possible advantages.[1–4] They are more efficient extractants for metals in strongly acidic solution and cheaper than the widely used 4,4,4-trifluoro-1-(2-thienyl)-1,3-butanedione, $C_4H_3SCOCH_2COCF_3$,[5,6] and the R substituents can be easily varied to optimize particular separations. One of the most powerful extractants is the butanoyl derivative (R = Pr)[7] and a method for separation of iron and uranium based on this reagent has been proposed.[2]

In order to understand the factors which determine selectivity it is necessary to examine the structures of both ligands and metal complexes. It has been suggested that the free pyrazolone ligands may be obtained in several tautomeric forms (e.g. **a–c**) by crystallization from various solvents under a variety of experimental conditions. As far as we are aware, however, only two compounds have been examined by X-ray crystallography, viz. the benzoyl derivative, which crystallizes as the NH tautomer **1b**, R = Ph, and the 1,3-butanedionyl (acetoacetyl) compound, which crystallizes as the OH tautomer **3c**, R = CH=C(OH)CH_3.[8] We describe herein the structure of the enol form **2c** of the butanoylpyrazolone and the synthesis, properties and structures of the iron(III) complexes $Fe(ab)_3$ (**5**) (abH = **2**) and **6** (abH = **4**). The crystal structures of two uranium complexes, viz. $[UO_2(ab)_2H_2O]$ (**7**) obtained from the acetylpyrazolone **4** and $[UO_2(ab)_2(PrOH)]$ from the benzoyl compound **1**, have been described elsewhere.[9]

EXPERIMENTAL

The ^1H and ^{13}C NMR data for samples in acetone-d_6 at 25°C were recorded on a Bruker WM360 instrument at 360 or 90.6 MHz, respectively; chemical shifts were relative to $SiMe_4$. The carbon atoms were numbered as in Figs 1–3.

1-*Phenyl*-3-*methyl*-4-*butanoylpyrazol*-5-*one* (2)

The synthesis of this compound has been described previously.[10] Yield: 85%. UV: λ_{max} 251 (ε 161), 287 nm (ε 6940 $dm^3\ mol^{-1}\ cm^{-1}$). IR (Nujol mull): 3100w (νOH), 2650wb (νOH···O), 1618s (νCO), 1590m, 1550b, 608w, 503w, 370w, 330 cm^{-1}

† Author to whom correspondence should be addressed.

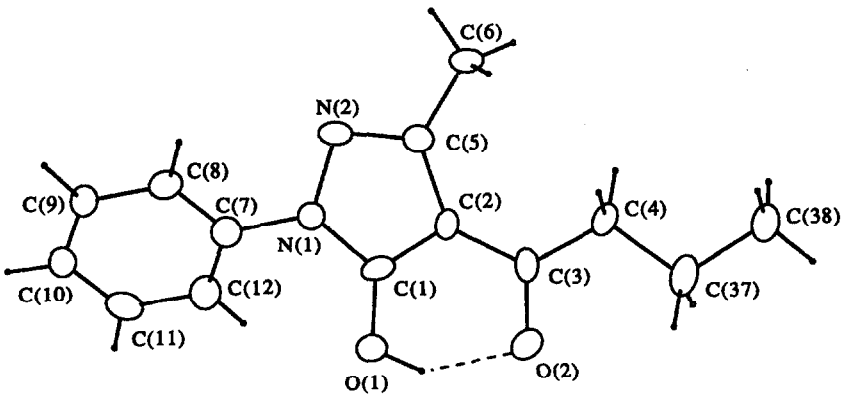

Fig. 1. The molecular structure of **2c**. Non-hydrogen atoms are drawn as 20% thermal vibration ellipsoids.

(w), (ligand). NMR: δ(H) 2.40 (s, 3H, Me), 2.78 (t, 2H), 1.64 (m, 2H), 1.01 (t, 3H), 7.17–7.97 (m, 5H), 12.26 (s, 1H, OH); δ(C), 14.0 C(38), 15.8 C(6), 18.6 C(37), 40.9 C(4), 104.6 C(2), 120.9 C(8, 12), 127.0 C(10), 129.9 C(9, 11), 138.7 C(7), 148.4 C(5), 162.2 C(1), 197.4 C(3). The pK_a in H_2O:dioxane (1:4), measured spectrophotometrically from the absorbance at 263 nm at a particular pH and the limiting values at low and high pH, was 4.19 ± 0.07.

phenyl-3-methyl-4-acetylpyrazol-5-onato)iron(III) (**6**) and an X-ray study showed that the *fac*-isomer had been obtained. Yield: 2.06 g, 95%; m.p. 256°C. Found: C, 61.2; H, 4.99; N, 11.9. Calc. for $C_{36}H_{33}O_6N_6Fe$: C, 61.6; H, 4.74; N, 12.0%. UV ($CHCl_3$): λ_{max} 250 (ε 5470), 291 (ε 20,900), 471 nm (ε 4760 $dm^3\ mol^{-1}\ cm^{-1}$). IR: 1603s (νCO), 300s (ν_{as} FeO), 282 cm^{-1} (w) (ν_s FeO). μ_{eff} 5.86 B.M.

Tris(1-*phenyl*-3-*methyl*-4-*butanoylpyrazol*-5-

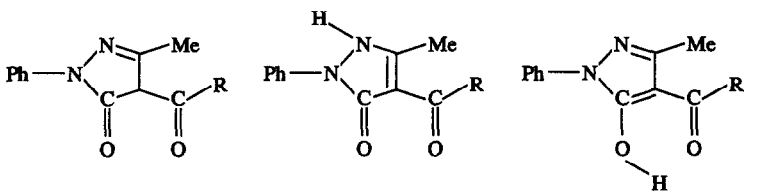

a **b** **c**

1: R = Ph; **2**: R = Pr; **3**: R = CH_2COCH_3; **4**: R = Me

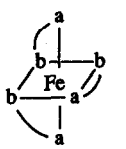

5

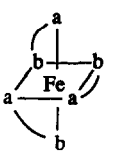

6

mer-form abH = **2**, R = Pr

fac-form abH = **4**, R = Me

$UO_2(ab)_2H_2O$
7
abH = **4**, R = Me

$UO_2(ab)_2PrOH$
8
abH = **1**, R = Pr

Iron complexes

A solution of $Fe(NO_3)_3 \cdot 9H_2O$ (1.25 g, 3.1 mmol) in water (50 cm^3) at 45°C was added to a stirred warm (45°C) solution of **4** (2.0 g, 9.3 mmol) in ethanol (50 cm^3). The mixture was kept at 45°C until a precipitate was obtained. This was filtered off, washed with water, recrystallized from butanol and dried in air. The dark red crystals were tris(1-*onato*)*iron*(III) (**5**). This compound was made similarly from **2** and isolated as dark red needles, which were shown to comprise the *mer*-isomer. Yield: 2.4 g, 99%; m.p. 162°C. Found: C, 63.8; H, 5.53; N, 10.6%. Calc. for $C_{42}H_{45}O_6N_6Fe$: C, 64.2; H, 5.77; N, 10.7%. UV ($CHCl_3$): λ_{max} 253 (ε 5760), 291 (ε 23,200), 463 nm (ε 4800 $dm^3\ mol^{-1}\ cm^{-1}$). IR: 1624m (νCO), 283 cm^{-1} (mb) (ν FeO). μ_{eff}: 5.81 B.M.

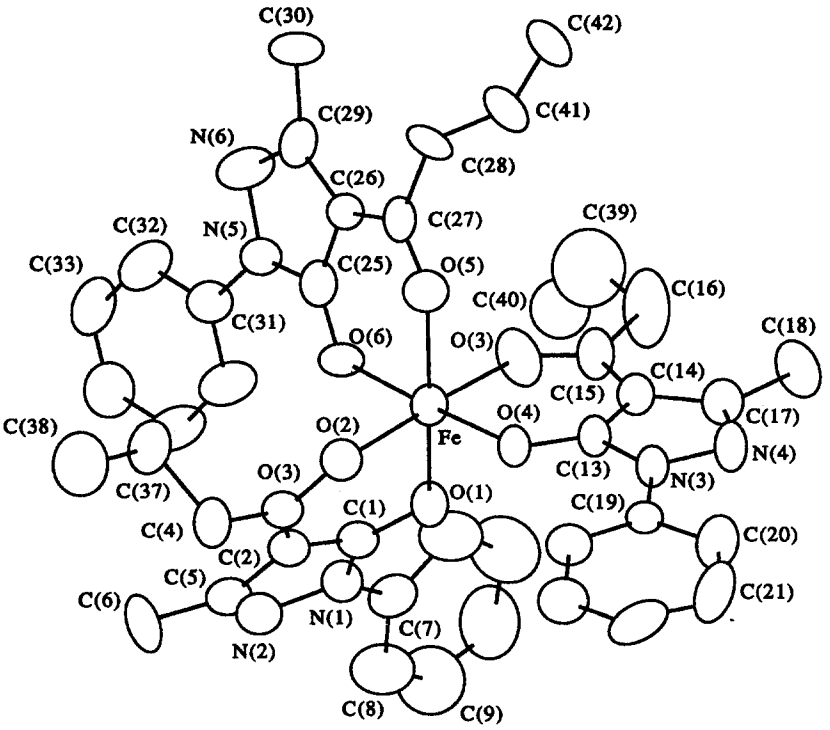

Fig. 2. The molecular structure of **5**.

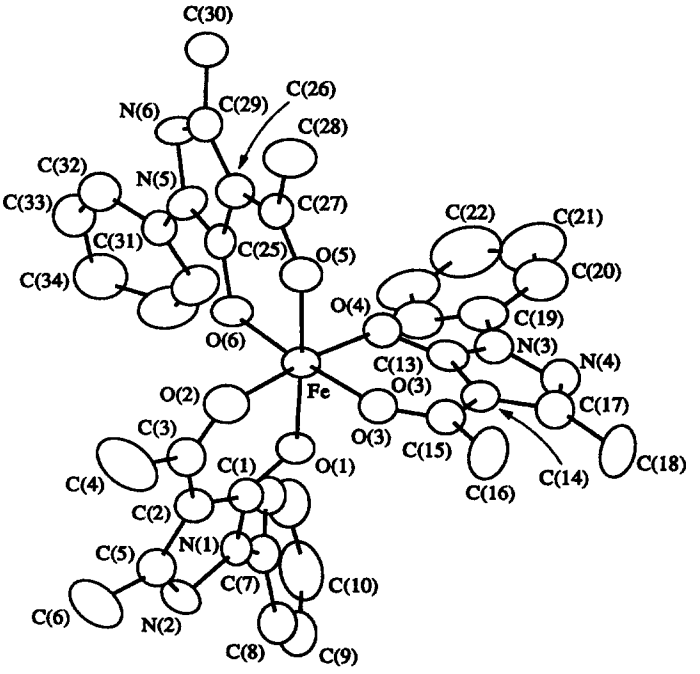

Fig. 3. The molecular structure of **6**.

Solvent extraction

Aqueous solutions of $Fe(NO_3)_3$ (5 cm^3), containing 10 ppm of iron and buffered to various pH, were shaken with a 0.02 M solution of **2** (5 cm^3) in xylene. Approximately 80% of the iron(III) was extracted at pH 0.5 and the extraction was almost quantitative between pH 1.4 and 4.3. When the complex was used for the spectrophotometric determination of iron(III) there was no detectable interference from Mg^{2+}, Al^{3+}, Zn^{2+}, Co^{2+}, Cu^{2+}, Ni^{2+}, Zr^{4+}, Cd^{2+}, Ba^{2+} and Pb^{2+}, present in each case in 500-fold excess. The formula of the complex in the organic layer was established as FeL_3 (LH = **2**) by Job's method[11] and the extraction constant $K = [FeL_3]_{org}[H^+]^3_{aq}/[Fe^{3+}]_{aq}[HL]^3_{org}$ at an ionic strength of 0.2 M was found to be $10^{0.5\pm0.1}$.

Crystal structures

Data were collected at 295 K on an Enraf–Nonius CAD4 diffractometer: those from **5** were of poor quality, perhaps because of disorder in the structure. Intensities, measured by a θ–2θ scan with $\Delta\theta = (0.8 \pm 0.35 \tan\theta)°$ and $2 < \theta < 25°$, were corrected for Lorentz and polarization effects but not for absorption. A MicroVax II computer and the Enraf–Nonius Structure Determination Package were used for structure solutions and refinement. The positions of the carbon, nitrogen and oxygen atoms of **2c** were found by MULTAN[12] and the structures of **5** and **6** were solved by heavy-atom methods. All the non-hydrogen atoms were refined by full-matrix least-squares techniques with anisotropic temperature factors, except for C(39) and C(40) of **5** for which the temperature factors were isotropic: C(40) was disordered between two sites. The hydrogen atoms of **2c** were located on a difference map and refined isotropically; those of the phenyl groups in **5** and **6** were placed at calculated positions (C—H = 0.95 Å) with $B_{iso} = 1.3\ B_{eq}$ for the attached carbon atom, where B_{eq} is defined as one third of the trace of the orthogonalized B_{ij} tensor. The other hydrogen atoms were omitted. More details are given in Table 1 and selected bond lengths and angles in Tables 2 and 3.

RESULTS AND DISCUSSION

The butanoyl compound was isolated from water–ethanol as colourless crystals. It was thought

Table 1. Details of structure determinations

	2c	**5**	**6**
Formula	$C_{14}H_{16}N_2O_2$	$C_{42}H_{45}N_6O_6Fe$	$C_{36}H_{33}N_6O_6Fe$
Crystal size (mm)	0.35 × 0.2 × 0.08	0.15 × 0.15 × 0.10	0.38 × 0.40 × 0.40
M	244.3	785.7	701.5
Crystal system	Orthorhombic	Triclinic	Monoclinic
Space group	*Pbcn*	$P\bar{1}$	*Cc*
a (Å)	16.183(3)	9.706(4)	18.322(5)
b (Å)	11.054(4)	13.358(6)	20.152(7)
c (Å)	14.404(3)	15.435(2)	9.384(8)
α (°)	90	99.46(2)	90
β (°)	90	91.98(2)	102.20(5)
γ (°)	90	92.55(3)	90
Z	8	2	4
U (Å^3)	2576.6	1970.1	3386.8
D_{calc} (g cm^{-3})	1.26	1.30	1.38
F(000)	1040	826	1460
μ(Mo-K_α) (cm^{-1})	0.8	4.3	5.0
Unique reflections	2584	6909	3074
Significant reflections [$I > \sigma(I)$]	750	3978	2538
R^a	0.040	0.103	0.041
R'^a	0.042	0.076	0.053
Parameters refined	227	490	440
Max. shift/e.s.d.	0.05	0.01	0.9
Max. difference density (e Å^{-3})	0.2	0.6	0.4

[a] $R = \Sigma\,||F_o| - |F_c||/\Sigma\,|F_o|$, $R' = (\Sigma\, w(|F_o| - |F_c|)^2/\Sigma\, w|F_o|^2)^{1/2}$. For **6** refinement with the opposite absolute structure gave $R = 0.042$, $R' = 0.054$.

Table 2. Intramolecular distances (Å) and angles (°) for **2c** with e.s.d.s in parentheses

O(1)—C(1)	1.319(5)	O(2)—C(3)	1.256(6)
N(1)—N(2)	1.396(5)	N(1)—C(1)	1.347(5)
N(1)—C(7)	1.426(6)	N(2)—C(5)	1.327(6)
C(1)—C(2)	1.386(6)	C(2)—C(5)	1.424(6)
C(2)—C(3)	1.433(6)	C(5)—C(6)	1.484(6)
C(3)—C(4)	1.484(7)	C(4)—C(37)	1.517(7)
C(37)—C(38)	1.529(8)	O(1)—H(01)	0.89(5)
O(2)···H(01)	1.81(5)	Mean C—C in Ph ring	1.382(7)
N(2)—N(1)—C(1)	110.5(3)	N(2)—N(1)—C(7)	119.0(3)
C(1)—N(1)—C(7)	130.2(4)	N(1)—N(2)—C(5)	105.6(3)
O(1)—C(1)—N(1)	124.0(4)	O(1)—C(1)—C(2)	127.8(4)
N(1)—C(1)—C(2)	108.1(4)	C(1)—C(2)—C(5)	104.7(4)
C(1)—C(2)—C(3)	120.1(4)	C(5)—C(2)—C(3)	135.1(4)
N(2)—C(5)—C(2)	110.9(4)	N(2)—C(5)—C(6)	119.1(4)
C(2)—C(5)—C(6)	129.9(4)	O(2)—C(3)—C(2)	118.1(4)
O(2)—C(3)—C(4)	120.6(4)	C(2)—C(3)—C(4)	121.3(4)
C(3)—C(4)—C(37)	115.9(4)	C(4)—C(37)—C(38)	112.6(4)
N(1)—C(7)—C(8)	119.3(4)	N(1)—C(7)—C(12)	120.0(4)
C(1)—O(1)—H(01)	106(3)	O(1)—H(01)···O(2)	144(5)
C(3)—O(2)···H(01)	104(2)	Mean C—C—C in Ph ring	119.9(5)

earlier[10] that the lack of colour indicated that the crystals comprised the keto form **2a**, but the structure determination described here shows that the enol form **2c** was obtained. The acylpyrazolone skeleton is planar (Fig. 1) with the phenyl ring twisted from the pyrazolone plane. The C—O and adjacent C—C and C—N bond lengths within the pyrazolone ring (Table 2) differ significantly from those in the benzoyl compound **1**, but are the same within the limits of error as those in the 1,3-butanedionyl compound **3**. The labile proton is attached to the pyrazolone rather than to the adjacent acyl carbonyl group and is linked to the acyl carbonyl by an intramolecular hydrogen bond. There are no intermolecular hydrogen bonds as found in **1**. It is difficult to deduce the structure of acylpyrazolones by IR measurements without confirmatory diffraction data,[4] but it is noteworthy that the absorptions at 3100 and 2650 cm^{-1} and the carbonyl peak at 1618 cm^{-1} found in the IR spectrum of solid **2c** are observed in other β-diketones which crystallize in the enol form.[13]

The butanoyl compound **2** is an extremely efficient selective extractant for iron(III), even in

Table 3. Mean bond lengths (Å) and angles (°) in **5** and **6** with e.s.d.s in parentheses

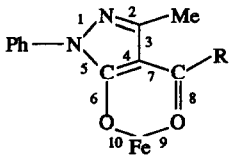

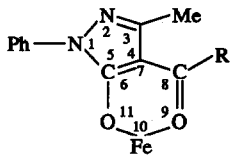

		5	6
1	N—N	1.413(8)	1.393(7)
2	N—C	1.317(9)	1.306(8)
3	C—C	1.435(6)	1.442(7)
4	C—C	1.406(10)	1.428(7)
5	N—C	1.351(9)	1.350(8)
6	C—O	1.285(8)	1.274(6)
7	C—C	1.400(10)	1.399(7)
8	C—O	1.275(8)	1.267(6)
9	Fe—O	2.016(5)	2.030(4)
10	Fe—O	1.983(5)	2.013(4)

		5	6
1	C—N—N	110.5(6)	111.9(4)
2	N—N—C	106.5(6)	106.2(4)
3	N—C—C	110.7(6)	111.5(4)
4	C—C—C	104.9(6)	104.0(4)
5	C—C—N	107.6(6)	106.3(4)
6	C—C—O	129.6(6)	130.3(5)
7	C—C—C	123.1(6)	122.6(5)
8	C—C—O	120.9(6)	121.4(4)
9	C—O—Fe	130.2(5)	131.3(3)
10	O—Fe—O	87.9(2)	88.6(1)
11	Fe—O—C	122.6(4)	123.4(3)

strongly acidic solution. In order to examine more carefully why this is so, we have isolated the wine–red complex $Fe(ab)_3$ (**5**), with abH = **2** (R = Pr). Complex **6** derived from **4** was also isolated: this is only 20% extracted with xylene at pH 0.5, but almost quantitatively in the pH range 2–4. UV spectra show that the ligand absorptions at 251 and 287 nm in the free ligands are also found in the complexes, suggesting that intraligand $\pi \rightarrow \pi^*$ transitions are almost unchanged. New peaks at longer wavelengths ascribed to ligand → metal charge-transfer transitions account for the colour of the complexes.

The structures of the iron compounds found by X-ray diffraction make possible a more precise comparison of bond lengths in coordinated complexes and complexes **7** and **8** where the presence of a heavy atom led to large uncertainties in estimated standard deviations. After coordination of the three bidentate enolato ligands there is no room for further coordination of solvent. The O—Fe—O angles in the metallocyclic rings are *ca* 88°, so there is only slight distortion from octahedral coordination at the metal. In contrast, the metal is seven-coordinate in the uranium derivatives **7** and **8**: U—O bonds are *ca* 0.3 Å longer than Fe—O bonds, so the O—U—O angles can be compressed to 72° to make room for coordination of H_2O or ROH. The mean bond lengths in the enol forms of the free pyrazolone ligands **2** and **3**[8] are insignificantly different from those in the iron complexes, except for the C—C bonds which are shared between the pyrazolone and metallocyclic rings. A comparison between the bond lengths in the ligand **2c** and the iron complexes **5** and **6** shows the effects of increased delocalization in the chelate ring with C—C and C—O bonds becoming more similar in length as the metal complexes are formed. The intramolecular hydrogen bond in **2c** is associated with a lengthening of the C—O bond of the acyl group [cf. 1.233(8) Å in **1**], so that it is almost the same as that in the iron complexes. In **3**, where there are two intramolecular hydrogen bonds to the central carbonyl, the lengthening is even more marked.[8]

It is not possible to be sure that the pattern of hydrogen bonds involving a particular pyrazolone ligand is the same in aqueous solution as it is in the crystalline state. However, the results here do suggest that if the enol form is present in solution, little overall reorganization is required to form the neutral iron complexes $[Fe(ab)_3]$.

It is interesting that changing the R group from butyl to methyl results in the isolation of the *fac*- rather than the *mer*-iron(III) complex. The crystallographic data give no explanation for this observation. Magnetic measurements indicate that the complexes are d^5 high-spin and therefore labile: *fac*-⇌*mer*-isomerization is thus expected to be facile. Which isomer is obtained on crystallization is probably determined by subtle differences in solubility. There are no significant differences between the bond lengths and angles in the coordination sphere and pyrazolone rings of **5** and the corresponding parameters in **6** (Table 3). The greater efficiency of **2** than that of **4** as an extractant is probably therefore a reflection of the higher solubility of the butanoyl complex in the organic layer.

Supplementary material. Tables of fractional atomic coordinates, bond lengths and angles, observed and calculated structure factors, hydrogen atom positions and temperature factors have been deposited with the Editor and are available on request.

Acknowledgement—We thank the Government of Saudi Arabia for financial support to S.S. Al-J. and the International Foundation for Science for a grant to A.B.U.

REFERENCES

1. B. S. Jansen, *Acta Chem. Scand.* 1959, **13**, 1890.
2. E. C. Okafor and B. A. Uzoukwu, *Radiochim. Acta* 1990, **51**, 167.
3. S. Umetani and H. Freiser, *Inorg. Chem.* 1987, **26**, 3179.
4. E. C. Okafor, *Spectrochim. Acta* 1981, **37A**, 939, 945.
5. Yu. A. Zolotov, V. G. Lambrev, M. K. Chmutova and N. T. Sizonenko, *Proc. Acad. Sci. U.S.S.R. (Chem.)* 1965, **165**, 1075.
6. G. N. Rao and H. C. Arora, *J. Inorg. Nucl. Chem.* 1977, **39**, 2057.
7. O. Navrátil and B. S. Jensen, *J. Radioanal. Chem.* 1970, **5**, 313.
8. M. J. O'Connell, C. G. Ramsay and P. J. Steel, *Aust. J. Chem.* 1985, **38**, 401.
9. E. C. Okafor, A. B. Uzoukwu, P. B. Hitchcock and J. D. Smith, *Inorg. Chim. Acta* 1990, **172**, 97.
10. B. S. Jansen, *Acta Chem. Scand.* 1959, **13**, 1668.
11. P. Job, *Ann. Chim.* (Paris) 1928, **9**, 113.
12. G. Germain, P. Main and M. M. Woolfson, *Acta Cryst.* 1971, **A27**, 360.
13. J. Emsley, *Struct. Bonding* 1984, **57**, 147.

Polyhedron Vol. 12, No. 22, pp. 2725–2730, 1993
Printed in Great Britain

0277–5387/93 $6.00+.00
© 1993 Pergamon Press Ltd

SYNTHESIS, STRUCTURE, SPECTRA AND METAL REDOX OF IMIDAZOLIUM TRIS(ARYLAZO OXIMATO)IRON(II): THE ASSOCIATION OF IMIDAZOLE WITH A TRIS CHELATE OXIMATO FACE AND ANALOGY WITH DISTAL IRON···IMIDAZOLE DISPOSITION

VADIVELU MANIVANNAN, SURAJIT CHATTOPADHYAY, PARTHA BASU and ANIMESH CHAKRAVORTY†

Department of Inorganic Chemistry, Indian Association for the Cultivation of Science, Calcutta 700 032, India

(*Received* 5 *May* 1993; *accepted* 28 *June* 1993)

Abstract—The reaction of $Na[Fe(RL)_3]\cdot H_2O$ with imidazole (im) in acidified methanol affords the green-coloured low-spin (t_2^6) complexes $Him[Fe(RL)_3]$, where $[RL^-]$ is $[RC(NO)NNPh^-]$ and R is Me, Ph, p-MeC_6H_4. The X-ray structure of the solvate $Him[Fe(p\text{-}MeC_6H_4L)_3]\cdot 2MeOH$ has revealed that the iron(II) atom is tris-chelated in facial geometry, the FeN_6 coordination sphere being distorted octahedral. Hydrogen bonding among the oximato oxygen, imidazole nitrogen and methanol oxygen atoms affords a centrosymmetric dimeric arrangement. The imidazole ring lies near the oximato periphery of the tris chelate. The different oximato functions are differently hydrogen bonded and the stronger the hydrogen bonding the longer the Fe—N(oxime) length. The shortest non-bonded Fe···N(im) length is 4.260(6) Å [motif Fe—NO···N(im)], which can be compared with the Fe···N(distal) length in oxyhaemoglobin, 4.34 Å, and oxymyoglobin, 4.53 Å [motif Fe—OO···N(im)]. The $Him[Fe(RL)_3]$ salts have low electrical conductivity in solution, showing that strong association persists in the dissolved state. An allowed band near 600 nm is assigned to the MLCT excitation $d\pi(Fe) \rightarrow \pi^*(azo)$ on the basis of an extended Hückel examination of a model system. A quasi-reversible stereoretentive one-electron couple, $[Fe^{III}(RL)_3]/[Fe^{II}(RL)_3^-]$, is electrochemically observable, the EPR spectrum of electrogenerated $[Fe(RL)_3]$ being axial ($g_{\parallel}$, ~2.0; $g_{\perp}$, ~2.1).

The common mode of imidazole (im) binding in metal complexes is direct coordination through a nitrogen atom. A relatively rare binding mode is shown in motif **1**, where the diatomic fragment XY coordinates to the metal through X and associates with the imidazole nitrogen through Y. An example is oxyhaemoglobin (or oxymyoglobin), in which the imidazole nitrogen of the distal histidine residue is hydrogen bonded to the iron-bound oxygen molecule, motif **2**.[1,2] While studying the interaction of imidazole with oximato complexes of iron we have come across the motif **3**, in which the NO fragment belongs to an oximato function. The synthesis and characterization of a family of such species are reported in this work. The X-ray structure of a representative member is described.

M—XY···N(im) **1** Fe—OO···N(im) **2**

Fe—NO···N(im) **3**

EXPERIMENTAL

Materials

Arylazo oximes, $Na[Fe(RL)_3]\cdot H_2O$, were prepared as reported.[3,4] The preparation of tetraethylammonium perchlorate (TEAP) and the purifica-

† Author to whom correspondence should be addressed.

tion of acetonitrile for electrochemical and spectroscopic work were performed as previously described.[5] All the other chemicals and solvents were of reagent grade and used as obtained.

Physical measurements and computations

UV–vis–NIR spectra were recorded on a Hitachi 330 spectrophotometer. Solution (10^{-3} mol cm^{-3}) electrical conductivities were measured on a Philips PR 9500 bridge. Electrochemical measurements were performed on a PAR model 370-4 electrochemistry system, as reported earlier.[6] All potentials reported in this work are uncorrected for junction contribution and referenced to a saturated calomol electrode (S.C.E.). The EPR spectra were recorded in the *X*-band with a Varian E-109C spectrometer fitted with a quartz Dewar flask for measurements at 77 K (liquid nitrogen) and dpph ($g = 2.0037$) was used for their calibration. Microanalytical data (carbon, hydrogen and nitrogen) were obtained with a Perkin–Elmer model 240C elemental analyser. Extended Hückel computations were performed using a variation of the ICON-8 software package originally developed by Hoffmann.[7]

Synthesis of the complexes

The same general procedure was followed for all the three complexes. Details are given for Him[Fe(PhL)$_3$]. To a methanolic solution of Na[Fe(PhL)$_3$]·H_2O (0.500 g, 0.65 mmol) was added $HClO_4$ (0.66 mmol) in methanol (10 cm^3). To the resulting brown solution was added imidazole (0.045 g, 0.66 mmol) and the solution was stirred for 15 min. The green solution was evaporated to dryness *in vacuo* and the solid obtained was washed with water and then with a 1 : 2 ethanol–water mixture. Finally, the green solid was dried *in vacuo* over boiling toluene; yield: 97%. Found: C, 62.9; H, 4.3; N, 19.1. Calc. for $C_{42}H_{35}N_{11}O_3Fe$: C, 63.2; H, 4.4; N, 19.3%.

The complexes Him[Fe(MeL)$_3$] and Him[Fe(*p*-$MeC_6H_4L)_3$] were synthesized similarly in 92% and 96% yields, respectively. Found: C, 53.2; H, 4.7; N, 23.1. Calc. for $C_{27}H_{29}N_{11}O_3Fe$: C, 53,0; H, 4.7; N, 25.2%. Found: C, 64.2; H, 4.9; N, 18.2. Calc. for $C_{45}H_{41}N_{11}O_3Fe$: C, 64.4; H, 4.9; N, 18.4%.

X-ray structure determination

Single crystals of Him[Fe(*p*-$MeC_6H_4L)_3$]·2MeOH were grown by slow evaporation of a methanol solution. Cell dimensions were obtained by the least-squares refinement of diffractometer angles of 30 automatically centred reflections. Data were collected at 296 K on a Nicolet R3m/V diffractometer with graphite monochromated Mo-K_α ($\lambda = 0.71073$ Å) radiation in the ω–2θ scan mode. Two check reflections measured after every 98 reflections showed no significant variations. Lorentz and polarization corrections as well as a semi-empirical absorption correction[8] were made. The structure was solved by direct methods and was refined by block-matrix least-squares procedures. All the non-hydrogen atoms were refined anisotropically. Hydrogen atoms were included at the calculated positions in the final refinement cycle with isotropic thermal parameters (0.08 $Å^2$). Crystal data and other details are collected in Table 1. Computations were performed on a MicroVAX II computer using the SHELXTL-PLUS program system.[9]

Tables of atomic coordinates, anisotropic thermal parameters, full listing of bond lengths and angles and observed and calculated structure factors are available as supplementary material from the Editor.

Table 1. Crystal data, intensity data collection and structural refinement for Him[Fe(*p*-$MeC_6H_4L)_3$]·2MeOH

Formula	$C_{47}H_{49}N_{11}O_5Fe$
Crystal size (mm)	0.36 × 0.42 × 0.50
Crystal system	Monoclinic
Space group	$P2_1/c$
a (Å)	9.407(7)
b (Å)	38.950(20)
c (Å)	13.197(9)
β (°)	110.92(5)
U ($Å^3$)	4516(5)
Z	4
M	903.8
D_c (g cm^{-3})	1.329
μ(Mo-K_α) (cm^{-1})	3.93
F(000)	1896
2θ range (°)	2–52
Total no. of reflections	9539
No. of unique reflections	8838
No. of observed reflections [$I > 3\sigma(I)$]	4273
Transmission factors	0.85–1.0
Weighing scheme (g) in $w = 1/[\sigma^2(F)+gF^2]$	0.00008
No. of parameters refined	577
Final R	0.0637
Final Rw	0.0689
Goodness-of-fit	1.66
Largest and mean Δ/σ	0.077, 0.003
Data-to-parameter ratio	7.4
Largest difference peak (e $Å^{-3}$)	0.56
Largest difference hole (e $Å^{-3}$)	−0.53

RESULTS AND DISCUSSION

Synthesis and structure

The oximato complex concerned is the tris-(arylazo oximato)iron(II) anion, $[Fe(RL)_3^-]$ (**4**) (R = Me, Ph or *p*-MeC_6H_4). The proven ability of **4** in sequestering metal cations via the pendent oximato oxygen atoms[10–13] prompted us to explore its interaction with protonated organic bases, imidazole (im) in the present case. The reaction of $Na[Fe(RL)_3]\cdot H_2O$ with imidazole in acidified methanol afforded green species of the composition (when dried *in vacuo*) $Him[Fe(RL)_3]$ in excellent yields. The complexes are diamagnetic, corresponding to a low-spin (t_2^6) configuration for the iron(II) atom.

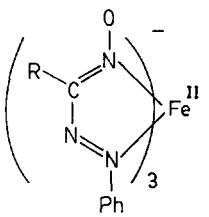

$Fe(RL)_3^-$

4

The complex with R = *p*-MeC_6H_4 afforded good single crystals in the form of a bis-methanol adduct. The X-ray structure (Figs 1 and 2) of the solvate has been determined. Selected bond parameters are listed in Table 2. The iron(II) atom is tris-chelated into facial geometry (Fig. 1). In the distorted octahedral FeN_6 coordination sphere, the Fe—N lengths lie in the range 1.905(4)–1.945(4) Å, showing no systematic difference between Fe—N(oxime) and Fe—N(azo). The bond parameters within the excellently planar chelate rings are comparable to those observed in the metal complexes of $[Fe(RL)_3^-]$.[10,12,13]

The centrosymmetric dimeric units (Fig. 2) are afforded through hydrogen bonding among the oximato oxygen, imidazole nitrogen and methanol oxygen atoms. The relevant distances are shown in Table 2. The imidazole ring is associated at the oximato periphery of the tris chelate via the imidazole N(11) atom, which is strongly hydrogen bonded to the oximato O(2) atom, the N(11)···O(2) length being 2.719(11) Å. The N(11) atom has a weaker contact with O(1), N(11)···O(1), 2.903(12) Å.

The net strength of hydrogen bonding (Fig. 1, Table 2) at the oxygen atoms of the oximato functions can be ordered as O(1) < O(3) < O(2). Interestingly, the stronger the hydrogen bond the longer the corresponding Fe—N(oxime) distance [Fe—N(3) < Fe—N(9) < Fe—N(6)]. The bond parameters within the imidazolium ion are normal.[14]

The non-bonded Fe···N(11) length in $Him[Fe(p\text{-}MeC_6H_4L)_3]\cdot 2MeOH$ is 4.260(6) Å. This can be compared with the Fe···N(distal) distances in oxyhaemoglobin and oxymyoglobin. From available coordinates,[2] these are calculated to be 4.34 and 4.53 Å, respectively.

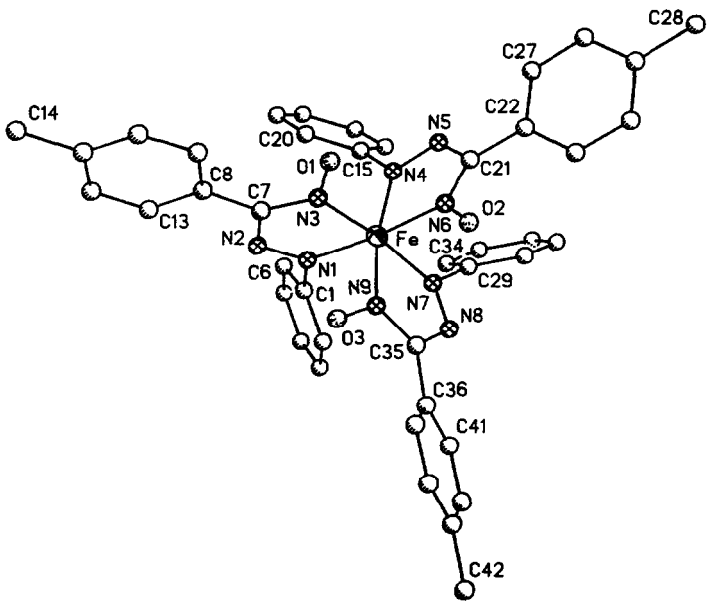

Fig. 1. Perspective view and atom labelling scheme of $[Fe(p\text{-}MeC_6H_4L)_3^-]$ in $Him[Fe(p\text{-}MeC_6H_4L)_3]\cdot 2MeOH$.

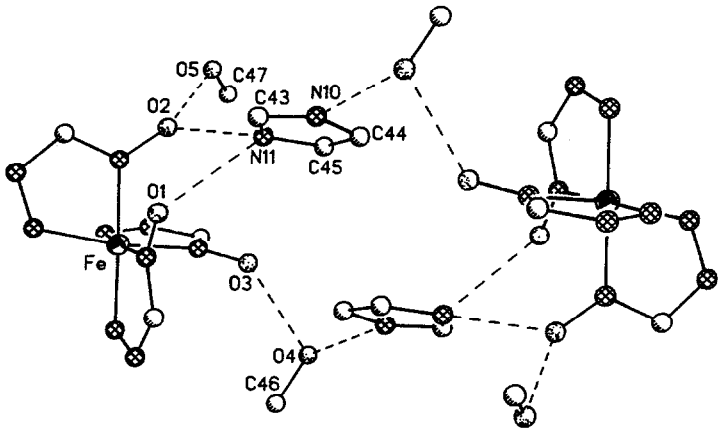

Fig. 2. A view of the hydrogen bonding in Him[Fe(*p*-$MeC_6H_4L)_3$]·2MeOH (for clarity, the aryl rings are not shown).

Table 2. Selected bond distances (Å) and angles (°)[a] for Him [Fe(*p*-$MeC_6H_4L)_3$]·2MeOH

Fe—N(1)	1.917 (5)	Fe—N(3)	1.905 (4)
Fe—N(4)	1.917 (4)	Fe—N(6)	1.932 (5)
Fe—N(7)	1.945 (4)	Fe—N(9)	1.919 (4)
N(11)—O(1)	2.903 (12)	N(11)—O(2)	2.719 (11)
O(3)—O(4)	2.733 (6)	O(2)—O(5)	2.706 (6)
O(4)—N(10A)	2.839 (9)		
N(1)—Fe—N(3)	79.4(2)	N(1)—Fe—N(4)	98.5(2)
N(3)—Fe—N(4)	94.1(2)	N(1)—Fe—N(6)	173.3(2)
N(3)—Fe—N(6)	94.8(2)	N(4)—Fe—N(6)	78.4(2)
N(1)—Fe—N(7)	100.8(2)	N(3)—Fe—N(7)	171.2(2)
N(4)—Fe—N(7)	94.6(2)	N(6)—Fe—N(7)	85.5(2)
N(1)—Fe—N(9)	90.4(2)	N(3)—Fe—N(9)	93.2(2)
N(4)—Fe—N(9)	169.4(2)	N(6)—Fe—N(9)	93.3(2)
N(7)—Fe—N(9)	78.0(2)		

[a] Estimated standard deviations are given in parentheses.

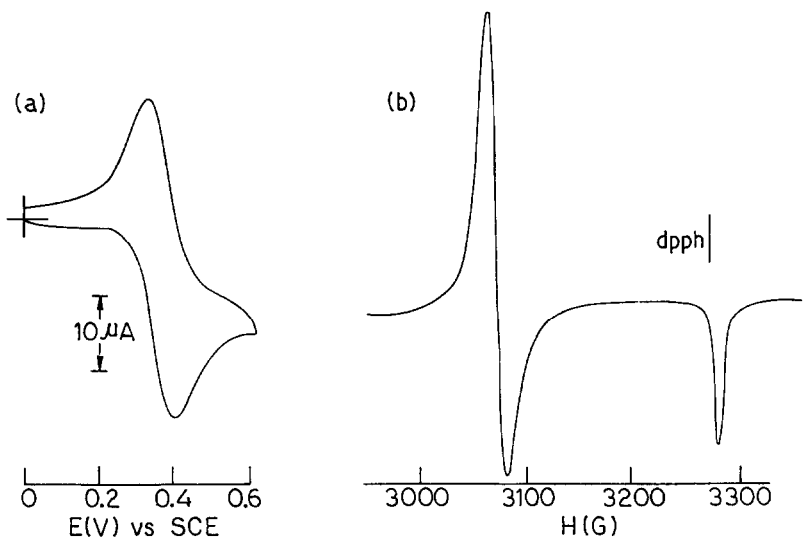

Fig. 3. (a) Cyclic voltammogram (scan rate 50 mV s^{-1}) of 10^{-3} mol dm^{-3} solutions of Him[Fe(PhL)$_3$] in acetonitrile (0.1 mol dm^{-3} NEt_4ClO_4) at a platinum electrode at 298 K; (b) *X*-band (9.1 GHz) EPR spectrum of [Fe(PhL)$_3$] (electrogenerated) in frozen (77 K) acetonitrile–toluene (1:1).

Table 3. Conductivity,[a] electrochemical,[b] electronic spectral[a] and EPR[c] data

Compound	Λ_M (Ω^{-1} cm^2 M^{-1})	$E_{1/2}$ (V)[d]	ΔE_p (mV)[e]	n[f]	λ (nm) (ε (dm^3 mol^{-1} cm^{-1}))	$g_\perp$[g] $g_\parallel$[g]
Him[Fe(MeL)$_3$]	21	0.33	100	0.95	950[h](300), 655[h](2450), 565(3300), 400(11,400)	2.161, 1.992
Him[Fe(PhL)$_3$]	19	0.37	80	0.96	930[h](200), 600(5450), 400(13,300)	2.131, 1.996
Him[Fe(*p*-MeC$_6$H$_4$L)$_3$]	30	0.30	80	0.91	925[h](300), 590(5900), 425(11,800)	2.131, 1.998

[a] In acetonitrile.
[b] In acetonitrile (0.1 M TEAP) at a platinum electrode with a S.C.E. reference.
[c] In frozen (77 K) acetonitrile–toluene (1:1) solution.
[d] From cyclic voltammetry at a scan rate of 50 mV s^{-1}.
[e] Peak-to-peak separation.
[f] n is the ratio of observed-to-calculated Coulomb counts.
[g] g values correspond to the oxidized species electrogenerated in acetonitrile solution.
[h] Shoulder.

Solution properties: conductivity, spectra and metal redox

Relevant data taken in acetonitrile solution are collected in Table 3. The low electrical conductivity of the salts show that strong [Him$^+$]$\cdots$[Fe(RL)$_3^-$] association persists in solution also. The green solutions display an allowed band at *ca* 600 nm with a shoulder at *ca* 900 nm.

Extended Hückel molecular orbital calculations on the hypothetical anion [FeL$_3^-$] (**4** with R and Ph replaced by hydrogen; C_3 symmetry imposed) has revealed that the HOMO is largely (66%) metal $3d\pi$ in character and the LUMO is a ligand orbital with 70% azo π^* character. The transition near 600 nm is assigned to an MLCT excitation, primarily $d\pi$(Fe) $\rightarrow$ π^*(azo) in character.

The salts display a quasi-reversible one-electron cyclic voltammetric metal redox response (Fig. 3) due to the [Fe^{III}(RL)$_3$]/[Fe^{II}(RL)$_3^-$] couple. The [Fe(RL)$_3$] complex ($S = 1/2$) can be generated in solution by constant potential (0.7 V) coulometry and in the frozen state (77 K) it has axial EPR spectra (Fig. 3) corresponding to facial geometry (effective C_3 symmetry). The [Fe^{III}(RL)$_3$]/[Fe^{II}(RL)$_3^-$] redox is thus stereoretentive.

CONCLUSIONS

In Him[Fe(RL)$_3$] the imidazole ring is associated at the oximato periphery of the facial iron(II) trisarylazo oximate. The shortest non-bonded Fe$\cdots$N(imidazole) length is comparable with distal Fe$\cdots$N distances in oxyhaemoglobin and oxymyoglobin. Strong [Him$^+$]$\cdots$[Fe(RL)$_3^-$] association persists in solution. The complexes display an MLCT (Fe $\rightarrow$ azo) transition in the visible region and undergo stereoretentive oxidation affording the axially symmetric [Fe(RL)$_3$].

Acknowledgements—Financial support received from the Department of Science and Technology, New Delhi, and the Council of Scientific and Industrial Research, New Delhi, are acknowledged.

REFERENCES

1. M. F. Perutz, G. Fermi, B. Luisi, B. Shaanan and R. C. Liddington, *Accts Chem. Res.* 1987, **20**, 309.
2. B. Shaanan, *J. Molec. Biol.* 1983, **171**, 31.
3. K. C. Kalia and A. Chakravorty, *J. Org. Chem.* 1970, **35**, 2231.
4. B. S. R. Raghavendra, S. Gupta and A. Chakravorty, *Trans. Met. Chem.* 1979, **4**, 42.
5. D. Datta, P. K. Mascharak and A. Chakravorty, *Inorg. Chem.* 1981, **20**, 1673.
6. P. Basu and A. Chakravorty, *Inorg. Chem.* 1992, **31**, 4980.
7. (a) R. Hoffmann and W. N. Lipscomb, *J. Chem. Phys.* 1962, **36**, 2179; (b) R. Hoffmann and W. N. Lipscomb, *J. Chem. Phys.* 1962, **36**, 3872; (c) R. Hoffmann and W. N. Lipscomb, *J. Chem. Phys.* 1963, **39**, 1397; (d) M. M. L. Chen and R. Hoffmann, *J. Am. Chem. Soc.* 1976, **98**, 1647.
8. A. C. T. North, D. C. Philips and F. S. Mathews, *Acta Cryst.* 1968, **424**, 351.
9. G. M. Sheldrick, SHELXTL-Plus 88, Structure Determination Software Programs. Nicolet Instrument Corporation, Madison, WI, U.S.A. (1988).
10. P. Basu, S. Pal and A. Chakravorty, *J. Chem. Soc., Dalton Trans.* 1991, 3217.
11. S. Pal and A. Chakravorty, *Inorg. Chem.* 1987, **26**, 4331.

12. S. Pal, R. N. Mukherjee, M. Tomas, L. R. Falvello and A. Chakravorty, *Inorg. Chem.* 1986, **25**, 200.
13. S. Pal, T. Melton, R. N. Mukherjee, A. R. Chakravorty, M. Tomas, L. R. Falvello and A. Chakravorty, *Inorg. Chem.* 1985, **24**, 1250.
14. (a) A. K. Abdul-Sada, A. M. Greenway, P. B. Hitchcock, T. J. Mohammed, K. R. Seddon and J. A. Zora, *J. Chem. Soc., Chem. Commun.* 1986, 1753; (b) D. L. Perry, D. P. Freyberg and A. Zalkin, *J. Inorg. Nucl. Chem.* 1980, **42**, 243; (c) M. N. G. James and M. Matsuskima, *Acta Cryst.* 1976, **B32**, 1708; (d) H. C. Freeman, F. Huq, J. M. Rosalky and I. F. Taylor Jr, *Acta Cryst.* 1975, **B31**, 2833.

Polyhedron Vol. 12, No. 22, pp. 2731–2736, 1993
Printed in Great Britain

0277–5387/93 $6.00+.00
© 1993 Pergamon Press Ltd

DIOXOMOLYBDENUM(VI) COMPLEXES OF NEW BINUCLEATING SCHIFF BASES DERIVED FROM METHYLENE- OR DITHIO-BIS(SALICYLALDEHYDE) AND VARIOUS AMINES†

MANNAR R. MAURYA,‡ DEENA C. ANTONY, S. GOPINATHAN‡ and C. GOPINATHAN

Inorganic Chemistry Division, National Chemical Laboratory, Pune 411 008, India

(*Received* 5 *May* 1993; *accepted* 25 *June* 1993)

Abstract—The syntheses of binuclear dioxomolybdenum(VI) complexes of the type $[(MoO_2)_2L]$, where L is a flexibly-bridged hexadentate tetraanionic Schiff base derived from the condensation of methylene- or dithio-bis(salicylaldehyde) with *o*-aminophenol, 2-aminoethanol, 2-amino-2-methyl propanol or 1-amino-2-propanol, are reported. The IR and NMR spectral data suggest an oligomeric structure in which each molybdenum ion achieves a pseudo-octahedral structure via Mo=O---Mo bridging. Treatment of $[(MoO_2)_2L]$ with pyridine leads to the formation of $[MoO_2)_2L(py)_2]$ in which pyridine binds at the sixth labile binding sites in both $[MoO_2]^{2+}$ units. $[(MoO_2)_2L(py)_2]$ is readily convertable into $[(MoO_2)_2L]$ at *ca* 180°C in a single endothermic step, as seen from their DTA analysis. The pyridine adducts show two IR absorptions at *ca* 900 cm^{-1}, attributable to a *cis*-MoO_2 structure, whereas the oligomeric complexes usually show one intense ν(Mo=O) band at 910–938 cm^{-1} and a broad but strong band at *ca* 820 cm^{-1} due to a weakened ν(Mo=O) band as a result of Mo=O → Mo interactions.

The discovery of molybdenum in a number of enzymes has led to the continued growth of the coordination chemistry of molybdenum.[1] The potential for biological and physiological activity and the industrial use of these complexes have also stimulated the discovery of a variety of molybdenum complexes in various oxidation states.[2] Amongst the −II to +VI oxidation states, the most stable is +VI, associated with the dioxo group. Although a number of reports are available in the literature dealing with mononuclear dioxomolybdenum(VI) complexes of tridentate Schiff base ligands, where one labile binding site allows the binding and displacement of various substrate molecules, such systems with binuclear dioxomolybdenum(VI) complexes are rare.[2c] The present report is mainly concerned with binuclear dioxomolybdenum(VI) complexes whose two labile sites are easily accessible within the molecule. The following tetraanionic Schiff base ligands (**A**) have been selected for the present study.

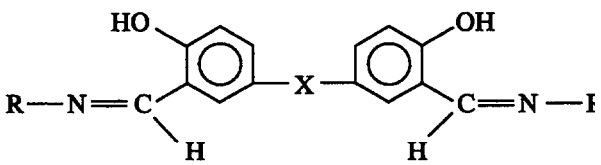

A

	X	R	Abbreviations
1	CH_2	*o*-C_6H_4OH	$CH_2(H_2sal\text{-}OAP)_2$
2	CH_2	CH_2CH_2OH	$CH_2(H_2sal\text{-}EA)_2$
3	CH_2	$C(CH_3)_2CH_2OH$	$CH_2(H_2sal\text{-}AMP)_2$
4	CH_2	$CH_2CH(CH_3)OH$	$CH_2(H_2sal\text{-}IPA)_2$
5	S—S	*o*-C_6H_4OH	$S_2(H_2sal\text{-}OAP)_2$
6	S—S	CH_2CH_2OH	$S_2(H_2sal\text{-}EA)_2$
7	S—S	$C(CH_3)_2CH_2OH$	$S_2(H_2sal\text{-}AMP)_2$
8	S—S	$CH_2CH(CH_3)OH$	$S_2(H_2sal\text{-}IPA)_2$

† NCL communication No. 5778.
‡ Authors to whom correspondence should be addressed.

EXPERIMENTAL

Reagents

All the reagents and solvents used were of analytical grade. *o*-Aminophenol, salicylaldehyde and acetylacetone were used after purification. Methylene-bis(salicylaldehyde)[3] and dithio-bis(salicylaldehyde)[4] were prepared following the literature procedures. $[MoO_2(acac)_2]$ was synthesized by the method described previously.[5]

Preparation of the Schiff bases

A solution of the appropriate amine (0.002 mol) in methanol (*ca* 10 cm^3) was added to a hot solution of the respective aldehyde (0.001 mol) in methanol (10 cm^3) and the reaction mixture was refluxed for 2 h on a water bath. After reducing the solvent to *ca* 5 cm^3 the solution was cooled to 10°C overnight. The separated solid product was filtered, washed with cold methanol and dried under reduced pressure at ambient temperature. Finally, the Schiff bases were recrystallized from methanol; yield: 50–80%.

Preparation of the complexes

$[(MoO_2)_2(CH_2\{sal\text{-}OAP\}_2)]$. The Schiff base $CH_2(H_2sal\text{-}OPA)_2$ (0.44 g, 0.001 mol) was dissolved in methanol (50 cm^3) by heating on a water bath and added $MoO_2(acac)_2$ (0.66 g, 0.002 mol) as a solid with vigorous shaking. The resulting turbid solution was filtered and then refluxed on a water bath for 6 h. After concentrating the solution to *ca* 10 cm^3 and cooling to 10°C overnight the separated solid was filtered, washed with methanol and dried at 100°C in air; yield 70%.

The other molybdenum complexes (listed in Table 1) were prepared following the above method, with slight modifications, in 50–70% yield.

$[(MoO_2)_2L(py)_2]$. These complexes were prepared in quantitative yield by dissolving $[(MoO_2)_2L]$ in a minimum amount of pyridine with heating on a water bath and then evaporating the excess pyridine *in vacuo*.

The analytical and physicochemical data of all the new Schiff bases and their $[(MoO_2)_2L]$ and $[(MoO_2)_2L(py)_2]$ complexes are presented in Table 1.

Measurements

Molybdenum was determined gravimetrically as dioxo-bis(8-quinolinolato)molybdenum(VI), as described previously.[6] Other elemental analyses were performed by the microanalytical section of this laboratory. The IR spectra were recorded as Nujol mulls and as KBr discs on a Perkin–Elmer model 1620 FT-IR spectrophotometer. The electronic spectra were recorded in DMF on a Shimadzu model UV-2101PC UV–vis scanning spectrophotometer. The ^1H NMR spectra were obtained on a Bruker WH-200 spectrometer in DMSO-d_6 and $CDCl_3$. Chemical shifts (δ in ppm) are reported relative to DMSO-d_6 (2.40 ppm) or $CDCl_3$ (7.24 ppm). The electrical conductance measurements were performed in 1×10^{-3} M DMF solutions using a Biochem model DC 808 digital conductivity bridge calibrated with potassium chloride solution. The mass spectra of the ligands were recorded on a Finnigan Mat model 1020 automated GC/MS spectrometer.

RESULTS AND DISCUSSION

Methylene- and dithio-bis(salicylaldehyde) behave like salicylaldehyde and react with amines in a 1:2 molar ratio to form the binucleating tetraanionic Schiff base ligands **1**–**8**. The mass spectral data of the representative ligands [e.g. molecular ion peak *m/z* of **1** at 438 (calc. 438), **3** at 398 (calc. 398), **5** at 488 (calc. 488) and 7 at 448 (calc. 448)] indicate the high degree of stability of the molecular ion to electron impact. These data also indicate that *para*-substituted methylene or disulphide groups are still attached to the two salicylaldehyde moieties. These ligands were further characterized by elemental analysis and other spectral techniques.

The tetraanionic binucleating Schiff base ligands **1**–**8** react with $[MoO_2(acac)_2]$ in a 1:2 molar ratio in refluxing methanol and complexes of the type $[(MoO_2)_2L]$ are formed as follows:

$$2[MoO_2(acac)_2] + LH_4 \xrightarrow[MeOH]{} [(MoO_2)_2L] + 4acacH.$$

Under these reaction conditions complete replacement of the bidentate acetylacetone groups occurs. The analytical data support the formulation of the complexes as $[(MoO_2)_2L]$ and not as $[(MoO_2)_2L \cdot 2MeOH]$, the expected octahedral complex. However, the coordination of methanol was observed in some complexes when dried only at ambient temperature. However, on drying at 100°C the complexes are invariably converted into a stable species, $[(MoO_2)_2L]$. Treatment of $[(MoO_2)_2L]$ with pyridine results in the formation of $[(MoO_2)_2L(py)_2]$, in which pyridine occupies the sixth coordination position in both $[MoO_2]^{2+}$ units. The $[(MoO_2)_2L]$ complexes do not lose weight on heating up to 200°C. However, the thermal analysis data for pyri-

Table 1. Analytical and physicochemical data of the ligands and complexes[a,b]

S. No.	Compound/ stoichiometry	Colour	M.p.	Found (Calc.) % C	H	N	Ω_M[c]
1	$CH_2(H_2sal\text{-}OAP)_2$	Orange	232	73.5	5.2	6.2	
	$C_{27}H_{22}N_2O_4$			(74.0)	(5.1)	(6.4)	
2	$CH_2(H_2sal\text{-}EA)_2$[d]	Yellow	92				
	$C_{19}H_{22}N_2O_4$						
3	$CH_2(H_2sal\text{-}AMP)_2$	Yellow	190	69.1	7.3	7.2	
	$C_{23}H_{30}N_2O_4$			(69.3)	(7.6)	(7.0)	
4	$CH_2(H_2sal\text{-}IPA)_2$	Yellow	102	68.3	6.9	7.3	
	$C_{21}H_{26}N_2O_4$			(68.1)	(7.1)	(7.6)	
5	$S_2(H_2sal\text{-}OAP)_2$	Red	220	64.2	4.1	5.8	
	$C_{26}H_{20}N_2O_4S_2$			(63.9)	(4.1)	(5.7)	
6	$S_2(H_2sal\text{-}EA)_2$	Orange	108	55.3	5.3	7.0	
	$C_{18}H_{20}N_2O_4S_2$			(55.1)	(5.1)	(7.1)	
7	$S_2(H_2sal\text{-}AMP)_2$	Orange	160	58.5	6.1	6.4	
	$C_{22}H_{28}N_2O_4S_2$			(58.9)	(6.3)	(6.2)	
8	$S_2(H_2sal\text{-}IPA)_2$[c]	Orange	52				
	$C_{20}H_{24}N_2O_4S_2$						
1a	$[(MoO_2)_2(CH_2\{sal\text{-}OAP\}_2)]$	Red	>250	47.3	2.9	4.0	5.6
	$C_{27}H_{18}N_2O_8Mo_2$			(47.0)	(2.6)	(4.1)	
1b	$[(MoO_2)_2(CH_2\{sal\text{-}OAP\}_2)(py)_2]$	Orange	>250	52.8	3.5	6.9	4.0
	$C_{37}H_{28}N_4O_8Mo_2$			(52.4)	(3.3)	(6.6)	
2a	$[(MoO_2)_2(CH_2\{sal\text{-}EA\}_2)]$	Orange	>250	38.2	3.2	4.7	8.0
	$C_{19}H_{18}N_2O_8Mo_2$			(38.4)	(3.0)	(4.7)	
2b	$[(MoO_2)_2(CH_2\{sal\text{-}EA\}_2)(py)_2]$	Yellow	>250	46.1	3.5	7.8	6.0
	$C_{29}H_{28}N_4O_8Mo_2$			(46.3)	(3.8)	(7.5)	
3a	$[(MoO_2)_2(CH_2\{sal\text{-}AMP\}_2)]$	Yellow	>250	42.2	4.0	4.1	5.0
	$C_{23}H_{26}N_2O_8Mo_2$			(42.5)	(4.0)	(4.3)	
4a	$[(MoO_2)_2(CH_2\{sal\text{-}IPA\}_2)]$	Yellow	>250	40.2	3.8	4.5	5.5
	$C_{21}H_{22}N_2O_8Mo_2$			(40.5)	(3.6)	(4.5)	
5a	$[(MoO_2)_2(S_2\{sal\text{-}OAP\}_2)]$	Red	>250	42.5	2.2	3.5	7.0
	$C_{26}H_{16}N_2O_8S_2Mo_2$			(42.4)	(2.2)	(3.8)	
5b	$[(MoO_2)_2(S_2\{sal\text{-}OAP\}_2)(py)_2]$	Orange	>250	48.5	3.9	6.5	3.5
	$C_{36}H_{26}N_4O_8S_2Mo_2$			(48.1)	(3.9)	(6.2)	
6a	$[(MoO_2)_2(S_2\{sal\text{-}EA\}_2)]$	Yellow	>250	33.1	2.3	4.7	9.0
	$C_{18}H_{16}N_2O_8S_2Mo_2$			(33.6)	(2.5)	(4.4)	
6b	$[(MoO_2)_2(S_2\{sal\text{-}EA\}_2)(py)_2]$	Yellow	>250	42.2	3.5	6.8	6.0
	$C_{28}H_{26}N_4O_8S_2Mo_2$			(41.9)	(3.3)	(7.0)	
7a	$[(MoO_2)_2(S_2\{sal\text{-}AMP\}_2)]$	Yellow	>250	37.9	3.2	4.4	3.0
	$C_{22}H_{24}N_2O_8S_2Mo_2$			(37.7)	(3.5)	(4.0)	
8a	$[(MoO_2)_2(S_2\{sal\text{-}IPA\}_2)]$	Yellow	>250	33.1	3.3	4.1	4.0
	$C_{18}H_{20}N_2O_8S_2Mo_2$			(33.3)	(3.1)	(4.3)	

[a] Abbreviations as listed earlier.
[b] Satisfactory molybdenum analysis of the complexes have also been obtained.
[c] Conductance values are in $\Omega\ mol^{-1}\ cm^2$.
[d] Elemental analysis could not be recorded.

dine adducts reveal a well-defined endothermic step at around 180°C, corresponding to the loss of two molecules of pyridine, which confirms the coordination of pyridine in $[(MoO_2)_2L(py)_2]$. The coordinated monodentate ligands in complexes of the type $[MoO_2L\cdot X]$ (X = monodentate ligand) are known to undergo dissociation on heating due to weak coordination and their labile nature.[7]

All the complexes reported here are diamagnetic, as expected for the $4d^\circ$ molybdenum ion. The low molar conductance values (3.0–9.0 $\Omega\ mol^{-1}\ cm^2$) of the complexes in DMF indicate their non-electrolytic behaviour. They are soluble in coordinating solvents such as pyridine, DMSO and DMF. The high decomposition temperature (>250°C) indicates the increased stability of the complexes.

IR studies

The IR spectra of the pyridine adducts exhibit two bands in the regions 920–936 and 905–915 cm^{-1}, due to the ν_{sym} and ν_{asym}(O=Mo=O) stretches, respectively. These data indicate the presence of a *cis*-MoO_2 structure as a *trans*-MoO_2 structure would only show one ν(O=Mo=O) band due to the asymmetric stretch.[1b] On the other hand, $[(MoO_2)_2L]$ complexes exhibit a sharp single band (but not in all the complexes) at 910–938 cm^{-1}, due to the ν(O=Mo=O) stretch, and a broad but strong band at *ca* 820 cm^{-1}, due to a Mo=O → Mo interaction.[1b] These observations suggest the presence of an oligomeric (pseudo-octahedral) structure for $[(MoO_2)_2L]$, in which each molybdenum ion achieves a pseudo-octahedral structure via oxo bridging.[7] Adduct formation with pyridine essentially shows the breaking of this bridge as the band at *ca* 820 cm^{-1} disappears and a new band appears at *ca* 910 cm^{-1} due to the ν_{asym}(O=Mo=O) stretch. This observation suggests bridging through the Mo=O → Mo moiety. The occurrence of the ν(C—O) (phenolic) band at almost identical positions in $[(MoO_2)_2L]$ and $[(MoO_2)_2L(py)_2]$ also suggests the presence of oligomeric bridges only through Mo=O → Mo, as oligomerization via the phenolic oxygen bridges would be expected to produce a substantial increase in the ν(C—O)(phenolic) stretch.[8]

The IR spectra of the Schiff bases show two medium intensity bands at *ca* 3200 and 2700 cm^{-1} (only one band at *ca* 2700 cm^{-1} in the Schiff bases derived from *o*-aminophenol), attributable to the ν(OH) band of alcoholic and intramolecularly hydrogen-bonded phenolic hydroxyl groups, respectively. These bands are absent in the spectra of the complexes, which indicates the deprotonation of the alcoholic and phenolic groups and coordination of the oxygen atoms to molybdenum. A strong band in the region 1630–1645 cm^{-1} is assigned to the azomethine ν(C=N) stretch and this band shifts to a lower frequency by 2–36 cm^{-1}, indicating the participation of the azomethine nitrogen atom in coordination.[9] Thus, the IR data suggest the dibasic tridentate and ONO donor behaviour of each Schiff base unit.

The coordination of pyridine is characterized by the shift of the ring breathing mode of pyridine, which occurs at 990 cm^{-1} in free pyridine,[10] to a

Table 2. IR and electronic spectral data (cm^{-1})

Compounds[a]	IR ν(C=N)	IR ν(O=Mo=O)	IR ν(Mo=O → Mo)	Electronic spectra (ε)[b]
1	1631			35,090 (35,350), 27,860 (48,330)
1a	1611	931, 911	851	37,880 (29,000), 32,310 (38,500), 28,410 (17,437), 23,360 (9875)
1b	1613	936, 906		37,880 (37,976), 31,055 (11,156), 27,250 (4855), 23,470 (462)
2	1634			37,170 (2663), 30,860 (9695), 23,810 (1413)
2a	1630	917	808	36,900 (25,000), 30,770 (4895), 29,240 (4845)
2b	1598	920, 902		36,500 (30,120), 30,580 (5204), 28,820 (5204)
3	1630			37,740 (14,490), 30,860 (9140), 23,980 (720)
3a	1626	928	820	37,240 (18,750), 29,850 (4836)
4	1644			37,660 (14,198), 30,960 (8521), 24,070 (354)
4a	1612	913	838	37,520 (1550), 30,170 (2480)
5	1633			34,720 (18,867), 28,090 (18,773)
5a	1606	938, 915	821	37,800 (38,062), 32,570 (38,875), 27,930 (18,757), 23,580 (8500)
5b	1609	922, 905		36,970 (7790), 32,260 (13,680), 27,780 (8173), 23,470 (3250)
6	1645			37,590 (11,539), 31,060 (6157)
6a	1643	910	820	34,720 (15,110), 31,250 (10,800)
6b	1640	922, 905		37,740 (3775), 31,450 (1259)
7	1643			34,960 (10,751), 30,400 (10,451), 24,690 (8105)
7a	1633	934	829	34,600 (16,850), 31,250 (12,136)
8	1643			37,380 (12,609), 30,260 (9160), 26,320 (6470)
8a	1641	924	823	37,740 (4700), 31,550 (1474)

[a] For abbreviations see Table 1.
[b] ε in $dm^3\ mol^{-1}\ cm^{-1}$.

Table 3. ^{1}H NMR spectral data (δ in ppm)[a,b]

Compounds[c]	—CH=N	Aromatic protons	—CH_2CH_2—	—CH_2—	—CH_3	—OH
1	8.90 (s, 2H)	6.88 (m, 6H), 7.13 (t, 2H), 7.29 (d, 2H), 7.36 (d, 2H), 7.45 (s, 2H)		3.88 (s, 2H)		9.71 (s, 2H), 13.61 (s, 2H)
1a	9.23 (s, 2H)	6.88 (m, 6H), 7.21 (t, 2H), 7.45 (d, 2H), 7.63 (s, 2H), 7.80 (d, 2H)		3.97 (s, 2H)		
1b	9.23 (s, 2H)	6.92 (m, 6H), 7.20 (t, 2H), 7.41 (m, 6H), 7.61 (s, 2H), 7.81 (t, 4H), 8.59 (b, 4H)		3.97 (s, 2H)		
2	8.47 (s, 2H)	6.80 (d, 2H), 7.15 (d, 2H), 7.26 (s, 2H)	3.35 (m, 8H)	3.80 (s, 2H)		4.26 (b, 2H)[d]
2a	8.70 (s, 2H)	6.82 (d, 2H), 7.32 (d, 2H), 7.35 (s, 2H)	3.95 (t, 4H), 4.35 (t, 4H)	3.88 (s, 2H)		
2b	8.70 (s, 2H)	6.85 (d, 2H), 7.40 (m, 8H), 7.82 (t, 2H), 8.57 (b, 4H)	3.97 (t, 4H), 4.37 (t, 4H)	3.90 (s, 2H)		
3	8.41 (s, 2H)	6.77 (d, 2H), 7.15 (d, 2H), 7.27 (s, 2H)	3.44 (s, 4H)	3.80 (s, 2H)	1.20 (s, 12H)	14.10 (s, 2H) 4.90 (b, 2H)[d]
3a	8.60 (s, 2H)	6.83 (d, 2H), 7.37 (d, 2H), 7.48 (s, 2H)	4.23 (s, 4H)	3.87 (s, 2H)	1.32 (s, 12H)	
4	8.43 (s, 2H)	6.76 (d, 2H), 7.17 (d, 2H), 7.25 (s, 2H)	3.82 (b, 4H)	4.75 (s, 2H)	1.07 (s, 3H), 1.12 (s, 3H)	13.50 (s, 2H)
4a	8.62 (s, 2H)	6.81 (d, 2H), 7.29 (d, 2H), 7.35 (s, 2H)	4.12 (m, 4H)	3.90 (s, 2H)	1.23 (s, 3H), 1.27 (s, 3H)	
5	8.80 (s, 2H)	6.72 (t, 2H), 6.87 (m, 4H), 7.10 (t, 2H) 7.35 (d, 2H), 7.50 (q, 2H), 7.77 (d, 2H)				9.56 (s, 2H), 14.15 (s, 2H)
5a	9.30 (s, 2H)	6.82 (t, 2H), 6.95 (m, 4H), 7.26 (t, 2H), 7.73 (d, 2H), 7.85 (q, 2H), 8.06 (d, 2H)				
5b	9.30 (s, 1H)	6.95 (m, 6H), 7.25 (m, 2H), 7.40 (t, 3H), 7.75 (m, 6H), 8.02 (m, 2H), 8.10 (d, 1H), 8.55 (b, 4H)				
6	8.35 (s, 2H)	6.60 (d, 2H), 6.81 (d, 2H), 7.20 (s, 2H)	3.25 (t, 8H)			4.70 (b, 2H)[d]
6a	8.75 (s, 2H)	6.90 (m, 2H), 7.58 (t, 2H), 7.72 (s, 2H)	4.08 (t, 4H), 4.45 (t, 4H)			
6b	8.75 (s, 2H)	6.95 (d, 2H), 7.38 (t, 2H), 7.62 (d, 4H), 7.73 (d, 2H), 7.81 (m, 2H), 8.55 (b, 4H)	3.97 (t, 4H) 4.40 (t, 4H)			
7	8.50 (s, 2H)	6.70 (d, 2H), 7.45 (d, 2H), 7.65 (s, 2H)	3.35 (s, 4H)		1.25 (s, 12H)	14.85 (s, 2H) 5.10 (b, 2H)[d]
7a	8.70 (s, 2H)	6.90 (d, 2H), 7.67 (d, 2H), 7.95 (s, 2H)	4.32 (s, 4H)		1.38 (s, 12H)	
8	8.10 (s, 2H)	6.25 (d, 1H), 6.50 (d, 1H), 6.95 (d, 1H), 7.12 (d, 1H), 7.18 (s, 1H), 8.15 (s, 1H)	3.55 (m, 2H) 4.40 (m, 2H)		0.75 (s, 3H)	14.0 (b, 2H)
8a	8.65 (s, 2H)	6.92 (d, 2H), 7.56 (d, 2H), 7.71 (s, 2H)	4.12 (m, 2H), 4.50 (m, 2H)		1.26 (s, 3H), 1.29 (s, 3H)	

[a] Letters given in parentheses indicate the type of signal. s = singlet, d = doublet, t = triplet, q = quartet, m = multiplet.
[b] CH resonance at 3.43 (m, 2H) in **4**, 4.44 (m, 2H) in **4a**, 3.07 (m, 1H) and 3.20 (m, 1H) in **8** and 3.57 (m, 2H) in **8a**.
[c] For abbreviation see Table 1.
[d] Alcoholic OH resonance.

higher energy by 15–20 cm^{-1}. In addition, the shift of the totally symmetric ring stretching mode at 1587 cm^{-1}, the in-plane antisymmetric ring stretching mode at 1438 cm^{-1} and the in-plane totally symmetric ring breathing mode at 1030 cm^{-1} to higher energy are indicative of the pyridine coordination to the molybdenum ion.

Electronic spectral studies

The electronic spectra of the complexes are recorded in DMF and the data are listed in Table 2. The Schiff bases exhibit two or three electronic spectral bands in the regions 34,960–37,740, 27,860–31,060 and 23,980–24,690 cm^{-1}. These bands are assigned to $\pi \rightarrow \pi_1^*$, $\pi \rightarrow \pi_2^*$ and $n \rightarrow \pi^*$ transitions, respectively[13]. There is no indication of bands due to hydrogen bonding and association in any ligand, which indicates the breaking of the hydrogen bonding in DMF. Usually this band appears in non-coordinating solvents. These ligand bands are also observed in the complexes, but there is no systematic trend in the change of energy. In addition, some complexes show a new band at 20,220–23,580 cm^{-1}, which is assigned to the ligand-to-metal charge transfer transition between the highest occupied ligand molecular orbital and the lowest empty *d*-orbital of molybdenum.

^{1}H *NMR studies*

Further evidence for the coordinating mode of the ligands is obtained from the study of their ^{1}H NMR spectra. The NMR spectra of the ligands and complexes are presented in Table 3. The ligands exhibit resonances due to the phenolic protons of the salicylaldehyde residue between 13.50 and 14.85 ppm as a singlet and an additional signal at 9.56–9.71 ppm in ligands **1** and **5** due to the phenolic proton of the *o*-aminophenol residue. In the ligands **2** and **6** the phenolic proton signal was not observed in the 0–15 ppm region. The absence of hydroxyl resonances in the spectra of the complexes indicates the coordination of the phenolic oxygen atoms to molybdenum after proton replacement.[11] The sharp singlet due to the azomethine proton shifts downfield, suggesting the coordination of the lone pair of the nitrogen of the azomethine group to the molybdenum atom. The Schiff bases do not show resonances due to alcoholic protons in $CDCl_3$ solution, which may possibly be due to intramolecular hydrogen bonding between the alcoholic proton and the azomethine group.[12] However, the spectra of Schiff bases (**2**, **3**, **6** and **7**) in DMSO show the alcoholic proton signal at *ca* 4.26–5.10 ppm, which is confirmed by D_2O exchange studies. The absence of this signal in the complexes suggests deprotonation as a result of complex formation. The complexes $[(MoO_2)_2L]$ when dried at 100°C did not show signals due to coordinated methanol, supporting the oligomeric structure.

The coordination of pyridine to the molybdenum ion in $[(MoO_2)_2L(py)_2]$ is evidenced by the appearance of two to three new signals in the aromatic region. Other signals in the complexes due to aromatic protons, —CH_3 protons, —CH— protons, —CH_2— protons and —CH_2CH_2— protons are observed in almost the same positions as in the respective Schiff bases. The occurrence of a singlet due to the —CH_2— protons attached to two aromatic rings at 3.80–3.97 ppm in the Schiff bases derived from methylene-bis(salicylaldehyde) and in their complexes indicates that the two Schiff base groups are still attached to the methylene group. Thus, the NMR data agree well with the conclusion drawn from the IR data.

Acknowledgements—MRM and DCA thank the Council of Scientific and Industrial Research, New Delhi 110 012, for the award of a Pool Officership and a Junior Research Fellowship, respectively.

REFERENCES

1. (a) R. C. Bray, *Enzymes*, Vol. 12, 3rd edn, p. 299 (1975); (b) E. I. Stiefel, *Prog. Inorg. Chem.* 1977, **22**, 1; (c) G. D. Lawrence and J. T. Spence, *Biochemistry* 1975, **14**, 3626; (d) G. D. Lawrence and J. T. Spence, *Biochemistry* 1977, **17**, 3087.
2. (a) R. A. D. Wentworth, *Coord. Chem. Rev.* 1976, **18**, 1; (b) R. Colton, *Coord. Chem. Rev.* 1987, **78**, 39; (c) A. Syamal and M. R. Maurya, *Coord. Chem. Rev.* 1989, **95**, 183.
3. C. S. Marvel and N. Tarkoy, *J. Am. Chem. Soc.* 1957, **79**, 6000.
4. P. A. Awasarkar, S. Gopinathan and C. Gopinathan, *Synth. React. Inorg. Met.-Org. Chem.* 1985, **15**, 133.
5. G. J.-J. Chen, J. W. Mcdonald and W. E. Newton, *Inorg. Chem.* 1976, **15**, 2612.
6. M. R. Maurya and C. Gopinathan, *Polyhedron* 1993, **12**, 1039.
7. (a) O. A. Rajan and A. Chakravorty, *Inorg. Chem.* 1981, **20**, 660; (b) A. Syamal and M. R. Maurya, *Synth. React. Inorg. Met.-Org. Chem.* 1986, **16**, 857.
8. A. Syamal and K. S. Kale, *Inorg. Chem.* 1979, **18**, 992.
9. P. Teyssie and J. J. Charette, *Spectrochim. Acta* 1963, **19**, 1407.
10. S. S. Singh and C. B. S. Sengar, *Ind. J. Chem.* 1969, **7**, 812.
11. E. C. Alyea, A. Malek and A. I. Kazi, *Trans. Met. Chem.* 1981, **6**, 223.
12. S. Gopinathan, M. P. Degaonkar, A. M. Hundekar and C. Gopinathan, *Appl. Organomet. Chem.* 1993, **7**, 63.
13. A. Syamal, O. P. Singhal and S. Banerjee, *Synth. React. Inorg. Met.-Org. Chem.* 1980, **10**, 243.

Polyhedron Vol. 12, No. 22, pp. 2737–2739, 1993
Printed in Great Britain

0277–5387/93 $6.00+.00
© 1993 Pergamon Press Ltd

COMMUNICATION

$[(PtMe_3)_3\{\mu\text{-I}, \mu\text{-S(CH}_2)_2NHEt_2\}_2]I$, THE FIRST PLATINUM THIOLATE COMPLEX WITH AN INCOMPLETE CUBANE STRUCTURE

WILLIAM CLEGG* AND KELLY ANNE FRASER

Department of Chemistry, University of Newcastle, Newcastle upon Tyne NE1 7RU, U.K.

and

NÚRIA DURAN and PILAR GONZÁLEZ-DUARTE*

Departament de Química, Universitat Autònoma de Barcelona, 08193 Bellaterra, Barcelona, Spain

(*Received* 2 *August* 1993; *accepted* 2 *September* 1993)

Abstract—The cluster cation of $[(PtMe_3)_3\{\mu\text{-I}, \mu\text{-S(CH}_2)_2NHEt_2\}_2]I$. CH_3CN has a cubane type structure, $[(PtMe_3)_4(\mu\text{-I}, \mu\text{-SR})_2]$, but lacking one $PtMe_3$ vertex. Each platinum atom exhibits octahedral coordination, one sulphur is triply bridging, the other sulphur and the two iodine atoms are doubly bridging.

Despite the wide diversity of structure types already established for metal thiolates,[1] only two have so far been observed for platinum(IV): cubanes $[(Me_3Pt)_4(\mu_3\text{-SR})_4]$, where R = Me[2] or Ph,[3] and thiolate-bridged mixed Pt(II)–Pt(IV) complexes of general formula $[(dppe)M(\mu_2\text{-SMe})_2PtXMe_3]$, with M = Pd or Pt, and X = Cl, Br or I.[4] Our interest in metal aminoalkanethiolate complexes, together with the scarcity of data on Pt(IV) thiolate complexes, encouraged us to study the reaction of tetrameric trimethylplatinum iodide with 2- and 3-aminoalkanethiols. These ligands can behave as simple thiols with a solubilizing and potentially ligating amine group, which becomes non-coordinating if it is protonated. Hence they give complexes different solubility properties from those of complexes of monofunctional thiols, thus facilitating the discovery of new structural types. Accordingly, previously unknown confacial bioctahedral diplatinum(IV) complexes with 3-aminoalkanethiolate bridges, $Na[(Me_3Pt)_2\{\mu_2\text{-SCH(CH}_2CH_2)_2NMe\}_3]$ and $[(Me_3Pt)_2\{\mu_2\text{-S(CH}_2)_3NHMe_2\}_3](BPh_4)_2$, have just been characterized structurally.[5] We now report the synthesis and crystal structure of an unprecedented complex, $[(Me_3Pt)_3\{\mu\text{-S(CH}_2)_2NHEt_2, \mu\text{-I}\}_2]I\cdot CH_3CN$, consisting of a Pt_3 cluster with an incomplete cubane structure.

The complex was prepared from the tetranuclear cubane-like $[(Me_3PtI)_4]$ by treatment with the aminothiol $HS(CH_2)_2NEt_2$ in methanol, and was recrystallized from isopropanol–acetonitrile solution. The crystal structure determination indicates that the complex consists of a trinuclear cluster cation $[(Me_3Pt)_3\{\mu\text{-I}, \mu\text{-S(CH}_2)_2NHEt_2\}_2]^+$ (Fig. 1), an I^- counterion, and a molecule of acetonitrile solvent. The cation can be described as a cubane-type $[(Me_3Pt)_4(\mu\text{-SR})_2(\mu\text{-I})_2]$ cluster, but lacking one Me_3Pt vertex group. Substitution of two of the iodide bridges of the starting material by thiolates has caused also loss of one of the trimethylplatinum units. The $Pt_3S_2I_2$ core is composed of a Pt_3 triangle and a distorted S_2I_2 tetrahedron. The cluster has an approximate mirror plane passing through Pt(3) and the two sulphur atoms. Each platinum atom has a distorted octahedral coordination, with a *fac* arrangement of the three methyl groups; each

* Authors to whom correspondence should be addressed.

octahedron shares two adjacent edges with the other two. Atoms S(1), I(1) and I(2) are doubly bridging, while S(2) is triply bridging; in the presence of a fourth Me_3Pt vertex, all these ligands would, of course, be triply bridging.

Values of individual bond lengths and angles for the cation are given in Fig. 1. Bond lengths and angles are essentially the same for the doubly-bridging and triply-bridging S atoms. Pt—C, Pt—S and Pt—I bond lengths, and angles within the $Pt_3I_2S_2$ core, are remarkably close to corresponding values in the complete cubane structures of $[(Me_3PtX)_4]$ (X = SMe,[2] SPh,[3] or I[6]), despite the lack of one Pt vertex and the mixture of bridging ligands in the current structure.

This structure is totally unprecedented among octahedrally coordinated metals and any type of thiolate ligands. A novel cadmium thiolate, $[Cd_3(SC_6H_2Pr^i_3)_7]^-$,[7] and the Fe_3S_4 cluster in *Desulfovibrio gigas* Ferredoxin II[8] are the closest examples of incomplete cubane clusters (similar Fe_3S_4 clusters are now known in about 20 proteins), even though in both cases coordination around the metal centres is essentially tetrahedral. For metals with octahedral coordination the present structure type is confined to early transition metal trinuclear cluster species. There are many molybdenum and tungsten trinuclear complexes with metal–metal bonding interactions and with oxo, sulphido, selenido, or halo ligands,[9] and a few structures of Cr, Mo and W are also known with carbonyl, alkoxo and alkylimido bridging ligands.[10] Several trinuclear complexes of niobium and tantalum, largely with halo and sulphido bridges, have also been structurally characterized.[11]

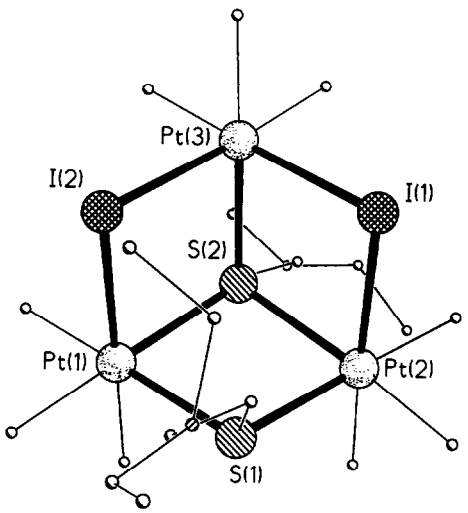

Fig. 1. Structure of the cation without hydrogen atoms, and with selected atoms labelled. Key dimensions: Pt(1)—S(1) 2.491(5), Pt(1)—S(2) 2.473(4), Pt(2)—S(1) 2.488(4), Pt(2)—S(2) 2.516(4), Pt(3)—S(2) 2.474(5), Pt(1)—I(2) 2.808(2), Pt(2)—I(1) 2.834(2), Pt(3)—I(1) 2.820(2), Pt(3)—I(2) 2.802(1) Å; S(1)—Pt(1)—S(2) 82.31(14), S(1)—Pt(1)—I(2) 94.61(11), S(2)—Pt(1)—I(2) 83.67(11), S(1)—Pt(2)—S(2) 81.49(14), S(1)—Pt(2)—I(1) 95.34(11), S(2)—Pt(2)—I(1) 81.76(11), S(2)—Pt(3)—I(1) 82.78(10), S(2)—Pt(3)—I(2) 83.77(10), I(1)—Pt(3)—I(2) 92.44(4), Pt(1)—S(1)—Pt(2) 97.8(2), Pt(1)—S(2)—Pt(2) 97.5(2), Pt(1)—S(2)—Pt(3) 104.0(2), Pt(2)—S(2)—Pt(3) 105.8(2), Pt(2)—I(1)—Pt(3) 89.51(4), Pt(1)—I(2)—Pt(3) 88.04(4)°.

EXPERIMENTAL

The complex was prepared by adding $[(Me_3PtI)_4]$ (0.205 mmol) to a filtered solution containing initially $HS(CH_2)_2NEt_2{\cdot}HCl$ (0.87 mmol) in dry and degassed acetonitrile (10 cm^3) and KMeO (0.85 mmol) in absolute methanol (0.25 cm^3). The reaction mixture was stirred under a nitrogen atmosphere for 5 days and then the solvent of the filtrate was evaporated. Subsequent additions of diethyl ether to the remaining oil yielded a yellow powder, which was treated with chloroform several times. After centrifugation, the solvent was decanted and the solid was dried *in vacuo* (yield 0.04 g, 11%). Alternatively, the same complex was obtained as a by-product in the synthesis of $[(Me_3Pt)_4\{\mu\text{-}S(CH_2)_2NEt_2\}_3(\mu\text{-}I)]$.[12] Yellow air-stable single crystals were produced by slow evaporation of an isopropanol solution containing a few drops of acetonitrile. Satisfactory analyses (C, H, N, S) were obtained.

Crystallography

The complex crystallizes as yellow blocks from isopropanol–acetonitrile solution. $[C_{21}H_{57}I_2N_2Pt_3S_2]I{\cdot}CH_3CN$, $M = 1408.8$, monoclinic, space group $P2_1/n$, $a = 11.301(2)$, $b = 20.455(4)$, $c = 16.884(3)$ Å, $\beta = 95.65(2)°$, $V = 3884.0(12)$ Å^3, $Z = 4$, $D_c = 2.409$ g cm^{-3}, $F(000) = 2576$. Reflections (9752) were measured on a Stoe-Siemens diffractometer with graphite-monochromated Mo-K_α radiation ($\lambda = 0.71073$ Å, $\mu = 13.29$ mm^{-1}) and on-line profile fitting.[13] Semi-empirical absorption corrections were applied and equivalent reflections merged to give 6814 unique data ($R_{int} = 0.080$, $2\theta_{max} = 50°$). Structure solution was by direct methods, refinement by full-matrix least-squares on F^2 for all measured data,[14] to give final $R' = [\Sigma w(F_o^2 - F_c^2)^2/\Sigma w(F_o^2)^2]^{1/2} = 0.1891$ for all data, conventional R [on F values for 4592 reflections with $I > 2\sigma(I)$] = 0.0568. Atomic coordinates, bond lengths and angles, and atomic displacement parameters have been deposited as

supplementary material at the Cambridge Crystallographic Data Centre.

Acknowledgements—We thank the UK Science and Engineering Research Council and the Ministerio de Educación y Ciencia (Spain, Grant PB90-0691) for financial support.

REFERENCES

1. I. G. Dance, *Polyhedron* 1986, **5**, 1037; P. J. Blower and J. R. Dilworth, *Coord. Chem. Rev.* 1987, **76**, 121.
2. G. Smith, C. H. L. Kennard and T. G. W. Mak, *J. Organomet. Chem.* 1985, **290**, C7.
3. D. C. Craig and I. G. Dance, *Polyhedron* 1987, **5**, 1157.
4. E. W. Abel, N. A. Cooley, K. Kite, K. G. Orrell, V. Sik, M. B. Hursthouse and H. M. Dawes, *Polyhedron* 1987, **6**, 1261.
5. W. Clegg, N. Duran, K. A. Fraser, P. González-Duarte, J. Sola and I. C. Taylor, *J. Chem. Soc., Dalton Trans.* 1993, in press.
6. G. Donnay, L. B. Coleman, N. G. Krieghoff and D. O. Cowan, *Acta Cryst. Sect. B* 1968, **24**, 157.
7. K. Tang, A. Li, X. Jin and Y. Tang, *J. Chem. Soc., Chem. Commun.*, 1991, 1590.
8. C. R. Kissinger, E. T. Adman, L. C. Sieker and L. H. Jensen, *J. Am. Chem. Soc.* 1988, **110**, 8721.
9. T. Shibahara, *Adv. Inorg. Chem.* 1991, **37**, 143.
10. D. J. Devenbourg, D. J. Zalewski, K. M. Sanchez and T. Delord, *Inorg. Chem.* 1988, **27**, 821; S. W. Kirtley, J. P. Chanton, R. A. Love, D. L. Tipton, T. N. Sorrell and R. Bau, *J. Am. Chem. Soc.* 1980, **102**, 3451; D. C. Bradley, R. J. Errington, M. B. Hursthouse and R. L. Short, *J. Chem. Soc., Dalton Trans.* 1990, 1043.
11. F. A. Cotton, M. P. Diebold, R. Llusar and W. J. Roth, *J. Chem. Soc., Chem. Commun.* 1986, 1276; F. A. Cotton, M. P. Diebold and W. J. Roth, *J. Am. Chem. Soc.* 1987, **109**, 2833; F. A. Cotton, M. P. Diebold, X. Feng and W. J. Roth, *Inorg. Chem.* 1988, **27**, 3413; F. A. Cotton, P. A. Kibala and W. J. Roth, *J. Am. Chem. Soc.* 1988, **110**, 298; E. Babaian-Kibala, F. A. Cotton and M. Shang, *Inorg. Chem.* 1990, **29**, 5148.
12. N. Duran and P. González-Duarte, unpublished results.
13. W. Clegg, *Acta Cryst. Sect. A* 1981, **37**, 22.
14. G. M. Sheldrick, SHELXS-86, program for crystal structure solution, University of Göttingen (1986); SHELXL-93, program for crystal structure refinement, beta-test version (1992).

Polyhedron Vol. 12, No. 22, pp. 2741–2743, 1993
Printed in Great Britain

0277-5387/93 $6.00+.00
© 1993 Pergamon Press Ltd

COMMUNICATION

A STERIC PREFERENCE FOR LINEAR VERSUS BENT IMIDO LIGATION? SYNTHESIS AND X-RAY CRYSTAL STRUCTURE OF $[Mo(NAr)_2(edtc)_2]$ (Ar = 2,6-^{i}Pr$_2$C$_6$H$_3$; edtc = S_2CNEt_2) CONTAINING TWO LINEAR IMIDO MOIETIES

THÉRÈSE A. COFFEY, GLYN D. FORSTER, GRAEME HOGARTH* and ANDREA SELLA

Chemistry Department, University College London, 20 Gordon Street, London WC1H 0AJ, U.K.

(*Received* 26 *July* 1993; *accepted* 31 *August* 1993)

Abstract—Reaction of two equivalents of ArNCO (Ar = 2,6-^{i}Pr$_2$C$_6$H$_3$) with $[MoO_2(edtc)_2]$ affords the bisimido complex $[Mo(NAr)_2(edtc)_2]$ shown by crystallography to contain two linear imido ligands; this is in contrast to the parent complex $[Mo(NPh)_2(edtc)_2]$ previously shown to contain both linear and bent imido groups.

Complexes containing the imido ligand continue to attract considerable attention, primarily since they are envisaged as potential amination and aziridination reagents for organic synthesis. It is well documented that, depending upon the metal–nitrogen–carbon angle, the ligand may act as either a 2- or 4-electron donor to a metal centre, and this is easily understood in terms of the simple valence bond models.[1] More recently, a number of studies have considered the bonding in such complexes in more detail and concluded that when more than one imido ligand is present, the donor ability may be intermediate between these two valence bond extremes.[2,3] An interesting dilemma arises for a molecule that contains two imido ligands, from which the metal requires only six electrons. This is the case for complexes of the stoicheiometry $[Mo(NR)_2L_2]$ (where L is a three electron donor ligand), since the MoL_2 moiety is a 12 electron fragment. To date only one complex of this type has been structurally characterized, namely $[Mo(NPh)_2(edtc)_2]$, shown to contain one bent and one linear imido ligand.[4] We now report the synthesis and structure of another compound of this stoicheiometry which differs only in the steric bulk associated with the aryl group, but adopts a structure in which both imido ligands are linear.

Addition of two equivalents of 2,6-diisopropylphenylisocyanate to a toluene solution of $[MoO_2(edtc)_2]$ affords after chromatography the bisimido complex $[Mo(NAr)_2(edtc)_2]$ **1** in 50% yield.† Addition of only one equivalent of arylisocyanate also yielded **1** as the major product and the mixed oxo-imido complex was not isolated, indicating that the second substitution process occurs considerably faster than the first.

$$MoO_2(edtc)_2 + 2\,ArNCO \rightarrow Mo(NAr)_2(edtc)_2 + 2CO_2$$

*Author to whom correspondence should be addressed.

†Complex **1** was characterized by elemental analyses and IR and NMR (^{1}H and ^{13}C) spectra.

Selected data: ^{1}H NMR. (C_7D_8, 373 K) δ 6.95 (*d*, 4H, *J* 7.6, m-C_6H_3), 6.80 (t, 2H, *J* 7.6, p-C_6H_3), 4.08 (septet, 4H, *J* 6.8, C*H*Me$_2$), 3.46 (q, 8H, *J* 7.0, C*H*$_2$Me), 1.19 (*d*, 24H, *J* 6.8, CH*Me*$_2$), 0.96 (t, 12H, *J* 7.0, CH$_2$*Me*); (C_7D_8, 253 K) δ 6.96 (*d*, 4H, *J* 7.6, m-C_6H_3), 6.84 (t, 2H, *J* 7.6, p-C_6H_3), 4.17 (septet, 4H, *J* 6.8, C*H*Me$_2$), 3.47 (sextet, 2H, *J* 6.8, C*H*$_2$Me), 3.14 (m, 4H, *CH*$_2$Me), 2.93 (sextet, 2H, C*H*$_2$Me), 1.28 (*d*, 12H, *J* 6.8, CH*Me*$_2$), 1.16 (*d*, 12H, *J* 6.8, CH*Me*$_2$), 0.81 (t, 6H, *J* 6.8, CH$_2$*Me*), 0.74 (t, 6H, *J* 7.0, CH$_2$*Me*); IR (KBr) 1267s, 1210m, 1149m, 1095w, 1075m, 962m, 847w, 755s cm^{-1}. Satisfactory elemental analyses were obtained.

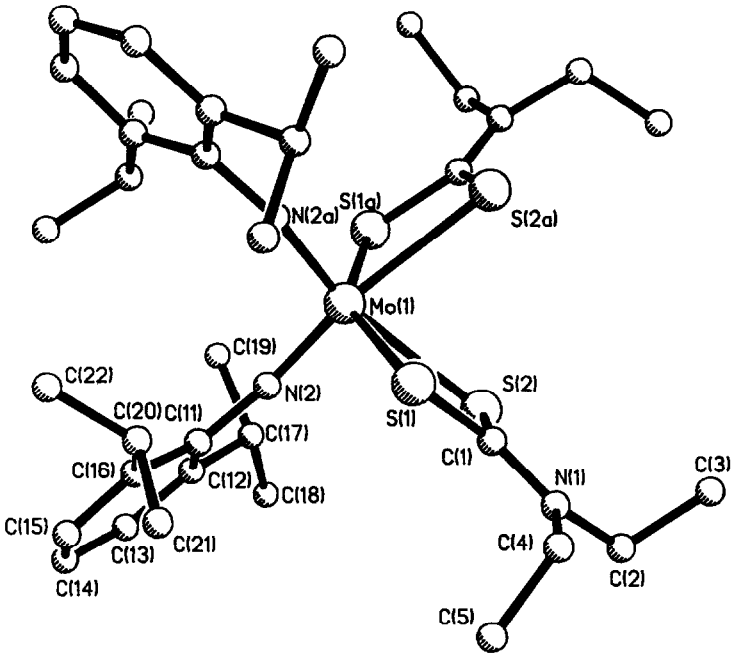

Fig. 1. Molecular geometry of **1**.

The structure of **1** has been determined crystallographically and is shown in Fig. 1.* As expected, the complex exhibits approximate octahedral coordination at molybdenum and contains a *cis* configuration of arylimido ligands [N(2)—Mo(1)—N(2A) 104.7(1)°]. The most surprising feature is that both are linear [Mo(1)—N(2)—C(11) 169.9(2)°], in marked contrast to the situation found in the parent complex $[Mo(NPh)_2(edtc)_2]$ which shows both linear [169.4(4) Å] and bent [139.4(4) Å] imido ligation (Fig. 2). Thus in **1** it appears that each imido ligand is acting as three electron donor to the molybdenum centre. For all known molybdenum imido complexes, the molybdenum–nitrogen bond length varies only within 0.1 Å, and thus this criterion alone is not necessarily a good measure of the donor properties of the imido ligand.[1] It is noteworthy however that in **1** the Mo(1)—N(2) distance of 1.766(2) Å is intermediate between those found in $[Mo(NPh)_2(edtc)_2]$, thus suggesting an intermediate bond order in **1**. A better insight into the molybdenum–nitrogen bond order can be gained in this instance by considering the *trans* influence of the imido ligand. Thus in $[Mo(NPh)_2(edtc)_2]$, while both the molybdenum–sulphur bonds *trans* to the imido ligands are elongated, that *trans* to the bent [2.755(2) Å] imido ligand, is considerably longer than that *trans* to the linear one [2.602(2) Å]. In **1** the *trans* molybdenum–sulphur bond is intermediate between these two extremes [Mo(1)—S(2) 2.672(1) Å], lending further weight to the postulation of two three electron donor imido ligands in **1**.

The concept of two imido ligands each acting as three electron donors is not new, indeed we ourselves have observed this behaviour in the somewhat related organometallic dimers $[CpMo(NAr)(\mu\text{-}NAr)]_2$.[2] The example reported here however

Crystal data: $Mo_1S_4N_4C_{34}H_{54}$, $M = 742.99$, monoclinic, space group C_2/c, $a = 16.336(2)$, $b = 12.977(2)$, $c = 19.230(2)$ Å, $\beta = 111.70(1)$, $U = 3788.7(9)$ Å^3, $Z = 4$, $T = 292$ K, $D_c = 1.30$ g cm^{-3}, $F(000) = 1568$, $\lambda = 0.71073$ Å, $\mu(\text{Mo-}K_\alpha) = 5.76$ cm^{-1}. Intensity data were collected on a crystal of dimensions 0.90 × 0.70 × 0.48 mm mounted on a Nicolet R3mV diffractometer, by the ω-2θ scan technique ($5 \leqslant 2\theta \leqslant 50°$). From 4593 measured data, 3059 with $I \geqslant 3\sigma(I)$ were considered observed. The structure was solved by direct methods and refined by full-matrix least-squares to R and R_w values of 0.031 and 0.034.

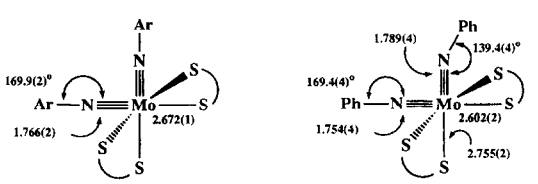

Fig. 2. A comparison of bond lengths and angles between **1** and $[Mo(NPh)_2(edtc)_2]$.

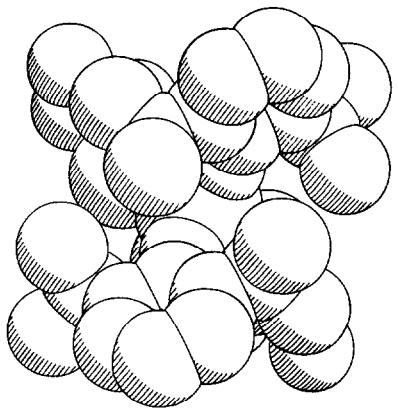

Fig. 3. Space filling diagram of **1**.

appears to be the first instance in which both possible configurations have been found within the same system. We believe that **1** adopts a configuration with two linear imido moieties due to steric effects. Figure 3 shows a space filling diagram for **1**. As can be clearly seen, a methyl from one isopropyl group lies above the arene ring of the second imido ligand, and sits in a pocket formed by its isopropyl groups. Adoption of a linear/bent structure would lead to steric clashes between two aryl groups, or between an aryl moiety and a dithiocarbamate ligand. We believe this conformation is maintained in solution since in the ^{1}H NMR spectrum at low temperatures two methyl environments are seen for both the isopropyl groups (in and out) and the dithiocarbamate ligands (up and down). Warming results in coalescence, until at 100°C a single resonance is observed for both of the different methyl environments. We attribute these spectral changes to two processes; geared rotation of the aryl groups about the N—C carbon bond, and rotation of the dithiocarbamates again about the C—N bond.

Complexes of the type $[Mo(NAr)_2L_2]$ are of particular interest as possible imido transfer agents due to the widespread use of the bisoxo complexes $[MoO_2L_2]$ in related oxidation processes.[5] We are currently investigating the reactivity of **1** in this respect, and it will be especially interesting to compare this with that of $[Mo(NPh)_2(edtc)_2]$, some reactivity studies of which have been reported.[6]

Acknowledgements—This work was supported by grants from SERC (studentship to G.D.F.), The Nuffield Foundation, The Royal Society, and University of London Central Research Fund.

REFERENCES

1. W. A. Nugent and J. M. Mayer, *Metal–Ligand Multiple Bonds*, Wiley Interscience, New York (1988).
2. M. L. H. Green, G. Hogarth, P. C. Konidaris and P. Mountford, *J. Chem. Soc., Dalton Trans.* 1990, 3781.
3. M. H. Schofield, T. P. Kee, J. T. Anhaus, R. R. Schrock, K. H. Johnson and W. M. Davis, *Inorg. Chem.* 1991, **30**, 3595.
4. B. L. Haymore, E. A. Maatta and R. A. D. Wentworth, *J. Am. Chem. Soc.* 1979, **101**, 2063.
5. R. H. Holm, *Chem. Rev.* 1987, **87**, 1401.
6. E. A. Maatta and R. A. D. Wentworth, *Inorg. Chem.* 1979, **18**, 2409.

Polyhedron Vol. 12, No. 22, pp. 2745–2747, 1993
Printed in Great Britain

0277–5387/93 $6.00+.00
© 1993 Pergamon Press Ltd

COMMUNICATION

CRYSTAL STRUCTURE OF TETRACAESIUMDIHYDROGENDECAVANADATE TRIHYDRATE, $Cs_4H_2V_{10}O_{28}\cdot 3H_2O$. A LAYERED CRYSTAL STRUCTURE OF DECAVANADATE

MASATO HASHIMOTO* and MAKOTO MISONO

Department of Synthetic Chemistry, Faculty of Engineering, The University of Tokyo, Hongo, Bunkyo, Tokyo 113, Japan

and

MITSUHIRO HIBINO, JUNKO OI and TETSUICHI KUDO*

Institute of Industrial Science, The University of Tokyo, Roppongi, Minato, Tokyo 106, Japan

(*Received* 7 *July* 1993; *accepted* 28 *August* 1993)

Abstract—The title compound $Cs_4H_2V_{10}O_{28}\cdot 3H_2O$ was obtained from a polyvanadate system containing H_2O_2. No peroxo group or hydrogen peroxide molecule was found in the structure. The polyanions are ordered parallel to the *bc*-plane forming a layered structure. The water molecules and the caesium ions make a hydrogen bonding network with decavanadate ions and each other to support the whole crystal structure.

We have studied polyacids of the early transition metal with peroxide ligands obtained from metal, metal oxide or metal carbide—H_2O_2 systems.[1] Structures of tungsten-, molybdenum- or niobium-based oxides from the calcination of alkaline metal salts of those acids have been determined by the powder X-ray diffraction method.[2] In this series of studies the title compound was obtained from vanadium metal—H_2O_2—Cs^+ system as single crystals and its structure was determined by single crystal X-ray diffraction.

EXPERIMENTAL

Preparation

The compound $Cs_4H_2V_{10}O_{28}\cdot 3H_2O$ was obtained by the following method: vanadium metal powder (325 mesh) 0.3 g was completely dissolved in 10 cm^3 of 30% hydrogen peroxide aqueous solution in an ice-cooled water bath. Then 1.5 g CsBr in 10 cm^3 water was added in small portions into the vanadium solution. Orange flakey crystals appeared after storage for a day at room temperature. Found: Cs, 34.9; V, 32.4; H_2O, 4.01. Calc. for $Cs_4H_2V_{10}O_{28}\cdot 3H_2O$; Cs, 34.4; V, 33.0; H_2O, 3.50%.

X-ray measurement and structure determination

A single crystal with dimensions $0.25\times 0.20\times 0.01$ mm was subjected to single crystal X-ray diffraction method. Intensity data were collected on RIGAKU AFC-5R automated four-circle diffractometer with graphite monochromated Mo-K_α radiation ($\lambda = 0.71069$ Å) at 296 K. Crystallographic data are: FW = 1545.1, monoclinic, $P2_1/c$, $a =$ 10.079 (3), $b = 14.116(2)$, $c = 11.544(1)$ Å, $\beta =$ 108.20(1)°, $V = 1560(1)$ Å^3, and $Z = 2$. Of total 3958 reflections, 1348 unique observed ones with $Io \geqslant 3.0\sigma(Io)$ and $4° \leqslant 2\theta \leqslant 55°$ were used for calculation by using TEXSAN.[3] Lorenz polarization correction was applied, anomalous dis-

*Authors to whom correspondence should be addressed.

persion factors including imaginary part were taken from International Tables for X-Ray Crystallography,[4] Cs and V atoms were refined anisotropically and oxygen atoms isotropically. The occupation factors of the oxygen atoms of water molecules were estimated from the water content by thermogravimetry and their thermal parameters. Full matrix least-squares refinement based on F gave $R = 0.068$ and $R_w = 0.079$ (sigma weight) for 128 parameters.

STRUCTURE DESCRIPTION AND DISCUSSION

An ORTEP[5] view of the decavanadate anion with atomic notation is shown in Fig. 1. Although H_2O_2 was used in the preparation no peroxo groups were found in the electron density map by the difference Fourier syntheses. The polyanion structure is similar to the normal decavanadate[6] and is different from the peroxodecamolybate structure.[7] The bond distances and angles of the V—O bonds are similar to those in another decavanadate.[6] Figure 2 shows the packing diagram of the crystal. The polyanions are arranged to form a layered structure through the centre of the crystal parallel to the *bc*-plane. Thus the interlayer distance is 9.57 Å, and, considering the van der Waals radius of the oxygen atom (*ca* 1.40 Å), the width of the interlayer space is about 1.8 Å. Molecules of the water of crystallization are almost on a plane sandwiched between the vanadate layers; two of four caesium cations are also located between the layers, *ca* 0.7 Å apart from the water plane, and another two are included in the vanadate layers. Interatomic distances (see Table 1) between the caesium cations and neighbouring waters of crystallization are 3.12(4) to 3.31(4) Å, and those between caesium and oxygen atoms of the polyanion shows 3.07(2) Å as the minimum. Those between each water of crystallization and the nearest oxygen in the polyanion are 2.70(4) and 3.08(4) Å, and the shortest distance between water of crystallization is 2.62(5) Å. These interatomic distances indicate that the

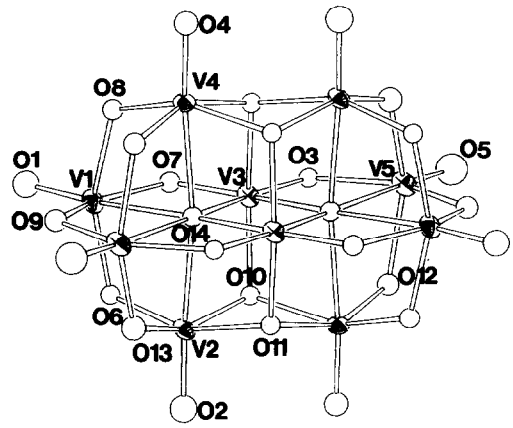

Fig. 1. Anion structure of the compound along with atomic notations.

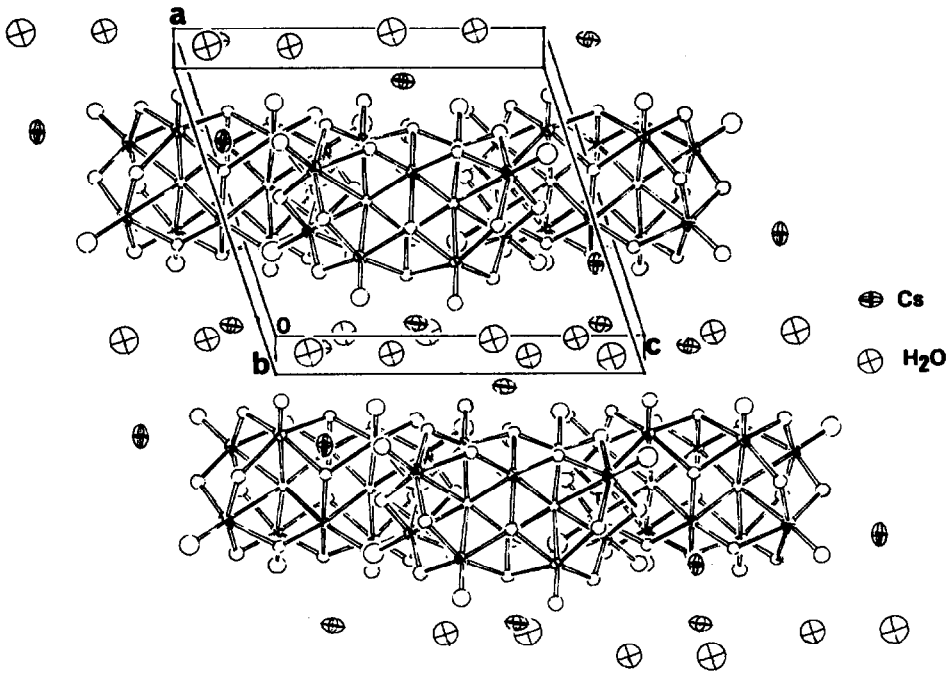

Fig. 2. Packing diagram of the compound.

Table 1. Selected interatomic distances (Å).

V1—O1	1.61 (2)	Cs2—O2[e]	3.09 (2)
V2—O2	1.58 (2)	Cs2—O4[f]	3.24 (2)
V3—O3	1.68 (2)	Cs2—O5[g]	3.12 (2)
V4—O4	1.58 (2)	Cs2—O7	3.10 (2)
V5—O5	1.60 (2)	Cs2—O101[f]	3.23 (3)
V4—O12	1.97 (2)	Cs2—O102[h]	3.31 (4)
V5—O12	1.98 (2)	O1—O3[i]	3.14 (3)
Cs1—O2[a]	3.17 (2)	O1—O5[c]	3.26 (3)
Cs1—O4[b]	3.24 (2)	O6—O12[g]	2.57 (2)
Cs1—O9	3.07 (2)	O8—O10	2.70 (4)
Cs1—O10[a]	3.24 (2)	O11—O101[f]	2.83 (3)
Cs1—O12	3.32 (2)	O13—O102[j]	3.08 (4)
Cs1—O13[c]	3.29 (2)	O101—O102	2.62 (5)
Cs1—O102	3.12 (4)	O102—O102[k]	3.07 (8)
Cs2—O1[d]	3.07 (2)		

Symmetry operations: [a]1−x, 1/2+y, 3/2−z; [b]x, 3/2−y, 1/2+z; [c]1−x, 1−y, 2−z; [d]x, 1/2−y, z−1/2; [e]x−1, 1/2−y, z−1/2; [f]−x, 1−y, 1−z; [g]1−x, y−1/2, 3/2−z; [h]−x, y−1/2, 3/2−z; [i]x, 1/2−y, 1/2+z; [j]1+x, y, z; [k]−x, 1−y, 2−z.

water molecules and caesium cations form the hydrogen bonding network among themselves or with decavanadate anion supporting the whole crystal structure. Some short interatomic distances were observed between neighbouring vanadate oxygens [O1—O3 3.14(3), O1—O5 3.26(3), O6—O12 2.57(2) Å]. The vanadium–oxygen bond length around bridging O6 are not elongated compared with another V—O(bridging) one, but those around O12 are relatively long. Terminal oxygen–vanadium distances of V1—O1, V5—O5 [1.61(2), 1.60(2) Å] are longer than two other V2—O2 and V4—O4 [1.58(2) Å each]. Considering these bond lengths and the influence of the hydrogen bonding with water molecule, but not with caesium cation which strongly correlated with O1, O2, O5, O7, and O9, bond orders[8] of O3 (1.39) and O12 (1.27) are remarkably smaller than those of other oxygen atoms, and this probably indicates that one of these oxygen atoms is protonated.

REFERENCES

1. T. Kudo and H. Okamoto, *Inorg. Chim. Acta* 1986 **111**, L27.
2. T. Kudo, J. Oi, A. Kishimoto and M. Hiratani, *Mat. Res. Bull.* 1991, **26**, 779.
3. TEXSAN, TEXRAY Structure Analysis Package, Molecular Structure Corporation (1985).
4. D. T. Cromer and J. T. Waber, *International Tables for X-ray Crystallography*, Vol. IV, Kynoch Press, Birmingham, U.K. (1974).
5. C. K. Johnson, ORTEP-II, ORNL-5138, Oak Ridge National Laboratory, Tennessee, U.S.A. (1976).
6. There are many examples of the structure determination. For example, V. W. Day, W. G. Klemperer and D. J. Maltbie, *J. Am. Chem. Soc.* 1987, **109**, 2991.
7. I. Persdotter, L. Trysberg and R. Stomberg, *Acta Chim. Scand.* 1986, **A40**, 83.
8. I. D. Brown and D. Altermatt, *Acta Cryst. Sect. B* 1985, **41**, 244.

Polyhedron Vol. 12, No. 22, pp. 2749–2751, 1993
Printed in Great Britain

0277–5387/93 $6.00+.00
© 1993 Pergamon Press Ltd

COMMUNICATION

SYNTHESIS AND X-RAY CRYSTAL STRUCTURE OF THE Sm-YLIDE COMPLEX, $[(C_5H_5)_3SmCH_2P(Me)Ph_2]$

WAI-KWOK WONG*

Department of Chemistry, Hong Kong Baptist College, Kowloon, Hong Kong

and

JINGWEN GUAN, JINSONG REN and QI SHEN

Laboratory of Rare Earth Chemistry and Physics,
Changchun Institute of Applied Chemistry, Academia Sinica,
109 Stalin Street, Changchun 130022, P.R.C.

and

WING-TAK WONG*

Department of Chemistry, University of Hong Kong, Pokfulam Road, Hong Kong

(*Received* 16 *June* 1993; *accepted* 11 *August* 1993)

Abstract—The interaction of $(C_5H_5)_2SmCl \cdot LiCl$ with one equivalent of $Li[(CH_2)(CH_2)PPh_2]$ in refluxing tetrahydrofuran gives the yellow complex $[(C_5H_5)_3SmCH_2P(Me)Ph_2]$ in 30% yield. The compound has been fully characterized by analytical, spectroscopic and X-ray diffraction methods.

Phosphorus ylides have been shown to possess an extensive coordination chemistry with main group and transition metal atoms and to form metal–carbon σ-bonds of unusual stability.[1] Schumann[2] and Gilje[3] have extended the ylidic chemistry to lanthanide and actinide metals, respectively. Gilje and co-workers have further demonstrated that the phosphorus ylidic ligand, depending on the reaction conditions, can act either as a monodentate or a bidentate ligand as shown below.[3a]

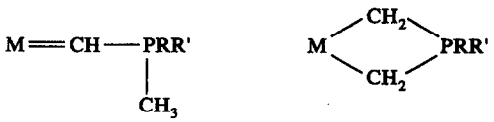

Recently we have described the preparation, solution dynamics and reactivities of a series of phosphorus ylidic organolanthanide complexes of the general formula $Cp'_2M[(CH_2)(CH_2)PRR'] \cdot (LiCl)_2$, ($Cp' = C_5Me_5$; M = Sm, Nd).[4] We are interested in examining the factors that affect the mode of coordination of the phosphorus ylidic ligand, particularly the steric and electronic effects of substituents of the cyclopentadienyl rings on the mode of coordination. In this communication, we report the result of the reaction of $(C_5H_5)_2SmCl \cdot LiCl$ with $Li[(CH_2)(CH_2)PPh_2]$.

The interaction of $(C_5H_5)_2SmCl \cdot LiCl$ with one equivalent of $Li[(CH_2)(CH_2)PPh_2]$ in refluxing tetrahydrofuran for 16 h, work up gave yellow crystals of stoichiometry $(C_5H_5)_3Sm[(CH_2)(CH_3)$

* Authors to whom correspondence should be addressed.

$PPh_2]\cdot C_4H_8O$, (**1**),* in 30% yield after recrystallization from a tetrahydrofuran–toluene mixture. Other than the resonances due to the tetrahydrofuran protons, the ^1H NMR of **1** exhibits a broad singlet, a multiplet, a doublet (J_{P-H} = 13.5 Hz), and a doublet (J_{P-H} = 8.0 Hz) of relative intensity 15, 10, 3 and 2 for the protons of the three Cp rings, the two phenyl rings, the methyl group, and the methylene group at δ 10.36, 7.17–7.60, 2.08, and 0.80 ppm, respectively. The $^{31}P\{^1H\}$ NMR spectrum of **1** exhibits a singlet at δ 21.2 ppm. The ^{31}P chemical shift is consistent with a ylide complex.[5] Based on the above spectroscopic data, **1** can be formulated as $[(C_5H_5)_3SmCH_2P(Me)Ph_2]$, a ylide complex having structure **A** as shown below.

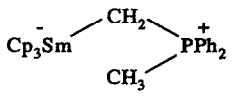

A

A similar structure has been proposed for $[(C_5H_5)_3LuCH_2PPh_3]$.[5] The structure of **1** was established by an X-ray diffraction study.† Crystals of stoichiometry $[(C_5H_5)_3SmCH_2P(Me)Ph_2]\cdot C_4H_8O$ suitable for X-ray diffraction study were grown from a solution of tetrahydrofuran. A perspective drawing and selected bond lengths and bond angles of **1** are shown in Fig. 1 and its caption.

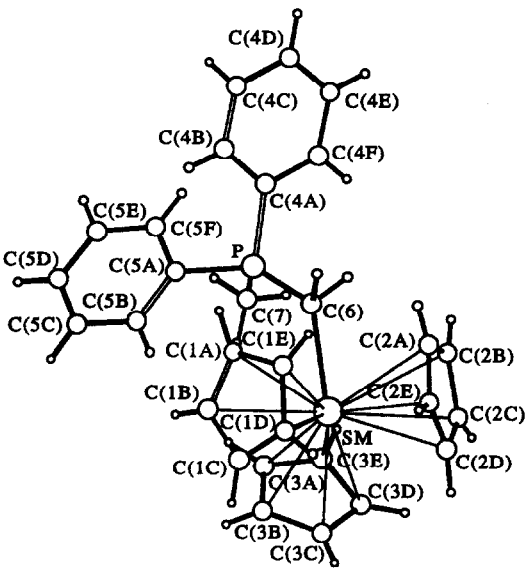

Fig. 1. A perspective view of the structure of $[Cp_3SmCH_2P(Me)Ph_2]$. Selected bond lengths (Å) and bond angles (°): Sm—C(6), 2.622(6); P—C(6), 1.734(6); P—C(7), 1.811(6); P—C(4A), 1.817(6); P—C(5A), 1.811(5); Sm—C(6)—P 138.2(2); C(6)—P—C(7), 112.2(3); C(6)—P—C(4A), 114.3(2); C(6)—P—C(5A), 113.3(1); C(7)—P—C(4A), 104.9(3); C(7)—P—C(5A), 106.5(2); C(4A)—P—C(5A), 105.0(3).

The solid state structure of **1** is consistent with the spectroscopic data and can be described as a distorted tetrahedron if one considers that the metal coordinated to the centroid of the cyclopentadienyl rings. The cyclopentadienyl rings are bonded in a η^5-fashion with Sm—C bond lengths ranging from 2.725(9) to 2.827(7) Å. The mean Sm—C distances for the three Cp rings are 2.75, 2.78, and 2.79 Å. These values are slightly longer than that of $[(MeC_5H_4)_2SmC{\equiv}CCMe_3]_2$ (2.71 and 2.72 Å)[6] and $(C_9H_7)_3Sm$ (2.75 Å),[7] and similar to that of $(C_5H_5)_3Sm(C_5H_5N)$ (2.75, 2.77, and 2.78 Å)[8] and $[(C_5H_5)_3Sm(\mu\text{-}Cl)Sm(C_5H_5)_3]^-$ (2.77 Å).[9] This is an agreement with structure **A** where a negative charge is delocalized on to the Sm metal. The Sm—C(6) distance is 2.622(6) Å and is longer than the Sm—C terminal distance in $(C_5Me_5)_2Sm(R)(THF)$ [R = Me, 2.484(14) Å;[10] R = Ph, 2.511(8) Å;[11] R = CH_2Ph, 2.528(8)[10] Å and shorter than the Sm—C bridging distance in $(C_5Me_5)_2Sm(\mu\text{-}Et)_2AlEt_2$ [2.662(4) Å].[12] This is consistent with the fact that the Sm—C(6) bond is a dative bond which should be weaker than a Sm—C σ-bond as in $(C_5Me_5)_2Sm(R)(THF)$ and stronger than an electron-deficient three centre-two electron Sm—C bridging bond as in $(C_5Me_5)_2Sm(\mu\text{-}Et)_2AlEt_2$. The P—C distances for the P—CH_2 and P—CH_3 groups are 1.734(6) and 1.811(6) Å, respectively. These

*$[(C_5H_5)_3SmCH_2P(Me)Ph_2]\cdot C_4H_8O$: Yellow crystals, m.p. 180–183°C. Found: C, 63.0; H, 6.1; Cl, 0.0; Sm, 23.6. Calc. for $C_{33}H_{38}OPSm$: C, 62.8; H, 6.0; Cl, 0.0; Sm, 23.8%. IR (cm^{-1}, in Nujol): 3087m, 3049m, 2883vs, 2844vs, 2721w, 1589w, 1576w, 1437s, 1416w, 1338w, 1317m, 1298w, 1157m, 1121m, 1109m, 1070w, 1010s, 994m, 931w, 898s, 886s, 846w, 773vs, 752vs, 738vs, 706m, 692s, 677w, 665w. $^{31}P\{^1H\}$ NMR (d_8-THF): 21.2(s) ppm. ^1H NMR (d_8-THF): Cp protons, δ 10.36 (15H, br s) ppm; phenyl protons, δ 7.17–7.60 (10H, m) ppm; methyl protons, δ 2.08 (3H, *d*; J_{P-H} = 13.5 Hz) ppm; methylene protons, δ 0.80 (2H, *d*; J_{P-H} = 8.0 Hz) ppm; THF protons, δ 3.54(m) and 1.70(m) ppm.

†Crystal data: $C_{29}H_{30}PSm\cdot C_4H_8O$, F_w = 632.01, triclinic, $P\bar{1}$ (No. 2), a = 10.760(6), b = 11.999(4), c = 12.441(6) Å, α = 74.84(3), β = 68.21(4), γ = 85.43(3), V = 1439.3 $Å^3$, Z = 2, $F(000)$ = 642, D_c = 1.458 $g\,cm^{-3}$, μ = 21.23 cm^{-1}. Crystal dimensions: 0.32 × 0.42 × 0.44 mm. Intensity data were collected on an Enraf-Nonius CAD4 diffractometer with grapahite monochromated Mo-K_α radiation (λ = 0.71073 Å) using ω–2θ scans ($2\theta_{max}$ = 50°). The structure was solved by a combination of Patterson and direct methods (DIRDIF) after an absorption correction (ψ-scan method) was applied and refined by full-matrix least-squares to give R = 0.035, R_w = 0.044 for 4085 independent observed reflections [$I > 3\sigma(I)$].

bond lengths are in very good agreement with comparable bond lengths in $(C_5Me_5)_2Lu[(CH_2)(CH_2)PMe_2]$[2a] [P—$CH_2$, 1.769(16) and 1.782(15) Å; P—CH_3, 1.816(22) and 1.823(23) Å] and $(C_5Me_5)_2U(Cl)[(CH_2)(CH_2)P(Me)Ph]$ [P—CH_2, 1.74(1) and 1.74(1) Å; P—CH_3, 1.77(1) Å].[3b]

In contrast to $(C_5Me_5)_2SmCl \cdot LiCl$ which reacted with $Li[(CH_2)(CH_2)PPh_2]$ to give the expected cyclic ylidic complex $(C_5Me_5)_2Sm(CH_2)(CH_2)PPh_2$,[4] interaction of $(C_5H_5)_2SmCl \cdot LiCl$ with $Li[(CH_2)(CH_2)PPh_2]$ gives the unexpected ylide complex $[(C_5H_5)_3SmCH_2P(Me)Ph_2]$. The result suggests that the nature of the products of the above reaction may be influenced by the substituents of the Cp rings. We are in the process of examining this effect.

Acknowledgement—W.-K. Wong thanks the Hong Kong Baptist College, the Hong Kong Research Grant Council, and the Croucher Foundation for financial support. W.-T. Wong thanks the Hong Kong Research Grant Council and the University of Hong Kong for financial support.

REFERENCES

1. H. Schmidbaur, *Acc. Chem. Res.* 1975, **8**, 62 and refs therein.
2. (a) H. Schumann, I. Albrecht, F. W. Reier and E. Hahn, *Angew. Chem. Int. Ed. Engl.* 1984, **23**, 522; (b) H. Schumann and F. W. Reier, *Inorg. Chim. Acta* 1984, **95**, 43 and refs therein.
3. (a) J. W. Gilje, R. E. Cramer, M. A. Bruck, K. T. Higa and K. Panchanetheswaran, *Inorg. Chim. Acta* 1985, **110**, 139; (b) R. E. Cramer, S. Roth, F. Edelmann, M. A. Bruck, K. C. Cohn and J. W. Gilje, *Organometallics* 1989, **8**, 1192 and refs therein.
4. W. K. Wong, H. Chen and F. L. Chow, *Polyhedron* 1990, **9**, 875.
5. H. Schumann and F. W. Reier, *J. Organomet. Chem.* 1984, **269**, 21.
6. W. J. Evans, I. Bloom, W. E. Hunter and J. L. Atwood, *Organometallics* 1983, **2**, 709.
7. J. L. Atwood, J. H. Burns and P. G. Laubereau, *J. Am. Chem. Soc.* 1973, **95**, 1830.
8. G. B. Deacon, B. M. Gatehouse, S. N. Platts and D. L. Wilkinson, *Aust. J. Chem.* 1987, **40**, 907.
9. H. Schumann, S. Nickel, J. Loebel and J. Pickardt, *Organometallics* 1988, **7**, 2004.
10. W. J. Evans, L. R. Chamberlain, T. A. Ulibarri and J. W. Ziller, *J. Am. Chem. Soc.* 1988, **110**, 6423.
11. W. J. Evans, I. Bloom, W. E. Hunter and J. L. Atwood, *Organometallics* 1985, **4**, 112.
12. W. J. Evans, L. R. Chamberlain and J. W. Ziller, *J. Am. Chem. Soc.* 1987, **109**, 7209.

Polyhedron Vol. 12, No. 23, pp. 2753–2762, 1993
Printed in Great Britain

0277-5387/93 $6.00+.00
© 1993 Pergamon Press Ltd

FUSED-RING METALLAMACROCYCLIC MERCURY/LANTHANIDE COMPLEXES FORMED BY FUSED-RING LACTAMS

DAVID M. L. GOODGAME,* STUART P. W. HILL, ROGER LINCOLN, MIGUEL QUIROS and DAVID J. WILLIAMS

Chemistry Department, Imperial College of Science, Technology, and Medicine, London SW7 2AY, U.K.

(*Received* 4 *May* 1993; *accepted* 28 *June* 1993)

Abstract—Mercury(II) acetate reacts with the fused-ring lactams (**I**) and lanthanide(III) nitrates, Ln = La–Gd (Pm not studied), to give $[LnHg_2L_4(NO_3)_3]_n$ and with Y and Ln = Tb–Yb to yield $[Y_2Hg_3L_6(NO_3)_6]_n$ and $[Ln_2Hg_3L_6(NO_3)_6]_n$, respectively. Each set of compounds forms an isostructural series. For the ligand **Ic** representative members of each series (Ln = Nd and Er, respectively) have been characterized by single-crystal X-ray diffraction methods. Both compounds form two-dimensional polymeric metallamacrocyclic arrays. They differ in the sense that the erbium complex comprises sheets of contiguous 48-membered rings, whereas in the neodymium compound two sizes of metallamacrocyclic coexist—one 48-membered and one 16-membered, which are fused together. The erbium ion is nine-coordinate and the neodymium atom 10-coordinate. The nitrate anions are involved in weak intra- and intermolecular interactions within the macrocycles.

Recently we reported the results of investigations into the ability of the anions of 2-oxazolidone[1,2] (**II**) and 2-azetidinone[1,3] (**III**) to link dissimilar metal ions to produce unusual new polynuclear compounds. The differences between the metal binding preferences of the deprotonated ring nitrogen and the exocyclic oxygen permit a heavy post-transition metal, such as mercury, to bind strongly to the nitrogen atom, leaving the oxygen atom free to coordinate to a wider range of other metal ions (e.g. transition metals[1] and lanthanides[2,3]).

The compounds formed thus far are very insoluble in common organic solvents due to their polymeric nature. To extend these studies we have examined the use of fused-ring lactams (**I**). These contain the same ambidentate N, O donor unit as the single-ring lactams for binding the respective metals and they also provide a bulky cycloalkyl group to favour enhanced solubility in common organic solvents. The ligand 2-azetidinone (**III**) possesses the largest HN—CO "bite" and thus favours the binding of two metals; also, it is the most acidic of the lactams [pK_a = 22.7]. Hence, the fused-ring ligands we have employed are based on this four-membered ring lactam. We report here the preparation and properties of complexes of **Ia–c** with combinations of mercury(II) and a range of lanthanide metal ions.

EXPERIMENTAL

Preparation of the ligands

The fused-ring lactams were prepared by modification of the methods of Jendralla[4] and Malpass[5] (Scheme 1).

Ia. Chlorosulphonyl isocyanate (7.1 g, 4.4 cm^3, 50 mmol) was added to dichloromethane (40 cm^3) cooled to −5°C under nitrogen. Cyclohexene (4.26 g, 5.25 cm^3, 52 mmol) was added dropwise through a syringe. The stirred mixture was allowed to warm to room temperature and then refluxed gently for 24 h. The progress of the reaction was followed by IR, by the disappearance of the isocyanate ν(C=N) band at 2200 cm^{-1} and the appearance of the lactam ν(C=O) band at *ca* 1810 cm^{-1}. When the reaction was complete, ice-cold water (40 cm^3) was added down the condenser dropwise with care,

*Author to whom correspondence should be addressed.

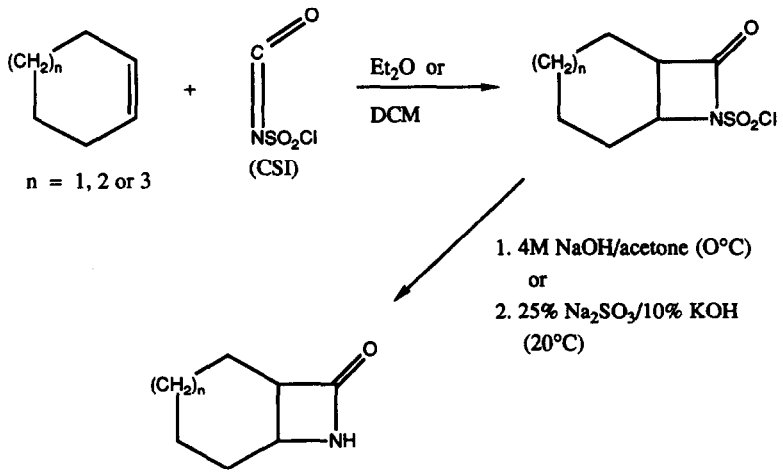

Scheme 1.

whilst keeping the flask in an ice/salt bath. The organic phase was separated, washed with ice-cold water (5×40 cm^3) and then dried over anhydrous sodium sulphate. After filtration, the solvent was removed under reduced pressure. The residue was dissolved in *n*-pentane (35 cm^3) to remove any unreacted cyclohexene and then cooled to between -40 and -70°C to crystallize the cycloadduct. The mother liquor was decanted off and any remaining solvent removed *in vacuo*.

The *n*-chlorosulphonyl-β-lactam was dissolved in diethyl ether (50 cm^3) and a solution of sodium sulphite heptahydrate (30 g in 100 cm^3 water) was added. The mixture was stirred for 2 h and 10% aqueous potassium hydroxide added dropwise to a constant pH of 7–8. The ether phase was separated, dried over anhydrous sodium sulphate and the solvent removed under reduced pressure. The resulting waxy, colourless solid was recrystallized from boiling hexane to produce colourless crystals (2.4 g, 37% yield). IR (cm^{-1}): 3420, 3265 (N—H); 1738 (C=O). NMR: δ_H (270 MHz, $CDCl_3$): 1.2–2.0 (8H, m), 3.22 [1H, ddt, H(1)], 3.84 [1H, m, H(6)], 6.19 [1H, s, H(7)]; δ_C (270 MHz, $CDCl_3$): 173.01 [C(8)], 48.23 [C(1)], 47.40 [C(2)], 26.24 [C(6)], 20.47 [C(3)], 19.55 [C(5)], 17.43 [C(4)].

For ligand **Ib** the same procedure was followed but using cycloheptene (5 g) (yield 3.7 g, 54%). IR (cm^{-1}): 3415, 3250 (N—H); 1746 (C=O). NMR: δ_H (270 MHz, $CDCl_3$): 1.2–2.0 (10H, m), 3.31 [1H, ddt, H(1), 3.82 [1H, m, H(7)], 5.90 [1H, s, H(8)]; δ_C (270 MHz, $CDCl_3$): 171.69 [C(9), 55.63 [C(1)], 53.84 [C(2)], 32.47 [C(7)], 32.18 [C(3)], 28.66 [C(6)], 25.75 [C(4)], 25.30 [C(5)].

For ligand **Ic** the same procedure was followed but using cyclooctene (5.72 g) and dry diethyl ether instead of dichloromethane (yield 5.9 g, 73%). IR (cm^{-1}): 3412, 3240 (N—H); 1750 (C=O); NMR: δ_H (270 MHz, $CDCl_3$): 1.2–2.0 (12H, m), 3.01 [1H, ddt, H(1)], 3.64 [1H, dq, H(8)], 5.91 [1H, s, H(9)]; δ_C (270 MHz, $CDCl_3$): 172.04 [C(10)], 54.63 [C(1), C(2)], 29.76 [C(8)], 29.66 [C(3)], 28.30 [C(7)], 26.74 [C(6)], 22.45 [C(5)].

Preparation of the complexes

The compounds HgL_2 (L = **Ia–c**) were prepared by mixing mercury(II) acetate (0.1 mmol) and the appropriate ligand (0.2 mmol) in methanol or acetonitrile (10 cm^3). The solid complexes separated when the solutions were left in a desiccator over concentrated sulphuric acid. The heterometallic complexes (Table 1) were prepared similarly but with the addition of the appropriate hydrated metal nitrate (0.05 mmol). The transition metal complexes were best prepared in acetonitrile. With the lanthanides from La to Gd the use of acetonitrile resulted in the immediate formation of powders, but crystals were obtained from a 50 : 50 mixture of acetonitrile/methanol; in methanol oils were produced. For yttrium and the lanthanides from Tb to Yb the best crystalline products formed from methanol, but the complexes may also be obtained from acetonitrile or acetonitrile/methanol mixtures. The products which formed were removed by filtration and allowed to dry.

Analytical data (Microanalytical Laboratory, Imperial College and Medac Ltd, Brunel University) are given in Table 1.

Crystallography

Crystal data. For $\{[NdHg_2(C_9H_{14}NO)_4(NO_3)_3]H_2O\}_n$ (**1**): $C_{36}H_{58}Hg_2N_7NdO_{14}$, M =

Table 1. Analytical data for the compounds formed by ligands **Ia–c**

Complex	Colour	Analysis (%)[a] C	H	N
Ligand **Ia** (= L)				
$HgL_2 \cdot H_2O$	White	35.8 (36.0)	4.7 (4.7)	5.8 (6.0)
$[LaHg_2L_4(NO_3)_3]$	White	27.4 (27.5)	3.4 (3.3)	7.9 (8.0)
$[CeHg_2L_4(NO_3)_3] \cdot H_2O$	White	26.9 (27.1)	3.3 (3.4)	7.7 (7.9)
$[PrHg_2L_4(NO_3)_3] \cdot H_2O$	Green	27.2 (27.0)	3.4 (3.4)	7.9 (7.9)
$[NdHg_2L_4(NO_3)_3] \cdot H_2O$	Lilac	26.8 (27.0)	3.4 (3.4)	7.9 (7.9)
$[SmHg_2L_4(NO_3)_3]$	White	27.2 (27.2)	3.2 (3.2)	8.0 (7.9)
$[EuHg_2L_4(NO_3)_3] \cdot H_2O$	White	26.7 (26.8)	3.3 (3.3)	7.9 (7.8)
$[GdHg_2L_4(NO_3)_3] \cdot H_2O$	White	26.9 (26.7)	3.3 (3.3)	7.8 (7.8)
$[Tb_2Hg_3L_6(NO_3)_6]$	White	25.1 (24.8)	3.0 (3.0)	8.2 (8.2)
$[Dy_2Hg_3L_6(NO_3)_6]$	White	25.5 (24.7)	3.1 (3.0)	7.7 (8.2)
$[Ho_2Hg_3L_6(NO_3)_6]$	Pink	24.8 (24.6)	3.1 (2.9)	7.9 (8.2)
$[Er_2Hg_3L_6(NO_3)_6]$	Pink	24.6 (24.6)	2.9 (2.9)	8.0 (8.2)
$[Tm_2Hg_3L_6(NO_3)_6]$	Pale green	24.4 (24.5)	3.0 (2.9)	8.1 (8.2)
$[Yb_2Hg_3L_6(NO_3)_6]$	White	24.0 (24.4)	2.9 (2.9)	7.4 (8.1)
$[Y_2Hg_3L_6(NO_3)_6] \cdot H_2O$	White	26.0 (26.1)	3.3 (3.3)	7.8 (8.7)
$[ThHg_2L_4(NO_3)_4]$	White	21.4 (21.6)	3.1 (2.6)	8.7 (8.4)
Ligand **Ib** (= L′)				
$HgL'_2 \cdot H_2O$	White	38.8 (38.8)	5.3 (5.3)	5.5 (5.7)
$[LaHg_2L'_4(NO_3)_3]$	White	30.2 (30.0)	3.8 (3.8)	7.4 (7.7)
$[CeHg_2L'_4(NO_3)_3] \cdot H_2O$	White	29.3 (29.6)	3.7 (3.9)	7.3 (7.5)
$[PrHg_2L'_4(NO_3)_3] \cdot H_2O$	Green	29.6 (29.6)	3.7 (3.9)	7.3 (7.5)
$[NdHg_2L'_4(NO_3)_3]$	Lilac	29.8 (29.9)	3.7 (3.7)	7.4 (7.6)
$[EuHg_2L'_4(NO_3)_3] \cdot H_2O$	White	28.9 (29.3)	3.6 (3.8)	7.2 (7.5)
$[Dy_2Hg_3L'_6(NO_3)_6]$	White	27.5 (27.1)	3.6 (3.4)	7.6 (7.9)
$[Tm_2Hg_3L'_6(NO_3)_6]$	Pale green	27.1 (26.9)	3.4 (3.4)	7.4 (7.8)
Ligand **Ic** (= L″)				
$HgL''_2 \cdot 0.5H_2O$	White	42.2 (42.0)	5.5 (5.7)	5.5 (5.4)
$[LaHg_2L''_4(NO_3)_3]$	White	32.4 (32.4)	4.2 (4.2)	7.6 (7.3)
$[CeHg_2L''_4(NO_3)_3]$	White	31.9 (32.4)	4.4 (4.2)	7.6 (7.3)
$[PrHg_2L''_4(NO_3)_3]$	Green	32.3 (32.3)	4.4 (4.2)	7.6 (7.3)
$[NdHg_2L''_4(NO_3)_3]$	Lilac	32.2 (32.3)	4.0 (4.2)	7.2 (7.3)
$[SmHg_2L''_4(NO_3)_3]$	White	31.9 (32.2)	4.3 (4.2)	7.9 (7.3)
$[EuHg_2L''_4(NO_3)_3]$	White	31.9 (32.1)	4.2 (4.2)	7.0 (7.3)
$[GdHg_2L''_4(NO_3)_3]$	White	32.2 (31.9)	3.9 (4.2)	7.3 (7.2)
$[Tb_2Hg_3L''_6(NO_3)_6]$	White	29.2 (29.3)	3.8 (3.8)	7.3 (7.6)
$[Dy_2Hg_3L''_6(NO_3)_6]$	White	29.7 (29.3)	4.0 (3.8)	7.7 (7.6)
$[Ho_2Hg_3L''_6(NO_3)_6]$	Pink	29.6 (29.3)	4.0 (3.8)	7.7 (7.6)
$[Er_2Hg_3L''_6(NO_3)_6]$	Pink	28.8 (29.2)	3.6 (3.8)	7.9 (7.6)
$[Tm_2Hg_3L''_6(NO_3)_6]$	Pale green	28.8 (29.2)	3.6 (3.7)	7.5 (7.5)
$[Yb_2Hg_3L''_6(NO_3)_6]$	White	28.9 (29.2)	3.8 (3.7)	7.5 (7.5)
$[Y_2Hg_3L''_6(NO_3)_6]$	White	31.5 (31.4)	4.3 (4.1)	7.8 (8.1)
$[Mn_2Hg_3L''_6(NO_3)_4] \cdot 2H_2O$	Pale pink	34.0 (34.0)	4.4 (4.6)	7.0 (7.3)
$[Co_2Hg_3L''_6(NO_3)_4] \cdot 2H_2O$	Pink	34.0 (33.8)	4.4 (4.6)	7.0 (7.3)
$[Cu_2Hg_3L''_6(NO_3)_4] \cdot 2H_2O$	Green	33.5 (33.7)	4.5 (4.6)	7.5 (7.3)
$[Cd_2Hg_3L''_6(NO_3)_4]$	White	32.4 (32.6)	4.2 (4.3)	7.5 (7.0)

[a] Calculated values are given in parentheses.

1358.3, triclinic, space group $P\bar{1}$, $a = 13{,}716(3)$, $b = 14{,}010(5)$, $c = 15.216(6)$ Å, $\alpha = 86.13(3)$, $\beta = 64.10(3)$, $\gamma = 89.80(2)°$, $U = 2623$ Å^3, $Z = 2$, $D_c = 1.72$ g cm^{-3}, μ(Mo-K_α) = 69 cm^{-1}, $\lambda = 0.71073$ Å, $F(000) = 1310$. Lilac-purple needles, crystal dimensions $0.08 \times 0.12 \times 0.25$ mm.

For $\{[Er_2Hg_3(C_9H_{14}NO)_6(NO_3)_6]\cdot CH_3OH\}_n$ (**2**): $C_{55}H_{88}Er_2Hg_3N_{12}O_{25}$, $M = 2253.7$, monoclinic, space group $P2_1/c$, $a = 14.933(2)$, $b = 15.638(2)$, $c = 16.213(3)$ Å, $\beta = 101.00(2)°$, $U = 3717$ Å^3, $Z = 2$, $D_c = 2.01$ g cm^{-3}, μ(Mo-K_α) = 85 cm^{-1}, $\lambda = 0.71073$ Å, $F(000) = 2156$. Pink needles, crystal dimensions $0.08 \times 0.10 \times 0.30$ mm.

Data collection and processing

Siemens P4/PC diffractometer, ω-scan method ($2\theta < 45°$), graphite-monochromated Mo-K_α radiation. For compounds **1** and **2** 9248 and 4854 independent reflections, respectively, were measured; 4526 [$|F_o| > 5\sigma(|F_o|)$] and 2778 [$|F_o| > 4\sigma(|F_o|)$] were considered observed and corrected for Lorentz and polarization factors. For **1** a Gaussian absorption correction (face-indexed numerical) was applied; minimum and maximum transmission factors 0.40 and 0.66; crystal **2** decomposed and absorption correction was not possible.

Structure analysis and refinement

Both structures were solved by the heavy-atom method, revealing the position of the mercury atoms. For **1** and **2** all non-hydrogen atoms were located from subsequent ΔF maps. In **1** there is disorder in all four of the eight-membered rings. In two of these the disorder was resolved into partial occupancy, alternate atom positions. In all four rings the atoms were refined isotropically, subject to a C—C distance constraint. A ΔF map also revealed the presence of two partial weight water molecules, which were refined isotropically. In **2** a ΔF map revealed the presence of a partial occupancy methanol molecule. This and all the other non-hydrogen atoms were refined anisotropically. The hydrogen atoms in both structures, with the exception of those of the partial weight water and methanol molecules, which could not be located, were idealized (C—H 0.96 Å), assigned isotropic thermal parameters, $U(H) = 1.2_{eq}(C)$, and allowed to ride on their parent carbons. Refinements were by full-matrix least-squares to give: for **1**, $R = 0.060$, $R_w = 0.058$ [$w^{-1} = \sigma^2(F) + 0.0007F^2$]; for **2**, $R = 0.064$, $R_w = 0.054$ [$w^{-1} = \sigma^2(F) + 0.0004F^2$]. The maximum residual electron densities in the final ΔF maps were 1.51 and 1.77 for **1** and **2**, respectively. The mean and maximum shift/error ratios in the final refinement cycle were: for **1**, 0.04 and 0.56; for **2**, 0.05 and 0.58. Computations were carried out on an IBM 386 PS2 computer using the SHELXTL-PC program system[6] and published scattering factors[7]. Important bond lengths and angles are listed in Tables 2 and 3.

RESULTS AND DISCUSSION

Two methods were used for the preparation of the ligands (**I**) (Scheme 1). The first step, which is common to both and has been employed in similar preparations,[8–12] is the direct reaction of the cycloalkene with chlorosulphonyl isocyanate (CSI) in diethyl ether (for **Ic**) or dichloromethane (for **Ia**, **b**). The second step, the reduction of the intermediate, can be performed in a number of ways.[10] The two usual methods include the use of cold 4 M NaOH/acetone[9] or aqueous sodium sulphite/KOH.[10] The former method suffers in that the final product is contaminated with by-products, causing difficulty in separation. We found the latter method to have the advantages of simplicity of the reaction and isolation procedures, mild reaction conditions and a good yield of pure product.

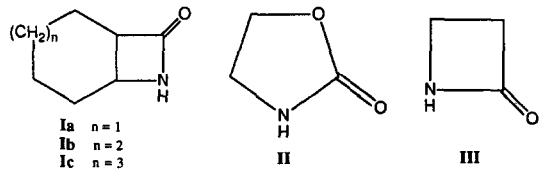

Reaction of the ligands **Ia–c** with mercury(II) acetate in methanol or acetonitrile gave the expected HgL_2 complexes as monohydrates with **Ia** and **Ib** and as a hemi-hydrate with **Ic**. Similar hydration was found for the analogous complex with 2-azetidinone and the role of the solvent water in that compound was elucidated by an X-ray structural study.[3]

The stoichiometries of the solid products obtained from the reaction of mercury(II) acetate, the fused-ring lactams **Ia** and **Ic** and yttrium(III) or lanthanide(III) nitrates depend on the lanthanide ion employed. Use of the trivalent lanthanide ions in the series lanthanum to gadolinium (promethium not studied) afforded the compounds $[LnHg_2L_4(NO_3)_3]_n$, whereas yttrium and the lanthanides in the series terbium to ytterbium inclusive gave compounds of the stoichiometry $[Ln_2Hg_3L_6(NO_3)_6]_n$. The size of the metal ion appears to influence which complex type is formed, with the change occurring on passing from Gd^{3+} to Tb^{3+}, and with Y^{3+} adopting the same type as the smaller lanthanide ions. In view of the similarity of

Table 2. Selected bond lengths (Å) and angles (°) for **1**

Hg(1)—N(1)	1.980(17)	Hg(1)—N(1A)	1.980(17)
Hg(2)—N(11)	2.036(17)	Hg(2)—N(11A)	2.036(17)
Hg(3)—N(21)	2.016(20)	Hg(3)—N(31)	2.033(18)
Nd(1)—O(2)	2.427(13)	Nd(1)—O(12)	2.418(17)
Nd(1)—O(22)	2.342(18)	Nd(1)—O(42)	2.563(19)
Nd(1)—O(43)	2.543(15)	Nd(1)—O(52)	2.591(16)
Nd(1)—O(53)	2.841(22)	Nd(1)—O(62)	2.636(19)
Nd(1)—O(63)	2.536(20)	Nd(1)—O(32A)	2.469(12)
O(32)—Nd(1A)	2.469(12)		
N(1)—Hg(1)—N(1A)	180.0(1)	N(11)—Hg(2)—N(11A)	180.0(1)
N(21)—Hg(3)—N(31)	179.2(9)	O(2)—Nd(1)—O(12)	69.9(5)
O(2)—Nd(1)—O(22)	81.8(5)	O(12)—Nd(1)—O(22)	82.4(6)
O(2)—Nd(1)—O(42)	128.0(5)	O(12)—Nd(1)—O(42)	149.3(5)
O(22)—Nd(1)—O(42)	76.9(6)	O(2)—Nd(1)—O(43)	138.4(5)
O(12)—Nd(1)—O(43)	136.4(6)	O(22)—Nd(1)—O(43)	125.7(7)
O(42)—Nd(1)—O(43)	50.4(7)	O(2)—Nd(1)—O(52)	73.7(5)
O(12)—Nd(1)—O(52)	135.0(6)	O(22)—Nd(1)—O(52)	117.6(6)
O(42)—Nd(1)—O(52)	75.4(6)	O(43)—Nd(1)—O(52)	66.0(5)
O(2)—Nd(1)—O(53)	64.2(6)	O(12)—Nd(1)—O(53)	129.4(5)
O(22)—Nd(1)—O(53)	71.1(6)	O(42)—Nd(1)—O(53)	64.1(6)
O(43)—Nd(1)—O(53)	93.4(6)	O(52)—Nd(1)—O(53)	46.5(7)
O(2)—Nd(1)—O(62)	116.4(6)	O(12)—Nd(1)—O(62)	70.4(5)
O(22)—Nd(1)—O(62)	137.4(5)	O(42)—Nd(1)—O(62)	111.2(5)
O(43)—Nd(1)—O(62)	66.7(6)	O(52)—Nd(1)—O(62)	104.6(6)
O(53)—Nd(1)—O(62)	151.0(5)	O(2)—Nd(1)—O(63)	73.6(5)
O(12)—Nd(1)—O(63)	76.9(6)	O(22)—Nd(1)—O(63)	152.1(5)
O(42)—Nd(1)—O(63)	129.0(5)	O(43)—Nd(1)—O(63)	82.1(6)
O(52)—Nd(1)—O(63)	68.1(6)	O(53)—Nd(1)—O(63)	108.4(6)
O(62)—Nd(1)—O(63)	50.3(5)	O(2)—Nd(1)—O(32A)	141.8(4)
O(12)—Nd(1)—O(32A)	78.0(5)	O(22)—Nd(1)—O(32A)	73.7(5)
O(42)—Nd(1)—O(32A)	74.6(5)	O(43)—Nd(1)—O(32A)	79.7(4)
O(52)—Nd(1)—O(32A)	144.0(5)	O(53)—Nd(1)—O(32A)	130.3(6)
O(62)—Nd(1)—O(32A)	69.1(5)	O(63)—Nd(1)—O(32A)	119.0(5)

the stoichiometries of the Hg/lanthanide complexes formed by **Ia** and **Ic**, we performed only a partial survey of the compounds formed by **Ib** (Table 1) and this ligand appears to follow the same pattern.

Reaction of mercury(II) acetate, ligand **Ic**, and the hydrated nitrates of manganese(II), cobalt(II), copper(II) and cadmium(II) gives the complexes $[M_2Hg_3L_6(NO_3)_4]\cdot 2H_2O$ (M = Mn, Co, Cu) and $[Cd_2Hg_3L_6(NO_3)_4]$. The electronic spectrum of the cobalt complex and the EPR spectra of the manganese and copper complexes pointed to the presence of distorted six-coordinate geometry about the transition metal ions, but crystals suitable for X-ray studies could not be obtained so their precise nature could not be determined.

Structural studies on the lanthanide complexes

X-ray powder diffraction measurements on the lanthanide complexes of **Ic** showed that all the compounds within each respective series, $[LnHg_2L_4(NO_3)_3]$ and $[Ln_2Hg_3L_6(NO_3)_6]$ are isostructural. The data, which were obtained photographically, were adequate to establish the isomorphous character of the related compounds, but not sufficiently resolved to permit accurate indexing and accurate lattice parameter determination. A representative member of each series, $[NdHg_2(C_9H_{14}NO)_4(NO_3)_3]_n$ (**1**) and $[Er_2Hg_3(C_9H_{14}NO)_6(NO_3)_6]_n$ (**2**), was obtained in a form suitable for single-crystal X-ray analysis.

Structure of $[NdHg_2(C_9H_{14}NO)_4(NO_3)_3]_n$ (**1**)

In the Nd complex (**1**) the lanthanide ion is bound to 10 oxygen atoms, four of which are from the lactam ligands [Nd—O 2.34–2.47 Å] and six from bidentate nitrate groups [Nd—O 2.54–2.84 Å]. The resultant coordination geometry is a distorted bicapped square anti-prism (Fig. 1). The principle cause of the distortion is the small "bite" of the

Table 3. Selected bond lengths (Å) and angles (°) for **2**

Hg(1)—N(11)	2.028(21)	Hg(1)—N(1A)	1.998(21)
Hg(2)—N(21)	2.059(21)	Hg(2)—N(21A)	2.059(21)
Er—O(2)	2.262(16)	Er—O(12)	2.274(17)
Er—O(22)	2.273(19)	Er—O(41)	2.395(19)
Er—O(42)	2.471(17)	Er—O(51)	2.522(15)
Er—O(52)	2.444(20)	Er—O(61)	2.412(21)
Er—O(62)	2.477(20)	N(1)—Hg(1A)	1.998(21)
N(11)—Hg(1)—N(1A)	172.9(8)	N(21)—Hg(2)—N(21A)	180.0(1)
O(2)—Er—O(12)	149.6(7)	O(2)—Er—O(22)	86.0(6)
O(12)—Er—O(22)	84.0(6)	O(2)—Er—O(41)	82.3(6)
O(12)—Er—O(41)	80.3(6)	O(22)—Er—O(41)	125.5(7)
O(2)—Er—O(42)	74.2(7)	O(12)—Er—O(42)	75.5(6)
O(22)—Er—O(42)	73.8(7)	O(41)—Er—O(42)	51.9(7)
O(2)—Er—O(51)	122.1(6)	O(12)—Er—O(51)	75.2(6)
O(22)—Er—O(51)	150.6(6)	O(41)—Er—O(51)	71.6(6)
O(42)—Er—O(51)	119.3(6)	O(2)—Er—O(52)	74.4(7)
O(12)—Er—O(52)	125.3(6)	O(22)—Er—O(52)	147.5(6)
O(41)—Er—O(52)	78.0(7)	O(42)—Er—O(52)	123.2(7)
O(51)—Er—O(52)	50.4(5)	O(2)—Er—O(61)	129.1(7)
O(12)—Er—O(61)	78.2(7)	O(22)—Er—O(61)	83.8(7)
O(41)—Er—O(61)	141.1(6)	O(42)—Er—O(61)	146.8(7)
O(51)—Er—O(61)	71.8(6)	O(52)—Er—O(61)	88.6(7)
O(2)—Er—O(62)	76.3(7)	O(12)—Er—O(62)	128.5(6)
O(22)—Er—O(62)	76.7(7)	O(41)—Er—O(62)	148.0(6)
O(42)—Er—O(62)	139.2(6)	O(51)—Er—O(62)	100.1(6)
O(52)—Er—O(62)	73.5(7)	O(61)—Er—O(62)	52.8(6)

bidentate NO_3 anions, which reduces the site symmetry to C_1. A similar coordination arrangement is observed in the thorium/mercury complex formed by 2-pyrrolidone,[13] but not, hitherto, in a lanthanide/mercury heterometallic complex.

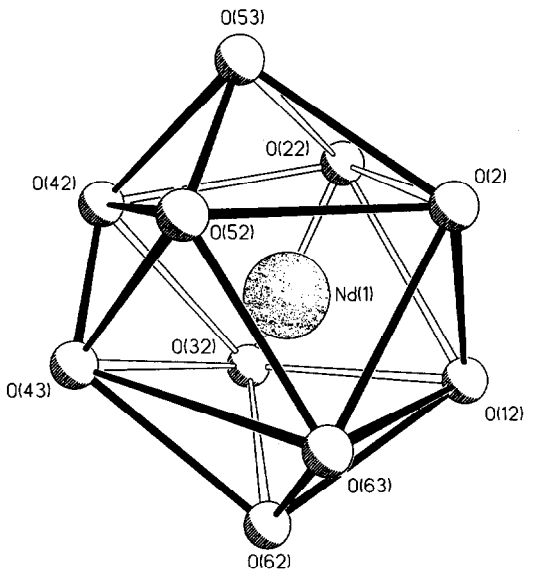

Fig. 1. The distorted bicapped square anti-prismatic coordination geometry about the Nd atom in **1**.

In the asymmetric unit (Fig. 2) the N—Hg—N units are essentially linear [180.0° at Hg(1) and Hg(2) and 179.2° at Hg(3)], with Hg—N distances in the range 1.98–2.04 Å. It is interesting to note that, although the crystal contains *cis*-fused lactam ligands of both chiralities, those bonded to any one Nd centre all have the same chirality.

Adjacent neodymium centres are linked via L—Hg—L bridges to form a polymeric array which is very different from those formed previously by lanthanide/mercury/lactam complexes (Fig. 3). Two of the HgL_2 units bridge centrosymmetrically-related neodymium centres, forming a 16-membered ring (A) containing two neodymium, two mercury, four carbon, four nitrogen and four oxygen atoms. The other two units, however, bridge via a glide-related neodymium centre to another lattice-translated neodymium atom, creating a 48-membered centrosymmetric macrocycle (B) which consists of six neodymium, six mercury, 12 carbon, 12 nitrogen and 12 oxygen atoms.

This coexistence of both 16- and 48-membered macrocycles, each with a common edge, is reminiscent of the structure found[2] for the gadolinium/mercury complex formed by **II**. In the latter case the 16-membered rings were offset with respect to each other. The array found for **1** also has some

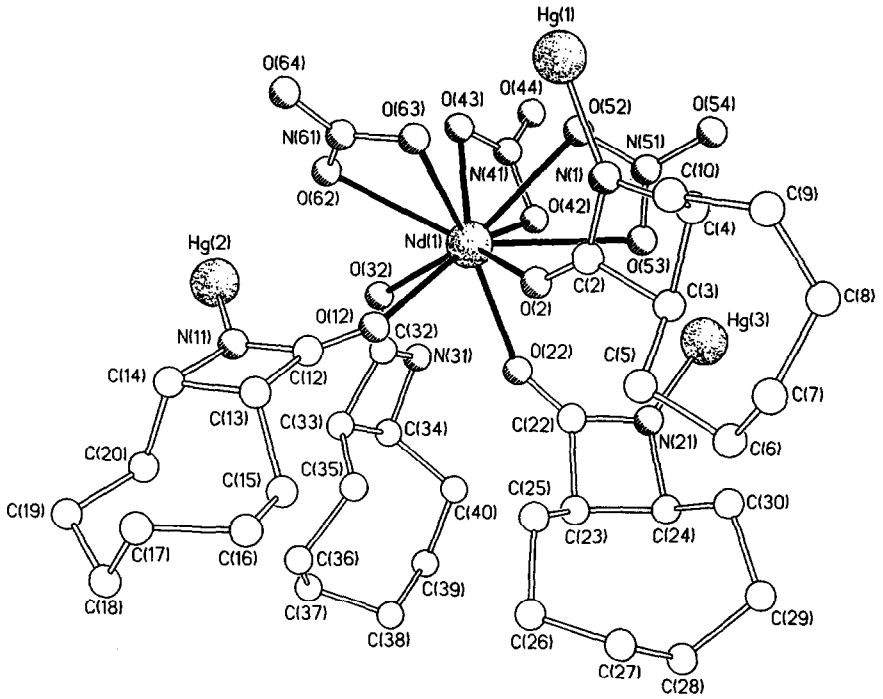

Fig. 2. The neodymium environment in **1**, showing the crystallographic numbering scheme.

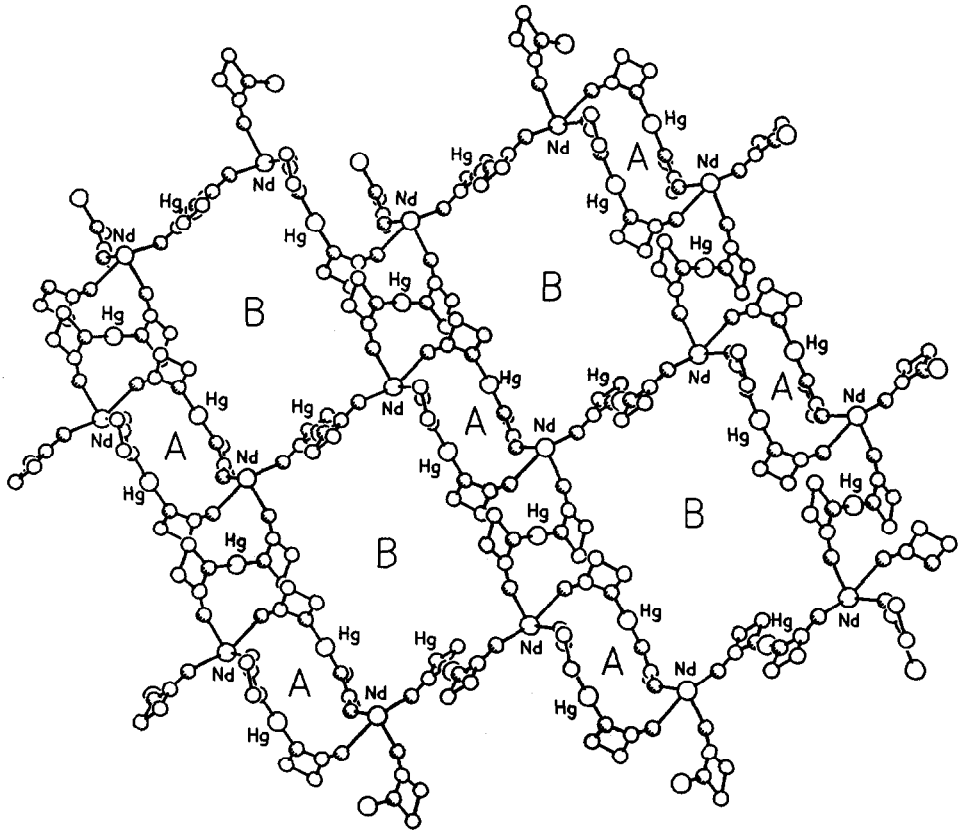

Fig. 3. Part of the contiguous array of fused 16- and 48-membered rings in the structure of **1**.

similarities to the structure of the terbium/mercury complex formed by 2-pyrrolidone[14] where an HgL_2 strut links separate 16-membered macrocycles to make a one-dimensional chain polymer. There, three carbonyl oxygens are bound to the lanthanide ion, whereas in **1** there are four. This additional carbonyl oxygen forms part of another HgL_2 strut, which joins the separate chains and, in so doing, generates the 48-membered macrocycle (Fig. 3).

There are two different dispositions of the lactam moieties about the mercury–nitrogen bonds in the HgL_2 units. The mercury atoms involved in the 48-membered macrocycle alone have organic ligands which are coplanar, whereas the lactams bound to the mercury atoms in the 16-membered rings have a large distortion from ligand coplanarity (114.7°). This latter arrangement is similar to those found in the 16-membered rings of the gadolinium/mercury complex with 2-oxazolidone, where angles of 119.8 and 122.3° are observed.[2] The shortest transannular Nd···Nd and Hg···Hg distances in **1** are 8.13 and 5.07 Å, respectively.

Structure of $[Er_2Hg_3(C_9H_{14}NO)_6(NO_3)_6]_n$ (**2**)

In **2** each erbium ion is bonded to nine oxygen atoms in a distorted tricapped trigonal prismatic geometry (Fig. 4). Three of the oxygen atoms are organic ligand carbonyl oxygens (Er—O 2.26–2.27 Å) and six are from the bidentate nitrate groups (2.40–2.52 Å).

In the asymmetric unit (Fig. 5) one of the HgL_2 units has linear N—Hg—N geometry, but the other is slightly bent [N(1A)—Hg(1)—N(11) = 172.9(8)°]. The Hg—N distances are in the range 2.00–2.06 Å. The HgL_2 units bridge adjacent erbium centres forming 48-membered metallamacrocycles which interlock at the erbium atoms, generating a sheet polymer (Fig. 6). This offset parquet-like pattern of fused metallamacrocyclic rings is very similar to that observed for the analogous complex formed by erbium with 2-azetidinone.[3]

In both **1** and **2** there are inter- and intramolecular stabilizing links between the nitrate anions and the mercury atoms in adjacent asymmetric units [in **1** Hg(1)—O(52) 2.82, Hg(1)—O(63) 2.88, Hg(2)—O(32) 2.90, Hg(2)—O(62) 2.85, Hg(3)—O(42) 3.02, Hg(3)—O(53) 2.76, Å; in **2** Hg(1)—O(22) 3.10, Hg(1)—O(41) 2.78, Hg(1)—O(51) 2.89, Hg(1)—O(63) 3.03, Hg(2)—O(42) 2.83, Hg(2)—O(53) 3.08 Å].

Both structures reported here consist of sheets of 48-membered rings, the only principal difference being in **1** the presence of an extra HgL_2 unit which links adjacent neodymium centres, forming an additional 16-membered macrocycle fused to the larger macrocycle. The X-ray powder studies show that this significant change in structural type occurs on passing from Gd to Tb within the lanthanide series, as the Gd complex is isostructural with **1** and the Tb complex is isostructural with **2**. In general terms, one can understand that the decrease in ionic size across the lanthanide series may result in fewer lactam ligands (three rather than four) being able

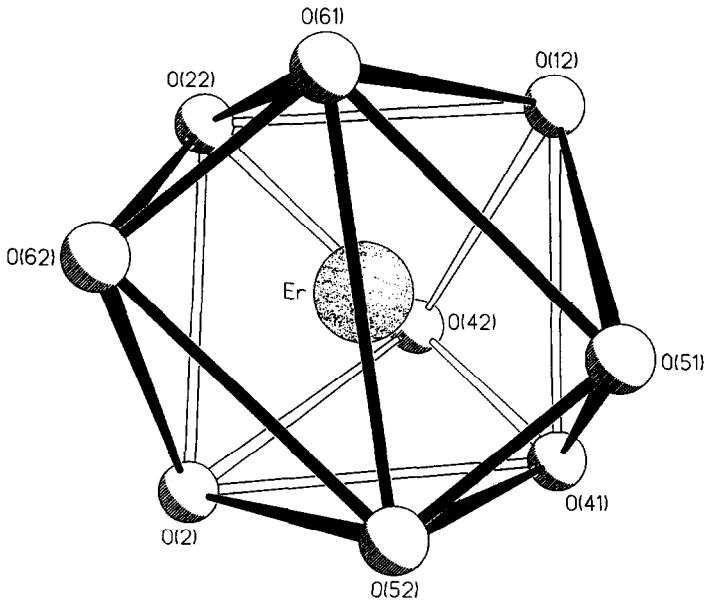

Fig. 4. The distorted tricapped trigonal prismatic coordination geometry about the erbium atom in **2**.

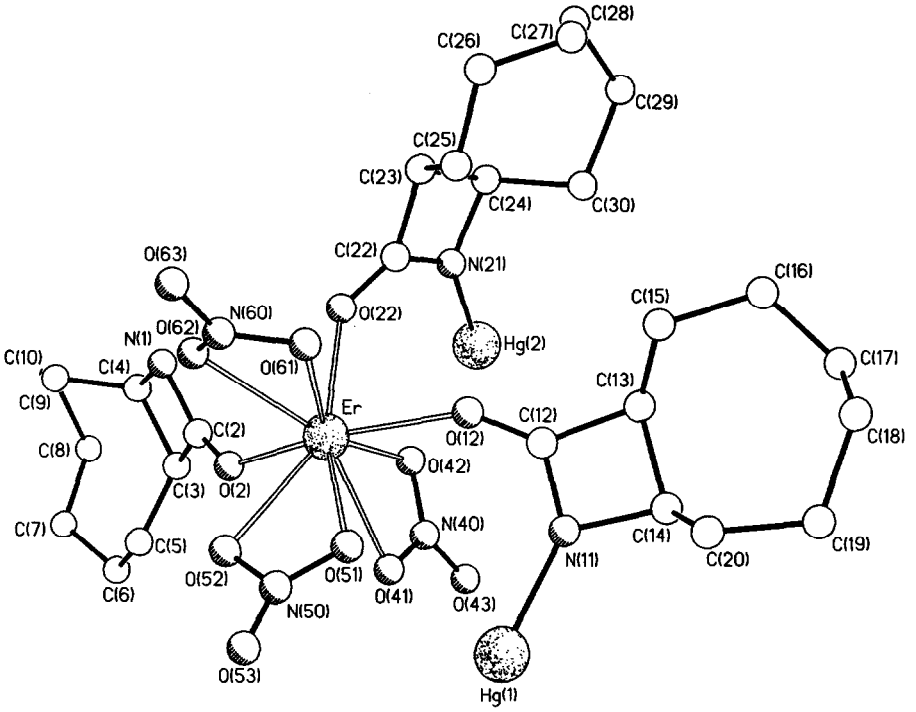

Fig. 5. The erbium environment in **2**, showing the crystallographic numbering scheme.

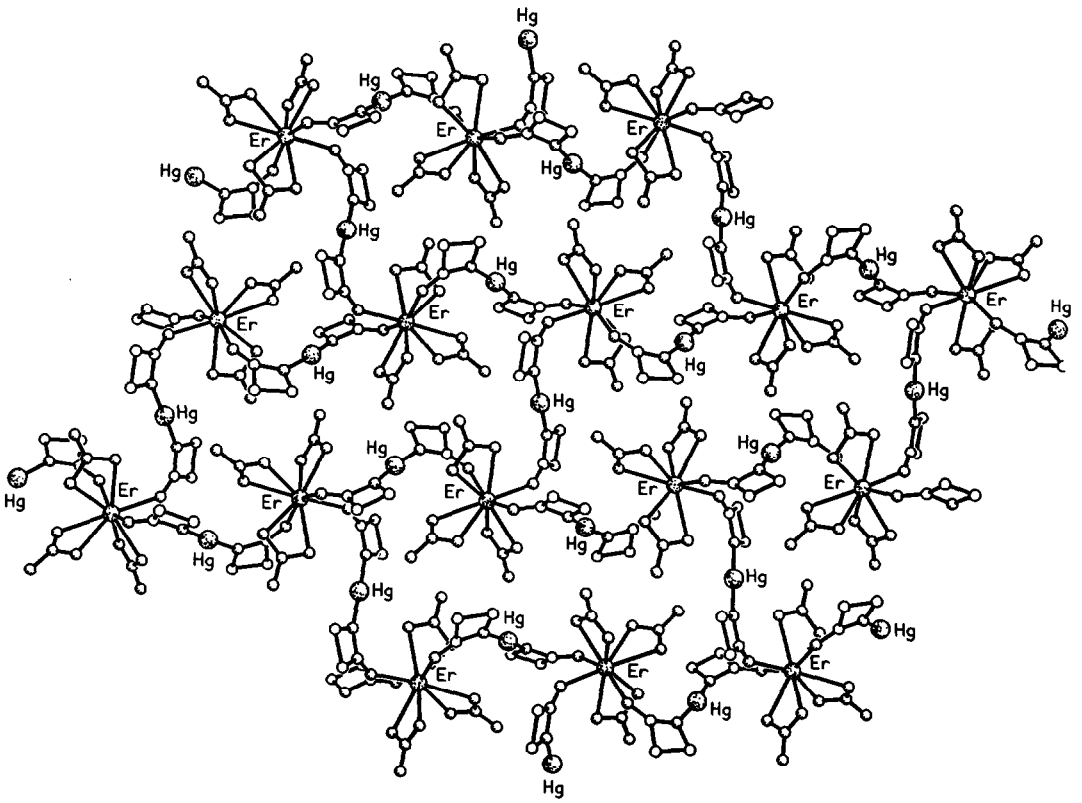

Fig. 6. Part of the contiguous, 48-membered, polymeric, macrocyclic array of **2**.

to be coordinated to the rare-earth metal centre. However, it is intriguing to find that the change in stoichiometry and the concomitant large change in polymeric structure occur at exactly the same point (Gd/Tb) with these more spatially-demanding fused-ring lactams as with 2-azetidinone itself[15] and with 2-pyrrolidone.[14]

Acknowledgements—We thank the SERC for a Research Studentship (to S.P.W.H.) and for the X-ray diffractometer and the British Council and the Spanish Ministry of Education and Science for the Fleming fellowship to M.Q.

REFERENCES

1. D. M. L. Goodgame, S. P. W. Hill and D. J. Williams, *Polyhedron* 1992, **11**, 1841.
2. (a) L. H. Carrad, D. M. L. Goodgame and D. J. Williams, *J. Chem. Soc., Chem. Commun.* 1991, 175; (b) L. H. Carrad, D. M. L. Goodgame, S. P. W. Hill and D. J. Williams, *J. Chem. Soc., Dalton Trans.* 1993, 1003.
3. D. M. L. Goodgame, A. M. Khaled, C. A. O'Mahoney and D. J. Williams, *J. Chem. Soc., Chem. Commun.* 1990, 851.
4. H. Jendralla and K. Laumen, *Chem. Ber.* 1983, **116**, 2136.
5. J. R. Malpass and N. J. Tweddle, *J. Chem. Soc., Perkin Trans. I* 1976, 874.
6. G. M. Sheldrick, SHELXTL, An Integrated System for Solving, Refining and Displaying Crystal Structures from Diffraction Data. University Göttingen, F.R.G. (1978); Revision 4.1 (1983).
7. *International Tables for X-ray Crystallography*, Vol. 4, pp. 99–149. Kynoch Press, Birmingham (1974).
8. R. Graf, *Leibigs Ann. Chem.* 1963, **661**, 111.
9. L. A. Paquette and T. Kakihana, *J. Am. Chem. Soc.* 1968, **90**, 3897.
10. T. Durst and M. J. O'Sullivan, *J. Org. Chem.* 1970, **35**, 2043.
11. L. A. Paquette, M. J. Broadhurst, C. Lee and J. Clardy, *J. Am. Chem. Soc.* 1973, **95**, 4647.
12. R. Graf, *Org. Synth.* 1966, **46**, 51.
13. D. M. L. Goodgame, D. J. Williams and R. E. P. Winpenny, *Polyhedron* 1988, **7**, 1807.
14. D. M. L. Goodgame, D. J. Williams and R. E. P. Winpenny, *J. Chem. Soc., Dalton Trans* 1989, 1439.
15. A. M. Khaled, PhD Thesis, London University (1991).

Polyhedron Vol. 12, No. 23, pp. 2763–2769, 1993
Printed in Great Britain

0277-5387/93 $6.00+.00
© 1993 Pergamon Press Ltd

SYNTHESIS AND LUMINESCENCE STUDY OF EUROPIUM COMPLEXES WITH 5,5-DIMETHYL-2,4-HEXANEDIONE AND VARIOUS ORGANIC BASES

DONJIN QIAN, ZHONG CHEN*† and SHUZHEN ZHANG

Department of Chemistry, Shandong University, Jinan, Shandong 250100, P.R.C.

and

J. VAN HOUTEN*

Department of Chemistry, St. Michael's College, Winooski Park, Colchester, VT 05439, U.S.A.

(*Received* 20 *April* 1993; *accepted* 28 *June* 1993)

Abstract—A series of europium(III) complexes with 5,5-dimethyl-2,4-hexanedione and various organic bases, $Eu(But\text{-}ac)_2OH$ and $Eu(But\text{-}ac)_3 \cdot B$, where But-ac = 5,5-dimethyl-2,4-hexanedionate, and B = 1,10-phenanthroline, 2,2′-bipyridine or 5-nitro-1,10-phenanthroline, were synthesized and characterized by elemental analysis, UV and IR spectroscopy and melting point data. IR data confirmed that the europium is coordinated via oxygen donor atoms to 5,5-dimethyl-2,4-hexanedione and via nitrogen donor atoms to the diimine bases. The $Eu(But\text{-}ac)_2OH$ complex appears to be polymeric. Luminescence spectra, lifetime and quenching studies are reported.

The narrow line emission of rare earth chelates, including β-diketonates, following irradiation with UV light has been studied intensely following the first report by Weissman[1] over 50 years ago. Interest in this phenomenon was stimulated by the potential use of these compounds as laser materials,[2,3] which prompted extensive investigations of fluorescence among these compounds, including studies of the mode of intramolecular energy transfer and metal ion excitation,[4–8] measurement of quantum efficiencies and lifetimes.[9] The efficiency of energy transfer depends on the nature of the metal–ligand bond and variations in luminescence intensity as a result of substitution in β-diketone ligands[10] have been attributed to changes in the donor ability of the diketonate oxygen atoms towards the europium.[11] A review of europium complexes with diketones and polyketones has been provided by Forsburg.[12]

Our studies have sought to broaden the knowledge of some areas of europium coordination chemistry. In this work we present the synthesis and luminescence of complexes with an unsymmetrical β-diketone, But-ac (5,5-dimethyl-2,4-hexanedione), and different organic Lewis base ligands which affect the luminescence of the complexes. The quenching of $Eu(But\text{-}ac)_2(phen)$ by naphthalene in methanol is also reported.

EXPERIMENTAL

Materials

Europium chloride was prepared from Eu_2O_3 (99.99%) supplied by Yue Long Chemical Plant, Shanghai, P.R.C. Other chemicals were analytical or reagent grade.

Methods

Elemental analyses (carbon, hydrogen and nitrogen) were performed using a Perkin–Elmer model

* Authors to whom correspondence should be addressed.
† Present address: Department of Chemistry, Teacher's College, Yangzhou University, Yangzhou 225002, P.R.C.

240-C elemental analyser. IR spectra were run on a Nicolet model 5-DX spectrophotometer. UV spectra and europium analysis[13] were performed on Hewlett–Packard models 8451A and 8452 UV–vis diode array spectrophotometers. Melting points were measured with an X-4 macro melting point appliance. Conductivities were measured using DDS-11A conductivity equipment. Luminescence spectra were measured with an SLM model 8000C spectrofluorometer and corrected for instrument response as a function of wavelength. Luminescence lifetimes were measured using a pulsed-nitrogen laser for excitation (337 nm) and monitoring the emission utilizing the SLM emission optics with the photomultiplier output fed into a Stanford Research Systems boxcar integrator for data reduction.

Synthesis of the ligand, 5,5-dimethyl-2,4-hexanedione, But-ac[14]

The syntheses of pinacol hydrate[15] and pinacolone[16] are essentially literature procedures. To synthesize 5,5-dimethyl-2,4-hexanedione, pinacolone (100 g) was added to water (1 dm^3) and distilled. Concentrated sulphuric acid (80 cm^3) was then added to the distilled liquid. Pinacolone was deposited, dried with potassium carbonate and redistilled at 104–108°C.

A piece of sodium ribbon (7.8 g, 0.34 mol) was placed in anhydrous ethyl acetate and the mixture was cooled. Pinacolone (34 g, 0.34 mol) was then added and after 2 h the sodium ribbon had disappeared. The mixture was placed in a boiling water bath to evaporate the solvent. After the solid had cooled for 45 min, ice-water was added. The organic layer was separated and washed with water. The water washings were combined with the aqueous layer and this was neutralized with acetic acid and treated with copper acetate solution. A blue copper salt was deposited. The copper compound was heated to 188°C, where it fused to a solid and then turned to a liquid at 190°C. Upon cooling, it reverted to a crystalline form. The crystals were mixed with ether and dilute sulphuric acid and the resulting liquid was purified by several distillations. A fragrant oil was obtained which boiled at 170–171°C (745 mm Hg).

Synthesis of bis(5,5-dimethyl-2,4-hexanedionato) hydroxoeuropium(III), $Eu(But\text{-}ac)_2(OH)$[10]

A sample (5 cm^3) of aqueous $EuCl_3$ (0.20 M, 1 mmol) was evaporated to dryness with gentle heating. The resulting solid $EuCl_3$ was dissolved in a minimum amount of water and 95% ethanol (5 cm^3) was added. A sample of 5,5-dimethyl-2,4-hexanedione (0.426 g, 3 mmol) was dissolved in more 95% ethanol (5 cm^3) and KOH (0.206 g, 3 mmol) was added to form the potassium salt of the β-diketone ligand. The ligand potassium salt solution was added dropwise to the $EuCl_3$ solution with stirring. Stirring was continued for 1 h after a white precipitate formed. The product was filtered, washed with methanol and ether and air-dried, yield 0.32 g.

Synthesis of tris(5,5-dimethyl-2,4-hexanedionato)1,10-phenanthrolineeuropium(III), $Eu(But\text{-}ac)_3(phen)$

A sample (5 cm^3) of aqueous $EuCl_3$ (0.20 M, 1 mmol) was mixed with 95% ethanol (10 cm^3) and 5,5-dimethyl-2,4-hexanedione (0.426 g, 3 mmol) was added. This solution was then mixed with methanol (10 cm^3) containing phenanthroline (0.198 g, 1 mmol). The pH of the solution was adjusted with KOH until a white precipitate formed. The mixture was stirred for 1 h, filtered and the solid was washed with ethanol and ether and air-dried, yield 0.64 g. The product was recrystallized from 95% ethanol.

Synthesis of tris(5,5-dimethyl-2,4-hexanedionato)5-nitro-1,10-phenanthrolineeuropium(III), $Eu(But\text{-}ac)_3(5\text{-}NO_2\text{-}phen)$

A sample (5 cm^3) of aqueous $EuCl_3$ (0.20 M, 1 mmol) was added to 95% ethanol (10 cm^3). A sample of 5-nitro-1,10-phenanthroline (0.241 g, 1 mmol) was then added to more 95% ethanol (10 cm^3), the mixture was heated to dissolve the ligand and then 5,5-dimethyl-2,4-hexanedione (0.426 g, 3 mmol) was added. The two solutions were mixed and the mixture was treated with NaOH (0.1 N) to form a pale yellow precipitate. The resulting suspension was stirred for 1 h, filtered, washed with ethanol and ether and air-dried, yield 0.52 g. The product was recrystallized from 95% ethanol.

Synthesis of tris(5,5-dimethyl-2,4-hexanedione)2,2′-bipyridyleuropium(III), $Eu(But\text{-}ac)_3(bpy)$

To a solution of 2,2′-bipyridine (1.56 g, 1 mmol) dissolved in 95% ethanol (20 cm^3) were added 5,5-dimethyl-2,4-hexanedione (0.426 g, 3 mmol) and europium nitrate (5 cm^3; 0.20 M, 1 mmol). The mixture was treated with NaOH (0.1 N) to form a white precipitate. The resulting suspension was stirred for 1 h, filtered, washed with ethanol and ether and air-dried, yield 0.54 g. The product was recrystallized from 95% ethanol.

RESULTS AND DISCUSSION

Properties of the complexes

The new complexes are all white solids, with the exception of the 5-nitro-phenanthroline complex which is pale yellow. Their elemental analysis, melting point, synthetic yield, conductimetric, and IR data are summarized in Table 1. The conductivity data indicate that the complexes are all non-electrolytes. They are insoluble in water, but they are dissolved by organic solvents such as methanol, ethanol, carbon tetrachloride, N,N-dimethylformamide and dimethylsulphoxide. They have constant composition and are stable to air, light and heat.

IR spectra of the complexes

The characteristic peaks and assignments of the IR absorption spectra of the complexes are given in Table 2.

The IR spectrum of Eu(But-ac)$_3$(phen) exhibits a methyl stretching band at 2965 cm^{-1}. The carbonyl peak of 5,5-dimethyl-2,4-hexanedione is shifted to 1597–1631 cm^{-1}, indicating chelation via the oxygens.[17] The characteristic C—N stretching of the 1,10-phenanthroline is absent, indicating chelation via the nitrogens. Other assignments are given in Table 2. On the basis of the IR data, the europium is assigned a coordination number of eight.

The crystal structure of the analogous complex Eu(acac)$_3$(phen) has been previously published.[18] That compound has a distorted square-antiprismatic geometry. The same geometry is assumed for the complexes reported in this study on the basis of the similarity of their vibrational and luminescence spectra.

Excited states

The UV absorption peaks of the complexes in ethanol are summarized in Table 3. The strong absorption at *ca* 270 nm is characteristic of the complexes since the europium(III) ion has no absorption in the 270–320 nm range.[19] That peak also appears in the excitation spectra and it is assigned as a ligand absorption. Absorption to the initially formed ligand singlet, S_1, excited state is followed by either non-radiative intersystem crossing to the ligand triplet manifold or by non-radiative or radiative decay (ligand fluorescence) back to the ground state. The latter processes quench any subsequent metal luminescence. If the ligand triplet is formed, it may undergo non-radiative energy transfer to the metal ion or undergo non-radiative or radiative decay (ligand phosphorescence) to the original ground state. Energy transfer to the metal ion produces an excited state, $^5D_0$, which may decay to the ground state $^7F_{0-4}$ with luminescence.

Luminescence studies

Emission spectra were recorded at room temperature and at 77 K using 345 or 350 nm excitation. Although all the spectra were recorded in the range 400–800 nm (25.0–12.5 kK), no emission peaks were observed outside the 14–18 kK range shown in Fig. 1. As expected, the emission intensity increases at 77 K and the bands are sharper and exhibit more detail than the room-temperature spectra. The details of the 77 K luminescence spectra of all the complexes are summarized in Tables 4–7. The room-temperature spectra of solid and DMSO solution samples exhibited the same features as those reported for 77 K. Band assignments were made by consideration of the calculated free ion energy levels

Table 1. Properties of the complexes

Complex	Elemental analysis Found (Calc.) C	H	N	Eu	Yield %	M.p. (°C)	Conductivity (Ω^{-1} cm^2 mol^{-1})
Eu(But-ac)$_2$(OH) $EuC_{16}H_{27}O_5$	42.7 (42.6)	6.1 (6.0)	— —	33.1 (33.7)	79	246	3.4
Eu(But-ac)$_3$(phen) $EuC_{36}H_{27}N_2O_6$	57.1 (57.2)	6.1 (6.3)	4.0 (3.7)	19.6 (20.1)	84	224	3.8
Eu(But-ac)$_3$(5-NO_2-phen) $EuC_{36}H_{46}N_3O_8$	54.3 (54.0)	5.7 (5.8)	5.3 (5.2)	19.2 (19.0)	63	208	4.0
Eu(But-ac)$_3$(bpy) $EuC_{34}N_{47}N_2O_6$	56.2 (55.8)	6.5 (6.5)	4.3 (3.8)	20.6 (20.8)	74	128	4.2

Table 2. IR spectral data (cm^{-1})

Complex	ν(OH)	$\nu(CH_3)$	ν(C═C + C═O)	ν(C—O + C═C)	δ(CH) + ν(C═C)	$\delta_a(CH_3)$	$\delta_s(CH_3)$	(CH) + (C═C)	(C—CH_3 + C═C)	(CH)	(Eu—O)
Eu(But-ac)$_2$(OH)	3440	2965	1631–1589	1517	—	1413	1354	1162	—	771	400
Eu(But-ac)$_3$(phen)		2965	1631–1597	1519	1453	1402	1357	1162	—	775	400
Eu(But-ac)$_3$(5-NO_2-phen)		2957 2925	1585	1516	1452	1413	1358	1160	1280	774–769	408
Eu(But-ac)$_3$(bpy)		2958 2953	1588	1516	1448	1413	1358	1160	1279	771	412

given by Dieke[20] and calculations on similar compounds by Filipescue *et al.*[21]

The excited-state spectra of the complexes show only small differences, with emission peaks belonging to the $^5D_0 \rightarrow {}^7F_{0-4}$ transitions, indicating that energy transfer in the molecule is fast[22] and that the effect of the ligands on the 4*f* electron levels is small. The peak patterns are consistent with square antiprismatic site symmetry.[23–25]

Although luminescence quantum yields have not been measured, when solid emission intensities were measured using sample plates under controlled excitation conditions, the luminescence intensities showed the following trend: Eu(acac)$_3$(phen) > Eu(But-ac)$_3$(phen) > Eu(But-ac)$_3$(bpy) > Eu(But-ac)$_2$(OH) > Eu(But-ac)$_3$(5-NO_2phen). Eu(acac)$_3$(phen), where acac is 2,4-pentanedione, was prepared by a published method.[10] The fact that the luminescence spectrum and intensity are similar for Eu(acac)$_3$(phen) and Eu(But-ac)$_3$(phen) indicates that asymmetry in the β-diketone has little effect on the excited state. However, introduction of the nitro group on the phenanthroline ligand results in an eight-fold decrease in luminescence intensity in the major band at 16.35 kK. The electron donor ability of 1,10-phenanthroline increases intramolecular energy transfer efficiency, resulting in a strong luminescence,[26] whereas introduction of the electron-withdrawing nitro group decreases luminescence, consistent with the accepted mechanism of rare earth ion luminescence. These data indicate that only organic bases whose triplet energy is close to the resonance energy of the europium ion will enhance the luminescence efficiency.[27]

Table 3. UV absorption features of the complexes (in ethanol at room temperature)

Complex	Wavelength (nm)	Extinction coefficient ($M^{-1}\,cm^{-1}$)
Eu(But-ac)$_2$(OH)	204	1900
	278	18,000
Eu(But-ac)$_3$(phen)	204	2400
	232	56,000
	266	63,000
Eu(But-ac)$_3$(5-NO_2-phen)	204	31,000
	234	34,000
	272	57,000
Eu(But-ac)$_3$(bpy)	204	22,000
	238	34,000
	280	57,000

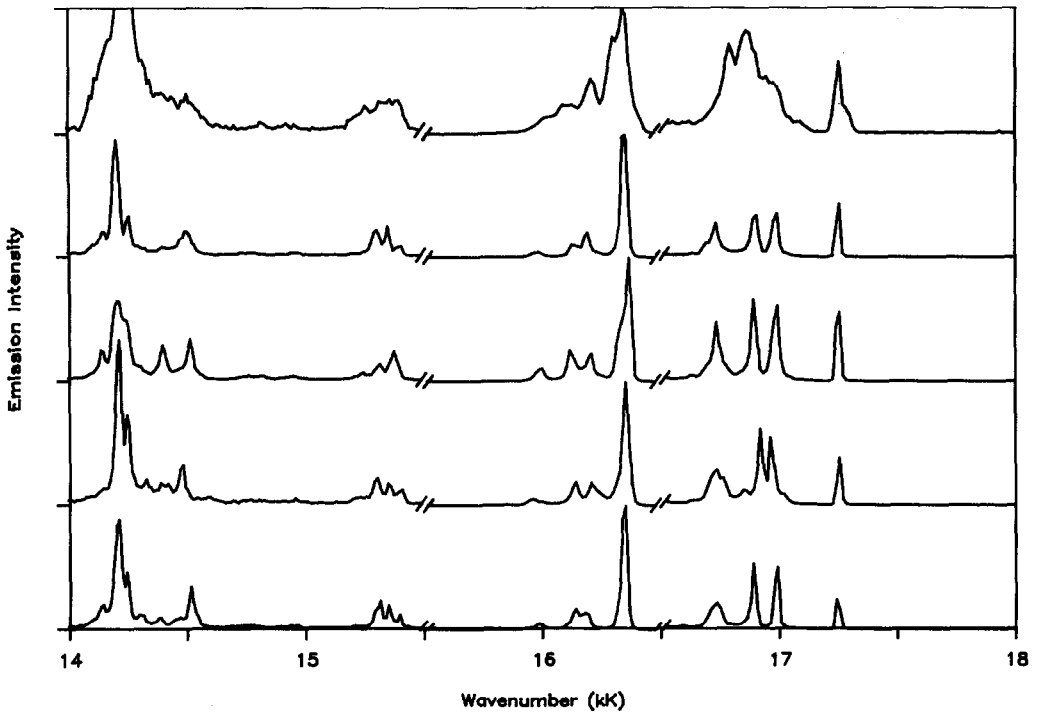

Fig. 1. Normalized, corrected emission spectra of the solid samples at 77 K, 0.5 nm resolution, 350 nm excitation. Top to bottom: Eu(But-ac)$_2$(OH), Eu(But-ac)$_3$(phen), Eu(But-ac)$_3$(5-NO$_2$-phen), Eu(But-ac)$_3$(bpy) and Eu(acac)$_3$(phen). The $^5D_0 \rightarrow {}^7F_2$ region (15.5–16.5 kK) of each spectrum has been attenuated by a factor of 10 in order to show the weaker peaks in the rest of the spectra.

Ethanol solutions of the complexes showed the same trend in luminescence intensity as was observed for the solids. Benzene and carbon tetrachloride solutions decreased luminescence intensities and lifetimes.

A Stern–Volmer plot of the quenching of Eu(But-ac)$_3$(phen) (1.40×10^{-4} M in methanol) by naphthalene is shown in Fig. 2. On the basis of the data in Fig. 2, the quenching is assumed to be both collisional and triplet quenching.[28]

Table 4. Luminescence transitions of solid Eu(But-ac)$_2$(OH) at 77 K

Wavelength (nm)	Wave number (kk)	Relative intensity	Assignment
579.5	17.25	0.06	$^5D_0 \rightarrow {}^7F_0$
593.0	16.86	0.08	$^5D_0 \rightarrow {}^7F_1$
595.5	16.79	0.07	
612.0	16.34	1.00	$^5D_0 \rightarrow {}^7F_2$
617.0	16.21	0.45	
620.0	16.13	0.24	
621.5	16.09	0.24	
649.5	15.40	0.03	$^5D_0 \rightarrow {}^7F_3$
653.0	15.31	0.03	
655.5	15.26	0.02	
689.5	14.50	0.03	$^5D_0 \rightarrow {}^7F_4$
703.5	14.21	0.17	

Table 5. Luminescence transitions of solid Eu(But-ac)$_3$(phen) at 77 K

Wavelength (nm)	Wave number (kk)	Relative intensity	Assignment
579.5	17.26	0.04	$^5D_0 \rightarrow {}^7F_0$
588.5	16.99	0.04	$^5D_0 \rightarrow {}^7F_1$
591.5	16.91	0.04	
597.5	16.74	0.03	
611.5	16.35	1.00	$^5D_0 \rightarrow {}^7F_2$
617.5	16.19	0.21	
620.0	16.13	0.11	
625.5	15.99	0.05	
651.5	15.35	0.03	$^5D_0 \rightarrow {}^7F_3$
653.5	15.30	0.02	
689.5	14.50	0.02	$^5D_0 \rightarrow {}^7F_4$
701.5	14.26	0.04	
704.0	14.20	0.10	

Table 6. Luminescence transitions of solid Eu(But-ac)$_3$(5-NO$_2$-phen) at 77 K

Wavelength (nm)	Wave number (kk)	Relative intensity	Assignment
579.5	17.26	0.06	$^5D_0 \rightarrow {}^7F_0$
588.5	16.99	0.06	$^5D_0 \rightarrow {}^7F_1$
592.0	16.89	0.07	
597.5	16.74	0.05	
611.0	16.37	1.00	$^5D_0 \rightarrow {}^7F_2$
617.0	16.21	0.23	
620.5	16.12	0.26	
625.0	16.00	0.11	
650.5	15.37	0.03	$^5D_0 \rightarrow {}^7F_3$
653.5	15.30	0.01	
656.0	15.24	0.01	
689.0	14.51	0.04	$^5D_0 \rightarrow {}^7F_4$
694.5	14.40	0.03	
704.0	14.21	0.07	
707.5	14.13	0.03	

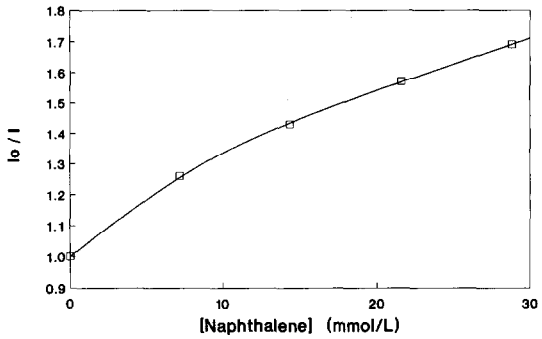

Fig. 2. Stern–Volmer plot of the luminescence quenching of Eu(But-ac)$_3$(phen) by naphthalene in methanol.

Table 8. Luminescence lifetime data for the solid samples

Complex	Lifetimes (ms) 77 K	Lifetimes (ms) Room temperature
Eu(But-ac)$_2$(OH)	0.45	0.38
Eu(But-ac)$_3$(phen)	0.80	0.79
Eu(But-ac)$_3$(5-NO$_2$-phen)	0.78	0.74
Eu(But-ac)$_3$(bpy)	0.85	0.79

Luminescence lifetime data for the $^5D_0$ level measured for solid samples at room temperature and at 77 K are summarized in Table 8. The lifetime of the Eu(But-ac)$_2$(OH) complex is approximately half that of the other complexes and very little temperature effect on the lifetime is observed. The structure of that complex is different from the others and it is probably polymeric.[10] The absence of any significant temperature effect on the lifetime is taken as an indication that a large number of vibrational quanta participate in the non-radiative decay process.[10]

Table 7. Luminescence transitions of solid Eu(But-ac)$_3$(bpy) at 77 K

Wavelength (nm)	Wave number (kk)	Relative intensity	Assignment
579.5	17.26	0.04	$^5D_0 \rightarrow {}^7F_0$
589.5	16.96	0.06	$^5D_0 \rightarrow {}^7F_1$
591.5	16.92	0.06	
597.5	16.74	0.02	
611.5	16.35	1.00	$^5D_0 \rightarrow {}^7F_2$
617.0	16.20	0.19	
619.5	16.14	0.19	
626.5	15.96	0.06	
649.0	15.41	0.01	$^5D_0 \rightarrow {}^7F_3$
651.5	15.35	0.02	
653.5	15.30	0.02	
690.5	14.48	0.03	$^5D_0 \rightarrow {}^7F_4$
702.0	14.25	0.07	
703.5	14.21	0.13	

Acknowledgements—Financial support was provided by the National Natural Science Fund of China, by St. Michael's College and by the National Science Foundation, RII-8610679 (Vermont EPSCoR).

REFERENCES

1. S. I. Weissman, *J. Chem. Phys.* 1942, **10**, 214.
2. E. J. Schimitschek, *Appl. Phys. Lett.* 1963, **3**, 117.
3. A. Lempicki and H. Samlson, *Appl. Phys. Lett.* 1963, **2**, 159.
4. G. A. Crosby and R. E. Whan, *J. Chem. Phys.* 1960, **32**, 614.
5. G. A. Crosby and R. E. Whan, *J. Chem. Phys.* 1962, **36**, 863.
6. S. T. Lyle, J. E. Newbery and A. D. Witts, *J. Chem. Soc., Dalton Trans.* 1972, 1726.
7. J. S. Curran and T. M. Shepard, *J. Chem. Soc., Faraday Trans.* II, 1973, **11**, 69, 126.
8. F. Halverson, J. S. Brineu and J. R. Leto, *J. Chem. Phys.* 1964, **40**, 2790.
9. M. J. Kleinerman, *J. Chem. Phys.* 1969, **51**, 2370.

10. L. R. Melby, N. J. Rose, E. Abramson and J. C. Caris, *J. Am. Chem. Soc.* 1964, **86**, 5117.
11. N. Filipescue, W. F. Sager and F. A. Serafin, *J. Phys. Chem.* 1964, **68**, 3324.
12. *Gmelin Handbuch der Anorgisches Chemie, 8th edn, Part* D5, Vol. D5, p. 39. Springer-Verlag, New York (1984).
13. *Practical Spectrophotometric Analysis of Elements* (Chinese), Translated by Z. Q. Min, Z. J. Fang and L. Y. Hua (1988).
14. S. W. Zhang, F. L. Tong and T. Zhang, *Handbook of Modern Chemical Reagents* (Chinese) (1987).
15. H. Gilman, *Org. Synth.* 1951, **1**, 459.
16. H. Gilman, *Org. Synth.* 1951, **1**, 462.
17. W. D. Horrocks Jr and M. Albin, *Prog. Inorg. Chem.* 1984, **31**, 1.
18. W. H. Watson, R. J. Williams and N. R. Stemple, *J. Inorg. Nucl. Chem.* 1972, **34**, 501.
19. S. L. Li and Y. S. Yang, *J. Inorg. Chem.* (*Chin.*) 1989, **4**, 84.
20. G. H. Dieke, *Spectra and Energy Levels of Rare Earth Ions in Crystals*, pp. 117–127. Interscience, New York (1986).
21. N. Filipescue, J. J. Degnan and N. McAvoy, *J. Chem. Soc. A* 1968, 1594.
22. S. Sato and M. Wada, *Bull. Chem. Soc. Japan* 1970, **43**, 1955.
23. C. Brecher, H. Samelson and A. Lempicki, *J. Chem. Phys.* 1965, **42**, 1081.
24. J. H. Forsberg, *Coord. Chem. Rev.* 1973, **10**, 195.
25. K. B. Yatsimirskii and N. K. Davidenko, *Coord. Chem. Rev.* 1979, **27**, 223.
26. *Gmelin Handbuch der Anorgisches Chemie*, 8th edn, Part D3, Vol. D3, pp. 65–297. Springer-Verlag, New York (1981).
27. M. Ngsee, H. W. Latz and D. G. Hendricker, *Inorganic Compounds with Unusual Properties* p. 214 (1976); R. B. King, *Advances in Chemistry Series No.* 150, American Chemical Society, Washington, D.C.
28. M. L. Bhaumik and M. A. El-Sayed, *J. Chem. Phys.* 1965, **42**, 787.

Polyhedron Vol. 12, No. 23, pp. 2771–2774, 1993
Printed in Great Britain

0277-5387/93 $6.00+.00
© 1993 Pergamon Press Ltd

SYNTHESIS AND CRYSTAL STRUCTURE OF TETRAHYDROFURFURYLCYCLOPENTADIENYL SODIUM TETRAHYDROFURANATE COMPLEX

SUOBO ZHANG and JUZHENG LIU

Department of Chemistry, Jilin University, Changchun 130023, P.R.C.

and

GECHENG WEI, GUANYIANG LIN and WENQI CHEN*

Changchun Institute of Applied Chemistry, Academia Sinica, Changchun 130022, P.R.C.

(*Received* 5 *April* 1993; *accepted* 28 *June* 1993)

Abstract—A tetrahydrofurfurylcyclopentadienyl sodium tetrahydrofuranate complex was prepared by the reaction of tetrahydrofurfurylcyclopentadiene with metallic sodium in THF. Its crystal structure was determined by X-ray analysis. In the crystal, the tetrahydrofuranate complex $C_4H_7OCH_2C_5H_4Na \cdot THF$ adopts a puckered chain structure with an η^5-$(C_4H_7OCH_2)C_5H_4$ ring connected by a bridging Na(THF) unit. The oxygen in the η^5-$(C_4H_7OCH_2)C_5H_4$ ring is coordinated to the sodium atom.

There is a rapidly growing interest in early-transition metal and lanthanide compounds with bidentate ligands, such as cyclopentadienyl ligands with built-in alkoxide or similar groups. Several papers have appeared describing the preparation of functionally-substituted cyclopentadienyl metal complexes,[1–3] the synthesis of tetrahydrofurfurylcyclopentadiene and its thallium complexes.[4] In this paper, we report the synthesis and crystal structure of its sodium complex.

EXPERIMENTAL

Synthesis of tetrahydrofurfurylcyclopentadiene

Tetrahydrofurfuryl chloride, was prepared according to the literature.[5] Sodium cyclopentadienide (0.2 mol) was prepared from sodium dispersion and cyclopentadiene in THF. Tetrahydrofurfuryl chloride (25.0 g, 0.207 mol) was added in a single portion and the solution was maintained at 60°C with stirring for 8 h. After cooling to room temperature, the solution was poured into water, the clear THF solution was separated, anhydrous $MgSO_4$ was added to dryness and then THF was distilled off from it. The residual solution was distilled under reduced pressure and a colourless distillate boiling at 48–56°C (0.1 mm Hg) was collected in a 40% yield.

Synthesis of tetrahydrofurfurylcyclopentadienyl sodium

Tetrahydrofurfurylcyclopentadiene (7.5 g, 0.05 mol) was dissolved in THF (50 cm^3). To the solution was added metallic sodium under an atmosphere of nitrogen and the reaction mixture heated to reflux for 8 h. The warm solution was filtered through Celite. When the resulting solution was cooled, colourless crystals were formed at 0 to −20°C, yield 50%.

Determination of the crystal structure

A single crystal with the dimensions 0.36 × 0.42 × 0.60 mm, suitable for X-ray analysis, was sealed under nitrogen in thin-walled glass capillaries. X-ray diffraction data were collected on a Nicolet XRD R_{3m}/E four-circle diffractometer at room

*Author to whom correspondence should be addressed.

temperature by the use of graphite monochromated Mo-K_α radiation, with a scan speed of 6° min^{-1} and scan range of 1.2°. One check reflection was measured after 70 reflections. A total of 2727 reflections were collected using the ω scan mode ($3° < 2\theta < 60°$), of which 1111 with $I > 3\sigma(I)$ were considered to be observed. The crystal data are listed in Table 1.

The crystal structure was solved by heavy atom methods using the SHELXTL program. The coordinates of the sodium atom, derived from a Patterson analysis, were used to calculate the Fourier map. Successive Fourier syntheses gave the positions of all the non-hydrogen atoms. The coordinates of the hydrogen atoms were added according to theoretical models. The atomic coordinates and anisotropic temperature factors for all the non-hydrogen atoms were refined by used block-diagonal least-squares. Further refinements led to final values of $R = 0.05$, and $R_w = 0.065$ ($w = 1/[\sigma^2(F_o)+0.00168F_o^2]$).

Table 1. Crystal data

Compounds	$[C_5H_4C_5H_9O]Na \cdot \{THF\}_n$
Molecular weight	244.4
Space group	$P2_1/n$
Cell constants	
a (Å)	9.048 (3)
b (Å)	9.587 (5)
c (Å)	16.716 (4)
β (°)	102.24 (3)
Cell volume (Å^3)	1417.08 (0.94)
Z	4
D_c (g cm^{-3})	1.15
μ (Mo-K_α) (cm^{-1})	1.1
F(000)	528
R	0.058
Rw	0.065
G	0.00168
$(\Delta/\sigma)_{max}$	0.03
S	1.43
$\Delta\rho_{max}$ (e Å^{-3})	0.16 to −0.30
Number of parameters refined	154

RESULTS AND DISCUSSION

The reaction of tetrahydrofurfuryl chloride with sodium cyclopentadienide in THF yielded, after work up and distillation, tetrahydrofurfurylcyclopentadiene with a small unreacted tetrahydrofurfuryl chloride contamination. The reaction of the mixture with metallic sodium gave $C_4H_7OCH_2C_5H_4Na \cdot THF$ [eq. (1)] and a small amount of $CH_2{=}CH(CH_2)_2CH_2ONa$ [eq. (2)].[5] The warm solution was filtered through Celite in order to remove the white precipitate of $CH_2{=}CH(CH_2)_2CH_2ONa$.

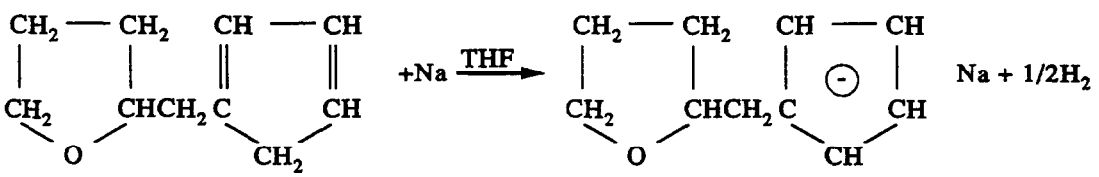

(1)

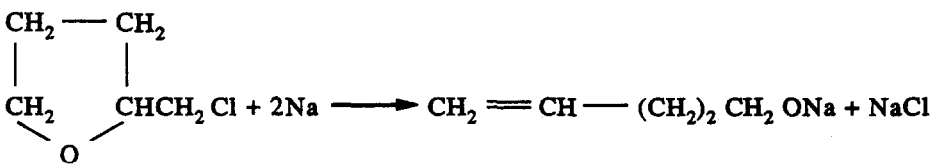

(2)

When the resulting solution was cooled, colourless rod-like crystals were formed. The stereoscopic drawing with the atom numbering scheme of the molecule is shown in Fig. 1. Selected bond lengths and angles are given in Tables 2 and 3.

In the molecule $C_4H_7OCH_2C_5H_4Na \cdot THF$, the central sodium atom is bonded to five carbon atoms and the oxygen atom of tetrahydrofurfurylcyclopentadienyl and one THF ligand is coordinated to each sodium atom. The skeletal structure consists of a puckered chain of sodium atoms, linked by bridging pentahapto-cyclopentadienyl groups inclined at 87.3° to the Na–Na axes (in $C_5H_5Na \cdot TMEDA$,[6] the angle is 88°), and there is a displacement from the ring centre. This slippage from the ideal η^5-geometry is attributed to non-bonded repulsions between adjacent $C_4H_7OCH_2C_5H_4$ rings. The puckering angle of Na—Na—Na is 139° (in $C_6H_5CH_2C_5H_4Na4 \cdot THF$,[7] the Na—Na—Na angle is 130°). The degree of puckering of the chain is indicative of

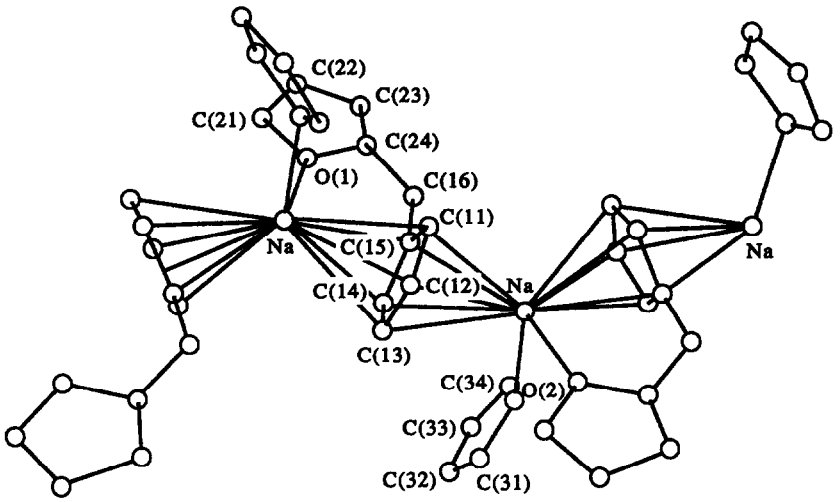

Fig. 1. Stereoscopic drawing of $C_4H_7OCH_2C_5H_4Na \cdot THF$.

Table 2. Bond lengths (Å)

Na—O(2)	2.424(3)	Na—C(11)	2.697((4)
Na—C(12)	2.860(5)	Na—C(13)	2.967(5)
Na—C(14)	2.880(5)	Na—C(15)	2.741(4)
O(1)—C(21)	1.411(6)	O(1)—C(24)	1.365(7)
O(1)—Na′	2.375(4)	O(2)—C(31)	1.387(6)
O(2)—C(34)	1.410(8)	C(11)—C(12)	1.382(7)
C(11)—C(15)	1.388(7)	C(11)—Na′	2.797(5)
C(12)—C(13)	1.359(7)	C(12)—Na′	2.898(5)
C(13)—C(14)	1.384(7)	C(13)—Na′	2.899(5)
C(14)—C(15)	1.392(6)	C(14)—Na′	2.788(4)
C(15)—C(16)	1.481(7)	C(15)—Na′	2.734(4)
C(16)—C(24)	1.413(7)	C(21)—C(22)	1.469(9)
C(22)—C(23)	1.489(9)	C(23)—C(24)	1.525(8)
C(31)—C(32)	1.534(10)	C(32)—C(33)	1.337(13)
C(33)—C(34)	1.383(10)		

Symmetry code: Na′: $1.5-x$, $-0.5+y$, $0.5-z$.

the distorted tetrahedral coordination of the metal atoms.

The distance from sodium to each of the carbons C(11)–C(15) is in the range 2.734(4)–2.899(5) Å. It is apparent that the influence of the Na—O_1 coordination produces significantly longer Na—C(12) and Na—C(13) bonds.

The Na—O(1) bond distance is 2.375(4) Å. The Na—O(2) bond length is 2.42 Å, which is considerably longer than those found in $(C_5H_4CO$ Me)Na · THF[1] (2.35 Å) and $(C_6H_5CH_2C_5H_4)$Na · THF[7] (2.337 Å). This is presumably due to the additional Na—O(1) coordination.

The best planes and torsion angles of some of the atomic groups are given in Table 4. As a rule, the smaller the deviations of the atoms from the best planes, the closer they are to a planar configuration. In view of this, the cyclopentadienyl ring, labelled

Table 3. Bond angles (°)

C(21)—O(1)—Na′	126.6(3)	C(24)—O(1)—Na′	118.7(3)
C(21)—O(1)—C(24)	112.1(4)	C(11)—C(12)—C(13)	108.2(5)
C(11)—C(12)—Na′	72.0(3)	C(13)—C(12)—Na′	76.5(3)
C(12)—C(13)—C(14)	107.5(4)	C(14)—C(13)—Na′	71.5(3)
C(13)—C(14)—Na′	80.4(3)	C(15)—C(14)—Na′	73.2(2)
C(11)—C(15)—C(14)	105.2(4)	C(11)—C(15)—C(16)	127.1(4)
C(14)—C(15)—C(16)	127.6(5)	C(11)—C(15)—Na′	78.0(3)
C(14)—C(15)—Na′	77.6(2)	C(15)—C(16)—C(24)	118.1(5)
O(1)—C(21)—C(22)	107.7(5)	C(21)—C(22)—C(23)	106.2(5)
C(22)—C(23)—C(24)	104.5(5)	O(1)—C(24)—C(16)	117.5(4)
O(1)—C(24)—C(23)	106.5(5)	C(16)—C(24)—C(23)	121.1(6)

Table 4. Best planes of rings and their torsion angles

Plane	Equation, atoms and deviation of atoms (Å)					Torsion angles (°)
1	$1.924x+8.850y+4.478z = 2.3732$					
	C(11)	C(12)	C(13)	C(14)	C(15)	
	0.005	−0.003	0.000	0.003	−0.005	
2	$8.535x-2.488y+0.042z = 6.5869$					88.4
	C(15)	C(16)	C(24)	O(1)	Na′	
	0.025	0.074	−0.216	0.191	−0.073	
3	$8.677x-0.574y+1.130z = 6.4936$					76.3, 12.2
	O(1)	C(21)	C(22)	C(23)	C(24)	
	0.068	−0.002	0.058	0.093	−0.100	

Table 5. Atomic coordinates ($\times 10^4$) and isotropic thermal parameters ($Å^2 \times 10^3$)

	x	y	z	U_{eq}
Na	8169(2)	2284(2)	2979(1)	58(1)
O(1)	7329(4)	−2087(3)	730(2)	84(1)
O(2)	10879(3)	2399(3)	3498(2)	75(1)
C(11)	6444(5)	128(4)	2288(3)	63(2)
C(12)	6738(6)	−349(5)	3087(3)	67(2)
C(13)	8207(5)	−766(5)	3286(3)	69(2)
C(14)	8827(5)	−553(5)	2607(3)	69(2)
C(15)	7736(5)	−3(4)	1972(3)	58(2)
C(16)	7877(7)	270(5)	1119(3)	92(2)
C(21)	7278(8)	−2977(6)	52(3)	104(3)
C(22)	7364(9)	−2100(7)	−658(3)	122(3)
C(23)	7593(6)	−645(7)	−344(3)	92(2)
C(24)	7255(8)	−713(6)	511(3)	115(3)
C(31)	11650(6)	1612(6)	4151(3)	91(2)
C(32)	13138(8)	1196(11)	3915(5)	182(5)
C(33)	13118(8)	1774(10)	3185(6)	164(5)
C(34)	11843(7)	2594(7)	2946(4)	108(3)

plane 1 in Table 4, is perfectly planar, whereas the other two rings are distorted to different extents from the ideal model. The normal of the cyclopentadienyl plane is almost perpendicular to that of the labelled plane 2. Atomic coordinates and isotropic thermal parameters are shown in Table 5.

REFERENCES

1. R. D. Rogers and J. L. Atwood, *J. Organomet. Chem.* 1982, **238**, 79.
2. R. Fandos, A. Meetsma and J. H. Teuben, *Organometallics* 1991, **10**, 59.
3. C. Qian, Z. Xie and Y. Huang, *J. Organomet. Chem.* 1987, **323**, 285.
4. T. E. Bitterwolf and K. A. Lott, *J. Organomet. Chem.* 1991, **408**, 137.
5. P. Gaubert, R. P. Linstead and H. N. Rydon. *J. Chem. Soc.* 1937, 1971.
6. T. Aogragi, H. M. M. Shearer, K. Wade and G. Whitehead, *J. Organomet. Chem.* 1979, **75**, 21.
7. B. Zhang, Z. Jin and W. Chen, *Chem. Res. Chin. Univ.* 1992, **8**, 15.

Polyhedron Vol. 12, No. 23, pp. 2775–2780, 1993
Printed in Great Britain

0277–5387/93 $6.00+.00
© 1993 Pergamon Press Ltd

DIVALENT COBALT, NICKEL, COPPER AND ZINC COMPLEXES OF TETRAAZA MACROCYCLES BEARING POLYAMIDE GROUPS: SYNTHESIS AND CHARACTERIZATION

MOHAMMAD SHAKIR,*† SAJI P. VARKEY and P. SHAHUL HAMEED

Division of Inorganic Chemistry, Department of Chemistry, Aligarh Muslim University, Aligarh-202 002, India

(*Received* 6 *April* 1993; *accepted* 25 *June* 1993)

Abstract—A new series of 14–20-membered tetraamide macrocyclic complexes, $[ML_1]Cl_2$–$[ML_8]Cl_2$, of cobalt(II), nickel(II), copper(II) and zinc(II) have been prepared via the template condensation of dicarboxylic acid with primary diamines. All the complexes are soluble in most polar solvents. The complexes have been characterized by IR, ^1H NMR, mass, ESR and electronic spectral studies and magnetic measurements. A square planar geometry for the complexes, $[ML_n]^{2+}$, where M = Ni^{II} and Cu^{II}, or a tetrahedral geometry for M = Co^{II} and Zn^{II} have been assigned. The electrical conductivity data in DMSO are as expected for 1:2 electrolytes.

Metal template syntheses of multidentate and macromonocyclic ligands have been established over the last two decades as offering high-yielding and selective routes to new ligands and their complexes. There have been recent interest in the study of macrocyclic complexes containing transition metals since they have been found to act as possible models for biochemically important proteins and enzymes.[1–4] Copper(II) peptide complexes have been studied extensively as models for copper(II)–protein interactions.[5,6] Macrocyclic polyamides of different ring sizes are now readily available by convenient methods as already reported.[7–13] In most cases the high dilution technique is employed for the cyclization process.[10] A series of polyamide macrocycles incorporating two α-phenylglycine units and a variable number of ethyleneoxy units have been reported[13] as new ionophore models and their transport studies showed that certain polyamide macrocycles mimic naturally-occurring cyclic ionophores (valinomycin, nonactin) in their ability to transport K^+ and Na^+ ions across the lipophilic membrane. A number of macrocyclic amides, containing oxygen or sulphur atoms as ring components through cyclization via aminolysis of the dimethyl esters of α,ω-dicarboxylic acid with polyethylenepolyamines, have been reported.[14] Generally, the macrocyclic polyamide ligand is prepared[14–16] by the reaction of polyamines with either the diester salt of a dicarboxylic acid or the dicarboxylic acid dichloride. In most cases the polyamide macrocycles thus formed on reduction with B_2H_6 or $LiAlH_4$ lead to the formation of their corresponding polyazamacrocycles,[14,17,18] which may be used to construct various macropolycyclic systems. Although a variety of macrocyclic moieties bearing the amide group have been reported, the tetraamides formed from the template condensation of dicarboxylic acid with primary diamines have not been reported so far. We report herein the metal ion-controlled syntheses and characterization of macrocyclic tetraamides from diacids and diamines.

EXPERIMENTAL

The metal salts $CoCl_2 \cdot 6H_2O$, $NiCl_2 \cdot 6H_2O$, $CuCl_2 \cdot 2H_2O$ and $ZnCl_2$ (all BDH) are commercially-available pure samples. The dicarboxylic acids malonic acid, succinic acid and glutaric acid

* Author to whom correspondence should be addressed.
† Present address: Institüt für Anorganische-Chemie der Universitat, Tammanstr. 4, D-3400, Göttingen, F.R.G.

(all Fluka) were used as purchased. The primary diamines 1,2-diaminoethane and 1,3-diaminopropane were purchased from E. Merck and used without further purification.

Synthesis of (2,4,9,11-*tetraoxo*-1,5,8,12-*tetraazacyclotetradecane*)*metal*(II) *chloride and* (2,4,10,12-*tetraoxo*-1,5,9,13-*tetraazacyclohexadecane*)*metal*(II) *chloride*, $[ML_1]Cl_2$ *and* $[ML_2]Cl_2$ (M = Co^{II}, Ni^{II}, Cu^{II} *and* Zn^{II}

To an ice-cold solution of metal salt (0.005 mol) in methanol (50 cm^3) was added either 1,2-diaminoethane or 1,3-diaminopropane (0.01 mol) dissolved in methanol (50 cm^3), followed by the addition of malonic acid solution (0.01 mol, 50 cm^3) in methanol. The resulting mixture was stirred continuously for *ca* 7 h. The resultant polycrystalline solid product was filtered, washed several times with methanol and dried *in vacuo*. All the experiments were performed under dry nitrogen.

Synthesis of (2,5,10,13-*tetraoxo*-1,6,9,14-*tetraazacyclohexadecane*)*metal*(II) *chloride and* (2,5,11,14-*tetraoxo*-1,6,10,15-*tetraazacyclooctadecane*)*metal*(II) *chloride*, $[ML_3]Cl_2$ *and* $(ML_4]Cl_2$ (M = Co^{II}, Ni^{II}, Cu^{II} and Zn^{II})

The procedure used for these complexes was the same as detailed above, using succinic acid rather than malonic acid as the diacid.

Synthesis of (2,6,11,15-*tetraoxo*-1,7,10,16-*tetraazacyclooctadecane*)*metal*(II) *chloride and* (2,6,12,16-*tetraoxo* - 1,7,11,17 - *tetraazacycloeicosane*)*metal*(II) *chloride*, $(ML_5]Cl_2$ *and* $[ML_6]Cl_2$ (M = Co^{II}, Ni^{II}, Cu^{II} and Zn^{II})

This preparation was analogous to the above, except glutaric acid (0.01 mol) was introduced.

Synthesis of (3,4,11,12-*dibenzo*-2,5,10,13-*tetraoxo*-1,6,9,14-*tetraazacyclohexadecane*)*metal*(II) *chloride and* (3,4,12,13-*dibenzo*-2,5,11,14-*tetraoxo*-1,6,10,15-*tetraazacyclooctadecane*)*metal*(II) *chloride*, $[ML_7]Cl_2$ *and* $[ML_8]Cl_2$ (M = Co^{II}, Ni^{II}, Cu^{II} and Zn^{II})

These complexes were also prepared using the above method with phthalic acid (0.01 mol).

The mass spectra (JMSD-300) and elemental analyses were obtained from the microanalytical laboratory of CDRI, Lucknow, India. ^1H NMR spectra in DMSO-d_6, using a Bruker AC 200E nuclear magnetic resonance spectrometer with Me_4Si as an internal standard, were obtained from GNDU, Amritsar, India. The metals and chloride were determined volumetrically[19] and gravimetrically,[20] respectively. The IR spectra (4000–200 cm^{-1}) were recorded as CsCl discs on a Perkin–Elmer 621 spectrophotometer. The electronic spectra of the compounds in DMSO were recorded on a Pye–Unicam 8800 spectrophotometer at room temperature. The ESR spectra were recorded on a Jeol JES RE2X ESR spectrophotometer. Magnetic susceptibility measurements were performed using a Faraday balance at 25°C. The electrical conductivities of 10^{-3} M solutions in DMSO were obtained on a Systronics type 302 conductivity bridge equilibrated at 25 ± 0.01°C.

RESULTS AND DISCUSSION

A new series of tetraamide macrocyclic complexes have been prepared by the template action of metal ions, as shown in Scheme 1.

The cyclic amide complexes corresponding to either a high-membered diacid or phenylene diamine under the same reaction conditions could not be formed, which may be due to the increased size of the macrocyclic cavity selectively needed for these metal ions. Most of the compounds were obtained in moderate yields (Table 1) and all were soluble in most polar solvents.

The results of the elemental analyses and the position of the molecular ion peaks in the mass spectra are consistent with their proposed 1:1 metal-to-ligand stoichiometry (Table 1). The observed molar conductance values of all the compounds indicate[21] that they are 1:2 electrolytes in DMSO (Table 1).

The IR spectra of all the macrocyclic complexes $[ML_1[Cl_2–[ML_8]Cl_2$, derived by the condensation of primary amines with dicarboxylic acids, show bands mainly in the regions 1680–1730, 1500–1520, 1240–1270 and 650–675 cm^{-1}, which may be assigned to amide I [ν(C═O)], amide II [ν(C—N) + δ(N—H)], amide III [δ(N—H)] and amide IV [ϕ(C═O)] vibrations, respectively.[9] All the complexes gave a single, sharp secondary amine peak, ν(NH), at *ca* 3220–3260 cm^{-1}, which is found to be lower by 40–60 cm^{-1} than the analogous metal-free tetraaza ligands.[22] This indicates that the amide nitrogens take part in coordination to the metal ions. This has been further corroborated by the appearance of bands at 340–380 cm^{-1} in the spectra of all the complexes, which may be assigned to ν(M—N) vibrations. However, the IR spectra of the complexes do not show bands which could be assigned either for primary amine or alcoholic groups, suggesting that the condensation has occurred.

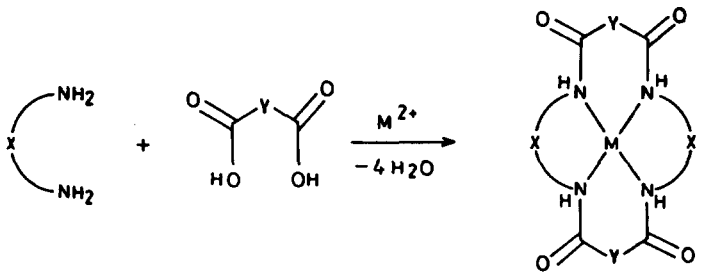

L_1, X = $(CH_2)_2$, Y = CH_2 L_5, X = $(CH_2)_2$, Y = $(CH_2)_3$

L_2, X = $(CH_2)_3$, Y = CH_2 L_6, X = $(CH_2)_3$, Y = $(CH_2)_3$

L_3, X = $(CH_2)_2$, Y = $(CH_2)_2$ L_7, X = $(CH_2)_2$, Y = C_6H_4

L_4, X = $(CH_2)_3$, Y = $(CH_2)_2$ L_8, X = $(CH_2)_3$, Y = C_6H_4

Scheme 1.

The ESR spectra of the polycrystalline copper complexes were recorded at room temperature and their $g_\parallel$, $g_\perp$, $A_\parallel$ and $A_\perp$ values have been calculated. All the complexes gave the same type of spectrum, although the spectrum of $[CuL_5]Cl_2$ and $[CuL_6]Cl_2$ showed no hyperfine splitting. The values of $g_\parallel$ and $g_\perp$ have been found to fall in the regions 2.01–2.05 and 2.17–2.24, respectively. However, hyperfine splittings have been observed for the complexes $[CuL_1]Cl_2$, $[CuL_2]Cl_2$, $[CuL_3]Cl_2$, $[CuL_4]Cl_2$, $[CuL_7]Cl_2$ and $[CuL_8]Cl_2$, where the $A_\parallel$ and $A_\perp$ values lie in the ranges 95–120 and 20–35 G, respectively. The large value of $A_\parallel$ along with the small value of $g_\parallel$ are quite consistent[23] with the square planar environment around the copper ion. The existence of $g_\parallel$ at lower values than $g_\perp$ for all the tetraazamacrocyclic complexes may be due to the presence of an unpaired electron in the d_{z^2} orbital, which is expected[24] for a ground state Cu^{2+} ion.

The ^1H NMR spectra of all the nickel(II) and zinc(II) complexes show a multiplet in the region 3.37–3.56 ppm, corresponding to CO—N—CH_2 (8H) protons.[8] However, a singlet in the regions 3.30–3.41 and 3.29–3.33 ppm and a multiplet in the region 3.20–3.24 ppm was observed for the respective complexes $[ML_1]Cl_2$, $[ML_2]Cl_2$, $[ML_3]Cl_2$, $[ML_4]Cl_2$ and $[ML_5]Cl_2$, $[ML_6]Cl_2$ and can be assigned to CO—CH_2—CO (4H), CO—$(CH_2)_2$—CO (8H) and CO—$(CH_2)_3$—CO (12H) protons, respectively.[8,25] The ^1H NMR spectra of $[ML_2]Cl_2$, $[ML_4]Cl_2$, $[ML_6]Cl_2$ and $[ML_8]Cl_2$ show multiplets in the region 1.98–2.12 ppm, corresponding to C—CH_2—C (4H) protons. A broad signal observed in all the complexes at 8.11–8.34 ppm may, unambiguously, be assigned to the amide CO—NH (4H) protons.[26] A multiplet was observed in the region 6.95–7.21 ppm for the complexes $[ML_7]Cl_2$ and $[ML_8]Cl_2$, corresponding to phenyl ring protons. However, no signals could be observed for primary amine or alcoholic protons.

The electronic spectra of the cobalt complexes show a band at 14,500–16,400 cm^{-1}, assignable to $^4A_{2g}(F) \rightarrow {}^4T_{1g}(P)$ transitions which is consistent with the tetrahedral environment around the cobalt ion.[27] The band below 11,100 cm^{-1} could not be recorded since it lies beyond the range of the instrument used. The observed values of the magnetic moments (4.2–4.6 B.M.) further confirm the tetrahedral geometry around the CO^{2+} ion.

The magnetic measurement studies on nickel(II) complexes suggest their diamagnetic nature which corresponds to the square planar geometry around the nickel(II) ion. The positions of the bands observed in the electronic spectra are in agreement with the transitions which support the magnetic measurement studies.[27]

The electronic spectra of the copper complexes exhibit a broad band centred at *ca* 16,000 cm^{-1}, assignable to $^2B_{1g} \rightarrow {}^2A_{1g}$ transitions. However, two weak shoulders appearing in the regions 21,000–22,400 and 11,500–12,600 cm^{-1} may be ascribed to $^2B_{1g} \rightarrow {}^2E_g$ and $^2B_{1g} \rightarrow {}^2B_{2g}$ transitions, respectively, suggesting a square planar geometry[27] around the copper(II) ion. The observed magnetic moment values (1.83–1.87 B.M.) further confirm the electronic spectral data.[27]

Table 1. μ_{eff} (B.M.), yield, m.p., colour, elemental analyses, molecular ion peaks and molar conductivity values of the compounds

Compound	μ_{eff} (B.M.)	Yield (%)	M.p. (°C)	Colour	Found (Calc.) (%)					(m/z) Found (Calc.)	Molar conductivity ($cm^2\Omega^{-1}mol^{-1}$)
					M	Cl	C	H	N		
$[CoL_1]Cl_2$	4.3	45	248	Reddish-brown	13.8 (14.5)	18.6 (18.4)	29.6 (31.1)	4.1 (4.1)	14.7 (14.5)	383 (386)	93
$[CoL_2]Cl_2$	4.2	55	220	Light orange	14.7 (14.2)	17.3 (17.1)	34.2 (34.8)	4.5 (4.8)	12.9 (13.5)	410 (414)	98
$[CoL_3]Cl_2$	4.4	40	270	Yellowish-orange	14.3 (14.2)	17.5 (17.1)	34.9 (34.8)	4.1 (4.8)	13.3 (13.5)	408 (414)	90
$[CoL_4]Cl_2$	4.2	50	265	Reddish-orange	13.8 (13.3)	16.2 (16.1)	38.4 (38.0)	5.4 (5.4)	12.6 (12.7)	436 (442)	100
$[CoL_5]Cl_2$	4.5	45	295	Light orange	12.8 (13.3)	15.8 (16.1)	38.1 (38.0)	5.4 (5.4)	12.8 (12.7)	438 (442)	95
$[CoL_6]Cl_2$	4.4	60	280	Light orange	12.6 (12.7)	15.3 (15.1)	41.0 (40.8)	5.6 (5.9)	11.5 (11.9)	468 (470)	98
$[CoL_7]Cl_2$	4.5	50	180	Yellowish-orange	11.5 (11.6)	13.6 (13.9)	47.2 (47.1)	3.6 (3.9)	10.9 (11.0)	512 (510)	105
$[CoL_8]Cl_2$	4.6	45	240	Light orange	10.9 (11.0)	13.4 (13.2)	48.9 (49.1)	4.4 (4.5)	10.6 (10.4)	532 (538)	100
$[NiL_1]Cl_1$	—	40	245	Light yellow	15.2 (15.2)	18.5 (18.4)	31.3 (31.1)	4.2 (4.4)	14.3 (14.5)	381 (385.6)	95
$[NiL_2]Cl_2$	—	45	310	Yellowish-green	14.3 (14.1)	17.3 (17.2)	34.4 (34.8)	4.8 (4.8)	13.4 (13.5)	412 (413.6)	100
$[NiL_3]Cl_2$	—	55	290	Light yellow	14.1 (14.1)	17.3 (17.2)	34.9 (34.8)	4.8 (4.8)	13.5 (13.5)	408 (413.6)	100
$[NiL_4]Cl_2$	—	40	320	Yellowish-green	13.3 (13.3)	16.2 (16.1)	38.1 (38.0)	5.3 (5.4)	12.5 (12.7)	438 (441.6)	105
$[NiL_5]Cl_2$	—	40	320	Light green	13.2 (13.3)	15.9 (16.1)	37.9 (38.0)	5.4 (5.4)	12.5 (12.7)	435 (441.6)	95
$[NiL_6]Cl_2$	—	45	295	Yellowish-green	12.3 (12.5)	15.4 (15.1)	40.8 (40.9)	5.9 (6.0)	11.8 (11.9)	463 (469.6)	110
$[NiL_7]Cl_2$	—	60	210	Yellowish-white	11.4 (11.5)	13.9 (13.9)	46.5 (47.1)	3.9 (3.9)	10.9 (11.0)	504 (509.6)	107

$[NiL_8]Cl_2$	—	45	280	Light yellow	10.9 (10.9)	13.3 (13.2)	48.9 (49.1)	4.4 (4.5)	10.6 (10.4)	536 (537.6)	112
$[CuL_1]Cl_1$	1.85	65	175	Light blue	16.1 (16.3)	18.2 (18.2)	30.5 (30.7)	4.1 (4.1)	14.3 (14.3)	385 (390.5)	104
$[CuL_2]Cl_2$	1.83	60	180	Dark blue	15.2 (15.2)	17.0 (17.0)	34.2 (34.4)	4.6 (4.7)	13.0 (13.4)	416 (418.5)	111
$[CuL_3]Cl_2$	1.87	55	190	Light blue	15.0 (15.2)	16.9 (17.0)	34.5 (34.4)	4.7 (4.8)	13.3 (13.4)	414 (418.5)	110
$[CuL_4]Cl_2$	1.84	55	150	Dark green	14.3 (14.2)	15.9 (15.9)	37.6 (37.6)	5.3 (5.4)	12.5 (12.5)	444 (446.5)	98
$[CuL_5]Cl_2$	1.84	50	148	Greenish-yellow	14.2 (14.2)	15.8 (15.9)	36.7 (37.6)	5.4 (5.4)	12.6 (12.5)	443 (446.5)	100
$[CuL_6]Cl_2$	1.86	60	160	Dark green	13.9 (13.4)	14.5 (14.9)	40.4 (40.5)	5.8 (5.9)	11.8 (11.8)	470 (474.5)	99
$[CuL_7]Cl_2$	1.85	70	170	Light green	12.2 (12.3)	13.7 (13.8)	46.5 (46.6)	3.7 (3.9)	10.8 (10.9)	513 (514.5)	108
$[CuL_8]Cl_2$	1.84	65	220	Greenish yellow	11.6 (11.7)	13.3 (13.1)	48.5 (48.7)	4.4 (4.4)	10.3 (10.3)	541 (542.5)	110
$[ZnL_1]Cl_2$	—	65	170	White	16.6 (16.7)	18.2 (18.1)	30.2 (30.6)	4.1 (4.1)	14.3 (14.3)	338 (392.4)	95
$[ZnL_2]Cl_2$	—	60	165	White	15.3 (15.5)	16.6 (16.9)	33.9 (34.3)	4.7 (4.8)	13.3 (13.3)	418 (420.4)	112
$[ZnL_3]Cl_2$	—	65	200	White	15.5 (15.5)	16.9 (16.9)	34.5 (34.2)	4.7 (4.7)	13.4 (13.3)	415 (420.4)	100
$[ZnL_4]Cl_2$	—	65	195	White	14.5 (14.6)	15.8 (15.8)	37.3 (37.5)	5.3 (5.3)	12.5 (12.5)	445 (448.4)	111
$[ZnL_5]Cl_2$	—	60	180	White	14.3 (14.6)	15.7 (15.8)	37.4 (37.5)	5.3 (5.3)	12.6 (12.5)	447 (448.4)	99
$[ZnL_6]Cl_2$	—	65	175	White	13.7 (13.7)	14.9 (14.9)	40.4 (40.3)	5.9 (5.9)	11.7 (11.7)	474 (476.4)	95
$[ZnL_7]Cl_2$	—	65	198	White	12.6 (12.7)	13.8 (13.7)	46.4 (46.5)	3.9 (3.9)	10.8 (10.8)	512 (516.4)	98
$[ZnL_8]Cl_2$	—	70	190	White	11.9 (12.0)	12.9 (13.0)	48.5 (48.5)	4.9 (4.4)	10.3 (10.3)	541 (544.4)	105

Acknowledgements—The Chairman, Department of Chemistry, AMU, CDRI and GNDU, is thanked for providing the necessary research facilities. Mr Saji P.V. is thankful to the Council of Scientific and Industrial Research, New Delhi, for financial assistance.

REFERENCES

1. R. R. Gagne, J. L. Allison, S. Gall and C. A. Kovac, *J. Am. Chem. Soc.* 1977, **99**, 7170.
2. R. R. Gagne, *J. Am. Chem. Soc.* 1976, **98**, 6709.
3. J. W. L. Martin, J. H. Johnston and N. F. Curtis, *J. Chem. Soc. Dalton Trans.* 1978, 68.
4. C. M. Deber, V. Madison and E. R. Blout, *Accts Chem. Res.* 1976, **9**, 106.
5. S. R. James and D. W. Margerum, *Inorg. Chem.* 1980, **19**, 2784.
6. E. J. Billo, *Inorg. Nucl. Chem. Lett.* 1974, **10**, 613.
7. J. F. Carvalho, S. Hui Khim and C. A. Chang. *Inorg. Chem.* 1992, **31**, 4065.
8. I. Tabushi, Y. Taniguchi and H. Kato, *Tetrahedron Lett.* 1977, **12**, 1049.
9. U. K. Pandey, O. P. Pandey, S. K. Sengupta and S. C. Tripathi, *Polyhedron* 1987, **6**, 1611.
10. S. J. Rodgers, C. Yuen Ng and K. N. Raymond. *J. Am. Chem. Soc.* 1985, **107**, 4094.
11. H. Kataoka and T. Katagi, *Tetrahedron* 1987, **43**, 4530.
12. A. G. Schultz, D. J. P. Pinto and M. Welch, *J. Org. Chem.* 1988, **53**, 1372.
13. M. Zinic and V. Skaric, *J. Org. Chem.* 1988, **53**, 2582.
14. I. Tabushi, H. Okino and Y. Kuroda, *Tetrahedron Lett.* 1976, **48**, 4339.
15. P. J. M. Lehn and F. Montavon, *Tetrahedron Lett.* 1972, **44**, 4557.
16. N. W. Alcock, P. Moorie, H. A. A. Omar and C. J. Reader, *J. Chem. Soc., Dalton Trans.* 1987, 2643.
17. P. B. Dietrich, J. M. Lehn and J. P. Sauvage, *Tetrahedron Lett.* 1969, **34**, 2885.
18. E. Graf and J. M. Lehn, *J. Am. Chem. Soc.* 1975, **20**, 5022.
19. C. N. Reilly, R. W. Schmid and F. A. Sadak, *J. Chem. Educ.* 1959, **36**, 619.
20. I. Vogel, *A Text Book of Quantitative Inorganic Analysis*, p. 433. Longmans, London (1961).
21. W. J. Geary, *Coord. Chem. Rev.* 1971, **7**, 82.
22. D. H. Cook and D. E. Fenton, *Inorg. Chim. Acta* 1977, **25**, L 95.
23. K. Miyoshi, H. Tanaka, E. Kimura, S. Tsuboyama, S. Murata, H. Shimizu and K. Ishizu, *Inorg. Chim. Acta* 1983, **78**, 23.
24. M. G. B. Drew, J. Nelson and S. M. Nelson, *J. Chem. Soc., Dalton Trans.* 1981, 1685.
25. R. M. Silverstein, G. C. Bassler and T. C. Morrill, *Spectrometric Identification of Organic Compounds*, 4th edn. John Wiley and Sons, New York (1981).
26. T. C. Woon and D. P. Fairlie, *Inorg. Chem.* 1992, **31**, 4069.
27. A. B. P. Lever, *Inorganic Electronic Spectroscopy*. Elsevier, Amsterdam (1968).

Polyhedron Vol. 12, No. 23, pp. 2781–2785, 1993
Printed in Great Britain

0277–5387/93 $6.00+.00
© 1993 Pergamon Press Ltd

SYNTHESIS AND MAGNETISM OF $[Cu_3^{II}Ln^{III}]$ HETEROTETRANUCLEAR COMPLEXES BRIDGED BY OXAMIDATE

YAN-TUAN LI,* ZONG-HUI JIANG, DAI-ZHENG LIAO,† SHI-PING YAN, SHU-LIN MA,‡ XIAO-YING LI§ and GENG-LIN WANG

Department of Chemistry, Nankai University, Tianjin, P.R.C.

(*Received* 5 *April* 1993; *accepted* 25 *June* 1993)

Abstract—Seven novel μ-oxamido heterotetranuclear complexes, namely $Cu_3(oxae)_3Ln(ClO_4)_3$ [Ln = La, Nd, Gd, Tb, Dy, Ho, Er; where oxae = N,N′-bis(2-aminoethyl) oxamido dianion] have been synthesized and characterized by elemental analyses, IR, conductivity measurements and electronic spectra. The magnetic susceptibility of $Cu_3(oxae)_3Gd(ClO_4)_3 \cdot H_2O$ was measured over the range 4–300 K and the observed data were successfully simulated by the equation based on the spin-Hamiltonian operator $[\hat{H} = -2J(\hat{S}_1\hat{S}_0+\hat{S}_2\hat{S}_0+\hat{S}_3\hat{S}_0)]$, giving the exchange integral J(Cu–Gd) = 2.72 cm^{-1}. This indicates a weak ferromagnetic spin exchange interaction between the Cu^{II} and Gd^{III} ions.

The study of polynuclear complexes with extended ligand bridges is an active area of coordination chemistry.[1] The main reason is probably that many metalloproteins and enzymes have multi-metal sites, which are essential for their biological and catalytic function.

In view of the effective bridging ability of the oxamido group, many efforts have currently been devoted to the synthesis of μ-oxamido complexes containing *d*-transition metal ions.[2–8] However, relatively few studies containing *d*-transition metal ions and lanthanide ions have been reported,[9,10] especially for tetranuclear complexes.

We first reported the synthesis and magnetism of the heterotetranuclear complexes[11] $Cu_3(oxpn)_3Ln(ClO_4)_3$ [Ln = Nd, Gd; oxpn = N,N′-bis(3-aminopropyl) oxamide] and as an extension of that investigation, we now report on seven novel heterotetranuclear complexes, $Cu_3(oxae)_3Ln(ClO_4)_3$ (Ln = La, Nd, Gd, Tb, Dy, Ho, Er) using N,N′-bis(2-aminoethyl) oxamido copper(II) [abbreviated as Cu(oxae)] as a starting material. The magnetic properties of the complex $Cu_3(oxae)_3Gd(ClO_4)_3 \cdot H_2O$ have also been studied.

EXPERIMENTAL

Materials

All of the reagents used were of analytical grade. The hydrated lanthanide perchlorates were prepared by general methods.[12] The starting material Cu(oxae) was synthesized by the literature method[13] from ethylenediamine, diethyl oxalate and copper hydroxide.

Synthesis of $Cu_3(oxae)_3Ln(ClO_4)_3$ (Ln = La, Nd, Gd, Tb, Dy, Ho, Er)

All seven complexes were prepared in a similar fashion and it will suffice to detail the typical preparation of $Cu_3(oxae)_3Gd(ClO_4)_3 \cdot H_2O$.

To a solution of Cu(oxae) (0.6 mmol, 141.5 mg) in absolute ethanol (20 cm^3) was added an absolute ethanol solution (10 cm^3) of $Gd(ClO_4)_3 \cdot 6H_2O$ (0.2 mmol, 112.8 mg) with stirring. After *ca* 1 h a small amount of violet–red precipitate formed and stirring was continued for 8 h. The violet–red microcrystals thus obtained were filtered, washed with

* Visiting scholar: Qufu Normal University.

† Author to whom correspondence should be addressed.

‡ Present address: Tianjin College of Commerce.

§ Visiting scholar: Tianjin Second Medical College, Tianjin P.R.C.

absolute ethanol and ether several times and dried *in vacuo*.

All the analytical data of the complexes are collected in Table 1.

Measurements

Elemental analyses for carbon, hydrogen and nitrogen were performed with a Perkin–Elmer elemental analyser Model 240. The metal contents were determined by EDTA titration.[14] The IR spectra were recorded with an IR-408 IR spectrophotometer on KBr discs. The electronic spectra (DMF solution) were measured on a Perkin–Elmer Hitachi-240 spectrophotometer. Molar conductances were measured with a DDS-11A conductometer. Variable-temperature magnetic susceptibilities (4–300 K) were performed at the Institute of Physics, Chinese Academy of Sciences, using the vibrating sample magnetometer CF-1 (sensitivity $m = 10^{-4}$ emu). Diamagnetic corrections were made with Pascal's constants[15] for all the constituent atoms and the magnetic moments were calculated by the equation $\mu_{eff} = 2.828(XT)^{1/2}$. The ESR spectra were measured with JES-FEIXG ESR-apparatus using *X*-band.

RESULTS AND DISCUSSION

General characterization

Elemental analyses have indicated that the reaction of Cu(oxae) with $Ln(ClO_4)_3 \cdot 6H_2O$ (Ln = La, Nd, Gd, Tb, Dy, Ho, Er) yielded the heterotetranuclear complexes $Cu_3Ln(oxae)_3(ClO_4)_3$. The presumed coordination environment of the complexes is shown in Fig. 1. For all the $Cu_3Ln(oxae)_3(ClO_4)_3$ complexes, the molar conductance values (see Table 2) fall in the expected range for 1:2 electrolytes,[16] which indicates that the two perchlorate anions are outside and only one perchlorate anion is inside the coordination sphere. The significant bands from the IR spectra for the complexes are collected in Table 2. It is noted that the carbonyl stretching vibration of the mononuclear fragment Cu(oxae) at 1615 cm^{-1} was con-

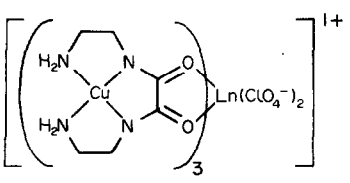

Fig. 1. Coordination environment of the complexes.

Table 1. Elemental analysis, yield and m.p. data of the complexes

Complexes	Colour	Yield (%)	m.p. (°C)	Found (%) C	H	N	Cu	Ln	Calc. (%) C	H	N	Cu	Ln
(1) $Cu_3Gd(oxae)_3(ClO_4)_3 \cdot H_2O$	Violet–red	58.5	312	18.3	3.2	14.1	16.1	13.3	18.3	3.2	14.2	16.1	13.3
(2) $Cu_3Nd(oxae)_3(ClO_4)_3 \cdot 2H_2O$	Purple–brown	59.6	345	18.1	3.4	14.1	16.1	12.1	18.2	3.4	14.2	16.1	12.2
(3) $Cu_3Tb(oxae)_3(ClO_4)_3 \cdot 3H_2O$	Purple	58.2	331	17.7	3.5	13.8	15.6	13.1	17.7	3.5	14.0	15.6	13.0
(4) $Cu_3La(oxae)_3(ClO_4)_3$	Violet	61.5	329	18.9	3.2	14.6	16.7	12.2	18.9	3.2	14.7	16.7	12.1
(5) $Cu_3Dy(oxae)_3(ClO_4)_3$	Violet–red	60.2	348	18.5	3.1	14.4	16.4	13.8	18.5	3.1	14.4	16.3	13.9
(6) $Cu_3Er(oxae)_3(ClO_4)_3$	Violet–red	59.5	325	18.4	3.1	14.3	16.3	14.3	18.4	3.1	14.3	16.2	14.5
(7) $Cu_3Ho(oxae)_3(ClO_4)_3$	Light purple	59.8	337	18.4	3.1	14.4	16.3	14.1	18.5	3.1	14.4	16.3	14.1

Table 2. Physical data for the complexes

Complex	Λ_M (Ω^{-1} cm^2 mol^{-1})	IR (cm^{-1}) —NH_2	C=O	ClO_4^-	UV ($\times 10^3$ cm^{-1})
Cu(oxae)		3250	1615		18.7
$Cu_3Gd(oxae)_3(ClO_4)_3 \cdot H_2O$	130	3250	1650	1100	18.5
$Cu_3Nd(oxae)_3(ClO_4)_3 \cdot 2H_2O$	138	3250	1650	1100	18.5, 13.6
$Cu_3Tb(oxae)_3(ClO_4)_3 \cdot 3H_2O$	160	3250	1650	1100	18.4, 22.3
$Cu_3La(oxae)_3(ClO_4)_3$	160	3250	1650	1100	18.4
$Cu_3Dy(oxae)_3(ClO_4)_3$	160	3250	1650	1100	18.3, 23.5
$Cu_3Er(oxae)_3(ClO_4)_3$	140	3250	1650	1100	18.4
$Cu_3Ho(oxae)_3(ClO_4)_3$	158	3250	1650	1100	18.4

siderably shifted towards higher frequencies in their tetranuclear complexes. It is likely that the bond order of C=O in the tetranuclear complexes is higher than that in the corresponding mononuclear complex Cu(oxae). This shift has often been used as definite proof of an oxamido-bridge.[17,18] On the other hand, the C=O deformation at 720 cm^{-1} of the Cu(oxae) complex disappeared in the spectra of the tetranuclear complexes. This fact may be attributed to the coordination of the carbonyl oxygen to the lanthanide(III) ions.[19] In addition, the —NH_2 vibration at 3250 cm^{-1} for Cu(oxae) was present for all the complexes and the splitting bands were observed at 1100 cm^{-1}, which are typical for the coordinated perchlorate ions.[17] This is consistent with the measured conductance data. The absorption maxima of the ligand field band due to copper(II) ions are summarized in Table 2. The electronic spectra show a band at (18.3–18.5) $\times 10^3$ cm^{-1} for all the tetranuclear complexes. The frequency is lower than that for the mononuclear copper complex (18.7 $\times 10^3$ cm^{-1}). Such a red shift of the *d–d* band may be attributed to the decreased planarity of the [CuN_4] chromophore on forming a tetranuclear complex with a lanthanide ion.[20] In addition, the band at 13,600 cm^{-1} for $Cu_3Nd(oxae)_3(ClO_4)_3 \cdot 2H_2O$ is assigned to the $^4I_{9/2} \rightarrow {}^4F_{7/2}$ hypersensitive transition of Nd^{III}, the band at 22,300 cm^{-1} for $Cu_3Tb(oxae)_3 \cdot (ClO_4)_3 \cdot 3H_2O$ to the $^7F_6 \rightarrow {}^5D_4$ hypersensitive transition of Tb^{III} and the band at 23,500 cm^{-1} for $Cu_3Dy(oxae)_3(ClO_4)_3$ to the $^6H_{15/2} \rightarrow {}^6F_{5/2}$ hypersensitive transition of Dy^{III}.[21]

Spin-exchange interaction of $Cu_3Gd(oxae)_3(ClO_4)_3 \cdot H_2O$

The temperature dependence of the magnetic susceptibility and magnetic moment for $Cu_3Gd(oxae)_3(ClO_4)_3 \cdot H_2O$ are shown in Fig. 2. The reason for the choice of gadolinium is the relative simplicity of its magnetic properties, which do not show large anisotropy effects as other lanthanides do. Gadolinium(III) is an f^7 ion; its ground state is $^8S_{7/2}$. Since the excited states are relatively high in energy, the zero-field splitting in the ground state

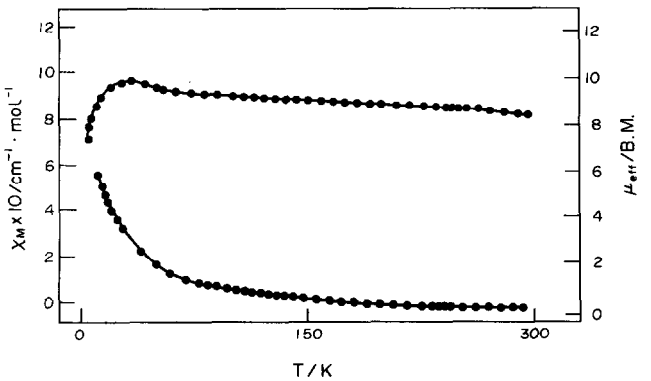

Fig. 2. Variable-temperature magnetic susceptibility and magnetic moment data for $Cu_3(oxae)_3Gd(ClO_4)_3 \cdot H_2O$; ··· experiment data and — — — calculated curves as described in the text.

is fairly small, so that $s = 7/2$ is a good quantum number.[22] From Fig. 2 it is noted that the effective magnetic moments increased with a decrease in temperature. This suggests a weakly ferromagnetic spin-exchange interaction between Cu^{II} and Gd^{III} ions.

In order to understand quantitatively the properties of spin-exchange interactions, the magnetic susceptibility expression for the Cu_3Gd system was derived by an extension of Kambe's approach.[23] The Hamiltonian expression for this system is given by:

$$\hat{H} = -2J(\hat{S}_1\hat{S}_0 + \hat{S}_2\hat{S}_0 + \hat{S}_3\hat{S}_0), \qquad (1)$$

where J is the exchange integral between Gd^{III} and Cu^{II}. The magnetic susceptibility and effective moment data were very successfully simulated by eq. (2), based on the Heisenberg model:

$$X_M = \frac{Ng^2\beta^2}{kT}\{[110\exp(24y) + 60\exp(14y) + 28\exp(6y) + 120\exp(17y) + 56\exp(9y) + 10]/[11\exp(24y) + 9\exp(14y) + 7\exp(6y) + 18\exp(17y) + 14\exp(9y) + 5]\} \qquad (2)$$

where, $y = J/kT$, X_M is the molecular susceptibility and the other symbols have their usual meanings. As shown in Fig. 2, good fits to the experimental data were obtained for $J = 2.72$ cm^{-1} and $g = 1.996$. The agreement factor F, defined here as $F = \Sigma[(X_M)_{obs} - (X_M)_{calc}]^2/\Sigma(X_M)_{obs}$, is then equal to 3×10^{-5}. The positive sign of J corresponds to a ferromagnetic Gd^{III}–Cu^{II} interaction. The small J value indicates a weak ferromagnetic spin-exchange interaction between Gd^{III} and Cu^{II} ions. This may account for the fact that the 4*f*-electrons are shielded by the outer shell electrons.[20]

We also previously investigated the magnetic behaviour of $Cu_3Gd(oxpn)_3(NO_3)_3$[11] [oxpn = N,N′-bis(3-aminopropyl)oxamido] and observed antiferromagnetic coupling between the Gd^{III} and Cu^{II} ions in this complex.

The two complexes $Cu_3Gd(oxpn)_3(NO_3)_3$ and $Cu_3Gd(oxae)_3(ClO_4)_3$ have essentially the same skeletal structure and their IR and electronic spectra are also similar. The main difference between $Cu_3Gd(oxpn)_3(NO_3)_3$ and $Cu_3Gd(oxae)_3(ClO_4)_3$ is that the chelate ring around the copper(II) consists 6–5–6 members in the former case and 5–5–5 members in the latter. The essential difference between the sign of the exchange parameter J in the two complexes indicates that the chelate ring arrangement may affect the nature of the exchange interaction. We have no reasonable explanation for this behaviour. Indeed, further investigations on these and similar systems are still required in order to obtain a reasonable explanation and are in progress.

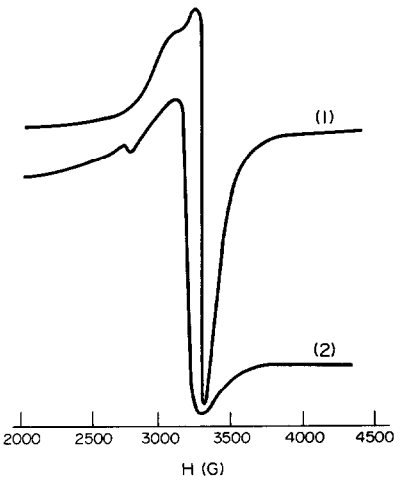

Fig. 3. *X*-band powder ESR spectra of (1) $Cu_3(oxae)_3$ and (2) $Cu_3Gd(oxae)_3(ClO_4)_3 \cdot H_2O$ at room temperature.

ESR spectra

The *X*-band powder ESR spectra at room temperature for $Cu_3Gd(oxae)_3(ClO_4)_3$ and Cu(oxae) are shown in Fig. 3. The spectra of the former are obviously different from that of the latter and exhibit a broad band, which also indicates a magnetic spin-exchange interaction between Gd^{III} and three Cu^{II} ions. According to Kambe's approach,[23] the four spins $S_{Gd} = 7/2$, $S_{Cu(1)} = S_{Cu(2)} = S_{Cu(3)} = 1/2$ coupled to yield the total spin state of one $S = 5$, three $S = 4$, three $S = 3$, one $S = 2$ and one $S = 1$. On the basis of Boltzmann's distribution all these states are in a thermal population at room temperature owing to very weak interactions ($J = 2.72$ cm^{-1}). Thus, the asymmetric broad signals may be ascribed to complexes in these spin states.

Acknowledgement—This project was supported by the National Natural Science Foundation of China.

REFERENCES

1. R. D. Willett, D. Gattesch and O. Kahn (Eds), *Magneto-Structural Correlations in Exchange Coupled Systems*, p. 523. D. Reidel, Dordrecht, Holland (1985).
2. L. C. Li, D. Z. Liao and G. L. Wang, *J. Struct. Chem. (Jiegou Huaxue)* 1991, **10**, 89.
3. D. Z. Liao, L. C. Li, Z. H. Jiang, S. P. Yan, P. Cheng and G. L. Wang, *Trans. Met. Chem.* 1992, **17**, 359.
4. D. Z. Liao, L. C. Li and G. L. Wang, *Polyhedron* 1991, **10**, 1785.

5. D. Z. Liao, B. Lin and G. L. Wang, *Acta Chim. Sin.* 1992, **50**, 269.
6. Z. M. Liu, Z. H. Jiang, D. Z. Liao, G. L. Wang, X. K. Yao and H. G. Wang, *Acta Chim. Sin.* 1991, **49**, 981.
7. Z. Y. Zhang, D. Z. Liao, Z. H. Jiang, S. Q. Hao, X. K. Yao, H. G. Wang and G. L. Wang, *Inorg. Chim. Acta* 1990, **173**, 201.
8. Z. M. Liu, D. Z. Liao, Z. H. Jiang and G. L. Wang, *Synth. React. Inorg. Met.-Org. Chem.* 1991, **21**, 289.
9. O. Guillou, P. Bergernt, O. Kahn, E. Bakalbassis, K. Boubekeur, P. Bataol and M. Guillot, *Inorg. Chem.* 1992, **31**, 110.
10. O. Guillou, O. Kahn, R. L. Oushoorn, K. Boubekeur and P. Batail, *Inorg. Chim. Acta* 1992, **119**, 198.
11. Z. M. Liu, D. Z. Liao, Z. H. Jiang, S. P. Yan and G. L. Wang, *Synth. React. Inorg. Met.-Org. Chem.* 1992, **22**, 1507.
12. J. R. Bethrendt and S. K. Madan, *J. Inorg. Nucl. Chem.* 1950, **20**, 195.
13. H. Ojima and K. Yamada, *Nippon Kaishi* 1968, **89**, 490.
14. J. J. Kinnunen and B. Wennerstrand, *Chem. Anal.* 1955, **44**, 33; G. W. C. Milner and J. W. Edwards, *Anal. Chim. Acta* 1958, **18**, 513.
15. P. W. Selwood, *Magnetochemistry*, pp. 78–91. Interscience, New York (1956).
16. W. J. Geary, *Coord. Chem. Rev.* 1971, **7**, 81.
17. W. Radecka-Paryzek, *Inorg. Chim. Acta* 1979, **34**, 5.
18. D. Z. Liao, L. C. Li and G. L. Wang, *Chin. J. Chem.* 1991, **9**, 410.
19. E. Lioret, Y. Jourmaux and M. Julve, *Inorg. Chem.* 1990, **29**, 3967.
20. M. Sakamoto, M. Takagi, T. Ishgimori and H. Okawa, *Bull. Chem. Soc. Japan* 1988, **61**, 1613.
21. A. M. Hamer and S. E. Livingstone, *Trans. Met. Chem.* 1983, **8**, 298.
22. A. Bencini, C. Benelli, A. Dei and D. Gatteschi, *Inorg. Chem.* 1985, **24**, 695.
23. K. Kambé, *J. Phys. Soc. Japan* 1950, **5**, 48.

Polyhedron Vol. 12, No. 23, pp. 2787–2789, 1993
Printed in Great Britain

0277–5387/93 $6.00+.00
© 1993 Pergamon Press Ltd

NOVEL STRUCTURE OF NICKEL(II) COMPLEX Ni(phth)(bpy)$(H_2O)_3$ ($phth^{2-}$ = THE DIANION OF PHTHALIC ACID; bpy = 2,2′-BIPYRIDINE)

FENG-CUN XUE,* ZONG-HUI JIANG, DAI-ZHENG LIAO, SHU-LIN MA,† SHI-PING YAN and GENG-LIN WANG‡

Department of Chemistry, Nankai University, Tianjin, P.R.C.

and

XIN-KAN YAO and RU-JI WANG

Central Laboratory, Nankai University, Tianjin, P.R.C.

(*Received* 23 *March* 1993; *accepted* 25 *June* 1993)

Abstract—In the title compound the coordination environment around nickel(II) is an octahedron composed of atoms N(1) and N(2) of 2,2′-bipyridine, O(5), O(6) and O(7) of three aquamolecules and O(3) of one carboxyl of the phthalate. The oxygen, O(1), of the other carboxyl of the phthalate does not coordinate to nickel(II). There is an electrostatic interaction between the negative ion of this carboxyl and the nickel(II) positive ion.

The phthalato ion is a bridging ligand and several binuclear and multinuclear complexes with phthalato bridges have been prepared in our laboratory.[1,2] In these complexes the phthalato bridges are in a bidentate coordination. However, to our knowledge no mononuclear nickel(II) complex with the phthalato ligand in a unidentate coordination has been reported. In this paper we report on the novel structure of a mononuclear nickel(II) complex, Ni(phth)(bpy)$(H_2O)_3$ ($phth^{2-}$ is the dianion of phthalic acid and bpy is 2,2′-bipyridine).

EXPERIMENTAL

Synthesis of Ni(phth)(bpy)$(H_2O)_3$

To $Ni(ClO_4)_2 \cdot 6H_2O$ (146 mg) stirred in ethanol (4 cm^3) was successively added a solution of the piperidinium phthalate (202 mg) in ethanol (6 cm^3) and bpy (62 mg) in ethanol (4 cm^3). After stirring for 10 h at room temperature, the solution was filtered and washed with water. The purple–blue filtrate was left for 3 days at room temperature. The blue crystals of the title complex, Ni(phth)(bpy)$(H_2O)_3$, were grown from an aqueous ethanol solution under vaporization.

X-ray diffraction of the title complex

Crystal data: $C_{20}H_{26}N_2NiO_9$, $Mr = 497.15$, triclinic, space group $P\bar{1}$, $a = 7.732(1)$, $b = 11.645(3)$, $c = 13.600(3)$ Å, $\alpha = 74.66(2)$, $\beta = 71.98(2)$, $\gamma = 73.11(2)°$, $V = 1093.5$ Å^3, $Z = 2$, $D_x = 1.51$ g cm^{-3}, $\mu = 9.41$ cm^{-1}, $F(000) = 520$. A total of 3192 reflections were collected with a single crystal of the dimensions $0.25 \times 0.3 \times 0.3$ mm on a CAD4 diffractometer with graphite monochromatized Mo-K_α ($\lambda = 0.71073$ Å) radiation using the ω–2θ scan mode in the range $2° \leqslant \theta \leqslant 25°$ at room temperature. Data were corrected for Lp factors and 2420 observed reflections [$I \geqslant 3\sigma(I)$] were used for the structure solution and refinement.

The structure of the complex was obtained by direct methods (MULTAN 82). The nickel atom was located from an E-map. The other non-hydrogen atoms were determined from successive difference-Fourier syntheses. The positions of the hydro-

* Visiting scholar: Hunan Normal University.
† Visiting scholar: Tianjin College of Commerce.
‡ Author to whom correspondence should be addressed.

Table 1. Selected bond lengths (Å) and angles (°)

Ni—O(3)	2.045(1)	Ni—O(7)	2.068(1)
Ni—O(5)	2.128(1)	Ni—N(1)	2.053(2)
Ni—O(6)	2.087(1)	Ni—N(2)	2.059(1)
O(3)—Ni—O(5)	87.71(4)	O(5)—Ni—N(2)	89.73(6)
O(3)—Ni—O(6)	93.24(4)	O(6)—Ni—O(7)	89.22(5)
O(3)—Ni—O(7)	87.30(5)	O(6)—Ni—N(1)	90.48(5)
O(3)—Ni—N(1)	93.36(6)	O(6)—Ni—N(2)	89.66(5)
O(3)—Ni—N(2)	172.37(5)	O(7)—Ni—N(1)	179.28(6)
O(5)—Ni—O(6)	177.30(6)	O(7)—Ni—N(2)	99.81(5)
O(5)—Ni—O(7)	88.29(4)	N(1)—Ni—N(2)	79.54(6)
O(5)—Ni—N(1)	92.00(5)		

Table 2. Least-squares plane data

Orthonormal equation of plane	$-0.6154(9)x+0.280(1)y-0.7369(8)z+9.695(8)=0$			
Atoms in the plane	O(5)	O(6)	O(7)	N(1)
Distance (Å)	0.0039	0.0040	−0.0040	−0.0039
Other atoms	Ni	O(3)	N(2)	
Distance (Å)	−0.0157	−2.0554	2.0110	

gen atoms of the phenyl and 2,2′-bipyridyl groups were calculated theoretically. The final refinement for the coordinates and anisotropic thermal parameters of all the non-hydrogen atoms and the isotropic thermal parameters of the hydrogen atoms by full-matrix least-squares methods converged to an unweighted R of 0.057 and a weighted R_w of 0.055 with $w = \exp[20*(\sin\theta/\lambda)^2]$.[3] The highest peak in the final difference-Fourier map had a height of 0.7 e Å^{-3}. All of the calculations were performed on a PDP 11/44 computer with the SDP software package.

Selected bond lengths and angles are given in Table 1 and the perspective view of the molecule is shown in Fig. 1.

RESULTS AND DISCUSSION

The coordination environment around nickel(II) is a distorted octahedron. The nickel atom lies generally in the least-squares plane composed of the atoms N(1), O(5), O(6) and O(7) (see Table 2). The other nitrogen atom of bpy, N(2) and O(3) of one carboxyl of the phthalate are in the axial positions. The axis does not show much distortion from linearity, N(2)—Ni—O(3)

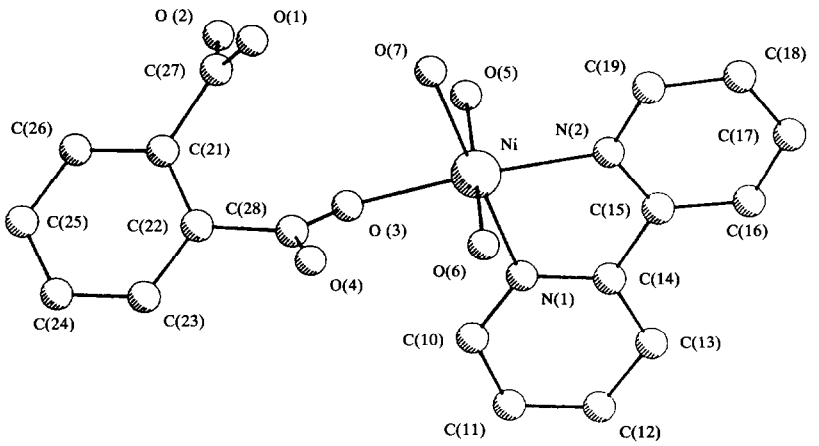

Fig. 1. A perspective view of the complex Ni(phth)(bpy)$(H_2O)_3$.

being 172.37(5)°. The nickel–nitrogen and nickel–oxygen [except O(5)] distances are almost equivalent [Ni—N(1) = 2.053(2), Ni—N(2) = 2.059(1), Ni—O(3) = 2.045(1), Ni—O(6) = 2.087(1), Ni—O(7) = 2.068(1) Å] and are shorter than the Ni—O(5) distance [Ni—O(5) = 2.128(1)]. Phthalic acid has two univalent negative "arms". It is a good bridging ligand which links with two metal ions via its two "arms".[2] In the present mononuclear complex an unstable seven-membered ring would be formed if phthalate chelated one nickel ion. Therefore, the novel structure of the present complex was obtained (Fig. 1). Only O(3) of one carboxyl group of the phalate coordinates to the nickel ion; O(1) of the other carboxyl group of the phthalate does not coordinate and we presume there is an electrostatic interaction between the negative ion of this carboxyl and the nickel ion. Three water molecules coordinate to nickel(II) to form an octahedral six-coordination environment.

REFERENCES

1. S.-L. Ma, D.-Z. Liao, Z.-H. Jiang, S.-P. Yan, F.-C. Xue and G.-L. Wang, *Synth. Rect. Inorg. Met.-Org. Chem.*, in press.
2. Z.-H. Jiang, S.-L. Ma, D.-Z. Liao, S.-P. Yan and G.-L. Wang, *J. Chem. Soc., Chem. Commun.* 1993, 745.
3. J. D. Dunitz and P. Seiler, *Acta Cryst., Sect. B* 1975, **29**, 589.

Polyhedron Vol. 12, No. 23, pp. 2791–2799, 1993
Printed in Great Britain

0277–5387/93 $6.00+.00
© 1993 Pergamon Press Ltd

COMPLEXES OF MOLYBDENUM(V) AND MOLYBDENUM(IV) WITH DITHIOCARBAMATES DERIVED FROM α-AMINO ACIDS. REACTION KINETICS IN ORGANIC SOLVENTS

BENIGNO MACIAS,† JULIO J. CRIADO and MARIA V. VILLA

Departamento de Química Inorgánica, Facultad de Farmacia, Avda. Campo Charro s.n., Universidad de Salamanca, 37007-Salamanca, Spain

and

LICESIO J. RODRIGUEZ

Departamento de Química Física, Facultad de Farmacia, Universidad de Salamanca, Spain

and

MANUEL CASTILLO

Departamento de Química Inorgánica, Facultad de Químicas, Universidad de Sevilla, Spain

(*Received* 23 *March* 1993; *accepted* 25 *June* 1993)

Abstract—The reaction between dithiocarbamate derivatives of α-amino acids (glycine, alanine, α-amino-butyric acid, norvaline, valine, norleucine, leucine and isoleucine) and sodium molybdate in acid medium leads to the formation of molybdenum(V) complexes with the general formula $[Mo_2O_3(dtc\ a.a.)_4]\cdot 2H_2O$ (a.a. = amino acid). The complexes were characterized by elemental analysis, FT-IR and uv–vis spectroscopies and XPS. They are binuclear complexes with a linear oxygen bridge, the dithiocarbamate moiety acting as a bidentate ligand and thus yielding a distorted octahedral coordination for the metal cation. In organic solvents, these compounds undergo a chemical transformation, yielding complexes with the general formula $[MoO(dtc\ a.a.)_2]$, whose synthesis is also described. These complexes were characterized using the same experimental techniques as above. The kinetics of transformation in organic media were studied, proposing a multi-step reaction mechanism, and the rate constants have also been determined.

Molybdenum is an essential trace element in living organisms, existing in active sites of molybdoenzymes, proteins which act on redox reactions. The study of the actual state (coordination geometry, oxidation state, etc.) of molybdenum in enzymes, as well as the mechanism followed by the reactions where these enzymes act, has attracted the attention of many researchers, mainly with a view to understanding the role played by molybdenum in these processes. Generally speaking, this type of work has been aimed in two directions: the study of the chemical environment of the molybdenum cations, through a direct study of molybdoenzymes using different analytical techniques (mainly EXAFS and EPR), and the synthesis and characterization of model compounds. For oxoenzymes it has been found that molybdenum cations are directly bonded to oxygen and sulphur atoms,[1,2] thus, most model compounds synthesized correspond to coordination compounds where the donor atoms are sulphur or oxygen.[2,3] On the other hand, an EPR signal characteristic of molybdenum(V) species has been recorded along the catalytic process, suggesting that a mononuclear complex of molybdenum(V) might be the active site in molybdo-

† Author to whom correspondence should be addressed.

enzymes since this signal is not recorded for binuclear complexes. In addition, binuclear molybdenum(V) complexes are rather stable and, therefore, only evolve to the +4 oxidation state with difficulty. This is the state shown by molybdenum in the reduced state of molybdoenzymes. For these reasons, a great deal of effort has been directed towards the synthesis of model compounds of molybdenum(V) with bulky ligands in order to avoid dimerization.[4-6] However, many binuclear complexes have been synthesized which are also able to participate in two-electron redox processes, similar to those found for molybdoenzymes and those with dithiocarbamate ligands.[3,4,7,8] Nevertheless, the organic chain linked to the dithiocarbamate moiety is also a hydrocarbon chain, despite the fact that in molybdoenzymes these are amino acid chains. In the light of this, in the present work a series of complexes was synthesized and characterized, using as ligands dithiocarbamate derivatives of α-amino acids, with the general formula:

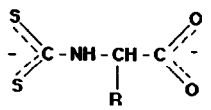

where R = H, glycine (gly); —CH_3, alanine (ala); —CH_2—CH_3, α-aminobutyric acid (α-ambut); —CH_2—CH_2—CH_3, norvaline (norval); —CH—$(CH_3)_2$, valine (val); —CH_2—CH_2—CH_2—CH_3, norleucine (norleu); —CH_2—CH—$(CH_3)_2$, leucine (leu); —CH—(CH_2—CH_3)(CH_3), isoleucine (isoleu). Our aim was to study the role played by the lateral chain in the amino acid on the donor properties of the dithiocarbamate ligand. Moreover, the presence of the carboxylate group may elicit important changes in the properties of the molecule, mainly with respect to the solubility of the compounds in polar solvents.

As described below, these ligands are readily prepared by reaction between the amino acid and carbon sulphide in basic medium, as described elsewhere.[9,10]

EXPERIMENTAL

Materials

All starting amino acids were in the DL form (except glycine) from Fluka; carbon sulphide and $Na_2MoO_4 \cdot 2H_2O$ were also from Fluka (p.a.). $MoO_2(acac)_2$ was from Aldrich and the organic solvents—acetone, absolute ethanol, diethyl ether, methanol and dimethyl formamide (DMF)—were from Carlo Erba (R.P.E.).

Physical measurements

Chemical analyses for carbon, hydrogen and nitrogen were performed on a 2400 elemental analyser from Perkin–Elmer, while sulphur was analysed in the CSIC laboratories (Barcelona, Spain). Molybdenum was determined on an I.C.P. spectrometer, Perkin–Elmer, model 2380 Plasma 2. The magnetic susceptibilities of the solids were determined following the Gouy method on a Stanton MC-5 microbalance, using $Hg[Co(SCN)_4]$ as a reference. FT-IR spectra were recorded in the 4000–275 cm^{-1} range on a Perkin–Elmer FT-IR 1730 instrument, coupled to a Perkin–Elmer 3600 Data Station by the KBr pellet technique. Electronic spectra were recorded on a Shidmazu UV-240 double beam spectrophotometer with an integrating sphere for solid samples, using MgO as a reference. The kinetics of transformation of the complexes in different organic solvents were studied using a Hitachi 150–20 spectrophotometer at 25°C. X-ray photoelectron spectra were recorded using Leybold–Heraeus LHS-10 apparatus, with Al-K_α radiation, at an intensity of 20 mA, under a pressure of 10^{-9} torr and using the C1*s* peak at 284.6 eV as a reference.

Preparation of the complexes

$[Mo_2O_3(dtc\ a.a.)_4] \cdot 2H_2O$ *complexes.* This series of compounds was prepared by direct reaction between sodium molybdate and the dithiocarbamate derivative of the corresponding α-amino acid. A fresh aqueous solution obtained by dissolving the sodium salt of the dithiocarbamate derivative of α-amino acid (8.8×10^{-3} mol, 10 cm^3) was slowly dropped into a vigorously stirred solution containing $Na_2MoO_4 \cdot 2H_2O$ (4.4×10^{-3} mol) in HCl (6 M, 10 cm^3). With long-chain amino acids a dark brown precipitate was formed. This was filtered, washed with doubly-distilled water and dried over P_2O_5. With the derivatives of glycine and alanine, however, cooling of the solution in an ice–salt freezing mixture was needed to attain precipitation of the complexes. The dark brown solids thus obtained were almost insoluble in water, but dissolved in organic solvents such as methanol, acetone and DMF. The data from the chemical analyses agree with the general formula $[Mo_2O_3(dtc\ a.a.)_4] \cdot 2H_2O$. The yield was *ca* 40% for compounds prepared with long-chain amino acids, but lower for those with shorter lateral chains.

The same compounds were also prepared starting from molybdenum(VI) acetylacetonate: $MoO_2(acac)_2$ (0.002 mol) was dissolved in methanol (10 cm^3) and doubly-distilled water (10 cm^3). The

solution was filtered and cooled at 0°C and then HNO_3 (1 M) was added until pH = 4.5–5 was reached. Another solution (also maintained at 0°C with a freezing mixture) containing the dithiocarbamate derivative (0.0015 mol in 10 cm^3 doubly-distilled water) was added to the former solution. A purple solution was formed immediately, giving rise to dark brown precipitates. When washed with water and dried over P_2O_5 these compounds were identical to those prepared following the above-described method. However, the yield was only 25–30%, depending on the length of the lateral chain.

[MoO(dtc a.a.)$_2$] *complexes.* Sodium molybdate (0.004 mol in 10 cm^3 doubly-distilled water) was added to the sodium salt of the dithiocarbamate derivative of the α-amino acid (0.008 mol, 25 cm^3) in a 500 cm^3 separation funnel. Diethyl-ether (50 cm^3) was then added to the separation funnel and portions of HCl (0.1 M, 5 cm^3) were then added. A violet precipitate was formed, which dissolved in the organic layer, giving rise to a green solution as more HCl (0.1 M) was added and the funnel vigorously shaken. After the addition of *ca* 40 cm^3 of the acid solution, the two phases separated and the evaporation of ether from the organic layer yielded a microcrystalline dark green powder. In this process, it is important that the ether should be added before the addition of the hydrochloric acid in order to avoid decomposition of the products formed. The chemical analyses for these solids are in agreement with the general formula [MoO(dtc a.a.)$_2$], although a slight excess of carbon and hydrogen suggests the presence of small amounts of ether, which is difficult to completely eliminate; yield 15–20%.

RESULTS AND DISCUSSION

Synthetic aspects and general characterization

Reaction of molybdenum(VI) with dithiocarbamates derived from α-amino acids in a medium of HCl (6 M) leads to a reduction of the metallic cation to molybdenum(V), probably according to the following reaction:

$$2Na_2MoO_4 + 6Na_2[SSC{-}NH{-}CH(R){-}COO] + 16HCl \rightarrow [Mo_2O_3(dtc\ a.a.)_4] + [HOOC{-}CH(R){-}NH{-}CS_2]_2 + 16NaCl + 5H_2O.$$

According to this reaction, one third of the dithiocarbamate is used to reduce molybdenum(VI) to molybdenum(V), probably accounting for the low yield achieved in this reaction. The formation of the disulphide has been confirmed experimentally, especially with the short-length derivatives, where a white crystalline powder is formed whose chemical analyses coincide with the percentages for this compound. The disulphide is also characterized by a strong IR band at 1250 cm^{-1} due to the C=S stretching mode, in addition to other bands characteristic of this substance.

Such a reduction of molybdenum(VI) species has been previously reported in the literature with some dialkyldithiocarbamates and also with alkylxanthates.[11] However, as our original aim was to synthesize molybdenum complexes in the three highest oxidation states of the element, we attempted to prepare molybdenum(VI) complexes by ligand substitution in $MoO_2(acac)_2$. The results were negative: in a neutral medium the ligands are not substituted and in an acidic medium molybdenum(VI) species are reduced, giving rise to the same compounds obtained using the former method.

In any case, the complexes are rather unstable in acidic solution, transforming to green compounds; this transformation was also observed in organic solvents. The above-described method, consisting of extracting the compound in diethyl-ether and a rapid removal of this solvent, allows the preparation of the compounds without decomposition. Unfortunately, due to this lack of stability, neither of the groups of complexes could be obtained in the crystalline state and hence the molecular structure could not be determined by X-ray diffraction. Electroanalytical methods such as cyclic voltammetry were also assayed, but non-reproducible curves were obtained, due to decomposition in solution during measurement.

It should be mentioned that all the compounds prepared are diamagnetic, a behaviour characteristic of binuclear molybdenum(V) compounds with a linear oxo bridge (Mo—O—Mo) and of oxomolybdenum(IV) complexes (d^2 configuration).

IR spectra

The positions of the most relevant bands recorded in the spectra of these compounds are given in Table 1. The band due to the C—N stretching is recorded between 1542 and 1500 cm^{-1}, indicating the double bond character already reported for dithiocarbamate complexes.[12] For the compounds prepared by extraction in ether, the bands are slightly shifted towards lower wave numbers, in agreement with the lower oxidation state of molybdenum in these compounds.[13,14] Contrary to the behaviour found with dialkyldithiocarbamate derivatives,[15] no steady change in the position of

Table 1. Proposed assignments for selected vibrational frequencies (cm^{-1}) in molybdenum complexes

	ν(C—N)	ν(N—H)	ν(C=O)	ν(C—O)+δ(O—H)	ν(Mo=O)	ν(Mo—O—Mo)	ν(S—Mo)
$[Mo_2O_3(dtc\ gly)_4]$	1542(vs)	3215(m)	1724(s)	1386(s), 1227(m)	939(s)	707(m)	358(m)
$[Mo_2O_3(dtc\ ala)_4]$	1538(vs)	3192(m)	1724(s)	1407(s), 1231(m)	938(m)	712(m)	358(w)
$[Mo_2O_3(dtc\ \alpha\text{-ambut})_4]$	1526(vs)	3206(m)	1723(s)	1408(s), 1253(m)	942(m)	707(m)	353(w)
$[Mo_2O_3(dtc\ norval)_4]$	1533(vs)	3192(m)	1723(s)	1412(s), 1238(m)	943(m)	737(m)	372(w)
$[Mo_2O_3(dtc\ val)_4]$	1525(vs)	3184(m)	1723(s)	1396(s), 1258(m)	943(m)	722(m)	391(w)
$[Mo_2O_3(dtc\ norleu)_4]$	1526(vs)	3188(m)	1723(s)	1411(s), 1224(m)	942(m)	729(m)	370(w)
$[Mo_2O_3(dtc\ leu)_4]$	1532(vs)	3190(m)	1724(s)	1409(s), 1242(m)	951(m)	726(m)	382(m)
$[Mo_2O_3(dtc\ isoleu)_4]$	1525(vs)	3198(m)	1719(s)	1413(s), 1250(m)	945(m)	728(m)	408(w)
$[MoO(dtc\ gly)_2]$	1515(vs)	3232(m)	1723(vs)	1395(s), 1225(m)	941(s)	—	353(m)
$[MoO(dtc\ ala)_2]$	1526(vs)	3221(m)	1719(vs)	1404(s), 1227(m)	968(s)	—	356(m)
$[MoO(dtc\ \alpha\text{-ambut})_2]$	1525(vs)	3203(m)	1719(vs)	1411(s), 1251(m)	973(s)	—	357(w)
$[MoO(dtc\ norval)_2]$	1505(vs)	3221(m)	1719(vs)	1411(s), 1236(m)	961(m)	—	371(w)
$[MoO(dtc\ val)_2]$	1510(vs)	3206(m)	1719(vs)	1394(s), 1261(m)	969(m)	—	394(w)
$[MoO(dtc\ norleu)_2]$	1505(vs)	3202(m)	1719(vs)	1407(s), 1223(m)	962(m)	—	355(w)
$[MoO(dtc\ leu)_2]$	1531(vs)	3191(m)	1719(vs)	1395(s), 1238(m)	971(s)	—	386(m)
$[MoO(dtc\ isoleu)_2]$	1500(vs)	3206(m)	1718(vs)	1390(s), 1248(m)	970(s)	—	407(w)

vs = very strong; s = strong; m = medium; w = weak.

the bands with the length of the side-chain is observed. This might be due to the presence of a relatively heavy carboxylic group in all ligands, which masks to some extent the changes in the point masses of these chains, thus decreasing the effect of the kinematic factor. In addition, the effect of the electronic factor cannot be exactly evaluated because of the presence of both linear and branched lateral chains in the series of complexes prepared.

Bands due to C=O stretching, at 1723 cm^{-1}, and to the coupled C—O stretching and O—H in-plane deformation, at 1400 and 1250 cm^{-1}, undoubtedly indicate the presence of the uncoordinated carboxylic group in all the compounds. According to Newton *et al.*,[16,17] bands due to the Mo=O stretching mode are recorded at 965 ± 8 cm^{-1} for molybdenum(IV) complexes with the general formula $MoO(LL)_2$ and 945 ± 16 cm^{-1} for oxygen-bridged molybdenum(V) complexes with the general formula $Mo_2O_3(LL)_4$. In all complexes prepared here, the bands are recorded within these wave number margins. The band corresponding to the single Mo—O bond in the bridging region is recorded at 730–700 cm^{-1}. Also, the band corresponding to the Mo—S stretching is recorded in the expected wave number range for molybdenum complexes containing sulphur donor atoms.[18–20]

X-ray photoelectron spectroscopy

Data for the complexes studied are included in Table 2. Energies for the N_{1s} level are slightly higher than those reported for other dithiocarbamates,[21] thus suggesting, in agreement with the FT-IR data, that the canonic form:

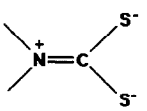

mainly contributes to the structure. Values for the S_{2p} level are high, but within the value range reported by Walton,[22] indicating the strong donor character of the sulphur atoms when bonded to the molybdenum atoms, although these values are similar to those reported for dithiocarbamate complexes of different metal cations.[23,24] As expected, Mo_{3d} values are lower for molybdenum(IV) complexes than for molybdenum(V), although the differences are not too great, as previously reported for complexes containing the S—Mo bond.[25,26]

Table 2. Binding energies (eV) of the relevant energy levels of molybdenum complexes

	$[Mo_2O_3(dtc\ a.a.)_4]$	$[MoO(dtc\ a.a.)_2]$
N_{1s}	400.0	400.1
S_{2p}	163.0	162.8
$Mo_{3d_{3/2}}$	234.1	233.7
$Mo_{3d_{5/2}}$	231.1	230.6

Electronic absorption spectra and transformation kinetics

The electronic spectra recorded for the complexes in solution were identical for a given solvent, with only very small differences due to the length of the side-chain, which slightly modifies the molar extinction coefficients (Table 3). For $[Mo_2O_3(dtc\ a.a.)_4]$ complexes, the strongest band is centred at 500 nm and can be associated with the presence of the linear Mo—O—Mo bridge, absent in binuclear complexes with two bridging oxygen atoms. Large molar extinction coefficients are also typical of this type of bridge.[11,27–29] The band at 365 nm in DMF and the shoulder close to 380 nm recorded when using acetone as a solvent must be originated by the same electronic transition, probably an S → Mo charge transfer process.[27,30] The remaining bands are deeply solvent-dependent and are probably due to electronic transitions between energy levels of the ligands. Using the diffuse reflectance technique the spectrum recorded in the solid state is very similar, indicating that the chemical environment of the molybdenum atoms would be rather similar in the solid state and in solution.

The spectra are more complicated for the $[MoO(dtc\ a.a.)_2]$ complexes. From the stoichiometry of these complexes and from data in the literature for similar compounds with the $[MoOS_4]$ moiety, it can be concluded that the geometry should be square-planar pyramidal, C_{4v}. Since the complexes are diamagnetic, from a simplistic point of view electron transitions from energy level b_2 to levels e, b_1 and a_1 would give rise to three bands in the spectrum, but the existence of electron repulsions, two-electron excitations, etc., complicates the spectrum. Thus, only the band at 585–600 nm can be ascribed to molybdenum *d–d* transitions, despite the extinction coefficient being rather high. The spectrum of the complex formed between molybdenum(IV) and diethyldithiocarbamate shows a band almost in the same position,[31] although other bands in the visible range are also expected. The shoulder at 370 nm can be ascribed to an S → Mo charge-transfer process and the remaining bands to intraligand transitions.

As mentioned above, we have observed that $[Mo_2O_3(dtc\ a.a.)_4]$ complexes are transformed to

Table 3. Electronic absorption data for molybdenum complexes

Solvent	$[Mo_2O_3(dtc\ a.a.)_4]$ λ (nm)	ε ($dm^3\ mol^{-1}\ cm^{-1}$)	Solvent	$[MoO(dtc\ a.a.)_2]$ λ (nm)	ε ($dm^3\ mol^{-1}\ cm^{-1}$)
DMF	500	1200–1400	Dimethyl-ether	590	150–250
	365	6500–7000		370(sh)	1600–1800
	270	22,000		270(sh)	8900
				245	12,200
				225(sh)	9100
Acetone	500	1300–1500	Acetone	585	180–240
	380(sh)	3500–4000		370(sh)	1200–1600
	325	6500–7000		330	2600
D.R.	510		D.R.	600	
	420(sh)			380	
	280				

D.R. = Diffuse reflectance; sh = shoulder.

$[MoO(dtc\ a.a.)_2]$, as shown by the shift of the main visible band of the former at *ca* 500 to 585 nm, characteristic of the latter complexes. This fact has been used to follow the kinetics of such a transformation. The changes are shown in Fig. 1 and these data can be used to follow the kinetics evolution, which was performed at both 500 and 585 nm. The intensity of the band at 500 nm decreases steadily (Fig. 2), while that of the band at 585 nm shows some oscillations, which complicates the analysis of such a transformation somewhat.

The change in absorbance with time [Fig. 3(a)] can be interpreted assuming that only the initial and the final species absorb at this wavelength, following first-order kinetics. In such a case

$$A - A_\infty = (A_0 - A_\infty)e^{-kt} \quad (1)$$

and then

$$\ln(A - A_\infty) = \ln(A_0 - A_\infty) - kt, \quad (2)$$

whose plot should be a straight line [Fig. 3(b)] and whose slope coincides with the rate constant. This is *ca* $1.2 \times 10^{-2}\ s^{-1}$ and does not depend on the concentration; the small differences found probably being due to the lack of stability of the dithiocarbamate derivatives in solution.

The behaviour shown by the band at 585 nm is rather more complicated. One can assume that a series of reactions occurs once the complex is dissolved, with the formation and disappearance of different intermediates whose specific absorptivities are sufficiently different for the total absorbance of

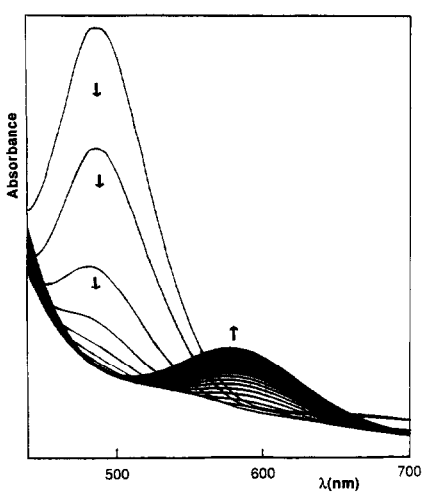

Fig. 1. UV–vis spectra showing the $[Mo_2O_3(dtc\ a.a.)_4] \rightarrow [MoO(dtc\ a.a.)_2]$ transformation. The interscan time was 1 min.

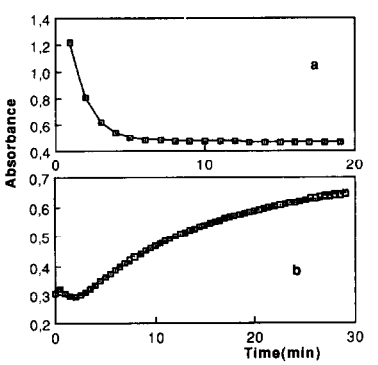

Fig. 2. Time-dependence of the absorbance of DMF solutions of $[Mo_2O_3(dtc\ a.a.)_4]$ complexes at (a) 500 and (b) 585 nm.

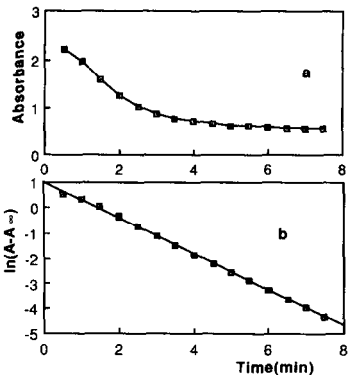

Fig. 3. (a) Time dependence of the absorbance at 500 nm of a DMF solution of the DL-norvaline complex (concentration = 1.4 g dm^{-3}). (b) Least-squares fit. The calculated equation for the straight line adjusted to the experimental data is $\ln(A-A_\infty) = 1.012-0.711t$.

the system to be subject to alternating variation. Disproportion of molybdenum(V) according to the reaction:

$$2Mo^{V} \rightarrow Mo^{VI} + Mo^{IV}$$

has been proposed for similar processes.[8,29,32] However, this does not seem to hold in this case as dithiocarbamate derivatives of α-amino acids already reduce molybdenum(VI) to molybdenum(V), which then undergoes a further reduction to molybdenum(IV) according to the reaction:

$$2Mo_2O_3(\text{dtc a.a.})_4 \rightarrow MoO(\text{dtc a.a.})_2 + MoO_2 + HOOC\text{—}CH(R)\text{—}NH\text{—}C(=S)\text{—}S\text{—}S\text{—}C(=S)\text{—}NH\text{—}CH(R)\text{—}COOH;$$

i.e. molybdenum(V) is reduced to molybdenum(IV) and the dithiocarbamate is oxidized to the disulphide. A tentative reaction scheme could be as follows:

$$Mo^{V}{}_2O_3(\text{dtc a.a.})_4 \xrightarrow{k_1} Mo^{V}{}_2O_3(\text{dtc a.a.})_2^* + 2(\text{dtc a.a.})^*$$

$$Mo^{V}{}_2O_3(\text{dtc a.a.})_2^* \xrightarrow{k_2} Mo^{VI}O_2(\text{dtc a.a.})^* + Mo^{IV}O(\text{dtc a.a.})^*$$

$$Mo^{VI}O_2(\text{dtc a.a.})^* + Mo^{IV}O(\text{dtc a.a.})^* \xrightarrow{k_3} MoO_2 + Mo^{IV}O(\text{dtc a.a.})_2$$

$$(2\text{dtc a.a.})^* \xrightarrow{k_4} (\text{dtc a.a.–dtc a.a.}),$$

which can be rewritten as:

$$C_1 \xrightarrow{k_1} C_2 + 2C_7$$

$$C_2 \xrightarrow{k_2} C_3 + C_4$$

$$C_3 + C_4 \xrightarrow{k_3} C_5 + C_6$$

$$2C_7 \xrightarrow{k_4} C_8,$$

where k_1, k_2 and k_3 are rate constants for reactions where species C_1, C_2, C_3, C_4 and C_5 (responsible for the absorption at 585 nm) participate. Thus, the total absorption would be:

$$A = \varepsilon_1(C_1) + \varepsilon_2(C_2) + \varepsilon_3(C_3) + \varepsilon_4(C_4) + \varepsilon_5(C_5), \quad (3)$$

where ε_i is the molar extinction coefficient of each species.

The rate equations for these processes would be:

$$d(C_1)/dt = -k_1(C_1) \quad (4)$$

$$d(C_2/)dt = k_1(C_1) - k_2(C_2) \quad (5)$$

$$d(C_3)/dt = d(C_4)/dt = k_2(C_2) - k_3(C_3)(C_4) \quad (6)$$

$$d(C_5)/dt = k_3(C_3)(C_4). \quad (7)$$

Unfortunately, integration of these equations to obtain a close mathematical equation involving the total absorbance, A, and time is impossible. We have, therefore, applied a numerical integration process based on Euler's method. According to this, if A_0 is the initial absorption at $t = 0$ and given values are assumed for the fit parameters (the rate constant k_1, k_2 and k_3 in our case), the specific absorptivities of the absorbing species can be written as a function of the specific absorptivity of the initial species ε_i; that is: $(\varepsilon_2/\varepsilon_1)$, $(\varepsilon_3/\varepsilon_1)$, $(\varepsilon_4/\varepsilon_1)$ and $(\varepsilon_5/\varepsilon_1)$. A sequential integration gives rise to the following equations:

$$C_1(i) = C_1(i-1) + k_1C_1(i-1)\Delta t, \quad (8)$$

$$C_2(i) = C_2(i-1) + [k_1C_1(i-1) - k_2C_2(i-1)]\Delta t \quad (9)$$

$$C_3(i) = C_3(i-1) + [k_2C_2(i-1) - k_3C_3(i-1)C_4(i-1)]\Delta t \quad (10)$$

$$C_4(i) = C_3(i) \quad (11)$$

$$C_5(i) = C_5(i-1) + k_3C_3(i-1)C_4(i-1)\Delta t, \quad (12)$$

where i is the corresponding iteration step, Δt is the step iteration time (we have taken 0.01 min) and hence, at iteration i time can be calculated as:

$$t(i) = t(i-1) + \Delta t \quad (13)$$

and

$$t(0) = 0 \quad (14)$$

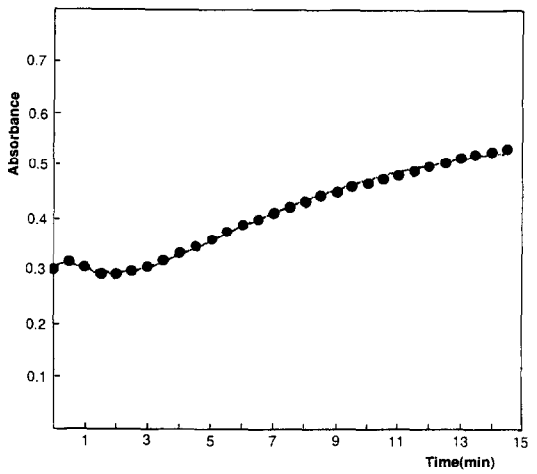

Fig. 4. Time dependence of the absorbance at 585 nm of a DMF solution of the DL-norvaline complex (concentration = 1.4 g dm^{-3}). The calculated parameters following the reaction scheme were: $k_1 = 0.476$, $k_2 = 2.20$, $k_3 = 0.686$; $\varepsilon_2/\varepsilon_1 = 1.03$, $\varepsilon_3/\varepsilon_1 = 0.108$, $\varepsilon_4/\varepsilon_1 = 0.665$ and $\varepsilon_5/\varepsilon_1 = 2.26$.

$$C_1(0) = C_1{}^0 \quad (15)$$

$$C_2(0) = C_3(0) = C_4(0) = C_5(0) = 0. \quad (16)$$

At a given time, the total absorbance is calculated as the sum of the absorbances of the different absorbing species.

The fitting process is controlled by comparing the absorbance values calculated with the experimental ones by the χ^2 parameter:

$$\chi^2 = \Sigma(A^2_{calc} - A^2_{exp}) \quad (17)$$

and the process is repeated until a minimum value for χ^2 is calculated. A computing program was used for this calculation. The application of this calculation to the molybdenum complexes studied in this work acceptably reproduces the kinetic evolution of the absorption of the band at 585 nm, as shown in Fig. 4 for the norvaline derivative. Rate constants and absorptivities are almost independent of the complex concentration, thus supporting the approximation used. On the other hand, the rate constant for the first step, k_1, almost coincides with that determined for the decomposition process studied from changes in the intensity of the band at 500 nm. The formation of the green complexes, $[MoO(dtc\ a.a.)_2]$, takes more time (*ca* 15 min) than the decomposition of the $[Mo_2O_3(dtc\ a.a.)_4]$ complexes.

Acknowledgements—Financial support from CAICYT (Grant No. 800-84) and from Universidad de Salamanca (Acciones Concertadas) is gratefully acknowledged. The authors thank Professor V. Rives (Universidad de Salamanca) for fruitful discussions.

REFERENCES

1. K. V. Rajagopalan, S. Kramer and S. Gardlik, *Polyhedron* 1986, **5**, 573.
2. R. H. Holm, *Coord. Chem. Rev.* 1990, **100**, 183.
3. E. I. Stiefel, *Prog. Inorg. Chem.* 1977, **22**, 1.
4. S. J. N. Burgmayer and E. I. Stiefel, *J. Chem. Educ.* 1985, **62**, 943.
5. M. Berg and R. H. Holm, *J. Am. Chem. Soc.* 1985, **107**, 917, 925.
6. J. A. Craig and R. H. Holm, *J. Am. Chem. Soc.* 1989, **111**, 2111.
7. P. W. Schneider, D. C. Bravard, J. W. McDonald and W. E. Newton, *J. Am. Chem. Soc.* 1972, **94**, 8640.
8. W. E. Newton, J. L. Corbin, D. C. Bravard, J. E. Searles and J. W. McDonald, *Inorg. Chem.* 1974, **13**, 1100.
9. M. Castillo, J. J. Criado, B. Macías and M. V. Vaquero, *Inorg. Chim. Acta* 1986, **124**, 127.
10. M. Castillo, J. J. Criado, B. Macías and M. V. Vaquero, *Trans. Met. Chem.* 1986, **11**, 476.
11. W. E. Newton, J. L. Corbin and J. W. McDonald, *J. Chem. Soc., Dalton Trans.* 1974, 1044.
12. D. A. Brown, W. K. Glass and M. A. Burke, *Spectrochim. Acta* 1976, **32A**, 137.
13. C. A. McAuliffe and B. J. Sayle, *Inorg. Chim. Acta* 1978, **30**, 35.
14. K. S. Jasim, C. Chieh and T. C. W. Mak, *Inorg. Chim. Acta* 1986, **116**, 37.
15. T. N. Srivastava, V. Kumar and R. B. Rastogi, *J. Inorg. Nucl. Chem.* 1978, **40**, 399.
16. W. E. Newton and J. W. McDonald, *J. Less-Common Met.* 1977, **54**, 51.
17. G. J. J. Chen, J. W. McDonald, D. C. Bravard and W. E. Newton, *Inorg. Chem.* 1985, **24**, 2327.
18. A. Nieuwpoort, J. H. E. Moonem and J. A. Cras, *Recl. Trav. Chim. Pays-Bas* 1973, **92**, 1086.
19. M. Chaudhury, *Polyhedron* 1986, **5**, 387.
20. S. Baran-Kumara and M. Chaudhury, *J. Chem. Soc., Dalton Trans.* 1991, 1149.
21. G. Polzonetti, C. Preti and G. Tosi, *Polyhedron* 1986, **5**, 1969.
22. R. A. Walton, *Coord. Chem. Rev.* 1980, **31**, 183.
23. C. Furlani, G. Polzonetti, C. Preti and G. Tosi, *Gazz. Chim. Ital.* 1983, **113**, 609.
24. A. A. Achilleos, L. R. Gahan, T. W. Hambley, P. C. Healy and D. M. Weedon, *Inorg. Chim. Acta* 1989, **157**, 209.
25. A. Müller, W. Jaegermann and J. H. Enemark, *Coord. Chem. Rev.* 1982, **46**, 245.
26. A. Müller, R. Jostes, W. Eltzner, C.-S. Nie, E. Diemann, H. Bögge, M. Zimmermann, M. Dartmann, U. Reinsch-Vogell, S. Che, S. J. Cyvin and B. N. Cyvin, *Inorg. Chem.* 1985, **24**, 2782.

27. R. N. Jowitt and P. C. H. Mitchell, *J. Chem. Soc.* (*A*) 1970, 1702.
28. A. T. Casey, D. J. Mackey, R. L. Martin and A. H. White, *Aust. J. Chem.* 1982, **25**, 477.
29. K. B. Pandeya and B. B. Kaul, *Synth. React. Inorg. Met.-Org. Chem.* 1982, **12**, 259.
30. M. W. Peterson and R. M. Richman, *Inorg. Chem.* 1982, **21**, 2609.
31. R. N. Jowitt and P. C. H. Mitchell, *J. Chem. Soc.* (*A*) 1969, 2632.
32. D. M. Baird, A. L. Rheingold, S. D. Croll and A. T. Dicenso, *Inorg. Chem.* 1986, **25**, 3458.

Polyhedron Vol. 12, No. 23, pp. 2801–2808, 1993
Printed in Great Britain

0277–5387/93 $6.00+.00
© 1993 Pergamon Press Ltd

MOLECULAR STRUCTURE AND CHARGE DISTRIBUTION IN COMPOUNDS OF THE 5*f*-ELEMENTS—VI. 1:1 ADDUCTS OF URANIUM(IV)-HYDROTRIS(3,5-DIMETHYLPYRAZOL-1-YL)BORATE-TRICHLORIDE WITH LEWIS BASES

R. MAIER, J. MÜLLER and B. KANELLAKOPULOS†

Kernforschungszentrum Karlsruhe, Institut für Heiße Chemie, Postfach 3640, 76021 Karlsruhe, F.R.G.

and

C. APOSTOLIDIS

Commission of the European Communities, JCR European Institute for Transuranium Elements, Postfach 2340, 76021 Karlsruhe, F.R.G.

and

A. DOMINGOS, N. MARQUES and A. PIRES DE MATOS

Departamento de Quimica, INCE, INETI, 2686 Sacavém Codex, Portugal

(*Received* 2 *February* 1993; *accepted* 25 *June* 1993)

Abstract—The 1:1 adducts of $UCl_3[HB(3,5\text{-}Me_2Pz)_3]$ with thf, pyridine (NC_5H_5), acetonitrile (MeCN), benzonitrile (PhCN), cyclohexylisocyanide ($C_6H_{12}NC$), triethylphosphate (tep), tributylphosphate (tbp) and triphenylphosphine oxide (tppo) have been prepared and characterized. The structure of the tep compound was determined by single-crystal X-ray analysis. The charge distribution within the molecules was determined and its correlation with spectroscopic data is discussed. The relative affinity of the Lewis base to the uranium central ion was determined by base exchange reactions and found to be tppo > RNC > RCN > tep > tbp > NC_5H_5 > thf.

During our investigations on polypyrazolylborates of the tetravalent actinides uranium[1–5] and neptunium,[6] we had found that the compound $UCl_3[HB(3,5Me_2Pz)_3]\cdot thf$,[7] which is an excellent precursor for the synthesis of a wide variety of uranium organocompounds easily loses the thf molecule by prolonged treatment *in vacuo* or by recrystallization from pentane solution. The same behaviour occurs with the analogous neptunium compound. In order to check if the lability of the thf molecule was due to steric crowding around the uranium(IV) ion or to the weakness of the thf—U bonding, we estimated the partial charge distribution in the molecule of the complexes with different Lewis bases; we realized that thf can be easily substituted by another Lewis base when the partial dipole moment between the central ion and the coordinating atom of the base is greater than that between the central ion and the oxygen of the thf molecule.

EXPERIMENTAL

Materials

All operations were performed under argon with the exclusion of oxygen and moisture using

† Author to whom correspondence should be addressed.

Schlenk-tube techniques. Thf, pentane and benzene were dried by refluxing under argon with potassium metal and were distilled before use. NCMe, NCPh, py and RNC were dried with $CaCl_2$ and distillated. $UCl_3[HB(3,5Me_2Pz)_3]$ (I) and $UCl_3[HB(3,5Me_2Pz)_3]\cdot$thf were prepared according to procedures described previously.[7]

Physical and analytical methods

IR spectra of the compounds embedded in KBr pellets were recorded with a Perkin–Elmer M283 spectrometer (4000–200 cm^{-1}). Electronic absorption spectra were recorded with a Lambda 9 Perkin–Elmer spectrophotometer on samples in solution and/or in KBr pellets. ^1H NMR spectroscopic investigations were performed in CD_3Cl with a Bruker AC-250 NMR spectrometer. The dipole moments of the adducts dissolved in benzene were measured with a DM 01 (2 MHz) WTW apparatus.

Synthesis of $UCl_3[HB(3,5Me_2Pz)_3]\cdot B$ **(II)** (B = MeCN, PhCN, Py, $C_6H_{11}NC$, tep, tbp *or* tppo)

One equivalent of the appropriate base B was added to a solution of I in benzene. After stirring overnight the solution was evaporated to dryness. The dried crude product was extracted with pentane and recrystallized several times before further investigaton or use.

Crystal and molecular structure of $UCl_3[HB(3,5Me_2Pz)_3]\cdot OP(OC_2H_5)_3$

Crystals of the compound, suitable for X-ray diffraction, were obtained by slow diffusion of n-pentane into a saturated solution of the compound in thf. A crystal was sealed in a thin-walled glass capillary in an argon-filled glove-box.

Data were collected at room temperature on an Enraf–Nonius CAD4 diffractometer with graphite monochromatized Mo-K_α radiation. Accurate cell dimensions were obtained from a least-squares refinement of the setting angles of 25 reflections with $14 < 2\theta < 28°$. Intensities were measured with an ω–2θ scan mode. A summary of the crystal data, data collection and refinement are given in Table 1. Data were corrected for Lorentz-polarization, linear decay and for absorption by empirical correction based on ψ-scans using the Enraf–Nonius program. The structure was solved by Patterson and Fourier methods and refined by full-matrix least-squares.[8] All but the methyl carbon atoms of the phosphate ligand were refined anisotropically and the hydrogen atoms were introduced in calculated positions, constrained to ride on their carbon and boron atoms with group U_{iso} values assigned. In the final difference Fourier map the highest peak was 1.6 e $Å^{-3}$ and was near the uranium atom. Atomic scattering factors and anomalous dispersion terms were taken from the International Tables of X-ray Crystallography. Tables of final atomic positional and thermal parameters, full lists of bond lengths and angles, equations of mean least-square planes and tables of F_o/F_c values have been deposited as supplementary material with the editor.

Table 1. Crystallographic data for $UCl_3[HB(3,5Me_2Pz)_3]OP(OC_2H_5)_3$

Formula	$UC_{21}H_{37}BN_6Cl_3O_4P$
Formula weight	832.70
Crystal system	Monoclinic
Space group (No.)	$C2/c$ (15)
a (Å)	16.839(3)
b (Å)	13.360(2)
c (Å)	28.516(6)
β (°)	92.90(2)
V(Å^3)	6407
Z	8
D_x (g cm^{-3})	1.709
Linear absorbance coefficient (cm^{-1}; Mo-K_α)	51.45
2θ range (°)	3.0–46
Decay corrections (min/max)	1.00009/1.09453
Range in absorption correction factors	0.7260/0.9991
Number of reflections $[F_o > 3\sigma(F_o)]$	3261
Number of parameters refined	327
Weighting scheme used: $w = [\sigma^2(F_o)+g(F_o)]^{-1}$ (g)	0.0003
Final R, Rw	0.059, 0.050

RESULTS AND DISCUSSION

The relative affinity of the Lewis bases towards the tetravalent uranium in the $UCl_3[HB(3,5Me_2Pz)_3]\cdot B$ compounds was determined by base exchange reactions.

$$UCl_3[HB(3,5Me_2Pz)_3]\cdot B + B' \longrightarrow UCl_3[HB(3,5Me_2Pz)_3]\cdot B' + B$$

was found to be:

$$tppo > C_6H_{11}NC > C_6H_5CN > CH_3CN > tep > tbp > py > thf.$$

Phosphine oxides were found to give the most stable coordination compounds, followed in base

strength by nitriles, phosphates, pyridine and thf. When stored under an argon atmosphere, the solid compounds remain stable. The green solids are very soluble in polar solvents.

The molecular structure and electric dipole moment of $UCl_3[HB(3,5Me_2Pz)_3]$ **(I)** *and* $UCl_3[HB(3,5Me_2Pz)_3]\cdot B$ **(II)**

The crystal and molecular structure of $UCl_3[HB(3,5Me_2Pz)_3]\cdot OP(OC_2H_3)_3$. As in the case of the thf compound,[7] the crystal structure of $UCl_3[HB(3,5Me_2Pz)_3]\cdot OP(OC_2H_3)_3$ consists of discrete molecules in which the uranium atom is seven-coordinate and displays capped octahedral (CO) geometry. The tridentate pyrazolylborate ligand and the three chlorine atoms define the two staggered triangular faces of the octahedron, the latter is capped by the phosphate oxygen. Figure 1 shows a PLUTO drawing of the molecule with the atomic labelling scheme. A view of the CO coordination polyhedron with edge lengths is given in Fig. 2. Selected bond distances and angles are given in Table 2.

The angles at the metal atom from the capping phosphate oxygen to the Cl(1), Cl(2) and Cl(3) atoms of the capped face are 76.0(2), 75.6(3) and 75.9(3)°, respectively, and to the three nitrogen atoms of the uncapped face are 137.5(3), 134.4(3) and 134.3(3)°. The average angles of 75.8° and 135.3° compare with the predicted values of 74.6° and 130.3° for the capped octahedral in ML7,[9] and with 74.6° and 134.4° reported for the related seven-coordinate $UCl_3[HB(3,5Me_2Pz)_3]\cdot$thf. A comparison of U—Cl and U—N bond lengths with those of the structure of $UCl_3[HB(3,5Me_2Pz)_3]\cdot$thf[7] also shows similar distances, so it may be assumed that all complexes of the $UCl_3{*}L\cdot B$-type **(II)** have the same molecular structure. The only difference between the two structures is in the

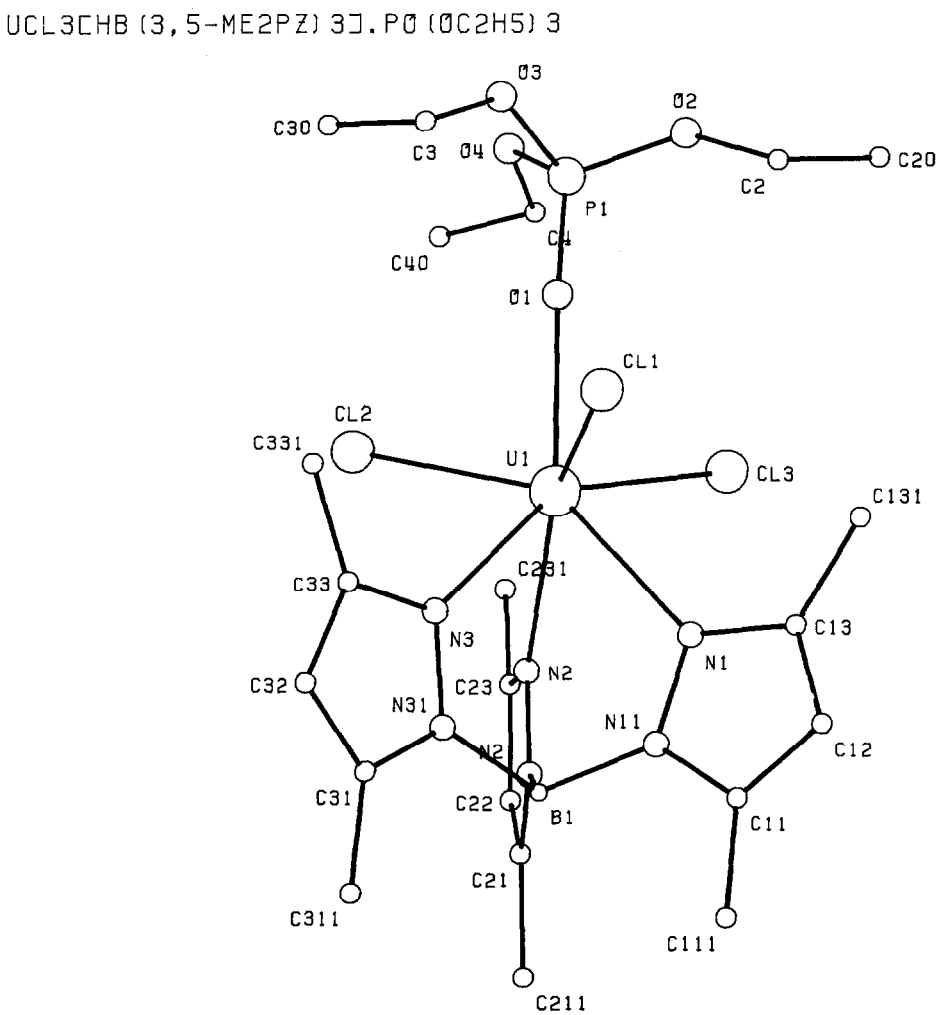

Fig. 1. The molecular structure of $UCl_3[HB(3,5Me_2Pz)_3]\cdot OP(OC_2H_5)_3$.

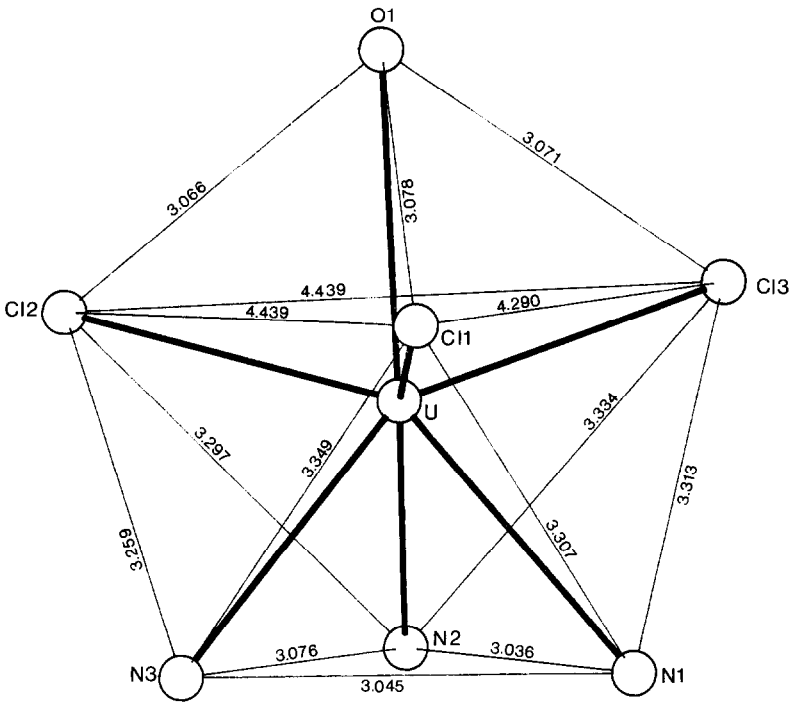

Fig. 2. Coordination polyhedron of $UCl_3[HB(3,5Me_2Pz)_3]\cdot OP(OC_2H_5)_3$.

U—O bond distance [2.373(7) Å in $UCl_3[HB(3,5Me_2Pz)_3]\cdot$tep, 2.546(4) Å in $UCl_3[HB(3,5Me_2Pz)_3]\cdot$thf.[7]

The crystal and molecular structure of the base-free compound $UCl_3[HB(3,5Me_2Pz)_3]$ is known.[5] The compound is six-coordinate and displays octahedral geometry, close to C_{3v} symmetry. The average U—Cl and U—N bond distances are comparable with those found for the complexes discussed above; the main differences between the two classes of compounds **I** and **II** being the Cl—U—Cl angles. For compound **I** the average angle is 97.0°, while for compounds **II** the corresponding angles are larger (114.7° for the tep,

Table 2. Selected bond lengths (Å) and angles (°) in $UCl_3[HB(3,5Me_2Pz)_3]\cdot OP(OC_2H_5)_3$

U—O(1)	2.373(7)	P—O(1)	1.44(1)
		P—O(2)	1.50(1)
U—Cl(1)	2.614(3)	P—O(3)	1.50(1)
U—Cl(2)	2.618(4)	P—O(4)	1.56(1)
U—Cl(3)	2.610(4)		
U—N(1)	2.526(10)		
U—N(2)	2.507(10)		
U—N(3)	2.496(10)		
Cl(1)—U—Cl(2)	116.0(1)	N(1)—U—N(2)	74.2(3)
Cl(1)—U—Cl(3)	110.4(1)	N(1)—U—N(3)	74.7(4)
Cl(2)—U—Cl(3)	116.2(2)	N(2)—U—N(3)	75.9(4)
O(1)—U—Cl(1)	76.0(2)	O(1)—U—N(1)	137.5(3)
O(1)—U—Cl(2)	75.6(3)	O(1)—U—N(2)	134.4(3)
O(1)—U—Cl(3)	75.9(3)	O(1)—U—N(3)	134.3(3)
U—O(1)—P	176.6(7)		

113.2° for the thf compound) in order to accommodate the base B.

The dipole moment of $UCl_3[HB(3,5Me_2Pz)_3]$ (= UCl_3*L). From the crystallographic data the partial charge distribution in the molecule can be estimated empirically. The permanent electric moment μ of a compound dissolved in a non-polar organic solvent can also be estimated from the permanent polarization $P_{2\infty}$ and the electronic polarization ${}_DP_E$ using the Debye equation.[10]

$$\mu^2 = (9kT/4\pi N_L)(P_{2\infty} - {}_DP_E)$$

The total dipole moment of compound **I** is given by the vectorial sum of the partial moments between the central uranium(IV) ion and:

(a) the chlorine atoms;
(b) the nitrogen atoms of the ligand *L (*L = $[HB(3,5Me_2Pz)_3]$; and
(c) the total negative ligand *L,

parallel and perpendicular to the C_3-axis of the molecule containing the uranium and the boron atoms and of the partial moment of the ligand *L:

$$\mu_{exp} = \Sigma\mu_{U-N(j)} \sin(\alpha_j - 90)^\circ + \cos(\alpha_j - 90)^\circ - \Sigma q_{eff(Cl^-)} r_{U-Cl} \sin(\Phi_i - 90)^\circ + \cos(\phi_i - 90)^\circ + q_{eff(*L^-)} r_{U-B}, \quad (1)$$

where, $q_{eff(Cl^-)} = 0.751\ e^-$, as has been calculated for uranium(IV)-chlorocomplexes,[6] $q_{eff(*L^-)} = 1.0\ e^-$, U—N(*j*), U—Cl(*i*), U—B distances in pm, α the C_3-axis–U—N angle and ϕ the C_3-axis–U—Cl angle in degrees, which are known from the crystallographic analysis. Due to the quasi-C_{3v} molecular symmetry of the compound, the sum of the vectorial parts of the partial moments $\Sigma r_{U-N(j)} \cos(\alpha_j - 90)^\circ$ and $\Sigma q_{eff(Cl^-)} r_{U-Cl(i)} \cos(\phi_i - 90)^\circ$ perpendicular to the C_3-axis are zero. The partial moment μ_{*L} of the ligand *L can be calculated; its value is almost zero also. Thus, eq. (1) gives:

$$\mu_{exp} = \Sigma\mu_{U-N(j)} \sin(\alpha_j - 90)^\circ - \Sigma q_{eff(Cl^-)} r_{U-Cl} \sin(\phi_i - 90)^\circ + q_{eff(*L)} r_{U-B} \quad (2)$$

The only unknown parameter in eq. (2) is now the partial moment $\mu_{U-N(j)}$ between uranium and nitrogen and can be calculated from (2):

$$\mu_{U-N(j)} = \{\mu_{exp} + \Sigma q_{eff(Cl^-)} r_{U-Cl} \sin(\phi_i - 90)^\circ - q_{eff(*L)} r_{U-B}\} / \Sigma \sin(\alpha_i - 90^\circ) = 1.40\,D \quad (3)$$

The dipole moment of UCl_3*L·B *compounds* (**II**)

The total dipole moment of compounds **II** can be calculated as discussed previously for the base-free compound by taking into account the moment contribution of the base molecule:

$$\mu_{exp} = \Sigma\mu_{U-N(j)}\{\sin(\alpha_j - 90)^\circ + \cos(\alpha_j - 90)^\circ - \Sigma q_{eff(Cl^-)} r_{UCl,i}\{\sin(\phi_i - 90)^\circ + \cos(\phi_i - 90^\circ)\} + q_{eff(*L^-)} r_{U-B} - \mu_{*L^-} - \mu_{U-B(base)} + \mu_{base}. \quad (3a)$$

Under the assumptions made for the base-free compounds eq. (3) can be written as:

$$\mu_{exp} = \Sigma\mu_{U-N(j)} \sin(\alpha_j - 90)^\circ - \Sigma q_{eff(Cl^-)} r_{UCl,i}\{\sin(\phi_i - 90)^\circ + q_{eff(*L^-)} r_{U-B} - \mu_{*L} - \mu_{U-B(base)} + \mu_{base}. \quad (3b)$$

Distances and angles are well known from the crystallographic analysis of the thf compound[7] and of the analogous tep-complex (this paper). The first four terms of eq. (3b) represent the partial moment of the "UCl_3*L" unity of the complex:

$$\mu_{"UCl_3*L"} = \Sigma\mu_{U-N(j)} \sin(\alpha_j - 90)^\circ - \Sigma q_{eff(Cl^-)} r_{UCl,i}\{\sin(\phi_i - 90)^\circ + q_{eff(*L^-)} r_{U-B} - \mu_{*L} \quad (4)$$

and is calculated to be 13.07 D for the thf compound and 13.11 D for the tep compound; $\mu_{"UCl_3*L"}$ can be treated as a constant because its value does not change with variation of the base B. Furthermore, the dipole moment of the free base, μ_B, is known from the literature or it can be easily measured experimentally; thus, the only unknown term in eq. (3b) is the partial moment μ_{U-base} between the uranium ion and the coordinated atom of the base B. The measured dipole moments of the free Lewis bases, μ_B, of the 1:1 adducts and the calculated partial moments, μ_{U-base}, are summarized in Table 3.

Table 3. Dipole moment of the UCl_3*L·B complexes and the free base B and partial electric moment for the coordinative uranium–Lewis base bonding

Base	μ_{exp} (D)	μ_B (D)	μ_{U-B} (D)
—	6.17	—	—
thf	7.05	1.65	7.67
py	7.09	2.10	8.08
tbp	7.69	3.18	8.56
tep	7.62	3.14	8.59
MeCN	7.75	3.35	8.67
PhCN	8.26	4.18	8.99
tppo	8.33	4.56	9.30
$C_6H_{11}NC$	8.27	4.57	9.37

Charge distribution and IR-spectroscopic investigations

The partial bonding moment $\mu_{U-B(base)}$ between the uranium ion and the coordinated atom of the base B increases with an increase in the electron-donor strength of the Lewis base B (Fig. 3).

Extrapolation of the linear μ_{exp} *vs* μ_{base} plot in Fig. 3 yields a dipole moment of 6.17 D. This electric moment corresponds to the moment of a molecule in which the uranium ion is coordinated to a hypothetical, non-polar Lewis base B (with $\mu = 0$). For this molecule a partial electric moment between the central ion and the hypothetical non-polar base of 6.90 D is obtained by extrapolation of the μ_{U-B} vs μ_B plot in Fig. 3. The same value is obtained by using eq. (3b):

$$\mu_{U-B(base)} = \mu_{\text{"}UCl_3{}^*L\text{"}} - \mu_{exp} + \mu_B = 6.90\,D$$

with $\mu_{\text{"}UCl_2{}^*L\text{"}} = 13.07$, $\mu_{exp} = 6.17$ and $\mu_B = 0.0$ D.

The interaction between the coordinated atom of a hypothetical, non-polar Lewis base and the uranium central ion (6.90 D) is strong enough to change the geometry of the UCl_3*L molecule into the coordination geometry of the UCl_3*L · B adduct, which means increasing the Cl—U—Cl angle from 97.0° to *ca* 114°. When a Lewis base B is coordinated to the UCl_3*L molecule, the electronic density of the uranium ion along the main symmetry C_3-axis in the UCl_3*L · B compound increases. An increase in the electron-donor strength of the coordinated base causes a decrease in the electronic inter action between the central ion and the pyrazolyl rings of the ligand *L and consequently, the interaction between the proton and the boron ion becomes weaker. This is reflected in the characteristic B—H vibration in the IR spectra. Compared with the B—H vibrational frequency of the base-free molecule **I**, the B—H frequencies of the adducts are shifted to lower energies (Table 4). The plot $\mu_{U-B(base)}$ vs $\Delta\nu_{B-H}$ $[\nu_{B-H(I)} - \nu_{B-H(II)}]$ demonstrates well the electronic interaction between the coordinated ligand and the uranium ion along the C_3-axis. If the interaction between the base B and the uranium ion is not too strong, a linear correlation between the bonding moment $\mu_{U-B(base)}$ and the frequency of the B—H stretch vibration ν_{B-H} was observed (Fig. 4).

The value of $\Delta\nu_{B-H}$ for the hypothetical compound in which the uranium ion is coordinated to a non-polar Lewis base ($\mu_B = 0$, $\mu_{U-B} = 6.90$ D) is 3.5 cm^{-1}. This difference in the B—H vibrational frequency corresponds to the change of the molecular geometry when UCl_3*L becomes UCl_3*L · B. An increase in the interaction strength between the Lewis base and the central ion causes a saturation effect in the μ_{U-B} vs $\Delta\nu_{B-H}$ plot (Fig. 4). The partial moment cannot increase beyond a maximum, because the uranium–base distance (r_{U-B}) is limited by the ionic radii of tetravalent uranium and the coordination atom of the base B.

The apparent discrepancy in the relationship between $\mu_{U-B(base)}$ and the ν_{B-H} vibrational frequency for the cyclohexylisonitrile and triphenylphosphine oxide complex [$\Delta\nu_{B-H(tppo)}$ >

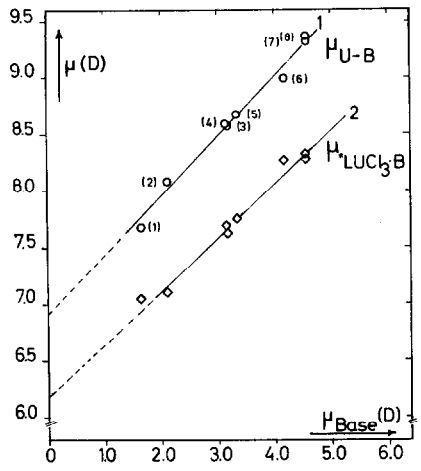

Fig. 3. Experimentally measured dipole moments (μ) of the $UCl_3[HB(3,5Me_2Pz)_3]$ · B complexes and calculated partial electrical moments (μ_{U-B}) between uranium and base as a function of the dipole moment of the free base [(1) thf; (2) py; (3) MeCN; (4) tep; (5) tbp; (6) PhCN; (7) $C_6H_{11}NC$; (8) tppo].

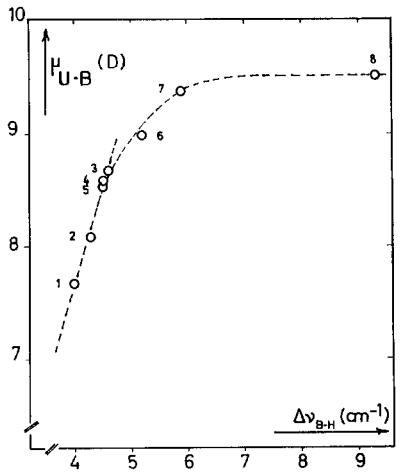

Fig. 4. The correlation between partial electrical moment μ_{U-B} and $\Delta\nu_{B-H}$ in the $UCl_3[HB(3,5Me_2Pz)_3]$ · B compounds [(1) thf; (2) py; (3) MeCN; (4) tep; (5) tbp; (6) PhCN; (7) $C_6H_{11}NC$; (8) tppo].

$\Delta\nu_{B-H(CNR)}$, while $\mu_{U-O(tppo)} < \mu_{U-C(C_6H_{11}NC)}$] is due to the back-bonding character of the isonitrile group through the electron density transfer into the anti-bonding orbitals of the isocyanide group. Therefore, the electron-acceptor character of the central ion and the partial bonding moment $\mu_{U-B(base)}$ are stronger in the isonitrile complex. The tppo molecule represents a very strong Lewis base without any π-acceptor back-bonding character and consequently, the $\Delta\nu_{B-H}$ value increases, whereas the partial electric moment $\mu_{U-B(base)}$ remains almost constant (saturation).

Electronic absorption spectra

The absorption spectra of all the UCl_3*L · B complexes in the region 1600–400 nm in the solid state (KBr matrix) and in benzene solution show the characteristic absorption band groups for uranium(IV) and are quite similar (Fig. 5); an indication of the similar coordination geometry around the uranium ion in all the compounds investigated. It can be assumed that all the analogous compounds

Table 4. Partial bonding moment μ_{U-B}, vibrational frequency of the B—H vibration and absorption band wavelength for the ^3F-term of the uranium ion of the UCl_3* L · B compounds

Base	μ_{U-B} (D)	ν_{B-H} (cm^{-1})	ν_{B-H} (cm^{-1})	λ (nm)
—	—	2565.0	—	1101.2
thf	7.67	2561.0	4.0	1168.0
py	8.08	2560.8	4.3	1169.9
tep	8.59	2560.5	4.5	1173.2
tbp	8.56	2560.5	4.5	1173.1
MeCN	8.67	2560.4	4.6	1174.4
PhCN	8.99	2559.8	5.2	1175.1
tppo	9.30	2556.5	9.5	1178.2
$C_6H_{11}NC$	9.37	2559.1	5.9	1176.5

are isomorphic (see crystal structure of UCl_3*L · thf and UCl_3*L · tep).

As can be seen in Fig. 5, the shape of the absorption band at 1170 cm^{-1} is sensitive towards the base B; the absorption energy changes with a change in the Lewis basity of the coordinated molecule (Table 4). The absorption band belongs to the ^3F-term of the $5f^2$ electronic configuration of the tetravalent uranium. Its energy must correlate with the electron-density along the C_3-axis of the molecule and with the partial electric moment $\mu_{U-B(base)}$. The bigger electronic density in the 1 : 1 adduct causes a lower absorption energy for the ^3F-term than in the base-free molecule, as is shown in the $\mu_{U-B(base)}$ vs $E_{^3F}$ plot of Fig. 6.

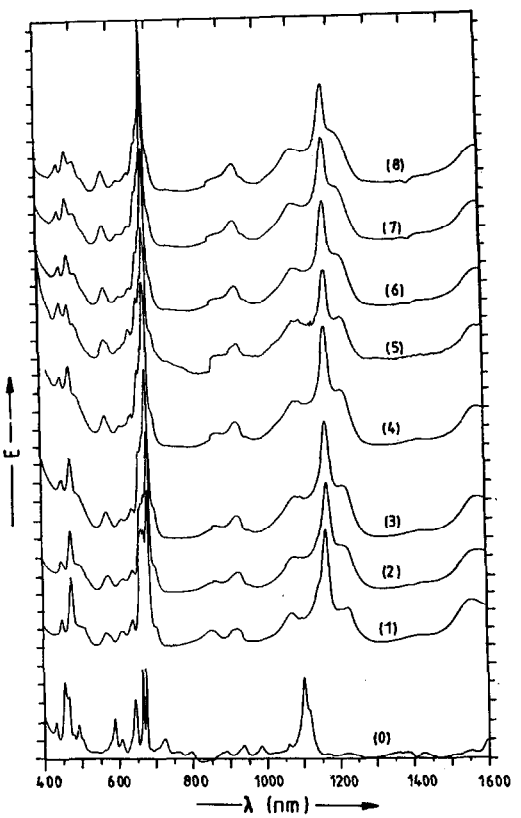

Fig. 5. Electron absorption spectra of the $UCl_3[HB(3,5Me_2Pz)_3]$ · B compounds [(0) base-free compound; (1) thf; (2) py; (3) MeCN; (4) tep; (5) tbp; (6) PhCN; (7) $C_6H_{11}NC$; (8) tppo].

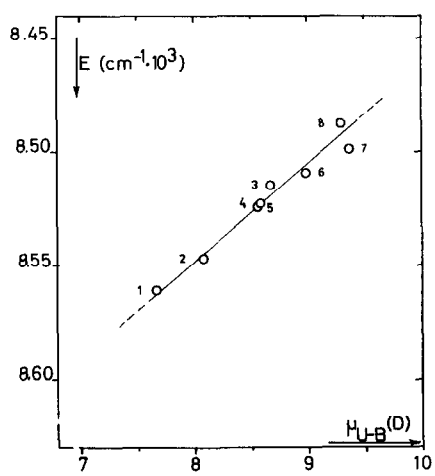

Fig. 6. The energy of the 1170 nm absorption band as a function of the dipole moment of the free base B [(1) thf; (2) py; (3) MeCN; (4) tep; (5) tbp; (6) PhCN; (7) $C_6H_{11}NC$; (8) tppo].

Extrapolation of the plot of Fig. 6 vs $\mu_{U-B(base)} = 0$ yields an energy of 8960 cm^{-1}, which is smaller than the absorption energy of 9081 cm^{-1} experimentally measured in L^*UCl_3. The energy difference, ΔE, between the extrapolated and measured value for the L^*UCl_3 compound is 121 cm^{-1} (= 1.447 kJ mol^{-1}) and corresponds to the energy which is needed to change the molecular symmetry by forming the 1:1 adduct $L^*UCl_3 \cdot B$, starting from L^*UCl_3.

^1H *NMR spectra*

As expected for C_{3v}-symmetry, in all the $UCl_3[HB(3,5MePz)_3] \cdot B$ compounds only one set of ^1H resonances was observed for the protons of $CH_3(3)$, $CH_3(5)$ and H(4) of the three pyrazolyl rings. Although the NMR spectra of all the compounds are similar, the chemical shifts of the protons of the pyrazolyl rings, especially those observed for the protons of the $CH_3(3)$ groups, vary over a wide range from −20 to −4 ppm. The chemical shifts of the resonances of the pyrazolyl protons of the different complexes at 300 K are summarized in Table 5. Measurements in $CDCl_3$ solutions at different temperatures show an almost linear correlation between the chemical shift and the temperature for all the adducts (Table 5).

Table 5. Partial bonding moment μ_{U-B} and chemical shift (δ) for protons of the three pyrazolyl rings in the $UCl_3{}^*L \cdot B$ compounds

Base	$\delta_{CH_3(3)}$ (ppm)	$\delta_{CH_3(5)}$ (ppm)	$\delta_{H(4)}$ (ppm)	μ_{U-B} (D)
thf	−4.2	2.9	7.7	7.67
py	−3.3	2.3	8.0	8.08
tbp	−10.8	3.8	7.6	8.56
tep	−10.9	3.8	7.6	8.59
MeCN	−4.8	4.1	7.5	8.67
PhCN	−5.2	4.2	7.4	8.99
tppo	−19.8	6.2	7.3	9.30
$C_6H_{11}NC$	−4.5	3.1	7.6	9.37

REFERENCES

1. J. Marçalo, N. Marques, A. Pires de Matos and K. W. Bagnall, *J. Less Common Met.* 1986, **122**, 219.
2. N. Marques, J. Marçalo, A. Pires de Matos, I. Santos and K. W. Bagnall, *Inorg. Chim. Acta* 1987, **137**, 309.
3. A. Domingos, J. Marçalo, N. Marques, A. Pires de Matos, J. Takats and K. W. Bagnall, *J. Less Common Met.* 1989, **140**, 271.
4. A. Domingos, J. P. Leal, J. Marçalo, N. Marques, A. Pires de Matos, I. Santos, M. Silva, B. Kanellakopulos, R. Maier, C. Apostolidis and J. A. Martinho Simoes, *Eur. J. Solid State Inorg. Chem.* 1991, **28**, 413.
5. A. Domingos, N. Marques and A. Pires de Matos, *Polyhedron* 1990, **9**, 69.
6. C. Apostolidis, B. Kanellakopulos, R. Maier, N. Marques, A. Pires de Matos and I. Santos, *20èmes J. Actinides*, 17–20 April, Prague (CS) (1990).
7. R. G. Ball, F. Edelmann, J. G. Matisons, J. Takats, N. Marques, J. Marçalo, A. Pires de Matos and K. W. Bagnall, *Inorg. Chim. Acta* 1987, **132**, 137.
8. G. M. Sheldrick, SHELX Crystallographic Program, University of Cambridge, U.K. (1976).
9. D. L. Kepert, *Inorganic Stereochemistry*. Springer Verlag, Berlin (1982).
10. The methods for the calculations are discussed in: B. Kanellakopulos, R. Maier and J. Heuser, *J. Alloys Compounds* 1991, **176**, 89.

Polyhedron Vol. 12, No. 23, pp. 2809–2813, 1993
Printed in Great Britain

0277–5387/93 $6.00+.00
© 1993 Pergamon Press Ltd

SYNTHESIS AND CHARACTERIZATION OF LANTHANIDE(III) COMPLEXES WITH 3,4-METHYLENEDIOXYBENZALDEHYDE THIOSEMICARBAZONE

SHREEDHAR D. DHUMWAD and T. R. GOUDAR*

Department of Chemistry, Karnataka University, Dharwad, India

(*Received* 20 *April* 1993; *accepted* 18 *June* 1993)

Abstract—New complexes of lanthanide nitrates with 3,4-methylenedioxybenzaldehyde thiosemicarbazone having the general formula $[Ln(LH)_2(NO_3)_2]NO_3$ (where Ln = La, Ce, Pr, Nd, Sm, Eu, Gd, Dy, Ho, Er, Yb and Y) have been prepared and characterized by elemental analysis, molar conductance, magnetic measurements, electronic, infrared, ^1H NMR, fluorescence spectra and thermal studies. Molar conductance studies indicate 1 : 1 electrolytic behaviour for these complexes. The spectral studies show that two thiosemicarbazone ligands and two nitrate groups are bound to the lanthanide ion in a bidentate fashion. TG and DTA studies indicate that these complexes are stable up to 255°C and do not contain water or alcohol molecules.

Thiosemicarbazones are amongst the most widely studied nitrogen and sulphur donor ligands. They are capable of acting as neutral or charged ligands. The importance of these compounds is mainly due to their anticarcinogenic,[1] antibacterial[2] and antifungal activities,[3] as well as their ability to form chelate complexes with transition metals.[4,5]

In cancer treatment it has been shown that the metal chelates are more potent than chelating agents.[6] The donor properties and biological activities of thiosemicarbazones of benzaldehyde and substituted benzaldehyde have been investigated in detail.[7,8] A thorough survey of the literature reveals that there is no report on the lanthanide complexes of 3,4-methylenedioxybenzaldehyde thiosemicarbazone (LH). This paper, therefore, describes the synthesis and characterization of lanthanide complexes with the above ligand.

EXPERIMENTAL

All the reagents used were of analytical grade. The ligand, LH, was synthesized by refluxing 3,4-methylenedioxybenzaldehyde and thiosemicarbazide (1 : 1 ratio) in absolute alcohol for 2 h and recrystallizing the product from ethanol,[9] m.p. 190–191°C.

Synthesis of the complexes

The following general procedure was used to isolate all the lanthanide(III) complexes. Lanthanide(III) nitrate (0.002 M) was dissolved in absolute alcohol (10 cm^3). The ligand, LH (0.004 M), dissolved in the same solvent (*ca* 20 cm^3) was added to the above solution with constant stirring. The mixture was refluxed on a water bath for *ca* 4 h and the pH of the mixture was then raised to *ca* 6.5 by the dropwise addition of alcoholic ammonia and again refluxed for 2 h. The solid complexes thus formed were filtered, washed with absolute alcohol and dried *in vacuo* at room temperature.

Physical measurements

Elemental analyses (C, H and N) were performed on an auto-elemental analyser, model 1106. The metal contents were estimated by complexometric EDTA titration using xylenol orange as an indicator[10] at pH 6. Sulphur was determined by the standard method.[11] Conductance measurements were performed on 10^{-3} M solutions of the complexes in methanol using an Elico conductivity

* Author to whom correspondence should be addressed.

bridge, type CM-82, attached to a dip type conductivity cell fitted with platinum electrodes (cell constant 0.51). The magnetic moments of the complexes were determined by the Gouy method at room temperature. The electronic spectra of the ligand and complexes were recorded on a Hitachi 150-20 spectrophotometer. IR and ^{1}H NMR spectra were recorded on a Perkin–Elmer model 337 spectrophotometer in Nujol mulls and a VXR 300S Varian supercon NMR spectrometer using DMSO-d_6 as a solvent, respectively. The fluorescence spectrum of the Eu^{III} complex was determined using a Perkin–Elmer MPF 3L fluorescence spectrophotometer from the solid compound by excitation with 400 nm radiation at room temperature. The thermal analyses, such as the TG and DTA measurements, were performed in static air, using a limiting temperature of 1000°C and a heating rate of 10°C min^{-1}.

RESULTS AND DISCUSSION

The stoichiometries of the complexes were confirmed by the elemental analyses reported in Table 1. All the complexes are air stable, non-hygroscopic and soluble in polar solvents. They are pale white to cream in colour, except praseodymium and neodymium which are green and violet, respectively. The complexes have the general formula $[Ln(LH)_2(NO_3)_2]NO_3$.

Molar conductance

The molar conductance data of the complexes are presented in Table 1. From these data it is clear that all the complexes show 1 : 1 electrolytic behaviour in methanol.[12]

The magnetic moments of these lanthanide complexes, recorded in Table 1, show little deviation from the Van Vleck values,[13] thereby indicating that the 4*f*-electrons do not participate in bond formation in these complexes. Thus, the magnetic moments of these complexes are within the range predicted and observed in compounds of the lanthanide ions.[14] The data also suggest that there are no metal–metal interactions or spin–spin coupling.

Electronic spectra

The ligand shows two absorption maxima, a sharp peak (of weak intensity) at 38,314 cm^{-1} due to the $\pi \rightarrow \pi^*$ transition and a broad peak (strong

Table 1. Analytical data, magnetic moment and molar conductance values of the new complexes

S. No.	Complex	Found (Calc.) (%) C	H	N	S	M	μ_{eff} (B.M.) at 302 K	λ_m (Ω^{-1} cm^2 Mol^{-1}) in 10^{-3} M Methanol
1.	$[La(LH)_2(NO_3)_2]NO_3$	27.8 (27.6)	2.3 (2.3)	16.4 (16.1)	8.4 (8.3)	17.4 (17.7)	Diamagnetic	83
2.	$[Ce(LH)_2(NO_3)_2]NO_3$	27.4 (27.6)	2.4 (2.3)	16.3 (16.1)	8.4 (8.2)	17.6 (17.9)	2.50	82
3.	$[Pr(LH)_2(NO_3)_2]NO_3$	27.6 (27.5)	2.4 (2.3)	16.3 (16.1)	8.6 (8.2)	18.6 (18.0)	3.54	83
4.	$[Nd(LH)_2(NO_3)_2]NO_3$	28.0 (27.4)	2.2 (2.3)	16.2 (16.0)	8.3 (8.1)	18.8 (18.3)	3.62	86
5.	$[Sm(LH)_2(NO_3)_2]NO_3$	27.6 (27.2)	2.4 (2.3)	16.0 (15.9)	8.5 (8.1)	18.4 (18.9)	1.68	84
6.	$[Eu(LH)_2(NO_3)_2]NO_3$	26.8 (27.1)	2.3 (2.3)	16.0 (15.8)	8.6 (8.0)	19.6 (19.1)	3.30	81
7.	$[Gd(LH)_2(NO_3)_2]NO_3$	26.3 (27.0)	2.2 (2.3)	15.4 (15.7)	7.6 (8.0)	19.0 (19.6)	7.82	85
8.	$[Dy(LH)_2(NO_3)_2]NO_3$	26.3 (26.8)	2.2 (2.2)	16.0 (15.6)	7.7 (7.9)	20.1 (20.2)	10.3	87
9.	$[Ho(LH)_2(NO_3)_2]NO_3$	26.3 (26.7)	2.2 (2.2)	15.3 (15.6)	7.8 (7.9)	20.0 (20.4)	10.72	85
10.	$[Er(LH)_2(NO_3)_2]NO_3$	26.2 (26.6)	2.3 (2.2)	15.3 (15.5)	7.6 (7.9)	19.9 (20.6)	9.38	89
11.	$[Yb(LH)_2(NO_3)_2]NO_3$	25.9 (26.4)	2.2 (2.2)	15.7 (15.4)	7.5 (7.8)	20.7 (21.2)	4.64	86
12.	$[Y(LH)_2(NO_3)_2]NO_3$	29.9 (29.5)	2.5 (2.5)	17.4 (17.2)	8.6 (8.7)	11.6 (12.1)	Diamagnetic	83

intensity) at 29,940 cm^{-1} due to the $n \rightarrow \pi^*$ transition. It was found that the electronic spectra of the lanthanide complexes are dominated by ligand absorption bands with a hyperchromic effect. The domination of the ligand absorption bands could be related to the high absorption coefficient of the ligand as compared with the Ln^{III} ions, which masks any splitting of the bands.[15]

IR spectra

The IR spectra of the ligand and complexes were recorded in the 4000–200 cm^{-1} range. The highest frequency of the ligand at 3450 cm^{-1} can be assigned to the asymmetric (N—H) vibration of the terminal $—NH_2$ group. The other bands at 3110 and 3280 cm^{-1} may be due to the vibration of the imino group and the symmetric (N—H) vibration of the terminal amino group. The absence of bands at 2650–2500 cm^{-1} in the ligand spectrum indicates that there is no S—H group in the free ligand in the solid state.[8] The band of strong intensity at 1580 cm^{-1} with a shoulder at 1650 cm^{-1} in the ligand spectrum may be assigned to the azomethine stretch. In all the complexes it undergoes a red shift by 20–30 cm^{-1}, indicating the participation of the azomethine nitrogen in coordination.[16] The band of medium intensity at 800 cm^{-1} with distinct shoulders at 815 and 845 cm^{-1} in the ligand spectrum may be assigned to pure ν(C=S). In all the complexes we found a band of strong intensity around 790 cm^{-1}, a band of medium intensity around 855 cm^{-1} and a new band of weak intensity around 760 cm^{-1}. In addition, the band position assigned to secondary (N—H) remained unaltered. These observations strongly suggest the coordination of thiocarbonyl sulphur to the lanthanide ion[17] (Table 2).

The complexes show six absorption bands near 1500, 1290, 1030, 820, 750 and 705 cm^{-1}, which are assigned to ν_4, ν_1. ν_2, ν_6, ν_3 and ν_5 vibrations, respectively, of the coordinated (C_{2v}) nitrate group.[18,19] The magnitudes of ν_4–ν_1 and ν_3–ν_5 are in the range 201–210 and 43–47 cm^{-1}, respectively, indicating that the nitrate groups are coordinated in a bidentate fashion. The band at 1350 cm^{-1} expected for ionic nitrate is not observed in the spectra as it might be obscured by the broad Nujol band in the range 1390–1340 cm^{-1}.

^1H NMR spectra

The methylene protons in the free ligand are represented by a sharp singlet at δ 6.08. The two doublets at *ca* δ 6.87 and 7.06 in the spectra of the ligand and the complexes are due to the two phenyl protons H(5) and H(6). This can easily be understood from the vicinal coupling constant ($J \approx 8.5$ Hz). The singlet at δ 7.55 is due to the third proton, H(2) of the phenyl ring. The signal for the azomethine proton is expected to appear at a lower field compared with the phenyl protons. Thus, the singlet at δ 8.02 due to the azomethine proton in the ligand spectrum is shifted downfield to δ 8.20–8.30 in the spectra of the diamagnetic complexes, showing its deshielding as a result of coordination through the nitrogen of the azomethine group to

Table 2. Important IR frequencies (cm^{-1}) of the ligand (LH) and its complexes

S. No.	Compound	ν(C=N)	ν(C=S)		NO_3^- ν_4	ν_1	ν_2	ν_6	ν_3	ν_5
1.	LH	1580s	800s 815sh 845sh							
2.	$[La(LH)_2(NO_3)_2]NO_3$	1560s	790s	855m 760w	1495s	1294s	1030m	820m	750m	705m
3.	$[Ce(LH)_2(NO_3)_2]NO_3$	1555s	790s	850m 760w	1495s	1290s	1030m	820m	750m	705m
4.	$[Pr(LH)_2(NO_3)_2]NO_3$	1560s	785s	850m 755w	1491s	1281s	1025m	815m	745m	700m
5.	$[Nd(LH)_2(NO_3)_2]NO_3$	1550s	790s	855m 755w	1500s	1295s	1020m	815m	745m	700m
6.	$[Sm(LH)_2(NO_3)_2]NO_3$	1570s	790s	855m 760w	1491s	1286s	1025m	820m	750m	705m
7.	$[Eu(LH)_2(NO_3)_2]NO_3$	1570s	785s	850m 760w	1500s	1290s	1025m	815m	750m	705m
8.	$[Gd(LH)_2(NO_3)_2]NO_2$	1565s	785s	855m 755w	1495s	1294s	1020m	820m	745m	705m
9.	$[Dy(LH)_2(NO_3)_2]NO_3$	1550s	790s	855m 760w	1495s	1294s	1030m	820m	750m	700w
10.	$[Ho(LH)_2(NO_3)_2]NO_3$	1560s	790s	850m 760w	1495s	1285s	1030m	820m	745m	700w
11.	$[Er(LH)_2(NO_3)_2]NO_3$	1555s	785s	855m 755w	1500s	1295s	1025m	815m	750m	705w
12.	$[Yb(LH)_2(NO_3)_2]NO_3$	1570s	790s	855m 760w	1500s	1299s	1020m	815m	750m	700w
13.	$[Y(LH)_2(NO_3)_2]NO_3$	1555s	785s	850m 760w	1500s	1290s	1030m	820m	750m	700w

s: strong; m: medium; w: weak; sh: shoulder.

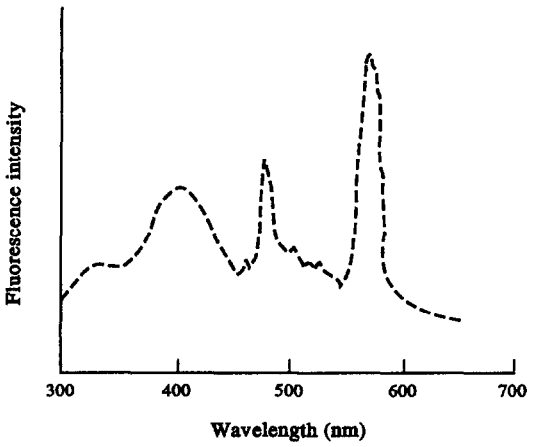

Fig. 1. Fluorescence spectrum of solid $[Eu(LH)_2(NO_3)_2]NO_3$ by excitation with 400 nm radiation at room temperature.

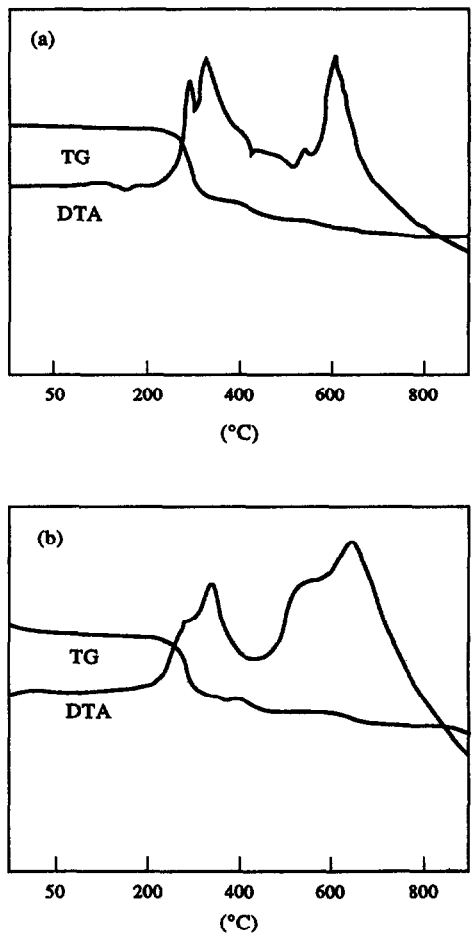

Fig. 2. TG and DTA of (a) Nd and (b) Dy complexes.

the metal ion. The spectra of thiosemicarbazones are expected to exhibit two resonances for the NH_2 protons, indicating hindered rotation about the C(S)—NH_2 bond due to its partial double bond character.[20] However, in the spectrum of the present ligand, there is only a singlet at δ 7.88 for the —NH_2 protons. This is not unexpected as one of these signals may be obscured by that of the aromatic protons, as in the case of benzaldehyde thiosemicarbazone. The secondary NH proton signal is found at δ 10.88 in the spectrum of the ligand. The shifting of secondary NH proton signal from δ 10.88 to 11.02 in the complexes indicates the coordination of the metal ion to the thiocarbonyl sulphur without deprotonation. Thus, IR and ^1H NMR spectral observations supplement each other.

Fluorescence spectrum of the europium(III) *complex*

The fluorescence spectrum of the europium(III) complex (Fig. 1) exhibits sharp emissions in the regions 475–515 and 560–570 nm. The more intense band observed in the 560–570 nm region is assigned to the transition $^7F_1 \leftarrow {}^5D_0$.[21] Comparatively weak bands between 475 and 515 nm may be assigned to phosphorescence emission.[22]

Thermal studies

The thermal analytical results of some complexes (Table 3 and Fig. 2) show that the complexes are stable up to 235°C. This observation shows that there are no water or solvent molecules in the lattice.

Table 3. Thermal analysis data for some of the complexes

S. No.	Complexes	Decomposition range in TG (°C)	Peaks in DTA (°C)
1.	$[La(LH)_2(NO_3)_2]NO_3$	240–650	295, 330, 570, 620
2.	$[Pr(LH)_2(NO_3)_2]NO_3$	245–640	285, 320, 580, 610
3.	$[Nd(LH)_2(NO_3)_2]NO_3$	245–645	295, 335, 575, 615
4.	$[Gd(LH)_2(NO_3)_2]NO_3$	250–630	285, 325, 580, 610
5.	$[Dy(LH)_2(NO_3)_2]NO_3$	250–640	290, 320, 560, 610

The complexes undergo complete decomposition in the region 620–650°C.

On the basis of elemental analysis, molar conductance, magnetic moments, IR, ^{1}H NMR and fluorescence spectra and thermal analysis, it is concluded that two LH ligands and two nitrate groups are bound to the lanthanide ion and another nitrate group is in the outer coordination sphere. Hence, the present complexes may be formulated as $[Ln(LH)_2(NO_3)_2]NO_3$. The lanthanide ions in the complexes exhibit coordination number eight.

Acknowledgements—The authors thank the authorities of BARC, Trombay, for providing library facilities. They are also thankful to Dr R. K. Dhumwad and other officials of BARC for their assistance in chemical analysis. One of the authors (S.D.D.) is grateful to the Chairman, Department of Chemistry, Karnatak University, for his constant encouragement during the course of these studies.

REFERENCES

1. L. Feedlander and A. Fraust, *J. Am. Chem. Soc.* 1952, **81**, 638.
2. N. P. Buu-Hoi, T. B. Voc and N. D. Xuong, *Bull. Soc. Chim.* 1955, **11**, 694.
3. J. M. Campbell, *Coord. Chem. Rev.* 1975, **15**, 279.
4. M. M. Mostafa, A. A. El-Asmy and G. M. Ibrahim, *Trans. Met. Chem.* 1983, **8**, 54.
5. K. M. Ibrahim, A. A. El-Asmy, M. M. Bekheit and M. M. Mostafa, *Synth. React. Inorg. Met-Org. Chem.* 1985, **15**, 1247.
6. J. A. Gim and H. G. Petering, *Cancer Res.* 1967, **27**, 1278.
7. T. Tunde, Bamgboye and O. A. Bamgboye, *Inorg. Chim. Acta* 1987, **133**, 247.
8. K. Balkrishnan and K. K. Aravindakshan, *J. Ind. Chem. Soc.* 1991, **68**, 187.
9. P. T. Peter Sah and T. C. Daniels, *Rev. Trav. Chim.* 1950, **69**, 1545.
10. F. J. Welcher, *The Analytical Use of EDTA*, Vol. 4. Van Nostrand, New York (1965).
11. A. I. Vogel, *A Text Book of Quantitative Inorganic Analysis*. ELBS, London (1978).
12. C. Bisi Casteelani and O. Carugo, *Inorg. Chim. Acta* 1989, **159**, 157.
13. D. M. Yost, H. Russell and C. S. Garner, *The Rare Earth Elements and Their Compounds*, Ch. 2. Wiley, New York (1947).
14. M. Karayannis, C. Mikulsi, L. L. Pytlewsi and M. M. Labes, *J. Less Comm. Met.* 1970, **20**, 29.
15. M. Mohan, J. P. Tandon and N. S. Gupta, *J. Inorg. Nucl. Chem.* 1981, **43**, 1223.
16. G. K. Joshi, M. P. Bhutra and S. N. Misra, *J. Inorg. Nucl. Chem.* 1981, **43**, 525.
17. M. Mashima, *Bull. Chem. Soc. Japan* 1964, **37**, 974.
18. B. M. Gatehouse, S. E. Livingstone and R. S. Nyholm, *J. Chem. Soc.* 1957, 4222.
19. N. F. Curtis and Y. M. Curtis, *Inorg. Chem.* 1965, **4**, 804.
20. C. Bellitto, D. Gattegno, A. M. Giuliani and M. Bossa, *J. Chem. Soc., Dalton Trans.* 1976, 758.
21. A. Musumeci and A. Seminara, *Inorg. Chim. Acta* 1981, **54**, L81.
22. C. B. Castfelani and O. Carugo, *Inorg. Chim. Acta* 1989, **159**, 161.

Polyhedron Vol. 12, No. 23, pp. 2815–2821, 1993
Printed in Great Britain

0277-5387/93 $6.00+.00
© 1993 Pergamon Press Ltd

SPECTRAL AND STRUCTURAL CHARACTERIZATION OF *TRANS*-DIBROMOBIS(2-BENZOYLPYRIDINE)COPPER(II) AND *TRANS*-DIAZIDOBIS(2-BENZOYLPYRIDINE)COPPER(II) [CuX_2(2-BENZOYLPYRIDINE)$_2$] (X = Br OR N_3)

FRANZ A. MAUTNER*

Institut für Physikalische und Theoretische Chemie, Technische Universität Graz, A-8010 Graz, Austria

and

MOHAMED A. S. GOHER* **and** AZZA E. H. ABDOU

Department of Chemistry, Faculty of Science, Alexandria University, P.O. Box 426, Ibrahimia, Alexandria 21321, Egypt

(*Received* 20 *April* 1993; *accepted* 15 *June* 1993)

Abstract—Complexes of copper(II) bromide and copper(II) azide with 2-benzoylpyridine (2-Bzpy), namely *trans*-dibromobis(2-benzoylpyridine)copper(II) (**1**) and *trans*-diazidobis(2-benzoylpyridine)copper(II) (**2**), have been prepared and characterized by spectroscopic methods and X-ray crystallography. The copper atom in centrosymmetric [$CuBr_2$(2-Bzpy)$_2$] (**1**) is six-coordinated by two nitrogen atoms [Cu—N = 1.970(4) Å] and two oxygen atoms [Cu—O = 2.407(4) Å] belonging to the two 2-Bzpy molecules and two *trans*-bromide atoms at Cu—Br distances of 2.468(1) Å. In the structure of complex **2**, [$Cu(N_3)_2$(2-Bzpy)$_2$], the copper atom which is also located at an inversion centre is six-coordinated by pairs of *trans*-N,O-bidentate chelating 2-Bzpy molecules [Cu—N = 2.005(3) Å, Cu—O = 2.467(3) Å] and the terminal azido ligands at Cu—N distances of 1.989(4) Å. The azido ligands are almost linear [N—N—N = 176.6(4)°] and asymmetric [N_α—N_β = 1.201(5) and N_β—N_γ = 1.158(5) Å]. The IR and electronic spectral data for both complexes are presented and discussed.

Monopyridyl ketones are potentially bidentate, or ambidentate, ligands which may show interesting coordination properties towards metal ions in the border region between class (a) and class (b) acceptors,[1] such as cobalt(II) and nickel(II). Plytzanopoulos *et al.*[2] and others[3–5] have reported complexes formed by first row transition metal ions with 2-benzoylpyridine (hereafter abbreviated as 2-Bzpy) and assigned the coordination geometry mainly on the basis of spectroscopic data. They found that 2-Bzpy acts as either a mono- or bidentate ligand in these complexes, depending on the central metal ions, the anions and the solvent used. Recent X-ray studies have shown that 2-Bzpy functions as an N,O-coordinating ligand in the polymeric complex Cu_3(2-Bzpy)$_2(N_3)_6$,[6] as well as in the dimeric complexes [Cu(2-Bzpy)$(N_3)_2]_2$[7] and [CuI(2-Bzpy)]$_2$.[8]

When a mixture of 2-Bzpy and copper(II) nitrate trihydrate and KI in aqueous/ethanolic medium was reduced by L(+)-ascorbic acid and the final mixture boiled and then allowed to stand over several weeks, an intramolecular oxidative cyclization of 2-Bzpy occurs and the complex [9H-indeno[2,1-b]pyridin-9-one)H]·CuI_2 is separated.[9] Trials to prepare the corresponding copper(I) azide complex led to the oxidation of copper(I) rather than 2-Bzpy, with the formation of a new 1 : 2 complex of copper(II) azide with 2-Bzpy. In the present paper we report our investigation of this complex along

* Authors to whom correspondence should be addressed.

with the corresponding 1 : 2 bromide complex elucidated by spectroscopic methods and X-ray crystallography. The latter complex has been described previously and suggested to possess a *cis*-octahedral structure.[2] As the IR and electronic spectra and other physical data of a sample prepared by us are very similar to those for the 1:2 azido complex having a *trans*-configuration, we have undertaken a reinvestigation of the bromide complex.

EXPERIMENTAL

Preparation of $[CuBr_2(2\text{-benzoylpyridine})_2]$ *complex* (**1**)

This complex was prepared by adding excess L(+)-ascorbic acid to a mixture of $Cu(NO_3)_2 \cdot 3H_2O$ (0.48 g, 2 mmol) and KBr (0.59 g, 5 mmol) in ethanol/aqueous medium (15/5 cm^3) followed by addition of 2-Bzpy (0.55 g, 3 mmol) dissolved in 10 cm^3 water. The final mixture was boiled for several minutes and then allowed to stand over several weeks. The complex was separated as dark green crystals. Found: C, 50.2; H, 2.9; N, 4.5; Br, 26.1; Cu, 11.1. Calc.: C, 48.9; H, 3.1; N, 4.7; Br, 27.1; Cu, 10.8%.

Preparation of $[Cu(N_3)_2(2\text{-benzoylpyridine})_2]$ *complex* (**2**)

Ethanolic solutions of copper(II) nitrate trihydrate (10 cm^3, 0.48 g, 2 mmol) and 2-Bzpy (10 cm^3, 1.10 g, 6 mmol) were mixed together, followed by addition of excess L(+)-ascorbic acid. To the resulting red solution, an aqueous solution of NaN_3 (5 cm^3, 0.26 g, 4 mmol) was added dropwise, and the final mixture boiled for several minutes and then allowed to stand over about 1 month in an open beaker. The complex was separated as dark green (almost black) crystals. Found: C, 55.7; H, 3.7; N, 22.1; Cu, 12.7. Calc.: C, 56.1; H, 3.5; N, 21.8; Cu, 12.4%.

X-ray crystallography

A modified STOE four-circle diffractometer was used for single crystal X-ray measurements. Lattice parameters were obtained by least-squares refinement of the diffraction data from 20 (compound **1**) and 18 (compound **2**) reflections in the 2θ range 8–18°. Data were collected at 300(1) K using graphite crystal-monochromatized Mo-K_α radiation ($\lambda = 0.71069$ Å) and the ω-scan technique. The intensities were corrected for Lorentz and polar-

Table 1. Crystallographic data and processing parameters of $CuBr_2(2\text{-benzoylpyridine})_2$ (**1**) and $Cu(N_3)_2(2\text{-benzoylpyridine})_2$ (**2**)

Compound	**1**	**2**
Chemical formula	$C_{24}H_{18}Br_2CuO_2N_2$	$C_{24}H_{18}CuO_2N_8$
Molecular weight	589.77	514.00
Crystal system	Monoclinic	Triclinic
a (Å)	7.401(3)	7.598(4)
b (Å)	20.690(7)	7.655(3)
c (Å)	7.403(3)	10.796(5)
α (°)		96.24(3)
β (°)	105.29(3)	110.10(3)
γ (°)		90.24(3)
V (Å^3)	1093.5(7)	585.6(5)
Space group	$P2_1/n$ (no. 14)	P-1 (no. 2)
Z	2	1
$F(000)$	582	263
D_{calc} (Mg m^{-3})	1.791	1.457
Approx. crystal size (mm)	$0.45 \times 0.20 \times 0.20$	$0.43 \times 0.20 \times 0.15$
Data collection limits	$\pm h, k, l$; $2\theta < 60°$	$\pm h, \pm k, l$; $2\theta < 55°$
Scan mode	ω-scan, $\Delta\omega = 1.5°$	ω-scan, $\Delta\omega = 1.75°$
Least squares parameters	151	169
$F_0 > 3\sigma(F_0)$	1214	1663
μ(Mo-K_α) (mm^{-1})	4.64	0.97
R	0.037	0.041
R_w	0.034	0.042
Weighting scheme	$1.521\sigma^{-2}(F_0)$	$1.591\sigma^{-2}(F_0)$
Residual electron density (e Å^{-3})	+0.56/−0.47	+0.34/−0.40

ization effects, and for absorption by an empirical method. Crystallographic data are given in Table 1.

The structures were solved by direct methods. Anisotropic displacement parameters were only applied to the non-hydrogen atoms in full-matrix least-squares refinements. The hydrogen atoms were included in the final refinement cycles on calculated positions. The programs DIFABS,[10] SHELX-76,[11] SHELXS-86,[12] PLATON[13] and THE XRAY SYSTEM[14] were used for computations. Analytical expressions of neutral-atom scattering factors were employed, and anomalous dispersion corrections were incorporated.[15] Selected bond distances and bond angles are given in Table 2. Positional parameters, anisotropic displacement parameters, hydrogen atom coordinates, a full list of bond lengths and angles and observed and calculated structure factors have been deposited with the Editor as supplementary material.

Spectral data

The IR absorption spectral bands are listed in Table 3, and electronic spectra of the solid complexes are shown in Fig. 5. The experimental procedures and instruments used for spectral and other measurements have been given previously.[16]

DISCUSSION

The interactions between copper(I) bromide or copper(I) azide and 2-Bzpy in the presence of the respective anions for a long time led to the oxidation

Table 2. Selected bond distances (Å), angles (°) and torsion angles (°)

$CuBr_2(2\text{-Bzpy})_2$ (**1**)

Br—Cu	2.468(1)	Cu—O(1)	2.407(4)
Cu—N(1)	1.970(4)	O(1)—C(6)	1.209(7)
C(5)—C(6′)	1.498(8)	C(6)—C(7)	1.484(8)

Br—Cu—O(1)	92.2(1)	Br—Cu—N(1)	89.4(1)
Br—Cu—O(1′)	87.8(1)	Br—Cu—N(1′)	90.6(1)
O(1)—Cu—N(1)	105.4(2)	O(1)—Cu—N(1′)	74.6(2)
Cu—O(1)—C(6)	107.2(4)	Cu—N(1)—C(1)	119.3(4)
Cu—N(1)—C(5)	120.9(4)	N(1)—C(5)—C(6′)	114.9(5)
O(1)—C(6)—C(7)	120.6(5)	O(1)—C(6)—C(5′)	118.9(5)
C(7)—C(6)—C(5′)	120.5(5)		

O(1)—Cu(1)—N(1)—C(5)	177.5(5)	N(1)—C(5)—C(6′)—O(1′)	20.2(8)
N(1)—C(5)—C(6′)—C(7′)	−158.9(5)	C(4)—C(5)—C(6′)—O(1′)	−158.8(6)
C(4)—C(5)—C(6′)—C(7)	22.1(9)	O(1)—C(6)—C(7)—C(8)	149.9(6)
O(1)—C(6)—C(7)—C(12)	−25.7(9)	C(5′)—C(6)—C(7)—C(8)	−29.3(9)

symmetry code: (′) $-x, -y, 1-z$

$Cu(N_3)_2(2\text{-Bzpy})_2$ (**2**)

Cu—O(1)	2.467(3)	Cu—N(1)	2.005(3)
Cu—N(11)	1.989(4)	O(1)—C(6)	1.231(5)
C(5)—C(6)	1.512(4)	C(6)—C(7)	1.483(5)
N(11)—N(12)	1.201(5)	N(12)—N(13)	1.158(5)

O(1)—Cu—N(1)	74.1(1)	O(1)—Cu—N(11)	85.0(1)
O(1)—Cu—N(1′)	105.9(1)	N(1)—Cu—N(11′)	92.2(1)
O(1)—Cu—N(11′)	95.0(1)	N(1)—Cu—N(11)	87.8(1)
Cu—O(1)—C(6)	104.3(2)	Cu—N(1)—C(1)	120.8(3)
Cu—N(1)—C(5)	120.1(2)	Cu—N(11)—N(12)	121.6(3)
N(11)—N(12)—N(13)	176.6(4)	O(1)—C(6)—C(7)	121.2(3)
N(1)—C(5)—C(6)	115.1(3)	O(1)—C(6)—C(5)	118.5(3)
C(5)—C(6)—C(7)	120.2(3)		

O(1)—Cu—N(1)—C(5)	11.1(3)	N(1)—C(5)—C(6)—O(1)	−24.7(5)
N(1)—C(5)—C(6)—C(7)	158.5(3)	C(4)—C(5)—C(6)—O(1)	149.7(4)
C(4)—C(5)—C(6)—C(7)	−27.1(5)	O(1)—C(6)—C(7)—C(8)	146.8(4)
O(1)—C(6)—C(7)—C(12)	−30.0(5)	C(5)—C(6)—C(7)—C(8)	−36.5(5)

symmetry code: (′) $-x, -y, -z$

Table 3. IR spectral data

Frequency (cm^{-1})			
2-Bzpy	1	2	Assignment
		2038 vs	$\nu_{as}(N_3)$
1663 vs[a]	1640 vs	1648 vs	ν(C=O)
1580 ms	1590 s	1590 s	pyridine ring
1560 m	1570 ms	1570 ms	vibrations
1430 ms	1440 ms	1440 ms	
1300 s	1320 s	1310 ms	
1220 s	1248	1255 ms	
995 s	1033 m	1028 m	
610 ms	655 ms	650 ms	
		610 w	$\delta(N_3)$
		365 ms	ν[Cu---N(N_3)]
	270 s	270 m	ν[Cu---N(L)]
	240 s	235 s	

[a] s = strong, m = medium, w = weak, v = very.

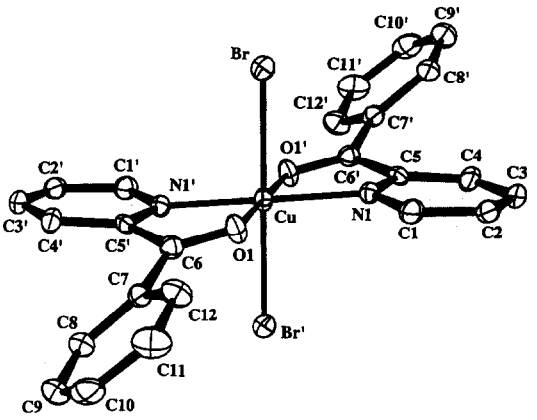

Fig. 1. Coordination figure and atom numbering scheme of $[CuBr_2(2\text{-Bzpy})_2]$ (**1**).

of copper(I) rather than the organic ligand, as found in the case of copper(I) iodide,[9] and afforded the eponymous copper(II) complexes. These complexes can also be prepared by direct interaction between the components or by mixing of copper(II) nitrate trihydrate and 2-Bzpy followed by addition of KX (X = Br or N_3) in ethanol. A sample of the 1:2 bromide complex was also prepared according to the method given previously.[2,3] X-ray powder diffraction patterns, IR and electronic spectral data of samples prepared by different procedures are so similar that we could not distinguish one from the other. One or the other of the title complexes are soluble in ethanol, acetonitrile, chloroform and DMF, and both gave non-conducting solutions in nitromethane as reported previously.[2,3]

Complex molecules of the bromide compound **1** have crystallographically imposed $\bar{1}$ symmetry. Figure 1 is a perspective drawing showing its *trans*-configuration along with the atom labelling. Taking the different size of ligating atoms into account, the coordination about the copper atom can be described as a tetragonal bipyramid with the oxygen atoms of the two 2-Bzpy ligands occupying the axial positions. This arrangement is different from that of *cis*-$Cu(2\text{-Bzpy})_2X_2$ (X = Cl or Br), the structure of which was inferred from IR and UV–vis spectra.[2,3] In accordance with the division of Cu—L distances into three ranges,[17] the measured axial Cu—Br bond of 2.468(1) Å is long and the equatorial Cu—N(2-Bzpy) bond of 1.970(4) Å is short, whereas the other Cu—O(2-Bzpy) bond of 2.407(4) Å is long. This long Cu—O distance, which reflects a weak interaction between the oxygen atom of 2-Bzpy and copper atoms, confirms the previous conclusion based on spectroscopic data.[2,3] A *trans* arrangement in other complexes of 2-Bzpy has been revealed in the structures of the $[Cu(2\text{-Bzpy})_2(H_2O)_2]^{2+}$ cation with intermediate Cu—O(aqua) bonds of 2.256(3) Å,[18] and $[Cu(2\text{-Bzpy})_2(ClO_4)_2]$ with long axial Cu—O(ClO_4) bonds of 2.485(17) and 2.492(7) Å.[19] The five-membered ring formed by copper atoms and the bidentate 2-Bzpy deviates from planarity [torsion angle N(1)—C(5)—C(6′)—O(1′) = 20.2(8)°].

Figure 3 illustrates the principal structural features of the $[Cu(N_3)_2(2\text{-Bzpy})_2]$ complex **2**, in which the copper atom is also located at an inversion centre. Each copper centre is coordinated by pairs of *trans*-N,O-bidentate chelating 2-Bzpy ligands [Cu—N = 2.005(3), Cu—O = 2.467(3) Å] and terminal azido ligands at Cu—N distances of 1.989(4) Å. The coordination about the copper atom can be described as a tetragonal bipyramid with the oxygen atoms of the 2-Bzpy ligands occupying the axial positions, very similar to the geometry around the copper atom in complex **1**. The five-membered chelate ring formed by copper atom and the bidentate 2-Bzpy also deviates from planarity [torsion angle N(1)—C(5)—C(6)—O(1) = −24.7(5)°]. The interaction between the copper atoms and carbonyl oxygen of the 2-Bzpy ligand is weaker than that in the case of the bromide complex, as indicated by the difference in Cu—O bonds in both compounds.

The terminal azido ligands are almost linear within experimental error [∠N—N—N = 176.6(4)°] and asymmetric [N_α—N_β = 1.201(5), N_β—N_γ = 1.158(5) Å]. The Cu—N(N_3) bond lengths match very well those reported in the structures of [CuBr(N_3)(tedt)] (tedt = 1,1,7,7-tetraethyldiethylenetriamine) [1.927(6) Å],[20] [Cu

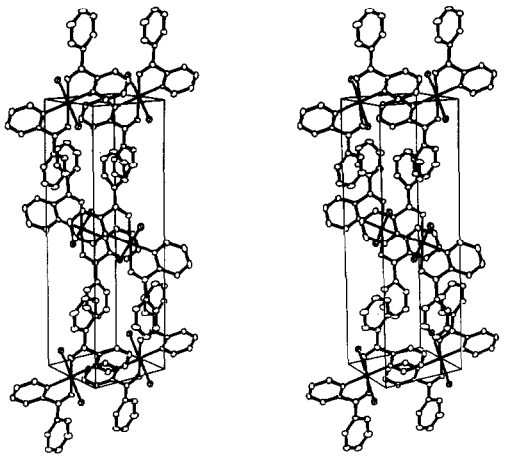

Fig. 2. $[CuBr_2(2\text{-Bzpy})_2]$: packing in the unit cell viewed approximately along [101].

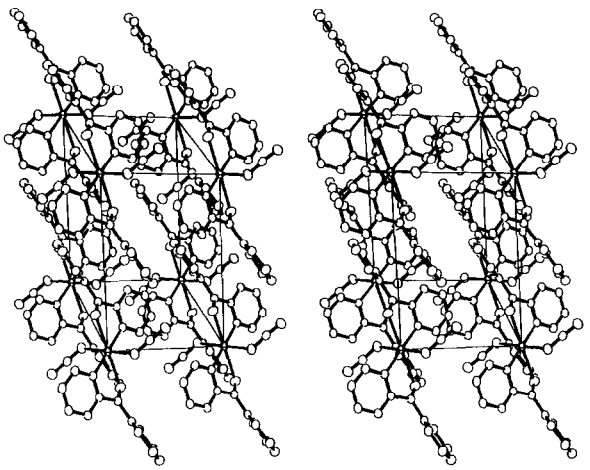

Fig. 4. $[Cu(N_3)_2(2\text{-Bzpy})_2]$: packing in the unit cell viewed down the *b*-axis.

$(pymep)(N_3)_2]$ (pymep = *N*-(2′-(6-methyl)pyridyl) (methylene-2-(2′-pyridyl)ethylamine) [1.986(7) and 2.039(8) Å][21] and $[Cu(N_3)_2$'diEten)] (diEten = *N*,*N*-diethylenediamine) [2.004(3) Å],[22] but are a little shorter than the corresponding values [2.015(3) and 2.176(3) Å] found in the structure of [Cu(2-pyridinecarbaldehyde)-histamine$(N_3)_2$],[23] all of which contain terminal azido ligands.

Stereoviews of the packing of both crystal structures are shown in Figs 2 and 4, respectively.

It is of interest to compare the 1 : 2 mixed ligand copper(II) azido complexes of pyridine,[24] 3-picoline,[25] 4-picoline[26] and 2-Bzpy. A common structural feature in this series of complexes is a six-coordination about the copper atom. The monomeric nature of the 2-Bzpy complex arises from the fact that the organic ligand acts as a bidentate, thus enforcing the two azides to function as terminal monodentate ligands. The organic ligand is monodentate in the first three complexes and the unsaturation in the copper sphere is satisfied by converting one or both azido groups from terminal to bridge mode. In the pyridine complex, as one of the two azides remains terminal, the other azide serves as a $\mu(1,1,3)$ bridging ligand, whereas the two azides function as $\mu(1,1)$ bridges in the 4-picoline complex and as $\mu(1,1)$ and $\mu(1,3)$ bridges in the 3-picoline complex, giving rise to polymeric structures for these three complexes.

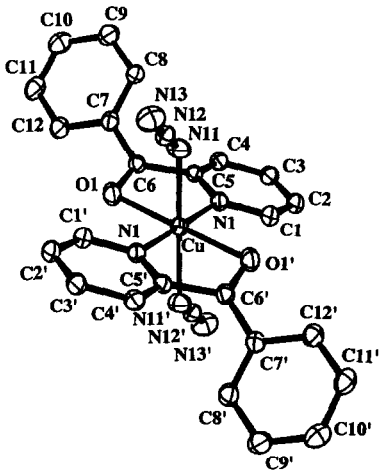

Fig. 3. Coordination figure and atom numbering scheme of $[Cu(N_3)_2(2\text{-Bzpy})_2]$ (**2**).

The IR spectral data given in Table 3 show a small decrease of ν(C=O) from 1663 cm^{-1} in free 2-Bzpy to 1640 and 1648 cm^{-1} in complexes **1** and **2**, respectively. Indeed, a substantial reduction of ν(C=O) with $\Delta\nu \cong 30$–70 cm^{-1} was observed for other metal complexes of 2-Bzpy and taken as good evidence for the coordination of the carbonyl oxygen.[2,3] The observed small decrease of ν(C=O) in the case of complexes **1** and **2** does not mean the exclusion of ν(C=O) from coordination. In fact, although a strong copper–carbonyl oxygen interaction occurs in the complex cation $[Cu(2\text{-bzpy})_2(H_2O)_2]^{2+}$, as indicated by the Cu—O distance of 2.068(2) Å, its spectrum shows only a very slight shift of ν(C=O) to 1555 cm^{-1}.[18] Thus the reduction of ν(C=O), together with the shift of pyridine ring vibrations to higher frequencies, suggests a simultaneous N,O-coordination of 2-Bzpy.

The crystal structure determinations show that complex **2** contains two crystallographically identical asymmetric terminal azido ligands with $\Delta d = 0.043$ Å (Δd is the difference between the N—N distances). Thus, only a single band associated with each of $\nu_{as}(N_3)$ and $\nu_s(N_3)$ is expected.

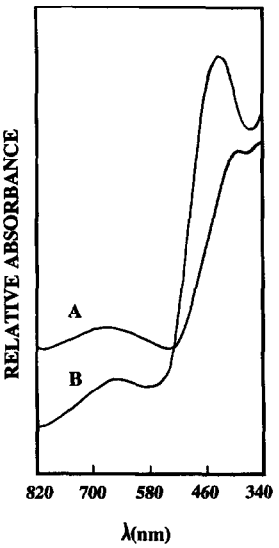

Fig. 5. Reflectance spectra of solid complexes: (A) $[CuBr_2(2\text{-Bzpy})_2]$ and (B) $[Cu(N_3)_2(2\text{-Bzpy})_2]$.

Moreover, from the relationship between Δd and $\nu_{as}(N_3)$ given earlier,[27,28] the single absorption band due to $\nu_{as}(N_3)$ is expected to be around 2043 cm^{-1}, a value which is very close to that of 2038 cm^{-1} given in Table 3. The strong absorptions of the ligand in the region 1350–1270 cm^{-1} masks the $\nu_s(N_3)$ absorption band.

The electronic spectra of complexes **1** and **2** are given in Fig. 5. The strong absorption bands at 25,640 and 23,255 cm^{-1} in the spectra of complexes **1** and **2**, respectively, are due to LMCT transitions from the bromide or azide to copper. The position of these bands indicates the influence of the azide group on the charge transfer as compared to the halide ions. Both complexes, however, exhibit an asymmetric *d–d* absorption band at 14,930 and 15,500 cm^{-1} for complexes **1** and **2**, respectively. For the bromide complex the previous value was 14,500 cm^{-1}.[2,3] These spectra are consistent with distorted octahedral copper(II) environments.[29,30] Previous studies[7,25,31–34] have shown that the electronic spectra of solid copper(II) azido complexes containing cyclic $Cu_2N_2(N_3)$ units usually exhibit a distinct absorption band in the vicinity of 17,000–20,000 cm^{-1}. The intensity of this band is so strong that it could not be attributed to *d–d* transitions. This band was considered as due to LMCT transition from bridging azides of the type $\mu(1,1)$ to copper(II).[35] The disappearance of any absorption in the range 17,000–20,000 cm^{-1} from the spectrum of complex **2** having only terminal azides, confirms our previous conclusion that the existence of such a band should be taken as strong evidence of the existence of binuclear cyclic Cu_2N_2 units, and hence at least two $\mu(1,1)$ bridging azido ligands.[35] The results given here may be of value in distinguishing between copper(II) azido complexes containing only terminal azide groups and those containing $\mu(1,1)$ bridging azido ligands.

Acknowledgement—The authors thank Prof. Ch. Kratky for the use of equipment.

REFERENCES

1. S. Ahrland, J. Chatt and N. R. Davies, *Quart. Rev. (London)* 1958, **12**, 265.
2. M. Plytzanopoulos, G. Pneumatikakis, N. Hadjiliadis and D. Katakis, *J. Inorg. Nucl. Chem.* 1977, **39**, 965.
3. R. R. Osborne and W. R. McWhinnie, *J. Chem. Soc. (A)* 1977, 2075.
4. A. W. Downs, W. R. McWhinnie, B. G. Naik and R. S. Osborne, *J. Chem. Soc. (A)* 1970, 2624.
5. J. D. Ortego and D. L. Perry, *J. Inorg. Nucl. Chem.* 1973, **35**, 3031.
6. M. A. S. Goher and T. C. W. Mak, *Inorg. Chim. Acta* 1985, **99**, 223.
7. T. C. W. Mak and M. A. S. Goher, *Inorg. Chim. Acta* 1986, **115**, 17.
8. M. A. S. Goher, A. E. H. Abdou, W.-H. Yip and T. C. W. Mak, *Inorg. Chim. Acta*, submitted.
9. M. A. S. Goher, A. E. H. Abdou and T. C. W. Mak, unpublished.
10. N. Walker and D. Stuart, *Acta Cryst.* 1983, **A39**, 158.
11. G. M. Sheldrick, SHELX-76, A Program for Crystal Structure Determination. University Chemical Laboratory, Cambridge (1976).
12. G. M. Sheldrick, SHELXS-86, Universität Göttingen (1986).
13. A. L. Spek, in *Computation Crystallography* (Edited by D. Sayre), p. 528. Clarendon Press, Oxford (1982).
14. J. M. Stewart, The X-RAY SYSTEM, version of 1976, Technical Report TR-466, University of Maryland, College Park (1976).
15. *International Tables for X-ray Crystallography*, Vol. IV, pp. 99, 149. Kynoch Press, Birmingham (1974).
16. M. A. S. Goher, R.-J. Wang and T. C. W. Mak, *Polyhedron* 1992, **11**, 829.
17. J. H. Brian, in *Comprehensive Coordination Chemistry* (Edited by G. Wilkinson, R. D. Gillard and J. A. McCleverty), Vol. V, pp. 596–597. Pergamon Press, Oxford (1987).
18. M. A. S. Goher, R.-J. Wang and T. C. W. Mak, *J. Cryst. Spectrosc. Res.* 1990, **20**, 265.
19. M. A. S. Goher, T. C. W. Mak, S. K. Hoffmann, to be published.
20. R. F. Ziolo, M. Allen, D. D. Titus, H. B. Gray and Z. Dori, *Inorg. Chem.* 1972, **11**, 3044
21. T. Rojo, J. I. R. Larramendi, J. I. Mesa, J. Via and M. I. Arriortua, *Polyhedron* 1990, **9**, 2697.

22. O. L. Casagrande, Jr., S. I. Klein, A. F. Mauro and K. Tomita, *Trans. Met. Chem.* 1989, **14**, 45.
23. Y. Nakao, M. Yamazaki, S. Suzuki, W. Mori, A. Nakahara, K. Matsumoto and S. I. Ooi, *Inorg. Chim. Acta* 1983, **74**, 159.
24. I. Agrell, *Acta Chem. Scand.* 1969, **23**, 1667.
25. F. A. Mautner and M. A. S. Goher, *Polyhedron* 1992, **11**, 2537.
26. M. A. S. Goher and F. A. Mautner, *Cryst. Res. Technol.* 1992, **27**, 817.
27. I. Agrell, *Acta Chem. Scand.* 1971, **25**, 2965.
28. M. A. S. Goher, *Acta Chim. Hung.* 1990, **127**, 213.
29. R. J. Dudley, B. J. Hathaway, P. G. Hodgson, P. C. Power and D. J. Loose, *J. Chem. Soc., Dalton Trans.* 1974, 1005.
30. B. J. Hathaway, *J. Chem. Soc., Dalton Trans.* 1972, 1196.
31. M. A. S. Goher and T. C. W. Mak, *Inorg. Chim. Acta* 1984, **85**, 117; *ibid.* 1984, **89**, 119.
32. M. A. S. Goher, R.-J. Wang and T. C. W. Mak, *J. Molec. Struct.* 1991, **243**, 179.
33. M. A. S. Goher and F. A. Mautner, *Z. Naturfor.* 1990, **46b**, 687.
34. M. A. S. Goher, *Rev. Inorg. Chem.* 1986, **8**, 102.
35. M. A. S. Goher, *Acta Chim. Hung.* 1988, **125**, 877.

Polyhedron Vol. 12, No. 23, pp. 2823–2829, 1993
Printed in Great Britain

0277–5387/93 $6.00+.00
© 1993 Pergamon Press Ltd

SYNTHESIS, SPECTROSCOPIC AND CRYSTAL STRUCTURE STUDY OF DI-μ(1,1)-AZIDO-μ(*O*,*O*)-NITRATO(*O*-NITRATO)TETRAKIS(3-PICOLINE)AQUADICOPPER(II) AND CATENA-DI-μ(1,3)-AZIDO-[DI-μ(1,1)-AZIDO-BIS(4-PICOLINE)DICOPPER(II)] [$Cu_2(N_3)_2(NO_3)_2$(3-PICOLINE)$_4(H_2O)$] AND Cu(4-PICOLINE)$(N_3)_2$

FRANZ A. MAUTNER*

Institut für Physikalische und Theoretische Chemie, Technische Universität Graz, A-8010 Graz, Austria

and

MOHAMED A. S. GOHER

Department of Chemistry, Faculty of Science, Alexandria University, Alexandria 21321, Egypt

(*Received* 30 *April* 1993; *accepted* 15 *June* 1993)

Abstract—Two mixed ligand complexes of copper(II) azide with 3-picoline and 4-picoline, namely di-μ(1,1)-azido-μ(*O*,*O*)-nitrato)(*O*-nitrato)tetrakis(3-picoline)dicopper(II) (**1**) and catena-di-μ(1,3)-azido-[di-μ(1,1)-azido-bis(4-picoline)dicopper(II)] (**2**), have been synthesized and characterized by X-ray crystallography. The structure of complex **1** consists of asymmetric dimeric units in which Cu(1) is six-coordinated to two nitrogen atoms from the picoline molecules, two nitrogen atoms of the two μ(1,1) bridging azido ligands and two oxygen atoms of the two nitrate anions. Cu(2) is also six-coordinated to two nitrogen atoms of the other two picolines, two nitrogen atoms of the two μ(1,1) bridging azido ligands, an oxygen atom of the aqua molecule and an oxygen atom of the μ(*O*,*O*) bridging nitrato group. The structure of complex **2** features distorted square pyramidal Cu^{II} coordination geometry, centrosymmetric di-μ(1,1) azido bridged Cu_2N_2 rings and di-μ(1,3) azido bridges which link the binuclear Cu_2(4-picoline)$_2(N_3)_2$ moieties into chains along the short *a*-axis. The IR and electronic spectra of the solid complexes are presented and discussed.

Copper(II) ion forms coordination compounds of a rich variety of stereochemistries.[1,2] The array of structural types are further enriched in copper(II) azide–nitrogen base adducts, owing to the variable manner of azide ligand binding[3] giving rise to the terminal end-to-end bridging and end-on bridging modes illustrated elsewhere.[4] Thus, the copper(II) ion is in a tetragonally distorted octahedral environment in the polymeric complexes Cu(py)$_2(N_3)_2$[5] and Cu$(NH_3)_2(N_3)_2$,[6] but adopts a distorted trigonal bipyramidal coordination geometry in the dimeric complex [Cu(pymep)$(N_3)_2]_2 \cdot 2H_2O$ (pymep = (*N*-(2′-6-methyl)pyridyl)methylene-(2,2′-pyridyl)ethylamine), in which the water molecules form hydrogen bonds with the azide groups.[7] Recently, we isolated and characterized the structures of polymeric Cu(3-picoline)$(N_3)_2$,[8] Cu(3-picoline)$_2(N_3)_2$[9] and Cu(4-picoline)$_2(N_3)_2$[10] complexes. The 1:1 copper(II) azide complex of 3-picoline possesses distorted trigonal pyramidal coordination polyhedra about the copper(II) ion and contains only

* Author to whom correspondence should be addressed.

μ(1,1) bridging azido ligands, whereas the 1:2 complex displays two crystallographically independent six-coordinate copper octahedra and contains μ(1,1) and μ(1,3) bridging azido groups. The 4-picoline complex, on the other hand, features oligomeric edge-sharing chains of polyhedra. Further work led to the synthesis of a new 1:1 complex of copper(II) azide with 4-picoline (hereafter abbreviated as 4-pic) and another new complex with 3-picoline (3-pic) of the composition $[Cu_2(N_3)_2(NO_3)_2(3\text{-pic})_4(H_2O)]$. The structure elucidation of these two complexes by X-ray and spectroscopic methods is presented in this report.

EXPERIMENTAL

Preparation of $[Cu_2(N_3)_2(NO_3)_2(3\text{-pic})_4(H_2O)]$ (**1**)

Copper(II) nitrate trihydrate (0.46 g, 2 mmol) dissolved in 30 cm^3 ethanol and 3-pic (0.93 g, 10 mmol) were mixed together followed by the addition of NaN_3 (0.13 g, 2 mmol) in 3 cm^3 water. The green coloured mixture was allowed to stand in an open beaker over two or three days until near dryness, upon which large black crystals separated. Crystals are sensitive to daylight and X-ray exposure. Found: C, 39.6; H, 4.3; N, 23.1; Cu, 17.5. Calc.: C, 39.7; H, 4.2; N, 23.2; Cu, 17.5%.

Preparation of polymeric $Cu(4\text{-pic})(N_3)_2$ (**2**)

Copper(II) nitrate trihydrate (0.96 g, 4 mmol) dissolved in 40 cm^3 ethanol and 4-pic (0.56 g, 6 mmol) were mixed together, followed by addition of NaN_3 (0.65 g, 10 mmol) in 5 cm^3 water. The brown mixture was allowed to stand over several weeks until black needles separated. Found: C, 30.0; H, 2.8; N, 40.5; Cu, 26.5. Calc.: C, 29.9; H, 2.9; N, 40.7; Cu, 26.4%.

Procedures and instruments used for other measurements are as described previously.[11]

X-ray crystallography

A modified STOE four-circle diffractometer was used for single crystal X-ray measurements. Orientation matrix and lattice parameters were obtained by least-squares refinement of the diffraction data from 24 (compound **1**) and 35 (compound **2**) reflections in the 2θ range 8–21°. Data were collected at 300(1) K using graphite crystal-monochromatized Mo-K_α radiation (λ = 0.71069 Å) and the ω-scan technique. The intensities were corrected for Lorentz and polarization effects, and for absorption.[12] For compound **1** an intensity decay correction was also included in the data reduction procedure (the intensity of three standard reflections dropped to 64% during X-ray exposure). Crystallographic data are given in Table 1.

The structures were solved by Patterson superposition methods and subsequent Fourier analyses. Anisotropic displacement parameters were applied to the non-hydrogen atoms in full-matrix least-squares refinements. The hydrogen atoms were included in the final refinement cycles on calculated positions. In order to improve the data/parameter ratio for the data set of compound **1**, atoms of nitrato groups were assigned with isotropic U values, and blocked-matrix least-squares techniques applied for refinements. The programs DIFABS,[12] SHELX-76,[13] SHELXS-86,[14] PLATON[15] and THE XRAY SYSTEM[16] were used for computations. Analytical expressions of neutral-atom scattering factors were employed, and anomalous dispersion corrections were incorporated.[17] Selected bond distances and bond angles are given in Table 2. Positional parameters, anisotropic displacement parameters, hydrogen atom coordinates, a full list of bond lengths and angles and observed and calculated structure factors have been deposited with the Editor as supplementary material.

DISCUSSION

Figures 1 and 2 illustrate the principal structural features of $[Cu_2(N_3)_2(NO_3)_2(3\text{-pic})_4(H_2O)]$ (**1**). The structure consists of asymmetric dimers. Both copper(II) atoms in each dimer, however, have distorted elongated octahedral environments. Cu(1) is coordinated to N(1) and N(2) of two picoline

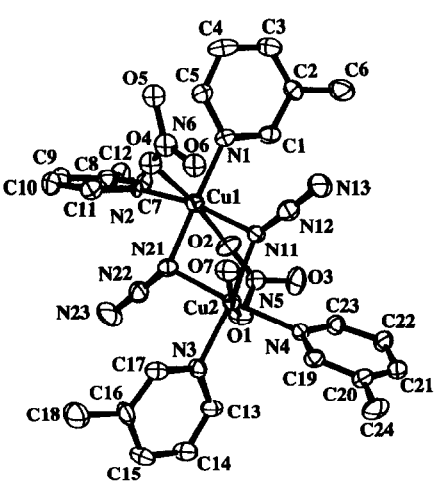

Fig. 1. The molecular geometry and atom numbering scheme of $Cu_2(N_3)_2(NO_3)_2(3\text{-pic})_4(H_2O)$ (**1**).

Table 1. Crystallographic data and processing parameters

Compound	**1**	**2**
Molecular formula	$C_{24}H_{30}Cu_2N_{12}O_7$	$C_6H_7CuN_7$
Molecular weight	725.67	240.71
Crystal system	Monoclinic	Triclinic
a (Å)	8.330(5)	5.288(1)
b (Å)	20.506(9)	9.675(2)
c (Å)	18.818(8)	9.925(2)
α (°)		110.38(2)
β (°)	98.04(3)	100.48(2)
γ (°)		92.37(2)
V (Å^3)	3183(3)	465.0(2)
Space group	$P2_1/c$ (no. 14)	P-1 (no. 2)
Z	4	2
$F(000)$	1488	242
μ(Mo-K_α) (mm^{-1})	1.40	2.32
D_{calc}/D_{obs} (Mg m^{-3})	1.514/1.51(2)	1.719/1.72(2)
Approx. crystal size (mm)	$0.60 \times 0.30 \times 0.25$	$0.60 \times 0.15 \times 0.15$
Data collection limits	$\pm h, k, l; 2\theta < 48°$	$\pm h, \pm k, l; 2\theta < 62°$
Scan mode	ω-scan, $\Delta\omega = 1.50°$	ω-scan, $\Delta\omega = 1.25°$
$F_0 > 3\sigma(F_0)$	2204	1724
Least-squares parameters	366	134
R	0.070	0.037
R_w	0.069	0.038
Weighting scheme	$6.335\sigma^{-2}(F_0)$	$1.327\sigma^{-2}(F_0)$
Residual extrema in final difference map (e Å^{-3})	+0.76/−0.46	+0.69/−0.37

molecules at Cu—N bond lengths of 1.986(10) and 1.980(10) Å, and two nitrogen atoms N(11) and N(21) of two μ(1,1) bridging azido ligands [Cu—N distances are 1.986(9) and 1.998(9) Å]. This copper atom further links two oxygen atoms of the two nitrato groups. The Cu(2) atom, on the other hand, is bonded to N(3) and N(4) of further 3-pic molecules with Cu—N bond lengths of 1.988(9) and 2.007(9) Å, and N(11) and N(21) of the two μ(1,1) bridging azido groups at Cu—N distances of 1.994(9) and 2.012(10) Å. The coordination number six of Cu(2) is completed through its binding to the aqua molecule [Cu(2)—O(7) = 2.338(8) Å] and the O(1) of a nitrato group with a long Cu(2)—O(1) bond length of 2.670(8) Å. The two nitrato groups, therefore, behave differently in this complex; one of them acts as a monodentate ligand bonded to Cu(1) and the other functions as a bridging bidentate group. The Cu—O distances with the $\mu(O,O)$ bridging nitrato ligand are much longer than the Cu—O distance with the monodentate nitrato group (Table 2).

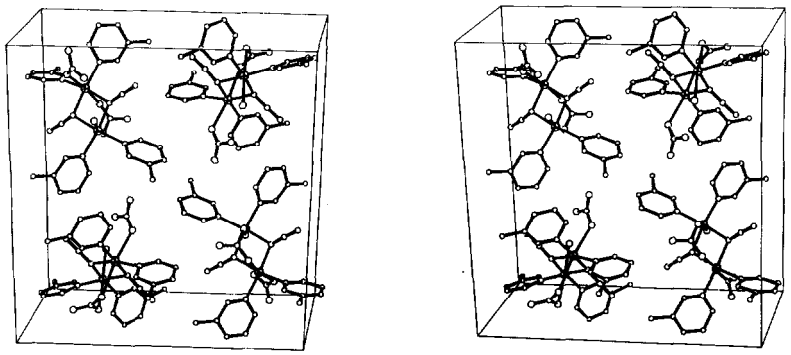

Fig. 2. Unit cell of $Cu_2(N_3)_2(NO_3)_2$(3-pic)$_4(H_2O)$ (**1**), viewed along the a-axis of the unit cell.

Table 2. Selected bond distances (Å) and bond angles (°)

$Cu_2(N_3)_2(NO_3)_2(3\text{-pic})_4(H_2O)$ (**1**)

Cu(1)—O(2)	2.691(8)	Cu(1)—O(4)	2.465(12)
Cu(1)—N(1)	1.986(10)	Cu(1)—N(2)	1.980(10)
Cu(1)—N(11)	1.986(9)	Cu(1)—N(21)	1.998(9)
Cu(2)—N(11)	1.994(9)	Cu(2)—N(21)	2.012(10)
Cu(2)—O(1)	2.670(8)	Cu(2)—O(7)	2.338(8)
Cu(2)—N(3)	1.988(9)	Cu(2)—N(4)	2.007(9)
O(1)—N(5)	1.26(1)	O(2)—N(5)	1.23(1)
O(3)—N(5)	1.21(1)	O(4)—N(6)	1.19(2)
O(5)—N(6)	1.24(2)	O(6)—N(6)	1.18(2)
N(11)—N(12)	1.21(1)	N(12)—N(13)	1.17(2)
N(21)—N(22)	1.22(1)	N(22)—N(23)	1.17(2)
Cu(1)···Cu(2)	3.087(3)		

O(2)—Cu(1)—O(4)	172.6(4)	O(2)—Cu(1)—N(1)	93.7(3)
O(2)—Cu(1)—N(2)	83.8(3)	O(2)—Cu(1)—N(11)	81.9(3)
O(2)—Cu(1)—N(21)	90.4(3)	O(4)—Cu(1)—N(1)	90.5(4)
O(4)—Cu(1)—N(2)	90.0(4)	O(4)—Cu(1)—N(11)	103.7(4)
O(4)—Cu(1)—N(21)	86.0(4)	N(1)—Cu(1)—N(2)	92.1(4)
N(1)—Cu(1)—N(11)	96.0(4)	N(1)—Cu(1)—N(21)	173.0(4)
N(2)—Cu(1)—N(11)	164.0(4)	N(2)—Cu(1)—N(21)	94.0(4)
N(11)—Cu(1)—N(21)	79.0(4)	N(11)—Cu(2)—N(21)	78.5(4)
N(11)—Cu(2)—O(1)	81.8(3)	N(11)—Cu(2)—O(7)	86.9(3)
N(11)—Cu(2)—N(3)	171.0(4)	N(11)—Cu(2)—N(4)	95.4(4)
N(21)—Cu(2)—O(1)	80.4(3)	N(21)—Cu(2)—O(7)	96.5(4)
N(21)—Cu(2)—N(3)	93.1(4)	N(21)—Cu(2)—N(4)	169.4(4)
O(1)—Cu(2)—O(7)	168.6(3)	O(1)—Cu(2)—N(3)	93.8(3)
O(1)—Cu(2)—N(4)	90.2(3)	O(7)—Cu(2)—N(3)	97.3(3)
O(7)—Cu(2)—N(4)	91.7(4)	N(3)—Cu(2)—N(4)	92.4(4)
Cu(2)—O(1)—N(5)	116.6(6)	Cu(1)—O(2)—N(5)	112.8(6)
Cu(1)—O(4)—N(6)	132.3(12)	O(1)—N(5)—O(2)	119.7(9)
O(1)—N(5)—O(3)	119.3(10)	O(2)—N(5)—O(3)	120.8(10)
O(4)—N(6)—O(5)	113.1(15)	O(4)—N(6)—O(6)	123.4(16)
O(5)—N(6)—O(6)	122.6(16)	Cu(1)—N(11)—Cu(2)	101.7(4)
Cu(1)—N(11)—N(12)	123.1(8)	Cu(2)—N(11)—N(12)	125.2(7)
N(11)—N(12)—N(13)	178.4(13)	Cu(1)—N(21)—Cu(2)	100.7(4)
Cu(1)—N(21)—N(22)	122.3(7)	Cu(2)—N(21)—N(22)	119.6(8)
N(21)—N(22)—N(23)	175.9(13)		

Cu(4-pic)$(N_3)_2$ (**2**)

Cu···Cu(c)	3.120(1)	Cu—N(1)	1.983(3)
Cu—N(11)	1.999(3)	Cu—N(21)	1.980(3)
Cu—N(23)	2.457(3)	Cu—N(11c)	2.005(3)
N(11)—N(12)	1.205(4)	N(12)—N(13)	1.130(5)
N(21)—N(22)	1.182(4)	N(22)—N(23b)	1.162(4)

N(1)—Cu—N(11)	172.9(1)	N(1)—Cu—N(21)	95.0(1)
N(1)—Cu—N(23)	93.4(1)	N(1)—Cu—N(11c)	95.3(1)
N(11)—Cu—N(21)	91.6(1)	N(11)—Cu—N(23)	87.3(1)
N(11)—Cu—N(11c)	77.6(1)	N(21)—Cu—N(23)	104.8(1)
N(21)—Cu—N(11c)	157.0(1)	N(23)—Cu—N(11c)	95.0(1)
Cu—N(11)—N(12)	125.6(3)	Cu—N(11)—Cu(c)	102.4(1)
Cu(c)—N(11)—N(12)	129.2(2)	N(11)—N(12)—N(13)	178.1(4)
Cu—N(21)—N(22)	124.8(3)	N(21)—N(22)—N(23b)	176.9(4)
Cu—N(23)—N(22a)	113.5(2)		

Symmetry code: (a) $x-1, y, z$; (b) $x+1, y, z$; (c) $-x, -y, -z$.

The Cu—N(3-pic) distances are very close to, whereas the Cu—N(N_3) distances in the Cu_2N_2 cyclic unit are shorter than, the corresponding values found in the structure of Cu(3-pic)$_2$(N_3)$_2$.[9] The latter Cu—N distances, however, fall in the range reported for similar bond distances in structures containing cyclic Cu_2N_2 units, e.g. Cu(4-methylquinoline)(N_3)$_2$ [1.972(6) and 1.974(5) Å],[18] Cu(2-picoline)(N_3)$_2$ [2.020(2) and 2.002(2) Å][18] and Cu(diethylnicotinamide)(N_3)$_2$ [2.006(2) Å].[19] The two azide ligands are almost linear [angle N(11)—N(12)—N(13) = 178.4(13)° and N(21)—N(22)—N(23) = 175.9(13)°] and asymmetric [N(11)—N(12) = 1.21(1) Å, N(12)—N(13) = 1.17(2) Å, and N(21)—N(22) = 1.22(1) Å, N(22)—N(23) = 1.17(2) Å]. These N—N distances correspond very well with the values reported for μ(1,1) bridging azido ligands in similar copper(II) azido complexes.[8,10,19]

A linear polymeric copper(II) complex, [Cu_2(N_3)$_2$(NO_3)$_2$(BET)$_2$]$_n$ (BET = $(CH_3)_3NCH_2CO_2$) was recently reported by Mak and co-workers.[20] Two different copper atoms, both featuring elongated octahedral environments, are simultaneously bridged by a μ(1,1) azido group, a μ(*O*,*O*) nitrato group, and a μ(*O*,*O*) carboxylato group of the betaine molecule. The apical sites of polyhedra are occupied by nitrato oxygen atoms [Cu—O from 2.419(4) to 2.446(3) Å]; the other Cu—N(O) bond lengths are in the range from 1.960(4) to 1.997(3) Å. The Cu···Cu separation of 3.436(1) Å is responsible for the unusually large Cu—N—Cu angle of 119.5(2)° of the symmetric bridging μ(1,1) azide group.

The principal structural features of the title complex (**2**) are illustrated in Fig. 3. The stereochemistry about each copper(II) atom is best described as distorted square pyramidal with basal bonds to N(11), N(21), N(1) and N(11c) in the range from 1.980(3) to 2.005(3) Å, and a longer apical bond of 2.457(3) Å to N(23). The 4-pic molecule coordinates the copper through N(1) with a Cu—N distance of 1.983(3) Å, which is very close to the corresponding Cu—N distances found in the structure of Cu(4-pic)$_2$(N_3)$_2$ [from 1.95(2) to 2.06(2) Å]. Centrosymmetric dimers are formed via μ(1,1) bridging azido groups N(11)—N(12)—N(13). The other azido group N(21)—N(22)—N(23b) functions as a μ(1,3) bridging ligand. As seen in Fig. 4, the structure contains chains of Cu_2N_2 units connected via two μ(1,3) azido groups along the short *a*-axis. The two independent azido groups are almost linear, and the N_α—N_β and N_β—N_γ bond lengths show a much smaller difference in the case of μ(1,3) bridging (Table 2).

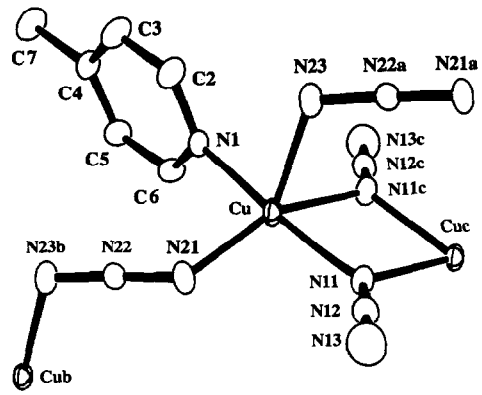

Fig. 3. Tetragonal pyramidal environment of the copper(II) centre and the atom numbering scheme of Cu(4-pic)(N_3)$_2$ (**2**) (symmetry code according to Table 2, b).

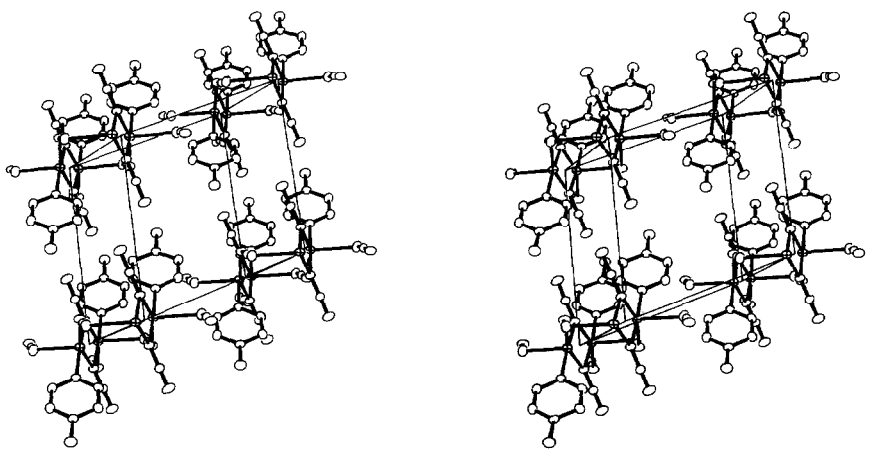

Fig. 4. Stereoplot of the structure of Cu(4-pic)(N_3)$_2$ viewed down approximately the *a*-axis of the unit cell.

The structure of the title complex **2** resembles that of di-μ(1,3)-azido-[di-μ(1,1)-azido-bis(2-picoline)dicopper(II)][18] (**3**), but also differs from it in several subtle aspects. Although complex **3** also exhibits distorted tetragonal pyramidal coordination about each copper atom, the Cu_2N_2 units are connected by μ(1,3) azido ligands to form layers of polyhedra, and the apical Cu—N distance is much shorter [2.273(2) Å] than the corresponding distance of 2.457(3) Å in **2**. The Cu(4-pic)$(N_3)_2$ complex also differs from the corresponding Zn(4-pic)$(N_3)_2$, although the zinc atom has a five-coordinate environment. In the latter complex, both azido groups function in the μ(1,1) fashion.[21]

Compared with other 1:1 complexes of copper(II) azide with substituted pyridine ligands, the structure of **2** differs from that of Cu(3-pic)$(N_3)_2$ (**4**), in which the coordination polyhedron of the copper atom is distorted trigonal bipyramid.[8] The structure of **4** contains three distinct μ(1,1) bridging azido groups; two azides bridge a pair of copper atoms forming a planar Cu_2N_2 ring and the third group asymmetrically links alternate copper atoms to yield an infinite zig-zag chain. The title complex **2** also differs from that of the polymeric 1:1 copper(II) azide complex of *N,N*-diethylnicotinamide.[19] In the latter complex, the coordination about each copper atom is an elongated octahedron with four short Cu—N bonds [from 1.979(5) to 2.006(5) Å] and two much longer axial Cu—N bonds [2.755(5) and 2.841(5) Å]. One of the two crystallographically independent azide groups acts as a μ(1,1) bridge, whereas the other is a μ(1,1,3) bridging group which interlinks the Cu_2N_2 units into a corrugated chain.

The interest in the IR spectra of these complexes lies mainly in the bands due to the nitrate groups and aqua molecule in complex **1**, in addition to those due to azido groups in both complexes. As seen from Table 3, the IR spectrum of complex **1** shows several bands due to the nitrato groups. The positions of these bands suggest that unidentate and bidentate types of coordinated nitrato groups are mixed in this complex, as has been found for other similar complexes.[22] The medium broad band with two peaks around 3400 and 3300 cm^{-1} indicates a hydrogen-bonded aqua molecule.[23,24] The IR spectrum of complex **1** also shows a very strong band at 2045 cm^{-1}, with a shoulder around 2060 cm^{-1} associated with the relation between the frequency of the asymmetric stretching vibration of azide groups and the difference between the two N—N distances (Δd).[25,26] The $\nu_s(N_3)$ is masked by the nitrate absorption. The IR spectrum of the solid complex **2** exhibits two well defined, very strong bands at 2070 and 2020 cm^{-1} due to the $\nu_{as}(N_3)$ modes of the N(11)—N(12)—N(13) and N(21)—N(22)—N(23b) groups, respectively. The appearance of the $\nu_s(N_3)$ mode as strong absorption bands in the region 1340–1280 cm^{-1} is strong evidence of the asymmetric nature of the azido ligands.

Table 3. IR spectral data

Frequency (cm^{-1})		
1	**2**	Assignments
2060 sh[a]	2070 vs	$\nu_{as}(N_3)$
2045 vs	2020 vs	
1480 m		A_1, B_2 of
1445 ms		NO_3 groups
1410 s		
1380 vs		
1280 m		
	1332 m	$\nu_s(N_3)$
	1290 s	
660 wm	610 w	$\delta(N_3)$
590 w	590 w	
360 m	393 m	ν(Cu—N_3)
345 m	360 m	
	340 m	
265 ms	270 ms	ν(Cu—L)

[a] s = strong, m = medium, w = weak, v = very, sh = shoulder.

The electronic spectrum (Fig. 5) of the solid complex **1** exhibits its *d–d* absorption band at 15,260 cm^{-1}, together with a distinct absorption band at 20,200 cm^{-1}. This result is consistent with distorted octahedral environments about the copper atoms.[27] For complex **2** the *d–d* band appears at 13,888 cm^{-1}, together with a distinct absorption band at 18,518 cm^{-1}. This *d–d* absorption band falls in the region frequently reported for five-coordinate

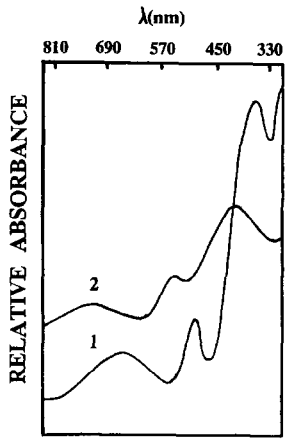

Fig. 5. Reflectance spectra of solid complexes. 1: [$Cu_2(N_3)_2(NO_3)_2$(3-pic)$_4(H_2O)$]; 2: Cu(4-pic)$(N_3)_2$.

copper(II) complexes.[1,2,28] The whole spectrum is very close to that reported for $Cu(3\text{-pic})(N_3)_2$, which features a distorted trigonal bipyramid.[8] The position of the *d–d* band, however, differs from those found for $[Cu(2\text{-ampy})(N_3)_2(H_2O)]_2$ (14,490 cm^{-1}),[29] Cu(Et-nicotinate)$(N_3)_2$ (12,048 cm^{-1}),[11] $[Cu(2\text{-Bzpy}(N_3)_2]_2$, (15,625 cm^{-1})[30] and $Cu(2\text{-pic})(N_3)_2$ (13,333 cm^{-1}),[18] all of which possess distorted pyramidal copper(II) atoms.

Acknowledgement—The authors thank Prof. Kratky for use of experimental equipment.

REFERENCES

1. B. J. Hathaway and D. E. Billing, *Coord. Chem. Rev.* 1970, **5**, 143.
2. B. J. Hathaway, *Coord. Chem. Rev.* 1981, **35**, 221.
3. Z. Dori and R. F. Ziolo, *Chem. Rev.* 1973, **73**, 247 and references therein.
4. M. A. S. Goher and T. C. W. Mak, *Inorg. Chim. Acta* 1985, **99**, 223.
5. I. Agrell, *Acta Chem. Scand.* 1969, **23**, 1667.
6. I. Agrell, *Acta Chem. Scand.* 1966, **20**, 1281.
7. T. Rojo, J. I. R. Larramendi, I. Duran, J. I. Mesa, J. Via and M. I. Arriortua, *Polyhedron* 1990, **9**, 2693.
8. M. A. S. Goher and T. C. W. Mak, *Inorg. Chim. Acta* 1984, **89**, 119.
9. F. A. Mautner and M. A. S. Goher, *Polyhedron* 1992, **11**, 2537.
10. M. A. S. Goher and F. A. Mautner, *Cryst. Res. Technol.* 1992, **27**, 817.
11. T. C. W. Mak and M. A. S. Goher, *Inorg. Chim. Acta* 1985, **99**, 223.
12. N. Walker and D. Stuart, *Acta Cryst.* 1983, **A39**, 158.
13. G. M. Sheldrick, SHELX-76, A Program for Crystal Structure Determination. University Chemical Laboratory, Cambridge (1976).
14. G. M. Sheldrick, SHELXS-86. Universität Göttingen, Germany (1986).
15. A. L. Spek, in *Computational Crystallography* (Edited by D. Sayre), p. 528. Clarendon Press, Oxford (1982).
16. J. M. Stuart, The X-RAY SYSTEM, version of 1976, Technical Report TR-466. University of Maryland, College Park (1976).
17. *International Tables for X-ray Crystallography*, Vol. IV, pp. 99, 149. Kynoch Press, Birmingham (1974).
18. M. A. S. Goher and F. A. Mautner, *Z. Naturfor.* 1991, **46b**, 687.
19. M. A. S. Goher, R.-J. Wang and T. C. W. Mak, *J. Molec. Struct.* 1991, **243**, 179.
20. M.-Y. Chow, Z.-Y. Zhou and T. C. W. Mak, *Inorg. Chem.* 1992, **31**, 4900.
21. F. A. Mautner, H. Krischner and Ch. Kratky, *Z. Naturfor.* 1988, **43b**, 253.
22. R. V. Biagetti and H. M. Heindler, *Inorg. Chem.* 1966, **5**, 383.
23. I. Nakagawa and T. Shimanouchi, *Spectrochim. Acta* 1964, **20**, 429.
24. K. Ichida, Y. Kuroda, D. Nakamura and M. Kubo, *Spectrochim. Acta* 1972, **28A**, 2433.
25. I. Agrell, *Acta Chem. Scand.* 1971, **25**, 2965.
26. M. A. S. Goher, *Acta Chim. Hung.* 1990, **127**, 213.
27. R. J. Fereday, *J. Chem. Soc. A* 1971, 3035.
28. E. D. McKenzie, *J. Chem. Soc. A* 1970, 3096.
29. M. A. S. Goher and T. C. W. Mak, *Inorg. Chim. Acta* 1984, **85**, 117.
30. M. A. S. Goher and T. C. W. Mak, *Inorg. Chim. Acta* 1986, **115**, 17.

Polyhedron Vol. 12, No. 23, pp. 2831–2839, 1993
Printed in Great Britain

0277–5387/93 $6.00+.00
© 1993 Pergamon Press Ltd

SYNTHESES, THERMAL BEHAVIOUR, AND SPECTROSCOPIC AND X-RAY STUDIES OF QUINOLINIUM SALTS OF NICKEL(II), PALLADIUM(II) AND PLATINUM(II) 1,2-DITHIOOXALATO-*S,S′* COMPLEXES. PACKING AND BONDING OF THE QUINOLINIUM BIS(1,2-DITHIOOXALATO-*S,S′*)NICKELATE(II)

PASCUAL ROMÁN,* JAVIER I. BEITIA and ANTONIO LUQUE

Departamento de Química Inorgánica, Universidad del País Vasco, Apartado 644, 48080 Bilbao, Spain

(*Received* 20 *April* 1993; *accepted* 15 *June* 1993)

Abstract—Three quinolinium (HC_9H_7N = Hquin) salts of planar inorganic dithiooxalato complexes: $(Hquin)_2[Ni(S_2C_2O_2)_2]$ (**1**), $(Hquin)_2[Pd(S_2C_2O_2)_2]$ (**2**) and $(Hquin)_2[Pt(S_2C_2O_2)_2]$ (**3**) were synthesized and characterized by elemental analysis, IR and UV–vis spectroscopies, thermal analysis (TG, DTG and DTA) and X-ray diffraction techniques. Spectroscopic data support the presence of the aromatic cation and the complex anion. The complexes show a high thermal stability and the thermal studies give evidence that the onset temperatures of their thermal decompositions, the corresponding reaction mechanism and the final solid products are strongly influencd by the atmospheric conditions, as well as the chemical and structural features of the starting compounds. X-ray diffraction analyses show that **2** and **3** are isomorphous with **1**, which crystallizes in the monoclinic space group $P2_1/n$ with $Z = 2$ so that the anion straddles a crystallographic centre of symmetry. The crystal structure of **1** is built up by layers of quasi-planar $[Ni(S_2C_2O_2)_2]^{2-}$ complexes (A) and quinolinium cations (C) stacked along the *c*-axis, following an $\cdots$ACCACC$\cdots$ sequence, with alternative interplanar spacings of 3.3–3.8 Å (A$\cdots$C) and 3.44 Å (C$\cdots$C), which suggest the existence of significant π–π and d_{z^2}–π interactions between the cations and the complexes' anions. These interactions, together with the electrostatic forces and an extensive network of hydrogen contacts, ensure the lattice cohesion and give the compound a three-dimensional character.

Recently, much attention has been devoted to the coordination chemistry of metal complexes involving sulphur donor ligands, due to the applications of these compounds in analytical chemistry, catalysis and their relevance to bioinorganic systems.[1] One of these sulphur donor ligands is the dithiooxalate dianion, in which the presence of four donor atoms and the possibilities of charge delocalization on its atoms results in a multifunctional ligand with unique coordination properties.[2–4]

On the other hand, oxidative thermal decompositions of various nickel, palladium and platinum complexes are used for the production of metal and metal oxides which are extensively applied as catalysts in a variety of important chemical processes.[5]

In this context we have studied the reaction between aromatic cations and several square-planar inorganic metal(II) 1,2-dithiooxalato-*S,S′* anions in order to obtain a deeper insight into the cation and metal effects on the crystal packing and the strength of the intramolecular interactions in this type of compound.[6–9] The present paper reports the syntheses, the chemical characterization and the thermal behaviour of quinolinium salts of 1,2-dithiooxalate-*S,S′* metalate anions, $[M(S_2C_2O_2)_2]^{2-}$, where M is Ni^{II}, Pd^{II} or Pt^{II}, as well as the crystal and

*Author to whom correspondence should be addressed.

molecular structure of the compound quinolinium bis(1,2-dithiooxalato-*S*,*S*′)nickelate(II).

EXPERIMENTAL

General and instrumental

The dithiooxalate ligand was used as purchased from Eastman Kodak. The potassium salts of the complex anions, $[M(S_2C_2O_2)_2]^{2-}$, were prepared according to the literature method.[10] Elemental analyses of carbon, hydrogen and nitrogen were performed on a Perkin–Elmer 240 analyser. Metal analyses were made on a Perkin–Elmer 360 Atomic Absorption/Flame Emission spectrometer. IR and UV–vis spectra were run on IR Beckman 4240 and Bausch-Lomb Spectronic 2000 spectrophotometers, respectively. Density values were measured by flotation in a mixture of CCl_4–$CHBr_3$. The thermoanalytical data (TG, DTG and DTA) were obtained, simultaneously, in argon and argon–oxygen atmospheres on a Setaram Tag 24 S16 thermobalance, with a heating rate of 5°C min^{-1}. X-ray powder diffraction patterns of **2**, **3** and the final products from thermal decompositions of compounds **1–3** were obtained on a Philips PW 1710 instrument with nickel-filtered Cu-K_α radiation. Diffraction patterns of thermal decomposition residues were compared with those obtained from the ASTM powder diffraction files of the Joint Committee on Powder Diffraction Standards (JCPDS).[11]

Synthesis of complexes

Quinolinium bis(1,2-dithiooxalato-S,S′)nickelate(II) $(HC_9H_7N)_2[Ni(S_2C_2O_2)_2]$ (**1**). An aqueous solution (25 cm^3) of quinolinium hydrochloride (0.60 g, 3.62 mmol) was added to 25 cm^3 of an aqueous solution of $K_2[Ni(S_2C_2O_2)_2]$ (0.55 g, 1.46 mmol) with stirring at room temperature. Immediately, an insoluble microcrystalline powder of **1** was obtained. Dark purple single crystals suitable for X-ray investigations were obtained by recrystallization from an H_2O–DMF (1 : 1, v/v) mixture, after 3 weeks. Yield: 0.62 g, 1.11 mmol, 76% based on nickel. Found: C, 47.3; H, 2.8; N, 5.0; Ni, 10.4. Calc. for $C_{22}H_{16}N_2NiO_4S_4$: C, 47.2; H, 2.9; N, 5.0; Ni. 10.5%. Selected IR data (KBr, cm^{-1}): 1600vs, 1545vs, 1425s [ν(C═O)]; 1075vs, [ν(C—C)+ν(C—S)]; 965s, 925s [δ(C—O)+ν_{as}(C—S)]; 575w, 443w [ν_s(C—S)]; 400m [ν_{as}(Ni—S)]; 352w [ν_s(Ni—S)].

Quinolinium bis(1,2-dithiooxalato-S,S′)palladate(II) $(HC_9H_7N)_2[Pd(S_2C_2O_2)_2]$ (**2**). This compound was synthesized from $K_2[Pd(S_2C_2O_2)_2]$ (0.50 g, 1.18 mmol) and quinolinium hydrochloride (0.45 g, 2.72 mmol) in water (50 cm^3) following the general method described for **1**. The resultant yellow precipitate was isolated by vacuum filtration, washed with EtOH and Me_2O and recrystallized from DMF. Unfortunately, yellow dark crystals were twinned and were not suitable for X-ray single crystal diffraction. Yield: 0.57 g, 0.93 mmol, 79.1% based on palladium. Found: C, 43.4; H, 2.6; N, 4.5; Pd, 17.6. Calc. for $C_{22}H_{16}N_2O_4PdS_4$: C, 43.5; H, 2.7; N, 4.6; Pd, 17.5%. Selected IR data (KBr, cm^{-1}): 1595vs, 1575vs, 1440w [ν(C═O)]; 1080vs [ν(C—C)+ν(C—S)]; 935m [δ(C—O)+ν_{as}(C—S)]; 570m [ν_s(C—S)]; 415w [ν_s(Pd—S)]; 340m [ν_{as}(Pd—S)].

Quinolinium bis(1,2-dithiooxalato-S,S′)platinate(II) $(HC_9H_7N)_2[Pt(S_2C_2O_2)_2]$ (**3**). Red crystals of this compound were prepared from $K_2[Pt(S_2C_2O_2)_2]$ (0.13 g, 0.25 mmol) and quinolinium hydrochloride (0.10 g, 0.60 mmol) in water (15 cm^3) by a similar procedure to above. Yield: 0.23 g, 0.37 mmol, 63% based on platinum. Found: C, 38.1; H, 2.4; N, 3.9; Pt, 27.9. Calc. for $C_{22}H_{16}N_2O_4PtS_4$: C, 38.0; H, 2.3; N, 4.0; Pt, 28.0%. Selected IR data (KBr, cm^{-1}): 1585vs [ν(C═O)]; 1085vs [ν(C—C)+ν(C—S)]; 950s [δ(C—O)+ν_{as}(C—S)]; 630w [ν_s(C—S)]; 465w [ν_{as}(Pt—S)]; 405w [ν_s(Pt—S)].

Crystallographic data collection and structural refinement of **1**

A dark purple prismatic single crystal of **1** (0.25 × 0.30 × 0.15 mm) was mounted on an Enraf–Nonius CAD4 four-circle diffractometer. Cell parameters and an orientation matrix for data collection, obtained from a least-squares analysis of the setting angles of 25 carefully centred reflections in the range 8–15°, correspond to the monoclinic space group $P2_1/n$. X-ray data were collected at 295 K using graphite-monochromated Cu-K_α radiation (λ = 1.54178 Å) and the ω–2θ scan technique. A total of 2160 independent reflections were measured in the range $2 \leqslant \theta \leqslant 72°$ ($0 \leqslant h \leqslant 14$; $0 \leqslant k \leqslant 10$; $-14 \leqslant l \leqslant 14$), 1865 of which, with $I > 3\sigma(I)$, were used in the development and refinement of the structure. The intensity data were corrected for Lorentz and polarization effects. An empirical absorption correction (μ = 49.885 cm^{-1}) following the procedure DIFABS[12] with minimum and maximum correction coefficients 0.765–1.231 was applied. The atomic scattering factors for neutral atoms and anomalous dispersion corrections for non-hydrogen atoms were taken from the *International Tables for X-ray Crystallography*.[13] The structure was solved by combination of Patterson and difference

Table 1. Crystal data for compounds **1–3**

Compound	**1**[a]	**2**[b]	**3**[b]
Formula	$C_{22}H_{16}N_2NiO_4S_4$	$C_{22}H_{16}N_2O_4PdS_4$	$C_{22}H_{16}N_2O_4PtS_4$
Formula weight	559.31	607.04	695.70
Space group	$P2_1/n$	$P2_1/n$	$P2_1/n$
a (Å)	11.428(3)	11.330(9)	11.631(9)
b (Å)	8.472(1)	8.469(7)	8.484(7)
c (Å)	11.721(1)	11.801(6)	11.894(7)
β (°)	100.48(1)	98.18(5)	99.03(5)
V (Å^3)	1115.9(3)	1120.7(9)	1159.2(9)
Z	2	2	2
D_x (g cm^{-3})	1.66	1.80	1.99
D_0 (g cm^{-3})	1.67(1)	1.78(2)	2.01(2)

[a] X-ray single crystal diffraction data.
[b] X-ray powder diffraction data.

Fourier methods and refined by full-matrix least-squares. Anisotropic thermal parameters were used for non-hydrogen atoms. A convenient weighting scheme[14] was used to obtain flat dependence in $\langle w\Delta^2F\rangle$ vs $\langle F_0\rangle$ and $\langle \sin\theta/\lambda\rangle$. All aromatic hydrogen atoms were clearly visible in a difference-Fourier synthesis and were refined isotropically. Last cycles of refinement lead to the discrepancy indices $R = 0.040$ and $R_w = 0.040$ for 183 parameters; goodness of fit = 0.99; maximum shift/error in the final cycle = 0.15 and the highest peak in the final Fourier difference map was 0.85 e Å^{-3}. Most calculations were carried out using the X-RAY76 System[15] running on a Micro VAX II computer. Final atomic positional and thermal parameters, together with observed and calculated structure factors, have been deposited as supplementary material with the Editor, from whom copies are available on request. Atomic coordinates have also been submitted to the Cambridge Crystallographic Data Centre.

Compounds **2** and **3** crystallized in insufficient quality to be studied by X-ray single crystal diffraction, but their cell parameters have been obtained by X-ray powder diffraction data. Table 1 summarizes the crystal data for the three compounds and shows that all of them are isostructural.

RESULTS AND DISCUSSION

Spectroscopic characterization

IR spectra of the three complexes certify the presence of the quinolinium cations, as shown by the corresponding bands at about 3000 cm^{-1} for the C—H groups, and the characteristic and very strong bands of quinolinium cations between 1650 and 600 cm^{-1}. IR assignments of the bis(dithiooxalato)metalate(II) anions have been made in the 1600–350 cm^{-1} region and a comparison of the results with the observed spectra of the reported compounds[6,7,16] leads to the assignments described in the Experimental section.

Table 2 lists the maximum peaks of the UV–vis spectra, as well as their assignments according to the literature.[2,17,18] The spectra of the three complexes show absorptions at *ca* 312, 299 and 223 nm, attributable to the $\pi \rightarrow \pi^*$ and $n \rightarrow \pi^*$ transitions of the quinolinium cations,[17] which are not affected by the complex anion. The rest of the spectral bands correspond to electronic transitions into the complex anions, with discrepancies due to the existence of different M—S bonds. For the $[Pd(S_2C_2O_2)]^{2-}$, the $M \rightarrow L(\pi^*)$ and $d_{xy} \rightarrow d_{x^2-y^2}$ bands are probably covered by the very intense $L \rightarrow M$ band at 276.7 nm.

Table 2. UV–vis spectra for compounds **1–3** [EtOH, λ nm ($\varepsilon \times 10^{-3}$, M^{-1} cm^{-1})]

1	**2**	**3**	Assignment
569.2 (2.2)		468.9 (4.7)	$M \rightarrow L(\pi^*)$
569.2 (2.2)		332.6 (3.2)	$d_{xy} \rightarrow d_{x^2-y^2}$
507.5 (3.0)		436.1 (5.7) 419.3 (4.9)	$M \rightarrow L(\pi^*)$
298.7 (27.2)	383.9 (7.7)		$L(\pi) \rightarrow M$
263.5 (22.8)	242.9 (21.0)	233.6 (27.4)	$L(\pi) \rightarrow L(\pi^*)$
225.5 (59.1)	276.7 (44.6)	228.2 (51.8)	$L(\sigma) \rightarrow M$
312.5 (21.6) 293.1 (26.2)	312.1 (15.0) 298.1 (19.8)	312.3 (7.7) 299.1 (7.5)	$\pi \rightarrow \pi^*$
223.1 (65.6)	223.5 (72.1)	223.5 (56.2)	$n \rightarrow \pi^*$

Thermal analysis

Very little has been published to date about the thermal decomposition of thioxalate complexes in general and 1,2-dithiooxalate complexes in particular.[8,9] The purpose of this study is to reveal the influence of the surrounding atmosphere and metal nature on the thermal decomposition, as well as to obtain different final products that may develop novel catalytic properties. Table 3 lists the steps, initial and final temperatures (°C), partial and total weight losses, enthalpy (endothermic or exothermic) and maximum peak for each step in the thermal decompositions of the three compounds in argon–oxygen and argon atmospheres.

The TG–DTA curves for the compounds in the oxidative and inert atmospheres are shown in Figs 1 and 2. Thermogravimetric curves indicate that the decompositions are not simple, and stable intermediate products are not found during the thermal processes since most of the stages were not resolved. Attempts to correlate the results with theoretical mass losses were not successful, except for the final solid products, which were identified by X-ray powder diffraction methods.

The thermal decompositions of the compounds are quite different in oxidative and inert atmospheres and the final residues depend on the starting compound. In an argon–oxygen atmosphere, the nickel complex is stable up to approximately 200°C, beyond which two abrupt weight losses take place corresponding to two exothermic peaks in the DTA curve, attributable to the pyrolysis of organic cations and the breakdown of the dithiooxalate ligands. The chemical analysis of the solid stable final residue, obtained above 270°C, gives no indication of carbon, nitrogen or hydrogen present in its composition and it was mainly identified as NiS by comparing its X-ray powder diffraction pattern with the Powder Diffraction File No 2-1280; however, its X-ray powder diffractogram also shows the presence of some diffraction maxima which could be identified according to different nickel oxides and sulphides (NiO, Ni_2O_3 and Ni_2S_3) presented in the JCPDS. In the inert atmosphere, **1** undergoes decomposition in a single step between 205 and 260°C, and the final black residue, whose elemental analyses did not reveal the presence of carbon, was identified as nickel(II) sulphide. In the oxidative atmosphere, **2** undergoes decomposition in one endothermic process followed by two exothermic ones. The final product obtained above 330°C was mainly identified as a mixture of palladium(0), palladium(II) oxide and palladium(II) sulphide. The elemental analysis of the final residue from the thermal decomposition of **2** in an inert atmosphere above 550°C gave no indication of carbon, nitrogen or hydrogen present in its composition, and it was

Table 3. Thermal analysis data for compounds **1–3** (°C)

	$Ar+O_2$					Ar			
Step	T_i	T_f	T_m[a]	Δm[b]	Step	T_i	T_f	T_m[a]	Δm[b]
Compound **1**									
1	200	245	240(+)	55.23	1	205	260	240(−)	83.05
2	245	270	265(+)	25.55					(83.05)
				(80.78)					
Compound **2**									
1	200	265	245(−)	68.40	1	205	280	260(−)	73.50
2	265	300	290(+)	3.13	2[c]	280	550		3.42
3	300	330	315(+)	6.57					(76.92)
				(78.10)					
Compound **3**									
1	175	255	250(+)	53.51	1	185	295	260(−)	52.32
2[c]	255	288		1.32	2[c]	295	555		5.60
3	288	308	300(+)	12.74	3[c]	555	850		13.20
4	308	350	330(+)	2.25					(71.12)
				(69.82)					

[a] Endothermic (−) or exothermic (+) process.
[b] Total mass losses are shown in parentheses.
[c] Progressive mass loss without clear peaks in DTG and/or DTA curves.

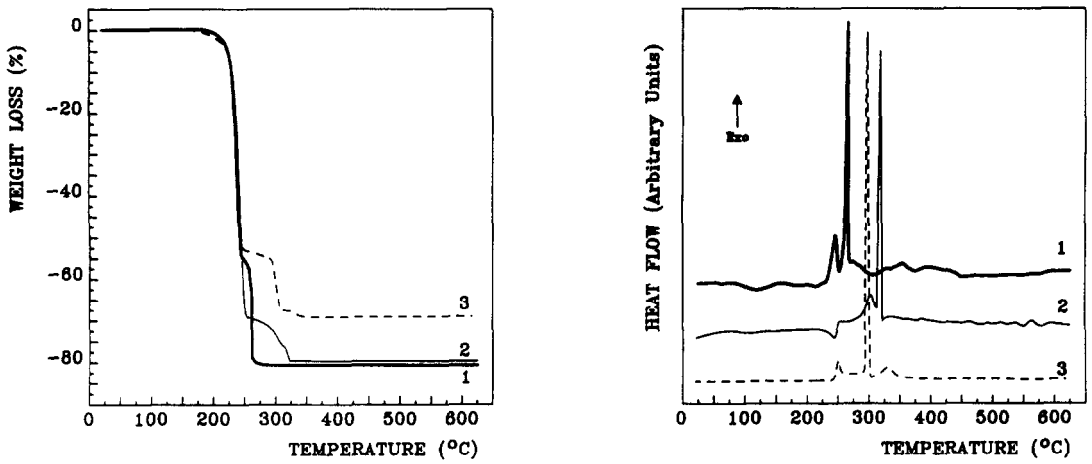

Fig. 1. TG (left) and DTA (right) curves for compounds **1**–**3** in an argon–oxygen atmosphere.

identified by its X-ray power diffraction pattern as palladium(II) sulphide. The thermal decomposition of the platinum complex in both atmospheres yielded platinum(0) as the final product.

X-ray structure determination

The asymmetric unit of **1** consists of one quinolinium cation and one-half of a complex anion, $[Ni(S_2C_2O_2)_2]^{2-}$, with the nickel atom lying on a centre of symmetry. Figure 3 shows the structures of the complex dianion and the cation with the atomic numbering scheme. Selected bond lengths, bond angles and the hydrogen contacts are listed in Table 4. The complex dianion is almost planar and the dihedral angle between the strictly planar NiS_4 group and the $S_2C_2O_2$ ligand mean plane [1.66(4)°] is in the lower end of the range previously observed for similar bis(dithiooxalato)metalate(II) anions in compounds also containing aromatic cations (1–9°)[6–9] and is considerably lower than those observed in analogous complexes containing large and bulky cations (7–20°).[19] The value of this angle is affected by a combination of factors, including the hydrogen contacts between the oxygen atoms and the hydrogen atoms of cations, as well as the π–π interactions between the aromatic cations and the dithiooxalate groups. Both of them may produce a displacement of the ligand atoms and a higher value of the dihedral angle between the MS_4 and the dithioxalate groups. Bond distances and angles within the dithioxalate group are comparable with those reported in the literature[2] and are consistent with the existence of a significant degree of delocalization throughout the S—C—O units in the dianion, with a single C—C bond of 1.549(5) Å. As far as the

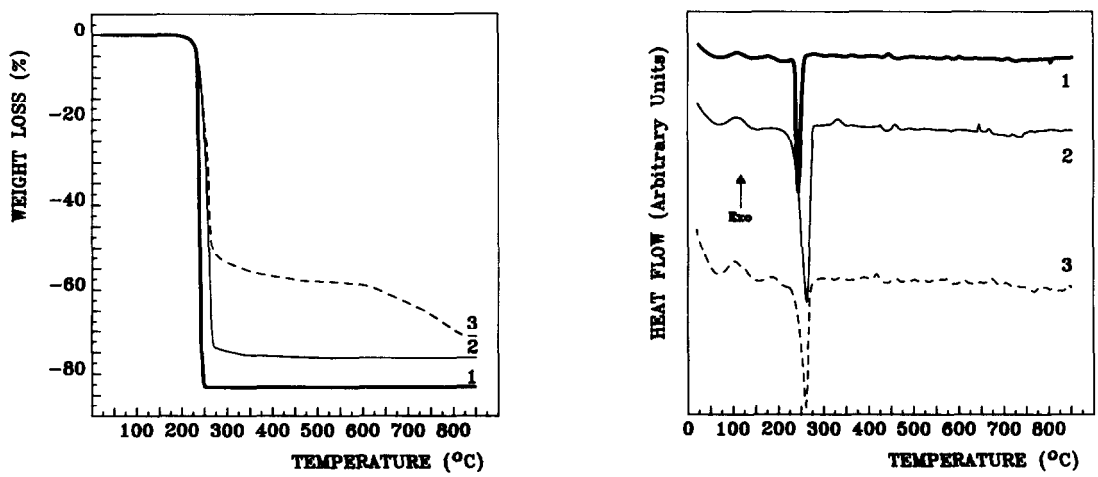

Fig. 2. TG (left) and DTA (right) curves for compounds **1**–**3** in an argon atmosphere.

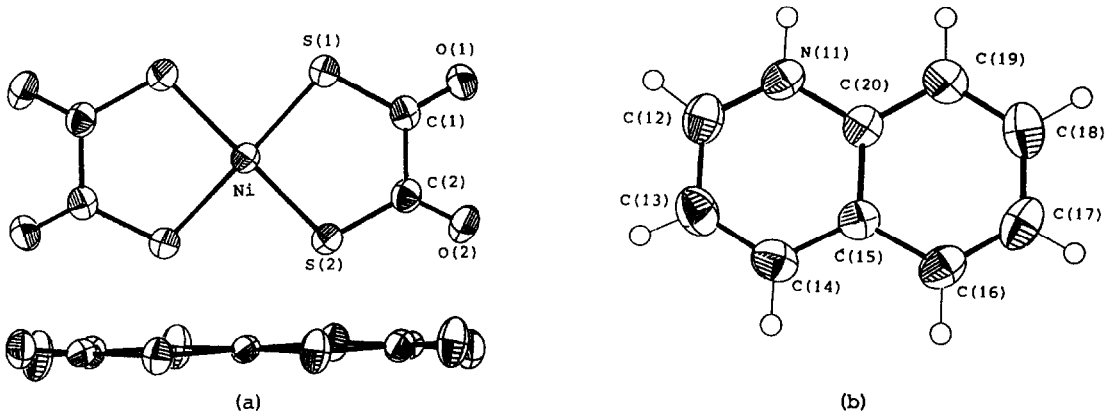

Fig. 3. An ORTEP view of the structure of: (a) the $[Ni(S_2C_2O_2)_2]^{2-}$ anion and (b) the quinolinium cation, showing the atom labelling scheme.

Table 4. Selected bond lengths (Å), bond angles (°) and hydrogen contacts for compound **1**

Anion			
Ni—S(1)	2.178(1)	S(1)—Ni—S(2)	92.10(4)
Ni—S(2)	2.162(1)	Ni—S(1)—C(1)	106.5(1)
S(1)—C(1)	1.711(4)	Ni—S(2)—C(2)	106.6(1)
S(2)—C(2)	1.716(4)	S(1)—C(1)—O(1)	125.0(3)
C(1)—C(2)	1.549(5)	S(1)—C(1)—C(2)	117.1(3)
C(1)—O(1)	1.228(4)	C(2)—C(1)—O(1)	117.8(3)
C(2)—O(2)	1.218(5)	S(2)—C(2)—O(2)	124.6(3)
		S(2)—C(2)—C(1)	117.5(3)
		C(1)—C(2)—O(2)	117.9(3)
Cation			
N(11)—C(20)	1.371(5)	C(12)—N(11)—C(20)	122.9(4)
N(11)—C(12)	1.321(5)	N(11)—C(12)—C(13)	120.3(3)
C(12)—C(13)	1.388(6)	C(12)—C(13)—C(14)	119.6(4)
C(13)—C(14)	1.369(6)	C(13)—C(14)—C(15)	120.3(4)
C(14)—C(15)	1.395(5)	C(14)—C(15)—C(16)	123.3(4)
C(15)—C(16)	1.415(6)	C(14)—C(15)—C(20)	118.8(3)
C(15)—C(20)	1.412(5)	C(16)—C(15)—C(20)	117.9(3)
C(16)—C(17)	1.348(6)	C(15)—C(16)—C(17)	120.4(4)
C(17)—C(18)	1.413(7)	C(16)—C(17)—C(18)	120.6(4)
C(18)—C(19)	1.364(6)	C(17)—C(18)—C(19)	121.0(4)
C(19)—C(20)	1.393(5)	C(18)—C(19)—C(20)	118.7(4)
		N(11)—C(20)—C(15)	118.1(3)
		N(11)—C(20)—C(19)	120.5(3)
		C(15)—C(20)—C(19)	121.3(3)

Hydrogen contacts

	X—H	X···O	H···O	∠X—H···O
N(11)—H(11)···O(1) (*1*)	0.94(5)	2.777(4)	1.85(5)	172(5)
C(19)—H(19)···O(1) (*1*)	0.96(5)	3.434(5)	2.74(5)	130(4)
C(12)—H(12)···O(1) (*2*)	0.94(5)	3.482(5)	2.56(5)	166(4)
C(13)—H(13)···O(2) (*2*)	0.92(5)	3.056(5)	2.37(5)	131(4)

Symmetry codes

(*1*) $\frac{1}{2}+x, \frac{1}{2}-y, \frac{1}{2}+z$ (*2*) $1-x, 1-y, 1-z$

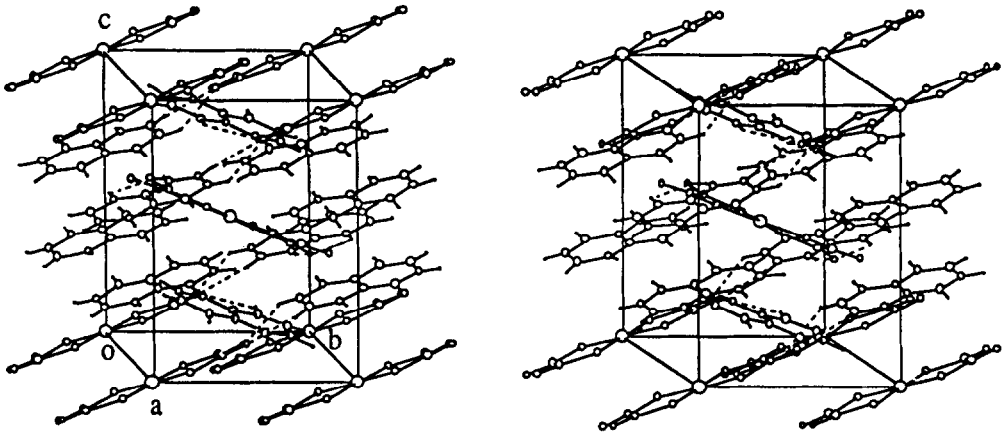

Fig. 4. Stereo packing diagram for $(HC_9H_7N)_2[Ni(C_2S_2O_2)_2]$ (hydrogen contacts: dotted line).

quinolinium cation is concerned, the two almost planar rings are tilted relative to one another by 1.5(1)° and show no abnormal geometry.[20]

The laminar structure of compound **1** is built up by mixed stacks of complex anions (A) and organic cations (C) developing along the *c*-axis, according to the scheme ··· ACCACC ··· (Fig. 4). The best A and C planes form a dihedral angle of 14.59(6)° and the mean plane of the anion is tilted by *ca* 24° with respect to the *ab* plane.

Of particular interest is the positioning of the anion which lies sandwiched between two quinolinium cations which are related by the centrosymmetric centre (Fig. 5a). The N-containing ring of the quinolinium lies up and down the NiS_4 plane (Ni ··· ring, 3.62 Å) and makes an angle of 76.4° with the nickel d_{z^2} orbital. A similar disposition is observed in metalloporphyrins, in which the metal atom lies above the centre of the porphyrin ring.[21] The second ring of the quinolinium cation is disposed above and below the dithiooxalate ligands, where a significant degree of electronic delocalization is present, with an interplanar space of 3.3–3.8 Å and a dihedral angle of 15.4°.

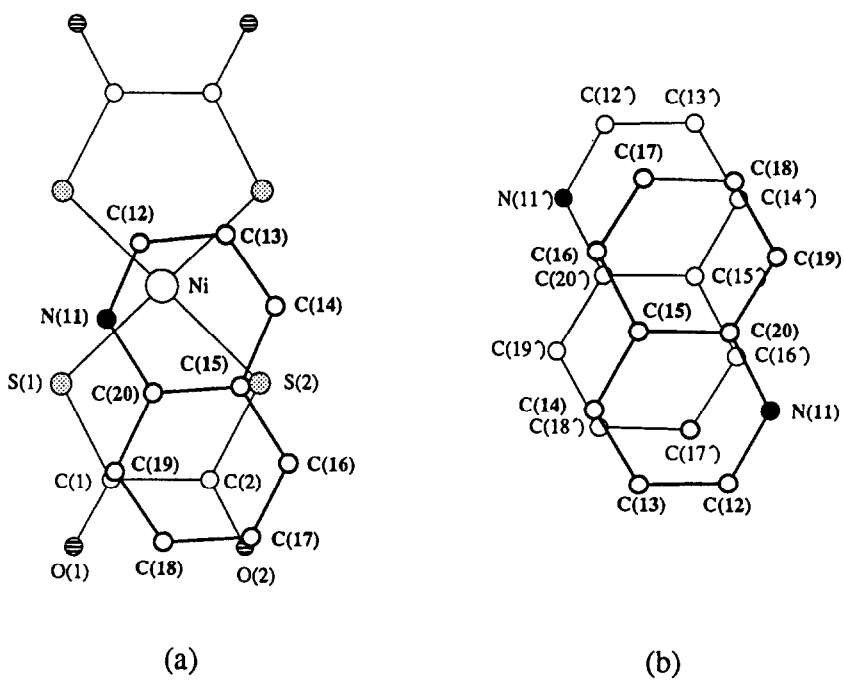

Fig. 5. Overlapping of anions and catons in the crystal structure of compound **1**.

Table 5. Packing interactions in some square-planar 1,2-dithioxalate-*S,S'* metalate(II) complexes of aromatic cations

Complex anion	Cation[a]	A—A[b]	C—C[b]	M—C[c]	L—C[d]	Ref.
$[Ni(dto)_2]^{2-}$	$DihypyH_2^{2+}$		3.7	3.4 (77.1)	3.4–3.7 (10.0)	3
$[Ni(dto)_2]^{2-}$	$QuinH^+$		3.4	3.6 (76.4)	3.3–3.8 (15.4)	This work
$[Ni(dto)_2]^{2-}$	$PyzH^+$	3.4			3.3–3.5 (5.4)	23
$[Ni(dto)_2]^{2-}$	PyH^+	3.6			3.4–3.5 (2.6)	6
$[Ni(dto)_2]^{2-}$	2-$MepyH^+$				3.3–3.6 (7.0) 3.4–3.7 (7.7)	9
$[Ni(dto)_2]^{2-}$	4-$MepyH^+$	3.7	3.6		3.3–3.6 (3.9)	23
$[Pd(dto)_2]^{2-}$	2-Am-3-$MepyH^+$	3.7			3.3–3.5 (2.3)	24
$[Pd(dto)_2]^{2-}$	3-$AmpyH^+$				3.2–3.4 (6.9) 3.2–3.7 (9.2)	8
$[Pd(dto)_2]^{2-}$	4-$AmpyH^+$		3.5	3.5 (87.6)		7
$[Pd(dto)_2]^{2-}$	Ttf^+		3.5		3.6 (4.0)	25
$[Pt(dto)_2]^{2-}$	Ttf^+		3.4			25

[a] $DihypyH_2^{2+}$: 6,7-dihydrodipyrido[1,2-a:2',1'-c]pyrazinium; $QuinH^+$: quinolinium; $PyzH^+$: pyrazinium; PyH^+: pyridinium; 2-$MepyH^+$: 2-methylpyridinium; 4-$MepyH^+$: 4-methylpyridinium; 2-Am-3-$MepyH^+$: 2-amino-3-methylpyridinium; 3-$AmpyH^+$: 3-aminopyridinium; 4-$AmpyH^+$: 4-aminopyridinium; Ttf^+: tetrathiofulvalenium.

[b] Interplanar distances (Å) between strictly parallel ions. A = anion, C = cation.

[c] Distance (Å) of metallic cation (M) to aromatic ring and angle (°) between the d_{z^2} orbital and the planar aromatic ring (C).

[d] Interplanar distances (Å) between organic cation (C) and dithiooxalate ligand (L).

The shortest contact, between C(1) and C(19), is 3.26 Å. The above described arrangement suggests the existence of significant interactions between the π systems of the aromatic cations, the metal d_{z^2} orbital and the partially delocalized structure of the dithiooxalate ligand. On the other hand, the two neighbouring cations in the same column, related by an inversion centre, show the usual *trans* conformation, with a lateral offset of 1 Å and an interstack distance of 3.44 Å (Fig. 5b). These values are comparable to those found in aromatic π systems (3.2–3.6 Å) with strong π–π interactions.[22]

Similar interactions have also been found in analogous dithiooxalate complexes containing aromatic cations, but they are affected by the nature and size of the cation. Table 5 shows different types of interaction in organoammonium dithiooxalate complexes. The π–π interactions between the π systems of the aromatic cations and the dithiooxalate ligands are the most usual ones and they are found in all the complexes except the 4-aminopyridinium salts. Only for the polycyclic cations and the 4-aminopyridinium cation does the arrangement suggest the existence of a significant interaction between their π systems and the metal d_{z^2} orbital.

In the crystal structure of **1**, there is an extended hydrogen bond network of the types N—H···O[26] and C—H···O[27] (Table 4). The ions situated in the same x level are linked by means of two hydrogen contacts between the hydrogen atoms of C(12) and C(13) of the quinolinium cation and two oxygen atoms of the same dithiooxalate ligand. The sheets placed in different x levels are connected by two hydrogen contacts involving the N(11) and C(19) atoms of the cation and the O(1) atom of the complex anion.

Acknowledgement—The authors would like to thank UPV/EHU (Grant No. 160.310-EA 166/92) for financial support.

REFERENCES

1. A Müller, *Polyhedron* 1986, **5**, 323; G. Wilkinson, R. D. Gillard and J. A. McCleverty (Eds), *Comprehensive Coordination Chemistry*, Vol. 6, pp. 541–1027. Pergamon Press, New York (1987); R. H. Holm, *Accts Chem. Res.* 1977, **10**, 427.
2. V. Deiztsch, P. Strauch and E. Hoyer, *Coord. Chem. Rev.* 1992, **121**, 43.
3. J. M. Gutiérrez-Zorrilla, P. Román and A. Gleizes, *C.R. Acad. Sci. Paris* 1987, **305**, 1353.
4. A. Gleizes and M. Verdaguer, *J. Am. Chem. Soc.* 1984, **106**, 3727.
5. P. A. Chaloner, *Coord. Chem. Rev.* 1990, **101**, 1.
6. P. Román, C. Bao, J. M. Gutiérrez-Zorrilla and A. Vegas, *J. Cryst. Spect. Res.* 1988, **18**, 207.

7. P. Román, J. I. Beitia, A. Luque and J. M. Gutiérrez-Zorrilla, *Mater. Res. Bull.* 1992, **27**, 339.
8. P. Román, A. Luque, J. I. Beitia and C. Guzmán-Miralles, *Polyhedron* 1992, **11**, 1883.
9. P. Román, J. I. Beitia, A. Luque and A. Aranzabe, *Polyhedron* 1993, **12**, 1345.
10. E. G. Cox, W. Wardlaw and K. C. Webster, *J. Chem. Soc.* 1935, 1475.
11. Powder Diffraction File of the Joint Committee on Powder Diffraction Standards, Sets 1–32. International Center of Diffraction Data, Swarthmore, PA, U.S.A: (1982).
12. N. Walker and D. Stuart, *Acta Cryst.* 1983, **A39**, 158.
13. *International Tables for X-ray Crystallography*, Vol. 4 (present distributor D. Reidel, Dordrecht). Kynoch Press, Birmingham (1974).
14. M. Martínez-Ripoll and F. H. Cano, PESOS, A program for the automatic treatment of weighting schemes for least-squares refinement. Instituto Rocasolano, CSIC, Madrid, Spain (1975).
15. J. M. Stewart, P. A. Machin, C. W. Dickinson, H. L. Ammon, H. Heck and H. Flack, The XRAY76 system. Tech. Rep. TR-446. Computer Science Center, Univ. of Maryland, College Park, MD, U.S.A. (1976).
16. D. Coucouvanis, N. C. Baezinger and S. M. Johnson, *J. Am. Chem. Soc.* 1973, **95**, 3875.
17. R. C. Weast and M. J. Astle (Eds), *CRC Handbook of Chemistry and Physics*, 59th edn. CRC Press, Boca Raton, FL, U.S.A. (1978).
18. A. R. Latham, V. C. Hascan and H. B. Gray, *Inorg. Chem.* 1965, **6**, 788.
19. P. Román, J. M. Gutiérrez-Zorrilla, A. Luque, J. I. Beitia, C. Guzmán-Miralles and M. Martínez-Ripoll, *Acta Cryst.* 1991, **C47**, 48; P. Román, A. Luque, J. M. Gutiérrez-Zorrilla, J. I. Beitia and M. Martínez-Ripoll, *Z. Kristallogr.* 1992, **198**, 213.
20. J. M. Savariault, J. Galy, J. M. Gutiérrez-Zorrilla and P. Román, *J. Molec. Struct.* 1988, **176**, 313.
21. C. A. Hunter, P. Leighton and J. K. M. Sanders, *J. Chem. Soc., Perkin I* 1989, 547.
22. C. A. Hunter and J. K. M. Sanders, *J. Am. Chem. Soc.* 1990, **112**, 5525.
23. R. Enjalbert, A. Gleizes, J. C. Trombe, M. L. Gutiérrez-Campo and P. Román, *J. Molec. Struct.* 1985, **131**, 1.
24. P. Román, J. I. Beitia and A. Luque, *Acta Cryst.* 1993, **C49**, 584.
25. C. Bellito, M. Bonamico, V. Fares, P. Imperatori and S. Patrizio, *J. Chem. Soc., Dalton Trans.* 1989, 719.
26. R. Taylor and O. Kennard, *Accts Chem. Res.* 1984, **17**, 320.
27. G. R. Desiraju, *Accts Chem. Res.* 1991, **24**, 290.

Polyhedron Vol. 12, No. 23, pp. 2841–2848, 1993
Printed in Great Britain

0277-5387/93 $6.00+.00
© 1993 Pergamon Press Ltd

CORRELATIONS BETWEEN BOND ORDER AND BOND LENGTH IN THE ELECTRON-DEFICIENT *CLOSO*-BORANES

JANE JOSEPH*

Department of Chemistry, Furman University, Greenville, SC 29613, U.S.A.

and

BENJAMIN M. GIMARC† and MING ZHAO

Department of Chemistry and Biochemistry, University of South Carolina, Columbia, SC 29208, U.S.A.

(*Received* 1 *April* 1993; *accepted* 15 *June* 1993)

Abstract—In the *closo*-boranes, the B—B bond distances vary widely, from 1.580 to 1.990 Å. These large variations are consistent with the notion of highly delocalized skeletal bonding in electron-deficient polyhedral clusters. In this paper, we show correlations between B—B bond distances and four different calculated bond order indices: (1) Wade's fractional bond orders; (2) Coulson's bond orders from three-dimensional Hückel MO theory; (3) Mulliken bond populations from extended Hückel MO theory; and (4) Mulliken bond populations from *ab initio* SCF MO calculations.

The *closo*-boranes, $B_nH_n^{2-}$, n = 5–12, have structures in which the boron atoms occupy the vertices of closed polyhedra with triangular faces and the hydrogens are attached, one per boron polyhedral vertex, in *exo*-positions projecting outward from each vertex.[1–8] Figure 1 displays these deltahedra and defines the numbering system for the polyhedron vertices. The $n = 5$ member of the series has not yet been prepared. It is included here because the isoelectronic and presumably isostructural carborane $C_2B_3H_5$ is known. Its structure is the trigonal bipyramid assumed for $B_5H_5^{2-}$ in Fig. 1.

The 25 different B—B bond distances in the *closo*-borane series exhibit a remarkable range, from 1.580 Å, one of four different distances in $B_8H_8^{2-}$, to 1.990 Å, one of nine distinct distances in $B_{11}H_{11}^{2-}$. Such variability is consistent with the notion of delocalized bonding in the *closo*-boranes. The numbers of edges connecting borons in the polyhedra far exceed the numbers of electron pairs available to form the bonds that must hold together the polyhedral structures. Consider the following arguments. In $B_nH_n^{2-}$ there are $3n+n+2 = 4n+2$ valence electrons. Of these, $2n$ electrons must be involved in the n normal, two-electron two-centre B—H bonds. Thus, $2n+2$ electrons or $n+1$ pairs remain for forming polyhedral skeletal bonds. However, each polyhedron contains $3n-6$ edges or bonds and for $n \geqslant 4$, for which these fomulae apply, the ratio

$$\frac{\text{number of skeleton electrons}}{\text{number of skeletal bonds}} = \frac{2n+2}{3n-6}$$

is always less than 2.0 and it declines with increasing n. Therefore, the *closo*-boranes are said to be electron deficient. Bonding has been discussed as combinations of two-centre and three-centre electron pair bonds, but a much more satisfactory description is based on molecular orbital (MO) theory, which assumes completely delocalized bonding across the surface of the polyhedron.[9,10]

In this paper, we attempt to correlate polyhedral B—B distances with several different calculated bond indices: (1) Wade's fractional bond orders; (2) Coulson bond orders calculated from three-dimensional Hückel theory; (3) Mulliken bond populations from extended Hückel theory; and (4)

* Present address: Department of Chemistry, Wake Forest University, Winston-Salem, NC 27109, U.S.A.

† Author to whom correspondence should be addressed.

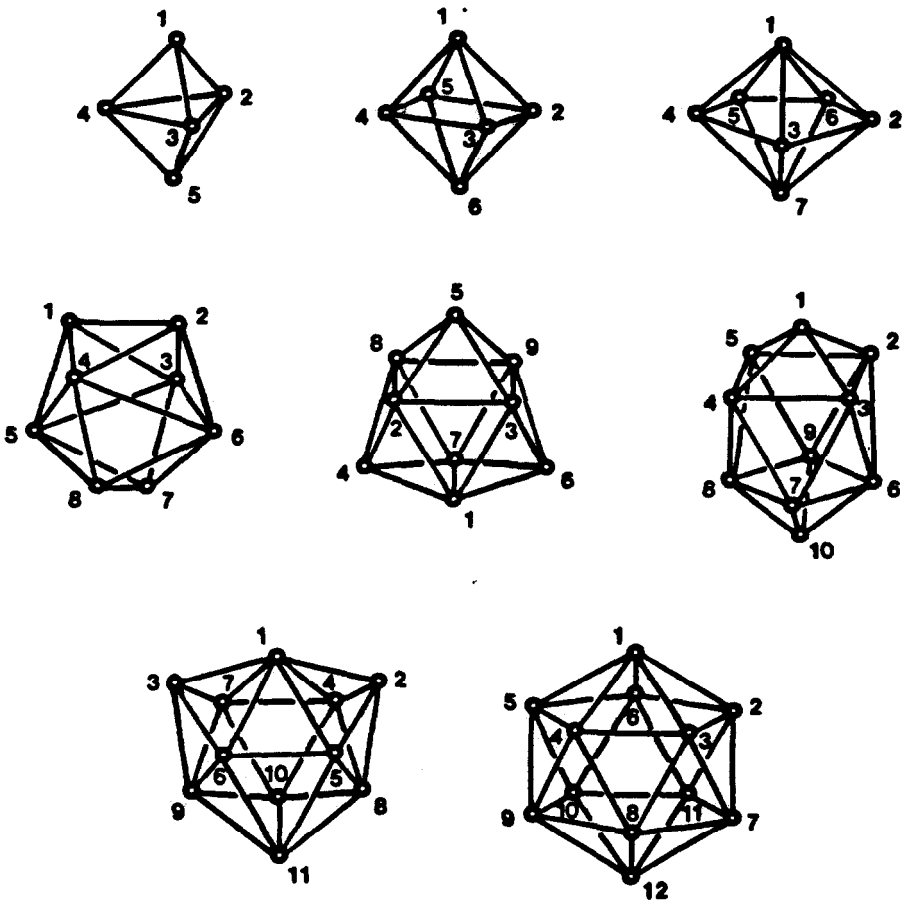

Fig. 1. The structures and numbering system for the *closo*-boranes, $B_nH_n^{2-}$.

Mulliken bond populations obtained from *ab initio* wavefunctions.

In connection with other work, we performed geometry optimized *ab initio* SCF MO calculations at the STO-3G level for the eight *closo*-boranes.[11] Table 1 compares B—B bond distances as obtained from our *ab initio* calculations[11] and from experiments.[2-8] Although the STO-3G basis set is minimal, the agreement between calculated and experimental distances is excellent, generally closer than 0.03 Å and in only two instances as large as 0.06 Å. Indeed, these differences appear to be no worse than those among different experimental determinations of the same distances where such comparisons are available. Furthermore, for each n, the order of bond distances, from shortest to longest, is the same for *ab initio* calculated distances as for experimentally determined distances. Because the *ab initio* distances form a complete set, including values for $n = 5$ and $n = 7$ for which no experimental results are available, we use the *ab initio* distances for comparison with various bond order indices described in this paper.

WADE'S FRACTIONAL BOND ORDER

Wade proposed a fractional bond order to account for variations in bond distances in the *closo*-boranes.[10] Suppose the $n+1$ skeletal electron pairs are evenly distributed over the n vertices of the polyhedron to give each atom $(n+1)/n$ electron pairs with which to form bonds. Further, suppose atom r shares its $(n+1)/n$ electron pairs with x_r neighbour atoms, where x_r is the degree of vertex r or the polyhedral coordination number of atom r. Atom r shares $(n+1)/nx_r$ electron pairs with each neighbour. Two adjacent vertices r and s share f_{rs} pairs of electrons, where

$$f_{rs} = \frac{(n+1)}{nx_r} + \frac{(n+1)}{nx_s} = \frac{(n+1)}{n}\left(\frac{x_r+x_s}{x_rx_s}\right).$$

A value of $f_{rs} = 1.0$ would mean one electron pair per bond or a normal single covalent bond linking atoms r and s. For the electron-deficient *closo*-boranes, f_{rs} turns out to be much less than 1.0. Thus, f_{rs} is the fractional bond order between atoms r and s. For example, in the trigonal bipyramid, $n = 5$,

Table 1. B—B bond distances (in Å) from geometry optimized *ab initio* SCF MO calculations and from experiment, and calculated bond orders from several models

Borane	B—B bond	Calculated distance	Experimental distance		Wade's fractional bond order (X_r, X_s)	Simple Hückel bond order	Extended Hückel[h,i] $B_nH_n^{2-}$	Extended Hückel[h,i] C_n^{2-}	*Ab initio*
$B_5H_5^{2-}$	1,2	1.607			0.700 (3,4)	2.053	0.7012	0.5968	0.3522
	2,3	1.820			0.600 (4,4)	1.587	0.3203	0.3363	0.0966
$B_6H_6^{2-}$	1,2	1.682	1.69[a]		0.583 (4,4)	1.833	0.5693	0.5694	0.2610
$B_7H_7^{2-}$	1,2	1.786			0.514 (4,4)	1.646	0.4262	0.3319	0.2017
	2,3	1.611			0.571 (4,5)	1.978	0.7208	0.6159	0.3295
$B_8H_8^{2-}$	1,2	1.580	1.56[b]		0.563 (4,4)	2.067	0.7345	0.5996	0.3496
	1,3	1.794	1.76		0.506 (4,5)	1.622	0.4639	0.3872	0.1907
	1,5	1.658	1.72		0.506 (4,5)	1.805	0.6211	0.5404	0.3217
	3,5	1.873	1.93		0.450 (5,5)	1.542	0.3777	0.3335	0.1620
$B_9H_9^{2-}$	1,2	1.930	1.97[c]	1.88[d]	0.444 (5,5)	1.485	0.4246	0.3346	0.1650
	1,4	1.682	1.70	1.71	0.500 (4,5)	1.761	0.5668	0.4906	0.2657
	1,7	1.781	1.77	1.81	0.444 (5,5)	1.568	0.4058	0.4043	0.1729
$B_{10}H_{10}^{2-}$	1,2	1.673	1.68[e]		0.495 (4,5)	1.782	0.5096	0.4806	0.2657
	2,3	1.826	1.82		0.440 (5,5)	1.553	0.4079	0.3661	0.1741
	2,9	1.795	1.80		0.440 (5,5)	1.580	0.5048	0.4319	0.2203
$B_{11}H_{11}^{2-}$	1,2	1.726	1.74[f]		0.455 (4,6)	1.563	0.5755	0.6295	0.2349
	1,4	1.990	2.01		0.400 (5,6)	1.432	0.2653	0.2368	0.1351
	2,4	1.634	1.66		0.491 (4,5)	1.871	0.6338	0.4834	0.3091
	2,8	1.746	1.77		0.491 (4,5)	1.684	0.4891	0.4078	0.1999
	4,7	1.847	1.85		0.436 (5,5)	1.615	0.5220	0.4915	0.1867
	4,8	1.783	1.78		0.436 (5,5)	1.464	0.4724	0.3907	0.1948
	4,10	1.775	1.78		0.436 (5,5)	1.569	0.5004	0.4409	0.2161
	8,10	1.760	1.77		0.436 (5,5)	1.613	0.5077	0.4344	0.2295
	10,11	1.821	1.78		0.436 (5,5)	1.544	0.4605	0.4120	0.1803
$B_{12}H_{12}^{2-}$	1,2	1.771	1.77[g]		0.433 (5,5)	1.607	0.4994	0.4142	0.2134

[a] Ref. 2; [b] Ref. 3; [c] Ref. 4; [d] Ref. 5; [e] Ref. 6; [f] Ref. 7; [g] Ref. 8.

[h] Bond distance deviations from standard 1.70 Å for $B_nH_n^{2-}$: $n = 8$, 1,3 = 1.7008, 3,5 = 1.7037; $n = 11$, 1,4 = 1.99, 2,4 = 1.7002, 4,8 = 1.6998, 8,10 = 1.703.

[i] Bond distance deviations from standard 1.54 Å for C_n^{2-}: $n = 8$, 1,3 = 1.5410, 3,5 = 1.5410; $n = 11$, 1,4 = 1.80, 2,4 = 1.5401, 4,8 = 1.5395, 8,10 = 1.5414.

and for atoms in the axial positions $x_a = 3$ and for the equatorial atoms $x_e = 4$. For axial–equatorial bonds,

$$f_{ae} = \left(\frac{5+1}{5}\right)\left(\frac{3+4}{3\times 4}\right) = 0.700,$$

and for equatorial–equatorial bonds,

$$f_{ee} = \left(\frac{5+1}{5}\right)\left(\frac{4+4}{4\times 4}\right) = 0.600.$$

These results look promising because axial–equatorial bonds in $B_5H_5^{2-}$ are shorter (1.607 Å) than the equatorial–equatorial bonds (1.820 Å). Fractional bond orders appropriately account for the trend.

Wade's fractional bond orders have their limitations. The assumption that the $n+1$ skeletal electron pairs are spread evenly over n vertices is generally not true. For example, in trigonal bipyramidal $B_5H_5^{2-}$ topology directs more electron density to the axial positions than to the equatorial sites. Only in the highly symmetric octahedral ($n = 6$) and icosahedral ($n = 12$) cases can the distribution of charge be uniform. Furthermore, working up fractional bond orders for the less symmetric polyhedra, one encounters instances in which distinctly non-equivalent bonds have the same x_r, x_s combinations and therefore the same fractional bond order. For $n = 11$, there are five different kinds of bonds between pairs of five-coordinate atoms, giving them all the same fractional bond

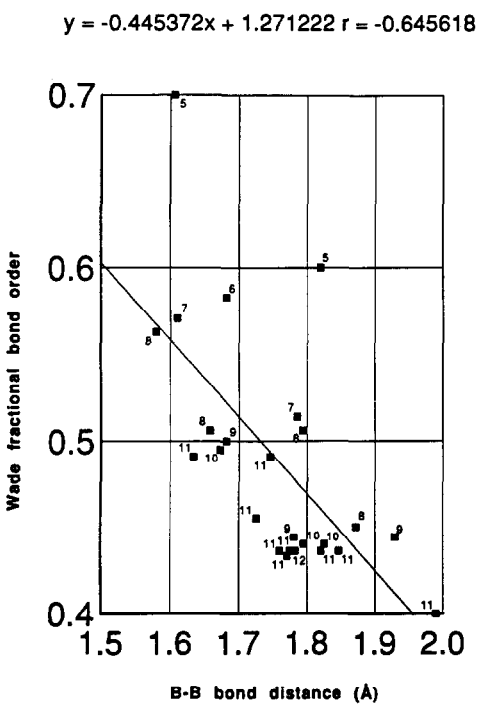

Fig. 2. Wade's functional bond order for $B_nH_n^{2-}$ polyhedra correlated with B—B bond distances. The number that accompanies each point indicates the size n of the polyhedron involved. One of the limitations of the Wade index is that in several instances it cannot distinguish among different bonds in the same polyhedron. For example, in the $n = 11$ polyhedron, there are five different bonds with the same fractional bond order.

order, $f_{rs} = 0.436$. These bonds range in length from 1.760 to 1.847 Å (experimental distances range from 1.77 to 1.85 Å). Wade's fractional bond orders for the *closo*-boranes are reproduced in Table 1. Figure 2 is an attempt to correlate fractional bond orders with corresponding bond distances. This figure includes a more extensive set of data than an earlier diagram prepared by Burdett.[12]

The f_{rs} function gives a qualitative rationale to bond distance trends. In f_{rs}, the factor $(n+1)/n$ decreases only slightly from $n = 5$ (1.200) to $n = 12$ (1.083). Larger changes occur in the factor $(x_r+x_s)/x_rx_s$, which is smaller for bonds that end at atoms with larger coordination numbers. Thus, in $B_5H_5^{2-}$ the axial–equatorial bonds (3,4-coordination) are shorter than the equatorial–equatorial bonds (4,4-coordination), while the reverse is true for the pentagonal bipyramidal $B_7H_7^{2-}$ (4,5 vs 4,4). For $B_{11}H_{11}^{2-}$, the model predicts the bonds with 5,6-coordination to have the smallest bond orders and therefore the longest bond distance in the whole series and this is born out in the bond distances. However, on the whole, fractional bond order–bond length correlations are not acceptable, as one can see from Fig. 2.

SIMPLE HÜCKEL THEORY

A model of the electronic structures for the *closo*-boranes was proposed by Wade,[10] with significant modifications by King and Rouvray.[13] According to this model, each of the boron atoms in the polyhedron contributes four valence atomic orbitals (AOs), one s and three p AOs, to the basis set for a total of $4n$ AOs. Imagine one of the p AOs at each vertex oriented along an axis such that it points toward the centre of the polyhedron. This is the radial AO. The other two p AOs are perpendicular to the radial axis and tangential to the surface of the polyhedron. These are the tangential AOs. The s AO and the radial p AO can be combined to form two sp hybrids, an internal hybrid pointing to the centre of the polyhedron and an external hybrid that points away from the polyhedral surface and towards the *exo*-hydrogen. The external hybrid is involved in normal localized two-centre, two-electron bonding between boron and hydrogen and its effect on polyhedral skeletal bonding can be neglected. The internal hybrid and the tangential AOs form a set of $3n$ AOs from which MOs can be constructed. These MOs then receive the $n+1$ delocalized skeletal electron pairs.

We have recently developed an MO method that combines the $3n$ tangential and internal orbitals according to the usual simple Hückel assumptions plus a few additional approximations that are completely within the spirit of simple Hückel theory.[14] This three-dimensional Hückel theory was developed specifically for applications to polyhedral cluster molecules. The additional assumptions involve the establishment of an internal coordinate system and the calculation of interactions between non-parallel internal and tangential AOs of adjacent vertices. Details and vital comparisons appear elsewhere.[14] The input for simple Hückel calculations consists of the number of delocalized electrons, the number of polyhedral vertices and an adjacency matrix that specifies neighbour–neighbour interactions between pairs of AOs.

In simple Hückel theory, the Coulson bond order p_{rs} between atoms r and s is defined as[15,16]

$$p_{rs} = \sum_i 2c_{ir}c_{is},$$

where c_{ir} and c_{is} are coefficients of AOs X_r and X_s in the MO $\phi_i = \Sigma_r c_{ir}X_r$ obtained from simple Hückel calculations and the summation is over all of the occupied MOs ϕ_i. Applications to many examples of planar conjugated hydrocarbons show that correlations of bond orders with bond lengths,

although far from perfect, are often useful and suggestive. Further correlations of this type have been made with comparable success for planar inorganic molecules that contain B—O and S—N bonds.[17,18]

Two-dimensional Hückel theory assumes only one AO per vertex and one pair of interacting AOs on bonded atoms. Three-dimensional Hückel theory involves three AOs per vertex and each of these can interact with AOs on neighbouring vertices in several different ways. Sums of contributions from each interacting AO pair produce total bond orders that are rather large. Typical values run from 1.5 to 2.0. Coulson bond orders for skeletal bonds for the polyhedral *closo*-boranes as obtained from three-dimensional Hückel theory appear in Table 1. Figure 3 shows how these values correlate with B—B bond distances.

EXTENDED HÜCKEL THEORY

The extended Hückel method is well known.[19] The *closo* boranes were among the first classes of molecules to be treated by this method.[20] In practice each boron or other main-group atom in the molecule contributes one s and three p AOs to the basis set. Hydrogen atoms are explicitly included and each hydrogen contributes its 1s AO. The coulomb integral for each AO is approximated by an empirical value of the valence state ionization energy for the orbital. Resonance integrals are taken as averages of the coloumb integrals of the two interacting AOs multiplied by computed AO overlap and perhaps another calibration parameter. Overlaps are distance-dependent quantities and bond distances enter the calculation as Cartesian spatial coordinates for each atom.

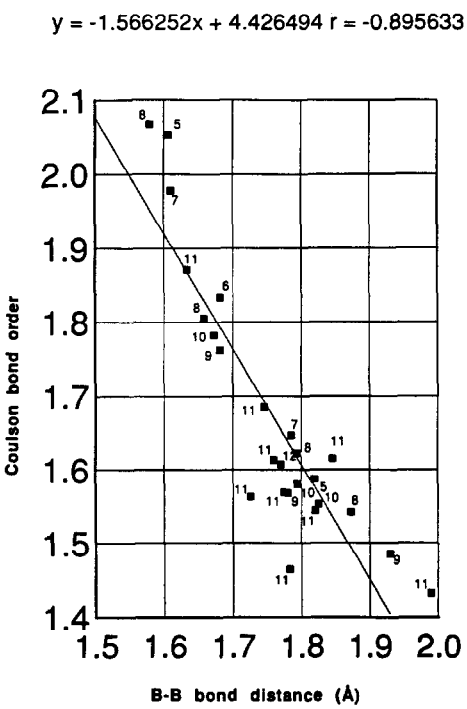

Fig. 3. Coulson's bond orders, obtained from three-dimensional Hückel MO calculations for the *closo*-boranes, correlated with B—B bond distances. The three-dimensional Hückel model includes no information other than atom connectivity or topology and electron count.

Mulliken described the overlap population[21,22] between a pair of AOs X_{rk} and X_{sl} on atoms r and s due to an electron in the MO ϕ_i as

$$p^i_{rksl} = 2c_{rki}c_{sli}S_{rksl},$$

where $S_{rksl} = \langle X_{rk}|X_{sl}\rangle$ is the overlap integral between the two AOs and c_{rki} and c_{sli} are the coefficients of the two AOs in ϕ_i. Summing over pairs of AOs on atoms r and s gives

$$p^i_{rs} = \sum_{k,l} p^i_{rksl}.$$

Summing over all MOs, each occupied by n_i electrons, gives the Mulliken overlap population between atoms r and s:

$$p_{rs} = \sum_i n_i p^i_{rs}.$$

Mulliken overlap populations are easily obtained from extended Hückel calculations.

Table 1 contains two sets of extended Hückel overlap populations, one for $B_nH_n^{2-}$ and another for the hypothetical isoelectronic and presumably isostructural C_n^{2-} polyhedra. We include the C_n^{2-} results to get a measure of the effect of neglecting the *exo*-hydrogens.

Since Mulliken overlap populations are proportional to AO overlaps, which in turn depend on interatomic distances, closer atoms might be expected to have larger bond orders than would atoms further removed from each other. Therefore, assigning different bond distances between atoms prejudices the outcomes of bond population calculations. To establish a uniform basis for calculations, we have assumed equal bond distances between all bonded atoms, even though the symmetry of most structures does not require all bond distances to be equal and experimental measurements and *ab initio* calculations demonstrate that those bonds are not of equal lengths. Indeed, for the eight- and 11-atom polyhedra, it is impossible to devise structures in which all bond distances are identical. For our extended Hückel calculations, we chose arbitrary but standard distances of 1.54 Å for C—C bonds and 1.70 Å for B—B bonds in all polyhedra. In the eight-atom cage, variations from

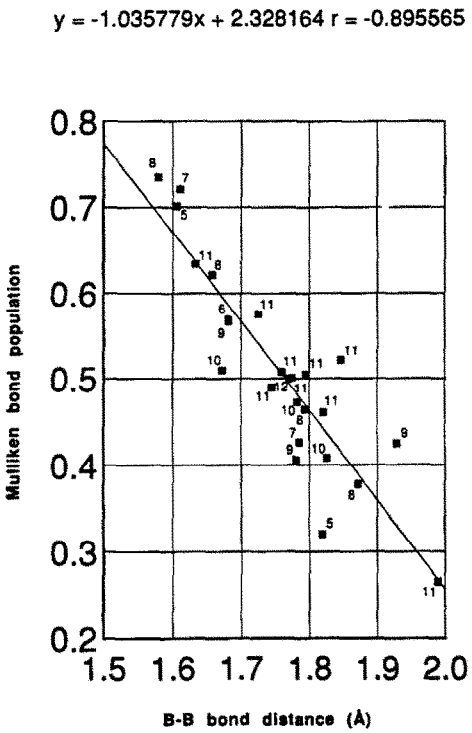

Fig. 4. Mulliken's bond populations from extended Hückel calculations for $B_nH_n^{2-}$ as functions of B—B bond distances.

the standard distances occur in the third or fourth decimal places. In the 11-atom polyhedron, deviations from standard distances are more serious. Since the 1,4-bond in the real $B_{11}H_{11}^{2-}$ turns out to be unusually long, indeed the longest of all B—B bonds in the *closo* borane series, we took long 1,4-distances in our calculations, allowing other distances to be within three or four decimal places of the standard values. Details are given in the footnotes to Table 1. Bond population–bond distance correlations appear in Figs 4 and 5.

AB INITIO BOND POPULATIONS

The STO-3G basis set *ab initio* SCF MO calculations that produced the table of geometry optimized B—B bond distances also gave comparable Mulliken bond populations.[11] These results appear in Table 1. Figure 6 plots *ab initio* bond populations against the optimized B—B distances.

DISCUSSION

How well do the various bond order indices agree with the reverse order of bond distances within each polyhedron of n vertices? Table 2 shows the irregu-

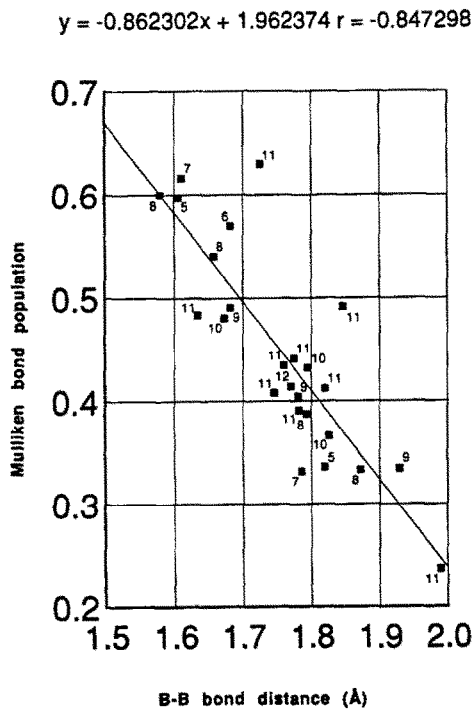

Fig. 5. Mulliken's bond populations from extended Hückel calculations for hypothetical C_n^{2-} clusters as functions of B—B bond distances in $B_nH_n^{2-}$.

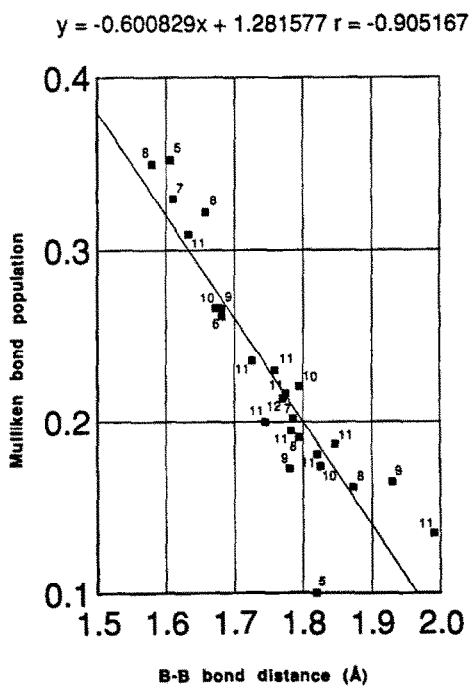

Fig. 6. Mulliken's bond populations from geometry optimized *ab initio* SCF MO calculations at the STO-3G level correlated with B—B bond distances determined by the same calculations.

Table 2. Irregularities in trends of decreasing bond orders with longer bond distances for polyhedra of given size, n

Wade's fractional bond orders		
$n = 8$	Distances:	1,2 < 1,5 < 1,3 < 3,5
	Bond orders:	1,2 > 1,5 = 1,3 > 3,5
$n = 9$	Distances:	1,4 < 1,7 < 1,2
	Bond orders:	1,4 > 1,7 = 1,2
$n = 10$	Distances:	1,2 < 2,9 < 2,3
	Bond orders:	1,2 > 2,9 = 2,3
$n = 11$	Distances:	2,4 < 1,2 < 2,8 < 8,10 < 4,10 < 4,8 < 10,11 < 4,7 < 1,4
	Bond orders:	2,4 = 2,8 > 1,2 > 8,10 = 4,10 = 4,8 = 10,11 = 4,7 > 1,4
Three-dimensional simple Hückel bond orders		
$n = 11$	Distances:	2,4 < 1,2 < 2,8 < 8,10 < 4,10 < 4,8 < 10,11 < 4,7 < 1,4
	Bond orders:	2,4 > 2,8 > 4,10 > 8,10 > 4,8 > 1,2 > 10,11 > 4,7 > 1,4
Extended Hückel bond orders, $B_nH_n^{2-}$		
$n = 9$	Distances:	1,4 < 1,7 < 1,2
	Bond orders:	1,4 > 1,2 > 1,7
$n = 11$	Distances:	2,4 < 1,2 < 2,8 < 8,10 < 4,10 < 4,8 < 10,11 < 4,7 < 1,4
	Bond orders:	2,4 > 1,2 > 4,7 > 8,10 > 4,10 > 2,8 > 4,8 > 10,11 > 1,4
Extended Hückel bond orders, C_n^{2-}		
$n = 11$	Distances:	2,4 < 1,2 < 2,8 < 8,10 < 4,10 < 4,8 < 10,11 < 4,7 < 1,4
	Bond orders:	1,2 > 4,7 > 2,4 > 4,10 > 8,10 > 10,11 > 2,8 > 4,8 > 1,4
Ab initio bond orders		
$n = 11$	Distances:	2,4 < 1,2 < 2,8 < 8,10 < 4,10 < 4,8 < 10,11 < 4,7 < 1,4
	Bond orders:	2,4 > 2,8 > 4,10 > 8,10 > 4,8 > 1,2 > 10,11 > 4,7 > 1,4

larities in trends. Not shown are the situations in which bond order–bond distance trends are in complete agreement. For example, for $n = 5$, all four methods give bond order indices such that 1,2 > 2,3, which is exactly the reverse of the bond distance trend: 1,2 < 2,3. Therefore, these agreements do not appear in Table 2. Only one distance is possible for the regular polyhedra $n = 6$ and $n = 12$. Since no internal trends exist for these cases, they are not listed in Table 2.

As shown in Table 2, the main difficulty with the Wade fractional bond order is its inability to distinguish between different bonds that link atoms of the same degrees. The worst case is $n = 11$. However, all models, including the *ab initio* bond orders vs *ab initio* distances, show reversals for the $n = 11$ polyhedron. One measure of order irregularities is the number of permutations required to put bond orders into the order dictated by bond distances. In this regard it takes three permutations to put the $n = 11$ bond orders into coincidence with bond distances for the three-dimensional Hückel, extended Hückel ($B_nH_n^{2-}$) and *ab initio* results. The extended Hückel bond orders for C_{11}^{2-} require six permutations.

Figures 2–6 show correlations of bond orders calculated by the various models applied here as functions of the 25 different polyhedral B—B bond distances that were previously determined by *ab initio* SCF MO calculations at the STO-3G level. We have attempted a linear fit among each set of points. Quality of fit is indicated by the correlation coefficient r reported with the equation of the line for each figure. It is likely that a linear relationship is not the most appropriate. For example, the points in Figs 3 and 6 might be better approximated by a quadratic curve, but in fact they are the two sets that best fit a linear plot. Other graphs show considerably more scatter. It is clear from the figures that bond order–bond distance correlations are only qualitative and, therefore, heroic attempts to fit points with many parameters is without justification. Perhaps not surprisingly, we obtain the best fit with Mulliken populations from the *ab initio* calculations that determined the distances (Fig. 6). Only slightly less satisfactory are the Coulson bond orders from three-dimensional Hückel theory (Fig. 3). It is gratifying that while they give almost as close a fit as the *ab initio* bond populations, the three-dimensional Hückel results contain no more

information, only molecular topology and electron count, than Wade's fractional bond orders (Fig. 2), which exhibit the greatest scatter. Not quite as good as the three-dimensional Hückel results are the extended Hückel–Mulliken bond populations for $B_nH_n^{2-}$ (Fig. 4). Still slightly less satisfactory are the extended Hückel results for C_n^{2-} plotted against B—B bond distances (Fig. 5). Part of the scatter among extended Hückel bond populations must be a result of the standard bond distances assumed to set up the structures for the calculations. Both sets of extended Hückel results would probably be improved by repeating the calculations using structures based on experiment or geometry optimized *ab initio* calculations. However, such a procedure would obviate the attractiveness of a computationally simple model. Points that lie farthest from the lines in all plots often come from the trigonal bipyramid ($n = 5$) and the octadecahedron ($n = 11$).

There has long been interest in correlating experimental bond distances with some sort of calculated bond index. Rarely have there been attempts to survey bond distance–bond index correlations among such a large number of bonds through a series of related molecules. The four indices we have considered here hardly exhaust the possible methods. All four indices are applicable to other classes of boranes, as well as to other cluster compounds. As chemists accustomed to counting bonds and electrons, it is satisfying to see that the Coulson bond orders, based on three-dimensional Hückel MO calculations and requiring as input information only atomic connectivity and electron count, perform almost as effectively in correlating bond lengths as do *ab initio* calculated Mulliken bond populations.

Acknowledgement—We are grateful to the National Science Foundation for partial support of this research through Grant Nos CHE-8703461 and CHE-9012216 to the University of South Carolina.

REFERENCES

1. R. E. Williams, Carboranes, in *Progress in Boron Chemistry* (Edited by R. J. Brotherton and H. Steinberg), Vol. 2. Pergamon Press, Oxford (1970).
2. R. Schaeffer, Q. Johnson and G. S. Smith, *Inorg. Chem.* 1965, **4**, 917.
3. L. J. Guggenberger, *Inorg. Chem.* 1969, **8**, 2771.
4. D. D. Brag, R. M. Kabbani and E. H. Wong, *Acta Cryst.* 1982, **B38**, 957.
5. L. J. Guggenberger, *Inorg. Chem.* 1968, **7**, 2260.
6. J. T. Gill and S. T. Lippard, *Inorg. Chem.* 1975, **14**, 751.
7. E. H. Wong, L. Prasad, E. J. Gade and M. G. Gatter, *Inorg. Chem.* 1983, **22**, 1143.
8. J. A. Wunderlich and W. N. Lipscomb, *J. Am. Chem. Soc.* 1960, **82**, 4427.
9. W. N. Lipscomb, *Boron Hydrides*. Benjamin, New York (1963).
10. K. Wade, *J. Chem. Soc., Chem. Commun.* 1971, 792; *Adv. Inorg. Chem. Radiochem.* 1976, **18**, 1.
11. J. J. Ott and B. M. Gimarc, *J. Comput. Chem.* 1986, **7**, 673.
12. J. K. Burdett, *Molecular Shapes: Theoretical Models of Inorganic Stereochemistry*, p. 255. Wiley, New York (1980).
13. R. B. King and D. H. Rouvray, *J. Am. Chem. Soc.* 1977, **99**, 7834.
14. M. Zhao and B. M. Gimarc, *Inorg. Chem.*, in press.
15. A. Streitwieser, Jr, *Molecular Orbital Theory for Organic Chemists*. Wiley, New York (1961).
16. C. H. Coulson, B. O'Leary and R. B. Mallion, *Hückel Theory for Organic Chemists*. Academic Press, New York (1978).
17. C. A. Coulson and T. W. Dingle, *Acta Cryst.* 1968, **B24**, 153.
18. B. M. Gimarc and N. Trinajstić, *Pure Appl. Chem.* 1980, **52**, 1443.
19. R. Hoffmann, *J. Chem. Phys.* 1963, **39**, 1397.
20. R. Hoffmann and W. N. Lipscomb, *J. Chem. Phys.* 1962, **36**, 3489.
21. R. S. Mulliken, *J. Chem. Phys.* 1955, **23**, 1883.
22. J. P. Lowe, *Quantum Chemistry*, p. 229. Academic Press, New York (1978).

Polyhedron Vol. 12, No. 23, pp. 2849–2856, 1993
Printed in Great Britain

0277-5387/93 $6.00+.00
© 1993 Pergamon Press Ltd

SYNTHESIS AND CHARACTERIZATION OF $[M(dmit)_2]^{2-}$ AND $[M(dmt)_2]^{2-}$ COMPLEXES (M = Se^{II} OR Te^{II}; dmit = 4,5-DIMERCAPTO-1,3-DITHIOLE-2-THIONE AND dmt = 4,5-DIMERCAPTO-1,2-DITHIOLE-3-THIONE)

JAI D. SINGH and HARKESH B. SINGH*

Department of Chemistry, Indian Institute of Technology, Powai, Bombay 400 076, India

(*Received* 5 *May* 1993; *accepted* 14 *June* 1993)

Abstract—Reactions of disodium salt of the ligands 4,5-dimercapto-1,3-dithiole-2-thione [H_2(dmit)] and 4,5-dimercapto-1,2-dithiole-3-thione [H_2(dmt)] with "sodium selenopentathionate"-3-hydrate [$Na_2Se(S_2O_3)_2]\cdot 3H_2O$ and "sodium telluropentathionate"-2-hydrate [$Na_2Te(S_2O_3)_2\cdot 2H_2O$, in the presence of cations Me_3Te^+, Ph_4As^+, $(C_5H_5)_2Co^+$ and PPN^+, yielded the corresponding complexes of stoichiometry [cation]$_2$[M(dmit)$_2$] and [cation]$_2$[M(dmt)$_2$]$_2$ (M = Se or Te). These complexes are thermally unstable and undergo redox decomposition in solution. Oxidation reactions of these complexes with iodine or tetracyanoquinodimethane afforded sulphocarbon C_6S_{10}. In order to study the oxidation–reduction process of these complexes, detailed electrochemical investigations have been carried out.

Square planar complexes, $[M(dmit)_2]^{n-}$, (M = d^8 metal; dmit = 4,5-dimercapto-1,3-dithiole-2-thione; n = 0–2), have attracted considerable attention recently.[1–3] This system has yielded several low temperature molecular metals and superconductors, namely [TTF][Ni(dmit)$_2$]$_2$,[4] [α-TTF][Pd(dmit)$_2$], [α′-TTF][Pd(dmit)$_2$]$_2$,[5] [Me_4N][Ni(dmit)$_2$]$_2$[6] and [Me_4N][Pd(dmit)$_2$]$_2$.[7] Molecular interactions through S···S contacts form effective conduction pathways in the crystals. The incorporation of tellurium in these systems may give rise to new unknown interactions, since tellurium is well known to participate in intermolecular interactions with sulphur. Recently, we prepared [Me_3Te][Au(dmit)$_2$] complex. The structure, as expected, exhibited several Te···S inter- and intramolecular interactions.[8] Hence it was decided to investigate further other systems containing tellurium as part of the cation and/or anion. Attention focussed upon **2** since the anion not only contained the more polarizable and large tellurium, but it was expected to be planar as well. Both Se^{II} and Te^{II} complexes with bidentate sulphur donor ligands have been shown to have trapezoid planar geometry around the central atom.[9–11] Furthermore, the presence of the dithiolene ligands may stabilize tellurium in unusual oxidation states (other than +II, +IV) similar to those observed for [Et_4N][Te(mnt)$_2$Cl] (mnt = 1,2-dicyanoethylene-1,2-dithiolate) where the effective magnetic moment of 1.5±0.1 BM has been interpreted in terms of the presence of an unpaired electron and a formal oxidation state of Te^{III}.[12] Recently, we[13] and others[14] have reported examples of Te^{III} derivatives. The majority of dmit complexes studied have involved transition metals. The dmit complexes of main group elements have attracted only limited attention; not a single dmit complex of selenium/tellurium has been reported. We reasoned that planar dmit complexes with Se^{II} and Te^{II} would have several features in common with transition metal dmit complexes and might lead to highly conducting complexes. We note that some examples of $[Se(dmt)_2]^{2-}$[15] and $[Te(dmt)_2]^{2-}$[16] have been reported; however, no attempt has been made to evaluate the efficacy of the systems as conducting solids. This paper reports the synthesis, chemical oxidation and detailed electrochemical study of the Se^{II} and Te^{II} complexes with dmit and dmt.

RESULTS AND DISCUSSION

The dithiolene complexes **1–11** were most conveniently prepared by the substitution reactions of labile Se^{II} and Te^{II} pentathionate complexes with

* Author to whom correspondence should be addressed.

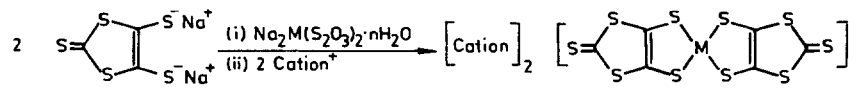

	M	Cation$^+$
1	Se	PPN^+
2	Te	PPN^+
3	Se	Ph_4As^+
4	Te	$(C_5H_5)_2Co^+$
5	Se	Me_3Te^+
6	Te	Me_3Te^+

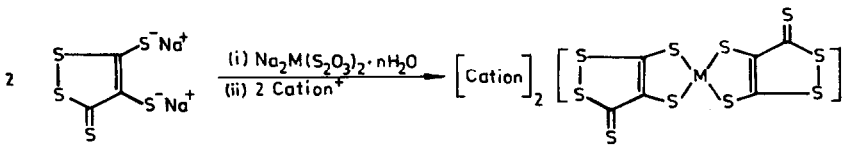

	M	Cation$^+$
7	Se	PPN^+
8	Te	PPN^+
9	Te	$(C_5H_5)_2Co^+$
10	Se	Me_3Te^+
11	Te	Me_3Te^+

[n = 2, M = Te; n = 3, M = Se]

Scheme 1.

disodium salts of the ligands 4,5-dimercapto-1,3-dithiole-2-thione [Na_2(dmit)] and its isomer, 4,5-dimercapto-1,2-dithiole-3-thione [Na_2(dmt)] (Scheme 1). The anionic complexes were isolated as salts with cations like Me_3Te^+, $(C_5H_5)_2Co^+$, Ph_4As^+ and PPN^+.

The complexes are orange–red to dark reddish brown in colour and are sharp melting solids (Table 1). The complexes with bulky cations like PPN^+, Ph_4As^+ and $(C_5H_5)_2Co^+$ are quite stable and remain unaffected by atmospheric oxygen and moisture for a long time. However, the complexes with the Me_3Te^+ cation are unstable and start to decompose after some time at room temperature; therefore, they were prepared and stored at 0°C under dinitrogen. The selenium complexes of both ligands, Na_2(dmit) and Na_2(dmt), were found to be relatively more stable as compared to their tellurium counterparts. The complexes have poor to moderate solubility in common organic solvents such as acetone, chloroform, dichloromethane, carbon disulphide, pyridine and dimethylformamide. The stability of the complexes in solution is rather poor. Solutions of the complexes decompose after a few hours at room temperature to give reduced metals. Attempts to isolate solid complexes with the smaller cations Me_4N^+ and Bu_4N^+ were unsuccessful. This is probably due to both low stability and high solubility of these complexes. Also, attempts to prepare the tellurium-containing thione **12** by 1:1 reaction of Na_2(dmit) and $Na_2[Te(S_2O_3)] \cdot 2H_2O$ afforded a yellowish-orange product of indefinite composition.

The complexes are well characterized by elemental analyses (C, H, N), IR, UV–vis spectroscopy and cyclic voltammetry studies. Attempts were made to record ^{77}Se and ^{125}Te NMR spectra in DMSO-d_6. The complexes, unfortunately, proved too insoluble to allow for meaningful measurements. Also in DMSO-d_6, considerable decomposition of the complexes was observed and a black–brown solid (probably metal) settled after some time.

The IR spectra of complexes (Table 2) exhibit the characteristic ν(C=C) stretching frequency at 1440 ± 10 cm^{-1} (for dmit complexes)[17] and 1320 ± 10 cm^{-1} with a shoulder at 1290 ± 10 cm^{-1} (for dmt complexes)[18] and are quite similar to those reported for tin[19] and indium.[20] These frequencies support the dianionic nature of the ligands. Upon oxidation, a negative shift in ν(C=C) is generally observed. The other bands associated with the ligands, ν(C=S) and ν(C—S) were observed in

Table 1. Characterization data for $M(dmit)^{2-}$ and $M(dmt)^{2-}$ complexes (M = Se or Te)

Complex	Colour	M.p. (°C)	Found (Calc.) (%) C	H	N
1	Red	95–97	60.1 (60.5)	4.0 (3.9)	1.6 (1.8)
2	Dark brown	85–88	57.1 (58.7)	3.8 (3.8)	2.8 (1.8)
3	Brick red	107–108	52.1 (52.4)	3.3 (3.2)	
4	Brown	117 (d)	34.5 (34.8)	2.2 (2.2)	
5	Light brown	123 (d)	16.6 (17.6)	2.0 (2.2)	
6	Brown	82–84 (d)	15.7 (16.6)	1.8 (2.1)	
7	Red–brown	188	60.2 (60.5)	3.8 (3.9)	1.8 (1.8)
8	Brick red	94–96 (d)	57.4 (58.7)	3.9 (3.8)	2.8 (1.8)
9	Brick red	136–137	34.0 (34.7)	2.3 (2.2)	
10	Dark brown	112 (d)	17.6 (17.6)	2.7 (3.2)	
11	Brown	126 (d)	16.5 (16.6)	2.1 (2.1)	

Table 2. IR frequencies (cm^{-1}) (KBr) and electronic absorption spectra

	IR, KBr (cm^{-1}) ν(C=C)	ν(C=S)	ν(C—S)	UV–vis, CH_2Cl_2 (nm) λ_{max}			
1	1450s	1070s, 1040s	880s	469	372	273	266
2	1450s	1060s, 1030s	925m	430	378	267	251
3	1450s	1080s 1040s	910m 880m	473	326	270	258
4	1430s	1050s 1020s	920s 865s	402	300	261	203
5	1420s	1050s 1030s	910s 890s	571	390	327	269
6	1430s	1070s 1050s	910m 900m	426	328	246	230
7	1320s 1280m	1060s 1040m	920s	417	292	266	206
8	1330s 1280s	1060s 1040s	930s	443	381	292	252
9	1320s 1290m	1050s 1020s	925s	421	330	260	201
10	1330s 1290m	1060	940s 910m	426	326	244	230
11	1330s	1055s	940s	431	328	251	216

the regions 1080–1020 cm^{-1} and 930–890 cm^{-1}, respectively.

The electronic absorption spectra show an intense band in the region 473–402 nm (Table 2) for both the dmit and dmt complexes. This is assigned to π–π^* transition of the ligand and is observed at 475 nm for $Na_2(dmit)$ in acetonitrile. A second π–π^* transition of the ligand is observed at 273–246 nm (for the dmit complex) and at ~ 292–244 nm (for the dmt complex). An intense band in the region 390–300 nm is assigned to the $M^{II} \leftarrow S$ charge transfer transition.[21]

The complexes, as expected, did not show an ESR signal and were insulated in the solid state, further supporting a dianionic nature of the ligand.

Chemical oxidation

Attempts were made to obtain odd-electron potentially conducting species, $[M(dmit)_2]^-$ and $[M(dmt)_2]^-$, where the formal oxidation state of selenium or tellurium would be III. Treatment of the $[M(dmt)_2]^{2-}$ complexes with iodine or TCNQ gave novel sulphocarbon C_6S_{10} (**13**), along with CS_2 insoluble polymeric sulphocarbon of the formula C_3S_x ($x = 5.5$; **14**). To the best of our knowledge,

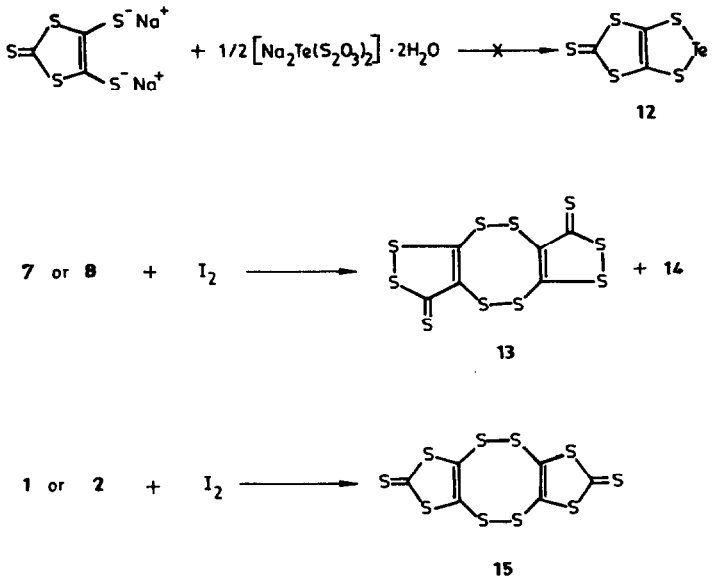

Scheme 2.

this is the first report on **13**, although its isomer (**15**) has recently been reported. Similarly chemical oxidation of the $[M(dmit)_2]^{2-}$ complexes with catalytic or excess of iodine led to the isolation of orange–red sulphocarbon C_6S_{10} (**15**) (Scheme 2), which was characterized by elemental analysis and comparing m.p. and IR with an authentic sample. It is worth noting that the results of chemical oxidation of the dmit complexes are in line with the conclusions from the electrochemical study (*vide infra*). These oxidation products do not exhibit an ESR signal.

Electrochemistry

Cyclic voltammetric studies of selenium and tellurium complexes are very few and are limited to only Te^{II} and Te^{IV} dithiocarbamates. Cyclic voltammograms of the complexes (**1–3**, **7–9** and **11**) have been obtained in dichloromethane and acetonitrile. Chemically and electrochemically irreversible reduction and oxidation processes can be inferred for all the complexes. In Table 3, electrochemical data are given for both reduction and oxidation steps.

$M(dmit)^{2-}$ *complexes.* The $M(dmit)^{2-}$ complexes (**1–3**; Fig. 1) in the direction of increasingly positive potentials reveal one electrochemically irreversible oxidation process in the range of +0.15 to +0.28 V. The sodium salt of the ligand $[Na_2(dmit)]$ also shows a single peak with peak potential at 0.07 V presumably corresponding to the formation of the oxidized derivative (**15**) (*vide supra*). In comparison to the sodium salt, the complexes are oxidized at more positive potentials. This oxidation behaviour of complexes is very similar to that of the ligand and the oxidation of the complexes is ligand-based only. We never observed any peak corresponding to Te^{II} or Te^{IV} species, although the +IV and +VI oxidation states are also well known for selenium and tellurium.

Unlike oxidation, the reduction process shows two peaks for the complexes at peak potentials in the range of −0.39 to −0.76 V. The reduction processes are also irreversible. The tellurium complexes show an interesting behaviour. An initial increase followed by a decrease in subsequent cycles of the reduction peaks was observed when the same solution was scanned several times (Fig. 2). A dark coating formed on the working electrode after the reduction process had been scanned and no follow-up peak, like $Te(dtc)_2$, was observed during oxidation.[22,23] The sodium salt of the ligand shows two irreversible reduction peaks at peak potentials of −0.46 and −0.78 V. Thus, in $M(dmit)^{2-}$ complexes the reduction processes are probably both ligand and metal based. The central metal is finally converted into the elemental form and the complexes do not show any indication of short-lived species formed by metal, similar to that reported for tellurium(II) dithiocarbamates,[22] during the electrochemical process. The data clearly indicate a metal dependence of the reduction potential. The ease of reduction decreases in the order Te > Se. It also appears that the solvent effect on the reduction of dithiolates has a profound effect.

$M(dmt)^{2-}$ *complexes.* The cyclic voltammetry experiments for the $M(dmt)^{2-}$ complexes (**7–9** and

Table 3. Cyclic voltammetric data[a] of $M(dmit)^{2-}$ and $M(dmt)^{2-}$ complexes

Compound	Solvent	Scan rate ($mV\ s^{-1}$)	Cyclic voltammetry			
			$Ep_{red}(1)$	$Ep_{red}(2)$	$Ep_{ox}(1)$	$Ep_{ox}(2)$
1	CH_2Cl_2[b]	50	−0.44	−0.76	+0.28	
	CH_2Cl_2	100	−0.39	−0.62	+0.20	
	MeCN	50	−0.6	−0.72	+0.26	
2	CH_2Cl_2	100	−0.49	−0.73	+0.15	
	MeCN	25	−0.57	—	+0.25	
	CH_2Cl_2[b]	50	−0.53	−0.72	+0.20	
3	CH_2Cl_2	100	−0.50	−0.72	+0.20	
7	MeCN	20	−0.35	−0.77	+0.40	+0.75
		50	−0.48	−0.79	+0.42	+0.80
		100	−0.61	−0.81	+0.47	+0.85
	MeCN[b]	25	−0.50	−0.87	+0.24	+0.65
	CH_2Cl_2	100	−0.39	−0.67	+0.38	
8	CH_2Cl_2	100	−0.50		+0.18	+0.50
	MeCN[b]	25	−0.46		+0.10	+0.72
9	CH_2Cl_2	25	−0.47	−0.91	+0.08	+0.50
11	MeCN	50		−0.62	+0.28	
	CH_2Cl_2	100	−0.32	−0.75		
$Na_2(dmit)$	MCN[b]	50	−0.46	−0.78	+0.07	
$Na_2(dmt)$	MeCN[b]	25			+0.3	+0.8

[a] Supporting electrolyte 0.1 Bu_4NPF_6 in CH_2Cl_2 or MeCN, $Ag^+/AgCl$ reference electrode.

[b] SCE reference electrode.

11) show two oxidation–reduction processes. The $Na_2(dmt)$ ligand in acetonitriles shows two oxidation peaks at peak potentials of +0.3 and +0.8 V. The complexes show similar behaviour, but the peaks are more prominent. The cyclic voltammogram of complex $(PPN)_2[Te(dmt)_2]^{2-}$ (**8**) showed one prominent irreversible reduction peak at −0.46 V with a very weak peak at −0.85 V. The

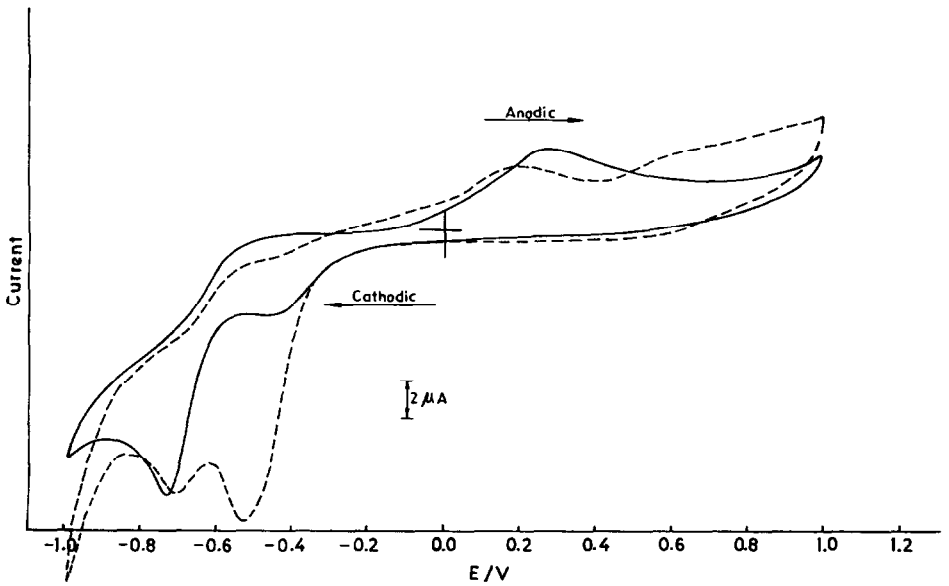

Fig. 1. Cyclic voltammograms for the reduction and oxidation of dmit complexes at platinum (– – –, **2**; ——, **1**) in CH_2Cl_2 solution containing 0.1 mol dm^{-3} $(C_4H_9)_4NPF_6$; SCE reference electrode, scan rate 50 $mV\ s^{-1}$.

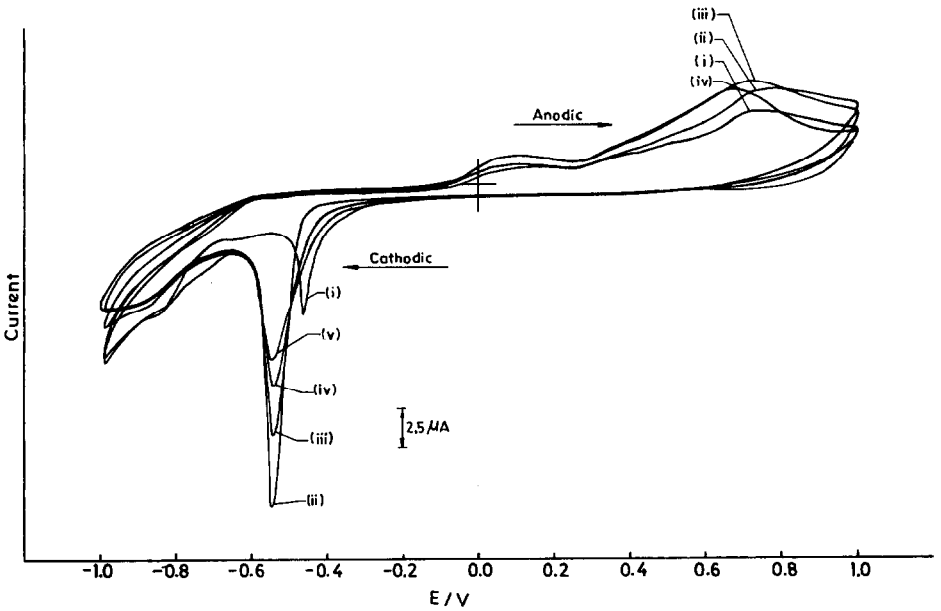

Fig. 2. Cyclic voltammograms for the reduction and oxidation of **8** when recycled in MeCN solution containing 0.1 mol dm^{-3} $(C_4H_9)_4NPF_6$; SCE reference electrode, scan rate 25 mV s^{-1}.

latter disappeared on recycling. However, the first peak at peak potential −0.46 V, similar to the Te $(dmit)_2$ complexes, first increases with shift (−0.54 V) and subsequently decreases by repeated recycling. The sharpness of the peak indicates metal deposition. In positive scan, two oxidation peaks at +0.1 V and +0.7 V were observed. Similarly for the complex $(PPN)_2[Se(dmt)_2]^{2-}$ (**7**), two prominent oxidation peaks at peak potentials +0.24 and +0.65 V were observed. The reduction peaks develop slowly on recycling of the solution during electrochemical study and becomes prominent after two or three recycles at −0.5 and −0.87 V (Fig. 3). Complex **11** showed a flat spectrum at positive potential, which may be due to rapid oxidation of the complex during electrochemical investigation, while the reduction process is prominent for the complexes **7** and **8**.

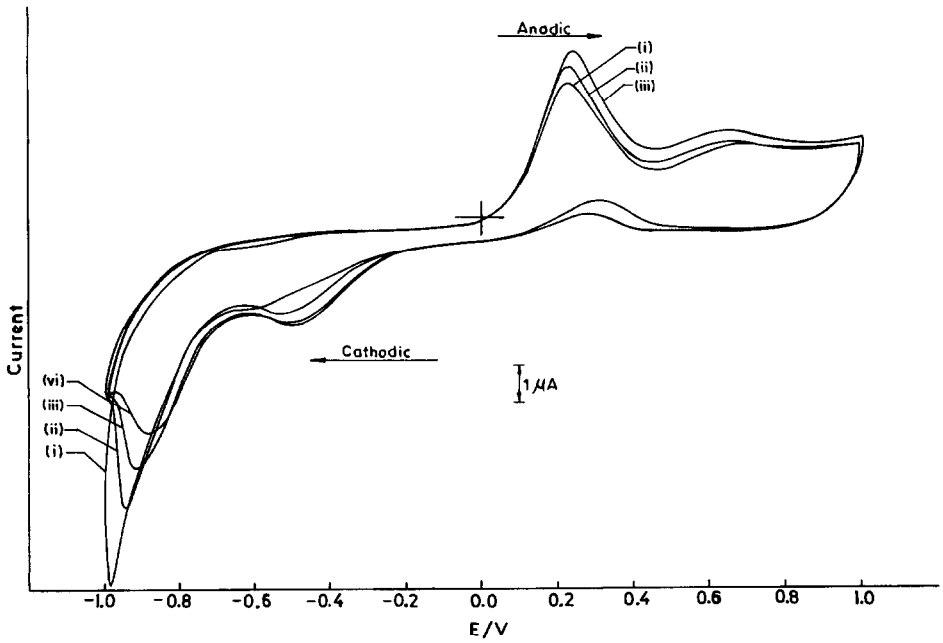

Fig. 3. Cyclic voltammograms for the reduction and oxidation of **7** when recycled in MeCN solution containing 0.1 mol dm^{-3} $(C_4H_9)_4NPF_6$; SCE reference electrode, scan rate 25 mV s^{-1}.

In summary, although planar dithiolene complexes which contain several chalcogen atoms (ligand, central metalloid ion and cation) have been prepared, no partially oxidized species could be isolated. Chemical and electrochemical methods to obtain partially oxidized species have led to the reduction of the central metalloid ion and oxidation of the ligands. Also, attempts to incorporate Te^{II} to isolate thione **12** have led to the reduction of the central metalloid ion. These results further emphasize the role of the transition metal ions (d^8) in obtaining highly conductive complexes. The problem with main group metal ions is probably the high reactivity associated with the unpaired electron on the main group metal ion which is present in a frontier orbital, whereas in a transition metal derivative, the unpaired electrons are in low-lying non-bonding *d*-orbitals.[24] The instability of odd-electron states in Main Group Chemistry is attributable not so much to thermodynamic facts, but rather to the kinetic reaction.

EXPERIMENTAL

General

Melting points were determined using a Ketan melting point apparatus and are uncorrected. Elemental analysis was performed on a Carlo Erba elemental analyser model 1106. IR spectra were recorded as KBr pellets on a Perkin–Elmer 681 IR spectrophotometer. UV–vis spectra were recorded on a Shimadzu UV-260 spectrophotometer (CH_2Cl_2 as solvent) and are reported as λ_{max}. ^{77}Se and ^{125}Te NMR spectral measurements were attempted on a Varian 90 MHz instrument in DMSO-d_6. Mass spectra were determined with a Shimadzu QP-1000 mass spectrometer operating at 70 eV and are reported as *m/z* (P, %). Solid state ESR spectra were investigated using a Varian E-112 ESR spectrometer. The solid state conductivities were measured on powdered samples at room temperature by the two-probe method. All electrochemical experiments were performed in a one-compartmental cell with platinum working electrode and platinum wire counter electrode. The reference electrodes were $Ag^+/AgCl$ or saturated calomel electrode (SCE). Measurements were done on an EG and G Princeton Applied Research, Potentiostat/Galvanostat Model 273. The solutions of complexes (5×10^{-4} mol dm^{-3}) with tetrabutylammonium hexafluorophosphate (0.1 mol dm^{-3}) as supporting electrolyte in dry dichloromethane (15 cm^3) were purged with dry nitrogen and a nitrogen blanket was kept over the solutions at all times. The sweep rate was varied from 25 to 100 mV s^{-1} over ranges of 0.0 to +1.0 V and 0.0 to −1.0 V.

All the reactions were carried out under a dry nitrogen–argon atmosphere. Solvents used were deoxygenated prior to use. Disodium salts of the ligands 4,5-dimercapto-1,3-dithiole-2-thione [H_2(dmit)][25] and 4,5-dimercapto-1,2-dithiole-3-thione [H_2(dmit)][18] were prepared by reported procedures. The complexes $Na_2[Se(S_2O_3)_2]\cdot 3H_2O$ and $Na_2[Te(S_2O_3)_2]\cdot 2H_2O$[26] were prepared as described. $Me_3Te^+I^-$ was prepared by the literature procedure[27] and converted to $Me_3Te^+Cl^-$ by reacting it with AgCl in methanol. Salts such as bis(triphenylphosphine)iminium chloride (PPN^+Cl^-) (Strem. Chem.), tetraphenylarsonium chloride ($Ph_4As^+Cl^-$) and cobaltecenium tetrafluoroborate $(C_5H_5)_2Co^+BF_4^-$ (Fluka) were used as received.

Synthesis

All the complexes were prepared in a similar fashion. Two examples are outlined below.

Preparation of $[(Ph_4As)_2][Te(dmit)_2]$. To a dark red solution of Na_2(dmit) (0.48 g; 2 mmol) in methanol (30 cm^3), was added a methanol (40 cm^3) solution of $Ph_4As^+Cl^-$ (0.98 g; 2 mmol), followed by the addition of $Na_2[Se(S_2O_3)_2]\cdot 3H_2O$ (0.40 g, 1 mmol) in methanol (20 cm^3). The reaction mixture was stirred for 1 h. Dilution of the reaction mixture with water gave the dark brown crude product, which was filtered off and dried. Recrystallization from acetone (without heating at any stage) afforded a crystalline solid.

Preparation of $[PPN]_2[Te(dmt)_2]$. $Na_2(Te(S_2O_3)_2]\cdot 2H_2O$ (0.43 g; 1 mmol) dissolved in methanol (40 cm^3) was added slowly to a mixture of Na_2(dmit) (0.48 g, 2 mmol) and PPN^+Cl^- (1.14 g, 2 mmol) in methanol (40 cm^3). The black finely crystalline compound which precipitated was filtered off, washed with water followed by isopropanol–ether and dried *in vacuo*. The complex was recrystallized by dissolving in pyridine followed by cautious addition of isopropanol till the solution became turbid. A dark red crystalline complex separated after ~ 2 h at 0°C.

Attempted synthesis of oxidized $[Te(dmt)_2]^{n-}$ $(n < 2)$

To an acetonitrile (25 cm^3) solution of $[PPN]_2[Te(dmt)_2]$ (0.319 g, 0.2 mmol) was added a solution of iodine (0.025 g, 0.025 mmol) in acetonitrile (15 cm^3). A yellow–orange product which was precipitated immediately was filtered off, washed with acetonitrile and dried *in vacuo*. Extraction of the crude product with CS_2 afforded an orange

coloured crystalline material (**13**) and a CS_2-insoluble red–brown product (**14**).

Compound **13**. Yield 12%, 0.07 g; m.p. 152–153°C. Found: C, 18.6. Calc. for C_6S_{10}: 18.4%. IR: 1310s, 1250m, 1210m, 1110s, 1040s, 940s, 820m. MS (*m/z*): 328 ($M^+ - 2S$, 53.3%).

Compound **14**. Yield, 0.01 g; m.p. 221°C (d). Found: C, 17.0. Calc. for $(C_3S_x)_n$ ($x = 5.5$): 17.0%. IR: 1470s, 1325m, 1255m, 1210m, 1115s, 1040s, 940s, 820m.

Similar oxidation reactions of $[PPN]_2[Te(dmit)_2]$ and $[PPN]_2[Se(dmit)_2]$ with iodine in a molar ratio of 1 : 2 in acetonitrile afforded **15**. Red solid, (0.06 g), m.p. 148–149°C (d) [lit.[28] 149°C (d)]. Found: C, 17.5. Calc. for C_6S_{10}: 18.4%. IR: 1470m, 1430s, 1250s, 1170m, 1105s, 1000m, 730m, 710s, 680s.

Attempted oxidation of $[PPN]_2[Se(dmt)_2]$ *with* 7,7,8,8-*tetracyano*-p-*quinodimethane* (*TCNQ*)

To an acetonitrile (30 cm^3) solution of $[PPN]_2[Se(dmt)_2]$ (0.15 g; 0.1 mmol) was added a solution of TCNQ (0.040 g; 0.2 mmol) in acetonitrile (15 cm^3). A yellow–orange compound which precipitated immediately was filtered off, washed with acetonitrile and dried *in vacuo* to give **13**.

Attempted aerial oxidation of $[PPN]_2[Se(dmt)_2]$

Air was bubbled into a solution of $[PPN]_2[Se(dmit)_2]$ (0.15 g, 0.1 mmol) in acetonitrile (30 cm^3) for 2 h. The resulting solution was concentrated *in vacuo* to give the starting material.

Acknowledgement—The authors are grateful to the Department of Science and Technology (DST), New Delhi for generous financial support.

REFERENCES

1. P. Cassoux, L. Valade, H. Kobayashi, A. Kobayashi, R. A. Clark and A. E. Underhill, *Coord. Chem. Rev.* 1991, **110**, 115.
2. R.-M. Olk, B. Olk, W. Dietzsch, R. Kirmse and E. Hoyer, *Coord. Chem. Rev.* 1992, **117**, 99.
3. V. E. Shklover, S. S. Nagapetyan and Yu. T. Struchkov, *Russian Chem. Rev.* 1990, **59**, 686.
4. L. Bossard, M. Ribault, L. Valade and P. Cassoux, *Physica B* 1986, **143**, 378.
5. L. Brossard, H. Hudequint, M. Ribault, L. Valade, J.-P. Legros and P. Cassoux, *Synth. Met.* 1988, **27**, 1315.
6. A. Kobayashi, H. Kim, Y. Sasaki, H. Kobayashi, S. Moriyama, Y. Nisho, K. Kajita and W. Sasaki, *Chem. Lett.* 1987, 1819.
7. A. Kobayashi, H. Kobayashi, A. Miyamoto, R. Kato, R. A. Clark and A. E. Underhill, *Chem. Lett.* 1991, 2163.
8. K. Swaminathan, P. Carroll, Kochurani, H. B. Singh and H. D. Bhargava, *Acta Cryst.* 1993, **C49**, 1243.
9. S. Husebye, in *Proceedings of the Fourth International Conference on the Organic Chemistry of Selenium and Tellurium* (Edited by F. J. Berry and W. R. McWhinnie), pp. 298–378. The University of Aston, Birmingham, U.K. (1983).
10. S. Husebye, *Phosphorus and Sulfur* 1988, **38**, 271.
11. L. Golic, W. Dietzsch, K. Kohler, J. Stach and R. Kirmse, *J. Chem. Soc., Dalton Trans.* 1980, 97.
12. G. Hunter, *J. Chem. Soc., Chem. Commun.* 1973, 624.
13. H. B. Singh and W. R. McWhinnie, *J. Organomet. Chem.* 1984, **264**, 305.
14. M. Bjorgvinsson, T. Heinze, H. W. Roesky, F. Pauer, D. Stalke and G. M. Sheldrick, *Angew. Chem. Int. Edn Engl.* 1991, **30**, 1677.
15. W. Dietzsch, R.-M. Olk, E. Hoyer, W. Meiler and W. Ropbien, *Magn. Reson. Chem.* 1988, **26**, 653.
16. W. Dietzsch, R.-M. Olk, E. Hoyer, W. Meiler and W. Robien, *Magn. Reson. Chem.* 1989, **27**, 500.
17. (a) H. Ushijima, S. Sudoh, M. Kojitani, K. Shimizu, T. Akiyama and A. Sugimori, *Inorg. Chim. Acta* 1990, **175**, 11; (b) G. Steimecke, H.-J. Sieler, R. Kirmse, W. Dietzsch and E. Hoyer, *Phosphorus and Sulfur* 1982, **12**, 237.
18. G. Steimecke, H.-J. Sieler, R. Kirmse and E. Hoyer, *Phosphorus and Sulfur* 1979, **7**, 49.
19. S. M. S. V. Doidge-Harrison, R. Alan Howie, J. T. S. Irvine, G. Spencer and J. L. Wardell, *J. Organomet. Chem.* 1991, **414**, C5.
20. R.-M. Olk, W. Dietzsch, R. Kirmse, J. Stach, E. Hoyer and L. Golic, *Inorg. Chim. Acta* 1987, **128**, 251.
21. G. Matsubayashi, K. Takahashi and T. Tanaka, *J. Chem. Soc., Dalton Trans.* 1988, 967.
22. W. Mazurek, *Inorg. Chim. Acta* 1989, **160**, 11.
23. A. M. Bond, D. Dakternieks, R. D. Giacomo and F. Hollenkamp, *Inorg. Chem.* 1989, **28**, 1510.
24. D. G. Tuck, *Coord. Chem. Rev.* 1992, **112**, 215.
25. (a) K. S. Varma, A. Bury, N. J. Harris and A. E. Underhill, *Synthesis* 1987, 837; (b) J. D. Singh and H. B. Singh, *J. Chem. Soc., Perkin I* 1992, 2913.
26. O. Foss, *Inorg. Synth.* 1953, **4**, 88.
27. M. L. Bird and F. Challenger, *J. Chem. Soc.* 1939, 163.
28. S. Kalyan Kumar, H. B. Singh, J. P. Jasinski, E. S. Paight and R. J. Butcher, *J. Chem. Soc., Perkin I* 1991, 3341.

Polyhedron Vol. 12, No. 23, pp. 2857–2867, 1993
Printed in Great Britain

0277–5387/93 $6.00+.00
© 1993 Pergamon Press Ltd

OXOVANADIUM(IV) AND AMINO ACIDS—VI. THE SYSTEMS GLYCYLGLYCINE AND GLYCYLGLYCYLGLYCINE+VO^{2+}; A POTENTIOMETRIC AND SPECTROSCOPIC STUDY

J. COSTA PESSOA* and S. M. LUZ

Centro de Química Estrutural, Complexo I, Instituto Superior Técnico, 1096 Lisboa Codex, Portugal

and

R. DUARTE and J. J. G. MOURA

Departamento de Química, Universidade Nova de Lisboa, 2825 Monte da Caparica, Portugal

and

R. D. GILLARD*

School of Chemistry and Applied Chemistry, University of Wales, Cardiff College, P.O. Box 912, Cardiff CF1 3TB, Wales, U.K.

(*Received* 6 *April* 1993; *accepted* 14 *June* 1993)

Abstract—The equilibria in the systems glycylglycine and glycylglycylglycine+VO^{2+} in aqueous solution have been studied in the pH range 1.5–4.5 by a combination of pH potentiometry and spectroscopy (EPR and visible absorption). The results of the various methods are made self-consistent, then rationalized assuming an equilibrium model including species MLH, ML_2H_2, MLH_{-1} and several hydrolysis products (where HL denotes glycylglycine or glycylglycylglycine); individual formation constants and absorption spectra are given. Plausible isomeric structures for each stoichiometry are discussed.

Knowledge of the complex equilibria of VO^{2+} in the presence of amino acids is relevant in understanding its possible interaction with likely biological ligands.

The first part of this study[1] introduced our work and gave detailed results for the system L-alanine+VO^{2+} in the pH range 2–12. Part II[2] involved the study of the L-serine and L-threonine+VO^{2+} systems, part III[3] L-aspartic acid+VO^{2+}, part IV[4,5] L-cysteine and D-penicillamine+VO^{2+}, and part V[6] the L-glutamic acid+VO^{2+} system. This paper reports our work on the glycylglycine and glycylglycylglycine+VO^{2+} systems by combining the results of potentiometric and spectroscopic techniques. Part of this work has been presented in preliminary form.[7] In common with biochemical studies, we abbreviate the HL forms of glycylglycine (I) and glycylglycylglycine (II) as glygly and glyglygly, respectively. When a shorter abbreviation is convenient, we use GG and GGG.

(I) (glygly or GG)

(II) (glyglygly or GGG)

* Authors to whom correspondence should be addressed.

To our knowledge the only report mentioning these systems is from Crans *et al.*[8] These authors used a phosphatase catalysed enzyme assay to determine the extent of interaction between 10^{-7}–10^{-5} M vanadium(IV) and selected organic molecules, namely glycine (gly), glycylglycine (glygly) and glycylglycylglycine (glyglygly). From the V_0/V_i ratios (V_0, rate of hydrolysis; V_i, inhibited rates) determined in the presence of these biomolecules, and assuming the formation of a single complex species in each case, Crans and co-workers[8] estimated formation constants of 5000, 20,000 and 40,000 for gly, glygly and glyglygly, respectively.

There are several experimental difficulties in studying the systems produced by oxovanadium(IV) and amino acids. These are discussed in Part I.[1] Our results with the glygly (and glyglygly) $+VO^{2+}$ systems differ greatly from those for the gly$+VO^{2+}$ or L-ala$+VO^{2+}$ [1] systems. For the vanadium(IV) concentrations used in our potentiometric and spectroscopic studies, it is possible with gly or L-ala to avoid vanadyl hydroxide precipitation by using relatively high ligand-to-metal ratios (L/M ratios). In contrast, with glygly or glyglygly, very extensive hydrolysis and precipitation of $VO(OH)_2$ occurs for pH > 4–5, even when using L/M ratios of 180.

As only pK_{a1} (terminal —COOH) and pK_{a2} (terminal —NH_2) can be determined, our calculations of formation constants correspond to the general reaction:

$$pM^{2+} + qL^- + rH^+ \overset{\beta_{pqr}}{\rightleftharpoons} M_pL_qH_r. \qquad (1)$$

For the formulations $(VO)_p$(GG or GGG)$_q H_r$ we normally use the abbreviation $M_pL_qH_r$. For each $M_pL_qH_r$ proposed in our final equilibrium models, possible stuctures are discussed.

EXPERIMENTAL

Materials and methods

All solutions were prepared in an inert atmosphere (high purity dinitrogen passed through soda lime and glass wool). All measurements were performed at 25°C with solutions containing 2.25 M $NaNO_3$.

Stock VO^{2+} and NaOH were prepared and standardized as described in part I.[1] Glygly and glyglygly (Sigma) for stock solutions were dried for several days (in a desiccator with silica gel *in vacuo*). Their purity was checked by HPLC (C_{18} column with several different eluents, one of them giving adequate selectivity to separate the *o*-phthalaldehyde derivatives of gly, GG and GGG), thin layer chromatography on silica plates and elemental analysis.

For potentiometric titrations we used a special glass vessel with a double wall, with entries for the glass electrode (Orion Ross/81-01) and reference electrode (Orion Ross/80-05), thermometer, nitrogen and base from the burette (Metrohm). A computerized system developed locally was used to control the titration conditions (e.g. the interval between the additions of base, criteria of stability of the point).[9] The e.m.f. measurements were made with a Crison 517 pH meter and the titrations were controlled by an IBM-PC XT computer. Visible spectra were recorded with a Perkin–Elmer lambda 9 spectrophotometer. Cell compartments were kept at 25°C with circulating water from a thermostatted bath. Unless otherwise stated, by visible spectra we always mean a representation of ε_m values vs λ [ε_m = absorption/($b \times C_{VO}$); b = optical path and C_{VO} = total oxovanadium(IV) concentration]. The X-band EPR spectra were recorded at 77 K (on glasses made by freezing solutions in liquid nitrogen) with a Bruker ESR-ER 200tt connected to a Bruker B-MN C5 EPR spectrometer and to a Bruker EPR data system (linked to an IBM AT computer).

The calibration procedure for pH measurements was described in Part I.[1] We continue to assume that the e.m.f. values (E) depend on [H^+] according to:

$$E = E^{0\prime} + Q \log [H^+] + J_H[H^+] + J_{OH}[OH^-]. \qquad (2)$$

As $J_H \sim 20$, the corrections in the acid range are significant only for pH < 2.0.

Eight titration curves ($0.02 < C_L < 0.07$ M; C_L = total peptide concentration) were obtained to determine the protonation constants in 2.25 M $NaNO_3$. NaOH (1.016 M) with a total ionic strength of 2.25 M was used as titrant.

As vanadyl hydroxide precipitates for pH > 4–5, even when using high L/M ratios, titrations of solutions containing glygly (and glyglygly) and VO^{2+} were only performed for $1.7 \leqslant$ pH $\leqslant 4.2$ (with $0.010 \leqslant C_{VO} \leqslant 0.022$ and $0.5 \leqslant$ L/M $\leqslant 6.0$).

Depending on C_{VO} and L/M ratio, for pH > 3.8–4.3 the e.m.f. readings become unstable. As in previous work,[1-6] such instability is probably due to oxidation and/or extensive hydrolysis of oxovanadium(IV).

Two types of sets of visible absorption spectra were recorded:

(a) varying the pH with approximately fixed total vanadium and peptide concentrations, at several ligand-to-metal ratios;

(b) at approximately fixed pH and total peptide

concentration and varying the total vanadium concentration (C_{VO}).

For the glygly + VO^{2+} system, a total of 63 visible absorption spectra were used for the calculation of spectra of individual species, with total concentrations in the range 3.3×10^{-3} M $\leqslant C_{VO} \leqslant$ 3.1×10^{-2} M and 1.8×10^{-2} M $\leqslant C_{GG} \leqslant 3.0 \times 10^{-1}$ M, respectively. Ligand-to-metal ratios were in the range $1 \leqslant L/M \leqslant 50$. For the glyglygly + VO^{2+} system, a total of 65 visible absorption spectra were used for the calculation of spectra of individual species, with total concentrations in the range 7.0×10^{-3} M $\leqslant C_{VO} \leqslant 3.0 \times 10^{-2}$ M and 1.4×10^{-2} M $\leqslant C_{GGG} \leqslant 1.8 \times 10^{-1}$ M, respectively. Ligand-to-metal ratios were also in the range $1 \leqslant L/M \leqslant 50$. The calculations were performed on results for 450–860 nm.

For the refinement of formation constants and calculation of spectra of individual species, the SUPERQUAD[10] and the SQUAD[11] programs were used. These were run in a Vax 780 DIGITAL computer.

For pH > 4–4.3, the bands in the experimental visible spectra are ill-defined, except when using quite high L/M ratios, e.g. L/M > 20–30, where accurate and reproducible spectra may be obtained till pH ~ 4.5. Further, inaccuracies in the calculation of the contributions of the hydrolysis of vanadium and/or oxidation of a small fraction of the total vanadium(IV) may have a substantial effect on the spectra and preclude a critical analysis of the results. We therefore present no results of calculation with SQUAD using visible spectra of solutions with pH > 4.5.

Using high L/M ratios, $VO(OH)_2$ dissolves for pH $\geqslant$ 7.5–8.0. However, as $pK_{a2} \simeq$ 8.3–8.4, the buffer effect of the R—NH_3^+ groups precludes the use of potentiometry. On the other hand, oxovanadium(IV) is quite extensively hydrolysed and visible absorption spectra are not very useful (see, for example, ref. 1). It is possible to use circular dichroism spectra to study such solutions for peptides such as gly–L-ala, L-alagly and L-ala–L-ala, but these will be discussed in a separate paper.[12]

RESULTS

EPR spectra

The X-band EPR spectra with frozen "solutions" containing GG or GGG and VO^{2+} at 77 K are typical VO^{2+} axial spectra. The field region that corresponds to $A_{\parallel}$ and $M_I = 5/2$ and 7/2 (3800/4300 G) gives more information about the type and number of species present.

For the glygly + VO^{2+} system, spectra were recorded with (1) L/M = 5, $C_{VO} \simeq 0.024$ M, $2.0 \leqslant$ pH $\leqslant 4.0$; (2) L/M = 20, $C_{VO} \simeq 0.017$ M, $1.5 \leqslant$ pH $\leqslant 4.4$; (3) L/M = 25, $C_{VO} \simeq 0.005$ M and $3.9 \leqslant$ pH $\leqslant 4.5$. For the glyglygly + VO^{2+} system, spectra were recorded with (1) L/M = 5, $C_{VO} \simeq 0.024$ M, $2.0 \leqslant$ pH $\leqslant 4.0$; (2) L/M = 15, $C_{VO} \simeq 0.026$ M, $1.5 \leqslant$ pH $\leqslant 4.4$; (3) L/M = 25, $C_{VO} \simeq 0.005$ M and $4.1 \leqslant$ pH $\leqslant 4.6$. For comparison, spectra were also recorded for the gly + VO^{2+} system with L/M = 5, $C_{VO} \simeq 0.038$ M and $1.5 \leqslant$ pH $\leqslant 4.2$.

Some spectra for the glyglygly + VO^{2+} system are included in Fig. 1. Results are similar for the glygly + VO^{2+} system and for the gly + VO^{2+} system

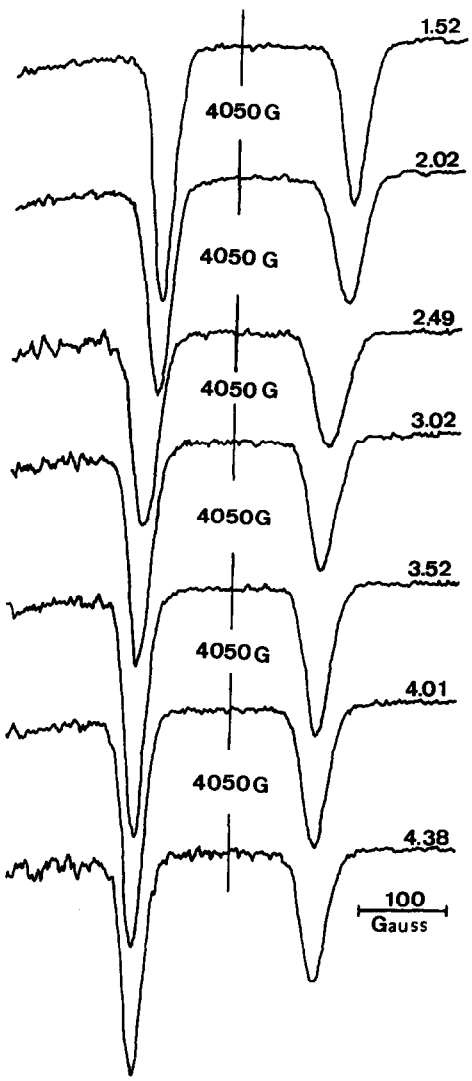

Fig. 1. First derivative EPR spectra (high field range, 3800–4300 G) of solutions containing glyglygly + VO^{2+} for 1.5 < pH < 4.4, L/M = 15 and $C_{VO} \simeq 0.026$ M. The pH corresponding to each spectrum is indicated.

Table 1. Vanadium hyperfine coupling constants and g values calculated[a] from the first derivative EPR spectra at 77 K of frozen "solutions" containing glygly (and glyglygly) + VO^{2+} with $C_{VO} \simeq 0.017$ M, L/M = 20 (GG) and $C_{VO} \simeq 0.026$ M, L/M = 15 (GGG)

	pH	$g_\perp$	$g_\parallel$	$A_\perp \times 10^4$ (cm^{-1})	$A_\parallel \times 10^4$ (cm^{-1})
glygly	1.5	1.982	1.926	71	183
	2.0	1.978	1.924	71	183
	2.5	1.976	1.930	67	181
	3.0	1.978	1.929	66	179
	4.0	1.976	1.928	65	177
	4.2	1.974	1.932	64	179
	4.4	1.971	1.929	62	177
glyglygly	1.5	1.979	1.924	71	183
	2.0	1.980	1.925	71	183
	2.5	1.977	1.930	67	181
	3.0	1.980	1.931	66	179
	3.5	1.981	1.929	66	176
	4.0	1.977	1.935	64	180
	4.4	1.975	1.931	64	178

[a] Absolute values of g and A ($\parallel$ and $\perp$) are probably within ± 0.007 and ± 1, respectively, of the tabulated values.

for pH <4.2. In all cases, as the pH is increased from 1.5 to 4, each spectrum appears like that of only one component but the peaks actually shift to lower field (in an approximately continuous manner). That is, in this pH range, more than one species exists with rather similar $A_\parallel$ values. For pH $\geqslant$ 4, the spectra practically coincide and apparently only one EPR component is detected, except for the gly + VO^{2+} system, where a distinct species may be clearly seen. Table 1 summarizes the relevant g and A ($\perp$ and $\parallel$) parameters calculated using an iterative procedure using the correct equations[13] based on Chasteen's method.[14]

Visible absorption spectra

The visible spectra recorded for solutions containing glygly + VO^{2+} are similar to those obtained for solutions of glyglygly + VO^{2+} in similar experimental conditions.

Figure 2 includes visible spectra of solutions of GG + VO^{2+} with an L/M ratio of 5 and Fig. 3 of GGG + VO^{2+} solutions with an L/M ratio of 20. For pH < 3, the spectra are similar (except for ε_m values) to those of aqueous oxovanadium(IV) solutions. For pH > 3, the spectra apparently reveal an increase of the ligand field around VO^{2+} as λ_{max} of band II[15] shifts to shorter wavelengths. The general

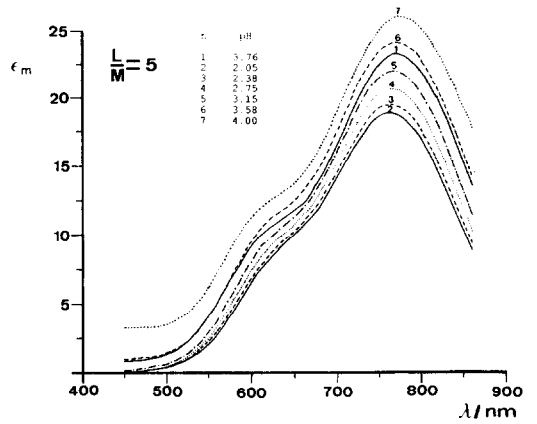

Fig. 2. Visible spectra of solutions containing glygly and VO^{2+} with L/M = 5 and $C_{VO} \simeq 0.016$–0.019 M. The pH corresponding to each spectrum is indicated. Spectrum 7 indicates hydrolysis of the complexes.

increase in ε_m (especially for $450 < \lambda < 650$ nm) in both systems for pH ~ 3.6–3.8 (for L/M = 2), 3.7–3.9 (for L/M = 5), 3.8–4.0 (for L/M = 10), 4.0–4.2 (for L/M = 20) and 4.4–4.8 (for L/M = 50) suggests hydrolysis of VO^{2+}. Addition of base to these solutions to increase the pH by 0.2 or more produces instability of the pH readings and after a while precipitation of vanadyl hydroxide. Even when using L/M ratios of 180, $VO(OH)_2$ precipitates for pH $\gtrsim$ 4.8.

Figure 4 gives examples of spectra at fixed pH varying the ligand-to-vanadium ratio at approximately fixed ligand concentration. For pH $\simeq$ 2.8, ε_m values hardly change as the metal concentration varies from 3.0×10^{-3} to 3.0×10^{-2} M (Fig. 4A) or from 3.4×10^{-3} to 2.4×10^{-2} M for the GGG + VO^{2+} or GG + VO^{2+} systems, respectively. For pH $\simeq$ 3.6, the ε_m values in the range 600–850 nm

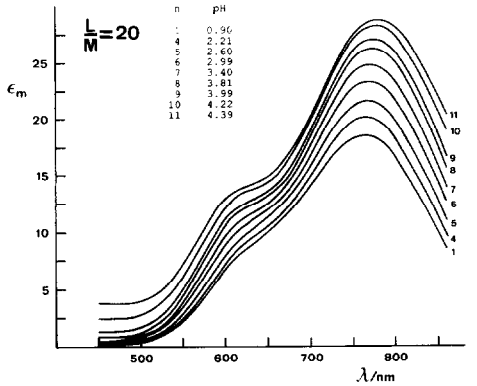

Fig. 3. Visible spectra of solutions containing glyglygly and VO^{2+} with L/M = 20 and $C_{VO} = 0.007$–0.009 M. Spectra 1–4 are similar to those of aqueous oxovanadium(IV) solutions.

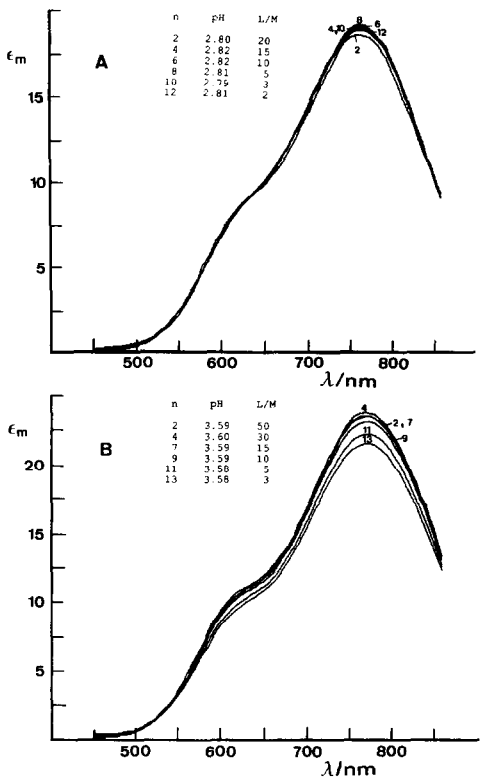

Fig. 4. Visible absorption spectra of solutions containing glygly and VO^{2+} at approximately fixed pH and ligand concentration, at several ligand-to-metal ratios. In A, the initial total vanadium concentration was 3.41×10^{-3} M and the L/M ratio was varied by successive addition of relatively concentrated oxovanadium(IV) solution. In B, the procedure was identical but the initial vanadium concentration was 3.28×10^{-3} M.

decrease about 3% as the L/M ratio varies between 50 and 10 and about 9% between 50 and 3; for solutions containing GGG and VO^{2+}, the corresponding ε_m decrease is about 1% and 6%, respectively. These results indicate that up to pH $\simeq$ 3.6, polymeric species do not form in significant concentration in the experimental conditions used.[1] The slight variations recorded are probably due to equilibria between complexes of different ligand-to-vanadium stoichiometry.

Potentiometry

From SUPERQUAD[10] in solutions containing 2.25 M $NaNO_3$ (at 25°C): $pK_{a1} = 3.31$, $pK_{a2} = 8.42$ and $pK_{a1} = 3.39$, $pK_{a2} = 8.30$ for glygly and glyglygly, respectively, values used in all calculations. These values compare well with literature[16] values; for glygly $pK_{a1} = 3.16$ and $pK_{a2} = 8.10$, and for glyglygly $pK_{a1} = 3.26$ and $pK_{a2} = 8.01$ ($I = 1$ M).

Vanadyl hydroxide precipitated for pH > 4–5, even for very high ligand-to-metal ratios, unlike several systems previously studied.[1-6] It was impossible to titrate in the pH range 4.5–7.5, where the ligands have no buffer effect. Therefore, a titration curve with L/M = 6 was the maximum ligand-to-vanadium ratio included in the calculations with SUPERQUAD for each of the systems.

In these experimental conditions, most of the vanadium(IV) is in the uncomplexed form, $VO(H_2O)_5^{2+}$. Further, the peptides are mainly or significantly in the protonated form, HL, in the pH range 2–4, so that no H^+ is involved in the formation of MLH or ML_2H_2. Consequently, the situation for calculating formation constants is unfavourable.

In the calculations with SUPERQUAD, only for MLH could $\log\beta$ be refined in a reasonably consistent manner: even this was not entirely satisfactory. In combinations of this species MLH with other reasonable guesses, e.g. ML, ML_2H_2, ML_2H, ML_2, MLH_{-1}, values of $\log\beta$ for groups of two or three (total) species could be refined, but not in a consistent way and with relatively high standard deviations (SDs). SUPERQUAD, therefore, afforded only preliminary results: model selection and calculation of formation constants were mainly based on the spectrophotometric results.

Spectrometry

In solutions of VO^{2+} and GG or GGG only vanadium complexes contribute to ε_m in the visible region. This fact removes the limitation (major, but not always appreciated) of potentiometry to those experimental conditions (L/M ratios and pH) where the ligand has no significant buffer effect. Therefore, when calculating formation constants based on visible spectra, we are better off for species that predominate in the pH range 2–4, because increasing the L/M ratio also increases the degree of complex formation.

As for the systems previously studied, the SQUAD program was run assuming many different models, taking combinations of plausible species (see above). For pH $\gtrsim$ 3.5–4.2 (depending on L/M ratio), hydrolysis products such as MH_{-1} and especially M_2H_{-2} may have significant concentrations. Therefore in many of these preliminary calculations $\varepsilon_{20\text{-}2}$ (and $\varepsilon_{10\text{-}1}$) and in some cases the corresponding values of $\log\beta$ were also included as parameters to be refined. These calculations suggested that standard deviations for $\log\beta$ and calculated ε, sum of squares and type of spectra calculated were more reasonable if the model includes

Table 2. Composition and formation constants of species in the glygly and glyglygly + VO^{2+} systems in the region $1.5 \leqslant pH \leqslant 5$[a]

Stoichiometry	glygly	glyglygly
MLH	10.3 (0.2)	10.1 (0.2)
ML_2H_2	19.5 (0.3)	19.4 (0.3)
MLH_{-1}	1.9 (0.3)	1.6 (0.3)
HL	8.42 (0.02)	8.30 (0.03)
H_2L	11.73 (0.03)	11.69 (0.03)

[a] Values for $\log\beta$ of eq. (1) are given (at 25°C and 2.25 M $NaNO_3$). Log β for vanadium hydrolysis products were:[1] −5.98, −6.95 and −22.22 for MH_{-1}, M_2H_{-2} and M_2H_{-5}, respectively.

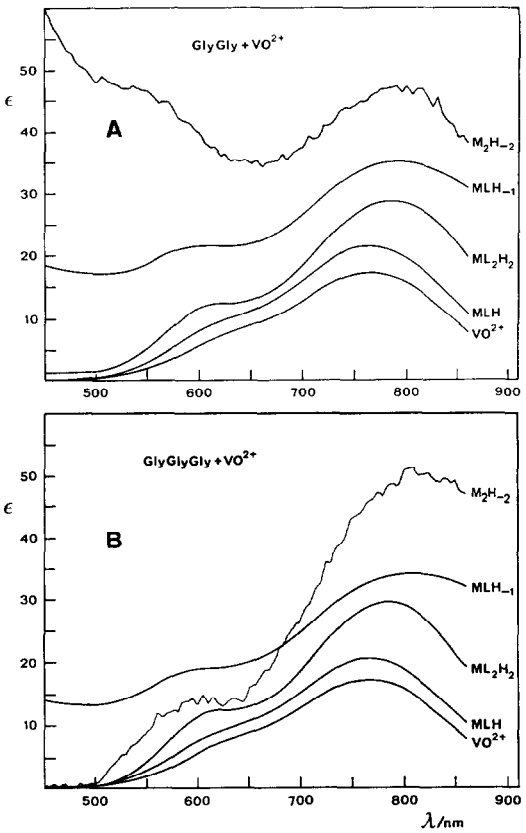

Fig. 5. Visible absorption spectra (calculated using the SQUAD program[11]—see text for details) for species that may form in solutions containing oxovanadium(IV) and glygly (A) or glyglygly (B) (high L/M ratios), using formation constants in Table 2 and experimental visible spectra in the pH range 2–4.5. Spectra for M_2H_{-2} were calculated with high SDs.

species MLH, ML_2H_2 and MLH_{-1}. For both GG and GGG + VO^{2+} systems, calculations involving models including ML, ML_2H, ML_2 or dimeric complexes generally gave unsatisfactory results.

Having obtained an order of magnitude of the appropriate values of $\log\beta$, we used a step-by-step procedure starting in the low pH region. Sets of experimental spectra were chosen where only $VO(H_2O)_5^{2+}$ and the MLH form are expected: $\log\beta_{111}$ and ε_{111} were refined. These agreed well with values obtained in the preliminary calculations described above and were included in the input file of SQUAD as fixed parameters for the next step. The SQUAD program was then run assuming many different models, taking combinations of ML_2H_2, ML, MLH_{-1}, ML_2H, ML_2 and dimeric species, and again the results suggest that besides MLH, only ML_2H_2 and MLH_{-1} should be included in the final equilibrium model.

Sets of experimental spectra were then chosen where M, MLH, ML_2H_2 and MLH_{-1} are expected to have significant concentrations and M_2H_{-2} is below 1%. SQUAD was run with $\log\beta_{122}$, $\log\beta_{11\text{-}1}$, ε_{122} and $\varepsilon_{11\text{-}1}$ as parameters to be refined and the β_{122} and ε_{122} obtained were taken as fixed for the next step. Taking the whole set of experimental spectra, $\log\beta_{11\text{-}1}$, $\varepsilon_{11\text{-}1}$ and $\varepsilon_{20\text{-}2}$ were refined; several calculations also included $\log\beta_{20\text{-}2}$ as a parameter to be refined. Table 2 includes the selected final equilibrium models incorporating both the potentiometric and spectroscopic results. For each of the $\log\beta_{xyz}$ values, plausible ranges are also given, established by a critical examination of all the calculations. The calculated spectra are given in Fig. 5.

The visible absorption spectra for M_2H_{-2} were calculated with high SD, both for GG and GGG + VO^{2+} systems. The spectra obtained for M_2H_{-2} in both calculations should coincide; therefore they could be considered as a good internal calibration pair of independent results. However, M_2H_{-2} is a minor species in the experimental conditions used for all spectra included in the input file of SQUAD: it is not possible to get reliable spectra for solutions where it has a significant concentration, as the pH readings are unstable and vanadyl hydroxide precipitates after a while. Recycling both sets of SQUAD calculations giving the values for M_2H_{-2} as fixed input can be done, but as calculated spectra reflect both the real spectrum for M_2H_{-2} and the "noise" in the SQUAD analysis, this precludes the quantitative use of these calculations to test the self-consistency of the results. Therefore, the fact that reasonable values are obtained for $\varepsilon_{20\text{-}2}$ indicates only that the models presented in Table 2 are correct. Calculations involving the refinement of $\log\beta_{20\text{-}2}$ also yielded satisfactory results.

Assuming SQUAD taking $\log\beta_{111}$, $\log\beta_{11\text{-}1}$, ε_{111}

and $\varepsilon_{11\text{-}1}$ as fixed and $\log\beta_{122}$ and ε_{122} (and also $\varepsilon_{20\text{-}2}$) as parameters to be refined gave results that agree quite well with those presented in Table 2 and Fig. 5, indicating that the various methods of calculation are self-consistent.

DISCUSSION

The proposed equilibrium models—the set of species (with plausible values for their formation constants)—to account for all the experimental potentiometric and spectroscopic results are given in Table 2. In the present systems potentiometry can only afford preliminary results: most of the calculations were based on spectrophotometric results.

Figure 6 gives the concentration distribution calculated for L/M = 20 for both systems and Fig. 7 a representation of (A) $\log\beta_{pqr}^{(GGG)}$ vs $\log\beta_{pqr}^{(GG)}$ and (B) $\log\beta^{VO}$ (GG and GGG) vs $\log\beta^{Cu}$ (GG and GGG). Such representations may help to indicate structures for each $M_pL_qH_r$ species in the models.

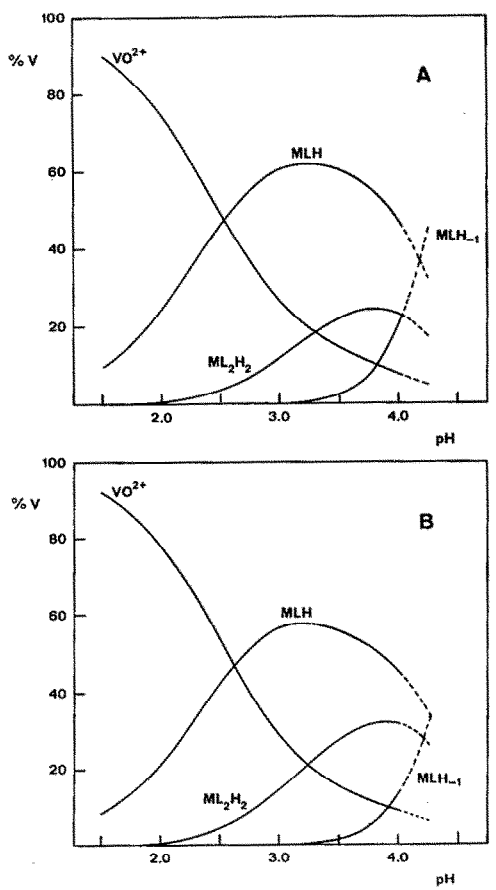

Fig. 6. Concentration distribution of the complexes formed in the glygly (A) and glyglygly (B)+VO^{2+} systems in solutions with $C_{VO} = 5\times10^{-3}$ M and L/M = 20, calculated[17] using β_{pqr} of the equilibrium models of Table 2.

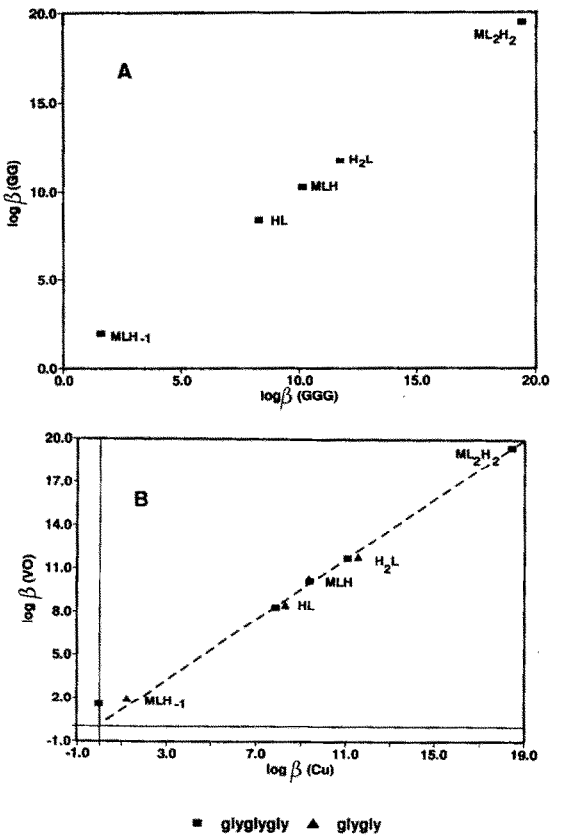

Fig. 7. Representation of: (A) $\log\beta_{pqr}^{GG}$ vs $\log\beta_{pqr}^{GGG}$ for vanadium complexes; (B) $\log\beta_{GG}^{VO}$ vs $\log\beta_{GG}^{Cu}$[18] and $\log\beta_{GGG}^{VO}$ vs $\log\beta_{GGG}^{Cu}$.[16] (▲) glygly; (■) glyglygly. In B, the straight lines are based solely on $\log\beta_{011}$, $\log\beta_{012}$ and $\log\beta_{111}$ (and also β_{122} in the case of glyglygly) and practically coincide for both systems.

The linear plots can also be used to estimate $\log\beta$ for vanadium or copper complexes as long as the coordination geometries are similar and one of the constants is known.

Structures

In relating the molecular structure of an aqueous species to its stability, it is generally useful to compare a spectroscopic property with that of the crystalline solid of known structure. Unfortunately, in our present studies of peptide complexes with oxovanadium(IV), there are as yet no well-characterized solid complex compounds, so there are no crystal structures to serve as points of reference. Our discussion of the structures of these species is based entirely on their properties in solution.

Four types of donor atoms, amino-N, carbonyl-O, amide-N and carboxylate-O, are present in simple peptides, such as glygly (**I**) or glyglygly (**II**): all are capable of metal ion coordination. The

basicity of various groups influences the coordination chemistry of these peptides: the amide group has an extremely weak basic character,[19–21] the pK_a values being of the order of 15. However, the pK_a values for amide deprotonation followed by coordination in copper(II) complexes is relatively low, 4.0 for GG and 5.2 for GGG; in Ni^{II} complexes it is ~ 9.3 for the first amide deprotonation and 10 for the second glygly bound.[19]

In discussing amino acid–vanadium(IV) coordination chemistry, comparisons are often made[1–6] with Cu^{II} and Ni^{II}. However, in the present systems vanadyl hydroxide precipitates for pH > 4–5, even when using high L/M ratios, and no such comparisons can be made.

For pH < 4–5, neither the EPR nor visible absorption spectra give any indication of deprotonation of the peptide group. Besides, if coordination in this pH range involves the amino group at some stage, this acts as an ineffective anchoring group for competition with vanadium hydrolysis, even when using high L/M ratios. Therefore the situation is quite different from that found for Cu^{II}, where a species ML forms with a coordination geometry of the type shown in **III**,[19–21] followed by the deprotonation and coordination of the peptide nitrogen at slightly acidic pH.

The situation is further complicated by the vanadyl ion being lop-sided: many of its chelates may give rise to more isomers than do apparently analogous mono-atomic metal centres such as the copper(II) ion; refs 1 and 15 briefly discuss this. Even in the absence of this extra isomerism, i.e. for monodentate ligands such as an amino acid or peptide via attached carboxylate, the common geometric isomers may both be present (if there are two such ligands).

We now discuss on the basis of Figs 5 and 7 and Table 2 the dominant structure for each stoichiometry. Potentiometry alone cannot of course distinguish structures of the same stoichiometry, except in favourable cases.

MLH. This stoichiometry probably has the α-COO^- group in an equatorial position. The visible spectrum of MLH is like those for the corresponding stoichiometries: MAH, MSH, MDH_2, MPH_2 and MEH_2 (L-alanine, L-serine, L-aspartic acid, D-penicillamine and L-glutamic acid, respectivcly), with amino acids monodentate via carboxylate.

Chasteen's method[14] gives estimated $g_\parallel \sim 1.935$ and $A_\parallel \sim 180 \times 10^{-4}$ cm^{-1} for this geometry. Consequently, values presented in Table 1 in the pH range 1.5–2.5 agree with those expected for solutions containing $VO(H_2O)_5^{2+}$ and MLH ($g_\parallel$ values somewhat lower than predicted).

Writing the formation as

$$VO^{2+} + nHL \overset{K_n}{\rightleftharpoons} VO(HL)_n^{2+},$$

$K_1 \sim 71$ and $K_1 \sim 69$ for glygly and glyglygly, respectively. These are higher than the corresponding K_1 values for several other amino acids, for gly (14.8),[22] L-ala (15.6),[1] L-ser (12.5),[2] L-thr (12.9),[2] D-pen (20.0),[5] L-cys (15.0)[5] and L-glu (9.3)[6] (the gly values relate to a different medium, 1 M $NaClO_4$), and of the same magnitude as K_1 for aspartic acid (78).[3]

K_1 values were reported as 186 and 245 for nickel complexes of GG and GGG, respectively, and $K_{ML} = 3.8$ for Ni^{II} binding at *N*-acetylglycine.[23] For Cu^{II}, several values have been reported for MLH complexes (L = GG or GGG) in the range $\log K_1 = 1.04–1.89$[16,18,24–28] and $\log K_{ML} = 1.3$ for monodentate coordination of *N*-acetylglycinate.[19] Apparently, the most reliable data come from the work of Shtyrlin *et al.*[18] for the Cu^{II}–glygly system, $\log \beta_{111} = 9.36$ and $\log K_1 = 1.04$ at 25°C and $I = 1.0$ M KNO_3. In that work the β_{111} value was determined from spectrophotometric data in calculations including spectra at high L/M ratios, where this complex has a significant concentration (for L/M = 1, MLH never exceeds 5% of the total copper).

In Fig. 8 we include a representation of $\log K_1$ vs pK_{a1} for vanadyl complexes involving the "monodentate" coordination of the carboxylate group. In this figure, "normal" values are expected to lie inside the region marked with dashed lines and it

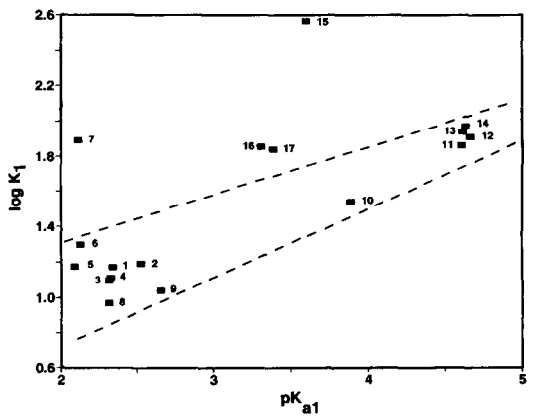

Fig. 8. Representation of $\log K_1$ (see text) vs pK_{a1} for vanadyl complexes involving the "monodentate" coordination of the carboxylate group. (1) Gly;[22] (2) L-ala;[1] (3) L-ser;[2] (4) L-thr;[2] (5) L-cys;[5] (6) D-pen;[5] (7) asp;[3] (8) L-glu;[6] (9) chloroacetate;[31] (10) chloropropionate;[29] (11) acetate;[29] (12) propionate;[30] (13) butyrate;[30] (14) isobutyrate;[30] (15) hydroxyacetate;[31] (16) glygly (this work); (17) glyglygly (this work).

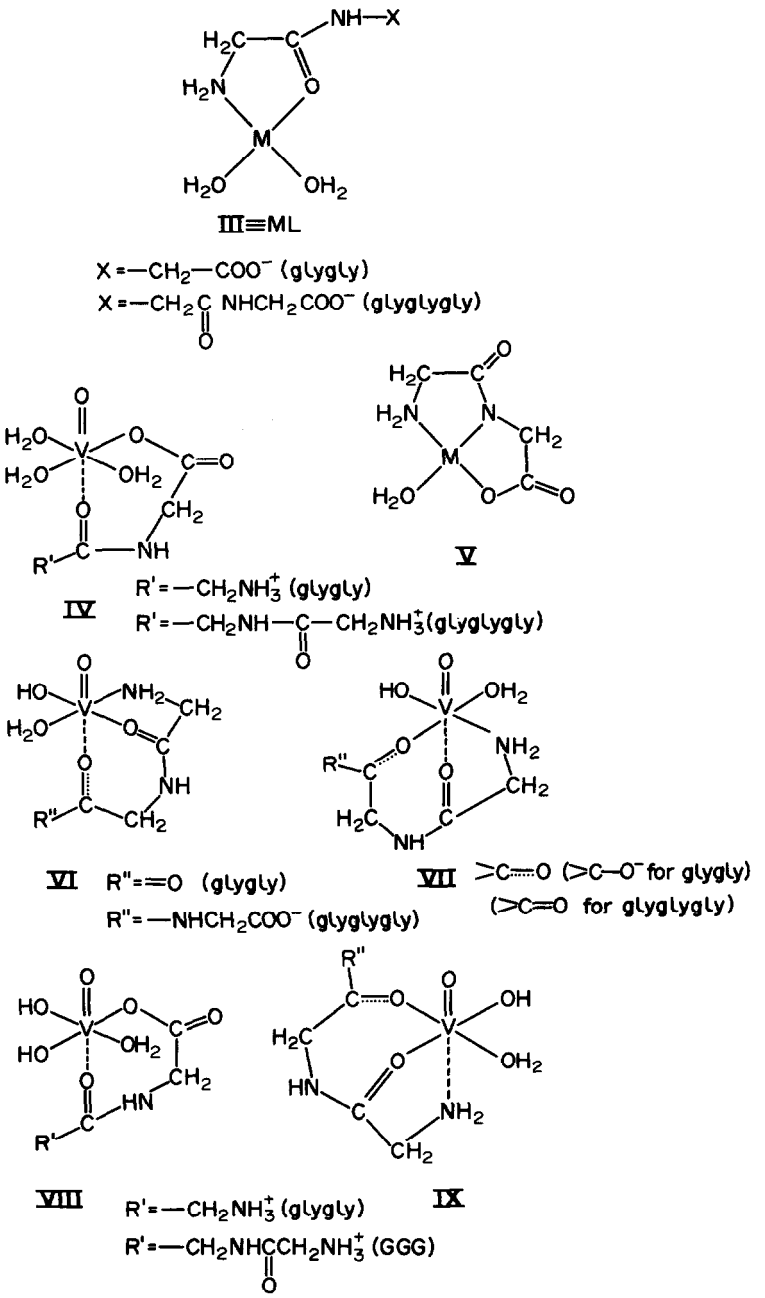

may be seen that values for glygly and glyglygly fall outside (above) this region. The fact that K_1 values for GG and GGG are considerably higher than those obtained for several other amino acids and carboxylates[29–31] cannot be easily understood. Shtyrlin *et al.*[18] argue that for Cu^{II}, coordination in the zwitterionic form (HL) is more favoured for dipeptides as compared to amino acids, because intramolecular hydrogen bonding between the $—NH_3^+$ group and the $—COO^-$ group of the non-coordinated zwitterion (cyclization) is more advantageous for amino acids owing to the steric requirements. The high K_1 values obtained may also arise from amide oxygen coordination. This requires the formation of a seven-membered chelate ring, which is unlikely for bidentate coordination in equatorial positions. However, if coordination is equatorial/axial as in **IV**, steric constraints appear to be much less, due to the much longer bonds typically formed in vanadyl axial positions, 2.3–2.4 as against 1.9–2.0 Å[15] in equatorial/equatorial. For glyglygly the coordination of the second amide oxygen in an equatorial position can also be envisaged.

ML_2H_2. This stoichiometry probably corresponds to complexes with two monodentate α-carboxylate groups coordinated equatorially. For

this coordination geometry, one can estimate[14] $g_{\parallel} \sim 1.937$ and $A_{\parallel} \sim 177 \times 10^{-4}$ cm^{-1}. The values presented in Table 1 in the pH range 2.5–3.5 consequently agree with those expected for solutions containing $VO(H_2O)_5^{2+}$, MLH and ML_2H_2 ($g_{\parallel}$ somewhat lower than predicted).

From Table 2, $K_1K_2 \sim 454$ and ~ 637 for glygly and glyglygly, respectively, again higher than the corresponding values for L-ala (30)[1], L-ser (24),[2] L-cys (45),[5] D-pen (70)[5] and L-glu (15).[6] Apart from differences in ε values, both visible spectra for ML_2H_2 are similar to those for the corresponding MA_2H_2, MS_2H_2, MP_2H_4 and ME_2H_4. K_2 values are ~ 6 and ~ 9 for GG and GGG, respectively. These are "normal" values, suggesting that coordination of a second ligand molecule involves monodentate coordination of the carboxylate group. At this point, we re-emphasize that the stoichiometry for each "species", $M_pL_qH_r$, corresponds to more than one isomer. Relative isomeric concentrations are independent of concentrations of metal, ligand and H^+, so our experimental techniques do not discriminate between them (in some cases, detailed study of the EPR spectra may ultimately help do this). Therefore, not only each formation constant, but also the visible (and CD) spectra reflect the features of each isomer in proportion to the relative importance. For example, in the case of ML_2H_2 stoichiometry, the value for β_{122}(*trans*) and the electronic spectra may involve contributions from both.

In the present cases, and for steric reasons, it is possible that the *trans* isomer predominates over the *cis*. However, three observations suggest that if different ratios of *cis* and *trans* isomers do indeed form in these various systems, these are not clearly reflected in the calculated visible absorption spectra and in the experimental EPR spectra:

(i) the similar types of visible absorption spectra for VO^{2+}, MLH and ML_2H_2 for both GG and GGG + VO^{2+} systems;

(ii) the similarity between the spectra calculated for MLH and ML_2H_2 and the corresponding species in most of the systems previously studied;[1–6] and

(iii) the type of EPR spectra obtained in the low pH region, where—as pH is increased—the spectrum appears like that of only one component but the peaks actually shift to lower field in an approximately continuous manner.

It is possible that CD spectra for peptides such as gly–L-ala, L-alagly and L-ala–L-ala[12] reflect these differences much more strongly than do visible spectra. However, because the systems are quite complicated, the differences found in CD spectra for the corresponding stoichiometries in the several systems studied[1–6] may also partly arise from mathematical artifacts, so that no safe conclusions can be made.

MLH_{-1}. Except for the absence of ML, species distributions as a function of pH for pH $\lesssim 4.5$ are quite similar in the VO^{2+} + GG and Cu^{2+} + GG[18] systems. Namely, for pH $\gtrsim 4$, the concentration of the MLH_{-1} stoichiometry increases steeply in both systems. However, while in the Cu^{2+} + GG (and GGG) system this stoichiometry corresponds to the formation of a complex such as **V**, in the VO^{2+} + GG (and GGG) systems, the spectroscopic results indicate that rather than deprotonation of the amide hydrogen in the pH range 4–5, hydrolysis occurs. Besides, the fact that the representations of $\log \beta_{11-1}$(VO) vs $\log \beta_{11-1}$(Cu), either for GG or GGG, lie above the straight line indicates different structures for Cu^{II} and VO^{II} complexes.

Several plausible structures, e.g. **VI–IX** may then be envisaged for this stoichiometry. In **VI** and **VIII**, coordination in an axial position may occur, although for **VI** this involves some steric constraints. For GGG there is still the possibility of coordination of the carboxylate group (in **VI**, **VII** and **IX**) in an equatorial position. The OH^- groups may be coordinated in different sites and the vanadyl group is lop-sided; therefore each structure **VI–IX** only indicates a type of coordination geometry corresponding to several isomers.

CD spectra of gly–L-ala, L-ala–L-ala and L-alaninamide + VO^{2+} solutions in the pH range 3.5–4.5 suggest[12] the formation of **VI** and, in the case of glygly, the coordination of the carboxylate group. Species **VI** may result from hydrolysis of complexes such as **III**. As mentioned above, our results suggest that complexes corresponding to ML stoichiometry do not form in significant concentrations in solutions containing GG or GGG + VO^{2+}. At pH values where ML could eventually form, hydrolysis occurs in competition with $-NH_3^+$ dissociation and in calculations with SQUAD only $\log \beta_{11-1}$ is refined in a consistent manner. Therefore, on increasing pH, MLH and ML_2H_2 form MLH_{-1} "directly".

Acknowledgements—J.C.P. and S.M.L. thank the Instituto Nacional de Investigação Científica, Fundação Calouste Gulbenkian, FEDER and JNICT (project STRIDE ref. STRDA/C/CEN/436/92 and CIENCIA/BD 859/90-RM) for financial support.

REFERENCES

1. J. Costa Pessoa, L. F. Vilas Boas, R. D. Gillard and R. J. Lancashire, *Polyhedron* 1988, **7**, 1245 (Part I).
2. J. Costa Pessoa, L. F. Vilas Boas and R. D. Gillard, *Polyhedron* 1989, **8**, 1173 (Part II).

3. J. Costa Pessoa, R. L. Marques, L. F. Vilas Boas and R. D. Gillard, *Polyhedron* 1990, **9**, 81 (Part III).
4. J. Costa Pessoa, L. F. Vilas Boas and R. D. Gillard, *Polyhedron* 1989, **8**, 1745.
5. J. Costa Pessoa, L. F. Vilas Boas and R. D. Gillard, *Polyhedron* 1990, **9**, 2101 (Part IV).
6. J. Costa Pessoa, J. L. Antunes, L. F. Vilas Boas and R. D. Gillard, *Polyhedron* 1992, **11**, 1449 (Part V).
7. (a) J. Costa Pessoa, R. D. Gillard and S. M. Luz, *Second Italian–Portuguese–Spanish Meeting in Inorganic Chemistry*, Alfa Mar, Algarve, Portugal (March 1992); (b) J. Costa Pessoa, R. Duarte, R. D. Gillard, S. M. Luz and J. J. Moura, *Third International Conference on the Chemistry of Early Transition Metals*, University of Sussex, Brighton, U.K. (July 1992).
8. D. C. Crans, R. L. Bunch and L. A. Theisen, *J. Am. Chem. Soc.* 1989, **111**, 7597.
9. J. Costa Pessoa and J. L. Antunes, unpublished.
10. (a) P. Gans, A. Sabatini and A. Vacca, *Inorg. Chim. Acta* 1983, **79**, 219; (b) P. Gans, A. Sabatini and A. Vacca, *J. Chem. Soc., Dalton Trans.* 1985, 1195.
11. (a) D. J. Leggett and W. A. E. McBryde, *Analyt. Chem.* 1975, **47**, 1065; (b) D. J. Leggett, *Analyt. Chem.* 1977, **49**, 276; (c) D. J. Leggett, S. L. Kelly, L. R. Shine, Y. T. Wu, D. Chang and K. M. Kadish, *Talanta* 1983, **30**, 579.
12. J. Costa Pessoa, S. M. Luz and R. D. Gillard, to be submitted.
13. L. Casella, M. Gullotti and A. Pintar, *Inorg. Chim. Acta* 1988, **144**, 89.
14. N. D. Chasteen, in *Biological Magnetic Resonance* (Edited by L. J. Berliner and J. Reuben), Vol. 3, p. 53. Plenum Press, New York (1981).
15. L. F. Vilas Boas and J. Costa Pessoa, Chapter on "Vanadium", in *Comprehensive Coordination Chemistry* (Edited by G. Wilkinson, R. D. Gillard and J. A. McCleverty), Vol. 3, pp. 453–583. Pergamon Press, Oxford (1987).
16. A. E. Martell and R. M. Smith, *Critical Stability Constants*, Vol. 1, pp. 322–323. Plenum Press, New York (1974).
17. D. D. Perrin and I. G. Sayce, *J. Chem. Soc. A* 1968, 53.
18. V. G. Shtyrlin, E. L. Gogolashvili and A. V. Zakharov, *J. Chem. Soc., Dalton Trans.* 1989, 1293.
19. H. Sigel and R. B. Martin, *Chem. Rev.* 1982, **82**, 385.
20. R. B. Martin, in *Metal Ions in Biological Systems* (Edited by H. Sigel and A. Sigel), Vol. 23, Ch. 5, p. 123. Marcel Dekker, Inc., New York (1988).
21. I. Sóvágó, in *Biocoordination Chemistry: Coordination Equilibria in Biologically Active Systems* (Edited by K. Burger), p. 139. Ellis Horwood, New York (1990).
22. I. Fábian and I. Nagypál, *Inorg. Chim. Acta* 1982, **62**, 193.
23. J. W. Bunting and K. M. Thong, *Can. J. Chem.* 1970, **48**, 1654.
24. L. Abello, M. Jonini, M. K. Onlaalon, R. Poisson and G. Lapluye, *J. Chim. Phys.* 1985, **82**, 1001.
25. R. Österberg and B. Sjöberg, *J. Biol. Chem.* 1968, **243**, 3038.
26. O. Yamauchi, Y. Nakao and A. Nakahara, *Bull. Chem. Soc. Japan* 1973, **46**, 2119.
27. D. L. Rabenstein and S. Libich, *Inorg. Chem.* 1972, **11**, 2960.
28. R. Tauler and B. M. Rode, *Inorg. Chim. Acta* 1990, **173**, 93.
29. A. Lorenzotti, D. Leonesi, A. Cingolani and P. Bernardo, *J. Inorg. Nucl. Chem.* 1981, **43**, 737.
30. A. Lorenzotti, D. Leonesi, A. Cingolani and A. Turolla, *Gazz. Chim. Ital.* 1983, **113**, 229.
31. A. Lorenzotti, D. Leonesi and A. Cingolani, *Inorg. Chim. Acta* 1981, **52**, 149.

Polyhedron Vol. 12, No. 23, pp. 2869–2875, 1993
Printed in Great Britain

0277–5387/93 $6.00+.00
© 1993 Pergamon Press Ltd

COMPLEXES OF NEW AMINE-NITROGEN SUBSTITUTED α-AMINE OXIME LIGANDS (*p*-AMINOBENZYL, *p*-NITROBENZYL AND *p*-(AMINOMETHYL)PHENYL SUBSTITUENTS): X-RAY STRUCTURES OF *p*-AMINOBENZYLAMINE OXIME DIHYDROCHLORIDE, $[Ni(AMINOBENZAO)_2]ClO_4$ AND $[Rh(NITROBENZAO)_2Cl_2]$

G. ERGUN EFE* and E. O. SCHLEMPER†

Department of Chemistry, University of Missouri, Columbia, MO 65211, U.S.A.

(*Received* 5 *February* 1993; *accepted* 14 *June* 1993)

Abstract—The syntheses and characterizations of two new amine oxime ligands are described. In addition, the crystal structure of the dihydrochloride salt of the previously reported 2-[*N*-(4-aminobenzyl)]amino-3-methyl-2-butanone oxime (aminobenzAO) is reported. This structure features a three-dimensional network of hydrogen bonds involving the amine and oxime groups, the chloride ions and the water molecule of crystallization. The crystal structure of the nickel(II) complex of this ligand, $[Ni(aminobenzAO)_2]ClO_4$, is reported. This structure features near square planar bonding of the two oxime nitrogen atoms and the two aliphatic amine nitrogen atoms to the nickel(II) atom with dangling aromatic amine groups. A strong intramolecular O---O hydrogen bond links the two *cis* oxime groups. Because of crystallization difficulty only a qualitative crystal structure of the rhodium(III) complex of the corresponding 4-nitrobenzyl ligand $[Rh(nitrobenzAO)_2Cl_2]$ is included. The octahedral structure is analogous to previously reported complexes with *cis* oxime nitrogen atoms, *cis* amine nitrogen atoms and *trans* chloride ligands.

Labelling of monoclonal antibodies with radioisotopes for imaging or therapeutic purposes continues to be under investigation in our laboratory for possible application in the field of nuclear medicine. One approach for labelling antibodies is the use of bifunctional chelating agents. These compounds can bind tightly to a metal ion and also covalently link with amino acid residues of the antibody. A review of the field has recently been given by Goldenberg.[1] We have been investigating the preparation of bifunctional chelating agents to complex the ^{105}Rh radioisotope[2–4] and have shown that rhodium readily forms a very stable bis complex with 3-amino-3-methyl-2-butanone oxime (α-amine oxime).[5] We recently reported the synthesis of a bifunctional ligand formed by adding a *p*-aminobenzyl substituent on the amine nitrogen of an α-amine oxime.[6] Radiochemical studies with the ^{105}Rh complex of this ligand were also reported. Here we report the crystal structures of the chloride salt as well as the nickel complex of that ligand. The syntheses of two more amine-nitrogen substituted ligands with *p*-nitrobenzyl and *p*-(amino)phenyl substituents are described. Low quality crystals of the rhodium complex of the *p*-nitrobenzyl substituted α-amine oxime could be isolated, and a crude structure was determined by X-ray diffraction.

EXPERIMENTAL

Preparation of the compounds

3-[N-(4-*Nitrobenzyl*) *amino*]-3-*methyl*-2-*butanone oxime* (p-*nitrobenzyl amine oxime*). 4-Nitrobenzylamine hydrochloride (2.20 g, 11.66 mmol) was dissolved in 70 cm^3 of water. NaOH (11.66 mmol) was added slowly and the solution was extracted with $CHCl_3$. $CHCl_3$ portions were col-

* Present address: Department of Chemistry, University of Southwestern Louisiana, Lafayette, LA 70504, U.S.A.

† Author to whom correspondence should be addressed.

lected, the solvent was evaporated and the resulting 4-nitrobenzylamine was dried (1.379 g, 9.072 mmol). The amine was dissolved in 50.0 cm^3 of absolute methanol, brought to 0°C in an ice bath and combined with 1.414 g (10.43 mmol) of α-chloro oxime. The mixture was brought to room temperature very slowly and then refluxed for 24 h. After the solvent was evaporated, the residue was dissolved in water and the free α-amine oxime was precipitated by the addition of KOH solution. The precipitate was recrystallized from ethanol. Yield was 58% after recrystallization, m.p. 135–136°C. ^{1}H NMR (DMSO-d^6): (a) 1.19s, 6H, (b) 1.71s, 3H, (c) doublet centred at 3.54 ppm, 2H, (d) triplet centred at 2.61 ppm, < 1H, (e) two doublets centred at 7.61 and 8.16 ppm, 4H, (f) 10.48s, 1H.

3-[N-(4-(2-*Aminoethyl*) *phenyl*) *amino*]-3-*methyl*-2-*butanone oxime*·HCl [*(aminoethyl)phenylamine oxime hydrochloride*]. 2-(4-Aminophenyl)ethylamine (1.32 ml, 1.36 g, 10 mmol) was put into 15 cm^3 of absolute methanol. α-Chloro oxime (1.35 g, 10 mmol) was added and stirred at room temperature for 18 h. The solvent was evaporated to dryness. The residue was an orange oily solid. It was dried under vacuum. The ^{1}H NMR spectrum indicated that the reaction mainly occurred through the aromatic amine, with a very small amount through the aliphatic amine. Comparison of the peak intensities showed that the product was mainly (> 80%) composed of that form. In melting point determination, a small part of the solid melted at 139–140°C, but the main portion melted at 149–150°C. ^{1}H NMR (DMSO-d_6): (a) 1.36s, 6H, (b) 1.69s, 3H, (g) broad multiplet around 2.78 ppm, (e) multiplet centred at 6.73 ppm, (h) broad, 8.12 ppm, 3H, (f) 10.60s, 1H.

[Ni(aminobenzAO)$_2$]ClO_4. Aminobenzyl amine oxime (0.0286 g, 0.129 mmol)[6] was dissolved in 2.5 cm^3 of ethanol, and $NiCl_2 \cdot 6H_2O$ (0.0285 g, 0.12 mmol) in 2 cm^3 of water was added. The pH was 6. The addition of $NiCl_2 \cdot 6H_2O$ changed the colour from light yellow to very dark yellow–orange. The solution was saturated with $NaClO_4$. Slow evaporation of the solvent first produced yellow crystals which were the protonated form of the ligand as indicated by ^{1}H NMR spectrum. A few days later, dark orange coloured crystals of the product formed. ^{1}H NMR (DMSO-d^6): (a,a') 0.93s and 1.43s, 12H, (b), 1.80s, 6H, (d) 5.31, 2H, (g) 4.73m, (e) two doublets centred at 6.67 and 7.41 ppm, (f) 18.31s, 1H. The (c) protons are covered by the H_2O signal at 3.30 ppm. IR (fluorolube mulls in NaCl cells): weak band at 1790 cm^{-1} due to short hydrogen bond between the oxime oxygens.

[Rh(nitrobenzAO)$_2$Cl$_2$]. NitrobenzAO ligand (0.374 g, 1.3 mmol)[6] in 10 cm^3 ethanol was combined with $RhCl_3 \cdot 3H_2O$ (0.153 g, 0.58 mmol) in 3 cm^3 water. The solution was refluxed for several hours, and the colour remained dark brown. Upon cooling, a brownish yellow precipitate formed and was collected by filtration. Yield was 51.5%. This precipitate was soluble in DMSO, $CHCl_3$, acetic acid, acetone, ethanol and methanol, but none of these solvents produced suitable X-ray crystals. Finally, poor quality crystals were obtained from ethyl acetate after the solution was left in the refrigerator for several days. The crystal used for the X-ray study contained approximately two molecules of ethyl acetate per rhodium complex, some of which was clearly lost in the analysed material. Found: C, 43.5; H, 5.1; N, 11.9. Calc. for $RhCl_2O_6N_6C_{24}H_{33} \cdot 0.5CH_3COOC_2H_5$: C, 43.4; H, 5.2; N, 11.7%. ^{1}H NMR (DMSO-d^6): (a,a') 1.21s and 1.39s, 12H, (b) 2.10s, 6H, (c) and (d) complex pattern at 4.18–5.31 ppm, 6H, (e) 7.38–8.18m, (f) 19.36–19.49 ppm. IR (fluorolube mulls in NaCl cells): weak band at 1792 cm^{-1} due to short hydrogen bond between the oxime oxygens.

[Rh(aminoethylphenAO)$_2$Cl$_2$]

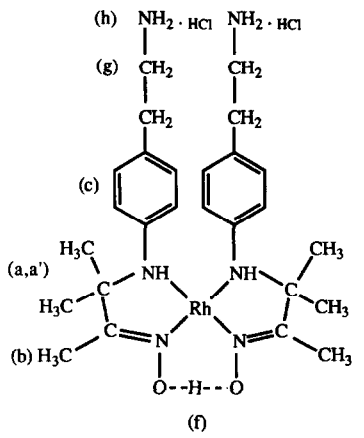

[Rh(aminoethylphenAO)$_2$Cl$_2$]. Aminoethylphen AO (0.104 g, 0.441 mmol) was dissolved in 6.5 cm^3 ethanol, and to this was added $RhCl_3 \cdot 3H_2O$ (0.058 g, 0.22 mmol) in 3 cm^3 of H_2O. The mixture was refluxed for 2 h and the pH dropped from 2 to 0.5. The pH was adjusted to 7 with NaOH, and refluxing was continued for 15 min. Evaporation of some of the solution yielded a dark yellow, finely divided solid which had very limited solubility in common solvents. Numerous attempts to grow crystals were unsuccessful. However, solubility in DMSO was sufficient to obtain the ^{1}H NMR spectrum of the HCl salt. The IR spectrum as a fluorolube mull showed the expected C—H and N—H stretching vibrations, as well as a weak bond at 1758 cm^{-1}, attributed to a strong

Table 1. Crystal data, data collection parameters and refinement parameters

	AminobenzAO · 2HCl · H_2O	Ni(aminobenzAO) · ClO_4 · H_2O	$Rh(nitrobenzAO)_2Cl_2$
Formula	$ON_3C_{12}H_{19} \cdot 2HCl$	$NiO_2N_6C_{24}H_{37} \cdot ClO_4$	$RhO_6N_6C_{24}H_{33} \cdot 2C_2H_5OOCCH_3$
Formula weight	312.2	617.8	851.6
Crystal size (mm)	$0.07 \times 0.10 \times 0.23$	$0.06 \times 0.24 \times 0.33$	$0.08 \times 0.30 \times 0.32$
Space group	$P\bar{1}$	$P2_1/c$	$P2_1/c$
a (Å)	10.013(3)	10.214(3)	15.800(9)
b (Å)	10.053(5)	19.985(1)	21.839(9)
c (Å)	9.858(5)	14.715(6)	12.341(6)
α (°)	116.60(5)	90	90
β (°)	117.99(4)	103.38(3)	110.44(5)
γ (°)	84.91(4)	90	90
V (Å^3)	774.2(5)	2922(4)	3990(6)
T (°C)	−130(5)	22(1)	22(1)
Z	2	4	4
D_{calc} (g cm^{-3})	1.340	1.405	1.417
μ (cm^{-1})	4.12	8.02	6.06
Rel. transmission factors	none (< 3% range)	95–100%	93–100%
Scan method	θ–2θ	θ–2θ	θ–2θ
Scan width (°)	$0.85 + 0.35 \tan\theta$	$0.75 + 0.35 \tan\theta$	$0.90 + 0.35 \tan\theta$
Scan time	to obtain 3% count. stat. to max of 90 s	to obtain 3% count. stat. to max of 90 s	to obtain 3% count. stat. to max of 90 s
2θ range (°)	4–45	4–43	4–40
Total refl. measured	2616	3666	4038
Total indep. refl.	2013	3435	3714
Indep. refl. with $I > 2\sigma$	1583	2589	1848
No. of variables	172	364	412
$R(F)$	0.055	0.042	0.072
$R_w(F)$	0.067	0.055	0.075
Max shift/err on last cycle	0.28	0.04	0.37

hydrogen bond between oxime oxygen atoms as normally observed for the *cis* bonded oxime groups in related complexes.[4] The NMR spectrum was assigned by comparison with the ligand spectrum and the spectrum of $[Rh(phenAO)_2Cl_2]$[4] as follows: (a,a') 1.09, 1.31s, 12H, (b) 2.21s, 6H, (c) broad multiplet 6.55–7.86, 8H, (f) 19.5s, 1H, (g) multiplet 2.99, 8H, (h) broad 8.37s, 6H (see structure above).

X-ray diffraction

Collection and reduction of X-ray data. X-ray data were collected on an Enraf–Nonius CAD4 automated diffractometer controlled by a Digital PDP 11/34 computer using Mo-K_α radiation ($\lambda = 0.7107$ Å) obtained from a graphite monochromator. Lattice constants were obtained by least-squares fit of 25 carefully centred reflections on each compound. The intensities of three standard reflections measured after every 7200 s of X-ray exposure showed no signficiant variation. Orientation was checked after every 200 reflections with the use of the same standards and all 25 original reflections were recentered when the measured deviation of any of the three standards exceeded 0.07°. The cell data, data collection parameters and refinement results for each structure are summarized in Table 1.

Solution and refinement of the structures. The structures were solved by conventional Patterson and Fourier methods. The full-matrix least-squares refinements minimized the function $\Sigma w(|F_o| - |F_c|)^2$, where $w = 1/\sigma^2(F_o)$, $\sigma(F_o) = \sigma(F_o^2)/2F_o$ and $\sigma(F_o^2) = [\sigma^2_{counting} + (0.04F_o^2)^2]^{1/2}$. Atomic scattering factors were taken from the *International Tables for X-ray Crystallography*[7] and included anomalous scattering contributions. Hydrogen atoms were located by difference Fourier methods or were placed in chemically reasonable positions with $B \sim 1.3 \times B$ of atom attached. For compounds **I** and **II**, positional and anisotropic thermal parameters of non-hydrogen atoms were refined in the least-squares cycles. The ethyl acetate molecules

were badly disordered in compound **III** and were placed with fractional occupancy (isotropic fixed *B*) to accommodate the electron density. This disorder and the related low quality of the data resulted in poor resolution of the entire structure. Thus, details of this structure are not well determined. Coordinates and thermal parameters for the three compounds are available.* The high thermal parameters for some of the atoms of compound **III** are a result of the low quality of the data set.

RESULTS AND DISCUSSION

Figure 1 shows a perspective view of the [Ni(aminobenzAO)$_2$]ClO$_4$. The structure of the compound consists of discrete, mononuclear, cationic nickel(II) complexes with the nickel atoms in a distorted square-planar configuration. The nickel atom coordinates to two amine nitrogens and two oxime nitrogens from the amine oxime ligands, forming two five-membered chelate rings. Also, the loss of an oxime hydrogen results in the other oxime hydrogen forming a hydrogen bond between the two oxime oxygens, closing a six-membered ring. The *p*-amino substituted benzyl groups on the amine nitrogens are in the *trans* position. The positive two charge of the nickel atom is balanced by the loss of one oxime hydrogen and a perchlorate ion. Three of the oxygens in the perchlorate ion [OS(2), OS(3), OS(4)] have second positions [OS(5), OS(6), OS(7)] occupied to the extent of 0.20. The crystal structure also contains a water molecule. The torsional angles indicate that the twist angles of the two methylene bridges from the molecular plane are the same, but the two ring planes make angles that are about 27° different with respect to the metal coordination plane. The dihedral angles between the least-squares plane of coordination and the phenyl rings confirm the results derived from the torsional angles. One of the phenyl rings is only 6.9(1)° away from being perfectly perpendicular to the coordination plane, while the other phenyl ring makes an angle of 51.3(1)° with this plane. The square plane around nickel is significantly distorted towards tetrahedral geometry. The *trans* N(1) and N(2′) atoms are 0.183(3) and 0.170(3) Å, respectively, above the plane and the *trans* N(1′) and N(2) atoms are 0.159(4) and 0.148(3) Å, respectively, below the plane. Pertinent intramolecular bond distances and bond angles involving non-hydrogen atoms are given in Table 2. The short intramolecular O---O hydrogen bond length in this compound is 2.404(4) Å. The only intermolecular contact less than 3.5 Å involving non-hydrogen atoms and non hydrogen bonding is the O(1)—C(3′) distance of 3.303(9) Å. The distances less than 3.3 Å and involving ClO$_4$ and water contacts with the molecule are: O(1′)—OW: 2.964(8) Å, N(1′)—OS(2): 3.30(1) Å, N(2′)—OS(2): 3.085(9) Å, N(3)—OS(1): 2.958(8) and N(3)—OW: 2.967(7) Å. There is a weak hydrogen bond between N(3) and OW as can be seen from the following distances: H(1)N(3)—OW: 1.84 Å, H(1)N(3)—N(3): 1.17 Å and the angle N(3)—H(1)N(3)—OW: 162°. Other weak hydrogen bonding interactions are as follows: HN(2′) interacts with OS(2) [HN(2′)—OS(2): 1.96 Å, HN(2′)—N(2′): 1.24 Å, N(2′)—HN(2′)—OS(2): 148°]; H(2)N(3) interacts with OS(1) [H(2)N(3)—OS(1): 1.81 Å, H(2)—N(3)—N(3): 0.89 Å, N(3)—H(2)N(3)—OS(1): 150°]; H(2)—N(3′) interacts with O(1′) [H(2)N(3′)—O(1′): 2.34 Å, H(2)N(3′)—N(3′): 1.06 Å, N(3′)—H(2)N(3′)—O(1′): 146°] and OW [H(2)N(3′)—OW: 2.96 Å, N(3′)—H(2)N(3′)—OW: 126°]. The hydrogen bonds involving OW as the donor are less well defined since hydrogen atoms on OW could not be satisfactorily located.

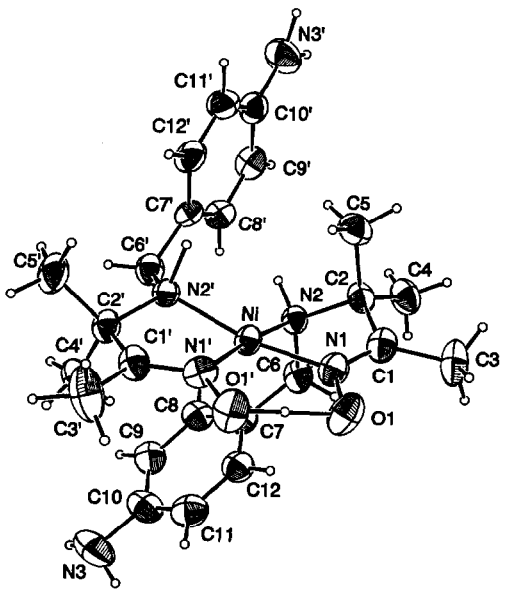

Fig. 1. Perspective view of [Ni(aminobenzAO)$_2$]ClO$_4$.

Figure 2 shows a perspective view of the aminobenzAO·2HCl molecule. Both of the amine nitrogens are protonated in the dipositive organic cation. The molecule forms a three-dimensional network of hydrogen bonds involving amine and oxime groups, chloride ions and water molecules. The crystal contains one water molecule per organic molecule. Pertinent intramolecular bond distances and bond angles involving non-hydrogen atoms are given in

*Atomic parameters, least-squares planes and complete tables of bond distances and angles are available through the Cambridge Crystallographic Data Centre.

Table 2. Selected bond distances (Å) and angles (°)

$[Ni(aminobenzAO)_2]ClO_4$			
Ni—N(1)	1.879(3)	N(1)—Ni—N(1′)	96.6(1)
Ni—N(1′)	1.855(3)	N(1)—Ni—N(2)	81.6(1)
Ni—N(2)	1.927(3)	N(1)—Ni—N(2′)	166.5(1)
Ni—N(2′)	1.949(3)	N(1′)—Ni—N(2)	172.9(1)
O—N(1)	1.351(4)	N(1′)—Ni—N(2′)	82.2(1)
N(1)—C(1)	1.282(4)	N(2)—Ni—N(2′)	101.2(1)
O(1′)—N(1′)	1.373(4)	O(1)—N(1)—C(1)	119.4(3)
N(1′)—C(1′)	1.285(4)	O(1′)—N(1′)—C(1′)	117.6(3)
AminobenzAO · 2HCl			
O(1)—N(1)	1.416(3)	O(1)—N(1)—C(1)	112.3(2)
N(1)—C(1)	1.267(4)		
$[Rh(nitrobenzAO)_2Cl_2]$			
Rh—Cl(1)	2.336(4)	Cl(1)—Rh—Cl(2)	177.8(2)
Rh—Cl(2)	2.324(4)	Cl(1)—Rh—N(1)	88.7(4)
Rh—N(1)	1.96(2)	Cl(1)—Rh—N(1′)	92.0(4)
Rh—N(1′)	2.04(1)	Cl(1)—Rh—N(2)	89.2(3)
Rh—N(2)	2.14(1)	Cl(1)—Rh—N(2′)	91.7(4)
Rh—N(2′)	2.20(1)	Cl(2)—Rh—N(1)	89.2(4)
		Cl(2)—Rh—N(1′)	88.9(4)
		Cl(2)—Rh—N(2)	90.0(4)
		Cl(2)—Rh—N(2′)	90.5(4)
		N(1)—Rh—N(1′)	93.9(7)
		N(1)—Rh—N(2)	81.9(6)
		N(1)—Rh—N(2′)	172.5(6)
		N(1′)—Rh—N(2)	175.6(6)
		N(1′)—Rh—N(2′)	78.6(6)
		N(2)—Rh—N(2′)	105.7(5)

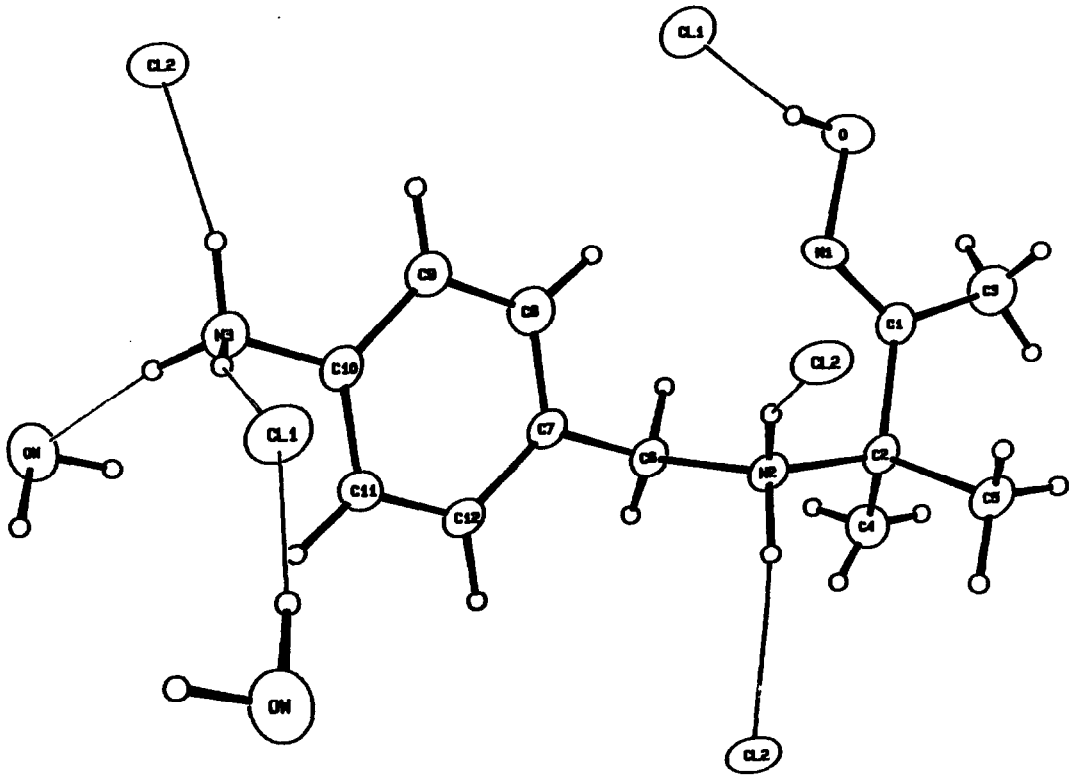

Fig. 2. Perspective view of aminobenzAO · 2HCl showing the hydrogen bond network.

Table 3. Bond distances and angles involved in hydrogen bonding interactions for aminobenzAO · 2HCl · H_2O

Interaction (X—H---Y)	X—H (Å)	H---Y (Å)	X—H---Y (°)
O(OH)---Cl(1)	0.84	2.26	154
OW—H(2)OW---Cl(1)	1.14	1.92	173
N(2)—H(1)N(2)---Cl(2)	0.97	2.21	164
N(2)—H(2)N(2)—Cl(2)	0.96	2.38	150
N(3)—N(1)N(3)---Cl(1)	0.91	2.22	164
N(3)—H(2)N(3)---OW	0.96	1.79	172
N(3)—H(3)N(3)—Cl(2)	0.97	2.25	168

Table 2. Bond distances and angles are rather normal. An interesting comparison is that of the oxime N—O [1.416(3) Å] and C=N [1.267(4) Å] with those in the nickel complex of 1.36(1) and 1.283(2) Å, respectively. Thus, the fully protonated oxime has a considerably longer N—O distance but only a slightly shorter C=N distance. The protonated aromatic amine nitrogen has a considerably longer C—N bond [1.448(4) Å] than the unprotonated counterpart in the nickel complex [1.390(2) Å]. Apparently there is significant π interaction of the amine lone pair of the latter with the aromatic system. Other distances in the uncomplexed ligand are very similar to those in the nickel complex. There are major differences in bond angles, particularly for those atoms involved in the chelate ring with the nickel(II) atom. The bond distances and the bond angles involved in the hydrogen bonding interactions (shown in Fig. 2) are summarized in Table 3. All of the amine and oxime hydrogen atoms and one of the water hydrogen atoms are involved in the hydrogen bonding network. Each chloride accepts three hydrogen bonds while the water is the acceptor for one hydrogen bond.

The ^{1}H NMR spectral results were given earlier in the preparation section. The most characteristic peaks of the ^{1}H NMR spectra of the ligands are the low field oxime proton signal around 10.5 ppm for the uncomplexed ligand and the high field signals due to the methyl protons. The formation of the complexes is generally revealed by the movement of the 10.5 ppm oxime peak to 18–19 ppm and by the splitting of the geminal methyl signal (singlet in the ligand) due to the different environments these methyl groups experience in the complex. That is observed here in going from the hydrochloride salt to the nickel complex. The IR spectrum of [Ni(aminobenzAO)$_2$]ClO_4 shows a broad, very weak band at 1790 cm^{-1}, due to the intramolecular O---O hydrogen bond, as normally found for this type of hydrogen bond.

The structural results for [Rh(nitrobenzAO)$_2$$Cl_2$] suffer from the disordered ethyl acetates of

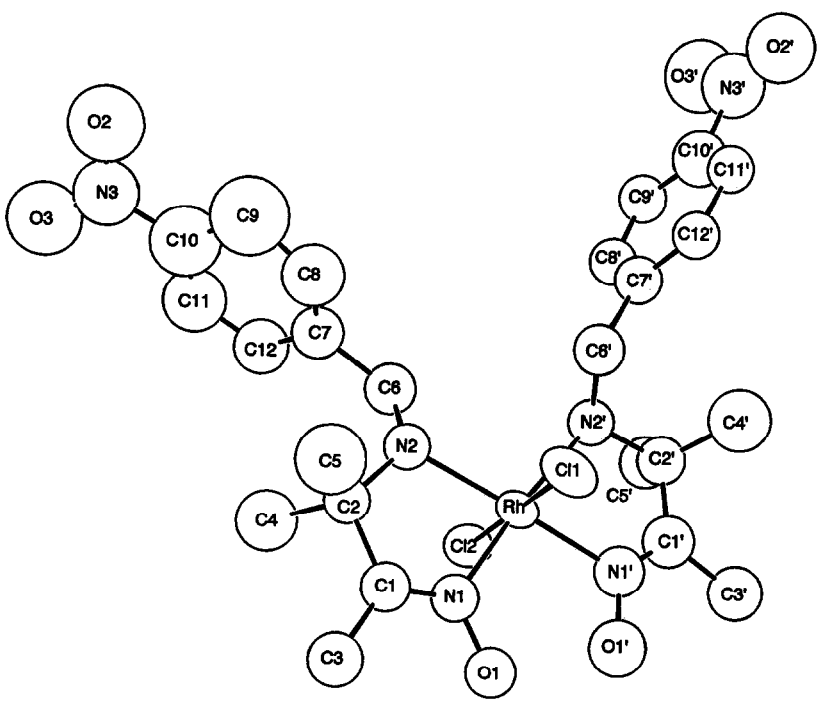

Fig. 3. Perspective view of [Rh(nitrobenzAO)$_2$$Cl_2$].

solvation. However, the immediate coordination of the rhodium(III) is clearly resolved (Fig. 3), as is all of the ligand geometry except for the nitro moiety on one of the benzyl groups. Despite the poor resolutions, the orientations of both benzyl groups are clearly defined. Pertinent bond distances and angles (Table 2) are generally reasonable (albeit of very low precision) except for those involving the poorly resolved nitro group [N(3), O(2), O(3)]. The phenyl rings make similar dihedral angles of 76.8(7)° and 75.4(5)° with the Rh, N(1), N(1′), N(2), N(2′) coordination plane. The latter is truly planar within experimental error.

The structures of the two metal complexes clearly demonstrate the steric freedom of the *para* substituents on the phenyl rings for possible use in additional reactions such as attachment to protein molecules.[4]

Acknowledgement—This work was supported by the U.S. Department of Energy Grant No. DEFG02-86ER60400.

REFERENCES

1. D. M. Goldenberg (Ed.), *Cancer Imaging with Radiolabeled Antibodies*. Kluwer Academic Publishers, Boston, MA (1990).
2. T. Lynde-Kernell and E. O. Schlemper, *J. Coord. Chem.* 1988, **16**, 347.
3. C. S. John, M. R. A. Pillai, J. M. Lo and D. E. Troutner, *Appl. Radiat. Isot.* 1989, **40**, 701.
4. G. Ergun Efe and E. O. Schlemper, *Polyhedron* 1992, **11**, 2447.
5. S. Siripaisarnpipat and E. O. Schlemper, *Inorg. Chem.* 1984, **23**, 330.
6. G. Ergun Efe, M. R. A. Pillai, E. O. Schlemper and D. E. Troutner, *Polyhedron* 1991, **14**, 1617.
7. *International Tables for X-ray Crystallography*, Vol. IV. Kynoch Press, Birmingham (1974).

Polyhedron Vol. 12, No. 23, pp. 2877–2881, 1993
Printed in Great Britain

0277–5387/93 $6.00+.00
© 1993 Pergamon Press Ltd

COMMUNICATION

METAL HYDROXYCARBENE-LIKE INTERMEDIATES IN THE HYDROCARBONYLATION OF ALKENES TO ALCOHOLS CATALYSED BY RHODIUM COMPLEXES

JOANNA K. MACDOUGALL, MICHAEL C. SIMPSON and DAVID J. COLE-HAMILTON*

Chemistry Department, University of St Andrews, St Andrews, Fife KY16 9ST, U.K.

(*Received* 10 *September* 1993; *accepted* 28 *September* 1993)

Abstract—Labelling studies show that aldehydes are not intermediates in the formation of heptanol from 1-hexene, CO and H_2 catalysed by $[RhH(PEt_3)_3]$ in ethanol, whilst studies of model intermediates suggest that ethanol hydrogen bonds to or even protonates an acyl oxygen atom to give a hydroxycarbene-like intermediate in the direct formation of heptanol.

Metal carbenes have been shown to be important intermediates in e.g. alkene metathesis, where the catalyst is a high oxidation state early transition metal complex.[1] However, they have not been identified as catalytic intermediates in reactions catalysed by platinum group metal complexes although we have suggested,[2] on the basis of model studies,[3] that carbon monoxide hydrogenation catalysed by ruthenium complexes may involve protonation of a formyl complex to give a hydroxycarbene intermediate and Consiglio and co-workers have suggested that related cyclic oxacarbenes may be intermediates in the stereoregular copolymerisation of CO and propene in the presence of palladium catalysts.[4] We now report studies which suggest that hydroxycarbene-like complexes are important intermediates in the hydrocarbonylation of alkenes to alcohols catalysed by e.g. $[RhH(PEt_3)_3]$ in alcoholic solvents.

We have recently reported[5] that, under hydroformylation conditions using $[RhH(PEt_3)_3]$ as catalyst precursor, alkenes give high selectivities to alcohols rather than aldehydes if the reaction is carried out in e.g. ethanol as solvent. In order to try to understand the reason for this unusual selectivity, we have carried out labelling studies and some stoichiometric reactions.

Hydrocarbonylation of 1-hexene using this system and D_2 in place of H_2 selectively produces $CH_3CH_2CH_2CH_2CHDCH_2CD_2OH/D$.† However, when the same catalyst system is used for the hydrogenation of heptanal using D_2 and CO in ethanol the product is a mixture of $CH_3CH_2CH_2CH_2CH_2CHXOH/D$ [X = H (60%) or D (40%)]. Experiments using H_2 in EtOD or D_2 in EtOD have confirmed that the source of added H on C_1 in the product of heptanal hydrogenation with CO/D_2 in ethanol is the alcoholic hydrogen atom of the solvent. If heptanal were an intermediate in the formation of heptanol from hexene then, when D_2 in EtOH is employed, some $CH_3CH_2CH_2CH_2CHDCH_2CHDOD$ would be expected in the product heptanol. Since this is not observed, we must conclude that the formation of heptanol from 1-hexene, CO and H_2 in this system does not pass through heptanal as an intermediate.

In order to seek for an alternative mechanism for the formation of heptanol from hexene in this system, we have carried out stoichiometric studies aimed at identifying the active species in the catalytic cycle. Thus, most hydroformylation mechanisms using complexes of the form $[RhH(CO)P_3]$ (P = tertiary phosphine) go through steps (loss of P, coordination of alkene and insertion of alkene into the M—H bond) which lead to intermediates

*Author to whom correspondence should be addressed.

†The branched product, $C_4H_9CH(CH_2D)CD_2OH$, is also formed.

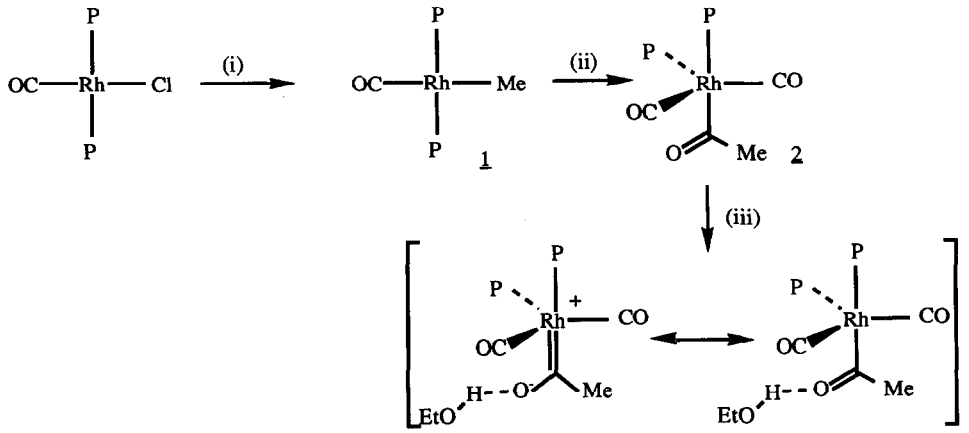

Scheme 1. Stoichiometric reactions of rhodium complexes. (i) MeLi, Et_2O; (ii) CO, toluene; (iii) EtOH; P = PEt_3.

of the form $[RhR(CO)P_2]$ (R = alkyl)[6]; CO coordination and insertion then give an acyl intermediate. In order to investigate these intermediates, we have synthesised $[RhMe(CO)(PEt_3)_2]$ (**1**)* by reaction of $[RhCl(CO)(PEt_3)_2]$ with MeLi and studied its chemistry. $[RhMe(CO)(PEt_3)_2]$ reacts with CO at 1 atm in toluene, thf or CH_2Cl_2 to give high yields of $[Rh(COMe)(CO)_2(PEt_3)_2]$ (**2**)* with the structure shown in Scheme 1. This compound is analogous to an intermediate identified by Brown and co-workers in hydroformylation of oct-1-ene catalysed by $[RhH(CO)(PPh_3)_3]$.[7]

On addition of ethanol (0.2 cm^3) to a solution of $[Rh(COMe)(CO)_2(PEt_3)_2]$ ($\sim$0.2 mol dm^{-3}) in toluene, thf, or CH_2Cl_2 (0.9 cm^3), important changes occur in the ^{31}P and ^{13}C NMR spectra. Although the general form of the spectra is the same, the resonance from one of the phosphorus atoms shifts to higher field, whilst the resonance from the acyl carbon atom shifts from 238.0 to 246.8 ppm (values given are for toluene but very similar values are obtained in thf or CH_2Cl_2). This large downfield shift (10.2 ppm if $[Rh(COMe)(CO)_2(PEt_3)_2]$ is dissolved in neat ethanol) is in the direction of the region where the carbenic carbon atom of alkyl hydroxycarbene[8] or alkoxycarbene[9] ligands are known to resonate (290–330 ppm). Figure 1 illustrates the effect on the chemical shift of the acyl carbon atom of $[Rh(COMe)(CO)_2(PEt_3)_2]$ of adding increasing amounts of ethanol. Analysis of these results indicates that the reaction involves 1 mol of ethanol per mol of complex and that the apparent equilibrium constant for the interaction is $\sim$0.3 dm^3 mol^{-1}. These measurements were made at -60°C and in all cases only one resonance was observed for the acyl C atom indicating that whatever the equilibrium process it is occurring rapidly on the NMR time-scale. Furthermore, the acyl species gives a non-conducting solution in ethanol. All of these results suggest that ethanol becomes hydrogen bonded to the acyl oxygen atom of the model complex, $[Rh(COMe)(CO)_2(PEt_3)_2]$ and this conclusion is supported by ^{13}C NMR studies on addition of CF_3CH_2OH to $[Rh(COMe)(CO)_2(PEt_3)_2]$ (Fig. 1). The overall shift of the resonance from the acyl C atom (19.7 ppm) is greater than for ethanol, as expected for the more acidic alcohol, but the apparent equilibrium constant is not greatly different.

In the catalytic cycle, the related intermediate to which oxidative addition of hydrogen will occur is the four coordinate $[Rh(COR)(CO)(PEt_3)_2]$. Having one less CO ligand, the electron density on the metal will be even higher than for $[Rh(COMe)(CO)_2(PEt_3)_2]$ and hence the oxygen atom of the acyl ligand will hold a higher negative charge. Hydrogen bonding by an ethanol molecule will be even stronger for this complex and may even lead

*NMR data: **1** (298 K, C_7D_8) ^{31}P 26.6 d, J_{RhP} = 140 ^1H, Rh-*Me* −0.36 *dt*, J_{RhH} = 1.6, J_{PH} = 8.2 ^{13}C Rh *Me* −4.2 *dt*, J_{RhC} = 20, J_{PC} = 13 Hz; Rh-*C*O 192.8 *dt*, J_{RhC} = 57, J_{PC} = 14. **2** (213 K, C_7D_8) ^{31}P 17.8 *dd*, J_{RhP} = 71, 12.1 *dd*, J_{RhP} = 140, J_{PP} = 36 ^1H RhCO*Me* 2.9s ^{13}C RhCO*Me* 53.8 dd, J_{RhC} = 32.7, J_{PC} = 4; Rh*C*OMe 238 *ddd*, J_{RhC} = 78, J_{PC} = 21, 9; Rh*C*O 200.5 *dt*, J_{RhC} = 75, J_{PC} = 20. **2** (213 K, C_7D_8+20% EtOH) ^{31}P 18.0 *dd*, J_{RhP} = 72; 10.3, J_{RhP} = 137, J_{PP} = 36 ^1H RhCO*Me* 2.7s ^{13}C RhCO*Me* 53.4 *d*, J_{RhC} = 30.2; Rh*C*OMe 246.8 *ddd*, J_{RhC} = 81, J_{PC} = 21, 9; Rh*C*O 199.9 *dt*, J_{RhC} = 73, J_{PC} = 21.

Fig. 1. Effect of adding ethanol (⊡) or trifluoroethanol (●) on the chemical shift of the acyl C atom of $[Rh(COMe)(CO)_2(PEt_3)_2]$. The shifts are to lower field. The initial solutions contained $[RhMe(CO)(PEt_3)_2]$ (0.15 g for EtOH, 0.10 g for CF_3CH_2OH) in thf (0.5 cm^3). They were treated with CO to give quantitative conversion to $[Rh(COMe)(CO)_2(PEt_3)_2]$ prior to addition of the alcohol.

to protonation to give a hydroxycarbene. Indeed, the difference between protonation and H-bonding is only a small shift in position for the potential well in which the H atom sits. Protonations of formyl or acyl oxygen atoms to give hydroxycarbene complexes are known in other systems, although strong acids are usually required.[3,10–12] Whether full protonation or strong hydrogen bonding occurs, the M—C bond will have significant double bond character making the acyl ligand more carbene-like. Many metal formyl complexes have short M—C bonds and long C—O bonds indicative of a similar contribution of an oxycarbene resonance form.[13]

After oxidative addition of H_2 to the four coordinate complex containing the carbene-like ligand, transfer of H to the carbene-like C atom would not lead to reductive elimination of aldehyde, but rather to the formation of a hydroxyalkyl complex which would reductively eliminate with the other H atom on the metal to give C_7 alcohols as the primary products (see Scheme 2).

Evidence that similar intermediates to those we have modelled are important under catalytic conditions is provided by ^{31}P studies of a reaction solution containing $[RhH(PEt_3)_3]$ in ethanol under 20 atm. of CO, H_2 and C_2H_4. After heating to 100°C and cooling to −60°C, resonances with similar chemical shifts and couplings to those from $[Rh(COMe)(CO)_2(PEt_3)_2]$ in ethanol are observed as significant features of the spectrum.* These presumably arise from $[Rh(COEt)(CO)_2(PEt_3)_2]$ with ethanol hydrogen bonded to the acyl oxygen atom.

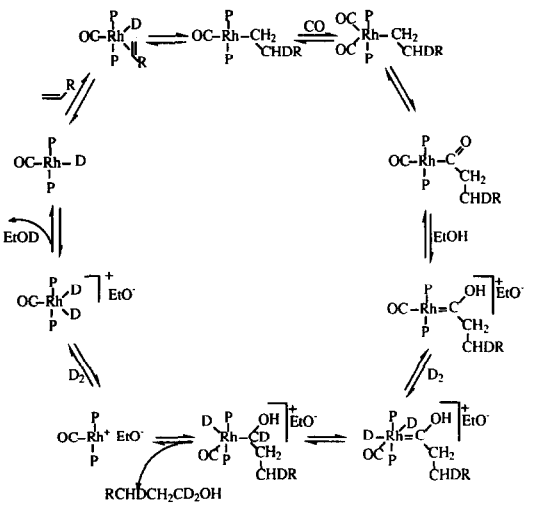

Scheme 2. Proposed mechanism for production of deuterated heptanol from 1-hexene, CO and D_2 catalysed by $[RhH(PEt_3)_3]$. $[RhHCO(PEt_3)_2]$ is formed from $[RhH(PEt_3)_3]$; deuterated 2-methylhexanol is produced *via* a similar mechanism involving Markownikoff insertion of the alkene into the M—H bond. Full protonation of the acyl is shown, although hydrogen bonding of ethanol to the acyl oxygen is also possible. P = PEt_3.

*^{31}P NMR (EtOH, 213 K) 17.2 *dd*, J_{RhP} = 68.5; 10.2 *dd*, J_{RhP} = 135, J_{PP} = 36.

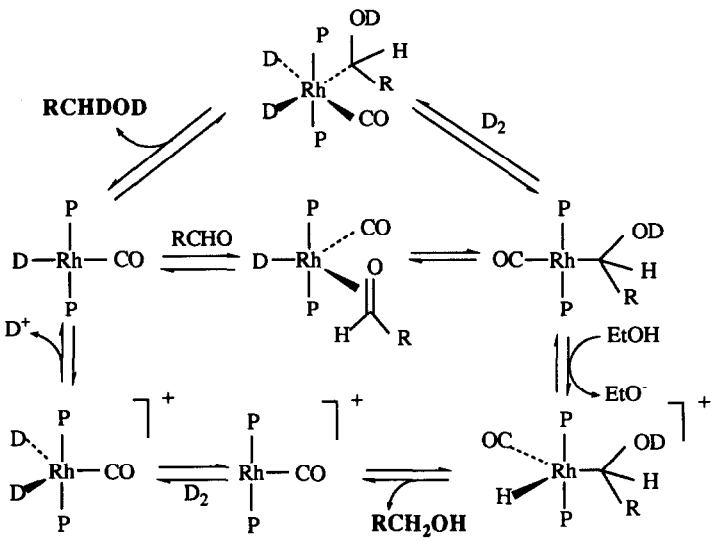

Scheme 3. Possible mechanism for production of $C_6H_{13}CHXOH/D$, X = H or D on hydrogenation of heptanal in EtOH catalysed by $[RhH(PEt_3)_3]$ with D_2/CO in the gas phase. P = PEt_3, R = C_6H_{13}.

Further support for the importance of hydrogen bonding or protonation in this system comes from observations of the products of hydrocarbonylation of 1-hexene in thf catalysed by $[RhH(PEt_3)_3]$. After 2 h, the products are aldehydes (100%) whilst if the same reaction is carried out in the presence of water (50%), alcohols are formed in substantial quantities (50%). The deuteration pattern for $(CH_3)_2CH$-CH_2OH produced on hydrocarbonylation of 2-propen-1-ol by rhodium–triethylphosphine complexes can also best be explained if ethanol protonates or hydrogen bonds to a related hydroxycarbene intermediate.[14]

Unfortunately, $[RhMe(CO)(PPh_3)_2]$ cannot be synthesized from $[RhCl(CO)(PPh_3)_3]$ and MeLi, so a direct comparison between the PPh_3 and PEt_3 systems cannot be made. However, solutions obtained from $[RhH(CO)(PPh_3)_3]$ and hex-1-ene under CO in toluene exhibit resonances* very similar to those of $[Rh(COMe)(CO)_2(PEt_3)_2]$. We tentatively assign them to $[Rh(C(O)hexyl)(CO)_2(PPh_3)_2]$. These resonances remain completely unchanged on addition of ethanol (20%) indicating that the electron withdrawing nature of PPh_3 means that there is insufficient negative change density on the acyl oxygen atom for significant hydrogen bonding to occur to ethanol. These results together with the mechanism of Scheme 2 explain why alcohol production occurs for trialkylphosphines but not for PPh_3. Since PPh_3 is a better π-acceptor than PEt_3, there is then less electron density on the acyl oxygen atom so that protonation is not favoured. C_7 aldehydes, together with acetals are the major products in this case.[5]

Finally, a possible mechanism, which explains the unusual labelling pattern obtained on hydrogenation of heptanal with CO/D_2 in EtOH is shown in Scheme 3. It assumes that insertion of the aldehyde into the Rh—D bond occurs to give a hydroxyalkyl intermediate and that protonation of this intermediate competes with oxidative addition of D_2. Reductive elimination from the cation will give $C_6H_{13}CH_2OH$, whilst reductive elimination from the dideuteride will give $C_6H_{13}CHDOH$.

Acknowledgements—We thank Dr M. Green and Dr A. Lucy for helpful discussions, Dr A. Lucy for high pressure NMR studies, the SERC and B.P. Research International for two studentships (J.K.M., M.C.S.) and Johnson Matthey plc for generous loans of rhodium salts.

*δ 24.7 *dd*, J_{RhP} = 132; 27.2 *dd*, J_{RhP} = 69, J_{PP} = 32. These figures differ significantly from those reported[7] for the analogous octene complex but we see no sign of resonances in the δ 30–36 region of the spectrum.

REFERENCES

1. R. H. Grubbs, *Prog. Inorg. Chem.* 1978, **24**, 1.
2. D. S. Barratt and D. J. Cole-Hamilton, *J. Organomet. Chem.* 1986, **306**, C41.
3. D. S. Barratt, C. Glidewell and D. J. Cole-Hamilton, *J. Chem. Soc., Dalton Trans.* 1988, 1079.

4. A. Batistini and G. Consiglio, *Organometallics* 1992, **11**, 1766.
5. J. K. MacDougall and D. J. Cole-Hamilton, *J. Chem. Soc., Chem. Commun.* 1990, 165.
6. I. Tkatchenko in *Comprehensive Organometallic Chemistry* (Edited by G. Wilkinson, E. Abel and F. G. A. Stone), Vol. 8, p. 101. Pergamon, Oxford (1982) and references therein.
7. J. M. Brown and A. G. Kent, *J. Chem. Soc., Perkins Trans II* 1987, 1597; *J. Chem. Soc., Chem. Commun.* 1982, 723.
8. J. T. Gauntlett, B. E. Mann and M. J. Winter, *J. Chem. Soc., Dalton Trans.* 1991, 1427
9. B. E. Mann and B. F. Taylor, *^{13}C N.M.R. Data for Organometallic Compounds*, Academic Press, London (1981) and references therein.
10. M. A. Lilger and J. A. Ibers, *Organometallics* 1985, **4**, 590.
11. M. L. H. Green, L. C. Mitchard and M. G. Swanwick, *J. Chem. Soc. A.* 1971, 794 and references therein.
12. K. R. Grundy and W. R. Roper, *J. Organomet. Chem.* 1981, **216**, 255.
13. J. A. Gladysz, *Adv. Organomet. Chem.* 1982, **20**, 1 and references therein.
14. M. C. Simpson, K. Porteous, J. K. MacDougall and D. J. Cole-Hamilton, *Polyhedron* 1993, **12**, 2883.

Polyhedron Vol. 12, No. 23, pp. 2883–2886, 1993
Printed in Great Britain

0277–5387/93 $6.00+.00
© 1993 Pergamon Press Ltd

COMMUNICATION

HYDROCARBONYLATION OF 2-PROPEN-1-OL CATALYSED BY TRIETHYLPHOSPHINE RHODIUM COMPLEXES—FORMATION OF 1,4-BUTANEDIOL AND MECHANISTIC STUDIES

MICHAEL C. SIMPSON, KAREN PORTEOUS, JOANNA K. MACDOUGALL and DAVID J. COLE-HAMILTON*

Department of Chemistry, University of St Andrews, St Andrews, Fife KY16 9ST, U.K.

(*Received* 10 *September* 1993; *accepted* 28 *September* 1993)

Abstract—In ethanol in the presence of $[Rh_2(OAc)_4]$ and PEt_3, 2-propen-1-ol (allyl alcohol) is hydrocarbonylated to a mixture of 1,4-butanediol and 2-methylpropanol; labelling and other studies indicate a mechanism for the formation of 2-methylpropanol in which key steps include protonation of an acyl intermediate by the solvent, dehydration of a bound hydroxycarbene intermediate, formation of a vinyl alcohol *via* an $\eta(1-3)$ allyl intermediate, tautomerization of the vinyl alcohol and hydrogenation of the 2-methylpropanal so formed.

We have reported that reaction of hexene with CO/H_2 in e.g. ethanol in the presence of rhodium catalysts containing PEt_3 gives C_7 alcohols as the products.[1] Labelling and model studies indicate that aldehydes are not intermediates in these reactions and that ethanol hydrogen bonds to or protonates an acyl intermediate to give a hydroxycarbene like species.[2]

We now report that the same catalytic system can be employed for the direct formation of 1,4-butanediol from 2-propen-1-ol (allyl alcohol) and that labelling studies, particularly on the formation of the other product, 2-methylpropanol, are also consistent with the proposed protonation of the acyl intermediate.

Reaction of CO, H_2 and 2-propen-1-ol in ethanol at 120°C in the presence of $[Rh_2(OAc)_4]$ and PEt_3 produces 1,4-butanediol and 2-methylpropanol as the major products (Table 1). 1,4-Butanediol is an important medium volume chemical, which is largely used for tetrahydrofuran synthesis.[3] A plant has recently been installed for its production from 2-propen-1-ol by hydroformylation followed by hydrogenation of the product, 4-hydroxybutanal. The direct synthesis of 1,4-butanediol from 2-propen-1-ol, avoiding the hydrogenation step, is therefore, potentially of considerable interest. 2-Methylpropanol has been observed as a hydroformylation product of 2-propen-1-ol and it has generally been assumed that it arises from dehydration of the branched aldehyde, 2-methyl-3-hydroxypropanal followed by hydrogenation.[4]

We have attempted to determine the mechanisms of formation of 2-methylpropanol and find that neither 2-methyl-2-propenal (methacrolein) nor 2-methyl-2-propen-1-ol (methallylalcohol) are intermediates in its production since neither of these gives more than traces of 2-methylpropanol under the reaction conditions.†

Clearly the product arises from dehydration at some stage in the cycle followed by hydrogenation. A plausible mechanism is shown in the scheme, particularly in view of our studies on other alkenes which suggest that alcoholic solvents protonate, or hydrogen bond to, the acyl oxygen atom of intermediates such as A.[2] Dehydration of the resulting

*Author to whom correspondence should be addressed.

†Methacrolein gives a series of products that have not been identified, whilst methallyl alcohol gives low conversions to 2-methylbutane-1,4-diol and 3-methyl-4-hydroxybutanal, with traces of 2,2-dimethylpropane-1,3-diol.

Table. 1 Products obtained from 2-propen-1-ol under hydrocarbonylation conditions[a]

Pressure (atm.)	[PEt_3] (mol dm^{-3})	Conversion (%)	2-methylpropan-1-ol (%)	1,4-butanediol (%)
10[b]	0.8	100	22	28
20	0.8	100	50	50
30	0.8	100	61	39
40	0.8	100	78	22
50	0.8	100	70	30
60	0.8	100	59	41
40	0.27	100	51	49
40	2.0	100	68	32

[a]$[Rh_2(OAc)_4]$ = 0.04 mol dm^{-3}; H_2 : CO (1 : 1); 120°C, 4 h, 2-propen-1-ol, 1 cm^3 (2.9 mol dm^{-3}) in ethanol, 4 cm^3.

[b]Other products account for *ca* 50% of the total. These include propan-1-ol, γ-butyrolactone and 2-methyl-2-pentenal.

hydroxycarbene would then give the unsaturated carbene species, **B**, with the formation of conjugated double bonds being a strong driving force. Hydrogen transfer would then give the hydroxyallyl intermediate, **C**. Further hydrogen transfer would then give 2-methyl-2-propen-1-ol but since this is not observed as a product and is not an intermediate on the pathway to 2-methylpropanol, we propose that this does not occur but rather that the hydroxyallyl group adopts an $\eta(1\text{–}3)$ bonding mode, **D**. Hydrogen transfer to the unsubstituted end of the allyl group would then give the vinyl alcohol, **E**, which would tautomerize to 2-methylpropanal. Finally, the 2-methylpropanal would be hydrogenated to the observed final product.

Evidence in favour of this mechanism includes the following:

(i) the same catalyst system does hydrogenate 2-methylpropanal to 2-methylpropan-1-ol, exclusively, under the hydrocarbonylation conditions.

(ii) In separate experiments, 2-methylpropanal was hydrogenated under the same conditions but using D_2 in place of H_2. The product is a mixture of $Me_2CHCHDOH/D$ (40%) and Me_2CHCH_2OH/D (60%), showing that some of the H incorporated onto the C atom attached to OHD derives from the gas-phase and some from the solvent (a similar labelling pattern is observed with heptanal and this has been attributed to competitive attack of H^+ and D_2 on a hydroxyalkyl intermediate).[2] Clearly, hydrogenation of the proposed Me_2CHCDO intermediate (as required in step V of the scheme) should lead to Me_2CHCD_2OH/D (40%) and Me_2CH-CHDOH/D (60%). The observed labelling pattern at this C atom is slightly higher in H than expected on this basis because of the larger concentration of OH in the solution (see below) but they are sufficiently close to give us confidence that one H/D atom on this C atom of the final product comes exclusively from the gas-phase (in step II) whilst the other arises from hydrogenation of the aldehyde (step V).

(iii) Under D_2, both of the methyl groups in the product 2-methylpropanol are $-CH_2D$ indicating that both added H atoms originate from the gas-phase. This is as expected, the transfers occurring directly from the metal in steps I and II of the scheme.

(iv) Under D_2 in C_2H_5OH there is no D incorporation onto the secondary C atom of the 2-methylpropanol. This could be explained either if the H atom remained on this C atom throughout the cycle (i.e. dehydration did not involve this H atom) or by the mechanism of the scheme; since the H atom on this C is derived from the solvent in the tautomerism of the vinyl alcohol (step IV). It is well known that this reaction occurs as shown in step IV of the scheme.

(v) Using D_2 in place of H_2 and EtOD in place of EtOH, substantial D incorporation (~50%) does occur onto the secondary C atom of the 2-methylpropanol. Incorporation of D is not 100% because (a) the alcoholic hydrogen in the solution is partly OD (from ethanol) and partly OH (from the substrate propenol) and partly because water (as H_2O or HDO) is released during the cycle and the H atoms in the water will exchange with the alcoholic OH. The exact

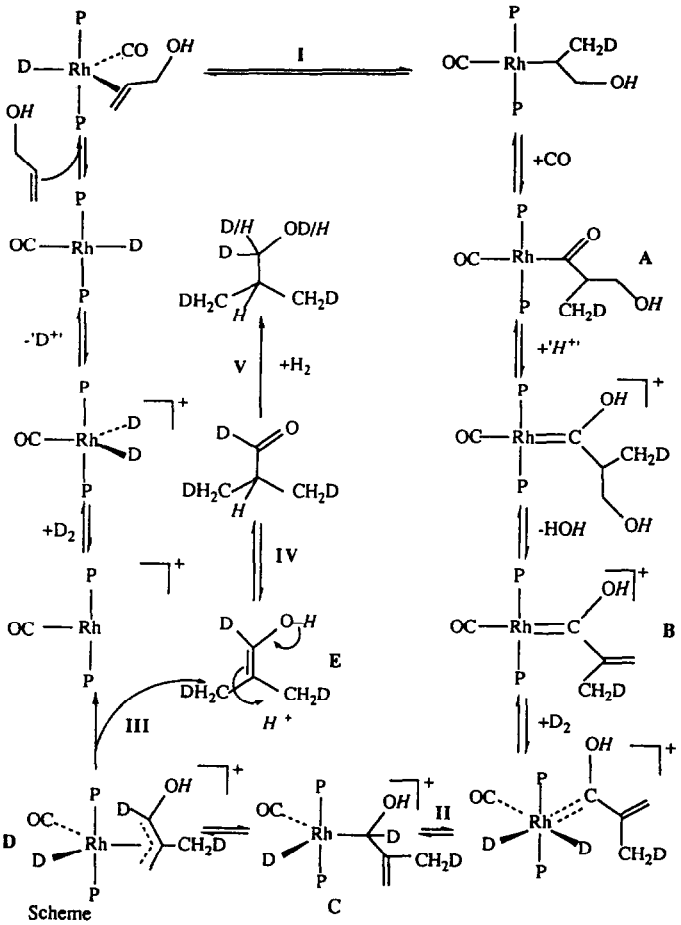

Scheme 1. Proposed mechanism for the formation of 2-methylpropan-1-ol from hydrocarbonylation of 2-propen-1-ol. Atoms labelled D arise exclusively from the gas-phase H_2 or D_2; atoms labelled *H* arise exclusively from the solvent OH or OD. Intermediates B to D are shown as cationic—they may have H bonding from the OH group to OEt^-.

percentage of D incorporation onto the secondary C atom can be modelled if a kinetic isotope effect (k_H/k_D) of 3–4 operates on the tautomerization reaction. Isotope effects in this range have been observed for ketonisation of allyl alcohols.[5,6]

These studies allow us to conclude (a) that the final step in the mechanism of formation of 2-methylpropanol is hydrogenation of 2-methylpropanal; (b) that the 2-methylpropanal is almost certainly formed by tautomerism of 2-methyl-2-propen-1-ol; (c) that dehydration of an intermediate must occur and that this intermediate is neither 2-methylpropane-1,3-diol (giving 2-methyl-2-propen-1-ol) nor 2-methyl-3-hydroxypropanol (giving 2-methyl-2-propenal). The dehydration must, therefore, occur from a metal bound intermediate and this cannot be the acyl species, (even though this too would give a conjugated double bond) since H transfer from the metal to this dehydrated species would give 2-methyl-2-propenal, which we have shown is neither a product nor an intermediate.

Overall, the evidence appears to support a mechanism involving steps similar to those shown in the scheme and hence to provide further evidence that this type of rhodium catalyst, containing trialkylphosphines, places sufficient electron density on the acyl oxygen atom to allow protonation of, or hydrogen bonding to, it by solvent alcohols.

Acknowledgements—We thank Drs M. Green and D. F. Foster for many helpful discussions, BP Research International and the SERC for a CASE studentship and Johnson Matthey plc for loans of rhodium salts.

REFERENCES

1. J. K. MacDougall and D. J. Cole-Hamilton, *J. Chem. Soc., Chem. Commun.* 1990, 165.
2. J. K. MacDougall, M. Simpson and D. J. Cole-Hamilton, *Polyhedron* 1993, **12**, 2877.
3. A. M. Brownstein, *Chemtech.* 1991, 506.
4. W. E. Smith, *Ger. Offen.* 1978, 275, 58473; see *Chem. Abstr.* 1978, **89**, 163050.
5. B. Capon and C. Zucco, *J. Am. Chem. Soc.* 1982, **104**, 7567.
6. S. H. Bergens and B. Bosnich, *J. Am. Chem. Soc.* 1991, **113**, 958.

Polyhedron Vol. 12, No. 23, pp. 2887–2890, 1993
Printed in Great Britain

0277-5387/93 $6.00+.00
© 1993 Pergamon Press Ltd

COMMUNICATION

TRANSITION METAL COMPLEXES OF DIALKYL α-HYDROXYIMINOPHOSPHONATES, A NOVEL CLASS OF METAL COMPLEXES

S. W. ANNIE BLIGH,* NICK CHOI, DONOVAN ST C. GREEN, HARRY R. HUDSON, CATHERINE M. McGRATH, MARY McPARTLIN and MAX PIANKA

School of Applied Chemistry, University of North London, Holloway Road, London N7 8DB, U.K.

(*Received* 6 *September* 1993; *accepted* 28 *September* 1993)

Abstract—A new range of dialkyl α-hydroxyiminophosphonates has been prepared and the first examples of metal complexes of this class of compound have been obtained; X-ray crystal structure analysis of the dichlorobis(diethyl *E*-(α)-hydroxyiminopropanephosphonate)nickel(II) complex shows a distorted octahedral coordination at the nickel atom giving two symmetry related diethyl-(*E*)-α-hydroxyiminopropanephosphonate ligands and two chlorine donors.

Bioactive phosphorus containing molecules have long been used in the fields of agriculture[1] and drug design, however their role as active ligands with biologically important metals[2] has yet to be fully exploited. α-Hydroxyiminophosphonic acid derivatives are widely known not only as intermediates in the synthesis of the important aminophosphonic acids,[3,4] but also as phosphorylating agents,[5] potential metalloenzyme inhibitors,[6] and as having fungicidal activity.[7] In this work the scope of these compounds has been extended considerably by the synthesis of a number of novel dialkyl derivatives. For the first time the potential of these dialkyl α-hydroxyiminophosphonates as ligands has been demonstrated by the successful synthesis of a range of transition metal complexes. X-ray structure analysis confirms the formation of a five membered chelate ring on coordination of diethyl *E*-(α)-hydroxyiminopropanephosphonate to nickel(II).

The new dialkyl esters were prepared by adaptation of a literature method.[8] Reaction of acylphosphonates with hydroxylamine, using 3 M HCl in the work up procedure, gives dialkyl α-hydroxyiminophosphonates with predominating *E* isomers and in good yield (>90%). $^{31}P(CDCl_3)$ NMR data of a number of these compounds are presented in Table 1. The ^{31}P assignment of the structural isomers was initially based on literature data[9] for related compounds and has been confirmed by a single crystal structure analysis† of diisopropyl *E*-(α)-hydroxyiminobenzylphosphonate L^2 (Fig. 1).

The solid state structure of L^2 consists spiral chains formed by hydrogen bonding between the phosphoryl and oxime group of adjacent molecules {H(O4)···O(1″)1.60Å}. The structure of the individual molecules of L^2, shown in Fig. 1, establishes a conformation ideally adapted to complex formation; the potential donor atoms, the oxygen atom of the phosphoryl and the nitrogen atom of the oxime, being *cis* to each other resulting in a preformed "chelate-bite" of 2.886 Å in the solid state. Very few compounds of this type are crystalline, but there have been two recent characterizations of the *E* and *Z* form of dimethyl α-hydroxyiminobenzylphosphonate[9] and diisopropyl *E*-(α)-hydroxyiminophthalimidopropylphosphon-

*Author to whom correspondence should be addressed.

†Crystal data: $C_{13}H_{20}NO_4P$, $M = 285.28$, orthorhombic, space group $P2_12_12_1$, $a = 10.264(3)$, $b = 19.243(3)$, $c = 7.803(2)$ Å, $U = 1541.17$ Å^3, $Z = 4$, $F(000) = 608$, $D_c = 1.229$ g cm^{-3}, μ(Mo-K_α) = 1.8 cm^{-1}, $\lambda = 0.71069$ Å. Final $R = 0.0774$ ($R_w = 0.0763$) for 1027 unique reflections with $I/\sigma(I) > 3$.

Table 1. The new dialkyl α-hydroxyiminophosphonate with the *E*:*Z* ratio deduced from ^{31}P NMR

L	R	R′	*E*:*Z*	^{31}P NMR δ*E*, δ*Z*
L^1	ethyl[14]	ethyl	78:22	12.03, 6.58
L^2	isopropyl	phenyl	80:20	7.62, 4.68
L^3	n-butyl	methyl	100:0	10.68
L^4	n-butyl	propyl	96:4	12.06, 7.08
L^5	ethyl	cyclopropyl	75:25	9.76, 6.44
L^6	isopropyl	2-ethoxycarbonylethyl	100:0	10.93

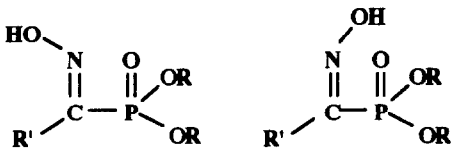

ate.[10] The equivalent bond lengths in these compounds do not differ significantly from those in L^2, but in both the *E* isomers *trans*-conformations of the potential donor atoms are observed. Interestingly for a monoalkyl α-hydroxyiminophosphonates where metal complex formation has been reported, X-ray structure analysis of the uncoordinated molecule also show a preformed chelate conformation similar to that in L^2.[11]

To date no examples of metal complexes of the bifunctional dialkyl α-hydroxyiminophosphonates have been reported, which is surprising considering that in addition to complexes of the monoalkyl esters,[11] both phosphoryl[12] and oxime[13] functional

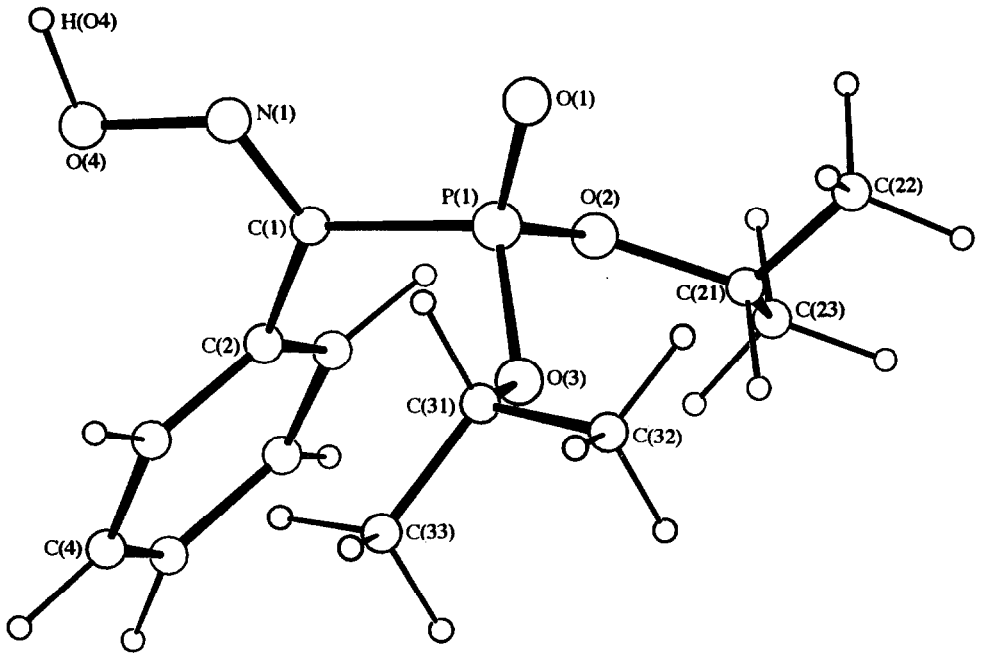

Fig. 1. The structure of diisopropyl *E*-(α)-hydroxyiminobenzylphosphonate. Selected bond lengths (Å) and angles (°): P(1)—O(1), 1.456(6); P(1)—O(2), 1.545(7); P(1)—O(3), 1.549(7); P(1)—C(1), 1.807(9); O(4)—N(1), 1.398(10); N(1)—C(1), 1.288(12); O(2)—P(1)—O(1) 117.2(4), O(3)—P(1)—O(1) 113.8(4), O(3)—P(1)—O(2) 102.7(4), C(1)—P(1)—O(1) 114.6(4), C(1)—P(1)—O(2) 100.2(4), C(1)—P(1)—O(3) 106.6(4), C(1)—N(1)—O(4) 110.3(7), N(1)—C(1)—P(1) 111.3(7).

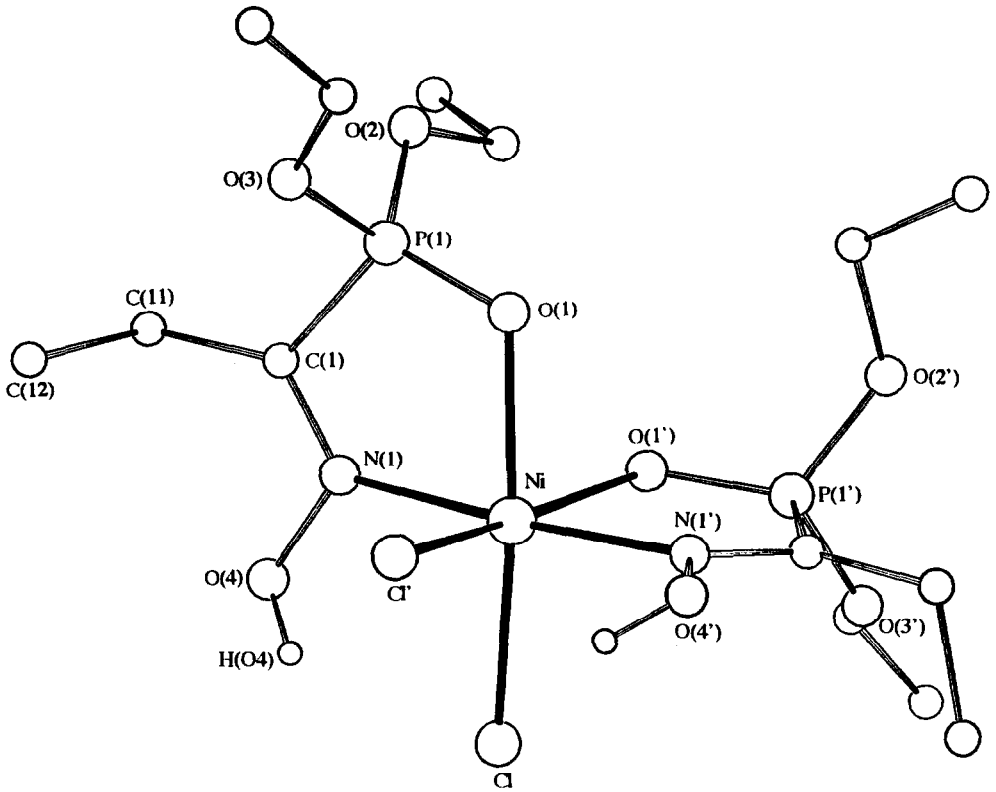

Fig. 2. The structure of the *cis* dichloro $NiL^1{}_2Cl_2$ showing the *E* isomeric form of the ligand. Selected bond lengths (Å) and angles (°): Ni—Cl, 2.346(4); Ni—O(1), 2.118(8); Ni—N(1), 2.036(9); P(1)—O(1), 1.478(8); P(1)—O(2), 1.550(9) and P(1)—O(3) 1.550(8); O(1)—Ni—Cl 168.3(2), N(1)—Ni—Cl 89.6(3), N(1)—Ni—O(1) 80.9(3), Cl—Ni—Cl′ 96.0(2), O(1)—Ni—O(1′) 83.1(4), N(1)—Ni—N(1′) 176.6(3), P(1)—O(1)—Ni 115.1(4), C(21)—O(2)—P(1) 120.5(7), C(31)—O(3)—P(1) 120.4(9), O(4)—N(1)—Ni 120.2(7), C(1)—N(1)—Ni 125.3(8).

groups can coordinate to metal ions. In this study it has been found that reaction of methanolic solutions of the diesters and the transition metal salt MX_2 gives ML_2X_2 (M = Co and Ni; L = L^1-L^6; X = Cl or NO_3).

All the cobalt(II) and nickel(II) complexes were characterized by satisfactory elemental analyses, and by liquid secondary ion mass spectrometry (LSIMS) which gave base peaks corresponding to $[M+H-Cl_2]^+$ in all cases. The infra-red spectra of the ligands and their metal complexes indicated that the oxime stretch at ν(C=N), 1614 cm^{-1} shifts to 1645 cm^{-1} on complexation and the two phosphoryl stretches at ν(P=O), 1173 and 1234 cm^{-1} condense and shift to 1164 and 1213 cm^{-1}. Magnetic moment measurements of CoL_2X_2 are 4.6 to 4.7 BM and NiL_2X_2 are 3.1 to 3.2 BM, which are in the normal range for six coordinate complexes of cobalt(II) and nickel(II). The formulation of the complexes has been confirmed by a single crystal structure analysis* of $NiL^1{}_2Cl_2$. This shows the *cis*-dichloro molecule of exact C_2 symmetry illustrated in Fig. 2, and confirms the *E* isomeric form of the phosphonate diester L^1. The atom pairs O(1), O(1′) and N(1), N(1′) from the two symmetry related chelating ligands coordinate in *cis* and *trans* configurations, respectively. The five membered chelate rings adopt an envelope conformation with maximum deviation from planarity of 0.125 Å for P(1). The oxime hydrogen atom is 2.26 Å from the coordinated chlorine atom, indicating strong intramolecular hydrogen bonding.

The selective complexation of the *E* isomers provides a useful method to separate the two isomeric forms and their biological activity can therefore be studied individually. Work is in progress in pre-

*Crystal data: $C_{14}Cl_2H_{32}N_2NiO_8P_2$, M = 547.96, monoclinic, space group $C2/c$, a = 8.980(2), b = 13.435(3), c = 21.218(3) Å, β = 94.864(2)°, U = 2550.65 Å^3, Z = 4, $F(000)$ = 1144, D_c = 1.427 g cm^{-3}, μ(Mo-K_α) = 11.0 cm^{-1}, λ = 0.71069 Å. Final R = 0.0725 (R_w = 0.0682) for 876 absorption corrected data with $I/\sigma(I) > 2.5$.

paring a range of lanthanide complexes for their potential applications as NMR shift and imaging agents.

Acknowledgements—We thank the PCFC for studentships (N. C. & C. M. M.), and the SERC for access to the Chemical Database Service at Daresbury.

REFERENCES

1. D. G. Cameron, H. R. Hudson, I. A. O. Ojo and M. Pianka, *Phosphorus and Sulfur* 1988, **40**, 183; *Handbook of Organophosphorus Chemistry* (Edited by R. Engel), Dekker, New York (1992).
2. P. J. Sadler, *Adv. Inorg. Chem.* 1991, **36**, 1.
3. S. Asano, T. Kitahara, T. Ogata and M. Mastsui, *Agric. Biol. Chem.* 1975, **37**, 1193.
4. L. Maier and P. J. Diel, *Phosphorus, Sulfur and Silicon* 1991, **62**, 15.
5. E. Breuer, R. Karaman, D. Gibson, H. Leader and A. Goldblum, *J. Chem. Soc., Chem. Commun.* 1988, 504.
6. E. Breuer, M. Safadi, M. Chorev, A. Vincze and P. Bel, *Tetrahedron* 1991, **47**, 1257.
7. N. K. Roy and H. K. Taneja, *Intern. J. Agric.* 1987, **5**, 215.
8. K. D. Berlin, R. T. Claunch and E. T. Gaudy, *J. Org. Chem.* 1968, **33**, 3090.
9. E. Breuer, R. Karaman, A. Goldblum, D. Gibson, B. V. L. Potter and J. H. Cummins, *J. Chem. Soc. Perkin Trans. I* 1988, 3047.
10. E. Breuer, M. Safadi, M. Chorev and D. Gibson *J. Org. Chem.* 1990, **55**, 6147.
11. D. Gibson and R. Karaman, *Inorg. Chem.* 1989, **28**, 1928.
12. R. Babecki, A. W. G. Platt and J. Fawcett, *J. Chem. Soc., Dalton Trans.* 1992, 675.
13. C. Lopez, S. Alvarez, X. Solans and M. Font-Bardia, *Polyhedron* 1992, **11**, 1637.
14. K. D. Berlin, N. K. Roy, R. T. Claunch and D. Bade, *J. Am. Chem. Soc.* 1968, **90**, 4494.

Polyhedron Vol. 12, No. 23, pp. 2891–2894, 1993
Printed in Great Britain

0277–5387/93 $6.00+.00
© 1993 Pergamon Press Ltd

COMMUNICATION

SYNTHESIS, X-RAY STRUCTURAL DETERMINATION AND COORDINATION CHEMISTRY OF 4′-FERROCENYL-2,2′:6′,2″-TERPYRIDINE

BRIAN FARLOW, TERENCE A. NILE* and JERRY L. WALSH*

Department of Chemistry, University of North Carolina at Greensboro, Greensboro, NC 27412, U.S.A.

and

ANDREW T. McPHAIL

Paul M. Gross Chemical Laboratory, Department of Chemistry, Duke University, Durham, NC 27706, U.S.A.

(*Received* 26 *June* 1993; *accepted* 7 *September* 1993)

Abstract—4′-Ferrocenyl-2,2′:6′,2″-terpyridine(Fctrpy) has been prepared from ferrocene carboxaldehyde and 2-acetylpyridine. A single crystal X-ray structure analysis indicates typical bond distances and angles with nearly coplanar aromatic rings. The angle between the cyclopentadienyl ring of the ferrocene moiety and the central pyridyl ring of the terpyridine is 19.2° Ruthenium complexes, $Ru(Fctrpy)_2^{2+}$ and $Ru(trpy)(Fctrpy)^{2+}$ (trpy = 2,2′:6′,2″-terpyridine) have been prepared and characterized electrochemically and spectrophotometrically.

The synthesis of substituted 2,2′:6′,2″-terpyridines is an area of great current interest.[1–4] The properties of transition metal complexes can be fine tuned by the use of substituents on the terpyridine ligands. We have synthesized a terpyridine ligand that contains a ferrocenyl moiety at the 4′ position. The ligand is unique in that the substituent itself can be modified *in situ* by oxidation of the ferrocenyl moiety to ferrocenium. We report here the synthesis and X-ray structural characterization of 4′-ferrocenyl-2,2′:6′,2″-terpyridine, Fctrpy, (**1**), its coordination to a ruthenium centre, and the properties of ruthenium complexes containing the Fctrpy ligand.

The ligand **1** was synthesized in two steps from ferrocenecarboxaldehyde using the elegant method reported by Constable, *et al.* who synthesized 4′-phenyl-2,2′:6′2″-terpyridine, 4′-Phtrpy, (**2**), from benzaldehyde.[3] Ferrocenecarboxaldehyde was reacted with two equivalents of 2-acetylpyridine, in the presence of base, to yield orange crystals of 2-ferrocenyl-1,5-bis(2-pyridyl)-1,5-pentanedione (**3**), in reasonable yield, eq. 1.

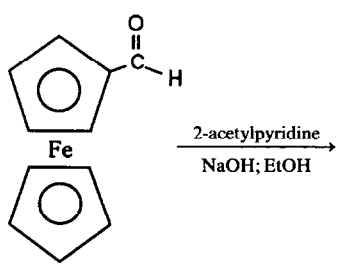

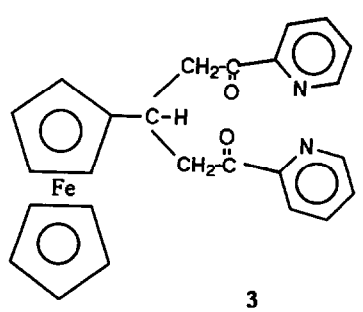

(1)

3

*Authors to whom correspondence should be addressed.

Table 1. UV-visible data[a]

Compound	λ_{MAX} ($\varepsilon \times 10^{-3}$)				
Ferrocene	—	438	322	—	—
trpy	—	—	—	278	—
Fctrpy	—	454 (2.5)	363 (6.1)	280 (107)	248 (107)
$Ru(trpy)_2^{2+}$	—	478 (14)	306 (61)	—	269 (39)
$Ru(trpy)(Fctrpy)^{2+}$	515 (sh)	478 (15)	306 (61)	—	270 (41)
$Ru(Fctrpy)_2^{2+}$	526 (15)	482 (15)	310 (60)	284 (44)	275 (49)

[a]Acetonitrile solvent.

The pentanedione was converted to **1** in good yield by reaction with ammonium acetate in refluxing ethanol in the air, eq. 2.

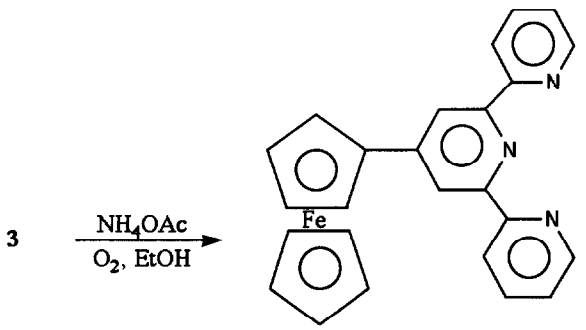

1 (2)

Both new compounds were characterized by ^1H NMR and microanalysis.*

The structure of **1** was confirmed by a single crystal X-ray structural determination.† An ORTEP view of **1** is shown in Fig. 1. As in the structure of **2**[3] the three pyridyl rings are in a *trans-oid* arrangement and are approximately co-planar: the angles between the central and the outer pyridyl rings average 7.3°, which is comparable to a value of 8.2° in **2**. The average C—C and C—N bond distances are 1.384±0.010 Å and 1.342±0.003 Å, respectively. These compare with values of 1.370±0.013 Å and 1.342±0.002 Å for **2**.[3] The terpyridine moiety is not co-planar with the ferrocenyl cyclopentadienyl ring, the dihedral angle between the two rings being 19.2°. For a series of closely related species **1**, **2** and 4-biphenylferrocene[5] (**4**), there is a correlation between the interannular bond distance and the twist angle. For **4**, **2** and **1**, the bond distances are 1.55 Å, 1.492 Å, and 1.471 Å, respectively, and the twist angles are 5.9°, 10.9°, and 19.2°. The larger twist angle occurs because of greater steric interactions between nonbonded hydrogen atoms as the interannular distance decreases. The ferrocene moiety has C—C bond distances of 1.416±0.008 Å, compared to 1.42±0.07 Å for **4**.

The properties of **1** are a combination of those of the constituent parts. The UV-visible spectrum of **1** essentially consists of π to π^* (trpy) bands[6] at 248 and 280 nm and ferrocene charge transfer bands at 351 and 452 nm[7] (Table 1). The red shift of the ferrocenyl bands of **1** relative to the 322 and 439 nm of ferrocene, and the reduction potential of the ferrocenyl moiety (0.57 V vs 0.41 V for ferrocene), reflect the electron withdrawing character of the trpy substituent.

Ruthenium complexes $[Ru(trpy)(Fctrpy)]^{2+}$ (**5**), and $[Ru(Fctrpy)_2]^{2+}$ (**6**), were prepared from Fctrpy and $RuCl_3 \cdot xH_2O$ or $Ru(DMSO)_4Cl_2$,[8] respectively. In the first case, a two step synthetic route through the intermediate $Ru(Fctrpy)Cl_3$ was used.[9] In each case, alcoholic solvents were used because use of DMSO or dimethylformamide lead to decomposition of Fctrpy to generate $Fe(trpy)_2$-type bypro-

*Characterization Data for **1**: Found: C, 72.2; H, 4.6; N, 9.9. Calc. for $C_{25}H_{19}FeN_3$: C, 72.2; H, 4.6; N, 10.0%. ^1H NMR [$(CD_3)_2CO$]: δ 4.12 (s, 5H); 4.54 (t, J = 2.0, 2H); 5.04 (t, J = 2.0, 2H); 7.45 (m, 2H); 7.98 (td, J = 7.9, 1.8, 2H); 8.62 (s, 2H); 8.71 (m, 4H). Characterization Data for **3**: Found: C, 68.4; H, 5.1; N, 6.3. Calc. for $C_{25}H_{22}O_2FeN_2$: C, 68.5; H, 5.1; N, 6.4%. ^1H NMR ($CDCl_3$): δ 3.51–3.71 (b, 4H); 4.05 (b, 1H); 4.18 (b, 9H); 7.49 (d, J = 8Hz, 2H); 7.80 (t, J = 8Hz, 2H); 7.97 (t, J = 8Hz, 2H); 8.67 (d, J = 8Hz, 2H).

†Crystal Data for **1** using Cu-K_α at T = 298K: Monoclinic, space group $P2_1/C(C_{2h}^5)$-No. 14, a = 7.898(2), b = 22.062(3), c = 11.405(2) Å, β = 107.21(1)°, V = 1898(1) Å^3, Z = 4, M_r = 417.30, D_{calc} = 1.460g cm^{-3}, 4084 reflections collected, R = 0.037 (R_w = 0.050) for 2406 [$I > 3.0\ \sigma\ (I)$] unique reflections.

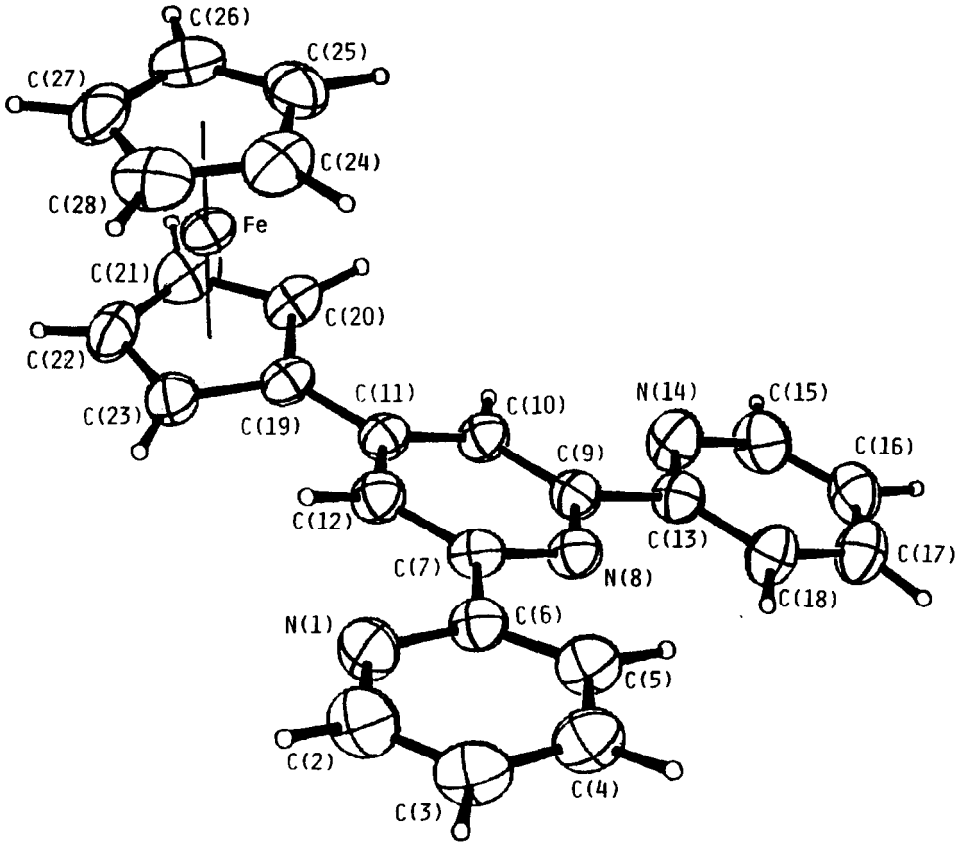

Fig. 1. ORTEP diagram (50% probability ellipsoids) of **1** showing the atom numbering scheme and solid-state conformation; small circles represent hydrogen atoms. Representative bond lengths and angles are included in the text.

ducts. Both **5** and **6** were characterized by ^{1}H NMR and microanalysis.*

The intensely red ruthenium complexes exhibit typical d(Ru)$\cdots\pi^*$(trpy) transitions around 480 nm and π(trpy)$\cdots\pi^*$(trpy) transitions in the UV region[4] (Table 1). Surprisingly, an additional absorption band is observed around 530 nm with an intensity proportional to the number of Fctrpy ligands. Other than $Ru(tro)_2^{2+}$ (tro = 4′-phenyl-2,2′:6′,2″-terpyridyl), for which absorption maxima at 490 nm (ε = 24,200) and 560 nm (ε = 8,000) are reported, substituted terpyridyl complexes of ruthenium(II) tend to exhibit a single maximum in the visible region.[4,6] The absence of a 530 nm band in free Fctrpy and its disappearance upon oxidation of the ferrocene site suggests that the 530 nm band may be a ruthenium-to-ferrocene charge transfer band and is presently under further investigation.

Results of cyclic voltammetric studies on Fctrpy, $[Ru(trpy)(Fctrpy)]^{2+}$, and $[Ru(Fctrpy)_2]^{2+}$ are listed in Table 2. The ferrocene moieties of each exhibit a reversible oxidation to ferrocenium at about 0.6 V and ruthenium(III/II) waves are observed at about 1.4 V (vs Ag/AgCl reference). The ruthenium(III/II) waves are irreversible due to deposition on the electrode and/or decomposition of the complex. Coulometric studies show that oxidation of $[Ru(trpy)(Fctrpy)]^{2+}$ at 0.8 V results in the loss of one electron whereas oxidation of $[Ru(Fctrpy)_2]^{2+}$ at the same voltage results in the loss of two electrons. This oxidation of the ferrocenyl moiety of $[Ru(trpy)(Fctrpy)]^{2+}$ or $[Ru(Fctrpy)_2]^{2+}$ leads to the loss of the 530 nm shoulder or maximum, respectively, in the visible spectrum and the d(Ru)$\cdots\pi^*$(trpy) band shifts

*Characterization Data for **5**: Found: C, 45.9; H, 3.1; N, 7.7. Calc. for $C_{50}H_{38}F_{12}FeN_6P_2Ru$: C, 46.1; H, 2.9; N, 8.1%. ^{1}H NMR [$(CD_3)_2CO$]: δ 4.37 (s, 5H); 4.78 (t, J = 2.0, 2H); 5.51 (t, J = 2.0, 2H); 7.3 (m, 4H); 7.76 (m, 4H); 8.06 (t, J = 4, 4H); 8.5–9.1 (m, 7H); 9.18 (s, 2H).

Characterization Data for **6**: Found: C, 48.6; H, 3.4; N, 6.2. Calc. for $C_{40}H_{30}F_{12}FeN_6P_2Ru$: C, 49.0; H, 3.1; N, 6.8% ^{1}H NMR [$(CD_3)_2CO$]: δ 4.36 (s, 5H); 4.77 (t, J = 1.8, 2H); 5.35 (t, J = 1.9, 2H); 7.18 (*ddd*, J = 5.7, 5.5, 1.7, 2H); 7.42 (*d*, J = 4.7, 2H); 7.94 (td, J = 7.9, 1.5, 2H); 8.64 (*d*, J = 7.2, 2H); 8.74 (s, 2H).

Table 2. Cyclic voltammetry data

Compound	$E_{1/2}$, volts vs Ag/AgCl			
	$Ru^{III/II}$	Fc^+/Fc	trpy Reductions	
Ferrocene	—	0.41	—	[a]
trpy	—	—	< -1.7	[a]
Fctrpy	—	0.57	< -1.7	[a]
$Ru(trpy)_2^{2+}$	1.19	—	$-1.19, -1.52$	[b]
$Ru(trpy)(Fctrpy)^{2+}$	1.42	0.59	$-1.21, -1.52$	[b]
$Ru(Fctrpy)_2^{2+}$	1.39	0.58	$-1.22, -1.52$	[b]

[a] CH_3CN/TEAP.
[b] CH_2Cl_2/TBAH.

to 501 nm. Oxidation of the ferrocenyl moiety apparently stabilizes the trpy π^* orbital, leading to a lower energy $d(Ru)\cdots\pi^*(trpy)$ transition. Comparison to ruthenium complexes of other substituted trpy ligands[4,6] suggests that the effect of the ferrocene or the ferricinium substituent is similar to that observed for other substituents. A weak absorption band is observed above 900 nm in $[Ru(Fctrpy)_2]^{4+}$, presumably a ruthenium(II)-ferrocenium intervalence transfer transition.

Attachment of a terpyridyl moiety to the ferrocene increases the ferrocenium/ferrocene reduction potential by about 0.17 V, independent of whether or not the terpyridyl is bound to a ruthenium(II) centre. This increase is similar to that observed for 3- or 4-ferrocenylpyridine[10] and considerably larger than the increase observed for phenylferrocene.[11]

Acknowledgements—The financial support of the American Chemical Society-Petroleum Research Fund and the Research Council of the University of North Carolina at Greensboro is gratefully acknowledged.

REFERENCES

1. (a) E. C. Constable and A. M. W. Thompson, *J. Chem. Soc., Dalton Trans.* 1992, 3467.
2. I. R. Butler, *Organometallics* 1992, **11**, 74.
3. E. C. Constable, J. Lewis, M. C. Liptrot and P. R. Raithby, *Inorg. Chim. Acta* 1990, **178**, 47.
4. (a) T. B. Hadda and H. Le Bozec, *Polyhedron* 1988, 7, 575; (b) E. C. Constable, A. M. W. Cargill Thompson, D. A. Tocher and M. A. M. Daniels, *New J. Chem.* 1992, **16**, 855; (c) R. P. Thummel, V. Hegde and Y. Jahng, *Inorg. Chem.* 1989, **28**, 3264; (d) J. R. Kirchhoff, D. R. McMillan, P. A. Marnot and J. P. Sauvage, *J. Am. Chem. Soc.* 1985, **107**, 1138.
5. F. H. Allen, J. Trotter and C. S. Williston *J. Chem. Soc. (A)* 1970, 907.
6. M. L. Stone and G. A. Crosby, *Chem. Phys. Lett.* 1981, **79**, 169.
7. Y. S. Sohn, D. N. Hendrickson and H. B. Gray, *J. Am. Chem. Soc.* 1971, **93**, 3603.
8. I. P. Evans, A. Spencer and G. Wilkinson, *J. Chem. Soc., Dalton Trans.* 1973, 204.
9. (a) H. F. Suen, S. W. Wilson, M. Pomerantz and J. L. Walsh, *Inorg. Chem.* 1989, **28**, 786; (b) B. P. Sullivan, J. M. Calvert and T. J. Meyer, *Inorg. Chem.* 1980, **19**, 1404.
10. (a) T. M. Miller, K. J. Ahmed and M. S. Wrighton, *Inorg. Chem.* 1989, **28**, 2347; (b) O. Carugo, G. DeSantis, L. Fabbrizzi, M. Licchelli, A. Monichino and P. Pallavieini, *Inorg. Chem.* 1992, **31**, 765.
11. (a) H. Grimes and S. R. Logan, *Inorg. Chim. Acta* 1980, **45**, L223; (b) M. M. Sabbatini and E. Cesaratti, *Inorg. Chim. Acta* 1977, **24**, L9.

Polyhedron Vol. 12, No. 23, pp. 2895–2898, 1993
Printed in Great Britain

0277–5387/93 $6.00+.00
© 1993 Pergamon Press Ltd

COMMUNICATION

FORMATION AND X-RAY STRUCTURE OF A NOVEL TETRADECANUCLEAR COPPER(I) CLUSTER COMPLEX $Cu_{14}(\mu_2\text{-}S)(SPh)_{12}(PPh_3)_6$

KALUO TANG,* TIANBING XIA, XIANGLIN JIN and YOUQI TANG

Institute of Physical Chemistry, Peking University, Beijing 100871, P.R. China

(*Received* 2 *July* 1993; *accepted* 3 *September* 1993)

Abstract—The neutral tetradecanuclear copper(I) thiolate cluster complex has been formed from the reaction of $(Ph_3P)_2Cu(S_2CSPh)$ with CH_2Cl_2 and MeOH and structurally characterized by X-ray diffraction analysis. The core of the $[Cu_{14}(\mu_2\text{-}S)(SPh)_{12}(PPh_3)_6]$ cluster consists of a sulphur ion at the centre of a cube of eight copper(I) atoms, which is inscribed into an icosahedron of twelve sulphur atoms. The other six copper(I) atoms form an octahedron and the icosahedron of S_{12} fits inside the octahedron of Cu_6.

The insertion reactions of CS_2 into Ag—S and Cu—S bonds have been studied by us in recent years.[1–6] We have found that silver or copper thiolate complexes react readily with CS_2 in the presence of PPh_3 to give almost the same structure of mononuclear product[1,6–8]

$$(MSR)_n + PPh_3 + CS_2 \leftrightarrows (Ph_3P)_2M(S_2CSR).$$
$$(M = Cu, Ag;\ R = aryl, alkyl)$$

This is a reversible reaction.[1,7] Recently, we also found some insertion products of this kind of reaction can easily react with various solvents to form unexpected cluster complexes. A novel tetradecanuclear silver cluster complex $[Ag_{14}(SPh)_{12}(PPh_3)_8Cl]^+Cl^-$ has been synthesized and structurally characterized.[9] In this communication we report the formation and crystal structure of a novel neutral tetradecanuclear copper(I) cluster complex $[Cu_{14}(\mu_2\text{-}S)(SPh)_{12}(PPh_3)_6]$.

The title complex was prepared as follows: the orange crystals of insertion product of CS_2 into Cu—S bond, $(Ph_3P)_2Cu(S_2CSPh)$, was readily obtained by stirring a solution of $(CuSPh)_n$ (0.173 g, 1 mmol) and PPh_3 (0.525 g, 2 mmol) in CS_2 (30 cm^3) for 4 h at room temperature and then cooling it to $-30 \sim -20$°C overnight. The crystal melts with effervescence at 101–104°C to a cream-coloured solid that subsequently melts at 165–167°C. This indicates that its structure is in agreement with that previously reported by Eller.[7] When the orange crystals of $[(PH_3P)_2Cu(S_2CSPh)]$ (30 mg) were dissolved in CH_2Cl_2 (4 cm^3), the initial orange colour of solution faded quickly. Then a layer of MeOH (12 cm^3) was placed above this solution and after two months colourless polyhedron-shaped crystals formed on the wall of the test tube. The crystals are air stable and decompose gradually above 140°C.

The crystal structure determination indicates that the complex is a neutral tetradecanuclear copper(I) cluster.† The core and the molecular structure are illustrated in Figs 1 and 2, respectively. Selected bond lengths and angles are given in Table 1. The molecule has a peculiar $Cu_{14}S_{12}$ cage which is composed of $Cu_8^{(I)}$, $Cu_6^{(I)}$ and S_{12} polyhedra centred around a sulphur ion. They are arranged in such a

*Author to whom correspondence should be addressed.

†The data were collected on a Siemens R3m/V diffractometer. The SHELXTL PLUS program was used to solve and refine the structure. Crystal data: $C_{180}H_{150}Cu_{14}P_6S_{13}$, M = 3805. 2, space group $P\bar{1}$, $a = 18.939(3)$, $b = 19.026(9)$, $c = 19.308(13)$ Å, $\alpha = 90.27(5)$, $\beta = 118.79(4)$, $\gamma = 119.95(3)°$, $V = 5000.03(5)$ Å^3, $D_c = 1.264$ g cm^{-3}, $Z = 1$, $F(000) = 1934$, $\mu = 1.68$ mm^{-1}. With anisotropic thermal parameters for all non-hydrogen atoms, the refinement yields the final discrepancy $R = 0.068$, $R_w = 0.068$ for 7647 observed reflections $[F > 4.0\ \sigma(F)]$ collected in the range $3.0 \leqslant 2\theta \leqslant 45.0°$ with Mo-K_α ($\lambda = 0.7103$ Å) at room temperature by the 2θ scan mode.

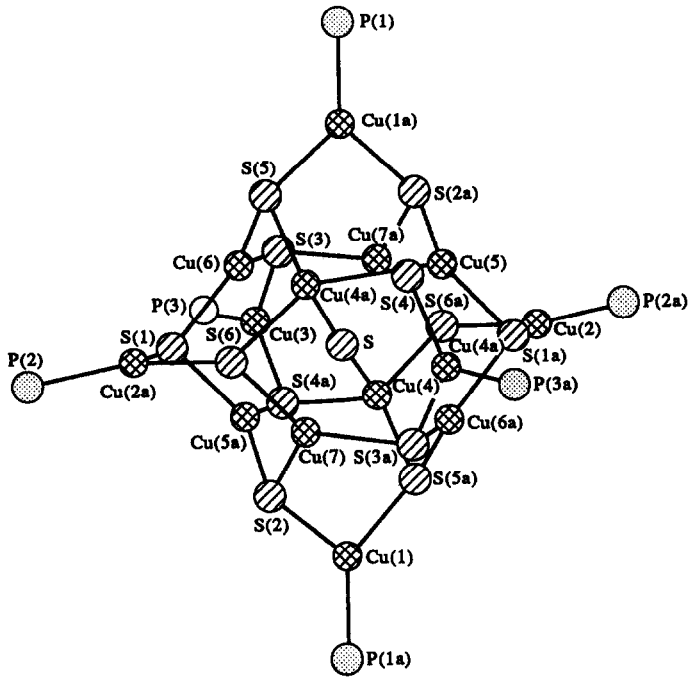

Fig. 1.

way that a cube of Cu_8 is inscribed into an icosahedron of S_{12}, which fits inside an octahedron of Cu_6. A single sulphur ion (S^{2-}) occupies the centre of the Cu_8 cube, whose vertices are at the centres of eight trigonal faces of the S_{12} icosahedron, the Cu atoms deviate only about 0.01 Å from the faces. Only two Cu atoms at either end of one diagonal of Cu_8 cube coordinate to the central S atom, the Cu—S bond lengths are 2.536 Å, and the other six Cu—S distances to this sulphur are around 2.8 Å,

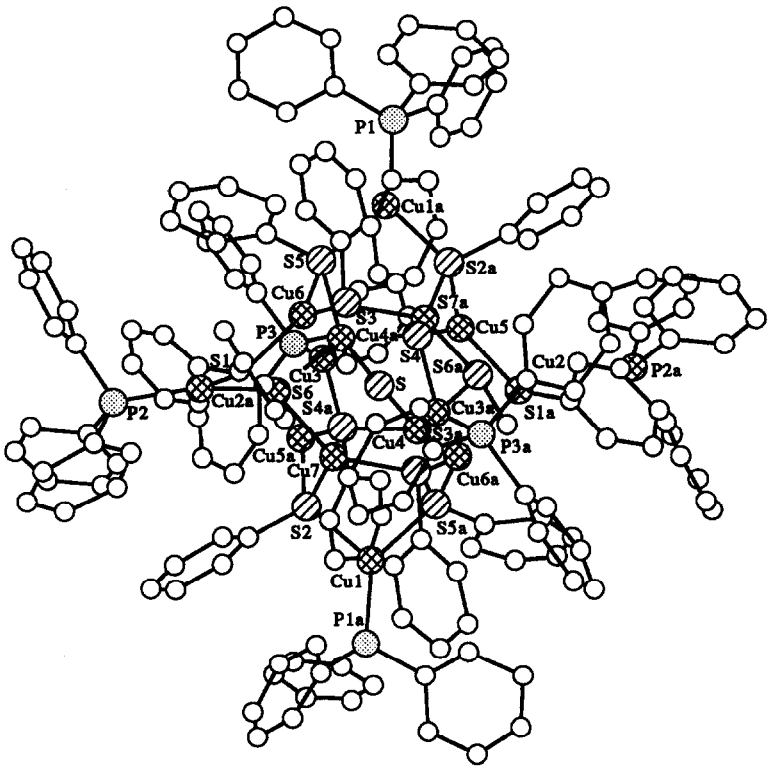

Fig. 2.

Table 1. Selected bond lengths (Å) and angles (°) of $Cu_{14}(\mu_2\text{-}S)(SPh)_{12}(PPh_3)_6$

Cu(1)—S(2)	2.283(3)	Cu(1)—S(5A)	2.270(5)
Cu(1)—P(1A)	2.220(6)	Cu(2)—S(3)	2.275(4)
Cu(2)—P(3)	2.205(6)	Cu(2)—S(4A)	2.257(6)
Cu(3)—S(1A)	2.269(5)	Cu(3)—S(6A)	2.264(4)
Cu(3)—P(2A)	2.225(4)	Cu(4)—S	2.536(2)
Cu(4)—S(4A)	2.299(5)	Cu(4)—S(5A)	2.299(6)
Cu(4)—S(6A)	2.302(5)	Cu(5)—S(4)	2.283(5)
Cu(5)—S(1A)	2.312(3)	Cu(5)—S(2A)	2.282(6)
Cu(6)—S(1)	2.294(5)	Cu(6)—S(3)	2.294(5)
Cu(6)—S(5)	2.287(5)	Cu(7)—S(2)	2.301(5)
Cu(7)—S(6)	2.296(3)	Cu(7)—S(3A)	2.293(4)

S(2)—Cu(1)—S(5A)	99.7(2)	S(2)—Cu(1)—P(1A)	126.2(2)
S(5A)—Cu(1)—P(1A)	133.6(1)	S(3)—Cu(2)—P(3)	125.9(2)
S(3)—Cu(2)—S(4A)	100.3(2)	P(3)—Cu(2)—S(4A)	133.4(2)
S(1A)—Cu(3)—S(6A)	99.2(1)	S(1A)—Cu(3)—P(2A)	126.1(2)
S(6A)—Cu(3)—P(2A)	134.2(2)	S—Cu(4)—S(4A)	97.9(1)
S—Cu(4)—S(5A)	98.8(1)	S(4A)—Cu(4)—S(5A)	117.9(2)
S—Cu(4)—S(6A)	98.0(1)	S(4A)—Cu(4)—S(6A)	118.2(2)
S(5A)—Cu(4)—S(6A)	117.8(1)	S(4)—Cu(5)—S(1A)	117.0(2)
S(4)—Cu(5)—S(2A)	125.2(1)	S(1A)—Cu(5)—S(2A)	117.8(2)
S(1)—Cu(6)—S(3)	117.5(2)	S(1)—Cu(6)—S(5)	125.8(2)
S(3)—Cu(6)—S(5)	116.7(2)	S(2)—Cu(7)—S(6)	117.2(1)
S(2)—Cu(7)—S(3A)	117.2(1)	S(6)—Cu(7)—S(3A)	125.6(2)
Cu(4)—S—Cu(4A)	180.0(1)	Cu(6)—S(1)—Cu(3A)	112.4(2)
Cu(6)—S(1)—Cu(5A)	93.2(1)	Cu(3A)—S(1)—Cu(5A)	113.6(2)
Cu(1)—S(2)—Cu(7)	113.6(2)	Cu(1)—S(2)—Cu(5A)	112.7(2)
Cu(7)—S(2)—Cu(5A)	92.6(2)	Cu(2)—S(3)—Cu(6)	113.2(2)
Cu(2)—S(3)—Cu(7A)	112.1(1)	Cu(6)—S(3)—Cu(7A)	93.7(2)
Cu(5)—S(4)—Cu(2A)	114.0(1)	Cu(5)—S(4)—Cu(4A)	84.6(2)
Cu(2A)—S(4)—Cu(4A)	116.8(2)	Cu(6)—S(5)—Cu(1A)	114.7(2)
Cu(6)—S(5)—Cu(4A)	83.8(2)	Cu(1A)—S(5)—Cu(4A)	116.8(2)
Cu(7)—S(6)—Cu(3A)	114.5(2)	Cu(7)—S(6)—Cu(4A)	84.3(1)
Cu(3A)—S(6)—Cu(4A)	117.4(2)		

which is longer than the normal Cu—S bond length. Therefore it is a distorted cube with slight compression along this diagonal. Twelve S atoms of thiolate ligands form an icosahedron, and these S atoms sit on the 12 edges of the Cu_8 octahedron. The bond angles of Cu—S—Cu average 172.1° (170.7–173.4°). Every thiolate S atom forms a bridge between two Cu atoms of the cube and one Cu atom of the octahedron. The Cu—S bond lengths vary from 2.257 to 2.312 Å. The six Cu atoms in the structure form the octahedron in such an orientation that each Cu atom of the octahedron centres above one of six faces of the Cu_8 cube, the distances average 3.09 Å. The Cu-centred trigonal icosahedronal face is approximately coplanar with a face of the Cu_6 octahedron. There is a terminal PPh_3 ligand on each of the vertices of the Cu_6 octahedron. The mean value of Cu—P bond length is 2.217 Å (2.205–2.225 Å). All copper atoms are trigonally coordinated except that the two coordinated by the central S atom are tetrahedronally coordinated. Furthermore, there are 12 $Cu_3(\mu_3\text{-}S)_3$ six-membered rings in the cluster, all of which are boat-like conformation. Viewing the whole molecule, we can find that all copper atoms are surrounded by the exterior phenyl groups, that is, the array of ligand substituents is on the surface of the molecule. So they protect the univalent metals sterically against oxidation or chemical attack.

The geometry of the core of $[Cu_{14}(\mu_2\text{-}S)(SPh)_{12}(PPh_3)_6]$ cluster resembles the geometries of the mixed-valent copper thiolate cluster compounds $[Cu_8^{(I)}Cu_6^{(II)}L_{12}Cl]$ (L = penicillamine (Pen)[10], α-mercaptoisobutyric acid (MIBA)[11], β,β-dimethyl cysteamine (DMC)[12]), and they have similar metal–metal and metal–ligand distances which are compared in Table 2. However, there are several main differences between our compound and mixed-valent copper thiolate cluster compounds. (i) Our compound is a neutral tetradeca-nuclear

Table 2. Comparison of metal–metal and metal–ligand distances in $Cu_{14}(\mu_2\text{-}S)(SPh)_{12}(PPh_3)_6$ within $[Cu_8^{(I)}Cu_6^{(II)}L_{12}Cl]$ compounds

		$Cu_{14}(\mu_2\text{-}S)(SPh)_{12}(PPh_3)_6$	$Cu_8^{(I)}Cu_6^{(II)}L_{12}Cl$		
			L = Pen[10]	L = MIBA[11]	L = DMC[12]
$^aCu_8$—S	range	2.282(6)–2.312(3)	2.21(2)–2.34(2)	2.26(2)–2.30(2)	2.268(5)–2.297(5)
	average	2.295	2.27	2.28	2.282
$^bCu_6$—S	range	2.257(6)–2.283(5)	2.26(3)–2.31(3)	2.23(2)–2.26(2)	2.269(6)–2.292(6)
	average	2.270	2.28	2.25	2.280
Cu_8—Cu_8	range	3.062–3.347		3.31(1)–3.38(1)	3.264(4)–3.341(3)
	average	3.207	3.30	3.35	3.3
Cu_6—Cu_6	range	6.514–6.754		6.29(1)–6.87(1)	6.645(4)–6.825
	average	6.637		6.6	—

$^aCu_8$ = the Cu atom in cubes.
$^bCu_6$ = the Cu atom in octahedra.

copper cluster, but all the mixed-valent copper thiolate clusters are anionic cluster complexes. (ii) All 14 copper atoms in our compound are of unitary valence, that is, univalent, but in the mixed-valent copper cluster compounds only eight of the 14 Cu atoms are univalent and the other six Cu atoms are bivalent. Therefore our compound is the first example of unitary valent neutral tetradecanuclear copper cluster to our knowledge. (iii) Instead of a chloride ion which is at the centre of mixed-valent copper thiolate clusters, a sulphur ion is at the centre of our cluster. And it is considered that the central S ion is essential for the formation of the whole structure. The initial presence of the central S ion was only fortuitous. It is estimated that the central S atom might be the result of nucleophilic reaction of PhS^- and CS_2, which are formed from dissociation of $(Ph_3P)_2Cu(S_2CSPh)$ in CH_2Cl_2 and MeOH solution. However, further investigation of the formation mechanism of the cluster is needed.

Acknowledgements—We wish to express our gratitude for financial support of this work by China's National Natural Science Foundation.

REFERENCES

1. K. Tang, Q. Xing, J. Yang, Q. Yang and Y. Tang, *Acta Chim. Sinica.* 1990, **48**, 242.
2. K. Tang, J. Yang, Q. Yang and Y. Tang, *J. Chem. Soc., Dalton Trans.* 1989, 2297.
3. K. Tang, D. Wu, X. Jin and Y. Tang, *Acta Chim. Sinica.* 1993, **51**, 52.
4. K. Tang, D. Wu, X. Jin and Y. Tang, *Heteroatom Chem.* 1992, **3**, 655.
5. K. Tang, D. Wu, X. Jin and Y. Tang, *J. Struct. Chem.* 1992, **11**, 314.
6. K. Tang. D. Wu, X. Jin and Y. Tang, *Acta Sci. Natur. Univ. Peking* 1992, **28**, 446.
7. P. G. Eller and R. R. Ryan, *Acta Cryst.* 1977, **B33**, 619.
8. A. Avdeff and J. P. Fackler Jr, *J. Coord. Chem.* 1975, **4**, 211.
9. X. Jin, W. Liu, K. Tang and Y. Tang, to be published.
10. P. J. M. W. L. Birker and H. C. Freeman, *J. Am. Chem. Soc.* 1977, **99**, 6890.
11. P. J. M. W. L. Birker, *Inorg. Chem.* 1979, **18**, 3502.
12. H. J. Schugar, C. C. Ou, J. A. Thich, J. A. Potenza, T. R. Felthouse, M. S. Haddad, D. N. Hendrickson, W. Furey Jr, R. A. Lalancette, *Inorg. Chem.* 1980, **19**, 543.

Polyhedron Vol. 12, No. 23, pp. 2899–2900, 1993
Printed in Great Britain

0277–5387/93 $6.00+.00
© 1993 Pergamon Press Ltd

COMMUNICATION

SYNTHESES AND X-RAY CRYSTAL STRUCTURES OF TETRAKIS(DIPHENYLAMIDO)NIOBIUM(IV) AND NIOBIUM(IV) AMIDO-HALIDE COMPLEXES

DAVID M. HOFFMAN* and SRI PRAKASH RANGARAJAN

Department of Chemistry, University of Houston, Houston, TX 77204, U.S.A.

(*Received* 17 *June* 1993; *accepted* 2 *September* 1993)

Abstract—The syntheses of three niobium(IV) amido complexes, tetrakis(diphenylamido)-niobium(IV), bis(bistrimethylsilylamido)dichloroniobium(IV) and bis(bistrimethylsilyl-amido)-dibromoniobium(IV), are reported as well as the X-ray crystal structure of the homoleptic amide.

The syntheses of homoleptic dialkylamido niobium(IV) complexes were first reported in 1962 by Bradley and Thomas.[1] Later, Bradley and Chisholm assigned a D_{2d} pseudo-tetrahedral structure for the compounds on the basis of electronic spectra, magnetic susceptibilities and ESR studies,[2] but a definitive structural characterization could not be carried out because the compounds are liquids. We report here the synthesis and X-ray structure of a new homoleptic niobium(IV) amide, tetrakis(diphenylamido)niobium(IV), and describe the syntheses of two niobium(IV) amido-halide complexes that may be of use in the synthesis of other four coordinate niobium(IV) compounds. Our interest in this chemistry was motivated by our use of $Nb(NEt_2)_4$ as a precursor to niobium nitrides.[3]

Thin purple–black plates of tetrakis (diphenylamido)niobium(IV), $Nb(NPh_2)_4$, were isolated in moderate yield (63%) by reacting $NbCl_4(thf)_2$ with four equivalents of $LiNPh_2$ in ether, stripping and extracting with benzene, and crystallizing from thf/acetonitrile (4:1). In the ^1H NMR (C_6D_6) only a single broad resonance at δ 9.5 is observed. The Evans' NMR method gives a room temperature magnetic moment of 0.98 BM.[4]

A plot of $Nb(NPh_2)_4$ from an X-ray crystallographic study is shown in Fig. 1.† The structure is best analysed in the context of the idealized D_{2d} structure **I**, which is close to the actual structure

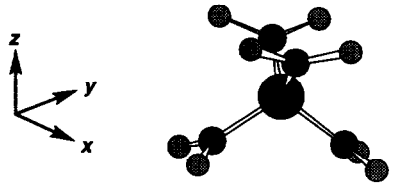

I

<N-M-N = 109.5°

*Author to whom correspondence should be addressed.

†Crystal data for $Nb(NPh_2)_4$ at −50°C, $C_{48}H_{40}N_4Nb$, thin purple–black plate, 0.44 × 0.24 × 0.04 mm, M = 765.83, triclinic, a = 10.596 (3), b = 11.622 (4), c = 16.177 (5) Å, α = 86.75 (2)°, β = 80.63 (2)°, γ = 80.33 (3)°, U = 1937 Å^3, space group $P\bar{1}$, Z = 2, D_c = 1.31 g cm^{-3}, μ(Mo-K_α) = 3.33 cm^{-1}. Data were collected on a Nicolet R3m/V diffractometer with graphite-monochromated Mo-K_α radiation (λ = 0.71073 Å) in the θ:2θ scan mode. Lorentz and polarization corrections were applied to the data. A total of 4157 reflections were collected in the range 4° < 2θ < 42°; 3195 unique reflections with $I > 3\sigma(I)$ were used in the structure solution. One of the phenyl groups (C7—C12) was found to be disordered over two slightly different positions, and this was treated by refining separate rigid bodies having 50% occupancies. Only one orientation is shown in Fig. 1. $R(F)$ = 0.031; $R_w(F)$ = 0.027. Atomic coordinates, bond lengths and angles, and thermal parameters for $Nb(NPh_2)_4$ have been deposited as supplementary material with the editor from whom copies are available on request. Atomic coordinates have also been deposited with the Cambridge Crystallographic Data Centre. Crystal data for $Nb[N(SiMe_3)_2]_2Cl_2$ at −50°C, $C_{12}H_{36}N_2Si_4Cl_2Nb$, dark blue block, 0.50 × 0.45 × 0.35 mm, M = 484.67, orthorhombic, a = 15.174 (5), b = 12.628 (5), c = 12.919 (4) Å, U = 2476 Å^3, space group Pbcn, Z = 4, D_c = 1.30 g cm^{-3}, μ(Mo-K_α) = 8.71 cm^{-1}.

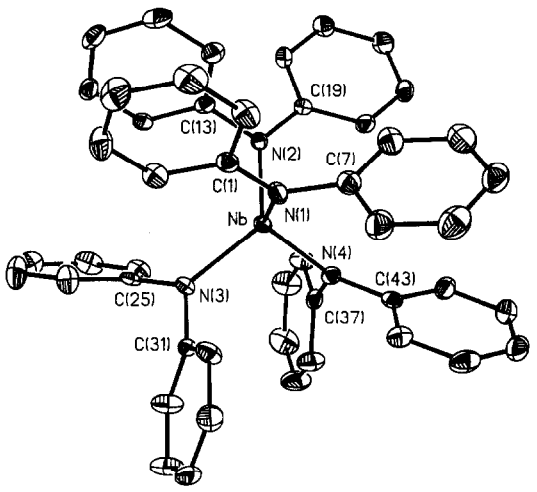

Fig. 1. Molecular structure of $Nb(NPh_2)_4$ (30% probability ellipsoids). Bond distances (Å): Nb—N(1) 2.028 (3), Nb—N(2) 2.029 (3), Nb—N(3) 2.029 (3), Nb—N(4) 1.985 (3). Bond angles (°): N(1)—Nb—N(2) 102.5 (1), N(1)—Nb—N(3) 108.2 (1), N(2)—Nb—N(3) 120.8 (1), N(1)—Nb—N(4) 116.7 (1), N(2)—Nb—N(4) 107.5 (1), N(3)—Nb—N(4) 101.9 (1), Nb—N(1)—C(1) 127.9 (2), Nb—N(1)—C(7) 112.8 (2), Nb—N(1)—C(7′) 117.7 (2), Nb—N(2)—C(19) 134.8 (2), Nb—N(2)—C(13) 106.3 (2), Nb—N(3)—C(25) 126.6 (2), Nb—N(3)—C(31) 119.2 (2), Nb—N(4)—C(37) 115.3 (2), Nb—N(4)—C(43) 131.2 (2), C(1)—N(1)—C(7) 117.1 (3), C(1)—N(1)—C(7′) 114.4 (3), C(13)—N(2)—C(19) 115.4 (3), C(25)—N(3)—C(31) 114.0 (3), C(37)—N(4)—C(43) 113.1 (3).

of d^2 $Mo(NMe_2)_4$.[5] In $Nb(NPh_2)_4$ the two N—Nb—N angles bisected by the $C_2(z)$ axis [N(1)NbN(2) and N(3)NbN(4)] are closed from 109.5° to an average of 102.2°. The closing of these two angles and a twist of the N(1)NbN(2) and N(3)NbN(4) blades by 8.2° from mutually perpendicular results in the two other pairs of N—Nb—N angles averaging 118.8° and 107.9°. The amido ligands are all close to planar, but the Nb—N—C angles vary widely (106–135°). Bond distances are unexceptional, although Nb—N(4) is nearly 10σ shorter than the average of the other three statistically equal Nb—N distances.

The orientations of the amido phenyl substituents are curious. The N(3) and N(4) amido ligand phenyl rings are rotated such that there is virtual C_2 symmetry in the $Nb(N(3)Ph_2)(N(4)Ph_2)$ moiety, an arrangement that minimizes interligand steric interactions between rings. On the other hand, the N(1) and N(2) phenyl substituents are oriented such that two of the rings [C(1) and C(13)] are in extremely close contact (≈3.2 Å), which would seem to maximize steric interactions.

It appears that steric interactions are the primary reason why the structure of $Nb(NPh_2)_4$ is substantially different from **I**, as evidenced by the wide variation in Nb—N—C angles. In this regard it should also be noted that a $(d_{x^2-y^2})^1$ configuration is expected for $Nb(NPh_2)_4$ (i.e. a $^2B_1$ or ^2A ground state in D_{2d} or D_2 symmetry, respectively),[5] and this does not provide a Jahn–Teller driving force for a distortion.

We have also prepared niobium(IV) amido halides. For example, dark blue crystals of $Nb[N(SiMe_3)_2]_2Cl_2$ were isolated in ≈60% yield by reacting $NbCl_4(thf)_2$ with two equivalents of $LiN(SiMe_3)_2$ in hexane/ether (2:1), stripping and extracting with hexane, and crystallizing from cold hexane. A similar procedure produced blue $Nb[N(SiMe_3)_2]_2Br_2$ in a comparable yield. In both preparations there is typically ≈10% contamination of the final product by $LiN(SiMe_3)_2$ which has proved difficult to remedy because of the similar solubilities of the lithium salt and niobium products. The ^1H NMR spectrum of $Nb[N(SiMe_3)_2]_2Cl_2$ in C_6D_6 has only a broad resonance centered at δ 1.9. An X-ray crystallographic study of $Nb[N(SiMe_3)_2]_2Cl_2$ indicates that the space group is the same as for $Ta[N(SiMe_3)_2]_2Cl_2$ and the cell constants are virtually identical,[6] suggesting that the two compounds are isostructural.

Acknowledgement—Financial support from the Robert A. Welch Foundation, the Texas Advanced Research Program, and the American Chemical Society-Petroleum Research Fund is gratefully acknowledged. DMH is a 1992–4 Alfred P. Sloan Research Fellow. We thank J. Korp for his technical assistance with the X-ray crystallographic analyses and his other helpful suggestions.

REFERENCES

1. D. C. Bradley and I. M. Thomas, *Can. J. Chem.* 1962, **40**, 449.
2. D. C. Bradley and M. H. Chisholm, *J. Chem. Soc. A* 1971, 1511.
3. R. Fix, R. Gordon, and D. M. Hoffman, *Chem. Mater.* 1993, **5**, 614.
4. D. F. Evans, *J. Chem. Soc.* 1959, 2003; D. H. Live and S. I. Chan, *Anal. Chem.* 1970, **42**, 791.
5. M. H. Chisholm, F. A. Cotton and M. W. Extine, *Inorg. Chem.* 1978, **17**, 1329.
6. D. M. Hoffman and S. Suh, *J. Chem. Soc., Chem. Commun.* 1993, 714.

Polyhedron Vol. 12, No. 23, pp. 2901–2903, 1993
Printed in Great Britain

0277–5387/93 $6.00+.00
© 1993 Pergamon Press Ltd

COMMUNICATION

SYNTHESIS AND X-RAY STRUCTURE OF THE POLYNUCLEAR COMPLEX BIS(μ-TRIFLUOROACETATO-O,O′)(1,10-PHENANTHROLINE)MANGANESE(II)

MARIUS ANDRUH, HERBERT W. ROESKY,* MATHIAS NOLTEMEYER and HANS-GEORG SCHMIDT

Institut für Anorganische Chemie der Universität Göttingen, Tammannstraße 4, D-37077 Göttingen, Germany

(*Received* 11 *August* 1993; *accepted* 31 *August* 1993)

Abstract—The reaction of $Mn(CF_3COO)_2$ (**1**) and 1,10-phenanthroline in 1 : 1 molar ratio yields the polynuclear compound $[Mn(CF_3COO)_2(phen)]_n$ **2**. The crystal structure of **2** reveals zig-zag infinite chains with *syn–syn* bridging trifluoroacetate ions.

The versatility of the carboxylate ligands, $RCOO^-$, has contributed over the past few years to the development of a rich co-ordination chemistry. Numerous complexes of a variety of metal ions have been prepared and structurally characterized. It is worth mentioning that some of these polynuclear compounds illustrate general structural types in modern inorganic chemistry.[1,2] The increasing interest in this chemistry is due to several reasons: (i) the carboxylate ions play a key role as ligands in many biochemical systems involving mono- or poly-metallic active sites; (ii) polynuclear carboxylates are good candidates for the investigation of exchange-coupling interactions between adjacent metal ions.

A successful strategy leading to polynuclear metal(II)carboxylates is the reaction of the corresponding salt with a bidentate organic ligand, LL, in a molar ratio preventing the formation of mononuclear species. It is difficult, however, to predict the nuclearity of the crystalline compounds. Taking into account the case of manganese(II) coordination chemistry, a survey of the recent literature reveals several interesting features. Lippard, Bino *et al.* have reported[3] the structures of two binuclear complexes with biological relevance: $[Mn_2(H_2O)(piv)_4(Me_2bipy)_2]$ and $[Mn_2(H_2O)(OAc)_4(tmeda)_2]$, both being rare examples of water-bridged dinuclear complexes. Two trinuclear species of the type $[Mn_3(RCOO)_6(bipy)_2]$ have been structurally characterized by Christou ($R = C_6H_5$)[4] and Kahn, Girerd *et al.* (the acetato analogue).[5] All these compounds have been obtained by keeping a manganese(II) to ligand LL molar ratio equal to 1 : 1. Another trinuclear compound, $[Mn_3(CF_3COO)_6(C_6H_5CN)_6]$, has been synthesized and characterized in our laboratory.[6]

Following our systematic structural investigation of trifluoroacetate manganese(II) complexes,[6,7] we now report here on the synthesis and X-ray structure of a new polynuclear complex of manganese(II): bis(μ-trifluoracetato-O,O′)(1,10-phenanthroline)manganese(II), $[Mn(CF_3COO)_2(phen)]_n$ (**2**).† The molecular structure of this compound has

* Author to whom correspondence should be addressed.

† 1,10-Phenanthroline monohydrate (0.4 g) was added with stirring to an aqueous solution (20 cm^3) containing $Mn(CF_3COO)_2$ (**1**) (0.56 g). Pale yellow fibrous crystals are obtained by slow evaporation of the resulting solution; yield 0.7 g (73%). Found: IR (KBr, cm^{-1}): 1802 w, 1718 vs, 1675 vs, 1625 m, 1591 m, 1519 s, 1444 s, 1348 s, 1197 vs, 1138 vs, 1049 w, 867 s, 847 vs, 795 vs, 774 s, 720 vs, 641 m, 607 m, 521 m, 421 m. Single crystals were obtained by slow diffusion of acetonitrile into the aqueous solution.

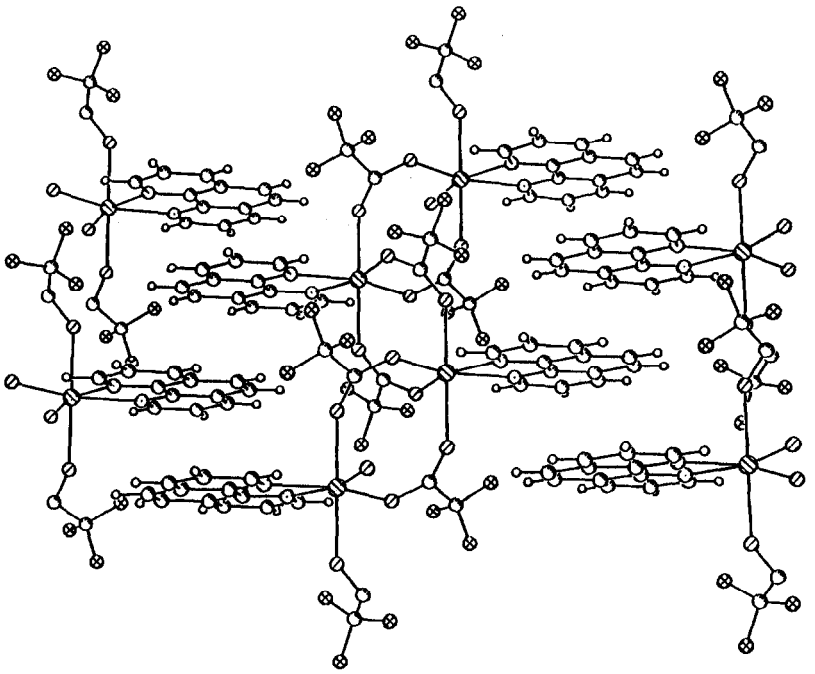

Fig. 1. View of the polymeric chain of **2** with neighbouring chains partially drawn.

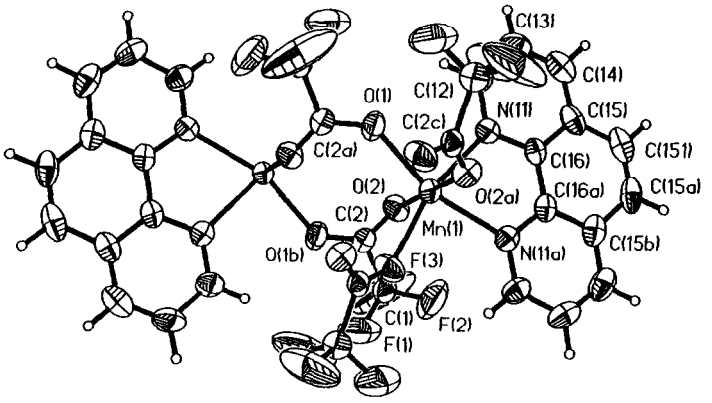

Fig. 2. A dimer of the asymmetric unit with atom numbering.

Table 1. Selected bond lengths [pm] and angles [°] for **2**

Mn(1)—O(1)	213.4(3)	Mn(1)—O(1)^a	213.4(3)
Mn(1)—O(2)	221.7(3)	Mn(1)—O(2)^a	221.7(3)
Mn(1)—N(11)^a	226.9(4)	Mn(1)—N(11)	226.9(4)
O(1)—Mn(1)—O(1)^a	107.1(2)	O(1)—Mn(1)—O(2)	94.87(14)
O(1)^a—Mn(1)—O(2)	85.17(13)	O(1)—Mn(1)—O(2)^a	85.17(13)
O(1)^a—Mn(1)—O(2)^a	94.87(14)	O(2)—Mn(1)—O(2)^a	179.9(2)
O(1)—Mn(1)—N(11)^a	162.13(13)	O(1)^a—Mn(1)—N(11)^a	90.09(13)
O(2)—Mn(1)—N(11)^a	91.25(12)	O(2)^a—Mn(1)—N(11)^a	88.69(12)
O(1)—Mn(1)—N(11)	90.09(13)	O(1)^a—Mn(1)—N(11)	162.13(13)
O(2)—Mn(1)—N(11)	88.69(12)	O(2)^a—Mn(1)—N(11)	91.25(12)
N(11)^a—Mn(1)—N(11)	73.3(2)	C(2)^b—O(1)—Mn(1)	132.6(3)

Symmetry transformations used to generate equivalent atoms: ^{a} $-x, y, -z + \frac{1}{2}$; ^{b} $-x, -y, -z$.

been determined by X-ray diffraction.‡ A view of the layered polymer is depicted in Fig. 1. A dimer of the asymmetric unit along with the atom numbering scheme is represented in Fig. 2. Selected bond distances and angles are given in Table 1.

The structure consists of *cis*-[MnN_2O_4] chromophores held by trifluoroacetate bridges, resulting in zig-zag infinite chains, which propagate in *c* direction and whose aromatic parts are parallel to [001] plane. The manganese(II) ion displays a (pseudo)-octahedral co-ordination, being linked to four O atoms of four CF_3COO^- ligands and to two N atoms of the phenanthroline ligand. The Mn—O distances are shorter than the Mn—N ones. The bridging mode of the trifluoroacetate ions is *syn-syn* bidentate asymmetric, with two short and two long Mn—O bonds (213.4 and 221.7 pm, respectively). The Mn···Mn distance (479.1 pm) is longer with respect to other bis- or tris(μ-carboxilato-O,O′) complexes of manganese(II).[3,5,6,10]

Although predictible, such a polymeric structure of metal(II) carboxylate complexes with bidentate ligands (phenanthroline and related compounds) has not been reported so far.

Acknowledgements—We are grateful to the Deutsche Forschungsgemeinschaft and VW-Stiftung for financial support. M. Andruh thanks the Alexander von Humboldt Foundation for a postdoctoral research fellowship.

‡ *Crystal data.* $C_{16}H_8F_6MnN_2O_4$, M = 461.18, monoclinic, space group C2/c, a = 1966.7(4), b = 1169.3(2), c = 751.0(2) pm, β = 100.96(3)°, V = 1.6955(6) nm^3, Z = 4, D_c = 1.807 Mg m^{-3}, $F(000)$ = 916; crystal size: 1.00 × 0.50 × 0.50 mm. Data were collected at 293 K on a STOE-AED four circle diffractometer (rev. 6.2), using Mo-K_α radiation. 2153 reflections (Θ = 3.59–22.48°) were measured. The structure was solved by direct methods (SHELXS-86)[8] and refined by full matrix least squares refinement on F^2 with SHELXL-92[9] to R = 0.0587 [for $I > 2\sigma(I)$] and wR_2 = 0.1339 (for all data). Atomic coordinates, thermal parameters and bond lengths and angles have been deposited at the Cambridge Crystallographic Data Centre.

REFERENCES

1. R. L. Rardin, W. B. Tolman and S. J. Lippard, *New J. Chem.* 1991, **15**, 417.
2. R. C. Mehrotra and R. Bohra, *Metal Carboxylates.* Academic Press, New York (1983).
3. S.-B. Yu, S. J. Lippard, I. Shweky and A. Bino, *Inorg. Chem.* 1992, **31**, 3502.
4. G. Christou, *Acc. Chem. Res.*, 1989, **22**, 328.
5. S. Ménage, S. E. Vitols, P. Bergerat, E. Codjovi, O. Kahn, J.-J. Girerd, M. Guillot, X. Solans and T. Calvet, *Inorg. Chem.* 1991, **30**, 2666.
6. K. Hübner, H. W. Roesky, M. Noltemeyer and R. Bohra, *Chem. Ber.* 1991, **124**, 515.
7. M. Andruh, K. Hübner, M. Noltemeyer and H. W. Roesky, *Z. Naturforsch. Teil B* 1993, **48**, 591.
8. G. M. Sheldrick, *Acta Cryst.* 1990, **A46**, 467.
9. G. M. Sheldrick, SHELXA 92, SHELXS 92 and SHELXL 92. Programs for absorption correction, crystal structure solution and refinement, University of Göttingen, (1992).
10. K. Wieghardt, *Angew. Chem.* 1989, **101**, 1179; *Angew. Chem., Int. Ed. Engl.* 1989, **28**, 1153.

Polyhedron Vol. 12, No. 24, pp. 2905–2911, 1993
Printed in Great Britain

0277–5387/93 $6.00+.00
© 1993 Pergamon Press Ltd

SOLUBILITIES OF CALCIUM SALTS OF DICARBOXYLIC ACIDS IN METHANOL–WATER MIXTURES; TRANSFER CHEMICAL POTENTIALS OF DICARBOXYLATE ANIONS

JOHN BURGESS* and DUNCAN N. DRASDO

Chemistry Department, University of Leicester, Leicester LE1 7RH, U.K.

(*Received* 26 *February* 1993; *accepted* 11 *August* 1993)

Abstract—Solubilities are reported of the calcium salts of a series of dicarboxylic acids, $HO_2C(CH_2)_nCO_2H$, with $n = 0$, 1, 2, 4, 8 and 12, and of cyclobutane-1,1-dicarboxylic acid in methanol–water mixtures containing 0–80% methanol. From these results, and known values for transfer chemical potentials for Ca^{2+}, transfer chemical potentials for the dicarboxylate anions have been calculated. The derived trends are discussed in terms of the hydrophilic/lipophilic properties of the anions and consequent preferential solvation.

The α,ω-dicarboxylic acids (**1**) furnish a homologous series whose character changes from strongly hydrophilic at the start (oxalate) to predominantly lipophilic for the higher members. All the acids with $0 \leqslant n \leqslant 8$ are commonly enough encountered to have trivial names; some higher members (n up to 14 and $n = 20, 22$) are also readily available. A number of these dicarboxylates and their calcium salts[1] are of pharmacological and biological relevance. Succinate, obtainable by distilling amber or by bacterial fermentation of tartaric or malic acids, assists the sometimes difficult[2] absorption of Fe^{2+} from the gastrointestinal tract,[3] azelate occurs in rancid fats, adipate (like oxalate) exhibits high oral toxicity. Thapsic acid occurs in *Thapsia garganica* ("Spanish Turpethroot", source of a resin used in plasters and a purgative) and in *Juniperus sabina* (whence "Oil of Savin", a multipurpose medicine for combatting intestinal worms, for controlling menstruation, for inducing sweating and a constituent in perfumery). Malonic, suberic, sebacic and pimelic acids are produced from malic acid (apples), cork, castor oil and atropine, respectively. Endothall, the rather more complicated dicarboxylic acid (**2**), is closely related to the beetle vesicant cantharidin and, in the form of its calcium salt, is an effective herbicide.[4] A number of cyclobutanedicarboxylate (CBDCA) (**3**), complexes of platinum, for example carboplatin (**4**),[5] zeniplatin (**5**), enloplatin (**6**) and the recently reported **7**,[6] are of proven or potential value in cancer chemotherapy.

The oxalate anion ($n = 0$) and its calcium salt are particularly important. Oxalate, as in for example rhubarb, inhibits the absorption of Ca^{2+} from the gastro-intestinal tract.[7] Calcium oxalate (as the monohydrate Whewellite or the dihydrate Weddellite) occurs in many plants[8] (cf. thapsic acid above), in the sap and as a calcium store. Calcium oxalate can appear as microscopic star-shaped crystals in the urine and is the main constituent of urinary calculi in man.[9,10]

Solvation is important in respect to these biologically and pharmacologically relevant areas, both in the obvious sense of being a key factor in determining (in-) solubility of the acids and their salts and in relation to absorption. This involves transport across membranes, whose ease is determined by the hydrophilic/lipophilic properties of the substrate,[11] as intimated for calcium oxalate and iron(II) succinate above. These properties are particularly relevant to the initial step in trans-membrane transport, viz. stabilization at the membrane–aqueous interface. Hydrophilic/lipophilic properties are generally assessed through determination of the water–1-octanol partition coefficient.[12] An alternative approach is to determine solubility or transfer chemical potential trends in alcohol–water mixtures.[13] The solubilities in the two pure components give an indication of the hydrophilic/lipophilic balance, HLB.[14] Any increase in

*Author to whom correspondence should be addressed.

1

n =	0	oxalic
	1	malonic
	2	succinic
	4	adipic
	5	pimelic
	6	suberic
	7	azelaic
	8	sebacic
	14	thapsic

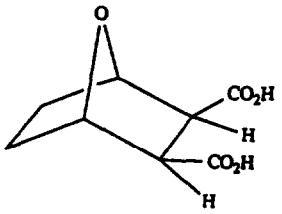

2

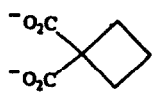

3

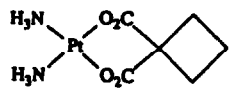

4

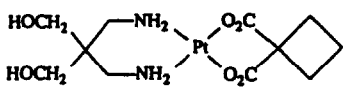

5

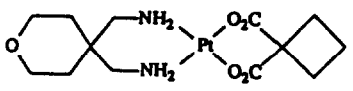

6

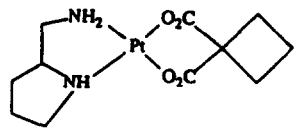

7

solubility in mixed solvents indicates favourable synergic solvation, i.e. hydration of hydrophilic regions by the water complementing solvation of lipophilic regions by the alcohol. Such synergic solvation has been demonstrated for, for instance, the ternary iron(II) complex $[Fe(CN)_2(bipy)_2]$, which has hydrophilic cyanide ligands balancing the very lipophilic surface of the coordinated 2,2′-bipyridyl ligands.[15]

Previous work in the area of the present paper has established solubilities of calcium oxalate in a series of primary alcohols and in ethanol–water mixtures[16] and the salting-in of calcium oxalate into aqueous solution by added sodium citrate.[17] We now report and discuss solubilities of the calcium salts of the dicarboxylic acids **1** with $n = 0$, 1, 2, 4, 8 and 12 and of CBDCA (**3**) in methanol–water. We thus derive, using established and estimated transfer chemical potentials for Ca^{2+},[18] transfer chemical potentials for the respective dicarboxylate anions and discuss the information these parameters provide on solvation of these anions.

EXPERIMENTAL

Preparation of salts

The dicarboxylic acids, and a sample of calcium oxalate, were obtained from Aldrich. Calcium salts were prepared by adding aqueous ammonia and a solution of the dicarboxylic acid (in water for the lower homologues, methanol for the higher) to a strong aqueous solution of calcium chloride. The products were washed with water and dried *in vacuo*. The calcium dicarboxylates studied here are almost all established compounds (although their numbers of waters of crystallization are not all firmly established, *vide infra*). We were unable to find a reference to the preparation of the calcium

Table 1. Solubilities (soly, expressed as ppm Ca) of calcium salts of dicarboxylic acids in water–methanol mixtures and derived transfer chemical potentials (Δ, in kJ mol^{-1} on the molar scale), at 298.2 K

Volume (% MeOH)	0	20	40	60	80	100
Oxalate						
ppm Ca	7.4[a]	2.2	0.86			
Δ		+6.0	+10.7			
Malonate						
ppm Ca	1010	252	64	14.9	3.4	1.42
Δ		+6.9	+13.6	+20.9	+28.2	+32
Succinate						
ppm Ca	3200	901	196	43	11.7	1.95
Δ		+6.3	+13.8	+21.4	+27.8	+37
Adipate						
ppm Ca	6830	2030	483	97	26	4.0
Δ		+6.0	+13.1	+21.1	+27.6	+37
Sebacate						
ppm Ca	330	164	83	52	31	16.7
Δ		+3.5	+6.9	+9.1	+11.7	+15
Dodecanedioate						
ppm Ca	6.3	4.5	3.7	3.2		
Δ		+1.6	+2.6	+3.2		
CBDCA						
ppm Ca	354	98	27	7.8	1.2	1.4
Δ		+6.3	+12.8	+18.9	+28	+27

[a] In agreement with values in refs 16 and 17.

salt of CBDCA in the literature and so characterized our product by microanalysis, as a dihydrate. Found: C, 33.0; H, 4.7. Calc. for $Ca(CBDC)2H_2O$: C, 33.0; H, 4.6%.

Determination of solubilities

A generous excess of calcium salt was agitated with the respective solvent medium in a thermostatted container for several days. Aliquots of the supernatant saturated solution were removed, diluted appropriately with water and analysed for calcium content by atomic absorption spectroscopy (Perkin–Elmer 1100B).

RESULTS AND DISCUSSION

Solubilities

The results of our solubility determinations are collected in Table 1. The values for calcium (ppm) are believed to be accurate to within *ca* 5%; a generous number of significant figures has been retained in the ppm and Δ values in this table; rounding off of Δ values to an appropriate number of figures has been carried out in Table 2. A selection of solubilities are plotted in Fig. 1 for ease of comparison. The solubility trends are all remarkably similar, except for the salts of the two most hydrophobic acids. In these cases the eight (sebacic) or 12 methylene groups significantly affect solubilities compared with the salts of the other acids.

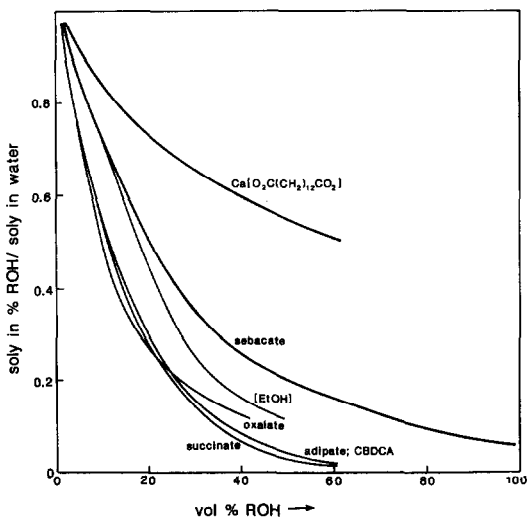

Fig. 1. Solubilities of calcium salts of dicarboxylic acids in alcohol–water mixtures, normalized for ease of comparison as quotients of solubility in mixed solvent divided by solubility in water; co-solvent methanol (thick lines) or ethanol (thin line); at 298.2 K.

Table 2. Transfer chemical potentials (Δ, in kJ mol^{-1}) for dicarboxylate anions form water in aqueous methanol, at 298.2 K on the molar scale, TPTB assumption (cf. text)

Volume (% MeOH)	20	40	60	80
$\Delta(Ca^{2+})^a$	+4.5	+8	+12	+17
$\Delta(oxalate^{2-})$	+1.5	+3		
$\Delta(malonate^{2-})$	+2	+6	+9	+11
$\Delta(succinate^{2-})$	+2	+6	+9	+11
$\Delta(adipate^{2-})$	+2	+5	+9	+10
$\Delta(sebacate^{2-})$	−1	−1	−3	−5
$\Delta(^{-}O_2C(CH_2)_{12}CO_2^{-})$	−3	−6	−9	
$\Delta(CBDCA^{2-})$	+2	+5	+7	+11

[a] Values derived as explained in text.

Favourable interactions between the methyl of the methanol and methylenes of the anion result in the solubilities of the calcium salts decreasing less markedly as the proportion of methanol in the mixed solvents increases. The effects of methanol and ethanol[16] as co-solvents are also compared, for calcium oxalate as solute, in Fig. 1. The addition of ethanol has, on a volume basis, slightly less effect than methanol, but it should be borne in mind that the water–ethanol solubilities were obtained at 20°C. An attempt was made to correlate solubilities with solvent dielectric properties for the ethanol–water solubilities, but there appeared to be no simple correlation.[16] However, a good correlation of solubility with reciprocal dielectric constant has been claimed for zinc and cadmium oxalates dissolved in a series of primary alcohols.[19] The rapidly decreasing solubilities of the calcium salts of the lower dicarboxylates as the proportion of methanol (or ethanol) increases reflects the strongly hydrophilic natures of Ca^{2+} and $^{-}O_2C(CH_2)_nCO_2^{-}$ (when $n = 0$ or is small). Decreasing solubilities of oxalic acid in the order[20]

water > methanol > ethanol > propanol

and solubilities of adipic acid in alcohol–water mixtures[21] similarly reflect the strongly hydrophilic properties of carboxylate moieties.

It is more difficult to comment satisfactorily on relative solubilities of a series of salts in a given solvent than on solubility trends for a given salt in a series of solvent media, since the solubility of a salt represents a balance between lattice energy and solvation of constituent ions. It is interesting to note (Table 1) that the solubilities of $Ca[O_2C(CH_2)_nCO_2]$ in water increase from $n = 0$ to $n = 4$, then decrease as n increases further. The low solubility of calcium oxalate ($n = 0$) presumably reflects its high lattice energy; the almost equally low solubility of the dodecanedioate must reflect poor hydration of this anion with its lipophilic $-(CH_2)_{12}-$chain.

Transfer chemical potentials: assumptions

Solubility trends are of interest and importance in their own right, but in order to obtain more detailed information on solvation it is useful to derive transfer chemical potentials (Δ) for the constituent ions. Transfer chemical potentials for electrolytes can be calculated from solubility products from the formula:

$$\Delta = -RT \ln\{(K_{sp} \text{ in medium 2})/(K_{sp} \text{ in medium 1})\}.$$

In the present case all transfer chemical potentials have been calculated from water as a reference solvent (medium 1). It is necessary to make some assumptions, detailed briefly here, in order to derive transfer chemical potentials for the constituent ions. Firstly, an extrathermodynamic assumption is essential to split whole salt values into individual ion contributions.[22] Here we shall use the well-established TPTB convention that transfer chemical potentials for $[Ph_4P][BPh_4]$ can be divided into equal contributions for the two large and lightly-solvated ions. As transfer chemical potentials are available on this assumption for Ca^{2+} from water into methanol–water mixtures, we can derive values for our dicarboxylate anions. We use published values in water-rich mixtures[18] and values estimated from published data on other M^{2+} ions at higher methanol contents;[23] Tissier's estimates in higher proportions of methanol[24] diverge increasingly towards intuitively implausible stabilization. Unfortunately, analogous calculations for oxalate to ethanol–water mixtures from published calcium oxalate solubilities[16] are not possible since transfer chemical potentials for Ca^{2+} are not available for this co-solvent, although they could in principle be estimated[25] using published solubilities of potassium sulphate[26] and calcium sulphate.[27]

The second assumption that has been made is that the ratios of the activity coefficients in mixed solvents to those in water are unity. This assumption is generally acceptable for sparingly soluble salts, as here, especially when solubilities decrease as the dielectric constant of the solvent medium decreases. Earlier workers have suggested[16] that ion association in calcium oxalate solutions in ethanol–water mixtures only becomes significant at dielectric constants below *ca* 60 (corresponding to approximately 50% methanol), although Nancollas predicted significant ion pairing even in water.[10] As the size of the dicarboxylate anion increases, the tendency to ion pairing will decrease, although this will be offset for the lower dicarboxylates by

increasing solubility. Overall, bearing in mind that our assumption involves *ratios* of activity coefficients rather than their absolute values, we do not expect ion association to have a major effect on our estimated transfer chemical potentials—perhaps introducing errors of 1 or 2 kJ mol^{-1}. The chemical potential of an uncharged ion pair would be expected to change less with change in solvent composition than the sum of the transfer chemical potentials of the two constituent ions.

The third assumption is that the solid phase in equilibrium with saturated solution is the same over the whole solvent composition range studied. The existence of various hydrates of calcium oxalate at first sight might appear to complicate matters, but published information on stability ranges[8,10,28] indicates that the monohydrate will be solid phase in contact with 0–40% methanol. Several other calcium dicarboxylates exist in hydrated forms,[29,30] so transfer chemical potentials to 100% methanol will not be directly obtainable. To test the validity of the assumption of constancy of solid phase in equilibrium with saturated solutions in media ranging from water to 80% methanol, thermogravimetric analyses were carried out on samples of the solid phases of three of the salts after completion of solubility determinations. As is shown by the results outlined in Table 3, the solid phase in equilibrium with saturated solution was the same for water and for 80% methanol for each of the three salts. As a by-product of the thermogravimetric experiments some light has been shed on the stoichiometry of some of the calcium dicarboxylates, over which there is some disagreement in the literature. Thus, Beilstein mentions a monohydrate of calcium sebacate, whereas earlier thermogravimetric analysis indicated a trihydrate.[31] Our results (Table 3) confirm the existence of both. In the case of calcium succinate, 1.5, 2 and 3 waters of crystallization have all been claimed. Our thermogravimetric results suggest that the trihydrate (of known structure[32]) loses two molecules of water between 100 and 150°C, with a resultant monohydrate losing its water of crystallization between 160 and 220°C. This indication of the existence of a monohydrate is supported by microanalysis of a sample of hydrated calcium succinate, which had been dried on a vacuum line. Found: C, 28.1; H, 3.2. Calc. for $CaC_4H_4O_4 \cdot H_2O$; C, 27.6; H, 3.4%.

Transfer chemical potentials: results

Transfer chemical potentials calculated from our measured solubilities with the use of the equation and assumptions given in the preceding section are given in Tables 1 and 2. The level of accuracy in the Δ values in Table 2 is believed to be between ± 0.5 and ± 1 kJ mol^{-1}. If, however, our choice of values for Ca^{2+} (cf. discussion above) is incorrect, individual values for Δ(dicarboxylate) will be in error by more than $\pm$ 1 kJ mol^{-1}. However, it should be stressed that differences between Δ values for dicarboxylates will still be accurate to ± 1 kJ mol^{-1} and that the pattern of trends discussed below will not be significantly affected. The transfer chemical potential trends for the dicarboxylates (Table 2) are shown in the context of a selection of other ions in Fig. 2. This shows the stabilization of the two most lipophilic dicarboxylates by methanol, but marked preferential hydration of the dicarboxylates up to adipate. The trend for cyclobutanedicarboxylate is very similar to that for its straight-chain analogue, adipate. The plot for oxalate appears to be out of the expected order. This may be due to errors introduced from non-conformance with one or more of the assumptions described above or, more likely, to strong preferential hydration. This would result in a very marked curvature of the complete (i.e. 0–100%) transfer chemical potential vs methanol content plot, so that the transfer chemical potential to pure methanol may well be large and positive. In water-rich mixtures the oxalate may

Table 3. Thermogravimetric results for calcium dicarboxylate hydrates

Anion	Medium[a]	Temperature range (no. of waters lost) (°C)
Malonate	Water	125–230 ($2H_2O$)
	80% methanol	130–210 ($2H_2O$)
Sebacate	Water	135–160 ($2H_2O$); 270–310 ($1H_2O$)
	80% methanol	130–160 ($2H_2O$); 280–320 ($1H_2O$)
1,12-Dodecanedicarboxylate		
	Water	120–150 ($1H_2O$); 270–320 ($1H_2O$)
	80% methanol	130–150 ($1H_2O$); 280–310 ($1H_2O$)

[a] Solid phase in equilibrium with saturated solution of calcium salt in solvent specified.

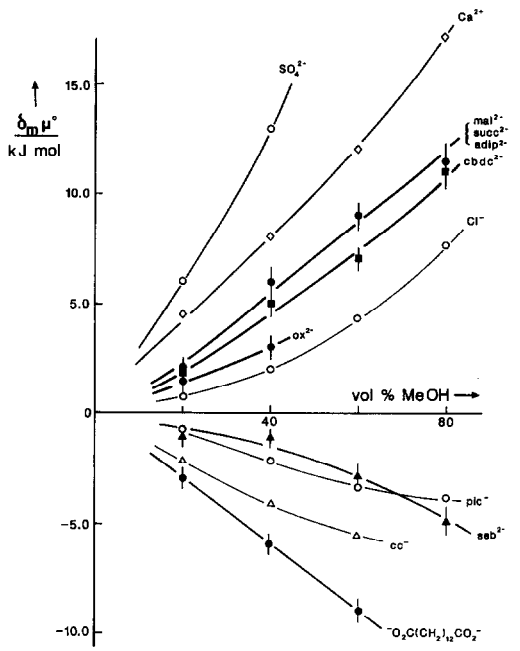

Fig. 2. Transfer chemical potentials for dicarboxylate anions (thick lines), for Ca^{2+}, and for a selection of other ions for comparison, for transfer to methanol–water mixtures; TPTB single ion assumption, molar scale, at 298.2 K. Abbreviations: pic = picrate, cc = chromone carboxylate.

retain its hydration shell essentially unchanged and thus be only slightly destabilized on the addition of methanol. Such behaviour has previously been described for the very hydrophilic cyanide and hexacyanoferrate(III) anions.[23] The more hydrophilic dicarboxylates have transfer chemical potential plots lying between those for chloride and for sulphate (Fig. 2); their smaller response than sulphate to increasing methanol content can readily be attributed to their larger size.

Transfer chemical potentials can be valuable in understanding solvent effects on reactivities, as they provide key information on initial state solvation.[33] Kinetics of hexachloroiridate(IV) oxidation of oxalate have been studied in dioxan–water mixtures[34]—it would be interesting to extend this kinetic study to methanol–water media so that an initial state–transition state analysis of reactivity could be carried out, to add to the body of information on hexachloroiridate(IV) oxidation of iodide and of catechol in several series of mixed aqueous solvents.[35]

Acknowledgements—We are most grateful to Dr S. H. Laurie and Mrs N. Garrington of the De Montfort University for arranging and carrying out the thermogravimetric analyses.

REFERENCES

1. E. Carafoli, G. Inesi and B. P. Rosen, in *Metal Ions in Biological Systems*, Vol. 17: *Calcium and its Rôle in Biology* (Edited by H. Sigel). Marcel Dekker, New York (1984).
2. R. R. Crichton and M. Charloteaux-Wauters, *Eur. J. Biochem.* 1987, **164**, 485.
3. R. G. Penn, *Pharmacology*, p. 138. Baillière, Tindall & Cassell, London (1970); E. F. Workman, G. Graham and G. W. Bates, *Biochim. Biophys. Acta* 1975, **399**, 254; T. H. Boswell, R. W. Charlton, J. D. Cook and C. A. Finch, *Iron Metabolism in Man*. Blackwells, Oxford (1979).
4. G. Smith, D. E. Lynch, C. H. L. Kennard and T. C. W. Mak, *Polyhedron* 1991, **10**, 1569.
5. For example, J. Reedijk, A. M. J. Fichtinger-Schepman, A. T. van Oosterom and P. van de Putte, *Struct. Bonding* 1987, **67**, 53.
6. K. Morikawa, M. Honda, K.-I. Endoh, T. Matsumoto, K.-I. Akamatsu, H. Mitsui and M. Koizumi, *J. Pharm. Sci.* 1991, **80**, 837.
7. R. S. Harris, *Adv. Chem. Ser.* 1970, **94**, 116.
8. L. Walter-Lévy and J. Laniepce, *Comptes Rend.* 1962, **254**, 296.
9. E. L. Prein and C. Frondel, *J. Urol.* 1947, **57**, 949.
10. B. Tomazic and G. H. Nancollas, *J. Cryst. Growth* 1979, **46**, 355.
11. W. D. Stein, *Transport and Diffusion across Cell Membranes*. Academic Press, New York (1986).
12. A. Leo, C. Hansch and D. Elkins, *Chem. Rev.* 1971, **71**, 525.
13. M. J. Blandamer and J. Burgess, *Trans. Met. Chem.* 1988, **13**, 1.
14. W. C. Griffin, *J. Soc. Cosmet. Chem.* 1954, **5**, 249; R. Sowada and J. C. McGowan, *Tenside Surf. Det.* 1992, **29**, 109; R. F. Rekker and R. Mannhold (Editors), *Calculation of Drug Lipophilicity*. VCH, Weinheim (1992).
15. J. Burgess, S. Radulovic and F. Sanchez, *Trans. Met. Chem.* 1987, **12**, 529.
16. J. A. Molzon, J. M. Lausier and A. N. Paruta, *J. Pharm. Sci.* 1978, **67**, 733.
17. D. J. Kok, S. E. Papapoulos, L. J. M. J. Blomen and O. L. M. Bijvoet, *Kidney Int.* 1988, **34**, 346.
18. M. J. Blandamer, J. Burgess, B. Clark, P. P. Duce, A. W. Hakin, N. Gosal, S. Radulovic, P. Guardado, F. Sanchez, C. D. Hubbard and E. A. Abu-Gharib, *J. Chem. Soc., Faraday Trans. I* 1986, **82**, 1471.
19. M. I. Lebedeva, B. I. Isaeva and L. S. Demchenko, *Russ. J. Inorg. Chem.* 1976, **21**, 729.
20. W. Timofeiew, Dissertation, Kharkov (1894); A. Seidell, *Solubilities of Inorganic and Metal-Organic Compounds*, 3rd edn, Vol. 1, p. 83. van Nostrand, New York (1985).
21. W. D. Bancroft and F. J. C. Butler, *J. Phys. Chem.* 1932, **36**, 2515.
22. Y. Marcus, *Ion Solvation*. Wiley, New York (1985).
23. M. J. Blandamer and J. Burgess, unpublished calculations.
24. C. Tissier, *Bull. Soc. Chim. France* 1988, 787.

25. D. L. Elvidge, PhD Thesis, Leicester (1988).
26. C. J. J. Fox and A. J. H. Gauge, *J. Chem. Soc.* 1910, 377.
27. T. Yamamoto, *Bull. Inst. Phys. Chem. Res.* (*Tokyo*) 1930, **9**, 352.
28. G. L. Gardner, *J. Cryst. Growth* 1975, **30**, 158.
29. A. Zell, H. Einspahr and C. E. Bugg, *Biochemistry* 1985, **24**, 533.
30. D. J. Hodgson and R. O. Asplund, *Inorg. Chem.* 1991, **30**, 3577 and refs therein.
31. K. C. Patil, G. V. Chandrashekhar, M. V. George and C. N. R. Rao, *Can. J. Chem.* 1968, **46**, 257.
32. A. Karipides and A. T. Reed, *Acta Cryst.* 1980, **B36**, 1377.
33. For example M. J. Blandamer and J. Burgess, *Trans. Met. Chem.* 1988, **13**, 1.
34. U. Chatterjee, S. Maiti and K. K. Sengupta, *Z. Phys. Chem.* (*Leipzig*) 1980, **261**, 1231.
35. M. J. Blandamer, J. Burgess, S. J. Hamshere, C. White, R. I. Haines and A. McAuley, *Can. J. Chem.* 1983, **61**, 1361.

Polyhedron Vol. 12, No. 24, pp. 2913–2919, 1993
Printed in Great Britain

0277–5387/93 $6.00+.00
© 1993 Pergamon Press Ltd

CRYSTALLOGRAPHIC EVIDENCE FOR DIFFERENT MODES OF INTERACTION OF BF_3/BF_4^- SPECIES WITH WATER MOLECULES AND 18-CROWN-6

H. FEINBERG, I. COLUMBUS, S. COHEN, M. RABINOVITZ, H. SELIG and G. SHOHAM*

Institute of Chemistry, The Hebrew University of Jerusalem, Jerusalem 91904, Israel

(*Received* 16 *June* 1993; *accepted* 6 *August* 1993)

Abstract—We report the crystal and molecular structures of the complex of 18-C-6 with $H_3O^+BF_4^-$ (I) and the complex of 18-C-6 with $BF_3OH_2 \cdot H_2O$ (II). The different modes of appearance of the "BF_3" species as BF_3, BF_3OH_2, $BF_3OH_2 \cdot H_2O$ and BF_4^-, as well as their structurally significant intermolecular and intramolecular interactions, are discussed. In complex **I** the oxonium ion is bound at the centre of the 18-C-6 macrocycle. The oxonium oxygen is located practically equidistant (2.68–2.73 Å) from the six macrocyclic ethereal oxygens. The BF_4^- counter-ion is positioned 7.3 Å away from the oxonium ion in the same general plane of the crown ether. This anion is not involved in any direct intermolecular contacts, a fact that may explain why it is spherically disordered. In complex **II** there is no guest molecule (or ion) present in the "cavity" of the macrocycle, but there are two hydrogen-bonded systems of $BF_3OH_2 \cdot H_2O$ that are interacting with the crown ether on either side of the general macrocyclic plane. Complex **II** features three types of hydrogen bonds—the O(water)-H···O(crown) bonds (2.83 and 2.85 Å), the O(water)···H-O(BF_3) bond (2.49 Å) and the O(BF_3)-H···O(crown) bond (2.65 Å). The strong intermolecular O(crown)···O(water)···O(BF_3) and O(crown)···O(BF_3) interactions stabilize the normally unstable $BF_3OH_2 \cdot H_2O$ species.

The H_2O/BF_3 has been the subject of numerous investigations.[1] Two complexes have been isolated from this system, $BF_3 \cdot H_2O$ and $BF_3 \cdot 2H_2O$. The latter complex is more stable, apparently due to the formation of the oxonium ion (H_3O^+), according to the following equilibrium:

$$BF_3 \cdot 2H_2O \leftrightarrow H_3O^+ + BF_3OH^-.$$

Above 20°C both hydrates decompose while releasing BF_3.[2] In the presence of HF, low melting phases of $H_3OBF_4 \cdot nH_2O$ ($n = 0$–3) have been shown to exist.[3] The complex $H_3O^+BF_4^-$ has also been reported by Christe *et al.*[4] but was not further characterized. This complex appears as a liquid at room temperature with a significant dissociation pressure. Its structure has been determined by Mootz and Steffen[5] by growing single crystals at low temperatures.

Some of the "BF_3" species have been shown to be significantly stabilized by macrocyclic ligands such as 18-crown-6. For example, the complex of H_3O^+/BF_4^- with 18-C-6 has been isolated, but its crystal structure has not yet been determined.[6] IR and Raman spectra indicate that a conformational change of the crown ether in this complex occurs over the temperature range -50 to -100°C. The symmetry of the crown ether appears to be relatively high at room temperature. It should be noted, however, that vibrational spectra do not yield precise enough information as to the relative geometry of the crown *vis-a-vis* the oxonium ion.[6]

In general, the possible structure of the oxonium cation (co-planar geometry vs pyramidal geometry) has been extensively discussed in the literature, as well as the influence of the coordination to a macrocyclic ring on its geometry. The distance between

*Author to whom correspondence should be addressed.

the oxygen of the oxonium and the plane defined by the hydrogen-bonded oxygens of the crown is 0.61 in $[H_3O^+/18\text{-crown-6(COOH)}_4]Cl$,[7] 0.439 in $(H_3O^+/\text{dicyclohexyl-18-crown-6})ClO_4^-$,[8] 0.09 in the complex $(H_3O^+/18\text{-crown-6})(Cl\text{-}H\text{-}Cl)$[9] and 0.1 Å in the complex $(H_3O^+/18\text{-crown-6})_2(Mo_6O_{19})$.[10] Thus, no clear-cut criteria can be formulated regarding which factors determine the exact geometry of H_3O^+ and whether the anion exerts any influence on the exact geometry of the H_3O^+ ion. Moreover, a number of crown ether complexes are known of the type 18-C-6/(H_2O·acid) (where the acid is HNO_3, H_2TiF_6 or H_3PO_4),[11] in which the oxonium plays no structural role at all. It should be noted, however, that on the basis of vibrational spectra it is believed that these acids are coordinated to the crown ether via water molecules.

In the present paper we report the crystal and molecular structures of the complex of 18-C-6 with an $H_3O^+BF_4^-$ species (**I**) and of the complex of 18-C-6 with a $BF_3{\cdot}OH_2{\cdot}H_2O$ species (**II**). These structures are then compared with the reported structure of the complex of 18-C-6/BF_3OH_2, in which BF_3 is covalently bonded to the oxygen atom of the water molecule, which is itself hydrogen bonded to the 18-C-6 molecule.[12] It is shown that the $BF_3{\cdot}OH_2$, $BF_3{\cdot}OH_2{\cdot}H_2O$ and BF_4^-/H_3O^+ species in these structures are rather different in appearance and geometry.

The coordination of these species relative to the macrocyclic ring are discussed in terms of the known conformations which this system can assume.[13] With relatively few exceptions, the coordination of an oxonium by the crown ether causes the latter to assume a relatively high symmetrical configuration approximating D_{3d} symmetry. The new structures reported here are the complex of 18-C-6 with an oxonium ion encaptured in the crown (complex **I**) and the complex of 18-C-6 with two water molecules hydrogen bonded on both sides of the crown ether (complex **II**). Both complexes show a similar configuration of the crown ether macrocycle.

EXPERIMENTAL

Preparation and crystallization of the complexes

18-Crown-6 was obtained from Aldrich Co. and used as supplied without further purification. Fluoroboric acid (*ca* 40% HBF_4), technical grade, was obtained from BDH Ltd. The complex of 18-crown-6 with BF_4^- (**I**) was prepared according to a previously described procedure.[6] Single crystals of **I** (thin plates of approximate dimensions $0.4\times0.4\times0.1$ mm) were obtained by slow evaporation from a methylene chloride solution. Single crystals of **II** (well formed with sharp edges, elongated trigonal prisms of approximate dimensions $0.5\times0.2\times0.2$ mm), were obtained from the same general procedure, with the fluoroboric acid mixture being slowly evaporated from a 1 : 1 (v/v) methylene chloride/carbon tetrachloride mixture. One of each of these single crystals was used for the complete crystallographic analysis. The crystals of **I** have a m.p. of 140–143°C,[6] while the crystals of the newly obtained complex **II** have a melting point of 85°C.

Crystal structure analyses

Crystal data. 18-crown-6/$BF_4^-{\cdot}H_3O^+$, $C_{12}H_{27}O_7BF_4$ (**I**), $M = 370.14$, tetragonal space group $P4_12_12$, $a = b = 10.575(3)$, $c = 16.471(3)$ Å, $V = 1842(1)$ Å^3, $D_c = 1.33$ g cm^{-3}, $Z = 4$, $\lambda(CuK\alpha) = 1.54178$ Å, $\mu(CuK\alpha) = 11.14$ cm^{-1}, $F_{000} = 784$, T = room temperature.

18-crown-6/2($BF_3{\cdot}OH_2{\cdot}H_2O$), $C_{12}O_{10}H_{32}B_2F_6$ (**II**), $M = 471.99$, triclinic space group $P\bar{1}$, $a = 8.366(2)$, $b = 10.405(2)$, $c = 7.344(3)$ Å, $\alpha = 108.79(2)°$, $\beta = 112.11(2)°$, $\gamma = 93.38(2)°$, $V = 549(1)$ Å^3, $D_c = 1.43$ g cm^{-3}, $Z = 1$, $\lambda(CuK\alpha) = 1.54178$ Å, $\mu(CuK\alpha) = 12.86$ cm^{-1}, $F_{000} = 248$, T = room temperature.

Data collection and processing. The molecular scheme and the numbering system for complexes **I** and **II** are shown in Figs 1 and 2, respectively. Diffraction data for both structures were measured on an Enraf–Nonius CAD-4 automatic four-circle

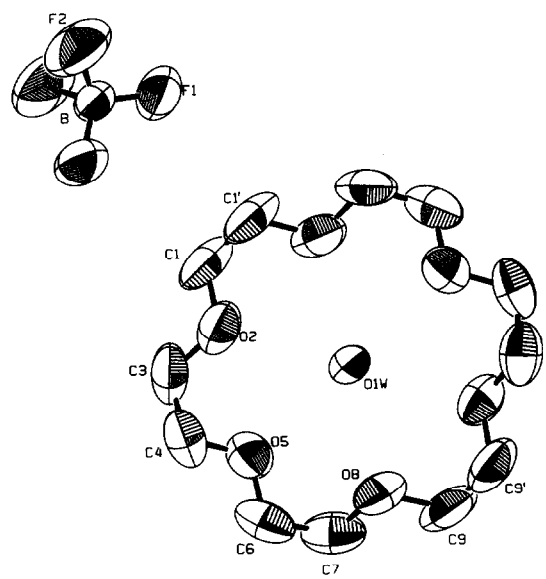

Fig. 1. The final crystal structure of the complex 18-c-6/$H_3O^+ \cdot BF_4^-$ (compound **I**).

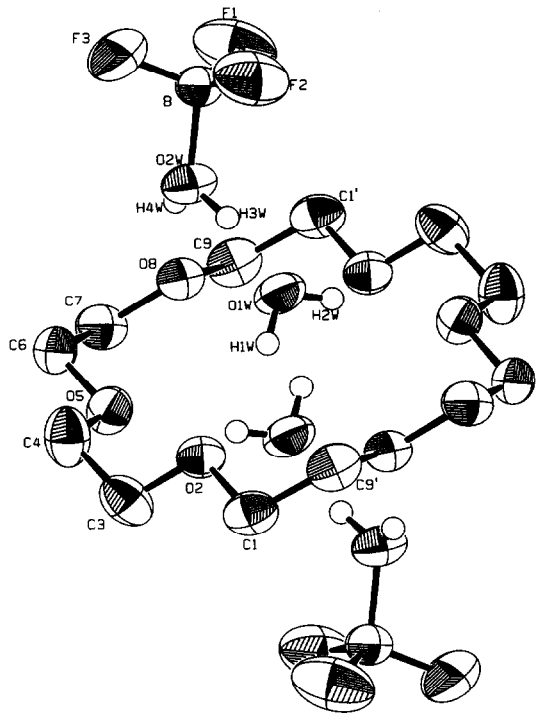

Fig. 2. The final crystal structure of the complex 18-c-6/2($BF_3OH_2 \cdot OH_2$) (compound **II**).

diffractometer. The lattice parameters and orientation matrix for the crystals were obtained using a least-squares procedure involving 25 carefully centred reflections in the range $25 < 2\theta < 40°$. Intensity data were collected in the $\omega/2\theta$ scan mode in the range $4 < 2\theta < 140°$, using a variable scan speed. The data were reduced and corrected for Lorentz and polarization effects.[14] An empirical extinction correction was applied, but due to the small absorption coefficient and insignificant radiation damage it was unnecessary to make corrections for radiation decay or absorption.

Crystal structure determination of **I**. Of the 2020 reflections which were collected, 1089 were unique ($R_{int} = 0.015$). Of these unique data only those 720 reflections with $I_o > 3\sigma(I_o)$ were included in further calculations. The structure was solved by direct methods (MULTAN-78).[15] The best phase set yielded a preliminary model with most of the non-hydrogen atoms of the molecule. The remainder of the non-hydrogen atoms were then located by successive cycles of least-squares refinement and difference electron density maps using standard Fourier syntheses and full-matrix least-squares techniques.[16] Most of the hydrogen atoms could be located in the difference electron density maps. Nevertheless, for convenience all of the hydrogen atoms in the initial model were calculated at idealized positions relative to their corresponding carbon atoms. All non-hydrogen atoms were refined using anisotropic thermal parameters. It should be noted that the crystallographic asymmetric unit of this structure is only one half of the complex (Fig. 1) and that both O_w (the water oxygen) and B are located at crystallographic special positions. During the course of refinement it was apparent that the BF_4^- group is disordered between several spherically related orientations around the boron atom. Three such orientations were assigned in the final model with the corresponding statistical occupancies of 0.45, 0.30 and 0.25 for the atom sets of F(1)—F(2), F(3)—F(4) and F(5)—F(6), respectively. The refinement of the structure converged smoothly to final crystallographic factors of $R = 0.072$ and $Rw = 0.10$. The final values of the thermal parameters of some of the atoms remained relatively high even at the final cycles of refinement, reflecting partial local disorder in several sites of the molecular system in the crystal. Nevertheless, in the final model there are no ambiguities as to the molecular structure of the entire complex or the conformation of the crown macrocycle.

Crystal structure determination of **II**. The integrated intensities of 2069 independent reflections were measured, of which only those 1924 reflections with $I_o > 3\sigma(I_o)$ were included in further calculations. The structure was solved by direct methods (MITHRIL).[17] The best phase set yielded very clearly all the non-hydrogen atoms of the molecule. For convenience, all hydrogen atoms of the crown ether were initially calculated at idealized positions relative to their corresponding carbon atoms. The hydrogen atoms of the BF_3OH_2 and the water molecules were located in the following difference electron density maps. The complete model was then refined by successive cycles of full-matrix least-squares techniques.[16] The positions of all non-hydrogen atoms were refined using anisotropic thermal parameters (nine parameters per atom), while the positions of all hydrogen atoms were refined with isotropic thermal parameters (four parameters per atom). The refinement converged rapidly to final crystallographic factors of $R = 0.061$ and $Rw = 0.123$. The relatively small thermal parameters of the atoms (Table S4) and the small ratios of shift/ESD in the last cycle of refinement (average of 0.0002) are evidence for the high quality of the diffraction data and the high accuracy in the final structure of **II**.

RESULTS AND DISCUSSION

Relevant bond lengths and angles for the structure of complex **I** are listed in Tables 1 and 2, respectively. Relevant bond lengths and angles for

Table 1. Relevant bond lengths (Å) for 18-C-6/$H_3O^+ \cdot BF_4^-$ (compound **I**)

C(1)—C(1′)	1.45(2)	C(7)—O(8)	1.432(9)
C(1)—O(2)	1.40(1)	O(8)—C(9)	1.445(9)
O(2)—C(3)	1.38(1)	C(9)—C(9′)	1.47(2)
C(3)—C(4)	1.49(1)	O(1W)—O(8)	2.684(6)
C(4)—O(5)	1.430(9)	O(1W)—O(2)	2.695(7)
O(5)—C(6)	1.403(9)	O(1W)—O(5)	2.733(5)
C(6)—C(7)	1.44(1)		

Estimated standard deviations in the least significant digits are given in parentheses.

Table 2. Relevant bond angles (°) for 18-C-6/$H_3O^+ \cdot BF_4^-$ (compound **I**)

C(1′)—C(1)—O(2)	107.5(7)	O(5)—C(6)—C(7)	107.9(7)
C(1)—O(2)—C(3)	108.8(6)	C(6)—C(7)—O(8)	108.7(6)
O(2)—C(3)—C(4)	111.0(6)	C(7)—O(8)—C(9)	112.8(6)
C(3)—C(4)—O(5)	108.1(6)	O(8)—C(9)—C(9′)	109.1(7)
C(4)—O(5)—C(6)	112.2(6)		

Estimated standard deviations in the least significant digits are given in parentheses.

the structure of complex **II** are listed in Tables 3 and 4, respectively. A stereoview of the crystallographic packing of the unit cell of **II** is shown in Fig. 3 and a side-view of the structure of **II** (including intermolecular hydrogen bond scheme) is depicted in Fig. 4.

In the complex of **I**, the crown adopts the most commonly encountered "round" conformation (D_{3d}-like symmetry[13]), where the oxonium ion is bound at the centre of the macrocycle (Fig. 1). The oxonium oxygen (Ow) is located practically equidistant (2.68–2.73 Å) from the six macrocyclic ethereal oxygens. Of the six macrocyclic oxygens, three alternating oxygens are pointing "down", while the

Table 3. Relevant bond lengths (Å) for 18-C-6/2($BF_3OH_2OH_2$) (compound **II**)

C(1)—O(2)	1.430(3)	O(2W)—B	1.510(3)
C(1)—C(9′)	1.493(4)	F(2)—B	1.361(3)
O(2)—C(3)	1.412(3)	F(3)—B	1.342(3)
C(3)—C(4)	1.490(4)	F(1)—B	1.338(3)
C(4)—O(5)	1.437(3)	O(1W)—O(5′)	2.831(3)
O(5)—C(6)	1.420(3)	O(1W)—O(2)	2.847(3)
C(6)—C(7)	1.495(4)	O(2W)—O(1W)	2.485(2)
C(7)—O(8)	1.425(3)	O(2W)—O(8)	2.652(2)
O(8)—C(9)	1.422(3)		

Estimated standard deviations in the least significant digits are given in parentheses.

Table 4. Relevant bond angles (°) for 18-C-6/2($BF_3OH_2OH_2$) (compound **II**)

O(2)—C(1)—C(9)	109.4(2)	C(1)—C(9)—O(8)	108.8(2)
C(1)—O(2)—C(3)	111.9(2)	O(2W)—B—F(2)	105.9(2)
O(2)—C(3)—C(4)	110.6(2)	O(2W)—B—F(3)	106.9(2)
C(3)—C(4)—O(5)	109.6(2)	O(2W)—B—F(1)	110.6(2)
C(4)—O(5)—C(6)	111.8(2)	F(2)—B—F(3)	107.4(3)
O(5)—C(6)—C(7)	109.1(2)	F(2)—B—F(1)	112.7(2)
C(6)—C(7)—O(8)	108.6(2)	F(3)—B—F(1)	113.0(3)
C(7)—O(8)—C(9)	112.9(2)		

Estimated standard deviations in the least significant digits are given in parentheses.

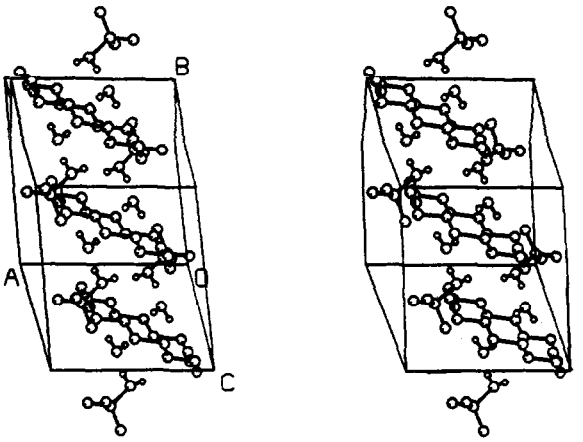

Fig. 3. Crystallographic unit cell packing of 18-C-6/2(BF_3OH_2·OH_2) (compound **I**). For clarity, only non-hydrogen atoms of the crown ring and all atoms of the BF_3OH_2·OH_2 species are shown.

other three oxygens are pointing "up". The planes formed by these two sets of oxygens are nearly parallel to each other (interplanar angle of 173°) and the oxonium oxygen is positioned between these two planes (0.175 Å below and above the two planes, respectively). Since we cannot locate the oxonium hydrogens in the electron density maps, we assume that the oxonium ion adopts two alternative orientations (each at 50% statistical occupancy) around its oxygen, such that two alternative sets of hydrogen bonds are formed. One such set of hydrogen bonds involves the three crown oxygens which point "down", while the other set involves the three oxygens which point "up". The BF_4^- counter-ion is positioned 7.3 Å away from the oxonium ion in the same general plane of the crown ether.

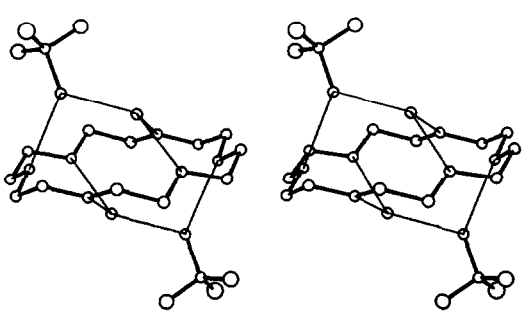

Fig. 4. Side-view of the structure of 18-C-6/2(BF_3OH_2·OH_2) (compound **II**), including the intermolecular hydrogen bonds (thin lines) O(1w)—O(2w), O(1w′)—O(2w′) = 2.49; O(1w)—O(2), O(1w′)—O(2′) = 2.85; O(1w)—O(5′), O(1w′)—O5 = 2.83; O(2w)—O(8), O(2w′)—O(8′) = 2.65 Å.

This anion is not involved in any direct intermolecular contacts, a fact that may explain why it is spherically disordered, as discussed above.

In complex **II** the macrocyclic ring of the crown ether appears also as the "round" conformation (conformer "A" D_{3d})[13] in a similar, yet not identical, conformation to the 18-C-6 ring of **I**. Here again, the crystallographic asymmetric unit is only one half of the complex (Fig. 2). There is a crystallographic centre of inversion at the centre of the macrocycle, although there is no ion or molecule in the "cavity" of the macrocycle. Two hydrogen-bonded systems of BF_3OH_2·H_2O interact with the crown ether on either side of the general macrocyclic plane (as demonstrated in Fig. 4). The six macrocyclic oxygens form a "chair shape" structure, where four of them [O(2), O(5) and their symmetry related atoms O(2′), O(5′)] form a perfect plane (plane *a*) and the other two oxygens are located 0.70 Å above [O(8)] and below [O(8′)] this plane. The two BF_3OH_2·H_2O systems which lie above and below plane *a* are diagonally oriented along the O(8)O(8)—O(8′) axis and located directly above O(8′) or O(8). The oxygen atom of the BF_3OH_2 species is hydrogen bonded to O(8′) (2.65 Å) of the crown ether and to the "free" water molecule via considerably shortened hydrogen bonds connecting it to the crown ring (2.49 Å). The water molecule is positioned 1.48 Å above plane *a* and interacts with O(2) and O(5′) via two specific hydrogen bonds. The O(1w)—O(2) and O(1w)—O(5′) distances are almost identical (2.85 and 2.83 Å, respectively) and the water hydrogens (which were clearly observed in the electron density maps) are located approximately along the O···O direction (± 20°), indicating a strong and symmetrical hydrogen bonding system. Such an arrangement is repeated, of course, on the other side of the macrocycle, such that the other BF_3OH_2·H_2O system is located below O(8) and hydrogen bonded through the water molecule to O(5) and O(2′). It is also hydrogen bonded to the crown's O(8) through the other hydrogen water in BF_3OH_2.

In these BF_3OH_2·H_2O systems the water oxygen is hydrogen bonded to the oxygen atom of BF_3OH_2. This hydrogen bond presents a short O_w···O distance (2.49 Å). The boron atom in the BF_3OH_2 moiety is almost tetrahedral (all angles are within the range 109 ± 4°), where the B—F(1), B—F(2), B—F(3) bonds (1.34–1.36 Å) are significantly shorter than the B—O bond (1.51 Å). This geometry of the BF_3OH_2 moiety is similar to that observed for BF_3OH_2 and $BF_3O(CH_3)H$ in the solid state determined at low temperature.[18] The recently determined structure of 18-C-6/BF_3OH_2 shows similar geometry of the BF_3OH_2 moiety,[12] yet the specific interactions to the

crown ether are significantly different. The main difference between complex **II** and the reported structure of 18-C-6/BF_3OH_2 is the insertion of an H_2O between the BF_3OH_2 and the crown ring. In complex **II** the water molecule features two hydrogen bonds to the macrocyclic ring—the O(1w)—H···O_c bonds (2.83–2.85 Å) and an additional bond to the oxygen atom of the BF_3OH_2 moiety, O(1w)···O(2w)—B (2.49 Å). Another difference between these two complexes is the BF_3OH_2/crown ratio. In complex **II** there are two BF_3OH_2·H_2O species bonded by one crown, while there is a 1:1 ratio in the 18-C-6/BF_3OH_2 complex. The solid-state structure of BF_3OH_2 with H_2O was determined at low temperature.[19] A comparison with the BF_3OH_2·H_2O moiety of complex **II** shows a significant difference in the distance between the two oxygens. In the solid-state structure of BF_3OH_2·H_2O the O···O distance is 2.63 Å, compared with a O···O distance of 2.49 Å in the complex structure of BF_3OH_2·H_2O with 18-C-6 crown ether. The strong intermolecular interaction in the latter stabilizes the normally unstable BF_3OH_2·H_2O system, as discussed above. The precise geometry required for such intermolecular hydrogen bonding may account for the fact that such a stabilized BF_3OH_2·H_2O complex has not been observed before. It is interesting to note that although the two BF_3OH_2·H_2O units associated with each crown ether are extended outwards (the relevant boron atoms are located *ca* 4.1 Å away from plane *a*), they are not involved in any additional intermolecular specific interactions in the crystal, as demonstrated in the unit-cell crystal packing (Fig. 3).

The present work shows that the normally unstable BF_3OH_2·H_2O system can be stabilized by its coordination to a crown ether. Hydrogen bonding obviously plays a major role, but no clear-cut pattern emerges as to what factors determine the stabilization of BF_3/BF_4^- species. Electrostatic effects appear to be of minor significance, since the covalently bonded species are at least as stable. Complex **I** has normal O···H bond distances similar to those found in other oxonium/crown-ether complexes. The oxonium ion is well shielded by the crown so that the BF_4^- ion is not involved in intermolecular contacts, perhaps accounting for the fact that it is spherically disordered.

It is of interest that in both cases the conformation adopted by the crown ether is independent of whether the oxonium ion is encapsulated in the cavity of the crown ether or whether the complex is formed outside of the cavity. The conformation adopted in all cases is the "round" D_{3d} or "D_{3d} like" conformation, which is the most commonly encountered and which has been calculated to be the conformer of lowest energy.[13] Such an observation is important not only for the evaluation of the specific case of the 18-C-6/oxonium (water) system, but also for other host–guest systems where multiple conformations of the host molecule are possible.

Supplementary material. A list of the coordinates of all atoms of **I** and **II** (Tables S1, S2), anisotropic temperature factors for non-hydrogen atoms of **I** and **II** (Tables S3, S4), all intramolecular distances in **I** and **II** (Tables S5, S6), all intramolecular bond angles in **I** and **II** (Tables S7, S8), all torsion angles for non-hydrogen atoms in **I** and **II** (Tables S9, S10), ESDs and interplanar angles for least squares planes in **I** and **II** (Tables S11, S12) and lists of observed and calculated structure factors for **I** and **II** (Tables S13, S14) are provided in the supplementary material (34 pages).

Acknowledgements—We gratefully acknowledge the comments of Professor D. Mootz on an earlier version of this manuscript which drew our attention to the relevant studies concerning the BF_3OH_2·H_2O species. We thank the Israeli Academy of Sciences (Grant No. 253/88 to GS), the Friends of the Hebrew University in England and Ms Myrtle Franklin, and the Bat Sheva de Rothchild Foundation for financial support. One of us (HF) thanks the Wolf Foundation for a predoctoral fellowship.

REFERENCES

1. N. N. Greenwood and R. L. Martin, *Q. Rev.* 1954, **8**, 1.
2. F. A. Cotton and G. Wilkinson, *Advanced Inorganic Chemistry*, 5th edn, p. 174. Interscience, New York (1988).
3. S. Pawlenko, *Chem. Ing. Tech.* 1968, **40**, 52.
4. K. O. Christe, C. J. Schack and R. D. Wilson, *Inorg. Chem.* 1975, **14**, 2224.
5. D. Mootz and M. Steffen, *Z. Anorg. Allg. Chem.* 1981, **482**, 193.
6. R. Chenevert, A. Rodrigue, M. Pigeon-Gosselin and R. Savoie, *Can. J. Chem.* 1982, **60**, 853.
7. J. P. Behr, P. Dumas and D. Moras, *J. Am. Chem. Soc.* 1982, **104**, 4540.
8. Y. A. Simonov, N. F. Krosnova, A. A. Dvorkin, V. V. Yashkin, V.M. Abashkin and B.N. Laskorin, *Dokl. Akad. Nauk. SSSR* 1983, **272**, 1129.
9. J. L. Atwood, S. G. Bott, A. W. Coleman, K. D. Robinson, S. B. Whetstone and C. M. Means, *J. Am. Chem. Soc.* 1987, **109**, 8100.
10. C. B. Shoemaker, L. V. McAfee, D. P. Shoemaker and C. W. Dekock, *Acta Cryst.* 1986, **C42**, 1310.
11. R. Chenevert, A. Rodrigue, D. Chamberland, J. Qullet and R. Savoie, *J. Molec. Struct.* 1985, **131**, 187.
12. S. G. Bott, A. Alvanipour and J. L. Atwood, *J. Inclus. Phenom.* 1991, **10**, 153.
13. M. Dobler, *Chimia* 1984, **38**, 415.

14. TEXSAN: Single Crystal Structure Analysis Software, Version 5.0. Molecular Structure Corporation, The Woodlands, TX 77381 (1989).
15. P. Main, S. E. Hull, L. Lessinger, G. Germain, J. P. Declercq and M. M. Woolfson, MULTAN 78, *A System of Computer Programs for the Automatic Solution of Crystal Structures from X-ray Diffraction Data*. Universities of York, U.K. and Louvain, Belgium (1978).
16. W. R. Busing, K. O. Martin and H. A. Levy, *ORFLS, A FORTRAN Crystallographic Least Squares Program*, Report ORNL-TM-305. Oak Ridge National Laboratory, Oak Ridge, TN, U.S.A. (1962).
17. G. J. Gilmore, *J. Appl. Cryst.* 1984, **17**, 42.
18. D. Mootz and M. Steffen, *Z. Anorg. Allg. Chem.* 1981, **483**, 171.
19. D. Mootz and M. Steffen, *Acta Cryst.* 1981, **B37**, 1110.

Polyhedron Vol. 12, No. 24, pp. 2921–2924, 1993
Printed in Great Britain

0277-5387/93 $6.00+.00
© 1993 Pergamon Press Ltd

STRUCTURES OF α-TRIS (2,4-PENTANEDIONATO) RUTHENIUM(III) AND TRIS(3-BROMO-2,4-PENTANEDIONATO) RUTHENIUM(III)

T. S. KNOWLES,* B. J. HOWLIN, J. R. JONES and D. C. POVEY

Department of Chemistry, University of Surrey, Guildford, Surrey GU2 5XH, U.K.

and

C. A. AMODIO

Department of Physical Sciences, St Mary's College, Strawberry Hill, Twickenham, Middlesex TW1 4SX, U.K.

(*Received* 16 *June* 1993; *accepted* 6 *August* 1993)

Abstract—Both title complexes have been synthesized and subsequently characterized by X-ray diffraction. Results available on the Cambridge Crystallographic Database (V.3) suggest that this is the first tris complex of a fully substituted 0,0′-bonded acetylacetone to be characterized as a crystal structure from X-ray methods.

One step catalytic procedures which lead to the regiospecific introduction of the isotopes (^{2}H, ^{3}H) of hydrogen are becoming increasingly attractive methods for incorporating the label in a wide range of organic compounds, particularly those of interest to the pharmaceutical industry and until recently, the preferred catalyst for this has been hydrated rhodium(III) chloride.[1] The discovery that ruthenium acetylacetonate complexes catalyse the regiospecific tritiation of aromatic carboxylates offers the dual advantages of improved specific activity and ease of chemical investigation owing to improved homogeneous retention. Only the ruthenium(III) complex of this ligand is known to catalyse the reaction; current work reflects modifications made to the catalyst structure and subsequent investigations in the potential for tritiation catalysis shown by homologous complexes. The apparently unique exhibition of catalytic behaviour by the ruthenium(III) complex suggested that structural considerations may be responsible, but this structure determination refutes such suggestions.

*Author to whom correspondence should be addressed.

EXPERIMENTAL

Syntheses

There are two routes to complex **I**, both involving refluxing hydrated ruthenium(III) chloride in aqueous solution. Route A proceeds via an ethanolic reduction to $[Ru_3Cl_{12}]^{2-}$ with the subsequent addition and reaction of the ligand with the cluster anion,[2] whereas in route B[3] the ligand is added directly to the solution of hot ruthenium(III) chloride.

$$RuCl_3 \cdot 3H_2O \xrightarrow[\text{(B) non-reductive addition}]{\text{(A) reductive addition}}$$

$$\underset{\text{(I)}}{Ru(acac)_3} \xrightarrow{\text{NBS, room temperature}} \underset{\text{(II)}}{Ru(3Br\text{-}acac)_3}$$

The microcrystalline product from route A was crystallized over the course of several days from ethanol, giving ruby–red prisms which were suitable for crystallographic analysis. It was subsequently found that route B gave a cleaner reaction and product and a better yield; thus, for the preparation of complex **II** the reaction of N-bromosuccinimide (NBS) with complex **I** prepared via route B was

Table 1. Summary of key crystallographic data

	Complex I	Complex II
Crystal description	Ruby prism	Hexagonal maroon plate
Crystal dimensions (mm)	0.5, 0.35, 0.075	0.65, 0.60, 0.425, 0.05
Data collection range (°)	$1 \geq \theta \geq 26$	$1 \geq \theta \geq 25$
hkl ranges	0–16, 0–18, 0–20	0–15, 0–11, −18 to +18
Total *hkl*	3778	3815
hkl [$I \geq , 3\sigma(I)$] (%)	2332 (62)	2649 (69)
Molecular formula	$RuC_{15}H_{21}O_6$	$RuC_{15}H_{18}O_6Br_3$
Mr	398.40	635.10
Crystal system	Orthorhombic	Monoclinic
Space group	*Pbca*	$P2_1/n$
a(Å)	13.468	12.798
b(Å)	16.566	9.980
c(Å)	15.364	15.809
β(°)	90.00	105.42
V(Å^3)	3427.9	1946.6
z	8	4
D(g cm^{-3})	1.544	2.170
F(000)	1624	1220
μ (Mo-K_α) (cm^{-1})	9.2	69.3
R	0.037	0.047
*R*w	0.047	0.073

employed.[4] Complex **II** gave maroon polyhedral plates when recrystallized from hot acetone.

Both cell determinations and data collections were performed on an Enraf–Nonius CAD4 four-circle diffractometer using graphite monochromated Mo-K_α radiation ($\lambda = 0.71069$ Å). In both cases, 25 reflections taken from the angular range $13 > \theta > 15°$ were used to determine the unit cell and no mechanical or chemical deterioration was observed in either case. Details of data collection and results for both complexes are summarized in Table 1.

For complex **I**, bond lengths and angles are summarized in Table 2 and those of complex **II** in Table 3.

Solution to crystal structures

Both structures were solved using the Enraf–Nonius Structure Determination package.[5]

Complex **I.** Solution of a three-dimensional Patterson synthesis gave a ruthenium position in the Harker plane (u, $\frac{1}{2}$, w) which refined to 34%. Iterative Fourier synthesis with isotropic refinement yielded a complete molecule with $R = 8.8\%$. Subsequent anisotropic refinement, of the ruthenium only, with the Killean–Lawrence weighting scheme[6] reduced R to 5.3%. Anisotropic refinement of the whole molecule converged to give a final R value of 3.7%. Figure 1 shows an ORTEP drawing of complex **I**.

Complex **II.** The direct methods program MULTAN[7] was used to provide four heavy atom positions which refined to $R = 32\%$. Further isotropic refinement with a single Fourier map yielded one ligand with R at 23% and then a single difference map provided the atomic complement necessary to complete the molecular skeleton, causing R to fall to 16%. Hydrogen atoms were added at calculated positions (bond length of 1 Å) and anisotropic refinement of the whole molecule using the Killean–Lawrence weighting scheme reduced R to

Table 2. Selected bond lengths (Å) and angles (°) for complex **I**

Ru—O(1)	1.998(3)
Ru—O(2)	1.991(3)
Ru—O(3)	2.008(3)
Ru—O(4)	1.990(3)
Ru—O(5)	2.005(3)
Ru—O(6)	1.998(3)
O(1)—Ru—O(2)	93.7(1)
O(3)—Ru—O(6)	92.5(1)
O(4)—Ru—O(5)	92.8(1)
O(1)—Ru—O(5)	178.5(1)
O(2)—Ru—O(3)	177.9(1)
O(4)—Ru—O(6)	178.8(1)

Estimated standard deviations are in parentheses.

Table 3. Selected bond lengths (Å) and angles (°) for complex **II**

Ru—O(1)	1.998(5)
Ru—O(2)	1.988(5)
Ru—O(3)	2.005(6)
Ru—O(4)	1.994(5)
Ru—O(5)	1.980(6)
Ru—O(6)	2.005(5)
C(12)—Br(1)	1.916(8)
C(36)—Br(3)	1.913(9)
C(45)—Br(5)	1.914(9)
O(1)—Ru—O(2)	91.3(2)
O(3)—Ru—O(6)	90.1(3)
O(4)—Ru—O(5)	92.0(2)
O(1)—Ru—O(5)	87.2(2)
O(2)—Ru—O(3)	89.4(2)
O(4)—Ru—O(6)	90.1(2)
C(1)—C(12)—Br(1)	116.8(6)
C(2)—C(12)—Br(1)	115.7(6)
C(1)—C(12)—C(2)	127.5(8)
C(3)—C(36)—Br(3)	115.9(7)
C(6)—C(36)—Br(3)	115.8(6)
C(3)—C(36)—C(6)	128.3(8)
C(4)—C(45)—Br(5)	116.2(6)
C(5)—C(45)—Br(5)	115.4(7)
C(4)—C(45)—C(5)	128.4(8)

Estimated standard deviations are in parentheses.

4.7%, at which the refinement converged. Figure 2 shows an ORTEP drawing of complex **II**.

RESULTS AND DISCUSSION

Following the discovery of tritiation catalysis shown by the ruthenium(III) complex, analogous

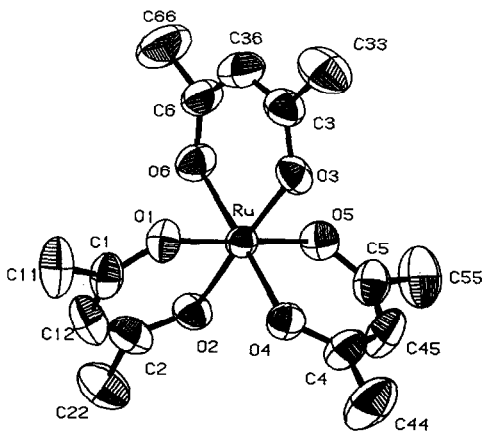

Fig. 1. ORTEP drawing of tris(2,4-pentanedionato) ruthenium(III) with 50% probability thermal ellipsoids.

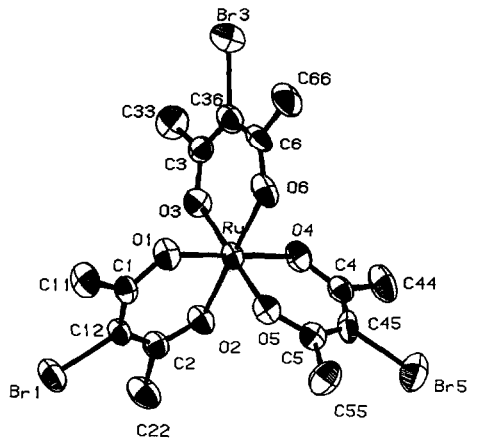

Fig. 2. ORTEP drawing of tris(3-bromo-2,4-pentanedionato) ruthenium(III) with 50% probability thermal ellipsoids.

chelates of a variety of closely related metals were investigated; none of these exhibited catalytic activity. A structural examination of those complexes tested, aided by the Cambridge Crystallographic Database (V.3),[8] revealed distortion in the structure of the racemic ruthenium complex which has already been reported to crystallize in the monoclinic space group $P2_1/c$.[9]

The redetermination of the structure of complex **I** resulted in the discovery of a dimorphic relationship which does not confirm the variation in ruthenium–oxygen bond lengths previously recorded. As the previous determination and labelling work both employed the commercially available compound, powder photographs were taken to investigate the relationship between these forms. The resulting photographs were identical, suggesting that structural irregularities do not account for the observed catalytic effect.

A dimorphic relationship in *Pbca* and $P2_1/c$ is observed in the acetylacetone complexes of vanadium(III)[10] and manganese(III);[11] by analogy, this is the α-form, the β-form being that previously reported. Furthermore, this ruthenium complex is isomorphic with the acetylacetone complexes of iron(III)[12] and scandium(III).[13]

In both structures the mean ruthenium–oxygen bond distance is 2.00 Å, which is within the range observed in other β-diketonato complexes of ruthenium(III)[14,15] and in agreement with the racemic and enantiomeric forms.[16] Evidence for pseudoaromatic character in both cases comes from the typical 0.01 Å shortening observed in ring carbon–carbon bonds in comparison to the terminal carbon–carbon bonds. In complex **II**, the mean carbon–bromine distance is 1.914(9) Å, which is

comparable to those observed in other substituted bromoaromatic systems.[17,18]

The structure of **II** represents a new development in the chemistry of acetylacetonate complexes; the only previous structural determinations are on the 3-methyl and 3-phenyl derivatives of copper(II).[19,20] There appears to be a slight reduction in the external angles at the 3-position in comparison to the aforementioned methyl derivative, but substitution of hydrogen by bromine at the 3-position does not affect the geometry.

Acknowledgements—We would like to thank Mr G. W. Smith for his kind guidance in overseeing the structural solutions, Dr J. H. Aupers for valuable discussion and helpful comments and Mr N. D. Wright for his instruction on the Cambridge Crystallographic Database.

REFERENCES

1. D. Hesk, J. R. Jones and W. S. Lockley, *J. Lab. Comp. Radiopharm.* 1990, **28**, 1427.
2. A. Endo, K. Shimizu, G. P. Sato and M. Mukaida, *Chem. Lett.* 1984, 437.
3. R. Grobelny, B. Jezowska-Trzebiatowska and W. Wojchiechowski, *J. Inorg. Nucl. Chem.*, 1966, **28**, 2715.
4. A. Endo, K. Shimizu and G. P. Sato, *Chem. Lett.* 1985, 581.
5. B. A. Frenz and Associates, *Enraf–Nonius Structure Determination Package*. SDP Users Guide Version 1.1a Delft, The Netherlands (1985).
6. R. C. G. Killean and J. L. Lawrence, *Acta Cryst.* 1978, **B25**, 1750.
7. P. Main, S. E. Hull, L. Lessinger, G. Germain, J. P. Declerqc and M. M. Woolfson, Multan 78, A System of Computer Programs For The Automatic Solution of Crystal Structures From X-Ray Diffraction Data. University of York, U.K. and Louvain, Belgium (1978).
8. F. H. Allen, S. A. Belard, M. D. Brice, B. A. Cartwright, A. Doubleday, H. Higgs, T. Hummelink, B. G. Hummelink-Peters, O. Kennard, W. D. S. Motherwell, J. R. Rodgers and D. G. Watson, *Acta Cryst.* 1979, **B35**, 2331.
9. G. K.-J. Chao, R. L. Sime and R. J. Sime, *Acta Cryst.* 1973, **B29**, 2845.
10. B. Morosin and H. Montgomery, *Acta Cryst.* 1969, **B25**, 1354.
11. J. P. Fackler and A. Avdeef, *Inorg. Chem.* 1974, **13**, 1864.
12. J. Iball and C. H. Morgan, *Acta Cryst.* 1967, **23**, 239.
13. T. J. Anderson, M. A. Neuman and G. A. Melson, *Inorg. Chem.* 1973, **12**, 927.
14. S. Aynetchi, P. B. Hitchcock, E. A. Seddon, K. R. Seddon, Z. Yousif and A. Zalal, *Inorg. Chim. Acta* 1986, **113**, L7.
15. Y. Hoshino, Y. Yukawa, T. Maruyama, A. Endo, K. Shimizu and G. P. Sato, *Inorg. Chim. Acta* 1990, **174**, 41.
16. H. Matsuzawa, Y. Ohashi, Y. Kaizu and H. Kobayashi, *Inorg. Chem.* 1988, **27**, 2891.
17. W. Harrison, S. Rettig and J. Trotter, *J. Chem. Soc., Dalton Trans.* 1972, 1852.
18. F. Toda, K. Tanaka and H. Ueda, *Tetrahedron Lett.* 1981, **22**, 4669.
19. I. Robertson and M. Truter, *J. Chem. Soc. A* 1967, 309.
20. J. W. Carmichael, L. K. Steinrauf and R. L. Belford, *J. Chem. Phys.* 1965, **43**, 3959.

Polyhedron Vol. 12, No. 24, pp. 2925–2928, 1993
Printed in Great Britain

0277–5387/93 $6.00+.00
© 1993 Pergamon Press Ltd

EQUILIBRIA IN COMPLEXES OF N-HETEROCYCLIC COMPOUNDS—LI.* SYNERGIC SOLUBILITY AND X-RAY CRYSTAL STRUCTURE ANALYSIS OF *MER*-CHLORO-OXALATO-TRIS-PYRIDINE-IRIDIUM(III), $[IrCl(py)_3(C_2O_4)]$

NICOLA S. A. EDWARDS, R. D. GILLARD,† MICHAEL B. HURSTHOUSE,† HARVEY F. LIEBERMAN and K. M. ABDUL MALIK

School of Chemistry and Applied Chemistry, University of Wales, P.O. Box 912, Cardiff CF1 3TB, U.K.

(*Received* 8 *June* 1993; *accepted* 6 *August* 1993)

Abstract—The title compound, *mer*-$[IrCl(py)_3(C_2O_4)]$, has been made by the reaction of the known *trans*-dichloro-tetrapyridine-iridium(III) chloride with ethanedioate ion(oxalate) in aqueous ethanol. A non-electrolyte, it resembles its rhodium eutrope in showing extraordinary synergic solubility in water: pyridine. An X-ray structure determination has confirmed the *mer* geometry.

Complex ions of rhodium (and to an extent iridium) with pyridine and with chelating dicarboxylates such as ethane-1,2-dioate (oxalate) have been well studied. A few mixed species, such as $[RhCl(py)_3(C_2O_4)]$ (**A**) are known. The unusual synergic solubility of this compound had been known for many years and we are trying to understand its molecular origin. We therefore synthesized the new iridium(III) mixed compound *mer*-$[IrCl(py)_3(C_2O_4)]$ (**B**) and report here some of its properties, including its structure. The known bromo-rhodium compound $[RhBr(py)_3(C_2O_4)]$ (**C**) is also further described with a convenient synthesis.

EXPERIMENTAL

Preparation of complexes

Mer-*Chlorotrispyridineoxalatoiridium(III)* (B). *Trans*-$[IrCl_2(py)_4]Cl \cdot 6H_2O$[2] (0.444 g, 0.614 mmol) and potassium oxalate (0.113 g, 0.614 mmol) were refluxed for 7 days in 50% ethanol solution (100 cm^3). Yellow needles (0.08 g) formed on cooling: these were collected by filtration. The filtrate was treated with an excess of ethanol to precipitate unreacted potassium oxalate. After filtration, the volume was reduced on a rotary evaporator when a further crop of crystals of the desired product was obtained (0.116 g). Yield: 58%. Found: C, 36.8; H, 2.8; N, 7.5. Calc. for $C_{17}ClH_{15}N_3O_4Ir$: C, 36.9; H, 2.7; N, 7.6%. IR: 1700m, 1670m, 1610m, 1245w, 1160w, 1072m-w, 1020w, 880w, 805w, 762m-w, 700s, 655w, 560w, 485w, 465w, 365w, 345s, 310w, 290w, 265m, 235w cm^{-1}.

A measurement of conductance (*ca* 10^{-3} M in aqueous pyridine) gave $\Lambda_m = 6.82$ S $mol^{-1}dm^3$. Complex **B** dissolves in boiling concentrated hydrochloric acid and on cooling, the solution yields the known complex $[IrCl_3(py)_3]$ as its *mer* isomer,[3] identified by its electronic spectrum in chloroform. Three bands were observed in the UV region at 320–317 shoulder, 266 and 238 nm. A visible absorption was also observed at 421–436 nm. These are in accordance with the electronic spectrum of the *mer*-$[IrCl_3(py)_3]$[4] isomer.

Mer-*bromotrispyridineoxalatorhodium(III)* (**C**). *Trans*-$[RhBr_2(py)_4]Br$ was prepared by boiling *trans*-$[RhCl_2(py)_4] \cdot 6H_2O$ with an excess of aqueous potassium bromide. After approximately 2 h the desired orange solid formed. This was collected by filtration, washed with ice-cold water and recrystallized from hot water; **C** was synthesized from it, *mutatis mutandis*, as with **A**.[2] Found: C, 40.3; H, 3.0; N, 8.3. Calc. for $C_{17}BrH_{15}N_3O_4Rh$: C, 40.18; H, 2.98: N, 8.27%. IR: 1703m, 1668m,

*See ref. 1.

†Authors to whom correspondence should be addressed.

1605m, 1242w, 1212m, 1153w, 1068m, 1015w, 881w, 796w, 775m, 761m, 708s, 697s, 686m, 651s, 553s, 480m, 470s, 412m, 360s, 350s, 275m, 251w cm^{-1}.

Electronic spectra were measured using a Kontron–Uvikon 930 UV–vis spectrophotometer. IR spectra were measured using a Perkin–Elmer 577 IR grating spectrophotometer, as Nujol mulls on caesium iodide plates; wave numbers are quoted to $\pm 2\ cm^{-1}$.

Crystallography

Data for compound **B** were collected on a FAST TV Area Detector diffractometer following previously described procedures.[5] The structure was solved and developed via the heavy-atom method and refined by full-matrix least-squares techniques. A correction for absorption was made using DIFABS.[6] All hydrogens were placed in idealized positions. Crystal data and details of the structure refinement are given in Table 1. Atomic coordinates, bond lengths and angles and thermal parameters have been deposited as supplementary material with the Editor. Atomic coordinates have also been deposited at the Cambridge Crystallographic Data Centre.

Table 1. Crystal data and details of structure refinement for *mer*-[IrCl(py)$_3$(C$_2$O$_4$)]

Formula	$C_{17}H_{15}N_3O_4ClIr$
Mol. wt	552.997
Crystal system	Orthorhombic
a (Å)	10.016(1)
b (Å)	12.059(3)
c (Å)	14.950(3)
V (Å^3)	1805.8(6)
θ range for cell (°)	1.5–25
Space group	$P2_12_12_1$
Z	4
D_c (g cm^{-3})	2.0341
$F(000)$	1056
μ (cm^{-1})	75.410
T (K)	298
θ range for data (°)	2.170–29.610
h_{min}, h_{max}	−12, 13
k_{min}, k_{max}	−15, 10
l_{min}, l_{max}	−14, 19
Total data measured	7717
Total unique	3677
R_{merge}	0.045
Total observed	3359
Significance test	$F_0 > 3\sigma F_0$
Absorption correction factors:	
min, max	0.884, 1.198
No. of parameters	250
ρ_{min}–ρ_{max} (e Å^{-3})	−1.53, 1.88
$(\Delta/\sigma)_{max}$	0.001
Weighting scheme	Unit weights
R	0.0420
ωR	0.0420

RESULTS AND DISCUSSION

The three compounds, [MX(py)$_3$(C$_2$O$_4$)] (**A**: M = Rh, X = Cl; **B**: M = Ir, X = Cl; **C**: M = Rh, X = Br) show synergic solubility in aqueous pyridine, as depicted in Fig. 1. The property was discovered[7] for the chloro-rhodium species and Reichardt[8] singled out this case in his discussion of solvent effects in organic systems. Chloro-oxalato-tris-pyridine-iridium(III) forms only slowly, even with ethanol present. Such a substitution at rhodium(III) centres is often strongly catalysed by the 2e-reductant ethanol, but that is not obvious here. Powder patterns show that compounds **A** and **B** are clearly isostructural (powder data have been deposited). The crystalline form which we have is isostructural with the well-known rhodium(III) eutrope. Our structure, therefore, confirms both that the rhodium compound is indeed the *mer* isomer and that its reaction [eq. (1)] with hydrochloric acid is, like many such acid displacements of oxalate in acid, stereoretentive: the product with an absorption at 428 nm was already known from spectroscopy to be the *mer* isomer.

$$mer\text{-}[RhCl(py)_3(C_2O_4)] + 2HCl \rightarrow mer\text{-}[RhCl_3(py)_3] + H_2C_2O_4 \quad (1)$$

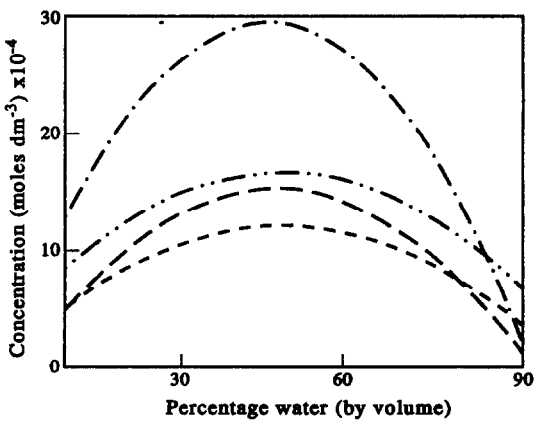

Fig. 1. Solubilities (given as concentrations of saturated solutions at 30° C) in water/pyridine of *mer*-[MX(py)$_3$(C$_2$O$_4$)]: ----, **A**(M = Rh, X = Cl$^-$); -------, **B**(M = Ir, X = Cl$^-$); -----, **C**(M = Rh, X = Br$^-$). The curve ---- is that reported[7] for **A**, *mer*-[RhCl(py)$_3$(C$_2$O$_4$)], measured at 15° C.

Table 2. Selected bond lengths (Å) and angles (°) for **B**

Ir—Cl	2.341(6)	Ir—O(1)	2.040(11)
Ir—O(2)	2.033(11)	Ir—N(11)	2.045(14)
Ir—N(21)	2.045(13)	Ir—N(31)	2.061(11)
O(1)—Ir—Cl	174.0(3)	O(1)—Ir—O(2)	83.0(5)
O(2)—Ir—Cl	91.1(4)	N(11)—Ir—Cl	89.9(5)
N(11)—Ir—O(2)	87.6(5)	N(11)—Ir—O(1)	90.0(5)
N(21)—Ir—Cl	91.3(4)	N(21)—Ir—O(1)	88.5(5)
N(21)—Ir—O(2)	88.5(5)	N(21)—Ir—N(11)	176.0(5)
N(31)—Ir—Cl	92.8(4)	N(31)—Ir—O(1)	93.2(5)
N(31)—Ir—O(2)	176.0(5)	N(31)—Ir—N(11)	93.4(6)
N(31)—Ir—N(21)	90.4(5)		

We have also shown this stereoretention for eq. (2):

$$mer\text{-}[IrCl(py)_3(C_2O_4)] + 2HCl \rightarrow mer\text{-}[IrCl_3(py)_3] + H_2C_2O_4 \quad (2)$$

Our crystals of the product from eq. (1) indeed have the well-known spectroscopic properties of *mer*-$[RhCl_3(py)_3]$ (e.g. *d–d* absorption at 428 nm). They have the same space group and unit cell as those studied in crystallographic detail elsewhere.[9] The available[9] crystal and molecular structure of *mer*-$[RhCl_3(py)_3]$, determined for a compound of unknown spectroscopic properties and provenance, is that of the isomer absorbing at 428 nm.

The vibrational spectra of **A** and **B** (as solids) are also very similar. The IR spectrum of **C**, the bromorhodium member, is closely similar, but its crystal lattice is entirely different (data deposited). Despite this (and it may be that a second dimorph crystallizes in this case alone), the solubility properties of all three are alike. The vibrational spectra of these $[MX(py)_3(C_2O_4)]$ complexes are superimposable to 360 cm^{-1}: the vibrations involving metal ions may be compared in **A**(Rh—Cl) and **B**(Ir—Cl), suggesting υ(Rh—Cl) at 318 ± 3 and υ(Ir—Cl) at 290 cm^{-1}. These frequencies are in line with others from the literature.

We interpret the synergism in solubility as representing the specific solvation of the polar meridian (P) by water and the non-polar (NP) meridian by pyridine. Describing the solvation enthalpies $\Sigma\Delta H$ as ΔH_P or ΔH_{NP}, in any solvent mixture we have:

$$\Sigma\Delta H = \Delta H_P + \Delta H_{NP}.$$

Using suffixes W for water and H for heterocycle, we see that:

$$\Delta H_{P(W)} \gg \Delta H_{P(H)}; \quad \Delta H_{NP(H)} \gg \Delta H_{NP(W)}.$$

Denoting the lattice enthalpy by U, dissolution occurs when

$$\Sigma\Delta H > U.$$

We believe that:

$$U > \Sigma\Delta H_W[= \Delta H_{P(W)} + \Delta H_{NP(W)}]$$
$$> \Sigma\Delta H_H[= \Delta H_{P(H)} + \Delta H_{NP(H)}]$$
$$\text{but} < \Sigma\Delta H_M[= \Delta H_{P(W)} + \Delta H_{NP(H)}],$$

where M refers to the mixture.

Our detailed thermodynamic and spectroscopic work on the molecular bases for these variations of ΔH will be published elsewhere.

Figure 2 shows the molecular structure of **B**. Table 2 contains selected bond lengths and angles. The measured iridium–chloride bond length of 2.341(6) Å compares well with those measured for $K_3[IrCl_6]$[10] (2.36 Å) and *trans*-$[IrCl_2(py)_4]Cl \cdot 6H_2O$(2.35 Å). The measured iridium–oxygen bond lengths are slightly longer in *mer*-$[IrCl(py)_3(C_2O_4)]$, at 2.033 and 2.040 Å, than in $K_3[Ir(ox)_3] \cdot 3H_2O$[11] (1.96 Å). In contrast, one of the Ir—N bond lengths in **B** (2.06 Å) is identical to one of the lengths in *trans*-$[IrCl_2(py)_4]Cl \cdot 6H_2O$. The

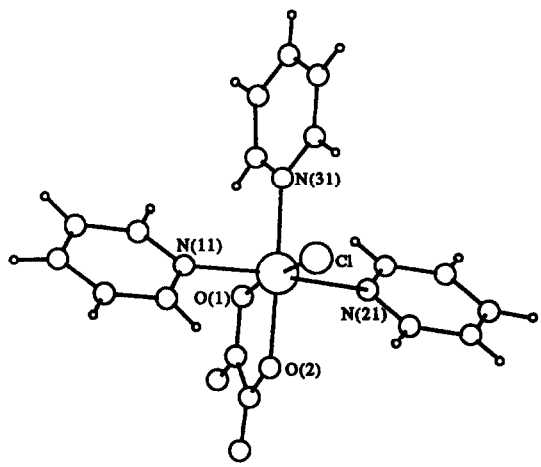

Fig. 2. The molecular structure of **B**.

Table 3. Pyridine ring orientations

	B	E	F	G	H
a*	138.36	130.08	42.48	49.00	65.09
b	79.68	136.20	110.10	43.47	48.58
c*	46.66	125.30	43.31	52.26	119.38

Values given are the dihedral angles between the pyridine ring planes and the meridional py_3MX plane. a* and c* are the outer rings and are interchangeable due to the "chemical" symmetry of the molecule. Similar values correspond to a propeller arrangement, approximate supplementary values correspond to different orientations relative to the meridianal plane.

B = This work; E = *mer*-$[CrCl_3(py)_3]$;[12] F = *mer*-$[InBr_3(py)_3]$;[13] G = *mer*-$[RhCl_3(py)_3]$;[9] H = *mer*-$[TlBr_3(py)_3]$.[14]

other Ir—N bond lengths [2.045(14) Å] are both shorter than those in *trans*-$[IrCl_2(py)_4]Cl \cdot 6H_2O$. A particular feature of this and related structures is the orientation of the pyridine rings with respect to the plane through the iridium and the three nitrogens. A comparison of data for these dihedral angles is given in Table 3.

REFERENCES

1. R. D. Gillard and S. H. Mitchell, *Polyhedron* 1989, **8**, 2649.
2. R. D. Gillard, S. H. Mitchell, P. A. Williams and R. S. Vagg, *J. Coord. Chem.* 1984, **13**, 325.
3. R. D. Gillard and S. H. Mitchell, *Polyhedron* 1989, **8**, 2245.
4. C. K. Jorgensen, *Acta Chem. Scand.* 1957, **11**, 151.
5. A. A. Danopoulos, G. Wilkinson, B. Hussain-Bates and M. B. Hursthouse, *J. Chem. Soc., Dalton Trans.* 1991, 1855.
6. N. P. C. Walker and D. Stuart, *Acta Cryst.* 1983, **A39**, 158.
7. R. D. Gillard, E. D. McKenzie and M. D. Ross, *J. Inorg. Nucl. Chem.* 1966, **28**, 1429.
8. C. Reichardt, *Solvent Effects In Organic Chemistry*. Weinheim, New York (1979).
9. K. R. Acharya, S. S. Tavale and T. N. G. Row, *Acta Cryst.* 1984, **C40**, 1327.
10. D. A. Rankin, B. R. Penfold and J. E. Fergusson, *Aust. J. Chem.* 1983, **36**, 863.
11. P. Herpin, *Bull. Soc. Franc. Min. Crist.* 1958, 245.
12. S. A. Howard and K. I. Hardcastle, *J. Cryst. Spectrosc.* 1985, **1**, 643.
13. R. W. H. Small and I. J. Worrall, *Acta. Cryst.* 1982, **B38**, 932.
14. S. E. Jeffs, R. W. H. Small and I. J. Worrall, *Acta Cryst.* 1984, **C40**, 1827.

Polyhedron Vol. 12, No. 24, pp. 2929–2932, 1993
Printed in Great Britain

0277–5387/93 $6.00+.00
© 1993 Pergamon Press Ltd

SYNTHESIS OF ISOCYANIDE COMPLEXES OF ZINC. THE MOLECULAR AND CRYSTAL STRUCTURE OF $Zn(SeC_6H_2Bu^t_3)_2(CNBu^t)_2$

MANFRED BOCHMANN,* GABRIEL C. BWEMBYA and ANNE K. POWELL

School of Chemical Sciences, University of East Anglia, Norwich NR4 7TJ, U.K.

(*Received* 8 *June* 1993; *accepted* 4 *August* 1993)

Abstract—The sterically hindered zinc chalcogenolato complexes $[Zn(EAr'')_2]_2$ (E = S, Se; Ar'' = 2,4,6-$Bu^t_3C_6H_2$) react with 1 equivalent of tert-butylisocyanide in non-coordinating solvents to give $Zn(EC_6H_2Bu^t_3)_2(CNBu^t)$ (**1**, E = S; **2**, E = Se) as thermally stable crystalline adducts; the compounds are thought to be chalcogenolato-bridged dimers. In the presence of excess isocyanide ligand the 1:2 adducts $Zn(EAr'')_2(CNBu^t)_2$ (**3**, E = S; **4**, E = Se) are isolated. The compounds represent the first examples of well-characterized isocyanide complexes of zinc. The X-ray structure of **4** showed that it is monomeric with a distorted tetrahedral coordination geometry of the metal centre, which reflects the steric requirements of the chalcogenolato and isocyanide ligands, respectively.

Isocyanides are among the most widely used ligands in transition metal chemistry. By contrast, isocyanide complexes of metals of the zinc triad are, to our knowledge, almost unknown. An incompletely characterized adduct with a zinc halide, $ZnBr_2(CNBu^t)_2$, has been reported[1] and a similar complex with ZnI_2 has been claimed in a patent.[2] As part of our search for potential single-source precursors for the deposition of II–VI semiconductor films from the gas phase[3] we have shown earlier that the coordinatively unsaturated zinc thiolato and selenolato complexes $[Zn(EAr'')_2]_2$ (E = S, Se; Ar'' = 2,4,6-$Bu^t_3C_6H_2$) readily react with O, N and P donor ligands to give three- and four-coordinate compounds[4–6] and react even with weak ligands such as ketones and aldehydes to give stable crystalline complexes.[7] We report here the synthesis and characterization of isocyanide complexes of bulky zinc chalcogenolato complexes.

EXPERIMENTAL

All operations were performed under dry argon using standard vacuum-line techniques. The complexes $[Zn(EAr'')_2]_2$ (E = S, Se; Ar'' = 2,4,6-$Bu^t_3C_6H_2$) were prepared as described previously.[4] Petroleum ether was distilled from sodium benzophenone under nitrogen. Bu^tNC (Aldrich) was dried over molecular sieves and distilled under nitrogen prior to use. Perkin–Elmer 684 (IR) and JEOL EX90Q and EX270 (^1H, ^{13}C NMR) spectrometers were used.

Preparation of $[Zn(SAr'')_2(Bu^tNC)]_2$ (1)

To a stirred suspension of $[Zn(SAr'')_2]_2$ (200 mg, 0.16 mmol) in petroleum ether (15 cm^3) at room temperature was added tert-butylisocyanide (27 mg, 0.32 mmol). The solid dissolved to give a clear colourless solution from which a white solid precipitated within a few minutes. After stirring the mixture for 2 h the precipitate was filtered off and recrystallized from hot toluene (5 cm^3) to give **1** as colourless crystals (83 mg, 0.06 mmol, 37%), dec. 200°C. The air-sensitive compound is soluble in chloroform and toluene. Found: C, 70.1; H, 9.7; N, 1.9; S, 9.7. Calc. for $C_{41}H_{67}NS_2Zn$: C, 70.0; H, 9.6; N, 2.0; S, 9.1%. IR (cm^{-1}): 2244 (s) [ν(CN)]. ^1H NMR (90 MHz, $CDCl_3$): δ 0.85 (s, 9 H, Me of Bu^tNC), 1.07 (s, 18 H, *p*-Bu^t), 1.45 (s, 36 H, *o*-Bu^t), 7.14 (s, 4 H, aryl). ^{13}C NMR (25 MHz, $CDCl_3$): δ 29.3 (Me of Bu^tNC), 31.6 (*p*-CMe_3), 32.0 (*o*-CMe_3),

*Author to whom correspondence should be addressed.

34.8 (*p*-CMe_3), 38.3 (*o*-CMe_3), 121.9 (*m*-C), 145.4 (*p*-C), 152.9 (*o*-C).

$Zn(SeAr'')_2(Bu^tNC)]_2$ (2)

In an analogous procedure, $[Zn(SeAr'')_2]_2$ (150 mg, 0.095 mmol) in petroleum ether (10 cm^3) was reacted with Bu^tNC (15 mg, 0.18 mmol) to give **2** as colourless crystals (56 mg, 0.035 mmol, 39%), dec 196–198°C. Found: C, 61.2; H, 8.5; N, 1.7. Calc. for $C_{41}H_{67}NSe_2Zn$: C, 61.8; H, 8.5; N, 1.8%. IR (cm^{-1}): 2218 (s) [ν(CN)]. ^1H NMR (270 MHz, $CDCl_3$): δ 1.04 (s, 9 H, Me of Bu^tNC), 1.28 (s, 18 H, *p*-Bu^t), 1.69 (s, 36 H, *o*-Bu^t), 7.37 (s, 4 H, aryl). ^{13}C NMR (25 MHz, $CDCl_3$): δ 29.4 (Me of Bu^tNC), 31.5 (*p*-C*Me*$_3$), 32.3 (*o*-C*Me*$_3$), 34.8 (*p*-*C*Me_3), 39.1 (*o*-*C*Me_3), 122.0 (*m*-C), 146.3 (*p*-C), 153.6 (*o*-C).

$Zn(SAr'')_2(Bu^tNC)_2$ (3)

To a stirred suspension of $[Zn(SAr'')_2]_2$ (198 mg, 0.16 mmol) in petroleum ether (15 cm^3) at room temperature was added tert-butylisocyanide (265 mg, 3.19 mmol). The solid dissolved to give a clear colourless solution, from which a white solid precipitated within a few minutes. Stirring was continued for 1 h. The precipitate was filtered off and recrystallized from warm toluene (5 cm^3) to give **3** as colourless crystals (93 mg, 0.12 mmol, 37%), dec. 192°C. The air-sensitive compound was soluble in dichloromethane, chloroform and toluene. Found: C, 70.5; H, 9.8; N, 3.4; S, 8.3. Calc. for $C_{46}H_{76}N_2S_2Zn$: C, 70.2; H, 9.7; N, 3.6; S, 8.2%. IR (cm^{-1}): 2223 (s) [ν(CN)]. ^1H NMR (270 MHz, CD_2Cl_2): δ 1.14 (s, 18 H, Me of Bu^tNC), 1.26 (s, 18 H, *p*-Bu^t), 1.62 (s, 36 H, *o*-Bu^t), 7.33 (s, 4 H, aryl). ^{13}C NMR (25 MHz, $CDCl_3$): δ 29.8 (Me of Bu^tNC), 31.6 (*p*-C*Me*$_3$), 32.1 (*o*-C*Me*$_3$), 35.0 (*p*-*C*Me_3), 38.6 (*o*-*C*Me_3), 122.3 (*m*-C), 145.4 (*p*-C), 153.2 (*o*-C).

$Zn(SeAr'')_2(Bu^tNC)_2$ (4)

The procedure given for **3** was followed to prepare **4** from $[Zn(SeAr'')_2]_2$ (394 mg, 0.28 mmol) and tert-butylisocyanide (458 mg, 5.51 mmol) as colourless crystals (218 mg, 0.248 mmol, 45%), dec. 190°C. The crystalline compound contains small amounts of hexane as one solvent of crystallization, most of which was released in prolonged evacuation at room temperature. Found: C, 63.4; H, 8.6; N, 3.3. Calc. for $C_{46}H_{76}N_2Se_2Zn$: C, 62.8; H, 8.7; N, 3.2%. IR (cm^{-1}): 2218 (s) [ν(CN)]. ^1H NMR (270 MHz, CD_2Cl_2): δ 1.18 (s, 18 H, Me of Bu^tNC), 1.27 (s, 18 H, *p*-Bu^t), 1.68 (s, 36 H, *o*-Bu^t), 7.35 (s, 4 H, aryl). ^{13}C NMR (25 MHz, $CDCl_3$): δ 29.8 (Me of Bu^tNC), 31.6 (*p*-C*Me*$_3$), 32.5 (*o*-C*Me*$_3$), 35.0 (*p*-*C*Me_3), 39.6 (*o*-*C*Me_3), 122.3 (*m*-C), 146.0 (*p*-C), 153.2 (*o*-C).

X-ray crystallography

Crystal data. $C_{46}H_{76}N_2Se_2Zn \cdot 1.6\ C_5H_{12}$, $M_r = 995.8$, monoclinic, space group $C2/c$ (no. 15), $a = 9.570(3)$, $b = 18.628(9)$, $c = 31.442(11)$ Å, $\beta = 94.63(3)°$, $V = 5587$ Å^3, $Z = 4$, $D_{calc} = 1.184$ g cm^{-3}, $F(000) = 2125$, μ(Mo-K_α) = 1.655 mm^{-1}.

Data collection and processing. Measurements were made on a crystal of the approximate dimensions 0.24 × 0.32 × 0.45 mm with a Siemens R3m/V diffractometer and graphite monochromated Mo-K_α radiation ($\lambda = 0.71073$ Å) using the ω-scan mode, scan range 0.60° in ω, scan speeds 3.00–19.53° min^{-1} in ω, $2 < 2\theta < 46°$, $-10 \leqslant h \leqslant 10$, $0 \leqslant k \leqslant 22$, $-37 \leqslant l \leqslant 37$. 4142 unique reflections, 1194 with $F_o > 6.0\sigma(F_o)$. The crystals deteriorated noticeably during data collection and a correction for this was applied, as well as Lorentz and polarization corrections.

Structure analysis and refinement. The structure was solved using the heavy-atom procedure and refined *via* full-matrix least-squares methods using SHELXTL programs. The zinc and selenium atoms were located from the Patterson map. Successive difference Fourier syntheses and full-matrix refinements revealed all other non-hydrogen atoms. There was evidence of the presence of disordered solvent molecules which were modelled with two fully occupied and four partially (1/2) occupied carbon sites per asymmetric unit. The marked deterioration of the crystal during data collection is probably partly the result of loss of this solvent. Hydrogen atoms were constrained to their calculated positions on carbons in the complex using a riding model and refined with fixed isotropic temperature factors. Only the zinc and selenium atoms were refined anisotropically, since more satisfactory refinement resulted from omitting the weak reflections and refining all but zinc and selenium isotropically in order to maintain a reasonable data/parameter ratio, rather than including these and refining all atoms anisotropically. A weighting scheme of the form $w^{-1} = \sigma^2(F) + 0.0070\ F^2$ was applied. The final difference-Fourier synthesis was essentially featureless, largest difference peak 0.69 e Å^{-3}, largest hole 1.14 e Å^{-3}. Final data: parameter ratio was 8.8:1, $R = 0.0876$, $R_w = 0.0922$.

Displacement factor coefficients, full lists of bond lengths and angles and F_o/F_c lists have been deposited with the Editor, from whom copies are available on request. Atomic coordinates have also been deposited with the Cambridge Crystallographic Data Centre.

Table 1. Selected bond lengths (Å) and angles (°) of **4**

Zn(1)—Se(1)	2.380(3)	Zn(1)—C(19)	2.131(23)
Zn(1)—Se(1A)	2.380(3)	Zn(1)—C(19A)	2.131(23)
Se(1)—C(1)	1.987(19)	C(19)—N(1)	1.093(28)
N(1)—C(20)	1.403(35)	C(20)—C(21)	1.394(56)
Se(1)—Zn(1)—C(19)	116.4(7)	Se(1)—Zn(1)—Se(1A)	119.8(2)
C(19)—Zn(1)—Se(1A)	105.4(6)	Se(1)—Zn(1)—C(19A)	105.4(6)
C(19)—Zn(1)—C(19A)	89.9(13)	Se(1A)—Zn(1)—C(19A)	116.4(7)
Zn(1)—Se(1)—C(1)	102.8(6)	C(19)—N(1)—C(20)	177.8(24)
Zn(1)—C(19)—N(1)	167.7(24)	N(1)—C(20)—C(21)	112.3(32)

RESULTS AND DISCUSSION

The addition of 1 equivalent of tert-butylisocyanide to a suspension of $[Zn(EAr'')_2]_2$ (E = S, Se) in petroleum ether at room temperature leads to the rapid formation of a clear solution, from which colourless crystals of $[Zn(EAr'')_2(CNBu^t)]_2$ (**1**, E = S; **2**, E = Se) are obtained (Scheme 1). The IR spectra of **1** and **2** exhibit the ν(CN) stretching modes at 2244 and 2218 cm^{-1}, respectively, and display the usual shift to higher frequency on coordination compared with the free ligand (2125 cm^{-1}). Although only one type of chalcogenolato ligands could be discerned by ^1H and ^{13}C NMR spectroscopy and molecular weight measurements do not give meaningful results because of the facile dissociation of donor ligands in solvents such as benzene, complexes **1** and **2** are thought to be dimeric on the basis of the small cone angle of the isocyanide ligands and the precedence for a similar dimeric structure in the case of the aldehyde complex $[Zn(SeAr'')_2(OCHC_6H_4OMe)]_2$.[7] Unfortunately crystals of **1** or **2** proved to be twinned and attempts at determining the crystal structures were unsuccessful.

Treatment of suspensions of $[Zn(EAr'')_2]_2$ in petroleum ether with an excess of Bu^tNC gives the 1:2 complexes $Zn(EAr'')_2(CNBu^t)_2$ (**3**, E = S; **4**, E = Se) as colourless crystals. The ν(CN) bands in the IR spectra are found at similar frequencies, 2223 and 2218 cm^{-1} for **3** and **4**, respectively. The crystal structure of **4** was determined (Fig. 1). Selected bond lengths and angles are given in Table 1.

The complex has a distorted tetrahedral geometry which reflects the steric requirements of the bulky selenolato and small isocyanide ligands. Hence, the Se(1)—Zn—Se(1A) angle is widened to 119.8(2)°, while the angle C(19)—Zn—C(19A) is only 89.9(13)°. The Zn—Se distance of 2.380(3) Å is slightly longer than the bond length between zinc and a terminal selenolato ligand in the related complex $[Zn(SeAr'')_2(OCHC_6H_4OMe)]_2$ (**5**) [2.345(3) Å], but significantly shorter than bridging Zn—Se distances (2.45–2.55 Å).[7] There is to our knowledge no precedence for a zinc complex π-bonded to carbon. However, the Zn—C(19) bond length to the isocyanide ligand appears to be rather long, 2.131(23) Å, when compared for example with the Zn—O distances to the aldehyde ligand in **5** [2.059(7) Å][7] and to the tetrahydrothiophene oxide ligand in $Zn(SeAr'')_2(OSC_4H_8)$ [1.925(14) Å].[6] The C(19)—N(1) bond length of 1.093(28) Å is short compared with transition metal isocyanide ligands, even those which lack *d*-electrons for back-bonding. Some structural parameters of isocyanide complexes are collected in Table 2 for comparison. The shortness of the C—N bonds, together with the long C—Zn distances, indicates that isocyanide ligands

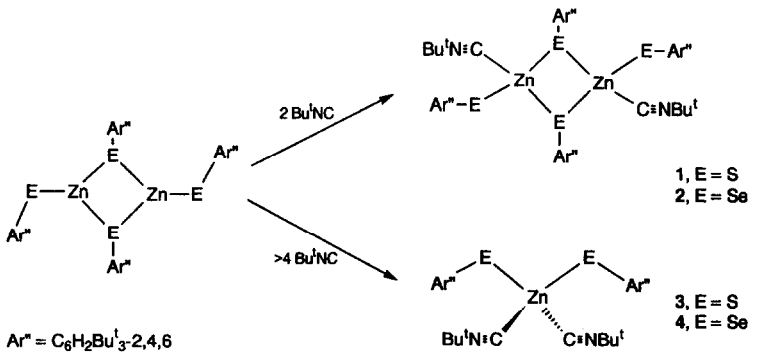

Scheme 1.

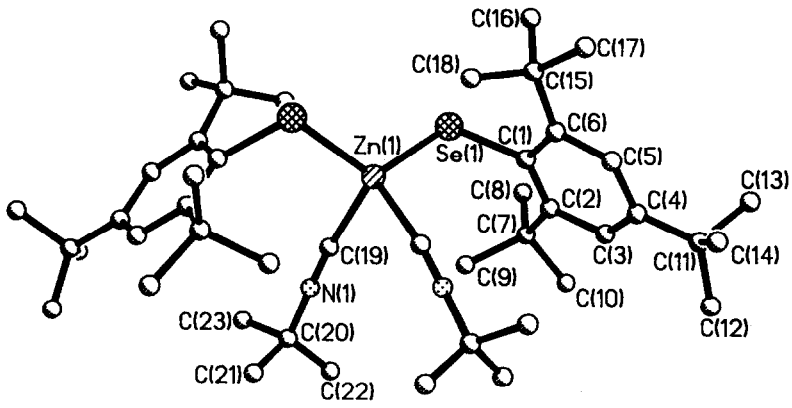

Fig. 1. Molecular structure of $Zn(SeC_6H_2Bu^t_3)_2(CNBu^t)_2$ (**4**), showing the atomic numbering scheme.

Table 2. Comparative data of selected tert-butylisocyanide complexes

Compound	d^n	ν(C≡N) (cm^{-1})	r(C≡N) (Å)	Ref.
$[Cp_2Ti\{\eta^2\text{-}C(NBu^t)Me\}(CNBu^t)]^+$	0	2190	1.150(6)	8
$Cp_2Ti(CO)(CNBu^t)$	2	2170	1.161(12)	9
$[V(CNBu^t)_6]^{2+}$	3	2197	1.150(12)	10
$[Mo(CNBu^t)_7]^{2+}$	4	2143, 2138	1.140(7), 1.165(8)	11
$Ru(PPh_3)(CNBu^t)_4$	8	2100, 2055, 1830	1.17(4), 1.19(4), 1.28(3), 1.22(3)	12
4	10	2218	1.093(28)	This work

in **4** are only weakly bonded to moderately strong Lewis acids such as zinc chalcogenolato ligands and are not stabilized by back-bonding contributions.

Acknowledgements—We are grateful to the Science and Engineering Research Council for support and to the Beit Trust for a studentship (to G.C.B.).

REFERENCES

1. J. A. McCleverty and N. J. Morrison, *J. Chem. Soc., Dalton Trans.* 1976, 2169.
2. A. G. Jones, A. Davison and M. J. Abrams, Eur. Pat. Appl. EP183,555.
3. M. Bochmann, K. Webb, M. Harman and M. B. Hursthouse, *Angew. Chem.* 1990, **102**, 703; *Angew. Chem., Int. Edn Engl.* 1990, **29**, 638; M. Bochmann and K. J. Webb, *Mater. Res. Soc. Symp. Proc.* 1991, **204**, 149; M. Bochmann, A. P. Coleman, K. J. Webb, M. B. Hursthouse and M. Mazid, *Angew. Chem.* 1991, **103**, 703; *Angew. Chem., Int. Edn Engl.* 1991, **30**, 973; M. Bochmann, A. P. Coleman and A. K. Powell, *Polyhedron* 1992, **11**, 507; M. Bochmann, K. J. Webb, J. E. Hails and D. Wolverson, *Eur. J. Solid State Inorg. Chem.* 1992, **29**, 155.
4. M. Bochmann, K. J. Webb, M. B. Hursthouse and M. Mazid, *J. Chem. Soc., Dalton Trans.* 1991, 2317.
5. M. Bochmann, G. Bwembya, R. Grinter, J. Lu, K. J. Webb, D. J. Williamson, M. B. Hursthouse and M. Mazid, *Inorg. Chem.* 1993, **32**, 532.
6. M. Bochmann, G. Bwembya, R. Grinter, A. K. Powell, K. J. Webb, M. B. Hursthouse and M. Mazid, *Inorg. Chem.*, in press.
7. M. Bochmann, K. J. Webb, M. B. Hursthouse and M. Mazid, *J. Chem. Soc., Chem. Commun.* 1991, 1735.
8. M. Bochmann, L. M. Wilson, M. B. Hursthouse and R. L. Short, *Organometallics* 1987, **6**, 2556.
9. L. B. Kool, M. D. Rausch, M. Herberholt, H. G. Alt, U. Thewalt and B. Honolt, *Organometallics* 1986, **5**, 2465.
10. L. D. Silverman, P. W. R. Corfield and S. J. Lippard, *Inorg. Chem.* 1981, **20**, 3106.
11. M. Novotny and S. J. Lippard, *J. Chem. Soc., Chem. Commun.* 1973, 202; F. D. L. Lewis and S. J. Lippard, *J. Am. Chem. Soc.* 1975, **97**, 2697.
12. J. M. Bassett, D. E. Berry, G. K. Barker, M. Green, J. A. K. Howard and F. G. A. Stone, *J. Chem. Soc., Dalton Trans.* 1979, 1003.

Polyhedron Vol. 12, No. 24, pp. 2933–2939, 1993
Printed in Great Britain

0277–5387/93 $6.00+.00
© 1993 Pergamon Press Ltd

FORMATION OF A NOVEL "BEDSPRING"-LIKE FRAMEWORK STRUCTURE BY A NEODYMIUM NITRATE COMPLEX WITH N,N′-BUTYLENEBIS(2-PYRIDONE)

DAVID M. L. GOODGAME,* STUART P. W. HILL and DAVID J. WILLIAMS

Chemistry Department, Imperial College of Science, Technology and Medicine, London SW7 2AY, U.K.

(*Received* 3 *June* 1993; *accepted* 4 *August* 1993)

Abstract—Reaction of N,N′-butylenebis(2-pyridone) (BBP) with hydrated $M(NO_3)_3$ salts (M = Y or a lanthanide ion) affords the complexes $M_2(BBP)_3(NO_3)_6$. Thorium(IV) nitrate and dioxouranium(VI) nitrate give $Th_2(BBP)_3(NO_3)_8 \cdot 0.5Me_2CO$ and $UO_2(BBP)(NO_3)_2$, respectively. X-ray diffraction studies on the Nd complex show it to contain arrays of contiguous 66-membered macrocyclic rings arranged so as to form an unusual "bedspring"-like network structure.

We recently reported a general strategy for the synthesis of polymeric complexes containing arrays of large metallomacrocyclic rings, by the use of bis(pyridone) (**I**) or bis(lactam) ligands (**II**).[1] In order fully to exploit this approach, which is proving to be very fruitful in generating a diversity of new compounds,[2] we are currently assessing how the choice of metal ion, anion and the nature of the bridge between the pyridone (or lactam) units influences the final, polymeric structure adopted. Variations in the ligand bridging unit can be in terms of the bridge length, flexibility or conformational preference(s). As part of this programme, we report here a new and unusual network structure adopted by some lanthanide complexes formed with N,N′-butylenebis(2-pyridone) (**I**, $n = 4$, BBP).

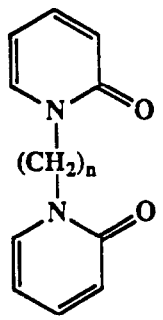

I

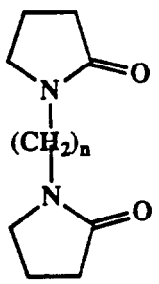

II

EXPERIMENTAL

Preparation of compounds

N,N′-butylenebis(2-pyridone). This was prepared by a literature procedure.[3] Pyridine (9.8 g, 0.125 mol) and 1,4-dibromobutane (15.1 g, 0.062 mol) were refluxed in ethanol (80 cm^3) for several hours. Concentration of the solution gave a white precipitate of the bis-pyridinium salt, which was oxidized to the bis-pyridone by reaction with potassium ferricyanide and sodium hydroxide. The product was extracted with chloroform; yield 55%. Found: C, 67.6; H, 6.7; N, 11.2. Calc. for $C_{14}H_{16}N_2O_2 \cdot 0.25H_2O$: C, 67.6; H, 6.6; N, 11.3%.

Metal complexes. The complexes obtained are listed in Table 1, together with their analytical data (Microanalytical Laboratory, Imperial College). They were prepared by reacting the appropriate

*Author to whom correspondence should be addressed.

Table 1. Analytical[a] data for the complexes

Complex	Colour	Analysis(%) C	H	N
$M_2(BBP)_3(NO_3)_6$				
M = Y	White	39.5	4.0	12.8
		(39.3)	(3.8)	(13.1)
La	White	36.5	3.4	12.0
		(36.5)	(3.5)	(12.2)
Ce[b]	White	38.4	3.7	11.9
		(38.4)	(3.8)	(11.6)
Pr[c]	Green	37.8	3.7	11.8
		(37.4)	(4.0)	(11.2)
Nd[c]	Lilac	37.1	3.7	11.2
		(37.2)	(3.7)	(11.6)
Sm	White	36.3	3.5	12.2
		(35.9)	(3.4)	(12.0)
Eu	White	35.7	3.3	11.7
		(35.8)	(3.4)	(11.9)
Gd	White	35.8	3.4	11.8
		(35.5)	(3.4)	(11.9)
Tb	White	35.6	3.4	11.6
		(35.4)	(3.4)	(11.8)
Dy	White	35.4	3.4	11.4
		(35.2)	(3.4)	(11.7)
Ho	Pink	35.3	3.4	11.4
		(35.2)	(3.4)	(11.7)
Er	Pink	35.3	3.4	11.6
		(35.0)	(3.3)	(11.7)
Tm	White	35.3	3.4	11.4
		(35.0)	(3.3)	(11.7)
Yb	White	35.0	3.3	11.3
		(34.8)	(3.3)	(11.6)
$Th_2(BBP)_3(NO_3)_8$[d]	White	30.5	2.9	11.2
		(30.3)	(3.0)	(11.4)
$UO_2(BBP)(NO_3)_2$	Yellow	26.4	2.5	8.4
		(26.3)	(2.5)	(8.8)

[a]Calculated values are given in parentheses.
[b]Formula: $M_2(BBP)_3(NO_3)_6 \cdot Me_2CO$
[c]Formula: $M_2(BBP)_3(NO_3)_6 \cdot 0.5Me_2CO$
[d]With 0.5 mol acetone of solvation.

hydrated metal nitrate and BBP in (1 : 2 mole ratio) in a mixture of methanol and 2,2-dimethoxypropane.

Crystallography

Crystal data for $Nd_2(BBP)_3(NO_3)_6$, $C_{42}H_{48}N_{12}Nd_2O_{24}$, $M = 1393.4$, monoclinic, $a = 16.252(7)$, $b = 9.599(6)$, $c = 17.466(9)$ Å, $\beta = 91.46(2)°$, $U = 2724$ Å^3, space group $P2_1/c$, $Z = 2$, $D_c = 1.699$ g cm^{-3}, μ(Mo-K_α) = 20 cm^{-1}, $\lambda = 0.71073$ Å, $F(000) = 1392$. Lilac–purple rhombic prisms, crystal dimensions 0.13 × 0.30 × 0.30 mm.

Data collection and processing

Siemens P4/PC diffractometer, ω-scan method ($4 < 2\theta < 50°$), graphite monochromated Mo-K_α radiation. 4802 independent reflections were measured, of which 3880 were considered observed [$|F_o| > 4\sigma(|F_o|)$] and corrected for Lorentz and polarization factors; no absorption correction was applied.

Structure analysis and refinement

The structure was solved by the heavy atom method. The non-hydrogen atoms were refined

Table 2. Selected bond lengths (Å) and angles (°) for **I**

Nd—O(2)	2.361(4)	Nd—O(12)	2.366(4)
Nd—O(22)	2.385(3)	Nd—O(31)	2.560(4)
Nd—O(32)	2.555(4)	Nd—O(41)	2.521(4)
Nd—O(42)	2.556(4)	Nd—O(51)	2.511(4)
Nd—O(52)	2.536(4)		

O(2)—Nd—O(12)	79.0(1)	O(2)—Nd—O(22)	153.4(1)
O(12)—Nd—O(22)	85.7(1)	O(2)—Nd—O(31)	72.5(1)
O(12)—Nd—O(31)	146.1(1)	O(22)—Nd—O(31)	127.4(1)
O(2)—Nd—O(32)	121.9(1)	O(12)—Nd—O(32)	153.5(1)
O(22)—Nd—O(32)	80.0(1)	O(31)—Nd—O(32)	49.4(1)
O(2)—Nd—O(41)	93.3(1)	O(12)—Nd—O(41)	128.2(1)
O(22)—Nd—O(41)	79.1(1)	O(31)—Nd—O(41)	72.3(1)
O(32)—Nd—O(41)	70.8(1)	O(2)—Nd—O(42)	80.8(1)
O(12)—Nd—O(42)	78.3(1)	O(22)—Nd—O(42)	74.7(1)
O(31)—Nd—O(42)	114.0(1)	O(32)—Nd—O(42)	118.5(1)
O(41)—Nd—O(42)	49.9(1)	O(2)—Nd—O(51)	126.0(1)
O(12)—Nd—O(51)	78.3(1)	O(22)—Nd—O(51)	70.8(1)
O(31)—Nd—O(51)	104.0(1)	O(32)—Nd—O(51)	76.0(1)
O(41)—Nd—O(51)	138.3(1)	O(42)—Nd—O(51)	139.3(1)
O(2)—Nd—O(52)	78.5(1)	O(12)—Nd—O(52)	81.0(1)
O(22)—Nd—O(52)	120.7(1)	O(31)—Nd—O(52)	75.7(1)
O(32)—Nd—O(52)	87.2(1)	O(41)—Nd—O(52)	148.0(1)
O(42)—Nd—O(52)	153.1(1)	O(51)—Nd—O(52)	50.0(1)

anisotropically. The positions of the hydrogen atoms were idealized, C—H = 0.96 Å, assigned isotropic thermal parameters, $U(H) = 1.2U_{eq}(C)$, and allowed to ride on their parent carbon atoms. Refinement was by full-matrix least-squares to give $R = 0.033$, $R_w = 0.033$ [$w^{-1} = \sigma^2(F) + 0.0005F^2$]. The mean and maximum shift/error in the final refinement were 0.000 and 0.002, respectively, and the maximum and minimum residual electron densities in the final ΔF map were 0.89 and -1.42 eÅ^{-3}, respectively.

Computations were performed on an IBM PS2 model 70 386 computer using the SHELXTL PC system[4] and published scattering factors.[5] Selected bond lengths and angles are listed in Table 2.

RESULTS AND DISCUSSION

Reaction of BBP with the hydrated nitrates of yttrium(III), the M^{3+} lanthanide ions and thorium(IV) in methanol/2,2-dimethoxypropane in each case afforded complexes with a 3:2 BBP:M ratio. In some cases, particularly with the larger metal ions, the solids initially isolated tended to retain some acetone of solvation, presumably formed from the reaction between the 2,2-dimethoxypropane and the water of hydration of the metal salts employed.

X-ray powder diffraction studies showed that the lanthanide compounds from Nd to Tb are isostructural. (The powder patterns of the Ho and Yb complexes are virtually identical to those of the earlier members of the series, but with a small displacement of some of the diffraction arcs. It is probable that they have essentially the same gross structure as the earlier lanthanide complexes but with a small difference in lattice size.)

A representative member of the series, the neodymium complex (**I**), was obtained in a form suitable for a single-crystal X-ray study. This analysis shows that the stoichiometry is $Nd(BBP)_{1.5}(NO_3)_3$. Each Nd atom is nine-coordinate, being bonded to one oxygen atom from each of three different BBP ligands and six oxygen atoms from three bidentate nitrate groups (Fig. 1). The geometry about the Nd centre is best described as very distorted tricapped trigonal prismatic, with O(2)O(12)O(52) and O(22)O(32)O(41) defining the trigonal faces and O(31), O(42) and O(51) as the face-capping atoms. The Nd—O distances are in the range 2.361(4)–2.385(4) Å to the carbonyl oxygens and 2.511(4)–2.560(4) Å to the nitrate oxygens. It is noticeable that the nitrate groups are concentrated in one coordination hemisphere, whilst the pyridones of the BBP ligands dominate the other.

The BBP ligands bridge adjacent Nd atoms to

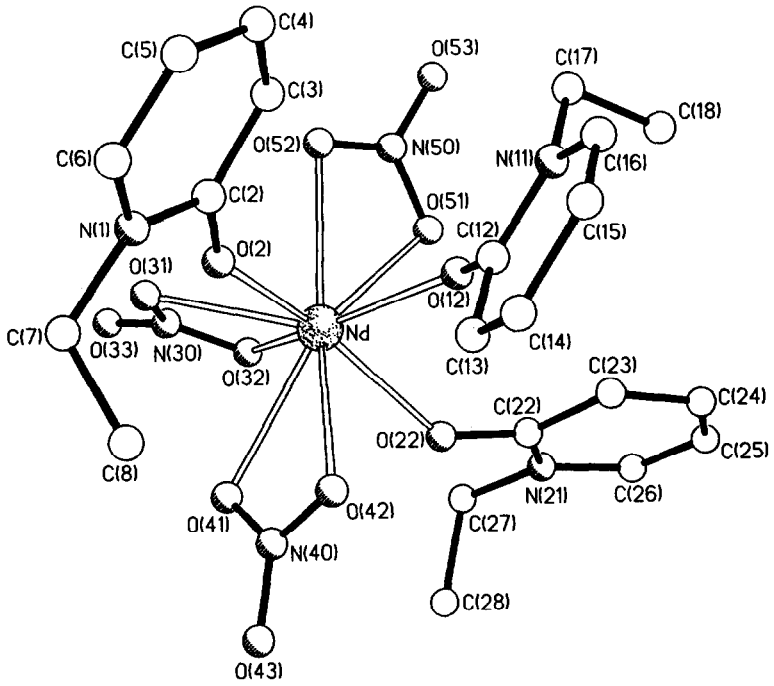

Fig. 1. The nine-coordinate neodymium environment in I showing the crystallographic numbering scheme.

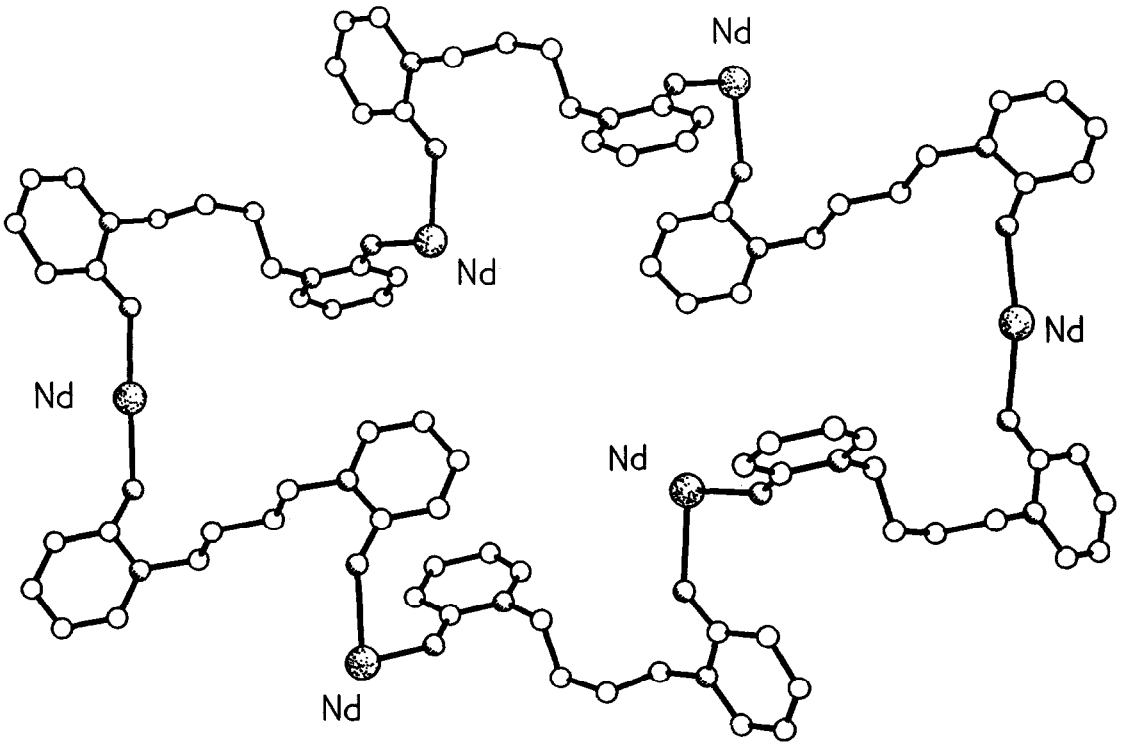

Fig. 2. The 66-membered metallomacrocyclic ring, which comprises the basic repeat unit in the structure of I. (The nitrate groups and one of the pyridone units bonded to each Nd atom have been omitted for clarity.)

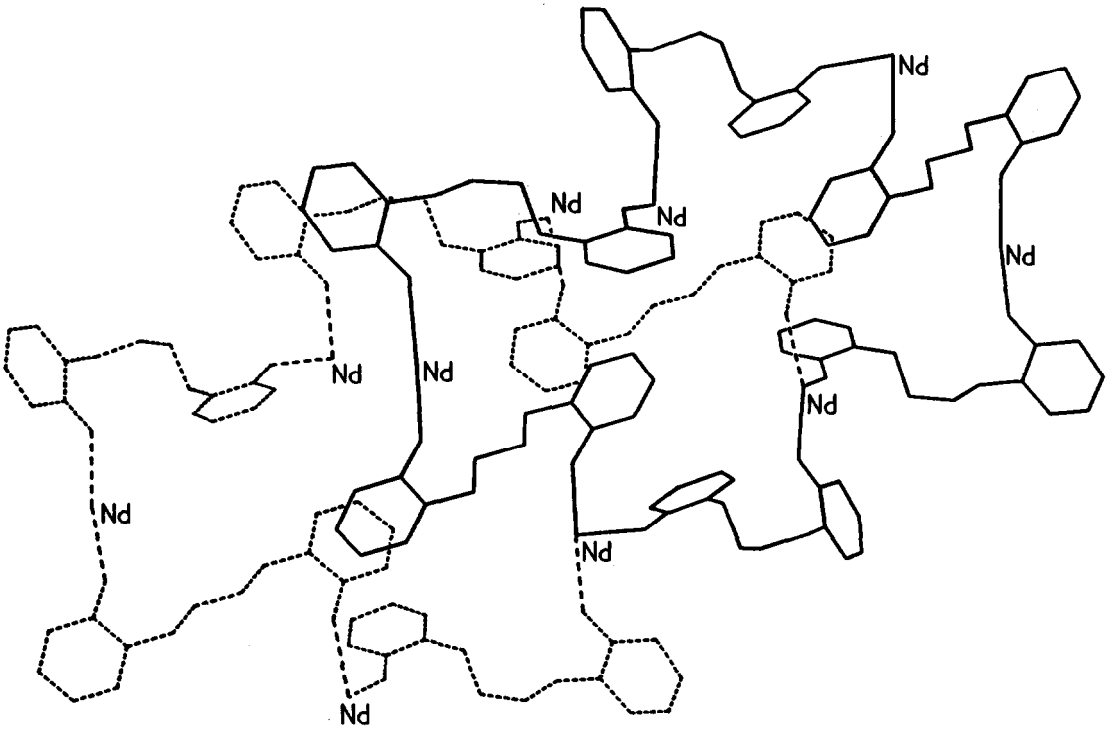

Fig. 3. Illustration of the way adjacent pairs of 66-membered rings are joined in the structure of **I**.

form a complex network of fused 66-membered metallomacrocyclic rings, each containing six neodymium, 12 nitrogen, 12 oxygen and 36 carbon atoms. The basic ring framework is shown in Fig. 2 in a simplified form, i.e. without the nitrate groups and without the BBP ligands which connect each Nd atom to two other, equivalent 66-membered rings. Within each 66-membered ring the $-(CH_2)_4-$ units of the 6 BBP ligands adopt two different conformations. In two of them the pyridone rings are essentially co-planar, but in the other four the rings are virtually orthogonal. Associated with these two geometries are two different butylene chain conformations. When the rings are parallel

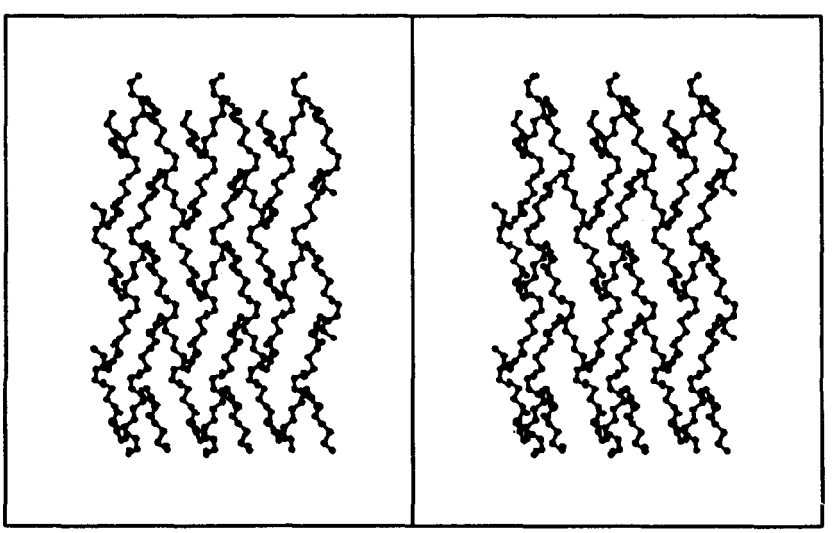

Fig. 4. Stereoscopic view down the crystallographic *a* axis of the polymeric units formed by **I** in the crystal.

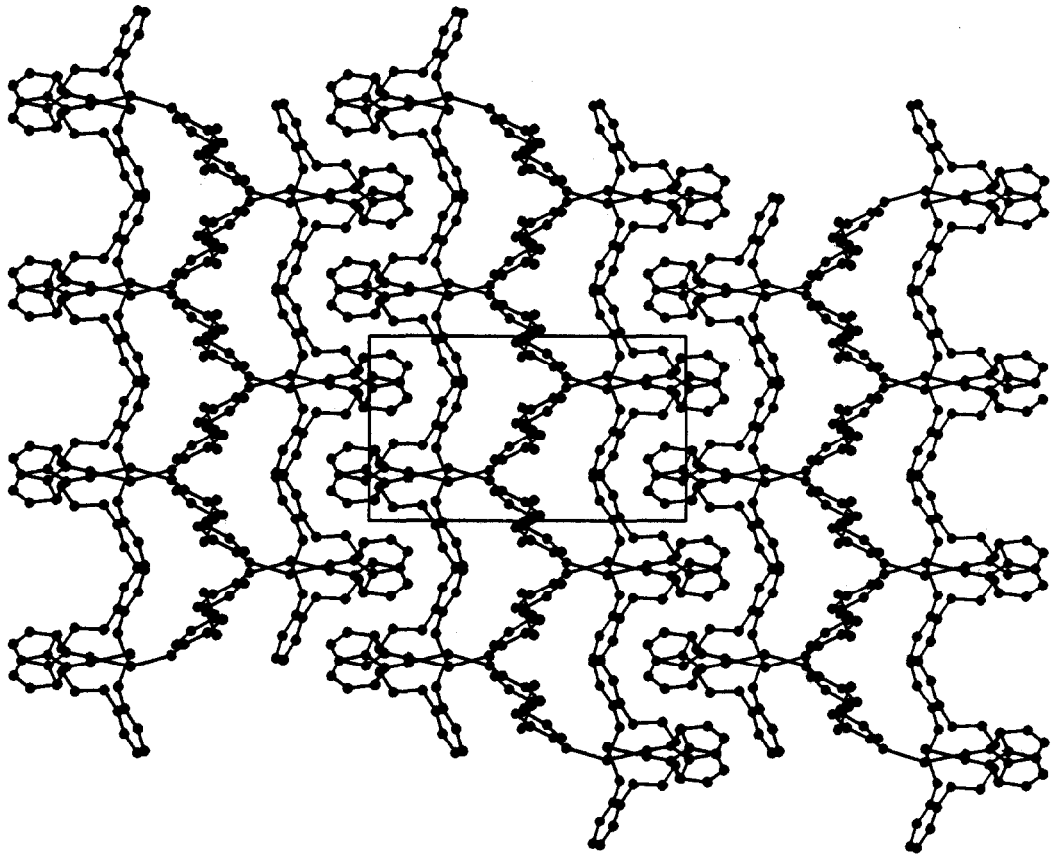

Fig. 5. Parallel projection down the crystallographic *c* axis of the interleaving sheets in **I** (nitrates omitted for clarity).

the chain adopts conventional all-*anti*-geometry, whereas when the rings are orthogonal the central CH_2—CH_2 bond is essentially *gauche*.

The nature of the linking of the 66-membered rings to form the contiguous network is somewhat complex. Figure 3 illustrates two such linked rings, both of which have identical conformations, and Fig. 4 shows a stereoscopic view (down the crystallographic *a* direction) of the extended network that results (the nitrates and parts of the phenyl rings have been omitted for clarity).

The network is not contiguous throughout the crystal. It comprises interleaving corrugated sheets that extend in the crystallographic *b* and *c* directions. Figure 5 is a projection of the structure down the crystallographic *c* direction and shows the interleaving of adjacent sheets that occurs within the (100) plane. Associated with this interleaving are parallel π–π stacking interactions between the pyridone rings of adjacent sheets. The interplanar separations are 3.37 Å, with a ring centroid–ring centroid distance of 3.9 Å.

It is interesting to compare the core geometry of **I** with that of the closely-related complex (**II**) formed by manganese(II) nitrate with N,N′-ethylenebis(2-pyridone) (**I**, $n = 2$).[1] In both instances, the oxygen donor atoms from the pyridone ligands adopt a meridional arrangement about the metal ion. Also, in the linking between adjacent metal centres in **I** and **II**, both orthogonal and essentially co-planar arrangements of pyridone rings are present. However, the final overall structures adopted are dramatically different, with chains of 36-membered macrocycles being formed in **II** in contrast to the 66-membered rings observed for **I**. It is not immediately obvious whether the difference in the arrays formed is due to the increase in the length of the spacer alkane groups or to the larger number of coordinated nitrates in **I**.

Acknowledgements—We thank the SERC for the X-ray diffractometer and for a research studentship (to S.P.W.H).

REFERENCES

1. G. A. Doyle, D. M. L. Goodgame, S. P. W. Hill and D. J. Williams, *J. Chem. Soc., Chem. Commun.* 1993, 207.
2. D. M. L. Goodgame, S. P. W. Hill and D. J. Williams, *J. Chem. Soc., Chem. Commun.* 1993, 1019.
3. J. A. Gautier and J. Renault, *Compt. Rend.* 1947, **225**, 682; *Rec. Trav. chim.* 1950, **69**, 421.
4. G. M. Sheldrick, SHELXTL PC, Version 4.2, Siemens Analytical Instruments Inc. (1990).
5. *International Tables for X-ray Crystallography*, Vol. 4, pp. 99–149. Kynoch Press, Birmingham (1974).

Polyhedron Vol. 12, No. 24, pp. 2941–2945, 1993
Printed in Great Britain

0277–5387/93 $6.00+.00
© 1993 Pergamon Press Ltd

SYNTHESIS AND X-RAY STRUCTURE OF AN ISOMERIC CYCLOPHOSPHAZENE COMPLEX CONTAINING ANTIMONY(III)

SUSHIL K. PANDEY, REINHARD HASSELBRING, ALEXANDER STEINER, DIETMAR STALKE and HERBERT W. ROESKY*

Institut für Anorganische Chemie der Universität Göttingen, Tammannstrasse, D-37077 Göttingen, Germany

(*Received* 3 *June* 1993; *accepted* 4 *August* 1993)

Abstract—The monosilylated acyclic phosphazene ligand $Me_3SiNP(NMe_2)_2NP(NMe_2)_2NH_2$ (**3**) has been synthesized and characterized. The reaction of **3** with antimony triacetate, $Sb(OOCMe)_3$, in refluxing toluene forms a cyclic phosphazene derivative, $[N\{P(NMe_2)_2NH\}_2Sb(OOCMe)_2]$ (**4**), which is characterized by elemental analyses, mass, IR and NMR spectroscopy and single-crystal X-ray structural analysis. Complex **4** crystallizes in the form of a *cis* and *trans* isomeric chain in the solid state.

In the past few decades a large amount of work has been carried out on various reactions of cyclophosphazenes.[1] Recently, the development of cyclometallaphosphazene chemistry has created a versatile field of research, particularly when transition metals are used as the building blocks for the cyclophosphazene skeleton.[2] These complexes have interesting structural aspects as well as physical properties.[3,4] A careful literature search shows the paucity of information on such derivatives where main group metals are part of the cyclophosphazene ring system. However, no such antimony(III) derivative has been reported.[1,5,6] In contrast, various derivatives having Sb—O and Sb—S units have been synthesized in recent years.[5,6] In this paper, we report on the synthesis and characterization of a monosilylated phosphazene ligand, along with the X-ray structure of a cycloantimony(III)phosphazene complex. We used antimony(III)acetate as a starting material knowing that the carboxylate moiety has shown various structural arrangements.[7]

RESULTS AND DISCUSSION

The monosilylated acyclic phosphazene ligand **3** was obtained as a viscous liquid in a two step synthesis (Ia and Ib). In the first step (Ia), the Bezman salt[8] (**1**) reacted with NaH with the evolution of hydrogen forming compound **2**, which on silylation with Me_3SiNMe_2 resulted in the formation of **3**.

Ia- $[N\{P(NMe_2)_2NH_2\}_2]^+Cl^- + NaH$

1

$$\xrightarrow[-NaCl\ -H_2]{toluene} HN[P(NMe_2)_2NH]_2$$

2

Ib- **2** $+ Me_3SiNMe_2 \xrightarrow[-HNMe_2]{}$

$$Me_3SiNP(NMe_2)_2NP(NMe_2)_2NH_2$$

3

Compound **3** was characterized by elemental analyses, mass, NMR and IR spectral data. It reacts with antimony(III)acetate, $Sb(OOCMe)_3$, in refluxing toluene in a 1 : 1 molar ratio resulting in the formation of the cycloantimony(III)phosphazene complex (**4**). The reaction can be depicted as below.

3 $+ Sb(OOCMe)_3 \xrightarrow[-MeCOOSiMe_3]{toluene}$

$$[N\{P(NMe_2)_2NH\}_2Sb(OOCMe)_2]$$

4

The reaction occurs with the elimination of 1 mol of $MeCOOSiMe_3$, which can be easily removed *in vacuo*. The product obtained is sufficiently pure for spectroscopic studies. However, it can be further purified by crystallization from n-hexane solution.

*Author to whom correspondence should be addressed.

Complex **4** is a white solid, moisture-sensitive and fairly soluble in organic solvents. The IR spectra of **4** shows the P—N bands in the 1170–1287 cm^{-1} region, which are in accordance with a P—N—P ring system. The C—O frequency appears at 1670 cm^{-1}, which is indicative of the monodentate nature of the acetate moiety. In the ^1H NMR spectra of **4** the presence of the —NH proton at 3.60 ppm and the disappearence of —$SiMe_3$ protons is observed. The —NMe_2 protons in **3** were found as double doublets in the 2.4–2.5 ppm region, while only one doublet is observed for **4**. The ^{31}P NMR chemical shift of **3** consists of two doublets (δ 11.6 and 23.3 ppm), due to the non-equivalent nature of phosphorus nuclei, while in complex **4** only one singlet is found (δ 25.6 ppm), which is indicative of one type of phosphorus nucleus.

X-ray structure of **4**

Suitable crystals were obtained by cooling the n-hexane solution of compound **4** to 0°C. This compound crystallizes as *cis* and *trans* isomeric chains in the solid state. The X-ray analysis of **4** shows two independent monomers in the asymmetric unit (Fig. 1). The backbone of these monomers consists of slightly twisted six-membered antimony diphosphatriazene ring systems. The average deviation from the best plane of the six-ring atoms is 15.8 (a) and 9.7 pm (b), respectively. The antimony atoms can be described as trigonal bipyramidal coordinate, with the lone pair stereochemically active in the equatorial position. The oxygen atoms of the axial coordinated acetate groups are bound in an average distance of 226 pm to the antimony atom. The average O—Sb—O angle is 162°. The Sb—N distances are 201 and 205 pm, respectively. The average N—Sb—N angle is 94°. This arrangement is in accordance with valence bond theory. The two independent monomers occur in two different conformations: in (a) the acetyl groups are oriented *trans* and in (b) they are oriented *cis* with respect to each other. The molecules are linked via NH···O··· hydrogen bridges to form infinite chains (Fig. 2). In the *trans* isomer one NH— and two acetyl groups and in the *cis* isomer two NH— and one acetyl group are involved in hydrogen bonding. The polymeric chain adopts the [$(cis)_2(trans)_2$] pattern. The centre of inversion is located between two *trans* and two *cis* isomers.

EXPERIMENTAL

General methods

All manipulations were performed under dry nitrogen using Schlenk, vacuum-line and glovebox techniques. Solvents were dried and degassed prior to use. IR and mass spectra were recorded on a Bio-Rad FTS 7 spectrophotometer and a Finnigan MAT system 8230, respectively. ^1H and ^{31}P NMR spectra were recorded on a Bruker AM 250 spectrometer using TMS and 85% H_3PO_4 as an external reference. Elemental analyses were obtained from the analytical laboratory, Institute of Inorganic Chemistry, Göttingen. Antimony(III) acetate was prepared using a literature method.[9]

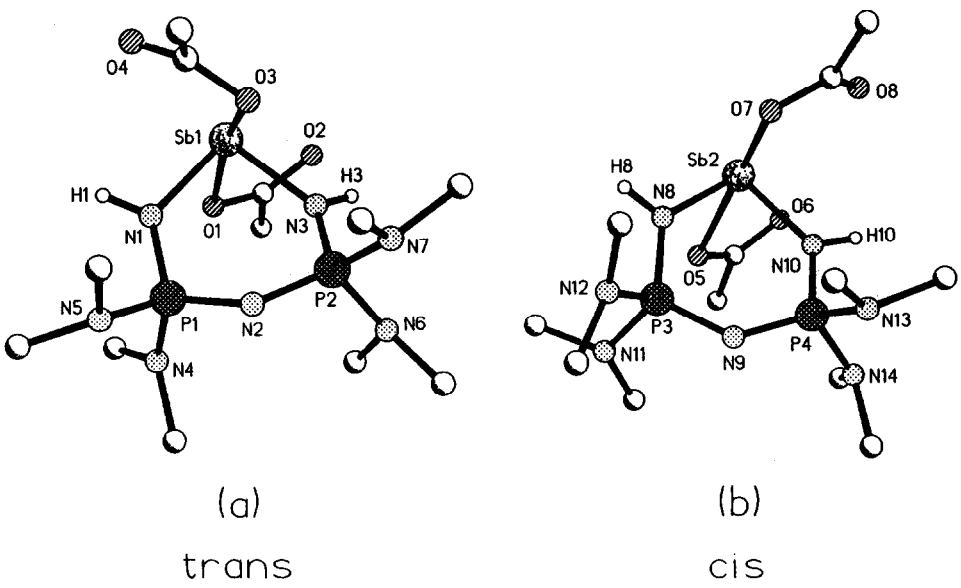

Fig. 1. Molecular structure of **4** having two independent *cis* and *trans* isomers.

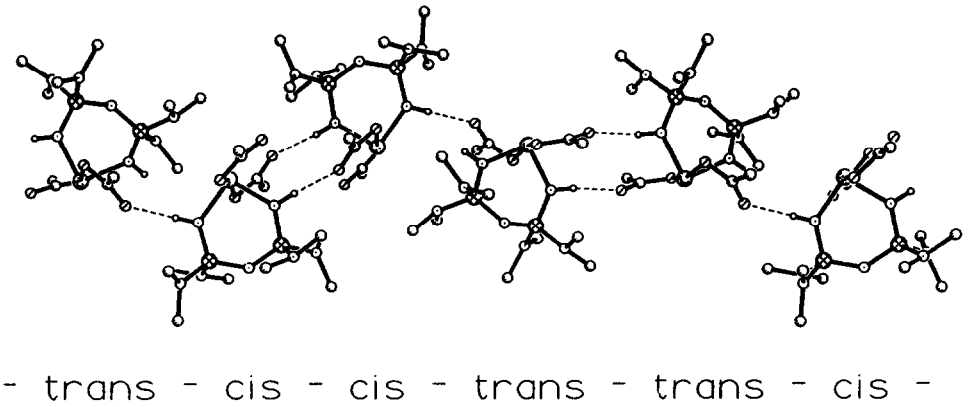

Fig. 2. Polymeric chain of **4** with a $[(cis)_2(trans)_2]$ pattern.

Crystallography

Intensity data for the crystal were measured at 153 K on a Stoe-Siemens AED diffractometer equipped with Mo-K_α radiation (graphite monochromator, $\lambda = 0.71073$ Å), employing the ω–2θ scan technique. The data sets were corrected for Lorentz and polarization effects. Crystal data are listed in Table 1. The structure was solved by direct methods[10] and each refined by full-matrix least-squares procedures on F^2.[11] All non-hydrogen atoms were refined with anisotropic displacement parameters and hydrogen atoms were set geometrically. A weighting scheme of the form $w^{-1} = \sigma(F_0^2)+(g1\ P)^2+g^2\ P$, with $P = (F_0^2+2F_c^2)/3$, was introduced for the structure. Selected bond lengths and angles are given in Table 2. Additional material available from the Cambridge

Table 1. Crystal data and structure refinement for **4**

Empirical formula	$C_{12}H_{32}N_7O_4P_2Sb$
Formula weight	521.81
Temperature (K)	153(2)
Wavelength (pm)	71.073
Crystal system	Triclinic
Space group	$P\bar{1}$
Unit cell dimensions:	
a(pm) 955.5(7)	α(°) 78.45(6)
b(pm) 1142.6(9)	β(°) 82.78(6)
c(pm) 2330(2)	γ(°) 76.39(4)
Volume (nm^3)	2.414(3)
Z	4
Density (calculated) (mg m^{-3})	1.437
Absorption coefficient (mm^{-1})	1.303
F(000)	1064
Crystal size (mm)	0.3 × 0.3 × 0.3
θ range for data collection (°)	4.05–22.59
Index ranges	$-10 \leqslant h \leqslant 10$, $-11 \leqslant k \leqslant 12$, $-21 \leqslant l \leqslant 25$
Reflections collected	8061
Independent reflections	6327 ($R_{int} = 0.0216$)
Absorption correction	Semi-empirical with 349 psi-scans
Max. and min. transmission	0.868 and 0.721
Refinement method	Full-matrix least-squares on F^2
Data / restraints / parameters	6327 / 92 / 553
Goodness-of-fit on F^2	1.037
Final R indices [$I > 2\sigma(I)$]	$R1 = 0.0258$, $wR2 = 0.0667$
R indices (all data)	$R1 = 0.0298$, $wR2 = 0.0693$
Largest difference peak and hole (e nm^{-3})	569 and −854

Table 2. Selected bond lengths (pm) and angles (°) for **4**

Sb(1)—N(1)	202.7(3)	Sb(1)—N(3)	203.2(3)
Sb(1)—O(3)	225.7(3)	Sb(1)—O(1)	226.9(3)
P(1)—N(2)	157.9(3)	P(1)—N(1)	161.6(3)
P(1)—N(4)	163.9(3)	P(1)—N(5)	164.7(3)
P(2)—N(2)	156.9(3)	P(2)—N(3)	162.1(3)
P(2)—N(7)	163.2(3)	P(2)—N(6)	164.9(3)
O(1)—C(1)	128.2(5)	O(2)—C(1)	123.7(5)
O(3)—C(3)	128.4(4)	O(4)—C(3)	123.3(5)
C(1)—C(2)	150.4(6)	C(3)—C(4)	150.4(6)
Sb(2)—N(10)	201.5(3)	Sb(2)—N(8)	205.0(3)
Sb(2)—O(7)	225.3(3)	Sb(2)—O(5)	226.0(3)
P(3)—N(9)	157.0(3)	P(3)—N(8)	160.6(3)
P(4)—N(9)	157.1(3)	P(4)—N(10)	161.1(3)
P(4)—N(14)	164.3(3)	P(4)—N(13)	165.5(3)
O(5)—C(13)	128.1(4)	O(6)—C(13)	123.9(4)
O(7)—C(15)	128.9(4)	O(8)—C(15)	123.2(4)
N(1)—Sb(1)—N(3)	93.36(13)	N(1)—Sb(1)—O(3)	85.61(11)
N(3)—Sb(1)—O(3)	81.36(11)	N(1)—Sb(1)—O(1)	82.96(12)
N(3)—Sb(1)—O(1)	85.54(12)	O(3)—Sb(1)—O(1)	162.06(9)
N(2)—P(1)—N(1)	113.9(2)	N(2)—P(1)—N(4)	111.3(2)
N(1)—P(1)—N(4)	107.8(2)	N(2)—P(1)—N(5)	106.0(2)
N(1)—P(1)—N(5)	110.8(2)	N(4)—P(1)—N(5)	106.9(2)
N(2)—P(2)—N(3)	111.9(2)	N(2)—P(2)—N(7)	107.9(2)
N(3)—P(2)—N(7)	113.9(2)	N(2)—P(2)—N(6)	116.5(2)
N(3)—P(2)—N(6)	103.0(2)	N(7)—P(2)—N(6)	103.4(2)
C(1)—O(1)—Sb(1)	109.3(3)	C(3)—O(3)—Sb(1)	108.3(2)
P(1)—N(1)—Sb(1)	127.7(2)	P(2)—N(2)—P(1)	130.0(2)
P(2)—N(3)—Sb(1)	128.9(2)	O(2)—C(1)—O(1)	122.6(4)
O(2)—C(1)—C(2)	120.4(4)	O(1)—C(1)—C(2)	116.9(4)
O(4)—C(3)—O(3)	122.6(4)	O(4)—C(3)—C(4)	120.9(3)
O(3)—C(3)—C(4)	116.5(4)	N(10)—Sb(2)—N(8)	94.75(12)
N(10)—Sb(2)—O(7)	87.41(11)	N(8)—Sb(2)—O(7)	82.02(11)
N(10)—Sb(2)—O(5)	85.86(11)	N(8)—Sb(2)—O(5)	81.22(11)
O(7)—Sb(2)—O(5)	161.34(8)	N(9)—P(3)—N(8)	112.8(2)
N(9)—P(3)—N(11)	106.4(2)	N(8)—P(3)—N(11)	115.6(2)
N(9)—P(3)—N(12)	116.6(2)	N(8)—P(3)—N(12)	104.0(2)
N(11)—P(3)—N(12)	101.3(2)	N(9)—P(4)—N(10)	113.3(2)
N(9)—P(4)—N(14)	115.3(2)	N(10)—P(4)—N(14)	105.7(2)
N(9)—P(4)—N(13)	106.9(2)	N(10)—P(4)—N(13)	113.6(2)
N(14)—P(4)—N(13)	101.6(2)	C(13)—O(5)—Sb(2)	107.8(2)
C(15)—O(7)—Sb(2)	107.1(2)	P(3)—N(8)—Sb(2)	128.7(2)
P(3)—N(9)—P(4)	135.3(2)	P(4)—N(10)—Sb(2)	130.4(2)
O(6)—C(13)—O(5)	123.1(3)	O(6)—C(13)—C(14)	120.5(3)
O(5)—C(13)—C(14)	116.4(3)	O(8)—C(15)—O(7)	122.8(3)
O(8)—C(15)—C(16)	120.6(3)	O(7)—C(15)—C(16)	116.7(3)

Symmetry transformations used to generate equivalent atoms.

Crystallographic data centre comprises atom coordinates, anisotropic displacement parameters and remaining bond lengths and angles.

Synthesis of $Me_3SiNP(NMe_2)_2NP(NMe_2)_2NH_2$ **(3)**

Compound **1** (0.9 g, 60 mmol) was refluxed with NaH (0.25 g, 6.3 mmol) in toluene (25 cm^3) for 6 h until the elimination of hydrogen gas ceased. The mixture was then cooled to room temperature and Me_3SiNMe_2 (0.7 g, 6 mmol) was added dropwise. The contents were further refluxed for 4 h, cooled to room temperature and filtered using a sintered glass funnel. All volatiles were removed *in vacuo* and then distilled. Compound **3** was obtained as a light yellow viscous liquid at 104°C and 0.1 mm.

Elemental analysis: Found: C, 36.3; H, 9.8; N, 29.6. Calc. for $C_{11}H_{35}N_7P_2Si$(355 g mol^{-1}): C, 37.2; H, 9.9; N, 27.6%. EI-MS, m/z(%): 355 (54) (M), 268 (100) ($M-2NMe_2+H$). ^1H NMR ($CDCl_3$): δ 0.09 (d, 9H, —$SiMe_3$), δ 2.48 (d, 12H, —NMe_2), δ 2.53 (d, 12H, —NMe_2) ppm. ^{31}P NMR ($CDCl_3$): δ 11.6 (d, P=$NSiMe_3$), δ 23.3 (d, P=NH) ppm. IR (Nujol): 3453m, 3200b, 2944vs, 2878vs, 2794s, 1630s, 1534m, 1282vs, 1239vs, 1189vs, 1148s, 979vs, 856s, 825s and 747s cm^{-1}.

Synthesis of $[N\{P(NMe_2)_2NH\}_2Sb(OOCMe)_2]$ **(4)**

A toluene solution (25 cm^3) of $Sb(OOCMe)_3$ (0.84 g, 2.8 mmol) was added to a toluene (25 cm^3) solution of **3** (1.0 g, 2.8 mmol). The contents were heated for 3 h and a clear colourless solution was thus obtained. All volatiles were removed under reduced pressure and a white solid remained, which was crystallized from n-hexane at 0°C; m.p. 72.5 °C. Elemental analysis: Found: C, 27.5; H, 6.2; N, 17.9; Sb, 24.2. Calc. for $C_{12}H_{32}N_7O_4P_2Sb$ (521.81 g mol^{-1}): C, 27.6; H, 6.1; N, 18.8; Sb, 23.3%. EI-MS, *m/z* (%): 461 (2) (M − MeCOO), 169 (100) [Sb(O) ($OOCCH_3$)]. ^1H NMR ($CDCl_3$): δ 1.90 (s, 6H, —MeCOO), δ 2.58 (d, 24H, —NMe_2, J=11.4 Hz), δ 3.60 (s, 2H, —NH) ppm. ^{31}P NMR ($CDCl_3$): δ 25.63 (s) ppm. IR (Nujol): 1670m, 1622s, 1556m, 1465vs, 1287mb, 1261m, 1183m, 1170m, 1062m, 980vs, 804m, 741vs, 671s, 620m, 486s and 462m cm^{-1}.

Acknowledgement—The authors gratefully acknowledge financial support from the Fonds der Chemischen Industrie and the Deutsche Forschungsgemeinschaft. One of the authors (S. K. P.) thanks the Alexander von Humboldt foundation, Germany for providing a post-doc fellowship.

REFERENCES

1. H. R. Allcock, *Phosphorus Nitrogen Compounds*. Academic Press, New York (1972).
2. H. W. Roesky, *Synlett* 1990, 651.
3. R. Hasselbring, H. W. Roesky and M. Noltemeyer, *Angew. Chem.* 1992, **104**, 613; *Angew. Chem., Int. Edn Engl.* 1992, **31**, 601; H. W. Roesky and M. Lücke, *Angew. Chem.* 1989, **101**, 480; *Angew. Chem., Int. Edn Engl.* 1989, **28**, 493.
4. H. W. Roesky, K. V. Katti, U. Seseke, M. Witt, E. Egert, R. Herbst and G. M. Sheldrick, *Angew. Chem.* 1986, **98**, 447; *Angew. Chem., Int. Edn Engl.* 1986, **25**, 477; H. W. Roesky, K. V. Katti, U. Seseke, H.-G. Schmidt, E. Egert, R. Herbst and G. M. Sheldrick, *J. Chem. Soc., Dalton Trans.* 1987, 847; K. V. Katti, H. W. Roesky and M. Rietzel, *Inorg. Chem.* 1987, **26**, 4032; K. V. Katti, U. Seseke, M. Witt and H. W. Roesky, *Phosphorus Sulphur* 1987, **30**, 421; M. Witt and H. W. Roesky, *Polyhedron* 1989, **8**, 1736.
5. D. A. Armitage, *Chem. Org. Silicon Comp* 1989, **2**, 1363; P. D. Lickiss, *Ann. Rep. Prog. Chem. Sect. B* 1989, **85**, 241.
6. L. D. Freedman and G. O. Doak, *J. Organomet. Chem.* 1991, **404**, 49.
7. R. C. Mehrotra and R. Bohra, *Metal Carboxylates*. Academic Press, London (1983).
8. I. I. Bezman and J. H. Smalley, *Chem. Ind.* 1960, 839.
9. F. Nerdel and J. Kleinwächter, *Chem. Ber.* 1957, **90**, 598.
10. G. M. Sheldrick, *Acta Cryst., Sect. A* 1990, **46**, 467.
11. G. M. Sheldrick, SHELXL-92 Program for Crystal Structure Refinement. University of Göttingen F.R.G. (1992).

Polyhedron Vol. 12, No. 24, pp. 2947–2953, 1993
Printed in Great Britain

0277–5387/93 $6.00+.00
© 1993 Pergamon Press Ltd

TERT-BUTYLBENZAMIDATE DIRUTHENIUM(II, III) COMPOUNDS. CRYSTAL STRUCTURE OF $[Ru_2(\mu\text{-}HNOCC_6H_4\text{-}p\text{-}CMe_3)_4(OPPh_3)_2]BF_4$

M. C. BARRAL, R. JIMÉNEZ-APARICIO,* J. L. PRIEGO, E. C. ROYER and F. A. URBANOS

Departamento de Química Inorgánica, Facultad de Ciencias Químicas, Universidad Complutense, Ciudad Universitaria, 28040 Madrid, Spain

and

A. MONGE and C. RUÍZ-VALERO

Instituto de Ciencias de los Materiales, sede D, C.S.I.C., Serrano 113, 28006 Madrid, Spain, and Laboratorio de Rayos X, Facultad de Ciencias Químicas, Universidad Complutense, Ciudad Universitaria, 28040 Madrid, Spain

(*Received* 3 *June* 1993; *accepted* 4 *August* 1993)

Abstract—The reaction between $Ru_2Cl(\mu\text{-}O_2CCH_3)_4$ and molten *p*-tert-butylbenzamide led to the formation of $Ru_2Cl(\mu\text{-}HNOCC_6H_4\text{-}p\text{-}CMe_3)_4$. The polymeric structure of this insoluble compound was broken with $AgBF_4$, in anhydrous thf, giving $[Ru_2(\mu\text{-}HNOCC_6H_4\text{-}p\text{-}CMe_3)_4(thf)_2]BF_4$. The reaction of this cationic complex with $OPPh_3$ gave $[Ru_2(\mu\text{-}HNOCC_6H_4\text{-}p\text{-}CMe_3)_4(OPPh_3)_2]BF_4$. The compounds have been characterized by elemental analysis, spectroscopic data and magnetic measurements and the crystal structure of $[Ru_2(\mu\text{-}HNOCC_6H_4\text{-}p\text{-}CMe_3)_4(OPPh_3)_2]BF_4$ was determined by X-ray crystallography. The asymmetric unit is composed of halves of two different crystallographically independent centrosymmetric cations. Each ruthenium(II,III) dimer is bonded to four bridging *p*-tert-butylbenzamidate ligands and to two axial triphenylphosphine oxide molecules. The Ru—Ru distances in the two dimeric cations of the unit cell are 2.281(2) and 2.280(2) Å. The compound has a non-polar 2 : 2 arrangement of the tert-butylbenzamidate ligands.

Since the reaction of $Ru_2Cl(\mu\text{-}O_2CCH_3)_4$ with molten trifluoroacetamide to give $Ru_2Cl(\mu\text{-}HNOCCF_3)_4$ was described,[1] several diruthenium(II,III) compounds with three atom-bridging ligands, with N,O- and N,N-atom donors, have been obtained.[2–15] Thus, with 2-hydroxypyridine and its derivatives, diruthenium(II,III) compounds containing four N,O-bridging units have been obtained.[2–5] In a similar way, with different aminopyridine ligands, several tetra-N,N-aminopyridinate compounds have been prepared,[5–7] although these ligands sometimes lead to partial substitution products.[8–11] By the same procedure, some tetraamidate complexes have also been obtained.[1,12–15]

Several X-ray crystal structure determinations of diruthenium(II,III) compounds with substituted 2-hydroxy-pyridinate[2,3,5] and 2-amino-pyridinate[5,7] ligands have shown that, in all cases, a completely polar 4 : 0 arrangement of the ligands was produced. However, in the case of tetraamidate complexes only the crystal structure of the polymer $Ru_2Cl(\mu\text{-}HNOCC_6H_4\text{-}p\text{-}Cl)_4$ is known and shows a non-polar 2 : 2 arrangement of the ligands. The low solubility of the tetraamidate complexes is probably the reason why only one crystal structure for these compounds has been described. In this paper, we

*Author to whom correspondence should be addressed.

report the synthesis, characterization and reaction with $AgBF_4$ of a new tetraamidate compound, $Ru_2Cl(\mu\text{-}HNOCC_6H_4\text{-}p\text{-}CMe_3)_4$. The synthesis, properties and crystal structure of the soluble (in polar organic solvents) $Ru_2(\mu\text{-}HNOCC_6H_4\text{-}p\text{-}CMe_3)_4(OPPh_3)_2]BF_4$ is also described.

RESULTS AND DISCUSSION

The reaction between $Ru_2Cl(\mu\text{-}O_2CCH_3)_4$ and $Me_3CC_6H_4CONH_2$ at 180°C for 72 h leads to the complete substitution of the acetate ligands, with the formation of $Ru_2Cl(\mu\text{-}HNOCC_6H_4\text{-}p\text{-}CMe_3)_4$ in a near quantitative yield. The compound is a brown solid, almost insoluble in all solvents tested, but slightly soluble in dmso. Due to this insolubility it has not been possible to obtain single crystals. However, elemental analysis, spectroscopic data and magnetic measurements indicate that the structure of this compound must be similar to the starting material $Ru_2Cl(\mu\text{-}O_2CCH_3)_4$, with two ruthenium atoms bonded to four bridging *p*-tert-butylbenzamidate ligands and to an axial chlorine atom, which links the dimetal units. This axial chlorine atom is abstracted by $AgBF_4$ in anhydrous thf, thus breaking the polymer structure to give $[Ru_2(\mu\text{-}HNOCC_6H_4\text{-}p\text{-}CMe_3)_4(thf)_2]BF_4$. This compound is soluble in most of the usual organic solvents, such as thf, dichloromethane, acetone, etc., and insoluble in petroleum ether and diethylether. The compound crystallizes from thf/petroleum ether (40–60°C), but easily loses thf. This facile loss of the coordinated thf has been previously observed in other thf adducts of diruthenium(II,III) carboxylate compounds.[16–20] The thf ligands can be substituted by $OPPh_3$, giving $[Ru_2(\mu\text{-}HNOCC_6H_4\text{-}p\text{-}CMe_3)_4(OPPh_3)_2]BF_4$. The solubility of this compound is similar to that of thf adduct and can be recrystallized from CH_2Cl_2/petroleum ether (40–60°C).

The IR spectra show, in all cases, corresponding absorption bands due to the *p*-tert-butylbenzamidate ligands. The absorption bands due to the thf molecules in $[Ru_2(\mu\text{-}HNOCC_6H_4\text{-}p\text{-}CMe_3)_4(thf)_2]BF_4$, similar to other thf adducts,[18–20] are absent when the IR spectrum is registered in KBr discs due to the lability of this ligand. In $[Ru_2(\mu\text{-}HNOCC_6H_4\text{-}p\text{-}CMe_3)_4(OPPh_3)_2]BF_4$ bands due to $OPPh_3$ are also observed. A strong band at 1100 cm^{-1} due to the BF_4^- group is also observed in the cationic compounds.

The magnetic measurements in the 70–290 K range (Table 1) show that the compounds obey the Curie–Weiss law over a range of temperatures. The

Table 1. Magnetic measurements at various temperatures

$Ru_2Cl(\mu\text{-}HNOCC_6H_4\text{-}p\text{-}CMe_3)_4$							
T (K)	287.8	273.8	243.9	229.0	214.0	184.3	169.4
$\chi_M \times 10^3$	5.96	6.38	6.94	7.44	8.26	9.61	10.05
μ (B.M.)	3.72	3.76	3.69	3.71	3.78	3.78	3.79
T (K)	154.5	124.6	108.4	94.8	83.8	76.9	
$\chi_M \times 10^3$	11.35	13.86	15.89	17.94	19.67	22.48	
μ (B.M.)	3.76	3.73	3.73	3.70	3.65	3.73	
$[Ru_2(\mu\text{-}HNOCC_6H_4\text{-}p\text{-}CMe_3)_4(thf)_2]BF_4$							
T (K)	288.8	267.0	246.9	227.3	208.1	188.2	168.8
$\chi_M \times 10^3$	7.44	7.85	8.19	9.09	10.01	11.35	12.83
μ (B.M.)	4.16	4.11	4.04	4.08	4.10	4.15	4.18
T (K)	148.6	128.6	108.9	89.1	79.3	75.5	
$\chi_M \times 10^3$	14.55	16.98	19.88	23.92	26.55	27.52	
μ (B.M.)	4.18	4.20	4.18	4.15	4.12	4.09	
$[Ru_2(\mu\text{-}HNOCC_6H_4\text{-}p\text{-}CMe_3)_4(OPPh_3)_2]BF_4$							
T (K)	291.5	270.2	241.5	220.2	211.4	181.7	161.6
$\chi_M \times 10^3$	7.45	8.11	9.23	9.96	10.11	12.28	12.49
μ (B.M.)	4.18	4.20	4.24	4.21	4.15	4.24	4.03
T (K)	150.5	131.7	112.5	99.4	86.96	77.89	
$\chi_M \times 10^3$	14.18	15.89	18.33	21.37	22.80	25.22	
μ (B.M.)	4.15	4.11	4.08	4.13	4.00	3.98	

magnetic moment corresponds to three unpaired electrons, which are in accord with the ground state configuration $\sigma^2\pi^4\delta^2(\pi^*\delta^*)^3$, similar to those described for the carboxylate compounds.[21]

The electronic spectra of the compounds show two bands. The band at 422–450 nm is assigned to a $\pi(Ru—O,Ru_2)\rightarrow\pi^*(Ru_2)$ transition, in agreement with Norman *et al.*[21] In $Ru_2Cl(\mu\text{-}HNOCC_6H_4\text{-}p\text{-}CMe_3)_4$ a strong absorption is observed at 320 nm (ε = 25,000 $dm^3\ mol^{-1}\ cm^{-1}$), which is consistent with those observed[15] in $Ru_2Cl(\mu\text{-}HNOCC_6H_4\text{-}p\text{-}Cl)_4$ and is assigned to a $Cl\rightarrow\pi^*$ or $Cl\rightarrow\delta^*$ transition. In $[Ru_2(\mu\text{-}HNOCC_6H_4\text{-}p\text{-}CMe_3)_4(thf)_2]BF_4$ and $[Ru_2(\mu\text{-}HNOCC_6H_4\text{-}p\text{-}CMe_3)_4(OPPh_3)_2]BF_4$ similar bands at 304 (18,240 $dm^3\ mol^{-1}\ cm^{-1}$) and 303 nm (21,400 $dm^3\ mol^{-1}\ cm^{-1}$), respectively, are observed, which could be due to an $O(OPPh_3)\rightarrow\pi^*$ or $O(OPPh_3)\rightarrow\delta^*$ transition.

The crystal structure of $[Ru_2(\mu\text{-}HNOCC_6H_4\text{-}p\text{-}CMe_3)_4(OPPh_3)_2]BF_4$ has been determined by X-ray diffraction. Some important bond distances and angles are listed in Table 2. In this structure the asymmetric unit is composed of halves of two different crystallographically independent centrosymmetric cations (**1** and **2**), with the inversion centre in the middle of the Ru—Ru bond. An

Table 2. Selected bond lengths and angles for $[Ru_2(\mu\text{-}HNOCC_6H_4\text{-}p\text{-}CMe_3)_4(OPPh_3)_2]BF_4$

Cation **1**		Cation **2**	
Ru(1)—Ru(1′)	2.281(2)	Ru(2)—Ru(2′)	2.280(2)
Ru(1)—O(11)	2.02(1)	Ru(2)—O(21)	2.03(1)
Ru(1)—O(13)	2.262(9)	Ru(2)—O(23)	2.28(1)
Ru(1)—N(12)	2.00(1)	Ru(2)—N(22)	2.01(1)
Ru(1)—O(12′)	2.04(1)	Ru(2)—O(22′)	2.03(1)
Ru(1)—N(11′)	2.01(1)	Ru(2)—N(21′)	1.99(1)
P(1)—O(13)	1.49(1)	P(2)—O(23)	1.50(1)
P(1)—C(123)	1.79(2)	P(2)—C(223)	1.79(2)
P(1)—C(129)	1.79(1)	P(2)—C(229)	1.79(2)
P(1)—C(135)	1.79(1)	P(2)—C(235)	1.78(2)
O(11)—C(11)	1.28(2)	O(21)—C(21)	1.30(2)
O(12)—C(12)	1.30(2)	O(22)—C(22)	1.29(2)
N(11)—C(11)	1.30(2)	N(21)—C(21)	1.29(2)
N(12)—C(12)	1.30(2)	N(22)—C(22)	1.30(2)
Ru(1′)—Ru(1)—O(11)	89.6(3)	Ru(2′)—Ru(2)—O(21)	91.2(3)
Ru(1′)—Ru(1)—N(12)	87.3(3)	Ru(2′)—Ru(2)—N(22)	82.1(4)
Ru(1′)—Ru(1)—O(12′)	91.2(3)	Ru(2′)—Ru(2)—O(22′)	90.3(3)
Ru(1′)—Ru(1)—N(11′)	88.6(3)	Ru(2′)—Ru(2)—N(21′)	87.8(4)
Ru(1′)—Ru(1)—O(13)	174.8(3)	Ru(2′)—Ru(2)—O(23)	174.9(3)
O(11)—Ru(1)—N(12)	91.3(5)	O(21)—Ru(2)—N(22)	90.3(5)
O(11)—Ru(1)—O(13)	95.5(4)	O(21)—Ru(2)—O(23)	92.1(4)
O(13)—Ru(1)—N(12)	93.8(5)	O(23)—Ru(2)—N(22)	95.7(5)
O(11)—Ru(1)—O(12′)	88.2(5)	O(21)—Ru(2)—O(22′)	90.4(4)
O(11)—Ru(1)—N(11′)	178.3(5)	O(21)—Ru(2)—N(21′)	178.6(6)
O(13)—Ru(1)—O(12′)	87.7(4)	O(23)—Ru(2)—O(22′)	85.8(4)
O(13)—Ru(1)—N(11′)	86.3(4)	O(23)—Ru(2)—N(21′)	88.9(5)
O(12′)—Ru(1)—N(11′)	91.8(5)	O(22′)—Ru(2)—N(21′)	90.6(5)
C(129)—P(1)—C(135)	106.5(8)	C(229)—P(2)—C(235)	106.5(8)
C(123)—P(1)—C(135)	108.3(8)	C(223)—P(2)—C(235)	103.8(9)
C(123)—P(1)—C(129)	106.8(8)	C(223)—P(2)—C(229)	108.9(9)
O(13)—P(1)—C(135)	111.0(7)	O(23)—P(2)—C(235)	113.1(8)
O(13)—P(1)—C(129)	110.6(7)	O(23)—P(2)—C(229)	108.5(8)
O(13)—P(1)—C(123)	113.3(8)	O(23)—P(2)—C(223)	115.5(8)
Ru(1)—O(11)—C(11)	120.0(1)	Ru(2)—O(21)—C(21)	117.0(1)
Ru(1)—N(12)—C(12)	125.0(1)	Ru(2)—N(22)—C(22)	123.0(1)
N(11)—C(11)—O(11)	119.0(1)	N(21)—C(21)—O(21)	121.0(1)
N(12)—C(12)—O(12)	118.0(1)	N(22)—C(22)—O(22)	118.0(1)

ORTEP view of the cation **2** is shown in Fig. 1. The differences between the two cations of $[Ru_2(\mu\text{-}HNOCC_6H_4\text{-}p\text{-}CMe_3)_4(OPPh_3)_2]^+$ are insignificant, except for the Ru—O_{axial} bond, which is slightly longer in cation **2**. Each ruthenium dimer is bonded to four bridging *p*-tert-butylbenzamidate ligands and two axial triphenylphosphine oxide molecules. The compound has a non-polar 2:2 arrangement of the ligands. This type of arrangement of ligands is the most common in other metals,[22–24] but in the case of ruthenium only has been found previously in the similar[15] $Ru_2Cl(\mu\text{-}HNOCC_6H_4\text{-}p\text{-}Cl)_4$.

The Ru—Ru distances in the two dimeric units are 2.281(2) and 2.280(2) Å. These Ru—Ru distances are similar to those observed[15] in $Ru_2Cl(\mu\text{-}HNOCC_6H_4\text{-}p\text{-}Cl)_4$ and are slightly longer than the same distances reported in the compounds with a totally polar arrangement of ligands.[2,3,5,7] On the other hand, these distances are longer than those found in the analogous carboxylate cation[20] $[Ru_2(\mu\text{-}O_2CC_6H_4\text{-}p\text{-}CMe_3)_4(thf)_2]^+$.

The Ru—O_{axial} distances, 2.262(9) (cation **1**) and 2.28(1) Å (cation **2**), are longer than those observed in $[Ru_2(\mu\text{-}O_2CCH_3)_4(OPPh_3)_2]^+$, which would indicate a lower acceptor character of $[Ru_2(\mu\text{-}HNOCC_6H_4\text{-}p\text{-}CMe_3)_4]^+$ than the $[Ru_2(\mu\text{-}O_2CCH_3)_4]^+$ unit.

EXPERIMENTAL

All reactions were performed under an inert atmosphere, using standard Schlenk techniques. Ruthenium trichloride, tertbutylbenzoic acid, silver tetrafluoroborate, thionyl chloride and triphenylphosphine oxide were purchased from commercial sources. The solvents were purified and distilled by standard methods. Methanol was used

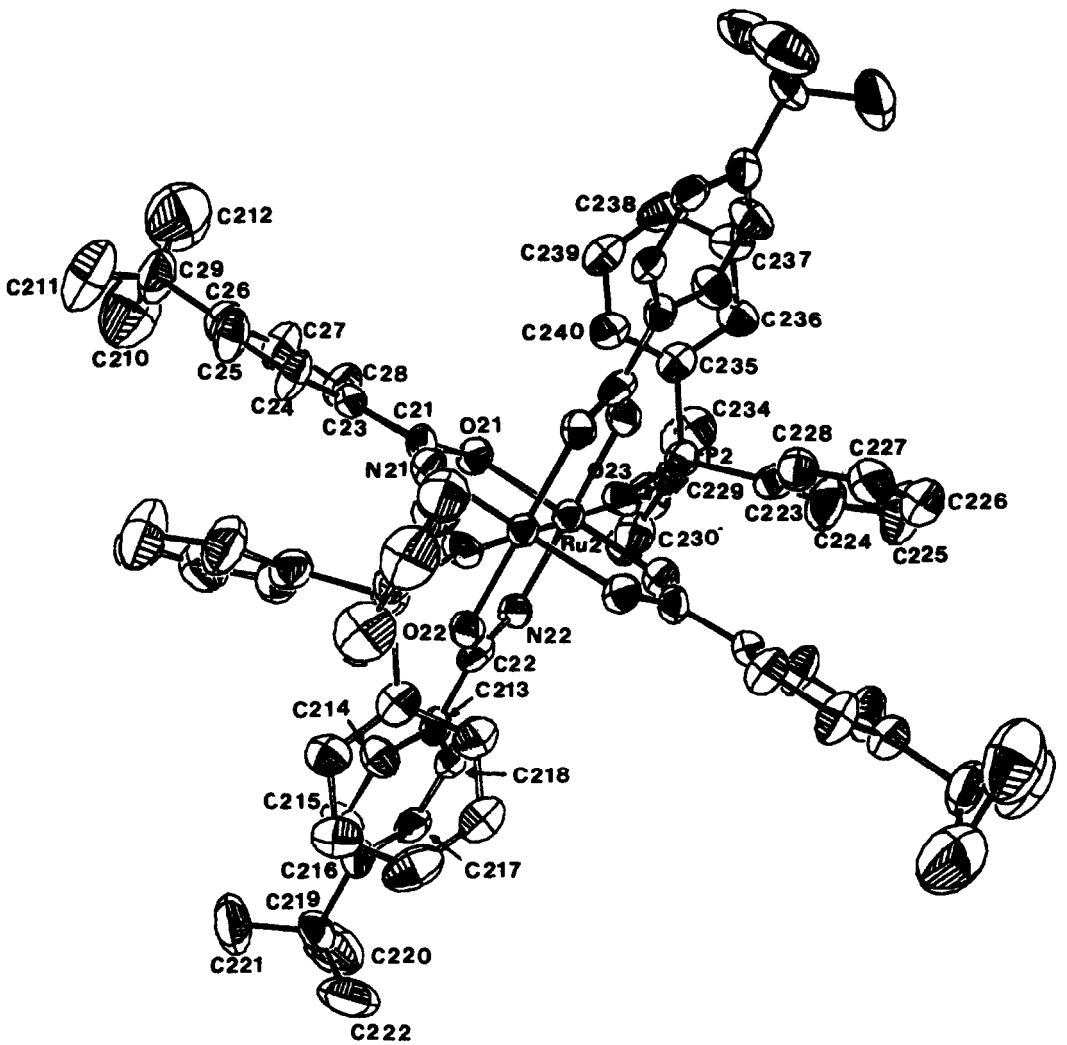

Fig. 1. ORTEP view of cation **2**, $[Ru_2(\mu\text{-}HNOCC_6H_4\text{-}p\text{-}CMe_3)_4(OPPh_3)_2]^+$. The hydrogen atoms are omitted for clarity.

without previous purification. $Ru_2Cl(\mu\text{-}O_2CCH_3)_4$ was prepared by the literature procedure.[25] Tert-butylbenzamide was prepared by the reaction of tert-butylbenzoic acid and thionyl chloride with the addition of NH_3 (ac.); the white solid obtained was recrystallized from hot methanol/water.

The IR spectra were recorded, as KBr discs, on Philips PU 9712 or Perkin–Elmer 1330 IR spectrophotometers. Magnetic susceptibility measurements were obtained using a fully automatic DSM 8 magneto-susceptometer, based on the Faraday methods. Electronic spectra in the 280–800 nm region were recorded on a gbc UV–vis 911 spectrophotometer. Elemental analysis for carbon, hydrogen and nitrogen were performed in the Microanalytical Service of the Complutense University of Madrid.

Synthesis of $Ru_2Cl(\mu\text{-}HNOCC_6H_4\text{-}p\text{-}CMe_3)_4$

$Ru_2Cl(\mu\text{-}O_2CCH_3)_4$ (0.1 g) and *p*-tert-butylbenzamide (5 g) were heated with stirring at 180°C (m.p. of *p*-tertbutylbenzamide-172°C) for 72 h. Excess ligand was removed by sublimation under reduced pressure, leaving a brown solid which was washed twice with acetone (10 cm^3) and dried *in vacuo*. Found: C, 55.3; H, 5.9; N, 5.4. Calc. for $Ru_2Cl(\mu\text{-}HNOCC_6H_4CMe_3)_4$: C, 56.1; H, 6.0; N, 5.9%. IR (KBr discs): 3390m, 3350m, 2960s, 2900m, 2860m, 1640m, 1610m, 1520m, 1480s, 1440vs, 1400s, 1360m, 1265m, 1210m, 1120s, 1100w, 1010m, 845m, 770w, 760m, 720s, 620m, 600m, 505m cm^{-1}. λ_{max} (nm) (ε, $dm^3\ mol^{-1}\ cm^{-1}$): 450 (658), 320 (25,000) (in dmso); due to the insolubility of the compound, the ε values are approximate.

Synthesis of $[Ru_2(\mu\text{-}HNOCC_6H_4\text{-}p\text{-}CMe_3)_4(thf)_2]BF_4$

A suspension of $Ru_2Cl(\mu\text{-}HNOCC_6H_4\text{-}p\text{-}CMe_3)_4$ (0.2 g, 0.21 mmol) in anhydrous thf (40 cm^3) was treated with $AgBF_4$ (0.041 g, 0.21 mmol). The mixture was stirred at room temperature for 24 h, leaving a red solution and a white precipitate of AgCl. The precipitate was removed by filtration over celite. The solution was concentrated under reduced pressure to half its initial volume and layered with petroleum ether (40–60°C). Red crystals of $[Ru_2(\mu\text{-}HNOCC_6H_4\text{-}p\text{-}CMe_3)_4(thf)_2]BF_4$ were formed, filtered and dried in a stream of nitrogen. Found: C, 53.2; H, 6.0; N, 5.0. Calc. for $[Ru_2(\mu\text{-}HNOC$

Table 3. Crystal and refinement data

Formula	$[Ru_2(ONHCC_6H_4\text{-}p\text{-}CMe_3)_4(OPPh_3)_2]BF_4$
Mr	1550.5
Crystal system	Monoclinic
Space group	*C*2/*c*
a (Å)	24.208(6)
b (Å)	24.46(2)
c (Å)	29.955(6)
β	110.36(2)
V ($Å^3$)	16,629(15)
Z	8
F(000)	6408
ρ (calcd) ($g\ cm^{-3}$)	1.24
Temperature (°C)	22
μ (cm^{-1})	4.5
Crystal dimensions (mm)	0.25 × 0.15 × 0.20
Diffractometer	Enraf–Nonius CAD4
Radiation	Graphite-monochromated Mo-K_α (λ = 0.71069 Å)
Scan technique	$\Omega/2\theta$
Data collected	(−28,0,0) to (28,29,35)
Reflections collected	15,670
Unique data	14,573
Unique data ($I \geq 2\sigma(I)$)	7028
R(int) (%)	1.8
Standard reflections	3
RF (%)	8.1
Average shift/error	0.11

$C_6H_4CMe_3)_4(thf)_2]BF_4$: C, 55.0; H, 6.2; N, 4.9%. IR (KBr discs): 3360s, 2980s, 2900w, 2860w, 1600m, 1520m, 1480s, 1440vs, 1400s, 1360m, 1265m, 1230w, 1195w, 1120vs, 1075vs br, 845s, 760m, 720s, 685m, 600m, 505m, 375w cm^{-1}. λ_{max} (nm) (ε, $dm^3\ mol^{-1}\ cm^{-1}$): 447 (658), 304 (18,240) (in MeOH).

Synthesis of $[Ru_2(\mu\text{-}HNOCC_6H_4\text{-}p\text{-}CMe_3)_4(OPPh_3)_2]BF_4$

To a thf solution (40 cm^3) of $[Ru_2(\mu\text{-}HNOCC_6H_4\text{-}p\text{-}CMe_3)_4(thf)_2]BF_4$ (0.2 g, 0.18 mmol) was added $OPPh_3$ (0.098 g, 0.36 mmol). The mixture was then stirred for 24 h at room temperature. The brown dark solution thus formed was pumped to dryness and the residue washed twice with diethylether. The solid was dissolved in dichloromethane and layered with petroleum ether (40–60°C), leaving dark red crystals of $[Ru_2(\mu\text{-}HNOCC_6H_4\text{-}p\text{-}CMe_3)_4(OPPh_3)_2]BF_4$, which were filtered and dried in a stream of nitrogen. Found: C, 60.9; H, 5.6; N, 3.1. Calc. for $[Ru_2(\mu\text{-}HNOCC_6H_4CMe_3)_4(OPPh_3)_2]BF_4$: C, 62.0; H, 5.6; N, 3.1%. IR (KBr discs): 3390m, 3360m, 3070w, 2975s, 2920m, 2880m, 1610m, 1580w, 1530m, 1490s, 1440vs, 1410s, 1370m, 1275m, 1200m, 1160s, 1150s, 1125vs, 1090s, 1075s br, 1000m, 850m, 780m, 765m, 750m, 725vs, 700s, 665m, 610m, 545vs, 515m, 470w, 380w cm^{-1}. λ_{max} (nm): 422 (690), 303 (21,400) (in MeOH).

X-ray structure determination

A summary of the fundamental crystal data is given in Table 3. A dark brown prismatic crystal was coated with epoxy resin and mounted on a kappa diffractometer. The cell dimensions were refined by least-squares, fitting the θ values of 25 reflections. The intensities were corrected for Lorentz and polarization effects. Scattering factors for neutral atoms and anomalous dispersion corrections for ruthenium and phosphorus were taken from the International Tables of X-Ray Crystallography.[26] The structure was solved by Patterson and Fourier methods. An empirical absorption correction[27] was applied at the end of the isotropic refinement.

A final refinement was undertaken with fixed isotropic factors and coordinates for all H atoms and unit weights.

A final difference synthesis showed no significant electron density. Most of the calculations were performed using the X-ray 80 system.[28]

Complete tables of distances and angles as well as atomic positional and thermal parameters and structure factors have been deposited as supplementary material.

Acknowledgements—We are grateful to the Dirección General de Investigación Científica y Técnica (DGICYT) (Spain) for financial support (project PB90 0020). Thanks are also due to Mr F. Rojas for his help in obtaining the magnetic measurements.

REFERENCES

1. T. Malinski, D. Chang, F. N. Feldmann, J. L. Bear and K. M. Kadish, *Inorg. Chem.* 1983, **22**, 3225.
2. A. R. Chakravarty, F. A. Cotton and D. A. Tocher, *Inorg. Chem.* 1985, **24**, 1263.
3. A. R. Chakravarty, F. A. Cotton and W. Schwotzer, *Polyhedron* 1984, **5**, 1821.
4. A. R. Chakravarty, F. A. Cotton, D. A. Tocher and J. H. Tocher, *Polyhedron* 1985, **4**, 1475.
5. A. R. Chakravarty, F. A. Cotton and D. A. Tocher, *Inorg. Chem.* 1985, **24**, 172.
6. D. A. Tocher, *Inorg. Chim. Acta* 1986, **115**, 51.
7. A. R. Chakravarty and F. A. Cotton, *Inorg. Chim. Acta* 1986, **113**, 19.
8. A. R. Chakravarty, F. A. Cotton and D. A. Tocher, *Inorg. Chem.* 1984, **23**, 4030.
9. A. R. Chakravarty and F. A. Cotton, *Inorg. Chim. Acta* 1985, **105**, 19.
10. A. R. Chakravarty, F. A. Cotton and L. R. Falvello, *Inorg. Chem.* 1986, **25**, 214.
11. H. J. McCarthy and D. A. Tocher, *Polyhedron* 1992, **11**, 13.
12. M. Y. Chavan, F. N. Feldmann, X. Q. Lin, J. L. Bear and K. M. Kadish, *Inorg. Chem.* 1984, **23**, 2373.
13. A. R. Chakravarty, F. A. Cotton and D. A. Tocher, *J. Am. Chem. Soc.* 1984, **106**, 6409.
14. A. R. Chakravarty and F. A. Cotton, *Inorg. Chem.* 1985, **24**, 3584.
15. A. R. Chakravarty, F. A. Cotton and D. A. Tocher, *Polyhedron* 1985, **4**, 1097.
16. A. J. Lindsay, G. Wilkinson, M. Motevalli and M. B. Hursthouse, *J. Chem. Soc., Dalton Trans.* 1985, 2321.
17. A. J. Lindsay, G. Wilkinson, M. Motevalli and M. B. Hursthouse, *J. Chem. Soc., Dalton Trans.* 1987, 2723.
18. F. A. Urbanos, M. C. Barral and R. Jiménez-Aparicio, *Polyhedron* 1988, **7**, 2597.
19. M. C. Barral, R. Jiménez-Aparicio, C. Rial, E. C. Royer, M. J. Saucedo and F. A. Urbanos, *Polyhedron* 1990, **9**, 1723.
20. M. C. Barral, R. Jiménez-Aparicio, J. L. Priego, E. C. Royer, E. Gutiérrez-Puebla and C. Ruíz-Valero, *Polyhedron* 1992, **11**, 2209.
21. J. G. Norman, G. E. Renzoni and D. A. Case, *J. Am. Chem. Soc.* 1979, **101**, 5256.
22. F. A. Cotton, P. E. Fanwick, R. H. Niswander and J. C. Sekotowsti, *J. Am. Chem. Soc.* 1978, **100**, 4725.
23. F. A. Cotton and T. R. Felthouse, *Inorg. Chem.* 1980, **19**, 320.

24. F. A. Cotton, W. H. Ilsley and W. Kaim, *Inorg. Chem.* 1980, **19**, 1453.
25. R. W. Mitchell, A. Spencer and G. Wilkinson, *J. Chem. Soc., Dalton Trans.* 1973, 846.
26. *International Tables for X-ray Crystallography*, Vol. IV, pp. 72–98. Kynoch Press, Birmingham (1974).
27. N. Walker and D. Stuart, *Acta Cryst.* 1983, **A39**, 158.
28. J. M. Stewart, F. A. Kundell and J. C. Baldwin, *The X-ray 80 System.* Computer Science Center, University of Maryland (1980).

Polyhedron Vol. 12, No. 24, pp. 2955–2960, 1993
Printed in Great Britain

0277-5387/93 $6.00+.00
© 1993 Pergamon Press Ltd

FLUORINATED TERTIARY ALKOXIDES OF SOME LANTHANIDES : TRIS-TRIFLUOROTERTIARYBUTOXIDES OF LANTHANUM, PRASEODYMIUM AND EUROPIUM

DONALD C. BRADLEY,* HALINA CHUDZYNSKA, MICHAEL B. HURSTHOUSE,† MAJID MOTEVALLI and RUOWEN WU

Department of Chemistry, Queen Mary & Westfield College, Mile End Road, London E1 4NS, U.K.

(*Received* 16 *July* 1993 ; *accepted* 28 *July* 1993)

Abstract—From reactions involving $M\{N(SiMe_3)_2\}_3$ (M = La, Pr and Eu) and trifluorotertiary butanol[$(CF_3)Me_2COH$; tftb.H], the compounds $[La(tftb)_3(thf)_{1.5}]$ (**1**), $[Pr(tftb)_3]$ (**2**) and $[Eu(tftb)_3]$ (**3**) have been isolated. From variable temperature ^1H and ^{19}F NMR studies it is suggested that **1** is a mixture of $[La_3(tftb)_9(thf)_2]$ (**1a**) and $[La_2(tftb)_6(thf)_4]$ (**1b**). X-ray crystallography has shown that **2** is the trimer $[Pr_3(tftb)_9]$ and variable temperature ^1H and ^{19}F NMR suggests that **3** is also a trimer, $[Eu_3(tftb)_9]$.

In a previous paper we reported on the synthesis of a number of fluorinated alkoxides of yttrium from reactions involving $Y\{N(SiMe_3)_2\}_3$ and fluoroalcohol.[1] With trifluorotertiarybutanol (tftb.H), the unsolvated compound $Y(tftb)_3$ was obtained from a reaction in benzene solution and from its ^1H NMR spectrum a trinuclear structure $[Y_3(\mu_3-tftb)_2(\mu\text{-}tftb)_3(tftb)_4]$ was proposed. When the reaction was conducted in thf, the product had the composition $[Y(tftb)_3(thf)_{2.5}]$, which was believed to be a mixture of the mononuclear $[Y(tftb)_3(thf)_3]$ and the dimer $[Y_2(tftb)_6(thf)_4]$. We now report the results obtained from the reactions of $M\{N(SiMe_3)_2\}_3$ (M = La, Pr and Eu) with tftb.H.

RESULTS AND DISCUSSION

The analysis of the product **1** of the reaction of $La\{N(SiMe_3)_2\}_3$ and tftb.H in thf corresponded to the formula $[La(tftb)_3(thf)_{1.5}]$. The complex ^1H NMR spectra in C_6D_6 or C_7D_8 were not completely resolved due to overlap of some of the tftb peaks with one of the thf peaks, but in $CDCl_3$ all peaks were separated and integration confirmed the presence of two tftb groups per thf ligand, in agreement with the elemental analysis. The low temperature (233 K) spectrum in $CDCl_3$ gave a set of five singlets (δ 1.76, 1.65, 1.61, 1.45 and 1.24) in the ratio 2 : 1 : 2 : 2 : 2, corresponding to a trinuclear species $[La_3(\mu_3\text{-}tftb)_2(\mu\text{-}tftb)_3(tftb)_4(thf)_2]$ (**1a**) related to the known structure of $[La_3(\mu_3\text{-}OBu^t)_2(\mu\text{-}OBu^t)_3(OBu^t)_4(Bu^tOH)_2]$.[2] In addition to the two peaks for thf (δ 3.80 and 1.90), the spectrum also showed a singlet at δ 1.30 due to tftb in another species, probably a dimer, $[La_2(tftb)_6(thf)_4]$ (**1b**). The ^{19}F NMR spectrum in C_7D_8 at 300 K also gave a set of five peaks in the ratio 1 : 2 : 2 : 2 : 2 which shifted slightly at low temperature (240 K), giving a ratio 2 : 2 : 1 : 2 : 2. Other peaks suggested the presence of another species besides the trinuclear compound. Interestingly, the ^1H spectrum in thf-d_8 at 305 K was dominated by a tftb peak at δ 1.21 in addition to the five smaller peaks for the trinuclear species at 1.61, 1.58, 1.52, 1.47 and 1.45. With thf as solvent it would be expected that an equilibrium between trinuclear (**1a**) and dimer (**1b**) species would be driven in favour of the dimer or even a mononuclear $[La(tftb)_3(thf)_3]$ species, thus explaining the strong peak at δ 1.21.

From the reaction of $Pr\{N(SiMe_3)_2\}_3$ and tftb.H in benzene, the pale green crystalline compound $[Pr_3(tftb)_9]$ (**2**) was isolated. The trimeric structure

*Author to whom correspondence should be addressed.
†Present address: Department of Chemistry & Applied Chemistry, University of Wales—Cardiff, PO Box 912, Cardiff CF1 3TB, U. K.

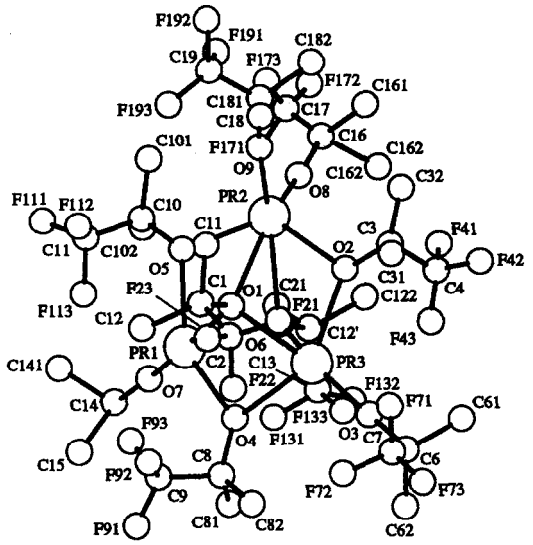

Fig. 1. X-ray single crystal structure of $[Pr_3(TFTB)_9]$.

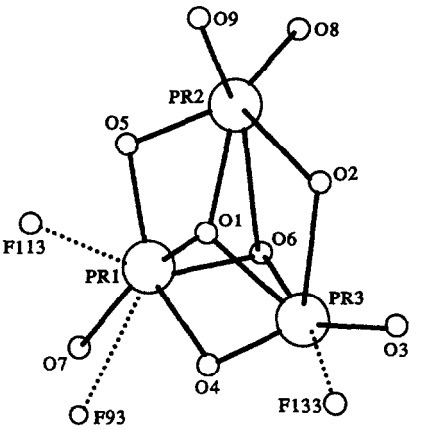

Fig. 2. The suggested coordination sphere of $[Pr_3(TFTB)_9]$.

(Fig. 1) was determined by single crystal X-ray diffraction. A preliminary account of the structure has been reported previously[3] and we now give full details (Tables 1–3). As can be more clearly seen in Fig. 2, showing the metal–oxygen framework, the trimeric structure is based on an isosceles triangle of metals capped by two μ_3-tftb ligands above and below the metal plane and by three μ_2-tftb ligands in the plane. One metal [Pr(2)] has two terminal ligands, giving it a distorted octahedral configuration, whilst the other two metals each have a single terminal ligand, giving five-coordinate structures. However, closer inspection shows that Pr(1) and Pr(3) are each interacting agostically with fluorine atoms. Thus, Pr(1) interacts with F(93) and F(113), whilst Pr(3) interacts with F(133), giving rise to distorted seven-coordination and six-coor-

Table 1. Crystal data, intensity measurements and structure refinement for $[Pr_3(tftb)_9]$ (**2**)

Formula	$C_{36}H_{54}O_3F_{27}Pr_3$
M	1566.056
Crystal system	Triclinic
Space group	$P\bar{1}$
a (Å)	10.992(2)
b (Å)	11.366(2)
c (Å)	23.404(9)
α (°)	75.04(2)
β (°)	102.86(2)
γ (°)	93.18(1)
U (Å^3)	2736.47
Z	2
D_c (g cm^{-3})	1.857
Radiation	Mo-K_α
λ (Å)	0.71069
Total no. of reflections	7846
No. of unique reflections	7612
No. of reflections used with $F_0 > 3\sigma(F_0)$	6085
No. of refined parameters	378
Weighting scheme parameter g in $w = 1/[\sigma^2(F)+gF^2)$	Unit
Final R	0.067
Final R_w	0.084

Table 2. Some bond lengths (Å) for $[Pr_3(tftb)_9]$ (3)

Pr(1)—O(7)	2.141 (0.012)	Pr(1)—O(1)	2.627 (0.011)
Pr(3)—O(3)	2.112 (0.012)	Pr(2)—O(1)	2.718 (0.013)
Pr(2)—O(8)	2.156 (0.014)	Pr(3)—O(1)	2.438 (0.010)
Pr(2)—O(9)	2.168 (0.011)	Pr(1)—O(6)	2.407 (0.010)
Pr(1)—O(5)	2.371 (0.012)	Pr(2)—O(6)	2.834 (0.010)
Pr(2)—O(5)	2.434 (0.011)	Pr(3)—O(6)	2.474 (0.010)
Pr(2)—O(2)	2.459 (0.011)	Pr(1)—Pr(2)	3.852 (0.001)
Pr(3)—O(2)	2.400 (0.013)	Pr(2)—Pr(3)	3.821 (0.001)
Pr(3)—O(4)	2.430 (0.013)	Pr(1)—Pr(3)	3.642 (0.001)
Pr(1)—O(4)	2.408 (0.012)	Pr(1)—F(93)	2.759 (0.016)
Pr(3)—F(133)	2.756 (0.012)	Pr(1)—F(113)	2.774 (0.010)
F(113)—C(11)	1.373 (0.029)	F(133)—C(13)	1.412 (0.025)
F(112)—C(11)	1.300 (0.028)	F(132)—C(13)	1.306 (0.024)
F(111)—C(11)	1.303 (0.026)	F(131)—C(13)	1.287 (0.030)

dination, respectively. The C—F bond lengths of these agostic fluorine atoms are significantly longer than the average C—F bond length of the CF_3 groups (Table 2). The agostic Pr(1)···F (2.774 and 2.759 Å) and Pr(3)···F (2.756 Å) distances are comparable with some of the longer Pr—O(μ_3) distances (2.834 and 2.718 Å). The Pr—O bond lengths involving the μ_3-tftb ligands show some interesting features. Thus the shortest bonds are to the "five-coordinated" metals [Pr(3)—O(1), 2.438 ; Pr(1)—O(6), 2.407 Å] and the longest are to the six-coordinated metal [Pr(2)—O(6), 2.834 ; Pr(2)—O(1), 2.718 Å]. Whilst the μ_2—O(4) bridging the "five-coordinated" metals is almost symmetrical [Pr(3)—O(4), 2.430 ± 0.013 ; Pr(1)—O(4), 2.408 ± 0.012 Å], the other μ_2 bridges are unsymmetrical [Pr(1)—O(5), 2.371 ; Pr(2)—O(5), 2.434 and Pr(2)—O(2), 2.459 ; Pr(3)—O(2), 2.400 Å]. As would be expected, the terminal Pr—O bond lengths are longer to the six-coordinated metal [Pr(2)—O(8) ; 2.156 ; Pr(2)—O(9), 2.168 Å] than to the "five-coordinated" metals [Pr(1)—O(7), 2.141 ; Pr(3)—O(3), 2.112 Å].

The ^1H and ^{19}F NMR spectra of $Pr_3(tftb)_9$ suggest that the trinuclear structure retains its integrity in solution. The paramagnetism of the Pr^{3+} ion causes large pseudo-contact shifts and at room temperature the ^1H spectrum (C_7D_8) shows five peaks at δ 52 (broad), 21, −18.5, −20 and −34.5 ppm in the ratio of 2 : 2 : 2 : 1. From the crystal structure, the terminal ligands are distinguishable into two sets, i.e. two bonded to Pr(2) and the two equivalent groups bonded to Pr(1) and Pr(3). The three μ_2 ligands are distinguishable in a 2 : 1 ratio and the two μ_3 ligands are equivalent, giving an overall 2 : 2 : 2 : 1 : 2 arrangement. The ^{19}F NMR spectra could also be interpreted on the basis of the crystal structure. The variable temperature spectra (C_7D_8) showed an interesting fluxional behaviour (Table 4 and Fig. 3). Thus, at 363 K there are four broad peaks in a 4 : 1 : 3 : 1 ratio which become narrower at 343 K, giving five peaks in a 2 : 2 : 1 : 3 : 1 ratio. At 313 K, there are again four peaks but in the ratio 2 : 2 : 3 : 2, whilst at 283 K the five line spectrum is in accordance with the crystal structure, giving the 2 : 2 : 2 : 1 : 2 ratio. Attempts to sublime compound **2** *in vacuo* were unsuccessful due to decomposition.

The europium compound $[Eu_3(tftb)_9]$ (**3**) was

Table 3. Some bond angles (°) for $[Pr_3(tftb)_9]$ (**2**)

O(4)—Pr(1)—O(5)	137.9 (0.4)	O(3)—Pr(3)—O(4)	108.1 (0.5)
O(2)—Pr(2)—O(5)	130.0 (0.4)	O(3)—Pr(3)—O(2)	110.5 (0.4)
O(2)—Pr(3)—O(4)	141.4 (0.4)	O(3)—Pr(3)—O(6)	144.3 (0.4)
O(1)—Pr(1)—O(6)	66.8 (0.3)	O(1)—Pr(2)—O(8)	152.6 (0.4)
O(1)—Pr(1)—O(7)	178.0 (0.5)	O(5)—Pr(2)—O(6)	69.4 (0.3)
O(1)—Pr(3)—O(3)	146.7 (0.4)	O(2)—Pr(2)—O(6)	67.9 (0.3)
O(6)—Pr(2)—O(9)	166.1 (0.4)	O(8)—Pr(2)—O(6)	93.4 (0.4)
O(7)—Pr(1)—O(5)	108.6 (0.5)	O(8)—Pr(2)—O(9)	100.2 (0.5)
O(7)—Pr(1)—O(4)	111.3 (0.5)	O(2)—Pr(2)—O(9)	104.4 (0.4)
O(7)—Pr(1)—O(6)	112.0 (0.4)	O(5)—Pr(2)—O(9)	111.1 (0.4)

Table 4. ^{19}F NMR spectra for $[Pr_3(tftb)_9]$ (**2**)

Temp. (K)	Chemical shifts	integration
363	−60, −111, −146, −190	4 : 1 : 3 : 1
343	−51, −71, −112, −152, −196	2 : 2 : 1 : 3 : 1
313	−47, −70, −163, −208	2 : 2 : 3 : 2
283	−41, −68, (−178, −180)[a] −220	2 : 2 : 2 : 1 : 2
253	−35, −66, −198, −201, −230	2 : 2 : 2 : 1 : 2

[a]Overlapping peaks.

obtained as pale yellow crystals from the reaction of $Eu\{N(SiMe_3)_2\}_3$ and tftb.H in benzene solution. The trinuclear structure proposed is based on the ^1H and ^{19}F NMR spectra. Thus, at room temperature, the ^1H spectrum gave five peaks at δ 46, 5, −17, −26 (v.broad) and −60 ppm in the ratio 2 : 2 : 2 : 2 : 1. The variable temperature ^{19}F spectra (Table 5 and Fig. 4) show interesting fluxional behaviour. Thus, at 373 K there are only three broad peaks in a 4 : 1 : 4 ratio, which become sharper on lowering the temperature to 343 K (four peaks in a 2 : 2 : 1 : 4 ratio). At 313 K, further splitting occurs and at 283 K the five line spectrum is fully resolved into a 2 : 2 : 1 : 2 : 2 pattern. The IR spectra of **2** and **3** are also very similar and there seems little doubt that these compounds have the same structure. Although $[Eu_3(tftb)_9]$ could not be sublimed *in vacuo* due to decomposition, a mass spectrum gave peaks at *m/z* 400.8, 398.8 and 396.8, corresponding to the isotopic species $^{153}Eu_2F_5^+$, $^{153}Eu^{151}EuF_5^+$ and $^{151}Eu_2F_5^+$. This suggests that fluorine abstraction from the ligand takes place in the mass spectrometer.

EXPERIMENTAL

All manipulations were conducted under dry nitrogen using vacuum-line, glove-box and Schlenk-style apparatus. Solvents were dried using the sodium ketyl of benzophenone and then distilled.

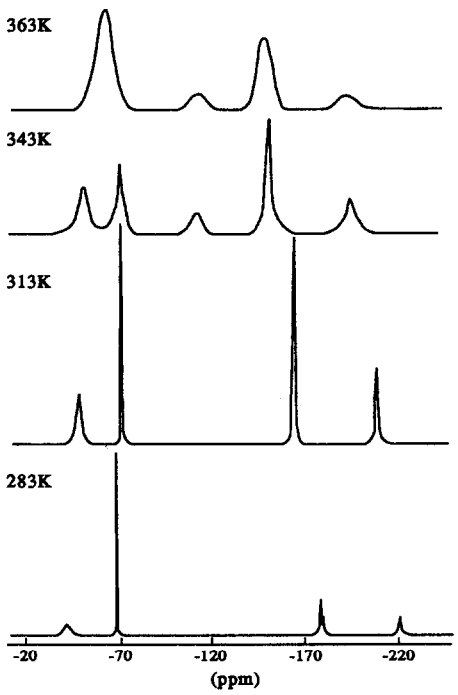

Fig. 3. The V.T. ^{19}F NMR spectra of $[Pr_3(TFTB)_9]$.

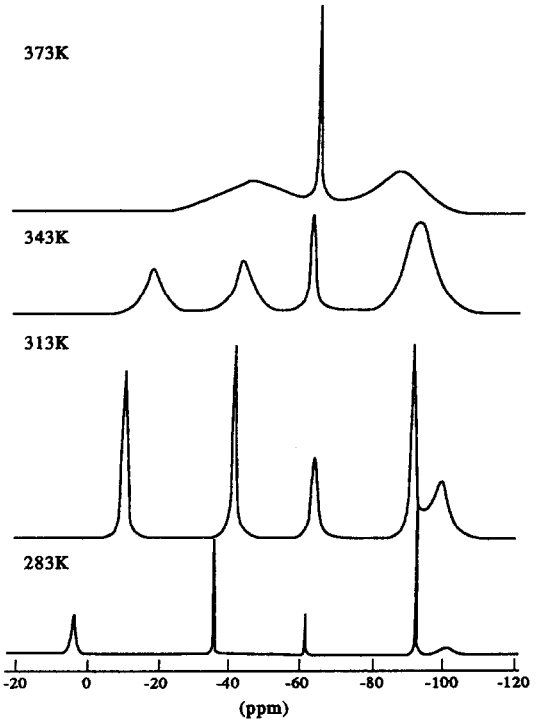

Fig. 4. The V.T ^{19}F NMR spectra of $[Eu_3(TFTB)_9]$.

Table 5. ^{19}F NMR spectra for $[Eu_3(tftb)_9]$ (3)

Temp. (K)	Chemical shifts	Integration
373	−49, −65, −87	4 : 1 : 4
343	−18, −44, −64, −94	2 : 2 : 1 : 4
313	−9, −40, −63, −91, −99	2 : 2 : 1 : 2 : 2
283	+4, −35, −60, −92, −102	2 : 2 : 1 : 2 : 2
253	+20, −28, −59, −94, −106	2 : 2 : 1 : 2 : 2

The trifluoro-tert.butanol (Fluorochem Ltd) was dried over molecular sieves. The metal tris-(bis-trimethylsilylamides) were prepared by reaction of the metal trichloride with $LiN(SiMe_3)_2$ as reported previously.[4]

NMR spectra were obtained using Bruker WM250FT and WH400FT spectrometers, using solvent signals from incomplete deuteration for ^1H chemical shifts (relative to TMS), with ^{19}F chemical shifts relative to $CFCl_3$. IR spectra were obtained as Nujoll mulls in the range 4000–200 cm^{-1} using a Perkin–Elmer FT1720 spectrometer. Attempts to obtain mass spectra were made using a Kratos MS50TC spectrometer operating at 70 eV. The carbon and hydrogen analyses were obtained commercially from either Microanalytical Services, University College, London or Butterworth Microanalytical Laboratories. Metals were determined gravimetrically as oxides.

Preparation of $[La(tftb)_3(thf)_{1.5}]$ (1)

$(CF_3)Me_2COH$ (2.1 g) in thf (10 cm^3) was added to a solution of $La\{N(SiMe_3)_2\}_3$ (3.0 g) in thf (100 cm^3) and left overnight. Solvent and $(Me_3Si)_2NH$ were then evaporated off *in vacuo* and the residue crystallized from a mixture of thf and pentane, giving **1** as white crystals (1.6 g, m.p. 78–86°C dec.). Found : La, 22.0 ; C, 33.4 ; H, 4.7. Calc. for $La\{OC(CH_3)_2(CF_3)\}_3(thf)_{1.5}$: La, 22.1 ; C, 34.4 ; H, 4.8%. ^1H NMR ($CDCl_3$) at 283 K : δ 3.85 (m, thf), 1.89 (m, thf), 1.77, 1.68, 1.63, 1.50, 1.44 (tftb-trinuclear), 1.31 (tftb-dinuclear) ; at 233 K : 3.80 (m, thf), 1.90 (m, thf), 1.76, 1.65, 1.61, 1.45, 1.24 (tftb-trinuclear), 1.30 (tftb-dinuclear). ^1H NMR (thf-d_8) at 305 K : δ 1.61, 1.58, 1.52, 1.47, 1.45 (tftb-trinuclear), 1.21 (tftb-dinuclear). ^{19}F NMR ($C_6D_5CD_3$) at 300 K : δ −76.91, −78.04, −78.16, −81.59, −82.64 (ratio 1 : 2 : 2 : 2 : 2) and small peaks at −79.50, −83.09 and −83.27 ; at 240 K : −78.42, −78.95, −79.43, −81.06, −81.76 (ratio, 2 : 2 : 1 : 2 : 2) and small peaks at −79.73, −82.48, −82.66, −82.91 and −83.16. IR : 1318m, 1207s, 1137vs, 1015s, 992s, 918w, 877s, 755m, 669w, 618s, 594m, 484m, 413w, 372wm 275w, 233w, 221m cm^{-1}.

Preparation of $[Pr_3(tftb)_9]$ (2)

$(CF_3)Me_2COH$ (5 cm^3) was added to a solution of $Pr\{N(SiMe_3)_2\}_3$ (1.8 g) in benzene (80 cm^3). After standing for 24 h the solution was concentrated at 70°C and allowed to cool. Pale green crystals of **2** were deposited (1.35 g, m.p. 180°C dec.). Found : Pr, 28.4 ; C, 27.2 ; H, 3.5. $Pr(tftb)_3$ requires : Pr, 27.0 ; C, 27.1 ; H, 3.5%. ^1H NMR ($C_6D_5CD_3$) at 300 K : δ 52 (12H), 21 (12H), −18.5 (6H), −20 (12H), −34.5 (12H). ^{19}F NMR data : see Table 4. IR : 1320s, 1261s, 1205s, 1147s, 1127s, 1015s, 990s, 886m, 872m, 801m, 753m, 723m, 677w, 612s, 586m, 506m, 490m, 373w cm^{-1}.

Preparation of $[Eu_3(tftb)_9]$ (3)

When $(CF_3)Me_2COH$ (5 cm^3) was added to a solution of $Eu[N(SiMe_3)_2]_3$ (2.2 g) in benzene (80 cm^3) there was an immediate colour change from orange to pale yellow. After standing for 24 h, the solution was concentrated and cooled to *ca* 5°C. Pale yellow crystals of **3** were deposited (1.2 g, m.p. 210°C dec.). Found : Eu, 29.2 ; C, 25.7 ; H, 3.9. $Eu(tftb)_3$ requires : Eu, 28.5 ; C, 27.6 ; H, 3.4%. ^1H NMR ($C_6D_5D_3$) at 300 K : δ 45.8 (12H), 5.0 (12H), −16.8 (12H), −26.0 (v.br, 12H), 39.8 (6H). ^{19}F NMR data : see Table 5. IR : 1320s, 1142s, 1017s, 988s, 885s, 754s, 723m, 677w, 613s, 586s, 511s, 492s, 481s, 424s, 375m cm^{-1}.

Crystal structure of $[Pr_3(tftb)_9]$ (2)

A preliminary account of the single crystal X-ray structure determination of **2** has already been reported.[3] The crystal structure parameters are given in Table 1 and the more important bond distances and bond angles are listed in Tables 2 and 3, respectively.

Acknowledgements—We thank the SERC and the British Council and Education Commission of the People's Republic of China (R. W.) for financial support. We thank Mr Peter Cook for mass spectral measurements, Mr Greg Coumbarides for the 250 MHz NMR spectra, Mr Peter Haycock of the University of London Intercollegiate Research Services (ULIRS) for the 400 MHz NMR spectra at QMW College, and Mrs Jane Elliot and Mr J. Cobb for the ^{19}F NMR spectra using the Bruker WM 250 MHz spectrometer (ULIRS) at King's College, London.

REFERENCES

1. D. C. Bradley, H. Chudzynska, M. B. Hursthouse and M. Motevalli, *Polyhedron* 1993, **12**, 1907.
2. D. C. Bradley, H. Chudzynska, M. B. Hursthouse and M. Motevalli, *Polyhedron* 1991, **10**, 1049.
3. D. C. Bradley, H. Chudzynska, M. E. Hammond, M. B. Hursthouse, M. Motevalli and R. Wu, *Polyhedron* 1992, **11**, 375.
4. D. C. Bradley, J. S. Ghotra and F. A. Hart, *J. Chem. Soc., Dalton Trans.* 1973, 1021.

Polyhedron Vol. 12, No. 24, pp. 2961–2964, 1993
Printed in Great Britain

0277-5387/93 $6.00+.00
© 1993 Pergamon Press Ltd

METATHESIS ROUTES TO TIN AND LEAD CHALCOGENIDES

I. P. PARKIN* and A. T. ROWLEY

Department of Chemistry, The Open University, Milton Keynes, MK7 6AA, U.K.

(*Received* 16 *June* 1993; *accepted* 15 *July* 1993)

Abstract—Thermal initiation (550°C) of a mixture of SnI_4 and Li_2E produces SnE_2 (E = O, S, Se). Similarly, $PbCl_2$ and Li_2E' produces PbE' (E' = O, S, Se, Te) via an exothermic solid state metathesis reaction. The PbE' and SnE_2 compounds were characterized by microanalysis, SEM/EDAX, FT-IR spectroscopy, magnetic moment measurements, X-ray powder diffraction and, in the case of tin, by solid state NMR.

Tin and lead chalcogenides are found as minerals and manufactured for semi-conductors, mosaic golds, pigments, photo-conductors and radio receivers.[1] Traditionally they are made by high temperature combination of the elements, by solution precipitation methods or by reaction of H_2E (E = S, Se, Te) on the metal.[2]

Self-propagating high temperature synthesis (SHS) methods to materials have been developed by Russian chemists[3] in the 1960s. These process involve initiating a solid-state reaction between pressed discs of the elements by means of an electric filament or an oven. Kaner *et al.*[4] and others[5] have utilized a similar idea by synthesizing transition metal chalcogenides via a solid state metathesis reaction involving sodium chalcogenides and metal halides. These syntheses have a number of advantages, firstly the reaction can be extremely rapid (2–3 s), secondly the by-product NaCl is easily removed by trituration, thirdly high purity crystalline products are produced and fourthly the reaction requires low energy initiation. Modifications to this technique have allowed control of crystallite size and morphology.[6]

Here we outline an extension of solid state metathesis reactions to main group metals in the synthesis of tin and lead chalcogenides.

EXPERIMENTAL

All reactions and preparations were carried out *in vacuo* or in a dinitrogen-filled dry box. Glass ampoules were made out of pyrex glass and were either flame dried *in vacuo* or heated to 400°C for 6 h prior to reaction. All solvents were degassed with dinitrogen. Methanol was distilled from MgI_2 and stored over 3 Å molecular sieves prior to use. Metal halides and Li_2O were purchased from Aldrich Chemical Co. and used as supplied. Lithium chalcogenides, Li_2S, Li_2Se and Li_2Te, were made by combining lithium and the chalcogenide in liquid ammonia followed by evaporation of the ammonia and thermolysis of the residue to 550°C for 10 h. X-ray powder diffraction patterns were obtained using a Seimens D5000 diffractometer using nickel filtered copper K_α (λ = 1.5406 Å) radiation; SEM and electron microprobe analysis on a Jeol JSM 820 equipped with Kevex program,[7] FT-IR as pressed KBr discs on a Nicolet 205 (CsI); magnetic susceptibility measurements were determined on a Johnson Matthey balance. Solid state ^{119}Sn MAS NMR spectra were obtained at 111.862 MHz at a spin rate of 12.25 kHz on the SERC machine at Durham University with chemical shift measurements given relative to $Sn(CH_3)_4$. Ultrasound sonication was achieved at 20 kHz using a Soniprep ultrasonic gun. Thermal initiation of the reactions was performed in a Lenton Thermal Design tube furnace.

Preparation of tin and lead chalcogenides

Lithium chalcogenide and anhydrous metal halide (SnI_4 or $PbCl_2$) were ground together using an agate pestle and mortar in a dinitrogen-filled dry box (such that the ratio of lithium to halide was 1 : 1). The powder was added to a thick-walled glass

*Author to whom correspondence should be addressed.

ampoule, sealed under vacuum and sonicated with an ultrasonic gun for 10 min. The ampoule was then wrapped in glass wool and placed in a conventional oven at 550°C for 5 h. The ampoule was removed from the oven, allowed to cool to room temperature and opened in a glove box. Trituration of the grey, orange or yellow solid with methanol, aqua regia, water or dilute HCl for 1 h produced a fine precipitate and a cloudy layer (Table 1). Evaporation of the methanol filtrate produces crystals of a white solid identified as LiCl or LiI by X-ray powder diffraction, lithium flame test and chlorine/iodine EDAX analysis. The coloured powders were identified as tin or lead chalcogenides by X-ray powder diffraction (Table 1), EDAX analysis, magnetic moment measurements, FT-IR and ^{119}Sn NMR. Ceramic yields, based on the metal after THF trituration, varied from 20% (Pb_2O_2Cl) to 80% (PbSe, SnS_2) depending on the sample.

RESULTS AND DISCUSSION

Reaction of SnI_4 or $PbCl_2$ with Li_2E (E = O, S, Se, Te) produces tin or lead chalcogenides and lithium halide via an exothermic solid-state metathesis reaction:

$$SnI_4 + 2Li_2E \xrightarrow{500°C} SnE_2 + 4LiI \quad (E = O, S, Se) \quad (1)$$

$$PbCl_2 + Li_2E \xrightarrow{500°C} PbE + 2LiCl \quad (E = S, Se, Te) \quad (2)$$

$$PbCl_2 + Li_2O \xrightarrow{500°C} Pb_2O_2Cl + LiCl + [Pb]. \quad (3)$$

After thermolysis the product was contained in fused grey, gold or orange lumps which showed a smooth morphology by SEM indicative of a coating of sublimed LiCl. Metal, chalcogenide and chloride were detected by EDAX analysis, which is consistent with the formation of a metal chalcogenide that contains amorphous lithium chloride on the surface. The metal chalcogenides were purified by trituration with methanol, aqua regia or dilute HCl (Table 1) to remove the LiCl, tin metal and unreacted metal halide, respectively. Characterization was by X-ray powder diffraction, magnetic moment measurement and solid state ^{119}Sn NMR spectroscopy.

The SEM profile of the triturated metal chalcogenides showed a rough porous surface, whilst the EDAX step analysis revealed only metal and chalcogen with no halide present (2–3% detection limit, except for Pb_2O_2Cl, where Cl was observed). The FT-IR spectra of the metal chalcogenides were featureless in the range 4000–400 cm^{-1}. No lithium (<0.1%) was detected by microanalysis for the triturated powders. The solid state ^{119}Sn NMR spectrum of SnS_2 showed a single resonance at −764 ppm, indicating that only one environment for tin is present in the lattice and that no detectable free tin is produced from the reaction of SnI_4 and Li_2S.

The X-ray powder diffraction data for the metal chalcogenides formed from reaction of Li_2E and $SnI_4/PbCl_2$ are summarized in Table 1. In general, after a reaction time of 4 h at 550°C, a crystalline metal chalcogenide was formed.[8] The crystalline size as determined by the Scherrer equation[9] based on the powder XRD line widths varied from 300 to 600 Å. The metal chalcogenides after trituration had no crystalline lithium halide present and showed the material as a single phase, SnE_2 or PbE.

Table 1. Crystallographic and experimental data from the reaction of SnI_4 and $PbCl_2$ with Li_2E (E = O, S, Se, Te)

Reagents	Work-up	Colour	Crystalline phase detected	Literature **a** spacing[8] (Å)	Observed **a** spacing (Å)	Crystalline size (Å)
$SnI_4 + Li_2O$	aqua regia	white	SnO_2[a] (tetragonal)	4.738	4.727	450
$SnI_4 + Li_2S$	methanol	gold	SnS_2 (hexagonal)	3.639	3.627	450
$SnI_4 + Li_2Se$	methanol	grey	$SnSe_2$ (hexagonal)	3.810	3.793	400
$PbCl_2 + Li_2O$	water	orange	Pb_2O_2Cl (tetragonal)	3.910	3.908	350
$PbCl_2 + Li_2S$	methanol	grey	PbS (cubic)	5.936	5.908	600
$PbCl_2 + Li_2Se$	methanol	grey	PbSe (cubic)	6.124	6.088	500
$PbCl_2 + Li_2Te$	dilute HCl	grey	PbTe (cubic)	6.459	6.437	450
$PbCl_2 + Li_2$(Se, Te)	dilute HCl	grey	Pb_2(Se, Te)		6.24	300
$PbCl_2 + Li_2$(S, Se)	dilute HCl	grey	Pb_2(S, Se)		5.99	450
$SnI_4 + Li_2$(S, Se)	dilute HCl	grey	Sn(S, Se)		3.71	400

[a]Before trituration tin metal was also detected by XRD.

In general, the reaction of SnI_4 or $PbCl_2$ with Li_2E involves no redox chemistry, with the metal in the same oxidation state as the starting material. The reaction times and crystallinity of the products were comparable for all the chalcogens studied; however, the yield of Pb_2O_2Cl was considerably lower than the rest at 20%. Formation of Pb_2O_2Cl involves oxidation at the metal and may form from a dispropotronation reaction with formation of some lead metal, although this was not detected by XRPD.

Analogous studies of reaction of sodium chalcogenides with transition metal halides showed that initiation can be achieved at room temperature by light grinding of the reagents.[4] No initiation of the reaction of $PbCl_2$ or SnI_4 and Li_2E could be achieved either by grinding or mixing the reagents or by means of a heated filament. The reactions required heating at 450–500°C to initiate; however, the presence of sublimed LiCl (b.p. = 1300°C) and occasional warping/pitting of the ampoules indicates that these reactions are exothermic and it is this that provides for a relatively rapid reaction generating crystalline products.

Hess' law calculations[10] of the reaction of metal halide and lithium chalcogenide indicate that the reaction is exothermic with $\Delta H \approx -200$ kJ mol^{-1}. The primary driving force for the reaction is due to the large lattice energy of the co-product LiX, which accounts for up to 80% of the reaction enthalphy.

Reaction of SnI_4 with mixed lithium chalcogenides $Li_2Se_{0.5}S_{0.5}$ proceeds analogously to the reactions to produce binary SnE_2 materials. The X-ray diffraction patterns of the mixed $Sn(S_xSe_y)$ materials are intermediate between and slightly broader than the patterns observed for the corresponding binary SnS_2, $SnSe_2$ materials. The EDAX step analysis of the mixed tin chalcogenide showed constant ratios of sulphur and selenium, indicating that an intermixed species was formed. Similar behaviour is observed for the reactions with $PbCl_2$ and $Li_2Se_{0.5}S_{0.5}$, $Li_2Se_{0.5}Te_{0.5}$ which formed the mixed species $PbSe_xS_y$ and $PbSe_xTe_y$, respectively. The composition of the mixed lead chalcogenide species as assessed from the lattice spacing, **a** (assuming Vegards' law[11]) and the EDAX analysis indicates that species of composition close to $PbSe_{0.5}S_{0.5}$ and $PbSe_{0.5}Te_{0.5}$ were formed. A representative powder pattern for $PbSe_{0.5}S_{0.5}$ is shown in Fig. 1.

Kaner[4] has suggested that reaction of MCl_5 and $Li_2S_xSe_y$ may proceed by formation of the salt LiCl, co-reduction to the metal and chalcogen followed by recombination of the metal and chalcogen promoted by the heat of reaction. This accounts for the slight differences in chalcogen ratio in a range of reactions.[12] The mixed chalcogenide reactions to form PbS_xSe_y showed that $x = y$. However, the amount of selenium incorporation (as assessed by EDAX and **a** value) was found to be slightly lower than that of sulphur, in agreement with Kaner's findings. Interestingly, reaction of SnI_4 with Li_2O formed some tin metal in the reaction, unlike the reactions for Li_2S and Li_2Se. If the partial reduction to the elements followed by recombination mechanism was correct, then combination of tin metal with O_2 (g) would be expected to be less likely than with sulphur or selenium.

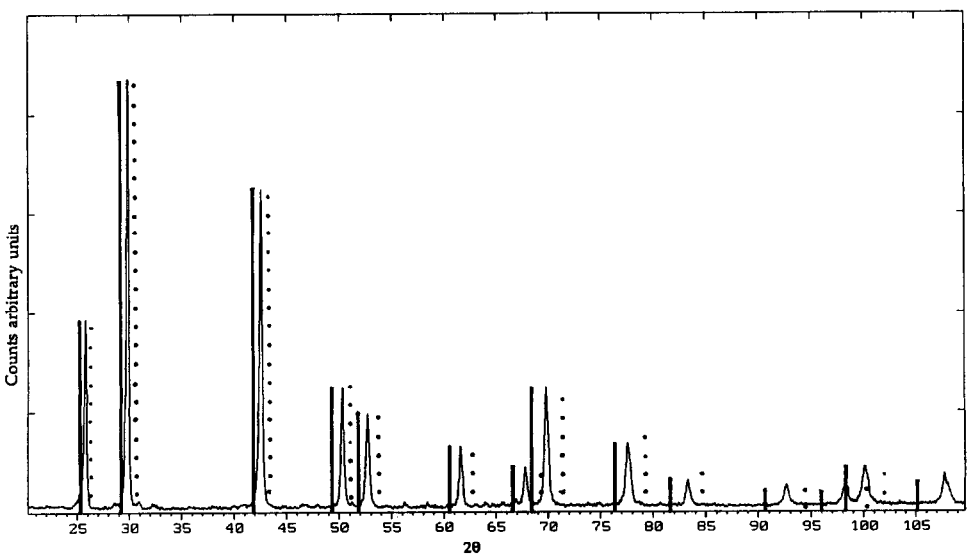

Fig. 1. X-ray powder diffraction pattern from reaction of Li_2(Se, S) and $PbCl_2$; standard patterns for PbS (—) and PbSe (···).

CONCLUSION

Solid state metathesis reactions offer a route to crystalline tin and lead chalcogenides via an exothermic reaction. The reactions are at lower temperature and reasonably rapid, requiring shorter annealing times than conventional preparations. The purity of the metal chalcogenide is high, with the by-product lithium halides either subliming out during the course of the reaction or being removed by trituration.

Acknowledgements—The Royal Society, Nuffield Trust, Leverhulme Trust, SERC (Fellowship to A.T.R.). Dr Apperley is thanked for obtaining the solid state NMR spectra.

REFERENCES

1. J. C. Bailar, H. J. Emeleus, R. S. Nyholm and A. F. Trotman Dickenson (Eds), *Comprehensive Inorganic Chemistry*, Vol. 2. Pergamon Press, Oxford (1973).
2. N. N. Greenwood and A. Earnshaw (Eds), *Chemistry of the Elements*. Pergamon Press, Oxford (1990).
3. V. J. Torbov, V. I. Chukalin and E. J. Yarembush, *Inorg. Mater.* 1970, **6**, 1559.
4. P. R. Bonneau, R. F. Jarvis and R. B. Kaner, *Nature* 1991, **32**, 2127; R. E. Treece, G. S. Macala and R. B. Kaner, *Chem. Mater.* 1992, **4**, 9.
5. A. Hector and I. P. Parkin, *J. Chem. Soc., Chem. Commun.* 1993, 1095.
6. A. Hector and I. P. Parkin, *J. Mater. Sci. Lett.*, in press.
7. Quantex 6.2, with Quantum detector Kevex delta 4.
8. PDF-2 database, International Centre for Diffraction Data, Swarthmore, PA 19081, 1990.
9. H. P. Klug and L. E. Alexander, *X-ray Diffraction Procedure for Polycrystalline and Amorphous Materials*, 2nd Edn. John Wiley, New York (1974).
10. D. D. Wagmann, W. H. Evans, V. B. Parker, R. H. Schumm, I. Halow, S. M. Bailey, K. Chumey and R. L. Nuttal, *The NBS Tables of Thermodynamic Properties*. American Chemical Society, Washington, DC (1982).
11. A. F. Wells, *Structural Inorganic Chemistry*, p. 1294. Clarendon Press, Oxford (1984).
12. P. R. Bonneau, R. F. Jarvis and R. B. Kaner, *Inorg. Chem.* 1992, **31**, 3127.

Polyhedron Vol. 12, No. 24, pp. 2965–2971, 1993
Printed in Great Britain

0277–5387/93 $6.00+.00
© 1993 Pergamon Press Ltd

RAMAN SPECTROSCOPIC CHARACTERIZATION OF HIGH TEMPERATURE $MGaCl_8$ (M = Nb, Ta) DINUCLEAR MOLECULAR COMPLEXES IN THE LIQUID AND GASEOUS STATE

S. BOGHOSIAN* and G. A. VOYIATZIS

Institute of Chemical Engineering and High Temperature Chemical Processes and Department of Chemical Engineering, University of Patras, P.O. Box 1414, GR-26500 Patras, Greece

(*Received* 2 *June* 1993; *accepted* 15 *July* 1993)

Abstract—Raman spectra were obtained at temperatures 375–650 K and pressures up to 4 atm from $GaCl_3$–$NbCl_5$ and $GaCl_3$–$TaCl_5$ binary mixtures in the liquid and vapour state. The data indicate formation of $NbGaCl_8$ and $TaGaCl_8$ liquid and vapour dinuclear addition complexes. The spectra were interpreted in terms of a C_{2v} configuration for the $MGaCl_8$ (M = Nb, Ta) molecules consisting of a MCl_6 octahedron sharing an edge with a $GaCl_4$ tetrahedron. A comparison of the spectral features of 1 : 1 $GaCl_3$–$NbCl_5$ and $GaCl_3$–$TaCl_5$ molten mixtures with the spectra of the corresponding polycrystalline samples indicates that the proposed identity for the complexes is maintained in all three phases. The $NbGaCl_8$ and $TaGaCl_8$ complexes exist in the liquid state in a wide temperature range beyond their melting points (125 and 150°C, respectively) and are shown to undergo dissociation to their components [Nb_2Cl_{10}(l)/$NbCl_5$(l), Ga_2Cl_6(l) and Ta_2Cl_{10}(l)/$TaCl_5$(l)] with increasing temperature. Both complex molecules are identified in the gaseous state in low percentages among the vapours of their components and are almost totally decomposed at temperatures higher than *ca* 325°C. The enthalpy of the reaction $TaCl_5(g)+1/2Ga_2Cl_6(g) \rightleftharpoons TaGaCl_8(g)$ was determined from accurate relative Raman intensity measurements as $\Delta H^0 = -38 \pm 2$ kJ mol^{-1}.

In the field of high temperature chemistry, the formation of metal halide complexes in the liquid and/or the vapour state has attracted a special interest due to potential applications in several technological problems. Comprehensive reviews on this apparently general phenomenon are available.[1–4] Raman spectroscopy has been used in the past as a powerful tool for establishing the vibrational and structural properties of a large number of liquid and/or vapour complexes as well as "adduct" compounds of inorganic salts at elevated temperatures.[1,2,5,6] It has also been demonstrated that in certain cases Raman spectroscopy can be used for establishing the stoichiometry and thermodynamics of formation of vapour complexes.[7,8]

The trihalides of aluminum, gallium, indium and iron are among the most commonly studied complex forming agents, since they form complex molecules with a variety of metal halides in the gas phase or in the condensed state.[1] Previous investigations concerning complex formation between trihalides and pentahalides involved vibrational, electronic and mass spectrometric studies as well as X-ray work in a limited number of systems. Particularly the $UAlCl_8$[9,10] and $TaAlCl_8$[11] vapour complexes have been identified, the $PCl_4^+MCl_4^-$ (M = B, Al, Ga) ionic structures are derived[12] and the $NbAlCl_8$ molecular complex in the solid, melt and vapour phases has been thoroughly characterized.[13]

The present work concerns the mixed halide complex compounds formed by $GaCl_3$ with $TaCl_5$ and $NbCl_5$ in the liquid, solid and gaseous state. Raman spectra of the formed complexes in the liquid and gaseous phases are obtained. The vibrational band frequencies of the complexes formed in the liquid or gaseous state are determined and possible complex structures are considered and discussed. Finally, for

* Author to whom correspondence should be addressed.

the $TaCl_5$–$GaCl_3$ vapour system the data obtained are shown to be suitable for a determination of the enthalpy of the reaction:

$$TaCl_5(g) + 1/2Ga_2Cl_6(g) \rightleftharpoons TaGaCl_8(g) \quad (1)$$

$$500\ K < T < 575\ K \quad 0.5\ atm < P < 1.5\ atm.$$

EXPERIMENTAL

High purity anhydrous $NbCl_5$, $TaCl_5$ and $GaCl_3$ were prepared from the corresponding Cerac/Pure Inc. reagents by repeated slow sublimations in fused silica tubes *in vacuo*. All handling of these chemicals took place in a nitrogen-filled glove-box with a water vapour content of less than 1 ppm.

The Raman (optical) cells containing the melt mixtures consisted of fused silica tubing (4 ± 0.1 mm o.d. and 2 ± 0.1 mm i.d., ~ 3 cm long). In the case of cells containing vapour mixtures, silica tubing with 20 ± 2 mm o.d., 18 ± 0.2 mm i.d. was used. Preweighed amounts of salts were transferred into clean, dry, flamed and degassed optical cells of known volume and sealed afterwards *in vacuo*. The salt mixtures were reacted inside a side tube (6 ± 0.1 mm o.d., 4 ± 0.1 mm i.d.), vapour transported into the main cell compartment and finally the side tube was sealed off. In this way a high degree of sample purity could be achieved. The ideal gas pressure, P_0, of each undissociated and non-reacted compound at a temperature T was calculated from the number of moles added to the cell.

Raman spectra were excited with the 514.5 and 488.0 nm lines of a 4 W Spectra Physics Ar^+ laser and the 647.1 and 676.4 nm lines of a Spectra Physics Kr^+ laser. The scattered light was collected at an angle of 90° (vertical scattering plane) and analyzed with a Spex 1403, 0.85-m double monochromator equipped with a −20°C cooled RCA photomultiplier and EG&G/ORTEC rate meter and photon counting electronics. The optical furnace for obtaining the high-temperature Raman spectra and the procedures for obtaining accurate relative Raman intensity data at high temperatures have been described in detail elsewhere.[14,7]

RESULTS AND DISCUSSION

The $GaCl_3$–MCl_5 (M = Nb, Ta) *molten systems*

Melts consisted of mixtures of pure gallium chloride, niobium pentachloride and tantalum pentachloride are considered as molecular liquids (Ga_2Cl_6, Nb_2Cl_{10} in equilibrium with $NbCl_5$ and Ta_2Cl_{10} in equilibrium with $TaCl_5$, respectively) and their Raman spectra are well characterized.[15–18]

Raman spectra of molten $NbCl_5$–$GaCl_3$ and $TaCl_5$–$GaCl_3$ mixtures have been recorded in the temperature range 390–580 K. Figure 1 shows representative Raman spectra obtained for $NbCl_5$–Nb_2Cl_{10}(l), Ga_2Cl_6(l) and for three different $NbCl_5$–$GaCl_3$ molten mixtures at 490 K. The spectra consist of superposition of bands due to the pure components plus several new bands, which are attributed to complex formation. The spectral data in Fig. 1 indicate that the predominant complex species is most probably a dinuclear addition compound of $NbCl_5 \cdot GaCl_3$ (m.p. $\sim$ 125°C) type, characterized principally by two strong polarized bands at 366 and 422 cm^{-1}. This is further justified by a study of temperature dependence measurements of Raman spectra obtained from a 1 : 1 molten mixture in the range 410–570 K (shown in Fig. 2). The spectral features in Fig. 2 reveal that: (i) in total eight bands can be assigned as due to the $NbGaCl_8$ liquid compound (see Table 1 for wave-numbers and polarization characteristics) and (ii) the intensities of the bands assigned to the complex are decreasing with increasing temperature, most probably due to thermal decomposition of the complex. At 410 K the strongest Ga_2Cl_6(l) and $NbCl_5$(l) bands at 96 and 395 cm^{-1} are observed as weak

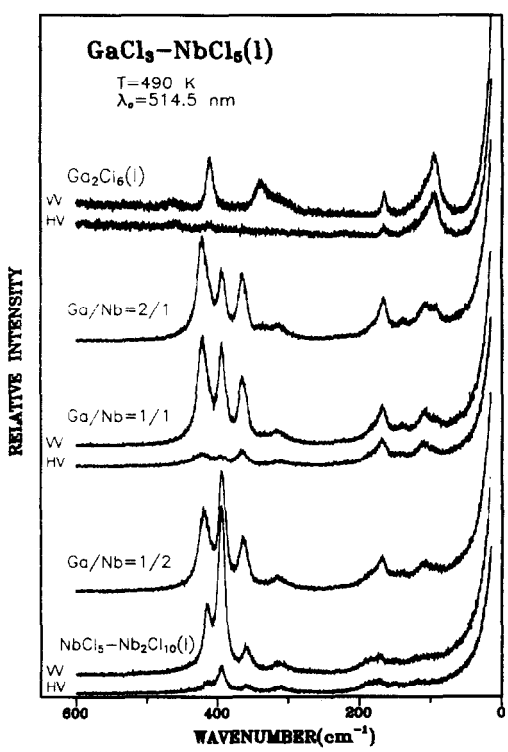

Fig. 1. Raman spectra of $GaCl_3$–$NbCl_5$ molten mixtures. Laser power, w = 15 mW; spectral slit width, ssw = 3.5 cm^{-1}; time constant, τ = 0.1 s; scan speed, ss = 1 cm^{-1} s^{-1}.

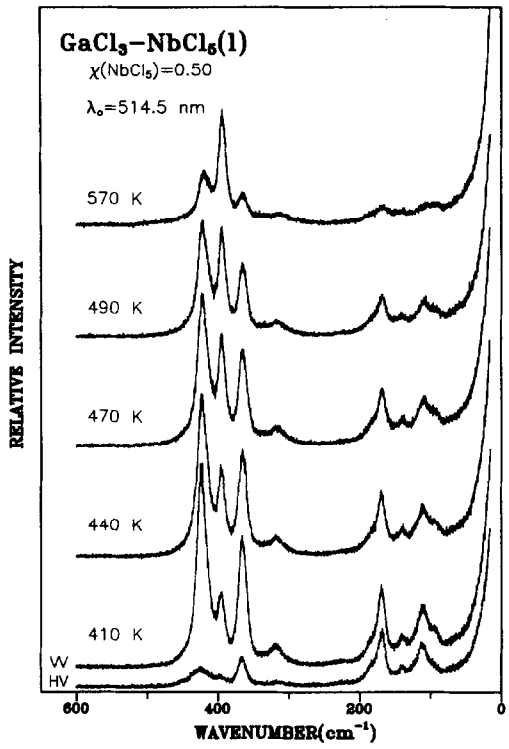

Fig. 2. Temperature dependence of Raman spectrum of liquid. $GaCl_3$–$NbCl_5$ mixture with $\chi(NbCl_5) = 0.50$. w = 15 mW; ssw = 3.5 cm^{-1}; $\tau = 0.1$ s; ss = 1 $cm^{-1}\,s^{-1}$.

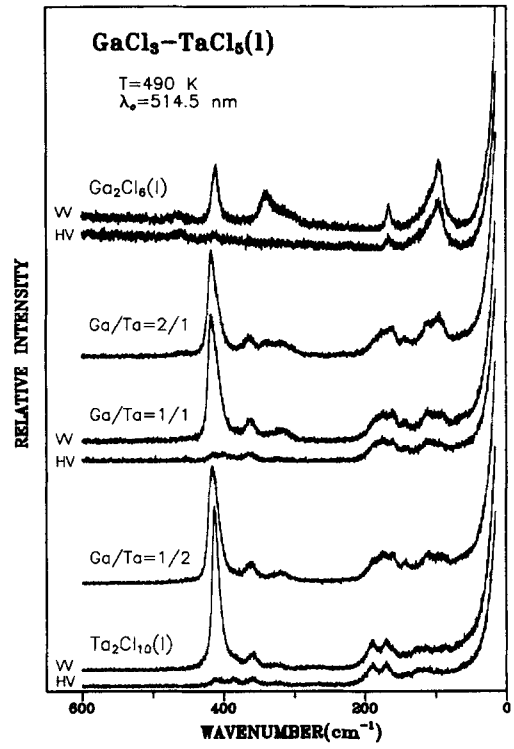

Fig. 3. Raman spectra of $GaCl_3$–$TaCl_5$ molten mixtures. w = 15 mW; ssw = 3.5 cm^{-1}; $\tau = 0.1$ s; ss = 1 $cm^{-1}\,s^{-1}$.

bands among the bands due to $NbGaCl_8$(l), which is the predominant species present. It is noteworthy that a temperature rise shifts also the dissociation equilibrium:

$$Nb_2Cl_{10}(l) \rightleftharpoons 2NbCl_5(l),$$

to the right. Thus, while at 500 K niobium pentachloride melts are considered as monomer-dimer mixtures, at 600 K the dimer is almost completely dissociated.[16]

Figure 3 shows representative Raman spectra obtained for Ta_2Cl_{10}(l), Ga_2Cl_6(l) and $TaCl_5$–$GaCl_3$ mixtures at 490 K. It should be pointed out here, that higher temperatures are needed to dissociate Ta_2Cl_{10} than to dissociate Nb_2Cl_{10}.[17] A careful comparison of the spectral features in Fig. 3 indicates that at least eight bands (attaining their maximum intensities in the spectrum with the composition: Ga/Ta = 1/1) can be assigned as due to a new complex species, presumably $TaGaCl_8$. Although there is an accidental frequency overlap of characteristic bands due to Ta_2Cl_{10} and Ga_2Cl_6 at ~ 412 cm^{-1}, one can easily observe by comparing the relative intensities of other bands of the different species that the spectral feature centred at ~ 417 cm^{-1} is mainly due to the $TaGaCl_8$ complex. Wavenumbers, polarization characteristics and species assignments of the observed bands in the $TaCl_5$–$GaCl_3$ molten system are summarized in Table 1. The temperature dependent features of the 1:1 $TaCl_5$–$GaCl_3$ liquid Raman spectra are similar to those of the $NbCl_5$–$GaCl_3$ system (Fig. 2) and are interpreted as indicating a thermal decomposition of the $TaGaCl_8$(l) to $TaCl_5$(l) and Ga_2Cl_6(l). The melting point of $TaGaCl_8$ was found to be ~ 150°C.

In summary, the molten MCl_5–$GaCl_3$ (M = Nb, Ta) mixtures in the composition and temperature range studied can be considered as molecular liquids consisting of Ga_2Cl_6, M_2Cl_{10}, MCl_5 and $MGaCl_8$ molecules linked by the equilibria:

$$2MGaCl_8(l) \rightleftharpoons M_2Cl_{10}(l) + Ga_2Cl_6(l)$$

$$M_2Cl_{10}(l) \rightleftharpoons 2MCl_5(l),$$

(M = Nb, Ta).

Raman spectra of polycrystalline 1:1 $NbCl_5 \cdot GaCl_3$ and $TaCl_5 \cdot GaCl_3$ were also recorded at room temperature. The observed wavenumbers are listed in Table 1.

Table 1. Raman spectal data obtained from (a) 1 : 1 $NbCl_5$–$GaCl_3$ and $TaCl_5$–$GaCl_3$ molten mixtures; (b) $NbGaCl_8$ and $TaGaCl_8$ vapour complexes and (c) $NbGaCl_8$, $TaGaCl_8$ polycrystalline samples[a]

$NbCl_5$–$GaCl_3$(l) 400 K < T < 575 K		$NbGaCl_8$(g) 485 K	$NbGaCl_8$(s) 300 K	$TaCl_5$–$GaCl_3$(l) 425 K < T < 575 K		$TaGaCl_8$(g) 485 K	$TaGaCl_8$(s) 300 K
ν(cm^{-1})	Molecular origin	ν(cm^{-1})	ν(cm^{-1})	ν(cm^{-1})	Molecular origin	ν(cm^{-1})	ν(cm^{-1})
			24m				30m
			39w				37sh
			45m				74w
			81m	93vw,dp	Ga_2Cl_6		90w
95vw,dp	Ga_2Cl_6		98w				96w
			104w				111w
			110w	113w,dp	$TaGaCl_8$		119m
110m,dp	$NbGaCl_8$		116s				129m
			123w	143vw,(dp)	$TaGaCl_8$, $TaCl_5$		153w
142vw,(dp)	$NbGaCl_8$		138m	160w,dp	$TaGaCl_8$		163m
			163s	174w,dp	$TaGaCl_8$		171w
169m,dp	$NbGaCl_8$		172s	186w,dp	$TaGaCl_8$		183m
186w,dp	$NbGaCl_8$		185m				190m
			221w				225w
310vw,dp	$NbGaCl_8$, $NbCl_5$		324vw				270w
318w,p	$NbGaCl_8$, Ga_2Cl_6			319w,p	$TaGaCl_8$, Ga_2Cl_6		318w
338vw,(p)	Ga_2Cl_6		359sh	339vw,br	Ga_2Cl_6		349sh
				358vw,(p)	Ta_2Cl_{10}		
366sp	$NbGaCl_8$	369w,p	362vs	364m,(p)	$TaGaCl_8$	370w,p	358s
395s,p	$NbCl_5$		390w				373w
			423m				382w
				410w,p	Ta_2Cl_{10}		399w
422s,p	$NbGaCl_8$	425sh,p	433vs	417vs,p	$TaGaCl_8$		412vs
							421m

[a] Abbreviations: s = strong, m = medium, w = weak, v = very, br = broad, sh = shoulder, p = polarized, dp = depolarized.

Vapour Raman spectra

Raman spectra of vapours over liquid mixtures Ga_2Cl_6–MCl_5 at temperatures between 453 and 573 K are mainly due to Ga_2Cl_6–$GaCl_3$(g) and MCl_5(g). The temperature dependent features of the Raman spectra of Ga_2Cl_6–$GaCl_3$ vapours are well established,[8] while niobium and tantalum pentachloride vapours are known to consist of monomeric MCl_5 molecules and their Raman spectra are described elsewhere.[18] Several gas-cells were prepared containing varying amounts of $GaCl_3$ and MCl_5. The chemicals were sublimed into the cells and the Raman measurements were made by using the techniques described in detail elsewhere.[7] The vapour Raman spectra obtained gave evidence of formation of vapour complexes. Figure 4 shows representative Raman spectra of $NbCl_5$–$GaCl_3$ vapours. Raman spectra of gaseous niobium pentachloride[18] and gallium chloride[8] are included for comparison. Two new polarized weak bands observed in spectra of $NbCl_5$–$GaCl_3$ vapours (marked by "C" in Fig. 4) at 369 and 425 cm^{-1} are attributed to vapour complexation. Figure 5 illustrates a similar behaviour exhibited in the $TaCl_5$–$GaCl_3$ vapour system. The spectra of $TaCl_5$–$GaCl_3$ vapour mixtures consist of superposition of bands due to $TaCl_5$(g) and Ga_2Cl_6(g)/$GaCl_3$(g) plus a new polarized band at 370 cm^{-1}. Another complex band is possibly obscured from the strong asymmetric doublet feature (centred at *ca* 407 cm^{-1}) due to the $\nu_1(A'_1)TaCl_5$ and $\nu_1(A_g)Ga_2Cl_6$ bands at 406 and 412 cm^{-1}, respectively.

A comparison of the spectral features in the MCl_5–$GaCl_3$ gaseous systems with the spectra of the corresponding liquids, indicates that most probably the vapour complexes also have a 1 : 1 stoichiometry. A temperature rise leads to thermal

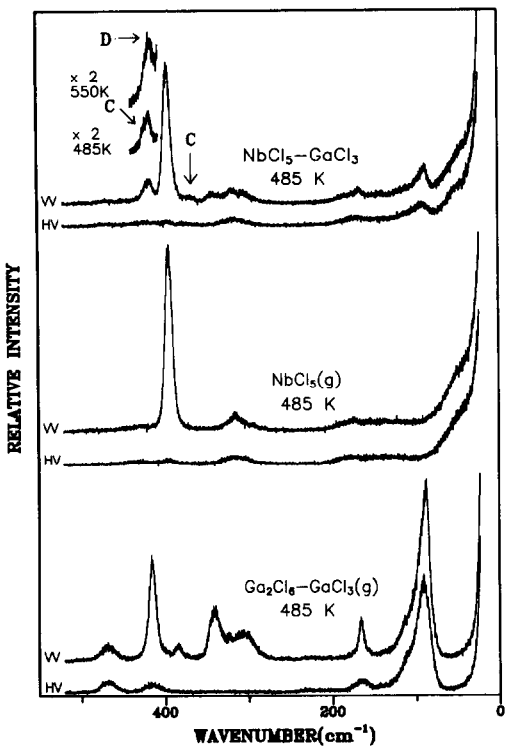

Fig. 4. Vapour Raman spectra of $Ga_2Cl_6/GaCl_3$, $NbCl_5$ and a $GaCl_3$–$NbCl_5$ mixture with $P_{0,NbCl_5} = 0.7$ atm. and $P_{0,Ga_2Cl_6} = 0.35$ atm. $\lambda_0 = 514.5$ nm; w = 420 mW; ssw = 5 cm^{-1}; $\tau = 0.15$ s; ss = 0.5 cm^{-1} s^{-1}.

decomposition of the $MGaCl_8$ vapour compounds (see Figs 4, 5).

Enthalpy of $TaGaCl_8(g)$ *formation.* Measurements of the vapour Raman spectra using different laser powers showed no changes in the relative intensities of the observed bands. On the other hand, changing the laser light frequency from red to blue altered the intensities of the $NbCl_5(g)$ and $NbGaCl_8(g)$ bands relative to those of the $Ga_2Cl_6(g)$ bands. As the frequency was changed from $\lambda_0 =$ 647.1 nm to $\lambda_0 = 488.0$ nm, the intensities of the ~ 425 cm^{-1} $NbGaCl_8$ and ~ 393 cm^{-1} $NbCl_5$ bands were almost tripled relative to those of $Ga_2Cl_6(g)$. This indicates preresonance enhancement of the $NbCl_5(g)$ and $NbGaCl_8$ fundamentals due to overlap of the excitation lines with the tail of the UV-absorption bands of the niobium vapour species.

On the other hand, no such overlap of the laser lines with the electronic bands of the tantalum vapour species could be observed. Therefore, contrary to the $NbCl_5$–$GaCl_3$ system, the procedure and method described in ref. 7 could be applied for determining the enthalpy of the gaseous reaction:

$$TaCl_5(g) + 1/2Ga_2Cl_6(g) \leftrightharpoons TaGaCl_8(g), \quad (1)$$

from a study of temperature dependence of the Raman intensities, I_i, of representative bands due to the participating species. Three different cells were made for studying the temperature dependence of the Raman spectra in the $TaCl_5$–Ga_2Cl_6 system. The first column in Table A (supplementary material, deposited with the editor) gives the characteristics of each cell. The intensity data obtained and the procedures used to derive band intensities that were not directly measured from the specta due to band overlaps are also described in Table A.

It is noteworthy that the Raman intensities listed in Table 1 were obtained under exactly the same experimental conditions (laser power, geometry of optics, position of cells), and thus they could be reproduced to within 2% and the relative Raman intensities of gases at different temperatures and pressures could be obtained within the same error.[7]

The calculation of the "second law" enthalpy is based on the following equation:[7]

$$R \ln K = R \ln [T^{\Delta n} K_f K_I] = -\Delta H^0 (1/T) + (\Delta S^0 - R \ln K_L), \quad (2)$$

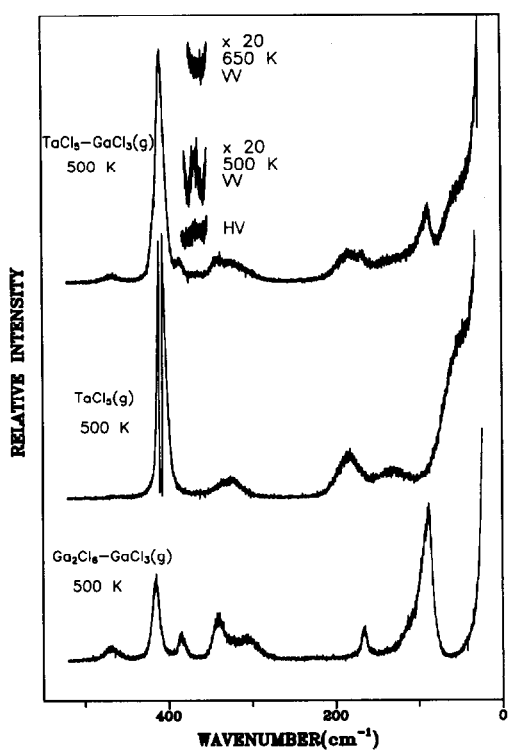

Fig. 5. Vapour Raman spectra of $Ga_2Cl_6/GaCl_3$, $TaCl_5$ and a $GaCl_3$–$TaCl_5$ mixture with $P_{o,TaCl_5} = 0.7$ atm. and $P_{0,Ga_2Cl_6} = 0.35$. $\lambda_0 = 514.5$ nm; w = 420 mW; ssw = 5 cm^{-1}; $\tau = 0.15$ s; ss = 0.5 cm^{-1} s^{-1}. Inserts show the Raman bands of $NbGaCl_8(g)$ at 425 cm^{-1} and $Ga_2Cl_6(g)$ at 412 cm^{-1} marked as "C" and "D", respectively.

where K_I is the quotient of the terms $I_i(v_i)$ (with v_i being the vibrational wave number) due to the gaseous species participating in reaction (1), K_f is the quotient of the terms $1-\exp(-hcv/kT)$ and K_L is a temperature-independent parameter involving the intensity of the excitation laser line, the molecular scattering properties and the sensitivity of the spectrometric system used.[7]

For the enthalpy of reaction (1) a plot (Fig. 6) of $R \ln K$, where $K = 1/T^{0.5}K_fK_I$, *vs* $1/T$ (i.e. eq. (2), $\Delta n = -0.5$), for all three cells used gives:

$$\Delta H_1^0 = -37.6 \pm 20 \text{ kJ mol}^{-1}.$$

Possible structures for $MGaCl_8$ (M = Nb, Ta) *complexes*

Formation of ionic $GaCl_2^+MCl_6^-$ or $GaCl_4^-MCl_4^+$ liquid compounds by chlorine ion transfer can be safely excluded because of the absence of the characteristic $NbCl_6^-$, $TaCl_6^-$ and $GaCl_4^-$ bands[2] from the spectra in Figs 1–4. Most probably, within the $MGaCl_8$ molecular unit, a $GaCl_4$ tetrahedron shares an edge with a MCl_6 octahedron (C_{2v} symmetry). The 24 vibrational modes of the $MGaCl_8$ complexes for such a molecular configuration can be classified according to:

$$\Gamma_{C_{2v},\text{vib}} = 9A_1 + 3A_2 + 6B_1 + 6B_2,$$

and are all Raman active. Identical structures have been established earlier for $NbAlCl_8$[13] and postulated for $NbGaCl_8$.[19]

Therefore, the bands at 422 cm^{-1} due to $NbGaCl_8$(l) and 417 cm^{-1} due to $TaGaCl_8$ (Table 1) can be assigned as due to the $\nu(M—Cl_{terminal})$ vibrations, of hexacoordinate Nb or Ta atoms while the bands at 366 cm^{-1} ($NbGaCl_8$) and 364 cm^{-1} ($TaGaCl_8$) can be due to $\nu(M—Cl_{bridging})$ modes. The positions of these bands are compatible with the proposed structures and lie—as it should be expected—very close to the respective bands due to the M_2Cl_{10}(l) dimers,[2] where an internal arrangement of two MCl_6 octahedra sharing an edge creates a similar environment around the metal atom as in the case of the $MGaCl_8$ complexes. Figure 7 shows molecular models for the $MGaCl_8$ complexes (C_{2v} symmetry) and the M_2Cl_{10} dimers (D_{2h} symmetry). Furthermore by considering the gaseous dissociation reaction:[11]

$$1/2Ta_2Cl_{10}(g) \rightleftharpoons TaCl_5(g), \quad \Delta H^0 = 25 \text{ kJ mol}^{-1},$$

the enthalpy of the following reaction can be derived in combination with the enthalpy of reaction (1):

$$1/2Ta_2Cl_{10}(g) + 1/2Ga_2Cl_6(g) \rightleftharpoons TaGaCl_8(g)$$
$$\Delta H^0 = -12.6 \pm 2.0 \text{ kJ mol}^{-1}.$$

The resulting value is rather small, indicating that the coordination number[3] and geometry[1] of Ta(V) and Ga(III) are not altered during the reaction. Thus, the tetrahedral coordination of Ga(III) in $Ga_2Cl_6(g)$[1] and the octahedral coordination of Ta(V) in $Ta_2Cl_{10}(g)$[1] are preserved in the $TaGaCl_8$ vapour complex (see Fig. 7).

It is noteworthy how little the $MGaCl_8$ strong bands shift from the liquid phase (422 and 366 cm^{-1}

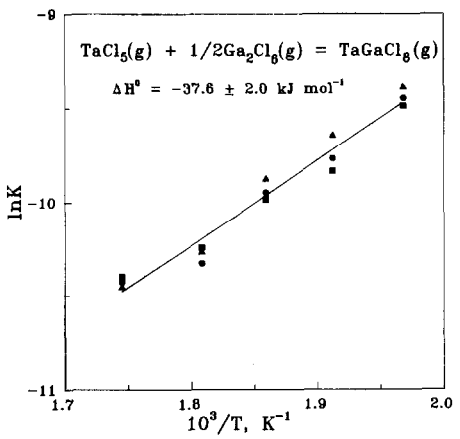

Fig. 6. Plot of ln K ($K = (1/T^{0.5})K_fK_I$ vs $1/T$ for reaction: $TaCl_5(g) + 1/2Ga_2Cl_6(g) \rightleftharpoons TaGaCl_8(g)$. Points indicate measurements from the different cells as follows: (a) cell I, ●; cell II, ■; cell III, ▲.

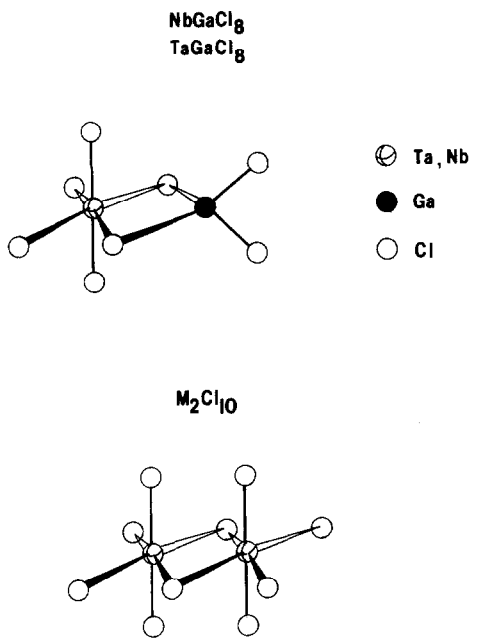

Fig. 7. Molecular models for $MGaCl_8$ (M = Nb or Ta) liquid and vapour complexes with C_{2v} symmetry and M_2Cl_{10} dimer vapour and liquid molecules with D_{2h} symmetry.

for $NbGaCl_8$, 417 and 364 cm^{-1} for $TaGaCl_8$) to the gas phase (425 and 369 cm^{-1} for $NbGaCl_8$, 370 cm^{-1} for $TaGaCl_8$) and to the crystalline phase (433 and 362 cm^{-1} for $NbGaCl_8$, 412 and 358 cm^{-1} for $TaGaCl_8$). This is interpreted as indicating that the proposed identity of the complexes is retained in all three phases.

Acknowledgement—The authors wish to thank Professor G. N. Papatheodorou for many helpful comments during the course of the present investigation.

REFERENCES

1. G. N. Papatheodorou, *Curr. Top. Mat. Sci.* 1982, **10**, 249.
2. M. Brooker and G. N. Papatheodorou, in *Advances in Molten Salt Chemistry* (Edited by G. Mamantov), Vol. 5, p. 27. Elsevier, New York (1983).
3. H. Schäfer, *Adv. Inorg. Chem.* 1983, **26**, 201.
4. K. Hilpert, *J. Electrochem. Soc.* 1989, **136**, 2099.
5. (a) G. N. Papatheodorou, L. A. Curtiss and V. A. Maroni, *J. Chem. Phys.* 1983, **78**, 3303; (b) T. Ostvold, E. Rytter and G. N. Papatheodorou, *Polyhedron* 1986, **5**, 821.
6. S. Boghosian, G. N. Papatheodorou, R. W. Berg and N. J. Bjerrum, *Polyhedron* 1986, **5**, 1393.
7. S. Boghosian and G. N. Papatheodorou, *J. Phys. Chem.* 1989, **93**, 415.
8. S. Boghosian, D. A. Karydis and G. A. Voyiatzis, *Polyhedron* 1993, **12**, 771.
9. D. M. Gruen and R. L. McBeth, *Inorg. Chem.* 1969, **8**, 2625.
10. G. N. Papatheodorou and D. A. Buttry, *Inorg. Nucl. Chem. Lett.* 1979, **15**, 51.
11. H. Schäfer and U. Florke, *Z. Anorg. Allg. Chem.* 1981, **479**, 89.
12. H. Gerding and J. C. Duinker, *Rev. Chim. Miner.* 1966, **3**, 815.
13. B. Krebs, H. Janssen, N. J. Bjerrum, R. W. Berg and G. N. Papatheodorou, *Inorg. Chem.* 1984, **23**, 164.
14. G. N. Papatheodorou, in *Proceedings of the 10th Materials Symposium on Characterization of High Temperature Vapors and Gases* (Edited by J. W. Hastie), NBS Publication 561. National Bureau of Standards, Washington, DC (1979).
15. E. Rytter, PhD thesis, Norwegian Institute of Technology (1974).
16. W. Bues, F. Femiray and H. A. Oye, *Z. Phys. Chem.* (Wiesbaden) 1973, **84**, 18.
17. R. Huglen, F. W. Poulsen, G. Mamantov and G. M. Begun, *Inorg. Chem.* 1979, **18**, 2551.
18. I. R. Beattie and G. A. Ozin, *J. Chem. Soc. A* 1691 (1969).
19. G. Okon, *Z. Anorg. Allg. Chem.* 1980, **469**, 68.

Polyhedron Vol. 12, No. 24, pp. 2973–2976, 1993
Printed in Great Britain

0277–5387/93 $6.00+.00
© 1993 Pergamon Press Ltd

SYNTHESIS AND X-RAY CRYSTAL STRUCTURES OF TETRAKIS-(2,2,6,6-TETRAMETHYLHEPTANE-3,5-DIONATO)BIS(2,2′-BIPYRIDYL)DIBARIUM $Ba_2(thd)_4(bipy)_2$ AND *catena*-[DODECAKIS(2,2-DIMETHYLPROPANOATO)BIS(2,2,6,6-TETRAMETHYLHEPTANE-3,5-DIONATO)TETRA(PYRIDINE)TETRA(AQUA)HEPTABARIUM] PYRIDINE SOLVATE $\{[Ba_7(piv)_{12}(thd)_2(py)_4(H_2O)_4]\cdot 2py\}$

ANDREI DROZDOV and SERGEI TROYANOV*

Department of Chemistry, Moscow State University, 119899 Moscow, Lenin Hills, Russia

(*Received* 21 *April* 1993; *accepted* 15 *July* 1993)

Abstract—Two new volatile mixed ligand barium complexes have been synthesized and their X-ray crystal structures determined. $Ba_2(thd)_4(bipy)_2$ (**1**) consists of dimeric molecules; with two barium atoms linked by four bridging Ba—O—Ba bonds. The structure of $\{[Ba_7(piv)_{12}(thd)_2(py)_4(H_2O)_4]\cdot 2py\}$ (**2**) contains Ba_3 units and separate Ba atoms which are connected into infinite chains through Ba—O—Ba bridges.

The search for new $Ba(thd)_2$ derivatives (Hthd = 2,2,6,6-tetramethylheptane-3,5-dione) more volatile than $Ba_4(thd)_8$ is rather important for the application of the MOCVD technique for $YBa_2Cu_3O_{7-\delta}$ thin films deposition. In the last two years a number of barium compounds containing both thd and O- and N- Lewis bases (e.g. H_2O, NH_3, CH_3OH etc) have been synthesized in laboratories in France,[1,2] the Netherlands[3] and the U.S.A.[4,5] In a previous paper[6] we discussed the crystal structures and thermal behaviour of $Ba_4(thd)_8$ and its derivatives containing the pivalate anion. Here we present two new compounds: an adduct of barium bis(2,2,6,6-tetramethylheptane-3,5-dionate) with 2,2′-bipyridyl (bipy) and a mixed ligand complex containing both thd-ligands and a number of pivalate anions (piv) as well as H_2O and pyridine (py) molecules. While the former compound consists of dimeric molecules, the latter contains infinite chains. For Ba-thd derivatives it is the first example of a polymeric structure.

EXPERIMENTAL

Synthesis

$Ba_2(thd)_4(bipy)_2$ (**1**) has been synthesized by the reaction of barium metal with the solution of Hthd and bipy (taken according to stoichiometry) in dry pentane–ether mixture (1 : 1) under dry nitrogen. Colourless crystalline plates formed by slow evaporation of the solvent. To isolate them from the air they were placed into glass capillaries.

$\{[Ba_7(thd)_2(piv)_{12}(py)_4(H_2O)_4]\cdot 2py\}$ (**2**). The colourless prismatic crystals of **2** were obtained from the pyridine solution of the product synthesized by the reaction between barium chloride and Hthd containing 3% admixture of pivalic acid in aqua-ethanol medium. As has been found previously, the dissolving of barium metal in this mixture of Hthd and Hpiv resulted in a mixed ligand compound $Ba_5(thd)_9(piv)$.[6]

Crystal structure determination

The experimental data for both structures were recorded using a CAD-4 diffractometer and Mo-K_α radiation. Cell data and details of the structure analysis are given in Table 1.

Compound **1**. The coordinates of the barium atoms were derived from an initial Patterson synthesis, and the positions of other atoms were found from subsequent difference Fourier synthesis. The structure was refined in anisotropic approximation for all barium, oxygen, nitrogen and non-terminal carbon atoms and isotropically for the other carbon atoms. The positions of H-atoms were not determined.

* Author to whom correspondence should be addressed.

Compound **2**. The structure was solved and refined via the direct methods followed by subsequent difference Fourier syntheses. We found that some ^{t}Bu groups are disordered about the threefold axes. The structure was refined by least-squares full matrix method with anisotropic thermal parameters for barium, oxygen, nitrogen and not disordered carbon atoms. Disordered carbon atoms were refined isotropically and their multiplicities were found for both positions.

Selected bond distances for **1** and **2** are listed in Tables 2 and 3, respectively. Positional and thermal parameters for both structures have been deposited at the Cambridge Structure Centre.

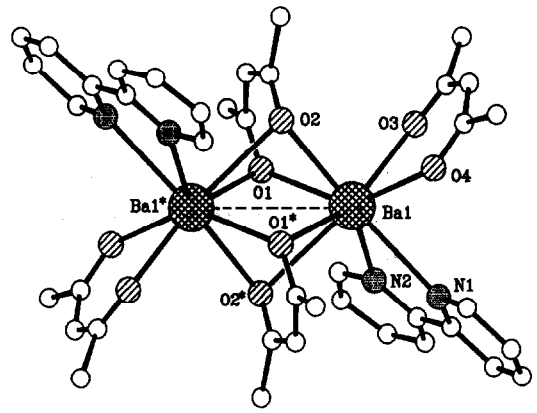

Fig. 1. A binuclear molecule in the crystal structure **1**. Terminal carbon atoms of ^{t}Bu groups are omitted.

RESULTS AND DISCUSSION

The structure of **1** is a packing of two crystallographically independent molecules $Ba_2(thd)_4(bipy)_2$. Two Ba atoms forming each dimer (Ba(1)···Ba(1′) 3.905 Å, Ba(2)···Ba(2′) 3.855 Å) are bound by two bridging thd ligands O(1), O(2); O(1′), O(2′) in the first dimer and O(5), O(6); O(5′), O(6′) in the second, with —OC—CH—CO— groups occupying positions in a plane nearly perpendicular to the line Ba···Ba (Fig. 1). The same type of tetradentate (O,O) bridging coordination of the thd anion has been recently found in a mixed ligand chelate $Ba_5(thd)_9(piv)$[6] (**3**) and adduct $Ba_2(thd)_4(NH_3)_4$[5] (**4**). While in the former chelate the ligands of this type link barium atoms in the square like framework, the latter binuclear complex **4** is much more similar to **1**; the place of the bidentate bipy ligand being occupied by two adjacent NH_3 molecules.

Two other thd anions in **1** (as well as in **4**) form usual bidentate O,O chelate rings; in **1** distances Ba—O being a little longer than in ammonia adduct

Table 1. Details of crystal determination and crystallographic data for **1** and **2**

Crystal data	**1**	**2**
Chemical formula	$C_{64}H_{92}N_4O_8Ba_2$	$C_{112}H_{184}N_6O_{32}Ba_7$
Formula weight	1320.10	3088.03
Crystal system	Triclinic	Monoclinic
Space group	$P\bar{1}$	$P2_1/n$
a (Å)	12.067(2)	17.331(3)
b (Å)	14.807(4)	18.194(1)
c (Å)	21.459(5)	22.871(3)
α (°)	92.40(2)	90
β (°)	105.56(2)	91.03(1)
γ (°)	104.31(2)	90
V (Å^3)	3555.0	7210.5
D_{calc} (g cm^{-3})	1.233	1.422
Z	2	2
μ(Mo-K_α) (cm^{-1})	11.47	19.43
Crystal size (mm)	0.2 × 0.2 × 0.4	0.3 × 0.3 × 0.1
Data collection and refinement		
θ_{max} (°)	22	22
Total data	9214	12,018
Observed data	4879 ($F^2 > 3\sigma$)	6144 ($F^2 > 3.5\sigma$)
No. of parameters varied	635	763
R	0.059	0.064
R_w	0.066	0.072

Table 2. Selected interatomic distances (Å) in structure **1**

Ba(1)···Ba(1)	3.905(1)	Ba(2)···Ba(2)	3.855(1)
Ba(1)—O(1)	2.79(1)	Ba(2)—O(5)	2.764(7)
Ba(1)—O(1′)	2.819(8)	Ba(2)—O(5′)	2.83(1)
Ba(1)—O(2)	2.76(1)	Ba(2)—O(6)	2.754(9)
Ba(1)—O(2′)	3.009(9)	Ba(2)—O(6′)	2.926(9)
Ba(1)—O(3)	2.656(8)	Ba(2)—O(7)	2.68(1)
Ba(1)—O(4)	2.62(1)	Ba(2)—O(8)	2.62(1)
Ba(1)—N(1)	2.94(2)	Ba(2)—N(3)	2.87(1)
Ba(1)—N(2)	2.90(1)	Ba(2)—N(4)	2.93(1)

Table 3. Selected interatomic distances (Å) in structure **2**

Ba(1)···Ba(2)	4.2726(9)	Ba(3)—O(4)	2.68(1)
Ba(2)···Ba(3)	4.213(1)	Ba(3)—O(8)	2.63(1)
Ba(3)···Ba(4)	4.260(1)	Ba(3)—O(10)	2.80(1)
Ba(2)···Ba(4)	4.377(1)	Ba(3)—O(11)	2.90(1)
Ba(4)···Ba(4)	4.446(1)	Ba(3)—O(13)	2.68(1)
		Ba(3)—O(14)	2.64(1)
Ba(1)—O(1)	2.80(0)	Ba(3)—O(16)	2.74(1)
Ba(1)—O(2)	3.02(1)		
Ba(1)—O(3)	2.67(1)	Ba(4)—O(5)	2.81(1)
Ba(1)—O(12)	2.74(1)	Ba(4)—O(5′)	2.729(9)
		Ba(4)—O(6)	2.85(1)
Ba(2)—O(2)	2.69(1)	Ba(4)—O(7)	2.75(1)
Ba(2)—O(3)	2.98(1)	Ba(4)—O(8)	2.84(1)
Ba(2)—O(4)	2.84(1)	Ba(4)—O(9)	2.78(1)
Ba(2)—O(6)	2.76(1)	Ba(4)—O(10)	3.08(1)
Ba(2)—O(10)	2.86(1)	Ba(4)—O(11)	2.93(1)
Ba(2)—O(11)	2.93(1)	Ba(4)—O(15)	2.75(1)
Ba(2)—O(12)	2.82(1)		
Ba(2)—N(1)	3.04(1)		
Ba(2)—N(2)	3.02(2)		

(average distances are 2.64 and 2.65 Å for two types of dimers in **1** and 2.60 Å for **4**). The slight elongation of Ba—O bonds in **1** compared to the ammonia adduct could be connected with the more rigid coordination of the chelating bipy ligand than NH_3. The lengths of Ba—O bonds forming bridges Ba—O—Ba lie between the limits of 2.76 and 3.01 Å in **1** being close to the range 2.77–2.87 Å in the ammonia complex. The elongation of the Ba—O—Ba bridges in the dimers results in a slight increase of distances Ba···Ba in chelate **1** (3.86 and 3.91 Å compared with Ba···Ba in **4** 3.83 Å). The last two positions in the coordination sphere of barium in **1** are occupied by two bipy molecules forming six-membered chelate ring, with average distances Ba—N in two dimers being 2.90 and 2.92 Å, respectively. The values of Ba—N distances are nearly the same in **4** (average 2.91 Å) but are longer in comparison with Ba—N(bipy) in $[Ba(bipy)_2(SCN)_2]$ (2.865 Å) consisting of infinite chains formed by the means of bridging SCN^- anions[7] (Ba—S is a very weak bridge: Ba—S distance is 3.36 Å).

The structure of **2** (Fig. 2) consists of triangular fragments Ba(2)Ba(3)Ba(4) with approximately equal sides (Ba(2)···Ba(3) 4.21, Ba(3)···Ba(4) 4.26, Ba(2)···Ba(4) 4.38 Å) linked into infinite chains on the one hand by the pairs of Ba(4)—O(5)—Ba(4′) bridges and on the other hand bound with Ba(1) atom lying in the centre of inversion and therefore being connected with the next triangular fragment. It is interesting to note that the ratio thd : piv in **3** (discussed in previous paper) is 9 : 1, while in **2** is almost the reverse—1 : 6, although the admixture of pivalic acid in Hthd was one and the same (3%). This may be connected with the influence of pyri-

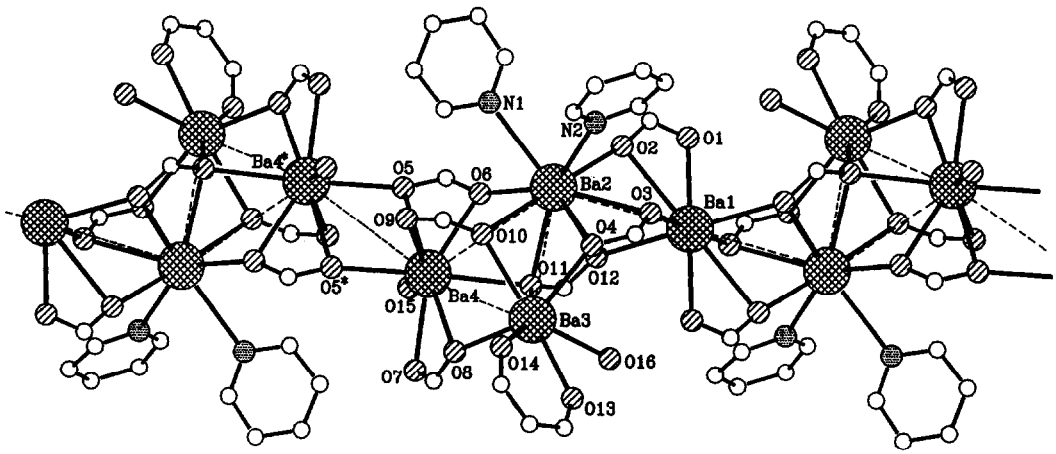

Fig. 2. A complex chain directed along the y-axis in the crystal structure **2**. Terminal carbon atoms of ^{t}Bu groups are omitted.

dine present in the system. Four barium atoms in the structure under discussion have different coordination spheres and CN's. The Ba(1) atom has a centrosymmetric coordination consisting of eight oxygen atoms from six piv-groups. The atoms O(1), O(1′), O(2), O(2′), O(3), O(3′), O(12), O(12′) connect Ba(1) with Ba(2) and Ba(2′) bridging two triangular units. The Ba(2) atom has a mixed coordination (CN = 9) formed by seven O-atoms from five piv anions and two N atoms of two py molecules, situated in *cis*-positions. The lowest CN of Ba(3) atom (CN = 7: four O atoms from four piv groups, two O atoms from thd and one $O(H_2O)$ atom) appears to be caused by the steric effect of thd ligand. It is common knowledge that barium requires high CNs; relatively low CN = 7 has been also found in sterically unsaturated $Ba_4(thd)_8$ obtained either by vacuum sublimation[1] or by crystallization from the pentane solution.[6] The Ba(4) atom possesses CN = 9, with the coordination sphere consisting of eight O atoms from five piv groups* and one $O(H_2O)$ atom. Two O(5)—Ba(4)—O(5′) bridges form a second linkage, connecting triangles Ba(2)Ba(3)Ba(4) into a chain.

Though the thd ligand forms a usual O,O bidentate six-membered chelate ring (Ba(3)—O(13) 2.68 Å, Ba(3)—O(14) 2.64 Å) one may distinguish four types of pivalate groups having different functions in the structure (Table 3). The groups of the first type form, besides a five-membered chelate ring, an additional bond with the other barium atom. Pivalate anions of both types 2 and 3 are tetradentate; two O atoms in every piv group of the second type possessing the same function in the structure (bidentate), while in the third type their functions are quite different (mono- and tridentate). The last type (4) of pivalate's coordination includes pentadentate ligand which links all four barium atoms. The piv group with similar function (which binds five barium atoms) has been found in the structure of the mixed ligand thd-piv complex **3**[6] (Table 3).

The longer Ba—N(py) distances in **2** (3.01–3.05 Å) in comparison with **1** and **4** are connected with the increase in coordination number in **2** CN(Ba(2)) = 9, in **1** and **4** and with the fact that the N atoms are not included in the chelate ring.

Thermal behaviour of chelates **1** and **2** is quite different. Thus, heating of the former compound in vacuum 0.01 torr results in the loss of bipy (80–90°C) followed by $Ba_4(thd)_8$ sublimation (200–220°C). The latter compound decomposes to $Ba_4(thd)_8$ (which sublimes in the same temperature range, vs) and barium pivalate, which can be partly sublimed at higher temperatures.

The results of crystal structure determinations for both homoligand and mixed ligand Ba-thd compounds allows us to make some previous conclusions concerning the influence of the type of additional ligand on the oligomerization degree and thermal stability of barium complexes. Thus, addition of N- and O-donor neutral chelating or macrocyclic ligands leads to decrease of oligomerization degree gradually from 4 in the case of $Ba_4(thd)_8$[1,6] to 2 in **1**, **2** and $Ba_2(thd)_4(diglyme)_2(H_2O)$[8] complex and even to mononuclear [$Ba(thd)_2(tetraglyme)$[8]]; the CN of barium increasing from 6, 7 in tetrameric barium dipivaloylmethanates to 8 in **1**, **4** and even to 9 in adduct with tetraglyme. In the case of negatively charged nonchelating additional ligands piv and OH^- the situation is more complicated. Being multidonor these anions link barium-thd fragments into pentameric units $Ba_5(thd)_9(piv)$[6] and $Ba_5(thd)_9(OH)(H_2O)_3$.[4] The piv ligands are multidonor and at the same time create less steric hindrances than the thd-ligand. The large number of piv-groups present in the structure leads to the higher oligomerization degree. According to this tendency even the presence of a great excess of py, which is a rather strong donor does not result in the formation of complexes with low nuclearity (structure of **2**). To make further investigations of these phenomena the structural studies of a greater number of mixed ligand barium compounds are required.

* If Ba(4)—O(10) distance (3.07 Å) is considered to be an interaction.

REFERENCES

1. A. Gleizes, S. Sans-Lenain and D. Medus, *C.R. Acad. Sci. Paris* 1991, **313**, 761.
2. A. Gleizes, S. Sans-Lenain, D. Medus and R. Morancho, *C.R. Acad. Sci. Paris* 1991, **312**, 983.
3. P. Sluis, A. L. Spek, K. Timmer and H. A. Meinema, *Acta Cryst.* 1990, **C46**, 1741.
4. S. B. Turnipseed, R. M. Barkley and R. E. Sievers, *Inorg. Chem.* 1991, **30**, 1164.
5. W. S. Rees Jr, M. W. Carris and W. Hesse, *Inorg. Chem.* 1991, **30**, 4479.
6. A. A. Drozdov and S. I. Troyanov, *Polyhedron* 1992, **11**, 2877.
7. W. H. Watson, D. A. Grossie, F. Vogtle and W. M. Muller, *Acta Cryst.* 1983, **C39**, 720.
8. A. A. Drozdov and S. I. Troyanov, *Koord. Khim.* (submitted).

Polyhedron Vol. 12, No. 24, pp. 2977–2980, 1993
Printed in Great Britain

0277–5387/93 $6.00+.00
© 1993 Pergamon Press Ltd

UV–VISIBLE SPECTROSCOPIC STUDIES ON THE PLATINUM-METAL PENTAFLUORIDES

ERIC G. HOPE

Department of Chemistry, University of Leicester, Leicester LE1 7RH, U.K.

(*Received* 1 *July* 1993; *accepted* 14 *July* 1993)

Abstract—The diffuse reflectance UV–vis spectra of RuF_5, RhF_5, OsF_5, IrF_5 and PtF_5 have been recorded for the first time and assigned on the basis of the strong-field model and optical electronegativity approach. The electronic transitions are interpreted in terms of a pseudo-tetragonally distorted octahedral field at the metal centres, which affords insights into the intense colours of these complexes.

The pentafluorides of the platinum metals, as rare examples of these metals in their +5 oxidation states, have been extensively studied. A range of physical properties has been described[1,2] while single crystal X-ray structure determinations on three of the compounds, ruthenium,[3,4] rhodium[5] and platinum,[6] illustrate their *cis*-octahedral bent fluorine-bridged tetrameric geometries. Most workers in this area have commented upon the intense colours of these species, in comparison to their related hexafluorometallate(V) derivatives, which are pale yellow or buff solids, and it is therefore surprising that the electronic spectra of the platinum-metal pentafluorides have received scant attention. Only two papers describe previous research in this area, a brief note on the electronic spectrum of liquid RuF_5[7] and a footnote to a preparative paper[8] describing limited electronic data for OsF_5 and IrF_5 in HF solution. Here we report and assign the electronic spectra for all the platinum-metal pentafluorides, which afford insights into their intense colours.

EXPERIMENTAL

The platinum-metal pentafluorides were prepared by literature routes; ruthenium and rhodium,[9] osmium,[10] iridium,[11] platinum[12] and stored in pre-passivated FEP (perfluoroethylene–propylene copolymer) containers in a dry-box. Commerical CaF_2 (BDH Ltd.) was dried in a furnace at 725 K and stored in the dry-box.

Electronic spectra were obtained from finely powdered neat $[MF_5]_4$ on dry CaF_2 in sealed silica cells. Spectra were recorded over the range 2000–200 nm (5000–50,000 cm^{-1}) on a Perkin–Elmer Lambda-19 instrument fitted with a diffuse-reflectance attachment, using the Kubelka–Munk function $F(R)$ available in the PECS software. Spectra were also recorded from samples exposed to moist air, to ensure that features in the reported spectra were not due to hydrolysis of these extremely moisture-sensitive materials.

RESULTS

The electronic spectra data are shown in Fig. 1 and recorded, with assignments, in Table 1. There is general agreement between these data and those reported previously over the limited range for RuF_5,[7] OsF_5 and IrF_5,[8] in view of the different physical states used whilst recording the earlier spectra.

The room-temperature magnetic moments of the platinum-metal pentafluorides, 3.06 BM (Ru),[3] 2.39 BM (Rh),[13] 2.06 BM (Os),[3] 1.32 BM (Ir)[11] and 2.05 BM (Pt),[14] are comparable to those reported[15–19] for the corresponding MF_6^- species, indicating that both types of metal(V) complexes have the same number of unpaired electrons. Hence, as might be expected, there is considerable correlation between the spectra for each platinum-metal pentafluoride and its hexafluorometallate. The intense low-energy bands which, as expected, move significantly to lower energy across each period (Ru → Rh, Os → Pt) are readily assigned as $\pi(F) \rightarrow$ metal charge-transfer for all these systems. The lowest energy charge-transfer transition may be treated by the optical electronegativity formula $E_{max} = 30{,}000\ \{\chi(F) - \chi(M)\}$[20] after corrections for spin-pairing and, for the 5*d* metals, spin-orbit effects have been

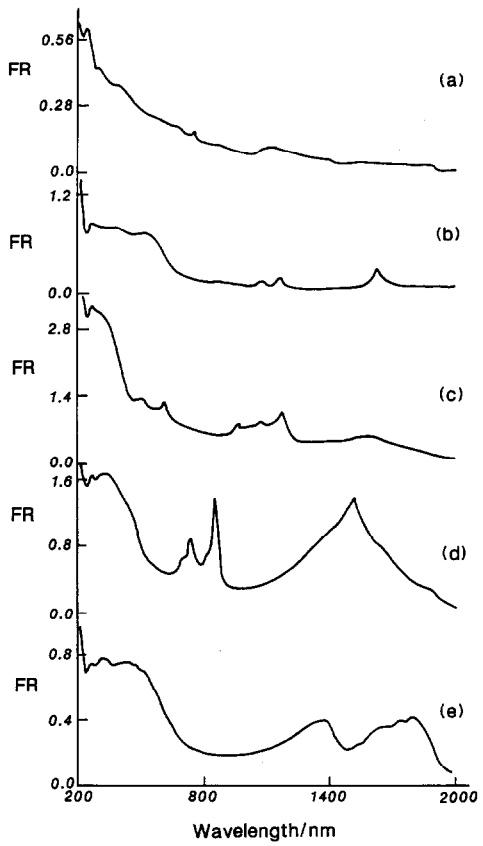

Fig. 1. Diffuse reflectance UV–vis spectra of: (a) RuF_5, (b) RhF_5, (c) OsF_5, (d) IrF_5 and (e) PtF_5 diluted in CaF_2.

considered. We follow convention[21] in not attempting to correct for the small spin-orbit effects in the 4*d* series. The relevant equations are therefore:

$$E_{obs} = 30{,}000\{\chi(F) - \chi(Ru)\} + 2D$$

$$E_{obs} = 30{,}000\{\chi(F) - \chi(Rh)\} + 4/3D$$

$$E_{obs} = 30{,}000\{\chi(F) - \chi(Os)\} + 2D - 2\xi$$

$$E_{obs} = 30{,}000\{\chi(F) - \chi(Ir)\} + 4/3D + \xi$$

$$E_{obs} = 30{,}000\{\chi(F) - \chi(Pt)\} + 2/3D + \xi.$$

D and ξ are not known accurately for these systems, but taking average values of $D = 3500\ cm^{-1}$ and $\xi = 3400\ cm^{-1}$, and $\chi_{opt}(F) = 3.9$, these equations afford $\chi_{opt}(Ru^V) = 2.7$, $\chi_{opt}(Rh^V) = 3.2$, $\chi_{opt}(Os^V) = 2.6$, $\chi_{opt}(Ir^V) = 2.9$ and $\chi_{opt}(Pt^V) = 3.3$. In view of the approximations inherent in these calculations, these values may be in error by ± 0.2, but they are nonetheless reasonable in comparison with the corresponding values for the M^{IV} and M^{VI} species.[9,22,23]

The remaining, weaker, higher energy features are either spin-forbidden intra-configurational bands arising from a redistribution of electrons within the spin-orbit split t_{2g}^n levels or spin-allowed *d–d* transitions between the t_{2g} and e_g levels. The intensity enhancement of the spin-forbidden transitions is, as expected, greater for the 5*d* than the 4*d* complexes as a result of larger spin-orbit coupling and, as observed previously for the platinum-metal hexafluorides,[9,22] the spin-allowed *d–d* transitions are either obscured by, or appear as shoulders on, the more intense charge-transfer transitions for the later metals in each period. The positions of each type of band are in similar spectral regions to those arising from the MF_6^- species, but each band appears more intense and shows considerable splittings. The more intense, split, spin-forbidden intra-configurational bands typically occur in the near IR/visible region of the spectrum and undoubtedly account for the intense colours of the platinum-metal pentafluorides.

These splittings and variations in band intensities may be accounted for by differences in the local site symmetry at the metal centres. All the MF_6^- complexes have a rhombohedral, $KOsF_6$-type lattice, in which the MF_6 unit is slightly distorted from a regular octahedron by compression along the trigonal axis, but with all the M—F bond distances approximately equal.[15,18,24,25] It was therefore assumed[23] that the analyses of the electronic spectral data of these complexes on the basis of O_h symmetry about the metal would be, and are, a satisfactory approximation. As mentioned above, the platinum-metal pentafluorides have *cis*-octahedral bent fluorine-bridged tetrameric structures in which the $M—F_{bridge}$ bonds are *ca* 10% longer that the $M—F_{terminal}$ bonds.[3–6] Since only the sum of the point charges on each axis determines the electronic structure of a given complex,[26] the symmetry groups of these *cis*-complexes are, in electronic spectroscopy terms, in practice tetragonally (D_{4h}) distorted. The increased intensities of the spin-forbidden transitions for the platinum-metal pentafluorides, as compared to the corresponding hexafluorometallates, may be ascribed to the greater influence of spin-orbit effects under the lower symmetry. Furthermore, descent in the double groups, $O^* \rightarrow D_4^*$, does indicate significant splittings as a result of the change in symmetry, e.g. for the d^3 systems, $(RuF_5)_4$ and $(OsF_5)_4$, the intra-configurational transitions are $^4A_{2g} \rightarrow {}^2E_g$, $^2T_{1g}$ and $^2T_{2g}$, which in the D_4^* double group give rise to eight possible states, $\Gamma_6+\Gamma_7$, $\Gamma_6+\Gamma_7+\Gamma_6$ and $\Gamma_7+\Gamma_6+\Gamma_7$, respectively. The complex theory behind spin-orbit split pseudo-tetragonally distorted octahedral complexes is unavailable, particularly when there is no information on the size of the pseudo-tetragonal splitting, so, the assign-

Table 1. Electronic spectra and assignments for the platinum-metal pentafluorides[a]

RuF_5	RhF_5	PtF_5
7300(sh), 8000(sh), 8500, 9000: $^4A_{2g}(\Gamma_8)\rightarrow{}^2E_g(\Gamma_8)$, $^2T_{1g}(\Gamma_6,\Gamma_8)$	5300, 5560, 6180: $^3T_{1g}(\Gamma_1)\rightarrow{}^3T_{1g}(\Gamma_3,\Gamma_5)$	
	8330, 8640, 8910, 9350: $^3T_{1g}(\Gamma_1)\rightarrow{}^1T_{2g}(\Gamma_5)$, $^1E_g(\Gamma_3)$	
13,200, 15,600(sh), 16,000: $^4A_{2g}(\Gamma_8)\rightarrow{}^2T_{2g}(\Gamma_7,\Gamma_8)$		
25,600 $^4A_{2g}(\Gamma_8)\rightarrow{}^4T_{2g}$	13,600, 14,600(sh): $^3T_{1g}(\Gamma_1)\rightarrow{}^5E_g(\Gamma_1,\Gamma_2,\Gamma_3,\Gamma_4,\Gamma_5)$	
32,000(sh) $^4A_{2g}(\Gamma_8)\rightarrow{}^4T_{1g}$	18,800 $^3T_{1g}(\Gamma_1)\rightarrow$lower $t_{2g}{}^3e_g$ triplet levels	
	25,000 $\pi(F)\rightarrow t_{2g}$(Rh)	
40,000 $\pi(F)\rightarrow t_{2g}$(Ru)	38,200 $\pi(F)\rightarrow t_{2g}$(Rh)	
~50,000 $\pi(F)\rightarrow t_{2g}$(Ru)		
OsF_5	IrF_5	PtF_5
	5460, 6160(sh), 6560, 7160: $^3T_{1g}(\Gamma_1)\rightarrow{}^3T_{1g}(\Gamma_3,\Gamma_5)$	5500, 5560, 5760, 5940, 6140, 6560, 6560, 7300, 8000(sh): $^2T_{2g}(\Gamma_7)\rightarrow{}^2T_{2g}(\Gamma_8)$
6300, 7200: $^4A_{2g}(\Gamma_8)\rightarrow{}^2T_{1g}(\Gamma_8)$		
8560, 9500: $^4A_{2g}(\Gamma_8)\rightarrow{}^2E_g(\Gamma_8)$		
	11,900, 13,600, 14,500(sh): $^3T_{1g}(\Gamma_1)\rightarrow{}^1T_{2g}(\Gamma_5)$, $^1E_g(\Gamma_3)$	
10,400 $^4A_{2g}(\Gamma_8)\rightarrow{}^2T_{1g}(\Gamma_6)$		
14,600, 20,100, 26,000(sh): $^4A_{2g}(\Gamma_8)\rightarrow{}^2T_{2g}(\Gamma_7,\Gamma_8)$	23,600 $^3T_{1g}(\Gamma_1)\rightarrow{}^1A_{1g}(\Gamma_1)$, $^5E_g(\Gamma_1,\Gamma_2,\Gamma_3,\Gamma_4,\Gamma_5)$	19,500(sh) $^2T_{2g}(\Gamma_7)\rightarrow{}^4T_{1g}(\Gamma_8,\Gamma_7,\Gamma_8,\Gamma_6)$
		23,500 $\pi(F)\rightarrow t_{2g}$(Pt)
	31,600 $^3T_{1g}(\Gamma_1)\rightarrow$lower $t_{2g}{}^3e_g$ triplet levels	32,000 $\pi(F)\rightarrow t_{2g}$(Pt)
38,900 $\pi(F)\rightarrow t_{2g}$(Os)	38,500 $\pi(F)\rightarrow t_{2g}$(Ir)	38,000 $\pi(F)\rightarrow t_{2g}$(Pt)

[a]Data recorded in diffuse reflectance in cm^{-1}).

ment of the observed bands to particular transitions in D_4* symmetry is not possible at this time.

Acknowledgements—I would like to thank the SERC for financial support and Johnson Matthey for the loan of platinum metals. I would also like to thank Prof. J. Evans for access to the Perkin–Elmer Lambda-19 UV–vis spectrometer at the University of Southampton and Dr W Levason for helpful discussions.

REFERENCES

1. R. D. Peacock, *Adv. Fluorine Chem.* 1973, **7**, 113.
2. D. J. Gulliver and W. Levason, *Coord. Chem. Rev.* 1982, **46**, 1.
3. J. H. Holloway, R. D. Peacock and R. W. H. Small, *J. Chem. Soc.* 1964, 644.
4. W. J. Casteel Jr., A. P. Wilkinson, H. Borrmann, R. E. Serfass and N. Bartlett, *Inorg. Chem.* 1992, **31**, 3124.
5. B. K. Morrell, A. Zalkin, A. Tressaud and N. Bartlett, *Inorg. Chem.* 1973, **12**, 2640.
6. B. G. Müller and M. Serafin, *Eur. J. Solid State Inorg. Chem.* 1992, **29**, 625.
7. R. D. Peacock and T. P. Sleight, *J. Fluorine Chem.* 1971, **1**, 243.
8. R. T. Paine and L. B. Asprey, *Inorg. Chem.* 1975, **14**, 1111.
9. A. K. Brisdon, P. J. Jones, W. Levason, J. S. Ogden, J. H. Holloway, E. G. Hope and G. Stanger, *J. Chem. Soc., Dalton Trans.* 1990, 715.
10. G. B. Hargreaves and R. D. Peacock, *J. Chem. Soc.* 1960, 2618; S.J. Mitchell and J. H. Holloway, *J. Chem. Soc. (A)* 1971, 2789.
11. N. Bartlett and P. R. Rao, *J. Chem. Soc., Chem. Commun.* 1965, 252.
12. W. E. Falconer, G. R. Jones, W. A. Sunder, M.J. Vasile, A. A. Muenter, T. R. Dyke and W. Klemperer, *J. Fluorine Chem.* 1974, **4**, 213.
13. J.H. Holloway, P.R. Rao and N. Bartlett, *J. Chem. Soc., Chem. Commun.* 1965, 306.
14. N. Bartlett, F. Einstein, D. F. Stewart and J. Trotter, *J. Chem. Soc., Chem. Commun.* 1966, 550.
15. E. Weise and W. Klemm, *Z. Anorg. Allg. Chem.* 1955, **279**, 74.

16. M. A. Hepworth, P. L. Robinson and G. J. Westland, *J. Chem. Soc.* 1954, 4269.
17. B. N. Figgis, J. Lewis and F. W. Mabbs, *J. Chem. Soc.* 1961, 3138.
18. V. Wilhelm and R. Hoppe, *J. Inorg. Nucl. Chem., Suppl.* 1976, 113.
19. A. K. Brisdon, J. H. Holloway, E. G. Hope and W. Levason, *Polyhedron* 1992, **11**, 7.
20. C.K. Jørgensen, *Orbitals in Atoms and Molecules*. Academic Press, New York (1962).
21. G. C. Allen and K. D. Warren, *Struct. Bond.* 1974, **19**, 105.
22. J. H. Holloway, G. Stanger, E. G. Hope, W. Levason and J. S. Ogden, *J. Chem. Soc., Dalton Trans.* 1988, 1341.
23. G. C. Allen, G. A. M. El-Sharkawy and K. D. Warren, *Inorg. Chem.* 1972, **11**, 51; 1973, **12**, 2231.
24. R. D. W. Kemmitt, D. R. Russell and D. W. A. Sharp, *J. Chem. Soc.* 1963, 4408.
25. N. Bartlett and D. H. Lohmann, *J. Chem. Soc.* 1962, 5253
26. C. J. Ballhausen, *Introduction to Ligand Field Theory*. McGraw-Hill, New York (1962).

Polyhedron Vol. 12, No. 24, pp. 2981–2987, 1993
Printed in Great Britain

0277–5387/93 $6.00+.00
© 1993 Pergamon Press Ltd

SYNTHESIS AND CHARACTERIZATION OF COPPER(I) HALIDE/PSEUDOHALIDE ADDUCTS OF 2-BENZOYLPYRIDINE AND X-RAY CRYSTAL STRUCTURE OF [DI-μ-IODO-BIS(N,O-2-BENZOYLPYRIDINE)DICOPPER(I)]

MOHAMED A. S. GOHER† and AZZA E. H. ABDOU

Department of Chemistry, Faculty of Science, Alexandria University, P.O. Box 426 Ibrahimia, Alexandria 21321, Egypt

and

WAI-HING YIP and THOMAS C. W. MAK†

Department of Chemistry, The Chinese University of Hong Kong, Shatin, New Territories, Hong Kong

(*Received* 5 *May* 1993; *accepted* 28 *June* 1993)

Abstract—Dark-brown copper(I) complexes of the type CuXL, for X = Cl, Br, I, SCN and N_3, and orange–yellow complexes of the type $(CuX)_2L$, for X = Cl or Br, where L = 2-benzoylpyridine, have been prepared and characterized. All complexes exhibit strong CT bands in the visible region and gave non-conducting solutions in acetone and nitrobenzene. The IR spectral data suggest that 2-benzoylpyridine acts as a monodentate ligand in the orange–yellow complexes and as a bidentate chelating ligand in the brown complexes, whereas bridging halides and pseudohalides exist in both types. The structure of the 1 : 1 black iodide complex, as determined by X-ray crystallography, features a discrete, centrosymmetric $[CuI(2\text{-benzoylpyridine})]_2$ molecule with a short Cu · · · Cu distance of 2.587(1) Å. Each copper atom in the dimeric molecule is tetrahedrally coordinated by two μ-iodine atoms and the carbonyl oxygen and nitrogen atoms of the chelating 2-benzoylpyridine ligand. The orange–yellow complexes display visible emission when excited in the UV region, whereas the brown complexes do not.

Complexes of copper(I) halides with unidentate nitrogen donor ligands have been observed to display a wide variety of stoichiometries, structures[1,2] and emission characteristics[3] in the solid state. Among other stoichiometries, the 1 : 1 : 1 copper–halide–base complexes most often occur with a cubane-like stereochemistry, as exemplified by $[CuIL]_4$ (L = pyridine,[4] morpholine[5]), or adopt a polymeric structure known as the ribbon or stair polymer as exemplified by $[CuX]_\infty$ adducts with pyridine,[6] isonicotinic acid,[7] methylcyanide[8,9] and benzonitrile.[10] Structures of the type CuXL–L, in which L–L is a bidentate ligand with hetero donor atoms, have been reported in the literature,[11–13] but definitive crystallographic data are lacking for these materials. X-ray structure determinations have been performed only for CuIL–L complexes, where L–L = methyl, isopropyl and n-butyl quinaldate.[14] These copper(I) iodide quinaldate complexes were found to display no visible emission when excited in the UV region.

Recently we reported the crystal structures of copper(I) chloride adducts of isonicotinic acid, $[CuClL]_\infty$,[7] nicotinic acid, $[CuClL_2]_\infty$[15] and 4-methylquinoline, $[Cu_2Cl_2L_3]$.[16] In the nicotinic acid complex the $(CuCl)_\infty$ chain takes the place of the Cu_2Cl_2 stair or ribbon in the isonicotinic acid adduct. The 4-methylquinoline complex comprises discrete centrosymmetric molecules with a Cu_4Cl_4 core of the step geometry.

†Authors to whom correspondence should be addressed.

Further work led to the isolation of copper(I) halide complexes of 2-benzoylpyridine (hereafter abbreviated as 2-Bzpy), a ligand which contains potential oxygen and nitrogen ligand sites. Some of these complexes exhibit solid-state emission at room temperature, whereas the others do not. We have now performed an X-ray structure determination of the title complex for which suitable crystals were available.

EXPERIMENTAL

2-Benzoylpyridine was obtained from Aldrich company and the other chemicals were of analytical grade quality.

Preparation of the complexes

(i) $(CuX)_2$(2-Bzpy) *complexes*, X = Cl *or* Br. A boiled ethanolic solution of 2-benzoylpyridine (10 mmol) was mixed with $Cu(NO_3)_2 \cdot 3H_2O$ (4 mmol) in ethanol and the subsequent addition of excess L(+)-ascorbic acid resulted in a clear dark brown solution. To this solution an aqueous solution of KX (X = Cl or Br) was added dropwise and the mixture was boiled for several minutes and allowed to stand over several hours to produce fine orange–yellow needles of the complex.

When NaN_3 solution was used in a similar way, the brown precipitate which was formed after a few minutes changed with time to a yellow precipitate. This yellow copper(I) azide compound was so easily oxidized that we could not isolate it by filtration.

(ii) Cu(2-Bzpy)X *complexes*, X = Cl, Br, I, SCN *and* N_3. An aqueous solution of $Cu(NO_3)_2 \cdot 3H_2O$ (5 mmol) was mixed with KX or NaX (X = Br, SCN or N_3), followed by the addition of L(+)-ascorbic acid. An ethanolic solution of 2-benzoylpyridine (8 mmol) was then added and the mixture stirred for *ca* 10 min. The final mixture was allowed to stand over several hours or days until a deep-brown crystalline product separated.

The chloro complex was prepared by the above procedure, except that $CuCl_2 \cdot 2H_2O$ was used instead of the nitrate salt.

Crystals of the dark-brown copper(I) iodide complex suitable for X-ray structure analysis were prepared by the procedure given for the orange–yellow complexes, except that a large excess of the ligand was added. Anisotropic thermal parameters and structure factors are available from the authors and also have been deposited with the Editor.

Elemental analysis results of the isolated complexes are given in Table 1.

Spectral data

The electronic spectral data of the complexes measured as solid Nujol mulls and some IR absorption bands are collected in Table 2. The experimental procedures and instruments used are as described previously.[17]

X-ray structure analysis of [CuI(2-benzoylpyridine)]$_2$

Intensities were recorded on a Nicolet R3m/V four-circle diffractometer[18] at 18°C and data collection and processing parameters are summarized in Table 3. The raw intensities were processed with

Table 1. Analytical data

Complex	Colour	M.p. (°C)	Analysis: Found (Calc.) (%) Cu	C	H	N	X
Cu(2-Bzpy)Cl	Deep brown needles	360	22.2 (22.5)	50.6 (51.1)	3.1 (3.2)	5.2 (5.0)	12.2 (12.6)
Cu(2-Bzpy)Br	Deep brown needles	116	19.1 (19.5)	44.6 (44.1)	2.9 (2.8)	4.4 (4.3)	24.2 (24.5)
Cu(2-Bzpy)I	Black blocks	128	17.3 (17.0)	38.4 (38.6)	2.2 (2.4)	3.4 (3.7)	32.7 (34.0)
Cu(2-Bzpy)SCN	Red–brown crystals	135 decomp	21.1 (20.8)	50.7 (51.2)	3.12 (3.0)	9.3 (9.2)	
Cu(2-Bzpy)N_3	Deep brown fine crystals	350	21.8 (22.0)	50.5 (49.9)	3.2 (3.1)	19.1 (19.4)	
$(CuCl)_2$(2-Bzpy)	Orange–yellow needles	66 decomp.	33.5 (33.3)	38.2 (37.8)	2.5 (2.4)	3.8 (3.7)	18.2 (18.6)
$(CuBr)_2$(2-Bzpy)	Orange–yellow needles	62 decomp.	27.3 (27.0)	31.0 (30.7)	2.1 (1.9)	3.5 (3.0)	33.9 (34.0)

Table 2. Electronic and IR spectral data

Compound	Maximum absorption (nm) (MLCT)	ν(C=O)	Vibration frequency (cm^{-1}) of the counter-ion	ν(Cu=L)
2-Bzpy		1663 s		
Cu(2-Bzpy)Cl	360–500 vs	1625 vs		270 ms
Cu(2-Bzpy)Br	330–480 vs	1630 vs		263 s
Cu(2-Bzpy)I	380–590 vs	1628 vs		265 s
Cu(2-Bzpy)SCN	350–500 vs	1635 vs	2105 vs, 2080 m [ν(CN)], 855 m, 745 m [ν(CS)], 430 m [δ(NCS)]	265 s
Cu(2-Bzpy)N_3	350–500 vs	1640 vs	2050 vs [$\nu_{as}(N_3)$], 620 w, 590 w [$\delta(N_3)$]	260 ms
$(CuCl)_2$(2-Bzpy)	410 s	1665 vs		270 s
$(CuBr)_2$(2-Bzpy)	410 s	1665 vs		265 s

s = strong, m = medium, v = very, w = weak.

Table 3. Data collection and processing parameters

Molecular formula	$(C_{12}H_9NO)CuI$
Molecular weight	373.64
Colour and habit	Black block
Crystal size (mm^3)	$0.24 \times 0.28 \times 0.36$
Crystal system	Monoclinic
Space group	$P2_1/n$ (No. 14)
Unit cell parameters	
a (Å)	7.210(1)
b (Å)	7.512(1)
c (Å)	22.605(2)
β(°)	92.75(1)
V (°)	1222.8(2)
Z	4
F(000)	712
D_{calc} (g cm^{-3})	2.030
Radiation (Å)	Graphite-monochromated Mo-K_α, $\lambda = 0.71073$
Standard reflections	(0, 1, 1); (0, 1, −4)
Intensity variation (%)	±1.1
Absorption coefficient (mm^{-1})	4.29
Mean μr	0.63
Transmission factors	0.155–0.231
Scan type and rate ° min^{-1})	ω-scan; 2.02–19.53
Scan range (°C)	0.80 below $K\alpha_1$ to 0.80 above $K\alpha_2$
Background counting	Stationary counts for one-fifth of the scan time at each end of the scan range
Collection range	$0 \leqslant h \leqslant 10$, $0 \leqslant k \leqslant 11$, $-34 \leqslant l \leqslant 34$; $2\theta_{max} = 65°$
Unique data measured	4426
Observed data with $\|F_o\| \geqslant 3\sigma(\|F_o\|)$, n	2790
No. of variables, p	145
Weighting scheme	$w = [\sigma^2\|F_o\| + 0.0005\|F_o\|^2]^{-1}$
$R_F = \Sigma\|\|F_o\| - \|F_c\|\|/\Sigma\|F_o\|$	0.048
$wR = [\Sigma w^2(\|F_o\| - \|F_c\|)^2/\Sigma w^2\|F_o\|^2]^{1/2}$	0.049
$S = [\Sigma w(\|F_o\| - \|F_c\|)^2/(n-p)]^{1/2}$	1.21
Residual extrema in final difference map (e$Å^{-3}$)	+0.92 to −1.07

the learnt-profile procedure[19] and an absorption correction was based on a pseudo-ellipsoidal fit to azimuthal scans of selected strong reflections over a range of 2θ values.[20,21]

The structure was solved by Patterson superposition and Fourier methods. All non-hydrogen atoms were subjected to anisotropic refinement. The aromatic hydrogen atoms were generated geometrically (C—H fixed at 0.96 Å), allowed to ride on their respective carbon atoms and included in structure–factor calculations with assigned isotropic thermal parameters.

All computations were performed on a DEC MicroVAX-II computer with the SHELXTL-PLUS system.[22,23] Analytical expressions of neutral-atom scattering factors incorporating the real and imaginary components of anomalous dispersion were employed.[24] Least-squares refinement converged to the R indices and other parameters, as listed in Table 3. Selected bond distances and angles are listed in Table 4, the atom labelling being shown in Fig. 1.

DISCUSSION

The reactions between the copper(I) halide and pseudohalide salts and 2-benzoylpyridine afforded the complexes given in Table 1. The orange–yellow copper(I) azide complex of 2-Bzpy formed in solution was too unstable to be filtered off. All other copper(I) complexes are coloured and stable against air oxidation when well dried. Solutions of these complexes are non-conducting in acetone and nitrobenzene.

The electronic spectra (Table 2) of these copper(I) complexes exhibit strong bands in the visible region, which are undoubtedly due to charge transfer transitions[2] from $Cu^{I}d^{10}$ to an empty π^*-orbital on 2-Bzpy. As found for other copper(I) complexes of similar ligands,[25,26] the λ_{max} value of the MLCT bands depends on the halide/pseudohalide ion as well as the ligand-to-metal molar ratio in the complex.

The IR spectra (Table 2) may distinguish between the bonding mode of 2-Bzpy in the yellow and brown copper(I) complexes. The spectra of the $(CuX)_2$(2-Bzpy) complexes show the ν(C=O) vibration at slightly higher frequencies than that of free 2-Bzpy, suggesting a unidentate ligand coordinating via its heterocyclic nitrogen atom only. On the other hand, the spectra of the brown complexes show a substantial downward shift of the carbonyl stretch by $\Delta\tilde{\nu} \simeq 25$–$40$ cm^{-1}, when compared with that of the uncoordinated ligand. This result indi-

Table 4. Bond lengths (Å) and angles (°)

Cu(1)—I(1)	2.599(1)	Cu(1)—O(1)	2.304(3)
Cu(1)—N(1)	2.035(4)	Cu(1)—I(1a)	2.555(1)
Cu(1)—Cu(1a)	2.587(1)	O(1)—C(6)	1.227(6)
N(1)—C(1)	1.340(6)	N(1)—C(5)	1.344(6)
C(1)—C(2)	1.376(8)	C(2)—C(3)	1.381(8)
C(3)—C(4)	1.376(7)	C(4)—C(5)	1.394(7)
C(5)—C(6)	1.499(6)	C(6)—C(7)	1.483(6)
C(7)—C(8)	1.382(8)	C(7)—C(12)	1.388(7)
C(8)—C(9)	1.375(8)	C(9)—C(10)	1.365(10)
C(10)—C(11)	1.362(11)	C(11)—C(12)	1.391(7)
I(1)—Cu(1)—O(1)	115.2(1)	I(1)—Cu(1)—N(1)	109.6(1)
O(1)—Cu(1)—N(1)	75.9(1)	I(1)—Cu(1)—I(1a)	119.7(1)
O(1)—Cu(1)—I(1a)	100.4(1)	N(1)—Cu(1)—I(1a)	125.8(1)
Cu(1)—O(1)—C(6)	110.5(3)	Cu(1)—N(1)—C(1)	123.8(3)
Cu(1)—N(1)—C(5)	117.7(3)	C(1)—N(1)—C(5)	117.3(4)
N(1)—C(1)—C(2)	123.6(5)	C(1)—C(2)—C(3)	118.3(5)
C(2)—C(3)—C(4)	119.7(5)	C(3)—C(4)—C(5)	118.1(5)
N(1)—C(5)—C(4)	122.9(4)	N(1)—C(5)—C(6)	114.7(4)
C(4)—C(5)—C(6)	122.3(4)	O(1)—C(6)—C(5)	118.4(4)
O(1)—C(6)—C(7)	120.1(4)	C(5)—C(6)—C(7)	121.5(4)
C(6)—C(7)—C(8)	118.1(4)	C(6)—C(7)—C(12)	123.6(4)
C(8)—C(7)—C(12)	118.3(4)	C(7)—C(8)—C(9)	121.5(6)
C(8)—C(9)—C(10)	119.6(7)	C(9)—C(10)—C(11)	120.3(6)
C(10)—C(11)—C(12)	120.5(6)	C(7)—C(12)—C(11)	119.7(5)

Symmetry transformation: a$(1-x, -y, -z)$.

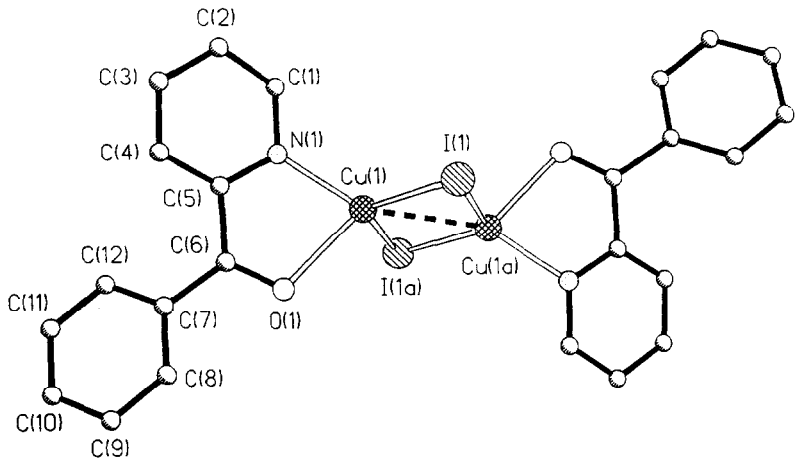

Fig. 1. Perspective view of the structure of the $[CuI(2\text{-benzoylpyridine})]_2$ dimer with atom labelling. The non-bonded interactions between the copper(I) atoms are indicated by a broken line.

cates the presence of N,O-bidentate 2-benzoylpyridine in such complexes, as found in the structure of $[Cu(2\text{-Bzpy})(N_3)_2]_2$,[27] with a similar downward shift of $\nu(C{=}O)$. The 1 : 1 thiocyanate complex shows two CN and two CS stretching bands, which are indicative of a μ(N,S)-thiocyanate ligand.[28] The dark-brown 1 : 1 azide complex on the other hand shows a very strong and sharp band at 2060 cm^{-1}, associated with the asymmetric stretch of the azide group, which is very similar to that reported for $[CuN_3(PPh_3)_2]_2$ having a $\mu(1,3)$-azido bridge.[29] The existence of this type of bridging azide in the 1 : 1 complex of 2-Bzpy is supported by the disappearance of symmetric stretching azide frequencies in the region 1275–1350 cm^{-1}. Accordingly, both complexes have the same bridging pseudohalide groups, assuming dimeric or polymeric structures with tetrahedral copper atoms in these 1 : 1 complexes.

In the far-IR spectra (400–200 cm^{-1}) of the brown and orange–yellow copper(I) chloride adducts of 2-Bzpy no bands could be attributed to terminal ν(Cu–Cl), which is suggestive of bridging chlorides in such complexes. For the brown copper(I) halide complexes with N,O-bidentate 2-Bzpy, we may assume dimeric or polymeric structures corresponding to those of 1 : 1 copper(I) iodide adducts of quinaldic acid esters having a chain of alternating copper and iodine atoms or planar Cu_2I_2 rhombohedra.[14] For the orange–yellow $(CuX)_2$(2-Bzpy) complexes with the N-monodentate 2-benzoylpyridine ligand, we may assume a polymer of chains linked side by side, as found in the structure of $[(CuI)_2(2\text{-Mepy})]$ (2-Mepy = 2-methylpyridine).[30] The bridging nature of the halide atoms in the brown 1 : 1 adducts is supported by crystal structure analysis of the iodide complex.

The present study has shown the title complex as $[CuI(2\text{-benzoylpyridine})]_2$ (Fig. 1), another example of a metal–halide–bidentate ligand with hetero atoms of the stoichiometry CuIL–L to be structurally characterized. This dinuclear complex is disposed about a crystallographic inversion centre with a planar Cu_2I_2 rhombohedral core of alternating copper and iodine atoms. The Cu—I distances of 2.555(1) and 2.599(1) Å are shorter than those usually observed for $[CuIL]_4$ cubes or polymeric pleated sheets where each copper atom has three iodine neighbours [av. 2.698(3)[31] and 2.706(3) Å,[32] respectively], but longer than those observed [2.388(2) Å][33] in CuI_2^- where copper has two neighbours (both iodine) and presumably exhibits multiple bonding character. The Cu—I bond lengths and I—Cu—I angles (Table 4), however, match the corresponding values reported for [CuI(isopropyl quinaldate)]$_2$ (2) and [CuI(n-butylquinaldate)]$_2$ (3) [Cu—I = 2.585(3) and 2.56(8) Å, I—Cu—I = 120.9(2) and 121.0(1)° for **2** and **3**, respectively] very well.[14] Each copper centre in the Cu_2I_2 unit is further coordinated by the carbonyl oxygen at Cu—O = 2.304(1) Å and the heterocyclic nitrogen at Cu—N = 2.035(4) Å, thus forming a five-membered chelate ring. The Cu—O distance is a little shorter than that found in complex **2** [2.33(1) Å], but a little longer than Cu—O [2.26(6) Å] in complex **3**, whereas the Cu—N distance agrees very well with corresponding values in both complexes [2.04(1) for **2** and 2.04(2) Å for **3**]. Similar Cu–carbonyl oxygen bond lengths in the complex of bis(10-methylisoalloxazine)[34] with copper(I) are

2.27(2) and 2.21(2) Å. In this complex a similar (—Cu···N=C—C=O—) five-membered chelate ring exists with both nitrogen and carbonyl oxygen coordinated to copper(I) [Cu—N = 1.94(2) and 1.92(2) Å].

Structures such as the title complex with a Cu_2I_2 rhombohedral unit are common in the literature of CuIL and $CuIL_2$ (L = nitrogen donor ligand), with Cu—Cu distances ranging from 2.535(9) Å in CuI(2,2,6,6-tetramethylpiperidine)[2] to 3.706(5) Å in CuI(2-Mepy).[35] It is noted that the smaller the bulk of the organic ligand, the closer the Cu···Cu distance. For example, the Cu···Cu separation in $[CuI(py)_2]$ is 2.699(5) Å,[35] whereas in [CuI(phenanthroline)$_2$] it reaches 3.083(3) Å.[36] The Cu···Cu distance of 2.587(1) Å found for the present complex is, however, comparable with values observed in other Cu_2I_2 rhombohedra, e.g. 2.544(2) Å in complex **2** and 2.53(1) Å in complex **3**.[14]

It is generally known that three structural features are identified with the emission spectra of solid-state CuX–ligand systems: (a) copper–copper distances of less than 2.8 Å lead to emission at 550–628 nm, attributed to metal–metal interactions;[31] (b) when copper links a ligand that permits charge-transfer transitions (MLCT); and/or (c) when aromatic ligands are packed in parallel planes separated by 3.225–3.279 Å, resulting in emission spectra of the ligand alone. Accordingly, the complex $[CuI(2\text{-Bzpy})]_2$ with a Cu···Cu separation of 2.587(1) Å is expected to demonstrate visible evidence of excitation of types (a) and (b), since both $[CuI(quin)]_4$ (Cu···Cu = 2.558(10) Å) and $[Cu_2I_2(quin)_4]$ (Cu···Cu = 3.364(5) Å) display room-temperature emission due to MLCT excitation.[37] However, neither the copper(I) iodide complex nor any of the brown 1 : 1 complexes of 2-Bzpy display emission at room temperature. This result resembles that reported for CuI (quinaldate) complexes,[14] where their non-emitting character was considered to be effected by the electron-withdrawing ester groups which alter the energy levels of the aromatic ring to make the excitation of greater energy or to make other radiationless decay mechanisms more efficient. Similar reasons may be suggested in the case of the brown complexes of 2-Bzpy. The lack of evidence of metal–metal interactions is apparently due to the alteration of the metal energy levels by the coordination to oxygen in such complexes. This view is supported by the observation of room-temperature emission of the orange–yellow $(CuX)_2$(2-Bzpy) complexes, where the metal centre is not coordinated to oxygen as inferred from the IR spectra. The chloride adduct displays poor emission, whereas the orange–yellow copper(I) bromide of 2-benzoylpyridine shows a broad-band emission with λ_{max} at 655 nm (excitation at 365 nm). The position of this emission band is somewhat higher than those reported for the tetrameric clusters of polymeric complexes of CuI with pyridines (emission from 550 to 628 nm)[38,39] or quinoline (emission around 620–632 nm).[31] Despite the lack of structural details of the bromide adduct, the 655 nm room-temperature emission may be suspected to arise from metal-centred excitation, since those assigned to metal–ligand charge-transfer excitations usually appear in the region 420–550 nm.[31,40]

REFERENCES

1. J. C. Dyason, P. C. Healy, L. M. Engelhardt, C. Pakawatchai, V. A. Patrick, C. L. Raston and A. H. White, *J. Chem. Soc., Dalton Trans.* 1985, 831.
2. P. C. Healy, C. Pakawatchi, C. L. Raston, B. W. Skelton and A. H. White, *J. Chem. Soc., Dalton Trans.* 1983, 1905.
3. H. D. Hardt, *Naturwiss.* 1974, **61**, 107.
4. C. L. Raston and A. H. White, *J. Chem. Soc., Dalton Trans.* 1976, 2135.
5. V. Schramm and K. Fischer, *Naturwiss.* 1974, **61**, 500.
6. E. Eitel, D. Oelkrug, W. Hiller and J. Strahle, *Z. Naturforsch., Teil B* 1980, **35**, 1274; J. A. Campbell, C. L. Raston and A. H. White, *Aust. J. Chem.* 1977, **30**, 1937.
7. M. A. S. Goher and T. C. W. Mak, *Inorg. Chim. Acta* 1985, **101**, L27.
8. M. Massaux, M.-J. Bernard and M. T. Le Bihan, *Bull. Soc. Fr. Mineral Crystallogr.* 1969, **92**, 118.
9. M. Massaux, M.-J. Bernard and M. T. Le Bihan, *Acta Cryst., Sect. B* 1971, **27**, 2419.
10. M. Massaux and M. T. Le Bihan, *Acta Cryst., Sect. B* 1976, **32**, 1586.
11. D. Datta and A. Chakravorty, *Inorg. Chem.* 1983, **22**, 1085.
12. M. A. S. Goher and A. Attia, *Polish J. Chem.* 1981, **55**, 289.
13. M. A. S. Goher and A. K. Hafez, *Bull. Soc. Chim. Fr.* 1980, I-287.
14. J. A. Tompkins, J. I. Maxwell and E. M. Holt, *Inorg. Chim. Acta* 1987, **127**, 1.
15. M. A. S. Goher and T. C. W. Mak, *Inorg. Chim. Acta* 1987, **127**, L13; 1988, **141**, 323.
16. T. C. W. Mak, M. A. S. Goher and A. K. Hafez, *Inorg. Chim. Acta* 1988, **146**, 103.
17. M. A. S. Goher and T. C. W. Mak, *Inorg. Chim. Acta* 1984, **85**, 117.
18. R. A. Sparks, in *Crystallographic Computing Techniques* (Edited by F. R. Ahmed), pp. 442–467. Munksgaard, Copenhagen (1976).
19. R. Diamond, *Acta Cryst., Sect. A* 1969, **25**, 43.
20. G. Kopfmann and R. Huber, *Acta Cryst., Sect. A* 1968, **24**, 348.
21. A. C. T. North, D. C. Phillips and F. S. Mathews, *Acta Cryst., Sect. A* 1968, **24**, 351.

22. G. M. Sheldrick, in *Computational Crystallography* (Edited by D. Sayre), pp. 506–514. Oxford University Press, New York (1982).
23. G. M. Sheldrick, in *Crystallographic Computing 3: Data Collection, Structure Determination, Proteins and Databases* (Edited by G. M. Sheldrick, C. Kruger and R. Goddard), pp. 175–179. Oxford University Press, New York (1985).
24. *International Tables for X-ray Crystallography*, Vol. IV, pp. 55, 99 and 149. Kynoch Press, Birmingham (1974) (Now distributed by Kluwer Academic Publishers, Dordrecht).
25. P. Krumholz, *Inorg. Chem.* 1965, **4**, 609; *J. Am. Chem. Soc.* 1960, **82**, 3000.
26. S. Kitagawa, M. Munakata and A. Higashie, *Inorg. Chim. Acta* 1982, **59**, 219.
27. T. C. W. Mak and M. A. S. Goher, *Inorg. Chim. Acta* 1986, **115**, 17.
28. A. P. Gaughan, R. F. Ziolo and Z. Dori, *Inorg. Chim. Acta* 1970, **4**, 640; M. A. S. Goher, *Coll. Czech. Chem. Commun.* 1977, **42**, 1478 and refs therein.
29. Z. Dori and R. F. Ziolo, *Chem. Rev.* 1973, **73**, 247 and refs therein.
30. J. Strahle, W. Hiller, E. Eitel and D. Oelkrug, *Z. Krist.* 1980, **53**, 277.
31. N. P. Rath, E. M. Holt and K. Taminura, *Inorg. Chem.* 1985, **24**, 3934.
32. N. P. Rath, J. L. Maxwell and E. M. Holt, *J. Chem. Soc., Dalton Trans.* 1986, 2449.
33. N. P. Rath and E. M. Holt, *J. Chem. Soc., Chem. Commun.* 1986, 665.
34. M. W. Wu and C. J. Fritchie Jr, *J. Biol. Chem.* 1975, **250**, 946.
35. J. C. Dyason, L. M. Engelhardt, P. C. Healy and A. H. White, *Aust. J. Chem.* 1984, **37**, 2201.
36. P. C. Healey, C. Pakawatchai and A. H. White, *J. Chem. Soc., Dalton Trans.* 1985, 2531.
37. N. P. Rath, E. M. Holt and K. Taminura, *J. Chem. Soc., Dalton Trans.* 1986, 12303.
38. H. D. Hardt and A. Pierre, *Inorg. Chim. Acta* 1977, **25**, L59.
39. K. Tanimura, W. A. Sibley and L. G. DeShayer, *Phys. Rev. B: Condens. Matter* 1985, **31**, 3980.
40. K. R. Kyle, J. DiBenedetto and P. C. Ford, *J. Chem. Soc., Chem. Commun.* 1989, 714.

Polyhedron Vol. 12, No. 24, pp. 2989–2993, 1993
Printed in Great Britain

0277–5387/93 $6.00+.00
© 1993 Pergamon Press Ltd

NMR STUDY OF NICKEL(II) SCHIFF BASE COMPLEXES WITH BENZOYL GROUPS AND LONG ALKYL CHAINS

MANABU FUJIWARA*

Department of Material Chemistry, Faculty of Science and Technology, Ryukoku University, Seta, Otsu 520-21, Japan

and

YOSHIHIDE ICHIKI and HISANOBU WAKITA

Department of Chemistry, Faculty of Science, Fukuoka University, Nanakuma, Jonan-ku, Fukuoka 814-01, Japan

(*Received* 5 *May* 1993; *accepted* 18 *June* 1993)

Abstract—The nickel(II) Schiff base complexes with 2-methylbutyl or 2-methylpentyl groups and their benzoyl derivatives have been prepared and characterized by ^1H and ^{13}C NMR spectroscopy. The structure of the benzoyl derivatives in chloroform solution can be estimated as follows: the donor set of N_2O_2 has a square planar coordination, the benzoyl substituents are perpendicular to the chelate plane and the long alkyl chains (2-methylbutyl or 2-methylpentyl groups) move segmentally to aproach the benzoyl substituents.

It is well known that weak interactions such as hydrogen bonds and hydrophobic interactions play an important role in most biological processes.[1] Recently, the hydrophobic interactions have been extensively studied and found to be applicable for selective syntheses of geometrical and optical isomers.[2]

In a previous paper[3] we prepared the nickel(II) Schiff base complexes with 2-methylpropyl(isobutyl) groups and benzoyl substituents and discussed their structures in solution from the results of their ^1H and ^{13}C NMR spectra and relaxation time (T_1) measurements. The results indicated that in the complex the donor set of N_2O_2 has a square planar coordination, the benzoyl substituents are perpendicular to the chelate plane and the isobutyl groups move segmentally so that they may approach the benzoyl substituents. The characteristic behaviour of the isobutyl groups in the complex could be affected by the so-called CH$\cdots\pi$ interaction[4] between alkyl and phenyl groups. However, as the isobutyl group is a rather short alkyl chain and its freedom of movement is not naturally high, the CH$\cdots\pi$ interaction is weak. Therefore, we decided that novel nickel(II) complexes with longer alkyl chains should be prepared and characterized. In this paper we report the preparation and characterization of the nickel(II) Schiff base complexes with both benzoyl substituents and 2-methylbutyl (isopentyl) or 2-methylpentyl (isohexyl) chains. Their structures and dynamics in chloroform solution will be discussed from the results of their ^1H and ^{13}C NMR spectra and ^{13}C relaxation time measurements. It will be made clear that the interaction between isopentyl or isohexyl groups and benzoyl substituents in nickel(II) Schiff base complexes affects the characteristic structure and dynamics of the long alkyl chains in chloroform solution.

EXPERIMENTAL

Preparation of nickel(II) *Schiff base complexes with isopentyl or isohexyl groups*

7-Methyl-2,4-octanedione and 8-methyl-2,4-nonanedione were prepared using the literature method.[5] The Schiff base ligands and their nickel(II) complexes [(2,7,12,17-tetramethyl-8,11-diazaocta-

* Author to whom correspondence should be addressed.

deca-5,14-dione-6,12-dienato)nickel(II), Ni(iso-Pe,Meen), and (2,8,13,19-tetramethyl-9,12-diaza-octadeca-6,15-dione-7,13-dienato)nickel(II), Ni (iso-Hx,Meen)] were prepared by refluxing an ethanol solution (200 cm^3) of 7-methyl-2,4-octanedione or 8-methyl-2,4-nonanedione (0.10 mol), ethylenediamine (0.05 mol) and nickel(II) acetate tetrahydrate (0.05 mol) for 1 h. The resulting solution was evaporated at reduced pressure and the residue was recrystallized from a mixed solution of ethanol and ether (1 : 1). The red–brown crystals were collected on a glass filter and dried *in vacuo*. The yields were *ca* 60%.

Preparation of benzoyl derivatives of nickel(II) *Schiff base complexes*

To a dry chloroform solution (500 cm^3) of the nickel(II) Schiff base complex (0.05 mol) mentioned above and excess trimethylamine (0.12 mol) was added excess benzoyl chloride [*m*-nitrobenzoyl chloride (*m*NB-Cl) or 3,5-dinitrobenzoyl chloride (DNB-Cl)]. The mixture was refluxed for 60 h and evaporated under reduced pressure. The residue was recrystallized from ethanol giving orange crystals in *ca* 50% yields. The results of the elemental analyses, IR and electronic spectral data of all the complexes indicate that they are pure and are consistent with their chemical structures (see Fig. 1). However, in the reaction of Ni(isoPe,Meen) with *m*NB-Cl, the reaction mixture of the parent complex, the mono-substituted complex and the di-substituted complex was obtained and attempts to separate pure Ni(isoPe,Meen)-*m*NB have been unsuccessful.

Measurements

The ^1H and ^{13}C NMR spectra and ^{13}C relaxation time (T_1) measurements were recorded using a JEOL FX-90 spectrometer at 90 MHz for ^1H and at 22.5 MHz for ^{13}C nuclei. Chloroform-d_3 ($CDCl_3$) and TMS were used as the solvent and internal standard, respectively. Each sample solution was almost saturated with the respective complexes.

RESULTS AND DISCUSSION

^1H *NMR spectra*

Figure 2 shows the ^1H and ^{13}C NMR spectra for Ni(isoPe,Meen)-DNB in $CDCl_3$. The chemical shift values for the ^1H NMR spectra of the nickel(II) Schiff base complexes in $CDCl_3$ are summarized in Table 1, except the signals due to the phenyl protons. For Ni(isoPe,Meen) the ^1H NMR spectrum has a doublet resonance due to the methyl protons of the isopentyl groups [CH_3(O)] at 0.88 ppm, a triplet due to the methylene protons on the 4-positions of the isopentyl groups, attached to the keto moiety [$^4CH_2$(O)] at 1.41 ppm, a singlet due to the methyl protons attached to the azomethine moieties [CH_3(N)] at 1.85 ppm, an overlapping multiplet resonance due to the methine and is neighbouring methylene protons of the isopentyl groups [$^3CH_2$+CH(O)] at 2.05 ppm, a singlet due to the methylene protons of the ethylenediamine moiety [CH_2(en)] at 2.99 ppm and a singlet due to the methine protons on the γ-positions of the chelate ring at 4.88 ppm. For its 3,5-dinitrobenzoyl derivative, Ni(isoPe,Meen)-DNB, a similar spectrum in a higher region was obtained (< 4.0 ppm), although the signals due to CH_3(N), CH_3(O), CH_2(O) and CH_2+CH(O) shifted to a higher field and the signal due to CH_2(en) to a lower field. The lower-field shift was caused by the electron-withdrawing effect of the DNB substituents and the higher-field shifts were as a consequence of a combination of the electron-withdrawing effect and the magnetic anisotropy effect of the DNB substituents; the latter is associated with the higher-field shift and the former with the lower-field shift. It is evident that the latter effect is stronger than the former in the case of Ni(isoPe,Meen)-DNB.

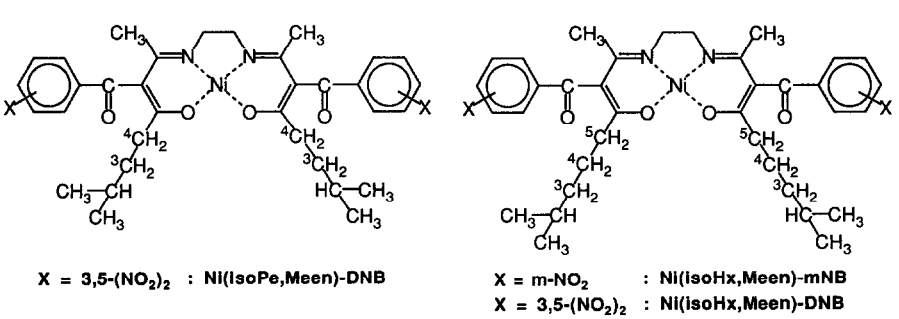

Fig. 1. Chemical structures of the nickel(II) Schiff base complexes with benzoyl substituents.

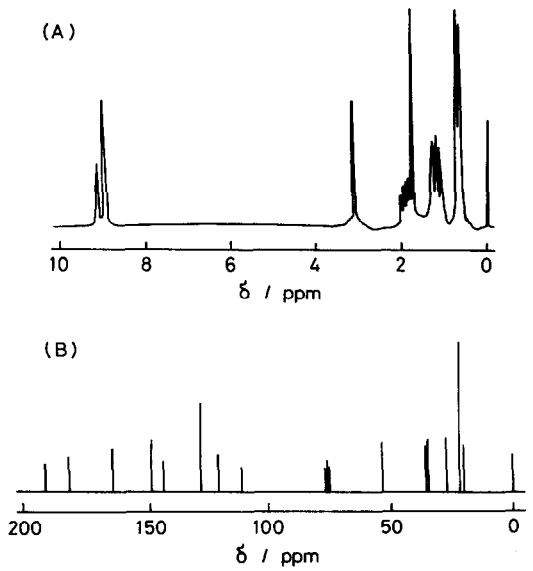

Fig. 2. (A) ^{1}H and (B) ^{13}C NMR spectra for Ni(isoPe, Meen)-DNB in $CDCl_3$.

On the other hand, for Ni(isoHx,Meen) the spectrum has a doublet resonance due to CH_3(O) at 0.86 ppm, a multiplet due to the methylene protons on the 4-positions of the isohexyl groups [$^4CH_2$(O)] at 1.24 ppm, a triplet due to the methylene protons on the 5-positions of the isohexyl groups [$^5CH_2$(O)] at 1.50 ppm, a singlet due to CH_3(N) at 1.86 ppm, an overlapping multiplet resonance due to $^3CH_2$+CH(O) at 1.97 pm, a singlet due to CH_2(en) at 3.01 ppm and a singlet due to the methine protons on the γ-positions of the chelate ring at 4.88 ppm. For its mNB and DNB derivatives, Ni(isoHx,Meen)-*m*NB and Ni(isoHx,Meen)-DNB, similar spectra in the higher region were obtained (< 4.0 ppm), although the signals due to CH_3(N), CH_3(O), $^4CH_2$(O), $^5CH_2$(O) and $^3CH_2$+CH(O) shifted to a higher field, except for CH_3(N) and $^3CH_2$+CH(O) in Ni(isoHx,Meen)-DNB, and the signals due to CH_2(en) to a lower field. The lower-field shifts were caused by the electron-withdrawing effect of the *m*NB and DNB substituents, respectively, and the higher-field shifts were as a consequence of a combination of the electron-withdrawing effects and the magnetic anisotropy effects by the *m*NB and DNB substituents; the latter effects are associated with the higher-field shift and the former effects with the lower-field shift. It is evident that the latter effect is stronger than the former in the case of Ni(isoHx,Meen)-*m*NB, but both are the same for the CH_3(N) and $^3CH_2$+CH(O) moieties in Ni(isoHx,Meen)-DNB.

^{13}C *NMR spectra*

The ^{13}C NMR spectrum of Ni(isoPe,Meen) in $CDCl_3$ has nine sharp signals at 20.9, 22.4, 27.8, 36.0, 36.4, 53.0, 98.4, 164.3 and 180.0 ppm, assignable to the methyl carbons attached to the azomethine moities [CH_3(N)], the methyl carbons of the isopentyl groups [CH_3(O)], the methine carbons of the isopentyl groups [CH(O)], the methylene carbons at the 4-positions of the isopentyl groups [$^4CH_2$(O)], the methylene carbons at the 3-positions of the isopentyl groups [$^3CH_2$(O)], the methylene carbons of the ethylenediamine moiety [CH_2(en)], the methine carbons at the γ-positions of the chelate ring, the azomethine carbons and the keto carbons, respectively. Similarly, the spectrum of Ni(isoPe, Meen)-DNB has 14 sharp signals. The higher-field peaks can be assigned to CH_3(N), CH_3(O), CH(O), $^4CH_2$(O), $^3CH_2$(O), CH_2(en), the quarternary carbons at the γ-positions of the chelate ring, the phenyl carbons of the DNB substituents (four signals), the azomethine carbons, the keto carbons and the carbonyl carbons of the DNB substituents, respectively. These results are consistent with the structure of the nickel(II) Schiff base complex shown in Fig. 1.

On the other hand, the ^{13}C NMR spectrum of Ni(isoHx,Meen) in $CDCl_3$ has 10 sharp signals at 20.7, 22.6, 28.0, 38.5, 39.0, 39.1, 53.2, 98.8, 164.4 and 181.1 ppm assignable to CH_3(N), the methyl carbons of the isohexyl groups [CH_3(O)], the methine carbons of the isohexyl groups [CH(O)], the

Table 1. ^{1}H NMR spectral data for nickel(II) Schiff base complexes

Complex	CH_3(N)	CH_3(O)	$^3CH_2$+CH(O)	$^4CH_2$(O)	$^5CH_2$(O)	CH_2(en)	CH
			δ (ppm)				
Ni(isoPe,Meen)	1.85	0.88	1.41	2.05		2.99	4.88
Ni(isoPe,Meen)-DNB	1.84	0.72	1.29	2.02		3.24	
Ni(isoHx,Meen)	1.86	0.86	1.50	1.97	1.24	3.01	
Ni(isoHx,Meen)-*m*NB	1.83	0.76	1.40	1.98	1.18	3.22	4.89
Ni(isoHx,Meen)-DNB	1.87	0.77	1.42	1.99	1.20	3.27	

methylene carbons at the 3-positions of the isohexyl groups [$^3CH_2(O)$], the methylene carbons at the 5-positions of the isohexyl groups [$^5CH_2(O)$], the methylene carbons at the 4-positions of the isohexyl groups [$^4CH_2(O)$], CH_2(en), the methine carbons at the γ-positions of the chelate ring, the azomethine carbons and the keto carbons, respectively. Similarly, the spectra of Ni(isoHx,Meen)-*m*NB and Ni(isoHx,Meen)-DNB have 17 and 15 sharp signals, respectively. The higher-field peaks can be assigned to CH_3(N), CH_3(O), CH(O), $^3CH_2(O)$, $^5CH_2(O)$, $^4CH_2(O)$, CH_2(en), the quarternary carbons at the γ-positions of the chelate ring, the phenyl carbons of the *m*NB or DNB substituents (six or four signals), the azomethine carbons, the keto carbons and the carbonyl carbons of *m*NB or DNB substituents, respectively. These results are also consistent with the structures of the nickel(II) Schiff base complexes shown in Fig. 1.

T_1 *measurements*

The T_1 measurements were obtained using the inversion recovery method[6] for the nickel(II) Schiff base complexes Ni(isoPe,Meen), Ni(isoPe,Meen)-DNB, Bi(isoHx,Meen) and Ni(isoHx,Meen)-*m*NB in $CDCl_3$ at 25.0°C. The T_1 data for the four nickel(II) complexes are listed in Table 2. It is considered that in large molecules, such as the nickel(II) complex investigated here, dipole–dipole relaxation is dominant.[7] It is difficult to extract intramolecular movements such as the distortion and the rotation of the benzoyl group, the segmental movements of the isopentyl or isohexyl groups from the whole movements of the complex molecule. However, the relative difference in intramolecular movements between Ni(isoPe,Meen) and Ni(isoHx,Meen) and/or the nickel(II) Schiff base complexes with shorter alkyl chains, Ni(Me,Meen) and Ni(isoBu, Meen), can be discussed qualitatively based on the T_1 data.[3] In addition, the difference between the parent complex and its benzoyl derivative can also be investigated. It is said that the larger the T_1 value of the ^{13}C atom, the faster its motion.

All the T_1 values of ^{13}C atoms were reduced greatly owing to the insertion of *m*NB or DNB groups in the nickel(II) Schiff base complex. This is caused by the reduction of movements such as translation and rotation for the whole complex molecule due to the increase in molecular weight. This effect can be extracted directly from the T_1 value of CH_2(en) because its molecular structure and intramolecular movement may be steady before and after the insertion of benzoyl groups. The T_1 values of CH_2(en) in Ni(isoPe,Meen)-DNB and Ni(isoHx,Meen)-*m*NB decrease to *ca* 30 and 40% of those in their parent complexes by the insertion of DNB and mNB substituents, respectively. However, the magnitude of the decrease in T_1 values for other carbons is not similar to that for CH_2(en).

The parent complexes, Ni(isoPe,Meen) and Ni(isoHx,Meen), exhibit similar T_1 values for the corresponding carbons and these results indicate that the isopentyl and isohexyl groups in Ni(isoPe, Meen) and Ni(isoHx,Meen) move segmentally.

Table 2. ^{13}C NMR spectral data and T_1 values for nickel(II) Schiff base complexes

Carbon	Ni(isoPe,Meen) δ (ppm)	T_1 (s)	Ni(isoPe,Meen)-DNB δ (ppm)	T_1 (s)
CH_3(N)	20.9	2.5	20.9	1.0
CH_3(O)	22.4	2.1	22.3	1.3
CH(O)	27.8	3.8	27.7	1.7
$^3CH_2(O)$	36.4	1.8	36.2	0.4
$^4CH_2(O)$	36.0	1.4	35.5	0.6
CH_2(en)	53.0	0.9	53.8	0.3
Carbon	**Ni(isoHx,Meen) δ (ppm)**	**T_1 (s)**	**Ni(isoHx,Men)-*m*NB δ (ppm)**	**T_1 (s)**
CH_3(N)	20.7	2.2	20.5	0.9
CH_3(O)	22.6	2.5	22.4	1.9
CH(O)	28.0	3.8	27.7	2.9
$^3CH_2(O)$	39.1	1.8	38.6	0.9
$^4CH_2(O)$	39.0	1.5	38.0	0.8
$^5CH_2(O)$	38.5	1.1	37.7	0.5
CH_2(en)	53.2	1.0	53.6	0.4

However, the activity of their segmental motion is slightly higher for Ni(isoHx,Meen) than for Ni (isoPe,Meen).

The T_1 values for CH_2(en), CH_3(N), $^4CH_2$(O) and $^3CH_2$(O) in Ni(isoPe,Meen)-DNB decrease remarkably to *ca* 30% in comparison with those for Ni(isoPe,Meen). However, the degree to which T_1 value decreases also decreases for CH(O) and CH_3(O), the end group of the isopentyl group, and in Ni(isoPe,Meen)-DNB is very low. The T_1 values for CH(O) and CH_3(O) reduce to *ca* 50 and 60% in comparison with those for CH(O) and CH_3(O) in Ni(isoPe,Meen), respectively. These results indicate that the intramolecular movements such as the segmental movements in the terminal moieties of the isopentyl groups in Ni(isoPe,Meen)-DNB are rather activated by the insertion of DNB substituents. This can be interpreted as follows: the CH(O) and CH_3(O) groups in isopentyl are attracted to the benzoyl substituents by the CH $\cdots \pi$ interaction.

On the other hand, for Ni(isoHx,Meen)-*m*NB the trend in T_1 values is almost equal to that for Ni(isoPe,Meen)-DNB, but the segmental movements for CH(O) and CH_3(O) of the isohexyl groups are rather more activated than those for Ni(isoHx,Meen). The T_1 values for CH(O) and CH_3(O) in Ni(isoHx,Meen)-*m*NB are slightly reduced (*ca* 80%) in comparison with those in Ni(isoHx,Meen). These results may be due to the same reason mentioned above for Ni(isoPe,Meen)-DNB and further indicate that the CH $\cdots \pi$ interaction is stronger between isohexyl and *m*NB groups than between isopentyl and DNB groups.

Structures and dynamics of nickel(II) *complexes in solution*

The structures and dynamics of nickel(II) Schiff base complexes in chloroform solution can be proposed from the results of the ^1H and ^{13}C NMR spectra and ^{13}C relaxation time measurements. In all the nickel(II) complexes studied, the donor sets of N_2O_2, which belong to three chelate rings, have a square-planar coordination. Their intramolecular movements are rather slow. For *m*NB or DNB derivatives, the inserted benzoyl groups are perpendicular to the chelate planes containing the nickel(II) ions. There is steric hindrance between the benzoyl groups and the adjacent methylene moieties [$^4CH_2$(O) or $^5CH_2$(O)] of isopentyl or isohexyl groups, respectively. Therefore, the benzoyl groups are inclined to approach the methyl groups attached to the azomethine moieties to avoid the isopentyl or isohexyl chains. This is the reason why the ^1H NMR signals due to CH_3(N) in the benzoyl derivatives were shifted to a higher field in comparison with those in the parent complexes. The isopentyl or isohexyl groups move segmentally so that they may chase the fleeing benzoyl groups. The movements of the terminal methyl moities and their neighbouring methine moieties are especially high so that they can experience the magnetic anisotropy effect of the benzoyl groups most strongly. Apparently, they are attracted by the benzoyl groups. Their results are different from those obtained for Ni(isoBu,Meen),[3] where the isobutyl groups move segmentally, but the movements of the methine moieties alone in the isobutyl groups are not activated but restricted by the benzoyl substituents. The large differences between the isobutyl group and the larger alkyl groups, isopentyl and isohexyl groups, in the molecular behaviour in chloroform would be mainly due to the differences in their freedom of movement; that for the isobutyl group is naturally low and those for the isopentyl and isohexyl groups are high. The isopentyl and isohexyl groups in the benzoyl derivatives of the nickel(II) Schiff base complexes are attracted to the benzoyl substituents by the CH $\cdots \pi$ interaction, especially on their terminal moieties, so that they segmentally move much more vigorously to experience the magnetic anisotropy effect of the benzoyl groups for a longer period. The CH $\cdots \pi$ interaction between the isoalkyl chains and benzoyl groups and the intramolecular movements of the isoalkyl chains in the nickel(II) Schiff base complexes in a non-polar solvent such as chloroform can be clarified by the results obtained in this study. In a polar solvent such as water, the CH $\cdots \pi$ interaction may be found to be much different in its nature and strength. Therefore, the preparation of water-soluble metal complexes with both alkyl and phenyl groups and their NMR investigation will be very interesting in the future.

REFERENCES

1. G. Nemethy and H. A. Scheraga, *J. Phys. Chem.* 1962, **66**, 1773.
2. H. Okawa, K. Ueda and S. Kida, *Inorg. Chem.* 1982, **21**, 1594.
3. M. Fujiwara, Y. Ichiki, S. Kinoshita and H. Wakita, *Polyhedron* 1991, **10**, 2833.
4. E. Freiden, *J. Chem. Educ.* 1975, **52**, 754; B. E. Fisher and H. Sigel, *J. Am. Chem. Soc.* 1980, **102**, 2998.
5. K. G. Hampton, T. M. Harris and C. R. Hauser, *Org. Synth.* 1967, **47**, 92.
6. S. Kinoshita and I. Masuda, *Polyhedron* 1985, **4**, 1245.
7. This assumption was confirmed by measuring the NOE factor (η). The values for these nickel(II) complexes were found to be within the 2.0 ± 0.1 range for all carbons.

Polyhedron Vol. 12, No. 24, pp. 2995–3002, 1993
Printed in Great Britain

0277–5387/93 $6.00+.00
© 1993 Pergamon Press Ltd

TECHNETIUM COMPLEXES WITH THIOETHER LIGANDS—III. SYNTHESIS AND STRUCTURAL CHARACTERIZATION OF CATIONIC NITRIDOTECHNETIUM(V) COMPLEXES WITH THIACROWN ETHERS

HANS-JUERGEN PIETZSCH* and HARTMUT SPIES

Forschungszentrum Rossendorf e.V., Institut für Bioanorganische und Radiopharmazeutische Chemie, D-01314 Dresden, POB 510119, Germany

and

PETER LEIBNITZ and GUENTER RECK

Bundesanstalt für Materialforschung, D-12489 Berlin, Germany

(*Received* 22 *February* 1993; *accepted* 15 *June* 1993)

Abstract—The first representatives of a new class of TcN complexes with thiacrown ethers have been prepared by ligand exchange reaction of $NBu_4[TcNCl_4]$ with 1,4,8,11-tetrathiacyclotetradecane (14S4), 1,5,9,13-tetrathiacyclohexadecane (16S4), 1,5,9,13-tetrathiacyclohexadecane-3,11-diole (16S4-$(OH)_2$) and 1,4,7,10,13,16-hexathiacyclooctadecane (18S6). The crystal structure of $[TcNCl(14S4)]TcNCl_4$ (**1**) consists of couples of independent cations with the metal in the oxidation state +5 and hexavalent $TcNCl_4^-$ anions. In the complex cation the metal is six-coordinated in a rather distorted octahedral geometry, being directly bound to four sulphur atoms from the macrocyclic ligand in the equatorial plane and to the nitrido atom and to one chlorine atom in the axial positions. The strong *trans* influence of the nitrido ligand causes an extreme lengthening of the Tc—Cl bond distance to 2.718 Å. The octahedral molecular structure of $[TcNCl(18S6)]TcNCl_4$ (**3**) is comparable with that of **1**, but only four sulphur atoms of the thiacrown ether form the equatorial plane, two sulphur atoms remain non-coordinated, and the nitrido and Cl^- ligands are in axial positions. The most interesting feature in the structure of $[TcNCl(16S4\text{-}(OH)_2)]Cl$ (**5**) is the observation of an exceptionally long Tc—N distance of 1.95 Å.

The chemistry of technetium is currently receiving considerable attention, mainly because of the pre-eminence of ^{99m}Tc in diagnostic medicine. This includes the search for new classes of technetium complexes and the evaluation of their ability to be used as diagnostic tracers.[1]

Although the high affinity of the soft sulphur donor atom to technetium is proved by a large variety of complexes with thiolate donor ligands, technetium complexes with neutral thioether ligands have scarcely been investigated until now. The number of fully characterized Tc/thioether compounds is rather limited. Recently reported complexes with the $Tc_2O_3^{4+}$ and the $O{=}Tc{-}O^{-2+}$ core,[2] compounds in which tetrathia ligands are coordinated to Tc^{3+} [3] and a Tc^{2+} complex with 1,4,7-trithiacyclononane,[4] demonstrate the pronounced capability of thioether ligands of binding technetium at different oxidation states.

An interesting extension involves the use of the nitrido technetium group in Tc/thioether chemistry. This core shows a high capacity to stabilize the metal in high oxidation states[5–7] and is known to form stable complexes with the tetraaza macrocycles 1,4,8,11-tetraazacyclotetradecane (cyclam),[8]

* Author to whom correspondence should be addressed.

Abbreviations: S_4, tetrathiacycloalkanes; 14S4, 1,4,8,11-tetrathiacyclotetradecane; 16S4, 1,5,9,13-tetrathiacyclohexadecane; 16S4-$(OH)_2$, 1,5,9,13-tetrathiacyclohexadecane-3,11-diole; 18S6, 1,4,7,10,13,16-hexathiacyclooctadecane.

1,4,8,11-tetraazacyclotetradecane-5,7-dione[9] and the analogous aza/thia ligand 1,4-diaza-8,11-dithiacyclotetradecane.[10].

In order to gain an insight into the effects on coordination geometry and complex stabilities of factors such as ring size and functional group substituent in macrocyclic polythioether ligands, we synthesized a number of technetium chelates with the thiacrown ethers 1,4,8,11-tetrathiacyclotetradecane (14S4), 1,5,9,13-tetrathiacyclohexadecane (16S4), 1,5,9,13-tetrathiacyclohexadecane-3,11-diole (16S4-$(OH)_2$) and 1,4,7,10,13,16-hexathiacyclooctadecane (18S6). Some representatives were characterized by X-ray crystal structure determination.

EXPERIMENTAL

The thiacrown ethers were obtained from Aldrich and used without further purification. UV–vis spectra were recorded on a Specord M 40 from Carl Zeiss Jena (solvent acetone). IR spectra were measured on KBr discs on a UR 20 spectrometer from Carl Zeiss Jena. The content of technetium was determined by liquid-scintillation counting.

Health precautions

In view of the radioactivity of ^{99}Tc, some health precautions were taken. All operations were carried out in a fume cupboard with gloves. ^{99}Tc is only a weak β^--emitter so that apart from some elementary precautions no further safety measures are required. Normal glassware gives adequate protection against the weak β^--emission. Bremsstrahlung becomes important if ^{99}Tc is handled on a larger scale.

Structure determination and crystal data

The X-ray data were collected at room temperature (296 K) on an automatic Enraf–Nonius CAD 4 diffractometer, using graphite monochromatized Mo-K_α radiation ($\lambda = 0.71073$ Å). A summary of the crystallographic data of the complexes is given in Table 1. The structure determination using a straightforward application of the direct method MULTAN 82 failed, therefore the structures were solved by the heavy atom technique. The positions of technetium were derived from three-dimensional Patterson functions. Subsequent difference Fourier syntheses containing additionally strong wrong maxima were interpreted by the program CELLGRAF.[11] In this way all non-hydrogen atoms were found.

After anisotropic refinement of the positions of the inner atoms, the hydrogen positions were calculated according to ideal geometries. Empirical absorption corrections with the program DIFABS[12] were made at two stages during the structure refinement. Most of the calculations were carried out in the Enraf–Nonius SDP system with some local modifications. Relevant bond lengths and angles are contained in Tables 2—4.

Atomic positional and thermal parameters, full lists of bond lengths and angles, and F_o/F_c values have been deposited as supplementary material.

Synthesis of [TcNCl(14S4)]$TcNCl_4$ (1), [TcNCl(16S4)]$TcNCl_4$ (2) *and* [TcNCl(18S6)]$TcNCl_4$ (3)

The appropriate thiacrown ether (130 μmol), dissolved in 1 cm^3 acetone, was added to 50 mg (100 μmol) $NBu_4[TcNCl_4]$, dissolved in 1 cm^3 acetone. After addition of 2 cm^3 methanol the colour changed to dark red–brown. Standing of the reaction mixture overnight yielded red crystals suitable for X-ray analysis.

Synthesis of [TcNCl(14S4)]BPh_4 (4)

1,4,8,11-Tetrathiacyclotetradecane (35 mg, 130 μmol), dissolved in 1 cm^3 acetone, was added to 50 mg (100 μmol) $NBu_4[TcNCl_4]$, dissolved in 1 cm^3 acetone. After addition of 51 mg (150 μmol) sodium tetraphenyl boranate in 2 cm^3 methanol the colour changed to light orange. Standing of the reaction mixture overnight yielded a beige microcrystalline powder, which was washed with diethylether.

Synthesis of [TcNCl(16S4-$(OH)_2$)]Cl (5)

1,5,9,13 - Tetrathiacyclohexadecane - 3,11 - diole (43 mg, 130 μmol), dissolved in 1 cm^3 acetone, was added to 50 mg (100 μmol) $NBu_4[TcNCl_4]$, dissolved in 1 cm^3 acetone. After addition of 2 cm^3 methanol the colour changed to dark red–brown and then to yellow. After standing overnight the mixture yielded small amounts of an orange–red powder and yellow crystals suitable for X-ray analysis.

RESULTS AND DISCUSSION

The ligand exchange reactions on $NBu_4[TcNCl_4]$ proceeding in acetone–methanol solutions at ambient temperature result in the formation of cationic complexes $[TcNCl(S_4)]^+$.

The crystalline compounds precipitate from the reaction mixtures in analytically pure form. The elemental analyses correspond to the formulations $[TcNCl(S_4)]TcNCl_4$ for 14S4 (1), 16S4 (2) and 18S6

Table 1. Experimental crystallographic data for [TcNCl(14S4)]$TcNCl_4$ (**1**), [TcNCl(16S4-$(OH)_2$)]Cl (**5**) and [TcNCl(18S6)]$TcNCl_4$ (**3**)

Crystal data			
Complex	**1**	**5**	**3**
Molecular formula	$C_{10}H_{20}S_4Cl_5N_2Tc_2$	$C_{12}H_{24}S_4Cl_2NO_2Tc$	$C_{12}H_{24}S_6Cl_5N_2Tc_2$
Molecular weight	671.790	512.169	763.879
a (Å)	13.215(2)	7.889(1)	12.942(6)
b (Å)	7.725(5)	10.802(5)	16.758(3)
c (Å)	21.606(2)	11.136(2)	11.577(6)
α (°)	90.02(2)	89.96(3)	90.06(2)
β (°)	105.82(1)	90.35(2)	95.45(4)
γ (°)	90.11(3)	90.02(2)	90.07(2)
V (Å^3)	2122.3	949.1	2499.6
Space group: no.	$P2_1/n$; 1014	Pc; 7	$P2_1/c$; 14
Z; $F(000)$; D_{calc}	4; 1316; 2.10	2; 520;. 1.79	4; 1508; 2.02
T (K)	296	296	296
Data collection			
Crystal size (mm^3)	$0.07\times0.30\times0.7$	$0.07\times0.13\times0.52$	$0.54\times0.18\times0.11$
λ, Mo-K_α (Å)	0.71073	0.71073	0.71073
μ (cm^{-1})	21.587	13.035	21.089
Data sphere (°)	$3 < 2\theta \leqslant 44$	$3 < 2\theta \leqslant 50$	$3 < 2\theta \leqslant 50$
Scan mode	ω–2θ	ω–2θ	ω–2θ
Scan rate (°/min)	variab. 1.1–4.8	variab. 1.2–4.8	variab. 1.2–4.9
Miller ind. range	h 0 to 13	h 0 to 10	h 0 to 15
	k 0 to 8	k 0 to 13	k 0 to 19
	l −22 to 22	l −14 to 14	l −13 to 13
Unique refl. meas.	3727	2331	4380
Unique refl. used [$I_o \geqslant 3\sigma(I)$]	3102	1601	3311
Check reflections	−2 3 −7	−2 2 −2	−5 −2 −1
	−5 3 2	−4 −2 −4	−6 −4 0
	−5 3 −3	−1 −5 1	−6 0 0
Absorpt. correction	yes	yes	
$R = \Sigma[\|F_o\| - \|F_c\|/\Sigma\|F_o\|$	0.027	0.046	0.035

Table 2. Selected bond lengths (Å) and angles (°) for [TcNCl(14S4)]$TcNCl_4$ (**1**)

Tc(1)—C(11)	2.718(1)	Tc(2)—Cl(2)	2.325(1)
Tc(1)—S(1)	2.414(1)	Tc(2)—Cl(3)	2.329(1)
Tc(1)—S(2)	2.411(1)	Tc(2)—Cl(4)	2.345(1)
Tc(1)—S(3)	2.405(1)	Tc(2)—Cl(5)	2.337(1)
Tc(1)—S(4)	2.408(1)	Tc(2)—N(2)	1.582(4)
Tc(1)—N(1)	1.615(3)		
Cl(1)—Tc(1)—S(1)	81.34(3)	S(3)—Tc(1)—N(1)	95.3(1)
Cl(1)—Tc(1)—S(2)	87.87(3)	S(4)—Tc(1)—N(1)	95.4(1)
Cl(1)—Tc(1)—S(3)	86.84(3)	Cl(2)—Tc(2)—Cl(3)	88.90(4)
Cl(1)—Tc(1)—S(4)	81.83(3)	Cl(2)—Tc(2)—Cl(4)	157.62(4)
Cl(1)—Tc(1)—N(1)	176.4(1)	Cl(2)—Tc(2)—Cl(5)	87.23(4)
S(1)—Tc(1)—S(2)	84.92(3)	Cl(2)—Tc(2)—N(2)	101.3(1)
S(1)—Tc(1)—S(3)	167.51(3)	Cl(3)—Tc(2)—Cl(4)	87.25(4)
S(1)—Tc(1)—S(4)	96.97(3)	Cl(3)—Tc(2)—Cl(5)	156.58(4)
S(1)—Tc(1)—N(1)	96.7(1)	Cl(3)—Tc(2)—N(2)	102.5(1)
S(2)—Tc(1)—S(3)	90.62(3)	Cl(4)—Tc(2)—Cl(5)	87.59(4)
S(2)—Tc(1)—S(4)	169.10(3)	Cl(4)—Tc(2)—N(2)	101.0(1)
S(2)—Tc(1)—N(1)	95.0(1)	Cl(5)—Tc(2)—N(2)	100.9(1)
S(3)—Tc(1)—S(4)	85.29(3)		

Table 3. Selected bond lengths (Å) and angles (°) for $[TcNCl(18S6)]TcNCl_4$ (3)

Tc(1)—Cl(1)	2.567(1)	Tc(2)—Cl(2)	2.352(1)
Tc(1)—S(2)	2.469(1)	Tc(2)—Cl(3)	2.334(1)
Tc(1)—S(2)	2.499(1)	Tc(2)—Cl(4)	2.345(1)
Tc(1)—S(3)	2.464(1)	Tc(2)—Cl(5)	2.338(1)
Tc(1)—S(4)	2.461(1)	Tc(2)—N(2)	1.611(4)
Tc(1)—N(1)	1.707(3)		
Cl(1)—Tc(1)—S(1)	87.82(4)	S(3)—Tc(1)—N(1)	95.2(1)
Cl(1)—Tc(1)—S(2)	81.65(4)	S(4)—Tc(1)—N(1)	90.6(1)
Cl(1)—Tc(1)—S(3)	83.96(4)	Cl(2)—Tc(2)—Cl(3)	87.87(5)
Cl(1)—Tc(1)—S(4)	86.82(4)	Cl(2)—Tc(2)—Cl(4)	161.22(5)
Cl(1)—Tc(1)—N(1)	177.4(1)	Cl(2)—Tc(2)—Cl(5)	85.81(4)
S(1)—Tc(1)—S(2)	82.76(3)	Cl(2)—Tc(2)—N(2)	100.5(2)
S(1)—Tc(1)—S(3)	171.30(4)	Cl(3)—Tc(2)—Cl(4)	90.57(5)
S(1)—Tc(1)—S(4)	99.99(3)	Cl(3)—Tc(2)—Cl(5)	160.08(4)
S(1)—Tc(1)—N(1)	93.1(1)	Cl(3)—Tc(2)—N(2)	99.7(1)
S(2)—Tc(1)—S(3)	93.21(4)	Cl(4)—Tc(2)—Cl(5)	89.39(5)
S(2)—Tc(1)—S(4)	168.05(4)	Cl(4)—Tc(2)—N(2)	98.3(2)
S(2)—Tc(1)—N(1)	100.9(1)	Cl(5)—Tc(2)—N(2)	100.0(1)
S(3)—Tc(1)—S(4)	82.42(3)		

(3), $[TcNCl(S_4)]BPh_4$ (4) and $[TcNCl(16S4\text{-}(OH)_2)]Cl$ (5) (see Table 5).

$$TcNCl_4^- \xrightarrow[\text{acetone–methanol}]{14S4/16S4/18S6\{+BPh_4^-\}} [TcNCl(S_4)]TcNCl_4/\{[TcNCl(S_4)]BPh_4\}$$

$1\,S_4$: 14S4 $\quad$ $4\,S_4$: 14S4

$2\,S_4$: 16S4

$3\,S_4$: 18S6

$$TcNCl_4^- \xrightarrow[\text{acetone–methanol}]{16S4\text{-}(OH)_2} [TcNCl(16S4\text{-}(OH)_2)]Cl. \quad (5)$$

From a mechanistic point of view it is interesting to note that the complexation reaction proceeds only after addition of methanol to the acetonic solution of the reaction participants. This may be explained by the fact that the exchange reaction is coupled with a reduction of Tc^{VI} and Tc^{V}, and methanol is assumed to be the reducing agent.

The exchange rates for the ligands 14S4, 16S4 and 18S6 are about 50%. The complex cations formed obviously combine with the precursor to produce an only slightly soluble salt, thus preventing further exchange. The reaction is practically quantitative in the presence of alternative counterions (e.g. BPh_4^-, PF_6^-).

The assumption that the solubility of the complexes formed in the reaction media governs the reaction route is supported by the reaction of 16S4-$(OH)_2$. The exchange reaction with this ligand, which bears two hydroxyl groups, is practically

Table 4. Selected bond lengths (Å) and angles (°) for $[TcNCl(16S4\text{-}(OH)_2]Cl$ (5)

Tc—Cl(1)	2.469(4)	Tc—S(3)	2.430(4)
Tc—S(1)	2.431(5)	Tc—S(4)	2.446(5)
Tc—S(2)	2.447(4)	Tc—N	1.95(1)
Cl(1)—Tc—S(1)	87.2(2)	S(1)—Tc—N	91.5(3)
Cl(1)—Tc—S(2)	89.0(2)	S(2)—Tc—S(3)	174.3(2)
Cl(1)—Tc—S(3)	85.3(1)	S(2)—Tc—S(4)	89.1(2)
Cl(1)—Tc—S(4)	87.8(2)	S(2)—Tc—N	91.6(3)
Cl(1)—Tc—N	178.6(4)	S(3)—Tc—S(4)	90.3(2)
S(1)—Tc—S(2)	90.7(2)	S(3)—Tc—N	94.1(3)
S(1)—Tc—S(3)	89.4(2)	S(4)—Tc—N	93.5(3)
S(1)—Tc—S(4)	175.1(2)		

Table 5. Yields and analytical data of the complexes **1–5**

Complex	Yield (%)	Elemental analysis[a] C	H	N	S	Cl	Tc	UV–vis, nm (log ε)
1	45	17.9 (17.7)	3.0 (2.9)	4.2 (3.9)	19.1 (18.8)	26.4 (25.7)	29.5 (29.2)	463 (3.2)
2	43	20.6 (21.0)	3.4 (3.2)	4.0 (3.7)	18.3 (17.8)	25.3 (24.7)	28.4 (28.1)	461 (3.2)
3	45	18.9 (18.4)	3.1 (3.0)	3.7 (3.4)	25.2 (24.9)	23.2 (22.8)	26.0 (26.2)	463 (3.2)
4	80	55.5 (54.9)	5.4 (5.2)	1.9 (1.7)	17.4 (16.8)	4.8 (5.2)	13.5 (13.2)	402 (3.4)
5	48	28.1 (27.5)	4.7 (5.1)	2.7 (2.2)	25.0 (24.2)	13.9 (14.1)	19.3 (18.9)	402 (3.4)

[a] Calc. (found).

quantitative in the absence of additional counterions.

The UV–vis spectra of all complexes without alternative counterions (**1–3**) are characterized by the absorption band of the $TcNCl_4^-$ moiety (λ_{max}: 404, 460 nm (sh) in acetone–methanol).

The IR spectra show less characteristic bands in the range between 1000 and 1100 cm^{-1}, which we assign to the TcN core of the complex cations, and additional peaks at 1080 cm^{-1} for compounds **1–3**, which contain he $TcNCl_4^-$ anion.

Structure of [TcNCl(14S4)]$TcNCl_4$ (**1**) *and* [TcNCl(18S6)]$TcNCl_4$ (**3**)

The molecular structures of compounds **1** and **3**, together with the atomic numbering schemes, are given in Figs 1 and 2. Selected interatomic distances and angles are summarized in Tables 2 and 3.

Compounds **1** and **3** consist of couples of independent cations with the metal in the oxidation state +5 and hexavalent $TcNCl_4^-$ anions. In both complex cations the technetium atom is six-coordinated in a rather distorted octahedral geometry, being directly bound in the equatorial plane to four sulphur atoms of the macrocyclic ligand. The nitrido and the chlorine atoms occupy the axial positions.

While the molecular cation **1** has a non-crystallographic mirror plane through Tc(1), N(1), Cl(1), C(4) and C(9), a mirror plane through Tc(1), N(1), Cl(1), S(5) and S(6) does not exist in **3**. The non-crystallographic symmetry was disturbed by a dislocation of the atoms C(5) and C(6) caused by packing of the molecules in the unit cell.

The technetium atom is displaced from the plane formed by the four sulphur atoms by 0.236 Å toward the N(1) atom in compound **1** and by 0.209 Å in compound **3**. The Tc(1)—N bond distances of 1.615 Å for **1** and 1.707 Å for **3** are consistent with the triple-bond distances found in all Tc^V–nitrido complexes structurally characterized.[13]

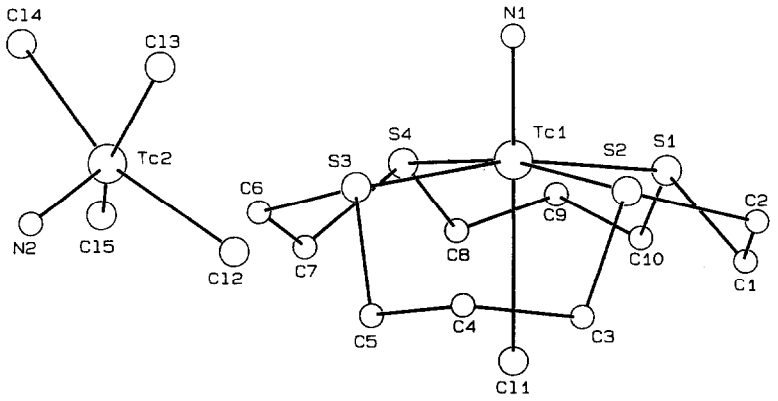

Fig. 1. CELLGRAF drawing of [TcNCl(14S4)]$TcNCl_4$ (**1**).

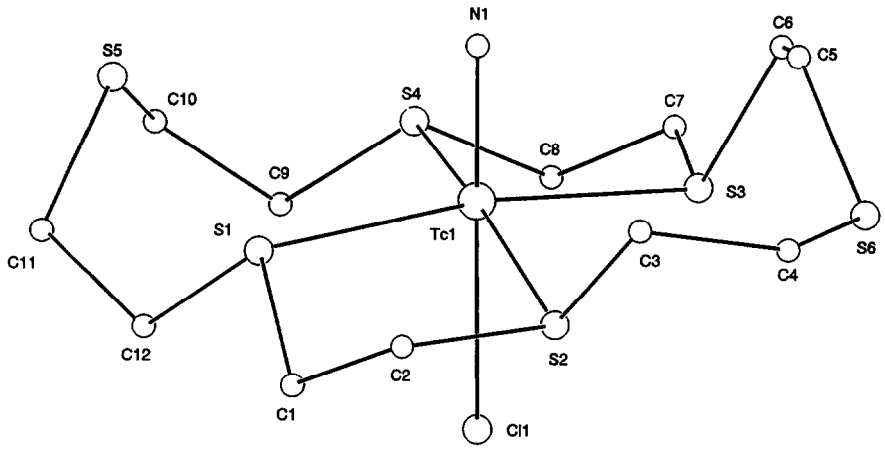

Fig. 2. CELLGRAF drawing of the molecular cation of $[TcNCl(18S6)]TcNCl_4$ (**3**).

The structure of **1** resembles closely that of the $[TcNCl(N_4)]^+$ cations (N_4 = 2 en, 1,5,8,12-tetraazadodecane).[14]

Structure of $[TcNCl(16S4\text{-}(OH)_2]Cl$ (**5**)

The octahedral molecular structure of **5** is comparable to that of $[TcNCl(14S4)]^+$: four sulphur atoms of the thiacrown ether form the equatorial plane, the nitrido and Cl^- ligands are in the axial positions (Fig. 3, Table 4). The metal is displaced from the equatorial plane by 0.114 Å toward the nitrogen atom. As found for **1**, the complex cation has a non-crystallographic mirror plane through technetium, nitrogen, Cl(1), C(2), O(2), C(8) and O(1).

In the crystal, the cations and the Cl^- counterions are connected by two symmetry-independent hydrogen bonds O(1)—H---Cl(2) (3.045 Å) and Cl(2)---H—O(2)′ (2.973 Å) forming chains in the [1 1 0] direction.

$[TcNCl(16S4\text{-}(OH)_2]Cl$ (**5**) differs from **1** and **3** concerning the extremely long Tc—N bond distance of 1.95 Å.

For all three compounds studied by X-ray analysis, coordination of technetium by four sulphur atoms in the equatorial plane was found to be the common feature, regardless of differences in ring size or the presence of two additional sulphur atoms in the ring of 18S6 or two hydroxyl groups in 16S4-$(OH)_2$.

The geometry of the distorted octahedral TcN complexes having a sixth, negatively charged ligand in the *trans* position to the TcN bond may be explained in terms of balancing the strong influence of the nitrido group, which destabilizes the octahedral coordination, and by the demand for an effective neutralization of the residual charge on the

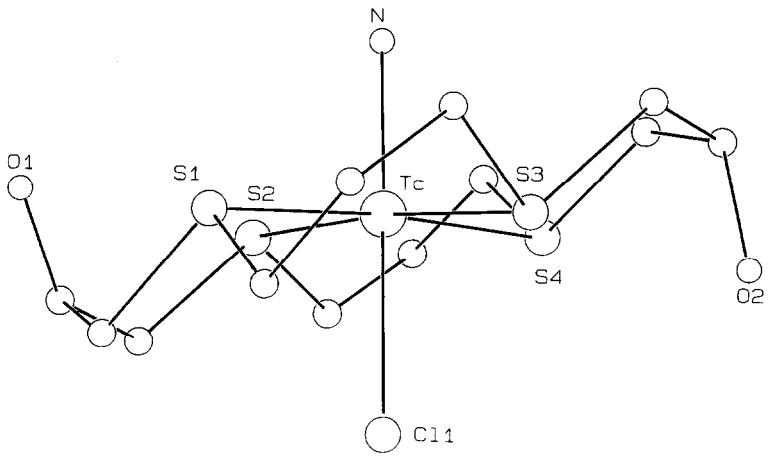

Fig. 3. CELLGRAF drawing of the molecular cation of $[TcNCl(16S4\text{-}(OH)_2]Cl$ (**5**).

Table 6. Bond lengths of Tc/Re nitrido complexes with *trans*-coordinated chlorine

Complex	Bond length (Å) Me≡N	Me—Cl	Ref.
$[TcNCl(en)_2]^+$	1.603	2.732	14
$[TcNCl(tad)]^+$	1.626	2.663	14
$[TcNCl_2(PMe_2Ph)_3]$	1.624	2.665	15
$[TcNCl(dmpe)_2]^+$	1.854	2.608	17
$[TcNCl(14S4)]^+$	1.615	2.178	This paper
$[TcNCl(18S6)]^+$	1.707	2.567	This paper
$[TcNCl(16S4\text{-}(OH)_2]^+$	1.950	2.469	This paper
$[ReNCl_2(PMe_2Ph)_3]$	1.660	2.633	19
$[ReNCl_2(PEt_2Ph)_3]$	1.788	2.563	20
$[ReNCl(dpae)_2]^+$	1.839	2.451	21

Abbreviations: en, ethylenediamine; tad, 1,5,8,12-tetraazadodecane; dpae, 1,2-bis(diphenylarsino)ethane; dmpe, 1,2-bis(dimethylphosphino)ethane.

TcN^{2+} group.[15] The *trans* influence of the nitrido ligand is, for example, apparent in $[TcNCl_2(PMe_2Ph)_3]$ in the *cis* and *trans* Tc—Cl bond lengths of 2.441 and 2.665 Å, respectively.

As shown in Table 6 for previously described complexes, as well as for compounds reported here, both the Tc—N and Tc—Cl bond lengths vary over a wide range. The same is true for the congener rhenium. Considerable Tc—N bond lengthening was found for $[TcN(dmpe)_2Cl]^+$ (dmpe = dimethylphosphinoethane; Tc—N bond distance: 1.85 Å)[16,17] and attributed to steric interactions between the nitrido group and the co-planar phosphorus atoms.[18]

Marchi *et al.*[14] have already pointed out that the lengths of the Tc—N and Tc—Cl bonds are inversely related. On the one hand, the strong *trans* influence of the nitrido ligand in $[TcNCl(en)_2]^+$ causes a considerable lengthening of the Tc—Cl bond distance at 2.732 Å, the longest Tc—Cl bond distance ever observed in technetium complexes.[14] On the other, the extremely long Tc—N bond distance in $[TcNCl(16S4\text{-}(OH)_2]^+$ (**5**) is accompanied by a decrease of the Tc—Cl bond to a distance normally found for equatorial bound chlorine (2.469 Å). This is also true of the TcN complexes contained in Table 6. The sums of the appropriate Tc—N and Tc—Cl bond lengths are relatively constant for compounds with "normal" Tc—N bond distances.

While the Tc—N bond lengths of **1** and **3** fall in the range between about 1.60 and 1.854 Å, the distance of 1.950 Å observed in the preliminary X-ray structural analysis of $[TcNCl(16S4\text{-}(OH)_2]Cl$ (**5**) is exceptionally long. This fact indicates a tendency to adopt a less distorted octahedral geometry. Accordingly, technetium is closer to the S_4 plane (0.114 Å) than found for **1** (0.236 Å) and **3** (0.209 Å). Whereas bond lengthening is accepted as a well known effect in these systems (see above), it is difficult to find a reasonable explanation for the extremely long Tc—N bond. Because the equatorial S_4 donor set is the same in the three complexes it is unlikely to attribute Tc—N bond lengthening to electronic donor atom influence. On the other hand, there is no evidence for hydrogen bonds between the hydroxyl groups of the ligand and the terminal nitrogen. The most likely explanation is to assume some disorder between the nitrido and the *trans*-chloro ligand, which causes an artifact in the X-ray structure determination. Such artifacts and disorders have been generally discussed in refs 22 and 23, for the Tc≡O bond distance in $[TcO(dmpe)_2(OH)]^+$[24] and by Baldas *et al.*[25] with regard to refs 16 and 17.

Additional X-ray crystal data can be obtained from Fachinformationszentrum Energie, Physik, Mathematik GmbH, D-76344 Eggenstein-Leopoldshafen, Germany, quoting CSD-No. 56459, and authors' names as well as the title of the paper.

Acknowledgements—This work was supported by the Fonds der Chemischen Industrie. The authors thank Dr J. Baldas (Yallambie, Australia) for helpful discussions.

REFERENCES

1. J. Steigman and W. C. Eckelman, *The Chemistry of Technetium in Medicine*, Nuclear Science Series. National Academy Press, Washington, DC (1992).
2. H. J. Pietzsch, H. Spies, P. Leibnitz, G. Reck, J. Beger and R. Jacobi, *Polyhedron* 1993, **12**, 187.
3. H. J. Pietzsch, H. Spies, P. Leibnitz, G. Reck, J. Beger and R. Jacobi, *Polyhedron* 1992, **11**, 1623.
4. D. J. White, H. J. Küppers, A. J. Edwards, D. J. Watkin and S. R. Cooper, *Inorg. Chem.* 1992, **31**, 5351.
5. J. Baldas, J. F. Boas, J. Bonnyman and G. A. Williams, *J. Chem. Soc., Dalton Trans.* 1984, 2395.
6. J. Baldas, F. Boas, S. F. Colmanet and G. A. Williams, *J. Chem. Soc., Dalton Trans.* 1991, 2441.
7. H. J. Pietzsch, U. Abram, R. Kirmse and K. Köhler, *Z. Chem.* 1987, **27**, 265.
8. S. A. Zuckman, G. H. Freeman, D. E. Troutner, W. A. Volkert, R. A. Holmes, D. G. van Derveer and E. K. Barefield, *Inorg. Chem.* 1981, **20**, 2386.
9. A. Marchi, R. Rossi, L. Magon, A. Duatti, U. Casellato, R. Graziani, M. Vidal and F. Riche, *J. Chem. Soc., Dalton Trans.* 1990, 19.
10. E. Ianoz, D. Mantegazzi, P. Lerch, F. Nicolo and G. Chapius, *Inorg. Chim. Acta* 1989, **156**, 235.

11. G. Reck and R. G. Kretschmer, CELLGRAF—A Program for Representation of Organic and Inorganic Crystal Structures. Analytisches Zentrum, Berlin (1989/1991).
12. N. Walker and D. Stuart, *Acta Cryst.* 1983, **A39**, 158.
13. M. Melnik and J. E. van Lier, *Coord. Chem. Rev.* 1987, **77**, 275.
14. A. Marchi, P. Garuti, A. Duatti, L. Magon, R. Rossi, V. Ferretti and V. Bertolasi, *Inorg. Chem.* 1990, **29**, 2091.
15. A. S. Batsanov, Y. T. Struchkov, B. Lorenz and B. Olk, *Z. Anorg. Allg. Chem.* 1988, **564**, 129.
16. C. M. Archer, J. P. Dilworth, M. McPartlin and J. D. Kelly, *Polyhedron* 1989, **8**, 1879.
17. C. M. Archer, J. P. Dilworth, D. V. Griffiths, M. McPartlin and J. D. Kelly, *J. Chem. Soc., Dalton Trans.* 1992, 183.
18. J. P. Dilworth, P. L. Dahlstrom, J. R. Hyde and J. Zubieta, *Inorg. Chim. Acta* 1982, **71**, 21.
19. E. Forsellini, U. Casellato, R. Graziani and L. Magon, *Acta Cryst.* 1982, **B38**, 3081.
20. P. W. R. Corfield, R. J. Doedens and J. A. Ibers, *Inorg. Chem.* 1967, **6**, 197.
21. V. W. Yam, K. Tam, M. Cheng, S. Peng and Y. Wang, *J. Chem. Soc., Dalton Trans.* 1992, 1717.
22. V. C. Gibson and M. McPartlin, *J. Chem. Soc., Dalton Trans.* 1992, 947.
23. G. Parkin, *Accts Chem. Res.* 1992, **25**, 455.
24. J. Vanderheyden, A. R. Ketring, K. Libson, M. J. Heeg, L. Roecker, P. Motz, R. Whittle, R. C. Elder and E. Deutsch, *Inorg. Chem.* 1984, **23**, 3184.
25. J. Baldas, J. F. Boas, S. F. Colmanet and G. A. Williams, *J. Chem. Soc., Dalton Trans.* 1991, 2441.

Polyhedron Vol. 12, No. 24, pp. 3003–3004, 1993
Printed in Great Britain

0277–5387/93 $6.00+.00
Pergamon Press Ltd

ANNOUNCEMENT

POLYHEDRON PRIZE FOR CREATIVITY IN INORGANIC CHEMISTRY 1993

It is with great pleasure that the selection committee for the *Polyhedron Prize* announce that the Prize for 1993 has been awarded to M. Frederick Hawthorne of the University of California, Los Angeles, "for his pioneering studies on boron hydrides, carborane complexes, and their uses in catalysis and biology radioimaging."

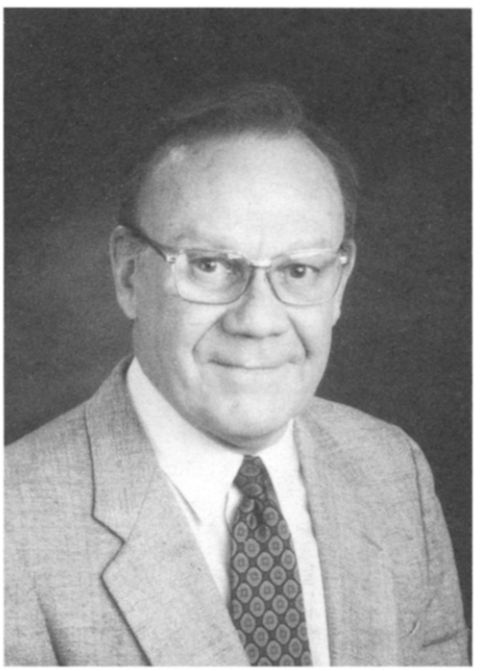

Dr M. Frederick Hawthorne, Professor of Chemistry at the University of California, Los Angeles, was born on August 24, 1928 in Ft. Scott, Kansas. He received his B.A. degree from Pomona College, Claremont, California in 1949 and his Ph.D. from UCLA in 1953 under the guidance of D. J. Cram. After postdoctoral work at Iowa State University with G. S. Hammond, he joined the Rohm and Haas Co. as a research chemist, working initially at the Redstone Arsenal Research Division in Huntsville, Alabama. Subsequently, he became a Laboratory Head in Philadelphia. It was in this period, as part of a high energy fuel program, that his research in the area of boron chemistry began. In 1962, Hawthorne left Rohm and Haas to join the Chemistry Department of the University of California at Riverside as a full Professor. He moved to his present position at UCLA in 1969.

Dr Hawthorne, more than any single individual, founded the field of modern borane and metallacarborane cluster chemistry. His research has provided the majority of seminal discoveries in this area, made at the interface of experimental chemistry and molecular structural theory. The wide range of cluster compounds and cluster fragment species that have

originated within Professor Hawthorne's laboratory has led to the development of principles governing the geometric and electronic relationships between a wide range of organic and inorganic molecules, and have served to link diverse regions of the periodic table of elements. His current research interests include "Anti-Crown" host–guest chemistry based upon electron-deficient macrocyclic mercuracarboranes, the development of radiometallacarborane reagents for the monoclonal antibody-mediated imaging and therapy of cancer, the discovery of new chemical methodologies for the selective delivery of boron-10 to tumours for the purpose of boron neutron capture therapy; and the use of ordered carborane arrays for the construction of supramolecular species.

Dr Hawthorne has received numerous awards and honours. He is a fellow of the American Academy of Arts and Sciences, and a member of the U.S. National Academy of Sciences. He has received the American Chemical Society awards for Research in Inorganic Chemistry (1973), and for Distinguished Service in the Advancement of Inorganic Chemistry (1988). He has also been an Alfred P. Sloan Fellow, received the Tolman Medal of the Southern California Section of the ACS, the Herbert Newby McCoy Award and the Bailar Medal. He was awarded a D.Sc. *honoris causa* from Pomona College in 1974 and a Ph.D. *honoris causa* from Uppsala University in 1992. He currently holds an Alexander von Humboldt U.S. Senior Scientist Award. In 1986 he received the Meritorious Civilian Service Medal from the U.S. Air Force. Dr Hawthorne has been the Editor-in-Chief of the American Chemical Society journal, *Inorganic Chemistry*, since 1969, and he is a member of the editorial boards of several other journals. He has published over 400 primary journal articles and holds numerous patents.

The *Polyhedron Prize* is awarded biennially and consists of a gold medal, a citation and U.S. $10,000.

Previous prize winners are:

1989 Professor Sir Geoffrey Wilkinson "for the outstanding contributions made to organometallic chemistry and the new horizons opened in this field".

1991 Professor Richard H. Holm "for his pioneering contributions to transition metal compounds with sulphur, thiolato and related ligands, in particular those cluster compounds of iron and molybdenum that have relevance to, and provide models for, species in biological systems such as ferredoxins, and for his continuing work in these areas and others such as oxygen and imido group transfer reactions".